

# IUGG 99

birmingham

abstracts

weeks A and B

including abstracts  
unavailable at time of  
original publication



international union of  
geodesy and geophysics

# Summary Listing

The Summary Listing gives an overview of all Symposia and Workshops the Associations are organising and/or are involved in. It also indicates the duration of each Symposia and Workshop. There is no indication of morning (AM) or afternoon (PM) when the Symposium lasts a full day. Please note that Inter Association Symposia and Workshops are listed as part of the Inter - Association programme and are repeated under the leading and sponsoring Associations.

## UNION LECTURES

UL1	MARS AND THE SEARCH FOR LIFE ELSEWHERE.....	A.1
UL2	THE STATE OF THE MANTLE - RECONCILING STRUCTURE AND PROCESSES.....	A.1
UL3	VOLCANIC HAZARDS, CITIES AND PUBLIC AWARENESS.....	B.1
UL4	VARIABILITY OF WEATHER AND CLIMATE.....	B.1

## UNION SYMPOSIA

U2	GLOBAL CHANGE AND PREDICTABILITY.....	A.1
U3	EARTH SYSTEM MODELS AND EARTH SYSTEM PREDICTABILITY.....	A.3
U4	MEGACITIES AND GEOPHYSICS.....	A.6
U5	GEOPHYSICAL HAZARDS AND RISKS: PREDICTABILITY, MITIGATION AND WARNING SYSTEMS.....	A.7
U6	VOLCANISM - MECHANISMS AND CONSEQUENCES.....	B.1
U7	INTEGRATED GLOBAL MONITORING NETWORKS.....	B.2
U8	GEOPHYSICAL ASPECTS OF THE COMPREHENSIVE TEST BAN TREATY.....	B.7

## INTER-ASSOCIATION SYMPOSIA AND WORKSHOPS

JSM01	MIDDLE ATMOSPHERE DYNAMICS AND CHEMISTRY.....	A.9
JSS02	PHYSICS AND CHEMISTRY OF THE EARTH'S INTERIOR.....	A.24
JSM03	ELECTRICAL DISCHARGES IN THE MIDDLE ATMOSPHERE.....	A.28
JSM04	HIGH-LATITUDE SURFACE/ ATMOSPHERE INTERACTION.....	A.30

JSP05	DATA ASSIMILATION IN METEOROLOGY AND OCEANOGRAPHY.....	A.32
JSA06	SPACE WEATHER FORECASTING AND EFFECTS.....	A.35
JSS07	ANISOTROPY: FROM MOUNTAIN BUILDING TO GEODYNAMO.....	A.41
JWM08	OROGRAPHIC PRECIPITATION: OBSERVATIONS, PROCESSES AND MODELLING, WITH FUTURE PLANS.....	A.44
JSA09	POLAR GEOPHYSICS.....	A.47
JSA10	PLANETARY EXPLORATION.....	A.52
JSG11	SEA-LEVEL CHANGES AND VERTICAL GROUND MOVEMENTS.....	A.56
JSH12	ICE SHEETS, OCEANS AND THE EARTH'S SHAPE: MODERN PERSPECTIVES ON SEA LEVEL.....	A.60
JSS13	CONSTRAINTS ON GLOBAL MANTLE CIRCULATION.....	A.62
JSG14	INSIGHTS INTO EARTH SYSTEM SCIENCE: VARIATIONS IN THE EARTH'S ROTATION AND ITS GRAVITATIONAL FIELD.....	A.66
JSA15	ELECTROMAGNETIC METHODS FOR MONITORING EARTHQUAKES AND VOLCANIC ERUPTIONS.....	A.73
JSA16	SOLAR VARIABILITY AND CLIMATE.....	A.84
JSA17	MANTLE-CORE STRUCTURE, PROPERTIES, COUPLING, AND THE GEODYNAMO.....	A.93
JSM18	ATMOSPHERIC AND OCEANIC CONNECTIONS BETWEEN THE POLAR REGIONS AND LOWER LATITUDES.....	A.95
JSA19	GEOPHYSICAL MEASUREMENTS RELEVANT TO HYDROGEOLOGICAL PROCESSES AND MODELLING.....	A.98
JSA20	MESOSPHERE-THERMOSPHERE IONOSPHERE COUPLING AND ENERGETICS.....	A.101
JSP21	SOURCES AND SINKS OF ENVIRONMENTALLY IMPORTANT SUBSTANCES (EXCLUDING CO <sub>2</sub> ).....	A.110
JSV22	OCEANIC, CONTINENTAL AND CONTINENTAL MARGIN VOLCANIC PROVINCES: OCEANIC PLATEAUS, FLOOD BASALTS AND SEAWARD-DIPPING REFLECTORS.....	A.113

JSP23	GEOPHYSICAL HAZARDS AND RISKS: PREDICTABILITY, MITIGATION AND WARNING SYSTEMS.....	A.116/B.16	JSS44	STRUCTURE OF THE CONTINENTAL LITHOSPHERE FROM INTEGRATED GEOPHYSICAL, GEOLOGICAL AND GEOCHEMICAL STUDIES.....	B.136
JSM24	WATER FLUXES AND WATER AVAILABILITY OVER CONTINENTAL REGIONS.....	B.32	JSA45	EFFECTS OF SOLAR VARIABILITY, SOLAR WIND AND HIGH ENERGY PARTICLES ON THE MIDDLE ATMOSPHERE.....	B.146
JSP25	OCEAN/ATMOSPHERE VARIABILITY AND PREDICTABILITY.....	B.36	JSS46	SEISMIC TOMOGRAPHY ON VOLCANOES AND VOLCANIC FIELDS.....	B.150
JSM26	CHEMISTRY AND TRANSPORT IN THE UPPER TROPOSPHERE AND LOWER STRATOSPHERE.....	B.52	JSV47	VOLCANO SEISMOLOGY.....	B.153
JSA27	HIGH-RESOLUTION GEOPHYSICAL STUDIES OF MINERALIZED ZONES.....	B.60	JSA48	CHARACTERIZATION OF THE LITHOSPHERE-ASTHENOSPHERE BOUNDARY.....	B.158
JSG28	PROBING THE ATMOSPHERE BY GP.....	B.62	JSP49	SMALL-SCALE FLOW, TURBULENCE, AND MIXING.....	B.161
JSV29	MAGMA PHYSICS VERSUS VOLCANO PHYSICS.....	B.68	<b><u>IAVCEI - International Association of Volcanology and Chemistry of the Earth's Interior</u></b>		
JSV30	ARC MAGMATIC ROCKS AS BUILDING BLOCKS FOR THE CONTINENTS.....	B.70	VS2	MAGMA FRAGMENTATION AND EXPLOSIVE ERUPTIVE FLOWS.....	B.167
JSS31	GEODETTIC CONSTRAINTS ON TECTONIC MODELS.....	B.76	VS3	ENVIRONMENTAL FORCING OF VOLCANIC ERUPTIONS.....	B.173
JSM32	SMALL-SCALE AND LAYERED PHENOMENA AROUND THE SUMMER MESOPAUSE.....	B.80	JSS02	PHYSICS AND CHEMISTRY OF THE EARTH'S INTERIOR.....	A.24
JWS33	NEW APPROACHES TO DATA COLLECTION, DATA PROCESSING AND DATA DISSEMINATION.....	B.82	JSS07	ANISOTROPY: FROM MOUNTAIN BUILDING TO GEODYNAMO.....	A.41
JWA34	LONG TERM OCEAN BOTTOM GEOPHYSICAL OBSERVATORIES.....	B.89	JSA09	POLAR GEOPHYSICS.....	A.47
JSA35	MIDDLE ATMOSPHERE ELECTRO-DYNAMICS: INFLUENCES AND PROCESSES.....	B.91	JSA10	PLANETARY EXPLORATION.....	A.52
JSV36	UNDERSTANDING VOLCANOES BY GEODESY, SEISMOLOGY, ELECTROMAGNETICS AND GEOCHEMISTRY.....	B.93	JSS13	CONSTRAINTS ON GLOBAL MANTLE CIRCULATION.....	A.62
JSA37	EARTH'S GRAVITY AND MAGNETIC FIELDS FROM SPACE.....	B.102	JSA15	ELECTROMAGNETIC METHODS FOR MONITORING EARTHQUAKES AND VOLCANIC ERUPTIONS.....	A.73
JSP39	DYNAMICS OF ROTATING AND STRATIFIED FLUIDS.....	B.105	JSA17	MANTLE-CORE STRUCTURE, PROPERTIES, COUPLING, AND THE GEODYNAMO.....	A.93
JSA40	SOLID EARTH GEOPHYSICAL DATA FUSION AND ANALYSIS METHODS.....	B.113	JSV22	OCEANIC, CONTINENTAL AND CONTINENTAL MARGIN VOLCANIC PROVINCES: OCEANIC PLATEAUS, FLOOD BASALTS AND SEAWARD-DIPPING REFLECTORS.....	A.113
JSM41	THE CONTRIBUTION OF SATELLITE OBSERVATIONS TO GLOBAL CLIMATE, OCEAN, AND TERRESTRIAL MONITORING.....	B.117	JSP23	GEOPHYSICAL HAZARDS AND RISKS: PREDICTABILITY, MITIGATION AND WARNING SYSTEMS.....	A.116/B.13
JSS42	TSUNAMI OBSERVATIONS, MODELLING AND HAZARD REDUCTION.....	B.126	JSM26	CHEMISTRY AND TRANSPORT IN THE UPPER TROPOSPHERE AND LOWER STRATOSPHERE.....	B.52
JSM43	BOUNDARY - LAYERS OVER COMPLEX TERRAIN AND HETEROGENEOUS SURFACES.....	B.134	JSV29	MAGMA PHYSICS VERSUS VOLCANO PHYSICS.....	B.68
			JSV30	ARC MAGMATIC ROCKS AS BUILDING BLOCKS FOR THE CONTINENTS.....	B.70

JSV36	UNDERSTANDING VOLCANOES BY GEODESY, SEISMOLOGY, ELECTROMAGNETICS AND GEOCHEMISTRY.....	B.93	JSG11	SEA-LEVEL CHANGES AND VERTICAL GROUND MOVEMENTS.....	A.56
JSM41	THE CONTRIBUTION OF SATELLITE OBSERVATIONS TO GLOBAL CLIMATE, OCEAN, AND TERRESTRIAL MONITORING.....	B.117	JSH12	ICE SHEETS, OCEANS AND THE EARTH'S SHAPE: MODERN PERSPECTIVES ON SEA LEVEL.....	A.60
JSS42	TSUNAMI OBSERVATIONS, MODELLING AND HAZARD REDUCTION.....	B.126	JSS13	CONSTRAINTS ON GLOBAL MANTLE CIRCULATION.....	A.62
JSS44	STRUCTURE OF THE CONTINENTAL LITHOSPHERE FROM INTEGRATED GEOPHYSICAL, GEOLOGICAL AND GEOCHEMICAL STUDIES.....	B.136	JSG14	INSIGHTS INTO EARTH SYSTEM SCIENCE: VARIATIONS IN THE EARTH'S ROTATION AND ITS GRAVITATIONAL FIELD.....	A.66
JSS46	SEISMIC TOMOGRAPHY ON VOLCANOES AND VOLCANIC FIELDS.....	B.150	JSA15	ELECTROMAGNETIC METHODS FOR MONITORING EARTHQUAKES AND VOLCANIC ERUPTIONS.....	A.73
JSV47	VOLCANO SEISMOLOGY.....	B.153	JSA17	MANTLE-CORE STRUCTURE, PROPERTIES, COUPLING, AND THE GEODYNAMO.....	A.93
JSA48	CHARACTERIZATION OF THE LITHO- SPHERE-ASTHENOSPHERE BOUNDARY.....	B.158	JSA19	GEOPHYSICAL MEASUREMENTS RELEVANT TO HYDROGEOLOGICAL PROCESSES AND MODELLING.....	A.98
JSP49	SMALL-SCALE FLOW, TURBULENCE, AND MIXING.....	B.161	JSV22	OCEANIC, CONTINENTAL AND CONTINENTAL MARGIN VOLCANIC PROVINCES: OCEANIC PLATEAUS, FLOOD BASALTS AND SEAWARD- DIPPING REFLECTORS.....	A.113

### **IASPEI - International Association of Seismology and Physics of the Earth's Interior**

ST1	THE NATURE OF SEISMIC SOURCES AND THE PREDICTION OF EARTHQUAKES.....	A.137	JSP23	GEOPHYSICAL HAZARDS AND RISKS: PREDICTABILITY, MITIGATION AND WARNING SYSTEMS.....	A.116
ST2	SEISMOTECTONICS.....	A.159	JSA27	HIGH-RESOLUTION GEOPHYSICAL STUDIES OF MINERALIZED ZONES.....	B.60
ST3	STRONG GROUND MOTION, EARTHQUAKE HAZARD AND RISK.....	A.177	JSV29	MAGMA PHYSICS VERSUS VOLCANO PHYSICS.....	B.68
ST4	EARTH STRUCTURE AND GEODYNAMICS.....	B.192	JSV30	ARC MAGMATIC ROCKS AS BUILDING BLOCKS FOR THE CONTINENTS.....	B.70
ST5	SEISMOLOGICAL OBSERVATION AND INTERPRETATION.....	B.211	JSS31	GEODETIC CONSTRAINTS ON TECTONIC MODELS.....	B.76
ST6	PHYSICS AND CHEMISTRY OF EARTH MATERIALS.....	A.172	JWS33	NEW APPROACHES TO DATA COLLECTION, DATA PROCESSING AND DATA DISSEMINATION.....	B.82
ST7	EDUCATION AND OUTREACH IN THE 21ST CENTURY.....	A.176	JWA34	LONG TERM OCEAN BOTTOM GEOPHYSICAL OBSERVATORIES.....	B.89
SW1	NEW SYSTEMATIC APPROACHES IN SEISMIC HAZARD AND EARTHQUAKE PREDICTION RESEARCH.....	B.224	JSV36	UNDERSTANDING VOLCANOES BY GEODESY, SEISMOLOGY, ELECTROMAGNETICS AND GEOCHEMISTRY.....	B.93
JSS02	PHYSICS AND CHEMISTRY OF THE EARTH'S INTERIOR.....	A.24	JSA37	EARTH'S GRAVITY AND MAGNETIC FIELDS FROM SPACE.....	B.102
JSS07	ANISOTROPY: FROM MOUNTAIN BUILDING TO GEODYNAMO.....	A.41	JSA40	SOLID EARTH GEOPHYSICAL DATA FUSION AND ANALYSIS METHODS.....	B.113
JSA09	POLAR GEOPHYSICS.....	A.47	JSM41	THE CONTRIBUTION OF SATELLITE OBSERVATIONS TO GLOBAL CLIMATE, OCEAN, AND TERRESTRIAL MONITORING.....	B.117
JSA10	PLANETARY EXPLORATION.....	A.52			



JSS42	TSUNAMI OBSERVATIONS, MODELLING AND HAZARD REDUCTION.....	B.126	JSH12	ICE SHEETS, OCEANS AND THE EARTH'S SHAPE: MODERN PERSPECTIVES ON SEA LEVEL.....	A.60
JSS44	STRUCTURE OF THE CONTINENTAL LITHO-SPHERE FROM INTEGRATED GEOPHYSICAL, GEOLOGICAL AND GEOCHEMICAL STUDIES.....	B.136	JSG14	INSIGHTS INTO EARTH SYSTEM SCIENCE: VARIATIONS IN THE EARTH'S ROTATION AND ITS GRAVITATIONAL FIELD.....	A.66
JSS46	SEISMIC TOMOGRAPHY ON VOLCANOES AND VOLCANIC FIELDS.....	B.150	JSM18	ATMOSPHERIC AND OCEANIC CONNECTIONS BETWEEN THE POLAR REGIONS AND LOWER LATITUDES.....	A.95
JSV47	VOLCANO SEISMOLOGY.....	B.153	JSP21	SOURCES AND SINKS OF ENVIRONMENTALLY IMPORTANT SUBSTANCES (EXCLUDING CO <sub>2</sub> ).....	A.110
JSA48	CHARACTERIZATION OF THE LITHO-SPHERE-ASTHENOSPHERE BOUNDARY.....	B.158	JSP23	GEOPHYSICAL HAZARDS AND RISKS: PREDICTABILITY, MITIGATION AND WARNING SYSTEMS.....	B.13

**IAPSO - International Association for the Physical Sciences of the Ocean)**

P07	STABLE ISOTOPES AND TRACE SUBSTANCES: THEIR USE IN OCEANOGRAPHY AND CLIMATE RESEARCH ON VARIOUS TIMESCALES.....	A.181
P08	BIOGEOCHEMICAL CONSTRAINTS IN THE OCEAN - CONTROLS, MODELLING AND PREDICTION.....	A.184
P09	ESTUARINE PROCESSES.....	A.186
P10	COASTAL AND SHELF PROCESSES.....	A.190
P11	CLOSED, SEMI-ENCLOSED AND MARGINAL SEAS: PHYSICAL, CHEMICAL AND BIOLOGICAL PROPERTIES.....	B.227
P12	GLOBAL WATER MASS ANALYSIS.....	A.197
P13	DYNAMICS OF POLAR OCEANS AND COUPLING TO SEA ICE.....	B.236
P14	HYDRAULIC CONTROL AND ENTRAINMENT IN STRAITS, SILL FLOWS, AND DENSITY CURRENTS.....	A.200
P15	OPTICAL OCEANOGRAPHY & UV RADIATION.....	B.242
P16	RECENT IMPROVEMENTS TO DEEP-SEA RESEARCH THROUGH USE OF SUBMERSIBLES, ACOUSTIC TOMOGRAPHY AND IN-SITU LONG TERM OBSERVATIONS.....	B.245
PW1	OCEANOGRAPHIC PROCESSES IN THE COASTAL SEAS AROUND DEVELOPING COUNTRIES.....	A.204
JSM04	HIGH-LATITUDE SURFACE/ ATMOSPHERE INTERACTION.....	A.30
JSP05	DATA ASSIMILATION IN METEOROLOGY AND OCEANOGRAPHY.....	A.32
JSA09	POLAR GEOPHYSICS.....	A.47
JSG11	SEA-LEVEL CHANGES AND VERTICAL GROUND MOVEMENTS.....	A.56

JSH12	ICE SHEETS, OCEANS AND THE EARTH'S SHAPE: MODERN PERSPECTIVES ON SEA LEVEL.....	A.60
JSG14	INSIGHTS INTO EARTH SYSTEM SCIENCE: VARIATIONS IN THE EARTH'S ROTATION AND ITS GRAVITATIONAL FIELD.....	A.66
JSM18	ATMOSPHERIC AND OCEANIC CONNECTIONS BETWEEN THE POLAR REGIONS AND LOWER LATITUDES.....	A.95
JSP21	SOURCES AND SINKS OF ENVIRONMENTALLY IMPORTANT SUBSTANCES (EXCLUDING CO <sub>2</sub> ).....	A.110
JSP23	GEOPHYSICAL HAZARDS AND RISKS: PREDICTABILITY, MITIGATION AND WARNING SYSTEMS.....	B.13
JSP25	OCEAN/ATMOSPHERE VARIABILITY AND PREDICTABILITY.....	B.36
JWS33	NEW APPROACHES TO DATA COLLECTION, DATA PROCESSING AND DATA DISSEMINATION.....	B.82
JSP39	DYNAMICS OF ROTATING AND STRATIFIED FLUIDS.....	B.105
JSM41	THE CONTRIBUTION OF SATELLITE OBSERVATIONS TO GLOBAL CLIMATE, OCEAN, AND TERRESTRIAL MONITORING.....	B.117
JSS42	STRUCTURE OF THE CONTINENTAL LITHOSPHERE FROM INTEGRATED GEOPHYSICAL, GEOLOGICAL AND GEOCHEMICAL STUDIES.....	B.126
JSP49	SMALL-SCALE FLOW, TURBULENCE, AND MIXING.....	B.161

**IAMAS - International Association of Meteorological and Atmospheric Sciences**

MI01	ATMOSPHERIC CHEMISTRY - CLIMATE INTERACTION, PT. I. AEROSOLS, CLOUDS AND CLIMATE.....	A.207
MI02	ATMOSPHERIC CHEMISTRY - CLIMATE INTERACTION, PT. II: TRACE GASES, AEROSOLS AND CLIMATE.....	A.214
MI03	THUNDERSTORM CHARGE AND DISCHARGE PROCESSES.....	B.217
MI04/MI10	CLOUDS - THEIR DYNAMICS, PHYSICS AND PARAMETERIZATION.....	B.268
MI05	WEATHER SYSTEMS - THEIR STRUCTURE, ORGANISATION AND INTERACTIONS.....	A.220
MI06	REMOTE SENSING OF THE ATMOSPHERE FOR WEATHER FORECASTING AND CLIMATE APPLICATIONS.....	B.282

MI07	ATMOSPHERIC SYNERGIES AND THEIR NUMERICAL SEPARATION.....	A.229	JSM01	MIDDLE ATMOSPHERE DYNAMICS AND CHEMISTRY.....	A.9
MI08	RADIATION AND CLOUDS IN POLAR REGIONS.....	A.230	JSM03	ELECTRICAL DISCHARGES IN THE MIDDLE ATMOSPHERE.....	A.28
MI09	RADIATIVE PROPERTIES AND REMOTE SENSING OF AEROSOLS.....	A.236	JSM04	HIGH-LATITUDE SURFACE/ ATMOSPHERE INTERACTION.....	A.30
MI11	NON-LINEAR DYNAMICS AND CLIMATE PREDICTION.....	B.288	JSP05	DATA ASSIMILATION IN METEOROLOGY AND OCEANOGRAPHY.....	A.32
MI12	SOURCES OF VARIABILITY IN THE MIDDLE ATMOSPHERE.....	B.291	JSA06	SPACE WEATHER FORECASTING AND EFFECTS.....	A.35
MC01	IMPROVEMENTS AND INTERCOMPARISONS OF CLIMATE SYSTEM MODELS AND THEIR COMPONENT MODELS.....	A.240	JSA10	PLANETARY EXPLORATION.....	A.52
MC02	DETECTION AND ATTRIBUTION OF CLIMATE CHANGE.....	B.249	JSH12	ICE SHEETS, OCEANS AND THE EARTH'S SHAPE: MODERN PERSPECTIVES ON SEA LEVEL.....	A.60
MC03	SUDDEN CLIMATE CHANGE.....	B.254	JSG14	INSIGHTS INTO EARTH SYSTEM SCIENCE: VARIATIONS IN THE EARTH'S ROTATION AND ITS GRAVITATIONAL FIELD.....	A.66
MC04	QUANTITATIVE PRECIPITATION FORECASTING.....	B.255	JSA16	SOLAR VARIABILITY AND CLIMATE.....	A.84
MC05	LAND-FALLING TROPICAL CYCLONES.....	B.258	JSM18	ATMOSPHERIC AND OCEANIC CONNECTIONS BETWEEN THE POLAR REGIONS AND LOWER LATITUDES.....	A.95
MC06	SYMPOSIUM ON THE QUASI-BIENNIAL OSCILLATION (QBO) AND INTERNAL GRAVITY WAVES.....	A.255	JSA20	MESOSPHERE-THERMOSPHERE-IONOSPHERE COUPLING AND ENERGETICS.....	A.101
MC07	RADIATIVE FORCING AND CLIMATE CHANGE.....	A.226	JSP21	SOURCES AND SINKS OF ENVIRONMENTALLY IMPORTANT SUBSTANCES (EXCLUDING CO <sub>2</sub> ).....	A.110
MC08	RADIATIVE EFFECTS OF WATER VAPOR IN CLIMATE MODELS.....	A.259	JSP23	GEOPHYSICAL HAZARDS AND RISKS: PREDICTABILITY, MITIGATION AND WARNING SYSTEMS.....	A.116
MC09	PLANETARY ATMOSPHERES AND THEIR EVOLUTION.....	B.259	JSM24	WATER FLUXES AND WATER AVAILABILITY OVER CONTINENTAL REGIONS.....	B.32
MC10	SUBTROPICAL ANTICYCLONE DYNAMICS.....	B.262	JSP25	OCEAN/ATMOSPHERE VARIABILITY AND PREDICTABILITY.....	B.36
MW01	INTERCOMPARISON OF TROPOSPHERE-STRATOSPHERE GCMS.....	A.262	JSM26	CHEMISTRY AND TRANSPORT IN THE UPPER TROPOSPHERE AND LOWER STRATOSPHERE.....	B.52
MW02	ON THE USE OF GLOBAL DATASETS TO VALIDATE AND IMPROVE ATMOSPHERIC PROCESSES IN CLIMATE MODELS.....	B.294	JSG28	PROBING THE ATMOSPHERE BY GPS.....	B.62
MW03	DEVELOPMENT OF HIGH RESOLUTION CLIMATE MODELS.....	B.296	JSM32	SMALL-SCALE AND LAYERED PHENOMENA AROUND THE SUMMER MESOPAUSE.....	B.80
MW04	TIDAL SIMULATION IN GLOBAL MODELS.....	A.264	JSA35	MIDDLE ATMOSPHERE ELECTRODYNAMICS: INFLUENCES AND PROCESSES.....	B.91
MW05	RADIATIVE PROCESSES IN THE MESOSPHERE AND LOWER THERMOSPHERE.....	A.265	JSV36	UNDERSTANDING VOLCANOES BY GEODESY, SEISMOLOGY, ELECTROMAGNETICS AND GEOCHEMISTRY.....	B.93
MW06	LOW FREQUENCY DYNAMICS IN THE MID-HIGH LATITUDES.....	A.267	JSP39	DYNAMICS OF ROTATING AND STRATIFIED FLUIDS.....	B.105
MW07	GRAVITY WAVE SOURCES AND PARAMETERIZATION.....	A.269			
MW08	QUASI-DECADAL OSCILLATION.....	A.271			

JSM41	THE CONTRIBUTION OF SATELLITE OBSERVATIONS TO GLOBAL CLIMATE, OCEAN, AND TERRESTRIAL MONITORING.....	B.117	JSG11	SEA-LEVEL CHANGES AND VERTICAL GROUND MOVEMENTS.....	A.56
JSM43	BOUNDARY - LAYERS OVER COMPLEX TERRAIN AND HETEROGENEOUS SURFACES.....	B.134	JSH12	ICE SHEETS, OCEANS AND THE EARTH'S SHAPE: MODERN PERSPECTIVES ON SEA LEVEL.....	A.60
JSS44	STRUCTURE OF THE CONTINENTAL LITHOSPHERE FROM INTEGRATED GEOPHYSICAL, GEOLOGICAL AND GEOCHEMICAL STUDIES.....	B.136	JSG14	INSIGHTS INTO EARTH SYSTEM SCIENCE: VARIATIONS IN THE EARTH'S ROTATION AND ITS GRAVITATIONAL FIELD.....	A.66
JSP49	SMALL-SCALE FLOW, TURBULENCE, AND MIXING.....	B.161	JSA19	GEOPHYSICAL MEASUREMENTS RELEVANT TO HYDROGEOLOGICAL PROCESSES AND MODELLING.....	A.98

### **IAHS (International Association of Hydrological Sciences)**

HS1	HYDROLOGICAL EXTREMES: UNDERSTANDING, PREDICTING, MITIGATING.....	B.301
HS2	INTERACTIONS BETWEEN THE CRYOSPHERE, CLIMATE AND GREENHOUSE GASES.....	B.306
HS3	IMPACT OF LAND-USE CHANGE ON NUTRIENT LOADS FROM DIFFUSE SOURCES.....	A.273
HS4	INTEGRATED METHODS OF CATCHMENT HYDROLOGY - TRACER, REMOTE SENSING AND NEW HYDROMETRIC TECHNIQUES.....	A.276
HS5	IMPACTS OF URBAN GROWTH ON SURFACE AND GROUNDWATER QUALITY.....	A.280
HW1	GLOBAL DATA BASES.....	A.285
HW2	HYDRO-ECOLOGY: RIVERINE ECOLOGICAL RESPONSE TO CHANGES IN HYDROLOGICAL REGIME, SEDIMENT TRANSPORT, AND NUTRIENT LOADING.....	B.309
HW3	HYDROLOGY OF ICE-COVERED RIVERS.....	B.312
HW4	REGIONALIZATION OF PARAMETERS OF HYDROLOGICAL AND ATMOSPHERIC LANDSURFACE MODELS.....	B.315
HW5	INTERACTIONS BETWEEN SURFACE AND GROUNDWATER - QUANTITY AND QUALITY.....	A.288
JSM04	HIGH-LATITUDE SURFACE/ ATMOSPHERE INTERACTION.....	A.30
JWM08	OROGRAPHIC PRECIPITATION: OBSERVATIONS, PROCESSES AND MODELLING, WITH FUTURE PLANS.....	A.44
JSA09	POLAR GEOPHYSICS.....	A.47
JSA10	PLANETARY EXPLORATION.....	A.52

JSP21	SOURCES AND SINKS OF ENVIRONMENTALLY IMPORTANT SUBSTANCES (EXCLUDING CO <sub>2</sub> ).....	A.110
JSP23	GEOPHYSICAL HAZARDS AND RISKS: PREDICTABILITY, MITIGATION AND WARNING SYSTEMS.....	A.116
JSM24	WATER FLUXES AND WATER AVAILABILITY OVER CONTINENTAL REGIONS.....	B.32
JWS33	NEW APPROACHES TO DATA COLLECTION, DATA PROCESSING AND DATA DISSEMINATION.....	B.82
JSM41	THE CONTRIBUTION OF SATELLITE OBSERVATIONS TO GLOBAL CLIMATE, OCEAN, AND TERRESTRIAL MONITORING.....	B.117
JSM43	BOUNDARY - LAYERS OVER COMPLEX TERRAIN AND HETEROGENEOUS SURFACES.....	B.134

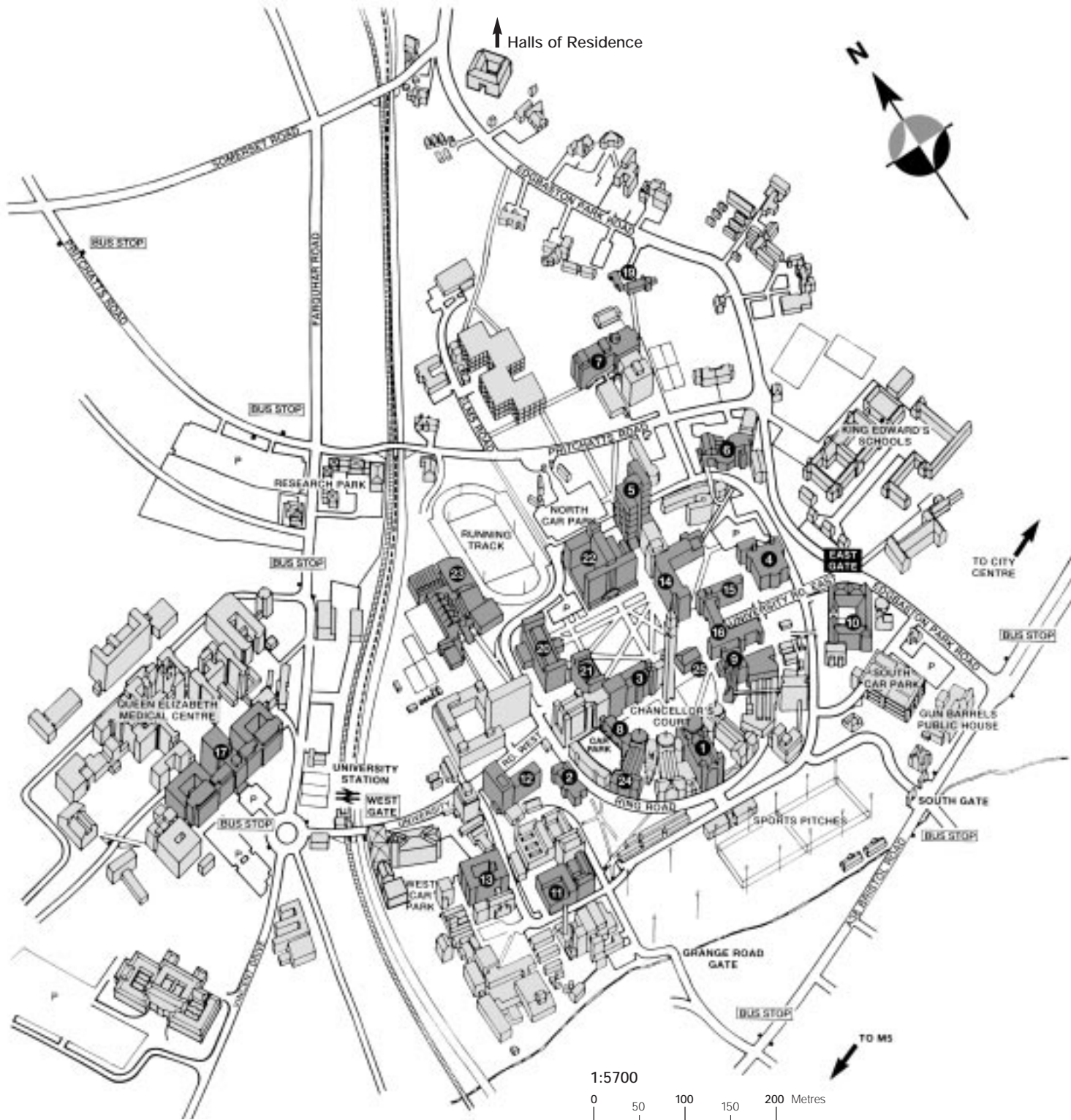
### **IAGA (International Association of Geomagnetism and Aeronomy)**

GA1.01	THE GEODYNAMO: THEORY, OBSERVATIONS AND MODELS.....	A.291
GA1.02	ELECTROMAGNETIC INDUCTION STUDIES.....	A.296
GA1.03	PALEOMAGNETIC FIELD BEHAVIOR.....	B.319
GA1.04	PALEOMAGNETISM: CONTRIBUTIONS TO TECTONICS.....	A.307
GA1.05	ROCK MAGNETISM: METHODS AND APPROACHES IN ROCK MAGNETISM (SESSION A) AND MAGNETIC PROPERTIES AS ENVIRONMENTAL PROXY PARAMETERS (SESSION B).....	A.315
GA1.07	SEPARATION OF INTERNAL AND EXTERNAL FIELD VARIATIONS.....	B.324
GA1.15	MAGNETOSTRATIGRAPHY AND TIME SCALES FROM EXCURSIONS TO SUPERCHRONS.....	B.326

GA2.01	IMAGING RIOMETERS, RADARS, AND D-REGION CHEMICAL MODELS.....	A.324	GA4.05	NEW INSIGHTS ON CORONAL HEATING AND SOLAR WIND ACCELERATION.....	A.368
GA2.02	ELECTRODYNAMIC PROCESSES IN THE GENERATION OF IONOSPHERIC IRREGULARITIES (OBSERVATIONS, THEORY, SIMULATIONS).....	B.328	GA4.06	REPORTER REVIEWS.....	B.381
GA2.03	TOWARD ANSWERING CRITICAL PROBLEMS IN IONOSPHERIC RESEARCH.....	B.335	GA4.08	INTERPLANETARY MEDIUM AND GEOPHYSICAL PHENOMENA DURING MAGNETIC STORMS.....	B.382
GA2.07	IONOSPHERIC IMPACT ON MAGNETOSPHERIC-IONOSPHERIC (M-I) COUPLING.....	A.326	GA4.09	TURBULENCE AND SOLITARY STRUCTURES IN SPACE PLASMAS: THEORY, EXPERIMENT AND ANALYSIS.....	A.370
GA3.01	REPORTER REVIEWS.....	A.330	GA4.10	PLANETARY ATMOSPHERES, IONOSPHERES, MAGNETOSPHERES AND SOLAR WIND INTERACTIONS.....	A.374
GA3.02	MAGNETOSPHERIC SUBSTORM ONSET: OBSERVATION, THEORIES, MODELS.....	B.338	GA5.01	GEOMAGNETIC OBSERVATORIES AND REPEAT SURVEYS: INSTRUMENTATION, PRACTICE, AND ANALYSIS (WITH CDC).....	A.379
GA3.03	DETERMINATION OF POLAR CAP BOUNDARY: IMPLICATIONS FOR MAGNETOSPHERIC ENERGETICS.....	B.346	GA5.06	PRODUCTION AND USE OF GEOMAGNETIC INDICES.....	A.384
GA3.04	GROWTH, PROPAGATION AND DAMPING OF ULF WAVES IN MAGNETOSPHERES.....	B.349	GA5.08	ANALYSIS AND INTERPRETATION OF OERSTED AND OTHER SATELLITE MAGNETIC FIELD SURVEY DATA.....	B.387
GA3.05	ACCELERATION, TRANSPORT AND LOSSES IN THE INNER MAGNETOSPHERE.....	B.357	GA5.09	NEAR-EARTH MAGNETIC REFERENCE FIELD MODELS.....	A.386
GA3.06	AURORA PROCESSES: MAGNETOSPHERE, IONOSPHERE-THERMOSPHERE COUPLING, ARCS AND MICROPROCESSES.....	A.331	GA5.11	CONTRIBUTION OF ROCK MAGNETISM (PETROPHYSICS) TO ANOMALY INTERPRETATION.....	A.388
GA3.07	FORESHOCK, BOW SHOCK, MAGNETOSHEATH, MAGNETOPAUSE, CUSP: STRUCTURE, TRANSIENTS AND WAVES.....	A.338	GA5.12	WORLD MAGNETIC ANOMALY MAPS DERIVED FROM MARINE, AIRBORNE AND SATELLITE DATA INTERDIVISIONAL COMMISSION ON HISTORY.....	A.390
GA3.08	MAGNETOTAIL DYNAMICS AND RELATIONSHIP TO HIGH-LATITUDE IONOSPHERIC PHENOMENA.....	A.350/B.364	GA6.01	LONG AND SHORT TERM VARIABILITY IN SUN'S HISTORY AND GLOBAL CHANGE.....	A.393
GA3.09	QUANTITATIVE TESTS AND INTER-COMPARISON OF SOLAR-TERRESTRIAL AND GEOMAGNETIC FIELD MODELS.....	B.370	GA6.02	400 YEARS OF GEOMAGNETISM.....	B.389
GA3.10	THE MAGNETOSPHERE AND IONOSPHERE UNDER NORTHWARD IMF.....	A.356	GA7.01	EQUATORIAL GEOMAGNETISM AND AERONOMY IN DEVELOPING COUNTRIES.....	A.400
GA4.01	CYCLE 23 SOLAR EVENTS AND HELIOSPHERIC CONSEQUENCES.....	A.360	JSM01	MIDDLE ATMOSPHERE DYNAMICS AND CHEMISTRY.....	A.9
GA4.02	CMES, ERUPTIONS AND FLARES: ONSETS AND RELATIONSHIPS.....	A.363	JSM03	ELECTRICAL DISCHARGES IN THE MIDDLE ATMOSPHERE.....	A.28
GA4.03	SOLAR MAGNETIC FIELD: REVERSALS, POLAR FIELD, DYNAMO.....	B.374	JSA06	SPACE WEATHER FORECASTING AND EFFECTS.....	A.35
GA4.04	ENERGETIC PARTICLES IN THE HELIOSPHERE: LOCAL AND INTERSTELLAR SOURCES, SOLAR CYCLE DEPENDENCE AND 3D STRUCTURE.....	B.377	JSS07	ANISOTROPY: FROM MOUNTAIN BUILDING TO GEODYNAMO.....	A.41
			JSA09	POLAR GEOPHYSICS.....	A.47
			JSA10	PLANETARY EXPLORATION.....	A.52
			JSS13	CONSTRAINTS ON GLOBAL MANTLE CIRCULATION.....	A.62



JSG14	INSIGHTS INTO EARTH SYSTEM SCIENCE: VARIATIONS IN THE EARTH'S ROTATION AND ITS GRAVITATIONAL FIELD.....	A.66	JSA48	CHARACTERIZATION OF THE LITHOSPHERE-ASTHENOSPHERE BOUNDARY.....	B.158
JSA15	ELECTROMAGNETIC METHODS FOR MONITORING EARTHQUAKES AND VOLCANIC ERUPTIONS.....	A.73	<b><u>IAG (International Association of Geodesy)</u></b>		
JSA16	SOLAR VARIABILITY AND CLIMATE.....	A.84	G1	POSITIONING.....	A.403
JSA17	MANTLE-CORE STRUCTURE, PROPERTIES, COUPLING, AND THE GEODYNAMO.....	A.93	G2	ADVANCED SPACE TECHNOLOGY.....	A.417
JSA19	GEOPHYSICAL MEASUREMENTS RELEVANT TO HYDROGEOLOGICAL PROCESSES AND MODELLING.....	A.98	G3	DETERMINATION OF THE GRAVITY FIELD.....	A.422
JSA20	MESOSPHERE-THERMOSPHERE-IONOSPHERE COUPLING AND ENERGETICS.....	A.101	G4	GENERAL THEORY AND METHODOLOGY.....	A.435
JSV22	OCEANIC, CONTINENTAL AND CONTINENTAL MARGIN VOLCANIC PROVINCES: OCEANIC PLATEAUS, FLOOD BASALTS AND SEAWARD-DIPPING REFLECTORS.....	A.113	G5	GEODYNAMICS.....	A.440
JSP23	GEOPHYSICAL HAZARDS AND RISKS: PREDICTABILITY, MITIGATION AND WARNING SYSTEMS.....	A.116	G6	GEODESY BEYOND 2000 - THE CHALLENGES OF THE FIRST DECADE.....	B.393
JSA27	HIGH-RESOLUTION GEOPHYSICAL STUDIES OF MINERALIZED ZONES.....	B.60	JSS02	PHYSICS AND CHEMISTRY OF THE EARTH'S INTERIOR.....	A.24
JSM32	SMALL-SCALE AND LAYERED PHENOMENA AROUND THE SUMMER MESOPAUSE.....	B.80	JSA09	POLAR GEOPHYSICS.....	A.47
JWS33	NEW APPROACHES TO DATA COLLECTION, DATA PROCESSING AND DATA DISSEMINATION.....	B.82	JSA10	PLANETARY EXPLORATION.....	A.52
JWA34	LONG TERM OCEAN BOTTOM GEOPHYSICAL OBSERVATORIES.....	B.89	JSG11	SEA-LEVEL CHANGES AND VERTICAL GROUND MOVEMENTS.....	A.56
JSA35	MIDDLE ATMOSPHERE ELECTRODYNAMICS: INFLUENCES AND PROCESSES.....	B.91	JSG14	INSIGHTS INTO EARTH SYSTEM SCIENCE: VARIATIONS IN THE EARTH'S ROTATION AND ITS GRAVITATIONAL FIELD.....	A.66
JSV36	UNDERSTANDING VOLCANOES BY GEODESY, SEISMOLOGY, ELECTROMAGNETICS AND GEOCHEMISTRY.....	B.93	JSP23	GEOPHYSICAL HAZARDS AND RISKS: PREDICTABILITY, MITIGATION AND WARNING SYSTEMS.....	A.116
JSA37	EARTH'S GRAVITY AND MAGNETIC FIELDS FROM SPACE.....	B.102	JSP25	OCEAN/ATMOSPHERE VARIABILITY AND PREDICTABILITY.....	B.36
JSP39	DYNAMICS OF ROTATING AND STRATIFIED FLUIDS.....	B.105	JSG28	PROBING THE ATMOSPHERE BY GPS.....	B.62
JSA40	SOLID EARTH GEOPHYSICAL DATA FUSION AND ANALYSIS METHODS.....	B.113	JSS31	GEODETIC CONSTRAINTS ON TECTONIC MODELS.....	B.76
JSS44	STRUCTURE OF THE CONTINENTAL LITHOSPHERE FROM INTEGRATED GEOPHYSICAL, GEOLOGICAL AND GEOCHEMICAL STUDIES.....	B.136	JWS33	NEW APPROACHES TO DATA COLLECTION, DATA PROCESSING AND DATA DISSEMINATION.....	B.82
JSA45	EFFECTS OF SOLAR VARIABILITY, SOLAR WIND AND HIGH ENERGY PARTICLES ON THE MIDDLE ATMOSPHERE.....	B.146	JSV36	UNDERSTANDING VOLCANOES BY GEODESY, SEISMOLOGY, ELECTROMAGNETICS AND GEOCHEMISTRY.....	B.93
			JSA37	EARTH'S GRAVITY AND MAGNETIC FIELDS FROM SPACE.....	B.102
			JSA40	SOLID EARTH GEOPHYSICAL DATA FUSION AND ANALYSIS METHODS.....	B.113
			JSM41	THE CONTRIBUTION OF SATELLITE OBSERVATIONS TO GLOBAL CLIMATE, OCEAN, AND TERRESTRIAL MONITORING.....	B.117



Halls of Residence



1:5700  
0 50 100 150 200 Metres

- Registration**
- 1 Great Hall, Aston Webb Building
- Union**
- 1 Great Hall, Aston Webb Building
  - 2 Old Gymnasium Posters
- IAG**
- 3 Law Buildings (office)
  - 4 Barber Institute
  - 2 Old Gymnasium Posters
- IAGA**
- 5 Muirhead Tower
  - 6 School of Education (office)
  - 7 Gisbert Kapp Building
  - 8 Hills Building
  - 4 Barber Institute
  - 2 Old Gymnasium Posters

- IAHS**
- 9 Physics West
  - 10 Guild of Students (office)
  - 4 Barber Institute
- IAMAS**
- 11 Mechanical Engineering (office)
  - 12 Haworth Building
  - 13 Chemical Engineering
  - 3 Law Building
  - 2 Old Gymnasium Posters
- IAPSO**
- 14 Arts Building (office)
  - 15 Watson Building
  - 16 Poynting Physics
- IASPEI**
- 17 Medical School (office)
  - 9 Physics West

- IIVCEI**
- 17 Medical School (office)
  - 9 Physics West
- ILP**
- 6 School of Education M35
- SCOSTEP**
- 6 School of Education M34
- IUGG Office**
- 21 Staff House
  - 19 Hornton Grange (meeting room)
- Exhibition**
- 20 University Centre
- Pressroom**
- 21 Staff House

- Business Centre**
- 21 Staff House
- Library**
- 22 Library
- Sports Centre**
- 23 Sports Centre
- IUGG99 Office**
- 24 Earth Sciences, Aston Webb Building
- Food and Drink**
- 10 Guild of Students
  - 20 University Centre
  - 21 Staff House
  - 25 Beer Tent

# Contents – abstracts week A

<b>U</b>	UL1	A.1	<b>P</b>	P07	A.181	<b>A</b>	GA1.01	A.291
	UL2	A.1		P08	A.184		GA1.02	A.296
	U2	A.1		P09	A.186		GA1.04	A.307
	U3	A.3		P10	A.190		GA1.05	A.315
	U4	A.6		P12	A.197		GA2.01	A.324
	U5	A.7		P14	A.200		GA2.07	A.326
			PW1	A.204	GA3.01	A.330		
					GA3.06	A.331		
					GA3.07	A.338		
<b>IA</b>	JSM01	A.9	<b>M</b>	MIO1	A.207	GA3.08	A.350	
	JSS02	A.24		MI02	A.214	GA3.10	A.356	
	JSM03	A.28		MI03	A.217	GA4.01	A.360	
	JSM04	A.30		MI05	A.220	GA4.02	A.363	
	JSP05	A.32		MI07	A.229	GA4.05	A.368	
	JSA06	A.35		MI08	A.230	GA4.09	A.370	
	JSS07	A.41		MI09	A.236	GA4.10	A.374	
	JWM08	A.44		MC01	A.240	GA5.01	A.379	
	JSA09	A.47		MC06	A.255	GA5.06	A.384	
	JSA10	A.52		MC07	A.256	GA5.09	A.386	
	JSG11	A.56		MC08	A.259	GA5.11	A.388	
	JSH12	A.60		MW01	A.262	GA5.12	A.390	
	JSS13	A.62		MW04	A.264	GA6.01	A.393	
	JSG14	A.66		MW05	A.265	GA7.01	A.400	
	JSA15	A.73		MW06	A.267			
	JSA16	A.84		MW07	A.269			
	JSA17	A.93		MW08	A.271			
	JSM18	A.95						
	JSA19	A.98						
	JSA20	A.101						
	JSP21	A.110						
	JSV22	A.113						
	JSP23	A.116						
<b>S</b>	ST1	A.137	<b>H</b>	HS3	A.273	<b>G</b>	G1	A.403
	ST2	A.159		HS4	A.276		G2	A.417
	ST6	A.172		HS5	A.280		G3	A.422
	ST7	A.176		HW1	A.285		G4	A.435
				HW5	A.288		G5	A.440
						<b>INDEX</b>	Alphabetical listing of authors	I.1

**Please Note:**  
Abstracts are divided into the equivalent of two published volumes for weeks A & B

## Key for Abstract Book

---

1. Symposia and Workshops are listed according to organising or leading Association, where:

UNION = U

INTER-ASSOCIATION = IA (IAVCEI, IASPEI, IAPSO, IAMAS, IAHS, IAGA and IAG)

IAVCEI = V

IASPEI = S

IAPSO = P

IAMAS = M

IAHS = H

IAGA = A

IAG = G

2. This Assembly has a much larger Inter-Association programme than usual. In the Abstract Books, these have only been listed as part of the Inter-Association programme and have not been repeated under the leading and sponsoring Associations, as has been done for the Programme Book.

3. Oral Presentations are listed according to time of presentation.

4. Poster presentations are listed:

- as part of the oral presentations if the convenor allocated a short presentation time or a scheduled viewing time
- at the end of the symposium if the convenor specified a particular half day for poster viewing, concurrently held to an oral session.
- at the end of the symposium if the convenor did not allocate a specific time for poster viewing; the posters are scheduled concurrently to the first half day of that symposia/workshop.

The organisers endeavour to leave posters up for the duration of the symposium or workshop they belong too. Please check the POSTER SCHEDULE, placed at the entrance of each lecture theatre and poster room, for final information.

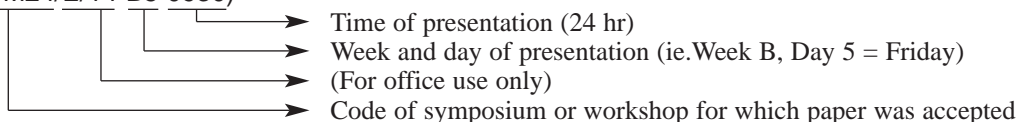
Convenors and Chairs, who have not already done so, are encouraged to specify at the beginning of their symposium or workshop a time when poster presenters are expected to be at their posters. Alternatively, poster presenters can make use of the 'I will be at my poster....' Messages available in each poster room.

## Key to Index

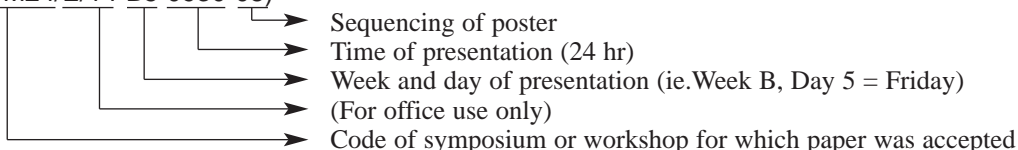
---

Authors are listed alphabetically, followed by the code of their abstract and indication of week, day and time of presentation, where:

SMITH, P (JSM24/E/14-B5 0930)



SMITH, P (JSM24/E/14-B5 0930-08)



N.B: IUGG cannot accept any responsibility for textual errors to the content of the submissions. Due to regional differences in software, some specific symbols may have been automatically substituted by the publishers native version.

IUGG apologise for any confusion that these errors may cause.



## UNION LECTURE 1

Tuesday 20 July

Location: Great Hall

0830

## MARS AND THE SEARCH FOR LIFE ELSEWHERE

EDWARD C. STONE, Jet Propulsion Laboratory, 4800 Oak Grove Drive, M/S 180-904, Pasadena, California 91109, USA, email: edward.c.stone@jpl.nasa.gov

Life thrives on Earth wherever there is water. As a result, the search for life elsewhere focuses on the search for water and the molecular building blocks of life. Mars once had flowing water, Jupiter's moon Europa may have water beneath its icy crust, and the surfaces of comets, Pluto, and Saturn's moon Titan are rich in the organic building blocks of life. Over the next twelve years we will explore each of these and bring back samples from several of them. We will also look for Earth-like planets orbiting nearby stars as we extend our search for life beyond the Solar System.

## UNION LECTURE 2

Thursday 22 July

Location: Great Hall

0830

## THE STATE OF THE MANTLE - RECONCILING STRUCTURE AND PROCESSES

B.L.N Kennett (Research School of Earth Sciences, Australian National University, Canberra ACT 0200, Australia, email: Brian.Kennett@anu.edu.au)

Over the last decade the rapid development of seismic tomography has provided a wealth of information on seismic wavespeed structure on a wide range of scales - from the local to the global. Increasingly information from P and S wave information is being combined to provide insight into the nature of the three-dimensional heterogeneity revealed in the tomographic images. Such seismic information provides a snapshot of Earth structure, whilst such major features such as subducting plates at depth reflect past environments. Geochemical probes can provide both a time component and considerable subtlety of insight into some aspects of the process which lead to the observed heterogeneity in surface samples.

The zones of strongest heterogeneity occur near the major boundaries, at the surface and the core-mantle boundary but there are other zones of significant variation, not just at the 660 km discontinuity which is commonly taken as the boundary between the upper and lower mantles. The newer views of the mantle are indeed more complex than the simple pictures drawn from radial reference models but offer greater concordance between geophysical and geochemical viewpoints.

## U2

Tuesday 20 July

## GLOBAL CHANGE AND PREDICTABILITY

Location: Great Hall

Tuesday 20 July AM

Presiding Chair: C.G. Rapley, (British Antarctic Survey, Cambridge, UK)

## THE EARTH SYSTEM AND GLOBAL CHANGE

U2/L/01-A2

0930

## THE EARTH SYSTEM: WHAT DO INTERMEDIATE COMPLEXITY MODELS TELL US?

Martin Claussen and Andrey GANOPOLSKI (both at Potsdam Institute for Climate Impact Research, PO Box 60 12 03, D-14412, Potsdam, Germany, Email: andrey@pik-potsdam.de)

Due to the large computational cost of the state-of-the-art models of different components of the climate system and biosphere, the development of integrated models of the Earth system up to now has been based on the so-called models of intermediate complexity. The main idea behind such models is to achieve a fast turnaround time by a reducing the resolution and complexity in the description of the individual processes, and at the same time retain a sufficient degree of realism ("as simple as possible but as complex as necessary"). This class of models allows us to perform many long-term simulations that advances our understanding of the Earth system. In particular, these models has been used for studying the role of different feedback and synergism between components of the Earth system. These models contribute to a better understanding of the stability of the climate and the mechanisms of abrupt climatic changes which took place in the past and may happen in the future. Finally, the models of intermediate complexity allow us to assess a very broad spectrum of scenarios of future climatic changes and to study the role of uncertainties in forcing scenarios and in the description of individual processes.

CLIMBER-2 model, developed at Potsdam Institute for Climate Impact Research, is an example of an Earth system model of intermediate complexity. This is a coarse resolution 2.5-dimensional geographically explicit model designed for long-term (up to a million years) simulations. The results from the model illustrate a potential of models of intermediate complexity for the study of the Earth system dynamics on different time scales, in particular the role of climate-biosphere feedback and the stability of thermohaline ocean circulation. The model has been used for paleoreconstructions and simulations of future climate change scenarios.

U2/E/09-A2

0950

## THE IGBP GLOBAL CARBON PROJECT: UNDERSTANDING THE BREATHING OF THE PLANET

W. Steffen, International Geosphere-Biosphere Programme, Royal Swedish academy of Sciences, Box 50005, S-10405 Stockholm, Sweden E-mail will@igbp.kva.se

The post-Kyoto world has put the planet's biogeochemical cycling into the forefront of international political and economic concerns, and has posed a considerable challenge to the international global change research programmes. The International Geosphere-Biosphere Programme (IGBP), in collaboration with its partner programmes the World Climate Research Programme (WCRP) and the International Human Dimensions Programme on Global Environmental Change (IHDP), is rising to this challenge by launching a major international research effort on the science of the global carbon cycle. The twin objectives of the IGBP Global Carbon Project are: (i) to produce a synthesis of our current understanding of the global carbon

cycle, including a fast-track scientific overview in time for inclusion in the IPCC special report on land-use change and forestry; and (ii) to develop an international framework for collaborative research on the carbon cycle; involving appropriate elements from IGBP, WCRP and IHDP, and to co-ordinate an international research effort under such a framework. This talk will focus on the current status of the IGBP synthesis effort on carbon, and will briefly outline the emerging framework for ongoing collaborative international research on the carbon cycle under the three international programmes. Critical aspects of the carbon cycle to be dealt with in the IGBP Global Carbon Project include palaeo-carbon studies, observational and process studies of oceanic carbon fluxes, coastal biogeochemical budgets, measurement of terrestrial carbon fluxes, reliability of the terrestrial carbon sink into the future (i.e., 'sink saturation'), effects of land-use/cover change on the carbon fluxes, and integrated modelling of the global carbon cycle.

U2/E/10-A2

1010

## ABRUPT CLIMATE CHANGE: UNDERSTANDING THE DYNAMICS OF THE EARTH SYSTEM

F. Oldfield, PAGES Core Project Office, Barenplatz 2, CH-3011 Berne, Switzerland  
E-mail: oldfield@pageibp.unibe.ch

It is only within the last few years that overwhelming evidence has accumulated pointing to the capacity of the climate system to undergo major changes on time-scales of less than a century, in some cases, less than a decade. The paper will outline four types of abrupt change and consider their possible future implications. On 'Milankovitch' timescales (tens to thousands of millennia), where external forcing through astronomically controlled changes in solar irradiance drives the rhythm of Earth System response, smooth changes in forcing across critical thresholds, trigger abrupt global responses, as may be seen at both the onset and termination of glacial periods. On sub-Milankovitch timescales – millennial and shorter – the best known and most dramatic changes are those that were first detected in the Greenland ice core record from the period of the last glacial (Marine Isotope Stages 2,3 and 4). These 'Dansgaard-Oeschger' oscillations appear to have involved changes in temperature over much of the Greenland ice cap of well over half the amplitude of the full range of temperature shift between full-glacial and Holocene optimum conditions. They were also marked by synchronous climate changes over much of the earth's surface. Their onset and termination appears to have taken place on decadal timescales in most cases. The best known and most fully understood of the major oscillations also includes the transition from glacial (Younger Dryas) to Holocene conditions and there is a growing body of evidence regarding the dynamical basis of the transition which took place over two or three decades at most.

The issue of abrupt changes during the Holocene (the last 11.5 kyrs) is a rather more controversial topic. A dominantly polar-centric view of variability has tended to foster the notion that the Holocene was a period of much reduced variability. This perspective is demonstrably false as soon as we turn to lower latitudes and consider hydrological, in addition to temperature, variability. During the first half of the Holocene, smooth changes in solar irradiance were accompanied by many kinds of earth system readjustment in the wake of the last glacial termination – the massive reduction in the extent of polar ice, especially in the Northern Hemisphere, a global rise in sea-level and dramatic changes in terrestrial...

Presiding Chair: H. Grassl

## THE VARIABLE OCEAN

U2/E/11-A2

1100

## GLOBAL OCEAN CIRCULATION

Harry L. Bryden Southampton Oceanography Centre, Southampton, SO14 3ZH UK  
E-mail: Harry.L.Bryden@soc.soton.ac.uk

In the past few years schematic diagrams of the global ocean circulation have become very popular. Rather than taking such sketches to be blueprints for the real ocean circulation, we should use them to help identify the key unknown elements of ocean circulation. In contrast to the simple sketches, measurements during the World Ocean Circulation Experiment reveal the complexity of the actual ocean circulation: maps of global sea surface height from satellite altimetry, basin-scale distributions of tracer fields in the interior ocean, and subsurface drifter trajectories demonstrate the richness of variability at a multitude of temporal and spatial scales. Simultaneously, numerical simulations of ocean circulation have been increasingly successful at representing present-day ocean circulation. Yet there remain fundamental questions as to what controls the strength of the ocean circulation, both the wind-driven basin-scale circulations and the global thermohaline circulation. Answering these questions is the key to understanding how the ocean circulation will evolve under changing climate conditions.

U2/E/12-A2

1120

## EVOLUTION OF THE 1997-98 EL NINO/LA NINA CYCLE

Michael J. McPhaden, NOAA/Pacific Marine Environmental Laboratory, Seattle, Washington 98115, USA. E-mail: mcphaden@pmel.noaa.gov

The 1997-98 El Nino, the strongest on record by some measures, has been called "The Climate Event of the Century". The event unfolded rapidly in the tropical Pacific beginning in early 1997, and by June 1997 sea surface temperatures in the eastern Pacific reached historic highs. By December 1997, 28-29°C surface water filled the equatorial basin. Then, in May-June 1998, SST dramatically plunged 8°C in 30 days along the equator in the eastern Pacific. The El Nino ended as suddenly as it began, replaced by La Nina conditions characterised by below normal sea surface temperatures and stronger than normal trade winds.

This presentation reviews the observations and forecasts of the 1997-98 El Nino/La Nina cycle in the tropical Pacific. A major contributor to recent progress in El Nino studies has been the development of an ocean observing system comprised of complementary satellite and in situ measurements.

The data from this observing system were used to initialise and validate model forecasts of the 1997-98 event, and to provide high definition monitoring of the event in real-time. The observations also provided new insights into the dynamics of coupled ocean-atmosphere interactions in the tropical Pacific, and highlighted issues concerning the relationship of El Nino to both shorter time scales associated with the intraseasonal Madden-Julian Oscillation, and longer time scales associated with interdecadal variability and global warming. Thus, while the 1997-98 El Nino/La Nina serves to emphasise fundamental advances made in seasonal-to-interannual climate research in the past 10-15 years, it also raises new challenging research questions for the future.

**U2/E/07-A2 1140****INTERANNUAL VARIABILITY OF THE OCEAN-ATMOSPHERE SYSTEM THROUGH GLOBAL GENERAL CIRCULATION MODEL RESULTS: THE TROPICAL PACIFIC OCEAN**

STEPHANE RAYNAUD, Sabrina Speich (both at Laboratoire de physique des Océans, Université de Bretagne Occidentale, UFR Sciences, 6 avenue Le Gorgeu - BP 809, 29285 BREST CEDEX - FRANCE) and Gurvan Madec (Laboratoire d'Océanographie DYnamique et de Climatologie, UPMC T26e4, boîte 100, 4 place Jussieu, 75252 PARIS CEDEX 05).

A global coupled General Circulation Model is used to study the interannual variability of the ocean-atmosphere system in the Pacific region. Two 40 years simulations are analysed in order to investigate the impact of the lateral diffusion of the ocean tracers (T & S) onto the climate variability in two different configurations: horizontal versus isopycnal diffusion.

The El Niño-Southern Oscillation (ENSO) phenomenon is clearly present but shows significantly different characteristics between the two runs, concerning the amplitude and the spectral properties. It can be attributed to a different mean state or to the direct effect of the isopycnal diffusion.

In this study, ENSO is regarded as combination of linear quasiperiodic modes perturbed by weak non-linearities, that we can identify with the Multichannel Singular Spectrum Analysis (MSSA). Applied to various fields, MSSA allows to find a qualitative and quantitative physical coherence in the cycle of each mode. Diagnostics of the tendency terms responsible for the sea surface temperature evolution are useful to evaluate the role of advection, air-sea fluxes and diffusion in the persistence of anomalies. Explanations are then purposed for the differences in the ENSO behavior of these two simulations.

**U2/E/08-A2 1200****ROLES OF BIOGEOCHEMICAL PRODUCTIVITY IN THE CARBON CYCLE USING A SIMPLE GLOBAL OCEAN MODEL**

MASAHIKO FUJII, Motoyoshi Ikeda and Yasuhiro Yamanaka (Graduate School of Environmental Earth Science, Hokkaido University, Sapporo 060-0810, Japan, email: fujii@ees.hokudai.ac.jp, mikedai@ees.hokudai.ac.jp and galapen@ees.hokudai.ac.jp)

A simple physical and biogeochemical ocean model is constructed. Horizontally, the global ocean is divided into four regions; i.e., the Pacific/Indian Ocean (PI), the Atlantic Ocean (AT), the Southern Ocean (SO) and the Greenland/Iceland/Norwegian Sea (GIN). The PI and AT are vertically continuous, while the SO and GIN are divided into two, the surface layers (50m thick) and the lower layers. This model is used to estimate the oceanic carbon cycle contributed by physical and biogeochemical processes. The physical parameters are chosen to represent the air-sea CO<sub>2</sub> flux, the thermohaline circulation, and vertical and horizontal diffusions. The biological productivity is controlled only by phosphate in the surface layers. The geochemical process is parameterized by a calcite productivity in the surface layers. The products are remineralized in the lower layers. The observed distributions of radiocarbon, phosphate and alkalinity are used as tracers to optimize the parameters. The total carbonate concentration is then calculated, and the vertical carbon flux is quantitatively estimated. A major feature is a clear contrast between the PI and AT; i.e., the total carbonate is richer in the PI than the AT, along with the other biogeochemical components. As the anthropogenic sources increase the CO<sub>2</sub> concentration in the atmosphere, the effects appear significantly in the AT, while a signal is extremely weak in the PI.

**Tuesday 20 July PM**

Presiding Chair: Jill Jaeger

**THE CRYOSPHERE AND ATMOSPHERE****U2/E/13-A2 1400****ASSESSMENT OF MASS BALANCE OF THE NOVAYA ZEMLA ICE SHEET BASED ON TWO CLIMATIC SCENARIOS**

Natalia Davidovich and Maria Ananicheva Institute of Geography, Russian Academy of Sciences, Staromonetny 29 Moscow 109017, Russia. E-mail: Maria@glacinfo.msk.ru

Fluctuations of the global thermal regime, recorded during the instrumental observation period of the last hundred years are better pronounced during the cold than warm period of the year; they are especially pronounced in high latitudes as e.g. the Atlantic sector of the Arctic. These changes are connected mainly with the atmospheric circulation and precipitation regime. Novaya Zemlya Archipelago is situated in a region of high oceanity and climatic fluctuations; it was subjected to significant variations in its glaciation regime. During the first half of the 20th century the type of ice sheet nourishment changed there at least twice. According to our calculations anomalies of winter precipitation of various signs and melting rates varying by 20-30% may lead to entirely different types of ice formations and therefore to significant changes in mass balance during one or two decades. Taking this into account, we tried to find out how a possible warming may affect the type of nourishment, mass balance and glacier runoff in the main glaciological zones of the Novaya Zemlya ice sheet.

We compare the results with the 1932-1962 sheet geometries for which detailed balance calculations are available. The GFDL model for the climate development, if the hydro-glaciological conditions are based on a change in winter temperature of 9.50C; this is quite realistic for the whole Novaya Zemlya region. However the rise of the summer temperature cannot be the same everywhere. Due to the negative feedback of the melting processes at the glacial surface, the warming over the ice sheet should be less than over ice-free land. Changes in precipitation on Novaya Zemlya predicted by the GFDL model led us to assume an increase of 25%.

The growth of the carbon dioxide and other greenhouse gases in the atmosphere during the epochs of global warming were most intense in the Cenozoic and took place 3-4 million years ago in the Young-Middle Pliocene, with a doubled CO<sub>2</sub>-concentration as compared to today. The mean temperature of the Northern hemisphere was about 50C higher than it is now, and in the Arctic there was no polar ice. Palaeoclimatic maps for this epoch which...

**U2/E/14-A2 1420****INDICATIONS OF THE EXTENT AND CAUSE OF GLOBAL TROPOSPHERIC OZONE POLLUTION**

PENKETT, Stuart(1) Reeves, Claire(1) Bauguitte, Stéphane(1) Green, Tim(1) Carpenter, Lucy(1) Law, Kathy(2) Evans, Mathew(2) Methven, John(3) Schmitgen, Sandra(4) Richer, Hannah(5) Dewey, Ken(5) Kent, Joss(5) Kaye, Andrew(6) Zanis, Prodromos(7), Schüpbach, Evi(7)& Monks, Paul(8)

(1)University of East Anglia, Norwich (UK); (2)University of Cambridge, (UK); (3)University of Reading, (UK); (4)KFA Jülich, (Germany); (5)MRF, Farnborough (UK); (6)NERC Scientific Services, Swindon (UK); (7)University of Bern, (Switzerland); (8)University of Leicester (UK)

Our understanding of the behaviour of ozone in the troposphere has been increased significantly in the last few years by experiments carried out on the ground and from aircraft,

and by indications of its global distribution from satellites. A number of factors are involved, including the development of instruments capable of studying the free radical chemistry associated with in-situ ozone production and destruction in real time, and the realisation that long-range intercontinental transport of ozone and other pollutants is occurring in both hemispheres on a large scale. This survey will show results collected in the atmosphere with increasing degrees of contamination from the marine boundary layer of the southern hemisphere to polluted air in the free troposphere over the Atlantic and the Alps, and to the more polluted boundary layer over the USA and Europe. The survey will also contrast the importance of transport as shown by trajectory analysis, with in situ production as a source of free tropospheric ozone. IGAC has played a major role in these developments, particularly in the background atmosphere; IGAC's role has been supplemented by information from satellites, from commercial aircraft and from national programmes designed to study air pollution.

**U2/E/15-A2 1440****PRECIPITATION FLUCTUATIONS OVER EASTERN EUROPE AS A REFLECTION OF GLOBAL ATMOSPHERIC CHANGES**

Valeria Popova Institute of geography, Russian academy of sciences, 29 Staromonetny per, Moscow 109017, RF, E-mail: climat@ipcom.ru

In order to determine statistical correlation between multyear precipitation fluctuation on the eastern Europe (Russian Plain) and atmospheric circulation processes the annual and seasonal data of spatial averaged precipitation on 30 regions of the Russian Plain for 1890-1985 so well as different kinds of indicator of circulation changes have been used. Data on circulation changes indicators include: archive of large-scale circulation processes in the extratropical zone on Northern hemisphere types by B.L.Dzherdzevsky, which covers each day of the 20th century, the meridional index by A.L. Katz estimated since 1950 and the anomalies of location variation of Iceland low pressure since 1890. It has been obtained patterns of correlation coefficient between precipitation fluctuation and each of circulation changes indicator. These patterns coincide to each other and show that the correlation is spatial distributed. It allowed to conclude that intensification of meridional atmospheric large scale processes cause the increase of precipitation on the east and south-west of Russian Plain and increase of precipitation on the northern-west is associated with intensification of zonal circulation. Peculiarities of distribution of the correlation coefficients between precipitation and circulation processes coincide with obtained earlier data on spatial structure of multyear precipitation fluctuation on the Russian Plain. These results explain the climatic cause of Caspian sea level fluctuations during 20th century because the main part of river Volga basin is located on the East of Russian Plain. It has been shown that present rise of Caspian Sea level is associated with the intensification of meridional atmospheric processes.

**U2/L/02-A2 1500****RECENT STRATOSPHERIC TRENDS**

Marie-Lise CHANIN (Service d'Aéronomie du CNRS, BP 3 Verrières-le-Buisson, France, email: chanin@aerov.jussieu.fr)

The stratosphere has shown the most spectacular anthropogenic changes of any atmospheric region. But even though the discovery of the Antarctic ozone hole, in 1985, triggered a strong interest in monitoring ozone all over the globe, changes in the vertical distribution of ozone are still poorly known, particularly around the tropopause, region where ozone changes have the strongest effect on climate. The stratosphere is shown to have cooled in the last decades, mostly as a consequence of ozone depletion. Both ozone and temperature trends have been updated recently as an initiative of the SPARC Project and the results, which are part of the recent WMO-UNEP Ozone Assessment, will be presented.

The radiative effect of water vapour makes it the most important of the greenhouse gases, and its concentration might be expected to change through the increase and subsequent oxidation of methane, as well as from changes in the atmospheric thermal structure. However the dataset available are scarce and too short to lead to concluding results. Where we stand on this issue will be discussed. During the last decade, the stratosphere has also experienced changes as a consequence of various naturally occurring effects. The impact of aerosols deposited in the stratosphere by the eruption of Pinatubo has been measured accurately and globally for the first time in surface temperature, in addition to its direct effect at other altitudes and its indirect effect through affecting stratospheric chemistry. It should be noted that the monitoring of any long term trend in background aerosol is difficult due to the long residence time of volcanic aerosol reaching the stratosphere (~5 years).

In addition to the rather direct radiative effects and the indirect chemical effects, there is also the possibility of more complicated changes occurring through changes in atmospheric dynamics. It is known that small changes in radiative forcing can have large effects on the dynamics of the winter stratosphere. Preliminary results on the activity of planetary waves, zonal mean wind and the occurrence of stratospheric warmings in the last decades will be presented.

Presiding Chair: W. Steffen

**HUMAN INFLUENCES AND THE FUTURE****U2/E/17-A2 1600****LAND COVER DYNAMICS IN AFRICA - OBSERVATIONS BY REMOTE SENSING AND SPATIAL MODELLING**

Eric Lambin, Department of Geography, University of Louvain, place Louis Pasteur, 3 B-1348 Louvain-la-Neuve, Belgium. E-mail: lambin@geog.ucl.ac.be

Quantitative data on where, when and why land-cover changes take place are still incomplete. Remote sensing techniques allow a systematic collection of data on land-cover changes at a range of spatial scales. Spatial modelling techniques, based on geographic information systems, can support a better understanding of the major determinants of land-cover change processes.

First, a continental-scale analysis of Africa was conducted, based on ten years of AVHRR remote sensing data, to detect land-cover change « hot spots ». Processes such as drought and fire impacts on vegetation, and forest clearings were identified at a broad scale. The results highlight the dynamic character of African ecosystems. Few areas in Africa are affected by continuous, unidirectional change processes.

Second, fine scale remote sensing data were used for validation and to better understand the land-cover change processes. A sample of fifteen intensive study sites, well-distributed across Africa, was selected. Time series of remote sensing data and long-term field data have been assembled to identify generic trajectories and processes of change.

Third, spatial statistical models of land-cover change were developed for each site. The approach consists in analysing the location of different categories of land-cover changes in relation to natural and cultural landscape attributes. One output is a projection of areas at risk of being affected by land-cover conversion in the future and the simulation of possible impacts.

U2/E/05-A2 1620

## CLIMATE CHANGE OVER MOZAMBIQUE AND SOME IMPACTS ON AGRICULTURE

ADAO HENRIQUE MATONSE ( Faculty of Natural Sciences & Mathematics, Pedagogical University, C.P. 0404, Maputo-6, Mozambique. Email: misa@zebura.ueem.mz)

According to IPCC, global temperatures have increased by over 0.5 °C since the nineteenth century, and may increase between 1.5 and 4.5 degrees by the doubling of CO<sub>2</sub> concentrations. Different GCMs are applied to produce climate change scenarios for the region of Mozambique. The results for the annual mean values, given by the models, indicate a sensitivity between 1.8 and 3.1 degrees, and a change in precipitation ranging from - 9 % to +11 %. The economy of Mozambique is based on agriculture which accounts for nearly half of the country's GDP, and 70 % of the foreign exchange earnings. The most important traditional food crops are maize, cassava, groundnut, rice, sorghum and millet. The absence of irrigation in Mozambique ( less than 2 % of the cultivated area is under irrigation) increases the sensitivity of crop yields to climatic variations. Possible impacts on agriculture are projected in terms of the productivity of maize, with the use of CERES- Maize model.

U2/E/16-A2 1640

## GLOBAL ENVIRONMENTAL CHANGE: THE HUMAN DIMENSIONS CHALLENGE

Jill Jaeger International Human Dimensions Programme Secretariat, University of Bonn, Nussallee 15a, D-53115 Bonn, Germany. E-mail: ihdp@umi-bonn.de

The realisation that human activities cause global environmental change, that individuals and societies can be affected by it and that they will develop responses has brought home forcefully the fact that studies of global environmental change must be broadly interdisciplinary, incorporating the social and natural sciences, and international. The range of social science disciplines involved in research related to global environmental change is large. The paper looks at the research challenges arising in studies of the causes, consequences and responses to environmental change, in understanding human attitudes and behaviour with respect to the environment, in dealing with questions of scale and with harmonising and integrating social science data. In the last 10 years interest has also focused on "sustainable development", for which there is a need for truly integrative assessments that combine various streams of knowledge from the social and natural sciences as well as the accumulation of experience in the implementation of local Agenda 21 and present it in a way that it can be useful in the decision-making process.

U3 Wednesday 21 July

## EARTH SYSTEM MODELS AND EARTH SYSTEM PREDICTABILITY

Location: Great Hall  
Location of Posters: Old Gym

Wednesday 21 July AM

Presiding Chair: G. Brasseur, National Centre for Atmospheric Research, Boulder  
Concurrent Poster Session

Introduction 0855

W. Richard Peltier (University of Toronto)

U3/W/17-A3 Invited 0900

## INSIGHTS FROM HIGH-SPATIAL RESOLUTION MODELING OF THE THERMOSPHERE-IONOSPHERE T.

L. KILLEEN (Space Physics Research Laboratory, Department of Atmospheric, Oceanic, and Space Sciences, University of Michigan, 2455 Hayward Street Ann Arbor, MI 48109-214, USA, Email: tkilleen@umich.edu), W. Wang and A. G. Burns (both at Space Physics Research Laboratory, Department of Atmospheric, Oceanic, and Space Sciences, University of Michigan, 2455 Hayward Street Ann Arbor, MI 48109-2143, USA, Email: wenbin@engin.umich.edu, aburns@umich.edu

Many important phenomena in the thermosphere/ionosphere system manifest themselves over mesoscales (10's to 100's of km) rather than over global scales (1000km). Features associated with such phenomena often remain unresolved by thermosphere-ionosphere models of conventional spatial resolution (standard grid spacings of 5degx5deg or 2.5degx15deg). High-latitude electrical dissipation (Joule heating) is a good example of a globally significant process that can and does vary considerably over scales of tens to hundreds of kilometers. In principle, mesoscale phenomena can be modeled using General Circulation Models (GCMs), but this requires increasing the resolution of the models greatly. The consequent increase in array size and running time can be prohibitive in terms of the computer resources required. The analogous problem is solved in the lower atmosphere by using local area models, when interaction with larger scale features is not important, and nested or adaptive grid models, when such interaction is important. Over the past 5 years, a nested grid model of the thermosphere and ionosphere (TING) has been developed and deployed to study mesoscale processes in the thermosphere-ionosphere. The TING model is based on the NCAR series of highly-developed thermosphere-ionosphere codes and has been parallelized for real-time use in a predictive mode. Results from the high-spatial-resolution (1.5x1.5deg grid) TING model calculations are presented and compared with their equivalent low-resolution counterpart calculations using identical inputs. Calculated Joule heat rates are significantly greater when the high resolution grid is used. Many other mesoscale features (low latitude troughs, electron temperature enhancements, tongues of ionization, etc.) are modeled at the higher resolution and can be investigated in detail using post-processor diagnostic codes. The paper will present an overview of insights derived from the use of high spatial resolution for coupled models of the thermosphere-ionosphere.

U3/W/10-A3 Invited 0930

## COUPLED CHEMICAL-DYNAMICAL MODELLING OF THE MIDDLE ATMOSPHERE

T.G. SHEPHERD (Department of Physics, University of Toronto, Toronto, Ontario M5S 1A7 Canada, email: tgs@atmos.physics.utoronto.ca)

The "middle atmosphere" is the name given to the stratosphere and mesosphere; it lies between the troposphere below and the thermosphere above. In the middle atmosphere,

chemical and radiative-dynamical processes all play equal roles in determining the atmospheric state, and coupled chemical-(radiative)-dynamical phenomena abound. The Antarctic ozone hole is but one example. The nature of chemical-dynamical coupling in the middle atmosphere presents many challenges for climate system modelling, because of space and time scale mismatches. In addition, because of the strong radiative-dynamical driving from the troposphere, comprehensive modelling of the middle atmosphere always includes the troposphere. This introduces a chemical interface (the chemical tropopause), separating the strongly layered stratosphere from the relatively well-mixed troposphere. This talk will describe some of the key aspects of chemical-dynamical coupling in the middle atmosphere, together with their implications for climate system modelling. Particular attention will be focused on those aspects affecting ozone and climate change. The points will be illustrated using observations as well as results from a comprehensive chemical-radiative-dynamical general circulation model of the troposphere-stratosphere-mesosphere system (the Canadian Middle Atmosphere Model).

U3/E/07-A3 Invited 1000

## MODELLING CHEMISTRY-CLIMATE FEEDBACKS

KATHY LAW (Centre for Atmospheric Science, University of Cambridge, Cambridge, CB2 1EW, U.K., Email: kathy@atm.ch.cam.ac.uk)

Atmospheric chemistry models of the troposphere and stratosphere have been developed to further our understanding about a wide range of important issues related to past, present and future changes in radiatively active trace gases, such as ozone and methane, and also, aerosols. Examples will be used to illustrate our current modelling capability. To date, chemistry transport models have been used to study particular feedbacks between chemical, dynamical and radiative processes. For example, the impact of ozone depletion on the stratospheric circulation. Other examples will be discussed. Current developments are focusing on the inclusion of atmospheric chemistry in global climate models in order to study the impact of changing trace gas and aerosol concentrations on the climate system and vice versa. Models are also being developed which link the atmosphere to the biosphere through interactive emissions of source gases (e.g. wetland emissions of methane).

U3/W/01-A3 Invited 1100

## THE NCAR CLIMATE SYSTEM MODEL

Byron A. Boville (National Center for Atmospheric Research, Box 3000, Boulder CO 80307 USA, email: boville@ucar.edu)

The NCAR Climate System Model (CSM) is a physical climate model containing component models for the atmosphere, land surface, ocean, and sea ice, communicating through a coupler. The CSM produces stable solutions for present (or pre-industrial) climate on multi-century time scales, without the need for flux corrections. Although the surface climate was stable, the initial version of the CSM had substantial deep ocean trends. Recent improvements in the model have significantly reduced the deep ocean trends. These improvements will be summarized and results from pre-industrial control simulations and from transient greenhouse gas forcing experiments will be discussed.

U3/W/07-A3 Invited 1130

## CAN WE ASSESS THE ROLE OF LAND-SURFACES ON CLIMATE CHANGE ?

Nathalie de Noblet (Laboratoire des Sciences du Climat et de l'Environnement, Unite mixte de Recherche CEA-CNRS, Bat. 709 / Orme des Merisiers , 91191 Gif-sur-Yvette, FRANCE, email: noblet@lscce.saclay.cea.fr)

Sensitivity experiments, using models of different complexity, have demonstrated the importance of biosphere/atmosphere interactions for climate studies. In addition there is evidence, from paleoecological data, that the global distribution of biomes has strongly varied through time. Therefore a full treatment of climate change, past or future, requires the use of integrated biosphere models. Coupled AGCM-Biome models have then been developed. Static biome models were first used, requiring as input an equilibrium state of the atmosphere. Such coupled models were applied to simulations of present-day climate, to test whether the AGCM was in equilibrium with the present-day land-surface conditions. Applications were also carried out for past climates : - accounting for feedbacks from vegetation redistribution during the last glacial period (115000 years ago) may have contributed to the build up of continental ice-sheet; - during mid-Holocene (6000 years ago), the orbitally-induced increase in African monsoon was enhanced by the subsequent growth of vegetation in the southern border of the Sahara. Some simulations of future climate change have recently been re-run accounting for the physiological response of plants to changes in the atmospheric CO<sub>2</sub> concentration. An additional warming of the whole globe has been found, the vegetation-induced response being larger in the tropics than in the mid to high latitudes. If we want to go a step further and evaluate the potential response of global ecological processes to anthropogenic perturbations, and its feedbacks to climate, the time behaviour of the biosphere must be examined. Coupled models such as those introduced above are therefore not applicable. Models that include the parameterization of vegetation dynamics are therefore being developed in several groups and will be briefly discussed.

U3/W/16-A3 Invited 1200

## A DYNAMICAL STABILIZING MECHANISM IN THE CLIMATE SYSTEM: RESULTS FROM A SIMPLE MODEL AND A GCM

J. R. BATES and V.A. Alexeev (Danish Center for Earth System Science, University of Copenhagen, Juliane Maries Vej 30, DK-2100 Copenhagen O, Denmark. email: jrb@gfy.ku.dk)

A fundamental problem in climate research is that of explaining how the Earth's climate remains stable on very long timescales. Positive feedback mechanisms such as the ice-albedo feedback and the lower tropospheric water vapour/infrared radiative (WVIR) feedback are known to exist which could, in principle, drive the climate system far from its observed mean state even in the absence of any external forcings. Extreme scenarios that have been envisaged are a completely ice-covered Earth and a runaway greenhouse such as seems to have occurred on Venus.

There is at present no generally accepted explanation for the stability of the Earth's climate, though a number of stabilizing mechanisms (based mainly on the radiative effects of clouds or upper tropospheric water vapour) have been proposed. Recently, a new stabilizing mechanism based on the linkage between the global atmospheric angular momentum (AM) cycle and the surface winds and evaporation has been proposed (Bates, 1999, Tellus in press). An empirical relationship found between the poleward AM transport across 30° and the difference between the mean height of the 500hPa surface in the tropics and extratropics has allowed a simple climate model to be constructed in which the surface fluxes of energy from the ocean surface are calculated explicitly. An analytical solution for perturbations about the model's equilibrium



climate has been obtained. This provides criteria for the stability of the model's equilibrium climate. The tendency towards instability resulting from the WVIR feedback is found to be overcome by the stabilizing influence of the evaporative heat loss determined by the atmospheric AM transport. Supporting evidence for the validity of the stabilizing mechanism is provided by experiments with a GCM in which the sea surface temperature is perturbed.

## Wednesday 21 July PM

Presiding Chair: R.A. Duce, Texas A & M University, USA

**U3/W/13-A3** Invited **1400**

### CLIMATE SYSTEM INTERACTIONS IN EL NINO/SOUTHERN OSCILLATION.

David Neelin, University of California, Los Angeles, USA, email: neelin@ucla.edu

The El Nino/Southern Oscillation (ENSO) phenomenon provides a prime example of a complex suite of interactions among climate system components. These include ocean-atmosphere interaction, interaction of convective ensembles with large-scale atmospheric flow, cloud-radiative interaction, the interactions involved in teleconnections, interaction of ENSO with Earth's seasonal cycle, and interaction of the slow components of the ocean-atmosphere system with weather. A combination of review and current work is presented, focusing on how to make a distinction among different degrees of coupling between subcomponents of the climate system within a phenomenon. ENSO may be said to be "strongly coupled" in the following sense: neither the time scale nor the spatial structure are characteristic of either the atmospheric or oceanic subsystem considered alone. While the ocean provides the memory of the system, it does so subject to the spatial structure of the wind stress. The atmosphere's adjustment by fast internal waves tends to set large spatial scales, but the specific structure depends on the interaction with the ocean. The characteristic timescale and spatial structure of ENSO may thus be considered fundamentally the product of coupling. On the other hand, while interactions of the ENSO phenomenon with both the seasonal cycle and weather are important, meaningful separations can be made. For instance, weather can be approximated as a noise product independent of ENSO in a climate model, and ENSO predictability in presence or absence of weather noise can be evaluated. The interaction between deep moist convection and large-scale atmospheric flow, as occurs in ENSO and other tropical phenomena is another example of strong coupling. Cloud-radiative interaction can play a significant role in ENSO teleconnections within the tropics, but it appears to be a modifying role rather than a fundamental one.

**U3/W/12-A3** Invited **1430**

### LOW FREQUENCY CLIMATE VARIABILITY AND ITS LINK TO THE OCEAN'S THERMOHALINE CIRCULATION

Andrew J. WEAVER (School of Earth and Ocean Sciences, University of Victoria, PO Box 3055, Victoria, BC, CANADA, Email: weaver@uvic.ca)

Climate records during the Holocene and the last glaciation have revealed substantial variability on decadal-millennial timescales. Both coupled atmosphere-ocean and uncoupled ocean-only models have also suggested mechanisms for this observed variability. Recent model results are presented to elucidate these mechanisms with special attention given to the role of the North Atlantic thermohaline circulation.

Initially, modelling evidence is given to suggest that the North Atlantic interdecadal variability, found in the GFDL coupled model, is a mode of the full coupled atmosphere-ocean-sea ice climate system. A follow-up analysis using the UVic coupled model suggests that interactions between the North Atlantic thermohaline circulation and Arctic sea-ice and freshwater export may play a crucial role in understanding this variability.

Recent numerical results from both coupled and uncoupled models are also presented to examine mechanisms for centennial-millennial timescale North Atlantic climate variability. Particular attention is given to understanding the observed millennial timescale Dansgaard-Oeschger variability during the last glaciation, its packaging into Bond Cycles and its association with Heinrich events.

**U3/L/01-A3** Invited **1500**

### MODELLING CRYOSPHERE-CLIMATE INTERACTIONS DURING THE LAST GLACIAL CYCLE

Paul J Valdes and Robin Glover (Department of Meteorology, University of Reading, Whiteknights, PO Box 243, Reading, RG6 6BB UK, email: P.J.Valdes@reading.ac.uk)

The last glacial-interglacial cycle presents a particularly challenging test of Earth System Models, and especially the coupling between the atmosphere-ocean system and the cryosphere-lithosphere system. General circulation models (GCM) have had particular problems in simulating the glacial inception period without having to invoke further feedbacks from vegetation. We will review this work and show new results from a cryosphere model forced by snapshot climate simulations from the UGAMP GCM. The work helps explain the problem of simulating glacial inception.

In addition, we will apply the same technique to the last glacial maximum and the subsequent deglaciation.

**U3/E/01-A3** Invited **1600**

### THE LATE PLEISTOCENE ICE-AGE CYCLE: AN ASTRONOMICALLY FORCED NONLINEAR OSCILLATION IN THE CLIMATE SYSTEM

Richard Peltier (Department of Physics, University of Toronto, Toronto, Ontario, M5S-1A7, Canada, email peltier@atmsop.physics.utoronto.ca)

The 100 kyr quasi-periodic oscillation of continental ice volume that has dominated climate variability since mid-Pleistocene time is entirely explicable as a nonlinear response of the system to orbital insolation forcing. A successful model of the phenomenon appears to require explicit treatment of atmospheric, cryospheric and solid-earth processes as well as an accounting for the amplification of the direct influence of insolation forcing due to the varying concentration of atmospheric carbon dioxide. I will describe a sequence of experiments with a model based upon this minimal mix of ingredients which explicitly predicts both the geographical regions that are subject to glaciation and deglaciation as well as the magnitude of the sea level depression that is observed to have attended ice-sheet growth.

**U3/W/04-A3** Invited **1630**

### THE COUPLED SYSTEM OF MANTLE CONVECTION AND LITHOSPHERIC PLATE TECTONICS: TOWARDS A SELF-CONSISTENT MODEL

Paul J. Tackley (Earth and Space Sciences Department, University of California, Los Angeles, CA 90095, USA, email: ptackley@ess.ucla.edu)

Lithospheric plate tectonics and mantle convection are different aspects of the same, coupled system, yet mantle convection simulations do not exhibit plate tectonic behavior unless it is imposed by the modeler, largely because 'realistic' temperature-dependent viscosity results in a stiff, immobile, rigid lid. Traditional methods of coupling 'plates' into mantle convection simulations involve the specification of plate boundaries as 'weak zones' or faults, or the specification of plates themselves as a velocity boundary condition. While such approaches have facilitated some important research, it is ultimately necessary to identify the correct 'self-consistent' description of plate tectonics and mantle convection, in which both components arise naturally out of a unified material description of rock deformation as a function of temperature, pressure, and stress. Field observations and materials science suggest that lithospheric strength may be dominated by ductile, semi-brittle deformation processes in the middle lithosphere, with brittle failure (faults) being important in the upper ~15 km, and viscous creep in the deep lithosphere and mantle. Thus, ductile shear localization in the mid-lithosphere may be the key process in the formation of weak plate boundaries. Possible localization mechanisms can be described using time-dependent evolution equations, allowing evolving lithospheric strength heterogeneity with long-term memory. Such descriptions are used to demonstrate the formation of weak transform boundaries in a 2-D model, and convergent, divergent and strike-slip boundaries in 3-D models. The role of elastic and brittle behaviors will also be discussed, as will future directions and philosophical issues.

**U3/W/02-A3** Invited **1700**

### NUMERICAL MODELLING OF THE GEODYNAMO AND CORE-MANTLE COUPLING

Jeremy BLOXHAM (Department of Earth & Planetary Sciences, Harvard University, Cambridge, MA 02138, USA. Email: Jeremy\_Bloxham@harvard.edu)

Of the various components of the Earth system, the most remote is the geodynamo operating in the Earth's core. The concomitant scarcity of observations is exacerbated not only by the complexity of the physics of the geodynamo but also by the inaccessibility of the dynamical regime of the core to direct numerical investigation. The almost vanishingly small role played by viscosity and the almost equally small, but nonetheless important, role played by inertia renders the system one that presents a great challenge to numerical studies.

Nonetheless, significant progress has been made over the last few years in the development of numerical models of the geodynamo, though none of the models is free of approximations, some of which are, unfortunately, introduced more for numerical expediency than for sound geophysical reasons. Here we review this progress and comment on the effect of these approximations on the solutions.

An additional complicating factor is that the geodynamo cannot be considered in isolation from the rest of the Earth system. The transport of heat from the core - which drives the geodynamo - is controlled by the mantle, and the pattern of mantle convection imposes lateral variations in the heat flux from the core. We show that this thermal core-mantle coupling influences the pattern of magnetic field at the core-mantle boundary, and that the pattern of mantle convection inferred from seismic tomography gives rise to a certain observed features in the magnetic field.

## Wednesday 21 July AM

**U3/E/02-A3** Poster **0900-01**

### THE REDUNDANCY IN NUMERICAL MODELS OF COMPLEX GEOPHYSICAL SYSTEMS

IRINA P. CHUBARENKO (P.P. Shirshov's Institute of Oceanology of Russian Academy of Sciences, Atlantic Branch, Prospect Mira, 1, 236000, Kaliningrad, Russia, E-mail: irina@ioran.kern.ru)

The majority of predicting models for complex geophysical systems (for example, for seaside lagoon) are based nowadays on the numerical solution of differential equations of movement, state or balance for some values. In doing so, some restrictions such as additional conditions and various approximations are applied because of the complexity of accurate decision. So, the numerical solutions obtained are not precise because of both restrictions of the problem statement (it is impossible to put down all the equations, managing the system), and its numerical realization (variety of approaches of the discretization of governing equations and time-space domain approximation). Besides, model solutions are always labour-consuming because of difficult procedure of calibration and verification, especially in the case of non-linear relationships using. The alternative approach to complex system model creation is to use modern philosophy of the processes hierarchy, scaling, fractal properties of natural processes and systems together with ideas of the redundancy within the model. In the work presented the ideas of redundancy are discussed in application to inter-disciplinary complex model creation. As for this case the redundancy of the model means the possibility to calculate some parameters of a system or process in different ways simultaneously. This approach has required research of peculiar problems: analysis and transmission of the information obtained in the models complex between various space and temporary scales, between different submodels of the process; advisable degree of redundancy; criteria for choosing of the simulated system development version.

**U3/E/03-A3** Poster **0900-02**

### GROUND-ATMOSPHERE-IONOSPHERE-MAGNETOSPHERE COUPLING CONCEPTION INCLUDING SEISMIC ACTIVITY

PULINETS S. A., Boyarchuk K.A., Hegai V.V., Shklyar D.R. (IZMIRAN, Troitsk, Moscow Region, 142092, Russia, E-mail: pulse@izmiran.rssi.ru)

During last 10 years the model of atmosphere-ionosphere coupling based on the quasi-electrostatic vertical atmospheric electric field penetration into the ionosphere was developed at IZMIRAN. The model consist of three parts: 1-electric field generation model, 2-electric field penetration at thermosphere-ionosphere heights, and 3-effects of electric field in the thermosphere-ionosphere. In the first part a model of ion kinetics in a near-ground layer of troposphere is considered. It explains the appearance of strong vertical electric field up to several kV/m near the ground surface. Second part with the help of existing model of atmosphere conductivity vertical distribution makes calculations of penetrated electric field at the heights from 90 up to 1000 km. It explains the transverse to geomagnetic field lines electric field ~ 1 mV/m at the ionospheric heights as a result of original vertical electric field ~ 1 kV/m at the ground surface. The third part demonstrates the effects of electron concentration modification over the vertical electric field source. Self-consistence of the model is substantiated by correspondence of the calculated parameters to the measured experimentally. Recently the model was supplemented by effects in magnetosphere (ion composition changes, VLF noises amplification), as well as by near-ground calculations (underwater effects, near-ground generation of ELF-VLF emissions). In present state the complete set of works could be regarded as complete conception of Ground- Atmosphere-Ionosphere-Magnetosphere Coupling based on the quasi-electrostatic vertical electric field effect.



**U3/E/04-A3** Poster **0900-03**

**CONCERNING SOME ASPECTS OF THE EARTH SYSTEM**

RASULOV D.Kh., Lange Institute of Hydrogeology and Engineering Geology Tashkent, Uzbekistan, e-mail: root@ariel.tashkent.uz

The work gives in details a new piezoelectric model of terrestrial magnetism which permits all the main features of geomagnetic field to be explained from the unified positions (see abstracts in GA1.01 and JSA37). In accordance with the model, owing to semi-diurnal rising tides, in the liquid Earth's core a toroidal flow in equatorial region which is normal to the geographic axis is to exist. Geomagnetic field inversion occurs when changing relatively mantle the direction of the core rotation angular velocity to the reverse one. The model permits some phenomena of the nature to be explained quite simply whose physics was not ascertained finely. One of this phenomenon is a fact of the constant presence of electric charge on the terrestrial surface. Today, in accordance with the model, negative charge will constantly flow to the surface of the Earth in the regions located at the low and middle latitudes. Again, positive electric charge stored at the rotation axis of the core. Owing to vertical atmospheric currents, an electric charge stored at the surface decreases, but because of rotation of the liquid core in the magnetic field it restores again.

**U3/E/05-A3** Poster **0900-04**

**FERTILIZER FEEDBACKS ON CLIMATE**

ROBERT DICKINSON, PAS Rm 480, P.O. Box 210081, University of Arizona, Tucson AZ, 85721, USA

Evapotranspiration is a key control on climate. Much of the transfer of water from soil to atmosphere passes through leaves where stomates control the rate. Recent formulations of leaf stomatal functioning implemented in climate models have followed a framework for photosynthesis first formulated by Farquhar, and have related stomatal controls on evapotranspiration to leaf carbon assimilation. However, the maximum photosynthetic capacity parameter of such formulations depends on the numbers of enzymes in the leaves that catalyze the leaf uptake of CO<sub>2</sub>. These enzymes, the most important of which is Rubisco, require substantial amounts of nitrogen for their construction. A model has been developed for coupled cycles of carbon and nitrogen integrated in a GCM climate model that illustrates the dynamics of such a system. Both soil plant exchanges and atmospheric sources and sinks are treated. This system has been built on BATS/CCM3 heritage code but is largely independent of that framework. The presentation title derives from the assumption that agricultural systems have a larger external source of nitrogen than do natural ones from which they are differentiated by their increased productivity and accompanying evapotranspiration. The presentation will address one of the more interesting physiological details that are treated, aspects that are still somewhat speculative, and comparison of the CCM3 15 year simulation with controls not including these interactions. An initial framework for the carbon aspects of seasonally varying leaf growth has been published in Dickinson et al., 1998, J. Climate.

**U3/E/06-A3** Poster **0900-05**

**ATMOSPHERIC OXYGEN RISE AT ABOUT 1.9 GA: REE (CE ANOMALY) EVIDENCE FROM CARBONATE SEDIMENTS**

QIU Yu-zhao and Fan Wen-ling (Institute of Geochemistry, Chinese Academy of Sciences, Guiyang 550002, CHINA)

More REE analyses of Chinese, South African and Australian Precambrian carbonate sediments confirmed and refined the preliminary idea suggested by Qiu (1987), which mainly based on rather limited samples of Chinese formations analyzed at Prof. Haskin's INAA lab. This result supports the traditional model of atmospheric oxygen evolution, i.e. the gradual increasing model, and is also in agreement with constraints indicated by other studies on temporal developments of BIFs, red beds, stratiform Cu deposits and Au-U conglomerates as well as the carbon isotope excursions all over the world. It may be more reasonable to consider an equilibrium state between atmosphere and upper hydrosphere (shallow sea water), in which most carbonates precipitated. As to the BIF, the formation condition should be more complicated. Therefore, unreliable is the model that argued Archean atmosphere to be in high oxygen level on the basis of negative Ce anomalies discovered in BIF ores. An oxygen fugacity vs pH value diagram has been constructed by means of thermodynamic calculation. Preliminary estimation for atmospheric oxygen level at about 1.9 Ga, when Ce(III) was oxidized to Ce(IV) in seawater or weathering surface, has been made for varied atmospheric CO<sub>2</sub> levels and pH values.

**U3/E/08-A3** Poster **0900-06**

**UNITED TIME SYSTEM OF EARTH SYSTEM MODEL**

Tarzadin ULAANBAATAR (Department of Earth Sciences, National University of Mongolia, email: numelect@maginet.mn)

In Earth System Model must incorporate Earth's basic support system: air, water, ocean and land, geophysical system: gravity, geoelectromagnetism, heliogeothermosphere, seismology and physics of Earth's interior, as well as biogeochemistry, climate system and society. For instance, the success of developing complete Earth System Model depends on the fundamental assumption, according to which all the sub-components of the Earth are necessary, at first, to be described by uppermost elementary parameters, at second, to be governed under a united time system based on the daily and yearly motions of the Earth in geographical coordinate system.

In this paper some laws and principles in hierarchy complexity in the thermal regimes on and near the Earth's surface, climate oscillation and daylight for reconstruction, estimation and predictability in different time interval of global, regional and local scales are described brand-newly by time of calculation, date, geographical latitude, terrain height and albedo.

Furthermore, their results and some proposed ideas for developing Earth System Model are shown. Among above mentioned systems the basic support system, heliogeothermosphere, climate system, biogeochemistry, gravity and their wide use in the service of humankind, as well as application in planetology, planetary-scale explorations of organic resources in earth's crust and so on are described.

**U3/P/01-A3** Poster **0900-07**

**ON THE SOUNDS OF THE CLIMATE SYSTEM'S DYNAMICAL STATUS AND EVOLUTION**

Peter CARL (Climate Dynamics Project, c/o Forschungsvorband Berlin, Hausvogteiplatz 5-7, D -10117 B Berlin, Germany, email: pcarl@ splim5. wias-berlin.de)

One of the intriguing questions in climate dynamics is concerned with low-dimensional contributions in the system's motion and predictability. Self-restriction in dimensionality is

bound to synchronisation - which offers a conceptual key when trying to identify the status and evolution of the Earth system. "Dynamic control" by the annual forcing constitutes the topological nature of its seasonal cycle. As studies with a conceptual GCM of about 4.000 d.o.f. have shown, the very existence of today's intraseasonal monsoon dynamics may indicate presence of a "route to chaos" via successive Hopf bifurcations in the atmosphere-land system. The resulting toroidal 'geometry of behaviour' in boreal summer provides a useful conceptual view on climate scales and phenomena across the annual forcing.

If the model does correctly exhibit monsoon onset as a 'hard', subcritical transition into a chaotic July regime, onset dates define natural Poincare sections that offer hints to the topology behind interannual climate dynamics, too. Reading this century's score of monsoon onsets from the southern tip of peninsular India by time-frequency methods comes up with that expectation. Moreover, the challenging methane anomaly of the early 90th presents itself as a phase coincidence across the annual forcing scale, announced in the monsoon series. Full modal structures unveil frequency relationships that point to organised yet highly complex, nonstationary dynamics.

**U3/P/02-A3** Poster **0900-08**

**GEOMAGNETIC CHARACTERISTICS OF THE DOJRAN LAKE AREA**

Todor Delipetrov (Faculty of Mining and Geology, University "Kiril and Metodij" Skopje, Stip, MK, email: todor@rgf.ukim.edu.mk); Krsto Blazev (Faculty of Mining and Geology, University "Kiril and Metodij" Skopje, Stip, MK, email: krsto@rgf.ukim.edu.mk) Deljo Karakasev (Faculty of Mining and Geology, University "Kiril and Metodij" Skopje, Stip, MK, email: karak@rgf.ukim.edu.mk)

Terrestrial measurements of the total vector of magnetic field were carried out in the 'area o the Dojran Lake. Study of data made possible to compile a map of the anomalies of total vector of magnetic field DT. The application of method of polynomial regression analysis as filter separated the regional DTR from local DT anomalies.

The map of local anomalies separates the eastern from the northern contour faults along which relative dip of the depression took place with relation to surrounding blocks of uplift.

The map of regional anomalies of the total vector of magnetic field DTR indicates that the field is fairly quiet or the gradient of the field above the lake is very low. Greater changes can be found in the northeast and southeast parts of the Dojran depression.

**U3/P/03-A3** Poster **0900-09**

**A MODEL FOR FLUID PORE PRESSURE AND ITS AFFECTION ON THE SEISMICITY IN THE SYSTEM**

Li LI and Guomin Zhang (Center for Analysis and Prediction, China Seismological Bureau, P.O. Box 166, Beijing 100036, China, email: zgm@cap.ac.cn); Yaolin Shi (Graduate School, University of Science and Technology in China,

A dynamic network is used to simulate the transportation and the diffusion of pore fluid in a seismogenetic system and the triggering effects of the variation in pore pressure on the temporal, spatial and magnitude distribution of earthquakes in the system are analysed in detail. The model contains 10 pre-existed seismic belts and there are 15 potential seismic sources in each belt. The whole system is a 2D netlike model that comprises of 150 Maxwell bodies, which will produce artificial catalogues with some definite boundary condition. Another Maxwell body is laid between every two neighboring sources in different belts, which is used as a coupled seismic source that will never break and as a passage for the stress and fluid between the potential sources in neighboring belts. Assumed that the pore fluid spreads in the system following the diffusion equation, i.e.,  $\frac{\partial p}{\partial t} = \nabla^2 p$ , where  $S$  is the temporal propagating coefficient of pore pressure,  $P$  is the pore pressure,  $Kx$  and  $Ky$  are the spatial propagating coefficient along  $x$  axis and  $y$  axis respectively, and  $A$  is for fluid source. The equation is dispersed according to the model used in this paper and solved in an implicit way. Based on the interpretation by Brace and Byerlee in 1996 (Brace, W.R and Byerlee, J.D., 1996) that the mechanism of the shallow shocks is the unstable stick slips and the experimental results by Ziqiang Guo et al in 1989, we assumed that there are no fluid sources in the system and the pore pressure within the broken seismic source decreases about 1/n of its strength immediately after the shock, while the pore pressures in its neighboring sources increase 1/4n of their strengths respectively, in spite of how many potential sources are around the broken one. The coefficient of  $n$  is the pore pressure response parameter of the system, which shows the influence intensity of the pore pressure on the strength of the seismic sources. The larger the  $n$  is, the smaller is the influence. The G-R relations, the  $\Sigma N - t$  and  $M-t$  curves of the artificial shocks are compared in this paper for the wet system in which the influence of the pore pressure is considered and for the dry system in which on fluid is transported. The result shows that the pore fluid and the derived pore pressure have triggered many shocks in the wet system. Under the pore pressure, the number of the shocks in the wet system is larger than that in the dry system and the maximum magnitude of the shocks is higher. The fluid in the system influences the seismicity in the 2D system totally, in temporal and spatial distribution and in the magnitudes and makes it more difficult to forecast the shocks in the system.

**U3/P/04-A3** Poster **0900-10**

**DEVELOPING EARTH SYSTEM MODEL THROUGH CHAOTIC DYNAMICS**

H.N. SRIVASTAVA (India Meteorological Department, New Delhi- 110003, India, e-mail: snb@imd.emet.in)

Earth atmosphere system has been investigated by integrating different observations derived from chaotic dynamics extending from earth's core to the outer atmosphere. Deeper insight has been provided through our results to distinguish earthquake dynamics on different type of plate boundaries. The atmospheric dynamics could be discussed through the strange attractor dimension of about 6 in respect of atmospheric pressure, maximum and minimum temperatures and monsoon rainfall. In the middle atmosphere, same order of predictability was found from ozone observations. However, ionospheric magnetospheric system had a low dimension of about 2 to 3. Using the concepts of compound chaos predictability of monsoon rainfall over India can be studied for Lorenz and Rossler Systems using any two parameters like ENSO and minimum temperature. However, since, this method can not be extended to more than two parameters, the question of earth system predictability appears to remain unresolved using this dynamical approach.

**U3/W/05-A3** Poster **0900-11**

**A NEW EARTH SYSTEM MODEL FOR THE LONG-TERM COEVOLUTION OF GEOSPHERE AND BIOSPHERE**

Siegfried Franck, Arthur Block, Werner von Bloh, Christine Bounama, Hans-Joachim Schellnhuber, Yuri Svirezhev (all at Potsdam Institute for Climate Impact Research, PF 601203, D-14412 Potsdam, Germany, email: franck@pik-potsdam.de)

We present a qualitative geosphere-biosphere model to analyse the evolution of the Earth system on a global scale from the geological past to the planetary future in 1.5 billion years. Our Earth system model consists of the components solid Earth, hydrosphere, atmosphere,

and biosphere. It evolves under the external influence of increasing solar luminosity. The model is based on a quasi-equilibrium formulation of the large-scale global carbon balance between the main sources and the main sinks as modified by the biosphere. To calculate the weathering rate we take into account the growth of continental area over geological time scales and extrapolate the present continental growth rate to the future. We determine the "terrestrial life corridor" for the existence of a photosynthesis-based biosphere in the dependence on the state parameters of the Earth system. In the case of the steady-state approximation without continental growth we reproduce the results of Caldeira and Kasting (1992) about the life-span of the biosphere. The consideration of continental growth in the new model gives a higher atmospheric carbon content for the past but a much stronger decrease for the future. This leads to a reduction of the life-span of the biosphere of up to some hundred million years. We calculate the habitable zone for the past, the present, and the planetary future. From this results we derive the optimum position for an Earth-like planet and calculate the maximum life-span of any photosynthesis-based biosphere.

**U3/W/06-A3** Poster **0900-12**

**THE GLOBAL MODEL OF THE EARTH'S ANOMAL STRUCTURE FROM THE MODERN SEISMIC, PETROLOGICAL AND GRAVITY DATA**

Susanna A. Kazaryan (Sternberg State Astronomical Institute, Universitetskij pr.13, Moscow, e-mail: kazaryan@sai.msu.ru), Nadejda A. Chujkova and Tatiana G. Maximiva (both at Sternberg State Astronomical Institute, Universitetskij pr.13, Moscow, e-mail: chujkova@sai.msu.ru)

The Earth's equivalent rock topography and depths of Moho discontinuity are represented as the spherical function expansion up to degree 30. The gravity field of the crust is calculated and subtracted from the Earth's global gravity field. The interpretation of the remaining anomalies sources is carried out. The coordinates of sources are determined from the map of the remaining gravity anomalies. The masses and depths are determined from the decision of the inverse problem. The obtained results show, that global gravity anomalies near Antarctica (negative) and Australia (positive) can be caused by the anomalies of the outer core boundary; positive anomaly near Caspian sea can be caused by the shift of the Earth's inner core; negative anomaly in Indian ocean corresponds to upper mantle' anomaly; positive anomaly in South Atlantic ocean corresponds to crust' anomaly.

**U3/W/08-A3** Poster **0900-13**

**DYNAMICS AND CHEMISTRY OF ATMOSPHERE AND OCEANS IN AN EARTH SYSTEM MODEL**

Carlos R. MECHOSO, J. D. Farrara, L. A. Drummond, R. P. Turco, M. Gupta, and J.A. Spahr (all at Department of Atmospheric Sciences, University of California, Los Angeles, CA 90095-1565, email: mechoso@atmos.ucla.edu); Y. Chao (Earth and Space Science Division, JPL, California Institute of Technology, Pasadena, CA 91109, email: yc@comp.jpl.nasa.gov) J. Demmel, H. B. Robinson, and K. Sklower (all at Department of Computer Sciences, University of California, Berkeley, CA 94720-1776, e-mail: demmel@cs.berkeley.edu)

This paper describes the methodology for design, code performance and preliminary results of an Earth System Model (ESM) developed by a team of Earth and computer scientists. The model is used for ensembles of climate simulations in high-end computing environments. The ESM has three modules: 1) "Models", 2) Distributed Data Broker (DDB), and 3) Verification, Analysis and Control System (VACS). Currently, "Models" includes an atmospheric general circulation model (UCLA AGCM), oceanic general circulation model (Parallel Ocean Program, POP), and atmospheric chemistry model (UCLA ACM). It will soon incorporate an oceanic chemistry model. DDB performs data exchanges and synchronizations between model subdomains based on a consumer-producer paradigm. VACS uses a Data Base Management System (DBMS) and a specialized data schema called "BigSur" to verify and analyze the model output, and has a web-based user interface to control model execution. Some of the model codes, particularly the AGCM, have been highly optimized with emphasis on algorithm improvement and load balancing. The AGCM (2.5 lon x 2 lat x 29 levels) with tracers CFC-11 and CFC-12, coupled to an Atlantic version of POP (1/6 lon x 1/6 lat x 37 levels) requires 47 s to simulate one day of climate on 756 processors of a CRAY T3E-600 (~40 GFLOPS). Selected model results will be presented at the Conference.

**U3/W/09-A3** Poster **0900-14**

**EURASIA MORPHOTECTONICS AND RELIEF OF THE GEOID AND THE CORE-MANTLE BOUNDARY**

Gennady F. UFIMTSEV. Institute of the Earth's Crust, Lermontov str. 128, 664033 Irkutsk, Russia. E-mail: ufim@gpg.crust.irkutsk.ru

1. In relief of geoid and the core-mantle boundary two associations of forms escape and their combinations are circumscribed by different groups of symmetry. In a sector of the West Pacific ocean, Indian ocean and Asia forms of relief of both surfaces are antisymmetric each other. In a sector of Atlantic region, Africa and America bilateral symmetry takes place. These sectors are divided by the Ural-Oman-Madagascar lineament ("axis") being in relief of both surfaces. This "axis" together with the East Asian lineament is the largest boundary in the post-gondwanian (Late Mesozoic and Cenozoic) Earth structure.
2. In the geoid relief the Urals-Oman-Madagascar "axis" is a slope of a geopotential surface. The meridional sutural block orogen of the Urals adjoins to its upper lip, but the extensive escarpment on the right-side of the Yenisei dividing young West Siberian and ancient Siberian platforms adjoins to its bottom. This escarpment is similar to the great escarpments of margins of the gonwanian continents.
3. The Ural-Oman-Madagascar axis divides Eurasia into two parts with mirror similar dislocation of main forms of tectonic relief: uplifted plains and plateau of the Siberian and Russian platforms, their marginal escarpments of the north-western Scandinavia coast and the northern slope of the Putoran plateau; young mobile belts of low base and mediterranean seas (Alpine belt and Mediterranean region, Indo-China and Zondian region); orogenic belts of high base (Iran and Asia Minor, Tibet-Himalayas); gondwanian subcontinents and their coastal great escarpments adjoined to Eurasia (Arabia and Hindustan). Rejuvenated orogenic belts spread on the east of Eurasia only and adjoin to the "cold" cap in a form of the largest depression of geoid surface.
4. The Pamirs-Punjabian and Assamian syntaxes are situated in the Ural-Oman-Madagascar and East-Asian slopes of a geopotential surface limits correspondingly which restrict the depression of geoid surface. This depression is divided into two steps. Plunging anticlines of the geoid's surface being connected with the Alpine-Himalayan mobile megabelt are disposed between them. The Himalayan front faced southward connects with steep scarp of the geopotential's surface.

**U3/W/14-A3** Poster **0900-15**

**THE PREDICTION OF THE REGIONAL NCEP ETA MODEL WITH DIFFERENT LAND SURFACE SCHEMES**

YONGKANG XUE, Y. Ji (both at Department of Geography, University of Maryland, College Park, MD 20742, USA Tel: 301-405-4050; fax: 301-314-9299, email:yxue@geog.umd.edu); E. Roger, T. Black, Z. Janjic and K. Mitchell (all at Development Division, NCEP, NOAA, Camp Springs, MD, USA)

Previous studies show that a coupled Eta/SSiB model is able to realistically simulate different climate scenarios. In these experiments, the model is only integrated for 48 hours. The forecast for June 1988 and July 1993 are averaged, respectively, to obtain the regional climate. However, because the model is initialized every 24 hours in these studies, the prediction for some hydrological variables, such as runoff, is mainly determined by the initial conditions. To understand the regional climate predictability, we have developed the Eta/SiB model for long term prediction studies. Long term numerical integrations are carried out for June and July 1998, June and July 1993, and June 1988 to investigate the time scale of the predictability for the Eta model. Both the 1993 and 1998 spring season have strong ENSO events. The summer of 1988 is extremely dry. The Eta/SSiB has reasonably good simulations for 1998 and 1988. The results from the Eta/SSiB are compared with the current Eta model simulations (with different land surface scheme). The preliminary results show that adequate simulations of large scale circulation, i.e., the low level jet and 200mb wind fields, are the key in successful North American regional climate prediction. The results also show that land

**U3/W/15-A3** Poster **0900-16**

**A TYPE OF COMPUTATIONAL CLIMATE DRIFT OF THE LARGEST SCALES MOTIONS IN BAROCLINIC PRIMITIVE EQUATIONS**

Qing ZHONG, Institute of Atmospheric Physics, Chinese Academy of Sciences, Beijing 100029, China, Email: zhongq@sgj50s.iap.ac.cn

A type of computational climate drift of the largest scales motions in baroclinic primitive equations system is newly revealed in this work. The origin of this computational drift is analyzed, and its unfavorable sequence in relation with predictability of numerical models for weather and climate is also discussed. Moreover, a new successful numerical technique to eliminate this kind of computational systematical error sources/sinks thereby largely reduce the total characteristic model errors in relation with the largest scales motions of atmosphere is discovered, formulated as well as numerically tested. In addition, some applications of this technique is also discussed as a new way to eliminate a corresponding type of computational systematic error source/sink in any Earth System Models, based on currently-used traditional type numerical techniques, with more sophisticated sub-components and thereby make further progress on the fundamental problem of Earth System predictability.

**U3/W/21-A3** Poster **0900-17**

**DEVELOPMENT OF SEISMIC RAPID REPORTING AND EARLY WARNING SYSTEM IN TAIWAN**

Yih-Min Wu(1), Jen-Kuang Chung(1), Tzay-Chyn Shin(1), Yi-Ben Tsai(2), and William H.K. Lee(3)  
1. Central Weather Bureau, 64 Kung Yuan Road, Taipei, Taiwan, 2. Institute of Geophysics, National Central University, Chung-li, Taiwan, 3. 862 Richardson Court, Palo Alto, CA 94303, USA

In 1994, two prototype seismic early warning systems have been implemented in Taiwan: (1) a rapid reporting system using a telemetered network of digital accelerographs spread over the entire island, and (2) an alert system exploring the use of modern technology for the highly seismic area of Hualien. After four-years operation, the rapid reporting system was successfully operated in the seismic monitoring system of the Central Weather Bureau (CWB) for felt earthquake observation (Taiwan Rapid Earthquake Information Release System, TREIRS). It has achieved in the determined of precise earthquake location and magnitude computation about in one minute after the earthquake origin times. On the other hand, the Healien alert system was phase-out in 1998 due to large uncertainty of source parameters determination caused by small station coverage, unsuitable automatic phase picker, and only using P waves in determining the magnitude, although it performed a very well reporting time. Recently, the Hualien alert system stations were equipped with the digital accelerograph and combined to the TREIRS system. By adding the Hualien alert system stations to the TREIRS system, we have obtained a good precision for source parameter determination and a well reporting time for Hualien area earthquake monitoring. During the experiment in the past several years, we benefited from these two prototype seismic early warning systems and optimized the TREIRS system. We are encouraged forwards in the development of seismic early warning system based on the successful experience.

**U4** **Thursday 22 July**

**MEGACITIES AND GEOPHYSICS**

Location: Great Hall

**Thursday 22 July AM**

Presiding Chair: TBA

**U4/W/04-A4** **0945**

**BASIC EARTH SCIENCES AND HAZARDS IN MEGACITIES**

Vladimir Keilis-Borok (International Institute of Earthquake Prediction Theory and Mathematical Geophysics, Russian Academy of Sciences, Warshavskoye shosse 79 kor.2, Moscow 113556, Russia, email: vkbork@mitp.ru)

The paper outlines the methodological background of the R&D aimed at containment of the hazards threatening the megacities. While each megacity is unique, this background is partly common for all of them. Three groups of problems are considered: 1) Geotechnical instability of a megacity. 2) Evaluation of possible damage to population, economy and ecology, the worldwide ripple effect included. 3) Disasters' prediction, preparedness, and (in some cases) control. New yet untapped possibilities for R&D in these problems come from integration of: 1) Modeling of "universal" scenarios of critical transitions, common for diverse chaotic systems, not necessary Earth - specific. 2) Modeling of Earth -specific scenarios, intervened with universal ones. 3) Joint phenomenological analysis of the relevant observed fields. 4) Probabilistic risk analysis. Important immediate promise comes from a proper choice of scaling.

**U4/W/06-A4 1015****VOLCANOES AND MEGACITIES**

Grant HEIKEN and Greg Valentine (Earth and Environmental Sciences Division, Los Alamos National Laboratory, Los Alamos, NM 87545, email: heiken@lanl.gov and gav@lanl.gov); Giovanni Orsi (Osservatorio Vesuviano, viale Gramsci, 17b, 80122 Napoli, Italy, e-mail: orsi@ischi.osve.unina.it)

Cities will continue to grow in the 21st Century as the living environment for most of humanity and as foci for the global economy. A volcanic eruption near a large city can have serious regional or global effects. Globally, there are 59 cities near potentially active volcanoes, including 2 megacities; the combined population at risk is over 50 million. As a result, more volcanologists are moving "into the city." There is a growing focus toward the integration of volcanic hazard studies with data-based models of urban infrastructure (e.g., transportation, energy, telecommunications, water distribution, and public health), and with the social and political framework. To prevent large-scale disasters in cities located on or near volcanoes, we must go well beyond the traditional hazard mapping and monitoring and involve the community in extensive education and public awareness campaigns. Risk evaluation must rely heavily on modeling and visualization of physical processes and their effects in a fashion that can be easily grasped by emergency planners, the insurance industry, policy makers, and the public. But it is not enough to focus individual disciplines such as volcanology on urban issues. We must take major steps toward integrating all the geophysical, atmospheric, hydrologic, and geological sciences for interdisciplinary approaches to solving the urban problems of vulnerability and sustainability. An additional but essential step is the integration of these physical sciences with the biological sciences and with infrastructure engineering and planning. IAVCEI therefore proposes to the IUGG that the years 2000-2010 be the "International Decade of Geosciences in the Cities," and that each nation select a "Decade City" for focused interdisciplinary study.

**U4/L/02-A4 Invited 1115****HYDROLOGICAL HAZARDS AND SUSTAINABILITY**

Erich J. PLATE (Universität Karlsruhe(TH), Kaiserstr.12, Tel. ++49-721-608-3814, Fax: ++49-721-661329, e-mail: erich.plate@bau-verm.uni-karlsruhe.de)

Cities and their environments strongly interact, what happens in the city affects the social and natural structure of its surroundings, and the surroundings influence the course of development of the city. The larger the city, the more far reaching is this interaction. Rural surroundings and city form a fairly rigid system of complicated interdependencies which is in a precarious balance and quite vulnerable to sudden changes, for example when a major natural disaster, such as a flood, strikes. The vulnerability is enhanced if large parts of the population are unable to cope with natural disasters. In particular the large megacities of the world in developing countries, have drawn very large numbers of poor people who settle in areas which are susceptible to floods and landslides.

There exists a direct link between natural disasters in large cities, and sustainability. An important criterion of sustainability of a society is its stability, which implies that a population is able to adjust to changes without social disruptions. The larger a city is relative to the total population of a country, the more does its stability determine the ability of the country for a sustainable development. The strong link of megacity stability and sustainable development has been emphasised by the International Decade of Natural Disaster Reduction (IDNDR).

**U4/E/04-A4 1145****GEOPHYSICAL STUDIES FOR THE EARTHQUAKE HAZARD MITIGATION IN BEIJING**

Yun-tai CHEN (Institute of Geophysics, China Seismological Bureau, Beijing 100081, People's Republic of China, email: chenyt@public.bta.net.cn)

The city of Beijing has a population of 12 million. It is among the megacities that historically and recently have been struck by destructive earthquakes occurred in its surrounding areas. With rapid development in economy during the past two decades, Beijing is vulnerable to earthquake. In order to mitigate earthquake hazard in Beijing, seismic activity monitoring in Beijing, especially in the earthquake-prone Yanqing-Huailai basin, 60km NW of Beijing is intensified. The potential seismic risk in the Yanqing-Huailai basin is estimated using the historical documents, tectonic stress field data, velocity structure of crust-upper mantle from deep seismic reflection and other geophysical measurements as well as the data of recent seismicity. It is inferred that an earthquake with magnitude 6.0 is likely to occur in the Yanqing-Huailai basin. We also carry out studies on the seismic ground motion in the Yanqing-Huailai basin. The results obtained indicate that the source spectrum of the earthquakes occurred in the Yanqing-Huailai basin can be described by a simple omega-squared model and that the quality factor, ranging from 140 to 360, for the SH waves in the Yanqing-Huailai basin are very low. Based on the geological and geophysical data, the shallow velocity structure model of the Beijing area is constructed and the characteristics of seismic ground motion in the Beijing area are modeled. It is found that the thick Tertiary sedimentary basin in the city of Beijing plays an important role in causing amplification of seismic signals. The peak ground acceleration and the total energy of ground motion in the Tertiary depression areas are much greater than that in the other area.

**U4/W/05-A4 1215****SAN SALVADOR, EL SALVADOR, A HIGH RISK, MULTIPLE HAZARD MEGACITY**

D J SOFIELD, J W Wallace, and W I Rose (Geological Engineering and Sciences, Michigan Technological University, Houghton, MI, 49931, email:djsiefiel@mtu.edu)

Volcanism and earthquakes are the most dire geological hazards that threaten San Salvador, El Salvador's largest city (population, 1.7 million), with a rapidly growing population, and few plans or resources for hazard mitigation.

Financial, transportation, and governmental centers of El Salvador all reside within San Salvador. The city lies on a plain within severe hazard zones of two active volcanoes (San Salvador to the W and Ilopango to the E) and also lies in a zone of major subduction earthquakes. In the past 60 Ka, a caldera 12 km E of the city now occupied by Lake Ilopango erupted at least four significant pyroclastic deposits, each of which blanketed the valley that San Salvador now occupies. The last of these eruptions devastated all El Salvador in AD 260 and drove pre-Classical Mayan civilization northward into the jungles. A dome eruption in 1880 and small seismic swarms beneath the lake indicate continuing unrest.

Neither San Salvador volcano nor its numerous flank vents has erupted catastrophically since European colonization, however numerous explosive eruptions occurred prior to that. San Salvador volcano erupted ash-rich tephra and pyroclastic flows 800 years ago and caused mudslides that would likely kill many thousands today. Because of the frequency of earthquakes, the people of San Salvador are much more aware of seismic risk than volcanic risk. The city has had to rebuild 7 times after earthquakes since 1712. The most recent devastating earthquake in 1986, killed 1500, injured 10,000 and left 100,000 homeless. Thick unconsolidated pyroclastic and tephra deposits amplify the effects of shallow-focus, moderate

magnitude earthquakes beneath the city. Timely international involvement could provide the impetus that San Salvador needs to begin effective hazard-assessment, monitoring, and educational programs. A significant part of this work will be to make the population of a volcanic country more aware of its vulnerability to volcanic hazards. The recent occurrence of hurricane Mitch offers an opportunity to advance all hazard work in Central America.

**U5****Thursday 22 July****GEOPHYSICAL HAZARDS AND RISKS: PREDICTABILITY, MITIGATION AND WARNING SYSTEMS**

Location: Great Hall

**Thursday 22 July PM**

Presiding Chair: Tom Beer, (CSIRO Environmental Risk Network, Australia)

**Opening 1400****U5/E/03-A4 1430****CRITICAL CONTRIBUTIONS OF GEOPHYSICS TO THE IDNDR**

Bruce A. BOLT (Department of Geology and Geophysics, University of California, Berkeley, CA, 94720, USA, email: boltuc@socrates.berkeley.edu)

The application of recent scientific and technological expertise in geophysics, geology, and geodesy has led to decisive steps forward during the IDNDR, particularly, basic research in physical modelling, surveillance instrumentation, including GPS satellite links, accessible computer networks and data bases, and user friendly software. The World Wide Web has proved a remarkable adjunct. Seismic intensity data are now accessible during and immediately after a strong earthquake through commercial technology, as used in California, Iceland, Taiwan, Mexico, Japan, and elsewhere. The advantages of digital recording for near real-time warning of and response to earthquakes, volcanic eruptions and tsunamis has become clear.

Advances in forecasting of the various hazards have been uneven, but issues have been clarified. Although prediction of eruption initiation has been advanced, that of earthquakes has not. Successful earthquake prediction is now seen as estimating realistic strong ground motions for engineering design and other risk mitigation. There are two main gaps: representative data bases and more relevant professional education. Liability from error is a problem. In all geophysical research germane to risk reduction and recovery response, there remains a need for precise definition of estimation procedures, and standardization of hazard parameters. Theoretical modelling of magma movements and tsunami and seismic waves in three-dimensional structures awaits acceptance as a reliable predictive tool in hazard mapping and in engineering. Widespread transfer to mitigation programs and public knowledge is still a challenge.

**U5/W/22-A4 1600****ATMOSPHERIC AND CLIMATIC HAZARDS**

Neville Nicholls, Bureau of Meteorology Research Centre, PO Box 1289K, Melbourne 3001, Australia

The last few years have seen enormous damage and loss of life from climate and weather phenomena. The most damaging have included the 1997/98 El Nino (with its near-global impacts), Hurricane Mitch, and floods in China in mid-1998. What have we learnt regarding the causes, variability, and predictability, of these phenomena? Do we understand how and why the frequency and intensity of such extreme climate and weather events varies from year-to-year and from decade-to-decade? Can we predict the occurrence of these extremes, and can we assist decision-makers to mitigate their damage? I will review what we have learnt in the last decade or so regarding the predictability of these climate and weather extremes. I will also discuss the impediments to the effective use of forecasts of these extremes to mitigate damage and loss of life.

**U5/L/02-A4 1700****HYDROLOGICAL HAZARDS AND RISKS**

Robert J. MOORE, Institute of Hydrology, Wallingford, Oxon, OX10 8BB, UK  
email: R.J.Moore@mail.nwl.ac.uk

Floods and droughts are hydrological hazards that result from extremes of meteorological conditions interacting with the terrestrial environment. Hydrological hazards in turn lead to hazards to man and the environment, including ecological systems involving the survival of plants and animals. The risk to the environment posed by hydrological hazards is reviewed from a perspective of scientific understanding, estimation, modelling, forecasting and management. Advances in the understanding of hydrological hazards and the development of improved methods to estimate the rarity of extremes and to mitigate their effects - through catchment planning, structural measures and forecasting-warming-control systems - are outlined. Future scientific challenges concerning hydrological hazards and risks that remain at the close of the IDNDR and the start of the new millennium are identified.





**JSM01** Monday 19 – Friday 23 July**MIDDLE ATMOSPHERE DYNAMICS AND CHEMISTRY (IAMAS, IAGA, SCOSTEP)**Location: Haworth Building 101 LT  
Location of Posters: Old Gym

Monday 19 July AM

Presiding Chair: Dave Fritts (Colorado Research Associates, Boulder, USA)

**PLANETARY WAVES****JSM01/W/42-A1** Invited **0830****MESOSPHERE MEAN STRUCTURE, PLANETARY WAVES, TIDES, AND WAVE-WAVE INTERACTIONS SIMULATED BY A MIDDLE ATMOSPHERE GCM**

W. NORTON (AOPP, University of Oxford, UK, email: wan@atm.ox.ac.uk) J. Thurn (Dept. of Meteorology, University of Reading, UK)

A global circulation model which extends from the surface to approximately 128 km has been used to examine the dynamics of the mesosphere. It is found that changes to the strength of parameterized gravity wave breaking has a strong influence on the mean structure of the mesosphere, for example, the temperature of the summer mesopause. Associated changes in the vertical shear of the summer mesospheric jet change the amplitude of the two-day wave which is generated through baroclinic instability.

It is shown that large two-day wave activity reduces the amplitude of the diurnal tide around the solstice. The interaction of the tides with the two-day wave produces other waves including a wave-number 4, 16 hour wave.

**JSM01/W/20-A1** **0900****EXCITATION MECHANISMS OF NORMAL MODE ROSSBY WAVES**

T. HIROOKA, T. Yonemitsu and Y. Miyoshi (all at Department of Earth and Planetary Sciences, Kyushu University, 6-10-1, Hakozaki, Fukuoka 812-8581, Japan, email hirook@geo.kyushu-u.ac.jp)

Normal mode Rossby waves are planetary-scale free or resonant oscillations of the atmosphere. Prominent among the waves are the three gravest modes of zonal wavenumber 1, which are called 5-day, 10-day and 16-day waves. As for the geopotential field, the 5-day and 16-day waves have symmetric structures with respect to the equator, while the 10-day wave has antisymmetric one. Although these waves frequently appear in the middle atmosphere, their excitation mechanisms have not been well understood. In this paper, the excitation mechanisms are investigated by a series of general circulation model experiments with different boundary conditions and physical processes. Results indicate that heating process due to the moist convection is essential for the excitation. Moreover, some different conditions are necessary for the excitation of individual modes, corresponding to each horizontal structure and travelling period.

**JSM01/W/103-A1** **0920****SIMULATION OF KELVIN WAVES IN THE MIDDLE ATMOSPHERE USING A GLOBAL MODEL OF PLANETARY WAVES**

A.I. POGORELTSEV (Institute of the Ionosphere, Ministry-Academy of Science of the Republic of Kazakhstan, Almaty, 480068, Kazakhstan; e-mail: pogor@ionos.alma-ata.su)

A 2D linearized numerical model of the global structure of planetary waves is used to simulate the propagation of Kelvin waves with zonal wave number one and period 4-, 8-, and 16-days (ultrafast, fast, and slow modes, respectively). The dependence of the vertical structure of Kelvin waves over the equator on the zonal mean wind is investigated through the comparison between the results of simulation for the windless atmosphere, and with taking into account the background wind distribution for solstice and equinox conditions. It has been shown that ultrafast mode is insensitive to zonal mean wind and propagates from the lower into the upper atmosphere without substantial attenuation. The propagation conditions of the slow and fast Kelvin waves are strongly dependent on the background wind and its vertical gradients, and these modes dissipate at the altitudes of the stratosphere and mesosphere. Eliassen-Palm flux divergence is used as a diagnostics of wave-mean flow interaction. It is found that zonal mean forcing due to dissipation of the slow and fast Kelvin waves does not exceed 1 m/s/day in the stratosphere and mesosphere. Ultrafast mode propagates into the lower thermosphere and provides substantial (about 10 m/s/day) eastward acceleration of the mean flow at the low latitudes in this region.

**JSM01/E/39-A1** **0940****OBSERVATIONAL VARIABILITY IN SIMULTANEOUS MEASUREMENTS OF MESOSPHERIC WINDS BY RADAR AND OPTICAL METHODS**

G J FRASER(1), S M Marsh(1), W J Baggaley(1), R G T Bennett(1), K A Deutsch(2), G Hernandez(2), B N Lawrence(1), M Plagmann(1), G E Plank(1) and R W Smith(3) (1) Dept. Physics and Astronomy, University of Canterbury, New Zealand (2) Graduate Program in Geophysics, University of Washington, Seattle, USA (3) Geophysical Institute, University of Alaska, Fairbanks, Alaska, USA

Observed differences between mesospheric wind measuring techniques may arise from a variety of sources including atmospheric variability, the physics of the technique being used, diurnal variations in sampling rate, the scale of the sampling volume and the duration of one observation. The nature and significance of differences will be illustrated by comparing measurements of the semidiurnal tide from 70 - 105km using an MF radar, a meteor wind radar (able to measure only the meridional component) and a Fabry Perot spectrometer. The two radar systems are at the same site near Christchurch, New Zealand, while the Fabry Perot spectrometer is situated 170km to the west of the radars. Results from this network, including meteor wind measurements near-coincident in time but at points up to 300km apart horizontally, will be presented to investigate any significant differences in the observed tide as the observation interval is increased from one day to one month.

**JSM01/E/47-A1** **1000****STUDIES OF STRATOSPHERIC DYNAMICS USING THE ALOMAR DOPPLER WIND AND TEMPERATURE SYSTEM**

DAVID REES (CASS, Utah State Univ. Utah State University, Logan, UT 84322-4405, USA) E-Mail: walnut1@easynet.co.uk, Gerd Baumgarten, PIBU, Germany, and Nick Lloyd, ISAS, Saskatchewan, CA.

Since early 1997, series of measurements of winds in the lower and middle stratosphere have been made using the Doppler Wind and Temperature System of the ALOMAR Facility in Northern Norway (69°N). These wind observations have been intercompared with nearby MST radar, radiosone and rocket measurements, validating the wind lidar technique and analysis procedures. The wind measurements are being used to describe the stratospheric transport appropriate to local measurements and studies of stratospheric ozone above Northern Scandinavia during the winter and spring periods in 1997 and 1998.

**JSM01/E/33-A1** **1050****PLANETARY WAVES STRUCTURE IN THE MIDDLE ATMOSPHERE IN 1991-1992 ON BASE OF DATA ANALYSIS AND MODELLING**

Alexei KRIVOLUTSKY, Tatyana Vyushkova (both Central Aerological Obs., Pervomayskaya Str.3, Dolgoprudny 141700, Moscow Region, Russia, email: alkriv@mycomp.netclub.ru) Dora Pancheva (Geophysical Institute, Sofia, Bulgaria) Pavel Vargin and Adolf Ebel (University of Cologne, Germany, email: pv@eurad.uni-koeln.de)

Global temperature (UKMO assimilated and UARS - ISAMS instrument), geopot. heights (UKMO), ozone content (UARS - MLS instrument), radio absorption and meteor radar data has been used for 1991-1992 interval to study motions structure in the middle atmosphere in this period. 2-D special statistical procedure was used for transient wave analysis using global UKMO data in the vertical range 0-50 km. Because of rather short temporal interval based on the observations from UARS MEM spectral technique was used also. Meteor radar data (at 95 km level over Bulgaria) were analysed using wavelet analysis to study temporal evolution of short-period waves in the meteor region. The results of such complex data base has revealed the presence of transient waves with periods: 2-3, 3-5 and 8-12 days. It should be mentioned that short period waves has a good manifestation in the mesosphere and lower thermosphere, but it is rather difficult to find these waves at lower levels. 2-D and 3-D model simulations has been used to support data analysis results.

**JSM01/W/67-A1** **1110****QUASI 16-DAY OSCILLATIONS IN THE MESOSPHERE AND LOWER THERMOSPHERE: MULTI-YEAR/MF RADAR OBSERVATIONS FROM THE ARCTIC TO SUBTROPICS, AND GSWM MODELING-RESULTS**

Y.LUO, A.H.Manson, C.E.Meek (Institute of Space and Atmospheric Studies, University of Saskatchewan, Saskatoon, Canada, email: luo@dasas.usask.ca); C.K.Meyer (HAO, National Center for Atmospheric Research, Boulder, USA); J.M.Forbes (Dept. of Aerospace Engineering Sciences, University of Colorado, Boulder, USA); C.M.Hall (Dept. of Physics, University of Tromsø, 9037 Tromsø, Norway); W.K.Hocking, J.MacDougall (Physics Dept., University of Western Ontario, London, Canada); D.C.Fritts, D.Riggin (Colorado Research Associates, Boulder, USA); G.Fraser (Physics Dept., University of Canterbury, Christchurch, New Zealand)

The daily mean winds observed by MF radars, located between the Arctic and the Subtropics (one is in southern hemisphere) are used to investigate the quasi "16-day" oscillations in the mesosphere and lower thermosphere. In Saskatoon (52N), the 16-day wave occurs there mostly in winter with maxima at 60-65 km and covers a large range of altitudes; in summer, however, it is much weaker and confined to ~85 km. The vertical wavelength in winter tends to be very long but in summer is a little shorter. The inter-annual variations of the 16-day imply certain associations with the equatorial QBO. Data from the other radar locations (Tromsø, 70N; London, 43N; Hawaii, 21N and Christchurch, 45S) are used for similar analysis of annual variations. The winter 16-day wave activity is very weak over Tromsø comparing to those over other sites; and the Hawaii shows relatively strong activity. The Global Scale Wave Model has been run to get the annual 16-day wave simulations from the ground to 200 km and for all latitudes of the globe. The comparison with the observation at Saskatoon indicates good agreement. Generally similar seasonal trends are seen by the other MFRs and GSWM, but differences in latitudinal and hemispheric responses are highlighted.

**JSM01/W/99-A1** **1130****NONLINEAR COUPLING OF PLANETARY WAVES AND TIDES OBSERVED BY METEOR RADAR IN THE LOWER THERMOSPHERE ABOVE BULGARIA**

Dora PANCHEVA (Geophysical Institute, Bulg. Acad. Sci., "Acad. G. Bonchev" str., bl.3, 1113 Sofia, BULGARIA; Email: dpanchev@geophys.bas.bg) Plamen Mukhtarov (Geophysical Institute, Bulg. Acad. Sci., "Acad. G. Bonchev" str., bl.3, 1113 Sofia, BULGARIA)

The variability of the atmospheric tides observed by meteor radar in the mesosphere/lower thermosphere region above Bulgaria during January, 1991 - June, 1992 demonstrates a complicated temporal behaviour. Waves with different dominant frequencies may occur at different time intervals. To investigate the localised variations of power within a time series of diurnal and semidiurnal tidal amplitudes, as well as of neutral wind, a Morlet wavelet transform is applied. The main periods observed in the variations of the tidal amplitudes and neutral wind are: about 2, 4-6, 8-10 and 14-18 days. The most regular oscillation presented in the neutral wind and in both tidal amplitudes is the well known "16-day wave". A process of a periodic frequency modulation of the 16-day wave with a modulating period of 2-3 months is visible. The nonlinear interaction between tides and planetary waves is studied by bispectral analysis. The results of this analysis indicate that the nonlinear interactions between semidiurnal tide and planetary waves with period in the range 2-20 days are stronger than those of the diurnal tide and planetary waves.

**JSM01/W/69-A1** **1150****SPATIAL STRUCTURE OF QUASI-2-DAY WIND VELOCITY VARIATIONS IN THE MESOPOUSE - LOWER THERMOSPHERE REGION**

B.L. Kashcheyev, A.N. Oleynikov, V.N. Oleynikov (Kharkov State Technical University of Radioelectronics, Ukraine, email:ort@khture.kharkov.ua) CH. JACOBI (Institute for Meteorology, University of Leipzig, Germany, email: jacobi@rz.uni-leipzig.de) Yu.I. Portnyagin, E.M. Merzlyakov, T.V. Solovjova (Institute for Experimental Meteorology, Obninsk, Russia, email: portnyagin@iem.obninsk.ru)

Quasi-2-day wind variations in the mesopause - lower thermosphere region were first detected by radio meteor investigations carried out by the Soviet equatorial expedition in Somalia (2 N, 45 E) from August 1968 to 1970. The period of these variations can differ from 48 hours for several hours. The origin of the quasi 2-day variations is not yet fully established, leading to continuous interest to this phenomenon. It is conjectured that the moment of quasi-2-day variations appearance is connected with the interplanetary magnetic field sign changes. The analysis of measurement results obtained at different sites (Kharkov, Mogadishu, Khabarovsk, Molodezhnaya, Collm etc.) showed that the disturbances with the quasi-2-day cycle exhibit the global nature of a westward propagating wave. Simultaneous measurements carried out in Kharkov and Khabarovsk in July-September, 1973 revealed a zonal wave number of 4.5 - 5, which is contrary to many observations revealing a zonal wavenumber of 3 - 4. In this paper the structure of quasi 2-day waves at different altitudes measured during radio meteor location

## INTER-ASSOCIATION

at Kharkov (1987-1988, 1998) and Mogadishu (1968-1970) is discussed. The higher intensity of the quasi-2-day variations in middle latitudes is observed in summer in July and manifests itself both in the zonal and meridional components. The second, smaller maximum of the quasi-2-day variations activity is sometimes observed in winter, namely in January. The amplitude changes from month to month can be described by the sum of mean annual, annual and semi-annual components.

**JSM01/E/05-A1**

**1210**

### THE SOUTHERN HEMISPHERE 2-DAY WAVE OF JANUARY 1998

G.O.L. JONES (British Antarctic Survey, Cambridge, UK) D. M. Riggin and D. C. Fritts (both at Colorado Research Associates, Boulder, CO80301, USA)

A quasi 2-day wave in the dynamics of the mesosphere is a common summertime occurrence. The phenomenon has been found to be particularly strong and stable in the southern hemisphere. We report on a 2-day wave which was clearly seen in the southern hemisphere during January, 1998.

Radar observations were made from several ground-based sites around the edge of the Antarctic continent providing information on both temporal and spatial variations. The wave was a significant feature of the mesospheric wind pattern for a 3-week interval. The relationship between the vertical structure of the wave's amplitude and the background wind and tides will be discussed. Possible links with other esospheric phenomena such as the summertime zonal jet will also be considered.

**Monday 19 July PM**

Presiding Chair: Julie Kalkalidis (Univ. of Michigan, Ann Arbor, USA)

### PLANETARY WAVES

**JSM01/W/36-A1**

**Invited**

**1400**

### PLANETARY WAVE VARIABILITY IN THE MLT: AN OBSERVATIONAL PERSPECTIVE

R. A. VINCENT, S. Kovalam, and I. M. Reid (Department of Physics and Maths Physics, University of Adelaide, Adelaide 5005, Australia, email rvincent@physics.adelaide.edu.au) D. C. Fritts and D. Riggin (Colorado Research Associates, Boulder, CO 80301, USA, email dave@colorado-research.com) T. Tsuda and T. Nakamura (Radio Atmospheric Science Center, Kyoto University, Kyoto, Japan, email tsuda@kurasc.kyoto-u.ac.jp)

Transient planetary waves, such as the quasi-2-day wave and the 6.5-day wave, are prominent features of the mesosphere and lower thermosphere. Ground-based radar observations in the Asia/Pacific region are used to describe the spatial and temporal variability of global-scale waves with periods from hours to days and their possible interactions with other atmospheric waves.

**JSM01/W/07-A1**

**1430**

### MODELLING THE DYNAMICS OF THE 2-DAY WAVE

Maisa ROJAS and Warwick Norton, Atmospheric, Oceanic and Planetary Physics Department, University, of Oxford.

Traveling planetary waves in the stratosphere and mesosphere in the Extended UGAMP GCM (EUGCM) have been analyzed. The frequency and wavenumber spectra for two years of the model run have been compared with meteor radar data from Aberystwyth. There is good agreement in periods of strong wave activity. Both data show a strong 2-day wave present during the summer months.

To understand the forcing mechanisms of this 2-day wave a linear instability calculation using zonal background fields from the EUGCM was performed. This used a two dimensional linearization of the primitive equations on the sphere. This showed for July a fastest growing mode of wavenumber 3 or 4 with period around 37 hours with a structure that peaks in the northern hemisphere at 60 degrees and 70 km height.

To examine the nonlinear evolution of the waves, the same zonally symmetric state, as used in the instability calculation, was used to initialize a Mechanistic model. This showed the growth to finite amplitude of the waves, including vortex merger, and decay; a 'baroclinic lifecycle' in the middle atmosphere. In the Mechanistic model one can observe the development of two independent waves with e-folding time of 4 days and 9 days and periods of 35 and 40 hours respectively.

The first one corresponds to the fastest growing mode of the instability calculation, even though this mode growth fastest it reaches finite amplitude and the dies, whereas the second persists for much longer reaching larger amplitude and has a more global structure, comparable to the 2-day wave in the EUGCM.

Analysis will be presented as to how these unstable modes relate to the Rossby-Gravity modes in the model.

**JSM01/W/100-A1**

**1450**

### ANNUAL VARIABILITY OF PLANETARY WAVES AS MODELED BY THE GLOBAL SCALE WAVE MODEL: EFFECTS OF MEAN WINDS, FORCING AND GRAVITY WAVES

Christian MEYER (High Altitude Observatory - National Center for Atmospheric Research, P.O.Box 3000, Boulder, CO, 80307, USA, email: meycerc@hao.ucar.edu)

Annual variations in the quasi 16-day and quasi 2-day wave are investigated using a 2-dimensional, steady-state, linearized, perturbation model. The effects of mean winds, location of forcing and the influence of internal gravity waves are explored. Background atmospheres based upon empirical models (HWM-93, MSIS) and satellite observations (JARS: HRDI) are utilized. Simple profiles of eddy diffusion, and those based upon a gravity wave parameterization are employed. When mesospheric wave signatures are significant, the interaction between the planetary wave and gravity wave are also examined.

It is seen that the mean winds have a significant effect on the month-to-month realization of the waves, and that the model predictions vary substantially as a function of background atmosphere that is used. By varying the location of the forcing it is possible to isolate what deltas in the mean wind fields are responsible for the majority of differences. The model predictions are compared to ground and space-based observations of the planetary waves.

**JSM01/W/107-A1**

**Invited**

**1510**

### TIDI - A TIMED DOPPLER INTERFEROMETER DESIGNED TO STUDY THE DYNAMICS AND THERMODYNAMICS OF THE MESOSPHERE AND LOWER THERMOSPHERE

T. L. KILLEEN, (Space Physics Research Laboratory, Department of Atmospheric, Oceanic, and Space Sciences, University of Michigan, 2455 Hayward Street Ann Arbor, MI 48109-214, USA,

Email: tkilleen@umich.edu), R. M. Johnson, W. Skinner, C. Edmonson, Q. Wu, R. Niciejewski, and S. I. Azeem (all at: Space Physics Research Laboratory, Department of Atmospheric, Oceanic, and Space Sciences, University of Michigan, 2455 Hayward Street Ann Arbor, MI 48109-214, USA)

The TIMED Doppler Interferometer (TIDI) will investigate the dynamics and energetics of the Earth's mesosphere and lower thermosphere - ionosphere. Launch is currently scheduled for May 18, 2000. TIDI measurements will enable a global description of the vector wind and temperature fields, as well as important information on gravity waves, species densities, airglow and auroral emission rates, noctilucent clouds, and plasma drifts. TIDI will scan the terrestrial limb through four identical imaging telescopes: viewing geometry will be at +/- 45 and +/- 135 degrees to the satellite velocity vector. Measurements will be combined to form horizontal velocity vector wind profiles. The vertical resolution will be 2.5 km at the lower altitudes and accuracies will approach 2 m/sec and 2 K for wind and temperature measurements under optimum viewing conditions. A novel adaptation of a circle-to-line interferometer design is incorporated into the detection system permitting simultaneous viewing through all four telescopes. This talk will describe the instrument design and capabilities and highlight anticipated scientific results. Attention will also be given to aliasing issues.

**JSM01/E/09-A1**

**Invited**

**1550**

### MEDIUM-SCALE WAVES TRAPPED AROUND THE MID-LATITUDE TROPOPAUSE

Kaoru SATO (Department of Geophysics, Faculty of Science, Kyoto University, Kyoto 606-8502, Japan, email: sato@kugi.kyoto-u.ac.jp)

Using recently available fine time resolution data from regional prediction model (time intervals of 3 h) and MST radar observation (3 min), medium-scale (zonal wavelengths of 2000-3000km) waves with periods of about 1 day trapped around the mid-latitude tropopause were discovered in early 1990's (Sato et al., 1993). Subsequent studies using 6 hourly objective analysis data and hourly regional climate model data showed that the medium-scale waves are ubiquitous in both hemispheres (Hirota et al., 1995; Yamamori et al., 1997; Yamamori and Sato, 1998; Sato et al., 1999). The eastward phase speed is about 20m/s which is twice as large as that of synoptic-scale (4000-5000km) waves. The wave structure is almost neutral.

The meridional gradient of quasi-geostrophic (QG) potential vorticity (PV) has a sharp positive peak in the vertical around the tropopause on the pole side of westerly jet, due to the westerly shear around a discontinuous change of static stability. The medium-scale waves can be regarded as neutral waves trapped in the positive maximum of PV gradient. The features of trapped waves analyzed using a 1-d QG model are similar to the observation. A re-examination of PV conservation equation indicates that the restoring effect to produce wave motions is attributed not to the meridional advection but to the vertical advection of background Ertel PV (Matsuno et al., 1999).

This theory shows that the intrinsic frequency does not depend on the wavenumber, namely, the intrinsic zonal group velocity is zero. This characteristic is consistent with 2-d spectra obtained by ECMWF global operational data. The intrinsic wave period is about 2 days suggesting possible contribution of medium-scale waves to the stratosphere and troposphere exchange.

**JSM01/W/47-A1**

**1620**

### PLANETARY WAVE INTERACTIONS IN THE ANTARCTIC STRATOSPHERE AND THEIR ROLE IN THE BREAKDOWN OF THE AUSTRAL POLAR VORTEX

Mark HARVEY (Cooperative Research Centre for Southern Hemisphere Meteorology, Building 70, 3rd Floor, Monash University, Clayton, Victoria 3168, Australia. Email: mark@vortex.shm.monash.edu.au)

Variations in zonal wave 1 geopotential height amplitude on timescales of 10-14 days have frequently been observed in the Antarctic winter and spring stratosphere. In a number of studies, these variations have been linked to interactions between stationary planetary wave 1 and eastward travelling wave 2. Results presented here indicate this process is a common feature, particularly during spring, and plays an important role in the seasonal breakdown of the Austral polar vortex. In many instances, such variations in zonally resolved waves appear related to irreversible 3-way interactions between a travelling and stationary anticyclone and the polar vortex. A few such episodes are discussed using both zonal and vortex-centred diagnostics.

**JSM01/W/28-A1**

**1640**

### A STUDY OF THE BREAKDOWN OF THE SOUTHERN HEMISPHERE POLAR VORTEX

Dr Gregory ROFF (Bureau of Meteorology Research Centre, Melbourne, Australia; CRC for Southern Hemisphere Meteorology, Monash University, Melbourne, Australia, email: greg@vortex.shm.monash.edu.au), Dr Elisa Manzini (Max Planck Institute for Meteorology, Hamburg, Germany, email: elisa@vortex.shm.monash.edu.au) and Mark HARVEY (CRC for Southern Hemisphere Meteorology, Monash University, Melbourne, Australia, email: mark@vortex.shm.monash.edu.au)

This study aims to investigate the role played by planetary - gravity wave interaction during the breakdown of the southern hemisphere stratospheric polar vortex, which generally occurs in October, using model simulations and observations.

The model simulations available are two versions of the MPI middle atmosphere ECHAM model (Manzini and McFarlane, 1998) as well as the BMRC atmospheric model, BAM, (Bourke 1998) which has recently been extended into the stratosphere. The model intercomparison enables us to obtain an indication of the robustness of the results as well as the dependence of the results on model features. The comparison with observations uses large scale analysed datasets (UKMO, NCEP-CPC, and GASP) to validate the simulated synoptic character of the circulation breakdown.

In this study we use elliptical diagnostics (Vaugh, 1997) to compare the simulated vortex breakdown with that shown in the observed datasets. The elliptical diagnostics are calculated for several levels in the atmosphere which enables us to follow the decay of the vortex as a function of both height and time.

**JSM01/W/05-A1**

**1700**

### STRATOPAUSE SUDDEN WARMINGS ON THE NORTHERN HEMISPHERE - WHEN DO THEY END UP IN A MAJOR STRATOSPHERIC WARMING?

P. BRAESICKE and U. Langematz Institut fuer Meteorologie, FU Berlin Carl-Heinrich-Becker-Weg 6-10, 12165 Berlin

Sudden warmings in the stratopause region are a well known phenomenon in middle atmosphere dynamics. The ability to observe these warmings in detail is limited. Using a ten year integration of the Berlin climate-middle atmosphere model the sudden warmings in the stratopause region and their relation to major stratospheric warmings will be analyzed. The good spatial and temporal resolution of the model can be used for a comprehensive hemispheric diagnostics. The magnitude and temporal development of the simulated events are in good agreement with observations. From the computation of the amplitudes of planetary



waves, the calculation of the EP flux diagnostics and the thermal budgets, we investigate the necessary conditions for stratopause warmings to propagate downward and end up in a major stratospheric warming. First results indicate that preconditioning of the lower stratosphere is an important factor.

**JSM01/E/01-A1****1720****TRAVELLING WAVE-PATTERNS BETWEEN TROPOSPHERE AND STRATOSPHERE**

Gerhard SCHMITZ, Norbert Grieger (Institut fuer Atmosphaerenphysik an der Universitaet Rostock, Schlosstr. 6, 18225 Kuehlungsborn, Germany, email: schmitz@iap-kborn.de)

The stratospheric circulation is determined by stationary and transient wave processes. On the basis of NCEP RE analyses geopotential fields, covering 1958-1997, travelling wave patterns between troposphere and stratosphere have been found using Principal-Oscillation-Patterns (POP)-method. The vertical propagation of these patterns depends on the analysed oscillation period and shows a distinctive dependence on the geographical longitude. Only over the North-Atlantic region, in the exit region of subtropical jet stream, travelling "wave packets" have been found, which propagate into stratospheric heights. The wave-patterns show characteristics of baroclinic wave life cycles with polewards respectively equatorwards directed Eliassen-Palm-Flux components. An interpretation of patterns has been given with model-experiments on the basis of a simple GCM. The difference in the vertical wave-energy-propagation over the North-Atlantic- respectively Pacific region is due to the regional zonal wind in the upper troposphere and have been discussed with a linear wave propagation model up to mesospheric heights, too.

**Tuesday 20 July AM**

Presiding Chair: Chris Meyer (NCAR/High Altitude Observatory, Boulder, USA)

**TIDES****JSM01/L/01-A2**

Invited

**0930****VARIABILITY OF SIMULATED MIGRATING AND NON-MIGRATING TIDES IN THE MLT REGION**

Saburo MIYAHARA (Department of Earth and Planetary Sciences, Kyushu University, Fukuoka 821-8581 Japan, email: sbm@rossby.geo.kyushu-u.ac.jp)

It is discussed about the variability of numerically simulated migrating and non-migrating tides in the MLT region, based on the recent analyses of output data of Middle Atmosphere Circulation Model at Kyushu University (MACMKU). It will be shown that non-migrating tides are highly variable for both the amplitudes and phases. Origin of the variability will be discussed related to excitation forcings.

**JSM01/E/07-A2****1000****AN EMPIRICAL GLOBAL MIGRATING DIURNAL TIDE WIND MODEL FOR THE UPPER MESOSPHERE/LOWER THERMOSPHERE**

Yuri PORTNYAGIN and Tatyana Solovyova (both at Institute for Experimental Meteorology, Lenin str. 82, 249020, Obninsk, Kaluga reg., Russia, email:portnyagin@iem.obninsk.ru)

An empirical climatic zonally averaged diurnal tide wind model for the 80-100 km height region is presented. The model is constructed from the fitting of monthly mean diurnal wind oscillation parameters measured by MF and meteor radars at more than 40 stations, well distributed over the globe. The model is constructed for all months of the year and extends from 80 deg.N to 80 deg.S. The height-latitude contour plots of monthly mean amplitudes and phases of the diurnal wind oscillations are analyzed to reveal the main features of the seasonal and latitudinal variations of these parameters. The results of a comparison between the presented ground-based model and those constructed using the UARS wind measurement data show some significant differences. Possible origin of these differences, including the effects of non-migrating diurnal tides, is discussed.

**JSM01/E/26-A2****1020****DIURNAL VARIATIONS IN THE RATE OF DISSIPATION OF TURBULENT ENERGY IN THE EQUATORIAL UPPER MESOSPHERE**

R.G. ROPER (School of Earth and Atmospheric Sciences, Georgia Institute of Technology, Atlanta, GA 30332-0340 USA, email roper@eas.gatech.edu) J.W. Brosnahan (LaSalle Research Corporation, 24115 Weld County Road 40, LaSalle, CO 80645-9521, email broz@csn.org)

The diurnal variations of the rate of dissipation of turbulent energy over Arecibo (18°N, 67°W) for the AIDA '89 campaigns from April 1 to 11 and May 2 to 9, 1969 have been estimated using a structure function approach applied to imaging Doppler interferometry (IDI) data. The source of the individual scatterers identified by IDI is postulated as resulting from wave-wave interaction within the gravity wave spectrum producing localized, decaying patches analogous to ocean whitecaps. There is a tendency for the turbulence to maximize in the morning and the evening. Values of the rate of dissipation of turbulent energy range from < 5 mW kg<sup>-1</sup> to 100 mW kg<sup>-1</sup>, with the latter probably an overestimate. Local Richardson numbers have been calculated, but it does not appear that the mean flow is the source of the turbulent energy, although the mean wind is capable of helping to destabilize the atmosphere. Emphasis is placed on the fact that any radar measurement of turbulence is an upper limit, because of the inhomogeneity of the turbulence in both space and time.

**JSM01/W/62-A2****1110****CORRELATIONS OF GRAVITY WAVES, TIDES AND PW IN THE MESOSPHERE: OBSERVATIONS USING MAINLY THE MLT-MF RADARS IN THE NORTH-AMERICAN/PACIFIC SECTOR**

Alan MANSON, Chris Meek (Institute of Space and Atmospheric Studies, University Of Sask., Canada, email: manson@dansas.usask.ca); Chris Hall (Auroral Observatory, University of Tromsø, Norway, email: chris.hall@phys.uit.no); Wayne Hocking, John MacDougall (Dept. of Physics and Astronomy, University of Western Ontario, Canada, email: whocking@danlon.physics.uwo.ca); Steve Franke, (Space Science and Remote Sensing Laboratory, University of Illinois, USA, email: sfranke@uiwpls.ece.uiuc.edu) Dennis Riggan, Dave Fritts (Colorado Research Associates, Boulder, USA, email: riggin@colorado-research.com) Bob Vincent (Dept. of Physics and Mathematical Physics, University of Adelaide, Australia, email: rvincent@physics.adelaide.edu.au) Maura Hagan (NCAR, Boulder, USA email: hagan@ucar.edu)

Measurements in the Mesosphere and Lower Thermosphere (MLT), from MF Radars (MFR)

located from the Arctic to the Tropics are used to study gravity waves (GW) and their variability : Tromsø, 70N, Saskatoon, 52N, London, 43N, Urbana, 40N, Hawaii, 22N, Xmas Is., 2N. GW-band time series (10-100min, 2-6 h), their spectra and their 12,24,48 h oscillations are used. 50d sequences of data from 3 seasons are selected, which themselves are marked by strong differences in winds and tides. The scenario at Saskatoon has recently been published (JASTP,60, p1089), and results from the other stations are quite similar: the modulation of GW by the longer period waves is quite spasmodic. Events of a few days are easily found, but the processes are generally intermittent, suggesting that the wave sources themselves are also intermittent in strength and direction. Results of the new correlation-vector technique, which locates the direction of highest correlation between the hourly mean winds and their variances, over 10 days, are also discussed; this method also assesses the GW modulation by all waves from GW, tides and PW (10d). Interesting differences emerge between high and low latitudes.

**JSM01/E/04-A2****1130****ON THE LONGITUDINAL STRUCTURE OF THE TRANSIENT DAY-TO-DAY VARIATIONS OF THE SEMIDIURNAL TIDE IN THE MID-LATITUDE LOWER THERMOSPHERE**

Eugeny MERZLYAKOV and Yuri Portnyagin ( both at Institute for Experimental Meteorology, Lenin str.82, 249020, Obninsk, Russia, e-mail: portnyagin@iem.obninsk.ru) Christoph Jacobi (Institute for Meteorology, University of Leipzig, Germany) Nicholas Mitchell ( Department of Physics, University of Wales, Aberystwyth, UK) Heinz Muller ( Cranfield University, RMCS Shrivenham, Swindon, UK) Alan Manson ( Institute for Space and Atmospheric Studies, University of Saskatchewan, Saskatoon, Canada) Antonina Fahrutdinova ( Kazan State University, Kazan, Russia) Werner Singer and Peter Hoffmann ( both at Institute of Atmospheric Physics, Kuehlungsborn, Germany)

During the DYANA campaign (January-March 1990) the coordinated meteor radar and MF wind measurements at the several mid-latitude stations (Sheffield, Kuehlungsborn, Collm, Obninsk, Kazan, Volgograd and Saskatoon) were carried out. All of these stations are situated in the Northern Hemisphere in a comparatively narrow mid-latitude belt. Using the S-transform technique the corresponding hourly mean wind data were analyzed to reveal the main features of the day-to-day semidiurnal tide wind variations and their longitudinal structure. It is shown that these variations have a periodic structure with the periods near to those simultaneously observed in the prevailing wind variations and of typical for the free (normal) atmospheric modes (about 5, 7, 10 and 16 days). The oscillations of the semidiurnal tide amplitudes as well as of the prevailing wind, have a definite transient nature, appear sporadically, existed during several periods and have a specific longitudinal structure.

For example, it is estimated that the near 7-day semidiurnal tide amplitude oscillation is westward-propagating one and has the zonal wave-number s=2 or 3 while the corresponding near 7-day oscillation of the prevailing wind is characterized by the zonal wave-number s=0. Some related problems of semidiurnal tide modulation by planetary waves are discussed.

**JSM01/W/104-A2****1150****FIRST AIRGLOW OBSERVATION RESULTS FROM 7.4 S**

R. A. BURITI (Dpto Física, CCT/UFPA, Campina Grande, PB, Brazil, 58109-970), H. Takahashi, D. Gobbi ( Instituto Nacional de Pesquisas Espaciais, INPE, Sao Jose dos Campos, SP, Brazil)

The Cariri Airglow Observatory has been started working since November, 1997. This observatory has a multi-filter photometer to measure the airglow emission intensities OI5577, OI6300, NaD, OH(6,2) band, O2 Atmospheric (0,1) band , and the OH and O2 rotational temperatures. The observatory is located at Sao Joao do Cariri, the driest region in the Northeast of Brazil at 7.4 S, 36.5 W. Continuous observation from day to day (13 days around the new moon period) make it possible to study nocturnal, day to day and seasonal variation of the airglow intensities. The nocturnal variations of the mesospheric emissions show strong seasonal dependence, maxima during the equinox and minima in the solstices, and the phase of maxima shifting from month to month. It indicates that tidal oscillation is important factor in the equatorial mesosphere. The thermospheric OI 6300 emission also shows significant seasonal variation. Salient features of the seasonal dependency will be presented and discussed in terms of the atmospheric dynamical processes.

**JSM01/W/11-A2****1210****TIDES (24-HOUR, 12-HOUR, 8-HOUR) AND TIDAL VARIABILITY IN THE MESOSPHERE AND LOWER THERMOSPHERE AT 53.5 DEG N, 3.9 DEG W BETWEEN 1990 AND 1994**

A.G. BEARD, N.J. Mitchell, P.J.S. Williams (Prifysgol Cymru Aberystwyth, Penglais, Aberystwyth, Ceredigion, SY23 3BZ, UK; email: agb@aber.ac.uk) and H.G. Muller (The Royal Military College of Science, Cranfield University, SN6 8LA,UK)

Four and a half years of data from a meteor radar based at Sheffield, UK representing measurements of neutral wind velocity in the meteor region above 53deg 27min N, 3deg 53min W, are analysed to produce tidal climatologies. The terdiurnal tide is a constant feature of the analysed neutral winds and its characterisation is given special consideration. Comparisons are made with other published studies and possible reasons for differences between them are discussed. Tidal variability is also studied both in the long-term and the short-term. Causes of this variability are discussed, including the possibility that some of the observed variability is an artefact of the analysis. The non-linear wave-wave interactions that could occur between the tides are considered and the possibility that the presence of a small winter quarterdiurnal (6-hour) tide could be partly due to such a coupling between the diurnal and terdiurnal tides is discussed.

**Tuesday 20 July PM**

Presiding Chair: Takuji Nakamura (Radio Atmospheric Science Centre, Kyoto University, Japan)

**GRAVITY WAVES****JSM01/W/03-A2**

Invited

**1400****GRAVITY WAVE MOMENTUM, HEAT AND ENERGY FLUXES IN THE MESOSPHERE**

R.L. WALTERSCHEID, The Aerospace Corporation, M2-260, P.O. Box 92957, Los Angeles, CA 90009 USA (email: Richard.Walterscheid@aero.org)

Gravity wave transports of momentum, sensible heat and energy alter the background atmosphere when waves violate the nonacceleration conditions. The wave fluxes of heat and momentum force the mean state by causing a redistribution of heat and momentum, while the energy flux adds heat to the mean state through the viscous dissipation of kinetic energy. Observations of wave fluxes indicate a strong influence of waves on the mean state of the middle atmosphere, especially the upper mesosphere. Recent and past measurements of wave fluxes and the implications of these measurements for the mesosphere will be reviewed.

**JSM01/E/03-A2** Invited **1430**

**A GLOBAL MORPHOLOGY OF GRAVITY WAVE ACTIVITY IN THE STRATOSPHERE REVEALED BY THE GPS OCCULTATION DATA (GPS/MET)**

Toshitaka TSUDA and Masahiro Nishida (Radio Atmospheric Science Center, Kyoto University Uji, Kyoto 611-0011, Japan, Email: tsuda@kurasc.kyoto-u.ac.jp, nishida@kurasc.kyoto-u.ac.jp) Christian Rocken and Randolph H. Ware (GPS/MET Project, GPS Science and Technology (GST) Program, UCAR, Boulder, CO 80307-3000, Email: rocken@unavco.ucar.edu, ware@unavco.ucar.edu)

Profiles of atmospheric temperature in the upper troposphere and stratosphere have been obtained by means of a radio occultation observation of GPS (Global Positioning System) signals (GPS/MET; GPS Meteorology) during April 1995 and February 1997. From each GPS/MET temperature profile we have extracted meso-scale temperature perturbations with a vertical scale ranging from 2 to 10 km, and defined the potential energy, Ep, from the temperature variance, which is assumed to be caused by atmospheric gravity waves. We have analyzed the latitude-longitude distribution of Ep at 20-30 km during northern hemisphere winter (from November to February). The large Ep values are generally detected at low latitudes between 25N and 25S, centered around the equator, and they are particularly enhanced over the regions of intense convections. Latitude and longitude variations of Ep are determined at 15-45 km altitude. At middle latitudes, Ep was larger in winter months in each hemisphere. Ep tends to become larger over continents than over the Pacific ocean, which suggests the generation of mountain lee waves due to interaction between the mean winds and topography.

**JSM01/E/12-A2** **1500**

**A STATISTICAL STUDY OF GRAVITY WAVES IN THE POLAR REGIONS BASED ON OPERATIONAL RADIOSONDE OBSERVATION DATA**

Motoyoshi YOSHIKI and Kaoru Sato (both at Department of Geophysics, Faculty of Science, Kyoto University, Kyoto 606-8502, Japan, email: yoshiki@kugi.kyoto-u.ac.jp)

Gravity waves in the Antarctic and Arctic lower stratosphere are examined based on operational radiosonde observation data at 32 stations over 10 years of 1987-1996. The rotation of hodograph with height indicates that most gravity waves propagate energy upward. Both potential and kinetic energies of gravity waves vary annually taking their maximum in winter in the Arctic and in spring in the Antarctic. The vertical flux of zonal momentum estimated using a statistical method by Vincent et al. (1997) which assumes universal gravity wave spectra is mostly negative and large in winter in both hemispheres, which shows the dominance of gravity waves propagating westward relative to the mean wind. The spring maximum as observed in gravity wave energy in the Antarctic is not clear in the profile of momentum flux. Momentum flux at Scandinavian stations is generally larger than that at Antarctic stations located at almost the same latitudes. In the Antarctic, the warming in the spring occurs earlier at higher altitude, and hence, the region with high static stability propagates downward. The region with large gravity wave energy in the spring propagates also downward following the movement of the high static stability region. Moreover, the high stability area moves horizontally gradually from 135E 50S to 45W 70S through the south pole in spring. The gravity wave energy enhancement coincides with the stability maximum at each station. The ratio of zonal to meridional wind variances depends strongly on location in the Antarctica, indicating that the dominant direction of gravity wave propagation is different.

**JSM01/W/40-A2** **1520**

**HIGH ARCTIC OBSERVATIONS OF GRAVITY WAVES AND STRATOSPHERIC WARMING**

Thomas J. DUCK (CRESTech & Dept. of Physics and Astronomy, York University, Toronto, Ontario, Canada, M3J 1P3; e-mail: tomduck@lidar.crestech.ca); James A. Whiteway (Dept. of Physics, University of Wales, Aberystwyth, Ceredigion, UK, SY23 3BZ; e-mail: jjw@aber.ac.uk); Allan I. Carswell (CRESTech & Dept. of Physics and Astronomy, York University, Toronto, Ontario, Canada, M3J 1P3; e-mail: carswell@lidar.crestech.ca)

Measurements of stratospheric temperatures and gravity wave activity have been obtained by a Rayleigh lidar stationed in the Canadian High Arctic at Eureka (80 N, 86 W) during each Winter since 1993. The stratospheric conditions above Eureka have proved to be particularly interesting due to the strong influence of the Arctic stratospheric vortex, an enormous cyclone some 4000 km across with peak wind speeds often in excess of 300 km/h. Movements of the vortex from its quiescent position over the pole have allowed measurements to be obtained inside the vortex core, within its Westerly jet, and outside of the vortex altogether. Observations in the vortex core and jet were collected and examined separately in an effort to resolve some average Wintertime trends in each region. During November and much of December, stratospheric temperatures in the vortex core were seen to remain at relatively constant and cool temperatures. However, a strong intra-vortex warming of roughly 30 K occurred annually in late December, and was sustained through the end of observations in late March. The warming first appeared in the upper stratosphere, and then propagated down to altitudes below 30 km. An increased level of gravity wave activity was detected in the vortex jet during the warming. The coincidence of these two events suggests that they were related by the principle of "downward control"; i.e., that increased gravity wave momentum deposition near the stratopause forced flow into the vortex core where it descended and warmed adiabatically. These observations have implications for our understanding of "sudden stratospheric warming" events, and the ozone depletion problem.

**JSM01/W/106-A2** Poster **1600-01**

**LARGE SCALE WAVES IN THE WINTER POLAR MESOSPHERE**

G. M. Fisher (Space Physics Research Laboratory, Department of Atmospheric, Oceanic, and Space Sciences, University of Michigan, 2455 Hayward Street Ann Arbor, MI 48109-214, USA, Email: fisherg@umich.edu), T. L. KILLEEN, R. J. Niciejewski, and Q. Wu, (all at Space Physics Research Laboratory, Department of Atmospheric, Oceanic, and Space Sciences, University of Michigan, 2455 Hayward Street Ann Arbor, MI 48109-2143, USA, Email: tkilleen@engin.umich.edu, niciejew@umich.edu, qwu@umich.edu)

Mesospheric wind data were measured by a Fabry-Perot Interferometer (FPI) at Resolute Bay, NWT, Canada (74 N). The OH(7,3) (892 nm) emission Doppler winds were analyzed for planetary scale oscillations throughout the months of December-March during 1995/96 and 1996/97. The FPI has a circle-to-line interferometric optical system (CLIO) which allowed for 9 orders of the OH(7,3) emission to be collected simultaneously by the CCD system. A full scan of the instrument involved measurements in the four cardinal directions and the zenith. Each of these scans required a 90 second integration. Winds were derived from the OH data (from a height of about 86 km) using a least squares fit. A Lomb-Scargle spectral analysis was performed to derive the frequency peaks present in the time series of the wind data. Large scale oscillations were observed within 2 years of data. Different techniques of analyzing non-linear interactions between planetary waves (16 day, 8 day, 5 day) and the 12 h wave were used. An analysis of the 12 h wave amplitude modulation and the frequency offset was performed.

**JSM01/W/72-A2** Poster **1600-02**

**CO-ORDINATED MESOPAUSE REGION WIND MEASUREMENTS OVER EUROPE IN SUMMER 1998**

Ch. JACOBI (Institute for Meteorology, University of Leipzig, Germany email: jacobi@rz.uni-leipzig.de) Yu.I. Portnyagin, E.M. Merzlyakov, T.V. Solovjova (Institute for Experimental Meteorology, Obninsk, Russia, email: portnyagin@iem.obninsk.ru) B.L. Kascheyev, A.N. Oleynikov (Kharkov State Technical University of Radioelectronics, Ukraine, email: ort@khture.kharkov.ua) D. Kürschner (Institute for Geophysics and Geology, University of Leipzig, Germany) N.J. Mitchell, A.G. Beard (Department of Physics, University of Wales, Aberystwyth, UK, email: njm@aber.ac.uk)

In July and August 1998, mesopause region wind measurements were carried out in by meteor radars at Obninsk, Russia and Kharkov, Ukraine, and by the LF D1 windprofiler at Collm, Germany. Two radars at Pykkvibaer, Iceland, and Hankasalmi in Finland also made additional measurements. The strongest feature within this period is a quasi 2-day wave that appeared in the second half of July. This wave was nearly phase-locked in the zonal component. Phase comparison between Collm, Obninsk, and Kharkov for the zonal component reveal a zonal wavenumber between 4 and 5. Comparison of the wave event with results from previous years shows the regular interannual variability of the quasi 2-day wave intensity, which is possibly connected with the solar cycle through wave-mean flow interaction in the stratosphere/mesosphere. The meridional phase during the event changes by about 0.25 h/day, so that the meridional period is slightly longer than the zonal one. The quasi 2-day wave event is connected with an increase of the semidiurnal tidal amplitude at Collm, but a decrease of the amplitude at Obninsk and - less strong - at Kharkov. This hints to a wave-tidal interaction through the modulation of the background wind field, which is influenced by the quasi 2-day wave.

**JSM01/W/102-A2** Poster **1600-03**

**THE RESONANT RESPONSE OF THE ATMOSPHERE TO THE LOWER BOUNDARY FORCING FOR WESTWARD ZONAL WAVE NUMBER ONE AND THE PERIOD VARIED FROM 6 TO 24 HOURS.**

A.I. POGORELTSEV (Institute of the Ionosphere, Ministry-Academy of Science of the Republic of Kazakhstan, Almaty, 480068, Kazakhstan; e-mail: pogor@ionos.alma-ata.su)

Experimental studies of the dynamics in the mesosphere and lower thermosphere (MLT) region show the presence of the large horizontal wind oscillations over South Pole with periods less than and/or about 12 hours (Hernandez et al., Geophys. Res. Lett., 20, 1787, 1993; Forbes et al., Geophys. Res. Lett., 22, 3247, 1995; Hermandes et al., Geophys. Res. Lett., 23, 1079, 1996; Portnyagin et al., Ann. Geophys., 16, 828, 1998). These oscillations were interpreted as manifestation of westward planetary waves with zonal wave number one, and a variety of mechanisms have been proposed to explain these observed features. Numerical simulations of the natural oscillations of the ionosphere-thermosphere- mesosphere system (Meyer and Forbes, J. Atmos. Solar-Terr. Phys., 59, 2185, 1997) provide strong evidence for a normal mode interpretation. However, the result of these simulations show that resonant atmospheric response at periods shorter than 24 hours is dominated only for the MLT forcing and is not observed in the case of the lower boundary forcing. Using a global model of planetary waves (Pogoreltsev and Sukhanova, J. Atmos. Terr. Phys., 55, 33, 1993), we investigate the resonant response of the atmosphere to the symmetric and asymmetric lower boundary forcing for westward zonal wave number one and the period varied from 6 to 24 hours. The results of simulations show that there is not any resonant response for periods between 14 and 24 hours, and that there exist well defined maxima in response at 13.7 and 9.0 hours for symmetric forcing and 10.9 and 7.5 hours for asymmetric forcing. These maxima can be identified with 1st and 2nd symmetric and asymmetric gravitational normal modes of the atmosphere. The dependence of the response magnitude on the latitudinal structure of the vertical motions at the lower boundary was investigated and it has been shown that relative value of the maxima is determined mainly by the projection of the lower boundary forcing onto the corresponding eigenfunction of Laplace's Tidal Equation. The vertical structure of the gravitational modes shows that magnitude of the horizontal wind perturbations increases with the altitude and relatively small disturbances in the lower atmosphere can provide substantial oscillations in the MLT region. These results provide further evidence for support a normal mode interpretation of the observed short period oscillations of the horizontal wind over South Pole.

**JSM01/W/93-A2** Poster **1600-04**

**SEASONAL VARIATIONS OF 3.0-3.8 DAY ULTRA KELVIN WAVES OBSERVED WITH A METEOR WIND RADAR AND RADIOSONDES IN INDONESIA**

Shuji YOSHIDA, Radio Atmospheric Science Center, Japan Email: yoshida@kurasc.kyoto-u.ac.jp

This presentation is concerned with observations of the long-term behavior of Kelvin waves with the wave period ranging from 3 to 4 days, which are generally called an ultra-fast Kelvin (UFK) wave. Horizontal wind velocity at 74--110 km altitudes observed with a meteor wind radar (MWR) near Jakarta (6.4S, 106.7E) for five years during November 1992 and December 1997 and daily radiosonde profiles in Bandung (6.9S, 107.6E) collected between October 1993 and March 1996 and have been analyzed. In the mesosphere and lower thermosphere (MLT) region, the UFK wave activity, defined by the spectral density of zonal wind perturbations at the 3.0--3.8 day period, clearly dominated by a semiannual periodicity, strongly suggesting an interaction between UFK waves and MSAO. However, an exact mechanism is uncertain. We also have investigated seasonal variation of 3.0--3.8 day oscillations of zonal winds in the stratosphere, excluding gravity wave components, but, we have not detected an evidence of semiannual periodicity. The UFK wave activity in the MLT region exhibited intraseasonal variations (20--33 days), which showed some correlation with the amplitudes of zonal wind in the troposphere.

**JSM01/W/98-A2** Poster **1600-05**

**A POSSIBLE MECHANISM FOR GENERATION OF 20- AND 30-HOUR WAVES IN THE NEUTRAL WIND OF LOWER THERMOSPHERE**

D. PANCHEVA (Geophysical Institute, Bulg. Acad. Sci., "Acad. G. Bonchev str.", bl.3, Sofia, Bulgaria) G. Beard (The University of Wales, Aberystwyth, Dept. of Physics, Aberystwyth, Ceredigion SY23 3BZ, U.K.)

A peculiar feature of dynamics in the mesosphere/lower thermosphere region above Bulgaria is the presence of strong oscillations with periods 20 hours and 30 hours, especially in the zonal wind component. Bispectral, correlogram and wavelet analyses of the data indicate that these signals are not simply the result of a nonlinear interaction between the diurnal tide and a 5-day wave. Bispectral analysis reveals that there is a strong interaction occurring involving the semidiurnal tide and the 20- and 30-hour signals. On the basis of this evidence, a mechanism is proposed in which the 20- and 30-hour waves, initially produced as "sum and difference" secondary waves by a 5-day wave/diurnal tide coupling, interact with the semidiurnal tide. The mathematical relationship between these waves results in a feedback mechanism being established in which energy from the semidiurnal tide is channelled into the 20- and 30-hour



waves. Wavelet analysis reveals a period in which the initial 5-day wave/diurnal tide coupling could have occurred. The correlogram analysis supports the proposed mechanisms and lends evidence against the theory that the large 20- and 30-hour waves are simply the result of a strong 5-day wave/diurnal tide interaction lower down in the atmosphere.

**JSM01/W/45-A2** Poster 1600-06

**SIMULTANEOUS MEASUREMENTS OF THE MESOPAUSE TEMPERATURE PROFILES WITH A SODIUM TEMPERATURE LIDAR AND THE OH(6,2) AND O2(0,1) ROTATIONAL TEMPERATURES AT 23 DEGREES**

S Paulo P. BATISTA, Barclay R. Clemesha, Delano Gobbi, Maria P. P. M Jorge, Hisao Takahashi and Igor Veselovskii (both at Instituto Nacional de Pesquisas Espaciais, C.P. 515, S. J. dos Campos, SP, BRAZIL) Email: pbatista@laser.inpe.br

The mesopause temperature profile has been measured at São José dos Campos (23.2 degree S, 45.9 degree W) for a total of 15 nights from July to October 1998. The technique used is the measurement of the Doppler temperature of the sodium atoms present in the atmospheric sodium layer with a Lidar. This Doppler temperature is measured by commuting the multi-line output of the laser separated by 1.98 pm between a position where the lines coincide or not with the NA D2 hyperfine lines by controlling the pressure in a Fabry-Perot interferometer. During 8 of the 15 days of Lidar temperature data, simultaneous measurements of the rotational temperature of the OH(6,2) band at 775.0 nm and the O2(0,1) Atmospheric band at 864.5 nm were obtained at a nearby station Cachoeira Paulista (22.7 degree S, 45.2 degree W), with a filtering filter photometer. There is a fair agreement between the OH temperature and the gaussian weighted temperature calculated using the Lidar temperatures centered on 87 km and with a half-width of 5 km, consistent with rocket measurements for the OH emission profile, for most of the days. But no consistent combination of height and half-width can reproduce the absolute value and variation of the O2(0,1) temperature, suggesting that transition probabilities used for determining the latter may need to be revised.

**JSM01/W/19-A2** Poster 1600-07

**THE MESOSPHERIC SODIUM LAYER AT 23°S**

Dale SIMONICH (Instituto Nacional de Pesquisas Espaciais-INPE, São José dos Campos 12201-970, SP, Brazil, email simonich@laser.inpe.br) Barclay Clemesha (Instituto Nacional de Pesquisas Espaciais-INPE, São José dos Campos 12201-970, SP, Brazil, email clem@laser.inpe.br)

We present here a comparison of 20 years of mesospheric sodium measurements (685 nights) with our previous paper covering the first 5 years of these measurements referred to as paper 1 (Simonich et al. J. Geophys. Res. 84.A4, p1543, 1979). The average of all of the daily profiles shows a small increase in the peak density (from 3 to 4 x 10<sup>9</sup> m<sup>-3</sup>) with a very similar shape i.e. a peak at around 91 km. (as opposed to 95 in paper 1) and a secondary maximum at about 85km. The center of mass of this layer was 93 km and its abundance was a little less than 5 x 10<sup>-13</sup> m<sup>-2</sup>. The monthly average profiles for these data show a somewhat different behaviour. Paper 1 showed a broad layer from equinox to equinox with a short minimum in December and slightly increased peak densities around the equinoxes. The more complete data still show a broad maximum but now the peak density is confined to the spring equinox (Southern Hemisphere) and is a little greater than in paper 1. The abundance curves are similar except for the larger abundance in September. Averaging the data into yearly profiles shows a mostly uniform profile with a minimum height in 1983 and a peak height in 1989. The peak density occurred in 84 and 89. There is a gradual rise in the layer from 85 to 89. The abundance seems to show a gradual overall reduction during the period. Fitting a DC level plus a 1 and 11 year cosines to the daily average abundance shows that there seems to be a solar cycle variation in the abundance. The curve has minimums of the 11 year cycle in early 77 and 88 while the minimums of the solar cycle occurred in mid 76 and early 86.

**JSM01/E/11-A2** Poster 1600-08

**SEASONAL VARIATIONS IN AIRGLOW INTENSITIES AND TEMPERATURES AT EL LEONCITO, 1997 - 1999**

Juergen SCHEER (PRONARP-CONICET, J. Alvarez 1218, 1414 Buenos Aires, Argentina, Email: jurgen@caerce.edu.ar)

A new run of airglow observations of the OH and O2 emissions and rotational temperatures from El Leoncito, Argentina, in the context of the Planetary Scale Mesopause Observing System, will have nearly completely documented the annual cycle of variations in the mesopause region. The emerging patterns of the intensity variations are different for both emissions. A seasonal oscillation with maxima in April and October and minima at the solstices dominate the behaviour of the O2 Atmospheric band. This is consistent with many previous observations of the green atomic oxygen line, also at similar Southern Hemisphere midlatitudes. The OH emission, also but more weakly dependent on the atomic oxygen concentration, shows a grossly similar behaviour, but with certain distinctive features, probably due to its lower altitude. The rotational temperatures lack the seasonal variations one would expect, at least for the 86 km level.

**JSM01/E/42-A2** Poster 1600-09

**WINDS AND WAVES AT 50-100 KM OBSERVED WITH MF RADAR AT POKER FLAT AND COMPARISON WITH SIMULTANEOUS RAYLEIGH LIDAR OBSERVATIONS**

Y. MURAYAMA, K. Igarashi, K. Mizutani (all at Communications Research Laboratory, Koganei, Tokyo 184-8795 JAPAN, email: murayama@crl.go.jp) Richard Collins (Geophysical Institute, University of Alaska Fairbanks, Fairbanks, AK 99775-7320 USA, email: rc@hoffa.gi.alaska.edu)

Poker Flat MF radar was constructed in October 1998, as part of the comprehensive arctic middle atmosphere observation program by Communications Research Laboratory of Ministry of Posts and Telecommunications of Japan, in co-operation with Geophysical Institute of Univ. of Alaska Fairbanks. The radar operates with the frequency of 2.43 MHz and peak power of 50 kW since then, which continuously conducts the mesospheric and lower thermospheric wind velocity observation, as well as differential absorption experiment (DAE) for D-region electron density estimation. The wind data in October-November 1998 showed surprisingly larger altitude coverage of 50-100 km (daytime) and 60-100 km (night time) than existing radars. Gravity wave and/or tidal structures can be seen with consistent behaviour of mean wind and fluctuation fields below and above the 60 km altitude. In this study, we conduct simultaneous observations with the MF radar and Rayleigh lidar both at Poker Flat in January 1999, to examine gravity wave fields in wind velocity and temperature, which should be connected by the polarization relation of the gravity wave. Also detailed analysis of the MF radar winds and vertical/temporal wave structure will be presented.

**JSM01/E/43-A2** Poster 1600-10

**OPTICAL AND RADAR MEASUREMENTS OF MESOSPHERIC TIDES AT DAVIS, ANTARCTICA.**

P.A. GREET (1), G.B. Burns(1), W.J.R. French(1), D.J. Murphy(1), P.L. Dyson(2), R.A. Vincent(3) (1) Australian Antarctic Division, Channel Highway, Kingston, Tas. 7050, Australia. (2) School of Physics, La Trobe University, Bundoora, Vic. 3083, Australia. (3) The University of Adelaide, Adelaide, South Australia 5005, Australia.

Davis, Antarctica (68.6°S, 78.0°E), hosts a number of instruments for middle and upper atmospheric studies including a high-resolution Fabry-Perot spectrometer (FPS), a Czerny-Turner grating spectrometer (CZT), and a medium-frequency (MF) radar. Observations of the OH (6-2) emission by the FPS yield mesospheric winds and OH intensities; by the CZT, OH intensities and rotational temperatures. The MF radar measures mesospheric winds from 80-100 km. The CZT and MF radar run routinely but the FPS data is campaign based and reliant on good optical observing conditions. A number of campaigns with reasonable FPS OH data have been obtained in 1997 and 1998. Tidal analyses of data from the three instruments will be presented.

**JSM01/W/50-A2** Poster 1600-11

**THE MEAN CIRCULATION, TIDES, AND PLANETARY WAVES IN THE EAST-SIBERIAN LOWER THERMOSPHERE**

Edward KAZIMIROVSKY and Galina Vergasova (Institute of Solar-Terrestrial Physics, Russian Academy of Sciences, P.O.Box 4026, 664033, Irkutsk, Russia, email:edkaz@iszf.irk.ru)

Ionospheric drift measurements in the LF range, which refer to altitudes between 80 and 100 km, enable the circulation in the lower thermosphere to be permanently monitored. From many years (1975-1996) of such continuous daily measurements on Observatory Badary near Irkutsk, Russia (52°N, 102°E) results have been obtained on prevailing zonal and meridional wind, semidiurnal tidal wind components and variations with planetary wave periods. We present the climatic norms for the wind field parameters, their seasonal, intraseasonal and inter-annual variations, their possible long-term trends and dependencies on the solar cycle. We consider the geographical nonzonality of the lower thermosphere wind field, including the response to the stratospheric quasi-biennial oscillations (QBO) and sudden stratospheric warmings.

**JSM01/E/10-A2** Poster 1600-12

**INTERANNUAL, SEASONAL AND INTERANNUAL VARIABILITIES IN LOW LATITUDE MESOSPHERIC TIDES**

S. GURUBARAN (Equatorial Geophysical Research Laboratory, Indian Institute of Geomagnetism, Krishnapuram, Tirunelveli 627 011, India, email gurubara@md3.vsnl.net.in) R. Rajaram (Indian Institute of Geomagnetism, Colaba, Mumbai 400 005, email rrajaram@iig.igm.res.in)

Atmospheric tides are one of the principal means of transferring energy and momentum between different regions of the atmosphere. Tidal perturbations, generated in the lower and middle atmosphere, grow in amplitude as they propagate upwards, and participate in governing the heat and momentum budgets of the upper atmosphere. Observational aspects of the tides were brought out in the past by the varieties of radars and instruments on board satellites. The studies revealed variability in mesospheric tides on different spatial and temporal scales. The causative mechanisms responsible for the tidal variabilities, however, are not known. The medium frequency (MF) radar observations of mesospheric tidal winds over more than five years, made from the low latitude site, Tirunelveli (8.7 degrees N, 77.8 degrees E), India, are reported in the present work. The variabilities on different time scales are examined in detail. The seasonal variabilities are rather complex. The prominent feature in the observations is the interannual variability in the diurnal tide. The tidal amplitudes are largest in the intraseasonal time scales in the zonal component than in the meridional component, the distinct periods observed being 90 and 60 days. Since similar variabilities are noticed in the mean zonal flow, tidal-mean flow interactions might have resulted in the observed intraseasonal variability in the tidal amplitudes.

**JSM01/E/06-A2** Poster 1600-13

**ON SOME VARIABILITIES IN MIDDLE ATMOSPHERE DYNAMICS OVER SOUTH EASTERN EUROPE**

Petio Simeonov, Staycho KOLEV and Lubka Milenkova (National Institute of Meteorology and Hydrology, Bulgarian Academy of Sciences, Sofia-1784, Bulgaria, email: Petio.Simeonov@meteo.bg, Staycho.Kolev@meteo.bg)

The basic wind and air temperature characteristics (representing the dynamic in the middle atmosphere) are obtained on the base of radio and rocketsounding data from Ahtopol station during December 1982 - March 1992.

The seasonal and annual vertical profiles of the wind (zonal and meridional components) up to 60 km are shown. Westerlies prevail in the annual distribution of zonal wind velocities. Mean monthly velocities vary between 9 and 57 m/s (in the summer) and reach up to 74 m/s in the winter. The values of meridional wind velocities are about 0 m/s up to 30 km altitude and reach up to 12 m/s over this level. The set of statistical characteristics are obtained concerning the time-space variability of the wind. The cross sections of monthly wind velocities distribution show the seasonal variability in middle atmospheric dynamics.

The temperature vertical profiles (seasonal and annual) are framed up to 75 km in the troposphere and stratosphere are framed. Annual and seasonal temperature trends at 25, 45 and 65 km levels are studied. The tendency of cooling in the high stratosphere is found out after 1985, more underlined in the springtime and summer season. The vertical cross section of monthly temperature distribution shows the seasonal passage in middle atmosphere over Balkan region in Southeastern Europe.

**JSM01/E/34-A2** Poster 1600-14

**MEAN WIND AND TIDAL FEATURES IN THE HIGH LATITUDE AS SEEN BY A NEW MF RADAR AT POKER FLAT, ALASKA (65.1N, 147.5W)**

Kiyoshi IGARASHI and Yasuhiro Murayama (both at Communications Research Laboratory, Koganei, Tokyo 184-8795, Japan, email igarashi@crl.go.jp) Done Rice and Brenton J. Watkins (both at Geophysical Institute, University of Alaska Fairbanks, Fairbanks, AK 99775-7320, USA, email ddr@flux.isr.alaska.edu)

We have constructed a new MF radar system at Poker Flat, Alaska (65.1N, 147.5W). This radar started operation on 16 October, 1998, for studies of the mesosphere and lower thermosphere region at high latitude as a collaboration project between Communications Research Laboratory, Japan and Geophysical Institute, USA. This radar is operated at frequency 2.430 MHz and peak power 50kW. Wind measurements by FCA and electron density measurements



## INTER-ASSOCIATION

by a differential absorption method are conducted alternately. From the first data in October, 1998 we found strong 12 hour oscillations and long-period oscillations in the mesospheric wind. In this paper we will introduce this new MF radar system and discuss features of mean winds, tidal and planetary waves in the high latitude based on this radar observations.

**JSM01/W/12-A2** Poster **1600-15**

### THE UARS REFERENCE ATMOSPHERE PROJECT

J.J. REMEDIOS, (Aopp, Dept. of Physics, Oxford University, Parks Road, Oxford OX1 3pu, U.K., E-Mail: J.Remedios1@Physics.Ox.Ac.Uk), D. Cunnold, H.J. Wang (Both At School of Earth and Atmospheric Sciences, Georgia Institute of Technology, Atlanta, Ga 30332-0340 U.S.A., E-Mail: Cunnold@Eas.Gatech.Edu), A.E. Dessler (Dept. of Meteorology, University of Maryland, College Park, Md 20742, U.S.A., E-Mail: Dessler@Atmos.Umd.Edu), J.C. Gille, W.J. Randel (Both At National Center For Atmospheric Research, Boulder, Co 80307, U.S.A., E-Mail: Gille@Acad.Ucar.Edu, Randel@Acad.Ucar.Edu), R.G. Grainger, S.M. Wheaton, (Both At Department of Physics And Astronomy, University of Canterbury, Private Bag 4800, Christchurch, New Zealand, E-Mail: R.Grainger@Phys.Canterbury.Ac.Nz), H.C. Pumphrey, Dept. of Meteorology, Univ. of Edinburgh, Edinburgh EH9 3Jz, Scotland, E-Mail: Hcp@Met.Ed.Ac.Uk).

The UARS (Upper Atmosphere Research Satellite) reference atmosphere project has developed a number of climatological datasets characteristic of the stratosphere (and mesosphere) during the UARS mission. These data are based on the unique, detailed, near-global observations from the chemical constituent sounders on UARS and include ozone and related chlorine and nitrogen species, sulphate aerosol, dynamical tracers and temperature. For this reason, they represent a major step forward in describing the middle atmosphere through simultaneous measurements of many species. The fields consist of monthly zonal means in both pressure and theta vertical co-ordinates where the theta co-ordinate data has been mapped using equivalent latitude techniques. Estimates of variability are also provided. The data will be presented along with methodologies and comparisons to previously available reference datasets. The new datasets will also be placed within the context of the atmospheric conditions prevailing during the UARS mission.

**JSM01/E/21-A2** Poster **1600-16**

### SEASONAL VARIATION OF GRAVITY WAVE ACTIVITY IN THE UPPER MIDDLE ATMOSPHERE IN CENTRAL EUROPE

Jaroslava Boskova, Jan LASTOVICKA (Institute of Atmospheric Physics, Bocni II, 141 31 Prague 4, Czech Republic, e-mail: jla@ufa.cas.cz)

The results of various authors on the seasonal variation of gravity wave activity in the middle atmosphere do not provide a consistent pattern. However, it is evident that the seasonal variation is height-dependent and it may be regionally dependent, as well, perhaps due to a regional variation of gravity wave sources. Here we analyze five years (1989-1993) of continuous gravity wave data inferred from the LF radio wave absorption in the night-time lower ionosphere (~90-100 km) in Central Europe (50N, 16E). Previous analyses were made only from the point of view of summer-winter difference on a substantially smaller data set. They did not find a detectable difference. They pointed out the importance of the effect of the length of night on the results due to limited persistency of wave events. This effect is now very carefully evaluated for the 5-year data series analysis.

**JSM01/W/74-A2** Poster **1600-17**

### WAVE ACTIVITY IN THE STRATOSPHERE OVER SPRING NORTH POLAR REGION DERIVED FROM OZONESONDE MEASUREMENTS AT FAIRBANKS IN APRIL 1997

Kazuo SHIBASAKI, Kokugakuin University, Email: skazuo@kokugakuin.ac.jp

Global distribution of gravity wave activity in the stratosphere is the key to understand the role of gravity wave on dynamical processes in the Earth's atmosphere. Recently many observational evidences have been reported on the behaviour of gravity wave activities. These data were obtained with a variety of instruments. However, few data have been collected in the polar region. We made ozonesonde measurements as a part of ADEOS validation campaign in Fairbanks, Alaska during April 1997. We present the characteristics of wave structure deduced from ozonesonde measurements made at collar region of northern polar vortex. Wave characteristics were examined using both the temperature and ozone vertical profiles. We show a spectral analysis result, which shows wave structures of a vertical wavelength of about 3km. These wavy structures may be attributed to gravity wave activity. Wavy structures are clearly recognized in the temperature profile. Although they are not so clear in the ozone profiles partly because of the variable layer structures of ozone in the lower stratosphere due to active horizontal transport process, a peak at wavelength of 3 km can be calculated from spectral analysis of ozone profiles. Correlation between the wavy structures seen in the temperature and ozone profiles is discussed in this paper. Also reported in this paper is the preliminary analysis result of the ozonesonde measurements scheduled to be carried out in mid-March 1999 at Fairbanks.

**JSM01/P/03-A2** Poster **1600-18**

### MESOSPHERE FRONTAL GRAVITY WAVES, AND SOLAR ECLIPSE AT NOON

J. Delloue (Valensole, Haute Provence, France), D.C. Fritts (Colorado Res. Ass., USA), Th. Farges (LDG/DASE-CB3, France), C. Lathuillere (LIS/Grenoble, France), G. Thuillier, S.A. Verrieres (CNRS, France) and P.M. VILA (CETP/CNRS, Saint-Maur-des-Fosses, France).

The traveling modes of ionospheric frontal wave have diverse source processes. The least elucidated are mesospheric shear effects now evidenced on the average Windii Hrdi data. We here present Summer midlatitude and associated low-latitude wind profiles from the Windii database. On the 11 August 1999 the Euro-pean zone swept by the noontime Solar Eclipse near 50°-80° North latitude will simultaneously create i) a deep conductivity shock at E-layer levels and ii) a subsequent bow-wave front at hundreds km distance from the edge of the totality zone. Traces of this front will be searched by the HF radar at Valensole (Haute Provence), and if possible in the early evening by the Michelson OHP interferometer (Manosque, Haute Provence, France). Experimental results from these experiments and from other European networks will be later usable to discuss the coupling model of Fritts (1993).

**JSM01/W/112-A2** Poster **1600-19**

### PRELIMINARY RESULTS OF THE AIRGLOW AND TEMPERATURE OBSERVATIONS BY MORTI AT THE ALMATY SITE (43.6 N, 76.6 E)

V.M. AUSHEV, A.I. Pogoreltsev, and V.V. Vodjanikov (all at Institute of the Ionosphere, Ministry-Academy of Science of the Republic of Kazakhstan, Almaty, 480068, Kazakhstan; e-mail: pogor@ionos.alma-ata.su); R.H. Wiens and G.G. Shepherd (both at Institute for Space and

Terrestrial Science, York University, 4850 Keele St., North York, Ontario, Canada, M3J 3K1, e-mail: rudy@stpl.cress.yorku.ca)

Preliminary results of analysis of the molecular oxygen nightglow emission rate and rotational temperature observed in Almaty by Mesopause Oxygen Rotational Temperature Imager (MORTI) during 1997-1998 period are discussed. The Lomb-Scargle periodogram analysis was applied to assess the statistically significant oscillations present in the data. A quadratic fit was subtracted from each data set to remove trends whose periods were commensurate with the data set length. Two groups of statistically significant peaks appear in the power spectra. The lower frequency group corresponds to the periods of 5-9 hours. These variations are most likely due to the tidal (6 and 8 hours) oscillations similar to reported by Wiens et al. (Geophys. Res. Lett., 22, 2637, 1995) and Ozonovich et al. (Planet. Space Sci., 45, 385, 1997) and/or perhaps due to the gravitational normal modes (Meyer and Forbes, J. Atmos. Solar-Terr. Phys., 59, 2185, 1997; see also Pogoreltsev, report submitted at this symposium). The higher frequency group corresponds to the periods of 2-3 hours, and these variations are due to the IGW propagation at the mesopause heights. COPHASE method proposed by Posmentier and Herrmann (J. Geophys. Res., 76, 2194, 1971) was applied to obtain IGW characteristics from MORTI data. It has been shown that the azimuth of wave propagation and the horizontal phase speed obtained by COPHASE technique are more reliable than estimations of these values obtained by least squares method, which is traditionally used for analysis of MORTI data.

**JSM01/W/66-A2** Poster **1600-20**

### EIKONAL SIMULATIONS OF THE SPECTRUM PRODUCED BY THE PROPAGATION OF SMALL-SCALE INTERNAL GRAVITY WAVES THROUGH LARGE-SCALE INTERNAL WAVE FIELDS

R.L. WALTERSCHEID, The Aerospace Corporation, M2-260, P.O. Box 92957, Los Angeles, CA 90009 USA (Richard.Walterscheid@aero.org)

A small-scale internal gravity wave packet sees a time- and space-dependent background as it propagates upward through a field of large-scale internal gravity waves. The time and space dependency of the background causes the wave packet to migrate in frequency-wave number space. In time-dependent wave backgrounds, waves can propagate through levels that would be critical in stationary horizontal flow. In wave backgrounds, wave removal at such levels depends on the initial wave-packet amplitude. We have performed eikonal calculations for large numbers of wave packets propagating through various realizations of background wave spectra. It is found that the migration of wave packets in both wavenumber and frequency and the initial wave amplitudes help shape the wave spectra.

**JSM01/W/22-A2** Poster **1600-21**

### QUASI-UNIVERSAL $M^2(-3)$ VERTICAL WAVENUMBER SPECTRA GENERATED BY ISENTROPIC ADVECTION BY A SUPERPOSITION OF SINUSOIDAL GRAVITY WAVE DISPLACEMENTS

Stephen D. ECKERMANN, E. O. Hulburt Center for Space Research, Code 7641.2, Naval Research Laboratory, Washington DC 20375

We present results of a two-dimensional model of isentropic advection of air parcels by a superposition of sinusoidal wave displacements due to hydrostatic gravity waves. Data are gridded at high vertical resolution and used to generate potential temperature, displacement and velocity perturbation profiles. As amplitudes increase, wave perturbation profiles distort due to advection of air parcels across the phase fronts of other waves. At saturation amplitudes near overturning, the spectra of these profiles attain quasi-universal  $M^2(-3)$  shapes similar to observations. Possible relationships to other theories of gravity wave spectra in the atmosphere and oceans will also be discussed.

**JSM01/W/64-A2** Poster **1600-22**

### SMALL SCALE WIND STRUCTURE IN THE MESOSPHERE

R. R. CLARK, (Electrical and Computer Engineering, University of New Hampshire, Durham, NH 03824, email: ron.clark@unh.edu) J. E. Salah, L. P. Goncharenko, (both at Haystack Observatory, Massachusetts Institute of Technology, Westford, MA 01886, email: jes@haystack.mit.edu)

Observations of small scale structure in the mesosphere winds with the UNH meteor wind and the Millstone IS radar will be presented. Attention is given to the measurement error associated with the radars and the possible errors introduced by known wind components. The spatial resolution of these measurements is approximately 2 km. The rms velocity errors vary but are generally 7 m/s for the meteor radar and 25 m/s for a 2 minute measurement with the IS radar. Observations have been made in a common volume with both instruments and both show random variations in the wind measurements that are greater than the predicted error from the measurement process. Measurements indicate that the roughness of the wind structure can change hourly. These results should be useful when one is trying to compare wind measurements made with instruments, which use different techniques.

**JSM01/W/91-A2** Poster **1600-23**

### SEASONAL VARIATIONS OF WIND VELOCITY AND TEMPERATURE VARIANCES OBSERVED WITH RADIOSONDES IN INDONESIA

Atsushi SHIMIZU, Radio Atmospheric Science Center, Japan, Email: shimizu@kurasc.kyoto-u.ac.jp

We continued radiosonde soundings once a day for about 30 months during October 19, 1993 and March 11, 1996, in Bandung, Indonesia (6.9 S, 107.6 E), and obtained total of 785 profiles of horizontal winds and temperature at 0--38km, and the same number of humidity profiles below 10 km. We first show in this presentation the climatological characteristics of zonal winds, precipitable water vapor content (PWC) and Brunt-Vaisala frequency squared,  $N^2$ , in the troposphere and lower stratosphere. PWC shows a clear annual cycle between dry and rainy seasons, centered in July-October and December-March, respectively. The  $N^2$  variations were particularly enhanced in the upper troposphere (11--14 km), and the seasonal cycle of  $N^2$  is anti-phase to that for PWC. We have further analyzed the seasonal variations of wind velocity and temperature perturbations with a vertical scale of 2 km, which is used as an index of gravity wave activity. Annual cycle of the gravity wave activity is clearly recognized in the entire troposphere, which is anti-phase to the seasonal variations of PWC, that is, it is in-phase to the  $N^2$  variation in the upper troposphere. The gravity wave energy seems to be proportional to the background  $N^2$  value, as suggested by a saturated gravity wave model. In the lower stratosphere the annual cycle of the gravity wave activity disappears, but the long-term variations are related to the QBO structure.

**JSM01/E/30-A2** Poster **1600-24****INITIAL RESULTS OF THE OPTICAL MESOSPHERE THERMOSPHERE IMAGERS (OMTI): SIMULTANEOUS IMAGING OBSERVATION OF FOUR AIRGLOW LAYERS AROUND THE MESOPAUSE**

Kazuo SHIOKAWA, Mitsumu Ejiri, and Tadahiko Ogawa (Solar-Terrestrial Environment Laboratory, Nagoya University, 3-13, Honohara, Toyokawa, Aichi 442-8507, Japan, Email: shiokawa@stelab.nagoya-u.ac.jp) Takuji Nakamura and Toshihata Tsuda (Radio Atmospheric Science Center, Kyoto University, Uji 611-0011, Japan, Email: nakamura@kurasc.kyoto-u.ac.jp) Rudolph H. Wiens (Center for Research in Earth and Space Science, York University, Ontario M8V 3E5, Canada, Email: rudy@stpl.cress.yorku.ca)

The Optical Mesosphere Thermosphere Imagers (OMTI) have been developed to investigate the dynamics of the upper atmosphere through nocturnal airglow emissions. The OMTI consist of an imaging Fabry-Perot interferometer, three all-sky cooled-CCD cameras, three tilting photometers, and a Spectral Airglow Temperature Imager (SATI) with two container houses to install them in. These instruments measure wind, temperature and 2-dimensional airglow patterns in the upper atmosphere at multi-wavelengths of OI (557.7nm and 630.0nm), OH(6-2) bands, O2(0,1) bands, and Na (589.3nm), simultaneously.

Using four all-sky cooled-CCD cameras (three from OMTI and one from Kyoto University), small-scale wave structures are observed in the airglow images at four wavelengths (OI, OH, O2, and Na emissions) around the mesopause region, during the Japanese PSMOS campaign on January-March, 1998 at Shigaraki (35N, 136E). We found an event during which gravity wave breaking occurs in the images. Vertical propagation and breaking of the gravity waves will be discussed using these image data and simultaneous wind and temperature data obtained by the MU radar.

**JSM01/W/108-A2** Poster **1600-25****WAVE STRUCTURES IMAGED NEAR INFRARED NIGHTGLOW AT YAKUTSK**

PP.AMMOSOV, G.A.Gavrilyeva (Institute of Cosmophysical Research and Aeronomy, 31, Lenin Ave., Yakutsk, 677891, Russia, e-mail: g.a.gavrilyeva@sci.yakutia.ru)

A digital all-sky imager for the study of the propagating internal gravity wave parameters and their sources is made and is installed at the station Maimaga ( $\lambda=63N$ ;  $\lambda=129,5E$ ;  $F=56$ ;  $L=199,7$ ). The instrument consists of the lens "fish eye" with angle of view  $180^\circ$  and CCD-camera which is cooled up to  $-50^\circ C$  and is interfaced with personal computer. Numerous wave patterns in the near infrared nightglow (600-1000) nm show that the short period gravity waves are commonplace over Yakutia. It is shown that in the most of cases the waves propagate to zonalward.

**JSM01/W/38-A2** Poster **1600-26****AVERAGE SEASONAL VARIATIONS OF IGW INTENSITY AND MOMENTUM FLUXES IN THE MESOSPHERE REGION FROM THE MU RADAR OBSERVATIONS IN 1986 - 1997**

Nikolai M GAVRILOV (Department of Atmospheric Physics, Saint-Petersburg University, Petrodvoretz, 198904, Russia, Email: gavrilov@snoopy.phys.spbu.ru); Shoichiro Fukao and Takuji Nakamura (both from Radio Atmospheric Science Center, Kyoto University, Uji, 611 Kyoto, Japan, Email: fukao@kurasc.kyoto-u.ac.jp)

Averaged seasonal variations of intensities of wind variations and vertical flux of horizontal momentum produced by internal gravity waves (IGWs) with periods 0.2 -- 1 hr and 1 -- 6 hr are studied at the altitudes 65 - 80 km using data of measurements with the Middle and Upper (MU) atmosphere radar at Shigaraki, Japan ( $35^\circ N$ ,  $136^\circ E$ ) during 1986 -- 1997. Simple numerical frequency filters are applied to separate wind variations having different periods. Wind variances and momentum fluxes are calculated using standard technique with pairs of the radar antenna beams inclined in opposite directions from zenith. Daily values of wind variances in every frequency band are averaged for each corresponding month over the whole period of the MU radar observations from 1986 to 1997. Mean IGW intensity has a maximum in summer and comparable maximum in winter, the winter values having big interannual variations. Mean zonal wave momentum flux is directed to the west in winter and to the east in summer - opposite to the mean wind in the middle atmosphere.

**JSM01/C/MW07/W/10-A2** Poster **1600-27****PARAMETERIZATION OF THE INTERNAL GRAVITY WAVE FORCING IN THE MIDDLE ATMOSPHERE**

A.BELYAEV (Fedorov Institute of Applied Geophysics, Rostokinskaya ul.9, Moscow 129128 Russia Email: belyaev@rc.msu.ru)

Momentum exchange between internal gravity waves and background atmosphere flow is simulated. Simulations using the original IGW parameterization allowing wave destruction on the critical levels are effected in the framework of the one-dimensional atmosphere model. It is shown that acceleration or deceleration of the background flow by wave forcing is depended on the direction of the mean wind vertical shift. Wave force has the same sign as the mean wind in the stratosphere and opposite in the upper mesosphere-lower thermosphere.

**JSM01/C/MW07/W/01-A2** Poster **1600-28****MOMENTUM FLUXES DUE TO OROGRAPHIC EFFECTS**

Rita Margarida CARDOSO (Centro de Geofísica da Universidade de Lisboa, R. da Escola Politécnica 58, 1250 Lisboa, Portugal, email: rcardoso@fc.ul.pt); Pedro M.A. Miranda (Faculdade de Ciências da Universidade de Lisboa, Campo Grande, Edifício C2, 1700 Lisboa, Portugal, pmiranda@fc.ul.pt)

The generation of gravity waves with wavelengths that allow for vertical transport of energy and momentum are one of the possible effects of orography. These waves may be responsible for dramatic changes in the flow around mountains. The horizontal dimension of the mountain plays an important role in the influence of the Coriolis force on the flow, and its height is crucial for determining flow splitting and wave breaking. In linear flow, the drag on the mountain due to an asymmetry of the pressure field around it, is equal to the upward flux of momentum due to gravity waves.

The present study focuses on the onset of different flow regimes due different horizontal mountain scales, including rotation, surface friction and thermal effects. Data from a field experiment in the Island of Madeira and from the PYREX campaign are used and compared with results from both linear and non-linear simulations of flow past realistic orography.

**JSM01/C/MW07/W/16-A2** Poster **1600-29****ALIGNMENT OF MOUNTAIN LEE-WAVES STUDIED USING MST RADAR AND NOAA AVHRR IMAGES**

R.M. WORTHINGTON (Department of Physics, University of Wales, Aberystwyth, Dyfed, SY23 3BZ, U.K.) email: rrw@aber.ac.uk

Alignment of atmospheric mountain-waves is a significant parameter in e.g. representation of wave drag in numerical weather models, and to predict PSCs or wave-breaking turbulence. The MST radar at Aberystwyth (52.4N, 4.1W) is used to measure long-term mountain wave alignment and its relation to background wind direction, using a method based on the tilting of VHF-radar scatterers by the mountain waves. Secondly, the alignment is also measured from wave clouds on more than 2 years of satellite images, and combined with UK Meteorological Office synoptic data. The two independent methods show the horizontal component of the mountain wave vector is, on average, aligned with the wind direction in the middle of the boundary layer, i.e. between the directions of the surface and geostrophic winds. For mountain waves above the Welsh mountains, the wind direction in the boundary layer appears to be a more important factor on the wave alignment than the direction of mountain ridges.

**JSM01/C/MW07/W/11-A2** Poster **1600-30****OROGRAPHIC BUOYANCY WAVES IN PRESSURE-CO-ORDINATE DYNAMICS**

Aarne MÄNNIK, (Tartu University, Tähe 4, Tartu, 51010, Estonia, email: aarne@aa.ee) Rein Rõõm (Tartu Observatory, Tõravere, Tartumaa, 61602, Estonia, email: room@aa.ee)

Estimation of the accuracy of different pressure coordinate models is carried out, modeling buoyancy wave generation by orography. Evaluated models are: the elastic nonhydrostatic model (EFM), the anelastic nonhydrostatic model (AEM) and the hydrostatic primitive equation model (HSM). These models are compared to the exact, nonfiltered, nonhydrostatic, pressure-coordinate dynamics (ExM). All model equations are linearized, a wave-equation for vertical displacements of air particles is derived, and stationary solutions for each model are compared for uniform flow over given smooth orography.

Modeling reveals that compressible (ExM, EFM) and incompressible models (AEM, HSM) are different at horizontal scales longer than 700 km. Differences are especially large in vertical velocity field (up to 100 %) at the medium and upper levels of the atmosphere, where incompressible models give systematic reduction of wave amplitudes. All models are effectively incompressible and coincide with high precision in the region 10 - 700 km. The first critical scale is at 10 - 20 km, below which the HSM fails. The second critical scale is at 100 m (moderate winds) - 1000 m (strong winds), below which the AEM becomes inconsistent with the other models in temperature fluctuation presentation. The EFM represents a universal approximation, valid at all scales.

**JSM01/C/MW07/E/01-A2** Poster **1600-31****THE FIRST DETECTION OF FREE OSCILLATIONS OF THE ATMOSPHERE IN THE 1 - 2 H PERIOD RANGE**

L.N. Petrova and G.M. SHVED (Institute of Physics, St.Petersburg State University, St.Petersburg-Petrodvoretz 198904, Russia, email: shved@lmupa.phys.spbu.ru)

The frequency spectra of seismic oscillations in the 1 - 2 h period range have been derived for four runs by seismograph with vertical pendulum in St.Petersburg (60N, 30E) of the 30-90 h duration. Oscillations with steady frequencies have been detected in the 0.155 - 0.290 mHz range. Most of them is thought to be global normal modes of the atmosphere. This conclusion bases on the following: (i) The number of the oscillations detected is approximately equal to a theoretically predicted number of the normal modes. (ii) In the 0.250 - 0.290 mHz subrange the oscillations are spaced at the 0.008 mHz intervals predicted.

**JSM01/C/MW07/E/02-A2** Poster **1600-32****PENETRATING THE EARTH'S FREE OSCILLATIONS WITH THE 54 MIN PERIOD INTO THE ATMOSPHERE**

G.M. SHVED, L.N. Petrova and O.S. Polyakova (Institute of Physics, St.Petersburg State University, St.Petersburg-Petrodvoretz 198904, Russia, email: shved@lmupa.phys.spbu.ru)

The most low-frequency mode of the Earth's free oscillations is the spheroidal mode 0S2 with period of about 54 min. The diurnal rotation of the Earth splits the mode 0S2 into 5 components spaced about 50 s apart, which are indexed by  $m = -2, -1, 0, 1, 2$  in order of increasing frequency. The synchronous measurements by a microbarograph and seismograph with vertical pendulum have been analysed to determine a phase difference between ground pressure oscillations and seismic oscillations at the frequencies of the 0S2 components. A certain phase relationship has been derived by comparing the phase difference for  $m=0$  with that for  $m<0$ . This relationship is a further proof of penetrating the Earth's 0S2 mode into the atmosphere. Moreover, it is the first observational manifestation of the second Pekeris normal mode of global atmospheric oscillations with the 54 min period.

**JSM01/C/MW07/W/23-A2** Poster **1600-33****OBSERVATIONS OF GRAVITY WAVE FLUXES AND TURBULENT DISSIPATION AT THE MU RADAR OBSERVATORY, JAPAN**

Dennis M. RIGGIN (Colorado Research Associates, Boulder, Colorado 80301, USA, email: riggin@colorado-research.com) Toshihata Tsuda (Radio Atmospheric Science Center, Kyoto University, Uji, Kyoto 611-0011, Japan, email: tsuda@kurasc.kyoto-u.ac.jp)

A measurement campaign was conducted with the MURadar at Shigaraki, Japan during Oct. 26-Nov. 5, 1996. The campaign combined high-resolution (150 m) Doppler wind radar measurements with temperature measurements made with the RASS (radio acoustic sounding system) and radiosonde balloon. In height, the RASS temperature measurements reached about 12 km, while the Doppler wind measurements extended into the lower stratosphere up to about 20 km. The results provide a comprehensive picture of the small-scale motion field with estimates of momentum flux, heat flux and the turbulent energy dissipation rate. The campaign was conducted during disturbed meteorological conditions characterized by a strong upper tropospheric jet and frontal passage. Relationships between the small-scale structure and the background fields are considered.

# INTER-ASSOCIATION

**JSM01/C/MW07/W/09-A2** Poster **1600-34**

## STUDIES OF ATMOSPHERIC GRAVITY WAVES AT MIDDLE-EUROPE AND NORTHERN SCANDINAVIA

Kathrin SCHULZ-SCHOELLHAMMER, Werner Singer, Peter Hoffmann, and Ralph Latteck, Leibniz-Institut fuer Atmosphaerenphysik an der Universitaet Rostock (e.V.), Schloss-Str. 6, D-18225 Kuehlungsborn, Germany

Gravity wave characteristics (e.g. vertical wave number spectra, propagation direction, momentum fluxes) have been derived from high-resolution balloon soundings of wind and temperature in the tropo- and lower stratosphere and from VHF radar measurements at mid latitudes (Lindenberg 52N14E, Kuehlungsborn 54N12E) and at arctic latitudes (Andenes 69N16E). A climatology of gravity wave activity over flat land terrain at Lindenberg has been established on the basis of a one year data set of 6-hourly soundings. The studies at arctic latitudes are restricted to wintertime and are directed to the relation between gravity wave activity and occurrence of polar stratospheric clouds. In addition, case studies on wave activity during the passage of fronts and during the presence of jet streams in the tropopause region will be discussed for both locations.

Wednesday 21 July AM

Presiding Chair: M. Joan Alexander (Colorado Research Associates, Boulder, USA)

## GRAVITY WAVES

**JSM01/E/17-A3** Invited **0830**

### HOW SIMPLE CAN SIMPLE GRAVITY WAVE PARAMETERIZATIONS AFFORD TO BE?

Christopher D WARNER and Michael E McIntyre, Centre for Atmospheric Science, D.A.M.T.P., University of Cambridge, Silver Street, Cambridge CB3 9EW, UK

An "ultra simple spectral gravity wave parameterization" (USSP) has recently been developed and tested in the UK Met. Office Unified Model. This parameterization has been developed from a full "power spectral" model of gravity wave spectral propagation and breaking by making simplifications analogous to those used in the popular Hines scheme. But such simplifications lead to significant discrepancies between simple gravity wave parameterizations, including full gravity wave models, and ours. We compare simple gravity wave models with our full model, and investigate strategies for improving simple models without incurring excessive additional computational cost.

**JSM01/W/31-A3** **0900**

### NUMERICAL STUDY OF THE LOCAL EFFECTS OF GRAVITY WAVE AND TIDAL INTERACTIONS

Han-Li LIU, Maura E. Hagan, Raymond G. Roble HAO/NCAR, Boulder, CO, USA

Gravity wave and tidal interactions may play an important role in the formation of the mesospheric inversion layer, and observations have also shown that this type of inversion layer is highly dynamic. Our work is a numerical investigation of such processes. We employed a two-dimensional nonlinear gravity wave/turbulence model along with global-scale wave model (GSWM-98) diurnal tidal winds and temperatures at different latitudes and different seasons to study the propagation of a gravity wave in a tidal wind field. A mesospheric chemistry model, adapted from the NCAR TIME-GCM, is coupled to the dynamics model and used to study the associated changes in chemical species and exothermic heating. Model results show that the gravity wave stability, momentum flux, and heat flux are strongly affected by the background mean state and tidal wind temperature, and are therefore seasonally and latitudinally dependent. The advective processes in the wave breaking region produce net cooling, while large non-uniform turbulence mixing can produce a large heating rate. Such processes may lead to an inversion layer (or layers) accompanied by cooling region(s). These region(s) descends with the breaking level(s), which are in turn dependent on the tidal wind and temperature. Therefore, such heating/cooling regions may bear the characteristics of the tidal wave. Furthermore, the inversion layer thus generated corresponds closely with mean wind acceleration and the wind shear associated with it, strong non-uniform turbulence layer, and chemical species changes. The wind, turbulence density, and species changes may be used as diagnostic parameters to test the theory with observations.

**JSM01/W/96-A3** **0920**

### A SPECIFIC INSTABILITY OF THE NONISOTHERMAL ATMOSPHERE

Olga SAVINA (Department of General and Applied of Physics, State Technical University, Minina st. 24, Nizhny Novgorod, 603600, Russia, Email: savina@appl.sci-nnov.ru)

In this work we discuss the problem of the instability of acoustic-gravity waves in the atmosphere with a realistic temperature distribution. For an analytical approximation of the real altitude profile of the atmospheric temperature we found an exact solution for the altitude dependence of a perturbation of the vertical speed in the atmosphere and an expression for the cut-off frequency of the fast branch of acoustic gravity waves. It is shown that this frequency can be smaller than the Brunt-Vaisala frequency. In this case the instability of acoustic gravity waves is possible. On the basis of these results we conclude that this instability realizes at altitudes about one hundred kilometers. It is shown that the frequency of these unstable waves is about the Brunt-Vaisala frequency and the increment of this instability depends on the temperature gradient.

**JSM01/W/18-A3** **0940**

### STUDY OF THE INTERNAL GRAVITY WAVES ABOVE ESRANGE (67.56 N, 21.04 E)

K. STEBEL and S. Kirkwood, IRF, Box 812, S-981 28, Kiruna, Sweden

Internal gravity waves are e.g. formed at orographic obstacles or at tropospheric weather systems. They effect the general circulation due to momentum and energy transport through the atmosphere. If they pass into the stratosphere localised cooling accompanied by rapid cooling rates can induce polar stratospheric cloud development, leading to an increased ozone reduction above the polar regions.

The 52 MHz MST radar ESRAD (ESRange RADar) is located at Esrange (67.56 N, 21.04 E), about 30 km east of Kiruna, in northern Sweden. It is in operation since July 1996. On many occasions quasi-stationary internal gravity waves have been identified in the radar data. Vertical velocity variations in a region just over the tropopause show the wave propagation to the stratosphere. The radar-data reveal the morphology of the tropopause and show frontal systems, which drift over the radar site. Additionally, we can observe evidence for the downward transport of lower stratospheric air into the troposphere.

The continuous operating VHF radar allows us not only to analyse individual cases but also to

study seasonal variations. Here, we present a radar study of the dynamics of the tropopause region above Esrange. We use weather chart and satellite images for interpretation of our data. The wave characteristics in the stratosphere are further studied utilizing radio- and ozonesonde data.

Presiding Chair: William Ward (CRESS/CRESTech, York Univ, Canada)

## PSMOS

**JSM01/W/30-A4** **1000**

### THE PLANETARY SCALE MESOPAUSE OBSERVING SYSTEM (PSMOS): OVERVIEW AND STATUS

Gordon G. SHEPHERD (Centre for Research in Earth and Space Science, YorkUniversity, Toronto, M3J 1P3, Canada, Email: gordon@windii.yorku.ca) and Maura Hagan (High Altitude Observatory, National Center for Atmospheric Research, Boulder, Colorado, USA Email: hagan@hao.ucar.edu)

The Planetary Scale Mesopause Observing System (PSMOS) is a new project approved by SCOSTEP, involving 53 scientists from 15 countries. It came about in part because of new information on planetary scale features observed with the UARS satellite, but more generally from a recognition of the impossibility of correctly resolving the spatial and temporal structures of these features with measurements from a single satellite. Thus the PSMOS project is founded on the basis of ground-based observations, organized into latitude bands, each with the best possible longitudinal coverage. Both radar and optical observations will be combined in this planetary scale description. The stations are organized into four zones; tropical, mid-latitude, mid-to-high latitudes and polar. Winds, temperatures and airglow emission rates will be measured from existing sites, but additional stations are being added to fill longitude gaps. The scientific results will include: 1. A determination of the dynamics of the mesopause region, by decomposition of the observations into the mean flow, planetary scale perturbations, tides and gravity waves, 2. A determination of the zonally averaged temperature trend, with its separation from the influence of solar variability and other dynamical effects and 3. A determination of gravity wave characteristics and their zonal variability, with a goal of identifying their sources. Following the official beginning of PSMOS activity at the DYSMER meeting held in Kyoto, Japan in March 1998, a major campaign has been initiated and six specific sub-projects identified. An overview of the objectives of PSMOS is presented, and the status of the current work described. For further information see: <http://www.hao.ucar.edu/psmos/home.html>

**JSM01/E/25-A3** **1020**

### PSMOS PROJECT ON DAY-TO-DAY VARIATIONS IN RELATION TO PLANETARY SCALE PROCESSES

Juergen SCHEER (PRONARP-CONICET, J. Alvarez 1218, 1414 Buenos Aires, Argentina, Email: jurgem@caerce.edu.ar) and Alan Manson (ISAS, University of Saskatchewan, 116 Science Place, Saskatoon, SASK, S7N-5E2, Canada, Email: manson@damnas.usask.ca)

We report on a project within the Planetary Scale Mesopause Observing System (PSMOS) destined to analyze sudden strong day-to-day variations and their relation to planetary scale dynamics. Day-to-day variations are believed to be a manifestation of planetary waves with periods of two days to more than a month. The airglow data set being accumulated at El Leoncito, since the start of PSMOS again contains a number of examples of very marked changes in nocturnal mean parameters that often persist for only one night, but that must be considered, due to the large number of individual measurements involved, as highly significant. Given the considerable amplitude of the variations, this is in fact the most reliable information that can be derived from the data. Radar observations are also showing the non-linear interactions between tides/PW which can lead to groups of days with unusually large wind perturbations. In a conventional spectral analysis, these events would either have an overwhelming impact, or would have to be eliminated as "outliers" or transients. The aim of the study is therefore to compare the occurrence characteristics of these powerful "transients" at different sites, their global distribution, and to investigate their relation to planetary scale phenomena. It includes different physical parameters, and is in principle not limited to optical and radar observations. The springtime transition is included in this study because it is phenomenologically, and probably also physically, related. This study is already under way, using the PSMOS database already acquired. We therefore expect to be able to present some first results.

**JSM01/C/GA2.15/W/80-A3** **1100**

### GRAVITY WAVE PARAMETERIZATION AND PSMOS STUDIES.

Nikolai M. GAVRILOV (Saint-Petersburg State University, Atmospheric Physics Department, Petrodvoretz, 198904, Russia, E-mail: gavrilov@snoopy.phys.spbu.ru) Mike J. Taylor (Utah State University, Space Dynamics laboratory, Logan, Utah, USA, Email: mtaylor@cc.usu.edu)

The main problems concerning parameterization of gravity waves (GWs) are discussed with reference to the PSMOS project. The key directions of GW studies essential for their parameterization include the following: (1) Coordinated observations of gravity waves (GWs) in the middle atmosphere with global networks of radar, optical and other facilities to map mesospheric GWs. (2) Study GW characteristics and climatology at different latitudes and longitudes. (3) Trends and interannual variations of GW activity from long-term data sets and their role in changes of general circulation and quasi-stationary planetary waves. (4) GW modulation by global-scale waves and GW influences on tidal and transient planetary waves. (5) Sources of mesospheric GWs located in the lower, middle and upper atmosphere. (6) GW breaking and the generation of turbulence. (7) Modeling and parameterization of nonlinear wave-wave and wave-mean flow interactions which involves GW parameterization into numerical models of general circulation, thermal regime and composition of the middle and upper atmosphere. Plans for GW studies aimed at developing realistic gravity wave parameterization as part of the PSMOS project are discussed with reference to current capabilities.

**JSM01/W/105-A3** **1120**

### OH ROTATIONAL TEMPERATURE MEASUREMENTS OF LONG AND SHORT PERIOD GRAVITY WAVES AT MID-LATITUDES USING THE CEDAR MESOSPHERIC TEMPERATURE MAPPER

M.J. TAYLOR and W.R. Pendleton, Jr., (both at Space Dynamics Laboratory and Physics Department, Utah State University, Logan, UT, USA, Email: mtaylor@cc.usu.edu)

A high sensitivity solid state "Mesospheric Temperature Mapper" has been used to investigate the rotational temperature signatures of long (several hour) and short (<1 hour) gravity waves induced in the OH (6,2) band emission at the ~87 km level. The imaging system is capable of measuring OH rotational temperature with a precision of better than 2 K every 3 minutes. Since its development in 1996/97 image measurements have been made from mid-latitude observatories at Bear Lake UT, Ft. Collins, CO and most recently from the Starfire Optical



Range, NM, USA. These observations have revealed a wealth of long and short period wave phenomena including marked terdiurnal oscillations in temperature around the spring and fall equinoxes with peak-to-peak amplitudes of 8-12 K and superimposed quasi-monochromatic wave events of periods as short as ~5 min. The relationship between the ~8-hour period waves and the diurnal and semi-diurnal tides will be discussed with reference to recent "24-hour" lidar studies of tides. The effects of the short-period gravity waves on the OH temperature and intensity will be discussed using novel two-dimensional maps of the wave field.

**JSM01/W/01-A3****1140****SEASONAL VARIATION OF GRAVITY WAVES OBSERVED WITH AIRGLOW IMAGING AT SHIGARAKI, JAPAN (35N, 136E)**

T. NAKAMURA, A. Higashikawa, R. Maekawa, T. Tsuda, (Radio Atmospheric Science Center, Kyoto University, Uji, Kyoto 611-0011, Japan, e-mail nakamura@kurasc.kyoto-u.ac.jp) M. Ejiri, M. Taguchi, S. Okano, (National Institute of Polar Research, Itabashi, Tokyo, Japan) K. Shiokawa, and T. Ogawa (STE lab., Nagoya University, Toyokawa, Aichi, Japan)

A long term CCD imager observation of OH airglow started in November 1996 at the MU radar site of Shigaraki, Japan. Gravity wave (GW) patterns in the images of the first 18 months have been analyzed. From more than 500 of GW events, seasonal variations of short period (5 - 30 min) and small scale (5 - 60 km horizontal wavelength) have been studied. For the waves with horizontal wavelengths larger than 17 km, horizontal propagation direction showed clear eastward/westward preference in summer/winter, respectively, suggesting that these waves are generated in the lower atmosphere and filtered out by the middle atmosphere winds. However, waves with shorter horizontal wavelengths did not show clear preferential direction as well as seasonal variation, which indicates that they are generated in the mesosphere. It is also notable that the waves with small horizontal wavelengths (<17km) and slow horizontal phase speeds (< 30 m/s) were mainly seen in summer/winter but not in equinoctial months. Intrinsic parameters of the waves are also studied using the wind measurement by the MU radar. Since January 1998, a new allsky imager of Kyoto Univ/NIPR and three other allsky imagers of Nagoya Univ. have been operated to observe allsky images of airglow around the mesopause region. 2-D and 3-D spectra of airglow images of OH, Na, O<sub>2</sub> and OI(5577) have been studied and seasonal variations have also been detected.

**JSM01/E/23-A3****1200****HRDI OBSERVATIONS OF THE O<sub>2</sub>(0,0) ATMOSPHERIC BAND NIGHTGLOW: A SEVEN-YEAR CLIMATOLOGY**

Julie F. KAFKALIDIS, Gregory M. Fall, Paul B. Hays (all at Space Physics Research Laboratory, University of Michigan, 2455 Hayward Street, Ann Arbor, MI 48109-2143, USA, email: juliek@umich.edu)

A climatology of an extensive multi-year and near-global data set of O<sub>2</sub> (0,0) Atmospheric band nightglow measurements collected by HRDI/UARS is presented. The measurements span all latitudes from 72S to 72N, and data are available for nearly all months between November 1991 and the present (1999).

Two operational modes on HRDI are used to observe the O<sub>2</sub> nightglow emission layer. A combined wind/photometric mode measured the emission brightness at low horizontal resolution (~500 km) from late 1991 through 1995, and intermittently thereafter. Much higher spatial resolution (~50 km) and a broader range of local time coverage has been achieved since March 1996 by using the HRDI photometer channel and sacrificing the ability to measure nighttime winds.

This seven-year climatology of the monthly averaged O<sub>2</sub> nightglow data greatly extends and expands upon an early survey of HRDI nightglow data by Burrage et al. (JGR 99, 15017-15023, 1994). We describe the brightness variations with latitude and local time with an emphasis on the seasonal and interannual variability revealed in this longer data set. In addition to tidal variations in the brightness (i.e. those dependent on latitude and local time), strong non-tidal variations are observed around the globe. A statistical method was used to separate these perturbations from the tidal and seasonal effects. Climatology of these perturbations is presented, and their possible origins in terms of gravity wave and planetary wave forcing are discussed. The daily variations accompanying these global patterns are rendered in fine spatial detail by the high-resolution data. Examining periods in which both high- and low-resolution data were gathered on alternating days assesses daily and small-scale variability within the monthly climatological average.

**JSM01/W/94-A3****1220****EVIDENCE FOR PLANETARY WAVE OSCILLATION OF THE UPPER ATMOSPHERIC AIRGLOW EMISSIONS OBSERVED FROM THE EQUATORIAL REGION.**

H. TAKAHASHI (Instituto Nacional de Pesquisas Espaciais, INPE, Sao Jose dos Campos, SP, Brasil, E-mail: hisao@laser.inpe.br), R. A. Burti (Universidade Federal de Paraiba, Campina Grande, PB, Brasil, E-mail: rburti@df.ufpb.br), D. Gobbi and P. P. Batista (both at Instituto Nacional de Pesquisas Espaciais, INPE, Sao Jose dos Campos, SP, Brasil, E-mail: delano@laser.inpe.br, pbatista@laser.inpe.br)

The upper mesospheric airglow emissions, OI 557.7 nm, NaD 589.3 nm, OH (6,2) and O<sub>2</sub> Atmospheric (0,1) band, and the thermospheric OI 630.0 nm emission have been measured by using a ground-based multichannel airglow photometer in the equatorial region, Sao Joao do Cariri (7 S, 37 W), Brazil. Good weather condition made it possible to study nocturnal and day to day variation of the emission rates continuously for more than 12 days per month from January to December 1998. It is found that there is an oscillation of 2 to 3 day period in the mesospheric emissions and 5 to 7 day oscillation for the thermospheric emission. The amplitudes of oscillation are larger at equinox condition than solstices. These long period oscillations are well known in the wind field as planetary waves. In case of the airglow, however, little observational evidence has been reported (Ward et al., GRL, 24, 1127-1130, 1997). Wave characteristics and source of the oscillation will be discussed.

**Wednesday 21 July PM**

Presiding Chair: Lesley Gray (Rutherford Appleton Laboratory, Didcot, UK)

**TRANSPORT AND MEAN FLOWS****JSM01/W/53-A3**

Invited

**1400****GRAVITY WAVE FORCING AND THE RESIDUAL CIRCULATION: SOME OBSERVATIONAL AND MODELING CONSTRAINTS**

M. J. ALEXANDER, L. Bruhwiler, and K. Hamilton

Constraints on gravity wave momentum fluxes in the lower stratosphere are now emerging that have implications for wave forcing in the middle atmosphere. The forcing drives mean-flow accelerations and zonal-mean meridional circulations known as the residual circulation. The constraints arise from the combined results of observational and modeling studies. Simple

models can relate an input gravity wave momentum flux spectrum as a function of phase speed to the effects of the dissipation of these waves in the middle atmosphere. Momentum flux as a function of phase is however difficult to determine from observations directly. Some techniques of combining modeling with observational constraints to constrain the momentum flux spectrum will be described. Another approach using global data to constrain large-scale wave effects on the mean and inferring the effects of the smaller-scale gravity waves as the residual will also be described. Preliminary tests of these constrained momentum flux spectra input into a gravity wave parameterization in a general circulation model will be shown with emphasis on the resulting residual circulation in both the stratosphere and esosphere.

**JSM01/E/31-A3**

Invited

**1430****DOWNWARD CONTROL AND THE ROLE OF GRAVITY WAVES IN MIDDLE ATMOSPHERE CLIMATE**

Bryan N. LAWRENCE (Department of Physics and Astronomy, University of Canterbury, Christchurch, New Zealand. Email: b.lawrence@phys.canterbury.ac.nz)

In this presentation results will be presented from a number of multi-year simulations of the middle atmosphere using a three-dimensional mechanistic model of the stratosphere and mesosphere. The model uses a prescribed tropospheric lower boundary, and has the Hines parameterization of gravity waves.

The control simulations use a geographically isotropic gravity wave source and two different upper boundary conditions for the parameterization. It will be seen that these control simulations differ from each other in a way that can be explained by using results from Downward Control theory. They also differ from simulations which have used latitudinal and time-varying gravity wave sources. Some simulations also exhibit systematic differences in planetary-wave behaviour which are attributed to the gravity waves changing the propagation regime in which the planetary waves exist. Other examples of wave-mean flow interaction will be shown, including the presence of a realistic QBO-like feature in these simulations.

**JSM01/W/63-A3****1500****WHERE IN THE MIDDLE ATMOSPHERE IS CHAOTIC ADVECTION RELEVANT?**

T.G. SHEPHERD, J.N. Koshyk (both at Department of Physics, University of Toronto, Toronto M5S 1A7 Canada, email tgs@atmosph.physics.utoronto.ca) and K. Ngan (Department of Geophysical Sciences, University of Chicago, Chicago, IL 60637 USA)

Several studies of tracer transport in the lower stratosphere have shown that horizontal tracer evolution is primarily controlled by the large-behaviour is consistent with the concept of "chaotic advection", wherein the Eulerian velocity field is spatially coherent and temporally quasi-regular on time scales over which the Lagrangian evolution is chaotic. In this study, winds from a middle atmosphere general circulation model are used to study tracer evolution in the stratosphere and mesosphere. It is found that the concept of chaotic advection is relevant in the stratosphere but not in the mesosphere. The explanation for this behaviour is the increased strength of gravity-wave activity in the mesosphere as compared with the stratosphere, which is reflected in shallower energy spectra and a stronger divergent component to the flow.

**JSM01/W/17-A3**

Invited

**1540****MECHANISMS FOR TRANSPORT OF TRACE CHEMICAL SPECIES IN THE MIDDLE ATMOSPHERE**

Anne K. SMITH, Atmospheric Chemistry Division National Center for Atmospheric Research Boulder CO 80307 USA

It is well known that the distribution of long-lived chemical constituents in the middle atmosphere such as water depends on transport by waves and the mean circulation. Transport can also have an impact on the distribution of shorter lived species whose photochemical time scales are a day or less. This paper will discuss transport mechanisms that are active in the middle atmosphere, with emphasis on the altitudes above the stratopause. Specific examples from observations and numerical models will illustrate transport by inertially unstable circulations and by migrating tides.

**JSM01/W/33-A3****1610****THE INTERACTION OF CHEMICAL HEATING AND MESOSPHERE / LOWER THERMOSPHERE CIRCULATION BY TRANSPORT OF ATOMIC OXYGEN**

Xun ZHU (JHU/APL, Johns Hopkins Rd., Laurel MD 20723-6099; Phone: 443-778-8764; e-mail: xzhu@grant.jhuapl.edu), Jeng-Hwa Yee (JHU/APL), Darrell F. Strobel (JHU)

Chemical heating in the upper mesosphere and lower thermosphere will influence the dynamical circulation in the mesosphere. Both the heating rate magnitude and its morphology are primarily determined by the atomic oxygen distributions. But, above the mesopause, the chemical timescale of the atomic oxygen is longer than the hemispheric exchange timescale by transport. Hence, the chemical heating above the mesopause will be determined by the dynamics. The JHU/APL fully coupled 2-dimensional model is used to study the interaction of between the chemical heating and mesospheric dynamical circulation. The model produces a latitudinal chemical heating rate that largely cancels the gradient in net radiative heating rate around the mesopause region. This interaction is also examined observationally with the chemical heating rates inferred from the nightglow emissions by the High Resolution Doppler Imager (HRDI) instrument onboard the UARS satellite. Furthermore, using the solar UV spectral irradiance measured by UARS instruments we also simulate the solar cycle variations in Lyman alpha radiation and in Schumann-Runge continuum and investigate its effect on the mesospheric circulation due to changes in the chemical heating rate.

**JSM01/W/24-A3****1630****ROLE OF THE NONLINEAR HADLEY CIRCULATION IN TROPICAL UPWELLING**

Kirill SEMENIUK and T. G. Shepherd (both at Department of Physics, University of Toronto, 60 St. George Street, Toronto, Ontario, M5S 1A7, Canada, email: kirill@atmosph.physics.utoronto.ca)

The Brewer-Dobson circulation is driven primarily by extratropical wave drag. This drag acts as a sort of "vacuum pump" in producing upwelling in the tropical stratosphere. It is believed to account for the seasonal cycle in temperatures above the tropical tropopause (Yulaeva et al., 1994) and the "tape recorder" effect in tropospheric water vapour transport into the stratosphere (Mote et al., 1996).

But the dynamics of tropical upwelling are not well understood. The latitudinal profile of the upwelling inferred from observations has the upwelling maximum occurring on the summer side of the equator. This pattern cannot be explained by the observed extratropical wave drag

distribution. Extratropical wave drag also cannot account for annual mean tropical upwelling which is suggested by the "tape recorder". Without nonlinearity or viscosity the annual mean meridional circulation obeys the downward control principle of Haynes et al. (1991) and is confined to the extratropical latitudes of the wave drag, which drives it. It is argued here that a key missing ingredient in explaining tropical upwelling is the balanced response to equatorially asymmetric radiative forcing, which Dunkerton (1989) termed the Nonlinear Hadley Circulation (NHC). Through nonlinearity, the NHC gives rise to annual mean upwelling at the equator. We examine the contribution of the NHC to upwelling and its interaction with the wave-driven circulation in a zonally symmetric model the existence of the NHC in a middle atmosphere GCM is also considered.

**JSM01/W/10-A3 1650**

**THE EXTENDED CANADIAN MIDDLE ATMOSPHERE MODEL: FIRST RESULTS**

William E. WARD (CRESS/CRESTech, York University, Toronto, Canada, email: william@stpl.cress.yorku.ca), V.I. Fomichev, S.R. Beagley, J.C. McConnell (all at EATS, York University, Toronto, Canada), N.A. McFarlane (CCCma, Atmospheric Environment Service, Victoria, Canada)

The Extended Canadian Middle Atmosphere Model is a general circulation model with an upper boundary at about 200km. It is a modified version of the Canadian Middle Atmosphere Model (CMAM). It is being developed to allow the investigation of phenomena near the mesopause without the influence of the sponge layer usually present in GCM's which extend to these heights. The model currently includes a full infra-red, UV and EUV radiative transfer model, a parameterized orographic gravity wave scheme and viscous and diffusive processes appropriate to the lower thermosphere. Gravity wave parameterizations and neutral chemistry near the mesopause are currently being implemented. The topic of this paper is the first runs of this model without these latter effects included. The general characteristics of the circulation, which develops under these conditions, will be discussed and compared to earlier runs of the CMAM under similar conditions.

**JSM01/W/46-A3 1710**

**COMPARISON OF SIMULATIONS WITH THE HINES GRAVITY WAVE DRAG PARAMETRIZATION AND RAYLEIGH FRICTION IN THE UKMO UNIFIED MODEL**

D. STAINFORTH, W. Norton (AOPP, University of Oxford, UK, email: das@atm.ox.ac.uk)

The Hines gravity wave drag parameterisation scheme from the ECHAM/MA model has been implemented in a 54 level version of the UKMO Unified Model with a top boundary near 0.01 hPa. The parameterised gravity waves are launched near the surface with a globally uniform strength. The sensitivity of the simulations to changes in gravity wave source strength has been examined. It has been found that limiting the maximum vertical wavelength of the parameterised gravity waves to around 20-km improves the simulation. Comparison with simulations of the Unified Model which use Rayleigh friction show that the Hines scheme correctly produces middle atmosphere jets which slope equatorward with height and produces a much better simulation of the breakdown of the southern hemisphere winter jet. The evolution of the tropical winds from different model runs will be presented.

**JSM01/W/44-A3 1730**

**CALCIUM IN THE UPPER ATMOSPHERE**

John PLANE and Rosemary Rollason (School of Environmental Sciences, University of East Anglia, Norwich NR4 7TJ, UK, email: j.plane@uea.ac.uk) Michael Gerding and Ulf von Zahn (Leibniz Institute for Atmospheric Physics, University of Rostock; Kuelungsborn, Germany)

A major question in the chemistry of the mesosphere is why calcium is depleted by more than two orders of magnitude compared to sodium and iron, all of which are produced by meteoric ablation. Furthermore, recent lidar measurements have shown that in contrast to the other meteoric metals, the Ca density actually increases in summer when the mesopause is coldest: We have carried out a laboratory kinetic study on the reactions of CaO together with an ab initio quantum calculations to establish the nature of the temporary reservoirs and sinks for the metal. The results indicate that switching between formation of calcium carbonate (CaCO<sub>3</sub>) and calcium hydroxide (Ca(OH)<sub>2</sub>) at low temperatures is the key to this mystery. A new atmospheric model of calcium will be presented which also includes a full treatment of the ion-molecule chemistry, since uniquely among the metallic ions, Ca<sup>+</sup> can be observed by lidar and a full set of simultaneous Ca/Ca<sup>+</sup> observations has been acquired.

**VARIABILITY AND TRENDS**

**JSM01/W/34-A3 Invited 1750**

**WATER VAPOUR TRENDS IN THE LOWER STRATOSPHERE: WHAT ARE THE DYNAMICAL IMPLICATIONS?**

Karen H. ROSENLOF (CIRES/University of Colorado/NOAA Aeronomy Laboratory Mail Stop R/E/AL6 325 Broadway Boulder, Colorado 80303 USA)

Trends in water vapor in the stratosphere may be an indication of temporal changes in tropical tropopause characteristics or in the large scale mean meridional circulation of the stratosphere. Satellite data (HALOE) and Northern Hemisphere middle latitude balloon data (CMDL) from the past 20 years show a slight increase with time in lower stratospheric water vapour. These trends are larger than accounted for by the observed increase in tropospheric methane over the same time period.

However, it is important to note that the magnitude of the water vapour trends from different instruments vary significantly. Additionally, in situ measurements taken from a NASA ER-2 high altitude aircraft do not show the same trends, and at some levels show a decrease. There are also substantial differences in the actual value of water vapour measured by in situ aircraft instruments during the same time period.

In this presentation, water vapour data from a variety of in situ and satellite sources will be compared. Both recent data and measurements published in scientific papers going back to the 1950's will be used in this study. The zonal mean circulation deduced from stratospheric water vapour measurements will be presented. Finally, possible mechanisms to explain the observed trends will be explored.

**VARIABILITY AND TRENDS**

**JSM01/W/52-A4 Invited 0930**

**VARIABILITY AND LONG-TERM TRENDS IN STRATOSPHERIC CONSTITUENTS**

William J. RANDEL (NCAR, PO Box 3000, Boulder, Colorado, 80307-3000, USA, email: randel@ucar.edu)

Long records of satellite constituent measurements show strong seasonal and interannual variations, which reflect transport and chemistry effects. Ozone and nitrogen dioxide observations from SAGE II, and long-lived constituents (CH<sub>4</sub> and H<sub>2</sub>O) from HALOE will be presented to document seasonal and interannual signals. The seasonal variations are closely tied to well-known stratospheric circulation patterns. One particularly large interannual signal is that associated with the stratospheric quasi-biennial oscillation (QBO), and the near-global QBO patterns in constituents are shown to be linked with QBO circulation anomalies. Low-frequency variations and trends in the constituent data will also be discussed.

**JSM01/E/37-A4 1000**

**A COMPARISON BETWEEN THE 70 HPA MONTHLY MEAN TEMPERATURE ANOMALY FIELDS FROM THE NCEP REANALYSIS AND MSU CHANNEL 4**

M.Alejandra Salles, Pablo O. CANZIANI, Rosa H. Compagnucci, Grupo de Atmosfera Media Departamento de Ciencias de la Atmosfera, Facultad de Ciencias Exactas y Naturales, Universidad de Buenos Aires, Pabellon II, Ciudad Universitaria, 1428 Capital Federal, Argentina

The monthly mean temperature anomaly fields at 70 hPa for the NCEP reanalysis are compared with those obtained by the MSU Channel 4. The aim of this study is to analyse the quality of the lower stratospheric temperature product of the NCEP reanalysis, given that this product, which spans the period 1958-1997, could be used to study periods before the MSU became operational in 1979. This is also an indirect contribution to the adjustment, on a climatic scale, of the model used in the reanalysis. In order to obtain the spacial patterns of the anomaly fields the T-mode Principal Component Analysis is applied i.e. the correlation between spatial fields used as variables. The NCEP reanalysis temperatures corresponding to the period 1979-1997 are considered and the annual cycle is removed, in a manner similar to that applied to the MSU data i.e. using the period 1982-1991 as the reference period. The results for both samples are compared and the main difference is that the reanalysis product overestimates the zonal flow, giving a larger weight to the corresponding anomaly pattern.

**JSM01/W/39-A4 1020**

**OZONE TREND ANALYSIS BASED ON EMPIRICAL ORTHOGONAL FUNCTIONS**

Frans J. M. ALKEMADE (IMAU, Instituut voor Marien en Atmosferisch onderzoek Utrecht, Postbus 80005, 3508 TA Utrecht, The Netherlands, Email: frans\_a@knoware.nl) Guus J. M. Velders (RIVM, Postbus 1, 3720 BA, Bilthoven, The Netherlands, Email: Guus.Velders@rivm.nl)

A new approach for ozone trend analysis, in connection with the isolation and identification of low frequency ozone fluctuations, is applied to the Nimbus7 TOMS data (version 7) from 1978 to 1992 and to the UARS/MLS data from 1991 to 1996. This new approach is based on the use of the Principal Components (PCs), found by an Empirical Orthogonal Function (EOF) decomposition, as representative functions in a Multi Linear Regression (MLR) analysis. The main results are: Apart from the commonly identified components of ozone variability (i.e. the seasonal cycle, the Quasi Biennial Oscillation (QBO), the El Nini/Southern Oscillation (ENSO), and the solar cycle), there exists a globally coherent oscillation in stratospheric ozone, having an average period of 1.7 +/- 0.15 year, and causing local deviations in the ozone field of up to 18 Dobson Units. Using EOF decomposition, a detailed spatial pattern in ozone of this oscillation could be extracted from the TOMS and UARS/MLS data. In terms of explained variability it is about half as important as the Quasi Biennial Oscillation (QBO). The 1.7 year oscillation can be identified as an interference effect between the QBO and the seasonal cycle. - A Multi Linear Regression (MLR) trend analysis that avoids the use of the commonly applied external representative functions (i.e. the 50 mbar Singapore zonal winds for the QBO, the 10.7 cm solar flux for the solar cycle, and the SOI-index for the ENSO), but is instead based on the first four Principal Components of the EOF analysis (associated to the three components of ozone variability mentioned above, plus the 1.7 year oscillation), leads to a more reliable trend detection in total ozone (in terms of smaller sigmas and a greater consistency). - The EOF based trend analysis leads to the detection of a significant ozone depletion (between 1987 and 1992) throughout the tropics, indicating an average ozone loss (between 30S and 30N of 0.9% +/- 0.2% per decade).

**TRANSPORT TIME SCALE**

**JSM01/W/06-A4 Invited 1100**

**TRANSPORT TIME SCALES IN THE MIDDLE ATMOSPHERE: THEORY, MODELS, AND MEASUREMENTS**

Darryn WAUGH (Department of Earth and Planetary Sciences, Johns Hopkins University, Baltimore, MD 21218, USA)

In this talk I will review the use of time scales to quantify the transport within the, real and simulated, middle atmosphere. The theoretical framework of a statistical distribution of transit times, the so called "age spectrum", will be discussed. The age spectrum provides information on the aggregated effect of the different transport processes within the middle atmosphere, and is a valuable tool for interpreting tracer data and diagnosing model transport. Tracer observations can be used to infer an aspect of the age spectrum, in particular the mean transit time (the "mean age"), or in some cases the shape of the spectrum. These observations can then be used to quantify the role of different transport processes; in particular the role of advection, vertical diffusion, and horizontal mixing within the tropical stratosphere. The observed time scales also provide stringent tests of model transport. This was highlighted in the recent NASA Models and Measurements II (MIMI) study, in which observations and over 20 models were compared and several deficiencies in the model transport identified.

**JSM01/W/25-A4 1130**

**LARGE SCALE TRANSPORT IN A MIDDLE ATMOSPHERE MODEL VISUALIZED BY A MULTI-YEAR SIMULATION OF THE SF6 TRACER**

E. MANZINI and J. Feichter (Max Planck Institute for Meteorology, Bundesstrasse 55, 20146, Hamburg, Germany)



A multi-year simulation of a passive tracer, with emissions linearly increasing with time aimed at representing the evolution of the sulfur hexafluoride, SF<sub>6</sub>, a compound of anthropogenic origin, has been performed. The general circulation model used is the MAECHAM4 model, middle atmosphere version with top at 80 km. General circulation models of the middle atmosphere are now starting to be coupled with models of the evolution of the chemical constituents of the atmosphere. Given the complex feedbacks in such coupled models, it is important to evaluate the transport characteristic with passive tracers, to focus on the role of dynamical processes and on the implications of model biases.

Comparison with measurements of SF<sub>6</sub> from aircraft mission (Project AIRSTREAM) indicates a good agreement between the simulated and observed vertical structure of the tracer concentrations in the upper troposphere and lower stratosphere. Given a reasonably realistic simulation of the SF<sub>6</sub> evolution, the multi-year simulation has been further analyzed. While most previous works have focused on events, here a climatological perspective is pursued. An attempt is made to evaluate the long term effect of the opposite drive of quasi-isentropic planetary wave mixing and residual mean circulation on tracer distribution. From the model results, subtropical and polar barriers in meridional transport can be detected in both the meridional gradient of potential vorticity and the relative change in latitude of the SF<sub>6</sub> concentration, thus providing a dynamical interpretation for the distribution of the age of stratospheric air evaluated from the SF<sub>6</sub> tracer. For comparison, the potential vorticity and its gradient are also computed from the ECMWF reanalysis (15-years). It has been found that the strength in the potential vorticity gradient and the location of its maxima in the model and in the reanalysis are in good agreement.

JSM01/W/41-A4

1150

### THREE-DIMENSIONAL SIMULATION OF LONG-LIVED AND SHORT-LIVED STRATOSPHERIC CONSTITUENTS MEASURED BY CRISTA

M. RIESE (Physics Dep., University of Wuppertal, Gauss-Str. 20, 42097 Wuppertal, Germany) X. Tie, G. Brasseur (National Center for Atmospheric Research, P.O. Box 3000, Boulder, Colorado 80307-3000, USA) D. Offermann, G. Lehmacher, and V. Kuehl (Physics Dep., University of Wuppertal, Gauss-Str. 20, 42097 Wuppertal, Germany)

The CRISTA experiment was flown on the Space Shuttle missions STS66 and STS85. During operating periods of about a week each, thermal emissions of several trace gases were measured with unprecedented horizontal resolution. The first flight was performed in early November 1994 during a period of disturbed dynamical conditions characterized by relatively large wave activity and associated exchange of tropical and extra-tropical air.

The detailed structure of the constituent distributions has been modeled with the NCAR ROSE model, which is driven by assimilated winds and temperatures provided by the UK meteorological office. The modeled trace gas distributions capture much of the measured structures. In addition, CRISTA trace gas data have been assimilated into the ROSE model by using a sequential technique. Some results are presented with emphasis on the nitrogen family and the partitioning of its members.

The assimilated distributions of long-lived species have been used for transport and budget studies based on the transformed Eulerian-mean (TEM) conservation equation. The high resolution distributions measured by CRISTA are ideally suited to assess effects of eddy transport, which are directly calculated from fluctuations of the measured trace gases, winds, and temperatures.

Resulting trace gas budgets of CFC-11 and methane will be discussed as well as forecast capabilities of the trace gas assimilation system.

JSM01/P/02-A4

1210

### INVESTIGATION OF HIGH-LATITUDE TRACER CHARACTERISTICS DURING FINAL WARMING IN THE SOUTHERN STRATOSPHERE BY USING ILAS AND OTHER SATELLITE DATA

Wookap CHOI and Sumi Kim (Department of Atmospheric Sciences, Soeul National University, Soeul, 151-742, Koera, Email: wchoi@plaza.snu.ac.kr)

Distributions of tracers in the stratosphere were investigated from November 1996 to June 1997 by analysing the Improved Limb Atmospheric Spectrometer (ILAS) and the halogen occultation experiment (HALOE) data. Both instruments are complementary in terms of the latitude coverage and their observations reveal the spatial distributions of tracers at different latitudes. Latitude-height and longitude-height sections were used to investigate characteristic behavior of tracers during the transition period between spring and summer. Concentrations of both tracers at high latitudes. The tracers also show temporal variations in wave number of the dominant planetary wave. The number one and two patterns repeat before the summer pattern finally sets in. The same feature is also observed in the geopotential height, potential vorticity and the meridional wind by the United Kingdom Meteorological Office (UKMO) data. Transport by eddy flux calculated by the UKMO and satellite data was also investigated following the changing wave pattern. Eddy flux plays significant role in transport of trace species in the meridional direction.

Thursday 22 July PM

Presiding Chair: A.R. Ravishankara (NOAA Aeronomy Lab, Boulder, USA)

## CONDENSED MATTER IN THE STRATOSPHERE

JSM01/W/21-A4

Invited

1400

### FORMATION OF AND REACTIONS ON CONDENSED MATTER

Thomas PETER (Institute for Atmospheric Sciences, ETH, Hoenggerberg HPP, CH-8093 Zurich, Switzerland, email: peter@mpch-mainz.mpg.de)

Within the last five years research on the thermodynamics, nucleation kinetics and chemical kinetics of the ternary system sulfuric acid/nitric acid/water in the temperature regime 180-300 K has laid the basis for understanding the microphysics and heterogeneous chemistry of stratospheric aerosol and cloud particles. Laboratory work, field studies and theoretical investigations revealed that ternary solution droplets do not freeze readily despite massive supercoolings with respect to acidic hydrates. At the same time the solubility of reactive gases like HCl and HOCl in the droplets increases dramatically under such conditions. The chemistry of heterogeneous chlorine activation, which is mainly responsible for the formation of the ozone hole, therefore takes place principally in/on the liquid phase, and not surface-catalyzed on solids as was thought not long ago. Conversely, the small number of frozen particles may assume large radii and sediment out, leading to denitrification, i.e. the removal of reactive nitrogen from the affected air masses. This may lead to an enhancement of ozone loss. The interplay between liquid and solid particles with their clearly separated influences on the ozone layer will be discussed. In a future stratosphere cooled by greenhouse gases, decreases in the chlorine atmospheric burden could be partly compensated by increases of chlorine processing in liquid particles and denitrification due to more frequent formation of solid particles.

JSM01/E/28-A4

1430

### CLOUD DETECTION IN THE UPPER TROPOSPHERE AND LOWER STRATOSPHERE BY CRISTA 1 AND 2

Reinhold Spang, Gunnar EIDMANN, and Dirk Offermann (Physik Department, University of Wuppertal, Gauss-Str. 20, 42097 Wuppertal, Germany, email: spang@wpos2.physik.uni-wuppertal.de)

The Cryogenic IR Spectrometers and Telescopes for the Atmosphere instrument (CRISTA) was flown in November 1994 and August 1997 during the space shuttle missions STS66 and STS85. CRISTA is a limb scanning experiment that measures the thermal emissions of 18 trace gases with high spatial resolution in three dimensions. During the second CRISTA mission a measurement mode with extra high spatial and temporal resolution was applied in the Indonesian sector of the tropics. First results will be shown.

Radiance fields and spectra show clear indications for deep convection clouds in the tropics (CRISTA 1/2). Cloud maps were derived on a daily basis. They are quite different in November and August. Comparisons with the AVHRR, GMS and GOES cloud observations and SAGE II observations of subsvisible cirrus clouds will be presented. Indications of different cloud types in the CRISTA data will be discussed. Backward trajectories are used to determine the origin of the cloud formation.

JSM01/W/08-A4

1450

### OBSERVATIONS OF POLAR STRATOSPHERIC CLOUDS.

J.J. REMEDIOS, (Aopp, Dept. Of Physics, Oxford University, Parks Road, Oxford OX1 3pu, U.K., E-Mail: J.Remedios1@Physics.Ox.Ac.Uk), A. Adriani (Cnr-Ifa, Via Del Fosso Del Cavaliere, 00133 - Roma, Italy, e-mail: adriani@atmos.ifa.rm.cnr.it), J. Ballard, RAL, Chilton, Didcot, Oxon OX11 0QX, U.K., e-mail: john.ballard@rl.ac.uk), G. Beyerle (AWI, Potsdam, Telegrafenberg, A43, D-14473 Potsdam, Germany, e-mail: gbeyerle@awi-potsdam.de), C. David (CNRS, Institut Pierre-Simon Laplace, Universite Paris VI - B.102, 75252 Paris Cedex 05, France, e-mail: christine.david@aero.jussieu.fr), D. Fonteyn (BIRA, Ringlaan 3, Brussels-1180, Belgium, e-mail: Dominique.Fonteyn@bira-iasb.oma.be), R.G. Grainger (Department of Physics and Astronomy, University of Canterbury, Private Bag 4800, Christchurch, New Zealand, e-mail: r.grainger@phys.canterbury.ac.nz), N. Larsen (DMI, Lyngbyvej 100, DK-2100 Copenhagen, Denmark, e-mail: nl@dmil.dk), M. Wirth, (Arbeitsgruppe LIDAR, DLR, Oberpfaffenhofen, D-82234 Wessling, Germany, e-mail: Martin.Wirth@dlr.de)

Within the last few years, it has become clear that there are still many difficult questions regarding the formation and composition of polar stratospheric clouds (PSCs). Although both observations and microphysical models have become more sophisticated, it has been difficult to consistently analyse the data to provide the most information obtainable from a particular measurement. Complicating factors include the large differences in wavelength coverage, spatial coverage and temporal sampling between various lidars, and between lidars and satellite instruments. The POSTCODE (Polar Stratospheric Clouds and Ozone Depletion) project is developing an integrated code capable of calculating microphysical, optical and chemical properties of the clouds. Examples of polar stratospheric cloud observations will be used to demonstrate the potential of this code, to illustrate the different attributes of lidar and satellite instruments, and to indicate our current understandings of PSC behaviour. An overview will be provided of the importance of measurement location, sampling, and ancillary chemical measurements, and of the chief questions concerning PSC formation.

JSM01/W/04-A4

1510

### THE SEASONAL EVOLUTION OF WATER VAPOR AND AEROSOLS IN THE ANTARCTIC AS OBSERVED BY THE POLAR OZONE AND AEROSOL MEASUREMENT (POAM III)

Gerald E. NEDOLUHA, Richard M. Bevilacqua, Karl Hoppel, Mark Daehler, Eric P. Shettle (Naval Research Laboratory, Code 7220, Washington DC 20375-5320, USA, Email: nedoluha@wvms.nrl.navy.mil), and Mike D. Fromm (Computational Physics, Inc., 2750 Prosperity Ave., Fairfax VA, USA)

The Polar Ozone and Aerosol Measurement (POAM) III has been making occultation measurements at high northern and southern latitudes since April 1998. We shall present measurements of stratospheric water vapor and aerosols from 65S-88S, illustrating descent in the vortex and dehydration in the lower stratosphere. In the upper stratosphere water vapor acts as a tracer, and in September and October the water vapor profile exhibits an unusual double peaked structure, with mesospheric air mixing in from midlatitudes providing a high altitude peak while air that has descended within the vortex produces a low altitude peak. In the lower stratosphere aerosol optical depth measurements begin to show a significant increase in June when the first PSCs appear, but dehydration does not occur until July when the aerosol optical depths begin to exceed a threshold value. The availability of simultaneous aerosol and water vapor measurements thus makes it possible to study the growth of PSCs, and to distinguish different types of PSCs by determining which ones cause significant dehydration. Most of the water vapour lost during PSC formation is not recovered when temperatures rise above the frost point in October, hence the PSC formation process appears to be a sink for middle atmospheric water vapor. Assuming that the POAM water vapour measurements are representative of water vapor within the vortex, we can estimate the importance of this process to the middle atmospheric water vapor budget.

## STRATOSPHERIC PHOTOCHEMISTRY

JSM01/W/60-A4

Invited

1550

### ATMOSPHERIC PHOTOCHEMISTRY OF OZONE IN THE NEAR-ULTRAVIOLET REGION

Yutaka. MATSUMI (Solar-Terrestrial Environmental Laboratory, Nagoya University, 3-13, Honohara, Toyokawa 442-8507, JAPAN, email: matsumi@stelab.nagoya-u.ac.jp)

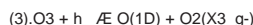
The overwhelming route to OH formation in the Earth's lower atmosphere is through the reaction of an electronically excited oxygen atom, O(1D), which is formed from the solar photolysis of ozone. Ozone in the stratosphere itself screens the atmosphere below from most solar UV radiation needed to produce O(1D). Therefore, how ozone dissociates when it absorbs the solar radiation in the longer wavelength edge of its absorption ( $\lambda > 300$  nm) is a crucial piece of information.

- (1)  $O_3 + h\nu \rightarrow O(1D) + O_2(a_1g)$
- (2)  $O_3 + h\nu \rightarrow O(3P) + O_2(X_3g)$

The channel (1) is important, since the product O(1D) can react with H<sub>2</sub>O and produce OH radicals, which has a photon energy threshold at 310 nm. The channel (2) does not result in the OH formation. Recent laboratory studies reveal that fairly amounts of O(1D) are produced in the O<sub>3</sub> photolysis even at wavelength longer than the threshold. In the wavelength range of 310-320 nm the O(1D) atoms are produced through the channel (1) by the efficient photoabsorption from the O<sub>3</sub> vibrationally excited states which are thermally populated in the atmosphere.

## INTER-ASSOCIATION

Furthermore, the O(1D) atoms are produced by the spin-forbidden channel above 320 nm:



These two processes were previously thought to be negligible. They could enhance the balance of OH formation, particularly at high latitudes in the troposphere from late autumn to early spring. This will affect the lifetime of short lived species such as CO, a common pollutant, and also control the cleansing power of the lower atmosphere at a level which was previously underestimated.

**JSM01/W/101-A5** Poster **1620-01**

### ON TRACER SENSITIVITY TO TRANSPORT COEFFICIENTS IN TWO-DIMENSIONAL MODELS

SHUHUA LI, CRC for Southern Hemisphere Meteorology, Monash University, Australia; Darryn W. Waugh, Department of Earth and Planetary Science, Johns Hopkins University, USA

Recent comparisons of modelled and observed stratospheric mean age show large differences between models and data as well as between individual models, indicating serious problems with model transport. We explore the sensitivity of the mean age to different components of the transport by examining the effect of varying the transport coefficients within a single two-dimensional model. The mean age is shown to be sensitive to changes in advective circulation or diffusion coefficients, with the sensitivity largest for changes in the circulation strength. In most cases the magnitude but not the spatial distribution of the mean age changes. However, if the horizontal mixing is made very small within middle latitudes or large within low latitudes there are large changes in the shape of age isopleths. The effect of these changes in transport on chemically-active long-lived tracers is also examined. It is found that the lower stratospheric concentrations are relatively insensitive to the transport changes if these changes do not alter the general shape of age/tracer isopleths. Significant changes occur only when the transport coefficients are modified so as to change the spatial distribution of the mean age (and chemical tracers).

**JSM01/W/48-A4** Poster **1620-02**

### ROUND-BASED MILLIMETER-WAVE MONITORING OF OZONE IN THE UPPER STRATOSPHERE AND MESOSPHERE AT TSUKUBA, JAPAN

Tomoo NAGAHAMA, Hideaki Nakane (National Institute for Environmental Studies, Onogawa 16-2, Tsukuba, Ibaraki 305-0053, Japan, email: nagahama.tomoo@nies.go.jp) Mariko Minomiya (Global Environmental Forum, Inarimae 24-18, Tsukuba, Ibaraki 305-0061, Japan) Hideo Ogawa and Yasuo Fukui (Department of Astrophysics, Nagoya University, Nagoya 464-8602, Japan)

We report on ground-based millimeter-wave observations of the upper stratospheric and mesospheric ozone conducted at the National Institute for Environmental Studies (NIES) in Tsukuba, Japan (36N, 140E) since October 1995. Spectral data were obtained by using the millimeter-wave radiometer equipped with the superconducting mixer receiver and the AOS spectrometer. Vertical profiles of ozone mixing ratio from 38 to 76 km were retrieved with an error of ~10%. In the time series of the ozone mixing ratio observed during more than 27 months, seasonal and short-term variations in the upper stratosphere and mesosphere are clearly detected. The annual variation is generally consistent with the climatological models, and the semi-annual variation in the upper mesosphere is similar to that of the SME data except that the ozone mixing ratio in the spring measured with SME is ~70% larger than that in autumn while those with the radiometer are almost same. Sudden enhancement of ozone in the upper stratosphere is well correlated with the decrease of temperature measured with the co-located lidar. Further details of the ozone variations and comparison with theoretical models are presented.

**JSM01/W/110-A4** Poster **1620-03**

### ROCKET MEASUREMENT OF MIDDLE ATMOSPHERIC OZONE CONCENTRATION PROFILE BY KSR-Y

Su Jeong Son, Yong Ha Kim (both at Department of Astronomy and Space Science, Chungnam National University, Taejeon, Korea, email: sjsong@jupiter.chungnam.ac.kr, yhkim@jupiter.chungnam.ac.kr); Jhoon Kim and Gwang Rae Cho (both at Korea Aerospace Research Institute, Taejeon, Korea, email: jkim@kari.re.kr)

KSR-Y (Korean-Scientific Rocket-영), a two-stage sounding rocket of KARI (Korea Aerospace Research Institute) was launched successfully at the Korean Peninsula on June 11, 1998. The apogee of the rocket was 137 km and the total flight time was 365 seconds. For the ozone measurement mission, 8-channel UV and visible radiometers were onboard the rocket. The rocket measured in situ stratospheric and mesospheric ozone density profile over Korea during its ascending phase using the radiometer and transmitted the data to ground station in real time. The maximum ozone density occurs near 25 km. Retrieved profile has a random error (1 $\sigma$ ) of approximately 15% for altitude below 20 km, 7% between 20-50 km and 10% greater than 50 km. Comparisons with Dobson spectrophotometer, ozonesonde, and HALOE onboard the UARS are shown together. Our results are in reasonable agreements with others.

**JSM01/W/51-A4** Poster **1620-04**

### DIABATIC CROSS-ISENTROPIC DISPERSION IN THE STRATOSPHERE

J.A. KETTLEBOROUGH, British Atmospheric Data Centre, Rutherford Appleton Laboratory, Chilton, Didcot, Oxon, OX11 0QX, UK

The evolution of tracers with respect to isentropic surfaces can be described by mean descent across the surfaces and dispersion about the surfaces. In some circumstances the dispersion can be modelled by a vertical diffusion coefficient.

Trajectories calculated from United Kingdom Meteorological Office analyses are used to determine the conditions under which a diffusive model is valid. When the dispersion is diffusive a diffusion coefficient is derived from the trajectory statistics. Trajectories have been calculated at different altitudes and different times of year. These calculations reveal the altitudinal and seasonal dependence of and interhemispheric differences between the derived diffusion coefficients.

**JSM01/W/09-A4** Poster **1620-05**

### WAVE-INDUCED TRANSPORT IN AN IDEALIZED STRATOSPHERE

D. PENDLEBURY and T. G. Shepherd (both at Department of Physics, University of Toronto, 60 St. George Street, Toronto, Ontario, Canada, M5S 1A7, email: diane@atmosph.physics.utoronto.ca)

The global mass circulation in the stratosphere is caused in part by the downward control principle introduced by Haynes et al. (1991). Extratropical stratospheric wave drag, produced by the breaking and dissipation of planetary waves, acts as a pump, drawing tracers from the

equator to the pole and resulting in the observed Brewer-Dobson circulation.

At present, the theoretical understanding of this process has limitations. Although it can be shown, under certain assumptions, that the Lagrangian velocities and the transformed Eulerian mean velocities are the same and correspond to the wave drag, it is not clear that this relationship holds in general. Thus, while the existence of the wave-induced circulation is not under debate, its quantitative determination remains problematic. Previous studies have been linear and used Newtonian cooling together with Rayleigh drag. While the relaxational character of the radiative cooling is a reasonably acceptable approximation, Rayleigh drag is not. It is quite clear that in the atmosphere the mechanism for planetary-wave dissipation is a nonlinear process involving wave breaking, the development of small scales and their subsequent dissipation.

This paper will detail some of the problems with the traditional assumptions and present numerical results using a 3D primitive equations model aimed at quantifying the connection between wave driving and Lagrangian transport in the strongly nonlinear regime. The effects of realistic radiative transfer, which act preferentially on the small vertical scales that develop due to the wave breaking process, are also considered.

**JSM01/W/23-A4** Poster **1620-06**

### A PRELIMINARY NUMERICAL EXPERIMENT OF AN ARCTIC OZONE LOSS BY THE CHEMICAL TRANSPORT MODEL

Toru SASAKI, Hisashi Kato, Atsuya Kinoshita, Kazuaki Akagi (Japan Meteorological Agency, Otemachi 1-3-4, Chiyodaku, 100-8122, JAPAN, Email: tsasaki@naps.kishou.go.jp) and Toshiki Iwasaki (Geophysical Institute, Graduate School of Science, Tohoku University, Aoba-ku, Sendai, 980-8578, JAPAN, Email: iwasaki@wind.geophys.tohoku.ac.jp)

We are developing a chemical transport model (CTM) for the purpose of operational analyses of stratospheric ozone at the Japan Meteorological Agency (JMA). The CTM consists of the transport model developed at the Meteorological Research Institute (MRI) and the chemical model developed at the National Center for Atmospheric Research (NCAR). The transport model is being improved at the JMA and Tohoku University (Iwasaki et al., 1999, submitted to MW03 session). The present version of the model has 16 layers between the surface and the altitude of 10 hPa, and 5 or 2.5 degree resolution in latitude and longitude. The chemical model considers about 40 species and their relating gas phase and heterogeneous reactions on the surface of PSCs and sulfate aerosols. The transport model uses the semi-Lagrange scheme in horizon and box scheme in vertical. The CTM uses the meteorological data from the numerical weather prediction model of the JMA.

Though the CTM is still on the developing stage, a preliminary numerical experiment for the period of 1997 northern winter/spring was done. Ozone depletion in the arctic region is partly simulated, but the loss amount is not enough, because of the insufficient chlorine oxygen density. The reason may be an insufficient transport of rich chlorine from the upper layer.

**JSM01/W/56-A4** Poster **1620-07**

### QUANTIFYING ATMOSPHERIC TRANSPORT WITH AIRBORNE TRACER OBSERVATIONS

F. L. MOORE 1,2, E. A. Ray 1,2, G. S. Dutton 1,2, D. F. Hurst 1,2, P. A. Romashkin 1,2, J. W. Elkins 2, D. W. Fahey 3, M. C. Volk 4, 1 CIRES, University of Colorado, Boulder, CO 803092 NOAA/CMDL, 325 Broadway, Boulder, CO 803033 NOAA/AL, 325 Broadway, Boulder, CO 803034 Institut fuer Meteorologie und Geophysik, Universitaet Frankfurt, Georg Voigt Strasse D-60325 Frankfurt am Main, GERMANY

The quality of an assessment of the environmental impact of existing aircraft and the proposed High Speed Civilian Transport (HSCT) fleet is limited by our ability to quantify stratospheric transport. The Lightweight Airborne Chromatograph Experiment (LACE) instrument, on board the Observations of the Middle Stratosphere (OMS) gondola platform, was designed and flown specifically to do this. LACE currently measures halon 1211, chlorofluorocarbons (CFC-11, CFC-113, and CFC-12), (CH3CCl3), carbon tetrachloride (CCl4), nitrous oxide (N2O), and sulfur hexafluoride (SF6) with a typical precision of between 1% and 4%. Mixing of air from mid-latitudes into the region of tropical upwelling with time scales between 1 and 2 years have been inferred from the LACE data by using a model analogous to the method of {Volk et al.} (Science, 272, 1763, 1996). The integrated fraction of mid-latitude air accumulating in the tropical upwelling region is also estimated to approach 50% at 20 km and up to 90% at 32 km. This quantifies the dominant mechanism for vertical transport of mid-latitude stratospheric pollutants to the upper stratosphere. The mean age of an air mass sampled in the stratosphere has been estimated from measurements of SF6 through the use of CMDL's historical record of the tropospheric global mean. This measured mean age is older than predicted by most models, particularly at altitudes above 20 km. Mean age estimates derived from LACE SF6 measurements are in agreement with mean age estimates from simultaneous CO2 measurements at all altitudes and latitudes, which do not contain vortex air. In vortex air, comparisons of mean age estimates derived from CO2 measured with an older mean age derived from SF6 data reveals a quantifiable (mesospheric) loss for SF6. An upper estimate of the SF6 global lifetime and estimates of mass flux across the vortex barrier are in principle possible.

**JSM01/E/13-A4** Poster **1620-08**

### TRACER TRANSPORT MECHANISMS IN THE SUBTROPICAL MIDDLE ATMOSPHERE

Lesley GRAY (Rutherford Appleton Laboratory, Chilton, Didcot, Oxon., OX11 0QX, U.K. Tel: +44 1235 446745, Fax: +44 1235 445848, e-mail: lesley.gray@rl.ac.uk).

Observations of long-lived trace gases from the Upper Atmosphere Research Satellite (UARS) exhibit an interesting 'staircase' feature in the Northern Hemisphere in winters in which the quasi biennial oscillation (QBO) is in an easterly phase. The staircase feature includes (a) an asymmetrical off-equatorial peak in the tracer isolines in the summer hemisphere above about 8 mb, with steep isolines over the equator forming a vertical 'equatorial cliff', (b) a region of almost horizontal isolines forming a 'subtropical ledge' between 8-15 mb and 0-20N, (c) a region of almost vertical isolines forming a 'subtropical cliff' in the Northern Hemisphere between approximately 20-30N and 15-70 mb. The origin of each of these features is investigated, using both observational data and model studies. The fact that the staircase feature is strongly asymmetric about the equator suggests that isentropic mixing may be responsible for this feature, since it is strong in the winter hemisphere and weak in the summer hemisphere. However, we use the model to show that advection by the local QBO-induced circulation is more important than isentropic mixing. In particular, the steep isolines that form the 'cliff' region are due to meridional overturning by the QBO circulation. They are not due to the sharpening of gradients at the subtropical edge of the surf zone caused by isentropic mixing.



**JSM01/E/38-A4** Poster **1620-09**

**A PRINCIPAL COMPONENT ANALYSIS OF TOTAL OZONE OVER THE SOUTHERN HEMISPHERE AS SEEN BY TOMS**

Pablo O. CANZIANI, Diego C. Araneo, Rosa H. Compagnucci, Grupo de Atmosfera Media Departamento de Ciencias de la Atmosfera, Facultad de Ciencias Exactas y Naturales, Universidad de Buenos Aires, Pabellon II, Ciudad Universitaria, 1428 Capital Federal, Argentina

The behaviour of the Southern Hemisphere total ozone as measured by the TOMS family of sensors is studied using the Principal Component Analysis method. The aim of the study is to determine the predominant structures in the distribution of the total ozone and the variability and trends since late 1978, when TOMS NIMBUS became operational. The results of the PC analysis are discussed to which are the dominant structures and variability with respect to the lower stratospheric temperature as measured MSU Channel 4 temperature retrievals. The role of changes in dynamics and chemistry on the variability of the ozone distribution is discussed.

**JSM01/E/36-A4** Poster **1620-10**

**TEMPERATURE TRENDS AT 70HPA USING MSU CHANNEL 4 RETRIEVALS**

Rosa H. COMPAGNUCCI, M.Alejandra Salles, Pablo O. Canziani, Grupo de Atmosfera Media Departamento de Ciencias de la Atmosfera, Facultad de Ciencias Exactas y Naturales, Universidad de Buenos Aires, Pabellon II, Ciudad Universitaria, 1428 Capital Federal, Argentina

MSU Channel 4 monthly temperature anomaly fields are used to analyse the trends in temperature in the lower stratosphere. Principal Component Analysis is used to study these fields over the Southern Hemisphere for the period 1979-1997. The time series at each grid point (i.e. 5184 pints for the 2.5x2.5 degree grid) are used as variables for the S-mode analysis. The first 5 components explain 75% of the observed variance and correspond to the predominant features if the temporal temperature in the Southern Hemisphere. The first and most importance variance corresponds to time series for grid points located at subtropical latitudes, and show the impact of the significant impact of two major volcanic events: the eruptions of El Chichon and Pinatubo. The 2nd principal component corresponds to temperature variability at high latitudes. It does not appear to show links with low latitude stratospheric processes. The 3rd and 4th components do not show any clear trends, while the 5th one yields a spectral peak in the same frequency band as the Quasi-Biennial Oscillation. The grid points associated with the latter are located at very low latitudes and those associated at mid-latitudes are in antiphase with respect to the equatorial grid points. It has been possible to identify real time series in the original data, which are in excellent agreement with the time series resulting from the PC analysis. It was possible to obtain regional characterizations of the behaviour of the temperature in the lower stratosphere over the Southern Hemisphere.

**JSM01/W/68-A4** Poster **1620-11**

**AN OZONE AND CLO MEASURING PROJECT AT LAS CAMPANAS OBSERVATORY IN CHILE**

Yasuo FUKUI, Hideo Ogawa and Kecheng Xiao (Three at Department of Astrophysics, Nagoya University, Nagoya 464- 8602, Japan), Yasunobu Iwasaka (Solar-Terrestrial Environment Laboratory, Nagoya University, Nagoya 464-8602, Japan), Hideaki and Tomoo Nagahama (Both at National Institute for Environmental Studies, Onogawa 16-2, Tsukuba, Ibaraki 305-0053, Japan)

In the last ten years, interests in measurements of stratospheric minor constituents have increased considerably. In 1997, Nagoya University and NIES started a joint research project to develop a high sensitive ground-based millimeter wave receiver capable of detecting thermal emission from the rotational lines of chlorine oxide(CIO) and other stratospheric minor constituents. We already constructed ozone sensors (110.8 GHz) employing SIS receivers. In this project, we shall develop a 200-300 GHz SIS receiver system. The receiver noise of SIS mixer is expected to be better than 50 K(SSB) at 230 GHz. In 1999, we will install this instrument at Las Campanas Observatory at altitude of ~2300m(S29, W71.) in Chile. This is a place suitable to measure CIO and ozone because of the dry weather. This project is a first dedicated effort to measure these stratospheric molecules in South America where the southern hemisphere vortex sometimes tends to move away from the South Pole, and should be able to provide valuable information on the behavior of CIO and ozone, helping our better understanding of the movement of the ozone hole.

**JSM01/W/14-A4** Poster **1620-12**

**WHAT CAUSES THE ARCTIC POLAR COOLING OF THE 1990'S?**

William J. RANDEL (NCAR, PO Box 3000, Boulder, Colorado, 80307-3000, USA, email: randel@ucar.edu) Darryn W. Waugh (Dept. of Earth and Planetary Science, Johns Hopkins University, Baltimore, MD, 21218, USA, email: waugh@jhu.edu)

Record cold temperatures have been observed in the springtime Arctic polar stratosphere during the 1990's. The 1990's decadal average temperature is significantly colder and the vortex persists longer into spring than can be explained by 'natural' year-to-year variability. This suggests a change in climate forcing in this region. Possible contributions to this forcing are analyzed, including: 1) coupling with the polar troposphere, 2) planetary wave forcing across the tropopause, and 3) radiative cooling due to ozone depletion and/or greenhouse gas increases. While each of these effects may contribute to the observed changes, close correspondence with trends in the Antarctic suggests that the radiative response to ozone loss is a major factor in the observed Arctic cooling.

**JSM01/W/70-A4** Poster **1620-13**

**LIGHTNING OVER THE NORTH ATLANTIC- IMPLICATIONS ON THE NITROGEN OXIDES (NOX) BUDGET AT CRUISING ATLANTIC**

Dominique JEKER and Johannes Staehelin (Institute for Atmospheric Physics, ETH Zuerich, 8093 Zuerich, Switzerland e-mail: jeker@atmos.unmw.ethz.ch and staehelin@atmos.unmw.ethz.ch)

In the frame of the EU project POLINAT 2 we carried out fully automated measurements of nitrogen oxides (NO, NO<sub>2</sub>) and ozone (O<sub>3</sub>) from aboard a commercial Swissair B-747 airliner on 85 flights between Zürich (Switzerland) and destinations at the Eastern United States in the period of August 13 to November 23, 1997. The tropospheric NO<sub>x</sub> concentrations exhibited a log-normal probability density function and confirm the patchy occurrence of large NO<sub>x</sub> plumes found during the NOXAR (Nitrogen Oxides and Ozone along Air Routes) campaign in 1995/96. In August of both years the plumes were concentrated above the US continent, suggesting that lifted air from the polluted planetary boundary layer and/or lightning produced NO lead to the characteristic maximal mean NO<sub>x</sub> concentration below the tropopause. In autumn and winter, large parts of the enhanced NO<sub>x</sub> concentrations can most probably be attributed to lightning activity and to air transported upward from the polluted US boundary layer, induced by convective motion and frontal activity above the warm Gulf Stream current. We present two

case studies of lightning events in thunderstorms above the North Atlantic where the relative importance of the ground sources is comparatively small and we show with images of the optical transient detector (OTD) satellite that the elevated NO concentrations can most probably be attributed to lightning activity. We then try to generalize the findings of these two case studies by statistically investigating the entire POLINAT 2 dataset.

**JSM01/E/44-A4** Poster **1620-14**

**REVISION OF THE O3 TREND ANALYSIS AT THE JUNGFRAUJOCH STATION**

M. DE MAZIÈRE, M. Van Roozendael, O. Hennen, (all at Belgian Institute for Space Aeronomy, Ringlaan 3, B-1180 Brussels, Belgium), P. Demoulin, and E. Mahieu (both at Institute of Astrophysics and Geophysics, University of Liège, 5 Avenue de Coïnte, B-4000 Liège, Belgium)

Two NDSC qualified instruments, namely a SAOZ and a Fourier-Transform spectrometer (FTS), measure vertical column amounts of O<sub>3</sub> on a regular basis at the International Scientific Station of the Jungfraujoch. The SAOZ O<sub>3</sub> time series is derived from UV-Visible zenith-sky measurements during every morning and evening twilight, and starts in mid 1990. The FTS time series contains daily averages of O<sub>3</sub> derived from high-resolution infrared solar absorption spectra on clear-sky days, and starts in 1985. For both techniques, the retrieval methods have been improved during the last years. In particular for the FTIR retrieval, a recently developed climatological tropopause dependent model for the a priori vertical O<sub>3</sub> profiles has been implemented. Here we present the homogenized time series, based on these latest algorithm revisions. The observed long-term O<sub>3</sub> trend above the Jungfraujoch will be discussed, and some particular periods like the aftermath of the Pinatubo eruption will be highlighted.

**JSM01/W/109-A4** Poster **1620-15**

**SAOZ NO2 MEASUREMENTS AT ABERYSTWYTH**

Aidan GREEN and Geraint Vaughan (both at Department of Physics, University of Wales, Aberystwyth, SY23 3BZ, UK, Email: acg@aber.ac.uk and gxv@aber.ac.uk)

The SAOZ UV-visible zenith-sky spectrometer has been measuring NO<sub>2</sub> vertical columns at Aberystwyth (52.4N, 4.2W) since March 1991. NO<sub>2</sub> is of interest due to its important role in the photochemistry of ozone. The spectrometer measures spectra of scattered sunlight from the zenith-sky, and NO<sub>2</sub> is derived from the region 405-498nm.

The time-series of data clearly shows the effect of the eruption of Mount Pinatubo in 1991, the increased level of stratospheric aerosol clearly causing a marked decrease in measured NO<sub>2</sub> levels. Also apparent is the gradual return to, and exceeding of, pre-Pinatubo NO<sub>2</sub> levels showing that the stratosphere was not free of aerosol even before Pinatubo.

**JSM01/L/01-A4** Poster **1620-16**

**OZONE DURING THE WINTERS 1991/92 TO 1998/99 : A COMPARATIVE STUDY**

F.M.O'Connor, G. Vaughan and M.Hatcher

Eight years of ozonesonde data and ECMWF potential vorticity fields are used to perform a comparative study of northern hemisphere winters in mid- and high latitudes. The effect of synoptic-scale dynamics on the ozone evolution in the lower stratosphere is removed by expressing ozone mixing ratio in isentropic-PV coordinates. Clear differences are revealed between different winters, especially at high latitudes where chemical destruction is greatest. This study is also extended to sub-tropical latitudes, where trends in ozone should be caused primarily by dynamics.

**Friday 23 July AM**

Presiding Chair: William Randel

(ACD National Center for Atmospheric Research, Boulder, USA)

**POLAR PROCESSES**

**JSM01/W/26-A5** Invited **0830**

**STUDIES OF POLAR PROCESSES IN THE LOWER STRATOSPHERE USING UARS MLS OBSERVATIONS**

Michelle SANTEE (Jet Propulsion Laboratory, Pasadena, CA, 91109, USA; email: mls@praxis.jpl.nasa.gov)

The Microwave Limb Sounder (MLS) experiments provide vertical profiles of atmospheric composition, temperature, and pressure by measuring millimeter- and submillimeter-wavelength thermal emission from the limb of Earth's atmosphere. The first MLS experiment in space was launched on the NASA Upper Atmosphere Research Satellite (UARS) in September 1991. One of the major objectives of UARS MLS is to improve understanding of stratospheric ozone, particularly the chlorine-catalyzed destruction of ozone in the polar regions of both hemispheres. In addition to measuring ozone, UARS MLS has obtained the first global observations of stratospheric CIO, the predominant form of reactive chlorine involved in ozone depletion. HNO<sub>3</sub>, which plays several pivotal roles in determining the cumulative amount of ozone loss, is also measured in the lower stratosphere. HNO<sub>3</sub> is a key component of the polar stratospheric clouds (PSCs) that form in the low temperatures of polar winter, on which the heterogeneous reactions leading to chlorine activation occur. In addition, photolysis of HNO<sub>3</sub> enables a major pathway for chlorine deactivation. It has been argued that denitrification, the permanent removal of reactive nitrogen from the lower stratosphere as HNO<sub>3</sub>-containing PSC particles gravitationally settle out, facilitates persistence of enhanced CIO abundances and thus increases ozone destruction. UARS MLS has obtained global measurements of O<sub>3</sub>, CIO, and HNO<sub>3</sub> through six complete annual cycles in both hemispheres (and is still taking data, although with greatly reduced sampling frequency), making this data set uniquely suited to addressing some unresolved issues in stratospheric ozone depletion. Here we review results from some recent analyses of UARS MLS data, which include inferring information about PSC composition and formation processes in both hemispheres, investigating the degree of denitrification in Antarctica and its influence on lower latitudes, studying interhemispheric differences and interannual variability in chlorine activation, denitrification, and ozone depletion and the relative importance of denitrification in regulating the extent and duration of enhanced CIO, and discussing the implications of these findings for future Arctic ozone loss.

**JSM01/E/19-A5** **0900**

**POLAR STRATOSPHERIC CLOUDS IN THE SOUTH POLAR REGION MEASURED BY CILAR 2**

Reinhold SPANG, Gunnar Eidmann, and Dirk Offermann (Physik Department, University of Wuppertal, Gauss-Str. 20, 42097 Wuppertal, Germany, email: spang@wpos2.physik.uni-wuppertal.de)

The CRyogenic IR Spectrometers and Telescopes for the Atmosphere instrument (CRISTA) was flown in November 1994 and August 1997 during the space shuttle missions STS66 and STS85. During the operation periods of around one week CRISTA has measured the thermal emissions of several trace gases with high spatial resolution in three dimensions. During the CRISTA 2 mission significant indications of polar stratospheric clouds were found in the south polar region. Two PSCs were observed with unexpectedly large horizontal dimensions (>2000 km). The temporal evolution of the clouds in the background temperature field will be presented as well as its influences on several trace gases (e.g. ozone, HNO<sub>3</sub> and ClONO<sub>2</sub>). One of the PSCs dissolves during two days. Possible mechanisms will be discussed. For a short time CRISTA has used a measurement mode with extra high spatial resolution (8 km long-track) in the region of the second cloud. This allows the observation of a possible inner structure of the PSC.

**JSM01/E/16-A5 0920**

**CHEMICAL-RADIATIVE INTERACTION IN THE WINTER POLAR STRATOSPHERE**

I.A. MACKENZIE and R.S. Harwood (both at Department of Meteorology, University of Edinburgh, JCMB, King's Buildings, Edinburgh, EH9 3JZ, UK, email: iam@met.ed.ac.uk)

Several recent northern and Southern Hemisphere winters were simulated with a mechanistic model of the middle Atmosphere incorporating a comprehensive, interactive Chemistry scheme. The extent of chemical feedback from stratospheric polar ozone depletion, i.e. self-perpetuation of the ozone destruction processes via the radioactively-induced Stratospheric cooling, is examined. Dynamical changes arising from the ozone loss and their impact on ozone transport in the polar region are also investigated. The results from the two hemispheres are compared, as are the results from northern hemisphere winters with different dynamical conditions as governed by the observed geopotential forcing applied to the model's lower boundary. The results suggest that, for different reasons, chemical feedback does not have a major impact on ozone destruction in either the current northern or southern winters. Nevertheless, there might be significant feedback if an unprecedented cold Arctic winter were to occur in the near future while the stratospheric chlorine and bromine loadings remain near their peak.

**JSM01/W/29-A5 0940**

**COUPLED CHEMISTRY IN THE CCSR/NIES AGCM AND THE IMPACT OF SULFATE AEROSOL ON CLIMATE**

Masayuki TAKIGAWA, Masaaki Takahashi ( both at the Center for Climate System Research, University of Tokyo, 4-6-1, Komaba, Meguro-Ku, Tokyo, 153-8904, Japan. e-mail: takigawa@ccsr.u-tokyo.ac.jp ; masaaki@ccsr.u-tokyo.ac.jp ) and Hideharu Akiyoshi ( National Institute for Environmental Studies, 16-2, Onogawa, Tsukuba-Shi, Ibaraki-Ken, 305-0053, Japan. e-mail: hakiyosi@nies.go.jp )

A new middle-atmosphere general circulation model that includes the photochemistry for ozone and other chemical species (25 photolysis and 59 gaseous reactions) has been constructed. The dynamical, radiative, chemical processes of the model are fully interactive. The chemical scheme treats Ox-HOX-NOx-ClOx chemistry for the stratosphere, and predicts the concentrations of 31 chemically reactive gases. Nineteen photolysis rates are calculated by using the chemical species predicted in the model. However, the absorption of shortwave radiation for wavelength less than 200 nm is neglected in the radiation scheme of the original CCSR/NIES AGCM. Therefore, four parameterized photodissociations are included in the GCM (e.g., the photolysis of the oxygen by the radiative absorption in the Schuman-Runge band). The distributions of long-lived species show good agreement with those from satellite observations in a climatological sense, and those of short-lived species are also compared to those observations. For example, the number density of OH in the upper stratosphere nearly equals to that from balloon observation. Simple SOx chemistry and the heterogeneous reactions with the stratospheric sulfate aerosols are being considered in the model. The effect of aerosols on the radiation is coupled to the radiation scheme in the GCM. The impact of the sulfate aerosols on the climate, after several years of the eruption of volcanos, will be estimated by using the model.

**JSM01/W/116-A5 1000**

**INTERANNUAL VARIABILITY OF ARCTIC POLAR VORTEX AND ITS EFFECTS ON OZONE**

Hideaki NAKANE, Alexei. Kournosenko, Alexander Lukyanov, Hideharu Akiyoshi (National Institute for Environmental Studies, 16-2, Onogawa, Tsukuba, Ibaraki 305-0053 Japan, e-mail: nakane@nies.go.jp) and M. Ninomiya (Global Environmental Forum, 24-18 Inarimae, Tsukuba, Ibaraki 305-0061 Japan, e-mail: ninomiya@nies.go.jp)

The minimum temperature in the Arctic polar vortex in winter-spring period is close to the threshold of generation of Polar Stratospheric Clouds (PSCs). This results in the large variability of ozone depletion in the Arctic region. We developed a method to visualize the duration, size and strength of the polar vortex and applied it to the 40 years NCEP data. The variability of the characteristics of the Arctic polar vortex will be discussed. Ozone vertical profile data obtained by long-term measurements were analyzed. The relations between the characteristics of the Arctic polar vortex and the variations in the ozone data will be discussed.

**JSM01/W/32-A5 Invited 1040**

**MODELLING OF OZONE WITHIN AND OUTSIDE THE POLAR VORTEX**

Martyn CHIPPERFIELD (The Environment Centre, University of Leeds, Leeds, LS2 JTT, UK, Email: martyn@lec.leeds.ac.uk).

The stratospheric circulation at high latitudes during winter is dominated by the polar vortex, a region of strong westerly winds which leads to some isolation of this air from mid-latitudes. Chemical ozone depletion is known to occur within both polar vortices during late winter and spring. This loss is triggered by cold temperatures which permit the formation of polar stratospheric clouds (PSCs). Within the strong Antarctic winter polar vortex, this chemical depletion removes essentially 100% of the ozone between about 15 and 22 km between late August and early October. The Arctic polar vortex is generally weaker, but displays much more interannual variability. This interannual variability modulates chemical loss (by controlling the extent of PSCs) but also modifies the absolute amount of ozone through different transport. A strong, isolated vortex leads to cold temperatures, but also results in only weak descent. Both of these processes act to cause low ozone columns.

I will discuss model studies which have quantified the springtime chemical ozone depletion within Arctic (and Antarctic) vortex. I will also discuss how transport affects ozone in the Arctic winter stratosphere. In particular, I will discuss how recent studies with a three-dimensional (3D) chemical transport model (CTM), reveal the relative contributions of chemistry and transport in producing the low average Arctic ozone columns observed during the mid-late 1990's. I will also discuss how polar ozone may evolve in the future, as stratospheric climate-change interacts with polar chemistry.

**JSM01/W/16-A5 1110**

**THE IMPACT OF OBSERVED OZONE AND CO2-TRENDS ON THE STRATOSPHERIC CIRCULATION IN THE BERLIN GCM**

Ulrike LANGEMATZ (Institut fuer Meteorologie, Freie Universitaet Berlin, Carl-Heinrich-Becker-Weg 6-10, 12165 Berlin, Germany email: lang@strat01.met.fu-berlin.de)

Recent assessments of stratospheric temperatures have revealed a cooling of the lower stratosphere over the Antarctic and in northern middle/high latitudes in the spring seasons. One explanation for this might be the radiative effects of a concurrent ozone decrease observed since 1979.

The question of a direct relationship between the observed ozone and temperature trends is studied here with the help of two 20-year integrations of the Berlin Climate-Middle-Atmosphere-model. A reference simulation using a climatological ozone distribution of the 1980s was compared with a run using an observed ozone trend scenario based on measurements between 1979 and 1996. The analysis focusses on radiative and dynamical interactions. Special attention will be paid to the impact of the ozone decrease on the interannual variability in the stratosphere, such as the occurrence of sudden stratospheric warmings and the timing of the polar vortex breakdown in spring. A possible modification of the ozone signal by the increasing amount of greenhouse gases will be investigated using a third model experiment, in which, in addition to the ozone change, the global CO<sub>2</sub> increase since 1979 was incorporated.

**JSM01/E/02-A5 1130**

**INTERANNUAL VARIABILITY OF VERTICAL DESCENT RATE IN THE ANTARCTIC POLAR VORTEX**

Nozomi KAWAMOTO (Department of Geophysics, Faculty of Science, Kyoto University, Kyoto 606-8502, Japan, email: kawamoto@kugi.kyoto-u.ac.jp) Masato Shiotani (Graduate School of Environmental Earth Science, Hokkaido University, Sapporo 060-0810, Japan, email: shiotani@ees.hokudai.ac.jp)

To estimate a descent rate in the Antarctic polar vortex, we analyze the long-lived trace gas data derived from the Halogen Occultation Experiment (HALOE) for the 6 year period 1992 to 1997. Comparing methane profiles between the Antarctic autumn (February-March) and spring (September-October), we calculated an average descent rate in the lower stratosphere for each of the 6 winters. We found that it shows large year-to-year variations (1.8-1.2 km/month) which consist of a decreasing trend and a biennial cycle for the period we analyzed. The Antarctic stratopause during the mid-winter in years with large descent rate is warmer than in years with small one. It brings early downward and poleward movement of the westerly jet in the upper stratosphere through the thermal wind relation. Consequently, in years with large descent rate, wave activity is enhanced in early winter and it remains until late winter resulting from wave-mean flow interaction. It is also found that the descent rate is larger when planetary-scale wave amplitude is larger over the winter season. The variability seen in the descent rate also corresponds to the QBO for this period. The descent rate is larger in winters of 1992, 1994 and 1996 when the equatorial zonal flow is in easterly phase of the QBO.

**JSM01/E/27-A5 1150**

**EVIDENCE FOR DYNAMICAL CHANGES AT THE EDGE OF THE ANTARCTIC STRATOSPHERIC VORTEX IN WINTER**

Howard ROSCOE, Catherine Fowler, Jonathan Shanklin, Jules Hill (All at British Antarctic Survey/NERC, Madingley Rd, Cambridge CB3 0ET, UK, email: h.roscoe@bas.ac.uk)

Measurements of ozone South of 60deg latitude in Antarctica during early winter show an increase, consistent with the observed descent of stratospheric air and the convergence, which must accompany descent aloft. In the 1960s and 1970s, the rate of increase of ozone at both Faraday (65degS) and Halley (76degS) was between 6.9 and 9.2 DU/month, with an estimated error of less than 3 DU/month (one-sigma). In the 1980s and 1990s, this increased to 18.6 q7.2 DU/month near the vortex edge at Faraday and at Syowa (68degS); but it decreased to -1.2 q4.7 DU/month at Halley in the vortex core. Either the rates of descent are now different inside and outside the stratospheric vortex in winter; or, more likely, the vortex edge now experiences greater convergence at the expense of the vortex core. The measurements (Lunar Dobson, plus SAOZ at Faraday in the 1990s) do not have sufficient time resolution to show whether the change is coincident with the appearance of the ozone hole or with increased CO<sub>2</sub>, except that the SAOZ measurements show the rate of increase to vary substantially from one year to another. GCM calculations by Mahlman et al (1994) predicted such a change due to the ozone hole, but it is not clear what mechanism in the model gave rise to the changes. Such feedbacks between chemistry or radiation and dynamics in the Antarctic stratosphere are important because they may affect recovery of the ozone hole as the provisions of the Montreal Protocol become increasingly effective.

**JSM01/W/02-A5 1210**

**TRANSPORT AT THE POLAR VORTEX EDGE AND THE INDUCED EXCHANGE OF MASSES**

R. ALFIER, Institut für Meteorologie, Freie Universität Berlin, Germany S. Leder, Institut für Meteorologie, Freie Universität Berlin, Germany S. Pawson, Universities Space Research Association, Greenbelt, USA K. Ketelsen, Cray Research Inc. München, Germany

The transport at the Polar Vortex Edge and the exchanged masses are investigated for typical dynamical situations in northern winter. Fine structures in the transport of tracers (like water vapour) have been modeled with a 3-dimensional model. Typical observed 200hPa geopotential height fields are used to force the model. The different amounts of exchanged masses are investigated in the experiments. The mechanistic (primitive equation) model was setup in a high resolution (1.4 deg X 1.4 deg horizontal; 1.6km vertical) form. With an accurate semi-Lagrangian transport scheme the model is well adapted for this studies.

Friday 23 July PM

Presiding Chair: Shigeo Yoden (University of Kyoto, Japan)

**OZONE CHANGES IN THE STRATOSPHERE**

**JSM01/W/37-A5 Invited 1400**

**OZONE LOSS IN THE ARCTIC STRATOSPHERE AS OBSERVED BY MATCH**

M. REX (Alfred Wegener Institute, now at JPL, 4800 Oak Grove Dr., Pasadena, CA 91109-8099, USA, e-mail: mrex@caesar.jpl.nasa.gov), P. von der Gathen, A. Schulz, J. Steger, H. Gernandt, N.R.P. Harris, E. Reimer, A. Beck, R. Alfier, M. Chipperfield, I. Kilbane-Dawe, M. Allaart, M. Alpers, H. De Backer,



D. Balis, B.R. Bojkov, G.O. Braathen, J. Cisneros, H. Claude, F. O'Connor, J. Davies, H. Dier, V. Dorokhov, H. Fast, A. Gamma, S. Godin, G. Hansen, E. Kyrö, Z. Litynska, I.S. Mikkelsen, M.G. Molyneux, G. Murphy, H. Nakane, C. Parronodo, F. Ravagnani, S.J. Reid, M. Rummukainen, P. Skrivankova, C. Varotsos, C. Vialle, P. Viatte, J. Wenger, V. Yushkov, C. Zerefos.

Wintertime ozone loss takes place in the stratospheric polar vortices of both hemispheres. Compared with the Antarctic, the ozone layer in the Arctic is much more variable and the degree of chemical ozone loss is smaller, making it more difficult to separate chemical ozone loss from changes due to dynamical influences and to quantify the chemical contribution to observed changes. In recent years, a number of techniques have been developed and now we are able to derive a detailed picture of the chemical ozone loss for a number of recent Arctic winters. The presentation will focus on the Match technique that is based on the coordinated launches of several hundreds of ozone sondes per winter from a network of about 35 stations in northern latitudes. With the Match technique it is possible to measure stratospheric chemical ozone loss rates as a function of time and altitude with high vertical resolution. Match campaigns have been used to quantify the chemical ozone loss for six Arctic winters since 1991/92. The degree of chemical ozone loss is highly variable from winter to winter with largest losses observed for the coldest stratospheric winters, when local chemical losses exceeded 60 % and ozone column losses of more than 30 % have been measured. The timing and vertical extent of the observed chemical ozone loss agrees qualitatively well with model predictions, however current chemical models considerably underestimate the observed rate of chemical ozone loss.

#### JSM01/W/61-A5 1430

##### SEASONAL EVOLUTION OF OZONE-METHANE CORRELATIONS IN THE POLAR REGIONS

D. SANKEY and T. G. Shepherd (Department of Physics, University of Toronto, 60 St. George street, Toronto, Ontario, Canada, M5S 1A7. email: sankey@mam.physics.utoronto.ca)

Correlations with long-lived chemical tracers are way of eliminating short-term dynamical ariability in the atmosphere. Plumb and Ko 1992) showed that a necessary condition to reduce a compact correlation between two tracers is that the lifetimes of the tracers involved must be longer than the quasi-horizontal mixing time. A recent application of such correlations is that of Mueller et al (1996), who used the evolution of a measured relationship between ozone and methane in the Arctic polar vortex to quantify the Arctic ozone loss due to chemistry alone. Their analysis assumes several things. One assumption is that a compact correlation exists when the initial measurement is made. This requires either that a correlation exists when the polar vortex is formed, which seems unlikely due to the short lifetime of ozone under sunlight conditions, or that a correlation forms in the early winter inside an isolated dark vortex. A second assumption is that a compact correlation is maintained even after the rapid destruction of ozone. There are not sufficiently extensive simultaneous measurements of ozone and methane to determine whether a well-defined correlation exists. Therefore data from a comprehensive middle atmosphere GCM (the Canadian Middle Atmosphere Model) are used to provide a surrogate dataset. The validity of the Mueller et al. approach is first examined by considering the correlations between ozone and methane in the Antarctic polar vortex. The Antarctic provides an ideal environment for compact correlations to occur because the vortex is much more stable than in the Arctic. The results suggest that although there is no correlation between ozone and methane when the vortex is formed, there is sufficient time for one to form through early winter. The situation for the Arctic vortex is much less clear due to the lower stability of the vortex.

#### JSM01/E/40-A5 1450

##### THE EFFECTS OF MIXING ON TRACER RELATIONSHIPS INSIDE THE POLAR VORTICES

Alan PLUMB (Massachusetts Institute of Technology, Cambridge MA, USA) Darryn Waugh (Johns Hopkins University, Baltimore MD, USA) and Martyn Chipperfield (University of Cambridge, UK)

Quantitative estimates of ozone loss and of denitrification within the polar vortices, whether based on trajectory-following or tracer correlation methods, implicitly ignore the effects of mixing. Accumulating observational evidence indicates that, on the contrary, mixing has a substantial impact on tracer budgets in the vortex. A single mixing event across the vortex edge will produce an anomalous mixing line, joining vortex and exterior air, on a tracer-tracer diagram. However, different lines would be produced at different altitudes, which the limited available observations indicate does not occur. A simple model of continuous mixing across the vortex edge shows that distinct tracer-tracer relationships are formed within the vortex, and that the separation from midlatitude relationships is greatest when the mixing is weak. The evolution of tracer relationships in a three-dimensional chemical transport model shows the development, though the winter, of anomalous relationships within the Arctic vortex.

#### JSM01/W/55-A5 1510

##### 4.5 YEARS OF OZONE LAYER OBSERVATIONS OVER LAUDER, NEW ZEALAND

E.J. BRINKSMA, J.W. Hovenier, W. Hogervorst (Vrije Universiteit, De Boelelaan 1081, 1081 HV Amsterdam, The Netherlands, Email: ellen@nat.vu.nl) D.P.J. Swart, J.B. Bergwerff (RIVM, Postbus 1, 3720 BA Bilthoven, The Netherlands)

Altitude profiles of the ozone density have been measured with lidar over Lauder, New Zealand (45S, 170E) since late 1994. An overview of these measurements will be presented, showing both the long-term (seasonal) variation and variations on a much shorter time scale. A few cases in which the ozone layer changed rapidly (timescale of days) will be highlighted. For example, the record low ozone column density that was observed in August of 1997 will be explained by first focusing on the ozone profiles, which indicate at which altitudes changes took place. Then, by an analysis of the potential vorticity and ozone fields, we will show that these changes were caused purely by an unusual dynamical situation: In the lower stratosphere tropical ozone poor air was observed over Lauder, while simultaneously high-latitude ozone poor air was observed in the middle stratosphere. Other cases that might be presented are the detection of laminae of chemically depleted ozone poor air, originating from the springtime vortex, and cases of rapid changes in the ozone column density.

#### JSM01/W/27-A5 1530

##### OZONE PROFILE TREND ANALYSIS OF THE SWISS RECORDS

Andrea K. WEISS and Johannes Staehelin (both at Institute for Atmospheric Physics, ETH, CH-8093 Zurich, Switzerland, email: weiss@atmos.univ.ethz.ch and staehelin@atmos.univ.ethz.ch)

Chemical destruction in the stratosphere and natural variability must be separated from methodical insufficiencies as well as instrumental drifts and shifts to prove ozone profile trends in order of some percent per decade. Height dependent ozone trends above Switzerland can be derived from the balloon soundings of Payerne, Umkehr measurements of Arosa, and satellite overpasses of SAGE and SBUV. We found striking differences between the trends derived from Umkehr measurements and

balloon soundings. This difference is not only present in Switzerland, but were noted also in global data in a recent assessment. The results are tuneable trends, especially for the climate relevant ozone in the height of the Troposphere.

With statistical homogeneity tests we identified breaks in the measurement series relative to each other. A trend analysis combining all methods is performed, showing the best possible estimates of ozone profile trends in Switzerland as well as the height dependent uncertainties.

#### JSM01/W/97-A5 Invited 1610

##### MIDDLE ATMOSPHERIC CHEMISTRY AND DYNAMICS: UNDERSTANDING THE DISTRIBUTION AND TRENDS OF STRATOSPHERIC OZONE

Roderic JONES (Cambridge University Centre for Atmospheric Science, Department of Chemistry, Lensfield Road, Cambridge CB2 1EW, UK, Email: rj1001@cam.ac.uk)

Stratospheric ozone provides an essential shield against short-wavelength solar radiation. In absorbing both solar and longwave IR radiation it has a major influence on the temperature structure and thus the circulation of the middle atmosphere.

Anthropogenic activity, coupled with natural events, have over the past decades lead to dramatic and highly significant changes in the distribution of stratospheric ozone, with negative ozone trends evident over large parts of the globe. The magnitudes of these trends vary with both latitude and altitude, reflecting the differing destruction mechanisms involved. It is now also appreciated that changes in lower stratospheric ozone may have ameliorated, albeit temporarily, the effects of greenhouse warming, while the potential effects of climate change on the distribution of stratospheric ozone have yet to be quantified reliably.

In this presentation, the chemical and dynamical factors which control the distribution and seasonal evolution of stratospheric ozone will be summarised. Our understanding of the origins of the observed trends in ozone will then be reviewed, and the current appreciation of likely future changes in ozone will be discussed.

#### JSM01/L/30-A5 1640

##### EFFECTS OF ELEVATED SULFATE AEROSOL ON MIDDLE ATMOSPHERE CHEMISTRY AND DYNAMICS: 3-D COUPLED MODEL SIMULATIONS

JASSIM AL-SAAD, R. Bradley Pierce (both NASA Langley Research Center, Hampton, VA, 23681, USA), T. Duncan Fairlie (STC, Hampton, VA), Mary Kleb, William Grose (both NASA Langley Research Center, Hampton, VA), and V. Lynn Harvey (SAIC, Hampton, VA)

The NASA Langley Research Center IMPACT model is used to examine the effect of enhanced stratospheric aerosol loading on the dynamical evolution and chemical composition of the stratosphere following a large tropical volcanic injection. The IMPACT model is a three-dimensional general circulation model (GCM) with coupled dynamics, radiation and chemistry. The chemistry component explicitly transports 24 chemical families and individual species, and includes parameterizations of heterogeneous chemical processes on sulfate aerosols and polar stratospheric clouds. The ozone distribution predicted by the model is used in the determination of stratospheric radiative heating. Aerosol perturbation simulations are compared with a multiple-year control simulation in which a background surface area density distribution is used. The influence of enhanced aerosol on heterogeneous chemical processing is simulated using a three-dimensional climatology of surface area density developed using observations made from the HALOE, SAGE II, and SAM satellite instruments following the June 1991 eruption of Mount Pinatubo. Radiative effects of the enhanced aerosol loading are represented by monthly-mean zonally-averaged heating perturbations obtained from a study conducted with the ECHAM-4 GCM. These simulations allow assessment of the relative contributions of heterogeneous chemical processing and direct aerosol radiative effects to the dynamical and chemical characteristics of the middle atmosphere. Model results are compared with observational data including TOMS total ozone and species observed by instruments on the UARS satellite.

#### JSM01/E/15-A5 1700

##### UPPER AND LOWER STRATOSPHERIC OZONE CHANGES 1979-1994: THE ROLES OF VARIABLE TRANSPORT AND TEMPERATURE

LINWOOD B. CALLIS (Atmospheric Sciences Division, NASA Langley Research Center, Hampton, VA 23681-0001, e-mail: lbc@jaguar.larc.nasa.gov)

Changes in upper and lower stratospheric ozone during the period 1979-1994 are imperfectly understood. Deviations in upper stratospheric O<sub>3</sub> cannot be fully explained by the effects of the solar UV variations and trace gas effects, and those in lower stratospheric O<sub>3</sub> cannot be fully explained by heterogeneous chemical destruction associated with Clx and Brx. In the present analysis SBUV and SBUV O<sub>3</sub> data are used with NMC temperature and layer thickness data, and MSU temperatures, to gain an understanding of the role variations in these quantities have on stratospheric O<sub>3</sub> changes. Trend analysis is carried out by least squares fitting of time series of O<sub>3</sub> with only constant, linear, and annual and semi-annual terms included. The residuals then contain the effects of the 11-year solar cycle, the QBO, and any other processes (dynamical or chemical) which may affect stratospheric O<sub>3</sub>. These residuals are analyzed with temperature and thickness data. In addition, diabatic transport fields have been diagnosed on a monthly basis from 1979 through 1996 using observed temperatures and climatological O<sub>3</sub>, CO<sub>2</sub>, and H<sub>2</sub>O distributions together with a radiative transfer code. These transport fields are discussed and have been used in a contemporary 2-D photochemical transport model to determine calculated O<sub>3</sub> trends due only to variations in the transport and temperature fields. The calculated results reveal significant trends and multi-year deviations in column and local level O<sub>3</sub> up to the global scale. These results are also discussed.

#### JSM01/W/15-A5 1720

##### CONSTRAINING UNCERTAINTIES IN THE PHOTOCHEMICAL MODELLING OF FUTURE OZONE CHANGES BY UARS OBSERVATIONS

Frans J. M. Alkemade (IMAU, Instituut voor Marien en Atmosferisch onderzoek Utrecht, Postbus 80005, 3508 TA Utrecht, The Netherlands, Email: frans\_a@knoware.nl) Guus J. M. VELDERS (RIVM, Postbus 1, 3720 BA, Bilthoven, The Netherlands, Email: Guus.Velders@rivm.nl).

The chemical modelling of stratospheric ozone depletion is analyzed (using the Cambridge/RIVM 2-dimensional chemical transport model) in order to find the connection between the uncertainties in a selected set of pivotal reaction rate constants and the associated uncertainty in the long term ozone change predictions. A comparison between the modelled 1992 atmosphere and the concentrations of a number of species measured by several instruments onboard the UARS satellite is used to constrain this uncertainty. Sensitivity studies for varying reaction rate constants are performed, aimed at the long term ozone change prediction and at the 1992 stratospheric concentrations. The main results are:- A long term ozone change prediction (from 2000 to 2050), based on the same reaction rate data and a specific emission scenario that are used by the ozone panel [WMO, 1999], contains an error of at least 100%, due to the reported uncertainties in the chemical input parameters.

## INTER-ASSOCIATION

A comparison between the model and the UARS data can constrain the uncertainties in a number of reaction rate constants that have a relatively large influence on the calculation of future ozone changes. The five most important are:

$\text{N}_2\text{O} + \text{O}(1\text{D}) \rightarrow 2 \text{NO}$  (error reduced from 30% to 7%)  
 $\text{O}_3 + \text{foton} \rightarrow \text{O}_2 + \text{O}$  (error reduced from 10% to 3%)  
 $\text{HCl} + \text{OH} \rightarrow \text{H}_2\text{O} + \text{Cl}$  (error reduced from 20% to 4%)  
 $\text{ClO} + \text{OH} \rightarrow \text{HCl} + \text{O}_2$  (error reduced from 100% to 8%)  
 $\text{NO}_2 + \text{foton} \rightarrow \text{NO} + \text{O}$  (error reduced from 10% to 7%)

- This reduction of the errors in the reaction rate constants reduces the associated error in the long term modelled ozone change by a factor of about two. The revised prediction for the percentage change in the globally averaged total ozone field (year 2050 ozone minus year 2000 ozone) now becomes: 1.6% +/- 0.8%. (It was 1.6% +/- 1.7%)

### JSM01/W/101-A5 1740

#### A THEORETICAL 2-D PHOTOCHEMICAL MODEL OF MINOR CONSTITUENTS DISTRIBUTION IN THE MIDDLE ATMOSPHERE

MANOHAR LAL and R. Rajaram, Equatorial Geophysical Research Laboratory, Indian Institute of Geomagnetism, Krishnapuram BO, Maharanagar PO, Tirunelveli-627011, India

Production and loss rate of several species belonging to NO<sub>x</sub>, HO<sub>x</sub>, and Ox group have been calculated using the family method. The computed production and loss rates have been used as input in solving the continuity equation of 2-D photochemical model. The continuity equation was solved by using alternating direction implicit method. Input parameters such as temperature, meridional velocity, vertical velocity were taken from CIRA-92. The vertical eddy diffusion coefficient was taken from Ebel, and the horizontal diffusion coefficient taken as a constant value of 10(9) cm<sup>2</sup>s<sup>-1</sup> in the present work. The chemical reactions and their reaction rates taken from JPL compilation. The photodissociation coefficients were used by the package developed by Arve Kylling and his group. We have derived the ozone and nitrogen dioxide latitude-altitude cross-sections and studied its diurnal and latitudinal variability. The ozone mixing ratio calculated by our model for 25 km altitude shows the value of about 2.4x10<sup>-6</sup> at equator and increases upto about 4.4x10<sup>-6</sup> at the polar region. Also the peak ozone density has been found at about 70 deg latitude. The present calculation does not, however, show any secondary peak in the mesospheric region.

### JSS02 Monday 19 – Tuesday 20 July

**PHYSICS AND CHEMISTRY OF THE EARTH'S INTERIOR (IASPEI, IAVCEI, IAG, SEDI)**  
Location: Medical School EG12 LT4  
Location of Posters: Arthur Thompson Hall

**Monday 19 July AM**

Concurrent Poster Session

### JSS02-A1 Introduction 1035

Raymond JEANLOZ (Dept. Geology and Geophysics, University of California, Berkeley, CA 94720-4767 USA)

### JSS02/E/05-A1 1045

#### PHYSICS AND CHEMISTRY OF THE EARTH'S INNER CORE

LARS STIXRUDE, Dept. of Geological Sciences, University of Michigan, Ann Arbor, MI 48109-1063, USA, stixrude@umich.edu

The structure of the earth's inner core is now known to differ from the homogeneous, isotropic picture we had only a decade ago. Recent seismological observations, when combined with knowledge of the physics of iron, have important implications for our understanding of the dynamics of the inner core, its interaction with the geomagnetic field, and its composition and temperature. The extreme pressure and temperature conditions of the inner core present substantial challenges. In this context, first principles theory provides the ideal complement to laboratory studies of iron, and a powerful probe of the earth's most remote regions. The first principles approach that we have used is based on Density Functional Theory and state-of-the-art computational methods for solving the quantum mechanical equations that reduce approximations to the minimum (LAPW). The theoretical results are found to be in excellent agreement with laboratory measurements, including the results of static and dynamic compression experiments, phase equilibria, and magnetism. Among the contributions of this approach to our understanding of the core are: 1) Placing new constraints on the crystalline structure of the inner core. The bcc phase can be essentially ruled out as an inner core constituent. The origin of its stability - its strong magnetism - vanishes at high pressure, rendering it mechanically unstable at core pressures. 2) An understanding of the first-order anisotropy of the inner core in the intrinsic crystalline anisotropy of iron. The single-crystal anisotropy of hcp iron agrees remarkably well with that observed for the inner core, indicating a strongly textured aggregate. 3) The composition of the inner core is found to contain a small amount of light alloying elements. Future directions, including the prediction of high temperature elasticity will be discussed.

### JSS02/W/14-A1 1115

#### PARAMETER DEPENDENCE OF CONVECTION DRIVEN SPHERICAL DYNAMOS WITH APPLICATIONS TO THE GEODYNAMO

F.H. BUSSE, E. Grote and A. Tilgner (Institute of Physics, University of Bayreuth, D-95440 Bayreuth, Germany. E-mail: busse@uni-beyreuth.de Telephone No: +49 921 553 329 Fax No: +49 921 552 999)

A systematic study of the generation of magnetic fields by convection flows has been done in dependence on the Taylor number T, the Rayleigh number R, the Prandtl number P and the magnetic Prandtl number P<sub>m</sub>. In different ranges of the parameter space dipolar, quadrupolar or hemispherical dynamos are preferred. The time dependence is usually chaotic, but steady (except for drifting nonaxisymmetric components) dynamos can also be found. The ratio of magnetic to kinetic energies exhibits the Prandtl number scaling expected on the basis of the magnetostrophic approximation, but other features indicate a significant dependence on P. Quadrupolar and hemispherical dynamos, for example, exhibit dynamo waves propagating in latitude which strongly depend on the inertial terms in the equations of motion. The results indicate that the geodynamo is characterized by a large effective Prandtl number suggesting

compositional buoyancy as dominant energy source. Effects of boundary conditions and buoyancy distributions will be discussed and be related to conditions in the Earth's core.

### JSS02/E/18-A1 1145

#### PHASE DIAGRAM OF IRON, REVISED-CORE TEMPERATURES

Thomas J. AHRENS Lindhurst Laboratory of Experimental Geophysics, Seismological Laboratory 252-21, California Institute of Technology, Pasadena, CA 91125 Kathleen G. Holland Sandia National Laboratory, MS George Q. Chen (Present address: The Santa Cruz Operations, Inc.)

Shock-wave experiments on iron preheated to 1573 K conducted from 14 to 73 GPa, yield new data for sound velocities in the gamma- and liquid-phases. Melting was observed in the highest pressure (~71 plus/minus 2 GPa) experiments at shock temperatures of 2775 plus/minus 160 K. This melting point is close to those measured by Boehler [1993], Saxena et al. [1993], and Jephcoat and Besedin [1997] and suggest the melting curve of gamma-iron is some ~500 degrees C lower than that of Shen et al. [1998] at 80 GPa. We speculate that the sub-solidus phase in the Earth's outer core could be the double hexagonally close-packed (d\_c hp) beta-phase [Saxena et al., 1996], and its onset would reconcile the static and dynamic data for iron's melting curve at core pressures. Based on upward pressure and temperature extrapolation of the melting curve of gamma-iron, the estimated inner core-outer core boundary (ICB) temperature is 5500 plus/minus 400 K, which is similar to earlier results based on gamma-iron data and well below temperatures inferred from shock-temperature data. The temperature at the core-mantle boundary (CMB) on the outer core side is then calculated to be 3930 plus/minus 630 K, and the thermal boundary layer at the core-mantle boundary has a temperature difference between 400 and 1400 C, considerably lower than 1000-2000 C range estimated by Williams [1998], based on the higher temperatures inferred from shock temperature data.

### JSS02/W/07-A1 1215

#### SIMULATING THE GEODYNAMO

Paul ROBERTS (Institute of Geophysics and Planetary Physics, UCLA, Los Angeles, CA 90095, USA, email: roberts@math.ucla)

Over the past four years, several groups have presented the results of their three-dimensional geodynamo simulations, some of which will be compared and contrasted in this presentation. The day seems to be approaching when comparisons between the behaviours of different simulations will reveal new facts about the deep interior of the Earth, now and in the geological past. Such information will follow from varying the parameters defining a model to make it behave increasingly like the observed geomagnetic field. An example is given in the second part of this presentation. Most geodynamo models are spherically symmetric in structure, but recently Glatzmaier, Coe and Roberts have investigated how lateral inhomogeneities in the thermal state of the lower mantle affect convection and field generation in the core. Eight different patterns of heat flux from the core to the mantle were imposed over the core-mantle boundary. Spontaneous reversals occurred in seven of these cases. The results provide insight into why the frequency of geomagnetic reversals, as seen in the paleomagnetic record, can be so different during different geological epochs. When the structure of the lower mantle constrains the pattern of heat flux from the core to differ significantly from what is preferred by the dynamics of the core, the fluid flow and magnetic field are considerably more stochastic than they are when in harmony. This results in more frequent magnetic reversals of longer durations, and during the constant polarity intervals between reversals a magnetic field of smaller intensity and greater secular variability is found. These and other results of varying the parameters of the Glatzmaier-Roberts geodynamo model will be described.

**Monday 19 July PM**

### JSS02/C/ST6/W/09-A1 1400

#### CHEMICAL BONDING AND ELECTRONIC STRUCTURE IN THE EARTH'S DEEP INTERIOR

David M. SHERMAN (Department of Earth Sciences, University of Bristol, Bristol UK BS8 1RJ; email: dave.sherman@bris.ac.uk)

During the past 50 years, it has been proposed that pressure-induced changes in the electronic structures of geochemical components affect the physics and chemistry of the Earth's mantle and core. Changes in chemical bonding may change the siderophile and lithophile behaviour of metals and consequently determine how elements such as K, Ni and Co are partitioned between the core and mantle. Arguments about the nature of the light element in the core rest on pressure-induced changes in bonding and phase equilibria in the Fe-S-O-Si system. Changes in the electronic structures of transition metal oxides and silicates must be known before we can predict transport properties such as radiative thermal conductivity and electrical conductivity. In recent years we have been able to address these fundamental problems in mineral physics through the application of first-principles electronic structure calculations using density functional theory. This talk will give an overview of the current state of approximation being used and an assessment of the reliability of calculated phase stabilities and elastic properties. Recent work, for example, has provided constraints on core composition. In the near future, ab initio calculated thermoelastic properties will allow us to fit PREM to a mineralogical model. More fundamentally, however, is the emerging qualitative picture that theory is giving us about the crystal chemistry and electronic structure in the Earth's mantle and core. In particular, transition metal oxides, silicates and sulphides show a breakdown of the ligand field theory (crystal field theory) picture and the onset of intermediate spin states stabilized by metal-metal bonding.

### JSS02/W/01-A1 1425

#### ON A FUZZY CORE-MANTLE BOUNDARY

Ed J. GARNERO (Arizona State University, Dept of Geology, BOX 871404, Tempe AZ 85287 USA, email: garner@asu.edu), Raymond Jeanloz (UC Berkeley, Dept of Geology and Geophysics, Berkeley, CA 94720 USA, email: jeanloz@uclink.berkeley.edu), Lianxing Wen (Carnegie Institute, Dept of Terrestrial Magnetism, 5241 Broad Branch Rd Washington DC 20015 USA, email: wen@clrs1.ciw.edu)

The detailed nature of Earth's core-mantle boundary (CMB) likely plays an integrated role in important processes related to the evolution and dynamics of the entire interior. Seismic imaging experiments of the CMB region have resulted in models of a thin (5-50 km) intermittent layer at the base of Earth's mantle having ultralow seismic velocities. The ultralow velocity zones (ULVZ) are generally located beneath lower mantle regions containing reduced wavespeeds, as depicted by tomographic studies. Studies of ULVZ have included analyses of SPdKS, PcP, ScP, and PKP, and argue for Vp depressions of 10% or more, relative to the overlying mantle, and Vs reductions of up to three times that of Vp; the possibility of a density increase in the ULVZ has also been explored. Partial melt of some lowermost mantle constituent has emerged as a likely explanation



of the ultralow velocities, with the strong possibility of a chemical contribution (such as byproducts from chemical reactions between the core and mantle). Subsequent work has demonstrated that strong trade-offs exist between ULVZ thickness and properties ( $V_p$ ,  $V_s$ , and density). Here we extend the trade-off space to include a "fuzzy CMB", i.e., a thin transition zone from mantle to core properties (around 2 km), and a thin zone in the outer core containing non-zero  $V_s$ , i.e., a core-rigidity zone (CRZ) of thickness less than a few km. 2-D synthetic seismograms demonstrate how non-planar structures (e.g., domes) can also enhance waveform anomalies. Anomalous ULVZ structure, a fuzzy CMB, or CMB underplating (CRZ) -- which could have significant implications for geomagnetism and geodynamics -- can individually or collectively perturb the seismic wavefield previously used to image ULVZ structure. Thus, given the uncertainties, a fuzzy CMB (with possible mantle or core-side boundary layer structure) can also explain the data. In non-ULVZ regions the CMB can be 'sharp', with transition thicknesses of a few hundred meters or less.

**JSS02/W/13-A1****1450****USING GEOMAGNETIC OBSERVATIONS TO INFER THE PROPERTIES OF MANTLE AND CORE MATERIALS**

Stephen ZATMAN (Department of Geology and Geophysics, University of California, Berkeley, California, 94720, USA, email:zacman@seismo.berkeley.edu)

The time varying geomagnetic field ought to be a useful tool for deducing the physical properties of the Earth's deep interior. In practice it has been difficult to use geomagnetic data in this way because it has not always been clear how to interpret the data. Attempts to do so have often led to findings that are more like suggestions than hard results. The answer is to find sensible questions whose answer can be directly related to observables in the field (and ideally observables with unique physical interpretations).

In order to do this, it is important to understand the core dynamics that cause the observed secular variation. The decadal variation is thought by many to be related to torsional oscillations (twisting motions between cylinders within the core about the axis of rotation): assuming that this is true allows us to estimate the timescale of magnetic diffusion within the mantle (by comparing estimates of the angular momentum in the core with changes in the mantle rotation rate), which constrains mantle conductivity. Application of this method suggests a diffusion timescale of around half a year. Buffett proposed that the core and mantle might be dynamically coupled via gravitational coupling of the inner core to lateral density variations in the mantle. It turns out that if true, this makes predictions concerning the variation of the magnetic field near the Earth's poles that depend on the viscosity of the inner core. Preliminary results suggest that the core is rigid on the timescale of motions within the core (perhaps 100-1000 years), although modelling difficulties may be hard to rule out.

**JSS02/C/ST6/W/01-A1****1515****EXTREMES IN COMPLEX STRUCTURES AT THE CMB**

D. V. HELMBERGER, I. Sidorin, L. Wen, S. Ni, J. Ritsema, and M. Gurnis Seismological Laboratory 252-21 California Institute of Technology, Pasadena, CA 91125, USA

We investigate some small scale seismic zones embedded in the large scale circum-Pacific Belt (Down-welling) and some slow zones beneath Europe and Africa (Up-welling) as delimited by long wavelength tomography. Using the results from dynamic modeling, Sidorin et al. (1998, 1999), we can perform a mapping of tomographic models into a physical model containing localized velocity gradients and a superimposed 1% phase change. This jump is temperature-dependent occurring 250 km above the CMB beneath the fastest regions (Caribbean, etc.) and drops to less than a 100 km away from these regions. The observed seismic triplication data, Scd, is explained well by 2D synthetics generated from these models showing its intermittent character which is controlled primarily by local velocity gradients. A review of the most anomalous seismic data and possible models associated with ultra-low velocity zones (ULVZ's) will be presented including distortions in SKS (SKPdS, etc.), precursors to PcP, ScS, PKP and anomalies in PKP branches. The African structure appears the most distinct with sharp features producing multi-pathed ScS and SKS behavior. Some 2D models are presented but these features prove difficult to constrain because of the overlying mega-plume complexity. Using forward modeling, we estimate that this structure extends halfway to the surface with rapidly varying ULVZ's at its base. As discussed in previous studies, some trade-offs occur in thickness but Gaussian-shaped structures with lateral dimensions of 50 to 300 km prove effective.

**JSS02/E/06-A1****1600****FINE-SCALE STRUCTURE AT THE CORE-MANTLE BOUNDARY**

Bruce BUFFETT (Department of Earth and Ocean Sciences, University of British Columbia, Vancouver, BC, V6T 1Z4, Canada, email: buffett@eos.ubc.ca)

Indications of unusual physical properties within a few tens of kilometers of the core-mantle boundary are found in several disparate observations. Waveforms of seismic waves that travel along partially diffracted paths indicate ultra low velocities in a layer that is probably less than 40 km thick. Independent observations of the Earth's nutation suggest high electrical conductivities in a layer that may be only a few hundred meters thick. Mechanisms that are proposed to explain these thin layers include partial melt in the mantle and chemical reactions between the mantle and liquid core. Ponding of partial melt at the base of the mantle is sufficient to explain the low velocity layer, but no entirely satisfactory explanation has been given for the anomalous conducting layer. Increases in conductivity due to partial melt appear to be too small and the conductive products of chemical reactions are not readily drawn into the mantle. We examine the possibility that a conducting layer develops at the top of the core through precipitation of dissolved mantle components. The combined effects of cooling and fractionation due to inner-core growth cause sediment of buoyant particles to settle at the top of the core. We assume that this layer of sediment forms a porous medium in which the high electrical conductivity is caused by liquid iron in the pore volume. Models for the Earth's nutation are used to establish the porosity, rheological properties and thickness of the layer needed to explain the observations. We use these estimates to infer the P and S wave velocities in the layer. Low P wave velocities relative to the overlying mantle occur because of the high density of liquid iron. Even lower S wave velocities are expected if the layer is poorly consolidated. Speculations about the evolution of porosity in the layer are based on comparisons of the rates of viscous compaction and sedimentation.

**JSS02/W/02-A1****1620****CORE-MANTLE: PHASE RELATIONS AND CHEMICAL INTERACTION**

Reinhard BOEHLER and Valerie Hillgren (both at Max-Planck Institut fuer Chemie, 55020 Mainz, Germany, email: boe@mpch-mainz.mpg.de)

In contrast to previous predictions, the solidus temperature of the lower mantle is substantially below the melting temperature of (Mg,Fe)SiO<sub>3</sub>-perovskite. New measurements on a pyrolytic

mantle composition in the diamond cell agree with the shock melting temperature for olivine, leading to a solidus temperature at the core-mantle boundary (135 GPa) of about 4300 K which is close to the core temperature. From these results recent observations of an ultra-low velocity zone at the bottom of the mantle may be explained by partial melting of normal mantle material. The eutectic melt is most likely rich in dense (Mg,Fe)O-magnesiowuestite which may gravitationally segregate from the less-dense perovskitic material.

New shock measurements on iron support the melting temperatures obtained from diamond cells, which leads to a rather simple phase diagram of iron. This weakens the case for a new high pressure phase observed in some cases in the diamond cell and yields a melting temperature at the inner core boundary near 5000 K. The Gruenisen parameter obtained from the Lindemann relation and the melting slope is in agreement with estimates using other methods.

We present new data on the chemical interaction of potential mantle and core materials. Oxygen and Silicon by themselves are soluble in liquid iron in only subpercent amounts. The solubility of oxygen increases in the presence of sulphur. Under increasingly reducing conditions silicon is dissolved but we also observe an increase in the solubility of calcium and this in conflict with geochemical observations. If during core formation silicon would have been dissolved in liquid iron under strongly reducing conditions, core and mantle would be in drastic disequilibrium. A chemical reaction would deplete the bottom part of the lower mantle in iron, and this is in conflict with the distribution of seismic velocities. Thus, a combination of oxygen and sulphur is likely to explain the density deficit in the outer core.

**JSS02/W/18-A1**

Invited

**1640****SOLUBILITY OF SILICON AND OXYGEN IN THE EARTH'S CORE**

C.K. Gessmann (1), (2), M. Kilburn (2), B.J. Wood (2) and D.C. RUBIE (1). (1) Bayerisches Geoinstitut, University of Bayreuth, D-95440 Bayreuth, Germany, (2) Department of Earth Sciences, University of Bristol, Wills Memorial Building, Queens Road, Bristol BS8 1 RJ, U.K., christine.gessmann@bristol.ad.uk.

In order to help identify the nature of the light component(s) in the Earth's core, we determined the solubilities of silicon and oxygen in liquid Fe-rich metal up to 23 GPa and 2400 °C using piston-cylinder and multi-anvil apparatus. Metal powders, doped with various siderophile and light elements were used as starting materials and were contained in MgO capsules. A wide range of oxygen fugacities was imposed by varying the composition of the starting material. The experimental results reveal that the solubilities of Si and O in liquid metal vary systematically as a function of pressure, temperature and oxygen fugacity. The solubility of Si increases significantly with decreasing oxygen fugacity (at constant P and T), with increasing pressure (at constant T and fO<sub>2</sub>) and with increasing temperature (at constant P and fO<sub>2</sub>). The solubility of O in liquid metal also increases with increasing temperature, but varies inversely with Si solubility as a function of fO<sub>2</sub> and pressure.

These results, if extrapolated to higher pressures and temperatures, suggest that significant amounts of Si can be dissolved in liquid metal even at 'moderate' oxygen fugacities, i.e. values that were likely during core formation. However, because of their inverse solubility behaviour, it is unlikely that the presence of both Si and O contribute significantly to the density deficit in the Earth's core. Additional model calculations based on available thermodynamic data allow extrapolation of these results up to core pressures and temperatures with the aim of better constraining the composition of the Earth's core.

**JSS02/W/11-A1****1700****THE EFFECT OF D<sup>\*</sup> STRUCTURE ON CORE PHASES: CONSEQUENCES FOR INNER CORE ANISOTROPY**

Ludovic Breger, Barbara ROMANOWICZ and Hrvoje Tkalcic (Seismological Laboratory, Univ. of California, Berkeley, CA, 94720, USA, email: barbara@seismo.berkeley.edu)

We have assembled a representative global dataset of differential PKP(AB)-PKP(DF) travel times to study structure and anisotropy in the deep inner core. The reference PKP(AB) phases, which sample the outer core, are known to be strongly affected by propagation through D<sup>\*</sup>, and this contributes to the dispersion in the measurements. On the other hand, recent results based on the study of S wave data indicate the existence of strong lateral variations in D<sup>\*</sup>, particularly in the vicinity of the two large low velocity "plumes" under the Pacific and Africa. By modifying an existing global tomographic model in a simple manner, which consists in saturating regions of low P velocity in D<sup>\*</sup> of amplitude larger than 0.8% to 2%, and adding patches of Ultra Low Velocity Zones (ULVZ) where they have been documented in studies by Garnero and collaborators, we show that we are able to explain most of the long wavelength trends as well as a large fraction of the dispersion in our global PKP(AB)-PKP(DF) dataset. In particular, our modified deep mantle model is able to explain the trend of travel time residuals with angle of the propagation path in the inner core with respect to the earth's rotation axis, without need for a contribution from inner core anisotropy. The uneven distribution of data, with most polar paths sampling D<sup>\*</sup> in the region of the giant plumes biases the observations, leading to an apparent trend with angle. We show that similar effects can explain the trends observed in PKP(BC)-PKP(DF) phases, and in particular are responsible for the different character of observations in the "western" and "eastern" hemisphere, as documented by Tanaka and Hamaguchi (1997). We therefore infer that inner core anisotropy may have been strongly overestimated, and that structure in D<sup>\*</sup> and the mantle is largely responsible for the travel time anomalies observed.

**JSS02/L/01****1720****COMPLEX STRUCTURES AT THE BASE OF THE MANTLE AS REVEALED BY SEISMIC PHASES SAMPLING THE DEEP MANTLE AND CORE**

Barbara Romanowicz, Ludovic BREGER and Hrvoje Tkalcic

A preferred interpretation of anomalous splitting of modes sensitive to core structure has been in terms of inner core anisotropy, providing a unified explanation of these data and observed trends in PKP waves, which travel faster on polar than on equatorial paths. We reexamine this interpretation, as well as alternative ones, in the light of our recent results which indicate that simple, smooth models of inner core anisotropy that might account for normal mode splitting are in contradiction with some PKP observations. By inverting a dataset comprising modes that are sensitive only to the mantle and outermost core as well as modes sensitive to both mantle, outer core and inner core structure, we show that (1) inner core anisotropy improves the overall fit to data compared to a model with aspherical structure restricted to the mantle; (2) when mode 3S<sub>2</sub> is excluded from the dataset, simple models with heterogeneity in the outer core fit the data consistently better than simple inner core anisotropy models; (3) when mode 3S<sub>2</sub> is included, overall residual variances are smallest for inner core anisotropy models. However, the splitting of 3S<sub>2</sub> is fit at the expense of that of the 5S mantle mode branch, sensitive to P-velocity in the mantle. (4) outer core models are more stable and consistent with each other than inner core models, when different subsets of core modes are inverted (i.e. modes with small versus large sensitivity in the inner core). (5) Lateral heterogeneity in the mantle alone (in particular D<sup>\*</sup>) cannot consistently account for the splitting of all modes. Simple anisotropic models of the inner core are therefore not sufficient to simultaneously explain the splitting of spheroidal mantle and core modes, and a combination of deep mantle and outer

core structure contributes significantly to the pattern of splitting. A possible model which could explain most of the core data could comprise a zone of low density material confined to the tangent Taylor cylinder in the outer core. On the other hand, preliminary tests indicate that 3S2 is particularly sensitive to shear in the outer core. We conjecture that a small amount of shear in a stagnant layer at the top of the outer core could help reconcile the splitting observations for 3S2 and other core and mantle modes

JSS02/E/14-A1

1740

#### IN SITU X-RAY OBSERVATIONS OF PHASE TRANSFORMATIONS IN MANTLE MINERALS AND ROCKS AT THE NEW SYNCHROTRON RADIATION FACILITY, SPRING-8

TETSUO IRIFUNE, Toru Inoue, Nobumasa Nishiyama, Koji Kuroda (Department of Earth Sciences, Ehime University, Matsuyama 790-8577, Japan, Email: irifune@dpc.ehime-u.ac.jp), Ken-ichi Funakoshi (Japan Synchrotron Radiation Research Institute, Kamigori 679-5198, Japan), Wataru Utsumi (Japan Atomic Energy Research Institute, Kamigori 679-5198, Japan)

Observations of phase transformations in olivine ( $Mg_2SiO_4$ ), pyroxenes ( $MgSiO_3$  and  $Mg_0.5Ca_0.5SiO_3$ ) and a pyrolyte composition have been successfully made at pressures to 25 GPa and temperatures to 2300K, using a combination of the newly constructed 1500 ton multianvil apparatus (SPEED-1500) and the third-generation large synchrotron radiation source (Spring-8). Precise determination of the phase boundaries of spinel to postspinel in  $Mg_2SiO_4$  and ilmenite to perovskite in  $MgSiO_3$  yielded Clapeyron slopes consistent with those of quench experiments (Ito and Takahashi, 1989), while there was significant discrepancy in the transformation pressures between these two studies.

The decomposition of  $Mg_0.5Ca_0.5SiO_3$  diopside and glass into  $MgSiO_3$  orthorhombic and  $CaSiO_3$  cubic perovskites was confirmed by the same technique, which is in contrast to some earlier results using quench technique. Further, the phase transformations in a pyrolyte composition were observed in a pressure range 20 - 25 GPa and at a temperature of 1873K, conditions close to those of the 660 km seismic discontinuity.

The results were generally consistent with those of quench experiments (Irifune, 1994), but the transformation pressures were again lower by 2 GPa than these results. Some geophysical implications and technical problems are discussed on the basis of the present in situ X-ray

Tuesday 20 July AM

JSS02/W/16-A2

0930

#### PHASE TRANSITIONS AND MINERALOGICAL COMPOSITION OF THE EARTH'S MANTLE

Jan MATAS (1), Yanick Ricard (1), Francois Guyot (2), and Philippe Gillet (1) (1) Ecole Normale Supérieure de Lyon, 46, allée d'Italie, 69007 Lyon, France. (2) Institut de Physique du Globe, 4, place Jussieu, 75005 Paris, France.

Several major discontinuities have been identified in the Earth's mantle. They are hypothesised to result from phase transitions of mantle rocks. A precise knowledge of the properties of mantle rocks at various pressures and temperatures is requested for determining the mantle composition and for evaluating the effects of phase transitions on the global dynamics. We propose a self consistent method for computing the thermodynamic properties of various solids at high pressures and at high temperatures. A numerical code based on a free-energy minimisation at various temperatures and pressures is developed for computing the equilibrium mineralogical composition for a given bulk mantle composition. Phase diagrams of mantle solid solutions are proposed for the system  $MgO$ ,  $FeO$ ,  $CaO$ ,  $Al_2O_3$ , and  $SiO_2$ . Comparing computed and observed transitions checks the thermodynamic models of mantle minerals. Several models of bulk mantle compositions, such as pyrolyte or piclogite, are considered. Various thermochemical and thermoelastic properties of the mantle are then obtained as a function of depth.

The mantle minerals are present in solid solutions and, thus, the phase transitions are not univariant. Our code allows us to compute corresponding thickness of major phase transitions. The decomposition of garnets into silicate perovskites and magnesiowüstite at the depth of 660 km, induces a thick discontinuity by about 40 km. Using the free-energy minimisation method, we compute adiabatic temperature profiles, which leaves mantle entropy constant with depth. Corresponding adiabatic density, bulk modulus and bulk sound velocity are deduced and compared to those deduced from seismological studies. Effect of latent heat of different phase transitions on the temperature profile, i.e. Verhoogen effect, is discussed in details. The temperature increases by about 50 K at the depth of 410 km due to the transition of olivine to wadsleyite. On the other hand, the decomposition of ringwoodite into silicate perovskite and magnesiowüstite at the depth of 660 km results in a temperature decrease by about 70 K.

JSS02/W/03-A2

1000

#### JOINT SEISMIC TOMOGRAPHY FOR P AND S VELOCITIES: CHEMICAL ANOMALIES IN THE LOWER MANTLE

G. MASTERS, H. Bolton, and Gabi Laske (IGPP, Scripps Inst. of Oceanography, U.C. San Diego SIO-0225, La Jolla, CA 92093; ph. 619-534-4122; e-mail: gmasters@ucsd.edu)

Over the past 15 years, we have accumulated large data sets of hand-picked long-period absolute and differential travel times, surface wave phase and polarisation, and free oscillation structure coefficients. These data have been inverted in a variety of ways for 3D structure in the mantle with our current modelling focussing on joint inversions of shear and bulk sound speed using models parameterised with 5 degree blocks. The resulting models are robust and are relatively independent of inversion technique provided that enough data of different types are included. The lower mantle of these (and almost all recent) models are characterised by slab-like fast regions surrounding broad regions of slow material with a strong increase in the amplitude of heterogeneity towards the base of the mantle with a particularly large increase in the amplitude of slow anomalies in S velocity. The bulk sound speed tends to be positively correlated with the shear velocity in the upper mantle but becomes increasingly negatively correlated as one descends through the lower mantle. This is largely due to the fact that the amplitudes of the broad slow P anomalies do not generally increase as rapidly as the amplitudes of the slow S anomalies. Our results admit the following general conclusions. The properties of the fast slab-like anomalies in the lower mantle are consistent with a thermal origin while the broad slow anomalies are at least partially chemical in origin or are associated with near-melting behaviour of some of their components. The near-melting explanation is less likely as there is no compelling evidence for low Q regions in the lower mantle, which would most likely accompany a region of partial, melt. We therefore speculate that the broad slow regions correspond to upwelling which is entraining chemical heterogeneity from the core-mantle boundary region. We also note that there is little evidence for a strong internal boundary layer separating the lower and upper mantle though we do observe some weak decorrelation of structure in this region.

JSS02/E/09-A2

1030

#### A GEODYNAMICALLY SELF-CONSISTENT MANTLE VISCOSITY PROFILE

J.X MITROVICA (Department of Physics, University of Toronto, Toronto, Canada, M5S 1A7, 416-978-4946, email: jxm@physics.utoronto.ca) A.M Forte (Institut de Physique du Globe de Paris, Dept. de Sismologie, 4 Place Jussieu, Paris 6, 75252 France) Karin Wiczerkowski (University of Muenster, Institute of Planetology, Wilhelm-Klemm-Strasse 10, Muenster D-48149, Germany)

One of the important outstanding issues in mantle rheology is the apparent disagreement between the radial viscosity profiles inferred on the basis of observables associated with mantle convection and glacial isostatic adjustment (GIA). We report here on ongoing efforts to address this issue using inverse procedures applied simultaneously to these two data sets. The GIA data set we employ includes post-glacial relative sea level variations at a globally distributed network of sites as well as a newly derived relaxation time spectrum for Fennoscandia. The convection observables include long-wavelength free-air gravity harmonics and plate motions. The inversions also incorporate geodetic constraints on CMB topography and a wide range of seismic data. We conclude that the discrepancy noted above is an artifact of model parameterisations used in previous studies; these parameterisations have not taken into account the unique revolving power of the two data sets. We find that a simultaneous reconciliation of the GIA and convection data sets (to a level similar to those obtained from independent inversions of the data types) is possible using multi-layer models characterized by a significant increase (1-2 orders of magnitude), with depth, in the mantle. Furthermore, we will present results based on regional subsets of the GIA data which indicate to what extent lateral heterogeneities in rheology need to be invoked to reconcile the totality of the GIA data set.

JSS02/W/12-A2

1115

#### PHASE TRANSFORMATIONS: IMPLICATIONS FOR MANTLE STRUCTURE

Donald J. WEIDNER (CHIPR and Dept. of Geosciences, State University of New York, Stony Brook, NY 11794, Email:dweidner@sunysb.edu) and Yanbin Wang (Consortium for Advanced Radiation Sources, The University of Chicago)

The role of phase transformations on radial and lateral velocity and density variations in the Earth's mantle is examined. Pyrolyte is taken as a reference chemical composition. Specific attention is given to the chemical interaction among the multiple components in the entire system. In particular, aluminum influences the width and depth of the 410-km discontinuity. The velocities and density at the 410-km discontinuity are rather insensitive to lateral variations of the temperature aside from the change in the depth of the discontinuity. Formation of  $CaSiO_3$  perovskite may be an important contributor to the 520-km discontinuity. Aluminum also plays a major role in defining the character of the 660-km discontinuity. Slight variations in Al content or temperature from the reference model changes the magnitude of the 660 velocity increase by a factor of two. Ilmenite forming phase transitions will introduce lateral velocity variations resulting from lowered temperatures that can be mistaken as a slab sitting on the 660-km discontinuity. These many different implications result from considering the whole chemical system.

JSS02/E/07-A2

1145

#### EFFECTS OF PHASE TRANSFORMATIONS ON LATERAL AND RADIAL VARIATION IN MANTLE RHEOLOGY

Shun-ichiro KARATO (University of Minnesota, Department of Geology and Geophysics, Minneapolis, MN 55455, U.S.A., Email: karato@tc.umn.edu)

Phase transformations are among the most important factors that may affect rheological properties of deep mantle thereby control the style of mantle convection. Phase transformations in a descending slab may cause rheological anomalies that may influence its fate upon subduction and could lead to deep earthquakes. Phase transformations in other general areas may cause global rheological layering that may affect the style of mantle convection. Using laboratory data and theoretical models, I will discuss some of the important issues on this topic. The most important is the development in high pressure, high temperature deformation technique which allows us to directly investigate the role of phase transformations on rheology. Such a technique allows us to investigate rheological properties at least up to 16 GPa and 2000 K. We now have direct experimental data on the effects of olivine-ringwoodite, olivine-wadsleyite transformations on rheology under the transition zone conditions. These studies show dramatic weakening associated with grain-size reduction, but both experimental and theoretical modelling show that such effects are sensitive to the temperature at which a phase transformation occurs. Combining these laboratory data with theoretical models of grain-size evolution associated with a phase transformation, we construct a model for rheological structure of subducted slabs. The model predicts that cold slabs are weaker than moderately warm ones and consequently the 660-km discontinuity will work as a rheological filter for convection current. The model also suggests a complicated rheological structure characterised by high energy dissipation in a wide (~40-50km) regions in a deep slab, providing a possible explanation for wide fault widths for deep earthquakes. Mineral physics basis for a possible weak layer in the deep mantle will also be discussed. "Transformational plasticity" (enhanced plasticity due to large internal stress/strain) and weakening due to grain-size reduction are shown to be difficult to cause global weak layer because these mechanisms work only at relatively low temperatures.

JSS02/W/06-A2

1215

#### SEISMOLOGICAL CONSTRAINTS ON UPPER MANTLE ANISOTROPY

Jean-Paul MONTAGNER, Laurent Guillot (all in Dept. Seismology, Institut de Physique du Globe, 4 Place Jussieu, 75252 Paris cedex 05, France, jpm@ipgp.jussieu.fr), Philippe Gillet and Daphne-Anne Griot (both at Laboratoire de Sciences de la Terre, ENS-Lyon, 46 Allée d'Italie, 69364 - Lyon cedex 07, France)

Mantle mineralogy and its different phase constituents are relatively well known. But the proportion of the different minerals and their lateral heterogeneities is still subject to debate. Isotropic velocity  $V_p$  and  $V_s$  alone, do not enable to separate temperature and chemical heterogeneities, but the joint use of  $V_p$ ,  $V_s$  velocities and anisotropic parameters enable to undertake such an investigation. First of all, we updated the elastic tensors of the competing petrological models (pyrolyte and piclogite). By considering a simple model of convection and by assuming some mechanisms of alignment of minerals, we show how to calculate the corresponding seismic observables, travel times of body waves and surface waves dispersion curves. It is demonstrated that seismic observations should enable to discriminate between different etiological models. A preliminary application to actual data will be presented.

Monday 19 July AM

JSS02/W/05-A1

Poster

0830-01

#### PERIDOTITE XENOLITHS FROM PLIOCENE BASANITE OF THE DZHILINDA RIVER



**(VITIM VOLCANIC FIELD): STRATIFICATION OF UPPER MANTLE AND CRYPTIC METASOMATISM**

Konstantin LITASOV, Yury Litasov, Vladimir Mal'kovets (Institute of Geology SB RAS, Koptuyga ave., 3, 630090 Novosibirsk, Russia, email: kostik@uigm.nsc.ru) Alexey Mekhonoshin (Institute of Geochemistry SB RAS, Favorsky st., 1a, 664033, Irkutsk, Russia, email: mekhonos@igc.irk.ru)

The abundant mantle xenoliths were found in Pliocene basanites of the Dzhlinda River (Vitim volcanic field). Two main and one detached peridotite groups were recognized: (1) spinel and garnet-spinel lherzolites with coarse-grained protogranular texture (two pyroxene temperature  $T=1060-1210^{\circ}\text{C}$ , Brey, Kohler, 1990); (2) spinel peridotites with various textures from protogranular to tabular equigranular ( $T=790-910^{\circ}\text{C}$ ); (3) mosaic equigranular lherzolite ( $T=710-750^{\circ}\text{C}$ ).

Trace element data were obtained by ion microprobe for 13 clinopyroxenes from different peridotite groups. Group 1 clinopyroxene shows HREE depletion due to a garnet control, Ba, Th, Nb depletion and Be, Zr, Ti negative anomaly. Group 2 clinopyroxene contains higher amounts of HREE and similar depletion and anomaly as in the group 1 for other elements. Both the groups also contain clinopyroxene moderately enriched in LREE. Texturally, it corresponds to deformed varieties of the group 1 and tabular equigranular varieties of the group 2. The group 3 clinopyroxene shows depleted patterns with positive Nb, Be, Ti anomalies and light negative Zr anomaly, suggesting rare HFSE cryptic metasomatism. Peridotite xenoliths of the Dzhlinda River are representatives of temperature-stratified mantle column with different degree signs of cryptic metasomatism caused by melt percolation. Our data for cpx may partly characterise metasomatizing agents. The first one causes light enrichment of peridotite in LREE. The second agent probably is a specific depleted HFSE- and Zn-bearing melt/fluid.

**JSS02/W/09-A1 Poster 0830-02****GEOCHEMISTRY OF LOWER CRUSTAL XENOLITHS FROM ALKALINE BASALTS, VITIM VOLCANIC FIELD, SIBERIA**

Konstantin LITASOV (Institute of Geology SB RAS, Koptuyga ave., 3, 630090 Novosibirsk, Russia, email: kostik@uigm.nsc.ru)

Among the lower crust-uppermost mantle xenoliths in Late Cenozoic alkaline basalts of the Vitim volcanic field (VF), three groups are recognised: (1) garnet granulites; (2) garnet-bearing clinopyroxenites and gabbro; (3) spinel websterites. T-P data evidence for the presence of intrusive bodies, lenses and veins of cumulate rocks at the depth 35-45 km in the lower crust along the Moho, which are underlay by spinel lherzolites. Calculated temperatures of cumulate formation range from 800 to 1200°C. Most of xenoliths have metamagmatic cumulative microstructure and their formation is corresponded to underplating of mantle melts.

Electron and ion microprobe study of clinopyroxene suggest that garnet clinopyroxenite and gabbro of group 2 correspond to most differentiated cpx-megacrysts ( $\text{Al}_2\text{O}_3=9-9.6$  and  $8-8.5\%$ ,  $\text{TiO}_2=1.5-1.8$  and  $1.6-1.8\%$ ,  $(\text{La}/\text{Yb})_n=9-16$  and  $5-6$  ppm,  $\text{Cr}=71-420$  and  $55-380$  ppm correspondingly). Spinel websterite of group 3 correspond to CrDi-pyroxenite (same  $\text{Al}_2\text{O}_3=5-7\%$  and  $\text{TiO}_2=0.3-0.7\%$ ,  $(\text{La}/\text{Yb})_n=0.7-1.6$  and  $0.3-2$ ,  $\text{Cr}=600-1200$  and  $1800-4000$  ppm). Garnet granulite of group 1 has intermediate characteristics but tend to Cr-rich group.

Using geochemical data we suppose that the formation of lower crustal rocks composing xenoliths of the VF is connected with following processes: (a) crystallization of last stage basaltic residue melts after megacryst series formation comagmatic to the host basaltic rocks (group 2); and (2) crystallization of melts comagmatic to the green series pyroxenites (group 3). The formation of garnet granulites of group 1 may be connected with both processes.

**JSS02/E/01-A1 Poster 0830-03****MONITORING OF SURFACE TILTS AND EFFECTIVE VISCOUS OF FAULTS ZONE**

Vladimir Timofeev (Institute of Geophysics UIGGM SB RAS, Pr.Koptuyg 3, 630090, Novosibirsk, Russia, email: sari@uigm.nsc.ru) Bernard DUCARME (Observatoire Royal de Belgique, Avenue Circulaire 3, 1180, Bruxelles, Belgium, email: B.Ducarme@oma.be)

Results of the monitoring of Baikal rift surface tilts (1985-1998) are discussed. Measurements with quartz tiltmeters were into 90-metres old underground gallery built in Archean marble rocks. The analysis of 13-years meridian's direction tilt and the seismological stress analysis are presented for Talaya station ( $51.68\text{ N}$ ,  $103.65\text{ E}$ ). Viscous Voigt-Kelvin model are used for the interpretation of tilt's data with north-south stress equal zero for post 1989 year's period. This result was used for effective viscous term determination for fault zone. The determination was made by attenuation tilt curve or by time delay curve at the period when the stress was equal zero. We determined the time delay term  $T=6$  years and the effective viscous term  $3 \times 10^{18}$  Paxis for main Sayan fault zone. The additional tectonic stress was determined from monitoring data. The tectonic stress was near 2 MPa.

**JSS02/E/02-A1 Poster 0830-04****INNER CORE'S SEISMIC VELOCITY ANISOTROPY IS CAUSED BY ITS ROTATION**

Bin LIU, Qunshan Zhang, Rongshan Fu (Dept. of Earth and Space Sci., Uni. of Sci. and Tech. of China, Hefei 230026, P. R. China)

The earth's inner core has a differential rotation relative to the outer earth with an angular velocity of about 3% faster. The relative linear velocity between solid inner core and molten outer core is the biggest at equator and zero at pole areas. According to the theory on crystal growth, when crystallising from molten, the crystal growth speed is proportional to the relative linear speed between solid and molten crystal. So when solid inner core grows in molten outer core, it grows faster at equator than at polar areas. Since the inner core is at a high pressure and high temperature condition, it shows intense plasticity in geological timescale. Under gravitational force the inner core remains quasi-orbicular, with a substance flow from the fast growing equator part to polar areas, forming an axisymmetric rheologic field. The accompanying axial symmetric stress field makes c-axes of hcp iron composing the solid inner core align with inner core's rotating axis, resulting in the observed seismic anisotropy in the inner core. The symmetric axis of the seismic anisotropy should coincide with the inner core's rotating axis. If it is true, as a deduction, the differential rotation observed by Song et al. (1996) and Su et al. (1996) is not really the rotation of the inner core relative to the outer earth and should be the precession of the inner core's rotating axis relative to the outer earth. Su et al. (1996) found that the angle between the inner core's symmetric axis of seismic anisotropy and the axis of the earth has an undulation with a period of about 8.39 years. This may be the nutation of the inner core's rotating axis accompanying the precession. Since the molten outer core is liquid with coefficient of kinematic viscosity can be as low as  $3 \times 10^{11} \text{ (7) m}^2 \text{ s}^{-1}$  -  $2 \times 10^{11} \text{ (5) m}^2 \text{ s}^{-1}$ , it is quite possible for the inner core to move almost freely inside the earth.

**JSS02/E/03-A1 Poster 0830-05****ALKALINE CARBONATE - SILICATE REACTIONS AT THE MANTLE - PLUME INTERFACE IN EXPERIMENTS UP TO 10 GPa: NEW MINERALS, LIQUID IMMISCIBILITY, DIAMOND - PRODUCING MELTS**

Yuriy LITVIN (Institute of Experimental Mineralogy, RAS, Chernogolovka, Moscow District - 142432, Russia, email: litvin@iem.ac.ru)

For simulating an interaction of alkaline - fluid agents of active plumes with the mantle wallrocks, the system  $\text{Mg}_2\text{SiO}_4$  (forsterite) -  $\text{K}_2\text{CO}_3$  -  $\text{Na}_2\text{CO}_3$  -  $\text{K}_2\text{SiO}_3$  was chosen. Melting relations of the system were experimentally studied at 4 GPa, 1100 - 1600°C at the forsterite -  $\text{K}_2\text{CO}_3$  -  $\text{K}_2\text{SiO}_3$  and forsterite -  $\text{Na}_2\text{CO}_3$  -  $\text{K}_2\text{SiO}_3$  joins. Essential distinction in chemical behaviour of K - and Na - carbonate agents, a responsibility of K - components for the processes of carbonation of the lithosphere and effects of carbonate - silicate liquid immiscibility which as discussed (Wyllie, 1996) are important in mantle petrology, the formation of plausible mantle minerals, such as  $\text{Ma}_2\text{MgSiO}_4$  silicate and  $\text{K}_2\text{Mg}(\text{CO}_3)_2$  carbonate (melt of the latter is effective for diamond growth) were revealed. The patterns of the mantle - plume interaction must be supplemented with the formation at 4 - 7 GPa and higher pressures of  $\text{Ma}_2\text{Mg}_2\text{Si}_2\text{O}_7$  phase (plausible mineral) together with pyropic garnet ( $\text{Mg}_2\text{Al}_2\text{Si}_3\text{O}_{12}$ ) and enstatite on the  $\text{Mg}_2\text{SiO}_4$  (forsterite) -  $\text{NaAlSi}_2\text{O}_6$  (jadeite) join (Gasparik, Litvin, 1997), and the peritectic reaction  $\text{Mg}_2\text{SiO}_4$  (forsterite) + alkaline melt =  $\text{Na}_2\text{Mg}_2\text{Si}_2\text{O}_7$  phase found in experiments on the  $\text{MgSiO}_3$  (enstatite) -  $\text{NaAlSiO}_4$  (nepheline) pseudo binary join (Litvin et al., in the press). Growth of diamond both spontaneous and seeded was discovered in experiments at 8 - 10 GPa in the  $\text{Na}_2\text{Mg}(\text{CO}_3)_2$  -  $\text{K}_2\text{Mg}(\text{CO}_3)_2$  - C system (Litvin et al., 1998) formation of which is realistic for the mantle - plume interface of the deep Earth's hot spots. The experimental data reported are applicable to the problem of primary stages of genesis of intraplate alkaline rock series and characterisation of the lithosphere - asthenosphere boundary.

**JSS02/E/04-A1 Poster 0830-06****INVERSION OF THE VISCOSITY STRUCTURE OF THE MANTLE**

Shaoxian ZANG and G. C. Chen (both at Department of Geophysics, Peking University, Beijing 100871, China, email: sxzang@ibmstone.pku.edu.cn)

Seismic tomographic results provided 3-D velocity structure of the mantle. How to use the seismic tomographic results to study the viscosity structure of the mantle has attracted big attention from geoscientists. In this paper the viscosity structure of the mantle was studied using the geoid anomaly and seismic tomographic data.

Firstly, the viscosity structures of eleven-homogeneous-layered mantle were studied. The density distributions for eleven homogeneous layers of mantle were obtained using the seismic tomographic results: MDLSH model (Tanimoto, 1990) and SH425.2 model (Su and Dziewonski, 1991). The viscosity distributions of eleven layers were obtained using geoid anomaly by genetic algorithm. The results for the two seismic models are basically coincident with each other. Secondly, for utilizing the 3-D seismic tomographic data, we divided the mantle into two parts according to the seismic tomographic data: Pacific area, where the velocity anomaly is negative and normal area, which excepts Pacific. Then density and the viscosity distribution of eleven layers for the two areas were obtained respectively by same data and algorithm as the first step. The result shows that the viscosity in the Pacific area is generally lower than another area. Finally, the result were discussed and pointed out some studies should be done such as seeking more accurate relation between velocity and density in the Earth's interior and more constrains on the viscosity structure.

**JSS02/E/08-A1 Poster 0830-07****PHYSICAL AND MINERALOGICAL MODELS OF THE MANTLE**

V. PANKOV, A. Kalachnikov and A. Babeyko (all at United Institute of Physics of the Earth, Russian Academy of Sciences, B. Gruzinskaya 10, Moscow, 123810 Russia, email: Pankov@uipe-ras.scgis.ru)

Based on experimental P-V data or evidence on bulk modulus and its pressure derivative, the method of potentials (Zharkov and Kalinin, 1971) is applied to the determination of equation of state (EOS) for a set of phases in the  $\text{MgO-FeO-SiO}_2$  system. The complete phase diagram is calculated by using the algorithm of Capitano and Brown (1987). Concentrations of phases and components in the mantle are estimated from its seismic and thermal models using the derived EOS' and phase stability fields. Depth distributions of various thermodynamic characteristics are calculated for the inferred compositional models. In certain cases, this approach allows estimation of the depth distribution of convective temperature gradient. Possible decomposition of perovskite to oxides at the mantle base and geodynamic consequences of the inferred models are discussed.

**JSS02/E/11-A1 Poster 0830-08****ELASTICITY AND ITS TEMPERATURE VARIATION OF MODIFIED SPINEL MEASURED AT AMBIENT CONDITION**

Isao SUZUKI, Norihito Mayama, Kousuke Shono, (Department of Earth Sciences, Okayama University, Okayama 700-8530, Japan, E-mail: isuzuki@cc.okayama-u.ac.jp) and Tomoo Katsura, Akira Yoneda (Institute for Study of the Earth's Interior, Misasa, Tottori 682-0193, Japan, E-mail: tkatsura@msewsl.misasa.okayama-u.ac.jp; yoneda@misasa.okayama-u.ac.jp)

The elasticity data of minerals such as olivine, modified spinel and spinel phases have basic importance to study the composition of the Earth's mantle. Here modified spinel with natural olivine components was synthesised at high pressure. The polycrystalline specimen was shaped into a sphere and elasticity was measured with the resonant sphere technique, RST. Temperature variations of frequencies of lower eight oscillatory modes were traced between 5 and 45 deg. C. Bulk and rigidity moduli change smoothly with temperature. The Anderson Gruneisen parameters have magnitudes of 4.6, 4 and 6.77, respectively for adiabatic and isothermal conditions. These values are compared with those of mantle candidate minerals. For example, the high temperature phase (>700 deg.C) of spinel  $\text{MgAl}_2\text{O}_4$  shows similar magnitudes of the parameters, 4.72 and 6.37, respectively.

**JSS02/E/13-A1 Poster 0830-09****INNER CORE ROTATION FROM GEOMAGNETIC ESTWARD DRIFT AND A STATIONARY SPHERICAL VORTEX IN EARTH'S CORE**

C. V. VOORHIES (Geodynamics Branch, Code 921, NASA's Goddard Space Flight Center, Greenbelt, MD 20771 USA; email: voorhies@geomag.gsfc.nasa.gov)

The idea that geomagnetic westward drift indicates convective levelling of the planetary momentum gradient within Earth's core is pursued in search of a differentially rotating mean state, upon which various oscillations and secular effects might be superimposed. The desired

## INTER-ASSOCIATION

state conforms to roughly spherical boundary conditions, minimises dissipative interference with convective cooling in the bulk of the core, yet may aid core cooling by depositing heat in the uppermost core and lower mantle. The variational calculus of stationary dissipation applied to a spherical vortex within the core yields an interesting differential rotation profile akin to spherical Couette flow bounded by thin Hartmann layers. Four boundary conditions are required. To concentrate shear induced dissipation near the core-mantle boundary, these are taken to be: (i) no-slip at the core-mantle interface; (ii) geomagnetically estimated bulk westward flow at the base of the core-mantle boundary layer; (iii) no-slip at the inner-outer core interface; and, to describe magnetic locking of the inner core to the deep outer core, (iv) hydrodynamically stress-free at the inner-outer core boundary. By boldly assuming the axial core angular momentum anomaly to be zero, the super-rotation of the inner core is calculated to be at most 1.5 degrees per year.

**JSS02/E/17-A1** Poster **0830-10**

**LOW-RESISTIVITY STRUCTURES AS CONVERTERS OF SEISMIC WAVES' ENERGY INTO ELECTROMAGNETIC SIGNALS.**

OLEG NOVIK (Moscow State Geol. Prospect. Acad., 117246, POB 51, Russia. email: onovik@glasnet.ru) Sergey Ershov (Keldysh Institute for Appl. Mathematics of Russian Academy of Sciences, Moscow) Irina Mikhaylovskaya (Moscow State University, email: irina@nw.math.msu.ru).

Trying to clear out the physical nature of electromagnetic (em) and temperature (t) signals observed in seismically active regions (some of them occurred to be precursors to earthquakes), we use the theory of magnetoelastocity to construct the mathematical model and calculate the elastic-em-t field interaction caused by displacements (ampl. freq. and duration are of order of a few cm, Hz and sec resp.) in the upper mantle domain of a model lithosphere zone containing the low-resistivity structures (LRS) in this domain and in the crust. According to MT-soundings in seismic regions, the LRSs' conductivity is 0.1 to 0.5 S/m and cross-section sizes and depths are of order of 10 km or more. It is clear from the computed pictures of the evolution of the interacting fields that em-signals arise near the contacts of the seismic waves' (s.w., from upper mantle in our runs) fronts with the boundaries of LRSs, as a result of their deformations in presence of geomagnetic field. The em-emission into atmosphere arises during the diffraction of s. w. by LRSs (60 pT at the Earth's surface and 10 pT at the height of 30 km). The t-signal (up to 0.02 K in the sedimentary layer) propagates together with the s.w. and is not influenced by ionosphere. The main frequencies of the computed em and t-signals (ULF field oscillations) are nearly the same as ones of displacements and are changing, together with the amplitudes, because of changing of displacements at the depth. The computed em and t-signals' amplitudes, frequencies, the delay of the seismic wave arrival at the surface in regard to em-signal and its delay in regard to beginning of displacements are of orders observed.

**JSS02/W/17-A1** Poster **0830-11**

**EVIDENCE FOR METASOMATISM OF THE TRANSITION ZONE BY CARBONATE MELTS ORIGINATING IN THE LOWER MANTLE**

Tibor Gasparik (CHiPR and Department of Geosciences, State University of New York, Stony Brook, NY 11794, USA, email: gasparik@sbmp04.ess.sunysb.edu)

Since the origin of some inclusions in diamonds can be traced to the lower mantle, the source of the kimberlitic melts carrying them to the surface should also be in the lower mantle. To test this hypothesis, experiments were conducted at 20-23 GPa and 1600-1700°C with simplified analog mantle compositions including carbonates. The experimental products contained small amounts of carbonate melt, suggesting that the temperatures in the transition zone (410-660 km) should be high enough to exceed the carbonate solidus. Starting material with a high content of MgSiO<sub>3</sub> and low concentrations of Na, K, Ca, Fe and Al produced mostly garnet at 22 GPa, but mostly MgSiO<sub>3</sub> perovskite and no garnet at 23 GPa. The main difference in the composition of the carbonate melts was in the sodium content, which was low at 22 GPa but high at 23 GPa. This is the well-known consequence of sodium being highly incompatible in perovskite but highly compatible in majorite garnet. Thus, the sodium-rich carbonate melts originating in the lower mantle do not have the kimberlite composition but could become kimberlitic on passing through the transition zone by losing sodium to majorite garnet. The resulting metasomatism taking place over a long period of time could modify the transition zone to sodium enriched compositions consistent with the compositions of inclusions in diamonds from the transition zone. For example, the origin of the NaPx-En garnet inclusion found by Wang and Sueno (Min. J. 18, 9, 1996), with the approximate composition 16 mol % Na<sub>2</sub>MgSi<sub>5</sub>O<sub>12</sub> and 84 % Mg<sub>4</sub>Si<sub>4</sub>O<sub>12</sub>, was experimentally constrained to the pressure range of 16-22 GPa. The type III inclusions reported by Hutchison (Ph.D. Thesis, 1997) have the composition of garnet coexisting with CaSiO<sub>3</sub> perovskite at 22 GPa (En40Di20Jd40).

**JSS02/L/02-A1** Poster **0830-12**

**DO MANTLE PLUMES CONTRIBUTE TO THE ORIGIN OF LIFE AND QUANTUM JUMPS IN THE EVOLUTION?**

U. RAVAL

Some plumes originate from deep interior e.g. D" layer. Since earth's core is relatively rich in Fe, Ni & S, their local concentrations may indicate plume activity. The thermo-chemical conditions - following magmatic upwelling consisting of pressured gas beneath ocean - could transform the prebiotic aminoacids into peptides. Some minerals in volcanic vents (pyrite etc.) can act as catalyst for production of ammonia from nitrogen. Association of plume and life processes is supported by: a) the taxa of the cellularly preserved filamentous microbes is found in Apex basalts from W. Australia and b) Stromatolites in Pilbara region occur in cherts of Warrawoona group. Other similar areas may be Onverwacht group (S. Africa), Garbenschieft (Greenland) and other LIPs. This suggests a significant role of plumes in the thermophilic origin of life.

Other significant correlations are i) plume event (2.7 Ga) which is characterised by suboxic and intense hydrothermal activity, highly sulphurous carbonaceous sediments (BIFs) and bacterial remains, ii) Stromatolite peak at ~1.2 Ga and iii) Pan-African thermal event at the PreCambrian-Cambrian boundary. Further, a strong association is evidenced between major biodiversifications and LIPs. These spatio-temporal correlations between plumes and fillips in the evolution deserve detailed follow ups.

**JSM03**

**Monday 19 July**

**ELECTRICAL DISCHARGES IN THE MIDDLE & LOWER ATMOSPHERE (IAMAS, IAGA)**

Location: Chemical Engineering G35 LT  
Location of Posters: Old Gym

**Monday 19 July AM**

Presiding Chair: R.A.Goldberg (NASA/GODDARD, Greenbelt, MD, USA)

**JSM03/L/01-A1**

**0900**

**EXPECTED TIME-VARIATIONS OF NEUTRON MONITOR COUNTING RATE CAUSED BY COSMIC RAY PARTICLE ENERGY CHANGE IN THE PERIODS BEFORE AND DURING THUNDERSTORMS**

LEV DORMAN (IZMIRAN, Technion and Israel Cosmic Ray Center, affiliated to Tel Aviv University; Current address: P.O.Box 2217, Qazrin 12900, ISRAEL; email: lid@physics.technion.ac.il); Irina Dorman (Institute of History of Science and Technology, Russian Academy of Science, Staropansky 1/5, Moscow 103012, RUSSIA); N. Iucci and M. Parisi (Terza Università di Roma, Dipartimento di Fisica "E. Amaldi", Via della Vasca Navale 84, 00146 Rome, Italy); G. Villoresi (IFI/CNR-Frascati c/o Terza Università di Roma, Dipartimento di Fisica "E. Amaldi", Via della Vasca Navale 84, 00146 Rome, Italy)

On the basis of theoretical model (Dorman and Dorman, 1995, 1999) of atmospheric electric field effect in the neutron monitor counting rate, we calculate the expected cosmic ray time variations in the periods before and during thunderstorms. According to Wallace and Hobbs (1977) the charge of clouds on the altitude 7-12 km can reach the value about +24 coulombs, and on lower altitudes about -20 coulombs. The rate of charge generation is about one (coulomb/cub.km)/min. Our calculations show that neutron monitors one minute data can be used to obtain important information on atmospheric electric field space-time distribution.

**JSM03/L/02-A1**

**0920**

**ON THE POSSIBILITY OF ATMOSPHERIC ELECTRIC FIELD EFFECT IN THE COSMIC RAY NEUTRON COMPONENT**

LEV DORMAN (IZMIRAN, Technion and Israel Cosmic Ray Center, affiliated to Tel Aviv University; Current address: P.O.Box 2217, Qazrin 12900, ISRAEL; email: lid@physics.technion.ac.il); Irina Dorman (Institute of History of Science and Technology, Russian Academy of Science, Staropansky 1/5, Moscow 103012, RUSSIA)

It is well known that about 0.07 of neutron monitor counting rate caused by negative soft muons captured by lead nucleons and formed mesoatoms with generation of several MeV energy neutrons from lead. In this case the neutron monitor or neutron supermonitor works as analyzer which detects muons of only one, negative sign. It is very important because the atmospheric electric field effect have opposite signs for positive and negative muons that main part of this effect in the muon telescope or in ionization chamber is compensated and we can observe only small part of total effect for one sign muons. On the basis of our general theory of cosmic ray meteorological effects with taking into account of negative soft muon acceleration and deceleration in the Earth atmosphere (in dependence of direction and intensity of electric field) we discuss the possibility of existing this effect in cosmic ray neutron component and made some rough estimations.

**JSM03/E/02-A1**

**0940**

**AN OVERVIEW OF PROCESSES AFFECTING THE GLOBAL ELECTRIC CIRCUIT**

M.J. RYCROFT (International Space University, Boul. Gonther d'Andernach, 67400 Illkirch, France, e-mail: rycroft@isu.isu.net.edu)

A review is attempted of the important physical processes in the atmosphere (e.g. aerosols, C.T.R. Wilson's currents upwards from thunderstorms, point discharge currents, fair weather air-Earth currents, cloud-to-ground lightning discharges) and the magnetosphere (e.g. interhemispheric coupling, dynamo actions) which - by Ohm's law and Maxwell's laws - maintain the ionosphere at a potential ~ + 250 kV with respect to the Earth. The diurnal and seasonal variations of the global electric circuit, temporal variations of atmospheric conductivity associated with energetic charged particle precipitation and different solar-terrestrial physics phenomena (e.g. Forbush decreases, solar cycle), and spatial variations (e.g. with altitude, geomagnetic latitude, geographic longitude) are considered. A conceptual model of the global electric circuit in terms of electrical resistances in series and in parallel, in parallel with capacitors representing atmospheric layers - a scale height apart, is developed. Its value is tested against observations both ancient and modern. Some interesting and important areas for future research on variations of the global electric circuits are suggested, such as effects associated with sprites (positive cloud-to-ground discharges), cirrus clouds and long term climate changes.

**JSM03/E/03-A1**

**1010**

**LIGHTNING-INDUCED DISTURBANCES OF THE MIDDLE ATMOSPHERE**

Umran S. INAN (Space, Telecommunications and Radioscience Laboratory, Stanford University, Stanford, CA 94305, USA, tel 650-7234994, fax 650-7239251, email: inan@nova.stanford.edu)

Electrodynamic coupling between tropospheric thunderstorms and the middle atmosphere, dramatically evidenced in sprites and elves, is now believed to widely occur, supported by both large and relatively small thunderstorm complexes. While initial observations of these luminous phenomena appeared to suggest that they were only triggered by positive cloud-to-ground discharges in mesoscale convective systems, it is now known that sprites can on occasion be also triggered by negative discharges and that elves may in fact be triggered much more often than previously believed, by nearly all positive and negative lightning discharges having peak currents in excess of several tens of kiloamperes. Furthermore, radio remote sensing observations of the lower ionosphere suggest that the ambient electron population may be quiescently heated throughout the many hour duration of a typical thunderstorm. Successive triggering of elves by electromagnetic pulses radiated by lightning discharges may also be accompanied by accumulation of ionization changes, leading to the production of ionospheric "bubbles" above thunderstorm regions. In this paper, we review recent experimental and theoretical results, with an eye towards assessing global effects of thunderstorm driven electrodynamic coupling between upper atmospheric regions.



**JSM03/W/04-A1** 1100**VLF SPRITES**

Prof Richard DOWDEN (LFEM Research)

Sprites are luminous columns stretching from thundercloud top (sometimes) to the base of the ionosphere and are associated with cloud-ground lightning. Sprite columns are highly conducting and so scatter VLF communications transmissions propagating in the Earth-ionosphere waveguide. Such scattered waves, interfering with the direct waves, produce "VLF sprites" as phase and amplitude perturbations of the VLF transmission. The VLF scattering is in all directions, almost equally on average, though the scatter pattern for any individual sprite has many lobes and minima as expected for the lateral structure of the sprite (e.g., random array of columns). The decay of the scattered signal, due to the decay of the sprite plasma, is logarithmic not exponential. This is expected for a vertically extensive (~40 km) plasma because, although the plasma at any given altitude decays exponentially, the decay rate decreases exponentially with altitude with a scale height of about 3.5 km. In contrast, scattering from plasma produced by electron precipitation is in the forward direction and the scatter signal decays exponentially. This is as expected for a smoothly varying, laterally extensive plasma body (or depression of the ionospheric base) of little vertical extension. The above description and explanation of VLF sprites is not generally accepted and so will be justified here.

**JSM03/E/05-A1** 1130**CURRENT IDEAS ABOUT JETS**

A I SUKHORUKOV (Max-Planck-Institute for Aeronomie, D-37191 Katlenburg-Lindau, Germany, email: sukhorukov@linmpi.mpg.de)

Blue jets are the narrowly collimated, a few km wide beams of light propagated from the top of the thundercloud to the top stratosphere with velocity of about 100 km/s [Wescott et al., GRL, 22, 1209, 1995]. Several ideas have been proposed to explain this unusual phenomenon. Most of them suggest that the blue jet is a likely manifestation of the breakdown phenomenon in the stratosphere. Yet the observations are still scarce, and the nature of the blue jets is still not clear. In this talk, an assessment will be given of the present state of the blue jet theories.

**Monday 19 July PM**

Presiding Chair: TBA

**JSM03/L/03-A1** 1400**LIGHTNING CONTINUING CURRENTS AS A SOURCE OF SPORADIC MAGNETIC EVENTS IN THE ULF FREQUENCY RANGE AND EXCITER OF IONOSPHERIC ALFVEN RESONATOR**

P.P. BELYAEV, S.V. Isaev and M.N. Yakunin (Radiophysical Research Institute (NIRFI), B. Pecherskaya St., 25, N.Novgorod, 603 600, Russia, Email: belyaev@nirfi.sci-nnov.ru)

Among a lot of natural sporadic emissions observed on the quiet magnetic background which originates from worldwide thunderstorm activity, we can consider an electromagnetic radiation of local (10-100km) thunderstorm cell as an extremely intensive sporadic event also. In case, the observed magnetic field spectral density can also be expressed as  $B(f) = B^* f^{-2}$  at the frequencies  $f$  higher than 1-2 Hz. Usually, a lifetime of this enhancement of magnetic noises, accompanying cell, is varied from 0.5 to 1.5 hours. The nature of a phenomenon consists in an excitation of magnetic fields by well known continuing currents of lightning flashes. Multicomponent measurements (two induction magnetometers, vertical electric field sensor, pressure sensor) carried out at the middle latitudes allowed us to separate the electromagnetic, acoustic and seismic phenomena produced by visible lightning flashes and to make simplest estimations of current amplitudes ( $I = 50-150$  A) and duration (0.1-2 sec). In accordance with approximation  $I(t) = I_0 [\exp(-t/\tau_1) - \exp(-t/\tau_2)]$ , where  $\tau_1 = (0.1-2)$  sec,  $\tau_2 = (0.05-0.1)$  sec, the ULF induction like magnetic field spectrum of a single flash is described by equation  $H(f) = H_0 / [(1/\tau_1 - 2\pi i f)(1/\tau_2 - 2\pi i f)]$  and we obtain the observed frequency dependence of magnetic field. Not every flash is accompanied by measurable continuing current. Frequently, in cases of well-structured thunderstorm clouds but without visible cloud-to-ground lightnings and thunders, intensive electric pulses were detected only in absence of observable magnetic activity. For daytime conditions, with moving away or decay of thunderstorm both, magnetic and electric intensities decreases, saving a smooth spectral form described above. In contrary, for nighttime one, for distance thunderstorm when lightnings are behind the horizon, magnetic spectra (never vertical electric one) of flashes exhibit clear evident resonance structure, the same as observed before formation of cell.

**JSM03/W/03-A1** 1420**3-D SIMULATIONS OF ELVES AND SPRITES**

H.L. ROWLAND, R.F. Fernsler, and C.L. Siefring (Plasma Physics Division, Naval Research Lab, Washington, DC 20375 USA, email: rowland@nrl.ppd.navy.mil)

We present the first 3-D simulations of the formation of elves and sprites by lightning discharges. The code is a full-wave model using Maxwell's equations. The currents are calculated using Ohm's law. The ionization, attachment, electron collision rate, and optical emissions are calculated from swarm data.

The threshold for breakdown and the formation of elves by the EMP of the lightning return stroke is in good agreement with theory and earlier simulations ( $I_0 > 1e5$  kA/s, where  $f$  is the frequency of the EMP and  $I$  is the current). A cloud-to-cloud discharge because of reflections from the ionosphere can form a pair of tubes at the bottom of the D region parallel to the direction of the discharge.

The threshold for the initial formation of sprites depends upon the D region electron density but is approximately  $LQ > 300$  km-C (where  $L$  is the length of the discharge and  $Q$  is the charge moved by the lightning current). The sprite forms around 80 km altitude. Larger  $LQ$  extends the sprite to lower altitudes. The altitude of the bottom of the sprite depends upon the feedback between the 3-D focusing of the quasistatic field by the sprite, which then lets the sprite form at a lower altitude.

**JSM03/E/07-A1** 1450**THREE-DIMENSIONAL SIMULATION OF UPPER ATMOSPHERIC IONISATION ABOVE A HORIZONTAL LIGHTNING DISCHARGE**

Michael J. RYCROFT (International Space University, Boul. Gonthier d'Andermarch, 67400 Illkirch, France); Mengu Cho (Kyushu Institute of Technology, 1-1 Sensui Tobata-ku, Kitakyushu 804, Japan)

In an attempt to understand the spatial structure of sprites, the effects of a horizontal lightning discharge on the upper atmosphere have been studied by a three-dimensional computer

simulation. The lightning discharge is modeled by a combination of the vertical return stroke current and the horizontal discharge, which travels with a finite velocity ( $6 \times 10^7$  m/s). The electromagnetic wave radiated by the lightning current heats the upper atmosphere and ionises it at heights of 75 km and above. Interference between the electromagnetic waves radiated by the discharge current, those reflected by the ground, and those reflected by the ionosphere produce a non-uniform ionisation pattern at heights above 80 km even for a single line current source in the thundercloud. Non-uniform ionisation due to such interference occurs with a spatial scale of a few km when the electromagnetic waves have strong components from 5 to 50kHz.

**JSM03/E/01-A1** 1510**TESTS OF C.T.R. WILSON'S PREDICTIONS FOR SPRITES BASED ON SCHUMANN RESONANCE OBSERVATIONS OF VERTICAL CHARGE MOMENTS**

Earle WILLIAMS (Parsons Laboratory, Massachusetts Institute of Technology, Cambridge, MA 02139 USA, email: earlew@ll.mit.edu)

Based on the simple observation that the electric field of an electrostatic dipole falls off less rapidly with altitude  $Z$  ( $-1/Z$  to the third power) than the dielectric strength of the atmosphere ( $\sim \exp(-Z)$ ), C.T.R. Wilson essentially derived quantitative criteria for sprites more than 60 years prior to their formal discovery. In this talk, observations of transient electromagnetic excitations of the Earth-ionospheric cavity from MIT's Schumann resonance station in Rhode Island, USA are described. Calibrated measurements of positive ground flashes coincident with sprites observed by W. Lyons and his colleagues from Colorado, USA are used in conjunction with the normal mode equations to infer the vertical charge moments for these energetic discharges. The observed charge transfer is found to be sufficiently fast to validate the electrostatic assumption in Wilson's theory. The observed charge moments (in the range 500 C-km to several thousand C-km) are not adequate to induce conventional air breakdown at observed sprite altitudes (~60km) but are sufficient to cause breakdown by the electron runaway process. Distinct differences in the charge transfer behaviour in ground flashes inducing sprites and elves will also be considered.

**JSM03/E/06-A1** 1600**SPACE-TIME STRUCTURES OF SPRITES AND ELVES OBSERVED AT COLORADO, USA AND HOKURIKU, JAPAN**

Hiroshi Fukunishi (Department of Geophysics, Graduate School of Science, Tohoku University, Sendai 980-8578, Japan, email: fuku@pat.geophys.tohoku.ac.jp)

To observe the rapid space-time structures of sprites and elves, we developed 16-channel array photometers using multianode photomultipliers and operated these photometers and CCD cameras at Yucca Ridge Field Station (40.7 N, 104.9 W), Colorado during the SPRITES'96, '97 and '98 campaigns. We also operated these instruments at Dodaira Observatory (36.0 N, 139.2 E) in December 1998 and January 1999, and succeeded for the first time in observing wintry sprites and elves above the Sea of Japan near the Hokuriku region. The obtained data clearly demonstrated that sprites can be classified into two categories, column-sprites and carrot-sprites, which exhibit different space-time development. Column-sprites are always accompanied by preceding elves and characterized by an initial downward development starting around 80-90 km altitude. On the other hand, carrot-sprites are characterized by an initial upward development starting around 50 km altitude and occurrences of preceding elves are rare. It was also found that the delay time from the onset of the causative sprites to the emission peak of sprites is almost constant (about 1 ms) for column-sprites, while it ranges from 2 to 150 ms for carrot-sprites. These differences can be interpreted by the difference in the time constant of charge removal by cloud-to-ground discharges in the quasi-electrostatic (QE) model proposed by Pasko et al. (1996, 1997). The development of elves is consistent with the electromagnetic pulse (EMP) model proposed by Inan et al. (1996).

**JSM03/W/05-A1** 1630**UNUSUALLY LOW ALTITUDE SPRITE EMISSIONS OBSERVED IN THE NITROGEN FIRST POSITIVE BAND EMISSION AT 665 NM**

M.J. TAYLOR and R.M. Dial (both at Space Dynamics Laboratory and Physics Department, Utah State University, Logan, UT, USA, Email: mtaylor@ccsu.edu), M. Heavner, D. Sentman, E. M. Wescott and D. R. Moudry (all at Geophysical Institute, University of Alaska, Fairbanks, AK, USA)

During the Sprites'96 campaign conducted at Yucca Ridge, Colorado over 500 Sprites were imaged in the nitrogen first positive band emission using an intensified Isocon TV camera and a bare CCD imager both fitted with band-limited interference filters centered at 665 nm. Many of the Sprites were found to exhibit "red" tendrill-like structures that extended down from the mesosphere well into the stratosphere, where the emission is expected to be strongly quenched, with some terminating below ~40 km. On at least two occasions a most unusual Sprite form was observed in addition to the main Sprite discharge. The red emission appeared to originate from well below the main body of the Sprite, in closer proximity to the cloud tops, and then to grow upwards to form a well-defined "narrow" channel with a broad "head" that terminated at tendrill heights. The University of Alaska has observed a similar event previously in white light during airborne observations. In this paper we discuss the properties of these unusual events focussing on their form, altitudinal extent and apparent temporal durations.

**JSM03/W/02-A1** 1650**HIGH SPEED VIDEO OF SPRITES AND ELVES**

Mark STANLEY, Paul Krehbiel, Marx Brook, Charles Moore, and William Rison (Physics Department, New Mexico Tech, Socorro, NM 87801, USA, email: stanley@ibis.nmt.edu). Bill Abrahams (Speed Vision Technologies, 990 Highland Drive, Suite 212m, Solana Beach, CA 92075, USA, email: speedwilly@aol.com)

In early October 1997, high speed light-intensified video was acquired which showed the development of sprites and elves at frame rates of 1000-4000 per second. The sprites began as a narrow and often non-continuous column at an altitude above 66 km. Most columns were at least partially composed of a highly transient luminous structure commonly known as a "tendrill" which propagated downwards at average velocities between 0.01 and 0.1 the speed of light. Tendrill luminosity was dominated by that from a compact downward-propagating head, which strongly suggests that tendrills are a form of streamer breakdown. In some sprites, upward developing structures forked outwards from within or below the column sometime after tendrills appeared. These structures propagated with average velocities approximately 0.1 that of light and were accompanied by significant persistence within the sprite's "head". The upward developing structures appear to be produced by fast streamer breakdown. Elves appear to develop horizontally away from the camera over the course of 1 millisecond with insignificant luminosity overlap between frames. A thin arc could be observed on the far side of the elf in later frames. The observed development sequence is in agreement with EMP-based theoretical predictions.



**ORAL AND POSTER PRESENTATION**

**JSM03/W/01-A1** **1720**

**OPTICAL FLARES IN NIGHT SKY RADIATION**

A.V.MIKHALEV and E.S.Kazimirovsky (Institute of Solar-Terrestrial, Russian Academy of Sciences, P.O.Box 4026, 664033, Irkutsk, Russia, email: mikhalev@iszf.irk.ru)

When investigating the optical self-radiation of the Earth's upper atmosphere at night, some publications point out the existence of irregular spikes on recorded optical signals interpreted as optical flares. This report analyzes and discusses the above mentioned phenomenon using data from ground-based photometer and TV observations of the Earth's upper atmospheric self-radiation in principal emission lines which were carried out in midlatitudes (52N, 103E) during 1987-1998.

Optical flares with durations of tens and hundreds of milliseconds are recorded in different ranges of optical spectrum, including near infrared and ultraviolet regions, have a diurnal and seasonal variations, and are recorded in the absence of thunderstorm activity over the region of observation. With the exception of the most intense flares, they have typical intensities comparable with night airglow intensities. The analysis of likely sources suggests what optical flares can be caused by cosmic X-ray and gamma-emission bursts, lightning discharges at high altitudes, microbursts of electron fluxes, and by other phenomena. The optical flares under discussion in this report are interpreted in terms of microbursts of precipitating electron fluxes and are likely to be associated with thunderstorm activity at a geomagnetically conjugate point of the terrestrial magnetosphere.

**JSM03/E/04-A1** Oral and Poster **1730**

**ROLE OF NEGATIVE IONS IN FORMATION AND DEVELOPMENT OF POSITIVE STREAMER OVER THUNDERCLOUD**

Andrew PASTERNAK(Space Research Centre, Bartycka Str.18-a,Warsaw, 00716, Poland, E-mail: andrew@cbk.waw.pl)

During last years different types of high altitude discharges are intensively investigated (Red Sprites, Blue Jets etc). Many theoretical models are proposed. In most cases authors propose huge electrical fields or high energy runaway electrons as initial conditions for streamer formation. Existence of large number of negative ions in atmospheric air (in value ranging from 100-1000 ions per sm<sup>3</sup>) can play important role in streamer development. Unfortunately, our knowledge about atmospheric ions behaviour is insufficient, especially in strong electrical field. In some experimental works it has been clearly demonstrated that the major source of initial electrons is by detachment from atmospheric negative ions which exist in the gap before the impulse is applied. The main mechanism of electron detachment is three-bodies collision but in strong electrical field negative ions can lose electrons without collisions, since energy of coupling is small. Such mechanism can be of vital importance in the streamer development. In this article a numerical model of the positive streamer formation has been developed consisting of conservation equation for electrons, positive and negative ions and Poisson equation. It's shown, that additional source of electrons has essential influence on picture of streamer generation.

**JSM04** **Tuesday 20 July**

**HIGH-LATITUDE SURFACE/ATMOSPHERE INTERACTION (IAMAS, IAPSO, IAHS)**

Location: Mechanical Engineering G34 LR

**Tuesday 20 July AM**

Presiding Chairs: A. Ohmura (Swiss Fed. Inst. of Tech., Zurich, Switzerland) and M.Kuhn (University of Innsbruck, Austria)

**EXCHANGE BETWEEN STABLE BOUNDARY LAYER AND SNOW AND ICE SURFACES**

**JSM04/W/02-A2** **0930**

**SURFACE-LAYER FLUX PROFILE RELATIONSHIPS IN THE ARCTIC FROM THE SEBA EXPERIMENT**

C. W. FAIRALL (Environmental Technology Laboratory, NOAA, Boulder, CO 80304, USA, email: cfairall@etl.noaa.gov) P. O. G. Persson (Cooperative Institute for Research in Environmental Sciences, NOAA/ETL, Boulder, CO 80303, USA, email: opersson@etl.noaa.gov) E. L. Andreas (US Army Cold Regions Engineering and Research Laboratory, Hanover, NH, 03755-1290, USA, email: eandreas@crrel.usace.army.mil) P. S. Guest (US Naval Postgraduate School, Monterey, CA, 93950, email: guestps@ibis.met.nps.navy.mil)

From November 1997 to October 1998 the Surface Heat Budget of the Arctic (SHEBA) surface flux group made a variety of micrometeorological measurements on the Arctic icecap as part of ice station SHEBA. The ice station was launched at 143 W and 75 N and ended at 166 W and 80 N. The measurements included 5 levels of sonic anemometers and mean T/RH sensors, one fast hygrometer, upward and downward solar and IR fluxes, and snow/ice temperatures. We believe this is the first multi-level set of eddy-correlation flux data obtained over an entire annual cycle on the ice cap. In this paper we will describe an analysis of the turbulence statistics and mean profiles in the context of Monin-Obukhov similarity theory. The emphasis will be on evaluation of various dimensionless stability functions. We will also discuss deficiencies of MO scaling and examine other types of scaling (e.g., the local similarity scaling of Nieuwstadt).

**JSM04/W/08-A2** **0950**

**AN EXTENDED SIMILARITY-THEORY FORMULATION FOR THE STABLY STRATIFIED ATMOSPHERIC SURFACE LAYER**

Sergej Zilitinkevich (Department of Earth Sciences - Meteorology, Uppsala University, Villavaegen 16, S-752 36 Uppsala, Sweden, email: sergej@big.met.uu.se) Pierluigi CALANCA (Department of Geography, Swiss Federal Institute of Technology, Winterthurerstr. 190, CH-8057 Zurich, Switzerland, email: calanca@geo.unm.w.ethz.ch)

A similarity theory formulation for the wind and temperature profiles in the stably stratified atmospheric surface layer (ASL) is developed with due regard to the effect of the free-flow

stability on the ASL. For the sake of simplicity the dry ASL is considered, although the treatment is immediately extended to cover the et ASLs. In the revised log-linear flux-profile relationships, empirical coefficients traditionally considered as universal constants, such as the slope factors in the z-less stratification layer (beyond the logarithmic layer), become functions of the dimensionless number  $S = N L/u^*$ , where N is the Brunt-Vaisala frequency in the free flow, L is the Monin-Obukhov length, and  $u^*$  is the friction velocity. This new formulation leaves room for occurrence of well-developed turbulence at much higher Richardson numbers,  $Ri$ , than has been suspected. Moreover, it results in a pronounced dependence of the turbulent Prandtl number,  $Pr$ , on  $Ri$  in a wide range of  $Ri$ , including the z-less stratification layer in correspondence with long-standing empirical evidence. The traditional Monin-Obukhov similarity theory disregards the above essential features of the stably stratified ASL. New data from measurements over a slightly inclined plateau in West Greenland provide experimental support for the proposed theory.

**JSM04/E/01-A2** **1010**

**AN INTERCOMPARISON BETWEEN THREE MODELS OF BLOWING SNOW IN THE ATMOSPHERIC BOUNDARY LAYER**

Jingbing XIAO (Dept. of Earth and Atmospheric Sciences, York University, 4700 Keele Street, Toronto, Canada, M3J 1P3, Email: jingbing@yorku.ca). Richard Bintanja (Institute for Marine and Atmospheric Research Utrecht, Email: r.bintanja@phys.uu.nl). Stephen Dery (Dept. of Atmospheric and Oceanic Sciences, McGill University, Quebec, Email: steph@zephyr.meteo.mcgill.ca). Graham Mann (Environment Centre, University of Leeds, Email: gm2@lec.leeds.ac.uk). Peter A. Taylor (Dept. of Earth and Atmospheric Sciences, York University, Toronto, Email: pat@yorku.ca)

Blowing snow is a common phenomenon in many high latitude regions. Over parts of the Arctic and Antarctica, climatology suggests that blowing snow can occur on one out of three days. During blowing snow events, the sublimation of blowing snow particles can be a significant source of water vapor and sink of sensible heat. Near the windy and relative warm coast of Antarctica, sublimation of suspended snow can reach 17 cm/year Snow Water Equivalent (SWE). Model simulations indicate that the vertically integrated sublimation rate can reach 2-4 mm/day SWE under strong wind conditions, corresponding to a heat flux of 72-128 W/m<sup>2</sup>. The physics of blowing snow is complex, and accurate blowing snow observations are hard to make. Several numerical models have been developed and their applications include helping to evaluate and design field experiments and to evaluate the sensitivity of the sublimation rate to various parameters. However, different models may give different results under given conditions. For example, the sublimation rate in a column of blowing snow calculated by the PBSM (Prairie Blowing Snow Model) is much higher than that estimated by a fetch dependent blowing snow model PIEKTUK-F when the wind speed is at 20 m/s under certain conditions (Dery et al., 1998). Hence, the model intercomparisons and verification become especially necessary. In idealised circumstances, blowing snow can be considered as a one-dimensional, time-dependent process. In this work, three one-dimensional time-dependent models have been intercompared. They are PIEKTUK-T developed by the group at York University in Canada (Dery et al., 1998), WINDBLAST developed by the group at Leeds University in United Kingdom (Mann, 1998) and SNOWSTORM developed by the group at Utrecht University in The Netherlands (Bintanja). These three models all show that the sublimation is a self-limiting process. As time increases after snow has become mobile, the sublimation rate first increases, reaches a maximum value and then decreases due to the increase of relative humidity and decreases of temperature. However, the value of the sublimation rate is not the same. Similarities and differences in model predictions will be reported and explanations considered.

**JSM04/W/09-A2** **1030**

**MESOSCALE MODELING OF GREENLAND'S KATABATIC WINDS AND THEIR INFLUENCE**

Keith M. Hines, Lin Li and David H. BROMWICH (all at Byrd Polar Research Center, The Ohio State University, Columbus, OH 43210, USA, e-mail: bromwich@polarmet1.mps.ohio-state.edu)

Simulations performed at 40 km resolution with the Penn State/NCAR MM5 modified for ice sheet meteorology detail the influence of Greenland's topography and katabatic winds on synoptic and mesoscale atmospheric phenomena in the North Atlantic sector. Months simulated include January 1990 during a winter with a large positive phase of the North Atlantic Oscillation and April and May 1997 at the time of the Katabatic Wind and Boundary Layer Front Experiment around Greenland (KABEG) study. The simulations are compared to standard meteorological analyses by ECMWF and to 1997 observations at automatic weather stations in Greenland. Additionally, the University of Bonn compares katabatic wind simulations with MM5 to similar simulations with the NORLAM model. The simulations detail the frequent track of cyclones to the east of Greenland and have demonstrated the need for very high vertical resolution to adequately capture the katabatic boundary layer.

**JSM04/E/06-A2** **1120**

**MEASUREMENTS AND NUMERICAL SIMULATIONS OF THE KATABATIC WIND OVER GREENLAND**

GUENTHER HEINEMANN and Thomas Klein, Universitaet Bonn, Auf dem Huegel 20, D-53121, Bonn, Germany

The katabatic wind system over Greenland is studied by means of surface and aircraft measurements, and by numerical simulations using the mesoscale model NORLAM. Measurements were carried out during the aircraft-based experiment KABEG'97 in the area of southern Greenland. The aircraft data allow the investigation of 3D structures of the katabatic wind, and can also be used for the validation of the boundary layer structures simulated by the numerical model. Comparisons of the numerical model results with AWS show good agreement in general. The validation of the simulations using aircraft profiles yields the result, that the correct simulation of the observed low-level jet in the stable boundary layer is highly sensitive to the correct simulation of the synoptic forcing above the boundary layer. The katabatic wind dynamics are also investigated using measurements and model results, showing that the classical katabatic force is the main driving mechanism for the flow regime.

**JSM04/E/09-A2** **1140**

**LONG-TERM MEASUREMENTS OF THE SURFACE ENERGY BALANCE AT HALLEY, ANTARCTICA**

J.C. KING and P.S. Anderson (both at British Antarctic Survey, Cambridge CB3 0ET, UK, email: j.c.king@bas.ac.uk)

Halley Research Station (75oS, 26oW) is situated on an expansive and uniform ice shelf and is thus an ideal location for making measurements of surface fluxes that are representative of a wide area. Continuous measurements of surface fluxes have been made at this site since 1995, using both eddy-correlation and profile techniques. Radiation measurements were added in 1996. We describe the instrumentation used and the problems encountered with making long-

term flux measurements in a harsh polar environment. Data from the first three years of measurements will be presented. During winter, the mean net radiative cooling of the snow surface exceeds the measured net turbulent heat flux plus snowpack heat flux by about 10 W/m<sup>2</sup>. Reasons for this apparent lack of closure of the surface energy budget are investigated.

**JSM04/W/07-A2****1200****IMPLEMENTING AND TESTING OF A NEW SNOW SCHEME SAST IN SIMPLIFIED SIMPLE BIOSPHERE MODEL (SSIB)**

Shufen Sun and YONGKANG XUE(both at Department of Geography, University of Maryland, College Park, MD 20742,USA Tel: 301-405-5880; fax: 301-314-9299,email: yxue@geog.umd.edu)

Based on up to date comprehensive and complex snow cover schemes, a Simple Snow-Atmosphere-Soil Transfer Model (SAST) has been developed. This model includes most important physical processes for simulation of seasonal snow cover change. The model also makes substantial simplification and improvement. For example, based on the analysis of the effect of vapor phase change and vapor movement on mass and energy balances, a formulation of effective heat conductivity has been derived which simplifies the description of complex processes without loss of accuracy. Base on analyses of diurnal and seasonal variations of snow temperature, an efficient snow cover layering system has been developed for better prediction. The volumetric specific enthalpy instead of temperature is used as the prognostic variable. It simplifies the formulations in phase change processes and reduces the computational procedures with an efficient implicit one step test numerical scheme. The SAST is coupled with SSIB to improve the SSIB prediction potential in snow cover regime. The coupled model includes the vegetation regime, snow cover regime and ground surface regime. Their physical properties are described by the mass and energy balance equations, respectively. Snow cover interacts with both vegetation cover above and ground surface below. In the coupled model, the snow surface temperature and canopy temperature are solved simultaneously to ensure the energy and water conservation in the vegetation-snow interface, which is crucial in the study of snow effects in global as well as regional climate models. The SAST model has been tested in off line model by using long term Russian and France field data. The results show its potential in predicting seasonal snow cover change. These two data sets along with the German snow data will be tested further to validate and evaluate the coupled SSIB/SAST model.

**JSM04/W/06-A2****1220****AIR-SNOWPACK CHEMICAL INTERACTIONS AT LOW ACCUMULATION RATE SITES IN ANTARCTICA**

Eric W. WOLFF, Anna E. Jones and Andrew M. Rankin (all at British Antarctic Survey, High Cross, Madingley Road, Cambridge CB3 0ET, UK, email: e.wolff@bas.ac.uk)

Understanding the processes that govern uptake of chemicals onto snow is fundamental to interpreting deep ice core records in terms of atmospheric chemical changes. For aerosol species, dry deposition processes dominate below a threshold snow accumulation rate. Ventilation by wind-pumping through topographic features is one dry deposition mechanism that could be important, but we show that it is unlikely to be at a site such as Dome C, Antarctica, which has a very low snow accumulation rate (about 30 kg m<sup>-3</sup>). We discuss the conditions (changed meteorology and surface roughness) that could make the wind-pumping mechanism dominate. For some gaseous species, post-depositional changes determine the ice core concentration. We investigate the case of nitrate, which shows large losses at a site such as Dome C, and discuss the possible controls on the nitrate concentration.

**JSM04/E/04-A2****1240****AIR-SNOW EXCHANGE STUDIES OF NITROGEN SPECIES AT NEUMAYER, ANTARCTICA.**

A.E. JONES, P.S. Anderson, H.K. Roscoe (British Antarctic Survey, NERC, Madingley Road, Cambridge, UK); R. Weller, H-W. Jacobi, G. Koenig-Langlo (Alfred-Wegener Institute, Am Handelshafen 12, Bremerhaven, Germany)

Processes of chemical exchange between air and snow surfaces at high latitudes will affect both ambient concentrations of trace gases and the incorporation of the chemical signature into ice cores. In order to understand both polar tropospheric chemistry and the ice core record it is therefore necessary to understand the complex exchange mechanisms involved at the snow/air interface.

We report here on measurements made during Austral summer 1999, at the German Antarctic research base, Neumayer. An earlier campaign, designed to study the speciation within the NOy family, detected a diurnal variation in NOy with apparent links to processes at the snow surface. As part of a follow up campaign, we made measurements at Neumayer specifically to look for fluxes of nitrogen species into and out of the snow pack, with high time resolution gradient measurements of NO and NOx combined with meteorological data to derive fluxes. We present our results, and discuss possible influences on local photochemistry and the ice core nitrate record.

**Tuesday 20 July PM**

Presiding Chairs: P. Wadhams (Cambridge University, UK),  
K. Steffen (University of Colorado, USA)

**POLAR OCEAN - ATMOSPHERE INTERACTIONS****JSM04/E/05-A2****1420****REDISTRIBUTION OF SOLAR RADIATION IN THE BARENTS SEA MARGINAL ICE ZONE DURING MELTING SEASON.**

Reinert KORSNES (Norwegian Polar Institute, Polar Environmental Centre, N 9005 Tromsø, Norway, Email: Reinert.Korsnes@npolar.no) Alexander P. Makshas ( Arctic and Antarctic Research Institute, 38 Bering str., St. Petersburg, 199397, Russia, Email: maksh@aaari.nv.ru)

Peculiarities of directional and spectral distributions of solar radiation under Arctic sea ice conditions are described based on field measurements during the Russian-Norwegian expedition "Barex-95" in the sea ice marginal zone of the Barents sea in the melting season. The results point out the importance of complex experimental investigations of radiation in the polar atmosphere under cloud and fog conditions. Cloud/fog conditions and the state of the sea ice surface control angular distribution of incoming solar radiation and its absorption by different types of sea ice covers (leads, melt ponds, wet snow and hummocks). A stochastic model of cloudy atmosphere is used to reproduce experimental data and to estimate sensitivity to angular and spectral distributions of solar radiation on the heat budget of the sea ice cover. An algorithm developed by Podgorny and Grenfell is modified to calculate melt pond bottom albedo and cardioidal radiance distribution parameters from hemispherical-directional reflectance distribution measurements.

**JSM04/W/05-A2****1445****A GCM STUDY OF THE SENSITIVITY OF THE ANTARCTIC SEA ICE DISTRIBUTION TO SNOW COVER**

Xingren WU (Antarctic CRC and Australian Antarctic Division, Hobart, Tasmania, Australia, email: x.wu@utas.edu.au) William F. Budd (Antarctic CRC, Hobart, Tasmania, Australia, email: w.f.budd@utas.edu.au) Victoria I. Lytle (Antarctic CRC and Australian Antarctic Division, Hobart, Tasmania, Australia, email: v.lytle@utas.edu.au) Robert A. Massom (Antarctic CRC, Hobart, Tasmania, Australia, email: r.massom@utas.edu.au)

This work estimates the effect of a snow layer and its depth on sea ice thickness accretion and ablation, using both a simple thermodynamic model and a coupled atmosphere-sea ice model including feedback and ice dynamics effects. The thermodynamic sea ice model is a 2-layer version model which treats snow, sea ice and snow-ice explicitly. The coupled model allows snow-ice to form when the snow cover is flooded. When snow is disregarded in the coupled model the averaged Antarctic sea ice becomes thicker. When only half of the snowfall predicted by the atmospheric model is allowed to accumulate on the ice surface, the sea ice gets thicker in most of the Weddell and Ross Seas but thinner in East Antarctic in winter, with the average slightly thicker. When twice as much snowfall as predicted by the atmospheric model is assumed to accumulate on the ice surface sea ice also gets much thicker due to the large increase of snow-ice formation. In this study we have also tested the use of a lower mean value of thermal conductivity of snow in the coupled model, namely 0.16 W/(mK) instead of the standard value 0.31. This value is based on the most recent observations in the eastern Antarctic and Bellingshausen and Amundsen Seas. We have found that the sea ice thickness distribution changes greatly, with the ice becoming thinner by about 0.2 m in the Antarctic and about 0.4 m in the Arctic on average.

**JSM04/E/03-A2****1510****ROUGHNESS-DEPENDENT AIR - SEA ICE MOMENTUM FLUXES IN LARGE-SCALE MODELS**

Nadja Steiner, Markus HARDER, Peter Lemke, Sandra Schuster (Institute of Marine Research at the University of Kiel, Germany, Duesternbrooker Weg20, D-24105 Kiel, Germany, email: nsteiner@ifm.uni-kiel.de, mharder@ifm.uni-kiel.de)

A quantitative relationship between observed sea-ice roughness and simulated large-scale deformation work is established in order to provide new means for model validation and a better representation of the sea ice component in coupled climate models. Sea ice roughness is introduced as an additional prognostic variable in the dynamic-thermodynamic Kiel Sea-Ice Simulation (KISS) with a viscous-plastic rheology. Ice roughness is defined as the accumulated work of internal forces acting upon an ice volume, given in energy per area. A fraction of this total deformation work is transformed into potential energy stored in pressure ridges. Observable quantities, such as mean pressure ridge height, ridge frequency as well as volumetric and areal fractions of deformed ice are derived from the simulated sea ice roughness by using observed ridge geometries and distribution functions. Roughness-dependent drag coefficients are introduced to account for the effect on the momentum exchange between ocean and atmosphere due to the form drag of roughness elements. Drag coefficients are parameterized as functions of deformation energy and ice concentration representing contributions of form drag due to pressure ridges and floe edges. This results in spatially and temporally varying drag coefficients, and yields significant differences in the magnitude and direction of ice drift velocities. A comparison with observed buoy drift velocities leads to an optimized parameterisation. The simulations indicate that the inclusion of sea-ice roughness provides for a more realistic representation of the boundary layer processes in climate models.

**JSM04/W/12-A2****1535****EVALUATION OF HEAT FLUXES IN THE WEDDELL SEA USING BUOY DATA**

O. EISEN (1) and C. Kottmeier (1,2) (1) Institute for Meteorology and Climate Research, Universität Karlsruhe, Kaiserstr. 12, D-76133 Karlsruhe, Germany, (2) Institute for Meteorology and Climate Research, Forschungszentrum Karlsruhe, Hermann-von-Helmholtz-Platz 1, D-72344 Eggenstein-Leopoldshafen, Germany.

The surface energy balance of open and refrozen leads in sea ice is evaluated for a good areal coverage in the Weddell Sea for the winter period using a kinematic-thermodynamic sea ice model forced by data from drifting buoys. Additionally, two case studies reveal the influences of oceanic heat flux and tidal motion in specific regions. The relative contribution of open and refrozen leads to the total net heat flux increases from 30 % (10 · 15 W m<sup>-2</sup>) in the eastern Weddell Sea to 70 % (30 W m<sup>-2</sup>) in the western Weddell Sea and is on average about twice the areal lead percentage. Both, atmospheric forcing and the lead percentage cause this pattern. The monthly winter ice production in leads increases from 10 cm in the eastern part to 30 cm over the western shelf. The oceanic heat flux reduces the ice production under thick ice significantly and thus emphasizes the importance of leads for the total ice production. In the western Weddell Sea leads induced by motion in the diurnal and semi-dinnal band contribute 7 % to net heat flux, 12 % to ice production and 37 % to the salt mass released during ice growth. The results emphasize the importance of leads for the interaction of ocean, sea ice and atmosphere.

**JSM04/W/01-A2****1620****INVESTIGATIONS OF ATMOSPHERE/ICE/OCEAN INTERACTIONS USING SATELLITE SOUNDER DATA IN POLAR REGIONS**

FRANCIS, Jennifer ( Institute of Marine and Coastal Sciences, Rutgers University, 71 Dudley Road, New Brunswick NJ 08901-8521 USA. E-mail:francis@imcs.rutgers.edu Telephone No: 732-708-1217 Fax No: 732-872-3088)

A wealth of new information is available from a recently completed 18-year data set of Arctic atmospheric and surface products derived from the TIROS Operational Vertical Sounder (TOVS). The TOVS Pathfinder data set comprises temperature and moisture profiles, cloud parameters, and surface characteristics at a 100-km spatial and daily temporal resolution, north of 60 degrees north latitude. We combine these fundamental variables with surface pressures and upper-level winds from the NCEP Reanalysis project to derive 10-meter wind fields, advected heat and moisture, and P-E. From the cloud information and atmospheric profiles we compute surface radiation fluxes. In this presentation we will describe the TOVS Pathfinder data set and present examples of air/ice/ocean exchange studies using these data.

**JSM04/W/04-A2 1645**

**AIR-SEA-ICE INTERACTIONS OVER THE RONNE POLYNIA, ANTARCTICA**

I. A. Renfrew and J. C. King, British Antarctic Survey, High Cross, Madingley Rd, Cambridge CB3 0ET, UK, email: i.renfrew@bas.ac.uk

Surface fluxes of heat and moisture are estimated for the coastal polynia that skirts the Ronne Ice Shelf, in the Weddell Sea, Antarctica. The air-sea-ice interactions of this region are responsible for changes in the surface waters that lead to the formation of Antarctic Bottom Water, an important water mass in the global thermohaline circulation. Automatic weather station (AWS) data have been used to generate a year long climatology of surface fluxes over the polynia. A simple one-dimensional convective boundary layer model has been developed. The model uses surface meteorological observations to grow a mixed layer over the polynia, and hence allow estimates of the surface sensible heat flux with fetch. The model has been tested with in situ data obtained from the Ronne Polynia Experiment (ROPEX) cruise of February 1998. The AWS data have been compared to ECMWF analysis products, with the aim of extending the flux climatology. Unfortunately the comparison illustrated a serious problem in the ECMWF model which was, until April 1998, treating the permanent ice shelves as sea-ice. This allowed an erroneous upward heat transfer through the sea-ice into the boundary layer, and meant that the model atmosphere was up to tens of degrees too warm.

**JSM04/W/10-A2 1710**

**AIR-SEA-ICE INTERACTION PROCESSES IN THE SOUTHERN OCEAN**

XIAOJUN, Yuan, Lamont-Doherty Earth Observation, email: xyuan@ldeo.columbia.edu

Air-sea-ice interaction processes in the Southern Ocean are investigated utilizing space-observed surface winds, sea ice concentration, and sea surface temperature (SST) from September through December, 1996. The sea ice edge (SIE) shows three ice-extent maxima around the Antarctic during September and October when sea ice coverage is maximum. They are located in the central Indian Ocean, east of the Ross Sea, and in the eastern Weddell Gyre. During September and October, most of the strong and long lasting storms initiate northeast of the three sea ice maxima. Such spatial distributions of storms and sea ice reflect coupling processes of the air-sea-ice interaction. A relatively stable, wave number 3 atmospheric circulation pattern that is believed to be fixed by the land-ocean distribution prevails during the ice maximum season. The ice-extent maxima coincide with strong southerlies and divergent wind fields associated with this pattern, which suggests that the mean atmospheric circulation determines the ice distribution. The ice-extent maxima can enhance the regional meridional surface pressure gradient and therefore strengthen the westerly winds north of the ice edge. The decreasing ice extent east of the ice maxima creates a local zonal thermal gradient which enhances local southerlies. This positive feedback between the wave pattern in the mean atmospheric circulation and ice distribution partially causes the eastward propagation of the ice maxima and also provides a favorable condition for cyclogenesis northeast of the ice-extent maxima. The mechanism of the cyclogenesis is the baroclinic instability caused by the cold air blown from the ice pack to the warm open-ocean waters. Where the SST is warmest off the SIE and the southerlies are the strongest, the potential for cyclogenesis is most likely. This is consistent with the observations.

**JSM04/W/11-A2 1735**

**AIR-SEA ICE INTERACTIONS SIMULATED WITH A REGIONAL CLIMATE MODEL FOR THE NORTH ATLANTIC AND THE ARCTIC**

Hauke BERNDT, Markus Harder, Michael Hilmer, Rolf Jürrens, and Peter Lemke (all at Institut für Meereskunde, Universität Kiel, Germany, email: hberndt@ifm.uni-kiel.de)

The atmospheric conditions in the Arctic and the Atlantic north of 35° N are investigated with the regional climate model REMO. REMO is based on the limited area numerical weather predictions system EM/DM of the Deutscher Wetterdienst (DWD). For the model the same physical parameterizations as implemented in the MPI global climate-model ECHAM4 are used. The modeled domain is resolved with a mesh of 145x121 grid points and a mesh-size of 0.5° on a rotated spherical grid. The model is forced with boundary conditions from the NCEP/NCAR-reanalyses project. Different validations of REMO have been performed by comparing the model results with meteorological observations from the cruise of RV/KNORR during February/March 1997 in the Labrador Sea, accumulation measurements of snow over the glacial areas of Greenland and observed and modeled precipitation over Greenland. Comparing our results with the forcing global dataset we see horizontal patterns with higher detailed structures e.g. of precipitation in the coastal regions of Greenland which lead to major improvements of the simulated hydrological cycle. Driving REMO with ice-thickness distributions from a viscous-plastic sea-ice model leads to more realistically results. With the implementation of partial ice cover for a better representation of the heat fluxes in mixed grid boxes of sea ice and open water we expect further improvements e.g. in the marginal ice-zone. This work is a first step towards a fully coupled regional atmosphere-ice-ocean climate model for the North Atlantic and Arctic which is going to be set up at the Institut für Meereskunde.

assimilation model were investigated through the identical twin experiments with varying the initial values of control variables, the observation period, and the spatial or temporal intervals of observation data. The main results are as follows: (a) the underestimated conditions of the initial values of the control variables tend to make calculation stable, (b) the appropriate temporal interval of the observation data is 1/5 times as short as the characteristic time scale of the forcing term (wind), (c) the surface current data is especially important in this type of wind forcing model, and (d) the observation period must be longer than the characteristic time scale of the forcing term. Next, the assimilation of in situ data was conducted by using the current data measured by HF ocean radar (-1m) and the moored currentmeter(-2, -5,-10m) in the sea off Fukushima, the open sea in the western Pacific. Two days data were assimilated when the continuous northern wind averaged 5m/s was dominant. The results showed the vertical eddy viscosity coefficients were of the order of 10<sup>-3</sup> (m<sup>2</sup>/s) and the surface wind drag coefficient was about 1.1 \* 10<sup>-3</sup> which were consistent with the past investigation results. One of the advantages of the data assimilation is to estimate the vertical or horizontal profile of the eddy viscosity coefficients.

**JSP05/E/02-A1 Invited 0850**

**ESTIMATES OF AIR-SEA HEAT FLUXES USING THE VARIATIONAL ASSIMILATION SYSTEM FOR THE 1-DIMENSIONAL MIXED LAYER MODEL**

YOICHI ISHIKAWA, Toshiyuki Awaji, Masatora Iida, Teiji In (Department of Geo physics, Kyoto University, Kyoto 606-8502, Japan, Email: ishikawa@kugi.kyoto-u.ac.jp), and Bo Qiu(Department of Oceanography, University of Hawaii at Manoa, Hawaii)

The ocean surface mixed layer plays a crucial role in the climate system through the air-sea interactions and hence it is strongly desired to construct the 4-dimensional data assimilation system capable of proving the integrated data set of the mixed-layer temperature and depth and the air-sea heat flux. In this study, a data assimilation system using the 1-dimensional bulk mixed layer model with the variation adjoin method is constructed to estimate the net air-sea heat flux as well as the mixed layer variables from observations of the mixed-layer temperature. When the mixed layer model is designed to reproduce the seasonal cycle of the mixed layer variability, it is required to use quite different equations governing the model variables in the deepening and the shoaling phase. Thus the data assimilation system shows strong non-linearity, causing a difficult situation in obtaining the optimum solution. In this study, the problem associated with the strong non-linearity is solved by the scaling of the gradient of the cost function, which has the potential to reduce the distortion of the Hessian matrix. Furthermore, the incremental method is applied to the minimisation of the cost function. To confirm the effectiveness of our approach, identical twin experiments are carried out by assimilating the simulated mixed-layer temperature into the model before conducting the assimilation of real data. The result shows that the RMS error of the estimated surface heat flux in our approach is 8 W m<sup>-2</sup>, while the RMS error using the previous approach is much larger, about 40 W m<sup>-2</sup>. Our assimilation system is applied to estimation of the net air-sea heat flux in the equatorial Pacific using the mixed layer temperature measured by the TOGA-TAO buoy. The estimated surface heat flux is compared with the heat flux obtained by in-situ observations, showing good agreement especially on seasonal time scales. The RMS difference between both values low-pass filtered over 90 days is 28 W m<sup>-2</sup>. Also, other mixed-layer variables such as the mixed-layer depth show very similar tendency to in-situ observations despite the assimilation of the mixed-layer temperature alone.

**JSP05/W/04-A1 0910**

**RECONSTRUCTION OF SUBSURFACE GEOCHEMICAL FIELDS USING ASSIMILATION OF UPPER OCEAN DATA**

M. IKEDA (Graduate School of Environmental Earth Science, Hokkaido University and Frontier Research System for Global Change, Sapporo, Japan, email: mikeda@ees.hokudai.ac.jp) and Y. Sasai (Graduate School of Environmental Earth Science, Hokkaido University)

Oceanographic data are collected much more extensively from the surface than subsurface. A data assimilation method is proposed for determining geochemical fields in the subsurface. The method is tested with a bulk mixed-layer model. The period from fall to winter and the subpolar North Pacific Ocean are chosen, in which the ocean interacts most extensively with the atmosphere via mixed layer development. In addition to physical properties, CO<sub>2</sub> and Alkalinity are also considered as model variables. Total carbonate and pCO<sub>2</sub> increase in fall through winter, as the mixed layer develops and entrain carbonate-rich subsurface water. A cost function has squared differences between data and a model solution. Initial values and subsurface properties are chosen as control variables. The seasonal evolutions of the physical properties are well reproduced even without data assimilation. If we attribute the mismatch of the chemical properties to the subsurface chemical data, zonal variabilities become remarkable in the subsurface ocean. The total carbonate is high in the northwest region, suggesting high biological productivity. In the eastern Pacific, alkalinity is low, suggesting high alkalinity pump effects.

**JSP05/E/08-A1 0930**

**INVERSE ESTIMATION OF SEA SURFACE HEAT FLUXES OVER THE EQUATORIAL PACIFIC OCEAN**

DONGLIANG YUAN and Michele Rienecker

In this study, we use the Poseidon quasi-isopycnal ocean model and the Reynolds weekly-mean sea surface temperature data combined with TOGA-TAO subsurface temperature observations to estimate the surface heat fluxes over the equatorial Pacific ocean. A variational data assimilation method optimizes the model initial temperature state and the sea surface heat fluxes simultaneously through assimilation of surface and sub-surface temperature data. Because the Reynolds sea surface temperature compilation is weekly, only monthly mean sea surface heat fluxes are obtained. The variational scheme is implemented on a thermodynamic sub-model of the Poseidon model. The velocity field that advects the temperature in the sub-model is provided by a full forward run of the model. After the variational assimilation, the optimized initial temperature state and the sea surface heat fluxes are substituted back into the full run of the forward model to modify the velocity fields used in the next round of variational assimilation. The iteration stops when the differences between two successive estimates of the sea surface heat fluxes satisfy a convergence criterion. The optimized sea surface heat flux will be compared with other estimates.

**JSP05/W/01-A1 0950**

**STRUCTURAL MODEL ERROR, THE LINEAR RANGE, AND VARIATIONAL ASSIMILATION**

J.A. HANSEN (1,2) and L.A. Smith (2) (1) Rutherford Appleton Laboratory, Space Science Department, Chilton/Didcot, OXON, OX11 0QX, UK, (2) Mathematical Institute, University of Oxford, Oxford, OX1 3LB, UK. E-mail: J.A.Hansen@rl.ac.uk Telephone No: (01235) 446 220 Fax No: (01235) 445 848

The perfect model assumption places an operational limit on four dimensional variational

**JSP05 Monday 19 – Tuesday 20 July**

**DATA ASSIMILATION IN METEOROLOGY AND OCEANOGRAPHY (IAPSO, IAMAS)  
Location: Poynting Physics S02LT**

**Monday 19 July AM**

Presiding Chair: Prof Motoyoshi Ikeda (Graduate School of Environmental Earth Science, Hokkaido University and Frontier Research System for Global Change, Sapporo, Japan)

**JSP05/E/04-A1 0830**

**ESTIMATION OF VERTICAL EDDY VISCOSITY COEFFICIENTS BY A ONE-DIMENSIONAL DATA ASSIMILATION MODEL WITH THE ADJOINT EQUATION**

Shin'ichi SAKAI (Environmental Science Department, Central Research Institute of Electric Power Industry, 1646 Abiko, Abiko City, Chiba, 270-1194, JAPAN, email: s-sakai@criepi.denken.or.jp)

The vertical eddy viscosity or the surface wind drag coefficients is significant parameter in the coastal ocean model. The field investigation of these parameters is however very difficult, so the actual value of these parameters are still unknown. A variational approach with the adjoint equation is useful to estimate these model parameters. At first, the basic behaviours of the



assimilation. Models are wrong. Four-dimensional variational assimilation assumes models are right, specifically a model trajectory exists which is consistent with observations and their associated uncertainty. When model error is large, minimising the cost function defined by model/data misfit can result in analyses that differ significantly from both observations and truth. We present the impact of different levels of structural model error in a simple model on 4D-Var assimilation results as a function of assimilation window length, and demonstrate the importance of the type of model error considered (structural vs. parametric). Model error also impacts the linearity assumption intrinsic to the 4D-Var approach. While a difference between the linearisation of a model about a model state and the linearisation of a system about a system state need not limit the 4D-Var minimisation process, it will impact the quality of uncertainty estimates produced by the resulting Hessian, and can limit the effectiveness of an incremental 4D-Var approach.

**JSP05/E/10-A1** Invited **1010**

#### 4 DIMENSIONAL DATA ASSIMILATION FOR THE LAND SURFACE PROCESSES

Ken-ichi Kuma Numerical Prediction Division Japan Meteorological Agency

For the atmosphere and the ocean, 4DDA is widely used to give the initial condition for the numerical integration. Although the land surface 4DDA has been recently introduced in several modelling centers, it is still far behind to the atmosphere and the ocean. Two main purposes for the land surface 4DDA are 1) Improvement of predictability for the atmosphere in various time scale and 2) Monitoring the land surface processes including hydrosphere, cryosphere, and biosphere for global domain. There are several difficulties for the land surface 4DDA. 1) Numerical model is not well defined by the physical law. 2) Observation and data exchanges are not well established. 3) Some processes highly depend upon locality. The most fundamental problem will be the issue related with the observation. If we consider the feasibility of the observation system, we must rely upon the remote sensing from the satellite as well as promotion of in-site data exchange. Passive microwave sensors provide the snow amount for dry snow, surface soil moisture for bare land surface. As to the canopy-covered region, the key information derived by the satellite is on photosynthesis process. Our ultimate goal for the land surface 4DDA is to assimilate the data related with photosynthesis process with the soil-vegetation-atmosphere transfer system model. This will enable us to monitor the carbon cycle as well as the hydrological cycle for the global domain.

**JSP05/W/17-A1** Invited **1050**

#### ATMOSPHERIC DATA ASSIMILATION AT JAPAN METEOROLOGICAL AGENCY (JMA)

Nobutaka MANNOJI ( Numerical Prediction Division, Japan Meteorological Agency, 1-3-4 Oote-machi, Chiyoda-ku, Tokyo 100-8122, JAPAN, email: nmannoji@npd.kishou.go.jp )

ERS-2 scatterometer data have been assimilated operationally in the T213L30 global model since July 1998. The feature in assimilating ERS-2 data at JMA is that not only the sea surface wind data but also the sea surface pressure data are assimilated. The sea surface pressure data are retrieved from the ERS-2 sea surface wind data referring to the surface pressure observation by buoys and ships. We found that that ERS-2 data have large positive impact in the Southern Hemisphere and small positive impact in the Northern Hemisphere and the Tropics, not only on the surface field but also on the upper air field. One-dimensional variational method (1DVAR) to assimilate TOVS radiance data is now being developed. An experiment in which retrieved temperature is assimilated through optimum interpolation method into the global model showed that 1DVAR has positive impact in the Southern Hemisphere, negative impact in the Tropics and neutral impact in the Northern Hemisphere. The method is being improved and will be in operation in 1999. Kanto Area Meso-scale Experiment (KAMEX), an observational system experiment (OSE) over Kanto Plain for meso-scale forecast, is now being performed. We are investigating impact of observational data such as the wind profiler, doppler radar, ACARS, sea surface wind by NSCAT and ERS-2, precipitable water by GPS and SSM/I, and moisture bogus data derived from GMS. Three-dimensional variational method for global analysis is now being developed with a low resolution (T63L30L) model. The method will be in operation in 2000 including variational assimilation of TOVS radiance data.

**JSP05/E/07-A1** Invited **1110**

#### MRI/JMA OPERATIONAL OCEAN DATA ASSIMILATION SYSTEM -COMPASS-K-

Masafumi KAMACHI (Meteorological Research Institute, 1-1 Nagamine, Tsukuba 305-0052, Japan, email: mkamachi@mri-jma.go.jp) Tsurane Kuragano and Jiang Zhu (both at Oceanographic Research Department, Meteorological Research Institute, 1-1 Nagamine, Tsukuba 305-0052, Japan, email: tkuragan@mri-jma.go.jp) Noriyo Yoshioka and Satoshi Sugimoto (both in the Japan Meteorological Agency, 1-3-4 Ohtemachi, Chiyoda-ku, Tokyo 100-8122, Japan, email: yoshioka@naps.kishou.go.jp) Francesco Uboldi (FISBAT-CNR, Dipartimento di Fisica, Via Imerio, 46, I-40126 Bologna, Italy, email: uboldi@pinochcio.fisbat.bo.cnr.it)

An ocean data assimilation system, COMPASS-K (the Comprehensive Ocean Modeling, Prediction, Analysis and Synthesis System in the Kuroshio-region), is developed at the Meteorological Research Institute. The system is for understanding ocean variability, an operational system in the Japan Meteorological Agency, and for the GODAE project.

The model is an eddy resolving version of an MRI-OGCM. Space-time decorrelation scales of ocean variability are estimated with TOPEX/POSEIDON (T/P) altimeter data. The scales show inhomogeneous and anisotropic features and give information about an error covariance matrix in an optimum interpolation process. Subsurface temperature and salinity fields are evaluated from T/P altimetry with a correlation scheme and assimilated into the model with a nudging scheme.

Seasonal and interannual variations in the western North Pacific are investigated. Realistic space-time distribution of the physical quantities, the path of Kuroshio and its separation from Honshu are captured well. The assimilation results give useful information about an effect of eddy-mean flow interaction to Kuroshio meander and dynamical insights of the separation.

**JSP05/E/03-A1** **1130**

#### TEST AND IMPLEMENTATION OF A MESOSCALE DATA ASSIMILATION CHAIN FOR VERY SHORT RANGE FORECAST PURPOSES.

Pier Paolo Alberoni, STEFANO COSTA, Tiziana Paccagnella, Paolo Patrino (both at Servizio Meteorologico Regionale, A.R.P.A. Emilia-Romagna, Bologna, Viale Silvani, 6, 40122 Italy, email: p.alberoni@arpamet.regione.emilia-romagna.it) Vincenzo Levizzani (Institute FISBAT-CNR, Bologna, via Gobetti 101, 40129, Italy, email: v.levizzani@fisbat.bo.cnr.it and EUMETSAT, Darmstadt, Germany)

The growth of observational capability over the last decades allows a detailed description of atmospheric structures, from large-scale phenomena to cloud features. The integrated use of whole information available bring together a NWP techniques, to produce very short range

forecast (vsrf) product operationally, is still now a challenge for the forecaster community. The coupling of a powerful mesoscale analysis tool with our limited area model (LAMBO) make up the base of SMR vsrf system.

The Local Analysis and Prediction System (LAPS) has been developed by NOAA-FSL as an integrated system to ingest and analyse meteorological data from different observational sources. The system is able to ingest all kinds of data routinely available, i.e. mesonet and regular surface data, radar and profiler data and satellite imagery. LAPS combines and harmonises the dataset to obtain surface and 3D fields of meteorological parameters, that is temperature, pressure, humidity, wind, cloud and other derived variables.

The resulting fields are finally fed into LAMBO, as a very detailed initialisation in order to produce a very short-range forecast. The analysis and assimilation cycles are carried out every hour. The overall system and some examples of forecast products will be presented.

**JSP05/W/10-A1** **1150**

#### FES98, A REVISED HYDRODYNAMIC AND ASSIMILATION MODEL FOR THE OCEANIC TIDES

F. Lyard (email: Florent.Lyard@cnes.fr), F. Lefevre (email: Fabien.Lefevre@cnes.fr), C. Le Provost (email: Christian.Le-Provost@cnes.fr) and F. Ponchaut (email: ponchaut@cnes.fr) (all at LEGOS/GRGS, UMR5566 CNES-CNRS-UPS, 14 Avenue E. Belin, 31400 Toulouse, France)

A new set of solutions from our FE hydrodynamic tidal model coupled with a revised data assimilation software has recently been made available as the FES98 solutions. The CEFMO model, previously used to compute the FES94.1 solutions, was improved to allow us to compute tidal solutions at a global scale without adding extra continuity conditions at the basin open limits. "Open limit constraints" free solutions, forced only by the astronomical potential and secondary effects (loading and self-attraction), were computed for the main tidal components. The assimilation method, based on the representer approach, has been used to compute the FES95.2 solutions in a multi-basin version also. Thus it was revised in a similar fashion as the hydrodynamic model. As an immediate benefit, the pathologic behaviour of the assimilation model over some places, due to the addition of continuity conditions into the assimilation problem, has vanished. For instance, the anomalous resonance observed over some specific coastal areas in FES95.2 were eliminated. A careful selection of in situ tide gauge data from different data banks (IAPSO, WOCE and BH) allowed us to build a collection of about 800 data for the assimilation model. Referred as FES98, the new assimilation solutions are available on a 0.25x 0.25 degrees gridded version of the full finite element solutions. They are totally independent of altimetric measurements, and are as much accurate as the best available altimetric empirical solutions. In addition to the new solutions, the assimilation model gives us some insight look on the model, like the prior and posterior error covariances. These aspects will be discussed as well as the FES98 model improvements compared to FES94 and FES95.

**Monday 19 July PM**

Presiding Chair: Dr MASA KAMACHI

**JSP05/W/16-A1** **1400**

#### EXPERIMENTAL SEASONAL CLIMATE FORECASTS

SEGSCHEIDER, J (European Center for Medium-Range Weather Forecasting, Shinfield Park, Reading, Berks, Rg2 9ax, UK. E-mail: ned@ecmwf.int Telephone No: 01180 9499 257 Fax No: 01180 986 9450)

Experimental seasonal climate forecasts as they are currently issued on a quasi-operational basis at ECMWF require an initialization. For the oceanic component of the coupled forecast system this is provided by an ocean analysis where subsurface temperature data are assimilated into a global ocean model using an optimum interpolation scheme. Altimeter data provide additional information about the upper ocean heat content. To make use of this information TOPEX/Poseidon and ERS1/2 data are assimilated into the HOPE ocean model by vertical adjustment of the density profiles. Coupled forecasts started from the so-obtained ocean analysis allow a first estimate of the impact on the forecasted SST. The analysis is global, but the focus of this study is the equatorial eastern Pacific, where impact of oceanic conditions on seasonal prediction of climate is largest. Cross-comparisons of TAO/XBT analysis with T/P sea level and T/P analysis with TAO/XBT temperatures show that both assimilation of subsurface temperature and altimeter data improve the ocean analysis as compared to the control (no assimilation). Forecasts of Nino 3 SSTA initialized from altimeter assimilation ocean analysis are closer to observed SSTA than the control forecasts, but because of the probabilistic nature of the problem it is not yet possible to decide whether forecasts are improved compared to those initialized from subsurface temperature assimilation analysis. However, some of the altimeter initialized forecasts are closer to observed SST than the best member of the ensemble of subsurface temperature initialized forecasts. Therefore, and to enlarge the ensemble spread of the forecasts in general, a combination of the two data sources in the ocean analysis will be a next step.

**JSP05/W/14-A1** **1420**

#### REVERSE INTEGRATIONS OF AN ICE-SHEET MODEL USING A KALMAN FILTER

RICHARD C.A. HINDMARSH, British Antarctic Survey, High Cross, Madingley Road, Cambridge, England CB30ET. E-mail: rcah@bas.ac.uk . Telephone No: +44 1223 221 495 Fax No: +44 1223 362 616

The best constraints of time-dependent ice-sheet behaviour come from the dated marginal retreat sequences following the last glacial maximum. Typically, they comprise geological deposits which define the margin position and which can be dated directly or correlated with dated sites using varve deposits. Excellent sequences are obtainable from Scandinavia and Northern America.

These sequences have been modelled using forward techniques, but the approach used in this paper is to use a Kalman filter integrated backwards in time to force the model to match the margin position. The ability of the Kalman filter to constrain dynamics on unstable manifolds means that reverse integrations of the essentially diffusive ice-sheet equation can be carried out in this way. The theory for applying the extended Kalman filter is outlined and some examples are presented.

**JSP05/W/15-A1** **1440**

#### REGIONAL STUDIES AND APPLICATIONS WITH A VARIABLE RESOLUTION STRETCHED GRID DATA ASSIMILATION SYSTEM

Michael FOX-RABINOVITZ (Department of Meteorology/ESSIC, University of Maryland, College Park, MD 20742, USA, Email: foxrab@atmos.umd.edu) Dick Dee and Lawrence Takacs (both at National Science Corporation, 6100 Chevy Chase Drive, Laurel, MD 20707, USA, Email: ddee@dao.gsfc.nasa.gov, Itakacs@dao.gsfc.nasa.gov)

The variable resolution stretched grid (SG) version of the Goddard Earth Observing System

## INTER-ASSOCIATION

(GEOS) Data Assimilation System (DAS) incorporating the GEOS SG-GCM, is used for regional analysis, forecast, and climate applications. The region of interest with enhanced horizontal resolution, mostly used in experiments, is a rectangle over the U.S. The SG-DAS is capable of reproducing regional mesoscale fields, patterns and diagnostics that are not produced by the medium uniform resolution run with the same amount of grid points as for the SG. The SG-DAS regional analyses and diagnostics are used for: validation of regional climate simulation experiments produced with the SG-GCM for the U.S.1988 summer drought; and are planned to be used for atmospheric chemistry transport experiments. Also, a case study is conducted on a super-typhoon development in December 1997. The SG-DAS appears to be a viable candidate for a variety of regional studies and applications.

**JSP05/W/11-A1**

**1500**

### CORRECTING SALINITY USING T-S RELATIONS DURING ASSIMILATION OF THERMAL PROFILE DATA.

ALBERTO TROCCOLI and Keith Haines , (Department of Meteorology, University of Edinburgh, King's Buildings - Mayfield Road, Edinburgh EH9 3JZ (UK). E-mail: alberto@met.ed.ac.uk Telephone No: 0131 650 5041 Fax No: 0131 650 5780)

Ocean data assimilation has been continuously investigated over the last decade. Most research has focussed on either satellite altimeter data or near surface temperatures, as measured by either expendable BathyThermographs (XBT) or moored buoys. Recently it has been realised that salinity also plays an important role determining density and circulation not only at high latitudes, (e.g. Reverdin et al., 1997), but also in the tropics (e.g. Dongyu, 1994). However, little attention has been paid to updating salinity (S) in ocean circulation models used for data assimilation (DA). This is mainly due to the paucity of salinity data. As a result, the easiest solution is usually adopted, namely salinity is left unmodified by DA (i.e. preserving the a priori S(z) profile). But this may lead to increased errors in the velocity field (Cooper, 1988). We will present a simple approach using in situ T-S relations to including salinity field adjustments when only temperature measurements are available. This DA method is then applied to an ocean general circulation model in a twin experiment framework. The true and the parallel runs differ by the external forcings. Simulated XBT data are inserted along selected sections. Results show that S(z) is generally largely improved along those sections. We also address how these changes reflect upon the downstream water properties and whether we can learn something useful from recording the modifications introduced by the assimilation.

**JSP05/W/18-A1**

**1520**

### DIAGNOSING VERTICAL VELOCITIES USING THE QG OMEGA EQUATION: AN EXAMINATION OF THE ERRORS DUE TO SAMPLING STRATEGY

J. T. ALLEN, D. A. Smeed, A. J. G. Nurser and J. W. Zhang (Southampton Oceanography Centre, Southampton , UK, SO14 3ZH, email: jta@soc.soton.ac.uk) M. Rixen (G.H.E.R., Universite de Liege, Belgium)

Vertical motion at the mesoscale plays a key role in ocean circulation, ocean-atmosphere interaction, and hence the control of climate variability. It is not yet possible to measure vertical velocities less than 1000 m day<sup>-1</sup> directly. However, by assuming quasi-geostrophic (QG) balance, they can be diagnosed from the geostrophic velocity field and suitable boundary conditions. Significant errors in the accuracy of this diagnosis arise from the necessary compromise between spatial resolution and synopticity of a hydrographic survey. Observations of a numerical ocean model have been made on similar temporal and spatial patterns to observations made of the real ocean during a typical mesoscale physics research cruise. The balance between the number of observations and the synopticity of observations effects the apparent flow and in particular the diagnosed vertical motion. A combination of effects can typically lead to errors of 85% in the estimation of net vertical heat flux. An analytical two layer model is used to understand the sources of the components of this error and suggest key parameters for the design of mesoscale sampling.

**JSP05/W/13-A1**

**1600**

### THE IMPACT OF ANISOTROPIC ERROR CORRELATION

R. SWINBANK (Universities Space Research Association, NASA Goddard Space Flight Center, Greenbelt, MD 20771, USA; email: swinbank@dao.gsfc.nasa.gov) L.P. Riishojgaard, R. Menard (both at JCET, NASA GSFC, Greenbelt, MD 20771, USA; email: riishojgaard@dao.gsfc.nasa.gov, menard@dao.gsfc.nasa.gov)

Most data assimilation systems assume isotropic forecast error correlations, but results from two dimensional Kalman Filter experiments indicate that the correlations can be far from isotropic. In this paper we use a simple two-dimensional data assimilation system, which analyses trace chemical species such as ozone, to assess different approaches to modelling the error correlations. We compare assimilation results using isotropic correlations with results obtained using different approaches to modelling anisotropic correlations: first, using correlations based on the concentrations of the trace chemicals, and secondly using an advective correlation model. We show that these relatively cheap ways of modelling anisotropic correlations give objectively better results than using isotropic correlations. We discuss the possible extension of these approaches to a full 3-D meteorological data assimilation system.

**JSP05/W/12-A1**

**1620**

### THE USE OF DIRECT NEURAL NETWORK INVERSE MODELS IN DATA RETRIEVAL AND ASSIMILATION

Dan CORNFORD and Ian T Nabney (Neural Computing Research Group, Aston University, Aston Triangle, Birmingham B4 7ET, UK, Email:d.cornford@aston.ac.uk)

The increasing volume of remotely sensed data available for use in Numerical Weather Prediction (NWP) models provides a challenge to data assimilation systems. It is not always feasible to assimilate the remotely sensed variables directly since their relation to the meteorological variables is typically complex and non-linear. Often the 'forward sensor model' relating the meteorological variables to the sensor measurements is available; however, inversion of this model is computationally expensive and often done in 'ad-hoc' ways. Using the example of satellite scatterometer data we show how direct neural network inverse models allow inference of the local conditional probability of a surface wind vector over the ocean given the local scatterometer observation. The inverse models can then be used in several ways: as preconditioners to any retrieval/assimilation algorithm; and, using the scaled likelihood method, for inference in a Bayesian retrieval procedure. The procedure we have developed permits the retrieval of the wind fields without background information, and can thus be performed independently of the NWP model. The Bayesian retrieval procedure uses a Gaussian Process based prior wind field model which resolves scales relevant to NWP models and has been extended to include fronts. Thus these winds could be used directly in the

assimilation procedure, saving time by considerably reducing the burden of forward model inversion in a variational assimilation system.

**JSP05/E/09-A1**

**1640**

### STATISTICAL ESTIMATION OF THE GRIN FUNCTION

Leonid I.Piterberg (Center of Applied Mathematical Sciences, USC, Los Angeles, USA, email: Piter@cams.usc.edu) Sergei V.SEMOVSKI (Limnological Institute SB RAS, P.O.Box 4199 Irkutsk 664033 Russia, email: Semovski@lin.irk.ru)

The general statement for heat transport is the equation  $dT/dt=LT+w$ . If linear operator L is independent of time, random field w is stationary by time and sequence of field observations  $T(x,y,t)$  is available, then statistical procedure is presented for estimation of Green function. Leith (1975) proposed method for delta-correlated noise, based on multivariate correlation matrix calculation. Piterberg & Semovski (1987) considered finite correlation case, the method is based on calculation of multivariate spectra. Grin function estimation can be used for simulation of transport for arbitrary initial conditions. Estimation of advection field, diffusion, feedback factors can be derived. However, the procedure can also used for "teleconnection" description. Some functionals, derived from Grin function estimation, can be used for description of different characteristics of process under study, including spreading of elementary heat impulse, "sensitivity" and "influence" functions. Examples of Grin function computation are presented for few model cases. Statistical estimation of Grin function has been used for description of anomalies formation of sea surface temperature for the North Pacific, global surface temperature analysis and "influence function" calculation for the Central Siberia.

**JSP05/W/05-A1**

**1700**

### THE DETERMINATION OF SURFACE IRRADIANCE DIURNAL CYCLES BY ASSIMILATION OF JOINT GROUND-BASED AND REMOTE SENSING DATA

Oleg Pokrovsky , Nadya Korolevskaya ( Main Geophysical Observatory, Karbyshev str.7, St.Petersburg, 194021, Russia, e-mail: pokrov@main.mgo.rssi.ru)

Subsystem of surface radiative budget (SRB) is one of the most important modules in global observational system (GOS). Ground-based actinometrical network (AN) does not meet such important requirements, as uniformly coverage and spatial density. Satellite data could be potentially to compensate the lack of observational information. Now AN and satellite data are used in separate mode. AN data are implemented for calibration and validation aims. But the most promising approach could be based on simultaneous assimilation of both kind of data, as only in this case known mutually supplement features (relatively high accuracy of AN data and global uniformly coverage, accompanied by increasing of spatial resolution and density of satellite data ) could give some synergy effect. Assimilation method should overcome principal difference of these two kind of data to supply the radiative fields, having sufficient diurnal resolution. It has been developed the retrieval method of diurnal cycles of surface radiation budget variables based on satellite observation dataset. The method has been examined by means of the simulation of satellite measurement dataset ERBE and ScaRaB. It has been elaborated a statistical model of surface downward irradiance (SDI) diurnal cycles including a classification into cases of the clear sky, overcast cloudiness and some cases of partly cloudiness. The complete set of classes changes in wide range from 3 in the winter up to 6 in the summer. To achieve an effective classification by using the method of the discriminant analysis it is necessary to have at least five satellite measurements per day in July and three instantaneous observations - in March. When the classification procedure has been performed it is necessary to consider the retrieval problem of missing diurnal cycle values. Having the 3-5 satellite observations during a day the retrieval of not only daily sums but also the diurnal distributions of irradiance could be effective. So, for example, in July the relative retrieval error decreases to 20-30 %, and in March - to 10-20 %. The study conducted has shown that some reserve for the increasing of the retrieval accuracy is connected to an optimum choice of satellite observation instants during a day.

**Tuesday 20 July AM**

Presiding Chair: Dr Keith Haines (Department of Meteorology, University of Edinburgh, King's Buildings, Edinburgh, EH9 3JZ, UK)

**JSP05/W/08-A2**

**0930**

### THE PERFORMANCE OF ALTIMETER DATA ASSIMILATION IN THE OCCAM GLOBAL OCEAN MODEL

Alan FOX and Keith Haines (Department of Meteorology, University of Edinburgh, King's Buildings, Edinburgh, EH9 3JZ, UK. Email: A.D.Fox@ed.ac.uk). Beverly de Cuevas and Dave Webb (Southampton Oceanography Centre, Empress Dock, Southampton SO14 3ZH, UK)

Sequential assimilation of TOPEX/POSEIDON and ERS-1 altimeter data every 10 days into the OCCAM 1/4 degree global ocean model has been performed from the beginning of 1993. The assimilation method uses mapped sea level anomalies provided by CLS and a mean sea level which has been corrected with hydrographic data in the western boundary current separation regions. An error analysis on the surface height fields is performed with the model errors calculated at low resolution on each assimilation using an adaptive method. Surface height updates thus calculated are projected vertically into the model interior using the Cooper and Haines water property preserving method. The principle aims of our assimilation system are two-fold: firstly, to produce improved analyses of surface and subsurface ocean fields; and secondly, using the analyses produce useful forecasts of the ocean. Changes to fields and transports introduced by the altimeter assimilation are highlighted via comparisons with an OCCAM control simulation. Bearing our aims in mind, the performance of the assimilating model is assessed by comparisons with independent XBT data and WOCE hydrographic and ADCP sections, and the ability of the system to predict sea level changes on the 10-40 day timescale is demonstrated.

**JSP05/W/07-A2**

**0950**

### ALTIMETER ASSIMILATION IN A GLOBAL OCEAN MODEL: MODEL ERROR ESTIMATION.

Keith Haines and Alan FOX (Department of Meteorology, University of Edinburgh, King's Buildings, Edinburgh, EH9 3JZ, UK. Email: A.D.Fox@ed.ac.uk)

Sequential assimilation schemes in oceanography rely on some estimation of model error at assimilation time. The Kalman Filter represents the optimal estimate, but remains computationally unfeasible in any realistic application. An alternative approach is described in which model errors are estimated by application of a simple consistency condition between the known model-data misfits and observational errors, and the unknown model errors at each assimilation time. This calculation is performed at low resolution and results in an adaptive estimate of model error.

The technique is described in relation to assimilation of mapped altimetry data into the OCCAM, 1/4 degree, 36 level, global ocean model. Surface height updates found using the estimated model errors are projected vertically into the interior using the Cooper and Haines water property preserving method. Results of experiments assimilating TOPEX and combined TOPEX+ERS1 altimetry data over the period 1993-1995 are shown. At various times short 'forecast' runs are also performed with durations of up to 2 months. In a useful dual application, the model error estimation procedure described can also be used to gauge forecast skill.

**JSP05/W/03-A2** 1010

#### WHAT CAN WE LEARN BY ASSIMILATING ALTIMETRY?

JENS SCHROETER, Bernadette Sloyan and Martin Losch (Alfred Wegener Institute for Polar and Marine Research, Postfach 12 01 61, 27515 Bremerhaven, Germany. Email: jschroeter@awi-bremerhaven.de Telephone No: +49-(0)471-4831 762, Fax No: +49-(0) 471-4831 797)

The assimilation of satellite altimetry referenced to a geoid is discussed. The first problem that stands out in this context is the geoid error which can dominate the sea-surface-height data to be assimilated and make this information almost useless. The second major problem is the fact that good resolution and high quality geoid models like EGM96 include information about an oceanic climatology. By assimilating altimetry referenced to such a geoid we implicitly assimilate ocean climatology. We apply a box-inverse model of the southern ocean and show how only the long wavelength information of the altimeter data can be used for assimilation. The change in the models inverse solution and in the associated error covariance is presented. The possible impact by future satellite gravity missions on our results will be discussed.

**JSP05/W/09-A2** Invited 1050

#### DATA ASSIMILATION FOR INITIALIZING COUPLED CLIMATE PREDICTIONS

Antonio J. BUSALACCHI (Laboratory for Hydrospheric Processes, NASA Goddard Space Flight Center, Greenbelt, MD, 20771, USA, Email: tonyb@neptune.gsfc.nasa.gov)

At the beginning of CLIVAR, data assimilation in support of coupled climate prediction is proving to be the link that binds the modeling and observational components of interannual climate research. Initialization studies of coupled ocean-atmosphere prediction models have become an active area of research in the past few years now that the Tropical Pacific Ocean Observing System has reached a mature stage of deployment. Data assimilation into coupled forecast models of seasonal to interannual climate variability can take the form of assimilation (OI or adjoint) in situ and remotely sensed data into the ocean model in a stand-alone mode to improve initial conditions (e.g., reduce systematic biases), for parameter estimation, or as part of a coupled initialization procedure. This presentation will discuss the prospects for improved prediction skill as a result of data assimilation approaches to initializing coupled climate models. Predictions of the 1997-1998 El Nino will be used to illustrate how forecast skill was enhanced as a result of various approaches to assimilating surface wind, sea level, subsurface thermal structure and sea surface temperature observations.

**JSP05/E/05-A2** 1130

#### ASSIMILATION OF ALTIMETER DATA IN A TROPICAL PACIFIC OGCM

PETER MCLEAN and Mike Davey, UK Meteorological Office, London Road, Bracknell, Berkshire, RG12 2SZ, UK

A Tropical Pacific OGCM has been used to simulate temperature and currents in this region. The OGCM used in the UK Met. Office has some systematic errors in common with other similar models, with sea surface temperatures having a warm bias in the central and eastern equatorial Pacific. The thermocline in the analysis is also too diffuse which in turn leads to a too weak equatorial undercurrent. Interannual variability of sea surface temperature in different regions of the equatorial Pacific follows the trends of observed anomalies, but underestimates some warm and cold events. Topex Poseidon altimeter data which is produced in gridded format by CLS was assimilated into the tropical Pacific OGCM to try to improve the analysis. Results suggest that there is a tightening of the thermocline so that subsurface temperatures more closely resemble those observed, and that sea surface temperature anomalies are closer to those observed for example during the 1997 El Nino event. However altimeter assimilation was found to be of less use away from the equator with little improvement in the analysis in the subtropical regions.

**JSP05/W/13-A2** 1150

#### VARIATIONAL ADJUSTEMENT OF TSUNAMI PARAMETERS BY ASSIMILATION OF TIDAL STATIONS DATA

Carlos A.L. PIRES (Centro de Geofisica da Universidade de Lisboa, Rua da escola Politecnica 58, 1250 Lisboa Codex, Portugal, email: cpirez@fc.ul.pt); Pedro A M Miranda (Centro de Geofisica da Universidade de Lisboa, Rua da escola Politecnica 58, 1250 Lisboa Codex, Portugal, email: pmiranda@fc.ul.pt)

Time series at tidal stations constitute a potential source of information that may be assimilated into oceanic models. That information is too restrictive to infer the full dynamical state of the sea with any assimilation technique. However, it can be relevant or even sufficient in cases where a simplified hydrodynamical model can be applied and initial conditions can be described by a small set of parameters. Both conditions are nearly satisfied in the case of large tsunami events. We develop a four-dimensional (4DVAR) data assimilation scheme for tsunami signs (after a tide removal) at tidal stations along the Iberian Peninsular and North Africa for the Goringe Bank large earthquake of February 1969. Observations are assimilated into a shallow-water model for a period covering the first two or three significant waves in each station. Minimisation is performed in a functional space of 9 parameters using the well known Okada formulas described a simple tsunami source. This method is able to recover parameter values that are comparable to those obtained by pure geophysical inversion techniques and can eventually be used to complement them.

**JSA06** Monday 19 – Tuesday 20 July

#### SPACE WEATHER FORECASTING AND EFFECTS (IAGA, IAMAS, SCOSTEP)

Location: Hills 212LT  
Location of Posters: Old Gym

Monday 19 July AM

Presiding Chair: D H Boteler (Geological Survey of Canada, Ontario, Canada)

**JSA06-A1** Introduction 0830

D.H.Boteler (Geographical Survey of Canada)

**JSA06/E/11-A1** Invited 0835

#### EFFECTS OF HIGH-ENERGY PARTICLES ON SPACECRAFT AND AIRCRAFT ELECTRONICS

D.J.RODGERS and C.S.Dyer (DERA, Farnborough, UK)

Spacecraft and high-altitude aircraft have, in common, a reliance on complex electronic systems and an environment bathed in ionising radiation. This environment comprises the trapped proton and electron populations of the Van Allen belts, solar energetic particles and galactic cosmic rays. Variations in these populations occur over a wide range of time-scales and present a challenging problem for space weather forecasting. In addition, secondary populations are generated by atmospheric and spacecraft interactions. Radiation effects include 'single event effects', total dose effects, noise and internal dielectric charging. These effects and resulting electronic anomalies are described with reference to in-flight observations.

**JSA06/W/03-A1** Invited 0855

#### SPACE ENVIRONMENT EFFECTS AND THE ANIK-F SATELLITE DESIGN

Robin GUBBY (Space Systems Department, Telesat Canada, 1601 Telesat Court, Gloucester, Ontario K1B 5P4, Canada, email: r.gubby@telesat.ca), Bill Willis, (Member of Technical Staff Survivability Activity, Hughes Space & Communications Company, 2060 E. Imperial Highway Los Angeles, California 90009, USA; email: www@mail.hac.com)

In spite of much knowledge gained over the past three decades, space environment effects continue to be a major cause of anomalies in communications satellites. The two most common causes of anomalies are surface charging and deep dielectric (dis)charging, but other effects, such as total radiation dose, must be accounted for in the design, particularly in the solar arrays and electronics. Many space environments are difficult to predict accurately, for example the peak intensity of the developing Solar Cycle 23, and in particular the radiation dose to be expected from it. The recent Leonid storm provides an example of the extreme variation possible between predictions and reality. In early 2000, Telesat Canada will launch the Anik-F satellite, which is currently under construction at Hughes Space and Communications Company, and which will be one of the most powerful communications satellites ever built. It is designed to operate trouble-free for at least 15 years. The ways in which the space environment can affect a satellite and how these effects will be countered in the Anik-F design are reviewed.

**JSA06/W/16-A1** 0915

#### CORRELATION BETWEEN MAGNETOSPHERE STORMS AND SPACECRAFT CHARGING FOR RUSSIAN HIGH ALTITUDE SATELLITES

Vladimir I. GUSELNIKOV and Yury M. Prokopyev (Novosibirsk State University, Pirogova 2, Novosibirsk, 630090, Russia, email: vgusel@phys.nsu.ru, uprok@phys.nsu.ru) Oleg S. Grafodatsky (Scientific Production Association of Applied Mechanics (NPO PM), Lenina 52, Krasnoyarsk-26, 662990, Russia, email: 434graf@npopm.krasnoyarsk.su)

During the 20 years, the interaction of magnetosphere plasma with space crafts has been investigated. We present here the results of high altitude spacecraft charging investigation for Russian high altitude satellites and mutual correlation between charging value and geomagnetic activity. The spacecraft charging experiments were made on the serial communication and navigation satellites GORIZONT, GLONASS, GALS, and EXPRESS designed by NPO PM. Electric field strength at various points of spacecraft, potential difference between its isolated parts, plasma fluxes and electromagnetic noise intensity in circuits and antennas were measured. The project "Patrol system" was started on space crafts EXPRESS-11 (1994-067A) and GALS-12 (1995-63A). Measurements of electric field strength were made by means of vibration type probes (DEP). The measured field range is 0-100 kV/m. We introduced an effective index ED (Electrisation Disturbances) for describing spacecraft charging. The index ED was calculated for flight data from both satellites on the base of the electric field strength value, frequency of polarity change, duration of high level period. We determined this parameter as a value in range from 1 to 10. Mutual correlation for D-index and Cp-index, ED-index and Ap-index were calculated. Correlation interval was ranged from -5 to +5 days. The correlation coefficient reach maximum at the interval equal zero. The noticeable maximum reflects presence of correlation between DE and Ap indexes. Correlation between DE and Cp indexes shows even bigger value.

**JSA06/L/06** Invited 0935

#### OBSERVATIONS OF HIGH-LEVEL CHARGING ON THE FREJA S/C IN POLAR LEO

WAHLUND, J-E; Carozzi, T; Eriksson, A.I.; Holback, B., and Wedin, L.(Swedish Institute of Space Physics, Uppsala, Sweden) Andersson, L.(Swedish Institute of Space Physics, Kiruna, Sweden) Cook, D. (Air Force Research Laboratory (AFRL), Hanscom AFB, MA, USA) Hilgers, A. (ESTEC, Noordwijk, Holland) Laakso, H. (Finnish Meteorological Institute, Helsinki, Finland) Svensson, U. (SAAB-Ericsson Space, Sweden)

A total of 291 charging events have been detected onboard the Freja spacecraft in the altitude interval 1000 - 1800 km from the time period October, 1992, to April, 1994, during declining solar activity conditions. The Freja satellite orbited Earth with a 63 degree inclination, and had 73 kg of state-of-the-art plasma instrumentation available for studying the characteristics of the charging events that occurred simultaneously as auroral inverted-V type energetic electron precipitation hit the spacecraft. Negative charging levels exceeding -2000 Volts were recorded despite the fact that the Freja spacecraft was designed to be as electromagnetically and electrostatically clean as possible with highly conductive ITO surface coatings among other precautions. Several of the plasma instruments experienced severe operation disturbances



## INTER-ASSOCIATION

during most charging events. Results from both a statistical investigation and a detailed charging event study will be presented. It is found that auroral inverted-V type electrons in the energy range above about 5 keV cause the charging on Freja. Most charging events occur during eclipse, even though a few existed during sunlight conditions when the energy peak of the inverted-V electrons was larger (10-15 keV). The cold thermal plasma density did not usually decrease significantly as compared to surrounding levels during the charging events. On the other hand, a threshold density of about 2000cm<sup>-3</sup> existed, above where no charging events occurred. The effect of the magnetic field and other possible secondary electron emission effects were investigated. We compared the observed results with the charging codes SURCHG and POLAR, which is presented in an accompanied abstract. The current feature of the Polar code could not fully account for the highest charging levels observed. We finally conclude that high-level charging is still of concern regarding operation of spacecrafts and payload in polar LEO.

**JSA06/W/11-A1** Invited **0955**

### LESSONS FROM CRRES ON SPACE RADIATION HAZARDS

D.H. BRAUTIGAM (Air Force Research Laboratory, Hanscom AFB, MA 01731, USA, email: brautigam@plh.af.mil)

The Combined Release and Radiation Effects Satellite (CRRES) was a unique experiment which provides valuable lessons about the space radiation environment and its effects on technological systems in space. The tremendous value of CRRES resides in the fact that it flew not only the technologies to be space-tested, but also an extensive suite of instruments to accurately specify the damage-causing radiation environment. CRRES was launched into a geosynchronous transfer orbit on 21 July 1990, one year following the maximum of solar cycle 22, and returned data for approximately 14 months. It was first exposed to eight months of a relatively quiet magnetosphere, followed by a very active six months which was initiated by the much documented March 1991 storm. This large magnetic storm, accompanied by a solar proton event, was responsible for creating a temporary proton and electron belt within the typically benign slot region. This very dynamic radiation environment, with its various particle populations, was responsible for a number of observable total dose effects, charging / discharging phenomena, single event effects, and assorted anomalies within the spacecraft instrumentation and technology test bed. This exceptional combination of technologies, instrumentation, and dynamic radiation environment will be reviewed, with attention given to lessons learned and how CRRES has changed our perspective on magnetospheric radiation hazards.

**JSA06/W/27-A1** **1035**

### GIC RISK IN THE UK: GEOMAGNETIC VARIATIONS, GEOLOGY AND SURFACE ELECTRIC FIELDS

David BEAMISH (Fluid Processes and Waste Management Group, British Geological Survey, Keyworth, Nottingham, NG12 5GG, England), Toby Clark, Ellen Clarke and Alan THOMSON (Global Seismology and Geomagnetism Group, British Geological Survey, West Mains Road, Edinburgh, EH9 3LA, Scotland. email: a.thomson@bgs.ac.uk)

The geomagnetic induced current (GIC) risk in the UK is assessed with reference to known examples of GICs in the power grid operated by National Grid plc. A simplified three-dimensional geology model is used to provide an indication of the surface electric field for various amplitudes and wavelengths of the external magnetic field variation. It is found that the conductivity contrast between seawater and the onshore geology produces enhanced E-fields around the coast. A simple measure of the power of the changing magnetic field is used to determine the risk to the power grid from rapid magnetic variations, according to season and local time. Monitoring and forecasting of this power index is suggested as a means of gauging the likely risk to high-cost power industry equipment.

**JSA06/L/02-A1** **1055**

### GIC IN NATIONAL GRID'S TRANSMISSION SYSTEM

Jon LAVER (The National Grid Company plc, Engineering & Technology, Kelvin Avenue, Leatherhead, Surrey KT22 7ST, U.K. Email: Jon.Laver@ngc.co.uk)

Some data from the previous sunspot maximum (Cycle 22) are available and briefly reviewed. Several incidents at the time were attributed to the effects of Geomagnetic Induced Currents (GIC) in the Transmission System. These are described in some detail together with the effects of several subsequent severe storms. National Grid is taking the forthcoming Cycle 23 seriously. Amongst several in-depth studies and initiatives taken include determining what the likely magnitudes and effects of the GIC will be on both primary plant (mainly Supergrid Transformers) and secondary plant (mainly protection equipment). Further studies have assessed what mitigation measures might be implemented.

Following upon the impact assessment study, a real-time data acquisition system is currently being commissioned at a number of sites. This will record quasi-DC currents in Supergrid transformers together with associated plant parameters, include some geophysical parameters, and will telemeter all this data back to a central system. A forecasting system is also being implemented, inputting available near real-time and forecast data. The physical model of the transmission system also constructed should then express this as equivalent surface electro-telluric fields throughout the country. Using this model's output together with conventional network analysis, magnitudes of induced quasi-DC currents in nodes of the transmission system may then be determined.

**JSA06/L/03-A1** Invited **1115**

### POSSIBILITY OF PREDICTING THE MAGNITUDE OF GIC IN PIPELINES

S. O. OGUNADE, (Department of Physics, Obafemi Awolowo University, Ile-Ife, Nigeria.)

In the equatorial and auroral zones Geomagnetically Induced Currents (GICs) are known to accelerate the corrosion process in oil and gas pipelines. Using a numerical model the horizontal H- and D-components of the magnetic field due to a buried pipeline under a sheet current source are obtained. A relationship is established between the horizontal components of the magnetic field obtained and the pipe-to-soil potential. A further relationship is found to exist between the pipe-to-soil potential and the current induced in the pipeline.

The pipe-to-soil potential measured for pipelines in Nigeria are correlated to Kp and Dst geomagnetic indices for the period 1993 to 1997. The trend of the result indicates a possibility of predicting the magnitude of geomagnetically induced currents in pipelines from real-time geomagnetic indices.

**JSA06/W/06-A1** **1135**

### APPLICATION OF DSTL THEORY TO STUDIES OF GEOMAGNETIC EFFECTS ON PIPELINE NETWORKS

Anitti PULKKINEN(1), David Boteler(2), Risto Pirjola(1), Ari Viljanen(1) (1) Finnish Meteorological Institute, Geophysical Research Division, P.O. Box 503, FIN-00101 Helsinki, Finland (2) Geomagnetic Laboratory, Geological Survey of Canada, 7 Observatory Crescent, Ottawa, Ontario K1A 0Y3, Canada

The expressions of the geomagnetically induced current in a pipeline and the voltage between the pipeline and the earth related to the current have a similar form whether they are derived from the Maxwell equations or from the transmission line analogy. This suggests that a pipeline can be represented as a transmission line, and geomagnetic effects can be calculated using the distributed source transmission line (DSTL) theory. The main advantage of the analogy is that we can use methods familiar from the circuit theory, e.g. the Thevenin theorem. Applying the Thevenin theorem we can model discontinuities of a pipeline which would be difficult if started directly from the basic electromagnetic theory. The latest achievements have been the modelling of branches of a pipeline network and inclusion of a non-uniform electric field. These new results make it possible to model the voltages and the currents produced in the entire pipeline network by realistic geomagnetically induced electric field.

**JSA06/E/09-A1** Poster **1155-01**

### 150 YEARS OF GEOMAGNETIC EFFECTS ON TECHNOLOGY

D. H. Boteler1, H. Nevanlinna2, J. Allen3, L. Morris3, G. Jansen van Beek1, R. Pirjola2 1 Geomagnetic Laboratory, Geological Survey of Canada, 7 Observatory Crescent, Ottawa, Ontario K1A 0Y3, Canada. 2 Geophysical Research, Finnish Meteorological Institute, P.O. Box 503, FIN 00101 Helsinki, Finland. 3 National Geophysical Data Centre, NOAA, 325 Broadway, Boulder, Colorado 80303, USA.

Geomagnetic effects have been observed on electrical systems since the early days of the telegraph. As each new system involving long conductors was laid across the earth's surface the engineers involved found that they had to contend with the effects of geomagnetic disturbances. Geomagnetically induced voltages on submarine phone cables caused voice transmissions to alternate between shrieks and whispers. Telluric currents in pipelines interfere with the corrosion prevention systems. Geomagnetically induced currents in power systems cause transformer saturation and harmonic generation leading to misoperation of relays, equipment damage and power blackouts. The largest magnetic disturbances that cause the worst effects are infrequent events so to assess their frequency of occurrence it is necessary to examine a long period of geomagnetic data. Thanks to the efforts of Mayaud we have the aa index of magnetic activity extending back to 1868. Now, using early recordings from the Helsinki magnetic observatory, equivalent 3-hourly activity values have been produced and used to extend the aa sequence back to 1844. To obtain representative measures of the activity in a geomagnetic disturbance a 24-hour running mean of these values is taken. The resulting aa\* index provides a record of geomagnetic disturbances throughout the whole period of electro-technological use on the earth.

**JSA06/E/13-A1** Poster **1157-02**

### EVALUATION OF TELLURIC CURRENT EFFECTS ON THE MARITIMES AND NORTHEAST PIPELINE

D. H. BOTELER (Geomagnetic Laboratory, Geological Survey of Canada, 7 Observatory Crescent, Ottawa, Ontario K1A 0Y3, Canada, email: Boteler@geolab.nrcan.gc.ca), R. Gummow (CORRENG Consulting Service Inc) B. Rix and R. Reid (Union Gas)

The Maritimes and Northeast Pipeline on the east coast of North America is being constructed through an area where large geomagnetic disturbances can be expected and where the electric fields produced will be amplified by the coast effect. In addition the water movement associated with the rise and fall of tides in the Bay of Fundy (the highest tides in the world) will produce significant tidal electric fields. Because of these factors it was decided to include consideration of telluric current effects in the design of the cathodic protection (CP) system for the new pipeline. An evaluation was made of the electric fields expected to be produced by geomagnetic disturbances and the tidal dynamo. A computer model was set up to examine the pipeline response to these electric fields. This allowed prediction of the pipe-to-soil potentials produced with different coating resistances and placement of insulating flanges and ground beds. The modelling capability allowed various cathodic protection schemes to be evaluated before construction and has resulted in a more efficient and cost effective CP design for the pipeline.

**JSA06/E/10-A1** Poster **1159-03**

### GEOMAGNETICALLY INDUCED ELECTRIC FIELDS AND CURRENTS IN PIPELINES

L. TRICHTCHENKO and D.H. Boteler (Geomagnetic Laboratory, Geological Survey of Canada, 7 Observatory Crescent, Ottawa, Ontario K1A 0Y3, Canada)

Variations of the Earth's magnetic field induce electric fields in pipelines. These induced electric fields drive currents along the pipeline that can interfere with the cathodic protection systems installed to prevent corrosion of the pipeline. For design of systems to counteract these effects it is necessary to be able to calculate the size of the currents that will be produced by different geomagnetic conditions. In this study we present the results of numerical modelling of the induced electric fields and currents produced in a long coated pipeline buried in the Earth. The effects of changes of the pipe parameters (pipe dimensions, conductivities, magnetic permeability) are studied. Calculations are made for different frequencies and characteristics of the source fields.

**JSA06/W/04-A1** Poster **1201-04**

### PROJECT ON GEOMAGNETICALLY INDUCED CURRENTS IN THE FINNISH NATURAL GAS PIPELINE NETWORK

ANTTI PULKKINEN(1), Kari Pajunpää(1), David Boteler(2), Ari Viljanen(1), Risto Pirjola(1) (1) Finnish Meteorological Institute, Geophysical Research Division, P.O. Box 503, FIN-00101 Helsinki, Finland (2) Geomagnetic Laboratory, Geological Survey of Canada, 7 Observatory Crescent, Ottawa, Ontario K1A 0Y3, Canada

This paper describes a study of geomagnetically induced currents (GIC) in the Finnish natural gas pipeline network being made by Gasum Inc., the pipeline owner, and the Finnish Meteorological Institute. The project involves theoretical studies and measurements of the currents and voltages produced in the pipelines during geomagnetic disturbances. The theoretical part of the project is performed by applying the distributed source transmission (DSTL) theory with new extensions developed in this study that make it possible to treat an entire pipeline network at the same time with a realistic non-uniform induced electric field. Profiles of GIC and voltage between the earth and the pipeline are calculated for different geomagnetic situations. Measurements are made of the voltage between the pipeline and the earth. The current along the pipeline is also measured by using two magnetometers: one near

the pipeline and the other is at the nearby Nurmijärvi Geophysical Observatory, so the difference of these two magnetic measurements is the magnetic field due to the current in the pipeline. The measured data will be combined with theoretical models to derive statistics of the GIC occurrence on the pipeline system.

**JSA06/W/07-A1** Poster **1203-05**

#### CHARACTERISTICS OF GEOMAGNETIC EVENTS CAUSING LARGE GEOMAGNETICALLY INDUCED CURRENTS

Ari VILJANEN, Olaf Amm and Risto Pirjola (Finnish Meteorological Institute, Geophysical Research, Division, P.O.B. 503, FIN-00101 Helsinki, Finland, email: ari.viljanen@fmi.fi)

Events of large geomagnetically induced currents (GIC) are studied by focusing emphasis on the relation between GIC and the local and global geomagnetic activity. From the local viewpoint, we especially attempt to describe the ionospheric currents which cause the largest GIC values. A global approach aims to clarify the possibilities of forecasting GIC. We present a rough classification of ionospheric currents associated with large GIC.

**JSA06/E/04-A1** Poster **1205-06**

#### IMPACT AND OBSERVATIONS OF GEOMAGNETIC SUBSTORMS IN A WIDE AREA DIFFERENTIAL GPS NETWORK

Susan SKONE (Department of Geomatics Engineering, University of Calgary, 2500 University Dr. NW, Calgary, Alberta T2N 1N4, Canada, email: sskone@ensu.ucalgary.ca)

The Global Positioning System (GPS) is a satellite navigation system, in which 24 satellites currently provide worldwide positioning capabilities. Due to the dispersive nature of the ionosphere, GPS signals experience ranging errors dependent on both the given signal frequency and ionosphere electron content. Such range errors translate into a degradation of positioning accuracies.

Dual frequency GPS receivers enable the estimation of absolute ionospheric range delay and total electron content (TEC) along the signal path. By using a number of GPS reference stations, each equipped with a dual frequency receiver, it is possible to estimate values of the vertical ionospheric TEC (in latitude and longitude) on a spherical shell. This type of ionosphere delay modelling is employed in Wide Area Differential GPS (WADGPS) Networks. Features such as the main ionospheric trough, and enhancements/depletions of electron density, are observed in the TEC maps during periods of enhanced auroral ionospheric activity.

In this paper, ionosphere TEC variations are investigated in the auroral region during periods of geomagnetic substorms, and the impact on WADGPS applications assessed. GPS observations from reference stations in the Natural Resources Canada wide area network are used, providing extensive coverage of the high latitude Canadian sector. A spectral analysis of the ionosphere TEC variations is also conducted, demonstrating the potential of identifying auroral disturbances associated with substorms in real-time from the GPS data. Correlations with space weather parameters from ground-based and space-borne magnetometers and imagers are illustrated. The ability to track substorm development over a large region, using GPS measurements from the network of reference stations, is also investigated.

**JSA06/W/29-A1** Poster **1207-07**

#### THE LARGE GEOMAGNETIC SUDDEN COMMENCEMENTS AT MOSCOW

Tamara KUZNETSOVA, Kharlampij Kanonidi (both at IZMIRAN, Troitsk, Moscow region, 142092, Russia, email: tvkuz@izmiran.rssi.ru)

A statistical study of geomagnetic sudden commencements (SCs) at observatory Moscow (geomagnetic latitude  $(g=51^\circ)$  since 1940 showed that the largest two SCs had amplitude in H-component equal to 305 nT and 250 nT. These SCs are observed on 9 May, 1992, UT=19h59m and on 13 June, 1990, UT=14h16m respectively. A detail analysis of these events showed that the disturbances connected with the SCs had global character on the Earth. An analysis of the amplitude distribution showed that amplitude of the SCs observed at the close MLT are linear proportional to the L-shell of the observatory on the Earth in range of  $L=1.6-6$ . Vector diagrams of the disturbances show that the polarization vectors are in agreement with superficially wave passing from the dayside magnetopause in antisunward direction. The amplitudes show dependence on MLT of SC observations. The solar sources of the SCs could be interplanetary shock waves generated by the flares. An analysis shows that velocities of the shock waves should be greater than 1000km/sec. These high amplitude SCs at Moscow are unusual phenomena. The SCs form instantaneously a radiation belt that exists more than a half year and they are potentially-damaging space weather events. Time delays between the SCs and beginnings of strong geomagnetic storms are analyzed. The other peculiarities of the events are discussed.

**JSA06/W/13-A1** Poster **1209-08**

#### SOLAR FLARE EFFECT CHANGES IN GEOMAGNETIC FIELD COMPONENTS AND IONOSPHERIC CHARACTERISTICS

I.M. VASILJEVIC (Geomagnetic Institute, 11306 Grocka, Belgrade, Yugoslavia, email: ivan@tehnico.net) L.J.R. Cander (Rutherford Appleton Laboratory, Chilton, Didcot, Oxon, OX11 0QX, UK, email: l.cander@rl.ac.uk)

This paper describes the results of the analyses of two solar flare effects (SFEs) on the geomagnetic field components variations and the key ionospheric characteristics at Observatory Grocka. Two periods in September 1991 have been considered: 9-14 and 24-29 covering geomagnetically disturbed period and periods prior and after the storm. The SFEs were identified by A3 method of absorption measurements. The results have shown that SFEs could be directly correlated with the changes in the ionospheric parameters but the same is not valid for the variations in the geomagnetic field components.

**JSA06/W/31-A1** Poster **1211-09**

#### TO EQUATORIAL SPREAD F USING MODELS OF THE LOW-LATITUDE IONOSPHERE AND ELECTRODYNAMICS

Dr Vince ECCLES

The fundamental processes of Equatorial Spread F (ESF) have been examined in detail for four decades. The gravitationally-driven Rayleigh-Taylor instability has long been identified as the initiating process. Likewise, controlling geophysical conditions of ESF have been identified: - large post-sunset vertical drift - conjugate sunsets - transequatorial winds - equatorial ionization anomaly conditioning However, forecasts of ESF occurrence and intensity of accompanying signal scintillation still are based on rough, but improving, probabilities from climatological

models. A physics-based model of the low-latitude ionosphere and its resulting R-T growth rates are used to examine predictors of ESF occurrence. In particular, the model is used to examine afternoon precursor observations that might be used to forecast ESF occurrence.

**JSA06/E/03-A1** Poster **1213-10**

#### GEOMAGNETIC SUBSTORM FORECASTING AT NETWORK OF HF RADIO PATHS

Donat V. BLAGOVESHCHENSKY (University of Aerospace Instrumentation, 67 Bolshaya, Morskaya Str., 190000, St. Petersburg, Russia, email:nataly@aari.nw.ru)

The emergence of active solar processes result in certain disturbances in the near-Earth environment. The disturbances manifest themselves first of all in the high-latitude ionosphere. Therefore the latter may serve as an object of studies in order to predict its state by means of radiophysical methods of investigation. Among them, one should specially single out the method of prediction with the help of a system of HF paths. The system represents a set of several paths of length up to 3000 km and of different directions but with one reception center located at a geomagnetic latitude  $?L = 60-65^\circ$ . The decimeter waves pass through the ionosphere, hence they are an effective tool to predict its state. The network of HF paths makes it possible to obtain and carry out an analysis of a complex of statistical characteristics of the SW signal envelope at the receiver output. The envelope characteristics of the signal are evaluated by a computer in on-line mode and include: m - the Nakagami law parameter, ? - the time correlation radius, ?X - the signal average, L1, L2, L3 - parameters of the process non-stationarity and so on. Their variations at different phases of a substorm reveal certain regularities. By our studies, two-three hours before the start of the decrease of the H-component of the Earth magnetic field, there is observed the growth of absolute values of all parameters. At about one hour before the substorm intensification there begins a sharp decrease in magnitudes of the characteristics considered, which reach their minimum at the expansion phase of substorm. Hence the forecasting of the substorm onset may be made about two hours before the breakup begins. At the recovery phase there is a gradual growth of the parameters back to their original values. Thus the suggested method of forecasting the geomagnetic substorm by the characteristics of propagating radio waves is important for investigation of potentially-damaging space weather events.

**JSA06/W/32-A1** Poster **1215-11**

#### AN IONOSPHERIC FORECASTING SERVICE BASED AROUND A NOVEL NONLINEAR TECHNIQUE CAPABLE OF USING BROKEN TIME SERIES

N M FRANCIS, P S Cannon \*(Defence Evaluation and Research Agency,D705, St. Andrews Rd., Malvern, Worcs., WR14 3PS, UK.Tel: +44 (0) 1684 896484, Fax: +44 (0) 1684 895241, email: nmfrancis@dera.gov.uk \*also at University Of Bath, UK.)

Recent advances in the fields of ionospheric and space weather forecasting have been possible due to the adoption of techniques derived from studies into artificial intelligence and non-linear dynamical systems theory. A common approach is that of using the Multi-Layer Perceptron (MLP) [1] to provide predictions based upon a time series input. However, we have adopted Radial Basis Function (RBF) Neural Networks (NN). The advantages of the latter over their MLP counterparts are outlined. This paper will describe an on-line WWW forecasting service of the ionospheric parameter foF2 for north western sub-auroral Europe. The forecast is based on data from the Chilton (UK) ionosonde. Scaled data can be routinely down-loaded from this ionosonde (and other Digisondes) and automatically processed by the forecasting algorithm. This algorithm produces hourly updated, nonlinear predictions for one to twenty four hours ahead, with data currently posted every 6 hours. In addition the pseudo-sunspot number derived from the forecast of foF2 is also posted. For algorithm evaluation purposes a wide complement of other algorithms are also available - although these are not available to the user. The paper will also review these and show comparative results. The user is, however, presented with a quantitative assessment of the efficacy of yesterdays forecast by reference to the measured values and the predicted monthly median values.

Of particular interest is the ability of this algorithm to deal with non-contiguous data sets, which are a recurrent problem in geophysical time series. Simple linear interpolation is undesirable because it can disrupt the delicate non-linear dynamics within the data, as well as degrading the performance of the nonlinear modelling process.

**JSA06/W/18-A1** Poster **1217-12**

#### SEDAT: SPACE ENVIRONMENT DATABASE

Mike HAPGOOD, Matthew Wild and Richard Stamper (CLRC Rutherford Appleton Laboratory, Chilton, Didcot, Oxfordshire, OX11 0QX, UK, email: M.Hapgood@rl.ac.uk ), Alain Hilgers, Hugh Evans and Norma Crosby (ESTEC, 2200 AG Noordwijk, The Netherlands, email: ahilgers@estec.esa.nl)

SEDAT is a project, funded by European Space Agency, which aims to develop a new approach to the engineering analysis of the spacecraft charged-particle environment. This project will (a) assemble a database containing a comprehensive set of data about that environment as measured in-situ by a number of missions and (b) develop an extensible set of engineering analysis software tools that can operate on data retrieved from the database. Thus the user will be able to select space environment data appropriate to the engineering problem under study and then apply appropriate tools. An important aspect of SEDAT is that the database and tools will be seamlessly integrated so that the tools can be applied within queries, i.e. the user can construct queries that operate on the values of engineering functions derived from database parameters (and not just on the values of database parameters). This approach differs from traditional space environment engineering studies. In the latter the space environment is characterised by a model that is a synthesis of previous observations. However, in SEDAT the environment is characterised directly by the observations. The poster will discuss the potential advantages of this new approach and describe the current state of the SEDAT project.

**JSA06/W/28-A1** Poster **1219-13**

#### WWW SERVICE FOR SPACE WEATHER FORECAST PROGRAM IN KOREA

Seok-HEE BAE , Hwang-Jae. Rhee and Yoo Sum Pyo (Radio Research Laboratory, 901 Hoge-2 dong, Dongahn-gu, Anyang, Kyunggi-do, 431-082, R.O.Korea, email: shbae@cc.ri.go.kr) , Kyung Seok. Cho and Guenho Lee (Ichon Branch of Radio Research Laboratory, 370-9, Shinpil-li Sulseong-meon, Ichon, Kyunggi-do 467-880, R.O.Korea, email: kscho@cc.ri.go.kr)

Radio Research Laboratory(RRL) has developed a space weather forecast program from 1994. The final goal of this program is to build up a realtime space warning system for space communication and satellite operation.

RRL have three ground observation systems to accomplish the goal: a solar radio spectrograph, geomagnetometers in three stations and an digital ionosonde. In addition, several researches have been performed for developing items as a part of space weather



## INTER-ASSOCIATION

forecast program. Until now, RRL had several projects for this program. That is a developed operational S/W for solar radio spectrograph, which obtained the information of solar activity in a near real time. And several researches make it possible to observe 210 degree geomagnetic field, to model a numerical scheme of the geomagnetic substorms. Others calculate a sun transit outage prediction for communication satellites and study the spacecraft charging effect due to the space plasma.

RRL is trying to make an effort to systemise the use of the research results and observation data through internet. The main service on our www website (URL: <http://spaceweather.rri.go.kr>) is to provide the ground based observation data for space environment research in a real time. That includes the solar radio spectrograph, 3 component geomagnetic field, and ionogram with ionospheric basic parameters. And another service contains current research area and contents as well as the results of some researches mentioned above. Others service has estimated 10.7 cm solar flux, dst index and so on for space researchers and satellite operators. For the public use, the home pages provide a monthly prediction of radiowaves propagation, weekly warning of radiowaves propagation disturbance and prediction of sun transit outage. Simple and interest topics on basic knowledge about space science are also described for the education.

**JSA06/W/17-A1** Poster **1221-14**

### SERVICES PROVIDED BY THE OTTAWA REGIONAL WARNING CENTRE OF ISES

Richard COLES, Hing-Lan Lam, Karen Harding, and David Boteler (all at Geological Survey of Canada, Geomagnetic Laboratory, 7 Observatory Crescent, Ottawa K1A 0Y3, Canada, email: [coles@geolab.nrcan.gc.ca](mailto:coles@geolab.nrcan.gc.ca))

The Ottawa Regional Warning Centre of the International Space Environment Service (ISES) operates several services that provide forecasts, warnings, and reviews of geomagnetic activity in the Canadian region. Long-term (up to 27 day) forecasts are issued at three-week intervals. Short-term (up to 48 hours) forecasts are issued every hour, and include magnetic storm warnings as appropriate. Reviews of recent past activity are incorporated into the hourly short-term bulletins. Forecasts and information on past activity are available via a variety of media, including World Wide Web, Internet ftp, fax, e-mail, mail and, for the short-term forecasts, a fully-automated voice service.

**JSA06/L/04-A1** Poster **1223-15**

### THE AUSTRALIAN SPACE FORECASTING CENTER (ASFC)

G. Patterson, R. Thompson, D. Cole, J. Kennewell, R. Luckhurst, P.WILKINSON (IPS Radio and Space Services, P O Box 1386, Haymarket, NSW 1240, AUSTRALIA)

IPS Radio and Space Services (IPS) is a Government Program within the Australian Commonwealth Department of Industry, Science and Resources. IPS supplies the Australian radio and space environment services for the Australian region of interest to customers operating in the fields of radio communications; land, sea and air transport; broadcasting; defence applications; spacecraft operations and geophysical exploration. Services are delivered in a variety of ways from normal postage to advice on the internet and cover a range of time scales from diagnostic climatology advice to real-time Web and e-mail based services. The immediate, and real-time services are distributed from the Australian Space Forecasting Center (ASFC). This is staffed during extended normal working hours and during weekends in the mornings. Advice offered by the ASFC is based on a range of data collected at IPS observatories as well as from overseas groups. As part of the International Space Environment Services (ISES), all these data are shared with other groups. The Australian observatories include two solar observatories at Learmonth and Culgoora and 15 ionospheric observatories spanning low to polar latitudes. Nine currently report real time observations. IPS has recently started collecting real-time geomagnetic data from four of these observatories. The ASFC services are mainly supplied from links to the IPS Homepage <http://www.ips.gov.au>. These services include real time maps of the local ionosphere as well as services based on the maps. There are also services based on the real time geomagnetic data to assist with aeromagnetic surveys and TEC advice based on local GPS observations. A special aspect of the services is that many are grouped under customer headings making ready access to key services easier.

**JSA06/E/12-A1** Poster **1225-16**

### SOLAR AND GEOMAGNETIC ACTIVITY DURING CYCLE 23

Richard THOMPSON (IPS Radio and Space Services, PO Box 1386, Haymarket, NSW 1240, Australia, email: [Richard@ips.gov.au](mailto:Richard@ips.gov.au)) and the Solar Cycle Prediction Panel

Predictions of solar and geomagnetic activity are crucial for the planning of satellite operations, especially for those in low earth orbit where atmospheric drag varies in response to activity on the sun. In 1996, and again in 1997 and 1998, a panel of international scientists met to review forecasts of solar and geomagnetic activity to be expected in Solar Cycle 23. The panel was organised by the US Space Environment Center under a contract from NASA. The panel examined the techniques used to predict the cycle and considered the many individual predictions. A consensus prediction was reached for a cycle of amplitude of 160 in sunspot number (with extremes of 130 and 190) and for time of maximum as April 2000 (with extremes of June 1999 and January 2001). This will make the cycle one of the largest on record and comparable to the last two solar cycles. The panel felt it unlikely that it would reach the amplitude of Cycle 19, the largest observed solar cycle. Examination of the early rise of Cycle 23 suggested that the date of solar minimum - the start of the cycle according to the traditional measure of the sunspot number (May 1996) - may not be a good guide. For this reason, the panel recommended that October 1996 be used as the "effective onset" of the cycle for all predictions requiring this information. The panel has made a prediction for the shape of Cycle 23 based on the average of recent cycles of similar amplitude. This profile is being used as the basis of a new service providing medium to long term predictions of smoothed sunspot number. A novel feature of the panel discussion was a prediction of geomagnetic activity to be expected over the cycle. Predictions were made using two techniques and, whilst they give different profiles, both indicate high levels during the years 1999-2004.

**JSA06/E/05-A1** Poster **1227-17**

### SOME PARTICULARITIES OF GEOMAGNETIC ACTIVITY TIME SCALES STATISTICS

V.G.VASILYEVA, N.S.Zaretsky, (Institute of Cosmophysical Research and Aeronomy, 677891 Yakutsk, Russia, email: [v.g.vasilyeva@sci.yakutia.ru](mailto:v.g.vasilyeva@sci.yakutia.ru))

Statistical characteristics of global and local disturbances with most intense and fast geomagnetic field oscillations are considered. This is 4-dimensional consideration. It seems like it is possible to get some more information due to fractal features of taken statistics either in space and time. And we have been trying to analyse power-like significance of disturbance duration scale what principally was stated earlier in Matsubara's analogy. Since

the fundamental feature  $E \sim T^{-1/t}$  has been understood as interaction intensification principle of ionospheric currents behaviour we could say the space weather forecasting makes deal with high "temperature", in its common sense.

Confirmation of existence of certain resonance fractals in magnetosphere the experimental data of geomagnetic activity indices are discussed.

**JSA06/E/01-A1** Poster **1229-18**

### FORECASTING THE MAGNETOSPHERIC AND IONOSPHERIC OF ENERGETIC ELECTRON FLUXES

MINEEV, Yu. V. (Skobel'syn Institute of Nuclear Physics, Moscow State University, Moscow 119899, Vorobjevy Gory, Russia, email: [mineev@srdlan.npi.msu.ru](mailto:mineev@srdlan.npi.msu.ru))

The connection between solar wind velocity variations and the dynamics of energetic electrons ( $E=0.03-3.0$  MeV) in magnetosheath, magnetopause, outer and inner radiation belts is considered. For the data on satellites "Prognoz", "Molnia", "Raduga" and "Sampex" analytical dependencies for electron flux density  $J$  on the magnetosheath, magnetopause and outer radiation belt were obtained for the solar wind  $V(t): J(t+d)=a+bV(t)$ , where  $t$ -time,  $d$ -delay time;  $a, b$ -coefficients, depending on position of satellites region of space. The equation has been obtained which takes into account parameters of the solar wind and determines time for energetic electron transfer from the magnetospheric boundaries to ionospheric altitudes. The obtained electron flux dependencies, including the maximal flux dependencies, from a value of the maximal velocity of the solar wind, may be used for short-time prognoses (about two-three days) of radiation condition and safety. This method is compared with other methods of space weather forecasting. A new system for the forecasting of radiation condition in near cosmic space is proposed. The scheme takes into account the above stated effect and other data, including geophysical one. The role of energetic electrons in processes of D-layer\_s ionisation, in an origin of the winter anomaly and in other phenomena in thermosphere and middle atmosphere is discussed.

**JSA06/E/06-A1** Poster **1231-19**

### NOWCASTING CONVECTION VELOCITIES IN THE HIGH-LATITUDE IONOSPHERE - A COMPARISON OF STATISTICAL CONVECTION MODELS

P. L. DYSON(1), M. L. Parkinson(1), P. R. Smith(1),(2), and R. J. Morris(3) (1)Department of Physics, La Trobe University, Victoria 3083, Australia (2)Department of Electronic Engineering, La Trobe University, Victoria 3083, Australia (3)Australian Antarctic Division, Kingston, Tasmania 7050, Australia.

The Weimer and IZMEM statistical convection models are driven with a time series of interplanetary magnetic field (IMF) measurements made onboard the Wind spacecraft. The model outputs are used to infer convection velocity at Casey, Antarctica (80.8S geomagnetic latitude), and then compared with measurements of Doppler velocity made using a Digisonde, and measurements of convection velocity made using a collocated magnetometer. During a single, representative campaign interval, Feb. 13-17, the Weimer model explained 10% (27%) of the variation in Doppler speed (direction) observed by the Digisonde, and 18% (14%) of the equivalent convection components observed by the magnetometer. This compares with IZMEM, which explained 8% (37%) of the variation in Doppler speed (direction) observed by the Digisonde, and 31% (34%) of the equivalent convection components observed by the magnetometer. In general, there was better agreement between convection direction than convection speed. The results of this study show that measurements of ionospheric velocity using different experimental techniques need heavy averaging to identify a common component of velocity controlled by the IMF vector.

**JSA06/L/09-A1** Poster **1233-20**

### AN ADJOINT METHOD OF CALCULATION OF ENERGETIC SOLAR-PARTICLE-EVENT EFFECTS ON THE EARTH'S ATMOSPHERE

K. O'BRIEN (Northern Arizona University, Flagstaff, AZ 86011 USA), Herbert H. Sauer (CIRES, University of Colorado, Boulder, CO 80303, USA; NOAA Space Environment Center, Boulder, CO 80303, USA)

High energy solar particles, produced in association with solar flares and coronal mass ejections, occasionally bombard the earth's atmosphere, resulting in radiation intensities additional to the already-present cosmic-ray dose rates. Access of these particles to the earth's vicinity during times of geomagnetic disturbance are not adequately described by using static geomagnetic field models. These solar fluxes are also often distributed non-uniformly in space, so that fluxes measured by satellites obtained at great distances from the earth and which sample large volumes of space around the earth cannot be used to predict fluxes locally at the earth's surface. We present here a method which uses the ground-level neutron monitor counting rates as adjoint sources of the flux in the atmosphere immediately above them to obtain solar-particle dose rates as a function of position over the earth's surface. We have applied this approach to the large September 29-30, 1989 event (GLE 42) to obtain the magnitude and distribution of the dose rates from an atypically large event. This approach could easily be adapted to the calculation of other atmospheric quantities of interest, such as ionization and energetic primary and secondary particle fluxes.

**JSA06/L/01-A1** Poster **1235-21**

### ON THE FORECASTING OF GREAT FLARE ENERGETIC PARTICLE EVENTS TO SAVE ELECTRONICS ON SPACECRAFTS

Lev DORMAN (IZMIRAN, Technion and Israel Cosmic Ray Center, affiliated to Tel Aviv University; Current address: P.O.Box 2217, Qazrin 12900, ISRAEL; email: [lid@physics.technion.ac.il](mailto:lid@physics.technion.ac.il))

The problem of influence of solar flare energetic particles (FEP) on micro-electronics code on spacecrafts is very important. Especially dangerous are single event phenomena (SEP)[1] which can destroy computer memories; according to [1] in the periods of great energetic particle fluxes is necessary to switch off some part of electronics to protect computer memories from SEP. How to predict this period of time? In principle it can be made by using high energy particles which came from the Sun much more early than main part of middle energy particles caused dangerous situation for electronics. The flux of these high energy particles is very small and can not be measured with enough accuracy on spacecrafts, but are measured continuously by ground based neutron monitors and muon telescopes with very small statistical errors. These predictions can be made exactly by the International Cosmic Ray Service[2], which could be organized in near future on the basis of world-wide network of cosmic ray observatories. For prediction of dangerous FEP events it is necessary to have 1-minute or 5-minute on-line data at least from several neutron monitors and muon telescopes. It is important that the accuracy of prediction increases with increasing of FEP event dangerous level. [1] J. Barak et al., 1995. Annual Report, Israel Atomic Energy Commission. [2] L.I. Dorman et al., 1993. Astrophys. and Space Sci., Vol. 208, p. 55.



JSA06/L/07-A1 Poster 1237-22

**COSMIC RAY FORBUSH-DECREASE AS A SIGNATURE OF SPACE DANGEROUS PHENOMENON AND POSSIBLE USE OF COSMIC RAY DATA FOR ITS FORECASTING**

Lev DORMAN (IZMIRAN, Technion and Israel Cosmic Ray Center, affiliated to Tel Aviv University; Current address: P.O.Box 2217, Qazrin 12900, ISRAEL; email: lid@physics.technion.ac.il), N. Lucci (Terza Università di Roma, Dipartimento di Fisica "E. Amaldi", Via della Vasca Navale 84, 00146 Rome, Italy), G. Villoresi (IFSI/CNR-Frascati c/o Terza Università di Roma, Dipartimento di Fisica "E. Amaldi", Via della Vasca Navale 84, 00146 Rome, Italy)

We consider the influence of space dangerous phenomenon as strong interplanetary shock waves caused a great cosmic ray Forbush-decrease on satellite electronics, as well as on people health and technology at ground level. The problem of influence of great magnetic storms accompanied by cosmic ray Forbush-effects was developed deeply by many authors (see review in [1] and references therein). The prediction of this dangerous phenomenon can be done by using cosmic ray data on preincrease effect and on the change of 3D cosmic ray anisotropy. We show that this prediction can be done accurately in the frame of International Cosmic Ray Service (ICRS) [2], which could be organize in near future. For prediction of dangerous Forbush-decreases it is necessary to have 1-hour on-line data. [1] N.G. Ptitsyna, G. Villoresi, L.I. Dorman, N. Lucci, M. I. Tyasto. 1998. "Natural and man-made low-frequency magnetic fields as a potential health hazard", Physics-Uspekh, Vol. 41, No 7, pp. 687-709. [2] L.I. Dorman, N. Lucci, G. Villoresi, 1993. Astrophys. and Space Sci., Vol. 208, p. 55.

JSA06/L/08-A1 Poster 1239-23

**NONSTATIONARY PROBLEM OF COSMIC RAY PREINCREASE EFFECT AND FORBUSH-DECREASE: AUTO-MODEL SOLUTION FOR FORECASTING USING**

Lev DORMAN (IZMIRAN, Technion and Israel Cosmic Ray Center, affiliated to Tel Aviv University; Current address: P.O.Box 2217, Qazrin 12900, ISRAEL; email: lid@physics.technion.ac.il), N. Lucci (Terza Università di Roma, Dipartimento di Fisica "E. Amaldi", Via della Vasca Navale 84, 00146 Rome, Italy), G. Villoresi (IFSI/CNR-Frascati c/o Terza Università di Roma, Dipartimento di Fisica "E. Amaldi", Via della Vasca Navale 84, 00146 Rome, Italy)

On the basis of Fokker-Plank equation with a boundary condition on the moving boundary (shock wave) we investigate nonstationary problem described the cosmic ray (CR) behavior before the interplanetary shock wave (CR preincrease effect) and after (CR Forbush-decrease). For this aim we transform the initial equation of partial derivatives from three variables (time, distance from the Sun and particle rigidity) to the ordinary differential equation of the second order from one auto-model variable. We found analytic solution for the auto-model problem with moving boundary (with conditions of continuity of CR density and equality of CR fluxes from both sides of the moving boundary) and describe the developing in time of the CR preincrease effect and Forbush-decrease in dependence of the shock wave speed and solar wind speed as well as values of diffusion coefficients before and after shock wave. Obtain analytic solution of CR preincrease effect in comparison with observation data can be used for forecasting of powerful shock waves caused a strong geomagnetic storms accompanied by great Forbush effects.

JSA06/W/21-A1 Poster 1241-24

**SUICIDE RISK DEPENDENCE ON HELIOGEOPHYSICAL ACTIVITY**

S.CHERNOUSS, V.Roldugin (Polar Geophysical institute, Apatity, 184200, Russia, email: SergeyChernouss@hotmail.com), E.Vlassova (The Kola Science Centre Hospital with Clinic, Apatity, 184200, Russia, email: Vlassova@vita.kolasc.net.ru), A.Ronkko (Labour Protection District of Lapland, FIN-941000 Kemi, Finland, email: Ahti.Ronkko@tsp.stm.vn.fi)

Statistical studies of suicides in Finland, from 1920 to 1996 in depending on heliogeophysical activity, is under consideration. Statistics relating to commission of suicide by males correlate with Wolf Numbers statistics of the Solar activity. Eleven year period is clearly distinguished in the suicide statistical data estimated by spectral and correlation analysis including MEM. It is shown that about 20% of male suicide commissions are connected with heliogeophysical disturbances. The problem of mechanism of the impact including cosmic rays, weather conditions and electromagnetic disturbances are discussed. Hypothesis of interference of the human brain alpha-rhythm and Schuman resonance frequencies could be acceptable explanation of the observed effect. Some indirect evidences of the situation are demonstrated.

JSA06/W/25-A1 Poster 1243-25

**SPACE WEATHER AFFECTS HUMAN BEINGS. EXPERIMENTAL CONFIRMATIONS.**

DMITRIEVA I.V., Khabarova O.V., Obridko V.N., Ragoulskaia M.V., Reznikov A.E. (The Institute of Terrestrial Magnetism and Radio Waves Propagation, Troitsk, Moscow region, email: bella@izmiran.troitsk.ru)

The results of experiment for determination of influence of geomagnetic field disturbances on a human organism are considered. We used method of electropuncture diagnostics by R.Voll for this aim. The method is based on measurement of conductivity in acupuncture points and is convenient by that allows to estimate deviations from the norm in functioning of various organs in same units. Local A-index is used as an indicator of geomagnetic field disturbance. The daily measurements of group (27 persons) have shown presence of a synchronous mass response of inspected people on magnetic storm. At first it is exhibited as sharp (within 3-4 hours) increase of conductivity of the all acupuncture points from normal values, that corresponds to a maximum of adaptational capabilities of an organism. And then - long duration (about 4 day) falling of conductivity that describes depression of all organs and systems of an organism. The reaction of adaptation on three magnetic storms of identical intensity going with an interval per week was registered for a half inspected people. It was found out, that the duration of depression phase and disbalance of an organism, intrinsic to this phase, depends extremely on a wholeness of an organism (that is on a power of ties between organs and co-ordination of their activity), but not on a type of disease.

JSA06/C/U4/E/02-A1 Poster 1245-26

**PEOPLE UNDER CONDITION OF ELECTROMAGNETIC CONTAMINATION OF MODERN MEGACITIES.**

Maria RAGOUSKAIA, Olga Khabarova and Vladimir Lubimov (all at The Institute of Terrestrial Magnetism, Ionosphere and Radiowaves Propagation, 142092, Moscow region, Troitsk, Russia; email: MARYL@izmiran.troitsk.ru), Yuri Gurfinkel (Central Clinical Hospital of Russia, 105203 Moscow, Russia)

The influence of space weather and high level of ambient electromagnetic noise of the modern megacities on a human health condition is considered. The method of electropuncture diagnostics based on measurement of electrical conductivity in acupunctural points (AP) of

skin is used for this aim. The daily measurements of electrical conductivity of 22 AP of constant group inspected (30 persons) are carried out simultaneously in centre of Moscow and in 20 kms from Moscow since March 1998. The obtained data are compared with data of geomagnetic field disturbance level, atmospheric pressure, temperature, humidity and ambient noise. It was found out, ambient electromagnetic noise influences an average level of the indications, characteristic of each inspected, due to downturn of conductivity values for a long time (months) rather genetically established level. As result there are the reduction of immunity, increased tiredness and irritability of the large cities inhabitants. The people that engage intellectual activity and chiefs of collectives as a rule easier adapt for conditions of the modern megacities. The response on electromagnetic disturbance of technical nature that close to intensity and frequency band of geomagnetic storms is similar to a response on magnetic storms of a natural origin. At first it is exhibited as sharp (within 3-4 hours) increase of conductivity of the all AP from normal values, that corresponds to a maximum of adaptational capabilities of an organism. And then - long duration (about 4 day) falling of conductivity that describes depression of all organs and systems of an organism.

JSA06/L/11 Poster 1247-27

**A PREDICTION METHOD OF GEOMAGNETIC DISTURBANCES BASED ON IPS OBSERVATIONS DYNAMICS FUZZY MATHEMATICS**

F. XUESHANG

A prediction method for geomagnetic disturbances, based on a combined approach of interplanetary scintillation (IPS) observations, dynamics of disturbance propagation and fuzzy mathematics, is suggested. Prediction test for 37 geomagnetic disturbance events caused by the solar storm-associated interplanetary disturbances, which could be identified by IPS observations during the period of 1984-1985, are made based on the membership functions established by using observational data on the solar storm, interplanetary and geomagnetic disturbances in 1966-1982.

JSA06/L/12 Poster 1249-28

**MAGNETOTAL ANALYSIS DURING GEOMAGNETIC PERTURBATIONS**

V. M. SILBERGLEIT

The auroral AE and the equatorial Dst indices with 1 minute time resolution were analyzed during three moderate geomagnetic storms. Different substorms periods are identified.

The distant Earth's magnetotail, using data from Geotail spacecraft are also studied. The existence of a Bz bipolar signature (a North then South turning of the magnetic field) and a pressure enhancement are observed. Those criteria indicate the existence of plasmoid events. In some cases, the plasmoids appeared as multiple events, perhaps due to multiple onset substorms. The geomagnetic indices show changes some minutes before magnetotail events.

Monday 19 July PM

Presiding Chair: D Baker (University of Colorado, Boulder, Colorado, USA)

JSA06/W/10-A1 Invited 1400

**GEOMAGNETIC FORECASTING - STATE OF THE ART**

BALCH, C (Space Environment Center, 325 Broadway, Boulder, CO 80303 USA. email:cbalch@sec.noaa.gov)

The prediction of geomagnetic conditions is an important part of the mission of the U.S. Space Weather Operations Center (SWO) in Boulder, Colorado. Geomagnetic activity is specified by means of the summary indices Kp and Ap (or real-time estimates thereof), and by probabilities for particular ranges of these indices (e.g. 'active', 'minor storm', and 'major storm' levels). These forecasts are based on available, timely observations of the Sun, the solar wind, and the magnetosphere. Solar observations include white-light, Helium 10830, and Hydrogen-Alpha images, x-ray images from Yohkoh/SXT. Images from SOHO were also quite useful when they were available. Solar wind conditions are monitored using real-time solar wind data from the ACE spacecraft. Magnetospheric conditions are evaluated primarily by means of a network of ground-based magnetometers.

Geomagnetic predictions produced by SWO consist of three types: daily forecasts, watches, and warnings. Daily forecasts and watches are predictions with lead times in excess of an hour; these products are necessarily restricted to inputs from observations of solar activity. Short term warnings, which can have a lead time of up to about forty minutes, are based on two additional inputs: 1) real-time solar wind measurements from the ACE spacecraft, and 2) an assessment of the current state of the magnetosphere.

In this talk I will give an overview of the observations and models that are available to the forecasters and I will discuss the various approaches used to synthesise the information into predictions. I will also review verification results as a means of measuring the success of current predictive techniques. Lastly I will identify what I perceive to be the key areas where significant progress can be made to advance the state of the art.

JSA06/W/20-A1 Invited 1420

**INTERPLANETARY MAGNETIC FLUX ROPES AS A TOOL FOR PREDICTING MAGNETIC STORMS**

Katsuhide MARUBASHI (Communications Research Laboratory, Koganei, Tokyo 184-8795, Japan, email: kmaru@crl.go.jp)

It has become increasing evident that the coronal mass ejection (CME) produces the interplanetary magnetic flux rope (henceforth called flux rope for simplicity). Flux ropes sometimes carry strong southward magnetic fields in the solar wind, and cause intense magnetic storms. In this sense, the flux rope is literally a tie to connect CMEs on the Sun and magnetic storms on the Earth.

When a flux rope encounters the Earth's magnetosphere, the variation of interplanetary magnetic field (IMF) is determined by many conditions. They include (1) the field intensity; (2) the size and orientation of the flux rope; (3) the bulk speed and expansion of the flux rope; (4) and which part of the structure passed the magnetosphere. The ability to forecast magnetic storms based on the physics of flux ropes depends on how such conditions can be predicted based on solar observations. We review our present knowledge of flux ropes and examine the possibility of forecasting magnetic storms based on the flux rope model. It is seen that we have enough evidence for the fundamental relationship between the magnetic structures of flux ropes and large-scale magnetic fields in the solar source regions of CMEs. We have to admit, however, that more precise knowledge about the propagation of flux ropes is needed in order to predict magnetic storms. An attempt is made to estimate how our present knowledge of flux ropes can assist forecasting magnetic storms.

# INTER-ASSOCIATION

**JSA06/W/23-A1** 1440

## FORECASTING HIGH LATITUDE SPACE WEATHER SOLELY FROM THE IMF/SW DATA

Vladimir PAPITASHVILI (Space Physics Research Laboratory, University of Michigan, Ann Arbor, MI 48109, USA, email: papita@umich.edu), Yohsuke Kamide (Solar-Terrestrial Environment Laboratory, Nagoya University, Honohara 3-13, Toyokawa, Aichi 442, Japan, email: kamide@stelab.nagoya-u.ac.jp), Federica Maruccci (CNR- Istituto Fisica dello Spazio Interplanetario, Tor Vergata, Via Fosso del Cavaliere 100, Roma 00133, Italy, email: federica@sunserv.ifi.rm.cnr.it)

The World Wide Web access to existing science-based models of the solar wind-magnetosphere-ionosphere interaction facilitates their usability for a variety of space weather applications. The Linear Model of Ionospheric Electrodynamics (LiMIE, <http://www.sprl.umich.edu/MIST>) utilises the IMF/SW data measured at L1 point by the NASA's spacecraft ACE. The input data are available from the NOAA Space Environment Center ([http://sec.noaa.gov/ace/ACERTsw\\_home.html](http://sec.noaa.gov/ace/ACERTsw_home.html)) in near-real time. The LiMIE specifies and then forecasts for ~1 hour ahead the ionospheric convection and field-aligned current distributions over both the Northern and Southern polar regions. The "snap-shot" maps are plotted in geographic co-ordinates or as the CGM Lat. - MLT polar dials. Other parameters (e.g., ion convection velocities, electric and magnetic fields, ionospheric currents, Joule heating and ground-induced current distributions) can also be plotted and statistical location of the auroral electrojets and pseudo-AE index can be estimated. The latter is important for electric and pipeline companies in northern Russia, Scandinavia, Canada, and United States. Forecasted ionospheric parameters over the Antarctic continent could be utilised for planning of scientific experiments and for estimating the radio wave propagation conditions. The LiMIE is made accessible also from the Solar-Terrestrial Environment Laboratory (<http://stesun8.stelab.nagoya-u.ac.jp>) and from the AGONET Data Analysis Facility (<http://sunserv.ifi.rm.cnr.it/~adaf>).

**JSA06/W/01-A1** 1500

## A COMPARISON OF SOLAR WIND PLASMA AND MAGNETIC FIELD CORRELATIONS

K. I. PAULARENA, J. D. Richardson, (M.I.T., Center for Space Research, Cambridge, MA, USA, 02139, email: kip@space.mit.edu), G. N. Zastenker and P. A. Dalin (both at Space Research Institute, Russian Academy of Sciences, Moscow, Russia, email: gzastenk@iki.rssi.ru).

Recent work examining the degree of correlation between 6-hour periods of solar wind plasma data measured by different spacecraft (IMP 8, WIND, INTERBALL-1, and ISEE-3) has shown that the level of correlation can vary from good ( $r > 0.8$ ) to quite poor ( $r < 0.1$ ). The degree of correlation is fairly strongly related to the standard deviation of density during the 6- hour period, and somewhat to the distance between the spacecraft along the Sun-Earth line. For distances larger than 220 Earth radii there is a steep fall-off in the average correlation from that observed with smaller inter-spacecraft separations. Nevertheless, at all separations there are times of good and times of poor correlation, implying that the scale of solar wind plasma homogeneity is quite variable. In an effort to understand what really drives the degree of correlation seen, a comparison is made between the observed interplanetary magnetic field (IMF) and plasma correlation. Results using a limited set of data (133 periods) from the WIND and INTERBALL-1 spacecraft show that good plasma correlation are observed 65% of the time that IMF correlation are good, while good IMF correlation are seen during only 44% of good plasma correlation periods. This result is particularly surprising since it was expected that all or almost all periods with good IMF correlation would also show good plasma correlation. Therefore, this study has been extended to a larger data set to provide more statistically robust comparisons and to examine whether other factors affect these results.

**JSA06/W/08-A1** 1520

## OPERATING AN AUTOMATED FORECASTING SERVICE - WHAT ARE THE PITFALLS?

Richard COLES (Geological Survey of Canada, Geomagnetic Laboratory, 7 Observatory Crescent, Ottawa K1A 0Y3, Canada, email: coles@geolab.nrcan.gc.ca)

In principle, an automated service of any kind has the promise of great efficiency and little human intervention. However, there are pitfalls. Canada has operated an automated magnetic forecasting and magnetic storm warning service since mid-1995. The Canadian service is committed to providing forecasts that are updated hourly every day of the year. To maintain such a service requires considerable effort, ingenuity, and expense. Any or all of the data streams (such as geomagnetic, solar wind, or solar) used by the forecasting process may fail or be interrupted. The forecasting process must be robust so that updates will continue to be issued. Backup systems or alternate paths for all stages in the process, including data telemetry and the provision of electrical power, are necessary. Current practice and future enhancements are presented.

**JSA06/W/09-A1** Invited 1600

## PROTON FLUENCE MODEL JPL1991: A REVIEW

Joan FEYNMAN (Jet Propulsion Laboratory, California Institute of Technology, 4800 Oak Grove Dr., Pasadena, CA 91109, USA, email: aruzmaikin@jplsp.jpl.nasa.gov)

The development of new technologies and the minimisation of sensors bring new requirements for our ability to predict and forecast hazardous space weather conditions. Of particular importance are protons of energies  $> 1$  MeV which cause single event effects, displacement and ionization damage, and pose a hazard to biological systems in space and to personnel in polar orbit. Sporadic high energy solar particle events are a main contributor to the fluences and fluxes of such protons. A statistical model, JPL 1991, developed for use in spacecraft design is now widely used in the community. I will review the model and its use, including extensions to high energies higher than 60 MeV. Predictions of the model will be compared to observations of solar particle events that have occurred since model development.

**JSA06/E/07-A1** Invited 1620

## RADIATION BELT MODELLING IN THE FRAMEWORK OF SPACE WEATHER EFFECTS AND FORECASTING

D. HEYNDERICKX and M. Kruglanski (BIRA/IASB, Brussels, Belgium)

The Earth's trapped radiation belts were discovered at the beginning of the space age and were immediately recognised as a considerable hazard to space missions. Consequently, considerable effort was invested in building models of the trapped proton and electron populations, culminating in the NASA AP-8 and AE-8 models that have been de facto standards since the seventies. The CRRES mission has demonstrated that the trapped radiation environment is much more complex than the static environment described by the old models. Spatial and especially temporal variations were shown to be much more important

than previously thought, and to require more complex models than those in use at that time. Such models are now becoming available, but they are as yet limited in spatial and temporal coverage. It is vital to co-ordinate future modelling efforts in order to develop new standard models. An overview of existing radiation belt models and future developments is presented.

**JSA06/W/02-A1** 1640

## STORM-ASSOCIATED ELECTRON FLUX CHANGES IN THE OUTER RADIATION BELT

Takahiro OBARA (Hiraoso Solar Terrestrial Res. Ctr., 3601, Isozaki, Hitachinaka, Ibaraki, 311-1102 Japan, email: T.Obara@crl.go.jp)

To forecast a relativistic electron flux in the outer radiation belt is one of the important aspects from the Space Weather point of view. Once a magnetic storm takes place, the relativistic electron flux decreases at the Geostationary orbit. This reduction is found to be a sudden earthward shift of the relativistic particles due to an increased electric field. It was also found that in case of major storms the outer radiation belt disappears entirely. After a disappearance of the relativistic electrons which can last as much as one day, an increase in the flux occurs in low L-shells (3-4) which propagates to higher L shells. There is a systematic tendency in the energy spectrum from 300 keV to 2.5 MeV; i.e. both decay and growth are severer for higher energy and a time delay of the recover is apparent for higher energy, suggesting some acceleration processes take place within the radiation belt. The increase sometimes exceeds the pre-storm levels. Investigation has been made on the correlation of the electron flux increase and the IMF Bz polarity together with AL index during the storm recovery phase. Result demonstrates that a larger flux enhancement occurred when the IMF was southward and AL index was quite large. Source particles are effectively supplied due to the southward IMF together with high magnetic activity, and they further are accelerated up to MeV range by some processes within the outer radiation belt. One candidate is a wave-particle interaction there.

**JSA06/W/14-A1** 1700

## SCOSTEP SPACE WEATHER WORKING GROUP AND SPACE WEATHER INFORMATION

HANNU KOSKINEN (Finnish Meteorological Institute, Geophysical Research, P.O.Box 503, FIN-00010 Helsinki, Finland, email: Hannu.Koskinen@fmi.fi, also at University of Helsinki), David Boteler (Geological Survey of Canada, Ottawa, Canada), Jih Kwin Chao (National Central University, Chung Li, Taiwan), Janet Kozyra (University of Michigan, Ann Arbor, Michigan, USA), Rainer Schwenn (Max-Planck- Institute für Aeronomie, Katlenburg-Lindau, Germany), Howard Singer (NOAA Space Environment Center, Boulder, Colorado, USA), Takashi Tanaka (Communications Research Laboratory, Tokyo, Japan), Oleg Troshichev (Arctic and Antarctic Research Institute, St. Petersburg, Russia), Phil Wilkinson (IPS Radio and Space Services, Haymarket, NSW, Australia)

During the 1997 IAGA meeting in Uppsala the Scientific Committee on Solar-Terrestrial Physics (SCOSTEP) decided to form a working group on space weather under the SRAMP program. In the acronym SRAMP, R stands for Results, A for Applications, and M for Modelling. In the present rapid growth of space weather the results of solar-terrestrial physics form the scientific basis, applications are a central goal, and major efforts are put into further development of models. The space weather working group has taken information spreading as the central theme of its mission. While there is much information around, it is often scattered and relevant information may be difficult to find. This applies to the whole information chain, including availability of data and up-to-date models, schedules of various observation facilities, joint observation or data analysis efforts, etc. The first tasks of the working group have been to create a www server that contains updated information on the major space weather campaigns and is linked to space weather servers world-wide and promote a Space Weather Month for the autumn of 1999, (for more information, see [http://aoss.engin.umich.edu/intl\\_space\\_weather/sramp/](http://aoss.engin.umich.edu/intl_space_weather/sramp/)).

Tuesday 20 July AM

Presiding Chair: E W Friday (Washington DC, USA)

**JSA06/W/22-A2** 0930

## SPACE WEATHER IMPACT ON HUMAN HEALTH IN THE NORTH

S.CHERNOUSS, M.Kuznetsova (Polar Geophysical Institute, Apatity, 184200 Russia, email: SergeyChernouss@hotmail.com), Yu.Fedorenko (Institute of the North Ecological Problem, Apatity, 184200 Russia, email: yura@ifjf.uib.no), E.Vlassova (The Kola Science Centre Hospital and Clinic, Apatity, 184200 Russia, email: Vlassova@vita.kolasc.net.ru)

The Report consists of two parts. The first one is a review of famous results that show negative impact of magnetic disturbances and Solar activity factors on human health. The second one describes new approach to the problem of the heliogeophysical factors impact on human health. It is based on simultaneous measurements of geophysical and human organism parameters at Kola peninsula in the Polar Geophysical institute. It would be possible to remark that studies of heliogeophysical attack on human body was studied occasionally at the West, meanwhile the heliobiology took an advantage since 30-s after Chizhevsky works in Russia. The most of published before results on the problem are based on hardship events. Cardiac diseases statistics give us undoubted evidences of geomagnetic storm influence on human health. Statistics of myocardial infarction also confirm strong influence of geomagnetic storms on human health. It was pointed out that the strongest impact on human health is observed at the North where auroral and magnetic disturbances are permanent. In this work we try to base the method of measurements of some parameters characterizing adaptation function of human being to compare those data with geomagnetic disturbances i.e. to avoid any diseases, myocardial infarction and other hard events in the studies. The report consist of description of ideology, methods and equipment to measure the response of human being to some outdoor factors first of all heliogeophysical disturbances, weather and environment conditions. The main idea is to obtain information about adaptation function of human being by real time measurements of heart rate variation parameters. We have used for that purpose cardiac rhythmology method originally was proposed by R.Baevsky in 60-s to check health of Russian astronauts on board of the Salute space vehicle. The local centre of cardiac measurements.

**JSA06/W/05-A2** 0950

## SPECIFICATION AND FORECASTING OF OUTAGES IN COMMUNICATION AND NAVIGATION SYSTEMS

SANTIMAY BASU and Keith M. Groves (Air Force Research Laboratory, VSBI, 29 Randolph Road, Hanscom AFB, MA 01731, U.S.A., email: santimay@aol.com) Sunanda Basu (National Science Foundation, Atmospheric Sciences Division, 4201 Wilson Boulevard, VA 22230, U.S.A., email: sbasu@nsf.gov)

The upper atmosphere above 100 km, called the ionosphere, is ionized and often becomes turbulent and develops electron density irregularities. These irregularities scatter radio waves to cause amplitude and phase scintillation and affect satellite communication and GPS



navigation systems. The effects are most intense in the equatorial region, moderate at high latitudes and minimum at middle latitudes. The thermosphere and the ionosphere internally control the generation of irregularities in the equatorial region and its forcing by solar transients is an additional modulating factor. On the other hand, the irregularity generation mechanism at high latitudes is driven by the magnetosphere and, therefore, high latitude scintillation can be tracked by following the trail of energy from the sun. The development of a global specification and forecast system for scintillation is needed in view of our increased reliance on space based communication and navigation systems, which are vulnerable to ionospheric scintillation. Such a system, called the Scintillation Network Decision Aid (SCINDA), has been developed for the South American sector. An international space weather initiative has been launched by SCOSTEP under the aegis of the S-RAMP group. It is hoped that during the proposed global campaign in September 1999, scintillation measurements will be performed at high and low latitudes and will contribute towards the development of a global scintillation specification and forecast system.

**JSA06/W/15-A2 1010**

**SHORT-TERM IONOSPHERIC AND TOTAL ELECTRON CONTENT FORECASTING OVER EUROPE**

L.R. CANDER, M.F. Levy and M.I. Dick (CRLC Rutherford Appleton Laboratory Chilton, Didcot, Oxon OX11 0QX, UK, email: lcander@rl.ac.uk), P. Muhtarov and L. Kutiev (Geophysical Institute, Sofia, Bulgaria, email: ikutiev@geophys.bas.bg), S.M. Radicella and B. Nava (ICTP Abdus Salam, Trieste, Italy, email: rsandro@ictp.trieste.it), R. Leitinger (University of Graz, Graz, Austria, email: leitinger@bkfug.kfunigraz.ac.at)

HF communications and GPS services can greatly benefit from accurate forecasts of ionospheric parameters (foF2, MUF(3000)F2 and FOT) and Total Electron Content (TEC) values in real-time mode. We describe an operational short-term forecasting tool for the European region based on continuous monitoring of the ionosphere. It is available on the World Wide Web for interactive use, at <http://www.rcru.rl.ac.uk/iono/maps.htm>. At any time, users may select a forecast map for 0 to 23 hours ahead, or browse through the archive of retrospective measurement maps. This paper outlines the basic principles of STIF (Short-Term Ionospheric Forecasting) and a technique to produce on-line forecast maps of vertical TEC over European region (100 W - 900 E, 300 - 700 N) and describes some of the on-line facilities. Statistical comparisons of maps obtained from forecast and measured values are discussed. European network of 23 ionospheric stations provide data every day as input parameters to an autoregressive extrapolation of foF2 and MUF(3000)F2 time series for each ionospheric station in the network. Kriging interpolation is used to get gridded values. TEC is obtained from a profiler based on a modified Di Giovanni - Radicella (DGR) model that has 5 semi-Epstein layers and uses ionospheric characteristics foE, foF1, foF2 and MUF3000(F2) as inputs. TEC maps are calculated with the last two characteristics given by STIF and simplified models for foF1 and foE values. The profiler has been adapted from the NeQuick model developed with ESA-ESTEC support.

**JSA06/L/05-A2 1030**

**INVESTIGATION AND FORECAST OF SPACE WEATHER EFFECTS ON SPACECRAFT SYSTEMS**

Yury ROMANOVSKY and Sergey Tasenko (both at Fedorov Institute of Applied Geophysics, Rostokinskaya 9, Moscow, 129128, Russia, email: hciag@sunny.aha.ru)

Method to investigate Space Weather (SW) effects on geostationary (GEO) and low Earth orbit (LEO) spacecrafts is developed. This method was applied to clarify SW effects on malfunctions and failures of <Electro> GEO satellite systems. Database on LEO spacecraft failures for period 1981- 1995 years is prepared. It is revealed that for this time interval about 20% of failures could be raised by SW effects. Codes and operational (short-term) prognostic models are developed for prediction of possible SW effects on LEO and GEO spacecrafts with usage of real time information on SW parameters. On the base of this prediction recommendations and proposals on spacecraft control are being formulated using artificial intelligence methods.

**JSA06/E/02-A2 1110**

**FUTURE RADIATION DAMAGE IN SPACE DUE TO THE SOUTH ATLANTIC ANOMALY**

J.R.HEIRTZLER (NASA Goddard Space Flight Center, Greenbelt, MD 20771, USA, email: jamesh@ltpmail.gsfc.nasa.gov)

Predictions of radiation damage for Low Earth Orbit (LEO) satellites now use semi-empirical models developed from prior satellite data. From these models it is clear that the low field strength of the South Atlantic Anomaly (SAA) controls where the maximum radiation damage occurs. One may make an estimate of future radiation damage to LEO spacecraft if one can predict the future of the SAA.

Although reliable maps of the geomagnetic field strength and its secular change have only been made in the last few decades, certain geomagnetic observatories in South America and Africa have recorded the geomagnetic field for a much longer time. These observatories show that the present geomagnetic field change has persisted for more than 100 years. In spite of the fact that a few observatories have shown sudden changes in secular variation, those around the SAA have shown a stable secular variation. Assuming that this will continue for the next 50 to 100 years one can show that the SAA will expand to cover most of the South Atlantic Ocean and will become much weaker. This will greatly intensify the radiation hazard in LEO, put significant new limitations on radiation-hardened hardware, severely restrict the length of time that humans can remain in orbit, and materially change the configuration of the radiation belts.

**JSA06/W/19-A2 Invited 1130**

**APPLICATION OF AI TO SPACE WEATHER FORECASTING**

LUNDSTEDT, H (Swedish Institute of Space Physics, Space Weather and AI Division, Scheelevägen 17SE-223 70 Lund, Sweden. email: hlundstedt@solar.stanford.edu or Henrik@astro.lu.se)

Intelligent hybrid systems (IHSs) represent not only the combination of different artificial intelligence techniques (neural networks, expert systems, fuzzy systems, genetic algorithms), but also the integration of intelligent techniques with mathematical and conventional statistical methods. Many of the physical processes, which cause the space weather, are complex, non-linear, highly dynamic and chaotic. The IHSs are therefore well suited for predicting and modelling the space weather.

The Lund Space Weather Model (LSWM) is based on such an intelligent hybrid system. The hybrid system predicts the space weather on time-scales from minutes to months. Real-time solar wind data from ACE has made real-time predictions possible. Several examples will be shown. The goal of the LSWM is not only to predict the space weather conditions and the effects on power systems, satellites, radio propagation conditions and avionics, but also to explain the predictions and effects. For that a close collaboration with the user and industry is needed.

The review will also include AI applications to space weather forecasting developed by other groups.

**JSA06/W/30-A2 1150**

**AUTOPREDICTION OF DST INDEX USING THE NEURAL NETWORKS AND THIER RELATIONSHIP WITH THE AURORAL ELECTROJET AND POLAR CAP INDICES**

Marina STEPANOVA and P. Perez (Universidad de Santiago de Chile, Ecuador 3493, Casilla 307, Santiago, Chile, email: mstepano@lauca.usach.cl, pperez@lauca.usach.cl)

The possibility of prediction of Dst variations using previous Dst values has been studied using a feedforward multi-layer perceptron. It was found that the Dst index can be auto-predicted well a few hours ahead. Both main and recovery phases of geomagnetic storms are accurately predicted up to 3 hours in advance. But, for more advanced predictions, a time shift between observed and predicted Dst minima is observed. The use of auroral electrojet indices as input has shown that there exists a slight relationship between these indices and Dst 1 at least one hour ahead. Weak and moderate geomagnetic storms are predicted well, but the predicted Dst values for more intense storms are less negative than observed minima, which may be related to the known saturation of auroral electrojet indices due to intense storm development. Prediction based on the PC index shows better correlation with Dst. Although the amplitude of Dst variation is not reproduced correctly, there is no time shift between measured and predicted location of Dst minima.

**JSA06/W/24-A2 1210**

**ADVANCES IN RING CURRENT INDEX FORECASTING**

PAUL O'BRIEN, (IGPP/UCLA, Los Angeles, CA 90095-1567, USA, email: tpouii@igpp.ucla.edu) Robert McPherron, (IGPP/UCLA, Los Angeles, CA 90095-1567, USA, email: rmcphe@igpp.ucla.edu)

The Ring Current is the largest global feature of a geomagnetic storm. The Dst Index measures its intensity and is used as an input to many models of geomagnetic activity. In order to use such models in real time, it is necessary to have Dst in real time. However, official Dst data are typically 30 days behind real time. At present, the Kyoto World Data Center provides the most up to date Dst proxies, which are typically 12 to 24 hours behind real time. Using ACE Real-Time Solar Wind data and a modification of the well-known Burton Equation, we are able to advance Dst from the twelve-hour lag of Kyoto to an actual one-hour forecast. The primary modification of the Burton Equation consists of a solar wind parameterization of the decay time. Performance measures are provided for the operational Dst forecast. Improvement over existing models is indicated by typical skill scores of 30% to 50% for individual storms.

**JSA06/W/26-A2 1230**

**MONITORING OF SPACE WEATHER WITH QUICK LOOK AE AND DST INDICES**

Toyohisa KAMEI and Tohru Araki (WDC-C2 for Geomagnetism, Graduate School of Science, Kyoto University, Sakyo-ku, Kyoto 606-8502, Japan, email: toyo@kugi.kyoto-u.ac.jp), Masahisa Sugiura (Research Institute of Science and Technology, Tokai University, 2-28 Tomigaya, Shibuya-ku, Tokyo 151-0063, Japan, email: sugiura@jspan.kugi.kyoto-u.ac.jp).

Responding to the growing demands for quicker availability of the Dst index, we have begun derivation of a Near Real-time (QL-) Dst index. This index has been available on the WWW page of WDC-C2 for Geomagnetism Kyoto (URL <http://swdccb.kugi.kyoto-u.ac.jp>) since October 1996. Through this page, the provisional Dst index and the Final Dst Index, to the extent that they are available, can also be accessed. Strong demands exist also for quicker derivation of the Auroral Electrojet (AE) indices. We are currently deriving Near Real-time (QL-) AE indices with eight of the twelve standard AE stations but with future plans on increasing the number of stations used for the derivation of these indices. However, regarding this program, we are facing serious problems with some of the stations. For instance, Cape Wellen, a Russian station, has been closed. Beginning January 1997, plots of the QL-AE indices are accessible through the same WWW page as the Dst index. These indices are updated frequently, with time delays typically from 3 hours to 3 days. Users are advised to use these QL indices for diagnostic purposes only, because the data used for the derivation of these quick-look indices are not adequately quality controlled. In particular, activity in QL-AE may often be underestimated due to insufficient station coverage. We recommend that for scientific analyses, the final Dst index which is usually published yearly with typically a 1.5 year delay, or the provisional Dst index which is normally made available within two months of the observation be used. Provisional AE indices have been published through 1994, and these data are accessible also through our WWW page.

**JSS07 Tuesday 20 July**

**ANISOTROPY: FROM MOUNTAIN BUILDING TO GEODYNAMO (ISAPEI, IAGA, IAVCEI, SEDI)**

Location: Medical School EF08 LT3  
Location of Posters: Arthur Thompson Hall

**Tuesday 20 July AM**

Presiding Chairs: J.M.Kendall (University of Leeds, UK), P.G. Silver (Carnegie Institute of Washington, USA) P.G. Silver, Carnegie Institution of Washington, Washington DC, USA  
Concurrent Poster Session

**JSS07-A2 Introduction 0930**

S. KARATO (Univ. Of Minnesota, USA)

**JSS07/L/04-A2 Invited 0935**

**ONE HUNDRED YEARS OF RESEARCH IN SEISMIC ANISOTROPY**

Klaus HELBIG, Kiebitzrain 84, 30657 Hannover, Germany, e-mail: helbig@real-net.de, and Edward Szaraniec, Cracow University of Technology, ul. Warszawska 24, 31-155 Krakow, Poland, e-mail: edszar@us.p.krakow.pl

The quest for geophysical knowledge is as old as mankind, but the first Geophysical Institute with a "Professor of Geophysics" as director was created as recently as November 1 1895,



when the Austrian Minister of Religion and Education appointed Maurycy Pius Rudzki as Distinguished Professor of Mathematical Geophysics and Meteorology to the newly established chair at the Philosophical Faculty of the Jagiellonian University of Cracow. Rudzki was 33 years old and had published 30 articles on a wide variety of subjects in mathematics, physics, geophysics, and geology.

Elastic anisotropy goes back at least to 1856, when William Thomson wrote his landmark paper, if not to 1837 and the treatises of Hamilton and McCullagh on optical rays in the (elastic) ether. Seismic anisotropy has started with Rudzki, who was interested in seismic wave types and in focal depths, both under the aspect of anisotropy of crust and mantle. The first publication we know is from 1898: "On the shape of elastic waves in rocks". The subject of this and several following articles is the description of the wave surface as a model for wavefronts in anisotropic media due to a point source (instead of the slowness surface). It took until 1911 until Rudzki solved the problem. In the absence of data, he assumed that the mantle had the properties of beryl (the five elastic constants were known by then). To construct the wave surface, he developed a parameter representation that is still in use today. In the course of his work he found what is known as the "fundamental inequality", and he was the first to point out that elastic waves in transversely isotropic media could have cusps, and thus there could be five direct arrivals at a single observation point.

**JSS07/E/02-A2 1005**

**ANISOTROPIC PORO-ELASTICITY (APE): A NEW UNDERSTANDING OF PRE - FRACTURING DEFORMATION IN CRUST AND MANTLE**

Stuart CRAMPIN (Department of Geology & Geophysics, University of Edinburgh, Edinburgh EH9 3JW, UK; email: scrampin@ed.ac.uk)

The fluid-saturated grain-boundary cracks and low aspect-ratio pores in almost all sedimentary, igneous, and metamorphic rocks in the Earth's crust are aligned by deviatoric stress. Sensitive to crack anisotropy, seismic shear-wave splitting polarised in the direction of maximum horizontal stress is seen in almost all rocks, with similar characteristics below about 1km-depth. The evolution of such microcracked rock can be modelled by anisotropic pore-elasticity (APE) where the driving force is fluid migration between neighbouring microcracks at different orientations to the stress field. APE modelling is tightly constrained yet matches a wide range of static and dynamic behaviour of shear-waves and cracks observed over several orders of magnitude in dimensions and frequencies, including the observed minimum of 1.5% and maximum of 4.5% shear-wave velocity-anisotropy of rocks in the crust. This means that pre-fracturing deformation of fluid-saturated crustal rock can be accurately modelled and the response to known changes calculated. (The success of the modelling is due to the critical non-linear behaviour of cracks in the crust which are always close to fracture criticality and fracturing.) The presence of water in mantle rocks is also well-established. In particular, small percentages of water lower the melting point of mantle rock so that pressure gradients in films of liquid melt are the preferred mechanisms for the turn-over in mantle convection currents. The mechanism for APE, flow of melt along pressure gradients between cracks at different orientations to the stress field, is a much more powerful mechanism than crystalline rotation. As a consequence, APE modelling applies to the upper mantle as well as to deformation of crustal rocks. The similar modelling explains the remarkable similarities between crustal and mantle shear-wave velocity anisotropy: approximately the same minimum velocity anisotropy, approximately the same maximum anisotropy and the same stress-aligned polarizations. These would not be expected for crystal-based anisotropy. The implications of APE-modelled upper mantle anisotropy is that shear-wave splitting is the result of current not paleo-stress effects.

**JSS07/E/09-A2 1025**

**CRUSTAL FRACTURE ANISOTROPY REVEALED AT THE TRENCH OUTER WALLS**

Kazuo KOBAYASHI (Japan Marine Science and Technology Center, 2-15 Natsumishima, Yokosuka 237-0061 Japan, email: kobayashik@jamstec.go.jp) and Masao Nakanishi (Ocean Research Institute, University of Tokyo, 1-15-1 Minamidai, Nakano 164-8639 Japan, email: nakanishi@ori.u-tokyo.ac.jp)

Mechanical anisotropy of the oceanic crust is manifested at the outer walls of the deep-sea trenches at which normal faults are formed under horizontal extensional force due to bending of the oceanic plate. We have examined its bathymetric evidence in the northwestern margin of the Pacific Ocean composed of a Pacific plate with magnetic lineaments trending in a direction of N70E. It is subducted along the Kuril, Japan, Izu-Bonin (Ogasawara) and Mariana Trenches, each having different trend of axis. At the western Kuril Trench with the trench axis trending N60E, a number of faulted escarpments parallel to the magnetic lineaments (type 1) are identified. At the Japan and Mariana Trenches trending in directions quite oblique to the magnetic lineations, majority of faulted scarps are parallel to the trench axis (type 2). At the Izu-Bonin Trench trending nearly perpendicular to the magnetic fabrics the outer trench walls consist of faulted escarpments with two proximate directions, one perpendicular to the magnetic lineations (type 3) and the other parallel to the trench axis (type 2). Type 3 scarps appear to be rejuvenated non-transform offsets. Observed results seem to indicate that a direction of magnetic lineations is the weakest, the offset direction is the second weakest and directions quite oblique to them are the hardest for fault generation.

**JSS07/P/01-A2 1105**

**THE FORWARD PROCEDURE OF CRUST ANISOTROPY FOR INTEGRATING RESEARCH BY SEISMIC WAVES AND ELECTRIC CONDUCTIVITY**

Li Qinghe & Ruan Aiguo (Lanzhou Institute of Seismology, China Seismological Bureau, Lanzhou, Gansu, 730000, P. R. China. e-mail: liqh@lzu.edu.cn)

Through discriminate the polarisations of fast and slow shear waves and the time delay between their arrivals recorded on seismic diagram, the characteristics of anisotropy can be ascertained. However, shear wave splitting is the total effect of ray path so it is difficult to decide the location where anisotropy is produced. The electric anisotropic layers with low accuracy can be distinguished through MT inversion. It is expected that when the elastic parameters and electric ones both present strong anisotropy, the combining explanation of the two methods could provide more clear image of media conditions such as the direction of fluid filled cracks align, stress status, conductivity, the location of some special layers and so on; when only one kind of parameters presents obvious anisotropy combining explanation at least could determine the type of anisotropy easily. The forward procedure as a base of inversion is following. (1) Firstly, the rocks characteristics from various elastic experiments and also from electric ones were analysed and summarised, then to seek some important parameters which strongly affect rocks elastic and electric anisotropic features. (2). Establish elastic and electric eigenfunctions of earth media respectively, which are controlled by some parameters sensitive to anisotropy. (3) Simulate the time delay, polarization and attenuation of shear-wave splitting and the MT response function at time for various models which consist of different parameters, layers structures and other factors. (4). Apply the combining explanation method to several practical examples to test above mentioned

**JSS07/W/01-A2 Invited 1125**

**MANTLE ANISOTROPY, DEEP GEOLOGY, AND MANTLE FLOW**

P. G. SILVER (Carnegie Inst. of Washington, DTM, 5241 Broad Branch Rd. NW Washington DC 20015) R. Russo (Dept. of Geological Sciences, Northwestern University, Evanston IL 60208)

The study of upper mantle anisotropy can address two fundamental issues: the mantle's contribution to continental geology, and the convective flow regime associated with plate tectonics. Mantle anisotropy beneath the continents is best revealed by shear-wave splitting. The fast polarisation direction and delay time can be used to constrain orientation and depth extent of deformed regions. The proliferation of portable, broadband experiments over the last decade has enabled the sampling of the mantle on spatial scales appropriate for examining geological variations. A survey of the available splitting data for the continents, both from permanent stations and portable deployments lead to two basic conclusions. First, the crust and mantle deform coherently during orogenies with this deformation being preserved as fossil anisotropy as far back as the early Archean. Second, there is no evidence for an asthenospheric decoupling zone between continental plates and the mantle below, suggesting that these plates are strongly coupled to general mantle circulation. Another area that can be explored is the mantle flow field associated with plate tectonics. Shear-wave splitting observations from a variety of oceanic environments: spreading ridges, hotspots, and beneath subducting slabs suggest a surprising diversity of flow behaviour. This ranges from the classic two-dimensional flow beneath ridges to a more complex three-dimensional sub-slab flow field found at many convergent margins.

**JSS07/E/11-A2 1155**

**LITHOSPHERIC ANISOTROPY CHANGE ACROSS THE EDGE OF THE CANADIAN SHIELD**

Goetz HR BOKELMANN (Department of Geophysics, Stanford University, Stanford, CA 94305-2215, USA, email: goetz@stanford.edu) Paul G. Silver (Dept. of Terrestrial Magnetism, Carnegie Inst. of Washington, 5241 Broad Branch Rd., Washington, DC 20015, USA, email: silver@pssl.ciw.edu)

We report travel times and shear-wave splitting from the Archean-Proterozoic Transect 1989. This type of data set recorded by a transect of portable broadband instruments allows us to make inferences about mantle structure in the region between Wyoming Craton and Superior Province of the Canadian shield, i.p. to study the relation of velocity variation in the continental upper mantle with surface geology, tectonic features and age provinces. The values are corrected for crustal contribution and inverted for the vertical path upper mantle delay  $\Delta t_{\text{UM}}$  under each station as well as azimuthal dependences of this quantity. The prominent feature in the upper mantle delays  $\Delta t_{\text{UM}}$  is the variation by at least 1.5 seconds for  $S_{\text{p}}$ , much of which occurs over a narrow zone of just a few hundred kilometres width. This suggests a major lateral upper mantle transition, which does not coincide with the surface geological edge of the Canadian shield but is located within the shield. This same transition is also observed in shear-wave splitting delay times. Surprisingly, however, the  $P$ -delays do not exhibit a corresponding variation. We address this apparent contradiction and show how it may be explained in conjunction with anisotropy in the subcontinental lithosphere. A simplified thermal model of the lithospheric transition zone, in which temperature controls the degree of alignment of crystal and thus seismic anisotropy, predicts this phenomenon.

**JSS07/P/03-A2 1205**

**THE EVIDENCE OF SHEAR WAVE SPLITTING OBSERVED ON THE RECORDS OF THE 1997 ZIRKUH (GHAEN-BIRJAND, EAST-CENTRAL IRAN) AFTERSHOCKS**

Z. ZARIFI (RAEESI) (Institute of Geophysics, University of Tehran, Tehran, Iran, email: zarifi@iman.ut.ac.ir); M. R. Gheitanchi and M. Raeesi (Both at the above address, email: mrgchec@chamran.ut.ac.ir and mraeesi@iman.ut.ac.ir)

On 10 May 1997 at 7:57:26.9 GMT a destructive earthquake occurred in Zirkuh (Ghaen--Birjand) region, east of Iran with  $M_s=7.3$ . Geophysics Institute of Tehran University recorded aftershocks of this event from 31 May 1997 to 25 June 1997, with three component digital seismographs. We searched for shear wave splitting in the aftershocks with magnitude less than 3 and incident angles less than critical angle;  $\arcsin(V_s/V_p)$ . We emphasized observation of particle motion of two horizontal components in a window including first arriving shear wave. Observation of no variety in particle motion in a range of time greater than sampling interval of recorded signal and less than about 200 ms was attributed to anisotropy. Then we used aspect ratio method to determine polarisation direction of fast shear wave and time delay between fast and slow shear waves. We found two directions for fast shear wave, including NE-SW and NW-SE. The dominant direction was NE-SW. This was compatible with direction of maximum regional stress that was mentioned by other researches in the region. As directions of fast shear wave suggest, here we have two sets of parallel cracks and we search about behaviour of shear wave in these two conjugate sets of cracks.

**JSS07/E/07-A2 1225**

**ALONG-STRIKE VARIATIONS IN THE ANISOTROPIC STRUCTURE OF THE HIKURANGI SUBDUCTION ZONE, NEW ZEALAND.**

Alex Brisbane, Graham Stuart, J-Michael KENDALL. School of Earth Sciences, University of Leeds, LS2 9JT, UK.

A model of subduction-zone anisotropy for the North-Island, New Zealand based on observations of seismic anisotropy from a variety of seismic phases is presented. We have analysed anomalous surface-wave polarisations and shear-wave splitting in local S-phases and SKS phases. Anomalous particle motions of the equivalent to fundamental-mode Love-waves imply anisotropy in the New Zealand crust and the subducted Pacific slab. Shear-wave splitting analyses of regional phases in the northern North-Island show no increase in delay times between the fast and slow shear-waves (0.21±0.03s) with increasing source depth, unlike previous observations in the southern North-Island, which display an increase in delay time to about 0.5s over 250km. Polarizations of the fast shear-waves are approximately parallel to the strike of subduction. In contrast, the SKS-splitting parameters do not vary significantly across the North-Island. A mean fast-slow delay time of 1.5±0.3s and a fast polarisation direction of 25-7deg, sub-parallel to the strike of subduction, was determined for the SKS observations. Modelling using reflectivity and ray theory was used to guide the interpretations. Both the surface-wave polarisation and local shear-wave splitting observations require an anisotropic (4%) New Zealand crust with a slow hexagonal-symmetry-axis dipping at 15-30° and a fast symmetry plane parallel to the strike of the subduction. This is compatible with the structural trends of the regional geology. The variation of the splitting delay times with source depth across the North-Island implies a horizontal symmetry axis in the subducted slab to the south, but an axis dipping parallel to the plate interface beneath the northerly regions. This variation reflects the change in intra-plate stress towards the South Island where the India-Australian and Pacific plates are locked. Beneath the slab, trench-parallel mantle flow is inferred from interpretations of 4% hexagonal anisotropy with a fast symmetry-plane parallel to the strike of subduction.

Tuesday 20 July PM

Presiding Chairs: L. Stixrude (Univ. of Michigan, USA),  
J-P. Montager (Inst. de Physique du Globe, Paris, France)**JSS07/W/07-A2** Invited **1400****HOW TO RELATE BODY WAVE AND SURFACE WAVE ANISOTROPY?**

Jean-Paul MONTAGNER (Dept. Seismology, Institut de Physique du Globe, 4 Place Jussieu, 75252 Paris cedex 05, France, email: jpm@ippg.jussieu.fr), and Daphne-Anne Griot (Laboratoire de Sciences de la Terre, ENS-Lyon, 46 Allée d'Italie, 69364 - Lyon cedex 07, France)

The seismic anisotropy turned out to be one of the most efficient tool for structural geologists and geodynamists developed during the last 30 years. Seismic anisotropy was evidenced in the upper mantle, primarily from two kinds of datasets, surface wave dispersion curves and body waves SKS data. First of all, the discrepancy between Rayleigh and Love wave dispersions makes it necessary to introduce transversely anisotropic medium with vertical symmetry axis characterized by 5 anisotropic parameters (A, C, F, L, N). Later on, the azimuthal dependence of Rayleigh wave and Love wave dispersion curves (at different periods) was largescale tectonic processes are taking place. We show that such is the case in Central Asia and Western USA.

**JSS07/E/08-A2** Invited **1430****NEW PROBES OF THE DYNAMICS OF EARTH'S DEEP MANTLE**

Lars STIXRUDE, Dept. of Geological Sciences, University of Michigan, Ann Arbor, MI 48109-1063, USA, email: stixrude@umich.edu

Seismological observations of elastic anisotropy in the deep mantle represent a potentially rich source of information on the dynamics and composition of this region of the interior. The anisotropy is determined by the elastic constants of the constituent minerals and their angular and spatial distribution. Our understanding of anisotropy in the deep mantle has been hindered by our ignorance of the relevant elasticity and deformation mechanisms at high pressure. We review recent results of first principle theory as applied to the prediction of elastic constants of important deep earth phases at high pressure. The foundation and implementation of the theoretical technique, the plane-wave pseudopotential method, is briefly discussed. The results show that predicted elastic constants are in good agreement with experiment: RMS deviations are typically a few percent, much of which can be accounted for by the difference in temperature between the athermal calculations and 300 K experiments. Predictions at high pressure show that anisotropy depends strongly on compression and that candidate deep mantle minerals are highly anisotropic. The theoretical predictions are discussed in terms of seismological observations, paying particular attention to the properties of aggregates. The properties of anisotropic mono-phase aggregates are estimated based on 1) theoretical results for single crystals, 2) simple models of flow in D" and 3) mineralogical deformation mechanisms. We find that the SH/SV anisotropy may be large for aggregates of Mg-silicate perovskite, periclase, and silica (6-8 % in magnitude) compared with that observed in D". While mono-phase aggregates of silica exhibit fast SH velocity at pressures corresponding to D", perovskite and periclase aggregates have slow SH velocities. We discuss the implications of these results for the origin of anisotropy in D".

**JSS07/L/03-A2** Invited **1500****DYNAMIC DISTRIBUTION OF MELT DUE TO DEFORMATION**

Mark E. ZIMMERMAN, Shun-ichiro Karato and David L. Kohlstedt (University of Minnesota, Department of Geology and Geophysics, Minneapolis, MN 55455, U.S.A., Email: mark@olivine.geology.umn.edu)

Our shear experiments on partially molten peridotites demonstrate the importance of deformation in the development of a melt preferred orientation (MPO). Deformation redistributes melt from a random array of tubules and wetted grain boundaries to aligned planar melt pockets extending over the scale of several grains. The dynamic distribution of melt, such as that produced in our shear experiments, will dramatically influence the seismic and transport properties of the mantle within zones of partial melting such as beneath mid-ocean ridges and in mantle wedges above subducting lithospheric slabs. For example, vertically aligned planar melt pockets beneath a mid-ocean ridge induce shear-wave splitting with the fast polarization direction parallel to the ridge axis and strong Rayleigh wave anisotropy in the same orientation. Consequently, seismic observations of deforming partially molten regions of the upper mantle should observe anisotropy due to alignment of melt as well as crystallographic alignment of olivine, assuming that the direction of wave propagation is appropriate and that the resolution of the seismic technique is sufficient.

For our shear experiments, olivine-basalt aggregates with an average grain size of ~20  $\mu\text{m}$  were deformed in a gas-medium apparatus at 1523 K and 300 MPa with shear stresses of 25 to 90 MPa to strains of 36 to 250%. To preserve the microstructures formed during deformation samples were quenched under load at 1-2 JK/s. The non-coaxial shear deformation produces a strong lattice preferred orientation (LPO) with the (010) of olivine rotated sub-parallel to the shear boundary at high shear strains. Olivine grains also exhibit a shape preferred orientation (SPO) reflecting the finite strain of the sample. Under hydrostatic conditions, the anisotropic surface energy of olivine-melt interfaces causes preferential wetting of the (010) of olivine. However, during shear deformation the effect of surface energy on MPO is surpassed by the influence of the differential stress

**JSS07/W/06-A2** **1520****MANTLE MICROGEODYNAMICS AND SEISMIC ANISOTROPY**GEOFFREY E. LLOYD School of Earth Sciences, The University, Leeds LS2 9JT, UK  
Email: g.lloyd@earth.leeds.ac.uk

The behaviour of the Earth's mantle remains a first order problem in the Earth Sciences. However, investigations are usually limited by restrictions imposed by scale. Mineral phase transformations, which are of primary significance in understanding mantle processes, can impact on all scales from the ionic to the geodynamic. A more comprehensive understanding of phase transformations, and hence mantle processes, can be achieved by combining investigations from different scales. Such an approach, referred to as 'microgeodynamics', is described here, in which crystal chemical modelling of phase transformations (ionic scale) and seismic anisotropy analysis of lithosphere structure (large scale) are combined via an interface provided by structural geology (intermediate scales). Significant recent advances in our understanding of mantle geodynamics have been gained from studies of seismic anisotropy. It is generally agreed that one major cause of seismic anisotropy is the preferred crystallographic alignment of anisotropic minerals during deformation or flow. Thus, understanding of seismic anisotropy requires knowledge of the deformation behaviour of rock-forming minerals and in particular their lattice preferred orientation (LPO) characteristics. In general, imposed environmental (i.e. pressure, temperature) and tectonic (i.e. stress, strain,

strain-rate, etc.) conditions determine how an individual mineral phase behaves (e.g. dislocation or diffusional creep, fracture, etc.). These deformation mechanisms are ultimately responsible for the development of specific structures; they also may be associated with LPO development. By accurately measuring the complete LPO for all mineral phases present, it is possible to predict most of the petrophysical properties (including seismic characteristics) of a mineral, rock or structure, and hence to explain any seismic anisotropy observed in terms of geodynamic processes. Modern advances in scanning electron microscopy (SEM) technology (specifically, electron backscattered diffraction, EBSD) now make it possible to routinely determine LPO and derive petrophysical properties for a wide range of minerals and polymineralic rocks. The crystal chemical modelling approach used to assist the seismic and microstructural (LPO) investigations is based on defining characteristic...

**JSS07/E/05-A2** **1540****LATTICE PREFERRED ORIENTATION IN DEEP MANTLE MINERALS AND IMPLICATIONS FOR DEEP MANTLE ANISOTROPY**

Shun-ichiro KARATO, Kyung-Ho Lee, Jeff Lawlis and Daisuke Yamazaki (University of Minnesota, Department of Geology and Geophysics, Minneapolis, MN 55455, U.S.A., Email: karato@tc.umn.edu) Dan Frost and Dave C. Rubie (Bayerisches Geoinstitut, Universität Bayreuth, Bayreuth, Germany)

Previous experimental studies of anisotropic structure formation in Earth materials have been limited to those in upper mantle or crustal materials. However, most of the key questions in global geodynamics center around the processes in the deep mantle including transition zone and the lower mantle. We have developed a new experimental technique of large strain, shear deformation under deep mantle conditions and applied it to investigate the lattice preferred orientation in wadsleyite, ringwoodite and (Mg,X)O with X=Fe or Ni. High pressure, temperature deformation experiments were conducted on these materials to large strain, typically ~100%. The lattice preferred orientations (LPO) of deformed samples were determined by EBSD (electron backscattered pattern) analysis. We chose those samples that show evidence of dislocation creep (high density of dislocations and wavy grain-boundaries). Using the measured lattice preferred orientation, we calculated elastic constant tensors and calculated the seismic anisotropy. Together with the earlier works on analog materials, we draw the following conclusions: (i) anisotropy in wadsleyite and particularly ringwoodite is weak even in the dislocation creep regime, (ii) (Mg,X)O develops strong lattice preferred orientation in the dislocation creep regime: at high pressures for Fe or Ni-rich composition, the {100} plane tends to be parallel to the flow plane whereas the {110} plane is subparallel to the flow plane at low pressures and for low Fe or Ni content, (iii) (analog) perovskite (CaTiO<sub>3</sub>) shows strong LPO when deformed in the dislocation creep regime. Seismic anisotropy caused by LPO in these minerals is calculated and the following geodynamic conclusions are obtained: (i) Majority of the deep mantle appears to deform by diffusion creep, whereas the bottom boundary layer (the D" layer) is likely to deform by dislocation creep. (ii) The observed regional variation in anisotropy in the D" layer is likely to reflect the regional variation in stress level and the azimuthal anisotropy provides constraints on the flow direction. (iii) If the bottom transition zone is anisotropic (VSH>VSV), it implies a presence of laminated structure presumably caused by the delamination of paleo-oceanic crust.

**JSS07/E/04-A2** Invited **1620****ANISOTROPY OF EARTH'S INNER CORE**

K C CREAMER (Geophysics Program, Box 351650, University of Washington, Seattle, WA, 98195-1650; email: kcc@geophysics.washington.edu)

Though the sampling is currently insufficient to obtain a robust image of the 3-D variations in anisotropy of the inner core, some robust conclusions can be inferred, and I speculate on a simple, but non-unique model, that is consistent with current observations. Thousands of differential travel times of the phases PKP (BC)-PKP(DF) and PKP(AB)-PKP(DF), picked by cross correlation by ourselves and other groups, provide compelling evidence that the inner core is strongly anisotropic with the fast direction parallel to the spin axis. Anisotropy is strong (2-4%) at depths from 100-400 km in the 240 deg longitude region from 160E to 360E to 40E (quasi-western hemisphere) and weak (0.5%) from 40E to 160E (quasi-eastern hemisphere). Below about 600 km depth into the inner core anisotropy appears strong (>2%) at all longitudes. The outer part (50-100 km) is not robustly imaged, but anisotropy appears weak here. The evidence for strong large-scale variation in anisotropy is compelling and must be incorporated in discussions of mechanisms for crystal alignment. On the other hand, the isotropic (Voigt averaged) velocities do not vary on this large scale, so there is no need to invoke lateral differences in temperature, chemistry, or density. I speculate on a new parameterization for the structure of the inner core, motivated by Song and Heimberger's [Science, 1998] inference from triplicated PKP (DF) arrivals that the inner core contains an internal discontinuity. Accordingly, I assume the inner core is divided into two regions, an upper inner core that is isotropic, and a lower inner core that is anisotropic. A model, characterized by velocity perturbations from model AK135 that are homogeneous within these two regions, can fit most of the features of my data set. The best fits are obtained when the discontinuity is less than 100 km from the inner core boundary beneath the Western Hemisphere, but more than 300 km deep in much of the Eastern Hemisphere.

**JSS07/E/01-A2** Invited **1650****ORIGIN AND IMPLICATIONS OF ANISOTROPY IN THE INNER CORE**

Bruce BUFFETT (Department of Earth and Ocean Sciences, University of British Columbia, Vancouver, BC, V6T 1Z4, Canada, email: buffett@eos.ubc.ca)

Accumulating evidence from the study of body waves and free oscillations provides compelling support for seismic anisotropy in the Earth's inner core. The origin of the anisotropy is generally attributed to a preferred orientation of the iron crystals, which comprise the inner core, but there is little consensus on the mechanism that produces this preferred orientation. Even the crystal structure of iron in the inner core is debated. Mechanisms that have been proposed to explain the alignment of iron crystals can be grouped into two categories. Those that produce alignment during solidification are not favoured because of the apparent absence of anisotropy in the top few hundred kilometres. More plausible explanations involve deformation of the inner core. Convection is possible at early times when the growth of the inner core was probably more rapid, but present-day estimates suggest that thermal and compositional stratifications are stable. An intriguing alternative can result from aspherical growth of the inner core. Viscous adjustment with strain-rates of order 10<sup>-18</sup> (1/s) can produce the observed crystal alignment by preferential growth of crystals in low energy orientations. However, low stresses cause the development of anisotropy by this mechanism to be prohibitively slow. Much larger stresses and strain-rates can be caused by rotation of the inner core through the aspherical gravitational field of the mantle. Total strains are small because the flow is periodic in time, but averaging over many revolutions can produce anisotropy with a cylindrical symmetry. Deformation of the inner core may also arise from Lorentz forces, depending on the strength of the magnetic field. In this talk I survey the relative importance of these various deformation processes and identify some of the difficulties that must be overcome to explain the origin of the anisotropy. Some



## INTER-ASSOCIATION

complications that arise in using the large-scale stress field to evaluate stresses at the scale of crystal grains are explored using analogous calculations for elastic inclusions.

**JSS07/W/03-A2** **1720**

### A LABORATORY MODEL FOR THE SOLIDIFICATION OF THE EARTH'S INNER CORE, AND THE INNER CORE'S SEISMIC ANISOTROPY

Michael BERGMAN (Physics Dept., Simon's Rock College, 84 Alford Road, Great Barrington, MA, 01230, USA, email: bergman@simons-rock.edu)

Although seismologists do not yet agree on the details of the depth dependence, the longitudinal variations, and perhaps the magnitude, to a first approximation the inner core has been inferred to be elastically anisotropic, with the direction parallel to the rotation axis fast. Many hypotheses have been suggested as a cause for the anisotropy, all involving a lattice preferred orientation, but the physical reality of many of them has not yet been demonstrated. Using ice as an analog material for high pressure, hexagonal closest packed iron, a series of laboratory experiments have been carried out in which salt-water is solidified from the center of a rotating, hemispherical shell. The experiments reveal more rapid growth of the solid nearer the pole than the equator, presumably because the Coriolis force inhibits convection within the tangent cylinder parallel to the rotation axis and circumscribing the inner core. Unlike in the Earth where pressure effects are important, in the experiments this leads to colder temperatures within the tangent cylinder. Because of the small length and time scales of the experiments it is not possible to study subsequent solid-state flow, but the experiments do demonstrate that the equilibrium solidification surface is not spherical. Using polarised light on thin sections of the ice, the columnar nature of the dendritic crystals is apparent, with the *a*-axes lying in the direction of growth. The laboratory model suggests how a solidification texture is frozen in, from which further textural changes might subsequently occur.

**JSS07/E/03-A2** **1740**

### ORIGIN OF SEISMIC ANISOTROPY IN THE INNER CORE: IMPLICATIONS FOR GEODYNAMO

Shun-ichiro KARATO (University of Minnesota, Department of Geology and Geophysics, Minneapolis, MN 55455, U.S.A., Email: karato@tc.umn.edu)

The strong interaction between inner and outer core of the Earth has been recognised in geodynamo modelling and the observed super-rotation of the inner core is considered to be a result of mechanical coupling through the stress caused by magnetic field (the Maxwell stress). Here I show that such a mechanical coupling through the Maxwell stress is also important in the large-scale, long-term deformation of the inner core that may be responsible for the observed nearly axi-symmetric seismic anisotropy. Toroidal magnetic field exerts large compressive stresses near the surface of the inner core that controls the geometry of flow. Inner core materials are squeezed from the regions of strong magnetic field to regions of weak magnetic field by the Maxwell stress, causing nearly axi-symmetric flow. The strain magnitude associated with this flow is significantly larger than those associated with other processes including the flow caused by gravitational interaction between the inner core and the mantle and the flow due to the anisotropic growth of the inner core. Therefore, the flow pattern and the resultant stress orientations in the inner core, which are likely to be related to the geometry of seismic anisotropy, should reflect the geometry of the magnetic field, particularly the toroidal field near the inner-outer core boundary. The flow causes melting and solidification at the inner-outer core boundary. This causes large release of latent heat that may affect convection pattern in the outer core and hence the geomagnetic field. The velocity of this flow is proportional to the Maxwell stress and inversely proportional to the viscosity of the inner core. For the reasonable range of parameters, the time scale of flow is estimated to be ~ 0.1-10 my, close to the time scale of geomagnetic field reversal (0.1-1 my). It is suggested that the feedback between the magnetic field and the flow-induced latent heat release may affect the geodynamo processes including reversal of the magnetic field. Thus the magneto-mechanical interaction between the inner and outer core may control a range of processes in the core including seismic anisotropy, super-rotation of the inner core and geodynamo. Seismic anisotropy of the inner core may provide a clue as to the generation of the geomagnetic field in the Earth.

## Tuesday 20 July AM

Presiding Chair: V.V. Kuznetsov (Russian Acad. of Sciences, Novosibirsk, Russia)

**JSS07/W/04-A2** **0930-01**

### MANTLE FLOW BENEATH ALTAI-SAYAN FOLDED BELT AND SURROUNDINGS (CENTRAL ASIA) FROM OBSERVATIONS OF SKS SPLITTING.

I. G. DRICKER, S. W. Roecker (both at E&ES, RPI, Troy, NY, 12180, USA, Email: ilya@geo.rpi.edu), L.P. Vinnik, Ye. A. Rogozhin, L. I. Makeyeva (all at IPE RAS, 10 B. Gruzinskaya, Moscow, 123810, Russia, Email: vinnik@synapse.ru).

We present measurements of anisotropy at 3 seismic stations (USK, AKT, TEL) in the Altai mountains, 3 stations in the Sayan mountains (TDZ, ERN, TLY), ELT in the Salair range, VEN in the boundary region between Altai and the West-Siberian plate, and NVS in the West-Siberian plate. Altai and surroundings are believed to be formed by Palaeozoic accretion of microplates and island arcs and reactivated in the late Cenozoic. Fast axes of anisotropy in tectonically active areas of Altai and Sayan strike NE-SW, whereas N-W fast axis is detected beneath the West-Siberian plate station NVS. We rule out the idea of frozen Palaeozoic anisotropy to be the cause of shear wave splitting, because detected fast axes are not parallel to the ancient tectonic trends not only in the area of active deformations, but also in the stable region to the North. In the active area fast directions of azimuthal anisotropy are oriented predominantly E-W, roughly parallel to the strikes of the mountain ranges. In addition, observed fast axes of anisotropy are parallel to the extensional axes of seismotectonic deformations obtained from fault plane solutions of local earthquakes. Delay times between fast and slow split waves vary from 1 to 1.5 s. This requires the anisotropic layer to be not less than 200 km thick, larger than the possible thickness of the subcrustal lithosphere. This is consistent with the observations in several other collisional belts, and can be interpreted as a passive reaction of the upper mantle to uniaxial compression or a flow parallel to the mountain belt

**JSS07/W/05-A2** **0930-02**

### PN ANISOTROPY IN THE UPPERMOST MANTLE BENEATH THE ITALIAN AREA

Giuliana MELE, Istituto Nazionale di Geofisica, E-mail: meleg@martel.ingr.it

Uppermost mantle anisotropy is imaged beneath the Italian area using Pn traveltimes residuals inverted with the anisotropic tomography technique of Hearn (1996). The resulting pattern of anisotropy in the uppermost mantle is closely related with the regional tectonic trend and surface geology. The fastest Pn velocity is perpendicular to the direction of compression that originated the two major arc structures of Italy, i.e., the northern Apennines and the Calabrian

Arc, deformed in Mio-Pliocene times. This suggests that the collisional processes that originated the two arcs have deformed a substantial portion of uppermost mantle. In the internal part of northern Apennines toward the Tyrrhenian Sea, presently dominated by normal faulting and graben tectonics, the direction of fastest Pn waves parallels the direction of extension. Low-velocity and high-attenuation zones in the uppermost mantle of Italy obtained both from tomography and shear wave attenuation are also shown.

**JSS07/W/08-A2** **0930-03**

### THE ANISOTROPY OF THE EARTH'S INNER CORE AND THE GEOMAGNETIC FIELD

Vladimir V. KUZNETSOV, Vsevolod V. Botvinovsky (Institute of Geophysics SB RAS, Koptyug av., 3, Novosibirsk 630090, Russia; e-mail: kuz@uigm.nsc.ru)

A model relating the cylindrical and the lateral anisotropy of the inner core to the circuit of the generation of the geomagnetic field is offered. The phenomenon of the anisotropy of the properties of the inner core consists in the fact that the time a seismic wave takes to traverse the core along the rotation axis is 1% less than the time taken in the equator plane. Another piece of evidence comes from the splitting of the Earth's eigen oscillation spectra. In addition to the velocity difference between traversing the core along and normal to the rotation axis, a lateral core anisotropy has been discovered both from function splitting and travel time data. The lateral anisotropy shows that the velocities of P-waves over the surface of the inner core at the regions, projected into the Earth surface at the Pacific and at the Atlantic oceans, are 0.2-0.4% less than these at the poles and at the continents. The circuit of generation of the geomagnetic field is based on the model of current differential loop looking like the double cylinder and taking place on the border of the inner core, at the F-layer, in the plane of equator. A model in which the cylindrical anisotropy of the core results from dissipative processes, accompanying the generation of the geomagnetic field. The attempt to explain the interrelation of the lateral anisotropy of the core and the morphology of the geomagnetic field is made.

**JSS07/E/10-A2** **0930-04**

### EXHUMATION HISTORY OF HP-HT ROCKS DEDUCED FROM PETROLOGICAL DATA IN A POLY-OROGENIC BELT: SOUTH CARPATHIANS, ROMANIA

IANCU VIORICA (Geological Institute of Romania, 1 Caransebes Street, Bucharest 32, Romania, RO-78344, Email: viancu@ns.igr.ro) Medaris Gordon Jr. (Dept. of Geology and Geophysics, Univ. of Wisconsin-Madison 1215 W., Dayton St., Madison, WI 53706, USA, Email: medaris@geology.wisc.edu) Ghent D. Eduard (Dept. of Geology and Geophysics, Univ. of Calgary, email: Ghent@geo.ucalgary.ca) Maluski Henri (Lab. De Geochronologie, Geochimie et Petrologie, Univ. Montpellier 2, email: maluski@dstu.univ-montp2.fr)

The South Carpathians resulted from Alpine polystage collision characterised by: a double verging orientation of the crustal bodies, delimited by thrust/overthrust planes, in an asymmetric, fan like, nape pile; a strong heterogeneity due to the alpine building and by the inheritance of a strong pre-Alpine anisotropy; important contrasts in the physical parameters of the metamorphic conditions correspond to the Alpine, Variscan and Pan-African cycles; the widespread occurrences of the HP/HT rocks occur only in the Variscan units of the Getic-Supragetic basement. The aim of this presentation is to emphasise: the spatial distribution and position of the HP/UHP and medium-HT rocks in the uppermost alpine units, with a sub-horizontal crustal tectonic layering. The Variscan polystage crustal thickening and subsequent thinning due to collaps (recently 40Ar/39Ar ages are 354-331 Ma) produced the anisotropy of the pre-Alpine basement and exhumed the high grade rocks from the roots of the belt. Well constrained PT conditions for eclogites and granulites are 550-7000C and for peridotites are cca. 12000C/25-32 Kb, which are comparable to those for similar rocks in the Variscan Bohemian Massif. The paleozoic crustal anisotropy can be explained by a complex, polystage tectono-metamorphic evolution, involving a "tectonic collage" or "mixing" of the crustal bodies; the exhumation processes of the HP rocks can be understood only by deciphering of the whole pre-Alpine history. The pre-331 Ma effects of thickening-thinning processes were followed by further uplift and erosion (cooling ages of 309-320 Ma, Dallmeyer et al., 1986). The presence of scarce allochthonous Carboniferous granites, large migmatitic areas, and "in situ" anatectic granitoids suggest the exhumation of magmatic root crustal domains at least in some units.

**JWM08** **Tuesday 20 – Wednesday 21 July**

### OROGRAPHIC PRECIPITATION: OBSERVATIONS PROCESSES AND MODELLING, WITH FUTURE PLANS (IAMAS, IAHS)

Location: Chemical Engineering 124 LT

**Tuesday 20 July AM**

Presiding Chairs: C SCHÄR, D WRATT

### FIELD EXPERIMENTS AND NUMERICAL MODELLING

**JWM08-A2** **0930**

C.SCHÄR

**JWM08/W/03-A2** **0940**

### OVERVIEW OF THE MESOSCALE ALPINE PROGRAM

Philippe Bougeault, Météo-France/CNRM, 42 Avenue G. Coriolis, TOULOUSE 31057, France. E-mail: philippe.bougeault@meteo.fr Telephone No: 33-56107-9358 Fax No: 33-56107-9626)

The Mesoscale Alpine Program is an international initiative to improve understanding of atmospheric and hydrological processes over the Alps and their prediction by numerical models. There are about 200 participants from 15 different countries. The main focus of the program are:

- 1) An extensive program of intercomparison of numerical models
- 2) The concentration of all existing measurements in a single data center
- 3) The realization of a major field campaign, featuring special atmospheric and hydrological measurements by a variety of platforms (research aircraft, doppler radars, airborne lidars and radiometers, profilers, etc...). This field experiment will take place from 7 September to 15 November 1999.

The talk will illustrate the general strategy and organization of the program, present a variety of on-going work, and highlight the plans for the upcoming field campaign.



JWM08/W/04-A2

1020

**OROGRAPHIC PRECIPITATION: RESULTS FROM SALPEX (THE SOUTHERN ALPS EXPERIMENT).**

Jeff Copeland, David Wratt, Warren Gray, Howard Larsen and Michael Revell (NIWA, Wellington, New Zealand, email: j.copeland@niwa.cri.nz). Geoff Austin (Physics Department, Auckland University, New Zealand, email: g.austin@auckland.ac.nz). Roddy Henderson and Richard Ibbitt (NIWA Christchurch, New Zealand, email: r.henderson@niwa.cri.nz). Jorgen Jensen and Sunhee Lee (CSIRO Atmospheric Research, Aspendale, Australia, email: jbj@atmos.dar.csiro.au). Niels Bormann, (Research School of Earth Sciences, Victoria University Wellington, Wellington, New Zealand, email: n.bormann@niwa.cri.nz).

This paper summarises orographic precipitation and river flow research results from New Zealand's Southern Alps. Important microphysical and dynamical processes influencing precipitation distribution have been identified through a synergy of SALPEX surface, radar and aircraft observations. The structure of air flow approaching the Southern Alps has been established, including blocking and formation of the barrier jet. Relationships between air mass properties and spillover (leeward precipitation intensity) have been determined. Observations and model studies are being used to test theories of mountain influence on frontal structure. Validation studies using SALPEX field campaign data show the RAMS mesoscale model has improved skill at predicting orographic rainfall over the global model in which it is nested. River flows predicted by the TOPMODEL hydrologic model driven by RAMS precipitation forecasts compare well with observations.

JWM08/E/07-A2

1040

**GPS PRECIPITABLE WATER MEASUREMENTS MADE DURING THE SALPEX'96 EXPERIMENT**

MARK FALVEY (School of Earth Sciences, Victoria University of Wellington, PO Box 600, Wellington, New Zealand, Email: mfalvey@gamma.gns.cri.nz) John Beavan (Institute of Geological and Nuclear Sciences, PO Box 30368 Lower Hutt, Wellington, New Zealand, Email: J.Beavan@gns.cri.nz) Niels Bormann (School of Earth Sciences, Victoria University of Wellington, PO Box 600, Wellington, New Zealand, Email: bormann@thor.niwa.cri.nz) Jeff Copeland (National Institute of Water and Atmosphere, PO Box 14-901 Kilbirnie, Wellington, New Zealand, Email: j.copeland@niwa.cri.nz) James McGregor (School of Earth Sciences, Victoria University of Wellington, PO Box 600, Wellington, New Zealand, Email: mcgregor@geo.vuw.ac.nz) David Wratt (National Institute of Water and Atmosphere, PO Box 14-901 Kilbirnie, Wellington, New Zealand, Email: j.copeland@niwa.cri.nz)

SALPEX'96 (Southern Alps EXperiment) was a three week long field experiment conducted in the South Island of New Zealand during October - November of 1996. A primary goal of the experiment was to examine the processes occurring during periods of high orographic rainfall, induced by north-westerly flow over the Southern Alps. The equipment deployed during SALPEX'96 included a set of eight GPS (Global Positioning System) receivers arranged in a transect across the mountains. The high quality GPS data collected has since been used to make hourly measurements of total precipitable water (PW) above each receiver site. We present here a validation of the GPS measurements by comparing with PW derived from radiosonde data collected at two of the GPS sites. We also investigate the correlation between PW and rainfall during selected storm events that occurred during the SALPEX'96 period. Finally we compare the GPS PW measurements with PW derived from RAMS (Regional Atmospheric Modeling System) mesoscale simulations of the SALPEX events. We examine the ability of the model to correctly capture the temporal evolution of the vapour fields and also to resolve the sharp PW gradients observed across the mountains during the storm events.

JWM08/E/06-A2

1120

**REAL-TIME FINESCALE NUMERICAL WEATHER PREDICTION DURING THE MAP FIELD EXPERIMENT**

R. Benoit (1), P. Binder (2), S. Chamberland (1), H.C. Davies (3), M. Desgagné (1), D. Lüthi (3), J. Schmidli (3), M. Sprenger (3), C. SCHÄR (3) schaar@geo.unmw.ethz.ch, S. Thomas (1) and E. Zala (2) (1 = Recherche en Prévision Numérique (RPN), Env. Canada, Dorval, Canada) (2 = Swiss Meteorological Institute (SMI), Zürich, Switzerland) (3 = Swiss Federal Institute of Technology (ETH), Zürich, Switzerland)

Further developments in numerical modelling and computer technology will soon allow for limited-area numerical weather prediction at a resolution of 1-2 kilometers. This advance opens exciting prospects for the prediction of orographic precipitation over complex terrain. The increase in resolution will allow for (i) a substantially improved representation of the underlying topography, (ii) the explicit (rather than parameterized) simulation of convective precipitation events, and (iii) the coupling with hydrological run-off models operating at the scale of individual catchments.

Within the Mesoscale Alpine Programme (MAP) attempts are underway to run the Canadian MC2 model in real time at a resolution of 2-3 km during the MAP field phase (August - November 1999). The MC2 model will be driven by a model chain consisting of a global model and a 14 km resolution mesoscale models in a one-way nesting mode. Current plans foresee a resolution of 2-3 km, a computational grid of ~300x300x60 gridpoints, and a computational domain covering the whole of the Alpine region.

Initial testing of such configurations is already well underway. An overview of the model configuration will be presented along with results from test cases of orographic precipitation events. Critical aspects that require particular attention in future research will also be discussed.

JWM08/E/02-A2

1140

**RAINFALL FORECASTS OVER THE NEW ZEALAND SOUTHERN ALPS FOR SALPEX'96: CHARACTERISATION AND THE IMPORTANCE OF ICE-SPECIES**

NIELS BORMANN NIWA/VUW Centre of Excellence, PO Box 14 901, Kilbirnie, Wellington, New Zealand/Aotearoa, email: n.bormann@niwa.cri.nz Crispin J. Marks NIWA Wellington, PO Box 14 901, Kilbirnie, Wellington, New Zealand/Aotearoa

Mesoscale and global-scale precipitation forecasts over the New Zealand Southern Alps are characterised and validated for the October/ November 1996 field campaign period of the Southern Alps Experiment (SALPEX) using rain gauge observations. SALPEX is a collaborative mountain meteorology project initiated to study processes through which the Southern Alps affect New Zealand weather and hydrology. The mesoscale forecasts are gained from a 48h, 20km configuration of the Regional Atmospheric Modeling System (RAMS). The contribution of the hydrometeor species snow, graupel, and aggregates on model precipitation in these forecasts is investigated by performing parallel month-long series of model experiments with and without these ice-species.

The rainfall predictions are satisfactory in general and the RAMS setup shows better skill in resolving heavy orographic precipitation than the global model, particularly when the full

RAMS microphysics scheme is used. The mesoscale model allows a better representation of the fine-scale orography of the Southern Alps. The results from RAMS show that heavy precipitation is strongly sensitive to the configuration of the microphysics scheme. It is essential to include processes related to snow, graupel, and aggregates in the model in order to reproduce the strong orographic enhancement observed and to improve rainfall forecasts in the lee of the Southern Alps. This suggests that these hydrometeor species play a key-role in determining the distribution of rainfall over the Southern Alps and affect the occurrence of spill-over across the alpine divide.

JWM08/E/05-A2

1200

**OROGRAPHIC RAINFALL AS SIMULATED BY THE NONHYDROSTATIC MODEL LM OF DWD**

J. Steppeler, (Deutscher Wetterdienst, Frankfurterstr 135, 63067 Offenbach, Germany), e-mail: jsteppeler@dwd.d400.de

Orographically induced rain simulated by the nonhydrostatic model LM of DWD is compared to observations. Model versions using horizontal meshes of  $dx=7$  km and  $dx=2.4$  km are used. For verification SYNOPSIS and the climatological observations as well as a dense network over the country of Baden-Wuerttemberg are used. The cases simulated comprise:

- The Rhine flooding case
- The Odra flooding
- The Brig case of MAP

For the Rhine flooding precipitation output of LM was used as input for a flood simulation runoff model in a cooperation with the country of Baden-Wuerttemberg. For the pegel of Karlsruhe the use of precipitation forecasts leads to an increase of useful flooding forecast time by 24 hrs. A selection of cases is presented where an increased model resolution produced improved orographic precipitation forecast.

JWM08/W/02-A2

1220

**MODELLING INTENSE OROGRAPHIC PRECIPITATION OVER THE TEVERE VALLEY: A CASE STUDY**

G. Pisacane, N. Tartaglione, P.M. Ruti - ENEA Roma A. Speranza - Un. di Camerino. E-mail: giovanna@mantegna.casaccia.enea.it Telephone No: +39 06 304 83570 Fax No: +39 06 304 83591

Orography has been demonstrated to play a fundamental role in determining both the intensity and distribution of precipitation. The Italian Peninsula is characterized by the presence of mountains along its whole length, in addition to the Alpine Chain, so that interaction between weather systems (fronts, cyclones, MCS) and orography may frequently take place. In the present work, a case study of heavy precipitation over the Tevere basin has been conducted, using the limited area model BOLAM to predict the meteorological fields of interest. An elongated front coming from the North-West crossed Italy on 5-6 December 1992. The associated pre-frontal low level jet, directed towards the North-East, impinged the Apennines over Central Italy, causing precipitation up to 40 mm/day over the whole basin. The event was characterized by two rainfall peaks, which in turn saturated the soil and caused saturation overland flow, in addition to large runoff volumes. We show the results of a high resolution (10 km) control run and some sensitivity experiments.

A comparison between rainfall data and simulated precipitation is presented. Future developments concern the application of rainfall forecast to a hydrological model in order to obtain flood prediction, whose skill dramatically depends on our ability to determine the correct relationship between precipitation and runoff.

Tuesday 20 July PM

Presiding Chairs: G. AUSTIN (Univ. of Auckland, New Zealand)  
H LANG (ETH Zurich, Switzerland)

**RAINFALL ANALYSIS AND RUNOFF FORECASTING**

JWM08/E/01-A2

Invited

1400

**STUDY ON THE USE OF OROGRAPHICAL DATA WITH SPATIAL ANALYSIS OF MONTHLY PRECIPITATION ON GLOBAL SCALE**

Bruno RUDOLF (Deutscher Wetterdienst, 63004 Offenbach a.M., Germany, Tel.: +49-69-8062-2765, email: brudolf@dwd.d400.de) and Franz M. Albrecht (Programm-und Gutachterservice, Frankfurt)

The measurement and mapping of precipitation is fundamental to meteorology, hydrology and to a number of other sciences. Precipitation data measured locally using raingauges need to be transferred to area-means in order to calculate water budgets or to compare the results from raingauge-measurements with satellite-based observations or numerical model results. Geometric spatial interpolation scheme are commonly used with global analyses. In order to reduce the interpolation error the use of precipitation-orography relationships was recommended. In order to find out the effect, a multivariate regression method has been established and tested with various orographical variables (elevation, slope, orientation, exposure, latitude, longitude, distance to coast).

First results of the tests have been: Application areas should not be larger than 250,000 km<sup>2</sup>, preferably smaller. The test analyses show remarkable variations of the regression fit. Correlations for longterm mean precipitation and orography are clearly higher than for individual monthly precipitation. The quality of the regression fit depends highly on the conditions in the individual regions and months, and varies between acceptable values and values near zero. For individual months, a fraction of the total variance of 5% to 50% only is described by regressions. In some regions the orographical variables are of nearly no importance. Most problems with the regression method occurred for the tropics and for Europe. North America with its large and significant north to south oriented structures shows the best evaluable relationships, the SALPEX'96 period. Finally we compare the GPS PW measurements with PW derived from RAMS (Regional Atmospheric Modeling System) mesoscale simulations of the SALPEX events. We examine the ability of the model to correctly capture the temporal evolution of the vapour fields and also to resolve the sharp PW gradients observed across the mountains during the storm events.

JWM08/E/03-A2

1440

**THE BIASED ASSESSMENT OF TOPOGRAPHY EFFECTS ON PRECIPITATION**

Boris Sevruk (Swiss Federal Institute of Technology, ETHZ, CH-8092 Zurich, Switzerland, email: sevruk@geo.unmw.ethz.ch)

The results of studies of the effects of topography on precipitation in the mountains are sometimes contradictory and confusing. In addition to the complex matter of precipitation processes and their regional character this is partly caused by different and/or subjective definitions and modifications and even combinations and number of topographic variables as used by individual authors to obtain the best results. A further bias is due to the systematic error of point precipitation measurement, particularly the wind-induced error and the prevailing

## INTER-ASSOCIATION

positioning of gauge sites in the high mountains in the valleys. Consequently, a valley gauge network must not be adequate for other topography elements (e. g. slopes) where other conditions could prevail. Moreover gauges situated on exposed slopes and in high altitude show larger wind induced error.

Problems exist also on the interrelation of topographic variables used as precipitation predictors in multiple regression analysis (e.g. altitude and distance to the mountainous ridge or altitude and slope). This indicates that results of studies of topography effects on precipitation are hardly transferable from one scale or region to others. Beside the region and weather situation they appear to depend on the general strategy of network design, the scale, the range of altitude and the method of selection and estimation of topographic variables. Principally, the relationships derived for large areas or valleys are scarcely adequate to be used for smaller areas or slopes. Examples from Switzerland will be presented.

### JWM08/W/13-A2 1500

#### ABOUT THE NECESSITY OF TOTALIZER MEASUREMENTS IN HIGH ALPINE REGIONS FOR CLIMATOLOGICAL PURPOSES

INGEBORG AUER (Central Institute for Meteorology and Geodynamics, Hohe Warte 38, 1190 Vienna, AUSTRIA, Email: ingeborg.auer@zamg.ac.at)

More than 120 totalizer gauges complete the Austrian precipitation network, especially in the high alpine regions. The majority of totalizers are installed at locations where it seems to be impossible to make daily gauge readings, however there are some places where parallel reading of rain gauges (tipping buckets or weighing gauges) and totalizers have been done since many years.

For financial reasons and often insufficient results there are tendencies to reduce the number of totalizer gauges. The paper intends to demonstrate that the advantages of totalizer measurements outweigh the disadvantages, that well done totalizer readings provide more reliable results than rain gauges and that totalizers are an indispensable component of the Austrian climatological network.

### JWM08/E/08-A2 1520

#### TOPOGRAPHIC EFFECTS IN PRECIPITATION CLIMATE AND VARIABILITY: ANALYSIS FROM HIGH-RESOLUTION RAIN-GAUGE OBSERVATIONS IN THE ALPINE REGION

Christoph FREI and Manfred Schwarb (Swiss Federal Institute of Technology (GI-ETH), Winterthurerstr. 190, CH-8057 Zurich, Switzerland, email: christoph.frei@geo.unm.ethz.ch)

Topographic effects on precipitation processes operate on a broad range of spatial scales. This study examines, for the region of the European Alps, the topographic influence as revealed in surface rain-gauge observations. Special consideration will be given to the organisation of the precipitation climate and frequency distribution in relation to the various scales of the ridge topography. The analysis is based on a comprehensive dataset of high-resolution observations (more than 6000 stations) with a typical inter-station distance of 10 kilometers covering the entire ridge and surrounding foreland regions. The dataset includes daily precipitation totals for a period of 20 years. The results of the statistical analyses reveal, on the ridge-scale, a pronounced upstream enhancement, shading of inner mountain areas and features of topographic channelling. On more local scales (a few kilometers) the relation to the underlying topography becomes weaker.

### JWM08/W/05-A2 1540

#### PRECIPITATION CLIMATE MAPS FOR THE ALPINE REGION. EVALUATION OF A HIGH-RESOLUTION ANALYSIS SCHEME USING COMPREHENSIVE RAIN-GAUGE DATA

Manfred SCHWARB (Swiss Federal Institute of Technology, Institute of Geography, Winterthurerstrasse 190, CH-8057 Zurich, Switzerland, email: schwarb@geo.unm.ethz.ch) Christopher Daly (Oregon State University, Department of Geosciences, 326 Strand Agricultural Hall, Corvallis, OR 97331-2204, U.S.A., email: daly@oce.orst.edu) Christoph Frei (Swiss Federal Institute of Technology, Institute of Geography, Winterthurerstrasse 190, CH-8057 Zurich, Switzerland, email: christoph.frei@geo.unm.ethz.ch)

Mapping of precipitation climate fields at spacial resolutions close to or finer than the resolution of observational networks requires the use of analysis schemes capable of representing local terrain effects upon precipitation. This study assesses the performance of a sophisticated statistical-geographical analysis approach for the entire region of the European Alps. A specific challenge of the region is the existence of pronounced and regionally variable topography-precipitation relationships, requiring special flexibility of the analysis scheme.

The analysis procedure being considered is the regression based model PRISM (Parameter-elevation Regressions on Independent Slopes Model), specifically developed for climate mapping over complex topography. The model applies linear regressions with elevation as a predictor. Variable weights are assigned to the point observations depending on topographic attributes of the stations' environment. The model is operated on a regular grid of 1.25 minutes resolution and makes use of a comprehensive dataset consisting of observations at more than 6000 rain-gauge stations. The model performance is quantified using cross validation results. The analysis method reproduces stable and realistic precipitation-height gradients and successfully reproduces regional variations of these gradients between the Alpine lowlands, the rim and the inner region of the ridge.

### JWM08/W/01-A2 1630

#### FLOW FORECASTING USING MESOSCALE PRECIPITATION PREDICTION

Roddy Henderson, Jeffrey Copeland, Richard Ibbitt, and David Wratt (National Institute of Water & Atmospheric Research Ltd. - NIWA, PO Box 14 901, Wellington, New Zealand, email: r.henderson@niwa.cri.nz)

The extreme nature of New Zealand's topography and precipitation, and lack of upstream information have made it difficult to forecast river flows beyond the nowcast (6-12 hour) time period. Mesoscale models nested within global forecasts can produce quantitative precipitation predictions of high spatial and temporal resolution and have the potential to provide forecasts up to two days ahead. A significant difficulty is validating these forecasts against rain gauges in regions of complex terrain.

One solution is to use observed riverflows as a measure of catchment integrated precipitation. This is particularly valid in catchments that have high runoff with little loss and short response times. We have applied this technique to 36 catchments in the Southern Alps for the SALPEX (Southern Alps Experiment) 1994 period using RAMS (Regional Atmospheric Modeling System) precipitation. The mean catchment integrated model rainfall was 65% of observed runoff with an R2 of 0.87.

The next step is to use the mesoscale model precipitation as input to a distributed hydrologic rainfall-runoff model (TOPMODEL). This approach has been tested on a range of New Zealand mountain catchments for several different events and the intensity and timing of the

forecast riverflow compares favourably with observed flows. A linked system holds the potential for use as an operational flow forecasting tool.

### JWM08/W/10-A2 1650

#### ON THE MODELING OF OROGRAPHIC PRECIPITATION AND ITS HYDROLOGICAL IMPLICATIONS

L.R. LEUNG, M.S. Wigmosta, and S.J. Ghan Pacific Northwest National Laboratory Richland, WA 99352, U.S.A. E-mail: ruby.leung@pnl.gov Telephone No: 1-509-372-6182 Fax No: 1-509-372-6168)

Surface topography explains a high percentage of spatial variability in precipitation over mountainous regions. The prediction of orographic precipitation has important implications to the prediction of surface hydrology such as snow cover and streamflow. An efficient way of modeling orographic precipitation is through subgrid parameterization. An example of such schemes has been developed and implemented in a regional climate model. The method aggregates subgrid variations in surface elevation to a limited number of elevation bands. An airflow model is used to determine the height rise or descent of air parcels as they encounter mountain barriers or valleys. A thermodynamic model is used to determine the temperature, humidity, and cloud water of the air parcels. Cloud, radiation, and surface processes are all calculated for each elevation band of each model grid cell. The prediction of surface variables such as temperature and precipitation is mapped from elevation bands to geographical locations during postprocessing to yield high resolution spatial distributions. This method has been evaluated by driving the regional climate model with large scale analyses for simulating precipitation over the U.S. Pacific Northwest. The model is found to correctly capture the surface temperature and precipitation variations as functions of surface topography over different mountain ranges, and under different climate regimes. The simulation has been used to drive a distributed hydrology model at two mountain watersheds in the Pacific Northwest. Simulation of snow cover and streamflow in these remote watersheds requires different degrees of accuracy and spatial resolutions in surface temperature and precipitation fields, which are neither widely observed nor easily predicted by models. A detailed case study using observed and simulated meteorology to simulate surface hydrology in those two watersheds will be described. Also will be discussed are the implications for assessing the impacts of climate variability and change on water resources in mountainous regions.

Wednesday 21 July AM

### JWM08/E/04-A3 Invited 0930

#### SOME QUESTIONS REGARDING OROGRAPHIC PRECIPITATION

Ronald B. Smith (Yale Department of Geology, P.O.Box 208109, New Haven, CT, 06520-8109, USA, email: ronald.smith@yale.edu)

A number of physical processes combine to make the phenomena of orographic precipitation rather varied and complex. This brief review will discuss only four of these processes: 1)the effect of latent heat on airflow splitting and/or focussing, 2)hydrometeor drift and spillover, 3)upstream effects and 4)seeding from higher clouds and cloud top processes. Results of some previous field projects around the world will be reviewed, including stable isotope data from surface precipitation. The influence of the scale, shape and latitude of various mountain ranges will be discussed.

### JWM08/W/16-A3 1020

#### NUMERICAL STUDY OF MOIST FLOW OVER AN ISOLATED 3-D TOPOGRAPHY

Mario MIGLIETTA (Institute for the Study of Atmospheric pollution and Agrometeorology, CNR-ISAATA, Strada Provinciale Lecce-Monteroni, 73100 Lecce, Italy, Email: miglietta@axple.le.infn.it) and Andrea Buzzi (Institute of Atmospheric and Oceanic Sciences, ISAO-CNR, Via Gobetti 101 - 40129 Bologna, Italy, Email: buzzi@ocean.fisbat.bo.cnr.it)

Orographic precipitation is intimately connected with the properties of flow regimes over orography in the presence of saturated atmospheric layers. The complexities related with the flow over mesoscale obstacles, even of idealised shape, in a moist atmosphere has limited the number of contributions on this subject to a few analytical and model simulation studies, mainly related to two-dimensional topography. On the other hand, analysis of numerical simulations of real events of heavy orographic precipitation have emphasised important dynamical effects of humid processes over flow patterns and precipitation. The present study is aimed at investigating moist effects in relation with orographic precipitation, as a function of different flow regimes, with particular attention devoted to upstream features. The effect of moisture is analysed with a systematic simulation approach, by estimating the role of different parameters like static stability, relative humidity, height and shape of the obstacle, in cases of highly idealised stratified flow over an isolated obstacle. A channel version of a meteorological model (BOLAM3), that includes a simplified treatment of microphysical processes, is employed. The simplest obstacle shape considered is that of a Gaussian mountain of circular horizontal section. Dry and moist flows are contrasted in different parameter regimes. The presence of humidity in the atmosphere, when saturated regions appear, can effectively modify the flow pattern in comparison with the dry case, given the same upstream values of wind and temperature profiles. In general, "flow over" is enhanced with respect to "flow around" in the moist case. This result can be interpreted, but only to some extent, in terms of variations of the local Froude number, which changes strongly from the dry case to the moist one. For example, in the moist case, nonlinear effects as the formation of stagnation regions upstream or of vortices downstream are confined to higher mountain cases than in the corresponding dry case. A decrease of the Froude number has the effect of increasing the volume of saturated air and the amount of precipitation. However, a complication arises because the volume of saturated air, where the decrease of the local Froude number takes place, is in itself a function of the flow regime that establishes near the obstacle. In this respect, the effects of variations of the shape of the mountain and of the humidity content in the upstream profile are examined.

### JWM08/W/09-A3 1030

#### OROGRAPHIC PRECIPITATION

A V COALS and S D Mobbs (The Environment Center, The University of Leeds, Leeds LS2 9JT, UK. E-mail: alison@lec.leeds.ac.uk Telephone No: 0113 233 1596 Fax No: 0113 233 6716)

Precipitation rates can be greatly enhanced by orographically-generated flows, but practical predictive models to date have been limited by the use of simple airflow models which are essentially dry. Airflow models for the flow of dry air over orography recently developed at The Environment Centre at the University of Leeds have been adapted in order to include moisture, thus allowing the prediction of the humidity field over complex terrain. Data obtained from experimental field work has been used as input. Verification of the moist flow model has been achieved by comparing the vertical velocities and humidity associated with gravity waves with actual measurements made by aircraft.



**JWM08/W/07-A3** 1120**LEE INTERNAL WAVES AND VORTICES IN A SLOPING INCIDENT FLOW**

Yuli D.Chashechkin (Laboratory of Fluid Mechanics of the Institute for Problems in Mechanics of the RAS, Moscow, prospect Vernadskogo, 101-1, 117526, Russia, E-mail: chakin@ipmnet.ru)

Pattern of three dimensional lee internal waves past a 3D body is calculated in linear approximation in the case when an arbitrary oriented uniform flow of a viscous stratified fluid with constant buoyancy frequency is incident upon an obstacle. Amplitude and phase characteristics and loci of caustic limited an area of wave propagation are found. Laboratory investigations of the pattern of flow past a sphere towing with constant velocity under an arbitrary angle to horizontal in a stratified brine are carried out using electrolytic precipitation, schlieren visualization and probe sounding techniques. Calculation results for the form of crests and troughs and for location of the boundary of the wave domain are in good agreement with experiment, whereas the calculated values of amplitude are underestimated. Distortion of the wave shape is used for calculation of a horizontal velocity profile in the vertical centreplane. Deformation of a shape of a pair bottom vortices with variations of an angle of the trajectory to horizon and internal Froude number are studied. Sharpening of an initial gradient inside a separating boundary current is measured by a narrow beam schlieren device. Flow regime diagram on the plane Froude number-Reynolds number is presented.

**JWM08/W/14-A3** 1140**STAGNATION POINTS IN 3-D MOIST MOUNTAIN FLOW**

QINGFANG JIANG and Ronald Smith Department of Geology, Yale University

The formation of stagnation points in airflow over mountains determines the onset of gravity wavebreaking and low level flow splitting. In this study, flow with uniform wind speed, a constant dry buoyancy frequency, and a deep moist layer, over a bell-shape mountain is investigated using a non-hydrostatic mesoscale model (ARPS). The control parameters of such a system are surface temperature, windspeed, and non dimensional mountain height. Two cases are considered here: a deep moist layer adjacent to the topography and a deep moist layer aloft above a shallow (2km) dry layer. It is demonstrated that in the absence of condensation or limited condensation, the speed extrema values collapse onto the 'universal curves' (Smith andGronas 1993). However, with increasing condensation, the wet curves depart from the dry 'universal curves'. This departure is caused by latent heating/cooling related to the condensation/evaporation process. The results question the idea that the wet dynamics can be predicted quantitatively by replacing the dry buoyancy frequency with a wet buoyancy frequency. With the moist layer adjacent to the topography, condensation occurs mainly over the windward slope and the peak. The release of latent heat helps flow to climb over a higher mountain and effectively delays the onset of both wave breaking and flow splitting. The maximum lee slope wind is also reduced significantly. It is found that the critical mountain height for windward stagnation is also approximately the mountain height to produce maximum precipitation. Beyond this height, lower level moist flow starts to split and less precipitation can be expected. With a moist layer aloft, condensation occurs mainly over the lee slope. It is found that the related latent heat release promotes wave breaking aloft and enhances the downslope wind maxima. However, it has little influence on windward stagnation. The steady precipitation rate is compared to a 'slab thermodynamic' model. The implications and applications to real situations are discussed.

**JWM08/W/08-A3** 1200**THE EFFECT OF OROGRAPHIC RESOLUTION ON EXTREME PRECIPITATION EVENTS: IMPLICATIONS FOR CLIMATE MODELS**

Deborah J. ABBS (CSIRO Atmospheric Research, Private Bag No. 1, Aspendale, Vic. 3195, Australia. Email: debbie.abbs@dar.csiro.au) Brian F. Ryan (CSIRO Atmospheric Research, Private Bag No. 1, Aspendale, Vic. 3195, Australia. Email: brian.ryan@dar.csiro.au)

The CSU Regional Atmospheric Modeling System (RAMS) has been used to model extreme precipitation events that have occurred along the steep, coastal escarpment of the Sydney-Illawarra region of south-eastern Australia. Results have been obtained at a horizontal resolution of 7 km. The synoptic-scale system considered in this presentation is of an east-coast low that was associated with 24-hr rainfall in excess of 300 mm. East-coast lows have been identified as the major cause of flood-producing rains on the east coast of Australia, and are characterized by heavy rainfall and strong winds.

For this study, simulations with high-resolution orography, GCM scale orography and no orography have been performed. In this presentation we will analyse the statistics of the 7 km RAMS simulations at horizontal scales of 300 km and 50 km. Parameters to be analysed will include cloud optical properties, cloud-top height, cloud cover, precipitation and phase. These statistics will be compared with observations.

**JWM08/W/11-A3** 1220**HIGH RESOLUTION ENSEMBLE PREDICITON WITH A LIMITED AREA MODEL**

Chiara Marsigli, ANDREA MONTANI, Fabrizio Nerozzi, Tiziana Paccagnella, Paolo Patrino (ARPA-SMR, Viale Silvani, 6, 40122 Bologna, Italy, Email: eps@metgranew.arpamet.regione.emilia-romagna.it), Roberto Buizza (ECMWF, Shinfield Park, Reading, UK) and Franco Molteni (CINECA, Via Magnanelli 6/3, 40033 Casalecchio di Reno, Bologna, Italy)

The aim of this work is to provide a contribution to the definition of a flood risk alarm system. The SMR-ARPA operational Limited Area Model (LAMBO) is nested on the ECMWF Ensemble Prediction System (EPS) and its capability to predict at the medium range (5 days ahead) and at high horizontal resolution (about 20 km) heavy rainfall events is investigated. Four case studies of flooding, selected from MAP case list, are examined. The clustering algorithm, using the 700 hPa geostrophic wind vector field as discriminant variable, allows to find, after 5 forecast days, different evolution scenarios, the most likely one being relative to the most populated cluster. For each case study, 5 different members of the EPS are selected and used as boundary and initial conditions for LAMBO integrations. In 2 case studies, the LAMBO-integrations, which correspond to the members of the most populated clusters, predict, to a very good degree of spatial accuracy, the heavy rainfall occurred. In the other cases, the LAMBO-spread of the ensemble is large enough so that the extreme events are predicted by at least one of the other members. The sensitivity to the choice of the variable for clustering the EPS members is also discussed.

Wednesday 21 July PM

**JWM08/L/02-A3** Invited 1400**THE PROCESSES INVOLVED IN THE OROGRAPHIC ENHANCEMENT OF PRECIPITATION AND THEIR DETECTION BY RADAR**

G.L. AUSTIN, J.Purdy, A.W Seed (Atmospheric Physics Group, University of Auckland, New Zealand, g.austin@auckland.ac.nz) and I Cluckie (Water Resources Group, University of Bristol)

In many parts of the world, including New Zealand, the annual distribution of rainfall is clearly intimately related to topography and wind direction. Climate change scenarios for New Zealand involve systematic changes in wind direction probabilities rather than direct surface heating. It thus becomes an important issue to discover quantitative relationships between topography and wind to predict climate and operational impacts on important activities such as agriculture and hydro-electric power generation. Two sets of high resolution radar and raingauge data from the SALPEX experiment are presented in the context of the other relevant meteorology. They represent the normal highwind speed Nor'wester which produces most of the rain in the South Island of New Zealand and a more unusual low wind speed event. Techniques for the determination of the detailed evolution of the precipitation processes involved are illustrated.

**JWM08/W/12-A3** 1440**OBSERVATIONS OF CONVECTION TRIGGERED BY WINDFLOW OVER HILLS**

Warren Gray (National Institute of Water and Atmosphere, PO Box 14 - 901, Wellington New Zealand, Email: w.gray@niwa.cri.nz)

The upmotion resulting from windflow over hills can lead to the triggering of convection in a potentially unstable flow. This can lead to an increase in rainfall over the hills compared to upwind regions. Two observational campaigns have been carried out in New Zealand, on two different scales of hills, to increase our understanding of the processes involved in the enhancement of rainfall over hills. The OPERA campaign studied rain over hills up to 1500m high and SALPEX studied rain over the Southern Alps, which have peaks in excess of 2500m.

High-resolution scanning radar data from OPERA show that convection tends to develop over the hills in conjunction with the passage of pre-existing showers. That is, showers pass over the hills from areas upwind, and as they pass more convective showers develop over the hills. This is commensurate with the concept that the pre-existing showers are marking areas of enhanced instability, which is then released by the upmotion of the flow over the hill. High-resolution rain gauge data show that, in general, that character of the showers over the hills is similar to those upwind, but the showers are more frequent over the hills.

Vertically pointing radar data and RHI scanning radar data from SALPEX show that the pre-frontal convection triggered by the windflow over the hill has echo top heights of only around 3 km, yet surface rainfall intensities can reach up to 100 mm h<sup>-1</sup>. Rain gauge data also shows that the rainfall becomes more variable as the flow moves towards the hill, but decreases nearer the crest. Numerical solutions to the windflow over the hill shows that, for stable flow, there is down motion aloft which would "cap" any rainfall formed at lower levels. This "capping" becomes stronger further towards the crest, and this could explain the more stratiform nature of the rainfall there.

**JWM08/W/06-A3** 1500**OROGRAPHIC INFLUENCES DURING WINTER PRECIPITATION EVENTS ON THE AVALON PENINSULA, NEWFOUNDLAND**

COLIN E. BANFIELD, David R.Hudak and Alan Thomson (Memorial University of New Foundland, Elizabeth Avenue, ST. John's, New Foundland A1B 3X9. E-mail:colinb@morgan.ucs.mun.ca Telephone No: 709-737-8981 Fax No: 709-737-3119)

Precipitation enhancement over a low coastal hill in winter is demonstrated for particular associations of synoptically determined onshore airflow and local geography encountered over southeastern Newfoundland. Four such cases are analysed, in which various sequences and combinations of precipitation types occurred at surface temperatures just below freezing during pre-warm front situations. Comparative surface gauge records from sites at the coast and hill summit, together with detailed volume scan data from a nearby Doppler radar, are employed to substantiate the interaction of local orography and meteorological factors. Although precipitation at the hill summit and upwind coast was of similar overall duration in each case, the observed surface rates on the hilltop exceeded those at the coast by approximately 1.0-4.0 mm hr<sup>-1</sup> during different stages of the events. Analysis of representative vertical cross sections of Doppler reflectivity patterns reveals that intensities are especially enhanced near the windward hill crest; this supports the observed association of periods of greatest enhancement with a local upslope wind component exceeding 20 m s<sup>-1</sup>. In the majority of these cases the enhancement is maintained primarily by the seeder feeder mechanism, which appears to be accelerated during transitions between precipitation types and when the surface warm front is 120-150 km distant. However, a preliminary phase of snowfall enhancement in advance of the main warm frontal clouds, due to the topographically-induced uplift of stable onshore airflow, was also observed.

**JWM08-A2** Introduction 1520**WORKING GROUP SESSION**

D. WRAIT

**JSA09** Tuesday 20 – Wednesday 21 July**POLAR GEOPHYSICS (IAGA, IAVCEI, IASPEI, IAG, IAPSO, IAHS, SCOSTEP)**

Location: Muirhead Tower, G08 LT

Location of Poster: Muirhead Tower, Student Room (1st floor)

Tuesday 20 July AM

Presiding Chair: Patrick T Taylor (NASA/GSFC, Greenbelt, MD, USA)  
Concurrent Poster Session**JSA09/E/12-A2** 0930**ACTIVE VOLCANOES OF THE ANTARCTIC PLATE**

Wesley E. LE MASURIER (Department of Geology, University of Colorado, Denver, Colorado, 80217-3364, USA, email: wlemasurier@carbon.cudenver.edu)

It has been estimated that there are 41 active volcanoes on the Antarctic plate, but there are only eight for which Holocene activity is unquestioned. This large uncertainty exists because direct observation is difficult, and because documenting Holocene activity by <sup>14</sup>C dating is not possible where no life forms exist. Fifteen of the 41 "active" volcanoes are in the West Antarctic rift system, including a recently discovered sub-glacial volcano inferred from



## INTER-ASSOCIATION

geophysical data. Twelve others are oceanic islands, 9 are in the South Sandwich arc, and 5 are on the Antarctic Peninsula. The Antarctic plate is almost completely encircled by mid-ocean ridges and has hardly moved since 85 Ma. This environment limits the mechanisms available to sustain volcanic activity on the continent. Thus, mantle plume activity and the interaction of transform faults with the rift system are the main mechanisms that have been invoked to explain volcanism in the rift.

The great enigma of Antarctic volcanism is the extent to which Cenozoic activity has occurred beneath thick ice cover, and the potential it, and associated high heat flow, may have to destabilize the West Antarctic ice sheet. Aeromagnetic surveys suggest the existence of  $10^6$  km<sup>3</sup> of subglacial volcanic rock, and it has been suggested that the aseismicity of the rift system may be related to magma overpressure. These portend significant subglacial volcanic activity (and high heat flow) in the future, but glaciologists are skeptical that these could be factors in the instability of the ice sheet. Until the potential effects of these factors are modeled, and the causes of the aeromagnetic anomalies verified, the question of how serious this threat might be will remain a matter of speculation.

### JSA09/W/14-A2

1000

#### ICE-VOLCANO INTERACTION DURING SUBGLACIAL ERUPTIONS IN TEMPERATE ICE CAPS IN ICELAND

Magnus T. GUDMUNDSSON (Science Institute, University of Iceland, Hofsvallagata 53, 107 Reykjavik, Iceland, email: mtg@raunvis.hi.is)

Subglacial eruptions occur in volcanic regions at high latitudes and at some large strato-volcanoes in other areas. About 11% of Iceland is ice covered and eruptions within ice caps have been frequent. Some of the most active volcanoes in Iceland are ice covered, notably the Grimsvotn volcano in the Vatnajökull ice cap and the Myrdalsjökull volcano. Jokullhaups associated with volcanic eruptions in Iceland may drain several cubic kilometers of water and discharge rates of order 100,000 m<sup>3</sup>/s have been reported. Landscape in the volcanically active zones is dominated by hyaloclastite ridges and tuyas, formed under the Pleistocene ice sheets. The first eruption within a large ice cap that could be monitored was the Gjalp eruption in Vatnajökull in 1996. About 0.4 km<sup>3</sup> of magma erupted in 13 days. Melting rates were very fast, 0.5-0.8 km/day for the first four days when the rate of eruption was highest. This high rate of melting suggests fragmentation of the magma and formation of hyaloclastites. Comparison of the Gjalp eruption with eruptions in the nearby Grimsvotn caldera, illustrates the effect of ice thickness on the response of the surrounding glacier. When the ice is thick, as in Gjalp (500-750 m), the ice deforms and flows into the depression created by melting and drainage. In Gjalp the depressions had a width of several kilometers but the glacier around the depressions was not affected. At known eruption sites in Grimsvotn, ice thickness is about 100 m. Openings are quickly melted in the ice, leading to explosive eruptions that disperse tephra over the ice cap. The ice surrounding the craters is mainly passive and suffers little deformation. Ice-volcano interaction, similar to that observed in Grimsvotn, occurs on ice covered strato-volcanoes in many parts of the world

### JSA09/W/08-A2

1045

#### ARCTIC GRAVITY PROJECT

Rene FORSBERG (Geodynamics Dept., KMS, Rentemestervej 8, DK-2400, Copenhagen NV, Denmark, email: rf@kms.dk) Steve KENYON (NIMA, 3200 S 2nd St, St. Louis, Mo., USA, 63118-3399, email: kenyon@nima.mil)

The gravity field of the Arctic Ocean region is of prime importance for global gravity field and geoid models, for providing information on the geology and tectonics of the Arctic Basin, and for navigation and orbit determination. Planned satellite gravity field missions such as CHAMP, GRACE and GOCE will all to a varying degree be strongly affected by the gravity field of the polar areas, especially for the satellites launched with a non-polar orbit, where a polar gap will remain in the coverage.

Ongoing gravity activities over many years have resulted in a nearly complete coverage of the Arctic with gravity field data. In recent years major airborne and surface survey activities have been carried out in the High Arctic and Greenland, US nuclear submarines have criss-crossed under the ice on scientific cruises, and Russia has continued a decade-long program of surface and airborne gravity measurements. Recently an international initiative, involving a.o. scientists from all circumarctic countries, has been taken to compile all available and releasable gravity data into a 5' uniform, public-domain gravity grid in year 2000. The paper will report on the progress of the project, and show examples from some recent airborne gravity survey activities.

### JSA09/E/02-A2

1115

#### POLAR GRAVITY MAPPING FROM FUTURE SATELLITE MISSIONS

C.K. SHUM (Department of Civil and Environmental Engineering and Geodetic Science, The Ohio State University, 470 Hitchcock Hall, 2070 Neil Avenue, Columbus, OH 43210-1275, USA, Email: ckshum@osu.edu) and Andy Trupin (School of Natural Science, Oregon Institute of Technology, Klamath, Oregon, USA, email: trupina@oit.edu)

By the beginning of the next Millennium, GRACE and CHAMP gravity mapping missions are expected to provide a three-fold improvement in our knowledge of the Earth's static gravity field to 1 cm accuracy in geoid at a wavelength of 300 km or longer, and to measure time-varying mass variations of the Earth system with a temporal resolution of days to weeks. With applications to the mass balances of the polar ice sheets, GRACE with a five-year mission is anticipated to provide a measurement accuracy corresponding to better than 0.01 mm/yr of sea level rise for each of Antarctica and Greenland ice sheets, over a spatial scale of 1600 km or longer. The orbital inclinations of GRACE/CHAMP would however limit the coverage of the polar ice caps to within +/- 87 degrees. In 2001, NASA will also launch IceSat, whose instrument Geoscience Laser Altimeter System (GLAS) will provide accurate measurements of ice elevation change. Radar altimeters are providing measurements of ice elevation change for interior of Antarctica and Greenland ice sheets. GPS measurements are providing crustal uplift information. In addition, cannon-satellites with satellite laser ranging are enabling determination of long wavelength gravity changes. In this paper, we will discuss the results of pilot studies for the anticipated improvement in the static and temporal gravity fields of the polar regions, and the ability of future satellite missions with combined use of in situ observations to potentially separate ice sheet mass balance, isostatic uplift, and changes in snow accumulation at the surface.

### JSA09/W/01-A2

1145

#### A HIGH RESOLUTION ARCTIC MARINE GRAVITY FIELD FROM ERS ALTIMETRY

Seymour LAXON, Neil Peacock (both at University College London, MSSL, Holmbury St. Mary, Dorking, RH5 6NT, email: swl@mssl.ucl.ac.uk) David McAdoo and Anahita Tikku, (both at U.S. National Oceanic and Atmospheric Administration, NODC/Lab for Satellite Altimetry, SSMC3, Silver Spring, MD, 20910, US, email: dave@comet.grdl.noaa.gov)

A new, detailed, high-accuracy gravity field has been derived from ERS-1 and ERS-2 satellite radar altimeter data over all Arctic seas south of 82 degrees north including permanently ice-covered seas. The entire ERS-1 Geodetic Mission and 22 cycles from the ERS-2 mission have been used in generating this field. In addition to using this larger data set, we have employed enhanced processing techniques, to retrack and reduce these ERS waveform data. Comparisons with airborne measurements show that this new Arctic gravity field resolves features down to crustal scales (i.e., spatial wavelengths as short as 20 km) representing a significant improvement over the 75 km resolution limit of our 1994 Science field (Laxon and McAdoo, Science, vol. 265, 621-624, 1994).

This gravity field should prove a particular help in unravelling the tectonic history and structure of the Canada Basin and Chukchi Borderland. For example, the gravity field clearly shows the anomalies associated with the Alaskan and Canadian continental shelf edges bordering the Canada Basin, shelf edge anomalies bordering the Eurasian Basin as well as a lineated low coincident with the Northwind Ridge. Anomalies and lineations arising from tectonic details imprinted in the seafloor can also be seen including: a north-south trending, negative lineation locating an apparent extinct spreading ridge in the middle of the Canada Basin. Other distinctive anomalies include those due to structures associated with crustal extension in the Chukchi Continental Borderland as well as on the Siberian continental margin and those overlying the active spreading ridge in the Eurasian Basin north of the Laptev Sea. At the other - or Atlantic end - of the Eurasian Basin, anomalies coincident with the Spitsbergen FZ and Lena trough can be seen.

### JSA 09/E/04-A2

1200

#### EARTH TIDES AND OCEAN TIDAL LOADING ON GREENLAND: CORRECTION OF SURFACE DEFORMATIONS BY TIDAL GRAVITY MEASUREMENTS

Gerhard JENTZSCH and Markus Ramatschi (both at Institute for Geosciences, FSU Jena, Burgweg 11, D-07749 Jena, email: jentzsch@geo.uni-jena.de), Per Knudsen (Geodetic Institute, National Survey and Cadastre, DK-2400 Copenhagen, email: pk@kms.dk)

Space and air borne observations of the earth concerning the changes of the Greenland ice cap are related to kinematic GPS measurements connected to fiducial sites. With regard to the accuracy of these measurements the time variation of the coordinates of the reference stations must be determined. Since most of the reference stations are close to the coast the correction applying standard ocean load models is not sufficient: Due to incomplete ocean tidal charts especially north of 60° and in shelf areas the computed loading signal does not explain the observation.

With our L & R tidal gravimeter ET 18 we performed gravity tidal measurements from 1993 to 1997 at four sites covering about one year each. The determination of the vertical deformation requires the separation of the Newtonian attraction from the observed load signal by model computations applying a local crust / mantle structure and a local distribution of the ocean tides derived from different models. The vertical deformations obtained for the main tidal waves of up to 35 mm explain about half of the observed effect in gravity only. Thus, the ocean tide models need improvement.

### JSA09/W/13-A2

1215

#### ANALYSIS OF GPS DATA OBSERVED BETWEEN 1997-99 ON PERMANENT STATIONS IN ANTARCTICA AND ITS VICINITY

Xin CHEN (1), Falko Menge (2), Hans Werner SCHENKE (1), Tilo Schoene (1), Guenter Seeber (2), Christ of Voelksen (2) ((1) Alfred Wegener Institute for Polar- and Marine Research, Columbusstrasse, D-27568 Bremerhaven, Germany, e-mail: Schenke@AWI-Bremerhaven.DE, (2) Institut fuer Erdmessung, Universitaet Hannover, Schneiderberg 50, D-30167 Hannover, Germany, e-mail: menge@mbox.ife.uni-hannover.de)

Under the scientific program GIANT (Geodetic Infrastructure of Antarctica, coordinated under the auspices of the SCAR Working Group on Geodesy and Geographic Information) several new permanent GPS stations were established in Antarctica and its vicinity during 1997 and 1998. The resulting network has enhanced our capability in monitoring crustal deformation in Antarctica. The new stations include: Jubany /Dallmann (DALL), Gough Island (GOUG), Sanae IV (VESL), General Belgrano II (BELG), Mawson (MAW1), Palmer (PALM), Syowa (SYO1), and Dumont d'Urville (DUM1).

The data were processed together with other existing permanent GPS-stations in Antarctica and several permanent IGS-stations in the southern hemisphere, using the GAMIT/GLOBK (Alfred Wegener Institute) and GIPSY-OASIS II (Institut fuer Erdmessung) software packages. Site position time series and site velocities were determined in the ITRF reference frame, and were then compared and analyzed with estimates from other sources.

### JSA09/L/02-A2

1230

#### PLATE DEFORMATIONS AND PLATE KINEMATICS OF ANTARCTICA DERIVED BY GPS

R. DIETRICH, R. Dach, J. Perl (TU Dresden, Institut für Planetare Geodäsie, D-01062 Dresden), H.-W. Schenke, T. Schöne, M. Pohl (Alfred-Wegener-Institut für Polar- und Meeresforschung, Columbusstraße, D-27568 Bremerhaven), J. Ihde, G. Engelhardt (Bundesamt für Kartographie und Geodäsie, Außenstelle Leipzig, Karl-Rothe-Straße 10, D-04105 Leipzig), G. Seeber, F. Menge, Ch. Völksen (Universität Hannover, Institut für Erdmessung, Schneiderberg 50, D-30167 Hannover), W. Niemeier, H. Salbach (TU Braunschweig, Institut für Geodäsie und Photogrammetrie, Gaußstraße 22, D-38106 Braunschweig), K. Lindner, H.-J. Kutterer, M. Mayer (Universität Karlsruhe, Geodätisches Institut, Englerstr. 7, D-76128 Karlsruhe), H. Miller, A. Veit (Universität München, Institut für Allgemeine und Angewandte Geologie, Luisenstraße 37, D-80333 München)

Repeated GPS observations are an efficient and accurate tool to study crustal deformations in polar regions. The results presented here are based on data obtained from 1995 until 1998 in the frame of the SCAR GPS Campaigns. A joint German research group contributed substantially to the field activities as well as analyzing the data with different software packages (BERNESE, GAMIT/GLOBK, GIPSY, GEONAP). The resulting network deformations can be used to relate the kinematics of the Antarctic plate to other major tectonic plates. Furthermore, regional deformation patterns, e.g. in the area of the Antarctic Peninsula, are obtained.

Tuesday 20 July PM

Presiding Chair: John Turner (British Antarctic Survey, Cambridge, UK)

### JSA09-A2

#### Introduction

1400

J. DUDENEY, (British Antarctic Survey)

### JSA09/L/01-A2

1415

#### THE GEOPHYSICS OF ARCTIC SEA ICE

Donald K. Perovich (USA CRREL, 72 Lyme Road, Hanover NH 03755, email: perovich@crrel.usace.army.mil)

Perennial sea ice covers much of the Arctic Ocean. The presence of the ice cover profoundly affects energy exchange between the atmosphere and the ocean. The energy exchange process is complicated by the considerable seasonal and spatial variability exhibited in the properties of the ice cover. For instance, due to a combination of thermodynamic and dynamic processes, ice thicknesses can range from open water to ridges tens of meters thick. Albedos decrease from peak values of 0.9 in the spring to minima of 0.4 at the height of the summer melt season. General circulation models indicate that Arctic sea ice may be a sensitive indicator of climate change. The sensitivity of the ice pack to climate changes is due in part to the ice-albedo and cloud-radiation feedbacks. This presentation will describe the key geophysical properties of the Arctic sea ice cover and summarize recent sea ice studies. Particular attention will be paid to sea ice feedback processes and the surface heat budget of the Arctic Ocean.

#### JSA09/L/03-A2 1445

##### GEOPHYSICS OF THE ANTARCTIC ICE SHEET

CHARLES R. BENTLEY, Geophysical and Polar Research Center, University of Wisconsin, 1215 W. Dayton St., Madison, WI 53706, USA; email: bentley@geology.wisc.edu

The Antarctic ice sheet contains sufficient ice to raise world-wide sea level by more than 60 m if melted completely; the amount of snow deposited annually on its surface is itself equivalent to over 5 mm of global sea level. Thus, the ice sheet could be a major agent of change for the present-day sea level, but it is still not known whether the ice sheet is growing or shrinking and the snow accumulation rate may be changing. The ice sheet is potentially subject to alteration in a modified climate; in fact, it may be shrinking now in response to the end of the last ice age. The West Antarctic ice sheet, which rests on a bed far below sea level, may be particularly capable of rapid retreat. Rates of discharge from some of the major ice streams have changed markedly in recent decades and the grounding line of one of them may be retreating rapidly. Measurements from satellites early in the 21st century are expected to settle the question of current growth or shrinkage, but prediction of the future will remain problematic for many years. Critical to improving our understanding of ice-sheet behavior is to learn more about the key physical processes that govern ice-stream dynamics. These include the interaction between an ice stream and its bed, which may vary with scale; complex temperature-dependent processes at lateral shear margins; interaction with ice shelves; and the spatial and temporal initiation of stream-like flow.

#### JSA09/L/04-A2 1515

##### ARCTIC METEOROLOGY AND CLIMATOLOGY : CURRENT UNDERSTANDING AND FUTURE DIRECTIONS

Amanda H. Lynch, University of Colorado, USA

The circulation and surface energy and mass balance of the Arctic atmosphere, land surface, sea ice and ocean system combine to have direct impacts on global climate. For example, the freshwater inputs via runoff and precipitation less evaporation (P-E) play a key role in maintaining the halocline, thereby influencing global ocean circulation as well as regional sea ice cover. The processes determining runoff and P-E include a complex series of feedbacks involving clouds, permafrost, atmospheric circulation, sea ice cover, and many other factors. In addition, the most recent IPCC assessment shows that the largest disagreement between coupled climate model simulations of present day climate remains the polar regions. The disagreement reflects the sensitivity of this interconnected system as well as our limited understanding.

Recent analyses of observations have identified interesting variations in the North Atlantic and Arctic Oscillations, the North Atlantic thermohaline regime, the sea ice distribution, precipitation, permafrost distribution and many other climate variables. It remains to be determined whether these variations are consistent with, or indicators of, the type of polar amplification predicted by global climate model experiments. This presentation will provide an overview of some current findings in the Arctic, and discuss future research directions.

#### JSA09/E/06-A2 1600

##### ANTARCTIC METEOROLOGY AND CLIMATOLOGY: RECENT DEVELOPMENTS AND OUTSTANDING PROBLEMS

J.C. KING (British Antarctic Survey, Cambridge CB3 0ET, UK, email: j.c.king@bas.ac.uk)

Over the past two decades, considerable progress has been made in understanding the processes that control the climate of Antarctica and couple this region with the rest of the global climate system. Technological developments have made it feasible to deploy automated measuring systems in previously inaccessible areas, while the wealth of data now available from satellite sensors permit continent-wide monitoring of key climatological variables. These advances in measurement technology have been paralleled by improvements in global and regional scale models that, for the first time, provide a synthesis of the workings of the Antarctic climate system. In this talk I will review the advances of the last two decades and will look at some problems that are still outstanding. These include identifying the causes of the recent warming seen in the Antarctic Peninsula and correctly parametrising the processes that control katabatic flow.

#### JSA09/W/12-A2 1630

##### THE APE-GAIA CAMPAIGN: AIRBORNE POLAR EXPERIMENT GEOPHYSICAL AIRCRAFT IN ANTARCTICA

Bruno CARLI and Ugo CORTESI (both at IROE-CNR, Via Panciatichi, 64 Firenze, Italy. E-mail: carli@iroe.fi.cnr.it, cortes@iroe.fi.cnr.it), Alberto ADRIANI (IFA-CNR Via del Fosso del Cavaliere, 100 Roma, Italy E-mail: adriani@atmos.ifa.rm.cnr.it), Cornelis Blom (IMK-FZK Postfach 3640, D-76021 Karlsruhe, Germany. E-mail: blom@imk.fzk.de), Stephan BORMANN (FZJ-ICG-1, 52425 Juelich, Germany. E-mail: S.Bormann@fz-juelich.de), Martyn Chipperfield (University of Cambridge, Cambridge CB2 1EW, U.K. E-mail: Martyn.Chipperfield@atm.ch.cam.ac.uk), Giorgio FIOCCO (University of Rome, Piazzale Aldo Moro, 2 Roma, Italy. E-mail: fiocco@g24ux.sci.uniroma1.it), Giorgio GIOVANELLI (FISBAT-CNR Via Gobetti, 101 Bologna Italy. E-mail: giorgio@atmosphere.fisbat.bo.cnr.it), Valentin MITEV (Observatory of Neuchatel Rue de l'Observatoire, 58 2000 Neuchatel, Switzerland. E-mail: mitev@on.unine.ch), Guido VISCONTI (University of L'Aquila, Via Vetoio 10, Coppito-L'Aquila, Italy. E-mail: guido.visconti@aquila.infn.it), Michael VOLK (University of Frankfurt, Georg Voigt Strasse, 14 D-60325 Frankfurt am Main, Germany. E-mail: M.Volk@meteor.uni-frankfurt.de)

In the frame of the "Airborne Polar Experiment" (APE) a Russian military plane M55 has been converted in a high flying research platform for investigations of the polar lower stratosphere and upper troposphere. A first campaign, carried out in the Arctic during the winter 1996-97 has proved the capability of M55-Geophysica aircraft to access altitude and geographical locations, which are difficult to reach with other platforms.

A new mission of the M55, supported by the Italian National Program for Antarctic Research

(PNRA), is now planned over the Antarctic Peninsula for the study of the chemical processes responsible for stratospheric ozone losses, its subsequent recovery and its interaction with mid-latitude air. The campaign, named APE-GAIA (Geophysica Aircraft In Antarctica), will be based in airport of Ushuaia, Argentina (Lat. 54°S, Long. 68°W) from 15 September to 15 October 1999 and will represent the first major mission with a scientific payload of both in-situ and remote sensing instruments conducted on board of a high altitude aircraft in the southern polar region.

#### JSA09/E/07-A2 1645

##### SIMULATED VARIABILITY AND TRENDS OF THE ARCTIC SEA-ICE COVER PROPERTIES

Michael Hilmer, Markus HARDER, Peter Lemke

The polar sea-ice caps have received special attention in the context of Global Warming. Especially focussing on detecting trends of the Arctic ice cover as an indication of Climate Change, it is essential to determine its natural variability. The temporal variations of the Arctic sea-ice cover properties, such as ice thickness and ice extent, are investigated with the dynamic-thermodynamic Kiel Sea-Ice Simulation (KISS). The model is integrated over 40 years (1958 to 1997) with a daily time step. Daily fields of surface wind and air temperature derived from the NCEP/NCAR.

Reanalysis Project provide the atmospheric forcing. The simulation yields both strong inter-annual variability and a statistically significant, decreasing trend in ice thickness. Largest inter-annual variations of the ice thickness occur in the Beaufort Sea and near the Siberian shelves. Statistically significant negative trends of the ice thickness mainly occur near the North Pole and in the Kara and Barent Seas where the inter-annual variability is small.

#### JSA09/E/01-A2 1700

##### GEOPHYSICAL METHOD OF DETERMINATION OF THE BASE PERMAFROST BOUNDARY IN HOLES

Boris SEDOV (North-East Interdisciplinary Research Institute, the Russian Academy of Sciences, Magadan, Russia)

During the development of deposits in criolitic zone ( production of coal, diamonds, placers etc.) there is a need to know the position of the base permafrost boundary (BPB) that in case of mineralized waters, does not coincide with 0<sub>is</sub> isotherm. To determine the position of the base permafrost boundary in the hole, geophysical method was used. This method makes possible to carry out the determinations with any possible precision. For this, multicore cable is installed into the hole after drilling. Every line of such a cable ends with electrode. The distance among the electrodes is chosen according to prescribed precision for (BPB) depth determination. During the recovery of rock temperature in frozen stratum, solution freezes in the hole. Ice is not formed under the BPB. Freezing- in of electrode into the ice increases the earth resistance.

#### JSA09/W/17-A2 1715

##### ANTARCTIC PHYSICAL OCEANOGRAPHY: INTERACTIONS WITH SEA ICE, ICE SHELVES AND ICE SHEETS

S.F. ACKLEY, (111 Villa Ann, San Antonio TX 78213, USA, email: jlongbotham@pol.net)

Within the world ocean, a significant fraction of the total water mass has had "contact" with the cold atmosphere in the Antarctic region, and is defined as Antarctic Bottom Water ( $T < 2^{\circ}\text{C}$ ). Sea ice affects significantly this water mass formation and its circulation in the polar oceans. The seasonal cycle of the ice cover modifies the large-scale density gradients due to the different locations of freezing and melting areas. Circulation beneath ice shelves results in cooling and freshening of water masses, while topography of ice shelves serves to steer water mass circulation, with consequences on their dynamics and thermodynamics. Investigations over the last two decades, when the few (but first) oceanographic expeditions to Antarctica during winter conditions have taken place have shown complex and sensitive interactions between the ocean circulation and sea ice and glacial processes. Event-driven processes originating in the sea ice and glacial ice account for significant variability in water mass modification. Sea ice-atmosphere interaction in the eastern Weddell Sea may, for example, account for the interdecadal variability in the occurrence of the deep water Weddell Polynya (1974-1976). When the Weddell Polynya occurred, total deep water formation of Antarctic Bottom Water was increased substantially, exceeding that occurring from interactions on the continental shelves alone. Ice Shelf Water, a constituent of Antarctic Bottom Water, is formed by modification of inward flowing waters from the continental shelves, that melt a portion of the ice shelves during their transit beneath them. The intensity of the circulation, and seasonal and interannual fluctuations, appear to be linked to the topography of the ice shelves, driven by glacial processes, and the properties of the continental shelf source waters, driven by sea ice formation in front of the ice shelves. Coastal polynyas, (found extensively around East Antarctica) can occur where glacial tongues from the ice sheet block the flow of sea ice.

#### JSA09/W/02-A2 1745

##### MODELLING OF THE ANTARCTIC CIRCUMPOLAR CURRENT: A COMPARISON OF FRAM AND EQUIVALENT BAROTROPIC MODEL RESULTS

Vladimir IVCHENKO (Jet Propulsion Laboratory/NASA, 300-323, 4800 Oak Grove Drive, Pasadena, CA 91109, USA. Email: voi@sundog.jpl.nasa.gov) Alexander Krupitsky (Lehman Brothers Holdings, Inc 3 World Financial Center, New York, NY 10285, USA. Email: akrupits@lehman.com); Vladimir Kamenkovich (Dept. of Marine Science, Institute of Marine Sciences, The University of Southern Mississippi, Stennis Sp.C., MS 39529, USA, Email:kamenkov@sunfish.ssc.usm.edu); Neil Wells (School of Ocean and Earth Sciences, Southampton Oceanography Centre, European Way, Southampton SO14 3ZH,UK. Email:n.wells@soc.soton.ac.uk)

Analyzing the Fine Resolution Antarctic Model (FRAM) simulations, Killworth (1992) noticed a strong tendency for self-similarity in the vertical structure of the velocity field of the Antarctic Circumpolar Current (ACC). Based on the self-similarity hypothesis, Krupitsky et al.(1996) developed an equivalent barotropic (EB) model of the ACC capable of describing the horizontal structure of the ACC. Compared to the multi-level-primitive-equation GCM, the EB model appeared substantially simpler and therefore useful in process-oriented and sensitivity studies. To assess the applicability of the EB model to the analysis of the horizontal structure of the ACC we performed the comparison of the EB model results with the time-mean depth-averaged results of the FRAM model. The horizontal structure of the ACC transport stream function appears reasonably similar in both models. The more detailed regional analysis shows a rather satisfactory agreement in the regions with pronounced topographic features (Crozet-Kerqueleen area, Macquarie-Ridge Complex and near Pacific-Antarctic Ridge, and to the east from the Drake Passage). In the regions with a more quiet topography (eastern part of the Indian Sector of the Southern Ocean, and in the Southeast Pacific Basin) the agreement is worse but still meaningful. It seems that the EB model satisfactorily describes the influence of the bottom topography on the ACC. It is known (Stevens and Ivchenko 1997) that the



## INTER-ASSOCIATION

averaged (over time, depth and a latitude circle) FRAM zonal momentum equation provides the balance essentially between the wind stress and the bottom pressure drag. The same averaged momentum balance is given by the EB model.

### Wednesday 21 July AM

Presiding Chair: R Dietrich (Technische Universität Dresden, Germany)

**JSA09/W/15-A3**

**0830**

#### TECTONICS AND SEISMICITY OF THE ANTARCTIC PENINSULA REGION

Stacey D. ROBERTSON, Douglas A. Wiens, and Gideon P. Smith (Department of Earth & Planetary Sciences, Washington University, St. Louis, MO, email: stacey@izu.wustl.edu), Emilio Vera (Universidad de Chile, Santiago, Chile), George Helffrich (University of Bristol, UK)

The purpose of the Seismic Experiment in Patagonia and Antarctica (SEPA) is to learn more about the seismic and tectonic characteristics of the South Shetland trench and Antarctic peninsula, which are largely unknown. It has been unclear whether subduction is still occurring in the South Shetland trench, and the level of tectonic activity in the backarc Bransfield Strait is also uncertain. Major changes in plate motions over the past 4 million years suggest that this region may provide important insights into several important processes, including very slow subduction, the initiation of rifting, and how plate tectonic systems change through time. The Antarctic portion of the SEPA deployment consists of seven broadband seismic instruments located in the Antarctic Peninsula - South Shetland Islands region. Three of these stations are at inhabited sites and receive occasional support throughout the year, and four are located at field sites which can only be reached during the Antarctic summer and which must receive all their power through solar power and banks of Carbonaire batteries. Fourteen ocean bottom seismographs were recently deployed in the South Shetland trench and Bransfield Strait in conjunction with Leroy Dorman of Scripps Institute of Oceanography. Although the South Shetland Island area displays a low level of seismicity in global catalogs, the data which we obtained from 1997 and 1998 indicates a high level of local seismicity (mb 2-4). Preliminary locations of these events indicate that the seismicity is concentrated in the South Shetland trench with a few earthquakes located in the Bransfield Strait. The seismicity of the South Shetland trench extends to depths of about 70 km, indicating that subduction is currently occurring. Some earthquakes are concentrated near large seafloor volcanoes along the central rift of the Bransfield Strait, suggesting current eruptive activity. We are also investigating mantle seismic anisotropy from shear wave splitting to provide constraints on the pattern of possible mantle flow through Drake Passage.

**JSA09/E/05-A3**

**0900**

#### SURFACE WAVE TOMOGRAPHY OF THE ARCTIC REGION

Michael Barmin, Anatoli LEVSHIN, Michael Ritzwoller, Alex Padgett (all at Department of Physics, University of Colorado at Boulder, Campus Box 390, Boulder, CO 80309, U.S.A., e-mail: levshin@lemond.colorado.edu)

Because of the station and earthquake distributions at high northern latitudes, the large-scale structure of the Arctic crust and uppermost mantle is best explored with surface waves. We report on the results of a study of surface wave dispersion at high northern latitudes. We have extended earlier studies of surface wave dispersion across Eurasia in three ways.

- (1) Data processing. We have obtained new Rayleigh and Love wave dispersion measurements at GSN, USNSN, and CNSN stations following about 300 earthquakes which occurred around the northern hemisphere from 1995 through 1997.
- (2) Isotropic dispersion maps. We have estimated broadband (20 s - 150 s) isotropic group velocity maps across the entire eastern hemisphere north of the equator and for the western hemisphere north of about 50 degree N latitude.
- (3) Azimuthally anisotropic dispersion maps. We have simultaneously estimated 2\*psi azimuthally anisotropic group velocity maps for the same region at the same periods. We report on the features that appear in the estimated isotropic group velocity maps and on the relation of these features to those apparent in other large-scale dispersion studies. The observed maps display the signatures of sedimentary and oceanic basins, crustal thickness variations, and upper mantle anomalies under both continents and oceans. For example, there are two significant Arctic oceanic low velocity anomalies at long periods. The first and more prominent is associated with the Iceland hotspot and the northward continuation of this anomaly adjacent to the Mohns Ridge toward the Fram Strait between Greenland and Svalbard. The second anomaly runs from the Laptev Sea to the Mendeleev Ridge. The latter anomaly is not obviously coincident with the seismically active Arctic Mid-Oceanic Ridge. At 150 s the low velocities are more nearly coincident with the aseismic Mendeleev Ridge. Finally, we report on the importance of the estimated azimuthal anisotropy in fitting the dispersion data and how its inclusion in the tomographic inversions affects the isotropic maps.

**JSA09/W/05-A3**

**0930**

#### AEROMAGNETICS IN ANTARCTICA.

Massimo CHIAPPINI (Istituto nazionale di Geofisica, Vigna Murata 605, 00143 Roma, Italy; Email: chiappini@ingrm.it) Fausto Ferraccioli (Dipteris Univ. Genova, Italy, email: magne@dister.unige.it) John Behrendt (INSTAAR - University of Colorado Boulder, CO 80309-0450 USA, Email: behrendj@stripe.colorado.edu) Julie Ferris (British Antarctic Survey High Cross, Madingley Road Cambridge CB3 0ET United Kingdom, Email: JFK@pcmail.nerc-bas.ac.uk).

The Antarctic continent is 99% covered with ice and is the most poorly understood region of the planet. International interest of Earth Sciences in the Antarctic is considerable because of the central role of its tectonics and geology in both Gondwana and Rodinia evolution. Remotely-sensed data, such as magnetic anomaly data provide one of the few ways to obtain geological information over much of the continent, helping to delineate major structural components of the continent, such as cratons, mobile belts, terranes and rifts. Consequently, numerous near-surface magnetic surveys have been carried out by the international community for site-specific geologic objectives.

Individual magnetic surveys are being combined into regional and ultimately continental scale magnetic synthesis for the Antarctic. In 1995, an international Working Group was established, and initiated efforts to develop an inventory of all magnetic data sources for the Antarctic region south of 60 degrees S, by means of a multinational cooperation called ADMAP, the Antarctic Digital Magnetic Anomaly Project. A number of Antarctic aeromagnetic surveys are reviewed, as a contribution to ADMAP's activities.

**JSA09/E/11-A3**

**1000**

#### A REVIEW OF MAGNETIC ANOMALY FIELD DATA FOR THE ARCTIC REGION: GEOLOGICAL IMPLICATIONS

Patrick T. TAYLOR (Geodynamics Branch, NASA/GSFC, Greenbelt, MD 20771, USA, email: ptaylor@ltpmail.gsfc.nasa.gov); Ralph von Frese and Daniel R. Roman (both at

Department of Geological Sciences, The Ohio State University, Columbus, OH 43210, USA, email: vonfrese@geology.ohio-state.edu); James J. Frawley (Herring Bay Geophysics, Dunkirk, MD 20754, USA, email: hbjiff@ltpmail.gsfc.nasa.gov)

Due to its inaccessibility and hostile physical environment remote sensing data, both airborne and satellite measurements, have been the main source of geopotential data over the entire Arctic region. Ubiquitous and significant external fields, however, hinder crustal magnetic field studies. These potential field data have been used to derive tectonic models for the two major tectonic sectors of this region, the Amerasian and Eurasian Basins. The latter is dominated by the Nansen-Gakkel or Mid-Arctic Ocean Ridge and is relatively well known. The origin and nature of the Alpha and Mendeleev Ridges, Chukchi Borderland and Canada Basin of the former are less well known and subject to controversy. The Lomonosov Ridge divides these large provinces. In this report we will present a summary of the Arctic geopotential anomaly data derived from various sources by various groups in North America and Europe and show how these data help us unravel the last remaining major puzzle of the global plate tectonic framework. While magnetic anomaly data represent the main focus of this study recently derived satellite gravity data (Laxon and cAduo, 1998) are playing a major role in Arctic studies.

**JSA09/E/09-A3**

**1015**

#### MAGNETIC AND GRAVITY COMPILATION OVER VICTORIA LAND (ANTARCTICA): SOME TECTONIC IMPLICATIONS AND PROBLEMS

Fausto FERRACCIOLI, Emanuele Bozzo, Massimo Spano (all at DIP.TE.RIS., Univ. Genova, Italy, email: magne@dister.unige.it) Massimo Chiappini (Istituto Nazionale di Geofisica, Rome, Italy, email: chiappini@marte.ingrm.it)

Victoria Land (VL) is a key area to study the geology of Antarctica and at a broader scale for the reconstruction of Gondwana assembly, evolution and dispersal. As a first step towards geophysically consistent models for the tectodynamical evolution of the region we compare magnetic and gravity patterns/trends with geologic and seismic constraints. After hypothesized rifting in Precambrian times at the East Antarctic Craton margin, the Early Cambrian to Carboniferous history features subduction, accretion and collision of terranes. Jurassic toleitic magmatism at the site of the later Transantarctic Mountains (TAM) was followed by amagmatic(?) crustal extension in the Cretaceous. Finally Cenozoic transtensional and transpressional reactivation of Paleozoic and Mesozoic faults was accompanied by rift-related alkaline magmatism and major uplift of the TAM. Prominent magnetic anomalies have previously been recognized to be associated to Cenozoic plutonism and volcanism. Now it is clear that the pre-existing lower Paleozoic architecture controls its location. New gravity and magnetic data leads to an improved imaging of the Mesozoic to Cenozoic Rennick pull-apart basin and its relationship to VL terrane boundaries. A major magnetic and gravity anomaly break is recognized to correspond to the western boundary of the Wilson Terrane. Extensive Jurassic magmatism focussed in this boundary zone. Open questions regard the nature of the Bowers/Wilson Terrane and the docking mechanisms to the East Antarctic Craton. Unravelling the late-Prerozoic to lower Paleozoic history of VL is still particularly intriguing.

**JSA09/W/21-A3**

**1045**

#### INTERPRETATION OF 'RECONSTRUCTED' MAGNETIC ANOMALY DATA FROM THE BARENTS SEA-EAST GREENLAND SHELF REGION

Jan R. Skilbrei (Geological Survey of Norway, po box 3006, N-7002, Trondheim, Norway, email: jan.skilbrei@ngu.no)

Potential field anomalies from the Barents shelf and the East-Greenland shelf is interpreted in a pre 'break-up' reconstruction. The geology of the Barents Sea and the Greenland margin is interpreted using the magnetic anomaly in this pre-Eocene context. The magnetic data has been compared with the seismic profiles and the gravity data in order to identify the structural highs and the sedimentary basins, and constrain the interpretation.

The Precambrian and Caledonian geology of Scandinavia and East Greenland is compared with the geophysical data in order to differentiate between intrabasement and suprabasement sources of the anomalies on the shelves. Long-linear anomalies are related to rift structures of the East Greenland shelf and the Barents Sea. A comparison with the Basin and Range Province of the western U.S. will be made, and the implications of the interpretations for the petroleum industry will be discussed. The lineament patterns as they are illustrated by the potential field images of shelves of the North-Atlantic region will be commented on.

**JSA09/W/18-A3**

**1100**

#### POLAR CRUSTAL ANOMALIES IN SATELLITE MAGNETIC AND GRAVITY OBSERVATIONS

Ralph R.B. VON FRESE, Hyung Rae Kim (both at Dept. of Geological Sciences, The Ohio State University, Columbus, OH 43210, USA, email: vonfrese@osu.edu, kim@geology.ohio-state.edu) Patrick T. Taylor (NASA Code 921, Goddard Space Flight Center, Greenbelt, MD 20771, USA, email: ptaylor@ltpmail.gsfc.nasa.gov)

Comparing satellite gravity data with terrain gravity effects can help sort crustal from subcrustal components. Crustal thickness variations may be estimated from the spectral correlation between the two data sets. Satellite gravity observations in combination with terrain gravity data may also be used to help estimate crustal components in satellite magnetic measurements. Here the first radial derivative of the terrain gravity effect may be used via Poisson's theorem for correlative potentials to sort crustal from noncrustal components in magnetic observations. Estimates crustal thickness variations and crustal components in satellite gravity and magnetic observations for the Arctic and Antarctic are presented.

**JSA09/W/10-A3**

**1115**

#### POLAR IONOSPHERES

Ted ROSENBERG (Institute for Physical Science and Technology, University of Maryland, College Park, MD 20742-2431 USA, email: rosenberg@uarc.umd.edu)

Quite recently, Newell [Eos, 79(51), 625, 1998] summarized evidence of the importance, even perhaps the controlling influence, of the ionosphere on magnetospheric dynamics, as manifested by the behavior of the aurora and other aspects of magnetosphere-ionosphere coupling. Changes in the background ionospheric conductivity affected by the amount of sunlight is thought to play the crucial role, with the flux of ionizing charged particles perhaps also having some significance. The two polar ionospheres are linked by the extension of the geomagnetic field into space which also provides a path for moving charged particles between hemispheres. Hence the importance of understanding the similarities and differences of the polar ionospheres. New facilities established in both polar regions in recent years have enabled extensive and simultaneous coverage of the polar ionospheres. The distributed high-latitude ground-based observations provide a valuable complement to the measurements being made in space. This has created new opportunities for global (including conjugate) studies of particle



precipitation, magnetic pulsations, ionospheric currents, radiowave emissions, and the structure and dynamics of the ionospheric plasma, as will be reported on here.

**JSA09/W/20-A3****1130****WHERE ARE THE MAGNETIC POLES ?**

Wallace H. CAMPBELL (World Data Center A for Solar Terrestrial Physics, NGDC / NOAA, 325 Broadway, Boulder, CO 80303-3328, USA, email: whc@ngdc.noaa.gov)

Cartographers indicate a specific location in the Northern and Southern Hemisphere of the Earth as the place of a "Magnetic Pole." To geomagnetic scientists, it is unclear what is the meaning or value of such map locations. "Magnetic" poles of differing location can be defined by the dip of the International Geomagnetic Reference Field, by a geomagnetic co-ordinate system, by the eccentric geomagnetic field axis or surface dip, by paleomagnetic evidence, or by local (induction anomaly and external disturbance sensitive) determinations of a vertical field. These differing pole locations can be tens of degrees apart. The locations are slowly varying in position over the years, although cartographers never attach dates to their "exact" poles. Contrary to some popular beliefs, the mapped spot is, most certainly, not the average global location toward which a compass points.

**JSA09/P/01-A3****1145****PECULIAR DECREASE IN THE MAGNITUDE OF VERTICAL GEOMAGNETIC FIELD NEAR THE MAGNETIC POLES IN SUMMER SEASON**

Naoshi FUKUSHIMA (Dept. of Earth and Planetary Physics, University of Tokyo, Tokyo 113-0033 Japan, email: fukushima@nipr.ac.jp)

This paper points out a remarkable decrease in the magnitude of vertical geomagnetic field Z (amounting to several tens of nT) observable only in the summer in the polar regions centering the northern or southern magnetic poles. This peculiar phenomenon was known since the Second International Polar Year 1932-1933, through an extensive analysis of world data by Vestine et al. compiled in the Carnegie Institution of Washington Publication No. 580 (1947). Later with the aid of the data during IGY 1957-58 and following years, Mansurov and Mansurova (1971) showed that the same kind of Z-decrease were also observed at Vostok, magnetic south pole station in the Antarctica. It is worth noting here that the geomagnetic anomaly maps published by Langel and Estes (Figs. 1b and 2b on pages 2497-8 in JGR 90 [1985] showing the calculated difference of Z-values at 500 km level from their model based on the Magsat data) show the greatest negative anomaly over Vostok, because the Magsat was operative during the austral summer.

The peculiar decrease in geomagnetic Z-field near the magnetic poles in summer seasons has been discussed at present even in connection with the earth's interaction with the solar wind, including the effect of IMF (Interplanetary Magnetic Field) Bz and By. However, it will be more essential for us to study a possible influence of ionized plasma produced in the sunlit polar ionosphere. We must bear in mind that the daily-mean energy received from the sun in the polar area at the summer solstice is even greater than at the equatorial region.

**JSA09/C/GA5.01/W/20-A3****1200****DETERMINATION OF THE MAGNETIC POLES LOCATION**

Vladimir V. KUZNETSOV, Vsevolod V. Botvinovsky (Institute of Geophysics SB RAS, Koptyug av., 3, Novosibirsk 630090, Russia; e-mail: kuz@uiggm.nsc.ru)

The idea of this model is that the magnetic pole drift is caused by change of the intensity of the main dipole field and the field of the global magnetic anomalies which are considered as sources that are quasi-independent from the main geomagnetic dipole field source. We have verified this hypothesis using the data of the geophysical magnetic observatories for the modern drift of the North magnetic pole (NMP) and the South magnetic pole (SMP). In particular, the NMP-1994 location was predicted by us. The observations of this location have confirmed our prediction with high accuracy. Based on the analysis of the magnetic observatories data, we have introduced a correction into the location of the NMP-1831 and the location of the SMP-1909. The application of our hypothesis has permitted us to explain the character of the magnetic pole motion during the reversal. The observations of the magnetic observatories and the hypothesis permit to interpret paleomagnetic data in a new way.

**JSA09/E/03-A3****1215****SUB-GLACIAL IMAGING IN SCHIRMACHER OASIS-WOHLTHAT MOUNTAINS REGION IN ANTARCTICA EMPLOYING HELI-MAGNETIC AND SURFACE GRAVITY SURVEYS**

Saurabh K. VERMA, H.V. Rambabu, and G.S. Mital (National Geophysical Research Institute, Uppal Road, Hyderabad-500 007, India, email: postmast@csngri.res.nic.in)

Helicopter-borne magnetic survey was carried out over an area measuring approximately 100 km x 85 km between the Schirmacher Oasis (SO) and Wohlthat Mountains (WM) during the Seventh Indian Antarctic Expedition. Two-dimensional spectral inversion of the data revealed gross features of the topography of the base of the glacier between SO and WM. Subsequently, during the Ninth Indian Antarctic Expedition, Helicopter-supported surface gravity measurements were done along five profiles over the glacial region. Modeling of these profiles provided additional information on the glacial depths, first order structural features, and moho thickness in the region.

Combined interpretation of the magnetic and gravity data has resulted in a more coherent model of the subglacial structure. Imaging of the magnetic map of the region highlights the prominent subglacial features including a graben like structure between SO and WM. Gravity modeling reveals the presence of faults in the subglacial basement that could be correlated with the known faults and structural trends observed in SO.

**JSA09/W/22-A3****1230****RESTORATION OF SPACE PARTICLE DATA COLLECTIONS**

Nickolay N. Kontor, Nickolay N. PAVLOV, and Elmar N. Sosnovets (Skobel'syn Institute of Nuclear Physics, Moscow State University, Moscow, 119899, Russia, email: nnpavlov@tasdp.npi.msu.su)

Since 1965, Theoretical and Applied Space Physics Division, Institute of Nuclear Physics, Moscow State University carries out monitoring of charged particles in space with use of Russian far spacecraft and satellites. Significant part of the data from old missions is stored only on paper, many data sets have been saved due to special issues published by the WDC-B. The data sets from both paper and old tapes needed to be restored and transferred to the modern computer media. This work has been supported by NASA, grant NAG5-4656. Useful collaboration with NSSDC has also made this project realizable. Assuming that similar projects are being currently launched by many research groups for the

sake of utilization of the benefits of the new Internet era we would like to share our experience in typical problems, common approaches and software tools used in our work. The main goal is to make the collection living and publicly accessible via Internet. Such issues as data input, data formats, file structure, use of database system, IDL, Java are concerned here. Interactive graphic rectification of raw data sets and creation of the proper documentation are highlighted as the most important for the solving of a key problem of data quality. A simple method of improving the ability of navigation within a multi-spacecraft data collection based on a plain ftp is discussed as well as our approaches to the effective graphic access to the data. Attaching of some simple tools for remote data analysis to the user interface is also considered as a way to make the services more attractive and useful.

**Tuesday 20 July AM**

Presiding Chair: Ralph von Frese (Ohio State University, USA)

**JSA09/W/16-A2**

Poster

**0930-01****FIRST ABSOLUTE GRAVITY MEASUREMENTS AT THE FRENCH STATION DUMONT D'URVILLE (ANTARCTICA)**

Martine Amalvict, Jacques HINDERER (both at Ecole et Observatoire des Sciences de la Terre, 5 rue Descartes, 67084 Strasbourg Cedex, France, e-mail: mamalvict@east.u-strasbg.fr)

We present the first series of absolute gravity measurements at the French station Dumont d'Urville in Antarctica. These measurements will be performed with a FG-5 (Micro-g Solutions Inc.) absolute gravimeter in a continuous way during a week in March 1999. We will report the conditions of the experiment for which a thermally regulated shelter has been built and discuss the quality of the results. A special attention will be paid to the influence of tidal ocean loading and different corrections according to existing models will be tested. We will also take this opportunity to establish a gravimetric link with a Scintrex CG3-M relative gravimeter to the tide gauge of Dumont d'Urville belonging to the ROSAME network in order to provide a geodetic reference. It is essential to be able to distinguish in the long term any vertical motion of tectonic origin from true sea level changes. A further use of our determination of the gravity field is to allow the establishment of a precise gravimetric calibration line between Hobart (Tasmania) and Dumont d'Urville which should be useful for the marine geophysics campaigns in this region.

**JSA09/W/07-A2**

Poster

**0930-02****INTRAMAP - INTEGRATED TRANSANTARCTIC MOUNTAINS AND ROSS SEA AREA MAGNETIC ANOMALY PROJECT: STATUS & PROGRESS**

Massimo CHIAPPINI (Istituto nazionale di Geofisica, Vigna Murata 605, 00143 Roma, Italy; Email: chiappini@ingm.it) Fausto Ferracoli, Emanuele Bozzo (DISTER, Univ. Genova, Italy, email: magne@dister.unige.it) Detlef Damaske (Bundesanstalt für Geowissenschaften und Rohstoffe Stillweg 2, 30655 Hannover Germany, Email: d.damaske@bgr.de) John Behrendt (INSTAAR - University of Colorado Boulder, CO 80309-0450 USA, Email: behrendj@stripe.colorado.edu)

Within the framework of the evolving Antarctic Digital Magnetic Anomaly Project (ADMMap), an international consortium called INTRAMAP was initiated in 1997. The aim of INTRAMAP is to compile the aeromagnetic, ground and marine magnetic data acquired throughout the "Ross Sea Antarctic sector" (60 degrees south and 135-255 E) including: the Transantarctic Mountains (TAM), the Ross Sea, Marie Byrd Land, the Pacific Coast, and also to begin the compilation effort to new data over the Wilkes Basin to be collected along the "backside of the TAM" which is the site of proposed future activities within joint Italian, US and German cooperations. Finally the integration of satellite and near-surface magnetic data will result in a compilation that accurately portrays the fullest possible spectrum of magnetic anomalies from the Antarctic lithosphere in the "Ross Sea sector". The final compilation will contribute both in delineating and in studying the major structural and geologic components of the Ross Sea Area. From the geodynamical point of view, the merged magnetic data will permit assessment of different tectonothermal provinces within the West Antarctic Rift System leading to regions of differential uplift along the TAM and in Marie Byrd Land. The status and progress of the project will be presented.

**JSA09/W/06-A2**

Poster

**0930-03****THE HYDROTHERMAL STRUCTURE OF POLYTHERMAL GLACIERS IN SVALBARD USING GROUND PENETRATING RADAR**

Anja PÄLLI (Department of Geophysics, University of Oulu, BOX 400, 90571 Oulu, Finland, E-mail: anjapa@paju.oulu.fi); John Moore (Arctic Centre, University of Lapland, BOX 122, 96101 Rovaniemi, Finland, E-mail: jmoore@levi.urova.fi)

A Ramac (Malå Geosience) Ground Penetrating Radar (GPR) working at 25, 50 and 200 MHz frequencies has been used to map the hydrothermal structure of two polythermal glaciers Hansbreen and Werenskjöldbreen and their tributaries in southeast Spitsbergen. The GPR data was compared with the data from several temperature boreholes instrumented with thermistors and with heights of water tables in moulins. The data collected is of high resolution and the cold ice temperate ice interface was easily detected in all the measured profiles. The bedrock reflection was detected almost everywhere. Many moulins and smaller water channels (probably of metre scale) seen as point reflectors were mapped. The GPR data shows that the hydrothermal structure of Hansbreen is highly variable both along the centre line and on transverse profiles. The temperate firn/cold ice transition appears to show a more gradual transition than observed on other glaciers in northern Svalbard. Water contents in cold and temperate ice were investigated by fitting hyperbolic model reflections to point reflectors. The water content in temperate ice varied from 0 to 2% but water contents up to 5% were calculated from areas associated with surface crevassing and moulins. Isolated point reflectors within the cold ice indicate large water filled bodies that are probably related to the regular drainage structure of the glacier.

**JSA09/W/11-A2**

Poster

**0930-04****DETERMINATION OF PLATE TECTONIC MOTION RATES IN THE REGION OF THE ANTARCTIC PENINSULA**

MICHAEL MAYER, Klaus Lindner, Hansjoerg Kutterer and Bernhard Heck (all at Geodetic Institute, University of Karlsruhe, Englerstr.7, D-76128 Karlsruhe, Germany, email: mmayer@gik.uni-karlsruhe.de)

The Geodetic Institute of the University of Karlsruhe (GIK) takes part in a bundle project called "Reference Network Antarctica II" which is sponsored by the Ministry of Science, Research, Education, and Technology of Germany (BMBF). Within this bundle project seven German institutions are co-operating in order to create a three-dimensional velocity field of the atlantic part of Antarctica. The basis and the motivation of this bundle project lays in the previous bundle project "Reference Network Antarctica" which was sponsored by the BMBF, too. The main goal of this bundle project was the creation of a highly precise three-dimensional reference network for the whole Antarctic continent. In the Antarctic summer 1994/95 simultaneous GPS observations (24 h per day, 21 days) were carried out at GPS stations situated on Antarctica

## INTER-ASSOCIATION

and on neighbouring tectonic plates to fulfill the main goal of the first bundle project. This work was done within the framework of the SCAR Epoch 95 Campaign (SCAR95). The GIK working group was responsible for preparatory investigations of the achievable point positioning accuracy by means of spectral analysis, and processing of the GPS observations based on the Bernese GPS Software Version 4.0 (BS). Furthermore several investigations were carried out concerning the accuracy of point positions (influence of atmospheric disturbances, ambiguity resolution strategies, effect of the selection of the ITRF-fiducials). Using the experiences gained from processing a network covering the complete southern hemisphere (SCAR95-data plus IGS-data) - characterized by inhomogeneous baseline lengths (from 1 km up to 4400 km) as well as by an irregular distribution of the sites showing high density in the area of the Antarctic Peninsula and the closeness of some network points to the geomagnetic pole in East Antarctica - the above mentioned second bundleproject was initiated.

**JSA09/W/03-A2** Poster **0930-05**

### HOW GEODETIC OBSERVATIONS CAN CONTRIBUTE TO THE DETERMINATION OF VERTICAL CRUSTAL DEFORMATIONS IN WEST GREENLAND INDUCED BY CHANGING ICE LOADS

Mirko SCHEINERT (Reinhard Dietrich Technische Universität Dresden, Institut für Planetare Geodäsie, D-01062 Dresden, Germany, e-mail:mikro@ipg.geo.tu-dresden.de)

Mass changes of ice sheets induce loading effects on the earth crust. These vertical deformations occur on different time scales. Viscous effects are due to the glaciation history, while elastic effects are mainly caused by recent ice mass changes. These different effects will be reviewed especially for West Greenland.

West Greenland provides a unique research field: large regions along the west coast are ice-free. This allows a comparably easy access to carry out geodetic field measurements in the immediate vicinity of the proceeding ice mass changes, which are the largest at the ice edge. In order to observe the ice-induced vertical deformations a special GPS network between the 61st and 69th parallel was set up. The first epoch observation of this network was carried out in 1995. These GPS observations were densified along the 67th parallel, from the coast up to the ice edge, in the subsequent years. Additional relative gravimetric observations in the region of Kangerlussuaq supplemented the GPS observations. The set-up of the investigations will be reported. The results of the regional observations obtained so far will be presented and discussed.

**JSA09/E/10-A2** Poster **0930-06**

### MORPHOMETRIC PATTERNS AND GEODYNAMICS OF THE LOMONOSOV RIDGE AND ADJUSENT BASINS

Elena DANIEL (All-Russia Research Institute for Geology and Mineral Resources of the World Ocean, 1, Angliysky pr., St.-Peterburg, 190121, Russia, email: dani@vniio.nw.ru)

The new computer bathymetry model reveals essential features of the ocean floor in more detail than in previously published small-scale bathymetric maps. The patterns of the ocean relief forms characterize the deep Arctic basin structures dynamic. Been situated between the Eurasian and Amerasian basins the Lomonosov Ridge has several bends through its extension. These bends coordinate with the such of the Gakkal Ridge and surrounded it basins. These bends are also accompanied by transverse extend line zones. These zones cross the Eurasian and Amerasian basins. The zones characterize ancient tectonic frame to with geometry of temporary spreading is submitted. In the seafloor relief these zones are presented by various forms having the same rout of extension and increased gradient in bathymetry. The escarpments with height of 500-600 m between plains are display of these zones. The plains are characterized by isobaths of 1,600; 2,200 m and of 2,700; 3,200; 3,800 m on the ridges and in the basins, respectively, with is the truth both from the Eurasia and North America point of view. The seismosounding data according the geotransect "De Long islands - Makarov Basin" (Krijukov et al., 1993) show that escarpments are the reflection of the earth crust flexures with accompany its rejuvenation. Probably the formation of the ocean in the Amerasian basin was together with long formation of the surrounded steps, relict of which are saved in temporary seafloor relief.

**JSA09/W/19-A2** Poster **0930-07**

### AEROMAGNETIC FEATURES OF ENDERBY LAND AND EASTERN DRONNING MAUD LAND: IMPLICATIONS FOR GONDWANA ASSEMBLY

Alexander V. GOLYNSKY (VNIIO Okeangeologia, 1 Angliysky Ave., 190121, St. Petersburg, Russia, email: sasha@gus1.vniio.nw.ru)

In the shield areas of East Antarctica (EA) interpretation of aeromagnetic data allowed to better define the boundaries between the Archean stable blocks and the Proterozoic mobile belts, and to trace these boundaries beneath the ice sheet. Four main boundaries of the EA Shield terranes are distinguished within Enderby Land and eastern Dronning Maud Land from the change of magnetic anomaly pattern. The boundary between the Napier terrane and the Rayner terrane is delineated by the oval band of high-intensity magnetic anomalies. The Napier terrane displays a complex magnetic grain which tends to reflect the lithology of granulites. Metasedimentary rocks and granitoids are associated with magnetic lows, whereas orthogneisses correlate with highs. A broad magnetic low, at least 100 km in width, is associated with the structural grain of the Rayner Complex originated during 1000 Ma event. The boundary between the Rayner - Lützow-Holm Bay (LHB) terranes is clearly visible on the map by distinction of trends. The elongated, fragmented magnetic highs and intervening lows of the LHB terrane is associated with the rocks metamorphosed under granulite facies conditions. Character of distribution and structural pattern of magnetic anomalies do not allow us to accept models of Gondwana reconstruction in which the LHB Complex in EA and Highland Group of Sri Lanka developed in the suture zone at the last phase the Pan-African orogeny and the Late Proterozoic supercontinent was separated by a missing ocean at the position of the LHB Complex. The absence of any well-defined anomalies coherently running in direction of proposed Cambrian orogenic belt allow us to joint to more appropriate conclusion of many authors that the 500 Ma event in East Antarctica was an intraplate phenomenon of Gondwana and restricted to minor though widespread activity.

**JSA09/W/04-A2** Poster **0930-08**

### THE GLENNY ANOMALIES OF ANTARCTICA AND SURROUNDING SEAS

Andrei N.Grushinsky (United Institute of Physics of Earth, Russian Academy of Science, B. Gruzinskaya, 10, Moscow 123810, e-mail: grush@upei-ras.scgis.ru, Pavel A.Stroev (Sternberg State Astronomical Institute, Moscow State University, Universitetsky pr., 13, Moscow 117899, e-mail: pstroev@sai.msu.ru) and Eugenij D.Koryakin (Sternberg State Astronomical Institute, Moscow State University, Universitetsky pr., 13, Moscow 117899, e-mail: koryakin@sai.msu.ru)

The gravitational effect of far zones and Glenny anomalies for Antarctica has calculated. This calculations take into account the thickness of sediments and their mean densities. The structure of the total correction for middle and far zones was analysed. The main features of

this correction is determined by the middle zone one. West Antarctica has a poorly effect on the form of middle zone correction isolines. This fact allows to suppose, that West Antarctica is an active continental margin. The field structure of the far zone gravitational effect connect with the distribution of continents and ocean on the Earth and have clearly expressed long-waved character. The influence of far zones manifests in the total correction by asymmetry: the values of correction for Pacific ocean sector some less, than for Indian ocean one. The structure of Glenny anomalies clearly enough indicates the main geological structures of Antarctica and allows to do some conclusions about the structure of its lithosphere. The Glenny anomalies correlation with heat flow was found for South ocean. The preliminary conclusions about isostatical models for different regions of Antarctica may be made from the considerable analysis. Authors are grateful to Russian Fundamental Investigations Foundation, which provided financial support (grant 98-05-64446).

**JSA09/C/VS1/E/01-A2** Poster **0930-09**

### SUBGLACIAL ERUPTION PILLOW LAVA BRECCIAS IN FUMAROLE BAY, DECEPTION ISLAND, ANTARCTICA:

CORINA RISSO, Alfredo Aparicio Yague, Antonio Delgado

The pillow lava breccia have a central part of massive columnar jointing pahoehoe lava with basaltic-andesite Composition. The external zone are composed by pillow lobes and fragments derived directly from the lobes during their development from the breaking up of the lava flow. The size of the pillows and lobes range from 0.10 to 4 m. Their shape varies from nearly spherical to elongate. The central zone, light brown, has porphyritic to cluster texture with plagioclase and clinopyroxene phenocrysts and glassy groundmass with plagioclase and clinopyroxene partially palagonitized. The external zone (0.5 to 0.8 cm) is characterized by a black obsidian rim. The small outcrop in Fumarole Bay, belongs to the "Conjunto Superior" and begins with base-surge deposits, poorly consolidated with reverse grading laminated bedding sets, deposited maybe during an explosive activity in a cupola of steam. To the top the participation of pillows and lobe fragments increase, followed by a massive lava flow and ending with strombolian deposits similar to others presents in others localities of the island. This sequence indicates the independence of water/snow/ice in the last stages of the eruption. High negative deuterium rates (d2H=-66,7/-61,4) indicates meteoric water contribution. The pillow lava outcrop is 50 m up to the actual sea level and in his original eruption position. According with this observations the eruption begun under a thin and shallow ice/snow cover.

**JSA10** Tuesday 20 – Wednesday 21 July

### PLANETARY EXPLORATION (IAGA, IAG, IASPEI, IAVCEI, IAMAS, IAHS, SCOSTEP)

Location: School of Education 135 LT

Location of Posters: Conference Room, School of Education

Tuesday 20 July AM

Presiding Chair: TBA

### MARS EXPLORATION

**JSA10/W/03-A2** **0930**

### NETLANDER : THE FIRST GEOSCIENCE NETWORK ON MARS

P.LOGNONNE (1), A.M. Harri (2), O. Marsal (3), F. Angrilli (4), B. Banerdt (5), J.P. Barriot (6), J.L. Bertaux (7), J.J. Berthelier (8), S. Calcutt (9), J.C. Cerisier (8), D. Crisp (5), V. Dehant (10), D. Giardini (11), R. Jaumann (12), Y. Langevin (13), M. Menvielle (8), G. Musmann (14), J.P. Pommereau (7), T. Spohn (15) and the Netlander team. 1) IPGP, 4 Avenue de Neptune, 94107 Saint Maur des Fosses Cedex, France, 2) FMI, Finland, 3) CNES, France, 4) Un. of Padova, Italy 5) JPL, USA, 6) OMP-GRGS, France, 7) SA, France, 8) CETP, France, 9) Oxford Uni., UK, 10) Royal Observatory of Belgium, Belgique, 11) Institut of Geophysics, Switzerland, 12) DLR/IPE, Germany, 13) IAS, France, 14) IGM, Germany, 15) IIP, Germany

The fundamental scientific objectives of the Netlander mission are to return the geophysical and atmospheric data necessary to perform a comparative study between Mars and the Earth. It will deploy in 2006 a network of 4 stations on the surface of Mars and will perform network science and multi-site observations.

The first objective will be the determination of the deep internal structure of the planet, especially the state and size of the core, the structure of the mantle and shape of discontinuities. It will be addressed by a package of VBB seismometer, magnetometer, and a geodetic experiment. A second specific objective will be the determination of the crustal and subsurface structure below all landing sites. It will use a package of a short period seismometer and a ground penetrating radar, in addition to the radar. A third objective will address the surface mineralogy and the geological context of the landing sites with a multi-spectral camera. A fourth objective will be performed by a package of multiple atmospheric sensors and finally, the planet ionised atmosphere will be studied jointly by the magnetometer and the measurement of the total ionospheric content.

The Netlanders, launched in 2005 with the Mars Sample Return mission on an Ariane 5, will be developed by CNES, FMI, DLR with significant contribution from NASA and possibly from new partners. The surface operations are expected to last over one Martian year, from August 2006 to July 2008, with an orbital support of the ESA Mars Express orbiter.

**JSA10/E/06-A2** **0945**

### THE NETLANDER MAGNETIC EXPERIMENT

M. MENVIELLE (CETP, 4 Avenue de Neptune, F-94107 SAINT MAUR CEDEX, FRANCE), G.Musmann (IGM/TU-BS, Braunschweig, GERMANY), M. Alexandrescu (IPG, Paris, FRANCE), J.J. Berthelier (CETP, FRANCE), K.H. Glassmeier (TU-BS, GERMANY), J.M.Knudsén (Copenhagen Univ., DENMARK), F. Kuhnke (TU-BS, GERMANY), U. Motschmann (TU-BS, GERMANY), K. Pajunpaa (FMI, Helsinki, FINLAND), J.L. Pincon (LPCE, Orléans, FRANCE), F. Primdahl (DTU, Lyngby, DENMARK), K. Schwingsenschuh (IWF, Graz, AUSTRIA), L. Szarka (GGKI, Sopron, HUNGARY)

The transient variations of the Mars magnetic field result from both the interaction between the planetary environment and the solar wind plasma (primary source) and induction in the conductive planet (secondary source). The main objective of the NetLander magnetic experiment is to make continuous recordings of the transient variations of the magnetic field at the Mars surface. It will therefore allow one to obtain a first description of the transient magnetic field of Mars, and then provide information on both the inner structure and the electro-dynamics of the ionised environment of Mars: - the depth of penetration of an electromagnetic wave in a conductive medium increases with decreasing frequencies:



the higher part of the frequency spectrum enables one to probe the uppermost kilometres of the crust, and the lower part enables one to probe the mantle down to a few hundreds of kilometres in depth. - as is the case for the Earth, different controlling plasma processes will lead to different current patterns inside the magnetosphere and therefore different magnetic signatures at the planetary surface. Continuous recordings of the transient variations of the magnetic field onboard landers will then provide constraints on the electrodynamic within an ionosphere-magnetosphere system in which the ionosphere lies at great heights relative to the dimensions of the magnetospheric cavity. Another objective of the NetLander magnetic experiment could be the investigation of the magnetic properties of the Martian surface rocks an/or dust and the search for and analysis of possible paleomagnetic signatures in the rocks. This would need to have the magnetometer sensor embedded in a magnetizing field coil and placed on the Mars surface: the field coil magnetizes the Martian surface while the fluxgate afterwards measures its magnetic response.

### JSA10/W/11-A2 1000

#### NETLANDER IONOSPHERIC AND GEODETIC EXPERIMENT

Jean-Pierre BARRIOT (Observatoire Midi-Pyrénées, 14, Av. E. Belin, Toulouse, France, email: Jean-Pierre.Barriot@cnes.fr) Veronique Dehant (Observatoire Royal de Belgique, Brussels, Belgium, email: veroniq@oma.be) Jean-Claude Cerisier (Centre d'Etudes des Environnements Terrestres et Planétaires, St-Maur des Fossés, France, email: cerisier@cetp.ipsl.fr) André Ribes (Centre National d'Etudes Spatiales, 18, Av. E. Belin, Toulouse, France, email: Andre.Ribes@cnes.fr)

The objectives of the NETlander Ionospheric and Geodetic Experiment (NEIGE) of the Mars Sample Return mission (MSR) is to obtain new information about the interior of Mars, surface/atmosphere interactions (e.g the seasonal cycling of CO<sub>2</sub>), and about the total electron content (TEC) of the Mars ionosphere. This information would be obtained from measurements of the Doppler shifts of the radio links between an orbiter and a network of four landers, and between the Earth and this orbiter. We detail both the technical and scientific aspects of this important experiment.

### JSA10/W/08-A2 1045

#### PYROCLASTIC FLOWS AND POSTERUPTIVE LAHARS AS THE RELIEF-FORMING FACTOR OF A MARS SURFACE

Alexander I. MALYSHEV (Institute of Geology and Geochemistry, Urals Branch of RAS, Pochtovy per 7, Ekaterinburg, SU-620151, Russia, email: root@igg.e-burg.su) Lidiya K. Malysheva (Kourovskaja astronomical observatory, Urals University, Lenina street 51, Ekaterinburg, SU-620083, Russia, email: lidiya.malysheva@usu.ru)

In the report the problem of an origin of channel-shaped valleys on the Mars surface is considered. Nowadays in the given area the concept of catastrophic freshet water flows dominates. The main reason for the benefit of the concept of Mars channels formation at the expense of catastrophic freshet water flows is the circumstance, that the researchers could not find any other substitution except water capable to production so powerful eroding influence and creation characteristic inner valley deposits. A serious drawback of the given concept is the fact, that the representations about the formation of Mars's channels under the influence of powerful current of large volumes of liquid water are incompatible with domination of low temperatures on the Mars surface. However alternative substations capable to make similar or even more powerful eroding effect, - pyroclastic flows and especially posteruptive lahars are well known for the researchers specializing on study of volcanic processes on the Earth. The pyroclastic flows are being formed during eruptions of large volumes of the heated fragmental material and have high mobility at the expense of the presence of the heated volcanic gases. Most powerful lahars, are being formed after the eruptions of pyroclastic or lava material in cases when at the area of eruption there is a plenty of frozen water. The presence on a Mars of very large volcanic structures, such as Nix Olimpica, and, possibly, a wide circulation of frozen water as rockforming mineral require more attentive attitude to an opportunity of large relief forms formation under the influence of pyroclastic flows and post eruptive lahars.

### JSA10/C/GA4.15/P/01-A2 1100

#### SAHARA CAMPAIGN FOR FIELD TESTING MARS EXPLORATION INSTRUMENTS FOR 2001-2005 MISSION ROVERS

M.A. Mosalam SHALTOU (National Research Institute of Astronomy and Geophysics, Helwan, Cairo, Egypt. Tel: (202) 2630833; Fax: (202) 5548020 Email: mamshaltou@rcu.eun.eg)

On July 4, 1997, NASA's Mars Pathfinder landed safely on the surface of the red planet, the first spacecraft to do so in 21 years. After this success, Mars exploration is a high priority program in the United States. There is a plan for testing instruments for a Mars Rover to be launched in the time period 2001-2005 in the Western Desert of Egypt. It is the driest Sahara in the world, and contains a variety of rocks and soil deposited by catastrophic floods early in the history as that occurred in the past history of Mars. Beside, dust storms for 50 scattered days during the year "El-Kamassen" similar in the dust storms in Mars. With The Planetary Society (TPS) in Pasadena, USA, currently, we are considering bringing a group of about 12 scientists, 5 from the United States (NASA-J PL), 3 from Russia (IKI), 1 from European Space Agency (ESA) and 3 from Egypt, to do Mars instruments testing in the very dry region of the Western Desert, at three different sites chosen by their analog with Martian Desert - like conditions, and contain subsurface water at different depths. The instruments to be tested will be electromagnetic sounder, magnetic coil, infra-red spectrometer, radiometer, co-ordination and GPS Navigation. The exception duration for testing is the Autumn of 1998.

### JSA10/L/01-A2 1115

#### EFFECT OF MARS' ATMOSPHERE ON NUTATION AND ROTATION

O.DE VIRON

Models of the atmospheric circulation of Mars will be used in order to compute the atmospheric torque acting on the planet, as well as the angular momentum changes. This effect can either perturb the rotation of Mars, or, if the diurnal time scale is considered in a frame tied to the planet, perturb the nutations (long periods in space). These computations are rather important in the frame of the NETlander Geodesy Experiment consisting of observing Mars' orientation in space during one Martian year. This experiment will give us information about the parameters of the interior of Mars that appear in the models. Mars' elasticity or inelasticity parameters are studied in the frame of long term effects. The amplitudes of the effects of the atmosphere on the Mars' rotation will be evaluated. Parameters related to the Free Core Nutation are considered at diurnal time scale. At that time scale, it is possible to compute an order of magnitude of the effects of the atmosphere on the nutations.

### JSA10/L/02-A2 1130

#### EFFECT OF MARS ICE CAP LOADING ON MARS' ROTATION.

O.DE VIRON

Models of Mars' ice cap are used in order to compute the changes in the loading effects (due to CO<sub>2</sub> sublimation and condensation) on Mars' rotation and polar motion. The response of the planet involves parameters of the interior as mantle inelasticity, core rheology. We have examined the response of Mars to the ice cap loading in order to compute the sensitivity of the potential observations to these parameters. Observing the effects of the sublimation and condensation of the ice cap on Mars' rotation would in principle give us the amount of ice changes with time and would also give information on Mars rheology. We examine the potentiality of the geodesy experiment of Netlander to detect these effects.

### JSA10/L/03-A2 1145

#### MARS' INTERIOR FROM NEIGE GEODESY

V. DEHANT, T.Van Hoolst, J.-P. Barriot et al.

The NETlander Ionospheric and Geodesy Experiment (NEIGE) consists in observing Mars' orientation in space by considering Doppler counting measurements. These measurements will give us the possibility to observe the polar motion, the rotation and the precession/nutations of Mars. We give here the objectives of NEIGE geodesy part and the order of magnitude of the expected motions. We show how this experiment will enable us to obtain important parameters on Mars' interior. In particular, we show how it would be possible to answer the question whether the core is liquid or solid. That question is in fact related to the existence or not of one important normal mode called the Free Core Nutation which only exists if the core is liquid.

Tuesday 20 July PM

Presiding Chair: TBA

### MERCURY, VENUS, MOON AND PLANETARY GEOPHYSICS

### JSA10/W/05-A2 1400

#### CORRELATION OF SURFACE FEATURES WITH GEOID IN THE APHRODITE-THEMIS-BETA REGION OF VENUS

Paul STODDARD (Dept. of Geology, Northern Illinois University, DeKalb, IL, USA, email: prs@geol.niu.edu) Donna Jurdy (Dept. of Geological Sciences, Northwestern University, Evanston, IL, USA, email: donna@earth.nwu.edu)

The recent Magellan mapping mission to Venus has returned a wealth of data. The apparently random distribution of impact craters indicates that the entire planet has been resurfaced over the last ca. 300-700 m.y. Studies of stratigraphic relationships show that certain Venusian terrain types tend to be older than others. Crater counts by terrain type also support a global terrain-based stratigraphy. In this vein, we look at distribution of coronae, craters, and chasmata in relation to the geoid and topography of Venus. The vast majority of chasmata fall along five great circle arcs with a combined length equivalent to that of the ridge spreading system on Earth. Furthermore, the gross similarity in morphology between these two suggests that chasmata may indeed be tectonically active regions. One unique region, bounded by Themis Regio, Beta Regio, and the eastern part of Aphrodite Terra, contains two major geoid highs at the intersection of three of these great circle arcs. One arc, extending 15000 km from Aphrodite to Themis, lies within 500 km of a line of 10 domal coronae (20% of the Venusian total). These coronae, distinguished by central uplift with no surrounding moat, may be the youngest of the coronal features, possibly even still active. In addition, craters near this arc are disproportionately embayed (30% compared to 6% planet-wide), and a first look at coronae in this region shows them to be linked morphologically to the location of chasmata. Alternatively, the arc extending 6000 km from Beta to Themis is heavily cratered with few coronae of any kind.

### JSA10/W/07-A2 1415

#### TECTONISM ON VENUS; AN EXPERIMENTAL AND IMAGE BASED STUDY

M.R.BALME (1,2), P. Sammonds (1) and C.Vita-Finzi (2) (1) Rock and Ice Physics Laboratory, University College London. email: m.balme@ucl.ac.uk (2) Centre for Planetary Studies, Department of Geological Sciences, University College London, London, England.

Enigmatic tectonic deformation has been observed in several regions of the volcanic plains of Venus. The 'Gridded-plains' of Guinevere Planitia, for example, are peculiar in that the fracture sets are orthogonal, but it is the close spacing (1-3km) of one of these sets that is most striking. Geophysical models of deformation are constrained by the physical properties of the plains material, which are currently only orders of magnitude estimates. To understand fully the tectonic setting, laboratory measurement of 'fracture-toughness' (an intrinsic material property) at Venusian surface conditions (90 bar of CO<sub>2</sub> at 450°C) are used to provide the data necessary to constrain fracturing models. We describe here the testing apparatus used in this investigation and the methodology for applying the results to Magellan imagery of tectonic features. Results at different temperatures and pressures are presented using Iceland basalt as the sample rock. Although the eruption of flood basalts is the preferred model for plains formation, some recent volcanic models suggest that large areas may have compositions that are more exotic. A programme of fracture toughness experiments using different candidate rocks coupled with image analysis is proposed. This will be used to constrain the choice of candidate plains material and therefore lead to refined models of formation and deformation.

### JSA10/W/06-A2 1430

#### ESA ADVANCED PLANETARY MISSION STUDIES: VENUS SAMPLE RETURN AND MERCURY SAMPLE RETURN

Lebreton J.-P. (1), Scoon G. (2), Lognonné Ph. (3), Masson Ph. (4), TAYLOR F. W. (5), Wänke H., (6), Coradini M. (7), and the VSR and MeSR Study Teams (1) Space Science Dept. of ESA, Solar System Division, ESTEC, P. O. Box 299, 2200 AG Noordwijk, The Netherlands (2) Scientific Project Dept, Future Project Office, ESA/ESTEC, P. O. Box 299, 2200 AG Noordwijk, The Netherlands (3) IPG, Paris (4) Univ. Paris-Sud (5) Oxford University (6) MPI Mainz (7) ESA/HQ, Science Directorate, 8-10 Rue Mario Nikis, F-75738 Paris Cedex 15.

Looking into the next decade, the Mercury Orbiter mission is the only future Planetary Exploration mission which has been identified as a potential element of ESA's Horizons 2000 Science programme. In order to prepare for the next steps in planetary exploration beyond the Mercury Orbiter mission, ESA is carrying out advanced studies of Planetary Sample Return Missions. The Venus Sample Return mission was first studied in early 1998 and was



## INTER-ASSOCIATION

completed in June 1998 with the publication of the study report ESA SCI(98) 3. A similar study is being undertaken for a Mercury Sample Return. The study was initiated in September 98 and is expected to be completed in February 1999. In this presentation we describe the scientific objectives of both missions and give an overview of the two baseline mission scenarios that have been identified. Although there are technical challenges that have to be worked before undertaking such ambitious missions, those initial studies demonstrate that such very exciting missions are within Europe's technical capabilities.

### JSA10/E/04-A2 1500

#### SPECTROPOLARIMETRIC INDEX OF THE LUNAR SOIL MATURITY

V.V.SHEVCHENKO, T.P.Skobeleva (Sternberg State Astronomical Institute, Moscow University, Universitetskii pr. 13, Moscow 119899, Russia, email: shev@sai.msu.su)

It was used a new calculations to obtain a number of spectropolarimetric ratio of the maximum degree of polarization values in blue and red parts of spectrum ( $P_{max}$  (419 nm)/  $P_{max}$  (641 nm)) for relief formations on the lunar surface. A new catalog contains 90 values of the ratio which characterize different features of the near side of the Moon (crater, mare and highland types). Distribution of the values has bimodal shape. The second mode of the distribution corresponds bright new formations (crater Proclus, swirl Reiner-gamma and others). The spectropolarimetric parameter has not any correlation with chemical composition of the regolith surface layer. The values of FeO content for Apollo and Luna landing sites were used to compare these characteristics. The values of  $Is/FeO$  (magnetometric index of the soil maturity) for Apollo landing sites were used for comparison of the spectropolarimetric index with average degree of the soil maturity. The corresponding diagram of dependance of the spectropolarimetric index from soil maturity shows a slight correlation between them. The values of average sized particles in the surface layer, which were obtained by remote method, were used to plot diagram of dependance of the spectropolarimetric index from granulometric characteristics of the local soil. The diagram shows an evident correlation between both parameters. The 2 last diagrams show dependance of the spectropolarimetric index from exposure age of the lunar surface layer. So, the spectropolarimetric ratio mentioned above can be used as synonymous parameter of soil maturity which is obtained by means of remote method from Earth or from lunar orbit.

### JSA10/E/01-A2 1515

#### LUNAR CRUST PETROLOGY AND STRATIGRAPHY FROM CLEMENTINE MULTISPECTRAL DATA

P. C. PINET, S. Chevrel, P. Martin, Y. Daydou; UMR 5562 /OMP/GRGS/CNRS, 14 Av. E. Belin, Toulouse, 31400 France.

Detailed remote sensing surveys have been conducted in the Humorum and Imbrium impact basin regions. Based on multivariate statistics and spectral mixture analyses, these studies deal with the characterization of the regional chemical composition (Fe and Ti content) and establish a first estimation of both the mineralogy and optical maturity state of the surface, on the basis of the spectroscopic properties. For Humorum basin, the combination of the results issued from the spectral mixture modelling with the regional geomorphologic and topographic information puts constraints on the emplacement of the different types of mare and highlands units, as well as on the stratigraphic and petrological crustal variations related to the basin formation, with for instance the detection of exposed anorthositic units as possible remnants of the primordial crust. For the Imbrium/Procellarum region, the Gruithuisen domes region is recognized as a candidate for an extended nonmare volcanism unit, suggesting that this style of volcanism (viscous flow of possible more silicic composition) might have occurred prior to the Iridium event (3.8 Ga ago) and could have been more widespread in the early part of lunar history than previously thought. Also the regional spectral variability of the Aristarchus volcanic Plateau is characterized and the spectroscopic mapping within Aristarchus crater reflects a petrological change with depth. The deepest material exposed in the uplifted central peak indicates an anorthositic horizon, overlain by an olivine/pyroxene-rich horizon, with a progressive change in the pyroxene/olivine ratio, the pyroxene abundance increasing as the depth decreases. These new results arise from the recent revival in lunar space exploration and will both benefit from (in terms of interpretation) and contribute (preparation and scientific goals) to the ongoing and soon-to-come missions to the Moon, such as Lunar Prospector, Lunar-A, Smart-1 and Selene.

### JSA10/W/10-A2 1600

#### USING THE MAGNETIC DATA FOR PROBING THE ELECTRICAL STRUCTURE OF A PLANET

P. TARITS, N. Grammatika (IUEM/UBO, Place Nicolas Copernic, F-29280, Plouzané, France, email: tarits@univ-brest.fr); M. Menvielle (CETP - 4 Avenue de Neptune, F-94107 Saint Maur cedex - France)

The magnetic field of a planet may result from two primary sources, convection in a conductive liquid core and the interaction between the planet and solar wind plasma, and from two secondary sources, the local magnetisation and electric currents induced in the planet by the transient magnetic fields of external origin. The external natural fluctuations (the primary source) of the magnetic field induce an internal response (the secondary source) that can be used to infer the electrical conductivity structure of the planet. The maximum depth resolved by the technique is a function of the longest period of variations of the external magnetic sources that may be recovered from the data. The external transient variations result from both the interactions between the planetary environment and the solar wind plasma. Traditionally, induction studies on Earth make use of magnetic data recorded continuously at stations set up at the Earth surface transitionally or permanently (the geomagnetic observatories). The upcoming of several magnetic satellite missions in the next years has triggered the interest of the electromagnetic induction community to use satellite data to investigate the electrical conductivity of the Earth. The satellite provides a complete coverage of the planet. Several studies both theoretical and with the 15 years old MAGSAT data have shown that the secondary induced field may be recovered from the satellite magnetic data and that electrical conductivity may be derived from them. There is therefore a great interest to apply a similar approach for the planetary exploration. Measuring the vector magnetic field in a satellite surveying the planet offers the unique opportunity to investigate at planetary scale the deep electrical conductivity structure. This parameter depends strongly on the temperature, partial melting, fluid phase as well as on the mineralogy and may provide strong constraints upon the mantle structure. One of the difficulties is the limited data about the primary field.

### JSA10/W/12-A2 1615

#### ELLIPSOIDAL HARMONIC EXPANSIONS OF THE GRAVITATIONAL POTENTIAL OF SMALL BODIES OF THE SOLAR SYSTEM: THEORY AND APPLICATION

Romain GARMIER (OMP, UMR5562, 14 avenue E. Belin 31400 TOULOUSE FRANCE, Email: garmier@boreal-ci.cnes.fr) Jean-Pierre Barriot (OMP, UMR5562, 14 avenue E. Belin 31400 TOULOUSE FRANCE, Email: jean-pierre.barriot@cnes.fr)

Small bodies of the solar system are now the targets of space exploration. Many of these bodies have elongated, non spherical shapes. Usual spherical harmonic expansions are not well suited for the modelling of spacecraft orbits around these bodies, as they can show strong divergence properties inside the smallest sphere enclosing the body.

An elegant remedy is to use ellipsoidal harmonics instead of the usual spherical ones, as the divergence is restricted to the smallest triaxial ellipsoid enclosing the body. We summarize mathematical properties of the ellipsoidal harmonics, and demonstrate their use with a simulation of the landing of the Rosetta module on the surface of comet Wirtanen.

### JSA10/C/GA4.15/P/02-A2 1630

#### SPACECRAFT'S ANOMALOUS ACCELERATION TOWARDS THE SUN

Probas RAYCHAUDHURI (Department of Applied Mathematics, Calcutta University, Calcutta 700 009, India. Email: prc@cucc.ernet.in)

Anderson et al. detected a mysterious phenomena that appears to slow down the spacecrafts and drag them off course (e.g., Pioneer 10, Pioneer 11, Galileo, and Ulysses etc.). The space probes appear to be experiencing an unexplained extra pull from the sun suggesting that an unknown force not known to the accepted laws of physics. In this paper I wish to point out that the unexplained extra pull is due to the contraction of solar core during the sunspot minimum period (about 4.6 years) in the solar activity cycle. During this period the solar core has extra tug throughout the solar system than the effects of gravity exerted by the sun in other times of the solar cycle. We show that the acceleration acting on the spacecraft with a magnitude of approximately  $8.16 \times 10^{-8} \text{sec/cm}^2$  directed towards the sun. This suggests that the anomalous acceleration towards the sun is the effect of solar core pulsation.

Wednesday 21 July AM

Presiding Chair: T.V. Johnson (JPL, Pasadena, USA)

### COSMOCHEMISTRY AND THE OUTER SOLAR SYSTEM

#### JSA10/E/02-A3 Invited 0830

#### COSMOCHEMISTRY FROM THE BEGINNING TO THE YEAR 2000

Jonathan I. LUNINE (Lunar and Planetary Laboratory, The University of Arizona, Tucson AZ 85721 USA, email: jlunine@lpl.arizona.edu)

Cosmochemistry--the study of the origin of the planets from chemical clues in samples and in remotely observed planetary environments is a field with a rich and convoluted history. The time available for this presentation does not permit a comprehensive and balanced historical treatment. To avoid the inevitable pitfalls of highlighting the work of a few at the expense of many other contributors, I focus on the overall development of ideas in the context of observational advances in the laboratory, at the telescope and in space. In the mid-twentieth century, increasingly detailed analyses of meteorite samples provided constraints on the solar nebula environment in the realm of the terrestrial planets. Simulations of nucleosynthetic processes in main sequence stars, supernovae and other stellar environments combined with meteorite analyses to provide a detailed picture, by the 1980's, of the timing and environment of solar system formation within a nascent molecular cloud. This picture was refined and bolstered by astronomical observations of cloud-forming regions, in which by the 1990's processes in planet-forming disks could be analyzed. Despite the fact that the vast majority of the solar system's mass lies in the outer planets, understanding of the cosmochemistry of the outer solar system lagged behind that of the inner because of the vast distances, which limited both remote observations and the capability to field spacecraft experiments in the region. A watershed event of 1995 was the direct sampling of Jupiter's atmosphere by the Galileo Probe, allowing noble gases and other spectroscopically inaccessible species to be measured. The start of the new millennium sees prospects for in situ measurements of comets and Titan, which along with more powerful telescopic studies will enable development of a cosmochemistry of the outer solar system commensurate with that of the inner.

#### JSA10/L/01-A3 Invited 0900

#### THE CASSINI/HUYGENS MISSION TO THE STURNIAN SYSTEM

D.L.MATSON (1) and J.P. Lebreton (2). (1) Jet Propulsion Laboratory, California Institute of Technology, Pasadena, CA 91106 USA. (2) Space Science Dept., ESTEC, Noordwijk, The Netherlands.

Cassini/ Huygens will carry out and in-depth exploration of the Saturnian system. On October 15, 1997 the spacecraft was launched in its interplanetary journey. On the way to saturn, Cassini/Huygens flybys Venus, twice (April 26, 1998; June 24, 1999), the Earth once (August 18, 1999), and Jupiter (December 30, 2000). On approach to Saturn a small satellite Phoebe will be encountered on June 11, 2004. Upon arrival at Saturn on July 1, 2004, Cassini/Huygens will fire its main engine and go into orbit about the planet. Huygens will be delivered to Titan on November 27, 2004. After deceleration in the upper atmosphere, Huygens will deploy a parachute system and its six instruments will make scientific measurements and observations as it descends to the surface. These data then will be transmitted to the Orbiter, which, in turn, will relay them to the Earth. The Orbiter will then commence a four year long tour of the Saturnian system. With its complement of 12 instruments, Cassini is capable of making a wide range of in situ and remote sensing observations. There will be repeated close flybys of Titan both to make measurements and for gravity assisted orbit changes that will enable Cassini to visit other satellites, various parts of the magnetosphere, and obtain occultations of the rings and atmospheres of Saturn and Titan. During the span of the mission, Cassini will also record temporal changes in many of the properties that it can observe. The presentation will emphasize current status and plans for the mission. (The Cassini mission is a joint undertaking by NASA and ESA. This work was carried out at Jet Propulsion Laboratory, California Institute of Technology, under contract to NASA

#### JSA10/W/01-A3 Invited 0930

#### EXPLORATION OF THE SATURNIAN SYSTEM WITH CASSINI RADIO SCIENCE

Arvydas J. KLIORIS (Jet Propulsion Laboratory, California Institute of Technology, Pasadena, CA 91109, USA, E-mail: akliore@jpl.nasa.gov)

The ongoing Galileo mission has provided many new insights into the Jovian system. Among them are new discoveries from the Radio Science investigations, including multiple measurements of the Jovian ionosphere, the ionospheres and plasma environments of Io, Europa, Ganymede, and Callisto, and the internal structure of the Galilean satellites. The Cassini spacecraft, which will be placed in orbit about Saturn in 2004, will conduct Radio Science investigations of many aspects of the Saturnian system with a radio instrument of unprecedented stability and versatility. It will use radio links at three wavelengths: S-band (13 cm), X-band (3.5 cm), and Ka-band (1 cm) to probe the atmospheres and ionospheres of Saturn and Titan and Saturn's rings by means of radio occultations, and to measure the masses and gravity fields of Saturn, Titan, and selected icy satellites by precision tracking. In addition, the stability of the radio instrument will be utilized to conduct a search for gravitational

waves during solar oppositions, and to precisely measure general relativistic effects during solar conjunctions during the interplanetary cruise prior to arrival at Saturn.

**JSA10/W/13-A3** Invited **1000**

**NITROGEN ISOTOPE FRACTIONATION AND THE CONSEQUENCES FOR TITAN'S ATMOSPHERIC EVOLUTION**

Helmut LAMMER (Institute for Space Research, Austrian Academy of Sciences, Elisabethstrasse 20, A-8010 Graz, Austria, EMail: helmut.lammer@oew.ac.at) Willibald Stumptner and Siegfried J. Bauer (both at Institute for Space Research, Austrian Academy of Sciences, and Institute of Meteorology and Geophysics, University of Graz, Halbaethgasse 1, A-8010 Graz, Austria, E-Mail: willibald.stumptner@oew.ac.at, siegfried.bauer@kfunigraz.ac.at), Tobias Owen (Institute for Astronomy, University of Hawaii, 2680 Woodlawn Drive, Honolulu, Hawaii 96822, USA, E-Mail: owen@hubble.ifa.hawaii.edu)

A nitrogen isotope anomaly on Mars has been established as the consequence of dissociative recombination in the Martian ionosphere. We have investigated the possible sources of nitrogen isotope fractionation in the Titan atmosphere where this molecule is the principle constituent. As on Mars, electron dissociative recombination of N<sub>2</sub><sup>+</sup> ions is one possible source, however, electron impact dissociation and atmospheric sputtering due to Titans location within Saturns magnetosphere also represent possible sources of isotope fractionation. Using a Monte Carlo method we have shown that electron impact dissociation of molecular nitrogen could lead to an isotope fractionation since the released energy of the newly born 14N isotope is slightly smaller than the necessary escape energy. The 14N isotope can therefore only escape from altitudes above the exobase level (1450 km) while the lighter 14N isotope can also escape from lower altitudes. This process may therefore be responsible for the observed enrichment of 14N on Titan, enabling us to estimate the total nitrogen reservoir required to produce the present atmosphere.

**JSA10/W/02-A3** Invited **1045**

**THE JOVIAN MAGNETOSPHERIC ENGINE**

C T RUSSELL (University of California, Los Angeles, CA, USA)

The energetics of the jovian magnetosphere are unlike those of any other magnetosphere in the solar system. The fuel for this gigantic engine is the mass loading deep in the planetary magnetosphere from the volcanic moon, Io. The energy gained by this fuel is drawn from the rotational energy of the planet extracted through the ionospheric currents that keep the magnetospheric plasma in rapid rotation. The magnetospheric plasma in turn accelerates the newly born ions erected from Io's neutral gas cloud. Once in the torus surrounding Io these circulating ions slowly but ever more rapidly drift outward. Once the dipolar magnetic field becomes too weak to confine this dense, rapidly rotating plasma, the configuration of the field becomes more disk-like and the field lines become much longer. Eventually the stretched out field lines "reconnect" across the current sheet producing magnetized islands that shed the mass down the tail that was long ago scavenged from Io. Empty flux tubes now make their way back into the interior of the jovian magnetosphere much as a conveyor belt returns to its loading point to pick-up another package but unlike most conveyor belts, the jovian magnetospheric circulation appears to be quite unsteady.

**JSA10/W/09-A3** **1115**

**THREE-DIMENSIONAL SPHERICAL SIMULATIONS OF MANTLE CONVECTION IN IO**

PAUL J. TACKLEY (Earth and Space Sciences Department, University of California, Los Angeles, CA 90095, USA), Gerald Schubert (Earth and Space Sciences Department and Institute of Geophysics and Planetary Physics, University of California, Los Angeles, CA 90095, USA), Gary A. Glatzmaier (Earth Sciences Department, University of California, Santa Cruz, CA 95064, USA), and J.Todd Ratcliff (Jet Propulsion Laboratory, Pasadena, CA, USA)

The Galilean moon Io has a very high heat flow of  $\sim 10^{14}$  W, much greater than Earth's, and should thus be undergoing very vigorous convection in its silicate mantle. Recent Galileo measurements suggest that Io may have an internally-generated magnetic field, indicating vigorous circulation in a liquid iron core. The pattern and dynamics of core convection are expected to be strongly influenced by the heat flow pattern at the core-mantle boundary imposed by mantle convection. Thus, we are performing simulations of Io mantle convection both to determine the heat flux variation at the CMB and to understand the distribution of surface heat flux and features. The heat source for Io's mantle convection is quite different from that of previously-simulated planetary mantles, being dominated by non-uniform internal (volumetric) heating due to tidal dissipation, rather than uniform volumetric heating from the decay of radiogenic isotopes. The distribution of tidal heating in Io's mantle is uncertain, with two end-member scenarios (Ross and Schubert, 1985) being dissipation in the entire mantle, or dissipation in a thin ( $\sim 100$  km thick) asthenosphere. We consider both end-members plus the "preferred" distribution of (Ross et al., 1990) comprising 1/3 mantle and 2/3 asthenosphere heating. The amount of tidal heat generation is extremely large and the associated (internally-heated) Rayleigh number is  $O(10^{12})$ , orders of magnitude larger than that of Earth, Venus or Mars, and larger than anything which can presently be simulated in 3-D. Results at Ra of  $O(10^6-10^8)$  indicate a large-scale flow pattern which is dominated by the pattern of tidal heating, with superimposed small-scale asthenospheric instabilities which become more pronounced as Ra is increased.

**JSA10/W/16-A3** Invited **1130**

**GALACTIC DUST MEASUREMENTS NEAR EARTH**

EBERHARD GRUEN, (MPI-Kernphysik, Heidelberg, Germany, Email: eberhard.gruen@mpi-hd.mpg.de) M. Landgraf (NASA JSC, Houston, TX., U.S.A.), H. Svedhem (ESA-ESTEC, Noordwijk, The Netherlands) and M. Horanyi (LASP, Boulder, CO., U.S.A.)

Galactic interstellar dust (ISD) is the major ingredient in planetary formation. However, information on this important material has been extremely limited. Recently the *Ulysses* dust detector has identified and measured interstellar dust outside 1.8 AU from the Sun at ecliptic latitudes above 50 deg. Inside this distance it could not reliably distinguish interstellar from interplanetary dust. From the *Hiten* satellite in high eccentric orbit about the Earth there are indications that ISD indeed reaches the Earth's orbit. The *Stardust* mission intends to analyze by an in-situ detector and to collect ISD between 2 and 3 AU from the Sun. Modeling the *Ulysses* data suggests that up to 30 % of dust flux with masses above  $10^{-13}$  g at 1 AU is of interstellar origin. In order to identify the ISD flux levels at 1 AU a mission is proposed that can identify and quantify interstellar dust flux in high-Earth orbit (outside the debris belts) and can provide chemical composition information of galactic dust. A mission scenario is described that allows us by in-situ dust measurements to distinguish interplanetary from interstellar dust and provide important physical and chemical information on ISD. In addition, crucial information is provided for follow-up missions to collect galactic dust in Earth orbit for sample return.

**JSA10/W/04-A3** Invited **1145**

**FUTURE EXPLORATION OF THE JOVIAN SYSTEM**

Torrence V. JOHNSON, Jet Propulsion Lab, Pasadena, CA 91109, USA. email: tjohnson@jpltvj.jpl.nasa.gov

Exploration of Jupiter's system began in 1610 with Galileo's first telescopic observations. The telescope remained the principle tool for Jupiter studies for more than 350 years before the first spacecraft missions to the giant planet were planned. Pioneers 10 and 11 opened the spacecraft era with flybys in 1973 and 1974 followed by Voyager 1 and 2 in 1979. Since December 1995 the Galileo spacecraft has orbited Jupiter sending back information about the planet, its moons and rings, and the magnetosphere. As we enter the next century, plans are being laid to continue Jupiter system exploration with a further extension of the Galileo mission, possibly allowing joint observations with the Cassini mission as it flies by in December 2000. Beyond that, a Europa orbiter mission is planned for launch in 2003, to study this fascinating moon and search for proof of a liquid ocean under its icy shell. Objectives, status and plans for these future explorations will be discussed in the context of what we have already learned about the system. This work was done at Caltech's Jet Propulsion Laboratory under a contract from NASA.

Wednesday 21 July PM

Presiding Chair: TBA

**SPACE EXPLORATION**

**JSA10/C/GA.4.15/P/03-A3** Poster **1400-01**

**THE MARTIAN EGYPTIAN DRILL PROJECT**

M.A. Mosalam SHALTOUT (National Research Institute of Astronomy and Geophysics, Helwan, Cairo, Egypt. Tel: (202) 2630833; Fax: (202) 5548020 Email: mamshaltout@frcu.eun.eg

During the fourth UN/ESA Workshop on Basic Space Science, held in Cairo, July 1994, the possible participation of Egypt in future Mars Rover mission was discussed. One concept suggested was that Egypt participate in these missions through involvement in the design, building and testing of a drill for obtaining sub-surface samples.

The Planetary Society (TPS), Sponsor of the UN/ESA Basic Space Science Workshop, is following up this suggestion. Society representatives Adriana Ocampo and Chris McKay, together with Egyptian Scientist Farouk El-Baz, and Society Executive Director Louis Friedman have begun organising a study of the concept. They informed the Space Research Institute (IKL) of the Russian Academy of Sciences about the idea, and they, in turn, formally invited the Egyptian ministry of scientific research to study the concept for potential use on the Russian Mars 2001 Mission. That study has now begun, under the direction of Dr. Farouk El-Baz and Prof M.A. Mosalam Shaltout. Of the many important scientific objectives of the Marsokhod mission, among the most interesting, is the analysis of sub-surface samples. Inclusion of same sort of drilling mechanism in the payload of such a mission would assist scientists in the investigation of volatile organic materials and mineralogy.

Twenty years ago, the arm on the Viking Mars lander was to obtain samples from depths up to 10cm. Today, a drill with the capacity of boring at least an order of magnitude deeper (more than one metre) would be essential to further research and investigation.

Egypt has expertise in drill development. A few years ago, as part of the archaeological exploration of the Pyramids, a sophisticated drilling system was developed to drill into and deploy a Camera into a sub-surface chamber without allowing air into the chamber. The drill perforated the limestone to a depth of 2m without the use of lubricants or cooling fluids that might have contaminated the Pit's environment, and successfully collected (six) samples.

This experience as well as more common terrestrial applications suggests that the necessary technology base for a drill development can be brought together. In the proposed application for the Mars 2001 Mission. A study team of Egyptian scientists, collaborating with American, Russian, AND European scientists, is now being organized.

**JSA10/W/14-A3** Poster **1430-02**

**A TWO DIMENSIONAL SIMULATION OF THE CONCERT EXPERIMENT (RADIO TOMOGRAPHY OF COMET WIRTANEN)**

Jean-Pierre BARRIOT (Observatoire Midi-Pyrénées, 14, Av E. Belin, Toulouse, France, email: Jean-Pierre.Barriot@cnes.fr), Wlodek Kofman (Laboratoire Images et Signaux, BP 46, St Martin d'Heres, France, email: wlodek.kofman@lis.inpg.fr)

We make in this poster two dimensional simulations of the mapping of the comet Wirtanen internal permittivity from CONCERT (Comet Nucleus Sounding Experiment by Radiowave Transmission) phase and amplitude measurements. We study the influence of a priori covariance matrices on the mapping process through Tikhonov or linear regression inverse formulas. We show that this a priori information permits a smooth imaging of the internal permittivity, sometimes affected by ghosts (false anomalies). We demonstrate that taking into account indirect propagation paths into the comet material (rays totally reflected by the comet surface) can alleviate this problem.

**JSA10/E/05-A3** Poster **1500-03**

**ON THE COMETARY ORIGIN OF THE LUNAR AND MERCURIAN POLAR ICE**

V.V.SHEVCHENKO (Sternberg State Astronomical Institute, Moscow University, Universitetskii pr. 13, Moscow 119899, Russia, email: shev@sai.msu.ru)

The most convincing model for the "swirls" (lunar and mercurian albedo anomalies) origin seems to be surface contact with the gas/dust coma of comets passing by or falling onto the bodies. It is possible to show that the most probable scenario for the water ice polar deposit origin is the falls of young comets onto the Moon (and possible onto Mercury) during comet showers. In particular the comet Hale-Bopp has become a sufficiently convincing confirmation of the existence of bodies with gigantic nuclei. Thus its parameters can serve as the first interaction data for the quantitative assessment of the lunar ice with a comet origin. The Hale-Bopp comet nucleus diameter was estimated to be about 40 km. Consequently after a similar body with a density of 0.1 g/cm<sup>3</sup> falls on the lunar surface a vapour cloud with a mass of about 3.4x10<sup>18</sup> g is formed. The water melting, surface, and crush-up energies are neglected. According to the above given assessment the mass of the volatile compounds which stay in the lunar environment will be 3.4x10<sup>17</sup> g. Assuming that these substances, distributed equally above the lunar surface, will further cool and deposit in the regolith upper layer, the assessed mass will be about 10E+10 g per a square kilometre. It is obvious that the subsequent preservation of the deposit is only possible in cold traps located near to the poles. Thus for the given assessments of the total area for both the southern and northern poles where the neutron spectrometer of the Lunar Prospector fixed the ice presence (3700 km<sup>2</sup>), the calculated mass of the volatile deposits of comet origin can be up to 10E+13-10E+14 g for each giant comet fall. These estimates fit the data obtained by the Lunar Prospector in the first approximation.



JSG11

Wednesday 21 – Thursday 22 July

THIS SYMPOSIUM IS DEDICATED TO THE MEMORY OF  
MOHAMMED EL-SABHSEA-LEVEL CHANGES AND VERTICAL GROUND MOVEMENTS  
(IAG, IAPSO, IASPEI, IAHS, ILP)

Location: Law Building 115 LR2

Location of Posters: Old Gym

Wednesday 21 July AM

Presiding Chair: Phil Woodworth

JSG11-A3

Introduction

0830

Phil Woodworth

JSG11/E/01-A3

0850

SEA SURFACE HEIGHT VARIABILITY DERIVED FROM ERS-2 ALTIMETER DATA NEAR CHINA SEA

HANJIANG WEN, H.Suenkel, Institute of Theoretical Geodesy, Steyrergasse 30, TU-Graz A-8010 Graz, Austria

A small area near China sea was used to study the sea surface height variability using one-year ERS-2 altimeter data. A local cross-over adjustment was carried out to reduce the residual radial orbit error, and the influence of the earth's geopotential model was also studied. Collinear analysis was then used to derive the RMS sea surface height variability, and seasonal variation of the sea surface was also compared.

JSG11/E/04-A3

0910

GLOBAL SEA LEVEL CHANGES FROM SATELLITE ALTIMETRY AND TIDE GAUGES

A. Cazenave, J.F. CRETAUX, K. Dominh and L. Soudarin (LEGOS-GRGS/CNES, 18, Avenue Edouard Belin, 31401 Toulouse Cedex 4, France, e-mail: anny.cazenave@cnes.fr)

Since late 1992, the global mean sea level variations are precisely monitored from space by the Topex-Poseidon (T/P) altimeter satellite. A mean sea level rise of  $1.8 \pm 0.2$  mm/yr is recorded between January 1993 and October 1998.

Excluding data since early 1997 which evidence the large rise and fall of the sea level associated with the 1997 El Niño, the global mean sea level rise measured by T/P, Poseidon reduces to  $\sim 1.0$  mm/yr. There is indication however that T/P underestimates the mean sea level rise by  $\sim 1.5$  mm/yr due to an instrumental drift of the onboard radiometer. By comparing sea level changes measured by T/P and tide gauges of the GLOSS network since early 1993, we confirm the presence of a sea level drift of  $\sim -1.8$  mm/yr between T/P and tide gauge measurements in agreement with independent estimates of the T/P radiometer drift. As a consequence, the global mean sea level monitored from space shows a rate of change of  $\sim 2.5$  mm/yr since early 1993. Attempt to understand this global sea level change in terms of thermal expansion and mass exchange with continental waters is also presented.

JSG11/E/09-A3

0930

FOURIER AND WAVELET ANALYSES OF TOPEX/POSEIDON-DERIVED SEA LEVEL ANOMALIES OVER THE SOUTH CHINA SEA - A CONTRIBUTION TO SCSMEX

Chenway Hwang and Sung-An Chen (both at Department of Civil Engineering, National Chiao Tung University, 1001 Ta Hsueh Road, Hsinchu 300, Taiwan. email: hwang@geodesy.cv.nctu.edu.tw)

We process 5.6 years of TOPEX/POSEIDON altimeter data and obtain time series of sea level anomalies (SLA) over the South China Sea (SCS). Fourier analysis shows that sea level variability of SCS contain major components with periods larger than 180 days. Tidal aliasing create 30 to 180-day components which can be misinterpreted as wind-induced variabilities. Continuous and multiresolution wavelet analyses of SLA show that sea level variability of SCS has monthly to interannual components, but with time-varying amplitudes. The sea level slope is 8 mm/year, possibly caused by decadal climate variation. Coherences of sea level with wind and sea surface temperature are significant only at frequencies lower than 2 cycles/year, and wavelet coefficients show high coherences at the interannual scales. Zero-crossing of SLA is highly correlated with the onset of the summer monsoon. The interannual variabilities of SCS sea level are correlated with ENSO, and most important is that when the El Niño-like wavelet coefficients change curvatures, an El Niño starts to develop, suggesting that real-time SLA over SCS or the western Pacific warm pool can provide a warning to the occurrence of an El Niño. This a contribution to SCSMEX.

JSG11/E/12-A3

0950

SEALEVEL VARIATION DATA EVALUATION IN INDONESIAN WATERS

Sobar SUTISNA (Center for Basicdata Survey, National Coordination Agency for Surveying and Mapping, P.O.Box 46/CBI, Cibinong 16911, INDONESIA, email: sobar@cbn.net.id) Mujiana and Bambang S. Pratomosunu (both at Center for Marine Mapping and Aerocharting, Bakosurtanal, P.O. Box 46/CBI, Cibinong 16911, INDONESIA)

Bakosurtanal (the National Coordination Agency for Surveying and Mapping of Indonesia) has today 28 tide stations in operation. The sealevel observation in the country are essential and are used for different purposes in both local and regional level as well as on a global scale. Tidal analysis were carried out using harmonic analysis method by treating the sum of a finite number of harmonic constituents whose angular speeds and phases are determined from the astronomical arguments.

This paper presents the results of analysis have been carried out at Bakosurtanal for all of the 28 tidal station data in order to determine mean sea level (MSL) position, to calculate low astronomical tide (LAT) and high astronomical tide (HAT) at each tide station locations. The possibility to define sealevel baseline data for sealevel rise monitoring in relation to climate change in Indonesia will also be discussed.

JSG11/W/03-A3

1010

A COMPREHENSIVE ANALYSIS OF THE TIDAL AND OCEANIC SIGNALS FROM THE WOCE SEA LEVEL OBSERVATIONS AND PRELIMINAR APPLICATIONS.

F. Ponchaut (email: ponchaut@cnes.fr), F. Lyard (email: Florent.Lyard@cnes.fr) and C. Le Provost (email: Christian.Le-Provost@cnes.fr) (all at LEGOS/GRGS, UMR5566 CNES- CNRS-UPS, 14 Avenue E. Belin, 31400 Toulouse, France)

A new sea level observation network initiated by the WOCE program is delivering hourly data from 150 ocean stations worldwide. A complete analysis of these data, the WSLA 98 data set (standing for WOCE Sea Level Analysis, 1998) was performed using a least-squares method allowing better accuracy over time series virtually unlimited in time (up to 13 years in this case). In addition to the classical tidal constants, the power density spectrum of the de-tided signal was computed and the 95% confidence intervals have been systematically estimated. Beyond the need for high accuracy de-tided sea level data, like in vertical ground movements applications, or for mean sea level monitoring purposes, the analysis outputs are a highly valuable material in the studies of the ocean waves, and in particular for the tidal modelling. The availability of confidence intervals allows to investigate more precisely the tidal waves of low amplitude, like long period or non-linear tides. For instance, the oceanic residual energy spectrum is used to select the tidal constant set needed to validate and compare the long period tide models. This selection is performed by eliminating stations where the oceanic continuum spectrum magnitude (around a given tidal frequency) is more than 25% of the corresponding tidal peak amplitude. It also gives the opportunity to prescribe realistic data error bars in the data assimilation models. This analysis intends to lead to a better exploitation of sea level observations, which contain highly valuable information in the tidal and non tidal domains. The authors emphasise the need for the WOCE Sea Level network to be maintained.

JSG11/W/04-A3

1030

SEPARATION OF THERMAL AND MASS SIGNALS IN SEA LEVEL VARIABILITY BY COMBINING SATELLITE ALTIMETRY AND XBT DATA

Don CHAMBERS, Jianli Chen, and Byron D. Tapley (University of Texas at Austin, Center for Space Research, R1000, Austin, TX, 78712, USA, Email: chambers@csr.utexas.edu)

Sea level variability can be measured quite accurately on regional and global scales with satellite altimetry. However, the altimeter measures the combination of changes caused by thermal and mass variations. In order to study the relative effect of mass or thermal variations, other measurements must be combined with altimetry. Expendable Bathothermographs (XBTs) dropped from ships measure temperature at depth, and can be integrated to compute the sea level variations due to thermal changes. However, the XBT casts are limited in both time and space. In this study, we interpolate XBT data for the period 1993 to 1997 to a uniform grid by using Empirical Orthogonal Functions computed from TOPEX/POSEIDON (T/P) altimeter data. The T/P and XBT sea level measurements are then compared on regional and global scales to determine the relative size of thermal to mass variability to the total signal. Interannual and annual variations in the global water mass balance are also studied by comparing the T/P and XBT measurements with output from various atmospheric and hydrological models.

JSG11/W/18-A3

1110

SEA-LEVEL CHANGES AND VERTICAL CRUSTAL MOVEMENTS IN THE SOUTHERN CARIBBEAN FROM SATELLITE ALTIMETRY, TIDE GAUGE RECORDS AND GPS HEIGHT DETERMINATIONS

Wolfgang BOSCH, Hermann Drewes, Klaus Kaniuth (all at Deutsches Geodaetisches Forschungsinstitut, Marstallplatz 8, D-80539 Muenchen, Germany, email: bosch@dgfi.badw-muenchen.de), Hans Kahle (Institut fuer Geodaesie und Photogrammetrie, ETH Hoenggerberg, HPV G 52, Zuerich, Switzerland, email: kahle@geod.ethz.ch), Napoleon Hernandez (Servicio Autonomo de Geografia y Cartografia Nacional, Av. Este 6, C.S.B., Edif. Camejo, Piso 2, Caracas 1010, Venezuela, email: hernandez.sagecan@conicic.vg)

The sea surface variability derived from four years of Topex/Poseidon altimeter data shows a heterogeneous feature in the southern Caribbean. The variations are analyzed and compared with records of tide gauges along the northern South American coast of the corresponding epoch. Long-term tidal records present a non-uniform behaviour ranging from  $-2$  mm/a decrease to  $+2$  mm/a increase of sea-level. To separate in the tidal records the sea-level changes from the vertical crustal movements, the tide gauges with extreme observed variations (Carupano, La Guaira, and Amuay, all at the Venezuelan coast) have been precisely determined in height by GPS measurements in three campaigns from 1993 to 1999. The results are analyzed together with the satellite altimetry data.

JSG11/W/19-A3

1130

THE INTEGRATION OF SEA-LEVEL MEASUREMENTS FROM SATELLITE ALTIMETRY SPANNING TWENTY-FIVE YEARS

Timothy J. URBAN, John C. Ries, Byron D. Tapley (all at University of Texas at Austin, Center for Space Research, 3925 W. Braker Lane, Suite 200, Austin, TX, 78759-5321, USA, e-mail: urban@csr.utexas.edu, ries@csr.utexas.edu, tapley@csr.utexas.edu), C.K. Shum (Ohio State University, 2070 Neil Ave., Columbus, OH 43210, USA, e-mail: ckshum@osu.edu)

Satellite altimeter data from the two and a half decades of data collection has been integrated into one data set for the purpose of monitoring long-term sea level. The satellites included are GEOS-3 (1975-1978), SEASAT (1978), GEOSAT (1985-1989), ERS-1 (1991-1996), TOPEX/POSEIDON (1992-present), and ERS-2 (1995-present). The historic data are improved with the most modern satellite orbits, media and geophysical correction models, yielding data sets as homogenous as currently achievable. Crossover and other analyses are performed to validate the correction models and resulting sea-level data. An accuracy assessment of the combined data is given, including orbit error and long-term analysis of altimeter corrections. Relative sea-level biases between satellite missions are determined through tide gauge and other analyses. Including gaps in the time series, a twenty-five year estimate of satellite-measured sea-level rise is produced.

JSG11/W/22-A3

1150

A GENERALIZED APPROACH TO THE CROSSOVER ANALYSIS OF ALTIMETRY DATA

Q.W. LIU and Y.Q. Chen (both at Department of Land Surveying &amp; Geo-Informatics, The Hong Kong Polytechnic University, Hunghom, Kowloon, Hong Kong, email: lsqliu@polyu.edu.hk)

The crossover adjustment has been extensively employed to correct altimetry data for the radial orbit error. The traditional procedure for the crossover adjustment is to use the difference of the sea surface height at crossover points to form the system equation and solve it by least squares. It is shown that the method is not effective in small ocean basins due to the few crossovers per track and to the relatively short tracks. An alternative approach is to make direct use of altimetry measurements at crossover points without differencing and to estimate simultaneously orbit parameters and mean sea surface heights in a single, unified adjustment. The rank defect inherent in the crossover estimation problem is overcome by introducing



additional constraints, as fixing certain number of parameters of non intersecting tracks (Schrama 1989), or adding an appropriate set of new constraints (van Gysen et al., 1997), or by combing the altimetry data with tide gauge station data (Fenoglio and Groten 1995). The purposes of our research are twofold. One is to theoretically generalize the existing crossover methods in order to provide a convenient theory for crossover analysis. It is shown that all the existing methods are special cases of our generalized approach developed by considering a weight for the estimated parameters of orbit error and mean sea surface height. Another is to practically compute a realistic estimate of the total radial orbit error and the mean sea surface. The detailed formula of the generalized approach is derived. Formulation and numerical example demonstrate its application.

**JSG11/W/21-A3****1210****LOCAL SEA LEVEL CAN BE MONITORED...**

Kyra VAN ONSELEN, Delft University of Technology, Email: onselen@geo.tudelft.nl

Local sea level can be monitored using a tide gauge, which relates sea level height variations to a local bench mark. In order to combine sea level height series for a number of tide gauges, the heights of these local tide gauge bench marks have to be determined in a common reference system. The geodetic measuring techniques used to perform these height connections will introduce measuring and systematic errors in the collection of sea level height series. The purpose of this work is to investigate how the detectability of a common pattern in sea level height series is influenced by the limited accuracy of the geodetic measuring techniques used to connect the tide gauges in height. Time series used are a combination of simulated patterns with periodic fluctuations obtained from actual tide gauge data. The effect of connecting the tide gauge bench marks is simulated based both on knowledge of error characteristics of geodetic measuring techniques and (differences) between actual sea level height series. Sea level height variation patterns under consideration are one common variation curve for all tide gauges, and a linear variation in this pattern for tide gauges situated along a specific coast.

**Wednesday 21 July PM**

Presiding Chair: R. Sabadini

**JSG11/E/10-A3****1400****DETERMINATION AND CHARACTERIZATION OF LONG-TERM MEAN SEA LEVEL CHANGE**

C. K. SHUM (Department of Civil and Environmental Engineering and Geodetic Science, The Ohio State University, 470 Hitchcock Hall, 2070 Neil Avenue, Columbus, OH 43210-1275, USA, Email: ckshum@osu.edu), Hong-Zeng Tseng (Ohio State University) Tim Urban and Byron Tapley (Both at University of Texas), Michael Anzenhofer GeoForschungs Zentrum Potsdam, Germany), and Philip Woodworth (Proudman Oceanographic Laboratory, Bidston, UK)

Recent studies of global sea level change have concluded that the global eustatic rate of sea level rise during the last century has been 1-2 mm/yr [Warrick et al., 1993]. Although there is no firm evidence of an acceleration in the rate of sea level rise over this time period [Woodworth, 1990], the projected future sea level rise is 13 +/- 4 cm during the next 40 years (1987-2027), and 61 cm over the next 100 years (1987-2087) [Woodworth, 1995]. Sea level change represents consequences of complicated interactions of the solid Earth-atmosphere-hydrosphere-ocean- cryosphere system and in part forced by human-originated greenhouse effect. Current long-term (40-100 years) sea level change estimates (e.g., IPCC studies) are primarily provided by long-term tide gauges located near coastal regions and continental margins. The estimate has deficiencies from local land movements (e.g., due to postglacial rebound and subsidence) and vertical datum knowledge, and the fact that the data only covers less than 5% of the global ocean. Satellite radar altimetry missions, both historic and current (Geos-3, Seasat, Geosat, ERS-1, TOPEX/POSEIDON, ERS-2, GFO-1, and future (Envisat, Jason-1, NPOESS), would provide global coverage but is deficiency both in data span (less than 10 years of continuous data), and the difficult in the knowledge of instrument biases. In this study, we attempt to use the available, improved processing of multiple mission altimeter measurements [Urban et al., abstract submitted to this session] and long-term tide gauges, to provide a combined analysis to examine the current rate of mean sea level rise. Second part of the study is intended to provide a characterization of the sea level change by using modern observations, including global sea surface temperature (spaceborne and in situ), ice extents [M. Anzenhofer et al., abstract submitted to session JSH12], postglacial rebound models, glacier and ice sheet mass balance data. Specific examples such as the sea level change in the China Sea region during the last decade will be discussed in the presentation.

**JSG11/P/01-A3****1420****INTERANNUAL AND ANNUAL SEA LEVELS IN THE SEISMIC AND TECTONIC ACTIVE ZONE IN THE NORTHWESTERN PACIFIC**

Shigehisa NAKAMURA (Famille Villa-A104, Tanabe 646-0031, Japan)

Interannual and annual sea levels in the seismic active zone is studied in order to realize what effects are seen just neoghbour the tectonic boundary. A special reference is that in the north-west Pacific. As for the problem of the tectonic effect to the apparent sea level at a tide station, a typical example of the 1995 seismic event can be introduced. The tide station of Kobe was strongly affected at the event, so that the marigram showed the patterns of the seismic motions and the successive upheaval as the vertical ground motion. This effect can be seen in the sea level variations of monthly mean or annual mean after processing the hourly read tide data. The interannual sea levels for about 100 years in the 20 century suggests the effect of under-ground waters and the effects of the crustal upheaval and the Kuroshio as an ocean current intensified in the western boundary of the Pacific. Spectral analyses are undertaken to demonstrate what specific variations of the spe(-trat patterns at several tide stations located just south of the tide station Kobe neighbour the boundary of the Eurasian tectonic plate. At the three tide stations located on the coast facing the Pacific, the spectral patterns are suggesting a significant effect of the Kuroshio meandering just off the tide stations. Successive studies should be followed after the year of 1999.

**JSG11/W/05-A3****1440****BIFROST PROJECT: FENNOSCANDIAN NETWORKS FOR CRUSTAL DEFORMATION AND SEA-LEVEL CHANGES**

J.M. JOHANSSON, H-G. Scherneck, G. Elgered (all at Onsala Space Observatory, Chalmers University of Technology, SE-43992 Onsala, Sweden, email: jmj@oso.chalmers.se) J.L. Davis, R.A. Bennett (both at Harvard-Smithsonian Center for Astrophysics, Cambridge, MA, USA, email: jdavis@cfa.harvard.edu); H. Koivula, M. Poutanen (both at Finnish Geodetic Institute, PL 15, FI-02431 Masala, Finland, email: hannu.koivula@fgi.fi) ; G. Hedling and B. Jonsson (both at National Land Survey of Sweden, SE-80182 G%ovle, Sweden,

email: gunnar.hedling@lm.se)

Project BIFROST (Baseline Inferences for Fennoscandian Rebound Observations, Sea level, and Tectonics) uses the continuous GPS observations in northern Europe to determine the 3-D motion associated with glacial isostatic adjustment. The backbone in this project is the permanent networks in Finland (FinnRef) and Sweden (SWEPOS). These networks has also proven to be an excellent tool for studying various effects of the environment near to the permanent sites.

In total, GPS-data from about 2000 days, have been acquired and analyzed. We have used different software packages and strategies. The entire data set has been analyzed with the GIPSY software package, both in a network solution as well as with the Precise Point Position method. Data from 1996 onwards have also been analyzed using the Bernese software, partly as a contribution to the EUREF permanent network and the IGS. Furthermore, periods of data have been analyzed with the GAMIT software package. The BIFROST project, the networks and their purposes are presented. We discuss the error budgets in an inter-comparison of analysis procedures. We discuss antenna and site related perturbations and methods for their reduction.

**JSG11/W/09-A3****1500****BIFROST PROJECT: 3-D CRUSTAL RATES INFERRED FROM GPS IN APPLICATION TO THE POSTGLACIAL REBOUND AND SEA-LEVEL IN FENNOSCANDIA.**

H-G. SCHERNECK, J.M. Johansson (both at Chalmers, Onsala Space Observatory, SE-439 92 ONSALA, Sweden, e-mail: hgs@oso.chalmers.se, jmj@oso.chalmers.se) M. Vermeer (Finnish Geodetic Institute, PL 15, FI-02431 Masala, Finland, e-mail: mv@fgi.fi) J.L. Davis, R.A. Bennett, G.A. Milne (Harvard-Smithsonian Center for Astrophysics, Cambridge, MA 02133, USA, e-mail: jdavis@cfa.harvard.edu, gmilne@cfa.harvard.edu, rbennett@cfa.harvard.edu) J.X. Mitrovica (Dept. Physics, University of Toronto, Toronto, Ontario, Canada M5S 1A7)

Since autumn 1993, the BIFROST project has provided daily GPS solutions of geodetic positions from a network of more than 40 stations covering a large area of the Baltic shield. This area is supposed to show large vertical motion due to glacial isostatic rebound after the deglaciation at the end of the pleistocene. This presentation will discuss the inference of three-dimensional rates of crustal motion at the GPS stations with respect to (1) a plate-fixed average as regards the horizontal components; (2) a geocentric reference in order to infer absolute changes of sea level from vertical crustal motion and models of geoidal rebound. We show that the horizontal strain rate pattern is largely dominated by unilateral extension and low in horizontal shear. As regards vertical motion a crucial issue is the stability of the geocentre in the GPS frame. We show results from Precise Point Positioning analysis which exhibits the problem more clearly than network solutions. We also show the importance to systematically reduce regional and local problems related to a number of surface loading problems.

**JSG11/E/05-A3****1520****BIFROST PROJECT: APPLYING 3-D CRUSTAL DEFORMATION DATA TO CONSTRAIN MODELS OF GLACIAL ISOSTASY IN FENNOSCANDIA**

Glenn MILNE, Jim Davis (Harvard-Smithsonian Center for Astrophysics, Cambridge, USA; e-mail gmilne@cfa.harvard.edu), Jerry Mitrovica (University of Toronto, Toronto, Canada), Hans-Georg Scherneck, Jan Johansson (Chalmers Institute of Technology, Onsala Space Observatory, Onsala, Sweden) and Martin Vermeer (Finnish Geodetic Institute, Masala, Finland)

The most recent solutions of BIFROST (Baseline Inferences for Fennoscandian Rebound, Sea-Level and Tectonics) project data for 3-D crustal-motion rates show a coherent picture that is clearly related to the glacial isostatic adjustment process. In this contribution, we shall present results from a series of both forward and inverse modeling calculations that adopt a spherically symmetric earth model with a compressible Maxwell viscoelastic rheology, a suite of different ice models and a sea-load model that is calculated by solving the sea-level equation in a gravitationally self-consistent manner. Our forward modeling analysis shows, in particular, that the data provide good constraints on the location of the center of mass and the large-scale geometry of the ancient Fennoscandian ice sheet. Also, the data are highly sensitive to viscosity variations within the upper mantle and, given the results of a simple sensitivity analysis, should provide a relatively firm lower bound on this parameter. An inverse analysis, based on ICE-1 [Peltier and Andrews, Geophys. J. R. astr. Soc., vol. 46, 1976] and an earth model with a 120 km elastic lithosphere and upper/lower mantle viscosities of  $1/2 \times 10^{21}$  Pa s, indicates that the data prefer a relatively 'soft' upper mantle ( $< 10^{21}$  Pa s) with a substantial increase in viscosity into the shallow lower mantle (viscosity within the deep mantle is not well constrained by the data). These general characteristics are consistent with a number of recently published viscosity profiles. We hope to present results from a new inverse analysis based on a viscosity profile that exhibits these general features and a recently published Fennoscandian ice model [Lambeck, Smither and Johnson, Geophys. J. Int., vol. 134, 1998].

**JSG11/W/02-A3****1540****MODELLING OF THE MULTIPLE PROCESSES AFFECTING SEA LEVEL RISE IN THE CENTRAL MEDITERRANEAN**

G. Di Donato, A.M. Negredo, R. SABADINI, L.L.A. Vermeersen, J.X. Mitrovica (Dipartimento Scienze Terra, Sezione di Geofisica, Università di Milano, Via L. Cicognara 7, I-20129 Italy, Email: stud1@sabadini.geofisica.unimi.it)

Geophysical modelling of tectonic mechanisms active in the central Mediterranean and of post-glacial rebound allows us to establish their relative contributions to sea-level changes. For a mantle stratified in viscosity, we obtain that the peak value of sea-level increase due to the two processes are comparable in magnitude, while its spatial variability portrays a different pattern. In the Adriatic sea, along the eastern part of the Italian peninsula, the effects of tectonic subsidence and post-glacial rebound sum up to a total sea-level increase that can be as high as 1 mm/yr. Both the amplitude of sea level rise and its spatial variability along the eastern coasts of Italy agree with secular sea-level changes inferred from archeological data, from Aquileia in the northern sector of the Adriatic sea to Egnatie in the southern part. Also in the historical cities of Venice and Ravenna model predictions agree with the data. The effects of a weak layer in the crust on the whole set of observables associated with glacial isostatic adjustment are also analyzed.

**JSG11/W/10-A3****1620****MANTLE VISCOSITY INFERRED FROM FENNOSCANDIAN STRAND LINE DATA**

Karin WIECZERKOWSKI (Institute of Planetology, University of Münster, Wilhelm-Klemm-Str. 10, D-48149 Münster, Germany) Jerry X. Mitrovica (Department of Physics, University of Toronto, 60 St. George Street, Toronto, Ontario M5S 1A7, Canada) Detlef Wolf (GeoForschungsZentrum Potsdam, Telegrafenberg, D-14473 Potsdam, Germany)

## INTER-ASSOCIATION

The postglacial rebound of the Fennoscandian shield has raised Holocene strandlines up to 200 m above the present sea level. The space-time distribution of these strandlines was used previously (e.g. McConnell 1968, JGR 73, 7089) to calculate the relaxation spectrum of rebound, i.e. the decay time of the uplift versus the wavelength of the deformation. Since it is unbiased by assumptions regarding the space-time history of the load, this spectrum has played a significant role in the inference of mantle viscosity. Previous relaxation spectra were derived on the basis of highly contentious hypotheses on strandline evolution (see Wolf 1996, GJI 127, 801). In this study we use strandlines based on more reasonable assumptions. Accounting also for the results of synthetic strandline calculations, we derive a new relaxation spectrum. Following Mitrovica & Peitler (1993, GJI 114, 45), we apply formal inverse theory to the new relaxation spectrum. In particular, we present estimates of the resolving power of the data as well as revised constraints, including uncertainties, on mantle viscosity. We find  $(5 \pm 1) \times 10^{20}$  Pa s in the depth range 100 to 500 km and  $(2 \pm 1) \times 10^{21}$  Pa s in the depth range 300 to 800 km.

**JSG11/E/08-A3**

**1640**

### MICROFOSSIL EVIDENCE OF LAND SUBSIDENCE OF THE 1964 EARTHQUAKE IN ALASKA

YONGQIANG ZONG and Ian Shennan Department of Geography, University of Durham, Durham, UK

Diatom and pollen assemblages from a number of outcrops and cores at Girdwood Flats and Kenai River, in the Cook Inlet, record four phases of relative land and sea-level movements. The first phase is the development of freshwater swamp above high marsh sediments during relative land uplift, caused by strain accumulation along the locked portion of the Alaska-Aleutian subduction zone. In phase two, diatom and pollen groups from the top few centimetres of the peat reveal relative sea-level rise (or relative land subsidence) prior to the main shock of the earthquake of March 1964. The third phase is rapid land subsidence, 1.7m at Girwood Flats and 0.5m at Kenai River, during the main shock that initiated intertidal silt sedimentation above the peat. The final phase is the colonisation of mudflat by saltmarsh communities during the post-seismic land uplift.

The concentrations of radionuclide  $^{137}\text{Cs}$  were measured to determine the time span of the second phase. The results suggest that the small land subsidence occurred about twenty years before the main shock in 1964, and was possibly a result of a major pre-shock.

The microfossil data compare favourably with sequences from Washington, Oregon and British Columbia that record late Holocene submergence events caused by large earthquakes. The results from Alaska raise the question whether pre-seismic sea-level rise (or land subsidence) represents any kind of warning of large earthquakes.

Co-workers include Dr. R. Combellick, Alaska Division of Geological & Geophysical Surveys, Fairbanks, Alaska, USA; Miss S. Hamilton and Ms M. Rutherford, Department of Geography, University of Durham, Durham, UK.

**JSG11/E/17-A3**

**1700**

### TECTONIC-HYDRO-CLIMATIC MECHANISM OF THE LEVEL FLUCTUATIONS IN THE INTRACONTINENTAL SEAS: THE CASPIAN

Dmitri A. LILJENBERG (Institute of Geography, Russian Academy of Science, 29, Staromonety per., 109017 Moscow, Russia, e-mail: geography@glas.apc.org)

A climatic concept has failed to predict a sudden and disastrous rise of the Caspian Sea level in 1978-95. As our recent studies show, the major impact to the Caspian Sea bath volume is caused by the lateral crustal motions in the Caucasian-Caspian nappe-overthrust domain. The lateral motions are parented by compression and tension produced by the Arabian Plate collision and are in complicated relations with hydro-climatic variations. The concurrent action of the tectonic and hydro-climatic mechanisms has also resulted in disagreement between Caspian transgressions and glaciation events. In the second half of the 20th century the Circum-Caspian was covered by repeated geodetic, sea-level, and seismic surveys with involvement of 10 geodynamic test areas. The resultant set of maps and profiles show the high mobility of the Circum-Caspian area, the reciprocal and variable contemporary motions, their dependence on the general morphostructure. Phases of the crustal extension and subsidence of the Caspian bath correlate with the sea-level drops in 1905-15 and 1929-40; the compression and uplifting correlate with the sea-level rise in 1978-95; but all level changes are independent of the actual sea water volume. The fluctuations of the sea level are in connection with the large-scale geodynamic processes, such as seismic activation in the Carpathians, Caucasus, and Asia Minor. The vertical motion rates make up few millimetres per tens of years, but can attain 5-7 cm/y. As recorded by trilateration and GPS surveys the lateral displacements are in the range of centimetres per year. The crustal motions, seismicity, mud volcanism, dynamics of subsurface fluids have a quasi-recurrence of 100-120, 80, 50-60, 35-40, 25-30, 10-20, 5-7, 2-3, and 1 year, which correlate with the hydro-climatic variations. Thus the Caspian Sea level fluctuations are caused by the integral tectonic-hydro-climatic mechanisms governed by the global processes.

**JSG11/W/06-A3**

**1720**

### HOLOCENE SEA-LEVEL CHANGES ALONG THE MEDITERRANEAN COAST OF ISRAEL - ARCHAEOLOGICAL OBSERVATIONS VERSUS ISOSTATIC MODEL

DORIT SIVAN and Avner Raban (both at the Center for Marine Studies, University of Haifa, Haifa, 31905 Israel, Email: Dsivan@research.haifa.ac.il). Shimon Wdowski (Department of Geophysics and Planetary Sciences, Tel Aviv University, Ramat Aviv, 69978, Israel, Email: Shimon@geol.tau.ac.il). Kurt Lambeck (Research School of Earth Sciences, The Australian National University, Canberra, ACT 0200, Australia, Email: Kurt.Lambeck@anu.edu.au) Ehud Galili (Marine Archaeology branch, Israel Antiquities Authority, P.O.B. box 180, Atlit 30350, Israel, email: Udi@israantique.org.il)

Underwater and coastal archaeological research conducted along the Mediterranean coast of Israel reveals significant sea-level changes during the Holocene. We consider the archaeological observations as upper and lower constraints of paleo sea-level. High resolution numerical models of sea-level change during the Holocene have been developed for the Mediterranean coast of Israel, and the predicted curves have been compared with field observations. The archaeological observations and the model curve are generally consistent indicating that sea-level rising rates along the Israeli coast were high and reached values of 7.5-9.0 mm/yr between 8,000-6,000 BP. The rate decreased to less than 1 mm/yr from 6000 BP. The close agreement between the modeled and the inferred curves also suggest that the local vertical crustal movements were low: less than 0.25 mm/yr, for the past 8 000 years.

**JSG11/W/12-A3**

**1740**

### SEA LEVEL CHANGES AND GEODYNAMICS

Nils-Axel Morner Paleogeophysics & Geodynamics, S-10691 Stockholm, Sweden, email: morner@pog.su.se

Sea level can only change within the limits set by the physical processes involved. Sea level changes is a multi-faceted problem, however, that calls for deep knowledge in a number of

different subjects and interacting processes. Sea level changes as a function of several different processes and by that it is, at the same time a remarkable measure of a number of different geodynamic processes. On the Ma-time scale, we are primarily dealing with long-term deformations of the ocean basin volume, the mass distribution and the rate of rotation. On the Ka-time scale, we are dealing with glacial eustasy and related effects on isostasy, rotation and geoid shape. On the Cy-time scale, we seem - though much debated - to be dealing primarily with changes in the distribution of ocean masses via changes in the oceanic circulation in a feed-back coupling with the Earth's rate of rotation. On the Yr-time scale, we are dealing with local dynamic factors, and in some places ENSO-effects, too. For different reasons and aspects, both geophysicists and geologists tend to oversimplify the picture, however. This is especially true when it concerns the changes during the last centuries and the expected future changes. Glacial eustatic changes virtually finished in Mid-Holocene time. The most powerful Late Holocene process of rapid changes in regional sea level refers to the variability in the main oceanic circulation system as a function of interchange of angular momentum between the solid Earth and the hydrosphere. The steric expansion of the water column is limited to individual oceanic layers with quite different recycling times. Only the surface layer can experience rapid changes in the order of are less than 10 cm in a century. If, on the whole, there was a global rise in sea level in the last 150 years, it cannot have exceeded 1.1 mm/yr. Evaluating the past and present changes in sea level, the expected changes in the near-future are estimated at "some 10 cm - at the most 20 cm - per century".

**Thursday 22 July AM**

Presiding Chair: H. Drewes

**JSG11/E/11-A4**

**0950**

### SCHEME OF THE CIRCUM-PACIFIC HIGH PRECISION SEA LEVEL GPS MONITORING NETWORK

Hu Jianguo, Chinese Academy of Surveying and Mapping

The circum-pacific high precision sea level GPS monitoring network (i.e. a net work combing GPS points with tide gauging) is proposed to establish according to this scheme. And at the same time, the satellite altimeter data is used to monitor the absolute changes of sea level in this area, to study the el niño, the movements of geological plates and other geodynamical matters, and to unify the vertical datum in the circum-pacific area. The network is composed of 41 points which lie in Asia, Australia, South America, North America, Antarctica and some islands around the Pacific Ocean. After all those points are Surveyed during the same period through GPS. This network will be put into the ITRF96 Reference Frame. It is supposed the horizontal precision of those points will be 5-8mm, the vertical precision 10-16mm.

**JSG11/E/15-A4**

**1010**

### GPS MONITORING OF VERTICAL GROUND MOVEMENTS AT UK TIDE GAUGE SITES SINCE 1990

Richard BINGLEY, Nigel Penna, Alan Dodson and Vidal Ashkenazi (IESSG, University of Nottingham, Nottingham, NG7 2RD, UK, Email: richard.bingley@nottingham.ac.uk), Trevor Baker (Proudman Oceanographic Laboratory (POL), Bidston Observatory, Birkenhead, Merseyside L43 7RA, UK, Email: tfb@pol.ac.uk)

Long term changes in mean sea level recorded by tide gauges are corrupted by vertical ground movements, which can be of a similar order of magnitude. Hence, to properly monitor changes in mean sea level, the rates of any vertical ground movements at tide gauge sites must be determined. The application of GPS to monitoring vertical ground movements at selected sites of the UK National Tide Gauge Network has been on-going at the IESSG and POL since 1990.

This work has closely followed the recommendations of the "Carter Reports" of 1989 and 1994, plus the more recent IGS/PSMSL workshop in 1997. Nine episodic GPS campaigns were carried out between 1991 and 1996, incorporating sixteen UK tide gauge sites. Since 1997, five of these sites have now been equipped with continuously operating GPS receivers (COGRs), which were some of the first to become operational at tide gauges in Europe.

This presentation charts the developments in using GPS at tide gauge sites, presents the results obtained in the UK from episodic GPS campaigns and COGRs, and discusses the contribution of these COGRs to a future European Sea Level Observing System (EOSS).

**JSG11/E/16-A4**

**1030**

### GROUND MOVEMENTS OF THE DORIS STATIONS DUE TO THE SEASONAL LOADING

LAURENT SOUDARIN, Anny Cazenave, and Jean-Francois Cretaux (Laboratoire d'Etudes en Geophysique et Oceanographie Spatiales, 18 avenue Edouard Belin, 31401 Toulouse cedex 4, France, email: Laurent.Soudarin@cnes.fr)

The ground positioning performances of the DORIS space system are at present at the centimeter level for the horizontal and vertical components (even subcentimetric for high-latitude stations), thanks to the combination of the data collected by the satellites carrying a DORIS receiver. Spot2, Spot3, and Topex/Poseidon data have been analysed over 1993-1997, and monthly positions computed for the about 50 stations of the permanent tracking network. Periodic variations are detected in the time series of the coordinate stations. In particular, a few mm annual signal is observed for a quarter of the sites. We investigate the atmospheric pressure loading effects which could cause the earth deformation signals observed. From the gridded surface pressure of the NCEP/NCAR reanalysis project, and the load Love numbers, we compute the crustal deformation by the atmosphere. We also investigate the loading deformation of snow and Continental hydrology.

**JSG11/W/01-A4**

**1050**

### MONITORING THE SEA-LEVEL AND VERTICAL CRUSTAL MOVEMENTS IN THE SOUTH ATLANTIC ALONG THE COAST OF ARGENTINA

Hermann DREWES, Wolfgang Bosch, Klaus Kaniuth (all at Deutsches Geoedatisches Forschungsinstitut, Marstallplatz 8, D-80539 Muenchen, Germany, email: drewes@dgfi.badw-muenchen.de); Claudio Brunini, Juan Moirano, Francisco Azpilicueta (all at Facultad de Ciencias Astronomicas y Geofisicas, Universidad La Plata, La Plata, Argentina, email: claudio@fcaglp.fcaglp.edu.ar)

Long-term tide-gauge records along the South Atlantic coast of Argentina show quite heterogeneous behaviour of sea-level variations ranging from -3.5 mm/a decrease to +5 mm/a increase. These signals are analyzed and compared with time series derived from six years Topex/Poseidon satellite altimetry data. Since December 1998, a selected number of representative tide gauges is monitored by repeated precise height determinations using the Global Positioning System (GPS). The ellipsoidal height of the sea surface at the tide gauges is compared with the sea surface height from satellite altimetry in order to detect systematic



effects. The repeated height determinations of the tide gauges will provide information about vertical crustal movements.

### JSG11/W/08-A4 1130

#### TECTONIC MOTION OF NY-ALESUND VLBI OBSERVATORY

Oleg TITOV (Astronomical Institute of Saint-Petersburg University, Bibliotechnaya sq., 2, Petrodvoretz, Saint-Petersburg, 198904, Russia, email: oleg\_titov@usa.net)

Ny-Alesund VLBI observatory has been operated since October, 1994. It is located on Svalbard archipelago which is an active tectonic area near edge of Eurasian plate. Therefore motion of the Ny-Alesund observatory is very complex. Natural deformation processes at the region could cause an unexpected shift of the site position. The previous estimates by GPS and VLBI technique sometimes show a disagreement between each other. About 150 single VLBI experiments has been processed by special software OCCAM to provide a detailed picture of the Ny-Alesund velocity drift in relation to conventional NNR-NUVEL-1A model. The five-years time series for vertical and horizontal components are presented. Generally, Ny-Alesund observatory moves in a good accordance with considered model. But it is suspected that seasonal effects in vertical component are able to distort the estimates of linear velocity. Origination of the seasonal effects is not clear up to now. Slow variations of longitude component are observed after removing of linear trend.

### JSG11/W/17-A4 1150

#### SEA LEVEL FROM GPS BUOYS

Authors: M. PARKE, C.K. Shum, K. Snow, K. Cheng (all at The Ohio State Univ., Columbus, OH) G. Mader and D. Martin (both at NOAA/NOS, Silver Spring, MD) F. Kelly and N. Guinasso (both at Texas A&M, College Station, Tx); G. Jeffress (Texas A&M, Corpus Christi, Tx) R. Gutierrez and B. Schutz (both at Univ. of Texas, Austin, TX) and J. Blaha (NRL, Stennis Space Center, MS)

Sea level measured from buoys can satisfy a wide range of oceanographic and geodetic requirements. In this talk we will address their roles in calibrating altimetric satellites, as "GPS tide gauges", spatial mapping of the sea surface for oceanographic and geodetic purposes, and in coastline mapping (in conjunction with other remote sensing techniques). Two experiments will be used for examples.

Between 19 April 1998 and 3 May 1998 a gps equipped buoy was taken on a Texas A&M hydrographic cruise. Data were taken using a gps buoy at 53 stations in conjunction with CTD measurements. All but one station were taken along altimeter ground tracks either for Topex/Poseidon or ERS-2. Two stations encompassed T/P overflights while one station encompassed an ERS-2 overflight. Other measurements along ground tracks were never more than about two days separated in time from the corresponding altimeter measurements. Data were taken in the El Dorado Eddy and the Fourchon Eddy with dynamic sea level signatures expected to be up to 20 cm and 60 cm respectively relative to the position of the mean sea surface. One station was taken near the center of the Fourchon Eddy (away from altimeter tracks) with an expected dynamic signal of about 80 cm.

A GPS buoy is being developed for deployment near a triple crossover point (a location where the three major altimetric satellite orbits cross: ERS, T/P, and GFO) as part of a plan for long term altimeter calibration and cross calibration.

### JSG11/W/23-A4 1210

#### LOCAL TIDE AND GEOID DETERMINATION FROM AIRBORNE GPS KINEMATIC POSITIONING AND LADS SURVEY

Shaowei Han, Chris Rizos and A. H. W. Kearsley (at School of Geomatic Engineering, The University of New South Wales, Sydney NSW 2052, Australia, email: s.han@unsw.edu.au, c.rizos@unsw.edu.au, w.kearsley@unsw.edu.au)

Airborne GPS kinematic positioning provides the geodetic height of the aircraft, and the Laser Airborne Depth Sounder (LADS) system can provide the distance between the aircraft and the sea surface. The height of the sea surface above the ellipsoidal model can then be determined, and this includes the local tide, local geoid, sea swell and noise. The local tide and local geoid can then be identified based the specific spectral features of the different components. In this paper, an experiment to test the utility of this concept using the Australian LADS system, together with state-of-the-art, geodetic GPS receivers, was carried out. The combination of an ambiguity recovery technique and a linear bias correction procedure has been used for this application to overcome the technical challenges of ambiguity resolution and cycle slip repair over distances many hundreds of kilometres. Finite Impulse Response filters are used to eliminate the measurement noise and sea swell distortion so that the local tide and geoid can be extracted. From a data analysis of this experiment, the accuracy of the local tide and geoid has been confirmed to be at the centimetre level from the comparison of four different sets of data in which three kinds of GPS receivers were involved. The comparison between the experimental results and theoretical computations of the local tide and geoid is attempted and commented upon.

Thursday 22 July PM

### JSG11/E/02-A4 Poster 1400-01

#### THE SEA LEVEL CHANGES AND VERTICAL GROUND MOVEMENTS IN THE SEA OF OKHOTSK

Olga Poezshalova and George SHEVCHENKO (both at Institute of Marine Geology & Geophysics, Russian Academy of Sciences, 693002, Nauki street, Yuzhno-Sakhalinsk, Russia, E-mail: tsunami@sakhmail.sakhalin.ru)

We examined the tendencies of changes of annual mean levels for different stations of the Okhotsk Sea. Parameters of linear trend were determined by least square method. The most expressed trends occurred at the stations of Kuril Islands. Annual mean levels in Severo-Kurilsk (Paramushir Is.), Matua (Matua Is.) and Malokurilsk (Shikotan Is.) decreased quickly (velocities is about 5 - 6 mm/year). That it speaks about uplifting of islands. However, Shikotan subsided at 50 cm after strong earthquake in October, 1994. The land subsidence looks in area of Kurilsk (Iturup Is.) and Yuzhno-Kurilsk (Kunashir Is.), particularly intensively this process proceed from 1955 to 1975. Analogous tendency observed in south-eastern coast of Sakhalin Island (Poronaysk, Vzmorye, Starodubskoye, Korsakov). That it speaks about subsiding of southern part of the Okhotsk Sea. The similar tendencies are not expressed at continental stations (Nagaeva bay, Okhotsk, Litke cape, Baydukov Island).

### JSG11/E/03-A4 Poster 1400-02

#### INTERDISCIPLINARY APPLICATIONS OF THE GPS ARRAY "CRETE"

Erricos C PAVLIS (JCET/UMBC, NASA Goddard, Code 926, Greenbelt, MD 20771, USA, email: epavlis@helmet.gsfc.nasa.gov) and Stelios Mertikas (Tech. Univ. of Crete, Chania, Greece)

A regional GPS array (CRETE) is being deployed over the past two years on the western side of the island of Crete, Greece. When complete, the array will consist of a continuously operating permanent site at the Technical University of Crete (TUC), Chania, Greece, and a number of other sites some of which will be permanent, continuously tracking while others will be visited periodically in "campaign style". We present here results from the expanded utility of this multipurpose GPS array. The Eastern Mediterranean area is one of great interest for its intense tectonic activity as well as for its regional oceanography. The contribution of the array to tectonics is the deformation field that can be inferred from the daily position time series. Another component of the project is the occupation the two tide-gauge sites at Souda Bay and Heraklion. We show here the so-far available position time series from Souda Bay. Tide-gauge monitoring has gained importance lately since tectonics contaminate the inferred sea level variations, and a global network of tide-gauges with long historical records can be used as satellite altimeter calibration sites for current and future missions (e.g. TOPEX/POSEIDON, GFO, JASON-1), a common IOC-GLOSS-IGS effort, already underway. Crete hosts these two tide-gauges, the oldest in the area, and our plans are to further expand the array to the south of the island with a new site on the isle of Gavdos. Gavdos is situated under a groundtrack crossing point of the T/P and JASON-1 orbits. It can be an ideal calibration site if the tectonic motions are monitored precisely. Our future plans include the deployment of additional instrumentation at this site (transponders, etc.) to ensure the best possible and most reliable results.

### JSG11/E/06-A4 Poster 1400-03

#### VERTICAL SITE MOTIONS FROM EUROPEAN VLBI CAMPAIGNS

James CAMPBELL, Axel Nothnagel, Klaus Boerger (Geodetic Institute, University of Bonn, D-53115 Bonn, Germany, email: campbell@picasso.geod.uni-bonn.de) Ruediger Haas (Onsala Space Observatory, Chalmers technical University, S-43900 Onsala, Sweden, email: haas@oso.chalmers.se) Paolo Tomasi, Istituto di Radioastronomia, CNR, I-40129 Bologna, Italy, email: tomasi@boira6.ira.bo.cnr.it) Dirk Behrend, Institut d'Estudis Espacials de Catalunya, Edif. Nexus, Gran Capita, 2-4, E-08034 Barcelona, Spain, email: behrend@ieec.fcr.es)

The European geodetic VLBI observations started in the late eighties and have been continuing through 1997 and 1998 at a rate of six experiments per year with six to nine stations in slightly different station configurations. The core network is formed by the stations of Onsala, Wettzell, Medicina, Matera, Noto and Madrid. More recently, the network has been considerably extended northward with the station of Ny Alesund on Spitsbergen and eastward with Simeis on Crimea, Ukraine. For those stations with a long enough observing record we present the results for the vertical site motions from the most recent analyses. Due to the high sensitivity of the vertical component to modelling of the atmospheric path delays, the level of significance of the vertical rates has been marginal up to now. Special attention has been given to the local effects at the sites such as telescope deformation due to temperature variations. At three stations repair works on the wheels and tracks have lead to defined height changes which can be seen in the time evolution of the vertical components. Local geodetic measurements have been carried out to establish these discrete vertical changes with high accuracy. The size of the vertical site velocities has been shrinking over the years to become more realistic with increasing length of the data set. The most apparent vertical change with respect to Wettzell, a site in Central Europe, happens at Medicina where we see significant and sustained subsidence of several mm/year. It is sure that the results derived from the VLBI campaigns will constitute a much needed basis for the geophysical interpretation of sea level changes and other vertical motion applications.

### JSG11/E/07-A4 Poster 1400-04

#### VERTICAL GROUND MOVEMENTS IN THE LOWER RHENISH EMBAYEMENT

Barbara GOERRES, James Campbell, Holger Kotthoff (all at Geodetic Institute, University of Bonn, D-53115 Bonn, Germany, email: goerres@picasso.geod.uni-bonn.de)

The Lower Renish Embayment is known for both its present-day seismo-tectonic activity and the extensive brown coal mining. The ground water withdrawal associated with the mining activities has produced widespread subsidence of several meters over a time span of 40 years. In parallel to the regular levellings in this area, a series of annual GPS-campaigns covering 13 simultaneously observed points has been started in 1993 in order to obtain vertical change by an independent technique. The size of the GPS network is about 100 km x 100 km. The initial goal of the project was to develop strategies to improve the accuracy (repeatability) of the vertical component measured by GPS. Apart from taking into account tropospheric refraction the observation sessions were extended to cover three entire days (3\*24h) and to go down to low elevations. In addition, all antennas were calibrated for phase center variations. Extensive tests revealed that the best repeatabilities are obtained with an elevation cutoff of 10 degrees. The data from six annual campaigns show significant height changes of up to 22 mm/y at three points. For all GPS points connected to the levelling network, the vertical velocities from GPS were in excellent agreement with the levelling results. In terms of wrms repeatability the vertical GPS results are at the level of 3 to 4 mm for each epoch and the velocities are at 1 to 2 mm/y. This confirms the validity of the chosen strategy and demonstrates the potential of GPS as a high precision tool for monitoring vertical change.

### JSG11/E/13-A4 Poster 1400-05

#### MODALISATION STOCHASTIQUE DES VARIATIONS DU NIVEAU D'EAU DANS L'ESTUAIRE DU SAINT-LAURENT, CANADA

MOHAMMED EL-SABH (email: mohammed\_el-sabh@uqar.quebec.ca), Karim Hilmi et J.P. Chanut (all at Département d'océanographie, Université du Québec à Rimouski, Rimouski, Québec, G5L 3A1, Canada)

Les enregistrements du niveau d'eau horaire à la station Québec Lauzon située à la tête de l'estuaire du Saint-Laurent, Canada, sont analysés à la fois dans le domaine fréquentiel (de 1970 à 1979) et dans le domaine temporel (durant l'année 1973). Les variations tidales expliquent 90 à 95% de la variabilité initiale de niveau d'eau observé entre 1970 et 1979. Les variations résiduelles (non tidales), de nature stochastique, peuvent contenir des valeurs irrégulières responsables des seiches et ondes de tempête. Bien que limitées à moins de 10% des variations initiales du niveau d'eau, ces variations résiduelles sont analysées et modélisées selon la méthodologie de Box et Jenkins afin d'identifier les facteurs environnementaux qui agissent de façon complémentaire sur le milieu marin. La réponse du niveau d'eau résiduel au forçage météorologique (pression atmosphérique et vents) se situe à une échelle de 2 à 28 jours; elle est de quelques heures à un jour pour les variations attribuables aux seiches longitudinales, aux cycles semi-diurne et diurne de la marée atmosphérique et aux périodes inertielles. Le débit d'eau douce contribue pour 29% à la



## INTER-ASSOCIATION

variabilité mensuelle du niveau d'eau résiduel, tandis que les vents et la pression atmosphérique y contribuent pour 8,9% et 8,1% respectivement. La composante U du vent, parallèle à la côte, agit davantage sur les variations du niveau d'eau résiduel que la composante V, perpendiculaire au rivage, avec une contribution approximative de 7%.

**JSG11/E/14-A4** Poster **1400-06**

### SUBSIDENCE PHENOMENON IN THE MONITORING OF SEA LEVEL RISE ALONG THE NIGERIAN COAST

DR. P.C. NWILO, Department of Surveying, University of Lagos, Yaba - Lagos, Nigeria, Tel + 234 1 821114 ext. 1865, fax + 234 1 2691315, Email: Library@rcl.nig.com

The Nigerian coast is low lying; the rocks are of sedimentary origin and recent. The coast is still undergoing natural compaction due to the weight of the sediments. This zone is the home to oil and gas exploitation in Nigeria. A number of highly populated cities such as Lagos, Port Harcourt, Bonny and Calabar obtain a large portion of water for industrial and domestic use from the bore holes that dot the coastal environment. There is, therefore, subsidence due to fluid extraction such as water, gas and crude oil.

Analysis of tidal data from Bonny for 19 years shows that the sea level is rising at about 1mm per annum. This rate of sea level rise does not take into account the subsidence phenomenon. Also, using over 40 years of tidal data for Takoradi, Ghana, it was obtained that the sea level was rising at the rate of 3.9mm per annum. This may represent the regional situation for the Gulf of Guinea coastal environment. The impact of sea level would be more devastating than currently envisaged due to subsidence.

Efforts to monitor subsidence along the Nigerian Coast using geodetic levelling methods have not been successful due to the difficult nature of the environment and lack of funding. There is, therefore, an urgent need for Federal Government, coastal states, the oil companies prospecting in the environment and the international community to show interest in subsidence monitoring along the Nigerian Coast. This can be done through the provision of funds for subsidence monitoring. Subsidence along the Nigerian Coast can be accomplished using the Global Positioning Methods. A clear indication of the rate of subsidence will help in the design of a national policy on managing the impacts of climate change along the coast of Nigeria.

**JSG11/W/07-A4** Poster **1400-07**

### TIDAL CHANGE IN THE YELLOW/EAST CHINA DURING THE LATE HOLOCENE

Katsuto Uehara (Research Institute for Applied Mechanics, Kyushu University, 6-1 Kasuga Koen, Kasuga, Fukuoka 816-8580 Japan, email: uehara@riam.kyushu-u.ac.jp)

One of the prominent features found in the present Yellow/East China Sea (YECS) is its large tidal influence. Maximum range exceeds 10m at the Korean coast and the vertical mixing effect of the tide is considered to be a significant factor to determine the circulation in the YECS (Lee, 1997). However, the tides in the past are expected to have different natures from today because the sea-level change is estimated to be more than 100m during the last 20000years. In particular, zonal asymmetry of the bottom topography become less evident in the lower sea-level stages because the present continental shelf extended in the western part of the YECS is mostly less than 60m deep.

In this study, two-dimensional tidal simulations are carried out for the ages of 0, 6, 9, 12 and 20 ka BP, in order to investigate the effect of the topographic change since the last glacial maximum. Several changes, including the reduction of the tidal range and the shift of the amphidrome points, are observed. Analyzing the results will not only provide a first scope to reproduce the paleotides of the Yellow/East China Sea, but also help us to understand the effect of the topography on the present tidal environment.

**JSG11/W/11-A4** Poster **1400-08**

### LONG-TERM SEA-LEVEL VARIABILITY IN THE BALTIC SEA AND ITS RELATION TO CLIMATE PHENOMENA

Dietrich, R. and LIEBSCH, G. Institut fuer Planetare Geodasie Technische Universitaet Dresden D-01062 Dresden Germany

Investigations concerning long-term sea-level variations require sea-level records of a high quality and reliability. Over the past years records with a homogenous local height reference were generated at several stations in the southern Baltic Sea. The measurements at these stations were initiated in the middle of the last century and are among the longest records in the Baltic Sea. Beside monthly mean sea-level records, which are in common use, records of monthly extreme sea-level values were created. On the basis of these records we will outline different aspects of the sea-level variability. This implies the analysis of - the mean sea-level records in the time domain as well as in the spectral domain and - potential changes of the extreme sea level with respect to the mean sea level. Furthermore, we will discuss possible relations between the sea-level heights in the Baltic Sea and the North Atlantic Oscillation (NAO), which is a large-scale alternation of atmospheric masses in the North Atlantic Sector.

**JSG11/W/13-A4** Poster **1400-09**

### CONTINUOUS GPS MONITORING AT BREST AND MARSEILLE GLOSS TIDE GAUGES

Serge Allain (1: SHOM, 13, rue du Châtelier BP 426, 29275 Brest, France), Claude Boucher (2: IGN/LAREG, 6-8, Avenue Blaise Pascal, 77455 Marne-la-Vallée, France), Serge Lannuzel (1), Didier Maillard (2), Bernard Simon (1) and Guy WOPPELMANN (\*)

Brest and Marseille are among the longest tide gauge time series available in the world, beginning in the early (1807) and late (1885) 19th century respectively. Time series spanning over at least 40 years are actually required to filter out the interannual and interdecadal sea level variability and to derive sea level trends which might be related to recent climatic changes. However, the long term signal inferred from tide gauge records is ambiguous : it includes eustatic sea level change as well as land movements. Space geodetic techniques like GPS can measure these components and have already been recommended by several international group of experts to monitor crustal vertical movements at tide gauge sites in a well defined and maintained geocentric reference system.

Brest and Marseille tide gauges are committed to the Global Sea-level Observing System (GLOSS). The French agencies, SHOM (Service Hydrographique et Océanographique de la Marine) and IGN (Institut Géographique National), are undertaking a close cooperation work to upgrade and fulfill GLOSS quality station requirements, especially the geodetic monitoring of the tide gauge zero. Both tide gauge stations have been equipped with continuous GPS receivers, since July 1998 in Marseille and since November 1998 in Brest. The hundred-year-old tide gauge in Marseille was repaired mid-1998 after the failure due to vandalism occurred in 1997. An acoustic one was purchased and installed in June 1998. This new tide gauge can provide numerical high frequency data.

The presentation will give a brief description of both coastal sea level observing stations : the

local environmental conditions and the instrumentation. GPS and tide gauge data analyses will be presented. A more comprehensive sea level picture will be addressed at both sites by the synergetic tide gauge GPS approach.

**JSG11/W/14-A4** Poster **1400-10**

### SPECTRAL ANALYSIS AND FILTERING BY TWO DIMENSIONAL FOURIER TRANSFORM OF SEA SURFACE TOPOGRAPHY OBSERVED BY TOPEX/POSEIDON ALTIMETRY.

Waldemar Popinski Department of Standards, Central Statistical Office, Al. Niepodleglosci 208, 00-925 Warsaw, Poland, Email: w.popinski@stat.gov.pl Wieslaw KOSEK Space Research Centre, Polish Academy of Sciences, Bartycka 18A, 00-716 Warsaw, Poland, Email: kosek@cbk.waw.pl

A method of spectral analysis and filtering of sea level anomalies obtained from Topex/Poseidon altimetric measurements is presented. Such sea level anomalies at a particular time moment create sea surface topography which can be analysed using the two dimensional discrete Fourier transform (DFT).

The original data called 'cycles' are defined on a rectangular grid in latitude-longitude domain and are transformed using the two dimensional DFT to corresponding wave-number domain. Filtering of the sea surface topography is achieved by multiplying the transformed data by a bivariate filter transfer function and next inverting the DFT.

These analyses enable detection of the most energetic waves in sea surface topography and estimating how much the sea level anomalies corresponding to different time moments are correlated along the meridian and parallel directions. It has been found that the correlation and coherence of the sea surface topography along the parallel direction is higher than along the meridian direction for the whole wave-number range and independently of time.

**JSG11/W/15-A4** Poster **1400-11**

### CHANGES IN SEA LEVEL, SEA SURFACE TEMPERATURE AND ATMOSPHERIC PRESSURE FROM SATELLITES.

Per Knudsen and Ole Baltazar Andersen (both at National Survey and Cadastre, Copenhagen NV, Denmark, email: pk@kms.dk, oa@kms.dk)

In studies of Global Change, sea surface temperature data may provide valuable information. Global sea surface temperature data may indicate changes in the heat budget of the oceans. Five years of sea surface temperature data and sea level height for the same period is analysed. Altimetry from the TOPEX/POSEIDON satellite will be used along with pressure observations provided in the T/P records and low resolution averaged sea surface temperature data from the ATSR 1 and 2 sensor onboard the ERS satellites and AVHRR data from the NOAA satellites.

The global and regional characteristics of the sea level trends and the trends in the sea surface temperature as well as trends in the atmospheric pressure during 1992-1997 are investigated. The changes in the sea level are compared with changes in sea surface temperature to decide whether the changes in sea level are related to changes in the heat content of the ocean. Spatial and temporal correlation between the signals are investigated, and a bivariate coherency analysis of the sea level together with the sea surface temperature is carried out at different spatial scales.

**JSH12** Thursday 22 – Friday 23 July

### ICE SHEETS, OCEANS AND THE EARTH'S SHAPE: MODERN PERSPECTIVES ON SEA LEVEL CHANGE (IAHS, IASPEI, IAG, IAPSO, IAMAS, CMG)

Location: Law Building 115 LR2

Location of Posters: Old Gym

Thursday 22 July PM

Presiding Chair: C.R. Bentley (University of Wisconsin, USA)

**JSH12/W/04-A4** Poster **1400-01**

### APPLICATION OF SAR INTERFEROMETRY TO DEM GENERATION OF ANTARCTICA

Taku Ozawa (The Graduate University for Advanced Studies, 1-9-10, Kaga, Itabashi-ku, Tokyo 173-8515, email: ozawa@nir.ac.jp); Koichiro DOI, Kazuo Shibuya (both at National Institute of Polar Research, 1-9-10, Kaga, Itabashi-ku, Tokyo 173-8515, email: doi@nir.ac.jp and shibuya@nir.ac.jp)

SAR interferometry is an effective tool for estimating ice sheet motion as well as generating a digital elevation model (DEM). There are few precise DEMs in Antarctica except for some restricted regions, because of logistic difficulties to make dense ground surveys. It is true that satellite radar altimetry provides us data to generate DEM in Antarctica, but more precise DEM is required for monitoring ice sheet motion by SAR interferometry. As a first step to estimate the ice sheet motion, we tried to generate DEM by SAR interferometry technique. We employed the 3-pass method to separate the topographic fringe and the displacement fringe which are mixed in a SAR interferogram obtained on the Antarctic ice sheet. As a test site, we selected the ice sheet and outcropped area in the vicinity of Syowa Station (69.0degS, 39.5degE), which is the wintering base for the Japanese Antarctic Research Expedition, and analysed three serial JERS-1 SAR images acquired on June 16, July 30, and September 12 in 1996. We successfully extracted the topographic fringe on a large part of the ice sheet in the image.

**JSH12/W/07-A4** Poster **1400-02**

### GEODETIC INDICATIONS ON RECENT ICE MASS CHANGES IN AN EAST ANTARCTIC REGION

Dietrich R. KORTH, W., Metzger, R., Perlt, J. (Institut fuer Planetare Geodasie Technische Universität Dresden, D-01062 Dresden, Germany)

During the last decade geodetic-glaciological investigations were carried out in Dronning Maud Land, Antarctica. The working area of about 300 by 300 square kilometres is located in the region of the Schirmacher Oasis (B=71° S, L=12° E). Different techniques were used to carry out observations, e.g. terrestrial geodetic measurements, static and kinematic GPS, tide gauge and SAR interferometry. As a result the flow of the inland and ice shelf glaciers has been completely studied. Detailed knowledge has been obtained on the ocean tide induced vertical motions of the ice shelf. Particular attention was paid to local rates of ice-sheet thickening or thinning. Such specific mass balances were derived from measurements along traverses crossing an ice stream. For one traverse running through an accumulation area the

results are disturbed by short-term fluctuations in snowfall and snow densification. Measurements in ablation areas with blue ice at the surface are not affected by these influence. A thinning of the glacier of about 10 centimetres per year was determined for a large blue ice region. A significant lowering of the level of lake Unterseer about 100 kilometres inland confirms this observed trend.

**JSH12/W/09-A4** Poster **1400-03**

#### COUPLED MARINE ICE-SHEET/EARTH DYNAMICS

Emmanuel LE MEUR, Richard Hindmarsh (both at British Antarctic Survey, Madingley Road, CB30ET Cambridge, U.K. Email: lemeur@nerc-bas.ac.uk; rcah@nerc-bas.ac.uk)

The West Antarctic ice sheet represents the only large marine icesheet on Earth. With most of the underlying bedrock below sea level, it strongly interacts with the sea which leads to specific ice dynamics and make these marine ice sheets potentially unstable. West Antarctica is believed to have substantially fluctuated during the last glacial/interglacial transition with a global sea level contribution of about 6 m. The question of its response to present-day conditions or to future environmental changes is therefore of major concern. Previous studies have shown the key effect on the ice dynamics from the free water depth at the grounding line. Like sea level change, by modifying this water depth, bedrock displacements make the grounding line migrate and can significantly modify the ice sheet configuration. This presentation describes a simple 1-D axisymmetric marine ice sheet model which couples with a spherical visco-elastic earth model. By incorporating a kinematic grounding line migration formula, the ice model is able to generate the ice sheet span in response to the sea level forcing, the ice flow and the bedrock characteristics. After testing the model response to some basic forcings we focus on the different effects resulting from including or excluding the bedrock response. The main effect of bedrock coupling consists of stabilizing the system by substantially reducing the grounding line migration. The overall time-dependent response of the system partly controlled by the delayed viscous mantle confirms the existence of specific ice/Earth dynamics and justifies the importance of realistic isostatics in ice sheet models.

**JSH12/E/05-A4** Poster **1400-04**

#### SPACEBORNE LASER ALTIMETRY OF THE POLAR ICE SHEETS

B. E. Schutz (University of Texas at Austin); C. R. Bentley (University of Wisconsin); R. Thomas (EG&G, NASA Wallops); J. Zwally (NASA Goddard)

In July 2001, NASA will launch a laser altimeter on ICES at into a near-circular, near-polar orbit to measure changes in polar ice-sheet topography. The ice sheet measurements will address fundamental questions about the growth or shrinkage of the polar ice sheets and their contribution to current and future global sea level change. The orbit inclination was chosen to provide coverage with the nominally nadir-looking altimeter, the Geoscience Laser Altimeter System, to a latitude of about 86 degrees. Exceptionally dense nadir tracks will occur at the high latitudes because of the orbit characteristics, thereby providing dense coverage of, for example, most West Antarctic features. The altimeter and related measurement systems have been designed to measure a secular height change with an accuracy of 15 mm/yr and over an area of 100 km x 100 km. This accuracy requirement was based on the analysis of van der Veen (1993) of the probability that a particular dh/dt is due to a real secular change in the ice sheet rather than arising from normal interannual variations in the snowfall. In the analysis of the results advantage will be taken of the synergy with the gravitational satellite GRACE to remove from the surface elevation changes any isostatic rebound signal that may exist. This paper will further describe the science requirements and the design considerations to meet the requirements, as well as the procedures planned for verification of the measurements and validation of the data products.

**JSH12/L/01-A4** Poster **1400-05**

#### CRUSTAL UPLIFT AND SEA LEVEL CHANGE AROUND SYOWA STATION, ANTARCTICA

K. KAMINUMA

There is a great deal of evidence concerning crustal uplift, after deglaciation, in the vicinity of Syowa Station (69.0S, 39.6E), East Antarctica, from geomorphological data as elevated beaches, marine terraces etc. The uplift of about 20 M was recognized during the last 600 years. Therefore the rate of uplift is estimated to be 3-6mm/y from geomorphological data. A tide gauge was installed at Syowa Station in 1966, and the observation has been continued currently. Sea level falling of 4.5mm/y was found using data 1975-1992. The falling rate is consistent with geomorphological data. Both data show that the crustal uplift is going on around Syowa Station at present. Micro seismic activity around Syowa Station are inferred to be caused by the tectonic stresses which are accumulated by the crustal uplift after deglaciation, as the location of the earthquakes are in the costal and offshore areas. Local earthquake activity corroborates the crustal uplift, and it is an intermittent phenomenon with 10-20 year interval. A trend of the falling sea level at Syowa Station at the rate of about 10mm/y was found by the detailed data processing using the well-controlled sea level data from 1981-1987. More than ten micro- and small- earthquakes were recorded at Syowa Station in 1987-1990. These earthquakes correspond well with the inferred crustal uplift of 10mm/y. Only one/two small/micro earthquakes per year were recorded at Syowa Station since 1990. A superconducting gravimeter (SG) was installed at Syowa Station since 1993. It is expected to detect the crustal uplift by SG. If the crustal uplift at a rate of 5 mm/y continues ten years, the total uplift obtained will be 5 cm, 15Gal in gravity change. This uplift is detectable by SG.

**Friday 23 July AM**

Presiding Chair: W.R. Peltier (Univ. of Toronto, Canada)

**JSH12/W/03-A5** **0830**

#### SIX YEARS OF DUAL FREQUENCY TOPEX ALTIMETER DATA OVER SOUTH GREENLAND

Benoit LEGRESY (1), Frederique Remy (1), Patrick Vincent (2) (1: UMR5566/GRGS (CNES-CNRS-UPS) 18 Av. E. Belin, 31401 Toulouse cedex 4 FRANCE) (2: CNES DGA/T/ED/LA/M 18 Av. E. Belin, 31401 Toulouse cedex 4 FRANCE E-mail: benoit.legresy@cnes.fr)

Since Topex/Poseidon was launched in 1991, it regularly releases altimetric data in C and Ku band every 10 days. As the satellite inclination only allows observations below 66 degree North latitude, only the southern part of the Greenland ice sheet is covered by a few tracks. The dual frequency altimetric information has been found useful for ice sheet surface properties investigation and for snow penetration induced error on the height measurement control. 6 years of data are now available. We have reprocessed the sensor level data of the

time series for 8 tracks that cross Greenland. It allows us to analyse the seasonal cycle of the measurement and its relation to the ice sheet surface conditions in the accumulation area.

The C-Band radar waves penetrate deep into the snowpack, of the order of 10 to 30 m for dry snow, while Ku-Band radar waves penetrate 5 to 15 m. Ku-Band measurements are more sensitive to surface snow metamorphism. The difference of penetration between the two frequencies is linked to snow grain size and stratification. We also used radiometer brightness temperature data at 18, 21 and 37 Ghz which are simultaneously acquired on-board Topex/Poseidon. We find that brightness temperatures are complementary to the altimetric measurement in order to characterise snow surface metamorphism. Finally the 6 year long measurements provided by Topex/Poseidon are well controlled and can be accurately interpreted despite the sparse coverage of the satellite.

**JSH12/W/05-A5** **0900**

#### ELEVATION CHANGES OF THE GREENLAND ICE SHEET FROM REPEATED GPS AND SAR INTERFEROMETRY

K. KELLER, R. Forsberg, C. S. Nielsen (KMS, Rentemestervej 8, DK-2400 Copenhagen NV, Denmark, email: kk@kms.dk) N. Gundestrup, C. C. Tscherning (Niels Bohr Institute, Univ. of Copenhagen, Juliane Maries Vej 30, DK-2100 Copenhagen O, Denmark, email: ng@gfy.ku.dk) S. N. Madsen, J. Mohr, J. Dall (Institute of Electromagnetic Systems, DTU, DK-2800 Lyngby, email: smn@emi.dtu.dk)

Elevations of the Greenland ice sheet has been measured repeatedly over several years at two sites at the centre of the Ice Sheet (at the GRIP drilling sites), and at a marginal ice cap in central East Greenland (Geikie Plateau). Repeated GPS measurements at the GRIP site since 1992 shows the ice sheet in this region to be essentially stable, with measured elevation changes and strain rates in good accordance with accumulation and ice flow models. Satellite and airborne SAR interferometry, and airborne laser altimetry, has additionally been used to study the coastal ice cap, primarily in order to evaluate accuracy of methods, as well as detect possible large yearly elevation changes in a region of high and variable yearly snow accumulation. The paper will present the project activities, methods and some recent results.

**JSH12/C/JSS31/E/05-A5** **0930**

#### ICE-3G RETREAT INCONSISTENT WITH GREENLAND OBSERVATIONS

R THOMAS and S Manizade (EG&G, NASA/WFF, Wallops Island, VA 23337, USA, email: thomas@osb.wff.nasa.gov; manizade@osb.wff.nasa.gov); W Krabill (Lab for Hydrospheric Processes, NASA/WFF, Wallops Island, VA 23337, email: krabill@osb.wff.nasa.gov); J Wahr, K. Larson, and S Gross (U. Colorado, Boulder, CO 80309, USA, email: wahr@lemond.colorado.edu; kristine@lemond.colorado.edu; sjg@quake.colorado.edu); T van Dam (Obs. Royal de Belgique, B-1180 Bruxelles, Belgium, email: tonie@oma.be); X Wu (JPL, Pasadena, CA 91109, USA, email: xpw@cobra.jpl.nasa.gov)

ICE-3G representation of Holocene retreat implies present-day isostatic uplift of the east and west coasts of southern Greenland by about 3-4 mm/yr if the present-day ice sheet is in balance. Satellite radar and aircraft laser altimeter surveys indicate overall balance for higher-elevation regions since 1978, with significant recent thinning nearer the east coast and areas of both thickening and thinning near the west coast. We would expect the areas of thinning to cause increased uplift rates, but continuous GPS measurements at Kangerlussuaq on the west coast, since 1995, and at Kulusuk on the east coast, since 1996, show subsidence of 7.7 +/- 2.6 mm/yr in the west and 6.1 +/- 5.1 mm/yr in the east. Kangerlussuaq is near to areas of ice that are approximately in balance and Kulusuk is close to ice that is rapidly thinning.

These observations suggest that either the Holocene retreat of the Greenland ice sheet differed significantly from that described by ICE-3G, and/or there was substantial thickening sometime between about 5000 BP and a few decades ago. We have used our observations of ice-surface elevation change and coastal subsidence to infer a range of ice-sheet histories and mantle-viscosity profiles that are consistent with those data, and these suggest that the southern part of the ice sheet may have been substantially thinner than at present at some time during the past few thousand years.

**JSH12/W/12-A5** **1000**

#### A RE-EVALUATION OF THE MASS BALANCE OF GREENLAND

Atsumu Ohmura and Pierluigi CALANCA (both at Department of Geography, Swiss Federal Institute of Technology, Winterthurerstr. 190, CH-8057 Zurich, Switzerland, e-mail: calanca@geo.unm.ethz.ch)

The present mass balance of the two major ice sheets, Antarctica and Greenland, is not known with sufficient accuracy. A re-evaluation of the mass balance of Greenland and its spatial distribution are presented. The accumulation is derived from direct observations. Compared to previous estimates, additional data for some 48 pits and 5 meteorological stations are included in the analysis. Moreover, care is taken to correct the precipitation measurements for the wind-induced defect, separately for the liquid and solid phases. The ablation is derived from the three-summer-months mean temperature. Finally, the calving rates are estimated from remote sensed data and the geometry of the outlet glaciers.

**JSH12/E/02-A5** **1100**

#### ICE CAP VOLUME CHANGE ON FRANZ JOSEF LAND DURING LAST 40 YEARS

Yuri Macheret, Andrey GLAZOVSKY (both at Institute of Geography, Russian Academy of Sciences, Staromonetny per., 29, 109017 Moscow, Russia, email: andrey@glazov.msk.ru); Julian Dowdeswell (Bristol Glaciology Centre, School of Geographical Sciences, University of Bristol, Bristol BS8 1SS, UK, email: j.a.dowdeswell@bristol.ac.uk); Michael Gorman (Scott Polar Research Institute, University of Cambridge, Lensfield Road, CB2 1ER Cambridge, U.K)

Airborne radio-echo sounding of 26 ice caps of various morphology and area (26 to 1.892 km<sup>2</sup>) was carried out on Franz Josef Land archipelago in 1994. Ice thickness data were obtained on 12 ice caps as maps and on 14 other ice caps as profiles. These data allowed to find the close empirical relationships between ice cap area and volume as well as between average and maximum ice thickness. These yield exponents for the power-law relations between volume-area of 1.312 and 1.228 and between maximum ice thickness-area of 0.295 and 0.245 for ice caps with and without outlet glaciers, and coefficients for the linear average-maximum ice thickness relation of 0.504 and 0.510, respectively. Relations between volume and area parametrized by maximum ice thickness provide exponents equal to 1.295 and 1.245, respectively. Using these empirical relations the ice volume of all ice caps on archipelago is estimated.

Total ice cap volume is estimated as 2105.9 km<sup>3</sup> in 1993 and as 2147.8 km<sup>3</sup> in 1953 with volume decrease during this period by 41.9 km<sup>3</sup> and area reduction by 209 km<sup>2</sup>. The volume decrease is equal to mean net specific mass balance -7.0 cm per year in water equivalent. Comparison of this value with mass-balance data of other authors suggests that the negative mass balance rate in the last 40 years has been approximately 3.3 times less than in 1930-

## INTER-ASSOCIATION

1960 which in turn agrees well with data on decrease of mean summer air temperature in compared periods on Franz Josef Land.

**JSH12/W/06-A5** **1130**

### SEA LEVEL CHANGE AND SEA-ICE VARIATIONS – A LINK?

ANZENHOFER, M (GeoForschungsZentrum Potsdam (GFZ), c/0 DLR, Postfach 1116, D-82230 Oberpfaffenhofen, Germany. E-mail: anzenhof@gfz-potsdam.de)

Model runs simulating future climate conditions assuming a further increase of atmospheric greenhouse gases show various asymmetries. Especially for the sea-ice extension, a decrease is expected for the North pole and an increase for the South pole. Time series of sea-ice extensions of both poles exist from passive microwave satellite observations from 1978 till now. Accurate sea level time series, however, only exist from 1992 on (the problem of linking Geosat and ERS or TOPEX data is still unsolved). Recent investigations have shown a surprisingly high correlation between sea level variations and sea-ice extension anomalies around Antarctica. The correlation time period was only 3 years long. The presentation will focus on an enhanced study of the correlation between vertical sea level and anomalies in spatial sea-ice distribution by the extension of the altimeter derived sea level data base, the analysis of North pole sea-ice, and the inclusion of sea surface temperature data.

**JSH12/W/01-A5** **1200**

### THE GLACIAL-INTERGLACIAL PARADOX

John A.T. BYE, (Flinders University, GPO Box 2100, Adelaide, Australia, 5001, email: John.Bye@flinders.edu.au)

Sea level variability during the Quaternary is simulated using a stochastic climate model and a sensitivity relation for the change in net oceanic evaporation due to a change in sea surface temperature, on the assumption that the greater part of the change in net oceanic evaporation causes changes in the land ice volumes, rather than being directly returned to the ocean by rivers. The analysis suggests that the observed sea level changes can be interpreted as due to the transfer of heat to the deep ocean from the surface mixed layer, arising from random radiation perturbations of the same variance as would give rise to the interannual variability of the global temperature series.

**Friday 23 July PM**

Presiding Chair: A. Ohmura (Swiss Fed. Inst. of Tech., Zurich, Switzerland)

**JSH12/E/04-A5** **1400**

### SCANDINAVIAN ISOSTATIC REBOUND: CONSTRAINTS ON THE LATE WEICHSELIAN ICE MODEL

Kurt LAMBECK (Research School of Earth Sciences, The Australian National University, Canberra, ACT 0200, Australia, email: Kurt.Lambeck@anu.edu.au)

Sea-level information from three different data sources have been combined to develop a comprehensive model of the isostatic rebound for Scandinavia in which it has been possible to separate effectively those parameters describing the earth response and those describing the ice sheet. The data sources used are: geological estimates of shoreline age-height relationships, the alternating marine freshwater stages of the Baltic Sea, and the recent tide-gauge and lake-tilt measurements. The essential glaciological result is an ice sheet that is distinctly asymmetrical over Scandinavia, with the ice over the southeastern and southern areas being relatively thin when compared with the ice over the north and west. Maximum ice thickness at about 18,000 years ago is unlikely to have exceeded 2000 m with the maximum ice cover occurring over northern Sweden rather than Finland. Earth model results include a well defined stratification in the mantle viscosity, consistent with analyses from other parts of the world.

The paradox is that glacial conditions (increase in ice volume) are favoured by positive (temperate) sea surface temperature anomalies, and interglacial conditions (decrease in ice volume) by negative (temperate) sea surface temperature anomalies. The evolution of both these regimes, which are inherently unstable, appears to be controlled by the deep water formation process, while albedo feedback is of minor importance.

**JSH12/W/13-A5** **1430**

### GRAVITATIONAL-VISCOELASTIC PERTURBATIONS OF A SPHERICAL EARTH WITH COMPRESSIONAL DENSITY STRATIFICATION

G. Li, D. WOLF (both at GeoForschungsZentrum Potsdam, Telegrafenberg, D-14473 Potsdam, Germany, email: dasca@gfz-potsdam.de)

We derive the analytic solution for the deformation and gravity change caused by the loading of a self-gravitating spherical earth model consisting of a viscoelastic mantle with compressional density stratification and a homogeneous inviscid core. The fundamental characteristics of the solution are evident in the Legendre-transform domain, where we show relaxation-time and amplitude spectra for the mantle and core modes that constitute the time-dependent part of the response. Following this, we predict in the space-time domain the radial displacement, the free-air gravity anomaly and the geoid height for an axisymmetric load model with parabolic cross-section and dimensions similar to those of the Laurentide ice sheet. A comparison with the corresponding predictions for an earth with homogeneous density in the mantle underlines the importance of allowing for the compressional density stratification when modelling load-induced gravitational-viscoelastic perturbations of the earth.

**JSH12/E/03-A5** **1500**

### THERMALLY INDUCED LATERAL VISCOSITY VARIATIONS AND POSTGLACIAL REBOUND: IMPLICATIONS FOR RELATIVE SEA LEVELS IN LAURENTIA

Patrick WU (Dept. of Geology & Geophysics, University of Calgary, Calgary, Alberta T2N-1N4, Canada, Email: ppwu@ucalgary.ca), John Wahr (Department of Physics, University of Colorado, Boulder, Colorado 80309 USA, Email: wahr@longo.colorado.edu), W.R. Peltier (Dept. of Physics, University of Toronto, Toronto, Ontario M5S-1A7, Canada, Email: peltier@atmosp.physics.utoronto.ca)

Quantifying lateral viscosity variations in the mantle is useful in understanding mantle dynamics. From seismic tomography, which maps the three dimensional structures in the mantle, one can convert lateral velocity variations to viscosity variations by simple scaling since both are affected by the same thermal structure. The assumption in doing so is that the contribution of lateral variations in chemical composition can be neglected. In reality, the viscosity variations obtained this way are only upper bound estimates. Let the ratio of the actual viscosity variation over this upper bound estimate be given by the factor Beta, the aim

of this work is to estimate the value of Beta from the postglacial sea level data in Laurentia. The finite element method is used to calculate the deformation and relative sea levels in a laterally and vertically heterogeneous flat Earth. The loading history is given by the realistic ICE4G model and its eustatic sea level loads. Several cycles of loading before the last glacial maximum are also included. The radial viscosity profile is assumed to be given by the VM1 or VM2 models of Peltier. The lateral viscosity variations are obtained by applying the simple scaling relation of Ivins & Sammis (1995) to Beta multiplied by the shear-wave velocity fluctuations in the S20A model of Ekstrom & Dziewonski (1998). A range of laterally heterogeneous viscosity models are constructed - each characterized by a different value of Beta. These viscosity models are tested to see which is consistent with the sea level data in North America. The maximum value of Beta that can explain the sea level data simultaneously will give the maximum contribution of thermal effects on lateral viscosity variation.

**JSH12/W/10-A5** **1600**

### GLOBAL GLACIAL ISOSTASY, SEA LEVEL AND GLACIOLOGY

Richard PELTIER (Department of Physics, University of Toronto, Toronto, Ontario, Canada M5S-1A7, email: peltier@atmosp.physics.utoronto.ca)

The global viscoelastic and gravitationally self consistent theory of the glacial isostatic adjustment process has recently been refined considerably so as to incorporate the influence of both time dependent coastlines and the feedback onto sea level of the earth's changing rotational state. Although the primary focus of the analyses that have been performed with this theory has been on the inverse problem for mantle viscosity, it has other, equally interesting, applications. For example it may be invoked to provide important constraints on both the origins of the global rise in sea level that is apparent on modern tide gauge recordings and on fundamental questions in glaciology. In the former area the strength of the rotational feedback on sea level turns out to be interesting, especially from the perspective of space geodesy (eg GRACE), whereas in the latter area its application has led to important constraints upon ice rheology.

**JSH12/W/14-A5** **1630**

### ANTARCTIC REBOUND AND THE TIME-DEPENDENCE OF THE EARTH'S SHAPE

Erik R. IVINS (JPL, Caltech, Pasadena, CA 91109-8099 USA, email: eri@scn1.jpl.nasa.gov); Thomas S. James (Geol. Survey of Canada, Sidney, BC, Canada, email: james@pgc.nrcan.gc.ca)

Great strides have been made during the past 30 years in refining models of the last global glaciation. The refinements draw upon a vastly expanded relative sea level and sedimentary core record. Furthermore, we now possess a sharpened understanding of the mechanisms that drive climate changes associated with deglaciation. Some 15 years ago, using only 5.5 years of ranging data, analyses of the acceleration in LAGEOS 1 nodal drift was used to infer that postglacial rebound was responsible for a secular change in the Earth's ellipsoidal shape [Yoder et al., 1983]. Today there exists a wealth of geodynamics satellite orbit data that constrain the secular time-dependence of the Earth's shape and low order gravity field, which includes mass redistribution from present-day glacier and great ice sheet imbalance and from postglacial rebound. We have shown that an unambiguous determination of the secular variation in the Earth's pear shaped harmonic ( $l = 3, m = 0$ ) might provide information that bears on the present-day mass balance of Antarctica. This issue is revisited in light of new constraints on glacial loading during the late-Pleistocene and Holocene. An especially critical issue for the interpretation of secular odd degree zonal harmonics,  $l = 3$  to  $7$ , is the timing and magnitude of the deglaciation of Antarctica from Last Glacial Maximum. We explore ways in which the recovery of secular variation in both zonal and non-zonal harmonics for  $l = 2$  through  $7$  can improve constraints on both rebound and present-day ice sheet balance.

**JSH12/W/11-A5** **1700**

### SURFACE TEXTURE AND ICE-STREAM BASAL DRAG/RICHARD

C.A. HINDMARSH, (British Antarctic Survey, High Cross, Madingley Road, Cambridge, CB3 0ET. E-mail: rcah@bas.ac.uk)

Ice streams are restrained by a combination of lateral drag and basal drag. Borehole observations from Ice-Stream B indicate little basal coupling, but the problem of whether ice-stream surface texture originates from internal rheological variations, basal topography or coupling of ice, till and water flows remains unresolved. If it is from such coupling, we conclude (i) that significant basal drag is present and (ii) this is dynamic and can change, implying that the basal resistance can change very fast, changing the rate of ice export to the sea.

This paper addresses the coupling of flows of ice, till and water, and the issue of whether such coupling provides mechanisms for meso-scale (kilometres to tens of kilometres) variability in ice-sheet flow and texture. The question of whether effective pressures at the ice-bed interface are statically or hydraulically controlled is examined in this paper. The answer is scale dependent, and has a significant effect on the relationship between ice surface and basal topography.

Linear stability analyses indicate that there appears to be sufficient variability in the ice-till water system to potentially explain texture in ice stream surfaces, variations in ice stream thickness of tens of metres not directly related to topography, and waves moving upstream or downstream. Most importantly, the ice-stream/bed system is shown to exhibit meso-scale variability simply by coupling ice-flow according to the shallow ice approximation, till flow according to the hydrostatic thin-till approximation and water flow according to an effective pressure-dependent hydraulics.

**JSS13** **Thursday 22 – Friday 23 July**

### CONSTRAINTS ON GLOBAL MANTLE CIRCULATION (IAPSEI, IAGA, IAVCEI, SED)

Location: Medical School Ext NG26 LT6

**Thursday 22 July PM**

Presiding Chair: John Woodhouse (Oxford University, UK)

**JSS13/W/02-A4** **Invited** **1400**

### MANTLE LAYERING WITHIN THE LOWER MANTLE

Stephen GRAND (Dept of Geological Sciences, University of Texas, Austin, TX 78712; steveg@maestro.geo.utexas.edu)

Recent tomographic images of the mantle clearly show that most slab enters the lower mantle below 700 km depth. Our most recent model of mantle shear wave speeds, based on the travel



times of multiply reflected S phases as well as ScS, SKS, and SKKS travel times, shows higher than average velocities beneath all subduction zones from 700 to about 1000 km depth. Above 700 km depth, high velocity anomalies are also seen but their volume is not large enough to account for the volume of slabs that have subducted during the last 40 Ma. We therefore conclude that the seismic anomalies seen from 700 to 1000 km depth are subducted slab remnants. Deeper than 1000 km, however, the pattern of fast anomalies is quite different. In the several subduction regions, for example beneath South America, Indonesia, the Kuriles, the Marianas, and Tonga-Kermadec, the high wave speed anomalies associated with subduction appear to terminate above about 1200 km depth. Other regions, particularly beneath Central and North America, Japan, and southern Eurasia show fast seismic velocities to much greater depths in the lower mantle, in some cases even reaching the core-mantle boundary. In these regions, however, the anomalies have their highest amplitudes and greatest widths in the range 1000 to 1500 km depth. In some cases there also appears to be a lateral offset of high wave speed anomalies above about 1300 km depth and below. Slow anomalies in the deepest mantle are very prominent beneath Southern Africa and the Cape Verde region. In both areas, however, the strong slow anomalies seen at depths below 1000 km or so, are not seen at shallower depths. An exception to this is beneath the East African Rift. The tomographic results seem to be most compatible with a barrier or impediment to flow at depths between 1000 and 1200 km depth. This is consistent with some other recent geophysical studies including the observation of a reflector near 1000 km depth beneath Indonesia by Kawakatsu and Niu (1994), a jump in viscosity near 1000 km depth inferred by Mitrovica and Forte (1997) and the study of the geoid and dynamic topography by Wen and Anderson (1998) who concluded that a barrier to flow is needed near 1000 km depth in order to fit both observables. The cause of such a boundary may be a chemical contrast or due to a phase change or viscosity change.

**JSS13/W/06-A4** Invited **1430**

#### GLOBAL TOMOGRAPHY IMAGES OF (PAST) SUBDUCTIONS AND UPWELLINGS

Harmen BIJWAARD and Wim Spakman (both at the Vening Meinesz School of Geodynamics, Institute of Earth Sciences, Utrecht University, Budapestlaan 4, 3584 CD, Utrecht, the Netherlands, email: bijwaard@geo.uu.nl)

Recent tomographic imaging of the Earth's mantle (Bijwaard et al., 1998) has provided detailed observations of (past) subduction zones as well as some prominent hotspot regions. This high-resolution tomography model was obtained through the application of nearly 8 million accurately processed P and pP phases and the implementation of an irregular model parameterization in which cell sizes were adapted to the amount of ray sampling. Observations in the upper mantle include thin zones of high P wavespeed associated with subduction. These 100-150 km thick anomalies generally continue into the transition zone where they may flatten on top of the upper-to-lower mantle discontinuity (660 km). Many of these anomalies (eventually) continue into the lower mantle as substantially thicker high velocity structures. In several instances, notably below the Aegean, the Sunda arc, South America, and Central America, these structures connect (at 1000-1300 km) with large-scale anomalies that have been associated with past subduction of the Tethys ocean and the Farallon plate. Below eastern Asia and Central America subduction-related anomalies seem to be continuing even further to the core-mantle boundary (CMB). Apart from subduction-related anomalies we find in several places deeply rooted low-velocity structures below prominent hotspots. Low velocities beneath the Africa rift, the Society Islands, Yellowstone, and Iceland can be traced to the lower mantle. Below Iceland estimates of the vertical resolution indicate that the observed structure is probably continuous from the CMB to the surface.

**JSS13/W/15-A4** **1500**

#### MANTLE CIRCULATION AS REVEALED FROM SEISMIC ANISOTROPY

Jean-Paul Montagner, Eleonore Stutzmann, Sebastien Chevrot (all in Dept. Seismology, Institut de Physique du Globe, 4 Place Jussieu, 75252 Paris cedex 05, France, email: jpm@ipgp.jussieu.fr), Goran Ekström (DEPS, Harvard University, Cambridge MA02138, USA), Lev Vinnik (IPE, Bolshaya Gruzinskaya 10, Moscow, Russia)

Whereas isotropic tomography only provides the location of seismic velocity heterogeneities, the anisotropic tomography is opening a new dimension by enabling to map the convective flow itself. So far, there are some good evidences of seismic anisotropy in the top 300km of the upper mantle and the bottom D"-layer, by using either the fundamental mode of surface waves or body waves. We present some new evidences of seismic anisotropy in the upper (410-660km) and lower (660-1000km) transition zones, obtained by different seismic waves. The normal mode dataset and converted P->S phases at 660km below the Grafenberg array and the GEOSCOPE station BNG, made it necessary the presence of seismic anisotropy on both sides of 660km discontinuity. Another way to get deep seismic anisotropy is to use overtones of surface waves. We will show how to map it by generalizing the technique developed by Stutzmann and Montagner.

All these investigations show that the presence of anisotropy is related to boundary layers and flow circulation in convective systems. In this framework, the transition zone turns out to be a secondary boundary layer in the mantle.

**JSS13/W/11-A4** **1520**

#### FINE DETAILS OF THE WADATI-BENIOFF ZONE UNDER INDONESIA: DIRECT EVIDENCE FOR MANTLE FLOW

H.-J. SCHOEFFEL and S. Das Department of Earth Sciences, University of Oxford, Parks Road, Oxford OX1 3PR, UK, email: hanns@earth.ox.ac.uk

The Indonesian subduction zone shows normal subduction under Java and Flores and very complex subduction beneath the Banda Sea. This region is the eastward extension of the Java subduction zone with an almost 180 degrees bend of the seismic zone, at depths down to 600km. Reliable hypocentral locations, especially depth, are essential to understanding this highly contorted zone and, thus, we use the procedure of Schoeffel and Das (1999) to achieve this. We use the JHD method, and handpicked arrival times for P, S, pP, sP, PcP and ScP phases from digitally recorded seismograms, together with agency reported times. Under Java and Flores, we find that (i) the portion of the arc between (110E-123E), and deeper than 500km, is dipping southwards at an angle of approximately 75 degrees, that is, in a direction opposite to the upper part of the north-dipping slab, (ii) east of about 108E, the seismic zone is wider near 670km than at 500km depth, with a thickness as wide as 100km below 600km. (i) suggests southward lateral flow in the mantle, relative to the plate motion vector here. P- and T-axes follow the general trend of down-dip orientation for deep and intermediate events, respectively. From the contortion of the seismic zone along the eastern portion of the Indonesian arc, we can estimate the average lateral shear strain rate in the 300-670km depth range to be of the order of 10e-16s, over the last 10-20 million years. Previous studies of the Banda arc show that it consists of 2 subducting plates. We suggest the plate underneath the Seram Trough subducts with a shallow angle to the SW down to 650km.

**JSS13/W/16-A4** **1540**

#### THREE-DIMENSIONAL MANTLE DENSITY STRUCTURE OBTAINED BY NORMAL MODE SPECTRAL MEASUREMENTS

Chaincy KUO and Barbara Romanowicz (both at UC Berkeley Seismological Laboratory and Department of Geology and Geophysics, University of California, Berkeley, California, 94720, USA, email: chaincy@seismo.berkeley.edu)

We present models of Vs, Vp, and density perturbations in the mantle, derived from spectra of the Earth's free oscillation spheroidal modes. Mantle heterogeneity from normal mode studies has been generally derived from "splitting coefficients", which represent an integration, over depth, of the lateral heterogeneity weighted in depth by the mode's sensitivity. The splitting coefficients, measured from individual mantle modes from observed spectra, are then inverted for mantle structure from this linear relationship. In contrast, we forego this intermediate stage of solving for splitting coefficients and invert directly for mantle structure from the spectral data for a sweep of mantle modes. In this manner, the inverse problem for structure becomes more constrained than the dual-stage inversion approach. Previous models determined from normal mode data were parameterized in terms of dln Vs, where aspherical structure in Vp and density were scaled to Vs structure, based on proportionality constants from studies by Li et al., 1991, for example. We demonstrate that this assumption is inadequate, and by preserving it, the final S-wave velocity model is contaminated by P-wave velocity and density structure. By setting the scaling relationships free, the model solutions resulting from independently and jointly inverting for dln Vs, dln Vp, and dln rho improves the correlation of S-wave velocity models with the existing Berkeley model derived from surface wave and body wave studies (SAW12D, Li and Romanowicz, 1996). We show that the Vp and density models elicited from these separate parameter inversions are valid.

In agreement with the study of Robertson and Woodhouse 1996, the Vs and Vp structure is found to correlate down to the mid-lower mantle, beyond which decorrelation of Vs and Vp dominates. Furthermore, in regard to the depths of correlation, the ratio of Vs to Vp root-mean-square amplitudes which we find are in concurrence with the determinations of the Robertson and Woodhouse 1996 paper. The density model is consistently robust, and presents high density features which coincide with the location of slabs in the upper mantle in the circum-Pacific region. A 3D mantle density model could provide a significant contribution to our understanding of mantle convection.

**JSS13/W/19-A4** **1620**

#### PKP PRECURSORS: FURTHER EVIDENCE FOR WIDESPREAD, WHOLE MANTLE CONVECTION

Michael A.H. HEDLIN and Peter M. Shearer (University of California, San Diego, La Jolla, CA, USA, 92093-0225, email: hedlin@ucsd.edu)

The recent global tomographic images of Grand, van der Hilst and their colleagues have revealed, with unprecedented clarity, large scale velocity variations in the mantle. In the mid-mantle, continuous, high-velocity trends are unmistakable and clearly correlate with known subduction zones such as the Tethys and Aegean trends in southern Eurasia and the Farallon trend in central America. These trends are believed to reveal subduction of slab material beneath the 660 km discontinuity into the mid-mantle. Beneath mid-mantle depths however the Eurasian trends become discontinuous and the question of whether the slabs remain intact and continue to subduct into the deepest mantle in these areas remains open for debate.

Precursors to the inner core phase PKP<sub>diff</sub>, which are due to scattering from velocity heterogeneity at the CMB and in the mantle, might provide further constraints on mantle convection. A recent analysis of GSN recordings by Hedlin et al. (1997) indicates the scattering that gives rise to the precursors occurs with equal strength at all mantle depths. Subsequent studies (Vidale & Hedlin, 1998; Hedlin et al., 1998) have used this model of global average scattering to identify regions that can be associated with anomalously strong or weak scattering. With ray-tracing it is possible to back-track precursors from the recording station into the mantle. Although vertical resolution is poor, it is possible to unambiguously associate early precursors recorded at all ranges, and all precursors that are recorded at ranges ranges < 137 deg. with scatteringbeneath the mid-mantle. Precursors are subject to ambiguity as to which end of the propagation path the scattering occurred but it is possible to limit this ambiguity with processing recordings that sample the same volumes of the Earth but by using dissimilar, i.e. crossing, paths. A global image of scattering strength which uses GSN recordings of precursors shows a possible correlation between mid-mantle velocity anomalies, such as the Aegean and Tethys trends, and unusually strong scattering beneath the mid-mantle. The precursors may be inferring indirectly the existence of these subductingtrends by detecting small fragments that are entrained with the slabs or the fragmentary remains of the slabs which are decimated by passage into the deepest mantle. Although this finding requires further study, this suggests that material from the Eurasian trends has subducted into the deepest mantle.

**JSS13/E/05-A4** **1640**

#### THE CAPABILITIES AND LIMITATIONS OF EXISTING NORMAL MODE CONSTRAINTS ON LONG-WAVELENGTH 3-D DENSITY STRUCTURE

Joseph Resovsky and Michael Ritzwoller (Department of Physics, University of Colorado, Boulder, Campus Box 390, Boulder, CO, 80301, email: resovsky@abdu.colorado.edu)

Descriptions of long-wavelength density heterogeneity are essential to modelling mantle dynamics, and new constraints on density provided by the latest catalogues of normal mode structure coefficients have been employed in several recent inversions for this structure. We demonstrate the capabilities and limitations of such inversions using set of more than 500 different inversions of normal mode data. First, we confirm the existence of a coherent signal from 3-D density structure and show that density models from normal mode inversions are robust with respect to the specification of other mantle structures. Second, we show that existing normal mode data do not yield density models that are robust with respect to the parameterization and damping of density heterogeneity. In particular, although normal modes clearly imply some decorrelation of shear velocity and density heterogeneity, the depth of such decorrelation is indeterminate. Finally, we demonstrate that this ambiguity may be reduced by applying emerging new normal model constraints on mantle structure and through using improved models of mantle discontinuity topography and 3-D velocity heterogeneity.

**JSS13/E/04-A4** **1700**

#### A TELESEISMIC SHEAR WAVE SPLITTING STUDY TO DETECT MANTLE FLOW AROUND SOUTH AMERICA THROUGH THE DRAKE PASSAGE

G. HELFFRICH (Earth Sciences, U. Bristol, Bristol, UK), D. Wiens (Earth & Planetary Sci., Washington U., St. Louis, MO USA) S. Barrientos, E. Vera (Dept. de Geofísica, U. Chile, Santiago, Chile)

Alvarez proposed the idea of mantle flow around South America to reconcile the demands of mantle mass conservation with the plate tectonically observed closing of the Pacific Ocean basin. Building on this notion, Russo and Silver (1994) studied South American shear wave

## INTER-ASSOCIATION

splitting and reported a pattern of fast polarization directions paralleling the western and northern coasts of South America. They interpreted the pattern as arising from anisotropy generated by olivine aligned by lateral flow. In this model, the flow is north-south around the buttress of the subducted lithospheric slab under South America's western coast, and east-west where the mantle material flows into the sub-Atlantic region around South America's cratonic roots through the Caribbean.

In the southerly reaches of South America's western subduction margin, the slab appears to be shorter and there are no cratonic roots. Thus, if mantle flow in fact occurs, it should flow under the Patagonian part of South America and through the Drake Passage. To test this prediction, in 1996-1998 we deployed broadband seismometers in Patagonia and Antarctica (the SEPA experiment) to look for the analogous pattern of shear wave splitting observed by Russo and Silver in northern South America. Preliminary results from stations around the Drake Passage/Scotia Plate yield splitting results typical of ~1 second continental splitting times except for PMSA, which is among the largest recorded (> 2 seconds). Drake Passage directions are mostly oblique to the E-W directions observed in Venezuela (Russo et al., 1996) and splitting times not as large (0.95 s average vs. 1.8 s). These observations suggest that a coherent, symmetric mantle flow structure is not present around South America like Alvarez envisaged, and that elimination of the shrinking volume of the sub-Pacific mantle must be achieved by a more diffuse circulation.

**JSS13/W/01-A4**

**1720**

### TOMOGRAPHIC IMAGES OF ANCIENT SUBDUCTED SLABS UNDER ASIA

Rob Van der Voo (Department of Geological Sciences, University of Michigan, Ann Arbor, MI, 48109-1063, U.S.A., email: voo@umich.edu); Wim Spakman and Harmen Bijwaard (both at Vening Meinesz School of Geodynamics, Institute of Earth Sciences, Utrecht University, Budapestlaan 4, 3584 CD Utrecht, the Netherlands, email: wims@geo.uu.nl)

The mantle under Siberia, the Indian subcontinent and the adjacent Indian Ocean reveals several zones of relatively high P-wave velocities at various depths, which can all be interpreted as remnants of subducted lithosphere ("slabs"). In the upper 600 km of the mantle under the Himalayas a slab appears to represent delaminated sub-continental mantle lithosphere that went down when Greater India continued to converge northward with Asia after about 45 Ma. High-velocity anomalies under Siberia occur at depths between 1500 km and the core-mantle boundary and are inferred to be remnants of Jurassic oceanic lithosphere, subducted when the Mongol-Okhotsk Ocean closed between Mongolia and Siberia by earliest Cretaceous time. This slab appears to join a "graveyard" (Wysesession, 1996) of slab remnants at the bottom of the mantle. Deep slabs under India and the Indian Ocean occur between 1000 and 2300 km and form three parallel WNW-ESE striking zones. We interpret these three zones as remnants of Paleo- and Neo-Tethys oceanic lithosphere, subducted between Late Jurassic and earliest Tertiary times, as southern Tibet, and later, India collided with Asia. Our interpretation implies (1) that most significant fast seismic anomalies in the lower mantle can be connected to past subduction, (2) that slab remnants in the mantle can still be recognized and interpreted some 150 million years or more after subduction ceased, and (3) that the mantle under Asia, which can be thought of as a growing "supercontinent", is characterized by dominant mantle downwelling.

**JSS13/C/ST2/W/25-A4**

**1740**

### REMNANT SLAB DYNAMICS FOLLOWING CONTINENTAL COLLISION

G.T. JARVIS (Department of Earth and Atmospheric Science, York University, Ontario, Canada M3J 1P3, email: jarvis@mantle.eats.yorku.ca) and J.P. Lowman (Institute of Geophysics and Planetary Physics, Los Alamos National Laboratory MS C305, Los Alamos, NM 87545, USA, email: lowman@lanl.gov)

A 2D numerical model of mantle convection, which incorporates rigidly moving surface plates, is used to study the effects of the accretion of a 2000 km wide block of continental crust, such as the Indian sub-continent, to the margin of a large stationary continent. This continental block is carried along with an oceanic plate towards a subduction zone at the leading edge of a much larger stationary continent, such as Asia. Prior to continental collision, subducted oceanic plate material under-rides the margin of the larger continent for several hundred kilometers before peeling away from the surface boundary layer and descending into the mantle as a cold narrow slab. Consequently, once the moving continental block arrives at the continental margin and closes over the original subduction zone the surface location of the continental suture lies several hundred kilometers away from the location of the cold remnant of the sinking slab. Convective flow in the subcontinental mantle adjusts to accommodate the change in mechanical boundary condition at the upper surface. We find that once the upper surface is immobilized, there may be a final pulse of vigorous subduction after which the continued descent of the cold slab is inhibited, and the cold remnant remains below the collision zone longer than expected based on 'normal' rates of subduction. Evolution of temperature and flow fields in the former subduction zone result in a relaxation of normal stresses at the upper surface and a consequent slow regional topographic uplift. Although the model is limited to two-dimensions, the observed time scales and orders of magnitude the observed variations are expected to be reasonably accurate.

**Friday 23 July AM**

Presiding Chair: Rob Van der Voo (University of Michigan, USA)

**JSS13/W/05-A5**

**Invited**

**0900**

### DYNAMICS OF CRETACEOUS VERTICAL MOTION OF AUSTRALIA AND THE ORIGIN OF THE AUSTRALIAN-ANTARCTIC DISCORDANCE

Michael GURNIS (Seismological Laboratory, California Institute of Technology, Pasadena, CA 91125 USA, email: gurnis@caltech.edu); Louis Moresi (Australian Geodynamics Cooperative Research Centre, CSIRO Exploration and Mining, Nedlands, WA 6009 Australia, e-mail: louis@ned.dem.csiro.au); R. Dietmar Mueller (Department of Geology and Geophysics, University of Sydney, Sydney, NSW 2006, Australia, e-mail: dietmar@es.su.oz.au)

We propose that the anomalous Cretaceous vertical motion of Australia and distinctive geochemistry and geophysics of the Australian-Antarctic Discordance (AAD) were caused by a subducted slab which migrated beneath the continent during the Cretaceous, stalled within the mantle transition zone, and is presently being drawn up by the South East Indian Ridge (SEIR). Using a three-dimensional model of mantle convection with imposed plate tectonics, we show that both the vertical motion of Australia and the distinct geochemistry and geophysics of the SEIR are related. The models start with slabs dipping toward the continent, but ~1,400 km from the present eastern margin. As Australia moves east in a hot-spot reference frame from 130-90 Ma, a broad dynamic topography depression of decreasing amplitude migrates west over the continent causing the continent to subside and then uplift. During this period most of the slab descends into the deeper mantle, but part of the cooler mantle becomes trapped within the transition zone above a viscosity jump and phase transition at 670 km depth. From 40 Ma to the present, wisps of this cool mantle are drawn up by the northward migrating ridge between Australia and Antarctica. This causes a circular dynamic topography depression to develop at the present position of the AAD. In addition, the

cool mantle leads to thinner oceanic crust. The method demonstrates the predictive power of mantle convection models when they incorporate plate tectonics.

**JSS13/W/17-A5**

**0930**

### LITHOSPHERIC STRESS FIELD AS A CONSTRAINT ON GLOBAL MANTLE CIRCULATION

Bernhard STEINBERGER and Harro Schmeling, (both at Inst. f. Meteorology and Geophysics, University Frankfurt, Feldbergstr. 47, 60323 Frankfurt, Germany, e-mail: steinber@geophysik.uni-frankfurt.de)

Lithospheric stresses have so far not been widely used as indicators of flow in the mantle beneath: it has been difficult to extract a large-scale stress field from stress measurements; the causes of lithospheric stresses have mostly been assumed inside the lithosphere; due to large uncertainties no good agreement between stresses predicted from mantle flow and observations could be achieved. The situation has however improved considerably during recent years: Seismic tomography can now give much better constraints on the driving forces of large-scale mantle flow, and an interpolated global stress map has been published.

Here we present a model of global mantle flow that gives a good agreement with an interpolated global stress distribution. The flow field is calculated with the method of Hager and O'Connell; driving forces are inferred from seismic tomography; for the surface boundary condition, the two limiting cases are a rigid lid, and the lithospheric plates moving freely in response to the forces acting on them. The model is similar to one that has been used to explain Africa's long-wavelength topography as dynamic topography, i.e. supported by internal flow. The agreement between predicted and observed stresses is particularly good in regions where lithospheric stresses and mantle tomography are well constrained (e.g. North America, Europe, East Asia). Our results clearly show that there is a long-wavelength lithospheric stress field that is due to flow in the underlying mantle. Except in regions of large continental topography (especially around Tibet) mantle flow is the dominant cause of this long-wavelength stress field. To further support our model we consider the distribution of hotspots and intraplate earthquakes: our model shows that most hotspots are located in regions of extensional stress and no hotspots are in regions of strong compression. A likely explanation for this observed distribution is that deep mantle plumes may not be able to penetrate a lithosphere that is strongly under compression. Our model also predicts high lithospheric shear stresses mostly in regions where the hazard due to intraplate earthquakes is considered high. We anticipate that it will be possible to use the large-scale stress field as a constraint to mantle flow. As a practical application, a model of mantle flow and induced lithospheric stresses will be able to better assess earthquake risk in intraplate settings.

**JSS13/W/09-A5**

**0950**

### THE HEAT FLOW CONSTRAINT ON RADIAL MIXING IN NUMERICAL MODELS OF MANTLE EVOLUTION

S. L. Butler and W. R. Peltier (both at Department of Physics, University of Toronto, Toronto, Canada, M5S 1A5, email: sam@atmosph.physics.utoronto.ca, peltier@atmosph.physics.utoronto.ca)

We demonstrate that when CMB temperature is fixed by the results of high pressure experiments in a spherical axisymmetric model of the thermal convection process then the total surface heat flow is considerably greater than that which is observed if the mantle rheology is Newtonian. In these analyses the radial variation of mantle viscosity is taken to be fixed by formal inversion of the constraints of glacial isostatic adjustment. The convection model then reconciles the observed heat flow if the degree of layering induced by the 660 km endothermic phase transition in our model is sufficiently strong. We present a suite of numerical simulations in which we characterize the effects of layered convection on surface heat flow. In particular, we determine that in order for the surface heat flow in our model to match that of the real Earth, the radial mass flux transiting the 660 km depth horizon must be only slightly greater than the extremely small values for this quantity that have been inferred on the basis of geochemical observations. The magnitude of the Clapeyron slope of the endothermic phase transition that is required to induce such strong layering is somewhat greater than high pressure experiments would suggest. We further demonstrate, however, that a decrease in viscosity in the region of the phase transition of the type that one would expect due to transformational superplasticity can significantly increase the ability of a phase transition to induce a layered style of flow. The strong layering required to reconcile the surface heat flow may then be compatible with the Clapeyron slope of the endothermic phase transition based on high pressure experiments.

**JSS13/W/14-A5**

**1010**

### MANTLE CIRCULATION MODELS AND TRUE POLAR WANDER

GREFF-LEFFTZ Marianne (Institut de Physique du Globe de Paris, Geomagnetism Department, 4 place Jussieu, 75252 Paris cedex 05, France) Bunge Hans-Peter (Department of Geosciences, Guyot Hall, Princeton University, Princeton, NJ 08544, United States)

Relative motion between hotspot and paleomagnetic reference frames is called true polar wander, to distinguish it from apparent polar wander, which is related to continental drift. Few studies have tried to link paleomagnetic constraints to a reference frame tied to vigorous mantle convection. Here we use a 3D spherical mantle circulation model to study the sensitivity and general character of true polar wander events during the past 100 million years, testing their dependence on a high viscosity lower mantle, the amount of core heat flux excavated by mantle plumes, or the buoyancy effects of mantle phase changes in the upper/lower mantle transition zone. The degree two geoid and the inertia tensor perturbations associated with these mantle density heterogeneities are computed and the Euler equations for conservation of angular momentum subject to the visco-elastic adjustment of the rotational bulge are solved at each time step. We find that the reorientation of Pacific plate motion from its formerly northward to a northwestward trend at 43 Ma, which initiated a system of new subduction zones in the western Pacific, produces a marked shift in the direction of predicted true polar wander at about 30 Ma, if the anomalous buoyancy effects from an endothermic phase change at 670 km depth are excluded. Otherwise, no cusp is produced, due to the dynamic compensation of newly subducted slabs in the transition zone. We also find that increasing the plume flux reduces the amount and rate of true polar wander, resulting in greater overall stability. These results indicate the potential of using mantle circulation models and observations from paleomagnetic and geochronological data to constrain the dynamic cause of true polar wander.

**JSS13/W/10-A5**

**Invited**

**1000**

### THE TECTONIC RECORD IN THE DEEP MANTLE

CAROLINA LITHGOW-BERTELLONI (Department of Geological Sciences, University of Michigan, Ann Arbor, MI 48019, USA, Email: crlb@umich.edu)

An important goal of the solid Earth sciences must be to understand how processes in the Earth's deep interior might be reflected in the surface geological record. Global tectonic



reconstructions used in connection with mantle flow models and the most recent images of the mantle from seismic tomography have allowed us to connect the tectonic record with structures in the deep mantle [e.g. Richards & Engebretson, 1992; Lithgow-Bertelloni & Richards, 1998; Bunge et al., 1998; Voo et al., 1998]. Moreover, simple dynamical flow models based on subduction over the last 200 Myr have successfully explained a variety of observations: the geoid [Ricard et al., 1993], present and past plate motions [Lithgow-Bertelloni & Richards, 1998], the Cenozoic true polar wander record [Richards et al., 1997], and continental flooding history [Lithgow-Bertelloni & Gurnis, 1997]. I will present a summary of the efforts to model global mantle circulation and related dynamical processes using the past 200 Myr of tectonics. I will also compare in detail to existing seismic tomographic models in an effort to interpret the observed seismic heterogeneity in relation to the tectonic record. I will examine the implications for global mantle circulation and address the question of whether dynamical barriers to flow are required by the observations, and therefore if the observed seismic heterogeneity is thermal or chemical in origin. Finally, I will show how the existing high-resolution tomographic models can provide important constraints to tectonic reconstructions when coupled with simple models of subduction history and mantle flow. I will look in particular at the evidence for changes in subduction polarity and cessation of subduction of the Phoenix plate under South America in the Mesozoic and whether the current tectonic reconstructions can be reconciled with the gaps in fast seismic heterogeneity seen in the tomography.

JSS13/W/03-A5

1130

## ABOUT THE SURVIVAL OF VISCOUS BLOBS IN THE MANTLE

Nicolas MERVEILLEUX DU VIGNAUX and Luce Fleitout (both at Laboratoire de Géologie de l'ENS, 24 rue Lhomond, 75005 Paris, France, email: nmerveil@jadeite.ens.fr)

The survival of blobs more viscous than the surrounding mantle is an important issue: the degassed harzburgite might be more viscous than the primordial mantle and this may affect its properties as a geochemical reservoir and also its gravitational segregation. It has been shown (Spence et al., *Geophys. J.*, 1988) that the deformation of a viscous blob is in first approximation proportional to its aspect ratio divided by its relative viscosity. Once submitted to a large strain, all blobs may have acquired a large aspect ratio so become easily deformed and mixed.

We study in a time-dependent laminar convective regime the deformation of blobs as functions of their viscosity and aspect ratios. The deformation is measured by small markers within the blobs. The deformation of the blobs is indeed inversely proportional to its relative viscosity but the aspect ratio has a moderate impact. The elongated blobs tend to buckle so that their effective aspect ratio becomes of the order of 1, or they separate in blobs of aspect ratio close to 1 rather than forming very elongated blobs. These results are analyzed with the help of numerical experiments where the blobs are submitted to pure and simple shears.

JSS13/W/13-A5

1150

## AN ULTRAFast PLUME UNDER GREENLAND?

Tine B. LARSEN (National Survey and Cadastre, Geodynamics Dept., Rentemestervej 8, DK-2400 Copenhagen NV, Denmark, e-mail: tl@kms.dk), David A. Yuen (Dept. of Geology and Geophysics and Minnesota Supercomputer Inst., 1200 Washington Ave. S, Minneapolis, MN 55415, USA, e-mail: davey@krissy.msi.umn.edu), and Michael Storey (Danish Lithosphere Centre, Øster Voldgade 10, DK-1350 Copenhagen K, Denmark, e-mail: ms@dlc.ku.dk)

Recent geochemical and geochronological data from the N. Atlantic region have placed strong constraints that copious amounts of hot magmatic material have been transported to the surface on a timescale of a few million years or less. A small, fast moving plume appears to be a more viable mechanism from these new observational findings than the traditional idea of a giant plume head with a diameter equal to or larger than the thickness of the entire upper mantle. In order to reconcile the idea of an ultrafast plume with the observed plate velocities, a physical mechanism is needed for inducing a separation of timescales between the plume speed and the surrounding mantle circulation. Thermal convection with a non-Newtonian temperature- and depth-dependent rheology has been found to provide such a mechanism wherein extremely fast plumes ascending at velocities between one to tens of meters per year can be produced in an otherwise slowly convecting mantle at cm/yr. This transport mechanism is capable of bringing up very hot matter from the transition zone to the lithosphere, where considerable melting would take place. Basalts of nearly the same age have been found in West Greenland, East Greenland, the Faeroe Islands and Scotland. It is thus possible to explain these semi-contemporaneous igneous events by a fast moving mantle plume spreading out below, upon surficial impact, with a horizontal velocity of around 0.5 m/yr. We discuss also the relationship of the upper-mantle plume under Iceland to the recent findings by seismic tomography of a deep mantle plume under Iceland and the presence of an ultra-low velocity zone at the very base of the mantle.

JSS13/E/01-A5

1210

## THREE DIMENSIONAL SPHERICAL EFFECT OF THE CIRCUM-PACIFIC LITHOSPHERE SUBDUCTION ON THE LARGE-SCALE MANTLE PLUME ACTIVITY

Takao EGUCHI (National Research Institute for Earth Science and Disaster Prevention, 3-1, Ten-nodai, Tsukuba, Ibaraki 305-0006, JAPAN, email: eguchi@geo.bosai.go.jp)

To make clear the basic and fundamental nature of mantle convection dynamics including unsteady large-scale plume activity, we must carry out numerical simulation with various initial and boundary conditions as well as constraints for rheology parameters such as viscosity and temperature, etc. Recently, Eguchi (1994) proposed a concept of "Jcool mantle doughnut" (CMD) with the great circle dimension surrounding the Pacific ocean, inferred from recent studies of the global seismic tomography and plate subduction history, etc. The CMD may involve the zone of major energy dissipation associated not only with the plate convergence but also with the global mantle downgoing flow.

To investigate unsteady recent mantle dynamics possibly influenced by the CMD, we developed a new code for 3-D numerical simulations of the spherical mantle convection. The basic three equations are for the continuity, the motion with the Boussinesq (incompressible) approximation, and the (thermal) energy conservation. The simulation code developed newly incorporates the spherical mantle layer with the temperature-dependent viscosity, etc. Our program is based on the finite difference method (Newton method) with the control volume technique. During the calculation, as for one of the initial condition, we inserted the relatively lower temperature material throughout at the equatorial zone, in addition to the horizontally uniform thermal field. We start the calculation with the zero initial velocity and displacement within the mantle layer. Thus, in our model, the equatorial zone is the centroid of the lithosphere downgoing and successive large-scale downwelling flow. The result shows that large-scale upwelling flows are exited at the latitude of 30-40 deg., after a certain period, as a response of the equatorial lithosphere subduction. North-south wider zone of equatorial subduction can shift the upwelling sites to the higher latitude to some extent. Our simulation result, however, constrains that the sites of the large-scale upwelling cannot reach the North and South poles.

JSS13/E/06-A5

1400

## MANTLE CONVECTION AND THE GENERATION OF THE PRINCIPAL GEOCHEMICAL RESERVOIRS

Uwe WALZER and Roland Hendel (both at Institut f. Geowissenschaften, Universitaet Jena, Burgweg 11, 07749 Jena, Germany, email: walzer@geo.uni-jena.de)

We investigate the evolution of the principal geochemical reservoirs of the mantle, the oceanic plateaus, the continents etc using new 2D-FD Oberbeck-Boussinesq convection models plus a fractionation mechanism. In one model a constant core-to-mantle heat flow is assumed, in the other model the CMB temperature is assumed to be constant. The fractionation generates the chemical diversity and an inhomogeneous mantle heat-source distribution, whereas the solid-state convection works toward homogenization. The deformation of the 410- and 660-km mineral phase change interfaces produces additional positive and negative buoyancy forces. A minor planar heat source at CMB creates the D" layer and thermal plumes. The pressure- and temperature-dependence of the viscosity is an essential feature of the models. Segregation takes place if the asthenospheric viscosity falls below a certain threshold. Oceanic plateaus, enriched in incompatible elements, develop leaving behind depleted parts of the mantle. A laterally moving continent grows by the accretion of oceanic plateaus. For the Phanerozoic we arrive at a mainly depleted upper half of the mantle and a predominantly pristine lower half of the mantle.

JSS13/W/18-A5

1420

## WHOLE MANTLE CONVECTION AND GEOCHEMICAL RESERVOIRS

Nicolas Coltice, Yanick Ricard and Philippe Gillet (Laboratoire de Sciences de la Terre; Ecole Normale Supérieure de Lyon; 46, allée d'Italie; 69364 Lyon cedex 07)

A wide range of geophysical observations suggests that slabs sink into the deep mantle. The injection of crustal and depleted material is of fundamental importance in understanding geochemical signature of oceanic basalts. In this study, we try to interpret the geochemical data (He, Sr and Pb) with a whole-mantle convection point of view. To propose a model of geochemical evolution of the mantle, we (a) try to understand the physical relationship between geochemical box models and fluid dynamic models in terms of mixing, (b) use geophysical observations and perform geochemical mass balance and geodynamical calculations to constrain mantle reservoirs and the fluxes between them. Using an inversion of a geochemical box model, we show that the geochemical features of hotspots can be related to recycled material, a mixture of oceanic crust and a high <sup>3</sup>He/<sup>4</sup>He component: ancient lithospheric mantle.

JSS13/W/08-A5

1440

## HELIUM ISOTOPE RATIO IN OCEANIC ISLAND BASALT: ITS ORIGIN AND CONSTRAINT ON MANTLE CIRCULATION

Yang WANG (Lab. for Geothermics, Institute of Geology, Chinese Academy of Sciences, P.O.Box 9825, Beijing 100029, China, email: thalassa@263.net)

The helium isotope ratio (<sup>3</sup>He/<sup>4</sup>He) in mid ocean ridge basalt (MORB) is ~8 RA (atmospheric <sup>3</sup>He/<sup>4</sup>He ratio); but <sup>3</sup>He/<sup>4</sup>He ratio in oceanic island basalt (OIB) exhibits geographic diversity, it is ~5-6 RA in the OIB which are mainly located in southern hemisphere, and ~10-35 RA in the OIB (i.e. Hawaiian, Loihi and Iceland) of northern hemisphere. This feature was previously explained by two layer steady state mantle model which requires a volatile degassed upper mantle, and a more volatile and high viscosity lower mantle. Nowadays, high resolution seismic tomography indicates the lithospheric plate penetrate the 670 km discontinuity, this should destroy the primitive isotopic composition of helium in the lower mantle. Numerical experiments on mantle convection by van Keken and Ballentine (1998) suggest that, <sup>3</sup>He/<sup>4</sup>He ratio remains relative homogeneous through the entire mantle over 4.6 Ga evolution, furthermore, degassing is more rapid in the case of high viscosity lower mantle. We consider a new model to explain the characters of <sup>3</sup>He/<sup>4</sup>He ratio in OIB. It is well known that the OIB of southern hemisphere has a lithophile-rich source which is the mixture of oceanic mantle and subducted continental material from Gondwanaland. Enriched U, Th in this source will produce more radiogenic <sup>4</sup>He than normal oceanic mantle after ~300 Ma (the time since the break-up of Gondwanaland), and result in low <sup>3</sup>He/<sup>4</sup>He ratio in southern OIB. The high <sup>3</sup>He/<sup>4</sup>He ratio of the OIB in northern hemisphere needs a source in which uranium and thorium is much depleted than normal oceanic mantle; and the ancient subducted oceanic lithosphere, which lose U and Th during subduction, is a possible candidate. After long period (e.g. 1-2 Ga), the source will have much less radiogenic <sup>4</sup>He and high <sup>3</sup>He/<sup>4</sup>He ratio. The calculation of van Keken and Ballentine (1998) also indicated that preservation time of chemical heterogeneity in mantle is 1-2 Ga. The geographic diversity in <sup>3</sup>He/<sup>4</sup>He ratio of OIB should be due to spherical harmonic degree l=2 pattern of mantle convection, which has hemispheric scale dimension. D.L. Anderson (1998) points out that the hotspots correspond to spherical harmonic degree l=6 pattern of convection, which means convection cell is of 6000 km dimension and its lower boundary is 670 discontinuity. Integrated his viewpoint and isotopic characters of He, Nd, Sr and Pb, we deduce that OIB in southern hemisphere is originated from the source stored in 670 discontinuity, and OIB in northern hemisphere from lower mantle; then the dominant circulation patterns in northern and southern hemisphere is very different.

JSS13/E/03-A5

1500

## HELIUM ISOTOPE CONSTRAINTS ON THE STRUCTURE AND EVOLUTION OF THE ICELANDIC MANTLE PLUME

HILTON, D.R., Scripps Inst. Oceanography, La Jolla, CA 92093 USA (email: dhilton@ucsd.edu) Gronvold, K., Nordic Volcanological Inst., Reykjavik, Iceland Macpherson, C.G., Royal Holloway, Univ. London, Egham, Surrey, UK

High and variable <sup>3</sup>He/<sup>4</sup>He ratios (> MORB He) throughout Iceland point to both a deep-seated origin of the Icelandic mantle plume - consistent with recent seismic studies which place its origin in the lower mantle or at the core-mantle boundary (Wolfe et al., 1997; Helmerger et al., 1998; Shen et al., 1998) - and to a complex history of mantle mixing and/or crustal interaction. To elucidate further details of the structure and evolution of the plume, we report new helium isotope data from two key areas in Iceland: (a) Vestfirðir, the oldest region of the Icelandic crust (~15 Myr) and the location of the highest geothermal <sup>3</sup>He/<sup>4</sup>He ratios observed to date (30RA; Hilton et al., 1998), and (b) Central Iceland, at the juncture of the western and northern rift zones and the hypothesised center of the Icelandic plume. Vestfirðir phenocrysts have <sup>3</sup>He/<sup>4</sup>He ratios up to 37RA - the highest ratio ever reported for Iceland. Central Iceland basalts have values up to 33RA and show a sharp discontinuity with lavas erupted ~100 km into the northern rift zone which have <sup>3</sup>He/<sup>4</sup>He ratios equal to MORB (~8RA). The new results, when combined with earlier studies (e.g. Polak et al., 1976; Condomines et al., 1983; Kurz et al., 1985; Hilton et al., 1990; Poreda et al., 1992), allow a detailed picture to be constructed of helium isotope variations throughout Iceland. This



## INTER-ASSOCIATION

distribution will be discussed in terms of the past and present-day history of impingement of the plume against the Icelandic crust, and the nature and spatial variability of mantle sources contributing to Icelandic volcanism.

**JSS13/W/12-A5**

**1520**

### **BUFFERING THE DEPLETED MANTLE WITH CRUST: AN INTERPRETATION FROM THE TRACE ELEMENT AND ND-HF- PB ISOTOPIC COMPOSITION OF MORB**

A.D. SMITH (Dept. Earth Sciences, Cheng Kung University, Taiwan;  
email: mochinn@mail.ncku.edu.tw)

The rate of isotopic evolution of the mantle of 2.2 epsilon Nd units per Ga through the Phanerozoic and Proterozoic and the shape of the modern MORB Nd-Hf isotopic array can be reproduced by subducted basaltic crust and sediment comprising 5-6% and 0.1-0.5%, respectively, by volume of the depleted mantle. Basalt and pelagic sediment generates the high 176Hf/177Hf-low 143Nd/144Nd part of the MORB array while basalt and turbidite generates the low 176Hf/177Hf-high 143Nd/144Nd signatures. In contrast, the rate of isotopic evolution of the Early Archean mantle as deduced from alumina-depleted komatiites corresponds to a scenario in which there is only limited crustal recycling into the depleted mantle, and is consistent with models for a voluminous early crust ~8% greater in volume than today. Depleted mantle Pb isotopic ratios are not correlated with Hf isotopes because of modifications to the U/Pb ratio on seafloor alteration and removal of these elements into the mantle wedge at subduction zones. However, variations in the efficiency of these mechanisms allows the buffering process to account for both the elongation of the MORB field toward HIMU and its tilt toward EM2 in Pb-Pb diagrams. The common argument that Ce/Pb-Nb/U ratios in MORB precludes buffering of the depleted mantle by crust is valid only for modern slab dehydration regimes. Melting of an ancient primitive mantle reservoir generates a depleted residue with higher Nb/U than the modern MORB-source. Remixing crust into this very-depleted reservoir produces the trend from high Nb/U-low Ce/Pb to low Nb/U-high Ce/Pb seen in MORB as tectonic regimes change from slab-melting to slab-dehydration regimes, with the greater retention of Pb in the slab under the former conditions accounting for elevated 207,208Pb/204Pb signatures in Precambrian mantle-derived rocks.

**JSS13/E/02-A5**

**1610**

### **EVIDENCE FOR A SMALL, GEOCHEMICALLY DISTINCT BODY IN THE MID-LOWER MANTLE**

SATOSHI KANESHIMA (Department of Earth and Planetary Sciences, Tokyo Institute of Technology, Meguro-ku, Oookayama, Tokyo 152, JAPAN, Email: kane@geo.titech.ac.jp) and George Helffrich (Geology Department, University of Bristol, Queens Road, Bristol UK, Email: george@geology.bristol.ac.uk)

We report observations which clearly show the presence of small-scale, geochemically distinct bodies in the mid-lower mantle. Our analyses of array data from western United States short period seismic networks detect S-to-P converted waves at a thin low seismic velocity sheet (with a velocity decrease from the surrounding mantle larger than 4%, and nearly 8 km thick) in the mid-lower mantle (1400 to 1600 km depth) east of the Mariana and Izu-Bonin subduction zones. The low velocity sheet dips nearly 40 degrees southward and is at least 500 km by 300 km. Its steep dip clearly rejects an origin as a pressure-driven phase transition, and its intensity and sharpness further imply a chemical rather than a purely thermal origin. Ancient oceanic crust subducted into the lower mantle would be the most plausible candidate for the low velocity sheet given its broad, thin extent. Previous seismic tomography studies do not predict significant velocity anomalies there. Plate reconstructions suggest the Indonesia slab may have been located above the site at 160 to 170 Ma. Laboratory estimates of thermoelastic properties currently available do not predict seismic velocity anomalies as large as the observation, but large uncertainties of shear velocity do not permit conclusive arguments. Undistorted sheets imply minor resistance to lower mantle slab penetration and may provide long-term geochemical reservoirs whose mixing into the mantle is not effective.

**JSS13/W/04-A5**

**1630**

### **GEOYNAMICAL IMPLICATIONS OF THE HETEROGENEOUS ELECTRICAL CONDUCTIVITY STRUCTURE OF THE MID-MANTLE**

Pascal TARITS (UBO/IUEM, UMR CNRS 'Domaines Oceaniques' Place Nicolas Copernic, Brest F-29280, France, E-mail: tarits@univ-brest.fr, Mioara Alexandrescu (IPGP, Observatoire Magnétique de Chambon La Foret, Beaune la Rolande F-45340, France, E-mail: mioara@ipgg.jussieu.fr)

In this study monthly mean values of the geomagnetic field from about 100 observatories have been analyzed. We selected time windows of 30-35 years which was appropriate for most of the available observatory data. The main field and the secular variation was removed using the model provided by Bloxham and Jackson (1992). A robust simultaneous spectral analysis in the time domain and in the spatial domain was carried out on the 3 components X, Y and Z at each observatory to obtain the internal and external magnetic potential coefficients. The transfer function between the internal and the external spectral components of the field was calculated robustly for periods between 2 months and 1 year. 3D conductivity models of the Earth were obtained from the non-linear minimisation of a penalty function between the data and the theoretical response of the model. The earth was parameterised with an homogeneous upper mantle down to 400 km and two heterogeneous layers each 250 km thick. Below these layers the Earth is assumed homogeneous. The heterogeneous conductivity is given on a grid 10 (north-south) by 20 (east-west) corresponding roughly to maximum wave numbers l=6-8. We compare the geodynamical implication of the models to other geophysical data.

**JSS13/W/07-A5**

**1650**

### **MAGNETIC FABRICS OF TROODOS OPHIOLITE REVEAL LOCALIZED FLOW PATTERNS**

Dr Graham Borradaile, Lakehead University, email: borradaile@lakeheadu.ca

Harzburgites exposed in the Troodos complex of Cyprus provide clear magnetic fabric patterns both from anisotropy of low field susceptibility (AMS) and anisotropy of anhysteretic remanence (AARM). AARM isolates the orientation distribution of ferromagnetic accessory minerals whereas AMS combines this with the contribution from paramagnetic mafic silicates. The two subfabrics differ somewhat due to differing ages of crystallization in noncoaxial flow. The magnetic fabrics define spatially varying flow patterns that indicate a general sense of regional tectonic flow. This helps to position the exposed rocks with respect to the spreading axis, a result that would be difficult to achieve by conventional petrofabrics, or other means.

**JSS13/L/01-A5**

**1710**

### **TOMOGRAPHIC CONSTRAINTS ON PAST PLATE MOTION MODELS**

H.-P. BUNGE (Dept of Geosciences, Princeton University, Princeton NJ 08544,  
email: bunge@geo.princeton.edu)

General circulation models are a flexible tool to probe mantle flow. In one of their most important applications they relate geologically derived past plate motion models explicitly to high resolution seismic mantle maps. Here we explore the approach using the 3D spherical TERRA mantle convection code. Allowing for more than 100 million grid points throughout the mantle, sufficient to fully resolve the lithosphere, we probe the circulation of the mantle to test both geodynamic and plate motion hypotheses with tomographic data. Our circulation experiments are highly successful in explaining a number of prominent seismic velocity anomalies in the deep mantle, especially those related to past subduction. They also confirm a simple whole mantle convection style with a substantial viscosity increase between the upper and lower mantle and little resistance from the endothermic phase transition. A significant amount of core heating is needed to explain anomalously slow mantle imaged under Africa and the Pacific. Importantly, we find that the most persistent discrepancy between geodynamic and seismic mantle models is entirely due to systematic errors in the current mesozoic and cenozoic plate motion input models suggesting to improve these models by using information from seismic tomography. We highlight the potential utility of the tomographic data by taking the late mesozoic subduction history of the western United States as an example. Allowing for a geologically inferred episode of low-angle subduction during the laramide, which uplifted much of the eastern front of the rocky mountains, we find a spectacular correlation between geodynamic and seismic images of the Farallon slab can be obtained. We also note that geodynamic mantle models must be evaluated by applying the same tomographic filtering that biases current seismic mantle models. By tracing seismic rays through our models, we critically reevaluate the common assumption of zero mean and Gaussian distributions in travel-time residuals.

**JSG14**

**Wednesday 21 July**

### **INSIGHTS INTO EARTH SYSTEM SCIENCE: VARIATIONS IN THE EARTH'S ROTATION AND ITS GRAVITATIONAL FIELD (IAG, IAPSO, IAMAS, IASPEI, IAGA, IAHS)**

Location: Poynting Pyshics  
Location of Posters: Old Gym

**Wednesday 21 July AM**

Presiding Chairs: J.O. Dickey, JPL/Caltech, Pasadena  
C.R. Wilson, NASA/HQ, USA

**JSG14/L/07-A3**

**0830**

### **EARTH ROTATION MONITORING: STATUS AND PROSPECTS**

Christoph REIGBER (GeoForschungsZentrum Potsdam, Div. Kinematics and Dynamics of the Earth, Telegrafenberg A 17, D-14473 Potsdam, Germany, e-mail: reigber@gfz-potsdam.de)

Rotation is the major feature of our planet's motion and its precise knowledge is required for various navigational, global geodetic and astronomical tasks. Irregularities in both the rotation rate and the position of the rotation axis in space are manifestations of changing mass redistributions within, on and outside of the planet and of torques acting on it. Their precise knowledge provide a unique and global measure of changes taking place in the various spheres of the Earth system.

International cooperative efforts for observing the Earth rotation date back almost exactly a century and have culminated in the space geodetic observation programs of the International Earth Rotation Service (IERS) which include satellite (SLR, LLR, GPS, DORIS) and radioastronomy (VLBI) based techniques. Analyses of the observations provide nowadays a monitoring of the Earth orientation and realizations of the terrestrial reference frame at the "0.3 mas accuracy level, corresponding to 1 cm on the Earth surface. This level of accuracy is continuously improving thanks to advances in technology, more robust tracking networks and improved data reduction and analysis techniques. The precise terrestrial reference frame sets the framework for regional networks being established for e.g. deformation monitoring, water vapor mapping and surveying tasks. The improved accuracy and temporal resolution of the Earth's rotation parameters is triggering investigations of their subdiurnal to multi-year variability caused by geophysical processes taking place in the Earth system components. In order to support such practical applications and frontier research activities best, the IERS is presently adjusting its structure and functions to the user needs. One of the major challenges for the future will be to realize within an integrated global geodetic monitoring system highly accurate, consistent, long-term Earth rotation series with very high temporal resolution. The presentation will describe the present status in monitoring the Earth rotation and is trying an outlook into near future developments and needs.

**JSG14/E/12-A3**

**0900**

### **ASSESSING THE PLANETARY ANGULAR MOMENTUM BUDGET WITH ATMOSPHERIC UPPER AIR AND OCEAN MODEL DATA**

DAVID A. SALSTEIN, Rui M. Ponte, Richard D. Rosen (Atmospheric and Environmental Research, Inc., 840 Memorial Dr., Cambridge, MA 02139, USA, email: salstein@aer.com) Detlef Stammer (Massachusetts Institute of Technology, Department of Earth, Atmospheric and Planetary Sciences, Cambridge, MA 02139, USA)

Atmospheric and oceanic information are used in combination with Earth rotation parameters to assess the angular momentum budget of the planet about the axis of rotation, on a variety of timescales. For the atmospheric data the 50-year long NCEP/NCAR reanalysis products capture variability at levels as high as 10 hPa. In addition, separate data sets of the stratosphere include comprehensive calculations on levels as high as 0.3 - 1 hPa. Because stratospheric winds vary strongly at semiannual, annual, and quasi-biennial timescales, incorporating these data is particularly important. We assess the regions within the atmosphere that have the strongest variations on intraseasonal, seasonal, and interannual timescales. In the last case, El Niño events are clearly related to the strength of the zonal circulation in the atmosphere. Available estimates of oceanic axial angular momentum, calculated from model-derived zonal current and mass fields, are also used to assess the role of the ocean in explaining some of the discrepancies still present in the solid Earth and atmosphere's combined angular momentum budget. In considering excitations for polar motion in the equatorial plane, atmospheric and oceanic effects can approach similar magnitudes on a number of timescales. Within the atmosphere, the mass field, related to surface pressure, is the agent that most

excites polar motion on subseasonal scales. We discuss the extent to which a closed budget is achieved within the estimated uncertainties in all momentum quantities, as a function of timescale.

JSG14/L/08-A3

0930

## INFLUENCE OF CORE DYNAMICS ON THE ROTATION OF THE EARTH

Gauthier HULOT (Institut de Physique du Globe de Paris, 4 Place Jussieu, 75252 Paris Cedex 05, France, email: gh@ipgg.jussieu.fr)

The visco-elastic body rotation of the Earth's mantle, usually referred to as the "Earth's rotation", is well known to display variations. These variations occur as a result of some mechanical forcing acting on the mantle and produced by both external interactions (Luni-Solar tidal forces) and internal interactions (with the fluid envelopes and the core). This forcing produces changes within the angular momentum of the mantle, which results in the observed changes within both the rate of rotation (Length of Day, LOD) and the position of the rotation axis. The present review will focus on the specific influence of core dynamics, thought to play a dominant role in modifying the Earth's rotation on decade time scales. We will briefly recall the two approaches currently used for studying this influence. One consists in inferring the core angular momentum (AM) from magnetic observations, assuming conservation of core+mantle AM and checking that variations within the Earth's rotation are correctly predicted. The other consists in searching for core-mantle coupling mechanisms that can produce such variations. We will then first focus on the LOD variations and present a set of results obtained by various teams. It will be shown that the AM approach clearly leads to the conclusion that core dynamics is responsible for the decade variations within the LOD. Results obtained through the second approach are not as clear cut, and arguments in favor or against each type of coupling (electromagnetic, topographic, or gravitational) will be discussed, together with the possible role of the inner core. We will next turn to the possible influence of core dynamics on the position of the rotation axis. This subject has received much less attention up to now. This is likely due to the combined facts that the dynamics of the core (under strong influence of the Coriolis forces) does not permit an easy approach of the problem in terms of AM conservation, and that the variation of the position of the rotation axis (usually determined in terms of the position of the pole of rotation within the mantle frame of reference) is not very well constrained on decade time scales. It will however be argued that core dynamics can also produce variations that are nearly compatible with the available observational constraints. Finally, the possible influence of core dynamics occurring on time scales less than one year (as testified by the occurrence of so-called geomagnetic jerks) will be briefly discussed.

JSG14/L/09-A3

1000

## NUTATIONS: OBSERVATIONS, THEORETICAL MODELING, AND IMPLICATIONS

P. M. Mathews, (Department of Theoretical Physics, University of Madras, Chennai 600025, India) email: mathews@imsc.ernet.in T. A. Herring, (Department of Earth, Planetary and Atmospheric Sciences, M.I.T., Cambridge, MA, U.S.A.), B. A. Buffett (Department of Geophysics and Astronomy, University of British Columbia, Vancouver, B.C., Canada)

The VLBI data available now permit estimation of the amplitudes of a large set of nutation terms with a formal precision much better than 10 except for a few terms. Recent advances in theory enable these estimates to be closely matched by model predictions. Apart from an excess (nonhydrostatic) flattening of the core mantle boundary (CMB), inferred earlier from nutation data, and the effects of mantle anelasticity and ocean tides on nutations, the couplings of the fluid outer core to the mantle and to the solid inner core through magnetic fields at the CMB and the inner core boundary (ICB) are found to have a significant role in accounting for the observations. The inner-core-induced normal mode (PFCN or FICN) plays an important part in this context. We shall present the estimates obtained for various parameters by a least squares fit of analytical theory to data, and their interpretation in geophysical terms. A precise estimate for the Earth's ellipticity, magnetic coupling parameters at the CMB and ICB and their implications, revision of the estimate for the CMB flattening, questions regarding the inner core flattening, and possibilities for constraining an elasticity and ocean tide models, will be discussed

JSG14/W/05-A3

Poster

1100-01

## CORE: 19+ YEARS OF VLBI UT1/LOD, AAM, EL NIÑO AND LA NIÑA

THOMAS A CLARK (Email: clark@tomcat.gsfc.nasa.gov), Chopo Ma (Email: cma@leo.gsfc.nasa.gov) and Ben Chao (Email: chao@denali.gsfc.nasa.gov), all at NASA/GSFC, Laboratory for Terrestrial Physics, Greenbelt MD 20771 USA.

Since 1980, the global VLBI network has produced more than 2000 one-day determinations of UT1 with a frequency of at least one measurement per week. The accuracy of the early measurements was hundreds of msec, while more recently ~5 msec is common. We have used this 19+ year record of UT1 to derive Length of Day (LOD), which mirrors changes in angular momentum in the fluids in earth's interior, atmosphere and hydrosphere. Observed decadal-scale variations arise largely from changes in the earth's core, and from global-scale climatic and ocean circulation variability which affect LOD with a peak-to-peak range ~1 msec over the 19+ year data set.

On shorter time scales, LOD is highly correlated with total atmospheric angular momentum (AAM). The annual average LOD signature due to AAM has a peak-to-peak amplitude ~900 msec. LOD is highly correlated with AAM derived from various global climate models (GCMs) and we present detailed comparisons with the NCEP GCM. We note that VLBI data has proven to be a useful, independent proxy for validation of various GCMs.

After removing the decadal and average annual components, LOD shows the interannual to intra-seasonal variability of the atmosphere. Of particular interest is the LOD signature of the 1997/8 El Niño/La Niña events when LOD increased ~ +400 msec in ~1997.2, followed by a ~-600 msec transition into La Niña in 1998.4, and with an integrated "sundial error" of ~-0.2 seconds. The observed LOD variations are highly correlated with conventional ENSO indices; it is rather remarkable that radio astronomical observations of quasars can be so closely correlated with barometric pressure differences between Darwin and Tahiti!

The VLBI community has begun a program that will improve the temporal coverage and accuracy of earth orientation measurements. The new Mark-4 VLBI data system will give a twofold increase in the sensitivity and a significant improvement in correlation capability. This program has been named CORE: Continuous Observation of the Rotation of the Earth.

JSG14/E/03-A3

Poster

1103-02

## BENEFITS FROM A COMBINED GPS/GLONASS ANALYSIS FOR EARTH ROTATION STUDIES

Markus ROTHACHER (Astronomical Institute, University of Berne, Sidlerstr. 5, M CH-3012 Berne, Switzerland, email: rothacher@aiub.unibe.ch) Robert Weber (Department of Advanced Geodesy, Technical University of Vienna, Gusshausstr. 27-29, A-1040 Vienna, Austria)

Since the start of the International GLONASS experiment (IGEX) in October 1998, the Center for Orbit Determination in Europe (CODE) is processing a global network of GPS/GLONASS receivers on a routine basis. This development opens up the possibility to study the benefits that may result from a combination of the IGEX solutions with the global GPS-only solutions (IGS network) for the estimation of earth rotation parameters (ERPs). An improvement in the ERP estimates is to be expected mainly because of the following circumstances: (1) by adding GLONASS data, the number of satellites involved increases from 27 (present GPS constellation) to about 41;(2) the different orbit inclinations of the two systems (55 and 65 degrees in the case GPS and GLONASS, respectively) should help to separate LOD and nutation rate estimates from variations in the orbital elements common to all satellites; (3) because the revolution periods of the GLONASS satellites, in contrast to those of GPS, are not in a 2:1 commensurability with the Earth's rotation, the impact of orbital biases on the determination of subdaily ERPs are less critical; (4) the improved satellite geometry should result in a better decorrelation of station heights and troposphere zenith delay parameters and thus, indirectly, to more accurate ERP estimates. RPs from combined GPS/GLONASS solutions will be presented and they will be compared to values from GPS-only solutions to assess the impact of the factors listed above.

JSG14/E/22-A3

Poster

1106-03

## COMBINATION OF VLBI, GPS AND SLR DATA AT THE OBSERVATION LEVEL-NEW RESULTS

Per Helge Andersen (Forsvarets forskningsinstitutt, P. O. Box 25, N-2007 Kjeller, Norway, and Institute of Theoretical Astrophysics, P. O. Box 1029, Blindern 0315, University of Oslo, Norway, email: per-helge.andersen@ffi.no)

A significant number of VLBI and SLR stations are equipped with GPS receivers. A few true fundamental stations with all three techniques even exist. Each technique has its strength and weakness with respect to the determination of geodetic parameters and together they complement each other in a way that should be fully taken advantage of in the data analysis. The simultaneous analysis of different data types at the observation level, due consideration of the physical interrelations, and presentation of results in a common reference system, are the main ideas behind the development of the GEOSAT software. A new and improved version of the software has been implemented with an automatic generation of 1) observation residuals and observation partial derivatives for VLBI, GPS and SLR, consistent at the 0.1 ppb level, and 2) a simultaneous arc-by-arc UD-filtering at the observations level. A very advanced multi-level (presently four parameter levels including stochastic parameter representations at each level) SRIF arc combination software for long-term solutions has been developed and validated. The main elements of the processing scheme will be presented. The first results with a simultaneous analysis of different space geodetic data types (VLBI, GPS, and SLR) at the observation level were presented at the IERS-98 symposium in Potsdam. That analysis was based on data from Jan 12 - Jan 23 in 1994. The analysis has recently been extended with significantly more observations. Results from the new analysis will be presented.

JSG 14/E/04-A3

Poster

1109-04

## MONITORING GLOBAL GEOPHYSICAL FLUIDS BY SPACE GEODESY

B. F. CHAO (Space Geodesy Branch, NASA's Goddard Space Flight Center, Greenbelt, Maryland 20771, USA; email: chao@denali.gsfc.nasa.gov), V. Dehant, R. S. Gross, R. D. Ray, D. A. Salstein, M. Watkins

Since its establishment on 1/1/1998 by the International Earth Rotation Service, the Coordinating Center for Monitoring Global Geophysical Fluids (MGGF) and its seven Special Bureaus have engaged in an effort to support and facilitate the understanding of the geophysical fluids in global geodynamics research. Mass transports in the atmosphere-hydrosphere-solid Earth-core system (the "global geophysical fluids") will cause the following geodynamic effects on a broad time scale: (1) variations in the solid Earth's rotation (in length-of-day and polar motion/nutation) via the conservation of angular momentum and effected by torques at the fluid-solid Earth interface; (2) changes in the global gravitational field according to Newton's gravitational law; and (3) motion in the center of mass of the solid Earth relative to that of the whole Earth ("geocenter") via the conservation of linear momentum. These minute signals have become observable by space geodetic techniques, primarily VLBI, SLR, GPS, and DORIS, with ever increasing precision/accuracy and temporal/spatial resolution. Each of the seven Special Bureaus within MGGF is responsible for calculations related to a specific Earth component or aspect -- Atmosphere, Ocean, Hydrology, Ocean Tides, Mantle, Core, and Gravity/Geocenter. Angular momenta and torques, gravitational coefficients, and geocenter shift will be computed for geophysical fluids based on global observational data, and from state-of-the-art models, some of which assimilate such data. The computed quantities, algorithm and data formats are standardized. The results are archived and made available to the scientific research community. This paper reports the status of the MGGF activities and current results.

JSG14/W/18-A3

Poster

1112-05

## THE ROTATIONAL AND GRAVITATIONAL EFFECT OF EARTHQUAKES

Richard GROSS (Jet Propulsion Laboratory, California Institute of Technology, 4800 Oak Grove Drive, Pasadena, CA 91109, USA, email: Richard.Gross@jpl.nasa.gov)

The static displacement field generated by an earthquake has the effect of rearranging the Earth's mass distribution and will consequently cause the Earth's rotation and gravitational field to change. Although the coseismic effect of earthquakes on the Earth's rotation and gravitational field have been modeled in the past, no unambiguous observations of this effect have yet been made. However, the Gravity Recovery And Climate Experiment (GRACE) satellite, which is scheduled to be launched in 2001, will measure time variations of the Earth's gravitational field to high degree and order with unprecedented accuracy. In this presentation, the modeled coseismic effect of earthquakes upon the Earth's gravitational field to degree and order 100 will be computed and compared to the expected accuracy of the GRACE measurements. In addition, the modeled second degree changes, corresponding to changes in the Earth's rotation, will be compared to length-of-day and polar motion excitation observations.

JSG14/E/15-A3

Poster

1115-06

## LONG-PERIOD TIDAL VARIATIONS OF THE EARTH'S ROTATION RATE

SHAILEN D. DESAI and Richard S. Gross (both at Jet Propulsion Laboratory, California Institute of Technology, Pasadena, CA 91109, U.S.A., email: Shailen.D.Desai@jpl.nasa.gov, Richard.Gross@jpl.nasa.gov), John M. Wahr (Department of Physics, University of Colorado, Boulder, CO 80309-0390, U.S.A., email: wahr@lemond.colorado.edu)

Long-period tidal variations of the Earth's rotation rate are caused by the redistribution of mass associated with the respective elastic solid Earth tides, the ocean tide heights, and the anelasticity of the Earth's mantle, and by the relative angular momentum associated with the long-period ocean tide currents. The dominant contribution, from the elastic solid Earth tides, is known to high accuracy from theoretical and numerical analyses. However, the lack of global observations of the long-period ocean tides has limited the accuracy of predicted contributions



## INTER-ASSOCIATION

from these ocean tides. The anelastic response of the mantle at frequencies smaller than the seismic frequencies are somewhat uncertain but could be inferred from observations of the long-period tidal variations of the Earth's rotation rate with improved predictions of the contribution from the ocean tides.

Almost global empirical models of the monthly and fortnightly ocean tides estimated from TOPEX/POSEIDON altimetry are used to predict their respective contributions to variations of the Earth's rotation rate. Observed long-period tidal variations of the Earth's rotation rate are estimated from the SPACE98 time series and the residual between these observations and the sum total of the predicted contributions from the elastic solid Earth tides and the ocean tides is used to infer anelastic properties of the Earth's mantle at the monthly and fortnightly periods.

**JSG14/L/01-A3** Poster **1118-07**

### TEMPORAL VARIATIONS OF OCEAN TIDAL TERMS IN UT1-UTC

Oleg TITOV (Astronomical Institute of Saint-Petersburg University, Bibliotechnaya sq., 2, Petrodvorets, Saint-Petersburg, 198904, Russia, email: oleg\_titov@usa.net)

Global redistribution of mass water causes a variations in Universal Time. VLBI technique allows to detect and estimate the corresponding oceanic tides with periods near 12 and 24 hours. Usually, scientists obtain the estimates using global set of VLBI data. Possibility of the tides variations from year to year is considered this paper. About 500 VLBI experiments (NEOS-A, CONT'96, etc.) from 1991 till 1998 year were analyzed. All reductional calculations have been made using OCCAM software. Least squares collocation method (LSCM) provides us the time series of UT1-UTC variations with high temporal resolution (one point for 3-5 minutes). The full number of points exceeds 100,000. Therefore the standard deviation of yearly estimates is reasonable. Variations of UT1-UTC obtained using the LSCM are in a good agreement with ones recommended by IERS Conventions. Estimates of main tidal terms in UT1-UTC independently for every year as well as for full set of data are presented. It is shown that the yearly estimates are slightly differ from each other. The various reasons of the effect are discussed.

**JSG14/W/09-A3** Poster **1121-08**

### ATMOSPHERIC ANGULAR MOMENTUM FUNCTIONS SIMULATED WITH THE JMA GLOBAL MODEL FOR THE PERIOD OF 1955-1994

I. Naito (National Astronomical Observatory, Mizusawa, Iwate, Japan), Y-H Zhou (Shang Hai Observatory, Shang Hai, China), M. Sugi (Meteorological Research Institute, Tsukuba, Japan), R. Kawamura (Toiyama University, Toyama, Japan), and N. Sato (Japan Meteorological Agency, Tokyo)

Axial and equatorial atmospheric angular momentum (AAM) functions calculated from an ensemble mean data of the three independent 40-year integrated values for the period of 1955-1994 under the observed near-global sea surface temperature (SST) condition by Japan Meteorological Agency (JMA) global model are discussed in comparison with those calculated from the reanalysis data during 1968-1994 of National Center for Environmental Prediction (NCEP) and from JMA's operational objective analysis data during 1984-1994 and the inferred functions during 1968-1994 from the observed length of day (LOD) and polar motion data, respectively. For comparisons in seasonal variation during 1984-1994, in general, the wind term for the axial AAM function agrees well with those from JMA's operational and NCEP's reanalysis data and roughly with the inferred function from the observed LOD. However, its semi-annual term is over-estimated, suggesting that the model unreliably simulates the subtropical zonal winds. On the other hand, the pressure term for the equatorial AAM function is considerably over-estimated with respect to those from JMA's operational and NCEP's reanalysis data, indicating that the SST driven global atmospheric motion induces too large seasonal variations in redistribution of atmospheric mass occurring mainly between the Eurasian Continent and the North Pacific Ocean.

**JSG14/W/14-A3** Poster **1124-09**

### SEASONAL-SCALE THREE DIMENSIONAL ANGULAR MOMENTUM BUDGETS FOR ATMOSPHERE-MANTLE SYSTEM

Yuichi Aoyama (School of Mathematical and Physical Science, The Graduate University for Advanced Studies, Mizusawa, 023-0861, Japan, email: aoyama@miz.nao.ac.jp) Isao Naito (National Astronomical Observatory, Mizusawa, 023-0861, Japan, email: naito@miz.nao.ac.jp)

Atmospheric contributions to seasonal variations of length of day (LOD) and wobble are evaluated during 1988 - 1997. The data sets used here are SPACE97 for LOD, EOP97C04 for wobble, and two atmospheric angular momentum (AAM) functions calculated from objective analysis data of Japan Meteorological Agency (JMA) and reanalysis data of National Centers for Environmental Prediction (NCEP). The axial AAM functions agree well in annual variation and roughly in semi-annual variation with inferred function from the observed LOD. However, there is a discrepancy between the equatorial AAM functions and the inferred function from the wobble in annual variation, where the wind terms show a considerable disagreement between JMA and NCEP, which arises mainly from tropospheric wind. Spatial distributions of regional wind contributions in annual variation to the LOD and the wobble are further discussed. In semi-annual variation for equatorial component, on the other hand, the AAM functions explain only a small part of the observed wobble, indicating that there remain a major other source.

**JSG14/W/23-A3** Poster **1127-10**

### ON THE CHANDLER WOBBLE AND ITS EXCITATION

Dr Aleksander Brzezinski

For the estimation of the Chandler wobble parameters it is important that the input time series expressing polar motion and its excitation are possibly long and homogeneous in time. The two series which seem to meet such requirements, hence are potential sources of new information about the Chandler wobble, are: 1) polar motion (PM) series spanning 1899.7-1992.0, derived from a new global adjustment of the optical astrometry observations by Vondrak et al. (1998), and 2) 40-years time series of the atmospheric angular momentum (AAM) estimates, computed on the basis of results of the NCEP/NCAR reanalysis project by Salstein and Rosen (1997). In this presentation we report an attempt to obtain from the new PM and AAM series improved estimates of the Chandler wobble parameters, the frequency of resonance F and the quality factor Q. Different stochastic models are used to express the wobble excitation. Finally, based on the AAM reanalysis data we address the problem, to which extent the observed Chandler motion can be explained by the atmospheric excitation.

**JSG14/L/03-A3** Poster **1130-11**

### VARIATIONS IN EARTH'S GRAVITATIONAL FIELD CAUSED BY THE POLE TIDE

S.R. DICKMAN (Department of Geological Sciences, State University of New York, Binghamton, NY 13902-6000, USA, email: dickman@bingvmb.cc.binghamton.edu)

The pole tide is the oceanic response to the Chandler wobble. The re-distribution of mass accompanying the pole tide causes periodic changes in Earth's gravity field. If the Chandlerian polar motion  $m$  is decomposed into prograde and retrograde components according to  $m = MP \exp(ist) + MR \exp(-ist)$ , where  $s$  is the Chandler frequency, then the pole tide's effects on gravity can be theoretically predicted in terms of MP, MR, and oceanic response factors.

I have employed a previously developed spherical harmonic dynamic ocean tide model to calculate the open-ocean response factors for the pole tide. Using these factors and the Chandler wobble amplitude observed over the past decade, I have computed the 14-month periodic contributions to the spherical harmonic coefficients of the gravitational potential. For example, including tidal loading of the underlying solid earth, the pole tide's contribution to  $J_2$  is typically  $\sim 1.3 \times 10^{-12}$ , whereas its contributions to  $C_{21}$  and  $S_{21}$  are typically  $\sim 3.6 \times 10^{-11}$  and  $\sim 2.2 \times 10^{-11}$ , respectively.

In addition to these results, I will also discuss how observationally based oceanic response factors -- determined, e.g., from satellite analyses or tide gauge data -- could be used to produce alternate estimates of the pole tide contributions to gravity. An illustration including the North and Baltic Seas, where the pole tide has long exhibited dramatic enhancements, will be presented.

**JSG14/L/04-A3** Poster **1133-12**

### BOUNDS ON CORE-MANTLE COUPLING AT SEASONAL PERIODS FROM COMBINED ROTATIONAL AND GRAVITATIONAL DATA

S.R. DICKMAN (Department of Geological Sciences, State University of New York, Binghamton, NY 13902-6000, USA, email: dickman@bingvmb.cc.binghamton.edu)

Excitation of variations in the Earth's rotation is often separated into 'matter' and 'motion' terms, which act to change Earth's inertia tensor and provide relative angular momentum, respectively. The outcome of any such excitation also depends on how well the core and mantle are rotationally coupled. Geophysicists have generally assumed zero axial coupling on time scales shorter than decadal. Recent work [Dickman & Nam 1995], in which observed and predicted tidal changes in the length of day were compared, found that such coupling is indeed weak on a nine-day time scale. However, the situation is unclear at longer periods. Knowing the frequency dependence of rotational coupling would yield more accurate estimates of excitation, and could provide clues to the state of Earth's deep interior.

A wide variety of processes -- some of which are not very well quantified -- contribute to seasonal changes in the length of day. Comparisons between observations and predictions, with the latter based on differing amounts of core-mantle coupling, may be too uncertain to allow the true extent of coupling to be resolved. Alternatively, recognizing that second-degree gravity coefficients reflect the total mass re-distribution contributing to rotational excitation [e.g. Eanes et al. 1997], we can incorporate the seasonal components of time-variable gravity data into our predictions, leaving only the 'motion' terms to be modeled (e.g. ocean currents) or measured (e.g. winds). Preliminary bounds on the extent of axial coupling at seasonal periods will be discussed.

**JSG14/E/08-A3** Poster **1136-13**

### ATMOSPHERIC FORCING OF POLAR MOTION AND CLIMATE PATTERNS

Jolanta NASTULA (Space Research Centre of the PAS, 00-716 Warsaw, Bartycka 18a, Poland, Email: nastula@cbk.waw.pl) and David A. Salstein (Atmospheric and Environmental Research, Inc. 840 Memorial Drive Cambridge, MA 02139, USA, Email: salstein@aer.com)

Atmospheric excitation of polar motion occurs by means of angular momentum exchange with the solid Earth in the equatorial plane. We assess such atmospheric forcing by comparing geodetic polar motion and atmospheric excitation functions. Atmospheric excitation of polar motion has different strengths on various time scales; we contrast the "subseasonal" and the "seasonal-interannual" regimes, with 150 days, the boundary between the two. Atmospheric excitation functions were computed from the new 50 year - long reanalysis system of the U.S. National Centers for Environmental Prediction and National Center for Atmospheric Research, which include effects of winds up to 10 hPa and surface pressure. In exploring how different regions were responsible for high frequency polar motion, we had already isolated the Eurasia, North American, and other regions as important for exciting high frequency polar motion, with the northern and central Eurasian region (EUR) especially prominent in this regard. Here we search for connections between EUR and certain well-known atmospheric behavior: the El Nino, the North Atlantic Oscillation, and the North Atlantic/Eurasian patterns. Additionally, empirical orthogonal function were computed for both temporal bands. The first such modes contain patterns with strong variations over southern oceans.

However, use of the inverted barometer correction (IB) reconfirm the overriding importance of Eurasia. Using the results of an ocean model run, we assess the regional variability of the excitation function within the oceans also.

**JSG14/W/15-A3** Poster **1139-14**

### INTERANNUAL VARIATIONS IN LENGTH-OF-DAY AND ATMOSPHERIC ANGULAR MOMENTUM WITH RESPECT TO ENSO CYCLES

Joachim Hoepfner (GeoForschungsZentrum Potsdam, Division 1: Kinematics and Dynamics of the Earth, Telegrafenberg, D-14473 Potsdam, Germany, email: ho@gfz-potsdam.de)

At interannual time scales, the excitation of variations in Length-Of-Day (LOD) is caused by two prominent signals in the atmosphere: The El Nino-Southern Oscillation (ENSO) and the Quasi-Biennial Oscillation (QBO). In this study, the axial Atmospheric-Angular-Momentum (AAM) component CH13 is related to changes in LOD. Focussing on the interannual variations in the solid Earth-atmosphere axial angular momentum budget, we consider the Low-Frequency Component and the Quasi-Biennial Oscillation in LOD and AAM in their temporal variability. In particular, we use the time series of LOD data of the series EOP (IERS) 97C04 from 1962 to 1998 and of CH13 data of the series AAM (NCEP) Reanalysis from 1958 to 1998, AAM (JMA) from 1983 to 1998, AAM (ECMWF) from 1988 to 1996, and AAM (UKMO) from 1986 to 1998. To separate the interannual signals, we have applied low-pass and band-pass filters. For comparison, the monthly data of the Southern Oscillation Index (SOI), as given by the NOAA by the difference in the surface pressure between Tahiti and Darwin, Australia, have been processed and are exhibited in the same manner. Concentrating on interannual time scales, the main results are quantitative estimates of the variability of two components, in particular of the Low-Frequency Component and the Quasi-Biennial Oscillation, in the LOD and AAM variations and also in the SOI variations and quantitative estimates of the total interannual AAM and SOI signals. Besides, the decadal LOD component is available as a function of time. The results show the character and the time evolution of the various portions. They should contribute to the problem of the interpretation concerning the interannual LOD changes associated with the global-scale ENSO cycles.

**JSG14/L/05-A3** Poster **1142-15**

### ATMOSPHERIC ANGULAR MOMENTUM VARIABILITY SIMULATED WITH THE ECHAM3-T21 GLOBAL CIRCULATION MODEL AND ITS INFLUENCE ON THE EARTH'S ROTATION PARAMETERS



JOCHEN ELBERSKIRCH, Andreas Hense (both at Meteorologisches Institut, Universität Bonn, Auf dem Hugel 20, 53121 Bonn, Germany, e-mail: jelbers@uni-bonn.de

The simulated Atmospheric Angular Momentum (AAM) budget of the ECHAM3-T21 global circulation model (GCM) is analysed. Five simulations with different initial conditions are forced by observed monthly means of sea surface temperature and global ice coverage (GISST-dataset from Hadley center, Bracknell) for the corresponding period from 1949 to 1994. The three components of AAM are compared to the Earth's rotation parameters (change of length of day and polar motion), respectively. A frequency analysis is performed with Fourier- and Wavelettransformation. The third component of simulated relative AAM for the mean of the five simulations shows significant variability on different timescales, particularly on the interannual timescale and it correlates very well with the timeseries of the change of LOD. The correlation of the other components are somewhat lower, which is not surprising. For the understanding of the physical process of the AAM transfer between atmosphere, ocean and solid earth, a canonical correlation analysis is carried out. This technique yields typical spatial anomaly patterns of maximum correlation between AAM and torques for all components. The application of lagged correlation analysis shows the spatial development of anomalous mountain torques if anomalies of relative AAM are existent. The mountain torque offers a very surprising pattern before and when the maximum anomaly of relative AAM occurs. To compare the results of the ECHAM3 model the NCEP Reanalysis data from 1958 - 1997 are also used.

**JSG14/L/08-A3** Poster **1145-16**

#### INTERANNUAL VARIABILITY IN EARTH ROTATION AND ATMOSPHERIC ANGULAR MOMENTUM: EL NIÑO CONNECTIONS

J. O. DICKEY (Jet Propulsion Laboratory, California Institute of Technology, 4800 Oak Grove Drive, Pasadena, CA 91109-8099; tel 818-354-3235; e-mail: jean.o.dickey@jpl.nasa.gov); P. Gegout (Ecole et Observatoire des Sciences de la Terre Laboratoire de Dynamique Globale, rue Rene Descartes 67084 Strasbourg Cedex, France; Tel: [33] 3 88 41 66; email: Pascal.Gegout@eost.u-strasbg.fr); S. L. Marcus (Jet Propulsion Laboratory, California Institute of Technology, 4800 Oak Grove Drive, Pasadena, CA 91109-8099; tel: 818-354-3477; e-mail: steven.l.marcus@jpl.nasa.gov)

Comparisons between length of day (LOD) and the strength of the ENSO cycle, represented by the Southern Oscillation Index (SOI), the difference in sea level pressure between Darwin and Tahiti series, have indicated striking agreement, with high interannual values of LOD generally coinciding with ENSO events. During an ENSO event, the SOI reaches a minimum, leading to an increase in atmospheric angular momentum (AAM) associated with the collapse of the tropical easterlies. Further increases in AAM may result from a strengthening of westerly flow in the subtropical jet streams. Conservation of total angular momentum then requires the Earth's rate of rotation to slow down, thus increasing LOD.

The impact of the 1997-98 ENSO event will be presented in context of angular momentum exchange utilizing LOD, SOI and AAM (both global and latitudinally banded) data. We have utilized the NCEP reanalysis from 1959 to 1998 from the surface to 100mb to examine the effect of the tropospheric zonal winds. Special emphasis will be placed on the globally coherent polarward propagation observed on interannual time scales; decadal variability will also be addressed. The techniques utilized include traditional recursive filter and multi-channel singular spectrum analysis (M-SSA); comparisons will be made with previous events, especially the 1982-83 event.

**JSG14/E/06-A3** Poster **1148-17**

#### OCEAN INDUCED VARIATIONS OF EARTH ROTATION ON TIME SCALES FROM HOURS TO YEARS - RESULTS FROM A NUMERICAL WORLD OCEAN MODEL

Juergen SUENDERMANN, Maik Thomas (both at Institut fuer Meereskunde der Universitaet Hamburg, Tropelowitzstr. 7, D-22529 Hamburg, Germany, email: suendermann@ifm.uni-hamburg.de)

The world oceans motion and mass fields cause significant variations of Earth orientation parameters on various time scales. Generally, these ocean induced changes are attributed either to tidal forces or variations of the general circulation. Analogously, numerical world ocean models can still be divided into Ocean General Circulation and tidal models. But it is questionable if the neglect of non linear interactions by a linear superimposition of both components of motion is accurate, especially with respect to frequencies that are typical for both circulation and tides. To include non linear interactions an OGCM is additionally forced with the complete astronomical tidal potential without decomposition into fourier components. Long-time integration and a time step of one hour offer a wide spectrum of analysis of ocean induced oscillations of Earth rotation. Time series of relative and rotational angular momentum resulting from three model runs from 1949 to 1994 with different forcing conditions are used to examine the role of the oceans with respect to excitation of polar motion and changes in length-of-day on time scales from hours to years. Since the model allows to treat the particular contributions of the three oceans separately, characteristic frequencies of global ocean basins can be identified.

**JSG14/W/10-A3** Poster **1151-18**

#### THE ROLE OF ATMOSPHERE AND OCEAN IN EXCITING VARIABILITY IN THE EARTH'S ROTATION AND GRAVITY FIELD

Thomas J. JOHNSON (U.S. Naval Observatory, 3450 Massachusetts Ave. NW, Washington, DC 20392-5420, USA, email: tj@casa.usno.navy.mil) Clark R. Wilson (NASA Headquarters, Code YS, 300 E St. SW, Wash. D.C. 20546; and The University of Texas at Austin, Austin, TX. 78712, email: cwilson@hq.nasa.gov) Benjamin F. Chao (NASA Goddard Space Flight Center, Code 926, Space Geodesy Branch, Greenbelt, MD 20771 email: chao@denali.gsfc.nasa.gov)

This research examines the role of the atmosphere and ocean in exciting the temporal variability in the Earth's rotation and gravity field. The main focus of this paper will be on the role of the ocean as predicted by 10 years of data products from the Parallel Ocean Climate Model. Unlike earlier rigid-lid models, this free-surface ocean model allows the estimation of the variability in the oceanic angular momentum and Stokes coefficients resulting from mass redistribution and relative motion that is more representative of the real ocean. First, we compare the atmosphere and ocean model's angular momentum time series to the polar motion and length of day variations. Then, we use the Stokes coefficients computed from the atmosphere and ocean model's mass redistribution to examine the Earth's temporally varying gravity field. These temporal variations are observable as variations in the Earth's geocenter location and as perturbations of an orbiting satellite's orbital elements. We also investigate the seasonal and interannual variability predicted by the atmosphere and ocean models. These comparisons can be useful in estimating the possible role of other geophysical processes, such as continental water storage in exciting the variations in the Earth's rotation and gravity field.

**JSG14/W/07-A3** Poster **1154-19**

#### HYDROLOGICAL AND OCEANIC EXCITATIONS OF EARTH ROTATION

C. R. Wilson [1,2,3] and J. L. Chen [1] Center for Space Research, University of Texas at Austin

[1] Department of Geological Sciences, University of Texas at Austin [2] NASA Headquarters, Washington D.C. [3]

Motion and redistribution of water on the continents and in the oceans are likely to be the major contributors to the residual polar motion excitation not accounted for by the atmosphere. We investigate continental water storage change and its excitation of polar motion and length-of-day (LOD) variation using both a data assimilating hydrological model and climatological average datasets. We estimate oceanic mass contributions to earth rotation changes from TOPEX/Poseidon sea level observations adjusted by a simplified steric sea level change model. The results are compared with the residual excitations after atmospheric contributions are removed using the NASA GSFC GEOS-1 atmospheric model. Our findings include the following: Continental water storage change plays an important role in exciting polar motion and LOD at seasonal time scales; hydrological models exhibit significant differences with regard to the predicted contribution to earth rotation changes, indicating the immaturity of understanding of the global hydrological cycle; The assimilated-data hydrological model provides generally better agreement with earth rotation observations; and non-steric sea level changes indicate a significant polar motion and LOD excitation source from ocean mass redistribution over a wide range of time scales.

**JSG14/W/08-A3** Poster **1157-20**

#### EARTH ROTATION AND OCEAN CIRCULATION INTERACTION

Nils-Axel Mörrer Paleogeophysics & Geodynamics, S-10691 Stockholm, Sweden, email: morner@pog.su.se

The ocean circulation is not only driven by thermo-haline forces. The interchange of angular momentum between the hydrosphere and the solid Earth is another fundamental factor. This can be demonstrated for the ENSO-events, for the last centuries' instrumental data, for decadal-to-century changes during the Holocene, for the high-amplitude climatic-eustatic changes some 13-10 ka ago, and for the main glacial/interglacial cycles. The oceans have a remarkable heat-storing capacity. Any change in the distribution of the water masses will have strong effects on the global climatic temperature distribution. The oceans contain huge masses of water of a reasonably high density that are constantly circulating both horizontally and vertically over the globe. Any irregularity in this circulation leads to a redistribution in total mass which affects the sea level and has to be compensated by an interchange of angular momentum between the hydrosphere and the solid Earth. This means that we in the recorded past changes in climate and in sea level can obtain information about possible past changes in ocean circulation, too. And this is exactly what our paleo-records seem to indicate. During sunspot minima, the solar wind intensity decreased (read by increased in-fall of cosmic ray increasing the <sup>14</sup>C production and <sup>10</sup>Be content) which led to a speeding-up of the Earth's rate of rotation affecting the ocean circulation so that the a major current like the Gulf Stream sent less warm equatorial water along its northern branch towards NW Europe at the same time as Arctic water penetrated further south giving rise to severe cold periods in NW Europe and warm period in S. Europe and N. Africa. The sudden changes in rotation at around 13,000 BP and 1000 AD, were both linked to trans-polar geomagnetic VGP-shifts and deformations of the gravitational potential surface besides their strong signals in the ocean circulation system.

**JSG14/W/04-A3** Poster **1200-21**

#### TEN-YEARLY POLAR MOTION CONNECTED WITH PRECIPITATION CHANGES OVER NORTH AMERICAN AND EURASIAN CONTINENTS

Tetsuya Iwabuchi (The Graduate University for Advanced Studies, Mizusawa, 023-0861, Japan, email: iwabuchi@miz.nao.ac.jp) Isao Naito (National Astronomical Observatory, Mizusawa, 023-0861, Japan, email: naito@miz.nao.ac.jp)

A hydrologic excitation model of ten-yearly polar motion appearing in the combined polar motion data of five-daily IPMS and SPACE94 during 1962-1995 is proposed. The model is based on the exponential decay of the land water storage supplied by precipitation. The NOAA monthly gridded precipitation anomaly data in 5 degrees-square are used for the model estimation. By assuming that the land water decreases exponentially with time, about 37% of the ten-yearly polar motion can be explained when decay parameter of 3.7 month. The seesaw-like changes of precipitation that efficiently excite the ten-yearly polar motion are also confirmed between the North American Continent and western region of the Eurasian Continent. From these results, a new look at the ten-yearly hydrological cycle system is advocated, which consists of atmospheric variations connected with the North Atlantic Oscillation, see-saw like sea level changes along both coastal regions in the North Atlantic Ocean, and precipitation changes in the North American Continent and the Eurasian Continent. The essential factor to determine the ten-year scale in the system is considered to be hydrological cycle in the two continent.

**JSG14/W/16-A3** Poster **1203-22**

#### INFLUENCES OF HYDROLOGICAL MASS REDISTRIBUTIONS ON EARTH ROTATION

R. DILL, H. Drewes, B. Richter, H. Schuh DGFI, Marstallplatz 8, D-80539 München, Germany email: dill@dgfi.badw.de

Hydrological processes cause local, regional and global redistributions of water masses which have an impact on the rotation of the Earth. We distinguish between direct and indirect influences of these mass motions on the rotation vector. Direct effects result from the displacements of water (matter term) which change the tensor of inertia of the whole Earth and from the velocity of water masses relative to a terrestrial reference frame (motion term). Redistributions of water masses influence also indirectly the Earth rotation by changing the tensor of inertia of the solid Earth due to load deformations. The indirect effects of atmospheric and oceanic loading and also the influence of small surface deformations caused by snow and ice loads or groundwater level variations are studied. Different realistic models of global snow cover are used to estimate and compare the magnitude of the resulting perturbations in Earth rotation. By a combined approach of atmospheric water balance, river runoff and sea level variation, the monthly continental ground water storage is determined. The influence of global and regional ground water variations will be discussed. Small regional effects are also looked at, especially the drying up of the Aral Sea and the filling of big new dams, like the proposed Three Gorges Dam in China.

**JSG14/P/01-A3** Poster **1206-23**

#### CLIMATE CYCLES IN VARIATIONS OF THE GRAVITY FIELD AND POLAR MOTION

Horst JOCHMANN (GeoForschungsZentrum Potsdam, Division of Kinematics and Dynamics of the Earth, Telegrafenberg, D-14473 Potsdam, Germany, email: rroni@gfz-potsdam.de)

Global change is accompanied by mass redistributions (e.g. mass exchanges between the hydrosphere and the cryosphere, and variations of the global atmospheric and oceanic circulations). These changes of the mass distribution at the earth produce temporal variations of

## INTER-ASSOCIATION

the earth's rotation and the gravity field. The discussions with respect to earth rotation are confined to polar motion, because the variation of this parameter is mainly caused by redistributions of masses, while length of day variations depend nearly completely on motion effects. So, polar motion is more closely related to gravity field variations than changes of the length of day. The amplitude spectrum of the temporal variation of polar motion contains well known climate cycles (e.g. 11, 13, 22, 35 and 80 years). Similar cycles are found in the atmospheric excitation function of polar motion. But, this excitation function can not be identified as the only source of these cycles. It was found that inner core motion contributes to a certain extent to the climate cycles in polar motion. Modern satellite missions (CHAMP and GRACE) will determine the gravity field with increased accuracy in near future. This allows a more accurate calculation of its temporal variation. Estimating the influence of long term atmospheric mass redistributions on the gravity field it could be shown that besides the dominating annual period a number of low frequent periods are expected to be contained in the gravity field. The amplitudes of these terms are in the same order of magnitude as the annual one and can be partly identified as climate cycles. The expected temporal behaviour of the Stokes coefficients infers the global property of the climate cycles.

**JSG14/W/12-A3** Poster **1209-24**

### EARTH ROTATION, ICE AGES AND SEA-LEVEL CHANGES: INFLUENCE OF MANTLE VISCOSITY AND SOLID-EARTH STRATIFICATION ON THEIR INTERDEPENDENCE

L.L.A. Vermeersen, R. SABADINI (Dipartimento di Scienze della Terra, Sezione Geofisica, Università di Milano, Via L. Cicognara 7, I-20129 Milano, Italy)

It has been realized long before the plate tectonics revolution of the sixties that there might exist close connections between changes in the position of the earth's rotation axis with respect to the earth's surface (polar wander), variations in sea level and the rise and decline of Ice Ages on geological time scales. Quantitatively, the modeling of these interrelationships has received renewed attention in the last few years, after initial attempts to relate these phenomena in the eighties by means of viscoelastic solid earth relaxation models had shown its feasibility. We show that the radial mantle viscosity profile and the layering of the solid earth have important influences on these interactions.

**JSG14/E/11-A3** Poster **1212-25**

### CORE MANTLE ANGULAR MOMENTUM EXCHANGE IN GEODYNAMIC MODELLING

Weijia Kuang and Benjamin F. Chao (Space Geodesy Branch, Code 926, NASA, Goddard Space Flight Center, Greenbelt, MD 20731, USA, email: Kuang@sanatfe.gsfc.nasa.gov)

Kinematic studies of geomagnetic data and Earth rotation observations have demonstrated that the decadal fluctuation of the length of day (LOD) results from the exchange of the angular momentum between Earth's core and the solid mantle. However, our knowledge about the dynamics responsible for the angular momentum exchange, i.e. the coupling torques across the core-mantle boundary (CMB), is limited in the past based on very simple theoretical models. To understand better the dynamics of the angular momentum exchange across the CMB, we introduce a heterogeneous mantle into our geodynamo model that simulates 3-D convective flow in the Earth's outer core. In the model, the mantle rotates subject to the coupling torques exerted on the CMB. In particular, we assume that the CMB is spherical but superimposed with a small amplitude (< 3 km), large scale (~ 1000km) and non-axisymmetric topography. We also assume that the electrical conductivity of the lower mantle (D'-layer) is finite and spatially variant. The heterogeneity introduced in the model follows the lower-mantle seismic tomography. With this model, we are able to study the topographic coupling and the magnetic coupling along with the convective flow in Earth's outer core. Furthermore, this model can be used to examine the effect of the couplings on the polar motion and nutations of the Earth.

**JSG14/W/06-A3** Poster **1215-26**

### THE EARTH'S POLAR ZONALITY MOTION DURING THE LATE WEICHSELIAN BASED ON PALAEOCRYOSPHERE STUDIES

Robert MOKRIK (Institute of Geology, Sevcenkos 13, 2600 Vilnius, Lithuania, email: mokrik@geologin.lt)

Periglacial periods during the Pleistocene in the Estonian Homocline have formed a permafrost up to 500m thick. Final phase of permafrost according to radiocarbon data had an extensive period of periglacial activity occurred 30-26 ka BP during the Huneborg-Denekamp Stadial time before Late Weichselian ice maximum. It is 6 ka BP earlier than in the West Siberian Craton (24-15 ka BP). That was related with polar zonality movement of the Earth. Permafrost processes caused metamorphism in the Cambrian-Vendian aquifer. As a result, the mineralization of groundwater decreased in comparison with the initial pre-Pleistocene period from 4-10 to 0.5-1 g/l. Hydrocarbonate-sodium chlorides prevail in the groundwater owing to degrees of calcium and magnesium carbonates and sulphates. The last cryogenese (30-26 ka BP) had lightened oxygen -18 isotope composition of groundwater at 2 per mil. The last Scandinavian Ice Sheet 11 ka BP had retreated northwards from the Estonian Homocline. It formed ice-dammed Baltic Ice Lake (BIL), having to 80m higher level in comparison with the Ocean. BIL took part in recharge of the Cambrian-Vendian aquifer for a short time. That is why an additional oxygen-18 lightening (1.5-2 per mil) of groundwater has been happened. Total isotope oxygen-18 lightening of groundwater during the Pleistocene is 13-14 per mil. Existence of the permafrost in Estonia is confirmed also by data of ratio uranium isotopes  $^{234}\text{U}/^{238}\text{U}$  activity in the Cambrian-Vendian aquifer. This ratio varies up to 40. These waters are unique in the European hydrogeological practice and reflect the cyclic cryosphere change during Quaternary. The permafrost in the Estonian domain caused great thermokarst activity which originated the valley shapes of lakes Peipus, Vortsjarv, Gulf of Parnu and Gotland Proper.

**JSG14/L/02-A3** Poster **1218-27**

### ON COSMOLOGICAL ORIGIN OF CERTAIN GEODETIC FEATURES OF THE EARTH

A.O. Adekugbe-Joseph (Center for Fundamental Study, P.O.Box 22415 University of Ibadan P.O., Ibadan, Oyo State, Nigeria. Email: nigeria@netbox.com)

The angle 66.5 degrees of inclination to the ecliptic of earth's rotational axis (rotational slanting of the earth), has been predicted accurately, and the ratio of polar diameter to equatorial diameter, (polar flattening of the earth), of 0.997 has been recalculated exactly, within a new cosmological model.

An instantaneous rate of increase of earth's radius of 0.108cm/yr, as well as instantaneous relative drift rate of 0.108y cm/yr of two points with longitudinal separation of  $\gamma$  degrees along the equator, have been calculated as consequences of the expansion of the earth with the universe in the new model. A remarkable agreement of the predicted rate of increase of earth's radius of 0.108cm/yr, earth's rotational slanting of 66.5 degrees and earth's polar flattening of 0.997 is shown.

The slight westward deflection in the north and eastward deflection in the south of continental

plates have also been explained as local consequence of the new cosmological model. These numbers as well as the westward deflection in the north and eastward deflection in the south of continental plates are increasing, but discernible changes occur in time scales of between 10 million and billion years only.

**Wednesday 21 July PM**

Presiding Chairs: C.R. Wilson , NASA/HQ, Washington D.C  
J.O. Dickey JPL/CALTECH, USA.

**JSG14/L/10-A3**

**1400**

### THE EARTH GRAVITY MODEL: STATUS AND PROSPECTS

Byron D. Tapley The University of Texas at Austin Center for Space Research R1000 Austin, TX 78712

The requirements for an Earth Gravity Model with both high spatial resolution and high accuracy have been articulated for over three decades. During the past decade, there has been considerable improvement in the global properties of the current models. A number of new, high accuracy tracking systems has provided data sets with enhanced accuracy and better global coverage. The use of satellite altimeter measurements has substantially improved the coverage over the oceans, and the release of several important gravity sets collected over the continents has allowed these improvements. Along with the improved models, the demands for gravity to support a number of important scientific investigations has increased. The utilization of the data from the highly successful TOPEX/Poseidon and ERS altimeter missions is still limited by geoid error. Further, the interest in mass variations within, and themass exchange between, the atmosphere, oceans and solid surface have lead to increased interest in the temporally varying characteristics of the gravity field. To satisfy the increased demands, there have been a number of new gravity mapping programs that span the spectrum from improved surface measurements to new exciting satellite missions. In this presentation, we summarize the status of current knowledge in the modeling of the earth's gravity field, note some of the limitations in the current data, discuss the current requirements and describe future opportunities to improve the gravity model. In particular, the promising suite of space missions, CHAMP, GRACE and GOCE, which are scheduled to be implemented during the first decade of the next century will be described and their contributions to the gravity model development will be discussed. Finally, the conceptual and computational challenges associated with these new data sets will be described.

**JSG14/L/11-A3**

**1430**

### OCEANOGRAPHY FROM GRAVITY MEASUREMENTS.

Chris W Hughes and Trevor F Baker (CCMS Proudman Oceanographic Laboratory, Bidston Observatory, Birkenhead, Merseyside L43 7RA, UK, Email: cwh@ccms.ac.uk, tfb@ccms.ac.uk)

In principle, measurements of the global gravity field should provide information about tides and ocean circulation. In practice, to date, this has been greatly complicated by the fact that terrestrial observations of time variations in these quantities have been at a limited number of sites, for which the movement of the observation point due to deformation of the earth must be taken into account. Satellite observations have the advantage of being global and decoupled from the solid earth, and have provided useful information about changes in gravity at tidal periods and in relation to post-glacial rebound, but are generally limited to very coarse spatial resolution. The launch in 2001 of a pair of satellites dedicated to monitoring the earth's gravity field and its variations on length scales down to 300 km will dramatically change the way such information can be used. Over the oceans it will be possible to invert this gravity information to give a measure of changes in ocean plus atmospheric mass distribution, and therefore in ocean bottom pressure. This is a fundamental quantity which relates not only to the moment of inertia of the ocean, but also to its coupling with the solid earth. New theoretical results suggest, and model diagnostics confirm, the important role of ocean bottom pressure in western boundary currents and at high latitudes, via a coupling of the oceanic angular momentum and vorticity balances. Results will be presented showing that it should be possible to use variations in global gravity to infer changes in abyssal ocean currents and important aspects of the thermohaline circulation - a unique ability for a remote sensing technology.

**JSG14/E/23-A3**

**1500**

### HYDROLOGICAL AND GLACIOLOGICAL APPLICATIONS OF GRACE; ESPECIALLY GRACE/GLAS SYNERGY AND ANTARCTIC MASS BALANCE

John Wahr (Dept of Physics and CIRES, U of Colorado, Boulder, CO 80309, US, email: wahr@lemond.colorado.edu) CHARLES BENTLEY (Dept of Geology and Geophysics, U of Wisconsin, 1215 West Dayton Street, Madison, Wisconsin 53706, US, email: bentley@geology.wisc.gov) Duncan Wingham (Dept of Space and Climate Physics, University College London, 17-19 Gordon Street, London, England WC1H 0AH, email: djw@mssl.ucl.ac.uk)

GRACE is a dedicated satellite gravity mission, approved and scheduled for a 2001 launch as part of NASA's Pathfinder Program and with assistance from DLR. GRACE will map the earth's gravity field to unprecedented accuracy and spatial resolution every few weeks. Time-variable gravity inferred from these measurements has applications for virtually all of the earth sciences, including hydrology, oceanography, glaciology, climatology, and solid earth physics. We will discuss the sort of hydrological and glaciological information that can be derived from the GRACE data. We will then concentrate specifically on using the data to learn about the mass balance of the Antarctic ice sheet. We will show that by combining GRACE data with laser altimeter measurements from NASA's GLAS mission, it should be possible to determine Antarctica's contribution to the present-day rise in global sea level to an accuracy approaching 0.2 mm/yr over a five year period.

**JSG14/W/19-A3**

**1600**

### GLOBAL AND REGIONAL GEOPHYSICAL PROCESSES AFFECTING THE GRAVITY FIELD AND ITS TIME VARIATIONS

R. SABADINI, L.L.A. Vermeersen, G. Di Donato (Dipartimento di Scienze della Terra, Sezione Geofisica, Università di Milano, Via L. Cicognara 7, I-20129 Milano, Italy, Email: bob@sabadini.geofisica.unimi.it); R. Devoti, V. Luceri, P. Rutigliano, C. Sciarretta (Telespazio, Matera, Italy); G. Bianco (ASI, Matera, Italy).

Integrated studies based on physical models of global and regional processes are of paramount importance to understand the complexities of the evolving Earth and, at the same time, to face the need of society to mitigate the consequences of environmental changes. Gravity data acquisition and modelling of global and regional geophysical processes at short and long time scales are keys to these issues. Joint inversions of secular changes in low degree harmonics of the geopotential based on new SLR analyses constrain the viscosity profile of the mantle and ongoing mass redistribution over the surface of the Earth, which is likely to be due to present-



day ice mass instabilities in alpine glaciers and/or to changes in the mass balance in Greenland and Antarctica. The rheological parameters inferred from the long wavelength, time dependent gravity field, and the density anomalies at crustal and lithospheric level, obtained from high resolution gravity space missions (GOCE), can be used as input lithospheric and mantle parameters in regional tectonic models. These allow to make predictions on important issues affecting our environment, such as sea level rise and stress accumulation in active seismic areas. Results are shown for the Mediterranean, severely affected by these natural risks.

**JSG14/E/14-A3** 1630

#### ABSOLUTE SEA LEVEL AND GLOBAL GLACIAL ISOSTATIC ADJUSTMENT

W.R. Peltier (Department of Physics, University of Toronto, Toronto, Ontario, Canada M5S-1A7, email: peltier@atmos.physics.utoronto.ca)

The global viscoelastic and self-gravitating theory of glacial isostatic adjustment (GIA), as recently reviewed in Peltier (1998, Rev. Geophys., 36, 603-689), has been extensively tested against a wide range of geological and geophysical observations. Since the future GRACE mission of NASA will deliver a rather high resolution model of geoid height time dependence and since a major, and perhaps dominant, contribution to this time dependence is expected to be due to the GIA process, we clearly require the best possible theoretical model of this field. Geoid height is of course synonymous with absolute sea level. I will describe a complete analysis of the expected signal that includes the full influence of rotational feedback due to the changes of earth rotation that accompany this dynamical process.

**JSG14/E/09-A3** Poster 1700-01

#### CHANGES IN THE GEOPOTENTIAL OBSERVED WITH SLR

C. COX, S. Klosko (Raytheon ITSS Corp., Greenbelt, MD 20770; 301-441-4010; email: ccox@magus.stx.com) B. Chao (Laboratory for Terrestrial Physics, NSAS/GSFC, Greenbelt, MD 20771)

Existing analyses of Satellite Laser Ranging (SLR) tracking data has yielded solution rates for low-degree zonals, in some cases up through J5. The secular zonal rate solution is improved using additional data and a new analysis technique applied in the processing of the SLR data. The new method effectively results in a continuous ephemeris in selected Keplerian orbit components, providing better estimates of the orbit plane accelerations, while retaining some of the accuracy of the shorter orbit solution arcs. The preliminary results of this technique, as applied to multiple satellite (LAGEOS, LAGEOS-2, Starlette, Stella, TOPEX/POSEIDON, and Ajisai) solutions for the secular rates will be presented. Additionally, the results of other new approaches for improving the resolution of the time varying gravity model by extending the temporal solutions to the low degree tesseral terms will be discussed. The secular zonal results, and those obtained earlier by Nerem and Klosko (1996) and Cheng et al. (1997) are combined with observed global sea level rise, and the secular polar motion rates in an inverse solution to provide constraints on geophysical models describing post-glacial rebound and ice sheet mass balances. Although the number of well resolved geopotential terms is limited, the inverse solutions are promising and provide results consistent with IPCC estimates of ice sheet mass balance and realistic contrasts between upper and lower mantle viscosity.

**JSG14/W/11-A3** Poster 1703-02

#### OBSERVING THE TIME-VARYING EARTH'S GRAVITY FIELD USING SATELLITE TRACKING DATA

M. K. Cheng and B. D. Tapley, Center for Space Research The University of Texas at Austin Austin, Texas 78759-5321, U.S.A., e-mail: cheng@csr.utexas.edu

Mass redistribution within the Earth causes the temporal variations in the Earth's gravity field. Analysis of the long-term satellite laser ranging (SLR) tracking data has provided the capability for measuring the time-varying Earth's gravitational field. In this paper, we present recent results for the secular rates of low degree and order geopotential coefficients and the seasonal variations of the zonal harmonics from analysis of over 23 years SLR data collected from 8 geodetic satellites, including Starlette, Ajisai, Stella, LAGEOS I and II, Etalon I and II, BE-C. In addition, DORIS data provide an important complement to the SLR data to monitor the temporal variations in the non-zonal terms. Comparisons of the results from analysis of the satellite tracking data and predicted from the geophysical models demonstrate that analysis of long-term SLR data can provide a global constraint on modeling of the long-term changes of the Earth system, such as the post glacial rebound and the mass balance of polar ice, and be able to observe the meteorological mass transport between the atmosphere, solid earth and ocean. The continuous long-term SLR data are invaluable for enhancing our understanding of the Earth system dynamics and its role of the meteorological excitation on the Earth's gravity field.

**JSG14/E/05-A3** Poster 1706-03

#### GEODETIC CONSTRAINTS ON MASS REDISTRIBUTION IN THE EARTH SYSTEM

Ericos C PAVLIS (JCE/UMBC, NASA Goddard, Code 926, Greenbelt, MD 20771, U.S.A., E-mail: epavlis@Helmert.gsfc.nasa.gov)

The continuous redistribution of mass within the Earth system causes concomitant changes in the Stokes' coefficients describing the terrestrial gravity field. Secular changes in J2 due to post-glacial relaxation have been observed since many years. Similar changes in J3 have been attributed to changes in the ice sheets of Greenland and Antarctica. Seasonal changes in these coefficients have also been closely correlated with mass transfer in the atmosphere and oceans. The system is also affected by the hydrological cycle, which however is the most difficult to measure accurately so far. It is thus important to find means to measure the total effect so that we can infer the least well-known component after subtraction of the other ones. Satellite laser ranging data to LAGEOS 1 and 2 have already contributed in this effort the most accurate results yet. The sparseness of the SLR data (due to the lack of several Lageos-like targets), places limits on the maximum resolution of these series of results. This new analysis doubles the resolution of our previous results and extends our series up to the recent past. This data set of the past six years has been analyzed in a consistent manner using NASA Goddard's GEODYN/SOLVE II software and following the IERS Conventions 1996. We present and discuss our low-degree Stokes' coefficients time-series with emphasis on the geocenter variations and compare them to those inferred geophysically. The spectral contents of the series are also compared and discussed.

**JSG14/W/24-A3** Poster 1709-04

#### SEASONAL VARIATIONS OF THE EARTH'S GRAVITY FIELD DETERMINED FROM SATELLITE LASER RANGING

R. S. NEREM, R. J. Eanes, P. F. Thompson, and J. L. Chen (all at the Center for Space Research, The University of Texas at Austin, Austin, TX, 78712, email: nerem@csr.utexas.edu)

Mass redistributes itself in the Earth system on a variety of temporal and spatial scales reflecting complex interrelated processes in the oceans, atmosphere, groundwater, glacial/polar ice, among others. The measurement of these variations is thus important for a variety of studies attempting to understand the interrelations of the different components of the Earth system, and how they may change with time due to anthropogenic influences. We have used Lageos-1 and Lageos-2 satellite laser ranging (SLR) data to determine long wavelength seasonal variations of the Earth's gravity field from 1993 to the present. Due to the altitude of these satellites, and the non-continuous nature of the measurements, these data can detect seasonal gravitational variations only for wavelengths of roughly 10,000 km and longer (a degree 4 spherical harmonic expansion). We have compared the observed annual variations for a complete 4 x 4 spherical harmonic expansion as observed by Lageos 1/2 SLR data to those predicted from a variety of atmospheric, oceanic, and hydrologic models. We have used the observed variations to optimally select the best set of model predictions. The correlation of the maps of the observed and modeled annual geoid variation is as high as 0.8, with an rms difference of close to 1 mm. Given the sparse temporal and spatial distribution of the SLR data, and the limitations of the geophysical models, we consider this agreement to be as good as can be expected before the launch of a dedicated satellite gravity mission. Similar results will also be presented for variations in the Earth's geocenter location. The implications of these results for planned future dedicated satellite gravity missions will be discussed.

**JSG14/E/02-A3** Poster 1712-05

#### GEOCENTER MOTION DETERMINED WITH GEODETIC DATA. COMPARISON WITH SURFACE LOADING DATA

J-F CRETAUX, A. Cazenave, L. Soudarin (LEGOS-GRGS/CNES, 18, Avenue Edouard Belin, 31401 Toulouse Cedex 4, France, e-mail: Jean-Francois.Cretaux@cnes.fr)

DORIS and SLR data were processed and combined in order to determine the Earth center of mass over the 6-year period from January 1993 to december 1998. The seasonal variations of the DORIS-SLR reference frame origin were computed by determining 3 translation parameters between monthly coordinates of the DORIS and SLR networks. These translation parameters are interpreted as the geocenter motions. These variations that are due to the mass redistribution inside the surface fluid envelopes of the Earth were compared to the variations of the 1 degree geopotential coefficients also computed with the same data. During the 1993-1998 period the geocenter coordinates obtained by space geodetic measurements were then compared to geocenter variation obtained from various geophysical sources, i.e. atmospheric pressure, ocean mass, and surface ground water load.

**JSG14/W/13-A3** Poster 1715-06

#### THE GRAVITY CHANGE INDUCED BY THE ANNUAL POLAR MOTION AND THE EFFECT OF SEA SURFACE HEIGHT VARIATIONS ON ITS CHANGE

Tadahiro SATO (National Astronomical Observatory, 2-12 Hoshigaoka-cho, Mizusawa-shi, 023-0861 Japan, e-mail: tsato@miz.nao.ac.jp) Yuichi AOYAMA (The Graduate University for Advanced Studies, 2-12 Hoshigaoka-cho, Mizusawa-shi, 023-0861 Japan, e-mail: aoyama@miz.nao.ac.jp) Masatsugu OOE (National Astronomical Observatory, 2-12 Hoshigaoka-cho, Mizusawa-shi, 023-0861 Japan, e-mail: ooe@miz.nao.ac.jp) Yoich FUKUDA (Graduate School of Science, Kyoto University, Kitashirakawa, Oiwake-cho, Sakyo-ku, Kyoto, 606-01 Japan, e-mail: fukuda@kugi.kyoto-u.ac.jp) Kazuo SHIBUYA (National Institute of Polar Research, 1-9-10 Kaga, Itabashi-ku, Tokyo, 173-8515 Japan, e-mail: shibuya@nipr.ac.jp)

Recent relative and absolute gravimeters have enough potential to detect such weak and long-period gravity change due to the effect of earth's polar motion for instance. In addition to the observations of polar motion itself at high precision, the observation of the polar motion effect on gravity gives us an important data to understand the characteristics of earth's behavior at a low-frequency band. The polar motion effect on gravity is mainly consisted of the three components of semi-annual, annual and Chandler (of 14 months). In this study, the annual component is mainly discussed based on the comparison of the 5-year observation from a superconducting gravimeter at Syowa Station, Antarctica. One great advantageous thing in the gravity observation at Syowa is that its observation is almost free from such irregular and long-term effects due to the variations in under ground water, which are one of the major noise sources in the measurement of polar motion effect. The observed gravity changes were compared with the theoretical estimated ones, i.e. the sum of the effects of solid tide, ocean tide, polar motion and SSH (Sea Surface Height) variations. The effect of SSH variations were estimated using the data obtained from POCM (Parallel Ocean Climate Model). Based on the SST (Sea Surface Temperature) data which were used to derive the POCM, the effect of SST variations on SSH was corrected. The comparison results suggest; (1) both the observed annual amplitude (1.2 micro Gals) and phase (25.5 degrees) measured by referring on an epoch of 2000, are well explained by the above four effects, and (2) the gravity effect of SSH variations (about 0.2 micro Gals in amplitude) plays an important role to explain the observed annual gravity change especially to its phase.

**JSG14/E/13-A3** Poster 1718-07

#### INTERANNUAL VARIABILITY OF THE EARTH'S GRAVITATIONAL FIELD: EL NINO CONNECTIONS

P. GEGOUT (Ecole et Observatoire des Sciences de la Terre, Laboratoire de Dynamique Globale, 5 rue Rene Descartes, 67084 Strasbourg Cedex, France; tel: [33] 3 88 41 66 94; email: Pascal.Gegout@eost.u-strasbg.fr); J. O. Dickey (Jet Propulsion Laboratory, California Institute of Technology, 4800 Oak Grove Drive, Pasadena, CA 91109-8099; tel: 818-354-3235; email: Jean.O.Dickey@jpl.nasa.gov); D. Dong (Jet Propulsion Laboratory, California Institute of Technology, 4800 Oak Grove Drive, Pasadena, CA 91109-8099; tel: 818-393-1827; email: dong@cobra.jpl.nasa.gov)

Temporal variations of the even zonal combination of the geopotential are investigated using the geodetic satellite Lageos I from 1980 to 1998. Our purpose is to investigate the interannual variability of the Earth's gravitational field and its connections with El Nino and La Nina, events. Gravity variations relative to redistributions of groundwater, atmospheric and oceanic masses are estimated and compared to Lageos I determination. After the removal of a composite seasonal cycle, the use of recursive filtering and multi-channel singular spectral analysis reveals strong similarities between observed interannual variability and El Nino Southern Oscillation proxies.



**JSG14/E/20-A3** Poster **1721-08****GRAVITY VARIATIONS COMPUTED FROM A COUPLED ATMOSPHERE-OCEAN MODEL**

Eric W. LEULIETTE and R. Steve Nerem (both at Center for Space Research, University of Texas at Austin, 3925 W Braker Lane Suite 200, Austin TX 78759, USA, email: leuliette@csr.utexas.edu) Gary L. Russell (NASA/Goddard Institute for Space Sciences, New York, NY 10025, USA, email: russell@giss.nasa.gov)

The Gravity Recovery and Climate Experiment (GRACE) will return high resolution measurements of the Earth's gravity field for five years beginning in 2001. The projected accuracy of this mission will allow for the observation of mass flow in various components of the coupled solid Earth/ocean/atmosphere system. General circulation models offer a way to assess the impact of these mass changes on the gravity field and the prospects for detecting climate signals in the gravity field. Using monthly-averaged fluid mass diagnostics from a coupled atmosphere-ocean model developed at GISS, we estimate the seasonal and secular geoid signals from sea level, snow, sea ice, soil moisture, and surface pressure can be compared to estimated errors for GRACE. We have used different climate scenarios to access the ability of gravity missions to identify climate change. All annual mass flows are well above the preliminary GRACE measurement errors at half wavelengths of 1000 to 10000 km. In addition, differences between the annual ocean column mass and snow mass annual as predicted by each model scenario (control versus %1 annual CO<sub>2</sub> increase), differ at amplitudes that are significant when compared to the GRACE errors. Mass flows with significant secular trends have been used to estimate the magnitude of climate change over five years. These redistributions should be detectable by GRACE in principle, although they can not be separated using GRACE data alone.

**JSG14/W/03-A3** Poster **1724-09****VARIATIONS OF GEOCENTER AND EARTH ORIENTATION DEDUCED FROM ESTIMATES OF OCEAN MASS REDISTRIBUTION**

Wolfgang BOSCH (Deutsches Geodätisches Forschungsinstitut, Marstallplatz 8, D-80539 München, Germany, email: bosch@dgfi.badw.de)

A consistent and homogeneous time series over more than six years is now available for global sea level variations monitored by Topex/Poseidon altimetry. The variations, dominated by a well known annual oscillation, are known to be caused by heating and cooling of the thermocline. The sea level variations therefore represent basically a volume change rather than a mass redistribution. We estimate the residual mass redistribution by using available climatologies to remove the steric effect and compute simultaneously the impact on both, variations of the Earth's center of origin and the Earth's orientation. The results are illustrated and analyzed on spatial and temporal scales.

**JSG14/W/01-A3** Poster **1727-10****FUTURE CONSTRAINTS FOR POST-GLACIAL REBOUND FROM GRACE**

Mark TAMISIEA and John Wahr (Department of Physics and CIRES, C.B. 390, University of Colorado, Boulder, CO 80309, USA, Email: tamisiea@colorado.edu)

GRACE, a dedicated gravity mission to be launched in 2001, will provide much more information on the secular change of the geoid coefficients than is currently available. Secular variations of the geoid could provide useful constraints for determining the radial viscosity profile of the earth from post-glacial rebound. However, other mechanisms such as hydrology, current ice mass changes, and sea level rise also cause such variations. With the new GRACE data, the spatial pattern of the variations may allow for separation of these mechanisms. In this talk, we create a synthetic geoid that includes various secular effects and determine the contamination of the post-glacial rebound signal from the other mechanisms' signals. We also begin to determine the extent to which the original input viscosity profile can be recovered.

**JSG14/W/20-A3** Poster **1730-11****ESTIMATION OF THE GRAVITY CHANGES INDUCED BY THE MASS VARIATIONS IN THE FLUID EARTH**

Yoichi Fukuda (Department of Geophysics, Graduate School of Science, Kyoto University, Japan, Kitashirakawa-Oiwakecho, Sakyo-ku, Kyoto 606-8502, Japan, email: fukuda@kugi.kyoto-u.ac.jp) Tadahiro Sato (National Astronomical Observatory, Mizusawa, 2-12 Hoshigaoka-chyo, Mizusawa-shi, 023-0861 Japan, email: tsato@miz.nao.ac.jp) Yuichi Aoyama (The Graduate University for Advanced Studies, 2-12 Hoshigaoka-chyo, Mizusawa-shi, 023-0861 Japan, email: tsato@miz.nao.ac.jp) Lorant Foldvary and Kazuo Tsutsui (both at Department of Geophysics, Graduate School of Science, Kyoto University, Japan, Kitashirakawa Oiwakecho, Sakyo-ku, Kyoto 606-8502, Japan, email: fl@kugi.kyoto-u.ac.jp)

The recent progresses of the precise gravity measurements using superconducting gravimeters and absolute gravimeters enable us to observe very weak gravity signals induced by the various kinds of dynamic processes in and on the Earth. Because gravity changes reflect actual mass movements, the data of gravity measurements give us useful information to understand the dynamic processes. As an experimental study, we estimated the gravity changes induced by the sea level variations. We first employed SSH (Sea Surface Height) variation data from POCM (Parallel Ocean Climate Model) to evaluate their gravity effects, and then applied the EOF analysis to investigate the characteristic of the gravity changes. The results show that one of the EOF components is strongly correlated with ENSO like SSH variations. The amplitude of expected gravity changes in the Pacific equatorial regions possibly reaches 2 to 3 micro Gals. This amount of amplitude could be enough detectable by a careful gravity observation. On the other hand, several satellite gravity missions are now under planning and some of them will soon be realized. Thus we also estimated the gravity effects of the sea level variations at the satellite orbit height level. Although the spatial coverage of the satellite gravity measurements are much superior than the ground measurements, the ground measurements are still important because of their high precision and temporal sampling rate. Using the simulated data set, we investigate the effective distribution of gravity observation points on ground. The same investigation has been carried out for gravity effects of the atmospheric pressure and soil moisture variations.

**JSG14/E/16-A3** Poster **1733-12****VARIATION OF THE GEOCENTER AT SECULAR AND GEOLOGICAL TIME-SCALE**

GREFF-LEFFTZ Marianne, Institut de Physique du Globe de Paris, 4 place Jussieu, 75252 Paris Cedex 05, France.

The degree one deformations of the Earth, in a reference frame related to the centre of mass of the planet, are computed using a theoretical approach (Love numbers formalism) at secular time-scale, where the Earth has a viscoelastic behavior and at geological time-scale, where the

mantle is a viscoelastic fluid. For a Maxwell model of rheology, the degree one relaxation modes associated with the viscoelastic Love numbers have been investigated : the Mo mode does not exist and there is only one transition mode (instead of two) generated by a viscosity discontinuity. The translations at each interface of the incompressible layers of the Earth's model (especially at the surface, at the Core-Mantle boundary (CMB) and at the Inner Core boundary (ICB)) are computed. They are viscoelastic when the Earth is submitted to Pleistocene deglaciation and of about the meter. In a quasi-fluid approximation (Newtonian fluid) because of the mantle density heterogeneity, their order of magnitude are of about 100 m at the surface, 1 km at the CMB and 10 m at the ICB (which is in a quasi-hydrostatic equilibrium at this time-scale).

**JSG 14/E/01-A3** Poster **1736-13****NON-TIDAL PLUMB LINE VARIATION: A NEW GEODYNAMICAL QUANTITY IN STUDYING THE VARIATIONS IN THE EARTH'S GRAVITATIONAL FIELD AND ITS ROTATION**

Zheng-xin LI (Shanghai Observatory, Chinese Academy of Sciences, 80 Nandan Road, Shanghai, 200030, China, email: lzx@center.shao.ac.cn)

Non-tidal plumb line variation (PLV) on ground is related to the variations of the Earth gravitational field but it remains unsolved whether or not one can actually measure them in practice. The paper describes the efforts in using the traditional techniques to detect the non-tidal PLV. Based on the results obtained recently at two different locations, Jozefoslaw of Poland and Yunnan of China, where parallel gravimetry and astrometry observations have been carried out more than 20 and 10 years, interannual PLV, in the order of 0.01"-0.02", have been discovered. It is clear now the existence of the non-tidal PLV at these two locations and the possibility in measuring them in practice by either of the two techniques at interannual time scales. Although only results of the two locations have been obtained, and only interannual part of the non-tidal PLV has been studied at the moment, it is already very interesting to see the correlation between the interannual PLV derived from some astrometric observations and a certain number of geodynamical quantities. It is quite possible that the non-tidal PLV discovered here will be used as a new geodynamical quantity one day with which the studying related to the variations in the gravitational field and its rotation might be carried out in a better way.

**JSG14/E/18-A3** Poster **1739-14****GLOBAL GRAVITY CAMPAIGNS - FROM THE GROUND (GGP) TO THE SKY (GRACE)**

DAVID CROSSLEY (Saint Louis University, Department of Earth and Atmospheric Sciences, 3507 Laclede Ave., St. Louis, MO 63103, USA, email: crossley@eas.slu.edu) Jacques Hinderer (Ecole et Observatoire des Sciences de la Terre, 5 rue Ren Descartes, 67084 Strasbourg, FRANCE, tel +33.88.60.50.63 fax +33.88.61.67.47 email: jhinderer@eost.u-strasbg.fr)

The GGP global geodynamics campaign is now returning high precision data from 17 superconducting gravimeter stations. These sites are clustered in Europe and Japan and more widespread in other parts of the globe. When the 6 years of the campaign are over we will for the first time be able to separate various types of global gravity signals, associated for example with rotation of the Earth, to local gravity changes caused by environmental factors. At the same time, the planned mission GRACE will look at the global gravity field in a very different way. Connecting the two campaigns is the need for ground truth for the GRACE mission. This talk will discuss ways in which the GGP sites, supplemented with absolute gravimeter measurements, may be useful to the GRACE mission.

**JSG14/W/02-A3** Poster **1742-15****A 750 DAY RECORD OF GRAVITY VARIATIONS AS SEEN BY A SUPERCONDUCTING GRAVIMETER (GWR C026) AND AN ABSOLUTE GRAVIMETER (FG5-206) IN STRASBOURG (FRANCE)**

Jacques Hinderer, Martine Amalvict, Jean-Paul Boy and Pascal Gegout (all at Ecole et Observatoire des Sciences de la Terre, 5 rue Descartes 67084 Strasbourg Cedex, France, e-mail: jhinderer@eost.u-strasbg.fr)

This paper is devoted to a comparative analysis of a 750 day long record of gravity changes as observed both by an absolute gravimeter (FG5 model 206) and a superconducting gravimeter (GWR model C026) which are operating in parallel in Strasbourg. This study extends previous related studies by adding one more year of relative and absolute gravity data at the same station. The relative gravity (as well as the atmospheric pressure) is sampled every 2 sec and numerically decimated to 1 min in agreement with the GGP (Global Geodynamics Project) recording standard. The absolute gravity values (with a drop repetition of 15 sec) consist in several days (about a week) of continuous measurements performed generally once every month. Two main objectives will be sought: on one hand, the alibration capability of AG/SG parallel registrations will be further tested, especially with respect to stability in time, duration requirement and precision; in particular, we will show the mean value of the scale factor resulting from a least squares adjustment using all the AG/SG values available during the 750 day time span. On the other hand, the absolute gravity values will be superimposed onto the continuous superconducting gravimeter observations in order to estimate long term gravity changes at our station. We will attempt to separate true (geo)physical effects from instrumental causes (e.g. drift of the cryogenic meter). A special attention will be paid to the gravity signature of the polar motion and to the respective capability of both types of instruments to exhibit it.

**JSG14/E/19-A3** Poster **1745-16****RELATIVE AND ABSOLUTE GRAVIMETERS IN LARGE AREAS**

A.Sas-Uhrynowski, Y.ZANIMONSKIY (Institute of Geodesy and Cartography, Warsaw, Poland, e-mail: zg@igik.edu.pl)

The advantages of the satellite missions to map the Earth's gravity field are increased with presence of the additional terrestrial data. Fast accumulation of the gravimetric data with high accuracy in special and least known areas especially is necessary. In this connection the traditional methods of gravimetric surveys should be improved. The modernization of the Polish Network shows that usage of relative gravimeters on a long (up to 350 km) distances between stations is quite effective. It is a great desire to use the Portable Ballistic Gravimeter as an additional device. This device was under R&D at the Institute of Geodesy and Cartography for a few years. It consists of an original parts and operates under special algorithm. The base of this algorithm is randomization of the systematic errors. PBG has been extensive field tested as autonomous as alongside other absolute gravimeters. The repeatability was estimated 0.01mGal for weekly and monthly intervals. Now we have the autonomous small-size and resistant to field conditions unit. The payment for this advantages is change of the instrument's metrological status. PBG is a working measuring instrument and it have to be calibrated at the standard such as Polish Gravity Reference Network. The relative connection is obtained by looping between two stations three days in a row. During this time PBG works automatically at the second consecutive station. The purpose of new algorithms for data processing is to bring together results obtained by means of so different instruments. Results of the recent measurements are going to discuss too.

## EVALUATION OF SIX YEAR SUPERCONDUCTING GRAVIMETER OBSERVATION AT GFZ POTSDAM SITE

JUERGEN NEUMEYER, Franz Barthelmes, Hans-Juergen Dittfeld (GeoForschungsZentrum Telegrafenberg A17, 14473 Potsdam, Germany, e-mail: neum@gfz-potsdam.de, bar@gfz-potsdam.de, ditti@gfz-potsdam.de)

The high accurate Superconducting Gravimeter TT 18 has been continuously recorded gravitational variations at GFZ Potsdam site for six years. This data set and environmental parameters recorded at the same time have been used for analysing the data and separation of different geophysical effects.

In a first step the short and long period Earth tides are analysed and the tidal parameters are compared with the Wahr Dehant model. Selected tidal parameters are used for determination of the complex eigenfrequency of the Earth's Nearly Diurnal Free Wobble and the result is compared with theory.

Gravity variations caused by atmospheric pressure, groundwater table and rainfall are estimated by using different approaches. The admittance coefficients are determined and the quality of the reduction is discussed.

After reduction of the environmental effects the polar motion is extracted from the residual data set and compared with smoothed records from space techniques. The free oscillation of the Earth caused by big Earthquakes is used for separation and splitting of the different modes. The decay of the modes is illustrated by means of the Wavelet Transform.

Finally an attempt is made for determination of the three translational modes of Earth solid inner core (Slichter Triplet) using the Cepstrum method.

## STUDY TO PROPOSE A GRAVITY NETWORK AS GROUND TRUTH FOR SATELLITE MISSIONS

Bernd RICHTER, W. Schwahn, D. Simon, R. Falk, H. Wilmes (all Bundesamt fuer Kartographie und Geodäsie, Richard Strauss Allee 11, D-60598 Frankfurt a.M. / Germany (email: richter@ifag.de)

Special satellite missions (CHAMP, GRACE) are initiated to study the fine structure of the Earth gravity field and its temporal variations. For the first time space borne derived gravity variations can be compared with series observed at the Earth surface. Various gravity variations and their contributions to the Earth borne and space borne sensors will be discussed. Due to the temporal resolution of the satellite data only gravity variations can be analysed which have a long-term periodical or non-periodical variation nature or a secular trend. As a test case periodical signals are preferable because of the higher sensitivity of models to periodical pattern. In addition the spatial disturbance for long-period variations is at least regional, usually of global character. The annual gravity variation is a potential candidate which should be detectable by satellite and ground borne.

## DETERMINATION OF GEOPENTIAL VARIATIONS USING SATELLITE LASER RANGING

Wu Bin , Pen Bibo , ZHU Yaozhong and Hsu Houze

The mass redistribution within the Earth produces variations of geopotential on a wide range of timescales. In this study, Lageos-1 and Lageos-2 satellite laser ranging (SLR) data from November 1992 to December 1997 are used to determine the variations of low degree harmonic coefficients of geopotential, J<sub>2</sub>, J<sub>3</sub> and J<sub>4</sub>. In the span of data, both Lageos-1 and Lageos-2 SLR data are available in every monthly arc analysis, which makes the disadvantage of single satellite geodynamic analysis overcome. Our results show that : 1) The harmonic coefficients J<sub>2</sub> and J<sub>4</sub> are determined in every monthly arc with low correlation by simultaneously using Lageos-1 and Lageos-2 SLR data. 2) The time series of J<sub>2</sub> mainly comprises an annual and a semi-annual variation. 3) The J<sub>2</sub> variation from two satellites SLR data instead of the effective J<sub>2</sub> from single satellite is used to calculate the change of length of day (LOD) caused by the mass redistribution within the Earth. Combining the LOD determined from space geodetic data and the result in this study, one can obtain the relative angular momentum contribution to the LOD and provide an observational constraint on the wind and ocean currents effects on LOD.

## CONSTRAINTS ON MANTLE ANELASTICITY FROM EARTH ROTATION AND TIDAL PARAMETERS

Yaozhong ZHU, Bin Wu and Bibo Peng

The response of the solid Earth to tidal forces is influenced, in part, by properties of the Earth's interior, which can be modeled with Love number. In this work, we compare the theoretical degree 2 Love numbers predicted by two frequency-dependent models of mantle anelasticity with the recently observed results derived from tides and the Earth rotation variations at M<sub>2</sub>, M<sub>f</sub>, M<sub>m</sub>, Chandler wobble and 18.6-year frequencies. The response of mantle anelasticity at different frequencies is analyzed, and the observed results of space geodesy are used to constrain the theoretical models of anelasticity. We find that Zschau's model can interpret the observed amplitude of anelastic Love number in the regime from the seismic frequency to the 18.6-year frequency. However, the theoretical Love number k<sub>2</sub> predicted by a single absorption-band model do not agree well with the observed values at M<sub>2</sub>, M<sub>f</sub>, M<sub>m</sub>, Chandler wobble and 18.6-year frequencies. Based on anelastic model and ocean tide model determined by Topex/Poseidon satellite altimetry data, we also present the theoretical values of the tidal response at M<sub>f</sub> and M<sub>m</sub> frequencies in consideration of mantle anelasticity and non-equilibrium ocean tide effects.

## ELECTROMAGNETIC METHODS FOR MONITORING EARTHQUAKES AND VOLCANIC ERUPTIONS (IAGA, IASPEI, IAVCEI)

Location: Hills 212 LT

Location of Posters: Old Gym

## A NUMERICAL APPROACH TO THREE DIMENSIONAL TECTONOMAGNETIC MODELING BY SURFACE INTEGRALS

Shin'ya SAKANAKA (Aso Volcanological Laboratory, Institute for Geothermal Sciences, Kyoto University, Choyo-son, Aso-gun, Kumamoto 869-1404, Japan, email: sakanaka@aso.vgs.kyoto-u.ac.jp).

Local geomagnetic changes are sometimes accompanied by tectonic activities such as earthquake occurrences, volcanic activities, and crustal movements. Mechanical stress change in the crust is expected as one of mostly probable causes of the local magnetic changes. In order to investigate such local magnetic changes, a new method of numerical calculation for tectonomagnetic modeling is developed and entailed problems in application of the method are discussed in this study. The new method in this study is based on surface integrals numerically estimated over the surface of a magneto-elastic medium, instead of volume integrals traditionally employed in this research field. At first, as an example of calculations for three dimensional tectonomagnetic models, magnetic changes due to an inclined columnar pressure source are evaluated in respect of several parameters. Next, making use of one of advantages of the surface integral method, which can treat arbitrarily shaped demagnetized areas, an effect of a combination of inflated and deflated sources with a demagnetized area is evaluated.

## SEISMOMAGNETIC EFFECT CONSIDERING THE INHOMOGENEOUSLY MAGNETIZED CRUST

Mitsuru UTSUGI and Yasunori Nishida (both at Division of Earth and Planetary Sciences, Hokkaido University, Sapporo 060-0810, Japan, e-mail: mithuru@ares.sci.hokudai.ac.jp and nishida@ares.sci.hokudai.ac.jp)

We present a new method to evaluate the geomagnetic change due to the inhomogeneously magnetized crust. From this method, quantitative analysis of the seismomagnetic effect can be made in the general geologic and tectonic situations in the Earth' crust. To represent the inhomogeneity of the crustal magnetization, we divide the crust into a number of compartments. Each compartment is assumed to have its own magnetic properties such as the magnetization and the stress sensitivity. Seismomagnetic field may be expressed by the summation of that from each compartment. In the present study, we used a cubic-shaped body as the compartment. The seismomagnetic field is expressed by the surface integral of a function including displacement and strain over the cubic body. In general, this finite integral cannot be solved analytically. However, the 2-D integral can be represented by analytical form using elliptic integrals to reduce the dimension of the integral to 1-D. Some model calculations reveal that the seismomagnetic fields are significantly enhanced near the place where the magnetic properties change sharply, as well as the place near the fault region.

## MAGNETIC FIELD GENERATION BY ELECTROKINETIC COUPLING IN 3-D RESISTIVITY STRUCTURES

Tsuneo ISHIDO (Geological Survey of Japan, 1-1-3 Higashi, Tsukuba, 305-8567, Japan, email: ishido@gsj.sci.gsj.go.jp)

The flow of a fluid through pores and cracks in a rock may transport electric charge along the flow path by the interaction of the moving pore fluid with the electrical double layer at the pore surface. This process is known as electrokinetic coupling. The total current density is composed of a drag current density caused by charges moved by fluid flow and a conduction current density caused by electric conduction. In order to evaluate the effects of complex 3-D resistivity structures on the generation of magnetic field at the ground surface, numerical simulations were performed. The present numerical approach simulates magnetic fields caused by subsurface fluid flow by a three-step process. First, it calculates the distributions of drag current, etc. from the underground conditions (pressure, temperature, salinity, flow rate, etc.) computed by thermohydraulic simulations. Second, it calculates the distributions of electric potential and conduction current within a 3-D finite-difference grid. Finally, it calculates the magnetic field distribution by applying the Biot-Savart law to the distributions of drag and conduction currents. The effects of inhomogeneous and anisotropic resistivity structures on the enhancement of magnetic signals on the ground surface, and its implications for earthquake-related magnetic anomalies will be discussed.

## ELECTROKINETIC PHENOMENA ON THE SURFACE OF PARTIALLY SATURATED ROCKS

Olivier GENSANE, Boris Konyukhov, Jean-Louis Le Mouel, Pierre Morat (Departement de Géomagnétisme et Paléomagnétisme, Institut de Physique du Globe de Paris, 4 place Jussieu , 75005 Paris, FRANCE, Email:gensane@ipgp.jussieu.fr)

A theoretical model and results of an experimental investigation of electrical self potential (SP) and conductivity (EC) variations on the surface of a partially saturated pillar under varying mechanical stress and atmospheric pressure in an underground limestone quarry are presented. The developed model is based on the theory of the electrical double layer and poroelasticity of partially saturated rocks. The obtained theoretical results show that SP and EC variations depend on the saturation coefficient and on the ratio of the conductive to total porosity. These results allow the local electrokinetic coupling coefficient to be obtained for partially saturated rocks as a function of the saturation, porosity and elasticity modulus. Experimental studies include SP and EC measurements on the surface of two limestone pillars. One of them is homogeneous and the other one contains a system of unstable cracks initiating mechanical stress variations. Obtained experimental results are in good agreement with the theoretical model. SP variations under varying atmospheric pressure are used for the estimation of the local electrokinetic coupling coefficient. Variations of the mechanical stress in the vicinity of active cracks are estimated using the local electrokinetic coupling coefficient and measured SP variations. These results are explained by existing fracture interaction models.

## ELECTROMAGNETIC SIGNALS RELATED TO MICROMOVEMENTS OF LIMESTONE BLOCKS: A TEST IN KARST CAVES (CENTRAL ITALY)

A. ERMINI (Department of Physics and Energy Science and Technology, University of Roma Tor



Vergata, Via di Tor Vergata, 00133 Rome, Italy); P. F. Biagi (Physics Department, University of Bari, Via Amendola 173, 70126 Bari, Italy); S.P.Kingsley (Sheffield Centre for Earth Observation Science, University of Sheffield, Hicks Building, Hounsfield Road, Sheffield S3 7RH, United Kingdom)

Since 1992 equipments for detecting electric and magnetic signals has been running inside two karst caves located in Central Apennines (Italy). The signals are recorded every ten minutes in the frequency range from some hundred Hz to some hundred kHz. On the occasion of rainfall, atmospheric pressure variations and heating we revealed electric and magnetic signals simultaneous with seismoacoustic (f=0.5, 25, 150kHz) signals. We propose a possible model to justify the observed phenomenology based on the micromovements of the limestone blocks that constitute the roof of the caves. The electrification on the new contacts created by micromovements of the limestone blocks can provide an adequate mechanism for generating charges. Such charges will redistribute in the caves so that charged capacitors can occur with respect to the floors of the caves. The moisture film on the walls of the caves can behave as a resistor and/or an inductance. In such a way equivalent RC or RCL circuits can be adopted and the electric and magnetic signals we recorded can be connected with the electric and magnetic energy stored in these circuits. Obviously, we have to suppose that several geometrically different capacitors become active in the caves during the phenomenology. The possibility that a similar phenomenology can happen wherever discontinuities as faults, geotectonic blocks and fractured zones exist seems to be realistic. In these cases, the electromagnetic energy recorded is mostly of radiating than stored type.

**JSA15/W/06-A3 1030**

**SELF-POTENTIAL ANOMALIES ON VOLCANOES**

M. J. S. JOHNSTON (U.S. Geol. Surv, Menlo Park, Ca 94025, USA, Email: mal@usgs.gov)  
J. D. Beyerle, and D. Lockner (both at U.S. Geol. Surv, Menlo Park, CA 94025)

Self-potential (SP) anomalies observed above suspected magma reservoirs, dykes, etc on various volcanoes (Kilauea, Mt Unzen - Japan, Piton de la Fournaise - Reunion Is., Miyake Jima - Japan) generate transient surface electric fields of tens of millivolts/km and generally have a positive polarity. Without a more plausible explanation, these SP anomalies are usually attributed to electrokinetic effects with poorly constrained properties. Contributions to electric fields might also be expected to result from fluid vaporization and gas transport away from hot dike intrusions, particularly since this vaporization process can dramatically change the local electrical resistivity structure. Laboratory observations of electric fields generated by pulses of fluid (water) through a hot rock at atmospheric pressure indicate the relative amplitudes of electrokinetic (EK) and fluid-vaporization (FV) potentials to be dramatically different and the signals are opposite in sign. Above vaporization temperatures, FV effects of positive sign in the direction of gas flow dominate, whereas, below these temperatures, EK effects of negative sign dominate. This suggests that the primary contribution to self-potential arises from gas-related charge-transport processes at temperatures high enough to produce vigorous boiling and vapor transport. At lower temperatures, the primary contribution is from electrokinetic effects modulated perhaps by elevation effects and low-temperature CO<sub>2</sub> and SO<sub>2</sub> gas flow. If charge generation is continuous, as could well occur above a newly emplaced dike, positive static potentials will be set up that could be sustained for many years, and the simplest method for identifying these hot, active regions would be to identify the SP anomaly they generate.

**JSA15/E/33-A3 1050**

**SELECTED RESULTS OF LABORATORY INVESTIGATIONS OF PULSE ELECTROMAGNETIC RADIATION FROM ROCKS SUBJECTED TO STRESS AND DESTRUCTION**

Michal STEFANIUK (Faculty of Geology, Geophysics and Environment Protection, University of Mining and Metallurgy, Al.Mickiewicza 30, 30-059 Krakow, Poland, Email: stefan@geolog.geol.agh.edu.pl); Tomasz Czerwinski (Geophysical Exploration Company, ul. Jagiellonska 76, 03-301 Warsaw, Email: pbg1@ikp.atm.com.pl)

The goal of the presented study was to examine a possibility of applying the electromagnetic emission from rocks into predicting rockbursts and other local geodynamic processes connected with deformation and destruction of rocks. A hand-operated press loaded rock specimens. Electromagnetic emission time-series were recorded with a two-channel equipment consisting of an EM field detector, a set of amplifiers and filters, and two digital recorders. The measurement stand was electromagnetically screened. Maximum amplitudes and spectra of recorded signals were then analysed. Rock samples of granite, syenite, sandstone, quartzite, marble, limestone, graphite, and black coal were examined. The comparative analysis of specific parameters of electromagnetic emission from different rocks was made. The coefficient of emissivity, characterising a tendency of rocks to generate electromagnetic radiation signals and the results of time-domain and frequency-domain signal analysis were subjected to the comparative analysis. The parameters were statistically processed and data files corresponding to each type of rock were compared. An attempt to evaluate a relation between the maximum signal amplitude and the strain applied to a rock sample was also made. As a result of the study, different tendencies of individual rocks to emit electromagnetic radiation were observed, the correlative dependence of the amplitude of signal emission on sample's strain was obtained, and the change of spectral composition of a signal, depending on a rock type, was evaluated. The obtained results characterise qualitatively and quantitatively the electromagnetic signal emission from selected rocks, and can make the basis for studying the genesis of this phenomenon.

**JSA15/W/11-A3 1110**

**ELECTRO-SEISMIC PHENOMENA IN SATURATED AND UNSATURATED SOIL**

Boris KONYUKHOV (Laboratoire de Geomagnetisme, Institut de Physique du Globe de Paris, 4, Place Jussieu, 75252 Paris cedex 05, FRANCE, E-mail: borisk@ipgg.jussieu.fr)

Electrokinetic phenomena coupled with seismic waves propagation in saturated and unsaturated soil are considered in a view of distant earthquakes registration. In fine-grained low permeability clayey soil the effect of the alternating electric potential generation is governed by the excitation of the colloidal-vibration potential. In high permeability soil such as a sand with a rigid matrix, this effect is related to the porosity streaming potential excitation. In the last case the generation of an alternative electric potential has been related to the expulsion of fluid from the permeable upper soil layer under the action of excess pore pressure caused by a propagating seismic wave. In sand-clay mixture the electro-seismic phenomena are more complicated and highly depend on a clay content. It is shown that in a sand-clay mixture, with the clay content lower than some critical value, electro-seismic phenomena are controlled by the colloidal-vibration potential generation and the streaming potential generation in the case of the clay content higher its critical value. The suggested models have obtained estimates of this electric field generated by seismic waves produced by different sources in the different type of soils, and physical properties of the soil measured in laboratory. The alternative electrical field is shown to be able to reach the value 10-4 V/m for natural microseism sources and 1.5 V/m for distant earthquakes.

**JSA15/E/04-A3 1130**

**STUDY OF BEHAVIOR OF PIEZO-COMPENSATING CHARGES IN SYNTHETIC ROCKS**

Tomonori MATSUDA, Hideki Sasaoka, Chihiro Yamanaka and Motoji Ikeya (Graduate School of Science, Osaka University, Machikaneyama, Toyonaka, Osaka 560-0043, Japan, E-mail: tomonori@ess.sci.osaka-u.ac.jp)

Free transient electric charges induced by stress reduction were measured for synthetic rocks made of cement and pieces of man-made piezoelectric ceramics or quartz crystals in different arrangements. We suggested an electromagnetical model of a fault, in which bound charges cancel the stress-induced piezoelectric polarization field around the fault zone [1]. When stress is changed by faulting or by micro fracturing of rocks, the piezoelectric polarization field changes giving free charges. Electromagnetic waves are generated by the change of the polarization. The peak height and the width of the electric pulse depend on the arrangement of ceramics [2]. Possible charge movements of (1) paraelectric orientation and (2) ferroelectric orientation are studied. The movement of bound charges was also simulated using a computer for these synthetic rocks containing one and two piezoelectric ceramics in different orientations. The effective piezoelectric coefficient of granite was obtained as 1.4x10<sup>-15</sup> C/N, which agrees well with theoretical estimation considering paraelectric, paired charges [3]. Some incredible legends on earthquake precursors have been explained as electromagnetic phenomena using numerical values of induced charges in these experiments [4]. Preseismic and coseismic electromagnetic nature might be clarified from the laboratory experiments.

**References:**

- [1] M. Ikeya and S. Takaki: Jpn. J. Appl. Phys., 35, Pt. 2, 355 (1996).
- [2] T. Matsuda, et al.: Chikyū Monthly, 20, 604 (1998), in Japanese.
- [3] H. Sasaoka, C. Yamanaka and M. Ikeya: Geophys. Res. Lett., 25, No.12, 2225 (1998).
- [4] M. Ikeya, T. Matsuda and C. Yamanaka: Proc. Japan Acad., 74, Ser. B, 60 (1998).

**JSA15/E/05-A3 1150**

**A POSSIBLE ROLE OF THE TWO-PHASE FLUID IN SEISMO-ELECTROMAGNETIC PHENOMENA**

Nadezhda YAGOVA (Institute of the Physics of the Earth, B.Gruzinskaya 10, Moscow, 123810, Russia, e-mail: vpilipenko@uipe-ras.scgis.ru) Viktor Yagov (Dept. of Thermophysics, Moscow Power Engineering Institute, Krasnokazarmennaya, 14, Moscow, 111250, Russia)

A new mechanism for the generation of electromagnetic fields in the Earth crust in the ULF/VLF frequency range is suggested. Among the possible mechanisms of the low frequency seismo-electromagnetic variations the electrokinetic effect seems to be one of the most promising. Some physical features which may strongly influence the fluid pressure gradients and thus field amplitudes are discussed. The rock pore water at seismogenic depths is highly mineralized. The realistic model of its phase state requires the account for at least 2 admixtures: carbon dioxide and NaCl. This leads to the existence of two-phase vapor-liquid mixture down to first ten kilometers. The following processes become important for the electrokinetic effect in the two-phase vapor-liquid mixture in the zone of super-critical to sub-critical phase transition: 1) The initial pressure/temperature impulse leads to the appearance of a segment with the sub-critical two-phase mixture. 2) Pressure impulses appear under bubble collapse, which leads to the impulsive fluid flow and changes the amplitude of the induced electric field. 3) The rock conductivity essentially changes if the diameters of a low-conductive bubble and of a pore are comparable. If the earthquake preparation is supported by microfracturing, the boundary between one-phase super-critical fluid and two phase vapor-liquid mixture displaces. The effect may be revealed in rock conductivity and in the ULF/VLF variations of the geomagnetic field.

**JSA15/E/46-A3 1210**

**CONVECTION CURRENT PRIOR TO RUPTURE IN SATURATED ROCKS**

Shingo YOSHIDA (Earthquake Research Institute, University of Tokyo, Tokyo 113-0032, Japan, also at Institute of Physical and Chemical Research (RIKEN), Email: shingo@eri.u-tokyo.ac.jp)

Laboratory experiments have been performed to clarify generation mechanism of seismo-electric signals. We pay attention to the interaction between rupture nucleation process and pore water movement. We have developed a triaxial apparatus specially designed for this purpose, in the framework of the International Frontier Program on Earthquake Research of the Institute of Physical and Chemical Research (RIKEN). This apparatus can deform rock specimen electrically isolated from the surroundings at a very slow strain rate (1<sup>-10</sup>/s). We use co-axial type feedthroughs which Nishizawa (1997) developed on the basis of a Bridgman's self-sealing mechanism. Using cylindrical specimen of intact rock saturated with water, we carried out deformation tests at a constant strain rate keeping constant confining pressure and pore pressure. During a deformation test, we continuously measured electric current through the specimen, or electric potential difference between top and bottom surfaces of the specimen. In addition, the differential stress, displacement, local strains, and pore fluid movement from the intensifier were recorded at a sampling frequency up to 1 kHz. The volumetric strain rate was obtained from the average of the strain measurements at four positions. We found that the convection current flow before the main fracture, showing good correlation with the volumetric strain rate and the water flow rate. The current density of the signal was about 1 mA/m<sup>2</sup>. This result suggests that the current is caused by an electrokinetic effect due to the water flow associated with accelerating evolution of dilatancy before the fracture.

**Wednesday 21 July PM**

Presiding Chairs: S. Uyeda (Tokai University, Japan),  
M.J.S. Johnston (US Geological Survey, Menlo Park, CA, USA)

**JSA15/W/33-A3 1400**

**INVESTIGATIONS OF TECTONOMAGNETIC VARIATIONS IN UZBEKISTAN AND EARTHQUAKE PREDICTION**

Vsevolod SHAPIRO (Institute of Geophysics, 100 Amundsen str., Ekaterinburg, 620016, Russia. Fax:+7 3432 678872, Email: seva@maglab.mplik.ru); Kakhar Abdullabekov, Mirzoid Muminov, Sabit Maksudov (Institute of Seismology, 3 Khurshid str. Tashkent, 700012, Uzbekistan. E-mail: root@seismo.tashkent.su)

Investigations of tectonomagnetic variations proved to be informative in the study of the modern geodynamic processes such as investigations of the seismotectonic processes, study of the earthquake (EQ) prediction and volcano eruption, and more sphere of application in geodynamics. Observations in situ during past several years have documented magnetic signals, which are attributed to precursory stress changes. The specific signatures of the geomagnetic variations in Uzbekistan were set up. The methods for forecasting of EQ's main parameters (magnitude M, time T and location L) were developed. Based on this approach we have predicted M, T and L for numerous EQs in Uzbekistan with M equal or above 4.0. A number of magnetic precursors of events in different regions of the globe were observed in



areas with weekly magnetised crust, that is practically excluded piezomagnetism as a source of observed variations. The ongoing efforts to identify "non-piezomagnetic" source is lead to conclusion about electric currents as an origin of observed variations. Lab and theoretical modelling is giving rise to deduction that one of the most probable sources of such variations is electrokinetic currents.

**JSA15/E/54-A3****1420****REGIONAL GEOMAGNETIC VARIATIONS AND TEMPORAL CHANGES OF SEISMIC ACTIVITY: OBSERVATION OF A SO FAR UNKNOWN PHENOMENON, ATTEMPTS OF INTERPRETATION**

Gerald DUMA (Central Institute for Meteorology and Geodynamics, Hohe Warte 38, A-1190 Vienna, Austria, email: duma@zamg.ac.at)

It will be demonstrated, that regional geomagnetic variations of high amplitudes can be correlated with the temporal changes of seismic activity in several main earthquake zones of Japan, China, California, Greece, Italy and Austria and in the volcano region of the Mt. Vesuvius. This applies to long term magnetic variations as well as to the diurnal magnetic changes (Sq-variations), the latter indicating a considerable impact of the external ionospheric electromagnetic field on the dynamics of the Earth's crust. Another observation makes this hypothesis more credible: the seismic activity in the volcano region of the Mt. Vesuvius exhibits a periodicity of about 11 years, in phase with the solar activity cycles (Duma, Vilardo, 1997). The observations can be best interpreted, both qualitatively and quantitatively, by the effect of a changing magnetization of crustal material and associated variations of tectonic stress. This phenomenon has been described by several authors in the period from 1960 to 1980 (e.g. F.D.Stacey, M.J.Johnston, T.Nagata, W.F.Kean and others), mainly based on laboratory results and not on magnetic measurements in earthquake zones. Results obtained e.g. by D.Beamish (1982, temporal variation of the lithospheric electromagnetic response function) and by F.Florindo and L.Alfonsi (1995, geomagnetic jerks and the occurrence of strong earthquakes) will be discussed in this context.

Although the present observations relate to the diurnal and long term range, they might possibly lead to a better understanding of related short term effects as well.

**JSA15/E/17-A3****1440****PRESEISMIC AND COSEISMIC GEOELECTRIC POTENTIAL CHANGES**

S. UYEDA, T. Nagao, Y. Orihara, I. Takahashi, T. Yamaguchi (RIKEN International Frontier Program on Earthquake Research, Tokai University, Shimizu 424-8610, Japan, email: suyeda@st.rim.or.jp); T. Mogi (Kyushu University); Y. Tanaka (Kyoto University); D. S. Widarto and E. M. Arsadi (RD Ctr for Geotechnology-LIPI, Indonesia)

Clear coseismic geoelectric potential changes have been observed for some earthquakes (EQ) by the VAN-type observation systems: 1) 1988 Jan. 24 M6.0 EQ in northern Okinawa Island by long-dipole network at about 50 km of epicentral distance (*r*). This EQ was preceded by a possible precursory change on Jan. 18. 2) 1996 March 6 M5.8 Yamanashi-ken Tobu EQ at *r*=10 km. This EQ was preceded by changes on Jan. 29 and Feb. 28. 3) Five EQ's off southern Sumatra Island in 1997 by short-dipole networks distributed in an area several kilometers wide at Liwa, southern Sumatra; Sept. 13 M5.0 EQ at *r*=147 km, Oct. 29 M5.7 EQ at *r*=152 km, Nov. 16 M5.5 EQ at *r*=5.5 km, Nov. 23 M5.1 EQ at *r*=174 km and Dec. 20 M5.0 EQ at *r*=146 km. None of these Indonesian EQs showed clear pre-seismic changes. 4) Less convincing coseismic change was observed for shallow 1997 May 22 M5.1 EQ by short and long dipoles in Kozu Island at *r*=6 km. This EQ, however, was preceded by a more convincing change on May 20. The changes were recorded by multiple dipoles simultaneously. Except the Indonesian cases, epicentral distance was small. Both preseismic and coseismic changes mentioned above were the only changes detected during the observation period of respective station. No changes were detected at more than one station and no station has experienced more than one sizable EQ so far. Simultaneous detection of changes at multiple stations and repeatability of correlatable changes and EQ are still to be awaited. Critics on the VAN - method often argue that if VAN's SES is generated by stress changes at EQ source, coseismic changes much stronger than SES should be observed, contrary to VAN's experience. Reception of the coseismic changes reported here do not seem to support the criticism, however, because within the timing precision of the recording system, the changes took place at the time of arrival of seismic waves. They may be so-called "seismo-electric effect". True co-rupture changes have not been observed at our frequency range (<Hz)

**JSA15/E/19-A3****1500****POSSIBLE ELECTROMAGNETIC PRECURSORS FOR 1995 HYOGO-KEN NANBU (KOBE) EARTHQUAKE**

Y. ENOMOTO (Mechanical Engineering Laboratory, Tsukuba, Japan); Y. Fujinawa (National Research Institute for Earth Science and Disaster Prevention, Tsukuba, Japan); M. Hata (Aichi Prefectural University, Aichi, Japan); M. Hayakawa (University of Electro-Communications, Chofu, Japan); Y. Kushida (Yatsugatake South Base Observatory, Kita-Koma, Japan); K. Maeda (Hyogo College of Medicine, Nishinomiya, Japan); T. Nagao (Tokai University, Shimizu, Japan); K. Oike (Kyoto University, Uji, Japan); T. Okamoto (Fukui College of Technology, Sabae, Japan); and S. UYEDA (RIKEN International Frontier Program on Earthquake Research, c/o Tokai University, Shimizu 424-8610, Japan, email: suyeda@st.rim.or.jp)

A synthesis of reported possible electromagnetic precursors related to the devastating 1995 M7.2 Hyogo-ken Nanbu (or Kobe) earthquake is presented. The data include: DC geoelectric potential change (Okamoto et al., 1996); ELF (223Hz) magnetic field peak (Hata et al., 1997); VLF (1-9kHz) Radio (Jav e pulse-like signal peaks (Fujinawa and Takahashi, 1995); Abnormal behavior of VLF (ca. 10 kHz) Omega wave transmission (Hayakawa et al., 1996); Peaks in the number of spike-like VLF (1-20kHz), and LF noise (163kHz) (Yamada and Oike, 1996); MF to HF (higher than 1 MHz) fluctuation of earth current (Y. Enomoto, pers. com.); 22.2MHz emissions (Maeda and Tokimasa, 1996); Back-scattered VHF FM-wave (77.1 MHz) (Kushida, 1996). These signals were interpreted either as emitted from the earthquake source area like in the VAN case, or as caused by pre-seismic ionospheric disturbances above the focal region. Many of the reported precursors in ELF to MF range occurred 7 days before the main shock and there seems to be a general tendency that higher frequency precursors occurred closer to the earthquake occurrence. Precaution against lightning discharges seems critically important as they generate similar signals. It was probably the first case where multiple electromagnetic methods detected possible precursors for one earthquake, some stations being hundreds of kms distant from the epicenter. Totality of the reported anomalous phenomena appears to warrant further investigation.

**JSA15/W/29-A3****1540****ELECTRIC AND MAGNETIC FIELDS ACCOMPANYING SEISMIC AND VOLCANIC ACTIVITY**

M. J. S. JOHNSTON and R. J. Mueller (U.S. Geol. Surv, Menlo Park, CA, 94025, USA, Email: mal@usgs.gov)

Continuous ground-surface observations of local magnetic and electric fields have been obtained in the near field of numerous felt earthquakes, near active faults and on volcanoes during the past 25 years. These data provide a reference set of data documenting the form and amplitudes of these fields during seismic and volcanic activity. The primary features of data taken along the San Andreas fault show that 1) near-fault magnetic field disturbances rarely exceed a few nanoteslas, 2) coseismic signals, with amplitudes from 0.7 nT to 1.3 nT, are routinely measured for earthquakes with magnitudes greater than 5.5, 3) preseismic signals of about 1.5 nT have been observed on just two occasions, 4) anomalies of a few nanoteslas are generated during aseismic strain events, and 5) near-fault electric field disturbances rarely exceed a few mv/km. These observations are generally consistent with seismomagnetic models based on geotectonically and seismically determined fault parameters for these events. Electrokinetic processes resulting from rupture of fluid filled compartments at hydrostatic to lithostatic pore pressures can generate transient signals in the frequency band 100 Hz to 0.01 Hz. Large-scale fluid driven processes are not evident in either near-fault magnetic field measurements or local strain measurements in the epicentral region minutes to weeks before large earthquakes. For volcanic events, contributions from different physical processes can be identified during the various eruption stages. Slow processes (weeks to months) include near-surface thermal demagnetization effects, piezomagnetic effects, and effects from rotation/displacement of magnetized material. Rapid processes (seconds to days) include piezomagnetic effects from instantaneous stress redistribution with explosive eruptions and electrokinetic effects from rupture of high fluid pressure compartments commonly encountered in volcanic regions. The most interesting signal in the Long Valley Caldera is a systematic decrease of 0.8-1 nT/year in magnetic field that has occurred in the caldera since 1989 in concert with inflation of the resurgent dome. The net change of 8 nT can be explained with a simple volcanomagnetic model involving pressure increase of 50 MPa/year at a depth of 7 km under the resurgent dome. This model is derived from the intrusion model that best fits the surface deformation data. Ionospheric disturbances generated by trapped atmospheric pressure waves are excited by earthquakes and volcanic eruptions and propagate to great distances.

**JSA15/E/08-A3****1600****VOLCANOMAGNETIC SIGNALS ASSOCIATED WITH THE QUASI-CONTINUOUS ACTIVITY OF MERAPI VOLCANO (INDONESIA): 1990-1998**

Jacques ZLOTNICKI (Laboratoire de Geophysique(a), UMR 6530, 3d av de la recherche scientifique 45071 Orleans cedex 02, France. Email: jacques.zlotnicki@cns-orleans.fr) Marcel Bof (L.E.T.I., Dsys, Cea Grenoble, 17 rue des Martyrs, 38054 Grenoble, France); Paul Yvetot(a), Laurent Perdereau(a) & Yochi Sasai (Earthquake Research Institute(b), Tokyo University, Japan)

Merapi volcano in Java Island (Indonesia) is an andesitic stratovolcano, which presents long periods of effusive activity during which an endogenous dome is continuously growing. The viscous lava dome gives rise to unstable blocks which collapse or to pyroclastic flows. When the volcano does not exhibit any surface activity, the overpressure within the volcano slowly increases. Depending on the quietness duration the unrest of the volcano can start with an explosive phase during which the former dome is partly destroyed. Different time constants magnetic variations are observed during the 1990-1998 period which includes one gas plume emission on August 26, 1990 and four eruptions on Jan., 1992, Nov., 1994, Jan. 1977, and July 1998. Compared with other types of active volcanoes the observed volcanomagnetic variations are very small, almost a few nanoteslas. To identify the variations associated with the global activity of the volcano from the signals correlated with each unrest phase, one has to dissociate the different time constant variations over the nine years time span. When long-term trends are removed from the magnetic field in each station of the network, an outstanding correlation between all the magnetic differences is emphasised. The variations point out cycles of activity that fit the stress field evolution within the edifice. Some of the volcanomagnetic variations are precursory signals as the three months decrease, up to 1.8 nT, preceding the 1992 eruption, or the long period decrease, of 2 nT in a remote station, before Jan., 1997 eruption.

**JSA15/E/30-A3****1620****COSEISMIC ELECTROMAGNETIC VARIATIONS MEASURED DURING AN ERUPTIVE PHASE OF MERAPI VOLCANO/CENTRAL JAVA**

Andreas MUELLER (GeoForschungsZentrum Potsdam, 14471 Potsdam, Germany, Email: grassus@gfz-potsdam.de)

During an eruptive phase of the Merapi volcano/Central Java in July 1998 magnetotelluric measurements were carried out in order to get structural information about the volcanoes interior. During the volcanoes activity in the campaign we decided to extend the measuring time at one side in order to observe electromagnetic changes connected to the eruption. A clear correlation was found between the electromagnetic variations and a nearby seismological station. While the correlation in the magnetic component can be explained by the movement of the induction coils in the earth's magnetic field the correlation in the electric channels remains unclear. Several mechanisms proposed by other researchers will be discussed here.

**JSA15/E/10-A3****1640****ELECTROMAGNETIC SIGNALS RELATED TO MARCH 9, 1998 ERUPTION OF LA FOURNAISE (REUNION ISLAND).**

Jacques ZLOTNICKI (Laboratoire de Geophysique(a), UMR 6530, 3d av de la recherche scientifique 45071 Orleans cedex 02, France. Email: jacques.zlotnicki@cns-orleans.fr) & Departement des Observatoires Volcanologiques(b), I.P.G.P., France) Jean Louis Le Mou & Jean Louis Cheminee(b), (I.P.G.P., Paris, France) Paul Yvetot(a) & Marie Hanne Ardisson(a), Michel Parrot (LPCE, Orleans, France) Thomas Staudacher (Observatoire du Piton de la Fournaise, Reunion)

La Fournaise volcano is a very active basaltic volcano, which has erupted in March 1998, after 6 years of quietness. First fissures opened on the north flank of the 2640m- high cone. After some hours, the effusive activity was located at the cone basis and gave rise to two cones. Two days later a small cone appeared on the Southwest cone flank, the activity of which subsided a few days later. On August 10, a new effusive activity appeared on the northern flank, outside Enclos Fouque caldera wall. The effusive activity lasted till October. Since several years a lot of magnetic (total field and components), telluric and Self-Potential recordings have been performed on this volcano. We will focus on the spatial and temporal variations: Magnetic signals, a few nT in amplitude, have appeared some weeks before the eruption; Magnetic signals were emphasised the day of the outburst, when the magma has migrated towards the ground surface. Amplitudes, up to 7 nT, were recorded; Telluric signals have been recorded in several autonomous stations. Some signals have appeared with a phase delay, depending on

## INTER-ASSOCIATION

the location of the station compared to the emplacement of the activity; Finally, SP signals, up to 2.5 V/km were recorded at the station located on northern cone foot.

**JSA15/E/40-A3** **1700**

### MOTIONALLY-INDUCED EM FIELDS: NATURAL NOISES FOR MONITORING MIYAKE-JIMA VOLCANO, IZU-BONIN ARC, JAPAN

Yoichi SASAI (Earthquake Research Institute (a), Univ. of Tokyo, Bunkyo-ku, Tokyo, 113-0032, Japan, email: sasai@eri.u-tokyo.ac.jp); Jacques Zlotnicki (Laboratoire de Geophysique (b), UMR 6530, 3d av de la recherche scientifique, 45071, Orleans, cedex 02, France); Makoto Uyeshima (a), Wataru Sekiguchi (a), Paul Yvetot (b), Yasunori Nishida (Graduate School of Science, Hokkaido Univ., Sapporo, 060-0810, Japan), Kunio Rikiishi (Fac. Sci. and Tech., Hirosaki Univ., Hirosaki, 036-8561, Japan); Yoshiharu Nagaya (Hydrographic Office, Japan Maritime Safety Agency, Chuoh-ku, 104-0045, Japan)

Miyake-jima is one of the most active basalt volcanoes in Japan. Since it has erupted at a rather regular interval in 1940, 1962 and 1983, the volcano is suggested now at a very preparatory stage to the next eruption. The typical activity is the flank fissure eruption: Basaltic magma rises up silently toward a depth of a few km below the summit and then extrudes rapidly by making tensile cracks. In order to monitor the gradual uprise of magma head, the EM observations started in 1995. Now we have 8 proton precession magnetometers, 2 short-span SP arrays, a continuous MT station and a long base-line SP array using telephone cables. Miyake-jima volcano is surrounded by the Pacific Ocean where the dominant ocean current Kuroshio, 100 km wide and 2 - 4 knots speed, flows changing its direction with time. The meander of Kuroshio results in magnetic field changes of more than 10 nT with a few months' duration along with the associated SP variations. They may completely obscure possible volcano-electromagnetic effects.

Electric potential differences by submarine cables and magnetic field data on nearby islands are available to investigate the nature of the motionally-induced fields. Analysis of tidally-induced magnetic fields on Miyake-jima island revealed a typical feature of the island effect, i.e. spatial discrepancy of the Z component amplitude due to distortion of induced electric currents by a resistive island. Electric field data from near-shore electrodes connected with telephone cables over the island seem to be effective for cleaning the irregular magnetic variations arising from meandering Kuroshio.

**JSA15/P/06-A3** **1720**

### VOLCANIC LIGHTNING

Stephen R. MCNUTT (Alaska Volcano Observatory, Geophysical Institute, Univ. of Alaska Fairbanks, P.O. Box 757320, Fairbanks, AK 99775, USA, email: steve@giseis.alaska.edu)

Volcanic lightning is a common yet poorly studied phenomenon. A literature search shows that lightning has occurred at more than 55 volcanoes in association with eruptions of various types and sizes; it is especially common during larger eruptions. Reports at night are slightly more numerous than those during the day, presumably because lightning is easier to see at night. Volcanic lightning was responsible for the only deaths reported at Paricutin from 1943-1952 and also killed one person during the eruptions at Rabaul in 1994. A particularly well documented case of lightning occurred at Mt. Spurr, Alaska in 1992. Lightning was detected on seismic stations as simultaneous spikes and simultaneous gain-ranging (a feature that normally lowers the gain at a station when the signal level begins to saturate). Spikes had typical durations of 0.04-0.05 sec. Using uniform criteria we found 28 lightning flashes in the June 27 eruption, 29 in the August 18 eruption, and 3 in the September 17 eruption. The August lightning was strongest, June the weakest, and September intermediate, using peak voltages on station RSO, 94 km away. In all three eruptions the first lightning was recorded 20-26 minutes after the onset of the eruption, suggesting that charge separation occurred in the convecting cloud rather than at the vent. Data recorded by a Bureau of Land Management lightning detection system for the August eruption showed negative polarities for the first 12 recorded flashes and a positive polarity for the last. This suggests a charge separation based on particle size. All three eruptions were quite similar with durations of 3.5-4 hours, and tephra volumes of 44-56 million m<sup>3</sup>. The August eruption, however, produced stronger volcanic tremor, 30 cm<sup>2</sup> reduced displacement as compared with 16 cm<sup>2</sup> for June, and thus tremor amplitude correlates crudely with lightning strength. The September eruption occurred during the coldest and driest atmospheric conditions, which may explain the small amount of lightning. In general, lightning is important because it can confirm that eruptions are in progress, although the information may be limited by the long delay from eruption onset to first lightning and the variability of eruptive and atmospheric conditions.

**JSA15/W/07-A3** **1740**

### IMAGING DEEP RESISTIVITY STRUCTURE OF ACTIVE FAULTS IN NE JAPAN: PRELIMINARY RESULTS

T. GOTO (Aichi Univ. Educ., Kariya, Japan, email: tgoto@aecc.aichi-edu.ac.jp); Y. Ogawa (Geol. Surv. Japan, Tsukuba, Japan); M. Mishina (Tohoku Univ., Sendai, Japan); M. Uyeshima (ERI, Univ. Tokyo, Tokyo, Japan); T. Kasaya, M. Ichiki, N. Oshiman (DPRI, Kyoto Univ., Uji, Japan); S. Sakanaka (AVL, Kyoto Univ., Kumamoto, Japan); Y. Takahashi, T. Nishitani (Akita Univ., Akita, Japan); Y. Takahashi, Y. Honkura (Tokyo Institute of Technology, Tokyo, Japan); H. Satoh (Hokkaido Univ., Sapporo, Japan); H. Murakami (Kochi Univ., Kochi, Japan)

Deep resistivity structure of active faults in NE Japan was investigated by wide-band magnetotellurics (MT). The study area is under compression tectonics. The thrust fault systems on both sides of the mountain range are believed to help uplift the mountain block. The recent deep reflection data support this idea. We had 15 MT sites aligned on a 45km profile running across the mountain range. We used simultaneously 5 sets of 5 component MT systems and 5 sets of telluric-only systems. Preliminary two-dimensional inversion results using TM mode revealed the deep sub-vertical conductors, which probably coincide with the deep active faults imaged by the reflection seismic experiments. Lower crustal conductor at around 20km depth also underlies the whole profile.

## Thursday 22 July AM

Presiding Chairs: J. Zlotnicki (Laboratoire de Geophysique, Orleans, France), S. Uyeda (Tokai University, Japan)

**JSA15/W/10-A4** **0900**

### VARIATION OF FREQUENCY CONTENT OF ELECTROMAGNETIC RECORD AT THE APPROACH AND AFTER THE 21 JULY 1995, M=5.7, YONGDEN EARTHQUAKE

Jacques Zlotnicki (CNRS, Laboratoire de Geophysique d'Orleans, 3D Avenue de la Recherche Scientifique, 45071 Orleans, Cedex 02, France, E-mail: jacques.zlotnicki@cnrs-orleans.fr); Vladimir KOSSOBOKOV (International Institute for Earthquake Prediction Theory and Mathematical Geophysics, Russian Academy of Sciences, 79-2 Warshavskoye Shosse, Moscow 113556, Russia,

E-mail: volodya@mitp.ru); Jean-Lois Le Mouel (IPGP, Laboratoire de Geomagnetisme, 4 Place Jussieu, 75252 Paris, Cedex 05, France, E-mail: lemouel@ipgp.jussieu.fr)

The frequency temporal analysis of electromagnetic field recorded during 05/30/95-08/18/95 at the site about a hundred kilometers to the north from the epicenter of the 21 July 1995 Yongden earthquake (China) has shown a clear systematic variation. In an ultra low range from 0.1 to 0.005 Hz a dramatic threefold decrease of the frequency of the maximal energy concentration is observed, i.e. from 0.05 on 05/30/95 to 0.015 Hz few hours before the earthquake. The decrease is a step-like, nearly monotonous and continues after the Yongden earthquake for about two weeks reaching the minimum of 0.01 Hz just before an abrupt disappearance. At the after the main seismic event stage the record shows three multiple frequencies of maximum energy concentration, thus suggesting a transition of the lithosphere crust system to a chaotic behavior. The results are subject to further understanding and interpretation. More data, both electromagnetic and seismic, are needed to outline the source of the observed phenomenon, its relation to tectonic environment and stress field, as well as to the universal scenarios of transition to a catastrophe.

**JSA15/P/03-A4** **0920**

### ANOMALOUS IONOSPHERIC SPORADIC E LAYERS OBSERVED BEFORE THE HYOGOKEN-NANBU EARTHQUAKE OF M 7.2

Tadanori ONDOH (Space Earth Environment Laboratory, Kitano, Tokorozawa, 359-1152, Japan, email: 77771903@people.or.jp)

Strong sporadic E layers of frequencies above 6.5 MHz (~100 km in altitude) were observed for 1300-1430 JST on January 15, 1995 at Shigaraki, 100 km northeast of the epicenter of the Hyogoken-nanbu earthquake which occurred at 0546 JST on January 17, 1995 near Kobe, Japan, and also at 1300 JST on January 15 at Kokubunji, 500 km east of the epicenter. The day of January 15, 1995 was a geomagnetically quiet one ( $\Sigma K=3$ ), and the local geomagnetic index for 12-15 JST on January 15 was  $K=0$  at Kakioka near Kokubunji. There was no solar flare during the daytime of January 15. The sporadic E layer normally appears during the daytime from April to August at mid and low latitudes in the northern hemisphere. Consequently, the anomalous sporadic E layers observed on January 15 seem to be a precursor ionospheric phenomenon of the Hyogoken-nanbu earthquake of January 17, 1996. Radon emanations of about 10 times the normal ion density were observed within 200 km from the epicenter before the Hyogoken-nanbu earthquake (Wadatumi 1998). However, the radon increase is too small to produce the anomalous sporadic E ionization, even if the radon emanations would go up to the ionosphere. Since the sporadic E layer is often observed simultaneously with strong lightning discharges in the tropical region, the anomalous sporadic E layers of January 15 could be caused by unknown seismic discharges.

**JSA15/W/30-A4** **0940**

### INVESTIGATION OF ELECTROMAGNETIC WAVE RADIATION IN THE VLF RANGE ASSOCIATED WITH EARTHQUAKES

Hisatoshi BABA, M. Sugiura, T. Asada (Research Institute of Science and Technology, Tokai University, 1117, Kitakaname, Hiratsuka, Kanagawa, 259-1292, Japan; ph:+81-463-58-1211; fax:+81-463-50-2034; E-mail: hbaba@keyaki.cc.u-tokai.ac.jp); M. Kawazoe (School of Engineering II, Tokai University, 2-28-4, Tomigaya, Shibuya, Tokyo, 151, Japan; 81-3-3467-2211); and S. Iizuka (Faculty of Marine Science and Technology, Tokai University, 3-20-1, Orido, Shimizu, Shizuoka, 424-8610, Japan; ph:+81-543-34-0411)

Investigations of electromagnetic radiation possibly associated with earthquakes have been made in the last two decades. In some studies the relation between the change in the electromagnetic noise level and the occurrence of earthquakes has been discussed. However, the discussions on the relationship between the changes in the noise level or the changes in the frequency of signals per hour and the occurrence of earthquakes were not sufficient, because wave forms of these signals were in most cases not recorded. In the present study, signals in the frequency range from 1 kHz to 10 kHz are recorded. Most of these signals have been determined to be atmospheric. Therefore one of the fundamental problems is to establish a method of delineating signals that are related to earthquakes from those that are not related to them. The location of the source of atmospheric signals generally changes every time, while signals associated with an earthquake appear to be generated in a definite area close to its epicenter. This feature, if established, would be useful in distinguishing signals related to an earthquake from atmospheric signals. In our instrument, signals are recorded digitally, and the direction of approach is calculated for each signal. During the one and one half years period of our observation we have obtained a result that among the four earthquakes that occurred during this period, three generated signals in the areas close to their epicenters several days prior to their occurrences. The magnitudes of these earthquakes were about 5, their depths 20 to 40 km, and the epicentral distances from our recording networks less than 100 km. We have concluded that these signals can be regarded as being precursors of the three earthquakes. Earthquakes, which occurred in the ocean floor, did not generate signals in the areas close to their epicenters. These earthquakes were of magnitude smaller than 4, more than 50 km in depth, or more than about 100km in distance.

**JSA15/E/49-A4** **1000**

### A COMPARATIVE STUDY OF THE LITHOSPHERE - IONOSPHERE COUPLING MECHANISMS

Michail GOKHBERG, Oleg Pokhotelov and Sergei Shalimov (all at Institute of Physics of the Earth, 123810 Moscow, Russia, Email: gokhberg@dir.iophys.msk.su; pokh@uipe-ras.scgis.ru)

A review of coupling mechanisms that could transform geophysical field anomalies generated at the source of seismic activity into large-scale ionospheric disturbances is presented. The problem is critically analyzed from different points of view, which involve magnitude and intensity of the possible sources in the lithosphere and on the Earth's surface, energy transfer upward into the ionospheric level (both dissipation and transformation into the ionospheric disturbances), the possibility of the ionospheric anomalies description in terms of unique model. Nonstationary boundary conditions that might modulate evaporation and outgassing rate are discussed. The latter processes can produce large scale atmospheric thermal and electromagnetic anomalies possibly related to the earthquake preparation and comprise greenhouse and radon gas anomalies. Two hypothetical coupling mechanisms are outlined: by electromagnetic low-frequency waves and by acoustic-gravity waves, which can be generated by the nonstationary atmospheric gas anomalies. The propagation of these waves through the atmosphere up to the ionospheric heights, and corresponding dissipation factors are considered. An efficiency of action by these waves from below upon the ionospheric plasma, and their possibility to cause observable ionospheric pattern is quantitatively estimated.



**JSA15/W/08-A4** **1040****SOME FEATURES OF THE ULF BAND ELECTROMAGNETIC FIELD CHANGES RELATED WITH EARTHQUAKE SWARM**

Yukio FUJINAWA, Takumi Matsumoto (NIED: National Research Institute for Earth Science and Disaster Prevention, E-Mail: fujinawa@bosai.go.jp), Koza Takahashi (CRL: Communications Research Laboratory), Hiroshi Itaka, Shigeru Yamane (ETL: Electrotechnical Laboratory), Takeshi Nakayama, Hideo Sakai (Toyama University), Toyooki Sawada (Kyoto University), and Yuji Enomoto (MEL: Mechanical Engineering Laboratory)

Electric field variations of dc, ULF (0.01-0.7 Hz), VLF (1-9 kHz) bands have been observed by using the borehole antenna at ten sites in Central Japan including the Hodaka site, Gifu Prefecture. Conspicuous anomalous changes were found at the Hodaka site to accompany with the nearby seismic activity at the border of Nagano, Gifu and Toyama. Prefectures occurred during the period from August to November 1998. The anomalous change correlated with the crustal activities is the second one during the observation period at Hodaka site since 1993. The first one was observed at the time of a small scale steam explosion in July 1996. The change is so clear that it is easy to discriminate from the normal calm state except very short duration of changes which were very probably induced by the large-scale lightning activities. The present electric field changes appeared in the whole three frequency bands of dc, ULF and VLF bands, but the former two bands dominated, and the VLF band appeared only at the occasion of conspicuous earthquake activities. The VLF band components were small in amplitude, so as not to be observed at nearby stations of distance about several tens kilometers with the result that the source were not located by the location system available now (Fujinawa et al., 1997). But it is suggested that the source of the VLF band was in the region of seismic activity. The vertical components provided larger signals in comparison with the horizontal components suggesting that the ULF and dc components are induced by the sources deep underground. The electric anomalous changes are suggested due to the electrokinetic effects related to the water flow activated by the magma injection around the zones. Strong similarities among the electric field anomalous changes hitherto reported by the VAN group (Varotsos et al., 1996), Uyeda group at the time of the off-Noto peninsula earthquake in 1993 (Nagao et al., 1996) and those at the Izu-Oshima observation sites at the time of small volcanic activity of 1990 in the Izu-Oshima island by us (Fujinawa et al., 1992) indicated that the anomalous electric signals associated with earthquake can be attributed to electric field changes induced by water flow causing earthquake in agreement with the seismogenetic process hypotheses on the basis of dominant role of fluids in the stress-concentrated region (e.g., Sibson, 1981; Bernard, 1992).

**JSA15/W/17-A4** **1100****MODELLING OF THE "TERMINATOR-TIME" EFFECT: CONSIDERATION OF A SUGGESTED EARTHQUAKE PRECURSOR**

Craig J. RODGER, and Mark A. Clilverd (both at UASD, British Antarctic Survey, Cambridge CB3 0ET, UK, email: cjr@mail.nerc-bas.ac.uk); Neil R. Thomson (Physics Department, University of Otago, Dunedin, New Zealand)

It has been reported that propagation of very-low frequency (VLF) waves in the Earth-ionosphere waveguide might provide an indication of imminent earthquakes. Such narrow band data from Inubo, Japan suggested that transmissions from Omega, Japan, 1000 km away, might be influenced by pre-earthquake processes. In this report the authors defined the Terminator Time (TT) as the time where a minimum occurs in the received phase (or amplitude) during sunrise and sunset. A few days before an earthquake the TT was observed to significantly deviate from the monthly averages, producing a longer "VLF day". The TT effect has been explained through some rather simple modelling by a 1-2 km drop in the VLF reflection height at the lower ionospheric boundary. Here we consider the application of more realistic propagation models to this situation. Comparisons are made between the more realistic models, those presented previously, and the effects of known influences upon the altitude of the lower ionospheric boundary.

**JSA15/W/31-A4** **1120****METHOD OF MEASURING "ABSOLUTE" VLF/LF PHASE (FREE OF NON-PROPAGATION EFFECTS) TO TEST FOR SEISMIC- INDUCED IONOSPHERIC PERTURBATIONS**

Richard DOWDEN and James Brundell, (LFOEM Research, 161 Pine Hill Rd, Dunedin, New Zealand.) Neil Thomson, (Physics Department, University of Otago, New Zealand.)

A seismic-induced ionospheric perturbation appears a few days before an earthquake and continues for days or weeks after the earthquake [1]. The perturbation induced by the Kobe earthquake was measured by the advance/retard of the terminator times (TT) of the 1000-km propagation of the 10.2 kHz transmission from Omega Japan (Tsushima) to Inubo. This perturbation was that expected if the VLF reflection height had decreased some 1-2 km [1]. If so, the corresponding midday phase change due to propagation of the VLF signal would have been 10° to 20°. Over several days, any slow phase drift due to propagation can be masked by phase drift in the receiver. Thus a receiver using a reference which is off frequency by only 1.5 parts in 10<sup>11</sup> (about that of a rubidium oscillator) logging the received phase of a perfect transmitter at exactly 10.2 kHz would see a spurious phase drift of 5°/day. This is about that of the Kobe effect due to propagation. This is why the TT method was used instead. However, a drift-free receiver can be made using an oscillator of only mediocre stability of only 1 part in 10<sup>6</sup> (about that of a cheap quartz wristwatch) provided the oscillator is reset to zero phase every second by GPS. The "selective availability" of GPS means that the individual GPS pulses can be early or late by up to 1 microsecond. This will introduce a phase jitter in even a perfect oscillator at 10.2 kHz of up to 3° but there would be no long term drift at all relative to GPS which can be the reference for all such receivers in a network. The phase jitter is reduced to below detectability if the phase received from a stable transmitter is averaged over several hours about midday. Phase records from such a drift-free receiver over some months show a slow phase drift of a few tenths of a degree per day due to the seasonal variation of the midday sun altitude. Large phase perturbations due to solar flares occur but these are easily allowed for. Departures from this seasonal drift, accumulating, say, 1° over a few days would be noticeable. This is less than a tenth of the effect of Kobe earthquake. A network of many receivers, each logging many transmissions, enables hemisphere-wide perturbations (e.g., solar flares) to be allowed for and also allows location of the perturbing source.

**JSA15/E/39-A4** **1140****STUDY OF IONOSPHERE DISTURBANCES, CALLED BY QUARRY EXPLOSIONS, IN RANGE OF EXTREMELY LOW FREQUENCIES**

Mikhail GOKHBERG (United Institute of Physics of the Earth, B. Gruzinskaya, 10, Moscow, 123810, Russia, e-mail: gokhberg@dir.iphys.msk.su); Alexander SARAIEV and Mikhail Pertel (St. Petersburg State University, Universitetskaya nab. 7/9, St. Petersburg, 190034, Russia, e-mail: aks@aks.usr.pu.ru)

Parameters of ionosphere processes are used for the study of wide class of seismic signals,

including the ionosphere precursors of earthquakes. One of the most effective ways of modeling of seismoionosphere connections is the influence on ionosphere by powerful explosion. Earlier for study of ionosphere disturbances was applied the method of soundings in megahertz frequency band. Very low frequencies 10-15 kHz (system "Omega") was used also. We studied the explosion acoustic influence on the propagation of extremely low frequencies (ELF) radio waves with use of the ELF radio station "Zevs", situated on Kola peninsula. Its operational frequencies changes from 30 up to 200 Hz, a long-range action makes about 10 000 km. The observation point was near St. Petersburg on distance 950 km from transmitter. Quarry explosions near transmitter, observation point and profile between them were taken into account. The amplitudes of electric and magnetic fields before explosions as background situation, and also in time and after explosions, as response on acoustic influence were registered. The disturbances of electric and magnetic field amplitude, observable after explosions, as oscillations with period about one hour, were registered. The depth of modulation reaches 15-35 %. The oscillations of such period in the ionosphere correspond to the phenomena, observable in the ionosphere before earthquakes. The obtained results indicate about perspective of use of the ELF-station "Zevs" for monitoring of ionosphere disturbances, connected with earthquakes preparation. The work was performed with the support of "Universities of Russia" program, N 2140.

**JSA15/E/09-A4** **1200****STATISTICAL PARAMETERS OF ULF ELECTROMAGNETIC NOISES AND SEISMICITY**

Nadezhda YAGOVA, Viacheslav Piliipenko (Institute of the Physics of the Earth, Moscow 123810, Russia, e-mail: vpiliipenko@uip-ras.scgis.ru); Kiyohumi Yumoto (Kyushu University, Fukuoka 81-812, Japan; e-mail: yumoto@geo.kyushu-u.ac.jp)

The analysis of ULF (ultra-low-frequency 0.001 - 0.1 Hz) geomagnetic noises at 3 low-latitude stations of the network "210 Magnetic Meridian" showed that their intensity is controlled mainly by the geomagnetic activity. For geomagnetically quiet conditions the ULF background amplitudes and spectral content remain stable for several months. The analysis of amplitudes and spectral slope of nighttime magnetically quiet ULF noises showed some middle-term (several weeks) enhancements at the low frequencies correlated with moderately strong (M>5.5) close-by earthquakes. No anomalous variations at the magnetically conjugated Australian stations were observed. These variations of ULF noise parameters have a local character and they cannot be explained by known magnetospheric or seasonal meteorological phenomena. The hypothesis about their possible seismic origin is discussed. The spectral features of these noises are in accordance with this suggestion. It is proposed that the existing global networks of magnetic stations could be effectively incorporated into seismic warning systems.

**JSA15/E/44-A4** **1220****NEW PECULIARITY OF THE NATURAL BACKGROUND ARJUND 1 HZ FREQUENCY RANGE**

Michail GOKHBERG, (Institute of Physics of the Earth, 123810 Moscow, Russia, Email: gokhberg@dir.iphys.msk.su)

In my report the diurnal and seasonal distribution of the wide band natural noise level in the frequency range 0.5-5 Hz are presented. These results are based upon the analysis of data during 1996-1997 obtained at two observatories: one is located in the center of European part of Russia (obs. Borok) and another one in the middle of Siberia (obs. Mondy). The correlation of intensity variation from the different parameters as index of geomagnetic activity, local temperature, clouds, rain precipitation, local storms, etc. are discussed. Strong variations of intensity are shown. The typical time scale corresponds to several gradations: hours, days and month. Such variation of intensity is related to the natural phenomena in the absence of seismic activity start to be a critical issue for the use of this frequency range for earthquake prediction. Some points of view and recommendation for discrimination possible anomaly related with earthquakes and the background intensity variation are presented. The special attention in the discrimination problem solving is paying to the simultaneous registration of electric and magnetic field components. The discrimination ability in this case is effectively enhanced.

Thursday 22 July PM

Presiding Chairs: S. Uyeda (Tokai University, Japan), M.J.S. Johnston (US Geological Survey, Menlow Park, CA, USA)

**JSA15/E/53-A4** **Poster** **1400-01****POSSIBLE TECHNIQUE FOR EM MONITORING OF UNDERWATER EARTHQUAKES AND TSUNAMI**

BOYARCHUK K.A. (General Physics Institute, 38 Vavilov Str., Moscow, 117942, Russia, Email:boy@kapella.gpi.ru); Pulinets S.A. (IZMIRAN, Troitsk, Moscow Region, 1420942, Russia, E-mail: pulse@izmiran.rssi.ru); Svirko Yu.P. (Applied Physics Department, University of Tokyo)

Electromagnetic field variations over the ocean can occur during earthquakes and tsunami because of the following effect. It is known that the acoustic wave propagation in an electrolyte solution, for example in ocean water, is accompanied by stimulation of a variable electric field inside a solution. The reason of given effect is the charge separation because of various weights and mobility of cations and anions. Owing to that the ions of different kinds are dragged in different way by driven solvent. Underwater earthquakes can cause strong perturbation of a water layer at the epicenter area, and the gear of transfer of energy from the oscillating bottom to a layer of a liquid can be a resonant type. Thus a layer of water by a depth about several kilometers is a natural resonator with a determined set of frequencies, lying in range of frequencies of seismic processes. Therefore effective transfer of energy from the driven bottom to the bulk of water is possible. The similar effect can be responsible for generation EM waves of a range 0.1 - 10 Hz in seismic regions. Thus the application of given effect for monitoring of geophysical hazards is possible.

**JSA15/W/18-A4** **Poster** **1400-02****ELECTRICAL POTENTIAL SIGNALS FROM FRACTURED CRUSTAL ROCKS**

O. C. CLINT (1), P. R. Sammonds (1), Yoshida, S (2), (1) Rock and Ice Physics Laboratory, University College London, London, UK. (2) Earthquake Research Institute, University of Tokyo, Tokyo, Japan

Fluid flow through porous rocks yields measurable electrical convection currents. The electrical potential anomalies due to this fluid flow depend on the applied pressure gradient. If the existing pore network of a rock medium changes during compaction and dilatancy, a corresponding electrical potential should be observed. We report results from triaxial deformation experiments on sandstone to investigate these expectations. The temporal electrical potential change and streaming potential were measured during constant strain rate experiments. Confining pressures were varied between 20MPa to 100MPa with pore fluid pressures ranging between 10MPa to 50MPa at room temperatures. Microseismicity was



recorded concurrently and analysed to provide information on the strain-induced micro-cracking. We show pre-cursory electrical potential signals can be observed from crustal rocks undergoing deformation and the effect of a varied range of pore fluid salinity is presented. Temporal variations of electrical potential difference change markedly during compaction and dilatancy. Microseismicity show an exponentially increasing event rate and decreasing b-value during this period. Our measurements can be interpreted using an electrokinetic model and suggest micro-cracking during dilatancy is a dominant source of the electrical phenomenon.

**JSA15/E/38-A4** Poster **1400-03**

**MODELING EXPECTED AND OBSERVED PIEZOMAGNETIC FIELD CHANGES IN THE LONG VALLEY CALDERA, CALIFORNIA**

Yoichi SASAI (Earthquake Research Institute, Univ. of Tokyo, Bunkyo-ku, Tokyo, 113-0032, Japan, email: sasai@eri.u-tokyo.ac.jp); Malcolm J. S. Johnston and Robert Mueller (both at US Geological Survey, 345 Middlefield Road, Menlo Park, CA 94025, USA); Yoshikazu Tanaka (Geothermal Research Center, Fac. Sci., Kyoto Univ., Choyo-son, Aso, Kumamoto, 869-1404, Japan); Jacques Zlotnicki (Laboratoire de Geophysique, UMR 6530, 3d av de la recherche scientifique, 45071, Orleans, cedex 02, France); Tadanori Goto (Dept. Environmental Earth Sci., Aichi Univ. Educ., Kariya, Aichi, 448-8542, Japan)

In Long Valley Caldera, remarkable changes in the total intensity have been observed, associated with a dramatic inflation near the central resurgent domes since 1989 (Mueller and Johnston, 1998). Total intensity changes during the first seven years can be interpreted in terms of piezomagnetism due to inflation of a spherical pressure source at a depth of 8 km. This same source explains the main features of the deformation data. However, neither the deformation data nor the magnetic data can be interpreted by such a single source model during heightened deformational and seismic activity in late 1997. In particular, the deformation data requires additional sources and can be satisfied by the addition of either an intrusive dyke at a depth of 4 km to 8 km, dipping by 45 degree located on the SE side of the main spherical pressure source, or a more complex model involving a combination of a deep-seated pressure source (depth 13 km) and slip on a vertical strike-slip fault with its top 4km deep beneath the south moat. We calculate the piezomagnetically generated magnetic fields expected from these models and compare these with the observed fields. Furthermore, we installed 5 proton magnetometers in the summer of 1998 to attempt to provide better differentiation between these two possible sources in the future.

**JSA15/E/27-A4** Poster **1400-04**

**HYDROTHERMAL SYSTEM AND FAULTING IN LONG VALLEY CALDERA INFERRED -BY SELF-POTENTIAL MAPPING**

Jacques ZLOTNICKI (Laboratoire de Geophysique(a), UMR 6530, 3d av de la recherche scientifique 45071 Orleans cedex 02, France. Email: jacques.zlotnicki@cnrs-orleans.fr); Tadanori Gotoh (Dept. Environmental Earth Sci., Aichi Univ. Educ., Kariya City, 448-8542, Japan); Malcolm Johnston (U.S. Geological Survey, Menlo Park, CA 94025, USA); Alban Mille(a) & Jean-Francois Delarue(a), Yoshikazu Tanaka (Beppu Geothermal Research Lab. of Kyoto Univ., Beppu, Japan); Yochi Sasai (Earthquake Research Institute(b), Tokyo Univ., Japan)

Long Valley caldera, located at the east of the Sierra Nevada, is a huge active volcanic complex. The caldera corresponds to an elliptical depression, about 32 km from the east to west by 17 km from north to south. Mainly on the northern, western and southern sides, 1000 m-high walls are encountered. After 250 years of relative inactivity, episodes of accelerated deformation with associated seismic swarms started in 1980 and have continued to the present. The net uplift of the resurgent dome in the centre of the caldera as a result of magma intrusion now exceeds 70 cm and affects more than 100 km<sup>2</sup>. During summer 1998, a large SP mapping of the central part of the caldera was completed through the region previously mapped by Anderson et al. (1976) to identify changes since that time. Profiles were also extended in the NW and SE directions past the caldera boundaries. The surveys were done along several kilometres long loops in order to check the closure errors. The measurement interval was 200 m and more than 80 km of profiles was measured. Large SP anomalies, up to 500 mV, were observed. Some of them present a negative linear relationship with the topography; we can associate these anomalies with the so-called "topographic effect". Other anomalies point out sharp flanks that could be associated with superficial faulting and hydrothermal activity. For instance, smooth SP anomalies are related to the Casa Diablo geothermal field.

**JSA15/E/01-A4** Poster **1400-05**

**THEORY OF SEMS AND REPRODUCTION EXPERIMENTS OF EARTHQUAKE-PRECURSOR LEGENDS (VIDEO)**

Motoji IKEYA, Chihiro Yananaka, Hiroshi Matsumoto and Synji Takakai (Department of Earth and Space Sciences, Graduate School of Sciences, Osaka University, 1-1 Machikaneyama, Toyonaka, Osaka 560, Japan)

Mysterious phenomena told as legends, proverbs and folk stories related to earthquakes and some of those reported retrospectively by citizens as precursors to the Kobe earthquake in 1995 have been examined and reproduced in electromagnetic (EM) experiments using a Van de Graaff generator and in rock-compression using 500 ton compression machine. (1) Unusual animal behaviour such as alignment and jumping of fish, both reported as precursors of the Kobe earthquake, were caused by pulsed electric fields. Rock fracture experiments produced EM waves and some unusual animal behaviour. (2) Malfunctioning of home electric appliances before the earthquake was reproduced, and so were noises on TV and radio, rapidly moving or stopping of the hands of a quartz clock, buzzing air-conditioner and refrigerator and so on. Laboratory experiments indicate that legends, proverbs and old sayings are not superstitions and can be reproduced and elucidated by intense seismic EM waves and appearance of pulsed charges at the epicenter. Physics, which produces SEMS, is due to the piezo-compensating charges released by stress changes. An ensemble of released charge pairs radiate EM waves resulting in pulsed EM waves whose propagation and attenuation were calculated. The scaling laws derived theoretically agree well with empirical ones. Physics of SEMS has quantitatively been established based on an electromagnetic model of a fault having piezoelectric quartz grains in the bedrock. M.Ikeya et al: Reproduction of mimosa and clock anomalies before earthquakes-Are they "Alice in Wonderland" syndrome? Proc. Japan Acad.74B (1998)60. M.Ikeya et al.: Pulsed electric field before Kobe and Izu earthquakes from seismically-induced anomalous animal behavior, Episodes20, (1997)253.

**JSA15/P/04-A4** Poster **1400-06**

**NEW METHODOLOGY FOR ANALYSIS OF ELECTROMAGNETIC FIELD DISTURBANCES AND EARTHQUAKES**

H.N. SRIVASTAVA (India Meteorological Department New Delhi-110003, India, e-mail: snb@imd.ernet.in)

There is growing observational evidence between electromagnetic field anomalies as precursory to earthquakes. However, the results are often considered as chance particularly

after the controversy about VAN predictions in Greece. Instead of applying a simple statistical methodology using Null hypothesis, a new method is proposed for interpretation of data which is based on the Principal components analysis. We need to choose physically linked parameters like specific area (including selectivity, if any), epicentral distance, focal depth, magnitude, source mechanism and other parameters to work out the loading factors in relation to the impending earthquakes. Case examples are given using observations to validate the new methodology.

**JSA15/E/13-A4** Poster **1400-07**

**PHYSICAL MECHANISMS FOR THE GENERATION OF ELECTROMAGNETIC FIELDS DURING EARTHQUAKES**

A. GUGLIELMI (Institute of Physics of the Earth, B. Gruzinskaya, 10, Moscow, 123810 Russia, Email: gugl@scgis.fisgeos.iitp.ru)

The theory describing the excitation of electromagnetic field by the earthquakes is outlined. The inertial, inductive, piezomagnetic and electrokinetic mechanisms are considered in details. The generation of electromagnetic waves in the ULF frequency band under the action of elastic waves and also due to the inelastic motion in an earthquake centre is studied. The solution of the problem on electromagnetic field of a propagating fault in the frame of two-dimensional model is presented. Particular attention has been given to the expressions describing the magnetic signal amplitude versus the magnitude of earthquake. The magnetic signal observed by Iyemori et al. at the 1995 Hyogoken-Nanbu earthquake (M = 7.2) is interpreted in the framework of the presented theory.

**JSA15/E/06-A4** Poster **1400-08**

**PHYSICAL MECHANISMS OF GENERATION OF ELECTROMAGNETIC ULF SIGNALS PRECEDING EARTHQUAKES**

Viacheslav PILIPENKO, Evgenij Fedorov (Institute of the Physics of the Earth, Moscow 123810, Russia, e-mail: vpilipenko@uipe-ras.scgis.ru); Vadim Surkov (Moscow Engineering Physics Institute, Moscow 115409, Russia; e-mail: vpilipenko@uipe-ras.scgis.ru)

The existing theories of the emergence of anomalous electromagnetic emissions and impulses in the ULF frequency range (up to 10 Hz) preceding earthquakes are critically revised. For a better physical insight simplified easy-to-use analytical estimates of the expected effects have been derived. The principal results of the existing numerical models are reproduced in a much simpler way without mathematical complexities. The considered phenomena comprise electrokinetic effects, seismo-inductive effects, filtration of underground fluid, charge relaxation related to micro-crack formation, large-scale current systems produced by dislocations or water evaporation, inductive effects caused by seismo-acoustic impulses from micro-cracks, plasma oscillations, etc. It is demonstrated that none of the theories can be fully adopted because of essential intrinsic difficulties. The comparative elementary analysis of the structure of hypothetical electromagnetic disturbances, produced by a lithospheric source, and of common electromagnetic noises suggests some simple technique for the discrimination of multi component signals from those two sources, based on the difference in their polarization structures.

**JSA15/E/15-A4** Poster **1400-09**

**ACTIVE ELECTROMAGNETIC MONITORING OF EARTHQUAKES**

Fedir DUDKIN and Valery Korepanov (Lviv Centre of Institute of Space Research, 5-A Naukova str., 290601, Lviv, Ukraine, e-mail: vakor@isr.lviv.ua)

Changes of electromagnetic (EM) fields during and before the earthquakes (EQ) have been clearly observed in many cases. The most difficult problem is to detect them because of very low level of these fields. Also any conclusion can be made today about the connection with seismic hazards of their other parameters such as frequency band, polarization etc. Because of this the extraction of noise-like seismogenic EM emission on the noisy EM background is an extremely complicated task.

A possibility of active EM sounding is investigated. It is widely used in geophysics for the study of crust deep conductivity structure. And it is also known that both the speed of seismic waves and the crust mean longitudinal conductivity can change before the EQ (Scholtz model), what is provoked by crust structural changes and hence can be very good observed in the regular field of artificial source. The development of local changes and irregularities (such as cracks and boundaries shifts) preceding the EQ also can be monitored using active EM sounding. This method has especially great advantages when the monitoring is executed near big cities or industrial centers where EQ effects are the most harmful. This is because having constant and known frequency of the monitored signal the well-developed methodology of synchronous detection can be applied, which is known to be able to extract useful signals with signal-to-noise ratio lower than 10-5. Some examples of cracks and inner boundary uplifts were calculated which show significant contribution in the sounding EM field changes for the deformations about some few hundreds of meters at the depth till 40 km.

**JSA15/E/36-A4** Poster **1400-10**

**MATHEMATICAL MODEL OF GENERATION AND PROPAGATION OF SEISMO-ELECTROMAGNETIC (EM) AND SEISMO-TEMPERATURE (T) SIGNALS**

Oleg NOVIK (Moscow State Geol.Prospect.Acad.,117246,POB51,Moscow,Russia email: Onovik1@glasnet.ru); Sergey Ershov (Keldysh Inst. for Appl. Math. of Russian Acad. Sci., Moscow); Irina Mikhaylovskaya (Moscow State University, email: irina@nw.math.msu.ru).

Our model medium includes: a) the lithosphere zone with the conductive layer (c.l., 0.1 S/m) in the upper mantle and the conductive block (c.b., 0.1 S/m) in the crust; b) the atmosphere zone up to the low boundary of the ionosphere domain D. As the matter of fact, the structures with the cross-section size 10 to 50 km and the conductivity of order above were discovered in most of seismic lithosphere zones at the depth >10 km. Proceeding from these data we construct the mathematical model and describe numerically and graphically the em- and t-signals caused, in presence of geomagnetic field, by the elastic (e) displacements of the bottom of the c.l. (during 5 sec, amplitude up to 3 cm, freq. up to 1.5 Hz). The signal forming includes: 1) the appearance of the em-signal (~150 pT during 1 sec after the beginning of the displacements); 2) the e-, em- and t-field diffraction on the c.b.; 3) the correspondence between the spatial structures of the e-, em- and t-waves and the correspondence between their spectra; 4) the saturation of the c.b. with the energy of the disturbed e-field; 5) the outrunning of the seismic wave by the em-wave (~0.1 sec per 1 km of the trace) and the emission into atmosphere (up to 60 pT at the earth surface and up to 10 pT at the height of 30 km); 6) the t-disturbance of the sedimentary layer (up to 0.02K); 7) the delay of the surface em-signal as regard to the beginning of displacements; 8) the change of the amplitudes and spectra of the surface em-t-signal after the change of the elastic displacements at the depth. These properties of the em-t-signal are similar by different input data of the computations.

JSA15/E/23-A4 Poster 1400-11

## ANOMALOUS PHENOMENA PRECEDING EARTHQUAKES

Igor I. ROKITYANSKY (Institute of geophysics, POB-338/7, Kiev-146, Ukraine, email: earth@igph.kiev.ua)

The concept of earthquake (EQ) unpredictability has grown over the last decade. According to A.Gusev (EOS,1998,10 Feb, p.71, 4 Aug, p.373), it can be expressed as follows: EQs are unpredictable within the framework of the present paradigm. A paradigm is a system of accepted ideas and laws considered by the scientific community as the truth for a certain period of time. A phenomenon that is unexplainable within the framework of the present paradigm can be labeled as an anomaly. When the quantity of anomalies reaches a critical value, the paradigm changes, opening a way for an explanation of the anomalies. EQ precursors offer a collection of anomalies: luminosity of the atmosphere, changes in ionosphere parameters, EM-emission, cloud lineaments, SES (Seismic Electric Signals). Three stages of paradigm changes are considered, and the conclusion is made that the second stage is necessary. This implies an expansion of physics via the introduction of new entities and laws. To support the conclusion, searches for other anomalies had been conducted. The results will be presented from metrology, bio-, geo-, astro- and nuclear physics, and chemistry. Speculative ideas concerning possible extension of physics are also reviewed.

JSA15/E/24-A4 Poster 1400-12

## MAGMA-INTRUSION SWARM GENERATION AS A PLAUSIBLE EXPLANATION OF SEISMIC ELECTRIC SIGNALS (SES) AND CRUSTAL EARTHQUAKES (EQ) IN GREECE

Igor I. ROKITYANSKY (Institute of geophysics, POB-338/7, Kiev-146, Ukraine, email: earth@igph.kiev.ua)

Crustal intrusions occur widely in the Earth's crust. In some places they form giant, radiating dike swarms (Earnst et al., 1995, Earth Sci.Rev.,v.39,1-58) extending up to 2,000 km from the center. Guterman & Khazan (1994, Geophys.J., v.16,N1,22-29) proposed the magma intrusion mechanism as an explanation for the recent strong shallow EQs. Proceeding from the two results, a model of the magma intrusion swarm is developed. It includes the mantle reservoir - plume head (MR), the deep channel (DC) from the MR to the central crustal chamber (CCC), and several chains of secondary crustal chambers (SCC) spreading quasi-radially from the CCC for up to hundreds of kilometers. A SES station placed in the vicinity of a DC or a CCC will be sensitive to magma flow toward any distant SCC. If conditions for an EQ in a peripheral chamber are favourable, the SES will also be recorded near the DC-CCC, even hundreds of kilometers away from an impending EQ. With four most effective SES stations (IOA, ASS, KER, PIR) in place in Greece, one can anticipate observing four principal intrusion swarms with DC-CCC in the vicinity of each of these stations. Mutual crossing and overlapping of the swarms can explain the puzzling characteristics of the SES: selectivity, lack of reversibility, and alternation. To progress from the outlined scheme to a meaningful pattern, all seismological, geo-electrical, geothermal, geodetic, and geological data obtained in Greece should be reviewed and utilized. The question to be answered is: what does the SES represent? Is it the magma flow, or the beginning of the flow, the process of the opening of the magma channels. To clear up the question, SES observations in volcanic areas would be helpful.

JSA15/E/60-A4 Poster 1400-13

## SPONTANEOUS POTENTIALS, GEOMAGNETIC ANOMALIES, ENDOGENOUS ENERGY, IONOSPHERIC COUPLING, AND SEISMIC AND VOLCANIC PRECURSORS

C. BELLECCI (II Università di Roma, Tor Vergata, Roma, Italy); G. M. Crisci (UNICAL, Arcavacata di Rende, Cosenza, Italy); G. P. Gregori (IFA-CNR, via Fosso del Cavaliere 100, 00133 Roma, Italy; e-mail: gregori@atmos.ifa.rm.cnr.it); V. Lapenna (ITAANA-CNR, Potenza, Italy); I. Marson (Università di Trieste, Italy); and G. Paparo (IDAC-CNR, Roma, Italy)

According to Gregori (PEPI, 77, 39, 1993), a great heterogeneity exists of the underground electrical circuits that relate the deep dynamo currents with shallow structures, such as even the magma chamber of volcanoes. Such an inference, provided it is correct, must imply: (1) that volcanism and geothermal heat flow are supplied (at least partially) by Joule's heating; (2) that the e.m. coupling between ground and ionosphere is quite different in different regions; (3) that the prime supply to volcanoes can be Joule's, and that its time variations ought to be closely correlated with the local spontaneous potentials, and with the geomagnetic secular variation (one should, however, also allow for different case histories to be supplied e.g. by frictional heat transformed from geodynamic energy); (4) that the geomagnetic anomalies within every volcanic area ought to reflect the geometry of the prime DC circuit that supplies its Joule's heating; (5) that the geo-e.m. precursors of either earthquakes or volcanic activity, either within ground or within the ionosphere and/or airglow, are not the same everywhere, due to the different morphologies of the underground circuits, and to their consequent ionospheric coupling (therefore, the well known controversi e s are nonsense). One seismic case history concerned with the Appennino Lucano is presented. An interdisciplinary experiment on the island of Stromboli is going to be started for checking whether such an entire interpretation is supported by observations, or not: the timing of Stromboli's explosions ought to be directly related to the variations of its spontaneous potentials.

JSA15/E/41-A4 Poster 1400-14

## ELECTRICAL SELF-POTENTIAL ON THE CENTRAL CONE OF ASO VOLCANO

Yoshikazu TANAKA (Aso Volcanological Laboratory, Kyoto Univ., Aso Kumamoto, 869-1404, Japan, email: tanaka@aso.vgs.kyoto-u.ac.jp); Hideaki Hase (AVL, email: hase@aso.vgs.kyoto-u.ac.jp); Takeshi Hashimoto (AVL, email: hasimoto@aso.vgs.kyoto-u.ac.jp) and Shinya Sakanaka (AVL, email: sakanaka@aso.vgs.kyoto-u.ac.jp)

Aso is one of the most active volcanoes in Japan. After huge eruptions occurred in 80,000 years ago, resurgent volcanism at many part of the cones finished in ages ago. Many hot springs were developed around west part, and the historical volcanic activities remain only at west flank of Mt.Nakadake. We conducted SP measurement in the summer of 1998 to reveal a geothermal activity of the volcano. Using CU-CUSO4 and Pb-PbCl2 electrodes, potential differences in each 100m were measured by a digital voltmeter with accuracy 1mV. Along a north-south route close to the active crater, the SP showed "W" character like change, namely, the SP decreased in proportion to height at the foot, but it changed to increase at 4km far point of the crater. The decrease rate is 150 mV/Km and increase rate is about 50-75 mV/Km. The decrease change is well known as a topographic effect caused by down flow of the ground water. While, the positive anomaly near the crater will be associated with upward fluid flow heated by magma. Thus, a monitoring of the SP will be useful to watch the volcanic activity.

JSA15/E/57-A4 Poster 1400-15

## TECTONOMAGNETIC INTERPRETATION OF LONG AND SHORT TERM CHANGES IN THE GEOMAGNETIC FIELD OBSERVED IN THE IZU PENINSULA

Naoto OSHIMAN (DPRI, Kyoto Univ., Gokasho Uji, Kyoto, 611, Japan, E-mail: g53032@sakura.kudpc.kyoto-u.ac.jp), Y. Sasai, Y. Ishikawa (ERI, Univ. of Tokyo) and Y. Honkura (Tokyo Institute of Technology)

Remarkable crustal activities, the anomalous crustal uplift and earthquake swarms, have continued for about 20 years in the Izu peninsula. The swarm activities, occurred off the coast of Ito intermittently since 1978, are interpreted as intrusions of magma or pressurized fluid. We have observed the total intensity of the geomagnetic field in the north-eastern part of the peninsula with a dense network of proton magnetometers since 1989. No remarkable swarm activities were observed there during the period from 1990 to 1992. However, after occurrence of a small swarm in Jan., 1993, five large activities were observed off the coast of Ito. At the closest observation site (KWN) to the swarm area, the total intensity changes showing a good correlation with occurrences of the swarm were observed. Namely, decrease in the total intensity at KWN, was observed before the occurrence of the swarm, and a recovery phase was observed after the activity. Another remarkable geomagnetic change is a long term change observed at one site located at northernmost area of our dense observation network. Decrease in the total intensity with almost constant rate has been observed since 1991. We try to interpret those long and short term geomagnetic changes in the Izu peninsula, on the basis of the thermal magnetic effect.

JSA15/W/14-A4 Poster 1400-16

## ELECTRICAL STRUCTURE OF ASO VOLCANO INFERRED BY BIPOLE-DIPOLE METHOD

HASHIMOTO.T, Hase.H., Sakanaka.S., Tanaka.Y., Masuda.H., Amita.K. (Institute for Geothermal Sciences, Graduate School of Science, Kyoto University, Choyo-son, Aso-gun, Kumamoto, 869-1404, JAPAN, Email: hashimoto@aso.vgs.kyoto-u.ac.jp); Kanda.W. (Sakurajima Volcano Observatory, Kyoto University); Djedi.S.W., Mogi.T., Ikoma.Y. (Faculty of Engineering, Kyushu University); Handa.S. (Department of Agriculture, Saga University); Shimozumi.M. (Politech College, Kitakyushu) Koyama.T., Ogawa.T., Kagiyama.T., and Masutani.F. (Earthquake Reserch Institute, Tokyo University)

We conducted a bipole-dipole electrical resistivity survey at Aso Volcano in December 1998. Aso is an active volcano with a large caldera, which locates at the central part of Kyushu island, southwestern Japan. Recently, Kaneshima et al. (1996) inferred a oblique crack vibrating at the depth of 1-1.5km beneath the active crater of Aso by means of broadband seismic observations. They speculated that ground water-heat interaction causes the intermittent vibration with a dominant period of 15 seconds. We are going to inspect this model from the viewpoint of electric or electromagnetic exploration. We deployed two transmission bipoles and 13 magnetic and telluric receivers around the central cones of Aso volcano. The amount of injection current was around 15(A). In the poster we will present the mapping of resistivity tensors. We will also propose a plausible model, which can satisfy both the seismic and electrical results in the asthenosphere.

JSA15/W/24-A4 Poster 1400-17

## SPATIAL AND TEMPORAL MAGNETIC ANOMALIES ON VOLCAN DE COLIMA, WESTERN MEXICO

H. LOPEZ-LOERA &amp; J. Urrutia-Fucugauchi, (Laboratorio de Paleomagnetismo, Instituto de Geofísica, UNAM, D. Coyoacan 04510 D.F., Mexico)

Volcan de Colima in western Mexico has been characterized by frequent eruptive events in historic time; present activity includes the episodic growth of a summit lava dome, intense fumarolic activity, and small lava, pyroclastic and debris flows. Volcan de Colima, which is one of the Decade volcanoes, forms the southern end of an elongated N-S volcanic complex that includes another tall stratovolcano Nevado de Colima. Total field magnetic measurements have been taken along a 45 km transect at various times since 1995. Three distinct sectors can be observed: Sector A between stations 10 and 23 km characterized by low amplitude, low frequency anomalies and no temporal changes, Sector N between stations 23 and 35 km characterized by low frequency anomalies and low amplitude temporal changes, and Sector C between stations 35 and 45 km over the volcano summit, characterized by low frequency, high amplitude highs and lows and large amplitude temporal variations. Sector A is on the volcano flank over volcanic conglomerates of the Atenquique Formation and the Nevado de Colima debris avalanche deposits. Sector N is over andesitic lavas and breccias. Sector C is over andesitic lavas and breccias on the summit caldera and active dome. Modeling suggests several source bodies extending several hundred meters deep. Temporal changes over sector C are possibly associated with thermal changes; particularly a magnetization/demagnetization process related to eruptive activity (magma movement, intense hydrothermal activity and groundwater circulation). A 1500-2500 nT composite magnetic low characterizes the present cone summit and avalanche caldera; the anomaly experiences consistent temporal changes superimposed over the high amplitude low frequency magnetic anomaly.

JSA15/W/02-A4 Poster 1400-18

## AUTOMATED SYSTEM FOR MAGNETIC SURVEILLANCE OF ACTIVE VOLCANOES

Ciro Del Negro (Istituto Internazionale di Vulcanologia - CNR, Piazza Roma 2, 95123 Catania, Italy, Email: delnegroc@iiv.ct.cnr.it); Fabrizio Ferrucci (Dipartimento di Scienze della Terra, Università della Calabria, Arcavacata di Rende, Cosenza, Italy, Email: f.ferrucci@unical.it); Rosalba Napoli (Istituto Internazionale di Vulcanologia - CNR, Piazza Roma 2, 95123 Catania, Italy, Email: napolir@iiv.ct.cnr.it)

Geomagnetic observations to monitor volcanic activities have been intensively carried out during the past decade. Significant correlation between volcanic activity and changes in the geomagnetic field were observed on several volcanoes. However, it is possible to assess that, in spite of the significant efforts devoted to establishing and expanding magnetic networks on volcanoes around the world, the limited availability in space and time of data substantially denied access to the quantitative evaluation of the dynamics of volcanoes, at temporal and spatial scales suitable for purposes of the mitigation of volcanic hazards. Our laboratory has been developing methods, hardware and know-how for the automated acquisition and management of data simultaneously acquired at a variety of remote magnetic stations. In order to provide a basis for short-term decision-making in the forecasting and control of volcanic activity linear and non-linear inversion techniques for the real-time processing of data have also been implemented. The developed system is entirely automated between the stages of data acquisition and processing. Memorised data are accessible by authorised external users via Internet. The on-line availability of crude or pre-processed data at authorised users connected to a wide-area network, fosters the possibility of monitoring active volcanoes without concentrating all human resources in a single observatory, at a given site. The system has been designed for uploading data at a distant user immediately after acquisition and re-



formatting. Then, data processed at the "distant desk" can be downloaded a few hours later and used by the personnel in charge of the volcano forecast on the spot.

**JSA15/E/59-A4** Poster **1400-19**

**GM COUNTING ANOMALY PRECEDING VOLCANIC SWARM WAS EXISTED AND TELLS PREPARING MECHANISMS OF QUANTAM AND GEOCHEMISTRY**

Masayasu HATA (Aichi Prefectural University, Aichi, Japan, email: hata@ist.aichi-pu.ac.jp); Ichi Takumi (Nagoya Institute of Technology, Aichi, Japan email: takumi@ics.nitech.ac.jp); and Yoshikazu Yamada (Tousei Electro-Beam Inc., Tokyo, Japan)

We have set up a Geiger-Muller counter vertically inside a closet of steel in thickness of 0.5mm, at the occasional volcanic swarm area of Cape Shiofuki in Itoh-city, Izu-peninsula, Japan. The counter often showed an anomalous peaky increase by about three times of the usual background level of 48cpm in the afternoon of 15 to 16 JST fairly accurately, for the period of one and half months preceding the swarm on April '98. The increase disappeared soon after the start of the swarm. Simultaneously observed ELF band magnetic flux showed the same tendency day after day, but with a different pattern and with a longer residual succession of the radiation after the swarm. The peaky pattern was considered owing to a high-energy radiation of probably light (electron) particle emitted from the deep crust, which was modulated by a surface induced current of the upper atmosphere current by the solar radiation. So, one another GM counter set up horizontally showed an inverse correlation with the original one. Further, the counting increase well correlated with the discharging current in the air and further negatively with the electric field of ELF band. This is estimated due to ionization of the air by the high-energy radiation from the earth crust.

**Friday 23 July AM**

Presiding Chairs: M.J.S. Johnston (US Geological Survey, Menlow Park, CA, USA)  
J. Zlotnicki (Laboratoire de Geophysique, Orleans, France).

**JSA15/W/12-A5** Poster **0830-01**

**ON SECULAR CHANGES IN THE MAGNETIC FIELD EXPECTED FROM SUBDUCTION PROCESS OF THE PHILIPPINE SEA PLATE IN THE SURUGA BAY AREA, JAPAN**

Yoshimori HONKURA and Naoto Imasaka (both at Department of Earth and Planetary Sciences, Tokyo Institute of Technology, Tokyo 152-8551, Japan, email: yhonkura@geo.titech.ac.jp)

Some local magnetic anomalies found in the the Suruga Bay where the Philippine Sea plate subducts beneath Japan have been interpreted as due to seamounts existing on the subducting Philippine Sea plate. In order to examine how these seamounts affect the generation of a great interplate earthquake at the Suruga trough, often referred to as the Tokai earthquake, we made a numerical simulation of earthquake generation, applying the rate- and state-variable friction law to the plate interface and incorporating the seamounts in the simulation as an additional normal stress exerted locally to the interface. Through this simulation we can estimate stress changes in the crust during a cycle of earthquake generation and hence changes in magnetization of the crust. The overriding plate mainly consists of accretionary sediments and their magnetization is weak, resulting in very small changes in the magnetic field which are hard to detect on the Earth's surface in general. However, anomalous changes in the magnetic field can be expected in the vicinity of the seamounts, because of their strong magnetization. Moreover, a notable stress change can also be expected in association with a pre-slip occurring in the vicinity of the seamounts some hours before the generation of an interplate earthquake. Numerical estimation shows that changes in the magnetic field on the Earth's surface associated with such a pre-slip are still small, but changes are abrupt and hence would be easiest detect.

**JSA15/E/07-A5** Poster **0830-02**

**ON THE CAUSE OF AN ANNUAL VARIATION IN THE GEOMAGNETIC TOTAL INTENSITY DATA**

Maroka NEKI, Tsuneomi Kagiya, and Hisashi Utada (Earthquake Research Institute, Univ. Tokyo, Tokyo 113-0032 JAPAN, email: neki@eri.u-tokyo.ac.jp, kagiya@eri.u-tokyo.ac.jp, utada@utada-sun.eri.u-tokyo.ac.jp)

Continuous measurement of the geomagnetic total intensity is now a powerful tool to monitor crustal activities. However, local geomagnetic data taken for that purpose often contain periodic variations of non-tectonic origin, such as an annual variation. In order to examine gradual geomagnetic changes relating to geothermal activity, for example, this may be a significant noise. This paper aims to clarify the cause of such a geomagnetic annual variation. We applied a hypothesis that a thermally induced magnetization change of near surface rocks causes this variation. We tested this hypothesis by using two datasets from different volcanoes, one from the Kirishima where magnetization is relatively weak (typically 1 A/m) and the other from Izu-Oshima with intense magnetization (typically 10 A/m). We measured magnetization and its temperature dependence of rock samples from the two volcanoes in the range 0-30 °C. We also obtained a total intensity anomaly map around magnetometer sites in each volcano where clear annual variations are seen. The short wavelength anomaly was then inverted to the equivalent source on the surface. We found that the observed annual variation in the total intensity can be quantitatively explained by an annual variation in the equivalent source due to temperature change. This result indicates that correction of this effect is necessary in order to extract a real tectonomagnetic signal.

**JSA15/P/05-A5** Poster **0830-03**

**SHORT-TERM PREDICTION OF ROMANIA'S VRANCEA EARTHQUAKES BASED ON ELECTROMAGNETIC PRECURSORS**

B.D.ENESCU, D.Enescu and A.P.Constantin (National Institute for Earth Physics, P.O. Box MG-2, Bucharest-Magurele, 76900 Romania, email: denescu@infp.ifa.ro)

The electromagnetic data used in this paper were recorded at Muntele Rosu Observatory during the periods from December 1996 to January 1997, and December 1997 to September 1998. This observatory consists of: 1) a three-axis magnetic field sensor, which is a Bartington-type MAG-03 MS; 2) nonpolarizable electric sensors; 3) a data - acquisition module, which is an MAG-03 DAM; 4) a computer for data storage and preliminary processing.

Data recording and preliminary processing yielded time variation diagrams of the magnetic and electric components; namely, three diagrams refer to the components of magnetic flux density, Bx, By and Bz, and two others to the horizontal components Ex and Ey of the electric field. The times when Vrancea earthquakes of magnitudes M > 3.9 occurred within these periods investigated are marked on the diagrams. The 3.9 magnitude was imposed as a threshold by the very records, which only showed significant variations in the run-up to Vrancea earthquakes of M > 3.9. The diagrams show that significant magnetic and electric anomalies (perturbations) arose prior to all Vrancea earthquakes of magnitudes M > 3.9 (in total 19 earthquakes) during the period of the

study. All but one of the anomalies (perturbations) occurred at similar precursor times (of order of days). Consequently, the results obtained in this paper prove that Vrancea earthquakes are preceded by electromagnetic anomalies that may be regarded as their short-term precursors.

**JSA15/P/01-A5** Poster **0830-04**

**ESTIMATION OF ELECTROMAGNETIC IMPEDANCE USING DATA RECORDED IN VRANCEA ZONE. AN ATTEMPT TO FILTER THE RECORDED SIGNALS**

B.D.ENESCU (National Institute for Earth Physics, P.O. Box MG-2, Bucharest-Magurele, 76900 Romania, email: benescu@infp.ifa.ro); D.Stanica (Romanian Institute of Geology, Caransebes Str. Nr.1, Bucharest, Romania); D.Enescu (see B.D.Enescu)

Some electromagnetic data recorded at Muntele Rosu Observatory (placed within the Vrancea seismic zone) are exposed to a mathematical treatment in order to filter the recorded signals and to estimate the magnetotelluric impedance. The signals obtained by means of this treatment are analysed with relation to Vrancea earthquakes occurred during the period of the study.

**JSA15/E/02-A5** Poster **0830-05**

**GEOELECTRIC POTENTIAL VARIATION MONITORING IN SOUTHERN SUMATRA, INDONESIA - CO-SEISMIC VARIATION**

Toru MOGI (Department of Earth Resources Eng., Kyushu University, Fukuoka 812-8581, Japan, email: tmogi@mine.kyushu-u.ac.jp); Yoshikazu Tanaka and Hideaki Hase (both at Aso Volcanological Laboratory, Kyoto University, Choyo-son, Aso-gun, Kumamoto Pref., 869-1400, Japan, tanaka@aso.vgs.kyoto-u.ac.jp); Edy M. Arsadi and Djedi S. Widarto (both at RD Ctr for Geotechnology-LIPI, Jalan Sangkuriang, Bandung 40135, Indonesia, widarto@bdg.centrin.net.id); Toshiyasu Nagao and Seiya Uyeda (both at RIKEN International Frontier Program at Tokai University, Shimizu 424-8610, Japan, suyeda@mail.st.rim.or.jp)

Five geoelectric potential monitoring stations have been in operation since September, 1997 in an area near Liwa town, southern Sumatra, Indonesia, to examine the relationship between geoelectric potential changes and earthquakes. Co-seismic geoelectric changes ranging between 1 and 8 mV/100m were observed for five mb<5 earthquakes at multiple stations during September and December, 1997. Co-seismic variations were observed for the following earthquakes (EQ); Sept.13 mb5.0 EQ at r=147km, Oct.29 mb5.7 EQ at r=152km, Nov.16 mb5.5 EQ at r=95km, Nov.23 mb5.1 EQ at r=174km and Dec.20 mb5.0 EQ at r=146km. In October 1998, in order to obtain more detailed information, the sampling interval was made from ten seconds to one second and simultaneous seismic monitoring was started at all sites. Co-seismic geoelectric potential changes were observed for nine more earthquakes during October to December 1998; (Sep.28 Mw6.5 EQ at r=993km, Oct.8 mb5.2 EQ at r=100km, Oct.21 mb5.1 EQ at r=148km, Oct.31 mb=5.3 EQ at r=590km, Nov.5 mb4.9 EQ at r=20km, Dec.7 mb5.2 EQ at r=99km, Dec.11 mb=5.4 EQ at r=97km, Dec.13 mb5.3 EQ at r=123km and Dec.20 mb5.6 EQ=r=210km) Comparing the potential change records and seismograms, we found that the onset time of potential change coincided with the arrival time of seismic wave and the amplitude of potential change, which was different from site to site, was correlated to the intensity of the ground motion.

**JSA15/E/28-A5** Poster **0830-06**

**DEVELOPMENT OF THE EARTH-RESISTIVITY MONITORING SYSTEM FOR DETECTING THE STRESS CHANGE OF EARTH'S CRUST**

Futoshi YAMASHITA and Takashi Yanagidani (both at Disaster Prevention Research Institute, Kyoto University, Gokasho, Uji, Kyoto, 611-0011, Japan, email: futoshi@rcep.dpri.kyoto-u.ac.jp)

We have developed the system which measured the earth-resistivity continuously and precisely with high stability, which means it becomes possible to monitor the stress state of Earth's crust via resistivity change. The principle of resistivity measurement is the same as the 4-pole method in electric prospecting. However, we use AC as current source in stead of DC in conventional methods. This system adopts an AC voltmeter with phase-sensitive-detection so-called lock-in amplifier, so it can precisely measure potential and current that flows through the Earth under very severe noise environments. It is verified by the laboratory tests that this system can make continuous resistivity measurements with 4 digits-precision with long-term stability. We are convinced of that this system can be applied to in-situ measurement, and have started the observations at several sites. The system have been measuring with high stability agreeable to our design, and at a site near the seaside, we have detected the daily resistivity change, which may be caused by tidal loading.

**JSA15/W/01-A5** Poster **0830-07**

**REMOTE OBSERVATIONS OF LIGHTNING DISCHARGES IN SEISMOACTIVE REGIONS**

SOBOLEV G.A., N.I.Migunov, and N.I.Rosanov (United Institute of Physics of the Earth, Russian Academy of Sciences, Moscow, 123810, B.Gruzinskaya 10, email: sobolev@uipe-ras.sgis.ru)

The hyperbolic system of passive radar location of lightning discharges was applied for the study of the relationship between earthquakes and powerful sources of natural radio emission. Within the territory, covered by an effective radius of monitoring of a recording system, were located all seismoactive regions of Eastern Europe. The detailed analysis on Northern Caucasus territory was chosen where a number of earthquakes took place with magnitude >4. Mainly the atmospheric were recorded varying from powerful cloud-to-ground discharges in the frequency range 0.5-50 kHz. In the recorded signals the amplitude of the first half-period was >2 V/m at the distance of 100 km from the source of radiation. The mean square error of determination of co-ordinates of the radiation sources was 5-10 km. The territory of the Northern Caucasus reveals zones where, by seismic data, are located the earthquake epicenters. According to the results of remote observations, the value was determined of the ratio of the number of lightning discharges in seismically active zones to the total number of lightning discharges in a seismically active region. A correlation is established between the changes in the value of this ratio and the periods of seismic activity in separate parts of the territory under control. In order to establish a similar dependence between the number of thunderstorms and the periods of seismic activity, the meteorological data on thunderstorms in seismoactive region are insufficiently informative. It is suggested that the recorded changes in the value of the relative intensity of the flow of natural radioemission can be accounted for by the effect of earthquakes on the electric state of the atmosphere near the ground. Ionisation and electrification of the boundary air layer in the periods of seismic activity is, apparently, followed by a considerable increase of the number of centers of condensation of water vapour with further formation of fog and other atmospheric phenomena. In this case, the development of cloudiness is limited and the electric conductivity of air is reduced, which facts can result in decrease of the number of lightning discharges in seismically active zones. Therefore, the results of electromagnetic monitoring of a seismically active region confirm the reality of connection between earthquakes and lightning discharges.



**JAS15/P/02-A5** Poster **0830-08**

**GEOMAGNETIC INVESTIGATIONS FOR MONITORING EARTHQUAKES IN BEIJING AREA, CHINA**

Zhan ZHIJIA, Gao Jintian, Zhang Hongli, Zhao Congli and Shen Wenzhi (All at: Institute of Geophysics, China Seismological Bureau, Beijing 100081, China)

In order to monitor the seismic activity, there is a dense seismomagnetic network in the Beijing area. The seismomagnetic precursor information was obtained before several earthquakes, which occurred in the Beijing and its neighbouring areas. According to the anomalous information of geomagnetic precursors, the M=4.5 Baodi earthquake on November 18, 1993, the M=4.3 Baodi earthquake on July 20, 1995 and the M=3.8 Baodi earthquake on July 28, 1998 were better predicted. There were the precursory anomaly with the amplitude  $f=5.2$  nT, the precursory time  $T=7$  months and the epicenter distance  $d=10$  km for the M=4.5 Baodi earthquake (1993); the anomaly with  $f=4.5$  nT,  $T=3$  months and  $d=15$  km for the M=4.3 Huailai earthquake (1995); and the anomaly with  $f=3$  nT,  $T=43$  days and  $d=10$  km for the M=3.8 Baodi earthquake (1998). After the M=6.2 Zhangbei earthquake of January 10, 1998 (about 180 km apart from Beijing), we set up the temporary seismomagnetic network in the western part of the Beijing area for monitoring the seismic activity. The research results of geomagnetic data showed that there was not any anomaly and we predicted no earthquake with  $M > 5.0$  in the Beijing area during January-February, 1998. The practical situation was consistent with the prediction. The investigation results show that the geomagnetic method has active effect and good prospect in earthquake prediction study. Therefore, the seismomagnetic precursor research should be strengthened in the future.

**JSA15/E/52-A5** Poster **0830-09**

**THE CRUST ELECTRICAL STRUCTURE SURROUNDING SOME EARTHQUAKE FOCI AND MTOBSERVATION BEFORE AND AFTER ZHANGBEI EARTHQUAKE**

Guoze ZHAO, Yan Zhan, Ji Tang, Qianhui Deng, Jijun Wang, Zhao Jiang and Guodong Liu (Institute of Geology, Seismological Bureau China, Beijing 100029, China, email: zhaogz@public.bta.net.cn)

MT measurements were carried out in some larger shock areas during the last a few years. They are Shacheng earthquake (M=7.0, 1720), Xingtai earthquake (M=7.2, 22/3/1966), Yanggao earthquake (M=6.1, 19/10/1989) and Zhangbei-Shangyi earthquake (M=6.2, 10/1/1998) that are in a seismic active region in northern part of North China. It is shown by MT data that first two earthquakes occurred in areas near the conjunction places of a detachment fault in the upper crust and steep vertical fault in the middle and lower crust. Great difference of the resistivity between both sides of the vertical faults appeared. The later two foci occurred near a boundary of two bodies with different conductivity features. After the main-shock of Zhangbei-Shangyi earthquake magnetotelluric measurements were carried out at the epicenter (site MMC) and at site 511 which is 26km south-east of the epicenter. MT data were previously obtained at site 511 in June 1, 1994. This site was again occupied in January 13 and 20, 1998 and the various data sets show significant changes in apparent resistivity and impedance phase following the earthquake. MT data were measured continuously at site MMC from 16 to 19 of January. No measurement had been carried out at site MMC before main shock, but a change of apparent resistivity was also observed. The apparent resistivity for the TE polarization (Rhoxy) at site 511 corresponding to NNW direction generally decreased on January 13 and 20, 1998 in comparison with the data observed in June 1, 1994. The greatest decrease appeared for MT periods of 0.2 sec to 2 sec and from 10 sec to 200sec. The maximum amount of decrease is about 30% at 0.5sec. The values of Rhoxy observed on January 20, 1998 are larger than those for January 13. On the contrary, for TM polarization (Rhoxy) corresponding to NEE direction, the resistivity generally increased before main-shock and then decreased after shock.

**JSA15/L/01-A5** Poster **0830-10**

**SEISMO-IONOSPHERIC EFFECTS DURING VIBROSEISMIC SOUNDING**

V.V. KUZNETSOV, S.Y. KHOMUTOV, V.V. Plotkin, O.M.Grekhov, A.F. Pavlov, A.N. Fedorov (Institute of Geophysics SB RAS, Koptuyg av., 3, Novosibirsk, 630090 Russia; e-mail: hom@uigm.nsc.ru)

The synchronous disturbances on the ionosphere were registered by the doppler sounding at the "Klyuchi" station (Institute of geophysics, Novosibirsk) when the seismic vibrator with 100 tons force amplitude mounted at the "Bistrovka" testing area of Siberian Branch of SB RAS (Novosibirsk) is operated. The vibrator generated the seismic oscillations in the sweep-mode with the frequency change from 6 to 9 Hz during about 45 min. The observed disturbances appeared as a outside frequencies in the Doppler spectrum. They drifted synchronously with seismic sweep-signal frequency with some time delay. The effect was noted during the daytime using the reflections from stable E-layer on the height about 100 km. It was absent during the night when the radioreflections are obtained for the sporadic Es- and F-layers. The distance between the ionosonde and vibrator is amount to about 50 km. The time delay between the initial sweep-signal and the its corresponding appearance in the ionosphere is estimated to 7-8 minutes. This is agreed with the time interval of the acoustic signal propagation to the radioreflection heights. It is noted that the similar infrasonic and seismic sweep-signals were detected by the ground measurements at the "Klyuchi" station.

**JSA15/W/04-A5** Poster **0830-11**

**MAGNETOTELLURIC MONITORING OF SEISMICITY IN THE NORTHERN GREECE IN ORDER TO IDENTIFY DISTURBANCES RELATED TO EARTHQUAKES.**

Cezary ROZLUSKI (Institute of Geophysics, Polish Academy of Sciences, ul. Ks. Janusza 64, 01-452 Warszawa, Poland; e-mail: cpr@igf.edu.pl)

A strong earthquake, followed by a sequence of aftershocks, occurred on May 13, 1995 in the northern Greece (Ms = 6.6, lat: 40.2 N, lon: 21.7 E). The magnetic (coils) and telluric (VAN dipoles) data from Ioanina (northern Greece) station have been analyzed in the frequency domain before and after the main shock. The single scalar parameter as a function of magnetic and electric field has been introduced in order to identify possible disturbances related to earthquake events in the area. It has been attempted to correlate that parameter with seismic activity. The seismic events have been chosen with selection criteria to distinguish those events, which are more likely, the source of magnetotelluric disturbances.

**JSA15/W/16-A5** Poster **0830-12**

**TOWARDS INCREASING RELIABILITY AND INFORMATIVENESS OF THE ELECTROTELLURIC MEASUREMENTS IN GEODYNAMIC MONITORING.**

Yeugeni CHIRKOV (United Institute of the Earth Physics of RAS, 10 Bolshaja Gruzinskaja, Moscow, 123810 Russia; email: chirkov@uipe-ras.scgis.ru).

The results of electrotelluric monitoring the aftershock's activity Djava-Racha earthquake (Caucasus, 1991) obtained by use two measurement arrays situated close together are presented. Experimental evidence of local nature of the majority signals (SES-type) has been given. Possible models of the relation between precursor signals and prepared earthquake are discussed. The model of electrotelluric measurements from the technical point of view is introduced. Multistage ways and means to increase reliability of electrotelluric measurements on a wide spatial scale are proposed. It is shown that the estimation of spatial characteristics of the source (type, position, moment) is very useful for eliminating the noise, isolating the signal and making theoretical estimation of signal's generation mechanism.

New way of measurements, informative parameters and technical means for estimation spatial characteristics of source are proposed. There are presented the results of mathematical imitation modeling and field experiments showed the efficient work of proposed system.

The possibility of various application proposed approach to electrotelluric measurements (cost-saving monitoring of large area, efficient ways for interpretation results of complex measurements, isolating the precursor signals, and experimental study of source location) are discussed.

**JSA15/E/58-A5** Poster **0830-13**

**SOME RESULTS OF MAGNETOTELLURIC MONITORING OF GEODYNAMICAL PROCESSES ON BISHKEK TEST GROUND**

Svetlana E. BALANDINA, Boris S. Svetov (both at Geoelectromagnetic Research Institute RAS, Troitsk, Moscow region, Russia, e-mail: svetov@geo.igemi.troitsk.ru)

In 1993-1998 continuous recording of 5 component of magnetotelluric (MT) variations (Hx, Hy, Hz, Ex, Ey) was performed in Bishkek (Kirgizstan), with a sampling rate equal to 0.1 Hz. This data set has been used for determination of time domain responses of transfer functions and of electromagnetic field of interior (geodynamical) origin. As it known the components of MT fields are connected by convolution relation of the type:  $H_z(E_{x,y})(t) = K_1(t) \cdot H_x(t) + K_2(t) \cdot H_y(t) + D(t)$ , where  $K_1$  and  $K_2$  - pulse responses of MT transfer functions and  $D(t)$  - is residual field of interior origin mainly. This equation is solved by iterative (adaptive) procedure. At a second stage, time variations of transfer functions and of residual field have been analyzed. MT data were averaged with sampling equal to 6 minutes, 1 hour and 1 day. Considerable variations of these values, with duration ranging from several hours to several months have been discovered. They are connected either to changes of the ionosphere current system or to changes of the geoelectrical section and to generation of electromagnetic fields in the Earth interior. We found no stable correlation between variations of MT data and individual seismic events (earthquakes). On the other hand a correlation between low pass filtered (three-month filter) MT data and energy of geodynamic process in the vicinity of measuring site has been established. The energy was determined using seismic events within 200-km radius around the MT site. More over MT data permit to forecast variations of the energy two months forward. These conclusions are preliminary because they were made on the basis of limited data series and on MT observation in one station only. They are illustrated by measured data and results of their processing.

**JSA15/W/25-A5** Poster **0830-14**

**EVOLUTION OF MAGNETOTELLURIC, MAGNETOVARIATIONAL AND TOTAL MAGNETIC FIELD PARAMETERS IN CENTRAL ITALY. RELATION TO LOCAL SEISMIC ACTIVITY**

Domenico DI MAURO, Giuliana Mele, Antonio Meloni, Paolo Palangio (Istituto Nazionale di Geofisica - via di Vigna Murata, 605 - Rome, Italy, e-mail: dimauro@ingrm.it) Tomasz Ernst, Roman Teisseyre (Institute of Geophysics, Warsaw, Poland, e-mail: ternst@igf.edu.pl)

Seven consecutive years (from the summer 1991 to the spring 1998) of magnetotelluric and magnetovariation measurements at Collemeluccio (41° 43N, 14° 22E, in central Italy) have been collected. These data analysed by means of tensor decomposition on the geoelectric potential and robust estimation on the geomagnetic field allowed the investigation of the electric properties at different times and spatial lengthscales. The MV analysis on the simultaneous data from the geomagnetic observatory at L'Aquila (42° 23N, 13° 19E about 100 km away from Collemeluccio) reveals lateral and in depth electrical conductivity heterogeneities. The variation of some indicators, which lead to the phenomenon of electromagnetic induction, are presented here in their time evolution while the non-inductive contribution has been compared to some tectonomagnetic field observations and to local and regional seismic activity. Tectonomagnetic field observations in central Italy were also made using data simultaneously recorded at four magnetometer stations, and using L'Aquila observatory as a reference for differentiation.

**JSA15/W/13-A5** Poster **0830-15**

**LIMITED PREDICTION OF THE EARTHQUAKES IN THE REGION OF LAKE BAIKAL**

Yili DASHEVSKII, Nina Nevdrova, Institute of Geophysics SB RAS, RUSSIA, Email: dashevsk@uigm.nsc.ru

In recent years we see a revival of interest in earthquakes prediction on the basis of some new trends. Instead of predicting the time, place and magnitude of a future earthquake, attempts are made to estimate an earthquake probability in a given window of time, place, and magnitude. It's evident that for a successful life-saving prediction we must consider a prediction methods, which are testable by others. This money-consuming approach is based on a sufficient data getting from different sources.

In parallel with this full-scale target a more conservative goal also exists. Sometimes the amount of monitoring data is insufficient to describe complex space-time-magnitude behavior of earthquake occurrence. In such a case all that is required is to obtain the prediction information which is in a correspondence with the quantity and quality of geophysical data. This type of prediction is given the name "limited prediction".

Long-term electrical and electromagnetic time-lapsed measurements are carrying out in the region of Lake Baikal. The objective is to find out the electrical and electromagnetic precursors for the earthquakes. We solve the inverse problem for electromagnetic data and correlate seismic events with the variations of electrical conductivity at different depths, inside the geological space. We considered about 600 earthquakes occurred within the area 300'300 sq. km in 1991-1996. Shlumberger monitoring array sensed 43 of them as conductance variations of tolerant shape at the depth 750m. Only earthquakes of energy class (K) and epicenter distance (R) which meet the condition  $0.6K - 3|R+8 > 0$  have been detected. We confirmed this practical relationship using theoretical evaluations of deformations within Baikal Rift Zone and consider it as a basis of a limited prediction in this area.

**JSA15/W/32-A5** Poster **0830-16**

**TECTONOMAGNETIC MANIFESTATIONS OF COMPRESSION EPISODE IN THE BAIKAL RIFT DURING 1992-1993**

Pyotr DJADKOV and Oleg Mikheev (both at Institute of Geophysics, av. Acad. Koptuyg, 3, Novosibirsk, 630090, Russia, E-mail: djad@uigm.nsc.ru)

On the basis of the tectonomagnetic monitoring information the episode of the horizontal

## INTER-ASSOCIATION

compression stress predominance was detected in the Baikal rift in 1992-1993. A number of unusual tectonomagnetic anomalies took place before, during and after this extraordinary occurrence. The beginning of this episode was related to the appearance of regional positive tectonomagnetic anomaly (with amplitude up to 2 nT under accuracy 0.1 nT) in 1992 in the Selenga depression where 60 stations of repeated and 4 stations of continuous observations are located. The confirmation of this episode of compression was found later in other information obtained by determinations of temporal variations of the earthquake focal mechanisms and extensometer observations. The number of the earthquakes with the thrust component of displacement in the earthquake sources reached 60 - 80 % in the Baikal rift zone, while such earthquakes occurred very rare in other periods. In the same time we observed the disappearance of the season changes in the difference of magnetic field between two stations Stvolovaya and Enhaluk at the Baikal coast. Before 1992 these season changes (1-1.5 nT) had the good correlation with the season variations of the Lake Baikal water level. After the compression episode the high-rate extension process which was confirmed by GPS- measurements was developed in this region in 1994-1995. In this period the 0.5-1 nT tectonomagnetic anomalies with duration of 2 to 4 weeks were accompanied the space-time clusters of the  $M = 3 - 4$  earthquakes at a distance up to 80 km.

**JSA15/E/43-A5** Poster **0830-17**

### BAIKAL: THE RESULTS OF MULTIDIMENSIONAL ANALYSIS OF THE TIME SERIES OF ELECTROMAGNETIC MONITORING SYSTEMS

MOROZ Y.U.F. (Institute of Volcanic Geology and Geochemistry, FED RAS.); Petropavlovsk-Kamchatsky, (683006, Russia. (4150058293) ; e-mail: ivgg@svyaz.kamchatka.su.); Mandelbaum M.M., (GFUGP "Irkutskgeofizika", Ministry of Natural Resources, I.P. Ministry of Natural Resources)

Monitoring the electromagnetic field with artificial source is being conducted at the eastern coast of Lake Baikal at the area of 60x60 km. A 200 kWt power generator is used as the source. There are 12 observational sites with the distance from one to 40 km between them. One site is located at the opposite shore of the lake. Measurements are made once a day. Depth of the controlled part of the earth crust does not exceed 2-3 km. The time period of monitoring is 18 years. Continuous time series of apparent resistivities, meteorological parameters, water level in Lake Baikal are studied using modern computer programmes for multidimensional analysis. As a result it was established that electric conductivity of rocks does not depend on the water level in Baikal, air temperature and atmospheric pressure. As a rule, regular variations in the range period from few days to a year are not observed in the behaviour of electric resistivity in the upper layers of the earth crust. However, in some cases variations are observed in power spectrum in the range period from 80 to 200 days and more. These variations have local character and are probably connected with the close-to-electrode processes. Increase of canonical coherence in the multidimensional series of apparent resistivities is observed before high seismicity in the Baikal rift zone. The increased coherence anticipates earthquakes of energy class 15 and more in the radius of 650 km. The anomalous effects are also revealed in the aggregate signal of multidimensional series of the apparent resistivities, which are connected, with the earthquakes of energy class 12 and 13. When the number of channels is increased the resolution of the aggregate signal increases as well, so that the effects may be observed of the earthquakes of energy class 10 and 11 with epicenters located near the test area. The canonical coherence and aggregated signal anomalies may serve as possible forerunners of large earthquakes in the Baikal rift zone.

## Friday 23 July PM

Presiding Chairs: J. Zlotnicki (Laboratoire de Geophysique, Orleans, France)  
S. Uyeda (Tokai University, Japan)

**JSA15/E/18-A5** Poster **1400-01**

### SOME MECHANISMS OF GEOMAGNETIC FIELD FLUCTUATIONS AND THEIRS STATISTICAL ANALYSIS

J.GORODISKY (Carpathian Branch of Subbotin Institute of Geophysics NASU, 3b, Naukova Str., 290601, Lviv, Ukraine, E-mail: valentyn@carp.lviv.ua)

As we already had shown the magnetic effect caused by electrokinetic processes on the surface of quasihomogenous halfspace isn't absent and statistical features of the anomalous Geomagnetic fields fluctuations contains information about the geodynamical processes evolution. We have analysed by the help of Monte-Carlo method the stochastic model of electrokinetic-magnetic effect in the quasihomogenous medium. The mechanism of electric currents spatial dividings is based on the effect of surface conductivity influence on the rock conductivity for microcapillary racks (d<50 mm). The main results are as follows. 1) The distribution of magnetic field changes as a result of random changes of microcapillars structure in case of constant value of the microcapillars space distribution dispersion is similar to the distribution of magnetic field in static case. The main feature of these distributions is symmetry of positive and negative values of effect. 2) In the case of nonconstant value of microcapillars space distribution dispersion the main feature of the distribution of magnetic field changes is asymmetry of positive and negative values of effect. The first result may be useful for the evaluation of natural magnetic noise when monitoring active faults by geomagnetic methods. The 2nd result we consider as a useful link for the magnetic image of tectonically active environments evolution constraining. Similar results we also obtained for the model that is based on the concentration mechanism of electric currents spatial dividing. It is significant, that in regions of active chemical transformations of magnetic minerals, the statistical analysis of anomalous geomagnetic field fluctuations also contains additional information about these processes activity. As we have shown such analysis is useful especially in the positive magnetic anomalies cases.

**JSA15/E/21-A5** Poster **1400-02**

### LOCAL GEOMAGNETIC FIELD CHANGES AND SEISMICITY OF ARMENIA

GRIGORIAN A.G., Nazaretnian S.N. (National Service of a Seismic Guard Rá, Leningradian,5, Gyumri, Armenia. email: serge@shirak.am) Skovorodkin Yu.P. (UIPE of RAS, B. Gruzinskaya, 10, Moscow, Russia. email: yupsk@uipe-ras.scgis.ru)

On the territory of Armenia the network of geomagnetic observatories is created which allows measuring the variations of components D, I and Z of Earth's magnetic field. The data of stations Jradzor, Garni and TÁvuch (30 km, 150 km and 200 km from epicenter of Spitak earthquake of 07.12.1988 y.) for time period 1986-1993 years are used in analysis. From these data the ratio of amplitudes A of variation of each component of the magnetic field synchronously measured by each pair of stations (parameter N(A)) is obtained for periods of variations 5-25 min, 30-60 min and 5-10 hours. From the beginning of observations up to moment of Spitak earthquake the trend in the behavior of N(A) is observed for all 3 components D, H, Z and for all periods of variations. On the background of trend the sharp changes of N(A) are observed during two intervals: from March to July of 1986 y and from February to December of 1988. The first sharp change of N(A) corresponds to Parvany earthquake (13.05.1986), the second one to Spitak earthquake (07.12.1988). The tendency of returning movement of parameter N(A) to the initial value is observed after Spitak earthquake.

It is supposed that the reason of parameter N(A) changes is the variation of electric conductivity of the rocks of terrestrial crust, which is created by the vertical filtration of high conducting fluids.

**JSA15/E/16-A5** Poster **1400-03**

### GEOMAGNETIC MONITORING FOR STUDYING MODERN GEODYNAMIC AND EARTHQUAKE PRECURSORS IN THE CARPATHIANS

Valentina KUZNETSOVA, Valentin Maksymchuk, Yuriy Gorodyski, Igor Dotsenko, Igor Chobotok (Carpathian Branch of Subbotin Institute of Geophysics NASU, 3b, Naukova str, 290601, Lviv, Ukraine, email: valentyn@carp.lviv.ua)

During the last 20 years geomagnetic monitoring have been held systematically in the territory of sesmoactive Transcarpathian Trough where every year 2-10 earthquakes of magnitude  $M=2.5-3$  occur. Maximal possible force doesn't exceed  $M=6$ . Geomagnetic monitoring consists of: 1) Repeat high-accurate plane and profile geomagnetic observations to study peculiarities of modern geodynamics and the block structure of lithosphere, as well as to determine zones of active tectonic faults. The zones of anomalous temporal geomagnetic changes with values of 2-7 nT/year have been mapped. 2) Regime continuous geomagnetic observations at a network of 4 stations both to study temporal changes in a broad frequency range and to search for earthquake precursors. During 1982-1997 24 anomalous effects were found, 15 of which were accompanied by earthquakes. Anomalous effects are characterised as follows: duration of 1.5-3 months, effect intensity - 2.5-5 nT, the earthquake moment mainly concerning the final stage or the post resumed field initial level. 3) Investigations of temporal changes of Wiese vector. Temporal changes corresponding to high seismicity activity period in the Carpathians region in 1990 are determined. The dynamic linearization zone is revealed. Physical mechanism of geomagnetic field anomalous temporal changes generation has been studied. Electrokinetic mechanism of anomalous magnetic effect generation for the quasihomogeneous medium is proposed and statistically studied.

**JSA15/E/14-A5** Poster **1400-04**

### USE OF APPARENT RESISTIVITY TIDES VARIATIONS FOR SEISMIC ACTIVITY MONITORING

Alexander SARAIEV, Mikhail Pertel (St. Petersburg State University, Universitetskaya nab. 7/9, St. Petersburg, 199034, Russia, e-mail: aks@aks.usr.pu.ru); and Zinoviy Malkin (Institute of Applied Astronomy RAS, nab. Kutuzova, 10, St. Petersburg, 191187, Russia, e-mail: malkin@ipa.rssi.ru)

A good correlation of apparent resistivity variations of electromagnetic soundings methods with artificial and natural fields in extremely low frequency range (units - thousands of a hertz) and earth tides deformations were observed. The apparent resistivity variations of 7-15 % were connected with deformations of 0.2 - 0.3 m. Both direct (rise of the earth surface and increase, lowering of the earth surface and decrease of apparent resistivity), and inverse relation were obtained. The various character of relations can be explained by a various degree of rocks water saturation. At small water content the fluid distribution in the rock has islands, not connected character. In case of compression the degree of fluid connections increases, the network of interconnected channels grows and rock resistivity decreases. On the contrary, at the biggest water content the fluid completely fills the rock pore space. At a pressure increase in this case happens compression of channels, and resistivity of the rock is grows. Tides effects should be taken into account for increase of electromagnetic soundings accuracy. The results can be used for the study of regularities of rocks geoelectric properties changes before earthquakes, for selection of tension sensitive zones and placing of the receiving devices, for choice of optimum frequencies for monitoring of a geoelectrical section intervals with the best tension sensitivity, and also for the taking into account of tides effects, as of the hindering factor at monitoring of seismic activity. This method of study of the earthquake precursors is oriented on large volumes of rocks in situ and has the possibility of realization of regular reproduced observations. The work was performed with the support of "Integration" grant, N 326.66.

**JSA15/W/21-A5** Poster **1400-05**

### EARTHQUAKE-ASSOCIATED PERTURBATION IN THE LOW-LATITUDE IONOSPHERE

Anna DEPUEVA and Nina Rotanova (both at IZMIRAN, Troitsk, Moscow Region, 142092, Russia, email: depueva@izmiran.rssi.ru)

Topside vertical sounding data were analysed in order to study earthquake-associated perturbations in the ionosphere. A few separate great earthquakes were considered, whose epicenters were situated inside a narrow zone close to the magnetic equator. It was shown that low-latitude ionosphere reacts on a forthcoming earthquake in a special way. Equatorial seismoionospheric effect manifest itself as electron density fall at the F-layer peak level and higher altitudes. Electron density spatial (longitude - latitude) distribution looks like a «funnel» over the earthquake preparation zone area. Some evidences in favour of the seismic origin of the above-said phenomenon will be presented including that arising from the method of natural orthogonal components application. A particular emphasis will be made on lithosphere-ionosphere coupling taking into account already known mechanism of E- and F-layers interaction due to vertical upward ExB plasma drift and diffusion over the dip equator.

**JSA15/L/02-A5** Poster **1400-06**

### ELECTROMAGNETIC AND PLASMA DISTURBANCES IN THE IONOSPHERE OVER EARTHQUAKE REGIONS

N.V. ISAEV and O.N. Serebryakova, (Institute of Terrestrial Magnetism, Ionosphere and Radiowave Propagation, 142092 Troitsk, Moscow Reg., Russia.)

The recent results of investigation of seismic-ionospheric effects are presented below. Data from the low-orbiting satellite COSMOS-1809 were used to search for a correlation between seismic activity and increases in ELF/VLF emissions for different regions. The data of 100 revolution of satellite were chosen for the analysis of ionospheric effects of this seismic activity. Analysis enables to draw the following conclusions. The electromagnetic emissions in the frequency range of 140-450 Hz are regularly observed within the L-shells with the root in the sesmoactive zone. Near a zone of seismic activity (??=?6) at the altitude - 950 km bursts of ELF radiation are observed at the frequencies  $f=140$  and 450 Hz in the magnetic and electric components. The radiation excess above the background level can reach more than an order of magnitude. The radiation bursts are observed minutes to hours beforehand an earthquake and during several hours after it. The sizes of the disturbed region are usually 400-600 km, and greater in the period of aftershock activity than during the earthquake development. The small-scale plasma irregularities  $dN_e/N_e$ ? 3-8% with characteristic scales 4-10 km along the orbit has been revealed in geomagnetic field tubes connected with epicentral region in which seismogenic ELF emissions were observed simultaneously. The empirical models of distribution of ELF-emissions for different regions were constructed on the basis of statistical study of these measurements. For these regions amplitude-spatial distributions of sesmoelectromagnetic radiation were constructed both for electric and magnetic components and distributions of the signal (-to-) noise ratio were constructed as well.



Analysis of seismogenic ELE/VLF radiation had shown that main signal characteristics (frequency, amplitude etc.) were sufficiently different for different seismo-active regions of the Earth. This fact is evidence of seismoelectromagnetic parameters dependence on physical-chemical properties of Earth's crust and lithospheric processes. Characteristic features of ELF/VLF radiation related to submarine earthquakes were exposed (radiation of higher frequencies, amplification of natural ELF/VLF radiation, take place, because electromagnetic connection between lithosphere and ionosphere is absent. The generation mechanism of earthquake-related small-scale plasma inhomogeneities was developed.

**JSA15/W/09-A5** Poster **1400-07**

#### MODELING OF POSSIBLE IONOSPHERIC PRECURSORS OF STRONG EARTHQUAKES

Vitali KIM and Valeri Hegai (both at IZMIRAN, Troitsk, Moscow Region, 142092 Russia, email: kimpv@izmiran.rssi.ru)

Possible changes of electron density in the nighttime mid-latitude ionosphere caused by seismogenic electric fields before strong earthquakes are calculated. The results indicated that the background electron density in the E region changes by 20-30% relative to its undisturbed value above the epicentral zone of forthcoming earthquake. In the middle part of E region, a dense layer of metal ions can be formed. Horizontal distribution of electron density in the F2 region is perturbed in non uniform manner within the area of horizontal size of about 400 km, he changes are stronger in the lower F2 region where irregularities of various scales (from 10 to 150 km) are developed in course of time. In the upper ionosphere, a geomagnetic field aligned inhomogeneity of plasma density is produced around the geomagnetic force line passing through the imminent earthquake epicentrum. It will result in enhancement of probability of whistler appearance in the forthcoming earthquake epicentral zone.

**JSA15/E/25-A5** Poster **1400-08**

#### SIMULTANEOUS VARIATIONS OF LOW FREQUENCY EMISSIONS AND PARAMETERS OF PLASMA AT UPPER IONOSPHERE HEIGHT OVER FUTURE EARTHQUAKE EPICENTRE

LARKINA V.I., Ruzhin Yu.Ya. IZMIRAN, Troitsk town, (Moscow Region, 142092, Russia)

At Low-Altitude Satellite above Earthquake Preparation Zones Abnormal Changes of Electromagnetic, Electrical and Magnetic Fields and Plasma parameters are found out. Simultaneous Changes of the Magnetic and Electrical Component of Field of Low Frequency Noise Intensity and Density and Temperature of an Environmental in a region above Earthquake Epicentre and in Magnetoconjugated Hemisphere are analysed by "Intercosmos" satellite Data. The Size of Zones of Plasma Parameters Change Registration connected with Processes of Preparation of Event (Earthquake) are determined. The Received Information are Necessary for Development and Creation Mechanizm of Penetration of Energy from Lithosphere in Ionosphere and Plasmasphere and for Creation of Seismic DangerousmPrognoz Methods.

**JSA15/E/48-A5** Poster **1400-09**

#### RELATION BETWEEN ELF AND VLF EMISSIONS ON THE INTERCOSMOS 24 SATELLITE AND CONCENTRATION OF RADON IN EARTHQUAKE REGIONS

Yu.M.MIKHAILOV, G.A.Mikhailova and O.V.Kapustina (Institute of Terrestrial Magnetism, Ionosphere and Radio Wave Propagation of Russia's Academy of Science, Troitsk, Moscow region, 142092, Russia, e-mail: yumikh@charley.izmiran.rssi.ru)

For study of ionosphere-lithosphere processes for the first time the comparative analysis has been carried out between radon concentration in seismoactive region and spectral characteristics of the ULF-ELF electromagnetic emissions, registered by satellite over the same seismoactive region. The regular observations data of radon level in the Kangra Valley, India, situated on the north boundary of the Indo-Australian plate were used. The choice of this place was done due to the storage time of alpha-track detectors, which registered radon concentration, being 1 day, lowest of all known stations. On the Intercosmos 24 satellite the electric component of ULF/ELF waves was registered with help of ten narrow band filters in the frequency range from 8 to 970 Hz. In days, when anomaly radon concentration bursts have been observed, simultaneous increasing of electric field on the factor more than ten at frequency 8 Hz and on the factor 2-3 in the intensity maximum from 150 to 623 Hz was observed. That effect was observed only at night and was localized exactly in space above the fault. In spectral distribution of emission maximum in the frequency range from 150 to 623 Hz was allocated, which coincided with the amplitude spectra maximum of fractional hop whistlers, observed on other satellites at night, and so with frequency distribution of atmospheric intensity in the waveguide Earth-ionosphere. This fact ensures statement, that the noises are generated by the lightning discharges, and their amplification simultaneously with radon anomaly bursts was due to decreasing of ELF-waves attenuation under influence of seismic nature electric field. That is a mechanism of the lithosphere-ionosphere interaction at the earthquake preparing phase proposed by the authors.

**JSA15/E/37-A5** Poster **1400-10**

#### THE EXPERIENCE OF SHORT-TERM EARTHQUAKE PREDICTION USING THE ELECTROMAGNETIC RADIATION METHOD AT NORTH CAUCASUS

Vitali A. MORGOUNOV (Institute of Physics of the Earth, Moscow 123810, B.Grusinskaya 10, Russia, email: vam@upei-ras.scgis.ru); Alexander G. Zdorov (Central Geological Expedition, Essentuki 357600, Kislovodskaya st. 203, Russia)

The experience of utilization of the electromagnetic radiation method (EMR) for scientific prediction of the earthquakes (EQ) is discussed. Prolonged observations from the network of stations carried out at North Caucasus at the test band (65x85 km), allowed to study peculiar local features in the generation of seismo-anomalous EMR and to begin the procedure of scientific prediction of local EQs of the background level. For the period of continuous registration of EMR (1990-1998), 16 seismic events occurred during which the observation stations were located within the EQ's preparation zone. 8 EQs were accompanied with clear EMR precursors. The useful signal exceeded the background values by up to 20 dB. The anomaly lasts up to two days, and the lead time of the signal before the event varies from two to four days. The intensity of EMR does not exhibit any explicit dependence on the EQ's magnitude, in agreement with the model of EM-radiators within the skin layer. Miss the target were registered in 8 cases, one as false alarm. Thus, the probability of correct "scientific alarms" of the time of the event could be estimated as  $W \sim 0.5$  for the region of a low seismicity, where  $M \sim 3-4$  is the long-awaited event. The probability of false alarm is very low  $W_f \sim 0.06$  for especially isolated events. All the EQs with  $M \geq 4$  were accompanied by clear-cut anomalous EMR spikes. The study of EM precursors of destructive seismic events during the last decades, testifies to the improvement of the method efficiency with the energy of EQ. 9 years of uninterrupted monitoring draw to the conclusion that on the average every next weak seismic event could be predicted.

**JSA15/E/51-A5** Poster **1400-11**

#### KAMCHATKA: THE RESULTS OF MONITORING LOW FREQUENCY ELECTROMAGNETIC FIELD OF THE EARTH

MOROZU YU.F., Institute of Volcanic Geology and Geochemistry, FED RAS. Petropavlovsk-Kamchatsky, 683006. Russia (4150058293); e-mail: ivgg@svyaz.Kamchatka.ru

The results of studying structure of the earth's electromagnetic currents and variations of the electromagnetic field are considered. The observational network is located within the subduction zone. It includes 4 sites at the distance of 50 to 120 km between them. Registration and transmission of the information is performed using radio telemetered system. Sampling frequency of the channels is one minute. The electromagnetic field structure has been studied in the range period from few hours to a year and more. Spectral-temporal characteristics, coherences, phase relationships and amplitude frequency functions between the components of the electromagnetic field have been studied using multidimensional analysis. The following anomalous effects, connected with large earthquakes and seismicity around Kamchatka (of almost 300km radius) have been detected. 1. Change to 180° of the phase relationship between yearly variations of the magnetic inclination and horizontal, vertical components of the magnetic field during the highest seismicity in 1996-1997 (over the period of 1990-1998). 2. Change to 90° of the phase relationship between yearly variations of the orthogonal component (NS and EV) of the earth's electric currents within the time intervals when large earthquakes of  $M=7.1$  and  $7.3$  occur. 3. Change of canonical coherence of yearly variations ( $T=12$  and  $24$  hours) of the Earth's electric currents and of variations of the geomagnetic field from the most common values of 0.8-1 to 0.3-0.5 values 10-30 days prior to the large earthquakes of  $M>7$ . 4. Occurrence of the bay-like disturbances in the earth's electric currents from 3-4 days up to one month and a half duration before the large earthquakes of  $M>7$ . 5. Occurrence of the oscillating-type quasi-periodical variations with the time period from 1 to 6 days prior to the large earthquakes of  $M>7$ .

**JSA15/E/20-A5** Poster **1400-12**

#### PULSED ULF EM SIGNALS - PRECURSORS FOR OPERATIVE MONITORING EARTHQUAKES

An. P. NAUMOV (D.I.Mendeleev Institute for Metrology, St. Petersburg, 198005, Russia, email: slovo@mail.line.ru)

We regularly observed Electromagnetic (EM) pulses of ULF range signals when working in the seismic dangerous regions of the Crimea and Tien Shan. Investigations of geomagnetic variations of these regions have confirmed tectonic nature of discovered signals. Their morphology was studied: the range of frequencies 0,001-5 Hz, the amplitude of almost square-wave pulses from 0.2 to 1-2 nT. Short pulses with an amplitude up to 20 nT and 6-20 seconds duration of the other origins (tectonic too) were observed in the form of pulse packets. Parallel synchronous work of several vector-magnetometers (3 or 4) in the area of coherent ULF signals allows to define coordinates of the source. The described signals appear before the seismic events: a time of signals gap always occurs prior to the moment of earthquake. Comparison of ULF signals and magnetic bay-like precursors also indicates correlation of observing results before earthquake. The measurements of ULF tectonic signals during of three-year interval show stability in time of the sources and their mode of the generation of ULF EM fields. The similar results with EM signals in the range of radio frequencies are discussed. Hence, there is a possibility to realise reliable operative monitoring of earthquakes by careful measuring of ULF EM signals-precursors.

**JSA15/E/45-A5** Poster **1400-13**

#### ANOMALOUS PARTICLE DIFFUSION ASSOCIATED WITH ATMOSPHERIC DISTURBANCES

Oleg POKHOTILOV, Vyacheslav Pilipenko (Institute of Physics of the Earth, 123810 Moscow, Russia, Email: pokh@upei-ras.scgis.ru); Michel Parrot (LPCE/CNRS, 3A, Avenue de la Recherche Scientifique 45071 Orleans Cedex 2, France, email: mparrot@cnrs-orleans.fr)

A new mechanism of the atmosphere-magnetosphere interaction, which might be called "acoustic-magnetospheric cyclotron accelerator" is proposed. The idea of this mechanism stems from the fact, that strong acoustical perturbations in the ionosphere (e.g., due to earthquakes, thunderstorms, etc.) may generate magnetic disturbances in the magnetosphere. We suggest the following scenario: strong acoustic oscillations, reaching the ionospheric E-layer, may result in the generation of the field-aligned currents. On one hand the magnetic effect of these currents in the magnetosphere has considerable magnitude. On the other hand the ground signature of these magnetic disturbances is essentially weaker. Alfvén waves, generated by acoustic disturbances in the upper atmosphere, may induce resonant energizing and subsequent diffusion of particles, trapped in the magnetosphere, across L-shells. This idea may be fruitful in the interpretation of some occasional increases in inner zone particle fluxes, which do not correlate with the solar or magnetospheric activities. Using this conception we provided a reasonable explanation for a number of satellite observations of occasional increases in inner zone particle fluxes which do not explicitly related to solar or magnetospheric processes.

**JSA15/W/20-A5** Poster **1400-14**

#### ELECTROMAGNETIC MONITORING BY THE METHOD OF RADIOTRANSLUCENT IN THE BAIKAL RIFT ZONE

Anatoly M. Popov and Alfred B. Baduev (Institute of the Earth's Crust, Irkutsk, Russia, email: popov@earth.crust.irk.ru); Nikolay A. Telpukhovskiy, Vadim M. Akulov and Anatoly V. Moshanov (East-Siberian Institute of physics-technical and radiotechnical measurements, email: eoprs@niifri.irkutsk.ru); Yuri B. Bashkuev and Mikhail G. Dembelov (Institute of Natural Sciences, Ulan-Ude)

In 1997 a highly exact amplitude and phase monitoring of electromagnetic signals from the standard radiostation RTZ-50 on the 50 kHz frequency was organized by the authors on the Irkutsk-Ulan-Ude direction crossing the southern part of the lake Baikal. The basis of the equipment complex consists of the quantum clock HP5061-A relatively to which the control (Irkutsk) and measurements (Ulan-Ude) of the phase of standard frequency have been carried out, PC IBM and other serial equipment. Digitization of the signals is conducted with the frequency 200 kHz. The control of the quantum clock's work relatively to the State standard is exercised by means of the satellite systems GLONASS or GPS.

The monitoring results have showed that the reflected signal from ionosphere is practically absent for the period of 4-5 hours of the world time. Therefore while being in search of the earthquake's precursors it's expedient to analyze the characteristics of the signals during the period of time closed to the indicated one. Basing on the values accepted within the 4-5 hours period the annual amplitude course (value 30 db) and signal phase (1,5 mks) were obtained. The calculations demonstrate that changes of the phase connected with the seasonal variations of the conductivity of the upper layer (winter-summer) aren't sufficient to create the anomaly's value which is being observed. Also the local anomalies timed to the earthquakes have been fixed that perhaps indicates their connection with the seismic processes.



**JSA15/E/31-A5** Poster **1400-15**

**IONOSPHERIC IMAGES OF STRONG EARTHQUAKES (EXPERIMENT AND THEORY)**

PULINETS S.A., Hegai V.V., Depuev V.Kh., Gaivornoskaya T.V., Legen'ka A.D. (IZMIRAN, Troitsk, Moscow Region, 1420942, Russia, E-mail: pulse@izmiran.rssi.ru) Liu J.Y. (National Central University, Jungli, Taiwan, E-mail: jyliu@jupiter.ss.ncu.edu.tw)

Many years of studies of the ionospheric precursors of strong earthquakes resulted in revealing of the ionospheric variations parameters set intrinsic exclusively to the seismic activity coupling processes. Spatial (latitude-longitude) and vertical distribution of the electron density, its behavior in local time and relatively to the anticipated earthquake instant, magnetically conjugated effects, ion composition variations - all together create the ionospheric image of the anticipated earthquake which couldn't be mixed with any other kind of the ionospheric variability. The self-consistent physical model of seismo-ionospheric coupling was created which is based on the effect of the strong quasistatic electric field generated in the future epicenter area. The model could be tested directly by experimental measurements, and many other effects observed over the area of the anticipated earthquake (for example, the ELF and VLF noises) could be explained by the model. The conception of the groundbased and satellite monitoring of the earthquake precursors is proposed. The special accent is made on the GPS/GLONASS ionospheric measurements.

**JSA15/E/55-A5** Poster **1400-16**

**TECTONIC FAULTS ACTIVITY AS A POSSIBLE SOURCE OF THE IONOSPHERE MODIFICATION**

PULINETS S.A., Kim V.P., Hegai V.V., Depuev V.Kh. (IZMIRAN, Troitsk, Moscow Region, 1420942, Russia, E-mail: pulse@izmiran.rssi.ru) Radicella S.M. (Abdus Salam International Center for Theoretical Physics, Trieste, Italy, E-mail: rsandro@ictp.trieste.it)

Ionosphere topside sounding data from the INTERCOSMOS-19 satellite have been utilized to study longitude distribution of the night-time midlatitude F2 region peak electron density NmF2 in the Southern hemisphere over the array of tectonic faults in the Andes area for low geomagnetic activity periods in July 1979 and in July 1980 when solar activity was high and nearly the same, however, in July 1980 there was intensified tectonic activity in the Andes area, and in July 1979 the tectonic activity was lower. The results show that in July 1980 the observed value of NmF2 as a function of longitude decreased by a factor of ~ 3 with the change of longitude from 280 to 295 E over the latitude range 30-45 S, whereas the appropriate longitude profiles of NmF2 observed in July 1979 and reproduced by the ionospheric model IRI-90 do not reveal any appreciable longitude variations above the Andes area. Using model simulation we interpret the observed longitude anomaly of NmF2 in July 1980 as a result of the F2 region modification caused by a hypothetical large-scale long-living perturbation of the vertical electrostatic field on the Earth's surface associated with intensified tectonic activity.

**JSA15/W/28-A5** Poster **1400-17**

**IONOSPHERE TOPSIDE SOUNDING DATA FROM THE INTERCOSMOS-19 SATELLITE**

Sergei PULINETS, (IZMIRAN, Russia, Email: pulse@izmiran.rssi.ru)

Ionosphere topside sounding data from the INTERCOSMOS-19 satellite have been utilized to study longitude distribution of the night-time midlatitude F2 region peak electron density NmF2 in the Southern hemisphere over the array of tectonic faults in the Andes area for low geomagnetic activity periods in July 1979 and in July 1980 when solar activity was high and nearly the same, however, in July 1980 there was intensified tectonic activity in the Andes area, and in July 1979 the tectonic activity was lower. The results show that in July 1980 the observed value of NmF2 as a function of longitude decreased by a factor of ~ 3 with the change of longitude from 280 to 295 E over the latitude range 30 - 45 S, whereas the appropriate longitude profiles of NmF2 observed in July 1979 and reproduced by the ionospheric model IRI-90 do not reveal any appreciable longitude variations above the Andes area. Using model simulation we interpret the observed longitude anomaly of NmF2 in July 1980 as a result of the F2 region modification caused by a hypothetical large-scale long-living perturbation of the vertical electrostatic field on the Earth's surface associated with intensified tectonic activity.

**JSA15/W/22-A5** Poster **1400-18**

**IONOSPHERIC ULF/ELF WAVE AND PLASMA EARTHQUAKE PRECURSORS: SATELLITE MEASUREMENTS AND ELECTRODYNAMIC MODEL**

Valery SOROKIN, Vitaly Chmyrev and Nikolay Borisov (Institute of Terrestrial Magnetism, Ionosphere and Radio Wave Propagation, Russian Academy of Sciences, IZMIRAN, Troitsk, Moscow Region, Russia, 142092, email: sova@izmiran.rssi.ru)

The satellite data are used as experimental basis for the electrodynamic model of earthquake precursors in the atmosphere and the ionosphere. According to this model the chain of processes forming the lithosphere - ionosphere coupling starts from the injection of radioactive substances and charged aerosols into the atmosphere prior to earthquake. This leads to increase of atmospheric conductivity and forms the vertical electromotive force in the near ground layer. Such modification of Earth - ionosphere electrical circuit results in change of vertical electric current in the atmosphere and the ionospheric electric field. Development of the acoustic-gravity wave instability stimulated by the increased DC electric field is followed by formation of horizontal periodic irregularities of the ionospheric conductivity. An excitation of such irregularities leads to formation of field - aligned currents and plasma density disturbances stretched along the geomagnetic field. When satellite crosses these structures it observes the small-scale plasma density fluctuations and ULF geomagnetic oscillations. The nature of seismic related ELF emissions in a frame of this model is connected with transformation of electromagnetic noises propagating in the Earth - ionosphere wave guide on the small - scale irregularities of ionospheric conductivity excited by AGW instability. The other effect of the electric field increase is an additional Joule heating of the lower ionosphere that results in an elevation of the F-layer maximum, a decrease of electron density in the maximum of this layer and a redistribution of ion composition in the upper ionosphere.

**JSA16** **Wednesday 21 July**

**SOLAR VARIABILITY AND CLIMATE (IAGA, IAMAS, SCOSTEP)**

Location: School of Education G33 LT

Location of Posters: Conference Room, School of Education

**Wednesday 21 July AM**

Presiding Chair: Judit. M. Pap (Department of Physics and Astronomy, University of California, Los Angeles, USA)  
Concurrent Poster Session

**JSA16/E/13-A3** Invited **0830**

**SCIENCE OVERVIEW OF INTERNATIONAL SOLAR CYCLE STUDIES (ISCS): 1998-2002**

S. T. WU (Center for Space Plasma and Aeronomic Research and Department of Mechanical and Aerospace Engineering The University of Alabama in Huntsville Huntsville, AL 35899 USA); V. N. Obridko (IZMIRAN, Troitsk Moscow Region, 142092, Russia); and M.A. Shea (Air Force Research Laboratory, 29 Randolph Road, Hanscom AFB, Bedford, MA 01731-3010, USA)

In August 1997, the Scientific Committee on Solar-Terrestrial Physics (SCOSTEP) initiated a program for the study of the rising phase of the 23rd solar cycle. This program, entitled "International Solar Cycle Study (ISCS)", consists of three working groups and one panel. These are: Solar energy flux study from the interior to the outer layer (WG1); Solar magnetic field variability study from the lower atmosphere through the inner corona (WG2); and Solar emissions, its origin and transport through the heliosphere (WG3). The Panel is Environmental Applications. In this paper we discuss the preliminary scientific results in the above mentioned topics during the early phase of the rising 23rd solar cycle. The programmatic aspects of ISCS will also be discussed.

**JSA16/W/18-A3** Invited **0900**

**TOTAL SOLAR IRRADIANCE: MEASUREMENTS AND RESULTS**

Claus FRÖHLICH (Physikalisch-Meteorologisches Observatorium Davos, World Radiation Center, CH-7260 Davos Dorf, Switzerland, email: cfrohlich@pmodwrc.ch)

Since November 1978 with the start of the NIMBUS7 total solar irradiance monitoring started a complete set of TSI measurements from space are available, yielding a time series of more than 20 years. From measurements made by five of these radiometers a composite record of solar total irradiance can be compiled. The radiometric, instrumental and operational influences and constraints are discussed in order to assess the precision and accuracy of this composite. Moreover, it is the basis for an evaluation of the influence of solar activity on total solar irradiance. An empirical model that parameterises the combined influences of dark sunspots and bright faculae features on solar irradiance is able to explain more than 95% of the variance. After removing the magnetic influence with the model, the remaining 'quiet sun' shows no trend over the whole period, indicating that the sun's output has not changed over the past two solar cycles.

**JSA16/W/36-A3** Invited **0930**

**VARIATIONS OF SOLAR SPECTRAL IRRADIANCE FROM THE NEAR UV TO THE INFRARED: MEASUREMENTS AND RESULTS.**

M. FLIGGE (ETH, Zurich, Switzerland), C. Frohlich (Physikalishes- Meteorologishe Observatorium Davos, Switzerland); J. Pap (University of California, Los Angeles, USA), and Sami Solanki (ETH, Zurich, Switzerland); and Ch. Wehrli (Physikalishes- Meteorologishe Observatorium Davos, Switzerland)

Solar spectral irradiance variations are known to exhibit strong wavelength dependence with the amount of variability increasing towards shorter wavelengths. The bulk of solar radiation occurs at visible wavelengths. The spectral radiation longward of 300 nm accounts for 99% of the total solar radiative output. Deposited in the Earth's troposphere and biosphere, this part of the solar irradiance spectrum determines direct solar radiative forcing and is therefore of particular interest for climate studies. In the following measurements of solar irradiance and irradiance variability from ear UV to the IR are reviewed with particular emphasis on the results obtained from the VIRGO (Variability of Irradiance and Gravity Oscillations) and SOLSPEC (Solar Spectrum Measurement) instruments.

Presiding Chair: Claus Frohlich  
(Physikalishes-Meteorologishe Observatorium Davos, Switzerland)

**JSA16/E/06-A3** Invited **1030**

**SOLAR UV AND EUV IRRADIANCE: MEASUREMENTS AND RESULTS**

Gary ROTTMAN and Thomas Woods (both at the University of Colorado, 1234 Innovation Dr., Boulder, CO 80303, USA; e-mail: gary.rottman@lasp.colorado.edu)

The ultraviolet ( $\lambda < 300$  nm) irradiance from the Sun is completely absorbed by the Earth's atmosphere; and although it comprises less than 1% of the total radiative output of the Sun, it enhances the effects of direct solar forcing. The irradiance at these short wavelengths has a dominant influence on the heating and composition of the atmosphere, and it thereby has indirect influence on greenhouse gas composition, wave activity and mean circulation, and perhaps on hydrological cycles. The bulk of the total solar irradiance (TSI) originates in the solar photosphere and varies by much less than 1%. In comparison, the ultraviolet irradiance, with its origin in the tenuous and magnetically active layers of the solar atmosphere, is far more variable - ~10% at 200 nm, a factor of 2 at 121 nm, and factors exceeding 10 in the EUV. Instruments and techniques steadily improve, and today a fairly consistent understanding of solar variability has emerged. This paper will review the following topics: 1) the state-of-the-art in measuring the Sun, 2) today's observational programs, and 3) the current understanding of both the magnitude and variability of the ultraviolet irradiance.

**JSA16/E/09-A3** Invited **1100**

**MODELLING OF SOLAR IRRADIANCE VARIATIONS**

Peter A. FOX, Oran R. White (both at High Altitude Observatory, National Center for Atmospheric Research, P.O. Box 3000, Boulder, CO 80307, Email: pfox@ucar.edu, orw@ucar.edu); Juan Fontenla (771 W. Dahlia, Louisville, CO 80027, Email: jfontenla@mho.net); Eugene H. Avrett and Robert L. Kurucz (both at Harvard Smithsonian Center for Astrophysics, 60 Garden St, Cambridge, MA 02138, Email: avrett@cfa.harvard.edu, kurucz@cfa.harvard.edu).

The study of solar radiative variability is of immediate importance and application to problems in terrestrial upper atmospheric chemistry and circulation. Over the past decade, regular measurement programs for parts of the solar spectrum have been established. However, the physical understanding of these measurements has not yet been achieved. To improve our understanding and to make quantitative estimates of this variability requires a study of the entire solar spectrum. Our approach to this requirement is to combine empirical image analysis with the theory for emission, absorption, and transfer of radiation in the solar atmosphere. Our ultimate goal is the successful combination of observed solar images with semi-empirical models and theory for calculation of a mixed line-continuum spectrum emitted from realistic representations of the observed solar disk. These pixel by pixel calculations properly weight the computed specific intensities for calculation of the Sun's irradiance at any particular wavelength and time. In this talk we present results and discussion of quantitative models of the total irradiance, specific spectral bands in the UV, IR and visible, and particular spectrum lines. The synthetically generated irradiances are presented for a range of realistic solar activity conditions, representing the quiet, moderate, and active Sun and are represented as images, spectra or irradiances and compared to extant observations.

**JSA16/W/16-A3** Invited **1130**

#### PHYSICAL ORIGIN OF LONG TERM IRRADIANCE CHANGES

Sabatino SOFIA (Department of Astronomy, Yale University, P.O. Box 208101, New Haven, CT 06520-8101, USA, Email: sofia@astro.yale.edu)

Various analyses of climate data carried out in recent years have provided convincing support for the existence of a solar component on timescales of decades to centuries. The amplitude of the activity-related modulation of total irradiance measured over the last 20 years appears to be insufficient to yield significant climate effects, at least according to most current climate models. Thus, either the model are significantly wrong (e.g. the spectral irradiance may produce climate change in excess of its energy content), or there must be a solar variability mechanism not connected to active regions and network. Theoretical considerations indicate that a variable, deep-seated magnetic field such as would be produced by the dynamo mechanism would modify (slightly) the structure of the whole Sun. As a consequence, all the global solar parameters (radius, temperature and luminosity) would be affected. Because the total irradiance depends on the solar luminosity, this could be the mechanism responsible for long term irradiance changes.

A variety of supporting evidence exists in confirmation of such mechanism, such as variations of the solar oscillation spectrum and possible variations of the solar radius. We will discuss the details of the mechanism, the supporting data, and the additional work required to understand its properties to the degree required to determine the climate implications.

**JSA16/W/39-A3** Invited **1200**

#### VARIABILITY OF SUNLIKE STARS

Richard R. RADICK (Air Force Research Laboratory, Space Hazards Branch, National Solar Observatory, Sunspot, New Mexico, USA, email: radick@sunspot.noao.edu)

Stars with approximately the same temperature, luminosity, chemical composition, and average activity level as the Sun may now readily be identified. The variability of several such sunlike stars has been monitored regularly in chromospheric Ca II HK emission for over three decades and photometrically for fifteen years; larger stellar samples have been observed less comprehensively. Similar solar time series exist. A comparison of solar variability with its stellar analogs indicates that the Sun's current behavior is not unusual among sunlike stars, although some observations do suggest that the amplitude of the Sun's cyclic variation, measured photometrically, may be smaller than its stellar analogs.

If the behaviour of a sample of sunlike stars is representative of the range for the Sun's possible behaviour, then it is instructive to examine not only how closely sunlike stars resemble the present-day Sun, but also how they differ. Thus, the behaviour of sunlike stars may provide insight about states of solar activity, such as Maunder minima, which have not been observed on the Sun during the modern era.

Wednesday 21 July PM

Presiding Chair: Juerg Beer (Environmental Physics, EAWAG, Switzerland)

**JSA16/E/07-A3** Invited **1400**

#### CLIMATE RESPONSE TO VARIATIONS OF THE SOLAR IRRADIANCE SINCE 1700 IN COUPLED AOGCM SIMULATIONS

Reinhard VOSS (Max-Planck Institut fuer Meteorologie, Bundesstr 55, D-20146 Hamburg, Germany, email: reinhard.voss@dkrz.de); Ulrich Cubasch (DKRZ, Bundesstr 55, D-20146 Hamburg, Germany, email: cubasch@dkrz.de)

In our study an atmosphere-ocean general circulation model (AOGCM) has been used to investigate the potential impact of variations of the solar irradiance on climate. Two different reconstructions of the solar irradiance for the period 1700 to 1992 (Hoyt and Schatten (1993), Lean et al. (1995)) have been used. For both reconstructed time series two AOGCM simulations have been performed. The results are compared to a control simulation with fixed solar irradiance and experiments with increasing CO<sub>2</sub> concentration. The AOGCM, which has been employed, is the ECHAM3/LSG in a T21 horizontal resolution (ca. 5.6 deg. in the grid space). In the solar runs long periodic fluctuations, which are mainly associated with the Gleissberg cycle, show the largest signal. The signal associated with the 11-year solar cycle is only weak. The temperature increase during the last century in the solar experiments is weaker than the observed warming. Assuming that the model forcing and response is realistic, other factors than the solar irradiance must contribute to the observed warming. In the troposphere the solar variability induces a temperature pattern similar to the one caused by the increase of atmospheric CO<sub>2</sub> concentration. The land-sea contrast is enhanced and the maximum warming in the free atmosphere is located in the upper tropical troposphere for increasing solar irradiance. In the stratosphere the impact of the solar variability on the temperature is small, whereas for the geopotential height in 30 hPa the correlations with the solar forcing exceed locally 0.9.

**JSA16/W/03-A3** Invited **1430**

#### THE EFFECT OF UV IRRADIANCE VARIATIONS ON THE EARTH'S ATMOSPHERE AND CLIMATE

Joanna D. HAIGH and Alice Larkin (both at Space and Atmospheric Physics, Blackett Laboratory, Imperial College of Science, Technology and Medicine, London SW7 2BZ, UK, email: j.haigh@ic.ac.uk)

Variations in solar ultraviolet irradiance have greatest impact in the middle and upper atmosphere. In the stratosphere UV increases result in heating, due to absorption by ozone and oxygen, and also in enhanced production of ozone which further modifies the solar and

infrared radiation balance. Previous studies have suggested that such changes in stratospheric thermal structure may impact the climate of the lower atmosphere through modification of the latitudinal structure of the radiative input and of planetary wave activity.

This talk will describe high spectral resolution calculations of the direct impact on radiative heating rate profiles of changes in the solar UV spectrum. The effects of such variations in heating rate on the climate of the middle and lower atmospheres of two different GCMs (the UGAMP UGCM and the UKMO Unified Model) will be described. The sensitivity of the simulations to the specification of ozone changes will also be discussed.

**JSA16/E/34-A3** Invited **1500**

#### EFFECT OF PARTICLE FLUX VARIATIONS ON CLIMATE

Egil FRIIS-CHRISTENSEN (Danish Space Research Institute, Juliane Maries Vej 30, DK-2100 Copenhagen, e-mail: efc@dsri.dk)

A number of studies have reported on a high correlation between solar activity variations and climate. Solar activity variations manifest themselves in different forms like variations in total solar irradiance, in variations in the UV range and in variations of the solar wind parameters. The correlations have indicated that a considerable part of the global warming during this century may have been caused by solar activity variations. Never the less, until now no single physical process has been proven capable of having the needed effect on climate. This presentation will review some of the available evidence that the cosmic ray flux through its modulation by the solar wind may contribute significantly to the formation of clouds. This will change the radiative properties of the atmosphere and hence the climate.

Presiding Chair: Sabatino Sofia (Department of Astronomy, Yale University, New Haven, USA)

**JSA16/W/21-A3** Invited **1600**

#### LONG-TERM SOLAR-TERRESTRIAL RECORDS FROM COSMOGENIC RADIONUCLIDES

Juerg BEER, (Environmental Physics, EAWAG, Duebendorf, Switzerland)

Direct solar terrestrial records are limited to the telescopic era starting at about 1600 AD. To extend these records further back in time one has to rely on proxies of solar and terrestrial parameters. Cosmogenic radionuclides proved to be useful tools for such a reconstruction of the solar variability over millennia. Cosmogenic radionuclides such as <sup>10</sup>Be, <sup>36</sup>Cl, and <sup>14</sup>C, are continuously produced by the interaction of cosmic ray particles with the atmosphere. Fluctuations the solar wind lead to magnetic modulation of the cosmic ray flux that induces corresponding changes in the production rates of these nuclides. As a consequence the production rate is high during periods of low solar activity and vice versa. After the production the fate of the radionuclides depends on their geochemical properties. <sup>10</sup>Be and <sup>36</sup>Cl are transported attached to aerosols or as a gas (<sup>36</sup>Cl) and after a mean residence time of 1 year they are removed from the atmosphere mainly by wet precipitation. <sup>14</sup>C, on the other hand, is oxidised to <sup>14</sup>CO<sub>2</sub> and exchanged with the biosphere and the ocean. In order to reconstruct the long-term solar variability archives are needed that store the radionuclides in a stratigraphically undisturbed way. The best archives are ice cores (<sup>10</sup>Be and <sup>36</sup>Cl) and tree rings (<sup>14</sup>C) respectively. During the last 10 000 years the <sup>14</sup>C tree ring record exhibits several peaks which can be attributed to quiet sun periods (e.g. Maunder minimum 1645 - 1715). Beside the well-known 11 year Schwabe cycle several periodicities in the range of decades to millennia can be found in all the radionuclide records which, most likely, represent solar variability. A comparison of the <sup>10</sup>Be and <sup>36</sup>Cl records with <sup>14</sup>C based on a carbon cycle model allows to separate production and system effects. Comparisons with climate records indicate that periods of high production rates (low solar activity) generally coincide with periods of cold climate. Potential and limitations of radionuclides to establish long-term solar terrestrial records are discussed.

**JSA16/W/43-A3** **1630**

#### LONG TERM SOLAR-TERRESTRIAL RECORDS FROM SEDIMENTS

G.CINI CASTAGNOLI, G. Bonino and C.Taricco (Dipartimento di Fisica Generale dell'Universit, Via P.Giuria 1, 10125 Torino, Italy and Istituto di Cosmogeofisica del CNR, Corso Fiume 4, 10133 Torino, Italy)

We discuss here the <sup>d18O</sup> and <sup>d13C</sup> profiles of Globigerinoides ruber measured in the GT90/3 shallow water Ionian sea core, dated with high precision. The core, extracted from the Gallipoli platform, is dated with high precision and sampled at 2.5 mm, corresponding to 3.87 years. The dating of the core has been performed by <sup>210</sup>Pb radiometric method and by a detailed tephroanalysis. The high precision of the core dating allows to transform the depth scale into a time scale with an accuracy of ~1%. The <sup>d18O</sup> and <sup>d13C</sup> profiles cover the period 1200-1975 AD. The long time series allows a) to obtain highly reliable results from spectral analysis and b) to evaluate the importance of the variations of solar origin with respect to the variation in the trend. <sup>d13C</sup> and <sup>d18O</sup> show an inverse relationship with a correlation coefficient of about -0.7. The spectral analysis of the <sup>d18O</sup> time series performed with different methods shows a dominant decadal periodicity, in antiphase with the sunspot solar cycle, while the <sup>d13C</sup> time series shows it in phase with the sunspot cycle. These components are identified at high significance level by Monte Carlo singular spectrum analysis (MC-SSA). The two records show the presence of the well-known climatic features of the Little Ice Age, the Maunder and the Sporer minima and the early 20th century global temperature rise. Yearly cloud coverage of the same region, deduced by annual percentage of rainy days recorded in Lecce (Puglia), and the annual average temperature measured in Reggio Calabria from 1875 to 1972 AD are compared to the <sup>d13C</sup> and <sup>d18O</sup> profiles. The cloud coverage decreases during this period, while <sup>d13C</sup> increases. This is in agreement with the fact that the light is the principal factor regulating <sup>d13C</sup> fractionation, mediated by symbiotic algae, as known from laboratory experiments performed at different light levels. We estimate an increase in insolation of about 10 W/m<sup>2</sup> during the century. The corresponding increase in <sup>d13C</sup> is of the order expected by controlled experiments. At the same time, air temperature rises, opposite to cloud coverage, and <sup>d18O</sup> decreases.

**DISCUSSION FUTURE DIRECTIONS** **1700**

Wednesday 21 July AM

**JSA16/E/43-A3** Poster **0830-01**

#### ANALYSIS OF THE ARCHIVES OF CA K OAR OBSERVATIONS

M. FOFI, I. Ermolli and M. Centrone (all at OAR - Osservatorio Astronomico di Roma, Roma, I-00136 Italia)

We present the first results of the analysis performed on historical Ca K filtergrams and PSPT

## INTER-ASSOCIATION

data obtained at the OAR. In particular we analyse Ca K (0.6 Å) full-disk filtergrams obtained from daily observations made during solar cycles 19 and 20 (1964-1979), in order to describe temporal variations of geometrical properties of the magnetic regions. We use PSPT 1k X 1k images, to calculate different descriptors that are correlated to various solar variability indices (radio flux, MgII, total irradiance and sunspot number).

**JSA16/E/42-A3** Poster **0830-02**

### SOLAR VARIABILITY ON SECULAR AND MILLENNIAL TIME SCALES FROM COSMOGENIC ISOTOPES AND THE SEARCH FOR CORRESPONDING CLIMATE SIGNALS

Werner MENDE, (NOAA SEC, 325 Broadway, 80303 Boulder CO USA, mende@bbaw.de)

The variability potential of the total solar irradiance (TSI) on time scales from days to millennial is considered and compared with the spectral variability of cosmogenic isotopes (10Be) and with 18O-ice-core records (SUMMIT, data to 60 kyr BP) in corresponding frequency bands. Low-frequency periodic components could be identified in cosmogenic isotopes and in 18O records the occasional modulation of these signals by the geomagnetic field is a strong argument in favour of the solar provenance of these components. These low-frequency periodicities can be used for the prediction of the solar activity in the range of the 11-year Schwabe cycle and beyond. An estimation of the TSI-variability on longer time scales could be obtained by extrapolation of the spectral shapes of the TSI measurements observed by satellites. After removal of broad spectral excess around the rotational frequency the 20-years TSI-spectrum can be considered as a 5/3-Kolmogoroff like spectrum and formally extrapolated to longer time scales. The slope of this extrapolation is in a good agreement with the slope of spectral variability observed in cosmogenic isotopes from Greenland ice-cores on millennial time scales. If the cosmogenic isotope variability is in a nearly linear relation to the TSI change, then this would be of relevance for climate change on secular time scales. Historical temperature records are compared with a reconstruction of TSI on the base of cosmogenic isotope records. The low-frequency solar components could be identified in various climate records by appropriate band filterings.

**JSA16/E/14-A3** Poster **0830-03**

### ON OSCILLATORY FEATURES IN CLIMATE DYNAMICS

Alina PRIGANCOVA (Geophysical Institute, Slovak Academy of Sciences, 842 28 Bratislava, Slovak Republic, E-mail: geofpria@savba.sk); Basil Petropoulos (Research Center for Astronomy and Applied Mathematics, Academy of Athens, 10573 Athens, Greece)

The global change approach to study the Sun-Earth system gives a growing amount of evidence that climate dynamics is affected by a great many of factors. The solar variability is very likely to be ranged among them. As a possible tracer of such an influence are characteristic features in climate dynamics presented by persistent peculiarities in its time structure. To illustrate time structure pattern on long-term scales the data on monthly averages of main meteorological parameters, air temperature T and precipitation totals P, for a number of observatories are used. The requirement for the length of individual time series to be as long as possible was utilised as a criterion for their option among available data from the world-wide network of observatories. That is most dense for the limited parts of the global territory. Mainly, observatories located in the latitudinal and longitudinal strips crossing Central Europe are considered to make it possible to do some generalisation on the modulation patterns in climate dynamics. The calculated annual and interannual anomaly field profiles are compared. Finally, there is presented a discussion on utilisation of features revealed for prognostic aims.

**JSA16/E/05-A3** Poster **0830-04**

### LONG - TERM VARIABILITY OF THE SOLAR WIND AND ITS CLIMATIC CONSEQUENCES

Alexander SHIROCHKOV and Ludmila Makarova (both at Arctic and Antarctic Research Institute, Saint - Petersburg, 199397, Russia, e-mail: shirmak@aari.nw.ru)

The Sun-Earth relationship as a factor capable to affect the Earth weather and climate has been studied for many years. A level of the Sun UV radiation (expressed as the sunspot number W) was used as the sole indicator of the amount of the Sun energy transferred to the Earth. The achievements and failures of such an approach are well known. On the other hand, the solar wind can provide substantial amount of energy into the Earth's atmosphere, which can influence the Earth's weather and climate under definite conditions. We explore the long - term temporal variations of the most geoeffective solar wind parameter - its dynamic pressure Psw for the whole satellite epoch (1960 - 1996). This parameter's changes in time do not coincide with the corresponding variations of the sunspot numbers. The Psw value determines a distance between the magnetosphere magnetopause and the Earth and this distance value is proportional to the energy amount transferred from the solar wind to the near- Earth space. We show that the Psw value (and subsolar distance between the magnetopause and the Earth) directly influences such hydrometeorological parameters as the stratospheric temperature, ozone content at stratospheric altitudes, structure of the tropopause, time of the spring change of the atmospheric circulation, and temperature anomalies on the Earth surface. Besides Psw value is closely connected with times of the spring openings of the arctic rivers as well as with the polar seas areas covered by the ice and the polar seas surface temperature anomalies. As the most probable physical mechanism responsible for these relationships a modified version of the global electric circuit where the magnetosphere magnetopause is an external element will be proposed.

**JSA16/E/17-A3** Poster **0830-05**

### THE EFFECT OF COSMIC RAY PRODUCED-CLOUDS ON CLIMATE

Blanca MENDOZA and Juan Ramirez, (Instituto de Geofísica UNAM, Ciudad Universitaria, 04510, Mexico D.F., Mexico, email: blanca@tonatihu.igeofcu. unam.mx Arturo Quintanar, Centro de Ciencias de la Atmosfera UNAM, CiudadUniversitaria, 045210, Mexico D.F., Mexico.)

Results, which assess the effect of the solar activity on climate, through the modulation of cosmic rays, are presented. In particular, a climatic model is developed where the clouds are included as forcings. It is assumed that the amount of cloudiness is modulated by the cosmic ray flux along the solar cycle.

**JSA16/E/35-A3** Poster **0830-06**

### WAVELET ANALYSIS OF THE SUNSPOT, GEOMAGNETIC AND CLIMATIC VARIATIONS IN ST.PETERSBURG

Dmitri I. PONYAVIN (Institute of Physics, University of St.Petersburg, 198904, Russia, e-mail: ponyavin@snoopy.phys.spbu.ru)

Wavelet transform analysis was applied to the sunspot, geomagnetic and air surface temperature variations recorded in St.Petersburg from 1775 to 1999. Patterns of wavelet transforms were compared, and coherence at different time and time-scales was found. A quasi 35- and 11-year oscillation of the sunspot and geomagnetic activity was approximately in phase with the air temperature data at least the later half of the 20th century.

**JSA16/E/37-A3** Poster **0830-07**

### THE SEPARATION OF ANTHROPOGENIC AND SOLAR VARIABILITY IN THE NORTHERN HEMISPHERIC TEMPERATURE RECORD ON A FILTER TIME SCALE OF 14 YEARS BASED ON THE FREQUENCY MODULATION FUNCTION OF THE SOLAR CYCLE AND COSMOGENIC ISOTOPES

Werner Mende, Rita STELLMACHER, (Freie Universitaet Berlin, Carl-Heinrich-Becker-Weg 6 - 10, D-12165 Berlin, email: mende@bbaw.de); Juerg Beer, (EAWAG Duebendorf, Switzerland)

The global and hemispheric temperature records are investigated on a decadal time scale. The most important forcing functions for temperature variability are characterised by proxy data. For the historic reconstruction of the solar forcing function cosmogenic isotopes and the frequency modulation function of the solar cycle (Sun melody) are used. The anthropogenic forcing function is parameterized by a hyperbolic model. Spectral filterings are used for a removal of all variability components with period lengths shorter than 6 years. For the separation of the different variability sources a nonlinear minimal-parametric model on a hemispheric aggregation level is used. The regression model is solved by a Levenberg-Marquardt procedure and the solution provides a relatively consistent picture of the contributions of the different variability sources to the observed climate variability on a filter time scale of 14 years. The results are in a good agreement with the global sensitivity of temperature against solar forcing given by general circulation models. Low-frequency variability components of the solar irradiance forcing function (88 years and longer) could also be identified in the hemispheric temperature records. Band filtering could separate the induced temperature variation. There is good phase coherence between the reconstructed solar forcing function and the corresponding frequency band in the temperature record.

**JSA16/E/21-A3** Poster **0830-08**

### LONG-TERM VARIABILITY OF SOLAR ACTIVITY AND ITS LINK TO SHARP CLIMATIC OSCILLATION DURING THE HOLOCENE

Oleg RASPOPOV, Oleg Shumilov (SPbF IZMIRAN, P.O.Box 188, St.Petersburg; 191023, Russia, e-mail:oleg@omr.izmi.ras.spb.ru); Valentin Dergachev (Physico-Technical Institute RAS, St.Petersburg, 194021, Russia); Bas Van Geel (University of Amsterdam, 1098 SM Amsterdam, the Netherlands); Johannes Van der Plicht (Center for Isotope Research, University of Groningen, the Netherlands); Hans Renssen (Free University, De Boelelaan 1085, 1081 HV Amsterdam, The Netherlands)

Recently obtained terrestrial, marine, and ice core data demonstrate the sharp climatic changes during the warm interglacial period of the last 12,000 years. These newly developed Holocene palaeoclimate records indicate that 2300-2400 years periodicity in the development of the most sharp cooling events took place. During the last 1000 years cooling events also showed 210 and 88-90 years periodicity. Analysis of geophysical, radiocarbon (<sup>14</sup>C), and <sup>10</sup>Be data demonstrated that mentioned cooling events are very well correlated with sharp increase of <sup>14</sup>C and <sup>10</sup>Be concentration. It means that the cooling events are correlated with the sharp increase of galactic cosmic ray fluxes and decrease of solar activity. Some recently obtained experimental data demonstrate that the galactic cosmic ray fluxes influence on optical properties and radiation balance of the atmosphere. The data indicates that cosmic ray enhancement leads to the temperature decrease in the middle and high latitudes. Thus periodically caused cooling events during Holocene can be connected with the decrease of solar activity. The decrease of solar activity leads to the increase of galactic cosmic ray fluxes and decrease of the solar radiation. Both these factors lead to solar radiation decrease near the Earth surface and thus create conditions for sharp climatic cooling. The work was supported by Russian Foundation for Basic Research and INTAS.

**JSA16/E/16-A3** Poster **0830-09**

### CLIMATIC FORCING OF THE ~ 2400-YEAR VARIATIONS IN THE RADIOCARBON CONCENTRATION OF THE EARTH'S ATMOSPHERE

Valentin A. Dergachev, Sergey S.Vasiliev (Both at: Ioffe Physico-Technical Institute RAS, Politekhnicheskaya 26, St.Petersburg, 194021, Russia, email: v.dergachev@pop.ioffe.rssi.ru); Oleg M. RASPOPOV (SPbF IZMIRAN, P.O.Box 188, St.Petersburg, 191023, Russia, email: oleg@omr.izmi.ras.spb.ru)

Spectral analysis of the available long-term series of the radiocarbon concentration based on the tree-ring count, using the classical harmonic methods of time series analysis, led to exhibition of spectral lines at a number of periods. However, the some harmonic features are not independent. Applying the methods of analysis on the non-stationary time series, as the frequency-time method and bi-spectral analysis to the radiocarbon concentration during the last 8000 years, we resolve a number of periods: 2400, 940, 720, 570, 500, 420, 360, 230, 210, 190 years. The strongest feature in this time series is a long period of ~ 2400 years. Analysis shows that the periods of 210, 420 and 720 years are primary. Besides, the primary periods are modulated by the long 2400-year period. Taking into account the structure of bi-spectrum, it was shown that the ~ 2400-year modulation have the climatic forcing.

**JSA16/E/24-A3** Poster **0830-10**

### ON THE INFLUENCE OF SOLAR RADIATION SCATTERING ON THE INTERPRETATION OF OZONE MEASUREMENT RESULTS

Olga ZYRYANOVA (Institute of ionosphere of Ministry of Sciences - Academies of Sciences of Republic Kazakhstan, Almaty, 480068, Kamenskoe Plateau e-mail: angel@ionos.alma-ata.su); Ibragim Suleimenov (Institute of ionosphere of Ministry of Sciences - Academies of Sciences of Republic Kazakhstan, Almaty, 480068, Kamenskoe Plateau e-mail: sul@ionos.alma-ata.su)

In present paper it is shown that well-known multi - wave ozone measurement technique based on the spectral data has a theoretical limit which is connected with light scattering processes. The role of such processes is of most significant in sunrise. It is shown that for the theoretical interpretation of experimental data obtained for large solar zenith angles one have to take into account superposition of light beams. These beams may be described as a result of solar radiation reflection from effective partly penetrable mirrors each of them is connected with the separate atmosphere layer. Reflection coefficient of such mirrors is determined by the value of scattering albedo.



JSA16/E/28-A3 Poster 0830-11

## THE MANIFESTATION OF SOLAR VARIABILITY IN CLIMATIC CHARACTERISTICS OF PREBAIKALIA

Gely Zherebtsov and Vladimir KOVALENKO (both at Institute of Solar-Terrestrial Physics SD RAS, P.O.B. 4026, Irkutsk, 664033 Russia, e-mail: uzel@iszf.irk.ru)

Evidence for the actual manifestation of solar variability in climatic characteristics of Prebaikalia (Irkutsk, Bratsk, and Zima) is presented. The relevant influence on ground air temperature is quantified. The study revealed a high degree of correlation (correlation coefficient is 0.97) between the mean power of solar activity cycle and the ground air temperature in Prebaikalia averaged over a solar cycle. It is shown that the main significant variations in air temperature in the region during 1881-1960 were caused by solar variability. The amplitude of temperature variations during this period was 1 degree. Since the 1960s till the present, with the influence of solar variability continuing, there has been a pronounced effect of another factor whose role is progressively increasing, and in the last decade it was even higher than the contribution of solar variability. During 1960-1997, the rise in temperature unassociated with solar activity was 1.7 degree. This new factor is most likely to be a global warming of the atmosphere. This assumption is consistent with model calculations indicating that the most drastic manifestation of a global warming should be expected in inland regions of Eurasia.

An analysis of seasonal variations in ground air temperature showed that the recorded variations are most pronounced during the winter-spring period and are most likely associated with a reduction in the stationary time of the Siberian anticyclone. This suggests that the global atmospheric circulation rather than a local change in the energy balance of the atmosphere constitutes the mechanism for the realisation of regional climate variability factors. An analysis is made of the relationship between solar activity characteristics and hydrometeorological parameters of Lake Baikal and the Angara river. The analysis revealed a high degree of correlation between the solar activity cycle length and long-term fluctuations of Lake Baikal's level, and the rate of water inflow to the lake and the duration of the unfrozen state of Baikal and the Angara. The origin and possible mechanisms of these correlations are discussed.

JSA16/E/27-A3 Poster 0830-12

## CHANGES OF SOLAR RADIATION INPUT IN THE LOWER ATMOSPHERE AS AN IMPORTANT LINK IN SOLAR-CLIMATE CONNECTIONS

Svetlana VERETENENKO and Mikhail Pudovkin (Institute of Physics, St.Petersburg State University, Ulianovskaya st., 1, St.Petersburg, Petrodvorets, 198904, Russia, e-mail: vereten@SV2135.spb.edu)

Variations of solar radiation input in the lower atmosphere caused by cloud cover changes associated with solar activity phenomena have been investigated at the network of actinometric stations of Russia. It was revealed that the half-yearly totals of global radiation, characterizing the entire amount of solar energy coming to the Earth's surface during cold or warm half a year, may be affected appreciably by galactic cosmic ray (GCR) variations, solar flare activity and auroral phenomena at high latitudes, their effects depending on the latitudinal belt and season. The negative correlation between the global radiation totals and the cosmophysical factors under study is observed in the high-latitudinal region, whereas at middle latitudes the solar radiation input was found to correlate with GCR intensity and solar flares. In turn the changes of the solar energy incoming the high-latitudinal atmosphere during a year are shown to influence the zonal circulation intensity in the following cold period. The results obtained allow us to conclude that the solar radiation input modulated by different solar activity phenomena through cloud cover changes seems to be an important factor affecting the troposphere dynamics and may be involved in the physical mechanism of solar activity influence on the lower atmosphere state.

JSA16/C/GA.07/E/26-A3 Poster 0830-13

## SOLAR ACTIVITY AND THE LOWER ATMOSPHERE STATE

Mikhail PUDOVKIN and Svetlana Veretenenko (Institute of Physics, St.Petersburg State University, Ulianovskaya st., 1, St.Petersburg, Petrodvorets, 198904, Russia, e-mail: pudovkin@snoopy.phys.spbu.ru)

The relationships between the solar activity associated variations of the cosmic ray fluxes and the state of the lower atmosphere are discussed. It is shown that the bursts of Solar Cosmic Rays, with the energy being enough to penetrate the stratosphere heights, cause the decrease of the solar radiation intensity at the Earth's surface, whereas the Forbush-decreases of the Galactic Cosmic Rays result in the increase of solar radiation intensity at latitudes higher than 60 degrees. Long-term variations of the solar radiation input in the lower atmosphere depending on the solar cycle phase, season and latitudinal belt are considered too.

The found changes of the solar irradiance are supposed to be caused by the variations of its scatter by some layer (homogeneous or in the form of clouds) at the heights of about 10 km. Results of the numerical modelling seem to confirm the suggested mechanism of the solar activity effects on the lower atmosphere circulation including the changes of the radiation budget due to the cloud cover variations.

JSA16/E/12-A3 Poster 0830-14

## SOLAR EXTREME ULTRAVIOLET MEASUREMENTS FROM THE NASA TIMED SATELLITE

Thomas N. WOODS, Frank Eparvier, Gary J. Rottman, Stanley C. Solomon (all at Laboratory for Atmospheric and Space Physics, University of Colorado, 1234 Innovation Dr., Boulder, CO 80303, USA; e-mail: tom.woods@lasp.colorado.edu); Scott M. Bailey (Center for Atmospheric Sciences, Hampton University); Raymond Roble, O. R. White (both at High Altitude Observatory, National Center for Atmospheric Research); Judith Lean (Naval Research Laboratory); W. Kent Tobiska (Federal Data Center, Jet Propulsion Laboratory).

The Solar EUV Experiment (SEE) on the NASA Thermosphere, Ionosphere, and Mesosphere Energetics and Dynamics (TIMED) mission will measure the solar vacuum ultraviolet (VUV) spectral irradiance from 0.1 to 200 nm. This solar radiation is the dominant global energy source for the heating of the thermosphere, creating the ionosphere, and driving the diurnal cycles of wind and chemistry in the upper atmosphere. The variability of the solar VUV irradiance over the 11-year solar cycle ranges from 10% to over a factor of 10, with more variability at the shorter wavelengths.

To cover the wide spectral range of 0.1 to 200 nm, two different types of instruments are used: a grating spectrograph for spectra above 25 nm and a set of silicon soft x-ray photodiodes with thin film filters for below 30 nm. Redundant channels of the spectrograph and soft x-ray photodiodes provide in-flight calibration checks on the time scale of a week, and annual rocket underflight measurements provide absolute calibration checks traceable to NIST photometric standards. Both types of instruments have been developed and flight proven as part of a NASA solar VUV irradiance rocket experiment. These solar rocket measurements in 1997 and 1998 will be presented.

The Applied Physics Laboratory (APL) is developing the TIMED spacecraft for a shared launch on a Delta vehicle at the Johns Hopkins University (JHU). The TIMED mission is being

planned as a two-year mission with a circular orbit altitude of 600 km and an orbit inclination of 74°. There are three other TIMED instruments, which measure the composition, temperature, infrared cooling, and winds in the upper atmosphere.

JSA16/E/11-A3 Poster 0830-15

## CALCULATION AND PROCESSING OF MT.WILSON SPOT, PLAGUE AND WEAK FIELD INDICES

Roger ULRICH, John Boyden, Daryl Parker, Judit Pap (all at the Department of Physics and Astronomy, University of California, Los Angeles, 405 Hilgard Ave., Los Angeles, CA 90095-1562, USA); Linton Floyd Code 7660, Naval Research Laboratory, Washington DC, 20375, USA)

The synoptic magnetograph observations at Mount Wilson Solar Observatory taken in the 525.0 nm line are used to derive spot (MWSI), plague (MPSI) and weak field indices (MWWI). The MPSI has been shown to be closely correlated with and a good surrogate for solar UV irradiance as measured by satellite instruments. The MPSI and MWSI together have been used to model total solar irradiance measurements from satellite observations.

The MWWI is a new index intended to represent the slow variability of the weak magnetic fields, which are likely connected with variations in both UV and total irradiance. The MPSI and MWSI are defined as the sum of the fields in all magnetograph pixels with fields in a certain range (e.g. between 10 and 100 gauss for the MPSI), divided by the total number of pixels while the MWWI is the ratio of the area covered by fields having absolute values between 4.8 and 5.2 gauss to the area covered by fields with absolute values less than 0.4 gauss. In this paper we describe the calculation and processing of these indices, including refinements of previous versions of the MPSI and MWSI which take into account changes in spectrograph instrumentation and observation protocols and which are intended to make the data base more internally consistent.

JSA16/E/22-A3 Poster 0830-16

## SOLAR ULTRAVIOLET IRRADIANCE: UARS SOLSTICE OBSERVATIONS

Gary ROTTMAN, Thomas Woods, Giuliana De Toma, Julius London, Marty Snow, Cindy Russell, Barry Knapp (at the University of Colorado, 1234 Innovation Dr., Boulder, CO 80303, USA; e-mail: gary.rottman@lasp.colorado.edu); Oran R. White (National Center for Atmospheric Research, PO Box 3000, Boulder, CO 80307-3000, USA)

The Solar Stellar Irradiance Comparison Experiment (SOLSTICE) on the Upper Atmosphere Research Satellite has made daily observations of solar ultraviolet irradiance since October 1991. The SOLSTICE spectrometer observes the Sun at wavelengths between 120 and 420 nm, and provides daily spectra with a spectral resolution of 1 nm. The UARS data record spans a time from near the maximum of solar cycle 22 in 1991, through solar minimum in about 1996-1997, and now into the new solar cycle 23.

Time series of SOLSTICE data have a long-term relative accuracy of 1 to 2%, although the short-term relative accuracy may often exceed 0.05%. These time series have been analyzed as a function of wavelength. They provide an estimate of the solar cycle change during the declining phase of cycle 22 and during the rising phase of cycle 23 (to the summer of 1999). Short and intermediate-term variations are examined, and are compared to the long-term records.

JSA16/E/23-A3 Poster 0830-17

## DETECTION OF CLIMATE OSCILLATIONS BY ENHANCED MONTE CARLO SSA

Milan Palus (Institute of Computer Science, Czech Academy of Sciences, Pod vodarenskou vezi 2, 182 07 Prague 8, Czech Republic, email: mp@uivt.cas.cz); Dagmar NOVOTNA (Institute of Atmospheric Physics, Czech Academy of Sciences, Bocni II/1401, 141 31 Prague 4, Czech Republic, email: nov@ufa.cas.cz)

Monte Carlo singular spectrum analysis (MC SSA), based on a so-called surrogate data technique, is a tool for detection of signals embedded in coloured noises, which are usually present in geophysical data. We propose to enhance the MC SSA by evaluating and testing the regularity of dynamics of the SSA modes against the coloured noises null hypothesis, in addition to the test based on variance. The method is illustrated in the detection of oscillations with a period of approximately eight years in historical surface air temperature records obtained from several European locations, as well as in the detection of approximately five-year cycles in the global surface air temperature series. The lengths of detected cycles related to the lengths of the periods in solar inertial motion and the possible solar-terrestrial relations are discussed.

JSA16/E/39-A3 Poster 0830-18

## WHAT CAN BE A MECHANISM UNDERLYING THE SUNSPOT CYCLE?

Milan Palus (Institute of Computer Science, Czech Academy of Sciences, Pod vodarenskou vezi 2, 182 07 Prague 8, Czech Republic, email: mp@uivt.cas.cz); Dagmar NOVOTNA (Institute of Atmospheric Physics, Czech Academy of Sciences, Bocni II/1401, 141 31 Prague 4, Czech Republic, email: nov@ufa.cas.cz)

A property of nonlinear oscillators - mutual dependence between their instantaneous amplitude and frequency is tested in the yearly and monthly records of the sunspot numbers using the histogram-adjusted isospectral surrogate data and the Barnes model as the ARMA surrogates. The instantaneous amplitudes and frequencies are obtained by means of the analytic signal approach using the discrete Hilbert transform. In several tests the amplitude-frequency correlations has been found significant on levels ranging from  $p < 0.03$  to  $p < 0.07$ , which supports the hypothesis of a driven nonlinear oscillator as a mechanism underlying the sunspot cycle.

JSA16/E/01-A3 Poster 0830-19

## SOLAR-FORCED COUPLED GCM EXPERIMENTS AND COMPARISON WITH OBSERVATIONS

William INGRAM, Simon Tett, Peter Stott (all at Hadley Centre for Climate Prediction and Research, Meteorological Office, London Road, Bracknell, Berks, RG12 2SY, UK); Myles Allen (Space Science Dept, Rutherford Appleton Laboratory, Chilton, OX11 0QX, UK &amp; Dept of Physics, University of Oxford); Gareth Jones and John Mitchell (both at Hadley Centre)

We have run the coupled model HadCM2 forced with reconstructed solar irradiance variations, both following Hoyt and Schatten (1993) and Lean et al (1995). For the twentieth century we have an ensemble of simulations with each, as well as volcanic and anthropogenic forcings. We have then used "optimal fingerprinting" to look in the twentieth century observations for the modelled response patterns in space and time, concentrating on the decadal time scale as having most general interest. There are serious issues of degeneracy (patterns resembling

## INTER-ASSOCIATION

linear combinations of each other), implying that investigations which do not include the full set of forcings could reach spurious conclusions. However, a solar contribution to the early-century warming is robustly detectable under the assumptions of the method (linearity, the accuracy of the modelled internal climate variability, and the accuracy of the modelled patterns of response, though not their amplitudes).

### JSA16/E/10-A3 Poster 0830-20

#### LONG-TERM VARIABILITY OF SOLAR PROTON FLUX AND ITS CONNECTIONS TO GLOBAL OZONE DISTRIBUTION

Alexei KRIVOLUTSKY (Central Aerological Observatory, Pervomayskaya 3, Dolgoprudny 141700, Moscow Region, Russia, alkri@mycomp.netclub.ru); Nina Perejaslova and Margarita Nazarova (both Institute of Applied Geophysics, Moscow, Russia)

Solar proton fluxes measured during 1969-1999 by Russian polar system of "Meteor" satellites and global total ozone distribution (ground based observations and TOMS data) were used to investigate long-term total ozone response to cosmic factors using linear regression simple and multiply statistical analysis. Yearly averaged data of total solar proton fluxes at different bands of energy and yearly averaged total ozone data for different latitudinal belts were used for analysis. Clear response of total ozone has been revealed for the years, which contain strong solar proton events (1972, 1989, 1991 and 1997). This response of total ozone depends on latitude strongly. The analysis has shown negative response at high latitudes and positive response for the lower latitudes both for Northern and Southern Hemispheres with zero effect at 40 N approximately. Local minimum of ozone response was found near by equatorial region. So that the response of total ozone to SPEs has global nature and was not concentrated near polar region. It is not easy to understand the evidence of solar particle influence at low latitudes. The positive sign of such response in this region also needs special attention based on photochemical modelling because of this result is in contrast to traditional conception of the ozone destruction by NOX. Some possible mechanisms are discussed.

### JSA16/C/GA4.07/E/25-A3 Poster 0830-21

#### ROLE OF SOLAR EUV AND SOFT X-RAY RADIATION PATROL FOR GLOBAL CLIMATE VARIABILITY INVESTIGATIONS

S.V. AVAKYAN (Aerospace Physical Optics Laboratory of S.I. Vavilov State Optical Institute, Tuchkov Lane 1, St. Petersburg, 199034, Russia, email: avak@soi.spb.su)

In the present paper process of excitation of the Rydberg atomic and molecular states should be taken into account in the solar-terrestrial connections as a source of the information at the ground on the solar shortwave activity (associated with the solar flares, solar cycles and solar rotation). This mechanism is associated with the sporadic ionospheric radio- and IR-emission in characteristic spectrum of Rydberg transitions. The principal geoeffective part of the solar spectrum can be exactly EUV and soft X-ray fluxes, because the variations of all types: cyclic, with solar rotation, and the most intensive - during large solar flares, in these spectral ranges of radiation have the highest amplitudes. Therefore the permanent monitoring of solar soft X-ray and EUV spectral radiation (of wavelengths less than 120 nm) for sufficiently long periods to fully assess the long-term climate variations is very important. At present in the world such a solar patrol does not exist but there is a plan of its realisation by development of the Project "Creation of the permanent space patrol of solar extreme ultraviolet and X-ray radiations". This Project was supported by the grant of International Science and Technology Center in 1996 and 1998/99. European Union financed these stages of our Project with the scientific collaborators from France and Germany. At present the EUV spectrometer (57(16) - 153 nm) and soft X-ray and EUV radiometer (0.14 - 135 nm) have been built and are now being tested and calibrated. In this paper the possible transfer mechanism of the upper atmosphere response on the solar activity to the ground is discussed and the connection of the future Solar Patrol Mission data with this problem is considered.

### JSA16/E/19-A3 Poster 0830-22

#### TOTAL SOLAR IRRADIANCE (TSI) VARIABILITY MEASUREMENTS FROM SPACECRAFT PLATFORMS

Robert B. LEE III (NASA Langley Research Center, Atmospheric Sciences Division, MS 420, Hampton, Virginia 23681-2199, USA, Email: r.b.lee@larc.nasa.gov); Robert S. Wilson, Aiman Al-hajjah, Jack Paden, Dharendra K. Pandey, and Susan Thomas (All at Science Application International Corporation (SAIC), Suite 300, One Enterprise Parkway, Hampton, Virginia 23666-5845, Email: r.s.wilson@larc.nasa.gov)

Long-term total solar irradiance (TSI) variability and the mean TSI magnitude were analyzed using TSI data sets from 1978-1998, spacecraft pyrheliometric missions Earth Radiation Budget Satellite (ERBS), Nimbus-7, Upper Atmospheric Research Satellite (UARS), and Solar and Heliospheric Observatory (SOHO) Spacecraft radiometers). The analyses suggest that the mean TSI value derived from each long-term spacecraft mission decreased chronologically from a high of 1371 Watts per square meter [1986 Nimbus-7 value] to a low of approximately 1365 Watts per square meter [1986 and 1996 ERBS values]. The ERBS pyrheliometer has produced the longest TSI spacecraft data set (October 1984 through January 1999). The recent UARS, Space Shuttle Atmospheric Laboratory for Applications and Science (ATLAS) Solar Constant (SOLCON), and SOHO measurements suggest that the most likely TSI magnitude is in the 1365-1366 Watts per square meter range at minimum solar magnetic activity as indicated by minimum sunspot numbers. The TSI long-term variability component was found to vary with a period of approximately 10 years. Between long-term minima (1986, 1996) and maximum (1989-1991) sunspot magnetic activity, the component varied as much as 2 Watts per square meter above its minimum magnitude. The TSI data sets were analysed to identify the possible existence of an additional TSI variability component with a period longer than 10 years as well as the effects of sunspot cycle length on TSI variability.

### JSA16/E/15-A3 Poster 0830-23

#### SOLAR FORCING OF GLOBAL CLIMATE AND ITS CONTRIBUTION TO ANDRONIAN WARMING

Paul E. DAMON and Alexei N. Peristykh (both at Department of Geosciences, University of Arizona, Tucson, Arizona, 85721 USA; e-mail: damon@geo.arizona.edu)

Before the beginning of the industrial age (ca. 1850), global climate during the past 8 millennia was surprisingly stable. d18O variation in Greenland ice cores during the past 8 millennia has not been very great despite the fact that the difference between d18O during summer and winter is as great as between Holocene and the Warm ice age and the effect on Greenland precipitation of about five air masses with more or less distinct d18O signatures [Cole, personal communication, 1988]. If we assume that the variations are due to changes in the temperature gradient alone, until the beginning of the industrial age, the temperature range for

the North Atlantic region was only ca. +/-0.5 °C and part of this is the result of changes in the Earth's orbit [Berger, 1988].

In contrast, the temperature rise since the beginning of the industrial period has been ca. 0.7 °C. Accompanying this period there has been an extinction of many faunal species, and large changes in river discharge with accompanying industrial metals and chemicals and other consequences. To our descendants looking back in time, the boundary between Holocene and the industrial stage of human history will represent a relatively sharp boundary that we will refer to as the beginning of the Andronian geologic stage.

At the end of the 19th century (ca. 1880), the Earth entered a Contemporaneous Solar Maximum (CSM) that seems to be equivalent to the Medieval Solar Maximum (MSM) [Jirikovic and Damon, 1994]. The MSM occurs between AD 1090 to AD 1270 [Stuiver et al., 1998]. The MSM is approximately equivalent to the "Early Medieval Warm Epoch" that lasted a few centuries around AD 1000-1200 [Lamb, 1965]. Because of the relative stability of global climate during the last 8000 years prior to the industrial era, it has not been possible to demonstrate that the "Early Medieval Warm Epoch" was global in extent [Hughes and Diaz, 1994].

We conclude that the Sun has contributed about 15% or 0.1°C to Northern Hemisphere warming to 1997.

### JSA16/E/40-A3 Poster 0830-24

#### RHYTHMS OF A SOLAR SYSTEM, EARTH ATMOSPHERE AND OCEAN CLIMATE

Boris SHERSTYUKOV (All-Russia Research Institute of Hydrometeorological Information-World Data Center, 6 Korolev St. Obninsk, Kaluga Reg. Russia, email: SBG@wdc.meteo.ru)

The external factors of Earth climate changes in the altitude zones 00-30, 30-60, 60-90 N and El Nino are considered. The analysis of the solar and geomagnetic activity indexes astronomical data and climate for 1900-1998 years is executed. In barycentric solar co-ordinate system the Earth disturbances under an operation varying asymmetry of a solar system, anomalies of orbital motion and oscillations of the Earth concerning a barycentre the Earth - Moon is shown, that the listed factors influenced for climate changes of 20-century in Northern hemisphere: in low altitudes - about 25 % of a general temperature variability, in mean altitudes 14 % and in high altitudes 8 %. The solar activity determines accordingly 16, 7, and 4 % of a temperature dispersion and its influence is increased in 1.5 times when asymmetry of planets configuration is increased too. Moon determines 17, 8, 4 % of dispersion and its influence more noticeably when asymmetry of planets configuration is absent.

The new method of detection and prognosis of rhythm is offered. The forecast of ocean temperature rhythm till 2008 composed and is shown that strong El Nino will be in 2000-2001 years.

### JSA16/W/11-A3 Poster 0830-25

#### SURROGATES FOR SOLAR UV/XUV IRRADIANCE

Linton FLOYD, Lynn Herring, Patrick Crane (all at Interferometrics Inc., Chantilly VA 20151, USA, Email: floyd@susim.nrl.navy.mil); Dianne Prinz (E.O. Hulburt Center for Space Research, Naval Research Laboratory, Washington, DC 20375, USA, Email: prinz@susim.nrl.navy.mil); D.L. Judge, H.S. Ogawa (both at Space Sciences Center, University of Southern California, Los Angeles, CA 90089-1341, USA, Email: djudge@lism.usc.edu)

We explore the level of correspondence between various solar indices (e.g. MgII core-to-wing ratio, F10.7 cm flux, and He 1083 nm equivalent width) and UV/XUV irradiances for 0.1-400 nm. The principal sources of data used in this analysis are from the Solar Ultraviolet Spectral Irradiance Monitor (SUSIM) and the CELIAS Solar EUV Monitor (SEM) aboard the Solar Heliospheric Observatory (SOHO). Responsivity degradation is accounted for in both instruments. Comparisons with results from other similar experiments are also presented. We find that variations in irradiances originating in the chromosphere and transition region are generally well described by the MgII index and that coronal irradiances are well described by F10.7. Both of these findings are consistent with those of other investigators. The continuum UV irradiance for wavelengths 160-263 nm is approximately linear with the MgII index. On the other hand, variations in the strong Ly- $\alpha$  emission line appear to be better fit by separate linear dependences on short- and long-term components of the MgII index. Other wavelength ranges possibly exhibiting this segmented MgII dependence are identified. The aggregate EUV/XUV irradiances as measured by the SEM zero-order channel from 1996 through mid-1998 are fit using a linear regression model involving MgII, F10.7, and GOES soft X-ray flux resulting in a correlation coefficient of 0.98.

### JSA16/W/41-A3 Poster 0830-26

#### POSSIBLE LINKS BETWEEN THE SUN'S RADIUS VARIATIONS AND THE EARTH'S CLIMATE EVOLUTION.

ROZELOT, Jean, (OCA/CERGA, Avenue Copernic, 06130 GRASSE, FRANCE, E-mail: rozeLOT@obs-azur.fr, Telephone: 33 4 93 40 53 53, Fax: 33 4 93 40 53 33)

The purpose of this paper is to investigate whether the effects of the Sun's radius variations influence some Earth climatic changes. For this purpose, we first describe the available data sets concerning the temporal dependence of the diameter of the Sun. The time series may be divided into three categories; (i) the measurements made by means of the solar astrolabes, for instance at the Calern Observatory or in Brazil; available data cover the time period ranging from 1777 up to now; (ii) the reconstruction of longer series, starting from the XVII th century but only concerning the "horizontal" apparent diameter and (iii) the recent measurements of any solar diameters which permits to determine the true shape of the Sun (the helioid). All these data are here for one of the first time briefly discussed to test their significance on solar luminosity models. Because both the irradiance and diameter variations are small, their climatic impact is difficult to quantify. However, the observed evolution of the Earth's global surface temperature seems strongly correlated with these solar diameter variations over decadal even longer period of time. Finally, we indicate which difficulties remain to explain on physical grounds. An analysis of this nature is obviously subject to several uncertainties; but we propose coupled modes as a basic effect to understand the link between solar diameter irradiance variations and temperature effects on decadal time periods.

### JSA16/E/32-A3 Poster 0830-27

#### CAII K IMAGING TO UNDERSTAND UV IRRADIANCE VARIABILITY

R. KARIYAPPA (Indian Institute of Astrophysics, Bangalore 560034, India)

Because the radiative output of the Sun is one of the main driving forces of the terrestrial atmosphere and climate system, study of changes in the solar energy flux integrated over the entire spectrum and in many spectral bands has recently become of interest. To identify and understand the underlying physical mechanisms of total solar and UV irradiance variability and to estimate the contribution of various chromospheric features to UV irradiance, detailed analysis of spatially resolved data is required. The various chromospheric features (plages,



network elements, intra network regions, background chromospheric regions and quiet Sun regions) have been segregated from Call K Spectroheliograms of NSO/Sac Peak and Kodaikanal Observatory. The different parameters of these chromospheric features have been derived, and compared with UV irradiance flux measured in MglI h & k lines by Nimbus 7 and NOAA 9 satellites to estimate the contribution of chromospheric features to UV irradiance variability. The important results of this detailed analysis of Call K Images together with UV irradiance data will be discussed in this paper.

**JSA16/W/33-A3** Poster **0830-28**

#### EVIDENCE FOR COSMIC TIMESCALES IN LAKE BAIKAL EVOLUTION

Vladimir F. Gelety and Gennady V. Kalmychkov (Institute of Geochemistry Irkutsk, Russia, email: gikil@igc.irk.ru); Alexander V. MORDVINOV (Institute of Solar-Terrestrial Physics, P.O. Box 4026, Irkutsk, 664033, Russia, email: avm@iszf.irk.ru); Anatoly M. Popov (Institute of the Earth's Crust, Irkutsk, Russia, email: popov@earth.crust.irk.ru)

It was shown earlier that the hydrologic regime and long-term evolution of Lake Baikal are sensitive to solar energy variations. The Lake is situated in the middle of the continent and water inflows into Lake Baikal from over the great region. Therefore Sun-climate relations appear clearly in temporal changes of parameters integrated over a bulk of water and accumulated from the great area. Continuous wavelet analysis was applied to study water level fluctuations in Lake Baikal. In the wavelet spectrum the 11-yr solar activity cycle is clearly delineated, besides usual meteorological timescales. Such influence of solar activity on water level is evidently caused through climatic changes. Wavelet analysis was also applied to study the records of biogenic silica concentration in the cores of bottom sediments obtained from the special drilling project at Lake Baikal. The previous studies of the cores revealed evolutionary changes of Lake Baikal during the past 5 million years. Diatom abundance in sediments shows dramatic changes on large timescales. Wavelet spectra demonstrate clearly unsteady and multiscale changes of biogenic silica. Wavelet spectra display also more-or-less regular changes induced by insolation changes according to the Milankovitch theory. Time scales at about 23, 41, 100, 400 and 800 thousand years were revealed earlier and appear in our spectra. Irradiance changes due to evolution of the Sun on geological timescale, if any, could be derived through comparison of these data and other records of geological or geophysical parameters sensitive to solar energy.

**JSA16/W/26-A3** Poster **0830-29**

#### TIME-FREQUENCY ANALYSIS OF TOTAL SOLAR IRRADIANCE VARIATIONS

Alexander V. MORDVINOV (Institute of Solar-Terrestrial Physics, P.O. Box 4026, Irkutsk, 664033, Russia, email: avm@iszf.irk.ru); Richard C. Willson (Center for Climate Systems Research, Columbia University 12 Bahama Bend, CA 92118 USA, email: acrim@pop.net)

Wavelet analysis was applied to study the time-frequency behaviour of a composite time series of total solar irradiance represented by the Space Absolute Radiometric Reference. Wavelet spectra accurately describe unsteady and multiscale changes of solar irradiance within a wide time-frequency range. Wavelet analysis was also applied to time series of both Photometric Sunspot Index and full-disk Calcium II K-line index to identify the contribution of sunspots and faculae to the time-frequency behaviour of the irradiance. In this analysis data from the web site of the World Radiation Center and from San Fernando Observatory were used. In the wavelet spectrum of the Photometric Sunspot Index the energy concentrates at a 27-day periodicity. In parallel with the rotational period the energy increases at 13, 40, 54 and 81 days. These timescales correspond to multiple and combinatory frequencies of the solar rotation frequency. Long-term changes due to activity complexes appear in the spectra as well. As the cycle progresses, wavelet spectrum of the calcium index shows an energy cascade towards greater time scales. This seems imply that facular and/or magnetic network characteristic timescale depends on the phase of the 11-yr cycle. Analogous patterns on timescales of several months are seen in wavelet spectra of total solar irradiance. Such energetic cascades characterise the relaxation of thermo-magnetic perturbations during the 11-yr solar cycle.

**JSA16/E/20-A3** Poster **0830-30**

#### VARIATION OF SOLAR CYCLE LENGTH BASED ON WEIGHTED WAVELET Z-TRANSFORM

Mezak A. RATAG and Suaydhi (Indonesian National Institute of Aeronautics and Space, Lapan JI. Junjuran 133, Bandung 40173, Indonesia, email: mezakr@indosat.net.id)

Time-variation of the solar cycle length has recently been suggested as having close association with climate. A number of methods to determine the cycle length have been proposed. They are mostly based on filtering techniques similar to the one employed by Friis-Christensen and Lassen (1991) or the median method developed by Mursula and Ulich (1998). These methods, however, have serious difficulties in defining the cycle length as well as in dealing with periodicities at both ends of the sunspot time series. In this paper we propose the use of weighted wavelet Z-transform (WWZ), applying the so-called Morlet wavelet, in determining the time-series of solar cycle length. This method is proven to be much better in overcoming the difficulties mentioned above. The resulting WWZ amplitude time-series is a very useful tool in comparing the behaviour of the 11-, 50-, 100-year and other cycles. It shows, for example, that the WWZ amplitudes of the 11- and the 100-year cycles - which presumably correspond to their relative significance - have approximately doubled during the last two centuries, while that of the 50-year cycle decreased to become about ten times lower than its values in 1700s.

**JSA16/E/03-A3** Poster **0830-31**

#### ON THE GLOBAL MANIFESTATION OF THE QUASI-10-DAY PERIODICITY

Nikolai KLOCHEK and Marina Nikonova (Institute of Solar-Terrestrial Physics, P.O.Box 4026, 57, email: klochek@iszf.irk.ru)

Quasi-10-day periodicity manifests itself in various processes on the Sun and in interplanetary space, such as solar radio emission, X-rays, dynamics of solar flares, solar wind density, cosmic ray rigidity and, especially total solar irradiance variability. It also presents in wave disturbances of the Earth atmosphere, ionospheric variations, the Earth's seismic noise, the Earth's global hydrocycle and some biological processes. All these facts suggest this periodicity to be global. Along with the assumption of the solar origin of this periodicity the question of the mechanism of its excitation is still open. On the other hand it should be noted that the variable stars of the type of classical cepheids, related to G2 spectral class in their average brightness have the same main period of pulsations. This fact suggests the excitation of this periodicity on the Sun to be related with the periodic variations of the opacity of subphotospheric layers that, in its turn, results in the periodic variations of the solar irradiance. If this mechanism is true then the global manifestation of the quasi-10-day periodicity may be explained.

**JSA16/E/04-A3** Poster **0830-32**

#### A NEW METHOD TO DETECT SOLAR VARIABILITY EFFECTS ON TREE-RINGS

Mezak A. RATAG (Indonesian National Institute of Aeronautics and Space, Lapan, Jl. Junjuran 133, Bandung 40173, Indonesia, email: mezakr@indosat.net.id)

A number of methods have been extensively used to detect possible impacts of solar variability on tree-rings. They are mostly developed on the basis of Fourier analysis. These methods are ideal tools if we are dealing with fluctuations characterised by truly or nearly constant period, amplitude, and phase. Periodic fluctuations, which behave as transient or nearly transient phenomena, will be very difficult to deal with. In many cases, the terrestrial data are in the form of unevenly sampled time series. These cause serious problems for the application of methods, which are based on Fourier analysis. Here we describe a new method to detect solar variability signals in tree-ring data, which is based on wavelet transform. Period analysis using the weighted wavelet Z-transform (WWZ), with Morlet wavelet, is applied to both the solar activity and the tree-ring time-series. The comparison of the results is made in WWZ time-frequency-amplitude space. This method is shown to be able to overcome the difficulties mentioned above. Various cycles can be analysed simultaneously.

**JSA16/E/44-A3** Poster **0830-33**

#### TOTAL SOLAR IRRADIANCE CHANGE ASSOCIATED TO QUIET SOLAR NETWORK

I. Ermolli (OAR - Osservatorio Astronomico di Roma, Roma, I-00136 Italia); F. BERRILLI (Dipartimento di Fisica, Università di Tor Vergata, Roma, I-00133 Italia); A. Florio (OAR - Osservatorio Astronomico di Roma, Roma, I-00136 Italia)

An estimate for the change in total solar irradiance due to quiet solar network during a 28 months period (Jul 1996 - Oct 1998) at the beginning of solar cycle 23 is presented. The valuation is based on measurements of the colour temperature for network and internetwork regions. These regions were identified with a numerical procedure applied on sub-arrays extracted from full-disk 1Kx1K CaK, Blue (409.6nm) and Red (607.2nm) continuum images obtained with the OAR-PSPT instrument. Our estimate for the change in total solar irradiance results of the order of 0.1%, and it is in good agreement with long-term irradiance variations measured from space.

**JSA16/W/07-A3** Poster **0830-34**

#### PHENOMENONS GEOPHYSICAL IN TREE-RINGS

Nivaor Rodolfo RIGOZO and Daniel Jean Roger Nordemann (both at Space Geophysics Division, National Institute for Space Research-INPE, CP 515, 12201-970, São José dos Campos, Brazil, E-Mail: rodolfo@dge.inpe.br)

Solar activity variations may be studied directly, through observations, or indirectly, through natural records which permit to extend the length of the time series well beyond the present and historical observations. Climatic natural records may be investigated to study the global and regional influence on climate of the variations of the energy emission by the Sun associated to its activity. Tree ring studies are usually used to determine or verify climatic factors which prevail in a given place or region and may cause tree ring width variations. Few studies are dedicated to the geophysical phenomena, which may underlie these tree ring width variations. Among these records, tree ring width series are of particular interest because of their availability, their regional coverage in continental areas and the possibility of very low cost methodologies for their study. The digitised images of polished dead tree slices are transformed by appropriate software into annual growth ring radial width. Samples may also be obtained from live tree by using an increment borer, but up to now higher facility and precision are achieved with polished slices than with drilled samples. Means of the time series and elimination of bias/tendencies are obtained from individual trees and local group, within dendrochronology norms. The search for periodicities is made by spectral analysis including maximum entropy and iterative regression methods. The first results obtained from *Auracaria angustifolia* specie (recently dead trees of maximum ages 200 yr.) from Santa Catarina States in Southern Brazil show periods of 84.2 to 85 yr., 46 to 50 yr., 24.6 yr., 10.6 yr. and 5.8 yr. which may be attributed to Gleissberg cycle, the 4th harmonic of the Suess cycle, the Hale cycle, the Schwabe cycles and the 2nd harmonic of the Schwabe cycle, and 4 and 6.9 yr. from El Niño kind of events.

**JSA16/W/22-A3** Poster **0830-35**

#### FORECAST OF THE MAJOR GEOMAGNETIC STORMS

Virginia SILBERGLEIT (Departamento de Física, Facultad de Ingeniería, UBA, Av. Paseo Colon 850, 1063-Buenos Aires, Argentina. Email: virginia@tormen.uba.ar)

Perturbed periods characterised by the maximum daily average AA index compiled from 1868 to 1992 are considered. The geomagnetic activity is studied by considering the even-odd effect with respect to sunspot cycles and applying Gumbel first asymptotic distribution extreme values.

The present study shows that the largest geomagnetic perturbed periods have different intensities depending on the parity of the solar cycles in which they occur.

**JSA16/W/17-A3** Poster **0830-36**

#### AN INVESTIGATION INTO SUNSHINE RECORDS FROM IRELAND AND THEIR LINK TO SOLAR VARIABILITY

ENRICH Palle and John Butler (both at Armagh Observatory, College Hill, BT61 9DG, Armagh, Northern Ireland. email: epb@star.arm.ac.uk)

We analyse the sunshine records made since the late 19th century in Ireland for evidence of a link between cloud factor and solar variability.

**JSA16/W/04-A3** Poster **0830-37**

#### ON THE RELATIONS BETWEEN SUNSPOT NUMBER

Konstantin N. VISHERTIN (Institute of Experimental Meteorology, SPA "Typhoon", Obninsk, Kaluga region, 82 Lenin Avenue, Russia, 249020, email: typhoon@meteo.ru); Boris G. Sherstukov (All Russia Research Institute of Hydrometeorological Information - World Data Center, Obninsk, Kaluga region, 6 Koroleva Street, Russia, 249020, email: sbg@meteo.ru)

The daily sunspot numbers spectral analyses have been made. The data from 1818 - 1998 have been transformed to standard variables and padded with zeros to provide a better resolution. The analyses have been carried out for the various sample lengths. The results obtained show



## INTER-ASSOCIATION

that 11-yr line is revealed as triplet with periods of 10.04, 10.94 and 11.96 yr, and there is harmonic structure for the periods range between about 5 and 40 yr. A fitting of the obtained sunspot number periodicities resulted in conclusion that solar activity periods are decrease from about 40 year to 27 days approximately as the second power of integer numbers.

**JSA16/W/14-A3** Poster **0830-38**

### "SOLAR ROTATION PERIOD INFERRED FROM A FEW UV LINES OBSERVED BY SBUV/2 ONBOARD NOAA11 SATELLITE"

Rajmal JAIN, Lokesh Bharti, Kandarp Bhatt (Udaipur Solar Observatory, Udaipur - 313001, INDIA); Richard. P. Cebula (Hughes STX Corporation, Greenbely, MD, USA)

Analysis of two time series of UV irradiance variation, one of 745 days during 1989-1991 and other of 898 days during 1991-1993, measured by SBUV/2 instrument onboard NOAA11 satellite, has been carried out for 13 UV lines. The chosen UV lines may be divided in two wavelength domain i.e below and above 290 nm. The UV lines with wavelength below 290 nm are: Ni XIII; Si IX; Fe XII; Mg II; Mg I; and Si I while above 290 nm are: Ca XII; Fe XIII; Fe I(M and N); Ni XVI and Ca H and K. The time series of UV irradiance variation in the core and in the wings of each selected line were subjected to Fast Fourier Transform. The power spectrum of each line shows 27-day solar rotation periodicity unambiguously, however more pronounced in the wavelength domain below 290 nm. The shorter period of about 14 days, related to the solar activity on the invisible hemisphere, is also evident. The power of fundamental 27-day period reduces appreciably from core to wing in each line as well as with increase in wavelength. The 27-day period varies from 30 to 27 days almost in each line during ascending phase of the sunspot cycle 22 i.e during 1989-94. Further, the Fourier analysis of both time series enabled us to detect distinctly the 76 and 154 days periods of solar activity. These periods, however, are more pronounced in the lines with wavelength >290 nm. Our study unambiguously reveals that amplitude and frequency of fundamental solar rotation period as well as other periods of solar activity strongly depend on the wavelength of UV line under study and sunspot number during the solar cycle.

**JSA16/W/10-A3** Poster **0830-39**

### "CORRELATION STUDY BETWEEN SUNSPOT AND RAINFALL IN SOUTHERN RAJASTHAN SUBTROPICAL REGION OF INDIA"

Rajmal JAIN and S. C. Tripathy

The cross correlation among 102 years rainfall data in Udaipur (southern Rajasthan) sub-tropical region and sunspots show the influence of solar activity on the climatic conditions of Udaipur. The periodicity obtained using rainfall and other data sets, such as, water storage of Jaisamand lake and gauge measurements of two rivers, Jakhm and karmoi, are similar to the periodicity of sunspots, which indicates a relationship between rainfall and sunspot activity. A period of about 27% is found to deviate from normal rains in the form of flood, excess and deficit of rains in Udaipur sub-tropical region. The possible physical mechanisms to explain sun-weather relationship in astro-physical context are discussed.

**JSA16/W/08-A3** Poster **0830-40**

### PROPOSED MECHANISM FOR EFFECTS OF GLOBAL ELECTRIC CIRCUIT ON CLOUD MICROPHYSICS

Brian A.TINSLEY, (University of Texas at Dallas, Richardson, TX 75083-0688 USA e-mail: Tinsley@UTDallas.edu); Kenneth V. Beard, (University of Illinois at Urbana-Champaign, Urbana, IL 61801)

The global atmospheric heat balance is sensitive to small changes in cloud albedo and opacity such as are produced by changes in the rate of production of ice from supercooled water at cloud tops. Also, the dynamics of winter storms respond to changes in precipitation efficiency resulting from changes in the production of ice. We have identified a hitherto neglected cloud microphysical process linking the rate of initial production of ice in many clouds to the vertical ionosphere-earth current density, Jz, that responds to changes in cosmic ray flux and to other solar wind and terrestrial inputs. (Tinsley will discuss the Jz response in the review JSA45). The cloud microphysical process entails an increase of the collision rate of 'evaporation aerosols' from the evaporation of smaller, electrically charged droplets with other, larger supercooled droplets at cloud tops. This increase is dependent on the electrostatic charge on the 'evaporation aerosols'. Sulphate and organic compounds scavenged by cloud droplets coat the 'evaporation aerosols' and condition them to be effective ice-forming nuclei. The 'evaporation aerosols' retain their initial charge for many minutes in the cloud environment. Image charge forces cause them to be strongly attracted to the droplets, whether the droplets are uncharged, or with like or unlike charges and ice nucleation is likely to occur on contact. We present numerical simulations showing that contact ice nucleation rates are dominated by image charge forces when the 'evaporation ice nuclei' carry only a few tens of elementary charges, and that this process

**JSA16/W/15-A3** Poster **0830-41**

### INCREASE OF THE TOTAL SOLAR IRRADIANCE SINCE THE LAST MINIMUM IN 1996

ANKLIN M (1), Fröhlich,C.(1), Willson R.C (2), Lee III, R (3), Wilson R.S (4) Crommelynck D(5), Dewitte S(5),1) Physikalisches-Meteorologisches Observatorium Davos, Dorfstr. 33, 7260 Davos Dorf, Switzerland, 2) Columbia University, 12 Bahama Bend, Coronado, CA, 92118, USA, 3) NASA Langley Research Center, Building 1250, Hampton, Virginia 23681-2199, USA, 4) One Enterprise Parkway, Suite 300, Hampton, Virginia 23666 ,USA, 5)Royal Meteorological Institute of Belgium, Av. Circulaire, 3 B-1180 Brussels

Total solar irradiance (TSI) has been monitored by the ACRIM II (Active Cavity Radiometer Irradiance Monitor), VIRGO (Variability of solar Irradiance and Gravity Oscillations) and ERBS (Earth Radiation Budget Satellite) experiments between 1996 - 1998. The anticipated increase if the TSI since the last minimum in the summer of 1996 has been observed. Small differences between these time series exist in the amplitude of the increase and in short term variability. Here we compare the VIRGO TSI with ACRIM II and ERBS. ACRIM II data is used to fill the gap in the VIRGO time series from June-October 1998, when SOHO was lost and no data could be received. Since VIRGO observes continuously it is possible to compare truly simultaneous observations, improving the quality of the comparison substantially. The main objective of the comparison is to get detailed information on the relative performance of the radiometers and to assess the confidential level of solar irradiance changes during the 1996-1998 period.

**JSA16/W/23-A3** Poster **0830-42**

### ON FINE STRUCTURE OF THE SOLAR CYCLISITY IN CONNECYION TO METEOROLOGICAL CYCLES

Edward KONONOVICH (Moscow University Sternberg Astronomical Institute, 119899, Moscow, Russia. E-mail: konon@sai.msu.su)

The beginning of the cycle 23 allows performing a comparison of the observed and predicted values of the Wolf numbers W given by various prognoses. The real value of such forecasting is the possibility to precisely the character of the current maximum of the long-term solar cycle known as a 80-100 year one. This maximum covers the recent 90-ies and coincides with the last highest 11-year cycles. The same pattern occurred for the previous 80-year cycle maxima in 1770 and 1850, when they coincided with the triads of high 11-year cycle maxima with numbers 2, 3, 4 and 8, 9, 10; in the same way there is a coincidence of series of the 11-year lowest maxima with 80-year minima at 1793 and 1894. The smoothed month mean W-values (since 1750) are considered to reveal different kinds of such triads. Their connection with meteorological cycle recognised by E.Bruckner (1890) is proved. The fine structures of deferent 11-year cycles are analysed by means of MME-method. The frequencies of the quasi-biannual cycle are revealed and considered.

**JSA16/W/05-A3** Poster **0830-43**

### QUASI-BIENNIAL CYCLICITY IN THE SOLAR-ATMOSPHERIC RELATIONS AT VARIOUS LATITUDES

Ruslan Smirnov (Fedorov Institute of Applied Geophysics, Moscow 129226, Russia); Edward KONONOVICH (Moscow University, Sternberg Astronomical Institute, 119899, Russia, e-mail: konon@sai.msu.su)

The structure of the relations between the geomagnetic activity variations represented by the mean aa index and the root-mean-square temperature anomalies in the low troposphere for the time interval 1874 - 1979 is considered over the periods 2 - 30 years. The data on temperature anomalies were used for the Polar Cap, and also for latitudes 65, 40 and 20 degrees. Frequency characteristics of the relations were obtained separately for January and July. The results have shown, that the high levels of the relations are characteristic for the Polar Cap and especially for the periods of quasi-biannual oscillations (QBO). The relation degrees for QBO as a whole decrease with transition to moderate and low latitudes. A scenario of QBO excitation based on the increasing of the meridional circulation form recurrency is suggested. The important role is played by the areas of baroclinic instability of the troposphere as cites of the tropospheric reaction on cyclic changes of the solar activity.

**JSA16/W/19-A3** Poster **0830-44**

### THE MIDDLE ATMOSPHERE AS A CONTROLLER OF THE SOLAR ACTIVITY INFLUENCE ON THE LONG-TERM VARIATIONS OF THE CLIMATE

Edward KONONOVICH (Moscow State University Sternberg Astronomical Institute, Moscow 119899, Russia, E-mail: konon@sai.msu.su); Nikolaj Shefov (Obukhov Institute of Atmospheric Physics, Russian Academy of Sciences, Moscow 109017, Russia, e-mail: meso@omega.ifaran.ru)

It is emphasised that the energy losses caused by the upward propagation of different kinds of the atmospheric waves generated in the troposphere is an important factor of the energy balance of the lower atmosphere. The modulation of the energy sink rate occurs due to the variation of wave transparency of the middle atmosphere. This variation is produced by the wind regime change. The letter, in its turn, is caused by different amount of the solar ultraviolet radiation absorbed by the atmosphere during different phases of the solar cycle: at cycle maximum UV radiation is larger. As a result the additional amount of energy absorbed per day at solar maximum is larger than that in minimum. The difference is about 6 per cent if measured in terms of the thermal energy of the atmosphere at 50-90 km height (its variation during the solar cycle is taken into account). In the same time it is known that the kinetic energy of the turbopause is mainly accumulated in the dynamic waves. As a result the thermal energy escapes from the atmosphere through the infrared emission of CO2 molecules due to the transfer process caused by conductivity. The variation of the atomic oxygen concentration at heights about 85- 100 km, caused by the change of the solar activity, significantly regulates the infrared energy losses. The above-mentioned process possibly increases the troposphere energy input because of decrease of sink of energy during the enhancement of the solar activity. This process may stimulate the long-term climatic variations of the energy balance in the middle and lower atmosphere. An estimation of the rate of energy sink shows that the cooling of the lower atmosphere by 1 K due to the decrease of the of solar activity level may occur during the time interval about 100 years. This is in an agreement with the conditions, which possibly took place during the Maunder Minimum in 1645-1715.

**JSA16/W/24-A3** Poster **0830-45**

### SOME VARIATION REGULARITIES OF BACKGROUND RADIATION AND ATMOSPHERIC TEMPERATURE

Yury SIZOV, Kharlampy Kanonidi and Konstantin Kanonidi (All at the Institute of Terrestrial magnetism, ionosphere and radio wave propagation (IZMIRAN), 142092 IZMIRAN, Troitsk, Moscow region, Russia; e-mail: sizov@izmiran.rssi.ru)

Background radiation and atmospheric temperature measured and registered by the data acquisition system at IZMIRAN continuously during 1998 are considered. It is shown that temporary lines of background radiation (BR) as well as atmospheric temperature (AT) demonstrate existence of time intervals when one can observe daily and seasonal variations. Disturbed BR interval events happen sometimes. Amplitudes of BR quiet daily variations are not stable and its pp values vary from 2 to 6 microRoentgen/hour (mCr/h). During disturbed intervals an amplitude of BR variations growth up to tenths mCr/h. The spectral analysis of BR temporary lines for every month has shown a presence of very stable 24-hour period. Besides it is happen rather often 4, 6, 8, 12 hour as well as 1.5, 2 days periods. BR spectrum contains some other periods but it varies from month to month. There are common periods (for example - 24 h) in BR and AT rhythms.

**JSA16/W/25-A3** Poster **0830-46**

### EXCESS ENERGY EMISSION BY ACTIVE REGIONS

Ada ORTIZ (Dept. d'Astronomia i Meteorologia, Univ. Barcelona, C/ Marti i Franques, 1, E-08028, Spain, email: aortiz@vega.am.ub.es); Vicente Domingo (ESA Space Science Dept/ESTEC, Noordwijk, Netherlands, email: vdomingo@so.estec.esa.nl); Blai Sanahuja (Dept. d'Astronomia i Meteorologia, Univ. Barcelona, C/ Marti i Franques, 1, E-08028, Spain, email: blai@am.ub.es); Thierry Appourchaux (ESA Space Science Dept/ESTEC, Noordwijk, Netherlands, email: thierrya@so.estec.esa.nl); Luis Sanchez (ESA/Space Science Dept. at NASA/GSFC, Greenbelt, Maryland, USA, email: lsanchez@esa.nascom.nasa.gov); Claus Frohlich (Physikalisches-Meteorologisches

Observatorium Davos, World Radiation Center, PMOD/WRC, Dorfstrasse 33, CH-7260 Davos-Dorf, Switzerland); Todd Hoeksema (Stanford University, Palo Alto, California, USA)

We study one of the isolated active regions that crossed the solar disk during the 1996 minimum of activity. Its passage during several Carrington Rotations allows us to analyse the evolution of the angular distribution of the excess radiance of the facular region. We evaluate the total (i.e. in all directions) emission of faculae, its spectral and temporal evolution and relate it to the solar surface magnetic field. To fulfil this goal we use the SOHO/VIRGO and MDI data. The results are compared with facular models through a compound model for the active region that takes them into account. The effect of the active region on the solar luminosity is discussed.

**JSA16/W/13-A3** Poster **0830-47**

#### SOLAR EUV VARIABILITY AS MEASURED BY SOHO/EIT

J.S. NEWMARK (SM&A Corp., NASA/GSFC, Code 682.3, Greenbelt, MD 20771, Email: newmark@eitv2.nascom.nasa.gov); J.W. Cook, J.D. Moses, L.E. Floyd (at Naval Research Laboratory, Washington, D.C 20375)

The Extreme-ultraviolet Imaging Telescope (EIT) on board the SOHO (Solar and Heliospheric Observatory) satellite provides wide-field images of the corona and transition region on the solar disc and up to 1.4 solar radii. Its normal incidence multilayer-coated optics select spectral emission lines from Fe IX,X (171 Å), Fe XII (195 Å), Fe XV (284 Å), and He II (304 Å) which allow us to describe Solar activity over a wide temperature range. We provide calibrated measurements of the Solar irradiance in all four lines for the first 2.5 years of the mission. Details concerning the calibration of the instrumental response are provided. Initial comparisons with SUSIM Lyman Alpha and Mg II indices are shown as well as comparisons with the SOHO SEM He II flux.

**JSA16/W/06-A3** Poster **0830-48**

#### RADIANCE OF THE QUIET SUN AT FAR-ULTRAVIOLET WAVELENGTHS MEASURED DURING THREE YEARS OF THE SOHO MISSION

Udo SCHÜHLE and Klaus Wilhelm (Max-Planck-Institut für Aeronomie, D-37191 Katlenburg-Lindau, email: schuehle@linmpi.mpg.de); Anuschka Pauluhn and Isabelle Ruedi and Sami Solanki (Institute of Astronomy, ETH-Zentrum, CH-8092 Zürich); Philippe Lemaire (Institut d'Astrophysique Spatiale, CNRS-Université Paris XI, F-91405 Orsay); Jörg Hollandt (Physikalisch-Technische Bundesanstalt, Abbstr. 2-12, D-10587 Berlin,

The SUMER spectrometer (Solar Ultraviolet Measurement of Emitted Radiation) on the Solar and Heliospheric Observatory (SOHO) measures the radiance of the solar spectrum in the far ultraviolet range between 66 nm and 161 nm with high spatial resolution since the start of the SOHO mission. The radiometric calibration of the instrument has been performed in the laboratory using a transfer source standard traceable to the primary source standard, the electron storage ring BESSY I. With the aim of a cross calibration among the ultraviolet instruments on SOHO an observational scheme had been designed which was reproducible with the quiet Sun as the source, and which was repeated regularly during the observational period of the SOHO mission. These observations were carried out about 20 times between 5. March 1996 and 6. November 1998 with the selected spectral lines of He I (58.4 nm), Mg X (60.9 nm and 62.5 nm), Ne VIII (77.0 nm), and N V (123.9 nm). Each measurement builds an average of about 20 minutes of the radiance of the quiet Sun network at the solar disk centre. After careful separation of the line emission from the superimposed contributions of different orders of the spectrometer and from the solar continuum, the spatially resolved measurements allow to draw a trend of the intensities of the quiet Sun network in these lines along the observational period between solar sunspot activity cycles 22 and 23.

**JSA16/W/02-A3** Poster **0830-49**

#### GEOMAGNETIC ACTIVITY AND ATMOSPHERIC PRESSURE FLUCTUATIONS

Yury SIZOV and Kharlampy Kanonidi (both at the Institute of Terrestrial Magnetism, Ionosphere and Radio Wave Propagation (IZMIRAN), 142092 IZMIRAN, Troitsk, Moscow region, Russia; e-mail: sizov@izmiran.rssi.ru)

Temporary lines of local three-hour, three hour ak- and daily average Ak-indices of geomagnetic activity (calculated on K- indices of "Moscow" magnetic observatory, IZMIRAN) and hourly average values of atmospheric pressure P on the data of cosmic rays "Moscow" station of IZMIRAN for 1994 - 1995 are considered. It is shown, that between the local ak-indices of geomagnetic activity and variations of atmospheric pressure exist relations, which are expressed in the following. During increase of geomagnetic activity (GMA) in an interval 44 considered cases of increasing GMA a level of atmospheric pressure during 1994 - 1995: decreased approximately in 40 % of cases; increased approximately also in 40 % of cases, i.e. up to 80 % of cases of long period changes of a level of atmospheric pressure (from 3 days up to 2-3 weeks) are definitely connected with GMA increasing. The oscillatory changes of the form of a P level with the periods 3 - 7 days were observed on a background changeable GMA or on a magnetic quiet background. The analysis of cross correlation functions specifies that between ak and P there is a dependence, what specify precise periodicity of these functions. By the spectral analysis of temporary lines and their correlation functions the common spectral maxima on the periods, common for both lines, are received. Under the diagrams of auto correlation functions two common periods are received: 14 and 27 day. The spectral analysis of cross correlation functions has allowed to reveal maxima on the periods: 5.4, 7.6, 9.2, 13.5, 28.1 day. The spectral analysis of temporary lines has shown presence of the following common periods: 3.7, 4.4, 5.5, 6.9, 7.9, 9.3, 13.2, 28 days.

**JSA16/W/09-A3** Poster **0830-50**

#### MODEL STUDY OF ATMOSPHERIC COMPOSITION AND TEMPERATURE BEHAVIOR DURING THE CURRENT 11-YEAR SOLAR ACTIVITY CYCLE

Igor KAROL, V.A. Frolkis, A.A. Kiselev (all at Main Geophysical Observatory, 7 Karbyshev Str., St.Petersburg, 194021, Russia; e-mail: karol@main.mgo.rssi.ru)

A model study of influence of the current 11-year solar activity cycle on both the atmospheric composition and radiative regime is actual for assessment of this natural and of anthropogenic inputs in the total ozone coming changes. The investigation is based on the estimations of i) solar spectrum intensity changes during its current cycle and ii) natural and anthropogenic air pollution from IPCC-92/95 scenarios. The radiative forcing due to the both above factors is calculated. Special attention is paid to study of the diurnal course peculiarities of the short-lived atmospheric radicals in the phases of 11-year solar cycle. Sensitivity of air compounds content to solar radiation changes is analyzed. For this the 2-D time dependent radiative photochemical channel model of the 0-50-km atmospheric layer and temperate latitudinal belt 30-60° N with fixed zonal and convective transport is used. The basic atmospheric reactions among the oxygen, nitrogen, hydrogen, carbon, chlorine and bromine compounds are considered. The

geographical inhomogeneity of pollution sources along latitudinal circle is accounted. The tropospheric water vapor conservation occurs according to the NCAR/NCEP data.

**JSA16/W/01-A3** Poster **0830-51**

#### INFLUENCE OF SOLAR VARIABILITY ON THE PRODUCTION OF ATOMIC OXYGEN O(1S) 558 NM EMISSION IN THE MIDDLE AND LOWER THERMOSPHERE

Gordon SHEPHERD and Rawatee Maharaj-Sharma (both at the Centre for Research in Earth and Space Science, York University, Toronto M3J 1P3, Canada, email: gordon@windch.yorku.ca)

The Wind Imaging Interferometer (WINDII) on the Upper Atmosphere Research Satellite measures winds from the Doppler shifts of five different emissions from the thermosphere and upper mesosphere. As part of the measurement process the volume emission rate (photon s<sup>-1</sup> cm<sup>-3</sup>) is accurately measured. This includes the atomic oxygen O(1S) emission at 558 nm, which during daytime is emitted over a large altitude range, from about 85 to over 250 km. Two distinct peaks in altitude are formed, one near 145 km (middle thermosphere) and the other near 100 km (lower thermosphere). Each involves very different production processes, so while both respond closely to solar variability effects, each is responding to different variability components of the solar spectrum. The correlation of these two emission regions with different solar indices is presented, for both daily averages, and for short term variations that include solar flares, which strongly (and only) affect the lower thermosphere peak. The relevant atmospheric processes are described.

**JSA16/W/12-A3** Poster **0830-52**

#### IRRADIANCE VARIATIONS DURING A PERIOD OF LOW SOLAR ACTIVITY IN 1996

Michael STEINEGGER (Institut fuer Astronomie, Universitaetsplatz 5, A-8010 Graz, Austria); Wolfgang Otruba (Sonnenobservatorium Kanzelhoehe, A-9521 Treffen, Austria); Peter Brandt (Kiepenheuer-Institut fuer Sonnenphysik, Schoeneckstrasse 6, D-79104 Freiburg, Germany); Zeki Eker (Department of Astronomy, King Saud University, Riyadh 11451, Saudi Arabia); Arnold Hansmeier (Institut fuer Astronomie, Universitaetsplatz 5, A-8010 Graz, Austria)

The last solar activity minimum around 1996 was characterised by several periods without any sunspots or faculae visible on the solar disk. Between these extremely quiet intervals, from time to time a single active region emerged and developed. The passage of these individual activeregions across the visible solar hemisphere was accompanied by a pronounced variation in the solar irradiance as observed by the VIRGO radiometers onboard SOHO. Making use of photometric full-disk observations of the Sun (e.g. MDI, RISE/PSPT, TON Ca II K) we try to reconstruct the temporal behaviour of the three spectral and the total irradiance channels measured by VIRGO. The aim of this project is to identify the different contributions of the sunspots, the faculae, and the network to the irradiance variations, and to study in detail the sunspot and facular contrasts at the different wavelengths.

**JSA16/W/20-A3** Poster **0830-53**

#### ANALYSIS OF THE SOHO/VIRGO TOTAL AND SPECTRAL IRRADIANCES BASED ON THE SOHO/MDI IMAGES

JUDIT PAP (University of California, Los Angeles, 405, Hilgard Ave., Los Angeles, CA 90095-1562); Michael Turmon (Jet Propulsion Laboratory, MS 126-347, 4800 Oak Grove Dr., Pasadena, CA 91109, USA); Richard Bogart (Center for Space Science and Astrophysics, Stanford University, Stanford, CA 94305, USA); Martin Anklin, Claus Frohlich, Christoph Wehrli (Physikalisch-Meteorologisches Observatorium Davos, CH-7260, Davos-Dorf, Switzerland); Linton Floyd (Naval Research Laboratory, Code 7660, Washington, DC 20375, USA); Ferenc Varadi (University of California, Los Angeles, 405 Hilgard Ave., Los Angeles, CA 90095, USA)

The Variability of IRradiance and Gravity Oscillations (VIRGO) experiment on SOHO has been measuring total solar and spectral irradiance since January 1996. The PMO6 and DIARAD instruments are monitoring total irradiance, whereas the SunPhotometer observes near-UV at 402 nm, visible at 500 nm, and near infrared at 862 nm. The VIRGO observations have shown that total solar and spectral irradiance vary in a similar fashion. The effect of sunspots, faculae and weak magnetic fields on the VIRGO irradiances will be estimated by means of the magnetograms and continuum images of the Michelson Doppler Imager (MDI) experiment on SOHO. The phase shift between the rise of VIRGO total irradiance and the SUSIM Mg core-to-wing ratio during the ascending phase of solar cycle 23 will also be examined.

**JSA16/W/38-A3** Poster **0830-54**

#### SOLAR TOTAL AND UV IRRADIANCE VARIATIONS MODELLED BY THE MT. WILSON MAGNETIC INDICES

JUDIT PAP, Roger Ulrich, John Boyden, Daryl Parker, Ferenc Varadi (University of California, Los Angeles, 405 Hilgard Ave., Los Angeles, CA 90095, USA); Claus Frohlich (Physikalisch-Meteorologisches Observatorium Davos, Dorfstrasse 33, CH-7260, Davos-Dorf, Switzerland); Linton Floyd (Naval Research Laboratory, Code 7660, Washington, DC 20375, USA); Larry Puga and Rodney Viereck (NOAA Space Environment Center, 325 Broadway, Boulder, CO 80303, USA)

Total solar and UV irradiances have been monitored from space for two decades. Observations of solar activity have been performed at the Mt. Wilson Observatory in the 525.0 nm magnetically sensitive Fe I line. From the Mt. Wilson observations we have derived the so-called Mt. Wilson Sunspot Index (MWSI), the Magnetic Plage Strength Index (MPSI) and the Magnetic Weak Field Index (MWF). MWF is a new data product representing the slow variability of the weak magnetic fields. In this paper we examine the variations in total irradiance and the UV irradiance as represented by the Mg II h & k as a function of solar cycle and compare their variations during solar cycles 21, 22, and 23. The contribution of sunspots, plages and the weak magnetic fields to the variations of total solar and UV irradiances will be estimated with advanced statistical methods.

**JSA16/C/GA4.07/W/34-A3** Poster **0830-55**

#### SOLAR VARIABILITY

Virginia SILBERGLEIT (Departamento de Fisica, Facultad de Ingenieria, UBA. Av. Paseo Colon 850 - 1063 - Buenos Aires, Argentina, email: virginiat@tormen.uba.ar); Silvia Gigola (Departamento de Matematica, Facultad de Ingenieria, UBA. Av. Paseo Colon 850 - 1063 - Buenos Aires, Argentina, email: sgigola@tron.fi.uba.ar); Ricardo Sime (Departamento de Matematica, Facultad de Ingenieria, UBA. Av. Paseo Colon 850 - 1063 - Buenos Aires, Argentina, email: rsime@tron.fi.uba.ar); Carlos D'Atellis (Departamento de Matematica, Facultad de Ingenieria, UBA. Av. Paseo Colon 850 - 1063 - Buenos Aires, Argentina, email: ceda@tron.fi.uba.ar)

The present article studies the sunspot numbers signal vs. time. According to the wavelet series, the intensity of the signal is considered as the coefficients of the series. The



## INTER-ASSOCIATION

multiresolution representation obtained from the wavelet transform and the corresponding digital filters derived allow time localisation of different development of the solar activity. The above mentioned study give us the opportunity to investigate the cause of the most perturbed geomagnetic periods.

**JSA16/C/GA4.07/W/37-A3** Poster **0830-56**

### INFLUENCE OF CLIMATIC CHANGES, SOLAR AND GEOMAGNETIC ACTIVITY ON DYNAMICS OF MAGNETIC PARAMETERS OF CONTEMPORARY SEDIMENTS

Kurazhkovskiy A.Yu., KURAZHKOVSKAYA N.A., Klain B.I. (everybody at Geophysical Observatory "Borok" of the United Institute of Physics of the Earth of Academy of Science of Russia, 152742 Borok, Yaroslavl, Nekouz, Russia, email: knady@borok.adm.yar.ru)

The results of investigation of correlative communications between magnetic parameters of contemporary sediments of Rybinsk reservoir and of the helio geophysical factors are given. The periodicity in dynamics of magnetic parameters of sediments, which coincide with 11-year's cycles of solar activity have been discovered. The back coupling between by planetary geomagnetic activity and quantity of a magnetization of ground sediments is detected. It was shown that periodicity and quantity of magnetic parameters of sediments depends from the temperatures of water, from a level of a reservoir and other geophysical conditions, in which occurred accumulation of sediments. Was found, that in the present region the dry and warm climate lead to decrease of a magnetisation and Koenigsberger's factor on quantity, and more wet and cold calls their increase.

The possibilities of application of obtained effects of dynamics of magnetic parameters of sediments for reconstruction and prognosis of regional climatic changes is considered.

**JSA16/W/35-A3** Poster **0830-57**

### VARIABILITY IN SOLAR ACTIVITY, GEOMAGNETIC FIELD AND GLOBAL TEMPERATURE DATA ON SHORT AND LONG TIME SCALES

Tamara KUZNETSOVA, Lev Tsurinik (both at IZMIRAN, Troitsk, Moscow region, 142092, Russia, email: tvkuz@izmiran.rssi.ru)

Two approaches can be used to extract deterministic and noise part in data sets. The first approach which may be called "nonlinear time series analysis" gives information about system dynamics. We applied alternative approach and tried to find "how much determinism" there is in data sets and whether this determinism can explain main regularities in data sets. The problems are trends and quasi-periodicities in many solar and climate processes. A method of nonlinear spectral analysis (called the method of global minimum: MGM) has been used to find periodicities in annual Wolf sunspot numbers (W) during the period 1700-1997. The longest set of magnetic observations on the Earth (D-component at Hartland, 1810-1995) is used for calculation of geomagnetic spectrum. The powerest trend at period T~204 yr. in W testifies to the existence of the slowest non-stationary processes in sunspot formation. It is shown a positive correlation of the trend changes and global climate changes: Little Ice Ages, global warming from the beginning of our century. Analysis of the geomagnetic spectrum shows that significant spectral peaks of the spectrum have solar origin at the studied time interval. But harmonics of the solar model that have analog in the geomagnetic spectrum are not the powerest (for instance, the power spectral peak in the solar spectrum at T=11.1 yr. is lower confidence limit in the geomagnetic one). Comparison of the reported spectrum of global temperature (SSR method) and geomagnetic one (MGM) shows that all significant spectral peaks of both spectra in the studied ranges of periods coincide (with accuracy of errors). Deterministic processes responsible for the climate and geomagnetic changes on the Earth have the same periodicities. The Earth's atmosphere and magnetic field are sensitive to the same part of deterministic band of solar activity, not the powerest in the solar activity spectrum of W.

**JSA16/C/GA4.07/W/28-A3** Poster **0830-58**

### A PARTIAL CORRELATION ANALYSIS OF STRATOSPHERIC OZONE RESPONSE TO THE SHORT-TERM SOLAR UV VARIATIONS WITH TEMPERATURE EFFECT REMOVED

Shuntai ZHOU and A J Miller (NOAA/NWS/NCEP, USA)

Although stratospheric ozone response to the 27-day solar UV variation has been detected from satellite ozone and UV data, the total response is modulated by the variations in temperature. Photochemical and radiative theory, along with previous data analysis, indicate that the temperature effect on this time-scale is essentially linear and can be separated statistically from the ozone effect. In this study we utilise the statistical estimation technique of partial correlations to separate ozone response to the 27-day solar variation. Our data set includes 2000 days of satellite UV, ozone and temperature data from the SBUV(2) and UARS measurements and the NCEP temperature analysis. We find that for the upper stratosphere, from 1 hPa to 5 hPa, the partial correlation coefficients of ozone and UV are considerably increased over the total correlation, there is no negative time lag (ozone leads UV), and the maximum ozone-UV correlation is obtained at a higher altitude compared with the previous total correlation analysis. In addition, we examine the ozone sensitivity to UV and temperature variations using linear regression with two independent variables. The results indicate that the upper stratospheric ozone variation can be very well represented by a linear combination of UV and temperature variations. The ozone sensitivity to UV or temperature is generally independent of time periods used for analysis, though solar UV and temperature variations may be very different for different time periods.

**JSA16/C/GA4.07/W/30-A3** Poster **0830-59**

### SOLAR AND GEOPHYSICAL DIGITAL DATA - WINDOWS ON OUR ENVIRONMENT

Helen COFFEY (Solar-Terrestrial Physics Division, NOAA National Geophysical Data Center, World Data Center A for Solar-Terrestrial Physics, 325 Broadway, Boulder, CO 80303 USA, email: hcoffey@ngdc.noaa.gov)

The Sun is the engine that drives the Earth's weather machine. The World Data Center (WDC) A for Solar-Terrestrial Physics maintains on-line digital archives for solar and geophysical databases via the Space Physics Interactive Data Resource (SPIDR) system and via ftp anonymous access. SPIDR is now available in Russia and Australia. A partial system resides at the WDC-C1 United Kingdom (UK). NOAA is using current technology to meet user requirements for data management, analysis, and distribution. The SPIDR system is being updated with new and improved technology. The available digital data will be reviewed, along with information about new developments occurring, such as including the Solar-Geophysical Data (SGD) databases in SPIDR. Users are asked for input on desirable future products and databases.

**JSA16/C/GA4.07/W/32-A3** Poster **0830-60**

### SOLAR CYCLE VARIATIONS OF SURFACE AIR TEMPERATURE

Katya GEORGIEVA, Boyan Kirov (both at the Solar-Terrestrial Influences Laboratory at the Bulgarian Academy of Sciences, Bl.3 Acad.G.Bonchev str., 1113 Sofia, Bulgaria, email: kgeorg@bas.acad.bg, bkirov@bgcict.acad.bg)

The influence of solar activity on weather and climate is one of the most controversial problems in Solar-Terrestrial physics. The main reason is that so far there is no convincing physical mechanism explaining such an influence, and, besides, the results themselves are rather ambiguous - some authors find a good positive correlation between solar activity and a given meteorological parameter, some find an equally good negative correlation, and some find no correlation at all. However, most of these studies use data for particular locations and/or for limited time periods. In the present paper long time series are examined of the global, hemispheric and zonal surface air temperatures, as well as from individual stations. It is found that the correlation between solar activity and temperature in the 11-year solar cycle changes in consecutive secular solar cycles - positive in the 18th Century, negative in the 19th and positive again in the 20th. This result pertains to both global and hemispheric (North and South) mean temperatures, and to individual midlatitude stations. As for the zonal temperatures, a good negative correlation at all latitudes is found in the 19th C, while in the 20th C the positive correlation is seen at low and midlatitudes, and lacks at high latitudes. This may mean that there are at least two mechanisms by which sun influences the climate, one of them working only at high latitudes and leading to negative correlation between solar activity and temperature in the 11-year solar cycle, the other one global and leading to correlation changing in sign in consecutive secular solar cycles, with the lack of correlation at high latitudes in the 20th C being the result of the competitive action of the two. Therefore, the physical mechanisms by which the solar activity influence atmosphere in the 11-year solar cycle could hardly be found without understanding the nature of the secular solar cycle.

**JSA16/C/GA4.07/W/31-A3** Poster **0830-61**

### IDENTIFICATION OF SOLAR IRRADIANCE FEATURES IN NSO MAGNETOGRAMS: HISTOGRAMS VS. MORPHOLOGICAL MASKS

Harrison P. JONES (NASA/Goddard Space Flight Center, Laboratory of Astronomy and Solar Physics, Southwest Solar Station c/o NSO, PO Box 26732, Tucson, AZ 85726, US, email: hjones@noao.edu) Karen L. Harvey (Solar Physics Research Corporation, 4720 Calle Desecada, Tucson, AZ 85718 US, email: kharvey@sprc.com)

Magnetograms obtained at the National Solar Observatory/Kitt Peak Vacuum Telescope (NSO/KPVT) form a useful data set to help identify and understand sources of solar irradiance variations. In this paper we compare two techniques for identifying relevant magnetic features in a subset of NSO/KPVT magnetograms obtained with the NASA/NSO Spectromagnetograph, which has been in daily operation since April 1992. One method, described by Harvey and White (1996), iteratively considers various morphological characteristics of the magnetogram to form spatial masks, which select such features as active regions, sunspots, and enhanced and quiet network. The other, described by Jones (1997), uses cuts in multidimensional histograms formed from the five cotemporal and cospatial spectromagnetograph images (line-of-sight magnetic flux and velocity, continuum intensity, equivalent width, and central line depth) to partition the data statistically. We spatially compare features determined by the two techniques for selected images and also compare histograms for data subsets marked by each of the Harvey and White masks to look for distinguishing thermodynamic characteristics and as a guide for refining the histogram classifications.

**JSA16/W/42-A3** Poster **0830-62**

### ON THE 10.4 YEAR SOLAR SIGNAL IN GLOBAL AIR TEMPERATURES: THE RELATIONSHIP TO LONG-TERM SOLAR ACTIVITY

Peter THEJLL, (Solar-Terrestrial Physics Division, Danish Meteorological Institute, Lyngbyvej 100, DK-2100 Copenhagen O, Denmark (email: thejll@dmi.dk))

The presence of a 'solar' signal in global air temperature records has been studied in depth by R.G. Currie, and others, for a considerable time. The approximately 10.4 year signal is present on most continents, shows periods of phase coherence between neighbouring stations, and phase changes at certain geographic locations and at certain times. The distribution of the signal has been linked, at least on the North American continent to mountain chains - lines of phase change lie along e.g. the Rocky mountains. A trend towards growing signal amplitude and latitude, in the USA, has been reported. In a new analysis of the high-quality data part of the Climatic Research Units temperature dataset the above properties of the signal are verified, and a new link to the geographic distribution of the signal is shown. Stations with a strong signal in the band near 10.4 years are also likely to be stations near an ocean shore or a large lake. The relevance to recent discoveries of correlations between climate factors and solar activity will be discussed, and the relationship between the strength of the periodic signal and the correlation with the long-term evolution of Solar Activity, in terms of the Solar Cycle Length, will be considered.

**JSA16/L/01/A3** Poster **0830-63**

### NIMBUS-7 SBUV SOLAR SPECTRAL UV MEASUREMENTS: 1979-1987

Richard P. CEBULA and Matthew T. DeLand

Absorption of solar ultraviolet (UV) energy plays a dominant role in the thermal structure, dynamics, and photochemistry of the Earth's middle atmosphere. The first continuous studies of solar UV irradiance were begun using satellite instruments during the late 1960s and early 1970s. These early measurements suffered from significant absolute calibration uncertainties and extensive sensor sensitivity drifts. Early estimates of solar cycle variation at wavelengths important to middle atmospheric photochemistry (e.g. 200-300 nm) hence differed by factors of 2-5.

The launch of Nimbus-7 SBUV in November 1978 represented a major step forward in our understanding of short and long-term solar variability. SBUV solar irradiance measurements covering the wavelength range 160-400 nm were made for more than 8 years, spanning the maximum and declining phases of solar cycle 21. Although SBUV did not incorporate an onboard calibration system, the frequency of solar observations was varied periodically during the mission. The resulting data form the basis of an empirical model that we use to characterize instrument changes. Our goal is to achieve a long-term accuracy approaching that which we have recently obtained for NOAA-11 SBUV/2 (approximately 1-2%, 2 sigma). We present a progress report on our instrument characterization efforts. At the current level of the analysis the SBUV data already dramatically improve the accuracy of estimated solar irradiance changes during solar cycle 21. For example, at 200 nm, pre-SBUV estimates of solar cycle variations ranged from essentially none to nearly a factor of two. The SBUV-estimated solar cycle 21 variation at 200 nm, 5-8%, is in substantial agreement with measurements of long-term solar change during solar cycle 22.



JSA16/L/02/A3 Poster 0830-64

## THE TOTAL SOLAR IRRADIANCE MISSION: 2) MEASUREMENT OF SOLAR SPECTRAL IRRADIANCE FROM 0.2 MM TO 2 MM

Gary ROTTMAN, Jerald Harder, and George Lawrence

The Total Solar Irradiance Mission, TSIM, is a satellite to be launched in 2001 as part of the Earth Observing System (EOS). The scientific payload will consist of two instruments, one to measure the Total Solar Irradiance (TSI) and the second to measure solar spectral irradiance in the range 200 nm to 2 mm. This paper describes the Spectral Irradiance Monitor, SIM, which is a prism spectrometer capable of covering the full spectral range 200 nm to 2 micron with a resolving power greater than 30. The optical design is a variant of a prism spectrometer first described by Fery in 1910 - the prism has a concave front surface and a convex, aluminized rear surface, and is therefore self-focusing. The absolute detector is a miniature, electrical substitution radiometer (ESR) with operation similar to the TIM detector described in the accompanying paper. The SIM is double redundant and self-calibrating. We plan to achieve an absolute accuracy of 0.3% (3s), and a precision and long-term relative accuracy of 0.01% per year. Details of our present understanding and characterization of the SIM will be provided.

JSA17 Wednesday 21 – Thursday 22 July

## MANTLE-CORE STRUCTURE, PROPERTIES, COUPLING, AND THE GEODYNAMO (IAGA, IASPEI, IAVCEI, SEDI)

Location: Muirhead Tower, G08 LT

Wednesday 21 July PM

Presiding Chair: G. Helffrich (Dept. of Geology, Univ. Bristol, UK)

JSA17/W/12-A3 1400

## CONSTRAINTS ON ELECTRICAL CONDUCTIVITY IN D''

Stephen GOOZOVAT and S.R. Dickman (Department of Geological Sciences and Environmental Studies, State University of New York at Binghamton, P.O. Box 6000, Binghamton NY 13902-6000 USA, email: dickman@bingvmb.cc.binghamton.edu)

Earth rotation studies in the past two decades have generally assumed zero axial coupling between the core and the mantle on time scales of less than a year. A recent study (Dickman & Nam 1995) comparing observed and predicted tidal changes in the length of day concluded that axial core-mantle torques are not likely to exceed  $3 \times 10^{18}$  Nm on a nine-day time scale. We are attempting to use this upper bound to constrain the electrical conductivity of the lower mantle. At these time scales, we expect our constraints to apply to the lowermost few tens of kilometers of D''.

In our approach we derive the field, H9, induced at the core-mantle boundary by the main field as the tidally deformed mantle periodically accelerates. On such time scales the diffusion of the induced field can be neglected. The axial torques produced by the interactions of H9 with the main field are then calculated for various epochs, for a variety of lowermost mantle conductivities. Our analysis will allow us to draw conclusions about the range of conductivities consistent with rotational observations.

JSA17/C/GA1.19/W/09-A3 1420

## ABOUT THE ELECTRICAL CONDUCTIVITY OF THE LOWER MANTLE

Mioara Manda ALEXANDRESCU (Institut de Physique du Globe de Paris, 4 Place Jussieu, 75252 Paris Cedex 05, France, email: mioara@ipgp.jussieu.fr); Dominique Gibert (Géosciences Rennes - CNRS/INSU, Université de Rennes 1, Bât. 15 Campus de Beaulieu, 35042 Rennes cedex, France, email: gibert@univ-rennes1.fr); Jean-Louis Le Mouél (Institut de Physique du Globe de Paris, 4 Place Jussieu, 75252 Paris Cedex 05, France, email: lemouel@ipgp.jussieu.fr); Gauthier Hulot (Institut de Physique du Globe de Paris, 4 Place Jussieu, 75252 Paris Cedex 05, France, email: ghulot@ipgp.jussieu.fr); Ginette Saracco (Géosciences Rennes - CNRS/INSU, Université de Rennes 1, Bât. 15 Campus de Beaulieu, 35042 Rennes cedex, France, email: saracco@univ-rennes1.fr)

It has recently been proposed that geomagnetic jerks observed at the Earth's surface could be viewed as singularities in the time behaviour of the geomagnetic field with a regularity of about 1.5 when wavelet-analysed. In the present paper we note that such a signal should have suffered some distortion when diffusing from the core-mantle boundary (CMB) through the conducting mantle. Assuming that the upper mantle is an insulator, and given the electromagnetic time constant of the mantle, we compute the distortion that a pure singularity introduced at the CMB suffers as it traverses the mantle. We compute this distortion through its effects on the so-called ridge functions extracted from the wavelet transform of the signal. This distortion is very similar to the small but significant one that we observe in real data. We therefore speculate that jerks must have been pure singularities at the base of the mantle and infer an average estimate for the mantle electromagnetic time constant from the way the signal is distorted by fitting the synthetic ridge functions to the experimental ones. Assuming, for example, a thickness of 2000 km for a uniform lower conducting mantle, we find an electrical conductivity smaller than 10 S/m. This value is in reasonable agreement with values derived from high pressure experiments for a silicate mantle.

JSA17/W/05-A3 1440

## GEOMAGNETIC SECULAR VARIATION IN THE ANTARCTIC REGION AND THE 1969.5 PULSE

GIANIBELLI, Julio C. (Dep. of Geomagnetism and Aeronomy, Faculty of Astronomical and Geophysical Sciences, La Plata University, Paseo del Bosque s/n, 1900 La Plata, Argentina, email: jcg@fcaglp.fcaglp.unlp.edu.ar)

The distribution of the South Hemisphere magnetic observatories in the antarctic and subantarctic region is heterogeneous. The trend in the vertical component of the magnetic field is positive, with the exception of two observatories, opposed longitudinally (Las Acacias-LAS and Canberra-CAN). The isoporic charts, previous and posterior to the field pulse about 1969.5, are showed. There are two isoporic foci in front to the Sanae Observatory, between 60° and 70° latitude and 0° and 330° longitude. The Walker and O Dea techniques to determine the magnetic field pulses are analysed.

JSA17/W/08-A3 1500

## THE RAPID DIFFUSION OF POLOIDAL MAGNETIC FIELD IN 3-D INHOMOGENEOUS MANTLE WITH GRADUALLY LATERAL VARIATION

Ma Shi-ZHUANG (Institute of Geophysics, Chinese Academy of Sciences, Beijing 100101, China, email: szma@c-geos.ac.cn)

In order to understand the magnetic field at core-mantle boundary, we have to continue down the observational data of geomagnetic field through conducting region of lower mantle. Had considered the limitation on variable scale from study of the Earth's deep interior, the author built a perturbation theory of electromagnetic field in 3-D inhomogeneous mantle with gradually lateral variation. It is unnecessary that the 1-D spherical symmetric distribution of the zero-degree approximation. As a direct application of the zero-degree approximation, it is presented how the gradually lateral variation of electric conductivity effect on anti-diffusion of poloidal magnetic field come from the outer core of the Earth.

JSA17/E/04-A3 1540

## PALEOMAGNETIC FIELD IN THE NEOGEA (~1700 MA) AND THE RELATIONSHIP BETWEEN PROCESSES NEAR THE EARTH'S CORE AND SURFACE

D.M.PECHERSKY (United Institute of Physics of the Earth, Ac. Sci., Russia)

The data on changes in geomagnetic field reversals, intensity and direction, organisms, and velocities of continental plate movements during the last  $\approx 1700$  m.y. are collected and analyzed. The following regularities were revealed: 1) long-term intervals of the steady field state with very rare reversals, spaced by 160-200 m.y. (a fractal dimension of about 0.9-1.0); 2) nearly chaotic field state, characterized by frequent reversals (a fractal dimension of 0.5-0.6); 3) in the first regime, the latitude dependence of variations in both intensity and direction are typical of dipole field, whereas in the second regime this dependence is different; 4) generally, the geomagnetic field exhibits no periodicity in its intensity, direction, and reversals throughout the Neogea: (a) in 95% cases, the "periods" consisted of only one or two oscillations, (b) oscillations of all geomagnetic elements with similar periods are commonly asynchronous, and (c) the "periods" often decrease or increase smoothly in time. The comparison of geomagnetic field pattern, on the one hand, and changes in the organic world and continental plate velocities, on the other hand, shows that either processes near the Earth's core and surface are synchronous ( $\pm 10$  my) or processes of the second group lag behind those of the first group (by  $40 \pm 20$  my). The first case implies the presence of an "external" mechanism with a characteristic time comparable with geological periods, the changes of the second group are due to an "internal" mechanism with a characteristic time comparable with geological eras. The value of this lag corresponds to a velocity of 4-10 cm/yr (this is the velocity of energy transfer from the mantle bottom to the Earth's surface). This value is in accordance with mean velocities of continental plate movements. However, there is no causal relation between the aforementioned processes. In Neogea, two time intervals are revealed that are characterized by specific behavior of all characteristics analyzed: (1) Phanerozoic-Riphean boundary interval and (2) Middle Riphean.

JSA17/W/06-A3 1600

## DOES THE GEOMAGNETIC SECULAR VARIATION ANTICIPATE OR CORRELATE WITH DECADE LENGTH OF DAY VARIATIONS?

Alexandra PAIS, Gauthier Hulot and Mioara Manda Alexandrescu (Institut de Physique du Globe de Paris, 4 place Jussieu, 75252 Paris Cedex 05, France, email: pais@ipgp.jussieu.fr)

In recent years, it has been pointed out that a secular variation indicator such as the secular variation of the declination in Europe, could be used to predict future changes in the length of day on decade time scales, because it essentially anticipates these changes by some 10 years (e.g. Le Mouél et al., 1992). In parallel, numerous studies have also shown that the secular variation could be used to compute core surface flows and to consequently predict, with no significant time delay, the instantaneous changes in the length of day (Jault et al., 1988, Jackson et al., 1993, Pais and Hulot, 1999). The present paper has two main purposes. One is to confirm the validity of both analyses, which is done by relying on a uniform set of annual means of geomagnetic field components for the period 1964-1996. The other one is to propose a simple explanation for the fact that the same magnetic data can be used to produce indicators that in one case anticipate and in the other correlate with no significant time offset the series of observed LOD decade variations. It will be argued that the reason for this is that the local value of the SV (hence of the SV of D) is mainly sensitive to the dominant non zonal core flows, which are responsible for the axial pressure torques acting on the mantle, while LOD instantaneous predictions (derived from core flows computations) are based on the weaker (but resolvable) zonal flows which reflect the dynamical, hence delayed, reaction of both the core and the mantle.

JSA17/E/01-A3 1620

## A NEW TOMOGRAPHIC MODEL OF D'' SHEAR VELOCITY AND ITS IMPLICATIONS

B. Y. KUO (Inst Earth Sciences, Academia Sinica, Taipei, Taiwan, ROC, email: byk@earth.sinica.edu.tw); E. J. Garnero (Berkeley Seismological Lab., University of California, Berkeley, CA 94720-4750, USA, email: eddie@seismo.berkeley.edu); T. Lay (Inst Tectonics, University of California, Santa Cruz, CA 95064, USA, email: thorne@es.ucsc.edu)

More than 1500 S-SKS times, tailored to reduce uneven sampling, yield a global image of D'' shear velocity variations that is robust up to degree 12. SKS-S times at distances beyond 95 degrees primarily sample the D'' region, with suppressed contributions from uncertainties in source location, origin time and upper mantle structures. We parameterise D'' shear velocity perturbation with (1) spherical harmonic functions and (2) equal-area blocks, and show that they yield practically indistinguishable results. Synthetic simulations demonstrate that a high degree (L) inversion followed by a low degree (L1) synthesis effectively filters out components most biased by the expansion truncation, and that the global maximum resolution supported by the geometry and quality of the present data set is not much higher than degree 12. Degree 12 models are constructed by performing inversions with  $L > 12$ , regularised so that when synthesised to  $L_1 = 12$  the rms magnitude is 1%. In our preferred model ( $L = 40$ ,  $L_1 = 12$ ), most surface hotspots and almost all of the "roots" of the hotspots in the lower mantle as predicted by global flow modelling are located in low velocity regions. Three strongly negative patches ( $< -2\%$ ) punctuating the Atlantic-Indian low velocity zone seem to be affiliated geographically to three separate groups of hotspot roots, and the Pacific corridor hosts dozens of S. Pacific plumes. Although there is no intrinsic difference in resolvability, parameterisation (1) is a better representation for long wavelength signals but (2) is more flexible for imaging small scale structure. To exploit regional high resolution and recover fine structure where the data permit, we remove the degree 12 aspherical reference model from the data and invert the residuals using 10 degree blocks. The hybrid model preserves robust power at low degrees on a global scale and at high degrees for regions where constraints are better than the global average.

**JSA17/E/05-A3 1640**

**AMPLITUDE OF CORE MANTLE BOUNDARY TOPOGRAPHY INFERRED FROM A STOCHASTIC ANALYSIS OF CORE PHASES**

Raphael Garcia (Observatoire Midi-Pyrenees and ENS Lyon, email: garcia@pontos.cst.cnes.fr); Annie SOURIAU (CNRS, Observatoire Midi-Pyrenees Toulouse, email: Annie.Souriau@cnes.fr)

In order to constrain the topography of the core-mantle boundary (CMB), which is an important parameter for Earth dynamics, we performed a stochastic analysis of the different core phases (PcP, PKP and PKKP), which sample the CMB as transmitted and/or reflected waves. Of particular interest is the underside reflected phase PKKP, which help discriminate between CMB topography and D" structure, and which has in addition a great sensitivity to the CMB topography at the underside reflected point. The analysis is performed on the travel time residuals of relocated events provided by Engdahl et al. (1998), with an additional set of 260 PKKP data of various origins. The estimated CMB topography variance has a significant signal in the 2-10 degree wavelength range we investigated, with root mean square of 2.2 +/- 0.2 km for wavelengths larger than 2 degrees. Despite a poor Earth sampling, interesting correlation are observed with mantle structure. In particular, mantle velocity heterogeneities and CMB topography variations are correlated, as expected from most geodynamical mantle models. Moreover, CMB topographic lows of 1-2 km are observed in regions 250-500 km wide below hotspots. A tentative inversion of CMB topography has been performed in the best sampled areas, i.e. those which are sampled by both underside reflected rays and transmitted rays.

**JSA17/W/03-A3 1700**

**ON THE SHORT SCALE TOPOGRAPHY OF THE CORE-MANTLE BOUNDARY**

Clement NARTEAU, Jean-Louis Le Mouel, Jean-Paul Poirier, Mikael Shirman (Institut de Physique du Globe de Paris 4 Place Jussieu, 75252 Paris cedex 05 France, email: narteau, lemouel, poirier, email: shnirman@ipgp.jussieu.fr)

We used a two-dimensional cellular automata method to study the short-scale roughness of the CMB. We consider the dissolution of the silicate rock of the lower mantle into the liquid iron of the core infiltrated along grain boundaries. We assume that a cubic centimetre of solid rock is dissolved in average in a time  $T_d$ , and we consider also the reverse process of crystallisation (with a time constant  $T_c$ ). We thus obtain a quasi steady-state depth for the CMB. We model three states in the cellular automata, according to the concentration of mantle material: solid (mantle), liquid, and saturated liquid. The evolution of the roughness of the interface is controlled both by diffusion of the dissolved elements and by their concentration in the upper outer core. We study the characteristic values of  $T_d$  and  $T_c$  in function of the intensity of the mixing process (buoyancy, force, diffusion) and the relationship between these time constants and the roughness of the CMB.

**Thursday 22 July AM**

Presiding Chair: G. Hulot (Institut de Physique du Globe, Paris, France)

**JSA17/W/15-A4 0930**

**CORE MOTIONS AND GEOMAGNETIC IMPULSES**

Mioara Manda ALEXANDRESCU (1), Minh Le Huy (2), Alexandra Pais(1), Jean-Louis Le Mouél(1) and Gauthier Hulot(1) (1) Institut de Physique du Globe de Paris, 4 Place Jussieu, 75252 Paris cedex 5, France, email: mioara.pais, lemouel, gh@ipgp.jussieu.fr); (2) Hanoi Institute of Geophysics - NCST, Nghia da - Tu Liem - Hanoi, Vietnam, email: lhmhinh@ipg.ncst.ac.vn)

The knowledge of geomagnetic field and its secular variation allow to compute the flow at the core surface. The poloidal and toroidal components of the fluid flow at the core-mantle boundary (CMB) at 50-year intervals have been calculated from different models over the last three centuries. The average motion on 300 years appears to be for the main fact symmetrical with respect to the equator. To time constant of degree 1 component of the motion is much larger than the time constant of the rest of the flow. We have also computed the acceleration field corresponding to the well-documented jerks of 1969, 1978, 1991. The geometry of these acceleration fields is the same, within a change of sign, for the three events. Moreover, this geometry has close connection with the geometry of the flow. In fact, the flow displays a kind of oscillation - non-sinusoidal - whose apexes are located at the jerk times. The corresponding mechanism and the effect of length of day oscillations are discussed.

**JSA17/W/13-A4 0950**

**FLUCTUATIONS OF THE PALAEOMAGNETIC FIELD: MANIFESTATIONS OF TIDALLY FORCED ELLIPTICAL INSTABILITY OF THE EARTH'S FLUID OUTER CORE?**

Behnam Seyed-Mahmoud, Keith ALDRIDGE and Gary Henderson (Dept. of Earth and Atmospheric Science, York University, Toronto, Canada; email: behnam@yorku.ca, keith@science.yorku.ca, gary@unicaat.yorku.ca)

The observed fluctuations in the intensity and inclination of the palaeomagnetic field over several thousand years (Laj and Kissel, 1999) may be due to a fluid instability excited in the Earth's outer core by the elliptical deformation produced in the mantle by the semi-diurnal tide. Our understanding of the elliptical instability derives not only from laboratory observations, but also from computations to predict the growth rate and velocity field at its onset. We have excited an elliptical instability in a rotating fluid shell through an elliptical distortion of its flexible inner boundary. Observations of the instability, and of the transition to turbulence that follows its onset, have been made using digital particle imaging velocimetry (DPIV). While the boundary distortion is applied continuously, two-dimensional Fourier transforms over a small region of the fluid show that the instability cycles through growth and decay. Laboratory observations show that, for a fluid shell with the same proportions as the Earth's outer core, the maximum growth rate of the fundamental instability occurs when the boundary distortion has a slight prograde rotation, close to that of the moon's orbit around the Earth.

**JSA17/C/GA1.19/W/11-A4 1010**

**SECONDARY FLOW INDUCED IN A FLUID CAVITY BY THE PRECESSION OF THE SPHERICAL CONTAINER**

Jérôme NOIR, Dominique Jault, Philippe Cardin (LGIT Grenoble, France)

They are already a few experiments on the flow in a rapidly rotating and processing spheroidal cavity (Malkus 1968, Vanyo et al 1995). The primary response was a solid body rotation. Superimposed on this main flow is a set of cylinders with alternatively positive and negative vorticity, aligned with the mean bulk rotation vector. We have endeavoured to understand better this geostrophic response. We began our study by the spherical case. Using the analytical determination of the solid body rotation by Busse in 1968, we investigate

numerically the viscous flow. For small rate of precession, the secondary flow is dominated by inertial-waves spanned by the boundary layer. Increasing and decreasing the viscosity we find critical values for which a geostrophic flow, similar to the cylinders observed experimentally, dominates the viscous response. We still discuss how results translate to the finite ellipticity case.

**JSA17/W/01-A4 1030**

**RESONANCES BETWEEN THE FREE-CORE-NUTATION AND THE SOLAR TIDAL WAVES IN THE GEOLOGICAL PAST**

GREFF-LEFFTZ Marianne (I.P.G.P., 4 place Jussieu, 75252 Paris Cedex 05, France); Legros Hilaire (E.O.S.T., 5 rue R. Descartes, 67084 Strasbourg Cedex, France)

We demonstrate how the knowledge of the temporal evolution of the terrestrial crust, the secular deceleration of the axial rotation of the Earth and the rotational eigen-mode of the core, may be inter-related, and how they can provide some information about the geodynamical history of the Earth. From the theory of the Earth's rotation for a simplified three elliptical layered Earth (mantle, fluid outer-core and solid inner-core), we compute the nearly-diurnal rotational eigenmode  $\lambda$  of the core. This mode can be excited by the solar tidal forces and its period varies weakly with time depending on the axial component of the rotation vector, and on the evolution of the size of the inner core. For models of secular deceleration of the Earth and of temporal evolution of the inner-core radius, we compute the dates of exact resonance in the geological past, between the nearly-diurnal luni-solar tidal waves and  $\lambda$  and we investigate, at these dates, the amplitude of the oscillations of the core and the dissipative frictional power at the fluid core's surface (Core-Mantle Boundary and Inner-Core Boundary). Finally, we discuss the influence of such a heat flux from the core at the CMB on the thermal D' layer, i.e., on the generation of deep mantle plumes, and on the dynamo processes within the fluid core, and we propose some correlation with surface observations.

**JSA17/C/GA1.19/W/07-A4 1050**

**GLOBAL MAGNETIC ANOMALIES AND FOCUSES OF A GEOMAGNETIC SECULAR VARIATIONS IN THE TERMS OF ROSSBY HYDRODYNAMICAL VORTICES**

Vladimir V. KUZNETSOV (Institute of Geophysics SB RAS, Koptyug av., 3, Novosibirsk 630090, Russia, e-mail: kuz@uigm.nsc.ru)

A model is offered in which global magnetic anomalies (GMA) and focuses of geomagnetic secular variation (FSV) are considered as sources that are quasi-independent from the source of main dipole magnetic field of the Earth. The GMA arise and exist as shallow-water Rossby hydrodynamical vortices in well-conducting medium of F-layer penetrated with outer magnetic field. It is possible if the thickness of F-layer is much less than the vortices sizes. The Canadian, Siberian and Antarctic GMA are anti-cyclonic vortices, and, on the contrary, the Brazilian GMA is cyclonic vortex. These vortices do not drift staying put not less than 12 Ma. But the FSV vortices drift along the equator westwards deflecting to the poles and then disrupt. Some hydrodynamic parameters of the F-layer substance are obtained from the drift velocities of FSV. The viscosity of F-layer substance is estimated as 107 Pa. The vortices of GMA are similar to Rossby vortices inside the atmospheres of large planets where the cyclone-anticyclone asymmetry is observed as well as in geomagnetic field.

**JSA17/C/GA1.19/W/10-A4 1130**

**EFFECT OF THE STRATIFIED OCEAN OF THE CORE UPON THE CHANDLER WOBBLE**

Stanislav I. BRAGINSKY (Institute of Geophysics and Planetary Physics, UCLA, Los Angeles, CA 90095, USA, email: sbragins@igpp.ucla.edu)

It is supposed that a stable stratified layer exists at the top of the fluid core; we call it the Stratified Ocean of the Core (SOC). The assumed model of the SOC has a sharp density drop on the boundary with the bulk of the core, and a homogeneous internal density gradient. The influence of the SOC upon the Chandler wobble is considered. It is shown that the action of Archimedean forces in the SOC creates inside this layer an additional fluid velocity of order of  $(C/2f)v$ . Here  $C$  is a relative density deficit in the SOC,  $v$  is velocity associated with the Chandler wobble without the SOC, and  $f$  1/400 is a frequency of Chandler wobble measured in cycles per day. The effect of the SOC on the Chandler wobble is small: it increases the period of the Chandler wobble by 1 day, and its contribution to the dissipation of the wobble energy is about four orders of magnitude smaller than the observed dissipation. A change of seismic velocity in the SOC due to a greater concentration of the light admixture is discussed. A comparison of conditions in the SOC with the conditions at the inner core boundary shows that an extra amount of the light fluid in the layer increases the seismic velocity; therefore, the SOC is a higher-velocity layer.

**JSA17/C/GA1.19/W/02-A4 1150**

**DIFFERENTIAL COOLING OF A HIDDEN ATMOSPHERE OF THE CORE**

John LISTER (Institute of Theoretical Geophysics, DAMTP, University of Cambridge, Silver St, Cambridge CB3 9EW, UK, email: lister@esc.cam.ac.uk)

Stratification of the fluid outer core below the CMB can be produced by a stabilising buoyancy flux across the CMB if either the heat extracted by mantle convection is less than that conducted up the core adiabat or if there is compositional transfer of a light component from the mantle to the core. The heat flux across the CMB is not spatially uniform, since the mantle cools parts of the core more strongly than others. Differential cooling of any stratified core layer would drive thermal winds analogous to the forcing of strong zonal winds in the Earth's atmosphere by the equator-to-pole variation in solar heating. Transport of heat can be achieved only by ageostrophic corrections to a leading-order geostrophic balance. While a geostrophic balance would predict flows which are orders of magnitude stronger than those observed by GSV, the magnetic braking inherent in a magnetostrophic balance reduces the predicted flows to the magnitudes observed and confines them to a shallow region at the top of the stratification. The existence of a stratified layer is thus consistent with the magnitude of GSV, but the frozen-flux assumption may have to be relaxed. If part of the CMB is cooled subadiabatically and part superadiabatically then any stratified region under the subadiabatic patch drains laterally into the adjacent deep superadiabatic convection. By this mechanism, any "Hidden Atmosphere" would drain to a depth of only a few kilometres and would not be significant.

**JSA17/W/04-A4 1210**

**THERMAL CORE-MANTLE INTERACTIONS AND THE GEODYNAMO**

Jeremy BLOXHAM (Department of Earth & Planetary Sciences, Harvard University, Cambridge, MA 02138, USA. Email: Jeremy\_Bloxham@harvard.edu)

Models of the magnetic field at the core-mantle boundary derived from recent and historical



observations reveal certain features in the field that are persistent over the 300 year time interval spanned by the observations. Bloxham & Gubbins (Nature, 1987) proposed that these features may be due to thermal core-mantle interactions: large lateral variations in temperature in the lower mantle (that are inferred from seismic tomography and from models of mantle convection) result in lateral variations in heat flux at the core-mantle boundary which affect the pattern of flow in the core. Indeed, they found some correspondence between the pattern of these features in the magnetic field and seismic tomography. Here we examine this proposal by imposing lateral variations in heat flux at the core surface in a numerical model of the geodynamo. In the simplest case, imposing variations given by just the  $Y(2,2)$  harmonic (with the phase as determined by seismic tomography), we find concentrations of flux at high latitude, symmetrically arranged in each hemisphere at longitudes corresponding to North America and to Siberia, similar to the pattern observed in the historical field models. Adding other harmonics yields other features identified in the field, including the central Pacific flux concentration.

JSA17/E/02-A4

1230

## GRAVITATIONAL LOCKING OF THE INNER CORE AND THE GEODYNAMO

Bruce BUFFETT (Department of Earth and Ocean Sciences, University of British Columbia, Vancouver, BC, V6T 1Z4, Canada, email: buffett@eos.ubc.ca); Gary Glatzmaier (Department of Earth Sciences, UC Santa Cruz, Santa Cruz, CA 95064, email: glatz@emerald.ucsc.edu)

Mass anomalies in the Earth's mantle distort the equilibrium shape of the inner core, producing topography on the inner-core boundary of roughly 100m (peak-to-peak). Gravitational forces on the aspherical inner core are strong enough to lock the rotation of the inner core to that of the mantle. However, relative rotation of the inner core is still permitted if the boundary topography adjusts during rotation to remain nearly fixed with respect to the mantle. Predictions of inner-core rotation from numerical simulations of the geodynamo have previously assumed that the inner core rotates freely in response to electromagnetic torque. In this study we present numerical simulations in which the influences of gravitational forces on the inner core are included. Allowances are also made for viscous relaxation of the inner-core shape. We use these calculations to explore several intriguing possibilities. First, a steady rotation of the inner core relative to the mantle requires persistent electromagnetic stresses on the inner core to overcome the gravitational restoring force. Lines of magnetic force that cross the inner-core boundary is stretched around the inner core, amplifying the azimuthal component of the field. Further amplification arises through the release of compositional buoyancy at the inner-core boundary, which lifts and twists the azimuthal field. The combination of these two effects is liable to produce strong dynamo action at the base of the fluid core. Second, we examine the influence of gravitational locking of the inner core on the dynamics of the overlying fluid motions. Conventional assumptions about the force balance in the outer core suggest that the geodynamo operates in a regime known as the Taylor state, but such a state may not be applicable to the entire outer core when the inner core is gravitationally locked to the mantle. We quantify these effects and make new predictions for the rotation rate of the inner core. We also look for evidence of gravitational oscillations about a steady rotation of the inner core, which would be manifest as changes in the length of day.

Environment Forecasts, 8 D Hui Si, Hai Dian District, Beijing, China, e-mail: linzh@polarmet1.mps.ohio-state.edu), David H. Bromwich and Keith M. Hines (both at Byrd Polar Research Center, The Ohio State University, Columbus, OH 43210, USA, e-mail: bromwich@polarmet1.mps.ohio-state.edu)

A previous observational study found a statistically-significant correlation between East Asian monsoon parameters and 10 years of observed Antarctic sea ice. This fascinating link is re-examined with the much longer record of Antarctic sea ice now available. The SIGRID sea ice data from 1973-1986, SSMR sea ice data from 1979-1987 and SSM/I sea ice data from 1988-1997 are correlated to precipitation records available from 364 stations over China. The sea ice data are also correlated to parameters of the monsoon pressure distribution as suggested by the earlier observational study. While the earlier study used sea ice with distinctive trends in the 10-year record, the present study has a sufficient sea ice record to reasonably capture interannual variations on the order of a decade or less. This new study complements earlier global climate modeling studies with the NCAR CCM2 as well as future modeling studies to be performed with the NCAR CCM3.

JSM18/W/17-A4

1120

## THIS STUDY EVALUATES THE RELATIONSHIP BETWEEN ANTARCTIC SEA ICE AND GLOBAL CLIMATE VARIABILITY

Xiaojun YUAN, Lamont-Doherty Earth Observatory of Columbia University, email: xyuan@ldeo.columbia.edu

This study evaluates the relationship between Antarctic Sea Ice and global climate variability. Temporal cross-correlations between Antarctic sea ice edge (SIE) anomaly and various climate indices are calculated. For the sea surface temperature (SST) in the eastern equatorial Pacific and tropical Indian Ocean, Southern Oscillation index, as well as the tropical Pacific precipitation, a coherent propagating pattern is clearly evident in all correlations with the detrended SIE anomalies (SIE\*). Correlations with ENSO indices imply that up to 30% of the variance in SIE\* is linearly related to ENSO. The SIE\* has even higher correlations with the SST in the tropical Indian Ocean. In addition, correlation of SIE\* with global surface temperature produces two characteristic correlation patterns: (1) an ENSO-like pattern in the tropics with stronger correlations in the Indian Ocean, and the Pacific and North American teleconnection (PNA) pattern in extra-tropics with stronger correlations in North America; and (2) a dipole like pattern in the tropical Atlantic with stronger correlations south of the equator. The SIE\* anomalies in the western Indian Ocean, eastern Pacific and Weddell Sea of the Antarctic polar ocean sectors show the strongest polar links to extratropical climate. Linear correlations between SIE\* in those regions and global climate parameters pass a local significance test at the 95% confidence level. The field significance is evaluated using colored noise that is more appropriate than white noise and shuffled noise. The fraction of the globe displaying locally significant correlations (at the 95% confidence level) between SIE\* and global temperature is significantly larger, at the 99.99% confidence level, than the fraction expected given colored noise in place of the SIE\*. Even so, one would still expect, by chance, to find a large number of significant correlations in any one individual correlation map.

JSM18

Thursday 22 - Friday 23 July

## ATMOSPHERIC AND OCEANIC CONNECTIONS BETWEEN THE POLAR REGIONS AND LOWER LATITUDES (IAMAS, IAPSO)

Location: Chemical Engineering 124 LT

Thursday 22 July AM

Presiding Chair: Robin D Muench (Earth and Space Research, Seattle, USA)

JSM18/E/05-A4

Invited

0940

## CHANGES IN THE NORTHERLY LIMIT OF ANTARCTIC SEA ICE SINCE THE 1930S

Peter WADHAM (Scott Polar Research Institute, University of Cambridge, Lensfield Road, Cambridge CB2 1ER, UK. email: pw11@cam.ac.uk).

A paper by de la Mare (Nature, 389, 57-59, 1997) utilises positional information from whaling ships to hypothesise that the latitude of the Antarctic ice edge retreated southward significantly during the 1960s, by nearly 3 degrees. In the current investigation, other sources of information about the Antarctic ice edge location have been examined, including the work of ships of the Discovery Committee. It has been found that although a southward shift did occur, it was not as great, or as sharply defined, as postulated in the paper. A possible reason for the discrepancy is changing patterns of whaling strategy during the 1960s based on a change in species composition of the prey. The implications of a southward ice edge shift for water mass modification are also discussed.

JSM18/W/05-A4

1020

## INFLUENCE OF THE VARIATION OF POLAR SEA-ICE EXTENT ON THE ATMOSPHERIC CIRCULATION, EL-NINO AND HYDROCLIMATIC REGIME OF THE YANGTZE RIVER BASIN

Gongbing Peng (Institute of Geography, Chinese Academy of Sciences, Beijing100101, P.R.China, email: zhangsh@reis.ac.cn)

Monthly anomalous data of Antarctic sea-ice extent from Jan., 1973 to Sept., 1997 and of Arctic sea-ice extent from Aug., 1901 to Aug., 1995 are used. They are then compared with corresponding data of the atmospheric circulation, El-nino and runoff of Yichang, Hankou and Datong, which represent hydroclimatic condition of upper, middle and lower Yangtze River basin respectively. The influences of the sea-ice extent on them have been revealed by means of cross correlation calculation and synoptic-climatic analysis. Special attention has been paid to the connections of South and North Pacific subtropic highs, sea-surface temperature and trade wind of equatorial East Pacific, El-Nino, Walker and Hadley cells with Antarctic sea-ice and to that of north polar vortex, meridional circulation of Asia, North Pacific subtropic high and El-nino with Arctic sea-ice.

The results show that the influences are significant. Several Synoptic climatic models have been established, dealing with the influence processes. It will be useful to hydroclimatic prediction.

JSM18/W/14-A4

1040

## CORRELATIONS BETWEEN CHINA MONSOON PRECIPITATION AND OBSERVED ANTARCTIC SEA ICE

Lin ZHANG (Department of Polar Research and Ocean Forecasts, National Research Center for Marine

JSM18/W/15-A4

1140

## ECMWF ANALYSES AND REANALYSES DEPICTION OF ENSO SIGNAL IN ANTARCTIC PRECIPITATION

David H. BROMWICH and Aric N. Rogers (both at Byrd Polar Research Center, The Ohio State University, Columbus, Ohio 43210, email: bromwich@polarmet1.mps.ohio-state.edu); Per Källberg (European Centre for Medium-Range Weather Forecasts, Shinfield Park, Reading, U.K., email: per.kallberg@ecmwf.int); Richard I. Cullather (Department of Aerospace Engineering Sciences, University of Colorado, Boulder, Colorado 80309, email: Richard.Cullather@colorado.edu); James C. White (Institute of Arctic and Alpine Research, University of Colorado, Boulder, Colorado 80303, email: jwhite@spot.colorado.edu); Karl J. Kreutz (Climate Change Research Center, Institute for the Study of Earth, Oceans and Space, University of New Hampshire, Durham, New Hampshire. Now at Department of Marine Chemistry and Geochemistry, Woods Hole Oceanographic Institution, MS #25, Woods Hole, Massachusetts 02543, email: kkreutz@whoi.edu)

The El Niño-Southern Oscillation (ENSO) signal in Antarctic precipitation is evaluated using European Centre for Medium-Range Weather Forecasts (ECMWF) operational analyses and ECMWF 15-year (1979-1993) reanalyses. Operational and reanalysis data sets indicate that the ENSO teleconnection with Antarctic precipitation is manifested through a positive correlation between the Southern Oscillation Index and West Antarctic sector (120° W to 180°, 75° S to 90° S) precipitation from the early 1980s to 1990, and a negative correlation after 1990. However, a comparison between the operational analyses and reanalyses shows significant differences in net precipitation (P-E) due to contrasts in the mean component of moisture flux convergence into the West Antarctic sector. An analysis of mean fields related to moisture convergence shows that there are significant differences in the average wind fields between the operational analyses and the reanalyses for the most reliable period of overlap (1985-1993).

Further, it is found that variations in net precipitation in this region are determined more by the structure of the flow pattern than by moisture content. Some of the differences in flow pattern are attributed to an error in the reanalysis assimilation of Vostok Station data that suppresses the geopotential heights over East Antarctica. Reanalysis geopotential heights are also suppressed over the Southern Ocean, where there is a known cold bias below 300 hPa. Deficiencies in ECMWF reanalyses result in a weaker ENSO signal in Antarctic precipitation and cause them to miss the significant upward trend in precipitation found in recent operational analyses. Ice core analyses reflect both the upward trend and ENSO teleconnection correlation pattern seen in net precipitation obtained from operational analyses. This study confirms the results of a previous study using ECMWF operational analyses that was the first to find a strong correlation pattern between the moisture budget over the West Antarctic sector and the Southern Oscillation Index.

JSM18/P/01-A4

1200

## A SEARCH FOR ENSO TELECONNECTION SIGNALS IN THE ANTARCTIC PENINSULA REGIONAL ATMOSPHERIC CIRCULATION AND CLIMATE IN THE AUSTRAL WINTER 1973-93

Steve Harangozo (British Antarctic Survey, Madingley Rd, Cambridge CB3 0ET, UK)

There is an increasing amount of evidence to implicate ENSO in modulating the surface climate in some parts of Antarctica on interannual time scales. The overall importance of ENSO in modulating interannual atmospheric circulation and climate variability is, however, far from clear at present. The way in which the ENSO signal becomes manifest in the Antarctic surface climate record remains an open question. This paper will present preliminary results of a study to detect ENSO signals in the atmospheric circulation and climate in the Antarctic Peninsula region of West Antarctica. The austral winter period (June-August) when interannual circulation variability is greatest is chosen for study. The study makes use of tropical SST data along with numerical analysed atmospheric circulation data.



## INTER-ASSOCIATION

Some of the key findings of this study to date are that: a) considerable variability exists in the winter extratropical atmospheric circulation between different ENSO warm events in the South Pacific/West Antarctica sector, b) the tropical climate/SST state in the central-western Pacific on seasonal time scales differs considerably between one ENSO warm event to the next and c) there is an apparent strongly linear association between seasonal climate/SST behaviour in the tropical Pacific and the South Pacific extratropical atmospheric circulation. These findings will be presented and their relevance for understanding interannual climate variability in the Antarctic Peninsula will be discussed.

### JSM18/E/01-A4 1220

#### INTERANNUAL PERIODICITIES IN ANTARCTICA, WITH COMPARISON TO THE SOUTHERN OSCILLATION

Greig THOMPSON (350 Salen Heights Avenue South, Salem, Oregon, 97302 USA, email: gthomp@cyberis.net) and Charles STEARNS (Space Science and Engineering Center, University of Wisconsin, 1225 West Dayton Street, Madison, Wisconsin 53706, USA)

Climatic data sets from 11 manned Antarctic stations covering the period from 1957 to 1991 were analyzed for interannual variability and possible relationship to the El Niño - Southern Oscillation (ENSO). Time series were constructed by removing the long term individual monthly means, centering and then normalizing by the standard deviation. This was done for surface temperature, pressure, potential temperature, coastal stations temperature average, coastal station pressure average, and the potential temperature difference between Scott Base and Amundsen-Scott station at the South Pole. Single Spectrum Analysis (SSA) uses data adaptive filters to discern quasi-periodic oscillations from noise in a time series. The data adaptive filters used were described by a set of mutually orthogonal vectors determined from the constructed time series under study. These base vectors were not necessarily sinusoidal and could therefore discern nonlinear aperiodic oscillations. The Maximum Entropy Method (MEM) of spectral analysis was used to resolve dominant quasi-periodic oscillations in the constructed time series. The MEM of estimating the spectral density fits an autoregression (AR) model to a series so as to maximize a lack of information (entropy) of the patterns in the time series. SSA indicated that for any one of the station time series at least 4.6% and at most 18% of the total variance was described by anharmonic components with a period between 18 and 59 months. Spectral analysis using MEM resolved dominant quasi-periodic oscillations of 27 and 55 month periods in the SSA-filtered Southern Oscillation Index (SOI), confirming earlier investigations. Temporal changes in the amplitudes of these oscillations coincide with ENSO events. The differenced potential-temperature time series between the South Pole and coastal stations showed interannual oscillations with periods on the order of the ENSO events.

Thursday 22 July PM

Presiding Chair: John Turner (British Antarctic Survey, Cambridge, UK)

### JSM18/W/03-A4 1400

#### SLOW OCEANIC TELECONNECTIONS LINKING THE ANTARCTIC CIRCUMPOLAR WAVE WITH TROPICAL ENSO

Ray G. PETERSON, Warren B. White (Scripps Institution of Oceanography University of California, San Diego La Jolla, California 92093-0230 USA email: rpeterson@ucsd.edu; E-mail: wbwhite@ucsd.edu)

A case study for the period 1982-1994 shows that a major source for the Antarctic Circumpolar Wave (ACW) is in the western subtropical South Pacific Ocean, where interannual anomalies in sea surface temperature (SST) and precipitable water (PrWat) form. Once established, these interannual anomalies, covarying with anomalies in sea level pressure (SLP), move south into the Southern Ocean. These covarying anomalies then propagate eastward around the globe as the ACW through a combination of oceanic advection by the Antarctic Circumpolar Current and ocean-atmosphere coupling (White et al., 1998). The coincidence of interannual anomalies in SST, SLP, and PrWat indicates the extra-tropical ocean and atmosphere are coupled on these time scales. Significant portions of the interannual SST signal propagating eastward around the Southern Ocean as the ACW propagate equatorward into the South Atlantic and Indian oceans, ultimately reaching the tropics in each basin some 6-8 years after appearing in the western subtropical South Pacific Ocean. This constitutes a slow oceanic teleconnection that is unique in climate dynamics, made possible by the continuity of Earth's oceans via the Southern Ocean. In the tropical Indian Ocean, these interannual anomalies propagate eastward and arrive at the Indo-Pacific transition in phase with the ENSO (El Niño - Southern Oscillation) signal in covarying SST and SLP propagating eastward from the Indian Ocean to the Pacific Ocean (Tourre and White, 1997). The interannual SST and PrWat anomalies that appear initially in the western subtropical South Pacific are directly linked with ENSO on the equator through anomalous vertical convection and a regional overturning Hadley cell in the troposphere, the same cell that initiates fast planetary waves in the atmosphere (Sardeshmukh and Hoskins, 1988) that transmit ENSO signals around the southern hemisphere on much shorter time scales.

### JSM18/E/03-A4 1420

#### EVIDENCE OF EL NIÑO-SOUTHERN OSCILLATION IN SURFACE METEOROLOGICAL DATA IN ANTARCTICA

Linda KELLER (Department of Atmospheric, Oceanic and Space Sciences, University of Wisconsin, 1225 West Dayton Street, Madison, Wisconsin, 53706 USA), George WEIDNER and Charles Stearns (both at Space Science and Engineering Center, University of Wisconsin, 1225 West Dayton Street, Madison, Wisconsin 53706, USA)

Meteorological measurements have been routinely made for some 40 years in Antarctica. For about half that period, automatic weather stations (AWS) have provided additional surface measurements at remote locations in Antarctica. Within this time span, there have been four El Niño events - 1982-83, 1986-88, 1991-92, and 1997-98. Signatures of the El Niño events have been observed in the surface meteorological data by several investigators and recently there have been studies concerning the teleconnections between the atmosphere at lower latitudes and the Antarctic atmosphere. Several studies have shown variability in meteorological data (temperature, pressure, precipitation, etc.) is correlated to the El Niño-Southern Oscillation (ENSO) phenomenon. Most of these studies have focused on particular regions of Antarctica. Since the number of surface observing stations has increased dramatically since the major ENSO event of 1982-83, we examine the records at new AWS sites for ENSO signatures along with the now longer record at long established AWS sites. In particular we are interested in comparing the two strong El Niño events of 1982-83 and 1997-98. Previous data indicated the Ross Ice Shelf is anomalously cold just prior to and during the early stages of ENSO events while stations on the high plateau of East Antarctica are anomalously cold during the later phase of the ENSO event. Results from the AWS will be included with observations from manned stations. The AWS data set for 1998 will be completed in the near future.

### JSM18/E/07-A4 1440

#### THE AGULHAS CURRENT SYSTEM: THE INFLUENCE OF EDDIES ON THE TIME-MEAN CIRCULATION DIAGNOSED FROM TWO GENERAL CIRCULATION MODELS

WELLS, N.C. (School of Ocean & Earth Sciences, Southampton Oceanography Centre, Southampton, S014 3ZH, email: ncw@mail.soc.soton.ac.uk), Ivchenko, V.O. (Jet Propulsion Laboratory, N.A.S.A., Pasadena, CA 91109, Best, S.E. (formerly of School of Ocean & Earth Sciences, Southampton Oceanography Centre, Southampton, S014 3ZH)

The Agulhas Retroflection region is analysed in two ocean general circulation models, (FRAM and POP). Both models are able to resolve some of prominent time-dependent features of the region, including the Agulhas rings which are shed off from the Retroflection region. In this paper an analysis of the energy budget over a 5 year period together with a stability analysis are used to determine the relative importance of barotropic and baroclinic instability processes in the two models. It is shown that both models have two quasi-zonal jets, a northerly westward flowing jet and a more southerly eastward flowing jet, which act as the entrance and exits of the Retroflection region respectively. Both jets are shown to be baroclinically unstable, and have growth rates and wavelengths consistent with those observed in both models. It is shown that this instability process is well resolved in the POP model, but is influenced by sub-grid scale viscosity in the FRAM model. The energy budget in POP demonstrates that the westward jet is intensified by reynold's stresses which arise from the eddies in that jet, whilst the eastward jet shows that the reynold's stresses act to diffuse the jet. In both jets the eddies are produced by a mixed barotropic- baroclinic instability, though the baroclinic instability transfers are significantly smaller than the barotropic instability. In FRAM, a similar response is observed.

### JSM18/W/06-A4 1500

#### MODELLING INTERHEMISPHERIC VARIABILITY DUE TO FLUCTUATIONS OF THE THC

Katrin MEISSNER, Holger Brix and Ruediger Gerdes (all at Alfred-Wegener-Institute for Polar and Marine Research, Bremerhaven, Germany, email: meissner@awi-bremerhaven.de)

Freshening of high latitude surface water can change the large scale oceanic transport of heat and salt. Atmospheric perturbations over the deep water production sites thus have a large scale response, establishing a kind of oceanic teleconnection with time scales of years to centuries. In a number of response experiments with a global coupled atmosphere-ocean-sea ice model, we here investigate the connections between northern and southern hemisphere sea surface conditions due to fluctuations of the thermohaline circulation. The atmospheric component of the model consists of the vertically integrated thermodynamic energy and moisture balance equations. The two-dimensional model calculates surface fresh water fluxes and surface heat fluxes over land, sea and ice areas. The sea ice component is a simple thermodynamic model while the ocean component is a full GCM based on MOM2.

### JSM18/W/04-A4 1520

#### HOW FURT STRESS IN THE SOUTHERN OCEAN LINKS WITH SVERDRUP BALANCE IN THE SUBTROPICS

Chris W. HUGHES (CCMS - Proudman Oceanographic Laboratory, Bidston Observatory, Birkenhead, Merseyside L43 7RA, UK, Email: cwh@ccms.ac.uk), and Beverly de Cuevas (Southampton Oceanography Centre, Empress Dock, European Way, Southampton SO14 3ZH, UK, Email: B.Decuevas@soc.soton.ac.uk)

There is a dichotomy in the way the ocean's response to wind forcing is usually interpreted, in which the Southern Ocean is considered quite separately from the rest of the world. The canonical balance for most of the world is Sverdrup balance in which the forcing is due to wind stress curl and interactions with bottom topography are ignored, coupled with viscous western boundary currents. In the Southern Ocean however, it is well established that interactions with the bottom topography are necessary to balance the zonal wind stress by topographic form stress. It will be shown here that this latter balance, which also holds in other ocean basins, implies a 'spin' pressure torque which upsets the Sverdrup balance at some longitude, and balances the wind stress curl in a zonal integral. At lower latitudes the spin pressure torque is concentrated near the western boundaries, producing nearly inviscid western boundary currents. This balance will be illustrated with diagnostics from an eddy-permitting global ocean model (OCCAM)

### JSM18/W/12-A4 1600

#### TIME-AVERAGED SUBANTARCTIC CYCLONIC ACTIVITY AS REVEALED IN A FOUR-DECADE REANALYSIS

Ian SIMMONDS and Kevin Keay (both at School of Earth Sciences, The University of Melbourne, Parkville, Victoria, 3052, Australia, email: ihs@met.unimelb.edu.au)

The high density of cyclones in the subantarctic region are known to be associated with the frequent severe weather conditions experienced over coastal Antarctica and the domain to the north. Such systems are also responsible for a large proportion of the transport of heat and moisture to the polar region effected by the atmosphere. Hence the study and documentation of the behaviour of these systems in the subantarctic is important for a number of reasons, among which is the fact that they form a 'bridge' between the Antarctic and the lower latitudes. We present a new climatology of subantarctic extratropical cyclones. This has been compiled by applying a state-of-the-art cyclone tracking scheme to the 6-hourly NCEP global reanalyses spanning the period 1958-1997. The greatest density of cyclones (exceeding 6 x 10<sup>-3</sup> cyclones (deg. lat.)<sup>-2</sup>) is found south of 60oS in all seasons and in the Indian and west Pacific Oceans in autumn and winter. In general, there is a net creation of cyclones (i.e., cyclogenesis exceeds cyclolysis) north of about 50oS, and a net destruction to the south of this latitude. Having said this, the most active cyclogenesis takes place south of 45oS. The NCEP reanalyses indicate that most SH cyclogenesis occurs at these very high latitudes, and the axis of the maximum lies on, or to the south of, 60oS. This is in agreement with the deductions of many modern studies of SH cyclone behaviour. The region is also host to even greater levels of cyclolytic activity. The presentation will consider measures of the importance and influence (e.g., for eddy fluxes) of cyclonic systems. It is suggested that the 'depth' of a system is a relatively bias-free and useful measure of a cyclone's status and effect on the circulation. The greatest climatological depths are seen to lie at about 60oS, well to the north of the circumpolar trough and of the region of greatest cyclone density.

### JSM18/W/09-A4 1620

#### DIAGNOSIS OF THE EXTRAORDINARY WINTER 1982 - 1983 SEASONAL ANOMALY FORMATION USING CYCLONE CLIMATOLOGY PARAMETERS OF THE GLOBAL ATMOSPHERE

Victor LAGUN, (Arctic and Antarctic Research Institute, 38 Bering str., St.Petersburg, 199397, Russia; e-mail: lagun@aari.nw.ru)

On the base of 1981 -1991 NCEP dataset the global distribution of the extra-tropical cyclone parameters is calculated using original numerical method of spatial cyclone position determination. The estimated parameters include temporal and spatial frequencies, the depth, the cyclone center location and pressure in the cyclone center, the square, the linear size, the shape, the drift velocity, the life time and storm track variability. These parameters are presented as a global distribution as well as integral hemispheric and global estimations. For the winter 1982-1983 of extraordinary weather conditions the seasonal anomalies for mentioned above synoptic climatology parameters are calculated relative to the mean decadal values. Studied decade was characterized by the increasing number of the intensive extra-tropical cyclones, accompanied by the increasing tendency of the surface temperature. The global distribution of the seasonal anomalies for the cyclone frequency, for the cyclone depth and for the drift speed is analysed. Regional features of the seasonal anomalies for Europe, North America and South Atlantic are discussed. The results are compared with the global diabatic energy source/sinks estimations and with the published results of this seasonal climatic event GCM simulations.

Friday 23 July AM

Presiding Chair: Charles R Stearns (University of Wisconsin, Wisconsin, USA)

JSM18/W/01-A4

1640

#### HEMISPHERIC CONNECTIONS WITH TEMPORAL CHANGES IN CYCLONE BEHAVIOUR OFF THE ANTARCTIC COAST

Ian SIMMONDS and Kevin Keay (both at School of Earth Sciences, The University of Melbourne, Parkville, Victoria, 3052, Australia, email: ihs@met.unimelb.edu.au)

We present an analysis of the variability and trends exhibited by many aspects of high southern latitude mean sea level extratropical cyclones during the period 1958-1997. The investigation is undertaken by applying an automatic finding and tracking scheme to the six-hourly 'reanalyses' produced by NCEP. The outcome of this is arguably the most reliable and extensive analysis subantarctic cyclone variability undertaken to date.

The annual average number of cyclones per analysis in the 50-70°S latitude band rose from the start of the period to a maximum of about 17 around 1970. Since then the numbers have shown an overall decline (by about 10%), the counts in the 1990s being particularly low. (Similar behavior was evident when the count was confined to the 30-50°S latitude band.) Least squares best fit to the time series exhibited a significant slopes of -0.58 cyclones analysis<sup>-1</sup> decade<sup>-1</sup>.

The overall structure of the time series of annual cyclone per analysis over 30-50°S and 50-70°S are similar, but their year-to-year changes are shown to be negatively correlated, and hence there tends to be an interannual compensation of cyclones density between the middle and higher latitudes.

A number of modelling studies have suggested that extratropical cyclone numbers may be expected to change under enhanced CO<sub>2</sub>. It is argued that under warmer conditions the specific humidity of the atmosphere increases and hence cyclonic eddies transport (latent) energy poleward more efficiently, and hence fewer are required. The SH mean annual surface temperature exhibits a minimum in the mid 1960s, and a fairly steady rise since then. The time series shows an out-of-phase relationship with that of the SH cyclone numbers and they possess a significant correlation coefficient of -0.79.

JSM18/E/06-A4

1700

#### EXTRATROPICAL INFLUENCES ON INTERHEMISPHERIC ASYMMETRY OF TROPICAL CLIMATE

Anthony J. BROCCOLI (NOAA/Geophysical Fluid Dynamics Laboratory, Princeton, NJ 08542, USA, email: ajb@gfdl.gov)

Evidence from a variety of climate simulations suggests a relationship between the latitude of the intertropical convergence zone (ITCZ) and the interhemispheric temperature contrast. To explore the role of extratropical forcing in this relationship, an atmospheric general circulation model is forced by prescribed sea surface temperatures (SSTs) in the extratropics and coupled to a mixed layer ocean elsewhere. The imposition of SST anomalies of opposite signs in the northern and southern extratropics induces substantial changes in tropical climate. The ITCZ shifts toward the warmer hemisphere, accompanied by tropical anomalies in meridional surface winds. Changes in atmospheric heat exchange between the tropics and midlatitudes are the likely cause of this shift. This linkage between extratropical forcing and tropical climate may be of importance in understanding past and future climates.

JSM18/L/01-A4

1720

#### INTERACTIONS BETWEEN THE LOWER LATITUDE CIRCULATION AND THE ANTARCTIC DURING PERIODS OF AMPLIFIED LONG WAVES

John TURNER (Ice and Climate Division, British Antarctic Survey, Cambridge, UK, email: J.Turner@bas.ac.uk)

Understanding the teleconnections between the Antarctic and lower latitudes is very important in interpreting correctly the global climate signals found in ice cores taken from the Antarctic ice sheets. However, the ice cores contain a wide range of signals from very local climate variations to those associated with the major global cycles. Some of the most pronounced signals are associated with periods of amplified long waves when mild, moist air masses can penetrate well into the interior of the continent giving some of the largest precipitation events found over the plateau. This talk will examine the nature of the synoptic events that can occur during periods of amplified long waves, including the occurrence of major storms in the coastal region, weather systems ascending onto the plateau and rapid warming taking place at interior locations. Selected cases will be presented using satellite imagery, model output, ice core accumulation data and synoptic observations from automatic weather stations. The climatological occurrence of such events will be considered along with their relationship to conditions at lower latitudes.

JSM18/E/04-A4

1740

#### HIGH LATITUDE THERMAL VARIABILITY IN RELATION TO LOWER LATITUDE

Tarzadin ULAANBAATAR (Department of Earth Sciences, National University of Mongolia, email: numelect@maginnet.mn)

A best way to show the climate teleconnection of high and lower latitudes is the creation of climate model covered Earth's surface by simple climatological parameters.

In result of my research works was born a 3D mathematical model of the air temperature regime on and near the Earth's surface. According to this model a thermal field exists near the Earth, i. e. this field includes the troposphere, earth surface and shallow layers of lithosphere, which is called heliogeothermosphere as wishing by Author. It is limited from depth of yearly

thermal influences into the shallow lithosphere to tropopause. In this interval the heliogeothermosphere consists of isothermal surfaces due to decreasing the temperature by atmospheric height. Shape of the heliogeothermosphere is more ellipsoid than Earth's. So, the isotherms cut the Earth's surface at certain geographical latitudes. In order to facilitate calculation we used following approach that we do not account atmospheric turbulence and its chemical content, therefore, the temperature gradient or distance between the isotherms is not changed. The isothermal surfaces show the connection of the high and lower latitudes. Temperature gradient fluctuates only in relation of sea level.

In this paper is presented that at a little fluctuation of the isothermal surface in lower latitudes drives dramatical shift of the geographical, climate and permafrost zones at high latitudes. Furthermore, the nature of thermal regime on and near the Earth's surface by length of daylight, daily and yearly motions of the Earth, terrain height, altitude of sun, geographical latitude and albedo of different objects) are shown in forms of equations and their terms.

JSM18/W/02-A5

Invited

0900

#### DECADAL CLIMATE FLUCTUATIONS IN THE ARCTIC AND CONNECTIONS TO LOWER LATITUDES

Lawrence A. MYSAK and Silvia A. Venegas, McGill University, Dept. of Atmospheric and Oceanic Sciences, 805 Sherbrooke St., W Montreal, QC H3A 2K6 Canada. E-mail: mysak@zephyr.meteo.mcgill.ca

During the past two decades there has been considerable research on identifying the nature and causes of interannual and interdecadal climate variability in the Arctic and high northern latitudes through the analysis of various atmospheric, oceanic, sea ice and hydrologic data sets. With the availability of longer records, it has become clear that the dominant signal of variability in the Arctic and subarctic has a decadal timescale. For example, the time expansion coefficients of the first empirical orthogonal function modes for the sea ice concentration (SIC), sea level pressure (SLP), 500-hPa height and 850-hPa temperature north of 45 degrees each exhibit an oscillatory pattern since the 1960s, with a period of around 10 years.

To further elucidate the nature of this decadal climate oscillation, we performed a combined complex empirical orthogonal function analysis of 40 years of SIC and SLP data which span the Arctic poleward of 45°N. The analysis indicates the over most of the duration of this climate cycle, the ice cover anomalies are created by the atmosphere (i.e., are wind generated), and change through ocean advection. However, it is suggested that during relatively short intervals the atmosphere could respond rapidly to changing sea ice conditions in the Greenland Sea, which results in reversals of the phases of the North Atlantic Oscillation, a familiar climate feature in the winter SLP. The evolving patterns of the SIC and SLP anomalies over the 10-year cycle can be succinctly described in terms of a new feedback, which has remnants of, but is quite distinct from that proposed some time ago by Mysak and his collaborators.

JSM18/W/07-A5

0940

#### CONNECTIONS BETWEEN AIR TEMPERATURE ANOMALIES IN THE ARCTIC AND LOWER LATITUDES: NATURAL AND GREENHOUSE COMPONENTS

N.Ye. KHARLANENKOVA, G.V. Alekseyev, R.V. Bekryayev (Arctic and Antarctic Research Institute, 38 Bering Street, St. Petersburg, Russia 199397, e-mail:alex@aari.nw.ru)

The spatial distribution of air temperature anomalies in the Arctic and adjacent latitudes at strong (exceeding RMS) deviations of air temperature means in the N 85-200 area based on the 1890-1998 data is characterized in the winter by two modes with the opposite in the sign anomalies. During the anomalously warm winter months the positive temperature anomalies occupy the Arctic region being most significant over the adjoining climatic cold sources on the Asian and North American continents whereas the weak negative anomalies are located above the temperate latitudes of the Atlantic and the Pacific Oceans (COWL structure). At strong negative anomalies of mean temperature in the winter negative anomalies are located above the Arctic region and the adjoining continental cold sources while the weak positive anomalies are observed above the oceans (WOCL-structure). Two types in the distributions of surface pressure and geopotential anomalies correspond to such temperature anomalies. In particular, the increase in the pressure difference between the centers of the Azore and Icelandic Highs (the North Atlantic oscillation index (NAO)) is obvious during winter warming with the reverse process occurring during cooling. The climatic signal from the other non-arctic impact on the Arctic atmosphere related to the ENSO phenomenon, is also noticeable, although it is much weaker compared to the NAO signal in the variability of mean winter air temperature at Arctic latitudes with a time scale of 5-6 years. The spectral analysis of relations between the air temperature anomalies in different latitudinal zones of the Northern Hemisphere revealed that both negatively and positively correlated components distributed by the periods of oscillations are present in the series of anomalies. A relative contribution of the former and the latter to the total dispersion of oscillations varies within a year with the positive correlation typically observed at low frequencies and negative at higher frequencies. It is demonstrated that the inverse relation between the air temperature anomalies in the Arctic area and in lower latitudes is mainly caused by the winter air exchange between them whereas the direct relations at low frequencies indicate the influence of global factors primarily of the increase in CO<sub>2</sub> content. The conclusions derived from the analysis of climatic data are confirmed by the analysis of data from long-term numerical experiments using the atmospheric circulation model. This study is supported by the INTAS N 97-1277 Project.

JSM18/W/10-A5

1000

#### A POSITIVE FEEDBACK MECHANISM BETWEEN THE OKHOTSK SEA ICE AND THE ALEUTIAN LOW

Yoshihiro TACHIBANA (JISAO Univ. of Washington, Box 354235, 4909 25 Ave NE Seattle, WA 98195-4235, USA, e-mail: tachi@atmos.washington.edu), Meiji Honda (Institute for Global Change Research/FRSGC, Tokyo, 105-6791, Japan, e-mail: meiji@frontier.esto.or.jp), Tatsuro Watanabe (Japan Sea National Fisheries Research Institute, Nigata 951-8121, Japan, e-mail: tatsuro@jsnf.affrc.go.jp)

We found a positive feedback that the Okhotsk sea ice enhances the Aleutian low while the enhanced Aleutian low also enlarges the sea ice in the Okhotsk Sea, using AGCM and ice-ocean model separately. The AGCMs with the boundary condition of widely covered ice over the Okhotsk Sea, and with that of slightly covered ice, respectively showed enhanced Aleutian low, and weakened one because of the different heat flux from the ocean due to the difference of ice coverage. Using the results of these two AGCMs as the boundary conditions of ice-ocean models in the Okhotsk Sea, we could simulate much larger ice area with the boundary condition of the strong Aleutian low than that of the weak Aleutian low. This ice difference is mainly because of the difference of northwestern wind that brings movement of sea ice toward the southern Okhotsk Sea and that brings cold air advection from Siberia toward the Okhotsk Sea, since Okhotsk Sea is to the west of the Aleutian low. Therefore, once the ice widely covers the Okhotsk Sea, the Aleutian low will be strengthened and this will also rebound upon



## INTER-ASSOCIATION

the ice again. In consequence, the Okhotsk sea ice amplifies the interannual variabilities of both the Aleutian low and the ice itself.

**JSM18/W/11-A5**

**1020**

### ARCTIC IMPACT ON THE NORTH ATLANTIC

MYAKOSHIN O.I., Alekseev G.V., Zakharov V.F. (The Arctic and Antarctic Research Institute Bering St. St., 38, 199347 St. Petersburg, Russia e-mail:alexgv@ari.nw.ru)

The North Atlantic region has a strong influence on Arctic climate, which is transferred through the atmospheric circulation variations connected with the dynamics of the North-Atlantic atmospheric action centers and through variations of the Atlantic water inflow to the Arctic Ocean. For the last 100 years significant natural climate fluctuations were observed in this region such as the warming of the 1930-1940s, the GSA and cooling in the late 1960s-early 1970s accompanied by the sea ice area variations. The climatic phenomenon of the GSA and the related cooling in the North Atlantic in the late 1960s-early 1970s developed under the influence of the increased inflow of freshened polar water and sea ice from the Arctic Ocean [Steffansson, 1969; Dickson et al., 1988; Mysak et al., 1990, S.Hakkinen, 1993]. However, the cause of this increase has not yet been unambiguously explained. An analysis of climatic conditions in the Arctic in the 1950s-1990s and the Soviet oceanographic survey data of the Arctic Ocean in 1955-1979 suggest the increased freshened influence of the Arctic Ocean on the North Atlantic region to be predominantly connected with more intense summer melting of snow, ice caps and sea ice in the Arctic in the late 1950s-1960s. During this period positive summer air temperature anomalies in the Arctic were observed, which were the largest in the Canadian-Greenland region where enormous snow and ice supplies accumulate. Favorable conditions for sea ice melting were observed in the Arctic Basin along with the increased river water flow to the Arctic Ocean. Since summer melting of snow and ice and the summer inflow of river water comprises the major portion of the total inflow of freshwater to the Arctic Ocean, the consequences of the increased summer inflow in the 1950s-1960s was manifested in a significant freshening of the upper layer in the Arctic Ocean in the early 1970s, especially in the region of the East Greenland Current outflow. What are the grounds to suggest a possible recurrence of the climatic scenario of the late 1960s-early 1970s in the North Atlantic? First, this is the increase of the summer air temperatures in the Arctic in the 1990s. Second, this is the increase of the sea ice export through Fram Strait [Vinje et al., 1997] and the increased sea ice cover extent in the West Atlantic in the mid-1990s. Third, there is a tendency for the decreased salinity of the upper layer in the Nordic Seas and finally a conclusion of the mathematical climate theory [Dymnikov, Volodin, 1998] about the similarity of the climatic system response to the natural and external impact.

**JSM18/W/08-A5**

**1100**

### CHANGES OF THE DEPOSITION OF SOLUBLE AND INSOLUBLE AEROSOLS ON EAST ANTARCTIC ICE DURING THE TERMINATION OF THE GLACIAL PERIOD AS RECORDED IN THE DOME SUMMIT SOUTH ICE CORE (DSS), LAW DOME, ANTARCTICA.

Mark A.J. CURRAN, Vin Morgan and Li Jun (Antarctic CRC & Australian Antarctic Division GPO Box 252-80, Hobart, 7001, Tasmania. Australia email: mark.curran@utas.edu.au) Jorgen Peder Steffensen (Dept. of Geophysics, University of Copenhagen, Juliane Maries Vej 30, DK-2100, Copenhagen Ø, Denmark)

Ice cores from polar ice sheets contain a wealth of information on past atmospheric conditions. Stratigraphical profiling of ice core impurities, along with the stable isotope ratio climate proxy  $^{18}\text{O}$ , make it possible to infer changes in the amount and composition of airborne material during past climate changes.

The Greenland ice core records all show that sudden climate oscillations (Dansgaard/Oeschger events) occurred during the last glacial period. The last of these oscillations was the warm Bolling/Allerød period (ca 14,500 B.P. - 12,500 B.P.) which was followed by a period of cold glacial conditions for ca 1200 years (Younger Dryas) before the final climate transition into the Holocene. Some of the fast climatic oscillations have also been recorded in Arctic ice cores, but in Antarctica they appear much less pronounced.

The  $^{18}\text{O}$  record shows that DSS core data extends back through the Holocene and the transition period and into the last Glacial cycle. We present dust (insoluble microparticle) and major chemical ionic species concentrations from the Law Dome Summit core, through the Last Glacial Maximum-Holocene transition period. This data will be compared with records from other Antarctic and Greenland core sites.

**JSM18/P/02-A5**

**1120**

### PARTICLE FORMATION IN THE MARINE BOUNDARY LAYER OVER ANTARCTICA: IMPLICATIONS IN CLIMATE CHANGE

V.K. SAXENA (Cloud-Aerosol Interactions Lab (CAIL), North Carolina State University, Raleigh, NC 27695-8208, U.S.A., email: saxena@eos.ncsu.edu)

We have characterized particle formation during flights (LC-130 aircraft) in the marine boundary layer over McMurdo and during ground based observations at Palmer Station. The following two features were observed at McMurdo: (1) The Aitken nuclei concentration showed a steady decrease up to 300m MSL and then a monotonic increase with altitude, the maximum ( $\sim 1300\text{cm}^{-3}$ ) was recorded at 2,500m MSL. (2) The cloud condensation nuclei (CCN) concentration varied from 50 to  $325\text{cm}^{-3}$ , the minimum occurred at 640 m MSL and the maximum at 830m MSL. At Palmer Station, we observed significantly different particle concentrations during January and February 1994. The January month was characterized by: (i) relatively constant temporal CCN concentrations, (ii) relatively constant equivalent potential temperatures, (iii) partly cloudy skies with respect to wind direction during the daytime, and (iv) winds predominantly from the east-southeast through the Southeast. In contrast, the month of February was characterized by: (i) relatively variable temporal CCN concentrations, (ii) variable equivalent potential temperatures, (iii) variable cloudy to overcast skies with respect to wind direction during the daytime, and (iv) winds predominantly from the northeast, southwest and northwest. Exceptionally elevated CCN concentrations were observed on Jan 17, 19, 20 and Feb 7, 1994 when the cloud base descended to the ground and dissipated under prevailing meteorological conditions. The most spectacular CCN enhancement event occurred on Jan 20 when the CCN concentrations were enhanced by factors of 4 and 7 respectively at 0.25% and 1.25% supersaturation (with respect to water) compared with the pre-event concentrations. Implications of these findings in enhancing the Antarctic cloud cover and its impact on the local radiation budget are discussed.

**JSM18/W/13-A5**

**1140**

### VARIABILITY OF METHANESULPHONIC ACID (MSA) IN A 27 YEAR ICE CORE RECORD FROM LAW DOME, EAST ANTARCTICA

Mark A.J. CURRAN (Antarctic CRC & Australian Antarctic Division, GPO Box 252-80, Hobart, Tas. 7001 Australia, email: mark.curran@utas.edu.au), Katrina L. Phillips (IASOS, University of Tasmania, GPO Box 252-77, Hobart, Tas 7001 Australia), Tas D. van Ommen and Vin Morgan (Antarctic CRC &

Australian Antarctic Division, GPO Box 252-80, Hobart, Tas. 7001 Australia), Anne Palmer (IASOS, University of Tasmania, GPO Box 252-77, Hobart, Tas 7001 Australia)

MSA is an atmospheric oxidation product of dimethylsulphide (DMS), and a component of Antarctic precipitation. DMS is produced by certain species of algae, via the breakdown of the algal metabolite dimethylsulphoniopropionate (DMSP). Antarctic ice core records of MSA thus provide a proxy for biological activity in the Southern Ocean, and a potential source of information on climate variability such as ENSO events and sea ice extent, and other factors influencing biological activity.

A 27 year record of MSA and other trace ions was extracted from a Dome Summit South (DSS) ice core, Law Dome, East Antarctica. The MSA record exhibited a persistent seasonality, with a distinct summer maximum usually flanked by two smaller peaks. This seasonal signal is apparently unique to Law Dome. The smaller peaks appear to occur in spring and late summer (or early autumn). The origin of the smaller peaks will be addressed by considering the seasonal and spatial variation in the source of DMS from the Southern Ocean and transport to Law Dome. The implications of using this MSA record as a proxy for ENSO and sea ice extent will be covered. The potential influence of post-depositional migration of MSA in the ice core record will be discussed.

**Friday 23 July PM**

Presiding Chair: C.R. Stearns

**PANEL DISCUSSION**

**1400**

### HOW DO WE ESTABLISH POLAR AND TROPICAL INTERACTIONS

DAVID BROMWICH, Ohio State University, Columbus Ohio, USA. PETER WADDAMS, Scott Polar Research Institute, Cambridge, UK. IAN SIMMONDS, University of Melbourne, Parkville, Victoria, Australia. LAWRENCE MYSAK, MCGILL University, Montreal, Canada

**JSA19**

**Friday 23 July**

### GEOPHYSICAL MEASUREMENTS RELEVANT TO HYDROGEOLOGICAL PROCESSES AND MODELLING (IAGA, IAHS, IASPEI, IAH)

Location: Muirhead Tower 424 LR5

Location of Posters: 422 LR4

**Friday 23 July AM**

Presiding Chairs: P Tarits (IUEM, Brest, France), D. Hyndman (Univ. of Michigan, East Lansing, USA)

**JSA19/W/06-A5**

**0900**

### GEOELECTRIC STUDIES IN QATAR PENINSULA

Nasser M. HASSAN (Geophysics Dept., Fac. of Sc., Ain Shams Univ., Egypt. e-mail: aboashor@asunet.shams.eun.eg) M. Sh. Diab (Geol. Dept., Fac. of Sc., Menoufia Univ., Egypt) Latifa Sh. Al Naimi (Minst. of Agri. and water Resources, Doha, Qatar)

Twenty seven vertical electrical soundings (VES's) were conducted in Qatar Peninsula. The well - known Schlumberger configuration was chosen and applied with maximum current electrode spacing of 1 Km to detect and estimate thickness of about 200m. Three profiles were constructed dissecting Qatar Peninsula in east, west directions, and comprise parts. From the geoelectric profiles, correlation with subsurface studies dominated lithologic units and their interpretations, an attempt has been made to divide the section into three major units based on the similarities in lithology, well logs and observed sedimentary structures. These units are the dolomite unit (Upper Dammam Formation), the evaporite unit (Rus Formation) and the chalky limestone unit (Umm er Radhoma Formation). Emphasis has been given to the water aquifers in the studied sections. Water quality and suitability for different purposes was also studied.

**JSA19/L/01-A5**

**0915**

### GEOPHYSICAL AND HYDROGEOLOGICAL STUDY TO DELINEATE THE GROUNDWATER AND SUBSURFACE GEOLOGIC STRUCTURES OF THE AREA AROUND THE TENTH OF RAMADAN CITY, EGYPT

Abdel-Rady, Hassaneen, Salah Osman and Tarek Abdel-Hafez (National Research Institute of astronomy and Geophysics, P.O. 11421, Helwan, Cairo, Egypt, email: arghareeb@frcu.eun.eg)

Fifty six vertical electrical soundings have been carried out to evaluate the extension of the Pleistocene aquifer and the geologic structures, which may affect the type of the groundwater. These VESes are interpreted qualitatively and quantitatively. The Pleistocene aquifer in the area is subdivided into four geoelectric zones. The first surface layer is composed of sands and gravels, with relatively high resistivity values and small thicknesses. The second zone is affected by large variations in the resistivity values, which may be due to lithologic variations within this zone. The third zone is considered to be the water-bearing horizon and composed of sands and gravels. The fourth zone is characterized by low resistivity values compared with clays, sandy clays and limestone. The area is found to be affected by about 20 faults, which may affect the extension, the thickness and the type of the groundwater, therefore twelve water samples were collected from the Pleistocene aquifer in the area. The water samples were analyzed to obtain the major anions and cations and also some trace elements to study the effect of the industrial waste products on the groundwater. Pleistocene groundwater aquifer is considered as free to semi-confined aquifer type. It is connected from the bottom by the Miocene formation. At the west the aquifer seems to be in direct connection with the Nile-Delta with limited entrance throughout faulting system, so the freshwater is governed by the flow from Ismailia canal and from the main Nile-Delta aquifer. This aquifer is recharged mainly from the seepage of the water of Ismailia canal and from the Nile-Delta through limited entrance of connection.

**JSA19/W/09-A5**

**0930**

### ESTIMATING AQUIFER PROPERTIES USING CROSSWELL GPR AND TRACER DATA

David W. HYNDMAN, Ruiqing He, and M.S. Phanikumar (Department of Geological Sciences, Michigan State University, East Lansing, MI 48824; email: hyndman@msu.edu)

Non-invasive characterisation methods, such as Ground Penetrating Radar (GPR), have the potential to provide detailed estimates of aquifer properties when used in conjunction with



solute tracer tests. Cross-well GPR tomography can provide detailed slowness and attenuation estimates along planes through an aquifer, however the relation between these properties and hydraulic conductivity is unknown. To address this problem, we are combining geophysical and hydrologic data in a joint inversion to estimate heterogeneous aquifer properties. We are estimating the flow and transport properties for the Schoolcraft aquifer in Southern Michigan, USA. This site is ideal for this investigation because a large number of direct hydraulic conductivity measurements were taken, which enables us to compare our parameter estimates with measured values. In addition, knowledge of heterogeneous conductivity values is useful for optimal remediation design at the site. At this site, joint geophysical and hydrologic inversion methods enable us to develop more accurate three-dimensional estimates of flow and transport properties in heterogeneous aquifers.

JSA19/W/13-A5

0945

#### DETAILED VLF-EM AND RMT METHODS APPLIED TO POROUS MEDIA AQUIFERS

K. KENNEDY and I. Müller (Hydrogeology Center, UniNeuchâtel, 11, rue Emile Argand, CH-2007, Neuchâtel, Switzerland, email: kkenedy@bigfoot.com)

Detailed Radio Magnetotelluric-Resistivity (RMT 12 to 240 kHz) and Very Low Frequency-Electromagnetic (VLF-EM) geophysical surveys were interpreted to characterize high permeability porous media depositional environments and paleogeography. Existing historic data for the prolific Seeland aquifer (Switzerland, BE) were too widely spaced to determine differences in important sedimentary structures, erosion surfaces and conductivity resulting from the area's complex peri-glacial history. First, continuous VLF-EM profiles and RMT soundings data identified geologic heterogeneity regionally over 3km at six sites. 1-D VLF-EM profiles showed variable resistivity, underlying aquitard depth and topography at four sites. 2-D RMT data (20m grid) confirmed sediment variability and yielded buried river channels and aquitard patterns. Of two sites with more uniform aquitard depth and topography, one was selected for VLF-EM and RMT (>800 points, 5m to 20m grid, 8000m<sup>2</sup>) measurements. These were used for a 3-D visual model of aquifer thickness (12m to 18 m), channel and ridge structures. Data interpretation showed regions with preferred permeability pathways (high resistivity). Field work took only 3 days and interpretation about two weeks. Wells drilled at 9 locations in the same area, now a ground water research field, confirmed aquifer depth, aquitard nature and consistency. A gravel aquifer resistivity correlation applied to a site flow and transport model will include the structure and permeability from this geophysical characterization combined with borehole and tracer test results. A detailed approach using these rapid, high-resolution RMT and VLF EM methods at regional and site-specific scales is an applicable technique in hydrogeology. Increasing vertical resolution can be done by incorporating recent advances in data interpretation developed jointly with our colleagues at Sopron (HU). In this way, multiple-frequency high resolution data at points can be efficiently interpreted.

JSA19/W/12-A5

1000

#### COMBINED GEOPHYSICAL INVESTIGATIONS FOR MAPPING MAJOR FAULT-BOUNDED DEEP AQUIFERS IN THE VIENNA BASIN

Kay ARIC (1), Kurt Decker (2), Alexander Roemer (3), David K Smythe (4). (1) Institute of Geophysics, University of Vienna, Althanstr. 14, A-1090 Vienna, Austria, email: kayihan.aric@univie.ac.at; (2) Institute of Geology, University of Vienna, Althanstr. 14, A-1090 Vienna, Austria; (3) Geological Survey of Austria, Rasumofskygasse 23, A-1031 Vienna, Austria; (4) GeoLogica Limited, 191 Wilton Street, Glasgow G20 6DF, UK

A combined geophysical approach including seismic and geoelectric measurements, together with gravity data, is used to map a deep aquifer of great economic importance for Vienna. The aquifer is formed by up to 140m of gravels filling the fault-bounded pull-apart Mitterndorf Basin of 50km length and up to 10km width. Pull-apart formation and Quaternary basin subsidence is related to active sinistral strike-slip faulting. The aquifer consists of Quaternary gravel intercalated with conglomerate layers, overlying over consolidated Tertiary shale, silt and sand. Geophysical measurements are used to map the surface topography of the underlying aquitard and to locate hydrologically relevant faults. A 500m seismic reflection profile was observed with dynamite source at a 40m shot and 10m geophone interval, to yield 3-fold subsurface coverage at 5m interval. Strong reflectors are observed at 80, 120, 220 and 380ms TWT. A 100-channel geoelectric profile about 2000m long was also observed with an electrode spacing of 20m. It crosses one end of the seismic profile. This yielded a synthesised expanding Wenner profile with a maximum electrode spacing in the centre of the line of 660m. Apparent resistivities decrease markedly from 400ohm.m at the surface to 10ohm.m at 250m depth. Our geophysical data complement existing 2-D hydrocarbon exploration seismic data which will allow us to map the down-section continuation of potential aquifer bounding faults.

JSA19/L/02-A5

1015

#### SEISMIC EVIDENCE FOR OVERPRESSURE AND FLUID MIGRATION WITHIN THE BARBADOS ACCRETIONARY COMPLEX

Sheila PEACOCK, Nathan Hayward and Graham K. Westbrook (School of Earth Sciences, University of Birmingham, Edgbaston, Birmingham B15 2TT, UK, email: s.peacock@bham.ac.uk)

Seafloor sediments involved in subduction are subject to a rapid increase in lithostatic stress due to forced burial, and to tectonic stress. The clay rich sediments at Barbados are overpressured because of low permeability and release of bound water from clays. Drilling and logging in accretionary complexes are difficult so seismic techniques are used to map porosity and fluid pressure and deduce the likely escape paths of the porewater.

At our site the toe of the Barbados accretionary complex consists of an upper accreted zone of stacked thrust slices, then a thin decollement zone, then an undisturbed zone of sediments riding down (at 20mm/year) with the subducting plate. A 3-D seismic reflection survey has been shot over this area and vertical seismic profiles and P waves from ocean bottom shots recorded in ODP borehole 949C within the 400-m thick accreted zone. We deduced velocity-overpressure relations from well logs to produce porosity and overpressure sections. These show a continuous zone of overpressure ( $\lambda$  - pore pressure/overburden pressure - up to 0.9) in the basal 80 m of the accreted sediments, above the decollement. The zone has low S-wave velocity and high Poisson's ratio (up to 0.477), probably indicating loss of cohesion. Above that, the thrust faults seen in the seismic section appear to act as barriers to flow, dividing the accreted sediments into packets of distinct pore pressure. Reflections from the decollement zone are modelled by a 12.5-m thick low velocity zone indicating porosity about 55% but the anisotropy seen in cores was not resolved.

JSA19/W/10-A5

1100

#### COMBINING GEOPHYSICAL, GEOMORPHOLOGICAL AND HYDROLOGICAL DATA TO INVESTIGATE THE STRATIFICATION OF AN AQUIFER

Gunnar LISCHIED (BITÖK, University of Bayreuth, 95440 Bayreuth, Dr.-Hans-Frisch-Str. 1-3, Germany, email: gunnar.lischied@bitok.uni-bayreuth.de)

Studies of subsurface solute transport and hydrochemical processes require information of the subsurface structure. Geophysical methods have proven their potential for this task. However, additional data are required for calibration. These can be provided, e.g., by drilling cores or borehole logs at a limited number of points. On the other hand, indirect methods provide less detailed, but spatially integrated information. In this paper geomorphological and hydrological data were used to check and to refine the interpretation of ground penetrating radar (GPR) data. The study was performed in a 0.55 km<sup>2</sup> forested catchment in the Steigerwald region, in the south west of Germany. Here biogeochemical processes have been investigated since 1994. The aquifer is about 60 m thick and consists of an interbedding of clayey and sandstone layers of several dm thickness each. To model solute transport, a detailed model of the subsurface structure is needed. To this end, a GPR survey was performed (50 and 200MHz antenna). Penetration depth was about 100ns, corresponding to 10m. Spacing of the survey lines was about 10 - 20m in the central part of the catchment.

Drilling cores were available only down to 3m depth. In addition, geodetic data were used, as the topography reflects the main features of the stratification. The same holds for the spatial and temporal pattern of groundwater discharge into the stream. Measuring discharge along the stream at different dates revealed zones of pronounced groundwater discharge. Finally, the spatial patterns of soil solution, groundwater and stream water quality data were used to check the stratigraphic model.

JSA19/W/07-A5

1115

#### PREDICTION OF HYDRAULIC PERMEABILITY FOR RESERVOIR SANDSTONES AND BASEMENT ROCKS BASED ON FRACTAL PORE SPACE GEOMETRY

Christoph CLAUSER and Hansgeorg Pape (both at: Joint Geoscientific Research Institute, D-30631 Hannover, Germany, email: c.clouser@gga-hannover.de Joachim Iffland (Geological Survey of Mecklenburg-Vorpommern, Pampower Str. 66/68, D-19061 Schwerin, Germany)

Estimating permeability from grain-size distributions or from well logs is attractive but difficult. In this paper we present a new, generally applicable, and relatively inexpensive approach which yields information on permeability on the core sample and on the borehole scale. The approach is theoretically based on a fractal model for the internal structure of a porous medium. It yields a general and petro-physically justified relation linking porosity to permeability, which may be calculated either from porosity or from the pore radius distribution. This general relation can be tuned to the entire spectrum of sandstones ranging from clean to shaly sandstones. The resulting expressions for the different rock types are calibrated to a comprehensive data set of petrophysical and petrographical rock properties measured on 640 sandstone core samples of the Rotliegend (Lower Permian) in northeast Germany. Permeability calculated with this procedure from industry porosity logs compares very well with permeability measured on sedimentary and metamorphic rock samples.

JSA19/W/08-A5

1130

#### 3-D ELECTROMAGNETIC IMAGING AND SELF POTENTIAL MODELLING: HYDROGEOLOGICAL CHARACTERISATION OF FISSURED CRYSTALLINE BEDROCK

Sophie HAUTOT, and Pascal Tarits, (IUEM/UBO, UMR CNRS 6538, Place Nicolas Copernic, F-29280 Plouzané, email: tarits@univ-brest.fr)

In crystalline bedrock geological context, fractured aquifers represent the main groundwater resources. Due to the complex geological structure three-dimensional (3-D) imaging tools are necessary to characterise the geometry of the fractures network. Electrical and electromagnetic sounding techniques are well suited to localise fractures because of the large electrical resistivity contrast between the fresh rock and the fractures in presence of water. Controlled source (EM31) and very low frequency (VLF) electromagnetic soundings were carried out in a test site in Western Brittany (France). The geological context of the area is a crystalline bedrock recovered by a few meters thick weathered layer. The 3-D interpretation of the electromagnetic data allowed us to obtain a 3-D model of the resistivity distribution down to about 50 meters. Our model suggests two structural units: an electrically resistive unit interpreted as a massive crystalline structure, and a conductive unit, interpreted as a fracture network. However, 3-D electromagnetic imaging does not allow determining if localised fractures are hydraulically active or not. A self potential (SP) survey was carried out to characterise the water flow in the weathered layer. The interpretation of the SP data allowed us to determine if the electrically conductive structures can be recharge zones or not. It is demonstrated that one of these structures is an active fracture.

JSA19/P/02-A5

1145

#### DELINEATION OF CORROSIVE GROUNDWATER ZONE USING RESISTIVITY METHOD

L.P. CHOURASIA (Department of Applied Geology, Dr. H.S. Gour University, Sagar, M.P. India)

Corrosion is basically an electrolytic process which severely attacks a metal surface. In order to study the effects of corrosion and incrustation characteristics of groundwater, geochemical methods are generally employed. Corrosive groundwater damages the iron pipes through which it is distributed. The use of resistivity method in corrosion related studies has been done in a part of Chambal-Sind drainage basin to demarcate the zone of corrosive groundwater. It has been correlated with the geochemical data. It is found that resistivity studies help in identifying the corrosive zone of groundwater as well as type of geologic formation and hence help in limiting the depth of well drilling.

JSA19/L/03-A5

1200

#### THE ATTENUATED RADAR WAVE MIGRATION WITH FINITE ELEMENT METHOD DI QINGYUN

WANG miaoyue (Institute of Geophysics, Chinese Academy of Sciences, Beijing, 100101, China)

Up to now, the GPR data is processed by means of the seismic programs. But the high frequency radar waves are different from the seismic waves in dynamic characteristics, it is strongly attenuated in earth media, and the attenuation function must be considered in inversion of ground penetrate radar wave.

First we derive the finite element equations for attenuated radar waves by Galerkin's method, especially give out thoroughly the attenuated coefficients. And second, we finished reverse time migration for no offset and offset GPR data with and without attenuated term. A series of model results show that the migration results are much better after considering attenuation. Two GPR profiles of Dynasty City in Shang Qiu of China are processed using the above method, the resolution of migration profile is improved much more. Our migration program with attenuated term processes one GPR profile for basement detection, the boundary of basement and a possible fault in middle is obvious. It proves that our work provides a possibility to improve the resolution of GPR profile and reliability of geological interpretation as long as the attenuation of radar wave is considered in data processing.

Friday 23 July PM

Presiding Chair: P Tarits (IUEM, Brest, France)

**JSA19/L/04-A5** Poster **1400-01****HYDROGEOLOGICAL AND HYDROCHEMICAL STUDIES ON THE DELTA OF NUWIEBA CITY, SOUTH SINAI**

Abdel -Rady HASSANCEN, Nagy Soliman and Ayman Abdel - Latiff (National Research Institute of Astronomy and Geophysics, P.O. 11421 Helwan Cairo, Egypt email: arghareeb@frcu.eun.eg)

The delta of Nuwieba City comprises Wadi Watier, Wadi Sada El - Sainra and Wadi El Sada El -Bada deltas from north to south. These wadis outlet to the Gulf of Aqaba. In this study thirtytwo drilled and hand dug wells are present in this delta reaching to the aquifer at variable depths. The direction of water flow takes the northwest and southeast directions and the water level decreases at the same direction. In this study ten isoparameters maps are constructed to show the horizontal distribution of the concentration of major cations and anions in the Quaternary aquifer. Hydraulic parameters of the aquifer in the hand dug wells are measured and show transmissivity ranging from 19.2 to 28.5 m<sup>2</sup>/day and storage coefficient ranging from 2.8 X 10<sup>-2</sup> to 4.4 X 10<sup>-2</sup>. The water type in the study area is Mg CL2 type of marine water genesis, except in some wells in delta of Wadi Sada El-Samra and delta of Wadi El-Sada El-Bada it is Na2SO4 type of meteoric water genesis, because it lies at the same main trends of these faults which constructed Wadi Sada El-Samra and Wadi El-Sada El-Bada. The hydrochemical computer program WATEQ was carried out to calculate the saturation indices for all minerals in the water samples. The saturation indices of these minerals are used to elucidate the water-rock and water-mineral interactions phenomena in the studied area. The results of this program, gave 18 minerals for the samples with special concentration according to the chemical characteristics for these samples. These resulting minerals are classified to carbonate minerals, chloride minerals sulphate minerals and hydroxyl minerals according to acidic radical and basic radical. Two hydrochemical profiles were constructed to show the water rock interaction and water minerals interaction, which gave indication that, the concentration of salts increased with water flow direction.

**JSA19/L/05-A5** Poster **1400-02****GEOPHYSICAL STUDIES FOR THE ENVIRONS OF THE ARCHAEOLOGICAL SITE OF ABYDOS AREA, SOHAG GOVERNORATE, EGYPT.**

Abdel-Rady HASSANEEN, El-Said El-Sayed and Mohamed Metwally (National Research Institute of Astronomy and Geophysics, P.O. 11421 Helwan, cairo, Egypt, email: arghareeb@frcu.eun.eg).

The Abydos locality is a famous archaeological site southwest of Balyana town, Sohag Governorate, Upper Egypt. It is located at the western boundary of the agricultural land of the Nile Valley and represents one of the most important holly burial grounds for kings and high court dignitaries in ancient Egypt, and also as a pilgrimage site for the religious Pharaohs for long time. The locality is liable to groundwater hazards on the archaeological burials due to the effect of the nearby agricultural and irrigation activities.

Vertical electric resistivity soundings were conducted. The layer resistivities were calibrated via the available boreholes data and geological information to relate them to the lithofacies units and to construct geoelectric sections across the area. The results helped to construct the isopach map for the Nile silt/clay cap (Holocene), that covers the sandy Pleistocene semiconfined aquifer and also indicated the free groundwater phreatic surface depth, which increases towards the elevated desertescarp.

The resistance geoscaning technique was applied at some localities of Abydos area. This technique proved to be a powerful mean in exploring the area for mapping the subsurface rock inhomogenities. Excavations in the area indicated numerous tombs and temples in many parts of the area. The resistance geoscaning examination of some parts of the unexplored localities is conducted depending on the marked resistance contrast between the buried stone and brick walls and the covering fill of sand, silt and clay.

**JSA19/L/06-A5** Poster **1400-03****SHALLOW GEOELECTRICAL STUDIES FOR PALEOTOPOGRAPHY AND ARCHAEOLOGICAL INVESTIGATIONS AT EL-SIMBELAWEIN DISTRICT, EASTERN NILE DELTA, EGYPT.**

Abdel-Rady HASSANEEN, Mohamed Abdalla and Ayman Taha (National Research Institute of Astronomy and Geophysics, P.O. 11421-Helwan, Cairo, Egypt, email: arghareeb@frcu.eun.eg)

The Middle Pleistocene Pre Nile sediments consisting of clay and silt cover the irregular surface of the Middle Pleistocene sands, as in Tell Timai locality and the environs of Tell Timai and Tell El-Ruba. These localities were covered with 76 Schlumberger vertical electrical sounding stations. Resistivities of the Quaternary sediments were calibrated with the corresponding lithofacies of the available boreholes data in the Eastern Nile Delta. Fourteen geoelectric resistivity cross-sections and eight interpreted resistivity slice maps as well as maps of palaeotopography of the Pleistocene sands and isopach map for the Holocene Nile sediments in the area of study were constructed. Exploration of a wide sand gezira related to the big sand buried ridge in which Tell Timai is located is depicted clearly from the palaeotopography of the Pleistocene sands and from the geoelectric sections. Also, the buried Mendisian Nile branch at the area of study has been traced.

The resistance geoscaning technique using the Geoscan RM-15 Resistance Meter applying the twin configuration was conducted at three sites in Tell Timai to detect the buried archaeological features. However, resistivity mapping using Wenner configuration and the Gga-31 Geoelectric DC-equipment was applied at one site to correlate resistance images with resistivity mapping.

**JSA19/W/11-A5** Poster **1400-04****THE HYDROGEOLOGICAL SECTIONS OF THE NORTH-EASTERN PART OF THE BUENOS AIRES PROVINCE (ARGENTINA), FROM AMT RESULTS**

SAINATO, Claudia M. (Fac. de Agronomía, University of Buenos Aires, Av. San Martín 4453 1417, Buenos Aires, Argentina, email: csainato@ciudad.com.ar) Pomposiello, M. C. (CONICET, Argentina) Landini, A. M. (Fac. de Agronomía, Univ. of Buenos Aires, Argentina) Galindo, G. (Fac. Ciencias Exactas y Naturales, Univ. of Buenos Aires, Argentina)

The shallow aquifers of the north-eastern part of the Buenos Aires Province has been described in previous studies. Free ground water presents good quality at some restricted zones, allowing its use for consumption. The field irrigation requires greater flows of water, perhaps from deeper aquifers.

Below the free groundwater level the aquifers have a multilayer character (Pampeano), with clay-sand sediments with low permeability and an increase of sand component with depth. Previous Audio magnetotelluric and DC soundings have shown an increase of salinity with depth with intercalation of more resistive layers which may be sand or calcareous crust. In this work, more AMT soundings have been performed, increasing the study area, in order

to have a better description of deeper aquifers and the different hydrogeological components of the basin.

The results coincide with previous hydrogeological studies. The Epiparaniana section reaches 170-260m depth, including the Pampeano aquifer with its base between 30 and 100m and the Puelches Formation, below the last one, which has variable thickness and bad quality water. Below this section, the Paranaiana Formation (Green Miocene) with clay and intercalation of sands shows very bad quality water and some resistive layers, perhaps hardpan. The Red Miocene with sandstones and clay is placed beneath the 400-500m.

**JSA19/W/04-A5** Poster **1400-05****HYDROGEOLOGICAL STUDY IN A PART OF THE NILE VALLEY, EGYPT**

Ahmed Mohamed Sobhy HELALY and Ahmed Sayed Ahmed Abu-El-Ata (both at Ain Shams University, Faculty of Science, Geophysics Department, Abbassia, Cairo, Egypt, email:helaly@asunet.shams.eun.eg).

The purpose of this work was to investigate the shallow section of the study area with respect to its groundwater aquifer conditions. That was through the use of the integrated shallow geophysical and some geological data. The subsurface stratigraphy in the study area is ranging from the deep Precambrian rocks up to the most recent Quaternary deposits, while the outcropped geological units are ranging in age from Middle Eocene to Quaternary. There are some detectable contrasts in the physical properties of the subsoil throughout the study area. So, the integrated use of electrical resistivity and gravity methods can be applied to investigate the subsurface lithological and structural manifestations which control the potentiality of the existing aquifer. The gravity method proved to be useful in mapping the buried rock topography and groundwater exploration in some geologic conditions, e.g. the occurrence of groundwater in the sands/gravels of buried stream valleys on the bedrock surface and/or bounded by much less permeable rock types. The gravity data was represented by the Bouguer gravity map which provided information about the general geologic conditions/structures in the study area and made possible estimates of depth to bedrock. The gravity method was devoted mainly to decipher the upper section of the study area that embraces the shallow Quaternary aquifer, through separating the residual gravity anomalies from the regional ones. These residual gravity anomalies have been subjected to further analysis to determine the extension of the water-bearing main aquiferous unit in terms of width and thickness. Furthermore, the probable paleocourse of the Nile River has been aligned. Then, for interpreting a multilayer electrical sounding curve, additional subsurface lithological information from wells/boreholes can be used for solving the problem of equivalence. But in case of absence of such data, the Dar Zarrouk parameters can be used to optimize the initial stages of resistivity interpretation. Such a procedure was...

**JSA19/W/03-A5** Poster **1400-06****INTEGRATION OF ELECTROMAGNETIC, S-P AND MAGNETOTELLURIC METHODS IN HYDROGEOLOGICAL INVESTIGATION.**

Fernando SANTOS, Rita Castro, Rita Nolasco, and Luís Mendes-Victor (Centro de Geofísica da Universidade de Lisboa, R. Escola Politécnica, 58, 1250 Lisboa, email: dfams fc.ul.pt) and Eugénio Almeida (Instituto Piilitecnico de Tomar)

At the Vilarelho da Raia area (northeastern Portugal), the youngest formations are sedimentary of Cenozoic age, having their maximum thickness along the central axis of the NNE-SSW depression. In the same area the oldest formations consist of a schisto-graywacke complex of Siluric age. A combined survey using electromagnetic, self-potential and magnetotelluric methods was carried out to delineate shallow and deep structures associated with the mineral water reservoir in Vilarelho da Raia depression.

The compiled SP and electromagnetic (electrical conductivity) maps correlated quite well with the spatial distribution of the knowledge fracturing. Nine magnetotelluric soundings were acquired in the frequency range of 180 to 0.01 Hz. The data set was analysed using the Groom- Bailey decomposition technique. A two-dimensional model was obtained by inversion of both E and B- polarisation. The geoelectrical structure of the main geological formations as well as the deep features of the main faults were well represented in the model.

**JSA19/W/02-A5** Poster **1400-07****THE STRUCTURE AND EVOLUTION OF THE EASTERN NANKAI TROUGH PRISM AS DERIVED FROM MCS REFLECTION DATA**

Shiguo WU, Narumi Takahashi, Hajimu Kinoshita, Yoshiyuki Kaneda, Izumi Sakamoto (Deep Sea Res. Dept., Japan Marine Science &amp; Technology Center, Yokosuka, 3270061, Japan, Fax: +81-468-5541, email: wushiguo@jamstec.go.jp)

We performed multi-channel seismic investigation during Cruise KH96-02 by R/V Hakuho-mura in 1996. Total 454 km Ggun seismic data has been acquired in order to detect the detailed structure and evolution of the eastern Nankai Trough prism, which is characterised by important active earthquake zone and widely cold seepage activity. Preliminary results show as follows: five deformation units have been divided. The five units are upper slope prism, accretionary basin, lower slope prism, trough and Zenisu Ridge from west to east, respectively. Tokai thrust fault is east boundary of upper slope prism. The fault extended to basement are important lithofacies boundary, which is suggested the Middle Miocene to Early Pliocene subduction zone from the lithofacies distribution and regional tectonics. More recently thrust system occurred between lower slope prism and trough, which express duplicated thrust and began from Late Pliocene. Tectonics of Zenisu Ridge is considered a new following subduction zone by many scientist, but we don't find compression structure in upper layers from seismic profiles. The subduction may happen more east because of collision between Izu-Bonin and Honshu Arcs. Therefore, it still needs more data to detect the possible subduction zone. The decollement surface has varied from west to east. The bend surface is resulted in the new compression by the deep subduction of Zenisu Ridge. The inner facies of the prism over the decollement surface occur slope apron, debris sediment and axial trench wedge sand and silty turbidites derived from the seismic facies. The gas hydrate surface can be seen in the some profiles, with depth variation from 0.4-0.6 sec. (two way time) below the seafloor.

**JSA19/W/01-A5** Poster **1400-08****REINTRODUCTION OF PHYSICS TO HYDRAULIC CONDUCTIVITY MODELING**

I. TCHIGUIRINSKAIA and F. J. Molz (E.E.&amp;S. Dept., Clemson University, 342 Computer Court, Anderson, SC29625, USA, email: iouliat@clemson.edu)

A fairly large body of observational evidence shows that the hydraulic conductivity (K) is extremely variable over a large range of scales. Pioneering attempts to capture the Log(K) variability rely naturally on the simplest scaling model, i.e. fractional Brownian motion. A class of fractal models, based on Levy-stable pdf's, was introduced to capture the 'fat tailed pdf's'. However, all these models could lead the anomalies in the resulting K field, obtained by exponentiation of Log(K). Indeed: (i) a scaling of the log(K) field does not imply in general a scaling of the K field; (ii) finiteness of some or all statistical moments of log(K) does not prevent



the K field from having all statistical moments divergent. We demonstrate that the fundamental condition of positiveness of K fields is naturally supported by an extension of Multifractal Fractionally Integrated Flux (FIF) models. Indeed, we propose an appropriate framework not only to interpretate the results of previous scaling analyses, but also to overcome (without artificial truncation) the fundamental problems, indicated above. Furthermore, we present an anisotropic version of this multifractal model in order to capture and to reproduce the anisotropy of hydraulic conductivity measurements. The theoretical findings are well supported by empirical evidence.

**JSA19/E/02-A5** Poster **1400-09**

#### MODELLING OF SEISMIC EFFECT ON GEOLOGICAL MEDIUM

A.V. MISHIN, T.V. Guseva, Yu.P. Skovorodkin (Institute of physics of the Earth, Russian Academy of Sciences, B.Gruzinskaya, 10, Moscow, Russia, 123810, email: mishin@redline.ru)

For determination of influence of a seismic waves on geologic medium we conducted full-scale modelling. A seismic waves on different geological structures made with the help of large industrial explosions or vibrational effect. The vibrations were carried out by stationary and mobile seismic vibrators on different frequencies. The complex monitoring has allowed to record diverse modifications of deformational, electromagnetic fields and local increments of gravity caused by the artificial effect on crust. The analysis of the results of the observations has shown, that in multiphase mediums there are two kinds of fluid transitions: oscillatory - in porous and translational - in permeable layers. As result of transitions of a liquid component relative to rigid skeleton there are electric currents of electrokinetic nature: variables - on frequency of vibration and quasi-constant - during filtration. During translational fluid movement the modification in space and time of liquid / gas ratio occurs due to a difference in phase velocity of filtration. As the corollary the effective density in the certain sites varies. The development of process proceeds after seismic effect decreasing gradually within several hours, that testifies a restoring an initial condition of a system rigid phase - fluid. We have conducted a number of successful experiments with vibration effects on petroleum deposits.

**JSA19/L/07-A5** Poster **1400-10**

#### METODOLOGY OF HIGH RESOLUTION COMPLEX OF ELECTRO-MAGNETIC METHODS FOR AQUIFERS STUDY

R.TURSUNMETOV Hidroingeo (64 Khodjibayev str. Tashkent, 700041 tel:(998 71) 162 74 68, fax:(998 71) 162 45 53)

Though electro-magnetic methods are for long time used for aquifers investigation, results can not always be used for study of ground water flow's filtration structure. On the other hand, methods developed for study of electro-magnetic properties of environment, connected with the real processes within this environment due to peculiarities of electro-magnetic fields distribution, were not applied sufficiently to the practical tasks resolution. In this connection, special theoretical and experimental investigations were carried out by the scientists of the GIDROINGEO institute in order to develop high resolution complex of electro-magnetic methods for aquifers study. On the base of these results the methodology of electro-magnetic investigations was developed, consisting of two stages. Within the first stage aquifer's lithology is being studied, which forms filtration characteristics of an aquifer. If on electric scanning curves an aquifer is mapped as a whole, it is possible to determine clay particales concentration. Aquifer homogeneity, e.g. availability of high and low resistance layers within the aquifer can be defined by frequency electro-magnetic scanning. Within the second stage electro-magnetic investigations were aimed to filtration characteristics of singled aquifers study. As an electro-magnetic parameters coefficient of electro-magnetic fields' heterogeneity and non-linear parameters of resistance and polarity were accepted, which characterize water flow movement within the porous media. Methodology of electro-magnetic fields space heterogeneity study was applied especially in vertical direction for decoding of environment's filtration properties. Moreover, methodology for determination of non-linear parameter of resistance, which describes interrelations between artificial field and natural electro-magnetic field, caused by ground water movement. Special installations were developed for determination of the electro-magnetic field's ellipse of heterogeneity and non-linear parameters of resistance. Thus, suggested complex permits to study aquifers with high reliability.

**JSA19/L/08-A5** Poster **1400-11**

#### TOWARDS AN INTEGRATED GEOPHYSICAL TECHNIQUES FOR HYDROGEOLOGICAL INVESTIGATION

MORUFFEEN A. Adabanija (Department of Pure and Applied Physics, Ladoke Akintola, University of Technology, P.M.B. 4000, Ogbomoso, Nigeria, email: Adebayo@Ibadan.skannet.com)

The ultimate goal of hydrogeological investigation is the exploration of aquifer. In this work, computer simulation has been designed to integrate the results of the geophysical exploration of aquifers. Templates overlaying approach vis-vis aerial photographs and satellite imagery as reconnaissance tool was used with geophysical borehole logs as reference. For the purpose of this exercise, GIS application package ARC/INFO was used as database for the templates which were obtained by synthesising the findings of the survey into Boolean grid. A new template was obtained by evaluating the resultant Boolean expressions of the overlaid templates. By this approach, the resolution of the images obtained and the capability of revealing subsurface structure was enhanced.

**JSA20** Thursday 22 – Saturday 24 July

#### MESOSPHERE - THERMOSPHERE - IONOSPHERE COUPLING AND ENERGETICS (IAGA, IAHS, SCOSTEP)

Location: School of Education 135LT  
Location of Posters: Conference Room

Thursday 22 July AM

Presiding Chair: J.M. Forbes, (Uni of Colorado, Dept of Aerospace Engineering, USA),

#### IONOSPHERE – THERMOSPHERE – MESOSPHERE INCLUDING VERTICAL COUPLING 1

Introduction **0930**

J.M.Forbes

**JSA20/W/25-A4** Invited **0935**

#### HYDRODYNAMIC TROPOSPHERIC WAVE SOURCES AND THEIR ROLE IN IGW CLIMATOLOGY OF THE UPPER ATMOSPHERE FROM THE MU RADAR OBSERVATIONS

Nikolai M. GAVRILOV (Department of Atmospheric Physics, Saint Petersburg, University, Petrodvorets, 198904, Russia, Email: gavrilov@snoopy.phys.spbu.ru) Shoichiro Fukao (Radio Atmospheric Science Center, Kyoto University, Uji, Kyoto 611, Japan, Email: fukao@kurasc.kyoto-u.ac.jp)

The results of measurements of generation of internal gravity waves (IGWs) in the troposphere by mesoscale dynamical processes with the MU radar are presented. Zonal and meridional horizontal nonlinear advective accelerations are estimated using 8 directions of the MU radar antenna beam. Seasonal variations of the intensity of tropospheric IGW sources are discussed using results of the observations in all seasons. A contribution of IGWs generated in the troposphere into dynamics of the mesosphere and lower thermosphere is considered by comparing the MU radar data with a theoretical model. Possible contribution of IGWs generated in the troposphere at middle and equatorial latitudes to interannual variations of the wave intensity and general circulation of the middle and upper atmosphere over the MU radar is discussed.

**JSA20/E/21-A4** Invited **1000**

#### TROPOSPHERIC EVENTS AND RELATED GRAVITY WAVE ACTIVITY EFFECTS ON THE IONOSPHERE

Petra SAULI, Josef Boska (Institute of Atmospheric Physics, Czech Academy of Sciences, Bocni II/1401, 141 31 Prague 4 - Sporilov, Czech Republic, e-mail: Pkn@ufa.cas.cz)

Short-time variability of the ionosphere was studied during campaigns of rapid sequence (repetition time 5 minutes) ionospheric soundings measured at the Puhonice Observatory (15E, 50N) and partly at the Ebro Observatory (0.5E, 41N) under the low solar and geomagnetic activity conditions with the aim to detect gravity wave activity at various heights and in different ionospheric parameters. The short repetition time of soundings allowed to detect significant gravity activity in the period range of 20-60 minutes. The effects of gravity waves were well expressed in the shape of electron density profile and in the differences between reflection heights at fixed frequencies. These effects display an evident height dependence. Some of the observed gravity wave events seem to be related to strong meteorological (tropospheric) events. Some details concerning the diurnal height dependence of the variation of electron concentration at the levels 150-205 km may be found in poster presented at the same session.

**JSA20/W/32-A4** **1025**

#### DIURNAL-, SEMIDIURNAL- AND PLANETARY-WAVE-PERIOD MODULATION OF GRAVITY-WAVE ACTIVITY IN THE MESOSPHERE AND LOWER THERMOSPHERE

V. St.C. Howells, N.J.MITCHELL, A. G. Beard (The University of Wales Aberystwyth, SY23 3BZ, UK, email: Nick.Mitchell@aber.ac.uk), H.G. Muller (The Royal Military College of Science, Cranfield University, SN6 8LA, UK)

Meteor-radar measurements of winds in the mesosphere and lower thermosphere were made over the UK from June 1989 to October 1994. Although individual gravity waves cannot easily be detected directly, the variance of the velocities is used as an indication of the overall activity of the gravity-wave field. The variances reveal a persistent diurnal cycle in wave activity with a maximum during the morning in winter and during the afternoon in summer. A time-series analysis also reveals occasions where strong modulation of the gravity-wave variance occurs at semidiurnal and planetary-wave periods. The seasonal behaviour of this modulation is investigated and possible mechanisms suggested.

Presiding Chair: A.D. Richmond

**JSA20/E/14-A4** **1110**

#### LUNAR TIDES IN THE MESOSPHERE AND LOWER THERMOSPHERE OVER COLLM

Robert STENING (School of Physics, University of New South Wales, Sydney 2052, Australia, email: R.Stening@unsw.edu.au); Christoph Jacobi (Institute for Meteorology, University of Leipzig, Stephanstr. 3, 04103 Leipzig, Germany, email: jacobi@rz.uni-leipzig.de)

Winds at heights of 85-105 km have been measured at Collm for many years using the D1 total reflection method. Although data are generally available only at night time the least squares analysis method of Malin and Schlapp can be used to extract lunar tides. We have thus been able to derive the mean seasonal variation of the phase and amplitude of the lunar tide in these winds. We have also obtained an estimate of some year-to-year variations which we compare with earlier results from Saskatoon in Canada.

**JSA20/W/51-A4** **1128**

#### THE SEMI-EMPIRICAL MODEL OF THE TURBULENT MESOSPHERE

Anzor R. GVELESIANI (Institute of Geophysics, Georgian Academy of Sciences, 1., M. Alexidze, Str., Tbilisi 380093, Georgia, email: vazha@excite.com)

It is discussed a mechanism of generation of the turbulence in the mesosphere and suggested its original semi-empirical theory with using the method of similarity and analysis of



## INTER-ASSOCIATION

dimensions. On the basis of general values: the rate of viscous dissipation of kinetic energy, the Brunt-Vaisala frequency and the rate of heat turbulent dissipation, - six parameters of fluctuations are obtained. It is established the connections between parameters of inertial subrange and buoyancy subrange and characteristics of maximal sizes of irregularities. It is also discussed the breaking problem of buoyancy waves in the mesosphere and the results of numerical calculations both of turbulent and buoyancy waves parameters in different conditions of geomagnetic activity.

### JSA20/W/22-A4 1146

#### A SPECTRAL STUDY OF PLANETARY WAVES AND TIDAL VARIABILITY: PLANETARY WAVE / TIDAL WAVE-WAVE COUPLING

A.G. BEARD, N.J. Mitchell, P.J.S. Williams (Prifysgol Cymru Aberystwyth, Penglais, Aberystwyth, Ceredigion, SY23 3BZ; email: agb@aber.ac.uk), H.G. Muller (The Royal Military College of Science, Cranfield University, SN6 8LA, UK)

Current theory predicts that a non-linear wave-wave interaction between a planetary wave and a tide should result in cyclical modulation of the tidal amplitude with a period equal to that of the planetary wave. Four and a half years of data from a meteor radar based at Sheffield, UK representing measurements of neutral wind velocity in the meteor region above 53 deg 27 min N, 3 deg 53 min W, are analysed to produce running (dynamic) periodograms to identify both longer-period (2-30 days) neutral-wind oscillations (e.g. planetary waves) and longer-period periodic variability in tidal amplitude measurements. These are used to study the relationship between periodic tidal amplitude fluctuations and contemporaneous, collocated observations of planetary waves. A bispectral analysis is also applied to the neutral-wind time series to identify quadratic non-linear interactions present in the data.

### JSA20/W/34-A4 1204

#### VERTICAL PROPAGATING CHARACTERISTICS OF WAVE OSCILLATIONS (FROM 2- TO 6.5-DAYS) IN THE IONOSPHERE OBTAINED FROM ELECTRON DENSITY PROFILES

David ALTADILL (Observatori de l'Ebre, CSIC-URL, Horta Alta 38, 43520-ROQUETES, SPAIN); Emil M. Apostolov (Geophysical Institute, Bulgarian Academy of Sciences, Acad. G. Bonchev Str. bl. 3, 1113 SOFIA, BULGARIA)

We present the climatology of quasi-periodic oscillations from 2- to 6.5-days in the ionosphere at the altitude range from 170 to 230 km during 1995. We investigate the characteristics of the oscillations from the true height electron density profiles obtained at the Observatori de l'Ebre (40.8N, 0.5E). We show that the oscillations are significant during time intervals when the planetary waves in the mesopause region display maximum amplitudes. We found several wave events of the oscillations, burst type, for which their vertical propagation is manifest in the ionospheric F region. Each event display different degree of dispersion and the observed changes of the electron density as function of the altitude show distinct dominant types of vertical propagation of the waves in the ionosphere. The potential mechanisms linking the planetary wave activity in the mesosphere with the wave events observed in the ionosphere are discussed in order to evaluate the most likely mechanism.

### ANNOUNCEMENT OF POSTERS 1230

### POSTER VIEWING 1235

Thursday 22 July PM

Presiding Chair: R. Sridharan (Physical Research Laboratory, Ahmedabad, India)  
Concurrent Poster Session

### IONOSPHERE - THERMOSPHERE - MESOSPHERE INCLUDING VERTICAL COUPLING 2

### JSA20/L/03-A4 Invited 1400

#### THERMOSPHERE-IONOSPHERE-MESOSPHERE, ENERGETICS AND DYNAMICS (TIMED) MISSION

J.H. YEE (JHU/APL, Laurel, MD 20723, USA, email: jeng-hwa\_yee@jhuapl.edu)

Thermosphere, ionosphere, mesosphere, energetics and dynamics (TIMED) is a NASA mission dedicated to the study of the Earth's mesosphere and lower thermosphere (60-180 km). It is also known that the global structure of this region can be perturbed during solar-terrestrial events, but the overall structure and dynamical responses of these effects are not completely understood. In order to develop and understanding of this complex region, the TIMED mission utilises well-co-ordinated measurements by both satellite-borne and ground-based instruments. Advances in remote sensing technology employed by TIMED enable us to explore this region on a global basis. An overview of the mission and its scientific objectives will be presented, followed by a description of the instruments, remote sensing techniques, and the measurements they will provide. TIMED is scheduled for launch in May 2000 into a 625 km, 72.40 inclination circular orbit. The overall plan for the collaboration with the ground-based observers and the status of its implementation will also be presented.

### JSA20/W/06-A4 1425

#### MESOSPHERIC SOLAR ENERGY DEPOSITION RATES AS DERIVED DIRECTLY FROM AIRGLOW OBSERVATIONS

Marty MLYNCZAK (Atmospheric Sciences, NASA Langley Research Center, Hampton, VA, 23681-2199, USA, email: m.mlynczak@larc.nasa.gov)

A new technique has been developed to determine directly the rates of energy deposition and atmospheric heating resulting from the absorption of solar ultraviolet radiation in the mesosphere, using measurements of the molecular oxygen airglow. This approach allows the deposition and heating rates to be derived independent of knowledge of the solar irradiance, the ozone abundance, and the temperature-dependent ozone absorption cross-sections. This technique has been applied using existing measurements of the infrared atmospheric band airglow at 1.27  $\mu$ m made by the Solar-Mesosphere Explorer (SME) satellite. Fifty-six months of data are analyzed and presented. The derived solar heating exhibits strong variations in altitude and season, with a semi-annual oscillation in heating present near the low-latitude mesopause and annual oscillations in heating present in the lower mesosphere. Comparisons between observed and modeled rates of energy deposition and heating are also presented.

### JSA20/W/19-A4 1450

#### INFLUENCE OF STRATOSPHERIC WARMINGS ON THE PLANETARY SCALE DISTRIBUTION OF ATOMIC OXYGEN IN THE LOWER THERMOSPHERE

Gordon SHEPHERD, Xialong Wang (both at Centre for Research in Earth and Space Science, York University, Toronto M3J 1P3, Canada, email: gordon@windii.yorku.ca)

Marked perturbations in the global scale distribution of lower thermospheric atomic oxygen are observed in the O(1S) 558 nm emission by the WINDII instrument on the UARS mission. These appear as wave 1 planetary scale perturbations, with a maximum emission rate near the longitude of maximum warming in the stratosphere, but with the lower thermospheric perturbation occurring a few days earlier. The perturbation extends from the poleward limit of WINDII observations (72 degrees) down to about 50 degrees latitude. A similar perturbation has been detected in relation to the final warming, which has been called the springtime transition; the similarities are discussed. The dynamical response of the lower thermosphere observed by WINDII is also described and discussed.

### JSA20/E/13-A4 1508

#### A COMPARISON OF TIDAL AND QUASI-TIDAL OSCILLATIONS IN THE LOWER THERMOSPHERE AS MEASURED SIMULTANEOUSLY BY EISCAT AT LONGYEARBYEN AND TROMSO

P.J.S. WILLIAMS (Prifysgol Cymru, Aberystwyth, Wales), M. Kunitake (CRL, Hiraiso Solar Terrestrial Research Center, Ibaraki, Japan), S.C. Buchert (STELAB, University of Nagoya, Japan), Tony van Eyken (EISCAT, Longyearbyen, Svalbard)

Incoherent-scatter measurements of ion velocity, made by the EISCAT radars observing along the magnetic field line, have been used to determine the meridional component of neutral wind velocity at a number of separate heights over the range 90 km to 120 km. Frequency analysis has been used to determine the amplitude and phase of the most prominent components at each height, including those with periodicities of 24, 12 and 8 hours. Since August 1998 such measurements have been made simultaneously at both Ramfjordmoen (69.6 degrees North) and at Longyearbyen (78.2 degrees North). For each component and at each height the ratio of the amplitudes observed at the two stations have been determined, as well as the differences in phase. The results have been compared with predicted values for tidal modes in an attempt to distinguish global modes and quasi-tidal oscillations at high latitudes.

### JSA20/W/30-A4 1526

#### COMPARATIVE STUDY OF NEUTRAL WIND AND TIDAL VARIABILITY IN THE LOWER THERMOSPHERE ABOVE U.K. AND BULGARIA

D. PANCHEVA, Pl. Mukhtarov (Geophysical Institute, Bulg. Acad. Sci., "Acad. G. Bonchev" str., bl.3, 1113 Sofia, Bulgaria); N.J. Mitchell, A.G. Beard, P.J.S. Williams (The University of Wales, Aberystwyth, Dept. of Physics, Aberystwyth, Ceredigion SY23 3BZ, UK); H.G. Muller (R.M.C.S., Cranfield University, SN6 8LA, UK)

The localised variation of power in the period range 1.5-30 days within a time series of diurnal and semi-diurnal tidal amplitudes, as well as of prevailing neutral wind, measured by meteor radar in the lower thermosphere above U.K. and Bulgaria during the time interval January, 1991 - June, 1992 is investigated by a Morlet wavelet transform analysis. There is a general coincidence between the observed dominant frequencies, however because of latitudinal and longitudinal differences between the two stations their temporal courses demonstrate some differences. By a cross-wavelet transform analysis the planetary waves and the time intervals when they exist simultaneously in the both studied time series are chosen. An attempt was made to estimate the wave number of the most well expressed planetary waves.

### JSA20/W/12-A4 1544

#### THERMOSPHERIC IN-SITU TIDES VERSUS THOSE PROPAGATING UPWARDS FROM THE LOWER AND MIDDLE ATMOSPHERE.

I.C.F. MUELLER-WODARG (A.D. Aylward Atmospheric Physics Laboratory University College London, 67-73 Riding House Street, London W1P 7PP, UK)

Purpose of this study is to investigate the relative importances of tides generated in the thermosphere at high latitudes ("auroral tides") and those originating from below the mesopause. We analyze output from the Coupled Thermosphere-Ionosphere-Plasmasphere Model (CTIP) for different levels of geomagnetic and tidal forcing which suggests that the role of in-situ thermospheric tides is often underestimated at mid- to high latitudes above the E-region.

### ANNOUNCEMENT OF POSTERS 1602

### POSTER VIEWING 1630

Friday 23 July AM

Presiding Chair: J.M. Forbes, (Uni of Colorado, Dept of Aerospace Engineering, USA)

### EQUATORIAL/TROPICAL COUPLING PROCESSES 1

### Introduction 0900

J.M. FORBES

### JSA20/W/15-A5 Invited 0905

#### THE SCOSTEP/EPIC PROJECT: EQUATORIAL PROCESSES INCLUDING COUPLING

Shoichiro FUKAO (Radio Atmospheric Science Center, Kyoto University, Uji, Kyoto 611-0011, JAPAN, email: fukao@kurasc.kyoto-u.ac.jp)

EPIC (Equatorial Processes Including Coupling) is one of four post-STEP programs sponsored by SCOSTEP. The equatorial region is the source of many unique atmospheric processes that couple the entire atmosphere vertically from the bottom to the top and horizontally from the equator to the poles. Despite its importance for global change, however, the equatorial atmosphere is not well studied and its coupling processes are poorly understood. The overall scientific objective of EPIC is to understand equatorial processes on all spatial and temporal scales occurring in the middle atmosphere and upper atmosphere/ionosphere, as well as their vertical coupling with atmospheric regions above and below. Coupling in the horizontal with the atmosphere/ionosphere at extratropical latitudes and between regions around the equator also needs to be studied. EPIC should become the core

program for studies of coupling processes in the equatorial atmosphere/ionosphere. Recognizing the necessity of motivating diverse science communities to work toward an interdisciplinary goal of interest, it was decided to adopt the following theme, which is related to almost all scientific questions raised to date, and can be pursued with the collaboration of all members: "Convective Processes and Influence on the Atmosphere-Ionosphere System." EPIC will operate during the period 1998-2002. It is chaired by Prof. S. Fukao in collaboration with Co-chairmen of Dr. J. M. Forbes and Dr. R. A. Vincent. A review of the project and its future perspectives will be presented.

**JSA20/W/07-A5** Invited **0930**

**CHARACTERISTICS OF GRAVITY WAVES GENERATED BY DEEP CONVECTION AND RELEVANCE TO MESOSPHERE DYNAMICS**

M.J. ALEXANDER (Colorado Research Associates, 3380 Mitchell Lane, Boulder, CO, 80301 USA  
Email: alexand@colorado-research.com)

Among the possible tropospheric sources of gravity waves, convection is a source likely to generate waves with the large horizontal phase speeds that would allow them to propagate to mesospheric and thermospheric altitudes. Measurements that directly link convection and middle atmosphere waves are still only few in number, and the parameters needed to evaluate the impact of these waves on the upper atmosphere are a challenge to determine observationally. Much of what is known about convectively generated gravity waves comes from model studies. Recent relevant model and observational results will be summarized that lead to some important constraints on the properties of convectively generated gravity waves and on their global-scale effects at tropical latitudes.

**JSA20/W/01-A5** Invited **0955**

**LONG-TERM STUDIES OF GRAVITY WAVE VARIABILITY IN THE EQUATORIAL MLT AND LINKS TO THE LOWER ATMOSPHERE**

Robert A. VINCENT (Department of Physics and Mathematical Physics, University of Adelaide, Adelaide 5005, Australia, email: rvincent@physics.adelaide.edu.au)

One of the most difficult problems in middle atmosphere dynamics is identifying the major sources of small-scale disturbances, such as gravity waves. Eight years of MF radar wind measurements in the mesosphere/lower thermosphere made at Christmas Island are used to study gravity wave variability on both long- and short-time scales. The location of Christmas Island in the equatorial central Pacific, remote from large landmasses, makes it ideal for investigating upward coupling from convective sources. Normally Christmas Island is located in a low-convection region, but during ENSO events convection is strongly enhanced in the central Pacific. Daily measurements of outgoing longwave radiation (OLR) are used as a measure of the strength of convection in the lower atmosphere and are shown to have a significant correlation with mesospheric gravity-wave activity. The filtering effects of the intervening wind systems, such as the QBO, are shown to be important and suggest that the wave sources are anisotropic.

**JSA20/W/54-A5** Invited **1020**

**NON-MIGRATING TIDES: A REVIEW OF THEORETICAL BACKGROUND AND A NUMERICAL SIMULATION**

Saburo MIYAHARA (Department of Earth and Planetary Science, Kyushu University, Fukuoka 821-8581 Japan, e-mail: sbm@rossby.geo.kyushu-u.ac.jp)

In the first half of this talk, Hough functions, equivalent depth, and vertical wavelength related to non-migrating tides in the atmosphere are reviewed based on the atmospheric tidal theory. It will be stressed that it is difficult to discriminate between migrating tides and non-migrating tides only by the vertical wavelength. In the second half of the talk, output data of the Middle Atmosphere Circulation Model at Kyushu University (MACMKU) are analyzed to study behavior of non-migrating tides in the MLT region. Utilizing the S-Transform method, it is shown that non-migrating tides show strong variability of amplitudes and phases than the migrating tides. Heating sources and non-linear interactions between tidal and planetary waves which can generate non-migrating tides in the model will be also discussed.

Presiding Chair: M.A. Abdu (Instituto Nacional de Pesquisas Espaciais, Brazil)

**JSA20/W/47-A5** Invited **1110**

**OUTSTANDING PROBLEMS IN THE ELECTRODYNAMICS OF THE EQUATORIAL IONOSPHERE-THERMOSPHERE SYSTEM**

M. A. ABDU (Instituto Nacional de Pesquisas Espaciais-INPE, São Jose dos Campo, SP, 12201-970, Brazil, email: abdu@dae.inpe.br)

Dynamic coupling of the atmospheric layers involving upward energy transport coupled with the locally active thermal tidal modes establish the wind system of the thermosphere whose interaction with the magnetized conducting ionospheric layers produces the dynamo electric fields that control the quiet time electrodynamic processes of the equatorial ionosphere-thermosphere system. Their well-known major manifestations are: the equatorial electrojet current system and its instabilities, plasma fountain and ionization anomaly with associated neutral wind and temperature anomalies, and plasma bubble irregularities. They underlie the strong electrical coupling of E and F layer processes in ways controlled by the conductivities and spatial gradients in them. The conductivity longitudinal gradients at the terminators control the sunset electrodynamic processes that is of fundamental importance to the problems of equatorial plasma bubble/spread-F phenomenon. A great deal of understanding on the quiet time/average behaviour of the different EITS phenomena are now available from past investigations. Little is known regarding the causes of their day-to-day variabilities under quiet conditions, in response to magnetospheric disturbances and forcing from lower atmosphere. Recent studies have provided evidence of significant longitudinal variations believed to be caused by the longitudinally dependent geomagnetic field configurations (such as the magnetic declination angle and the south Atlantic magnetic Anomaly). This paper will focus on the roles of electrodynamic processes vis-a-vis the neutral dynamics in the variabilities of the major EITS phenomena on, including those in response to magnetospheric disturbances and as a function of longitude.

**JSA20/W/20-A5** Invited **1135**

**EFFECT OF SPACE WEATHER RELATED PROCESSES IN THE LOW LATITUDE THERMOSPHERE IONOSPHERE SYSTEM**

R. SRIDHARAN, Alok Taori, D. Chakrabarty, H. Chandra, Som kumar Sharma, R. Narayanan (Physical Research Laboratory, Ahmedabad - 380009, IDIDA.

Though the low latitude Thermosphere – Ionosphere system (TIS) is normally shielded by the geomagnetic fields, from the highly energetic particles from the sun, electrodynamic and neutral dynamic coupling of the high and low latitude regions enables the transfer of energy and momentum to the latter. As a consequence a variety of complex processes occur in the low latitude TIS after a time delay. The effects are generally more pronounced in the thermosphere. One of the unique data set from Mt. Abu (24.6N, 73.7E) and Ahmedabad (23N, 72.6E) a pair of low latitude stations corresponding to the 6th Jan 1997 space weather event, revealed that the OI 630.0 nm dayglow intensity registered an enhancement by a factor of 2 - 2.5 on 11th Jan in the morning hours, as compared to 9th and 12th Jan i.e. one day later than the day when the auroral activities were noticed at as low as 55 N latitudes, on the day when the magnetosphere was compressed to < 6 R<sub>E</sub>. However the ionosphere didn't reveal any dramatic changes for the same period. Interestingly another low latitude station Kolhapur (16.8N, 74.2E), closer to the equator, revealed an opposite trend for the 630.0 nm thermospheric dayglow for another space weather event during Feb 97. Plausible explanations for such preferential behaviour of the thermospheric dayglow would be presented and discussed.

**JSA20/W/41-A5** Invited **1200**

**MID AND LOW LATITUDE RESPONSE OF THE THERMOSPHERE AND IONOSPHERE TO GEOMAGNETIC STORMS**

Timothy FULLER-ROWELL, G. Millward, M.V. Codrescu (all at NOAA Space Environment Center and CIRES, University of Colorado, Boulder, CO 80303, USA, email: tjfr@sec.noaa.gov, gmillward@sec.noaa.gov, mcodrescu@sec.noaa.gov)

At mid-latitudes a significant fraction of the ionospheric response to geomagnetic storms can be explained by thermospheric wind and composition effects. The electrodynamic component has yet to be quantified. At low latitude the response is complicated by stronger coupling with electrodynamics. Penetration electric fields, followed by the arrival of wind surges, changes in global circulation, and subsequent composition changes, all act to alter low latitude electrodynamics. The ionosphere responds to all these processes, but the balance between them has yet to be quantified.

**ANNOUNCEMENT OF POSTERS** **1225**

**POSTER VIEWING** **1230**

**Friday 23 July PM**

Presiding Chair: S. Fukao  
Concurrent Poster Session

**EQUATORIAL/TROPICAL COUPLING PROCESSES 2**

**JSA20/E/12-A5** Invited **1400**

**GEOMAGNETIC FORCING OF THE EQUATORIAL THERMOSPHERE-IONOSPHERE SYSTEM: A STUDY OF THE DISTURBANCE PERIOD 7-13 MARCH 1994**

J. Hanumath SASTRI (Indian Institute of Astrophysics, Bangalore 560 034, India); V.V.Somayajulu (Space Physics Laboratory, VSSC, Trivandrum 695 022, India); K. B. Ramesh, H. N. R. Rao, J. V. S. V. Rao (Indian Institute of Astrophysics, Bangalore 560 034, India)

We present salient features of the behaviour of the thermosphere-ionosphere (TI) system in the Indian equatorial region during the prolonged disturbance period of 7-13 March 1994. A multi-experiment (FPI, ionosonde and HF Doppler radar) database is used for the study. The average nighttime (1930-0430 IST) thermospheric temperature, <T<sub>n</sub>> varied from 701 K to 914 K on individual nights of the disturbance period. There is no evidence for any persistent change in <T<sub>n</sub>> on disturbed nights compared to quiet nights. <T<sub>n</sub>> is nevertheless reduced on three nights (8, 11 and 13 March) corresponding to the recovery phase of Dst index. The agreement between the measured and MSIS model T<sub>n</sub> is better on disturbed nights than on quiet nights. The nighttime pattern of meridional winds showed several interesting features which include strong surges in equatorward winds and quasi-periodic wind oscillations with a period of about 3-hr, with a corresponding feature in T<sub>n</sub>. The F region vertical plasma drift pattern at Kodaikanal showed unambiguous effects of short-lived (2-3 hrs) electric field perturbations on some of the disturbed nights. These and other results are compared with earlier work and discussed in the light of current understanding of the disturbance-time behaviour of the equatorial TI system.

**JSA20/W/26-A5** **1425**

**MODELLING STUDIES OF THE ELECTRODYNAMIC COUPLING BETWEEN THE EQUATORIAL IONOSPHERE AND THERMOSPHERE USING CTIP**

G. H. MILLWARD, T.J. Fuller-Rowell (both at Space Environment Center, 325 Broadway, Boulder, CO 80303, USA, email: gmillward@sec.noaa.gov)

The CTIP (Coupled Thermosphere Ionosphere Plasmasphere) model has undergone a significant enhancement with the addition of the equations for a full electrodynamic coupling between ionosphere and thermosphere at equatorial latitudes. The new enhanced model has been used to investigate the vertical component of the resulting equatorial ionospheric ExB drift and its changes according to season, F10.7, geographic longitude, and also the effects (in separate experiments) of the forcing from lower-thermosphere tides and a large geomagnetic storm. Results from the model will be presented and compared with the latest measurements. In addition, the causative factors for the production of a 'post-sunset enhancement' of the vertical ExB drift (seen clearly in the model) will be addressed.

**JSA20/W/16-A5** **1443**

**ON THE VARIABILITY OF EQUATORIAL PLASMA MOTIONS**

B. G. FEJER, L. Scherliess (Center for Atmospheric and Space Sciences, Utah State University, Logan, Utah 84322-4405, USA, email: bfejer@cc.usu.edu)

We use incoherent scatter radar observations from the Jicamarca Observatory to examine the variability of the equatorial plasma drifts driven by ionospheric dynamo and disturbance dynamo electric fields. The average vertical plasma drifts during the March and September equinoctial periods are significantly different for low solar flux conditions, but are nearly identical during high solar flux periods. Our measurements suggest that over Jicamarca, the transition from the southern hemisphere summer to winter takes place over a relatively short period of time (about 4 weeks). These transitional periods are characterized by very large day-to-day variability. Since, on these occasions, the F-region dynamo contributions are expected to be identical, this effect is probably due to changes in the lower thermospheric wind forcing. The vertical daytime plasma drifts show significantly larger day-to-day variability during solar minimum than near

## INTER-ASSOCIATION

solar maximum. Preliminary TIEGCM results suggest that this could be explained by the effect of the (2,2) semidiurnal tidal mode. Large short term variability also occurs near sunset possibly due to gravity waves and/or changes in the relative efficiencies of the E- and F-region dynamo. During disturbed conditions, the efficiency of the disturbance dynamo electric fields near sunset is strongly season and solar cycle dependent. The evening disturbance dynamo zonal electric fields drive downward plasma motions which maximize during solar maximum equinoctial conditions over Jicamarca. We will also discuss possible seasonal and solar cycle effects on the efficiency of prompt penetration zonal electric fields at the equator.

### JSA20/P/01-A5 1501

#### MODELING OF THE PENETRATION OF HIGH-LATITUDE ELECTRIC-FIELD TO LOW LATITUDES FOR NON-STEADY CONDITION.

A.T. KOBEA (UFR SSMT/Laboratoire de Physique de l'Atmosphère, 22 B.P. 582 Abidjan 22, Côte d'Ivoire (West Africa), email: kobeat@syfed.ci.refer.org); C.Peymirat (CETP-CNRS, Centre Universitaire, 10-12 Avenue de l'Europe, 78140 Velizy, France); A.Richmond, R. G. Roble (High Altitude Observatory, National Center for Atmospheric Research, Boulder, Co. 80307-3000, U.S.A., e-mail: richmond@hao.ucar.edu); C. Amory-Mazaudier, J. Vassal (both at CETP-CNRS, Observatoire de Saint Maur, 4, avenue de Neptune F-94107 Saint-Maur-Des-Fossés, France, email: Christine.Mazaudier@cetp.ipsl.fr); H.Lühr (Institut für Geophysik und Meteorologie der Technischen Universität Braunschweig, Mendelssohnstraße 3, 38106 Braunschweig, Germany)

Auroral and equatorial magnetometer data are used to study a direct penetration of polar electric field at the equator. First, an observed case of apparent overshielding is modeled with the Magnetosphere-Thermosphere-Ionosphere-Electrodynamics General Circulation Model (MTIE-GCM). Although no particular attempt was made to match the model conditions to the observations, the simulated equatorial H variation is in acceptable agreement with the observed H disturbance at the equator both for the magnitude and the duration. Subsequently to that event, a quasi-periodic DP2 fluctuations (period of 30-40 min) appears coherently at the equator with an enhancement ratio of 4 compare to the magnitude at sub-auroral latitude.

The excellent correlation coefficient(0.9) between the high latitude variation and the equator can be explained as an instantaneous extension of the ionospheric current generated by magnetospheric electric field. The mid-latitude and the equator fluctuate coherently with the afternoon vortex which seems to extend in wide latitudinal range (67°- 120°) in regard to the twin-vortex pattern resulting from the AME procedure run. The polar cap potential variation inferred from the AMIE pattern tends to lag behind the electric field at the equator whereas it tends to be advanced in phase with respect to the auroral oval field; such behavior is expected from the dynamics of the Region 2 currents which tends to shield electric field penetration across the latitude of Region 2 currents.

### JSA20/W/21-A5 1519

#### LOW-LATITUDE IONOSPHERIC ELECTRIC FIELD INFERRED FROM ION DRIFT MEASUREMENTS OF THE ROCSAT-1 IPEI PAYLOAD

H. C. YEH, S. Y. Su (both at Institute of Space Science, National Central University, Chung-Li, Taiwan, email: yeh@jupiter.ss.nctu.edu.tw); R. A. Heelis (William B. Hanson Center for Space Sciences, The University of Texas at Dallas, Richardson, Texas, 75803, USA)

The ROCSAT-1 satellite is scheduled to launch in January 1999 with a nominal mission time of 2 years. The Ionospheric Plasma and Electrodynamics Instrument (IPEI) onboard ROCSAT-1 consists of 4 sensors to take in-situ measurements of ion density, temperature, composition and drift velocity over a large dynamic range with high sensitivity. As ROCSAT-1 is maintained in a circular orbit with an altitude of 600 kilometers, and an orbital inclination of 35 degrees, observations with global coverage in local time and longitude are available every 52-day period. Furthermore, since the IPEI payload will normally be operated with 100% duty cycle, the ROCSAT/IPEI can provide a fairly complete set of ion drift data for the low-latitude ionosphere during its mission lifetime. In this report, we analyze four months of ion velocity data from ROCSAT-1 to compile a preliminary global electric field model at 600 km altitude. The dependencies of electric field structure on latitude, longitude (and geomagnetic field configuration), local time, and geomagnetic activity are examined in detail. Electric field mappings along the realistic geomagnetic field lines are performed for the purpose of comparing ion  $E \times B$  drift with conductivity-weighted neutral wind at various altitudes along the magnetic flux tubes covered by the ROCSAT orbits. As the IPEI data are accumulated the electric field model will be improved and contribute more to studies of thermosphere-ionosphere coupling at low latitudes.

### ANNOUNCEMENT OF POSTERS 1555

### POSTER VIEWING 1630

**Saturday 24 July AM**

Presiding Chair: J. Lastovicka

(Institute of Atmospheric Physics, Bocni II Prague, Czech Republic)

### IONOSPHERE & THERMOSPHERE: HIGH LATITUDES AND DISTURBED CONDITIONS

#### Introduction 0900

J. Lastovicka

### JSA20/W/18-A6 Invited 0905

#### E-REGION IONOSPHERIC TOMOGRAPHY

L. KERSLEY (Department of Physics, University of Wales, Aberystwyth SY23 3BZ, UK, e-mail: lek@aber.ac.uk)

Radio tomography has matured into an established experimental technique for imaging the spatial structure of ionospheric electron density. The method uses observations recorded at a chain of receiving stations of total electron content, measured by means of radio transmissions from a satellite in low Earth orbit. The resultant data set is then inverted in a reconstruction algorithm to create an image in two dimensions of the plasma density. The bulk of the ionospheric plasma is concentrated in the F-layer and radio tomographic techniques are now well established for the imaging of F-region features. However, at high latitudes precipitation of energetic particles may result in 'auroral-E' ionisation that can make a significant contribution to the total content. With appropriate selection of the reconstruction process the structuring of this E-layer plasma can be imaged, thus providing spatial information about features in the electron density that complement results from other experimental techniques. The paper reports experimental work directed towards the imaging of the ionosphere at high latitudes, where the validity of the technique has been verified by means of independent

measurements from the EISCAT and ESR incoherent scatter radars. Observations made at a chain of stations (Ny Ålesund, Longyearbyen, Björnåya and Tromsø) in the European Arctic have been used to investigate features in the cusp, polar cap and auroral ionospheres. Results are presented in which 'auroral-E' ionisation imaged by tomography is related to both optical observations and satellite measurements of precipitating particles.

### JSA20/W/49-A6 0930

#### DETERMINATION OF E-REGION CONDUCTIVITY FROM FAR ULTRAVIOLET IMAGES

Larry J. PAXTON (email: larry.paxton@jhuapl.edu); Daniel Morrison (email: daniel.morrison@jhuapl.edu); Gerald J. Romick (email: Gerald.Romick@jhuapl.edu); Ching I. Meng (email: ching.meng@jhuapl.edu) (all at The Johns Hopkins University Applied Physics Laboratory 11100 Johns Hopkins Rd., Laurel, MD 20723, USA); Douglas J. Strickland (email: strick@euler.cpi.com); Scott Evans (email: evans@euler.cpi.com) (both at Computational Physics, Inc. 2750 Prosperity Ave Ste 600, Fairfax, VA 22031, USA)

United States High latitude inputs to the coupled thermosphere-ionosphere system are important factors in determining the response of the atmosphere at low and mid-latitudes as well as at high latitudes. Local heating by particle precipitation and Joule heating are two of the major high latitude influences on the neutral atmosphere composition. Imaging in the Far Ultraviolet (110 to 180 nm) is commonly used to provide estimates of the magnitude of these inputs. The measurements are inherently a column-integrated one since the observed radiance represents the integral of the altitude dependent source and transmission functions. To first order, observations in two wavelength regions (one wavelength interval or "color" where atmospheric optical absorption is important and one "color" where it is not) are required in order to provide some information on the precipitating particles' energy distribution and the magnitude of the flux of those particles. Broadband or single "color" imagery can yield some information on the magnitude of the incoming flux but can not provide much quantitative information. Furthermore, the choice of a single color must be considered very carefully: for example, the relatively bright OI 130.4 nm emission feature will show reduced spatial structure due to multiple scattering effects. In this paper we discuss how accurately the ionization rate profile in the E-region can be deduced using multiple "colors" (i.e. simultaneous measurements of OI 135.6, LBH short (140 to 150 nm), and LBH long (165 to 180 nm)) and the role of proton precipitation (seen using HI 121.6 nm) as a source of additional ambiguity. From the ionization rate profile, a time dependent electron density profile can be calculated. The Hall and Pedersen conductivities couple the neutral atmosphere to these calculations through collisional terms. Assumptions about the distribution function (i.e. Maxwellian or Gaussian) of the precipitating electrons or neglecting to allow for the presence of precipitating protons leads to uncertainties of a factor of two in the height-integrated conductivity and larger errors in the altitude distribution. We will discuss the implications of modeled and observed changes in the neutral atmosphere on the estimated conductivity profile.

### JSA20/W/40-A6 Invited 0948

#### GLOBAL JOULE HEATING AND THE THERMOSPHERE-IONOSPHERE RESPONSE

G. CROWLEY (Southwest Research Institute, San Antonio, TX, USA; email: crowley@picard.space.swri.edu); C. Fesen, O.Kivanc (UT Dallas, Richardson, TX, USA); T. Immler, A. Ridley (Southwest Research Institute, San Antonio, TX, USA); R.G. Roble, A.D. Richmond, B.A. Emery (HAO-NCAR, Boulder, CO, USA); D.J. Knipp (US Air Force Academy, Colorado Springs, CO, USA)

Joule heating is a key element of thermosphere-ionosphere-magnetosphere coupling. At high latitudes, the local Joule heat input can exceed the daytime solar input. Joule heating provides more than 10 percent of the global average energy input to the thermosphere, and plays major role in determining the global temperature, wind, density and compositional structure of the thermosphere. This in turn drives the global structure of the ionosphere. Currently our knowledge of Joule heating at both a particular location and globally is uncertain by factors of 2 to 10. Numerical experiments illustrating the effect of these uncertainties on the global atmospheric structure will be discussed. Both quiet and storm conditions were simulated using the NCAR TIE-GCM. Dramatic differences result from only factors of 2 changes in the Joule heat inputs. For space weather modelling, these results illustrate the importance of accurately defining the high latitude inputs, and of fully coupling the ionosphere and thermosphere. Comparison of the Joule heating computed by the TIEGCM and AMIE versus ground-based and space-based measurements reveals some of the problems which need to be addressed in the specification of Joule heating and magnetosphere-ionosphere-thermosphere coupling.

### JSA20/W/53-A6 1013

#### DETECTION OF GEOMAGNETIC STORM EFFECTS ON LOWER THERMOSPHERIC WINDS AT MIDLATITUDES

Joseph E. SALAH (Haystack Observatory, Massachusetts Institute of Technology, Westford, MA 01886 USA, email: jsalah@haystack.mit.edu); Larisa Goncharenko (Haystack Observatory, Massachusetts Institute of Technology, Westford, MA 01886 USA, email: lgoncharenko@haystack.mit.edu)

Several sets of observations of neutral winds in the lower thermosphere have been obtained by the Millstone Hill incoherent scatter radar (42.6N, 71.5W) during geomagnetic storms of different intensity. The reliable detection of the storm effects on midlatitude winds in the altitude region 100-130 km is difficult, and a search for such effects during the CEDAR/LTCS campaigns over the past ten years does not reveal strong evidence for a response to the storm at these altitudes until the intensity of the storm exceeds a Kp of 6 and is long lasting. Observations made during two campaigns, June 1991 and September 1998, where the disturbances were intense, illustrate this conclusion. The primary finding is that the effects are best seen in the zonal wind component with enhanced westward motions during the most intense storm in June 1991. Evidence of flywheeling of the winds in the lower thermosphere on the day following the end of the geomagnetic storm is seen, as predicted by some general circulation models. Opportunities for collecting additional observations to investigate this important topic are planned and will be discussed.

### JSA20/W/17-A6 1031

#### LATITUDINAL AND GEOMAGNETIC ACTIVITY VARIATIONS IN LOWER THERMOSPHERIC NEUTRAL WINDS OBSERVED OVER SONDRE STROMFJORD AND MILLSTONE HILL

R. M. JOHNSON, S. M. I. Azeem (both at Space Physics Research Laboratory, The University of Michigan, 2455 Hayward, Ann Arbor, MI 48109, USA, Email: rmjohnsn@umich.edu); L. P. Goncharenko, J. E. Salah (both at Haystack Observatory, Massachusetts Institute of Technology, USA)

Neutral winds deduced from measurements obtained during Lower Thermospheric Coupling Study (LTCS) campaigns at two incoherent scatter radar (ISR) sites, Sondre Stromfjord in Greenland and Millstone Hill in U.S.A, are compared in the light of model results to examine the latitudinal variation of lower thermospheric semidiurnal oscillations. Both Sondre



Stromfjord and Millstone Hill observations indicate large variability in the tidal oscillations during winter whereas the results obtained during summer LTCS campaigns show more consistent amplitude and phase structure. Average seasonal amplitude and phase structures obtained from the radar measurements are compared with model predictions of expected semi-diurnal amplitude and phase profiles at the two different latitudes of the radars. The effects of geomagnetic activity on the semi-diurnal tidal oscillations are assessed and compared with model predictions and previous results.

**JSA20/E/18-A6** 1118

#### THERMOSPHERIC AND IONOSPHERIC DYNAMICS IN THE AURORAL REGION

Hiroyuki SHINAGAWA, Shin'ichiro Oyama, Satonori Nozawa, Ryoichi Fujii (Solar-Terrestrial Environment Laboratory, Nagoya University, Toyokawa 442-8507, Japan, email: sinagawa@stelab.nagoya-u.ac.jp); Mamoru Ishii (Communications Research Laboratory, Tokyo 184-8795, Japan, email: mishii@crl.go.jp)

Dynamics of the thermosphere and the ionosphere in the auroral region is quite complicated. There have been a number of reports on strong vertical neutral winds mainly in the auroral region. The magnitude of the vertical winds sometimes exceeds 100 m/s, suggesting that particle precipitation heating as well as Joule heating could cause extremely large upwelling and downwelling of the thermosphere. Behavior of the ionosphere associated with strong neutral winds also appears to be complex. Although such small-scale variation is likely to be confined in the auroral region, those events are expected to produce equatorward propagating gravity waves. It is also possible that such small-scale phenomena influence the global structure and dynamics of the thermosphere-ionosphere system. Two- and three-dimensional non-hydrostatic thermosphere-ionosphere models are used to investigate small-scale variation of the thermosphere and the ionosphere associated with local auroral activities. The results are compared with neutral and ion velocities measured by Fabry-Perot Interferometers and the EISCAT radar. In this paper, emphasis is placed on coupling of the thermosphere and the ionosphere in the auroral region. Interaction processes between the global wind system and the locally generated winds are also discussed.

Presiding Chair: G. Crowley

**JSA20/E/04-A6** 1136

#### THERMOSPHERIC WIND FIELD OVER MAWSON AND DAVIS, ANTARCTICA; SIMULTANEOUS OBSERVATIONS BY TWO FABRY-PEROT SPECTROMETERS OF L630 NM EMISSION

P.A. GREET (1), M.G. Conde (2), P.L. Dyson (3), J.L. Innis (1), A.M. Breed (1), D.J. Murphy (1) ((1) Australian Antarctic Division, Channel Highway, Kingston, Tas. 7050, Australia. (2) Geophysical Institute, University of Alaska, Fairbanks, USA. (3) Department of Physics, La Trobe University, Bundoora, Vic. 3083, Australia)

The thermospheric oxygen I630 nm emission has been observed using high-resolution Fabry-Perot spectrometers at Mawson (67.6°S 62.9°E) and Davis (68.6°S 78.0°E), Antarctica. A new technique, combining the results from the two instruments, is used to derive vector wind fields. The technique is described and applied to five nights of simultaneous cardinal point data obtained in 1997. Solar flux was low during this interval, typically  $F_{10.7} = 75$ . Of the five nights two were magnetically disturbed and three were quiet. The disturbed nights were compared to a TIEGCM model run and reasonable agreement was found in the first half of the night. On one of the disturbed nights a closed evening circulation cell and cross-polar jet could be identified in our data. On none of the nights was a morning circulation cell evident. Auroral imager data were used to locate the auroral oval. For several hours around magnetic midnight the auroral oval produces a doldrums in the thermospheric winds. Auroral doldrums are not described by the model. Auroral doldrums are also seen on the quiet nights which otherwise maintain approximately antisunward flow

**JSA20/E/17-A6** 1154

#### A LARGE VERTICAL WIND IN THE THERMOSPHERE AT THE AURORAL OVAL/POLAR CAP BOUNDARY SEEN SIMULTANEOUSLY FROM MAWSON AND DAVIS, ANTARCTICA.

J.L. Innis (1), P.A. GREET (1), D.J. Murphy (1), M. Conde (2), P.L. Dyson (3) ((1) Australian Antarctic Division, Channel Highway, Kingston, Tas., 7050, Australia. (2) Geophysical Institute, University of Alaska, Fairbanks, Alaska, USA. (3) Department of Physics, La-Trobe University, Bundoora Campus, Vic., 3083, Australia)

Ground-based Fabry-Perot spectrometer observations from the Australian Antarctic stations of Davis and Mawson show an upward wind  $\geq 100$  ms in the thermosphere at  $\sim 240$  km altitude on the night of Day of Year 159 in 1997. The wind was from a region located to the poleward of the poleward edge of the discrete auroral oval, and is identified as a further event of the type seen at Mawson, and elsewhere, in earlier work. The upward wind was first seen over Davis station at  $-22$  UT. As the auroral oval moved northward the region of upward wind followed, and was seen at Mawson (some 5 degrees magnetically north of Davis) just over 1 hour later. It is shown that the presence of the large upward wind does, at times, affect the derived horizontal wind. Correcting the affected measurements for the non-zero upward wind leads to a much smoother (less divergent) horizontal wind field. The area of the region of upward wind over Mawson and Davis on this night is estimated as  $\sim 6 \times 10^4$  km<sup>2</sup>. The estimated power required to drive the upward wind over this area at 240 km altitude is of order  $6 \times 10^9$  W. This represents a significant fraction of the power input at high-latitudes during quiet geomagnetic conditions.

**JSA20/E/02-A6** 1212

#### A STUDY OF THE STRONG MAGNETIC STORMS BY THE CLUSTER ANALYSIS

Pavlina K. IVANOVA (Geophysical Institute Bulg. Acad. Sci., Akad. G. Bonchev str., bl.3 Sofia 1113, Bulgaria, email: pivanova@geophys.bas.bg)

The problem of the Solar-Terrestrial interactions is presented in the following manner: to find the interplanetary medium parameters, which determine Geomagnetic activity (GA) and to work out an algorithm for the Geomagnetsphere storm (GMS) prediction. The GMS causal dependences on the processes running in the interplanetary environment are included in the present analysis of the problem. We should consider the Dst-variations of the geomagnetic field as the accumulation of a great number of disturbances which reflect different in time and space operating processes. The magnetic storms, which have occurred in 1978-1979, have been analysed, i.e. close to the maximum of the 19th cycle of solar activity. First the =D3outer environment where the storm occur has been analysed. The results obtained indicate the conditions under which it occurs. After that the main phase is considered and finally the recovery phase. The clusters obtained show not only the inner structure of the investigated SSC but also the change the functional connections between the different studied parameters participating in the SSC.

**JSA20/W/52-A4** Poster 1200-01

#### THE THEORY OF MID-LATITUDE IONOSPHERIC LONG-PERIOD VIBRATIONS

Khantadze, Anzor GVELESIANI, Z. Kobaladze, Z. Ioseliani (Tbilisi State University, I., Chavchavadze Ave., Tbilisi 380028, Georgia Institute of Geophysics, Georgian Academy of Sciences, I., M. Alexidze Str., Tbilisi 380093, Georgia, email: vazha@excite.com)

Numerous ionospheric observations of mid-latitude long-period vibrations travelling horizontally allow to separate: a) background vibrations at quiet and moderate geomagnetic disturbances and b) separate splashes of magnetic storms, earthquakes and artificial explosions. The linear theory of these observations is suggested when Rayleigh and ion frictions are taken into account. From the dispersion relation are obtained two types of waves: a) slow Rossby's waves travelling to the West caused both by anisotropy of Coriolis force and geomagnetic field; b) fast planetary waves, caused only by the gradient of geomagnetic field travelling both to the East and to the West. The values of the velocities of the latter waves are more on the night side than on the day side. Parameters of these waves are in good agreement with the parameters of mid-latitude ionospheric long-period vibrations and may be attributed to the background vibrations, caused by the gradient of geomagnetic field. It is shown identity of these waves with drift waves in an inhomogeneous magnetoactive plasma.

**JSA20/W/04-A4** Poster 1200-02

#### A NEW COUPLED MESOSPHERE / THERMOSPHERE MODEL

M. J. HARRIS(1), A. D. Aylward(1), N. F. Arnold(2), (1) : Atmospheric Physics Laboratory, University College London; (2) : Radio and Space Science Group, University of Leicester.

The upper mesosphere / lower thermosphere is an important transition region in the coupling of the upper and middle atmospheres. In order to help study the dynamics and energetics of this system, a 3-D time dependant Coupled Mesosphere and Thermosphere model (CMAT) has been developed, extending and updating the existing thermospheric code to incorporate mesospheric dynamics, energetics and chemistry. Some general output and a preliminary study of minor constituent response to tidal forcing will be presented.

**JSA20/W/39-A4** Poster 1200-03

#### SIMULATION OF LARGE-SCALE DYNAMICS IN THE MESOSPHERE AND LOWER THERMOSPHERE WITH THE DOPPLER-SPREAD PARAMETERIZATION OF GRAVITY WAVES

R. A. AKMAEV (Department of Aerospace Engineering Sciences, CB-429, University of Colorado, Boulder, CO 80309-0429, USA, email: akmaev@spb.colorado.edu)

The Doppler-spread parameterization of gravity wave (GW) spectra developed by C. O. Hines has been implemented into the Spectral Mesosphere/Lower Thermosphere Model. Special attention has been devoted to different ways of parameterization of eddy mixing associated with saturation and breaking of gravity waves in the mesosphere and lower thermosphere (MLT). Simulations for solstice and equinox conditions have been conducted. The role of gravity-wave imposed drag and mixing in maintaining the global-scale dynamics and structure in the MLT and their seasonal variations is discussed. The modeling results are compared with simulations using a different ("Lindzen type") GW parameterization and with empirical models and observations.

**JSA20/E/10-A4** Poster 1200-04

#### FIRST E-REGION OBSERVATIONS OF TIDES IN THE LOWER THERMOSPHERE USING THE EISCAT SVALBARD RADAR

P.J.S. WILLIAMS (Prifysgol Cymru, Aberystwyth, Wales), M. Kunitake (CRL, Hiraso Solar Terrestrial Research Center, Ibaraki, Japan), S.C. Buchert (STELAB, University of Nagoya, Japan), Tony van Eyken (EISCAT, Longyearbyen, Svalbard)

The EISCAT Svalbard Radar made the first E-region measurements free of ground clutter in August 1998 with three days of observation with the radar pointing along the magnetic field line. This was followed by a two-day run of the common programme CP1 and a one-day run of the UK/Japan Special Programme TIDE. An analysis of the periodic components of field-aligned ion velocity provided the amplitude and phase of the meridional tides at 78 degrees North at heights between 93 and 120 km. The dominant oscillations at most heights show periods of 24, 12 and 8 hours, with height profiles of amplitude- and phase very similar to those of the corresponding tidal modes observed at lower latitudes. In addition, at heights below 100 km there is a prominent 10-hour oscillation similar to that observed near the South Pole. At the lowest heights there is also evidence of a planetary wave with periodicity between 2 and 3 days. Over the same period the amplitude of the semi-diurnal tide shows a strong day-to-day variation, compatible with modulation at a period of 2-3 days.

**JSA20/W/02-A4** Poster 1200-05

#### A '30 DAY' OSCILLATION IN THE MLT WINDS: OBSERVATIONS IN EUROPE, JAPAN AND CANADA

Y. LUO, H.H. Monson, C.E. Meek (Institute of Space and Atmospheric Studies, University of Saskatchewan, Saskatoon, Canada, email: luo@dansas.usask.ca); K. Igarashi (Communications Research Lab., Tokyo, Japan); Ch. Jacobi (Institute for Meteorology, University of Leipzig, Leipzig, Germany)

A long period oscillation has been identified in the winds observed by radars (MF, LF) in the northern hemisphere. Although initially thought to be anormal mode planetary wave, spectral analysis at three sites (Saskatoon 107W, 52N; Collm 15E, 52N; Yamagawa 130E, 31N) has shown that the oscillation is a common feature of the winter atmosphere, and has strong amplitudes throughout the mesosphere ( $\sim 10$ m/s) and lower thermosphere ( $\sim 5$ m/s). The phase variations at the various sites are similar, and not consistent with a freely propagating wave. Comparisons with geomagnetic and solar wind parameters suggest that the oscillation is related to solar activity and the solar rotation period. Forcing mechanisms are discussed.

**JSA20/W/13-A4** Poster 1200-06

#### SPRINGTIME TRANSITION IN UPPER MESOSPHERE TEMPERATURE

Marianna SHEPHERD, Gordon Shepherd, Shengpan Zhang, Boedjanti Prawirosoehardjo (Centre for Research in Earth and Space Science, York University, 4700 Keele Street, Toronto, Ontario, Canada, M3J1P3, Email: marianna@windii.yorku.ca.), Patrick Espy (Department of Physical Sciences, Embry-Riddle Aeronautical University, Daytona Beach, FL, USA, Email: espy@db.erau.edu)

## INTER-ASSOCIATION

Observations from the wind imaging interferometer (WINDII) on the upper atmosphere research satellite and three optical ground stations have revealed a 'springtime transition' in atomic oxygen. The transition is characterized by a rapid 2-day rise in the night-time oxygen nightglow emission rate by a factor of 2 to 3 followed by a subsequent decrease by a factor of 10 in the same period of time indicating a depletion of atomic oxygen that persists for days. The current study examines signatures in the upper mesosphere temperature field (70-95 km height), derived from the WINDII Rayleigh scattering observations, that are possibly associated with the springtime depletion of the atomic oxygen. Comparisons with ground-based airglow rotational temperatures and optical emissions are presented and discussed. Data from the northern springtimes of 1992 and 1993 are reported upon in detail.

**JSA20/E/22-A4** Poster **1200-07**

### SPATIOTEMPORAL DETAIL IN METEOR WINDS FROM HALLEY, ANTARCTICA

Martin JARVIS (British Antarctic Survey, Madingley Road, Cambridge, CB3 0ET, UK)

Meteor echoes have been extracted from SuperDARN HF radar data from Halley, Antarctica (76xS, 27xW) to produce an archive going back 10 years from which meteor winds can be derived. Although the SuperDARN radars provide no meteor height discrimination they have the unique advantage that their fan-like array of 16 beams gives spatial information on the derived mesospheric wind field. Examples of these wind fields are presented and, having removed the dominating semidiurnal and diurnal tides, the remaining wave signatures and intraseasonal variations are discussed.

**JSA20/W/55-A4** Poster **1200-09**

### THE VARIABILITY IN THE AIRGLOW INDUCED BY THE VERTICAL MOTION ASSOCIATED WITH TIDES.

Tai-Yin HUANG (CRESS, York University, 4700 Keele St., North York, Ontario, M3J 1P3, Canada. Email: taiyin@stpl.cress.yorku.ca)

Variability in the airglow was often observed and yet its origin is still not fully understood. Various studies suggest that the variability might be induced by the vertical motion associated with tides. Green line volume emission rate data at 5577 Å and meridional winds measured around fall equinox 1995 by the Wind Imaging Interferometer (WINDII) on the Upper Atmosphere Research Satellite (UARS) were analyzed. Atomic oxygen mixing ratio was derived from the volume emission rate using MSIS-90 model as the background atmosphere. Green line volume emission rate has a cubic dependence on the concentration of the atomic oxygen, thus any variation in the concentration will be amplified in the variations in the volume emission rate. Tidal amplitudes, phases and the background fields were derived using the least mean squared fitting method. Our studies show that the variations in the mixing ratio are consistent with the vertical motion associated with tides.

**JSA20/W/11-A4** Poster **1200-10**

### AN INVESTIGATION OF THE UPPER ATMOSPHERIC OPTICAL RADIATION IN THE LINE OF ATOMIC OXYGEN 557.7 NM IN EAST SIBERIA

A.V.Mikhalev, I.V.Medvedeva, A.B.Beletsky, E.S.KAZIMIROVSKY (Institute of Solar-Terrestrial, Russian Academy of Sciences, P.O.Box 4026, 664033, Irkutsk, Russia, email: mikhalev@iszf.irk.ru)

The results of photometer observations of the Earth's upper atmospheric radiation in the line of atomic oxygen 557.7 nm that were conducted in East Siberia (52N, 103E) during 1997-1998 within the PSMOS program are presented. The seasonal and diurnal dependencies for this emission are discussed. Anomalously high values of 557.7 nm emission are recorded in the winter months (end of January - beginning of February) of 1998, which are likely to be associated with the stratospheric warming observed in the East-Siberian region during this period.

**JSA20/W/09-A4** Poster **1200-11**

### WINDS AND TEMPERATURES AROUND THE SPORADIC SODIUM LAYERS OBSERVED WITH THE MU RADAR AND SODIUM LIDARS

T. NAKAMURA, H. Miyagawa, T. Tsuda (Radio Atmospheric Science Center, Kyoto University, Uji, Kyoto 611-0011, JAPAN, e-mail: nakamura@kurasc.kyoto-u.ac.jp); M. Abo, C. Nagasawa (Graduate School of Electrical Engineering, Tokyo Metropolitan University, Hachioji, Tokyo, Japan); T. D. Kawahara, K. Kobayashi, T. Kitahara, and A. Nomura (Faculty of Engineering, Shinshu University, Nagano, Japan)

Simultaneous observation of mesopause region have been carried out with the MU radar at Shigaraki (34.9N, 136.1E) and two Na lidars in Shigaraki and in Hachioji (35.6N, 139.4E). From lidar data, 15 events of sporadic sodium layer (Nas) were detected. Dynamical parameters, such as wind shears, temperatures, and indices for stability, at around the time and height of Nas have been observed by the MU radar. There are some cases indicating the strong westward shear or temperature enhancement accompanied Nas events, as reported by previous studies, but the statistical study for the all 15 events suggested that strong total wind shear correlates well with the Nas occurred at Shigaraki and Hachioji (mid-low latitudes) but no other clear correlations are found, which is similar to the study from the lidar observations in Hawaii (22N) during ALOHA-93 campaign.

**JSA20/W/03-A4** Poster **1200-12**

### CONSTITUENT OBSERVATIONS IN THE PRESENCE OF LARGE SCALE VERTICAL MOTIONS.

William E. WARD (CRESS/CRESTech, York University, Toronto, Canada)

In the mesosphere and lower thermosphere significant vertical motions occur as the result of the large amplitude tides and planetary waves present at these heights. In addition, the mixing ratio profiles of a number of constituents have significant gradients with height. These two aspects of this region result in significant variations in the concentration of these constituents at a given height. As a result interpretation of constituent observations must be made with care taking into account the variations associated with these motions. In this paper, the effects of these motions will be described and a strategy for correctly interpreting constituent observations at these heights outlined. These considerations are particularly important for the interpretation of the atomic oxygen distribution and its associated airglow in the mesopause region because of the strong vertical gradient in the atomic oxygen mixing ratio between 80 and 100 km.

**JSA20/W/29-A4** Poster **1200-13**

### SOLAR WIND INDUCED PERTURBATIONS IN THE METEOR REGION AS DETERMINED BY SPECTRAL WIDTH VARIATIONS IN THE SUPERDARN HF RADARS

Neil ARNOLD, Terry Robinson, Mark Lester, Paul Byrne and Peter Chapman (all at Department of Physics and Astronomy, University of Leicester, Leicester, LE1 7RH, UK, email: nfa1@ion.le.ac.uk)

Near range echoes from meteors in the SuperDARN oblique HF radar network allow the Doppler shift of the neutral winds to be measured near the mesopause. Information about the spectral width of the echoes is used to infer the mean altitude of the neutral wind layer as it is related to the ambi-polar diffusion coefficient. We show that the spectral width, and hence the observed height of the meteor region, is sensitive to a number of parameters such as operating frequency, zenith angle and season. A correction parameter is needed to provide long-term wind measurements at a constant height or pressure. In addition, the mean spectral width has been found to increase significantly during an interval of high geomagnetic activity. The data was consistent with modelled temperature variations in the upper mesosphere and lower thermosphere region. The technique is thus of value in monitoring the response of the atmosphere to changes in the solar wind at a number of Arctic and Antarctic stations.

**JSA20/E/26-A4** Poster **1200-14**

### SEPARATING NON-PROPAGATING FROM FRONTAL THERMOSPHERE GRAVITY WAVES

Th. Farges (LDG/DASE CEB3, France), J.P. Villain (LPCE Orleans, France), A. Bourdillon (Univ. de Rennes, France), P. VILA, (CETP/CNRS, St Maur des Fosses, France)

A re-activated Y-shaped bistatic network around Francourville (with 150 km reflection distance from the central transmitter and with zenithal probing) should contribute (from early 1999 on) to a discrimination of high latitude traveling disturbances against the ionospheric gravity wave activity generated in the local mesosphere below. High latitude sources can be composites of auroral electric and thermodynamic disturbances (K.D. Cole, 1996) with obvious DP1 origin, but also "quiet activity" source couplings (which can include large-scale stratospheric post-storm effects and local stratospheric jet-streams). Among the coupling processes, the disturbance dynamo and its fronts traveling to equatorial latitudes is of major concern for ionosphericists. On the basis of recent Windii and Hrdi average variations we also extract some particular European and Afro-Atlantic Windii data. The major solar eclipse of 11 August 1999 must provide a free special disturbance of all-levels supersonic shocks that should help testing: i) a twin dynamo and near-total sunset and sunrise noontime front, ii) the E-F near-simultaneous electric field coupling with unstable distribution above new layers, iii) the two lateral (lower midlatitude and higher latitude) "bow"-wave fronts of mesospheric origin. The perfectly defined scale and timing of the eclipse perturbation will be a great advantage for discriminating among these various contributions.

**JSA20/C/JSM01/E/32-A4** Poster **1200-15**

### THE INFLUENCE OF ION COMPOSITION ON THE SPECTRUM OF PLASMA IRREGULARITIES INDUCED BY NEUTRAL TURBULENCE IN THE MID-LATITUDE SPORADIC-E LAYER

Yurij KYZYUROV (Main Astronomical Observatory NASU, Kiev, 252650, Ukraine, email: kyzzyurov@mao.kiev.ua)

In the present report an analytic expression describing the spectrum of plasma density fluctuations generated by neutral air turbulence in the mid-latitude sporadic-E layer is discussed for the cases of different ion composition of the layer. The expression was derived from the system of 3-fluid equations taking into account processes of diffusion and recombination, in assumption that plasma density is a passive scalar field and turbulence of neutral gas is a Kolmogorov type one. The analysis of the irregularity spectrum under different values of the recombination coefficient shows that the presence of slowly recombining ions in the sporadic-E increases the slope of spectrum and the rms level of plasma density fluctuations created by atmosphere turbulence.

**JSA20/L/01-A4** Poster **1200-16**

### HORIZONTAL SHEAR FLOW AS A REASON OF FORMATION OF LARGE SCALE TIDS WITH SMALL PERIODS

Goderdzi DIBEBULIDZE, Stephan Chilingarashvili, Avtandil Pataraya (Town Department of Abastumani Astrophysical Observatory, A. Kazbegi ave.2a, 380060 Tbilisi, Georgia, email: gocha@dtapha.kheta.ge)

The ambipolar diffusion equation for the height distribution of electron density at the ionosphere F2-layer is solved by presence of neutral horizontal shear flow. By using this nonstationary solution the reaction of F2-region electron density on the evolution of atmospheric gravity waves (AGW) is investigated. The evolution of the AGW and the corresponding behavior of the height distribution of the F2-region electron density are described by characteristic time,  $t_a$ , of transient development of shear waves in horizontal shear flow. For great times  $t \gg t_a$  the gravity wave frequency tends to the isothermal Brunt-Vaisala frequency, which appears in the F2-layer by wavelike behavior of hmF2 and NmF2 with periods close to 16-20min, when the scale height of the neutral gas is  $H=60$ km. The shear wave which is due to the presence of horizontal shear flow, gives sufficient changes of the height profile of electron density for times of  $t < t_a$ . The intensity of mid-latitude F-region oxygen red line OI 630.0nm emission as an indicator of the propagation of the large scale TIDs with periods of 16-20min at magnetic disturbed days is used.

**JSA20/W/27-A4** Poster **1200-17**

### INVESTIGATION OF THE NATURAL VARIABILITY IN EXOSPHERIC HYDROGEN EMISSIONS

S. NOSSAL, F.L. Roesler (Both At Department Of Physics, University of Wisconsin, 1150 University Ave., Madison, WI 53706, USA, email: nossal@wisp5.physics.wisc.edu, roesler@wisp.physics.wisc.edu), J. Bishop (Computational Physics Inc., 2750 Prosperity Avenue, Suite 600, Fairfax, VA 22031, USA, email: jbishop@euler.cpi.com), R.J. Reynolds (Astronomy Department, University of Wisconsin, 475 N. Charter St., Madison, WI 53706, USA, email: reynolds@fosters.astro.wisc.edu)

The Wisconsin H-alpha Mapper (WHAM) is a ground-based Fabry-Perot instrument which has been making extensive high resolution observations of exospheric hydrogen Balmer-alpha emission intensities over the past two years. WHAM is remotely operable and is located at the Kitt Peak Observatory near Tucson, Arizona to take advantage of its high altitude and clear sky conditions. The majority of the WHAM exospheric data are the terrestrial byproduct of WHAM observations being taken to make an all-sky map of the interstellar medium hydrogen Balmer-



alpha emission. We have been using the exospheric Balmer-alpha component, present in all of the interstellar Balmer-alpha data, to systematically investigate the natural variability in these emissions over differing solar-geophysical conditions and a wide range of viewing geometries. We are now using these data to test exospheric model predictions. A long term goal of the WHAM and similar measurements is to use them to aid in separating natural variability from anthropogenic perturbations to the Balmer-alpha emissions. Exospheric hydrogen densities are predicted to increase by about 30-50% with a doubling in the tropospheric concentration of methane. We are carefully calibrating the WHAM data and are studying small scale effects on the data so as to make the WHAM data set a resource for future long term climatic comparisons. Interpretation of the exospheric Balmer-alpha emission data is complicated by the fact that the intensity which we observe is a function of both the exospheric hydrogen density structure and the magnitude of the solar excitation flux. We have begun using the *lyao\_rt* radiative transport model developed by one of us (JB) to untangle these dependencies in the data. At low shadow heights (below 1000 km), photoelectron impact excitation of Balmer-alpha is also important. In this presentation we will compare WHAM exospheric Balmer-alpha emission data with predictions from the *lyao\_rt* model incorporating the contributions from photoelectron impact. We vary the solar-geophysical inputs and the MSIS90 thermospheric boundary conditions through a range of geophysically reasonable values to explore their effect on the fits to the data. The signal-to-noise of the WHAM observations is sufficient to distinguish goodness of fit between model scenarios using different geophysical parameters as inputs. Also included in this presentation will be a brief overview of the WHAM exospheric observational and analysis program as well as the Fabry-Perot annular summing technique used to acquire the data.

**JSA20/E/08-A4** Poster **1200-18**

#### GEOMAGNETIC VARIATIONS CAUSED BY QUASI-TWO-DAY WAVE OF THE NEUTRAL WIND IN THE LOWER THERMOSPHERE

Manabu KUNITAKE (Hiraiso Solar Terrestrial Research Center, Isozaki, 3601, Hitachinaka, Ibaraki, 311-1202, Japan, Email: kunitake@crl.go.jp); Hiroshi Tachihara and Kiyohumi Yumoto (both at Department of Earth and Planetary Science, Kyushu University 33, 6-10-1, Hakozaki, Fukuoka, 812-0053, Japan, email: tachi@geo.kyushu-u.ac.jp, yumoto@geo.kyushu-u.ac.jp)

Quasi-Two-Day (QTD) geomagnetic variations can be seen in globally for January, 1993. In the interval, the neutral wind in the lower thermosphere has a large activity of the Quasi-Two-Day wave. The hypothesis that the geomagnetic variations are driven by the thermospheric wind is examined by comparison between the characteristics of the wind variations and those of geomagnetic variations. Three components at 20 ground stations were analyzed.

(1) The major component is Y(EW) near the equator region, contrasting to that the major is X(NS) or Z(vertical) in the low and middle latitudes. (2) The geomagnetic variation in the low latitude regions in the southern hemisphere shows some phase shifting along longitudes systematically. East squares fitting to the phase distribution results in that the zonal wave number of the variation is about three. These characteristics are consistent with the characteristics of neutral wind variation.

(3) In the western pacific longitudinal zone, the phase comparison of X(NS) component of the geomagnetic variation between hemispheres shows that the variation is not out-of-phase but in-phase. After comparing it with the wind pattern, it means that the interhemispheric coupling through geomagnetic field lines which connect both hemispheres should be taken into consideration in this case.

**JSA20/W/31-A4** Poster **1200-19**

#### BEHAVIOUR OF SUBAURORAL LOWER THERMOSPHERE AND MESOPAUSE TEMPERATURE DURING POLAR STRATOSPHERE WINTER STRONG WARMINGS

S. V. NIKOLASHKIN, V. M. Ignatyev, V. A. Yugov, V. N. Alexeyev (Institute of Cosmophysical Research and Aeronomy, 31, Lenin ave., Yakutsk, 677891, Russia, email: s.v.nikolashkin@sci.yakutia.ru)

The relationship between temperatures of stratosphere (~24 km), mesosphere (~87 km) and lower thermosphere (~97 km) on data of the Fabry-Perot interferometer temperature measurements in night atmosphere by thermal broadening of OI 557.7 nm emission in 1979-1991, and spectrograph data on intensity distribution of rotational structure of the band OH(6.1) in 1965-1970 near Yakutsk (62N, 129.7E) is studied.

It is shown that in a few days after beginning of the moment of winter strong (major) warming peak in the polar stratosphere is observed the temperature decreasing in a subauroral mesopause and lower thermosphere. The intensity and the time of beginning of these atmosphere layers cooling depends on warming magnitude in stratosphere.

The obtained result points out on existence of role of large-scale wave processes in a formation of mesosphere and lower thermosphere temperature regime in winter period.

**JSA20/W/46-A4** Poster **1200-20**

#### ARTIFICIAL PERIODIC INHOMOGENEITIES: STUDIES AND OUTLOOKS

N.V.BAKHMETEVA, V.V.Belikovich, E.A.Benediktov, A.V.Tolmacheva (Radiophysical Research Institute, Nizhny Novgorod, Russia, e-mail: natali@nirfi.sci-nnov.ru)

The review of the experiments being performed at SURA heating facility using artificial periodic inhomogeneities (API) is presented. The formation of the API and measurements of the ionospheric and atmospheric parameters using the API are discussed. The API have been studied only at NIRFI for 15 years old. Some interesting results were obtained: 1) The relative concentration of negative oxygen ions in the D-region; 2) A model of the D-region; 3) Irregular structure of the lower ionosphere including the separation of the regular E-layer, the sporadic layers, additional layers in the valley; 4) The neutral temperatures and densities at the height region at 100-120 km were measured; 5) Vertical motion velocities and the parameters of the internal gravity waves in the D- and E-regions of the ionosphere were obtained; 6) Seasonal-daily variation of the vertical velocity at the heights 70-120 km were studied; 7) Parameters of the internal gravity waves and its spectral characteristics; 8) N(h)-profiles in the interlayer valley between E- and F-regions were measured and the appearance sporadic layers was testified; 9) Some data of electron and ion temperatures in the F-region. Use API could make it possible to study coupling between ionospheric layers. The work is supported by Russian Foundation of Basic Research under grants N 96-05-65130 and 97-05-64392.

**JSA20/E/27-A4** Poster **1200-21**

#### EARLY RESULTS FROM THE TERRIERS MISSION

S. CHAKRABARTI, D. Cotton, T. Cook, A. Stephan, J. Vickers, V. Taylor, S. Stephan, F. Kamalabadi, J. Baumgardner, M. Mendillo, W. Oliver (all at Center for Space Physics, 725 Commonwealth Avenue, Boston University, Boston, MA 02215; email: supc@bu.edu) P. Bernhardt (Naval research Laboratory, Washington, D. C. 20375) J. Foster (Haystack Observatory, Westford, MA 01886)

The Tomographic Experiment Using Radiative Recombinative Ionospheric EUV and Radio Sources (TERRIERS) is a small satellite mission whose primary goal is to understand the ionosphere-Thermosphere-Sun coupling through simultaneous observations of Extreme Ultraviolet (EUV) emissions. It has been shown that one feature (30.4 nm) of the highly variable solar EUV emissions is responsible for approximately 50% of all photoelectron flux responsible for many airglow emissions. TERRIERS will use a newly developed optics-free spectrometer to observe solar flux in 20 - 50 nm. A single-element imaging spectrograph will observe airglow in the 80 - 140 nm range where emission features from most of the atmospheric species are present and a dual frequency radio beacon will measure Total Electron Content (TEC) simultaneously from several ground stations. In addition, ground based optical spectrograph and incoherent scatter data will be used in observational campaigns. TERRIERS will be placed in a 550 Km altitude, 8:30AM/8:30PM circular orbit. Because it will be in a sun-synchronous, polar orbit, it will have the opportunity to study many geophysical phenomena such as Equatorial Spread F, mid-latitude trough and aurora. It is scheduled for launch in April, 1999. As an example of thermosphere-ionosphere coupling, we will examine the 83.4nm dayglow which is produced primarily by photoionization of atomic oxygen. The photons undergo multiple scattering by O+ ions and are absorbed by molecular nitrogen, oxygen and atomic oxygen gas. Thus, a complete description of 83.4nm airglow requires a knowledge of the coupling between solar EUV, and thermospheric and ionospheric density profiles. In this talk we will present TERRIERS observations of 83.4nm airglow.

**JSA20/W/42-A4** Poster **1200-22**

#### API TECHNIQUE AND STUDIES OF THE IRREGULAR STRUCTURE OF THE LOWER IONOSPHERE

N.V.BAKHMETEVA, V.V.Belikovich, E.A.Benediktov, A.V.Tolmacheva (Radiophysical Research Institute, Nizhny Novgorod, Russia, e-mail: natali@nirfi.sci-nnov.ru)

The artificial periodic inhomogeneities of the ionospheric plasma (API) have been discovered in 1975 in the experiments on the ionospheric plasma modification by a powerful radio emission. More than ten new methods of the different ionospheric parameters measurements are developed. For example, API technique allows to study the irregular structure of the lower ionosphere including the sporadic layers and to determine the turbulent velocities and the turbopause height. The measurements of amplitude and phase of scattering signals from API with height resolution equal to 1.2 km have been carried out in August, 1996 using SURA heating facility. The analysis discover that the height dependence of the relaxation time of the scattering signal shows an inclination at a height of about 100 km. The height of the inclination corresponds to the turbopause height where the turbulent mixture finishes and diffusion separation begins. The vertical component of turbulent velocities below this height have been determined. Besides it was detected the inhomogeneity of some height profiles of the relaxation time above 100 km. The analysis shows that local maxima of relaxation time are accompanied by the increase of the amplitude of a scattering signal. We suppose that sporadic E layers may be caused of the local maxima. The work is supported by Russian Foundation of Basic Research under grants N 96-05-65130 and 97-05-64392.

**JSA20/W/43-A4** Poster **1200-23**

#### RELATIONSHIP THE SUBAURORAL MIDDLE ATMOSPHERE TEMPERATURE WITH SOLAR ACTIVITY AND QBO PHASES

S. V. NIKOLASHKIN, V. M. Ignatyev, V. A. Yugov and V. N. Alexeyev (Institute of Cosmophysical Researches and Aeronomy, 31, Lenin ave., Yakutsk, 677891, Russia, e-mail: s.v.nikolashkin@sci.yakutia.ru)

The subauroral lower thermosphere and mesosphere temperature relationship with solar radi flux density on wavelength 10.7 cm (F10.7) and quasi-biennial oscillations (QBO) phases based statistical analysis of the optical measurements data are studied.

It is showed that (1) in winter exists the negative correlation between subauroral lower thermosphere temperature and F10.7 index; (2) in the west phase of QBO between F10.7 index and temperature variations are observed a positive correlation at stratosphere and negative - at the mesopause and lower thermosphere. In the east phase for stratosphere and lower thermosphere is observed the negative correlation but for mesopause - weak positive one. This result points out on existence of the dynamic relationship between considered atmosphere layers.

**JSA20/E/03-A4** Poster **1200-24**

#### DIURNAL HEIGHT DEPENDENCE OF THE VARIATION OF ELECTRON CONCENTRATION AT THE LEVELS 150 KM - 205 KM DEDUCED FROM VERTICAL IONOSPHERIC SOUNDING DATA

Petra SAULI, Josef Boska (Institute of Atmospheric Physics, Czech Academy of Sciences, Bocni II/1401, 141 31 Prague 4 - Spriřov, Czech Republic, e-mail: Pkn@ufa.cas.cz)

Analyses of the height dependence of the variation of electron concentration are based on the ionosonde data measured at the observatory Pruhonic (15E, 50N). The campaign was run under low solar and geomagnetic activity conditions on 27 October - 7 November 1997. Repetition time of 5 minutes of the vertical ionospheric sounding was used during the campaign. The short-time deviations from a smoothed diurnal behaviour were derived to demonstrate the short-time variability of the electron concentration at levels from 150 km to 205 km. The average deviations show expressive height and diurnal variation. A large increase of deviations with height appears to be regular feature in the range 170-185 km. Height dependence of the gradient of the electron concentration was studied, as well. This gradient reveals among others a strong diurnal variation.

**JSA20/E/08-A4** Poster **1200-25**

#### GEOMAGNETIC VARIATIONS CAUSED BY QUASI-TWO-DAY WAVE OF THE NEUTRAL WIND IN THE LOWER THERMOSPHERE

Manabu KUNITAKE (Hiraiso Solar Terrestrial Research Center, Isozaki, 3601, Hitachinaka, Ibaraki, 311-1202, Japan, Email: kunitake@crl.go.jp); Hiroshi Tachihara and Kiyohumi Yumoto (both at Department of Earth and Planetary Science, Kyushu University 33, 6-10-1, Hakozaki, Fukuoka, 812-0053, Japan, email: tachi@geo.kyushu-u.ac.jp, and yumoto@geo.kyushu-u.ac.jp)

Quasi-Two-Day (QTD) geomagnetic variations can be seen in globally for January, 1993. In the interval, the neutral wind in the lower thermosphere has a large activity of the Quasi-Two-Day wave. The hypothesis that the geomagnetic variations are driven by the thermospheric wind is examined by comparison between the characteristics of the wind variations and those of geomagnetic variations. Three components at 20 ground stations were analyzed. (1) The major component is Y(EW) near the equator region, contrasting to that the major is X(NS) or Z(vertical) in the low and middle latitudes. (2) The geomagnetic variation in the low latitude regions in the southern hemisphere shows some phase shifting along longitudes systematically. East squares fitting to the phase distribution results in that the zonal wave number of the variation is about three. These characteristics are consistent with the characteristics of neutral wind variation. (3) In the western pacific longitudinal zone, the phase



## INTER-ASSOCIATION

comparison of X(NS) component of the geomagnetic variation between hemispheres shows that the variation is not out-of-phase but in-phase. After comparing it with the wind pattern, it means that the interhemispheric coupling through geomagnetic field lines which connect both hemispheres should be taken into consideration in this case.

**JSA20/W/56-A4** Poster **1200-26**

### PARAMETERISATION OF THE LOCAL AND NONLOCAL PROCESSES IN THE THERMOSPHERIC ENERGY BUDGET BASED ON DE-2 SATELLITE DATA

Tarun Kumar Pant and R. SRIDHARAN (Physical Research Laboratory, Navrangpura, Ahmedabad - 380 009, India)

It is known that the in situ [e.g. DE-2 (WATS)] satellite measured thermospheric temperatures over low latitudes exhibit significant deviations from the thermospheric model (MSISE-90) predictions. The existence of such deviations between the two can be due to two main factors. One is that, all the processes and energy inputs for quiet and disturbed geophysical conditions are not adequately accounted for by the model, especially so, for low latitudes. The other factor is that the low latitude thermosphere ionosphere system (TIS) is continuously under the influence of many large scale local processes which might contribute significantly to its thermal balance but are not yet accounted for by the MSIS model. The process of Equatorial temperature and wind anomaly (ETWA) is perhaps one of the most important aspect in this context. In the present study, a method for parameterisation of the energy inputs during varying geophysical conditions in terms of rate of change of magnetospheric ring current based on the characteristic thermospheric response time during different seasons has been developed. It is proposed that the various current systems operative in the ionosphere and magnetosphere at anytime could be used as an indices for the fast temporal changes occurring in the neutral temperatures. It has been found that these changes could be represented by the temporal rate of change in the ring current index i.e. Dst. Further, to parameterise the ETWA associated temperature variations, the DE-2 satellite data on composition and temperature has been made use of. Since, the process of ion-drag and chemical heating are expected to be important for the generation of ETWA, an estimation of the contributions from both these processes was made. The final exercise dealing with all the three i.e. the current systems, ion-drag and chemical heating which contribute towards the low latitude thermospheric temperatures and its variabilities was performed for a representative location for more than 30 days during year 1981-82. The estimated contributions were added to the standard MSIS model which is taken as the base purely accounting for the solar controlled processes. After the inclusion of all the three terms to the model, the observed temperatures and their variabilities are reproduced fairly well on most of the occasions except for a few exceptions. Even on the very few exceptional cases, the variabilities are fairly well reproduced leaving the difference only in the absolute magnitude. This has to be necessarily due to an significantly long duration and which has not yet been accounted for. These results, first of their kind, would be presented and discussed.

**JSA20/W/08-A4** Poster **1200-27**

### A COMPARISON OF HIGH-LATITUDE THERMOSPHERIC ION AND NEUTRAL TEMPERATURES FROM GROUND BASED MEASUREMENTS

K. Cierpka, M. KOSCH, M. Rietveld, K. Schlegel and T. Hagfors (Max-Planck-Institut fuer Aeronomie, Max-Planck-Str. 2, 37191 Katlenburg-Lindau, Germany, email: cierpka@linmpi.mpg.de)

Direct measurements of neutral temperature in the lower and upper thermosphere are obtained by a Fabry-Perot interferometer (FPI) located within the Scandinavian auroral zone. The EISCAT radar, located only 50 km westward from the FPI, provides measurements of ion temperatures in the E- and F- region as well as ionospheric electric fields. FPI neutral temperatures are compared with MSISE90 model predictions and EISCAT ion temperatures for different altitude ranges. Without an external energy source, the ion and neutral temperature should be equal. Significant enhancements of the ion temperature over the neutral temperature indicate Joule heating, a parameter which EISCAT can estimate. For periods when electric field data are available, the ion energy equation is used to predict the effect of Joule heating. This is compared to measured temperature differences.

**JSA20/W/08-A4** Poster **1200-28**

### PERTURBATION OF ELECTRON DENSITY DISTRIBUTION IN THE DAYTIME MID-LATITUDE F2 REGION IONOSPHERE ASSOCIATED WITH A GIANT THUNDERCLOUD

Vitali KIM, Valeri Hegai (both at IZMIRAN, Troitsk, Moscow Region, 142092 Russia, email: kimvp@izmiran.rssi.ru)

Changes of electron density in the daytime mid-latitude F2 region ionosphere associated with dc giant thundercloud electric fields penetrated into the ionosphere are calculated. It is obtained that the F2 region electron density is noticeably disturbed within an area with horizontal dimensions of about 500 km. The horizontal distribution of electron density in the perturbed area becomes irregular in course of time. The irregularities' sizes range from 15 to 150 km one hour after thundercloud formation. The changes of electron density are stronger in the upper F2 region where their amplitude can be as large as 40% relative to undisturbed values of electron density.

**JSA20/E/11-A4** Poster **1200-29**

### RESEARCH OF TROPOSPHERIC FRONTS AND INTERIOR GRAVITY WAVES INFLUENCE ON IONOSPHERIC IRREGULARITIES BEHAVIOUR

Oleg A. Litvinenko, Roman O. KRAVETZ, Svetlana K. Panishko (URAN-4 observatory, Radioastronomical institute, Pushkinskaya str. 37, 270011 Odessa, Ukraine. Email: uran@paco.net)

The radioastronomical monitoring of ionosphere by the radio telescope URAN-4 (Odessa, Ukraine) is used for observation of mean-scale ionospheric irregularities. The observations were carried out in decimeter radiorange. Ground-base sounding of an ionosphere on fixed frequencies was simultaneously carried out. By means of a measurement of the dopler frequency shift of reflected signals this mode allows to discover large-scale periodic ionospheric irregularities which are identified as interior gravity waves. The joint analysis of time series of intensity and characteristic sizes variations of ionospheric irregularities and time series of intensity and phase of interior gravitational waves was carried out. Correlation between these time series was not detected. In difference from gravitational waves, tropospheric fronts rendered the strong influence on a behaviour of ionospheric irregularities, which we has observed with the help of radio telescope.

**JSA20/E/07-A4** Poster **1200-30**

### AGW SPECTRA IN THE ELECTRON DENSITY

Joseph Boska (Intitute of Atmospheric Physics, Academy of Sciences, Bocni II cp 1401, 14131 Praha 4, Czech Republic, email: boska@ufa.cas.cz); Diego MARIN, Gloria Miro and Benito A de la Morena

(all at Atmospheric Sounding Station El Arenosillo, National Institute of Aerospace Technology, Ctra. San Juan-Matalascanas km. 33, 21130, Mazagon-Huelva, Spain, email: marinsd@inta.es); Miguel Herraiz (Geophysics and Meteorology Dp., Faculty of Physics, Complutense University, 28040, Madrid, Spain, email: mherraiz@eucmax.sim.ucm.es); Edward Kazimirovsky (Siberian Institute of Terrestrial Magnetism, Ionosphere and Radio Propagation, Academy of Sciences, 664033, PB 4026, Irkutsk, Russia, email: edkaz@iszf.irk.ru)

The datasets of 5-min measurements by ionosondes in El Arenosillo, Spain (37.1° N; 6.75° W; 41.37° dipole geom. lat.) allow to use ionospheric parameters data for the studying the gravity wave activity in the midlatitude upper ionosphere in the period range 5 - 120 min. The comparison of data has revealed some features of the resulting AGW spectra including similarity and some distinctions possibly caused by AGW dependence on the season, latitude, and regional peculiarities of the lower atmosphere.

**JSA20/W/48-A4** Poster **1200-31**

### THE RESPONSE OF THE TOPSIDE IONOSPHERE TO THE TOTAL SOLAR ECLIPSE OF FEBRUARY 26, 1998

B. MACPHERSON, S. A. Gonzalez, M.P. Sulzer (all at National Astronomy and Ionospher Center, Arecibo Observatory, HC3 Box 53995, Arecibo, PR 00612 U.S.A. Email: bmacpher@naic.edu, sixto@naic.edu, sulzer@naic.edu); G. J. Bailey (The Upper Atmosphere Modelling Group, Applied Maths Department, The Hicks Building, University of Sheffield, Sheffield, England. Email: g.bailey@sheffield.ac.uk); F. Djuth (Geospace Research, Inc., El Segundo, California, U.S.A. Email: djuth@netcom.com); R. Rodriguez (Plasma Physics Division, Naval Research Laboratory, Washington, D.C., U.S.A. Email: rodriguez@ccf.nrl.navy.mil)

The Arecibo Incoherent Scatter Radar was used to observe the response of the topside ionosphere during the total solar eclipse of 26 February, 1998. The path of totality passed south of Puerto Rico with the maximum degree of obscuration at Arecibo being 90%. The data were taken using an experimental technique which allows measurements from around 146 km to 2400 km altitude. This paper will present what we believe to be the first observation of the response of the topside ionosphere to a solar eclipse. These results, together with the lower altitude measurements, will be used to study the coupling and energy transfer of the F-region and topside ionosphere during the eclipse.

**JSA20/W/45-A4** Poster **1200-32**

### VARIATIONS OF TOTAL ELECTRON CONTENT DURING A GEOMAGNETIC STORM IN ARGENTINA

Blas Fde Haro Barbás, Victor H. Ríos, Antonio Pérez Gómez, Marcelo Santillán (Laboratorio de Técnicas Satelitales, Av. Independencia 1800, CP (4000), S. M. de Tucumán, Argentina)

In the present work we studies the variations of total electron content (TEC) caused by a happened geomagnetic storm between days 9 to the 12 of April of 1997 by means of the analysis of data pertaining to three Argentine permanent stations: Tucumán (-26,3 Lat; -65,13 Long), San Juan (-31,4 Lat; -68,23 Long) and Tierra del Fuego (-54,4 Lat; -68,56 Long); and its corresponding comparison with the measurements of such days obtained during 1998. The determination of the TEC became from measurements of observable of code and the phase of the signals transmitidas by the satellites of the Global Positioning System GPS. It is possible to be observed that the values obtained during the days of the storm exceed approximately in a 30% to the values corresponding to the quiet days. Also the variation of the TEC with the latitude due to the different geographic positions from the analyzed stations is observed.

**JSA20/W/44-A4** Poster **1200-33**

### PROPAGATION OF MAGNETIC STORMS EFFECTS ON IONOSPHERE FROM HIGH TOWARDS LOW LATITUDES

O.M.Pirog, N.M.Polekh, L.V.Chistyakova , and E.S. KAZIMIROVSKY (Institute of Solar-Terrestrial Physics, 664033 Irkutsk, P. O. Box 4026, Russia, e-mail: edkaz@iszf.irk.ru)

Magnetic storm effects on ionosphere were investigated. Data from ionospheric stations located in the range of longitudes 90°-175° E and invariant latitudes 51°N-51°S were used in this study. The intense magnetic storms were considered, which were observed at the equinox period, but correspond to different solar activity. At all stations, one day before the storm and during initial phase (daytime), foF2 increased significantly, then at midlatitudes it was decreasing with the progression of the storm, and during the explosive phase it dropped by a factor of 1-1.5 as against the undisturbed level. Negative disturbances were also observed at night. At low latitudes, the storm maximum and the recovery phase (daytime) showed abrupt changes in foF2 relative to the undisturbed level, with an amplitude of up to 3 MHz and a period of up to two hours. A change of the character and sign of disturbances occurs at latitudes corresponding to L<1.5. Es of auroral type, was observed to L=2 in the storm maximum. The above mentioned effects are most pronounced during minimum SA. The observed variations of ionospheric parameters were caused by a strong contraction of the magnetosphere and by the equatorward displacement of the main ionospheric trough. The ring current energy dissipation affects the global circulation rearrangement of the upper atmosphere, the neutral component at midlatitudes starts to change its composition thus affecting foF2 variations. During the main phase, a contraction of the plasmapause can lead to observed wave-like changes in electron density in the F2-layer maximum at low latitudes.

Friday 23 July PM

**JSA20/W/37-A5** Poster **1200-01**

### KELVIN WAVES IN THE MESOSPHERE AND THERMOSPHERE

J.M. FORBES (Department of Aerospace Engineering Sciences, Campus Box 429, University of Colorado, Boulder, CO 80309-0429, USA); M.E. Hagan (High Altitude Observatory, National Center for Atmospheric Research, P.O. Box 3000, Boulder, CO 80307, USA)

Satellite and radar observations near the equator have established the existence of "ultra-fast" Kelvin waves in the mesosphere and lower thermosphere (40 to 110 km), with periods between about 3 and 6 days and vertical wavelengths in excess of 20 km. Using the global-scale wave model (GSWM) we simulate the propagation of Kelvin waves in the presence of realistic mean winds and dissipation from the troposphere to the upper thermosphere. We consider waves with periods of 3 and 6 days and zonal wavenumbers, s=1 and s=2. By calibrating the tropospheric latent heat source to match observed amplitudes, we are able to provide realistic estimates of the penetration of these waves above 110 km and to predict their latitudinal structures. Temperature and wind amplitudes achieved by the 3-day s=1 wave exceed 20 K and 30 m/sec in the 100 to 150 km regime. Significant interhemispheric asymmetries are found and attributed to the interplay between Doppler-shifting of the wave period and the accompanying influences of eddy and molecular dissipation. The mean-flow accelerations due to dissipation of these Kelvin waves are also estimated.

JSA20/W/10-A5 Poster 1200-02

**COORDINATED OBSERVATIONS OF QUASI-2-DAY OSCILLATION IN EQUATORIAL ELECTROJET STRENGTH AND MESOSPHERIC WINDS**

S. GURUBARAN, T. K. Ramkumar, S. Sridharan (Equatorial Geophysical Research Laboratory, Indian Institute of Geomagnetism, Krishnapuram, Tirunelveli 627 011, India, email: gurubara@md3.vsnl.net.in) R. Rajaram (Indian Institute of Geomagnetism, Colaba, Mumbai 400 005, India, email: rrajaram@iig.iiigm.res.in)

The quasi-2-day oscillation (QTDO), believed to be a manifestation of the westward propagating mixed Rossby-gravity normal mode with zonal wavenumber 3, is an ubiquitous feature of the middle atmosphere. Several studies in the past indicated that the QTD type of oscillations exist in the ionospheric parameters. Though these features are thought of originating in the mesospheric QTD wind oscillation, the mechanisms for producing them are not known. Observations of mesospheric winds with a medium frequency (MF) radar operated from Tirunelveli (8.7 degrees N, 77.8 degrees E, geographic, 0.3 degree N dip), India, since the middle of 1992, are being made use of in the present work and the characteristics of the quasi-2-day oscillation in zonal and meridional winds are brought out. The equatorial electrojet (EEJ) strength, derived from ground-magnetic field variations, is determined for the same period, and the QTDO events are identified. It is noted that there is a reasonable correlation between the occurrence times of the QTDO in the EEJ strength and the mesospheric winds, as revealed by the observations.

JSA20/W/23-A5 Poster 1200-03

**DAYTIME MESOPAUSE 'OH' ROTATIONAL TEMPERATURES FROM EQUATORIAL AND LOW LATITUDES USING GROUND BASED OPTICAL METHODS**

R. SRIDHARAN, Alok Taori (Physical Research Laboratory, Ahmedabad -380009, INDIA)

In spite of the crucial role played by the mesopause in coupling the lower and upper atmosphere, this region is one of the least explored due to its relative inaccessibility. Mesopause temperature is one of the sensitive parameters, that gives clues to the complex processes occurring there in. Till recently, the ground based optical methods had been restricted only to clear sky, moonless periods of a night. In this paper we present some of the first of its kind results, on the daytime mesospheric OH (8,3) rotational temperatures, estimated from the measurements of the relative intensities of the rotational lines in the same vibrational band, using the unique multiwavelength daytime photometer from Tirunelveli (8.7N, 77.8E) and Kolhapur (16.8N, 74.2E). After validating the initial results using near simultaneous WINDII data, continuous data have been obtained from both the locations revealing - (1) Significant deviations (+/- 30K) from the models on several occasions and also large day to day variabilities and (2) Oscillatory features with periods ranging from 0.5 - 6.0 h. The data were subjected to spectral analysis on all the days. It is seen that periods ranging from 0.5 - 1.5h stood out prominently. These unique results would be presented and discussed.

JSA20/E/24-A5 Poster 1200-04

**PLAUSIBLE EXPLANATION FOR THE EQUATORIAL TEMPERATURE AND WIND ANOMALY (ETWA) BASED ON CHEMICAL AND DYNAMICAL PROCESSES**

Tarun Kumar Pant, R. SRIDHARAN (Physical Research Laboratory, Navrangpura, Ahmedabad - 380 009, India)

One of the important discoveries based on the Dynamics Explorer (DE-2) data in the recent years had been the Equatorial temperature and wind anomaly (ETWA) [Raghavarao et al. 1991], which is a perfect example for a closely coupled interacting equatorial thermosphere ionosphere system (TIS) and has important implications with regard to the overall energy budget of low latitude TIS. Earlier attempts to theoretically simulate ETWA had been with limited success. In order to fully understand the processes involved in the generation of ETWA, so as to be able to parameterise the same, a detailed exercise was undertaken using DE-2 satellite data. It has been shown that both the Chemical heating due to the exothermic reactions and the frictional heating due to the ion-drag effects, contribute significantly to the generation of ETWA. Simultaneously measured ionospheric and thermospheric parameters both during day and night time by DE-2 have been made use of in coming to the above conclusion. This enables one to quantify their contribution and paves the way for taking into account the local processes while formulating models for the equatorial thermosphere.

JSA20/W/05-A5 Poster 1200-05

**LONG TERM VARIATIONS IN THE EQUATORIAL F-REGION USING OI 630NM OBSERVATIONS**

FAGUNDES, P.R., (Instituto de Pesquisas e Desenvolvimento, IP&D/UNIVAP, Av. Shishima Hifumi, 2911, Urbanova - S. José Campos, SP, Brazil-CEP 12244-000, email: fagundes@univap.br); Y. Saha, A.A. Pimenta, J.A. Bittencourt, H. Takahashi (Instituto Nacional de Pesquisas Espaciais, INPE, CP 515, S.P. S. J. dos Campos -Brazil-CEP 12201-970)

The OI 630 nm nightglow emission is widely used to monitor thermosphere/ ionosphere processes as well as large scale ionospheric plasma irregularities (plasma bubbles). Simultaneous observations of the OI 630 nm emission using multi-channel tilting filter-type zenith photometers have been carried out in Brazil at Cachoeira Paulista (22.7°S, 45.0°W) and Fortaleza (3.9°S, 38.4°W) during the last solar cycle. Also, an all-sky (180° field of view) imaging system for observing the OI 630 nm nightglow emission is operational at Cachoeira Paulista. The observed averaged intensities changes from 60(±44) R to 223(±90) R at C.P. and from 70(±40) R to 50(±41) R at Fortaleza between years of low to high solar activity, respectively, suggesting that the equatorial ionospheric anomaly region (C.P.) is more affected by the solar flux changes than the equatorial region (FOR.). Also, it was noticed that during the solar activity maximum the frequency of occurrence plasma bubbles are larger than during the low solar activity.

JSA20/E/16-A5 Poster 1200-06

**DP2 ELECTRIC FIELDS IN THE MIDNIGHT DIP EQUATORIAL IONOSPHERE**

J. Hanumath SASTRI (Indian Institute of Astrophysics, Bangalore, India); H. Lühr (GeoForschungsZentrum Potsdam, Germany); H. Tachihara, T. I. Kitamura (Department of Earth and Planetary Sciences, Kyushu University, Hakozaki, Fukuoka, Japan); J.V.S.V. Rao (Indian Institute of Astrophysics, Bangalore, India)

Measurements with a HF Doppler sounder at Kodaikanal (10.2N, 77.5 E, dip 4 N) revealed conspicuous quasi-periodic fluctuations (period 25-35 min) in F region vertical plasma drift, Vz, in the interval 1916-2026 UT on 23 December 1991 (Ap=14, Kp < 4-). The fluctuations in F region vertical drift are found to be coherent with variations in north-south (Bz) component of interplanetary magnetic field (IMF) and with geomagnetic H/X components at high-middle

latitude locations both in the sunlit and dark hemispheres. They are also coherent with H-field variations in the dip equatorial region on the dayside. We interpret the disturbance in F region vertical plasma drift over Kodaikanal as the signature of DP2 electric field fluctuations in the midnight dip equatorial ionosphere.

JSA20/W/24-A5 Poster 1200-07

**EQUATORIAL PLASMA BUBBLE DEVELOPMENT AND ZONAL DRIFT DURING THE 26 AUGUST 1998 MAGNETIC STORM**

M. A. ABDU, H. Talahashi, I. S. Batista, E. R. de Paula, J. H. A. Sobral, N. B. Trivedi and A. F. Medeiros (Instituto Nacional de Pesquisas Espaciais- INPE, São Jose dos Campos, Brazil)

Equatorial ionospheric plasma bubble development and dynamics during the major magnetospheric storm of 26 August 1998 are investigated based on the data collected by two digisondes, an all-sky 630nm imager, GPS scintillation receivers and two magnetometers operated in the equatorial and low latitude sites in Brazil. The disturbances in the auroral electrojet activity (represented by AE indices) and associated disturbances in equatorial magnetograms had their onsets at 11UT on the 26th. Large enhancements in these disturbances produced large equatorial F region vertical plasma drift (eastward electric field) in the evening sector over Brazil which triggered a series of intense plasma bubbles, the event lasting the entire night, as observed by the all-sky imager at Cachoeira Paulista and digisondes at the equatorial site, Sao Luiz, and at the low latitude site, Cachoeira Paulista. Under quiet conditions plasma bubbles do not generally occur over Brazil in August. A notable aspect of the dynamics of the bubbles on the night of 26-27 Aug. was their westward zonal drift, in contrast to the well-known eastward drift observed under quiet conditions. The analysis to be presented will focus on the possible causes of the bubble westward drift as arising from (a) Hall electric field arising from prompt penetration magnetospheric electric field interacting with the enhanced ionospheric conductivities produced by storm associated particle precipitation in the South Atlantic magnetic anomaly zone as recent evidences have suggested (Abdu et al., Geophys. Res. Lettrs. 25, p.4137, 1998) and/or (b) disturbance dynamo associated westward thermospheric winds resulting from the storm associated heating of the high latitude I-T.

JSA20/E/06-A5 Poster 1200-08

**AN EQUATORIAL AND LOW LATITUDE TIME-DEPENDENT IONOSPHERIC MODEL**

Scott DANN, Robert Stening (School of Physics, University of New South Wales, Sydney, 2052, Australia, email: sadn@newt.phys.unsw.edu.au)

A new version of the Chan and Walker model has been developed, capable of running under a variety of solar activity levels and at any longitudinal sector. The model solves the plasma continuity equation for the total ion density, as well as the equations of motion of the neutral species to obtain a self consistent estimate of the neutral wind velocities. The non-linear terms in the neutral equations of motion pose a particular problem in this type of model, which uses input thermospheric data. By solving for the neutral wind velocities, this model lends itself to studying the symmetry of the equatorial anomaly. The effects of trans-equatorial meridional winds and the resulting interhemispheric transport of ionization, often give rise to large asymmetry in the development of the anomaly crests, the maximum crest electron densities and the latitudinal extent of the plasma fountain.

JSA20/W/50-A5 Poster 1200-09

**SIMULTANEOUS GPS AND OI 6300 ALL-SKY IMAGING OBSERVATIONS DURING LARGE SCALE EQUATORIAL IONOSPHERIC IRREGULARITIES**

FAGUNDES, P.R. (Instituto de Pesquisas e Desenvolvimento, IP&D/UNIVAP, Av. Shishima Hifumi, 2911, Urbanova, S. José dos Campos, SP, Brazil-CEP 12244-000, fagundes@univap.br); E. R. de Paula, Y. Saha, (Instituto Nacional de Pesquisas Espaciais, INPE, CP 515 - S.P. São José dos Campos, Brazil-CEP 12201-970)

Global Position System (GPS) is now a days the most common instrument for navigation and the coordinates of any location on the earth (latitude longitude and altitude) can be obtained using the GPS. However, it is well known that equatorial large scale ionospheric irregularities have strong influence on transionospheric radiowave communications and on GPS performance causing amplitude and phase fluctuations in radiowaves crossing these irregularities. The equatorial F-region irregularities have scale sizes from meter, or less, to large scale plasma depletions, or bubbles, extending north-south to a few thousands of kilometers (aligned to the earth's magnetic field lines) with east-west widths of few hundred kilometers. The large scale irregularities are monitored at Cachoeira Paulista (23 S, 45 W) by an all-sky (180 field of view) imaging system for observing the OI 630 nm nightglow emission and the observations provide informations about the size, position and dynamics of these irregularities. Since these irregularities affect the performance of the GPS, we carried out an analysis of the simultaneous observations of the GPS data (latitude, longitude and altitude) and all-sky imaging to estimate deviations in the GPS data during different geophysical conditions. In this paper we present the GPS performance with/without large scale ionospheric irregularities and quiet/disturbed geomagnetic conditions.

JSA20/W/28-A5 Poster 1200-10

**THE IONOSPHERIC PLASMA AND ELECTRODYNAMICS INSTRUMENT (IPEI) ONBOARD ROCSAT-1: MISSION OPERATION AND DATA PRESENTATION**

H. C. YEH, S. Y. Su, J. M. Wu, Y. C. Yeh, C. K. Chao (all at Institute of Space Science, National Central University, Chung-Li, Taiwan, email: yeh@jupiter.ss.ncu.edu.tw) R. A. Heelis, B. J. Holt, C. R. Lippincott, and R. A. Power (all at William B. Hanson Center for Space Sciences, The University of Texas at Dallas, Richardson, Texas, 75803, USA) Y. S. Chang and W. L. Chiang (both at National Space Program Office, National Science Council of ROC, Hsin-Chu City, Taiwan)

The newly launched ROCSAT-1 is the first scientific satellite program of the Republic of China (ROC) on Taiwan. The satellite is in circular orbits at 600 km altitude with inclination of 35 degrees. The mission lifetime will be 2 years with 4 years as the design goal. The ROCSAT-1 program is managed by the National Space Program Office (NSPO) of ROC. There are two major mission objectives. The first is to successfully develop, launch, and operate a Low Earth Orbiting scientific satellite. The second is to conduct three scientific experiments using three separate instruments onboard the spacecraft in the areas of ocean color imaging, space telecommunications, and solar terrestrial physics. The Ionospheric Plasma and Electrodynamics Instrument was selected as the sole solar-terrestrial physics payload. The IPEI payload consists of an ion trap, a retarding potential analyzer and a pair of ion drift meter. These sensors are designed by the University of Texas at Dallas to measure ion density, temperature, composition and drift velocity with unprecedented spatial resolution and sensitivity. In anticipating significant contributions of ROCSAT-1 IPEI to the understandings of low-latitude ionosphere physics, we introduce to interested scientists, the instrument



## INTER-ASSOCIATION

capabilities, mission operations and data management of the IPEI payload. In particular, we will present examples that typify the IPEI data. We will also discuss procedures for campaign mode operation and the level of data access for general users.

**JSA20/W/33-A5** Poster **1200-11**

### EQUATORWARD PENETRATION OF ELECTRIC FIELDS ASSOCIATED WITH REGION-1 AND 2 FIELD-ALIGNED CURRENTS DURING DP2 AND SUBSTORM EVENTS

Takashi KIKUCHI (Communications Research Laboratory, Koganei, Tokyo 184, Japan, e-mail: kikuchi@crl.go.jp), Hermann Luehr (GeoForschungsZentrum, Potsdam, Germany), Kristian Schlegel (Max-Planck Institut für Aeronomie, Katlenburg-Lindau, Germany), Hiroshi Tachihara, Manabu Shinohara, and Tai-Ichi Kitamura (Kyushu University, Fukuoka 812-81, Japan)

During a substorm event on April 20, 1993, a negative magnetic bay occurred in the afternoon sector at mid to equatorial latitudes. The negative bay at low latitudes is caused by a 3-D current in the magnetosphere, but the large amplitude at mid and equatorial latitudes suggests major contribution of DP currents. The temporal variations of the electric field measured by the EISCAT radar (66 cgmlat) and of the magnetic X-component at Nurmijarvi (56 cgmlat) are coherent during the DP2 fluctuation event preceding the substorm (correlation coefficient  $r = 0.71$ ), while the coherency is broken during the substorm event ( $r = 0.26$ ). The breaking of the coherency infers a secondary electric field associated with the R2 field-aligned current (FAC) which tends to shield the convection electric field associated with the R1 FAC from the lower latitude ionosphere. From the IMAGE magnetometer array the R1 and R2 FACs are inferred at 73 and 61.5 cgmlat, respectively. Quantitative analysis is made to obtain electric fields associated with the R1 and R2 FACs basing on the EISCAT and magnetometer observation at Nurmijarvi. The R2 FAC grows in concert with the R1 FAC, with a correlation coefficient of  $r = 0.92$  and a time delay of 17 min. The DP current component of the negative bay is primarily caused by the substantial decrease in R1 FAC, but the delayed growth of the R2 FAC contributes considerably to the enhancement of the negative bay at subauroral and equatorial latitudes.

**JSA20/C/GA2.02/W/20-A5** **1200-12**

### RESPONSE FEATURES OF THE IONOSPHERE OVER FORTALEZA (DIP 3S) TO VERY INTENSE GEOMAGNETIC STORMS

J. H. A. SOBRAL, M. A. Abdu, W. D. Gonzalez, Alicia C. de Gonzalez (all four at the Instituto Nacional de Pesquisas Espaciais, São José dos Campos, S.P, Brazil), B. T. Tsurutani (Jet Propulsion Laboratory, Pasadena, California, U. S. A.)

Disturbed ionospheric F-region height drifts and peak electron density changes observed at Fortaleza, to events of very high intensity and long time duration of magnetospheric storms that occurred in December 1980, April 1981 and September 1982, are analyzed. All the magnetic storms considered here are the result of the transit at Earth of magnetic clouds. The interplanetary magnetic field (Bz) data from the ISEE-3 satellite, the auroral activity index AE, and the ring current index Dst are used as indicators of the magnetospheric conditions, and the ionospheric response features are analyzed using the F-layer critical parameters h'F, h'F3, hpF2 and foF2. An attempt is made to identify the origin of electric fields responsible for the disturbed F-layer alterations.

**JSP21** **Thursday 22 – Friday 23 July**

### SOURCES AND SINKS OF ENVIRONMENTALLY IMPORTANT SUBSTANCES (EXCLUDING CO<sub>2</sub>) (IAPSO, IAMAS, IAHS, IABO)

Location: Arts Building 120 LT

**Thursday 22 July AM**

Presiding Chair: Dr D Smythe-Wright  
(Southampton Oceanography Centre, Southampton, UK)

**JSP21/C/U4/W/03-A4** **0910**

### EVIDENCE FOR VOLCANIC INFLUENCE ON MEXICO CITY AEROSOLS

G. B. RAGA (Centro de Ciencias de la Atmósfera, Universidad Nacional Autónoma de México, Ciudad Universitaria, 04510, México DF, México, email: raga@servidor.unam.mx); G. L. Kok (National Center for Atmospheric Research, Boulder, CO 80303, USA, email: kok@ucar.ncar.edu); D. Baumgardner, A. Báez and I. Rosas (all three at: Centro de Ciencias de la Atmósfera, Universidad Nacional Autónoma de México, Ciudad Universitaria, 04510, México DF, México, email: darrel@servidor.unam.mx)

In situ measurements of sulphur dioxide (SO<sub>2</sub>), carbon monoxide (CO) and sulphate mass provide evidence that aerosol composition in Mexico City is affected by emissions from the neighbouring volcano, Popocatepetl. The data suggest that there are two distinct pathways by which SO<sub>2</sub> is incorporated into particulates. Periods of high humidity, fog, and rain are accompanied by elevated sulphate mixing ratios, attributed to aqueous chemistry. Similarly, elevated sulphate concentrations in low humidity periods appear to be a result of adsorption onto existing particles. These two mechanisms are important for understanding the processes associated with particle formation in this highly polluted urban area. Under the influence of volcanic emissions, SO<sub>2</sub> concentration is more than four times the average value and particulate sulphate is a factor of 2 larger.

**JSP21/E/02-A4** **0930**

### CURRENT AND LONG TERM TRENDS OF CFC REPLACEMENT CHEMICALS AT CAPE GRIM, TASMANIA

Georgina STURROCK and Paul Fraser (CSIRO Atmospheric Research/CRC Southern Hemisphere Meteorology, Aspendale, Victoria 3195, Australia, email: g.sturrock@bom.gov.au); Simon O'Doherty and Peter Simmonds (School of Chemistry, University of Bristol, Bristol, UK); Ben Miller and Ray Weiss (Scripps Institution of Oceanography, University of California at San Diego, La Jolla, California, USA); Ron Prinn (Department of Earth and Planetary Sciences, Massachusetts Institute of Technology, Cambridge, Massachusetts, USA); David Oram (School of Environmental Sciences, University of East Anglia, Norwich, UK)

The refrigeration/air conditioning and foam plastics industries are using HCFCs and HFCs as interim and long-term replacements, respectively, for the ozone depleting chlorofluorocarbons (CFCs). The tropospheric removal of HCFCs and HFCs by reaction with hydroxyl radicals is significant and thus they cause less ozone depletion and global warming than the CFCs they replace. Nevertheless some of the HCFCs reach the stratosphere, resulting in limited ozone destruction, especially over the next 20 years. Both HCFCs and HFCs contribute to global

warming - in particular the HFCs.

Monitoring the early accumulation in the background atmosphere of the CFC replacement chemicals is important, as it ensures that any unexpected increase in their levels will be detected early, possibly avoiding a repetition of the CFC pollution problem which was not detected until there had been significant accumulation in the atmosphere, resulting in unavoidable environmental damage, for example the Antarctic ozone hole.

Tropospheric data are being collected for the CFC replacement species using identical instrumentation and methodologies at mid-latitude sites in the Northern (Mace Head, Ireland, 52N) and Southern (Cape Grim, Tasmania, 41S) Hemispheres, as part of the long-term Advanced Global Atmospheric Gases Experiment (AGAGE) program designed to determine global trends and ultimately atmospheric lifetimes or emissions of CFCs, HCFCs and HFCs. In situ measurements are achieved using state-of-the-art instrumentation with high-resolution capillary gas chromatographic (GC) separation and mass spectrometric (MS) detection.

**JSP21/W/13-A4** **0950**

### TROPOSPHERIC CONCENTRATIONS OF THE CHLORINATED SOLVENTS, PERCHLOROETHENE AND TRICHLOROETHENE, MEASURED IN THE REMOTE NORTHERN HEMISPHERE.

Claudia H. DIMMER, Peter G. Simmonds, Graham Nickless. (School of Chemistry, University of Bristol, Bristol, BS8 1TS, UK, email: c.dimmer@bris.ac.uk); Archie McCulloch. (ICI Chemicals & Polymers Ltd, P.O. Box 13, The Heath, Runcorn, Cheshire, WA7 4QF, UK.)

A fully-automated twin ECD GC system with sample enriching Adsorption-Desorption front end was deployed on two major field campaigns - Ny-Ålesund, Svalbard, (July to September 1997), and the RRS Discovery CHAOS cruise of the N.E. Atlantic, (April to May 1998). Concentrations of an extensive suite of halocarbons were detected at 50 minute intervals at pptv levels of concentration. The results obtained for the chlorinated solvents, perchloroethene (PCE), and trichloroethene (TCE) will be presented. Trajectory sector analysis sorting, and filtering to remove local pollution events enabled baseline concentrations for each compound to be defined, and ratios between PCE and TCE for polluted air masses to be determined. Background PCE and TCE concentrations of 2.68 and 0.26 pptv respectively were recorded in Ny-Ålesund. During pollution incidences, concentrations rose to 7.41 (PCE) and 2.89 pptv (TCE). The cruise data showed average concentrations ranging from 5.71 (PCE) and 1.43 pptv (TCE) for air masses originating over the N. Atlantic and Arctic open oceans, to 11.46 (PCE) and 5.75 pptv (TCE) for polluted air masses from Northern Europe. The significance of local contamination was highlighted and the concentrations compared to data obtained at Mace Head, Ireland, and to atmospheric concentrations calculated from the audited emissions data.

**JSP21/L/01-A4** **1010**

### REGIONAL AND BACKGROUND MEASUREMENTS OF HALOMETHANES AT CAPE GRIM, TASMANIA

Michelle COX (CRC for Southern Hemisphere Meteorology, Monash University, Wellington Road, Clayton, Victoria, 3168, Australia, email: michelle.cox@dar.csiro.au); Paul Fraser and Georgina Sturrock (CRC for Southern Hemisphere Meteorology/CSIRO Atmospheric Research, PMB1 Aspendale, Victoria, 3195, Australia, email: paul.fraser@dar.csiro.au); Steve Siems (Mathematics Department, Monash University, Wellington Road, Clayton, Victoria, 3168, Australia, email: siems@monsoon.maths.monash.edu.au)

Chlorine and bromine species are the major catalysts for the significant, anthropogenically-enhanced, stratospheric ozone destruction that has occurred over the past two decades. The synthetic chemicals that provide the major halogen sources are the chlorofluorocarbons (CFCs) and halons. However approximately 20% of stratospheric chlorine and 50% of stratospheric bromine are derived from halomethanes, largely methyl chloride (CH<sub>3</sub>Cl) and bromide (CH<sub>3</sub>Br), which have both natural and anthropogenic sources. The atmospheric behaviour, sources and sinks of these halomethanes are not well understood. In an attempt to reduce the uncertainties associated with these species, an in-situ measurement project for CH<sub>3</sub>Cl, CH<sub>3</sub>Br, CH<sub>2</sub>Cl<sub>2</sub> (dichloromethane) and CHCl<sub>3</sub> (chloroform) was established at Cape Grim in late 1997, using state-of-the-art GC-MS instrumentation developed at the University of Bristol as part of the global AGAGE (Advanced Global Atmospheric Gases Experiment) program. In this paper, the temporal behaviours of these species in the background atmosphere are described and low level trajectories are used to investigate the pollution episodes and to help identify possible source regions. Trajectories from two high-resolution regional climate models (DARLAM - Division of Atmospheric Research Limited Area Model (CSIRO) - and LAPS - Limited Area Prediction System (BMRC)) are compared.

**JSP21/W/11-A4** **1050**

### A FIRN AIR RECORD OF CHLORINATED AND BROMINATED ORGANIC COMPOUNDS AND HCFCs SINCE THE 1950'S IN TWO HEMISPHERES

WT STURGES, DE Oram, H McIntyre, SA Penkett (School of Environmental Sciences, University of East Anglia, Norwich NR4 7TJ, UK, email: w.sturges@uea.ac.uk), A Fabre, J Chappellaz, JM Barnola (Laboratoire de Glaciologie et Géophysique de l'Environnement, CNRS, 54 Rue Molière, Domaine Universitaire, 38402 St-Martin-d'Hères Cedex, FRANCE), E Atlas, V Stroud (National Center for Atmospheric Research, Boulder, CO 80307-3000, USA)  
R Mulvaney (British Antarctic Survey, High Cross, Cambridge, CB3 0ET, UK)

The histories of a number of HCFCs and chloro-bromo-carbons, dating back to the 1950's, have been examined in firn air from Canada and Antarctica. Many of the replacement compounds for CFCs such as HCFC-22, HCFC-141b, HCFC-142b, HCFC-21 HCFC-123 and HFC-152a show trends dating back to the late 1950's or early 1960's. Comparisons between hemispheres for the shorter-lived species reveals evidence for changing interhemispheric ratios, suggesting possible changes in global sinks. Trends for methyl chloroform, chloroform, dichloromethane, tetrachloroethylene, 1,1,2-trichloroethane and 1,1,2,2-tetrachloroethane show clear maximum Northern Hemispheric (NH) concentrations in the early 1980's (early 1990's for methyl chloroform). The lower levels in the Southern Hemisphere (SH) can be largely attributed to transport from the NH. Current estimates of oceanic sources of these compounds appear to be too high in many instances. Methyl chloride appears to have grown slightly in the SH, possibly due to biomass burning. Organobromines are separated into those showing trends due to anthropogenic sources (methyl bromide, dibromoethane), and those which have no trend and are evidently of entirely natural origin (dibromomethane, chloro-bromo-methanes, etc.). There appears to be a significant source of several organohalogen within the firn itself.

**JSP21/W/12-A4** **1110**

### NEW CONSTRAINTS ON GLOBAL AND HEMISPHERIC LOSS RATES OF METHYL CHLOROFORM

Stephen A. MONTZKA, James H. Butler, and James W. Elkins (NOAA/CMDL, ms: R/E/CG1, 325



Broadway, Boulder, CO 80303, email: smontzka@cmdl.noaa.gov, jbutler@cmdl.noaa.gov, jenkins@cmdl.noaa.gov.

The atmospheric residence time for many CFC-replacements and other reduced gases is determined primarily by the abundance of the hydroxyl radical. Accordingly, an accurate understanding of the burden of OH on global and hemispheric scales is essential for gauging the environmental effects of these gases. Estimates of the global mean hydroxyl radical concentration have been made in the past by inferring residence times or lifetimes for CH<sub>3</sub>CCl<sub>3</sub> and 14CO from consideration of global measurements and sources. As emissions of methyl chloroform become insignificant, owing to the limits outlined in the Montreal Protocol on Substances that Deplete the Ozone Layer, atmospheric measurements of this gas will allow for refined estimates of its lifetime on global and hemispheric scales. From our measurements of CH<sub>3</sub>CCl<sub>3</sub> at 7-9 remote sampling locations, the decrease observed between 1997 and 1998 corresponds to an e-folding time of  $5.7 \pm 0.3$  yr. Because the data suggest that industrial emissions are not yet zero, this e-folding time represents only an upper limit to the global atmospheric lifetime of CH<sub>3</sub>CCl<sub>3</sub>. This upper limit, however, is independent of accuracy associated with calibration gas standards and industrial emission estimates. Additional consideration of our data allows us to estimate an upper limit of approximately 4.8 yr to the lifetime of CH<sub>3</sub>CCl<sub>3</sub> in the Southern Hemisphere. This limit is also quite insensitive to calibration accuracy, emission estimates, and hemispheric exchange rates. Finally, we explore the utility of our measurements to discern relative differences

#### JSP21/W/09-A4 1130

##### CHANGES IN STRATOSPHERIC OZONE INDUCED BY CHANGES IN NATURAL ORGANOHALOGEN EMISSIONS

K. KOURTIDIS, C. Tourpali, C. Zerefos and D. Balis (Aristotle University of Thessaloniki, Laboratory of Atmospheric Physics, 54006 Thessaloniki, Greece, email: kourtidi@ccf.auth.gr)

We present here model simulations with a 2-D CTM that deal with the effect on stratospheric ozone of changes in the tropospheric abundance of the natural organohalogen methyl chloride (CH<sub>3</sub>Cl) and methyl bromide (CH<sub>3</sub>Br). The simulations include a 5-fold increase in the tropospheric CH<sub>3</sub>Cl abundance, a 5-fold increase in the tropospheric CH<sub>3</sub>Br abundance, and combined 5-fold increases in the tropospheric levels of both substances in both the unperturbed pre-industrial atmosphere and the industrial atmosphere. Thirty-fold increases in the tropospheric levels of both substances in the unperturbed pre-industrial atmosphere have also been simulated. The simulations for a combined 5-fold increase in both substances in a pre-industrial atmosphere show significant depletion of ozone at high latitudes during the spring season, that are mostly confined in the 30-55 km altitude region, while 30-fold increases are shown to significantly affect the global ozone layer. The results for 5-fold increases are also discussed in view of the effect of the calculated ozone changes in the radiation reaching various atmospheric levels in the 10-40 km altitude region. Possible mechanisms that could have led to changes of the simulated magnitudes in the tropospheric natural organohalogen abundance in the past are also discussed.

#### JSP21/L/06/A4 1140

##### TRENDS IN HALOCARBON RELEASES FROM ANTHROPOGENIC, NON-COMBUSTION SOURCES

A. MCCULLOCH

A large number of halocarbons are manufactured industrially and used in society to provide specific effects such as refrigeration and solvent cleaning. In many cases, release of these chemicals into the atmosphere is a fundamental part of the way that they are used and occurs in quantities sufficient to be detected remotely. In order to assist in the Advanced Global Atmospheric Gases Experiment, manufacturers have cooperated to collect production and sales data for several decades and have developed technically based emission functions. Thus the quantities of individual halocarbons released into the global atmosphere can be estimated with comparatively small uncertainty. The compounds included in this exercise are the CFCs (11, 12, 113, 114 and 115) – CCl<sub>2</sub>F<sub>2</sub>, C<sub>2</sub>Cl<sub>3</sub>F<sub>3</sub>, C<sub>2</sub>Cl<sub>2</sub>F<sub>4</sub>, C<sub>2</sub>ClF<sub>5</sub>, Halons (1211 and 1301) – CBrClF<sub>2</sub>, CBrF<sub>3</sub>, methyl chloroform – CHCl<sub>3</sub>, as well as the halocarbon CFC replacements, HCFCs (22, 124, 141b, 142b) CHClF<sub>2</sub>, C<sub>2</sub>HClF<sub>4</sub>, C<sub>2</sub>H<sub>3</sub>Cl<sub>2</sub>F, C<sub>2</sub>H<sub>3</sub>Cl<sub>2</sub>F, C<sub>2</sub>H<sub>3</sub>ClF<sub>2</sub>, and HCFC-134a C<sub>2</sub>H<sub>2</sub>F<sub>4</sub>. In a parallel exercise, production, sales and emissions data for trichloroethene, tetrachloroethene and dichloromethane have been developed. The global and regional emissions of all these compounds will be discussed, together with methods to distribute those emissions latitudinally and longitudinally. Chloroform and carbon tetrachloride releases arise mainly as unintentional by-products and the quantities and distribution have been estimated by far less rigorous methods. Nevertheless, the values are consistent with the observations and will be discussed here.

#### JSP21/W/02-A4 1150

##### THE INFLUENCE OF DIURNAL VARIATIONS IN THE CONCENTRATION OF HALOCARBONS ON AIR-SEA FLUX CALCULATIONS

Katarina ABRAHAMSSON, Anja Ekdahl and Anders Lorén (Department of Analytical and Marine Chemistry, Chalmers University of Technology, SE-412 96 Göteborg, Sweden)

Diurnal variations in concentrations of volatile halogenated organic compounds have been studied in a rock pool and in open ocean. The concentrations were measured every hour or every other hour at six different occasions during a cruise in the Atlantic sector of the Atlantic Ocean, as well as every hour during one occasion in a rock pool at the Canary Islands. We will present results that show that the variations in concentrations of halocarbons correlate with photosynthesis and respiration. The levels of halocarbons vary considerably during a 24 hour period even in the open ocean, for example for diodomethane, bromoform and trichloroethylene the concentrations varied with a factor of 90, 8 and 10 respectively. The diurnal variations are characterised by rapid increases and decreases in concentrations, just within a few hours, and calculations of the air-sea flux cannot account for the observed losses.

Thursday 22 July PM

Presiding Chair: TBA

#### JSP21/W/08-A4 1400

##### ON THE FLUXES OF SHORT-LIVED ORGANOCHLORINE COMPOUNDS BETWEEN THE OCEAN AND ATMOSPHERE.

Robert M. MOORE, (Department of Oceanography, Dalhousie University, Halifax, N.S. Canada, B3H 4J1, email: rmoore@is.dal.ca)

Measurements of dichloromethane, chloroform, trichloroethylene and tetrachloroethylene were made, at the same time as several naturally-produced trace gases, in the ocean water

column during cruises in the western Atlantic in 1997, and, as part of the GAS EX98 experiment, north of the Azores in 1998. While it is evident that the gases were supersaturated at the ocean surface, and that the ocean was therefore acting as a source to the atmosphere, it will be shown that it is more difficult to establish whether the gases are produced within the ocean or are, at least in part, anthropogenic. All of these compounds are expected to have seasonally varying concentrations in the atmosphere as a result of their short lifetimes (ca. 7 – 150 days) with respect to loss by reaction with the OH radical. This can, depending on the lifetime of the gas in seawater, drive a wintertime flux of a gas from atmosphere to ocean, and a reverse flux during summer. The effects of any biological production or consumption of the gas in the ocean will be superimposed on the physically driven fluxes.

#### JSP21/W/03-A4 1420

##### SOURCES AND SINKS OF HALOGENATED GASES IN THE NORTH ATLANTIC OCEAN

Denise SMYTHE-WRIGHT, Stephen Boswell and Russell Davidson (Southampton Oceanography Centre, Empress Dock, Southampton SO14 3ZH)

Following the Montreal Protocol on ozone depleting gases and continuing concern over greenhouse warming, attention is now being focused on the new anthropogenic CFC 'replacements' and other radioactively-active and ozone-depleting gases which initially were given little regard; for example, hydrohalomethanes, haloforms and methylhaloforms. Evidence suggests that the ocean is both a source and a sink of such compounds but the specific sources (and sinks) within the ocean are poorly understood. While it is possible to measure variations in the seawater concentrations, little is known about seasonal and geographical variation, or about biological production or release (ie during the growth and mortality of planktonic organisms). Results from 3 RRS Discovery cruises covering winter, summer and spring biological conditions will be presented to show that there is a direct relationship between the distribution of methyl chloride, methyl bromide and methyl iodide and biological production, depending on season and geographical location. For example up to 40% methyl bromide supersaturation (with respect to the atmosphere) has been observed off the coast of Greenland and in excess of 1000% methyl iodide supersaturation in the subtropical gyre. Speciation studies indicate that the methyl bromide production may be related to a bloom of *Nitzschia* spp while the methyl iodide may result from a prochlorophyte source, but the mechanism by which the compounds are produced is still unclear.

#### JSP21/L/02-A4 1440

##### METHYL BROMIDE AND METHYL CHLORIDE EMISSIONS FROM COASTAL SALT MARSHES

ROBERT C. RHEW, Benjamin R. Miller, and Ray F. Weiss (Scripps Institution of Oceanography, University of California at San Diego, La Jolla, CA 92093-0220; 619-534-2599, email: rob@gaslab.ucsd.edu)

Field measurements show that coastal salt marshes are large natural sources of methyl bromide and methyl chloride and may contribute significantly toward balancing the known global budgets of these compounds. We chose to investigate salt marshes for methyl halide emissions because they are known to be regions of high primary productivity and high halide concentrations. Flux chamber deployments were carried out between June and December 1998, in two southern California coastal salt marshes. Measured net fluxes show that methyl bromide and methyl chloride are emitted from all vegetation zones of both salt marshes, with greater emissions in the growing season than in the non-growing season. The greatest emissions of these methyl halides are from the middle to upper-middle zone of the salt marsh and are associated with high carbon dioxide respiratory emissions and high densities of above-ground green biomass. Furthermore, there is a strong correlation between the molar fluxes of methyl bromide and those of methyl chloride, pointing to a common mechanism of production and release. The average molar ratio of chloride ion to bromide ion in seawater is about 600, while the average ratio of emissions of methyl chloride to methyl bromide from the salt marsh is roughly 20. Therefore the mechanism appears to favor the production of methyl bromide over methyl chloride, an observation consistent with the biosynthesis of these compounds by enzymes isolated from certain plants and wood-rot fungi. Estimated global extrapolations indicate that coastal salt marshes represent the largest natural terrestrial source of methyl bromide and methyl chloride identified thus far. Although salt marshes comprise less than 0.1% of the global surface area, they may produce roughly 10% and 5% of the total annual fluxes of methyl bromide and methyl chloride, respectively.

#### JSP21/W/17-A4 1500

##### PRODUCTION AND EMISSION OF METHYL CHLORIDE IN THE SURFACE OCEAN

Daniel B. KING (NOAA/CMDL, Boulder, CO 80303, USA and CIRES, University of Colorado, Boulder, CO 80309, USA, email: dking@cmdl.noaa.gov); James H. Butler (NOAA/CMDL, Boulder, CO 80303, USA, email: jbutler@cmdl.noaa.gov); Jürgen M. Lobert (Center for Clouds, Chemistry, Climate, SIO/UCSD, La Jolla, CA 92093, USA); Shari A. Yvon-Lewis (NOAA/AOML/OC, Miami, FL 33149, USA); Stephen A. Montzka and James W. Elkins (NOAA/CMDL, Boulder, CO 80303, USA)

Methyl chloride (CH<sub>3</sub>Cl) is the primary natural source of organic chlorine in the atmosphere. As anthropogenic sources of atmospheric, organic chlorine are reduced in the future, the relative contribution of CH<sub>3</sub>Cl to chlorine in the stratosphere will increase. However, there are currently significant uncertainties associated with the global budget of atmospheric CH<sub>3</sub>Cl. The oceans are a substantial source, as is biomass burning, and perhaps wood-rotting fungi. The oceanic contribution alone is difficult to quantify, and extrapolations of the known oceanic sources of CH<sub>3</sub>Cl cannot currently account for the estimated oceanic emission to the atmosphere.

In an attempt to understand the oceanic processes driving the production and emission of CH<sub>3</sub>Cl, we examined the relationship between its air-sea flux and a variety of physical and chemical oceanic properties. A total of four field campaigns was conducted in the Atlantic, Pacific, and Southern Oceans, in open ocean, upwelling and coastal environments. CH<sub>3</sub>Cl was supersaturated in most of the waters, with higher degrees of saturation in warmer waters. Data from these campaigns are used to derive a correlation between the flux and temperature, along with other physical and chemical properties. The contributions of the chemical degradation of CH<sub>3</sub>Br and CH<sub>3</sub>I to the production of CH<sub>3</sub>Cl are estimated for the four field campaigns and compared to the total air-sea flux of CH<sub>3</sub>Cl.

#### JSP21/W/05-A4 1520

##### THE OCEANIC CONTRIBUTION TO ORGANIC BROMINE IN THE ATMOSPHERE

Shari YVON-LEWIS (NOAA/AOML, Miami, FL 33149, USA, email: Shari.Yvon-Lewis@noaa.gov); James Butler, Daniel King, Stephen Montzka (NOAA/CMDL, Boulder, CO 80303, USA, email: jbutler@cmdl.noaa.gov); Jose Rodriguez (RSMAS, Univ. of Miami, Miami, FL 33149, USA); Jürgen Lobert (C4/SIO, Univ. of California San Diego, La Jolla CA 92093, USA); Malcolm Ko (AER Inc, Boston, MA 02139, USA)

## INTER-ASSOCIATION

The ocean delivers considerable organic bromine into the troposphere. Although many of the oceanic, bromine-containing compounds are short-lived in the troposphere, they can be convected periodically into the stratosphere, where they contribute to the destruction of stratospheric ozone. Methyl bromide (CH<sub>3</sub>Br) and the halons are recognized as being the primary carriers of bromine into the stratosphere, but contributions from other compounds may be significant. Some of these other trace gases include CH<sub>2</sub>Br<sub>2</sub>, CHBr<sub>3</sub>, CH<sub>2</sub>BrCl, CHBr<sub>2</sub>Cl, and CHBrCl<sub>2</sub>. All of these gases are produced to some extent in the ocean and their collective sea-air flux is of the same order as the total flux of CH<sub>3</sub>Br from all sources.

We have been measuring CH<sub>3</sub>Br, CH<sub>2</sub>Br<sub>2</sub>, CHBr<sub>3</sub>, and other bromine-containing compounds in air and surface seawater samples on research cruises in the Pacific, Atlantic, and Southern Oceans since 1994. Results show CH<sub>3</sub>Br undersaturations throughout much of the ocean, suggesting that the ocean is a net sink for this brominated trace gas. However, results for CH<sub>2</sub>Br<sub>2</sub>, CHBr<sub>3</sub>, and the other bromine-containing compounds show these trace gases to be supersaturated throughout much of the ocean, often with higher degrees of saturation in the tropics and subtropics. These data are presented here and will be used in conjunction with a 2-D model to examine the role that the oceans play in the cycling of atmospheric organic bromine.

JSP21/W/15-A4

1600

### SEASONAL AND TEMPORAL VARIABILITY IN THE DISTRIBUTION OF METHYL BROMIDE IN THE SURFACE OCEAN

James H. BUTLER (NOAA/CMDL, 325 Broadway, Boulder CO, 80303, USA; email: jbutler@cmdl.noaa.gov; +01-303-497-6898); Daniel B. King (University of Colorado/NOAA, CIRES; Boulder CO 80309, USA); Shari A. Yvon-Lewis (NOAA/AOML, Miami, FL 33149, USA); Jürgen M. Loberg (C4/SIO, Univ. of California San Diego, La Jolla CA 92093, USA); Stephen A. Montzka, James W. Elkins (NOAA/CMDL, Boulder CO, 80303, USA)

The ocean is both the largest known source and the second largest known sink for methyl bromide (CH<sub>3</sub>Br) in the atmosphere, yet we still don't fully understand how the ocean regulates the atmospheric burden of this gas. Consequently, we cannot predict accurately how oceanic fluxes of methyl bromide will respond to global change. First-order calculations suggest that the steady-state, net flux of CH<sub>3</sub>Br from the ocean will act in opposition to changes in the atmospheric burden. The distribution of the oceanic sources and sinks of this gas, however, lacks uniformity on both small and large scales. The open oceans are typically undersaturated in CH<sub>3</sub>Br, with coastal waters commonly supersaturated. Warm waters tend to be undersaturated and cooler waters can be super- or undersaturated, but there are significant exceptions to these generalities. Although the chemical degradation of dissolved CH<sub>3</sub>Br is predominantly a function of sea-surface temperature, production appears to be mainly biological, and there is strong evidence for biological degradation as well. Here, we examine the distribution of methyl bromide from recent studies of its saturation in the Pacific, Atlantic, and Southern Oceans to examine spatial and temporal dependencies upon its net flux and, consequently, its production and degradation.

JSP21/W/07-A4

1620

### DEGRADATION OF METHYL BROMIDE IN SURFACE WATERS OF ATLANTIC AND PACIFIC OCEAN (8N TO 45N)

Ryszard TOKARCZYK, Eric Saltzman (RSMAS, Univ. of Miami, FL-33149, USA, email: rtokarczyk@rsmas.miami.edu, esaltzman@rsmas.miami.edu)

Methyl bromide is both produced and destroyed in the surface ocean, at rates which significantly impact its tropospheric burden and lifetime. Recycling of methyl bromide within the water column limits emissions from this source into the atmosphere and enhances the removal of atmospheric methyl bromide derived from anthropogenic or terrestrial biospheric emissions. Methyl bromide is destroyed in the ocean by chemical and biological processes. In this study seawater samples were incubated with <sup>13</sup>C-labelled methyl bromide in order to measure the degradation rate, with the goal of determining the relative importance of chemical and biological processes. Degradation rates were measured during the GASEX-98 cruise across the Atlantic and the western Pacific coast (May-July 1998). Total measured degradation rates averaged from 0.17 to 0.31 per day. Methyl bromide degradation was faster in the Caribbean Sea and the coastal Pacific waters, than in the Atlantic. Temperature seems to be the primary factor controlling degradation rates in the mid-latitude ocean. On average, biological degradation contributed only 1-5% to the total degradation rates in these waters, but its contribution increases with decreasing temperature.

JSP21/W/01-A4

1640

### ARE SOILS A GLOBALLY SIGNIFICANT SINK FOR ATMOSPHERIC CARBON TETRACHLORIDE AND METHYL CHLOROFORM?

James D. HAPPELL (Department of Marine and Atmospheric Chemistry, University of Miami, 4600 Rickenbacker Cswy, Miami, Florida, 33149, USA, email: jhappell@rsmas.miami.edu); Douglas W.R. Wallace (Abteilung Meereschemie, Institut fuer Meereskunde, Duesternbrooker Weg 20, 24105 Kiel, Germany, email: dwallace@ifm.uni-kiel.de)

Evidence will be presented that suggests that soils are a globally significant sink for atmospheric carbon tetrachloride (CT) and methyl chloroform (MC). Soil gas profiles of CT and MC obtained from temperate and sub-tropical forests and lawns indicate rapid removal of CT and MC in the top 30 cm of soil. The concentration of CT and MC in the soil gas decreased by up to 75 % and 50 % relative to the respective atmospheric concentration in the top 30-cm of the soil. CFC-11, CFC-12 and CFC-113 were also measured and there was no evidence for the removal of these compounds. These data and the changes in the soil gas profile during and after a large rain storm at one site will be used to speculate on likely removal mechanisms for CT and MC.

The soil gas profiles will also be used to calculate the flux of CT and MC into soils, and the flux estimates will be scaled up to give a preliminary estimate of the global soil sink strength for these compounds. Because estimates of the ODP and GWP for CT and MC are based on their atmospheric lifetimes, which in turn are based on estimates of their sources and sinks, a globally significant soil sink would require a reevaluation of their ODPs and GWPs. Changes in the atmospheric lifetime of MC will also affect the deduced concentration of tropospheric OH, because the global mean OH concentration is estimated from the MC lifetime. If the deduced OH concentration changes so will the estimated lifetime, ODP and GWP of other radiatively and/or chemically important gases (CH<sub>4</sub>, HCFCs, HFCs, CO, NO<sub>x</sub>, SO<sub>2</sub>, etc) oxidized by OH.

JSP21/E/03-A4

1700

### AN INVESTIGATION INTO THE RELEASE OF HALOCARBONS BY PHYTOPLANKTON CULTURES

Cristina F. PECKETT(1,2), Denise Smythe-Wright (2) and Duncan A. Purdie (1). (2)George Deacon Division for Ocean Processes, (1) School of Ocean and Earth Science, University of Southampton,

Southampton Oceanography Centre, Empress Dock, European Way, Southampton, SO14 3ZH, email: crfp@soc.soton.ac.uk.

Halogenated methanes are known to contribute significantly to ozone destruction in the stratosphere and to play an important part in tropospheric chemistry. The oceans act as both a source and a sink for these halogenated methanes, and marine organisms are possibly a major oceanic source. This paper describes the results of an investigation into the release of a suite of halogenated methanes by a number of different phytoplankton species in culture. Cultures were grown for about four weeks in specifically designed, gas-tight glass vessels, which hold 1 litre of culture, leaving over 1 litre of headspace for gas exchange. The headspace was sampled every two days and analysed using a GC-ECD or GC-MS. Culture growth was monitored by cell counts and chlorophyll analysis. Species tested include *Isochrysis galbana*, *Phaeocystis pouchetii*, *Chaetoceros* sp., *Emiliania huxleyi*, *Thalassiosira gravida* and *Prochlorococcus marina*. Methyl chloride, methyl bromide and methyl iodide production has been detected for most species and some negative production, i.e. apparent uptake of halocarbons by the culture has also been observed. DMS production has also been detected. The mechanisms behind halocarbon production by phytoplankton are poorly understood. Further experiments are planned involving nutrient manipulation, the use of axenic cultures and grazing experiments. It is anticipated these will allow the mechanism of halocarbon production by marine phytoplankton to be investigated and results from some of these experiments will be discussed. The pattern of halocarbon production during the growth cycle will be compared between species and the significance of this halocarbon production on a global scale will be discussed.

JSP21/L/03-A4

1720

### THE QUANTIFICATION OF DIMETHYLSULPHIDE

ARCHER SD, Stelfox CE, Burkill PH, (Centre for Coastal and Marine Science, Plymouth Marine Laboratory, Prospect Place, West Hoe, Plymouth PL1 3DH, UK); Malin G, Steinke M, Liss PS. (School of Environmental Sciences, University of East Anglia, Norwich NR4 7TJ, UK)

Microzooplankton herbivory is one process by which dimethylsulfoniopropionate (DMSP) contained in phytoplankton, is converted to dimethylsulfide (DMS). Several previous studies have illustrated the extent of conversion of algal DMSP to DMS as a result of grazing by microzooplankton in laboratory cultures. However, few if any studies have demonstrated or quantified this process in natural waters. We have developed a new approach in the laboratory that has been applied to natural waters to quantify DMS production by microzooplankton. The model is based on the dilution technique that is used routinely to determine the impact of microzooplankton grazing on phytoplankton. The modified dilution approach provides simultaneous estimates of microzooplankton grazing rate, phytoplankton specific growth rate, grazing-mediated production of DMS and dissolved DMSP and the production/loss of DMS and dissolved DMSP in the absence of grazing.

During field studies in the southern North Sea and Iceland Basin in 1998, we found that microzooplankton were active grazers in waters containing DMSP-rich *Phaeocystis* spp. and autotrophic dinoflagellates. Our modified dilution technique was used to quantify this grazing impact and to estimate the production of DMS and dissolved DMSP that resulted from the grazing. Variations in the production of DMS and dissolved DMSP due to grazing reflect the differences in plankton composition between experiments. The experiments confirm the importance of bacterial processes to dissolved DMSP and DMS turnover and provide an indication of these rates in relation to grazing-mediated production. An impression of the relative importance of microzooplankton grazing to the DMS budget in each region was possible. We suggest that the technique provides a useful means by which some of the complex processes involved in the production of DMS in natural waters can be quantified and modelled.

Friday 23 July AM

Presiding Chair: Dr J Butler (NOAA/CMDL, Boulder, Colorado, USA)

JSP21/L/04-A5

0930

### OBSERVATIONAL CONSTRAINTS ON THE GLOBAL BUDGET OF ATMOSPHERIC NITROUS OXIDE

James W. ELKINS, James H. Butler, and Thayne M. Thompson (Climate Monitoring and Diagnostics Laboratory, National Oceanic and Atmospheric Administration, Boulder, Colorado, USA, email: jelkins@cmdl.noaa.gov, jbutler@cmdl.noaa.gov, thompson@cmdl.noaa.gov)

Nitrous oxide (N<sub>2</sub>O) is a significant contributor to the radiation budget of the atmosphere and to the depletion of stratospheric ozone (O<sub>3</sub>). N<sub>2</sub>O is a strong greenhouse gas and it is the major source of ozone-depleting nitric oxide in the stratosphere. Increased levels of atmospheric N<sub>2</sub>O may delay the recovery of the O<sub>3</sub>-layer even though mixing ratios of the chlorofluorocarbons (CFCs) are decreasing. The relative effect of N<sub>2</sub>O in depleting stratospheric ozone also could increase in the future because methane has now reached steady state in the atmosphere; methane is the primary source of water that aids in tying up free chlorine. Our group has been monitoring N<sub>2</sub>O from ground-based stations since the mid-1970's and, in recent years, has developed small gas chromatographs for sampling N<sub>2</sub>O in the atmosphere from airborne and shipboard platforms. While trends over the past 20 years tend to be relatively constant, there have been some significant variations over short periods. This talk will focus on the observational constraints on the global budget of atmospheric N<sub>2</sub>O from measurements made from tall towers, baseline stations, aircraft, balloons, and ships.

JSP21/W/04-A5

0950

### FACTORS GOVERNING THE OCEANIC NITROUS OXIDE SOURCE AND DISTRIBUTION

P. SUNDHARALINGAM (Department of Earth and Planetary Sciences, Harvard University, Cambridge, MA 02138, USA, email: pns@europa.harvard.edu); J. L. Sarmiento (Atmospheric and Oceanic Sciences Program, Princeton University, Princeton, NJ 08544, USA, email: jls@splash.princeton.edu)

N<sub>2</sub>O is a radiatively important trace gas and also plays a significant role in stratospheric ozone depletion. The major contributors to the atmospheric budget are biological processes in soils and water. The oceanic source displays a high degree of spatial and temporal variability, making it difficult to derive reliable flux estimates from sparse surface measurements. Furthermore, the main formation mechanisms responsible for marine N<sub>2</sub>O remain subject to some uncertainty. In this study, ocean general circulation model (OGCM) simulations of the marine N<sub>2</sub>O distribution are employed to evaluate current understanding of the dominant formation processes and to estimate the magnitude of the global sea-air flux. N<sub>2</sub>O is modelled as a non-conserved tracer in a global OGCM and subject to biological sources and sinks in the ocean interior and gas-exchange at the surface. A comparison of two source presentations is presented; the first is based on observed correlations between excess N<sub>2</sub>O and AOU, and models N<sub>2</sub>O production as a linear function of organic matter remineralisation. The second parameterization incorporates, in addition, behaviour suggested in recent studies, namely, enhanced N<sub>2</sub>O production at low oxygen concentrations. Simulation results indicate that both parameterizations are able to reproduce the large-scale features of the observed distribution,



i.e., high surface supersaturations in regions of upwelling and biological productivity, and values close to equilibrium in the oligotrophic sub-tropical gyres. However, inclusion of a dependence on a depth varying quantity in the relationship between N<sub>2</sub>O production and remineralisation (as, for example, in the oxygen dependent case) is more successful in reproducing the structure of the observed deep N<sub>2</sub>O distribution. These simulations yield an estimate for the global open ocean water column N<sub>2</sub>O source of 3.8 Tg N per year (range 2.7 - 8.0 Tg N).

**JSP21/L/05-A5****1010****NEW SOURCES AND SINKS OF NITROUS OXIDE**

Sheo S. PRASAD (Creative Research Enterprises, P.O. Box 174, Pleasanton, CA, USA, email: ssp@CreativeResearch.org)

Nitrous oxide (N<sub>2</sub>O) is an important greenhouse gas, since it is about 300 times more efficient than CO<sub>2</sub> on per molecule basis and its atmospheric loading is rising. The current belief is that N<sub>2</sub>O has no atmospheric sources. However, recent observations of N<sub>2</sub>O isotopic anomalies and reviews of earlier laboratory experiments suggest the existence of significant atmospheric photochemical production of N<sub>2</sub>O. The talk will review these breaking developments and the experimental study, which shows that vibrationally highly excited O<sub>3</sub> reacting with N<sub>2</sub> in the gas phase produces N<sub>2</sub>O at an atmospherically significant rate. Kinetically, this result closely parallels the recently reported N<sub>2</sub>O production from vibrationally highly excited ClO. If we accept the 1990 IPCC position on the N<sub>2</sub>O source-sink budget, then the new atmospheric source bridges the source deficit. On the other hand, if the current IPCC position of a nearly balanced source-sink budget is accepted, then the new source implies that either the current methodology for estimating the surface emission is over-estimating this emission, or there is a significant missing sink. It will be further argued that this missing sink, if it is really there, must be a surface sink. Laboratory experiment based speculations about its nature, and suggestions for new field and laboratory experiments will be presented.

**JSP21/W/06-A5****1050****LIGHT NON-METHANE HYDROCARBONS IN THE OCEAN - AN OVERVIEW**

J. RUDOLPH (Centre for Atmospheric Chemistry and Chemistry Department, York University, 4700 Keele Street, Toronto, Ontario, M3J 1P3, Canada, email: rudolphj@yorku.ca)

Emissions from the ocean into the atmosphere are a source of a substantial number of different non-methane hydrocarbons (NMHC). However, the magnitude of this source is still under debate with estimates of global emission rates ranging from a few Tg/yr to over 50 Tg/yr. Since the atmospheric residence time of most non-methane hydrocarbons does not allow for long-range transport, oceanic emissions will determine the abundance of NMHC in the remote marine atmosphere. The oceanic emission rates of light alkenes, derived from oceanic concentrations and air-sea transfer formulations are in the range of several Tg/yr. The oceanic production rates derived from laboratory experiments and field observations are somewhat higher, suggesting that emission to the atmosphere is not the sole loss process for hydrocarbons produced in the ocean, although the difference between both estimates is statistically not significant. Total oceanic emissions of all non-methane hydrocarbons are estimated to be somewhat less than 10 Tg/yr. Consequently oceanic NMHC emissions have only a minor impact on the chemistry of the remote marine atmosphere. However, oceanic emissions have to be considered if measurements of reactive in the marine atmosphere are used to study atmospheric processes.

**JSP21/E/04-A5****1110****ON INTERPRETING THE SEASONAL CYCLE IN AGAGE METHANE OBSERVATIONS AND VARIATIONS IN THE METHANE COLUMN**

D.CUNNOLD (School of Earth and Atmospheric Sciences, Georgia Tech, Atlanta, GA 30332-0340, USA Email: cunnold@eas.gatech.edu); P.Steele, P.Fraser, R.Prinn, P.Simmonds, R.Weiss and L.Emmons

Measurements of methane at the AGAGE sites are reported and compared against results from the CMDL network. Simultaneous measurements of the CFCs and CH<sub>3</sub>CCl<sub>3</sub> are used to constrain the OH distribution and transport in models in order to better isolate the effects of regional sources on the observed seasonal cycle in methane. Results from a 2D model are reported and the 3D MOZART model is now being used to test the conclusions. The MOZART model is also being used together with the ground-based observations to investigate likely sources of variability in observations of vertical column methane which will be made by upcoming satellite experiments such as MOPITT.

**JSP21/W/16-A5****1130****METHANE EMISSION REDUCTION IN WASTE MANAGEMENT**

Percival THOMAS (Department of Environmental Management and Ecology, La Trobe University, P.O. Box 821, Wodonga, Victoria 3689, Australia)

Methane is considered as one of the main greenhouse gases because of its ability to trap much of the outgoing earth's radiated energy forming a thermal blanket around the globe, raising its temperature. It is produced in large quantities under anaerobic conditions in garbage dumps, swamps and cattle feedlots. Methane which is more potent than carbon dioxide in causing global warming has an atmospheric residence time of 10-12 years as compared to carbon dioxide's residence time of about 100 years, and reduction of methane from the atmosphere should produce an immediate beneficial effect. Solid waste landfills are found in every country where tonnes of garbage are disposed of each year. Gas produced from these sites consists of about 45-55% methane, which is also a useful source of energy, and therefore, control of atmospheric emission can have an added benefit if the energy content is utilised. In many developing countries the level of income of the people is so low that they cannot afford to pay for the conventional energy sources, and methane collected from garbage dumps can be a cheap source of energy. In most cases revenues from the sale of methane will offset the cost associated with the operation of the landfill.

**JSP21/W/10-A5****1150****NON-CONTROLLED EMISSION OF METHANE, CARBON DIOXIDE, AND OTHER TOXIC GASES FROM LANDFILLS**

Noemi LIMA, José M. L. Salazar, Nemesio Pérez (Environmental Research Division, ITER, 38594 Granadilla, Tenerife, Canary Islands, Spain, email: nlima@iter.canaria.es); Candelaria Perdigon, Ana Martinez-Zubieta (Faculty of Chemistry, Univ. La Laguna, 38206 La Laguna, Tenerife, Canary Islands, Spain); and Pedro A. Hernández (Laboratory for Earthquake Chemistry, Univ. Tokyo, Tokyo 113, Japan).

Landfills work as chemical and biological reactor where biogas and leachates are the products. CH<sub>4</sub> and CO<sub>2</sub> are major components of biogas, which also contains other trace gas

components. These gas species are atmospheric contaminants which must be collected and either flared or utilized for the production of energy. Landfill gas extraction system recover just 35 to 50 % of the total production of biogas at landfills, but significant amounts of non-controlled emissions of major and trace biogas components could be released to the environment in the form of diffuse degassing. The goal of this study is to evaluate the non-controlled emission of biogas in Arico's landfill, where biogas extraction system is not operative yet. Arico's landfill has an extension of 350,000 m<sup>2</sup> and 1,170 tons of urban solid wastes, which contains 48 % of organic matter, are daily deposited. Diffuse emission of CO<sub>2</sub> levels were measured at 525 sites by means of a NDIR spectrometer and ranged from 0.8 to 32,868 g-m<sup>-2</sup>-d<sup>-1</sup>. Spatial distribution of diffuse emission of CO<sub>2</sub> indicates that biogas degassing is not uniform all over the landfill. The total output of CO<sub>2</sub> released to the atmosphere from Arico's landfill is about 150 t-d<sup>-1</sup>. The total output of biogas can be estimated by taking into consideration the CH<sub>4</sub>/CO<sub>2</sub> molar ratio of the biogas; this amount is about 423 t-d<sup>-1</sup>. Trace components emission levels are 11 t-d<sup>-1</sup> of H<sub>2</sub>O, 153 t-yr<sup>-1</sup> of VOCs, 0.9 t-yr<sup>-1</sup> of C<sub>2</sub>HCl<sub>3</sub>, 2.5 t-yr<sup>-1</sup> of C<sub>2</sub>Cl<sub>4</sub>, and 1.1 kg-yr<sup>-1</sup> of As. Significant amounts of non controlled emission of toxic gases to the surrounding environment suggest important environmental and engineering implications. In addition, generation of methane from numerous anaerobic wastewater treatment ponds, sludge digesters and artificial wetlands designed to treat wastewater needs attention, if a country has to maintain its commitment to the United Nations Framework on Climate Change.

**JSP21/W/14-A5****1210****ESTIMATION OF THE METHANE EMISSIONS FROM THE WEST SIBERIA WETLANDS AND OIL AND GAS DEPOSITS BY THE 3D REGIONAL CHEMICAL TRANSPORT MODEL**

Svetlana JAGOVKINA, Igor Karol, Vladimir Zubov (Main Geophysical Observatory, Karbyshev str. 7, 194021, Russia, email: karol@main.mgo.rssi.ru); Victor Lagun (Arctic and Antarctic Research Institute, Bering str. 38, 199397, Russia, email: lagun@aar.i.nw.ru); Eugeny Rozanov (University of Illinois at Urbana-Champaign, IL 61801, USA, email: rozanov@uiatma.atmos.uiuc.edu)

Methane is one of the most important greenhouse gases, but some its source intensities are not well known. The 3-D regional transport chemical model of the troposphere with the calculated PBL and wind fields of the above layers from data bases is used for estimation of methane fluxes from West Siberia Region (58-730N x 62-810E). The model has 0.5x10 resolution, 10 layers up to 1 km and 10 layers in the troposphere. Databases of the wind and temperature fields are created from the data from Russian meteorological stations located in the considered and adjacent areas. The estimations of the methane fluxes from gas deposits, as well as from the wetland are made on the base of the data for three periods (July 1993, June 1996 and May 1997) of airborne and ground surface methane concentration measurements. The results of the model estimations are compared with published data of the methane fluxes from Canadian and Alaska wetlands and the input of West Siberia Region into the global methane budget is evaluated.

**JSV22****Friday 23 July****THIS SYMPOSIUM IS DEDICATED TO THE MEMORY OF KEITH COX****OCEANIC, CONTINENTAL AND CONTINENTAL MARGIN VOLCANIC PROVINCES: OCEANIC PLATEAUS, FLOOD BASALTS AND SEAWARD-DIPPING REFLECTORS (IAVCE, IASPEI, IAGA,ILP)**

Location: Medical School, EF08 L73

Location of Posters: Medical School, Arthur Thompson Hall

**Friday 23 July AM**

Presiding Chairs: J.R. Hopper (Danish Lithosphere Centre, Copenhagen, Denmark), M.F. Coffin (Inst. for Geophysics, University of Texas, Austin, USA)  
Concurrent Poster Session

**LARGE IGNEOUS PROVINCES 1****JSV22/W/08-A5****0900****THE USE OF CONTINENTAL FLOOD BASALTS TO PROVIDE CONSTRAINTS FOR OFFSHORE HYDROCARBON EXPLORATION: A CASE STUDY ON THE HUAB BASIN, NW NAMIBIA**

Dougal JERRAM (Dept. of Geological Sciences, University of Durham, South Rd, Durham, DH1 3LE, UK, email: D.A.Jerram@dur.ac.uk); Nigel Mountney (Department of Earth Sciences, Keele University, Keele ST5 5BG, UK); John Howell (Department of Earth Sciences University of Liverpool, Brownlow St, Liverpool L69 3BX, UK); and Harald Stollhofen (Institut für Geologie, Universität Würzburg, Pleichervall 1, D-97070 Würzburg, Germany).

Of increasing interest in the petroleum sciences is the effect and interaction of igneous rocks with petroleum reservoirs and sediments. Currently there is continued exploration interest in the Atlantic margin and offshore NW Scotland areas, where basins have been effected by the Tertiary Igneous Province, and where there is considerable difficulty in imaging under the basalt units. Continental Flood basalt provinces, e.g. the Etendeka Province NW, Namibia, can potentially be used to provide field outcrop databases to aid exploration and provide realistic numbers for geological modelling. The Huab Basin in NW Namibia, is used as a case study to highlight the use of detailed fieldwork in understanding the development of such provinces and their relation to the underlying sedimentary sequences, providing important information e.g. geometry, size and thickness of flow units etc., and enabling simple 3-D models to be produced. Here an active aeolian sand sea (erg) was progressively engulfed by lavas of the Etendeka Flood Basalt Province. This has resulted in the unprecedented preservation of large parts of the active dune system, the occurrence of a variety of sediment interlayers and examples of the dynamic interaction between lava and aeolian/fluvial sands. The stratigraphic relationship in the Huab Basin is a potential analogue for the offshore Kudu Gas Province, as well as providing many examples of how igneous rocks intrude and invade an extensional basin during passive rifting and continental break-up. The contact between the lavas and the sediments is of particular interest. These regions are indurated, often with carbonate cements, and show systematic thickness variation of the indurated zone with respect to lava flow thickness. This suggests that the lavas have a marked 'baking' effect on the sands, although at this stage the full dynamics of that effect are poorly understood. In other places strong silica cements are present, and in one example a pure quartzite layer is produced.



**JSV22/W/02-A5 0920****ETENDEKA IGNEOUS PROVINCE: INSIGHTS INTO CONTINENTAL BREAKUP PROCESSES**

J.S. MARSH, (Department of Geology, Rhodes University, Grahamstown, 6140 South Africa)

Eight mafic and 17 silicic and geochemically distinct magma types occur in the Etendeka Igneous Province. Mafic magmas have sources dominated by components of a plume (Tafelkop), the asthenosphere (Horingbaai) and mantle lithosphere (Khumib, Tafelberg, Albin, Kuidas, Huab, Esmeralda). Silicic magmas (60-72% SiO<sub>2</sub>) have sources in old continental crust or underplated Etendeka basalt. Geographic and stratigraphic distribution of these types gives insight into magmatic processes on a breakup continental margin. Amongst early eruptives, plume-derived magmas are localised in a narrow zone, orthogonal to the breakup margin, at least 300 km S of the plume axis as defined by its trace in adjacent oceanic lithosphere, i.e. the Walvis Ridge. Late-stage asthenospheric dykes are confined to the same zone, as are generation and eruptive/emplacement sites of large-volume, crustally-derived silicic magmas. Implications: this was a major weak or thin zone in continental lithosphere towards which plume-head material was channelled to shallow depth with subsequent melting and emplacement of melts into continental crust. Later, asthenospheric mantle was also channelled into this zone to produce Horingbaai dykes as continental lithosphere moved away from the plume head. High-Ti Khumib basalts, derived from enriched lithospheric mantle, thicken northwards towards the plume axis and dyke distributions suggest main eruptive sites over the plume axis. Thus, an important thermal influence of the plume, in conjunction with lithospheric thinning, is to produce significant melting of the subcontinental lithosphere. Such lithosphere is also incorporated into the plume and subsequently sourced for some Walvis Ridge basalts (DSDP 525A). Continental crust (early to late) and underplated basalt (late) are also melted to produce a number of giant (1000-10000 cubic kms) and compositionally discrete silicic magma systems. Within the continental breakup zone the flux of silicic magma into the upper crust may match that of mafic magma.

**JSV22/E/07-A5 0940****UPPER MANTLE STRUCTURE OF PLATEAU-BASALTS AREAS IN THE SIBERIAN CRATON**

Nina PAVLENKOVA (Institute for Physics of the Earth, B.Grusinskaja 10, 123810 Moscow, Russia, email: Ninel@Pavlenkova.msk.ru) Galina Pavlenkova (GEON Centre, Chisty 4,119034 Moscow, Russia)

One of the largest area of the continental plateau-basalt covers the eastern part of the Siberian Craton. The flood-basalt penetrate the Paleozoic sediment of the Tunguss basin. The area is characterized by specific pattern of the magnetic field and by ed with nuclear explosions, cross the area and characterize the upper-mantle structure down to depth of 700 km. Some peculiarities were determined in the lithosphere structure of this area. Two blocks with anomalous high velocities (8.5-8.6 km/s) were outcrops in the crust and upper mantle structure are observed: decreasing of the velocities in the middle crust, inclined crustal and upper-mantle reflectors dipping to the north, a reflectivity zone (bright spot) at depth of 300-350 km. These structural peap transportation of fluids and flood-basalts to the surface through the cold lithosphere.

**JSV22/W/06-A5 1000****INTRA-PLATE VOLCANISM IS IN RIFTS OR DERIVED FROM DEEP OR SHALLOW MANTLE PLUMES**

K. BURKE (Geosci, Univ.Houston, Tx 77204-5503, USA email: kburke@uh.edu)

Rifts, which form where plates are locally in extension, are the sites of most intraplate volcanism. Much of the rest can be ascribed either to deep or to shallow mantle clearly recognised on the African plate which has been at rest wrt the mantle circulation for the past 30 My. Modellers have shown that a distinctive pattern of shallow mantle circulation develops under plates that are at rest. Much African plate volcanism began ~ 30 Ma when that plate stopped moving and is therefore attributable to plumes of a shallow mantle convection system. Plumes under the African plate have generated elevations and small volumes of HIMU-derived basalt with low 3 He values. Exceptions are the Afar, whose vast volume shows that it alone comes from depth, Tristan which is ancient (130 Ma), and Reunion, Shona, Bouvet and perhaps also Ascension which have 3 He values MORB. Initial eruptions of these four plumes are all < 2 My old perhaps indicating that at their initiation plumes of shallow origin may briefly tap a reservoir isolated from the MORB, HIMU, low 3 He sources that dominate the convecting upper mantle. Shallow plumes may also underlie slowly moving parts of the Antarctic, Caribbean and Eurasian plates but the occurrence of volcanism in rifts and Eurasian plates but the occurrence of volcanism in rifts within broad plate boundary zones has made shallow plume recognition harder than on the African plate.

**JSV22/E/14-A5 1050****HAWAII'S HOT SPOT, AND THE "ELECTROCARDIOGRAM" OF THE EARTH ARE LIP'S ITS "HEARTBEATS"?**

Giovanni P. GREGORI (IFA-CNR, via Fosso del Cavaliere 100, 00133 Roma, Italy; e-mail: gregori@atmos.ifa.rm.cnr.it); Wen Jie Dong (Lanzhou Institute of Plateau Atmospheric Physics, Academia Sinica, Lanzhou, Gansu Province, P. R. of China, e-mail: hxy@ns.lzb.ac.cn)

The geographical location and dating of the islands and seamounts of the Hawaii - Emperor Seamount chain allow for inferring the time variation of the magma emplacement rate during the last ~70 Ma. A trend resembling an electrocardiogram is thus found, with three heartbeats, with a return time every ~27.4 Ma. The available dating of all known LIP's appears consistent with the guess that every LIP perhaps occurred on the occasion of one such heartbeat. In any case, as far as the last ~70 Ma are concerned, a detailed analysis was carried out relating such Earth's electrocardiogram with the timing of the geomagnetic reversals, and with a tide-driven dynamo (Gregori, PEPI, 77, 39, 1993), and with its Joule's heating generation and propagation up to Earth's surface. Similar analyses from other hot spot trails ought to confirm such a feeding mechanism and its respective time variation, mechanism that, provided it is correct, should hold on the planetary scale.

**JSV22/E/09-A5 1110****INDIRECT EVIDENCES OF JURASSIC VOLCANICS IN NORTH ARABIAN SEA AND RELATED TECTONICS ON ADJOINING INDIAN CONTINENT**

D.C. MISHRA (National Geophysical Research Institute, Uppal Road, Hyderabad 500 007, India, email: postmast@csngri.res.nic.in)

Analysis of airborne/marine magnetic anomalies of the north Arabian sea delineates two ridges oriented NE-SW with basic intrusive rocks at depths of approximately 1.0 km and 5.0

km located offshore (Pakistan) and Saurashtra (India) respectively. The former coincides with the known Murray ridge while the latter offshore Saurashtra extending towards the Owen fracture zone is known as Saurashtra ridge. The observed magnetic anomalies can be accounted only by remanent magnetisation with a direction of magnetisation corresponding to high latitudes in the southern hemisphere. Seismic velocities reported along profiles offshore Karachi, Kutch and Saurashtra indicate volcanic activities of early-Jurassic time which may constitute a part of these magnetic ridges and floor of the north Arabian sea. This volcanic activity of Jurassic time show sea ward dipping reflectors and appears to be related to the break-up of Africa from the Indian plate and may be contemporary to Karoo and post karoo volcanics of east Africa. Saurashtra and Kutch on shore are also characterised by similar structural trends namely NE-SW and E-W respectively and depict several contemporary tectonic activities including Mesozoic sediments and intrusives of almost same period which might be related to the break-up of Africa from the Indian plate.

**JSV22/E/02-A5 1130****GLOBAL TEPHRA LAYERS FROM THE ETHIOPIAN TRAPS : A CLUE TO EVALUATE TRAP CLIMATIC IMPACT**

Yannick Touchard, Pierre ROCHETTE (CEREGE, BP80 13545 Aix en Provence Cdx 4, France, email: rochette@cerege.fr), Marie-Pierre Aubry (ISEM case 64 34095 Montpellier Cdx 5) and Franck Bassinot (LSCE 91198 Gif-sur-Yvette cedex)

A precise stratigraphic study of the Ethiopian traps have demonstrated that the emplacement of the main flood sequence has occurred at 30 ±0.5 Ma (Ar/Ar dating) and within magnetochron 11, with a maximum duration of either 0.8 or 1.9 Myr, depending on the magnetostratigraphic solution chosen. Four acidic tephra layers have been found in leg 115 sediments, 2600 km to the SE, with magnetostratigraphic ages synchronous with acidic layers of the traps section (in the 0.8 Ma solution). This support the "short" hypothesis, leading to magma production rate >1.6 km<sup>3</sup>/yr. The Ethiopian origin of the tephra material (glass shards) have been confirmed by distribution of major and trace elements together with isotopic studies. For the first time, trap products are found within distant marine sequences, allowing to discuss with much more confidence the climatic impact of trap atmospheric emissions. Perfectly synchronous susceptibility peaks -interpreted as the results of volcanic input- are found in the South Atlantic 522 site. Together with the characteristics of interplate global atmospheric circulation, this strongly suggests that the glass shards have been disseminated globally, at least in the intertropical band, during explosive eruptions largely exceeding the Toba tuff eruption. A sudden global cooling should therefore be associated with each tephra layer. However the well established global cooling event Oi2 appears below the tephra layers, that is during the early flood basalts emplacement. Micropaleontological evidences and deltaO18 stratigraphy will be used to discuss these correlations.

**JSV22/L/01-A5 1150****INTRUSIVE-SPLITTING OF TECTONIC PLATES AND LOG-JAM SEGREGATION OF MAGMAS: A NEW MECHANISM FOR INTRAPLATE MAGMATISM ON EARTH AND IN OTHER TERRESTRIAL BODIES**

Miles OSMASTON (The White Cottage, Sendmarsh, Ripley, Woking, Surrey GU23 6JT, UK, email: miles@osmaston.demon.co.uk)

The base of a large plate may be put into extension mechanically or by the penetration of cooling. Mantle cannot be split at low strain rates but its viscosity is highly temperature-sensitive and dependent on local composition. These may then combine to result in rapidly concentrated upward-necking of the plate. Sub-plate material thus drawn upward will undergo pressure-relief melting and eventually endow the column with net buoyancy to extend the narrow split up to the surface. Melt segregation will occur by a log-jam mechanism, well-known to grouting engineers and in other fields, in which the solids inevitably jam in the crack if they are bigger than 20-25% of the crack width. In our diapiric/intrusive column the jam will form when the solids grow again at shallower levels where wall cooling becomes important. The diapiric column will force melt through the jam. Continued opening of the crack will be offset by wall accretion; the jam will continually reform and permit the segregation of flood basalts. Rupturing of jams provides a source of xenoliths. The self-generated diapiric capability of the column in the crack results in pressure around its base being sub-lithostatic, so low- melting and diffusible-gas mantle constituents will be drawn from a wider zone than the main melting, giving the magma a 'plume' signature (e.g. 3He and 87Sr) that is not of lower mantle origin. The mechanism offers a simple account of the alk-thol-alk-neph OIB sequence and of alkali basalts that precede or follow tholeiitic flood basalts. It also seems applicable to any terrestrial bodies with thermally shrinking global lithospheres.

Friday 23 July PM

Presiding Chairs: J.R. Hopper (Danish Lithosphere Centre, Copenhagen, Denmark), J. Marsh (Dept. of Geology, Rhodes University, South Africa)

**LARGE IGNEOUS PROVINCES 2****JSV22/E/05-A5 1400****COMPUTER ANIMATION OF GONDWANA DISPERSAL AND THE HISTORY OF IGNEOUS EXTRUSION IN THE INDIAN OCEAN**

Colin REEVES and B.K. Sahu (International Institute for Aerospace Survey and Earth Sciences (ITC), Kanaalweg 3, 2628 EB Delft, The Netherlands. email: reeves@itc.nl)

Perceptions of geological phenomena can be clarified by their visualisation in time through computer animation. Thanks largely to interpretation of the Geosat ocean-floor topography data, the spreading history of the Indian Ocean now has far fewer uncertainties. In broad lines, four distinct but individually long-lived regimes of plate tectonism can be described quantitatively and animated using appropriate Euler poles. One of these regimes, which included several minor plate re-organisations, occurred largely during the Cretaceous Normal Superchron and so left little record in the marine magnetic anomalies, adding to the uncertainties of earlier work.

Ocean floor and continental geological features have been digitised with precision, ascribed to their respective plates and programmed to appear at appropriate times using the Cambridge Atlas and Timetrek software. The animation demonstrates graphically the relation in space and time between the igneous events of (1) Karroo-Ferrar volcanism, (2) dyke injection in southern Africa, (3) Rajmahal-Bunbury-Kerguelen basalts and the Ninety-East Ridge, (4) the Etendeka-Parana-Walvis Ridge complex and (5) the Deccan-Seychelles-Reunion hotspot in relation to the several spreading regimes and their respective plate boundaries and time intervals. The appearance, progress and disappearance of suspected hotspots and mantle plumes can also be visualised schematically. The eye of the beholder may be inspired to new and better-conceived interpretations by viewing this geological pageant.

JSV22/L/05-A5

1420

## THE KERGUÉLEN PLATEAU AND BROKEN RIDGE LARGE IGNEOUS PROVINCE: INITIAL RESULTS OF OCEAN DRILLING PROGRAM LEG 183

Millard F. COFFIN (Institute for Geophysics, The University of Texas at Austin, 4412 Spicewood Springs Road, Building 600, Austin, TX 78759-8500, USA, email: mikec@ig.utexas.edu); Fred Frey (Department of Earth, Atmospheric, and Planetary Sciences, Massachusetts Institute of Technology, Cambridge, MA 02139, email: fafrey@mit.edu); Paul Wallace (Ocean Drilling Program, Texas A&M University, College Station, TX 77845, email: Paul\_Wallace@odp.tamu.edu); and Ocean Drilling Program Leg 183 Scientific Party

Most of the Kerguelen Plateau and Broken Ridge formed as a single giant oceanic plateau in Cretaceous time. During Ocean Drilling Program Leg 183 (December 1998-February 1999), we cored igneous basement rock and sediment from five sites on the Kerguelen Plateau and two closely spaced sites on Broken Ridge. Initial analyses of basalt, other igneous rock, and interbedded and overlying sediment shows that: (a) The uppermost crust of this very large igneous province (LIP) formed in several, probably discrete episodes. The southern Kerguelen Plateau formed at ~110 Ma; the central Kerguelen Plateau, Broken Ridge, and Elan Bank at ~85 to ~95 Ma; and the northern Kerguelen Plateau at ~35 Ma. (b) High melt production rates of the Kerguelen hot spot formed several subaerial landmasses that gradually subsided below sea level through time. For example, terrestrial sediment containing wood fragments overlies subaerially erupted lava flows on the central Kerguelen Plateau. (c) Explosive eruptions of volatile-rich magmas marked the terminal phase of volcanism forming Elan Bank, and the central and northern Kerguelen Plateau sectors. (d) Continental crust comprises parts of the Kerguelen Plateau and Broken Ridge. For example, clasts of garnet-biotite gneiss in a braided river conglomerate are intercalated with basalt flows on Elan Bank.

JSV22/E/13-A5

1440

## GEOPHYSICAL/MORPHOTECTONIC ANOMALIES ALONG THE EDGE-OF-THE-INDIAN SHIELD AND INDIAN OCEAN HOTSPOTS

U. RAVAL and K. Veeraswamy (National Geophysical Research Institute, Hyderabad, India)

During 125-60 Ma, encompassing its break-ups the 'Greater' Indian lithosphere seems to have been influenced by 2-4 hotspots lying within (20-50) S & (55-70) E, which may perhaps represent a superplume. Further a number of gravity highs could be noted along the edge-of-the-Indian-shield which, it is suggested, may have developed, at least partly, due to modification of continental lithosphere (CL) by plumes. Their occurrence near continent-Ocean transition may be attributed to juxtapositioning of break-ups (at 130, 90, 64 Ma) with plumes. The gravity highs over thick sedimentary basins imply large subsidence and foundering of high density material due to say gabbro-eclogite transformation. Other density materials due to say gabbro-eclogite transformation. Other geophysical anomalies also appeared to be associated with these gravity highs e.g. a) high velocities beneath Mahanadi & Cambay, b) magnetic highs over Mahanadi and offshore regions & western Rajasthan and c) high heatflow and seismicity along the Cambay. This emphasizes that plume-CL and plume-ridge interactions could manifest not only as magmatism but also as geophysical features due to heat & mass transfer, which may be of economic significance as well.

JSV22/E/06-A5

1500

## ST. MARY ISLES OFF INDIA - REMNANTS OF MARION PLUME

K.V. SUBBARAO (Department of Earth Sciences, Indian Institute of Technology, Mumbai (Bombay) 400 076, India. E-mail:subbu@geos.iitb.ernet.in)

The 90 Ma old acid rocks of the St. Mary Isles of Western Continental Margin (off Mangalore Lat. 30 degree 20; Long. 74 degree 41) of India are characterised by the presence of highly evolved dacites and rhyolites (Mg<sup>30</sup>), Ti-enriched (~4%) tholeiites and alkali dykes (ne- and ol-normative), with narrow range of Sr87/Sr86 (0.7053-0.7058) covering all rock types. The palaeomagnetic pole of these islands (8 degree, 45 degree West (dp = 8 degree, dm = 6 degree); ancient latitude 26 degree S) does not fall on the apparent polar wandering curve obtained for the Deccan Traps (~65Ma) and Rajmahal Traps (~188 Ma). Based on nearly similar age (~90 Ma), chemical Sr isotopic composition and ancient latitudes for both the St. Mary Isles and early Cretaceous rocks of Madagascar, we propose that the former bears an important signature of the breakup of Madagascar and India around 90 Ma vis-à-vis Marion hot spot; but totally unrelated to the Deccan and Reunion activity. Thus the early Cretaceous St. Mary volcanism appears to represent amixture of Madagascar lithospheric mantle and Southwest Indian Ridge mantle. We will discuss the effects of overprinting of three plume activities (Kerguelen-Marion-Reunion) during the past 20 Ma and related thermal effects on the Indian lithosphere.

JSV22/E/15-A5

1550

## GEOCHEMICAL EVIDENCE FOR CENOZOIC MANTLE PLUME IN THE SOUTH CHINA

Jian-Ren MAO, Kui-Yuan Tao, Guang-Fu Xing, Yu Zhao and Zhu-Liang Yang (Nanjing Institute of Geology and Mineral Resources, 534 East Zhongshan Road, Nanjing, P.R.China, email: nigmr@public1.ptt.js.cn)

The authors discuss the geochemical characteristics of Cenozoic basalts in the South China Sea basin, Hainan Island, Leizhou Peninsula and Longhai-Mingxi in Fujian Province. They may be divided mainly into two periods: mid-Miocene (20-10Ma) and Pliocene-Pleistocene (<5Ma). These basalts are almost consistent with OIB which are more enriched in HFSE, especially in Nb,Ta,U. It is considered that the Polynesian basalts are probably formed by upwelling from the core-mantle boundary superplume, and the Hawaiian basalts are probably formed by the low-velocity column of the upper mantle. The occurrence of both the Polynesian-type and the Hawaiian- or MORB-type lavas in the South China Sea basin may imply that OIB may be produced on an oceanic ridge and that entrainment of upper mantle material may be caused by a rising superplume of lower-mantle origin. The basalts in Hainan Island and Leizhou Peninsula may have a similar origin. The within plate basalts about same contemporaneity in Longhai-Mingxi have high =E2=96=B37/4Pb, =E2=96=B38/4Pb and Nb/Zr ratios=EF=BC=8Cshowing they are totally Polynesian-type basalt. The special geochemistry of Cenozoic basalts may indicate the speciality of mantle source-"quasi-OIB-type" enriched mantle. The origin of the basalts may be attributed to (1) the eclogite residue after the partial lower-mantle; (2) the continental crust contribution through delamination of the lithosphere (including the lower crust); (3)the upwelling of a deep-mantle superplume.

JSV22/E/18-A5

1610

## MESOZOIC PETRO-TECTONIC ASSOCIATIONS AND RECORDS OF THE GEODYNAMIC PROCESSES IN SOUTHEAST CHINA

Kui-Yuan TAO, Jian-Ren Mao, Zhu-Liang Yang, Yu Zhao, Guang-Fu Xing and Huai-Min Xue (Nanjing Institute of Geology and Mineral Resources, 534 East Zhongshan Rd., Nanjing, P. R. China, email: nigmr@public1.ptt.js.cn)

According to the researches on the ages of volcanic/intrusive rocks-compositions (rock series and associations), the tracing isotopic geochemistry (Sr and Nd) and the geotectonic orientation etc., the authors have summarized the petro-tectonic associations during 250-80Ma and have divided the volcanic-intrusive rocks in the region into five petro-tectonic associations and three rock provinces, then have discussed the magmatic source regions as well as the crust-mantle interaction and their contributions. The authors have proposed that the original cause for the complex nature of various rock associations in the region may be derived from the composite of the dynamic system, i.e., the Tethys tectonic regime and the Paleo-Pacific Ocean tectonic regime. The authors also considered that the study of the mechanism for the transition and continuation of the two dynamic systems would be the link for the plate tectonics and deep processes. The Southeast China would become one of the best regions for the study of the ocean-continent transitive terrain in the world.

JSV22/W/05-A5

1630

## EPISODIC SILICIC VOLCANISM ALONG THE PALAEO-PACIFIC MARGIN OF GONDWANA; PLUME AND SUBDUCTION INFLUENCES

Teal RILEY, Philip Leat and Bob Pankhurst (British Antarctic Survey, Natural Environment Research Council, High Cross, Madingley Road, Cambridge, CB3 0ET, UK, email: t.riley@bas.ac.uk)

Jurassic magmatism in western Gondwana produced the most voluminous episode of continental volcanism in the Phanerozoic. During the Early-Middle Jurassic, some 2-3 million km<sup>3</sup> of dominantly basalt and to a lesser extent rhyolite, were erupted onto a supercontinent in the early stages of break up. Ninety percent of the volcanic rocks were emplaced during a short, 2-3 Ma burst (ca. 183 Ma). The major silicic portion of the Gondwana magmatic province is exposed in Patagonian South America, and an extension into the Antarctic Peninsula would increase the strike length along the active Pacific margin by ca. 2000 km. The volcanic rocks of Patagonia have been collectively termed the Chon-Aike Province and constitute one of the world's most voluminous silicic provinces. The volcanic rocks are predominantly pyroclastic, dominated by ignimbrite units of rhyolite composition. Volcanic rocks exposed along the east coast of the Antarctic Peninsula (Mapple Formation) are also dominated by rhyolitic ignimbrite flows, with individual units up to 80 m in thickness, and a total thickness of ca. 1 km. The ignimbrites vary in degree of welding, from high-grade rheomorphic ignimbrites with parataxitic textures, to unwelded, lithic-rich ignimbrites. The silicic rocks from Patagonia and the Antarctic Peninsula are chemically and isotopically indistinguishable and have a similar Middle Jurassic eruptive age, which strongly suggests a continuum between the two regions. Granitoid plutonic rocks of similar Middle Jurassic age and with identical isotopic (Sr and Nd) characteristics are also exposed extensively along the east coast of the Antarctic Peninsula and an identical source region to the volcanic rocks seems likely.

JSV22/P/01-A5

1650

## DEEP STRUCTURE OF THE LITHOSPHERE BENEATH THE BASALTIC PROVINCES IN THE TRANSITIONAL ZONE FROM EURASIAN CONTINENT TO THE PACIFIC OCEAN

A.G.RODNIKOV (Geophysical Center, Molodezhnaya, 3,Moscow, 117296, Russia, email: gcras@wdbc.rssi.ru)

Research was carried out along tree geotraverses made on the base of complex interpretation of geological and geophysical data. The first geotraverse across the structures of the Sikhote Alin, Japan Sea, Honshu Island and Northwest Pacific Ocean was prepared jointly with Japanese scientists. The second geotraverse across the North China Plain, East China Sea, Philippine Sea and Mariana Island Arc was carried out jointly with Chinese and Japanese specialists. The third geotraverse being under preparation now runs across the Sikhote Alin, Sea of Okhotsk, Kuril Island and Pacific Ocean. Volcanic rocks in the marginal sea basins occur predominantly as pillow lavas indicating submarine eruption. Most basalts are classified as olivine tholeiites. They form a series of N-and T-type MORB to E-type MORB. The general characteristics of the deep structure of the basaltic provinces of the marginal seas in the transitional zone from Eurasian continent to the Pacific Ocean are as follows: (1) the deep basins of the marginal seas overlie the asthenospheric diapir; (2) rift structures or spreading centers are in the base of deep basins; (3) active volcanism is present at the initial stage on the formation of a deep basins; (4) the hydrothermal activity with the sulfide deposits is observed in the rift structures. Probably, the asthenospheric diapir is a channel through with the hot mantle fluids rise from the asthenosphere into the deep basin.

Friday 23 July AM

Presiding Chair: J.R. Hopper (Danish Lithosphere Center, Copenhagen, Denmark)

## LARGE IGNEOUS PROVINCES

JSV22/W/03-A5

Poster

0900-01

## STRUCTURAL-AGE RELATIONS AND PETROGEOCHEMICAL DIFFERENCES OF DOLERITES AND GABBRO IN OPHIOLITES OF THE URALS (RUSSIA)

Igor V. SEMYONOV, Yuri L. Ronkin (Institute of Geology and Geochemistry Urals Branch of Russian Academy of Sciences, Pochtovy 7, 620151 Ekaterinburg, Russia, email: root@igg.e-burg.su)

The biggest in the world the ophiolite complex stretching almost for 2500 km along the Urals presents itself the preserved fragment of the Urals Paleozoic ocean - a part of Paleo-Tethys Ocean. In different degree preserved blocks of paleoceanic spreading structure as the enclosing rocks for the sheeted dyke complex there have been served already substantially deformed and cold rocks of dunite-harzburgite and dunite-clinopyroxenite-gabbro associations. On the contact with the bodies of gabbro and other rocks of these associations everywhere dolerite dykes have the edge hardened zones. Nowhere one could observe reverse relations - reliable hardened edge parts of bodies or the massifs of gabbro and ultrabasites on the contact with paleoceanic tholeiitic basalts of any facial nature. On their chemical and rare-earth contents dolerites sharply differ from gabbro. For example, dolerites an all petrochemical parameters are comparable with tholeiites of MOR and possess tholeiitic trend of differentiation (in parameters f-SiO<sub>2</sub>), while gabbro of both gabbro-ultrabasite associations have quite an opposite trend, not characteristic to magmatic series at all. Dolerites possess REE distributions close to chondrite or with obvious lack of light rare earths, while gabbro of dunite-harzburgite association have mainly W-like distributions of REE and dunite-clinopyroxenite-gabbro - distributions of REE with gradual increase of all the more lighter REE. The work has been done with RFFI (Russia) support - grant N 98-05-64809.



JSV22/E/03-A5 Poster 0900-02

**CRUST MANTLE INTERACTION AND ITS CONSTRAINTS ON THE FORMATION OF GIANT DEPOSITS – A CASE STUDY OF THE SHIZHUYUAN TUNGSTEN DEPOSIT, HUNAN PROVINCE, CHINA**

Zhao ZHENUA, Bao Zhiwei, Zhang Boyou, Xiong Xiaolin (Guangzhou Institute of Geochemistry, Chinese Academy of Sciences, Guangzhou, 510640, China)

In recent years, our systematic investigation and some others' on the Shizhuyuan giant tungsten deposit, Hunan Province, China, have shown that there is a strong and prolonged crust-mantle interaction in this area, and played an important role in the ore-forming processes. The main geology and geochemistry evidences are as follows: 1. The Shizhuyuan giant tungsten deposit occurs in rift-like environment; 2. The Qianlishan granite which closely associated with the ore-formation is subalkaline with high Ga/Al\*10000 values (average 3.85), low (18O values (5 ~ 7)k#, varied (87Sr/86Sr#)i (lower case) (0.7032 ~ 0.73282), high 143(upper case) Nd/144 (upper case) Nd (0.512112~0.512344) and (epsilon) Nd(T) = -4~-8; 3. Apart from granite, alkaline rocks, basaltic rocks and diabase are closely associated with ore formation temporally and spatially; 4. The Sr, Nd, and Pb isotopic compositions of the alkaline rocks and basaltic rocks and spinel lherzolite inclusions in the basaltic rocks show that the regional mantle was fertilized; 5. Isotopic compositions and trace elements of the ores show that mantle material played a role in the metallogeny: (1) Pb isotope compositions of the ores and the lower initial 187Os/186Os ratios of molybdenite in the ores (2.17(0.08) show clearly mantle material input; and (2) the ores are strongly enriched in volatile components such as F, Cl, B.

JSV22/E/10-A5 Poster 0900-03

**MANTLE METASOMATISM AND MANTLE ZONING BENEATH THE VIRUNGA VOLCANIC RANGE (CENTRAL-EASTERN AFRICA)**

A.B. KAMPUNZU (Department of Geology, University of Botswana, Private Bag 0022, Gaborone, Botswana. E-mail: Kampunzu@noka.ub.wb)

The Virunga volcanic range is the best example of extensional perpotassic igneous province around the world. It is located in the western branch of the East African Rift System and straddle the boundaries between Democratic Republic of Congo, Rwanda and Uganda. This volcanic province includes eight major volcanoes, two of them (Nyiragongo and Nyamulagira) being active volcanoes. The main rock types in this volcanic province are basanites, nephelinites, leucitites, mellilitites, tephrites, K-hawaiites, K-mugearites, K-benmoreites, trachytes and phonolites.

The geochemical investigation of mafic rocks with more than 5% MgO indicates a major increase of CaO, P2O5 and rare earth elements correlated to a decrease of SiO2, Al2O3, K2O and radiogenic isotope compositions from the east to the west of the volcanic province. This variation of composition of mafic rocks is shown to be the result of a zoning of the mantle source. This zoning is inherited from a ca 800 Ma old mantle metasomatism induced by the injection of alkaline-carbonatitic melts within the Proterozoic subcontinental lithosphere. The belt of Neoproterozoic alkaline-carbonatitic complexes aligned along the western branch of the East African Rift System strongly supports this model.

JSV22/C/U6/L/02-A5 Poster 0900-04

**ORIGIN CONDITIONS FOR VITIM BASALTS**

ASHCHEPKOV I.V. (United Institute of Geology Geophysics and Mineralogy, SD RASC, Email: gamet@uiggm.nsc.ru)

Liquidus thermobarometry for Vitim basalts suggest that in initial stage Bereya block hydrous OIB picrite basalts (mg170) came from depth of 40-60kbar heated to 1500°C. Associated Hi-K silicic basalts differentiated in the crust. The main plateau (14-7Ma) (mg165-60) basanites with the slightly convex down LMREE part originated from peridotites gently U shaped and Cpx deficient as result of melt percolation in 32-25kbar interval while more differentiated are close to Ga-Sp boundary. Subalkaline ol-basalts interacted with peridotites ascending from garnet to spinel facie with the relic garnet revealing more gentle PT pass. Typical Quaternary OIB Ne-mela-hawaiites (25-15 kbar) and more differentiated Ne-leico-hawaiites with hydrous phases demonstrate more cold conditions of differentiation. The later are contaminated in host peridotites as well as Miocene basanites mixed with the DM (MORB0 type mantle). Geochemistry of HFSE elements suggest primary OIB type magmas in 1st and last stages to be individual representing head and tail of the small plume. Megacrystalline pyroxenite assemblages demonstrate intermediate heating conditions between basalts and iherzolites and mixing signatures being originated in pre-eruption small magma chambers or large veins.

JSP23 Friday 23 – Tuesday 27 July

**GEOPHYSICAL HAZARDS AND RISKS: PREDICTABILITY, MITIGATION, AND WARNING SYSTEMS (IAPSO, IASPEI, IAVCEI, IAHS, IAMAS, IAG, IAGA, IUGG TSUNAMI COMMISSION, ILP)**

Location: Poynting Physics S02 LT

Location of Posters: Bridge Poynting/Watson

Friday 23 July AM

Presiding Chair: T BEER (CSIRO Atmospheric Research, Aspendale, Australia)  
Concurrent Poster Session**HAZARD AND RISK ASSESSMENT, RISK MITIGATION AND MANAGEMENT**

JSP23/C/U5/P/01-A5 Invited 0830

**ATMOSPHERIC HAZARDS ASSOCIATED WITH THE EL NINO/SOUTHERN OSCILLATION PHENOMENA: A SYNTHESIS**

Madhav L. KHANDEKAR (Consultant, Baird &amp; Associates, Ottawa, Ontario, CANADA, L3R 7Z5)

The ENSO phenomenon – spreading of warm water from the equatorial central Pacific to the equatorial South American coast and associated global weather anomalies – is now identified as the strongest signal in the global climate system after the annual cycle. The term El Niño refers to the spreading of anomalously warm water off the coast of Ecuador and Peru and associated weather anomalies over the west coasts of the Americas. The Southern Oscillation is the atmospheric counterpart of El Niño and refers to the slowly varying atmospheric pressure differential over the eastern and western regions of the tropical Pacific. The two phenomena

together are now popularly known by the acronym ENSO (El Niño/Southern Oscillation). The appearance of warm water off the coast of South America and associated changes in the regional weather patterns were known to Peruvian fishermen for over 400 years. The landmark papers of Jacob Bjerknes in the Nineteen Sixties provided a physical link between ENSO and weather anomalies over the entire equatorial Indo-Pacific basin. Several studies inspired by Bjerknes' landmark papers and reported in the last twenty-five years have documented a link between ENSO and global weather anomalies.

This paper provides an overview of global weather anomalies and associated atmospheric hazards in the context of the ENSO phenomena. The paper further presents several examples of atmospheric hazards associated with extreme weather events and their relationship to the various phases of ENSO. The importance of monitoring various phases of the ENSO phenomena through suitable atmospheric and oceanic indices will be discussed in the context of long-range weather forecasting.

JSP23/W/04-A5 0910

**ENSO AND 'ENSO-LIKE' IMPACTS ON INTERANNUAL TO SECULAR TIME SCALES**

Robert J. ALLAN (CSIRO Atmospheric Research, Aspendale, Victoria 3195, Australia, email: rob.allan@dar.csiro.au); Ian N. Smith (CSIRO Atmospheric Research, Aspendale, Victoria 3195, Australia, email: ins@dar.csiro.au).

Efforts to improve our understanding of the various types of natural variability inherent in the global climate system have included a growing focus on the El Niño Southern Oscillation (ENSO) phenomenon and lower frequency 'ENSO-like' decadal to secular scale fluctuations. Signal detection analyses applied to global historical sea surface temperature and mean sea level pressure anomalies, reveal significant climatic signals operating on quasi-biennial, inter-annual, decadal multi-decadal and secular time scales. The ENSO signal is seen to consist of quasi-biennial (QB) and lower frequency (LF) components that interact to produce important modulations of the phenomenon. 'Protracted' El Niño and La Niña episodes are found to be a consequence of the 'phasing' of quasi-decadal and inter-decadal 'ENSO-like' signals with the QB and LF ENSO components. Further climatic modulations are provided by 'ENSO-like' phenomena operating on multi-decadal time scales. The secular trend, reflecting the observed global warming signal, reveals neutral to slightly 'La Niña-like' conditions in the Pacific sector. The impact of the above climatic signals can be seen in the patterns of correlation with global precipitation and mean surface land temperatures. Significant contributions to rainfall and land temperature variability are evident, not just in known 'ENSO-sensitive' regions. In addition, El Niño and La Niña episodes on inter-annual time scales can be both synchronous and asynchronous with 'El Niño-like' and 'La Niña-like' signals on various decadal to multi-decadal time scales, resulting in the range of fluctuations seen in many rainfall and temperature impacts over time.

JSP23/L/01/A5 0930

**HAZARD AND RISK MITIGATION BY IMPROVING THE CULTURE OF SOCIETY AND OF THE DECISION MAKERS**

FABRIZIO FERRUCCI and Giovanni P. Gregori

Hazard and risk management requires a precise preliminary assessment of their respective formal definition, sources and causes. The natural environment, likewise demography, territory use, and energy consumption, are not steady in time. They rather experience a continuous transformation or evolution. Every so-called natural catastrophe is a strict need by natural reality. Neither it makes sense to search for a forerunner (that in a strict sense can be given, at most, only with some relevant error bar, that makes a forecast of little practical help). Moreover, a prevision is often useless in terms of concrete reduction of causalities and/or damages. The entire problem rather emphasises per se the great need for improving the consciousness of the specific characteristics of every type of natural catastrophe, and of the ways by which its consequences can be prevented or minimised. A forgotten aspect of human history is concerned with the epoch when mankind got the consciousness of space orientation, and much later also of absolute time. Similarly to this, at present there is a great need for educating both society and decision makers about the correct cultural approach to Nature, to environmental knowledge, and to territory management. All this appears the unique concrete viable approach for solving the threaten by the progressively stronger impact of mankind on environment, a factor that is closely and unavoidably related to the same progress of civilisation. Several case histories will be specifically discussed.

JSP23/W/31-A5 0950

**FLOOD EVENTS IN THE RHINE RIVER BASIN: GENESIS, INFLUENCES AND MITIGATION**

Markus DISSE (German Federal Institute of Hydrology, P.O. Box 309, D-56003 Koblenz, Germany, Email: disse@bafg.de); Heinz Engel (German Federal Institute of Hydrology, P.O. Box 309, D-56003 Koblenz, Germany)

The catchment of the river Rhine can be distinguished in 4 main subcatchments: the alpine region with the river Aare as the main tributary and downstream the lower mountain regions of the tributaries Neckar, Main and Moselle. These four basins clearly generate different hydrographs. Due to the geographical circumstances, the average discharge maximum shifts from summer towards winter downstream the Rhine. However, spatial and temporal precipitation patterns have a strong influence on the individual flood. The particular genesis of recent and historical floods will be discussed. Besides the climatological causes a brief overview of the manmade alterations to the river system itself (Rhine and tributaries) and to the linked catchments are given and their effect will be indicated. However, up to now the influence of land surface and river training measures on flood conditions in the Rhine basin has not exactly been quantified. Therefore, the Dutch-German project LAHoR has been established within the framework of the EU-project IRMA (INTERREG II C Rhine Maas Activities). The results of this project may give efficient advice for the "Action Plan on Flood Defence" of the International Commission for the Protection of the Rhine (ICPR), which is briefly introduced. In this plan a multidisciplinary approach to mitigate floods is suggested that can yield to synergic effects between flood prevention, water management, regional planning, agriculture, forestry and ecological demands.

JSP23/E/37-A5 1010

**THE SUVA EARTHQUAKE RISK MANAGEMENT SCENARIO PILOT PROJECT (SERMP) - MITIGATION OF EARTHQUAKE AND TSUNAMI RISKS FOR THE CITY OF SUVA, FIJI**

Jack RYNN (Centre for Earthquake Research in Australia, PO Box 276, Indooroopilly, Brisbane, Queensland 4068, Australia, email: sally.brown@uq.net.au); Poasa Raveo (Department of Regional Development and Multi-Ethnic Affairs, Government of the Republic of Fiji, PO Box 2219, Government Buildings, Suva, Fiji); Atu Kaloumaira (South Pacific Disaster Reduction Management Office, c/o UNDP, Private Mail Bag, Suva, Fiji, email: atu@sopac.com.org)



The 1953 Suva earthquake (ML 5.6) and associated tsunami is a stark reminder of the vulnerability of the City of Suva to such natural hazards. Through the UN IDNDR program, per the 1994 "Yokohama Statement", the Government of the Republic of Fiji took the challenge to counter mitigation strategies. SERMP was a co-operative effort of the Government, UNDP-UNDHA and international consultants. A specific methodology was developed to address definitive project components of hazard, vulnerability and risk assessments, mitigation measures, response planning, public awareness, policy support and dissemination of findings. Wide-ranging outcomes for both earthquake and tsunami, of risk assessments, loss estimations, disaster planning, risk management and tsunami warning, with 90 recommendations, were documented as an "information resource." These were implemented as "practical applications" in building codes, GIS, land use planning, disaster plans, training, emergency management and community education. A Sub-Regional Seminar and exercise "SUVEQ 97" were conducted. SERMP also demonstrated mitigation measures to decision makers in all Pacific Island Countries.

**JSP23/W/19-A5****1050****THE AUSTRALIAN ENVIRONMENTAL RISK MANAGEMENT FRAMEWORK**

Tom BEER (CSIRO Atmospheric Research, Aspendale, 3195, Australia, email:Tom.Beer@dar.csiro.au)

Environmental risk management deals with impacts on the environment, as well as with impacts on organisations that disturb the environment. Management options are based on a measure of the risk, which is obtained through an analysis of both the likelihood and the consequences of the impact. Many of the concepts, and much of the terminology, of environmental risk assessment have arisen from its use by the US EPA as an objective tool that provides information on which to base environmental decisions. A key step in the United States was to maintain a clear separation between risk treatment and risk assessment. Risk treatment is an activity undertaken by decision-makers and managers, whereas risk assessment is an activity undertaken by technicians. Many workers have argued that one cannot maintain such a clear distinction and a conference of the Australian Academy of Science developed an Environmental Risk Management framework. Australia has been reluctant to embrace the US-inspired clear distinction between risk treatment and risk assessment. Australia has, instead, combined risk assessment (envisaged as a combination of risk analysis and risk evaluation) and risk treatment within a generic risk management framework that has been incorporated into the Australian/New Zealand Standard on Risk Management, AS/NZS 4360. This presentation synthesises the Australian Risk Management and Environmental Risk Management frameworks.

**JSP23/W/02-A5****1110****CAUSE-EFFECT MODELS OF LARGE LANDSLIDES**

Ewald P. BRUECKL (Vienna University of Technology, Gusshausstrasse 27-29, A-1040 Vienna, Austria, email: ebrueckl@ luna.tuwien.ac.at)

Within the scope of IDNDR cause-effect models of large landslides are being developed to estimate potential danger. This work is based on structural exploration of the landslides mainly by seismic methods. Information about the status of deformation is got by comparison of the actual topography with a reconstruction of the original topography, GPS and SAR interferometry. Geological and geomorphological evidence, as well as relevant information from other geoscientific disciplines, is included. The Finite Element method is used to model the initial phase of a mass movement. Later on this modelling will be extended to the quasi-stationary creep phase and the transition from creeping to rapid sliding.

Three large landslides within the crystalline rocks of the Eastern Alps have been investigated since 1997. The largest one is the Koefels landslide with a total volume of 3.9 km<sup>3</sup> and a potential energy release of 5\_10<sup>16</sup> Joule. Refraction and reflection multi-component seismic techniques were applied successfully to resolve structure and elastic parameters of the landslide masses. For the modelling of the initial phase of the landslides by the Finite Element method a strain softening behaviour of the rock mass has been assumed. The development of softened or fractured zones according to the structures obtained by the seismic measurement was simulated.

**JSP23/L/04-A5****1130****PSEUDOSCIENCE U.N. DOCUMENT: GEOMAGNETIC FORECASTING OF EARTHQUAKES AND METEOROLOGICAL DISASTERS**

Wallace H. CAMPBELL (World Data Center A for Solar-Terrestrial Physics, NGDC / NOAA, 325 Broadway, Boulder, CO 80303-3328, USA, e-mail: whc@ngdc.noaa.gov)

The United Nations recently published a "Manual on the Forecasting of Natural Disasters: Geomagnetic Methods" (1998) by Chinese and U.N. authors that stretches the imagination with prediction of earthquakes and Meteorological disasters. A careful reading of this document reveals an illusionary approach to the subject with no valid supporting evidence of prediction capability. The "mathematical" section simply copied well-known formulae that provided no scientific details of any physics connecting changes in geomagnetic recordings and subsequent localized disastrous earthquakes or meteorological events. The presented data indicated that 82.3 % of the recorded earthquakes did not correspond well to predictions. The authors ignored the recommendations and testing suggestions of a 1996 international London meeting, Assessment of Schemes for Earthquake Prediction. The manual provides clear and reliable evidence of the improper use of public funds for building hopes of disaster relief with projects totally lacking in scientific merit.

**JSP23/W/26-A5****1150****25 SECONDS FOR BUCHAREST**

Friedemann WENZEL, Mihnea C. Oncescu, Michael Baur and Frank Friedrich (University of Karlsruhe, 76128 Karlsruhe, Germany, email: fwenzel@epiwap1.physik.uni-karlsruhe.de); Constantin Ionescu (National Institute for Earth Physics, P.O. Box MG-2, 76900 Bucharest, Romania, email: viorel@infp.ifa.ro)

The Romanian capital Bucharest faces a significant earthquake hazard with a 50% chance for an event in excess of 7.6 moment magnitude every 50 years. Within the last 60 years Romania experienced 4 strong Vrancea earthquakes: Nov. 10, 1940 (Mw = 7.7, 160 km deep); March 4, 1977 (Mw = 7.5, 100 km deep); Aug. 30, 1986 (Mw = 7.2, 140 km deep); May 30, 1990 (Mw = 6.9, 80 km deep). The 1977 event had catastrophic character with 35 high-rise buildings collapsed and 1500 casualties, the majority of them in Bucharest. A group of civil engineers and seismologists from the National Institute of Earth Physics (NIEP) in Romania and Karlsruhe University in Germany propose an Early Warning System (EWS) for the capital city of Bucharest. The group studied the seismological boundary conditions of an EWS for the Romanian capital of Bucharest. The earthquakes threatening the capital are intermediate deep events with magnitudes close to Mw = 8.0 at an almost fixed epicentral distance of about 150 km. The travel-time difference between the destructive S-wave arriving in Bucharest and the

epicentral P-wave is always greater than 25 s, which represents the maximum possible warning time. Moreover source mechanisms are extremely stable for larger and smaller events so that a projection of the level of ground motion to be expected in Bucharest can be based on the amplitude of the epicentral P-wave rather than on cumbersome determination of magnitude and depth. This feature allows the design of a simple, robust and fast EWS. With 25 s, a system with the largest warning time after the Seismic Alarm System for Mexico City could be established. Even this small time window can provide opportunities to automatically trigger measures such as, shutdown computers; re-route electrical power; shutdown airport operations; shutdown manufacturing and high-energy facilities; stop trains; shutdown gas distribution; alert hospital operating rooms; open fire station doors; start emergency generators; stop elevators in a safe position; issue audio alarms; maintain safe-state in nuclear facilities. The value of an EWS can be judged on the basis of an application specific costs-benefit analysis, but simple considerations suggest that it will be cost-efficient.

**JSP23/E/31-A5****1210****GLOBAL VOLCANIC SIMULATOR: ERUPTION FORECASTING AND URBAN PLANNING OF DENSELY POPULATED AREAS**

Flavio DOBRAN (Global Volcanic and Environmental Systems Simulation, 32-50, 34 Street, Long Island City, New York 11106, Email: dobran@idt.net)

A Global Volcanic Simulator consists of physico-mathematical models of the volcano that are effectively implemented for solution on distributed or parallel computers. Such a simulator can be used to forecast future eruptions and for studying their effects on people and infrastructures for the purpose of mitigating eruption consequences. Current simulator for Vesuvius models magma reservoir volume, temperature, and pressure changes, variable rates of magma supply into the chamber, and varying elastic, plastic, and heat transfer characteristics of magma reservoir surroundings. Different types of magma ascent models allow for time-varying and non-isothermal simulations, including magma flow regime changes and melting of conduit walls. These models have been used to forecast that a plinian or subplinian eruption of Vesuvius will occur within the next 100 years and that the pyroclastic flows from column collapses can destroy the surrounding territory in several minutes. The simulator is also being employed to study the effects of different eruption scenarios on the territory and how this territory can be protected by engineering intervention measures. Computer simulations of possible eruptions of Vesuvius are also being utilised to sensitise the population of the area. A useful simulator requires reliable geological and geophysical data of the volcano's internal structure, whereas the verification and validation of complex physical models on computers presents both computational and physical modeling challenges that are described in: Dobran, F., Theory of Structured Multiphase Mixtures, Springer Verlag, New York, 1991; Dobran, F., Global Volcanic Simulation of Vesuvius, Giardini, Pisa, 1993; Dobran, F., Etna: Magma and Lava Flow Modeling and Volcanic System Definition Aimed at Hazard Assessment, Topografia Massarola Offset, 1995.

**Friday 23 July PM**

Presiding Chair: Prof. Dr.F Wenzel (Universitaet Fridericiana Karlsruhe, Germany)

**JSP23/E/20-A5****1400****EXTRATROPICAL EVOLUTION OF TROPICAL CYCLONES AS AN UNEXPLORED HAZARD IN MIDDLE AND HIGHER LATITUDES**

Jenni L. EVANS (Department of Meteorology The Pennsylvania State University University Park PA 16802, USA.)

A recent climatology of extreme rainfall incidence in the northeast United States (including New England) reveals that the passage of a tropical cyclone is the cause of major rainfall events every 2-3 years over most of this region. Locations such as Boston and Cape Cod are particularly susceptible, with individual events resulting in twice their monthly rainfall due to a single tropical cyclone passage every 5-6 years. At the time that these tropical cyclones are delivering such copious rainfalls, they are typically undergoing complex structural changes that are poorly understood.

The lifecycle of the tropical cyclone through to a hybrid or truly extratropical cyclone and the associated rainfall evolution will be elucidated here and a theoretical underpinning provided.

**JSP23/C/U5/E/14-A5****1420****NATURAL DISASTERS: A POSTGRADUATE PROGRAM AT UNIVERSITY OF KARLSRUHE**

Jens MEHLHORN, Frank Fiedrich and Fritz Gehbauer (Institute for Construction Equipment and Construction Management, University of Karlsruhe, Am Fasanengarten, 76126 Karlsruhe, Germany, email: mehlnhorn@imbdec1.bau-verm.uni-karlsruhe.de)

According to the United Nations the annual financial loss as a result of natural disasters increased from 50 billion to 360 billion US-dollar during the last 35 years. This fact presents a tremendous challenge to politics, society, and the scientific community. Disaster related research has to be increased. On the basis of fundamental research new knowledge will be created and used to develop practical tools for hazard and risk assessment. More effective measures for reducing this risk can be taken and the performance of emergency response can be improved. These steps towards a better understanding of disaster causes and effects and improved disaster management have been demanded since the UN-decade IDNDR (International Decade for Natural Disaster Reduction) started in 1991. The Postgraduate Program Natural Disasters has to be seen in this context. A total of 15 institutes of different fields work together in this project involving five departments of the university.

The research projects include topics like Modelling of Hazard and Risk, Development of Disaster Scenarios, Mitigation Aspects and Economic Consequences of Natural Disasters. During the first period the activities concentrate on floods, earthquakes, strong rainfalls and land-slides. Natural sciences like physics, hydrology, meteorology and geosciences give a contribution to the basic understanding of the disaster process. Mathematics and computer sciences are used for complex models, for modelling fuzzy and imprecise information and for forecasts. With the help of economics the risk can be quantified and evaluated. In addition the institutes dealing with engineering aspects develop measures and tools for risk mitigation.

**JSP23/C/U5/W/13-A5****1440****WORLD MAP OF NATURAL HAZARDS – A DEPICTION OF THE GLOBAL DISTRIBUTION OF SIGNIFICANT HAZARDS AND THEIR INTENSITY**

G. Berz, S. Ehrlicher, T. Loster, E. Rauch, A. Siebert, J. Schimetschek, J. SCHMIEDER, A. Smolka and A. Wirtz (Munich Re, Geoscience Research Group, D-80791 Munich, Germany, Tel. 0049-89-3891-5291, Fax: 0049-89-3891-5696, E-mail: info@munichre.com)

For over 25 years now Munich Re's Geoscience Research Group has been looking at natural hazards throughout the world. Twenty years ago it summarised the overall results of its work

## INTER-ASSOCIATION

in the first edition of the World Map of Natural Hazards. The map represents a unique source of information for numerous insurance companies, engineering offices, planning authorities, geoscientists, schools and interested lay people world-wide. For the recently released third edition all the basic data was for the first time captured and analysed using Munich Re's geographical information system (GIS). The resulting maps were created using digital cartography. Four auxiliary maps have supplemented the new edition. The earthquake and windstorm zones contained in the previous editions have been updated, refined and augmented. There are also details of other significant natural hazards like severe rainfall, storm surges, hail and lightning. A particularly interesting innovation is the auxiliary map on climate change. It deals on the one hand with the effects of El Niño, which generated so much interest and concern internationally in 1997/98 and was responsible for numerous natural catastrophes. Even more important are the effects that are to be expected from the emerging phenomenon of global warming, which will be accompanied by more frequent and more dramatic natural catastrophes in many parts of the world and will lead to a distinct long-term deterioration in the risk situation. The accompanying publication provides a detailed catalogue of historic natural catastrophes that have occurred in countries all over the world, grouped by continent and listed chronologically with additional information on the number of deaths and the economic losses.

**JSP23/C/U5/W/11-A5**

**1500**

### ASSESSMENT OF HYDROLOGICAL HAZARDS OF VOLCANIC ALLUVIAL FANS

Kazuo OKUNISHI (Disaster Prevention Research Institute, Kyoto University); Gokanoshō Uji, (611-0011 Japan, Email: okunishi@slope.dpri.kyoto-u.ac.jp); Hiroshi Suwa (Disaster Prevention Research Institute, Kyoto University, Gokanoshō Uji, 611-0011 Japan, Email: suwa@slope.dpri.kyoto-u.ac.jp)

Alluvial fans on the foot of volcanoes have high hazard potential because of frequent inundation of debris flows and floods accompanying marked topographic changes. However, the social needs for the development of such lands are ever increasing, because of their high demand for recreational and touring sites. Assessment of hazard potential and regulation of land use are thus urgent problems. We propose fundamental principles for the assessment of hazard potential on the basis of a case study carried out at the Kikkakezawa Fan on the southern foot of Mt. Yatsugatake, central Japan. Existing villages are located below a major spring zone in the alluvial fan, which is fed by the groundwater in the volcanic body. Construction of a new road stimulated land developments along it and further upstream. It has been found that the debris-flow deposits had covered the fan in three geologically distinct ages. The ages of the deposits of new-age and middle-age debris flows are estimated on the basis of aerial photographs and a field investigation to assess their recurrence interval. The three kinds of debris flows are characterized by relative height from the current stream bed and by the area of deposition. Since the hazard assessment is needed for any part of the fan for any time span of the planned land use, it is advisable to define and assess the hazard potential of a fan from which the risk is calculated taking account of the location in the fan, and the time-span and the mode of the planned land use.

**JSP23/E/54-A5**

**1520**

### THE ADVANTAGES OF HOLONIC DESIGN FOR WARNING AND ALARM SYSTEMS

Gary GIBSON (Seismology Research Centre, 2 Park Drive, Bundoora, Victoria 3083, Australia, email: gary@seis.com.au)

Warning and alarm systems are near real-time monitoring systems. They may be adversely affected by the events they are seeking to detect, such as a communication failure caused by an earthquake. Holonic systems were developed in manufacturing engineering, and require that each system element involves both task performing and decision making. A holon is an intelligent system element, either human or computer based, that is normally in communication with other holons. A holon is AUTONOMOUS (it can perform tasks alone if communications fail) and COOPERATIVE (overall results are enhanced when holons help each other, and it monitors the health of neighbouring holons, providing an immediate alarm if a failure is detected, and may attempt to compensate for any loss of function). Holonic systems are designed so that no elements or communication links are critical. It must be accepted that any particular component will fail, and the system must be designed to cope with this. The Internet is a system designed to continue in operation after individual components have failed. An holonic system is one, which self-organises and evolves to dynamically optimise survivability, adaptability, flexibility, efficiency and effectiveness. Earthquake and tsunami warning and alarm systems are ideally suited to holonic design. They use "Event Oriented Seismology", requiring minimal data flow. Each seismograph may be event triggered, may record continuously and only transmit selected waveform segments on request, and/or may transmit minimal continuous data to facilitate event detection. They respond to requests or issue messages to other holons in the system. Communication can vary from the Internet, to slow digital radio links, or even dial-up telephone. A system is holonic if each element sends and receives information to and from other elements, but continues to function autonomously when communications fail. Any system failure should be immediately reported by one or more system elements. Holonic systems may be very economical because they only perform the tasks that are required. Compared with continuously tele-metered data from non-holonic digitisers, there is a dramatic reduction in total data flow, and usually in operating cost, with enhanced reliability and flexibility.

**JSP23/C/U5/W/08-A5**

**1600**

### URBAN LOCAL EARTHQUAKE DISASTER RISK INDEX

Yang TING (Geophysics Institute, China Seismological Bureau, Now at Shanghai Seismological Bureau, No.87, Lanxi Rd, Shanghai, China, 200062, Email: tyang@263.net); Zhu Yuanqing (Shanghai Seismological Bureau, No.87, Lanxi Rd, Shanghai, China, 200062)

In many modern cities, especially megacities with low seismicity, there exist a lot of hidden disadvantages, except for the frequency of historical earthquake and ground shaking level, that may amplify the influence of earthquakes and cause a catastrophe to them. The Urban Local Earthquake Disaster Risk Index (ULEDRi), which is firstly presented by authors, will highlight those disadvantages with an easily understandable form for city decision-makers, planners, organizations and individuals. ULEDRi is a variation of EDRI, which is a new approach that can directly compare the relative overall earthquake disaster of megacities worldwide, and describe the relative contributions of various factors to that overall risk. Unlike EDRI, whose study unit is the greater metropolitan area, ULEDRi uses the local area of an urban, e.g. administrative district, postal area, as its unit of study. What's more, depended on the demand of users, ULEDRi's study unit can be a larger one (e.g. every administrative district of city), or a smaller one (e.g. several blocks). As a result of this difference between EDRI and ULEDRi, the objectives, uses and developing approach of ULEDRi will differ distinctly from those of EDRI. ULEDRi involves a large amount of knowledge about earthquake disaster of a wide range of disciplines, and the factors that contribute to overall ULEDRi of a city include those of geophysics, geology, engineering, residents, socio-economics, culture and so on. ULEDRi has the following potential uses. First, this kind of index can serve as a simple tool to directly compare the relative overall earthquake disaster risk of different local area of a city, so

the decision-makers and administrators can find where the most dangerous local area is when an earthquake affects the city. Second, through disaggregated ULEDRi, the users can find the reason why a local region has a high overall ULEDRi, and which factor is the most important one that causes this. For city planner and disaster manager, the information will be significant in urban function planning and disaster mitigation. Third, any organization and individual will be able to refer to the index in allocating resources and increasing awareness of disaster. As a sample, ULEDRi of Shanghai, which is based on several districts, has been constructed, and its feasibility and potential application have also assessed.

**JSP23/C/U5/E/16-A5**

**1620**

### THE GSHAP WORLD MAP OF SEISMIC HAZARD

D. GIARDINI (ETH, 8093 Zurich, Switzerland, email: giardini@seismo.ifg.ethz.ch); G. Grunthal (GFZ, Potsdam, Germany); H. Gupta (NGRI, Hyderabad, India); D. Mayer-Rosa and S. Sellami (ETH, Zurich, Switzerland); K. Shedlock (USGS, Boulder, USA); P. Zhang (SSB, Beijing, China); T. Annaka (Tokyo Electric Power Services, Japan); M. G.-Ashtiany (IEES, Tehran, Iran); K. Atakan (Bergen University, Norway); S. Balassanian (NSSP, Yerevan, Armenia); P. Basham (CTBTO, Vienna, Austria); C. Dimate (Ingeominas, Bogota, Colombia); M. Erdik (Kandilli Obs., Istanbul, Turkey); M. Garcia (CSIC, Barcelona, Spain); Giesecke (CERESIS, Lima, Peru); K. McCue (AGSO, Canberra, Australia); R. McGuire (Risk Engineering, Boulder, USA); R. Musson (BGS, Edinburgh, UK); S. Riad (Assiut University, Cairo, Egypt); D. Slejko (OGS, Trieste, Italy); V. Ulomov (JIPE, Moscow, Russia)

The Working Groups of the GSHAP regions: Central-North America, Central-Northern Europe, Eastern Asia, Northern Eurasia, Ibero-Maghreb, Adria, the working Groups of the projects: PILOTO, CAUCAS, RELEMR, SESAME, PAIGH-IDRC, EU-QSEZ-CIRPAN.

The Global Seismic Hazard Assessment Program (GSHAP) was launched in 1992 by ILP and ICSU and endorsed as a demonstration program by the UN/IDNDR. The GSHAP promoted a regionally co-ordinated, homogeneous approach to seismic hazard evaluation. Regional activities were concluded in 1992-98; the results have now been compiled in a uniform set of databases and in a world map of seismic hazard expressed in PGA. Support for the GSHAP implementation was provided by ING, Roma, by national and regional institutions, by IASPEI, UNESCO, ICSU, ILP, IDNDR, EU, NATO, INTAS and IGCP. All GSHAP materials (regional report, maps, datasets) can be retrieved on the GSHAP web site at <http://seismo.ethz.ch/GSHAP/>. The GSHAP world map of seismic hazard will be presented for the first time at the IUGG assembly and will be available for distribution at the assembly.

**JSP23/E/33-A5**

**1640**

### RISK ASSESSMENT AND MANAGEMENT IN RUSSIA

Shakhramanjan M.A.(1), Nigmatov G.M.(1), Larionov VI (1), FROLOVA N.I.(2), Suchzhev S.P.(3), Ugarov A.N.(3) Agency on Monitoring and Forecast of Emergency Situations, Ministry of Emergency Situation of Russian Federation (2)Seismological Center of IGE, Russian Academy of Sciences (3) Extreme Situations Research Center

At present in Russia the new technologies and procedures of natural and technological disasters monitoring and forecast of their consequences are elaborated and implemented, they are the following: procedure for individual seismic risk and losses assessment and identification of effective response scenarios; technology of operative zonation of the territories according to the rate of forest fires and flooding hazards; procedure of complex risk assessment and mapping with taking into account different natural and technological hazards; technology of estimation of buildings and structures' stability and earthquake resistance with the help of mobile diagnostic complexes; technology of operative monitoring of the territories with the use of remote sensing. All the technologies and procedures are realised on the basis of modern geographical information systems (GIS). The main blocks of the special GIS is described. The examples of individual seismic risk computations for different earthquake prone areas and cities of the Russian Federation, as well as for other countries are given. The influence of secondary engineering geological processes (landslides and liquefaction) is considered. The procedure of acceptable seismic risk level estimation is proposed. The examples of complex risk estimations are also given for the areas where different natural hazards (earthquakes, volcanic hazard, tsunami, flooding, hurricanes and storms, avalanches, forest fires) are possible. The preventive measures plans and measures for reduction the risks from separate hazards are proposed. The maps of operative zonation of the territories according to the rate of forest fires and flooding hazards are presented for some regions of Russia and other countries. The application of the obtained results to disaster management practice may increase significantly the efficiency of measures aimed at risk reduction for population in urban areas.

**JSP23/E/39-A5**

**1700**

### EARTHQUAKE RISK ASSESSMENTS AND PRACTICAL APPLICATIONS FOR EARTHQUAKE MITIGATION STRATEGIES IN AUSTRALIA

Jack RYNN (Centre for Earthquake Research in Australia, PO Box 276, Indooroopilly, Brisbane, Queensland 4068, Australia, email: sally.brown@uq.net.au)

In response to the United Nations IDNDR program, the Australian IDNDR Co-ordination Committee of Emergency Management Australia facilitated the earthquake zonation mapping of urban areas in Australia as one of its initial projects. The catalyst for this was the devastating 28 December 1989 Newcastle earthquake. A specific methodology was developed which has been expanded to address the national requirements for earthquake mitigation strategies. This involves a multidisciplinary approach integrating, both quantitatively and qualitatively, earth science, engineering, socio-economic, humanitarian, disaster planning, emergency management and community aspects. The results are compiled as an "information resource" in terms of hazard and vulnerability assessments and the integrated risk assessments, earthquake scenarios, potential ground motions and possible damage situations relative to the built and natural environments and the community, the outcomes are translated into practical applications to address awareness and preparedness for earthquake codes,

**JSP23/W/11-A5**

**1720**

### HYDRODYNAMIC SIMULATION EXTREME STORM SURGES IN AZOV AND CASPIAN SEAS

Olga TIKHONOVA, Sergei Popov, Guennady Safronov, Oleg Zilberstein (State Oceanographic Institute, Kropotkinski per. 6, 119838, Moscow, Russia, email: oleg@soins.msk.ru)

Problems of storm surges description and prediction are very important because surges often lead to loss of human life and bring substantial damages to national economies. Thus for prevention their fatal consequences it is necessary to forecast storm surges according to available operative meteorological information and to calculate the storm surges characteristics. Besides of that, each extreme storm surge case is very important for determination of long return period characteristics of sea level and currents for hydrodynamic



support hydro-technical engineering and marine shelf oil and gas exploration. Design and installation of stationary shelf oil platforms require information about vertical structure of currents. These characteristics are obtained by the 3D hydrodynamic model simulation. In this paper a non-linear 2D and 3D hydrodynamic models were applied for calculation of some extreme storm surges in Azov and Caspian Seas (including the catastrophic cases). The regime of sea level variations was investigated.

GIS mapping, education and training, loss reduction, disaster planning and emergency management. Such projects have been undertaken in the urban areas of Sydney, Southeast Queensland, Newcastle and Melbourne. Particular effort is directed towards real-time simulated earthquake exercises in co-operation with emergency services authorities. Collaboration with several international organisations and other risk projects in Australia is continuing. Although Australia is a moderate seismicity active interplate regime, the record of albeit "rare" earthquake disasters pointedly attests to the need for mitigation strategies.

**JSP23/E/40-A5****1740****TOWARDS REAL-TIME MONITORING OF LAVA EFFUSION RATES DURING VOLCANIC ERUPTIONS**

Andrew HARRIS and Luke Flynn (HIGP/SOEST, University of Hawaii, 2525 Correa Road, Honolulu, HI 96822, USA, email: harris@kahana.pgd.hawaii.edu)

Determining volumetric effusion rates for lava flows is an important but challenging task. Effusion rates are a major consideration in considering the potential threat posed by a lava flow. For channel-fed flows, higher effusion rates produce flows that are longer, more rapidly moving, voluminous, and aerially extensive than those with low effusion rates. High effusion rate flows thus have greater potential to inflict damage on distant communities with less advance warning. To calculate effusion rates we use satellite-derived (TM and AVHRR) thermal data in a heat balance. High spatial resolution TM data are collected infrequently, but allow high precision. Using TM data for active flows at Kilauea, Hawaii, we obtain effusion rates of  $1.76 \pm 0.57$  and  $0.78 \pm 0.27$  cubic meters per second on 23 July and 11 October 1991, respectively. These rates compare with field measurements of  $1.36 \pm 0.14$  and  $0.89 \pm 0.09$ . Using lower spatial resolution weather satellite (AVHRR) data collected at higher spatial resolution (>1 image per day), we obtain similar but more poorly constrained effusion rates. However, comparison with ground-based and TM data for eruptions at Kilauea, Krafla and Etna show that the AVHRR-derived time series reliably show waxing and waning phases of effusive eruptions with high temporal precision.

All of our systems are automated, and with direction reception of TM and AVHRR at the University of Hawaii we anticipate providing a web-based real-time lava flow monitoring tool. This will display current effusion rate time series, up-dated within minutes of satellite overpass at least once every 6 hours for AVHRR, once every 8 days for TM. This system will be similar to our GOES-based real-time hot spot monitoring site at <http://volcano1.pgd.hawaii.edu>.

**Saturday 24 July AM**

Presiding Chair: A Ansal (Istanbul Technical University, Istanbul, Turkey)  
Concurrent Poster Session

**SEISMIC RISK MAPS AND SCENARIOS: TOOLS FOR THE PROTECTION AGAINST EARTHQUAKES****JSP23/W/17-A6****0830****THE LONG AND WIDING ROAD FROM EARTHQUAKES TO DAMAGE**

A. Ansal (Istanbul Technical University, Faculty of Civil Engineering, Maslak, Istanbul 80620, Turkey, tel: (90)-212-285 3702, fax: (90)-212-2856006, e-mail: ansal@itu.edu.tr); D. SLEJKO (Osservatorio Geofisico Sperimentale, P.O.Box 2011, 34016 Trieste, Italy, tel: (39)-40-2140248, fax: (39)-40-327307, e-mail: dslejk@ogs.trieste.it)

The impact of destructive earthquakes has two faces: one in the short term and the other in the long term. The first is given by the number of victims, damaged structures and direct economic losses. The second is given by the negative influence on the social structure in the following years. Although the direct economic losses can be absorbed by the country, especially with international support, in most cases the social structure suffers permanent damages. The recent earthquakes of Northridge and Kobe have shown the long term problems caused respectively to the insurance companies and private habitants. This is one of the reasons why in seismically active countries (e. g.: Italy), a general private insurance against natural calamities is now being implemented. The knowledge on seismic risk is, therefore, fundamental for loss reduction. Seismic hazard maps at national level are the basic tool for defining the national seismic zonation which is relevant for planning adequately new settlements and constructing properly new buildings. The choice of the hazard parameter to consider for zonation is critical when the description of the whole contents of the seismic excitation is desired. However, these maps are only valid at large scales and local effects are not taken into consideration. Seismic risk maps at national scale are strategic for planning the policy for retrofitting old buildings in the presence of limited investments: their definition in a quantitative manner remains mainly a research topic for the difficulty of quantifying properly the ingredients. Risk scenarios at regional to local scale are very popular in recent years as they have the potential to limit earthquake victims and structural damage when a dangerous event is presumed to take place. In fact, based on the information and analysis concerning earthquake resistance capacity of existing buildings and structures, strengthening and retrofitting programmes can be optimised. The good knowledge ...

**JSP23/E/34-A6****0850****DETERMINISTIC VS. PROBABILISTIC EARTHQUAKE HAZARDS AND RISKS**

Robin K. MCGUIRE (Risk Engineering, Inc., 4155 Darley Ave, Suite A, Boulder, Colorado, 80403, USA, email: mcguire@riskeng.com)

Deterministic vs. probabilistic approaches to assessing earthquake hazards and risks have differences, advantages, and disadvantages that often preclude the use of one over the other. Factors that influence the choice include the decision to be made (i.e. the purpose of the hazard or risk assessment), the seismic environment (whether the location is in a high, moderate, or low seismic risk region), and the scope of the assessment (a single-site risk, a multi-site risk, or risk to a region).

Decisions coming from earthquake assessments include selection of design or retrofit criteria and levels, financial planning for earthquake losses, and planning for emergency response and long-term recovery. The more quantitative the decision to be made, the more appropriate is probabilistic hazard and risk assessment.

For high seismic regions (e.g. California or Japan) where the largest earthquakes occur every 100-300 years), a deterministic scenario for the largest event will allow details to be examined such as ground motion effects caused by rupture propagation. In low seismic regions, extreme deterministic scenarios will have probabilities of occurrence that are too low to be useful for most decision purposes.

Specific site analyses generally require a probabilistic approach. Multiple-site analyses (e.g. for a portfolio of exposed or insured properties, or a lifeline) often require a probabilistic analysis because of multiple variables and complexities of the system, and a deterministic check can be misleading. Regional assessments often benefit most from deterministic models.

**JSP23/C/ST3/E/21-A6****0910****METHODOLOGICAL CONSIDERATIONS OF PROBABILISTIC SEISMIC HAZARD MAPPING**

R.M.W. MUSSON (British Geological Survey, West Mains Road, Edinburgh, EH9 3LA, UK, Email: R.Musson@bgs.ac.uk)

The study of seismic hazard is perhaps the most practically oriented aspect of earthquake seismology. As such, it should not be treated in an idealised or academic manner, but with regard to the needs of the consumers of the final product. This has important consequences when it comes to the topic of probabilistic seismic hazard maps. Who are these for? Historically, early studies of probabilistic seismic hazard tended to be done for engineers for specific design requirements. Consequently, there has been a tendency to treat seismic hazard maps as a sort of pan-national study for engineers, who can identify the design requirements for any site by picking them from the map. A dissenting point of view argues that seismic hazard maps are by their very nature too generalised to be used in this way; that such maps provide a first indication of relative hazard and should not be a substitute for site studies. There are, therefore, a number of interesting and important methodological questions to be asked: what are the practical differences in undertaking a seismic hazard map from calculating hazard for a site? Should probabilistic seismic hazard maps have the same degree of conservatism as site studies? How can seismologists meet the needs of different audiences? An engineer may think in terms of ground acceleration, but this parameter probably means little to people in other professions who still need access to seismic hazard data, but in a form they can understand. These are questions that need to be addressed directly; one should not leave them to be answered by default.

**JSP23/E/03-A6****0930****EARTHQUAKE SCENARIOS FOR SWITZERLAND**

FAEH, D., Bay, F., Giardini, D., Kind, F., Mayer-Rosa, D., Sellami, S. (Swiss Seismological Service, ETH Zurich); Lang, K., Bachmann, H., Wenk, T. (Institute of Structural Engineering, ETH Zurich); Noack, T., Huggenberger, P. (Institute of Geology, University of Basel)

The goal of our project is to develop a method for the estimation of expected damage from earthquakes. The presentation is giving an overview of the state of the project, which includes, the modelling and mapping of ground motion on a regional scale for the area of Switzerland, and on a local scale for the Basel area, the classification of the vulnerability of buildings to earthquake ground motion for some target areas, and the realization of scenarios. We will present the deterministic seismic hazard in form of scenario ground motion maps. This can be done on a regional scale or on a local (microzonation) scale. On the regional scale the scenario ground motion maps should include significant earthquakes in a regional sense. Maps will then display ground motion with different probabilities of occurrence in different locations. On a local scale, ground motion scenario maps are most appropriately computed for single possible earthquakes, and these maps can be combined with a vulnerability assessment of existing structures. In this combination the scenario maps include the level and duration of shaking. Furthermore they make it possible to identify localities where ground is likely to fail through liquefaction or landslides, and they enable us to pinpoint structures that are likely to be severely damaged and to find weak links in life-line structures. Such studies can be done with different levels of detail. The project will contribute to the necessary seismic upgrading of existing buildings, as well as to reliable earthquake resistant design of new structures, to the education of the general public, the emergency planning and it will serve as a reminder that there is a large difference between what is expected from probabilistic maps and what is a possible event.

**JSP23/E/08-A6****0950****REGIONAL AND LOCAL SEISMIC HAZARD ASSESSMENT**

A. MARCELLINI, R. Daminelli, G. Franceschina e M.Pagani (Istituto di Ricerca sul Rischio Sismico, CNR, via Bassini 15, 20133 Milano, Italy, e-mail: marcel@irrs.mi.cnr.it)

Site effects can produce, at a local scale, abrupt changes of the ground motion as also instability phenomena such as landslides and soil liquefaction; microzonation studies are the scientific response for the evaluation and mitigation of this kind of phenomena. Seismic microzonation generally produces on a municipal scale Landuse planning criteria and defines seismic actions for engineering purposes. Seismic codes instead, are issued on the basis of Seismic Hazard studies, that is, seismic actions and seismic zonation are a direct consequence of a probabilistic seismic hazard, generally assessed considering a 474 yr R.P. In other words seismic actions assessment is biased by the inefficiency of seismic hazard evaluation procedure to account properly of parameters controlling the ground motion, mainly due to the limited number of factors used in the attenuation laws. It should be pointed out that till now this limits appears unavoidable due to the scarcity of strong motion recordings. Microzonation investigation can overcome these limitations, but only if the reference input motion is properly assessed by adopting the same level and the same criteria of protection used to issue seismic codes at national level. The case study here presented refers to a zonation and microzonation investigation performed in the Forlì provincia (Emilia-Romagna) for the purposes of seismic prescriptions to be issued both at regional and local level and we will main focus on the importance of multiple approach for the definition of the reference input motion.

**JSP23/C/U5/W/06-A6****1010****NEAR-FIELD GROUND MOTIONS**

N. AMBRASEYS (Imperial College, London)

The assessment of earthquake hazard of interest to the engineer must be based on the analysis of reliable observational data than on statistics of many records and seismological parameters of questionable quality. Theoretical methods for the prediction of ground motions have become highly developed, whilst knowledge of the observational material is usually lacking. Differences between attenuation laws arise from the size and distribution of the sets of data used in their derivation and from the use of different magnitude scales, which introduce significant bias in the results. In addition, the correction of records and the modelling of attenuation laws and fitting method used to regress the data are sources of systematic errors. Taking some of these differences into consideration we find no significant variation of attenuation laws among different regions for shallow earthquakes, and a remarkable agreement between attenuation laws derived for Europe, western North America and New Zealand. They are all within the standard deviation of the determinations, which are not better than by a factor of 1.7 for accelerations. The importance of the vertical acceleration needs further investigation. However, the observation that the ratio of peak vertical zero-period or



## INTER-ASSOCIATION

spectral value, to that of the horizontal, can be larger than 1.0 does not necessarily imply large vertical accelerations or spectral ordinates, most certainly when these maxima occur simultaneously. Also the assessment of peak and spectral ground displacements, which is of some engineering importance, needs further investigation. Near-field ground motions from medium and large magnitude earthquakes associated with surface faulting or, from sites on low-strength deposits, contain a significant component of permanent displacement, not accounted or in standard base-line correction procedures. An answer to these question is needed in order to rank these effects among other variables, and clarify the need to include or exclude them from building codes.

### JSP23/W/18-A6 1050

#### ASSESSMENT OF STRONG EARTHQUAKE GROUND MOTIONS FOR NEAR-FAULT CONDITIONS

Mustafa ERDIK, Eser Durukal (Bogazici University, Kandilli Obs. And Earthq. Res. Inst. 81220 Cengelkoy, Istanbul, Turkey, email: erdik@boun.edu.tr, durukal@boun.edu.tr)

Near-fault ground motions are strongly influenced by the earthquake faulting mechanism. Especially, the motions with periods above 1s may follow certain radiation patterns, predicted by equivalent double-couple source models, and exhibit distinct long period pulses with amplitudes depending on the orientation of the site with respect to the rupture direction. Widely used predictive earthquake engineering tools, such as empirical attenuation relationships and spectral shapes fail in the assessment of such near fault motions. Deterministic theoretical predictions of the ground motion can be achieved by convolution of the Green's Functions and the slip function. Such deterministic predictions cannot be extended into the frequency regions above 1Hz, since, high frequency ground motions are controlled by the heterogeneities in the fault rupture, which cannot be accounted for in a deterministic manner. This requires either the use of stochastic source models or the stochastic treatment of the high frequency components in the ground motions.

Based on these developments a state-of-the-art hybrid procedure is developed for the assessment of the time history of the DBE (or SEE) ground motion for important engineering structures near major faults. The essential elements of the procedure can be listed as follows:

(1) Assessment of the source parameters of the DBE motion associated with the corresponding return period for specific conditions of site and seismicity; (2) Deterministic assessment of the low frequency (DC-1Hz) ground motion, at the outcrop of a reference soil layer, due to rupture of seismic faults using numerical simulation; (3) Use of a Boore (1983) type stochastic simulation method to complement the deterministic low frequency ground motion with high frequency (1Hz- 50Hz) components; (4) Combination of the two parts of ground motion to yield a site-specific simulation for a frequency range of DC-50 Hz.; and (5) Site response analysis, if required, to include the local wave propagation effects in the soil media above the reference soil layer.

An example that illustrates the application of this procedure is provided.

### JSP23/E/01-A6 1110

#### MODIFICATIONS TO SEISMIC HAZARD DUE TO SITE-CITY INTERACTION

Pierre-Yves BARD, Philippe Gueguen (Laboratoire Central des Ponts- et-Chaussées and Observatoire de Grenoble, BP 53 - 38041 Grenoble Cedex - France,

email: Pierre-Yves.Bard@lgit.obs.ujf-grenoble.fr); Jean-François Semblat (LCPC, 58 Bd Lefebvre, 75732 Paris Cedex 15 - France); Martin Cardenas and Francisco Chavez- Garcia (Coordinación de Ingeniería Sísmologica, Instituto de Ingeniería, UNAM, Ciudad Universitaria, Apdo. Postal 70-472, Coyoacan, 04510 Mexico, D.F)

Soil-structure interaction has long been known to significantly affect the seismic behavior of large buildings on soft soils. A few observations, and several computations as well, recently indicated the possibility for significant feed-back effects from buildings into the soil: the waves radiated back into the soil from the soil-structure interface are trapped in the surface layers when the impedance contrast at depth is large enough, so that the building is acting as a secondary source of surface waves. This phenomena has been shown to be maximum in case of coincidence between the building and ground natural frequencies: the worst case corresponds to the matching of fundamental frequencies, and induces ground motion modifications of at least 30 % in time-domain amplitudes within distances up to 5 to 10 times the building base dimensions. The question then arises of the possibility of large-scale site-city interaction due to the quasi-random superposition of such phenomena for a large number of buildings in a given city, or in a given quarter, which, in turn, raises two issues: Is the "free-field record" concept relevant in such areas? And will the construction or destruction of some buildings modify locally the hazard? The aim of the presentation is not to answer these questions, but simply to briefly review the reasons why these issues have to be addressed, and to present some preliminary, first order computations exhibiting significant effects not only for "exceptional" configurations such as Mexico City, but also for much more common situations with "ordinary" sediments and "ordinary" buildings.

### JSP23/W/20-A6 1130

#### THE CYCLIC BEHAVIOUR OF SOILS AND EFFECTS OF GEOTECHNICAL FACTORS IN MICROZONATION

Atila ANSAL (Istanbul Technical Uni, Civil Engng., Maslak, Istanbul, Turkey, email:ansal@itu.edu.tr)

The behaviour of soils subjected to cyclic loading is briefly reviewed. The results obtained from cyclic triaxial, simple shear and torsional hollow cylinder tests conducted on undisturbed, normally consolidated clay samples subjected to different shear stress amplitudes and different loading patterns are summarised. Results of the tests conducted under uniform cyclic stresses to evaluate "cyclic yield stress" and "threshold cyclic shear stress" are presented. The effects of cyclic loading on static shear strength and induced settlements due to pore water pressure dissipation are discussed. Cyclic tests performed to evaluate the liquefaction susceptibility of laboratory prepared and undisturbed sands and silty clayey sands are briefly reviewed in the light of the findings reported in the literature.

Geotechnical site conditions is one of the main factors controlling earthquake forces affecting structures. Therefore, in analysing the observed damage in previous earthquakes and for microzonation studies, this factor and its coupled effect with earthquake source characteristics need to be evaluated. The earthquake source characteristics induced by a tectonic source mechanism are on macro level and are not sufficient to explain the variations in structural damage observed within short distances. On the contrary, the geotechnical site conditions that can be very different due to changes in the thickness and properties of soil layers, depth of bedrock and water table, can have more dominant influence on damage distribution. In addition the effect of coupling between site and source characteristics may modify earthquake ground motion characteristics significantly. There are large numbers of instrumental field observations obtained during recent earthquakes reflecting the coupled effects of geotechnical site and earthquake source characteristics. During earthquakes soil layers are subjected to multi-directional cyclic stresses with different amplitudes and frequencies that lead to cyclic deformations and to changes in stress-strain and strength properties of soil layers. Extensive laboratory, model and field studies were conducted concerning response of soils subjected to

cyclic stresses. Significant improvements were achieved in the field of insitu tests to obtain more reliable soil properties. Numerous analytical and empirical relationships were developed to model the behaviour of soil deposits subjected to earthquake excitations. From an engineering perspective, it is possible to investigate the properties of geo-technical site conditions in detail and analyse the response of soil layers with sufficient accuracy.

### JSP23/E/05-A6

1150

#### LOCAL SITE EFFECTS AND DYNAMIC SOIL BEHAVIOUR

Erdal SAFAK (U.S. Geological Survey, Box 25046, MS 966, Denver, CO 80225, USA, email: safak@usgs.gov)

Amplitudes of seismic waves increase significantly as they pass through soft soil layers near the earth's surface. This phenomenon, commonly known as site amplification, is a major factor influencing the amount of damage on structures. It is crucial that site amplification is accounted for when designing structures on soft soil sites. The characteristics of site amplification, at a given site, can be estimated by analytical models, as well as field tests. Analytical models require as inputs the geometry of all soil layers from surface to bedrock, their dynamic properties (e.g., density, wave velocity, damping), and the incident bedrock motions. Field tests involve recording and analyzing the dynamic response of sites to artificial excitations, ambient forces, and actual earthquakes. The most reliable estimates of site amplification are obtained by analyzing the recorded motions of the site during earthquakes.

This paper presents a review of the models and methods that are used to characterise site amplification, and introduces some new ones with better theoretical foundations. The models and methods discussed include spectral and cross-spectral ratios, response spectral ratios, constant amplification factors, parametric models, physical models, time-varying filters, methods for downhole records, single-station methods, and generalised inversion techniques. The paper also examines the validity of one-dimensional models, in comparison to 2D and 3D models, and shows the effects of surface waves and surface-to-bedrock topography on site amplification estimates. The paper concludes that probabilistically cross-spectral ratios give more reliable estimates of site amplification than spectral ratios. Spectral ratios should not be used to determine site amplification from downhole-surface recording pairs because of the feedback in the downhole sensor. Response spectral ratios are appropriate for low frequencies, but overestimate the amplification at high frequencies. One-dimensional site amplification models are not appropriate for sites in deep sedimentary basins that are susceptible to generating surface waves. The surface topography...

### JSP23/E/44-A6

1210

#### THREE DIMENSIONAL PLATE KINEMATICS IN ROMANIA

Georg Dinter (Department of Geodesy, University of Karlsruhe, D-76128 Karlsruhe, Germany, email: dinter@gik.uni-karlsruhe.de); Guenter SCHMITT (Department of Geodesy, University of Karlsruhe, D-76128 Karlsruhe, Germany, email: schmitt@gik.uni-karlsruhe.de)

Since 1996 the Collaborative Research Center (CRC)461 "Strong Earthquakes: A Challenge for Geosciences and Civil Engineering" is funded by the Deutsche Forschungsgemeinschaft (German Research Foundation) as a German Contribution to the UN initiative "International Decade of Disaster Reduction" (IDNDR). A central project of this CRC is the subproject B1 "Three dimensional Platekinematics in Romania" which is installed to detect borders of the geotectonic plates in Romania, to quantify their three dimensional movement rates and to determine in detail the deformation of each geotectonic unit in the Vrancea Region as a contribution to the research of the tectonic cause of the intermediate depth earthquakes in this region. These aims shall be accomplished by repeated GPS-measurements in a network which has been installed in 1997 and measured until now in 1997 and 1998. This network is consisting of 26 stations, covering an area of 250 x 380 km with the Vrancea area as the centre. The frame is given by six stations of the CEGRN (Central European Geodynamic Regional Network) of the CEI-Initiative CERGOP, for which co-ordinates and velocities in a global tectonic scenario are available. The paper gives information about the tectonic background, the geodetic network, the GPS-measurements and the achieved accuracy's and first results of deformation analyses.

Saturday 24 July PM

Presiding Chair: D Slejko (Observatorio Geofisico Sperimentale, Trieste, Italy)

### JSP23/L/06-A6

1400

#### EVALUATION OF VULNERABILITY OF CIVIL ENGINEERING STRUCTURES

Mauro DOLCE (Department of Structures, Soil Mechanics, Applied Geology, University of Basilicata, Potenza, Italy)

The impact of earthquakes on man-built systems (buildings, groups of buildings, lifelines, cities, etc.) is usually expressed in terms of losses. Loss assessment is a highly complicated task, involving, besides structural engineering and seismology, many disciplines such as geotechnical, transport, hydraulic and electrical engineering, geology, urban planning, social and economic sciences, etc. However most of the losses results from the consequences of direct damage to civil engineering constructions, particularly buildings. The evaluation of their seismic vulnerability is then a fundamental step in the process of determining the impact of earthquakes on man-built systems. This is usually assessed in terms of seismic risk in a period of time (e.g. one year, hundred years), i.e. in terms of probability or of expectation of losses during that period due to all the possible arriving earthquakes. This representation is very general but presents many drawbacks such as the difficulty of interpreting the results in practical terms and the difficulty of expressing and quantifying losses for territorial systems. In fact they are highly dynamical systems, whose future developments are difficult to forecast, particularly after the occurrence of an earthquake. A long term loss prediction is therefore not much significant, if it is referred to the current situation or even to the current trend.

Recently the interest of researchers and operators has been focused on risk scenarios, where the impact of a given earthquake is investigated and quantified. This approach permits to better understand the behavior of the built environment under study and to take the countermeasures aimed at reducing its impact. Scenarios can be prepared considering different aspects of the earthquake consequences. Different levels of accuracy can be assumed in the preparation of a scenario, starting from the assessment of shaking intensity and characteristics, through damage prediction up to loss assessment. Obviously the accuracy levels in the different steps must be consistent.

The assessment of damage to constructions deserves a special attention. In this respect, two ...

### JSP23/L/07-A6

1420

#### FROM VULNERABILITY OF OBJECTS TO VULNERABILITY OF SYSTEMS

Carlo GAVARINI (Universita' La Sapienza, Roma, Italy)

First of all the paper outlines the current conceptions relevant to vulnerability of constructions, describing the various approaches and the different research levels, then, in the second part,

a more global vision is developed in which the constructions belonging to an aggregate, or a centre, or a city, or a territorial area, are considered as a part of a vulnerable system, with all the complexity that it brings about, in terms of different variables that must be taken in consideration, properties and values that are in danger, disciplinary, cultural and historical aspects that must not be ignored.

Assessment of vulnerability is strictly connected with another basic problem, risk mitigation, that will be briefly considered in the third part, analysing the interrelations between vulnerability and environment aggressions. Also here we must point out how today it is a common exigency, also as regards technical codes, to abandon the sectional vision of objects considered separately and to promote instead the above mentioned 'picture in picture' vision applied to systems, better said to complex systems, specially when the areas in question are rich with particular 'objects' with a 'cultural value', such as historical buildings and monuments.

Lastly, in the fourth part, we return to deal with single objects, giving a short account of problems specific to monuments and in particular to churches subjected to seismic actions; referring to studies regarding the Cathedral of Noto, partially collapsed in 1996 and now in course of reconstruction.

The need for experiments, either real or virtual, is recognized as a key for understanding and classifying the...

**JSP23/E/19-A6****1440****LOSS ESTIMATION: A POWERFUL TOOL FOR RISK ASSESSMENT AND MANAGEMENT**

Fouad BENDIMERAD (Risk Management Solutions, Inc., 149 Commonwealth Drive, Menlo Park, CA 94025, USA; email: fouadb@riskinc.com)

Earlier loss estimation studies were limited to investigating particular scenarios and were carried out by highly specialized experts. Today, loss estimation techniques are translated into efficient software applications that are accessible by a large constituency of end-users. These techniques offer a high level of analysis sophistication and enable users to perform various "if-then" scenarios to study the sensitivity of the results, to develop a better understanding of the outcomes and to gain insight on the consequences of the findings and decisions.

Loss estimation techniques have benefited from the advances in information technology. Modularity, encapsulation and a new generation of computer codes such as C++, provide a logical and flexible structure for organizing the analytical procedures involved in loss estimation. These techniques organize the multitude of analytical calculations into modules that are logically inter-related by hierarchical rules. This flexible architecture permits ease in development, testing, validation, maintenance and upgrade. The study region is divided into geographical units (Geo-Units) such as postal codes or census tracts. The data, calculations and results are then associated with the centroid of the Geo-Unit. The aggregated results from the Geo-Units yield the results for the study region. Geographical Information Systems (GIS) and Relational Database Management Systems (RDMS) are used to organize data in data warehouses, to manipulate data during analysis, and to associate results to geographical regions from which they can be queried, aggregated and/or mapped. GIS and RDMS also allow for easy display of input and output (in standard reports and maps) providing a critical functionality for communication of outcomes to end-users. Loss estimation has become a critical tool to the insurance industry and is quickly being adopted by a wide range of users including emergency managers and planners. The key to this expansion is the integration of new information technologies that gave these techniques greater analytical capabilities, flexible architecture, and user-friendliness.

**JSP23/C/U5/E/15-A6****1500****GLOBAL SEISMIC HAZARD AND RISK ASSESSMENT**

YONG CHEN, Qi-fu Chen, Ling Chen, Juan Li and Jie Liu (No. 63, Fuxing Avenue, China Seismological Bureau, Beijing 100036, P. R. China)

A global seismic hazard assessment was conducted using the probabilistic approach in conjunction with a modified means of evaluating the seismicity parameters. This method is applicable to both oceanic and continental regions, and for any specific duration of time. It can be used for those regions without detailed geological information or where the relation between existing faults and earthquake occurrence is not clear.

Most seismic risk studies use a probabilistic approach in which predicted damages in various categories of structure and facilities in the region in concern are estimated and added together to obtain a total loss for particular intensity ranges. We have used an alternative means of estimating earthquake losses based on several macroeconomic indices such as the gross domestic product (GDP) and population. A global seismic loss map is then compiled.

The expected losses (in USD) of selected countries and regions for the next 50 years are as follows:

World 949 (USD), Asia 563 (USD), European 184 (USD), N.America 115 (USD), S.America 60 (USD), Oceania 12 (USD), Japan 390 (USD), USA 66 (USD), China 17 (USD)

**JSP23/W/16-A6****1520****SEISMIC HAZARD MAPPING FOR ADMINISTRATIVE PURPOSES**

L. Peruzza (C.N.R. Gruppo Nazionale Difesa Terremoti, c/o OGS, Trieste, Italy); A. Rebez and D. SLEJKO (Osservatorio Geofisico Sperimentale, Trieste, Italy, tel: (39)-40-2140248, fax: (39)-40-327307, e-mail: dslejk@ogs.trieste.it)

Local site conditions strongly influence the seismic hazard assessment, even if done using standard probabilistic techniques, with average soil classification. GIS applications, nowadays, enhance these variations, without entering into a detailed microzonation study, that is not possible at wide, regional scale. On the other side, the administrative border of municipalities remains the basic units to face the problems of legislative measurements devoted to risk evaluation and reduction. The aim of this paper is to present maps of different hazard parameter devoted to better represent the free field shakeability in NE Italy. The dominant soil in each municipality has been classified, taking into account the location of buildings and structures: then soil dependent hazard estimates have been performed and mapped, according to the some of the criteria leading the new proposal of seismic classification in Italy.

**JSP23/W/29-A6****1600****EARTHQUAKE HAZARD ASSESSMENTS FOR THE GULF OF CORINTH (CENTRAL GREECE) AND KRESNA REGION (SW BULGARIA)**

Vladimír SCHENK, Zdeka Schenková and Pavel Kottbauer (all at Institute of Rock Structure and Mechanics, Academy of Sciences, CZ-182 09 Praha 8, The Czech Republic, email: schenk@irm.cas.cz)

The earthquake hazard calculations were realised for two seismically high-active European zones, for the area round the Gulf of Corinth (Central Greece) and for the Kresna region (SW Bulgaria). To make reliable earthquake hazard calculations all available data were collected. For

the Gulf of Corinth data of the National Observatory of Athens compiled by Drakatos, Kalogerias and Papadopoulos and as well the published earthquake catalogues, geological and geophysical materials (Ambraseys & Jackson 1990, Ganas & White 1996, Hatzfeld et al. 1990, Makropoulos 1985, Papazachos 1988, Papazachos & Kiratzi 1993, 1996, Papazachos et al. 1991, 1996, Shebalin et al. 1974) were applied. Simultaneously, for the Kresna region similar available data of the Geophysical Institute, Bulgarian Academy of Sciences, were sent to us by Rangelov and Shanov. All these data allowed seismogenic zones with respect to earthquake occurrence and main tectonic structures to be delineated, dependent events from independent ones to be identified, an earthquake regime per requested observation period and/or a size of the area to be normalised, a maximum possible earthquake to be assessed and an acceptable attenuation law to be applied. Every quantity was statistically tested in order to be possible to introduce the logical tree of the input parameters to the hazard calculations. A reliability of the earthquake hazard calculations in common practice will be discussed. The presented calculations were realised under the EC INCO-Copernicus ASPELEA Project No ERBIC 15CT97 0200.

**JSP23/C/U5/W/09-A6****1620****EARTHQUAKE DISASTER MITIGATION AND EMERGENCY RESPONSE SYSTEM (EDMERS) OF SHANGHAI BASED ON GIS**

YANG TING (Geophysics Institute, China Seismological Bureau. Now at Shanghai Seismological Bureau, No.87, Lanxi Rd. Shanghai, China, 200062, Email: tyang@263.net) Zhu Yuanqing and Song Jungao (Both at Shanghai Seismological Bureau, No.87, Lanxi Rd. Shanghai, China, 200062)

As the largest city of China, Shanghai is also under the earthquake threat. In order to understand how severe disaster Shanghai will be suffered and what should be done by government when a possible earthquake affects the city, the Earthquake Disaster Mitigation and Emergency Response System (EDMERS) has been developed based on Geographic Information System (GIS). The EDMERS mainly includes two subsystems and several databases. The first subsystem, rapid earthquake damages estimation subsystem, will provide the rapid estimation of all kinds of earthquake damages according to the real earthquake parameters, (the origin time, epicenter location and source depth) which determined by Shanghai Telemetry Seismic Network in minutes while a destructive earthquake occurs. The second subsystem is the emergency response, in which the following emergency responses should be completed in time after a shock: determining the rescue scheme, evacuating victims, coping with dangerous materials, making decisions against fire following earthquake. The databases of EDMERS include building information, lifelines, soil conditions, aerial photographs, historical earthquake catalogues and so on. The following features of EDMERS should be highlighted: first, making use of GIS can enable the system to process the spatial data in a reasonable way, for example, The overlay and buffer functions of GIS can deal with the comprehensive effect of damage of buildings and lifelines. The network analysis of ARC/INFO can be directly used in emergency response such as victim evacuation and pathfinding. Second, emergency response can carry out on the base of real damage conditions by integrating damage estimation subsystem and emergency response subsystem. Third, using remote sensing, namely aerial photograph as an auxiliary tool, make EDMERS visual, vivid and informative.

**JSP23/E/15-A6****1640****FIELD SURVEY OF TSUNAMI DISASTER IN PAPUA NEW GUINEA ON 17 JULY 1998**

Yoshiaki KAWATA ( Research Center for Disaster Reduction Systems, DPRI, Kyoto University, Gokasho, Uji, Kyoto 611-0011, Japan, email: kawata@drs.dpri.kyoto-u.ac.jp)

On the evening of Friday 17 July at about 7:30 p.m. a breaking wave from a massive tsunami swept across the sand bar that forms the outer margin of Sissano Lagoon, west Sepik, PNG. Initial reports claimed that the wave was between 7 and 10m and that up to 3,000 persons were killed or missing. This seemed to be an unusually damaging tsunami given the size of the earthquake. Members of the International Tsunami Survey Team decided that a field survey was necessary as soon as possible to try and determine the true value of the maximum run-up and to accurately map the run-up distribution along the coast. The first surveys to the Sissano region confirmed the 7 - 10m wave reports and even found place where the waves were larger - up to 15 m. The severe damage and extreme wave heights were confined to a relatively short (30 km) stretch of coast between Aitape and Sissano Village. The survey was conducted by a multi-national team with representatives from Japan, the United States, Australia, and New Zealand. The team was broken up into two groups, the Japanese and everyone else. By the numerical estimation, it is impossible to get such gigantic tsunamis with the earthquake magnitude of 7.0. We found many marks of liquefaction at the sand bar and many residents reported that they had three earthquakes and middle one was the most severe. Therefore, we concluded that the earthquakes were not slow earthquake. Numerical simulation models of submarine landslide show good agreement with tsunami heights and their longshore distribution.

**JSP23/C/U5/E/23-A6****1700****PRECISE TOPOGRAPHIC AND GEOPHYSICAL SURVEYS OFF SISSANO LAGOON, NORTHERN PAPUA NEW GUINEA**

TAKESHI MATSUMOTO(1), David Tappin(2) and R/V KAIREI KR98-13 Cruise Scientific Party 1) Japan Marine Science and Technology Center (JAMSTEC), 2-15, (BNatsushima-cho, Yokosuka 237-0061, Japan (2) British Geological Survey, Keyworth, Nottingham, UK

The northern coast of Papua New Guinea suffered from a M7.1 earthquake and aftershock events which occurred on July 17, 1998. A large-scale tsunami also occurred just after the earthquakes. KR98-13 Cruise by the Research Vessel KAIREI was carried out in January 1999 in order to locate the possible seismic faults and/or underwater landslides as the source of tsunami. Precise topographic and other geophysical mapping off Sissano Lagoon, in the area of 200km (E-W) and 120km (N-S), was completed after the 9 days' survey. The study area is characterised by enormous amount of fan sediment supply from Sissano Lagoon, deep-sea canyons on the shelf, arc-shaped slump and offshore strike-slip faults. Straight small-scale submarine canyons and valleys are eroding the shelf slope. The meandering canyon is located on the old shelf to the north of Aitape. Topographic features caused by landslides are recognised at numerous sites of the study area. Most of them are old, and the most recent is located 25km north-east off the Sissano Lagoon. The most prominent of the many tectonic faults located in the study area is E-W trending escarpment, the length of which is about 40 kilometres, recognised 25 kilometres north of Sissano Lagoon.

The result of simplified numerical modelling of tsunami propagation by use of the new bathymetric data shows that the distribution of maximum wave height is in good agreement with the observation. This suggests that the bottom topographic feature is an important factor to amplify the wave and to generate the focused tsunami runup, and that both earthquake faulting and underwater landslide should be taken into account as possible origins of the tsunami.



**JSP23/C/U5/W/19-A6** 1720**SUPER DENSE REAL-TIME MONITORING OF EARTHQUAKES: SUPREME**

Fumio YAMAZAKI (Institute of Industrial Science, The University of Tokyo, 7-22-1 Roppongi, Minato-ku, Tokyo 106-8558, Japan, email: yamazaki@iis.u-tokyo.ac.jp); Yoshihisa Shimizu, Wataru Nakayama and Ken-ichi Koganezumi (all at the Center for Supply Control and Disaster Management, Tokyo Gas Co., Ltd., 1-5-20 Kaigan, Minato-ku, Tokyo 105-8527, Japan, email: yshimizu@tokyo-gas.co.jp)

To cope with earthquake-related secondary disasters, city gas companies in Japan have promoted several countermeasures in the last two decades: increasing seismic resistance of facilities and pipelines, segmentation of gas networks into blocks, earthquake monitoring by seismometers, installation of intelligent gas meters with a seismic sensor etc. As one of such earthquake countermeasures, Tokyo Gas Company introduced an earthquake monitoring and rapid damage assessment system, SIGNAL, with 331 SI-sensors, which measure the peak ground acceleration (PGA) and spectrum intensity (SI) at district regulator stations. The strong motion indices and the results of damage estimation are used for the decision-making whether or not to shut off gas supply.

Recently Tokyo Gas further developed new SI-sensor, having several new functions with the much cheaper price. The new SI-sensor can store acceleration time histories in its IC memory and send monitored strong motion indices to the Supply Control Center through public telecommunication lines. The new sensors will be installed at all the 3,600 district regulator stations with in the next 8 years. The new SI-sensor network is named SUPREME (Super-Dense Real-time Monitoring of Earthquakes), which may be the most dense seismic monitoring network in the world. The data from the network will significantly contribute to the strong ground motion research as well as promote seismic safety of the greater Tokyo Metropolis.

**JSP23/W/00-A6** 1740**APPLICATION OF POTENTIAL FIELD ANALYSIS ...IN INTRAPLATE SEISMIC RISK ASSESSMENT**

GUO

Abstract not available at the time of going to press

**Monday 26 July AM**

Presiding Chair: S. McLean (NGDC/NOAA, Boulder, Colorado, USA)  
Concurrent Poster Session

**NEW PHENOMENA, APPROACHES AND TECHNIQUES****JSP23/C/U5/W/18-B1** Invited 0830**POTENTIAL OF DISRUPTION OF HUMAN ACTIVITIES ON EARTH AND IN SPACE AS A CONSEQUENCE OF THE INTERACTION BETWEEN THE SOLAR CORONA AND EARTH'S MAGNETIC FIELD**

Gordon ROSTOKER (Department of Physics, University of Alberta, Edmonton, Alberta, Canada T6G 2J1, email: rostoker@space.ualberta.ca)

Over the past few decades, mankind has become increasingly dependent on various technologies which have helped greatly to improve the standard of living around the world. Two examples of such technologies that have had an enormous impact on human activities are global communications and the provision of readily available electric energy through the development of large transmission grids. Unfortunately, with the advent of new technologies comes human dependence on them. The use of satellites for communications and position finding purposes serves as a useful example of this dependence. It is now recognised that both geostationary communications satellites and the position-finding GPS satellites are vulnerable to the energetic electron environment in which they orbit. In this paper I shall outline the nature of this vulnerability and what the consequence of the loss of these satellites might be. As well, it is worth noting that large fluctuations in the geomagnetic field at auroral latitudes can induce electric currents in large power transmission grids sometimes causing them to be disabled for significant periods of time. I shall describe the nature of this problem and how space researchers are attempting to develop techniques to predict the potential for power outages. These practical manifestations will be presented in the context of the physical processes through which the solar corona interacts with the earth's magnetic field.

**JSP23/W/00-B1** 0910**REVEALING TEMPORARY MAGNETIC VARIATIONS ASSOCIATED WITH GEODYNAMIC PROCESSES**

EPPELBAURN

Abstract not available at the time of going to press

**JSP23/W/07-B1** 0930**DESTRUCTIVE ATMOSPHERICALLY-GENERATED LONG WAVES: SEPARATION BETWEEN SOURCE AND TOPOGRAPHY**

S. MONSERRAT (1), A.B. Rabinovich (2) and B. Casas (1). (1) Instituto Mediterráneo de Estudios Avanzados, IMEDEA, (CSIC-UIB), Palma de Mallorca, SPAIN, dffsmt4@ps.uib.es, (2) Tsunami Center, P.P. Shirshov Institute of Oceanology, Moscow, RUSSIA

Destructive long waves caused by atmospheric disturbances (meteotsunamis) present a significant threat for the Mediterranean coast, in particular, for the Iberian Peninsula and the Balearic Islands. Ciutadella Harbour, Menorca Island, is the place where extreme oscillations, locally known as 'rissaga waves', occur most frequently. The understanding of their origin and generation mechanism is a key scientific and applied problem. A method was first elaborated to suppress the influence of the initial source in order to isolate the general topographic function. The next step was to separate the resonant influence of the outer shelf from the local coastal features (bays or inlets). This second step allows reconstructing the corresponding admittance functions for any bay or inlet, which may be afterward used to predict amplification of meteotsunami but also of tsunami waves in a given location. The data of LAST-97 hydrophysical experiment (June-September, 1997) gave us a good opportunity to test this. A set of bottom pressure recorders were deployed on the shelf of Menorca Island, in two neighboring inlets of this island (Ciutadella and Platja Gran), and in Palma Bay (Mallorca Island); a number of precise microbarographs were working simultaneously. The first step of our analysis allowed reconstructing the open-sea source spectra for several abnormal seiche events recorded in the region of Ciutadella which, after compared with the observed atmospheric spectra, were used to estimate the so-called 'transfer function' between the atmosphere and the sea surface. This function is clearly related to the topography of the

source area, but when computed for Ciutadella region, the transfer function was quite similar for different rissaga events suggesting consistency of the basic parameters (phase speed and direction of propagation) of the atmospheric waves generating large seiches. This fact can be used to predict the sea-level spectrum at a given location with the knowledge of the atmospheric pressure spectrum only. The second step of...

**JSP23/L/05-B1** 0950**ASSESSMENT OF GEOMAGNETIC HAZARD TO POWER SYSTEMS**

D. H. BOTELER (Geomagnetic Laboratory, Geological Survey of Canada, Observatory Crescent, Ottawa, Ontario K1A 0Y3, Canada)

During severe geomagnetic disturbances electric currents induced in high voltage power transmission systems can cause transformer saturation resulting in transformer heating, generation of harmonics and increased reactive power demand. These effects can damage transformers, cause misoperation of protective relays and, in the worst case, cause power blackouts. An extensive study has been made to assess the geomagnetic hazard to power systems in Canada. Data from the Canadian Magnetic Observatory Network and conductivity models for different parts of Canada were used to calculate the electric fields produced during different levels of geomagnetic activity. This was combined with statistics on the occurrence of geomagnetic disturbances to determine the electric fields the power systems could expect to experience, on average, once a year and once every ten years. These electric field values were then used as input to power system models which calculated the corresponding levels of geomagnetically induced currents (GIC) in each power system.

**JSP23/W/22-B1** 1010**THE SATELLITE CONCEPTION FOR MONITORING OF IONOSPHERE EXCITATION BY SEISMIC OR TECTONIC PROCESSES.**

Vladimir DOKUKIN, Victor Oraevsky, Yury Ruzhin and Vladimir Alekseev (IZMIRAN, Troitsk-town, Moscow Region, 142092, RUSSIA; E-mail: ruzhin@izmiran.rssi.ru)

The deep tectonic faults are known to be zones of concentration of stresses, canalisation of fluids, aerosols and gases, change of magnetisation and electro-conductivity of rocks, appearance of high electrical potentials and so on. Also the tectonic faults are associated with the geodynamical structures which form the zones of elevated seismicity (quakes or volcanic eruptions) or zones of dangerous natural hazards. The results of joint processing of the data of low-frequency emission, corpuscular flows as well as temperature and density of plasma permitted us to reveal the previously unknown effect of the generation of low frequency noises in space over the deep faults of the earth crust. The developing now in Russia method of ionosphere tomography also is very perspective for that. The system of the small satellites can be especially important for revealing and research of global and regional net of geological faults in an effort to plan searches of mineral resources and to forecast destructive earthquakes (volcanic eruptions). The first microsatellite COMPASS, weighting about 80 kg, is planned to launch to the circular orbit with height 400 km and inclination 790 for development of the methods of monitoring and forecasting of natural disasters on the base of co-ordinated monitoring at the Earth and from space the pre-earthquake phenomena. COMPASS is composed of several sensors associated to a data processing unit and a large memory in order to record the information all around the Earth independently from telemetry station. The details of the measurements, instruments and general conception of the microsatellite system based on the COMPASS mission are presented in the report.

**JSP23/W/09-B1** 1050**AIR QUALITY AS A GEOPHYSICAL HAZARD**

Tom BEER (CSIRO Atmospheric Research, Aspendale, 3195, Australia, email: Tom.Beer@dar.csiro.au)

Geophysical hazards are usually considered to be earthquakes, volcanic eruptions, landslides, floods, droughts, tsunamis, storm surges, wildfire, tropical cyclones and extreme weather events. Air pollution is not normally considered to be a geophysical hazard. This view has arisen because the causes of air pollution – industrial and motor vehicle emissions – are not geophysical in nature. However, as air pollution regulations succeed in reducing the amount of pollutant emissions, air pollutant episodes become sporadic in nature, and their occurrence depends on a particular combination of meteorological factors. Analyses of air pollution episodes and hospital admissions indicate that there is a significant increase in morbidity and mortality as a result of air pollution episodes. Time-series studies undertaken in Sydney have shown that particulate matter, ozone and nitrogen dioxide are the pollutants that are primarily responsible for adverse health effects. Air quality forecasting systems can play an important role in mitigating the adverse effects of air pollution. The forecasts will affect the behaviour of susceptible individuals, and thus reduce adverse health effects. The outputs from forecasting systems can also be used to provide improved estimates of the total exposure to air pollutants of the inhabitants who are at risk. Such improved estimates can then be used in conjunction with longitudinal studies of health effects to obtain better understanding of the complex interaction between air quality and health. This presentation will illustrate the manner in which air pollution depends on meteorology, review some of the data concerning the resulting health effects, and discuss the future research needed for a better understanding of the interaction between air quality and human health.

**JSP23/W/13-B1** 1110**MULTIFRACTAL ANALYSIS OF TROPICAL ATMOSPHERIC STRUCTURES AND TYPHOONES GENERATION.**

I. TCHIGUIRINSKAIA (E.E.&S. Dept., Clemson University, 342 Computer Court, Anderson, SC29625, USA, E-mail: iouliat@clemson.edu); D. Schertzer (L.M.M., Université Pierre et Marie Curie, 4 Place Jussieu F-75252 Paris Cedex 05, France); S. Lovejoy (Physics Dept., McGill University, 3600 University st., Montréal, Qué., H3A 2T8, Canada)

During the last past ten years numerous investigations have been lead on the tropical atmospheric structures: boundary layer coherent structures, tropical storms and typhoons. Emphasis has been often placed on the structural conditions of generation of typhoons. Contrary to other approaches, we investigate this question on a large range of scales and intensities, trying to understand the crucial relationships between extremes events (such as typhoons) and more average ones, how the latter can build up to the appearance of the former. We chose thus a universal multi-fractal approach, since in this case the mean as well as the extreme events are ruled by three fundamental multi-fractal exponents determining the infinite hierarchy of singularities of the field and their corresponding co-dimensions. We analysed data sets obtained during two aircraft expeditions over South China Sea in 1988 and 1989 (Karmazin and Mikhailova, 1991). Measurements were usually done everyday from July to October on 8 or 11 levels from 50 meters up to 5 km heights, every 125 ms along 40 km in the horizontal for each level across the largest clouds bands. In the latter case, some flights were carried at a



distance of Ed typhoon center as close as 7 km. Although variations of the estimates of the multi-fractal exponents are present, they do not seem to be significant, since these values remain close to those obtained in mid-latitude boundary layers or wind tunnel experiments (Schmitt et al. 1992). In conclusion, we discuss the rather low critical order of divergence of statistical moments  $q_D=7$  which rules the self organised criticality of extreme wind shears, temperature gradients and generation of related structures, in particular typhoons.

**JSP23/W/32-B1****1130**

### LARGE-SCALE EVOLUTIONARY PROCESSES IN HAZARD SYSTEMS OF EARTHQUAKES, A PHENOMENOLOGICAL MODEL BASED UPON SELF-ORGANIZED CRITICALITY [SOC]

Natalia SMIRNOVA, Vladimir Troyan (both at Institute of Physics, University of St.Petersburg, St.Petersburg 198904, Russia, e-mail: nsmir@snoopy.phys.spbu.ru); Masashi Hayakawa (The University of Electro-Communications, Chofu, Tokyo 182, Japan, e-mail: hayakawa@whistler.ee.ucc.ac.jp); Thomas Peterson (TFPLAB, Cleveland, Ohio 44124-5441, U.S.A., e-mail: TFPLAB@aol.com); Yuri Kopytenko (St.Petersburg Filial of IZMIRAN, St. Petersburg 191023, Russia, e-mail: galina@admin.izmi.ras.spb.ru)

The concept of self-organised criticality (SOC) is now widely used for the interpretation of the behaviour of natural hazard systems. This concept was recently introduced by the present authors as a way to search for earthquake precursory signatures. Here, we continue to consider earthquake region processes on the basis of the SOC concept. We suggest a phenomenological model for large-scale evolutionary processes that occur between violent earthquake episodes. Four principal stages of evolution are proposed and analyzed. They are: random chaos, subcritical, critical, and super-critical. External stimuli such as geomagnetic storms, sharp temporal and spatial variations in atmospheric pressure, and ULF impulses are considered as driving forces for a "cellular automata" process in active seismic regions. We discuss the possibility of using fractal characteristics of signals to study the critical dynamics of a hazard system. The important fingerprints of SOC - temporal and spatial fractal structures are analyzed using seismic and ULF electromagnetic data timed to violent earthquakes near Guam (August 8, 1993,  $M = 8.0$ ) and Kobe (January, 16, 1995,  $M = 7.2$ ). The research was supported by NASDA (Japan) and Russian Foundation for Basic Research (Grants No. 98-05-65554 and 99-05-NNN).

**JSP23/W/10-B1****1150**

### ON CONNECTION BETWEEN THE SEISMICITY SPACE-TEMPORAL CHARACTERISTICS AND THE EARTH ROTATION

Boris W. LEVIN (\*Shirshov Oceanology Institute of RAS and Russian Foundation for Basic Research, 32a Leninsky prosp., Moscow, 117334 Russia; levin@rbr.ru) Yegueny Chirkov (\*\*Union Institute of the Earth Physics of RAS, 10 Bolshaja Gruzinskaja, Moscow, 123810 Russia; chirkov@uipe-ras.scgis.ru)

An importance of the Earth's rotation influence to earthquakes occurrence was noted by I.Kant (1756), I.R.Mayer (1893), G.H.Darwin (1908) and was often discussed by geophysicists at present time. Supposing the unpredictability of natural hazards is connected partially with our poor understanding of the planetary processes role, we investigated a geographical distribution of the earthquakes. Using the catalog NEIC, we had created the histograms of the earthquake numbers and its energy as a function of a latitude  $F$  from 90 deg. N to 90 deg. S at period of 1900-1993. We had found that the latitude distribution of the event numbers  $N(F)$  is similar to the curve describing a dependence  $R^2(F)$  or  $I(F)$  where  $R$  is a distance from the axis of rotation and  $I$  is an inertia momentum of mass unit. Also we discovered the local maximum of the seismicity on so-called "critical latitude" 35 deg. N which was first mentioned by geographer A.Veronne (1912) and was calculated by F.Krasovsky and V.Magnitsky (1941) as a specific parallel for the Earth figure theory. The preliminary analysis of the seismicity-time dependence (more than 100000 events with  $M > 4.0$ ) for different latitude layers showed that the seismicity varies with main period of near 6 years practically at all latitude layers of the Earth.

**JSP23/E/02-B1****1210**

### VOLCANIC RISK ASSESMENT AND ZONATION OF THE MAIN ERUPTIVE HAZARDS IN TENERIFE (CANARY ISLANDS)

Vicente ARANA and Alicia Felpeto (Dept. Volcanologia, Museo Nacional de Ciencias Naturales, Jose Gutierrez Abascal 2, 28006 Madrid, Spain); Mar Astiz (Dept. Matematica Aplicada, E.T.S. Arquitectura, U.P.M., Avda. Juan de Herrera, 4, 28040 Madrid, Spain, email: civgy@pinar1.csic.es); Francisca Gomez (Centro di Studio per la Geologia Strutturale e Dinamica dell'Appennino, CNR, Pisa Italy); Alicia Garcia and Ramon Ortiz (Dept.Volcanologia, Museo Nacional de Ciencias Naturales, Jose Gutierrez Abascal 2, 28006 Madrid, Spain, email: mcng92@pinar1.csic.es and mcnor72@pinar1.csic.es)

Taking into account that the island of Tenerife is a complex case, that one unique volcano and a unique eruptive style cannot be considered, the methodology developed in this paper to define a volcanic hazard-risk zonation in the island consists of: (1) Definition of the different hazards. (2) Numerical gradation of the probability of occurrence of each phenomenon by area. (3) Selection of the areas that show the higher probability of being emission centres. (4) Numerical simulation of the effects of an eruption of the corresponding eruptive style in those areas. The steps (1), (2) and (3) are based on the extensive knowledge of the eruptive activity of Tenerife Island and structural parameters. The results obtained from these three steps and the hazard map are implemented in a GIS and also used for the organisation of the surveillance network in terms of efficiency.

**Monday 26 July PM**

Presiding Chair: B Scott (GNA, CRI, New Zealand)

**JSP23/W/80-B1****1400**

### STRESS CHANGES AT THE SOUTH ICELAND SEISMIC ZONE - A MODEL FROM 1706 UP TO THE PRESENT FOR BETTER HAZARD ESTIMATION

Frank ROTH (Section "Earthquakes & Volcanism", Division "Solid Earth Physics and Disaster Research", GeoForschungsZentrum, Telegrafenberg, D-14473 Potsdam, Fed. Rep. of Germany, email: roth@gfz-potsdam.de)

The South Iceland Seismic Zone is situated between two sections of the mid-Atlantic ridge, i.e. the Reykjanes Ridge SW of Iceland and the Eastern Volcanic Zone on the island. It is a transform zone, though no typical one, as it is not connecting both rifts at right angles. Following this hypothesis, earthquakes should occur on EW-trending left-lateral shear faults, equivalent to conjugate, NS-oriented right-lateral, rupture planes. In fact earthquakes take place on NS-oriented faults, which are indicated by intensity and aftershock distributions, as well as by surface fault traces.

The stress field permanently generated in the fault zone by opening of the adjacent ridges with

slightly more than 2 cm per year is computed and superimposed with the stress field changes induced by a series of 11 earthquakes ( $M \geq 6$ ) between 1706 and 1912. For these, different rupture depths are assumed, depending on the distance to the rifts. Finally, the post-seismic stress field of 1912 is extrapolated to the present, to see where highest stresses might have accumulated. In addition, the influence of loads at the Eastern Volcanic Zone on the stress field in the seismic area is studied.

The modelling shows that the stress is released by the series of events in the whole area, even though the ruptures planes are located on parallel NS-striking zones. The pre-seismic stress level for most events is high and pretty stable with the exception of situations when several strong shocks occur over a time span of several days, i.e. display typical main shock-aftershock patterns.

**JSP23/C/U5/W/03-B1****1420**

### INITIAL STRUCTURES AND PACKING TRANSFORMATIONS OF LOESS DEPOSITS: IMPLICATIONS FOR THE ANALYSIS OF CATASTROPHIC MASS MOVEMENTS

Eleanor PARKER and Tom Dijkstra (Coventry University)

Gradual settlement from aeolian suspension means that loess particles generally form very open initial packing. There is less than 50% solids in a unit volume of soil - unless there is too much water or additional stress which will cause particles to settle in a much denser state. As long as the deposit remains relatively dry, cementation and other bond types will maintain the open structure; the loess is metastable. The potential of metastable loess to collapse is impressive. Rapid transformations from undisturbed packing with dry densities of about 1.3 Mg/m<sup>3</sup> (void ratio  $e \sim 1$ ), to more closely packed 'deformed' fabrics with dry densities of about 1.65 Mg/m<sup>3</sup> ( $e = 0.65$ ) after collapse. At failure, significant pore volume reductions (often more than 10%) result in considerable rapid increases in pore pressures (principally related to water pressures, but in loess air pressures are also important). Such pore pressures are necessary ingredients to produce very mobile mass movements, usually in the form of flowslides. In situations where pore pressure dissipation is impaired, a lowering of the shearing resistance may last long enough to allow long run-outs and high sliding velocities. The study material is Chinese loess from Gansu province, but there are important parallels with similar collapsible deposits such as the brickearths of South East England.

**JSP23/C/U5/E/04-B1****1440**

### EARTHQUAKES PREDICTABILITY: A CASE STUDY

Valery KOREPANOV, Yevhen Klymovych and Pavlo Maltsev (Lviv Centre of Institute of Space Research, 5-A Naukova str., 290601, Lviv, Ukraine, e-mail: vakor@isr.lviv.ua); Masashi Hayakawa (Dept. of Electronic Engineering, University of Electro-Communications, 1-5-1 Chofugaoka, Chofu, Tokyo 182-8585, Japan, e-mail: hayakawa@whistler.ee.ucc.ac.jp); Katsumi Hattori (International Frontier Program on Earthquake Research, Institute of Physical and Chemical Research (RIKEN), c/o Earthquake Prediction Research Center, Tokai University, 3-20-1, Orido, Shimizu 424, Japan, e-mail: hattori@ior.d.u-tokai.ac.jp); Victor Tregubenko (Kyiv Branch of Ukrainian Geology Research Institute, 78 Avtozavodska str., 252144 Kyiv, Ukraine, e-mail: direct@kgou.ru.kiev.ua)

It is accepted that large earthquakes (EQ) are accompanied by different electromagnetic phenomena. They are also found to precede the EQ and the most debatable question is whether they can be used as EQ precursors. Two of such positive examples for EQ with  $M$ ; 4.5 are investigated: near Matsushiro (Japan) 01.07.1998 and near Crimea peninsula (Ukraine) 16.10.1998. In both cases three components of magnetic fluctuations only were studied: for Matsushiro in frequency band from 0.01 to 30 Hz and for Crimea the DC magnetic field was sampled once per 10 seconds. For Matsushiro EQ some preceding events were extracted: short spikes with some features deviating from noisy background and also about 50% overall growth of daily averaged amplitude of ELF emission. For Crimea EQ the variations of mean longitudinal conductivity of the crust were calculated. The resulting curves excellently suit the Scholtz dilatant-diffusional model: for 15 days averaged variations of the conductivity deflection from the mean value before earthquake was about 6% what was fairly beyond mean error  $\sim 1.2\%$ . Still higher was the deflection for daily averaged variations: more than 25%. The peculiarities of the study and processing methodology are discussed.

**JSP23/C/U5/L/01-B1****1500**

### MACRO SCALE MODELLING OF CATASTROPHIC NATURAL HAZARDS

Adrian STEWART, and Dr Claire McQueen, (EQE International Ltd, 500 Longbarn Boulevard, Warrington, WA2 0XF, UK. Tel:- +44 1925 838372, fax +44 121987 654, Email: astewart@eqe.co.uk, cmcqueen@eqe.co.uk.)

Economic losses from Natural disasters over the last few decades have been enormous, as demonstrated by Hurricane Andrew in the US. The impact on the Global economy can reverberate for years after a single event. Assessing the risk to regions and countries is essential in the context of enabling International Organisations, Governments an International Industry and Commerce to plan, mitigate and manage losses.

In terms of risk from damaging earthquake or windstorm events, the risk is a function of the hazard intensity combined with the vulnerability of the properties within any given unit or area. The deterministic results of such studies may also be combined With expected frequencies to obtain probabilistic estimates of risks. In order that the losses expected within an area from an event be estimated accurately, the vulnerability functions and hazard models should be representative of the scale of the are that they are located in. Scale is an important issue. The Hazard Model needs to reflect the reduced risks expected over larger areas. However, the detail needs to remain in order that the spatial resolution of the hazard across an area is accurately represented. The question is whether vulnerability and hazard models can be created for a specific scale, or whether it is possible to calculate losses on a detailed grid and aggregate consistently at any macro scale.

**JSP23/W/39-B1****1520**

### SPACE PRECURSORS OF EARTHQUAKE REGISTERED BY SATELLITE AT GEOMAGNETICALLY CONJUGATED AREAS

Yuri RUZHIN, Vera Larkina and Anna Depueva (IZMIRAN, Troitsk-town, Moscow Region, 142092, RUSSIA; email:ruzhin@izmiran.rssi.ru)

There is some progress in investigations of space plasma precursors of earthquake (EQ) - the magnetic conjugation of VLF pre-seismic emission on satellite orbits was found in both hemispheres. It means that some signature of precursor could be found inside the geomagnetic flux tube (shell) which connected with both conjugated ionosphere regions where the VLF precursors on satellite orbits were registered. Satellites INTERCOSMOS-18 and ALOUETTE data were analyzed from this point of view. Conjugated EQ-precursors are found in very low frequency (VLF) emission and ionosphere F2-layer plasma parameters. It should be pointed out that F2-precursors appears some days before the earthquake, manifest

## INTER-ASSOCIATION

themselves as an plasma anomaly like Appleton anomaly if epicenter of future earthquake is situated near magnetic equator. It is shown that the electric field less than one mV/m have to be generated in the ionosphere. Then we'll be able to observe the above ionosphere phenomena as an equatorial earthquake forerunners. We are able to show that VLF precursors which appears some hours before the earthquake are localized close to magnetic shell corresponding to future earthquake epicenter and have a belt-like structure (longitude aligned on more than some tens thousands kilometers) in bot hemispheres. In the presented work relationship of VLF fields intensity and spectra with energetic electrons flux density are investigated over epicentral zone of the prone earthquake. On the base of our estimations and phenomenological development of the event in the ionosphere (plasmosphere) over the seismic region and over magnetically conjugated region the possibilities of the seismoionospheric anomalies (space precursors of EQ) generation are discussed.

**JSP23/C/U5/W/10-B1**

**1600**

### THE CENTRAL POSITION OF GEOPHYSICS FOR THE EVALUATION OF THE NEAR-FUTURE AND ESPECIALLY THE DISTANT FUTURE

Nils-Axel MÖRNER, (Paleogeophysics & Geodynamics, S-10691 Stockholm, Sweden, email: morner@pog.su.se)

Geophysics and its paleogeophysical expressions over past periods will always play a central role for all types of predictions and estimations of the future. This applies for the near-future and its evaluation based on our understanding of the natural variability in environmental parameters on a decadal-to-century time scale, and its interaction with induced anthropogenic factors. On the 104-105 year time scale, the seistrial mechanical calculation of the so-called Milankovitch variables form a strong basis in climate prediction. Distant predications and evaluations are, in general, neither simple nor straight-forward. Still, there is a desperate need for safety predictions over 104-106 year time scale when it concerns the long-term stability and safety of high-level nuclear waste repositories. This has added a completely new dimension to geophysics. For a "safe" final bedrock deposition of high-level nuclear waste, we need guarantees for the immense time period of "hundreds of thousands of years". No one can, of course, give meaningful guarantees over such long time periods. The Fennoscandian crystalline bedrock is, by no means, as stable and reliable as sometimes claimed. Only some 10,000 years back in time, the seismic activity was (as a function of the extreme rates of glacial isostatic uplift amounting as much as some 10 cm per year) tremendously high; in amplitude as well as in frequency. In such an environment – to be repeated at the next future ice age – we can, of course, give no guarantees for a waste disposal in the bedrock; on the contrary, most facts suggest that it would be seriously damaged. In the absence of a true long-term safety, we can only propose that the waste produced: (1) is kept at a minimum, (2) is stored under constant control, and (3) is kept accessible for reparations as well as possible future innovations of how to render the waste harmless.

**JSP23/E/14-B1**

**1620**

### LONG-TERM HAZARD FROM RIVER-BED AGGRADATION FOLLOWING VOLCANIC ERUPTIONS

Thomas C. PIERSON (U.S. Geological Survey, Cascades Volcano Observatory, 5400 MacArthur Blvd., Vancouver, WA 98661, USA, email: tpierson@usgs.gov)

Explosive volcanic eruptions can provide immense volumes of readily erodible volcanoclastic sediment to drainage basins on or near source volcanoes. Posteruption rainfall, or other types of rapid runoff, mobilizes sediment from hillslopes or from source deposits in upper valleys, episodically moving it downstream during periods of high discharge (probably as long, slow-moving sediment waves). Depending on the volume of sediment added to a fluvial system, this sediment mobilization can result in dramatic and hazardous vertical aggradation of river beds. Data from recent historical eruptions at Mount Pinatubo (Philippines), Mount St. Helens (USA), and other volcanoes demonstrate that river-bed aggradation can occur rapidly (at varying rates as high as 0.4 m/day) in channels up to hundreds of meters wide over extensive downstream reaches in the first year or two following an eruption. Although periods of aggradation may be interrupted by irregular periods of degradation (channel downcutting), river-bed elevations may show net rises of as much as 20 to 30 m within only a matter of months within 50 km of source, and net aggradation of at least 8 m has been documented as far as 280 km from source. Under these conditions, floods and lahars need not have extraordinarily high discharges to be able to reach and inundate previously safe homes, roads, and farmland. Aggradation may continue for decades before sediment supply from the disturbed areas decreases enough to allow rivers to incise back down to previous bed levels. Tree-ring data from terraces along the Sandy River, 80 km downstream from Mount Hood (USA) indicate that significant reincision (about 8 m or nearly 50 percent) occurred within about 40 years of the ~200 yBP eruption of Mount Hood, and the river nearly regained its original bed level within about 60 years. Efforts to mitigate river-bed aggradation hazards, such as has been done at Mount St. Helens, should be planned with knowledge of this potentially long-term impact on fluvial systems.

**JSP23/C/U5/W/17-B1**

**1640**

### A SEA LEVEL-WAVE JOINT DISTRIBUTION FOR SEVERE STORM SURGE HAZARD ASSESSMENT USING OFFSHORE PLATFORM DATA

Le KENTANG (Institute of Oceanology, Chinese Academy of Sciences, Qingdao 266071, PRC, email: ktle@ms.qdio.ac.cn)

Generally speaking, the direct economic losses from a severe storm surge disaster consist mainly of that from sea water flooded over land and that from damage caused by high sea. However, the traditional method for storm surge hazard assessment in China is to construct one or two single-parameter distributions by using historical sea level and/or wave data at some coastal stations and/or ocean stations. In this case, apparently, both sea level data and wave data at these stations must be long enough to estimate the return periods needed for mitigation. However, the existing data of sea levels and waves at most of these stations can't meet the needs of the estimation. In this paper we presents a method to construct the sea level-wave joint distribution for severe storm surge hazard assessment by using a couple of years data on such a stations. Using a one-year platform data in the Bohai Sea, an example is given to illustrate the capabilities of this methodology.

**JSP23/C/U5/E/08-B1**

**1700**

### STATISTICAL METHODS FOR SLUSHFLOW SITUATIONS RECOGNITION, MONITORING AND FORECASTING

Pavel CHERNOUSS and Olga Tyapkina (Center of AvalancheSafety,"Apatit" JSC, 33a, 50 years of October St.,Kirovsk, Murmanskregion184230, Russia, e-mail: P.Chernous@apatit.murmansk.su); Erik Hestnes and Steinar Bakkehoi (both at NorwegianGeotechnicalInstitute, P.O. Box 3930 Ullevål Hageby, N-0806, Norway, e-mail: eh@ngi.no)

Slushflows - flowing mixtures of water and snow - are a hazardous phenomena in mountainous regions all over the world. They are most frequent in higher latitudes, i.e. in Norway, Iceland, USA(Alaska),Canada and Russia (northern and eastern parts). Slushflows exert high destructive forces and they are almost unpredictable due to inadequate studies. The work is an attempt to classify meteorological situations at different heights above sea level on "slushflow" and "non-slushflow" with linear discriminant analysis and Bayes'formula. Standard meteorological observations were used as primary parameters to describe the situations. Classification was made on daily base. Data for the mountain regions of Norway and the Khibini Mountains in Russia were taken to derive the classification rules and to carry out a verification of the methods. Different sets of parameters were tried to find out most informative ones. Two parameters have been chosen -daily water income (designed parameter) and snow cover thickness. Classification accuracy, obtained with independent data, was better than 75% for both types of the situations. For more detail slushflow danger monitoring one day moving average values are used. There are two ways to transform the diagnostic methods into forecast ones- by using of forecasted parameters as predictors or by extrapolation of situation probabilities. The methods are an effective tool for slushflow forecaster and realized as software package for the real-time work at the Center of Avalanche Safety of "Apatit" JSC.

**JSP23/W/23-B1**

**1720**

### PRESEISMIC ELECTROMAGNETIC SIGNALS GENERATED IN ATMOSPHERE

Yuri RUZHNIN (IZMIRAN, Moscow, 142092,RUSSIA; E-mail: ruzhnin@izmiran.rssi.ru); Costas Nomicos (Technological Educational Institute of Athens, GREECE); Filippos Vallianatos (Technological Educational Institute Chania branch, Crete, GREECE)

Electromagnetic (EM) precursors of Earthquakes (EQ's) are modern possibility to monitor pre-earthquake situation and to improve the EQ forecast. Its nature up to now is under the question. The EM signals registered (before the EQ) onboard of satellites is the object of intensively investigations during last decade. Here we overview of EM seismo precursors and present situation with its explanation but the high frequency (HF) precursor (43MHz and 51MHz) is main point of our presentation. It is showed that precursor type HF signals are appeared before the EQ for one-three days and the some new peculiarity is found. This is under horizon epicenter position for main part of events under question. It means that emitted volume must be located at some altitude in atmosphere or ionosphere. The another unusual result is that such pre-seismic signals are responsible for seaquakes (not, as usually, for the earthquakes!). In result, we made conclusion about existing of some thunderstorm type activity above the sea level before the seismic event. It means that above sea level (up to 3-8 kilometers) the space charge cloud would be generated at one-three days before the active seismicity (under sea floor). Based on above mentioned we can supposed that probably this is new pre-seismic signature which will be used in future EQ forecast. Some additional experimental facts and mechanisms are discussed to explain this HF precursor (EM signals) generation above the epicenter of future seismic activity.

**JSP23/W/87-B1**

**1740**

### SIMULATION OF THE DARWIN OBSERVATION OF THE 1835 CHILEAN EARTHQUAKE

GALIEV

Abstract not available at the time of going to press

**Tuesday 27 July AM**

Presiding Chair: Chen Yong (Seismological Bureau, CHINA)  
Concurrent Poster Session

### DETECTION, MONITORING, EARLY WARNING AND PREDICTION

**JSP23/E/18-B2**

**0930**

### MONITORING THE CURRENT SUMMIT ERUPTION OF MOUNT ETNA USING INFRARED SATELLITE DATA FROM THE ERS ATSR-2

Rob WRIGHT, David Rothery, Stephen Blake (Department of Earth Sciences, The Open University, Milton Keynes MK7 6AA, UK, email: r.wright@open.ac.uk); Martin Wooster (Department of Geography, King's College London, Strand, London, WC2R 2LS, UK)

After the unusually quiet period that followed the end of the 1991 to 1993 eruptions, magmatic activity resumed within Etna's summit crater complex in July 1995. All four summit craters have been characterised by strombolian activity while between July 1997 and July 1998 the South East crater was also the site of sustained lava effusion. Intense paroxysmal explosions have also occurred intermittently from the North East crater and La Voragine.

In March 1998, at the request of the Italian Civil Protection Authority, the European Space Agency commissioned the "Empedocles" project. This aim's to assess the role that satellite remote sensing can play in monitoring the volcano, and understanding the nature and future evolution of the current activity. Using data acquired by the ERS-2 along Track Scanning Radiometer (ATSR) we show how the amount of short-wave infrared radiance emitted from the summit crater complex has fluctuated since July 1996. The data reveal patterns that correlate well (on a weekly time scale - ATSR acquires data ~ every 3 days) with Etna's general level of activity as documented in field reports. Examining the amount of radiation emitted at different wavelengths allows us to distinguish activity associated with high temperature vents from that associated with lava flows. By applying rank order statistics to the ATSR data-set we have inferred changes in the level of activity on Etna that may reflect changes in the eruptive state of the volcano.

**JSP23/C/U5/W/07-B2**

**0950**

### THE SPACE VOLCANO OBSERVATORY (SVO) PROJECT

Pierre BRIOLE (Institut de Physique du Globe, 4 Place Jussieu, F-75005 Paris, email: briole@ipgg.jussieu.fr) and the SVO science team

1500 volcanoes on the earth are potentially active. One third of them have been active during this century and about 70 are presently erupting. At the beginning of the third millennium, 10% of the world population will be living in areas directly threatened by volcanoes. Presently, in spite of the efforts of many countries, only a few volcanoes are monitored by modern observatories. Even in the best equipped of them, real-time data acquisition on the active parts of the edifices during crisis is an extremely difficult and risky task. The only way to provide global, continuous, real-time and all-weather information on volcanoes is to combine observations from space and from the ground. Spaceborne observations (with satellites, helicopters, drones, balloons,...) are mandatory and complement the ground ones that can be implemented on a limited set of volcanoes. A project called SVO (Space Volcano Observatory) has been proposed to the European Space Agency to remotely monitor the deformations and thermal changes of the highest active areas of the volcanoes (lava lakes, lava domes, lava

flows, eruptive vents...). These zones are unstable and often deform significantly prior to paroxysmal events (sudden collapses, flank pyroclastic flows, ...). They are also remote and dangerous and cannot be easily equipped with ground equipment. We propose to map at high resolution (1.5m pixel size) the topography and the thermal changes (for pixels above ~ 450°C) of active volcanic areas with a return time of one to three days and an image size of 6 x 6km. Those variations will put constraints on the physical and dynamic processes of the system. Other applications like landslide monitoring, will be possible. The requirement of fast data processing and interpretation imply the set up of several ground-based stations for data collection. The 12-15 major volcanological observatories of the world could host those receiving stations.

**JSP23/E/42-B2****1010****VOLCANIC RISK AND EMERGENCY PLANS OF THE NEAPOLITAN VOLCANOES**

Lucia CIVETTA (Co-ordinator of the technical committee for preparation of the emergency plans Osservatorio Vesuviano, via Manzoni, 249, 80123 Naples, Italy e-mail:civetta@osve.unina.it)

The volcanoes of the Neapolitan area, Vesuvius, Campi Flegrei and Ischia, have generated more than 100 explosive eruptions in the past 10 ka. However, they can lie dormant for many centuries and the great risk posed by volcanic activity in the region was, therefore, not always apparent. Vesuvius has exhibited various types of activity in the past 25 ka. Plinian and subplinian explosive eruptions occurred every few millennia or few centuries, respectively. Strombolian activity, lava effusions and phreatomagmatic eruptions usually follow the plinian and subplinian eruptions until conduit closes. Since the last eruption of 1944, Vesuvius has not shown signs of unrest. Only moderate seismicity and fumarolic emission testify the current state of activity of the volcano. The Vesuvius eruptive history however suggests that the longer is the quiescent period, the more violent is the renewal of the activity. The last eruption of the Campi Flegrei caldera occurred in 1538 AD, at the north-western edge of the La Starza resurgent block. Since that time, after hundreds of years of subsidence, two bradyseismic events occurred in 1969-70 and 1982-84, which totalled a net vertical uplift of 350 cm of the central caldera block, at the harbour of Pozzuoli. The last eruption of Ischia occurred in 1302 AD, at the edge of the resurgent Mt. Epomeo block. Since that time intense fumarolic activity, hot springs and seismicity characterise the island current state. Intense urbanisation and inadequate planning of the Neapolitan territory have significantly contributed to the increment of the volcanic risk since the fifties. In response to the increasing volcanic risk, in 1993 the Minister for Civil Defence appointed a commission to prepare the emergency plan of the Vesuvian area that was completed at the end of 1995. In 1996 the Minister of Civil Defence appointed a new Commission to update the emergency plan of Vesuvius and prepare the scenario of the expected eruption at the Campi Flegrei Caldera and define the guidelines for the Campi Flegrei emergency plan.

**JSP23/E/26-B2****1050****VOLCANIC HAZARD MAPS OF TENERIFE ISLAND (CANARY ISLANDS)**

Alicia FELPETO, Vicente Araña (Dep. Vulcanology, Museo Nal.Ciencias Naturales, CSIC, J. Gutiérrez Abascal, 2, 28006 Madrid, Spain, email: mcnafe66@pinar1.csic.es); Mar Astiz (Dep. Matematica Aplicada, E.T.S.A. Universidad Politécnica, Avda. Juan de Herrera 4, 28040 Madrid, Spain); Francisca Gómez (Centro de Studio per la Geologia Strutturale e Dinamica dell'Apennino, CNR, via Santa Maria, Pisa, Italy); Alicia García, Ramón Ortiz (Dep. Vulcanology, Museo Nal. Ciencias Naturales, CSIC, J. Gutiérrez Abascal 2, 28006 Madrid, Spain)

The first steps for the generation of volcanic hazard maps of Tenerife consists of the definition of the most significant hazards and the selection of the most suitable areas for containing emission centres, taking into account all the data of the eruptive history of the island. Then, for the evaluation of the effects of an eruption, a numerical model for each hazard has been chosen. The application of the different models allows the computation of the probability of each point of the island being affected by each type of eruption, and so, building up the volcanic hazard maps. The methodology proposed, integrated on a GIS framework, allows the automation of the generation of hazard maps for more specific studies of smaller areas of the island or specific risk scenarios. It also represents the starting point for developing risk maps.

**JSP23/C/U5/E/20-B2****1110****MAPPING AND MONITORING OF VOLCANOES USING SPACE-BORNE SAR**

Woolil M. MOON, Lanying Feng and (Geophysics, The University of Manitoba, Winnipeg, Canada R3T 2N2 (email: lfeng@gis.geop.umanitoba.ca, wmoon@cc.umanitoba.ca); DUK-JIN-KIM, K.H. Choi, C.W. Lee and Woolil M. MOON (Earth System Science, Seoul National University (email: wmoon@eos1.snu.ac.kr, djkim@eos1.snu.ac.kr); J. L. Lizeca (SERGEOMIN, La Paz, Bolivia ("Jose Luiseca" abtema@coord.rds.org.bo

In this study, we have investigated several active volcanic areas (Baiktu-san (China-Korea border), Cerro Caquella (Bolivia), and Halla-san (South Korea)) using RADARSAT and JERS-1 SAR data for their geological characteristics and for their application criteria in view of natural hazard monitoring. Baikтусan is located at the junction of northeastern edge of Huabai tectonic block of the Eurasian continent and mid-Cenozoic off-shore Pacific volcanic zone, and have gone through several stages of crustal evolution. According to historical records, Baikтусan had a major eruption in 1002 AD, and several minor eruptions in 16th and 18th century. However, the strategic location of Baikтусan at the political boundary between P. R. China and North Korea, has resulted in a situation with rather poorly surveyed geology maps and inconsistent geological interpretation of recent volcanic activities. The Halla-san volcano has not been active during the historical time, but it is the main feature of the Jeju Island (a volcanic island), which has recently been rapidly developed for increasing human settlement. In the Cerro Caquella region, which is a remote barren Andean range, a detailed DEM could be extracted to investigate morphological changes associated with active volcanic activities, in addition to correlation of the DEM with respect to several other geological and geophysical data collected over the study area. Several sets of JERS-1 SAR and RADARSAT data are acquired for this study with the objectives of investigating the surface geology of Baiktu-san and Halla-san volcanoes and the surrounding area to delineate consistent geological and volcanic characteristics. Both traditional geological remote sensing approach and the space-borne InSAR (SAR interferometry) approach were used (i) for structural geological interpretation of the study area using the pre-processed SAR data, and (ii) for correlation of the interferogram fringe pattern...

**JSP23/C/U5/W/02-B2****1130****THE MONTSERRAT VOLCANO ALERT AND WARNING SYSTEM**

Lloyd L. LYNCH (Seismic Research Unit, University of the West Indies, St. Augustine, Trinidad W.I., email: sru@wow.net)

From the onset of the Soufriere Hills volcano eruption on July 18, 1995, to the waning stages of the eruption almost three years later most areas of the more developed half of the island of

Montserrat faced the threat of devastation. The relatively small size of the island, its complex political and governance structure, and the demographic setting in relationship to the threatening volcano were factors which all combined to make the management of the crisis one of the most challenging of the twentieth century. Compounding matters, was the fact that the eruption followed a style for which there was no well-documented precedent. As in most volcanic crises, an alert and warning system was instituted primarily to facilitate risk and emergency management. The system employed was an adoption of the generic alert and warning system popularised by the UN Volcanic Emergency Handbook. In this article the Montserrat volcano alert and warning system is modelled as network of closely interrelated functional entities comprising of a management subsystem, a detection subsystem and a response subsystem. This provides a comprehensive abstraction of the functions and interaction between the administrative authorities, scientists and the public during the eruption. With aid of this model a detailed analysis of the strengths and shortcomings of the system is performed and presented. Attempt is also made to document the major changes within the subsystems during the crisis. There were several. Among the most remarkable were the many changes in the management personnel such as chief minister, governor and chief scientists. Throughout the crisis key institutions such as the Montserrat Volcano Observatory and the Emergency Operation Center also endured constant evolution. Operational and decision-making policies and procedures within these institutions encountered numerous revisions. Generally, these changes were intended to facilitate the tacit objective of local authorities to maximise life safety while retaining a sustainable level of functionality on the island. In the absence of...

**JSP23/W/24-B2****1150****A DEVELOPING VOLCANIC CRISIS IN DOMINICA, LESSER ANTILLES**

John B. SHEPHERD, Lloyd L. Lynch, Mark Stasiuk, Joan L. Latchman (Seismic Research Unit, UWI, St. Augustine, Trinidad, e-mail: johnbshepherd@hotmail.com); Joseph M. Devine (Brown University, Providence, R.I. USA)

The island of Dominica is in the centre of the volcanically active Lesser Antilles island arc. The island is approximately 35 km long by 12 km wide and is composed entirely of Pleistocene to recent volcanoes. Earthquake swarms have been reported from Dominica since it was first settled by Europeans. These originate in all parts of the island but are most common in the southwestern part of the island where there are at least three volcanic vents which have erupted in the last few thousand years.

The most recent swarm began in September 1998 and is continuing. By January 10 1999 over 1,000 shallow volcanic earthquakes had been recorded by a nine-station digitally recording short period seismograph network. Over 300 earthquakes had been felt in the southwestern part of Dominica causing significant damage. Epicentres were initially located close to Morne Plat Pays volcano but during the swarm have spread to the most of the southwestern region. Focal depth are in the range 1-5 km and are becoming shallower as the swarm progresses. GPS measurements have detected widespread inflation of the epicentral region. An extensive programme of geological mapping is in progress and a response plan has been developed by the civil authorities.

**JSP23/C/U5/W/14-B2****1210****THE SEISMIC ALERT SYSTEM IN MEXICO CITY AND THE SCHOOL PREVENTION PROGRAM**

ESPINOSA ARANDA J M, A Jimenez, G Ibarrola, F Alcantar, A Aguilar, M Inostroza, S Maldonado Director, (Centro de Instrumentacion y Registro Sismico, A.C. Anaxagoras #814, C.P. 03020, Mexico, D.F. E-mail: cires@cires.org.mx Home page: http://www.cires.org.mx;); R Higuera (Director, Direccion de Emergencia Escolar Subsecretaria de Servicios Educativos del Distrito Federal Secretaria de Educacion Publica Callejon de Torresco #12, C.P. 04010, Mexico, D.F. E-mail: rhiguera@yahoo.com)

The Seismic Alert System (SAS) is a public service developed with the sponsorship of the City Government Authorities, with the aim to mitigate seismic disasters. Since August, 1991, after 88 months of continuous operation, the SAS has been capable to detect 714 seismic events in the Guerrero Coast; 12 of them so strong to trigger general alerts in Mexico City, 34 restricted, and one false general alert. The warning ranges strong or restricted correspond to seismic magnitude forecasted greater than 6, or greater than 5. During the "Copala" M7.3 earthquake, in September 14, 1995 the SAS was activated and issued a general warning signal in Mexico City, 72 seconds prior to the "S" ground motion first arrivals. This earthquake warning reached an estimated population of more than 4 million citizens. The response of children in schools was massive because of the application of an earthquake hazard reduction program. The Copala earthquake helped us to identify the societal response strengths and weaknesses to the earthquake early warning signal. The long-term plan of hazard mitigation of the National Ministry of Public Education, Secretaria de Educacion Publica (SEP), has created awareness to earthquakes in the children that have assisted in these years to various school levels. Even though they did not suffered the disastrous consequences of the 1985 earthquake, they are more aware than the average people that lived through that disastrous event, who still are not trained.

**Tuesday 27 July PM**

Presiding Chair: J M Espinosa-Aranda  
(Centro de instrumentacion y Registro Sismico, Mexico)

**JSP23/W/12-B2****1400****SEASONAL WARNING FOR CLIMATIC HAZARDS: PROSPECTS AND RESPONSES**

T.DOWNING (Environmental Change Unit, 1A Mansfield Road, Oxford, OX1 3TB, Email: tom.downing@ecu.ox.ac.uk)

With climate change, there is increasing concern that climatic hazards will become more frequent and more severe. One of the most promising developments is seasonal climate forecasts. Already forecasts are operational in many parts of the tropics and sub-tropics, and particularly for droughts and floods associated with ENSO events. Prospects for further development of seasonal forecasting for a range of climatic hazards are reviewed, illustrated with case studies in Africa and Europe. A critical evaluation of the utility of seasonal forecasts centres on vulnerability, communication channels, and effective responses. In contrast to short-term prediction, seasonal forecasts raise new issues of preparedness and the use of information.

**JSP23/E/10-B2****1420****CHANCES FOR A LONG TIME FORECAST OF SEVERE STORM EVENTS IN WESTERN EUROPE WITH RESEPT FOR THE NORTH ATLANTIC OSCILLATION**

Mattius KLAWA, Uwe Ulbrich and Johannes Wefers (Institut fuer Geophysik und Meteorologie, Kerpener Str. 13, 50923 Koeln, Germany, e-mail: mklawa@meteo.uni-koeln.de, phone: 49 (0)221/470-3689)

The North Atlantic Oscillation is the dominant variability pattern in sea level pressure over the North Atlantic. Spectral analyses of the variations of this pattern show peaks on seasonal,



yearly or decadal time scales. Also research proved influence of the NAO on the North Atlantic Stormtracks and on the European climate e.g. rainfall rates, winter temperatures in western Europe. In this presentation extreme storm events in western Europe are evaluated with respect to the NAO. Probabilities for extreme storm events on time scales of 5-10 years dependent on the NAO are estimated. In combination with daily weather regimes (since 1881) the long time series of the NAO pattern (since 1865) is used for a more detailed analyses on European weather events. In a first step damaging storms named by reinsurance companies and meteorological extreme events are compared. Weather regimes associated with these events are used for a description for the atmospheric circulation over Europe and to find out common features of periods around storm events. In a final step the probabilities for storm events are evaluated and interpreted.

**JSP23/E/29-B2 1440**

**FRACTURE CRITICALITY: A NEW CRITERIA FOR MONITORING THE ONSET OF EARTHQUAKES AND FRACTURING**

Stuart CRAMPIN (Department of Geology & Geophysics, University of Edinburgh, Edinburgh EH9 3JW, UK; email: scrampin@ed.ac.uk)

Seismic shear-wave splitting, diagnostic of distributions of stress-aligned fluid-saturated grain-boundary cracks and low aspect-ratio pores is seen with very similar characteristics in almost all igneous, metamorphic, and sedimentary rocks with a few well-understood exceptions. There is a minimum shear-wave velocity anisotropy of about 1.5% and a maximum of about 4.5% in intact un-fractured rock below about 1km in the crust. Theory and both field and laboratory observations suggest that this maximum value is close to the level of fracture criticality, associated with the percolation threshold, where rocks are so heavily fractured that shear-strength is lost, through-going fractures propagate, pore-fluids disperse, and earthquakes and fracturing occur. The evolution of such fluid-saturated rock can be modelled with anisotropic poro-elasticity (APE), where the driving mechanism is fluid migration by flow or diffusion along pressure gradient between neighbouring grain-boundary cracks and pores at different orientations to the stress field. APE shows that shear-wave splitting is controlled by the same parameters as control pre-fracturing deformation so that shear-wave splitting can be used to monitor directly the approach of fracture criticality before earthquakes or other failures by fracturing. The high seismicity of SW Iceland and the extensive SIL seismic network now allow changes in shear-wave splitting before earthquakes to be observed routinely with hindsight. A real-time "stress-forecast" in a narrow magnitude/time window was made with forecasts 17, 15, and 3 days before a M=5 earthquake on 13 November 1998. The key feature is monitoring the increase of stress in the relatively-undisturbed rockmass away from the complications of the earthquake source, and estimating the time at which induced cracking reaches the level of fracture criticality. By monitoring the build-up of stress, such stress-forecasts can give (potentially reliable) estimates of time and magnitude of future earthquakes but cannot give estimates of location. However, forecasts may well stimulate local studies, as was the case in Iceland, where investigations by the Icelandic Meteorological Office correctly identified the rupturing fault.

**JSP23/W/01-B2 1500**

**THE COASTAL OCEAN MONITORING AND PREDICTION SYSTEM FOR WEST FLORIDA**

MARK E. LUTHER, David Burwell, Meredith Haines, Nan Schmidt, Mark Vincent, Robert Weisberg, and Huijun Yang (University of South Florida Department of Marine Science, 140 Seventh Avenue South, St. Petersburg, FL 33701; Tel: 727/553-1528; Fax: 727/553-1189; E-mail: luther@marine.usf.edu)

Florida is the United States' fourth most populous state, with 80% of the population living in a coastal county. Several recent storms have brought large, unpredicted flooding to Florida's west coast. The coastal sea level response to tropical and extra-tropical storms results from wind forcing over the entire continental shelf. Much of the local response may actually be due to storm winds quite distant from the local area of concern; a case in point being tropical storm Josephine, a modest storm that nevertheless caused extensive flooding in the Tampa Bay area. The University of South Florida is implementing a real-time Coastal Ocean Monitoring and Prediction System (COMPS) for West Florida that will provide additional data needed to give more accurate predictions of ocean storms and coastal flooding by storm surge. This system consists of an array of instrumentation both along the coast and offshore combined with numerical circulation models and builds upon existing in-situ measurements and modelling programs funded by various state and federal agencies. This observing system fulfils all of the requirements of the Coastal Module of the Global Ocean Observing System (CMGOOS). Data and model products are disseminated in real-time to federal, state, and local emergency management officials via the internet (URL <http://comps.marine.usf.edu>).

**JSP23/W/03-B2 1520**

**EARTHQUAKE PREDICTION AND EARTHQUAKE PREPAREDNESS: CURRENT POSSIBILITIES FOR THE PACIFIC RIM**

Vladimir KOSSOBOKOV, Vladimir Keilis-Borok, (International Institute for Earthquake Prediction Theory and Mathematical Geophysics, Russian Academy of Sciences, 79-2 Warshavskoye Shosse, Moscow 113556, Russia, E-mail: volodya@mitp.ru); John Healy (USGS, Menlo Park, CA 94025, USA, E-mail: jhhealy@aol.com); Donald Turcotte (Department of Geological Sciences Cornell University, Ithaca, NY 14853-1504, USA, E-mail: Turcotte@Geology.Cornell.edu)

The recent results of real-time testing in the Pacific Rim, 1992-1998, have established the high statistical significance of intermediate-term predictions of the largest earthquakes by algorithms M8 and MSc. Among predicted are all earthquakes of magnitude 8 or greater. Predictions are completely reproducible and use precursory activation of seismic static at different space and time ranges to reduce consecutively time and space where disastrous earthquake has to be expected. Although the predictions are of limited accuracy they do create a possibility to prevent part of the damage. This encourages a multi-scale approach to mitigate earthquake disaster. In general, earthquake predictions range from a zero-approximation of seismic zoning through long- and intermediate- to short-term ones. Accordingly, the preparedness measures range from building code, to simulation alarms and reinforcement of high-risk facilities, to the imminent "red alert" (e.g. evacuation of population and introduction of martial law). Different time from decades to seconds is required to undertake different measures; having different cost, they can be realistically maintained during different time periods and in the territories of different size. The key to damage reduction in the area of concern is escalation or de-escalation of preparedness measures depending on the current state of alert. That is the standard practice for mitigation of other major disasters, wars included. The interface between prediction and preparedness is delivered by the recent development of optimal strategies based on a trade-off between total volume of alert and rate of failures-to-predict. We demonstrate case histories of intermediate-term predictions that would have led to preventing a considerable part of losses by low-key safety measures.

**JSP23/E/06-B2 1600**

**SANARIS PROJECT: A SATELLITE NETWORK FOR NATURAL RISKS MONITORING**

Marta TARRAGA (Dept. Volcanologia, Museo Nacional de Ciencias Naturales, Jose Gutierrez Abascal 2, 28006 Madrid, Spain, email: mcnt184@mncn.csic.es); Alicia Garcia, Ramon Ortiz, Rafael Abella and Javier Peña (Dept. Volcanologia, Museo Nacional de Ciencias Naturales, Jose Gutierrez Abascal 2, 28006 Madrid, Spain, email: mcnp182@mncn.csic.es)

A new satellite communication system specifically designed for low-rate data applications has been developed and prototyped. A validation project is proposed to install a pilot network to be operated during 6 months. One of the target markets related to volcanoes has been selected, so a group of users is integrated in the project. A specific application for this market will be developed regarding data acquisition, processing, storage and dissemination to distant users. The feasibility of using the new satellite system to provide a new Eutelsat service for low-rate data applications will be evaluated from the pilot network performance. According to the Department of Volcanology (M.N.C.N.-C.S.I.C.) experience on the development of systems for volcano monitoring, its role in the project will be: -Co-ordinate the definition of users requirements for the pilot application. Installation of the digital seismic stations. -Maintenance of Teide and/or Timanfaya stations (Canary Islands).

**JSP23/C/U5/E/06-B2 1620**

**EFFECTIVE EARTHQUAKE MONITORING PROCESS FOR EMERGENCY RESPONSE ON RESCUES (EMPEROR)**

Yutaka NAKAMURA (System and Data Research Co. Ltd., SDR Bldg., 3-25-3 Fujimidai, Kunitachi-shi, Tokyo, 186-0003, JAPAN, E-mail: yutaka@sdr.co.jp)

It has been widely recognised that systematical and continuous monitoring of earthquakes is necessary for the early warning. In this presentation an effective earthquake monitoring process is proposed. DI, Damage Intensity of seismic motion, is defined as an inner product of acceleration vector and velocity vector at each time step dt. The multiplication of DI with mass received seismic motion, indicate the power of the motion act to the object. DI-value, defined as maximum of DI, is generally appeared after S-wave arrival. When P wave arrives, DI increases drastically, and after S wave arrival DI reaches to its maximum value, DI-value, soon. P wave Index, PI-value, is defined as maximum DI of P wave part. This value is suggested to be used for P wave alarm. DI-value is related with seismic intensity. DI-value has a very important practical advantage, since it can be calculated in real-time soon after the P wave arrives. Additionally, DI-value has a clear physical meaning and it is strongly related with the earthquake damage. This can be concluded as, with the continuous observation of DI, earthquake alarm can be issued efficiently and damage can be estimated precisely. According to combination of S wave and P wave alarms, early and/or reliable alarm is realised. P wave alarms can be issued when PI-value over the pre-set level, and S wave alarm can be issued when ordinary monitored values or DI-value exceed pre-set level. Combining PI, DI values together with K values is promising for the future early warning systems, since it has been clarified with both methods that it is possible to estimate the vulnerabilities of all ground and structures concerned and it is possible to issue the alarm before the real damage occurs.

**JSP23/W/06-B2 1640**

**HIGH RESOLUTION AEROMAGNETIC SURVEY FOR CONCEALED FAULTS IN THE FUKUI PLAIN, CENTRAL JAPAN**

Shigeo OKUMA, Masahiko Makino and Tadashi Nakatsuka (Geological Survey of Japan, 1-1-3 Higashi, Tsukuba, Ibaraki, 305-8567 Japan, email: okuma@gsj.go.jp)

Geological Survey of Japan (GSJ) has conducted a helicopter-borne high-resolution aeromagnetic survey in the Fukui Plain, Central Japan, to better understand concealed faults associated with the 1948 Fukui Earthquake (June 28, 1948, M=7.3) which brought disastrous damages to this area. The survey was flown along east-west flight lines at an altitude of 150 m above terrain and spaced 300 m apart with a Cesium Vapour magnetometer with a sensitivity of 0.01 nT at a sampling interval of 0.1 second and a differential GPS system. The compiled total intensity map of IGRF residuals shows interesting magnetic features as follows: 1) A broad magnetic high area occupies the western half of the plain with a sharp NNW-SSE trending boundary to the east, which corresponds well to the assumed location of the concealed Fukui Earthquake fault. 2) Three distinctive dipole magnetic anomalies lie in the magnetic high area, two of which lie at the northern edge of the area, implying the existence of intrusions associated with the Awara Hot Spring. 3) Magnetic lows are dominant along the coast line of the Sea of Japan and in its offshore areas, suggesting the existence of reversely magnetised volcanic rocks which lie offshore and maybe outcrop along the coast line.

**JSP23/E/27-B2 1700**

**LAND SUBSIDENCE OF JAKARTA (INDONESIA) AND ITS GEODETIC-BASED MONITORING SYSTEM**

Hasanuddin Z. ABIDIN, I. Meilano, M. A. Kusuma, J. Kahar (Department of Geodetic Engineering, Institute of Technology Bandung, Jl. Ganesha 10, Bandung, Indonesia, email: hzabidin@indo.net.id and hzabidin@gd.itb.ac.id); Rochman Djaja (National Coordinating Agency for Surveying and Mapping, Cibinong, Bogor, Indonesia); Samsul Hadi (Jakarta Provincial Agency of Surveying and Mapping, Jakarta, Indonesia)

Jakarta is the capital city of Indonesia with population of about 12 million peoples, inhabiting the area of about 25-km by 25-km. It has been reported for quite sometimes that several places in Jakarta are subsiding at different rates from place to place. Up to the present times, however, there has been no definitive, detail, and comprehensive information about the characteristics and pattern of land subsidence in Jakarta areas. Usually the land subsidence in several places of Jakarta is estimated using their geological parameters or inferred from the ground water level observations. In order to give a better picture about these land subsidence phenomena in Jakarta, the geodetic-based land subsidence monitoring system has been implemented. The system is based on GPS and levelling measurements. In this paper the land subsidence study in the city of Jakarta using repeated GPS and levelling surveys will be described and discussed. The land subsidence characteristics of Jakarta and its surrounding area are investigated using the data from three repeated GPS surveys conducted in 1994, 1997, and 1998 and four repeated levelling surveys performed in 1982, 1991, 1993, and 1997. The main goal of this land subsidence study is to understand the characteristics of land subsidence in Jakarta area and their generating forces and factors. Therefore, in this paper, the geological, geophysical, and hydrological aspects of Jakarta area would also be investigated and correlated with the geometrical changes information obtained from geodetic based systems. The paper would be sum up with some closing remarks.

JSP23/W/38-B2

1720

**INTERNATIONAL TECTONIC REAL TIME RADON OBSERVATION AND TRANSMISSION - RELIMINARY RESULTS OF GEODYNAMIC MONITORING.**

G.SOBOLEV (United Institute of Physics of the Earth, RAS, Moscow, Russia, email: sobolev@uipe-ras.scgis.ru); S.Balassanian (National Survey for Seismic Protection, Yerevan, Armenia, email: presidnt@nssp.yerphi.am); A.Belayev (Vernadsky Institute of geochemistry and analytical chemistry, RAS, Moscow, email: abelyaev@chat.ru); S.Bushati (Center of Geophysical and Geochemical Exploration, Tirana, Albania, email: bushati@cgge.tirana.al); E.Lagios (Department of Geophysics and Geothermy, National & Kapodistrian University of Athens, Athens, Greece, email: elagios@atlas.uoa.gr); R.A.Nicholson (British Geological Survey, Keyworth, Nottinghamshire, NG125GG, United Kingdom, email: RAN@wpo.nerc.ac.uk); A.Ponomarev (United Institute of Physics of the Earth, Moscow, email: avp@uipe-ras.scgis.ru); A.Pronin (Geological-technical Scientific Industrial Enterprise "Geotekhvims", Naro-Fominsk, Russia); G.Sideris, F.Zervos (GeoMentor, European Economic Interest Grouping, Athens, Greece, email: geomen@otenet.gr).

Seismic activity is a potential threat to populations and commerce throughout the world. Geophysical-geological research institutes and commercial companies in Greece, France and the UK are collaborating with similar organisations from Russia, Armenia and Albania, under the EU-funded Inco-Copernicus (Framework IV) programme, to develop new techniques for the automatic acquisition of gas geochemical data from remote sites using gas-sensing probes and telemetry. The data are being integrated with seismic information acquired in parallel, and used to determine whether or not the technique is a suitable method for monitoring ground disturbance associated with tectonic events. A number of data loggers (transducers/detectors) have already been installed since 1998 at specific locations (base stations) selected by the Project scientists in Caucasus (Southern Russia and Armenia), Greece, Albania and Scotland (UK). The seismic and gas-hydrogeochemical maps as the results of geophysical prospecting were used to select eligible sites for radon monitoring. Each base station includes two data loggers with the latest version of the Barasol MC radon probe incorporating sensors for barometric pressure and temperature combined with local rainfall measurements. These parameters are being transferred to attached cordless modems and are transmitted via INMARSAT global satellite communication system to Greece (Project co-ordinator) where all data are collected for joint processing. Signal processing software has been developed on the base of standard and original approaches. The spectral composition and structure parameters of obtained time series are determined by applying descriptive statistics, causal analysis and methods of the dynamic theory systems. The first stage realisation of Project indicates that telemetry systems are operating satisfactorily and the data are collecting, but that longer-term monitoring is necessary to link seismic measurements to radon exhalations and consider mentioned data acquisition-broadcasting system as real warning system.

JSP23/C/U3/W/21-B2

1740

**DEVELOPMENT OF SEISMIC RAPID REPORTING AND EARLY WARNING SYSTEM IN TAIWAN**

Yih-Min WU, Jen-Kuang Chung, Tzay-Chyn Shin (Central Weather Bureau, 64 Kung Yuan Road, Taipei, Taiwan, email: ludan@sz2.cwb.gov.tw); Yi-Ben Tsai (Institute of Geophysics, National Central University, Chung-li, Taiwan); William H.K. Lee (862 Richardson Court, Palo Alto, CA 94303, USA)

In 1994, two prototype seismic early warning systems have been implemented in Taiwan: (1) a rapid reporting system using a tele-metered network of digital accelerographs spread over the entire island, and (2) an alert system exploring the use of modern technology for the highly seismic area of Hualien. After four-years operation, the rapid reporting system was successfully operated in the seismic monitoring system of the Central Weather Bureau (CWB) for felt earthquake observation (Taiwan Rapid Earthquake Information Release System, TREIRS). It has achieved in the determined of precise earthquake location and magnitude computation about in one minute after the earthquake origin times. On the other hand, the Hualien alert system was phased out in 1998 due to large uncertainty of source parameters determination caused by small station coverage and only using P signal in determining the magnitude. Although it performed a very well reporting time (less than 10s after the earthquake origin time). Recently, the Hualien alert system stations were equipped with the digital accelerograph and combined to the TREIRS system. By adding the Hualien alert system stations to the TREIRS system, we have obtained a good precision for source parameter determination and a well reporting time for Hualien area earthquake monitoring. During the experiment in the past several years, we benefited from these two prototype seismic early warning systems and optimised the TREIRS system. We are encouraged forwards in the development of seismic early warning system based on the successful experience

Friday 23 July AM

**HAZARD AND RISK ASSESSMENT, RISK MITIGATION AND MANAGEMENT**

JSP23/W/30-A5

Poster

0830-01

**MISLEADING SIGNALS IN HAZARD CATALOGS**

Allen M. HITTELMAN (NOAA's National Geophysical Data Center (NGDC), World Data Center-A (WDC-A for Solid Earth Geophysics, 325 Broadway, Boulder, CO 80303, U. S. A., email: ahittelman@ngdc.noaa.gov); Lowell S. Whiteside and James F. Lander (Co-operative Institute of Research in Environmental Sciences, NOAA, 325 Broadway, Boulder, CO 80303, U. S. A., email: lws@ngdc.noaa.gov)

The primary purpose of natural hazard data catalogs is in the mitigation of future disasters. It is hoped that future natural disasters can be anticipated and populations warned if long term catalogs, which record the regional periodicity of events, are available. While such long-term variations in hazard are possible, we show that many current catalogs of natural hazard data may not be satisfactory to determine whether they actually occur.

Most hazard catalogs cover periods of less than 200 years and are reasonably complete and accurate for only the past 20-50 years. Such catalogs are not sufficient to investigate long term hazard variations. Earthquake, tsunami and volcanic catalogs, acquired and integrated at NGDC, illustrate artificial long-term variations created by cultural and scientific reporting changes, which can introduce unanticipated cyclical variations in the catalogs. These inconsistencies are often related to changes in the way magnitudes are calculated, evolving network equipment, network discontinuities of operation and personnel.

JSP23/W/35-A5

Poster

0830-02

**DISASTERS CAUSED BY CATASTROPHIC STORMS AND THEIR PREVENTION IN SMALL CATCHMENTS IN THE QIN MOUNTAINS**

Guozhang FENG (College of Water Resources and Architectural Engineering, Northwestern Agricultural University, Yangling, Shaanxi, 712100, China, e-mail: gfeng@public.xa.sn.cn)

Catastrophic storms often cause flash floods and corresponding geophysical hazards in the Qin Mountains in Shaanxi Province, China. The disasters are difficult to be prevented due to their rare occurrence, extremely high severity, non-predictability and too short warning time. The 980709 storm, occurred in a small area in the southeast of the Qin Mountains on 9 July 1998, is the maximum storm event in the records in the region and has an investigated maximum point storm rainfall of approximately 2122 mm during 6 hours and 40 minutes at one of two storm centers, and 1511 mm during 11 hours and 30 minutes at another center. The areas involved inside the isohyets of 1500 mm, 1000 mm, 500 mm and 50 mm's storm rain, are 31.4 km<sup>2</sup>, 45.5 km<sup>2</sup>, 86.8 km<sup>2</sup> and 847.1 km<sup>2</sup>, respectively. The storm formed enormous flash floods, landslides, mud-rock flows and aggradation of the riverbeds. As a combined consequence of the storm related disasters, 82 people and over 2000 thousands livestock were lost, over one hundred families were homeless, and most of the farmlands with growing crops were destroyed in the disaster involved two small catchments, especially in their densely populated valleys. Similar disasters with relatively lower severity frequently occur in the Qin Mountains even during the periods of general storms.

Reconstruction and protection of the areas both under and facing the damages are considerably important. Based on the natural and socio-economic features in the damaged and relevant areas, some integrated reconstruction and protection strategies for mitigation of the disasters and sustainable development of the region as an optimal eco-socio-economic system are proposed. The strategies consist of appropriate flood control standards, optimal land uses, reasonable economic structures, and safe residences and environments, in which some detail measures of engineering and non-engineering are involved. The strategies may be suitable to the similar catchments in the Qin Mountains.

JSP23/W/08-A5

Poster

0830-03

**VOLCANIC HAZARD ASSESSMENT FOR A PROPOSED HIGH-LEVEL RADIOACTIVE WASTE REPOSITORY AT YUCCA MOUNTAIN, NEVADA, USA**

Charles CONNOR and Brittan Hill (CNWRA, Southwest Research Inst., 6220 Culebra Rd, San Antonio, Tx, 78238, USA, e-mail: cconnor@swri.org); Andrew Woods and Steve Sparks (Centre for Geophysical and Environmental Flows, University of Bristol, Bristol, UK, e-mail: a.w.woods@bristol.ac.uk)

The proposed high-level radioactive waste repository at Yucca Mountain, Nevada, USA, is located within a geologically active basaltic volcanic field. Probabilistic volcanic hazard models for future eruptions through the proposed repository depend heavily on spatial controls on basaltic volcanism, including: Pliocene-Quaternary vent clustering, development of volcanic vent alignments, and localisation of vents along normal faults. When these spatial controls on past volcanism are considered, the probability of volcanic eruptions through the repository is estimated to be 10<sup>-7</sup> to 10<sup>-8</sup> annually, or 1:1000 during the 10,000 yr performance period for the repository. This estimate is greater than some previous estimates that do not consider structural controls on basaltic volcanism explicitly, primarily because of the location of the proposed repository within a broad density low produced by a half-graben. Modification of spatial hazard models to include this structure, which appears to have controlled past volcanism, provides a mechanism to link patterns in basaltic volcanic activity and crustal extension in a quantitative hazard assessment for the first time. This technique may be widely applicable to assessment of volcanic hazards resulting from small-volume basaltic volcanic fields.

JSP23/P/05-A5

Poster

0830-04

**A SEISMIC HYDRAULIC BEARING**

Federico BARTOLOZZI (Civil Engineering an Independent Researcher, via dei carracci 4, 21100 varese, Italy, email: ciuciuza@iol.it)

The proposed bearing consists of two parts. The fixed part, connected to the building is a steel sliding surface in the shape of a spherical bowl with a safety side spandrel. The movable part, connected to the foundation-soil complex, consists of a movable steel ball (rolling friction) in direct contact with the overhanging spherical bowl; alternatively, the ball may be fixed and coated on the top with Teflon (sliding friction). The lower part of the ball is linked to a movable cylindrical piston housed in the central chamber of a hydraulic device, also having two lateral symmetrical chambers with movable pistons, subjected to the elastic reactions of pre-stressed springs. Two holes connect the lateral chambers with the central one. During an earthquake, the horizontal displacement of the foundation-soil complex slightly affects the rest state of the building and the corresponding seismic energy in the building is negligible. The vertical displacement of the foundation-soil complex does not notably alter the rest state of the building, where there is no danger of resonance occurring due to the damping action of the liquid contained in the hydraulic device. The main advantages of the seismic insulation system, characterised by this type of bearing, are: 1. self-catering of the building after an earthquake; 2. possibility of application to modern and old buildings with any planimetric shape; 3. negligible pendulous effect in the building; 4. economical competitiveness with the existing aseismic systems both with partial and total absorption of seismic energy; 5. negligible psycho-physical effects for the inhabitants.

JSP23/P/04-A5

Poster

0830-05

**SELF-CENTERING ASEISMIC SYSTEM WITH ELASTIC BEARINGS AND HYDRAULIC DAMPERS**

Federico BARTOLOZZI (Civil Engineer and Independent Researcher, via dei Carracci 4, Varese, Italy, email: ciuciuza@iol.it)

The theoretical and experimental analyses emphasise the following characteristics of the proposed system: 1. the self-centring of the building after an earthquake; 2. the undulatory seismic energy in the building is constant and about 1% of the weight, by using bearing with sliding friction (pure Teflon). It is negligible, by using bearings with rolling friction (steel balls). In addition, it is independent on the seismic frequency and the soil displacement; 3. the vertical seismic energy in the building is minor and it increases both with the increase of the ratio between the frequencies (phase opposition) and with its decrease (phase); 4. the building remains almost motionless (negligible displacement) with respect to the horizontal translation of the foundation-soil complex for all values of the direction angle of the motion, of the soil displacement and acceleration; 5. in the interval of emergency vertical seismic frequencies, including the resonance frequency, the automatic starting of the dampers occurs. They progressively decrease the dynamic strain of the springs, which are integral parts of the bearings; 6. because of the sub-undulatory shock, the total load on the bearings increases for upward soil displacements and it decreases in the contrary case, both in phase and in phase opposition conditions; 7. the experimental tests, executed with reference to the undulatory shock, confirm the theoretical results.



**JSP23/W/00-A5** Poster **0830-06**

**A PROPOSAL FOR COASTAL SAFEGUARDS**

MARABINI

Abstract not available at the time of going to press

**JSP23/W/37-A5** Poster **0830-07**

**ABOUT THE ENSO IMPACTS IN NORTH-EASTERN ARGENTINE**

Norberto O. GARCIA and Maria del Valle Venencio (Facultad de Ingeniería y Cs. Hidricas - Univ. Nac. del Litoral, CC 495 - (3000), Santa Fe, Argentina. E-mail: nogarcia@fich.unl.edu.ar)

Frequently the North-eastern Argentine Republic is affected by floods on the riversides of the Paraná river, originated in the precipitation on the High Basin, and/or floods caused by the local rainfalls. With the same recurrence characteristic, drought situations take place that also affects the region, going from an extreme to the other in a short time generating emergencies totally different, but equally serious.

The present work makes an analysis of the extreme situations of the Paraná River associating them with the development of the sea surface temperatures on the Pacific Equatorial Ocean (EL NIÑO, LA NIÑA and neutral years). In this sense was found, as it was hoped, that most of the EL NIÑO events were associated with extraordinary floods of the Paraná river; although there were some floods that they were associated with the neutral phase (1959). The phase LA NIÑA (cold events) not always was associated with notable low waters of the river.

The behaviour of the precipitations over the region was non-homogeneous, and not always coincident with what it was hoped from a statistical point of view (Ej. 1983). The situation of EL NIÑO 1997/98 was permanently scanned and climatologically predicted through several models. So much in the river such as in the region the forecasts were completed acceptably. While, the socio-economic impact of the extreme events was very graphically shown in the means of communication.

**JSP23/E/53-A5** Poster **0830-08**

**ESTIMATION OF SEISMIC INTENSITY ATTENUATION LAWS FOR BANAT REGION**

AURELIAN PANTEA and Iren-Adelina Moldovan Ivan (National Institute for Earth Physics, P.O. Box MG-2, Bucharest-Magurele, Romania, e-mail: pantea@infp.ifa.ro and iren@infp.ifa.ro)

An attenuation relationship for macroseismic intensities for Banat (Romania) crustal earthquakes has been developed. We have used a data base including macroseismic maps from 21 earthquakes occurred during the period 1900 to present with MGR>4.0. The general form of the attenuation relation used is:  $\log(I) = f_1(M) + f_2(r, E) + f_3(r, M, E) + f_4(F) + e$  (where: I is the macroseismic intensity, M is the earthquake magnitude, r is the hypocentral distance, E is the tectonic environment, f<sub>4</sub>(F) is a function of fault type and "e" is a random variable representing the uncertainty in log(I)). Comparison with other attenuation relationships have been made.

**JSP23/E/48-A5** Poster **0830-09**

**TROPICAL CYCLONE RISK ASSESSMENT**

M.V.RODNIK (Geophysical Center, Russ. Ac. Sci., 117296 Moscow, Molodezhnaya 3, rodnik@wdbc.rssi.ru); G.S.Golitsyn (Inst. of Physics of Atmosphere, Russ. Ac. Sci., Moscow); V.F.Pisarenko (Intern. Inst. of Earthquake Prediction Theory and Math. Geophysics, Russ. Ac. Sci., Moscow); M.I.Yaroshevich (NPO Taifun, Rosgidromet, Obninsk, Russia)

A method of statistical estimation of tropical cyclone hazard is suggested. Probabilities of exceeding of certain levels of wind velocity (quantiles of distribution function) at a given area for given time intervals T are evaluated. The evaluation is based on the following velocity/distance relation:  $V(R) = V_{max} * (R_{max}/R)^{2.2}$ , where R<sub>max</sub> is the radius of central part of tropical cyclone where maximum of wind velocity V<sub>max</sub> at given moment is observed. Accuracy of this relation is estimated by an error with standard deviation 7 knots. Suggested method is applied to typhoons in the Western Pacific, 1950-1988. The used catalog contains 1013 events. The 50%-quantiles (medians) and 90%- and 95%-quantiles of maximum possible wind velocity for time intervals T=1, 2, 5, 10 and 20 years at 4 areas were evaluated: Tokyo, Hong-Kong, Taiwan Isl., and Vladivostok. Problem of possible temporal change in the typhoons regime is discussed in connection with the solar activity and El-Niño regime. The suggested typhoons risk assessment method can be useful for insurance industry and administration in areas subjected to tropical cyclones.

**JSP23/E/11-A5** Poster **0830-10**

**LARGE SCALE DESTRUCTIONS OF BUILDINGS, THEIR CONNECTION WITH GROUNDS SPECTRAL PECULIARITIES DURING THE SPITAK EARTHQUAKE OF 12.07.1988 IN LENINAKAN (NOW GIUMRY), ARMENIA**

Hrachya ABRAHAMYAN (Institute of Geophysics & Engineering Seismology, NAS RA, Leningradian 5, Gyumri, 377515 Armenia, email: iges@shirak.am)

Severely consequences of Spitak catastrophic earthquake force us to carry out the investigations revealing the causes of much more in quantity destructions. The most interesting aspect of testing the possibility of microvibrations using for prediction the grounds frequency characteristics is the comparison of buildings destructions measure by the grounds frequency elective property giving through the microvibrations. During the earthquake of December 7, 1988 with M=7.0 the full destruction of frame-panel 9-storey buildings (from 138 buildings in Leninakan were undamaged only 6) and frame-stone 5-storey buildings (from 335 buildings were undamaged 87) was observed.

Registrations of buildings natural oscillations before the earthquake and grounds dominant periods by microvibrations after the earthquake showed that statistically the largest amount of destructions were obtained on the parts of town where the grounds natural dominant periods T were approximately of 0.5-0.6 sec for five-storey frame-stone buildings. On the grounds with T=0.2-0.38 for nine-storey buildings and T=0.2-0.3 for five-storey buildings damages were been of least amounts. Natural periods of nine-storey buildings are of 0.5-0.6 and of five-storey buildings are of 0.25-0.4. The high damages may be explained by strong influence of oscillations due to resonance phenomenon when the ground natural dominant periods tally with the buildings natural periods.

In seismic microzonation of region the possible spectrum of disastrous earthquake must be assessed. By this assessment only the grounds frequency peculiarities may be compared with buildings frequency characteristics. Such a complex approach only enables us to solve correctly the task of connection of possible damages by grounds frequency characteristics. Neglect of this factor will bring to tragic consequences such that were been in Leninakan.

**JSP23/E/32-A5** Poster **0830-11**

**MINERAL PATHOGENIC DEPOSITS INTO A HUMAN ORGANISM AS A SIGN OF NATURAL HAZARDS**

Nadezhda PAL'CHIK (United Institute of Geology, Geophysics and Mineralogy of Siberian Branch of RAS, Koptjug prosp. 3, Novosibirsk 630090, Russia; email: nadezhda@uiggm.nsc.ru)

It is known that minerals exist not only into the Earth's crust but also into all human organisms. The physiogenic minerals contained into teeth and bones (as an apatite) are discovered also into pathogenic formations which can be found into different organs and tissues of a human body. We show, using the X-ray diffraction and the infra-red spectroscopy methods, that the apatite is present into urinary calculi, gallstones, dental stones, salivary calculi and also calcified cardiac valves as only phase of a mineral formation. Observations show that the full pathogenic mineralization of all living tissues of an organism occurs in some cases. Such peculiar natural hazard and its geographical distribution require a special attention and further investigation.

**JSP23/W/60-A5** Poster **0830-12**

**NEGATIVE IMPACT ON HUMAN HEALTH FROM GEOPHYSICAL RISK FACTOR AT THE NORTH**

VASSOVA

Abstract not available at the time of going to press

**JSP23/W/61-A5** Poster **0830-13**

**GEOPHYSICAL RISK FOR HEALTH IN THE CIRCUMPOLAR AURORAL BELT**

VINOGRADOV

Abstract not available at the time of going to press

**JSP23/E/30-A5** Poster **0830-14**

**ASSESSMENT OF LANDSLIDE HAZARDS USING GEOPHYSICAL TOMOGRAPHIES**

Simeon KOSTYANEV, Petar Srefanov and Peshka Stoeva (University of Mining & Geology, Sofia-1100, Bulgaria, e-mail: skost@staff.mgu.bg)

Landslides and unstable slopes are among the major natural and man-made hazards affecting mankind and yet their causes, their consequences for human life and property, and possible strategies for mitigating their effect are not very well understood. We will note, that only in Bulgaria there are over thousand active landslides on populated and health resort areas. The material and social losses have not been calculated yet. But in preliminary data they are enormous. Numerous and dangerous are the landslides and unstable slopes in open-cast coal-mines too.

In this paper we offer methods for combined application of high-resolution electrical tomography and seismic ray tomography for characteristic of landslide hazards and unstable ones. The major aim here is to predict where and when landsliding will occur, establishing their variability in space and time, and appraising their impact on the natural and socio-economical environment.

The above methods are applied for the studying of concrete landslide in Bulgarian Black sea coast and on some unstable slopes in an open-cast coal-mine of Maritza-Iztok area. This combined application of electrical and seismic tomography for assessment of landslide hazard is very useful.

**JSP23/E/45-A5** Poster **0830-15**

**SEISMICITY AND SEISMIC HAZARD STUDIES IN EGYPT AND SURROUNDING COUNTRIES**

Samir RISAD (Geology Department, Assiut University, Egypt), Mahmoud Ghalib (Geophysics Department, Cairo University, Egypt)

The tectonic setting of the Eastern Mediterranean Region is complicated because of the interacting effect of the principal plates: Africa, Eurasia and Arabia. The highest level of activity occurs at the northern margin of the Arabian plate, where it collides with Turkey and Iran. Strong earthquakes also occur along the western edge of the plate, along the Sea rift and the axis of the Red Sea Gulf of Aden. Egypt has a historical record of earthquake activity extending over the past 4,800 years. The most devastating earthquake in the recent history of Egypt, Dahshour earthquake, occurred some kilometers south of Cairo on the 12th of October 1992 damaged over 1,000 schools and other buildings, and injured over 7,000 people. In addition, other significant earthquakes occurred during this century interrupting the socio-economic development process of Egypt. Vulnerability to earthquakes increases steadily as urbanisation and development occupy more areas that are prone to the effects of significant earthquakes. The uncontrolled growth of cities in such areas are often associated with the construction of seismically unsafe buildings and infrastructures, mostly due to the insufficient knowledge of existing seismic hazard. Moderate and even small earthquakes may turn catastrophic in highly populated areas with poor building construction practice. In addition to the direct socio-economic impact of an earthquake, the long-term effects (the disruption of the economic chain, human resettlement, the reconstruction to modern standards) may last decades and absorb a considerable part of the national budget. In the absence of strong motion records a possible alternate method for seismic risk evaluation is the study of the attenuation of intensity with distance. For this purpose isoseismal maps for 17 historical and instrumental earthquakes that occurred in different parts of Egypt were analysed. Relations for intensity attenuation in different direction for different regions were obtained and have been used to calculate maximum intensity values all over Egypt. In addition, peak ground acceleration maps were produced for exposure time 10, 25, 50, 100 and 250 years, making use of an updated earthquake catalogue for Egypt. More than 20 seismogenic zones in and around Egypt were involved in the calculations. Hazard studies in Egypt were carried within the framework of the regional ICGP Project 382, entitled "Seismotectonics and Seismic Hazard Assessment in the Mediterranean Basin (SESAME)", and in co-ordination with the activities of RELEM Project. The results on Egypt were integrated with other available data for the surrounding countries.

**JSP23/E/55-A5** Poster **0830-16**

**DIRECT AND INDIRECT LOSSES DUE TO EARTHQUAKES**

KOFF G.L. (1), Lobatskaya R.M. (2), Frolova N.I. (3). (1) Institute of Lithosphere, Russian Academy of Sciences, Moscow, Russia, (2) Irkutsk University, Irkutsk, Russia, (3) Seismological Center of IGE, Russian Academy of Sciences, Moscow, Russia

The stability of urban area development is strongly depended on the hazardous natural processes. In order to secure the stable development of the territory the expected losses due to future events should be estimated. Direct and indirect economic losses are distinguished.



We understood direct economic losses due to natural processes as losses in economy within the current reproductive cycle which are expressed in terms of annual indexes of social economic development. All other losses are referred to indirect ones. They do not influence directly on the achieved results in the economy in the current year. The indirect losses is an estimation of negative consequences resulted from secondary effects. In contradiction to direct losses, indirect ones may arise and manifest within the long time interval. The indirect losses may not have a definite place in space and are usually characterised by cascade effects. Four main groups of factors, which influence upon direct and indirect economic losses due to earthquakes and other natural processes are distinguished; they are the following: origination, susceptibility, cycles and state. Different factors and their influence on losses due to earthquakes are analyzed. For different urban areas it is possible to construct in advance the index system which will allow to estimate the value of mentioned factors. Than it is possible to identify zones according to the weights of different factors which may be used in order to improve prevention, mitigation and response from future events. The system analysis of existing connections of urban areas with other regions will allow to estimate the rate of possible instability of the territory in the case of emergency and to obtain more reliable estimations of acceptable level of economic and ecological risks.

**JSP23/C/U5/W/16-A5** Poster **0830-17**

#### RECENT ANOMALOUS GEODYNAMICS OF PLATFORM FAULTS AS THE NEW ECOLOGICAL RISK FACTOR

CHURIKOV V.A., Kuzmin Yu.O. (both at United Institute of Physics of the Earth, Recent Geodynamic Lab., B. Gruzinskaya Str. 10, Moscow, Russia, email: vt.churik@relcom.ru)

New data on the existence of recent superintensive deformations (SD) of the ground surface are obtained for fault zones in aseismic regions (Russian platform, Pripyatskaya depression (Belorussia), Turanskaya platform (Turkmenistan) and etc.). These deformations have amplitude approximately 20 - 50 ppm, extension 0.1-1.0 km, velocity of vertical and horizontal displacements up to 5 - 7 cm per year. They have a pulsating character (the duration of the impulses of the activity of 0.5 - 1.5 year). These anomalous deformations call into existence the ecological risk of two types. 1. Direct - by the plums of anomalous fluids during the periods of activating fault zones; 2. Indirect - by the casualties of ecologically dangerous objects (wells on oil field and gas deposits, pipelines, underground depots of gases and toxic wastes, atomic power stations and etc.). The mechanism of SD-processes is suggested based on the parametrical excitation ( the induction) of anomalous deformations in fault zones. In this case, the induction is evoked by small disturbances with nature and technogenic origins.

**JSP23/L/08-A5** Poster **0830-18**

#### DISASTER MITIGATION PROGRAMMES FOR EARTHQUAKES, CYCLONES, DROUGHTS AND LANDSLIDES

H.N. SRIVASTAVA (India Meteorological Department, New Delhi-110003, India, email: snb.imd.ernet.in)

Peninsular India earthquake of September 1993 (Latur, Magnitude 6.3) which caused the death of about 10,000 persons and major damage to stone built mud houses led to the development of a World Bank aided project for relief and rehabilitation work besides reconstruction of cheaper but safe dwellings in the area. Under this project, broad band digital seismographs (GSN) were installed in India to improve earthquake risk assessment. Issue of warnings about the land fall of tropical cyclones through INSAT based disaster warning system have helped in saving the lives of people living in coastal areas of peninsular India. Improvement of the rainfall measurements through another World Bank Project for the peninsular India will enable us to study agricultural droughts with greater reliability. Recent landslides and floods in Garhwal and Kumaon regions during May, 1998 in Himalaya which have taken a heavy toll of life and property during August, 1998 have focussed the need for a coordinated approach for landslide zonation integrating seismological, meteorological, remote sensing and other observations.

**JSP23/P/03-A5** Poster **0830-19**

#### TOWER OF PISA: STABILITY RESTORATION PROPOSAL TO SAFEGUARD AGAINST SEISMIC RISK

Federico BARTOLOZZI (Civil Engineer and Independent Researcher, via dei Carracci 4, 21100 Varese, Italy, email: ciuciuza@iol.it)

The proposed technique includes the solution of two problems. The former immediately provides to the removal of the instability due to the rotation in the north-south direction. The second problem consists in preserving the stability against the occurrence of two different phenomena: 1. the restarting of the instability, caused by a possible uneven subsidence of the foundation soil; 2. the instability consequent to an earthquake. Both phenomena could be avoided with the following complex operations: 1. planning and laying of a sub-foundation with geometrical and structural characteristics which ensure the stability of the foundation soil; 2. operation for preserving or decreasing the present inclination and, even, operation for conferring the perfect verticality, as well as, if wanted, the counter-inclination; 3. interruption of the solidarity between the building and the sub-foundation-soil complex, by using multidirectional movable bearings with low sliding or rolling friction, with or without dissipators of sub-undulatory seismic energy and laying laterally or rigid connections with alternative function of elastic linkages. This technique has two important advantages: 1. possibility to remove a future rotation of the Tower, due to an eventual subsidence of the soil; 2. easy maintenance of the sub-foundation structural elements, of the movable bearings and the side connections. The technique permits the removal only of the present instability, disregarding the seismic risk. In this case it is evidently less complicated and expensive. In addition, all operations for preserving or decreasing the present inclination and, even, for conferring the verticality and the counter-inclination are possible.

Saturday 24 July AM

#### SEISMIC RISK MAPS AND SCENARIOS: TOOLS FOR PROTECTION AGAINST EARTHQUAKES

**JSP23/C/U5/E/09-A6** Poster **0830-01**

#### THE PREDICTABILITY OF EARTHQUAKE: TWO RECENT CASES IN YUNNAN, CHINA

Lin RONGHUI ( Seismological Bureau of Yunnan Province, Kunming 650041, CHINA); Tel: 86-871-3312339 Fax: 86-871-3315049 E-mail: ydj@public.km.yn.cn

China is one of few countries, which have the stipulation for issuing earthquake prediction and put it in practice. In the past three decades, the Chinese scientists did predict a few events of

a certain type and with obvious characteristics. Though on a largely empirical basis such experience is a wealth, as the standpoint of practice should be first and fundamental in the theory of knowledge. The Menglian M7.3 earthquake occurred in the Sino-Burmese border (21°59'N; 99°04'E) at 05:46:41.21aon July 12, 1995. Predictions of the intermediate-term (>1 year), short-term(3 months) and immediate-term (1 day before the mainshock) were made by analyzing in detail the observed seismic and precursory anomalies. The outcome of the prediction effort was only really significant when the immediate-term prediction was made at site just one day ahead of time. The Lijiang M7.0 earthquake occurred in 27°18'N; 100°13'E at 19:14:18.11aon Feb. 3 1996. The observed precursory signals laid bases for making the intermediate- and short-term predictions. Yet, at the time of impending stage, a failure was made to locate the event, due to the superposition of post-precursors caused by Wuding earthquake (M=6.5) which occurred in central Yunnan in later October 1995.

**JSP23/C/U5/E/07-A6** Poster **0830-02**

#### CHARACTERISTIC PRECURSORS OF THE 1996 LIJIANG, YUNNAN, EARTHQUAKE (M=7.0)

Lin RONGHUI (Seismological Bureau of Yunnan Province, Kunming 650041, CHINA); Tel: 86-871-3312339 Fax: 86-871-3315049 E-mail: ydj@public.km.yn.cn

The Lijiang M7.0 earthquake occurred in Yunnan (27°18'N;100°13'E) at 19:14:18.11aon Feb. 3, 1996. Before the event, precursory anomalies in the regional seismicity pattern were characterized as the absence of moderate-strong and small events around the source area. Since 1925, an average interval between  $M_L$  6.0 events was 6.4 years in the Lijiang area, northwest Yunnan, with the longest lasting 15 years. The latest Yanyuang M6.7 and Ninglang M6.4 events in the area occurred in 1976, surpassing the longest interval. Along the northern segment of the Zhongdian-Dali seismic belt  $M_L$  5.0 events were absent from 1983 to 1993, forming a gap of 150 km long. From 1990 to 1995, small events of  $M_L$  3.5 were also absent in the source area ( $i$ ≐760km). Activity of small events began to increase in the Yongsheng earthquake window ( $i$ ≐77km) in Dec.1995 and Jan.1996. Around the Eryuan area ( $i$ ≐122km), a foreshock swarm with the maximum magnitude 3.6 occurred on Dec.10, 1995. In addition, in the short and impending stage from Dec.1995 to Jan. 1996, 6 items of abnormal precursors were observed at 7 stations, namely the water level at Jianshui; water temperature at Liuku, Gangyuan, and Lincang; tilt at shipping; water quality (ion of HCO<sub>3</sub>-1) at Longling; and short leveling and short base line at Yongsheng. Besides, anomalous variations were also obtained from a synthetic analysis of precursory network data in the Lijiang area (which is consisted of 17 deep wells, 20 Radon points, 6 mercury points and 28 hot springs), and from the mobile gravity measurements in the networks of Western Yunnan Test Site before the event. Together with the seismic anomalies, all laid bases for making the intermediate (1-3 years)-, medium-short (1 year)- and short-term (months) predictions. Yet, at the time of impending stage, a failure was made to locate the event, due to the superposition of post-precursors caused by Wuding earthquake (M=6.5) which took place in later Oct. 1995.

**JSP23/C/U5/E/10-A6** Poster **0830-03**

#### RECENT CRUSTAL MOVEMENTS AND SEISMIC ACTIVITY STUDIES IN THE ASWAN REGION, EGYPT

Abdel Monem S. MOHAMED (National Research Institute of Astronomy and Geophysics, Helwan, Cairo, Egypt, email: moonm98@yahoo.com)

Aswan region is one of the most important regions in Egypt and because it encompasses the vital engineering structure of the High Dam, it has been selected as a pilot project for the present study. Such a choice has been motivated by the fact that both geodetic and seismic data needed for the current investigation have been collected and become available from the Aswan region. So, the main objectives of the current research is to unify the results of the crustal movements and seismic studies which have been made in the Aswan region. This has been done for reaching the best understanding about the geodynamics of the area through investigating the relation between the crustal movements, seismic activity and earthquake occurrence and also for detecting the precursory events associated with earthquake occurrence. For the purpose of monitoring earthquake activity continuously around the Aswan Lake, a radio-telemetry network of 13 seismic stations was established. For monitoring the recent crustal movements several local geodetic networks were established around active faults in the area. Regional geodetic network covering the whole area of the northern part of Aswan Lake was established.

These studies use the seismicity recorded by the Aswan network from December 1981 to December 1997 and analyses different aspects of the data. Geodetic data were collected from local and regional geodetic networks. These studies were initiated to obtain an improved understanding of the seismotectonics in the Aswan region because this information is of importance in assessing the seismic risk.

**JSP23/C/U5/E/19-A6** Poster **0830-04**

#### SEISMICITY OF IRANIAN PLATEAU AND ITS BORDERING REGIONS

Arezou DOROSTIAN (Department of Geophysics, Azad University, North Tehran Branch); M. R. Gheitanchi (Institute of Geophysics, Tehran University, email: mrghchee@chamran.ut.ac.ir)

During the 20th century, from Jan.1, 1900 to Dec.30, 1998, nearly 5100 earthquakes of magnitude 4 and above occurred in the region of 20-40° N and 40-75° E. The area lies along the Alpine-Himalayan belt and surrounded by active seismic faults. This study shows a general aspect of seismicity of different parts of Iranian plateau and bordering regions. Historical and Instrumental data have been collected from several different sources. In order to minimize the uncertainty in magnitude estimation we present a uniform magnitude scale for the calculation of earthquakes. Seismicity maps for periods of time before 1965 and after that in five-year intervals were constructed. Seismic activity in some areas has changed with time. Within major seismic zones, large earthquakes fill gaps in the seismicity pattern. A grid interval of 0.5-degree in Lat. and Lon. covered the whole area. The seismic energy and strain release in each quadrangle were computed for each interval up to 29 years from 1970 to 1999. Maps of tectonic flux and two and three dimensional energy maps were constructed to define the distribution of seismic zones in the area and to give a dynamic measure of their variation. The a and b values for 99 years period are same for some seismotectonics provinces of area and the regions of homogeneous seismicity were constructed. The frequency distribution of earthquakes of different magnitude is discussed. Recurrence curves support a high level of activity for the Zagros zone and they indicate a lower rate of activity for northern Iran faults zone than for other areas in the region. Recurrence curves for central Iran area indicate that the rate of activity in a given region may remain practically constant over periods at least as long as a century, whether or not large earthquakes occur in the region during those periods. Comparisons between seismic hazard, energy maps, faults location and earthquake epicenters distinguish areas which will be damaged or have a heavy casualty.

**JSP23/L/01-A6** Poster **0830-05**

**EXPERIENCES GAINED IN THE RESPONSE TO THE EARTHQUAKE EARLY WARNING SIGNAL IN THE UNIVERSIDAD AUTONOMA METROPOLITANA, CAMPUS IZTAPALAPA IN MEXICO CITY**

Delfino LASCARES, Universidad Autonoma Metropolitana, Iztapalapa Av. Michoacan y Purisima, Col. Velfina, Delegacion Iztapalapa, C.P. 09340, A.P. 55-535, Mexico D.F. Tels. 724-46-98, FAX 724-46-88, email: held@xanum.uam.mx.

Since June 1997 a radio receiver of the Seismic Alert System of Mexico, City (SAS) was installed in the Universidad Autonoma Metropolitana, Campus Iztapalapa and an integral program for hazard mitigation has been applied in the campus. The population reached by the early warning signal is about 17,000 students and academic personnel, with an average nearby population of 45,000 people. To date 7 early warning signals have been received. During these early warning that occurred in working hours, evacuation has been carried out in an average time of 30 to 60 seconds. Surveys show that, since the SAS warning operation the attitude of the near by population toward earthquake prevention has changed. To date 90 percent of the population respond to the early warning signal. The Seismic Alert System (SAS) was developed by the Centro de Instrumentacion y Registro Sismico (CIRES). The alerts have provided as much as 30 to 60 seconds average in advance warning, before the ground motion sake reach Mexico City.

**JSP23/C/U5/E/05-A6** Poster **0830-06**

**PRECURSORY SEISMIC SIGNALS DURING THE 1998 GUAGUA PICHINCHA CRISIS**

HUGO A., Mario C. Ruiz, Minard L. Hall, Monica Segovia, Alexandra Alvarado, Acinoe Calahorrano, Darwin Villagomez, Diego Viracucha, Patricia Mothes, Andres G. Ruiz, Daniel Andrade; (Instituto Geofisico, Escuela Politecnica Nacional, P.O. Box 17-01-2759, Quito, Ecuador; e-mail: geofisico@accessinter.net)

The Geophysical Institute in Quito, Ecuador, began the instrumental monitoring of Guagua Pichincha volcano in 1981. Until 1988, activity was characterized by a small number of earthquakes and sporadic phreatic explosions, which generated an explosion crater approximately 200 meters in diameter in the bottom of the caldera. In 1988, a swarm of VT earthquakes occurred 9 km southeast of the caldera at a depth of 8-12 km. Moderate phreatic explosions were detected in 1990, 1993, 1995, and 1997 during periods of rain. Between December 1997 and April 1998, three VT earthquake swarms were registered underneath the caldera, and in June 1998, an important swarm of VT earthquakes began 15 km northeast of the caldera. This swarm lasted until October, and at its height more than 100 earthquakes per day with a magnitude between 2.5 and 4.0 were noted. Furthermore, since June 1998, there have been hybrid earthquakes at depths less than 9 km.

A subduction earthquake with a magnitude of 7.1 occurred on the Ecuadorian coast 220 km from the volcano on 4 August. On 7 August, almost continual explosive activity began at Guagua Pichincha. This activity was characterized in the initial weeks by explosions followed by various days/hours of tremors. Between 7 October and 22 November, the tremors were shorter, with frequencies between 1.8 and 2.0 Hz. Between 22 November and 19 December, the number of explosions diminished with cycles of tremors between 28 and 32 hours. A new cycle of activity began on 19 December with spasmodic tremors and strong explosions followed by short episodes of tremors (<10 minutes) with frequencies of 1.6 Hz. In addition, earthquakes characterized by narrow spectrum (between 2 and 5 Hz) have been registered since 10 September. These earthquakes have originated at shallow depths under the caldera and have accompanied periods of intense phreatic activity. Guagua Pichincha's continuing activity is attributed to various pulses of intrusion of small magmatic bodies, a process, which could ultimately result in a volcanic eruption.

**JSP23/C/U5/E/12-A6** Poster **0830-07**

**THE HYDROPHYSICAL METHOD OF TSUNAMI ESTIMATION**

Yury KOROLYOV and Alexander Poplavsky (Institute of Marine Geology and Geophysics, Sakhalin Scientific Centre, Nauki st., Yuzhno-Sakhalinsk 693002, RUSSIA, email: tsunami@sakmail.sakhalin.ru)

The estimation of tsunami danger is based on seismological data at present. It doesn't take into account inhomogeneity of tsunami source, directivity of tsunami, diffracting effects, which may both amplify and attenuate tsunami waves, and duration of tsunami. Therefore it gives some erroneous forecasts. Information of some level gauges placed on sea may confirm or refute tsunami danger. The hydrophysical method of tsunami estimation using information of some remote level gauges is based on well-known reciprocity principle. This method needs in minimal seismological data (time of beginning and co-ordinates of earthquake), data on sea level in three points and numerical "mareograms" in these points and in point to be warned. These "mareograms" must be obtained by tsunami simulation from some model tsunami sources placed on earthquake epicentre. This method takes into account inhomogeneity of tsunami source, directivity of wave radiation, different diffracting and resonance effects. As a result the time of tsunami attack, form, heights and number of tsunami wave and duration of tsunami alarm are determined. This hydrophysical method will improve the reliability of tsunami warning and allow a creating of networks of local tsunami warning systems. This work was supported by grant 97-05-96625 from Russian Foundation for Basic Researches.

**JSP23/E/56-A6** Poster **0830-08**

**HISTORICAL DOCUMENTATION OF THE SEISMICITY OF LESVOS ISLAND (E. AEGEAN, GREECE) IN THE SECOND HALF OF THE 19TH CENTURY: COMPARISON WITH THE INSTRUMENTAL PERIOD DATA**

Vicki KOUSKOUNA (Department of Geophysics & Geothermy, University of Athens, 157 84 Athens, Greece, email: vkouskou@atlas.uoa.gr); Kostas Taxeidis (Psichari 20, Mytilini 81 100, Greece); Kostas Macropoulos (Department of Geophysics & Geothermy, University of Athens, 157 84 Athens, Greece, email: kmacrop@atlas.uoa.gr)

A total number of 32 earthquakes from Lesbos island for the period 1851-1899 are listed in the existing published catalogues, five of which were destructive and were felt in the Eastern Aegean and Minor Asia. A detailed investigation carried out on the island revealed new, local sources of information (manuscripts, newspapers, etc.) reporting the earthquakes of Lesbos. These sources, together with the existing ones, present a more complete seismic picture of the island, and almost double the total number of its earthquakes, i.e. 34 new single earthquakes (or series of earthquakes) were located, one of which (in 1882) was damaging. The seismicity of the island in the 20th century, as derived from instrumental data, for a time window of 50 years, was compared to the above mentioned period, in an effort to: a) re-evaluate the parameters of the known, major destructive earthquakes by adding the new sources of information, and b) answer to certain questions of tectonic character, i.e. the existence of foreshock/aftershock activity and its characteristics. In this sense, the catalogue of earthquakes of the area is extended backwards up to 1850, and the completeness of its seismicity is tested.

This enables the creation of an artificially complete data set, which will therefore contribute to more realistic local seismic hazard assessment and microzonation studies.

**JSP23/E/38-A6** Poster **0830-09**

**MODULE AND GRADIENT HIGH-SENSITIVITY MEASUREMENTS OF GEOMAGNETIC FIELD VARIATIONS AT THE SEISMIC RESEARCHES**

Oleg KUSONSKI (Observatory Arti, Institute of Geophysics, Urals Branch of Russian Academy of Sciences, Geophysics Str., 2a, Arti, Sverdlovsk region, 623350, Russia); Vladimir Sapunov and Olga Dekusar (Ural State Technical University, Quantum Magnetometry Lab, Mira St., 19, Ekaterinburg, 620002, Russia)

The researches are carried out at the observatory Arti (WDC's mnemonic is ARS, coordinates are 56°25.8' N, 58°33.7' E) that is located on the Predursky pericratonic trough of the East-European platform. This area is seismically active. Observable here earthquakes have both natural and industrial origin. The last is connected with production of minerals and oil. The magnetic field of this region is characterized by presence of anomaly up to 1200 nT. The module and gradient variations are measured by the proton Overhauser's magnetometer POS-1 with resolution 0.001 nT (sensitivity up to 0.02 nT and 0.01 nT/meter at single measurement). At the same time a registration of super-long-period seismic oscillation (SSO) are made by the ARU IRIS station. A gradiometer allows to control the real measurement sensitivity for absolute value of magnetic fields and to locate geological and technogeneous effects caused by a near zone. The submitted methods and equipment allow to study geoblocks movements creating intensive deformations of mountain breeds, geoblocks response to tectonic factors, SSO excitation mechanism, trigger factors of earthquakes. The data can essentially soften dramatic and economic consequences of earthquakes at the mining enterprises of Ural.

**JSP23/E/45-A6** Poster **0830-10**

**OBSERVED AND PREDICTED INDUCED SEISMIC IMPACTS IN PREADRIATIC COASTAL AREA OF ALBANIA**

Siasi KOCIU (Seismological Institute, Tirana, ALBANIA, email: kociu@sizmo.tirana.al)

Albania, situated on Western Balkans, with a coastal line of 470 km long, represents an attractive area for the future development of tourism. Adriatic seacoast of Albania with many, as one of the most populated areas of the country (where more than 70% of the population is concentrated, with many inhabited centers as those of Durres and Vlora towns in seacoast and Shkodra, Fieri and Tirana (capital), not far away (20-40 km), from the seacoast), represents one of the most hazardous seismic zones of the country, where many seismic impacts were observed during the past earthquakes and may be developed during expected future earthquakes.

Preadriatic area as a flat area filled mainly by recent very poor Quaternary sediments of thickness down to 100-150 m, with shallow underground water level, represents an area where a lot of soil in stabilities were observed during past earthquakes and can be observed in the future. Based on seismic hazard assessment procedures at local level for two of the biggest coastal cities of Albania (Durres and Vlora) it is shown that during the expected strong earthquakes induced seismic impacts as liquefaction of sands, new and induced landslides and appearance of fault rupturing on free surface can be observed not only along Adriatic seacoast, but especially within urban areas of these two cities.

**JSP23/E/07-A6** Poster **0830-11**

**THE RISK OF LARGE VOLCANIC ERUPTIONS AND THE IMPACT OF THIS RISK ON FUTURE OZONE DEPLETION**

Howard ROSCOE (British Antarctic Survey/NERC, Madingley Rd, Cambridge CB3 0ET, UK, email: h.roscoe@bas.ac.uk)

Ozone depletion at mid-latitudes due to reactive halogens from man-made halocarbons is enhanced by the increase in stratospheric sulphate aerosol, which follows large volcanic eruptions. Mid-latitude ozone depletion due to halocarbons almost doubled for the two to three years following the eruption of Mt Pinatubo in 1991. Although the Montreal Protocol is expected to reduce amounts of halocarbons in the atmosphere during the next century, the predicted reductions are such that stratospheric ozone will be at risk from such depletion enhancement for the next 50 years. Volcanological mechanisms, models, and measurements in ice cores, suggest that large volcanic eruptions are random and that their global rate is constant over periods of a few centuries. From the rate of large eruptions observed in ice-cores, the probability of one or more eruption, the size of Pinatubo or larger, is 58% in 50 years. This probability is large enough that it should be taken into account in predictions of future ozone loss. Several of the eruptions in the ice-core record were many times larger than Pinatubo, so that a more comprehensive analysis, which also included the probability of eruptions as a function of size, would be beneficial.

**JSP23/E/47-A6** Poster **0830-12**

**STATISTICS OF EARTHQUAKE HAZARDS**

M.V.RODKIN (Geophysical Center, Russ. Ac. Sci., 117296 Moscow, Molodezhnaya 3, email: rodkin@wdcb.rssi.ru); V.F.Pisarenko (Intern. Inst. of Earthquake Prediction Theory and Math. Geophysics, Russ. Ac. Sci., Moscow)

Earthquake tolls and economic losses in 1900-1996 years are examined in connection with earthquakes regime and economic conditions in different regions. It was shown that while the number of events with small and moderate number of victims and losses increase with time in a non-linear manner the large losses that constitute the major part of the total number of victims and losses have a linear increase with time. The non-linear increase with time of the total number of victims and losses is caused mainly by the Pareto-law distribution of losses from earthquakes, thus a high non-stationarity of regime of hazards assumed by a few authors is apparent. The limitations inherent to the Pareto-law distribution of losses are discussed and the value of maximum possible seismic hazard is evaluated. The connection of regime of seismic disasters with regional economic situation is discussed also. It was shown that while the losses from earthquakes have a tendency to increase with time, the number of victims and losses we normalised with the national income per capita have a tendency to decrease. A prognosis of number of victims and losses from earthquakes till 2020 year is presented.

**JSP23/E/51-A6** Poster **0830-13**

**INTERNATIONAL GPS TEST-AREA FOR DEFORMATION FORERUNNERS OF EARTHQUAKE STUDY**

Mikhail PRILEPIN (United Institute of Physics of the Earth, B.Gruzinskaya Str., 10, 123810 Moscow, Russia, email: prilepin@uipe-ras.sgis.ru)



One of the reasons why the problem of earthquake prediction is far away from the solution stipulated is the lack of real international co-operation on experimental study and evaluation of significance of different forerunners. Many scientists today share the opinion that deformation forerunners are primary and their study can help in understanding the processes of preparation of earthquakes and prediction of event. The favorable factor nowadays is the availability of very effective GPS technology for the study of deformation forerunners on large territory with high accuracy and with the possibility for automatization of gathering and processing of the data. The next step in instrumentation is combining GPS with SAR interferometry, which is making the first but a very successful step toward the study of geokinematics. In the report discussed, the items dealing with the determination of the epicenter position, magnitude and time of shock using the data accumulated on GPS networks of different levels developed in seismically active areas. The consideration about the selection of place for a test-area, its status, sequence of development of the GPS networks, transition of data, gathering of auxiliary data and activity of the center for processing and analyzing the data are discussed. The consideration about the possibility of united study of different kinds of forerunners: seismic, geoelectromagnetic, variation of ground water level and emanation of noble gases are also presented shortly.

**JSP23/C/U5/P/01-A6** Poster **0830-14**

#### THE THREE STRONG EARTHQUAKES, NORTH CHINA, CHINA AND ITS STRUCTURAL SIGNIFICANCE

Lu PEILING (Centre for Analysis and Prediction, CSB, Beijing (100036), China, Tel: 010-88015557, Fax: 010-68218604)

Abstract The seismic activities before and after strong earthquakes, the source mechanism of mainshocks, and the geological structure of the epicenter area of three strong earthquakes (the 1976(M7.8) Tangshan, the 1989(M6.1)Datong-Yanggao and the 1998 (M6.2)Zhangbei-Shangyi earthquake) have been investigated. The structural significance of the three strong events is also discussed. The results show that 1. In according to the seismic activities before and after mainshocks, three strong events occurred in the north margin of North China faulting block area. The occurrence of three events was resulted from the most recent abrupt slip on a NE-trending Changdong fault zone, a NE-trending Shanxi graben zone and a NWW-trending Zhanjilakou-Bohai fault zone, respectively. 2. In according to the mainshock location, the events was in the intersecting area of the faults, therefore its sequences have the rich aftershock action, the most of strong aftershocks and the energy attenuation slow. 3. The source mechanism solutions of mainshocks are in agreement with the regional stress field with the P axis in the NEE-SWW direction of North China, but there are a difference in the fault motion type, 1976 event shows the northeastern striking high-angle strike-slip faulting mechanism, 1989 event has the strike-slip with the normal faulting motion, and 1998 quake is the thrust fault type. Those might correspond upon the structure of the epicenter area. 4. The epicenters is in or near Cenozoic-aged faulting basins with the Cenozoic -aged basels, the genesis of the strong earthquakes which are derived from basels may be the rising model of the hot material. Due to an action of the local hot stress the earthquakes occurred. 5. The mainshock faults are not at a great active structure, even there is not active fracture in the surface of the epicenter area.

**JSP23/C/U5/P/04-A6** Poster **0830-15**

#### SEISMIC HAZARD ASSOCIATED WITH SUBMARINE NEOTECTONIC FAULTS IN GREECE

Joanna PAPOULIA (National Center for Marine Research, Agios Kosmas, Hellinikon, 16604 Athens, GR)

Seismic hazard analyses are associated with large uncertainties when historical data are insufficient to define seismicity rates. These uncertainties may be decreased however in areas where seismicity is shallow, and produced by Quaternary faulting, by incorporating geological data in the analysis of seismic hazard. A tool towards the integration of the so-called prior information of seismicity, obtained from geological data, with historical observations is the Bayesian probability theory. This theory is tested here to estimate the seismic hazard associated with submarine active fault zones in the area of Greece. Prior estimates of seismicity are developed from slip rate measurements obtained from offsets of geological formations. The analysis demonstrates the importance of uncertainty in the Bayesian estimate of seismicity, and subsequently in the estimate of seismic hazard.

**JSP23/C/U4/E/03-A6** Poster **0830-16**

#### GUAGUA PICHINCHA: MANAGING THE CRISIS

HUGO A. YEPES; Instituto Geofísico, Escuela Politécnica Nacional, P.O. Box 17-01-2759, Quito, Ecuador; e-mail: geofisico@accessinter.net

Guagua Pichincha is a dacitic volcano located 12 km west of Quito (pop. 1.2 M.), the capital of Ecuador. It has erupted five times in the last 1,030 years (970, 1560, 1575, 1582, and 1660), with a recurrence period of approximately 500 years during Holocene. In July/August 1998, there was a commencement of seismic and explosive activity at levels superceding those seen since the installation of the monitoring network in 1988. The increased activity, which peaked during late September, precipitated the declaration of a yellow alert by the city of Quito on 1 October.

The Geophysical Institute, drawing on its experience and expertise, acted as a catalyst for the city's actions given the city's lack of preparedness and inability to initially grasp the gravity of the situation. The initial step for the government in dealing with the crisis was the designation of the mayor of Quito as the overall response coordinator. The city established an operations/information center; determined populated areas at risk; identified public sectors likely to be affected; and cleared debris from flow areas and potential evacuation routes. Contingency planning included one evacuation drill; periodic meetings of governmental entities; solicitation of heavy equipment and medical supplies from foreign governments and NGOs; the development of ways to minimize impact to the water supply, power grid, and telecommunications; and the planning for ash removal, police deployment, evacuation of aircraft, ingress/egress of the city, and procurement of food and fuel. Educational efforts comprised press conferences, briefings, and press bulletins.

Any crisis has its difficulties. Some problems are unavoidable, some can be mitigated by adequate funding, and others are preventable. Problems encountered by the city have included the inability to control rumors, inability of the government to ameliorate the public's linkage of the alert declaration to local political events, poor management of the initial alert declaration, confusion over alert level definitions, difficulty in maintaining public interest over the long term, the release of overly technical information to the public, delays in developing contingency/evacuation plans, reluctance to disclose all available information on potentially affected areas, the ill-defined role of the operations center, inadequacies in the call-down list, a failure to publicize an alarm system, and insufficient funding. Yet despite these problems, the city has made great progress in recognizing the hazard and addressing the risk.

**JSP23/C/U4/W/01-A6** Poster **0830-17**

#### VOLCANIC HAZARD ASSESSMENT AT THE DENSELY INHABITED ISLAND OF ISCHIA

Sandro de VITA, Giovanni Orsi (Osservatorio Vesuviano, 80056 Ercolano -NA- Italy, email: devita@osve.unina.it) Fabio Sansivero (Dip. Geofisica e Vulcanologia. Un. "Federico II", 80138 Napoli, Italy)

Ischia is a volcanic island located in the north-western corner of the Gulf of Naples. Volcanism begun more than 150 ka B.P. and the last eruption took place in 1302 A.D. The largest caldera forming eruption generated the Mt. Epomeo Green Tuff and occurred 55 ka B.P. Resurgence of the central part of the caldera begun around 28 ka B.P. and caused a net uplift of about 900 m of the Mt. Epomeo block. It occurred through a simple-shear mechanism that determined the conditions for magma to rise to surface only along normal faults within the eastern sector of the resurgent block. Almost all the volcanic vents of the last period of activity (10 ka B.P.-1302 A.D.) are located in the eastern part of the island. During this period 46 eruptions, effusive and explosive, occurred mainly between 2.9 ka B.P. and 1302 A.D. Effusive eruptions produced lava flows and domes; explosive eruptions formed tuff-rings, tuff-cones, and variably dispersed pyroclastic deposits. Eruptions were separated by periods of quiescence that lasted up to few centuries. Slope instability, likely triggered by resurgence dynamics, generated landslides and mud-flows shortly before and after eruptions. The magmatic system is still active, as testified by the intense historical, volcanic and seismic activity, and by widespread thermal springs and fumaroles. The island is inhabited by about 50,000 peoples that greatly increases during summer. Farming, wine industries and a complex network of commercial exchanges with the near city of Naples, contribute to determine a high volcanic risk in this area.

**JSP23/W/72/C/U4/W/03-A6** Poster **0830-18**

#### EVIDENCE FOR VOLCANIC INFLUENCES ON MEXICO CITY AEROSOLS

G. B. RAGA (Centro de Ciencias de la Atmósfera, Universidad Nacional Autónoma de México, Ciudad Universitaria, 04510, México DF, México, email: raga@servidor.unam.mx), G. L. Kok (National Center for Atmospheric Research, Boulder, CO 80303, USA, email: kok@ucar.ncar.edu), D. Baumgardner, A. Báez and I. Rosas(all three at: Centro de Ciencias de la Atmósfera, Universidad Nacional Autónoma de México, Ciudad Universitaria, 04510, México DF, México, email: darrel@servidor.unam.mx)

In situ measurements of sulfur dioxide (SO<sub>2</sub>), carbon monoxide (CO) and sulfate mass provide evidence that aerosol composition in Mexico City is affected by emissions from the neighboring volcano, Popocatepetl. The data suggest that there are two distinct pathways by which SO<sub>2</sub> is incorporated into particulates. Periods of high humidity, fog, and rain are accompanied by elevated sulfate mixing ratios, attributed to aqueous chemistry. Similarly, elevated sulfate concentrations in low humidity periods appear to be a result of adsorption onto elevated particles. These two mechanisms are important for understanding the processes associated with particle formation in this highly polluted urban area. Under the influence of volcanic emissions, SO<sub>2</sub> concentration is more than four times the average value and particulate sulfate is a factor of 2 larger.

**JSP23/C/U4/W/05-A6** Poster **0830-19**

#### SAN SALVADOR, EL SALVADOR, A HIGH RISK, MULTIPLE HAZARD MEGACITY

D J SOFIELD, J W Vallance, and W I Rose (Geological Engineering and Sciences, Michigan Technological University, Houghton, MI, 49931, email:djsosiel@mtu.edu)

Volcanism and earthquakes are the most dire geological hazards that threaten San Salvador, El Salvador's largest city (population, 1.7 million), with a rapidly growing population, and few plans or resources for hazard mitigation. Financial, transportation, and governmental centers of El Salvador all reside within San Salvador. The city lies on a plain within severe hazard zones of two active volcanoes (San Salvador to the W and Ilopango to the E) and also lies in a zone of major subduction earthquakes.

In the past 60 Ka, a caldera 12 km E of the city now occupied by Lake Ilopango erupted at least four significant pyroclastic deposits, each of which blanketed the valley that San Salvador now occupies. The last of these eruptions devastated all El Salvador in AD 260 and drove pre-Classical Mayan civilization northward into the jungles. A dome eruption in 1880 and small seismic swarms beneath the lake indicate continuing unrest. Neither San Salvador volcano nor its numerous flank vents has erupted catastrophically since European colonization, however numerous explosive eruptions occurred prior to that. San Salvador volcano erupted ash-rich tephra and pyroclastic flows 800 years ago and caused mudslides that would likely kill many thousands today. Because of the frequency of earthquakes, the people of San Salvador are much more aware of seismic risk than volcanic risk. The city has had to rebuild 7 times after earthquakes since 1712. The most recent devastating earthquake in 1986, killed 1500, injured 10,000 and left 100,000 homeless. Thick unconsolidated pyroclastic and tephra deposits amplify the effects of shallow-focus, moderate magnitude earthquakes beneath the city. Timely international involvement could provide the impetus that San Salvador needs to begin effective hazard-assessment, monitoring, and educational programs. A significant part of this work will be to make the population of a volcanic country more aware of its vulnerability to volcanic hazards. The recent occurrence of hurricane Mitch offers an opportunity to advance all hazard work in Central America.

Monday 26 July AM

#### NEW PHENOMENA, APPROACHES AND TECHNIQUES

**JSP23/W/28-B1** Poster **0830-01**

#### METHODS OF EXTREME SEA LEVEL AND CURRENTS VALUES CALCULATION

Oleg ZILBERSTEIN, Guennady Safronov, Sergei Popov, Mikhail Chumakov (all at State Oceanographic Institute, Kropotkinski per. 6, 119838, Moscow, Russia, email: oleg@soins.msk.ru)

Hydrometeorological support for marine branches of the economy and safety of human activities on offshore regions requires knowledge of the main marine parameters (in particular sea level and current extreme values). As a rule long-term observations in offshore regions are absent. The most dangerous rise and fall of sea level and also extreme currents are result from the combined effect of tides and storm surges. A special automated technology including hydrodynamic and probabilistic modelling was developed. On the basis of historical information and observation series analysis for region of interest, extreme storm cases with corresponding weather maps are selected. Following computation of earth-surface level wind and atmospheric pressure gradients are produced. On the base of this information the hydrodynamic calculation of storms and summary (accounting tides) sea level oscillations and currents are calculated with help of verified 2D and 3D hydrodynamic models. Baroclinic models are actively used last years. With the help of produced probability models, which are based on Gumbel low and Langbein relationship, the results of numerical modelling are processed and long-return period characteristics of sea level and currents at different horizons are determined. Produced complex of models and methods is successfully used within



## INTER-ASSOCIATION

researches and survey for number of designing objects in Barents, Kara, Baltic, Caspian, and Sea of Okhotsk. This approach allows us to produce computer maps of long return period characteristics of sea levels and current

**JSP23/W/33-B1** Poster **0830-02**

### SEARCH FOR THE EARTHQUAKE PRECURSORY SIGNATURES BASED ON FRACTAL ANALYSIS OF THE ULF GEOMAGNETIC DATA

Natalia SMIRNOVA (Institute of Physics, St. Petersburg University, St. Petersburg, 198904, Russia, e-mail: nsmir@snoopy.phys.spbu.ru); Masashi Hayakawa and Tetsuya Ito (The University of Electro-Communications, Chofu, Tokyo 182-8585, Japan, e-mail: hayakawa@whistler.ee.ucc.ac.jp)

An attempt to use fractal methods of time series analysis for searching the earthquake precursory signatures is fulfilled on the basis of ULF geomagnetic data obtained during Guam earthquake (EQ1) on August, 8 1993 (M=8) and Biak earthquake (EQ2) on February, 17 1996 (M=8). The observing places were situated both near the epicenters (Guam, 65 km off EQ1 and Biak, 100 km off EQ2) and far away (Darwin, 1200 km off Biak EQ). The chosen period covered a few months before and after the earthquakes in order to reveal the large-scale dynamics of scaling (fractal) characteristics of the pulsations. It is revealed that in the seismotectonic region the ULF spectrum of emissions exhibits a power law behavior which is typical for self-organized critical dynamics. For Guam EQ the slopes of spectra and the fractal dimensions of ULF time series manifested stochastic fluctuations between values 2.5-0.7 with pronounced tendency for slope to decrease and for fractal dimension to increase in the process of the earthquake preparation. Taking into account the certain value of the critical slope we suggest that the gradual increase of the intervals with slopes less than this critical one prior to the earthquake may be considered as an earthquake precursory signature. The peculiarities revealed on the basis of ULF data of Guam EQ is verified on the materials of Biak EQ. The fractal properties of ULF emissions in seismotectonic and seismotectonic regions are compared. The research was supported by Grant 98-05-65554 from Russian Foundation for Basic Research.

**JSP23/C/U5/E/13-B1** Poster **0830-03**

### RESEARCH ON CORRELATION OF ASTRONOMIC FACTORS AND EARTHQUAKES

Hu HUI; Li Yongsheng (Yunnan Observatory, Academia Sinica, Kunming, 650011 China)

The effect of astronomical factors on the major earthquakes in China and the world is discussed in detail in this paper. The results show that the major earthquakes, especially the ones of above magnitude 7.0 are evidently affected by the astronomical factors, such as the Earth rotation, solar activities and lunar orbital motion. Only different seismotectonic belts or zones have different responses to an astronomical factor. The node of the lunar orbit with the earth's orbit regresses towards the west on the ecliptic, with a period of 18.6 years. The precession of the lunar ascending node causes the inclination between the moon's path and the equator to change continuously from 18.28 to 28.58 degrees. The seismic activities of the main seismic belts in the world are obviously affected by the period of 18.6 years and only their active periods appear alternately, which shows that different locations of the moon correspond to different seismic belts or regions on the Earth. This bears analogy to the fact that the change Earth's climate with a period of a year is caused by the different quantities of arrival of solar radiation due to the inclination of the ecliptic to the equator.

In China, 8 seismic events over M 8.0 occurred since 1820 happened to be during the acceleration of the Earth rotation (DAER). Among the 106 events over M 7.0 occurred in the 20th century, 72% were during the DAER and 71% happened when the inclination changed from the maximum to minimum. Most of the events happened in the descending phases of solar activities.

**JSP23/E/16-B1** Poster **0830-04**

### POINT-LIKE PROCESSES AND CATASTROPHE PREVISION

Giovanni P. GREGORI (IFA-CNR, via Fosso del Cavaliere 100, 00133 Roma, Italy; e-mail: gregori@atmos.ifa.rm.cnr.it)

A frequent approach when attempting at managing a natural catastrophe is in terms of a numerical model, by which we try at forecasting its occurrence in space and time. Sometimes this results to be difficult or even unrealistic. On a more pragmatic ground we can rather appeal to a formal analysis of the historical time series of every catastrophe of concern. Only approximately, however, such series can be likened to a point-like process, because the "detector-mankind" experienced substantial changes vs. time. Nevertheless, such algorithms can be approximately applied by means of a few suitable assumptions. Four basic viewpoints can be considered: (i) either by assuming that phenomena are periodic; (ii) or by assuming that an event occurs only whenever some energy threshold is attained (calorimetric criterion); (iii) or by assuming that it occurs only whenever the system experiences some abrupt change of its boundary conditions; or (iv), whenever no such algorithm is viable due to scanty observational information, just by applying the box counting method, or some other more or less related and/or equivalent fractal algorithm. The mutual relations, advantages, and drawbacks of either one such approach are briefly discussed, with a few applications. They already lead to an apparently successful long-range forecast of a large flood in northern Italy occurred in 1994, and to the prevision of the next explosive eruption of Vesuvius. But, the success of every such application is closely determined by the quality of the historical database, or by the physical information that is fed into the analysis, rather than by mathematics that per se have only to be concerned with avoiding that some arbitrary non-physical input is added, based only on the human need for simplicity.

**JSP23/W/88-B1** Poster **0830-05**

### SIMULATION OF ANOMALOUS BEHAVIOUR DURING THE NORTHBRIDGE 1994 EARTHQUAKE

GALIEV

Abstract not available at the time of going to press

**JSP23/E/22-B1** Poster **0830-06**

### PHASE OF MOON, INCLINATION OF MOON'S PATH WITH EQUATOR AND STRONG EARTHQUAKES IN YUNNAN

Li XIAOMING (Yunnan Observatory, Chinese Academy of Sciences, P.O.Box 110, Kunming; Yunnan Province, 650011, P.R.China)

Yunnan Province lies in the southwestern part of China, adjoining the juncture of the Eurasian plate and Indian plate, with the complicated geological structure, frequent seismic activities and the Mediterranean seismic belt passing through the province itself. It is found from the analyses that the rate of recurrence of earthquakes has close correlation to the position of the

Moon at the last quarter and especially near the new Moon and the last quarter of the Moon earthquakes occur frequently. In the 19th and 20th centuries the rates of recurrence of the earthquakes with M 6.2 near the two phases of the Moon are respectively 6.2 times and 4.5 times as frequent as the average rate of recurrence, having a stripe-shaped distribution and the major earthquakes with M 7.0 almost occurred in the maximum and minimum year of the inclination and within two years after or before it in particular. As for the solar and lunar tidal forces, most of the earthquakes occurred in the time interval when the horizontal component of the tidal force made the greatest change. This shows that an earthquake can be excited by the position of the Moon and the tidal forces of the Sun and the Moon.

**JSP23/E/46-B1** Poster **0830-07**

### IMPACT OF THE HYDROLOGIC EXTREMES OVER THE WATER TABLE IN THE "PAMPA HUMEDA" (ARGENTINA) AND ITS RELATIONS WITH THE ENSO

Maria del Valle VENENCIO and Norberto O. Garcia (Facultad de Ingenieria y Cs. Hidricas - Univ. Nac. del Litoral, CC 495 - (3000) Santa Fe, Argentina. - E-mail: mvv@fich.unl.edu.ar)

This paper aims to create the bases in order to carry out, starting from seasonal and interannual climate prediction, a seasonal and interannual prediction of availability of groundwater resources coming from the unconfined aquifer in the productive areas of the "Pampa H=FAmeda" in the Argentine Republic.

The regional averages of the depth of the unconfined aquifer get rid suppose affected only for climatic variations. Also, the use of the groundwater resource is considered constant. Keeping in mind that the several water resources states in the region obeys several relationships between the variables precipitation, evaporation and evapotranspiration, it was carried out a serial water balance and correlations between the variability of the precipitation and the depth of the unconfined aquifer.

So, we can say that the precipitation produces decreasing or rising water level. As it was demonstrated the relationship between the ENSO and the precipitation on the Southeastern South America (SSA) by several authors, presently work was aimed to establish relationships between the water table and the ENSO. This correlation also provides useful information about the predictability of the future piezometric levels for sustainability of groundwater resources. Then, the main conclusion of this work is that the water table level is predictable in function of a predictor like El Nino.

**JSP23/E/04-B1** Poster **0830-08**

### LONG REPOSE PERIODS IN THE ERUPTIVE HISTORIES OF RECENT KAMCHATKA VOLCANOES: WHAT VOLCANO CAN BE RECOGNIZED AS EXTINCT?

Vera PONOMAREVA, Olga Braitseva, Ivan Melekestsev (Institute of Volcanic Geology and Geochemistry, Piip Ave., 9, Petropavlovsk-Kamchatsky, 683006, Russia, email: ponomareva@geology.ru) Leopold Sulzerzhitsky (Geologic Institute, Pyzhevsky per., 7, Moscow, 109017, Russia, email: sulzer@ginran.msk.ru)

Detailed studies of the eruptive histories of Kamchatka volcanoes, based on geologic mapping, tephrochronology and radiocarbon dating, allowed us to document main repose periods in the lives of most Holocene volcanoes and monogenetic volcanic fields, and to determine their duration. It appeared that dormant periods as long as 500-1000 years were common in the lives of the volcanoes of various morphology, types of activity, and composition of eruptives. The best known example is Bezymianny volcano which was silent for about 1000 years before the 1955-56 large eruption. Longer repose periods up to 2000-3000 years were not rare. The longest repose periods - about 3500 years - were recorded at Kikhpinych and Diki Greben' volcanoes; after a long dormancy both volcanoes were able to resume their activity. These data suggest that at least in Kamchatka a volcano should be considered potentially active (and thus, potentially hazardous) if it was proved to produce at least one eruption within the last 3-4 thousand years. This approach has allowed us to add some more names to the list of active volcanoes: Taunshits, Khodutka, Diki Greben', Khangar volcanoes, which have been considered extinct and were not included in any catalogues of active volcanoes, appeared to have large eruptions within the last 3000 years, as well as Tolmachev Plateau and some other volcanic fields.

**JSP23/E/57-B1** Poster **0830-09**

### THE CELLULAR AUTOMATA MODEL SCIARA FOR LAVA FLOW SIMULATION: APPLICATIONS AND RESULTS

G.M. CRISCI, A. Di Francia, S. Di Gregorio, F. Nicoletta\*, R. Rongo, W. Spataro (Dip. di Scienze della Terra Dip. di Matematica \*Dip. di Chimica ersità della Calabria, I 87036 Arcavacata, Italy)

Cellular Automata (CA) represent a parallel computational method in alternative to differential equations, for modelling very complex phenomena, whose evolution can be considered based exclusively on local interactions. The CA model SCIARA for the simulation of lava flow was developed and subsequently improved several times by our research group. A lava flow is described in SCIARA as a system with discrete time and space; the space is represented by regular cells (square or hexagonal) two-dimensional cells, whose specifications (substates) describe the main physical characteristics of the corresponding portion of space: altitude and, for each lava layer, lava thickness, temperature, lava outflows toward the adjacent cells; furthermore a division in lava layers can be considered in a refinement of the model. The CA evolves changing the state of all cells simultaneously at discrete times. Input for each cell is given by the states in the adjacent cells; the evolution of the phenomenon is mainly given by the computation of the outflow from the cells and the change of the remaining substates. SCIARA was applied in different times to 1986/7 and 1991/2 Mount Etna eruptions. The results were satisfying within limits to forecast the lava flow path, according to the surface covered by lava. The main parameters of the model for Etna lavas were found; then simulations were performed in order to evaluate the risk in some inhabited Etna area (the towns of Nicolosi, Pedara and S. Alfio) considering future catastrophic events. We consider the evolution of SCIARA, the main results and a critical discussion for a further improvement of the model, its limits in the application.

**JSP23/W/89-B1** Poster **0830-10**

### UNFAMILIAR HORIZONTAL WAVES IN UPPER LAYERS EXCITED BY ACCELERATION AND OTHER EFFECTS

GALIEV

Abstract not available at the time of going to press

**JSP23/C/U5/E/18-B1** Poster **0830-11**

### LAVINA - A COMPUTER TOOL FOR AVALANCHE FORECASTER

Pavel CHERNOUSS and Evgeny Mokrov (Center of Avalanche Safety, "Apatit" JSC, 33a, 50 years of October St., Kirovsk, Murmansk region 184230, Russia, e-mail: P.Chernous@apatit.murmansk.su);

Alexander Perlikov (Institute of Ecology, Kola Science Centre of the Russian Academy of Sciences, 14a, Fersmana St., Apatity, Murmansk region 184200, Russia)

LAVINA is a software package which assist avalanche forecaster to evaluate avalanche risks. It is an integrated system consist of two main units permitting evaluate probabilities of avalanche occurrence and dynamical parameters of possible avalanches. Probability of avalanche occurrence is evaluated for a whole region or for a separate starting zone. In the first case standard meteorological data and snow drift measurements are used for different types of discriminant analysis and pattern recognition algorithms. Diagnostics is carried on each third hour as current measurements have being made. Probabilistic and categorical conclusions on avalanche releases are the results of data treatment. There is an opportunity to display ten situations closest to current one from archive. Statistical simulation applied to snow thickness, density and shear strength is used for evaluation of snow cover stability in a separate starting zone. The areas of instability of different probabilities are displayed at a computer monitor. The dynamical parameters of a probable avalanche – maximal speed and impact pressure, are calculated at any given point of the avalanche path. LAVINA as a part of computer assisted work place of an avalanche forecaster is in operation at the Center of Avalanche Safety since 1991. The results of its exploitation are discussed and the ways of its improving are considered.

**JSP23/E/52-B1** Poster **0830-12**

#### INFLUENCE OF MACROSEISMIC INTENSITY ATTENUATION IN SEISMIC HAZARD EVALUATION FOR FAGARAS (ROMANIA) CRUSTAL SOURCES

IREN-ADELINA MOLDOVAN (IVAN) and Aurelian Pantea (National Institute for Earth Physics, P.O. Box MG-2, Bucharest-Magurele, Romania, e-mail: pantea@infp.ifa.ro and iren@infp.ifa.ro)

An important step for the correct assessment of seismic hazard is the interpretation of the macroseismic effects distribution from a given seismic zone, as well as the good evaluation of seismic intensity attenuation laws. The attenuation was analysed as a function of distance and azimuth, using nine attenuation laws.

The present paper is a study of macroseismic intensity attenuation laws, using 5 crustal earthquakes (MGR>4.0) occurred in Fagaras(Romania) seismic zone, along the following azimuths: E, W, N,S,NE,SW,NW,SE. The evaluation of macroseismic intensity attenuation laws for Fagaras region was imposed by the necessity of seismic hazard assessment in this high seismic potential zone the largest event occurred in this zone: MGR =6.4;  $l_0=IX$ .

**JSP23/W/90-B1** Poster **0830-13**

#### COMPARISON BETWEEN TWO SYSTEMS OF BASE SEISMIC INSULATION

Federico BARTOLOZZI (Civil Engineer and Independent Researcher, via dei Carracci, 21100 Varese, Italy, email: ciuciuza@iol.it)

One of the proposed systems is with four rigid movable bearings and the other one with four elastic bearings. The two systems share the following characteristics: 1. self-centring of the building after an earthquake; 2. extreme economical competitiveness with all the existing anti-seismic systems, due to the considerable decrease of the seismic energy in the building, which makes possible the use of slenderer carrying structures. The differences between the above systems are: 1. a pendulous effect in the building, during an earthquake, in the system with rigid bearing. It is characterised by a very small vertical rotation of the building, which varies in average from a few seconds to some minutes with soil displacements included between some millimetres and about 150 mm. In addition, this effect is extremely limited and has no repercussions of psycho-physical character for the inhabitants of the building; 2. the verticality and the immobility of the building with respect to the horizontal translation of the foundation-soil complex in the system with elastic bearings. The vertical elastic strain of the springs compensates the variations of rigid deflection relative to the bearings, due to the inclination of their sliding surfaces. The vertical component of the of the motion, due to the sub-undulatory shock, varies only partially the building behaviour because of two phenomena: minor vertical translation of the building and resonance possibility. In order to prevent the resonance danger, each bearing is equipped with two or four frequency converters automatically started up when the emergency situation, defined by the equality between the vertical component of the earthquake frequency and the building vertical natural frequency, becomes imminent.

**JSP23/C/U5/W/05-B1** Poster **0830-14**

#### HIMALAYS CRUST DEFORMATION REGION, RADON EMANATION AND SEISMO WAVE EFFECTS

Vladimir ALEXEEV, Yury Mikhailov (Institute of Terrestrial Magnetism, Ionosphere and Radio Wave Propagation of Russia's Academy of Science, Troitsk, Moscow region, 142092, Russia, e-mail: yumikh@charley.izmiran.rssi.ru)

The Himalays form is available region for study of the deformation processes of continental crust during collision orogeny. Simple shear dominant strains have developed new fabrics parallel to the main thrust zone. Radon fields [1] and aerosols create anomalous electric fields, which may change properties of upper wall of wave-guide earth ionosphere. This process leads to change of penetration of ELF-VLF waves through lower ionosphere and evolution of spectral characteristics of electromagnetic emissions, registered on satellites [2].

1 Virk H.S., Singh B. Correlation of radon anomalies with earthquakes in the Kangra Valley, Nucl. Geophys. 1992 V.6. N2. P.293-300.

2 Yu.M.Mikhailov, G.A.Mikhailova, O.V.Kapustina. Relation between ELF and VLF emissions on the Intercosmos 24 satellite and concentration of radon in earthquake regions. SSA 15 /GA 118 report of XXII IUGC General Assembly

**JSP23/W/34-B1** Poster **0830-15**

#### PHENOMENOLOGICAL MODEL OF THE LARGE-SCALE EVOLUTIONARY PROCESSES IN A HAZARD SYSTEM OF THE EARTHQUAKE BASED ON THE SOC (SELF-ORGANIZED CRITICALITY) CONSIDERATION

Natalia SMIRNOVA, Vladimir Troyan (Institute of Physics, University of St.Petersburg, St.Petersburg 198904, Russia, e-mail: nsmir@snoopy.phys.spbu.ru); Masashi Hayakawa (The University of Electro-Communications, Chofu, Tokyo 182, Japan, e-mail: hayakawa@whistler.ee.ucc.ac.jp); Thomas Peterson (TFPLAB, Cleveland, Ohio 44124-5441, U.S.A., e-mail: TFPLAB@aol.com), and Yury Kopytenko (St.Petersburg Filial of IZMIRAN, St. Petersburg 191023, Russia, e-mail: galina@admin.izmi.ras.spb.ru)

The concept of self-organised criticality (SOC) is now widely used for interpretation of the natural hazard system behaviour. That concept was included as one of the principal point in a complex approach proposed recently by the present authors for searching the earthquake precursory signatures. Here we develop consideration of the processes in the earthquake regions on the basis of SOC concept. We suggest a phenomenological model for large-scale evolutionary processes occurring between two violent earthquakes. Four principal phases of

the evolution: random chaos, subcritical, critical and supercritical stages are proposed and analysed consistently. The external stimuli such as geomagnetic storms, sharp temporal and spatial variations of atmospheric pressure, ULF impulses and others are considered as a driving force for "cellular automata" process in a seismoactive region. The important fingerprints of SOC - fractal structures in space and time are analysed using seismicity data and the ULF electromagnetic data timed to violent earthquakes near Guam (August 8, 1993, M = 8.0) and Kobe (January, 16, 1995, M = 7.2). A possibility to use the fractal characteristics of signals to study critical dynamics of a hazard system is discussed. The research was supported by NASDA (Japan) and Russian Foundation for Basic Research (Grants No. 98-05-65554 and 99-05-NNN).

**JSP23/E/24-B1** Poster **0830-16**

#### DYNAMICS OF SELF-DEVELOPING NATURAL PROCESSES AND PROSPECTS OF ITS USE FOR THE FORECAST OF GEOPHYSICAL CATASTROPHES

Alexander I. MALYSHEV (Institute of Geology and Geochemistry, Urals Branch of RAS, Pochtovy pr 7, Ekaterinburg, SU-620151, Russia, email root@igg.e-burg.su)

Study of patterns of fore-culmination activations present a great interest for the forecast of geophysical catastrophes, such as disastrous earthquakes, strong volcanic eruptions, rock bumps, landslides etc. During the study of Bezymyannyi volcano eruptions in 1980-1987 the fact of hyperbolic activation before explosive-effusive eruptions was established. Further studying of the revealed regularities and their comparison with empirical dependencies of the development of various natural processes allowed to conclude that there is a wide class of self-developing natural processes, the dynamics of which is described by non-linear differential equation of the second order. The attempts of using these regularities for the forecast of eruptions were quite successful, however the accuracy of the forecast for the time of eruption did not exceed a semi-quantitative level. At present the methods, allowing confidently to reveal the laws of the development of natural processes, have been developed. As it is shown on the example of a number of Bezymyannyi and Shivelutch volcanic eruptions, for the class of eruptions, having stable fore-culmination preparation, this technique allows increasing accuracy of paroxysm time forecast up to a quantitative level.

The forecast of destructive earthquakes is more complicated. Ivan Tikhonov and me have analyzed the fore-shock-aftershock sequences of destructive earthquakes in southern Kuril arc area. It was established that the development of both of fore-shock, and aftershock sequences corresponds to the equation of the dynamics of self-developing natural processes. However the fore-shock sequences are more poorly expressed. Probably, some updating of seismic observations is required for getting more stable results. The obtained results make it possible to assume that the methods are a perspective for the forecast of these geophysical catastrophes.

Tuesday 27 July AM

#### DETECTION, MONITORING, EARLY WARNING AND PREDICTION

**JSP23/W/25-B2** Poster **0830-01**

#### EXCESS AND DEFICIENT RAINFALL YEARS OVER INDIA DURING 1871-1996: A BRIEF APPRAISAL

A. A. MUNOT (Indian Institute of Tropical Meteorology Dr. Homi Bhabha Road, Pashan, Pune-411 008, India, e-mail: munot@tropmet.ernet.in)

India, being an agricultural country has its economy closely linked with the performance of the summer monsoon (June-September) which gives 75-90 % of the total annual rainfall. Timely onset and normal distribution of rain in the summer monsoon season generate good amount of food production whereas erratic behavior of monsoon which leads to drought/flood over the country has an adverse effect on the food production and in turn on the economy of the country. Because of this, year to year variation of monsoon rainfall becomes the subject of immense importance. In view of this in this paper an attempt is made to study the inter-annual variability of summer monsoon rainfall for the period 1871-1996. On an average India as a whole receives 852.4 mm of monsoon rainfall with a standard deviation of 84.7 mm and coefficient of variation of 9.9 %. Excess and deficient rainfall years over the country are identified using suitable criterion. There are 22 deficient and 19 excess rainfall years during 1871-1996. The total area of the country under deficient rainfall conditions as well as under excess rainfall conditions have been computed for all the deficient/excess rainfall years. The mean area of the country under deficient rainfall condition in a deficient rainfall year is found to be 42.8% whereas the mean area of the country under excess rainfall condition in a excess rainfall year is found to be 35.7 %. Out of 22 deficient rainfall years, during four years viz. 1877, 1899, 1918 and 1987 more than 60 % area of the country suffered from deficient rain. Similarly out of 19 excess rainfall years during four years viz. 1892, 1917, 1961 and 1988 more than 40 % of the total area of the country was under excess rainfall conditions. Conditional probabilities have been computed for all-India rainfall to be deficient or excess on the basis of June, July and June + July rainfall. It is observed that by the end of July it is possible to anticipate with reasonable degree of accuracy how the performance of the monsoon will be at the end of September, whether it will be normal, deficient or excess. Based on these assessments precautionary measures can be taken in case of monsoon being abnormal.

**JSP23/C/U5/E/11-B2** Poster **0830-02**

#### SHORT-TERM EARTHQUAKE PREDICTION: METHODOLOGICAL ADVANTAGES AND WARNING SYSTEM.

Vitali A. MORGOUNOV (Institute of Physics of the Earth, Moscow 123810, B.Grusinskaya 10, Russia, email vam@uipe-ras.scgis.ru)

What is preferable: to use a chance to win or full ignorance of impending hazard?! Are the cases of real predictions only a blind luck or it is a step to solve the problem? At what extend the uncertainty relation Cognoscibility/Unpredictability of Earthquakes could be improved? Between polar opinions like the dismal prospects for real improvement of the unpredictability (London, November, 7-8, 1996) and unique practical success in China in 1975,1997 there exist a optimum way to solve the most important part of the problem. Progress in the study of short/immediate precursors could be one of the possible path to get over the obstacle due to the following advantages. 1. The final stage of preparation of impending earthquake is characterised by a substantial activation of the process while it's strain rate increase by the orders of magnitude and considerably increase signal-to-noise ratio. That is favourable for identification of critical state of the focal zone through the ground measurements of geophysical fields, in particular by electromagnetic emission, generated by the stress-strain rate of the rock. 2. The avalanche creep process and the worked out instrument make possible to advance the effectivity of the method in relatively short period of time in seismic active areas during the background seismicity (M=3-4). 3. The short-term methods suggest the practical utilisation to prevent the casualties and ecological catastrophes. The EM method, experimental results, and Hardware-Software System "Alarm-Seismo" as an acceptable warning instrument are discussed. The System consists of the network of N slave controllers and master station, where in a real time regime the data is processing by PC computer. The



## INTER-ASSOCIATION

distance between the slave stations is defined by the magnitude of expected earthquake, tectonic and geological peculiarities of the region, relief.

**JSP23/W/99-B2** Poster **0830-03**

### MONITORING OF NATURAL HAZARDS USING MULTI-SENSOR DATA

Ramesh P. SINGH, Sudipa Roy and N.C. Mishra (all at Department of Civil Engineering, Indian Institute of Technology, Kanpur - 208016, India, email: ramesh@iitk.ac.in)

The data recorded by the Special Sensor Microwave Imager (SSM/I), IRS-P3 MOS, IRS - LISS and NOAA AVHRR Data over India have been analysed. The brightness temperature deduced from SSM/I data over snow covered region show distinct behaviour which is attributed to the variable snow thickness and snow melting. The routine analysis of SSM/I data will give fairly good idea of snow avalanches and flooding of the river as a result of snow melting. The daily or weekly variations of brightness temperature, liquid water path (LWP) and total precipitable water (TPW) over Arabian sea and Bay of Bengal has given an anomalous characteristics of a tropical cyclone which hit the coast of Bangladesh. The normalised vegetation index (NDVI), vegetation condition index (VCI) and temperature condition index (TCI) deduced from NOAA-AVHRR give information about the vigor of the vegetation which can be used in monitoring of drought conditions. The IRS-P3 MOS data in 14 bands along path 95 of winter and summer seasons have been used in classifying water bodies. The spectral reflectance deduced in 14 bands give information about the water quality> The characteristic peaks in the spectral reflectance data give idea about the type and distribution of contamination in water bodies. The IRS-LISS data has been used for mapping of the lineaments which can be used for the evaluation of seismic hazards of any region. In the present paper the use of multi sensors data will be illustrated and discussed in monitoring various types of natural hazards.

**JSP23/W/100-B2** Poster **0830-04**

### GEOPHYSICAL HAZARDS: MITIGATION AND WARNING SYSTEMS IN INDIA

K.S. MURTY (E-3 Vishnukamal Apts., 160 Shivajinagar, Nagpur, 440 010 India)

In the last two decades, India was hit by several natural disasters of which the Andhra cyclone of 1977, the Uttarkashi earthquake of 1991, the Latur earthquake of 1993 and the Andhra cyclone of 1996 are typical geophysical phenomena that caused destruction of property and loss of life on a large scale. Relief measures were taken up by government and non-government agencies, while long-term measures like construction of cyclone shelters and new villages to house the affected population were initiated. Cyclone warning systems, flood warning systems, and seismological network in areas that are prone to these geophysical hazards have been set up. Besides, improved infra-structures like road construction have been made part of the development programmes of the concerned areas. These steps have considerably reduced loss of life in some of the more recent natural disasters the country faced.

**JSP23/E/12-B2** Poster **0830-05**

### AN EMPIRICAL DISPERSION RELATION FOR SEISMIC SIGNALS AND EARTHQUAKE PREDICTIONS

Boris W. LEVIN (Shirshov Oceanology Institute of RAS and Russian Foundation for Basic Research, 32a Leninsky prosp, Moscow, 117334 Russia, email: levin@rbr.ru); Elena V. Sassorova (State Oceanographic Institute, 6 Kropotkinsky per., Moscow, 119838 Russia; sazor@geoph.ioras.msk.ru)

We show that faint seismic signals radiated from an earthquake source and acoustic signals foregoing a compression failure of laboratory rock samples can be written by common empirical relationship for waves of period T and length L, as follows  $T^2 = d L$ , where d is dimension coefficient. This leads us to some empirical dispersion relation for seismic signals that is defined by expression  $W^2 = 2^*3.14^* A k$ , where W is frequency, k – wave number, A – acceleration of stress force. The attempt to find such dispersion relation with theoretical way was made by L.Brevdo (1998) because similar function may, on his opinion, lead to an effective method of some earthquake prediction. We used special developed software package for data processing of 200 earthquake records and had found more than 30 events in which digital records the seismic foregoing signals were discovered. The period-length relation for these signals was well described by presented expression. Although the expression should be studied for using in condition of real seismic region, the presented method can sometimes be used to further improve earthquake disaster mitigation practices.

**JSP23/C/U5/W/04-B2** Poster **0830-06**

### A VOLCANO MONITORING AND TSUNAMI WARNING SYSTEM FOR GRENADA AND THE SOUTHERN GRENADINE ISLANDS

Lloyd L. LYNCH, John Shepherd, and Chandradath Ramsingh (Seismic Research Unit, University of the West Indies, St. Augustine, TRINIDAD, email: sru@wow.net).

We propose to develop and establish a volcano monitoring and tsunami warning system for Grenada and the southern Grenadine islands. This region is located close to the Kick 'em Jenny (KeJ) submarine volcano, which has erupted ten times since it was first identified in 1939. Studies that have been done to assess the explosive potential of this volcano and to assess the vulnerability of the East Caribbean Islands to tsunamis, have identified it as a prime tsunami-genic source with Grenada and the southern Grenadines being most vulnerable to its hazards. The studies have also revealed that East Caribbean islands are exposed to tsunamis from other potential sources but to a lesser extent and that the existing regional seismograph and volcano monitoring efforts could be extended and reinforced to mitigate the effects of hazards from KeJ and tsunamis.

The primary aim objective of the volcano monitoring and tsunami warning system is therefore to maximise life safety by providing some level of advanced warning to the vulnerable population. The system is composed two critical components. The first is an integrated network of instruments to detect and rapidly evaluate the nature of increased volcanic activity at the KeJ and events of tsunami generating potential (such as sub-marine landslides or large earthquakes). An array of tide gauges will also be used to track the progress of any sea wave that may be generated. The second component of the system is a set of definitive procedures on how to respond to a tsunami-genic event. All data from the network will be tele-metered to a permanently manned monitoring and warning center to be established near the north coast of Grenada. Warning and alert activities will be co-ordinated through this center. Selected data channels will be relayed to the headquarters of the regional earthquake and volcano-monitoring agency - the Seismic Research Unit (SRU). This agency will widely support the warning center in the areas of equipment installation and maintenance, data processing and interpretation, and staff training. The SRU also plans to assist in educating vulnerable communities about other mitigation techniques that can be used to complement the proposed system.

**JSP23/E/49-B2** Poster **0830-07**

### TOWARDS UNDERSTANDING LAHAR-TRIGGERING MECHANISMS AT RUAPEHU

Vincent NEALL and Jerome Leconte (Institute of Natural Resources, Massey University, Private Bag 11 222, Palmerston North, New Zealand, email: V.E.Neall@massey.ac.nz); Katy Hodgson (Natural Resources Engineering/Environmental Management and Design Division, Lincoln University, P.O. Box 84, Canterbury, New Zealand, email: Hodgsonk@ke.linc.linc.ac.nz)

Over 20 major lahar deposits have been mapped and described from the past 2,000 year B.P. record at Ruapehu. In historical time, a number of different lahar-triggering mechanisms have been observed, so it is pertinent to ascertain how the prehistoric lahar record originated and how this relates to lahar magnitude. We are beginning to recognise specific signatures in the lahar/tephra record that fit models for lahar generation at this volcano. Lahar deposits immediately preceding tephra eruptions are consistent with volcanic activity emptying the crater lake until dry eruptions can occur with resultant ash showers as exemplified by the 1995 eruptions. Lahar deposits immediately following tephra eruptions are consistent with post-eruptive rain-triggering events mobilising tephra accumulations high on the cone. Lahar deposits containing fragile volcanic bombs are clearly indicative of explosion events and eruption-generation of the lahars. Others will be non-eruptive collapse events due to failure of the crater lake wall for a variety of reasons. Currently our programme seeks to: (1) use all sedimentological parameters to characterise the lahar deposits; (2) use petrological matching of lahar clasts to lava flows on the edifice; (3) integrate the complex lahar and tephra record and; (4) provide further precise dating, to elucidate how prehistoric lahars over the last 2,000 years were generated. We thereby hope to understand the environmental conditions one may expect to lead to, or cause any future laharc event.

**JSP23/W/27-B2** Poster **0830-08**

### ERUPTION FORECASTING AT CERRO NEGRO VOLCANO, NICARAGUA, USING TIME-VOLUME RELATIONSHIPS

Brittain HILL, Charles Connor (CNWRA, Box 28510 San Antonio TX USA 78228, E-mail: bhill@swri.edu)

At the scale of sub-duction-zone tectonics, magma production rates appear constant relative to eruption recurrence rates. Differentiation and mixing processes obscure magma production rates in the mantle, making time-volume relationships complex at differentiated volcanic systems. Cerro Negro (CN) volcano in Nicaragua, however, has erupted relatively homogeneous high-Al basalt 22 times since forming in 1850 A.D. Small petrogenetic variations at CN are produced through minor crystal fractionation+accumulation. Waxing activity from 1850-1900 is followed by a steady-state eruption rate of  $1.8 \times 10^6 \text{ m}^3/\text{yr}$ . Relatively constant petrogenesis of CN basalt suggests eruption rate is controlled by the mantle replenishment rate and thus may follow simple time-volume predictable patterns. Empirically, large-volume eruptions at CN since 1900 are followed by long quiescence, whereas short quiescence follows small-volume eruptions. The timing of CN eruptions  $>5 \times 10^6 \text{ m}^3$  has a linear relationship ( $r^2=0.97$ ) with cumulative volume at the time of each eruption. Eruptions in 1992 and 1995 are successfully forecast within 1 yr of the actual eruption using these relationships. The 1971 eruption occurred 12 yr earlier than expected, also earlier than forecast using a 95% confidence interval (1973-1996). The 1968 eruption occurred 8 yrs

**JSP23/E/23-B2** Poster **0830-09**

### GEODETTIC MONITORING OF FOGO ISLAND (CAPE VERDE ARCHIPELAGO) FOR VOLCANIC HAZARD REDUCTION

Sandra I N HELENO, Joao L Matos and Joao F B D Fonseca (IST, Av Rovisco Pais, 1, 1049-001 LISBOA, Portugal, email: sasilva@alfa.ist.utl.pt); Jos N P Lima and J P Osorio (Centro de Geodesia, Instituto de Investigacao Cientifica e Tropical, Rua da Junqueira, 534, 1300 LISBOA, Portugal, email: cgeod@www.ict.pt); Inocencio J M Barros and Arlindo Rosario (LECV, CP 114, Praia, Republic of Cape Verde, email: lec.mit@mail.cvtelecom.cv); Antonio Berberan (LNEC, Av. Brasil, 101, 1799 LISBOA, Portugal, email: berberan@lnecc.pt); Simon J Day, Benfield Greig Hazard Research Centre, UCL, Gower Street, London WC1E6BT, UK, email: s.day@ucl.ac.uk)

As part of a broader hazard reduction project in Fogo Island, N Atlantic, (Fonseca et al., this issue), a programme of periodic GPS and levelling observations was initiated, with a view to the forecasting of impending eruptions by the detection of associated anomalous crustal deformations. In addition, the data will be used in the characterization of the possible flank instability of the volcanic edifice (Day et al., this issue), which may in itself constitute a significant hazard to the population of the island (33000 inhabitants). This poster describes the observational infrastructure built in the island (23 observation points), emphasising the volcanological criteria behind its design, the care taken in the selection of sites with adequate geology, and the stability requirements of the monuments. Results from the Zero Epoch campaign (September 98) are presented and discussed earlier than forecast, but within a 95% confidence interval (1967-1994). Several intervening small-volume eruptions before the 1968 and 1971 events likely triggered the larger eruptions before source replenishment was complete. The  $8 \times 10^6 \text{ m}^3$  of basalt erupted during 1995 activity at CN indicates the next significant eruption is most likely in 2000+/-1, with a 95% confidence interval to 2006 in the absence of intervening small-volume eruptions. The work reported here was supported by the U.S. Nuclear Regulatory Commission (Contract NRC-02-97-009). This work is an independent product of the CNWRA and does not necessarily reflect the views or regulatory position of the NRC.

**JSP23/E/50-B2** Poster **0830-10**

### GLOSEISRISK: A SIMPLIFIED APPROACHING TOOL FOR GLOBAL SEISMIC RISK

QI-FU CHEN and Jie Liu (P. O. Box 166, Center for Analysis and Prediction, CSB, Beijing 100036, P. R. China, email: cqf@ip.cap.ac.cn); Yong Chen (No. 63, Fuxing Avenue, China Seismological Bureau, Beijing 100036, P. R. China, e-mail: yongchen@public.bta.net.cn); Ling Chen (Institute of Geophysics, CSB, Beijing 100081, P. R. China)

A simplified methodology of seismic hazard and risk assessment has been developed by IASPEI working group chaired by Prof. Yong Chen. The new approach includes two analysis methods: One is the seismic hazard analysis method by using earthquake catalogs as basic data and taking area model as potential earthquake sources. A technique is also developed providing the method for integrating individual influences of area sources, near and far, more active or less, into the probability distribution of seismic intensity or peak ground acceleration. Second method addresses exposure bypasses the data collection problems of the traditional method by employing a macroscopic indicator to represent the total exposure directly. The earthquake losses are assessed quickly and approximately by using social wealth represent by Gross Domestic Product and population data.

GloSeisRisk is application software based on Geographic Information System, which is designed to perform analysis and demonstration of seismic hazard and risk with the simplified methodology. The GIS-based GloSeisRisk offers a simplified approach modeling earthquake



hazard assessment, loss estimation and earthquake scenario analysis. The GloSeisRisk includes the data analysis and processing programs for seismic catalogue, GDP and population and the seismic risk estimation functions respectively. It can also illustrate the data distribution and seismic risk maps for different print output. The data can be updated readily from available resources in this application tool and easy to update seismic risk analysis.

**JSP23/C/U5/E/21-B2** Poster **0830-11**

**SCIENCE OR CHANCE? SCORING THE CHINESE ANNUAL EARTHQUAKE PREDICTION FROM 1990 TO 1997**

Yaolin SHI (Graduate School, University of Science and Technology of China, Academia Sinica, Beijing 100039, China, email: shiy1@sun.ihep.ac.cn); Jie Liu and Guomin Zhang (Center for Analysis and Prediction, Chinese Seismological Bureau, Beijing 100036, China, email: liujie@cap.ac.cn)

China is the only country in the world that has an official institution dedicated to precursor monitoring and earthquake prediction. About 800 observational stations spread over China, where more than 1700 pre-cursorial elements are monitored on regular basis. Every January, the Chinese (State) Seismological Bureau holds a national consultation meeting on prediction of major earthquake of the year. Deterministic predictions are made in the meeting. Possible risk areas for the year are circled out. These predictions are reported in official documents to the State Council, though kept confidential during the predicted year to avoid unnecessary social panic. In this study, we apply a scheme of success rate score (R-score) to evaluate the disclosed annual predictions in the 90s. A random guess leads to an R-score of 0 and a complete successful prediction has an R-score of +1. The average R-score of the annual prediction in China in the 90s is about 0.10. The probability in achieving equal or better results by random guess for an averaged year is quite high, about 1/3. However, the probability for random prediction to get equal or better scores in 8 successive years is very low, only  $1.5 \times 10^{-4}$ . In conclusion, we believe that earthquake prediction in China is not by chance, even though it is still in a very preliminary stage to fit the definition of science.

**JSP23/E/35-B2** Poster **0830-12**

**CONTRIBUTION OF GEOPHYSICAL INVESTIGATION TO SOLVE AN ENGINEERING PROBLEM, SOUTH EL-KHARGA OASES, EGYPT**

Maher A. MESBAH (Department of Geological and Geophysical Engineering; Faculty of Pet. and Min. Eng., Suez, Suez Canal University, e-mail: mmesbah@frcu.eun.eg)

A severe subsidence in the ground has been occurred during the passing of heavy machines which are used in the foundation processes of the base and the sub-base of El-Kharga-Paris railway proposed site. The current geophysical study is directed to determine the causes of this civil engineering problem. Therefore, geoelectrical resistivity measurements were done by measuring 25 vertical electrical soundings (VESes) along the proposed line. Also, the previous regional gravity and magnetic surveys were examined in order to obtain the maximum information content from the measured resistivity soundings. In the light of the previous geological, geophysical and geotechnical studies in the area, the measured VESes were manually and automatically processed and interpreted in the light of the drilled boreholes. The analysis and the interpretation of the obtained results should that the maximum monitored depth is 42 m. The resulted geoelectrical models reflects that 3 to 4 geoelectric layers can be determined. A dry surface inhomogeneous layer formed from alluvium deposits covers the investigated site. This surface layer is followed by a soft to hard clay layer. The second geoelectric layer is followed by a hard and compacted clay layer and it was monitored at the most of VESes and didn't at some of them. Therefore, the bedrock layer needed to be a sub-base (or a base) for foundation didn't monitored along the investigated site and special construction requirements are necessary to overcome this conditions of the base.

**JSP23/E/36-B2** Poster **0830-13**

**AUSTRALIA'S IDNDR PROGRAM FOR MITIGATION OF GEOPHYSICAL HAZARDS**

Jack RYNN (Member Australian IDNDR Co-ordination Committee, Centre for Earthquake Research in Australia, PO Box 276, Indooroopilly, Queensland 4068, Australia. email: sally.brown@uq.net.au); Alan Hodges (Chair Australian IDNDR Co-ordination Committee, Director General Emergency Management Australia, PO Box 1020 Dickson, ACT 2602, Australia. Email: ahodges@ema.gov.au); Pip Marks, (Manager Australian IDNDR Co-ordination Committee, Emergency Management Australia, PO Box 1020 Dickson, ACT 2602, Australia. Email: pmarks@ema.gov.au)

Following the proclamation by the United Nations of the International Decade for Natural Disaster Reduction (IDNDR) 1990 - 2000, the Australian Committee was established within Emergency Management Australia (EMA) to pursue the ideals and goals of IDNDR pursuant to mitigation measures of natural disasters in Australia. More than 120 projects were successfully undertaken directly relating to the IDNDR targets of risk assessment, mitigation measures (awareness, disaster planning, education, dissemination of information, community involvement) and warning systems, natural hazards. The multi-disciplinary approach involved government agencies (national, state and local), NGO's, academia and the private sector. The Australian projects include tropical cyclone workstation, risk assessments for storm surge and tsunami, earthquake mitigation of cities, flood and landslide awareness, wildfire prediction and warnings, economic guidelines for loss reduction, medical training package, media campaigns, education curricula and community awareness campaigns. Co-operative efforts with 7 Pacific Island countries through the Pacific Region IDNDR (per 1994 Yokohama Statement) completed projects on cyclone, flood, earthquake, tsunami, landslide and volcano. Planning is in progress to continue the IDNDR concept into the 21st century.

**JSP23/E/27-B2** Poster **0830-14**

**VIGIL - A WARNING SYSTEM FOR VOLCANIC ERUPTIONS IN FOGO ISLAND, NORTH ATLANTIC**

Joao F B D FONSECA and Sandra I N Heleno (both at Physics Department, IST, Av Rovisco Pais, 1, 1049-001 LISBOA, Portugal, email: fonseca@alfa.ist.utl.pt) Peggy Hellweg and Horst Rademacher (both at Geo Enterprises Orinda, 57 Overhill Road, Orinda, CA 94563-3122, USA, email: HRademacher@compuserve.com) Steve Pauly and Bruce Pauly (both at Digital Technology Associates Inc, USA, 1330A Galaxy Way, Concord, CA94520, USA, email: dta\_pauly@compuserve.com) Nicolas d'Oreye (ECGS, Walferdange, G.D.L., email: nicolas.doreye@ecgs.lu) Inocencio J M Barros and Arlindo Rosario (both at LECV, CP 114, Praia, Republic of Cape Verde, email: lec.mit@mail.cvtelecom.cv)

The low-energy strombolian eruption of April 95 in Fogo Island (North Atlantic), following 44 years of quiescence, enhanced the awareness of the risk posed to its 33,000-strong population by the volcanic activity (average interval between eruptions of about 20 years). This created the conditions for the implementation of a volcanological monitoring routine, presently being tested.

This presentation will describe the main components of the monitoring instrumentation,

namely, a combined network of broad-band (Guralp CMG-40T) and short-period (Guralp CMG-40T-1) seismic stations, and a network of resistive tiltmeter (AGI702) stations. All the data collected, both in Fogo Island and in the neighbouring Brava Island, are transmitted in real-time to the data acquisition and processing laboratory (located in Praia, Santiago Island) using spread-spectrum transceivers and combiner-repeater modules. Additionally, a network of 23 high-precision geodetic monuments was built in Fogo Island to allow the periodic surveying with GPS receivers and EDM.

**JSP23/C/U5/W/01-B2** Poster **0830-15**

**SPACE - GEODETIC MONITORING OF LANDSLIDE MOVEMENTS USING GPS TECHNIQUES**

PRUTIGLIANO, F. Vespe (Centro di Geodesia Spaziale P.O. BOX Aperta, 75100 - Matera ITALY, email: rutigl@asi.it); F. Cafaro, C. Cherubini (Politecnico di Bari - Istituto di Geologia Applicata e Geotecnica, Via Orabona 4, 74100 Bari, Italy)

The use of GPS techniques in monitoring natural hazards like volcanic deformations or landslide motions can be a powerful way to improve disaster mitigation. In this work the experimental setting up of a GPS-based system able to monitor landslide motions is reported. The first step of this work consists in evaluating how much a small simulated landslide movement can be mirrored by GPS data. The landslide simulation has been necessary to calibrate the hardware and the software used in this analysis. The experiment has been done using an array of six receivers placed in a small area around the CGS (Center of Space Geodesy) near Matera, Italy. One receiver has been assumed as reference, working permanently during the whole campaign. The other sites have been occupied for eight hours three times each, in order to obtain an evaluation, of the baseline length between all the receivers and the reference one before and after the displacement of the antenna of a known quantity (few cm). The main topics under investigation in this step have been:

a) The minimum observation time needed to obtain an estimation accuracy level suitable to this application (2-3 cm)

b) The possibility of using one frequency (L1) instead of two frequency (L1/L2) GPS receivers without loss of accuracy in the estimation of the movements

The second step of the work consists in the planning of a system to constrain solidly the GPS antenna to the ground, necessary to be sure that the possible motions detected with the GPS are representative of the real motion of the landslide.

IA



**ST1** **Monday 19 – Thursday 22 July****THE NATURE OF SEISMIC SOURCES AND THE PREDICTION OF EARTHQUAKES**Location: Medical School Ext NG26 LT6  
Location of Posters: Arthur Thompson Hall**Monday 19 July AM**

Presiding Chairs: D. Booth, D. Rhoades (Inst. of Geological and Nuclear Sciences, NZ)

**QUANTITATIVE TESTING OF HYPOTHESES OF PRECURSORS****ST1/W/67-A1** **1050****CO- AND POSTSEISMIC GROUND WATER CONDUCTIVITY ANOMALIES RELATED TO DISTANT EARTHQUAKES**

Heiko WEITH, Claus Milkereit, Rongjiang Wang and Jochen Zschau (all at GeoForschungs Zentrum Potsdam, D-14479 Potsdam, Germany, email: radon@gfz-potsdam.de); Valerie Igumnov, Ashot Avanesian and Serguei Balassanian (all at National Survey for Seismic Protection, Yerevan, Armenia, email: ird@nssp.yerphi.am); Ulrike Maiwald and Asaf Pekdeger (both at FU Berlin, FR Rohstoff- und Umweltgeologie, Malteser Str. 74-100, D-12249 Berlin, Germany, email: rike65@zedat.fu-berlin.de)

In 1996, 1997, and 1998 three co/post-seismic conductivity anomalies were observed at an artesian well in southern Armenia related to earthquakes with epicentral distances of 30, 185, and 205 km, corresponding MB magnitudes of 4.8, 5.6, 5.8, and depths of 61, 10, 33 km, respectively. In all cases the conductivity sharply dropped between 20 and 60 minutes after the event by 12, 12, and 23  $\mu\text{S}/\text{cm}$ . We call this drop "co-seismic" to distinguish it from a nearly exponential decay during the succeeding 4 weeks, which is observed for the first two events (no data for the last event). The total conductivity drops - from the beginning of the anomaly until the start of the recovery about 1 month later - are 120 and 60  $\mu\text{S}/\text{cm}$  for the first two events. The co- and post-seismic strains calculated for the site Kajaran are between 10-9 and 10-8 for the three mentioned seismic events, they are below 10-9 for all other earthquakes between December 1995 and August 1998. The strains were calculated for a model with an elastic upper crust overlying a Maxwellian lower crust using the dislocation theory. How can strain events below 10-8 reduce the specific electrical conductivity of a mineral water by 5 to 10 %. To our present knowledge the answer might be related to the special site conditions. We propose a mixture process between different water types, which is obviously very strain sensitive.

**ST1/W/42-A1** **1110****STATISTICAL ASSESSMENT OF SEISMICITY PATTERNS IN ITALY: ARE THEY PRECURSORS OF SUBSEQUENT EVENTS?**

M. MURRU, R. Console, C. Montuori (Istituto Nazionale di Geofisica, Roma, Italy, email: Murru@ing750.ingrm.it)

The variations of seismicity rate in Central Apennines prior to the event of 26 September 1997 (at 00:33 UTC) with  $M_L=5.6$  have been analysed by statistical methods, with the purpose of pointing up eventual periods of quiescence. The analysis was carried out on the instrumental catalogue of the National Institute of Geophysics, covering the period from 1 January 1975 up to the date of the above mentioned event. In a preliminary phase, the catalogue was declustered using the Reasenberg algorithm. After that, eventual magnitude shifts due to variations in the modalities of observation have been individuated and corrected. The subsequent analysis, carried out making use of the Zmap software package, has put in evidence that the main shock of 26 September was preceded by a 2.5 years period characterised by absence of events of magnitude larger than 3.2, in an area approximately 20 x 40 km wide, including the epicentre of the main shock. The statistical methodology shows that only 1/103 of the space-time volume analysed in this study, exhibited quiescence of the same level. The study of seismicity rate change correlated to previous main shocks in a larger area of Central Apennines shows that none of them was preceded by a seismic quiescence, specially close to the epicentre of the main shock, and lasting until the time of occurrence of the main shock as in the 1997 case. Actually, we found other patterns of precursory quiescence with different time or space distribution. We conclude that precursory quiescence is a real feature of Central Apennines seismicity, but it is difficult to define a simple hypothesis, which applies to the generality of cases and can be tested before implementation in a system of earthquake risk mitigation.

**ST1/W/23-A1** **1130****PERFORMANCE AND SIGNIFICANCE OF AN EARTHQUAKE PREDICTION MODEL**

David RHOADES (Institute of Geological and Nuclear Sciences, P.O. Box 30-368, Lower Hutt, New Zealand, email: d.rhoades@gns.cri.nz) Frank Evison (School of Earth Sciences, Victoria University of Wellington, P.O. Box 600, Wellington, New Zealand, email: Frank.Evison@vuw.ac.nz)

The performance of a prediction model can be compared to that of the stationary Poisson model, or any other well formulated model, using a likelihood ratio test and an independent catalogue. The significance and power of a test can be determined by means of Monte Carlo simulations. Under the precursory swarm model, major shallow earthquakes are predictable, with respect to time, location and magnitude, by means of prior earthquake swarms. In New Zealand, an early form of the model failed the performance test, which showed that the model should have allowed for the clustering of swarms and of major earthquakes. The revised model performed inconclusively, the test showing that the swarm precursor is a characteristic of subduction zones. This led to the discovery of the precursory quarm, which is a more protracted, quasi-swarm phenomenon, in the region of continental collision. As a result of these tests, the New Zealand model is now similar to that which had been formulated earlier for Japan. In Japan, a performance test is proceeding satisfactorily. Two separate major earthquakes have occurred, both preceded by swarms. Monte Carlo simulations were carried out after the second New Zealand test, and revealed the significance and power of the test as a whole, as well as the significance of the individual major earthquake occurrences. These results confirmed the need to revise the hypothesis. In the Japan test, Monte Carlo simulations show that the results as a whole are already statistically significant.

**ST1/W/14-A1** **1150****HYDROGEOCHEMICAL SEISMIC PRECURSORS IN KAMCHATKA**

P.F. BIAGI (Physics Department, University of Bari, Via Amendola 173, 70126 Bari, Italy) A. Ermini (Department of Physics and Energy Science and Technology, University of Roma Tor Vergata, Via di Tor Vergata, 00133 Rome, Italy); S.P.Kingsley (Sheffield Centre for Earth Observation Science, University of Sheffield, Hicks Building, Hounsfield Road, Sheffield S3 7RH, UK); Y.M.Khatkevich and

E.I.Gordeev (Experimental and Methodical Seismological Department, Geophysical Service Russian Academy of Science, Pijp Av. 9, Petropavlovsk-Kamchatsky 683006, Russia)

For many years, hydrogeochemicals have been collected with a mean sampling frequency of three days in the form of the pH value and of the most common ions and gases in the groundwater of three deep wells in the south area of the Kamchatka peninsula, where the capital city Petropavlovsk is located. In the last decade five earthquakes with  $M>6.5$  occurred at distances less than 250 km from the wells. These earthquakes were powerful enough for them to be considered as potential precursor sources. Having filtered the hydrogeochemical data, we considered each signal having an amplitude three times the standard deviation to be an irregularity and we defined as an anomaly the existence of an irregularity occurring simultaneously in more than one parameter at each well. Then, on the basis of past results worldwide and of the time recurrence of the previous earthquakes, we chose 158 days as the maximum temporal window between a possible anomaly and the subsequent earthquake. We identified 12 anomalies with 8 possible successes and 4 failures as earthquake precursors and we obtain a probability of 67% that any given hydrogeochemical anomaly is an earthquake precursor. Out of five earthquakes considered capable of producing precursors we obtained precursors in all the cases. A very few probability exists that the precursors signals are by chance.

**ST1/E/85-A1** **1210****STATISTICAL EVALUATION OF PRECURSORS: BACK TO BASICS**

PASCAL Bernard, (Institut de Physique du Globe de Paris, 4 Place Jussieu, 75252 Paris, France, email: bernard@ipgp.jussieu.fr)

The aim of this paper is to show that a significant part of the controversial arguments on the statistical evaluation of precursors and predictions and in particular for the VAN method are due to the semantic fuzziness of what is a valid prediction method, and on the inadequation of the proposed evaluation of significance levels. Some of these points are well known, but they seem to be too often forgotten, and thus need to be recalled in their simplest form. First, it is well known that in a prediction method, one should distinguish the first step, i.e., the statistical validation of precursory phenomena (existence of the precursor), from the second step, i.e., statistical validation of the method (cost-benefit evaluation); consequently, a number of recent discussions on the number of missed events are pointless, as the latter is not directly relevant to the first problem. Second, in the first step, for evaluating the significance level of observed successful alarms, the probabilities of a chancey result are often calculated after selecting alarm subsets for different magnitude thresholds, the lowest magnitudes providing the less significant results. This is usually not appropriate, and one should instead select alarm subsets according to their probability of success, with various probability thresholds. Third, still in the first step, the standard probability gain of the alarm sequence is often provided, but its meaning in terms of significance level of precursors is usually not given. This however can be done by evaluating the statistical properties of its distribution, which is easily achieved when the individual probabilities of success of all alarms are known. This later approach has the advantage of been only weakly sensitive to the maximal probability threshold defining the alarm subset selected for evaluation.

**ST1/E/59-A1** **1230****GENERAL EARTHQUAKE MODELS: PROCESSES, PATTERNS AND PREDICTABILITY**

John B. RUNDLE, (Department of Physics, C4/CIRES, University of Colorado, Boulder, CO, email: rundle@cires.colorado.edu); William Klein (Department of Physics, Boston University, Boston, MA); Geoffrey Fox (Department of Physics, Syracuse University, Syracuse NY)

The General Earthquake Model (GEM) paradigm is directed towards the development of realistic, high performance computational simulations of earthquake processes on individual and systems of faults within the earth's crust. As a part of this project, it will be necessary to push forward ideas and technologies that will allow large groups of scientists to interact within an object oriented, collaborative software environment on a geographically diverse set of computational hardware. As a part of the development of these models, advances in a number of areas will be necessary. These technologies, which have in general not been contemplated for use in earthquake related problems, include: Fast Multipole Methods, that have been used extensively in gravitational N-body problems and in computational fluid mechanics; Karhunen-Loeve Expansions, and other pattern recognition, feature extraction, mode shaping and "data mining" techniques; Data Assimilation Methodologies, that permit "model steering" and model adaptation; Analysis Techniques, that originate from statistical field theoretic analyses of random field systems; Computational, Web-Based Collaboratory Software, whose development will be driven by the advent of web-based computing approaches. In this talk, we describe these approaches, as well as the need for coarse-grained models and simulations that capture the basic physical processes. We present a summary of ideas that describe the nucleation, growth, and arrest of earthquakes on individual faults, and the space-time patterns they produce on systems of faults. Finally, we describe how some of these methods might be used in the future to forecast the progression of patterns through pattern state space.

**Monday 19 July PM**

Presiding Chairs: M.Ohnaka (University of Tokyo, Japan), R.Teisstyr

**EARTHQUAKE NUCLEATION TO DYNAMIC RUPTURE****ST1/E/02-A1** **1400****QUANTUM MODEL OF SEISMIC CODA WAVES GENERATION**

Marius ANGHEL (National Institute for Earth Physics, P.O. Box MG-2, 76900 Bucharest, Romania, email: anghel@infp.ifa.ro); Olivia Bazacliu (National Institute for Earth Physics, P.O. Box MG-2, 76900 Bucharest, Romania, email: olivia@infp.ifa.ro)

The quantum model of the tectonic seismic source (Anghel, 1998 - Ph. D. Thesis) is applied to the study of the interaction of the phonon flow (radiated during the earthquake process) with the heterogeneities of the medium between the focus and station. The quantum model starts from the quantum coherence of the atoms in the source before the Megascopic Quantum Tunneling. The quantum coherence is also characteristic for the phonon radiation. The coda waves are formed at macroscopic scale (observatory scale) by the secondary phonons that result from the interaction of the primary phonons with the atoms composing the medium heterogeneities. As a consequence of these interactions, the quantum coherence of the phonons is destroyed and the seismic energy is attenuated, due to both the absorption of a part of phonons by the atoms in the medium and inelastic collisions with them during the propagation. From the analysis of the phonon number - frequency distribution we can deduce several properties known from observations, such as coda spectrum independence of the source - station distance, coda wave envelope stability and dependence of the coda absolute amplitude of the total number of phonons radiated by the source (which is equivalent with the radiated seismic energy).



ST1/W/68-A1

1420

## SIMULATIONS OF SPONTANEOUS RUPTURES ON INHOMOGENEOUS FAULTS

Ruth A. HARRIS (U.S.G.S., M.S. 977, 345 Middlefield Rd, Menlo Park, CA 94025; email: harris@usgs.gov), Steven M. Day (Dept. of Geological Sci., San Diego State University, San Diego, CA 92182)

Although 2D and 3D numerical simulations of spontaneous (unforced) earthquake ruptures are becoming more common, most of these simulations still assume that the earthquake occurred on a single fault plane, in a homogeneous medium. However, observations show that many earthquakes do not occur on single fault planes, or in homogeneous rock. For example, the 1992 Landers, California earthquake was a multi-fault rupture, as shown by geological and seismological data

[Sieh et al., Science, 1993], and the fault material was heterogeneous [Li et al., Science, 1994]. We have assumed a slip-weakening fracture criterion and investigated the 2D and 3D cases of a rupture encountering a stepover in a strike-slip fault, and of a rupture in a bi-material setting. Among our observations: (i) For simple, uniform stress drop configurations, 3D model predictions of the likelihood that a rupture jumps a wide stepover are similar to those obtained in 2D by Harris et al., GRL, 1991 and Harris & Day, JGR, 1993. ii) When a rupture does jump, rupture of the second fault occurs preferentially at very shallow depth for compressional stepovers, and at shallow to moderate depths, depending on S value and previous earthquake history for dilatational stepovers. iii) Repeated earthquakes on faults similar to those at Parkfield, CA and at Landers can produce events that jump across a stepover alternating with those that do not, similar to the pattern observed in these two earthquake-prone regions. iv) For the bi-material case, ruptures can propagate bilaterally, with the rupture velocity depending on both the direction of propagation and the material-velocity contrast. v) There can be a reduction in the normal stress, but its absolute value is not yet resolved. vi) Complexity is produced in the seismograms, but there is no healing. These examples show how basic features observed in the field add major complexity to dynamic simulations.

ST1/W/08-A1

1440

## USING OF STAGES OF THE EARTHQUAKE SOURCE PREPARATION TO REVEAL POTENTIAL SOURCES

G.A. SOBOLEV (United Institute of Physics of the Earth, Russian Academy of Sciences, Moscow, 123810, B.Gruzinskaya, 10, Russia, email: sobolev@uipe-ras.scgis.ru)

The results of the laboratory monitoring presume that a macrorupture is preceded by the characteristic stages of acoustic emission. Among them are acoustic quiescence, migration of activity to the place of the future macrorupture accompanied by the appearance of clusters, foreshock activation. These stages indicate the development of mechanical instability in the area of the macrorupture. In the laboratory experiments, the duration of these stages falls within the minute range; under mine conditions with destruction of rock massifs it reaches hours and days. During the strong earthquakes preparation in seismotectonic regions it is likely that the instability stages may take months and years. We have tested the validity of these propositions by analysing the seismic regime of Kamchatka earthquakes with magnitudes more than 7 that occurred during the last seven years. We used the regional catalogue, which was uniform for this period, starting with energy class  $K \geq 8.5$ , i.e., magnitude  $M \geq 2.5$ . The occurred earthquakes were preceded by seismic quiescence and foreshock activation, which were revealed by using the RTL prognostic and the DS localisation parameters. The quiescence areas appeared in the time intervals ranging from 35 to 16 months before the corresponding earthquake and covered the areas with linear dimensions of about 200 km. The earthquake epicentres were located on the edge of the quiescence anomalies. The areas of foreshock activation occurred in the time interval from 23 to 4 months before the corresponding earthquake and covered areas with linear dimensions of about 50 km. The earthquake epicentres were located within the areas of foreshock activation. A year prior to all these earthquakes, there also appeared, in their epicentral areas, single clusters of two and more earthquakes of energy class  $K \geq 10$ , i.e., of magnitude  $M > 3.5$ . The anomalies of the phenomena indicated above, not accompanied by strong earthquakes, were also recorded. Their analysis implies that though the study of these stages of seismic regime does not guarantee against false anomalies and missing the individual earthquakes, still their combination is helpful in establishing potential sources and keeping track of their development.

ST1/W/61-A1

1500

## DYNAMIC TRIGGERING OF SEISMICITY IN GRANITE

R. Paul YOUNG, Calum Baker, James Hazzard, Dave Collins and Will Pettitt (all at Department of Earth Sciences, University of Keele, Staffordshire, UK, email: r.p.young@keele.ac.uk)

There is a growing body of evidence that spatial and temporal patterns of seismicity can be influenced by static and dynamic stress changes arising from other earthquakes, both local and distant. Such influences have important implications for seismic hazard but the key factors are hard to assess due to a lack of instrumentation in key areas and problems in distinguishing these triggered seismic events from those that would have occurred anyway. In this paper we show new evidence for dynamic triggering from modelling studies, laboratory experiments and field investigations. Dynamic modelling of wave interaction from microcracking, using the Particle Flow Code, is shown to trigger new cracks and seismicity. These results are compared to experimental acoustic emission studies of rock mechanical tests of granite samples, which were used to validate the modelling results. In the field, induced seismicity from excavations at the Underground Research Laboratory in Canada are shown to interact/communicate with acoustic emission activity at the grain boundary/microcrack scale.

ST1/W/46-A1

1520

## GROUND ROTATIONAL MOTIONS RECORDED IN NEAR-SOURCE REGION OF EARTHQUAKES

Minoru TAKEO (Earthquake Research Institute, University of Tokyo, 1-1-1, Yayoi, Bunkyo, Tokyo 113-0032, Japan, email: takeo@eri.u-tokyo.ac.jp)

Large rotational motions excited by earthquakes are recorded during two earthquake swarms at offshore Ito in Izu peninsula, Japan, which occurred in March, 1997 and in April, 1998. The purpose of this paper is to report the characteristics of the rotational ground motions excited by the earthquakes, and to estimate spatial changes of slips for small earthquakes. The largest rotational velocity recorded at KAW is  $2.6 \times 10^{-2}$  rad/s around the north-south axis during an earthquake of magnitude 5.2 at 14:09 (GMT) on March 3, 1997. The largest earthquake with a magnitude of 5.7 occurred at 3:51 on March 4 (GMT), 1997, whose rotational motions around the vertical axis was  $3.3 \times 10^{-3}$  rad/sec. Considering a spatial variation of slip velocity which directly relates to excitation of a rotational motion, we apply simple point source models to the largest event and the second largest event in the swarm of 1997, and succeed in explaining the observed rotational motions around the vertical axis. These results suggest that the fault slip of the at a shallower part (about 3km deep) of the fault during the second largest event.

ST1/E/33-A1

1600

## ON THE PRELIMINARY RUPTURE OF THE EARTHQUAKE

Yasuhiro UMEMA and K. Kitada (both at Disaster Prevention Research Institute, Kyoto University, 611-0011, Gokasho, Uji, Kyoto, Japan, email: umeda@rcp.dpri.kyoto-u.ac.jp)

For the large shallow earthquakes, the preliminary rupture process precedes a large complex rupture called "an earthquake bright spot". The preliminary rupture differs from the nucleation process which is aseismic process observed on the rock experiment. The preliminary rupture is normal earthquake and it produces the seismic waves. On the surface of the earthquake bright spot, severe shaking dislodges almost all of boulders. Sometimes an initial faulting steps over to another faulting accompanying with a lot of cracks. Aftershock gap is also found in this spot. The duration time (T sec) of the preliminary rupture proportion to the earthquake moment ( $M_0 : N_{BI} \cdot (B_m)$ ). The relationship of  $\text{Log}M_0 = 3\text{Log}T + 18.1$  shows that the longer duration time of the preliminary rupture induces the larger earthquake. However, this relationship holds on the large earthquakes or the main shocks. Almost of the earthquake swarms, aftershocks and micro-earthquakes have not the preliminary rupture process. The earthquake having the clear preliminary rupture phase is found only 9 percent in the earthquake, swarm (2.5  $B_{BI} \cdot (B_M \cdot B_{BI} \cdot (B_{4.7} \cdot B_{BI} \cdot (B_{in}$  the east of Izu peninsula, Japan. They distribute a little apart from the earthquake swarm area.

ST1/E/90-A1

1620

## A UNIFIED COMPREHENSION FOR FRICTIONAL SLIP FAILURE, SHEAR FRACTURE OF INTACT ROCK, AND EARTHQUAKE RUPTURE: SIGNIFICANCE OF THE UNDERLYING PHYSICAL LAW

M. OHNAKA(1), A. Odedra(1,2), and L.-f. Shen(1) (1)Earthquake Research Institute, The University of Tokyo, Yayoi 1-1-1, Bunkyo-ku, Tokyo 113-0032, Japan, email: ohnaka-m@eri.u-tokyo.ac.jp) (2)University College London, and BG plc Exploration and Production, 100 Thames Valley Park Drive, Reading, Berkshire RG6 1PT, UK, email: odedra.a@bgep.co.uk

There are increasing amounts of circumstantial evidence that the earthquake rupture at crustal depths is a mixed process between what is called frictional slip failure and fracture of intact rock mass. In fact, what is called a 'barrier' or 'asperity' on earthquake faults can be a local patch of high rupture growth resistance whose strength equals the strength of intact rock. In addition, a large earthquake tends to nucleate at depths corresponding to the brittle-plastic transition regime where the frictional strength conforms to the shear fracture strength of intact rock, since the lithostatic pressure and temperature are high enough at these depths. Hence, if there is a constitutive law that governs the earthquake rupture, the law should be formulated as a unifying constitutive law that governs both frictional slip failure and shear fracture of intact rock mass.

Two kinds of laboratory experiments have been performed to reveal the constitutive property of frictional slip failure on a preexisting fault, and that of shear fracture of intact rock at lithospheric conditions. Combining these data on constitutive properties of friction and fracture leads to the conclusion that the constitutive law should be formulated primarily as a slip-dependent law, and also leads to an important finding that the slip-dependent constitutive law parameters are mutually not independent, but related to one another by a universal relation, which plays a fundamental role in unifying shear fracture of intact rock and frictional slip failure, and as a consequence, earthquake rupture. The relation found here specifically prescribes the relation between the scale-dependent constitutive parameter  $D_c$  (critical slip displacement) and the characteristic length representing geometric irregularity of the rupturing surfaces, and allows to scale scale-dependent physical quantities (such as the shear fracture energy, the nucleation zone size and its duration) consistently in quantitative terms, because the characteristic length in general increases with an increase in the fault size for natural earthquakes. A unified comprehension can thus be provided for the shear rupture of any size scale - from small scale in the laboratory to large scale in the crust as an earthquake source.

ST1/W/69-A1

1640

## SOURCE PARAMETERS OF SMALL EARTHQUAKES ALONG ATOTSUGAWA FAULT ZONE, CENTRAL JAPAN

ANSHU Jin(1, 2), Cesar Moya(3), Masataka Ando(2) (1) Geoscience Center, JNC, Japan; (2) RCEP, DPRI, Kyoto University, Japan; (3) University of Costa Rica, Central America.

Site response and source parameters are determined, simultaneously, for 102 events along Atotsugawa Fault zone recorded at 9 stations, in Hida region, central Japan by applying a Genetic Algorithm. To avoid the high frequency leaking, multi-taper technique is used for FFT for a 5 s time window starting at 0.1 s before S-onset. We adopt the circular crack model (Brune, 1970) to describe the source in frequency domain by 3 parameters, namely, the flat level of the displacement spectrum,  $W_0$ , the corner frequency,  $f_c$ , and the high frequency decay rate,  $n$ . The source parameters of 102 events and site response for each of the 9 stations are determined by using a GA approach running up to 600 generations. We divided the earthquakes into 10 subgroup, and apply the GA approach to each subgroup in order to check the stability of the solutions. The results show that (1) the site amplification for each station varies within a factor of 4; (2) for the source parameters, the variations of  $W_0$ ,  $f_c$ , and  $n$  are 4-6%, 4 Hz, and 0.5, separately. The resultant source parameters show that the events located on Mozumi fault tent to have higher stress drop and the events located on the creep section and the southwest ends, where the fault dismissed into an inactive volcano, have lower stress drop. After carefully check on the effects from using different Q model, the seismic scaling is discussed by combining with some previous estimation.

ST1/W/56-A1

1700

## RELATIONS OF THE HARD-CORE ALLOMORPHER ROCK FRACTURES AND THE EVOLUTION CHARACTERISTICS OF THE DEFORMATION DYNAMIC IMAGES

ZHENGYUAN Li, Shuoyu Zhou and Yun Wu (all at Institute of Seismology, China Seismological Bureau, Xiao Hong Shan, Wuhan, China 430071) Zhaoyong Xu (Seismological Bureau of Yunnan Province, Kunming, China 650041)

The fracture processes of the deformation dynamic image can directly reflect the rock evolution situation under pressure, which is the effective method for monitoring the fracture process. It has been spreadly applied in the earthquake prediction. Since the rock samples of the hard-core allomorpher under pressure display more complicate evolution image than the homogeneous one, it is much closer to the real generating earthquake process. From the experimental results of the rock samples, this paper gives the following recognitions for the characteristic of the deformation image.

1. display twice linear-nonlinear elastic variation. After the process, the rock will be fracture.sixty percent, the deformation stability will be weak, namely the empty space of deformation. If the pressure loading is more than a ninety percent, the deformation stability is

variable on the different gradient strips, and then gets into fracture situation. The process of the hard-core allomorpher sample rock is similar with the micro-fracture, from the image of the empty space to strip.

2. Comparing with the generating earthquake model of the hard-core allomorpher rock and the solid model, this paper proves the coincidence with the real earthquake cases happened in Tangshan ( $M_s=7.8$ ,  $39^\circ 38' N$ ,  $118^\circ 11' E$ ) and Lanchang-Gengma ( $M_s=7.6$ ,  $22^\circ 54' N$ ,  $100^\circ 06' E$ ). Therefore, we suggest three characteristic stages of the deformation dynamic images: the structure stage, loading stage, and fracture stage, and also explain the behavior of the image of the generating earthquake and the theory of the fracture.

ST1/E/44-A1

1720

#### MICROMECHANICS OF CHANGES IN TRANSMISSION WAVES ACROSS A FAULT WITH APPLICATION OF SHEAR LOADS AND PRECURSORY SLIPS

Naoto YOSHIOKA and Akihiro Suzuki (both at Yokohama City University, Seto 22-2, Kanazawa-ku, Yokohama, 236-0027, Japan, email: yoshi@yokohama-cu.ac.jp) Koji Iwasa (Earthquake Research Center, Association for the Development of Earthquake Prediction, Sarugaku-cho, 1-5-18, Chiyoda-ku, Tokyo, 101-0064, Japan, email: iwasa@erc.adep.or.jp)

We have performed an observatory experiment to detect precursory slips prior to a dynamic rupture (stick-slip event) by transmission waves across a simulated fault. The results have been reported elsewhere (GRL, 25, 3907, 1998), which show two distinctive features: (1) the amplitude of the first arrivals of transmitted waves significantly increases with application of shear stress, and (2) the increasing rate of seismic sequences there. The last seismic swarm occurred in 1997. More than 170 events were located in a very narrow area. The wave forms and earthquake recurrence graph were investigated. Great similarity exists in the wave forms for most of the swarm events. Nevertheless, the old sequences in this region were reviewed and an attempt to find a probable relation between them and the strong events was made.

ST1/W/01-A1

1740

#### COMPLEXITY IN RECURRENCE OF LARGE EARTHQUAKES IN AND AROUND THE JAPANESE ISLANDS: A SIMULATION WITH INTERACTING FAULT SYSTEM MODEL

MANABU Hashimoto (DPRI, Kyoto University, Uji, Kyoto 611-0011, Japan, email: hasimoto@rcp.dpri.kyoto-u.ac.jp)

I present the results of simulation of large earthquakes in and around the Japanese islands with a model incorporating interactions between inter- and intraplate faults. I adopt a back-slip model obtained by the inversion of geodetic data by Hashimoto and Jackson (1993) for the fault system model. There are 104 faults and each fault is divided into  $2 \times 2$  segments along the length and width directions, respectively. I also made a simulation with original fault system model and compared the results. Interaction between these segments are calculated as changes in Coulomb Failure Function for preferred slip of each fault due to forward- / back-slip of all faults in the model under the assumption of purely elastic half space. Back-slip is assumed to be constant, so that CFF of each fault increases linearly. When cumulative CFF of a particular fault reaches its threshold, that fault slips forward and stress is redistributed until no more forward slip occurs. In this model threshold is assumed to be 0.5 MPa and 2 MPa for interplate and intraplate faults, respectively. Initial stress of each fault is given randomly between 0 MPa and its threshold. I also deviate initial stress and back-slip rate by 1 % and 10 %, respectively, of all faults in order to investigate dependence of resultant seismicity on these two parameters. Results of simulation suggest (1) Recurrence interval of large events which rupture whole fault area is longer (~1000yrs) than that in case of the model with undivided faults. (2) Amplitude of CFF changes on some faults fluctuate with as long period as 2000 yrs. (3) Small errors in initial stress and back-slip rates cause significant difference in simulated seismicity after hundreds of years, which cast a serious problem on long-term forecast of earthquake occurrence.

Tuesday 20 July AM

Concurrent Poster Session

#### PANEL DISCUSSION ON EARTHQUAKE PREDICTION

PANEL DISCUSSION

1050

Max Wyss: Geophysical Institute, University of Alaska, USA. P. Bernard: Institut de Physique du Globe de Paris, France. R. Console: Istituto Nazionale di Geofisica, Italy. Harsh Gupta: National Geophysical Research Institute, India. Stuart Crampin: Department of Geology and Geophysics, University of Edinburgh, UK. David Jackson: Department of Earth and Space Sciences, UCLA, USA. Keilis-Borok: International Institute for Earthquake Prediction Theory and Mathematical Geophysics, Russia. Sobolev G.A.: United Institute of Physics of the Earth, Russia. J. Zschau: Geoforschungszentrum, Potsdam, Germany. Frank Evison, Institute of New Zealand.

Tuesday 20 July PM

Presiding Chairs: Max Wyss (University of Alaska, USA), P. Bernard (Inst. de Physique du Globe de Paris, Paris, France), R. Console (Nazionale di Geofisica, Roma, Italy)  
Concurrent Poster Session

#### EARTHQUAKE NUCLEATION TO DYNAMIC RUPTURE

ST1/E/43-A2

1400

#### MEDIUM TERM FORECAST OF 1988 NORTHEAST INDIA EARTHQUAKE REVISITED

Harsh K GUPTA, (National Geophysical Research Institute Hyderabad-500007, India)

Northeast India is seismically one of the most active intra-continental regions in the world. It has been a site of several earthquakes including four earthquakes exceeding magnitude 8 during the last 100 years. Gupta and Singh (1986) systematically analyzed the time series of earthquakes associated with several main shocks in an area bound by  $20^\circ$  deg N and  $32^\circ$  deg N latitude and  $88^\circ$  deg E and  $100^\circ$  deg E longitude and found \*1. Moderate magnitude to great earthquakes in the northeast India region are found to be preceded, generally, by well defined earthquake swarms and quiescence periods. 2. On the basis of an earthquake swarm and quiescence period, an area bound by  $21^\circ$  deg N and  $25^\circ 1/2$  deg N latitude and  $93^\circ$  deg E and  $96^\circ$  deg E longitude is identified to be the site of a possible future earthquake of  $M 8 \pm 1/2$  with a focal depth of  $100 \pm 40$  km. This earthquake should occur any time from now onwards. Should it not occur till the end of 1990, this forecast could be considered as a "false alarm". This medium-term earthquake forecast came true with the occurrence of a  $M 7 1/2$  earthquake on August 6, 1988. Table 1 gives the parameters of forecast and occurrence.

TABLE 1. Forecast of August 6, 1988, Earthquake

Earthquake Parameters	Prediction, (Gupta and Singh, 1986)	Occurrence NEIS, (Preliminary Determination),
Epicenter	$21^\circ$ deg N- $25^\circ 1/2$ deg N $93^\circ$ deg E- $96^\circ$ deg E	$25.116^\circ$ deg N $95.171^\circ$ deg E
Magnitude(M)	$8 \pm 1/2$	$7 1/2$
Depth	$100 \pm 40$ km	115 km
Time	February 1986 – December 1990	August 6, 1988, (00:36:26.9 G.C.T.)

The original paper by Gupta and Singh was published in 1986. This was also presented at the 19th IUGG General Assembly at Vancouver in 1987. The forecast of this earthquake was based on the concept of precursory swarms and quiescences preceding main-shocks. It is worthwhile noting that in the entire region under study the only place where an earthquake exceeding  $M 7$  occurred since 1952 is in the area where forecast was made. At the time of writing this abstract, more than 10 years have passed after the occurrence of August 6, 1988 earthquake of  $M 7.5$ . In this paper the details of making this forecast and possible use of such medium-term forecasts are presented.

ST1/W/41-A2

1420

#### THE STATIONARY POISSON RATE AT WHICH INTERMEDIATE DEPTH EARTHQUAKES ARE PRODUCED CONTRASTS SHARPLY WITH PRE- AND POST MAIN SHOCK SEISMIC QUIESCENCE

Max WYSS, Yozo TOYA and Stefan WIEMER (Geophysical Institute, University of Alaska, Fairbanks, 99775, email: max@giseis.alaska.edu.)

We investigated the question of how stationary the production of the background seismicity is for deep and intermediate earthquakes. For shallow earthquakes it is difficult to reliably separate the independent (background) seismicity from the dependent component (fore-, aftershocks and swarms), but the majority of the deep seismic zones are free from obvious earthquake clusters. Using data from local, regional and global seismograph networks we selected earthquakes in about 100 volumes at depths deeper than 60 km, of which only approximately 10 to 15 % contained obvious clusters. We used 500 events per sample and divided the time covered by the catalog (10 to 30 years) into 100 intervals. Chi square tests applied to the distribution of the seismicity rates within these volumes revealed that for most of them one cannot reject the null hypothesis that the production rate is a stationary poissonian process. For a number of data sets we attribute the deviation from a poissonian process to changes in the re-portion procedure. Like aftershock sequences clearly deviate from the stationary production of seismicity, the phenomenon of after-quiescence is obvious in some cases. For example the December 1994 off-Sanriku  $M 7.5$  earthquake induced a quiescence down-dip from its rupture area that lasted several years, and a 1993  $M 4.8$  Parkfield earthquake induced a quiescence lasting several years in the northern part of its rupture area and north of it. Similarly precursory quiescence is a phenomenon not unlike foreshocks, both due to redistribution of stress during the preparation process for the main rupture. There are now approximately a dozen main shocks for which we mapped statistically uniquely significant precursory quiescence in great detail. The tectonic settings of these include strike-slip and thrusting along plate margins, as well as normal and reversed faulting in mountain belts. Not all significant quiescence are followed by main shocks, and not all main shocks are preceded by significant quiescence.

ST1/W/43-A2

1440

#### EARTHQUAKE PREDICTION: RECENT RESULTS AND WHAT COMES NEXT

Vladimir KEILIS-BOROK, Vladimir Kossobokov, Irina Rotwain, Alexandre Soloviev (all at International Institute for Earthquake Prediction Theory and Mathematical Geophysics, Russian Academy of Sciences, 79-2 Warshavskoye Shosse, Moscow 113556, Russia, E-mail: volodya@mitp.ru); Andrei Gabrielov (Departments of Mathematics and Geophysics, Purdue University, W. Lafayette, IN 47907-1395, USA, E-mail: agabriel@math.purdue.edu)

The worldwide test of several algorithms for intermediate-term earthquake prediction validates the underlying paradigms derived from phenomenology and modeling: 1) The area where premonitory phenomena are formed is much larger than the source of a subsequent large earthquake. 2) These phenomena include specific transformations of background seismic static. 3) They are partly similar in a wide range of conditions - from fractures of samples in laboratory experiments, through earthquakes to starquakes. 4) Some of premonitory phenomena that we encountered in seismology are universal symptoms of critical transitions, common for a wide class of chaotic systems.

The accuracy of the existing earthquake prediction algorithms is limited and allows only a partial damage reduction. However, the accumulated experience suggests a way to develop a next generation of prediction methods with about fivefold increase of accuracy and transition to short-term prediction. The following possibilities emerge: integration of modeling with phenomenology; combination of universal and Earth-specific premonitory phenomena; use of a multitude of relevant fields with common scaling and common symptoms of critical transition; identification of the current state of criticality of an active lithospheric volume; prediction of transition from one state of criticality to another ("prediction of predictability"). The theoretical base and practice in linking prediction and preparedness are discussed. The following possibilities emerge: integration of modeling with phenomenology; combination of universal and Earth-specific premonitory phenomena; use of a multitude of relevant fields with common scaling and common symptoms of critical transition; identification of the current state of criticality of an active lithospheric volume; prediction of transition from one state of criticality to another ("prediction of predictability"). The theoretical base and practice in linking prediction and preparedness are discussed.

ST1/W/52-A2

1500

#### EARTHQUAKE-PREDICTION RESEARCH IN A NATURAL LABORATORY-PRENLAB

RAGNAR Stefansson (Geophys. Dep. of Geophysics, Icelandic Met. Office, 150 Reykjavik, Iceland email: ragnar@vedur.is) Reynir Bodvarsson (Dep. of Geosciences, University of Uppsala, Sweden, email: rb@geofys.uu.se)

The PRENLAB project is a multidisciplinary and multinational project in earthquake prediction research, focussing at crustal processes in the seismic and rift zones of Iceland. The idea is that various conditions prevailing in Iceland, ranging from well exposed geology to frequent short term variations in strain rate can be utilized to obtain significant understanding of crustal processes leading to large earthquakes. Results of various approaches of the PRENLAB project will be described. Mapping of faults by



microearthquake technology with 10m relative accuracy, and by geologists of surface exposures. Results of deformation studies by GPS and SAR are presented. Build up of stresses approaching breaking strength, observed by S-wave splitting, by seismicity and based on fault plane solutions will be presented. Results will be presented of various studies, seismological and geological related to the effects of fluids in fault zones. Modelling of earthquakes based on deformation measurements as well as on studies of the related small earthquakes will be described, also observations of stress changes and instability related to the earthquake nucleation process.

The application of the results for warning purposes is discussed.

ST1/W/63-A2

1520

## GLOBAL EARTHQUAKE FORECASTS: HYPOTHESES AND TESTS

David D. JACKSON and Yan Kagan (both at Department of Earth & Space Sciences, UCLA, Los Angeles, CA 90095-1567, USA; email: djackson@ucla.edu)

We present a global model of earthquake potential, defined here as the probability of occurrence per unit area, magnitude, time, and focal mechanism parameters. The model is based on the occurrence of past earthquakes only, with no information, at present, on plate tectonics, faults, earth structure, etc. We assume that the earthquake potential is separable into factors depending on location, magnitude, and time respectively. The magnitude distribution is assumed fixed (a Gamma distribution with a corner magnitude of about 8.5) and the time function is constant within yearly intervals, so that for a given year the earthquake potential is uniquely defined by a spatial function. That spatial function is assumed to be a weighted average of previous earthquake occurrence, where the weighting kernel decreases with distance and increases in proportion to magnitude. There are only three variable parameters in the model, corresponding to a distance scale, the rate of decrease with distance of the spatial function, and an aspect ratio defining the degree of directionality of the spatial kernel. Once the parameters are specified, the model can be tested unambiguously against future earthquake occurrence using a likelihood test. After successful retrospective tests, we began forward testing at the beginning of 1999. Testing will be based on a likelihood value obtained by evaluating the earthquake potential function at the site of each qualifying earthquake.

ST1/W/53-A2

1600

## A SIMPLE AND TESTABLE EARTHQUAKE FORECAST HYPOTHESIS

R. CONSOLE and M. Murru (both at Istituto Nazionale di Geofisica, Via di Vigna Murata 605, 00143, Roma, Italy, email: console@ing750.ingrm.it, Murru@ing750.ingrm.it)

Earthquakes are regarded as the realization of a point process modeled by a generalized Poisson distribution taking into account the past history. No hypothesis is evoked on the physical model of such a process. We assume that the Gutenberg-Richter law describes the magnitude distribution of all the earthquakes in a sample, with a constant b-value. We model the occurrence rate density of earthquakes in space and time as the sum of two terms, one representing the independent, or spontaneous, activity, and the other representing the activity induced by previous earthquakes. The first term depends only on space, and is modeled by a continuous function of the geometrical co-ordinates, obtained by smoothing the discrete distribution of the past instrumental seismicity with a suitable kernel function. The second term depends also on time, and it is factorized in two terms that respectively depend on the space distance (according to an isotropic normal distribution) and on the time difference (according to the generalized Omori law) from the past earthquakes. Under this hypothesis, all the earthquakes may potentially induce subsequent events, and all the earthquakes are subject to induction from the previous ones, so that the distinction between foreshocks, main shocks and aftershocks is meaningless. Knowing the expected rate density, the likelihood of any realization of the process (actually represented by an earthquake catalogue) can be computed straightforwardly. In the first application of the model on a computer code, we assume that all the parameters involving time dependence are space-independent. This algorithm can be used in two ways: (a) during the learning phase, for the maximum likelihood estimate of the few free parameters of the model, and (b) for hypothesis testing. The latter should be carried out on a new and independent set of data, having fixed the values of all the parameters. The test can be run in real time. Few months of seismological observations in an active region proved to be usually sufficient for showing the superior significance level of this time-dependent model with respect to a simple time-independent Poisson distribution.

ST1/E/57-A2

1620

## A "STRESS-FORECAST" EARTHQUAKE IN ICELAND

Stuart CRAMPIN, Theodora Volti (both at Department of Geology & Geophysics, University of Edinburgh, Edinburgh EH9 3JW, UK, email: scrampin@ed.ac.uk) Ragnar Stefansson (Iceland Meteorological Office, Bustadavegur 9, 150 Reykjavik, Iceland; email: ragnar@vedur.is)

Stress-aligned shear-wave splitting is seen with similar behaviour in almost all rocks below about 1km-depth. Shear-wave splitting is very sensitive to microcrack anisotropy and the splitting is a result of propagation through the effective anisotropy of the stress-aligned fluid-saturated grain-boundary cracks and low aspect-ratio pores present in almost all sedimentary, igneous, and metamorphic rocks. These fluid-saturated cracks are very compliant and the evolution of fluid-saturated cracked rock can be modelled by anisotropic poro-elasticity (APE), where the driving mechanism is fluid migration along pressure gradients between neighbouring grain-boundary cracks and pores at different orientations to the stress field. APE-modelling matches observations in both field and laboratory and suggest that small changes in stress modify crack geometry and the consequently modify shear-wave splitting. In the past, changes in shear-wave splitting before earthquakes have been seen (with hindsight) on five occasions worldwide. Changes in shear-wave splitting before earthquakes are now observed routinely (with hindsight) before larger earthquakes in the highly seismic transform zone of the Mid-Atlantic Ridge onshore in SW Iceland. Consequently, it was only a question of time before a real-time stress-forecast could be made. Changes before an earthquake were recognized at three seismic stations in a 70km line in SW Iceland and stress-forecasts were issued to the Icelandic authorities on 27th and 29th October and on 10th November. The final forecast was that a  $M \geq 5$  earthquake could occur soon or a  $M \geq 6$  event before four months if stress continued to increase. Three days later, on 13th November 1998, a  $M=5$  earthquake occurred near the middle of the three stations where changes had been observed. Local investigations approximately identified the source location. Note that routine stress-forecasting for a vulnerable location, without such a high level of swarm activity, would require cross-well seismicity between deviated boreholes. We shall present the theory and assumptions for stress-forecasting earthquakes, and present the data for this first stress-forecast event.

ST1/E/81-A2

1640

## TOWARDS THE PREDICTION OF THE TOKAI EARTHQUAKE

Naoyuki Kato (Department of Environmental Geology, Geological Survey of Japan, Ibaraki, Tsukuba, Higashi, 1-1-3, 305-8567 Japan, email: nkato@gsj.go.jp); Shozo Matsumura and Shin-ichi Noguchi (both at Earthquake Research Center, National Research Institute for Earth Science and Disaster Prevention, Ibaraki, Tsukuba, Ten-nodai, 3-1, 305-0006 Japan, email: shozo@geo.bosai.go.jp; shin@geo.bosai.go.jp); Takeshi Sagiya (Geographical Survey Institute, Ibaraki, Tsukuba, Kitasato, 1, 305-0811 Japan, email:sagiya@gsi-mc.go.jp); Stefan Wiemer (Geophysical Institute, University of Alaska, Fairbanks, USA, email: stefan@giseis.alaska.edu); Akio YOSHIDA (Seismological and Volcanological Department, Japan Meteorological Agency, Tokyo, Chiyoda, Ote-machi, 1-3-4, 100-8122, Japan, email: akio.yoshida-a@met.kishou.go.jp)

Since 1976, when Ishibashi stated that the expected Tokai earthquake should be impending and advocated the necessity of countermeasures against the anticipated disaster, dense networks of seismographs, volumetric strainmeters, tiltmeters, extensometers, tide gauges and ground water monitors were deployed in the Tokai region. The various geophysical data are telemetered to the headquarter of JMA, and are continuously monitored. Because the expected Tokai earthquake is a great interplate earthquake, we think it is vitally important to elucidate the coupling state between the oceanic and the continental plates. So far we estimated the region where the two plates are strongly coupled by investigating the characteristics of the spatial distribution of source mechanisms and the hypocentral distribution of earthquakes in the subducted slab and in the upper crust. Moreover, it has now become possible to estimate changes of the back slip between the two plates using the data of GPS stations densely distributed in the Tokai region. Our strategy for a successful prediction of the Tokai earthquake is the following: First, we study the evolution of the interplate coupling state. Then, by comparing our estimate on the coupling state with the results of computer simulations of the subduction process, we try to estimate how far the plate interface has matured towards the occurrence of the Tokai earthquake. Finally, based on the evolving understanding of the coupling state, we endeavor to identify short-term precursors in real time.

ST1/W/54-A2

1700

## QUANTITATIVE TESTING WORLDWIDE SEVERAL EARTHQUAKE PREDICTION ALGORITHMS

Vladimir KOSSOBOKOV, Irina Rotwain, Olga Novikova, Inna Vorobieva, Leontina Romashkova (all at International Institute for Earthquake Prediction Theory and Mathematical Geophysics, Russian Academy of Sciences, 79-2 Warshavskoye Shosse, Moscow 113556, Russia, E-mail: volodya@mitp.ru)

We summarize our experience in predicting of large catastrophic earthquakes worldwide. Our approach is based on theoretical implications that come from non-linear dynamics of chaotic systems. The prediction algorithms were designed mainly by using generic pattern recognition methods. The predictions by such algorithms are completely reproducible and scale with the magnitude of the incipient earthquake. Their spatial accuracy is limited although could be improved significantly by additional analysis, in some cases, to the size of incipient earthquake as exposed by distribution of aftershocks. Their temporal accuracy is intermediate term, i.e. of the order of years. Although of limited accuracy, the predictions create a possibility to prevent part of the damage. The interface between prediction and preparedness is delivered by the recent development of optimal strategies based on a tradeoff between total volume of alert and rate of failures-to-predict. We briefly discuss a novel understanding of seismic process as an essential part of dynamics of a hierarchical system and outline how the predictions of the current limited accuracy could be implemented on practice.

ST1/E/89-A2

1720

## ANALYSIS OF SEISMICITY AROUND THE WESTERN KANAGAWA, CENTRAL JAPAN FOR EARTHQUAKE PREDICTION

Toshikazu TANADA (Hot Springs Research Institute of Kanagawa Prefecture, Iriuda 586, Odawara, Kanagawa, JAPAN (B0031; email: read35@mail.dddd.ne.jp)

It has pointed that the M7 class earthquake might occur in near future around western Kanagawa Prefecture, southwest Kanto district, central Japan and named after the place of this hypothetical earthquake as the "Western Kanagawa Prefecture Earthquake(WKPE)". In order to investigate the mechanism of WKPE, we have carried out continuous monitorings of seismicity and crustal deformation (borehole tilt meters, GPS and EDM instruments, groundwater levelling) since 1989, which covers the anticipated rupture zone estimated from historical data.

Analysis of seismicity are summarized as follows. (1)The cutoff depth of seismicity varies 6-16km from the center to the eastern flank of Hakone volcano. According to tomographic image, the relative low velocity zone extend to a depth 5-10km in this eastern flank, but high velocity zone to depth 10-15km. As large crustal earthquakes around volcanoes were reported to occur at the steeply changing zone of cutoff depth or in the periphery of low velocity zones in Japan, these relationship between seismicity and crustal structure are important to reveal the place where M7 class earthquakes might occur. (2)A seismic quiescence had been continued since the end of 1930's to early 1990's. But a remarkable seismic recovery has been recognized since the early 1990's with a successive occurrence of M4-5 earthquakes in the area surrounding the eastern flank of Hakone volcano. (3)In 77 years, the 1994 earthquake(M4.8) with focal depth of 6km occurred at the southern part of the Hakone volcano where Kita-Izu fault systems cross the somma. The focal area was clearly separated from the volcanic earthquake swarm area. As Hakone volcano is supposed to be a possible indicator of crustal stress, this event can be interpreted as caused by a stress increase with collision of the Philippine Sea plate. These analyses of seismicity would provide us with important information for forecasting crustal activity.

ST1/E/38-A2

1740

## MONITORING SEISMICITY IN THE TOKAI AND KANTO REGIONS OF JAPAN - THE SEISWATCH APPROACH

Kohji HOSONO, Kenji Maeda, and Akio Yoshida (Seismology and Volcanology Dept., JMA, Tokyo; e-mail: hosono@eqvol.kishou.go.jp); Shozo Matsumura and Shin-ichi Noguchi (Earthquake Research Center, NIED, Tsukuba, Japan); Stefan Wiemer (Institute of Geophysics; ETH Hoenggerberg, CH-8093, Zurich, Switzerland);

Modern seismic networks such as the JMA and NIED networks in Central Japan record tens of thousands of earthquakes every year. To continually and efficiently monitor this seemingly overwhelming stream of data we have designed an advanced seismicity analysis software package, SEISWATCH. The two primary objectives of our project are: (1) To monitor the health of the entire recording system by identifying artificially introduced changes in reporting and temporal changes in the magnitude of completeness; (2) To identify unusual patterns in seismicity which may be related to precursory processes. From numerical simulations and



selected case studies we expect characteristic anomalies in seismicity patterns, such as seismic quiescence and neighboring rate increases, to occur in the years to months before a large and potentially disastrous interplate earthquake. However, these precursory changes are likely to be spatially and temporally complex in appearance. We therefore regularly and automatically map several seismicity parameters in three dimensions and monitor the spatial and temporal variations of the seismicity rates in different magnitude bands, the magnitude of completeness, and the earthquake size distribution. By comparing the largely independently completed seismicity data sets of JMA and NIED in real time, we have a unique opportunity to identifying artificial rate changes in either catalog. In addition, having two independent data sets greatly improves the reliability of potentially observed precursors. SEISWATCH identifies anomalous patterns, establishes their significance in comparison to the background, and will send out automatic alert messages. SEISWATCH also provides an interactive interface to further analyze seismicity. Observed anomalous seismicity patterns are then interpreted in conjunction with the dense geodetic observations and with numerical simulations of the subduction process.

Wednesday 21 July AM

Presiding Chairs: D.Simpson, and S.Talebi  
Concurrent Poster Session

## TRIGGERED/INDUCED EARTHQUAKES

ST1/E/63-A3

0830

### PROBLEMS OF INDUCING SEISMICITY, CONTROLLED RELEASE OF TECTONIC ENERGY AND SEISMIC HAZARD REDUCTION

Alexei NIKOLAEV and Nikolai Tarasov (both at Joint Institute of Physics of the Earth, Bolshaya Gruzinskaya 10, 123810 Moscow, Russia, email: alex@nikavs.msk.su)

Influence of underground nuclear explosions and powerful electric pulses on seismic flow shows that during the very last period of the strong earthquake preparation process, source zone is getting more and more sensitive to external impacts of different nature. This create a favorable conditions for triggering strong earthquakes using controlled seismic and electric sources like explosions, powerful seismic vibrators and electric generators.

The other way is to initiate systematically an activity of weak and moderate earthquakes to speed up the release of tectonic energy and mitigate the magnitude of strongest earthquakes. The regime of artificial impacts on the Earth crust must be in concordance with natural processes like Earth tides, changes of atmospheric pressure, variations of the Earth rotation speed and others.

Problem of controlled release of tectonic energy and seismic hazard reduction is realistic both from point of view of specific instruments - powerful seismic vibrators and electric generators which are already designed, and from point of view of theoretical and experimental experience. It should be one of central seismological problems of the next century.

ST1/W/58-A3

0850

### INDUCED SEISMICITY IN THE NETHERLANDS; ROSWINKEL A CASE STUDY

Bernard DOST, Hein Haak (KNMI, Postbus 201, 3730 AE De Bilt, the Netherlands)

Since 1992 the region around Roswinkel (Dr.) experienced 23 earthquakes of magnitudes between 0.8 and 3.4. Most locations and magnitudes are determined using a network of 8 borehole seismograph stations in operation since 1995. The depth of these earthquakes is 2 km and their origin is related to local gas exploitation. Since waveforms of all events show a high correlation at each seismograph station, a high resolution technique of relative locations could be applied.

The last five events were recorded in a triangular network of accelerometers, installed in the region in 1997, 2-4 km from the epicenter. These data enable an absolute high resolution location and relative locations could be anchored. The recorded peak horizontal accelerations for the largest event amounts to 0.3g at a dominant frequency of 10 Hz. This last event caused damage to buildings in the region. Results will be shown of a magnitude calibration within the region, determinations of relative locations and source parameters of events around Roswinkel.

ST1/W/10-A3

0910

### CHANGES IN EFFECTIVE STRESS DUE TO DIFFUSION OF METEORIC WATER - LARGE ENOUGH TO TRIGGER EARTHQUAKES?

Malte WESTERHAUS, Birger-G. Luehr, Jochen Zschau (all at GeoForschungsZentrum Potsdam, Telegrafenberg, Haus E, 14473 Potsdam, Germany, email: tilt@gfz-potsdam.de)

Data sets from the interdisciplinary Turkish-German Project on Earthquake Research indicate that the state of deformation along a 200km long segment of the North-Anatolian Fault Zone is not stable over time. A dominant feature of various (quasi-) continuously recorded parameters and derived transfer functions, including microseismic activity, are variations with annual periodicity. We assume that these variations are induced by pore pressure disturbances that are caused by the annual recharge of groundwater and propagate downwards by diffusion. The relation between the tectonic loading rate as obtained from geodetic measurements, and the background seismicity gives the opportunity to check whether the small annual changes in crustal stress/strain are sufficient to induce earthquakes. Taking stream flow as a measure of the pressure time function at the surface, pore pressure transients at depth are calculated. Units of stream flow are converted into units of pressure by a linear regression to variations in the hydraulic head of a confined aquifer. A phase lag of 5 months exists between the rate of the surface water input and variations of microseismic activity. With a mean hypocentral depth of 8 km, the best fitting pore pressure curve at depth yields a hydraulic diffusivity of 0.75 sq.m/s, which is close to the results obtained from studies on reservoir induced seismicity and hydroseismicity elsewhere. The pressure amplitude variations in this depth correspond to about 12% of the tectonic strain rate. Assuming that seismicity is a function of strain rate, the hydrologically induced changes in strain could explain 40% of the observed annual rate changes in the microseismic activity. We conclude that the crust might be in a critical condition, and even small changes in the state of deformation potentially have a strong influence on its physical properties.

ST1/W/51-A3

0930

### SCALING RELATIONSHIPS FOR INDUCED SEISMICITY IN THE FREQUENCY BAND 1-250KHZ

Will PETTITT, James Hazzard, R. Paul Young and Dave Collins, The Department of Earth Sciences, Keele University, Staffordshire, UK. Email: w.s.pettitt@keele.ac.uk

We investigate the scaling relationship between high-frequency acoustic emissions (AEs), at frequencies between 30 and 250KHz and lower frequency microseismic events (MS) at

frequencies between 1 and 10KHz. Induced seismicity data from the Underground Research Laboratory (URL) in Canada are used for this investigation. At the URL, similar volumes have been monitored from grain boundaries to induced microcracks and fractures. We have analysed AEs occurring in very tight spatial and temporal clusters. Each cluster is associated with failure along a fracture plane and is coincident with a much more energetic MS event. The source mechanics of both the MS event and AEs have been analysed using a moment tensor inversion technique allowing a comparison of the mechanics of failure observed on the same fracture but at widely different source scales. Dynamic numerical modelling has been used to model the failure process and has been related to the in situ results. The models simulate blocks of granite made up of thousands of individual particles bonded together at points of contact. This micromechanical modelling approach allows for a direct comparison between small-scale AEs, associated with individual bond breakage, and larger scale ruptures caused by the interaction of these. It is found that the AEs show similar mechanics to the MS events even though the MS events exhibit a much larger magnitude and source dimension. Larger scale failure is shown to be an interaction of much smaller failure on the same fracture. It is proposed that the AEs are created as the fracture plane weakens preceding an MS event and then occur afterwards as the fracture returns to equilibrium.

ST1/E/75-A3

0950

### EVALUATION OF FAILURE MECHANISMS FOR MINING INDUCED MICROSEISMICITY

C-I. TRIFU, V. Shumila, and T.I. Urbancic (Engineering Seismology Group Canada Inc., 1 Hyperion Court, Kingston, ON, Canada, K7K 7G3)

Moment tensor inversions are calculated for over 100 microseismic events ( $M = -2$  to 0) recorded at Kidd Creek Mine, Ontario, based on time domain equivalent low-frequency spectral displacements and first motion polarities as determined from wave energy functionals (P- and S-waves) and polarization criteria (S-waves). The mine has an underground 64 channel microseismic array, including 8 triaxial accelerometers located within 200 x 200 x 300 m volume at depth. Previous studies have shown that failure mechanisms can be robustly evaluated from 6 to 8 triaxial recordings. This study, consisting of work in progress, attempts to analyze the relationship between the shear and tensile components of failure and the presence of large fault structures at depth. The dependence of source parameters (e.g., source radius, Es/Ep, stress release, seismic efficiency) on resulting failure mechanism is also studied. Finally, the possibility of using the above approach for the automatic characterisation of event mechanisms is investigated.

ST1/E/67-A3

1010

### STUDY OF WATER LEVEL CHANGES IN DEEP BORE WELLS IN SEISMICALLY ACTIVE KOYNA-WARNA REGION OF WESTERN INDIA

R K CHADHA, H K Gupta (both at National Geophysical Research Institute, Uppal Road, Hyderabad-500 007, India, email: postmat@csngri.res.nic.in), H J Kumpel (University of Bonn, Nussallee 8, D-53115,Bonn, Germany, email: kuempel@geo.uni-bonn.de), I.Radhakrishna and Subhash Kushwaha (both at National Geophysical Research Institute, Uppal Road, Hyderabad-500 007, India)

Twenty one bore wells were drilled in the seismically active Koyna-Warna region in western India to study causal relationship between water level fluctuations in the wells and earthquake occurrences in the region. A clear steplike change of the order of 3 to 7 cm was observed after an earthquake of M 4.4 on April 25, 1997, 5 km from two observation wells situated within the active seismic zone, identified in this region. The influence of earth tides, barometric pressure, rainfall and groundwater exploitation on the observed water level change was considered to rule out nontectonic causes related to this earthquake. Since most of the wells which are being monitored respond to earth tides, they are considered sensitive indicators to crustal strain and hence to tectonic strain due to earthquakes. Long-term monitoring of these wells thus provides useful input to identify the possible medium and long term precursors for earthquakes. In this paper, we present the water level data from the observation wells in Koyna-Warna region and discuss tidal, barometric and earthquake related signatures.

Presiding Chairs: G.A. Sobolov (United Institute of Physics of the Earth, Moscow, Russia), J. Zschau (GFZ Potsdam, Germany)

## SPACE-TIME PATTERNS OF SEISMICITY AND RELATED FIELDS

ST1/E/17-A3

1050

### THERMAL WATERS MONITORING OF THE 1997-1998 CENTRAL ITALY SEISMIC SWARM

G. MARTINELLI (Regione Emilia Romagna, Serv. Cartogr. e Geologico, v.le Silvani 4/3, 41100 Bologna, Italy); email: gmartinelli@mo.nettuno.it F. Italiano and S. Francofonte (both at Istituto di Geochimica dei Fluidi, C.N.R., via U. La Malfa 153, 90146 Palermo, Italy); Email: italiano@igf.pa.cnr.it P.M. Nuccio (Dipartimento C.F.T.A., Università di Palermo, via Archirafi 36, 90123 Palermo, Italy).

A seismic sequence struck Central Italy starting on September 26, 1997. The sequence began on September 4 with a MI 4.4 foreshock and some of the following earthquakes were characterized by magnitudes between 5 and 6. A possible clue of the reactivation process is also recognizable in a seismic swarm occurred at about 40 Kms. during May 1997. On the basis of previous studies the May 1997 swarm renewed the interest on chemically and thermally anomalous waters of Umbria Region and allowed the collection of samples before the September 1997 swarm. Thermally and chemically anomalous spring waters were collected in previously identified sites during the period 1997-1998. Seismogenic process influenced chemical composition and temperature of thermal waters allowing to distinguish anomaly patterns induced by seismic events occurred at different depths. Analytical patterns recognized in local gaseous emissions support the hypothesis that changes in crustal permeability occurred. Crustal permeability changes were found influenced by focal mechanism and/or depth of seismic events. Possible precursory geochemical patterns are discussed.

ST1/W/57-A3

1110

### MONITORING OF FAULT MOVEMENTS BY USE OF MICROEARTHQUAKES

Ragnar SLUNGA (Dep. of Earth Sciences, Uppsala University) Reynir Bodvarsson (Dep. of Earth Sciences, Uppsala University) Bjorn Lund (Dep. of Earth Sciences, Uppsala University)

Fault slip may be stable and not only unstable as in earthquakes. The commonly observed time clustering of microearthquakes, often over distances large compared to the earthquake sizes, is probably sometimes related to deformation expressed by stable brittle aseismic slip on faults. The SIL system produces absolute and high accuracy relative locations for selected groups of events. Fault plane solutions and dynamic source parameters for all detected microearthquakes are estimated in near-real time (within a few minutes of the earthquake). Based on both the

relative locations and the fault plane solutions one can conclude on which fracture the earthquake slip occurred. This makes it possible to monitor the movements of the faults and fractures, identified by the multievent locations if detectable microearthquakes are generated by the fault slip. This is one of the ideas behind the PRENLAB project, as it has been suggested that slip weakening may be important in the geomechanical process leading to major earthquakes. This means that in such cases a major earthquake will be preceded by a phase of accelerating stable fault slip. If this slip is indirectly detected and followed by the microearthquake activity it opens a possibility for earthquake warning before a major earthquake. Examples of this analysis will be given in this presentation. The results support the well known observation that fault slip on part of a fault increases the probability for slip on neighboring parts ("domino" effect).

ST1/W/24-A3

1130

#### QUANTITATIVE REPRESENTATION AND EVALUATION OF SEISMIC ACTIVITY AROUND ACTIVE FAULTS

Ryohei NISHIDA, Jun'ichi Ozaki, Michiru Asai (these at Faculty of Engineering, Tottori Univ., Koyama-cho, Tottori, Japan, e-mail: nishidar@cv.tottori-u.ac.jp), Kunihiko Watanabe, Yukihito Imada (both at Disas. Prev. Res. Inst., Kyoto Univ., Gokasho, Uji, Japan)

A quantitative method for evaluating seismic activity along active faults is proposed. By applying GIS, an objective evaluation of the seismic activity of the fault can be done without difficulty. (A) How widely an active fault affects the seismic activity of its surrounding area. Procedure is as follows: 1)  $S_i$  is defined as the area whose distance from the fault ranges from  $i-1$  to  $i$  kilometers.  $R_i$  (= km, discrete value) is defined as the representative distance of area  $S_i$ . 2)  $E_i$ , whole seismic energy released in  $S_i$  area, can be obtained. 3)  $D(R_i)$ , defined by  $E_i/S_i$ , is the seismic energy density of area  $S_i$ .  $D(R_i)$  is a function of  $R_i$ . 4)  $R_e$  is defined as the distance that  $D(R_i)$  first becomes to be independent of  $R_i$ .  $R_e$  is the important value that the influence of the fault reaches. As a result,  $R_e$  values of active faults in southwestern Japan are ranging from 3 to 6 km, not depending on the fault length. Namely, active faults generate seismic activities in the area less than 6 km from the fault. (B) Quantitative evaluation of seismic activity of an active fault zone. Earthquake generating capabilities of active faults can be evaluated by comparing seismic energy density  $D(R_i)$ . We obtained  $D(R_i)$ s of more than 20 active faults in southwestern Japan and b-values of G-R's of these areas. This analysis is carried out by considering fault types, magnitude ranges and hypocenter depths. This method can be used as an objective parameter which represents the seismo-generating capability of an active fault. Furthermore, it may represent the condition of tectonic stress accumulation of an active fault zone.

ST1/W/39-A3

1150

#### ABOUT NATURE OF CALDERA LONG VALLEY (NORTH CALIFORNIA)

V.I. LYKOV, A.O. Mostryukov, V.F. Ruban (Geophysical observatory Borok, Branch of the United Institute for the Earth's Physics, RAS.)

The authors developed a method for assessment the rigidity of seismoactive rock massifs according to a primary type of seismogenic destruction. Background seismicity was used as a source of information. In present work the method has been tested on an object which is a magmatic epicentre. Monitoring of its activity is conducted by geodasical, hydrochemical and seismic measurements.

ST1/W/26-A3

1210

#### SEISMICITY PATTERN DYNAMICS FOR CALIFORNIA FAULT SYSTEMS

K. F. TIAMPO, J. B. Rundle and S. J. Gross (all at CIRES, University of Colorado, Boulder, CO, USA; Email: kristy@fractal.colorado.edu); W. Klein (Dept. of Physics, Boston University, Boston, MA)

The California fault system demonstrates complex space-time seismicity patterns that include repetitive events, precursory activity and quiescence, as well as aftershock sequences. Our research suggests that a new pattern dynamic methodology can be used to define a unique, finite set of seismicity patterns for a given fault system. Similar in nature to the empirical orthogonal functions historically employed in the analysis of atmospheric and oceanographic phenomena (Preisendorfer, 1988), this method derives the eigenvalues and eigenstates from the diagonalization of the correlation matrix using a Karhunen-Loeve expansion (Fukunaga, 1990). This pattern dynamic technique has been successfully applied to the study of numerically modeled seismicity for fault networks similar in character and extent to those found in California (J.B. Rundle, et al, submitted to Phys. Rev. E, 1998). We implement this same methodology in order to analyse historical seismicity in California in an attempt to derive space-time eigenvalue patterns for the San Andreas fault system. The data has been converted to recognized fault segments for central and southern California. The significant eigenstates for this relatively short period of time can be directly correlated with the known California faults and associated events.

ST1/E/45-A3

1230

#### SPATIAL-TEMPORAL-ENERGY CHARACTERISTICS OF SEISMICITY OCCURRING DURING THE SEISMIC CYCLE: A REAPPRAISAL

Omar J PEREZ, (Dpt. Earth Sciences, Simon Bolivar University, Baruta, Apdo. 89000, Caracas 1080A, Venezuela, e-mail: ojperez@usb.ve)

We analyze the spatial-temporal-energy distribution of seismicity ( $M_s > 6$ ;  $h < 70$  km) occurring in the focal and adjacent regions of all the eleven great ( $M_w > 7.8$ ;  $M_o > 5 \times 10^{20}$  N-m) pure shallow thrusting interplate events that occurred along simple plate boundaries in the Circum-Pacific from 1985 to 1997, in the decades preceding and following every main shock. For this purpose we revised and constructed a new world seismicity catalog (1950-1997;  $M_s > 6$ ;  $h < 70$  km) by removing a series of heterogeneities in the earthquake reporting and magnitude determination through time (Perez, O. J., Bull. Seism. Soc. Am., 1999, in press), including a heavy overestimation of the  $M_s$  assigned to shocks in the range  $6 < M_s < 7$  in the period 1950 to 1963, with respect to the  $M_s$  calculated since 1964. This new catalog lists nearly all and only those shallow shocks with  $M_s > 6$  that occurred in the world since 1950. Our findings indicate that, contrary to what predicted by the seismic gap theory, significant seismic activity occurs inside or close to the rupture of a forthcoming great shock during many decades prior to it, whereas little or no activity occurs in the adjacent segments of the plate boundary. Observations corresponding to two complete seismic cycles in the period 1950-1997 in the Kurile Is. (1969-1994; 1963-1991/95) indicate that this significant ( $M_s > 6$ ) activity is fairly continuous or random in time and takes place during large portions of the cycle. In some cases a small period of quiet is observed prior to the main shock. It appears that those seismic gaps showing significant activity for many decades are more likely to break in the near future than those not showing it. Finally, we also observe that also contrary to the seismic gap theory, the main epicentral regions of giant ( $M_w > 8.5$ ) shocks are in general the location of events with  $M_w = 7$  to 8, in the decades following their occurrence.

#### SPACE-TIME PATTERNS OF SEISMICITY AND RELATED FIELDS

ST1/W/28-A3

1400

#### THE EARTHQUAKE: A CRITICAL, PREDICTABLE PHENOMENON

Frank EVISON (Institute of Geophysics, Victoria University of Wellington, P.O.Box 600, Wellington, New Zealand, email: Frank.Evison@vuw.ac.nz) David Rhoades (Institute of Geological & Nuclear Sciences, P.O.Box 30-368, Lower Hutt, New Zealand, email: d.rhoades@gns.cri.nz)

A three-stage model of seismogenic faulting - crack formation, fracture and healing - represents a major earthquake as part of a complex, long-term seismicity anomaly. Within the affected space, conditions of self-organised criticality are maintained on a medium scale during the seismogenic process, compared with a small scale before and after. The process begins with a major crack formation, which activates a medium-scale fractal set of faults, and raises the level of seismicity accordingly. Earthquake triggering is also facilitated, producing swarm-like anomalies of seismicity, interspersed with relative quiescence. The completion of this episode of medium-scale faulting satisfies Mogi's uniformity criterion, and enables the large-scale earthquake to occur. This occurrence again activates a medium-scale fractal set of faults, and aftershocks occur in rapid sequence, triggered both by the mainshock and by one another. Finally, the scale of seismicity reverts to the original low level. Observed occurrences of the long-term seismicity anomaly are well displayed by the cumag statistical technique, which is a form of the cusum technique, modified to indicate magnitudes. Both sets of medium-level earthquakes are closely related to the mainshock. Thus the precursor set is a long-range predictor of the mainshock, with respect to location, time and magnitude, just as the mainshock is a short-range predictor of the set of aftershocks.

ST1/W/44-A3

1420

#### WHAT PARAMETERS CONTROL THE RECURRENCE INTERVALS FOR GREAT SUBDUCTION EARTHQUAKES?

MASATAKA ANDO and Sou Nishimura (Disaster Prevention Research Institute, Kyoto University, Uji, Kyoto 611-0011, Japan email: ando@recep.dpri.kyoto-u.ac.jp)

Along the Nankai trough of subduction boundary between Philippine sea plate and Eurasian plate, off the coasts of Honshu and Shikoku, Japan, great subduction earthquakes ( $M > 8$ ) occurred with an interval of about 100 years. We found 10 great earthquakes in historical documents in past 1300 years. The seismic coupling rate, seismic moment release relative to the relative plate motion along the subduction boundary, is calculated to be 70 to 100% for the area between 132E and 139E, estimated from the recent GPS observation. However, the seismic coupling rate suddenly decreases at 132E from east to west. The seismic rate east of 132E is estimated to drop down to 10 % from the analysis of GPS displacement and the recurrence intervals of subduction earthquakes. A remarkable difference between the tectonic boundary is found in seafloor sediments on the subducted slab: muds are dominant to the west and coarser volcanic sediments to the east. The sediments in the seismogenic zone may control the seismic coupling of the inter plate earthquakes. This is due to Kyushu-Palau ridge, occupying in the western Philippine sea plate, meets obliquely with the subduction boundary at around 132E. It plays a role of a barrier for separating the sedimentary basins.

ST1/W/22-A3

1440

#### AFTERSLIP FOLLOWING THE 1978 MIYAGI-OKI, NORTHEAST JAPAN, EARTHQUAKE REVEALED FROM TIDE-GAUGE AND LEVELLING DATA

Hideki UEDA, Masakazu Ohtake and Haruo Sato (Graduate School of Science, Tohoku University, Aoba-ku Sendai 980-8578, Japan, email: ueda@zisin.geophys.tohoku.ac.jp)

The Miyagi-Oki earthquake of June 12, 1978 ( $M=7.4$ ) ruptured a portion of the plate boundary of the subducting Pacific plate in the region east off northeastern Honshu. Based on the analysis of tide-gauge observation and precise levelling data, we found a significant post-seismic crustal deformation following the earthquake. The post-seismic deformation, which lasted at least 4 years, is successfully interpreted by the occurrence of aseismic afterslip following the main shock. Our inversion analysis indicates that the area of afterslip nearly coincides with the main shock fault plane, but the afterslip area is further extended to shallower portion of the plate boundary. The total moment release including the afterslip amounts to  $5 \times 10^{20}$  Nm, which is roughly twice the co-seismic moment release. Similar afterslip have been reported for the 1994 Sanriku-Oki earthquake ( $M=7.5$ ), and two other large earthquakes which occurred to the north of the 1978 Miyagi-Oki earthquake. These observations suggest that the occurrence of large afterslip may be a common nature for the subduction plate boundary in the northeastern part of Japan.

ST1/E/14-A3

1500

#### POSSIBLE SEISMICITY AND ELECTRICAL EARTHQUAKE PRECURSORS IN A SOC SYSTEM: THE 17-1-1983, M7 KEFALLINIA EVENT, GREECE

A. TZANIS, K. Makropoulos (both at Dept. of Geophysics & Geothermy, Univ. of Athens, 157 84 Zografou, Greece, E-mail: atzanis@atlas.cc.uoa.gr) and F. Vallianatos (Technological Educational Inst. of Crete, Chania Branch, Crete, Greece, E-mail: fvallian@teihn.gr)

A characteristic signature of the earthquake preparation process, (assuming it is a self-organised critical point system), is power-law acceleration in regional seismic energy release strongly diverging towards the main event. In a SOC system this would include all scales of fractures. At the very terminal phase, a crack propagation avalanche may be expected, after which the system has reached the critical point and instability is imminent. The time function of crack propagation processes may be modelled with a limited class of characteristic transient bay-like shapes, featuring a corner frequency and inverse power energy distribution law. Electrification processes due to crack propagation may generate electrical precursors with similar characteristics. Such phenomena may have preceded the  $M7.1$ , 17-1-83 Kefallinia earthquake. These included stable and persistent increase of the regional b-values, indicating changes in the stress state of the crust via long range interactions, reversing immediately after the event. A power law acceleration of seismic release was also observed, which could be modelled to yield a time-to-failure of 1983.0. On 15-1-83 a transient ULF electrical signal was independently observed approx. 120km from the epicentre, consistent with the crack propagation model above. The aftershock sequence was also associated with a number of (alleged) electrical precursors following a fractal-like amplitude-magnitude relationship, which may theoretically be shown to result from the fractal geometry of their sources. In this case, a set of diverse 'precursors' could be accommodated within the model of SOC crustal processes. We discuss whether the same may be possible in the general case.



ST1/E/83-A3

1520

**THE LIMITATION OF H/V RATIO IN ESTIMATING THE SITE RESPONSE OF LAYERED MEDIUM**

Hung-Chie CHIU, (Institute of Earth Sciences, Academia Sinica, P.O. Box 1-55 Nankang, Taipei, Taiwan, R.O.C., email: chiu@earth.sinica.edu.tw); Ta-liang Teng (Department of Earth Sciences, University of Southern California, Los Angeles, CA 90089-0740, email: lteng@codu.usc.edu); Xiaofei Chen (Department of Geophysics, Peiking University, Beijing, China, email: xfchen@pku.edu.cn)

Spectral ratio between horizontal and vertical components (H/V ratio) has been widely applied to site response estimation recently. However, the physical basis behind this ratio is still unclear. Furthermore, most studies indicated that the H/V ratio only can predict the fundamental resonant frequency but very few researchers claimed that this ratio could estimate the amplification factor. Although many researchers have attempted to verify this method, none of them have fully explored this problem. This paper presents an extensive analysis of the H/V ratio and gives one possible approach to verify the controversial assumptions that made for developing the H/V method. We also give a reasonable explanation to the observations. According to our analyses, the H/V ratio can well estimate the fundamental resonant frequency for a simple layered model with a simple source, and this method may fail in all other cases because of noise, multi-layered-medium or complicate-source effects. Numerical validation based on synthetic seismograms also supports our assessment.

ST1/W/17-A3

1600

**NONRANDOM PATTERNS IN THE OCCURRENCE OF THE WORLD STRONGEST EARTHQUAKES**

W. MARZOCCHI (Osservatorio Vesuviano, Via Manzoni 249, 80123 Napoli, ITALY)

For a long time, the spatiotemporal independence of the world largest earthquakes was a paradigm in seismology. Even if in the last years some researchers raised doubts on its validity and suggested the existence of triggered seismicity at great spatiotemporal distances, the lack of convincing and statistically significant phenomenological evidence lead to a long standing scepticism about this issue.

The aim of this work is to fill this gap by searching for non-random patterns in the occurrence of the strongest shallow earthquakes of this century. A new multivariate approach, which simultaneously accounts for the spatial and temporal aspects of the earthquakes occurrence is developed.

The results indicate that the strongest earthquakes do not occur randomly. Besides to influence the seismicity at small distance and time, the strongest events extend their reach even to 5000-10000 km, and 20-25 years later. These non-random patterns have a very low probability to be observed by chance. This behaviour is discussed and interpreted in terms of the post seismic stress transfer through a viscous asthenosphere in a planet lying in a critical state. This result provides new insights, which could be profitably used, at least in principle, in the seismic risk mitigation of many areas of the world.

ST1/E/46-A3

1620

**SOURCE PARAMETERS AND AFTERSHOCK CHARACTERISTICS OF THE 1997 STRONG EARTHQUAKES IN GREECE**

G.N.STAVRAKAKIS (Institute of Geodynamics, National Observatory of Athens, 11810 Athens, Greece, E-mail: g.stavr@ege.lados.gein.noa.gr); N. Voulgaris (University of Athens, Dept of Geothermy and Geophysics, Athens, Greece); G.Chouliaras and G. Drakatos (both at the Institute of Geodynamics, National Observatory of Athens, 11810 Athens, Greece)

In 1997, strong seismic activity took place in different seismotectonic regions of Greece (13-10-1997, Ms=6.6 in southern Greece; 5-11-1997, Ms=5.6 in Central Greece; 14-11-1997, Ms=5.8 in the northeastern Aegean Sea; 18-11-1997, Ms=6.4 in the Ionian Sea). Broadband waveforms recorded by the IRIS network for these main shocks, have been used to compute the far-field displacement spectra and the source parameters (fault dimensions, stress drop, seismic moment, average displacement and seismic energy). In addition digital short period waveforms recorded by the Greek National Seismographic network have also been analysed and the computed source parameters are compared to those computed from the broadband data. The relationship of the seismic source parameters and the aftershock pattern regarding its spatial and temporal characteristics is also investigated.

ST1/E/52-A3

1640

**SEISMOTECTONIC DEFORMATIONS ON THE REGION TAVR-CAUKASUS**

GYODAKYAN Naira, (Institute of Mechanics, Moscow State University, I chourinskiy ave, Moscow, Russia), GYODAKIAN Eduard, (Institute of Geophysics and Engineering Seismology of the National Academy of Sciences of the Republic of Armenia, Leningradian 5, Giumry, 377515 Armenia)

In the present work the seismotectonic processes connected with the unelastic deformations arising in the Earth's crust large blocks on areas of strong earthquakes are examined. On a basis of the analysis the knowledgements about the seismic flow of mountain mass are fixed. The estimation of deformation processes is done by the data of focal mechanisms of the strong earthquakes taken place on investigated region for the period from the period from 1970 to 1996. In this work the analysis of deformations relative speed is carried out using the tensor of seismic moments, of occurring on the investigated region strong earthquakes. Components of deformations and deformations speeds are determined both for region as a whole and for separate elements with the equal area on the Earth's surface. The intensity of deformations and speed of deformation are calculated as well as the class of the environment tense condition for separate elements. It is revealed the orientation of the main axes of deformation tensor is various for different elements that testifies to the complicated geodynamic structure of the region under investigation.

ST1/E/70-A3

1700

**SEISMICITY VARIATIONS UNDER ELECTROMAGNETIC IMPACT USING MHD-GENERATOR**

N.T.Tarasov and N.V.Tarasova (both at Joint Institute of Physics of the Earth, Russian Acad. Sci., 10 Bol. Gruzinskaya Str., Moscow, 123810 Russia, E-mail: tarasov@uipe.uas.ru)  
A.A.Avagimov and V.A.ZEIGARNIK (both at Institute for High Temperatures - Association, Russian Acad. Sci., 13/19 Izhorskaya Str., Moscow, 127412 Russia, Email: zeig@termo.msk.su)

The analysis is presented of the seismicity variations within a seismoactive region of the Northern Tien Shan and adjacent areas; the variations are connected with the impact of high-power electrical pulses produced by MHD-generator. The data are engaged of long-standing

earthquake prediction monitoring based on regular deep electrical soundings by high-power single pulses. Pronounced spatial and temporal variations of the seismic regime are detected; after the MHD-runs, the seismicity level (in terms of quake number) becomes distinctly higher than the same before the runs. The total energy release in the form of weak earthquakes after all 85 runs is estimated to be 5-6 orders of magnitude more than the total energy inserted by the MHD-generator into its load. Instant seismicity activation occurs on the 2nd-4th day after the run and lasts for several days. The most distinct is the effect within the upper 5-km layer of the earth crust. The results obtained are similar to those for a seismoactive region of Pamirs. The electromagnetic impact serves as a trigger initiating the seismic energy release, which is accumulated in the media during the tectonic processes.

The principal result lies in the possibility of controlled external impact on natural seismic process and triggering the release of accumulated energy in the form of relatively weak quakes. The possible physical model of the phenomenon is under discussion.

ST1/P/13-A3

1720

**RESEARCH ON TEMPORAL AND SPATIAL DISTRIBUTION, EVOLUTIONARY CHARACTER AND MECHANISM OF CRUSTAL DEFORMATION FIELD BEFORE AND AFTER THE TANGSHAN EARTHQUAKE**

Shuoyu ZHOU, Shunying Shi, Ping Shuai (all at Institute of Seismology, China Seismological Bureau, Wuhan, 430071, China)

According to the data of precise releveling and deformation measurement across faults, the temporal and spatial evolution process of crustal deformation field in the focal and peripheral regions of the Tangshan earthquake (1976, Ms=7.8), from 22 years before the earthquake to 9 years after, is described with the method of crustal deformation pattern dynamics. The crustal unstable zones first occur in the exterior, and then surround the focal region by contracting from the exterior to the interior, when the focal region appears to be unstable but does not lose stability. After the transient stable state, the second unstable process from the exterior to interior appears, which results in the instability of focal region. "Deformation gap", "earthquake gap" and "locked fault zone" occur before instability, and their spatial distribution overlap, but their occurrence times have little difference. The earthquake occurs after the impending pre-slide of the faults in the focal region. The studied results of the evolution process of crustal deformation field are identical with each other and with that of numeric simulation of crustal stress field, which supports the evolution model of seismogenic system with a strong body as its core.

ST1/W/13-A3

1740

**FORESHOCK DISTRIBUTION OBTAINED BY SYNTHETIC SEISMICITY BASED ON A STATISTICAL MODEL**

Kenji MAEDA (Meteorological Research Institute, 1-1, Nagamine, Tsukuba, 305-0052, JAPAN; e-mail: kmaeda@mri-jma.go.jp); Rodolfo Console (Istituto Nazionale di Geofisica, Via di Vigna Murata, 605, Rome, ITALY; e-mail: console@ing750.ingrm.it); and Yasuhiro Yoshida (Meteorological Research Institute, 1-1, Nagamine, Tsukuba, 305-0052, JAPAN; e-mail: yyoshida@mri-jma.go.jp)

It is well known that the space-time distribution of foreshocks obtained by superposing many foreshock-mainshock pairs within a few days before a mainshock shows that the number of foreshocks increases acceleratively as the time and the location approach a mainshock (e.g. Jones, 1985). Two different explanations are possible to interpret the distribution (Maeda, 1999). The first one is that the accelerative increase of instability or stress in the region causes the accelerative increase of foreshocks, and the other one is that a foreshock is the cause of a stress change in the region and it triggers a mainshock. The second explanation, which may be a little hard to understand, is compatible with the relationship between a mainshock and aftershocks, when an aftershock happens to become larger than the mainshock. To show the second explanation more explicitly, we analysed the synthetic seismicity data produced by a statistical model (Console, 1998). The statistical model used in this study assumes a random occurrence of events with the Poisson distribution and an induced seismicity with a circular normal space distribution and the Omori time distribution, combined with the Gutenberg-Richter frequency-magnitude distribution. Note that the model does not assume an increasing time distribution before an event. The results show that the synthetic data also exhibits the accelerative increase of time distribution of superposed foreshocks.

Tuesday 20 July AM

Presiding Chairs: D. Booth, D. Rhoades (Inst of Geological and Nuclear Sciences, NZ)

QUANTITATIVE TESTING OF HYPOTHESES OF PERCURSORS

ST1/E/60-A2

Poster

0930-01

**POTENTIAL PRECURSORS OF 1998 ZHANGBEI M=6.2 EARTHQUAKE IN CHINA**

QI-FU CHEN (P. O. Box 166, Center for Analysis and Prediction, China Seismological Bureau, Beijing 100036, P. R. China, email: cqf@ip.cap.ac.cn)

The 1998 Zhangbei M6.2 earthquake occurred on northwest of Beijing on January 10 with 49 death and 816 million RMB losses. Its focal mechanism shows a NNE-striking right-lateral faulting or EW-striking faulting at a depth of 10 km. There are some potential precursors are identified from various earthquake-monitoring networks in north of China for the Zhangbei earthquake. A swarm event with magnitude 4.0 which belongs to breaking out earthquake occurred in Beijing on Dec. 16 of 1996 maybe a symptom for a magnitude 6 or above in a future. Then an isolated earthquake with magnitude 4.2 occurred in Zhangjiakou on May 25 of 1997. The interval of earthquake quiescence with ML $\geq$  4.0 in north of China is beyond 90 days found on Dec. 31 of 1997. The quiescence is also identified by SEISMOLAP. The water table of Wuliying located on Beijing showed notable anomaly, which maybe classified into medium and short-term precursory variation. It is also observed other anomaly variations of CO<sub>2</sub> and electromagnetic radiation from Huailai station, and ground tilt from Chicheng station. Specially, there are clear demarcation lines of shift time from the lowest Z-value in geomagnetic stations around China on Dec. 17, 18 and 19 in 1997.

Those potential precursors were examined with long term data. The probability increase of earthquake occurrence is tens with those potential precursors. It is very difficult, even now, to make an exact prediction for this earthquake with those potential precursors, especially for its location. The reason is that the earthquake occurred in the Tertiary basaltic region without recognized active faults.

ST1/W/38-A2

Poster

0930-02

**APPLICATION OF TIME-TO FAILURE MODEL TO PRECURSORY SEISMIC ACTIVATION ON KAMCHATKA AND IN ITALY**

R. Di Giovambattista (Istituto Nazionale di Geofisica, Via di Vigna Murata, 605, I-00143 Roma, Italy. E-mail: digiovam@mare.ingrm.it); G.A.Sobolev (Institute of the Physics of the Earth, B/Gruzinskaya 10 123810 Moscow, Russia. E-mail: sobolev@uipe-ras.scgis.ru.); Yu. S.TYUPKIN (Geophysical Center, Molodezhnaya 3, 117296 Moscow, Russia E-mail: tyupkin@wdch.ru)



Suppositions that potential sources of earthquakes form a fractal manifold and that the process of seismic release is accelerated before a strong earthquake and is concentrated in the neighborhood of its hypocenter lead to a time-to-failure model of precursory seismic activation. Log-periodic time-to-failure model is used for analysis of a process of a strong earthquake preparation. A cumulative sum of square root of seismic energy  $Q(t)$  of events preceded time  $t$ , is used for the study. Log-periodic term is considered as perturbation. The application of the model to a retrospective precursory seismic activation on Kamchatka and in Italy give a scattering of predicted time of main shocks from few days to a half of year and an error of predicted energy class  $<0.5$ . A real time application of the model for prediction of strong earthquake is labored if the location of predicted event is unknown. The model may be useful in combination with other earthquake prediction approaches. The work was supported by Russian Basic Research Foundation.

**ST1/W/48-A2** Poster **0930-03**

**ANALYSIS OF NON-TYPICAL SEISMIC MOMENT TENSORS AS A POSSIBLE PRECURSORS OF STRONG EARTHQUAKES**

YUNGA S. (Institute of physics of the Earth, Moscow, 123810, B.Gruzinskaya, 10, Email: syunga@uipe-ras.scgis.ru)

The temporal-spatial variations of focal mechanisms and seismic moment tensors are studied retrospectively in a set of points corresponded to the epicentres of strong earthquakes. The study focuses on the local variation of the state of stress in a region of strong earthquake preparation where stress state disturbances theoretically evaluated as a result of re-activation of localised deformation bend or large-scale faults.

Investigation of numerous seismic moment tensors in terms of seismotectonic strain rates in Kuriles-Kamchatka region is performed. Seismotectonic strain rate tensor is determined as a normalised sum of local seismic moment tensors for a representative number of seismic events within 1.3 degree vicinity of each point. Analysis is based on scalar product of tensors under investigation. Temporal variations are investigated on the basis of comparison individual seismic moment tensor and seismic strain rate tensor obtained through this averaging procedure. This technique, together with the construction of classification diagrams of fault plane solutions enables us to rapidly examine the stress-field pattern and further discuss the deformation modes of faulting and fracturing, which may take place at a local scale. Local variations of stress field may be considered as an additional tool in solving earthquake prediction problem. It is found that foreshocks source mechanisms were untypical for the zones of two recent large earthquakes with  $M=8$ : the October 4, 1994 Kurile Islands earthquake and the December 5, 1997 Kamchatka earthquake. A geologic interpretation of the temporal-spatial focal mechanism variations is proposed to highlight the role played by major structural discontinuities in the local variations of the stress regime. This research was partly supported by R.F.B.R., grant N 98-05-65159.

**ST1/E/29-A2** Poster **0930-04**

**ABOUT THE PROBLEM OF THE CORRESPONDENCE OF DATA USED FOR THE ANALYSIS OF PHYSICAL STATE OF THE EARTH**

Anatoly DYCHENKO, (Department of Mechanical Engineering, Ukrainian State University of Food technologies, Volodymyrska St., 68, Kyiv, 252610, Ukraine, tel.: 380 (44) 558 8313, fax.: 380 (44) 212 4267, E-mail: dychenko@uduff.niit.kiev.ua)

The natural processes and phenomena, proceeding on the Earth are caused by the influence of global space surrounding the Earth. The physical state of global space changes continuously, which leads to continuous changes in geometric and physical parameters of the Earth as a part of the uniform global system. Therefore all natural processes, proceeding on the Earth, are connected with each other in time by cause-and-effect relationship.

To investigate physical state of the Earth it is necessary to use a great many real input data. Obtaining such data is often connected with significant difficulties and material expenditures and frequently requires long-term research work. The problem is, that the input data used for studying the state of the Earth should correspond to one certain moment of time. Otherwise the cause-and-effect relationships between phenomena can be lost, which leads to the complexity of their detection and to the initiation of essential errors in the analysis of physical state of the Earth corresponding to the moment of time considered.

The calculations carried out using a mathematical model, describing the geometric shape of the Earth, show, that even minor changes in exterior action in the scale of the Earth can lead to the results appreciable for the mankind.

**ST1/E/84-A2** Poster **0930-05**

**PROBABILISTIC FILTERING USING STOCHASTIC MODELS OF EARTHQUAKE PRECURSORS ANOMALIES: CASE STUDIES AND RESULTS**

Stefan SHANOV (Geological Institute of Bulgarian Academy of Sciences, Acad.G.Bonchev Str., bl.24, 1113 Sofia, Bulgaria, email: shanov@geology.bas.bg)

The published data for the behavior of the known earthquake precursors (phenomenological approach) have shown the complexity of the claimed prognostic anomalies and their variations in amplitude and length, as well as their deformation by irregular noises of different genesis. For increasing of the quantity of forecasting it can be used the probabilistic filtering. The Method of Inverse Probability needs of stochastic model of the expected prognostic anomaly. This method is applied in order to detect a comparatively weak efficient signal against strong, disturbing noises. The stochastic model could be created using the data records of the precursor before earthquakes above chosen magnitude level and inside given territory around the monitoring point. The imposed restrictions to the stochastic anomaly model are: 1) The noise correlation time interval has to be at least two times shorter than the length of the anomaly model; 2) The anomaly should faded several days (or months) before the earthquake; 3) The anomaly model needs to have a variation equal to 1. The data for comparing are normalized by their standard deviation. The correlation is obtained by interval, constant step multiplication of the observed values by the ordinates of the stochastic anomaly model, and by summarizing the product obtained. For the purpose of the prediction this amount is attributed to the final measurement. The curve plotted, using the values of the cumulative function, will contain the entire information of effective anomalies. The final result is given as a probability for the existence of the expected precursor anomaly on the records. Results from monitoring of thermal water level variations in a borehole (short-term prediction) and extensometric measurements on active fault (intermediate-term prediction) show the high performance of the method used.

**ST1/E/86-A2** Poster **0930-06**

**IMPLICATIONS OF MOMENT RELEASE RATES FOR SEISMIC SOURCES**

L. R. JOHNSON and R. M. Nadeau (both at Center for Computational Seismology and Seismological Laboratory, University of California, Berkeley, CA 94720 USA)

Measurements of moment release rates for sequences of small repeating earthquakes are used to estimate the seismic parameters source area, slip, and recurrence interval. Such parameters exhibit a systematic dependence upon source size over a range of ten orders of magnitude in seismic moment that can be described by three simple scaling relationships. These scaling relationships have implications for the repeat time of earthquakes, average stress drop, strength of the fault, and heat generated by earthquakes. They suggest a model for earthquakes that involves a highly heterogeneous fault on which the earthquake process is controlled by small strong asperities that occupy less than 1% of the area. Such heterogeneity helps to explain many apparent contradictions about earthquakes, such as their apparent weakness, the absence of heat flow anomalies, and the presence of pseudotachylites. Field data from exhumed fault zones are used to complement the seismic measurements, provide further constraints on the fine scale features in the earthquake source region, and constrain the energy budget of the earthquake process. Numerical calculations are used to study the dynamic interaction of a heterogeneous stress field and simulate the radiated elastic waves.

**ST1/W/30-A2** Poster **0930-07**

**PRECURSORY GEOCHEMICAL SIGNATURES OF RECENT EARTHQUAKES IN THE NORTHWESTERN IBERIAN PENINSULA**

José M. L. SALAZAR, Nemesio M. Pérez (both at the Environmental Research Division, ITER, 38594 Granadilla, Tenerife, Canary Islands, Spain; e-mail: jsalazar@iter.canaria.es); George Igarashi (Laboratory for Earthquake Chemistry, Univ. Tokyo, Bunkyo-ku, Tokyo 113, Japan); Hiroshi Wakita (Gakushuin Women's College, 3-20-1 Toyama, Shinjuku-ku, Tokyo 162, Japan); and Sun'ichi Nakai (Earthquake Research Institute, Univ. Tokyo, Yayoi, Tokyo, Japan)

Significant CO<sub>2</sub>-rich ground water and alkaline sulphide spring discharges occur in the NW part of the Iberian Massif, the largest outcrop of the Hercynian orogenic belt in Europe. Most of the CO<sub>2</sub>-rich ground waters are discharged along old NNE-trending faults, which had been reactivated during the Quaternary. Recent seismic activity in the region might be related to these NNE trending faults. In the search for precursory geochemical signatures related to recent major earthquakes in Galicia, secular variation analysis of dissolved Cl<sup>-</sup> in commercial, bottled, and mineral-CO<sub>2</sub>-rich ground water exploited at Cabreira's well (SW of Galicia) have been performed. Temporal variations of Cl<sup>-</sup> concentrations showed a uniform pattern from February to August 1995, about 24 mg/L. By the end of August, Cl<sup>-</sup> contents increased and reached relatively high Cl<sup>-</sup> levels (>26 mg/L) almost two months before two magnitude 4.6 earthquakes occurred on November 29 and December 24, 1995. In April 1996, Cl<sup>-</sup> content went back to background levels. After the finding of this sensitive well, in April 1997 a continuous radon monitoring system was installed at Cabreira. The initial results showed a significant increase of dissolved gas radon reaching levels up to 70,000 cph four weeks prior to the magnitude 5.1 earthquake of May 21, 1997. The radon peak lasted until early May when radon activity levels were about 30,000 cph. Data after July 1997 showed background radon values about 25,000 cph with daily variations much smaller than previous observed anomalous changes.

**ST1/W/32-A2** Poster **0930-08**

**SEISMIC SHORT-TERM PRECURSORS OF VOLCANIC ERUPTIONS AND EARTHQUAKES**

Victor V. MYACHKIN, Lidia B. Slavina (both at Institute of Physics of the Earth, Russian Academy of Sciences, Bolshaya Gruzinskaya 10, Moscow 123810, Russia, e-mail: myachkin@uipe-ras.scgis.ru)

A method of medium- and short-term prediction of strong earthquakes, volcanic eruptions and rock bursts is proposed. It is based on study of dispersion of P and S wave travel times from weak local earthquakes located in a concrete active seismic region. An algorithm and programs for calculation of the prediction curve are developed. The method was used in various cases: volcanic eruptions in Kamchatka: the Large Tolbachik Fissure Eruption in 1975, several eruptions of Klychevskoi Volca - no, the eruption of Karymsky Volcano in January, 1996), before the Spitak earthquake of 7.12.1988, in the Kopet-Dag region for a long period of time, and during preparation of a rock burst. A precursor occurs 5-45 days before a strong event. Duration of the alarm interval depends on intensity of the earthquake under preparation and on remoteness of the observation station from the source. Duration of precursor manifestation decreases at a station near the forthcoming event. This method can be successfully used as for a network of regional stations, so for a telemetric network, in the last case online regime of data obtaining and calculations is possible.

**ST1/E/15-A2** Poster **0930-09**

**CLOUDINESS REVEALS CRUST FAULTS AND FORECASTS EARTHQUAKES (RESULT OF A NUMEROUS-EVENT ANALYSIS)**

Vladimir A. ALEKSEEV (Institute of Terrestrial Magnetism, Ionosphere and Radio Wave Propagation, Russian Academy of Sciences (IZMIRAN), Troitsk, Moscow region, 142092 Russia, email: ogm@fly.trinit.troitsk.ru), Tamara N.Bibikova and Tamara A. Proskuryakova (both at Department of Physics, Lomonosov Moscow State University, Vorob'evy Gory, Moscow, 119 899, Russia, email: ann@geos34.phys.msu.su)

During field works in the seismological region of Crimea peninsula, we studied sharply outlined clouds (sometimes these clouds were of a layered structure). The method of stereophotogrammetrical shooting (with 2% precision) was used. We find that the clouds nearly follow the fault line revealed by the seismic method. We suppose these "tectonic clouds" are due to the injection of submicronic aerosols during the process of degasation in tectonic active zones, the aerosols being the centres of condensation of atmospheric water vapours. The events of 296 earthquakes, which occurred during 50 years, are investigated. We demonstrate the overall enhancement of cloudiness before earthquake. There are two pronounced maximums of the cloudiness, the first being in the diapason 66 - 42 hours before the beginning of the earthquake and the second being in the diapason 30 - 24 hours. The majority of the clouds are of thunderstorm character. This shows enhancement of electric field intensity, thus supporting the idea about aerosols injections. Similar form of clouds occurs in Taiwan and New Zealand. Also we show some data on temperature variation preceding the earthquake. Observing the specific temperature variation and the cloudiness over crust faults is appropriate for monitoring the Earth's surface with a system of small satellites to evaluate seismic hazards.

ST1/E/48-A2 Poster 0930-10

## TIME SERIES ANALYSIS OF THE RADON CONTENT IN GROUNDWATER AND OTHER GEOCHEMICAL PARAMETERS MONITORED IN THE LABORATORI NAZIONALI DEL GRAN SASSO (ITALY)

Francesco Bella (Physics Department, University "Roma Tre", via della Vasca Navale, 84, 00146 Roma, Italy, email: bella@fis.uniroma3.it); and Wolfgang PLASTINO (Physics Department, University "Roma Tre", via della Vasca Navale, 84, 00146 Roma, Italy, email: plastino@fis.uniroma3.it)

Physics Department of the University "Roma Tre" performs, beginning from the May 1996, measurements of the radon content in groundwater and other geochemical parameters in the L.N.G.S. to study the following topics: a) correlations between the possible variations of the radon with the stress-strain processes of the rock; b) study of the diffusive processes of the radon related to the water geochemistry. This monitoring activity is a part of the geophysical and geochemical research of the Gran Sasso aquifer, the most important of the central Italy. Then, we have planned and realized a multiparametric equipment and we have set up in the underground laboratory of the Istituto Nazionale di Fisica Nucleare. The geochemical measurements carried out in the L.N.G.S. seem to point out a good reliability and stability of the automatic equipment and a correlation with the local seismicity and with the seismic sequence of the Umbria earthquake.

ST1/E/53-A2 Poster 0930-11

## VARIATIONS OF APPARENT RESISTANCE: EARTHQUAKES PRECURSORS OR SEASONAL EFFECTS?

A.V. Descherevsky, (Russia, Moscow, Bolshaya Gruzinskaya 10, Union Institute of Physics of the Earth, email: deshere@upei-ras.wscgis.ru); A.Ya. SIDORIN (Russia, Moscow, Bolshaya Gruzinskaya 10, Union Institute of Physics of the Earth, email: sidorin@upei-ras.wscgis.ru)

Statistic structure of variations of apparent electrical resistance of rocks observed in Garm by long-standing dipole soundings is surveyed. By method of mid-seasonal function the seasonal component of time series is recognized, and its functions are observed. Using the data of long-standing vertical sounding with the distance of 6 m to 3 km between the feeding AB dipoles, the dependence of phase and amplitude seasonal components from the dimensions of using adjustments (sounding depth) are studied. It was determined the seasonal variations of apparent resistance observed with the help of dipole adjustment (placing) with about 6 km distance are lagged behind the variations of surface layer resistance on approximately 4 months. Amplitudes of seasonal variations decrease smoothly with the increasing of the distance; if the distance becomes more than 3km the amplitude extremely increases. Residual series, received after the filtration of primary series of seasonal component, have the peculiarities of flicker-noise. The result of this residual series analysis by formalized method on the basis of quantum (photon) detector is the definition that during the "anomalous" periods of low values of apparent resistance the strong local events have occurred twice more frequently than during the background values of this parameter. Thus, the prognostic significance of the observed resistance variations has been confirmed.

ST1/E/87-A2 Poster 0930-12

## THE RIFT OF CORINTH (GREECE): A EUROPEAN OBSERVATORY FOR CRUSTAL INSTABILITIES AND EARTHQUAKE PRECURSORS

P. BERNARD (I.P.G.P., 4 Place Jussieu, 75252 Paris, France; ph. 33-1-44-27-24-14; email: bernard@ipgp.jussieu.fr); J. Vandemeulebrouck (L.I.G., Université de Savoie; email: jvandem@univ-savoie.fr); J.-C. Gariel (I.P.S.N./C.E.A.; email: gariel@tokyo.farcea.fr); S. Abbad (INFOTERE, France); K. Makropoulos (Seismological Laboratory, University of Athens; email: kmacrop@cc.uoa.gr); G. Veis (Dionisos Satellite Observatory, National Technical University of Athens); G. Stavrakakis (National Observatory of Athens; email: g.stavr@egeledos.gein.noa.gr); F. Scherbaum (University of Potsdam; email: fs@geo.uni-potsdam.de); B. Ducarme; M. VanRuyambeke (all at Observatoire Royal de Belgique; email: vruymbek@mailserv.oma.be)

The rift of Corinth is one of the most active continental structure of the Euro-Mediterranean region. Its opening rate is 1 to 1.5 cm/year, with an associated strain rate of 10-6/year, and 6 earthquakes with magnitude larger than 5.8 in the last 35 years. The European GAIA project (1996-1998) has allowed the installation of a multiparameter geophysical observatory continuously monitoring the activity of the rift, complementing the seismometer and accelerometer arrays: shallow borehole tiltmeters, strainmeters and tiltmeters in a cave, radon probes in soil near fault zones and in karstic springs, and magneto-telluric and radio stations. Its aim is to detect and analyze short-term crustal instabilities within the long-term deformation context of the whole seismic cycle: coseismic and postseismic perturbations from large earthquakes, aseismic instabilities and clusters of small earthquakes, and possible precursory instabilities. The paper presents the recent achievements of the GAIA project, and mentions the objectives of a future project proposing a "Multiborehole Observatory in the Gulf of Corinth" (Cornet et al., 1997).

ST1/C/JSS02/E/17-A2 Poster 0930-13

## LOW-RESISTIVITY STRUCTURES AS CONVERTERS OF SEISMIC WAVES' ENERGY INTO ELECTROMAGNETIC SIGNALS

OLEG NOVIK (Moscow State Geol. Prospect. Acad., 117246, POB 51, Russia. email: onovik@glasnet.ru) Sergey Ershov (Keldysh Institute for Appl. Mathematics of Russian Academy of Sciences, Moscow) Irina Mikhaylovskaya (Moscow State University. email: irina@nw.math.msu.ru)

Trying to clear out the physical nature of electromagnetic (em) and temperature (t) signals observed in seismically active regions (some of them occurred to be precursors to earthquakes), we use the theory of magnetothermoelasticity to construct the mathematical model and calculate the elastic-em-t field interaction caused by displacements (ampl., freq. and duration are of order of a few cm, Hz and sec resp.) in the upper mantle domain of a model lithosphere zone containing the low-resistivity structures (LRS) in this domain and in the crust. According to MT-soundings in seismic regions, the LRSs' conductivity is 0.1 to 0.5 S/m and cross-section sizes and depths are of order of 10 km or mo-re. It is clear from the computed pictures of the evolution of the interacting fields that em-signals arises near the contacts of the seismic waves' (s.w., from upper mantle in our runs) fronts with the boundaries of LRSs, as a result of their deformations in presence of geomagnetic field. The em- emission into atmosphere arises during the diffraction of s. w. by LRSs (60 pT at the Earth's surface and 10 pT at the height of 30 km). The t-signal (up to 0.02 K in the sedimentary layer) propagates together with the s.w. and is not influenced by ionosphere. The main frequencies of the computed em and t-signals (ULF field oscillations) are nearly the same as ones of displacements and are changing, together with the amplitudes, because of changing of displacements at the depth. The computed em and t-signals' amplitudes, frequencies, the delay of the seismic wave arrival at the surface in regard to em-signal and its delay in regard to beginning of displacements are of orders observed.

This page may be copied freely

Tuesday 20 July PM

Presiding Chairs: M. Ohnaka, R. Teisstyr

EARTHQUAKE NUCLEATION TO DYNAMIC RUPTURE

ST1/E/27-A2 Poster 1400-01

## INFLUENCE OF CHANGES IN THE GEOMETRIC SHAPE OF THE EARTH ON THE INITIATION OF COMMON AND LOCAL CENTERS OF STRAIN

Anatoly DYCHENKO, (Department of Mechanical Engineering, Ukrainian State University of Food technologies, Volodymyrska St., 68, Kyiv, 252610, Ukraine, tel.: 380 (44) 558 8313, fax.: 380 (44) 212 4267, E-mail: dychenko@duft.niit.kiev.ua)

Each geometric shape is characterized only by its inherent metric properties. The changes in the geometric shape lead to the changes in metric properties, which under the conditions of real physical rigid body results in inevitable initiation of centers of strain. For example, a maximum volume at a minimum area of surface characterizes a body of spherical shape. The deformation of a spherical body under the change of its shape for the ellipsoidal one leads to a modification of relationship volume / area of the surface and modification of lengths of characteristic lines on the body's surface. Continuous deformation of the Earth under the influence of constant changes in an exterior force field also results in the initiation of common and local centers of strain in the body of the Earth. Depending on the peculiarities of deformation both contracting, and stretching strains of high intensity arise in the rigid basis of the Earth resulting in local manifestations, sometimes disastrous for mankind. Detecting small (related to a determining size of the Earth) deformations, and correspondingly arising deformation strains is possible only in the case when the mathematical means used for processing and analysing of input data allow to obtain results of required exactitude. Such exactitude can be provided by the new analytical technique based on the natural unity of spatial and other physical parameters.

ST1/E/34-A2 Poster 1400-02

## PHYSICAL GEOMETRY OF ACTUAL SPACE

Anatoly DYCHENKO, (Department of Mechanical Engineering, Ukrainian State University of Food technologies, Volodymyrska St., 68, Kyiv, 252610, Ukraine, tel.: 380 (44) 558 8313, fax.: 380 (44) 212 4267, E-mail: dychenko@duft.niit.kiev.ua)

When studying the influence of geometric shape of a body on physical processes, proceeding in it, there is a necessity for describing the relation between geometric and other physical parameters. Existing geometric mappings of real physical space cover only the relations and shapes of objects and phenomena similar to spatial ones but regardless their concrete physical content. It superimposes essential restrictions at a research.

To analyse the influence of geometric shapes of real bodies on physical processes proceeding in them and to determine the field of distribution of physical parameters in these bodies, the principles of physical geometry have been developed. The physical geometry reflects the organic natural constraint between spatial and other physical parameters. The initial geometric concepts of elementary geometric objects are defined proceeding from a physical state of real space elements, whose geometric mappings these objects are.

The use of physical geometry when investigating the influence of geometric properties on physical processes has allowed to improve the accuracy of some existing theoretical provisions, to reveal the reasons of erroneous results of determination of physical state of system as a whole when analysing the system in its separate elements, and to develop a new technique for analysing distribution of interior forces in bodies of complicated geometric shape.

ST1/W/12-A2 Poster 1400-03

## A MODEL FOR FRACTURING PROCESS OF INTACT ROCKS UNDER AXIAL LOADING OF COMPRESSION: THE SIZE-EFFECT OF STRENGTH FOR FRACTURE OF SPECIMENS

Kiyohiko YAMAMOTO (Graduate School of Science, Tohoku University, Sendai, 980-8578 JAPAN, email: yama@aob.geophysics.tohoku.ac.jp)

A simple model called strength distribution model has been proposed to elucidate the process to the macroscopic fracture, or the fracture of an intact rock specimen, under tri-axial loading of compression. This model is constructed on the assumptions as follows: 1) A specimen consists of small volume elements of the same size. 2) Fracture of an element, or a micro-fracture, occurs according to the Coulomb's criterion, where the internal friction coefficient is taken to be proportional in magnitude to the cohesion force. 3) The strength distribution for the elements is expressed by a power function. 4) The applied load to a specimen is equally shared among the elements that have remained un-fractured. The model provides the analytical expression for the relation between density of micro-cracks and applied stress and that for the relation between a decrease in the macroscopic strength and an increase in the average size of generated micro-cracks. It has already been confirmed that the former expression well explains the experimental data. The analytical expression for the size-effect of macroscopic strength is derived by assuming that the average size of micro-cracks is proportional to specimen volume. There exist the experimental data obtained for quartz diorite and coal under uni-axial loading. Although an abundance of tensile micro-cracks are generated in specimens under uni-axial loading, the expression is fitted to these data on the idea that tensile micro-cracks are generated due to the tensile stresses locally induced by shear micro-fractures even under uni-axial loading. It is found that the expression can be well fitted to the data in the wide range of specimen volume over more than 3 order of magnitude. This result together with the previous one shows the validity of the present model. This validity of the model implies that the internal friction coefficient is not an essential physical constant but a variable with regard to specimen size.

ST1/E/74-A2 Poster 1400-04

## COMPREHENSIVE SOURCE ANALYSIS EMPLOYING A UNIVERSAL KINEMATIC MODEL

Yeugeny Chirkov, Nadezhda KONDORSKAYA, Ilya Zyrkis, Natalia Lagova, and Yelena Khrometskaya (all at the Russian Academy of Sciences Institute of Physics of the Earth, 123810, GSP, Moscow, Russia)

The elaboration of physical models is one possible way to get the understanding of the complicated processes that occur within the earthquake source. A kinematic model of earthquake source is presented which allows to obtain analytical approximation of P-waves in the teleseismic zone (with respect for attenuation and instrument characteristics) in the form of finite series. The model's time function is physically substantiated (finite, continuous and differentiable), and its parameters have been determined via simultaneous approximation of



source P-waves in the teleseismic zone and in a wide azimuth range. Seismic moment has been assessed employing a nonconventional method and with the help of kinematic model presented herein.

The model, by analogy with seismic moment, allows to describe frequency spectrum of the earthquake's source emission in terms of conventional parameters, that is dimensions of the rupture, maximum speed of displacement, initial and final speed of fracturing. An algorithm is presented for automated selection of source P-waves.

Model's applicability is illustrated on the example of the Racha-Djava earthquake (Caucasus) of April 29, 1991 ( $M_s = 6.9$ ). The work has been carried out with support of the Russian Fund for Fundamental Research.

**ST1/E/26-A2** Poster **1400-05**

#### RESPONSE OF SPRING SYSTEMS TO EARTHQUAKES IN ARMENIA

V. LEONARDI (Magmas et Volcans UMR 6524 & CNRS, Clermont-Ferrand, France, email: leonardi@opgc.univ-bpclermont.fr); A. Tovmassian (National Survey for Seismic Protection of the Republic of Armenia, 4 Yerevan 375054 Armenia)

This study presents the relationship between local seismicity and springs discharge, in which the microseismicity modifies the state of stress of the aquifer matrix and these modifications of the local stress control the aquifer behaviour from an example of a basaltic reservoir crossed by a seismic fault. Along the right-lateral Garni seismic wrench fault, the distribution in space and time of more than 500 micro-earthquakes has been studied providing a pattern of stress distribution. Together with this tectonic survey, the hydrographs of springs issuing from an aquifer located in basaltic lava flows and crossed by the fault have been gauged for four years. According to its tectonic, geologic and hydrodynamic properties, the reservoir has been divided in several parts. The hydrological behaviour of the reservoir and of each of its parts has been modeled, based on the rainfall and hydrodynamic properties of the basaltic reservoir and of nearby reservoirs. The model allows us to define the "normal behaviour" of the springs, when their discharge is not affected by an earthquake. Anomalies to the normal hydrodynamic curves are defined, and correlated to small ( $M < 3.5$ ) earthquakes along the Garni fault. We propose that the circulation of underground water in the area around the fault depends largely on the fracture pattern of the basalts and the aquifer basement, as pointed out from field observations. Changes in springs discharge are explained by variations in the state of stress around the Garni fault, induced by the alternation of elastic strain and stick-slip movement on the fault and by creep far from the fault. A model of stress distribution correlated with microseismic activity is proposed which explains changes in fracture characteristics before and after earthquakes.

**ST1/E/30-A2** Poster **1400-06**

#### A DYNAMIC MODEL FOR INTERSEISMIC VARIATION IN GROUND DEFORMATION RATES

Nipun KAPUR, (Department of Earthquake Engineering University of Roorkee, Roorkee - 247 667 India)

Geodetic observations during earthquake cycle at a number of fault / subduction zones show variation in ground deformation rates. A rapid post seismic to low preseismic values is characteristic of deformation rates. A dynamic model is proposed in which nonlinear friction and material response during interseismic period along the Main Thrust Zone (MTZ) contributes to the characteristic strain rates. Such, nonlinear time dependent interseismic phenomenon may be active for both situations of a locked as well as unlocked MTZ as hypothesized in various subduction models. The model exclusively explains slow preseismic strain rates. Moreover it infers that an unlocked interseismic MTZ does not rule out the possibility of strain accumulation.

**ST1/E/54-A2** Poster **1400-07**

#### TUNNEL EFFECT OF FRACTAL FAULT AND TRANSIENT S-WAVE VELOCITY RUPTURE (TSVR) OF IN-PLANE FAULT

LI SHI-YU and Chen Yun-tai Chen (Institute of Geophysics, China Seismological Bureau, Beijing 100081, China, email: lisy@cdsindm.csb.gov)

Transient S-wave velocity rupture (TSVR) means the velocity  $v$  of fault propagation is between S-wave velocity  $v_s$  and P-wave velocity  $v_p$ . Its existence in the rupture of in-plane fault was proved, but there are two difficulties, i.e. initialisation difficulty and divergence difficulty in 2-D LEFM model. The initialisation difficulty means, when  $v \ll v_R$  (Rayleigh wave velocity), the dynamic stress strength factor  $K_2(t)$  is  $\ll 1$ , and change from positive into negative in the forbidden of  $(v_R, \dots)$ . The divergence difficulty means  $K_2(t) \rightarrow \infty$  when  $v \rightarrow v_p$ . Here we introduce the concept of fractal and tunnel effect of fault. As we know,  $v$  is differentiate of the length of the fault respect to time, so  $v$  is also fractal. The tunnel effect means the dynamic rupture cross over the interval of the cracks, and the coalescence of the interval is slower than the propagation of disturbance. Suppose the area of earthquake nucleation is critical or sub-critical propagation everywhere. The arriving of disturbance triggers or accelerates the propagation of cracks tip, and the observation system can't distinguish the front of disturbance and the tip of fracture. Then the speed of disturbance may be identified as velocity of fracture velocity, and the phenomenon of TSVR appears, which is an apparent velocity. The dual character of rupture velocity means that the apparent velocity of fault and the real velocity of micro-crack extending, which are different in physics, but are unified in rupture criterion. Introducing the above concept into the calculation of  $K_2(t)$ , the difficulty of initialisation can be overcome, and the integral equation of triggering the initialization of TSVR is given quantitatively. By solving this equation, the lower limit of TSVR is  $1.1053 v_p$ , then the divergence difficulty is also overcome. TSVR is unstable solution, and may degenerate to sub-Rayleigh wave velocity rupture immediately where the non-critical condition can be measured. The results of this paper show that the initialisation and continuum depends on the condition of earthquake nucleation area.

**ST1/E/55-A2** Poster **1400-08**

#### INFLUENCE OF LOADING RATE ON THE STABILITY OF A UNIFORM FAULT WITH VARYING NORMAL STRESS

Changrong HE, Shengli Ma (both at Institute of Geology, China Seismological Bureau, Beijing 100029, China, email: rmlab@public.bta.net.cn)

We analyzed the stability and dynamic motion of a single degree of freedom spring-slider system as a model of a uniform fault with a rate- and state-dependent friction law that the effect of normal stress. When the fault is inclined to the driving direction, critical stiffness that separates stable sliding and cyclic stick-slip is velocity-dependent. Moreover, the critical stiffness decreases with increasing velocity. Accordingly, higher velocity stabilizes a system for a predetermined stiffness lower than the critical value and may change the motion from cyclic stick-slip to stable sliding, and vice versa. Our numerical simulations in full dynamic motion confirmed such transition, and agree well with the analytical result. Sensitivity of such transitions to change of loading rate is also discussed. The sensitivity depends on how close the stiffness is to the critical point and on the fault angle. A higher angle

between the maximum principal stress and the fault surface favors the transition, i.e. a smaller change in loading rate can activate the transition with a higher angle. Nonlinear analysis is also discussed on the boundary in rate change that separates stable sliding mode and single triggered instability when the system stiffness is greater than the critical value.

**ST1/E/61-A2** Poster **1400-09**

#### SOURCE RETRIEVE BY EMPIRICAL GREEN'S FUNCTION DECONVOLUTION IN VRANCEA REGION (ROMANIA)

Mihaela Popa (National Institute for Earth Physics, P.O. Box MG-2, 76900 Bucharest, Romania, email: mihaela@inf.ifa.ro); Mircea RADULIAN (National Institute for Earth Physics, P.O. Box MG-2, 76900 Bucharest, Romania, email: mircea@inf.ifa.ro)

Vrancea seismic region is characterized by a highly confined subducted focal volume in the depth range between 60 to 200 km, where strong earthquakes ( $M_w$  max of 7.7-7.9) occur. The seismicity rate is relatively high (around 10 events/month with  $M_L > 3$ ) for such a small volume. At present a network of 14 short-period Teledyne S13 stations (vertical component) and a network of 30 K2 accelerometer stations (three components) are monitoring the Vrancea seismic activity. They offer a sufficient number of digital waveforms within a magnitude range from 3.0 to 7.0 suitable for application of the EGF deconvolution.

The source parameters (seismic moment, source size and stress drop) are determined for a set of 30 intermediate-depth earthquakes, localized all along the subducting slab. Most of the sources are simple unipulse-like with relatively short rupture duration. It is assumed that the existence of a fluid-assisted faulting mechanism at intermediate depth can explain the particularities of the Vrancea source. In a few cases significant source directivity effects are detected for moderate size events ( $M_w \sim 5$ ). Scaling of the seismic moment with magnitude, source dimension and stress drop is analyzed. Possible dependencies on depth of the source parameters and scaling properties are discussed in correlation with the distribution of the seismicity and energy along the subducting lithosphere.

**ST1/E/79-A2** Poster **1400-10**

#### SOURCE PARAMETERS OF CRUSTAL EARTHQUAKE SEQUENCES IN THE FOREDEEP AREA OF EASTERN CARPATHIANS BY EMPIRICAL GREEN'S FUNCTION DECONVOLUTION

Emilia POPESCU (National Institute for Earth Physics, P.O. Box MG-2, 76900 Bucharest, Romania, email: epopescu@inf.ifa.ro) Mircea Radulian (National Institute for Earth Physics, P.O. Box MG-2, 76900 Bucharest, Romania, email: mircea@inf.ifa.ro)

Source parameters of a few earthquake sequences of moderate-size ( $M < 5$ ) crustal earthquakes occurred in the foredeep area of Eastern Carpathians (Romania) are retrieved using the empirical Green's function (EGF) technique. The digital waveforms recorded by Romanian local seismic telemetered network are considered. To apply the EGF deconvolution, we select for each studied sequence pairs of main and Green's events with similar location and focal mechanism. The apparent source time function and source spectrum of the main event are obtained using the seismograms of adjacent small events as empirical Green's functions. The deconvolved pulses and spectra are implicitly corrected for instrument and propagation effects. The analysis of the retrieved parameters outlines a heterogeneous faulting process in the seismic source. Scaling relationships between seismic moment, magnitude, source dimension, stress drop, peak velocity parameter are estimated. They agree also with a complex rupture process in the focal area. The SW-NE trend of the epicenter distributions for the earthquake sequences in the foredeep area is related to a dominant crustal fault orientation and a specific focal mechanism. Our results are finally discussed in connection with the seismicity and seismotectonics of the Eastern Carpathians foredeep area and the possible relation with the subducting process at the Eastern Carpathians arc bend (Vrancea).

**ST1/E/80-A2** Poster **1400-11**

#### CRUSTAL STRUCTURES AND DYNAMICS OF THE 1983(MS6.6) TUAN GIAO EARTHQUAKE EPICENTRAL REGION

Cao Dinh TRIEU and Nguyen Xuan Binh (Institute of Geophysics, VNCST, P.O.Box 411 Buu Dien Ho, Hanoi, Vietnam)

In this paper, the authors present a solution of source process of the Tuan Giao earthquake and its tectonic implication. The crustal structures and Dynamics of the Epicentral Region are also described. Based on obtained analytical results, the following conclusion can be made:

1. Epicentral area of Tuan Giao earthquake located in northwest margin of M River zone and coincided with uplifted zone of lower boundary surface of the earth crust, where shifting amplitude into both sides of the Son La fault reached value of 2-3 km.
2. The Son La fault strongly activated during Mesozoic-Cenozoic period and Neotectonic and neotectonic movement. Uplifting movement into northeast part of the fault reached value of about 1-2 mm/year.
3. The largest surface ruptures were characterized by system of 3 parallel fracture which have an azimuth 130°, a width 10-17 cm, and a length of about 200 m, that continuously distributed at the total length of at least 20 km. The surface ruptures, at smaller level, has maximum length a fracture about 20 m of which direction is NW-SE, concentrated at the displacement on surface pure right lateral strike-slip was observed.
4. The fault plane solution from the inversion teleseismic body waves indicates pure right-lateral strike-slip, striking N290E, which the fault orientation in this area. The focal mechanism determined from the P-wave first motion data has the different strike N120E. This fact suggests that the initial rupture occurred at the fault with the different from that of the main rupture.

**ST1/W/47-A2** Poster **1400-12**

#### EXPERIMENTAL STUDIES ON CONSTITUTIVE PROPERTIES FOR THE SHEAR FAILURE OF ROCK IN SEISMOGENIC ENVIRONMENTS

Aitaro KATO, Mitiyasu Ohnaka, and Hiromine Mochizuki (Earthquake Research Institute, University of Tokyo, Tokyo 113-0032, Japan, email: akato@eri.u-tokyo.ac.jp)

Elaborate laboratory experiments have been performed to evaluate in quantitative terms how the constitutive property for shear failure of intact granite is affected by seismogenic environments with increasing depths. In the present experiments, we simply assumed the crust to consist of granite, the lithostatic pressure gradient to be of 30 MPa/km, and the temperature gradient to be of 30C/km. We further assumed the interstitial pore water pressure to be hydrostatic (its gradient of 10 MPa/km) in one series of experiments, and suprahydrostatic (24 MPa/km) in another series of experiments. Tsukuba granite was selected for the present experiments, and the shape of test samples was a circular cylinder (40 mm long and 16 mm in diameter). All the tests were conducted at the strain rate of  $10^{-5}$ /sec. It has been confirmed by these experiments that all the test results can well be represented in terms of the slip-dependent constitutive law. The experiments showed that the peak shear strength increases linearly with depth shallower than 10km, while it becomes virtually constant at deeper



depths. The critical slip displacement was virtually constant over the depth range up to 12km, beyond which it increased with depth. These results clearly show that mechanical instability is suppressed at depths greater than 12km, which corresponds to the brittle-plastic transition regime.

**ST1/W/55-A2** Poster **1400-13**

**SOURCE PARAMETERS BY SPECTRAL ANALYSIS OF OCEANIC EARTHQUAKES RECORDED AT GAURIBIDANUR SEISMIC ARRAY, INDIA**

Imtiyaz A. PARVEZ (Department of Geology, Kumaun University, Nainital, INDIA. Presently at the Department of Earth Sciences, University of Trieste, ITALY, email: parvez@geosun0.univ.trieste.it); Avadh Ram (Department of Geophysics, Banaras Hindu University, Varanasi - 221 005, INDIA)

A study of source parameters from the Andaman Sea and Carlsberg Ridge earthquakes in a narrow azimuthal range using the Gauribidanur Seismic Array (GBA) data in southern India has been carried out. Nine earthquakes from Andaman sea and eight from Carlsberg Ridge in the magnitude range of 4.5<math>M\_b</math>5.4 recorded by the short-period digital seismometers of 1 sec period at the rate of 20 samples/s have been used. The earthquakes from both regions are at an epicentral distance of about 17 degree from GBA. The Fourier displacement spectra of P-waves are estimated for 512 samples in time domain to the frequency domain and analysed with respect to Brune's model. A systematic and uniform approach to the problem of determining the corner frequency ( $f_c$ ) and low frequency spectral level has been used by computing theoretical spectra in frequency domain and compared with observed one. It is interesting to note the characteristic of the seismic sources of two different oceanic regions having the identical distances and similar path with recording instrument alike. The seismic moment and stress drop for the Andaman sea earthquakes are estimated as 4.8E+22 to 4.8E+23 dyne-cm and 14-78 bars, respectively. The source radius, apparent stress and energy released are estimated as 1.10-1.41 km, 1.49-8.04 bars and 2.5E+17 to 1.3E+19 ergs, respectively. For the Carlsberg Ridge, seismic moment and stress drop are estimated as 4.8E+23 to 8.3E+23 dyne-cm and 81-116 bars, respectively. The source radius, apparent stress and energy released are estimated as 1.36-1.47 km, 8.38-11.88 bars and 1.3E+19 to 3.2E+19 ergs, respectively. The source parameters versus magnitude have also been plotted to find out the empirical relationships and compared for the two regions. It has been observed that all the source parameters of the Carlsberg Ridge are showing higher stress drop as compared to the Andaman regions may be because the two areas have evolved from different geological and tectonic processes.

**ST1/W/04-A2** Poster **1400-14**

**ACOUSTIC AND ELECTROMAGNETIC DISTURBANCES DURING VIBROSEISMIC SOUNDING**

V.V. Kuznetsov, V.V. Plotkin, S.Y. KHOMUTOV, O.E. Grekhov, A.F. Pavlov, A.N. Fedorov (Institute of Geophysics SB RAS, Koptuyug av., 3, Novosibirsk 630090, Russia; e-mail: hom@uigm.nsc.ru)

The powerful seismovibrators can be considered as controlled sources of the seismic energy. They can be used for the researches of the mechanisms of the earthquake precursors. The observations of a disturbances of the acoustic, electric and magnetic fields at various distances from a source during the operating of the seismovibrators in a sweep-mode (the frequency range is 6-11 Hz) are performed. The used seismovibrators are the centrifugal vibrosources with the sinusoidal vibrational action onto the ground of 100 and 40 tons. The signal in the vertical component of the atmospheric electric field at the distances up to 2 km is detected. This signal has near zero delay with respect to session beginning and advances beyond the acoustic and seismic signals. It can specify an electromagnetic nature of disturbances of the electric field. The infrasonic signal is reliably registered on distances up to 50 km. In some cases depending on acoustic signal magnitude the seismic signal with the same arrival times is registered. The amplitude of infrasonic signals depends on the meteorological conditions along a path of its propagation. The measurements with the remote infrasonic sensors have allowed to determine a path of the acoustic wave from vibrosources to sensors. The disturbances caused by the seismovibrators were also registered in a telluric field at distance up to 2 km from source.

**ST1/E/78-A2** Poster **1400-15**

**FRACTAL DISTRIBUTIONS OF THE EARTHQUAKE SEQUENCES IN BANAT AND CAMPULUNG-FAGARAS SEISMIC REGIONS (ROMANIA)**

Emilia Popescu (National Institute for Earth Physics, P.O. Box MG-2, 76900 Bucharest, Romania, email: epopescu@inf.ifa.ro); Mircea RADULIAN (National Institute for Earth Physics, P.O. Box MG-2, 76900 Bucharest, Romania, email: mircea@inf.ifa.ro); Ana Utale (National Institute for Earth Physics, P.O. Box MG-2, 76900 Bucharest, Romania)

Fractal characteristics of time, space and size distributions of earthquake sequences in two regions of increased seismic activity, located at the eastern and western extremities of the Southern Carpathians (Romania) - Campulung-Fagaras and Banat - are analyzed. Campulung-Fagaras area is situated close to Vrancea subduction region. Here the largest shallow earthquakes on the Romanian territory are observed ( $MW = 6.5$ ). The last large shock was recorded on January 26, 1916 ( $MW = 6.5$ ). Banat area is situated at the contact of the Pannonian basin and Carpathians orogen and is characterized by a relatively high seismicity in the upper crust ( $h < 10$  km;  $MW < 6$ ). Two important earthquake sequences occurred between July 1991 and June 1992 in Banat region and between May and June 1993 in Campulung-Fagaras are considered. A number of 1134 events with  $1.5 < MW < 5.8$  are identified in the first case, and 318 with  $1.2 < MW < 5.2$  in the second. Fractal properties of the time, space and size distributions are outlined and compared for the two seismic processes. The fractal dimension of the temporal distribution is in the range  $0.14 < D < 0.25$  in both cases. The fractal dimension of the epicenter distribution and the b-slope of the frequency-magnitude distribution, as functions of time, are positively correlated for the Banat sequence and negatively for the Câmpulung-Fagaras sequence.

**ST1/W/62-A2** Poster **1400-16**

**REGISTERED TWO DISTINCT WAYS OF RELEASING ACCUMULATED POTENTIAL ENERGY: SEISMICITY AND "FAULT SUPERINTENSIVE MOVEMENTS"**

CHURIKOV V.A., Kuzmin Yu.O. (both at United Institute of Physics of the Earth, Recent Geodynamic Lab., B. Gruzinskaya Str. 10, Moscow, Russia, email: vt.churik@relcom.ru)

Data obtained in the geodynamic polygon of Kamchatka (Russia) by multiple repeated high-precision vertical geodetic observations with great detail in time and space in fault active zone are discussed. The data processing, measurements and analytical methods that were originally used for small local levelling profile in fault zones have been elaborated. As a result of analysis are be found very localized superintensive deformations of the ground surface in

fault zones with amplitude approximately 5 - 10 cm per year. Accurately located superintensive movements correspond to extension fracture local fault zones has been identified along the profile. Correlation between the deformation rate and seismic activity allowed us to distinguish direct and inverse correlation types. In the direct correlation, the main deformational event precedes the seismic event (deformation forerunner of an earthquake, in our case M 7.1, 1992 March 2, 82 km from the profile), while in the inverse type the redistribution of accumulated energy is expressed by both the seismic process and the fault superintensive movement. Hence, while executing observations for predicting destructive earthquakes, one should take into consideration the correlation character between seismic activity and contemporaneous superintensive movements in the fault zones.

**ST1/W/06-A2** Poster **1400-17**

**IDENTIFY THE CHANGE OF SHEAR-WAVE SPLITTING ON MARBLES WITH LOADING IN LABORATORY**

Yuan GAO (Center for Analysis and Prediction, China Seismological Bureau, 100036 Beijing, China/Graduate School, University of Science and Technology of China, Email: geo\_yuan@yahoo.com /ygao@tomo.ig.erdw.ethz.ch); Shi-yu Li (Institute of Geophysics, China Seismological Bureau, 100083 Beijing, China) Hui-lan Zhou (Graduate School, University of Science and Technology of China, 100039 Beijing, China)

We have done a laboratory test on measuring shear-wave splitting change with loading pressure on marbles. The data acquisition is performed by a triggering digital waveform acquirer of frequency of 20 million Hz. Using the probes of three components, the signal source of shear wave could be changed in frequency, the waves which propagate through the sample rock could be received well by probes at three channels.

This experiment is focused on the change of pattern of shear-wave splitting when the loading pressure is changed. We selected two groups of marbles. One of groups is composed of intact marble samples which just show original parallel structure, without original cracks. With the increment of pressure from free status, the shear-wave shows the splitting and increment. When near to the critical state in which samples will be destroyed, the time delays of shear-wave splitting do not change regularly increasing with loading. Those changes for samples are different with each other. The pattern is characterized as more complexity. Another groups of marble samples are composed of those with original parallel cracks. No loading, we directly detect the shear-wave splitting. Results show obvious azimuthal anisotropy. Splitting phenomena of shear-wave were also observed.

Although we did this experiment in single-axis loading, not in condition of a triaxial stress cell. The critical patterns of marbles are very complicated. The results suggest that the critical change of shear-wave splitting could be observed. However, it is possible to identify the change before a large event with the observation on shear-wave splitting.

**ST1/E/58-A2** Poster **1400-18**

**SOURCE COMPLEXITY OF THE CAP - ROUGE EARTHQUAKE - MODERATE EARTHQUAKES YIELD THEIR SECRETS**

John ADAMS (Geological Survey of Canada, 7 Observatory Crescent, Ottawa K1A 0Y3 Canada, email: adams@seismo.nrcan.gc.ca) and R.A.W. Haddon (32 Mahuta Road, Five Mile Bay, RD2, Taupo, New Zealand)

The mbLg 5.1 Cap-Rouge earthquake is the largest well-instrumented earthquake in southeastern Canada since the (similar-sized) 1990 Mont-Laurier earthquake. It occurred on 971106 at 0234, 22 km under the western suburbs of Quebec City (46.80N, 71.42W, see www.seismo.nrcan.gc.ca). The mainshock ( $Mw$  ca. 4 1/2) was well recorded by seismographs at >100 km, and by the Quebec City analog strong motion instrument (11 km). The network recorded 15 aftershocks of magnitude 2.9 - 1.3 and field instruments recorded 20 smaller aftershocks, the tight cluster of the latter establishing the hypocentre. A P-nodal mechanism (by A. Bent) indicates primarily reverse faulting, from geological arguments likely on a plane dipping 70 degrees southeast and striking N50E. We have interpreted spectral ratios and forward modelled the source (compare Haddon and Adams, GJI 129:235). Derived source spectra vary for various azimuths and show spectral scalloping, a source interference effect implying a double event. Spectral modeling indicates a pair of sources with the second about 1.0km southwest of the first and delayed by 0.6 sec. The strong motion time history supports a double source. Consequences of the interference for moment determination and Q determination will be presented. The spectral characteristics of this model are fully consistent with the Haddon 1996 (BSSA 86:1300) source scaling model. Complexity like this makes simplistic interpretations of "the" source in terms of Brune-type models extremely misleading. Taken with the results of the Mont-Laurier mainshock, Saguenay mainshock, Saguenay foreshock (also a double event), and other mbLg>4.5 earthquakes studied, we find this complexity pervasive for eastern Canada. If such complexity exists for many Mw 4.5 earthquakes in other areas, conclusions about average rupture velocities as inferred from the size and duration of rupture will be inaccurate and may account for the unusual properties claimed for the "nucleation zones" of M>6 earthquakes.

**ST1/P/09-A2** Poster **1400-19**

**GROUND MOTION COMPUTATION AND MODELLING OF CONTROLLED AND NATURAL SOURCES**

Soma Chatterjee; Avadh RAM (Both at Department of Geophysics, Banaras Hindu University, Varanasi-221005, India; tel: +91 542 317123; fax: +91 542 317074; email: aram@banaras.ernet.in)

Physics of earthquake processes and crustal stresses and its mechanism may be investigated in formulating any programme towards earthquake hazard and risk estimation or for earthquake prediction. In order to assess the quantum of strain energy released during an earthquake, the nucleation process of the fault and the final rupture must be given due consideration. The seismodynamics and numerical earthquake prediction methodologies are being contemplated. The problem of source characterization and theoretical estimation of ground motion in the vicinity of the source under controlled media have also been considered. The spherical cavity model emplaced in a homogeneous, ideally elastic and infinite medium, has been chosen to compute the elastic wave motion. A modified pressure function has been used for computation of ground motion. The effect of transmission path and some other factors have also been considered. The analytical expressions for reduced displacement potential as source function, radial displacement and velocity for any yield in a given medium have been derived using the Duhamel's integral. The results are compared with observed data. Further earthquake source modelling and computation of relevant ground motion using body wave waveform modelling technique has also been carried out. Two different fault systems i.e. the one associated with Bihar earthquake of January 15, 1934 and the other with the recent event of Jabalpur earthquake of May 22, 1997, have been mapped in detail. These fault systems have also been simulated. A comparison of the model parameters for two different source processes has yielded very interesting results which may provide a clue in solving the

**ST1/W/15-A2** Poster **1400-20**

**SEISMIC MOMENT TENSORS ISOMETRIC HYPER-SPHERICAL REPRESENTATION**

YUNGA, S. (Institute of physics of the Earth, Moscow, 123810, B.Gruzinskaya, 10, Email: syunga@uipe-ras.scgis.ru)

A new system of parameters describing seismic moment tensors is suggested. Classification of seismic moment tensors is considered on this basis. Typical geometrical configurations are constructed, from one side, with the help of the set of synthetic planar faults: a horizontal fault, a vertical fault, an oblique fault, and, from the other side, using the synthetic slip vectors of horizontal, vertical or oblique orientations. Parametrization of normalized deviatoric moment tensor is obtained by specific spectral decomposition, in terminology of Trusdell. Parametric representation is calculated through angular parameters. It is found that in application to the problem of classification the results of parametrization are geometrically obvious. The suggested set of angles may be considered as spherical coordinates of unit radius-vector in the 4D space. Thus, a parametric representation of seismic moment tensor in spherical coordinates as a point of a 3D surface of a hyper-sphere in 4D space, preserving scalar product is established. Optimum graphic representation of initial data on seismic moment tensors, as well as results of its summation, is obtained. This can be used effectively in seismotectonic deformation study, as well as in statistical analysis of moment tensors. This research was partly supported by R.F.B.R., grant N 98-05-65159.

**ST1/W/35-A2** Poster **1400-21**

**STRESS REDISTRIBUTION IN A SCALING ORGANIZATION OF FRACTURE TECTONICS (S.O.F.T)**

Clement Narteau (1), Peter SHEBALIN (2), Mathias Holshneider (1), Jean-Louis Le Mouél (1) Claude Allègre (1); (1)Institut de Physique du Globe de Paris, IGP, B.P.89, 4 Place Jussieu, 75552 Paris Cedex 5, France, e-mail: narteau@ipgp.jussieu.fr; (2) International Institute of Earthquake Prediction Theory and Mathematical Geophysics, Russian Academy of Sciences, 79/2, Varshavskoye shosse, 113556 Moscow, Russia, e-mail: shebalin@mitp.ru

We consider here simple case of friction in a pre-fractured medium between two tectonic plates which move in horizontal plain with a constant relative velocity. Sliding can occur in a system of many parallel plains. We model this system (its horizontal plain) with a 2-D hierarchical system composed of embedded cells.

Nucleation of sliding occurs in the lowest level cells with a probability depending on the local stress. Each fracture propagates through the hierarchical system according to the S.O.F.T rule (Allègre et al. 1995) applied now in a time interval defined according to the cell size and the fracturing velocity. Sliding of different sizes introduces a self similar stress redistribution in adjacent cells with the scaling of absolute values according to the intensity stress factor. In this simple model with few parameters, we obtain an inverse power-law cascade of fracturing which gives foreshocks before strong earthquakes, power-law post-seismic decay of aftershocks and seismic cycle. In our system the aftershock sequences are obtained without any supplementary artifice; they are due to stress relaxation of non-broken parts in the main shock fault and also due to stress maximums formed by the fault on a distance.

**ST1/W/27-A2** Poster **1400-22**

**SOURCE RUPTURE PROCESS IN THE DIFFERENT FREQUENCY RANGES FOR THE 1997 YAMAGUCHI, JAPAN, EARTHQUAKE (MW 6.0)**

Satoshi IDE (Earthquake Research Institute, Univ. of Tokyo, 1-1-1, Yayoi, Bunkyo, Tokyo, 113-0032, JAPAN, email: ide@eri.u-tokyo.ac.jp)

It is sometimes claimed that an earthquake rupture process looks different depending on analyzed frequency ranges. To investigate the kinematics and dynamics of the earthquake source, I made the analyses of spatio-temporal distribution of earthquake rupture in the different frequency ranges using the same waveform inversion method except for Green's functions. In the relatively high frequency range more than about 1 Hz, it is difficult to calculate accurate Green's function using layered structure. Therefore, for the analysis in high frequency range (0.5 - 2.0 Hz) the empirical Green's functions (EGF) are used, while the theoretical ones are used for low frequency (0.1 - 0.5 Hz) analysis. The studied event is the 1997 Yamaguchi earthquake occurred in western Japan. The data is the strong motion records of Kyoshin-NET, National Research Institute for Earth Science and Disaster Prevention, Japan. The spatio-temporal slip distribution on an assumed fault plane is determined by waveform inversion method of Ide and Takeo (1997). In different frequency ranges and different EGF events, five solutions are obtained. All results have three distinct subevents. Spatially, the slip in the high frequency solution locates near the edge of the slip region of low frequency result. The slip-rate time function at each point on the fault plane in high frequency result tends to have narrow peak at the rupture initiation, while that in low frequency result has smoothed shape and long duration. These suggest that we can see the migration of rupture front using high frequency waveform. Dynamic behavior is also studied using finite difference method for each result. In this calculation, slip and stress relations show larger slip-weakening rate,  $d(\text{stress})/d(\text{slip})$ , in the high frequency result.

**ST1/W/50-A2** Poster **1400-23**

**ESTIMATES OF FAULT GEOMETRIES AND RUPTURE VELOCITIES FOR SMALL EARTHQUAKES USING STOPPING PHASES**

Kazutoshi IMANISHI and Minoru Takeo (both at Earthquake Research Institute, University of Tokyo, 1-1-1, Yayoi, Bunkyo, Tokyo, JAPAN, Email: imani@eri.u-tokyo.ac.jp; takeo@eri.u-tokyo.ac.jp)

Dimensions of small earthquakes have been investigated based on corner frequencies of source spectra or pulse widths of waveforms assuming a rupture velocity, a specific shape of fault surface and orientation of fault plane. Since these assumptions can lead to large errors, most previous estimates of the fault dimensions of small earthquakes are unreliable. In this study, we propose a method to estimate fault geometries (dimensions, shapes and orientations of fault plane) and rupture velocities for small earthquakes using stopping phases. We assume that the fault surface is bounded by an ellipse and that rupture initiates at one focus of the ellipse. In this model, we found that there exist two high-frequency stopping phases whose difference of the arrival times are dependent on rupture velocity, the radius of major semi-axes of ellipse and its ellipticity. These parameters are estimated by nonlinear least-square inversion method. We also determine the fault plane from two nodal planes by comparing the residual at each nodal plane. We apply this method for several small earthquakes occurred around the source area of 1984 Western Nagano earthquake (M=6.8). The result indicates that rupture velocities and rupture

**ST1/L/01-A2** Poster **1400-24**

**MEDIUM-VELOCITY IMPACTS ON GRANITE: GENERATION OF HIGHLY MOBILE POSITIVE HOLE CHARGE CARRIERS**

Friedemann FREUND and Alexander S Bradley, (NASA Ames Research Center, Moffett Field, CA 94035-100 USA)

Impact experiments were conducted on a 25x25x20 cm block of granite from Barre, Vermont, USA, using the NASA Ames Vertical Gun Range (AVGR) with 6.3 mm Al spheres, in the 1.4-1.6 km/sec range plus two shots at 4.45 and 5.64 km/sec which led to disintegration of the block. The granite block, sitting on a grounded Al metal plate, was equipped with (i) three magnetic pick up coils, a first on 10 cm above the plane of impact to measure the electromagnetic (EM) emissions from the plasma plume, a second one at mid-height and third one at the bottom to measure the EM emission from within the block, (ii) three capacitive sensors in the plane of impact, at mid-height and at the bottom, and (iii) two contact electrodes, one at the top in the plane of impact and another one at the bottom, both connected to ground through 2.4 Mohm resistances. After impact the on-set of the EM emission from within the block propagated at the speed of sound, ringing at distinct frequencies in the 10-30 KHz range, decaying within less than 1 msec. The capacitive sensors recorded trains of 20 micro seconds long voltage pulses travelling down the block at the speeds of P wave (6 km/sec) and S wave (3.4 km/sec) and up again with the reflected waves, due to piezoelectric signals from quartz crystals. At the same time the capacitive sensors registered a positive voltage building from within the rock over 600-800 micro seconds and decaying over 2-3 msec. The contact electrodes recorded a current flowing into the rock and decaying over a similar time interval. The current drawn by the bottom contact electrode was modulated by wide amplitude variations, also seen in the response from the capacitive sensors, in particular at mid-height and at the bottom. These observations are consistent with shock-activation of highly mobile positive hole charge carriers  $h_v$ , e.g. defer electrons in the O 2- sub lattice (O-) from pre-existing electrically inactive dormant precursors, presumably preoxy links (O-O-), in the constituent minerals. Activated by the shockwave throughout the volume, the insulating granite becomes momentarily semiconducting. As the  $h_v$  charges spread to the surface and the resulting positive voltage exceeds the potential barrier at the metal-to-semiconductor contact, the Al metal ground plate acts as a gate injecting bursts of electrons across the interface of the rock.

**ST1/E/31-A2** Poster **1400-25**

**NEW TECHNIQUE FOR ANALYSING STRESS-STRAIN STATE OF THE EARTH AS A UNIFORM SYSTEM**

Anatoly DYCHENKO, (Department of Mechanical Engineering, Ukrainian State University of Food technologies, Volodymyrska St., 68, Kyiv, 252610, Ukraine, tel.: 380 (44) 558 8313, fax.: 380 (44) 212 4267, E-mail: dychenko@udufu.niit.kiev.ua)

Principally new technique for determining analytically the distribution of values of physical parameters in real bodies depending on geometric properties of a body's shape and on the physical factor acting on the shape has been developed. The new technique excludes static uncertainty of existing mathematical models. This allows to receive analytical results of a high exactitude, adequate to an initial problem, and also to analyse the stress-strain state of systems of various geometry and to investigate both elastic systems, and systems which do not possess elastic properties. The new technique allows to analyse the stress-strain state of the Earth as a uniform system and can become the basis for creating new methods for long-term prediction of the stress-strain state of the Earth's crust, dynamics of atmosphere and hydrosphere. The application of the given technique when studying physical state of the Earth allows to use in the most comprehensive way the information contained in processed input data and to reduce largely unproductive expenditures of material tools, expended for their deriving. The new technique is an effective analytical tool for the deepening of existing and deriving of new knowledge about the real physical world.

**ST1/E/08-A2** Poster **1400-26**

**SOURCE PARAMETERS OF THE TWO RECENT SCR EARTHQUAKES IN THE INDIAN SUBCONTINENT**

M. RAVI KUMAR, D. Sarkar (both at National Geophysical Research Institute, Uppal Road, Hyderabad 500 007, India, email: postmast@csngri.ren.nic.in) and S. J. Duda (Institute of Geophysics, University of Hamburg, Bundesstrasse 55, 20146, Hamburg, Germany, email: duda@dkrz.de)

The Latur earthquake of 29 September, 1993 with an Mw of 6.2 and the Jabalpur earthquake of 21 May, 1997 with an Mw of 5.8 are two examples of the recent SCR earthquakes in the Indian subcontinent. From the P- wave portions of the broad-band data from several stations of the IRIS and GEOSCOPE networks, we derive the parameters like corner frequency, seismic moment, energy, fault length, stress drop and apparent stress, of these earthquakes using the concept of magnitude spectrum (Duda and Yanovskaya 1993, 1994). This study reveals that for each of these earthquakes, the corner frequency estimates from different stations are relatively consistent. While the fault length for the Latur earthquake is found to be 4.8 km, a larger fault length of about 5.7 km is estimated for the Jabalpur earthquake, although the moment magnitude of the latter is smaller. Also, the Latur earthquake indicates a stress drop and apparent stress, which are 5 times higher, compared to the Jabalpur earthquake. These observations support the view that the Latur earthquake could have occurred due to a relatively new fault in the Deccan traps, while reactivation of a pre-existing fault in the Narmada-Son lineament zone is responsible for the Jabalpur earthquake.

**ST1/E/22-A2** Poster **1400-27**

**EARTHQUAKE AS A FINAL STAGE OF CREEP**

Vitali A. MORGOUNOV (Institute of Physics of the Earth, Moscow 123810, B.Grusinskaya 10, Russia, email: vam@uipe-ras.scgis.ru)

Critical stresses in the interior before the shock are favorable for development of the last, accelerated stage of creep. Creep process, being the more general phenomenon do not always ends with seismic event, that is the physical basis of occurrence of false alarm. Thus, earthquakes can be considered as a display of the general creep motions in the Earth crust, which is important for estimations of reliability of the short-term forecast of earthquakes. Great variety of the earthquake precursor's signature is one of the obstacles to understand the mechanism of its generation. The results of experimental study of short-term precursors carried out in different seismic regions during earthquakes of various energy, depths and at epicentral distances are discussed. The comparison of the records of different geophysical parameters showed that the upper layers of the Earth crust follow after the dynamic of stress-strained state in the focal zone. Consideration of the process of tertiary creep under relaxing load makes possible to explain in the term of Relaxation Creep Model different images of the registered pre-seismic short/immediate-term anomalies in geophysical fields like abnormal electromagnetic and acoustic emission, atmospheric-electric and geochemical parameters at the period just before the earthquake. The experimental estimations of the prognosis probability of the time of impending earthquake in a short-term scale are submitted.

ST1/W/11-A2 Poster 1400-28

## AN ANALYSIS OF THE STAGES OF ACOUSTIC ACTIVITY IN THE LABORATORY EXPERIMENT

SOBOLEV G.A., Ponomarev A.V. (United Institute of Physics of the Earth, Russian Academy of Sciences, Moscow, 123810, B.Gruzinskaya, 10, Russia, email: sobolev@uipe-ras.scgis.ru)

The distribution of hypocenters of acoustic signals of the different energy classes was studied in the course of artificially restrained formation of a macrodestruction source in a granite sample deformed under triaxial compression. The formation of the source is followed by a sudden rise in acoustic activity and by reduction of the external load. The relative frequency of appearance of signals of low energy classes is concurrently reduced, whereas that of higher energy classes increases. The change in this parameter is observed prior to reduction of the outer load, i.e., it represents the prognostic indicator. The distribution of acoustic signals within the zone of the forming source and outside it is different. Inside the source zone, the relative frequency of the appearance of signals of low energy classes is reduced and, consequently, it increases in the outer zone. The signals of high energy classes are characterised by inverse relation. The formation of the source, therefore, takes place during transition of cracking from the lesser to the larger scale level. The development of the source has the stage of acoustic quiescence, during which again occurs the relative increase in the frequency of appearance of signals of low energy classes. The chains of clusters of acoustic signals of different energy classes were investigated. Their appearance precedes both the formation of the zone of the source on the whole and the separate large events within the source. This approach allows to indicate the deterministic part of acoustic activity and thus create the more predictable model of process. The distribution of hypocenters of clusters indicates the area of the future source. It is presumed that the effects and stages of acoustic activity recorded in the course of the analysis of data of the laboratory experiment can be applied to reveal the earthquake sources and to keep track of their development. The work is supported partly by RFBR grants.

ST1/W/16-A2 Poster 1400-29

## EFFECTS OF LARGE SHEAR LOAD PERTURBATIONS ON FRICTION AND HEALING IN SIMULATED FAULT GOUGE

Stephen KARNER and Chris Marone (both at Dept. Earth, Atmospheric and Planetary Sciences, MIT, 77 Massachusetts Ave, Cambridge, MA, USA, Email: slk@bera.mit.edu)

Many characteristics of faulting can be described by the laboratory based rate and state friction laws. However, few laboratory studies have investigated the frictional response to large, rapid loading variations likely to occur in the spatio-temporal vicinity of dynamic rupture. To explore the effects of large loading perturbations on fault restrengthening, we have performed experiments on layers of quartz fault gouge in a biaxial testing apparatus at room-temperature and humidity. We modified the conventional slide-hold-slide (SHS) technique by rapidly reducing shear load prior to holds, and we vary shear load for holds (thold), hold time (th), loading rate, and initial layer thickness (T0). Healing (Dm) is defined as the difference between reload peak friction and pre-hold sliding friction. For all tests, gouge layers dilate during reloading and the amount of dilatancy is greater for larger Dm. With decreasing thold, we observe a systematic increase in Dm and layer compaction. For increasing T0, we observe a similar increase in Dm and layer compaction. For zero-load SHS tests we observe decreasing Dm and increasing layer compaction for longer th. This time-dependent weakening is a consistent feature of our zero-load SHS data, independent of loading rate and T0. Direct measurement across gouge layers show a reversal of slip direction as shear load is reduced (10's  $\mu$ m). This observation, coupled with our compaction data, suggest that gouge deformation during hold cycles occurs in two stages: 1. during unloading, considerable gouge compaction and some slip reversal promotes large initial restrengthening dependent only on thold and T0; 2. during holds, time-dependent gouge compaction is associated with processes that counteract the initial restrengthening, resulting in time-dependent weakening. We have performed numerical simulations using the Dieterich (1979) and Ruina (1983) rate and state friction laws and find that healing predictions do not match the systematic observations from our data. The Dieterich law underpredicts the observed thold dependence of healing, while the Ruina law fails to match the trend. Neither law predict the healing levels nor the time-dependent weakening shown by our data.

ST1/E/05-A2 Poster 1400-30

## SOURCE PARAMETERS OF WEAK CRUSTAL EARTHQUAKES OF VRANCEA (ROMANIA) INFERRED BY WAVEFORM INVERSION

Luminita ARDELEANU and Mircea Radulian (both at National Institute for Earth Physics, P.O. Box MG-2, 76900 Bucharest, Romania, email: ardel@infp.ifa.ro) Jan Sileny (Geophysical Institute, Acad. Sci. Czech Republic, Prague, Czech Republic, email: jsil@blboun.ig.cas.cz) Giuliano Francesco Panza (Department of Earth Sciences, University of Trieste, 34127 Trieste, Italy, email: panza@geosun0.univ.trieste.it)

The inversion of high-frequency waveform data is used to determine the source parameters (seismic moment tensor, hypocenter depth, source time function) and their reliability, for 14 shallow, weak events, distributed in the crustal seismogenic zone, located at the major bending of the Carpathians Mountains. The source is described by the unconstrained moment tensor, which is subsequently decomposed in a volumetric (V) component, a compensated linear vector dipole (CLVD) and a double couple (DC). The Green's functions needed to extract the moment tensor rate functions from the observed seismograms are computed using the multimodal summation method in layered anelastic media. The observed data are digital waveforms recorded by the Romanian telemetered network (epicentral distances up to 150 km). Using four-station configurations the method allows to get the focal mechanism of small events, for which the standard procedures, based on amplitudes of first arrivals, are not providing reliable determinations. To diminish the effects of the inexact structural modelling, consequence of the few available data, an averaging procedure is used to constrain reasonably the source mechanism and the source time function.

ST1/E/09-A2 Poster 1400-31

## A NEW LIGHT ON ARRESTING MECHANISM OF DYNAMIC EARTHQUAKE FAULTING

Nobuki KAME (Department of Earth and Planetary Sciences, Faculty of Science, Kyushu University, 6-10-1 Hakozaki, Higashi-ku, Fukuoka 812-8581, Japan, Email: kame@geo.kyushu-u.ac.jp) and Teruo Yamashita (Earthquake Research Institute, University of Tokyo, 1-1-1 Yayoi, Bunkyo-ku, Tokyo 113-0032, Japan, Email: tyama@eri.u-tokyo.ac.jp)

Classic analyses have shown that dynamic growth of a shear crack cannot be arrested in a uniformly stressed elastic medium with homogeneously distributed fracture strengths. This leads to a general supposition that earthquake rupture growth is arrested by inhomogeneities in the distributions of strengths or stresses. We propose a novel idea for arresting mechanism

of dynamic crack growth in the simulation with no constraints on the crack geometry. Our analysis shows that the arresting occurs spontaneously soon after crack bending even in the homogeneous medium and that inhomogeneities are indispensable not for stopping crack growth, but for its promotion.

ST1/E/07-A2 Poster 1400-32

## PERIOD DOUBLING OF STICK SLIP CAUSED BY HETEROGENEITY IN FRICTION

SHENGLI MA and Changrong He (both at Institute of Geology, China Seismological Bureau, Beijing 100029, China, email: tplabssb@public.bta.net.cn)

Period doubling bifurcation of stress drop is one of nonlinear dynamic phenomena in transition from stable sliding to stick-slip of rock friction. It has been suggested that the onset of period doubling is dependent on stiffness, constitutive parameters and load point velocity. We find in our frictional experiment on medium-scale samples that period doubling bifurcation of stick-slip occurs due to macroscopic heterogeneity of the sliding surface under conditions for typical stick-slip. The strain measurement shows that the period doubling bifurcation of stress drop results from the alternate occurrence of strain release along whole fault and that along parts of fault, i.e. strong patches of fault. To better understanding the physics of period doubling as a possible phenomenon in a fault system with two strong patches as has been simulated by the experiment, we conduct numerical analysis using a two-block model based on the rate- and state- dependent friction law. We get a result that is the most analogous to the experimental result. The simulation result indicates that strong block is active in producing stress drop and weak block only triggers stress drop. Based on detailed analysis of the simulation result, the interaction between two blocks and the mechanism of period doubling of stick-slip are discussed.

ST1/E/23-A2 Poster 1400-33

## STATISTICS OF APPARENT STRESS VALUES AND THE EARTHQUAKES GENERATION MODEL

M.V.RODGIN (Geophysical Centre, Russ. Ac. Sci., 117296 Moscow, Molodezhnaya 3, email: rodkin@wdcb.rssi.ru)

Seismic stresses (apparent stress values, stress-drops) have typically unexpected low values and change in a very wide bounds. This poses a problem do these characteristics have a real physical meaning. The problem was examined using the apparent stress values calculated from the Harvard CMT catalogue and from the regional Russian network. Firstly, the tendency of change of typical stress values was examined. It was shown that despite of a very high variability of apparent stress values the typical stress values display a close correlation with the fluid regime as it is suggested for the Earth's crust and subduction zones. Thus, it is reasonably that variations in stress values have a physical sense also. Distribution of apparent stress values obey the lognormal law. This distribution was imitated by the cascade scheme similar to multifractal approach. Difference in strength of rigid asperities and soft zones was modelled this way. It was shown that the used model describes a few empirical relations between earthquake size and apparent stress value. Thus the used model seems reasonable and thus strength of earthquake source zone is a multifractal. Physical models that could explain the multifractal strength distribution and the revealed tendency in change of typical apparent stress values are discussed.

ST1/E/35-A2 Poster 1400-34

## STUDY OF LONG-RANGE INTERACTION BETWEEN SYNTHETIC EARTHQUAKES IN THE MODEL OF BLOCK STRUCTURE DYNAMICS

Alexandre SOLOVIEV and Inessa Vorobieva (International Institute of Earthquake Prediction Theory and Mathematical Geophysics, Russian Academy of Sciences, Varshavskoye sh. 79, kor. 2, Moscow, 113556 Russia, email: soloviev@mitp.ru, vorobiev@mitp.ru)

The phenomenon of long-range interaction between earthquakes is studied by means of modeling of block structure dynamics. Absolutely rigid blocks separated by thin plane faults are considered in the model. The interaction of the blocks along the fault planes and with the underlying medium is viscous-elastic. The velocity vectors, which define the motion of the structure boundaries and of the medium underlying the blocks are, input model parameters. When for some part of a fault plane the ratio of the stress to the pressure exceeds a certain strength level a stress-drop ("a failure") occurs in accordance with the laws of dry friction; it can cause failures in other parts of the same fault or within other faults. In the model the failures represent earthquakes, so a synthetic earthquake catalog is produced. Numerical experiments with simple block structures show that there is the long-range interaction between synthetic earthquakes. This is detected by statistical analysis of the synthetic earthquake catalogs obtained. At the same time increasing the strength level for individual faults to prevent earthquake occurrence on them affect pronouncedly earthquake flows on other faults. This means that the long-range interaction found in the observed seismicity could be explained by considering lithosphere blocks being absolutely rigid in comparison with fault zones, separating them, and the underlying medium.

ST1/E/47-A2 Poster 1400-35

## NEW MECHANISM OF GENERATION OF LOW FREQUENCY VIBRATIONS DURING THE SEISMIC RUPTURE PROCESS IS PREZENTED AS THE MOVING DEFORMATION WAVE

V.V. AKSENOV (1), V. Rudajev (2) and J. Kozak (3) United Institute of Physics of the Earth, Russian Academy of Sciences, 10 B. Gruzinskaya, Moscow, 123810, Russia (2) Institute of Rock Structure and Mechanics, Academy of Sciences of the Czech Republic, V Holesovickach 41, 182 09 Prague 8, Czech Republic

The long period waves, preliminarily stress drop were registered by laser velocimeter method in shear-slip modeling experiments. Single polar wave profile were always observed after integration. The wave amplitude is reduced with distance from fault zone and became zero. Spectral structure of acoustic signal is changed from anomaly low frequency at fault to standard high frequency with distance from foci. These phenomena were observed while carrying out field experiments (rock burst). The observed long period waves in fault zone is interpreted like moving deformation waves. It is represented a contact interaction of two solid bodies at their relative motion by the scheme of contact interaction of mass having slender deforming lines. Relationships between relative velocity and motion value of a contact surface arbitrary point and geometrical form of deformation transverse and longitudinal waves, their velocities and contact lengths are reported. Forms of longitudinal and transverse waves at displacement motion are observed on different models. Deformation wave velocity; velocity and value of displacement of a contact surface of arbitrary point in the course of moving wave of deformation are determined experimentally. Theoretically estimated and experimentally observed spectra of oscillations have been presented. Physical interpretation of observed (laboratory experiments, rock bursts, aftershocks) modulated oscillations, in the shape of interaction of elastic waves and deformation ones is given.



## ST1/E/50-A2 Poster 1400-36

## ON THE 3-D FRACTURE AND ITS IMPLICATION TO EARTHQUAKE NUCLEATION

Li SHI-YU, Yin Xiang-chu and Liu Qi-liang (Institute of Geophysics, China Seismological Bureau, 5 Minzuxueyuan Nanlu, Haidian District, Beijing 100081, China, email: lisy@cdsindmc.css.gov); Teng Chun-kai (Institute of Geophysics, Chinese Academy of Science, Beijing 100101, China)

The three-dimensional fracture of rock and other material was investigated. Series of fracture experiments on the extension of oblique non-penetrating cracks in plate specimens of rocks and other brittle solids under uniaxial compression was carried out. These cracks are in the category of compound mode  $\phi_0$ - $\phi_6$ . The main feature of extension is that a set of non-coplanar double-curvature sub-cracks and a couple of main crack occur along the crack front. The shape of fracture is asymmetric, which is different from mode  $\phi_0$  and mode  $\phi_1$ - $\phi_6$ . The normal stress criterion of a 3-D brittle fracture of continuum is developed based on the Griffith-Irwin theory. As the results of new method, the shapes of the initial fracture surfaces are described as wide-angle cone with its initial point as its apex. These cones straddle the crack front, and their outline is quasi-helical. Every generatrix of the cone is normal to the maximal principle stress at that point. These results are in good agreement with all the previous experimental results.

There are several characteristics of 3-D fracture, e.g., the initial fractures distribute closely with similar shape. They form self-similar construction, and the number of fractal is about 1.0. In the dynamic process (video recording), the fractures grow one and another but not simultaneously. These characteristics may be significant to the nucleation of the earthquake to interpret the distribution shape of faults (e.g., appearing as en-echelon in the surface of the ground in earthquake center) and the non-coplanar of multiple shocks.

## ST1/E/56-A2 Poster 1400-37

## STRAIN FIELD CHANGES DURING FAULT FORMATION, GROWTH, AND SLIP PROCESSES - AN EXPERIMENTAL STUDY

Hironori KAWAKATA (Disaster Prevention Research Institute, Kyoto University, Gokasho Uji, Kyoto, 611-0011, Japan, email: kawakata@rcep.dpri.kyoto-u.ac.jp); Akio Cho (Geological Survey of Japan, Tsukuba, Ibaraki, 305-8567, Japan, email: cho@gsj.go.jp); Takashi Yanagidani and Mitsuhiro Shimada (both at Disaster Prevention Research Institute, Kyoto University, Gokasho, Uji, Kyoto, 611-0011, Japan, email: yasan@rcep.dpri.kyoto-u.ac.jp, shimada@rcep.dpri.kyoto-u.ac.jp)

We analyzed the tangential strain of fault in granite samples, and the onset of relative displacement on experimentally formed faults during triaxial compression tests. We obtained samples having experimentally-formed faults produced by fault-formation processes in a laboratory. The samples were recovered after the peak stress level had been reached, but before the samples were bisected in the triaxial compression tests. After attaching strain gauges around the fault trace on the sample surface, parallel to the fault trace or transversely across it, the samples were compressed again in the same way as previously. Tangential strain localized around fault tips in accord with the static strain deviation due to slip on a fault in an elastic medium. Localization near the fault nucleation region preceded peak stress. Tangential strain never localized at a point which had previously experienced localization, when the sample was again loaded. Our results also show that the onsets of relative displacement (slip) were behind the fault tips.

## ST1/E/66-A2 Poster 1400-38

## PORE CREATION DUE TO FAULT SLIP IN A FLUID-PERMEATED FAULT ZONE AND ITS EFFECT ON SEISMICITY - GENERATION MECHANISM OF EARTHQUAKES

Teruo YAMASHITA (Earthquake Research Institute, University of Tokyo, 1-1-1 Yayoi, Bunkyo-ku, Tokyo, Japan, email: tyama@eri.u-tokyo.ac.jp)

Spatio-temporal variation of rupture activity is modeled assuming fluid migration in a narrow porous fault zone formed along a vertical strike-slip fault in a semi-infinite elastic medium. Pores are assumed to be created in the fault zone by fault slip. Principle of the effective stress coupled to the Coulomb failure criterion introduces mechanical coupling between fault slip and pore fluid. The fluid is assumed to flow out of a localized high-pressure fluid compartment in the fault with the onset of earthquake rupture. The duration of earthquake sequence is assumed to be much shorter than the recurrence period of characteristic events on the fault. The rupture process is shown to be significantly dependent on the rate of pore creation. If the rate is large enough, a foreshock-main shock sequence is never observed. When an inhomogeneity is introduced in the spatial distribution of permeability, high complexity is observed in the spatio-temporal variation of rupture activity. For example, frequency-magnitude statistics of intermediate-size events is shown to obey the Gutenberg-Richter relation. Rupture sequences with features of earthquake swarm can be simulated well when the rate of pore creation is relatively large. For example, such sequences generally start and end gradually, and no single event dominates in size in each sequence. In addition, the  $b$  values are shown to be unusually large. These are consistent with seismological observations on earthquake swarms.

## ST1/W/45-A2 Poster 1400-39

## A MECHANICAL MODEL FOR EARTHQUAKE NUCLEATION

F. Fattori SPERANZA, V. Sgrigna (both at Dipartimento di Fisica, Universita' Roma Tre, Via della Vasca Navale 84, 00146 Roma, Italy, email: SPERANZA@amaldi.fis.uniroma3.it, Sgrigna@amaldi.uniroma3.it); M. Caputo (Dipartimento di Fisica, Universita' degli Studi "La Sapienza", Ple Aldo Moro 2, 00185 Roma, Italy); R. Console (Istituto Nazionale di Geofisica, Via di Vigna Murata 605, 00143 Roma, Italy)

A 3-D model is developed in order to simulate the occurrence of earthquakes in a seismogenic region characterised by a domain of both parallel and collinear interacting faults, spatially non-homogeneous. The Amonton's law with non-constant friction coefficient is applied to the fault domain. Each fault is supposed to be constituted by a matrix of  $n \times m$  square elements of equal dimensions. Both cohesion and friction coefficient increase with depth up to 20 km, which is a good representation of the observed seismogenic layer. At greater depths, it is supposed that many earthquakes with very small magnitude are nucleated with the condition that cohesion and friction values are much smaller than those assumed for the upper layer. In this way, the  $a$ -seismic creep is simulated. Every fault surface element is supposed to be locked until the occurrence of a seismic event (e.g. non seismic slip takes place in the seismogenic layer). We assume that the friction coefficient is not slip- and rate- dependent, but that it is time-dependent. The time intervals corresponding to the variation of friction are chosen randomly in the range 10-100 year, which is the period necessary to allow the stress to reach the fault strength. Empirical features as the Gutenberg-Richter's relationship and the Omori's Law are expected to be fit by our model. Further refinement of the model is obtained by applications to experimental data.

## EARTHQUAKE PREDICTION

## ST1/W/65-A3 Poster 0900-01

## MEDIUM TERM FORECAST ON NOVEMBER 18, 1997, M=6.7 EARTHQUAKE IN GREECE

ZAVYALOV A.D. (United Institute of Physics of the Earth, Russian Academy of Sciences, str.B.Gruzinskaya, 10, 123810 Moscow, Russia, tel. +7(095)254-2478, fax +7(095)254-2478, email: zavyalov@uipe-ras.scgis.ru.

In the beginning of 1997 the MEE algorithm (Map of Expected Earthquakes), based on physics of a seismic source, results of physical modelling and research of a seismic regime, was used for maps of expected earthquakes computation for Greece. The informational basis of work was the catalogue of earthquakes for 1964-1995 (about 55 thousands of events), kindly given by the Greek colleagues from the Geophysical Laboratory Aristotel University of Thessaloniki. The algorithm allows calculating the maps of spatial distributions of conditional probability of strong earthquake appearance with use of a complex of geology-geophysical prognostic indicators, each of which has the certain physical sense. Two types of indicators are used: dynamic, fast varying on the time intervals, that are essentially smaller as compared with time preparation of strong earthquake, and quasi-stationary, slowly changing its values. As dynamic prognostic parameters  $b$ -value, density of seismogenic ruptures  $K_{sr}$ , number of weak earthquakes, released seismic energy of weak events  $E^{**2/3}$  were selected. A role of a quasi-stationary indicator performed the map of seismotectonic faults of Greece. The retrospective analysis of maps of expected earthquakes has shown, that 48% of target earthquakes with  $M_b=5.5$  happen in areas with conditional probability  $P(D1|K)>70\%$ . The square of these zones does not exceed 20% from total square of observation area. On the last map of expected earthquakes with the prognostic period 1996-2002 a number of zones with increased probability of target earthquake appearance in them are revealed. The obtained results were presented on the S7 symposium on 29-th General Assembly of IASPEI in August 1997 (Greece, Thessaloniki). In one of zones located in 200 km to a southwest from Athens, on November 18, 1997 has taken place earthquake with  $M=6.7$ . The work has been executed under financial support of RFBR, project 94-05- 16114.

## ST1/W/49-A3 Poster 0900-02

## THE USE OF AN OUTLIER DETECTING METHOD IN TIME SERIES OF CONTINUOUS DAILY MEASUREMENTS OF UNDERGROUND WATER LEVEL AND TEMPERATURE IN EARTHQUAKE PREDICTION INVESTIGATION

D. Arabelos, G. ASTERIDIS, M. Contadakis (all at Department of Geodesy and Surveying, Aristotle University of Thessaloniki, Univ. Box 444, GR-540 06 Thessaloniki, Greece, email: aster@eng.auth.gr); G. Zioutas (Division of Computational Methods and Programming, General Department, Faculty of Technology, University of Thessaloniki, Greece); Xu Daoyi, Zhang Cunde, Zheng Binghua (Department of Geology, State Seismological Bureau, 100029 Beijing, China)

Two years continuous daily measurements of underground water level and temperature have been performed in four selected shallow wells in a seismic area close to Thessaloniki, Greece. A graphical method has been applied for the analysis of these water level and temperature time series in order to detect outliers. The magnitude of the changes of the underground water level, characterized as outliers, varies from 3 to 10 cm, and the corresponding changes of the temperature varies from 0.3 to 0.8 degree centigrade. Combining the resulting outliers with the seismic activity observed in the same time period and in the same area, a high correlation was found in the case of the water level time series. In the case of the water temperature time series the correlation was lower. Most of the outliers were detected in a time interval which varies from 1 to 7 days before or after the earthquakes. The strongest outliers found, correspond to earthquakes with  $M > 3.0$ . The software developed is able to detect outliers, in the time series of continuous daily measurements, at the time of their occurrence, using only the previous observations. This is very important in studying precursory phenomena of forthcoming earthquakes.

## ST1/W/64-A3 Poster 0900-03

## AN ANALYSIS OF LONG-TERM SEISMIC QUIESCENCE BEFORE THE GREAT HYOGO-KEN NANBU, JAPAN, EARTHQUAKE ON JANUARY 17, 1995

FU ZHENGXIANG and Liu Geiping ( Center for Analysis and Prediction, China Seismological Bureau, 63 Fuxing Avenue, Beijing, 100036, China, Email: fzx@ip.cap.ac.cn); Ando Masataka, (Research Center for Earthquake Prediction, DPRI, Kyoto University, Japan)

The great Hyogo-ken Nanbu, Japan, earthquake 7.2 on January 17, 1995 was located at 34.595 N, 135.036 E. The aftershock area of about 25km x 70km trended northeast to southwest. The aftershock area is considered to be the source area of the mainshock, where the temporal variation of seismicity before the mainshock has been studied here. The earthquake data ( 1976.1 to 1995.1 ) used come from the seismic data-base compiled by DPRI, Kyoto University, Japan. The minimum magnitude of completeness was considered as 2.0 by the magnitude - frequency relation. The research show that there was a period of about 6.5 years of seismic quiescence from July 25, 1988 to January 16, 1995, the seismic rate in the period decreased by 34 percent comparing to a background seismicity rate from January 1, 1976 to July 24, 1988; the difference between the rates in two periods is obviously at the significant level 90 -- 95 % by statistically Z--test method, the calculated Z value is equal to 1.78. The seismicity had an increase in a short-term of several days prior to the mainshock occurrence.

## ST1/E/24-A3 Poster 0900-04

## PREDICTION MODELS OF THE TIEN-SHAN SOURCE ZONES LOCATION

Elena MUSIENKO (Institute Of Seismology, Nas Kyrgyz Republic, Asanbai 52/1, 720060 Bishkek, Kyrgyzstan, email: kis@imfiko.bishkek.su; itmc@imfiko.bishkek.su); Alexander Lobanchenko (Institute of Geology NAS Kyrgyz Republic, Erkindik avenue 30, 720000 Bishkek, Kyrgyzstan)

The approach to modeling mathematically the source zones location was applied at the Tien-Shan region. We used method of purposeful classification and objectives ordering to calculate possible  $M_{max}$  through polymasured linear correlation between geological and geophysical parameters and the strongest earthquake sources ( $M > 6.0$ ) space distribution. 24 primary parameters were selected to characterize the deep structure, recent tectonics and seismicity at the region. We chose four reference patterns at the three main Tien-Shan tectonic areas which are significantly different. The estimation of correlations between parameters mentioned above and strongest earthquake sources space distribution has shown that number of parameters and their informative weights are not the same for different reference patterns. However following four parameters: small earthquakes density on 100 sq.km; summary velocities of the vertical tectonic motions for Recent period; transformed gravity field and  $V_p$  velocities for the upper

crust (depth is about 30 km) remained among informative ones invariably. Quality of recognition of the source zones location depended on choice reference pattern. From 55% to 77% strong events ( $M > 6.0$ ) occurred in past were discerned by 4 prediction models. Numerical models included past and new sources zones that are similar in general.

**ST1/W/07-A3** Poster **0900-05**

#### PHYSICS OF THE SEISMIC SOURCE AND EARTHQUAKES PREDICTION

Ponomarev A.V., Sobolev G.A., Tyupkin Yu.S., ZAVYALOV A.D. (all from United Institute of Physics of the Earth, Russian Academy of Sciences, str.B.Gruzinskaya, 10, 123810 Moscow, Russia, tel. +7(095)254-2478, fax +7(095)254-2478, email: zavyalov@uipe-ras.scgis.ru.)

The complex of laboratory and field researches of physical substantiation of new methods of seismic hazard evaluation and prognosis of earthquakes was carried out.

It was established as result of laboratory experiments, that the model of a seismic source passes some main stages during its development: accumulation of small-sized ruptures up to a critical level; association of cracks with formation larger and localization of this process in a zone of an unstable strain. These stages are accompanied by prognostic effects of clusterization of acoustic emission, quiescence and foreshocks activation.

On a basis of the physical modelling regularities the algorithms were offered and the programs for revealing places of the developing sources, time and magnitude of appropriate earthquakes were compiled. The medium term forecasts in real time of two earthquakes with  $M=7.0$  (June 21, 1996) and  $M=7.7$  (December 5, 1997) on Kamchatka are carried out. The information basis of work was the regional catalogue of earthquakes (more than 60 thousands of events) and laboratory catalog of acoustic emission (more than 100 thousands of events). The suggested approach is shown to be effective for using in real time warning systems. The work has been executed under financial support of RFBR, projects 96-05-65439, 97-05-65906 and 99-05-65447.

**ST1/W/34-A3** Poster **0900-06**

#### PREDICTION OF THE LARGEST EARTHQUAKES WORLDWIDE SINCE 1985

Vladimir KOSSOBOKOV, Leontina Romashkova (both at International Institute for Earthquake Prediction Theory and Mathematical Geophysics, Russian Academy of Sciences, 79-2 Warshavskoye Shosse, Moscow 113556, Russia, E-mail: volodya@mitp.ru)

The hierarchical approach to earthquake prediction has been statistically verified at the 99% confidence level recently. It became possible due to the on-going systematic real-time testing in the Pacific Rim and to abnormal rise of global seismic energy release during 1993-1996 that produced enough magnitude 8 events for the conclusion. Statistical validity of predictions by the reproducible algorithms M8 and MSc confirms the underlying paradigms: existence of robust premonitory seismic patterns, large size fault system involved in formation of the phenomena at the scale of years, their partial similarity in a wide range of tectonic environment, and their certain universality. We have analyzed in detail case histories of all the recent great earthquakes (with magnitudes 8 or above) within space-time of intermediate-term predictions in attempt to find short-term rise of seismic activity close to the epicenter of approaching large earthquake. This phenomenon is observed before some of the great earthquakes (e.g. 4 October 1994, Shikotan Island,  $M=8.2$  event), but in some cases it is hard to reveal due to evident incompleteness at small magnitudes of the global data bases available. Thus, in such regions better catalogs of earthquakes are needed for next refinement of intermediate-term predictions on a regular basis. On the background of intermediate-term prediction the short-term precursors could become distinguished. Without the intermediate-term stage they could be lost easily in the seismic static.

**ST1/W/60-A3** Poster **0900-07**

#### EARTHQUAKE PREDICTION CASE HISTORIES IN VRANCEA (ROMANIA) AREA

V. MARZA (Seismological Obs., Univ. of Brasilia, Brasilia-DF, Brazil, email: marza@unb.br); V. Burlacu (Center for Monitoring Research, Arlington, VA 22209, email: burlacu@cmr.gov); H. Sandi (INCERC, Bucharest, Romania, email: sandi@cons.incerc.ro); H. Shimamura (Lab. for OBS, Hokkaido Univ., Sapporo, Japan, email: shima@obs.sci.hokudai.ac.jp); A. Pantea (Seismological Lab., NI[R&D]EP, Bucharest, Romania, email: pantea@infp.ifa.ro)

Vrancea Seismogenic Zone [VSZ] is a conspicuous active area in terms of its: (A) extraordinary seismotectonic characteristics (extremely compact subcrustal source, impressive seismic energy release rate or a rare 'event' in terms of hypothesis of a terminal phase of detachment of a subducting slab), (B) outstanding persistent and highly recurrent seismicity [SE] displaying a remarkable regularity in occurrence of large events and manifestation of a plethora of (geo)physical precursors [PRs]; (C) severe socio-economic impact (i.e., 4-5 damaging events a century) with huge felt and meizoseismal areas. During the 1985-1989 period a joint Japanese-Romanian earthquake prediction [EqP] program was underway in VSZ and along the time EqP and hazard evaluations were carried by various teams as well.

The last two major VSZ events, i.e., the 1977 ( $M_w=7.4$ ) and 1986 ( $M_w=7.2$ ) were successfully forecasted and respectively anticipated. The forecasting (long term EqP) of the 1977 event was based on salient regularity patterns in long-term strong SE (cyclicality and paired occurrences) displayed by all large events ( $M_w \geq 7$ ) during a time span more than a millennium. The anticipation (medium term EqP) of the 1986 event was based on a variety of precursory SE patterns including: preseismic quiescence, hypocentral migration, b-slope change etc ('a priori' reported), but also other PRs: seismic (e.g., foreshocks), geophysical (an underground microtemperature anomaly or a telluric current observation) and biological ones, or parameterized EqP algorithms were observed.

Currently a forecast for the next major ( $M_w \geq 7$ ) VSZ event is attempted with the approximate time window:  $2006 \pm 7$  yr and magnitude range  $M_w=7.3 \pm 0.3$  unit; obviously the space interval is not crucial as the spatial extent of the VSZ is only  $80 \times 35$  km<sup>2</sup> (certainly the depth range should be of more interest, but this parameter could be inferred when some physical PRs, e.g., seismic quiescence, would be detected). All the above case histories are presented, discussed, refined and evaluated for their causal, informational and predictive potential. Finally we like to emphasize (based on past history) the good prospects and likelihood for observation of PRs and predictability of VSZ major events and in turn we advance/contemplate the following...

**ST1/P/05-A3** Poster **0900-08**

#### STUDY ON THE QUASI DYNAMIC FACTORS IN THE APPLICATION OF EARTHQUAKE PREDICTION

Wang LINYING, Zhu Chuangzhen and An Zenwen (Institute of Geophysics, China Seismological Bureau, Beijing, 100081, China, email: Zhucz@ihw.com.cn)

Earthquake process consists of a complex macro-system, based on the concept of modern

physics, there are two fundamental features of macro-system: dissipation and catastrophe. Dissipative function is illustrated by invariability of time-inversion during the violating rule of macroscopic movement, while, catastrophe means that a series of instability corresponding to the violation of symmetry in time. Thus, it is essential in earthquake prediction research, to probe the dissipative function in the preparatory process of earthquake and instability of temporal evolution. It is reasonable to assume that the earthquake preparatory system develops into a self-organized critical state just prior to the occurrence of large earthquake than the characteristics of system should be indicated by special dynamic patterns. In the paper we pay more attention to the selection of relatively independent predicting factors from non-linear dynamics point of view, as well as to the efficiency of prediction through strict stochastic test. Considering the clustering, orderliness and instability shown in the precursory seismic pattern, seismic entropy, multi-fractal dimensions, algorithmic complexity and Hurst index are selected as predicting factors. By use of scanning analysis, more than hundred earthquake cases in Chinese Continent have been studied from 1970 to 1998 and rigorous statistical test is carried out to estimate the efficiency of earthquake prediction. The results indicate that the factors selected above exhibits a certain efficiency of prediction than the random forecast, and false alarm can be greatly reduced by using multi-factor comprehensive prediction method.

**ST1/E/41-A3** Poster **0900-09**

#### THE EARTH TIDE OBSERVATION IN CHINA AND ITS APPLICATION STUDIES ON PREDICTION OF EARTHQUAKE

Yaibin ZHANG, Jun Jiang, Shengle Li, and Daihong Yan (all at Institute of Seismology, China Seismological Bureau, Wuhan, 430071, China)

There are more than 100 observation stations of the earth tide (tilt, strain and gravity) in China, they belong to the Seismological Bureau of China and about 40 stations are in good working. Their main purpose is for monitoring and observing of the seismic precursor and predicting of earthquake. In this paper, the progressive development of studies how to use the earth tide observation on earthquake prediction in China is introduced systematically in several aspects as below:

(1). The analysis of the earth-tide observation data and study on catch information of precursor abnormal. The main methods are: (a). The characteristic parameters that relate to the elasticity of crust media are analyzed based on the tide theory. The results can show the effect of elasticity change in the seismic process. (b). By using of some mathematical methods such as fit-testing, filtering, testing, spectral analysis etc, to catch the interference information in observation by that seismic effect. (c). The application of the theory of response ratio by tidal load and unload. (2). The statistical analysis results of the scope of monitor ability of the earth tide observation. (3). The testing evaluates of the various precursory parameters. (4). The synthetic analysis method of the precursors information. (a). To get physical characteristic parameters synthetically from earth tides observations considering its physical properties. (b). Synthesis many different observational anomalous information in some spots or area. (5). The study on some examples of earthquake. (a). The analysis on precursors of the Ms 7.0 Lijiang earthquake took place in Feb, 1996 is carried on by using the earth-tide observations in Yunnan and Sichuan area, China. (b). To show the analysis results of precursory anomalous of Ms 6.2 earthquake happened in Zhangbei, Hebei province, China in 1, 1998.

**ST1/W/73-A3** Poster **0900-10**

#### RELIABILITY OF FORECAST AND LUNAR HYPOTHESIS OF EARTHQUAKES

Yury A. BRAGIN, Oleg A. Bragin (both at Novosibirsk State University, 630090 Novosibirsk, Russia, email: obragin@phys.nsu.ru); Vasily Yu. Bragin (United Institute of Geology, Geophysics and Mineralogy, Ac. Koptyug prospekt, 3, 630090 Novosibirsk, Russia)

It is established that the global component of a geoelectrical field contains electrical precursors of earthquakes. We isolated these precursors and observed that they arise in some tens hours before the earthquakes manifest itself on a surface of the Earth. The comparison of time when a precursor appears and the real earthquake occurs revealed the following experimental facts. (1) If during the forecasted period no electrical precursors of the large amplitude appeared, then no strong earthquakes occurred on the Earth at this time. There were no exceptions from this statement for four years of permanent monitoring. (2) Time interval between the moment of registration of an electrical precursor and the moment of appropriate earthquake is approximately constant. (3) As a first approximation, the magnitude of an electrical precursor is proportional the earthquake magnitude expressed in Mb. The last two statements allow forecasting the time and magnitude of earthquakes with reliability 60-70%. The unreliability arises mainly due to lacking of global information about powerful earthquakes. On the basis of prevailing positive experience of the forecast one can make the conclusion about presence of a periodic factor, that influences substantially on the earthquake dynamics. We believe the lunar influence is this factor. At the certain stage of formation of earthquake the processes in seismically stressed points become especially sensitive to periodic change of gravitational influence of the Moon.

**ST1/E/16-A3** Poster **0900-11**

#### THE PREDICTION OF EARTHQUAKES (PE) AND EM PARAMETERS OF SEISMIC SOURCES (SS)

A. P. NAUMOV ( D.I. Mendeleev Institute for Metrology, St. Petersburg, 198005, Russia, email: slovo@mail.line.ru )

Many field observations of electromagnetic (EM) tectonic signals, which researchers realized for last 20 years in different regions, have shown a direct relation of these signals with the possibility of PE. We shall select only some observations as undoubted possibility short-term PE on EM and magnetic signals within the range of frequencies from 0 to 10 Hz, when high-speed magnetometers with the optical pumping (MOP) can be applying. The installation of the vector MOP in the corners of equilateral triangles with sides 20-50km gives the possibility to define power, time and coordinates of the sources of expecting earthquakes on results of components measurements in the zone of coherent EM signals. This measurements made with MOP allows to cover seismic hazards area using a small number of instruments. Nature of SS can be better understood, if we produce the physical models of SS and process of earthquake. This model-process consist of several stages: the first - accumulation of tectonic energy (months, years); the second - preseismic preparation, when all precursors are registered (hours, weeks); etc. Specific sequence of the EM tectonic signals corresponds to each stage. We considered different aspects of both models, made quantitative estimates some EM parameters of SS in all stages. Differences between EM tectonic signals and signals of ionosphere are discussed.



ST1/C/JSA10/W/15-A3 Poster 0900-12

**A POSSIBILITY OF SHORT-TERM PREDICTION OF ORIGIN TIME FOR DISASTROUS EARTHQUAKE IN SOUTHERN KURIL ARC**

Ivan Tikhonov (Institute of Marine Geology and Geophysics, Far East Branch of RAS, Yuzhno-Sakhalinsk, Nauka street, 693002 Russia, email: tsunami@sakmail.sakhalin.ru); Alexander MALYSHEV (Institute of Geology and Geochemistry, Urals Branch of RAS, Pochtovy per 7, Ekaterinburg, SU-620151, Russia, email: root@igg.e-burg.su)

Satisfactory origin time estimations for disastrous earthquakes with  $M \geq 7.5$  were obtained from a retrospective short-term prediction in the studied region on the basis of mathematical modeling. The following parameters of seismic process were investigated: a cumulative sum of the number of shocks, the similar sum for energy of earthquakes and square root from the energy. We analyzed the total seismic events flux within the region for magnitude  $M \geq 4.0$  since 1962. The algorithm was designed to imitate real time processing. The average relative prediction error is within the interval 18-49 %. The first satisfactory results are gained not earlier than 100 days before the main shock, however, in one anomalous case - 2.7 days before. This technique has been tested for more than 10 years and now is fit for experimental predictions of Kuril earthquakes. We plan to combine it with intermediate-term prediction algorithms (first of all with the M8 algorithm), that gives a significant reduction of failures-to-predict. We have now good possibilities to realize a prediction scheme in two steps: intermediate first and then short-term. Thus, the alarm is declared by the M8 algorithm since 1996 to 2001 within the studied region for earthquakes with  $M = 7.5-7.9$ . Trial calculations show, that our prediction methods, probably, will be perspective for using in other regions.

ST1/E/49-A3 Poster 0900-13

**FORESHOCK ACTIVITY BEFORE THE STRONG EARTHQUAKE AS A PRECURSOR FOR LONG TERM EARTHQUAKE PREDICTION**

PHAM DINH NGUYEN, Pham Quang Hung, Nguyen Dinh Xuyen, Institute of Geophysics Vietnam National Center for Natural Science and Technology, Cau Giay - Hanoi - Vietnam.

Using the seismological data of ISC in the period 1965-1993 the authors have studied the variation of seismic activity in the focal area of earthquakes ( $M_b \geq 5.0$ ) in the region limited by  $20N \leq \text{lat.} \leq 30N$  and  $95E \leq \text{long.} \leq 105E$ . Seismic activity is characterized by total of number  $N$  of earthquakes in interval of time  $dt = 5$  years and its variation is expressed in the graphs ( $N$ ,  $t$ ), where  $t$  is observation time. We can see on the graphs that the foreshock activity is clearly observed in many cases, among them are all the cases of earthquakes of magnitude  $M_b \geq 6.0$ . This activity may be begun about 10 or 15 years before the main shock. In this period the seismic activity is gradually increased. The observed fact indicates that the foreshock activity is a precursor for long term earthquake prediction.

ST1/E/42-A3 Poster 0900-14

**SUCCESSFUL PREDICTIONS FOR THE KRONOTSKY EARTHQUAKE DECEMBER 5, 1997,  $M=7.9$ , KAMCHATKA, AND FOR ITS STRONG AFTERSHOCKS  $M_6$ .**

Sergei A. FEDOTOV, Sergei D. Chernyshev, Jury D. Matvienko, and Nikolai A. Zharinov (Institute of Volcanology, Far East Division, Russian Academy of Sciences, Petropavlovsk-Kamchatsky, 683006 Russia, email: volcan@svyaz.kamchatka.su)

Successful long-term and mean-term seismic prediction for the Kronotsky earthquake December 5, 1997,  $M=7.9$ , occurred in subduction zone near the Kronotsky peninsula, Kamchatka and for its strong aftershocks,  $M_6$  has been made by four different methods at the Institute of Volcanology, FED RAS. Their combination includes next ones: long-term seismic prediction based on features of seismic gaps and seismic cycle, algorithm M8, repeated geodetic measurements, application of the found average sequence of aftershocks  $M_6$  which follow Pacific earthquakes  $M-8$ .

Regular long-term seismic prediction for Kamchatka made in June, 1997 has shown that the area of the Kronotsky peninsula has become one among two most probable places of earthquakes  $M > 7.7$  in Kamchatkan seismic zone for the next 5 years. This result was reported on June 19, 1997.

Algorithm M8 was used to determine mainly probable time intervals for events  $M_{7.5}$  near Kamchatka. It was reported in April 1996 that such interval for the area of the Kronotsky peninsula is between July 1, 1993 and June 30 1998.

Different geodetic observations were repeated since 1971 at the Ust-Kamchatsk geodetic polygon at distance 100km from the epicenter of the Kronotsky earthquake. Contraction of all measured lines (4-10-6) was detected here at the end of November 1997. Conclusion was made and reported on December 4 1997 one day before the Kronotsky earthquake that earthquake  $M > 7.0$  is preparing in its area.

Expected number and magnitudes of strong aftershocks  $M_6$  were predicted correctly after the main shock of the Kronotsky earthquake for the first days, weeks, months and year of aftershocks.

ST1/P/06-A3 Poster 0900-15

**A METHOD TO EXPRESS THE PATTERN OF SEISMICITY ANOMALY BEFORE STRONG EARTHQUAKES AND ITS PREDICTIVE VALUE**

Hong CHEN (Institute of Crustal Dynamics, China Seismological Bureau, Beijing, 100085, China; E-mail: hongchen@sdb.cdi.ac.cn, tel: 0086-010-62913865-2107)

Seismic quiescence and seismic clusters within the preparation area of earthquakes are one of the anomalies before strong earthquakes. Here we proposed a method to express seismic quiescence and seismic clusters on a map at the same time and we hope that would be useful to determine the future earthquake position. Two parameters were defined as:

Here  $N_{ij}$  is the number of earthquake with magnitude  $M \geq m$  in  $i$ -th space and  $j$ -th time interval, and is the average earthquake number of many years in the same space grid.  $E_{ij}$  is the equivalent magnitude of seismic strain release in  $i$ -th space and  $j$ -th time interval, and is the average equivalent magnitude of many years in the same space grid. China was divided into three seismic areas according to its seismicity level and detection level. Each seismic area was divided into a  $1^\circ \times 1^\circ$  grid,  $_N$  and  $_E$  were calculated for each grid using seismic data from 1970 to 1998 ( $M \geq 2.5$ ), and the contour maps of  $_N$  and  $_E$  were got for each time interval (one year). The results show that from 1970 to 1998 there were 68 earthquakes magnitude greater than 5.0 occurred in North part of China, values of  $_N$  and  $_E$  within the preparation area of 48 earthquakes are great or low obviously. We also calculated another two seismic area of China. We analyzed if it is possible to use those patterns of seismicity anomaly to determine future earthquake position.

ST1/W/66-A3 Poster 0900-16

**SOME EVIDENCE FOR PREMONITORY CHANGES IN SEISMICITY FOR THE 1995 HYOGO-KEN NAMBU EARTHQUAKE: (2) FRACTAL DIMENSION AND ITS CORRELATION WITH B-VALUE**

Bogdan ENESCU (National Institute for Earth Physics, Bucharest, Magurele, P.O. Box MG-2, Romania, e-mail: benescu@infp.ifa.ro) Kiyoshi Ito (Disaster Prevention Research Institute, Kyoto University, Gokanoshio Uji, Kyoto, 611-0011, Japan, e-mail: ito@rcpe.dpri.kyoto-u.ac.jp)

Using the same catalogue as in the first part of our study (but without declustering), we continue our search for possible precursory changes associated with Hyogo-ken Nambu Earthquake. This time we focus our attention on fractal dimension (correlation dimension,  $D_2$ ) evolution in time and the correlation between  $D_2$  and  $b$ -value and its evolution in time. We use for the computation of  $D_2$  the sphere counting method and for  $b$ -value determination we use the maximum likelihood approach. In order to see reliability and robustness change of the results, we compute the above functions using different initial inputs; time windows of 100, 200 and 400 events and different minimum magnitudes. The obtained results show that the time evolution pattern of the computed parameters is changing before the Hyogo-ken Nambu Earthquake. We observe also that, for all the period considered, the change of  $D_2$  and  $b$ -value in time correlates quite well with seismicity evolution (occurrence of events of magnitude bigger than 4, aftershocks and preshocks, earthquake swarms). Approximately 7 years before the Hyogo-ken Nambu Earthquake the correlation between  $D_2$  and  $b$  value is changed from weak negative to moderate positive. We propose some possible physical explanations for this new earthquake precursor: the correlation between  $D_2$  and  $b$ .

ST1/E/28-A3 Poster 0900-17

**LOCAL PROBABILITY OF A MAJOR EARTHQUAKE: AN ALTERNATIVE METHOD TO ESTIMATE LOCAL SEISMIC HAZARD, THE EXAMPLE OF GREECE**

G.CHOULIARAS (Institute of Geodynamics, National Observatory of Athens, 118 10 Greece, Email: gchoul@mail.totenet.gr); M. Wyss (Geophysical Institute, University of Alaska, Fairbanks, USA), S.Wiemer (Meteorological Research Institute, JMA, Tsukuba, Japan); George Stavrakakis and G.Drakatos (both at Institute of Geodynamics, National Observatory of Athens, 118 10 Greece)

We assume that the frequency-magnitude relationship contains information about the probability of occurrence of main shocks,  $P(M)$ , in the volume for which it is valid and that in some areas one can estimate from its parameters  $a$  and  $b$  the probability for a main shock. In small volumes, comparable in size to crustal asperities, are studied separately, one finds that  $a$ - and  $b$ -values vary strongly over distances of just a few kilometers. That means that  $P(M)$  must vary locally also strongly and we introduce the notion of  $PL(M)$ , the local probability of a main shock. It is this variation that we intend to map, and we explore its potential for better estimating the local probability for a main shock for the Greek area. The local probability of a main shocks that we estimate may be useful for identifying locations where major earthquakes are most likely, and from where ruptures of large earthquakes may emanate. We don't argue that the standard engineering approach of estimating accelerations should be replaced by estimating  $PL(M)$ . Instead, we propose that  $PL(M)$  gives a complimentary estimate of seismic hazard, and that in the future the standard engineering approach may be improved by using local  $a$ - and  $b$ -values within the seismic source volumes, instead of bulk values.

ST1/E/73-A3 Poster 0900-18

**THE SEISMIC RISK MAP OF VIETNAM USING THE GUMBEL'S THEORY**

PHAM QUANG HUNG Nguyen Ngoc Thuy Institute of Geophysics Vietnam National Center for Natural Science and Technology, Cau Giay, Hanoi, Vietnam.

In this work, a seismic risk map of Vietnam is constructed using the modified first asymptotic distribution of the extreme values theory. On the basis of the earthquake catalogue of Vietnam the earthquakes with  $M > 4$  of the studied territory was obtained and analyzed. The maximum potential earthquakes that are expected to occur with a 10% exceeding probability within 50 years are estimated in eight seismic provinces. Finite seismic sources of maximum expected potential earthquakes are assumed as seismogenic faults or points located randomly within the meizoseismal areas in each seismic province. Maximum ground acceleration for all points on a grid:  $0.16$  degree  $X$   $0.16$  degree (geographical coordinate) are computed by using Boore's attenuation equation and the results are contoured on the seismic risk map of Vietnam.

ST1/W/16-A3 Poster 0900-19

**EARTHQUAKE PREDICTION: PROBLEMS AND RESULTS**

Oleg KHAVROSHKIN, Vladislav Tsyplakov and Natalia Vidmont (United Institute of Physics of the Earth, Russian Academy of Sciences, B.Gruzinskaya 10, 123810 Moscow D242 Russia, Email: khavole@uipe-ras.segis.ru)

The history of the problem mentioned in the head is full of dramatic collisions. Methods of many branches of modern science are applied for its solving. Thus, we shall invent general aspects of this problem without detail: 1. The monitoring of the energetic state of investigated region. 2. Physical models. 3. The paradigm of the prediction and courses of its deadlock. 4. Nets of seismic stations. 5. What to do: abandonment of the old paradigm, the prediction in the open non-linear system, etc.

The analysis based on the scheme proposed leads to sad prognosis on complete decision of the problem in nearest 10-20 years. The only way is to abandon on the existing paradigm and development of the scheme of operative prediction of individual using (OPIU). We propose the scheme of OPIU that can be realized just now. It is based on the analysis of the emission seismic response of geophysical media in the region learned by the user, to local variations of strained state. We suppose that the great part of seismological information is contained in the emission seismic noise. Thus, this noise must be recorded in dangerous areas permanently.

ST1/W/72-A3 Poster 0900-20

**SEISMIC SEQUENCES IN RILA MOUNTAIN**

Blagovesta Babachkova, Tatiana TOTEVA, Snezhina Rizikova (Department of Seismology, Geophysical Institute, Ak.G.Bonchev Str., Block 3, 1113 Sofia, Bulgaria, email: toteva@nlcv.net)

This study aims to investigate the sequences in Rila mountain region. The area mentioned above is interesting for some reasons: the lack of strong earthquakes, but this region is closed to active areas especially Kresna seismic zone - the most active region in Bulgaria (Rila region is included in Knopoff space window for 1904 earthquake,  $M=7.8$ ). Another reason for investigating the Rila Mountain is the observed seismic sequences there. The last seismic swarm occurred in 1997. More than 170 events were located in a very narrow area. The waveforms and earthquake recurrence graph were investigated. Great similarity exists in the waveforms for most of the swarm events. Nevertheless, the old sequences in this region were reviewed and an attempt to find a probable relation between them and the strong events was made.



ST1/L/02-A3 Poster 0900-21

**MODEL FREE SEISMIC HAZARD EVALUATION AND ITS APPLICATIONS IN MINING INDUCED SEISMICITY**

Stanislaw LASOCKI Andrzej Kijko.

Statistical procedures which are used for the evaluation of seismic hazard assume that the analytical forms of the distribution functions of seismic event magnitude are known. The distribution functions are usually derived from the Gutenberg-Richter relation or its modifications. In most cases, for magnitudes in the middle of the range of distribution, the choice of the model is not crucial, however, it can have a significant effect on estimates related to the upper tail of the distribution which determine the values of seismic hazard parameters. Hence, for example, the occurrence of so called "characteristic" events can drastically change the tail of the magnitude distribution and influences the values of hazard.

The presently used models of magnitude distribution are unable to account for these and other non-linear effects in frequency-magnitude relations, well documented in both natural and mine induced seismicity. It was therefore decided to replace analytical models of the magnitude distribution by kernel-based distributions, which are data-based and non-parametric. To describe the probability density function (PDF) of seismic event magnitudes we chose the Gaussian kernel function and the smoothing factor estimated by means of the least-square minimization of the mean integrated square error. An analysis of several cases of seismicity induced by mining in South African gold mines and Polish copper mines showed that the model-free approach provides much better fit of the estimated PDF of magnitudes to observations and significantly changes the hazard estimates. In some cases the largest event probability obtained from the non-parametric considerations turned out to be changed by several dozens times with respect to its estimate achieved from the Gutenberg-Richter relation based approach.

Thursday 22 July AM

Presiding Chairs: D. Simpson, S. Talebi

**TRIGGERED/INDUCED EARTHQUAKES**

ST1/W/21-A4 Poster 0930-01

**TOWARDS AN AUTOMATIC APPROACH FOR SEISMIC MOMENT TENSOR INVERSION OF MINE-INDUCED MICROSEISMIC EVENTS**

Douglas ANGUS (Queen's University, Kingston, Ontario, Canada, K7L 3N6, Email: angus@geol.queensu.ca); C.-I. Trifu and V. Shumila (both at E.S.G. Canada Inc., Kingston, Ontario, Canada, K7K 7G3)

The seismic moment tensor is a valuable tool in the evaluation of seismic source mechanisms because it is the most general representation of any indigenous source. For that reason a seismic moment-tensor inversion approach has been developed by E.S.G. Canada Inc. for retrieval of source mechanisms of mine-induced microseismic data. This method is unique because it is based on a time-domain calculation/evaluation of the seismic moment-tensor components.

The limitations and applicability of this moment-tensor inversion method is tested using a waveform simulation program. This waveform simulation algorithm is sophisticated enough to test the inversion approach for the retrieval of geometrical as well as shear and non-shear components of failure. The results from the waveform simulation tests indicate that the seismic moment-tensor inversion approach is reliable so far as retrieving the geometrical aspects of the seismic source are concerned. Inversions for the double-couple and so-called general mechanism are shown to be robust for the various wavetype solutions, under reduced array coverage, hypocentral mislocation and the addition of Gaussian-normally distributed noise. Errors in first-arrival polarities and low-frequency displacement amplitude are very influential, though. Although for manually processed data these effects can be significantly reduced, it is anticipated that for automatically processed data that they become quite problematic.

The tests conducted with simulated waveforms indicate that the inversion approach is valid in principle. These tests, however, are only preliminary and more work is needed to completely sanction this method as a standard technique in microseismic source analysis. This is not to suggest that doubt exists about the principles and direction of the method, but simply is a reflection of the sophistication and intricacy of the algorithms and software.

ST1/W/25-A4 Poster 0930-02

**STATISTICAL EVALUATION OF POTENTIAL FOR PREDICTION: THE CASE OF A PARAMETRIZATION OF EPICENTER DISTRIBUTION OF MINING INDUCED SEISMIC EVENTS**

Anna LASKOWNICKA and Stanislaw Lasocki (both at Department of Geophysics, University of Mining and Metallurgy, al. Mickiewicza 30, 30-059 Krakow, Poland, email: anial@geol.agh.edu.pl, lasocki@geol.agh.edu.pl)

Candidates for precursors to targets of prediction are mostly inferred from the knowledge about a physical process controlling the studied phenomena. Before, however, such a candidate is introduced to the prediction system it is reasonable to test its potential for prediction - a step which is often omitted but which can both save further efforts in case of rejection and provide hints on construction of a prediction algorithm in case of acceptance. In our opinion a parameter can be regarded as having the potential for prediction if its values prior to the occurrences of targets of prediction differ statistically significantly from its values at random moments. In many instances simple statistical procedures can determine whether the parameters has a feature like that.

It is expected that an occurrence of a strong event in the local mining induced seismicity is preceded by certain alterations of epicenter distribution of smaller events. Three parameters defined on series of epicenters of successive events were selected as candidates for precursors to strong tremors: the directional coefficient of the temporary linear trend of epicenter distribution, the root-mean-square dispersion around the trend and the statistical coefficient of seismic diffusion. Seismic series connected with individual mining stopes were used to build appropriate experimental and control groups of the parameter values. The study of potential for prediction of every parameter involved comparing locations of the parameter distribution in experimental and control groups by means of the Wilcoxon matched-pair test. If the locations did not differ the Shapiro-Wilk's and Kolmogorov-Smirnov tests were used to check overall differences in the distributions. All three parameters turned out to change significantly before strong event occurrence.

ST1/P/02-A4 Poster 0930-03

**EARTHQUAKE PRECURSORY MODEL FOR KOYNA RESERVOIR, INDIA**

H.N. SRIVASTAVA and S.N. Bhattacharya (both at India Meteorological Department, New Delhi-110003, India, e-mail: snb@imd.emet.in)

Koyna region continues to be seismically active with the recurrence of earthquakes of magnitude 5.0 from time to time, which may cause some damage. Based on 12 parameters

for 10 months prior to the occurrence of the largest magnitude earthquakes namely number of microearthquakes at Koyna observatory, earthquakes of magnitude 2.0 to 2.9, earthquakes of magnitude  $\geq 3.0$ , total number of epicentres, sense of first motion C, D and percentage ratio C/D at Koyna, and Dilatation at Pune, largest magnitude earthquake, total seismic energy released, reservoir height and change of level per month, a predictive model has been developed using Principal Component Analysis for Koyna reservoir and neighbourhood. This technique has provided deeper insight about the role of different parameters preceding earthquakes of same magnitude in different years. It is shown that the methodology provides an operational model for prediction of earthquakes in Koyna region similar to that used in long range weather forecasting before the southwest monsoon.

ST1/W/20-A4 Poster 0930-04

**SOME ASPECTS OF RESERVOIR INDUCED SEISMICITY IN BRAZIL WITH EMPHASIS ON RECENT CASE HISTORIES**

Vasile MARZA, Lucas Barros, Jose Eduardo Soares &amp; Juraci Carvalho (all at Seismological Obs., University of Brasilia, Brasilia-DF, Brazil, e-mail: marza@unb.br or obsis@unb.br); Marcelo Assunção (Geophysical Department, IAG, University of São Paulo, São Paulo, SP, email: marcelo@iag.usp.br)

The realm of the reservoirs induced seismicity [RIS], has started to mature after more than a half century of investigation and with the increase of both the number and size of reservoirs worldwide RIS turned in a serious issue for its environmental, societal and economic impact. By the other hand, the phenomenology of RIS process is considered a bridge between the laboratory scale and the natural extreme scale in modelling the seismogenesis. In Brazil the matters of RIS have been approached during the decade of '70s when the seismographic monitoring of reservoirs has begun, but during the '80s the interest became greater.

The paper attempts to accomplish a synopsis of the main 15 case histories of RIS in Brazil, to discuss its features (with a taxonomic goal) and to analyze the most recent RIS cases observed in Brazil during 1998, i. e., the principal events at Tucuruí (PA) on March 02 (magnitude 3.6) and Nova Ponte (MG) May 22 (magnitude 4.0). The main findings of the our work should be: (1) manifestation of a particular category of RIS at some Brazilian reservoirs, i.e., repetition of the mainshocks at a specific reservoir, which we coin it as "repetitive cycle"; (2) a conspicuous time-space precursory seismicity pattern, associated to the 1998 Nova Ponte mainshock, displaying the following stages: early foreshocks - seismic quiescence - immediate foreshocks - mainshock - aftershocks, and a nonrandom spatial configuration of the event population.

ST1/E/16-A4 Poster 0930-05

**INDUCED SEISMICITY AS MANIFESTATION OF FINE STRUCTURE OF GEODYNAMIC PROCESSES**

Alexei NIKOLAEV and Vsevolod Nikolaev (both at Joint Institute of Physics of the Earth, Bolshaya Gruzinskaya 10, 123810 Moscow, Russia, email: alex@nikavs.msk.su)

Weak natural and man-made impacts on the Earth's crust - the Earth tide, changes of the Earth rotation velocity, variations of atmospheric pressure, filling of reservoirs, oil, gas and minerals extraction, water pumping in and out, strong earthquakes and underground nuclear explosions - display in their influence upon seismicity.

Sensitivity of seismicity towards inner actions and its response to it - the induced seismicity - has pronounced non-linear character, and is dependent upon fine structure of medium, its stress condition and mechanical instability.

Typical of this reaction is its time changing sensitivity to the outer processes conditioned by temporal changes of stress field in lithosphere; sequence of periods of organized and chaotic behaviour; pronounced connection with separate periodic components of the Earth tide. These qualities allow to reveal typical features of time-spatial dynamics of the stress field, the rate and direction of creep, movement of crustal blocks.

The induced seismicity caused by the Earth tide shows that gravitational action of the Sun and the Moon is one of the causes of tectonic movements performed by wave transfer of substance. The fine structure of these movements has the same character as that of the induced seismicity: frequency-selective response to weak inner impacts, spatial mosaic, time instability.

ST1/E/20-A4 Poster 0930-06

**EVALUATION OF INDUCED SEISMIC RISK IN THE AREA OF SHURTAN GAS FIELD (SOUTH UZBEKISTAN)**

NURTAEV B.S., Plotnikova L.M.(Institute of Geology and Geophysics, Academy of Sciences of Uzbekistan, Tashkent 700041, 49 N.Khodjibaeva, email: nurtaev@rubin.gov.uz)

The severe earthquakes  $6.0 < M < 7.3$ , which are occurred last years in regions of major oil and gas field extraction in USA, Italy, Turkmenistan, Uzbekistan, Russia testify possible influence of engineering activity of man on isostatic and hydrodynamic seismic zoning results for providing seismic safety of constructions. For development of efficient methods of seismic hazard assessment, particularly in the regions of large gas and oil fields it is necessary at first to do the following: a) to construct correct geodynamic model of region; b) to develop the model of induced We would like to present results of investigations of main peculiarities of seismic process changes due to technogenous and endogenous factors for the region of large gas field Shurtan(South Uzbekistan). Analysis of structural and tectonic setting conditions of earthquakes connected with world large gas oil fields and comparison with exploitation regime has revealed at least two main regularity 1) tectonic compression conditions and 2) initial gas-oil pre Expected parameters of maximal probable endogenous and technogenous earthquakes in geological and tectonic conditions of gas field were obtained, taking into account existing regime of exploitation.

ST1/E/40-A4 Poster 0930-07

**STUDY OF SEISMIC EFFECTS OF MINE BLASTING ON STRUCTURES AT GOL-E-GOHR IRON ORE MINE S. E. IRAN**

Ahmad Sadikhohi and Abdolrahim JAVAHERIAN (both at Institute of Geophysics, Tehran University, P. O. Box 14155-6466, Tehran, I. R. Iran, email: javaheri@chamran.ut.ac.ir)

In most open pit mines, explosives are used for crushing materials. The seismic waves generated by these explosions can cause damage to near structures, especially in large mines with great blastings. In Gol-e-Gohar iron ore mine, almost 26000 kg of explosives is used for each blasting. To investigate the effect of blasting on the structures, we recorded seismic signals of two normal explosions by several digital recording systems. Each recording system consisted for a digital data acquisition part and a three component seismometer. The three component of each seismometer were aligned in vertical, radial (towards the blasting location) and tangential directions. For the first explosion, we used a dispersed array of seismometers to find 2-D model of peak particle velocity (horizontal model), which led us to radiation pattern of explosion. This pattern was determined for each component of particle velocity. For the

second blasting, seismometers were aligned in a line to study the effect of distance on the particle velocity. So we enabled to draw the variations of peak particle velocity versus distance. This study showed that normal explosions in Gol-e-Gohar iron ore mine have no destructive effect on near structures due to safety standards.

**ST1/E/72-A4** Poster **0930-08**

**CHARACTERIZING HYDRAULIC FRACTURE BEHAVIOUR USING MICROSEISMICITY**

T.I. URBANCIC, C-I. Trifu, V. Shumila, (Engineering Seismology Group Canada Inc., 1 Hyperion Court, Kingston, ON, Canada, K7K 7G3, email: urbancic@esg.ca ) J.T. Rutledge (Los Alamos National Laboratory, Earth and Environmental Sciences Division, Los Alamos, N.M., USA, 87545, email: rutledge@seismo5.lanl.gov ) R.J. Zinno (Union Pacific Resources Co., 777 Main St., Fort Worth, Texas, USA, 76102-5398, email: DickZinno@upr.com )

Temporal-spatial variations in event locations, source parameters, and in frequency-magnitude parameters (occurrence rate of seismic activity and b-value) are evaluated for a catalogue of 994 microseismic events (-2.0 # M # -0.5) associated with the Cotton Valley (East Texas, USA) fracture treatment of May 14, 1997. The treatment was carried out between 2756 and 2838 m depth and consisted of three separate injection phases. Event locations were obtained based on P- and/or S-wave arrivals and direction vectors, to an accuracy of 14 to 24 m. Spatially, the event locations were contained within the perforation interval, and outlined a hydraulic fracture 560 m in length and 60 m in width, that was symmetric about the treatment well (TW), and followed the predicted N70E trend. Nearly 50% of the events occurred over the short interval 90m to 120m east of TW. Over this interval, b-values were above 1 during the initial two injections, S- to P-wave energy release values (Es/Ep) were small (<10), and occurrence rates increased relative to other parts of the fracture. During the third injection, the fracture growth eastwards was accompanied by b-values above 1 and Es/Ep values ranging from 20 to 30, suggesting that the failures within the treatment contained non-shear components near TW and were more shear-like with distance east of TW. To the west of TW, b-values ranged from 0.5 to 1 for all three injections, however, the third injection was accompanied by an increase in occurrence rate. Based on these observations, we suggest that microseismic event locations can be used to define the overall dimensions of the hydraulic fracture, and that source and frequency-magnitude parameters can potentially be used to identify differences in fracture growth and failure mechanisms.

**ST1/E/77-A4** Poster **0930-09**

**EARTHQUAKES TRIGGERING OTHER EARTHQUAKES AS A PRECURSORY PROCESS**

G. A. PAPAPOULOS (Institute of Geodynamics, National Observatory of Athens, 118 10 Athens, Greece, email: g.papad@egedlos.gein.noa.gr)

Observations made in California, Greece and elsewhere about earthquake clusterings occurring beyond chance in adjacent or spatially isolated seismic zones, at distances ranging usually between 200 km and 900 km, indicate that some earthquakes are triggered by other earthquakes. When this domino-like phenomenon takes place as a synchronization between two particular zones, then the triggering earthquake is bearing a precursory nature to the triggered one. A geophysical mechanism has been developed to explain (1) how after some initiation the process is accelerating leading to the clustering by rupturing a number of near to failure prestrained regions, and (2) why a preferential correspondence occurs in the case of synchronization. The value of the above observations and modelling for earthquake prediction is discussed on the basis of earthquake triggering examples from Greece. This is a contribution of the ASPELEA Project supported by EU-DGXII - Inco Copernicus, Contract n. IC-15CT-97-0200.

**ST1/W/33-A4** Poster **0930-10**

**MAN-MADE RISE OF THE LAKE BAIKAL WATER LEVEL AND THE M=6.8 BAIKAL'S EARTHQUAKE OF AUGUST 29, 1959 : COINCIDENCE OR REGULARITY ?**

Pyotr DJADKOV (Institute of Geophysics, av. Acad. Koptuyg, 3, Novosibirsk, 630090, Russia, E-mail: djad@uiggm.nsc.ru)

The M=6.8 earthquake of August 29, 1959 occurred in the central part of Lake Baikal near the Selenga river delta at depth of 18 km during the initial period of man-made rise of Lake Baikal water level under filling of reservoir of the Irkutsk water-power station. Selenga delta has high level of seismic activity which is developed during the periods of increase of seismic activity in the all Baikal rift zone as a rule. It was showed earlier that the influence of the water level variations on seismicity of this region occurred exactly during the such seismic active periods [Djadkov, 1997]. The M=6.8 earthquake of 1959 took place in time of high seismic activity (1957-1962) in Baikal rift zone and the main energy source of this event was caused by the crustal stress redistribution in this period. However the time of this earthquake fell on the first stage finish of quick rise of the Baikal water level in period of May to September 1959. The quick water level rise was caused summation of the man-made rise and the natural season rise of water level. So far as the induced or triggered seismicity depend clearly on the rate of water load in this place [Djadkov, 1997] the moment of the 1959 earthquake had the close connection with one. So although the energy source of the 1959 earthquake was caused mainly by the high regional seismic activity in 1957-1959 the man-made rise of the Lake Baikal water level could initiate this earthquake and besides the such rise could increase its magnitude.

**ST1/W/40-A4** Poster **0930-11**

**REGIONAL SEISMICITY TRIGGERED BY THE GREAT HYOGO-KEN NANBU, JAPAN, EARTHQUAKE, ON JANUARY 17, 1995**

Fu ZHENGXIANG and Liu Geiping (Center for Analysis and Prediction, China Seismological Bureau, 63 Fuxing Avenue, Beijing, 100036, China. Email: fzx@ip.cacp.cn)

The great Hyogo-Ken Nanbu, Japan, earthquake with magnitude 7.2 on January 17, 1995 was located at 34.595 N, 135.036 E. The focal mechanism of the mainshock is a right-lateral strike-slip faulting with trend of N40E. The aftershock area extended about 70km trending northeast to southwest. The regional seismicity triggered by the mainshock is studied here. The studied region is defined as an area of 33 – 37 N, 133 – 138 E around the mainshock epicenter and divided into 16 sub-regions. The earthquake data (1976.1 to 1996.6) used come from the seismic data bank compiled by Disaster Prevention Research Institute, Kyoto University, Japan. The minimum magnitudes of completeness ranging from 1.0 to 3.5 for the different sub-regions are determined by using the earthquake magnitude – frequency relation. The research results show that (1) the high seismicity triggered by the mainshock were observed in 10 sub-regions, where the differences on seismicity rates before and after the triggering time are obviously at the significant level 95% or more by using statistically Z - test method, the maximum of rate changes occurred in the sub-regions near to the aftershock area, the sub-regions of triggered seismicity go as far as about 250 – 280 km from the mainshock epicenter; (2) the high triggered seismicity happened respectively in the first, second and fifth day after

the mainshock for 3 sub-regions adjacent to the aftershock area, the triggered seismicity delayed several ten days for other sub-regions far an away; (3) the magnitudes of triggered events are not more than 5.4. The triggering mechanisms are also discussed.

**ST1/E/01-A4** Poster **0930-12**

**INDUCED EARTHQUAKES ACCOMPANIED BY THE WATER INJECTION EXPERIMENT AT THE NOJIMA FAULT ZONE, JAPAN**

Keiichi TADOKORO, Masataka Ando, and Kin'ya Nishigami (Disaster Prevention Research Institute, Kyoto University, Gokasho, Uji, Kyoto 611-0011, Japan, email: tad@rcep.dpri.kyoto-u.ac.jp; ando@rcep.dpri.kyoto-u.ac.jp; nishigami@drs.dpri.kyoto-u.ac.jp)

After the 1995 Hyogo-ken Nanbu (Kobe) earthquake of M7.2 occurred on January 17, a scientific drilling program called the "Nojima Fault-zone Prove" was carried out at the Nojima fault ruptured during the mainshock. A water injection experiment was executed by the program during the two periods, February 9-13 and March 16-25, 1997. Pressured water (~4 MPa) injected out from one of the three boreholes drilled by the program at depths between 1480 and 1670 m. The total amount of injected water was 258 cubic meters. A seismic observation network was deployed and increase in earthquake was observed 4-5 days after the beginning of each water injection. Because the seismicity increased in the region not far from the injection holes, around 3 or 4 km from the injection point, these earthquakes were likely to be induced by the water injections. Most of the earthquakes were located between 2 and 4 km in depth and had magnitudes ranging from -2 to +1. The values of intrinsic permeability of  $10^{-2}$ - $10^{-3}$  darcy were obtained from the induced seismicity change. The coefficient of friction in an area where the induced earthquakes occurred was estimated to be less than 0.3. The hypocenters of induced earthquakes migrated with speeds of ~5-40 m/h. The speed decreased with time, suggesting diffusion of water. Twenty earthquake clusters were found in terms of waveform similarity. Migration speed of the earthquakes within each cluster also estimated by cross-spectrum method. Moreover, source parameters were computed. The seismic moment ranged from  $10^9$  to  $10^{11}$  N-m. Small values of stress drop,  $10^3$ - $10^5$  Pa, were obtained.

**ST1/W/09-A4** Poster **0930-13**

**SEISMIC MIGRATION IN A MINING INDUCED ENVIRONMENT: A CASE OF SPACE-TIME FRACTALITY**

David MARSAN, Chris Bean (both at Geology Dept., University College Dublin, Belfield, Dublin 4, Ireland); Sandy Steacy, John McCloskey (both at the School of Environmental Studies, Univ. of Ulster, Coleraine, N. Ireland).

It is observed that the seismicity recorded in Creighton Mine, Canada, in a 6 month period, exhibits scaling both in time (from 1 mn to about 2 weeks) and in space (from the observational resolution of 10 m up to the size of the mine, about 500 m). Temporal migration of earthquakes away from any given earthquake is also statistically observed. We show that both observations are equivalent in terms of dynamical behaviour of the mining system, and argue that space-time fractality is the pertinent framework to explain and model such behaviour. This model is exploited in order to provide an original method for predicting seismicity level in the mine, based uniquely on scaling.

Presiding Chairs: G.A. Sobolev and J. Zschau

**SPACE-TIME PATTERNS OF SEISMICITY AND RELATED FIELDS**

**ST1/W/37-A4** Poster **0930-14**

**ACOUSTIC EMISSION AT MATSUSHIRO. ASSOCIATION WITH NEARBY EARTHQUAKES**

Andrei V. GORBATIKOV (Institute of Physics of the Earth, B.Gruzinskaya 10, Moscow, Russia, email: avgor70@hotmail.com); Oleg Molchanov (Earth Observation Research Center, NASDA, Tokyo, Japan, email: oleg@eiocr.nasda.go.jp); Masashi Hayakawa (University of Electro-Communications, Chofu, Tokyo, Japan, email: hayakawa@whistler.ee.ucc.ac.jp); Seiya Ueda, Katsumi Hattori, Toshiyasu Nagao and Paul Maltsev (all RIKEN, Earthquake International Frontier Project, Shimizu, Japan, email: hattori@iord.u-tokai.ac.jp)

Acoustic Emission (AE) intensity was recorded at Matsushiro station (Nagano Prefecture, Japan) in the special tunnel inside rocky mountain at depth about 100 meters. Sensitive 3-component AE receiver with frequency response proportional to cube of frequency and four narrow-band filters: 30, 160, 500, 1000 Hz was used. We analyzed the envelopes of the filters averaged in 30-minute samples for 7 months period from February to August 1998. 11 nearby (20km<D<70km) quite strong (3.8<Ms<5.2) and shallow (H<35km) earthquakes happened during this period and we tried to find an association of AE intensity with them. We found definitely AE response on the earthquakes, appearing as increasing of AE intensity. The amplitude of AE increases about 12 hours before earthquakes and decreases afterwards in a similar manner. We conclude, some process of earthquake preparation and some process of post-earthquake relaxation invoke that. This AE response depends on frequency (signal to noise ratio decreases with increase of frequency). The observational results are in agreement with simple theoretical model of propagation the seismic perturbations from the epicenter area. For noise conditions present at Matsushiro, characteristic radius of sensitivity for AE response on earthquake was estimated. It is ~100 km for an earthquake Ms=5 (direct observations), and it is expected to be ~250 km for earthquakes Ms=6. But multi-station observations are needed for more reliable evaluations. The evident ULF magnetic emission accompanying AE was found for July 1, 98 event.

**ST 1/E/64-A4** Poster **0930-15**

**CRUST DEFORMATION PROCESSES IN STRONG EARTHQUAKES FOCAL ZONES OF TIEN-SHAN (ON SEISMOLOGICAL DATA)**

Nailya BAGMANOVA (Institute of seismology, National Academy of Science, Asanbai 52/1, Bishkek 720060, Kyrgyz Republic, email: kis@imfiko.bishkek.su)

We study the crust deformation style observed in focal zones of 9 strong earthquakes (M=5) which have struck Tien-Shan for the period 1978-1992. Initial data were focal mechanisms data for 2500 earthquakes with 1.7<M<5. Six components of strain tensor, intensity of shear strains, orientations of principal strain axes have been calculated. Were revealed the specific features in crust deformation style during a number of years prior to strong event occurrence. Deformation style as result of strong earthquakes seems to be different of that in source zones during earthquakes preparation period. North Tien-Shan and South Tien Shan seismogenic zones serve as examples of difference in styles of crust deformation.



ST1/W/19-A4 Poster 0930-16

## ON A RESONANT PHENOMENA IN THE FLUID-SATURATED GEOPHYSICAL MEDIUM

Dr. Alexey L. SOBSEVICH and Prof. Leonid E. Sobisevich (Institute of Physics of the Earth, Russian Academy of Sciences B.Gruzinskaya 10, Moscow 123810, Russia email: alex@uipe-ras.scgis.ru)

The new approach to understanding the conditions of interaction and transformation of geoaoustic fields is proposed. It is shown that resonance interactions can play the main role in fluid-saturated medium. The reaction of porous fluid-saturated medium to weak seismic force, when the solid phase shifting can be neglected, was studied. The analysis shows the existence of slow waves of porous pressure in fluid-saturated medium. The speed of propagation of such waves can be up to 10 m/sec and depends on the structure of porous medium and some parameters of the fluid. The theoretical model of slow waves of porous pressure is developed. This model may be used for prediction of seismic events.

ST1/E/19-A4 Poster 0930-17

## GENERALIZED RYDELEK-SACKS TEST FOR DISTINGUISHING BETWEEN PERIODIC AND RANDOM PATTERNS IN SEISMICITY

ZHONGLIANG WU (Institute of Geophysics, China Seismological Bureau, 100081 Beijing, China, email: wuzl@cdsindm.csb.gov)

In the study of geodynamics and earthquake prediction, one of the tricky things is to distinguish between periodic and random patterns in the activity of strong earthquakes using undersampled data, namely a few tens of events. For distinguishing the periodicity of strong earthquakes on the time scale of decades, we generalized the Rydelek-Sacks test (Rydelek and Sacks, 1989) to explore whether or not a time series is modulated by a periodic process. The test is conducted by comparing the phasor walkout of seismicity with theoretical results, given a certain statistical significance. The phase angle is defined by the origin time of earthquakes relative to a reference time scale. Using this method we tested two hypotheses in geodynamics and earthquake prediction study. One is the hypothesis of Romanowicz (1993) proposing that great earthquakes alternate in a predictable fashion between strike-slip and thrusting mechanisms on a 10 to 30 year cycle. The other is the observation that strong earthquakes in and around China have a period of ten years. The test obtains a negative conclusion for the former hypothesis and a positive conclusion for the latter, with 95% statistical significance. The result is of help in the modeling of geodynamics and the estimation of seismic hazard.

ST1/E/18-A4 Poster 0930-18

## NONLINEAR ANALYSIS OF CAUCASIAN EARTHQUAKES' TEMPORAL AND SIZE DISTRIBUTION

Teimuraz MATCHARASHVILI, Tamaz Chelidze, Zurab Javakhishvili (Institute of Geophysics, Georgian Ac. Sci. 1, Alexidze str. 380093 Tbilisi, Georgia. e-mail: tmnat@hotmail.com)

It is well known that earthquakes' size, time, space and space-time distributions obey power law. At the same time precise details of underlying dynamics is not quite clear. We apply tools of nonlinear dynamics theory, such as correlation dimension, "surrogate" data analysis etc., as well as positive Lyapunov exponent calculation for investigation of dynamical characteristics of earthquakes' temporal distribution in Caucasian region. In this study we have considered interearthquake time intervals sequences for different areas and magnitude windows. We have found significant evidence for low dimensional nonlinear structure of earthquakes' time distribution, obtained by consideration of time interval sequences between all events, encountered in the original catalogue above threshold magnitude. At the same time, based on phase randomised and Gaussian scaled surrogate tests, existence of nonlinear structure in selected sequences of time intervals between independent events as well as between aftershocks (events were picked out from the original catalogue) were rejected. It seems that such kind of filtration of the original catalogue destroys the existing temporal structure. Unlike selected interaftershock time interval sequences, time interval sequences between Racha earthquake original aftershocks reveal clear evidence of nonlinear structure. Caucasian earthquakes size distribution also was investigated. It has been shown that distribution of earthquakes' magnitudes for all considered sequences of magnitudes and magnitude windows reveal high dimensional nonlinearity. These results show that well known scaling laws of earthquakes time and size distribution have different underlying dynamics and from the point of view of prediction of hazardous events must be considered separately.

ST1/E/21-A4 Poster 0930-19

## PAIRS OF LARGE EARTHQUAKES AND GEODYNAMICAL PROCESSES IN CENTRAL AND SOUTH ASIA

Yuri Kopnichev and Inna SOKOLOVA (Complex Seismological Expedition, Joint Institute of Physics of the Earth, Kamo str. 8a, Talgar, Almaty region, 483310 Kazakhstan, email: adm@cse.academ.alma-ata.edu)

Pairs of large earthquakes (M-7.0) were observed in Central and South Asia: a deep-focus Hindu Kush earthquake followed by a shallow event during an interval varying from a few weeks to 4.5 months. Distances between epicenters of these events were within a range of 300-1450 km. Strong shallow earthquakes after deep-focus Hindu Kush events have occurred in the regions of the Kopet Dag, Iran, Turanian plate, Hindu Kush, the South Tien Shan, and the Himalaya. The probability of occasional occurrence of 9 pairs of such earthquakes since the beginning of this century is insignificant. We have established, that these events occur only during episodes of long-term (a few years) increase of the Earth's rotation speed. To interpret this effect, we have considered temporal variations of shear wave attenuation field structure in the earth's crust and upper mantle, which are connected with active fluid migration within large deep fault zones. For this purpose seismograms of local explosions at a small quarry in the region of the North Tien Shan (1965-1995) have been analyzed. Using coda analysis, we have shown, that during periods of increasing the Earth's rotation speed, and especially after the strongest Hindu Kush earthquakes, the fluid field comes to "excited" condition in the earth's crust and upper mantle. This stipulates a sharp acceleration of formation processes of large shallow earthquakes sources in most prepared areas. The data obtained may testify that the information on preparing deep-focus Hindu Kush earthquakes is passed through active deep fault zones due to relatively effective system of hydrodynamical ties.

ST1/E/32-A4 Poster 0930-20

## RELATIONSHIP BETWEEN THE DEEP CRUSTAL FEATURES IN VELOCITY AND THE REPLICATION OF STRONG EARTHQUAKES IN XINGTAI AREA

Jing-yuan YIN and Shi-rong Mei (Both at Center for Analysis and Prediction, CSB, 63 Fuxing Avenue, 10036 Beijing, China, email: jy55@hotmail.com)

The explosion sounding and seismic tomography analysis implied that most of the strong

earthquakes taken place in the North China would be found in the transition zones between the regions with high velocity and the ones with lowvelocity. The source for strong earthquakes would locate in generally in segment between the lower wall of the shallow shovel-like normal fault and the upper part of a steeply inclined fault deeply buried in the crust. Furthermore, upward movement of upper mantle with the irruption of some material from mantle to crust would be found in the Mohodiscontinuity near the epicentral area of strong earthquakes.

By comparing the distribution of main shock and after shock with the detailed tomography data for Xingtai epicentral regions, a new idea on the preparation of strong earthquakes was suggested and a model based upon this idea was presented. The effect of the inhomogeneity of the crust structure on the crustal stress field was calculated by using 3-D finite element method in a model with certain boundary constraints and conscientious selection of mechanic parameters of inhomogeneous media on the basis of the exploration data associated with the deep structures about the meizoseismal regions. The simulation is examined by Xingtai earthquake sequence and the results coincide quite well with its spacial distribution.

ST1/E/37-A4 Poster 0930-21

## COMPREHENSIVE SPACE-TIME PATTERNS OF SEISMICITY AND RELATED GEOPHYSICAL FIELDS AND EARTHQUAKE PREDICTION

Yueqing Zhu, Shirong Mei, Guomin Zhang, Ruying Xing (Center for Analysis and Prediction, China Seismological Bureau, P.O.Box 166 Beijing, 100036, email: zhuyq@sun.ihep.ac.cn)

Frequent occurrence of strong quakes has been forcing Chinese government and seismologists work hard for warning people before a catastrophic event coming. During the last years a lot of station networks have been established and running continuously for monitoring fault activity and earthquake generation process and so a huge of documents, experiences and lessons have been accumulated. Both of these provides good conditions for studying earthquake prediction.

Based on the results of these studies combining with some results of existing physical modeling of seismic source process at home and abroad, the Authors have done a series of researches on comprehensive space-time patterns of seismic and related geophysical fields during the last 30 years, so a series of combining patterns for predicting strong earthquakes with different scales of space-time-magnitude by different sets of indicators with relevant Certainty Factors(CF) have been obtained, then several relevant software systems for describing these patterns have been developed and tested and checked with about 100 strong cases, a group of CFs of these patterns have also been got. Based on the later results some prediction software systems have further been formed and put into practical works. A continuous 5 years practical results of them have shown that it is a feasible strategy for predicting strong earthquakes, specially for long-term and medium-term predictions.

ST1/E/37-A4 Poster 0930-22

## COMPREHENSIVE SPACE-TIME PATTERNS OF SEISMICITY AND RELATED GEOPHYSICAL FIELDS AND EARTHQUAKE PREDICTION

Yueqing Zhu, Shirong Mei, Guomin Zhang, Ruying Xing (Center for Analysis and Prediction, China Seismological Bureau, P.O.Box 166 Beijing, 100036, email: zhuyq@sun.ihep.ac.cn)

Frequent occurrence of strong quakes has been forcing Chinese government and seismologists work hard for warning people before a catastrophic event coming. During the last years a lot of station networks have been established and running continuously for monitoring fault activity and earthquake generation process and so a huge of documents, experiences and lessons have been accumulated. Both of these provides good conditions for studying earthquake prediction.

Based on the results of these studies combining with some results of existing physical modeling of seismic source process at home and abroad, the Authors have done a series of researches on comprehensive space-time patterns of seismic and related geophysical fields during the last 30 years, so a series of combining patterns for predicting strong earthquakes with different scales of space-time-magnitude by different sets of indicators with relevant Certainty Factors(CF) have been obtained, then several relevant software systems for describing these patterns have been developed and tested and checked with about 100 strong cases, a group of CFs of these patterns have also been got. Based on the later results some prediction software systems have further been formed and put into practical works. A continuous 5 years practical results of them have shown that it is a feasible strategy for predicting strong earthquakes, specially for long-term and medium-term predictions.

ST1/E/51-A4 Poster 0930-23

## NEW NATURE OF AFTERSHOCK SPATIAL DISTRIBUTION, EARTHQUAKE FAULT LENGTHS AND SECONDARY DISASTER PREVENTION

Kazuyoshi NANJO and Hiroyuki Nagahama (both at Institute of Geology and Paleontology, Graduate School of Science, Tohoku University, Sendai 980-8578, JAPAN, email: nanjo@dges.tohoku.ac.jp)

We present new nature of aftershock spatial distribution on the upper limits of aftershock magnitude. This nature gives a useful information about the prevention of secondary disaster by aftershocks.

Consideration of recent earthquake sequences suggests that aftershocks can be even more damaging than main shock in some sense. In order to prevent the secondary disaster by aftershocks, we need to know the spatial distribution of potential of how large aftershocks a main shock can trigger. The potential can be evaluated by the upper limit of aftershock magnitude. Here we examined the upper limits of aftershock magnitude as a function of hypocenter distance from main shock. To examine them, we used aftershock sequences following six main shocks (magnitude of 5.2 to 6.8) occurring in Japan inland from 1983 to 1987. The upper limits of the magnitude do not monotonically decay with increasing distance from main shock hypocenter, but show systematically two peaks at characteristic distances equivalent to earthquake fault length in Japan inland and to maximum earthquake fault length of world earthquakes. The distances of the two peaks from main shock hypocenter can be regarded as especially 'dangerous distances' from the view point of secondary disaster prevention. Moreover, the magnitudes of the two aftershocks giving the peaks correlate positively with those of the main shocks. These magnitude correlations are similar to Bath's law. Thus, our results indicate that the 'dangerous distances' and the aftershock magnitudes at the 'dangerous distances' can be predicted from a main shock.

We derive that Japan inland earthquakes occur under a local tectonic condition from the earthquake fault lengths in Japan inland. Furthermore, according to the energy efficiency of fracturing, earthquake fault lengths necessarily can not be larger than the maximum earthquake fault lengths.



**ST1/E/65-A4** Poster **0930-24**

**MAJOR EARTHQUAKES IN SOME AREAS OF CHINA AND LUNISOLAR TIDAL GENERATION FORCE**

HAN YAN-BEN (Beijing Astronomical Observatory, Chinese Academy of Sciences, Beijing 100012, P.R. China, email [hyb@class1.bao.ac.cn](mailto:hyb@class1.bao.ac.cn)) Li Zhi-an (Department of Astronomy, Beijing Normal University, Beijing 100875, P.R. China)

Although the force which leads to occurrence of earthquake is mainly from the interior of the Earth, some forces from other sources will probably trigger the earthquake when the stress has been accumulated to critical state at the focus fault. The relationship between major earthquakes occurred in some seismic areas in China has been analyzed. The result shows that dates of the earthquakes closely related to the variation of a certain component of the force. Probably the result will be significant for providing information on prediction of shorter dangerous period, about one week in each month, when the earthquake prediction lasting several months was made by other methods.

**ST1/E/68-A4** Poster **0930-25**

**CHANGES IN MATERIAL PROPERTIES BEFORE MAJOR EARTHQUAKES**

Tetsuo TAKANAMI (Institute of Seismology and Volcanology, Graduate School of Science (B Hokkaido University, Sapporo, 060-0810, Japan, email [ttaka@eos.hokudai.ac.jp](mailto:ttaka@eos.hokudai.ac.jp)) I. Selwyn Sacks (DTM, Carnegie Institution of Washington, 5241, Broad Branch Rd., NW, Washington, DC 20015, USA, email [sacks@dtm.ciw.edu](mailto:sacks@dtm.ciw.edu))

Observations of changes in seismicity before great earthquakes have long examined for precursory behavior. We report on five examples where the change in seismicity suggest change in fault zone properties. Taylor et al. 1991, Takanami et al. 1991 and Takanami et al. 1996 reported that the region surrounding the eventual earthquakes, became quiescent for earthquakes larger than  $m=3$ , even though smaller events seemed unaffected. While the aftershock zone shows no significant change in seismicity for the decade prior to the earthquake, the region surrounding this zone has significantly decreased seismicity for events larger than  $m=3$  for one to three years before the earthquake. In these cases, the seismicity of the surrounding region returned to normal background after the large quake. Assuming that the driving forces are essentially uniform, either the surrounding zone has to weaken, or somehow else allow aseismic slip or the eventual fault zone has to stiffen. If the fault zone becomes stiffer than the surrounding areas, more of the forces due to plate motion will be supported or resisted by the stiffer zone, thus somewhat destressing the adjacent regions. The edge of the stiffened zone would have a stress concentration which could give rise to "Mogi donut" type seismicity.

**ST1/E/69-A4** Poster **0930-26**

**THE RELATION BETWEEN THE ENERGETIC PARAMETERS OF ALBANIA EARTHQUAKES**

Sulstarova Eduard and PECCI Veronika; Institute of Seismology, Tirana, Albania, e-mail: [vera@sizmo.tirana.al](mailto:vera@sizmo.tirana.al)

In the framework of Project "Seismic Zonation of the Albania Republic in scale 1:200 000" it is under the process of re-evaluation all the earthquake focal parameters of Albania and its surroundings. Among these re-evaluation we are also reconsidering the energetic focal parameters - magnitudes (MS, Mb, ML), seismic intensity in epicenter (I<sub>0</sub>), seismic moment (M<sub>0</sub>), the length and width of fault (L, W), the area of the fault (S) as well as the stress drop. For the re-evaluation of energetic focal parameters of earthquakes besides the source data used in our previous works, we are also using many others sources of information coming from Seismological Bulletins and from other different authors. The region being studied is taken from the parallels 39-43degree North and meridians 18.5-22.0 degree East. We have been investigated the data for the seismic moment (M<sub>0</sub>) for strong earthquakes with magnitude MS > 5.0. From the above mentioned data we have found the relations between them (I<sub>0</sub> - MS, I<sub>0</sub>-Mb, I<sub>0</sub>-ML; MS - Mb, MS - ML; ML - Mb; MS - Mo; etc.). It also been studied the influence of focal mechanism in the length and width of the fault. The relations between energetic focal parameters of the earthquakes are of great importance for the homogenous of all the seismological material for the compilation of the New Catalogue of Albanian Earthquakes and the Assessment of the Seismic Hazard.

**ST1/E/71-A4** Poster **0930-27**

**ANOMALOUS LAND UPLIFTS AND SEISMICITY IN THE EASTERN PART OF THE ALPINE BELT**

Vladimir KAFTAN and Yuriy Kuznetsov (both at Central Research Inst. of Geodesy, Air Survey and Cartography, Onezhskaya, 26, 125413 Moscow, Russia, email [V.Kaftan@relcom.ru](mailto:V.Kaftan@relcom.ru))

Regional characteristics of Caucasus land movements are determined thrice. Maps of recent vertical crustal movements of Eastern Europe published in 1971 and 1986 and Map of velocities of recent crustal movements in the Caspian region (preliminary and final variants of 1994 and 1995) demonstrate large zones of anomalous uplifts with the rates of 10-15 mm/year near Greater and Lesser Caucasus ridges. So large rates can not explained by precision levelling errors of both, random and systematic, characters. The accuracy of velocity determination varies from 0.2 to 2.5 mm/year and reliability of the results is undoubted. Mean dates of the first and second epochs of levelling were 1924-1947, 1941- 1970 and 1960-70 - 1980-90 for each map respectively. The latest Map of the recent crustal movements of the Carpatho-Balkan Region showed great uplifts too.

This uplift were preceded to the great earthquakes in the Vrancha region. This behaviour is closed to the Caucasus anomalous vertical crustal movements. Spatial and temporal analysis of vertical land movements comparing with the seismicity behavior shows that large uplifts precede the largest Caucasus and Carpathian earthquakes occurring near such anomalous zones. The interesting fact is that there are many events of the anomalous uplifts occurs all over the world. This phenomenon have been occurred in the regions of Japan, South California and China. Decades of publications describe this events and their relation with the seismicity.

**ST1/E/76-A4** Poster **0930-28**

**FORESHOCK-AFTERSHOCK SEQUENCES OF DESTRUCTIVE EARTHQUAKES IN SOUTHERN KURIL ARC AREA**

Alexander I. MALYSHEV (Institute of Geology and Geochemistry, Urals Branch of RAS, Pochtovy per 7, Ekaterinburg, SU-620151, Russia, email: [root@igg.e-burg.su](mailto:root@igg.e-burg.su)) Ivan Tikhonov (Institute of Marine Geology and Geophysics, Far East Branch of RAS, Yuzhno- Sakhalinsk, Nauka street, 693002 Russia, email: [tsunami@sakmail.sakhalin.ru](mailto:tsunami@sakmail.sakhalin.ru))

Revealing and study of empirical dependencies of natural processes allowed to conclude that there is a wide class of self-developing natural processes, the dynamics of which is described by the non- linear differential equation of the second order. At present the methods, allowing confidently to revealing the regularities of the development of natural processes, have been developed. On example of the foreshock-aftershock sequences of destructive earthquakes in southern Kuril arc area it was established, that the development of both of foreshock, and aftershock sequences corresponds to the equation of the dynamics of self-developing natural processes. The following parameters of Nseismic process were investigated: cumulative sum of the number of shocks, the similar sum for energy of earthquakes and square root from the energy. We have analyzed the total seismic events flux within the region for the magnitude  $M \geq 4.0$  since 1962. We have determined a range of the most probable parameters of this equation and we hope that the future researches will allow reducing this range. The logarithmic dependencies of the development of foreshock-aftershock sequences upon time are being met most frequently. However the foreshock sequences are more poorly expressed. Probably, some updating of seismic observations is required for getting more stably results for foreshock sequences. It is caused by the necessity of study of weak seismicity anticipating destructive earthquakes. Nevertheless the obtained results allow to assume, that the methods are perspective for the forecast of disastrous earthquakes.

**ST1/E/82-A4** Poster **0930-29**

**CASCADE EARTHQUAKES IN ALBANIA**

Betim MUCO (Seismological Institute, Tirana, Albania, e-mail: [betim@sizmo.tirana.al](mailto:betim@sizmo.tirana.al))

A complex web of active faults is distributed throughout all the territory of Albania. The intersection of northwest-trending Adriatic and Ionian longitudinal fault system and northeast-trending shear fault systems, dominates Albanian tectonics and gives rise to recent seismicity backed mostly by the confrontation between Adria microplate and Albanian orogen. Sometimes, activation of some active faults produces the earthquake activity in a neighbor one and this process could continue as a cascade through other faults. This may cause the migration of seismic activity from one system of faults to another and sometimes could lead to wrong deduction about the proper fault responsible for an earthquake. Based on the available data from the records of Albanian Seismological Network, since 1976, some cases of the so-called cascade earthquakes for Albania are evidenced in this approach trying to explain also their mechanism.

**ST1/E/88-A4** Poster **0930-30**

**THE PROPERTIES OF THE LOW-FREQUENCY SEISMIC SIGNALS FOREGOING A MAIN SHOCK**

Boris W. Levin (\*Shirshov Oceanology Institute of RAS and Russian Foundation for Basic Research, 32a Leninsky prosp., Moscow, 117334 Russia; [levin@rfr.ru](mailto:levin@rfr.ru)) Elena V. SASSOROVA ( State Oceanographic Institute, 6 Kropotkinsky per., Moscow, 119838 Russia; [sasor@geoph.ioras.msk.ru](mailto:sasor@geoph.ioras.msk.ru))

The low-frequency seismic signals foregoing a main shock may be considered as a local sign of the earthquake preparation. More than 30 events with low frequency forecasting signals were detected by a special developed software package (above 200 event records were data processing). These signals have a period from 3 to 200 s and forecast time before P-wave arrival in area from 20s to 1.5 hours. The foregoing low-frequency signals were detected only for the events with epicentral distance no more than 1000 km. The classification of the forecasting signals was proposed. The properties of low frequency signals vary over a wide range. The signal properties from the same region vary but slightly. Thus the connection between the signal type and the event localization was noted. Analysis the signals and records of the acoustic waves from laboratory experiments provided confirmation that a period of radiated signal and an oscillator size are connected by empirical relation. The seismic foregoing signal parameters are depended on the regional characteristics (the oscillator size, features of the environment, structure of the earth crust). Thus the global problem of the prediction search may be replaced by the set of the local problems for each seismoactive region.

**ST1/P/03-A4** Poster **0930-31**

**SEISMICITY AND CORRELATION COEFFICIENT OF MOHO-DISCONTINUITYRELATIVE TO SOME GEOPHYSICAL PARAMETERS FOR THEREPUBLIC OF MACEDONIA**

Todor DELIPETROV, Krsto Blazev Delipetrov (Faculty of Mining and Geology, Uni "Kiril and Metodij" Skopje, Stip,MK, Email: [todor@rgf.ukim.edu.mk](mailto:todor@rgf.ukim.edu.mk));

Defining the seismicity of a given area is similar to that of earthquakes. In order to do it successfully it is necessary to know seismicity demonstrated so far. Available knowledge indicates that earlier active areas should be expected to be as such in the future. With regard to the geophysical approach in modelling the seismicity of a certain area it is necessary to know the geological structure, tectonic processes, geophysical fields in the region under consideration and further afield. Analysis of the model of earlier earthquakes registered indicates that the hypocentres of the territory of the Republic of Macedonia are situated in the Moho-discontinuity. The dependences of the depth of Moho-discontinuity on the height of the relief and Bouguer's anomaly or their correlation coefficients are analysed from that aspect . It is the opinion of the present authors that defining the moho-discontinuity and its correlation relationship with Bouguer's anomaly and the height of the relief can be used in the assessment for possible seismic energy in the earth's crust above moho-discontinuity.

**ST1/W/18-A4** Poster **0930-32**

**ON SOME ANOMALY PHENOMENA APPEARANCE DUE TO ACTIVE INFLUENCE ON A REAL GEOPHYSICAL MEDIUM**

Dr. Alexey L. SOBSEVICH and Prof. Leonid E. Sobisevich Institute of Physics of the Earth, Russian Academy of Sciences B.Gruzinskaya 10, Moscow 123810, Russia email: [alex@uipe-ras.scgis.ru](mailto:alex@uipe-ras.scgis.ru)

Modern technology of usage of powerful seismic vibrators allows to simulate earthquake conditions. Using this technique were studied earthquake precursors such as: change of water-level in a bore-hole, resonant response of the medium upon powerful vibration, generation of seismic noise by the zone of dilatancy. The explanations to a number of anomaly phenomena caused by resonant interactions in the layered geophysical medium are considered. At the same time the results of experimental observations over some geophysical phenomena discovered are considered. The conditions of interaction between the source of seismic oscillations and the geophysical medium in case of existence of the resonant structures are studied. The case of the source positioned onto a boundary of a half-space and the resonant structure located underneath in the near-field of the source is considered. Given theoretical study allows to perform immediate numerical estimations. The possible relation between the theoretical study and experimental facts is a subject for discussion.

ST1/E/10-A4 Poster 0930-33

## VARIATION OF AUTOCORRELATION FUNCTION'S FIRST ZERO CROSSINGS IN SEISMOLOGICAL TIME SERIES

Teimuraz MATCHARASHVILI, Tamaz Chelidze, Zurab Javakhishvili (Institute of Geophysics, Georgian Ac. Sci. 1, Alexidze str. 380093 Tbilisi, Georgia. e-mail:tmnat@hotmail.com)

It is widely accepted that lithospheric processes underlying earthquake generation are complex and highly nonlinear. Complete evaluation of such processes by tools of nonlinear time series analysis is too difficult task, due to complicated inherent dynamics and shortness and noise problems in time series analysis. Therefore, approaches based on linear properties of generally nonlinear data bases remain important. Autocorrelation function, characterising the resemblance of signal with itself, is one of such tools. Nonlinear time series analysts often use autocorrelation function's first zero crossing as an average measure of linear independence of the observations. In general linear independence between data, like any other linear or nonlinear property of time series can change depending on their length. So in the present study we have analysed the variation of autocorrelation function's first zero crossing as a measure of evolution of linear independence of time series data, by addition in tens of subsequent events, beginning from the first 100 data of the observations. Namely, there were considered variability of Caucasian earthquakes' magnitude and interevent time intervals sequences linear independence measure by addition successive 10 events from earthquake catalogue. It was found that linear independence of interevent time intervals strictly increases after large earthquakes; that can be related to the temporal clustering of earthquakes' aftershocks. On the other hand variation of linear independence of magnitude sequences before large events, and in most cases also after the events, does not change practically. These results confirm differences in dynamical properties in earthquakes' temporal and size distribution, found by nonlinear approach.

ST1/E/11-A4 Poster 0930-34

## SPACE AND TIME PATTERNS OF THE SEISMICITY OF THE VRANCEA REGION, ROMANIA

Luminita ARDELEANU (National Institute for Earth Physics, P.O. Box MG-2, 76900 Bucharest, Romania, email: ardel@infp.ifa.ro)

The seismic region of Vrancea is located in a tectonically complicated area, at the contact between the Eastern European plate, Moesian, Black Sea and Intra-Alpine subplates; this complex junction is considered as a continental-type collision, with a paleosubduction from NE to SW.

The seismicity studies show distinctive characteristics of the seismogenic zone of crustal earthquakes (hypocentral depths between 0 and 60 km) relative to the seismogenic zone of intermediate-depth earthquakes (hypocenters in the depth range from 60 to 200 km): the seismic activity in the crust is moderate (maximum MS magnitude less than 5.5) and it is mainly located within the foredeep region, in front of the bend of the Eastern Carpathian Arc; the subcrustal seismicity is almost vertically distributed in the deeper seismogenic segment, in a volume with a well confined epicentral area which includes the major Vrancea earthquakes (1 - 6 events with magnitude MW greater than 7 each century).

To study the space and time seismicity patterns, a parameterization derived from the Weibull distribution is used. The space-time distribution of the shallow earthquakes (local magnitudes greater than 2.0) show a strong clustering tendency, while the subcrustal mainshock sequences (local magnitudes greater than 2.5) are modelled by a completely random pattern. The time occurrence of moderate and strong intermediate depth earthquakes (local magnitudes greater than 5.5) shows also a completely random pattern.

ST1/E/12-A4 Poster 0930-35

## NONLINEAR STRUCTURE OF EARTHQUAKES' SIZE AND TIME DISTRIBUTION BEFORE AND AFTER LARGE CAUCASIAN EVENTS

Teimuraz MATCHARASHVILI, Tamaz Chelidze, Zurab Javakhishvili (Institute of Geophysics, Georgian Ac. Sci. 1, Alexidze str. 380093 Tbilisi, Georgia. e-mail:tmnat@hotmail.com)

It is known that seismological data bases both from qualitative and quantitative point of view are as a rule not sufficient for proper investigation of lithospheric dynamics even for lowdimensional processes. Therefore, similar to other fields, evaluation of nonlinear structure of geophysical data seems to be a more appropriate approach. In this study we have continued qualitative and quantitative investigation of dynamical properties of Caucasian region earthquakes' temporal and size distributions in order to evaluate the contribution of lithospheric processes taking place before and after strongest regional events in observed lowdimensional structure of general seismic dynamics. Dynamical characteristics of seismic processes before and after Daghestan, Paravani and Racha strongest events were investigated by means of nonlinear time series analysis tools, such as correlation dimension algorithm and surrogate data analysis test, using magnitude and interevent time intervals sequences as "time series". It was found that, similar to integral dynamics of regional seismicity, magnitude sequences before and after strongest events remain high dimensional in contrary to revealed low dimensional nonlinear structure of interevent time intervals distribution, although in the last case there is no evidence for deterministic chaos. It means that qualitatively dynamics of earthquake generating lithospheric processes did not change after large events. At the same time, for both earthquakes' size and temporal distributions, nonlinear structure of lithospheric processes before and after large events quantitatively are significantly different.

ST1/E/13-A4 Poster 0930-36

## AN APPRAISAL OF OBSERVED TRANSIENT 'ELECTRICAL EARTHQUAKE PRECURSORS': PHYSICAL PROPERTIES AND IDENTIFICATION

A. TZANIS (Dept. of Geophysics &amp; Geothermy, Univ. of Athens, 157 84 Zografou, Greece. E-mail:atzanis@atlas.cc.uoa.gr) and F. Vallianatos (Technological Educational Inst. of Crete, Chania Branch, Crete, Greece, E-mail:fvallian@teihann.gr)

The quest for observation and study of transient Electrical Earthquake Precursors (EEP) has been vigorous in the past and has produced a prolific variety of signal shapes and durations. To date however there exists no universal theory to describe the mode of appearance and expected waveforms, nor proven techniques to identify and discriminate precursors from noise. Earlier attempts to appraise a signal based on electric field observations only, could only determine whether it was produced from known local sources. Identification was not possible, save for the abstract assumption that a non-local signal ought to have been generated by some distant earthquake source. Statistics were used to establish the association of signals with earthquakes but given the insufficient understanding of their nature, this has led to vigorous controversy and debate. Herein we attempt to appraise a different classes of transient signals observed in Greece and abroad, especially those used in publicised short-term prediction. We base our investigations on their physical characteristics (e.g. shape,

duration, properties of their magnetic companion) and attempt to assess whether their sources can be consistent with what is expected from known physics of the earthquake focus and associated electrification processes within the fundamental concept of self-organised criticality. We conclude that only a limited class of the observed signals can be consistent such properties: they can be theoretically modelled and have characteristic transient bay-like shapes, featuring a corner frequency and inverse power energy distribution law. Other types of signals such as single or multiple pulses with shapes like spikes, delta functions or boxcars cannot be produced by such a system. A number of examples is presented and discussed.

ST1/E/36-A4 Poster 0930-37

## FREQUENCY ANALYSIS OF SEISMIC SOURCES AT GOL-E-GOHAR IRON ORE MINE, S.E. IRAN

FARHAD JAVADI and Abdolrahim Javaherian (both at Institute of Geophysics, Tehran University, P. O. Box 14155-6466, Tehran, I. R. Iran, email: javaheri@chamran.ut.ac.ir)

The effect of seismic waves on the stability of structures and buildings is very important. In open pit mines, it is interesting to study the effect of vibrations produced by blasting and mine utilities on the surface structures. The study of microtremors is also helpful in determining the natural frequency and noise level of the site. Fundamentally, assessment of seismic waves and their effect on structures requires to determine their frequency content.

In this research, the frequency content of main seismic sources at Gol-e-Gohar iron ore mine (blasting, mine utilities and microtremors) is studied. To do this, we recorded seismic signals for three days, using several digital recording systems. Due to short duration of blasting, we extracted part of the seismogram containing the event to determine its amplitude spectrum. In this way, the frequency range of two normal mine explosions was detected. In contrast to blasting, vibrations of utilities and microtremors are almost permanent. So it's necessary to study variations of their frequency content against time to specify dominant frequency ranges. In this case, we divided each seismogram to several windows, with 20 second length and calculated amplitude spectrum of each window, separately. Then using three dimensional graphs, showing variations of amplitude against frequency and time (window), dominant frequency ranges were determined. We also performed a qualitative interpretation on the effect of distance from the source, on the frequency range of seismic waves for explosions and mine utilities.

ST1/E/03-A4 Poster 0930-38

## IONOSPHERE RESPONSE ON CURRENT PROCESSES IN LITHOSPHERE

LARKINA V.I.(1), MIGULIN V.V.(1), SERGEEVA N.G.(2), SENIN B.V.(3). (1) IZMIRAN, Troitsk town, Moscow Region, 142092, Russia, (2) Polar Geophysical Institute, Murmansk, Halturina Str.15, 183010, Russia, (3) SouzMorGeo, Gelendzik

Low-frequency Emission Investigations at Low-Altitude Satellites has shown, that Electromagnetic Processes, registered in the Ionosphere can be connected with Processes in Lithosphere. We find out Changes in the Low Frequency Emission Field (0,1-20 kHz) registered onboard "Intercosmos 19" Satellite at its Flight above Deep Lithospheric Faults in a Region of Barentz and Kara Seas. Magnetic and Electrical Components of Emission Field are registered. We carry out the Correlation Analysis of magnetic and electrical component emission bursts. The Correlation Coefficient exceeded 0,72. It speaks that observable Emissions are Electromagnetic.

Complex Researches of Plasma Parameters and Low Frequency Emissions above Deep Fault Regions are Fulfilled. Over the one We marked Low Energy (50 and 120 eV) electron flow Bursts and Environmental Temperature Bursts.

Correlation Analysis Results have shown that Best Correlation take place between the Particle Bursts and Low Frequency Emission electrical Component one. Zones of Abnormal bursts Observations above Fault Zones are appreciated. Different Character of Noise bursts above Compressing zZones and Stretching Zones is found out. Conformity and Distinction of the plasma Parameter Changes and Geological Structures on the Estimate of Barentz-Kara sea Region are found out. Interpretation of Received Results is given.

ST1/E/03-A4 Poster 0930-39

## IONOSPHERE RESPONSE ON CURRENT PROCESSES IN LITHOSPHERE

LARKINA V.I.(1), MIGULIN V.V. (1), SERGEEVA N.G. (2), SENIN B.V. (3), (1) IZMIRAN, Troitsk town, Moscow Region, 142092, Russia, (2) Polar Geophysical Institute, Murmansk, Halturina Str.15, 183010, Russia, (3) SouzMorGeo, Gelendzik

Low-frequency Emission Investigations at Low-Altitude Satellites has shown, that Electromagnetic Processes, registered in the Ionosphere can be connected with Processes in Lithosphere. We find out Changes in the Low Frequency Emission Field (0,1-20 kHz) registered onboard "Intercosmos 19" Satellite at its Flight above Deep Lithospheric Faults in a Region of Barentz and Kara Seas. Magnetic and Electrical Components of Emission Field are registered. We carry out the Correlation Analysis of magnetic and electrical component emission bursts. The Correlation Coefficient exceeded 0,72. It speaks that observable Emissions are Electromagnetic.

Complex Researches of Plasma Parameters and Low Frequency Emissions above Deep Fault Regions are Fulfilled. Over the one We marked Low Energy (50 and 120 eV) electron flow Bursts and Environmental Temperature Bursts.

Correlation Analysis Results have shown that Best Correlation take place between the Particle Bursts and Low Frequency Emission electrical Component one. Zones of Abnormal bursts Observations above Fault Zones are appreciated. Different Character of Noise bursts above Compressing zZones and Stretching Zones is found out. Conformity and Distinction of the plasma Parameter Changes and Geological Structures on the Estimate of Barentz-Kara sea Region are found out. Interpretation of Received Results is given.

ST1/W/03-A4 Poster 0930-40

## WHY DOES COEFFICIENT C IN THE MODIFIED OMORI LOW STRONGLY DEPEND ON THE MAGNITUDE CUT-OFF OF THE AFTERSHOCKS?

Peter SHEBALIN (International Institute of earthquake prediction theory and mathematical geophysics, Varshavskoye shosse, 79/2, Moscow 113556, Russia, e-mail: shebalin@mitp.ru); Nikolay Tsybine (Federal Research Institute for Aviation Systems, Ministry of Economics of Russian Federation, 7 Victorenko st., 125319 Moscow, Russia)

For large aftershock sequences after strong earthquakes we observe that in most cases parameter c in the modified Omori law ( $N(t) \sim 1/(t+c)^p$ ) depends exponentially on the magnitude cut-off of the aftershocks. The larger magnitude aftershocks are taken in estimation, the larger value of c is obtained. In some cases the estimated value of c can reach many hours.

The evident reason of this is the lack of events in the catalogue right after strong events.



Smaller aftershocks are easier to be "lost". Some aftershocks can not be identified because they are "shaded" by stronger events on the seismograms. In some cases large number of aftershocks can also "overload" data processing, and as the result the catalogue is not complete. But those factors can not explain very large values of the parameter  $c$ . We suggest the explanation by presenting aftershock sequence as self-exciting process. In this case even weak "shading" of small events by stronger ones can be enough to obtain large estimated values of  $c$ . We simulated aftershock sequences using epidemic-type model (as proposed by Ogata for the seismicity of a region) and adding the "shading" time intervals after events depending on their magnitude. We succeeded to obtain for real and simulated catalogues of aftershocks of Landers, Northridge and other earthquakes good coincidence of all Omori law parameters, including  $c$ , at a large spectrum of the magnitude cut-off. In addition, the estimations of correlation dimension of temporal distribution of aftershocks also well coincide for real and artificial data.

**ST1/W/36-A4** Poster **0930-41**

#### TEMPORAL FEATURES OF SEISMICITY IN THE AREAS OF TWO STRONG EARTHQUAKES OCCURRENCE IN THE REGION OF KAMCHATKA AND KURILE ISLANDS

Alexander LUTIKOV, Joint Institute of Physics of the Earth, RAS, Moscow, (B.Gruzinskaya, 10, Moscow, Russia, Email: ail@uipe-ras.scgis.ru)

The areas of occurrence of three strong earthquakes in Kamchatka, Kuril Islands and Taiwan have taken place in the last decade (South Kuriles 1994 ( $M_s=8.1$ ); Kronotskoye (east coast of Kamchatka) 1997 ( $M_s=7.9$ ) earthquakes) are identified from a statistical analysis of numerous seismic moment tensors time series in terms of its two invariants (the ordering index  $K$  ( $0 < K < 1$ )), which is determined as ratio of the average seismic moment per year matrix norm to the seismic moment average matrix norm per year, and cumulative scalar seismic moment -  $M_o(t)$  per year. The last parameter was used only for Kronotskoye earthquake. For this purpose the CMT-catalog (research group from Harvard University) and regional catalog of Kamchatka have been used. The basic conclusions of this work amount to the following: 1. Time series of ordering index  $K$  shows the statistically significant changes before earthquakes: the phase of increasing the value of  $K$  (duration - 3-5 years) replaces the short phase of its falling down (1-1.5 years before earthquake). This demonstrates the complicated process of seismicity order and chaoticity in strong earthquake areas of preparation. 2. Statistically significant minima of cumulative seismic moment of about 5 year duration before the Kronotskoye earthquake can be considered seismic quiescence. It is interesting that the phase of seismic quiescence for this earthquake coincides with phase of increasing the value of  $K$ .

**ST1/W/71-A4** Poster **0930-42**

#### CN MONITORING OF SEISMICITY IN THE ITALIAN AREA

ANTONELLA PERESAN (Department of Earth Sciences, University of Trieste, via Weiss 4, 34127 Trieste, Italy, Email: anto@geosun0.univ.trieste.it) Giuliano F. Panza and Giovanni Costa (both at Department of Earth Sciences, University of Trieste, via Weiss 4, 34127 Trieste, Italy) and at The Abdus Salam International Centre for Theoretical Physics, SAND Group, Trieste, Italy) Irina M. Rotwain (Russian Academy of Sciences, International Institute of Earthquake Prediction Theory and Mathematical Geophysics, Varshavskoye, 79/2, 113556 Moscow, Russia and The Abdus Salam International Centre for Theoretical Physics, SAND Group, Trieste, Italy)

A regionalization, strictly based on the seismotectonic zoning and taking into account the main geodynamic features of the Italian area, is used since 1997 for the application of CN algorithm to the Italian territory. The monitoring of seismicity is performed using the Italian catalogue CCI1996 updated with the Preliminary Determinations of Epicentres (PDE) from NEIC. In order to obtain a catalogue as homogeneous as possible, the completeness of PDE data and the relations between different kind of magnitudes reported in the CCI1996 and PDE catalogues have been analysed. A rule for the choice of magnitude priority in PDE, similar to that used for CCI1996, has been formulated. The results obtained in the forward monitoring appear to substantiate the robustness of the algorithm with respect to this change in the catalogue. Results updated at January 1, 1999 show that no alarm is given for the monitored regions, though the reliability of predictions for the Southern region is still insufficient, due to the low completeness level of the catalogue. More updated results will be provided at the meeting, since the monitoring is performed with a time step of two months.

A comparison of the performances of CN algorithm with the different regionalizations proposed up to now for the Italian territory, indicates that the regionalization based on the seismotectonic model should be preferred.

**ST1/P/07-A4** Poster **0930-43**

#### CHARACTERISTICS OF STRONG EARTHQUAKES IN EAST CHINA AND ITS APPLICATION

Chen YUWEI and Huang Xiongang (Seismological Bureau of Anhui Province, Hefei, China, Email: anhuisig@public.hf.ah.cn)

Earthquake is a complicated phenomenon in nature. Individual earthquake happens with great uncertainty, studying integrate features of earthquakes and subtracting precursory information from them would be an effective way in earthquake prediction research.

Taking tectonics characters in consideration, authors analyse the temporal-space distribution of earthquakes ( $M > 5.0$ ) and seismicity patterns in East China qualitatively. It is shown that the activity of strong earthquake indicates an alternative features between active and perigram analysis of historical earthquake series, it is found that the distribution of earthquakes illustrates the clustering and linear features along longitude and latitude, it is also shown the characteristics of oriented migration with strong earthquakes. Finally, the variation of regional stress field and some precursory information for strong earthquakes are obtained by analysis of evolution of seismicity patterns.

**ST1/W/73-A4** Poster **0930-44**

#### COMPARISON OF THE COSEISMIC RUPTURE WITH THE AFTERSHOCK DISTRIBUTION IN THE HYUGA-NADA EARTHQUAKE OF 1996

Yuji YAGI, Masayuki Kikuchi, Shingo Yoshida, (Both, Earthquake Research Institute, University of Tokyo, Yayoi 1-1-1, Bunkyo-ku, Tokyo 113-0032, Japan; e-mail yuji@eri.u-tokyo.ac.jp) and Takeshi Sagiya (Geographical Survey Institute, Katagou 1, Tsuba 305-0811, Japan; e-mail sagiya@gsi-mc.go.jp)

On October 19, 1996, a large underthrusting earthquake, the Hyuga-nada, Japan, earthquake occurred along the southern end of Nankai trough. About two months later, a second large earthquake occurred in the adjacent region. We retrieved waveforms recorded at K-NET in Kyushu and GPS data at the network of Geographical Survey Institute. We employed a multiple-time window inversion to determine the temporal and spatial distribution of fault slip.

The main source parameters obtained for the first mainshock are: (strike, dip, rake) = (210, 12, 81); the seismic moment  $M_o = 2.7E19Nm$ ; the rupture area  $S = 15km \times 25km$ , and the source duration  $T = 17s$ . For the second main-shock, (strike, dip, rake) = (210, 12, 87); the seismic moment  $M_o = 1.5E19Nm$ ; the rupture area  $S = 18km \times 18km$ , and the source duration  $T = 15s$ . The coseismic rupture areas do not overlap the aftershock areas, while the aftershock areas of the two events mutually overlap. This implies that the common aftershock region takes a role of barriers to dynamic rupture. It is also seen that the aftershock area expanded during the first one day.

**ST1/W/72-A4** Poster **0930-45**

#### SEISMIC SEQUENCES IN RILA MOUNTAIN

Blagovesta Babachkova, Tatiana TOTEVA, Snezhina Rizikova (Department of Seismology, Geophysical Institute, Ak.G.Bonchev Str., Block 3, 1113 Sofia, Bulgaria, toteva@nlcv.net)

This study aims to investigate the sequences in Rila mountain region. The area mentioned above is interesting for some reasons: the lack of strong earthquakes, but this region is closed to active areas especially Kresna seismic zone - the most active region in Bulgaria. (Rila region is included in Knopoff space window for 1904 earthquake,  $M=7.8$ ). Another reason for investigating the Rila mountain are the observed seismic sequences there. The last seismic swarm occurred in 1997. More than 170 events were located in a very narrow area. The wave forms and earthquake recurrence graph were investigated. Great similarity exists in the wave forms for most of the swarm events. Nevertheless, the old sequences in this region were reviewed and an attempt to find a probable relation between them and the strong events was made.

**ST1/W/02-A4** Poster **0930-46**

#### LOCALIZATION OF SEISMICITY BEFORE STRONG KAMCHATKA EARTHQUAKES

ZAVYALOV A.D. and Nikitin Yu.V. (both United Institute of Physics of the Earth, Russian Academy of Sciences, str.B.Guzinskaya, 10, 123810 Moscow, Russia, tel.+7(095)254-2478, fax +7(095)254-2478, email: zavyalov@uipe-ras.scgis.ru)

Shrinkage of cracking process to a plane of a future main line rupture and its consequent localization near this plane are qualitatively described by avalancheunstable cracking model (IPE-model). This phenomenon is marked in laboratory on rock samples. In the present work the outcomes of researches on detection of the indicated effect under preparation of strong earthquakes in Kamchatka seismoactive region are shown. As a basic data the catalogue of Kamchatka earthquakes and also information about source mechanisms of the 10 Kamchatka earthquakes with an energy class  $K > 14.0$ , occurred in central part of Kamchatka seismoactive region were used. In the work the space-time behaviour of distance  $R$  from a center of gravity of a hypocenters cloud up to the 1-st source plane of appropriate earthquake, and also distribution of seismogenic ruptures density  $K_{sr}$  were considered. As research area for each strong earthquake the stratum by a breadth 50km, including the 1-st source plane, was selected. It is established that long before strong events in the area of their hypocenters distribution of parameters  $K_{sr}$  and  $R$  along source plane have a casual character. Immediately before earthquake in hypocentral area of a main event there are one or two zones, where the parameter  $R$  accepts the minimum values ( $R < 5km$ ). It testifies that the seismic events are strapped to one among source planes of the future main earthquake. Its hypocenter places or in one from zones of minimum values of a parameter  $R$ , or between them. In turn aftershocks of the first day of a main event envelope square between these zones, mainly placing there, where the parameter  $K_{sr}$  accepts minimum values. However, hypocenters of main events are in zones of minimum values just of a parameter  $R$ . It is possible to suppose, that the seismicity is located close to source plane of the future main line rupture, and, apparently, the area of such localization determines a site of future hypocenter of strong earthquake (site of a beginning of destruction process). After a main event in the area of low values of parameter  $K_{sr}$ , close located to hypocenter of a main event, aftershocks are happening and finally finish process of destruction, connected to this earthquake. The work has been executed under financial support of RFBR, projects 94-05-16114 and 96-05-65439.

**ST1/W/29-A4** Poster **0930-47**

#### MONITORING CRUSTAL STRESS VARIATIONS DURING EARTHQUAKE SEQUENCES CULMINATING IN A LARGE, $M > 5.0$ , EARTHQUAKE

BJÖRN LUND, Sverker Olsson, Reynir Bödvarsson and Ragnar Slunga (Dep. of Earth Sciences, Uppsala University, Villav. 16, 752 36 Uppsala, Sweden, email: bl@geofys.uu.se)

Real-time monitoring of the state of stress in the crust would be a very valuable aid in earthquake prediction. We invert microearthquake focal mechanisms to estimate the stress tensor, using a range of acceptable focal mechanisms for each event to account for the errors in the focal mechanism estimates. The stress tensor inversion is rather time consuming so to minimize the number of events included in each new stress estimation we have developed a new event selection method. The selection method rejects new events that have focal mechanisms similar to events already included by correlating the new event's amplitudes with those of the old events. Only if the amplitudes, or polarities, indicate that the event would contribute significant new information to the stress estimation is the event included. Sequential stress tensor estimates are compared at the 10%, 68% and 95% confidence levels in directions of the principal stress axis, the maximum horizontal stress and the relative size of the intermediate principal stress and we have designed criteria to distinguish significant changes in the stress state. The stress tensor inversion with the new event selection criterion was applied to two earthquake sequences in the Hengill region in Iceland. We investigate temporal variations in the crustal state of stress during a three month period before, and one month after, two large, magnitude  $> 5.0$ , earthquakes.

**ST1/W/31-A4** Poster **0930-48**

#### AIC ANALYSIS OF CATEGORICAL DATA FOR EARTHQUAKES AND VELOCITY STRUCTURES IN THE NORTH CHINA

SUN Ruomei, SHI Yaolin, LIU Jie, 1) Sun Ruomei in the Institute of Geophysics, Chinese Academy of Sciences, Beijing, 100101, email@sun.ihep.ac.cn, 2) Shi Yaolin in the Graduate School, University of Science and Technology of China, Academia Sinica, Beijing, 100039, email: shiy1@sun.ihep.ac.cn, 3) LIU Jie in the Center for Analysis and Prediction, CSB, Beijing, 100036 email: liujie@ip.cas.ac.cn

The North China plain is an economic flourishing area with high population and large cities, it is also an area of the highest seismic risk in eastern China. Here we quantitatively analyzed the relation between the occurrence of strong earthquakes and the tomographic velocity structure in North China by using the AIC (Akaike Information Criterion) analysis method for categorical data. We will list results of AIC values, single explanation variables first, such as the velocity or velocity gradient in each layer to show their relation with earthquake occurrences, then, combinations of two, three, or more explanation variables. The



corresponding interval division of explanation variables are also given. Finally, all possible variable combinations are listed by AIC order. The results indicate that areas of low P-wave velocity in the lower crust and the top of upper mantle and areas of high S-wave horizontal gradient in the upper and lower crust are correlated with earthquakes of magnitude greater than 5-6. The correlation may be related to the geodynamics of Cenozoic thinning of the lithosphere and upwelling of mantle materials. Zones lateralinhomogeneous in crustal structure and thermal state is prone to occurrence of strong earthquakes.

**ST1/W/59-A4** Poster **0930-49**

**MULTIFRACTALITY IN AFTERSHOCK SEQUENCES CORRESPONDING TO SHALLOW EVENTS IN THE SOUTH-AMERICAN SUBDUCTION ZONE**

Ana M. Osella (Dto. de Física - Fac. de Cs. Exactas y Naturales - Univ. de Buenos Aires - Ciudad Universitaria - Pab. 1 - 1428 - Buenos Aires - Argentina, email:osella@df.uba.ar); Nora C. SABBIONE (Dto. de Sismología - Fac. de Cs. Astr. y Geofísicas - Univ. Nac. de La Plata - Paseo del bosque s/n - 1900 - La Plata - Pcia de Buenos Aires - Argentina, email:nora@fcaglp.unlp.edu.ar); Daniel Cernadas (Dto. de Física - Fac. de Cs. Exactas y Naturales - Univ. de Buenos Aires - Ciudad Universitaria - Pab. 1 - 1428 - Buenos Aires - Argentina, email: cernadas@df.uba.ar)

The spatial distribution of aftershocks following large earthquakes may give information about the behavior of the seismic zones and the physical state of the crust. The low possibilities for modeling the evolution of the fields of stresses and strains make it necessary, at least in a first approach, to face the problem in a statistical way. In the present paper we apply this kind of approach to analyze the aftershock activity corresponding to large and shallow earthquakes occurred in the South-American subduction zone. The degree of clustering of the different events are described through a multifractal analysis and complemented with the pair analysis technique and regional values previously obtained. Monofractality together with low values of D seems to be related to the presence of complex sets of faults responsible of the events, while the multifractal behavior with higher values of D could indicate the presence of a dominant fault around which the aftershocks are clustered. From these results, the behavior of D when applied to aftershock sequences appears to be related to the mechanisms associated to the rupture history and therefore may contribute to propose more realistic models of the seismic sources.

**ST1/P/12-A4** Poster **0930-50**

**RESEARCH ON DYNAMIC PATTERNS AND PARAMETER CHARACTERS OF CRUSTAL DEFORMATION FIELD BEFORE AND AFTER STRONG EARTHQUAKE**

Shuoyu ZHOU, Yun Wu, Ganjin Deng (All at Institute of Seismology, Chia Seismological Bureau, Wuhan, China)

Based on the dynamic monitoring of crustal deformation, the parameter for the dynamics pattern and fractal dimension of crustal deformation field and the integral activity level of many faults etc. before and after the Tangshan(1976) AND Lijiang(1996) strong earthquakes and others are studied by using the method of pattern dynamics. It is exposed that two time-space characters, the ordered dimension drop for the deformation field and the accelerated motion of multi-fault before an earthquake, are probably caused by the deformation localization and fault softening after the seismogenic process enters the nonlinear stage. They could be an important seismic precursor if they occurred before strong earthquakes.

**ST1/E/04-A4** Poster **0930-51**

**THE LITHOSPHERE AND ATMOSPHERE INTERACTION ACTIVITY AND ITS POSSIBLE CONNECTION WITH COSEISMIC PROCESS**

Viktor A. Volkov (United Institute of Physics of the Earth, Russian Academy of Sciences, Bol'shaya Gruzinskaya str., 10, Moscow, 123810 Russia); Mstislav N. DUBROV and Rostislav F. Matveev (both at Institute of Radioengineering and electronics, Russian Academy of Sciences, ac. Vvedensky sq., 1, Fryazino, Moscow region, 141120 Russia, email: mnd139@ire216.msk.su)

The lithosphere-atmosphere interactive disturbances are investigated. The joint data analysis of synchronous operating and spatial distanced at 140 km laser strainmeter, tiltmeter, and seismogram has been performed. The ultra long period (3 min...6 hours) oscillations of the Earth together with the atmospheric pressure microvariations in the same period range are analysed. Strain-to-pressure ratio at 2-3 m depth varies within  $(2-4) \cdot 10^{10} \cdot (-8)$  /mbar during the year and is one order greater than such ratio at 15 m underground. The dynamic disturbances in atmosphere have the wave microstructure and are accompanied by complicated earth strains, tilts, and gravity variations. These interactive <waves> propagates along the atmosphere-earth boundary with the velocities of 30 - 50 km/h. Being partial coherent they would produce the obstacles into the precise geophysical data acquisition. However the correct knowledge of those ground motions would bring the new technique for earth material testing. We have observed the essential growth of 4-5 hour period disturbances during 2 days before the earthquake March 25, 1998, Mp.s=7.0-7.9. The intensity of atmosphere-lithosphere interaction has to be compared with the Earth's seismic activity. The vertical strains and underground water regime should be investigated.

**ST1/E/06-A4** Poster **0930-52**

**HYBRID LG + RG AND LG + SN DATA AT REGIONAL DISTANCES: IMPLICATIONS FOR SOURCE SPECTRA AND INFERRED SEISMIC MOMENTS**

R.A.W. Haddon (32 Mahuta Road, Five Mile Bay, RD2 Taupo, New Zealand), John ADAMS (Geological Survey of Canada, 7 Observatory Cres., Ottawa K1A 0Y3 Canada, email: adams@seismo.nrcan.gc.ca), and Hilmar Bungum (NORSAR, PO Box 51 N-2007 Kjeller Norway)

While seismic moments are reliably determined from teleseismic P or S waves clearly separated from surface waves, at regional distances the surface waves and the Lg coda overlap, constituting hybrid data. Attempts to infer source spectra and seismic moments using vertical and/or randomly-oriented horizontal component data must take cognisance of the commonly large spectral amplitude contributions from the surface Rayleigh wave Rg for frequencies below about 1 Hz (depending on focal depth). We have computed synthetic wave trains containing Lg + Rg at regional distances for sources at various depths in layered crustal models using a precise f-k method and then computed their amplitude spectra. For Green's function sources we see prominent spectral humps due to Rg with spectral amplitudes as much as about an order of magnitude higher than the associated Lg spectral amplitudes for frequencies between about 0.05 and 1.0 Hz (depending on focal depth). The overall effect of the humps is to elevate spectral levels for low frequencies and to produce spectral "sags". The elevated spectral levels and the "sags" have nothing to do with real source spectra, but are simply artifacts resulting from invalid interpretation of hybrid data and the invalid neglect of excitation, transmission, and surface transfer effects associated with Rg, in particular. For moderate distances (R>250 km, say) and high frequencies (>6 Hz) the phases Lg and Sn cannot be separated and so Lg + Sn wave trains also

constitute hybrid data. Neglect of this fact results in invalid Q models for Lg and significant invalid trade-off effects between inferred attenuation and inferred source spectra. Important consequences of our interpretation are: (1) that seismic moments calculated from the elevated spectral levels (between say 0.05 and 0.2 Hz) without regard to the physics pertaining to Rg overestimate moment magnitude by up to one unit for large (M>6, say) events (depending on focal depth and other factors); (2) high frequency source spectral amplitudes proposed by some authors may be associated with magnitudes up to one unit lower; (3) significant systematic errors in both attenuation and source spectra result from the indiscriminate use of Lg + Sn hybrid data; and (4) claims that the Haddon (BSSA, 1996) source model overpredicts motions at all periods, are unfounded.

**ST1/E/62-A4** Poster **0930-53**

**ANOMALOUS STRAIN-SENSITIVITY OF ELECTROMAGNETIC PARAMETERS IN A FAULT ZONE**

A.A.VAGIMOV (Institute for High Temperatures - Association, Russian Acad. Sci., 13/19 Izhorokaya Str., Moscow, 127412 Russia, Email: rickman@hedric.msk.su)

The results are presented of temporal dynamics of electrical conductivity, electric and magnetic fields obtained from the combined observation systems in the Central-Copetdagh seismic active region.

Levels are determined of relative strain-sensitivity for anomalous variations of the electrical conductivity as well as quantitative relations between dynamical parameters of the electromagnetic process.

For low-resistive, low-magnetic sedimentary rocks, the anomalies of electrical conductivity, electric and magnetic fields are shown to be spatially localized and connected with the fault zones. The governing role is elicited of a fluid dynamics process for structure forming of temporal variations of the electromagnetic parameters for a fault zone.

On the base of reversed problem solution, parameters are determined of an anomaly constituting body. The determined mechanisms are considered of the anomaly variation generation.

**ST1/E/74-A4** Poster **0930-54**

**ANOMOLOUS STRAIN SENSITIVITY OF ELECTROMAGNETIC...**

RANGUELOV

Abstract not available at time of going to press

**ST1/E/75-A4** Poster **0930-55**

**INITIAL DATA FOR THE MAGNITUDE REVALUATION OF THE EARTHQUAKES...**

RANGUELOV

Abstract not available at time of going to press

**ST1/C/GA4.10/E/01-A4** Poster **0930-56**

**COSMIC PHENOMENA AND THE PROBLEM OF EARTHQUAKES...**

Marina Despotashvili, Nodar Khazaradze, Nugzar Nachkebia and Luli SHATASHVILI (Cosmic Ray Department, Institute of Geophysics, Georgian Academy of Sciences, 1 M. Aleksidze st.; Tbilisi 380093; Georgia, email: lkh@cosmr.acnet.ge); David Sikharulidze (Department of Earthquakes, Institute of Geophysics, Georgian Academy of Sciences, 1 M. Aleksidze st.; Tbilisi 380093; Georgia)

It has been shown that a number of revealed anomalous diurnal variations of cosmic rays (CR) corresponds to the periods of the Earth's passage through the neutral sheet of interplanetary magnetic field (IMF). The unusual diurnal CR variations are called the cases when anomalous increases of b (b is the ratio of CR diurnal variation neutron component amplitude to that of hard component) are observed. It is suggested that in these cases CR diurnal variation hard component amplitude increases due to the heating of the Earth's upper atmosphere.

The frequency distribution histogram of destructive earthquake cases in relation with the moments of Earth's passage through the neutral IMF sheet is presented. The given histogram with pronounced maximum of the distribution gives the evidence that a lot of cases of the destructive earthquakes coincide with the moment of Earth's passage through the neutral IMF sheet. Analyzing complex diagrams of b magnitude decrease cases compared to the moments of Earth's passage through the neutral IMF sheet, to the moments of new Moon and full Moon as well as to the perigee and apogee, it is shown that large destructive earthquakes occur preferentially in the cases, when several (two or three) above-mentioned factors are superimposed.

**ST2** **Wednesday 21 – Friday 23 July**

**SEISMOTECTONICS (IASPEI)**

Location: Medical School, EG12 LT4

Location of Posters: Medical School, Arthur Thompson Hall

**Wednesday 21 July AM**

Presiding Chairs: J.M. Lees (Yale University, New Haven, USA),  
Sun Ruomei (Science Academy of China, Beijing, China)

**SEISMOTECTONICS OF WESTERN PACIFIC/ASIA**

**ST2/L/04-A3** **0830**

**SEISMIC COUPLING AT SUBDUCTION ZONES - ITS MECHANICAL CAUSE AND FAR-REACHING GEOLOGICAL CONSEQUENCES**

Miles OSMASTON (The White Cottage, Sendmarsh, Ripley, Woking, Surrey GU23 6JT, UK, email: miles@osmaston.demon.co.uk)

The phenomenon known as seismic coupling, first recognized by Kanamori more than 20 years ago, has increasingly emerged as a tendency for the subduction interface slip to become locked by some kind of asperity, then sheared off by a major interface slippage, to be followed by a 'normal-fault' event and the re-locking of the interface. Seismic coupling is primarily confined to zones where the subducting plate is <70Ma old. The big question has been 'How do the repeated asperities arise?' The seismicity present to considerable depths within downbending plates led me to outline a step-faulting mode of downbend (IGC92, IASPEI94) in which repeated increments of

step-fault throw generate locking asperities at the interface. The shearing of these asperities would have the effect of transferring hanging-wall material to the downgoing plate and thus of advancing the hanging-wall-controlled position of interface downbend beneath the margin.

This contribution will elaborate upon this model (including the provision of outer rises without elastic support) and illustrate the huge tectonic significance of the resulting basal subduction tectonic erosion (STE) that has emerged from my study of subduction orogens and collision orogens, now ranging in age from the present to the Archaean. STE is to be seen as one of the great tectonic processes of the Earth and, as such, intensive study of its seismological manifestation - seismic coupling - is well warranted, hopefully also leading to improved understanding of seismic hazard. A highly STE-specific form of tectonic melange, generated by it, will also be illustrated.

**ST2/W/13-A3****0845****SIDE EDGE OF KAMCHATKA SLAB: 1998-1999**

Jonathan M. LEES, Jeffrey Park, Vadim Levin, Valerie Peyton (all at Department of Geology and Geophysics, Yale University, New Haven, CT, 06511 email: lees@love.geology.yale.edu) Evgenii Gordeev, Alexei Ozerov and Victor Chebrov (all at Russian Academy of Sciences, Petropavlovsk-Kamchatsky, Kamchatka, Russia)

In August of 1998 a joint team of Yale University and Russian Academy of Science investigators installed a broad band array of 15 seismic stations spanning the length of Kamchatka. The purpose of the array is to investigate the possibly torn edge of the Pacific plate as it subducts beneath the Kamchatka Arc at its northern terminus where the Bering fault intersects with the Kamchatka Arc. Connecting the western Aleutian oblique subduction zone to the arc-perpendicular Kamchatka subduction presents certain spatial difficulties in accommodating excess slab material as it bends around the corner. Our model, eliminates this problem by proposing a tear in the slab between Adak Island and Ključevskoi Volcano in Kamchatka. Shallowing of seismicity, unusual volcanic products, high heat flow in the Komandorsky basin each contribute to the accumulated data suggesting the torn slab model is correct. One objective of the large scale array is to determine flow in the upper mantle associated with slab roll back as material is ejected from beneath the Kamchatka slab around the edge of the slab beneath the Komandorsky Basin. If our model is correct we expect a consistent pattern of anisotropy as flow curls around the edge of the slab, heating and ablating the cold lithosphere as it plunges into the mantle. On a local scale, seismic investigations of the exploding Karymsky and Ključevskoi volcanoes are providing insights into volcano dynamics and the relationship of the subducting plate and surficial eruption products. We will present a first look at the data addressing these issues and present our initial interpretation.

**ST2/E/39-A3****0900****THE RELATIONSHIP BETWEEN LARGE SHALLOW INTRAPLATE EARTHQUAKES AND THE INTERPLATE DEEP-FOCUS EARTHQUAKES IN AND NEAR THE KOREAN PENINSULA OF THE FAR EAST**

SO GU KIM, Lhasuren Erendenedalai, Seoung Kyu Lee, and Jiseok Song (The Seismological Institute, Hanyang University, Ahnsan, Kyonggi-do, 425-791, South Korea, Tel: +82-345-400-5532, Fax: +82-345-400-5830, email: sogukim@mail.hanyang.ac.kr)

We often have large shallow intraplate-earthquakes in the Far East, NE China, SW Japan and Korea, outside the plate boundary. We investigate the relation between large shallow earthquakes and large deep-focus earthquakes in the East Sea (Japan Sea) in this study.

From shear-wave splittings of SKS and S(SCs) for deep-focus earthquakes, the orientation of the fast shear-wave accords with that of Pacific plate movement, NW in the inner continent of NE China and Korea, while it is NS in the outer continent of the Sakhalin and Japan regions, which may be related to the steep dipping of the Pacific plate. Using the 3-D velocity tomography of the crust and upper mantle in and near the Korean Peninsula, the high velocity of the lithosphere slab is found to subduct beneath the Eurasian plate in the NW direction. 660 km ? and 410 km ? discontinuities are also found to be in the inner continent and in the East Sea (Japan Sea), respectively.

Most of large deep-focus earthquakes may induce large shallow earthquakes in the Far East seismic regime because the energy density of deep-focus earthquakes is captured over 1000 km of epicentral distance and accelerate the regional stress of this regime. From principle of energy conservation, the kinetic energy of the earthquake is transformed to the elastic potential energy, which may strongly influence the seismicity in and near the Korean peninsula.

**ST2/E/45-A3****0915****DEPTH DISTRIBUTION OF STRESS FIELD IN THE HOKKAIDO WADATI-BENIOFF ZONE AS DEDUCED BY INVERSION OF EARTHQUAKE FOCAL MECHANISMS**

Cenka CHRISTOVA (Geophysical Institute of Bulgarian Academy of Sciences, 1113 Sofia, Bulgaria, email: cenka@geophys.acad.bg) Theodoros Tsapanos (Aristotle University of Thessaloniki, Geophysical Laboratory, 54006 Thessaloniki, Macedonia, Greece, email: tsapanos@geo.auth.gr)

This study is based on the detailed geometry of the Hokkaido Wadati-Benioff zone (HWBZ) and the paleosubduction zone (HPSZ) as delineated by Hanus & Vanek. CMT solutions and the inverse technique of Gephart and Forsyth (1984) were incorporated for determining the best fit principle stress directions  $s_1$ ,  $s_2$ ,  $s_3$  and the ratio  $R=s_2-s_1/s_3-s_1$  for 20 km depth intervals in the HWBZ and for the HPSZ, considered as a whole body. The maximum compressive stresses  $s_1$  in all considered depth ranges towards SE trend dip less than 300, indicating the NW-SE convergence between the Pacific and Eurasian lithospheric plates. The depth layer 100- 120 km and HPSZ are exclusions, the dip/az of  $s_1$  being 42/201 and 30/270, respectively. In all considered depth intervals the minimum compressive stresses  $s_3$  are steeper than 45. A tendency of clockwise rotation of  $s_3$  from NW (along dip of the subducting plate) to NNE (along strike of the subducting plate) and a decrease of plunge with increasing depth is observed. Exclusions are the 120-220 km layer and HPSZ, where  $s_3$  are almost horizontal. The results are discussed in the light of depth distribution of seismogenic properties in the HWBZ.

**ST2/E/20-A3****0930****A NEW GRAVITY ANOMALY - IMPLYING STRUCTURES OF SEISMOGENIC LAYERS IN JAPAN**

Naomi Gennai and Yoshiteru KONO (both at Graduate School of Natural Science and Technology, Kanazawa University, Kanazawa, 920-1192, Japan, email: ngen@hakusan.s.kanazawa-u.ac.jp)

Most earthquakes are occurring within the upper part of the Earth's crust. At the Earth's surface, active faults are indicative of the past seismic activity. On the other hand, gravity anomalies represent the total attraction from shallow as well as deep structure. In particular, gravity anomalies around the Japanese Islands are strongly influenced by complex geological structures within the upper crust and also by undulations of the Moho and Conrad discontinuities and subducting lithosphere (slab). If we can extract the gravity contribution due only to the upper

crust, it may give us information on the geologic structure of seismogenic layers. For this purpose, we apply geophysical gravity reductions to observed gravity anomalies. The reduction procedures begin with the conventional Bouguer anomalies. In contrast to many other geophysical reduction procedures, we start reductions with the gravity contribution of deeper layers. First, we calculated the gravity contribution of subducting slabs beneath the Japanese Islands. Upper surfaces of the slabs are well defined by tracing the upper boundary of hypocenters of deep earthquakes. We evaluated the contribution of the slabs by considering their three-dimensional configuration, thickness and density contrast with the surrounding asthenosphere. Second, reductions due to undulations of the Moho and Conrad discontinuities were performed by employing seismological tomography models. When we subtract gravity contributions due to subducting slabs and undulating Moho and Conrad discontinuities from observed Bouguer anomalies, the resultant gravity anomalies mainly come from upper part of the crust, say shallower than about 14 km. We call the new gravity anomalies thus obtained the "Conrad-Moho-Slab Residual Bouguer Anomaly (CMS-RBA)". The CMS-RBA shows many steep horizontal gradient zones that presumably indicate block boundaries of seismogenic layers. The CMS-RBA was compared with distributions of surface geology, of active faults, of seismicity, and of crustal displacement vectors derived from dense GPS observations. Good correspondence was obtained between the CMS-RBA and those observables, indicating that the CMS-RBA is a useful information for studying active geological structures.

**ST2/W/35-A3****0945****CRUSTAL DEFORMATION OF SEISMIC AND ASEISMIC SUBDUCTION ZONES**

Takeshi SAGIYA (Geographical Survey Institute, Tsukuba 305-0811, Japan, e-mail: sagiya@gsi-mc.go.jp)

Recent space-based geodetic measurements revealed seaward motion of aseismic island arcs such as Ryukyu and Mariana. Marine terraces found in some of the islands are evidences of Quaternary uplifts. These crustal deformations may have a close relationship with geological features like back-arc opening, but physical mechanism is not solved. At aseismic subduction zones, interplate coupling is considered to be very weak. So we calculate crustal deformation due to steady plate subduction along a curved plate boundary in a three-dimensional elastic layer overlying a viscoelastic substratum, based on a dislocation model for plate subduction developed by Sato and Matsu'ura (1988, 1993). The calculated deformation field shows seaward motion and uplift of the island arc and the result may possibly give an explanation for the observed deformation. Curvature of the island arc is an important factor determining the style of deformation. On the other hand, at seismic subduction zones, we need to estimate inhomogeneous distribution of relative displacement and its temporal variation on the plate boundary surface in order to understand the plate subduction process through a whole earthquake cycle. It can be estimated through an inversion analysis of geodetic data taking viscoelastic effects of asthenosphere into account. Four-dimensional (three in space and one in time) inversion technique of geodetic data is now being developed, and it is to be applied for geodetic data during last 100 years along the Nankai trough, southwest Japan.

**ST2/E/05-A3****1000****THE INTERACTION BETWEEN PHILIPPINE SEA PLATE AND EURASIA PLATE AND ITS EFFECT ON THE STRESS FIELD IN EASTERN PART OF CHINA**

Shaoxian ZANG and Q.Y. Chen (both at Department of Geophysics, Peking University, Beijing 100871, China, email: sxzang@ibmstone.pku.edu.cn)

The Euler parameters of the Philippine Sea plate were studied using the slip vectors of earthquakes obtained from CMT data from 1977 to 1996. Some slip vectors which were used by other authors were also used. According to the deformation within Philippine Sea plate the slip vectors were selected and considered in different way. The Euler parameters were calculated in Nuvel-1A framework firstly, then in 14 plates framework, the Okhotsk sea plate was added. The relative movement between Philippine Sea plate and Eurasia plate were obtained.

The stress field in eastern part of China, Taiwan area, Ryukyu island arc and Okinawa trough was obtained using focal mechanisms of earthquakes, it was found that the stress field in Taiwan and southeastern part of mainland of China is coincident with one another, but different from eastern part of mainland; the stress field in eastern part of the mainland of China, Ryukyu island arc and Okinawa trough are different with one another.

By comparison of the principal compressional axes of the stress field with the direction relative movement of the plates as well as the tectonic structure, such as rifting in Okinawa trough, subduction in Ryukyu arc, collision in Taiwan and strike slip fault in Philippine island. It was found the Philippine Sea plate has less influence on the stress field in eastern part of China except the area near Taiwan.

**ST2/E/01-A3****1100****EXTRUSION OF SOUTH CHINA BLOCK AND SLIP RATE OF MAIN ACTIVE FAULTS IN VIETNAM**

Trinh PHAN-TRONG, (1), Robin LACASSIN (2), Phillippe Herve LELOUP(2), Paul TAPPONNIER(2), (1) Institute of Geological Science, NCNST, Vien Dia Chat, Nghia Do, Cau Giay, Hanoi. Fax : 84 4 8362886, E-mail: pptrinh@referer.edu.vn (2) Institut de Physique du Globe, 4 Place Jussieu, 75005 Paris.

The continental extrusion that pushed Indochina Southeast wards along the Red River shear zone was a major event in South East Asia. In North Vietnam, various structures associated with strike-slip motion occurred in the first phase of extrusion. More recently (late Cenozoic) the sense of movement on this fault has changed. Paleostress analysis indicate that since the Miocene two main tectonic phases affected. Several active faults associated with the phase 2 are clear in North Vietnam. Amongst these, two main zones seem to be relatively fast movement: the Red River fault zone and Dien Bien Phu fault. In North Vietnam, the Red River fault zone splays into two major active fault branches. The Red River branch that limits to the SW the metamorphic massif of Day Nui Con Voi, follows the Red River valley. The Song Chay river branch, very clear in the geomorphology, is located NE of Day Nui Con Voi. Towards the SE, the Red River itself splays into several faults. The two major one being respectively located NE and SW of the Red River. Right lateral strike-slip offsets of these faults are determined by analyzing tributaries, stream channels, Quaternary alluvial fans, river valley from LANDSAT, SPOT images, detail topographical maps and field observations. Along the SW fault of the Red River, right lateral offsets of stream channels range among 220 and 700 m (mean offsets of 313 m). Drainage offsets (250 - 450 m) are found on the NE branch. Geomorphology and topographical offset suggest that these strike-slip movements are combined with normal slip. Along the Song Chay branch, right lateral offsets of rivers range among 250 and 1000 m (mean value of 566m). Clear evidence of the active strike-slip movement is also found on the conjugate Dien Bien Phu fault, there, measured left-lateral offsets of river rang between 270 and 790 m. Slip rate may be estimate using 2 different approaches. Assuming that major phase of incision visible in this area, close to the Red-river delta is due to the onset of Wurm glaciation and to sea level drop (100 Kyr), slip rate of  $3.1 \pm 0.9$  mm/yr. (SW Red River branch),  $3.6 \pm 1.1$  mm/yr. (NE Red River branch),  $5.6 \pm 2.3$  mm/yr. (Song Chay branch) and  $5.3 \pm 2.6$  mm/yr. are estimate. Using average length of offset channels and a minimum rate of 100mm/yr. for river propagation, slip rates are...



ST2/E/08-A3

1115

## CRUSTAL STRUCTURES AND DYNAMICS OF THE 1983 (MS6.6) TUAN GIAO EARTHQUAKE EPICENTRAL REGION, VIETNAM

Cao Dinh Trieu and Nguyen Xuan Binh (Institute of Geophysics, VNCST, P.O. Box 411 Buu Dien Bo Ho, Hanoi, Vietnam, email: trieu@igp.ac.vn) P.O. Box 411 Buu Dien Bo Ho, Hanoi, Vietnam, email: trieu@igp.ac.vn)

In this paper, the authors present a solution of source process of the Tuan Giao earthquake and its tectonic implication. The Crustal structures and Dynamics of the Epicentral Region are also described. Based on obtained analytical results, the following conclusions can be made: 1. Epicentral area of Tuan Giao earthquake located in northwest margin of Ma River zone and coincided with uplifted zone of lower boundary surface of the earth crust, where shifting amplitude into both sides of the Son La fault reached value of 2-3 km. 2. The Son La fault strongly activated during Mesozoic-Cenozoic period and Neotectonic and recent movement. Uplifting movement into northeast part of the fault reached value of about 1-2 mm/year. 3. The largest surface ruptures was characterized by system of 3 parallel fracture which have an azimuth, a width 10-17 cm, and a length of about 200 m, that continuously of distributed at the total length of at least 20 km. The surface ruptures, at smaller level, has maximum length a fracture about 20 m of which direction is NW-SE, concentrated at the northwest part of the epicenter area. The surface break have a type of tension. As to the displacement on surface pure right lateral strike-slip was observed. 4. The fault plane solution from the inversion teleseismic body waves indicates pure right-lateral strike-slip, striking N290E, which is consistent with the fault orientation in this area. The focal mechanism determined from the P-wave first motion data has the different strike N120E. This fact suggest that the initial rupture occurred at the fault with the different from that of the main rupture.

ST2/E/33-A3

1130

## DISTRIBUTION OF EARTHQUAKE FOCI AND DEEP STRUCTURE OF SUMATRA-JAVA-LOMBOK PLATE MARGIN

Ales SPICAK, Vaclav Hanus and Jiri Vanek (Geophysical Institute, Bocni II, 141 31 Prague 4, Czech Republic, email: als@ig.cas.cz); John Milsom (University of London, Gower Street, London WC1E 6BT, UK)

The detailed study of the geometrical distribution of earthquakes in the Sumatra-Java-Lombok region allowed the authors to distinguish the foci belonging to the recent Wadati-Benioff zone from those occurring in the continental wedge. The morphology of the Wadati-Benioff zone, its geometrical parameters and the variable depth of its penetration into the upper mantle were established. The existence of an intermediate-depth aseismic gap in the Wadati-Benioff zone was observed and its spatial relationship with young calc-alkaline volcanism was confirmed. The subduction process was correlated with the stratigraphy and geology of the region. The duration of the present cycle of subduction was estimated to be 6-8 Ma. The occurrence of Oligocene volcanism and the location of deep earthquakes point to the existence of a Tertiary subduction zone underlying the present slab. The seismotectonic pattern of the continental wedge was described by well-defined seismically active fracture zones, the orientation and tectonic function of which were checked by fault plane solutions. Considerable shallow and intermediate seismic activity was observed in the vicinity of the Java-Sumatra trench. The distribution of these earthquakes along the trench is not continuous forming seismically active segments separated by aseismic regions or by transverse seismically active fracture zones. All the segments are inclined to the Euro-Asian continent. Fault plane solutions of associated earthquakes indicate normal faulting. The existence of this seismoactive belt can be explained either as a gradual bending of the present subduction zone at the trench or as a manifestation of a new cycle of subduction of the Indo-Australian plate.

ST2/E/60-A3

1145

## EVIDENCES FOR CESSATION OF INDIAN PLATE SUBDUCTION IN THE BURMESE ARC REGION

N. Purnachandra Rao and M. Ravi KUMAR (both at National Geophysical Research Institute, Uppal Road, Hyderabad 500 007, India, email: postmast@csngri.res.nic.in)

The issue of whether subduction is still active in the India-Burma plate boundary zone continues to be a matter of controversy. In this study, we demonstrate that the subduction in the Burmese arc may no longer be active. A classification of the thrust, strike-slip and normal type of earthquakes in the major subduction zones worldwide, indicates that the number of thrust type earthquakes far exceeds those of the other types, comprising about 75% on an average. In the Burmese arc, however, the strike-slip mechanism is found to be dominant. Also, the P-axis orientations of thrust type earthquakes along all the major subduction zones are in close agreement with the predicted NUVEL1 plate motion vectors. On the contrary, in the Burmese arc region, the P-axes are oriented predominantly in the NNE direction, concurrent with the predicted India-Eurasia plate motion vector, rather than eastward, as would be expected in the case of an active subduction. Further, we find that in an east-west depth section, there is a distinct segregation of strike-slip earthquakes in the upper half of the subducted slab (0-90 km) and the thrust type, exclusively in the lower half. This can be explained only in terms of shearing of the Indian plate past the Burmese plate in the zone of contact, and compression of the lower portion of the slab against the asthenosphere, in the NNE direction. Computation of strain rates in the Burmese arc region indicates a ratio of 4:1 for NS-EW convergence, in agreement with the above results. In conclusion, the Burmese arc region is a special situation in where there is a subducted slab, but the direction of plate motion is not down-dip. Instead, the subducted Indian lithospheric slab is sheared past the Burmese plate in the NNE direction.

ST2/E/52-A3

1200

## GEOLOGIC SETTING OF STRONG EARTHQUAKES IN THE EAST-NORTH CHINA

SUN Ruomei and LIU Futian (both in the Institute of Geophysics, Science Academy of China, 100101 Beijing, CHINA, email: sunrm@sun.ihp.ac.cn)

The east-north China is one of high seismicity areas in China. During the past 1000 years more than 200 earthquakes with magnitude M(5.0, 58 with magnitude M(6.0 and 15 with magnitude M(7.0 occurred. The 1976 Tangshan earthquake (M=7.8) is in the area. The catalogues of last 1000 years are compared with tomographic images. The results are:

- (1) Hypocenters of most of strong earthquakes distribute near the boundaries between different high velocity blocks or in the transitional zones from high to low velocity on the side of high velocity in the upper crust. Projected locations of strong shocks on the image of the lower crust distribute in transitional zones from low to high velocity at the side of low velocity.
- (2) More deep geologic setting of strong earthquakes is as follows. Seismicity distributes in the area, where the lithosphere is thin. The thickness of lithosphere of the east-north China has thinned since early Tertiary basalt eruptions, composed by theolite and olivine, occurred in several episodes, now about 80km.(3) The 1976 Tangshan earthquake is not located near any

known large surface fault, but in sharp velocity gradient zones both in horizontal and vertical cross sections. It might be the result of expansion of covered fault. (4) Seismicity, focal depth and mechanism of the Buohai bay link with upwelling of hot material of mantle and extensional crust there.

ST2/W/03-A3

1215

## NUMERICAL CALCULATIONS ON TECTONIC STRESS FIELD OF CHINESE MAINLAND AND ITS NEIGHBORING REGION AND THEIR APPLICATIONS IN EXPLANATION OF SEISMIC ACTIVITY

MINGRUO JIAO, Guomin Zhang, Shi Che, Jie Liu (Center for Analysis and Prediction, SSB, Beijing 100036, China)

This paper made a numerical simulation to the basic tectonic stress field of Chinese mainland and its neighboring land using the visco-elasticity finite element pattern and the new published displacement rate result. Main contents include the simulation of maximum shear stress and its varying rate, the maximum shear strain and its varying rate, the shear strain energy density and its varying rate. In view of the highly seismic inhomogeneous distribution character in space and time in Chinese mainland and its neighboring area, the normalized background energy value was given by normalized treatment to the earthquake energy release in eastern and western parts of Chinese mainland, obtaining the normalized background energy values. And the comparison of the simulation result with the active seismicity was made. The results show that the simulation values can explain well the earthquake distribution character of Chinese mainland and its neighboring area.

Key words: tectonic stress field, numerical simulation, seismic activity, Chinese mainland

Wednesday 21 July PM

Presiding Chairs: Rongsheng Zeng (China Seismological Bureau, Beijing, China), U. Raval (National Geophysical Research Institute, Hyderabad, India)

SEISMOTECTONICS OF ASIA

ST2/W/01-A3

1400

## EPISODE OF COMPRESSION IN THE BAIKAL RIFT ZONE IN 1992-1993

Pyotr DJADKOV (Institute of Geophysics, av. Acad. Koptuyg, 3, Novosibirsk, 630090, Russia, E-mail: djad@uiggm.nsc.ru), Valentina Melnikova and Vladimir Sankov (both at Institute of the Earth's crust, Lermontova str., 128, Irkutsk, 664033, Russia, E-mail: vimel@crust.irk.ru), Vladimir Timofeev (Institute of Geophysics, av. Acad. Koptuyg, 3, Novosibirsk, 630090, Russia, E-mail: sari@uiggm.nsc.ru)

The Baikal region is the typical continental rift, where the high seismic activity and the explicit predominance of the normal focal mechanisms are observed. The episode of compressive horizontal strain predominance was detected in the Baikal region in 1992-1993 by the geophysical methods of the crustal stress and strain monitoring: the tectonomagnetic observations in the central part of the Baikal rift, the determinations of changes of the focal earthquake mechanisms in time for all Baikal region, the extensometer measurements at station Talaya near the south part of Lake Baikal. During the March 1992 to July 1993 the number of the earthquakes with the thrust component of displacement in the earthquake sources reached 60 - 80 % , while such earthquakes occurred very rare in other periods. After the compressive episode we observed the process of the high-rate extension during 1994-1995, when the normal and strike-slip displacements in the earthquake sources occurred only. The GPS-observations were begun in 1994. These observations showed high rate of the Baikal rift's opening (~ 10-15 mm/y) for period of 1994-1996 [ Calais et al., 1997]. The most probable cause of the compressive strain episode in the Baikal rift in 1992-1993 is the irregularity of development of geodynamic process in the West-Pacific subduction zones.

ST2/E/40-A3

1415

## SEISMIC DEFORMATION AND THREE DIMENSIONAL VELOCITY STRUCTURE IN THE TIEN SHAN, PAMIR AND WESTERN CHINA

Lira MUNIROVA, (Institute of Seismology, Bishkek 720060, Kyrgyzstan, E-mail: kis@imfiko.bishkek.su) Tatyana Yanovskaya ( St.Petersburg State University, Dept. of the Earth, St.Petersburg, 198904, Russia, email: yanovs@snoopy.phys.spbu.ru)

Focal mechanisms and velocity structure were used for analysis of the rheology in the region and the kinematics of the deformation. All the available data recorded by local seismological networks deployed in Kyrgyzstan (North Tien Shan) were used as the database for body waves velocity structure inversion. This database consisted on about 20000 P and 10000 S arrival time readings from local earthquakes recorded between 1967 and 1998. Also we present a study of the dispersion characteristics of intermediate period (5-60s) Rayleigh and Love waves propagating across the region for tomographic imaging. Broad-band waveform data of the events from distances from 300 to 1500 km from 1992 to 1998 recorded at 10 stations KNET. Group velocities of both Rayleigh and Love waves are used in a tomographic inversion to obtain group velocity maps. The source parameters of moderate- to large-sized earthquakes and the spatial distribution of earthquake hypocenters are used to investigate the active tectonics and three dimensional configuration of the lithosphere in the Tien Shan region. Theoretical relationships allow the distributed deformation due to seismic activity to be quantified on the basis of the analysis of moment tensors. This method was applied to a data set consisting of seismic events that have occurred in the past 21 yr in the Tien Shan region. As data was used the Centroid Moment Tensor Catalog prepared at Harvard University, covering the last 21 yr. Focal mechanism solutions of events beneath Tien Shan show thrust faulting with approximately E-W oriented P-axes on the North Tien Shan, N-S oriented P-axes on the South Tien Shan. Events beneath Pamir show some strike-slip faulting on the eastern and northern edge of the Pamir on the border with Western China (Tarim) and Tien Shan. The high velocities of the deformation also are occurred on the Pamir, Tien Shan, Tarim boundary. The most of strike-slip events were associated with high gradient and low velocity zone.

ST2/E/57-A3

1430

## EVOLUTION CHARACTERISTICS OF CRUSTAL DYNAMICS IN THE NORTH AND EAST MARGIN OF QING-ZANG(TIBET) PLATEAU

Xie Furen, ZHANG Shimin, Shu Saibing, Dou Suqin (Institute of Crustal Dynamics, CSB, Beijing, 100085, China)

The analysis result of tectonic stress field evolution based on faults slip data and crustal deformation characteristics suggest that the north and east margin of Qing-Zang plateau was subjected to an omnibearing compression caused by the collision of India plate with Qing-Zang block approximately from Pliocene to early Pleistocene, when the tectonic stress field was featured by a maximum principal compression stress perpendicular to the boundary of the



plateau and the stress regime was basically of reverse faulting type. Since the end of early Pleistocene, India plate continues to push northward and the compressional deformation of the plateau crust increases continuously and is transmitted through the northern margin of Qing-Zang block to further north. At the same time, the crustal thickening in southeast Qing-Zang decreases rapidly towards east margin indicating that the eastward

**ST2/E/19-A3****1445****THE LATEST TECTONIC DEFORMATION AND CRUST MOVEMENT, SOUTHEASTERN MARGIN OF QINGHAI-TIBET PLATEAU**

XUHUI SHEN (Center for Analysis and Prediction, Chinese Seismological Bureau, 100036, Beijing, China) Yipeng Wang (Institute of Geology, Chinese Seismological Bureau, 100029, Beijing, China)

The tectonic deformation and crust movement since 30KaBP is the latest period of neotectonism in southwest of China, the southeastern margin of Tibet plateau. According to existing materials, there displays clear stratigraphic unconformity, sedimentary facies change and briefly sedimentation hiatus in this period. In the respect of tectonic geomorphology, it shows tectonic basin altering and river system modifying, such as regional tectonic basins shrivel, partly embryonic basin forming, river courses rejoining-up, river capture, watersheds migrating and some superimposed valleys forming and so on. And in the respect of tectonic deformation, there shows regional stratigraphic unconformity and light fold, and some major fault zones display clear tenso-shear sliding. Tectonic deformation since 30KaBP mainly shows co-existing of escape tendency from Qinghai-Tibet Plateau and complicated inner deformation of Chuandian Region. The escape rate of Chuandian Rhombus-shaped Block is 5.4-7.6mm/a at the northwest part, and 3-3.8mm/a at the center, and only 2.0mm/a at the southeastern corner. The complicated inner deformation shows regional uplifting, block rotation and partly extension and so on. The dynamic mechanism of present crust movement may sum-up as top layer of crust slide relatively to lower layer, progressive deformation since neotectonism and two-way horizontal compressional field.

**ST2/E/35-A3****1500****SEISMOLOGICAL EVIDENCE FOR THE MULTIPLE INCOMPLETE CRUSTAL SUBDUCTIONS IN HIMALAYA AND SOUTHERN TIBET**

RONGSHENG ZENG (Institute of Geophysics, China Seismological Bureau, Beijing, 100081, People Republic of China, email: zengrs@public.bta.net.cn)

Geological evidences indicated large -scale shortening by thrust faultings in Himalaya, such as MCT and MBT. The thrust faulting near Yaruzampbo suture was also observed. However, it is still unknown to what depth those thrust faultings have been going down into the crust or mantle. Investigations of the earthquakes show that the thrust faultings underneath MCT, MBT and Yaruzampbo suture are closely related to the multiple crustal subductions in Himalaya and southern Tibet. They provide important constraints for the collision process between India and Eurasia. Seismological evidences also show that the crustal subductions have extended to a depth of 80 to 100 kms, and then stopped. The incomplete subductions in those places suggest that the incoming Indian plate is too light, and prevents it going further down. The multiple crustal subductions are compatible to the multiple episodes of the geological activities in Himalaya and southern Tibet. Firstly, the crustal subduction was produced at Yaruzampbo suture, and stopped at a depth of 80-100 kms. Then it migrated to the south, and another new subduction was started successively at MCT and MBT respectively. They also stopped at a depth of 80-100 kms. Beside the steep north-dipping seismic zones in Himalaya and Yaruzampbo suture, another gentle south-dipping seismic zone, extending from Tangula Shan mountain at the surface to the Moho at Yaruzampbo suture was also observed. It can be interpreted as an obduction at Tangula Shan mountain. The multiple incomplete crustal subductions in Himalaya and Yaruzampbo suture highly suggest that the incoming Indian crust has been splitted apart from its upper mantle, which may be subducted deeper into the Eurasian mantle.

**ST2/W/20-A3****1515****ON STRAIN RATE OF SOUTH INDIAN PENINSULA AND SLIP RATE OF GARHWAL HIMALAYAN THRUSTS USING GPS**

John Paul, Ananda M B, Dileep Kumar and Vinod Gaur (Centre for Mathematical modelling and computer simulation, Bangalore, India, email: jpaul@cmmacs.ernet.in)

Global positioning system measurements in south Indian peninsula and garhwal himalaya has thrown significant light on the knowledge of deformation mechanisms in south Indian peninsula and Garhwal Himalaya. A network of 12 points south of Bangalore have suggested a shear strain rate 0.002 microstrain/year suggesting regional stability. Baseline repeatabilities were between 3 - 7 mm. Bernese Processing Engine was used to process the data. Measurements were carried out in Garhwal Himalaya to partition the Indo-Eurasian slip rate. GPS points measured are spread across the main boundary thrust and main central thrust where deformation may be taking place currently. Baseline repeatabilities obtained were between 4 - 9 mm. Results show a 14 mm/yr slip across the main boundary thrust between India and Eurasia and 18 mm/yr slip across the main central thrust.

**ST2/E/23-A3****1600****SHALLOW EARTHQUAKE SWARMS IN STABLE CONTINENTAL REGIONS**

Amy BROWN and Gary Gibson (both at Seismology Research Centre, 2 Park Drive, Bundoora, Victoria 3083, Australia, email: gary@seis.com.au)

A feature of seismicity in some stable continental regions is the occurrence of shallow earthquake swarms. These swarms involve many hundreds of events up to about magnitude ML 3.0 to ML 4.0, usually with several events almost as large as the largest in the sequence. They usually start with a few very small events, then build up in frequency and magnitude over a few weeks, with peak activity lasting a few days. The activity then decays over a period of months or years, perhaps with a reduction in the relative number of small to large events (a decreasing b-value). These events often occur at very shallow depths, within a kilometre or two of the surface. This means that events smaller than ML 1.0 are often felt within about a kilometre or two from the epicentre. They often occur where granitic rocks outcrop, or are near to the surface. This suggests that shallow swarms may be associated with movement on "joints" within the granite. Such swarms occur every couple of years in eastern Australia, and there have been recent examples in central and southern India. In these regions, the proportion of felt earthquakes that are members of shallow swarms is much higher than in more active regions. This is possibly because earthquakes are rarely felt in continental regions, so the small events are more likely to be reported. Alternatively, it could be because high horizontal compressive stress within continents allows accumulation of strain energy at very shallow depths. Modern portable digital seismograph systems have been installed in dense arrays above recent swarms. High sample rates and high precision timing can be used to locate events to a precision

of 100 metres or better, in both epicentre and depth. It has then been possible to associate the activity with a regional fault, previously either known or unknown. Examples include swarms at Bradford Hills and Eugowra in eastern Australia.

**ST2/E/27-A3****1615****SEISMICITY AND POSSIBLE METAMORPHISM BENEATH MOBILE BELTS**

U. RAVAL, National Geophysical Research Institute, Hyderabad-500 007, India.

In this study it is suggested that prograde metamorphism might occur even within the fault-infected crustal column along the continental margins which have undergone severe extension. Because under some situations the necessary (P,T) conditions may be fulfilled at: (i) deeper crustal levels due to large thermal inputs, and (ii) intermediate crustal depths due to additional pressure caused by large compressions across fault-zone provided sufficient amount of hydrous-minerals (e.g. serpentinites) are present particularly in the fillings along the fault and fracture. Such fillings might arise following decompressional melting during the thermal and extensional activities along the continental margins and/or mobile belts. Anomalous gravity and magnetic signatures in the Koyrna region support the intrusive activity due to decompression. Substantial heat and mass transfer, into the crust, is expected since western margin of India where Koyrna region lies, has undergone two continental breakups (at ~90 M.a. and 64 Ma.) and has also been affected very largely by outburst and trace of the Reunion mantle plume (between 66 - 60 M.a.). This thermal input will elevate the crust-mantle isotherms to much shallower levels so that (P,T) conditions necessary for the prograde metamorphism might get fulfilled, even if transiently, and result in release of fluid. The latter would result in substantial variation of pore-fluid pressure and an interplay before lithostatic pressure and tensile strength. In light of this possibility, the metamorphically released deep-seated fluid along the faults of the rifted margins as well as mobile belts need to be evaluated more carefully. Apparently development of the low seismic velocities and high electrical conductivity anomalies/layers in such seismic zones could be the result of such release of fluid.

**ST2/E/42-A3****1630****BEHAVIOUR OF HELIUM FLUX IN SEISMIC FAULTS : SOME EXAMPLES FROM STABLE CONTINENTAL REGIONS OF INDIA**

R SRINIVASAN, G V Rao, G K Reddy and R U M Rao (National Geophysical Research Institute, PO Bag 724, Uppal Road, Hyderabad 500 007, India, email: postmast@csngri.ren.nic.in)

Helium flux through seismic faults has been measured in the meizo-seismal areas of the 1997 Jabalpur (Mw 5.8), the 1993 Latur (Mw 6.1), the 1900 Coimbatore (Mw 5.7) and the 1967 Koyrna (Mw 6.3) earthquakes. The first three were caused by thrusting, along the Narmada south, the Killari and the Bhavani faults respectively and the Koyrna by strike slip, along the Donechiwada fault. The Latur and the Koyrna are shallow focus (< 10 km) and the Jabalpur and the Coimbatore are deep focus (~30 km) earthquakes. Surface rupturing occurred only in the case of the Latur and the Koyrna events. The fault scarp at Killari and an area of 300 x 200 m in its immediate vicinity, recorded up to several tens of ppm helium over and above the regional background level. Outside this zone no excess helium was recorded over secondary fissures. Intermittent monitoring of helium flux over the last five years shows a waning tendency, though higher than background levels still persist. At Koyrna, helium anomalies up to 7 ppm have been picked up, even after 27 years, with the peaks aligning over the enechelon fissure representing the surface rupture zone. The Koyrna region is an interesting zone with several M > 4 events continuing to occur.

Our observations thus show: 1) shallow earthquakes that produce surface ruptures facilitate excessive helium leakage discerning of which would clearly establish the fault that caused the earthquake; 2) excessive helium leakage may wane with time in some cases indicating annealing of the fault or persist in areas of continued seismicity as at Koyrna; 3) faults of deep focus earthquakes, which do not reach the surface, as expected, do not appear to have associated helium anomalies, as is to be expected.

**ST2/E/10-A3****1645****THREE DIMENSIONAL P-WAVE VELOCITY STRUCTURE OF CRUST AND UPPER MANTLE BENEATH THE KOYRNA SEISMIC ZONE**

D.SRINAGESH and K.S.Prakasam (both at National Geophysical Research Institute, Uppal Road, Hyderabad-500 007, India, email: postmast@csngri.ren.nic.in)

P-wave teleseismic tomography of Koyrna Seismic Zone has been studied through inversion of teleseismic travel times from a 20 station digital network. Tomographic images reveal presence of lateral velocity variations (5% to 6%) between Koyrna Seismic zone and the adjoining region. The high velocity heterogeneity (1%-3%) in the crust straddles the Koyrna Seismic zone and further, extends into the mantle up to a depth of 75 km below which the array configuration fails to resolve this heterogeneity. This high velocity anomaly is flanked by lower velocities both in the crust and upper mantle. The high velocity region is also reflected by positive residual Bouguer gravity indicating a deeper source. The high velocity and high density geological feature suggests a tectonic cause for sustained seismicity in Koyrna region.

**ST2/E/24-A3****1700****SEISMICITY, CRUSTAL RHEOLOGY AND THREE DIMENSIONAL P- AND S-WAVE VELOCITY IMAGES BENEATH KOYRNA SEISMIC ZONE (DECCAN VOLCANIC PROVINCE)**

S.K. SINGH, D. Srinagesh and S.S. Rai (All at National Geophysical Research Institute, Uppal Road, Hyderabad-500 007, India, email: postmast@csngri.ren.nic.in)

We present results from 20 short period triaxial digital seismic stations operated during April 1996 to December 1997 in Koyrna seismic zone covering an area of 60x80 sq.km. Joint hypocentral location of more than 700 local earthquakes confined to an area of 11x25 sq.km. reveals fragmentation in the seismicity pattern - a NE-SW trend approximately dips 45x in NW direction whilst the two NW-SE trends are near vertical. The depth distribution of earthquakes shows more than 90% of the seismicity is confined to the depth range of 3-10 km with the base of seismogenic zone at 11 km. Lack of shallow seismicity up to 3 km indicates a mature fault system with well developed gouge zones which inhibit shallow earthquake nucleation. Reference 1-D velocity model of P and S waves show an increase in velocity indicating absence of LVZ within the seismogenic crust (up to 10 km). Local earthquake travel time 3-D inversion for P and S waves show about 2% higher velocity seismogenic crust (up to 10 km) beneath the epicentral tract relative to 2 to 3% lower velocity in the adjoining region. Presence of high P and S velocity beneath earthquake epicentres negates presence of fluid saturated/over pressured zone. The high velocity region is also manifested by a positive residual Bouguer gravity anomaly and a high gradient in magnetic anomaly indicating presence of significant inhomogeneity in the Koyrna Seismic Zone. Based on seismicity, crustal rheology and 3-D velocity images we infer segmented and matured seismogenic fault systems in Koyrna region where the seismicity is possibly controlled by strain build up due to competent lithology in seismic zone.

ST2/L/01-A3 1715

## SOURCE CHARACTERISTICS AND FOCAL MECHANISM SOLUTIONS OF FOUR KOYNA-WARNA (WESTERN INDIA) EARTHQUAKES OF 1997 AND 1998 THROUGH INVERSION OF WHOLE BROADBAND WAVEFORM DATA

S.N.BHATTACHARYA, Seismological Observatory, India Meteorological Dept., New Delhi 110003, India.

The area just south of Koyna dam in Maharashtra state of Western India remains active since the occurrence of 1967 earthquake of magnitude 6.5. Since then the activity has extended 30 km southward to Warna reservoir. Source characteristics and fault plane solutions of a few moderate size earthquakes near Koyna dam have been obtained earlier. It is necessary to evaluate the same for small earthquakes particularly those which are occurring around Warna reservoir. During 1996-97, ten seismological observatories in the Peninsular India have been upgraded with broadband digital seismographs. Since the upgradation 4 small earthquakes of magnitude 3.9 and above have occurred in this area and these were well recorded by the upgraded observatories at Karad and Pune which are at a distance 45 to 154 km from epicentres. The ground displacement waveforms are compared with best fitting synthetic ones to obtain rise time, seismic moment and fault plane solution. The rise time of the earthquakes varies between 0.2 and 0.3 s. The seismic moment obtained has been used to obtain Mw which is only 0.1 to 0.2 higher than the corresponding ML. The earthquake on 1997 April 25, which is close to Warna reservoir, shows normal faulting along a NW striking plane. However, the other 3 earthquakes on 1997 March 20, 1998 February 11 and 14 which occurred close to Warna reservoir, show mainly left lateral strike component along a near vertical fault in NNE direction. Thus earthquakes around Warna reservoir are generally occurring along a near vertical fault in a NNE direction with a left lateral strike slip.

ST2/E/18-A3 1730

## SEISMICITY OF THE DECCAN VOLCANIC PROVINCE - AN EVALUATION OF SOME ENDOGENOUS FACTORS

K.V. Subbarao (Department of Earth Sciences, Indian Institute of Technology, Mumbai (Bombay) 400 076, India, e-mail: subbu@geos.iitb.ernet.in) T.M. Mahadevan (Sree Bagh, Ammankoil Road, Cochin - 682 035, India)

The seismotectonics of the western pericontinental belt of active rifts (BARS) extending from the Cambay basin in the north, southwards along the country west of the Nasik-Mahabaleshwar line (NML) of volcanic eruption centres seem to have been inherited through the evolutionary stages of the initial thermal doming and uplift at the peak of Deccan volcanism (~ 65 Ma) and subsequent thermal subsidence. The west coast plains (Konkan) and the offshore region subsided more, being predominantly the area of asthenospheric upwelling along and close to the centre of rifting and later due to offshore sediment loading. The western Ghat region forming the eastern collar of the main rift zone maintained higher elevations due both to underplating and the support of the cratonic interior. The Deccan Volcanic Province along with the rest of the shield, has however, passed from the early dilational to a compressive regime due to the impact of the plate boundary and other neotectonic forces. Any uplift, tectonic, isostatic or thermal has to operate in the non compressional set up. The thick basalt and sedimentary cover strengthen basement faults old and new stressed to near failure. Seismicity, therefore results through an interplay of these forces, some of which may compliment and others cancel each other. In areas of thick cover, earthquakes occur when the compressive neotectonics, uplift and importantly the fluid pressure amidst faults compensate the strengthening influence of the overburden cover and destabilize weak faults. There are pointers in the differences in the seismicity of these different lithospheric segments (such as BARS, Son-Narmada-Tapti belt etc.) that the seismogenic forces could operate differently in each of them.

ST2/E/55-A3 1745

## CHARACTERISTICS OF THE SURFACE DEFORMATION ASSOCIATED WITH THE 1819 KUTCH (INDIA) EARTHQUAKE AND THEIR BEARING ON THE FAULT BEHAVIOUR

C.P. RAJENDRAN and Kusala Rajendran (Centre for Earth Science studies, Trivandrum, India 695 031, tel +91 471 442451, fax +91 471 442280.) email: geo@giasmd01.vsnl.net.in

The 1819 Kutch, northwest India, earthquake is a significant intraplate event that caused extensive changes in topography, damming of a river and widespread liquefaction. A remarkable feature of the Kutch earthquake is the formation of an elevated tract of land known as the 'Allah Bund'. This feature remains an object of scientific interest although no survey has been made since 1846. Our field studies indicate that the maximum throw during the 1819 earthquake may have been ~3m, which varies along the strike and reduces to <0.50 m at the eastern terminus of the fault; lateral extension of the fault is ~100 km and is about 15-20 km wide. Fault geometry based on the field data suggests that 1819 event occurred on a reverse fault. Assuming a northward dip of 40 degree and a focal depth of 15 km, the epicenter would be at a point 18 km north of the maximum throw. Using this geometry, we calculate the moment magnitude of the 1819 event to be MW 7.8. The morphological features at the Runn of Kutch suggest the presence of multiple scarps formed by similar size events. Stratigraphic and trench log data support the occurrence of at least two events prior to the 1819 earthquake. Available radiocarbon age data along with the historical information suggest a recurrence period of ~1000 years for the large earthquakes in the Runn.

Thursday 22 July AM

Presiding Chairs: M.R. Gheitanchi (Geophysics Institute, University of Teheran, Iran), T. Taymaz (Dept. of Geophysics, Istanbul Technical University, Turkey)

SEISMOTECTONICS OF EURASIA

ST2/W/16-A4 0930

## SEISMOTECTONICS OF LARGEST EARTHQUAKE SOURCES IN NORTHERN EURASIA AT 1866-1997

Evgeny ROGOZHIN, Sergei Yunga (both at Institute of physics of the Earth, Moscow, 123810, B.Gruzinskaya, 10, Email: evgrog@uipe-ras.scgis.ru; syunga@uipe-ras.scgis.ru)

The largest earthquakes of northern Eurasia in the past two decades (the Kaspian, Spitak, Racha, Zaisan, Susamyr, Shikotan, Kobe, Neftegorsk, and Kronotsk events) are investigated on the base of integrated geological-seismological works in the near-field zone and data from the IRIS global seismographic network. Field investigation in near zone and study of aftershocks process and geological structures at large earthquake sources supply information concerning fault dimensions, type and amplitude of displacements on faults. It is shown that based on geological observations directly calculated characteristics of seismic sources are largely consistent with the source parameters estimated seismologically. Our study also showed that focal mechanisms of the largest earthquakes are clearly

correspond to low-magnitudes populations of fault plane solutions and regularly associated with regional geological structures. Low-magnitude earthquakes are not random events, but are regular manifestations of seismotectonic deformation and contemporary geodynamic.

In each considered case mechanism of large earthquake source is consistent with the deformation pattern of weak and moderate shocks in source region. This feature is suggested to consider as discriminative factor for recognizing characteristic earthquakes and their maximum magnitude. Acknowledgments. This work was partly supported by the Russian Foundation for Basic Research, grants 98-05-65159 and 99-05-64582.

ST2/P/10-A4 0945

## THE CASPIAN REGION: INTERACTION BETWEEN THE BRITTLE AND DUCTILE LAYERS AND EARTHQUAKE RISK

Nadezhda Kondorskaya (United Institute of Physics of the Earth, Russian Academy of Science, Moscow, Russia, email: strachov@dir.iephys.msk.su) Leonid LEVIN (Centre GEON Regional Geophysical and Geoenviromental Data, 119034, Chisty per., 4, Moscow, Russia, email: moscow@geon.msk.su.) Leonid Solodilov (Centre GEON - Regional Geophysical and Geoenviromental Data, 119034, Chisty per., 4, Moscow, Russia, email: moscow@geon.msk.su)

Seismicity of the Caspian region is due to an action of a combination of geodynamic processes, namely, a collision of plates, subduction of the above - asthenosphere layer of the mantle, upwelling of the asthenosphere above old and recent zones of subduction, horizontal displacements of blocks along the lineaments; mud volcanism in the South Caspian basin. It has been established, on the base of the <<Caucasus>> catalog including the data on earthquakes as of 1998, that 90% of released seismic energy is related to reologically brittle layers which, like in other regions of plate collision, are developed at two levels - the crustal and mantle. Distribution of earthquakes at these levels is controlled by a change in strained state of the ductile layer in time and space. A study of interaction between brittle and ductile layers based on the data of distribution seismic wave's energy and thermal regime of the tectonosphere has revealed a number of indicators for an estimation of earthquake risk.

ST2/E/17-A4 1000

## DOES TURAN BLOCK MOVE TOWARD IRAN?

M. RAEESI (Geophysics Institute, Univ. Of Tehran, Tehran, Iran, email: mraeesi@iman.ut.ac.ir) M. R. Gheitanchi and Z. Zarifi (Raeesi) (Both at the above address, email: mrghchee@chamran.ut.ac.ir and zarifi@iman.ut.ac.ir)

In most researches Turan Block which is part of Eurasian plate is considered fix and geological structures in northeastern Iran are regarded as the result of compression of Iran plate to Eurasia. On Feb. 4, 1997 at 10:37:47.1 GMT a damaging earthquake (Ms 6.7) occurred in northeastern Iran in Bojnourd area. Harvard CMT solution includes two nodal planes; the first 148/80NE and the second 56/83NW. With regard to field observation the first nodal plane is the break surface. As most of earthquakes in NE Iran the quake had a right-lateral strike-slip surface rupture. Institute of Geophysics of Tehran University installed a temporary seismic network for monitoring aftershocks. More than 90% of aftershocks located at northeast of the surface rupture, in other words the northeastern block is hanging-wall and this is contrary to SW to NE compression vector which is considered for the region. Clearly it must be said that this event shows a compression vector from NE to SW. This study focuses on mechanism of moderate to great earthquakes and geological structures with skepticism to previous results and considering new viewpoint.

ST2/P/12-A4 1015

## CRUSTAL SEISMIC VELOCITY STRUCTURE WITH LOCAL EARTHQUAKE TOMOGRAPHY IN NW IRAN BY AZARBAIJAN LOCAL ARRAY DATA

HAMID ZANDIFAR (Dept. of Geophysics, Exploration Directorate, NIOC, 1863, Tehran,Iran) Mohammad Reza Gheitanchi (Division of Earthquake Seismology, Institute of Geophysics, Tehran University, P.O.Box 14155-6466, Tehran, iran)

Inadequacy of standard crustal models is one of the main sources of errors in locating earthquakes. Relocating will be meaningful if a more accurate crustal model is available. Each earthquake include the data set which required for determining the crustal structure. The principal data gathered in a @croequake monitoring network of seismograph stations are first P arrival times form local earthquakes. In order to study the crust in this research we have used the method of two stations which is independent of mislocation errors. The various types of P phases of given earthquakes from Azarbaijan array have been calculated which the event and stations locations make a straight line on map- Then a primary model was made by a thickness approximation of different layers of crust based on previous studies and also velocity approximation. The events with magnitude between 2 and 4 were selected. Finally main method LET (Local Earthquake Tomography) applied to draw velocity profiles at different depths and directions. These profiles dete@nd the trend of velocity and crustal changes under Azarbaijan array. The damping factor was 10 and the value of RMS changes from 0.001 to 1. 17 sec. Compression caused by Arabian plate to southern part of Eurasia in a south-north direction have formed the Azarbaijan miicrator. The results of study shows a changes of P-wave velocity near surface from 4.8 to 5 km/s. There is no increase in P-wave velocity at depth of 5 km. In deeper depth, 25 km velocity changes from 5.8 to 6.6 km/s, and velocity variation curve pattern is same as upper layer. The thickness of first layer of model changes from 4.5 to 6.3 km and the highest thickness is located in North, North east part. The second layer thickness changes from 18 to 22 km and relative to upper layer is uniform. The highest thickness at this layer is located in northern part.

ST2/E/15-A4 1100

## SEISMOTECTONICS OF THE EASTERN ANATOLIA: SOURCE PARAMETERS OF LARGE EARTHQUAKES OBTAINED FROM INVERSION OF TELESEISMIC BODY-WAVEFORMS

Tuncay TAYMAZ (Department of Geophysics--Seismology Section, Istanbul Technical University (ITU), Maslak-80626-Istanbul, Turkey, e-mail: taymaz@sariyer.cc.itu.edu.tr)

This presentation is concerned with the active tectonics of the eastern Anatolia. The North and East Anatolian Fault Zones accommodates most of the observed motion between the Arabian plate, and the apparently little-deforming interior of central Turkey and Eurasian plate in the eastern Anatolia.

The direction of overall slip across these zones are crucial to the determination of the slip rate on them. I have studied 1966 Varto sequence, 1967 Pulumur, 1976 Caldiran-Muradiye, 1983 Narman-Horasan, and 1992 Erzincan earthquakes in details to improve our understanding of collisional continental tectonics taking place. The waveforms used in this research include the WWSSN, and the digitally recorded seismograms of the DWWSSN, SRO, ASRO, GEOSCOPE, and IRIS networks. I compared the shapes and amplitudes of long period P- and SH-waveforms recorded in the distance range 30—90 degrees, for which signal amplitudes were large enough, with synthetic waveforms. The minimum misfit solutions obtained by the

inversion of teleseismic body waveforms are better constrained than those of the previously published first motion, and Harvard Centroid-Moment Tensor (CMT) solutions. These data allow us to discuss the slip vectors in the earthquakes with much more confidence.

**ST2/E/14-A4 1115**

**SOURCE PARAMETERS OF CAUCASIAN EARTHQUAKES**

Onur Tan and TUNCAY TAYMAZ (both at Department of Geophysics--Seismology Section, Istanbul Technical University (ITU), Maslak-80626-Istanbul, Turkey, e-mail: taymaz@sariyer.cc.itu.edu.tr)

This presentation is concerned with the active tectonics of the Caucasus, and consists of studies of two moderate earthquakes. In the Lesser and Greater Caucasus, major structures trend west-northwest, and focal mechanisms indicate primarily thrust faults striking parallel to the mountains, with shallow-dipping planes dipping to the north. Observed convergence along the Eurasian and Arabian plate boundaries is further partitioned into almost pure shortening by thrusting in the Greater Caucasus, and pure right-lateral strike-slip motion in eastern Turkey. We used long-period P- and SH-waveforms and first motion polarities of P waves to determine the source parameters of July 16, 1963 (Western Greater Caucasus, to: 18:27:18.4, Ms=6.5) and July 28, 1976 (Eastern Greater Caucasus, to: 20:17:44.0, Ms=6.1) earthquakes. We compared the shapes and amplitudes of long period P- and SH-waveforms recorded by WWSSN stations in the distance range 30--90 degrees, for which signal amplitudes were large enough, with synthetic waveforms. The minimum misfit solutions obtained by the inversion of teleseismic body waveforms are better constrained than those of the previously published first motion, and Harvard Centroid-Moment Tensor (CMT) solutions, and are in good agreement with local geometry of the faults.

**ST2/E/09-A4 1130**

**SEISMIC ACTIVITY OF MOSHA-FASHAM FAULT IN THE VICINITY OF TEHRAN, BY A LOCAL NETWORK**

B. Akasheh (Institute of Geophysics, University of Tehran, Iran) M.R. Gheitanchi (Institute of Geophysics, University of Tehran, Iran, email: mrghchee@chamran.ut.ac.ir)

Historical documents of seismic activity in Iran back to more than two thousands years indicated that Tehran region has experienced great earthquakes, frequently. Micro-seismic studies by several researchers, during the past three decades also confirm that Tehran is seismically active region. It is approved that Mosha-Fasham active fault, having a fault length about 175 with a high seismic potential, can be dangerous for the city of Tehran. Therefore, in a research program, by analyzing the records of a local mobile seismic network, detailed information related to the rate and process of the fault activity are obtained.

**ST2/P/09-A4 1145**

**ANALYSIS OF CONTINENTAL DEFORMATION BASED ON SEISMIC AND NON-SEISMIC DATA IN SOUTH-SOUTHWEST OF IRAN**

BEHZAD ALAEI (Dept. of Geophysics, Exploration Directorate, NIOC, 1863 TEHRAN, IRAN) Mohammad Reza Gheitanchi (Division of Earthquake Seismology Institute of Geophysics, Tehran University, P.O.Box 14155-6466, Tehran, Iran)

The differences of continental deformation with general rules of plate tectonics have been known for many years and several authors have mentioned the diffuse nature of today deformation in continents. So the continental deformation should be studied with continuum mechanics. The mathematical method in order to calculate deformation parameters is mainly based on thin sheet model. The Zagros mountains form the northern border of Arabian plate which thickens due to collision of Arabia and Eurasia. The components of two tensors one M moment rate when all deformation is seismic and the other one the moment rate tensor of whole deformation caused by continent collision have been calculated and also correlated. The calculations show that how many percent of deformation which took place in the collision zone is seismic. Based on the study maximum deformation which can be related to earthquakes is about 15% and rest of deformation is non-seismic. Temperature-related deformation in deeper parts of earth such as creep on faults and folding are main controllers of deformation. Strain rate tensor components, velocity gradient and uplift rate have also been measured. We have used the earthquake data in two ways. Earthquakes after 1977 which their moment data are present and for older earthquakes relationship between Ms and scaler moment can be used. The uncertainties are the short time duration of recorded earthquakes and the other one is the effect of smaller earthquakes. In modern earthquakes also there is uncertainty in depth determination. The relationship between deformation and stress in Zagros area shows that the style of deformation is not basement involved and deforming of sedimentary cover is independent of basement and appear in the form of folding which in structural point of view is a good opportunity for hydrocarbon generation and accumulation.

**ST2/E/29-A4 1200**

**SEISMOTECTONICS OF SAHNEH FAULT, MIDDLE SEGMENT OF MAIN RECENT FAULT, ZAGROS MOUNTAINS, IRAN**

NOORBAKHSH MIRZAEI (Institute of Geophysics, Tehran University, Tehran 14394, Iran, email: nmirzaei@chamran.ut.ac.ir) Mohammad Reza Gheitanchi (Institute of Geophysics, Tehran University, Tehran 14394, Iran, email: mrghchee@chamran.ut.ac.ir)

A detailed structural analysis and short term micro-earthquake survey in a small region covering Sahneh Fault segment of Main Recent Fault of Zagros mountains, in western Iran, indicate that the Sahneh Fault is an active second order structure of transpression (positive flower structure) type with presently low level of seismic activity. Meizoseismal regions of historical earthquakes, macro-seismic epicenters of pre-instrumental (1900--1963) earthquakes, as well as location of micro-earthquakes together with structural geology of the region, strongly suggest that the study region should be considered as a localizing structure, so that seismic activity of the region can not reliably be correlated to any known active faults. Present micro-seismic activity is concentrated in the area bounded by southern part of Sahneh Fault and northern elongation of Nahavand Fault, that covers the meizoseismal regions of the Farsinaj earthquake of 13 December 1957 (Ms=6.9). Focal mechanisms of earthquakes and structural analysis confirm the prominent right-lateral strike-slip deformation along Sahneh Fault that is in consistent with relative motion between Arabian Plate and Central Iran Micro-continent.

**ST2/W/19-A4 1215**

**INVESTIGATION OF THE ACTIVE FAULT SYSTEM DIRECTED ON NE-SW AT THE NORTHERN PART OF NAFZ-ADAPAZARI AND ITS ELONGATION INTO THE BLACK SEA**

Naside OZER, Demir Kolcak (both at Department of Geophysical Engineering, Faculty of Engineering, University of Istanbul, Avcilar, 34850, Istanbul, Turkey, Email: naside@istanbul.edu.tr), Recep Cakir, S.Shelton Alexander (both at Department of Geosciences, The Pennsylvania State University, 308 Deike Building, University Park, PA 16802, USA, Email: recep@essc.psu.edu, shel@essc.psu.edu), Erdinc Yigitbas (Department of Geology, Faculty of Mining, Istanbul Technical University, Maslak, Istanbul, Turkey) and Ali Elmas (Department of Geological Engineering, University of Istanbul, Avcilar, 34850, Istanbul, Turkey)

The North Anatolian Fault Zone (NAFZ) is a seismically active right lateral strike slip fault extending E-W direction in Northern Turkey. The NAFZ splits into different branches and the characteristics of tectonic regime changes at Adapazari-Sapanca. Our study takes place at the northern part of this region. The present study aims to clarify the micro seismic activity detected within the area bordered by Kandira, Akcakoca, Black Sea continental shelf and the NAFZ-Izmit Bay, and also its significance in the geological evolution of the region.

The relocation of the earthquakes recorded by the local seismic network of the Turkish-German "Earthquake Research Project" shows NE-SW lineaments at the area which was previously regarded as connection between the Marmara Sea and the Black Sea Basin, prior to the development of Istanbul strait.

In this study, the correspondence between the seismic active zones observed on seismicity map with structural lines lying in the area between Adapazari and Karasu investigated together with their geological relation to the Black Sea and Marmara Sea basins. For this purpose genesis of this lineaments studied incorporating detailed geological and geophysical data and Landsat TM.

**ST2/W/27-A4 1230**

**OBSERVATION OF THE ADANA-CEYHAN EARTHQUAKE JUNE 27, 1998**

Naside OZER and Oguz Gundogdu, (both at Department of Geophysical Engineering, Faculty of Engineering, University of Istanbul, Avcilar, 34850, Istanbul, Turkey, Email: naside@istanbul.edu.tr, gundogdu@istanbul.edu.tr)

The Adana-Ceyhan earthquake (June 27,1998) occurred at northeastern land of the Mediterranean Sea and had magnitude Ms=6.2(USGS), M=6.3(KOERI) and Mw=6.3(USGS). 146 people were killed and over a thousand injured by this earthquake. According to the preliminary determination of General Directorate of Disaster Affairs about 9500 buildings were heavy, 2000 moderate and 40000 slight damaged.

Concerning our observations on the field, structures and questionnaires at 72 villages and towns, macroseismic epicentre is near southern part of Abdioglu village (35.56E, 36.89N). Source of faulting is in Cukurova Basin and faulting could not be traced due to relatively great thickness of alluvial deposits and source depth. The faulting traced place to place about 15kms from southern Abdioglu village to Yeni Kucuk Kapili Ciftligi at South and to Yakapinar at North. Any recent activity and displacement could not be observed on the Misis Fault Zone.

Damage in Ceyhan is over expected as far as alluvial deposit and under ground water level of few meters increased the intensity and caused to the severe damage in this area. Sandblowing and liquefaction observed along the Ceyhan River about 45-50kms and some other place in Cukurova Basin. Unexpected damages in some villages and towns mostly caused by soil conditions. So, soil investigation should be taken into account more seriously as well as geological, geophysical and geotechnical aspects.

**Thursday July 22 PM**

Presiding Chairs: C. Papazachos (ITSAK, Thessaloniki, Greece), K. Abou Elenean (Nat. Res. Inst. of Astronomy and Geophysics, Helwan, Egypt)

**SEISMOTECTONICS OF THE MEDITERRANEAN**

**ST2/W/14-A4 1400**

**TRANSPRESSIONAL TECTONICS IN SOUTHERN AEGEAN**

LOUVARI E., Kiratzi A. and Papazachos B. (All at Geophysical Laboratory, Aristotelian University of Thessaloniki, PO Box 352-1, Thessaloniki 54006, Greece, email: louvari@lemnos.geo.auth.gr, kiratzi@geo.auth.gr)

Southern Aegean has experienced a large number of destructive earthquakes during the last decades mainly due to the interaction between the Aegean and the African plate. To gain quantitative insight into the active tectonics of the area, new fault plane solutions based on body-waveform modeling were computed, including the last two major earthquakes of 13 Oct., 1997 (Mw=6.3) and 18 Nov., 1997 (Mw=6.5), located south of Peloponnese and south-west of Zante, respectively. The source parameters of the 18 Nov. 1997 earthquake revealed a complex pattern. Two sources were determined at the depth of ~31 Km. The time shift between the two sources was ~9 sec and the separation distance ~30 Km. The first source showed a low angle thrust fault while both sources were characterized by a considerable strike-slip component. Distribution of earthquake epicenters, fault plane solutions of small earthquakes, sea bottom topography and GIS analysis were used complementary to the above to define the orientation of the active zones.

All the data show that low angle thrust faults, in many cases having a considerable strike-slip component, coexist with high angle strike-slip faults and normal faults. P-axes mainly trend NE-SW and dip to the SW. Along the Hellenic trench T-axes trend NE-SW to SE-NW, while EW arc-parallel extension dominates along the accretionary prism.

**ST2/E/61-A4 1415**

**THE ACTIVE DEFORMATION FIELD OF THE AEGEAN DETERMINED FROM SEISMICITY AND GPS DATA**

Costas PAPAACHOS (Institute of Engineering Seismology and Earthquake Engineering-ITSAK, PO Box 53, Finikas, GR-55102, Thessaloniki, GREECE, e-mail: costas@itsak.gr)

A model is derived for the deformation velocity and strain rate field in the crust of the broader Aegean area. Using the most reliable seismological (seismicity, fault plane solutions, etc.) and GPS data, the complete main characteristics of the crustal deformation field are retrieved. Comparison between the results obtained from the two data sets, seismological and GPS, shows a very good agreement as far as the deformation pattern is concerned. The largest part of the total deformation (GPS data) is expressed seismically. This "efficiency index" becomes significantly smaller in the southern Aegean-Hellenic Arc area. The final deformation field is more detailed than previous deformation models. According to the results, western Turkey moves towards the W-SW, with respect to stable Europe, with an average velocity of 25mm/yr, which changes in the Aegean where N-S extension dominates and the deformation velocities increase. The deformation reaches an average velocity of 30-35mm/yr in the southern Aegean. This increase further



supports the idea that the Aegean should not be considered as a part of a single Anatolia-Aegean microplate which has been suggested to perform an almost rigid body rotation. The rotational component of the velocity field, which is also retrieved, shows a clockwise rotation in central and SW Aegean and an anticlockwise rotation in the SE Aegean. This rotation is in excellent agreement with the available palaeomagnetic data while some previous estimates showed a clockwise rotation throughout the whole Aegean area. The proposed model predicts a crustal thinning for the back-arc Aegean region, except along the outer Hellenic Arc where crustal thickening is observed, in excellent agreement with the crustal thickness variations determined for the area.

ST2/W/11-A4

1430

## THE FINAL STAGE OF PLATE BREAK-OFF

Friedemann WENZEL, Blanka Spener, and Frank Lorenz (all at Geophysical Institute, Karlsruhe University, Hertzstr. 16, 76187 Karlsruhe, Germany, email: fwenzel@gpiwapl.physik.uni-karlsruhe.de), Victor Mocanu (Faculty of Geology and Geophysics, Bucharest University, Str. Traian Vuia 6, 70139 Bucharest, Romania, email: mocanu@ter1.sbn.ro)

When convergence of lithospheric plates ceases and the suction force of the subducting plate becomes negligible, the subducting slab moves into an almost vertical position. Wortel and Spakman pioneered the idea of slab detachment, based on tomographic images of the upper mantle beneath the Mediterranean area: At some point of weakness, the slab starts to detach horizontally. However, to date little attention has been paid to the terminal phase of break-off. What happens at the very last 'moment' before the entire subducted material of a closed ocean is separated from the overlying lithosphere and ready to sink into the mantle? Where is this geodynamic scenario observable? We show evidence that this process is active beneath the Romanian southeastern Carpathians, an area called Vrancea. The main observations that support this hypothesis are: (1) Geological evidence for ocean closure around the Carpathian Arc that progressed along the arc and terminated about 9 m.y. ago at Vrancea. Although crustal deformation has simmered on a small scale ever since, real action has taken place in the mantle, where delamination started through mass, heat, and fluid transport and also by significant strain deforming subducted portions of the lithosphere. The latter process can be quantified by seismological data. (2) Vrancea subcrustal seismicity displays extraordinary characteristics such as localization of earthquakes in an extremely small source volume and massive release of seismic energy (four events with magnitudes in excess of 6.9 within 50 years). Epicenters of Vrancea earthquakes are confined to an area of about 30 x 70 km and occur between 70 and 200 km depth within an almost vertical column. (3) Recent tomographic inversion of regional and teleseismic P-wave arrival times recorded by the Romanian network of seismological stations confirm that the intermediate depth seismogenic volume shows high velocities. As on a global scale, all images of active subduction zones are characterized by high P-wave velocities we interpret this as strong evidence for a remnant piece of a slab of lithosphere beneath Vrancea.

ST2/E/41-A4

1445

## NUMERICAL STUDY OF INTERMEDIATE-DEPTH SEISMICITY IN THE VRANCEA REGION

Alik ISMAIL-ZADEH, Vladimir Keilis-Borok and Alexander Soloviev (all at International Institute of Earthquake Prediction Theory and Mathematical Geophysics, Russian Academy of Sciences, Varshavskoye shosse 79, kor. 2, Moscow 113556, Russia, email: aismail@mitp.ru)

The earthquake-prone Vrancea region is modelled as a system of absolutely rigid blocks separated by infinitely thin plane faults. The interaction of the blocks along the fault planes and with the surrounding medium is assumed to be a viscous-elastic. The displacements of the block system are caused by motions of boundary blocks. The velocities of the motions are found from a model of mantle flows induced by a sinking slab beneath the Vrancea region. When a ratio of stress to pressure for some portion of a fault plane exceeds a certain strength level, a stress-drop ('earthquake') occurs. As a result of the numerical simulation a catalog of synthetic earthquakes is produced. Several numerical experiments for various model parameters show that the spatial distribution of synthetic events is significantly sensitive to the directions of the block movements. Small variations in a slab rotation control the pattern of the synthetic seismicity. The results of the analysis show that the catalogs obtained by the simulation of the block structure dynamics have certain features similar to those of the real earthquake catalog of the Vrancea region.

ST2/L/02-A4

1500

## DEPTH DISTRIBUTION OF STRESS FIELD IN THE HELLENIC AND TYRRHENIAN WADATI-BENIOFF ZONES

Cenka CHRISTOVA (Geophysical Institute of Bulgarian Academy of Sciences, 1113 Sofia, Bulgaria, email: cenka@geophys.acad.bg)

The study is based on the detailed morphology of the Hellenic (HWBZ) and Thyrrenian (TWBZ) Wadati-Benioff zones which allows to discriminate earthquakes that belong to the subducting plate from those bound to the overriding one. The inverse technique of Gephart and Forsyth (1984) was used for determining the best fit principle stress directions  $s_1$ ,  $s_2$ ,  $s_3$  and the ratio  $R=s_2-s_1/s_3-s_1$  for 40 km and 100 km depth intervals in the HWBZ and the TWBZ, respectively. The depth behavior of maximum and minimum compressive stresses in the considered Wadati-Benioff zones is different. In the HWBZ the maximum compressive stresses  $s_1$  (all considered depth ranges) are of NE trend (normal to the strike of the western subduction flank and along strike in the eastern flank), indicating the NW-SE convergence between the African and the Eurasian plates; the plunge decreases with increasing depth.

The minimum compressive stresses  $s_3$  are along dip; the plunge increases with increasing depth. The 50-100 km layer of TWBZ is characterized by along strike  $s_1$  and along dip  $s_3$ . Within the two deeper layers  $s_1$  are along dip and  $s_3$  are almost horizontal and normal to the strike of the subducting plate.

ST2/W/34-A4

1515

## ACTIVE DEFORMATION IN THE ALPS-DINARIDES JUNCTION (NE ITALY)

Peter SUHADOLC, Abdelkrim Aoudia (both at Department of Earth Sciences, University of Trieste and Abdus Salam International Center for Theoretical Physics - SAND Group, Trieste - Italy, Email: suhadolc@geosun0.univ.trieste.it) and Alexei Kiryushin (Institute of Earthquake Prediction and Mathematical Geophysics, Moscow, Russia, Email: kiryush@mitp.ru)

The Alps-Dinarides junction, NE Italy, is an active part of the Adria-Eurasia collision zone. It is dominated by a NNW-SSE convergence. The Alpine structures are represented by E-W trending thrusts and folds that link towards the east with NW-SE Dinaric structures. Until recently, identification and understanding of active geological structures in this area were hindered by the lack of reliable and organised seismological data, the complex geological setting and the very dense vegetation cover. This zone has been the site of the 1976 6.5Ms Friuli thrust faulting earthquake and of the 1998 5.7Ms Bovec (NW Slovenia) strike slip faulting

earthquake. We use high resolution DEM, field geology, long period surface waves inversion, joint hypocenter determination and a robust statistical method for stress tensor reconstruction to identify active geological structures and understand the present day kinematics in this region. We show: 1) evidence of active folds and flexural-slip anticlines along the E-W striking structures, where the most frontal structure has been reactivated by the 1976 Friuli earthquake; 2) how the drainage and the moraines know about fold growth in this area; 3) evidence of two active parallel strike slip faults on the Dinaric system inferred from a combined study of: the 1998 Bovec earthquake, the local microearthquakes polarity data and the DEM; and 4) that the inherited geological structures are controlling the present day fault geometry and behaviour. Clearly, most of the geological and geomorphological evidences we discuss are in an active piedmont area, at the foot of a major continental mountain range.

ST2/W/06-A4

1600

## SEISMOTECTONICS OF THE BETICS AND ALBORAN SEA (WESTERN MEDITERRANEAN)

E. Buforn, A.M. NEGREDO and A. Udías (Department of Geophysics, Faculty of Physics, Universidad Complutense de Madrid, Av. Complutense s/n, 28040 Madrid, Spain, Email: figeo07@sis.ucm.es)

The two principal characteristics of the seismicity of the Betics an Alboran sea area: earthquakes of moderate magnitude ( $M < 5.5$ ) and focus at shallow ( $h < 30$  km), intermediate ( $30 < h < 150$  km) and deep depth ( $h = 650$  km). Most of shallow shocks on the Betics have normal faulting mechanism with small component of strike-slip. In the Alboran sea, shallow earthquakes show predominantly strike-slip solutions. Intermediate depth events show vertical tension axes, indicating vertical extension. Focal mechanisms of deep events show the tension axes dipping about 45 degrees to East. The most striking feature of the area is the presence of E-W extension in the internal Betics and Alboran sea, in contrast with the general NW-SE compressive stresses associated with the convergence between Africa and Eurasia. To investigate the possible tectonic mechanisms responsible for the described pattern, we have applied to the study area numerical finite element models using the thin plate approximation. Model predicted principal stress direction and velocity distribution are compared with seismotectonic and geodetic data.

ST2/E/36-A4

1615

## SEISMOTECTONICS OF THE HERCYNIAN BELT IN NW SPAIN. A GEOPHYSICAL INTERPRETATION

Julio MEZCUA (Instituto Geografico Nacional, 28003 Madrid, Spain, e-mail: julio@ign.es) Juan Rueda (Instituto Geografico Nacional, 28003 Madrid, Spain, e-mail: juan@ign.es)

The recent increase of moderate seismicity in the Hercynian belt in NW Spain started January 1979 and continuing up to present, having a maximum event on 21 May 1997 of 5.1 magnitude, near the Sarria tertiary basin. In order to characterize the seismicity of the region a comprehensive revision of both historical and instrumental seismicity had been performed, including the calculation of 16 new focal mechanisms. The seismotectonic interpretation had been possible incorporating not only the tectonics of the tertiary basin generation but also the crustal models obtained by gravity and aeromagnetic studies. The result points out that under a NNW-SSE stress field, a crustal layer of a few kilometers thick underthrusting in E-W direction is responsible of that activity and may be interpreted as a reactivation of the tertiary basin formation.

ST2/E/47-A4

1630

## SEISMICITY, FOCAL MECHANISMS AND SOURCE PARAMETERS IN SOUTH OF PORTUGAL AUGUSTO

J. S. FITAS, M. Bezzeghoud, J. F. Borges, (Dept. de FEdsica, Apt 2E 94, 7002-554, C9vora, Portugal, tel 351 66 744616, email: mourad@uevora.pt). F. Carrilho and L. Senos (Instituto de Meteorologia, Rua C do Aeroporto, 1700, Lisboa, Portugal, tel 351 1 848 39 61, email: fernando.carrilho@meteo.pt).

The Algarve province in the southern region of Portugal, where important historical seismic events took place, presents a potentially moderated and high seismic hazard. To reach a better understanding of seismicity in Algarve and its Atlantic adjacent zone, a project was implemented from January 1996 till December 1998. The results already obtained correspond to a period of three years of seismological observations. (1) The recorded spatial distribution of seismicity shows clearly five subregions: Monchique, Portimao, Loule (continental seismicity), South Faro and Golf of Cadiz (Atlantic seismicity). A more recent calculation of the parameters of Gutenberg-Richter distribution for all region is presented ( $a=3D3.27$  and  $b=3D0.74$ ). (2) The anelastic attenuation, Q factor ( $Q=3DQ_0^{**v}$ ), following the analysis of the high frequency of seismic code a (regional values of  $Q_0$  and  $v$ ) has been estimated. (3) Source parameters, seismic moment, stress drop and source radius of 12 earthquakes (with M ranging from 2.0-3.5) occurred in this region, have been determined by analysing the P-waves spectra. The computed seismic moment ranges from  $8.0 \cdot 10^{11}$  to  $3 \cdot 10^{13}$  Nm, the static stress drop ranges between 1 and 10 bars and show an increasing trend with the earthquake size. (4) Focal mechanisms determined from 9 events, with magnitudes between 2.0 and 3.5, show that is region is under horizontal pressure about NW-SE direction, resulting in strike-slip motion. This sense of motion is consistent with the general relative motion of Eurasia and Africa.

ST2/P/02-A4

1645

## EARTHQUAKE POTENTIAL ALONG THE SEISMOGENIC GEOLOGICAL STRUCTURE OF ORAN (ALGERIA): THE MURDJADJO ANTICLINE IS IT ASSOCIATED TO A BLIND FAULT?

Yousef BOUHADAD & Djamel El-Foul (National Center of Applied Research in Earthquake Engineering (CGS) 1, Rue, Kadour Rahim, H. Dey Algiers- Algeria).

We have studied the Geological structure of Oran which consists of an asymmetric fold-the Murdjadjo anticline. We analysed its relationships with the historical seismicity of the region, particularly the Oran earthquakes of 1790 ( $I=X$ ) and December 1959, ( $M=4.5$ ). During the October 9, 1790 about 3000 human lives were claimed following strong earthquake which hit the Town of Oran. New field observations indicates that the Murdjadjo anticline of about 32 km of length and a direction of  $NO50$  is faulted in it's Southeastern flank. The faulted flank bound to the North the quaternary basin of Mletta which is characterised by a high subsidence (more than 400 m of quaternary deposits). The direction of isoseismal maps of historical earthquakes are elongated in the direction of the anticline.

Quaternary terraces are observed along the Oued El Malah River (alluvial terraces) and along the coast (marine terraces where Neo-Tyrrenian deposits are observed at altitude of 8 to 10 m above sea level). The Northwestern part is marked by small basins triggered by secondary normal faults (Ain Turck plain). Analysis of drainage network suggest that the fault present also a senestral strike component. The geological structure of Oran present analogies with the oued Fodda fault that produced the El-Asnam earthquake of October 10, 1980 of magnitude  $M_s=7.3$ . In term of seismic hazard the blind fault could produce in the future strong earthquakes of magnitude greater than 6.5.

ST2/E/07-A4

1700

**SESTRESS FIELD PATTERN IN EGYPT AND ITS ADJACENT AREAS BASED ON EARTHQUAKE FOCAL MECHANISMS**

K. ABOU ELENEAN (Nat. Res. Inst. of Astronomy and Geophysics, Seismology Department, Helwan, Egypt) Abou El Ata (Ain Shams University, Faculty of Science, Geophysics Department, Cairo, Egypt) C. Christova (Seismology Department, Geophysical Institute, Bulgarian Academy of Science) E. IBRAHIM (Nat. Res. Inst. of Astronomy and Geophysics, Seismology Department, Helwan, Egypt)

The distribution of earthquake epicenters, geological and structural setting and earthquake focal mechanisms are used for division the area into different seismic zones. The stress tensors are deduced from earthquake focal mechanisms using Gephart and Forth (1984) inversion technique for the different seismic zones. The results indicate a dominant tension stress affecting the NE corner of the African plate, which may be related to the counterclockwise of African plate with the respect to Eurasia or to the suggested radial extension centered on Cameroon. The stress field is changing to compression to the north along the subduction zones beneath the Hellenic and Cyprean arcs.

ST2/E/51-A4

1715

**FOCAL MECHANISMS OF SMALLER EARTHQUAKES CLOSE TO VBB KOTTAMIA STATION, EGYPT**

K. ABOU ELENEAN (National Research Institute of Astronomy and Geophysics, Helwan, Cairo, Egypt) R. Arvidsson (Department of Earth science, Uppsala Univ. Villavagen 16, S-752 36 Uppsala) O. Kulhanek (Department of Earth science, Uppsala Univ. Villavagen 16, S-752 36 Uppsala)

The three components of the VBB Kottamia station are used to determine the focal mechanisms of smaller local events up to a distance of 200 km. The digital data is band pass filtered and the inversion is done to get the double couple solutions at different depths of each event. The root mean square errors between the observed and synthetic at different depths are calculated to find the best fit solution. The synthetic seismogram is derived for the best fit solution at different frequency bands (.01-.1, .01-.2 and .01-.5 Hz). The solution gives a good match between the observed and synthetic is selected for each event. The focal mechanisms for the events located along the Suez gulf show normal faulting mechanism which reflect that the rifting process is still be active along the gulf. These solutions give planes trending parallel to the gulf. The solutions of the events to the west of the gulf indicate normal faulting with slight horizontal movement along planes trending WSW-ENE, NW-SE and NNE-SSW. The mechanisms of the events located along the northern extension of the gulf (west of Bitter Lake) show normal faults mostly directed E-W.

ST2/E/49-A4

1730

**PROBABLE ORIGIN OF THE ABU DABBAB EARTHQUAKE SWARMS IN THE EASTERN DESERT OF EGYPT**

E. M. IBRAHIM (National Research Institute of astronomy and Geophysics, Seismology Department, Helwan, Cairo, Egypt, email: seism01@frcu.eun.eg) I. Yokoyama (Higashi 1-17-7-1304, Kunitachi, Tokyo 186-0002 Japan)

Earthquake swarms accompanied with sound at Abu Dabbab in the Eastern Desert of Egypt have been known since the beginning of the 20th century. One of their characteristics is a periodic clustering for a long period, probably for a century. After 1970, the swarms have been instrumentally observed and discussed by several authors. Some of them proposed that the origin of the swarms was attributable to igneous activity in the Precambrian basements, showing an analogy with the activity at rifted margin of the Red Sea. In the present paper, the authors try to review and supplement the previous studies of the Abu Dabbab swarms and to discuss the circumstantial evidence to investigate their origin. The authors analyze the seismograms registered at the nearest station to the epicentral area by local seismic network for a limited period: the m-values in relation ship between maximum trace amplitude and frequency are discussed for the purpose of studying characteristics of the earthquake swarms. To find similarity, if any, among the Abu Dabbab swarms and others, four swarms are exemplified: the 1907-1915 Vogtland earthquake swarms (Germany), the 1930 Ito earthquake swarms (Japan), the 1965-1970 Matsushiro earthquake swarms (Japan), and the 1992 Al-Udayn earthquake swarms (Yemen). To explain the origin of the Abu Dabbab earthquake swarms, circumstantial evidence is examined from the standpoints of tectonics, geology and volcanology. From the discussion, it is concluded that the origin of the Abu Dabbab earthquake swarms is probably igneous.

ST2/W/09-A4

1745

**SOURCE PARAMETERS AND TECTONIC IMPLICATION FOR THE TWO CONGO EARTHQUAKES OF MARCH AND APRIL, 1998**

ATALAY AYELE, Geophysical Observatory, Addis Ababa University, Box. 11 76, Addis Ababa, Ethiopia, tel + 251 1 11 72 53, fax +251 1 55 21 12, email: observatory.aau@telecom.net.et

Two earthquakes occurred in Congo, in March and April, 1998. These two events are reported to have comparable size (5.5mb) and nearly same epicentral location, farther west of the western branch of the East African Rift System. The area is not much associated with the major rift trends in East Africa and the occurrence of seismic events is relatively sporadic. P-wave first motion readings from Broadband stations and waveform data at teleseismic distances are employed to study the fault mechanism and other source parameters of these earthquakes.

The preliminary result shows that the two earthquakes have similar rupture process with slight variation. The duration of each event is less than 2 secs. and the scalar seismic moment  $M_0$  is in the order of  $2-3 \times 10^{17}$  Nm. The style of the dominant deformation is thrust type, which is not common in the East African Rift System. A compressive stress environment possibly created by the extensions of the Atlantic ridge and the East African Rift System may influence this type of rupture process.

Friday 23 July AM

Presiding Chairs: E. Hauksson (Caltech, Pasadena, USA),  
H. Bungum (NORSAR, Kjeller, Norway)

SEISMOTECTONICS OF NORTH AMERICA/FENNOSCANADIA

ST2/W/12-A5

0830

**STRUCTURAL AND TECTONIC SETTING OF THE DYNAMICS OF SEISMICITY**

Vladimir KEILIS-BOROK, Irina Rotwain, (both at the International Institute of Earthquake Prediction Theory and Mathematical Geophysics, Russian Academy of Sciences, Warshavskoye shosse 79 kor.2,

Moscow 113556, Russia, email: vkborok@mitp.ru) Dmitry Rundkvist (State Geological Museum, Russian Academy of Sciences, Mokhovaya 11 kor. 2, Moscow 103009).

Dynamics of seismicity is to a large extent controlled by the structure of the tectonic blocks&faults system, comprising the seismically active lithosphere. We describe powerful mechanism of such control concentrated to a large extent in the fractured zones (nodes) surrounding the faults intersections. This includes reconstruction of the system, nucleation of the earthquakes, emergence of transient asperities and weak links and, premonitory phenomena, specific to geometry of the system. Model of this mechanism brings together the data on the movements in a broad velocity range - from seismicity, to creep, to GPS, to neotectonics, - and possibly also the data on fluids migration. Pilot applications of similar approach to intraplate regions are discussed, North American platform included.

ST2/W/08-A5

0845

**NEW INSIGHTS INTO THE SEISMOTECTONICS OF NORTHEAST PACIFIC OCEAN SPREADING CENTERS, TRANSFORM FAULTS, AND MICROPLATES USING HYDRO-ACOUSTIC MONITORING METHODS**

Robert P. DZIAK and Christopher G. Fox (OSU/NOAA, Marine Science Center, Newport, OR 97365 U.S.A., email: dziak@pml.noaa.gov)

Since August 1991, NOAA/PMEL has been monitoring seismicity from the northeast Pacific Ocean using the U.S. Navy's SOSUS hydrophone array. Oceanic earthquakes are detected on the hydrophone array using the acoustic Tertiary (T-) wave that propagates within the ocean's low-velocity sound channel. Use of T-waves for detecting and locating northeast Pacific ocean earthquakes has lowered the regional detection threshold to mb-1.8. Optimum hydrophone array distribution coupled with precise ocean sound-speed models has resulted in low-error epicentral locations with excellent correspondence to active seafloor faults and volcanic features. During the past 8 yrs, three major seafloor spreading episodes have been detected, two along the Juan de Fuca Ridge in 1993 and 1998, and one along the Gorda Ridge in 1996. Each spreading event was characterized by: 1) Several hundred earthquakes that occurred for 1-3 weeks, 2) low-magnitude ( $M_w < 3.5$ ) events that went undetected by land-seismic networks, and 3) earthquake epicenters that migrated, during the first few days, distances of 35-65 km along the ridge segments. Earthquake epicenter migration was inferred to be the lateral injection of a magma dike into the shallow ridge crust, which was later supported by extensive field observations. The Blanco Transform Fault (BTF) and Sovanco Fracture Zone (SFZ) are two major right-lateral transforms within the optimum coverage of the SOSUS array. Hydroacoustic monitoring of BTF seismicity has shown evidence of tectonic earthquake sequences limited to individual strike-slip fault segments, and volcanically active pull-apart basins. Moreover, acoustic locations of large BTF events ( $4 < M_w < 7$ ) show good correlation of earthquake source parameters to geologic structure. In December 1991, >700 earthquakes were detected along the Heck Seamounts, a chain parallel to and south of the SFZ. The acoustic location of a ( $M_s=6.0$ ) strike-slip event within the swarm suggests the initiation of a previously unrecognized transform segment. In 1991-1992, a band of acoustically detected microseismicity ( $M_w < 3.5$ ) was located within the outer-rise of the Gorda Plate. The microseismicity ceased following the occurrence of a large thrust earthquake at the adjacent subduction zone.

ST2/W/07-A5

0900

**ESTIMATES OF STRESS DIRECTIONS BY INVERSION OF EARTHQUAKE FAULT PLANE SOLUTIONS IN THE CENTRAL WASHINGTON CASCADE MOUNTAINS (USA)**

GIAMPICCOLO E., Gresta S., Malone S.D. and Musumeci C., Istituto di Geologia e Geofisica - Universit di Catania, Corso, Italy, 55. email: EliGIAMP@mbox.unict.it

The tectonic setting of north-western United States is dominated by the interaction between three plates. The small oceanic Juan de Fuca plate subducts beneath the North American one which, on a larger scale, is moving to the south-east relative to the Pacific plate. While the Cascade Range volcanoes result from the subduction process, crustal tectonics are dominated by N-S compression due to the North American Pacific plates interaction. In this study we used ca. 800 earthquakes recorded between 1980-1998 in the central Washington Cascade Mountains to investigate, on a local scale, how uniform the regionally dominant north-south compressive stress field is and if there are some changes that can be associated with local structures. Earthquake locations from the Pacific Northwest Seismograph Network (PNSN) catalogue were grouped into four different zones. Two of them are referred to the volcano body of Mount St. Helens (last eruption in October 1986) and to the Mt. Rainier one (last eruption more than 200 years ago). The other two seismic zones run NNW-SSE and are located respectively 5 km to the north of Mt. St. Helens (St. Helens Seismic zone or SHZ) and 15 km to the west of Mt Rainier (Western Rainier Seismic Zone or WRSZ). The stress field inferred from the focal mechanisms of different subsets was calculated using the Gephart and Forsyth technique. As in previous similar studies we found that the maximum compressive stress axis ( $s_1$ ) in the Mount Rainier area is nearly horizontal and trending ca. N-S and NNE-SSW, in all but one subset. In fact, events beneath Mount Rainier (0-5 km) show a near vertical  $s_1$  suggesting that gravitational forces dominate the maximum compressive stress. For other subsets the minimum compressive stress axis ( $s_3$ ) deviates from vertical to horizontal for events in the depth range of 10-14 km in the WRSZ. We hypothesize that the change in orientation of  $s_3$  for the 10-14 km depth range in the WRSZ is probably due to the influence of the nearby Mount Rainier magmatic system as suggested from the deep low-frequency or long-period (LP) earthquakes located in the south-west part of Mount Rainier summit. In the Mt. St. Helens area we found a uniform stress field along the SHZ, with the maximum principal stress  $s_1$  oriented horizontally in a NNE-SSW direction and the minimum principal stress  $s_3$  oriented ENE-WSW, consistent with the regional tectonics of the Washington part of North America. No evidence is found of stress change as a function of the depth and the subdivision in subsets does not appreciably change the results. Contrarily, earthquakes directly under the volcano body Mount St. Helens (0-10 km) show some variability of the stress field as function of space and time, related to magmatic processes occurring within the conduit.

ST2/E/34-A5

0915

**DEEP CRUSTAL STRUCTURE OF THE SAN ANDREAS FAULT SYSTEM IN CENTRAL CALIFORNIA AND ITS RELATION TO THE GENERATING PROCESS OF M6-7 EARTHQUAKES**

Kin'ya NISHIGAMI (Disaster Prevention Research Institute, Kyoto University, Gokasho, Uji, Kyoto 611-0011, Japan, email: nishigam@drs.dpri.kyoto-u.ac.jp)

We estimated 3-D distribution of coda scatterers in the crust in central California by using an inversion analysis of coda envelopes from local earthquakes. 3,801 seismograms of the Northern California Seismic Network were analyzed. The San Andreas fault and other sub-parallel faults seem to be almost vertical from a surface to about 15km depth. The scatterer distribution also shows a sub-horizontal detachment structure connecting the San Andreas fault (SAF) and the Hayward-Calaveras faults (HCF) in the lower crust, and some deeper heterogeneous structure at 30-45km depths below the detachment. This image suggests the



sub-horizontal detachment structure may transfer the shear stress due to a continuous slip across the Pacific-North American plate boundary to the bottom of the SAF and the HCF. Segmentation structure of the SAF is also estimated from south of San Francisco to San Juan Bautista. Partially locked segments with a horizontal length of about 20-30 km are ruptured during respective M6-7 earthquakes and the segment boundaries are estimated to be weak zones characterized by stronger scattering and stationary micro-seismicity. The segment boundaries estimated by the present analysis almost exactly agree with one of those proposals estimated from the slip distribution of the great 1906 San Francisco earthquake as well as the fault geometry, although the segment boundaries along the SAF in and around the San Francisco Bay area are still under discussions and speculative.

ST2/W/10-A5

0930

## SEISMOTECTONICS OF SOUTHERN CALIFORNIA: RECENT DEVELOPMENTS

E. HAUKSSON, J. Hardebeck, J. Nazareth Seismological Laboratory, Caltech, Pasadena, CA, 91125 USA; L. Jones U.S. Geological Survey, 525 S. Wilson Av., Pasadena, CA, 91106, USA

Near the US Mexico international border, the Pacific North America plate boundary is characterized by extensional tectonics as it emerges from the Gulf of California, reflected by dextral fault steps in Imperial Valley. To the north of Los Angeles the big bend of the San Andreas causes compressional tectonics to west, within the Pacific plate. A separate zone of right-lateral shear and some extensional tectonics extends into the North America plate, referred to as the eastern California shear zone. We synthesize seismicity, Vp and Vp/Vs velocity structure, and state of stress along these tectonic features. The heterogeneity of the crustal structure as imaged in both the Vp and Vp/Vs models is larger within the Pacific plate than the North America plate reflecting regional asymmetric variations in the crustal composition and past tectonic processes. Similarly, the spatial distribution of the seismicity reflects shallower seismicity within the North America plate and more complex three-dimensional distribution within the Pacific plate. The change in depth of seismicity appears to coincide with the major northwest striking strike-slip faults such as the San Andreas, San Jacinto, and Elnsinore faults. The most complex three-dimensional seismicity distributions within the Pacific Plate are in areas of compressional tectonics. We have inverted for the state of stress from focal mechanisms to determine the predominant type of faulting and the orientations of the three principal stresses. The predominant orientation of the maximum principal stress varies from due north to 30deg east of north. The small scale spatial variations in the stress state may be affected by presence of high pressure pore fluids and proximity to the active fault strands of the San Andreas fault.

ST2/E/44-A5

0945

## LATERAL VARIATION OF SEAFLOOR ROUGHNESS NEAR THE TRENCH AND LARGE EARTHQUAKE OCCURRENCE ALONG THE MEXICAN SEGMENT OF THE MIDDLE AMERICAN TRENCH

Carlos A. MORTERA-GUTIERREZ (Instituto de Geofísica, Universidad Nacional Autónoma de México, Cd. Universitaria, D.F., C.P. 04510, México, email: carlosm@ollin.igeofcu.unam.mx)

The lateral variation in surface roughness of the subducting plate along the western margin of Mexico is examined in correlation with the mode of large-earthquake occurrence along the northern segment of the Middle American Trench (MAT). From the seafloor topography derived from satellite altimetry and topographic profiles, the occurrence of large earthquakes correlates with regions where the surface roughness of the ocean bottom near the trench is greater. Along the MAT, the seafloor roughness near the trench is greater to the east and west of the Guerrero Seismic Gap (GSG) region. In the Jalisco-Colima-Michoacan segment, west of the GSG, horsts and grabens trending diagonal to the trench dominate the ocean bottom roughness near the trench. In the Guerrero-Oaxaca segment to the east of GSG, the seafloor roughness contains linear trends of fracture zones striking nearly normal to the trench. The region where the ocean bottom is relatively smooth along the MAT coincides with the region of seismic quiescence along the Guerrero coast. It has been proposed for the Japan Trench where the seafloor roughness is smooth that the subducted seafloor form a homogeneous, strong contact zone in the plate interface and that the seismogenic zone extends to greater depths. Therefore it is expected that large thrust earthquakes should occur in the deeper part of the seismogenic plate interface (e.g. 1968 Tokachi-oki event). However the reverse is observed for the Mexican subduction zone. In the GSG region, it is observed that no large earthquake have occurred along the plate interface zone. Whereas in the regions of rough surface along the Japan Trench, the subducted structures (e.g. horsts and grabens, seamount chains and fracture zones) create zones of sufficient contact with the overriding plate at shallow depths of the plate interface zone, causing large tsunami-earthquakes (e.g. 1896 Sanriku event) and large normal-faulting intraplate events (e.g. 1933 Sanriku event). Both areas of rough-seafloor along the MAT correlate well with regions where: (1) large normal intraplate earthquake have occurred in the subducting plate (e.g. 1997 Michioacan event of Mw 7.1), (2) large underthrust earthquakes have occurred in the shallow region of the plate interface zone (e.g. Jalisco 1932 event with a magnitude of 8.1, 1957 San Marcos of Mw 7.8, 1995 Colima-Jalisco event of Mw 8.0), and (3) tsunamis have been seismically generated (e.g. 1978 Oaxaca event of Mw 7.8, 1985 Michioacan event of Mw 8.3, 1995 Colima-Jalisco event of Mw 8.0).

ST2/W/05-A5

1000

## THE WESTERN GUERRERO, MEXICO, SEISMOGENIC ZONE FROM THE MICROSEISMICITY ASSOCIATED TO THE 1979 PETATLAN AND 1985 ZIHUATANEJO EARTHQUAKES

D.A. NOVELO-CASANOVA and C. Valdes-Gonzalez (both at Instituto de Geofísica, UNAM, Mexico 04510 D.F., Mexico, email: david@ollin.igeofcu.unam.mx)

The Western Guerrero, Mexico, seismogenic zone was completely ruptured by the 1979 (Ms=7.6) Petatlan and 1985 (Ms=7.5) Zihuatanejo earthquakes. Hypocenters of the Petatlan aftershocks define an approximately 10-km-thick Wadati-Benioff zone of high seismic activity and a thinner seaward region that is primarily an extension of the deeper part of the 10-km-thick zone. The aftershocks of the Zihuatanejo earthquakes occurred in the seaward portion of the same epicentral region but the hypocenters were shallower. The spatial distribution of the closely timed microseismicity following the two earthquakes outlines a seismogenic zone which begins at about 40 km from the trench axis of the Western Guerrero subduction region and extends approximately 90 km. These results indicate that the maximum possible size of thrust earthquakes in the Guerrero seismic gap is of Mw ~ 8.4.

ST2/W/18-A5

1015

## FOCAL MECHANISM STUDY IN COSTA RICA AND VICINITY, CENTRAL AMERICA

Ronnie QUINTERO and Federico Guendel (OVSCORI, Costa Rica, email: rq@geofys.uu.se)

We have relocated 1698 earthquakes which have occurred in Costa Rica and vicinity. Relocated earthquakes were used to investigate the fault plane solution within the mentioned area. The analysis was made using the polarities of first motions of P waves. The area in study is characterized by the subduction of the Cocos under Caribbean plate. Therefore the dominant fault plane solutions are reverse fault with some anomalies caused by the subduction of sea mounts and a truncurrent plate boundary that traverses central Costa Rica from west to east. These anomalies produces normal and strike slip faulting, especially along the frontal arc in central Costa Rica.

ST2/L/03-A5

1030

## SUBDUCTING PLATE MORPHOLOGY AND ITS RELATED SEISMICITY: NEW BATHYMETRIC EVIDENCE FROM THE TONGA AND MIDDLE AMERICA TRENCHES

Nancy KANJORSKI: Scripps Institution of Oceanography, UCSD, La Jolla, CA 92093

The extreme geometry of the Tonga trench creates significant changes in the seismicity of the subduction zone. The northern bend to the west is known to add a strike slip component of motion to the numerous earthquakes in this region. New bathymetric data of this area illustrates the physical manifestation of this seismicity in magnificent faulting along the outer rise over a series of extensional "tear" faults. This influence of plate geometry on the activity of the subduction zone persists over 150 km east of the trench. However, we find that the exceptional Tongan type crook in the axis is perhaps unnecessary to influence the outer rise morphology and subduction seismicity. A comparison between the curvature of the Tonga trench and the muted bend of the Southern Mexico trench off Oaxaca is instructive as both display similar trench morphology and seismicity.

The Mexico trench has always been a region of interest for its patterns of seismicity. Here along the trench a subdued bend of the axis creates some notable outer rise weaknesses evident in unique faulting and anomalous seismic activity. The weakened subducting crust with its rough inherited

volcanic terrain allows for regular moderate stress release along the interplate thrust zone. Around the bend to the east the background seismicity common along much of the Middle America Trench is tranquil. The few larger historical events in this area display components of strike slip activity. Missing here from the outer rise are the perpendicular scarps which enhance the seismicity north of the bend. Dividing these two territories the trace of an extensional tear fault like that of the northern Tonga Trench fractures the outer swell of the subducting plate. This Puerto Angel Fault extension has created deep outer rise sediment ponds which run along the sinuous scarp. It is likely that, as recognized in the Tonga trench, the Mexico trench exhibits seismicity related to the subducting plate weakness and geometry.

ST2/W/28-A5

1115

## SEISMOTECTONICS OF THE NORTHEASTERN UNITED STATES

John E. EBEL (Weston Observatory, Department of Geology and Geophysics, Boston College, Weston, MA 02493, USA, email: ebel@bc.edu)

The northeastern United States is an intraplate region with low or moderate seismicity located on a passive margin. Earthquake activity is scattered broadly across the region, from the coastal areas through the Appalachian orogen and into the precambrian craton. The principal stresses associated with the earthquakes are consistent with those from plate driving forces. Regional seismic network monitoring is being carried out to determine which geologic structures are seismically active and how large an earthquake can occur on those structures. Currently, there have been insufficient data collected to determine which specific structures are seismically active. On a regional basis, most of the modern earthquakes are occurring on or near structures that formed or were reactivated during Mesozoic rifting. These structures include faults, dikes and uplifts. Since some of these faults are hundreds of kilometers in length, major earthquakes (M7+) may be possible at a number of localities in the region, although with a relatively low frequency of occurrence.

ST2/E/50-A5

1130

## SEISMICITY AND RHEOLOGY OF THE CHARLEVOIX SEISMIC ZONE, QUEBEC, CANADA

G. RANALLI (Department of Earth Sciences, Carleton University, Ottawa, Canada K1S 5B6; email: granalli@ccs.carleton.ca) M. Lamontagne (Geological Survey of Canada, 1 Observatory Crescent, Ottawa, Canada K1A 0Y3; email: maurice@seismo.mrcan.gc.ca)

The Charlevoix Seismic Zone (CSZ) is the most active seismic zone of Eastern Canada, with five historical earthquakes in the 6-7 magnitude range and high background activity (about 1500 shocks with magnitude 0 to 5 from 1977 to 1997). Epicenters define a 30x85 km ellipse along the St. Lawrence River 100-150 km downstream of Quebec City. The hypocentre distribution shows an increase with depth to a peak at 10-12 km, followed by a decrease: 99% of all events are shallower than 25 km. Most events occur in highly fractured volumes that are sometimes bounded by regional faults.

The temperature at a depth of 25 km is estimated to be between 220 and 360 C. Values in the upper range coincide with the brittle/ductile transition if the rheology of the lower crust is quartz-controlled. However, most interpretations of the CSZ require a more basic lower crust. Consequently, neither the peak nor the cutoff of seismicity in the CSZ appear to be related to the transition to bulk ductility.

Focal mechanism solutions show predominantly reverse faulting on steeply dipping planes. The reactivation of these fractures requires high pore fluid pressure and/or low friction coefficient. If earthquakes in the CSZ are a consequence of frictional Coulomb failure, the evidence points to the occurrence of relatively high fluid pressures (~ 60-90 of lithostatic) in the lower crust.

ST2/E/32-A5

1145

## NEW SEISMIC ACTIVITY IN THE NORTH ATLANTIC RIDGE

Bela Assinovsky (Geodynamical Laboratory, CAO RAS, Bolshoi pr.50G, V.O., 199034, Saint-Petersburg, Russia, email: bela@ba2248.spb.edu)

Connection of two global North Atlantic and Arctic ocean rift systems it is known to have distinctive features as rapid change of submeridional rift strike to subparallel and closeness to the Svalbard High with its continental type of crust. The earthquake data of the 20th century from the Knipovich Ridge and Spitsbergen fracture zone and the seismic process trend of the region are examined. According to seismic, morphological and geophysical information complex combination of some rift and transform fault zones is recognized here. The seismicity of these zones is distinguished by many parameters: 1. earthquake concentration density 2. source depth 3. seismic regime 4. laws of seismotectonic deformation release. For example, transform fault zone spaced more closely to the Svalbard High is characterized by occurring of rare but large earthquakes, focal depth about 20 km and nonlinear mode of seismic energy



release . Reciprocating migration of earthquake sources with  $M_b > 5$  along the North Atlantic ridge strike is studied. Two slow channels ( $V = 3-10$  km/y) with sources that travel to the south direction and one quick channel ( $V = 40$  km/y) with of earthquake sources that travel to the of rift split direction are marked out in the time-space field by numerical method. At the intersection of these channels the largest event of region of 28 March 1998  $M_b = 5.9$  occurred. All together four large ( $M_b = 5.7-5.9$ ) earthquakes occurred within the Knipovich rift zone and Spitsbergen Fracture zone during the last 6 years, all of them had focal mechanisms of the same type – predominance of right-side strike slip along the main faults. In total these sources migrated along half-round way clockwise from the north of the Knipovich Ridge to central part of it and then to the north to the parts of Spitsbergen Fracture zone. The described seismic activity was predicted earlier (B. Assinovsky "Earthquakes in the Barents Sea").

ST2/E/31-A5

1200

## SEISMOTECTONICS OF THE NORWEGIAN CONTINENTAL MARGIN

H. BUNGUM (1,2), C. Lindholm (1), O. Eldholm (2) and E. Hicks (1,2) 1. NORSAR, Kjeller, Norway 2. University of Oslo, Oslo, Norway

The Norwegian continental margin is less seismically active than some other passive margins, but still highly active on a northern European scale, with historical earthquakes up to magnitude 6, and with some 60 earthquakes above magnitude 2.5 every year. Historical data and more recent instrumental studies using dense networks of stations and arrays have shown that the seismic activity is concentrated to the local zones along the margin and to coastal regions, but with seismic activity also in the Viking and Central Grabens and the Oslo Rift zone. The earthquake depths vary from about 30 km (offshore) to shallow microactivity at around 5 km in coastal regions, reflecting not only the varying physical properties of the crust but also a regional differentiation of deformation processes with depth. The stress field complies in general with the ridge push force, but with significant contributions also from regional and local sources of stress (including lateral density inhomogeneities, deglaciation, sediment loading, and topographic effects), the latter in fact being necessary for explaining the earthquake activity. The relative importance of these local sources of stress is supported by several cases of 90 degree stress reversals relative to the ridge push direction. One of the most significant local sources of stress has been found to be the rapid deposition of late Pliocene-Pleistocene glacial sediments, particularly in parts of the Lofoten and Norway ocean basins and below thick glacial depocenters on the margin, where the excess load has enhanced the local stress field, and consequently the seismic activity. In contrast, crustal underplating may contribute to crustal strengthening and thereby less seismicity, in particular at marginal highs. We suggest that increased stress due to appreciable post-glacial rebound gradients in the coastal region also may be a contributing factor.

ST2/E/11-A5

1215

## CONCENTRATED EARTHQUAKE ZONES ON THE NORWEGIAN CONTINENTAL MARGIN

HICKS, E.C. (1,2), C.D. Lindholm (1) & H. Bungum (1,2) 1. NORSAR, Kjeller, Norway; 2. Dept. of Geology, University of Oslo, Norway

The Norwegian continental margin is comprised of a complex system of deep rifted sediment basins and adjacent highs. The southern parts of the margin are dominated by Triassic to early Cretaceous rift basins in the North Sea, while the Mid-Norwegian margin to the north sustained rifting mainly in Late Cretaceous to Paleocene, leading up to the continental breakup and opening of the North Atlantic ocean with associated volcanic activity. Earthquake swarms in coastal areas of Mid- and Northern Norway are known to occur fairly regularly, the Ms 5.8-6.2 earthquake of 1819 was also located in this area, while the southern parts of the Mid-Norwegian coast have lower levels of activity. Since 1997, a local network in the Rana area (Northern Norway) has located a large number of small, shallow coastal earthquakes (magnitudes up to  $M_l 2.8$ ). Several new focal mechanism solutions with inverted (90 deg. rotation) horizontal stress directions compared to the regional case have also been determined. The earthquakes show a complicated spatio-temporal activity pattern, with the activity distributed among several distinct groups, all having similar NW-SE elongated trends. There does not appear to be any connection between the observed earthquakes in this area and the nearby Baasmoen fault, a major fault thought to have been postglacially active. The northern parts of the North Sea have the highest levels of seismic activity in Fennoscandia. Recently, a new local network (in the Bremanger area) has provided new insight into this activity through improved location and detection capabilities. Although detailed correlation of earthquakes and faults is always difficult due to hypocenter location uncertainties and problems in tracing the fault plane with depth, new detailed fault mapping in this area combined with improved earthquake data may be able to provide more insight into the interaction of existing faults and seismic activity.

ST2/W/23-A5

1230

## HIGH SEISMO-TECTONIC ACTIVITY IN SWEDEN AT THE TIME OF DEGLACIATION AS RECORDED BY MULTIPLE PALEOSEISMIC EVIDENCE

Nils-Axel MOERNER Paleogeophysics & Geodynamics, S-10691 Stockholm, Sweden, email: mornner@pog.su.se

Today, Fennoscandia is characterized by a low to moderately low seismic activity. At the time of deglaciation, the situation was quite different, however: the whole region was characterized by both large and frequent earthquakes. The rate of isostatic uplift then amounted to some 10 cm per year (i.e. about 10 times as high as the present sea floor spreading rates). In Sweden, we have the possibility of utilizing the varve chronology for the dating of paleoseismic events. This means that we can achieve an annual resolution despite ages in the order of 10,000 years. This technique has successfully been applied to some regions in Sweden. In the Stockholm region, we have been able to date an extremely large paleo-seismic event to the autumn of varve year 10,430 BP. This event caused liquefactions and varve disturbances over an area of about 60 x 320 km, which exceeds the liquefaction distribution of the famous Alaska 1964 event. We have also been able to identify multiple events re-occurring about every 20 varve (~10,490, 10,469, 10,447, 10,430, ~10,410 BP) indicating an unusually high frequency of the event, too. A Holocene event occurred along the same fault zone at about 3500 BP. At Iggesund, we have recorded heavy bedrock deformations in association with strong sediment deformations from both ground shaking and tsunami waves, and turbidites over an area of 60 x 210 km at varve 9663 BP. Other high-amplitude events are the Åspö event at ~12,200 BP, the Kinnarumma event at ~11,700 BP, the Billingen event at ~10,400 BP, the Gillberga event at ~10,000 BP, the Lansjår event at ~9,150 BP and the Pärve event at ~9,000 BP (Ref.: Quaternary Science Reviews 15: 939-947, 1996). They occur all over Sweden. Our paleoseismic records give a totally new situation for issues of a long-term deposition of high-level nuclear waste in the bedrock.

## SEISMOTECTONICS

ST2/W/26-A5

Poster

1400-01

## LONG-PERIOD AFTERSHOCKS OF A MODERATE-SIZE EARTHQUAKE NEAR THE IWATE VOLCANO, NORTHERN JAPAN, OBSERVED BY A BROADBAND SEISMIC ARRAY

Masahiro KOSUGA, Kazutoshi Watanabe, Yoshimichi Senda, and Hisayuki Sakoi (all at Faculty of Science and Technology, Hirosaki University, Hirosaki 036-8561, Japan, email: mkos@cc.hirosaki-u.ac.jp)

We have examined the origin of long-period (LP) aftershocks associated with a moderate-size ( $M = 6.1$ ) earthquake that occurred on September 3, 1998, to the south of Iwate volcano in northern Japan. The broadband array was deployed to observe volcanic tremors and low-frequency earthquakes near the volcano whose activity has increased from the beginning of 1998. We could obtain array recordings of many aftershocks with epicentral range from 15 to 30 km. The noticeable feature of aftershocks is the existence of LP events aligned along the eastern margin of the aftershock zone. LP phase that appears about 10 s after the P-wave is characterized by a predominant period of 2 s, larger amplitude than that of S-wave, and long (> 20 s) duration. From the semblance analysis we found that the LP phase comes from the direction of epicenter. The facts of large slowness and retrograde particle motion suggest the wave type of Rayleigh wave. The basin structure extended to the east from the aftershock zone probably play a key role to enhance the surface wave, however, UP Diliman campus, Diliman, Quezon City 1100, Philippines) we used hypocentral (1619 to 1997) ...and focal mechanism (1963 to 1997) data in order to characterize the tectonic configuration of northern Luzon and refine a model for describing the geometry of the subducted slab of the Eurasian plate beneath the northern segment of the Manila Trench. We considered the bend in the trench line of the Manila Trench at 20°N lat, the collision and subduction of an extinct mid-oceanic-ridge at 16-17°N lat and the intraplate deformation pattern in the North Luzon Ridge region in depicting a new model that will be consistent with most of the observed features and phenomena in the study area. The model suggests the collision and subsequent partial subduction of a buoyant plateau at around 20°N lat to explain the sharp bend in the trench line, the complicated deformation pattern on the overriding plate fronting the bend and the shallow dip of the subducted slab beneath this zone. The shoaling of the dip of the slab may be due to the buoyancy effect of the subducted part of the buoyant plateau. The change in...

ST2/W/21-A5

Poster

1400-02

## AN ALTERNATIVE MODEL FOR THE GEOMETRY OF SUBDUCTING SLABS IN NORTHERN LUZON, PHILIPPINES

BARTOLOME C. BAUTISTA (1,2), Ma. Leonila P. Bautista1, (2) and Kazuo Oike (1) (1), Dept of Earth and Planetary Sciences, Graduate School of Science, Kyoto University, Sakyo, Kyoto, Japan, 606-8502; (2), Philippine Institute of Volcanology and Seismology, C. P. Garcia Avenue, UP Diliman campus, Diliman, Quezon City 1100, Philippines)

We used hypocentral (1619 to 1997) and focal mechanism (1963 to 1997) data in order to characterize the tectonic configuration of northern Luzon and refine a model for describing the geometry of the subducted slab of the Eurasian plate beneath the northern segment of the Manila Trench. We considered the bend in the trench line of the Manila Trench at 20°N lat, the collision and subduction of an extinct mid-oceanic-ridge at 16-17°N lat and the intraplate deformation pattern in the North Luzon Ridge region in depicting a new model that will be consistent with most of the observed features and phenomena in the study area. The model suggests the collision and subsequent partial subduction of a buoyant plateau at around 20°N lat to explain the sharp bend in the trench line, the complicated deformation pattern on the overriding plate fronting the bend and the shallow dip of the subducted slab beneath this zone. The shoaling of the dip of the slab may be due to the buoyancy effect of the subducted part of the buoyant plateau. The change in dip shifted the position of the magma generation level towards the east and may have led to the subsequent extinction of the western chain of volcanic centers and the eastward shift of active volcanism in the region. A tear in the slab is also inferred to be present as evidenced by the observed gap in strain energy release and the abrupt change in dip from shallow to steep south of 18°N lat. The gap in seismicity and strain energy release (65-300 km depth) at around 17°N lat may be used to infer the trajectory and location of the subducted extinct mid-oceanic-ridge. The subducted ridge is still probably hot and is deforming plastically causing the aseismic behavior. The subducted part of the mid-oceanic ridge may serve as the weakest zone where this tear could be localized. The tear may also explain the cause of the abrupt termination of the eastern chain of volcanoes south of 18°N lat. The above model, which is a refinement of the model introduced by Yang et al (1996) is consistent with the observed seismicity and deformation pattern, bathymetric features, spatial distribution and geochemical character of volcanism in northern Luzon.

ST2/W/04-A5

Poster

1400-03

## DECAY OF MICRO-EARTHQUAKE SEISMICITY ACTIVATED BY STATIC STRESS CHANGE

Mamoru NAKAMURA (Department of Physics and Earth Sciences, University of the Ryukyus, Senbaru, Nishihara-cho, Okinawa, 9030213, Japan, email: mnaaka@sci.u-ryukyuu.ac.jp)

Background seismicity of micro-earthquakes activates occasionally in the surrounding of the mainshock area after the large earthquake. The activated background seismicity decays with time. We investigated the index of decay of activated background seismicity (p value) using 1995 Hyogo-ken Nanbu (Kobe) earthquake, Japan and 1989 Loma-Prieta earthquake, California. The micro-earthquake seismicity changed in the surrounding of the aftershock area of the Kobe earthquake. The background seismicity in this area activated five times higher than that before the mainshock. We obtain the estimate of p value in Ohmori formula for the activated background seismicity. Hypocenter data we used are catalogued by DPRI, Kyoto University. The p values scatter from 0.5 to 0.9. These values are much lower than that obtained from aftershock decay (usually  $p = 0.9-1.5$ ). We compare them with change of the CFF using dislocation model by Hashimoto et al. (1996), which is estimated using geodetic data. High p value ( $p = 0.9$ ) is obtained in a region where the increase in CFF is large (100 kPa), and low p ( $p = 0.5$ ) is obtained in a region where that is small (50 kPa). Next we compare the activation of seismicity with CFF change for 1989 Loma-Prieta earthquake. We pick up the seismically active area along the San-Andreas fault from southern part of the aftershock area. We divide this into three segments with the length of 10 km. We calculate change of the CFF using dislocation model by Lisowski et al. (1990), which is estimated using geodetic data. Finally, we compare the change of CFF with p-value at each segment. We use the seismicity data catalogued by NCEDEC. High p value ( $p = 0.7$ ) is obtained in a region where the increase in CFF is large (130 kPa), and low p ( $p = 0.4$ ) is obtained in a region where that is small (70 kPa). These suggest that the low decay of activated seismicity would usually occur when seismicity has changed by small CFF change and degree of the decay is inversely proportional to the increase in CFF.

ST2/E/58-A5 Poster 1400-04

## CONFIGURATION OF THE PHILIPPINE SEA PLATE UNDER THE TOKAI REGION, SOUTHERN COASTAL AREA OF CENTRAL JAPAN, AND THE SEISMICITY IN THE SLAB

Satoshi HARADA (Seismology and Volcanology Research Department, Meteorological Research Institute, Ibaraki, Tsukuba, Nagamine, 1-1, 305-0052 Japan, email: sharada@mri-jma.go.jp) Akio Yoshida (Seismological and Volcanological Department, Japan Meteorological Agency, Tokyo, Chiyoda, Ote-machi, 1-1-1, 100-8122 Japan, email: akio.yoshida-a@met.kishou.go.jp)

Relation between configuration of the oceanic plate and the seismicity in it is investigated for the Philippine Sea slab subducted under the Tokai region, southern coastal area of central Japan. The upper surface of the slab is delineated by tracing an envelope of the hypocentral distribution of earthquakes in the cross section for each parallel narrow region taken east-west and north-south direction, respectively. A noticeable feature of the configuration is that the slab warps downward in the middle of this region. That is, the slab deepens toward west in the eastern part and inclines northward in the western part. The deepest portion of the Tokai slab exists in the northwest. We consider that the above-described configuration of the slab and the result obtained by an analysis of the GPS data which the direction of the relative motion between the subducting Philippine Sea slab and the overriding continental plate changes clockwise are related each other. According to the back-slip analysis of the interplate coupling the slab moves westward in the eastern Suruga Bay region, while it subsides more northerly in the western part (Sagiya, 1998). On the other hand, the seismicity in the slab is high in a relatively narrow zone of NNW-SSE direction in the western part of the Tokai region. When the seismicity in the slab is compared with the above-described configuration of the slab, we find a noticeable feature that the seismicity is high around the area where the slab changes its gradient steeply. This correspondence between the shape of the slab and the distribution of seismicity indicates that seismogenic stress field in the slab is mainly originated by the bending of the slab at each local site in the course of the subduction process. The fact that the earthquake mechanisms in the high seismicity zone are mostly normal fault type (Noguchi, 1996) also supports the idea

ST2/E/30-A5 Poster 1400-05

## SEISMIC ACTIVITY ALONG ATOTSUGAWA FAULT, CENTRAL JAPAN, AND ITS RELATION TO CREEP MOVEMENT AND TECTONICS

Kiyoshi ITO (Disaster Prevention Research Institute, Kyoto University, Uji Kyoto, Japan, 6110-0011, email: ito@rcep.dpri.kyoto-u.ac.jp) Hiroo WADA (Kamitakara observatory, Disaster Prevention Research Institute, Kyoto University, Kamitakara, 506-1317 Gifu Pref., Japan, email: hiroo@ktj.rcep.dpri.kyoto-u.ac.jp)

Activity of microearthquakes along the Atotsugawa fault, a prominent active fault in northwest Honshu, is relatively high and well concentrated at the surface fault compared to other active faults in Japan. Although a large inland earthquake of M7.0 occurred in 1858, at the fault, aftershock activity must be low because of long time after the main shock. Besides, a creep movement was found at a northwestern portion of the fault from the surveys with electro-optical distance-meters. Some new seismic stations were set to make clear the seismicity, in particular focal depth distribution of microearthquakes along the fault. Focal depth distributions, obtained from new data show, are deeper by about 2-3km than those determined without temporary stations. Moreover, few events have been located in the upper crust down to 8-9km deep beneath the creep portion of the fault. This detailed hypocenter distribution suggests heterogeneous stress state or barriers along the fault. Cutoff depth of seismicity also changes along the fault, and it is deepest in the creep portion as about 18km. The heat flow value near the area is about 75mW/m<sup>2</sup>, which is rather high and corresponding cutoff depth is usually 10-15km. The focal depths are deeper than the usual value in this area. On the contrary, seismicity is also high but the cutoff depth is less than 10km at both ends of the fault, where there are active volcanoes. The displacement pattern derived from GPS surveys is changed at the fault. Thus, the fault seems to play an important role in the deformation of the area.

ST2/E/22-A5 Poster 1400-06

## UPPER AND LOWER CUTOFF DEPTHS OF SEISMICITY AND ITS RELATION TO TECTONICS OF JAPAN

Kiyoshi ITO (Disaster Prevention Research Institute, Kyoto University, Uji Kyoto, Japan, 611-0011, email: ito@rcep.dpri.kyoto-u.ac.jp) Shuichi NAKAMURA (Mitsubishi Research Institute Inc., 2-3-5 Ohte-machi, Chiyoda-ku, Tokyo, Japan, 100-8141, email: shuichi@mri.co.jp)

Upper and lower cutoff depths of seismicity have been determined from many microearthquake hypocenters in the inland area of Japanese Island. More than 150,000 determined hypocenters were used for the determination of depths, D10%, D50% and D90%, i.e. the depths above which 10, 50 and 90% events occur in the grid of 0.25x0.25 degree latitude and longitude. D10, D90 and D50% roughly correspond to the upper, the lower and the mean depths of seismogenic layer, respectively. Regional variations in the D90%, as well as D10% and 50%, are well correlated with topography, and also with the thermal structure of the crust. Active faults and large inland earthquakes occurred in the area of steep changes in the seismogenic layer. This shows the deformation of the island arc is closely related to the thickness of the seismogenic layer, or brittle regime in the crust. Strain pattern derived from repeated GPS survey shows the changes relating to D90%. Moreover, the upper cutoff depth (D10%) is well correlated with D90% and D50% and the average thickness between D10% and D90% is about 10km. This suggests that not only the lower cutoff depth but also the upper cutoff are related to the thermal structure of the crust.

ST2/E/37-A5 Poster 1400-07

## SEISMOTECTONICS OF CONVERGENT PLATE MARGINS AND CHRONOLOGICAL EVOLUTION OF SUBDUCTION

Ales SPICAK, Vaclav Hanus and Jiri Vanek (Geophysical Institute, Bocni II, 141 31 Prague 4, Czech Republic, email: als@ig.cas.cz)

The study of geometry of distribution of earthquake foci in convergent plate margins, if based on a large body of high-quality seismological data, enables us to investigate the morphology and the basic parameters of the Wadati-Benioff zone, to elucidate the character of seismicity in the continental wedge above the Wadati-Benioff zone, to correlate the position of present and ancient volcanic events with the morphology of the Wadati-Benioff zone and with the seismicity of the continental wedge, and to contribute to the knowledge of deep structure of different regions of convergent plate margins and of chronological evolution of subduction. From the distribution of earthquake foci inside the Wadati-Benioff zone an intermediate-depth aseismic gap can be observed, the position of which correlates with the position of active volcanism on the surface. On the basis of the distribution of earthquakes in the continental wedge above the subduction zone, seismotectonics of the continental lithosphere can be derived. Groups of deep earthquakes clearly divided by a vast region without earthquakes and

shifted in the relation to the active subduction zone in several convergent plate margins, interpreted as remnants of paleosubduction zones buried in the upper mantle, give a possibility to speculations on the chronological evolution of subduction zones and on the geodynamic development of respective regions. The applicability of the above method is exemplified in the areas of Andean South America and in the Indonesian island arc.

ST2/W/33-A5 Poster 1400-08

## GPS DERIVED SLIP RATE ALONG THE KARKORAM FAULT IN THE INDO-EURASIAN CONTINENTAL COLLISION ZONE

Sridevi jade (C-MMACS, NAL Belur Campus, Bangalore-560037,India) Bhat, B.C (Indian Institute of Astrophysics,Bangalore,India) Anand,M.B.(C-MMACS, NAL Belur Campus, Bangalore-560037,India) Gaur,V.K.(C-MMACS, NAL Belur Campus, Bangalore-560037,India)

The long Karakoram fault stretching for over 1000km from Pamir to Manasarovar in Tibet is a right lateral strike slip fault and a major feature of continental deformation north of the Himalaya. Current Estimates of annual slip along the fault, regarded as facilitating the eastward extrusion of Tibet in response to the continued Indo-Eurasian convergence, based on geological investigations, however, vary from 3 to 30mm/yr. This paper presents slip rates along the Karakoram fault based on GPS monitoring of sites in Ladakh since 1997.

ST2/E/54-A5 Poster 1400-09

## ON SEISMODYNAMIC OF CENTRAL ASIA

A.R.YARMUKHAMEDOV (Institute of Seismology, Khurshid str.3, 700128 Tashkent, Uzbekistan, email: root@seismo.tashkent.su)

In contrast to the traditional statistical study of the seismic regime for the seismogeodynamic approach development we consider seismic phenomena of different scale as an indivisible dynamic system taking into account peculiarities of the hypogene structure, crustal dynamics, stress state, processes of deformation and geophysical fields caused by the processes. The regional determinate seismogeodynamic model characterizing nature and spatial distribution of the seisdangerous zones (junctions) in Central Asia is developed and maps of junctions and recent geodynamic activity was constructed proceeding from the above-stated preconditions. The Central Asia recent crustal geodynamic activity is estimated for the first time through the integral index of the geologo-geophysical parameters and the territory under investigation is zoned on the basis of the index. It is noted that seismicity as a process is connected with the areas of high geodynamic activity and orders of blocks of different activities. Sources of destructive and disastrous earthquakes in Central Asia and Uzbekistan in particular spatially and genetically are connected with junctions. Data about the Gazli (1976 and 1984, M=7.1-7.3), Tashkent (1966, M=5.6), Nazarbek (1980, M=5.3), Tavaksei (1977, M=5), Chimion (1982, M=6.2), Pap (1984, M=5.2), Kairakum (1985, M=6.0), Khumsan (1987, M=5.0), Shamaldysai (1988, M=5.0), Izbastkend (1992, M=6.8) earthquakes can be the confirmation of the fact. Energetics of the seismotectonic process depends not only on internal structure of the lineaments and processes in them but also on the geoblock dynamics, their displacement and interaction. Character of seismicity within the young Turan platform and in genesis of the Tien-Shan and Pamirs depends on their geodynamic and structural-tectonic conditions.

ST2/E/28-A5 Poster 1400-10

## NEOTECTONIC STRUCTURE AND SEISMICITY OF THE INTERIOR TIEN SHAN

Alexander MIKOLAICHUK and Oksana Lesik (both from the International Research Center - Geodynamic Proving Ground in Bishkek, 720049, Bishkek-49, Kyrgyzstan, email: mav@laurel.gdirc.ru)

The Tien Shan orogenic belt is bounded by major fault zones along the north and south margins as well as by the Talas-Ferghana dextral strike-slip fault, which separates the Western and Central segments of this orogen. These fault zones are delineated by seismically active zones. All historically documented destructive earthquakes are localized within these zones. The remaining portions of the Tien Shan were traditionally considered to be less active sites of neotectonic deformation and seismicity. The Suisamyrt earthquake (1992, M=7.3) in the interior of the Tien Shan demonstrated that this traditional seismotectonic concept was flawed, highlighting the need to identify the active geological structures which are responsible for the high seismicity of this region. Two east-west trending strike-slip faults and linked northwest striking reverse faults and overthrusts were mapped in the areas bordering the Suisamyrt earthquake zone. The mapped tectonic structure of this region resembles a series of rhomboidal uplifted (push-up) blocks separated by asymmetric depressions filled by Neogene and lower Pleistocene sediments. Results of detailed seismic observations conducted from 1967 to 1997 for the territory are considered. These push-up blocks are clearly shown on epicentrum field as seismic or aseismic areas. One of these blocks provides a strong match with the focal zone of the Suisamyrt earthquake. It was completely aseismic before 1992. These data suggest that other presently aseismic push-up blocks could produce strong earthquakes in the future. Paleoseismic dislocations features are often found within such tectonic units.

ST2/E/26-A5 Poster 1400-11

## CONTEMPORARY DEFORMATIONS AND SEISMICITY AT THE TIEN-SHAN

Nelly Bagmanova, Zoya Kalmetieva and ELENA MUSIENKO (all at THE INSTITUTE OF SEISMOLOGY, NAS KYRGYZ REPUBLIC, ASANBAY 52/1,720060 BISHKEK,KYRGYZSTAN, email: kis@imfiko.bishkek.su; itmc@imfiko.bishkek.su;)

Components of strain tensors determined from fault plane solutions (more than 5000 events since 1938) show general east-west extension as well south-north shortening across Tien-Shan resulted India-Eurasia plates convergence. However there are separate areas where total sub-horizontal extension or compression or south-north extension take place during the last 60 years. At the same time geodetic and GPS measurements reproduce annual modifications of velocity vectors on horizontal and vertical components against a background of present uplift of the range. Inversion of vertical tectonic motions on surface produced corresponding alternation of fault plane solutions types for small events (3.0<M<6.0) into the crust. Faulting associated with major earthquakes M>6.0 revealed predominant component of thrust on planes trending east-northeast-west-southwest. However strike-slip component on plane trending east-west prevails at the area of the Tien-Shan and Pamir convergence. Space distribution of the Tien-Shan major earthquakes M>6.0 points out that most events occur within large faults zones demarcated areas which have been undergoing contrast vertical tectonic motions since late Oligocene or rather between faults segments that differ by styles of tectonic deformation for the last 60 years. In distinction from strong earthquakes M>6.0 small events demonstrate various patterns of fault plane solutions and happen everywhere at the region.



**ST2/E/25-A5** Poster **1400-12**

**THE PECULIARITIES OF THE DENSITY SECTIONS OF THE STRONG EARTHQUAKES FOCUS ZONES IN THE NORTH TIEN-SHAN**

Oksana M. LESIK (Experimental-Methodical Expedition of Joint Institute of High Temperatures RAS, 720049, Bishkek-49, Kyrgyzstan, e-mail: olesik@gdir.ru) Kanatbek E. Abdrakhmatov (Institute of Seismology, NAS, Asanbai 52/1, 720060, Bishkek, Kyrgyzstan, e-mail: kis@imfiko.bishkek.su) Apas B. Bakirov (Institute of Geology, NAS, av. Erkindik, 30, 720481 Bishkek, Kyrgyzstan, e-mail: bakirov@geol.freenet.bishkek.su)

Recently to study the distribution of density the results from a seismic tomography study on P-wave as well as S-wave velocities were used. Using empirical formula on the relationship between velocity and density their distribution has been calculated. Zoning of different density types of crust (Lesik, 1998), the density characteristics of the "crust-mantle" transition (Sabitova, Lesik, 1997) was carried out for the Tien-Shan. In this study, we are considering the peculiarities of the density sections of the seismic focus zones of the strong earthquakes (M > 6) which had happened in the North Tien-Shan. It is an actual problem to reveal the inverse low density layers which promote both the realization of the subhorizontal displacements and the relative autonomous movement of the layers during deformation events. Joint analysis of obtained results with the neotectonics data (dynamic characteristics of the newest structures, active faults and blocks, their relationship etc) allowed to conclude about the geodynamic conditions in the focus zones of the strong earthquakes in the North Tien-Shan.

**ST2/W/22-A5** Poster **1400-13**

**RATES OF CRUSTAL DEFORMATION IN EASTERN ANATOLIA**

Gürnh BA\_CI (General Directorate of Disaster Affairs, Earthquake Research Department, Ankara, TURKEY, e-mail: seis@sismo.deprem.gov.tr) The purpose of this study is to investigate the seismicity of Eastern Anatolia.

Earthquakes located in the region between 35 N - 44 N latitude and 34 E - 46 E longitudes are investigated for this purpose. Eastern Anatolia is located between the Eurasian, African plates. It is "squeezed" and driven by the stresses exerted on it through the northward movements of the Arabian and African plates. The Earthquake epicenters covering the period 1900-1998, delineate the major fault zones and show the great activity and seismicity in Eastern Anatolia. Seismic moment values and fault plane solutions for large earthquakes which occurred in Eastern Anatolia are used to calculate the average rate of deformation in the area. The seismic moment tensor Mij is the most direct measure of deformation associated with earthquakes. The moment tensor Mij can be described when the strike, dip and rake of the fault are known in addition to the scalar value Mo. Eastern part of North Anatolian Fault Zone (NAFZ), Northeast Anatolian Fault Zone (NEAFZ), East Anatolian Fault Zone (EAFZ) and Çaldıran Fault Zone (CFZ) are selected as seismotectonic zones with high seismic activity. The results show that the deformation in the eastern part of NAFZ is taken up by extension on EW direction 28mm/yr and as compression an NS direction at a rate of 18 mm/yr. The average right-lateral displacement rate is about 33mm/yr. In the EAFZ, the EW extension at a rate of about 7.5mm/yr. The average left-lateral motion has a rate of about 3.5 mm/yr. The deformation rate in NEAFZ is 20 mm/yr with compression in the NS direction and left-lateral displacement rate is 2.5 mm/yr justifying the left-lateral strike-slip fault mechanism. NS compression rate in CFZ is 40 mm/yr. Right-lateral deformation rate in CFZ having right-lateral strike-slip fault mechanism is calculated as 15 mm/yr. As a result of NS compression in all zones, thickening rates are found as 0.16 mm/yr in eastern part of NAFZ, 0.12 mm/yr in NEAFZ, 0.40 mm/yr in EAFZ and 1.15 mm/yr in CFZ, respectively. P.S. POSTER presentation

**ST2/E/06-A5** Poster **1400-14**

**SEISMOTECTONICS OF THE TEHRAN REGION**

Mohammad Ashtari JAFARI (Institute of Geophysics, University of Tehran, P.O.Box 16765-533, Tehran 16, Iran, email: mjafaree@chamran.ut.ac.ir)

The city of Tehran (13 million of inhabitants) is located at the southern foothills of the central Alborz mountains over Quaternary alluvial sediments. This is an area of active deformation as attested by the nearby active faults and historical seismicity. A permanent seismological network has been installed since 1996 in order to monitor the regional seismic activity and several hundreds of earthquakes are located every new year. We present preliminary results regarding the local velocity structure, and discuss the seismicity and focal mechanisms in relation with tectonic information

**ST2/W/32-A5** Poster **1400-15**

**COMPOUND POISSON PROCESS APPLIED TO AFTERSHOCK SEQUENCE MODELS**

DRAGOMIR GOSPODINOV, Geoph.Inst.Bulgarian Ac.Sci., Akad.G.Bonchev str. bl.3, Sofia, Bulgaria

Some applications of marked Poisson process are presented to analyze catalog data for aftershock sequences. In most cases when studying aftershock occurrences as a stochastic process, only their behaviour in time is considered. It has always been of interest to try to enrich time models of aftershocks with information about other parameters i.e. to develop space-time models or the ones relating the occurrence times with a quantity, representing the size of an event (magnitude, intensity or energy). A compound Poisson process has been used to model cumulative energy release of events in several aftershock sequences, following the assumption of their independence. Results reveal, that there are some discrepancies between the model and the real processes, pointing that not always the assumption of independence is true. On the whole results reveal, that marking of the process is a helpful instrument, enabling us to catch some features of the seismotectonic process underlying the data.

**ST2/W/10-A5** Poster **1400-16**

**SEISMOTECTONIC RE-INTERPRETATION OF THE ZONE ALONG THE STRUMA LINEAMENT**

Savka Dineva and Dimitar Mihaylov (both at Geophysical Institute, BAS, Ac.G. Bonchev street bl.3, 1113 Sofia, Bulgaria. E-mail: dgm-sid@geophys.bas.bg), TORILD VAN ECK (Seismological Division, Royal Netherlands Meteorological Institute, PO Box 201, 3730 AE De Bilt, The Netherlands. E-mail: vaneck@kmi.nl)

The Serbo Macedonian Massif and the Rhodope Massif are separated by the NNW-SSE oriented Struma lineament. The neotectonics along this old fault zone is complicated. Presently, seismic activity suggests mainly activity on more recent SW-NE oriented faults instead of on the known N-S oriented older faults. Also the strong April 1904 earthquakes near Kresna most probably occurred along a SW-NE oriented fault zone. We reanalysed arrival time data and focal mechanisms from the region. A combined relocation and velocity inversion

of more than 20,000 phase observations have resulted in a new crustal velocity model estimate and relocation of about 1000 small events in the region. Stress tensor inversion using 180 focal mechanism solutions provide an estimate of the present day stresses within the crust in this region. Finally an effort has been made to relate known surface faulting with the relocated seismic activity and stress tensors. Our results may have significant impact on the seismic hazard estimates in the region.

**ST2/L/05-A5** Poster **1400-17**

**SEISMIC ACTIVITY IN THE WESTERN BOHEMIA**

Vladimir NEHYBKA, Zuzana Skacelova, Jan Svancara (Institute of Physics of the Earth, Masaryk University, Tvrdého 12, 602 00 Brno, Czech Republic, Email: nehybka@ipe.muni.cz, zuzka@ipe.muni.cz, svancara@ipe.muni.cz)

Institute of Physics of the Earth has been acquiring data in Western Bohemia since April 1991. The monitoring network consists of five stations. The registration is continuous with the digital recording of selected parts of the seismic signal. The purpose of the measurement is to map the active tectonic lines from their seismic manifestations. Western Bohemia is known by the swarm type seismic activity from the former times; the last strong swarm was in years 1985-86, the last swarm with the big number of the weaker earthquakes was in January 1997. We have registered thousands of earthquakes in the time period 1991-1998 and we have observed seven areas with the occurrence of the seismic activity. The main activity is in the Nový Kostel vicinity. The epicenters in this area seem to map some tectonic lines. We constructed maps of the epicentres on the locality of Western Bohemia. The data obtained from the comparison of surface manifestations and seismological results indicated connection with the Mariánské Lázně deep fault. The synthetic map shows the comparison of the seismic data with the gravimetric measurement.

**ST2/W/30-A5** Poster **1400-18**

**MASCARA EARTHQUAKE OF AUGUST 18TH 1994, MW= 5.8 (MS=6.0), IN THE CONTEXT OF THE QUIETNESS OF THE ORANIE REGION, ALGERIA**

Abdelhakim Ayadi (Dept. E.S.S./C.R.A.A.G., BP 63 Bouzaréah, 16340, Algiers, Algeria, e-mail: ess1@ist.cerist.dz) Seid Bourouis (Departement de Géophysique, C.R.A.A.G., BP 63 Bouzaréah 16340, Algiers, Algeria) Farida OUSADOU (Dept. E.S.S./C.R.A.A.G., BP 63 Bouzaréah, 16340, Algiers, Algeria, e-mail: ess3@ist.cerist.dz)

A seismic event of magnitude M=5.6 (C.R.A.A.G., Algiers) struck Mascara province (western part of Algeria) on August 18th 1994. This event is the strongest one censused in the Oranie region since that of May 21st 1889. The earthquake was located by C.R.A.A.G., using data of the ASTN network stations, at 00.30°W and 35.40°N with a depth of 10 km. From August 18th to August 23rd we have recorded many aftershocks among them we have 16 events with magnitude ranging between 3.9 and 5.1. The maximum observed intensities map (MOI) made for Algeria (Bezzeghoud et al., 1996) shows that the Mascara region is located in a X intensity's zone, which explain partially the damages caused by the 18/08/1994, M=5.6 event. The gravity and the seismotectonic maps and also the focal solution have been used to better understand the source origin of that event.

**ST2/W/17-A5** Poster **1400-19**

**SURFACE FAULTING AND ACTIVE TECTONICS IN THE UPPER ATERNO VALLEY (CENTRAL ITALY)**

BLUMETTI, A.M. (DSTN - Servizio Sismico Nazionale, Via Curtatone, 3, 00185, Roma)

Surface faulting effects are still not widespread documented in Italy. By now they were recognised in the Fucino basin (Michetti et al., 1995), in Irpinia (Pantosti & Valenzise, 1990) and in other very few areas. On the other hand many geomorphological features of the Apennine and particularly along fault generated range fronts, emphasize a very recent tectonic activity presumably connected with repeated surface faulting events. The long Italian historical record reports many seismic events of intensity >IX MCS; this gives the possibility of comparing the geological effects described in such reports with the mentioned features of the relief. The area investigated in this study is the Upper Aterno Valley, a tectonic depression bounded to the NE by two NW-SE trending normal faults which generate the Mt. Marine and M. Pettino fault escarpments, belonging to the Gran Sasso structure. These range fronts and the relative piedmont belt show many evidences of Upper Pleistocene-Holocene tectonic activity. In this area the seismic catalogue recorded some events of very high intensity: (1349 e 1461, I = X MCS; 1703 e 1762, I = IX MCS). In particular, during the January -February 1703 seismic sequence spectacular geological effects occurred (Blumetti, 1995). In this study, geological and morphological evidence of active tectonic processes will be shown, and slip rates, size, and recurrence intervals of major earthquakes discussed.

**ST2/E/56-A5** Poster **1400-20**

**FAULT DETECTION BY MIGRATION OF EARTHQUAKE EPICENTERS: CASE STUDIES FROM ALBANIA**

Betim MUCO (Seismological Institute, Tirana, Albania, e-mail: betim@sizmo.tirana.al)

It is well known that not all the active faults display themselves on the earth surface. Many of them are the so-called blind or hidden faults. In this case the accurate determination of earthquake parameters and focal mechanism solutions are the most important means to give insights on these faults where the earthquakes are buildup and release their energy. Analysing the migration of epicenters for the earthquakes, which belong to the same active tectonic fault, one can get information on the geometry and kinematic characteristics of the hidden faults. The method of fault detection by lineaments of consecutive epicenters of micro-earthquakes is of importance because it can give the information on active faults for relatively short period of data and time, without waiting the occurrence of high magnitude earthquakes. Using the above method, some segments of active faults are revealed for Albania. A verification of these lineaments with long-term observation of the seismological data and tectonic consideration it is also provided here.

**ST2/E/53-A5** Poster **1400-21**

**SEISMOTECTONIC PECULIARITIES INFLUENCE OF THE STRONG VRANCEA EARTHQUAKES ON MACROSEISMIC EFFECT ON MOLDAVIAN TERRITORY**

Anatol DRUMEA and Nila Stepanenko (both at Institute of Geophysics and Geology Moldavian Academy of Sciences), Academy str. 3, Kishinev, MD-2028, Moldova; email: drumea@geo.moldova.su

On the basis of the detailed study of four strong Vrancea earthquakes, observed in XX century, were made the conclusions about the peculiarities of source zone's tension conditions. The



study results indicated that in case of 4.03.1977 earthquake the rupture was multishock and has been spread from north-eastern border of focal zone from the depth of about 90 km to south-west direction and the depth reached 120 km. The first shock of 1990 seismic double, observed 30.05, was located nearly in the same place, but its rupture has been spread on the opposite direction, i.e. north-east. The second shock, taking place on 31.05, spread towards south-west (as 4.03.1977 earthquake). The 30.08.1986 earthquake occurred in the south-western limit of Vrancea active zone and its depth was about 140 km. The rupture spread toward north-east. As a result the intensive macroseismic action and significant Doppler's effect created by 30.08.1986 shock, the damage was twice stronger in Moldova, then in 1977 one, in spite of smaller magnitude. The hypocenter of 10.11.1940 earthquake took place in the south-west border of focal zone and rupture spread toward north-east (by analogy with 1986 earthquake). Two weeks before the main shocks of 1940 and 1986 events there were observed foreshocks. The additional analysis of the strong earthquakes of XIX century and detailed investigation of the manifestations of such events in XX century revealed the effect of mutual repelling preceding and following events and alternate focal depth. It was determined, that the most dangerous for the territory of Moldova are the seismic sources having the strike slip in azimuthal range 30-60 of degrees.

**ST2/E/48-A5** Poster **1400-22**

#### RELOCALIZATION OF SEISMIC EVENTS IN SOUTH PORTUGAL

Fernando BORGES, and M R Duque, (Departamento, de Fisica, Universidade de Evora, Rua Ramalho59, 7000, Evora, Portugal, tel 351 66 744616, email: jborges@uevora.pt). Fernando Carrilho, (Instituto Nacional de Meteorologia e Geofisica, rua C do Aeroporto, 1700, Lisboa, Portugal, tel 351 1 848 39 61, email: fernando.carrilho@meteo.pt).

The Southern of Portugal is a region of significant seismic activity, and it can be divided into two areas: Atlantic underwater adjacent zone and continental zone. The first one is characterized by a more intense instrumental and historical seismicity, which is strongly correlated to the border zone between Euroasian and African plates. The second zone is characterized by a seismicity of low or moderate magnitudes (often less than 5) and with epicenters concentrated in three areas: The Algarvian coast, the Evora region and, the Low Valley Tagus zone. Most of these events, mainly those that possess low magnitude or poor azimuthal coverage, present high localization errors. The present study is an attempt to use the data collected by the National seismic network in order to improve the epicenter and hypocenter localization. So we used different models of the crust based in refraction profiles, and we are also employed a technique of simultaneous inversion for hypocenters and velocity models.

**ST2/E/38-A5** Poster **1400-23**

#### SOURCE OF THE ML 5.2 EARTHQUAKE OF 1994 SEPTEMBER 1 IN THE BITOLA REGION, REPUBLIC OF MACEDONIA

Vera CEJKOVSKA (Seismological Observatory, P.O.Box 422, Faculty of Natural Sciences and Mathematics, Ss Cyril and Methodius University, 91000, Skopje, Republic of Macedonia, email: vcejkovska@seismobsko.pmf.ukim.edu.mk) Lazo Pekevski and Dragana Cernih (both at Seismological Observatory, Faculty of Natural Sciences and Mathematics, Ss Cyril and Methodius University, Skopje, Republic of Macedonia)

A P-nodal solution has been obtained for the earthquake occurred in the Bitola region (Republic of Macedonia) on 1 September 1994, at 16h 12min 40.40s UTC, with magnitude ML = 5.2 and without any evidence of surface rupturing. The solution has been discussed in the view of the neotectonic conditions in the Bitola region and compared with the observed macroseismic effects and aftershocks distribution. Assuming the P-nodal planes as two possible fault planes, synthetic far-field seismograms of the main shock and aftershocks have been generated and compared with the empirical far-field seismograms. In result, a choice for a fault plane has been made, suggesting a normal left-lateral fault, striking toward WNW, as a source of the main shock. That seismic source has been recognized in the neotectonic Pelister fault. The contribution of the Pelister fault to the historical and recent seismic activity in the Bitola region has been discussed.

**ST2/E/21-A5** Poster **1400-24**

#### REGIONAL CENTROID MOMENT TENSORS OF THE MEDITERRANEAN AREA AND THEIR TECTONIC IMPLICATIONS

PONDRILLI S. (Istituto Nazionale di Geofisica, Rome, Italy; e-mail: pondrix@ing750.ingrm.it) Boschi E. (Istituto Nazionale di Geofisica, Rome, Italy) Dziewonski A., Ekström G. (both at Department of Earth and Planetary Sciences, Harvard University, Cambridge, Massachusetts) Mazza S., Morelli A. and Piomallo C. (all at Istituto Nazionale di Geofisica, Rome, Italy)

The complex active tectonics associated with the convergence of the Africa and Eurasia plates, and the relative motion of a few microplates, characterise the Mediterranean region and produce its high level of seismicity, mostly of moderate energy. Earthquake focal mechanisms contribute to the determination of the current mode of crustal and lithospheric deformation. Together with geodetic data they allow the study of regional tectonic strains and strain rates. Teleseismic observations are routinely used to determine focal mechanisms of events with Mw>5.5 worldwide, but for smaller events, regional and local records are needed. We routinely calculate Regional Centroid Moment Tensors (RCMT) for seismic events of the Mediterranean area with moderate magnitudes (4.5-5.5), using intermediate period surface waves recorded by MEDNET and other observatories located at regional distance. Seismograms are collected automatically in nearly real time. Moment tensor results from more than one year of near real time RCMT computations, in addition to additional results for selected moderate earthquakes of last few years, have considerably increased the available catalog of earthquake focal mechanisms for the Mediterranean area.

**ST2/E/04-A5** Poster **1400-25**

#### THE ALGIERS EARTHQUAKE OF 4 SEPTEMBER 1996: SEISMOTECTONIC ASPECT

Said MAOUCHE, Djillali Benouar, Assia Harbi and Hadj Benhallou

On the 4th September 1996, a moderate earthquake struck the sahel of Algiers. Taking into account the type of damaged buildings, maximum intensity has been estimated at  $I_0 = VII$  (MSK) at Ain Benian in the Wilaya of Algiers. The main shock was felt with same intensity in most of the localities around Algiers. According to the Center of Research in Astronomy, Astrophysics and geophysics (CRAAG, Algeria), the local magnitude was calculated at  $M_l = 5.7$  and  $M_b = 5.5$  (IPG at Strasbourg, France). It seems that the main shock was not preceded by any kind of premonitory sign; but it was followed by a long sequence of aftershocks continuing until late November, 1996. The aftershocks distribution of this earthquake occupies a large area at west of Algiers and off-shore zone of about 20 Km long, the focal mechanism of this event exhibits an reverse fault. The earthquake was associated with landslides and rockfalls along the coast as well as about 6 Km west of Ain Benian; but no sign of liquifaction was

revealed. From seismotectonic point of view, the Mitidja basin constitutes a part of the folds and thrust geological structures that belong to the Tellien Atlas mountains. This region is characterised by a fold and thrust geological domain which displays domain which displays active reverse or thrust faulting related to the folding trending NE-SW. This active structures have "en echelon" distribution in the intermountain basins where young quaternary deposits are deformed by the compressional tectonic process.

**ST2/E/03-A5** Poster **1400-26**

#### RELOCATION OF THE BOVEC 1998 EARTHQUAKE SEQUENCE: IMPLICATION FOR ACTIVE TECTONICS IN NW SLOVENIA

Jure Bajc (1,2), Abdelkrim Aoudia (1,3), Peter SUHADOLC (1), Mladen Zivcic (2) ADDRESSES: (1) Department of Earth Sciences, University of Trieste, Via E. Weiss 1, 34127 Trieste, Italy, (2) Geophysical Survey of Slovenia, Pot na Golovec 25, 1000 Ljubljana, Slovenia, (3) The Abdus Salam International Center for Theoretical Physics, Miramir, P.O.Box 586, 34100 Trieste, Italy

On April 12th, 1998, an M=5.7 strike-slip faulting earthquake has occurred in NW Slovenia. The main shock has been followed by a series of aftershocks, the strongest one exceeding M=4. Three local networks (Slovenian national seismic network, Osservatorio Geofisico Sperimentale seismometric network, and Dipartimento di Scienze della Terra, Universita' di Trieste accelerometric network) provide a set of high-quality recordings of these events on a local scale (epicentral distances < 150 km). The main shock and related aftershocks have been relocated with a modified joint hypocentral determination method that is based on numerically calculated travel times, using a 1D velocity model, while the lateral velocity variations are accounted for by usual station-phase corrections. Improved locations are combined with digital elevation model analysis and field investigations to get a better insight into active tectonics of the area and its implications on earthquake hazard. In particular, the significance of the Idrija fault is reconsidered and its seismogenic potential is discussed.

**ST2/E/59-A5** Poster **1400-27**

#### SEISMOTECTONIC MODEL OF THE FAULTING DURING THE 1986 STRAJITZA EARTHQUAKE SEQUENCES (BULGARIA)

Stefan SHANOV (Geological Institute of Bulgarian Academy of Sciences, Acad.G.Bonchev Str., bl.24, 1113 Sofia, Bulgaria, email: shanov@geology.bas.bg)

According to the seismotectonic prognosis for Gorna Oriahovitza seismic zone (Northern Central Bulgaria), based on the evaluation of the seismotectonic potential and the fault setting, earthquakes of M=5.6-6.0 may be expected in the fault knot near the town of Strajitza. This prognosis was confirmed by the 1986 earthquakes. A comparison of the tectonic setting with all seismological data and the fault-plane solutions of nine consecutive earthquakes of magnitudes  $M_s$  more than 3.0 permits to create a model of the progressing of the process of faulting in the time and the space. The process was initiated in the fault knot and advanced to NE. The fault-plane solutions confirmed the earthquake capability of the lineaments, detected by analyzing the geological, geophysical and remote-sensing data. The principal axes P and T of the solution for the strongest earthquake with magnitude 5.6 coincide with the reconstructed regional trend of maximum and minimum tectonic stress axes. The process fades south-southwestwards and this indicates the screening role of some lineaments for the stress redistribution. The model is in a good agreement with the idea for the hierarchical system of the Earth's crust blocks. The smallest blocks are volumes of low energy accumulation and the appropriated earthquake mechanisms follow the local stress field peculiarities. The strongest earthquake mechanism reflects the regional tectonic stress field.

**ST2/W/15-A5** Poster **1400-28**

#### TECTONIC SETTING OF WEST QARUN AREA, WESTERN DESERT, BASED ON AEROMAGNETIC AND SEISMIC STUDIES

Nasser M. HASSAN ( Geophysics Dept., Fac. of Sc., Ain Shams Univ., Egypt. Email: aboashor@asunet.shams.eun.eg); Mohamed F. Mohamed., Hussein Hammouda ( Expl. Dept., GUPCO, Egypt. )

The study area is located in the North Western Desert of Egypt between Latitudes 29°24' N and 29°47' N and longitudes 29°00' E and 29°24' E. Comprehensive interpretation of aeromagnetic and seismic surveys were attempted to delineate the main tectonic trends that affected the area and its structural frame work.

A basement tectonic map was established; the Basement depth ranges between 4 and 4.6 Km. Sixty four migrated seismic lines were interpreted using the available well velocity surveys and synthetic seismograms to identify seven selected horizons from the Cretaceous to the Basement. Two way time maps, interval velocity maps, two dimensional depth conversion and seismic depth maps for all the interpreted horizons were constructed. In addition, three geoseismic cross sections were generated and the magnetic basement tectonic map was interpreted for better understanding of the structural setting of the study area.

The study revealed that the study area is characterized by complex step faults, horsts, grabens and flower structures of different trends; Syrian arc, Suez and Aqaba trends

**ST2/E/13-A5** Poster **1400-29**

#### SOURCE PARAMETRES OF SEPTEMBER 3, 1968 BARTIN (SW BLACK SEA) AND OCTOBER 5, 1977 KURSUNLU (NAF) EARTHQUAKES FROM INVERSION OF TELESEISMIC BODY-WAVEFORMS

TUNCAY TAYMAZ and Onur Tan (both at Department of Geophysics--Seismology Section, Istanbul Technical University (ITU), Maslak-80626-Istanbul, Turkey, e-mail: taymaz@sariyer.cc.itu.edu.tr)

This presentation is concerned with the active tectonics of the SW margin of Black Sea, and consists of studies of two moderate earthquakes. Seismic activity occurs at shallow depths along the Turkish margin of the Black Sea, and the relation of this activity to the North Anatolian Fault is not clear. The source mechanisms of these earthquakes are therefore crucial for understanding the present tectonics and recent evolution of the Black Sea. We used long-period P- and SH-waveforms and first motion polarities of P waves to determine the source parameters of September 3, 1968 (Bartın-NW Turkey,  $M_s = 6.6$ ) and October 5, 1977 Kursunlu (NAF,  $M_s = 5.8$ ) earthquakes. Bartın earthquake is the largest instrumentally recorded earthquake to occur, and provides first evidence for active thrust faulting along the SW-Black Sea margin. We compared the shapes and amplitudes of long period P- and SH-waveforms recorded by WWSSN stations in the distance range 30-90 degrees, for which signal amplitudes were large enough, with synthetic waveforms. The minimum misfit solutions obtained by the inversion of teleseismic body waveforms are better constrained than those based solely on first motion polarity readings and other reported solutions. The Black Sea appear to be closing under north-south compression.

**ST2/W/24-A5** Poster **1400-30**

**RELATIVE FAULT STRENGTH IN THE TJÖRNES FRACTURE ZONE, NORTH ICELAND, AS INFERRED FROM STRESS TENSOR INVERSION OF MICROEARTHQUAKE FOCAL MECHANISMS**

Björn LUND and Ragnar Slunga (Dep. of Earth Sciences, Uppsala University, Villav. 16, 752 36 Uppsala, Sweden, email: bl@geofys.uu.se)

Using micro-earthquake focal mechanisms we are studying the relative strength of faults in two major fault zones in the Tjörnes Fracture Zone (TFZ) of Northern Iceland. The TFZ is a transform zone that connects the Kolbinsey Ridge with the Icelandic Northern Rift Zone. Most of the transform motion is accommodated by the well developed, 7-9 Ma old, right-lateral, Husavik-Flatey Fault (HFF). We inverted focal mechanisms from the HFF for the local stress tensor using two different criteria to select the fault plane from the two nodal planes. First a stability constraint was used that selects the nodal plane with the highest instability;  $I = -\frac{\sigma_1 - \sigma_3}{2}$ , in the tested stress field as the plane most likely to fail. For the second inversion we used information from high accuracy relative location of the events, fitting groups of events to common faults, to pick the correct nodal plane. Although the stress states resulting from the two inversions are similar, we infer a strike-slip state of stress with the maximum principal stress being approximately horizontal and in the direction N 165 - 175 E, the instability criterion frequently selects the wrong nodal plane. The correct fault planes, which are parallel to the strike of the HFF, are thus not the most likely to fail in the estimated stress field but since they do fail we infer that the HFF is a relatively weak fault. The weakness can be explained either as a zone of low coefficient of friction in the vicinity of the fault or as an increase in pore pressure in the fault zone. We estimate the necessary decrease/increase of these parameters. Preliminary results from a similar study on the Grimsey lineament, also in the TFZ approximately 40 km to the north of HFF but considered a feature with very recent tectonic activity, show that the fault planes there are at high angles to the overall trend of the lineament. Stress tensor inversion show that these planes also are the most unstable in the stress field, i.e. there are no indications of weak faults. Combining the methods of high accuracy relative locations with stress tensor inversion using the instability criterion might thus prove a feasible way of detecting mature fault systems or oppositely areas of recent or diffuse seismicity.

**ST2/E/43-A5** Poster **1400-31**

**NEOTECTONICS IN NORWAY: NEONOR**

H. BUNGUM, E. Hicks, C. Lindholm, (NORSAR, Kjeller, Norway; HB and EH also at University of Oslo, Norway) O. Olesen, J. Dehls, L. Olsen (Norwegian Geological Survey, Trondheim, Norway) L. Bockman (Norwegian Mapping Authority, Hænefoss, Norway) F. Riis (Norwegian Petroleum Directorate, Stavanger, Norway)

The NEONOR project is a multidisciplinary research project conducted in cooperation between a number of research institutes in Norway and funded by both public institutions and private industry. The project is aimed in general at delineating and understanding recent crustal deformations, with more specific aims on driving processes, migration of crustal fluids (including hydrocarbons), and geohazard implications. A comprehensive review and analysis of earlier claims for neotectonic phenomena in Norway has been conducted, resulting in positive evidence for neotectonic faults in Masi and Kefjord and for recent crustal deformation also in Rana, Steigen and Melfjord. Other claims have been classified either as gravitationally induced faults, erosion along older zones of weakness, overburden draping of underlying bedrock features, and stress release features. The project also includes other geological and geophysical investigations, including detailed seismological studies (new arrays in northern and western Norway), geodetic measurements at several locations (GPS, triangulation, levelling) and mapping of recent offshore faulting. The 3-year (1997-99) project will publish a new 1:3,000,000 scale neotectonic map of Norway.

The detailed studies have shown that there exist two systems of postglacial faults. The Stouragurra (Masi) Fault consists of large scale (up to 10 metre) NE-SW trending reverse faults while the Nordmannvikdalen (Kefjord) Fault in Troms is one or two minor (1-2 metres offset and 2-3 km length) NW-SE trending normal faults. The faults are interpreted to represent a conjugate set, with normal faults perpendicular to the extensive system of NE-SW trending reverse faults in northern Fennoscandia. Trenching of the Stouragurra Fault indicates formation during one seismic event during or immediately after deglaciation (9,300 years BP). Dating of several large rock avalanches in the vicinity of the Nordmannvikdalen indicate a similar age for this faulting.

**ST2/E/12-A5** Poster **1400-32**

**EARTHQUAKE FOCAL MECHANISMS AND STRESS IN NORWAY**

HICKS, E.C.(1,2), H. Bungum (1,2) & C.D. Lindholm (1) 1. NORSAR, Kjeller, Norway 2. Dept. of Geology, University of Oslo, Norway

A total of just under 100 earthquake focal mechanism solutions from onshore and offshore parts of Norway have been analyzed with regard to crustal stress orientation. The study area was divided into six areas assumed to have a relatively homogeneous stress field, each containing between five and 25 focal mechanism solutions. Inversion of the focal mechanism data within each group for stress was performed, yielding a stress tensor representative for each of the six areas.

Overall, it appears that the regional stress field in Norway has a NW-SE to WNW-ESE orientation of the maximum horizontal stress direction, which can most likely be attributed to the gravitational effect of the mid-Atlantic ridge, the "ridge-push" effect. However, certain areas show a 90 degree rotation (or inversion) of the horizontal stress directions. This is particularly evident for parts of the Northern North Sea and coastal areas in Northern Norway, and is to some extent observable in the Oslo Rift area. This indicates significant influences from regional and/or local stress sources. These same areas also have elevated levels of seismic activity compared to the regional activity.

**ST2/E/46-A5** Poster **1400-33**

**ON THE METHOD OF SEISMIC REGIONALIZATION OF THE FENNOSCANDIAN SHIELD**

BELA ASSINOVSKAYA (Geodynamical Laboratory, CAO RAS, Bolshoi pr.50G, V.O., 199034, Saint-Petersburg, Russia, email: bela@ba2248.spb.edu)

The seismic regionalization methods are probably the least developed and formalized among the all seismic hazard assessment stages. Due to this fact certain regions especially with weak seismic activity areas such as the Fennoscandian Shield seem groundlessly large and generalized. Whereas the maximum earthquake magnitude (Mmax) is low as for the Fennoscandian Shield the simple cell square for assessment of Mmax should not exceed the area 10x10 km. Development of Mmax determination method described by us earlier is suggested. The method is based on the geological information and the most possible full data on the rock mechanical properties of the crust simple cell. This work uses relationships between accumulated energy and calculated strike slip rock strength at the depth of

earthquake sources taking into account pressure and temperature. In the Fennoscandian Shield conditions Early Proterozoic granite batholith intrusions formed in compression environment have the most seismotectonic potential that becomes less as geometry intrusion changing. Gneissic rocks with the same quartz contents as in granite, have lesser strike slip strength. The method was used to estimate Mmax in the region of seismic profile Kostamuksha -Pechenga on the north-east of the Fennoscandian Shield.

**ST2/W/31-A5** Poster **1400-34**

**THE MARCH 25, 1998 BALLENY ISLAND EARTHQUAKE: GREAT EARTHQUAKE CAUSED BY POSTGLACIAL REBOUND**

Seiji TSUBOI (Department of Geoscience, National Defense Academy, Yokosuka 239-8686 Japan, e-mail: tsuboi@cc.nda.ac.jp) Masayuki Kikuchi and Yoshiko Yamanaka (both at Earthquake Research Institute, University of Tokyo, Tokyo 113 Japan, e-mail: kikuchi@eri.u-tokyo.ac.jp) Masaki Kana (National Institute of Polar Research, Tokyo Japan, e-mail: kanao@nipr.ac.jp)

A large Mw=8.1 earthquake occurred off southeast coast of Antarctica near the Balleny Island region on March 25, 1998. We inverted teleseismic body-wave records to determine the rupture pattern using an iterative deconvolution method. The source parameters obtained are: the centroid depth=31 km; (strike, dip, rake)=(288, 87, -2); the seismic moment M0=2.1x10<sup>21</sup> Nm (Mw=8.1); the length L and the width W of the fault: L=140 km and W=40 km; the average slip D=5.4 m. This earthquake occurred in the mid-plate but there has been no reports of such large earthquakes in this region ever before. Furthermore, the source mechanism cannot be related to the plate motion inferred from the nearby transform faults. Therefore this earthquake should not be considered as a usual tectonic event. Here we show that the compressional axis of our source mechanism coincides with the horizontal crustal motion predicted by the Earth's response to present-day and past ice mass changes in Antarctica. Our result suggests that the 1998 Antarctica earthquake is caused by the postglacial rebound in the Antarctica.

**ST2/W/37-A5** Poster **1400-35**

**SEISMOTECTONICS OF THE SOUTH SANDWICH ISLAND ARC**

ANYA M. READING, University of Edinburgh, Dept. of Geology and Geophysics, Grant Institute, West Mains Road, Edinburgh, EH9 3JW, UK

The South Sandwich Plate lies in the South Atlantic bounded to the west by a spreading ridge and the Scotia Plate. To the east, the South American Plate is subducted, forming the South Sandwich Arc; a simple but relatively unstudied area of active intra-oceanic tectonics.

As well as data from the global seismic network, this work uses local earthquake records from broad-band stations on three of the South Sandwich Islands and records from ocean-bottom seismometers deployed across the arc. These were recorded as part on a multi-disciplinary geological and geophysical campaign undertaken by British Antarctic Survey in early 1997. Seismicity results are obtained from OBS instruments below the threshold of the global network and together with structural information from travel-times and dispersion modelling are interpreted in terms of spreading ridge and slab roll-back dynamics and likely mantle flow beneath the arc.

**ST6** Monday 19 – Tuesday 20 July

**PHYSICS AND CHEMISTRY OF EARTH MATERIALS (LINKED TO JSS02)**

Location: Medical School EG12 LT4  
Location of Posters: Arthur Thompson Hall

Monday 19 July AM

**ST6/P/01-A1** Poster **0830-01**

**VELOCITIES OF SEISMIC WAVES IN ANDESITE ROCKS OF NORTH-WEST IRAN**

Mino KOSARIAN, Saeed Amiri, and Majid Nabi-Bidhendi (all at the Institute of Geophysics, Tehran University, P.O. Box 14155-6466, Tehran, Iran, email: minoo@iman.ut.ac.ir)

In this paper based on the results obtained from laboratory measurements of compressional and shear-wave velocities on 15 different andesite rock samples in both dry and saturated states a few relationships have been found between physical properties of the rocks. A pair of piezoelectric transducers with the central frequency of 63 kHz is employed to measure P-wave velocities. Similar transducers but with the central frequency of 33 kHz have been used for S-wave velocity measurements. The cubic samples are prepared in various sizes between 45 mm and 55 mm. Dry samples are made by placing them in a 70 C oven for 24 hours. The velocity measurements are made in both dry and saturated states under low axial stress. Our data show excellent linear relationships between P and S-wave velocity for both dry and saturated states as follows:

$$\begin{aligned} V_p &= 1.45 V_s + 0.65 & (\text{dry}) & R = 0.93 \\ V_p &= 1.61 V_s + 0.38 & (\text{sat.}) & R = 0.97 \end{aligned}$$

Where velocities are in km/s and R is the correlation coefficient. Also the data demonstrate excellent linear relationships between bulk modulus normalised by density and Vp as follows:

$$\begin{aligned} K/p &= 2.56 V_p + 3.90 & (\text{dry}) & R = 0.87 \\ K/p &= 2.53 V_p + 3.85 & (\text{sat.}) & R = 0.90 \end{aligned}$$

Where density,  $\rho$ , is in g/cm<sup>3</sup> and bulk modulus, K, is in kbar and Vp is in km/s.

**ST6/P/02-A2** Poster **0830-02**

**COMPOSITE LOGS INTERPRETATION OF SOME BOREHOLES IN CENTRAL IRAN AND RADIOACTIVE MINERAL EXPLORATION**

FYEGANI (Atomic Energy Organisation of Iran, P O Box 14155-1339, Tehran, Iran) B.A. Feizabadi and M. Nabi-Bidhendi (both at Institute of Geophysics, Tehran University, P O Box 14155-6466, Tehran, Iran, email: mnbhendi@chamran.ut.ac.ir)

At the end of ground survey for testing acquired data, it is customary to drill some boreholes in estimated targets. Due to economical condition, it is obvious to get the most information from the drilled boreholes in order to have a clear and meaningful profile of intersected layers. It could then be possible to locate the coordinates of the next boreholes precisely.

In this article the composite logs of six boreholes are interpreted. The composite logs consist of electric, IP, SP, density, porosity, natural gamma-ray, spectral gamma-ray, magnetic susceptibility, deviation, caliper and temperature logs. The main aim of this survey is uranium and radioactive Minerals exploration. In addition to geological column which is obtained

directly from the cored samples, the geophysical column is drawn by correlating the different logs. It is observed that the latter method exhibits more accurate and detailed information. Based on geophysical column the radioactive zones and uranium mineralization layers are identified and then by borehole to borehole correlation the uranium orebody is outlined. Although an excellent coincidence of these two columns is observed, the fine discrimination of the layers by geophysical column is more significant.

**ST6/P/03-A2** Poster **0830-03**

**SPATIAL-TEMPORAL FEATURES OF CHANGES IN THE CONDITION OF THE ROCK MASSIF IN THE CONTOUR ZONE**

V.N. TATARINOV (Geophysical Center, Russian Academy of Sciences, Molodezhnaya, 3, Moscow, 117296, Russia), T.A. Gupalo, N.I. Seleznev (VNIIPromtehnology, Ministry of Nuclear Power, Kashirskoe shosse, 36, Moscow, Russia)

The processes resulting in restructuring of local stress fields and structural discontinuity of rocks around mine openings and producing force effect on rock massif composed of structural blocks of different hierarchy have been studied. Result are presented of the study of the effect of explosion mining of ores on rock distribution in dynamic representation. Force effects of explosion mining as well as natural tectonic processes are manifested as stepped in spatial and cyclic in time dislocation of zones of relative packing and failing towards the worked out room. The developed methods of geophysical observation of the effect of space-time changes on stress fields in the contour zone of a blocks rocks during explosion mining of ores can be applied for solution of a wide range of practical problems in the mining industry.

The established time regularities in geophysical fields and in the deformation of rock massif, parameters like the velocity of dislocation of failure zones, effective radius of their development in the massif, the distance to the packing zone shield, especially when predicting rock bump strength, and geometrical parameters of sites where the changes of geophysical fields characterizing the condition of separate structural blocks of the massif occur can serve as prognostic criteria for dynamic destruction of rocks. New data have been obtained on the deformation in the contour zone of large-diameter chambers in which hazardous techniques are used under prolonged effects of high temperature and rock pressure.

**ST6/W/02-A1** Poster **0830-04**

**STRESSES IN A SUBDUCTING SLAB IN THE PRESENCE OF A METASTABLE OLIVINE**

WEDGE J.P. DEVAUX, L. FLEITOUT (Laboratoire de Geologie, 24 Rue Lhomond, 75005 Paris, email: devaux@jadeite.ens.fr), G. Schubert (ESS, UCLA, Los Angeles CA 90095-1567), C. Anderson (LANL, Los Alamos NM 87545)

The transformation of olivine to spinel in a subducting slab gives rise to thermal strain, transformation strain and buoyancy stress inside this slab. We use a finite element method to solve the mechanical equation and we follow the evolution of the stresses inside the slab during its descent. We use a viscoelastic rheology with a viscosity that depends on pressure, temperature and grain size. The stresses due to buoyancy are found to be negligible compared to the internal stresses due to the phase transformation. A zone of very high differential stress coincides with the olivine spinel phase boundary. This zone is associated with large down-dip compressive stresses inside the metastable olivine wedge, and large down dip tensile stresses in the spinel region, along the wedge. If we assume that the failure criterion can be related to the differential stress, our model is in agreement with the patterns of deep seismicity. However, patterns of deep seismicity cannot reflect buoyancy stress, which are negligible compared to the internal stresses.

**ST6/W/03-A1** Poster **0830-05**

**FRACTAL MICROSTRUCTURE OF ROCKS OF KAINUU SCHISTS BELT (FINLAND). RESULTS FROM INTERPRETATION OF SVEKA AND EL DEEP SEISMIC SOUNDING PROFILES**

Elena KOZLOVSKAYA (Department of Geophysics, University of Oulu, POB 3000, FIN-90401 Oulu, Finland, e-mail: elena@babel.oulu.fi), Jukka Yliniemi (Sodankylä Geophysical Observatory, Oulu Unit, POB 3000, FIN-90401 Oulu, Finland, e-mail: jyl@babel.oulu.fi)

The wide range of velocities associated with Earth materials makes it difficult to relate seismic data to specific lithologies. A review of geological parameters show that depth, lithology and age are not as specifically related to velocities as are the physical parameters of density, elastic constants, and porosity. The former, in turn, are strongly influenced by the rock microstructure (pore shapes, pore size distribution, grain-to-grain contacts etc.). Recent theoretical investigations of rock physical properties have shown that the real rocks can be adequately described by structural fractal models. The assumption of a fractal geometry is in accordance with the experimental data about real rock structure. The fractal conception gives possibility to connect rock microstructure with rock elastic properties and with macroproperties like seismic P- and S-wave velocities and seismic anisotropy. In our investigation we make an effort to use the fractal model for elastic properties of porous rock and to estimate the microstructure of rocks of Kainuu Schists belt from experimental seismic data of SVEKA and EL deep seismic sounding profiles in Finland. The results of modeling are proposed for discussion.

**ST6/W/04-A1** Poster **0830-06**

**TITANATE PEROVSKITES AT HIGH TEMPERATURE: THERMOELASTICITY, SHEAR MODULUS DISPERSION, ATTENUATION AND MICRO-CREEP**

Sharon Webb, IAN JACKSON and John Fitz Gerald (Research School of Earth Sciences, Australian National University, Canberra ACT, Australia)

Ultrasonic measurements of the bulk and shear moduli for polycrystalline specimens of Ca- and Sr-titanate perovskites to ~500°C provide additional insight into the high-temperature thermoelastic behaviour of oxide (and by analogy silicate) perovskites. Torsional micro-creep and seismic frequency forced oscillation tests demonstrate strong viscoelastic relaxation at high temperature in each of these fine-grained materials, resulting in large reductions in shear modulus G (by >70%) and enhancement of its temperature sensitivity as much as 10-fold relative to ultrasonic values. The temperature of onset of this frequency dependent behaviour is grain-size dependent. The frequency-dependent and time-dependent data have been described in terms of the elastic, anelastic and viscous components of deformation using the Andrade model. The relatively smooth variation with temperature of G and 1/Q for Ca-titanate suggests that its high temperature phase transitions have little effect on the viscoelastic behaviour.

In the absence of melt films, twinning and dislocations, the long-timescale viscoelastic deformation of Sr-titanate is attributed to grain-boundary sliding accommodated by lattice or grain-boundary diffusion, controlled by the slowest diffusing species, which is expected to be either Sr or Ti. The low viscosities determined for the Ca-titanate samples, together with the

low values (with respect to the extrapolated ultrasonic data) of shear modulus associated with Andrade model fits to the data suggest that its long-timescale viscoelastic deformation may reflect relatively faster grain-boundary diffusion of the slowest moving species through the thin (<2 nm) melt films and larger impurity segregations present in these samples. Implications for the seismic properties of the lower mantle will be discussed.

**ST6/W/05-A1** Poster **0830-07**

**PROCEDURE AND APPARATUS TO MEASURE ELASTIC, DEFORMATIONAL AND TEXTURAL-STRUCTURAL CHARACTERISTICS OF ROCKS AND MINERALS UNDER HIGH THERMODYNAMIC CONDITIONS IN THE NEUTRON BEAM**

Efimova G.A., Kireenkova S.M., and SOBOLEV, G.A. (United Institute of Physics of the Earth, Russian Academy of Sciences, Moscow, 123810, B.Gruzinskaya 10, email: sobolev@uipe-ras.scgis.ru) Ivankina T.I., Nikitin A.N. (Joint Institute of Nuclear Research, Dubna, Moscow Region, 141980)

Unique procedure and apparatus are described that are applied to measure a set of physical parameters of rocks and minerals under high temperatures in the neutron beam. The freshness of this procedure is that it allows us with the same material to conduct research on physical properties of rocks and minerals under high thermodynamic parameters in combination with the studies of rocks and minerals texture and structure by neutron diffraction. As distinct from traditional methods this procedure enables continuous recording of all investigated parameters. The cylindrical samples from natural marble consisting only of calcite were chosen for first experiments. The samples were 20 mm long with diameter 16mm. A experimental run comprised loading up to 20 MPa, step by step temperature increase, recordings of strain, ultrasonic wave velocities and diffraction patterns. Comparison of preliminary measured diffraction spectra of chamber without sample and sample showed that diffraction peaks of material used for chamber did not overlap the main peaks of calcite. The changes of diffraction pole figures were obtained as result of loading and heating of the samples.

**ST6/W/06-A1** Poster **0830-08**

**SHOCK INDUCED MELTING OF MGSI<sub>3</sub> PEROVSKITE AT 100 GPa AND -5000 K: A NEW CONSTRAINT ON LOWER MANTLE TEMPERATURE**

J. A. Akins, T.J. Ahrens (both at Lindhurst Laboratory of Experimental Geophysics, Seismo Lab, Caltech, Pasadena, CA 91125, USA, Email: jakins@gps.caltech.edu), G. Jyoti (present address: High Pressure Physics Division, Bhaba Atomic Research Centre, Trombay, Mumbai 400085, INDIA)

New equation of state (EOS) and shock temperature data have been obtained, using a 25mm light gas gun, for MgSiO<sub>3</sub> (glass) shocked into the shock pressure range > 80 GPa where densities and current knowledge of the MgSiO<sub>3</sub> phase diagram indicate that the perovskite structure is stable. Initial experiments have sampled the region in which the shock temperature decreases from 5650 +/- 553K at 97GPa to 5050 +/- 465K at 107 GPa. This observation is qualitatively similar to experiments on alkali halides, SiO<sub>2</sub> shocked into the stishovite range, and our recent experiments on Mg<sub>2</sub>SiO<sub>4</sub> shocked into the MgSiO<sub>3</sub> (perovskite) + MgO (periclase) range. This phenomenon results from superheating of the solid, over a pressure range of 5 - 15 GPa, followed by melting. The comparison of V(partial P/partial E), at constant V, between the glass data and previous ceramic data indicates a Grüneisen parameter (gamma) of 1.18 +/- 0.30 at a density of 4.67 g/cm<sup>3</sup>, corresponding to approximately 45GPa and 1100km depth in the Earth, based on PREM. We expect these data, along with future data, to better constrain the adiabatic temperature profile of the lower mantle as well as provide a long sought independent determination of the melting curve of MgSiO<sub>3</sub>. Previous static melting data differ by approximately 2000K when extrapolated to the CMB. As present data suggest melting of MgSiO<sub>3</sub> perovskite occurs at ~5000 K at 100 GPa it appears highly unlikely that the ULVZ, at the base of the mantle, is due to MgSiO<sub>3</sub> perovskite melt. The slope of our preliminary melting curve is similar to (Brown and Shankland, 1981) mantle adiabat with a homologous temperature, T/T<sub>m</sub>, of ~ 0.46.

**ST6/W/07-A1** Poster **0830-09**

**IS HYDROUS PHASE MORE COMPRESSIBLE?**

Lin-gun LIU (Institute of Earth Sciences, Academia Sinica, Taipei, Taiwan, R.O.C. 11529, email: lliu@earth.sinica.edu.tw)

Raman study of both anhydrous and hydrous alpha, beta and gamma phases of Mg<sub>2</sub>SiO<sub>4</sub> provides us with the unique opportunity to compare the compressional behavior between anhydrous and hydrous phases. It is generally believed that hydrous phases are more compressible than anhydrous phases. The data combining both compression and elasticity studies of the above mentioned materials showed that the hydrous phases are more compressible than the anhydrous phases. On the other hand, the data of pressure dependence of Raman frequency of these materials do not substantiate the convention that hydrous phase should be more compressible. Instead, the latter data seem to suggest that hydrous phases are slightly less compressible than anhydrous phases, if the pressure variation of vibrational frequencies depends solely on volume.

**ST6/W/08-A1** Poster **0830-10**

**THE INFLUENCE OF METAMORPHISM PROCESSES ON ROCKS PHYSICAL PROPERTIES ON EXAMPLE OF COLA SUPER DEEP BOREHOLE**

G.A.Efimova (United Institute of physics of the Earth, Russian Academy of Sciences, 123810 Moscow, B.Gruzinskaya, 10, e-mail: slavina@uipe-ras.scgis.ru)

The practical works with the samples from super deep boreholes have shown that the elastic waves velocities of rocks determine by "mineral skeleton" of rocks. The measuring of the longitudinal waves velocities were conducted by ultrasonic method in the high-pressure cell known as cylinder-piston up to 1.5 GPa. It was established that elastic waves velocities of rocks of Cola super deep borehole from different facieses of metamorphism depend from second processes taking place in rocks under action of metamorphism. The rocks having the same compositions have the same meanings of physical characteristics.

**ST6/W/11-A1** Poster **0830-11**

**THE MICROSCOPIC ORIGIN OF THERMAL CRACKING IN ROCKS STUDIED BY TIME-OF-FLIGHT NEUTRON DIFFRACTION**

P.G. MEREDITH (1), K.S. Knight (2), S.A. Boon (1) and I.G. Wood (1), (1) Department of Geological Sciences, University College London, London WC1E 6BT, UK, (2) ISIS Facility, Rutherford Appleton Laboratory, Didcot, Oxfordshire, UK. (E-mail: p.meredith@ucl.ac.uk)

Recent research focused on mid-ocean-ridge processes and geothermal energy extraction



has highlighted the importance of thermal cracking as a rock deformation mechanism in regions of high geothermal gradient and heat flow. In particular, thermal cracking can lead to significant reductions in bulk strength, and to dramatic increases in fluid transport properties. We report results from an experimental programme that made use of time-of-flight neutron diffraction to study the microscopic origin of thermal cracking in a pure quartzite. The High Resolution Powder Diffractometer (HRPD) at the Rutherford Appleton Laboratory was used to measure the thermal strain in (i) quartzite cores, and (ii) finely ground quartzite powder, as a function of temperature over the interval 293K to 573K. It was observed that the powder expanded more than the cores over the same temperature interval. The difference in thermal strain between rock powder and solid rock is due to the internal self-constraint experienced by the solid rock, and generates a differential thermal stress in the rock cores. The onset of thermal cracking was monitored by continuous recording of acoustic emission (microseismic) output, and was seen to commence at some critical value of this differential thermal stress. Calculation of the critical stress for the onset of thermal cracking showed that it corresponded closely to the bulk tensile strength of the quartzite.

**ST6/W/12-A1** Poster **0830-12**

**PHYSICAL PROPERTIES AND COMPOSITION OF CARBONATE ROCKS: CASE STUDY FROM ESTONIAN LOWER PALAEOZOIC SEDIMENTARY BASIN**

Alla SHOGENOVA (Institute of Geology at Tallinn Technical University, 7 Estonia Avenue, EE10143, Tallin, Estonia, Email: alla@gi.ee.

Petrophysical properties and chemical composition of some 600 samples of Ordovician and Silurian rocks of different genesis were studied and compared using regression and factor analysis. Lower, Middle, Upper Ordovician and Silurian data sets were analyzed and compared. The most important factors influencing the physical properties of carbonate rocks were revealed. These are clay content, dolomitization and porosity. Increase in the clay content causes the increase in primary porosity decrease in density, P-wave velocity, apparent resistivity and increase in magnetic susceptibility in most of Ordovician and Silurian limestones. Dolomitization of rocks causes increase in secondary porosity, grain density and magnetic susceptibility of Lower and Middle Ordovician rocks. The influence of widespread dolomitization and that associated with fracture zone were studied and compared for different groups of properties. The properties of different age limestones are controlled most of all by clay content. The properties of different age and genesis dolomites vary more and depend on the composition of dolomitization fluids and on the secondary porosity caused by leaching of the rocks during dolomitization. The differences between properties of limestones and dolomites are the most contrast in the Middle and Lower Ordovician rocks and they are the least contrast in the Upper Ordovician and Silurian sequences. But there were found the most porous dolomites. Their porosity is close to that in the Lower and Middle Ordovician fracture zones. The most contrast chemical parameters in the different rock groups were found to be iron and manganese. They increase in the most studied dolomite types. The physical properties of different genesis limestones and dolomites may be used to distinguish different rock types and their genesis.

**ST6/W/14-A1** Poster **0830-13**

**THE ELASTIC AND DEFORMATIONAL CHARACTERISTICS OF SALTS AND THEIR CHANGES DURING PROCESS OF PHASE TRANSITIONS AT HIGH PRESSURES.**

S.M. KIREENKOVA (Institute of Physics of the Earth, Russian Academy of Sciences, B.Gruzinskaya 10, 123810 Moscow, Russia, Email: kireenk@ipmet.ru)

The experimental study of processes of earthquake preparation of geophysical methods has allowed to establish that the properties of geomaterials within area of a future source undergo significant changes. From this point of view the processes of solid phase transition occurring at high pressures and temperatures and accompanied by anomalous changes of the physical properties of rocks and minerals are of prime interest. The behavior of salts have been demonstrated with ammonium iodide that is the rocks analog, of a NaCl structure. The elastic waves velocities and density of the pressing ammonium iodide were determined by the impulse ultrasonic method in the process of pressing inside a device of the cylinder-piston type at pressures up to 700 MPa. The jump changes of the elastic waves velocities were observed during phase transition under pressure. The change of values of longitudinal waves velocities during transition amounted 0.25 km/s and in shear waves velocities to 0.16 km/s and the change in the decrement volume amounted, on the average, to 30%. The deformational characteristics samples were determined at different values of constant hydrostatic pressure and additional axial compression with a constant rate 0.000018 mm/s. A decrease of strength characteristics of ammonium iodide in the process of phase transition takes place during its deformation at the constant hydrostatic pressure of 12.5 MPa. Variations of the physical parameters of geomaterials, in the main of deformational characteristics during phase transitions at high pressure, serves as a criterion of quantitative estimation of the conditions for the preparation of an earthquake.

**ST6/E/03-A1** Poster **0830-14**

**THERMAL CONDUCTIVITY OF ROCKS IN THE AREA OF THE KOLA SUPERDEEP WELL (SG-3)**

Yuri POPOV and Raissa Romushkevich (Moscow State Geological Prospecting Academy, Miklukho-Maklai str., 39-1-191, Moscow 117485, Russia, email: Yupopov@mgga-sec.msk.ru) Christoph Clauser (Joint Geoscientific Research Institute (GGA), Stilleweg 2, D-30655 Hannover, Germany; email: c.clauser@gga-hannover.de)

22 boreholes with a depth of 250-2000 m surrounding the Kola superdeep borehole (SG-3) were chosen to study geothermal parameters of this strata. Rocks intersected by these boreholes include diabases, tuffs, sandstones, phyllites, gabbro, serpentinites, chlorite-talk and chlorite-amphibolite shists, gneisses, amphibolites. Thermal conductivity was measured with the optical scanning device on 1375 cores. The principal components of the tensor of thermal conductivity was found to be in a range of 1.05-7.11 W/(m<sup>2</sup>K). Anisotropy is often significant and reaches factor of two. In most cases thermal conductivity varies within a range of 2-5 W/(m<sup>2</sup>K) along the boreholes. Local variations and trends along the boreholes are significant but not straightforward to interpret for most of the boreholes. For gneisses and amphibolites of the Archean complex we found the thermal conductivity of our samples to be larger by about 20 % compared to previous measurements on samples from the SG-3 borehole below 6800 m. This may be due to the decompression and mechanical wear of the cores from the SG-3 borehole experienced. We gratefully acknowledge financial support for this project by the European INTAS organization (project INTAS-93-273-ext) and by the German Science Foundation (DFG) under grant CL 121/4-1.2.

**ST6/E/05-A1** Poster **0830-15**

**COMPOSITIONS IN YOUNG OROGENIC CONTINENTAL CRUST BENEATH TAIWAN**

DER-RU SONG and Kuo-Fong Ma (both at Institute of Geophysics, National Central University Chung-Li, Taiwan, ROC, e-mail: fong@sal.gep.ncu.edu.tw) Lin-Gun Liu (Institute of Earth Sciences, Academia Sinica, Taiwan, ROC)

Recently, three dimensional seismic velocity structure beneath Taiwan had been fully investigated. The results show obvious velocity contrast between the foreland and the hinterland of the Taiwan Orogenic belt at various depths. On the basis of the geophysical observation and comparison, we obtained the bulk crustal compositions under the young orogenic belt of Taiwan by comparing the tomographic inverted P-wave velocities with the measured P-wave velocities of relevant metamorphic rocks at the pressure and temperature conditions corresponding to the crust. The crustal composition derived in the present study is correlated to general lithologic categories rather than a specific rock type. The results were also further constrained by geological and geophysical data available in the area and the Poisson's ratio derived from reliable S-wave. It is concluded that, generally, the foreland of Taiwan is composed of a mafic bulk crust. The distribution of the crustal SiO<sub>2</sub> is comparable with that of global observation for Mesozoic-Cenozoic Contractions and rift margins. The crust having a sialic bulk composition in hinterland is the main character in responds to the lower crustal velocity.

**ST6/E/06-A1** Poster **0830-16**

**TEMPERATURE DEPENDENCY OF STRENGTH OF GRANITE AT HIGH CONFINING PRESSURE AND MICROMECHANICS**

Mitsuhiro SHIMADA (Research Center for Earthquake Prediction, Disaster Prevention Research Institute, Kyoto University, Uji, Kyoto 611-0011, Japan, email: shimada@rcpe.dpri.kyoto-u.ac.jp) Junlai Liu (Department of Earth Sciences, Changchun University of Science and Technology, Changchun 130026, P. R. China, email: jliu@public.cc.jl.cn)

Triaxial testing on a dry granite (Man-nari granite) was conducted at a confining pressure of 1500 MPa and temperatures to 600\_°C (with an averaged strain rate of approximately 2 x 10<sup>-6</sup> s<sup>-1</sup>). All the experiments fall in the high-pressure type fracture regime, which occurs when the compressive strength equals the frictional strength. The experiments were conducted with small temperature intervals at a fixed confining pressure to ascertain an unusual behavior of strength in our previous experiments temperature with a trend. The trend is similar to that for Westerly granite obtained previously. The strength values between 200\_°C (Band 280\_°C, however, deviate from the trend and very low with a minimum at around 250\_°C. The rock exhibited macroscopically brittle fracture behavior accompanied by occurrence of AE events and stress drop up to 530\_°C. However, it deformed microscopically with several factors for crystal plasticity with increasing temperature. Micromechanical studies suggest that the unusual behavior of strength is caused by switching the dominating factors from the activation of crack groups to the inhibition of them and the dominance of crystal plasticity. If we estimate the lithospheric strength using these results and our previous assumption that the high-pressure type fracture occurs in the crust considering the size effect of rock strength, a low-strength zone between 8 and 12 km depth is suggested. This suggestion could provide an alternative explanation for the brittle-ductile hypothesis for seismogenic zones in the crust: earthquakes could occur or nucleate more easily where the strength is low. that the strength of the granite at 250\_°C (B appears to decrease with increasing confining pressure or to have a minimum value in the high-pressure type regime whereas those at 100\_°C (Band 300\_°C increase with increasing confining pressure. The strength of the granite decreases with increasing

**ST6/E/08-A1** Poster **0830-17**

**MONITORING OF GEOMATERIAL STRESS STATE TIME DEPENDENCIES ON A BASIS OF THE SURFACE INFRA-RED EMISSION MEASUREMENTS**

Vladimir I. SHEININ, Edward A. Motovilov and Alexander A. Morozov A.A. (Gersevanov Research Institute of Basements and Underground Structures, 2-nd Institutskaya str.,6, 109428, Moscow, Russia, E-mail: geo-mech@rinet.ru)

A new technique has been elaborated to detect changes of the stress state in geomaterials and to describe the stress variations quantitatively by the processing of surface infra-red (IR) flux power records. The method is based on the known thermodynamical effects. Changes of the stress tensor first invariant at a point of an elastic medium being deformed "adiabatically" produce temperature variations proportional to the invariant variations with the factor depending on physical properties of the medium. These variations generate the IR-flux power changes which are practically proportional to the stress variations as well. The method efficiency is demonstrated in laboratory geomechanical experiments for samples of rock under temporarily changing uniaxial compression. It has been shown that one can treat conditions as "quasiadiabatic" if the stress state changes quickly enough. The features of IR-signal components (i.e. carrying signal, noise and summand defined by heat change) have been considered. Original devices and facilities allow to read and then to process the radiation flux changes with amplification factor up to ten million. The multichannel analogue-to-digital converter was used so that one can get synchronous radiometric and "key" tensiometric data records. The experimental series with the impulse and oscillation loading of samples shows a satisfactory coincidence of the IR-radiometric and tensiometric descriptions of the stress state "time histories". Possible schemes, involving IR-radiometer, are considered for monitoring variations of instrumentation. The work is supported by the Russian Foundation for Basic Researches.

**ST6/JSS02/W/19-A1** Poster **0830-18**

**SIMULTANEOUS ULTRASONIC MEASUREMENTS OF X-RAY DIFFRACTION AT HIGH PRESSURE AND HIGH TEMPERATURE FOR MAJORITE GARNET**

Gabriel GWANMESIA, (Department of Physics & Pre-Engineering, Delaware State University, Dover, DE 19901, email: ggwanmesia@dsc.edu), Baosheng Li and Ganlin Chen (both at ChiPR and Mineral Physics Institute, SUNY at Stony Brook, Stony Brook, NY 11794-2100), Jun Liu and Robert C. Liebermann (both at ChiPR and Department of Geosciences, SUNY at Stony Brook, Stony Brook, NY 11794-2100)

Precise determination of the elastic properties of the mantle minerals at pressure and temperature conditions of the Earth's interior is very important for understanding the composition of the mantle. In our laboratory, we have developed techniques to measure elasticity of mantle minerals up to 8 GPa and 1500K using simultaneous ultrasonic velocity measurements and X-ray diffraction studies in a DIA-type, cubic anvil high pressure apparatus (SAM85) installed at beamline X17B at NLSL in Brookhaven National Laboratory. Ultrasonic measurement is implemented by mounting an acoustic transducer at the back of the WC anvil and including a buffer rod inside the cubic boron epoxy pressure medium. X-ray diffraction spectra from both the sample and NaCl were recorded at elevated pressures and temperatures from which the unit cell volumes of the sample and cell pressures were retrieved.

Using this technique, compressional ( $V_p$ ) and shear ( $V_s$ ) wave velocities measurements and equation of state (P-V-T) study for MgSiO<sub>3</sub>-majorite garnet have been conducted on a polycrystalline specimen previously hot-pressed at 18 GPa and 2100 K; the bulk density is 99.7% of the single crystal X-ray value. Compressional and shear wave velocities at ambient P and T agree with single crystal data within 1%. Complete P-V-T and  $V_p$  and  $V_s$  data have been collected up to 8 GPa and 1000 K along several decompression/heating/cooling cycles. Analyses from present P-V-T and acoustic measurements provide independent determination of elastic moduli and their pressure and temperature derivatives for this phase which is believed to be a major component of the transition of the Earth's mantle.

ST6/L/02-A1

Poster

0830-19

### SOME NEGLECTED THERMOPHYSICAL PROPERTIES OF PLATE MATERIALS AND THEIR WIDER SIGNIFICANCE

Miles OSMASTON

Phase changes. Geophysical treatments of thermal subsidence, doming or uplift usually refer solely to the thermal expansivity of silicate rock. If it is found that not enough heat can have been conducted in, it is common to invoke advective introduction of the heat (e.g. delamination, plumes). Similarly, in the case of ocean floor subsidence, measured heat flow out to 50-60Ma is less than half what the observed subsidence would require with pure thermal contraction, so hydrothermal extraction of heat has been invoked. Solid-state phase changes, e.g. spinel-to-garnet peridotite, are, however, an inescapable consequence of cooling or heating the mantle and are enormously (>10x) more efficient at converting joules to volume change. Low velocity zone (LVZ). It now seems that up to ~3% interstitial melt can be held without migration, so volcanism should not be regarded as a foregone conclusion. Water partitions strongly into the interstitial melt so the water-weakening of the mineral fabric is removed, possibly making the LVZ more resistant to creep than if no melt were present (Karato 1986). This contradicts the perception that the LVZ is, by definition, a mobile zone. The thermal conductivity of silicate melt is at least 10x less than that of upper mantle minerals, lowering LVZ thermal conductivity by up to 30%, so thermal gradient in an immobile LVZ will be markedly superadiabatic, affecting temperatures throughout the mantle. Here I will suggest in outline how to accommodate the impact of these matters upon the interpretation of Earth behaviour, and aim to do so in more specific detail in other symposia at this meeting.

Tuesday 20 July PM

ST6/E/04-A2

1400

### DYNAMICS OF MANTLE PLUME: FIELD EVIDENCE AND EXPERIMENTAL CONSTRAINTS

Eiichi TAKAHASHI (Earth &amp; Planetary Sci., Tokyo Inst. of Tech., 2-12-1 Ookayama, Meguroku, Tokyo 152-8551, Japan, Email: etakahas@geo.titech.ac.jp)

Recently, the role of recycled oceanic crust in the magma source region of LIP (large igneous provinces) have been reemphasized (i.e., Hauri, 1996; Takahashi et al., 1998). In order to constrain the chemistry and temperature of the hot rising material (mantle plume), detailed field works have been carried out in Koolau and some other Hawaiian shield volcanoes. Based on the petrology of the Koolau lava and high-pressure melting experiments on them, we propose a model that the Hawaiian plume had a potential mantle temperature (PMT) of only 1350°C in the Koolau stage (ca 2.5 Ma) and the primitive Koolau magma was formed by extensive melting of recycled old oceanic crust but not ambient peridotite. This PMT is much lower than the estimate for the modern Hawaiian plume by Watson & McKenzie (1991, PMT=1558°C) assuming homogeneous peridotite source. Our experiments (melting of basalt/peridotite hybrid source at 3 GPa) show that only slight temperature increase (50deg) will shift the Koolau type primary melts (SiO<sub>2</sub>=53, MgO=7 wt.%) to the parental Mauna Loa and Kilauea type melts (SiO<sub>2</sub>=49, MgO=14) when solidus origin of the mantle plume and the mechanism of its upwelling transport. Presence or absence of the old oceanic crust in the plume heads will explain chemical diversity and the contrasting melt productivity between hot spots (e.g., Iceland vs. Azores). Mantle upwelling flows are expected to obtain extra buoyancy at a round 650-700km because of the phase transition from the perovskite dominant to majorite dominant facies. Subducted old oceanic crust residing at the base of the upper mantle due to the neutral buoyancy may be easily entrained in this upwelling flow.

ST6/E/09-A2

1420

### MELT STRUCTURE IN FE-FES BINARY SYSTEM AT HIGH PRESSURE

Satoru URAKAWA (Department of Earth Sciences, Okayama University, Okayama 700-8530, Japan, email: afeg0320@cc.okayama-u.ac.jp) Kenichi Funakoshi (Japan Synchrotron Radiation Research Institute, Mihara 679-5198, Japan, email: funakoshi@sp8sun.spring8.or.jp) Keiji Kusaba (Institute for Material Research, Tohoku University, Sendai 980-8577, Japan, email: kusaba@jpnimr.tohoku.ac.jp) Hideo Ohno and Osamu Shimomura (Spring-8 Japan Atomic Energy Research Institute, Mihara 679-5198, Japan, email: simomura@sp8sun.spring8.or.jp)

The physical properties of molten iron alloy, such as density and viscosity, are important to elucidate the formation and the dynamics of the earth's core. Thus, it is expected to reveal these properties at high pressures. Structural study is essential to understand the physical properties of melt. In order to clarify the relations between physical properties and structure, we have conducted some experimental studies on molten iron alloy at high pressures. Here we report the results of structural study using synchrotron radiation.

X-ray diffraction experiment of melt in the Fe-FeS system was carried out up to 5 GPa by the energy dispersive method. Total radial distribution function was derived from X-ray diffraction profiles. We found the change of melt structure with sulfur content between Fe and FeS. Structure of molten iron alloy is very simple, which corresponds to low viscosity for Fe-FeS eutectic melt measured by Dobson et al. (1998).

ST6/W/10-A2

1440

### DYNAMICS OF HCP TRANSITION METALS AT ULTRAHIGH PRESSURES

Andrew JEPHCOAT (Department of Earth Sciences, University of Oxford, Oxford OX1 3PR, UK, email: andrew@earth.ox.ac.uk) Helmut Olijnyk (Department of Earth Sciences, University of Oxford, Oxford OX1 3PR, UK, email: helmuto@earth.ox.ac.uk)

Despite recent experimental progress towards measuring the physical properties of iron at core conditions, the crystalline structure of solid core phases remains unknown, making it difficult to interpret seismological evidence for the elastic anisotropy of the inner core. Recent elastic constant measurements for hcp iron (assumed to first order to dominate inner-core properties) have highlighted significant differences with parallel theoretical predictions of the elastic moduli suggesting a need for improvements in the theoretical treatment and/or a re-examination of models for the origin of the seismic velocity anisotropy of the inner core. Experimental measurements related directly to lattice-dynamical properties have not been

available up to the present time at high compressions, but recent work has shown that the transverse-optical, doubly-degenerate (E<sub>2g</sub>) phonon mode in hcp transition metals is Raman-active and can be measured at high pressure in the diamond-anvil cell (DAC) with sensitive CCD detectors. If theoretical techniques reproduce the observed room-temperature pressure dependence of these modes in various metals, confidence in the elastic-constant calculations at core conditions would be substantially increased.

We report on studies of several hcp transition metals by Raman scattering techniques in the DAC up to 100 GPa under hydrostatic and nonhydrostatic pressure conditions. The pressure response of the E<sub>2g</sub> phonon mode in metals includes normal behaviour (positive pressure shift) as well as anomalies involving splitting and negative pressure shifts. (For Fe and Re, well studied by x-ray diffraction and observed to remain hcp to 200-300 GPa, there is no information on their high-pressure dynamics. Measurement of the hcp phonon in Fe should be possible above 12 GPa at room temperature, where the fcc-hcp transition occurs; the Re phonon mode shows normal hard-mode behaviour with pressure. Calculations of selected phonon frequencies and their pressure dependence have recently been performed for Re, Fe and Zn and are compared with the new experimental data.

ST6/E/11-A2

1500

### IN SITU X-RAY DIFFRACTION STUDY OF THE POST SPINEL TRANSFORMATION KINETICS IN MG2SIO4

Kubo Tomoaki, Eiji OHTANI, Akio Suzuki, Kiyoshi Fujino(1), Takumi Kato(2), Satoru Urakawa-Institute of Mineralogy, Petrology, and Economic Geology, Tohoku University, Sendai 980-8578, Japan; (1) Department of Earth and Planetary Sciences, Hokkaido University, Sapporo 060-0810, Japan; (2) Institute of Geoscience, University of Tsukuba, Tsukuba 305-0006, Japan; Department of Geosciences, Okayama University, Okayama 700-0082, Japan

The postspinel transformation is believed to be the cause of the 660 km seismic discontinuity. In order to evaluate the effects of the postspinel transformation on the dynamics of the slab descending into the lower mantle, we studied the kinetics of the phase transformation of Mg<sub>2</sub>SiO<sub>4</sub> on the basis of the high pressure and temperature in situ X-ray diffraction experiments. The experiments were conducted using "SPEED1500" and "MAX90" multianvil high pressure apparatus installed in the synchrotron radiation beam line BL04B1 at SPRing-8 and BL14C at the Photon Factory, respectively. We observed that spinel Mg<sub>2</sub>SiO<sub>4</sub> dissociates metastably into MgSiO<sub>3</sub> ilmenite and periclase, and stishovite and periclase in the stability field of perovskite and periclase. These metastable assemblages nucleate at the grain boundary between spinel grains and grow with the lamellar texture. The spacing of the lamellae composed of the post-spinel phases decreases with the overpressure, and it reduces to less than 0.5 micrometers at the overpressure of 1 GPa. Existence of this very fine grained lamellae of the post spinel phase strongly suggests that there is a transformation superplasticity around 660 km discontinuity due to significant grain size reduction by the transformation. We measured the growth rate of the post spinel phase transformation and analyzed by the diffusion-controlled model. The activation energy of the growth is estimated to be 350(+240)KJ/mol. The present results give basic data to constrain the post-spinel phase transformation kinetics in the descending slabs.

ST6/W/13-A2

1520

### APPLICATIONS OF IMPULSIVE STIMULATED SCATTERING AT ELEVATED PRESSURE AND TEMPERATURE

J. Michael Brown (Geophysics Program, University of Washington, Seattle, WA 98195 USA Email: brown@geophys.washington.edu)

Dynamic processes within Earth, including heat removal through large-scale convection within the mantle and magnetic field production in the core via the geodynamo, are intrinsically regulated by the physical properties of constituent materials. Such properties are dependent on intermolecular interactions at short distances. To a large extent, the physics that has been successful in rationalizing condensed matter behavior near ambient conditions has been simplistically extrapolated to deep Earth conditions of reduced intermolecular distances. New experimental confrontation with theory is now possible using a family of time-domain optical techniques. These methods, "holographic grating spectroscopy", "thermally stimulated Brillouin scattering", "laser-induced phonon spectroscopy," and "impulsive stimulated scattering," are exploited in determination of a set of equilibrium and dynamic properties of solids and fluids at elevated pressure and temperature. The experiments and selected results are discussed in the context of a renewed need to improve theory essential in understanding Earth processes.

ST6/E/10-A2

1540

### HYDROLYTIC WEAKENING IN FORSTERITE

John BRODHOLT (Dept. of Geological Sciences, UCL, Gower Street, London WC1E 6BT, UK) and Keith Refson (Department of Earth Sciences, University of Oxford, Oxford OX1 3PR, UK)

Even small amounts of water can profoundly effect the physical properties of minerals. In olivine less than 1 H in every 1000 unit cells acts to increase creep rates of dunite by about two orders of magnitude. Although the mechanism for this is not known, it is not unreasonable to suggest that it is in some way related to an increase in vacancy population. In order to understand this better we have performed ab initio pseudopotential calculations within the generalised gradient approximation on protonic defects in Mg<sub>2</sub>SiO<sub>4</sub> forsterite. Three mechanisms for incorporating protons are considered: a) interstitial, b) binding at cation vacancies, and c) binding at silicon vacancies. Assuming the existence of both Si and Mg vacancies, on energetic considerations, protons will initially populate Si vacancies until there are three protons in the vacancy. At this point the addition of one more proton (to make a hydrogarnet substitution) is energetically unfavourable in comparison to populating the Mg vacancy, and the next two protons will enter the Mg site. Interstitial protons will be very rare. Since it is greater than 3 eV more favourable to put the first proton into the Si vacancy than the magnesium site, the presence of water will certainly act to increase the population of silicon vacancies. In fact in the presence of water, the energy required to form a Si vacancy is about the same as to form a Mg vacancy. This is in stark contrast to dry olivine where Si vacancies are many eV less favourable. If creep is rate limited by the diffusion of the slowest species, silicon in olivine, then increasing the Si vacancy concentration could provide a mechanism for hydrolytic weakening.

ST6/C/JSS02/W/04-A2

Invited

1620

### SHEAR ATTENUATION IN UNIFORM, FINE-GRAINED FERROMAGNESIAN OLIVINE AND OLIVINE-MELT AGGREGATES: GRAIN BOUNDARY RELAXATION AND THE PHYSICAL SIGNIFICANCE OF THE ANDRADE MODEL OF VISCOELASTICITY

Reid F. COOPER and Tye T. Gribb (both at Department of Materials Science &amp; Engineering, University of Wisconsin, Madison, WI 53706, USA, e-mail: cooper@engr.wisc.edu)

High-temperature (1100-1300°C), driven (10-3-100 Hz) torsional attenuation and creep



experiments have been performed on uniform, fine-grained (d~3mm) olivine aggregates and texturally equilibrated olivine-basaltic partial melts. Both materials demonstrate mechanical linearity: for these conditions, inelastic deformation is accomplished via ionic diffusion. The materials display relatively high  $QG^{-1}$  values ( $-2 < \log_{10} QG^{-1} < 0.5$ ) that are but moderately dependent upon frequency, with  $QG^{-1} \sim 0.35$ . The partial-melt material displays but a modest increase in shear attenuation ( $-0.35 \log$  units in  $QG^{-1}$ ), with no change in the form of the attenuation "band." Predictions of the  $QG^{-1}$  behavior based on the Laplace transform of the best-fit Andrade function replicate exactly the directly measured  $QG^{-1}$ . Although the anelastic portion of the Andrade function (i.e.,  $gxy,a = b \ln$ ) is numerically equivalent to an infinite distribution of compliances, our controlled-microstructure material and fully linear rheology indicate that the observed attenuation and creep behaviors cannot be attributed to spatial variations, e.g., in grain size or in density of lattice dislocations. The Andrade function here attests, rather, to an intrinsic aspect of diffusional creep: the redistribution of grain boundary traction via chemical diffusion. The effect on  $QG^{-1}$  of the melt phase is related solely to its modest impact on the aggregate viscosity; there is no unique shear-attenuation signature of equilibrated, grain-scale melting. Comparison of our results to other experimental studies, and their extrapolation to geological conditions, raises the suggestion that subgrain boundary dynamics may play a significant role in seismic-frequency absorption in the upper mantle.

**ST6/C/JSS02/W/15-A2** Invited **1640**

#### HIGH-TEMPERATURE VISCO-ELASTIC RELAXATION IN SYNTHETIC OLIVINE AGGREGATES: INFLUENCE OF GRAIN SIZE AND BASALTIC MELT FRACTION

B.H. Tan, I. JACKSON, J.D. Fitz Gerald, U. Faul, H. Kokkonen and G.R. Horwood (all at Research School of Earth Sciences, Australian National University, Canberra, ACT 0200, Australia, E-mail: ian.jackson@anu.edu.au Telephone No: +02 624 92498 Fax No: +02 627 98253)

Progress made since our preliminary report (Tan et al., GRL, 24, 1055-1058, 1997) of forced oscillation tests on a dense hot-pressed aggregate of San Carlos olivine of composition Fo90 and grain size 0.05 mm will be described. Additional specimens have been synthesised from San Carlos- derived material, in both Fe and Ni/Fe containers, with and without added basaltic melt. The use of synthetic sol-gel precursors is also being investigated. Microstructural studies have continued in parallel with further torsional forced oscillation and microcreep measurements and developments in data processing in an attempt to identify the mechanism(s) contributing to the observed viscoelasticity.

All specimens so far examined have been shown to be of low dislocation density. It therefore appears unlikely that dislocations are responsible for the high-temperature relaxation in these relatively fine-grained materials, and grain boundaries have therefore become important targets for closer examination. The levels of impurity in the nominally melt-free synthetic Fo90 specimens are generally low with small pockets of quenched melt glass located mainly in the grain-edge triple junctions at an overall concentration of ~0.01 %. Significant grain-boundary enrichment in Al and Ca point to impurity segregations, and the probable existence everywhere of reasonably continuous but very thin (< 2 nm) grain boundary films. The unrelaxed shear modulus and viscosity associated with both the Andrade and generalised Burgers fits to the torsional microcreep data are lower than those inferred from short-period (ultrasonic) and large-strain creep tests, respectively. Both 'discrepancies' can be explained by invoking the presence of thin grain-boundary films of relatively low viscosity. The strength of the 'high-temperature background' relaxation varies inversely with grain size and is increased by the addition of basaltic melt.

**ST6/E/01-A2** **1700**

#### ELASTIC NONLINEARITY AND SLOW DYNAMICS IN ROCKS

James A. TenCate, Eric Smith, Loren W. Byers, Thomas J. SHANKLAND, and Paul A. Johnson (all at Earth and Environmental Sciences Division, MS D443, Los Alamos National Laboratory, Los Alamos, NM, 87545 USA, Email: shankland@lanl.gov)

As revealed by longitudinal bar resonance experiments, materials such as sandstone and concrete show a rich diversity of nonlinear elastic behavior. As a function of increasing drive level, resonance frequencies shift downward by as much as several percent, the resonant lineshape changes, and harmonics and slow dynamics appear. Slow dynamics [Geophys. Res. Lett., 23, 3019-3022, 1996] refers to the following sequence: a large strain applied to a rock ("conditioning") reduces its modulus (i.e., it behaves like a softer spring); if the strain is applied for several minutes, the rock remains "soft" even after the strain is removed; the rock eventually recovers to its initial stiffness. In order to explore the mechanisms of nonlinear response including slow dynamics, we performed experiments to study conditioning and recovery, processes that appear to be asymmetric. Conditioning takes place quickly, but recovery of the elastic modulus as measured by drift of the resonance peak takes place in two stages. After the conditioning strain is removed, the modulus first quickly recovers most of its initial stiffness. However, the next stage of recovery to the original modulus takes minutes to hours, depending on the length of time the conditioning strain was applied. In this stage, resonant frequency goes as  $\log(\text{time})$ . Logarithmic time-dependence is a phenomenon associated with static friction and restoration of surface contacts, which in rocks probably take place at contacts across crack surfaces. Not only do these effects help reveal the causes of nonlinearity, they can be of use in evaluating damage to materials.

**ST6/C/JSS02/W/08-A2** Invited **1720**

#### SOUND VELOCITIES AND ELASTICITY OF MANTLE MINERALS AT HIGH PRESSURES AND TEMPERATURES, AND IMPLICATIONS FOR MANTLE COMPOSITION

J D BASS and S V Sinogeikin (both at: Department of Geology, University of Illinois, 1301 W. Green St., Urbana, IL 61801 USA; E-mail: bass@hercules.geology.uiuc.edu)

The most direct and detailed observations on Earth's interior consist of seismologically determined velocities as a function of depth, including velocity anisotropy and heterogeneity. Experimental advances within the mineral physics community have progressed to the point that direct measurements of elastic wave velocities on mantle minerals are now being performed at high pressures and temperatures. This technological progress permits a more direct comparison between laboratory velocity measurements on minerals and the seismic properties of the Earth than was possible even just a few years ago, and suggests that inferences about mantle mineralogy can be made with a higher degree of certainty. In our laboratory we have been performing high pressure and high temperature measurements of sound velocities on single-crystal samples by Brillouin scattering, utilizing a diamond anvil pressure cell and resistance heating. Experimental studies have been completed on ringwoodite (the high-pressure spinel-structured polymorph of olivine), pyrope garnet, and MgO, all of which are thought to be important components of the mantle. Experiments on other high-pressure silicates of importance to the mantle, such as majorite, are in progress and will be presented. The results presently available allow us to investigate the possibility of chemical stratification in the mantle. In particular, the increases in velocity across the 410 and 660 km discontinuities, and the high gradients of velocity with depth in the transition zone are diagnostic of the mineralogy of this region. Measured pressure derivatives of velocity for the high-pressure polymorphs of olivine and for garnet do not match velocity gradients in the

transition zone. The general conclusion to be drawn from the high-pressure velocity measurements is that it is difficult to reconcile the velocity structure of the transition zone with a uniform pyrolyte composition for the mantle.

**ST6/C/JSS02/W/19-A2** **1740**

#### CORRELATION OF MAGNITUDE AND T-DEPENDENCE OF HIGH PRESSURE VISCOSITY OF FE LIQUIDS WITH SULFUR CONTENT

SECCO, Richard ( Bayerisches Geoinstitut, Universitdtt Beyreuth, Beyreuth D-95440 GERMANY. E-mail: Richard.Secco@Uni-Bayreuth.DE Telephone No: 49-(0)921-553729 Fax No: 49-(0)921-553769)

The viscosity of liquids in the Fe-S system at high pressures are being experimentally determined using the electro-detection method. The method was developed for in-situ sphere speedometry measurement and is based on the detection of time resolved sphere position from an electrical resistance anomaly produced by an insulating sphere passing through a pair of Fe electrodes located in the conducting liquid sample. The experiments are carried out in 1000 ton multi-anvil and cubic-anvil presses with heating rates as high as 2500C/min using LaCrO3 or Nb furnaces and W/Re or Pt/Pt-Rh thermocouples. Spheres of ruby or sapphire, 0.5-0.7 mm diameter, are used in BN contained samples of 2.5 mm diameter and 2.5-3.5 mm height. There is no evidence of reaction between the sphere and melts on the time scale and at the P,T conditions of the experiments. Comparison of Fe-S melt compositions with 20.7wt%S and 27wt%S in the ranges 5-8 GPa and 1050-1300C show that the higher S content melt has a higher viscosity by 2-3 ln units. The T-dependence of viscosity also appears to correlate positively with S content and this relationship is preserved on comparison with 1 atm viscosity data on pure liquid Fe. This is consistent with the large viscous activation energy values obtained for 27wt%S in an earlier study and the interpretation of S content control on the viscosity through the size of viscous flow units.

**ST7** **Tuesday 20 July**

#### EDUCATION AND OUTREACH IN THE 21ST CENTURY

Location: Physics West  
Location of Posters: Old Gym

**Tuesday 20 July AM**

Presiding Chairs: V.M. Hamza, (Observatorio Nacional – CNPq, Rio de Janeiro, Brazil)  
W.H.K. Lee, (U.S. Geological Survey, U.S.A.)

**ST7/E/03-A2** **0930**

#### INTERNATIONAL TRAINING COURSES ON SEISMOLOGY AND SEISMIC HAZARD ASSESSMENT

PETER BORMANN (GeoForschungsZentrum Potsdam, Division on Solid Earth Physics and Disaster Research, Telegrafenberg E428, D-14473 Potsdam, Federal Republic of Germany, email: course@gfz-potsdam.de)

The post-graduate International Training Courses on Seismology and Seismic Hazard Assessment are run annually for participants from developing countries in the framework of the UNESCO educational and know-how transfer programme, the IDNDR and the IASPEI Sub-Committee on Training. Since 1992 they are carried out alternately every second year in Germany as world-wide open courses and in developing countries, respectively, as regional courses, e.g. 1993 in India, 1995 in Nicaragua, 1997 in Kenya and 1999 in China. Sometimes, these regular 5-weeks courses are, on special request, complemented by thematically focussed regional 2-weeks courses (e.g. in 1993 in Iran and in 1998 in India). In total, 440 participants from 77 countries attended these courses since 1980. But none the less, the number of applications still exceeds every year by far the number of fellowships (20-25) available.

The courses are strictly praxis-oriented. The approach is learning-by-doing. Accordingly, about 40 per cent each of the time is allocated for introductory lectures, which provide the theoretical basis and interdisciplinary problem understanding, and for practical exercises, respectively, on all fundamental tasks of seismological observatory practice and seismic hazard assessment. This is complemented by extended workshop discussions and by field excursions to relevant institutions, seismological stations and data analysis centers as well as to famous seismotectonic features and sites of earthquakes or volcanic eruptions. The paper outlines the course philosophy, programme and approach, evaluates their effectiveness and demonstrates the course web-page.

**ST7/E/04-A2** **0950**

#### THE NEW IASPEI MANUAL OF SEISMOLOGICAL OBSERVATORY PRACTICE

PETER BORMANN (GeoForschungsZentrum Potsdam, Division on Solid Earth physics and Disaster Research, Telegrafenberg E428, D-14473 Potsdam, Federal Republic of Germany, email: course@gfz-potsdam.de)

The last edition of a Manual of Seismological Observatory Practice dates back to 1979. It covered analog techniques only and is out of stock. Since that time, computer and communication technologies as well as the availability of modern broadband sensors have revolutionized seismological observatory practice. Related know-how is chiefly available in industrial countries only. Besides this, classical university curricula do not provide suitable education and training of observatory personnel. Therefore, the IASPEI Commission on Practice has launched an initiative to produce within the next few years a New Manual of Seismological Observatory Practice (NMSOP). It will be developed step by step as an electronic database and is freely accessible, together with the old manual, via Internet. The systematic tutorial body of the manual, complemented by index search, annexed job-related worksheets and data bases, extensive references and contact addresses of authors, institutions, firms etc. will make it in future easy to assist station operators and analysts in their daily work and to retrieve relevant pieces of information or teaching/training modules tailored to specific needs. A later publication of a condensed NMSOP version as a text book is envisaged.

The paper outlines the philosophy, structure and list of contents of the NMSOP and demonstrates its use by way example. A more comprehensive web-side demonstration and user/contributor guidance will be given in a complementary presentation by E. Bergman.



ST7/E/08-A2

1010

## TRAINING FOR HAZARD MITIGATION IN CENTRAL AMERICA

Jens HAVSKOV (Institute of Solid Earth Physics, Allegaten 41, 5007 Bergen, Norway, email: jens@ifj.ubi.no Conrad Lindholm (NORSAR, Box 51. 2007 Kjeller, Norway, email: conrad@norsar.no

Earthquake hazards is common in the developing countries which are often the countries which least can afford the mitigation of natural hazards. The University of Bergen and NORSAR has for the last 8 years been involved in a project of earthquake disaster prevention in Central America. The project involves the aspects of improving instrumentation, determination of earthquake parameters, calculating seismic hazard, doing microzonation for city planning and providing formal education on the MSc and PhD level. Our main experience is that, for educational programs in hazard mitigating, to have any effect at all, they must include all elements starting with basic training on a technical level to formal training on a PhD level and the effort must be long term and include human network building. There must also be a minimum level of infrastructure so that the level of training matches the possibility of using that training. In our opinion, far too much money is wasted in international high quality training and educational programs because the training received does not match possibilities in real life. Obviously this kind program cost more than just a training course, but if we want to be serious about hazard mitigation, our experience is that all the above mentioned elements must be included.

ST7/L/01/C/U1-A2

1050

## WINDOWS TO THE UNIVERSE - A GLOBAL RESOURCES FOR EARTH AND SPACE SCIENCE EDUCATION FOR THE GENERAL PUBLIC AND THE PRECOLLEGE ENVIRONMENT

Dr. Roberta Johnson, Dr. Janet Kozyra, Ms. Jennifer Leonard, Mr. Ryan Deardorff, Mr. Mike Burek, Dr. Terry Weymouth (all at The University of Michigan, 2455 Hayward, Ann Arbor, MI 48109, email: rmjohns@umich.edu), Dr. Claudia Alexander (Jet Propulsion Laboratory, Pasadena, CA), Dr. Jon Linker (SAIC Corporation, San Diego, CA), Mr. David Mastie (Ann Arbor Public Schools, Ann Arbor, MI)

Windows to the Universe is a NASA-supported award-winning Internet-based learning system on the Earth and space sciences for students, teachers, and the general public. The web site (<http://www.windows.umich.edu>) is used extensively in the home environment, classrooms, hands-on science museums, and libraries worldwide, by users with ages ranging from 5 to 85. The web site, composed of ~4500 html files, ~4700 image files, currently serves about 190,000 visitors per month. The web site is truly interdisciplinary, integrating science content with content on the humanities, and provides interactive activities designed to draw users into further learning and exploration of the Earth and space sciences. Content on the site is presented at three levels of sophistication approximating the upper elementary, middle, and high school levels. In addition, a supplementary CD is available that allows most images on the site to be accessed from the users local CD drive rather than potentially time-consuming internet transfer. Resources for educators are also provided, including easy to use classroom activities, extensive science standards-based search capabilities, and an area for sharing information with other teachers.

ST7/W/06-A2

1110

## A STUDY OF AWARENESS ABOUT NATURAL DISASTERS

Noriko SUGI (Kyoritsu Women's University, Moto-hachioji, Hachioji, Tokyo 193-8501, JAPAN, Email: sugi@s1.kyoritsu-wu.ac.jp)

To study how ordinary public is aware of natural disasters, we have made questionnaires repeatedly to students at Kyoritsu Women's University since the occurrence of the 1995 Hyogo-ken Nanbu Earthquake, which caused a huge damage to the central area of southwest Japan. The students did not experience the earthquake nor had seen a big damage by any natural disaster. By summing up their answers, we examined what are important to inform to and to educate the broader public in the 21st Century. One of the questions in the questionnaires was "Which disasters in the world made the strongest impressions on you?" Many of the students cited the 1995 Hyogo-ken Nanbu Earthquake, the 1993 Hokkaido Nansai-oki Earthquake accompanied by a large tsunami, and the 1991 Eruption of Unzen Volcano accompanied by pyroclastic flows. The factors that impressed people about disasters, such as time or place they occurred, number of people who suffered damage and kinds of damage, were investigated. Another question was "What do you think are the significant remaining problems related to the Hyogo-ken Nanbu Earthquake?" After one year, the most common answers were those related to reconstruction of the victims' normal daily lives. As time goes by, those answers changed to concern for disaster prevention.

ST7/E/06-A2

1130

## QUALITATIVE AND SEMI-QUANTITATIVE SEISMOLOGY

ZHONGLIANG WU (Institute of Geophysics, China Seismological Bureau, 100081 Beijing, China, email: wuzl@cdsindmc.css.gov)

The qualitative and semi-quantitative aspects of physics and seismology plays an important role in the education of modern seismology which is characterized by quantitative and computational modeling. Besides the usually cited qualitative skills in physics, such as dimensional analysis, estimation of the order of magnitudes, qualitative analysis of differential equations, and using of simple system, and so on, qualitative and semi-quantitative knowledge in seismology also includes the empirical approaches in seismological observation and practice, visualization of seismological phenomena, and the universalities in the extreme simple dynamic models (toy models) of earthquakes. It is specially important that seismology is facing to some outstanding problems, e.g., the prediction of earthquakes, in which the qualitative and empirical understandings are of help in the identification, formulation, and solution of seismological problems. In this presentation we try to figure out some of the important topics in qualitative and semi-quantitative seismology. Also, it is worth pointing out that with the development of high-technology, qualitative and semi-quantitative knowledge becomes of more use not only in education but also in research.

ST7/W/01-A2

1145

## THE NEED FOR EARTHQUAKE EDUCATION IN ITALY

Laura Alfonsi (Istituto Nazionale di Geofisica, Roma, Via di Vigna Murata 605, 00143 Roma, email: alfonsi@ing750.ingrm.it)

In a densely populated country such as Italy, where culture and social structures are strongly connected, any natural event is potentially a disaster. The impact on the community of the

1997-98 Umbria seismic sequence will be briefly outlined enhancing how the lack of earthquake culture and education in the media, politicians and population can somehow increase the earthquake impact.

ST7/E/05-A2

1200

## SCIENTIFIC CORRESPONDENCE IN SEISMOLOGY: ITS SCIENTIFIC AND HISTORICAL VALUE

Graziano FERRARI (S.G.A. Storia Geofisica Ambiente, Bologna, Italy, email: ferrari@sga-storiageo.it)

Among the historical documentary materials produced by earth scientists the epistolary correspondence is of importance both for the outline of their biographies and for the reconstruction of the theoretical and experimental paths of the disciplinary history of seismology. This correspondence between seismologists is an important source of instrumental and descriptive data on the earthquakes of the past. Often, it contains references to seismic effects, to descriptions of instruments or of their adaptations, and to interpretations. In Italy, for the period from 1850 to 1940 alone, have been identified about 30,000 letters, of which only a part has been catalogued and used. Unfortunately, this particular kind of documentation is too often at the high risk of being lost or destroyed as it is being unrightfully considered of little interest by the more recent generations of seismologists. Recent experiences within specific projects of study and recover carried out in Italy and in the rest of the world have allowed the possibility to re-establish the just value of this documentation. There will be presented some results of an original method to catalogue the historical-scientific processing applied to files of correspondences between Italian and foreign seismologists.

ST7/E/07-A2

1215

## THE NEW IASPEI SUB - COMMITTEE "HISTORICAL INSTRUMENTS AND DOCUMENTS IN SEISMOLOGY": AIMS, OBJECTIVES AND FIRST RESULTS

Graziano FERRARI (S.G.A. Storia Geofisica Ambiente, Bologna, Italy, email: ferrari@sga-storiageo.it)

At the end of 1998 a Sub-Committee IASPEI was created within the Committee Education, aimed at promoting: (1) research, inventory, and restoration of historical instruments, recordings, station bulletins, papers, and scientific correspondence, (2) preservation and reproduction of seismograms and historical documents, especially scanning/digitizing into computer files, (3) experimentation of techniques for the scientific investigations of all historical seismic data. The Sub-Committee draws the inspiration for its own aims and objectives from the recent experiences carried out in Italy within the TROMOS project realised by SGA for the Istituto Nazionale di Geofisica (National Institute for Geophysics) and in Europe within the WG ESC "History of Seismometry". Some of the objectives are: (a) to create a database of seismic observatories, including their histories, installed instruments and activity period, access to the recordings and related documents, (b) to produce biographies of the deceased scientists who contributed significantly to seismology and earthquake engineering, including their life, work, and publications, (c) to collaborate with local historians of science and of scientific instruments, (d) to compile and edit materials for inclusion in the "International Handbook of Earthquake and Engineering Seismology", a Centennial Volume of IASPEI to be published in 2001. The first results of the activity of the S-C will be presented and discussed.

ST7/L/01-A2

1230

## AN INVENTORY OF SPANISH OLD SEISMOGRAPHS

Josep BATLLO (Escola Universitaria de Ciències Empresarials Dr. Manyà, E-43500 Tortosa, Spain, Email: jbo@tinet.fut.es)

A new, exhaustive, catalogue of old seismographs operated at Spanish sites is presented. It has been intended to be useful not just for historians, but mainly for researchers dealing with old data and seismograms recorded by such instruments. As a result, the beginning of instrumental seismology in Spain shows now a much more lively and complex process than expected. The catalogue summarises more than one hundred instruments and includes recording sites up to now forgotten. A cataloguing card has been elaborated for every seismograph. It contains the main physical characteristics, recording characteristics and periods, ground motion response, bibliography, hand written documents, actual condition and other data of interest for the instrument. Also, photographs of such described instruments, if available, have been included and referenced. Instruments have been classified according to its design: warning devices, seismoscopes, vertical pendulums, conic pendulums, inverted pendulums, electromagnetic, etc. Main features of the elaborated catalogue and results, concerning to the historical seismometry in Spain as well to the possibilities of its use on further studies are presented.

ST7/L/02-A2

1250

## VESUVIUS 2000: A VOLCANIC RISK MITIGATION INITIATIVE FOR A MEGACITY OF THREE MILLION PEOPLE

Flavio DOBRAN

Millions of people surround very dangerous volcanoes where effective risk mitigation strategies cannot be based on unreliable predictions of eruptions, poor evacuation infrastructures, and inadequate volcanic risk education of the population. Over three million people surround Vesuvius and Phlegrean Fields in the Bay of Naples, and an even greater number surround many other volcanoes in Mexico, the Philippines and elsewhere. Computer simulations and past eruption history of Vesuvius strongly suggest that a large explosive eruption will occur in the next 100 years and that it is necessary to prepare the territory through information campaigns and provision of economic incentives.

The ultimate objective of VESUVIUS 2000 is to produce an accurate probabilistic risk assessment, or expected human, material, socio-economic, environmental, and cultural losses due to future eruptions, for the purpose of reorganizing the Vesuvius area and creating a security culture. Solicitations of Italian and European Union institutions for collaboration has only produced frustration and demonstrated that its leaders prefer to hide behind an unreliable evacuation plan that only provides an illusion of safety. This plan, promoted by the volcanologists within the Italian government, is a shameful consequence of a special interest group that is protecting the politicians from taking a direct responsibility for the Vesuvius area. Further details are available on the Internet (<http://idt.net/~dobran>).

ST7/W/02-A2

1400

**WEB-BASED EDUCATIONAL TOOLS IN AND ITS POTENTIAL USE IN PUBLIC AWARENESS PROGRAMS**

VALIYA M. HAMZA, Observatório Nacional - CNPq, Rio de Janeiro, Brazil

At present most of the web-based courses are academic oriented while facilities for interactive learning by the public is limited. Such difficulties are being overcome with recent advances in the use of server-side CGI (common gateway interface) scripts that allow inquiry-based interactive learning more effective than is possible in conventional systems. Thus various aspects of natural phenomena and their environmental impacts can be illustrated on the web, in the form of simulations in response to user inputs. Examples of virtual geothermal measurements (VGM) are presented which demonstrate how interactive techniques can be used to examine environmental consequences of human activities that lead to long term changes in vegetation cover and accumulation of greenhouse gases. Trial experiments with VGM also reveal that facilities for stimulating creative thinking can be setup more easily in web-based systems than in those which emphasize traditional teaching techniques. The fact that web-based information packages can be developed at relatively low cost has important implications for setting up cost-effective programs aimed at improving education and public awareness of the environment and of natural hazards. For example, maintaining infrastructures for education, information and training for such tasks as disaster preparedness, early warning and mitigation are turning out to be relatively expensive operations for institutions in developing countries. On the other hand, developing web-based informative and educational packages require no significant additional investments in infrastructure or personnel and can be carried out promptly by many of the scientific and educational institutions. A major advantage of web-based programs is the efficiency and ease with which background information can be made available to the general public, properly blended with links to more detailed educational material. This approach minimizes the need for qualified personnel necessary to develop detailed informative material at the initial stages. In addition, availability of properly designed introductory material, should allow inexperienced users in gaining familiarity in using web-tools and to acquire confidence in facing more elaborate learning tasks based on context-sensitive queries and answers.

ST7/L/02-A2

1415

**CONTRIBUTIONS TO A HISTORY OF EARTHQUAKE PREDICTION RESEARCHES**

Giovanni MARTINELLI, (Regione Emilia-Romagna, Serv.Cartogr. e Geol., Bologna, Italy, email: email: g.martinelli@mo.nettuno.it)

Data coming from observations lasted 25 centuries have been systematized in the last 120 years and have become the object of applied research in the last 30 years in coincidence with a better understanding of physical and chemical phenomena which accompany earthquake occurrence.

The main procedures of diffusion of knowledges on earthquake prediction researches in space and time have been reconstructed. Scientific and economic constraint factors that caused difficulties or accelerations in seismic precursors researches have been investigated and commented. Future research tendencies are also described and commented.

ST7/L/03-A2

1430

**TROMOMETRIC MEASUREMENTS AS A TOOL FOR CRUSTAL DEFORMATION INTERPRETATION**

Graziano Ferrari (S.G.A. Storia Geofisica Ambiente, Bologna, Italy, email: ferrari@sga-storiageo.it); Dario ALBARELLO, (Dip. Scienze della Terra, Universit=E0 di Siena, Italy, email: Dario@ibogfs.df.unibo.it) Giovanni Martinelli, (Regione Emilia-Romagna, Serv.Cartogr. e Geol., Bologna, Italy, email: g.martinelli@mo.nettuno.it)

In the past and still today crustal deformation has been considered as a powerful tool in the understanding of seismogenetic processes. In 1870, Timoteo Bertelli, inspired by the observation of small and natural movements of pendulums recorded by scientific and historical witnesses, began in Florence his first elementary observations by using a vertical pendulum and a magnifying lens. Thanks to his collaboration with Michele Stefano de Rossi which started in 1873, Bertelli came to the definition of the standard tromometer: a pendulum of 150 cm. in length and 100 gr. of mass whose horizontal shifts were observed through a microscope tube and a prism. The great simplicity and economy of the construction made this instrument easily widespread in many private, ecclesiastic and public observatories. Perhaps for the first time an actual network was established for the instrumental observation of earthquakes. In 1880 31 standard tromometers were being used in various Italian observatories. Between 1873 and 1930 more than 100,000 observations were performed. Previous researches have demonstrated that these data are highly useful for the identification of preseismic or coseismic phenomena. The results of a statistical analysis of a set of data collected in Florence, Bologna and other localities from 1878 until 1887 are presented and compared with the local seismic activity.

ST7/E/10-A2

1445

**CREATION OF 'GEOLOGICAL MENTALITY' DURING EDUCATIONAL PROCESS AT THE HUMANITARIAN FACULTIES IN RUSSIAN UNIVERSITIES.**

Nicolai V.Koronovsky (Faculty of Geology, Moscow State Lomonosov University, Moscow 119899, Russia, E-mail: koronovsky@dynamo.geol.msu.ru)

The matter of this thesis - teaching experience of different geological courses to humanitarian students of such specialties as historians, biologists, lawyers, economists, linguists and others. The main purpose of the courses of various duration (from 12 to 48 hours) for students and graduates is to give them knowledges about basic elements of geology such as Earth origin, structure and composition, evolution; to get them know different geological processes that are most affectable on human life: earthquakes, land-slides, floods and other natural hazards. We pay particular attention to modern methods of effective predictions and prevention of geological hazards.

ST7/P/01-A2

1500

**PUBLIC EDUCATION AND AWARENESS OF EARTH AND ENVIRONMENT: THE INDIAN CONTEXT**

K.S. Murty, (E-3 Vishnukamal Apts., 160 Shivajinagar, Nagpur 440 010, India)

There is a traditional way of predicting natural disasters in India. Ancient classical works like the 'Brihat Samhita' of Varahamihira (5th century A.D.) have chapters devoted to cloud formation, rainfall, groundwater studies and earthquakes. The almanacs in regional languages do predict these phenomena fairly accurately, though not perhaps the exact date and time. Indeed, agricultural operations in India are still guided by these fore casts. However, modern education in related sciences has created greater public awareness among the general public, apart from the fact that topics of geological background have been included in the syllabi at school, college and post-graduate levels. Almost a decade ago, a debate was launched on the Integrated Economic and Environment Accounting Framework for India. The public consciousness has also grown to such an extent that mass resistance to projects that could cause great environmental consequences the Chipko movement and the Narmada Protest being the direct results of degradation of the Himalayas, location of Tehri and Narmada dams in seismically active areas. TV, Radio and other mass media are used to warn people of impending floods and cyclones so that they could be evacuated to safer places. Remote sensing techniques have helped in studying soil erosion, forest cover loss and related phenomena and informing the general public. Environmental education with reference to conservation, ecology and health has been introduced at formal and informal levels.

ST7/P/02-A2

1515

**PROPOSAL ON EARTHQUAKE EDUCATIONAL PROGRAMMES FOR INDIA AND NEIGHBOURING COUNTRIES**

H.N. SRIVASTAVA (India Meteorological Department New Delhi- 110003, India, e-mail: snb@imd.ernet.in)

Damaging earthquakes in India and neighbouring countries occur not only near the Indian Eurasian Plate boundary but also within the Indian Plate. Larger destruction due to the earthquakes in these countries occur in villages, urban slum and hilly areas which is attributed to lack of education, financial constraints and lack of availability of cheaper designs of dwelling units to suit the local environment. Even in cities, awareness about earthquake resistant designs is lacking.

The programme to face disaster mitigation needs to introduce earthquake safety rules right from primary and secondary schools and adult education centres. Since radio and television are now very common in India, frequent educational programmes through these media is essential. Also since more and more people are now joining computer-oriented management courses, a package needs to be designed for specialised programmes in such institutions. Refresher courses in Government and autonomous institutions may also be introduced so that very large trained manpower is available for disaster mitigation efforts.

ST7/E/11-A2

1530

**EDUCATION ON SEISMIC AND NATURAL HAZARD MITIGATION IN SOUTH EAST ASIA**

PHAN-TRONG Trinh, Institute of Geological Science, NCNST, Nghia do, Cau Giay, Hanoi, E-mail: pptrinh@refer.edu.vn, Fax: 84 4 8362886

South east Asia region with population of 530 Million is one of highest risk of natural hazard in the world. Many countries are threatened every time by storms, floods, earthquakes, volcanic eruptions, landslides and coastal zone erosions. The Asian Disaster Preparedness Center (AIT) have effected the Asian Urban Disaster Mitigation Program strike the education to reduce the vulnerability of urban areas and commitment to earthquake mitigation. We suggest here to extent the education system on seismic and other natural hazard for secondary school and publics by media and telecommunication. The education for public will focus on how self protection with Hazard and management plan of emergency works after destructive hazard to reduce hazard losses. This education will present in text book for secondary school and in the scientific education program of Television and radio. We suggest also the cooperation between scientific institutions in ASEAN countries for training post-graduate and high level education in seismic hazard assessment with the support from IASPEI training committee and experts form other institutions in Asia such as IIEE, CSB, ERI, INCEDE... in parallel with training course organising every years, internet will be a powerful tool for education. In near future this communication technique is a cheapest way for education for large region although it is rather expensive currently for certain countries in ASEAN such as Vietnam. It will be used not only for transferring lectures but also softwares, examples, data and examinations. We could think of the system " request - answer " at the first stage by E-mail. One regional center for hazard education is responsibility to answer the questions of students in collaborating with experts. For seismic and natural hazard, the lectures will cover not only on seismic data but also geological data. We expect 4 main points will be paid more attention in seismic and natural hazard education: 1. The linking between paleoseismicity, seismotectonics, active tectonics, seismicity, geochemistry ( Radon, Hydrogen) and some other advance techniques such as GPS, GIS, RADA interpherometry, remote sensing. 2. the combination between probabilistic and deterministic approach in estimation of seismic and natural hazard. 3. estimation of the losses ( property and lives ) is the complex result of seismic and natural hazard, population, housing structures, facilities, experiences... 4. As other developing countries, we need the know - how transfer from IASPEI and institutions of developed countries. The transfer of sources of some basic softwares such as EQRISK will speed up the rapid progress of seismic and natural hazard mitigation in the region.

Presiding chair: V.M. Hamza, Observatorio Nacional - CNPq, Rio de Janeiro, Brazil

ST7/W/03-A2

Poster

1605-01

**SCHOOL SEISMIC NETWORK IN EUROPE BY SCHOOLS FOR SCHOOLS**

Jean-Luc BERENGUER (Centre International de Valbonne, France) Anne Deschamps, Antony Lomax, Jean Virieux (Geosciences Azur, Universite de Nice-Sophia Antipolis, France) Antonella Bobbio, Andre Herrero, Aldo Zollo (Dipartimento di Scienze Fisiche, Universita di Napoli "Federico II") Anne-Marie Bruyas, Angela Palma (European Services, Fondazione IDIS-Citta della Scienza, Italy) Marc Daignieres, Erik Doerflinger (Geophysique, Tectonique et Sedimentologie, Universite de Montpellier II, France) Jean-Francois Karczewski (DT-INSU/CNRS, France) Bernard Dost(Orfeus Data Center, The Netherlands)

A dedicated seismic station has been designed for schools and has been presented at the last IASPEI meeting. The features of this station are high dynamic recording (24 bits with 5 bits of electronic noise), broadband sensor (from 10 Hz to 300 sec), gps time reference, continuous time serie in a cyclic buffer, post triggering through telephon maintenance with possible on-line extraction of data signals.

This station has been installed in different schools both in France and in Italy. These stations through a seismic network have recorded different local, regional and teleseismic events. The extraction of these events has been organized in an automatic way through seismic catalogs. Different illustrations of school applications as velocity wave estimation, comparison of seismic waveforms between stations, localization of events will be presented.

ST7/W/04-A2

Poster

1605-02

**EDUCATIONAL NETWORK OF THE GEOLOGICAL FACULTY OF THE MOSCOW STATE UNIVERSITY**

Pavel Pletchov, Dmitry Koshchug (both from Geological department, Moscow State University, Moscow, Russia E-mail: lym@ccas.ru)

The Educational Network (EduNet), which includes some multimedia lecture courses, was created on the basis of Geological Department local area network. All lecture courses are represented via Internet as an HTML files and has a multimedia support (sound, video etc.). Hypertext connections of summaries of different courses allow creating more than simple archive of the courses. By the hypertext links, we have an opportunity to create union educational network (WWW-system) with common navigation, across and thematic searches, common database of definitions etc. Besides, a manual management (insert, update and support) of Educational Network too hard. We need to use the automatic system with next properties: Each part of EduNet is a valuable information resource, which interconnected to other resources via common and thematic searches and hyperlinks EduNet supports a free and convenient access for lecturer to edit and update his lecture courses and supplementary materials. The new course of lectures would be conformably inserted to EduNet. All interconnection to other information resources would be created automatically EduNet has a common navigation scheme for quick search of needed information resource. All navigation pages would be dynamic and would have both thematic and across search systems. Some aspects of multimedia courses creation, lecture-to-lecture interconnections, common navigation scheme would be discussed in this presentation.

**ST7/W/05-A2 Poster 1605-03**
**NATURAL HAZARDS EDUCATION ON THE WEB**

Paula K. Dunbar, and ALLEN M. HITTELMAN (both at NOAA's National Geophysical Data Center, 325 Broadway, Boulder, CO 80303, USA, email: ahittelman@ngdc.noaa.gov)

Each year natural disasters take a huge toll in deaths and injuries, property damage, and economic loss. Much of this devastation can be reduced through existing mitigation techniques and greater public awareness of them. The National Geophysical Data Center (NGDC) is using state-of-the-art World Wide Web tools for natural hazards education and public outreach.

NGDC acquires, processes, and analyzes technical data that are useful in natural hazards risk assessment. These include earthquake, tsunami, and volcano data. Interactive search and retrieval capabilities via the Web are now available for these datasets. A three-CD collection of hazards slides is also available online. Photographs of damage caused by natural hazards represent a unique form of data that capture the transient consequences of Earth's periodic upheavals. They not only remind us that such events can and probably will recur, but that we should be prepared to handle their consequences in the future.

NGDC recently created an online "Natural Hazards Quiz" to test the user's "Natural Hazards IQ." The quiz presents multiple-choice questions on all types of natural hazards. The questions range in difficulty and include historic, mitigation, and scientific information.

The Natural Hazards Data Resources Directory is also available online. The Directory includes information on more than 230 organizations that provide natural hazards data and information.

**ST7/E/02-A2 Poster 1605-04**
**DISTURBED GEOPHYSICAL FIELDS AND FUNCTIONING OF NEURORECEPTORS**

NONNA S. VASILYEVA-VASHAKMADZE (Tbilisi State University, I. Chavchavadze Ave., Tbilisi 380028, Georgia, email: vazha@excite.com) Anzor Gvetsiani (Institute of Geophysics, Georgian Academy of Sciences, I. M. Alexidze Str., Tbilisi 380093, Georgia, email: vazha@excite.com)

In view of importance of helio-geophysical disturbed field influence on men and animals problem investigation - electro-magnetic, acoustic waves emission accompanying earthquakes, thunderstorms, magnetic storms, etc. - it is carried out the theoretical, by quantum electrodynamics and quasi-classical mechanics methods, study of the neuroreceptors functioning dynamics in chemical synopsis. As experiments and observations show external disturbed fields can penetrate into the central nervous system (CNS) across the isolating layer of glia. In those cases when the glia is not enough developed or it is exhausted or at anomalous external fields, resonance frequencies, when their intensity exceeds the protective barrier then direct influence on the CNS takes place, clearing up as encephalogram change. According to the suggested model theoretical values of synaptic receptors parameters (at a state of rest), in particular, of acetylcholin neuroreceptor for human CNS are calculated. It is shown that the frequencies of electro-magnetic and acoustic and infraacoustic radiation was respectively of order about 9 and less and 3-2 and less are active and can initiate the generation and spreading of nerve impulses in the same parts of the cerebral brain and disturb the CNS normal functioning.

**ST7/E/09-A2 Poster 1605-05**
**A MACROSEISMIC NETWORK OF SCHOOLS FOR THE COLLECTION OF EARTHQUAKES EFFECTS IN A LARGE CITY**

Andrea TERTULLIANI (Istituto Nazionale di Geofisica, Via di Vigna Murata, 605, 00143 Roma, Italy, email: tertul@ing750.ingrm.it) Francesca Funicello, Stefano Donati and Francesca Cifelli (all at Dept. of Geology, University of Roma Tre, Largo S. L. Murialdo, 00146 Roma, Italy, email: sdonati@uniroma3.it)

In order to obtain a realistic picture of the distribution of earthquake effects in large urban areas it is necessary to apply a suitable kind of macroseismic survey taking into the right account the distinctive features of modern megacities. To outreach such an objective a cooperation among Istituto Nazionale di Geofisica, University of Roma Tre and many roman high schools has been created, compounding scientific results and didactical development in earthquake preparedness. By using limited man-power and money we involved in the macroseismic survey the students of a sample of high schools (14-19 years). The schools were previously selected to obtain the best geographical distribution and to achieve us the creation of a macroseismic network in the urban area. Schools headmasters and teachers were previously contacted by our staff, providing them information about the aim of the study and the method. Two high density macroseismic surveys were for the first time performed to evaluate the intensity of shaking in the city of Rome (Italy) during the September 1997-March 1998 Umbria-Marche (Italy) sequence. At last the involved students resulted over 2000, with a final density of observation points never reached before in the city of Rome for earthquake surveys. From the scientific point of view the results are in the high definition of the intensity points distribution, basic for site response analysis especially in large urban areas; besides valuable results arise in the educational and didactical field, with a development of the attention to preparedness topics, mainly due to the direct and practical involvement of young people into the research. We feel that this effort will be fruitful in the future as it would be an important corner-stone in the growing awareness about information, training and mitigation of geohazards, combining educational and scientific goals.

**ST 7/E/01-A2 Poster 1605-06**
**A NEW METHOD FOR IMPROVEMENT OF EDUCATION, INFORMATION AND TRAINING IN THE FIELD OF EARTH AND ENVIRONMENTAL SCIENCES**

Tarzadin ULAANBAATAR (Department of Earth Sciences, National University of Mongolia, email: numelect@maginnet.mn )

A best way to improve education, information and training in all levels of persons and to better serve society in the new century is to show mathematically the nature of Earth, geophysical systems, climate system and environmental sciences. The conditions of their wide use are to be of very elementary mathematics and described by uppermost simple parameters for facility to understand, be interested everybody from ordinary public, through schools and apprenticeship, to more research-oriented university studies or to application-oriented post-graduate training.

In this paper geometry in daylight, thermal regimes, climate conditions on and near the Earth's surface, and some methods of their applications in society described brand-newly by time of calculation, date, geographical latitude, terrain height and albedo. Furthermore, results are shown in comparison with observed data and calculations and model results of other researchers.

All of these are summarized in a monograph, some chapters of which seem to be selected for ordinary public, elementary schools and apprenticeship, some for research-oriented university studies and others for application-oriented post-graduate training.

**ST7/L/04-A2 Poster 1605-07**
**EDUCATION AND OUTREACH IN THE 21ST CENTURY: TOWARDS HIGH-LEVEL RESEARCH ORIENTED EDUCATION IN DEVELOPING COUNTRIES**

Author: Isaiiah Tumwikiriz, Uganda National Seismological Network, Geological Survey and Mines Department, Ministry of Energy and Mineral Development, P. Box 9 Entebbe (Office) or Box 404 Entebbe (Private) Uganda.

Education is crucial for a society. It is through education that human capital of the society is developed. The quality of labour, productivity in all sectors of the economy, social services, welfare, all depend on the education and its policy of a country. Investment in education promotes innovativeness due to the desire for economic improvement hence accelerated growth and development. In this paper, an effort is made to analyse the level of research oriented education activities in the developing countries; and at the same time the portion of the Gross National Product (GNP) invested in such activities as compared to the developed countries. The paper also looks into the extent of internal and external inabilities that challenge the Research Oriented Education (ROE) today and perhaps will remain bottlenecks in Education Outreach in the 21st Century. The author also summarises the lessons learnt from international efforts towards the high-level research education activities in developing countries. In the conclusion, developing countries therefore must create an atmosphere that encourages to work in partnership with the owners of technologies so as to promote international technology transfer that will enable in building up ROD infrastructure. This certainly will require the developing countries develop a S&T culture through national policies, but remains a question of political will and innovativeness.

**ST7/L/02-A2 Poster 1605-08**
**VESUVIUS 2000 EDUCATIONAL ACTIVITIES FOR SECURITY CULTURE**

Flavio Dobran (Gianfranco Gambardella, Anna Ibello, Ida Mascolo, Global Volcanic and Environmental Systems Simulation, P.zza Matteotti, CP418, 80133 Napoli, Italy, Email: dobran@idt.net)

Vesuvius is a volcano in the Bay of Naples that is surrounded by about three million people. Computer simulations and past eruption history strongly suggest that a large explosive eruption will occur in the next 100 years. In the past such eruptions devastated the territory, but today they would also produce a human catastrophe because of the widespread abusive urbanization of the area and lack of security culture among its people. The central objective of the VESUVIUS 2000 initiative is to produce risk mitigation guidelines for the Vesuvius area aimed at informing the population about the potential risk of future eruptions and how this risk can be reduced through the reorganization of the territory and establishment of security culture. The basic premise of the initiative is that a secure cohabitation of people with volcano is possible and that this cohabitation can produce socio-economic, scientific, and cultural benefits without creating adverse effects to the environment. For this purpose, a Global Volcanic Simulator which physically models the entire volcano is being developed and computer simulations of possible eruptions used to study their effects on the territory and how it can be reorganized and the people protected. The development of a proper educational methodology for the Vesuvius area is fundamental for establishing new habits of mind conducive for the creation of security culture. For this purpose we have been conducting public seminars in town halls, churches, private clubs, military establishments, schools, private residences, and producing written and visual material. On the anniversaries of large eruptions of Vesuvius (August 24, 79, and December 16, 1631) we have been issuing international appeals and involving Vesuvius area schools in sharing their cultural works associated with their environment. We have also produced educational material directed at better acquainting school teachers on the interdisciplinary issues of their environment. Much of this information has been available on the Internet (<http://idt.net/~dobran>) since 1995 and has been often visited by children and adults from around the world.





P07

Wednesday 21 July

**STABLE ISOTOPES AND TRACE SUBSTANCES: THEIR USES IN OCEANOGRAPHY AND CLIMATE RESEARCH ON VARIOUS TIMESCALES**

Location: Arts Building 120 LT

Location of Posters: Arts Building 126 LR2/101LR4

Wednesday 21 July AM

Concurrent Poster Session

Introduction

0900

P07/L/01-A3

0905

**CIRCULATION FEATURES IN THE ARCTIC OCEAN REVEALED BY THE NUCLEAR FUEL REPROCESSING TRACERS, 129I AND 137Cs**

John N. SMITH - Marine Environmental Sciences Division, Bedford Institute of Oceanography, Dartmouth, N. S., Canada B2Y 4A2

The development during the past 10 years of analytical techniques to measure 129I by accelerator mass spectrometry has led to recent advances in its use as an oceanographic tracer, particularly in the Arctic Ocean. This stems from the fact that large quantities of 129I ( $t_{1/2} = 16 \times 10^6$  y) have been discharged from the Sellafield (UK) and La Hague (France) nuclear fuel reprocessing plants into the Irish Sea and English Channel, respectively since the 1960s. Together with 137Cs ( $t_{1/2} = 30$  y), derived mainly from Sellafield, the 129I reprocessing signal is transported into the North Sea and Norwegian Coastal Current and then enters the Arctic Ocean through Fram Strait and the Barents Sea where both tracers reflect the circulation of Atlantic-origin halocline and intermediate water. Measurements of 129I and 137Cs, combined with a knowledge of the historical record of reprocessing plant discharges, can be used to identify a given year of transport through the Norwegian Coastal Current (NCC), thereby permitting the determination of a transit time from the NCC to a given sampling location, similar to a ventilation age determined using atmospherically-derived tracers such as tritium and chlorofluorocarbon compounds (CFC's). One difference is that the release rate of 129I from La Hague and the dynamic range of the tracer pair for transit time measurements is rapidly increasing while the input functions for many ventilation tracers are leveling off or decreasing owing to global constraints placed on their production and usage. Measurements of 129I and 137Cs conducted on seawater samples collected during icebreaker and US Navy nuclear submarine cruises (SCICEX program) to the Central Arctic Ocean since 1993 provide a basis for evaluating the utility of these tracers. 129I results in halocline waters clearly delineate the front between Atlantic-origin water having an elevated 129I reprocessing signal ( $> 100 \times 10^7$  at/l) and Pacific-origin water labeled mainly by fallout ( $< 5 \times 10^7$  at/l), that is aligned with the Mendeleev Ridge. Low 129I levels ( $< 2 \times 10^7$  at/l) measured in Atlantic and intermediate water in the Northern Canada Basin and over the Alpha Ridge indicate that ventilation rates are extremely low ...

P07/W/06-A3

0935

**USING CHEMICAL TRACERS TO ASSESS OCEAN MODELS**

Matthew H. ENGLAND Centre for Environmental Modelling and Prediction (CEMAP), School of Mathematics The University of New South Wales, NSW 2052 Australia and Ernst Maier-Reimer Max Planck Institut für Meteorologie, Hamburg, Germany

Geochemical tracers can be used to assess the simulated circulation in ocean models. Tracers that have been used in this context include tritium, chlorofluorocarbons, natural and bomb-produced radiocarbon; and, to a lesser extent, oxygen, silicate, phosphate, isotopes of organic and inorganic carbon compounds and certain noble gases (e.g., helium and argon). This paper reviews the use of chemical tracers in assessing the circulation and flow patterns in global and regional ocean models. It will be shown that crucial information can be derived from chemical tracers that cannot be obtained from temperature-salinity (T-S) alone. In fact, it turns out that a model with a good representation of T-S can have significant errors in simulated circulation, so checking a model's ability to capture chemical tracer patterns is vital. Natural chemical tracers such as isotopes of carbon, argon, and oxygen are useful for examining the model representation of old water-masses, such as North Pacific and Circumpolar Deep Water. Anthropogenic or transient tracers, such as tritium, chlorofluorocarbons, and bomb-produced 14C are best suited for analysing model circulation over decadal time-scales, such as thermocline ventilation, the renewal of Antarctic Intermediate Water, and the ventilation pathways of North Atlantic Deep Water and Antarctic Bottom Water. Tracer model studies have helped to reveal inadequacies in the model representation of certain water-mass formation processes; for example, convection, downslope flows, and deep ocean currents. They show how coarse models can chronically exaggerate the spatial scales of open ocean convection and deep currents, while underestimating deep flow rates and diffusing downslope flows with excessive lateral mixing. Higher resolution models typically only resolve thermocline ventilation because of shorter integration times, and most resort to high-latitude T-S restoring to simulate reasonable interior water-mass characteristics. This can be seen to result in spuriously weak chemical tracer uptake at high latitudes due to suppressed convective overturn and vertical motion. Overall, the simulation of ...

P07/W/17-A3

0955

**WATER MASS FORMATION AND CIRCULATION IN THE SOUTHERN AND SOUTHERN INDIAN OCEANS: RESULTS FROM STABLE OXYGEN ISOTOPES**

M.P.MEREDITH, K.J.Heywood, R.D.Frew and P.F.Dennis

Measurements of the stable isotopes of oxygen made from samples collected on the Antarctic Deep Outflow Experiment (ADOX) cruises in the Southern Ocean and southern Indian Ocean, February to March 1993 and 1994, are discussed. The data are used in conjunction with hydrographic data to infer characteristics of the formation and mixing of water masses found in the region. The isotopically heaviest waters of the survey were found at the surface of the Madagascar Basin, a consequence of evaporation-induced enrichment of the heavier molecule. The isotopically lightest waters were found on the continental shelf of Antarctica, adjacent to the Princess Elizabeth Trough (PET); these waters are made isotopically light by the injection of around 1% of glacial ice melt, and are probably advected to the region from further east by the current associated with the Antarctic Slope Front. They appear to be locally disassociated from the Antarctic Surface Water and Winter Water (WW) further north in the PET. The WW of the Enderby Basin is isotopically lighter than the PET WW, and also fresher, indicating the presence of an additional component of glacial ice melt or high-latitude precipitation. North of the Antarctic Circumpolar Current (ACC), the delta 18-O of the surface waters show a strong correlation with salinity, but extrapolate to an apparent freshwater

endmember which is too isotopically light to be reasonable; advection and mixing of the water masses dominate over the local water balance at this location. The Subantarctic Mode Water of the southern Indian Ocean lies on the line of the surface waters in salinity-delta 18-O space, a consequence of its formation at the surface of the region by deep convection. The Antarctic Intermediate Water also lies on the same line, but this is somewhat coincidental since it does not originate in the region. Consequently, the observation does not, in fact, imply formation by local deep convection. There is no evidence in the data from the two repeated surveys of the Crozet-Kerguelen Gap to suggest interannual variability in the amount of glacial ice melt contributing to Antarctic Bottom Water (AABW) formation in the Weddell Sea. A previous hypothesis based on a subset of the data used here...

P07/W/08-A3

1015

**TRACER STUDIES OF ARCTIC SEA-ICE GROWTH AND ABLATION**

H. EICKEN (Geophysical Institute, University of Alaska, Fairbanks, AK 99775-7320, USA, Email: hajo.eicken@gi.alaska.edu), S. Pfirman (Barnard College, Columbia University, New York, NY 10027-6598, USA), H. R. Krouse (University of Calgary, Calgary, T2N 1N4, Canada), C. Haas, J. Freitag, A. Mackensen (Alfred Wegener Institute, D-27515 Bremerhaven, Germany)

In conjunction with ice sampling, stable-isotope and fluorescent tracer studies can yield substantial insight into the processes controlling growth and ablation of the Arctic sea-ice cover. Similar to drifting buoy measurements, the isotopic record of sea-ice cores extracted from the pack ice may provide time series of parameters relevant in the context of ocean-ice-atmosphere interaction. Drawing on field studies the following research will be discussed.

- (1) Stable-isotope measurements (delta-18O and delta-D) allow discrimination between the contribution of meteoric (precipitation, snow meltwater, river water) and marine waters to the total ice volume. In the Eurasian Arctic, with its substantial inflow of river water onto the shelves, this helps in identification and tracking of coastal ice into the deep basins. Based on a linear-mixing/fractionation model, the stable-isotopic composition of sea ice has furthermore been utilized to reconstruct the formation and growth of sediment-laden ice in the Laptev Sea.
- (2) For a given parent water-mass composition, the growth-rate dependent fractionation of stable isotopes during ice accretion allows a reconstruction of the growth history and - through integration of surface-energy balance data - the oceanic heat flux at the base of the ice cover. In the Transpolar Drift, where isotopic gradients in the surface water are associated with the entrainment of Atlantic water into the Arctic halocline, the isotopic ice-core record may provide insight into the spatial and temporal variability of entrainment processes.
- (3) The pronounced isotopic contrast between snow and ice meltwater and the strong seasonality of the melt signal can furthermore be utilized in studies of meltwater dispersal in the ice cover and the underlying water layers. Recent work at the SHEBA field site has demonstrated the great potential of fluorescent tracers in determining lateral and vertical advection of meltwater and associated heat transport through the ice cover on time scales ranging from hours to several weeks. It was shown that hydraulic properties and processes may play an important role in controlling the evolution of summer ice albedo.

P07/W/14-A3

1035

**THE APPLICATION OF RADOTRACEDERS TO A STUDY OF BLACK SEA CIRCULATION: VALIDATION OF NUMERICAL SIMULATIONS AGAINST OBSERVED WEAPON TESTING AND CHERNOBYL 137CS DATA**

J. V. STANEVA, E. V. Stanev (both at the University of Sofia, 5 J. Bourchier Street, Sofia 1126, Bulgaria, Fax: +359-2-9625276; e-mail: joana@phys.uni-sofia.bg); Ken. O. Buesseler (Department of Chemistry and Geochemistry, Woods Hole Oceanographic Institution, Clark-447, Woods Hole, MA 02543 USA); Hugh D. Livingston (IAEA Marine Environment Laboratory, Monaco)

In this paper, we use the distribution of the artificial radionuclide, 137Cs, to investigate mixing and ventilation in the Black Sea. Time-series data of vertical radionuclide distributions are combined with model simulations in order to follow the magnitude and depth of penetration of surface ocean water into intermediate depths, below the oxic/anoxic interface. Simulated data are produced by a three-dimensional circulation model that includes a new parameterization of the Bosphorus inflow/plume to simulate the effects of Mediterranean water on internal mixing. A radioactive tracer model for pre-Chernobyl 137Cs (weapon testing 137Cs) and Chernobyl 137Cs is coupled to the circulation model. The model results are compared to field data collected between 1986 and 1992. The main output from the simulations is the identification of the contribution of entrainment in the mixing of surface waters into subsurface layers. The trend of tracer penetration into the deeper layers following isopycnal surfaces is well demonstrated in the model and is consistent with the known circulation and physics of the Black Sea. The correlation between the activities of radionuclides and salinity, found in the field data, is supported by the simulations. These model results illustrate that the time-space abundance of the existing field data is sufficient for reconstructing the distribution of tracers in space and time, provided reliable estimates of Black Sea circulation exist.

P07/L/02-A3

1125

**REGIONAL AND INTERANNUAL DATA ARCHIVED BY DRIFTING ARCTIC SEA ICE**

S. PFIRMAN (Barnard College, Columbia University, New York, NY 10027-6598, USA, Email: spfirman@barnard.columbia.edu); H. Eicken (Geophysical Institute, University of Alaska, Fairbanks, AK 99775-7320, USA); R. Colony (International ACSYS Office, Postboks 5072 Majorstua, N-0301 Oslo, Norway); P. Schlosser (Lamont-Doherty Earth Observatory of Columbia University, Palisades, New York, 10964); I. Rigor (University of Washington, Polar Science Center, 1013 NE 40th Street, Seattle, WA, 98105); R. Morlock (Lamont-Doherty Earth Observatory of Columbia University, Palisades, New York, 10964); D. Bauch (GEOMAR, Kiel, Germany)

Arctic sea ice drift trajectories coupled with measurements of d18O values in cores from multiyear ice floes can provide information on regional and interannual variations in sea surface d18O values. The isotopic composition of newly formed sea ice is influenced by the parent water d18O composition and fractionation during ice formation. Under floe ice accretion can be estimated by an ice growth model. Drifting sea ice trajectories are reconstructed from the International Arctic Buoy Programme database. Stepping back along the trajectory, sea surface d18O values are derived from either the measured profiles or a gridded compilation of measured sea surface d18O values. Comparison of the two approaches yields information on regional and interannual variations in sea surface d18O along the drift trajectories as well as ice accumulation and hence heat flux along the drift track. Errors include: 1) errors in ice floe trajectories, 2) volume averaging in core samples, and 3) misrepresentation of energy balance terms at the upper or lower surface.

**P07/W/15-A3 1145****ADDITION OF GLACIAL MELT WATER TO ANTARCTIC SHELF WATERS DERIVED FROM HELIUM ISOTOPES**

Peter SCHLOSSER (email: [peters@ldeo.columbia.edu](mailto:peters@ldeo.columbia.edu); Department of Earth and Environmental Sciences, Columbia University, NY; Lamont-Doherty Earth Observatory of Columbia University), Roland Hohmann, Andrea Ludin, and Ralf Weppernig (all at Lamont Doherty Earth Observatory, POB 1000, Palisades, NY, 10964)

The ice shelves surrounding Antarctica contain about 10 percent of atmospheric air. During melting of the glacial ice a significant fraction of this air is dissolved in the sea water. Helium has the lowest solubility among the gases contained in air. Therefore, the melt water is highly supersaturated in helium. The helium signal imprinted by addition of glacial meltwater can be detected in large portions of the shelf region of the Southern Ocean.

Here we present He-4 data from all sectors of the Southern Ocean and interpret them in terms of addition of glacial meltwater to the shelf waters, as well as the deep and bottom waters. An attempt is made to quantify the flux of glacial meltwater into the individual water masses around Antarctica. Where available, the helium data are compared to stable isotope ratios of water.

**P07/E/04-A3 1205****ANALYZING ANTARCTIC BOTTOM WATER FORMATION IN A GLOBAL ICE-OCEAN MODEL USING PASSIVE TRACERS**

Jean-Michel CAMPIN and Hugues Goosse (Institut d'Astronomie et de Géophysique G. Lemaître, Université Catholique de Louvain, 2 ch. du cyclotron, 1348 Louvain-la-Neuve, Belgium, email: [campin@astr.ucl.ac.be](mailto:campin@astr.ucl.ac.be) and [hgs@astr.ucl.ac.be](mailto:hgs@astr.ucl.ac.be))

Antarctic Bottom Water (AABW) is formed near Antarctica. In those regions, the brine released on the continental shelf during ice formation is responsible for an increase of the water salinity. After mixing with ambient water (mainly Circumpolar Deep Water) at the shelf break this salty and dense water sinks along the shelf slope and invades the deepest part of the global ocean. Ocean General Circulation Models generally fail to represent this mechanism correctly. Two potential causes of this problem are a too simple parameterization of the sea-ice influence and the difficulty to simulate the downward movement of the dense water along the slope in large-scale models. In the present study, AABW formation is analyzed in a global coupled ice-ocean model which takes into account these two processes: the sea-ice component has a representation of both thermodynamic and dynamic processes and the ocean component includes an explicit parameterization of downsloping flows. The investigation of the T-S properties of the water masses in the Southern Ocean shows that the model is able to reproduce the main characteristics of AABW although regional differences are not well represented. In addition, the CFC concentrations computed by the model compare favorably with observations. They depict the pathway of the newly formed bottom water and offer a quantitative estimate of the recent ventilation of the Southern Ocean. The simulated natural C14 distribution extends this estimation to longer time scales and provides supplementary information concerning the water masses involved in AABW formation.

**P07/W/11-A3 1225****AN OXYGEN ISOTOPE DATA SET FOR MARINE WATERS: DEEP CONVECTION IN THE NE PACIFIC?**

Grant R. BIGG (School of Environmental Sciences, University of East Anglia, Norwich, NR4 7TJ, U.K., email: [g.bigg@uea.ac.uk](mailto:g.bigg@uea.ac.uk)); Eelco J. Rohling (School of Ocean and Earth Sciences, University of Southampton, Southampton Oceanography Centre, Southampton SO14 3ZH, U.K., e-mail: [ejr@soc.soton.ac.uk](mailto:ejr@soc.soton.ac.uk))

The proportion of  $^{18}\text{O}$  in a sample of seawater is an excellent tracer of its past history as, away from the surface, it is conservative and also non-dynamical. The range of values in source waters is also large, and the accuracy achievable in modern measurement high. Here we bring together for the first time a global dataset of over 6000 individual measurements from the past 40 years. The properties of this dataset are described. Noteworthy features include the hitherto unnoticed, but distinctive, contribution of Pacific intermediate water to the  $^{18}\text{O}$ :salinity relationship, and different origins of the deeper waters of the Atlantic and Pacific Oceans. As an illustration of the contribution that this dataset could make to oceanography we examine evidence in the  $^{18}\text{O}$  distribution for at least occasional deep convection in the Gulf of Alaska of the North-east Pacific.

Wednesday 21 July PM

**P07/E/01-A3 1400****ENVIRONMENTAL CONTROL ON MEDITERRANEAN SALINITY AND  $\Delta^{18}\text{O}$** 

Eelco J. ROHLING (School of Ocean and Earth Science, Southampton University, Southampton Oceanography Centre, Southampton SO14 3ZH, United Kingdom, email: [E.Rohling@soc.soton.ac.uk](mailto:E.Rohling@soc.soton.ac.uk))

A simple box-model presenting the long-term average Mediterranean is developed that resolves, within one system, for change in both salinity (S) and  $\Delta^{18}\text{O}$ . In spite of its basic configuration and schematic input, the model successfully approximates: (1) present-day Atlantic-Mediterranean salinity and  $\Delta^{18}\text{O}$  contrasts (using relative air humidity of 70%); (2) millennium-scale variability in Mediterranean inflow volume as also inferred from micropaleontological records; and (3) general changes in basin-average planktonic foraminiferal carbonate  $\Delta^{18}\text{O}$  since the last glacial maximum. This justifies the use of the model to explore the nature and principal causes of temporal changes in Mediterranean S and sea-water  $\Delta^{18}\text{O}$  (SM and dM, respectively). The model indicates that dM shows temporal variability of much greater amplitude than SM. Relative to the present, reversed Atlantic-Mediterranean  $\Delta^{18}\text{O}$  gradients may have occurred, while present-day type salinity gradients were maintained, albeit somewhat weakened. A strong temporal variability is observed of the non-proportionality between dM and SM responses to forcing by an internally consistent set of environmental changes. Consequently, the results suggest that oxygen isotope results cannot be used to reliably approximate paleosalinity change in the Mediterranean. However, oxygen isotope residuals still hold vital information on interactions between the freshwater cycle and advective processes, and so remain an important element in studies of the (paleo-)circulation state of the basin. From foraminiferal carbonate  $\Delta^{18}\text{O}$  records, it has been inferred that distinct dM depletions occurred during sapropel deposition. The model results immediately imply that such depletions are possible only if run-off at those times was isotopically more depleted than today. The model results also allow speculation on the nature of particularly strong depletions such as observed in sapropel S5 from the penultimate interglacial maximum. These can no longer be interpreted as immediate evidence of major freshening of Mediterranean surface waters, but might equally likely have resulted from slight (of order 5%) increases in relative air humidity over the basin, relative to the present.

**P07/E/03-A3 1430****HOLOCENE MONSOONAL AND UPWELLING RECORDS DERIVED FROM THE MARGIN SEDIMENTS OF THE EASTERN ARABIAN SEA**

B.L.K. SOMAYAJULU, A. Sarkar, R. Agnihotri, R. Ramesh, K. Dutta, R. Bhushan. Oceanography & Climate Studies Area, Physical Research Laboratory, Ahmedabad 380 009, India, e-mail: [soma@prl.ernet.in](mailto:soma@prl.ernet.in) A.J.T. Jull, G.S. Burr (NSF Arizona AMS Facility, The University of Arizona, Tucson, AZ 85721, USA, e-mail: [AMS@physics.arizona.edu](mailto:AMS@physics.arizona.edu))

Eastern continental margins of the Arabian Sea viz. West Coast of India experience widely varying annual rainfall, ~30 cm at 22°N to ~250 cm at ~9°N peaking to ~400 cm at ~13°N. Between ~200 m and ~1000 m, the waters are perennially anoxic and upwelling induced biological productivity results in high concentrations Corg (~2% - ~6%) in the underlying sediments. Five of the ten gravity cores dated by AMS  $^{14}\text{C}$  on planktonic foraminiferal separates yielded fairly uniform sedimentation rates (4-100 cm/k yr) three of which have so far been studied for paleomonsoonal and productivity and/or upwelling trends using  $\delta^{18}\text{O}$ ,  $\delta^{13}\text{C}$ , Corg, Sr/Al, Ba/Al as proxies.

We infer that the Evaporation-Precipitation (E-P), decreased steadily during the last 10 Ka, indicated by  $\delta^{18}\text{O}$  of G. sacculifer, after correcting for SST variations, which are minor. Such a trend is also shown on Corg (%) and Sr/Al, indicators of productivity. Significant periodicities of 700 and ~1450 years seen in  $\delta^{18}\text{O}$  record indicating possible teleconnection with the North Atlantic Oscillation.

**P07/W/09-A3 1450****TESTING ASSUMPTIONS FOR STABLE ISOTOPE PROXY DATA: WHAT CAN MODELS TELL US?**

Gavin SCHMIDT (NASA Goddard Institute for Space Studies and Center for Climate Systems Research, Columbia University, 2880 Broadway, New York, NY 10025, USA, Email: [gschmidt@giss.nasa.gov](mailto:gschmidt@giss.nasa.gov))

The ratio of oxygen isotopes ( $\text{O-18}$  to  $\text{O-16}$ ) in foraminiferal carbonate deposits in ocean sediments and corals is a record of both the ambient ratio of the oxygen isotopes in the surrounding seawater and the temperature-dependent fractionation that occurs as the carbonate precipitates from the seawater. In addition, the record contains influences of thermocline or seasonality changes on planktonic foraminiferal ecology. All these factors are functions of climate.

We attempt to untangle these competing effects using results from the GISS global ocean model with water isotope tracers, in conjunction with simple ecological models that forward model the isotopic signals recorded in the carbonate. Models of planktonic foraminiferal abundance estimate the distribution in the vertical over time as a function of monthly column temperature, season, light intensity and density stratification. Carbonate is assumed to precipitate in isotopic equilibrium contemporaneously with abundance. Comparisons with core-top data show reasonable matches when conditions typical for *N. pachyderma* (l), *G. bulloides* and *G. ruber* (white) are used.

Time series of these virtual proxy data as the model climate changes are then examined to investigate the accuracy of derived climatic variables (SST, SSS) and the sensitivity of the results to changes in the assumptions concerning foraminiferal growth and seawater isotopic variation. Error estimates for paleo-temperatures and paleosalinity records are given for different regions. Errors due to measurements are generally negligible, however, errors due to the "goodness of fit" of various regressions used in calculations can be significant. In regions such as the North Atlantic, co-variance of  $\delta^{18}\text{O}$  and temperature are the biggest source of error in paleo-temperature reconstructions. For paleo-salinity calculations, the largest errors occur because of the differences between temporal and spatial  $\delta^{18}\text{O}$ : salinity relationships and through the use of non-concurrent temperature measurements.

**P07/W/10-A3 1510****HIGH-RESOLUTION CORAL  $\delta^{14}\text{C}$  RECORDS FROM THE TROPICAL AND SUB-TROPICAL PACIFIC: RECONSTRUCTING OCEAN DYNAMICS.**

T.P. GUILDERSON (Center for AMS, LLNL, Livermore CA), D.P. Schrag (Harvard Univ., Cambridge MA), M. Kashgarian, and J. Southon both at (Center for AMS, LLNL, Livermore CA).

We have generated several new near-monthly resolution, coral-based, post-bomb radiocarbon ( $\delta^{14}\text{C}$ ) time series from the subtropical and tropical Pacific. In general, the subtropics (Hawaii, Rarotonga) have higher  $\delta^{14}\text{C}$  reflecting the stability of the gyres and high air-sea exchange.  $\delta^{14}\text{C}$  in the eastern equatorial Pacific (Galapagos) are lower and reflect the subsurface pathway of the Equatorial Undercurrent and entrainment of deeper thermocline waters which feed the upwelling in this region. Radiocarbon values in the "warm pool" region (Nauru) are intermediate between the higher subtropics and those in the east. The long-term trend reflects the invasion of bomb-  $^{14}\text{C}$  into the surface ocean. The post-bomb maxima in the subtropics is reached in the early 1970s whereas at Nauru and Galapagos it is delayed by 10 years. The delay is a consequence of the subsurface history of waters upwelling in the east and the subsequent advection and mixing of these waters in the west. Superimposed upon the long term trend is seasonal to interannual variability. The patterns of radiocarbon variations in the Galapagos timeseries can be explained in terms of variability in the intensity of upwelling and changes in source water feeding the upwelling. During ENSO warm events, the depth of the thermocline increases in the east so that Ekman pumping no longer brings water from the undercurrent to the surface. This creates high  $\delta^{14}\text{C}$  anomalies in the coral timeseries which are most pronounced from July through September. Large interannual variability is observed in the Nauru record and also follows ENSO. During ENSO warm phases  $\delta^{14}\text{C}$  is higher reflecting the reduction of low- $^{14}\text{C}$  water upwelling in the east and the invasion of subtropical water into the western equatorial tropical Pacific. Warm events tend to be sharply terminated with sharp overshoots. These series of coral records demonstrates the potential for using radiocarbon time series for documenting variability in Pacific shallow circulation over interannual and decadal timescales. Timeseries such of these hold great promise to augment ontime surveys such as GEOSECS and WOCE.

**P07/W/19-A3 1550****RIVER, SEA-ICE, AND PACIFIC WATER MASS COMPONENT SEPARATION FROM ATLANTIC WATER IN THE ARCTIC OCEAN USING  $\Delta^{18}\text{O}$  AND  $\text{PO}_4^{3-}$** 

Brenda EKWURZEL (email: [ekwurzel1@lnl.gov](mailto:ekwurzel1@lnl.gov)), Peter Schlosser (email: [peters@ldeo.columbia.edu](mailto:peters@ldeo.columbia.edu)), Rick G. Fairbanks (email: [fairbank@ldeo.columbia.edu](mailto:fairbank@ldeo.columbia.edu)), and Rick Mortlock (email: [mortlock@ldeo.columbia.edu](mailto:mortlock@ldeo.columbia.edu)), (all at Lamont-Doherty Earth Observatory, POB 1000, Palisades, NY, 10964, present address for Ekwurzel: Lawrence Livermore National Laboratory, POB 808, Livermore, CA 94551)

Immense river discharge combined with the small ocean basin volume gives the Arctic Ocean the distinction of having the highest percentage of river runoff of all the world ocean basins. The resulting surface mixed layer and highly stratified halocline form a low salinity layer of



water with temperatures close to the freezing point that overlie the more saline and warmer layer of Atlantic origin. Three freshwater sources maintain the halocline: river runoff, sea ice meltwater, and the low salinity Pacific Water entering through the Bering Strait.

Identifying the freshwater components in the halocline provides a clue to possible causes for the diminished halocline observed over the past few years. We use delta O-18, PO4\* (= PO43- + O2/175 - 1.95 micro mol/kg), and salinity to quantify the spatial and temporal distribution of freshwater sources in the halocline. Fractionation between the heavier and lighter oxygen isotopes due to temperature and distance from the source area results in significant depletion of O-18 in Arctic River runoff relative to Standard Mean Ocean Water. The phase transition during sea ice formation fractionates the oxygen isotopes and can be used to separate the sea ice component. The large range between the nutrient-rich Pacific Water PO4\* (~ 2.4 micro mol/kg) and the three other components (range: 0.1-0.7 micro mol/kg) make it a good tracer for the Pacific Water component.

River runoff circulation in the Kara Sea in 1993 exhibited a cyclonic circulation from the Ob and Yenisey rivers, plus a net eastward flow toward the Laptev Sea. River runoff exhibited a net eastward surface circulation in the Laptev and East Siberian Sea, with a northeastward component flowing toward the Lomonosov Ridge and Mendeleyev Ridge region in 1994...

**P07/W/02-A3****1620****CONSTRAINING OCEAN GENERAL CIRCULATION MODELS USING CFC OBSERVATIONS**

Suzanne GRAY (Department of Meteorology, University of Reading, Earley Gate, Reading RG6 6BB, UK, Email: S.L.Gray@rdg.ac.uk) Thomas Haine (Atmospheric, Oceanic and Planetary Physics, Department of Physics, University of Oxford, UK).

We have developed and tested an inverse method, based on Green's functions, for using transient tracer observations to constrain Ocean General Circulation Models. The method has been tested using a North Atlantic configuration of MICOM (the Miami Isopycnic Coordinate Ocean Model) with 4/3 degree resolution. A substantial quantity of North Atlantic CFC-11 and CFC-12 data has been collated. The fluxes of these tracers into the ocean and the errors in the fluxes and in the tracer data have also been estimated.

Systematic differences can be seen between the observed CFC concentrations and an optimal prediction of these concentrations by the model. The errors in these predictions (due to errors in the assumed tracer flux into the ocean) and in the observations are incorporated into the inverse calculation to yield a quantitative measure of the degree of fit between the predictions and the observations. A poor fit is a consequence of deficiencies in the model circulation and may be due to processes which are not well parameterized in the model. We find that the model circulation is inconsistent with the CFC dataset, the estimated tracer fluxes, and the estimated errors on scales of order a few 100 km.

**P07/W/03-A3****1640****STABLE ISOTOPES OF OXYGEN IN SEAWATER IN THE NORDIC SEAS AND NORTHEAST ATLANTIC**

Karen J. HEYWOOD, Michael P.Meredith, Timothy A. Winters, Paul F.Dennis (School of Environmental Sciences, University of East Anglia, Norwich NR4 7TJ, email: k.heywood@uea.ac.uk)

We present analysis of the stable isotopes of oxygen (O18 and O16) in seawater samples collected in 1991, 1996, 1997 and 1998 in the Nordic Seas and Northeast Atlantic. Most of the work has been undertaken through the EU MAST programme VEINS (Variability of Exchanges in Northern Seas).

In Fram Strait, preliminary calculations of the flux of meteoric water and sea ice melt out of the Arctic show a strong meteoric outflow, and negative sea ice meltwater. Negative values imply sea ice formation, equivalent to 4 m of ice. Just southwest of Svalbard, observations in the Storford plume of bottom water indicate that while the surface water is predominantly fresh due to sea ice melt, the bottom water is fresh due to mainly meteoric input (probably glacial melt from Svalbard).

Results from Denmark Strait show that between August 1972 (GEOSECS data) and August 1991, the core of Labrador Sea Water (LSW) had both freshened and increased in O18, due to changes in the formation properties of LSW. Because there is a change in O18, the freshening of LSW must be due to the inclusion of meteoric water precipitation or runoff from land/ice) and not due to changes in sea ice melt quantities or locations. In the deep water overflows, the O18 data indicate that the water has undergone sea ice freezing processes during its formation, showing that sea ice formation is an important component of the deep convection process.

In contrast, deep waters in the Faeroe-Shetland Channel are diluted with fresh water or meteoric origin (probably Arctic precipitation) and no influence of sea ice freezing processes is required. Isotope ratios in the European Shelf Edge Current, observed in the Faeroe-Shetland Channel and the Rockall Trough, imply influence of water from the Mediterranean.

**P07/W/05-A3****1700****AN ESTIMATE OF THE ANTHROPOGENIC OFFSET OF OCEANIC DELTA C-13 (DIC) BASED ON THE VENTILATION OF THE CALIFORNIA CURRENT AT 42°N**

J.D. ORTIZ 1, A.C. Mix2, P. Wheeler2, and R.M. Key3, 1Lamont-Doherty Earth Observatory of Columbia University, 2College of Oceanic and Atmospheric Sciences, Oregon State University, 3Department of Geosciences, Princeton University

Nutrient and delta C-13 (DIC) measurements from depth profiles down to 2,500 m at four stations across the California Current (42°N) constrain the magnitude of the oceanic anthropogenic delta C-13 (9DIC) shift (denoted Delta delta C-13a-p). At these stations, nitrate, rather than phosphate, provides the strongest correlation to delta C-13 (DIC). Values of Delta delta C-13a-p vary systematically as a function of water mass, similar to the pattern of Delta C-14 and Tritium penetration for these waters. Near surface waters of potential density (sq) < 25.1 and within the Shallow Salinity Minimum (sq 25.1 to 26.5) have a mean Delta delta C-13a-p offset of -0.6 +/- 0.24. This estimate is within the range of surface water values cited by Beveridge and Shackleton [1994] and suggests that near-surface waters obtain their anthropogenic signature by direct contact with the atmosphere, while waters of the Shallow Salinity Minimum (SSM) obtain their anthropogenic signature through winter ventilation of outcropping isopycnal surfaces. Below the SSM, a simple scaling argument suggests that the anthropogenic signature is transmitted diffusively across the North Pacific Intermediate water (NPIW). Our results suggest the magnitude of Delta delta C-13a-p in well ventilated waters is essentially constant, and decreases diffusively into less well ventilated waters.

**P07/W/18-A3****1720****HELIUM-3 BALANCE OF THE UPPER WATERS OF THE WEDDELL SEA: IMPLICATIONS FOR OCEANIC HEAT FLUXES**

Roland HOHMANN and Peter Schlosser (Lamont-Doherty Earth Observatory of Columbia University, Route 9W, Palisades, NY 10964-8000, USA, email: hohmann@ldeo.columbia.edu)

To a large extent the hydrographic structure of the upper waters of the Weddell Sea is the result of atmosphere/ice/ocean interaction. During winter, a seasonal ice cover develops over the marginally stable ocean surface layer. Brine release during sea ice formation induces convection in the Winter Mixed Layer (WML) which leads to the erosion of the pycnocline that separates the WML from the underlying Weddell Deep Water (WDW) and to subsequent entrainment of relatively warm, salty, low-oxygen and 3He-rich WDW into the WML. In summer, after the melting of the sea ice cover, warm and fresh Antarctic Surface Water (AASW) is formed by addition of sea-ice meltwater to the WML water and by solar heating. The remnant water of the WML is preserved as Winter Water (WW) and centers around 80 to 100 m depth. It is not possible to determine the rate of WDW entrainment into the WML directly from temperature and salinity, because the heat transferred into the WML by WDW entrainment is lost to the atmosphere by heat flux through the sea ice cover and leads, and the mixed layer salinity is altered by sea ice formation and melting. An alternative method is provided by the evaluation of gas balances (e.g. 3He) of the upper layers in the ice-covered regions. If we assume that the elevated 3He concentrations of the WML are chiefly the result of entrainment of 3He-rich WDW into the WML and that gas exchange is to a large extent suppressed by the sea-ice cover, we can convert the observed 3He excess into the apparent fraction of WDW contained in the WML and calculate entrainment rates and heat fluxes. Data obtained from samples collected during the Winter Weddell Sea Project (ANT V/2, 1986), the drift of Ice Station Weddell (ISW, 1992), and the Antarctic Zone Flux Experiment (ANZFLUX, 1994) provide a consistent picture of the entrainment of WDW into the WML and the oceanic heat fluxes in the central Weddell Sea during winter. The fraction of WDW in the WML derived from the 3He excess in the surface layer increases with latitude and reaches 20-30% at 68°S...

**P07/W/07-A3****1740****WATER MASS ANALYSIS IN THE WESTERN EQUATORIAL PACIFIC USING ANTHROPOGENIC TRACERS**

Olaf KLATT, Birgit Klein (both at Institute of Environmental Physics, Department of Tracer Oceanography, P.O. Box 330440, 28334 Bremen, Germany, Email oklatt@physik.uni-bremen.de)

During R/V Sonne cruise 113 in late 1996, in the Western Equatorial Pacific, hydrographic properties were measured as well as (anthropogenic) tracers (Chlorofluorocarbons (including CCl4), Tritium, Helium). The goal of the tracer analysis is to further our knowledge about intermediate and deep waters in this area of investigation. The anthropogenic origin of CFCs and tritium makes them useful tools to investigate water mass formation and spreading. Making use of the different input-function of the above mentioned tracer one can distinguish temporal and spatial differences in the spreading of water masses. Whereas CFCs allow a temporal differentiation, tritium measurements allow a spatial distinction of the formation areas. Helium marked the water masses at the bottom of the ocean due to the geothermal activity of the East Pacific Rise, hence it is qualified for the deduction of spreading of deep water. We found elevated CCl4 concentrations at the bottom north of the Caroline Seamounts. The presence of higher CCl4 concentrations at the bottom is interpreted as a signature of the spreading of Lower Circumpolar Deep Water (LCDW) in a western boundary current. It has been postulated that a deep boundary current should exist north of the Caroline Seamounts in which a faster advection of LCDW could be expected. The tracer measurements indicate the boundary current must include a component of LCDW which is younger than 80 years. The different behaviour of CFC and tritium leads to a large dynamical range with respect to the ratio of CFC-11 and tritium. By means of this ratio we are able to separate intermediate water masses of North Pacific origin from those of South Pacific origin.

Wednesday 21 July AM

**P07/W/01-A3**

Poster

**0900-01****210PB BALANCE IN THE SEDIMENT AND WATER COLUMNS OF THE EAST SEA**

Deok-Soo Moon (Chungnam National University, Dept. of Oceanography, Taejeon, Korea, 305-764; E-mail: s\_dsm@hanbat.chungnam.ac.kr) and Kee-Hyun Kim (Chungnam National University, Dept. of Oceanography, Taejeon, Korea, 305-764; E-mail: khkim@hanbat.chungnam.ac.kr)

The balance of radioactive lead in the East Sea was constructed by comparing the deficiency of 210Pb in given water column (its supply from the atmosphere and in situ decay of 226Ra) with inventories of excess 210Pb in underlying sediments. The scavenging effectiveness defined as the ratio of 210Pb deficiency in water column to total supply into sediment column, was estimated to be 82-98 % in regions as the shelf of Korea Strait and upper slope of Ulleung Basin, and less than 82 % in the central Ulleung Basin. These high scavenging effectiveness in coastal regions indicates that 210Pb adsorbed onto sinking particles is actively removed from water column by scavenging. A estimation of the relative importance of vertical and lateral processes in 210Pb scavenging is derived from the ratio of sediment 210Pbex inventories to the deficiency of 210Pb in the overlying water column. The 210Pbex fluxes in coastal sediment were deposited in the range of 116-170 %, compared to the values estimated from 210Pb deficiency relative to 226Ra profiles with the atmospheric flux. This is interpreted as evidence that the sea floor of these regions are supplied much fine sediment in the past 100 years compared to other regions. The increased 210Pb deliveries to these areas located in outflow of the Nakdong river is a consequence of sediment focusing in the last century, rather than surface productivity. In contrast, sediments in the central Ulleung Basin were accounted for only 35 - 70 % of the 210Pb scavenged from the overlying water column, and the remainder were transported to sinks outside the area. The data coverage is insufficient to permit a quantitative mass balance to be constructed, but cores taken in areas of frequent bottom disturbances and underlying the relatively high productivity waters have surpluses of 210Pbex.

**P07/W/04-A3**

Poster

**0900-02****FRESHWATER BALANCE OF THE LABRADOR SEA**

Samar P. Khatawala, Peter Schlosser, Richard G. Fairbanks, and Richard Mortlock  
Lamont-Doherty Earth Observatory of Columbia University, Palisades NY 10964, USA

Oxygen isotope (H2O18/H2O16)/salinity data are used to identify freshwater sources to the Labrador Sea. The dominant freshwater source for the low-salinity Labrador and West Greenland Currents is runoff into the Arctic Ocean. It is estimated that 2-3.5 m of freshwater is extracted from the water column on the Labrador Shelf to form sea ice, a process which significantly modifies the isotope-salinity characteristics of waters on the Labrador Shelf, as well as further downstream on the Scotian Shelf, Gulf of Maine, and Middle Atlantic Bight. In

the interior Labrador Sea, low-salinity water originating in the Arctic is diffusively mixed in from the boundaries and is of primary importance in freshening the upper 200m. Sea ice meltwater is added to the surface ocean by local melting of sea ice, and its influence is restricted to the upper 10-15m. We also examine the impact of interannual variations in sea ice formation on (a) the strength and T/S properties of the Labrador Current, and (b) exchange rates between the Shelf and open ocean. These results have important implications for convection in the Labrador Sea.

**P07/W/12-A3** Poster **0900-03**

**TRANSPORT OF ICELAND SCOTLAND OVERFLOW WATER FROM THE ICELAND BASIN TO THE WESTEUROPEAN BASIN**

Uli FLEISCHMANN, Reinhold Bayer, Alfred Putzka

Increased values of freon (CFC-11) and tritium at the western flank of the Mid Atlantic Ridge at 48° N (WHP A2 section) hint to newly ventilated Iceland Scotland Overflow Water (ISOW). This water has passed the Gibbs Fracture Zone (52° N) and flows topographically leaded towards the south along the Mid Atlantic Ridge. By comparison of the tracer concentrations in the eastern and western part of the eastern basin a surplus of tracers is determined. This surplus is used to calculate a CFC-11/tritium ratio age for the ISOW, which is compared with the CFC-11/tritium ratio age of the ISOW on the section WHP A1 (58° N) distance of the two sections, the area covered by the measurements with a tracer surplus on the WHP A2 section and the fraction of ISOW resulting from the ratio dating on A2 result in a lower limit for the transport of newly ventilated ISOW past the Gibbs Fracture Zone of (1.08±0.20) Sv.

**P07/W/13-A3** Poster **0900-04**

**ASSIMILATING A GLOBAL OCEAN OXYGEN-18 ISOTOPE DATA SET INTO AN OCEAN GENERAL CIRCULATION MODEL**

Martin WADLEY and Grant Bigg (both at School of Environmental Sciences, University of East Anglia, Norwich, UK, email: m.wadley@uea.ac.uk) Eelco Rohling (Southampton Oceanography Centre, Southampton, UK)

A global ocean oxygen-18 isotope data set (Bigg and Rohling, 1999) has provided a new method of validating ocean general circulation models (OGCMs). An OGCM is forced at the surface to the observed oxygen-18 isotope distribution, and the resulting modelled sub-surface distribution compared with observations. In regions of agreement between the modelled and observed values the OGCM provides a valuable tool for interpolating between sparse observations. However, in regions of disagreement between the modelled and observed oxygen-18 distributions, the use of this extra passive oceanic tracer provides a useful tool for understanding the weaknesses of the OGCM, and evaluating improvements.

**P07/W/16-A3** Poster **0900-05**

**A RESISTANCE METHOD OF TRACER DATA ANALYSIS.**

Mikhail Vladimirovich ANISIMOV, P.P Shirshov Institute of Oceanology, Nakhimovskiy pr.,36, Moscow 117851, Russia

A one-dimension task of radioactive tracer transfer is considered. The purpose is to find a space distribution of transfer coefficient, when discrete observations of concentration are available. The base is using of a "resistance" value, which is bound with transfer coefficient like an electrical resistance with conductivity. The method seems to be simple and flexible and applied to RN-222 data in the ocean.

**P07/E/02-A3** Poster **0900-06**

**STRUCTURE AND VARIABILITY OF THE THERMOHALINE FIELDS AND THE CHARACTERISTICS OF THE CURRENTS IN THE ARGENTINE ISLANDS (THE WESTERN SHELF OF THE ANTARCTIC PENINSULA) IN MARCH 1998**

Juriy ARTAMONOV, Pavel Lomakin, Irina Orlova, Juriy Popov, Vladimir Ukrainsky (all at Marine Hydrophysical Inst., 2 Kapitanskay str., Sevastopol, 335000, Crimea, Ukraine; email: ocean@mhi2.sebastopol.ua. Tel: 380 (0692)522236, Fax: 380 (0692) 444253).

The thermohaline structure and the characteristics of the currents in the region of the Argentine Island shelf on the base of CTD- and current observations during the Second Ukraine Antarctic Expedition (March 1998) are analyzed. It is shown that the vertical thermohaline structure had 2-layer stratification, which is typical for the Antarctic shelf water in the autumn season. Tidal activity is the essential factor induced variability in the thermohaline fields. Part connected with this phenomenon in the summary dispersion of the temperature and salinity on the synoptic temporal scale is estimated as 50 – 70%. Tidal currents are produced by the semi-diurnal and the diurnal tidal waves. Semi-tidal waves spread from NNW to SSE, diurnal waves – from WNW to ESE. Tidal and remainder currents were very weak. Their speeds were not more than 2-4 cm/s. Reverse and elliptic tidal currents were fixed.

**P07/W/20-A3** Poster **0900-07**

**FLOW THROUGH BATHYMETRIC CHANNELS AT THE MOUTHS OF ESTUARIES**

R. P. Mied, R. A. Handler, and T. Evans, Naval Research Laboratory Remote Sensing Division Washington, D.C.20375

In-situ observation and remote sensing imagery indicate the presence of velocity convergences located over bathymetric channels in the mouths of tidal estuaries. In the Chesapeake Bay for example, there are three such features which extend partially or completely through the mouth of the Bay. As such, they are riven by strong tidal forcing, and convergent features are formed over them. In this talk, we present numerical simulations performed to investigate these velocity structures in an estuary with a channel in an otherwise flat bottom.

The equations of motion are solved using a fully spectral code in the vertical plane (x-z) on a rotating earth. No along-channel flow variations (in the y direction) are permitted. The bottom bathymetry is generated by using a unique virtual surface approach (Goldstein et al., J. Comp. Phys., 105, 1993) in which the no-slip bottom is generated using feedback forcing. A Gaussian-shaped channel is employed to simulate typical bathymetry observed in estuarine regions. In the along-channel direction, a constant pressure gradient is imposed and the flow is integrated until a steady state results.

The simulations are performed at high Rossby number (of order unity) based on the width of the groove and a typical surface velocity. Simulations show the development of a localized surface jet co-located with a bottom feature. This bottom feature takes the form of a recirculation cell, and results from the coupling of the along-channel flow with the motion in the vertical plane. The associated across-channel surface flow in the vicinity of the jet exhibits

convergent and divergent regions, which correlate reasonably well with features observed in radar imagery. Their position and strength are seen to vary with the along-channel Reynolds number, Ekman layer thickness, and aspect ratio of the channel.

**P07/L/03-A3** Poster **0900-08**

**THE TRANSFER OF 99TC FROM SELLAFIELD TO THE ARCTIC**

Peter Kershaw (a), Lars Foyn (b), Gordon Christensen (c), Kins Leonard (a), Hilde Elise Heldal (b), Per Varskog (c); Centre for Environmental, Fisheries and Aquaculture Science (CEFAS), Pakefield Road, Lowestoft, Suffolk, NR33 0HT, UK, (b) The Institute of Marine Research, Nordnengaten 50, P.O. Box 1870, N-5024 Bergen, Norway, (c) Institute for Energy Technology, P.O. Box 25, Kjeller, Norway

Substantial increases in the discharge of 99Tc occurred in the mid-1990's, from the Sellafield nuclear fuel reprocessing plant in the UK, against the overall trend of most other radionuclides. 99Tc is long-lived radionuclide which normally is considered to behave conservatively in seawater and is readily taken up by the brown seaweed *Fucus* sp. The "pulsed" release of 99Tc in 1994-96 has provided a new opportunity to study transport pathways and transit times from the Irish Sea to other parts of the NE Atlantic and Arctic Oceans. The distribution of 99Tc has been mapped from a series of RV cruises, extending from the Irish Sea to Fram Strait and the Barents Sea. A comparison is made between the response of seawater concentrations and those in *Fucus vesiculosus* (used as a bio-accumulator) to variations in the release rates. Transit times within UK waters and the North Sea from the 99Tc data were significantly shorter than rates reported previously using other radiotracers. The possible reasons for this are discussed, together with the scope for continuing to follow this tracer as it enters the Eurasian Basin.

**P08**

**Tuesday 20 July**

**BIOGEOCHEMICAL CONSTRAINTS IN THE OCEAN: CONTROLS, MODELLING AND PREDICTION**

Location: Arts Building 1390

**Tuesday 20 July AM**

Presiding Chairs: W I Jenkins (University of Southampton, Southampton Oceanography Centre, UK) and D Smythe-Wright (George Deacon Division, NERC, Southampton, UK)

**P08/E/02-A2** **0930**

**ROLES OF BIOGEOCHEMICAL PRODUCTIVITY IN THE CARBON CYCLE USING A SIMPLE GLOBAL OCEAN MODEL**

Masahiko FUJII, Motoyoshi Ikeda and Yasuhiro Yamanaka (Graduate School of Environmental Earth Science, Hokkaido University, Sapporo 060-0810, Japan, email: fujii@ees.hokudai.ac.jp, mikedai@ees.hokudai.ac.jp and galapai@ees.hokudai.ac.jp)

A simple physical and biogeochemical ocean model is constructed. Horizontally, the global ocean is divided into four regions; i.e., the Pacific/Indian Ocean (PI), the Atlantic Ocean (AT), the Southern Ocean (SO) and the Greenland/Iceland/Norwegian Sea (GIN). The PI and AT are vertically continuous, while the SO and GIN are divided into two, the surface layers (50m thick) and the lower layers. This model is used to estimate the oceanic carbon cycle contributed by physical and biogeochemical processes. The physical parameters are chosen to represent the air-sea CO<sub>2</sub> flux, the thermohaline circulation, and vertical and horizontal diffusions. The biological productivity is controlled only by phosphate in the surface layers. The geochemical process is parameterized by a calcite productivity in the surface layers. The products are remineralized in the lower layers. The observed distributions of radiocarbon, phosphate and alkalinity are used as tracers to optimize the parameters. The total carbonate concentration is then calculated, and the vertical carbon flux is quantitatively estimated. A major feature is a clear contrast between the PI and AT; i.e., the total carbonate is richer in the PI than the AT, along with the other biogeochemical components. As the anthropogenic sources increase the CO<sub>2</sub> concentration in the atmosphere, the effects appear significantly in the AT, while a signal is extremely weak in the PI.

**P08/W/06-A2** **0950**

**BIOGEOCHEMICAL VARIABILITY AND THE NORTH ATLANTIC OSCILLATION**

Michael J. FOLLOWS, Stephanie Dutkiewicz, John C. Marshall (Program in Oceans, Atmospheres and Climate, Massachusetts Institute of Technology, Cambridge, MA 02139, USA); Watson W. Gregg (NASA/Goddard Space Flight Center, Maryland, USA)

Through better understanding of interannual and decadal climatic and biogeochemical variability in the observed record we seek to identify patterns and mechanisms which may be important in global climate change. Time-series observations of biogeochemical indicators in the North Atlantic ocean exhibit significant interannual and decadal variability which, in some cases, correlate with indices of regional climate such as the North Atlantic Oscillation (NAO) index. Remote observations of ocean colour indicate that interannual changes are manifested with coherent patterns on the gyre and basin scale.

We examine the hypothesis that biogeochemical variability in the surface ocean may, in part, be a response to variability in ocean circulation and mixing and thus reflect the large-scale patterns associated with the dominant atmosphere-ocean climate regimes of the region. We use a North Atlantic biogeochemical model driven by twelve-hourly, observed, surface wind-stress and heat fluxes, examining the variability of export and primary production and surface gas exchanges on interannual timescales. We find basin wide patterns in the biogeochemical variations of the model. These patterns resemble those in the physical forcing associated with the North Atlantic Oscillation.

In a model with highly idealised biological cycle, variability in surface heat fluxes and associated convective mixing result in significant variability of nutrient supply and export production on year to year time-scales even in the subtropical gyre where the longer term balances are dominated by advective processes. Introducing an explicit ecosystem model in order to address remote ocean colour observations, biophysical interactions result in a more complex relationship between chlorophyll, primary production and physical forcing.



P08/W/04-A2

1010

## NUTRIENT SUPPLY TO THE UPPER NORTH ATLANTIC OCEAN: A MODEL STUDY

A. OSCHLIES, W. Koeve (Institut fuer Meereskunde, D-24105 Kiel, email: aoschlies@ifm.uni-kiel.de); V. Garcon (UMR5566/LEGOS, F-31401 Toulouse, email: garcon@pontos.cst.cnes.fr)

A high-resolution coupled biological-physical model of the North Atlantic is used to investigate regional patterns of nitrogen supply and primary production. For the subtropical gyre, episodic nutrient pulses by eddy-induced upwelling have been suggested to explain why geochemical estimates of nitrate supply to the euphotic zone are an order of magnitude higher than biological and physical ones. This is investigated by varying the level of activity in the model by assimilating altimeter data and by changing the parametrization of horizontal friction. It is found that eddies contribute about one third of the nutrient input into the subtropical Atlantic. The associated mechanisms of the eddy-induced supply are discussed in relation to that of mean advection and different representations of subgrid-scale diapycnal mixing. At higher latitudes, the main pathway of nutrient supply is via deep winter mixing which, after rapid shallowing of the mixed layer, leads to a spring bloom. When forced with daily atmospheric fluxes from the ECMWF reanalysis, the model shows both typical spring blooms characterized by a rapid development of a shallow phytoplankton bloom which is terminated by depletion of nutrients, as well as transient blooms characterized by intermittent chlorophyll maxima separated by phases of a deepening mixed layer. Both simulated scenarios agree well with observations taken at the JGOFS NABE (47N, 20W) site in 1989 and 1992, respectively. The interannual differences in spring bloom development, corresponding nitrate supply, and primary and export production are shown to be closely related to surface heat flux patterns.

P08/E/07-A2

1050

## THE VARIABILITY OF EXPORT PRODUCTION OVER THE NORTH ATLANTIC

ALISON J. McLAREN, Richard G. Williams (Oceanography Labs., University of Liverpool, Liverpool, L69 3BX, U.K.); Michael J. Follows (Program in Oceans, Atmospheres and Climate, MIT, Cambridge, MA 02139, USA.)

The dominant physical processes that supply nutrients to the pelagic ecosystems are advection by the circulation and convective mixing. The variability of these physical processes is predicted to cause changes in export production. Follows and Marshall (1999) show that changes in convection linked to the North Atlantic Oscillation (NAO) affect the interannual variability of export production. However, it is unclear which physical process will cause the longer term variability in export production.

An idealised ocean basin model is used to investigate the variability of export production during a five year period with the same NAO phase. The model results suggest that the initial change in the export production in a subtropical gyre is controlled by the anomalous convective supply of nutrients. However, after several years, the anomalous export production is caused by the advective supply of nutrients. During NAO conditions, the changes in advection and convection reinforce each other to enhance or reduce export production over the subtropical gyre. In contrast, the advective and convective changes oppose each other in the subtropical gyre. A method is developed to quantify the variability of the horizontal Ekman advection of nutrients using available data for the North Atlantic; this Ekman supply is particularly important along the flanks of the subtropical gyre (Williams and Follows, 1998). The Ekman nitrate supply into the subtropical gyre is found to follow the NAO cycle and vary annually by up to 40% from the annual mean during 1945-93. This variable Ekman supply is expected to cause changes in the export production when the NAO remains in the same phase for several years.

P08/W/09-A2

1110

## REDFIELD RATIOS IN THE DEEP EASTERN NORTH ATLANTIC

Uli FLEISCHMANN, Alfred Putzka and Alexander Sy

The Redfield ratios for the deep eastern North Atlantic are a difficult subject because of the complex mixture of water masses. This mixture is analysed with a quantitative water mass analysis for a collection of hydrographic data from the deep eastern North Atlantic between 10° N and 60° N. A multiparameter approach was used for this based on the parameters potential temperature, salinity, oxygen and nitrate. A consumption quantity which accounts for oxygen consumption ( $\Delta O$ ) and nitrate ( $\Delta N$ ) remineralisation is included in the analysis. The ratio of  $\Delta O:\Delta N$  in the consumption quantity is varied in the range from 8:14. A  $\Delta O:\Delta N$  ratio of 9 is found to be the best estimate from considerations of the phosphate values, their remineralisation and the quality of the representation of the mixture. The resulting range of the Redfield ratios for the deep eastern North Atlantic is 1:(14.9-15.8):(132-150) for  $\Delta P:\Delta N:\Delta O$  with an optimum at 1:15.3:137.

P08/W/02-A2

1130

AN EVALUATION OF GAS-EXCHANGE PARAMETERIZATIONS USING A GLOBAL MODEL OF THE OCEANIC N<sub>2</sub>O FLUX AND DISTRIBUTION

P. SUNTHARALINGAM (Department of Earth and Planetary Sciences, Harvard University, Cambridge, MA 02138, USA, email: pns@europa.harvard.edu); J. L. Sarmiento (Atmospheric and Oceanic Sciences Program, Princeton University, Princeton, NJ 08544, USA, email: jls@splash.princeton.edu)

A significant source of uncertainty in deriving large-scale oceanic flux estimates directly from surface partial pressure anomalies arises from the parameterization of the gas-exchange coefficient relating the two quantities. In this study, global ocean general circulation model simulations of the marine nitrous-oxide distribution and sea-air flux are used in conjunction with observations of surface N<sub>2</sub>O partial pressures to evaluate the performance of two commonly used wind-speed dependent parameterizations, namely, Wanninkhof (1992), and Liss and Merlivat (1986).

The net global marine N<sub>2</sub>O flux of the ocean model is determined by an embedded biological source function and constrained independently by observations of excess N<sub>2</sub>O and Apparent Oxygen Utilization (AOU) at depth. The model transfer of this predetermined N<sub>2</sub>O source across the sea-air interface under different gas-exchange parameterizations gives rise to different surface distributions of the air-sea partial pressure anomaly. These are then compared to observational values to evaluate the success of each gas-exchange formulation. Results indicate that the larger averaged transfer coefficients provided by the Wanninkhof (1992) parameterization produce modeled N<sub>2</sub>O partial pressure anomalies closer to the observed levels. The sensitivity of our conclusions to the assumptions of the underlying biological and circulation models will also be discussed.

P08/W/03-A2

1150

## AIR-SEA EXCHANGE COEFFICIENTS OF GASES

David WOOLF (School of Ocean and Earth Science, University of Southampton, Southampton Oceanography Centre, European Way, Southampton SO14 3ZH, UK, email: dkw@mail.soc.soton.ac.uk)

Some recent laboratory experiments give new insights into the kinetics of air-sea gas exchange. Processes and rates of gas exchange are investigated in two sets of experiments. In the first set, gas transfer is measured at moderate wind stress, with and without artificial bubble plumes. The gas supply to the bubbles is manipulated, allowing the contribution of sub-surface bubbles (bubble-mediated transfer) and surface exchange (including that resulting from surfacing bubble plumes) to be separated. In the other experiments, gas transfer is measured at high wind stresses, but low rates of bubble entrainment (relative to the ocean).

Tuesday 20 July PM

P08/W/07-A2

1400

## COUPLED PHYSICAL/BIOLOGICAL MODELLING IN THE ANTARCTIC POLAR FRONT

CH. DIETERICH; I. Hense; R. Redler (Alfred Wegener Institute, 27568 Bremerhaven, Germany); C. Böning (Institute für Meereskunde, 24105 Kiel, Germany)

During JGOFS cruises in the Atlantic sector of the Southern Ocean relatively high chlorophyll concentrations were observed along the Antarctic Polar Front. It has been hypothesized that small-scale variability plays a major role in setting up the prerequisites for phytoplankton growth. Enhanced vertical transports of nutrients and trace elements along the front, mesoscale upwelling and shallow mixed layers promote phytoplankton blooms.

To investigate the influence of mesoscale dynamics on the regional ecosystem we use a coupled physical/biological model. The physical model is a primitive equation model encompassing the South Atlantic Frontal System from about 60S to 40S, run in both eddy-resolving and non eddy-resolving resolution. It has been developed in the framework of FLAME (Family of Linked Atlantic Model Experiments). The physical model is coupled with an ecosystem model, with special emphasis on the regional phytoplankton community. In sensitivity studies with the physical model we examine the impact of mesoscale variability on phytoplankton dynamics.

P08/W/08-A2

1420

## A COUPLED PHYSICAL-CHEMICAL-BIOLOGICAL MODEL OF THE INDIAN OCEAN

P.S.SWATHI and M.K.Sharada (CSIR Centre for Mathematical Modelling and Computer Simulation NAL Belur Campus, Bangalore 560 037, India, e-mail: swathi@cmmacs.ernet.in, sharada@cmmacs.ernet.in); K.S.Yajnik (Regal Manor, 2/1 Bride St., Langford Town, Bangalore 560 025, India, e-mail: ksy@letterbox.com)

A coupled physical-biological-chemical model for studying the time-variation of primary productivity and air-sea carbon-dioxide exchange in the Indian Ocean is being developed at C-MMACS. The physical model is based on the Modular Ocean Model, Version 2 (MOM 2) and the biological model describes the non-linear dynamics of a 7-component system. The chemical model includes dynamical equation for the evolution of dissolved inorganic carbon (DIC) and total alkalinity. The interaction between the biological and chemical model is through the Redfield ratio. The CO<sub>2</sub> content of the surface layer is obtained from the chemical equilibrium equations of Peng et al, 1987. Transfer coefficients for air-sea exchange of CO<sub>2</sub> are computed dynamically based on the wind speeds. The coupled model reproduces the strong upwelling blooms seen during the SW Monsoon and the weak blooms in the Northern Arabian Sea in winter caused by convective overturning. The Bay of Bengal is strongly affected due to the low salinity in the area leading to a much smaller pCO<sub>2</sub> concentration than the Arabian Sea. On an annual scale the entire Indian Ocean is an out-gassing region for air-sea CO<sub>2</sub> transfer.

P08/W/01-A2

1440

## TESTING THE IRON HYPOTHESIS IN SITU IN THE PACIFIC AND ANTARCTIC OCEANS

Cliff LAW and Phil Nightingale (CCMS, Plymouth Marine Laboratory, Prospect Place, West Hoe, Plymouth, Devon PL1 3DH, UK, Email: csl@ccms.ac.uk., pdn@ccms.ac.uk. A. Watson (School of Environmental Sciences, University of East Anglia, Norwich, NR4 7TJ, UK, Email: a.watson@uea.ac.uk. P. Boyd (Centre of Excellence for Chemical and Physical Oceanography, University of Otago, Dunedin, NZ, Email: P.Boyd@alkali.otago.ac.nz).

Iron (Fe) limitation of phytoplankton productivity in the High-Nutrient Low-Chlorophyll regions of the oceans has long been suspected. However, it is only with the in situ releases into the surface waters of the equatorial Pacific within IronEx1 and IronEx2 that this has been proved conclusively. The strong response of the phytoplankton to iron addition, with chlorophyll increasing 30-fold and a decrease in surface fCO<sub>2</sub> of 70 &#61549;atm during IronEx2, supports previous observations that iron flux may influence atmospheric CO<sub>2</sub>. However increased iron fertilisation of the Equatorial Pacific may be relatively insignificant in terms of the global ocean sink. Instead consideration of ocean circulation suggests that it is the Southern Ocean where Fe-induced increases in productivity may impact the ocean carbon sink. The first in situ release of iron into the surface waters of the Antarctic took place during the SOREE cruise to the south of the Polar Front at 61-62S in February 1999. The response of the biota and the biogeochemistry will be reviewed, with re-assessment of the role of Fe in limiting productivity and the ocean carbon sink.

P08/E/04-A2

1500

SPATIO-TEMPORAL VARIABILITY OF PCO<sub>2</sub> IN THE MEDITERRANEAN SEA

Milena BEGOVIC and Claire Copin-Montégut (Laboratoire de Physique et Chimie Marines, Université Pierre et Marie Curie, Observatoire Océanologique de Villefranche-sur-Mer, 06238 Villefranche-sur-Mer Cedex, France, email: milena@obs-vlfr.fr)

Time series observations provide valuable insights into the natural seasonal variability of the oceanic carbon cycle. Monthly measurements of hydrography and biogeochemical properties have been made in the central part of the northwestern Mediterranean Sea (Ligurian Sea), in the course of the DYFAMED (France-JGOFS) operation. The annual cycle of the Ligurian Sea is defined from well-mixed conditions in winter to a progressive stratification in spring and early summer and a strong thermohaline stratification in summer and fall. So hydrological and trophic conditions encountered along the year are representative of conditions existing in large areas of the world ocean (from mesotrophy to oligotrophy). Continuous underway measurements of the partial pressure of CO<sub>2</sub> in surface water have been made monthly since February 1998, from the Riviera coast to the DYFAMED site (56 km off Nice, 43°25' N, 7°52' E) and twice a year



to Calvi (Corsica, 42°34' N, 8°45' E).

Characteristic seasonal patterns were observed along these transects. The changes in pCO<sub>2</sub> ranged in 1998 from ~315 µatm in winter, to ~450 µatm in summer. Winter mixing induced high variations of pCO<sub>2</sub> in surface waters. In February and March, the coldest waters were supersaturated with respect to the atmosphere. These cold waters result from the mixing of surface water with deep water up-welled at sea surface. On the other hand, waters of any tenth degrees warmer were largely under-saturated with CO<sub>2</sub>. This under-saturation results from the biological production, which has been emphasised by up-welling of nutrient-rich waters. Surface sea waters were under-saturated until the end of May, and become supersaturated as a consequence of the summer warming. But if pCO<sub>2</sub> values calculated at the same temperature are compared, a general trend toward a decrease in pCO<sub>2</sub> with temperature since winter months is observed. This decrease can be explained by the biological production in surface water, which should stop when surface water becomes depleted in nutrients. When surface waters are super-saturated, gas exchange of CO<sub>2</sub> with the atmosphere is not sufficient to explain this decrease. So in fact, the biological uptake of CO<sub>2</sub> should continue in absence of nutrients, which has been also observed during previous studies in the same region.

P08/E/03-A2

1520

#### MODELLING THE VERTICAL BIOCHEMICAL STRUCTURE OF THE BLACK SEA: DYNAMICAL COUPLING OF THE OXIC, SUBOXIC AND ANOXIC LAYERS

Temel OGUZ (Middle East Technical University, Institute of Marine Sciences, Erdemli, Icel, Turkey, e-mail: oguz@ims.metu.edu.tr); Hugh W. Ducklow (Virginia Institute of Marine Sciences, The College of William and Mary, Gloucester Point, VA, USA, e-mail: duck@vims.edu); Paola Malanotte-Rizzoli (Massachusetts Institute of Technology, Department of Earth, Atmospheric and Planetary Sciences, Cambridge, MA, USA, e-mail: rizzoli@mit.edu); James W. Murray (University of Washington, School of Oceanography, 104 Ocean Teaching Building, Seattle, WA 98195-7940, USA, e-mail: jmmurray@ocean.washington.edu)

The upper layer biogeochemical structure of the Black Sea is simulated using a one dimensional vertically-resolved coupled physical-biochemical model. The physical model involves the mixed layer dynamics endowed with Mellor-Yamada turbulence parameterization, and is coupled with the biochemical model by the specification of water column eddy diffusivity and temperature structures. Its biological component considers two phytoplankton species groups (flagellates and diatoms), three zooplankton size groups (micro-, meso- and macrozooplankton), bacterioplankton, particulate and dissolved organic materials. They are complemented by the equations for the ammonium, nitrite, nitrate as well as for the dissolved oxygen, hydrogen sulphide and additional ones for major redox reactions taking place across the suboxic-anoxic interface. The model is thus able to represent different biochemical processes interacting with each other in different parts of the water column, and allows a dynamical coupling between the euphotic zone, the oxycline/upper nitracline layer, the suboxic and the anoxic layers.

P08/E/01-A2

1600

#### THE POSSIBLE RELATIONSHIP BETWEEN EUTROPHICATION AND SUB-OXIC ZONE OF THE BLACK SEA

Sergey K. KONOVALOV (Marine Hydrophysical Institute, Kapitanskaya 2a, Sevastopol 335000, Crimea, Ukraine, email: sergey@alpha.mhi.iuf.net); James W. Murray (School of Oceanography, University of Washington, Box 357940, Seattle, WA 98195-7040, USA, email: jmmurray@ocean.washington.edu)

Sub-oxic zone of the Black Sea appears to be related to the nature of oxygen/sulfide interactions rather than eutrophication of this marine basin. The existing hypotheses on the nature of the sub-oxic zone cannot solve the main question about the redox imbalance of this zone. It is known that the downward diffusive flux of oxygen at the upper boundary of sub-oxic layer is 10-times larger than the upward diffusive flux of sulfide at the lower boundary. To solve the redox balance we have proposed the presence of other sinks of oxygen, beside oxidation of sulfide. We have analyzed existing data on the distributions of oxygen, sulfide, nutrients, temperature and salinity in the Black Sea from 1960 to 1995. We highlight a number of observations regarding temporal variations in the structure of sub-oxic zone and adjacent layers of water: different dynamics of the upper and lower boundary of sub-oxic zone, a correlation between the intensity of eutrophication and distribution of oxygen in the layer of the oxycline, significant correlation between apparent oxygen utilization and nitrate concentration in the middle oxycline, and a highly significant correlation between changes in distribution of nutrients. These observations suggest that about 90% of that oxygen should be consumed during oxidation of sinking particulate organic matter rather than oxidation of the upward flux of sulfide from the anoxic zone. This hypothesis highlights new links in the oxic/anoxic ecosystem of the Black Sea. It demonstrates that the entire biogeochemical structure of the Black Sea depends on the intensity of eutrophication.

P08/E/05-A2

1620

#### COMPARATIVE RELIABILITY ASSESSMENT OF VARIOUS METHODS OF PRIMARY PRODUCTION MEASUREMENTS

GORIOUNOVA V.B., Sapozhnikov V.V. (All Russian Federal Research Institute of Fisheries and Oceanography, V.Krasnoselskaya 17, Moscow, 107140, Russia, e-mail: vera@pisarev.msk.ru)

The comparative measurements of primary production (PP) with different methods: oxygen, radionucleic and with the help of sounding device PrimProd, were made during ecosystem cruise in the Norway Sea. Preliminary analysis of data showed, that the absolute values, received with the help of oxygen methods exceed those of PrimProd by 3-4 times. However, the sounding device PrimProd was calibrated using radionucleic method, and even more significant difference was obtained while comparing the results of oxygen and radionucleic methods. Radionucleic estimation of PP value was made in small volume bottles (100 ml), that provided hypertrophic growth of microheterotrophic organisms onto the walls of the bottles and so the results become lower. The sounding device PrimProd have certain advantages: it gives the opportunity of PP measuring "in situ" not only at the day time, but at night as well; it also allows more correct computation of integral PP value in photic layer. Received results were compared with the distribution of nutrients, dissolved oxygen and main hydrophysical parameters. Hydrophysical parameters' influence on the formation of mesoscale ecosystems with different values of PP is shown.

P08/W/05-A2

1640

#### EARLY DIAGENETIC CHANGES IN THE SHELF SEDIMENTS OF THE NORTH JAPAN SEA

K. ABDULLA BAVA and Ken Ikehara (Marine Geology Department, Geological Survey of Japan, 1-1-3 Higashi, Tsukuba, 305-8567 JAPAN. Phone: +81-298-543627 Fax: +81-298-543589 Email: bava@gsj.go.jp)

The exchange of dissolved substances across the sediment-water interface is an important process affecting the chemical composition of water bodies. This is particularly important for coastal marine environments, where nutrient regeneration in benthic sediments can supply a significant fraction of the nutrient requirements of primary producers in overlying water. In this investigation, sediment cores and its associated pore waters were collected from shelf region of North Japan Sea to understand the characteristics in the vertical profile of this highly productive marginal sea. Seven cores were collected using Multiple Corers and sectioned with an interval of 0.5 cm up to 10 cm and with 1 cm afterwards. Physico-chemical parameters such as Eh, pH, total C and N in the sediments and Fe, Mn, Ca, Mg, Si, Sr, Zn, NO<sub>2</sub>, NO<sub>3</sub>, PO<sub>4</sub>, and NH<sub>4</sub> in the pore waters were measured.

A general downward decrease of Eh, NO<sub>2</sub>, NO<sub>3</sub> and increase of pH, NH<sub>4</sub>, PO<sub>4</sub> in their vertical pore water profile, and C and N depletion downward in the sediment column, indicate the microbial degradation of the organic matter and remineralization. In our results, significant enrichment of NO<sub>3</sub> in interstitial waters is recorded in a thin layer of 0 to 2 and 0 to 7.5 cm in the shallower sediments and a layer of 0 to 13 cm layer in the case of deeper sediments. The sharp decline of NO<sub>3</sub> values and the uniformly very low NH<sub>4</sub> profiles at surficial levels are also noted. The consistent NH<sub>4</sub> minimum in the upper sedimentary layer is mainly caused by the chemical removal of NH<sub>4</sub> by oxidation to NO<sub>2</sub> and NO<sub>3</sub>. The increase in PO<sub>4</sub> concentration in interstitial waters with depth can be explained due to the release of PO<sub>4</sub> during mineralization of organic matter and dissolution of phosphorus bearing solid phases in the existing reducing condition. Fe and Mn distribution in the pore waters are controlled by the redox condition of the sediment. The distribution of the other elements are influenced by mobility of the Fe and Mn and their relation to other parameters are also discussed in the paper.

P08/P/01-A2

1700

#### THE STUDY OF RED TIDE FORECAST MODEL IN THE YANGTZE ESTUARY

Wang Zhengfang (Second Institute Oceanography, SAO 310012 Hangzhou PRC) I v haiYan Zhang qing lu yong (Second Institute Oceanography, SAO 310012 Hangzhou P.R.CHINA)

The study about red tide short time forecast model was carried on the Yangtze river estuary on May to August 1995 to May to September 1997. In the seasons of easy discoverable red tide, some of chemical and physical times, such as: water depth, water temperature, transparent degree, water colour, specific gravity, dissolved oxygen, chemical oxygen consumption, nutrients (N,P) were determined in the studied sea area. The result was indicated that suit to short time forecast about red tide in the Yangtze river estuary. The model is Z = SAL-3. 96DO-26. 97pH-5.42PO<sub>4</sub>-P.

P09

Monday 19 – Tuesday 20 July

#### ESTUARINE PROCESSES (IAPSO/IABO)

Location: Watson Building G23 LTA

Monday 19 July AM

Presiding Chair: M.C. Piccolo (Inst. Argentino de Oceanografía, Bahía Blanca, Argentina)

P09/W/02-A1

0910

#### OBSERVATION-BASED VERTICAL TURBULENT FLUXES OF MOMENTUM AND MASS IN A PARTIALLY MIXED ESTUARY

Hartmut PETERS (Rosenstiel School of Marine and Atmospheric Science, University of Miami, USA, email: hpeters@rsmas.miami.edu); Helmut Baumert (Hydromod Scientific Consultants, Wedel, Germany, email: baumert@hydromod.de)

Profiling microstructure measurements were made during 5 cruises in the Hudson River Estuary off Manhattan in 1994/95. Some 6000 drops taken in a relatively straight and uniform section of the estuary with typically 15 m depth cover fortnightly and tidal cycles in stratified and sheared flow of 1-2 m/s. Observed mixing characteristics show pronounced tidal and fortnightly variability, mixing across the estuarine halocline being strongest during ebbs on spring tide. The vertical (diapycnal) fluxes of momentum and mass can be estimated from the measured viscous dissipation rate, shear and stratification using a simple model for the flux Richardson number as function of the gradient Richardson number. The estimated turbulent momentum flux, or stress, and mass flux as well as the dissipation rate are related to the estuarine momentum, mass and energy balances.

P09/W/03-A1

0930

#### CIRCULATION AND MIXING IN A HYPERSALINE LAGOON

C. D. Winant, Scripps Institute of Oceanography, Centre for Coastal Studies-0209, 9500 Gilman Drive, La Jolla, CA 92093-0209. USA. E-mail: cdw@coast.ucsd.edu

Laguna San Ignacio is a coastal lagoon located along the Pacific coast of the Baja California peninsula in Mexico. Evaporation exceeds precipitation all year, and the total evaporation exceeds 2 m a year. The concentration of salt in the lagoon has been found to remain steady, therefore a net flux of salt into the lagoon must be returned to the open ocean through circulation and mixing processes. Observations made over a year-long period reveal three mechanisms responsible for this return of salt. Near the ocean, tidal pumping dominates the mixing processes. Midway between the ocean and the closed end of the lagoon, a buoyancy-driven two-layer flow carries relatively fresh ocean water into the lagoon at the surface, while salty, denser water returns to the ocean near the bottom. Near the closed end of the lagoon, where depths are shallow and wind forcing is large, a horizontally variable circulation develops which carries relatively fresh water towards the closed end over the deeper channels near the central axis, and saltier water towards the ocean over the shallower areas near the sides of the lagoon.

P09/W/07-A1

0950

## TIDAL CIRCULATION AT THE QUEQUEN GRANDE ESTUARY (ARGENTINA) MOUTH

Diana G. CUADRADO and Gerardo M.E. Perillo (both at Instituto Argentino de Oceanografía, CC 107, 8000 Bahía Blanca, Argentina, and Departamento de Geología, Universidad Nacional del Sur, San Juan 670, 8000 Bahía Blanca, Argentina, e-mail: cuadrado@criba.edu.ar, perillo@criba.edu.ar)

The Quequén Grande Estuary is located at SW of the Buenos Aires Province, Argentina. The Quequén Harbour, one of the most important harbours in Argentina, is placed at the mouth of the estuary. To accommodate the large cargo vessels that operate there, the estuary has been dredged to 12-m depth from the mouth to a distance of 2-km headward. Natural depths in the river upstream of this limit are 2-4 m. Therefore, a major step separates both reaches. We hypothesise that this abrupt change in depth introduce major disturbances in the tidal circulation within the harbour. Profiles of current velocity and direction as well as salinity and temperature were made for over a tidal cycle at three stations. One current station was placed over the step (riverside) another was placed immediately after the step (harbour side), whereas the third one was located at the harbour mouth. From the analysis of the data, we found a three layer circulation system marked by a strong stratification of the water column. There is an upper layer (1-1.5 m thick) with almost freshwater during all the tidal cycle and with water flowing seaward. A second layer is 2-3 m thick and has salinities that vary with tidal stage and with reversing current. Whereas, on the two stations located within the harbour, there is a lower layer 6-8 m thick in which the salinity is quite homogeneous on the order of 35 and practically no currents. A situation that it is not observed in the river station. A possible explanation for the phenomena is the influence of the in the tidal wave propagation within the estuary that may induce a standing wave by reflection against the step.

P09/W/11-A1

1010

## FLOW THROUGH BATHYMETRIC CHANNELS AT THE MOUTHS OF ESTUARIES

R. P. MIED, R. A. Handler, and T. Evans, Naval Research Laboratory Remote Sensing Division Washington, D.C.20375

In-situ observation and remote sensing imagery indicate the presence of velocity convergences located over bathymetric channels in the mouths of tidal estuaries. In the Chesapeake Bay for example, there are three such features, which extend partially or completely through the mouth of the Bay. As such, strong tidal forcing drives them, and convergent features are formed over them. In this talk, we present numerical simulations performed to investigate these velocity structures in an estuary with a channel in an otherwise flat bottom.

The equations of motion are solved using a fully spectral code in the vertical plane (x-z) on a rotating earth. No along-channel flow variations (in the y direction) are permitted. Using a unique virtual surface approach (Goldstein et al., J. Comp Phys., 105, 1993 generates the bottom bathymetry.) in which the no-slip bottom is generated using feedback forcing. A Gaussian-shaped channel is employed to simulate typical bathymetry observed in estuarine regions. In the along-channel direction, a constant pressure gradient is imposed and the flow is integrated until steady state results.

The simulations are performed at high Rossby number (of order unity) based on the width of the groove and a typical surface velocity. Simulations show the development of a localised surface jet co-located with a bottom feature. This bottom feature takes the form of a recirculation cell, and results from the coupling of the along-channel flow with the motion in the vertical plane. The associated across-channel surface flow in the vicinity of the jet exhibits convergent and divergent regions, which correlate reasonably well with features observed in radar imagery. Their position and strength are seen to vary with the along-channel Reynolds number, Ekman layer thickness, and aspect ratio of the channel.

P09/E/04-A1

1050

## STUDIES ON ESTUARINE MIXING ZONES AND CIRCULATION ON CONDUCT OF DESILTING ACTIVITIES

K.RASHEED and A.N. Balchand (Department of Physical Oceanography, Cochin University of Science and Technology, Fine Arts Avenue, Cochin 682 016,INDIA, email: oceans@md3.vsnl.net.in)

In tropical regions, large volume of freshwater and heavy loads of suspended sediments ultimately reach the coastal seas through narrow tidal inlets backed by extensive water bodies where complex estuarine processes occur. Sedimentation is one of the conundrums facing most of such locations and in cases of harbours added significant is attributed. In order to counteract sedimentation, planners and policy makers usually adopt dredging measures of varied degree and applications. Dredging operations in the mixing zone have proven effects to alter the circulation pattern, tidal flushing action, influence the bed load movement and distribution of suspended solids. As a case study, the features at Cochin estuary, the second largest port along the southwest coast of India is reviewed. This study brings out the various processes in the context of desilting at this estuarine harbour and attempts to explain particularly the changes in circulation pattern, salinity and suspended solids in the mixing zone under changing hydraulic conditions. The positive and negative aspect of dredging as well as the impact assessment for the region is comprehensively presented.

P09/E/06-A1

1110

## RESIDUAL CIRCULATION IN AN ELONGATED INVERSE ESTUARINE SYSTEM: THE GULF OF SUEZ, EGYPT

MOHAMMED EL-SABH (email: mohammed\_el-sabh@uqar.quebec.ca), M.A. Rady (both Département d'océanographie, Université du Québec à Rimouski, Rimouski, Québec, G5L 3A1, Canada, T.S. Murty (Baird & Associates, 1145 Hunt Club Road, Suite 1, Ottawa, Ontario, K1V 0Y3, Canada, and J.O. Backhaus (Institut für Meereskunde der Universität Hamburg, Hamburg 13, Germany

A three-dimensional non-linear hydrodynamical numerical model has been used to study the water movement in the shallow Gulf of Suez at the northern end of the Red Sea. The computational grid used to schematize the Gulf has a horizontal resolution of 3x3 km and levels at 5, 15, 30 and 60m in the vertical. The simulations were carried out separately for tidal forcing and wind forcing. Further, in each case, stratified conditions were considered to represent the state of the Gulf during late summer periods. In the case of wind-induced circulations, a uniform wind speed of 5 m/s was applied over the Gulf, blowing from NW, N and NE directions. The results suggest that the dynamics of the Gulf of Suez are governed by the interaction of wind and density forcing. Only occasionally, for instance in the vicinity of headlands and islands, tidal residuals are of similar importance. For the overall residual currents, it was found that the typical (quasi) baroclinic two-layered inverse estuarine circulation observed in the Gulf of Suez can be produced under the combined action of M2-tide and winds blowing steadily from the north-eastern direction. Northwestern and northern winds produced the reverse pattern.

P09/E/08-A1

1130

## PHYSICAL PROCESSES IN INVERSE ESTUARINE SYSTEMS

MOHAMMED EL-SABH (Département d'océanographie, Université du Québec à Rimouski, Québec, G5L 3A1, Canada, email: mohammed\_el-sabh@uqar.quebec.ca), Than H. Aung (National Tidal Facility, The Flinders University of Australia, Adelaide, S.A.-500, Australia, T.S. Murty (W. Baird & Associates Coastal Engineers Ltd, 1145 Hunt Club Road, Suite 1, Ottawa, Ontario, K1V 0Y3, Canada

An inverse or negative estuary is a semi-enclosed sea or embayment within which loss of fresh water is more than the gain by runoff and precipitation combined. The tide-averaged internal circulation comprises as outflow of saline water near the bottom and an inflow of less saline water near the surface. Inverse estuaries are not common features of the world's coastal environment and one can distinguish two subsets according to geographical location. The first subset includes those estuaries in which fresh water removal is the result of an excess of evaporation over precipitation. These mostly occur in low latitudes of both hemispheres and are associated with arid conditions (e.g. the Red Sea, the Mediterranean, the Arabian Gulf, the Adriatic and the South Australia gulfs). The second subset covers those estuarine systems in which fresh water removal is achieved by freezing and the production of sea ice, which involves rejection of salt from the ice crystal lattice and hence increases the salinity of the underlying fluid. This type is therefore confined to high latitudes and principally the polar regions (e.g. the Weddell Sea, the Ross Sea and the Beaufort Sea). Although there have been many observational and numerical studies of the dynamics of classical positive estuaries since Pritchard's pioneering work in the early 1950's, inverse estuaries have received relatively little attention. This paper reviews available literature relating to physical processes in several inverse estuarine systems and provides a framework for better understanding their characteristics and dynamics, hence providing another perspective on estuarine processes in general.

P09/P/02-A1

1150

## ESTUARINE PROCESSES AND GEOMORPHOLOGY, KARNATAKA COAST, INDIA

K S JAYAPPA (Marine Geology Faculty, Mangalore University, Mangalagangotri-574199, Karnataka, India, email: jayappa@mnglr.ernet.in).

Estuarine siltation especially during SW monsoon is a common processes of southern Karnataka coast. The two main sources of sediment input are river discharge and littoral drift. Because of continuous accumulation of sediment, the draft required for navigation is reduced and capsizing of fishing boats and loss of lives has become a frequent phenomenon. To achieve minimum depth for navigation, the channels need to be dredged regularly. To avoid littoral drift entering the estuaries, construction of breakwaters is necessitated.

Erosion of beaches close to river mouths is more complex than that of open beaches. It is more complex due to the presence of forces like tidal and fluvial currents in addition to storm waves, longshore currents and influence of man-made structures. Most of the marshy and swampy zones bordering the estuaries are getting silted. Mangroves covering tidal creeks and estuarine borders act as land builders, natural buffers and give protection to the coastline against stormy winds and floods.

Migration of estuaries and confluence of two or three of them before debauching into the sea and occurrence of various types of spits are the peculiarities of this coast. Spits indicate secreting tendency of beaches. Migrations of estuaries are mainly due to longshore drift while evolution of spits are due to longshore and river drifts. The net drift has been inferred to be southerly on the basis of accretion on updrift and erosion on downdrift directions of barriers, shifting of estuarine mouths, heavy mineral distribution, length of drift sectors and longshore sediment transport studies.

Monday 19 July PM

Presiding Chair: C.D. Winant (Scripps Inst. of Oceanography, La Jolla, CA, USA)

P09/W/01-A1

1420

## CURRENT OBSERVATIONS OFFSHORE BAHIA BLANCA ESTUARY, ARGENTINA

M. Cintia Piccolo and Gerardo M. E. Perillo (both at Instituto Argentino de Oceanografía, CC 107, 8000 Bahía Blanca, Argentina and Universidad Nacional del Sur, email: plcicolo@criba.edu.ar)

Continuous current measurements at two stations offshore Bahía Blanca Estuary (Argentina) in late spring, 1993 were employed to analyse the magnitude and relative importance of tidal and wind driven motion in the area. Hourly wind and tides were obtained from an oceanographic tower located at the mouth of the estuary and from three coastal navigation lights that cover all the coast of the study region.

Subtracting the tidal components from the original records revealed non-tidal flow. Instantaneous motion is characterised by semidiurnal tidal currents of 5-56 cm s<sup>-1</sup> amplitudes. Mean velocities at both stations (located at both sides of the estuarine mouth) were 22.6 and 22.1 cm s<sup>-1</sup>, respectively. Winds were strong practically during all the measurement period being always higher than 18-m s<sup>-1</sup> from the SE. Tidal and higher frequencies motions were smaller than the instantaneous and well correlated with the prevailing winds.

P09/W/04-A1

1440

## EFFECT OF THE EARTH FS ROTATION ON THE CIRCULATION IN ROFIS

AKIHIDE KASAI (Graduate School of Agriculture, Kyoto University, 606-8502, Japan, email: kasai@kais.kyoto-u.ac.jp) Edward Hill (School of Ocean Sciences, University of Wales, Bangor, LL59 5EY, U.K.) Tateki Fujiwara (Graduate School of Agriculture, Kyoto University, 606-8502, Japan) John Simpson (School of Ocean Sciences, University of Wales, Bangor, LL59 5EY, U.K.)

Recent surveys in various channel-type ROFIs (regions of freshwater influence) have shown considerably different flow patterns in each. A simple model including viscous effects and the Earth's rotation is proposed to explain these differences and to examine the along-channel flow pattern. Model results show that the flow pattern is strongly dependent on the Ekman number. With a large Ekman number, the system is governed by gravitational circulation and thus the along-channel density gradient is important. However, the contribution by the baroclinic component becomes large when the Ekman number is small. Density structure and residual currents were observed on the two sections in the Kii Channel, Japan. Since the Ekman number is O(10<sup>-2</sup>) in the channel and the current is highly dependent on the across-channel density structure, the flow pattern was different from those observed in many classical drowned river valley estuaries. The along channel flow in the Kii Channel was successfully reproduced by the model based on the observed density field. The model can be applied to the other ROFIs and satisfactorily explained their flow patterns. In Delaware Bay or Chesapeake Bay, contrary to the Kii Channel, shallow depth makes large Ekman numbers (~1) and the barotropic flow penetrates in the whole water.

**P09/W/10-A1 1500****OBSERVATIONS OF FRONTOGENESIS IN DIFFERENT ESTUARINE SYSTEMS**

Arnold Valle-Levinson, Center for Coastal Physical Oceanography, old Dominion University, Crittendon Hall, 768 52nd Street, Norfolk, Virginia 23529 USA, email: arnoldo@ccpo.odu.edu

Underway current velocity profiles obtained in two different estuaries (the James River and the lower Chesapeake Bay) and one coastal lagoon (Yavaros Bay in Mexico) are used to depict the appearance of surface lateral flow convergences during both flood and ebb stages of the tidal cycle. Lateral surface flow convergences appear over the edges of the channels and are produced by the phase lag of the flow in the channel relative to the shoals. In the three systems studied, flood convergences consistently develop on the right edge of the channel (looking into the estuary) in the late tidal stages. Ebb convergences appear over the left edge of the channel soon after maximum currents. Most of these convergences cause fronts in the density field and flotsam lines that also appear over the edges of the channel and that last less than two hours. In the lower Chesapeake Bay, the position of the fronts is compared to concentrations of measured near-surface chlorophyll and optical backscatter (a proxy for zooplankton). This work shows that the strength of lateral convergences along the estuary is proportional to the tidal amplitude and the channel steepness. It also suggests that the convergences are produced mainly by the tidal flow interacting with the channel-shoal bathymetry, i.e., that they do not require the presence of density gradients.

**P09/W/14-A1 1520****UPWELLING IN A SEMI-ENCLOSED COASTAL SEA INDUCED BY INTERMITTENT INTRUSION OF OCEANIC WATER**

SHIGEO KAKEHI (Graduate School of Agriculture, Kyoto University, Sakyo-ku, Kyoto 606-8502, Japan, email: kakehi@kais.kyoto-u.ac.jp) Tateki Fujiwara (Graduate School of Agriculture, Kyoto University, Sakyo-ku, Kyoto 606-8502, Japan, email: fujiwara@kais.kyoto-u.ac.jp) Satoshi Sato (Hydrographic Department Maritime Safety Agency, Japan, Minato-ku, Nagoya, 455-8528, Japan, email: sstasato@cue.jhd.go.jp) Sugiyama Youichi (Electric Technology Research Department, Chubu Electric Power Co., Inc., Midri-ku, Nagoya, 459-8522 Japan, email: Sugiyama.Youichi@chuden.co.jp)

Estuaries are affected by not only river but also ocean. Estuarine circulation, one of the dominant flows in estuaries, is the mechanism which steadily transports and lifts nutrient-rich deep water to the euphotic zone. In contrast, oceanic water may intrude intermittently into estuaries and induce sporadic upwelling. Because of the difficulty of observing the intermittent intrusion of oceanic water, its magnitude and its effect on estuarine ecosystems remain unknown.

CTD and ADCP surveys were conducted in Ise Bay, Japan, on 29 and 30 October 1994. The data observed by mooring system in center of the bay showed that oceanic water flowed into the bay on 29 October. The water, influenced by earth's rotation, flowed in along the bottom along the eastern edge of the bay. The upwelling velocity at each 1m is estimated from volume flux by residual current at 5.7m/d on 29 October, the day on which large scale intrusion occurred. This value exceeds 10 times the upwelling velocity estimated from salt budget under the steady state assumption. This suggests that upwelling induced by intermittent intrusion is larger in magnitude than that driven by the mean estuarine circulation. It is considered that large amounts of nutrients are supplied to the upper layer by this upwelling. This indicates that the intermittent intrusion plays an important role on the primary production in estuaries.

**P09/W/08-A1 1600****INTERNAL SEICHES IN THE QUEQUEN RIVER ESTUARY, ARGENTINA**

Gerardo M. E. PERILLO and M. Cintia Piccolo (both at Instituto Argentino de Oceanografía, CC 107, 8000 Bahía Blanca, Argentina and Universidad Nacional del Sur, email: perillo@criba.edu.ar)

Quequén River Estuary is one of the largest of the Buenos Aires Province (Argentina) containing one of the most important grain and fisheries harbour of the country. The last 2000 m of the estuary have been dredged to 12 m to accommodate the large cargo vessels. The average river headward of the dredging border is almost 4 m, which resulted in a 8 m step between them.

Historical tidal records from the gage located at mid distance from the mouth and the step present short period (3-25 min) fluctuations superimposed over the regular tide. These fluctuations are almost permanent with and amplitude of 4-10 cm. However, there are examples of large fluctuations up to 1.5 m that have produced serious consequences to loaded vessels.

Two tide gages sampling at 1-min interval were located at the mouth and at the step (on the harbour side) for a period of 1 month. Although no major fluctuations occurred both gages have registered the same fluctuations but displaced 3-6 min being earlier at the step. CTD data gathered at 1.5 m depth for one tidal cycle presented a similar fluctuation that occurs at a strong halocline that is present almost all the time at that depth.

**P09/E/07-A1 1620****LOW FREQUENCY RESPONSE OF BAIE DES CHALEURS, CANADA, TO WIND FORCING**

MOHAMMED EL-SABH (Département d'océanographie, Université du Québec à Rimouski, Rimouski, Québec, G5L 3A1, Canada, email: mohammed\_el-sabh@uqar.quebec.ca) Diane Lavoie (Institut Maurice-Lamontagne, B.P. 1000, Mont-Joli, Québec, G5H 3Z4, Canada)

The response of the Baie des Chaleurs (BdC), a large-scale stratified estuarine system in eastern Canada, to the passage of three storms in 1990 is discussed. Current meter, sea-level data and time-series temperature observations are analyzed and compared with output from a 3-layer numerical model. The model incorporates realistic coastal geometry and is driven by wind stress calculated from observed winds. The results show that the kinetic energy is dominated by a low frequency periods of 5-12 d, with the strongest signal at 10-12 d. This corresponds to similar variability in the synoptic wind forcing due to the rapid propagation of extratropical cyclones and the passage of pressure systems over the Gulf of St. Lawrence, including the BdC. The spectra for temperature show similar features, with the strongest signal near the density interface. The 5-12 d peak may also be related to fluctuations in the Gaspe Current, near the entrance of BdC, which are likewise correlated with wind stress at the NW of the Gulf of St. Lawrence. Further data analysis show a relationship between upwelling coastal wave propagation and alongshore wind stress in the north shore of the bay. The corresponding wave, with phase speed of 0.50 m/s, can be interpreted as a coastally trapped wave with the characteristics of a baroclinic Kelvin wave. Results from the numerical model show good agreement with observed currents in the bay during the height of the storms.

**P09/W/05-A1 1640****OBSERVATIONS AND MODEL STUDY OF THE DNIEPER-BOOG ESTUARY**

V. Serenko and V. Kovba (both at Main Ecological Inspection, Kiev, Ukraine) J. Greenfield (EPA, Athens, GA, USA) and J. Marlar (EPA, Athens, GA, USA, retired) R. Demchenko, V. Maderich, N. Margvelashvili, M. ZHELEZNYAK (all at Institute of Problems of Mathematical Machines and Systems, Glushkov pr., 42, Kiev, 252187, Ukraine; E-mail: mark@immsp.kiev.ua)

The Dnieper-Boog Estuary (DBE) located on the north-west coast of the Black Sea, is the sea's largest estuary. It is plagued with problems caused by the man-made alterations. The most important factor, which changed state of whole ecosystem, was construction of the Kakhovka Reservoir dam at approximately 60 km from the mouth of the Dnieper. Industrial and agricultural development are also significant factors. The results of observations and simulations of water quality using 1985-1998 data are presented. The two- and three-dimensional real time models, consisting of linked hydrodynamic and water quality models were applied to the DBE. The submodel of water quality simulates the transport and transformation reactions of four interacting systems: phytoplankton kinetics, the phosphorus cycle, the nitrogen cycle, and the dissolved oxygen balance. The models were calibrated using historical data from 1985 and 1987. New field data collected in 1998 by the joint USA-Ukraine project were used for verification of the models. The models reproduced the behavior of the main nutrients as well as the summer hypoxia. A set of numerical experiments was carried out to predict and assess the impact of the Kakhovka Reservoir operational mode on the environmental situation in the downstream river/estuary system. The preliminary results of this study demonstrate that decisions involving complex environmental problems can be addressed with the coupled hydrodynamic and water quality models.

**Tuesday 20 July AM**

Presiding Chair: G.M.E. Perillo (Inst. Argentino de Oceanografía, Bahía Blanca, Argentina)

**P09/W/06-A2 0850****HYPOXIA IN THE GULF OF MEXICO: POLITICAL MANIFESTATIONS OF SCIENTIFIC AMBIGUITY**

TODD M. KENNEDY and Timothy W. Lyons (Department of Geological Sciences, University of Missouri, Columbia, MO 65211, USA, Email: c694575@showme.missouri.edu)

Seasonal occurrence of hypoxia has been observed in the Gulf of Mexico since 1985. The hypoxic zone extends for up to 18,000 sq. km and encompasses up to 80% of the total water column. Hypoxia has already caused massive fish kills, significantly impacting the economy of the Gulf region and disturbing the trophically linked aquatic community. While the magnitude of hypoxia and its effects are well documented and undisputed within the scientific community, and although fertilizer usage has been identified as a contributor, there is significant scientific uncertainty in the causal relationship between upstream nutrient sources and downstream eutrophication.

Separation between cause and effect and uncertainty in the linkages between complex coupled systems is manifested in the current approaches to remediation: (1) treatment of symptoms rather than causes, (2) allocation of limited resources to address hypoxia in the context of related coastal issues [e.g., harmful algal blooms] that are politically more visible but may ultimately represent red herrings, and (3) failure to co-ordinate currently isolated efforts to address what is likely a diverse nonpoint-source pollution issue. Most intriguing about the latter is that lack of co-ordination may exacerbate hypoxia. Insular upstream efforts to reduce the flux of a specific nutrient may shift biological production downstream, facilitating accelerated oxygen consumption in the Gulf. The dilemma lies with co-ordinating the regulatory response within the time frame of the problem in an atmosphere of scientific uncertainty and disparate political and societal agendas.

**P09/W/12-A2 0910****INTRUSION OF OCEANIC WATER INTO ISE BAY AND ITS INFLUENCE ON HYPOXIA**

TETSUYA TAKAHASHI (Graduate School of Agriculture, Kyoto University, Sakyo-ku, Kyoto 606-8502, Japan, email: tetsuya@kais.kyoto-u.ac.jp) Tateki Fujiwara (Graduate School of Agriculture, Kyoto University, Sakyo-ku, Kyoto 606-8502, Japan, email: fujiwara@kais.kyoto-u.ac.jp)

Ise Bay is a semi-enclosed sea connected with the Pacific Ocean through Irako Strait and has an area of 1700 square km and mean depth of 30 m. A large amount of fresh water (annual mean: 600 cubic m/s) flows into the head of the bay and water in the bay is strongly stratified. In contrast the water column is well mixed at the bay mouth (Irako Strait) because of strong tidal stirring. This heterogeneity of stratification leads to a horizontal density gradient and strong estuarine gravitational circulation.

Below the pycnocline in the bay, severe hypoxia occurs during the summertime every year. This hypoxic water mass is cold and isolated from the surrounding waters. The supply of oxygen to the hypoxic water mass is restricted to the intrusion of the well mixed water in Irako Strait. The mixed water intrudes into the bay along isopycnals. We define the intrusion depth as the depth where the water density equals that of the intruding mixed water. The temporal variation of the intrusion depth explains the temporal and spatial variation of hypoxia. When the mixed water intrudes into the middle layer in the bay, the hypoxia progresses below the intrusion depth, and when it intrudes into the bottom layer, the hypoxia disappears. The age of the intruded water, which is defined as elapsed time after the intrusion, is estimated from the water temperature. The age explains 80% of variance in the concentration of oxygen in the bay. This indicates that physical processes can explain the major part of the behaviour of hypoxia and that the seasonal variation in density difference between the bay and shelf waters plays an important role in the development of hypoxia in Ise Bay.

**P09/W/13-A2 0930****INFLUX OF NITROGEN AND PHOSPHORUS FROM THE OUTER OCEAN INTO EUTROPHIC ESTUARIES DRIVEN BY ESTUARINE CIRCULATION**

Tateki FUJIWARA, Tetsuya Takahashi and Natsuko Uno (all at Graduate School of Agriculture, Kyoto University, Sakyo, Kyoto 606-8502, Japan, email: fujiwara@kais.kyoto-u.ac.jp, tetsuya@kais.kyoto-u.ac.jp, uno@kais.kyoto-u.ac.jp)

Nitrogen and phosphorus from human activity make estuaries eutrophic. In highly populated bay areas, such as Tokyo Bay, Ise Bay and Osaka Bay in Japan, red tide may occur throughout the year near the bay head, where large amounts of terrestrial N and P collect. Until recently it has been widely believed that the greater part of this inflow of N and P is transported to the open ocean by water exchange between the bay water and oceanic water. However, the research necessary to verify this hypothesis has not been carried out because of the difficulty of observation. We developed a method to directly measure the flux of N and P, and applied it to surveys at various cross-sections in Osaka Bay-Kii Channel System, and obtained results contrary to the previous hypothesis. We found that N and P flow into the System from the outer ocean, and their



fluxes exceed the terrestrial N and P loads.

The inflow of these oceanic nutrients is caused by the coexistence of two factors: the estuarine circulation (inflow in the lower layer and outflow in the upper layer) and nutrient depletion in the upper layer by the photosynthesis. Both phenomena are common in many stratified estuaries. We can therefore estimate that the inflow of the oceanic nutrients is not a unique but rather common phenomena.

**P09/E/02-A2**

**0950**

**A MULTI AND INTERDISCIPLINARY APPROACH IN STUDY OF ESTUARINE PROCESSES IN A TROPICAL WATERBODY**

A. N. BALCHAND, K. J. Ajith, K. Rasheed, M. G. Sreedevi, M.S. Madhusoodanan, J. K. Jossia, T.K. Anujee, P.R.Saritha and T.T.M. Asharaf (Department of Physical Oceanography, Cochin University of Science and Technology, Fine Arts Avenue, Cochin 682 016, India, email: oceans@md3.vsnl.net.in)

Tropical waterbodies exemplify complex biogeochemical processes coupled with extensive geomorphological variability capable of signaturing sensitive land sea boundary changes and (hydrological) impacts of any climate change. In addition, anthropogenic demands and varied uses have now left a very clear impression on the aquatic scenario with distinguishable marks of past two decades or more of activities. The estuarine system is currently subjected to a systems approach methodology to unravel the environmental features that has a bearing on the coastal seas. The steps covered include (1) periodic update on embank features (2) land use and practices in hinterland development (3) water resources and management plans (4) hydrological impact assessment (5) assessment of geomorphologic features (6) study of biogeochemical processes (7) identifying sensitive variables and (8) prospective planning and developmental measures. The scenario of the Cochin estuary on the tropical maritime boundary of southwest coast of India is drawn up as an illustrative case study to impress the complexities of these coastal environments.

**P09/E/03-A2**

**1010**

**ORGANIC CONTAMINANTS AND HEAVY METALS IN THE CONWY ESTUARY, NORTH WALES**

Yang P Liu, JUN L ZHOU, Tim Dunn School of Ocean Sciences, University of Wales Bangor, Menai Bridge, Anglesey LL59 5EY, UK

The Conwy Estuary is one of the largest and most westerly of the major estuaries of the North Wales coast, and drains an area of about 660 square kilometres from its source at Llyn Conwy in the mountains of Snowdonia. The estuary has rarely been studied for the presence of organic and inorganic contaminants, which may arise from the surrounding farming and mining activities, and sewage discharges. The present project aims to fill in gap in our knowledge by determining the levels of heavy metals and polycyclic aromatic hydrocarbons (PAHs), polychlorinated biphenyls (PCBs), organochlorine insecticides in water, suspended particulate matter and sediments. Results show the levels of heavy metals and organic contaminants in water are seasonally dependent, with high levels in summer and relatively low levels in winter. Metal levels suggest strong influence from mining activities, while PAH levels indicate the importance of river and sewage inputs as well as atmospheric deposition. Contaminant levels in sediments exhibit homogeneous distributions suggest strong circulations of sediment population within the estuary. The ratios of individual PAHs in sediment point to the dominance of inputs by urban activities. Finally the results are incorporated into the Estuarine Contaminant Simulator (ECOS) for simulation and prediction purpose.

**P09/W/09-A2**

**1050**

**BIOGEOCHEMICAL LOADING VIA GROUNDWATER DISCHARGE TO ESTUARIES: BARATARIA BASIN, LOUISIANA (USA)**

Jaye E. CABLE (Department of Oceanography & Coastal Sciences, Coastal Ecology Institute, Louisiana State University, Baton Rouge, Louisiana, USA 70803, email: jcable@unix1.sncc.lsu.edu) L.V. Inness (Institute for Environmental Studies and Department of Oceanography & Coastal Sciences, Louisiana State University, Baton Rouge, Louisiana, USA 70803; email: linniss@unix1.sncc.lsu.edu) E.M. Swenson and R.E. Turner (both at Coastal Ecology Institute, Louisiana State University, Baton Rouge, Louisiana, USA 70803)

Submarine groundwater inputs to marine and fresh waters are receiving increasing attention within the United States and other countries as techniques are developed to better assess this elusive component of hydrologic budgets. Techniques that have been applied to quantify this flow include seepage meters, piezometers, and naturally occurring tracers. Several studies have demonstrated the importance of groundwater inputs to estuaries and coastal waters. In fact, these subsurface flows to estuarine surface waters can be surprisingly high. Biogeochemical budgets in estuaries often neglect groundwater inputs due to the difficulty associated with quantifying this input. The overall objective of this research is to contribute to our understanding of nutrient inputs to Barataria Basin via subsurface waters using the natural tracers,  $^{222}\text{Rn}$  ( $t_{1/2} = 3.83$  days) and  $^{226}\text{Ra}$  ( $t_{1/2} = 1620$  years). A geochemical mass balance of these tracers, in conjunction with standard hydrological techniques, provides an estimate of the magnitude of groundwater inputs to the water budget of this important estuarine watershed. Nutrient concentrations (N, P) measured at each station during the study provide an assessment of the nutrient loading from groundwaters to surface waters in the basin. Key questions include (1) what are the regional magnitudes and variations (temporal and spatial) of groundwater inputs to the estuary; and (2) how does temporal variability in groundwater input affect the nutrient loading to wetlands and lakes within the Barataria Basin?

**P09/L/04-A2**

**1110**

**LINKING OFFSHORE IMPACTS TO MAINLAND WITHDRAWALS FROM REGIONAL AQUIFERS**

Sydney T. Bacchus (Institute of Ecology, University of Georgia, Athens, Georgia, 30602-2202; e-mail: sbacchus@arches.uga.edu)

Adverse impacts to surface resources beyond the points unsustainable groundwater withdrawals from the Florida aquifer have been documented throughout Florida. Unsustainable withdrawals from the same regional karst aquifer on the mainland of southeast Georgia have resulted in an estimated decline in the potentiometric surface of approximately 9 m on Cumberland Island. The majority of this largest, barrier island off the coast of Georgia was designated as a National Seashore in 1972, with 3,600 ha of the federally owned tract identified as a "Wilderness Area", to "preserve the scenic, scientific, and historical values" of this natural resource. A ground reconnaissance conducted in the vicinity of the interior "Wilderness Area" wetlands on Cumberland Island, where the greatest potential for adverse impacts related to groundwater withdrawals was predicted to occur, revealed extensive environmental damage and sinkhole-like depressions. Groundwater discharges from submarine springs and seeps are known to have decreased due

to groundwater mining on the mainland, but quantification is difficult. The hypothesis is proposed that the documented damage to the National Seashore, in addition to large scale damage to estuarine and marine resources are linked to wide-spread fluid extraction throughout the Atlantic and Gulf Coastal Plains. Detailed, multidisciplinary investigations are recommended to determine the magnitude and extent of the damage and what corrective measures can be taken.

**P09/L/01-A2**

**1130**

**BAROTROPIC CIRCULATION IN BAHÍA BLANCA ESTUARY (ARGENTINA). 1: TIDAL RESPONSE**

Elbio D. PALMA (Dpto. de Física, Universidad Nacional del Sur. Avda. Alem 1253. (8000). Bahía Blanca)

The Bahía Blanca Estuary lodges in its margins a major petrochemical industrial park, a thermoelectric plant, and an important deep-water harbor system. A better understanding of the physical properties of the estuary will certainly help in solving the pollution and dredging problems of the region. In this study the tidal wind driven response of the estuary is analyzed with a finite difference two-dimensional barotropic model which has an embedded algorithm that handles tidal flat covering and uncovering. The model is verified by comparing observed and computed water elevations in some stations. The model results show that the incident tidal wave from the Atlantic is delayed considerably as it enters the estuary channels. The wave amplitude is amplified towards the head, with channel convergence prevailing over bottom and lateral friction. A comparative study between sea surface elevation and currents lag confirms the existence of a standing wave in the main navigation channel. Experiments with the prevailing NW winds show minor modifications of surface elevations in the outer estuary and of tidal currents in the inner main channel. The simulation with the strongest SE winds ('sudestadas') produce the highest sea level changes in coastal areas, with important consequences for harbor activities.

**P09/L/02-A2**

**1135**

**BAROTROPIC CIRCULATION IN BAHÍA BLANCA ESTUARY (ARGENTINA). 2: RESIDUAL CURRENTS**

Elbio D. PALMA (Dpto. de Física, Universidad Nacional del Sur. Avda. Alem 1253. (8000). Bahía Blanca)

Tidally driven residual circulations are persistent features that contribute to the overall long-term distribution and transport of water properties. In this study we develop a depth-averaged model that includes tidal flats covering and uncovering to examine the residual circulation in Bahía Blanca estuary (Argentina). The model is integrated with appropriate boundary conditions to study the residual through-flow and the generation of residual eddies. The qualitative nature of the residual gyres is consistent with those discussed by several authors for similar coastal locations. Sensibility of the results to spatial resolution and horizontal mixing parameters are also analyzed by numerical experimentation. The dominant physical mechanism is explained by transport of vorticity from the oscillating flow to the mean field by barotropic rectification of the tidal wave. Finally, the effects of the dominant winds on the residual currents are discussed. The results stressed the importance of the open boundary treatment when studying wind driven residuals.

**P09/L/03-A2**

**1140**

**MODELLING OF THE VERTICAL CIRCULATION IN QUEQUEN HARBOR (ARGENTINA)**

Elbio D. Palma and G.M. E. Perillo<sup>2,3</sup> (1Dpto. de Física, Universidad Nacional del Sur. Avda. Alem 1253. (8000). Bahía Blanca. 2Instituto Argentino de Oceanografía Florida 400 Edificio E1. (8000) Bahía Blanca. Argentina. 3Dpto. de Geología, Universidad Nacional del Sur. San Juan 870, 8000 Bahía Blanca, Argentina.)

It has been observed that the vertical circulation in Quequén Harbor is strongly influenced by a steep bathymetric slope (step) located at the junction of the main harbor with the river. In this study a numerical model is used to examine the dynamics induced by tides and freshwater discharge in the system and to investigate the influence of the step on the circulation. Residual currents and salinity distribution obtained with the model show a two-layer circulation pattern where relatively low salinity water flows out at the surface and compensating high salinity waters from the shelf flows at the bottom. However, the model results also show that the presence of the steep slope can generate internal waves that modified the two-layer circulation mode. Sensibility experiments conducted changing the step position and depth confirms its strong influence on the harbor dynamics. During slack water time the model results show a re-circulation pattern at the base of the step. Further numerical experiments including passive tracers in the model show that this re-circulation modifies the vertical distribution of dissolved and suspended estuarine constituents.

**P09/E/01-A2**

**1145**

**THE INFLUENCE OF THE TIDES ON THE CIRCULATION OF A TWO-SILLED FJORD**

Michael W. STACEY (Department of Physics, Royal Military College of Canada, Kingston, Ontario, K7K 7B4, Canada. Email: stacey-m@rmc.ca) Yves Gratton (INRS-Océanologie, 310 Allée des Ursulines, Rimouski, Quebec, G5L 3A1, Canada. Email: yves\_gratton@uqar.quebec.ca)

A laterally integrated, two-dimensional numerical model has been used with observations of velocity, temperature and salinity to study the influence of the M2 tide on the circulation in the Saguenay Fjord. The fjord has two sills, an outer sill (approx. 30 m deep) near its mouth, and an inner sill (approx. 60 m deep) about 20 km further up-fjord. The inner sill separates the inner and outer basins of the fjord. Both basins are about 250 m deep. The fjord is highly stratified, so vigorous internal motions are generated by the interaction of the tide with the sills of the fjord. The M2 tidal velocity near the surface, and over the deepest part of the outer basin, can be greater than 1 m/s.

The M2 tide has a very significant influence on the sub-tidal circulation because much of the energy associated with the tidally-generated internal motions is dissipated in the outer basin, so there is significantly more vertical mixing there than in the inner basin. The resulting horizontal pressure gradient causes a significant (10-20 cm/s) mean bottom flow of water from the inner into the outer basin across the inner sill. Upon entering the outer basin, this water sinks almost to the bottom. This 'reverse renewal', caused by the excessive tidal mixing in the outer basin, is evident in both the observations and the simulation.

According to the numerical model, M2 tidal energy is withdrawn from the surface tide at a rate of about 50 MW. The rate of withdrawal would be about five times less if the fjord were unstratified. Most of the energy withdrawn from the surface tide is fed into the internal tide.

**P10** **Wednesday 21 – Friday 23 July****COASTAL AND SHELF PROCESSES (JOINT IAPSO/IABO)**

Location: Watson Building G23 LTA

Location for Posters: Bridge Poynting/Watson

**Wednesday 21 July AM**

Presiding Chair: John Johnson (University of East Anglia, Norwich, UK)

**PROCESSES AND CIRCULATION AT THE SHELF SLOPE (1)****Introduction** **0900**

John JOHNSON

**P10/E/23-A3** **Invited** **0910****FORCED TRANSPORT ACROSS THE CONTINENTAL SLOPE**

John HUTHNANCE (CCMS Proudman Oceanographic Laboratory, Bidston Observatory, Birkenhead, Merseyside L43 7RA, UK)

Ocean-shelf exchange is of interest as a component of the global cycling of nutrients and organic carbon (for example) and specifically for the fuelling of high primary production in shelf seas. Several ocean margin experiments concerned with this question have estimated significant cross-slope fluxes, especially down-slope export of particulate matter. However, large-scale flow across the continental slope is inhibited by geostrophy, and recent studies have suggested "shut-down" of the up- or down-slope Ekman transport below unforced along-slope flow.

External forcing appears to provide a means of resolving this apparent contradiction via sustenance of cross-slope circulation (in an up-welling or down-welling sense) including a bottom Ekman layer. The oceanic density field and associated pressure gradients, as well as winds, may provide such forcing. A parallel question is the form of boundary condition that the shelf and slope provide for ocean circulation.

These questions are explored with semi-analytic and fully prognostic numerical models. The models also indicate the importance of a non-uniform slope and of the coast which respectively aid and hinder cross-slope circulation.

**P10/W/08-A3** **0950****FLOW STRUCTURE AND SEASONALITY IN THE HEBRIDEAN SLOPE CURRENT**

ALEJANDRO J. SOUZA (Centre for Coastal &amp; Marine Sciences, Proudman Oceanographic Lab., Bidston Observatory, Birkenhead L43 7RA, UK, email: ajso@ccms.ac.uk) John H. Simpson, M. Harikrishnan and J Malarkey (all at School of Ocean Sciences, University of Wales Bangor, Menai Bridge, Anglesey LL59 5EY, UK).

We report on new determinations of the intensity, structure and variability of the slope current based on the 16 months of observations with ADCPs and conventional current meters on a cross-slope section at the Hebridean shelf edge during the SES programme.

After removal of the tidal signals, the mean flow over the upper slope is found to be closely parallel to the topography with speeds of ~20 cms<sup>-1</sup>. The flow extends down to depth of 500 m and is predominantly barotropic especially in winter when the flow is practically uniform between 350 m and the surface. In summer, there is a significant baroclinic component with a pronounced maximum in current at a depth of about 200 m but more than 80% of the kinetic energy is in the barotropic component. Flow in the core of the current is highly persistent with the Neumann's steadiness  $St > 0.8$  in summer. The cross-slope profile of sea surface elevation, computed from the mean barotropic currents, shows a consistent relation to seabed topography through the seasonal cycle. Long term averages of the cross-slope components are generally small (~2cms<sup>-1</sup>) with some indication of persistent down-slope flow in the bottom Ekman layer.

Measurements with shipboard ADCP on sections at intervals along the slope show a high degree of continuity in the structure of the flow. The core of the flow appears to be related to a weak positive salinity anomaly and a depression of the 9.5\_C isotherm near the shelf, but there is no strong correlation between the core of the slope-current and the core of the salinity anomaly. It is proposed that this may be due to differences in the cross-stream diffusion of salt and momentum which have different boundary conditions at the slope.

The observations suggest JEBAR as possible forcing mechanism for the slope current, but care should be brought to this assumption as other constraints, like homogeneous vorticity can produce a similar cross-shelf structure of the slope current.

**P10/L/03-A3** **1010****COASTAL CURRENTS DRIVEN BY WIND AND ALONGSHORE GRADIENT IN WINDCURL**

DR LIE-YAUW OEY (Princeton University, Atmospheric &amp; Oceanic Sci Program, Sayre Hall, Forrestal Campus, Princeton University, Princeton, NJ 08544, NJ 08544 USA, email: lyo@splash.princeton.edu)

When wind distribution along a coast is anisotropic, such that its cross-shore scale is smaller than its alongshore scale, the forced Kelvin wave consists of forcing by both the wind and alongshore gradient of the windcurl. The resulting evolution of the current on both the f-plane and beta-plane will be discussed, and ideas are applied to the observed seasonal variation of the coastal currents off the Southern California Bight, USA.

**P10/W/09-A3** **Invited** **1050****TRANSPORT AND RECIRCULATION IN UPWELLING FILAMENTS**

E.D. BARTON, E. Navarro Perez, R. Torres Almaraz (all at School of Ocean Sciences, University of Wales, Bangor, Menai Bridge, Anglesey LL59 5EY, UK, Email: oss041@bangor.ac.uk)

The offshore flow in upwelling filaments represents a plausible pathway for exchange between continental shelf and oceanic waters, mainly but not exclusively on the Eastern Boundaries of the oceans. However, compensating and possibly continuous return flows may result in no net offshore transport of nutrients or biogenic material. Two recurrent filaments, near 28N and 41N in the NW African and Iberian upwelling regimes, are examined to investigate the nature of the flow. One filament occurs in a relatively steady, possibly year round upwelling, while the other is located in a region of seasonal and intermittent upwelling. Both systems exhibit similar structure, despite having possibly different formation mechanisms, and both are associated with a well defined return flow on their equatorward flank. However, the time scales for circulation through the filament and return are significantly different in each location (7 and 20

days, respectively). This has clear implications for the transport of any non-conservative property advected around the system. In the NW African case, there is evidence that the filament interacts with offshore eddies generated by the Canaries archipelago to produce a net enrichment of island waters.

**P10/W/12-A3****1130****MODELLING THE CAPE GHIR FILAMENT**

Ian STEVENS and John Johnson (both at School of Mathematics, University of East Anglia, Norwich, NR4 7TJ, UK, email: i.stevens@uea.ac.uk)

Satellite imagery reveals the presence of a cool filament extending offshore from the coast of Morocco at Cape Ghir out into the Atlantic Ocean to the north of the Canary Islands. The filament appears to be a permanent feature with a seasonal variation in its zonal extent which is maximum in late summer.

A primitive equation model at 1/12° resolution covering the region between the Gulf of Cadiz and the North West African coast and including the Canary Islands has been constructed to investigate the generation mechanism of the filament.

The model reproduces seasonal variations in the surface temperature signal of the filament which compare well with the satellite observations, and also provides a description of the vertical structure of the hydrology and velocity field. Anticyclonic and cyclonic eddies trapped to the north and south of the Cape Ghir Plateau are produced in the model and these may play a role in the generation of the filament.

**P10/W/05-A3****1150****STRATIFICATION PATTERNS AND PROCESSES ON THE INNER CONTINENTAL SHELF OF THE MIDDLE ATLANTIC BIGHT**

John BRUBAKER (VIMS, School of Marine Science, College of William &amp; Mary, Gloucester Point, Virginia, 23062, USA, Email: brubaker@vims.edu)

Patterns of density stratification and dynamic stability over the inner shelf in late summer to early autumn have been investigated in a field program in the Mid-Atlantic Bight off the coast of North Carolina. Temperature, salinity, and velocity data sets from repeated shipboard surveys over a grid of stations and from an array of moored instrumentation provided complementary perspectives. In this inner shelf environment, stratification was influenced significantly by variations both in temperature and in salinity. The relative influence was quantified through computation of the separate thermal and haline contributions to the potential energy anomaly integral, which compares the potential energy of the observed, stratified water column to the potential energy it would have if it were well mixed. In August, stratification at offshore distances < 10 km was due primarily to vertical salinity structure, whereas at distances > 15 km thermal influence was usually dominant. By October, the role of thermal structure had been reduced drastically. In addition to the vertically integrated energy measure for characterizing the water column as a whole, local stratification and stability were examined in terms of buoyancy frequency and gradient Richardson number estimates. Various spatial configurations were observed, with a thermocline and halocline sometimes distinct and sometimes merged. In August, localized velocity shear layers often coincided with sharply defined pycnoclines. With respect to Richardson number values, these stratified shear flows were usually stable, although the stability was often only marginal and some instances of likely instability in limited spatial regions were observed. In October, the regions of low Richardson number were more extensive. Key physical processes underlying the variability of stratification include fresh water influence from the Chesapeake Bay outflow and wind-driven currents, particularly at the synoptic scale on which upwelling and downwelling circulation patterns redistributed the buoyancy associated with the Bay plume.

**P10/E/10-A3****1210****OCEANIC INTERNAL SOLITARY WAVES: AN ANALYTICAL MODEL FOR KDV SOLITON PACKETS**

John R. APEL (Global Ocean Associates, P.O. Box 12131, Silver Spring, MD 20853, USA; 1-301-460-7018 (V); 1-301-460-9775 (F); e-mail: globocen@erols.com)

A new analytical model for oceanic internal solitons has been constructed that is based on (a) an approximate "dnoidal" solution to the Korteweg-De Vries wave equation, and (b) solutions to the Taylor-Goldstein equation for the vertical structure function. A finite-length wave packet results that has most of the salient properties of solitons generated at continental shelf breaks and oceanic sills: rank-ordered non-linear oscillations; a packet that propagates at speeds above the long-wave linear speed; increasing numbers of oscillations and packet lengths as time goes on; and a long-term depression of the pycnocline at the rear of the packet. The packet properties derive from imposition of a shocklike initial condition which evolves into a nonlinear undulatory internal bore that decays toward a linear state at its trailing edge. Input data include the vertical density and background velocity profiles, and specification of a numerical amplitude. The resultant solitons have properties that agree quantitatively with observed packets in the New York Bight and the Sulu Sea. The solution is extended to the full cycle of the internal tide by modeling the recovery of the "solibore" trailing edge to its equilibrium state over the semi-diurnal tidal cycle. The theory connects a wave number scale  $ko$  with the amplitude  $eta$ ; from knowledge of the density and background velocity fields, and the variation of wavelengths within the packets, it is possible to construct the entire subsurface hydrodynamic field with the model. The wavelength variations come most conveniently from satellite imagery such as that from synthetic aperture radar. Thus from density data (either concurrent or historical) and a SAR image, one may arrive at reasonable estimates of the internal hydrodynamics. Predictive models can follow from the formulation. Based on a collection of images gathered from around the world, a global atlas of internal solitons is being prepared for publication.

**Wednesday 21 July PM**

Chair: Des Barton (University of North Wales, Bangor, UK)

**PROCESSES AND CIRCULATION AT THE SHELF SLOPE (2)****P10/W/18-A3****Invited****1400****RECENT DEVELOPMENTS IN WIND-FORCED UPWELLING AND DOWNWELLING**

John MIDDLETON (School of Mathematics, University of New South Wales, Sydney 2052, Australia, Email: john.middleton@unsw.edu.au)

A numerical study is made of the dynamics of the circulation that arises from forcing by a steady, uniform alongshore wind over a uniform zonal shelf in the southern hemisphere. Both upwelling and downwelling favourable winds are considered.

In the former case, the results show that most of the upwelling is confined to the region inshore

of the shelfbreak. Over the slope and within the region of wind-forcing the circulation is found to be dominated by the growth of both an anticyclonic and a cyclonic eddy, an offshore flow, and downwelling. The results are fundamentally different to the upwelling described by 2-dimensional models or by 3-dimensional linear dynamics. Two new mechanisms related to the surface mixed layer are identified as being responsible for these features of the upwelling circulation. First, the offshore advection of alongshore momentum within the surface mixed layer (SML) is shown to accelerate the alongshore current near the eastern end of the region of wind-forcing leading to a sharpening of the cross-shelf gradient of sea level, and an excess in the alongshore transport. This excess transport acts to raise sea level, leads to downwelling below the base of the SML and the growth of the anticyclonic eddy. A simple scaling is given to show that the nonlinear effects will be important for narrow, strongly stratified shelves. A second important effect is argued to result from the geostrophic cross-shelf flow that is associated with the alongshore gradients of density within the SML.

The downwelling circulation obtained by simply reversing the sign of the wind stress is also examined. Over the first 10 days, when the system is largely linear, the circulation is simply the reverse of that found in the upwelling case. However, after this time, the downwelling and upwelling circulations are notably different, and the former is dominated by the development a bottom mixed layer (depth 70m) rather than the SML. Through thermal-wind shear, an Undercurrent (UC) over the slope evolves, the bottom Ekman transport becomes small and negative leading to the detachment of flow near the shelf break, localised spreading of isopycnals and further intensification of the UC. Finally, some recent modelling developments are presented for the seasonal circulation within the Great Australian Bight. The models are nested inside the Semtner-Chervin 1/4 degree output, and contain 150X60 cells in the horizontal with 40 sigma cells in the vertical.

**P10/W/26-A3****1440****INTERANNUAL CHANGES IN THE EAST AUSTRALIAN CURRENT AS INFERRED FROM INFRARED SATELLITE IMAGERY**

W.J. EMERY (CCAR Box 431, U. Colorado, Boulder, Co., 80309 USA) and J. Wilkin (Univ. of Auckland, SEMS, Tamaki Campus, Private Bag 92019, Auckland, New Zealand)

A five-year time series of infrared satellite images is used to compute surface currents using the Maximum Cross Correlation (MCC) technique in the area off southeast Australia. All pairs of images between 4 and 24 hours separation are used to compute surface currents. A relaxation step is added to the selection of the maximum correlation greatly reducing the errors in selecting the correct end point of the vectors. In addition next neighbor filtering can now be done in time as well as in space also improving the resulting vector velocity field. The need to prefilter cloudy pixels is a limiting factor in the application of the MCC technique. The MCC surface current fields are then mapped using optimum interpolation (OI) constrained to yield a surface stream function resulting in a smooth surface current field dominated by eddies and variable mean flow. These OI current maps are used to compute Empirical Orthogonal Functions (EOFs) of the East Australian Current region. These EOFs characterize both seasonal and interannual variations in the surface currents. Wavenumber/frequency spectra are used to find the fundamental time and space scales characteristic of the East Australian Current region.

**P10/L/06-A3****1500****THE RESPONSE OF SEMI-ENCLOSED SEAS TO SYNOPTIC ATMOSPHERIC FORCING**

Christopher N.K. MOOERS, HeeSook Kang, and Lianmei Gao (OPEL/RSMAS, University of Miami, 4600 Rickenbacker Cswy., Miami, FL 33149-1098, USA, email: cmoers@rsmas.miami.edu, hkang@rsmas.miami.edu, lgao@rsmas.miami.edu)

Semi-enclosed seas are under the influence of atmospheric forcing (wind stress, surface pressure, heating/cooling, and evaporation/precipitation) on a variety of space and time scales from mesoscale to synoptic scale to intra-seasonal, seasonal/annual, inter-annual, and so forth. Here, the primary interest is in the oceanic response to synoptic scale forcing. Because of the joint effects of Earth's rotation, ocean density stratification, and continental margin topography, the response of semi-enclosed seas to synoptic forcing can be rich, ranging from transient coastal upwelling or downwelling, to coastally trapped waves, storm surges, transient jets and fronts, transient surface and bottom mixed layers, convection/ventilation, and so forth.

Numerical simulations (using POM) of the response of the Japan (East) Sea to wintertime extratropical cyclone/cold front outbreaks, and the Intra-Americas Sea to summertime tropical cyclones, are used as examples. The synoptic atmospheric forcing (with mesoscale resolution) utilized is provided by relatively new sources; e.g., a spaceborne scatterometer (NSCAT) and a mesoscale atmospheric model (MM5). By comparing with the response to more conventional, lower-resolution atmospheric forcing fields, the sensitivity of semi-enclosed seas is illustrated. Conversely, the space-time-amplitude resolution and accuracy requirements of atmospheric forcing for quality simulations of semi-enclosed seas circulation are beginning to be better defined by these response studies.

Looking ahead, the new sources of synoptic atmospheric forcing information (with mesoscale resolution) offer the potential for driving simulation and predictive models of circulation in semi-enclosed seas with higher accuracy on a routine (operational) basis.

**P10/E/17-A3****1520****CIRCULATION PATTERNS OVER THE PETER THE GREAT BAY SHELF AND ADJACENT JAPAN SEA AREA**

Vladimir Ponomarev, and Olga TRUSENKOVA (both at Pacific Oceanological Institute, 43 Baltiyskaya, Vladivostok, 690041, Russia, e-mail: archer@linkor.ru, ponomarev%dan86@poi.marine.su)

The dynamic processes associated with synoptic wind forcing and generation of topographic eddies and streamers over the Peter the Great Bay shelf and adjacent Japan Sea area are studied. The strong northern winds are typical for a cold season over the studied sea area. These winds generate upwelling and intensive water exchange between the Bay and open sea area. Satellite and CTD observations show the eddy structure of upwelling and synoptic scale multiple fronts over the shelf and continental slope. We simulated the circulation patterns in this area using the MHI numerical model developed by Naum Shapiro (Marine Hydrophysical Institute, Sebastopol, Ukraine, 1992-1998). It is the layered model based on the primitive equations and free surface boundary condition; temperature and salinity within layers and layer thickness are functions of time and horizontal coordinates. Interfaces between layers are allowed to bend up and down and layers themselves can degenerate by acquiring negligible thickness. This makes the MHI model an appropriate tool for simulation of synoptic scale vertical circulation. Numerical experiments were performed under forcing of synoptic north-western wind characterized by a strong jet directed along the axis of the Peter the Great Bay. Synoptic-scale dipole circulation patterns and streamers were obtained over the continental slope, associated with strong upwelling in the cyclonic eddy and downwelling in the anticyclonic one. Evolution of these structures and the Peter the Great current system was shown under alternative wind forcing.

**P10/E/22-A3****1600****COASTAL PROCESSES INVOLVED IN THE FORMATION OF ANTARCTIC BOTTOM WATER**

Ann-Marie M. WONG and Jason H. Middleton (School of Mathematics, University of New South Wales, Sydney, AUSTRALIA)

Antarctic Bottom Water (AABW) is the dense water mass found at the bottom of the ocean basins around the world. The major sources of AABW are the Weddell Sea and the Ross Sea, both of which are characterised by wide continental shelves and land barriers, confining the circulation of the water on the shelf so that it becomes very saline. This shelf water forms an integral part of AABW.

The region off the coast of Wilkes Land has been identified as a source of AABW. In the past this region was not considered as a significant source of AABW but more recent research suggests otherwise. Wilkes Land does not have the land barrier confining the circulation to the shelf which plays a significant role in the circulation in the Weddell Sea and Ross Sea. The region off the coast of Wilkes Land is characterised by deep depressions on the shelf, strong katabatic winds and polynyas which are believed to contribute to the formation of AABW.

A numerical modelling study of the coastal processes off Wilkes Land is being undertaken using the Princeton Ocean Model (POM). The model has been configured to capture the essential features of this region including the deep reverse sloping shelf, brine production, strong katabatic winds and coastal trapped waves. The effects of these factors on the formation of AABW are analysed from the model results.

**P10/W/19-A3****1620****CHARACTERISTIC PATTERNS OF CIRCULATION OFF THE COAST OF CALIFORNIA**

C. D. WINANT (Scripps Institute of Oceanography, Centre for Coastal Studies-0209, 9500 Gilman Drive, La Jolla, CA 92093-0209, USA, E-mail: cdw@coast.ucsd.edu)

The ocean circulation along the central and southern California coast is described in terms of a few characteristic flow patterns based on a five-year set of moored observations, drifter releases, and ship-borne surveys. The observations were carried out over the Pacific continental shelf north of Los Angeles for a distance of approximately 300 km. The characteristic patterns are similar to the synoptic patterns used by meteorologists to forecast weather. A cyclonic eddy located in the western end of the Santa Barbara Channel is the most persistent feature of the observations and is present in all patterns. In spring and summer, when winds are persistently equatorward and upwelling favorable, the current pattern is equatorward as well. Whereas in the fall and winter, when the equatorward winds have relaxed, currents shift to poleward. Two indices of forcing, the local wind stress and the alongshore pressure gradient, appear to be useful predictors of the circulation pattern.

**P10/W/17-A3****1640****SUMMER MARINE BOUNDARY LAYER DYNAMICS AROUND PT CONCEPTION, CALIFORNIA**

Clive DORMAN (Center for Coastal Studies, Scripps Institution of Oceanography, University of California San Diego, La Jolla, CA 92092-0209, USA, email: cdorman@ucsd.edu ORNIA)

A climatology is based upon a net of twenty four surface stations on land, islands, buoys and platforms around the Santa Barbara Channel/Santa Marina Basin in Southern California. Radar profiler and soundings sampled the upper air. Marine layer winds accelerate around Pt Conception to reach a maximum in the western mouth of the Santa Barbara Channel, then decelerate toward the east. This wind speed maxima is also one of the two monthly mean, summer wind speed maxima along the west coast of the United States. A sea level pressure is lowest on the north side of the channel and on the eastern end. An air temperature inversion base in the Southern California area is lowest and strongest in the western mouth of the Santa Barbara Channel. Stratus clouds are a minimum in the western portion of the Channel. The low level atmospheric structure in the vicinity of the Santa Barbara Channel is explained as a transcritical expansion fan in the marine boundary layer.

**P10/W/20-A3****1700****OBSERVATIONS AND SIMULATIONS OF THE CALIFORNIA CURRENT**

Robert L. HANEY (Department of Meteorology, Naval Postgraduate School, Monterey, CA 93943-5114, USA, email: haneyr1@met.nps.navy.mil) David E. Dietrich (Center for Air Sea Technology, Mississippi State University, Stennis Space Center, MS 39529, USA, email: dietrich@nmia.com) Robert A. Hale (Department of Meteorology, Naval Postgraduate School, Monterey, CA 93943-5114, USA, email: hale@met.nps.navy.mil)

Major observational programs in the California Current (CC) during the last 15 years have greatly increased our knowledge of the quantitative nature of this important eastern boundary ocean current. In response to strong upwelling favorable winds in spring, a surface intensified baroclinic equatorward jet, with cold offshore-directed filaments and unstable frontal eddies, develops next to the coast. The jet moves offshore during summer and fall, and is replaced by a poleward Davidson Current next to the coast in winter. There is also a seasonal signal and limited offshore propagation (to only about 128W) of surface eddy kinetic energy (EKE), with the decrease of surface EKE west of 128W attributed to an unspecified dissipation process. To help interpret the new observations, long term simulations of the CC are carried out using the DieCAST regional model. In most of the simulations, the wind stress is prescribed from monthly climatology, while the buoyancy flux is computed by damping to the mean annual cycle of temperature and salinity at the surface. The simulations reproduce the main features of the annual cycle described above, however the decrease of surface EKE west of about 128W in the simulations is due to the vertical redistribution of EKE to the deep ocean, not dissipation. Adding a realistic wind enhancement offshore of each coastal headland produces both local and remote changes to the above annual cycle.

**P10/W/29-A3****1720****USE OF MMS/SCRIPPS OCEANOGRAPHIC DATA FOR OIL SPILL RISK ANALYSIS AND OIL SPILL RESPONSE IN THE SANTA BARBARA CHANNEL-SANTA MARIA BASIN AREA**

David R. Browne

In 1991, the Minerals Management Service (MMS) entered into a Cooperative Agreement with the State of California-Scripps Institution of Oceanography (Scripps) to conduct physical oceanographic studies to determine potential environmental impacts of offshore oil and gas activities in the Southern California Bight. The result is the Santa Barbara Channel-Santa Maria Basin (SBC-SMB) Circulation Study in the primary area of active federal oil and gas



leases. Field measurements extend from April, 1992, to November, 1999, with the objective of determining characteristic flow fields and their forcing mechanisms in the SBC-SMB area for MMS oil spill risk analysis and strategic planning purposes. Six characteristic surface circulation flow patterns identified through the SBC-SMB Circulation Study are discussed in terms of their relative impact on oil spill transport. This background knowledge of characteristic flow patterns, together with real-time acquisition of currents, winds, satellite imagery, and surface drifter tracks from the study's field array is proving helpful to industry and agency tactical oil spill response efforts. During actual oil spills in the SBC-SMB area, real-time estimates of synoptic flow patterns have been used to predict, with reasonable accuracy, oil spill trajectories in this complicated oceanographic environment. Trajectory prediction performance as a result of using real-time and climatic data in past actual oil spills and oil spill drills is presented.

Thursday 22 July AM

Chair: John Middleton (University of New South Wales, Sydney, Australia)

## MESOSCALE CIRCULATION ON THE SHELF (1)

P10/L/01-A4

0930

### A CASE STUDY OF BORA-DRIVEN CURRENTS AND PO OUTFLOW SPREADING OVER THE ADRIATIC SHELF (16-20 JANUARY 1987)

Gordona Beg PAKLAR (Institute of Oceanography and Fisheries, Set. I. Mestrovica 63, 21000 Split, Croatia, email: beg@jadran.izor.hr), Vlad Isakov and Darko Koracin (both at Desert Research Institute, P.O. Box 60220, Reno, NV 89506-0220, USA, email: darko@dri.edu), Vassiliki Kourafalou (National Centre for Marine Research, Elliniko, Athens 166-04, Greece, email: villy@erato.fl.ncmr.gr), Mirko Orlic (Andrija Mohorovicic Geophysical Institute, Faculty of Science, University of Zagreb, Horvatovac bb, 10000 Zagreb, Croatia, email: orlic@olimp.irb.hr)

The bora over the Adriatic sea induces strong transient currents whose horizontal variability is mainly controlled by an orographically-induced wind-curl effect. Until now, numerical models with resolution fine enough to resolve the alongshore variability in the bora wind field were forced with suddenly applied climatological wind, and inertial effects were not considered. In the present study we use the space- and time-varying hourly winds simulated by Mesoscale Model 5 with 9 km resolution to analyze the bora wind episode of 16-20 January 1987 and to reproduce its influence on the sea with Princeton Ocean Model. Infrared (IR) satellite imaged taken after the long lasting bora event reveal a cyclonic gyre traced by the Po River cold water. Although the bora wind, being of the NE direction, may be expected to induce downwelling on the western Adriatic coast, due to its alongshore variability the bora instead drives the Po River water away from the coast. The Po River was introduced in our model as an extra volume in the continuity equation and, moreover, was assumed to have zero salinity and 5 degrees C lower temperature than the sea water. The Advanced Very High Resolution Radiometer (AVHRR) sea surface temperature measured on 9 January was used to initialize the model, whereas temperature was assumed to be vertically uniform in accordance with some simultaneous bathythermograph measurements. AVHRR sea surface temperatures of 21 and 22 January were used to verify the model results. Initial salinity fields were obtained via a 10 days simulation, with the river discharge being the only forcing and neglecting the temperature changes. The results of the numerical simulations with space- and time-varying wind show current field resembling the cyclonic gyre visible on IR satellite images. Modeled sea surface temperatures show a smaller cyclonic gyre with lower temperature gradients than observed. In order to explain the discrepancy, in our final numerical simulations we explore a positive feedback mechanism: Po- influenced cold water enhance the stability of the overlaying atmosphere and locally reduce the wind stress which, in turn, reinforce the wind-curl effect over the Northern Adriatic.

P10/W/27-A4

0950

### INTERNAL KELVIN WAVES OBSERVED AND MODELLED IN THE ZADAR AND PA\_MAN CHANNELS (EAST ADRIATIC)

Ivica VILIBIC (Hydrographic Institute of the Republic of Croatia, Zrinsko Frankopanska 161, 21000 Split, Croatia, email: dhi-oco@dhi.tel.hr)

An experiment was organised during summer 1994 in the Zadar and Pa\_man Channels (50 km long, 2-7 km wide, 8-50 m deep), placed in the inner Croatian waters. The experiment comprised 29 STD stations and 7 current-meter moorings (current-meters in the surface and bottom layers). Due to vertical stratification, various baroclinic processes were detected. An oscillation with 4-day period and 10 cm/s maximum current amplitude was extracted from the data, being parallel with the coastline and having bottom current which opposes to the surface one. Consequently, it is related to internal Kelvin waves, as the internal Rossby radius was a slightly lower than the channel width in its greater part. The waves were modelled in two ways: (1) using two-dimensional two-layer linear analytical model of a rectangular bay, imposing nodal line at the mouth and radiation condition on its shallowest part (head), and (2) using one-dimensional two-layer defect-like model of a bay which allows for the variable topography. The first model successfully reproduced the phase changes in the channels, energy loss throughout the head and inclination of the current vector close to the mouth, while the second gives a more realistic along-channel distribution of the currents, being largest exactly where they are observed. The oscillation has a respectable horizontal transport for such small channel area (maximum about 5E8 m<sup>3</sup>/cycle), therefore, this should be taken into account, especially if the area is prone to the industrial pollution.

P10/E/02-A4

1010

### THE CONTRIBUTION OF MIXING PROCESSES TO 3-D CIRCULATION IN THE SHALLOW ARABIAN GULF

CHERYL ANN BLAIN (Ocean Dynamics and Prediction Branch, Oceanography Division (Code 7322), Naval Research Laboratory, Stennis Space Center, MS 39529-5004, Email: blain@nrlssc.navy.mil)

Within the Arabian Gulf, mixing over the water column is achieved by way of three primary forcings: tides, winds, and evaporation. The contribution of each of these mechanisms to the 3-D, seasonal mean circulation is presented. Numerical simulations of the nonlinear, 3-D shallow water dynamics are achieved through application of the Dartmouth finite element coastal ocean model. This free surface, 3-D circulation model includes tidal dynamics, wind and buoyancy driven flows, and level 2.5 advanced turbulence closure. An examination of mixing dynamics at both basin and localized scales is possible due to the variable grid resolution employed. Diagnostic (prescribed mass variable fields) and prognostic (with advection and mixing of the mass variables) computations in combination with the modularity of the model allow forcing mechanisms to be considered independently and together in this study of mixing over the shallow shelf water. Asymmetry of the shelf bathymetry between the bounding coasts of the Gulf lend additional complexity to the mixing and circulation patterns present.

P10/E/12-A4

1050

### BOILS AND EDDIES IN TIDAL FLOWS

W.A.M.NIMMO SMITH, S.A.Thorpe and A.Graham (School of Ocean and Earth Science, Southampton Oceanography Centre, European Way, Southampton SO14 3ZH, UK.)

The processes which lead to dispersion by tidal flows in shelf seas are poorly understood, in spite of their great importance in the spread of oil spills and the distribution of sediment, phytoplankton blooms or larvae. Here we describe acoustic and visual observations of large 'boils', regions of local upwelling, in strong quasi-steady tidal currents in the well-mixed and unstratified southern North Sea. The diameter of the boils is about equal to the water depth and at any one time they affect about 25% of the water surface. The typical time for which their effect persists at the surface is at least 7 min. Comparison of these observations with measurements reported in rivers and laboratory channels, the evident presence of sediment in the boils seen at the surface, and the frequent bifurcation of sediment patches, together offer strong evidence that the boils originate as turbulent bursts and ejections from the strongly sheared boundary layer near the sea bed, and that eddies appear after the erupting water reaches the surface. Buoyant material (oil) is pushed radially outwards and accumulates into filaments around the edges of the boils. The acoustic signal from the boils is strongest principally around their up-wind edge, pointing to an accumulation or increased production of bubbles in a region of convergence with associated wave steepening and breaking along this edge. A simple calculation shows that the effect of the boils on lateral dispersion of buoyant material is consistent with other observations. The boils contribute to surface renewal, and may therefore enhance the fluxes of gases between the atmosphere and the unstratified shelf-seas. They produce a patchy structure in, for example, the colour of the water surface which may bias the measured average values of sea-surface parameters detected by satellite or other 'remote' sensors.

P10/W/13-A4

1110

### OBSERVED TIDAL MODULATIONS IN THE EASTERN NORTH SEA

Vibeke HUESS, Danish Meteorological Institute, Lyngbyvej 100, DK-2100 Copenhagen, Denmark. Email: vh@dmi.dk Ole B. Andersen, Kort- og Matrikelstyrelsen, Rentemestervej 8, DK-2400 Copenhagen, Denmark. Email: oa@kms.dk

During 1997 the GEOid and Sea level Of the North Atlantic Region (GEOSONAR) project deployed an off-shore tide gauge station at Horns Rev, situated 60 km west of Esbjerg at the Danish North Sea coast. The pressure gauge was employed for 8 months, before disappearing. At the harbour of Esbjerg tide gauges have been deployed for many years. The objective of establishing the pelagic tide gauge station in the eastern North Sea was to identify the influence on the existing on-shore tide gauges by the local effects such as wind set-up and wave reflections. Additionally the pelagic gauge was positioned close to a TOPEX/Poseidon crossover as well as an ERS satellite ground track, and the sea level information provided by the station is used to validate the altimetry data. The aim of this presentation is to investigate the tidal and non-tidal variations observed by the near coastal and the on-shore tide gauge, respectively. The tides in this region are influenced by non-linear tidal effects, due to the non-linear shallow water processes. Besides the higher harmonics with amplitudes up to 6 cm (M4), annual modulations of the major ocean tide constituents apparently due to interaction with the wind driven effects are observed. These annual modulations change the amplitude of the major astronomical constituents by up to 20 % in amplitude (K1), whereas the largest constituent (M2) is only modified by 5 % in amplitude.

P10/W/22-A4

1130

### THREE-DIMENSIONAL MODELING OF TIDAL CURRENTS AND SEASONAL CIRCULATION ON THE EASTERN SCOTIAN SHELF

Guoqi HAN and John W. Loder (both at Coastal Ocean Sciences, Fisheries and Oceans Canada, Bedford Institute of Oceanography, Dartmouth, Nova Scotia, B2Y 4A2, Canada, Email: ghan@emerald.bio.dfo.ca)

Tidal currents and seasonal-mean circulation on the eastern Scotian Shelf are studied using a three-dimensional, nonlinear finite-element model with a level 2.5 turbulence closure scheme. Tidal currents are moderate over the outer shelf banks, and weak over the inner shelf except for the northeastern tip of the Shelf. The seasonal-mean circulation for four bimonthly periods (centered on February 1, May 1, August 1 and November 1) exhibits dominant and persistent southwestward nearshore and shelf-break currents, embedded with anticyclonic (cyclonic) gyres over outer-shelf banks (inner-shelf basins) and onshore/offshore exchange along cross-shelf trenches. The model transport of the nearshore and shelf-break currents shows prominent seasonal and alongshelf changes. The baroclinic component dominates the nearshore current, while the shelf-break current is sensitive to barotropic boundary inflows through Cabot Strait and on the southern Newfoundland Shelf. Tidal mixing plays an important role over the outer shallow banks, even though tidal rectification is generally weak in the entire region. The solutions are in approximate agreement with observed transports and currents for the primary flow features.

P10/L/05-A4

1150

### INERTIAL OSCILLATIONS NEAR THE CRITICAL LATITUDE FOR DIURNAL RESONANCE

John SIMPSON, Tom Rippeth, (University of Wales, Bangor, School of Ocean Sciences, Menai Bridge, Anglesey, U.K., e-mail: j.h.simpson@bangor.ac.uk), Pat Hyder, Ian Lucas (Fugro Geos Ltd)

Oscillations at, or close to, the inertial frequency are widely observed in shelf seas where frictional damping is weak. In the vicinity of latitudes 30 deg. N and S, such motions may become significantly enhanced by a resonance in which the local inertial frequency coincides with that of diurnal forcing. Under these conditions, regular daily variations in wind stress tend to produce large anticyclonic motions which may extend throughout the water column as shown, for example in Craig (1989; Continental Shelf Research 9(4),343-358 and 9(11), 965-980)

In this contribution we shall examine new data sets from three low tidal energy locations close to the critical latitude including one in the southern hemisphere. The measurements have been made through the full depth of the water column with bottom mounted ADCP's and, in one case using HF radar to measure surface currents. At each of the locations we shall identify the vertical structure of the flow and the response to forcing by windstress in the diurnal and inertial bands. Analytical and numerical models of increasing subtlety will be used to elucidate an explanation of the characteristic surface to bottom phase shift observed in all three cases. In all three locations, we shall demonstrate that near-inertial motions make a major contribution to the total kinetic energy of the flow and must, therefore, be considered as an important candidate source for vertical mixing. Shear production of turbulent kinetic energy will be examined both directly from the observations and from the models of flow structure.

**P10/W/02-A4** 1210**A GENERALIZED SET OF EQUATIONS FOR COASTAL OCEAN CIRCULATION AND ITS APPLICATION TO THE EAST CHINA SEA**

Shizuo FENG, Dexing WU, Hui Wang and Kai Wang (Institute of Physical Oceanography, Ocean University of Qingdao Qingdao, 266003, CHINA)

A turbulent closure three-dimensional nonlinear baroclinic coastal water system, in which tidal currents and a quasi-steady flow are dominant over the flow field and supposed to be of the same order of magnitude, is presented and examined. In view of dominant tidal currents, associated with tides as gravitational long waves, the scale analysis on the system reveals a small parameter characterizing and measuring the order of nonlinear convection, and using a perturbation approach with the small parameter the coastal water system is systematically treated. The inter-tidal transport equations for the tidally time-averaged concentration, temperature, salinity, turbulent kinetic energy and its dissipation rate are derived, in which the convective transport velocity is the sum of velocity of the dominant quasi-steady flow and the mass transport velocity and is termed a "generalized mass transport velocity". The generalized mass transport velocity as a solenoid can be viewed as a Eulerian field variable and the aggregate of such local velocities can be specified as a Eulerian field of flow of an incompressible fluid. A set of field equations governing the generalized mass transport velocity is derived and a turbulent closure problem for the coastal ocean circulation of which the velocity is embodied by the generalized mass transport velocity, nonlinearly coupled with the dominant tidal circulation through the eddy viscosity, is proposed and used to describe and understand the dynamics of the wind-, density- and tide-driven circulation and the inter-tidal transport processes. Based on the set of field equations, the nonlinear effects of the convection and the sea surface elevation of the quasi-steady flow on the circulation and, in particular, the dynamic mechanism of the nonlinear coupling between the tidal and the tidally time-averaged circulation are revealed and examined. Finally, a preliminary application of the proposed model to simulating the winter-time and the summer-time circulations in the East China Sea and to understanding their dynamics is briefly described and discussed.

Thursday 22 July PM

Presiding Chair: Chris MOOERS (University of Miami, Florida, USA)

**MESOSCALE CIRCULATION ON THE SHELF (2)****P10/E/16-A4** 1400**THE CONTRIBUTIONS OF NONLINEAR HYDRODYNAMIC PROCESSES TO WAVE-INDUCED NEARSHORE CIRCULATION**

Mark Cobb (Sverdrup Technology, Inc. (ASGMS), MSAAP Building 9101, Door 136, Stennis Space Center, MS 39529, USA, Email: cobb@alaska.nrlssc.navy.mil) Cheryl Ann Blain (Ocean Dynamics and Prediction Branch, Oceanography Division (Code 7322), Naval Research Laboratory, Email: blain@nrlssc.navy.mil)

In the nearshore environment there are a number of nonlinear hydrodynamic processes (wave-current interactions, nonlinear bottom stress, advection, diffusion/dispersion, and tides) that play a significant role in determining the surface elevation and current velocity. A better understanding of nearshore circulation is crucial to problems concerning coastal zone management such as sediment transport, pollutant transport, water quality, and ship navigation. The contributions of each of these nonlinear processes are considered within the context of wave-induced nearshore flow. Three scenarios are investigated for the cases of a planar, colinear, and sinusoidal beach using a 2-dimensional finite element hydrodynamic model based on the shallow water equations, ADCIRC-2DDI. The three scenarios consist of applying a surface wave stress without wave-current interactions, including wave-current interactions through only the bottom stress, and examining both effects together. For each case, the nonlinear processes are analyzed both individually and collectively from offshore to nearshore and under varying wave conditions in order to determine their contribution to nearshore circulation. Within the context of this study, computed longshore currents were validated by comparison to measured values at Leadbetter Beach, CA in 1980.

**P10/W/16-A4** 1420**AN ASSESSMENT OF LOCAL COASTAL DYNAMICS OBSERVED WITH HIGH FREQUENCY RADAR**

Colin Y. SHEN and Robert A. Fusina (Code 7250, Naval Research Laboratory, Washington, D. C. 20375 USA); Lynn K. Shay (Department of Meteorology and Physical Oceanography, Rosenstiel School of Marine and Atmospheric Science, University of Miami, Miami, Florida 33149 USA)

An assessment is made of the dominant processes governing the circulation in a 30 km by 40 km area off the coast of Cape Hatteras, North Carolina, where surface current velocity vectors have been obtained using shore-based high frequency radars in the High Resolution Remote Sensing experiment in 1993. Although the currents in this region are constantly under the influence of winds and tides, frequent intrusion of energetic flows into the area, apparently mostly of Gulf Stream origin, is shown to have a strong influence on the current variability. Analysis of vorticity and divergence shows that the flow intruding into the area is strongly rotational with positive vorticity. This rotational motion is not in geostrophic balance with the surface pressure gradient, and an inertial oscillation is often excited as a result, with vorticity and divergence oscillating 90° out of phase. On average, the geostrophic imbalance generates a net surface flow divergence which, in turn, induces negative vorticity that more than offsets the positive vorticity advected into the region. However, vertical viscous transfer of positive vorticity from subsurface to surface is shown to be required to complete the surface vorticity balance; the same energetic cyclonic shear flows that intrude into the area are suggested as the source of the subsurface vorticity, as these flows of Gulf Stream origin are known to be subducted under buoyant shelf water.

**P10/E/01-A4** 1440**NEW DATA ON NONLINEAR INTERNAL WAVE EVOLUTION FROM OBSERVATIONS ON SHELF OF THE SEA OF JAPAN**

Andrey SEREBRYANY (N.N. Andreyev Acoustics Institute, Moscow 117036, Russia, email: aserebryany@glasnet.ru)

The process of internal tide propagation on a shelf leading to generation of soliton-like internal waves was investigated by means of special field experiment which we carried out in the Sea of Japan. During period of 24 hours research vessel with towed temperature line sensor performed 10 non-stop repeated runs along a section oriented across the shelf. These measurements were supplemented with CTD zond survey along the section made just before and after the towing and 12-hour observation by line temperature sensor in the point of the section on shallow water made from anchored vessel after the towing and the survey. On the

basis of the measurements we obtained the picture describing internal wave field evolution on a shelf. It was observed that generation of intense internal wave trains took place in the shallow water zone at a distance of 5-6 km from the shore. Observed intense internal waves are soliton-like. They propagated toward the shore. The most significant fact we found was connected with an interesting phenomena of alternative displacement up and down of the internal wave train as a "hole body" by long-period internal movements on the thermocline. This process leads to the strengthening of nonlinearity of internal waves and can create for them a radically new nonlinear effect.

**P10/E/14-A4** 1500**A NESTED BASIN/COASTAL CIRCULATION MODEL FOR EAST ASIAN REGIONAL SEAS**

Peter C. CHU, S.L. Lu, and Y.C. Chen

A nested basin/coastal model is developed to study the east Asian regional seas and shelf processes. The Princeton Ocean Model (POM) with 23 sigma levels conforming to a realistic bottom topography is used for the study. The horizontal resolution is 1 deg by 1 deg for the Pacific basin module, and 0.25 deg by 0.25 deg for the coastal module including JES. The open boundaries for the coastal module are 150 deg E and 15 deg S. The model simulates realistic circulation pattern and thermohaline structure. Comparison between the model results with observations is also given.

**P10/P/01-A4** 1520**THE KUROSHIO EAST OF TAIWAN AND IN THE EAST CHINA SEA IN SUMMER 1997\***

Yaochu YUAN (Second Institute of Oceanography, SOA, P O Box 1207, Hangzhou, 310012, China, email: yuanyc@zgb.com.cn); Yonggang Liu and Jilan Su (both at Second Institute of Oceanography, SOA, P O Box 1207, Hangzhou, 310012, China, email: sujil@zgb.com.cn); Arata Kaneko (Department of Environmental Sciences, Faculty of Engineering, Higashi-Hiroshima 739, Japan, email: akaneko@ipc.hiroshima-u.ac.jp)

On the basis of hydrographic data obtained from two cruises during June and July of 1997, a modified inverse method is used to compute the Kuroshio east of Taiwan and in the East China Sea, respectively. It is found that: 1) The net northward volume transport (VT) of the Kuroshio through Section K2 southeast of Taiwan is about  $37.5 \times 10^6$  during July of 1997. In comparison with VT of the Kuroshio through Section K2 during October of 1995 and May-June of 1996, this value of VT of the Kuroshio decreases obviously, i.e.: VT of the Kuroshio southeast of Taiwan decreases obviously during 1997 stronger El-Nino year. 2) There is not a branch of the Kuroshio east of Taiwan to flow northeastward to the region east of Ryuku Island during July and of 1997. 3) During July of 1997 there is an anticyclonic eddy east of the Kuroshio and a countercurrent east of this anticyclonic eddy. 4) There is an anticyclonic recirculating gyre south of Miyako Island and southeast of Okinawa Island during July of 1997. The net northward VT of the Kuroshio through Section PN in the East China Sea is about  $26.3 \times 10^6 \text{ m}^3/\text{s}$  during June of 1997. 5) The comparison between the above computed results and the ADCP observed currents show that they agree quite each other.

**P10/E/05-A4** 1600**VARIABILITY IN Pycnocline Diffusivity in the Seasonally Stratified Shelf Seas of Western Europe**

T. P. RIPPETH (School of Ocean Sciences, University of Wales Bangor, Menai Bridge, Anglesey, LL59 5EY, UK. M. E. Inall, SAMS, CCMS Dunstaffnage Marine Laboratory, PO Box 3, Oban, Argyll, PA34 4AD, UK.) J. H. Simpson (School of Ocean Sciences, University of Wales Bangor, Menai Bridge, Anglesey, LL59 5EY, UK.) John Howarth (CCMS Proudman Oceanographic Laboratory, Bidston, Merseyside, L43 7RA, UK. Neil Fisher, School of Ocean Sciences, University of Wales Bangor, Menai Bridge, Anglesey, LL59 5EY, UK.)

The determination of vertical mixing rates in the stratified water column is one of the key objectives of shelf sea Physical Oceanography with important applications in many aspects of Biological Oceanography. Recent developments in turbulence probe technology have allowed direct estimation of the vertical profile of dissipation, from which it is possible to determine the eddy diffusivity  $K_z$  via the Osborne relation;  $K_z = 0.2 E / N^2$ ;  $E =$  energy dissipation rate;  $N =$  Brunt-Vaisala frequency.

In this paper we shall present observations of the vertical structure of the dissipation of turbulent kinetic energy, made using a Fly Profiler, over 25 hour cycles, at a number of contrasting thermally-stratified sites in the shelf seas of north western Europe. The dissipation observed in the pycnocline region varies from 10-6 Wm-3 at a low energy site in the northern North Sea station, to 10-2 Wm-3 at a station located near to the continental shelf edge during a period of intense internal wave activity. These direct measurements of  $E$  are combined with  $N^2$  based on T and S measurements also made by the FLY, to estimate the diffusivity  $K_z$ . The variability of the pycnocline  $K_z$  and its dependence on spatial differences in wind and tidal stirring at the contrasting sites will be considered along with the question of whether mixing rates in the stratified regime respond significantly to the springs-neaps cycle in the tidal flow.

**P10/E/21-A4** 1620**CURRENT PROFILES DURING THE BREAKDOWN OF STRATIFICATION IN THE NORTH SEA**

John HOWARTH (Centre for Coastal and Marine Sciences, Proudman Oceanographic Laboratory, Bidston Observatory, Birkenhead, Merseyside, L43 7RA, UK, email: mjh@ccms.ac.uk)

Two sets of current and temperature profile measurements have been made in the northern North Sea during the breakdown of stratification between September and November, in 1991 and 1998. At the two sites which were close together, about 20 miles apart, tidal currents were weak and water depths over 100 m so that the surface and benthic boundary layers were initially well separated. During both sets of measurements the thermocline substantially weakened and deepened as a result of heat loss at the sea surface. There was no exchange of heat downwards across the thermocline and by the end in neither case had the water column become fully mixed. The first set of current measurements has been analysed in terms of barotropic dynamics, inertial currents and near surface shear. The inertial currents were first mode baroclinic and were well modelled by a two-layer local wind driven model. Shears across the thermocline of 0.02/s over 10 m were measured. Near surface shear was confined at most to the top 25 m even during the largest storms and was correlated with the wind stress. The largest shear between 2 and 25 m below the surface was 0.01/s. During the second set of measurements turbulence dissipation measurements were also made. An interesting contrast between the two sets is that for the first the water column was homohaline whereas for the second there was a surface to bed salinity difference of more than 0.5.



P10/W/06-A4

1640

## SEASONAL EVOLUTION OF THE IRISH SEA COLD POOL GYRE

K.J. HORSBURGH and A.E. Hill (School of Ocean Sciences, University of Wales Bangor, Menai Bridge, Anglesey, LL59 5EY U.K.)

An extensive cruise program in 1994, 1995 and 1996 provided observations which describe the seasonal evolution of the three-dimensional density field in the western Irish Sea. A cold, dense pool flanked by strong, near-bed horizontal density gradients was present from May until October in 1995. The trajectories of 55 satellite-tracked Argos drifters demonstrated the existence of the cyclonic circulation pattern that constitutes the western Irish Sea gyre and defined the gyre's full spatial extent. Several distinct recirculation paths were observed and the implications for planktonic organisms of the seasonal variability in circulation is discussed. Drifter speeds were in good agreement with geostrophic calculations based on the density field. The dynamical significance of strong near-bed density gradients, or bottom fronts, is highlighted. The gyre is a special case of a class of intense, organised, density-driven flows in shelf seas and the ability of numerical models to properly simulate such baroclinic circulations is critical. The results of a primitive equation model are compared with the seasonal observations. The model reproduces well the spatial pattern of heating, the residual flows and furthermore provides some new dynamical insights into shelf sea frontal processes.

P10/E/08-A4

1700

## FRONTS AND WATER MASSES IN THE NORTHERN SOUTH BRAZIL BIGHT

Belmiro M. CASTRO and Luiz B. Miranda (both at Oceanographic Institute, University of Sao Paulo, Praca do Oceanografico, 191, 05508-900, Sao Paulo, SP, Brazil, email: bmcastro@usp.br)

Data from seven consecutive seasonal (summer/winter) hydrographic cruises are used to study the seasonal stratification cycle in the northern part of the South Brazil (23.4S-23.7S). Three shelf regions have been identified: Inner Shelf (IS), Middle Shelf (MS) and Outer Shelf (OS).

The IS outer limit changes seasonally: it reaches the 20-40 m isobath during summer (10-30 km from the coast) and the 50-70 m isobath during winter (40-80 km from the coast). The IS Coastal Water is separated from the lower layer MS South Atlantic Central Water (SACW) by a bottom thermal front. The presence of the SACW is associated with intrusions towards the coast of slope waters. The intrusion scale is larger during summer than during winter due to seasonal changes in the wind forcing. The MS extends offshore to the 70-90 isobaths (60-80 km from the coast) during summer, being very narrow during winter. The main characteristic of the MS is the high stratification during summer, due to the presence of a seasonal thermocline. Estimates for the thermodynamical and dynamical processes able to vertically mix the water column show that were not for the SACW intrusions during summer the MS would be almost homogeneous, not presenting the dominant seasonal thermocline. The MS is separated from the OS by a surface saline front which is located in the transition region between two upper layer water masses: the MS Coastal Water and the Tropical Water. The latter is one of the two water masses transported by the Brazil Current in the region, the other being the lower layer SACW. The OS extends from the surface saline front to the shelf break. Stratification in the OS does not vary much during the year, being a thermocline present all the time.

P10/E/15-A4

1720

## THE INFLUENCE OF PATOS-MIRIM LAGOON DISCHARGE ON THE THERMOHALINE REGIME OF THE SOUTH BRAZILIAN SHELF

Peter O. ZAVIALOV (Shirshov Institute of Oceanology, Moscow, Russia, email: zavialov@mi.ras.ru) Osmar O. Moller Jr (University of Rio Grande, Rio Grande, Brazil, email: osmar@calvin.ocfis.furg.br)

Patos-Mirim lagoon is a large choked freshwater lagoon connected to Southwestern Atlantic through a narrow and relatively deep Rio Grande channel. It is known that the discharge from the lagoon contributes significantly into the regional heat and mass budgets (e.g. Zavialov et al., 1998, J. Phys. Oceanogr., 28, 545-562) and is among principal factors controlling the thermohaline regime of the southern Brazilian shelf. However, the Patos-Mirim plume has never been mapped in detail. A helicopter/ship CTD survey of the inner shelf south of the estuary was conducted in September, 1998. Profiling was performed simultaneously by the helicopter and the Brazilian R/V "Comandante Varela". The total number of CTD stations was 21. The collected data revealed extremely stable salinity-controlled stratification within the plume which largely suppressed vertical mixing. Despite of the initial southward momentum of the plume waters, south of the estuary the thermohaline signature of the plume is observable only within a distance of 5-15 km from the and separates from the coast. Thus the hypothesis that relates low salinity values observed on the inner southern Brazilian shelf south of Rio Grande to Patos-Mirim discharge is not supported by our data. Rather, this low salinity belt can be related to Plata river discharge transported by a northward coastal current.

Analysis of local historical data revealed anomalously strong secular warming trend of SST (up to 1.6 degrees C per 100 years) in the area adjacent to the estuary. This may be related to a human impact upon the freshwater discharge from the lagoon.

Friday 23 July AM

Presiding Chair: Juergen SUNDERMANN (University of Hamburg, Germany)

## FLUXES OF MATTER AND PRIMARY PRODUCTION (1)

P10/W/03-A5

Invited

0850

## SIMPLIFYING PELAGIC BIOLOGY FOR COUPLED MODELS

TETT, P.1, Wild-Allen, K.1 &amp; Wilson, H.2,1 1. Department of Biological Sciences, Napier University, Edinburgh, U.K. 2. School of Ocean Sciences, University of Wales, Bangor, U.K.

Marine pelagic ecosystems contain many hundreds of species and very large numbers of individuals. Although the life of each individual and the dynamics of each population can be described by a small set of rules, marine ecologists have achieved no consensus about a way to model system dynamics. There is no ecological equivalent of physical oceanographers' basic hydrodynamic equations. Nevertheless, models must simplify the complexity of real marine pelagic ecosystems. But how much? A series of biological models with increasing numbers of state variables will be used to discuss necessary complexity and to illustrate biogeochemical (element-conserving) and ecological (semi-freely dynamically interacting) models of the marine microplankton, defined as all organisms less than 200 µm. One endpoint of the series is a model with two microplankton compartments, which is able to represent the annual sequence from Spring, diatom-dominated plankton to a Summer Microbial Loop community. This model has been coupled to a depth-resolving physical framework which includes deposition to and resuspension from the sea-bed. Simulations will be shown for sites in the North Sea, and compared with observations.

P10/W/23-A5

0930

## A COUPLED PHYSICAL-BIOLOGICAL MODEL FOR THE SEASONAL CYCLES OF CHLOROPHYLL AND NUTRIENTS IN THE FIRTH OF CLYDE

JAE-YOUNG LEE and Paul Tett (Department of Biological Sciences, Napier University, 10 Colinton Road, Edinburgh EH10 5DT, UK, Email: j.lee@napier.ac.uk and p.tett@napier.ac.uk)

The Firth of Clyde, located on the west coast of Scotland, receives anthropogenic nutrients from the discharge of the Clyde and other rivers draining much of agricultural and industrial western central Scotland. As a result of these discharges, the Firth of Clyde is enriched in nutrients from agricultural fertilisers and domestic sewage.

A coupled physical-biological model has been constructed to aid understanding of the effects of these nutrients on the biota and oxygen demand. The physical model consists of a set of compartments with turbulent and advective exchanges driven dynamically by density differences and supplies of turbulent kinetic energy. It is forced by freshwater discharge to the Firth of Clyde, meteorology, and boundary conditions in the North Channel. The model was used to quantify the effect of various physical processes during the seasonal cycle, and extended to construct a budget of nutrients for the Firth.

The biological model divides organic particulates into microplankton (phytoplankton plus bacteria and protozoa) and detritus. It has two microplankton compartments, a diatom dominated (or 'diatomy') compartment and a small-cell dominated (or a 'flagellatety') compartment. It cycles carbon, nitrogen and silicon through microplankton, defecated-detritus, phyto-detritus, mesozooplankton and dissolved nutrients compartments.

Climatologically- and meteorologically-forced simulations of several seasonal cycles were compared with historic data, for dissolved oxygen, dissolved nutrients and chlorophyll, in the Firth of Clyde with the aim of using the model as a tool to predict the effects of the perturbations induced by Man or Nature. The importance of coagulation processes for the termination of diatom spring-bloom in the region has been investigated.

P10/W/15-A5

0950

## MODELLING THE AGGREGATION AND SEDIEMNTATION OF PLANKTON

WILD-ALLEN, Karen (Dept. of Biological Science, Napier University, Edinburgh, UK, Email: k.wild-allen@napier.ac.uk)

Variations in aggregation parameters were found to influence the functional group dominance of a mixed population of marine microplankton in a model system. The model cycles organic carbon, nitrogen and silica through microplankton, detritus and dissolved nutrient pools in a 1-D depth-resolving framework forced by turbulent diffusivity. The microplankton are modelled as two mixed populations of pelagic micro-organisms (<200 µm) which include photo-autotrophic micro-algae, cyanobacteria and heterotrophic bacteria and protozoa. One population is dominated by diatoms and includes silica dynamics, and the other by flagellates. This formulation allows a full range of pelagic micro-organisms to be modelled in a computationally efficient manner. Detritus is generated as a by-product of zooplankton grazing and by aggregation of diatom-type microplankton into phyto-detritus which sinks rapidly (100m/day). Seasonal cycles of biomass show Spring and Autumn blooms with a shift from diatom to flagellate dominated communities as aggregation parameters increase. At higher rates of aggregation the Autumn bloom is larger and increasing amounts of nutrients in the euphotic layer remain unused. These results demonstrate the influence of aggregation processes in all parts of the pelagic system. This is important in relation to change in species balance in eutrophication, and in the export of organic material from the oceans surface.

P10/W/28-A5

1010

## THE ROLE OF TURBULENCE IN DRIVING PRIMARY PRODUCTION AT SHELF SEA FRONTS

Jonathan SHARPLES, (Southampton University School of Ocean and Earth Science, Southampton Oceanography Centre, Empress Dock, Southampton, SO14 3ZH, UK, email: j.sharple@soc.soton.ac.uk)

Shelf sea, or tidal mixing, fronts mark the physical transition between mixed and stratified water columns during summer in temperate shelf seas. These fronts are also known to be regions of enhanced primary productivity compared to the mixed and stratified waters on either side. This productivity requires an input of new nutrient (nitrogen) into the photic zone at the front, but the mechanisms behind this nutrient supply are not yet well understood. A simple model of the physical structure of a front, using a turbulence closure scheme to describe the temporal and spatial variability of vertical turbulent exchange, has been coupled to a model of primary production to simulate possible nutrient supply mechanisms. Two processes are investigated: nitrogen supply through the weakening stratification associated with the front, and spring-neap variability of frontal position leading to a fortnightly replenishment of surface nitrogen within the transition zone. The basic result shows that consideration solely of the cross-frontal change in vertical turbulent mixing is sufficient to explain typical observations of phytoplankton biomass, with both surface frontal and sub-surface thermocline concentrations being predicted. The addition of spring-neap tidal variability results in fortnightly pulses of frontal productivity and biomass, again similar to available observations. The model results are then used to further investigate nitrogen fluxes, nitrogen uptake, and phytoplankton growth rates within the front, leading to two important conclusions. First, for a phytoplankton with a deep critical depth, the vertical flux of nitrogen into the frontal photic zone is dominated by the flux of algal nitrogen rather than the direct physical mixing of dissolved inorganic nitrogen. This could help explain why recent estimates of dissolved nitrogen fluxes at a front are less than the estimated nitrogen requirements of the frontal productivity. Second, the total annual production at a front is altered significantly when spring-neap variability in the tidal mixing is included. For a phytoplankton with a deep critical depth, total production is predicted to be 20% less with a spring-neap cycle. For a phytoplankton with a shallow critical depth, total annual production with a spring-neap cycle increases by 50%. Consequences of these results for the design of experiments aiming to quantify annual production in shelf waters will be discussed. The conclusions can also be applied to ocean fronts in general, rather than being limited to tidal mixing fronts in shelf seas.

P10/E/06-A5

1050

## HORIZONTAL TRANSPORT OF MARINE ORGANISMS RESULTING FROM INTERACTION BETWEEN DIEL VERTICAL MIGRATION AND TIDAL CURRENTS OFF THE WEST COAST OF VANCOUVER ISLAND

C.L. SMITH (Institute of Ocean Sciences, Sidney, B.C., Canada, email: smithcl@dfp-mpo.gc.ca) A.E. Hill (School of Ocean Sciences, University of Wales, Bangor, Wales, U.K.) M.G.G. Foreman (Institute of Ocean Sciences, Sidney, B.C., Canada) M.A. Peña (Institute of Ocean Sciences, Sidney, B.C., Canada)

This paper examines horizontal transport of marine organisms, resulting from the interaction between diel vertical migration (DVM) and numerically generated tidal and buoyancy currents



for the continental shelf and slope off Vancouver Island, Canada. DVM behaviour is simulated by migrating particles which are in the surface layer at night and near the bottom during the day. Eight tidal constituents, the tidal residual and typical summer buoyancy flows are calculated for the region using a 3-D barotropic finite element model. The interaction of these tides with migrating particles is investigated using the finite element model and Lagrangian particle tracking techniques in spatially heterogeneous tidal and buoyancy flows. DVM-tidal interaction alters the horizontal distance particles travel compared to non-migrating particles. We show that the K1 tidal constituent dominates transport patterns, producing regions of convergence and divergence, and on and offshore transport along the continental shelf. During April and May, particles are transported from offshore onto the southern shelf and into Juan de Fuca Strait. From June to October, this pattern is reversed and there is a general offshore migration of particles. As the K1-DVM beat period is exactly 1 year, these patterns are reversed 6 months later, and do not change from year to year. When a typical summer buoyancy flow is included, the effect of DVM-tidal interactions is reduced, with buoyancy flow dominating transport of particles over most of the domain. However, cross shelf transport resulting mostly from K1-DVM interaction is shown to be important in the southern shelf in the La Perouse Bank area. This process may provide a partial explanation of observed changes in seasonal and interannual zooplankton biomass in the region.

P10/E/09-A5

1110

#### STARTING OF PHYTOPLANKTON SPRING BLOOM IN THE NORTHERN NORTH SEA (FLADENGROUND)

DILEK H.TOPCU, Birgit Mieding, Uwe H.Brockmann, Venugopalan Ittekkot (all at University of Hamburg, Centre for Marine and Climate Research, Inst. for Biogeochemistry and Marine Chemistry, Martin-Luther-King-Platz 6, 20146 Hamburg, Germany, e-mail: fg8z001@public.uni-hamburg.de)

In the Fladenground in 1976 the start and development of the phytoplankton spring bloom was studied in the frame of an international project (FLEX76). In March/April 1996 the starting conditions of the blooming were investigated again. Along a transect from the German Bight to the Fladenground different blooming situations were found: blooming in the shallow German Bight and nutrient reduced water masses originating from the continuous production on the Doggerbank, interrupted by vertically mixed water masses without blooming indications. Only in the Fladenground chlorophyll maxima, reaching 0.15 (g/L, developed in depths between 10 and 40 m, showing during a 4 days lasting drift experiment diurnal variation, coupled with a weak vertical temperature gradient of 0.1 to 0.40C, and decreases of nitrate and silicate, and increase of particulate carbon and phosphorus, reflecting the start of net production and the beginning of phytoplankton spring bloom. During this situation also a fluctuation of dissolved total amino acids (0.05 to 4 (mol/L) and to some degree also of DON (3 to 8 (mol/L) was observed, indicating the modification of water chemistry right up from the beginning of spring bloom.

P10/E/07-A5

1130

#### CONVERSION OF NUTRIENT ELEMENTS N AND P IN THE ELBE RIVER PLUME, GERMAN BIGHT

UWE H.BROCKMANN, Thomas Raabe, Andreas Starke (all at University of Hamburg, Centre for Marine and Climate Research, Inst. For Biogeochemistry and Marine Chemistry, Martin-Luther-King-Platz 6, 20146 Hamburg, Germany, e-mail: brockmann@rz.uni-hamburg.de)

In the German Bight within the propagating river plume of the Elbe during summer 1994 and spring 1995 drift experiments were performed in order to study the conversion of nutrients, dissolved and particulate organic matter. In spite of moderate changes of the water masses, marked by the drifter, the succession of nutrient uptake, formation of particulate matter in the mixed layer and modification of the dissolved organic fraction of N and P could be followed. The drift experiments lasted 9 and 10 days and were accompanied by repeated investigations of the surrounding area. By this, the extension of the river plume and the regional representativity of the development in the drifting field could be identified. During spring at the central drift station nitrate decreased with 2.5 (mol/l d, partly compensated by an increase of 1.8 (mol/l d PN, phosphate decreased by 0.05 (mol/l d coupled with an increase of 0.03 (mol/l d of PP. Due to the accelerated remineralisation during summer there was a net nitrate decrease of 0.04 (mol/l d observed but a PN increase of 0.11 (mol/l d. Phosphate decrease (0.02 (mol/l d) was larger than the PP increase (0.002 (mol/l d) at this time. However, in the bottom water increases of nutrients were observed, especially for phosphate. During summer nutrient concentrations in the bottom layer were higher than in the mixed layer, reflecting the more important regeneration mode during this season. Mainly during spring the conversion rates at the drift station in the river plume corresponded to overall net conversion in the German Bight.

Friday 23 July PM

Presiding Chair: Paul Tett (Napier University, Edinburgh, UK)

#### FLUXES OF MATTER AND PRIMARY PRODUCTION (2)

P10/E/03-A5

1400

#### DYNAMICS OF FINE SEDIMENTS IN SHELF SEAS: OBSERVATIONS, PROCESSES AND MODELLING

Juergen Suendermann (Zentrum fuer Meeres- und Klimaforschung, Universitaet Hamburg, Troplowitzstr. 7, 22529 Hamburg, Germany, email: suendermann@ifm.uni-hamburg.de)

The global change of our environment is a consequence of variable matter fluxes between land and ocean. An essential part of these fluxes is represented by the transport of suspended particulate matter (SPM). SPM consists of anorganic and organic constituents, and its dynamics is determined by physical and biological processes and their interactions. Field observations show a distinct dependency of SPM concentrations on currents and waves as well as on input from rivers and land. The key processes of SPM transport are sinking, deposition and resuspension. They are controlled by the current regime (advection, turbulence, orbital motion) and by biological factors as aggregation, filtration or bioturbation. A high-resolving 3D Lagrangean tracer model will be presented containing all these components. The time scale covered ranges from hours to years. The model is applied to the North Sea, to the Bohai Sea (China), to the German Bight and to the river Elbe. The numerical results are discussed and interpreted against observational data of SPM concentrations and bottom sediments.

P10/W/01-A5

1420

#### APPLICATION OF A 3-D HYDRODYNAMIC-WATER QUALITY COUPLED MODEL TO KOREAN WATERS IN THE YELLOW SEA

CHANG S. KIM (Korea Ocean R&D Institute, Coastal Engineering Division, 1270 Sadong, Ansan,

425-170, South Korea. Email: surfkim@kordi.re.kr)

A 3-D hydrodynamic-water quality coupled model is used to simulate the impact of river discharge, nutrient loads and dynamic forcings on the variability of coastal waters. The model consists mainly of two modules; hydrodynamics and water quality parts. Both modules are directly coupled in computation scheme. The hydrodynamic model is originated from the Blumberg-Mellor algorithm and extended at Virginia Institute of Marine Science, USA to include further processes such as tidal flat, etc. The water quality module has been adapted from the CE-QUAL-ICM developed by the WES of US Army Corps of Engineers. The module deals with 25 state variables including temperature, salinity, DO, nitrogen, phosphate, suspended matter, etc. The coupled model has been applied to the waters of Kyunggi Bay, where rivers flow in with terrain nutrient loads. The model uses the curvilinear grid system with grid size ranging from 200 m to 9 km. The study area shows the maximum tidal range of approximately 11 m and wide tidal flats. This study shows the result of the model implementation for the water quality prediction in macro-tidal coastal and shelf waters off Korea.

P10/E/13-A5

1440

#### PROCESSES CONTROLLING THE DISTRIBUTION OF SOLID RUN-OFF OF THE TUMANNAYA RIVER (PETER THE GREAT BAY, JAPAN SEA)

Alexander Moshchenko, Konstantin Feldman (both at Institute of Marine Biology, Russian Academy of Sciences, Far-Eastern Branch, Palchevskogo str., 17, 690041 Vladivostok, Russia, email: inmarbio@mail.primorye.ru). Gennady YURASOV, Nikolay Vanin (both at Pacific Oceanological Institute, Russian Academy of Sciences, Far-Eastern Branch, Baltiyskaya Str., 43, 690041 Vladivostok, Russia, email: pacific@online.marine.su)

The region studied extent is 30 km offshore and 35 km northward from the mouth of the Tumannaya River. It includes the territory of the Far Eastern State Marine Reserve. Presumable economical development of the Tumannaya River mouth area requires to study how to minimize possible anthropogenic impact on environs. That's why the processes defining natural sedimentation in the coastal area are to be important for understanding of possible unfavorable consequences for the region. Bottom sediments of the region studied are presented by a complex of terrigenous deposits from coarse sands to aleurites-pelites. The content of fine fractions varies from 1 to 45%. Their distribution have distinctive contagious character. Along with that the spots of aleuro-pelites prevailing are found closely to the mouth of the Tumannaya River and at 20-25 km off north-eastward. Results of numerical modeling of circulation on a basis of shallow water equations and instrumental observations reflect in whole the features of sediments distribution. Due to monsoon climate the maximal values of solid run-off of the Tumannaya River are observed during summer period, when the winds of the southern routes are prevailed. The schemes of circulation are defined mainly by the bottom relief features and the wind direction. For the south-western winds the transportation of suspensions and pollutants occurs north-eastward along the coastline. During the south-eastern winds an anticyclonic eddy is formed over the northern part of the region studied that also produces favorable conditions for sedimentation northward from the mouth of the Tumannaya River. But most unfavorable consequences for Marine Reserve should be expected in summer season during moderate and strong south-western wind.

P10/E/18-A5

1500

#### INFLUENCE OF CLIMATIC AND OCEANOGRAPHIC PROCESSES ON FORMATION OF COASTAL SUBWATER LANDSCAPES AND CONDITION OF BENTHOS (BLACK SEA)

Alexei PETROV, Vladimir Shalyapin and Sergey Ignatyev (all authors at Institute of Biology of the Southern Seas, 2, Nakhimov av., 335011 Sevastopol, Ukraine, email: benthos@ibss.iuf.net)

The large-scale subwater landscape/ecological investigation have been made in 1993-96 along the coastal zone of SW Crimea at 0-40 m depth. In hydrological regime of this area role of breeze effect is very significant. Daily alterations in spatial pattern of wind currents define the unsteadiness of thermocline structure mostly revealed in early summer period. Such fluctuations impact on hydrological and biological peculiarities. To differentiate landscape facies, the data on hydrodynamics, seabed microrelief and slope, grain-size structure of bottom substrate as well as quantitative characteristics of phyto- and zoobenthos were used. As a result, 7 different bottom landscapes were distinguished. In the shallow (2-8 m depth) water areas with maximum hydrodynamic load (current velocities fluctuated 0.35 to 0.60 m/s) geomorphology were represented only by cliff and rocks sloping down at 8-140 and covered by *Cystoseira* spp. and mussels. Within 10-15 m depth a steepness of underwater slope reduced to 4-7° and velocity of wind currents to 0.12-0.23 m/s. Mosaic pattern of grounds promotes development of landscapes with high diverse in such groups of benthos as mobile predatory ectobionts and less abundant sessile filter-feeders. Sandy and silty grounds covered by meadows of eelgrass *Zostera* spp. Below 18-20 m depth, where the steepness does not exceed 1-2° and velocity of currents 0.03-0.05 m/s, a fine sand facies with admixture of shell debris and silt prevailed. Phytobenthos is scarce; in zoobenthos endobenthic suspension-feeders, epibenthic mobile deposit-feeders dominate. Comparative temporal analysis of landscapes patterns and condition of biota has manifested that about 15% of coastal rocky substrates covered earlier by brown algae and mussels have been destroyed due to anthropogenic eutrophication of water areas and hydrotechnical construction and replaced by cenoses wherein indicators of eutrophication (green algae) prevail. Biodiversity of soft-bottom macrobenthos also reduced and degradation of sensitive to eutrophication indicator species has been observed. The processes of mudding leads to expand a bottom areas covered with *Zostera* growth that contributes to accumulation of organic matter and formation of unfavorable oxygen conditions in such sites, gradual degradation of benthic assemblages associated with meadows of eelgrass.

P10/W/24-A5

1520

#### THE INTERACTION OF SHALLOW WATER AND COULOMB-DAMPED POROELASTIC BED

Mian Li (Institute of Mechanics, CAS, Beijing 100080, China, Email: rxzhu@mail.c.geos.ac.cn)

In many cases of coastal engineering, e.g., constructions of coastal structure and breakwaters, pipe lines, etc., Correct estimations of the dynamic behavior of seabed and propagating water wave are very important. However, due to the fact that in most cases the seabed is permeable and deforming, and the water wave, in general, is nonlinear, the studies of the interaction between the water waves and seabed are very complicated.

Now the theory of shallow water waves has been applied and the seabed is regarded as compressible and deformable. Not only the wave propagation over coulomb-damped poroelastic bed has been considered, but also the porous pressure in the seabed take into account. Nonlinear shallow water equation of boussinesq type and nonlinear dispersion relation for shallow water are derived. It is found that wave damping is agreement with the experiments, as the coulomb friction between grains is considered. Porous pressure in sand and clay has been calculated. There is an extreme value of porous pressure in some depth of clay bed and the depth is compared with the resonant depth.

**P10/E/11-A5** Poster **1600-01**

**TIDAL AND SUBTIDAL CIRCULATION ON THE SOUTH BRAZILIAN CONTINENTAL SHELF**

O. MOLLER Jr., D. Urbano Neto (both at Lab. Oceanografia Fisica, Depto. Fisica, Universidade do Rio Grande, 96201-900 Rio Grande, RS, Brazil; email: osmar@calvin.ocfis.furg.br)  
P. Zavialov (Shirshov Institute of Oceanology, Moscow, Russia; email: zavialov@mi.ras.ru)

In order to characterize the water circulation and dynamics of Rio Grande do Sul continental shelf, time series of current and wind vectors covering a period from March to May of 1997 are analysed. A mooring station with two current meters that registered hourly values of current velocity and direction at the depths of 15 m and 45 m was deployed in the point 32 41'S, 51 27'W. The results indicate that the prevailing current direction was to NE despite of the predominantly NE winds. This indicates a geostrophic flow related to the cross shore density gradient and local sea surface elevation forced by freshwater discharge from Patos Lagoon and Plata River. The wind forcing resided mostly at the synoptic time scale in the range between 3 and 10 days. The tidal influence was small.

**P10/W/21-A5** Poster **1600-02**

**NUMERICAL STUDIES OF UPWELLING OFF ZHEJIANG AND FUJIAN**

Yiyong LUO and Guangyao YU Institute of Physical Oceanography, Ocean University of Qingdao Qingdao, 266003, CHINA

The waters off Zhejiang and Fujian in the East China Sea have anomalously low temperatures and high nutrients during summer. The contribution of tidal current, wind stress and Taiwan Warm Current (TWC) to the anomaly of temperatures and nutrients is individually discussed by using a three dimensional numerical model as well as field observations. The result reveals that there exists a tide-induced upwelling stripe off Zhejiang and Fujian, and its large ranges appear off Zhoushan Islands and north of Fujian where the tidal currents are strong and the variations of bottom topography are large. The result also shows that there exist wind-driven and TWC-driven upwelling stripes off Zhejiang and Fujian, and their ranges are more and more smaller from the south to the north. The computed largest upwelling, 0.0005cm/s for tidal current, occurs in upper layer (10-20m), 0.001cm/s for wind stress in middle layer (20-30m) and, 0.001cm/s for TWC in bottom layer (below 30m). The combination of tide-induced, wind-driven and TWC-driven upwelling provides the mechanism for producing the observed cold water anomaly off Zhejiang and Fujian. In addition, the source of these anomalous waters is discussed by using the Eulerian-Lagrangian method. Results show that the anomalous waters originate from Kuroshio subsurface waters climbing up the continental shelf northeast of Taiwan Island.

**P10/W/11-A5** Poster **1600-03**

**MODEL OF WATERS CIRCULATION ON A CONTINENTAL SHELF WITH THE HIGH SPATIAL RESOLUTION (ON AN EXAMPLE OF THE BARENTS AND KARA SEAS)**

SEMYONOV G.A., Bezgreshnov A.M. ( both at Arctic and Antarctic Research Institute, Bering st., 38, St.-Petersburg, Russia, 199397. E-mail: geosem@ecoshelf2.spb.org)

The calculation of currents on a grid with the high spatial resolution imposes, as a rule, restriction on the sizes of modeling area, that results in appearance of opened (liquid) borders of a model domain. On opened borders the budget of a liquid either are unknown, that calls the inadequate results of computation of currents in shelf zones. The merging of global and regional model grids does not result in significant reduction of an error in the task of determine of the fluxes on borders of a grid with the high resolution. In order to prevent the specified above difficulties in simulation of circulation of waters and ice, and also for calculation of fluxes of solid substance and various pollutants for Barents and Kara seas the non-uniform model grid in spherical system of coordinates with a pole located in a point 65° N and 60° E was designed. The modeling area covers all Polar Ocean. The horizontal resolution of this grid varies from 4 km in a coastal zone up to 19 km in a strait between Spitsbergen and Franz-Josef Land and reaches 120 km in Bering and Danish straits. The vertical resolution of the model grid is the 20 levels. For calculation of water circulation, fluxes of solid substance and pollutants is constructed the efficient numerical model. Step of integration on time can change from 0.5 till 12 hours. This model based on the complete equations of hydrothermodynamics of ocean with used of a hydrostatics and Boussinesque approximation with free surface, with registration of tidal component and parameterization of upper mixed layer. Also in model took into account the flux of energy from broken of superficial wind's waves.

The simulation of waters circulation in Barents and Kara seas for average year, for separate seasons and for differences state of atmosphere parameters are carried out. The analysis of water circulation in upper and bottom layers of the specified seas is executed.

**P10/E/20-A5** Poster **1600-04**

**PROCESSES OF VERTICAL EXCHANGE IN SHELF SEAS (PROVCESS)**

John HOWARTH (Centre for Coastal and Marine Sciences, Proudman Oceanographic Laboratory, Bidston Observatory, Birkenhead, Merseyside, L43 7RA, UK, email: mjh@ccms.ac.uk)

Vertical exchanges are principally controlled by the water column's turbulence characteristics. Turbulence is generated at the sea surface, by winds and waves, and at the bed, by friction. At the pycnocline turbulence levels are reduced and vertical fluxes can be inhibited. Turbulence characteristics therefore depend on and affect the water column's thermodynamics and dynamics and their interaction with the sea bed and surface.

An aim of the project is to test turbulence closure models, which are commonly used to quantify fluxes in shelf sea environmental models of, for instance, heat, of particles and of nutrients into the photic zone. Of particular importance are fluxes across the thermocline and the determination of which processes control nutrient recycling in the benthic boundary layer where a key will be to distinguish processes in the water column from those in the fluff layer formed by freshly deposited particulates, from those in the compacted sediment.

Measurements of turbulence dissipation rate throughout the water column and intensity over a wide frequency range, and of fluxes near the sea bed are being made at two contrasting sites in the northern North Sea. The first set of measurements were made during the autumnal breakdown of stratification in the northern North Sea in 1998 and the second, at a shallow high tidal energy site in the southern North Sea, will be in spring 1999. The project will contribute to the development of robust water column plankton shelf sea models tested over a range of turbulence environments.

**P10/W/04-A5** Poster **1600-05**

**USING SURVEYS OF AN UPWELLING JET NEAR A CAPE TO EVALUATE LAYERED MODELS OF JET SEPARATION**

Andrew C. DALE and John A. Barth (both at College of Oceanic and Atmospheric Sciences, Oregon State University, 104 Ocean Admin Bldg, Corvallis, Oregon 97331-5503, USA, E-mail: acd@oce.orst.edu)

During the upwelling seasons of 1994 and 1995 the coastal upwelling jet off Cape Blanco on the Oregon coast was surveyed using a CTD mounted on an undulating SeaSoar vehicle and shipboard ADCP. The observed fields show a tendency towards intensified upwelling in the lee of the cape accompanied by separation of the jet from the shelf and flow into the deep ocean. It is clear, from SST images, that these features are typical of the region. Layered models governed by potential vorticity conservation predict the evolution in structure of a coastal jet as it encounters gradual changes in topography, latitude and coastline curvature. The applicability of such models to the Cape Blanco region is investigated in the light of three dimensional dynamical fields derived from the survey data. A significant feature of the models is that when a jet passes a topographic anomaly (such as a constriction of shelf width) its structure can smoothly distort to a new downstream state. This happens when the flow is exactly critical to long coastal-trapped waves, a condition that is especially likely to be satisfied at some time by an upwelling jet as it evolves during the course of an upwelling season. Such a critical transition can lead to strongly enhanced upwelling in the lee of a cape and may be interpreted as jet separation. The likelihood of wave criticality is here determined by direct calculation of coastal-trapped wave phase speeds for the observed stratification and jet structure. The premise of potential vorticity conservation is also investigated for the alongshore scales of interest.

**P10/L/04-A5** Poster **1600-06**

**SHELF WAVES AS A CONTROL OVER THE FLOW, TEMPERATURE AND NUTRIENT SUPPLY IN SALDANHA BAY, SOUTH AFRICA**

Grenville NELSON (Sea Fisheries, Department of Environmental Affairs, Cape Town.)

Saldanha Bay is a semicircular indentation on the west coast of South Africa centered on latitude 330 5'S with an area 1.41x108 m<sup>2</sup>. A lightly dredged central channel drops from 12m at the centre of the bay to 40m at the mouth, which is some 6 to 7km wide. The adjacent narrow shelf supports the passage of energetic barotropic coastal-trapped waves, with a period of 5 to 6 days. The cross-shelf component of these waves acts to drive cold water into the bay below the wind influenced layer on the eastward phase. This is the dominant driving mechanism controlling temperature and nutrient supply and consequently primary productivity. The energetic six-day period waves appear to be forced by the synoptic pressure field over the southeast Atlantic. Also present in the spectra are less energetic waves at three and four days. These are the freely propagating coastally trapped waves generated locally by wind, and when their phase corresponds to that of the forced wave, the amplitude is great enough to produce a shelf wave penetration of 4km into the bay. Under these conditions, upwelling favourable winds exacerbate the inward movement of bottom water, which is entrained into the surface layer in the shallowest parts.

Tidal flow, generally of little significance on this coastline, can be an important factor in this bay at the spring tide. A tidal lagoon of area 5.3x107m<sup>2</sup> connects with the eastern part of the bay.

**P10/E/04-A5** Poster **1600-07**

**INDIRECT OBSERVATIONS OF DEIL MIGRATION ON THE HEBRIDEAN CONTINENTAL SHELF**

T.P. RIPPETH and J.H. Simpson (School of Ocean Sciences, University of Wales Bangor, Menai Bridge, Anglesey, UK, LL59 5EY.)

In this poster we shall consider the interpretation of measurements of vertical velocity and backscatter intensity, made using an acoustic doppler current profiler (ADCP) moored on the Hebridean Continental Shelf. The existence of vertically migrating scatterers is inferred from both the backscatter signal intensity and vertical velocity data, which indicates migration rates of 2-3 cm/s, and shows consistency between the displacement deduced from the vertical velocity and the observed movement of scatterers from the near bed to the near-surface region, evident in temporal variations in the backscatter signal intensity. Independent evidence that the observed vertical velocities are largely due to movements of the acoustic scatterers relative to the water is obtained through comparison of the ADCP vertical velocity data with vertical velocities inferred from the movement of the thermocline. The close phase locking between the motion and sunset and sunrise times has led us to interpret the signal in terms of the diel migration of zooplankton. Although no biological samples were collected during this study, previous surveys of the area have identified species of copepod and euphausiid that are known to migrate. The 12 days of data available show an initial period, during which there was a strong vertical migration signal, and a later period, during which the signal was not clear. By combining the observed vertical velocity and horizontal velocity components in a particle tracking model, it is demonstrated that the change in the migration signal may be a result of the advection of the patch of migrating zooplankton away from the ADCP, during the later part of the observational period.

**P10/E/19-A5** Poster **1600-08**

**ANALYSIS OF THE GEOMORPHOLOGICAL TRENDS FOR THE SOUTHERN CURONIAN SPIT LAGOONIC COAST**

TATIANA A. DORMOLENKO, Boris V. Chubarenko (P.P.Shirshov's Institute of Oceanology of Russian Academy of Sciences, Atlantic Branch, Prospect Mira, 1, 236000, Kaliningrad, Russia, E-mail: chuboris@ioran.kern.ru)

The Curonian spit is the largest (near 100 km) accumulative coastal macro-form in the South-Eastern Baltic and separates the Curonian lagoon from the Baltic Sea. It is mostly covered by forest but also has the areas of opening dune and the wetlands. The sand basis of the Curonian spit determines both the high velocity of shore-line shape changing and the instability of the vegetation free areas. The objective of this work consists in the quantification and analysis of the morphological trends of the Curonian spit lagoonic littoral from 1955 till 1994 years and assessing the influence of dune stripes on these trends. Practically important problem is the evaluation of the dune cells nourishment distribution downwards the underwater coastal slope and especially alongshore from open dune cells. Such knowledge is necessary for the optimization of trees planting program aiming to dunes fixation and for the using of the open dune stripes to compensate the shore erosion. The temporal variations (1955-1995) of the coastline, depths of 1, 2, 3 meters and underwater deposit volume were numerically appraised on the basis of comparative cartometric survey for the Curonian spit lagoonic coast. The analysis was executed for the set of sequential sites of the littoral, which were selected by coastline partition with a number of shore-normal cross-sections. The main geomorphological trends for the indicated above period were quantified. The shore-line of dune cells has promoted into lagoon and the littoral of these cells has got more shallow. The coastal line and littoral of the other cells have been eroded. The influence of dune nourishment on the stability of the coastline and littoral sites adjacent to dune cells was assessed. The trends in the alongshore and downwards sediment distribution were revealed.



P10/L/02-A5 Poster 1600-09

**OBSERVATIONS OF SEDIMENT RESUSPENSION AND TRANSPORT IN THE COASTAL AND BOTTOM BOUNDARY LAYERS OF LARGE LAKES WITH ACOUSTIC DOPPLER CURRENT PROFILERS**

SALYOR, James H. and Gerald S. Miller (Both at: National Oceanic and Atmospheric Administration, Great Lakes Environmental Research Laboratory, 2205 Commonwealth Blvd., Ann Arbor, MI 48105; e-mail: saylor@glertl.noaa.gov)

Data from Acoustic Doppler Current Profilers (ADCP) deployed in the nearshore region of southeastern Lake Michigan provide evidence of sediment resuspension and the cross-shelf transport of these materials during episodes of winter wind storms. Significant increases (+20 dB) in echo intensity and current velocity correlate well with satellite imagery of a sediment-laden plume transporting material in a cyclonic flow around the basins perimeter. A decrease in echo intensity to near background levels following the resuspension event suggests that the larger particles settle out, leaving the very fine material that remains visible in satellite imagery for many days. In Lake Champlain, a long, narrow and deep lake that forms the boundary between the states of New York and Vermont, bottom sediment resuspension caused by surges and gravity currents in the density-stratified lake water has also been documented in acoustic profiler records. Although no concurrent measurements of Total Suspended Material have been achieved in either lake, the ADCP results show that resuspension events can be detected using these instruments. With calibration of sediment concentration and echo intensity at each site, it appears that quantitative values of sediment fluxes can be determined.

P12

Monday 19 July

**GLOBAL WATER MASS ANALYSIS**

Location: Arts Building 120 LT

Location of Posters: Arts Building 120 LT and 101 LR4

Monday 19 July AM

Presiding Chair: Matthew England

**WATER MASS FORMATION PROCESSES**

P12/W/03-A1

0830

**SOME HISTORICAL, THEORETICAL AND APPLIED ASPECTS OF QUANTITATIVE WATER MASS ANALYSIS**

Matthias TOMCZAK (School of Earth Sciences, The Flinders University of South Australia, GPO Box 2100, Adelaide SA 5001, Australia, Email: matthias.tomczak@flinders.edu.au)

The concept of water masses is reviewed from the point of view of quantitative water mass analysis. A theoretical framework is presented which describes the life history of water masses in terms of formation, consolidation, ageing and decay. Water masses are described as physical entities and compared with their atmospheric counterparts (air masses). The classical temperature-salinity diagram is expanded into the mathematical concept of water types in an n-dimensional parameter space. Water types and their standard deviations are introduced as the foundation for quantitative water mass analysis. The relationship between parameter space and physical space is established through the definition of water type density. Mode Waters are discussed as regions in physical space with a minimum in water type density. Some unresolved issues of the structure of the oceanic thermocline are discussed in this context. The definition of water masses is extended to include water masses in the surface mixed layer where air-sea exchange processes continuously modify water mass properties. The paper concludes with a brief discussion of the representation of water masses and their evolution in numerical models.

P12/W/07-A1

0850

**SUBDUCTION RATES FOR THE SOUTHERN INDIAN OCEAN THERMOCLINE**

J. KARSTENSEN and D. Quadfasel 1) Institut für Meereskunde, University of Hamburg, Germany 1) now at: NBI/AFG, University of Copenhagen, Denmark

Using a kinematic as well as a transient tracer/oxygen approach, the subduction rates for water into the southern Indian Ocean thermocline were calculated and compared. For both techniques, the rates were found to be of the same magnitude with respect to the error margins. Comparing Ekman and Ekman-lateral induced rates in density increments of the winter mixed layer, the side-by-side existence of Indian Central Water and Mode Water is evident. The total volume of subducted water into the permanent thermocline was found to be 32 Sv for the density range 25.3 to 26.9 kg/m<sup>3</sup>. This is comparable to recent estimates for the North Atlantic (27 Sv) and North Pacific (35 Sv) Ocean. However, the proportion of the lateral volume transport in the Indian Ocean (21 Sv) is twice as large compared to the northern hemisphere oceans (NA 9.5 Sv; NP 10.1 Sv). This is in agreement with the large volume of Mode Water, which can be found in the Indian Ocean. The formation of the Mode Water through mid-latitude convection is located south of the subtropical front, whereas its subduction in the thermocline is lateral, as a combination of the eastward flow field along the front combined with the southern tilting of the front. Relating the rates to tracer distribution in the winter mixed layer depth, enabled us to determine source tracer characteristics of the Mode and Central Water, respectively. The characteristics may be used for further water mass mixing analysis.

P12/W/22-A1

0910

**TWO VARIETIES OF SUBTROPICAL LOWER WATER (SLW) IN THE SOUTH PACIFIC: THEIR ORIGIN AND DISTRIBUTION**

Serguei SOKOLOV and Stephen Rintoul (both at CSIRO Marine Research and Antarctic Cooperative Research Centre, GPO Box 1538, Hobart, Australia, email: Serguei.Sokolov@marine.csiro.au and Steve.Rintoul@marine.csiro.au)

Two varieties of SLW are present throughout the western part of the South Pacific: a cool, fresh variety is situated north of New Zealand, and a warm, salty variety is found north of Fiji and the New Hebrides. New data from a roughly meridional WOCE section P11 along 155E between the Subtropical Front and Louisiade Archipelago at 12S occupied in winter 1993 help refine some details of the SLW origin and distribution in the region. The warm and salty northern variety of SLW is formed in the central South Pacific near the Society Islands where a surface salinity maximum coincides with a maximum in evaporation minus precipitation. The

subsurface salinity maximum of the SLW in the western South Pacific is a result of these high salinity surface waters being carried west in the northern arm of the subtropical gyre and under-riding lighter, low salinity water produced by an excess of precipitation over evaporation in the western tropical Pacific. South of 25S on P11 the salinity maximum reaches the sea surface marking the northern boundary of the cooler, fresher, denser southern variety of SLW. The southern boundary of the southern SLW on P11 is marked by the strong near-surface horizontal salinity gradient associated with part of the Subtropical Front at 38S. The formation region of the southern type of SLW - the Central Tasman Sea - also coincides with a maximum excess of evaporation over precipitation. This region also experiences strong cooling by the atmosphere, driving winter convection. Deep mixing during winter increases the oxygen content of the surface layer. The water which feeds the formation zone of southern SLW is the northern variety of SLW. Cooling and evaporation convert about 5 Sv of northern SLW to southern SLW in the Tasman Sea. Ventilated SLW carried eastward by the EAC spreads around the subtropical gyre of the South Pacific and is driven northward beneath the Tropical Convergence zone by Ekman pumping (Morris et al., 1996). The high-oxygen southern SLW under-rides the newly formed northern SLW in the central Pacific. The two super-posed varieties of SLW are carried westward to the Coral Sea in the SEC along the northern flank of the subtropical gyre. Here the two components of SLW are separated by only 40-60 m in depth and become almost indistinguishable within the cyclonic gyre of the Coral Sea. The total net inflow of SLW into the Coral Sea in the neutral density layer between 23.6 and 26.8 is 32 Sv, with 10.1 Sv re-circulating in the Gulf of PNG and entering the Solomon Sea. The remainder of the SLW turns south to feed the EAC.

P12/W/02-A1

0930

**THE ORIGIN OF WATERS OBSERVED ALONG 137°E**

Frederick BINGHAM (UNC-Wilmington, Wilmington, NC 28403 USA; Email: binghamf@uncwil.edu) Toshio Suga and Kimio Hanawa (both at: Department of Geophysics, Tohoku University, Sendai 980-77 Japan; Email: suga@pol.geophysics.tohoku.ac.jp)

Using the World Ocean Atlas data set, we examine the origins and flow paths of waters observed along 137°E section in the western North Pacific. The method of Bingham (1999) was used to trace waters from 137°E back through the subtropical gyre to their outcrops. We divide the water masses observed along this section into four zones. (1) There is a zone of waters that connect directly to areas of surface subduction, chiefly the water mass known as North Pacific Tropical Water. Working backward along geostrophic streamlines, we find the locations of the outcrops of these waters. Subducted waters are aged using this technique and found to be between 0.5 and 35 years old by the time they reach 137°E. For this subducted regime, waters on a given isopycnal observed along 137°E increase in age with decreasing latitude, with waters at the southern end of the section being 2-3 times older than waters at the northern end. (2) There is a recirculating zone, where waters do not have any direct contact with the surface. Some of these recirculating waters, particularly the North Pacific Intermediate Water are strongly influenced by surface processes outside the subtropical gyre, but are not subducted by Ekman pumping. (3) There are North Pacific Subtropical and Central Mode Waters, which have direct contact with the surface, but mainly through buoyancy forcing rather than Ekman pumping. And (4) there is a seasonal thermocline, where waters are strongly influenced by surface heating and cooling, and isopycnals can disappear during the winter. We use these generalizations to characterize water mass variability observed in the PR-1 hydrographic section along 137°E.

P12/C/JSP21/E/01-A1

0950

**INTERPRETATION FOR THE FORMATION OF THE CFC MAXIMUM IN THE NORTH PACIFIC**

Sachiko OGUMA, Yutaka Nagata (both at Marine Information Research Center, Japan Hydrographic Association, Tokyo 104-0061, Japan) Goro Yamanaka (Oceanographic Division, Meteorological Research Institute, Tsukuba 305-0052, Japan) Toshio Suga and Kimio Hanawa (both at Department of Geophysics, Graduate School of Science, Tohoku University, Sendai 980-8578, Japan)

Chlorofluorocarbon (CFC) maximum layers have been found in the broad area of the Subtropical North Pacific. By using the results which contain the distributions of current and temperature and its variation, obtained by an Ocean General Circulation Model (OGCM) developed by Yamanaka (1997), and by giving spatial (depending on surface temperature) and temporal variations of CFC at the sea surface, we calculate CFC distributions in the North Pacific, and compare them with the observed CFC distribution, especially in the cross-section along 30N. The main feature of the CFC distribution including its maximum layer is well reproduced. In order to find the source area of CFC maximum layer water, trajectory analysis is also made. It is shown that the CFC maximum layer water is originated near the bottom of the winter mixed layer near 39N of the central part of the North Pacific, along the line of outcrop of 25.8 sigma<sub>theta</sub> isopycnal surface. However, the distribution derived from an assumption that the CFC concentration is simply advected along trajectories by keeping the values in the injected area is much different from that reproduced in our model which includes the effect of eddy-diffusion. Distribution of CFC concentration would depend not only on advection but also on eddy-diffusion. Using a simple box model checks the relative importance of the advection to diffusion. It is suggested that this ratio is different between in the upper half and in the lower half of the CFC maximum layer. The position of the CFC maximum layer may be located between the regimes where diffusion is dominant and where advection is dominant.

P12/E/03-A1

1010

**PHYSICAL MECHANISMS OF NORTH PACIFIC INTERMEDIATE WATER FORMATION**

Nikolai A. MAXIMENKO (Shirshov Institute of Oceanology, Russian Academy of Sciences, 36, Nahimovskii prospect, Moscow 117851, Russia, email: maximenko@stream.sio.rssi.ru)

Results of isopycnal analysis of mean distribution of seawater properties in the North Western Pacific along with the propagation of seasonal signal point at the western part of the Kuroshio Extension as a formation area of the North Pacific Intermediate Water (NPIW). In addition to critical analysis of conventional theory of dominant role of lateral mixing, some new hypotheses are forwarded. Among them are: cabbelling and frontal convection, density-driven intrusions, geostrophic adjustment both in the confluence zone of subarctic and subtropical water masses and downstream the current (due to dissipation of its zonal momentum), non-turbulent vertical transfer of zonal momentum (wave radiation and baroclinic interaction, resulting in "form drag"- type effects), interaction between thermocline and deep circulation. In all the cases specific forcing may appear in NPIW layer, making it drifting geostrophically equatorward. Developed is a scheme of measurements and historical data reanalysis that may verify the importance of this physical mechanisms.



<b>Introduction</b>	<b>1030</b>
---------------------	-------------

<b>P12/W/15-A1</b>	<b>Poster</b>	<b>1030-01</b>
--------------------	---------------	----------------

**VARIABILITY OF THE NORTH ATLANTIC WATER MASS STRUCTURE AND CIRCULATION**

S.A.DOBROLIUBOV (Department of Oceanology, Moscow State University, Vorobievsky Gory, Moscow, 117234, Russia, e-mail: dobro@ocean.geogr.msu.ru), A.V.Sokov and V.P.Tereschenkov (both at P.P.Shirshov Institute of Oceanography, Nahimovskiy pr., 36, Moscow, 117851, Russia, e-mail: bobag@gulev.sio.rssi.ru)

Interdecadal changes of thermohaline characteristics and circulation of the intermediate and deep waters in the North Atlantic are considered. The results are based on the comparison of the Russian 1997 survey of 60N and WOCE AR5 with historical data. Significant changes of intermediate and deep waters T,S properties are found, accompanied by changes of the cross section mass, heat and freshwater fluxes. The earlier determined intensification of the Meridional Overturning Circulation (MOC) in the 80-s is confirmed. The MOC strengthening is accompanied by the rapid decrease of the recirculation flows and the formation of the well-defined two-layer structure of the MOC. The derived changes of the thermohaline structure suggest that at the phase of intensified MOC the preferable direction of the Labrador Sea Water spreading is north-east into the Irminger Basin, while at the period of reduced MOC the LSW flows preferably to the east and south-east. Enhancement of the southward freshwater transport in the Denmark Strait was closely correlated with the intensification of the northward meridional heat transport; the latter varied from 0.28 PWt to 0.38 PWt at 60N.

<b>P12/W/16-A1</b>	<b>Poster</b>	<b>1030-02</b>
--------------------	---------------	----------------

**INTERDECADAL CHANGES OF MASS AND MERIDIONAL HEAT TRANSPORT IN THE NORTH ATLANTIC**

A.V.SOKOV, V.P.Tereschenkov (P.P.Shirshov Institute of Oceanography, Nahimovskiy pr., 36, 117851, Moscow, Russia; e-mail: sokov@gulev.sio.rssi.ru) and S.A.Dobroliubov (Department of Oceanology, Moscow State University, Vorobievsky Gory, Moscow, 117234, Russia, e-mail: dobro@ocean.geogr.msu.ru)

Estimates of meridional mass and heat transports across the planes of transatlantic hydrographic sections along 24.5N, 36N, 48N and 59N (computed for the three time periods 1957-1962, 1981-1982 and 1991-1993) are considered. The intensity of the Meridional Overturning Circulation (MOC) didn't change significantly at 59N during the whole time period. While remarkable changes were detected to the south from 59N. Strengthening of MOC occurred at 48N and 36N in 1981-82 (19Sv and 20Sv respectively) against 14Sv and 12Sv in 1991-93 and 9Sv and 8Sv in 1957-59. Intensification of MOC at 24.5N is less profound. The results demonstrate negative correlation between the variability of MOC and Labrador Sea Water (LSW) production rate. The MOC intensification observed in 1980s corresponds to the increase of the mass transport in the Denmark Strait Overflow waters (DSOW) layer at 59N and is accompanied by the increase of the Antarctic Bottom Water (AABW) transport at 24.5N and its upwelling in the area between 24.5N and 36N. During the weak MOC (in the 1990s) the LSW production reached its maximum, the transport of DSOW reduced and the AABW penetrated further to the north than 36N.

<b>P12/W/12-A1</b>	<b>Poster</b>	<b>1030-03</b>
--------------------	---------------	----------------

**INTERANNUAL VARIABILITY OF THE UPPER OCEAN CIRCULATION AT 36N IN THE ATLANTIC OCEAN**

V.P.TERESCHENKOV (P.P.Shirshov Institute of Oceanography, Nahimovskiy pr., 36, Moscow, 117851, Russia, e-mail: bobag@gulev.sio.rssi.ru) and A.V.Arkipkin (Department of Oceanology, Moscow State University, Vorobievsky Gory, Moscow, 117234, Russia, e-mail: arkip@ocean.geogr.msu.ru)

Interannual changes of the ocean steric height at 36N in the Atlantic ocean are considered. The study is based on the temperature and salinity observations in the upper 2000m layer collected by repeated surveys of the cross-ocean hydrographic section during 1972-1984 time period. Variability of the upper layer steric height is inspected in terms of water mass properties variability. Special attention is paid to the evolution of subtropical (18 degree) and subpolar mode waters and Mediterranean waters, regarding their remote relation to the changes of the atmospheric conditions over the sites of their origin. The changes of the upper ocean zonal pressure gradients are discussed in sense of North Atlantic circulation features, such as Gulf Stream, its recirculation jets and Azore Current.

<b>P12/E/01-A1</b>	<b>Poster</b>	<b>1030-04</b>
--------------------	---------------	----------------

**WATER MASS, TEMPERATURE, SALT AND HEAT EXCHANGE OF ANTARCTIC AND NORTH ATLANTIC BASINS**

ANISIMOV M.V., Ivanov Yu.A., Lebedev K.V. and M.M. Subbotina P.P.Shirshov Institute of oceanology, 117851, Nakhimovskiy pr.36, Moscow, Russia, Tel.: (095)124-7729; fax: (095)124-5983; e-mail: MMS@sio.rssi.ru, MVA@sio.rssi.ru

On the base of ocean general circulation model with using of climatological massive (Levitus, 1994), we calculated temperature, salinity, density, free surface level and current fields in the North Atlantic and Arctic basins. We defined the integral mean annual and mean seasonal characteristics of water mass, salt and heat transports. Also we fulfilled the analysis of inter seasonal redistribution of water mass, salt and heat transports for climatic seasons. Estimates of climate averaged variability of integral transports were made.

<b>P12/E/06-A1</b>	<b>Poster</b>	<b>1030-05</b>
--------------------	---------------	----------------

**THE SPREADING OF RED SEA OVERFLOW WATERS IN THE INDIAN OCEAN**

LISA M BEAL and Amy Ffield (Lamont-Doherty Earth Observatory, Palisades, NY 10964, USA. Email: lbeal@ldeo.columbia.edu)

As a result of its remarkably high salinity and low oxygen content, remnants of Red Sea Waters (RSW) have been identified in the southwest Indian Ocean, over 50f south of their source. Here we describe the mean pathway for the spreading of RSW throughout the Indian Ocean. A comprehensive set of observations is used, taken from the National Oceanographic Data Center archives and from the World Ocean Circulation Experiment Hydrographic Program for the Indian Ocean. The analysis suggests that the large scale salinity and oxygen distribution of the Indian Ocean is stationary at intermediate depth, indicating that there is little monsoon or interannual variability. From property maps the spreading of RSW appears to be

favoured along the western boundary, particularly south of the westward flowing South Equatorial Current, where there is a clear tongue of RSW spreading through the Mozambique Channel and into the Agulhas Current. The property distributions imply a predominantly diffusive mixing regime in the ocean interior with a stronger advective component at the western boundary. The evidence for a long-time-mean pathway for RSW into the Agulhas Retroflection region suggests a consistent supply of saline intermediate waters which may be captured in Agulhas Rings and exported to the South Atlantic. A quantitative estimate of the transport of RSW in the Agulhas Current at 32S suggests that almost all of the Red Sea outflow waters end up in the WBC.

<b>P12/E/02-A1</b>	<b>Poster</b>	<b>1030-06</b>
--------------------	---------------	----------------

**WATERMASS STRUCTURE AND TRANSPORT IN THE INTERMEDIATE LAYERS OF THE SOUTH INDIAN OCEAN**

BENNY N. PETER & Vimal Kumar (Department of Physical Oceanography, Cochin University of Science & Technology, Fine Arts Ave, Cochin, India 682016, email: benny@md2.vsnl.net.in)

The watermass assembly in the intermediate layers of the South Indian Ocean and its exchange with the Antarctic Ocean (at 32 degree south) is described in the present study. The hydrographic data procured from the National Oceanographic Data Center, Washington, USA and National Research Institute of Far Seas Fisheries, Shimizu, Japan are used. Isanosteric Analysis is employed to identify the watermass movement. The distribution of potential temperature, salinity and depth on 140, 120, 100, 80, 60 ct/ton surfaces are presented. The method introduced by Montgomery and Stroup(1962), depicting the transport in the T-S diagram, is adopted to quantify the watermass exchange. The watermasses in the South Indian Ocean is much influenced by the Indonesian Throughflow, even in the intermediate layers. Also, the cross equatorial spreading is weakened towards deeper levels. The intrusion of Antarctic waters are more confined to the central part, while the return flow is taking place near the continental boundaries. The Indonesian Throughflow adds more low saline cool water to the South Indian Ocean. The thermohaline front which separates the cool, less saline Pacific and saline, warm Indian waters is weakened with respect to depth. In the intermediate layers a net southward transport of 5.84Sv is observed. The major contribution of low saline Antarctic Intermediate Water towards north is confirmed from the flux distribution in the T-S diagram.

<b>P12/E/07-A1</b>	<b>Poster</b>	<b>1030-07</b>
--------------------	---------------	----------------

**WATER MASSES OF COASTAL REGIONS OF THE FAR-EASTERN (THE JAPAN, OKHOTSK, AND BERING) SEAS**

Gennady YURASOV ( Pacific Oceanological Institute, Russian Academy of Sciences, Far-Eastern Branch, Baltiyskaya Str., 43, 690041 Vladivostok, Russia, email: pacific@online.marine.su) Yury Zuenko (Pacific Fishery and Oceanography Research Institute, Shevchenko Alley, 4, 690600 Vladivostok, Russia).

General principles of water mass analysis based on statistical methods are applied to all listed seas. Materials of the long-term seasonal surveys of coastal regions are examined for this purpose. Using proposed technique a classification of water masses and types of water vertical structure was conducted.

Influenced by the same formation mechanism at all seas the water masses produce an estuarine (at the Okhotsk Sea only), coastal, shelf and subarctic types of the vertical structure. All of them have their attributed stratification degree and characteristics of water masses. In the regions of complete tidal mixing the water masses are homogenous from the sea surface to the bottom. The same named water masses for each of the listed seas are differed each other by values of their parameters (temperature, salinity, depth) and sizes of their extension. During winter season at all three seas the water masses of higher density are being formed. As a result of convection and mixing these waters ventilate deep layers. Particularly this mechanism develops at the Japan Sea where the shelf is of insignificant extent. It is supposed that the higher density waters of the Okhotsk Sea ventilate the layer of lower salinity in the North Pacific Ocean.

<b>P12/W/19-A1</b>	<b>Poster</b>	<b>1030-08</b>
--------------------	---------------	----------------

**A THREE-LAYER MODEL FOR THE STUDY OF TIDALLY INDUCED DENSITY CURRENTS**

Rainer Weigle, Peter BRANDT, and Angelo Rubino (Institut für Meereskunde, Universität Hamburg, Troplowitzstr. 7, D-22529 Hamburg, Germany, Email: brandt@ifm.uni-hamburg.de)

The dynamics of tidally induced internal waves is investigated by using a numerical three-layer model based on the weakly nonlinear, weakly non-hydrostatic Boussinesq equations. Numerical solutions of the three-layer Boussinesq equations are compared with analytical solutions of different equations describing internal solitary waves in a two-layer system. In contrast to the two-layer models, the three-layer model is capable of describing the evolution of sub-surface jets. As a result of the three-layer model these jets develop undulations that finally disintegrate into internal solitary waves. Several characteristics of these waves, like e.g., wave amplitude and distance between the first two solitary waves of a wave train are studied as a function of the initial jet velocity and the stratification. Results of the numerical simulations are compared with results of high resolution in-situ measurements carried out north and south of the Strait of Messina, in the European Mediterranean Sea. Implications of the presented study for a possible inversion of sea surface manifestations of oceanic internal waves into characteristics of the interior ocean are discussed.

<b>P12/W/20-A1</b>	<b>Poster</b>	<b>1030-09</b>
--------------------	---------------	----------------

**GROWTH MECHANISM OF TOPOGRAPHIC INTERNAL WAVES GENERATED BY AN OSCILLATORY FLOW**

Tomohiro NAKAMURA and Toshiyuki Awaji (Department of Geophysics, Graduate School of Science, Kyoto University, Kyoto 606-8502, Japan, Email: nakamura@kugi.kyoto-u.ac.jp)

A new amplification mechanism for topographic internal waves generated by tidal flow is presented to reveal the unknown growth processes of the internal waves in the Kuril Straits (about 47N in the North Pacific) reported by Nakamura et al. (1998). According to their investigation, the nature of the wave properties is determined by the nondimensional parameter  $(k U_0/\sigma_f)$ , where  $k$  is the curvature of topography,  $U_0$  is the flow speed amplitude, and  $\sigma_f$  is the frequency of tidal flow, through which the topographic internal waves can be classified into the three wave types; (1)unsteady lee waves ( $k U_0/\sigma_f \gg 1$ ), (2)mixed tidal lee waves ( $k U_0/\sigma_f \sim 1$ ), and (3)internal tides ( $k U_0/\sigma_f \ll 1$ ). Notably, their numerical model showed that the growth processes of the first two waves were quite different from those predicted by conventional internal wave theories, thus suggesting the presence of another criterion for wave amplification. For this issue, our theoretical investigation based on the ray tracing of individual waves generated at various time reveals the following interesting facts. Unsteady lee waves are always amplified when the maximum frequency is sufficiently smaller than the buoyancy frequency (i.e.,  $\sigma_f \ll k U_0 \ll N$ ), because their phase speeds and amplitudes are equal

and proportionate to the tidal flow speed at their generation, respectively. Fast mixed tidal lee waves are also effectively amplified as well as unsteady lee waves, when the rotation effect is significant (i.e.,  $f \sim \sigma_f \sim k U \ll N$ ). Accordingly, amplification of unsteady lee waves and fast mixed tidal lee waves can occur even if the conditions indicated by previous theories (i.e., the critical slope and the critical Froude number) are not satisfied. Since our theoretical model covers generation and amplification processes of topographic internal waves in a broader parameter range than before, it may contribute to a better understanding of the Boundary Mixing processes.

**P12/W/06-A1** Poster **1030-10**

**WATER MASS, TEMPERATURE, SALT AND HEAT EXCHANGE OF ANTARCTIC AND NORTH ATLANTIC BASINS**

Anisimov M.V., IVANOV Yu.A., Lebedev K.V. and SUBBOTINA M.M. P.P.Shirshov Institute of Oceanology

On the base of ocean general circulation model with using of climatological massive (Levitus,1994) we calculated temperature, salinity, density, free surface level and current fields in the North Atlantic Antarctic basins. We defined the integral mean annual and mean seasonal characteristics of water mass, salt and heat transports. Also we fulfilled the analysis of interseasonal redistribution of water mass, salt and heat transports for climatic seasons. Estimates of climate averaged variability of integral transports were made.

Presiding Chair: Bernadette Sloyan

**WATER MASS CLIMATOLOGY**

**P12/E/04-A1** **1110**

**WORLD OCEAN THERMAL STRUCTURE**

Peter C. CHU, Chenwu Fan, and Hui Liu

We used gradient criteria to establish a global ocean mixed layer depth (MLD), thermocline depth (THD), and thermocline strength (THS) data sets from the National Oceanographic Data Center (NODC) 4.5 million temperature profiles. The annual cycles of MLD, THD, and THS of the world ocean are described based on climatological monthly-mean MLD fields. The interannual variabilities of MLD, THD, and THS are obtained from zonally averaged monthly mean fields as well as the latitudinally averaged (10 deg N and 10 deg S) monthly mean fields. The ocean interannual thermal variability is closely related to El Nino, North Atlantic Oscillation (NAO), and Great Salinity Anomaly in the Arctic regions.

**P12/W/11-A1** **1130**

**WATER MASS CHANGES IN THE SCOTIA SEA**

David P. STEVENS (School of Mathematics, University of East Anglia, Norwich NR4 7TJ, email: D.Stevens@uea.ac.uk) Karen J. Heywood (School of Environmental Sciences, University of East Anglia, Norwich NR4 7TJ, email: k.heywood@uea.ac.uk)

In March-April 1999 two South Atlantic WOCE sections, A21 (Drake Passage) and (part of) A23 (35 degrees west), will be reoccupied as a component of ALBATROSS (Antarctic Large-scale Box Analysis and The Role Of the Scotia Sea). WOCE section A21 was occupied in February 1990 and section A23 was occupied in March 1995. Early results from ALBATROSS will be presented. In particular we will focus on an analysis of differences between ALBATROSS and the earlier WOCE sections. Both the WOCE and ALBATROSS data include a full suite of chemical tracers (such as CFCs and nutrients) as well as traditional hydrography. Assessments will be made of the role of the observed water masses in climate variability.

**P12/W/10-A1** **1150**

**WATER MASS CHANGES IN THE NORTH AND SOUTH PACIFIC OCEANS BETWEEN THE 1960'S AND 1985-94, IMPLICATIONS FOR CLIMATE CHANGE**

Annie P.S. WONG (IASOS, University of Tasmania, GPO Box 252-77, Hobart, 7001, Australia), Nathaniel L. Bindoff (Antarctic CRC, GPO Box 252-80, Hobart, 7001, Australia, email: N.Bindoff@utas.edu.au) and John A. Church (Antarctic CRC and CSIRO Marine Research, GPO Box 1538, Hobart, 7001, email: john.church@marine.csiro.au).

Comparisons have been made along five modern hydrographic sections with historical data to investigate water mass changes in the North and South Pacific Oceans. The five modern hydrographic sections were sampled in the decade 1985-94, while the historical data were mostly from the 1960s.

Below the seasonal mixed layer, statistically significant temporal differences in temperature and salinity have been detected in the water masses that occur in the top 2000 dbar of the water column. These differences in water mass property changes are assumed to result from changes in sea surface conditions at the formation regions.

Of the observed temporal differences, the ones with largest scale are from the shallow salinity maxima of North Pacific Subtropical Water (NPSTW) and South Pacific Subtropical Water (SPSTW), and the intermediate salinity minima of North Pacific Intermediate Water (NPIW) and Antarctic Intermediate Water (AAIW). The two salinity maxima, NPSTW and SPSTW, also show signs of salinity increase, while the two salinity minima, NPIW and AAIW, have become warmer and fresher. Since NPSTW and SPSTW originate under the high evaporative cells of the central North and South Pacific, and NPIW and AAIW acquire their properties near the polar gyres, these changes in the ocean interior imply an increase in evaporation over the mid-latitudes, and an increase in precipitation over the high-latitudes regions in both hemispheres. Taken together these results imply a strengthening of the hydrological cycle over the North and South Pacific Oceans. Output from coupled climate model for increasing atmospheric CO<sub>2</sub> level show that the model ocean responds with a warming of the water column. Superimposed on this background warming trend is a decrease in salinity in the salinity minima of the Pacific (AAIW and NPIW) which corresponds to near-surface freshening where their respective isopycnals outcrop. Hence the freshening signature that has been detected in NPIW and AAIW from observational data is qualitatively consistent with the results from this climate model for increasing atmospheric CO<sub>2</sub>.

**WATER MASSES IN MODELS**

**P12/W/23-A1** **1400**

**WATER MASS ANALYSIS IN OCEAN MODELLING**

Matthew H. ENGLAND, Centre for Environmental Modelling and Prediction (CEMAP), The University of New South Wales, Sydney NSW 2052, Australia email: M.England@unsw.edu.au

Water mass analysis forms a vital component of ocean model assessment. I will present an overview of the fidelity of models in the context of the global scale water masses, summarising the key processes and parameterisations required for large-scale simulations of water mass renewal. I will also outline how ocean modellers try to verify water mass formation processes in global ocean simulations. Proxy model diagnostics of ventilation rates, such as "age" and age distributions, will also be discussed in the context of ocean model assessment.

**P12/W/05-A1** **1420**

**USE OF PASSIVE TRACERS TO ANALYSE WATER MASSES IN CONTROL AND TRANSIENT CO<sub>2</sub> SIMULATIONS**

Siobhan P. O'FARRELL, CSIRO Atmospheric Research Aspendale, 3195, Australia. email : Siobhan.O'Farrell@dar.csiro.au

Due to the high frequency component of atmospheric forcing, the ocean response when coupled to an atmospheric model differs from that seen with imposed surface boundary conditions. In particular, the rates of convection, depth of mixed layer, and meridional overturning rates are altered at high latitudes under coupled conditions. A passive tracer has been used in the ocean model to explore differences between spin up and coupled experiments as an analogue to some of the chemical species that are regularly measured on ocean hydrographic sections. There are two versions of the ocean model, a version with standard horizontal diffusion and a second with the Gent and McWilliams eddy mixing. Simulations with both ocean versions have included tracers for 50 years in the coupled ocean atmosphere model and in ocean-only runs. The tracer output is discussed in terms of water masses for individual ocean basins.

Additionally, there are 50 years of tracer data from a transient CO<sub>2</sub> experiment with the coupled model. The tracer was released at a time when the CO<sub>2</sub> level is held constant in the atmosphere at double the value of the control simulation, after the ocean adjustment to the new surface conditions has slowed. A further set of passive tracer data is now being gathered in a transient simulation, as CO<sub>2</sub> is increased from 1880 levels to those projected for the end of the next century. Both these tracer data sets will be used to examine how different water masses in the ocean are responding to the climate change signal.

**P12/W/13-A1** **1440**

**RENEWAL AND MODIFICATION OF ANTARCTIC INTERMEDIATE WATERS**

Bernadette SLOYAN, Alfred Wegener Institute for Polar and Marine Research, Postfach 12 01 61, D-27515 Bremerhaven, GERMANY

Subantarctic Mode water (SAMW) and Antarctic Intermediate water (AAIW) are characterized by a dissolved oxygen maximum and salinity minimum north of the Antarctic Polar Front zone (APF). These water masses move eastward with the Antarctic Circumpolar Current (ACC) and northward into the adjacent Atlantic, Indian and Pacific subtropical Oceans. Along this circulation path significant property changes occur to both water masses. Many mixing mechanisms and their principal location, which results in the observed property changes, have been suggested.

Estimates of interior and air-sea diapycnal fluxes for the southern oceans, across neutral surfaces identifying SAMW and AAIW, are derived from basin-scale budgets of mass, heat and salt using a box inverse model. The diapycnal fluxes quantify mixing occurring in the subtropical oceans and across the APF. The inferred fluxes help us explain the property changes in SAMW and AAIW observed across each ocean basin.

**P12/W/04-A1** **1500**

**ZONAL FLUXES IN THE DEEP LAYERS OF THE SOUTH ATLANTIC**

Michael VANICEK (Department of Marine Physics, Institut fuer Meereskunde Kiel, Duesternbrooker Weg 20, 24105 Kiel, Germany, email: mvanicek@ifm.uni-kiel.de) Gerold Siedler (Department of Marine Physics, Institut fuer Meereskunde Kiel, Duesternbrooker Weg 20, 24105 Kiel, Germany, email: gsiedler@ifm.uni-kiel.de)

The circulation of the North Atlantic Deep Water (NADW) in the South Atlantic is determined from hydrographic, nutrient, and tracer data from WOCE and other high quality pre-WOCE sections using a linear box-inverse model. Multiple linear regression, which makes use of the correlation between different parameters, is applied to infer the missing parameters in the bottle data set. This interpolation technique also enables us to include the nutrient and tracer measurements in the inverse model with a spatial resolution of the corresponding CTD data. The data define a set of 126 closed boxes on which conservation requirements are imposed. A detailed water mass analysis is performed, incorporating the tracer information from the whole South Atlantic, to determine the vertical boundaries of these boxes. As a result the water column is divided into 11 layers which are defined by neutral densities. Constraints for the inverse model are an integral meridional salt and phosphorus transport, the overall salt and silica conservation, as well as flow conditions inferred from moored current observations. The results are analysed with an emphasis on the zonal spreading of the NADW. A clear meridional separation in the direction of the zonal NADW transports can be observed. Quantitative estimates are given.

**P12/E/05-A1** **1520**

**MEAN CIRCULATION AND TURBULENCE IN THE EASTERN NORTH ATLANTIC, FROM A REGIONAL NUMERICAL MODEL**

Thierry PENDUFF (Laboratoire des Ecoulements Geophysiques et Industriels, BP53 38041 Grenoble Cedex 9, France, email Thierry.) email: Penduff@hmg.inpg.fr Alain COLIN DE VERDIERE (Laboratoire de Physique des Océans, Université de Bretagne Occidentale, BP 809, 29280 Brest cedex, FRANCE, email: acolindv@univ-brest.fr) Bernard BARNIER (Laboratoire des Ecoulements Geophysiques et Industriels, BP53 38041 Grenoble Cedex 9, France, email: Bernard.Barnier@hmg.inpg.fr)

An eastern North Atlantic regional configuration of SPEM model is used to study the general circulation in the basin, the mesoscale turbulence, and the interactions between these two

scales. Contrary to previous studies, and to ensure consistency between lateral forcing and inner dynamics, the velocity field along the wide open boundaries is largely determined by the model itself. This approach can therefore be considered as a prognostic alternative to inversions; after stabilization, the general circulation is qualitatively and quantitatively close to available data. It is shown that in the North Atlantic Current, baroclinic instability generates eddies that in turn strengthen the mean flow, and that these processes are intensified on the polar side of the fronts; available data seems to confirm this features.

### P12/W/08-A1 1600

#### INFLUENCES ON NEAR-SURFACE VELOCITY FIELDS DUE TO STRONG VERTICAL MIXING IN THE INDONESIAN SEAS

Masatora IIDA, Toshiyuki Awaji, Yoichi Ishikawa, Kazunori Akitomo, Teiji In, Nobumasa Komori, Takaki Hatayama, Tomohiro Nakamura (Department of Geophysics, Graduate School of Science, Kyoto University, Kitashirakawa-Oiwake, Sakyo, Kyoto 606-8502, Japan, email: iida@kugi.kyoto-u.ac.jp), and Bo Qiu (Department of Oceanography, University of Hawaii at Manoa, 1000 Pope Rd., Honolulu, Hawaii 96822, U.S.A., email: bo@iniki.soest.hawaii.edu)

Impacts of strong vertical mixing caused by tidal mixing in the Indonesian Seas are investigated with emphasis on how much this regional mixing has influences on the near-surface velocity fields over the Pacific and Indian Oceans by using an extended reduced gravity layer model, which is basically similar to that of McCreary and Kundu (1989) but is widely extended. Our reduced gravity layer model has dynamically two and thermodynamically three active layers. The first dynamical layer has two thermodynamical layers; the upper one is called the 'mixed layer' which includes a bulk mixed layer model based on Kraus-Turner thermodynamics, and the lower one is called the 'fossil layer'. Within this layer, no vertical temperature gradients exist but horizontal gradients do. This means that density can vary within the layer. In addition, our layer model can deal with vertical heat / momentum exchanges due to entrainment / detrainment.

Using this layer model, we have performed two numerical experiments with and without strong vertical mixing in the Indonesian Seas. Comparison between both results revealed many interesting facts about the influences of the regional vertical mixing on the near-surface velocity fields of the equatorial Pacific and Indian Oceans. For example, the South Equatorial Current in the Pacific Ocean is much intensified, leading to the significant increase in transport of the South Pacific water into the Indonesian Seas. This is very consistent with the observational result revealed by Ffield and Gordon (1992). Our detailed analysis showed that such an increase in the volume transport of the South Pacific Water flowing into the Indonesian Seas is associated mainly with the occurrence of upwelling Kelvin waves in the western equatorial Pacific due to the effect of strong vertical mixing in the Indonesian Seas and their propagation along the equator.

### P12/W/21-A1 1620

#### THE EFFECT OF THE SUBTROPICS ON THE TROPICAL SALINITY FIELD

Masami NONAKA (Institute of Low Temperature Science, Hokkaido University, Sapporo 060-1809, Japan, Email: nona@lowtem.hokudai.ac.jp) Kensuke Takeuchi (Institute of Low Temperature Science, Hokkaido University, Sapporo 060-1809, Japan, Email: takeuchi@lowtem.hokudai.ac.jp)

In higher latitudes, more saline water compared with that in the tropics is supplied through the sea surface and is advected to the tropics by the ocean circulation connecting the subtropics and the tropics. Using an ocean general circulation model (GCM) which has realistic topography and is forced by the climatological data, we examine the effect of water directly transported to the tropics on the tropical salinity fields and the reason for the discrepancy between the salinity and tritium fields' properties: Tritium indicates an interior route to the equator in the Northern Hemisphere, but high salinity water does not indicate it. The results of our GCM show that the water subducted into the subsurface from the high sea surface salinity (SSS) regions in the subtropics is advected to the tropics, forming a high salinity tongue. In the Southern Hemisphere, the high salinity tongue extends directly to the equatorial region, but in the Northern Hemisphere it extends to the western boundary. In the Northern Hemisphere, water subducted from the low SSS region in the eastern part of the subtropics and water whose salinity is lowered by mixing with the eastern low salinity water extend to the equatorial region through the interior ocean, forming a low salinity tongue. The ocean circulation in our GCM follows an interior route from the North Pacific to the equator, consistent with the subsurface tritium field, and, at the same time, reproduces the properties of the subsurface tropical salinity field. Because the northern interior route transports only low salinity water, the northern high salinity tongue does not follow an interior route and is discrepant from the tritium fields. The discrepancy is caused by the difference of the sea surface distribution: High SSS exists in the western boundary exchange window in the Northern Hemisphere, while sea surface tritium has its maximum near the eastern boundary within the interior exchange window. Here, water subducted from the western boundary (interior) exchange window is transported to the equatorial region through the western boundary region (the interior ocean) in the subsurface layer.

### P12/W/18-A1 1640

#### WATER MASS TRANSFORMATIONS IN THE NORTH PACIFIC OCEAN

Dr Maxim YAREMCHUK, International Pacific Research Center

A dynamically consistent state of the North Pacific ocean has been obtained by the variational assimilation of climatological data into a non-linear steady state circulation model. The assimilated data include Da Silva heat, freshwater and momentum fluxes at the ocean surface, WOCE hydrology, five year (1992-1997) mean Topex-Poseidon altimetry and MEDS surface drifter trajectories, averaged over the period 1990-1996. Advective balance residuals in the optimized fields of potential temperature and salinity are treated as transformation rates of water properties caused by local diffusive and mixing processes. Statistical analysis of these "elementary" transitions in the temperature-salinity space provides their decomposition into transformation rates between the basic water masses of the North Pacific ocean. The analysis shows in particular, that North Pacific Intermediate Water (NPIW) plays a central role in the water mass balance of the region. Isopycnal flow patterns identify intensive NPIW divergences east of Southern Kuril Islands and Hokkaido. A much weaker possible source of NPIW is located in the Alaska Gyre. Zonal mean circulation of the optimal state exhibits 8.5 Sv of the deepwaters inflowing from the south which are then involved into the meridional upwelling of 14 Sv between 30-50N. A weaker (5 Sv) overturning cell exists north of 50N which is driven by the downwelling of the north Bering Sea waters.

### REGIONAL WATER MASS STUDIES

### P12/W/09-A1 1700

#### ORIGIN OF DEEP AND BOTTOM WATER IN THE SOUTHWEST PACIFIC

Serguei SOKOLOV and Stephen Rintoul (both at CSIRO Marine Research and Antarctic Cooperative Research Centre, GPO Box 1538, Hobart, Australia, emails: Serguei.Sokolov@marine.csiro.au and Steve.Rintoul@marine.csiro.au)

The majority of the hydrographic stations occupied in the Tasman/Coral Sea have been shallow (<1500 m deep). As a result, there has been little discussion of the deep circulation. Recent high quality deep hydrography, including WOCE P11, helps refine some details of the deep water circulation in the region. According to P11 data, there are two major sources of the deep water in the Coral and Solomon Seas: the "southern" source supplied from the East Australian Basin and the "eastern" source entering the Coral Sea from the east. About 3 Sv of deep water is carried into the Coral Sea by a deep western boundary current in the Cato I. Trough from the Tasman Sea, and about 6 Sv (relative to the bottom) of deep and bottom water recirculate in the Coral Sea across P11. The deep and bottom water entering the Coral Sea from the east are derived from the CDW spreading north from the ACC as a western deep boundary current along the Tonga-Kermadec Ridge, through the Samoa Passage, and finally across the equator to the North Pacific. While the densest water in the boundary current is prevented from spreading to the west by topography, lighter CDW spreads west in the East Mariana Basin and also supplies deep water to the eastern Coral Sea and the Solomon Sea. The deep waters in the Solomon Sea are horizontally homogeneous throughout the basin, and the theta-S curves found for the New Britain Trench and near the northern entrance to the Solomon Sea at the Vitiaz Strait, St. Georges Channel and the Solomon Strait are almost identical to those found in the South Solomon Trench. This is a clear indication that the deep waters in the Solomon Sea enter from the east. The CDW entering from the east is cooler and fresher than water entering the Coral Sea from the East Australian Basin. The distribution of silica in the South Pacific also supports this view. CDW entering the Pacific from the Southern Ocean is initially low in silica (<90, see e.g. Schmitz, 1996), while North Pacific DW can have values as high as 180. The low silica in the Coral Sea Basin is an indicator of the "southern" source of deep water supplied from the Tasman Sea, while the higher values in the eastern part of the Coral Sea reflect deep water inflow derived from the "eastern" source.

### P12/W/17-A1 1720

#### STRAIT OF SICILY WATER MASSES

Alex WARN-VARNAS (Naval Research Laboratory at Stennis, USA, email: varnas@nrlssc.navy.mil), Allan Robinson, Jurgen Sellschopp, Wayne Leslie, Pat Haley, Carl Lozano, and Steve Piacsek

We have derived a water mass model for the Strait of Sicily, based on 1994 and 1995 cruise data. The model consists of seven water masses, suggested by the measured shapes of the vertical temperature and salinity profiles. The core of the Atlantic water is distributed below the surface as a shallow layer, in a depth range of 40 to 100 meters, with a salinity minimum. Upper and surface layers above and a mixed region below cap it. At the bottom Levantine water is present with a transition region above. Between the mixed and transition region there is, on occasion, a fresher water layer. The structure and statistics of the water masses is analyzed in terms of their temperature, salinity, and depth parameters. Objective analysis of the temperature, salinity, and depth parameters is performed in latitude and longitude. The water masses are tracked in terms of their parameter signatures. Changes in temperature and salinity distributions are interpreted. 2-D ellipses that represent the water masses, in terms of mean and standard deviation, are derived in a space of temperature, salinity, and depth. Their axes are the standard deviations of parameter space ranges. The areas of the ellipses are compared against the temperature and salinity distributions. The water mass composition ratios are computed and analyzed. Hypotheses and mechanisms for the origin and mixing of water masses are suggested. The temporal and spatial variability of the volume flows associated with the major water masses is studied via high horizontal resolution, 5km, and 64 level ocean model using 6-hour forcing and an embedded mixed layer.

### P14 Thursday 22 July

#### DYNAMICS OF SEA ICE AND OCEAN IN POLAR SEAS

Location: Poynting Physics, S02 LT  
Location of Posters: Bridge Poynting/Watson

Thursday 22 July AM

Presiding Chair: M.C. Gregg (University of Washington, USA)

#### HYDRAULIC CONTROL AND ENTRAINMENT IN STRAITS, SILL FLOWS AND DENSITY CURRENTS

Introduction 0950

P14/W/10-A4 Invited 1000

#### REVIEW OF HYDRAULICS AND HYDRAULIC CONTROL IN THE OCEAN

Larry Pratt (Woods Hole Oceanographic Ins., Woods Hole, MA. 02543, USA. email: lpratt@whoi.edu)

A review of recent progress in understanding the hydraulics of strait and sill flows is given. Areas of interest include hydraulic control in the presence of continuous stratification, linking controlled flows to forcing and dissipation in upstream and downstream basins or marginal seas, hydraulic jumps and bores, rotation, and time-dependence. Also mentioned will be some longstanding problems whose importance is widely recognized but which have proved difficult to understand. These include hydraulic control in the presence of rapidly fluctuating currents, the presence of critical layers in 'hydraulically critical' flow, and the role of friction in rotating, hydraulically-driven flows. Finally, I will review two classes of hydraulic problems having well-developed theories but, at present, little or no observational support. These are coastal hydraulics and potential vorticity hydraulics.

P14/E/04-A4 Invited 1040

#### CIRCULATION IN STRAITS - A REVIEW OF RECENT OBSERVATIONAL STUDIES

Stephen P. MURRAY (Coastal Studies Institute, Louisiana State University, Baton Rouge, Louisiana 70803, USA, email: smurray@unix1.sncc.lsu.edu)

The important role of sea straits in controlling exchange between marginal seas and ocean basins and between adjacent ocean basins is well established, but in the last 20 years, modern instrumentation has provided a new depth of insight into the controlling processes. The Gibraltar Experiment (1985-86), for example, allowed a vast improvement in the determination of mass and salt transport between the Mediterranean and the Atlantic Ocean, leading to a significant revision in the Mediterranean evaporation rate. The Experiment also determined that as much as one-half of the exchange across the Gibraltar sill is controlled by



tidal covariance (Bryden et al. 1994). Additionally, barotropic fluctuations caused by atmospheric pressure differences between the basins can cause transport fluctuation as much as 1 Sv—as large as the mean flow. A recent study in the Bab el Mandab Strait (linking the Red Sea and Indian Ocean), employing moored ADCPs, has documented the seasonal transport cycle of the two-layer regime that is present most of the year and the three-layer regime that prevails in summer. Highly energetic low frequency fluctuations in the transport are largely controlled by direct wind driving, producing both barotropic and baroclinic responses. A strong (0–0.8 Sv) seasonal modulation in the deep high density outflow is related to the annual cycle of the winds in the Arabian Monsoon but the controlling dynamics remain unclear. In addition to the above settings forced by the thermohaline, wind, and atmospheric pressure effects, other straits (e.g. in the Indonesian Archipelago) are controlled by inter-ocean basin sea level differences at the seasonal scale and coastal Kelvin waves at the intraseasonal line scale. These and other examples from the Bosphorus and Straits of Otranto, of Sicily and Hormuz, are discussed, compared, and summarized in terms of regional forcing mechanisms.

**P14/W/14-A4** Invited **1140**

#### ASPECTS OF STRAIT DYNAMICS STUDIED BY NUMERICAL LAYERED MODELS

Angelo RUBINO and Peter Brandt (both at the Institut für Meereskunde, Universität Hamburg, Troplowitzstr. 7, Hamburg, Germany, Email: rubino@ifm.uni-hamburg.de) Stefano Pierini (Dipartimento di Fisica, Università dell'Aquila, Via Vetoio, I-67010 Coppito (l'Aquila), Email: pierini@cds.unina.it)

Different multi-layer numerical models are employed for the study of three straits of the western Mediterranean Sea: the Strait of Gibraltar, the Strait of Sicily, and the Strait of Messina. The Strait of Gibraltar, that connects the Mediterranean Sea and the Atlantic Ocean, is investigated with the help of two different two-layer models. By using a one-dimensional, nonlinear, weakly non-hydrostatic model the generation and propagation of internal bores caused by the interaction of the barotropic tide with the Camarinal Sill and their disintegration into trains of internal solitary waves is simulated. The results are compared with different remote sensing data. By using a nonlinear, hydrostatic, two-dimensional boundary-fitted coordinate model, two-dimensional aspects of the strait dynamics induced by topography and earth rotation are simulated. In particular, it is shown that within the strait different areas in which the flow is supercritical exist, characterized by a complex temporal evolution. The Strait of Sicily, that connects the western and eastern Mediterranean basins is investigated with the help of a nonlinear, hydrostatic three-layer model. The layers represent waters of Atlantic origin, the Levantine intermediate water, and deep waters of the Mediterranean Sea. Quasi-stationary circulation patterns representing aspects of an idealized thermohaline circulation are produced by steady fluxes imposed at the open boundaries. The model is capable of capturing several features of the observed circulation in the area of the Strait of Sicily. The Strait of Messina, that connects the Tyrrhenian and Ionian seas, is investigated with the help of two different models. The first model is a one-dimensional, two-layer coupled model. In the region of the strait sill the complex interaction of the lower layer with the topography induced by a strong barotropic tide is simulated by using a frontal model that, due to a numerical technique for the treatment of movable lateral boundaries, is capable of describing the dynamics of water layers having a localized extension. Outside the sill region the disintegration of the internal tidal bores produced in the sill region into trains of internal solitary waves is simulated by coupling to the generation model a nonlinear, weakly nonhydrostatic model. The results are compared with high-resolution in-situ and remote sensing data. The second model is a three-layer, nonlinear, weakly non-hydrostatic model. Using this model, the observed jet-like structure of the tidal flow outside the sill region is simulated.

**P14/E/02-A4** Invited **1210**

#### ENTRAINMENT BY OVERFLOWS AND DENSITY CURRENTS, A REVIEW

JAMES F. PRICE, Woods Hole Oceanographic Inst., Woods Hole, MA, 02556 USA (email: jprice@whoi.edu)

Simulation of past or future climate will require ocean general circulation models (OGCMs) having comprehensive physics, and including a realistic treatment of the most important marginal sea overflows. This presents a considerable challenge since the scales and dynamics inherent to marginal sea overflows are different from that of the general circulation over most of the open ocean. Overflows are density-driven bottom currents that have small vertical scales, being typically about 100–200 m thick, and currents that are  $O(1 \text{ m s}^{-1})$ . As they descend into the ocean they may mix intensely with overlying oceanic water, typically doubling their initial transport and diluting their tracer properties. Because of these distinctive scales and dynamics, realistic marginal sea-ocean exchange and deep water production do not arise spontaneously in large-scale OGCMs, even those with the greatest resolution. Consequently, it will be necessary to parameterize marginal sea processes in OGCMs. The aim of this review will be to describe what an ideal parameterization should do, and to consider some candidates.

**Thursday 22 July PM**

Presiding Chair: E. OZSOY (Institute of Marine Science, Middle East Technical University, Turkey)  
Concurrent Poster Session

**P14/W/08-A4** **1400**

#### HYDRAULIC CONTROL IN THREE-LAYER EXCHANGE FLOWS AND APPLICATION TO THE BAB AL MANDAB

David SMEED and Gregory Lane-Serff, Southampton Oceanography Centre, University of Southampton, Southampton, SO14 3ZH UK.

There is a strong seasonal variation of the flow in the strait of Bab al Mandab. In winter dense salty water leaves the Red Sea and fresher surface water enters the Red Sea from the Gulf of Aden. In the summer the outflow of dense salty water is much reduced, the direction of flow in the surface layer is reversed and a sub-surface layer of cool fresh water enters the Red Sea between the two outflowing layers. A model of hydraulic control in three-layer exchange flows has been developed. The model predicts the observed flow regimes and supports the hypothesis that upwelling, dependent upon the monsoon, in the Gulf of Aden is primarily responsible for the seasonal variation. The model has applications to other strait and sill flows. The problem has been examined further in a series of laboratory experiments. Measurements of the exchange fluxes and interface heights agree well with the model predictions.

**P14/W/05-A4** **1420**

#### THE CONTINUOUS DYNAMICAL MODES OF THE BAB AL MANDAB AND THEIR HYDRAULIC INTERPRETATION

Heather E. DEESE (Woods Hole Oceanographic Ins., Woods Hole, MA, 02543, USA, email: hdeese@mit.edu); Larry J. Pratt (Woods Hole Oceanographic Ins., Woods Hole, MA, 02543, USA, email: lpratt@whoi.edu); Steve Murray (Coastal Studies Institute, Louisiana State University, Baton Rouge, LA, USA, email: smurray@lsuvax.sncc.edu); William Johns (RSMAS, University of

Miami, Miami, FL, USA, email: johns@ibis.rsmas.miami.edu)

The continuous dynamical modes of the exchange flow in the Bab al Mandab are computed in an attempt to assess the hydraulic character of the flow at the sill. Hydrographic and direct velocity measurements taken from April to November of 1996 using moored CTDs and a bottom-mounted ADCP are first used to construct monthly mean density and velocity profiles. Next, an extended version of the Taylor-Goldstein equation is solved for the phase speeds and vertical structures of the first and second internal long wave modes. The 'extended' equation takes cross-strait topography into consideration. The sill flow is found to be subcritical during each month, but it hovers near a critical state with respect to the second internal mode during the non-summer months. A series of calculations using idealized velocity and buoyancy frequency profiles are presented to illustrate the effects of the topography on the vertical modes. Wave speeds are also calculated for a variety of instantaneous conditions at the extremes of the tidal cycle. The results indicate that the tides often push the flow into a critical or supercritical regime with respect to the second mode and, somewhat less frequently, with respect to the first mode. We can only speculate on the connection between classical hydraulic control and the observed intermittent critical and supercritical conditions. A series of calculations using idealized velocity and buoyancy frequency profiles are also presented to illustrate the effects of the topography of the vertical modes.

**P14/E/06-A4** **1440**

#### INVESTIGATING THE FEEDBACK BETWEEN STRAIT EXCHANGE AND WATER FORMATION USING A HYDRAULICALLY CONTROLLED BOX MODEL OF THE MEDITERRANEAN

Stephan MATTHIESEN and Keith Haines (Dept. Meteorology, Univ. Edinburgh, James Clerk Maxwell Building, Edinburgh EH9 3JZ, UK, email: stephan@met.ed.ac.uk and kh@met.ed.ac.uk)

We have built a 2 layer model consisting of a hydraulically controlled strait coupled to a 2 box model of the Mediterranean. This is the simplest system that can respond to changes in the strait flow. Unlike most previous models which have assumed maximal exchange at all times, our model also allows the exchange to become submaximal. A wide range of strait cross sections can be accommodated in the model. For the maximal regime, the model includes a hydraulic jump towards the Mediterranean with the possibility of mixing. The model is used to investigate the feedback between the water formation processes in the basin and the strait dynamics and the relevant timescales. We discuss the implications of the fact that the adjustment time for salinity changes is of the order of decades, while the adjustment time for water budget changes are of the order of years. This study also addresses the stability of the maximal and submaximal regimes for different situations. In most cases, the water formation rate inside the basin determines whether the strait flow is maximal or submaximal. When mixing in the hydraulic jump is included, the system can exhibit stable multiple equilibria for the same net evaporation over the basin, where one state is submaximal with weak mixing, and the other maximal with strong mixing. Comparisons with GCM simulations are also shown.

**P14/W/11-A4** **1500**

#### LARGE AMPLITUDE INTERNAL WAVES IN THE STRAIT OF GIBRALTAR

Harry L. BRYDEN and Brian A. King (both at Southampton Oceanography Centre, Southampton, SO14 3ZH UK, email: h.bryden@soc.soton.ac.uk or b.king@soc.soton.ac.uk)

Large amplitude internal waves are generated close to the time of high tide at or near the sill in the Strait of Gibraltar, particularly during strong Spring tides. We examined the subsurface characteristics of these large amplitude waves using new technology including calibrated, three-frequency backscatter profiles from an EK500 and accurate velocity profiles from shipboard ADCP measurements combined with three-dimensional differential GPS navigation as well as using a slowly-towed CTD package to measure the hydrographic properties of the interface between inflowing Atlantic water and outflowing Mediterranean water. In the early morning hours of 4 successive days over Easter weekend 1998, 100 m amplitude waves propagated eastward past the nearly stationary ship at locations east of the sill. Maxima in the vertical profiles of backscatter, particularly at 38 kHz, provided dramatic, real-time portraits of the waves. The maxima in backscatter, however, appear to be a feature of the Mediterranean layer and not a feature of the interface as the maximum lies 20 m below the 38-isohaline; furthermore, the backscatter maximum appears to vanish before the complete wave train has passed so it is an unreliable indicator of the waves. More robust signatures of the waves are measured by the shipboard ADCP: upward and downward vertical velocities as large as 50 cm s<sup>-1</sup> are an outstanding feature of the waves and the depth of the maxima in the vertical shear of the eastward current from the ADCP tracks the lower part of the interfacial region (salinity of about 37.7) for much longer periods than does the backscatter.

On 14 April the large amplitude waves are observed at two along-strait locations separated by 15 km and 2 hours implying an eastward propagation speed of about 2 m s<sup>-1</sup>. As the waves propagate over 15 km, their amplitude, maximum vertical velocity, and maximum steepness decrease by about 30% from 120 m to 80 m, from 50 to 35 cm s<sup>-1</sup>, and from 0.7 to 0.5. As a measure of nonlinearity, horizontal advection accounts for about half of the local time changes in interface depth while vertical velocity accounts for the remainder.

**P14/W/12-A4** **1520**

#### GROWTH MECHANISM OF TOPOGRAPHIC INTERNAL WAVES GENERATED BY AN OSCILLATORY FLOW

Tomohiro NAKAMURA and Toshiyuki Awaji (Department of Geophysics, Graduate School of Science, Kyoto University, Kyoto 606-8502, Japan, Email: nakamura@kugi.kyoto-u.ac.jp)

A new amplification mechanism for topographic internal waves generated by tidal flow is presented to reveal the unknown growth processes of the internal waves in the Kuri Straits (about 47N in the North Pacific) reported by Nakamura et al. (1998). According to their investigation, the nature of the wave properties is determined by the nondimensional parameter  $(k U_0 / \sigma_f)$ , where  $k$  is the curvature of topography,  $U_0$  is the flow speed amplitude, and  $\sigma_f$  is the frequency of tidal flow, through which the topographic internal waves can be classified into the three wave types; (1) unsteady lee waves ( $k U_0 / \sigma_f \gg 1$ ), (2) mixed tidal lee waves ( $k U_0 / \sigma_f \sim 1$ ), and (3) internal tides ( $k U_0 / \sigma_f \ll 1$ ). Notably, their numerical model showed that the growth processes of the first two waves were quite different from those predicted by conventional internal wave theories, thus suggesting the presence of another criterion for wave amplification. For this issue, our theoretical investigation based on the ray tracing of individual waves generated at various time reveals the following interesting facts. Unsteady lee waves are always amplified when the maximum frequency is sufficiently smaller than the buoyancy frequency (i.e.,  $\sigma_f \ll k U_0 \ll N$ ), because their phase speeds and amplitudes are equal and proportionate to the tidal flow speed at their generation, respectively. Fast mixed tidal lee waves are also effectively amplified as well as unsteady lee waves, when the rotation effect is significant (i.e.,  $f \sim \sigma_f \sim k U_0 \ll N$ ). Accordingly, amplification of unsteady lee waves and fast mixed tidal lee waves can occur even if the conditions indicated by previous theories (i.e., the critical slope and the critical Froude number) are not satisfied. Since our theoretical model covers generation and amplification processes of topographic internal waves in a broader parameter range than before, it may contribute to a better understanding of the Boundary Mixing

processes.

**P14/E/10-A4** **1540****FLOW IN THE SILL REGION OF THE CLYDE SEA.**

Rik MIDDLEY & John Simpson (School of Ocean Sciences, University of Wales, Bangor, Gwynedd LL57 2DG, U.K. email: oss088@sos.bangor.ac.uk)

Observations of the vertical structure and currents in the Clyde Sea over a seasonal cycle identified the sill as a region of major uncertainty. At times when the cross-sill density difference was maximum, the rate of exchange was below average, indicating that other forces control exchange. Renewal was generally episodic, indicative of wind induced exchange, and in the summer, when horizontal gradients were minimal, persistently high rates of exchange were observed.

New observations in the sill region in 1995 were used to construct a dynamical schematic of the structure. In March, a rapid cross-sill exchange (flows ~10 cm<sup>-1</sup>), which appeared to be essentially estuarine, and influenced by rotation, was observed. In contrast, in September cross-sill flows were observed to be relatively weak and spatially complex. A 3-dimensional model was used to confirm that changes in wind direction could substantially increase or diminish exchange by enhancing or blocking the estuarine circulation, and the summer time retreat of the front at the mouth of the Clyde, due to low freshwater inflow, could enhance exchange by increasing the availability of saline water over the sill.

**P14/E/03-A4** **1620****MODELING OF MEDITERRANEAN OUTFLOW IN THE BLACK SEA. DEPENDENCE ON TOPOGRAPHY**

Elissaveta PENEVA and Emil Stanev (both at Dept. of Meteorology and Geophysics, University of Sofia, Sofia 1126, Bulgaria, email: elfa@phys.uni-sofia.bg, stanev@phys.uni-sofia.bg)

Numerical simulations of Mediterranean outflow in the Black Sea using reduced gravity model with horizontal resolution of 600 m have been carried out. The Mediterranean water spreads in the neighbouring Black Sea as gravity plume accelerated by the large density contrasts and topography slopes. This process is of major significance for the deep and intermediate water mass formation in the Black Sea. A number of numerical experiments have been run in attempt to better understand the topographic control of the current. In the reference experiment we use realistic topography and the model is tuned to adequately simulate the observed characteristics of gravity currents. Idealistic topography  $H=H(y)$ , consisting of Bosphorus exit, shelf, continental slope and abyssal plain, is constructed in such a way that the geometric parameters of topography elements (slope and length) are comparable to the real ones. In order to investigate the impact of roughness on the gravity current simulations are carried out with idealistic but rough topography with roughness characteristics similar to observed ones. Additional experiments with deviating element in north-western direction after Bosphorus exit were run too in order to study the effects of Bosphorus underwater extension. The results show that the entrainment rate reaches its maximal values over the continental slope due to the acceleration of the plume. The roughness affects both entrainment rates and dispersive properties of the model. It was also found that the presence of Bosphorus underwater channel in north-western direction is quite significant for the dynamics of gravity currents.

**P14/E/05-A4** **1640****FLOW AND MIXING IN THE BOSPHORUS**

Michael GREGG (University of Washington Seattle, WA 98105 USA); Emin Ozsoy (Middle East Technical University Erdemli, Turkey)

Current meter moorings and high-resolution surveys during late summer of 1994 in the Bosphorus revealed important details of the exchange flow between Mediterranean and Black Sea waters. We conducted the surveys with a narrowband ADCP, a high-frequency acoustic backscatter system, and a microstructure profiler carrying a CTD. The flow was quasi-steady and mixed most vigorously south of the principal contraction in the strait. The mixing was demonstrated by trains of billows, density overturns, high dissipation rates, and rapid thickening of the interface between the surface and bottom layers. Nevertheless, composite Froude numbers were much less than critical through the Contraction and may have been critical only several kilometers south of the Contraction, when the surface layer became too thin and shallow for us observe its speed.

**P14/W/16-A4** **1700****THE BOSPHORUS STRAIT MIXING AND THE DENSE WATER OUTFLOW ON THE BLACK SEA SHELF: EXPERIMENTS AND MODELLING**

Emin OZSOY (Institute of Marine Sciences, Middle East Technical University, P.K. 28 Erdemli - Icel 33731 Turkey, Email: ozsoy@ims.metu.edu.tr), Daniela Di Iorio (NATO SAACLANT Undersea Research Centre Fine Scale Acoustics and Oceanography Group, Viale S. Bartolomeo 400, 19138 La Spezia (SP), Italy, Email: daniela@saclant.nato.int), Michael Gregg (College of Ocean and Fishery Sciences, 522 Henderson Hall, University of Washington, 1013 NE 40th Street Seattle Washington 98105-6698, Email: gregg@apl.washington.edu), Sciences, 522 Henderson Hall, University of Washington, 1013 NE 40th Street Seattle Washington 98105-6698, Email: gregg@apl.washington.edu), Jan Backhaus (Institute for Oceanography, University of Hamburg, Troplowitzstr. 7, D-22529, Hamburg, Germany Email: backhaus@dkrz.de).

The exchange and mixing of waters from the Black Sea and the Mediterranean Sea occurs throughout the Turkish Straits, and intensively in the Strait of Bosphorus. Entrainment and mixing processes are studied through the Bosphorus, and on the Black Sea continental shelf / slope, based on the historical data base and the high-resolution intensive data sets obtained in 1994 and 1996. The changes in water properties along the Strait and in the outflow regions are characterized by distinct entrainment / mixing regimes, such as near the southern end of the Bosphorus, within the northern reach of the Strait and across the northern sill and the shelf region. A reduced gravity model of the dense bottom current is employed to study the flow across the northern shelf and to the continental slope. The flow is shown to be very sensitive to chosen parameters, to the environmental conditions in the Black Sea, and especially to the accurate representation of the bottom topography. High resolution, improved topographical data constructed from adcp and swath echosounder measurements are used to improve model predictions. Measurements of hydrographic and current features are used for verification of the results.

**P14/W/15-A4** **1720****A COMPARISON OF LARGE EDDY SIMULATIONS WITH OBSERVATIONS FROM THE CENTRAL CONTRACTION IN THE STRAITS OF BOSPHORUS**

HARVEY SEIM, Skidaway Institute of Oceanography, Savannah, Ga 31411, USA, email: seim@skio.peachnet.edu Kraig Winters, Applied Physics Laboratory, University of Washington, Seattle, WA, USA and Centre for Water Research, University of Western Australia, Nedlands, Australia, email: winters@cw.r.uwa.edu.au

Large eddy simulations of an internal hydraulic control at a contraction are found to support both maximal and submaximal exchange flows. The model results are compared with observations collected from intensive shipboard sampling by Gregg and Ozsoy of the central contraction in the Straits of Bosphorus. A two layer decomposition of both the model results and the observations facilitates comparison with two-layer inviscid hydrostatic theory. A three layer decomposition, in which the upper and lower layer are well-mixed and the third layer comprises the interface between them, highlights the extent and location of mixing between layers. The comparison suggests the flow in the contraction is submaximal exchange, and that this can occur without flooding other hydraulic controls along the Strait, but that this configuration still generates copious mixed fluid.

**Thursday 22 July PM**

Presiding Chairs: M.C. Gregg (University of Washington, USA), E. OZSOY (Institute of Marine Science, Middle East Technical University, Turkey)

**P14/E/07-A4** **Poster** **1400-01****ROLE OF DENSITY CURRENTS IN STRAIT DYNAMICS AT COCHIN INLET- SOUTHWEST COAST OF INDIA**

K. J. AJITH and A.N. Balchand (Department of Physical Oceanography, Cochin University of Science and Technology, Fine Arts Avenue, Cochin 682 016, INDIA. email: oceans@md3.vsnl.net.in)

The shores of the tropical regions are embedded with tidal inlets that are grouped under straits as the dynamics of these inlets mimic flow patterns similar to that which occur in larger straits. As these inlets serve as openings of estuaries in many instances, the dynamics of two layer exchange present a vivid analytical situation brought about by the circulation of coastal waters vs. inland runoff. Also the physical configuration of the inlet controls the amount of exchange between the protected embayment and the coastal sea. The southwest coast of India, often a region of many geomorphologic features is no exception, where Cochin inlet (9°58'N, 76°14'E), provides an insight on the strait dynamics. This paper elucidates information on the inflow and outflow transport rates by density currents due to the change in sigma-t with appreciable salinity differences. A monthly sigma-t analysis at Cochin inlet authenticates the variation in density currents with seasonal changes in mixing. The tidal conditions and freshwater influence is also considered while analysing the strait dynamic features of this tropical tidal inlet. The study also covers aspects on the influence of land sea exchange of material and the role of inlet hydraulics in the protection of the embayment within.

**P14/E/01-A4** **Poster** **1400-02****A 3-LAYER HYDRAULICALLY CONTROLLED BOX MODEL OF THE RED SEA AND BAB AL MANDAB STRAITS**

David COBBY (ESSC, Univ. Reading, Harry Pitt Building, 3 Early Gate, Reading RG6 6AL, UK, email: dmc@mail.nerc-essc.ac.uk) Keith Haines and Stephan Matthiesen (Dept. of Meteorology, Univ. Edinburgh, James Clerk Maxwell Building, Edinburgh EH9 3JZ, UK, email: kh@met.ed.ac.uk and stephan@met.ed.ac.uk)

We have built a 3 layer model for the Red Sea in which the inflow and outflow of the layers is controlled hydraulically. The Bab al Mandab Strait connecting the Red Sea to the Gulf of Aden exhibits a 2 layer anti-estuarine exchange in winter which becomes a 3 layer flow in summer under the influence of summer Monsoon winds which raise an intermediate water mass up in the Aden Gulf, which then penetrates into the Red sea. The main control for the hydraulic flows is taken at a sill and narrows which are assumed coincident. Other controls and associated hydraulic jumps are detected by their influence on the flow rates. Our model simulates the full seasonal cycle of flow as the Gulf of Aden intermediate water level is raised and lowered outside the straits. The layers inside the Red Sea exchange water through mixing and E-P water conversions and maintain both mass and salt budgets. The results are compared to observations from both current meter in the strait, layer thicknesses and sea level changes. The impact of the summer season 3-layer flow on the average properties of the waters inside, and emerging from, the Red Sea is discussed.

**P14/W/01-A4** **Poster** **1400-03****CONTROL OF CONVECTIVELY DRIVEN EXCHANGE FLOW IN A SILL-ENCLOSED SEA**

TIMOTHY D. FINNIGAN and Gregory N. Ivey (both at Department of Environmental Engineering, Centre for Water Research, University of Western Australia, Nedlands, WA 6907, Australia email: finnigan@cw.r.uwa.edu.au)

Flux of buoyancy through the surface of a semi-enclosed or marginal sea, due to cooling or evaporative processes, generally results in a circulation within the sea and an exchange of fluid with the adjoining water body (ocean). The Red and Mediterranean Seas are well known examples of systems exhibiting this type of circulation. We describe laboratory experiments of the flow in an idealized semi-enclosed sea, with a configuration similar to the natural examples, where the sea is uniform in width and separated from an ocean by a shallow sill. Steady withdrawal of buoyancy by cooling at the sea surface results in turbulent convection and an associated lateral buoyancy gradient across the sill. A mean flow is thus driven into the sea near the surface becoming progressively more dense as it traverses the length of the sea before turning 180 degrees and flowing back out of the sea at depth. This circulation persists above a deep stagnant layer trapped behind the sill.

The net effect of the surface buoyancy flux is reflected in the density of the lower outflowing layer at the sill. The two-layer exchange at the sill is hydraulically controlled and thus coupled with the surface buoyancy forcing through the density signature in the lower layer. The hydraulic control, the mean flow, and the mixing are linked in a complicated non-linear feedback loop. We present observations of the mean and turbulent fields, obtained through particle tracking methods, and interpret the effect of mixing on the control condition and the outflow density and volume flux. In addition, the long-term erosion of the deep stagnant layer is described and related to the geometric scales of the sea and the buoyancy forcing.

**P14/L/01-A4** **Poster** **1400-04****EVOLUTION OF SALINATION OF THE BLACK SEA DURING HOLOCENE**

Mehmet Karaca, Eurasia Inst. of Earth Sciences, ITU Maslak 80626 Istanbul Turkey, Achim Wirth and Michael Ghil, Dept. of Atmospheric Sciences and Inst. of Geophysics and Planetary Physics, UCLA Los Angeles, CA 90095 USA

The evolution of the Black Sea's salinity after the opening of the Bosphorus about 7500 years



ago is investigated using a simple two-box model. The model consists of watermass and salt conservation equations, allows for changes in thermocline depth. The paleoceanographic box model is forced by the present-day Mediterranean inflow and outflow, and atmospheric forcings. Analytic solutions for the evolution of the box volumes are given. Model salinities reach 90% of their present-day values in both boxes about 2,500 years after the opening of the Bosphorus. The evolution of salinities is shown to be almost independent of the evolution of the box volumes and the results are shown to agree with the existing paleoceanographic proxy records.

**P14/W/03-A4** Poster **1400-05**

#### SILLS AND INTERNAL BORES

Gregory LANE-SERFF (School of Ocean and Earth Science, University of Southampton, Southampton Oceanography Centre, Southampton, SO14 3ZH, UK, email: gfl@soton.ac.uk)

Flows through straits and over sills are often strongly modulated by the tide. Basing calculations on mean conditions and treating the flow as steady may significantly underestimate the mixing that takes place in straits. A common feature of tidally modulated strait flows is the generation of internal bores. It is important to determine how much of the mixing takes place during transient events (such as the passage of an internal bore and its associated internal waves) compared with the mixing that occurs at other times. A striking example of a tidally generated internal bore is that in the Strait of Gibraltar, where the interface between the outflowing Mediterranean water and the inflowing Atlantic water can oscillate by 100 m or more in the vertical over periods of only a few minutes as the bore passes. Oceanographic measurements of the internal bore in the Strait were recovered during a cruise in 1998 led by Dr H L Bryden, using acoustic backscatter, ADCP and an oscillating CTD package. The simultaneous use of these different types of observations allows a comprehensive description of the internal bore to be made. The flow in a two-layer system with a combination of sill and internal bore is also analysed mathematically using shallow water equations and hydraulic control theory. The theory gives predictions for the dependence of bore speeds and layer depths on the initial stratification and the net flow through the strait. The same system is modelled in the laboratory using tanks of saline solution of different density. The laboratory experiments are recorded on a video system and processed to give quantitative information about the flow. The laboratory experiments also give information about the character of the bore, whether it is abrupt or marked by a series of internal waves (undular bore). For the undular bores, the experiments give the amplitudes and wavelengths of the waves. The results from all these methods of investigating unsteady flow through straits are compared, and we outline directions for future research.

**P14/W/04-A4** Poster **1400-06**

#### QUASI-STATIONARY TWO-LAYER EXCHANGE FLOWS THROUGH LONG STRAITS

Vladimir MADERICH (Institute of Mathematical Machine and System Problems NASU, Glushkova pr. 42, Kiev 252187, The Ukraine. Email: vlad@maderich.pp.kiev.ua)

Quasi-stationary water exchange through the narrow strait with two-layer flow structure and net barotropic transport was investigated both experimentally and theoretically. The experimental facility consisted of the tank that was divided on two basins, connected by a shallow and narrow rectangular channel. One basin was heated at the bottom. Another basin was cooled at the top. The results of measurements were given for the short, intermediate and long straits in dependence on the magnitude of the net barotropic transport. The measured depths of interface and volumetric flow rate in the laboratory analog agree reasonably well with computed by a laminar hydraulic model that based on the principle of maximal exchange. The influence of the sills placed inside of the long strait, on the exchange was studied. The results showed strong influence of the position of sill on the exchange in the long straits. These results have been extended on the sea straits with predominated turbulent bottom and interfacial friction. Finally, the response of the chain of the seas connected by the long straits to the seasonal variations of the freshwater budget was investigated for the case Black Sea - Bosphorus - Marmara Sea - Dardanelles - Mediterranean Sea. The one-and-a-half-dimensional sea models supplemented the strait models. The computations showed a complicated response of exchange flows and level in adjacent seas on the seasonal forcing.

**P14/E/08-A4** Poster **1400-07**

#### TRANSFORMATION OF ATLANTIC WATERS IN THE BARENTS SEA AND THEIR FLOW TO THE EURASIAN BASIN THROUGH ST. ANNA TROUGH

URSULA SCHAUER (Alfred-Wegener-Institut fuer Polar- und Meeresforschung, D-27515 Bremerhaven, Germany, email: uschauer@awi-bremerhaven.de Bert Rudels (Finnish Institute of Marine Research, FIN-00931 Helsinki, Finland) Harald Loeng (Institute of Marine Research, N-5024 Bergen-Nordnes, Norway) Robin Muench (Earth & Space Research, Seattle, WA 98102-3699 USA) Jim Swift (UCSD Scripps Institution of Oceanography, La Jolla, CA 92093-0214, USA)

The ventilation of the Arctic Ocean basins is largely associated with the input of water from the Barents and Kara Seas. Using hydrographic observations, made in the Barents Sea and along the shelf edge of the Kara Sea between 1991 and 1996, and time series of current, temperature and salinity from moorings in the eastern Barents Sea, we discuss the flow and the modification of the water masses between the western Barents Sea and the St. Anna Trough. The inflow of warm, saline Atlantic-derived water from the Norwegian Sea and the low salinity Norwegian Coastal Current feed a permanent eastward flow. An additional input of fresh water is melted ice which is advected from the central Arctic Ocean and the Kara Sea. These three water masses are modified through cooling and the freezing/melting cycle. Two distinct modes are formed, which leave the Barents Sea eastward and descend down the St. Anna Trough. The lighter mode is winter water of low salinity, thus confined to the upper layers, which leaves the Barents Sea seasonally at temperatures close to freezing point. The largest and most dense contribution consists in more saline but only moderately cold bottom water which is formed in the polynya west of Novaya Zemlya through highly brine-enriched water. Subsequent lateral mixing with warmer Atlantic water feeds a bottom-intensified flow throughout the year. At present conditions, both modes form a low salinity input of about 2 Sv to intermediate depths of the Arctic Ocean.

**P14/W/09-A4** Poster **1400-08**

#### VARIATIONS IN THE MAIN KUROSHIO PATH SOUTH OF JAPAN

Yoshihiko SEKINE (Institute of Oceanography, Faculty of Bioresource, Mie University, 1515 Kamihama, Tsu Mie 514-8507 Japan.)

Characteristics of the variation in the Kuroshio path south of Japan is studied by use of the observational distance of the main Kuroshio path from Japanese Coast over the period of 1975 - 1993. It is pointed out that a large meander formed in 1975 has a larger distance from the Japanese coast from Murotomisaki ( Muroto Pen.) to Daihozaki ( Daiho Pen.), while its

distance from coast in east of Omaezaki (Omae Pen.) is small. In contrast to this, large meanders formed after 1980 show an opposite tendency to have short distances from coast from Murotomisaki to Shionomisaki (Shiono Pen.), while they have larger distance from eastern area of Omaezaki. It is also resulted from the correlation analysis of the distances of the main Kuroshio path from Japanese coast that the path pattern of the large meander path formed in 1975 has a tendency to shift westward, while that formed after 1981 has a tendency to shift eastward. It is shown that the flow pattern of the large meander path is different before and after 1980. It is also resulted that there exists one month ( two months) time lag between sea level difference across Nishinoomote - Naze that represents the surface volume transport of the Kuroshio and distance of the main Kuroshio axis off Toimisaki (Murotomisaki), which indicates that an increase in current velocity of the Kuroshio occurs before formation of the small meander of the Kuroshio and its eastward shift. Some other results that give important suggestion on the Kuroshio path dynamics are also detected.

**P14/W/06-A4** Poster **1400-09**

#### MODELLING STUDIES ON ASPECTS OF THE DYNAMICS OF THE STRAIT OF SICILY

S. PIERINI (Dipartimento di Fisica, Università dell'Aquila, Via Vetoio, I-67010 Coppito (l'Aquila) Italy, Email: pierini@cds.unina.it) A. Rubino (Institut für Meereskunde, Universität Hamburg, Troplowitzstrasse 7, D-22529 Hamburg, Germany, Email: rubino@ifm.uni-hamburg.de)

In order to describe aspects of the baroclinic dynamics of the Strait of Sicily a high resolution multi-layer model has been implemented in a central Mediterranean region including the Tyrrhenian and the Ionian Sea. Three layers have been considered representing waters of Atlantic origin (MAV), the Levantine Intermediate Water (LIW) and deep waters of the Mediterranean. Quasi-stationary circulation schemes representing the effect of an idealized Mediterranean thermohaline circulation are produced by steady fluxes imposed remotely along the open boundaries. In order to follow the evolution of the oceanic response, a norm in the space of the flow patterns in each layer is defined. Thus, by studying the temporal evolution of the "distance" between our numerical solution and the initial motionless state we identified an initial adjustment time of 1-2 months followed by a very slow evolution of the system in which dissipating mechanisms appear to play a major role. We therefore selected our quasi-stationary states just after the adjustment phase. Such states can be interpreted as possible dynamic scenarios of the seasonal variability. In the simulations an inflow of MAV and an outflow of LIW through the Strait of Sicily, an outflow of MAV and an inflow of LIW through the Ionian boundary and an outflow of MAV through the Corsica channel are imposed, resulting in a vanishing total net transport in each layer within the basin. For realistic values of the imposed transports the model captures some of the main features of the observed circulation in the area of the Strait of Sicily, such as: (a) the separation of the Algerian current into two branches (one directed toward the Tyrrhenian and the other toward the strait) of relative intensity in agreement with observations; (b) a secondary bifurcation of MAV within the strait giving rise to a southward moving current which follows the Tunisian continental slope and to a current that, after flowing south-eastward along the southern Sicilian coast, travels northward as a coastally trapped current; (c) a bifurcation of LIW at the strait level leading to a main current directed toward the Strait of Sicily and to a weaker current crossing the strait and bending eastward along the northern Sicilian coasts. Variations of the boundary fluxes in the MAV and LIW layers have also allowed to determine that the horizontal distribution of the MAV flow across the Strait of Sicily does not exert a relevant influence on the circulation in the zone of interest, and that the bifurcation of the Algerian current strongly depends on the LIW transport, i.e. the Tyrrhenian branch of the MAV decreases as the LIW transport decreases.

**P14/W/07-A4** Poster **1400-10**

#### A THREE-LAYER MODEL FOR THE STUDY OF TIDALLY INDUCED DENSITY CURRENTS

Rainer Weigle, Peter BRANDT, and Angelo Rubino (Institut für Meereskunde, Universität Hamburg, Troplowitzstr. 7, D-22529 Hamburg, Germany, Email: brandt@ifm.uni-hamburg.de)

The dynamics of tidally-induced internal waves is investigated by using a numerical three-layer model based on the weakly nonlinear, weakly non-hydrostatic Boussinesq equations. Numerical solutions of the three-layer Boussinesq equations are compared with analytical solutions of different equations describing internal solitary waves in a two-layer system. In contrast to the two-layer models, the three-layer model is capable of describing the evolution of sub-surface jets. As a result of the three-layer model these jets develop undulations that finally disintegrate into internal solitary waves. Several characteristics of these waves, like e.g., wave amplitude and distance between the first two solitary waves of a wave train are studied as a function of the initial jet velocity and the stratification. Results of the numerical simulations are compared with results of high resolution in-situ measurements carried out north and south of the Strait of Messina, in the European Mediterranean Sea. Implications of the presented study for a possible inversion of sea surface manifestations of oceanic internal waves into characteristics of the interior ocean are discussed.

**P14/E/09-A4** Poster **1400-11**

#### MODELLING THE RIFT-VALLEY FLOW OF THE MID-ATLANTIC RIDGE

A.M. THURNHERR, K.J. Richards, and M.M. Lam (School of Ocean and Earth Sciences, Southampton Oceanography Centre, Southampton SO14 3ZH, UK)

The hydrography and flow field of the AMAR segments of the Mid-Atlantic Ridge (35 Deg 35' N - 36 Deg 45' N) were investigated by analysing CTD data from two hydrographic surveys, a set of LADCP profiles, and data from an array of moored current meters deployed for one year. The bathymetry of the rift valley can be approximated as a sequence of deep basins separated by shallow sills. Hydrographic sections across these sills show potential density contours consistent with unidirectional, hydraulically controlled, along-valley flow. This is supported by the current meter observations, which show unidirectional flow of order 0.1 Sv along the valley throughout the one year deployment. Based on the T/S characteristics of the rift-valley water as well as direct density observations, the flow is most likely fed by an inflow sill on the eastern valley wall of the southernmost basin of the segment.

Based on these observations a simple basin/sill model for the along-valley flow is constructed. Topics to be studied using this model include: the timescales of the flow; the nature and variability of its forcing; the most likely destiny of the rift-valley water; and the sensitivity of the flow to rift-valley processes, such as the localized hydrothermal density flux which occurs just upstream of one of the sills studied.



P14/W/02-A4 Poster 1400-12

### LATERAL CIRCULATION DRIVEN BY AN OVERFLOW

Jody M. KLYMAK and Michael C. Gregg (both at APL/U. of Washington, 1013 NE 40th St., Seattle, WA 98105; 206-543-1300; e-mail: jklymak@apl.washington.edu)

The importance of interfacial stress and entrainment on the dynamics of an overflow is generally recognized. Interfacial stress slows the overflow, while mixing dilutes it and makes it lighter. However, the importance of stress and mixing on the water above an overflow is not usually discussed.

Recent observations in Knight Inlet (B.C.) show that an overflow can drive strong recirculations. We believe that shear instabilities along the top of the overflow accelerate the overlying water. This acceleration is local because it only occurs over the overflow, which creates a cross-channel divergence in the overlying water. A matching pair of recirculations transport water across the channel to fill this divergence. These recirculations strongly affect the flow in Knight Inlet. For instance, they draw mixing ingredients into the flow laterally, they bias volume budgets, and they confuse determinations of the level of no-motion which has traditionally been used to define the vertical extent of an overflow.

We hypothesize that these recirculations are a general phenomena in supercritical flows. First, supercritical flows are often susceptible to shear instabilities which exchange momentum and fluid between the overflow and the overlying water. In addition, supercritical flows are too fast to allow pressure signals to propagate back upstream. This means that the local acceleration in the lee of the sill cannot change the flow upstream of the sill crest, and the increased flow can only be supplied by circulation in the lee of the sill. Since the major overflows are almost all supercritical at some point, we expect that they all drive lateral recirculations.

PW1

Saturday 24 July

### OCEANOGRAPHIC PROCESSES IN THE COSTAL SEAS AROUND DEVELOPING COUNTRIES

Location: Watson Building G23 LTA

Saturday 24 July AM

Presiding Chair: S.V. Durvasula, (Kuwait Institute of Scientific Research, Kuwait)

PW1/E/04-A6 0900

### MULTI-PHASE DISTRIBUTION OF ORGANIC MICROPOLLUTANTS IN XIAMEN HARBOUR, CHINA

J.L. Zhou (1), Z. Zhang (2), K. Maskaoui (2) and H. Hong (1) School of Ocean Sciences, University of Wales Bangor, Menai Bridge, Anglesey LL59 5EY, UK, (2) Environmental Science Research Centre, Xiamen University, Xiamen 361005, P.R. China

Abstract 2. Xiamen Harbour, In Xiamen Special Economic Zone of the People's Republic of China, was studied for its water and sediment quality, by determining the levels of 16 polycyclic aromatic hydrocarbons (PAHs), 12 polychlorinated biphenyls (PCBs) and 18 organochlorine insecticides in water, porewater and sediment samples from nine stations in the Harbour. Total PAH concentrations varied from 106 to 945 ng/l in water, 0 to 3548 ng/l in porewater, and 247 to 480 ng/g dry weight in surficial sediments. Total PCB levels varied from 0.12 to 1.69 ng/l in water, 2.67 to 34.80 ng/l in porewater, and 0 to 0.32 ng/g dry weight in sediments. The levels of all insecticides were in the range 6.60 - 19.56 ng/l (water), 11.93 - 78.53 ng/l (porewater), and 0 - 0.58 ng/g dry weight (sediment). The levels of total hexachlorocyclohexane (HCHs) in sediments varied from 0 to 0.14 ng/g dry weight, and those of total DDTs were in the range 0 - 0.06 ng/g dry weight. The micropollutants were present in higher levels in porewater than in surface water, due to the preference of these hydrophobic compounds for sedimentary phase than for water. Such a concentration gradient imply a potential flux of pollutants from sediments to overlying water. The levels of pollutants in sediments were one to several orders of magnitude lower than those in 1993, suggesting their decreased inputs in recent years and possible degradation over a period of time. Further work is needed to quantify the levels of these contaminants in suspended particulate matter, which are currently below the limits of detection.

PW1/W/05-A6 0920

### TROPICAL REGIONS OF FRESHWATER INFLUENCE

ALEJANDRO J. SOUZA (Centre for Coastal & Marine Sciences, Proudman Oceanographic Lab, Bidston Observatory, Birkenhead, L43 7RA, UK email: ajo@ccms.ac.uk) and John H. Simpson (School of Ocean Sciences, Menai Bridge, Anglesey, LL59 5EY, UK).

The processes involve in the dynamics of Regions of Freshwater Influence (ROFIs) have been studied for some time in the first world countries, this has lead to basic understanding of this systems. But the Mayor ROFIs are located in tropical regions and predominantly third world countries in America, Asia and Africa, most of these systems are little studied and insitu data is scarce or non existant. The study of tropical ROFIS is of great importance to the global ecology as is here that there is great diversity of marine organisms live or develop, at the same time these regions are subject to important fisheries and in some cases are subject to large inputs of agrochemicals, as in the case of west Mexico and Mozambique. This calls for a knowledgable mangement of the Tropical ROFIs, which only be possible if the knowledge aquired in developed countries is transferred to underdeveloped countries.

PW1/P/01-A6 0940

### MANGROVE DENUDATION AND ECOLOGICAL CHANGES IN A BAY-ESTUARY SYSTEM ON THE EAST COAST OF INDIA

Raman A.V., Frank Dehairs\*, Chandramohan, P., Dipti Raut, Murthy, N.V. S. S., Rohini, T. and Satyanarayana, B. (Marine Biological Laboratory, Department of Zoology, Andhra University, Visakhapatnam-530 003, India, email: pcmavr@md2.vsnl.net.in) \*Department of Analytical Chemistry (ANCH), Virje Universiteit Brussel, Pleinlaan 2, B-1050 Brussels, Belgium, email: fdehairs@vub.ac.be)

Kakinada Bay, a shallow (<5 m) bar-built water body on the east coast of India, underwent many topographical changes attributable to port expansion programmes and industrial development recently. The Bay which covers an area of approximately 132 sq.km. is surrounded by extensive estuarine areas with enormous mangrove vegetation mainly, *Avicennia*, *Excoecaria*, *Rhizophora*, *Aegiceras*, *Lumnitzera*, *Cerriops* and others. In recent years, there has been a spurt in shrimp farming activity in this area which resulted in the

destruction of much of this vegetation, the impingement being very severe in some localities. Investigations during the last three years (1994-1997) revealed appreciable changes in water quality and organisms in the Bay and tributaries, Coringa and Gaderu, as a result of these activities. In Coringa-Gaderu region close to shrimp farms, a several fold increase in nitrate (max. 83.52 µg.at/1) and phosphate (max. 41.6 µg.at/1) levels was noticed. Several species of phytoplankton notably *Navicula*, *Skeletonema costatum*, *Pleurosigma angulatum* and *Nitzschia closterium* occur here often in bloom proportions (8,000 cells/ml). Within the Bay, regions once supported dense assemblages of benthic organisms (molluscs) *Anadara*, *Placuna*, *Tonna* and *Turritella* have now given place to different species owing to changes in sediment nature. Over the years, population size of these species decreased as a result of over exploitation commercially. The paper purports to draw comparisons between this study with those conducted in 1959-1964 attributing changes to anthropogenic effects during the intervening years.

PW1/W/02-A6 1000

### OVERTURNING LENGTH SCALE AS AN INDICATOR OF THE WASTEWATER NEAR FIELD

Vlado MALACIC (Marine Biological Station, National Institute of Biology, Piran, 6330, Slovenia, email: malacic@nib.si)

During a period of calm weather and stratified water column of a shallow (depth = 21 m) semi-enclosed sea, six surveys of the wastewater near-field of two adjacent submarine diffuser outfalls, with a low sewage outflow rate (usually less than 220 l/s), were conducted with a fine-scale CTD probe. The survey area of 780m x 740m was monitored with the free-falling probe at 30-31 stations. Vertical velocity of the probe was nearly constant, 1 m/s, and the data was retrieved at a frequency of 50 Hz, providing a vertical resolution of 2.5 cm.

When using a fine-scale CTD it has been observed that from the vertical distribution of 'virtual' displacements (Thorpe displacements) of particles with a sampled density, by which each particle would gain a statically stable position, the length scale of overturning events could be estimated, through an appropriate averaging process.

Within the turbulent wastewater field the fluctuations of temperature were of the order of 0.1°C, and of salinity less than 0.05 psu, generating overturning. The vertical extent of the overturning events could well be determined using the maximum vertical displacement, or the Thorpe length scale. Both scales also indicate the thickness of the neutrally buoyant subsurface wastewater field. Distribution of these length-scales over the diffusers show a clear picture of the wastewater field(s) of a thickness smaller than 1m in windless, stratified conditions, which is otherwise hard to obtain without costly experiments (dye tracers).

PW1/P/03-A6 1120

### OCEANOGRAPHIC PROCESSES AND IMPACT OF HUMAN ACTIVITY ON COASTAL EROSION: A CASE STUDY FROM KARNATAKA, INDIA

K S JAYAPPA (Marine Geology Faculty, Mangalore University, Mangalagangothri-574199, Karnataka, India, email: jayappa@mnglr.ernet.in)

Complex nearshore processes change continually and derive their energy from waves and currents. Variations in energy distribution within the surf zone cause transport of sediment alongshore and offshore. Beach erosion in Karnataka has become a severe problem since last two decades. It is estimated that out of 290 km, 80 km is vulnerable to erosion during SW monsoon. The factors which are responsible for erosion of this coast are: storm waves, tidal and longshore currents, wave refraction (all natural), construction of ports, harbours, breakwaters, seawalls, damming of rivers and sand mining (all man-made). Of these, the man-made erosion and steps taken for its prevention are important ones to be attended immediately. In recent years, coastal communities are inhabiting newly developed coastal landforms. Beach erosion is part of a cyclic process and maintains a seasonal balance between erosion and accretion, but in some cases net erosion or accretion takes place. Erosion of beaches could be minimised by preventing (1) human interference with coastal processes, (2) inhabitation of fragile zones, and (3) sand mining from beaches and estuaries. Seawalls which are used as erosion management tools, often complicate the erosion problem or shift the erosional sites to adjacent areas. In general, the cost of seawall construction and maintenance is greater than the value of the property saved. In some cases they have been destroyed by huge waves thereby recreational potentials of beaches are lost and posed a severe threat for shore-based fishing activity.

PW1/E/02-A6 1140

### ON THE ISTRIAN COASTAL COUNTERCURRENT

Nastjenjka Supic (Centre for Marine Research, Rudjer Boskovic Institute, G. Paliaga 5, 52210 Rovinj, Croatia, email: supic@cim.irb.hr) Mirko ORLIC (Andrija Mohorovicic Geophysical Institute, email orlic@olimp.irb.hr) Danilo Degobbis (Centre for Marine Research, Rudjer Boskovic Institute, email: degobbis@cim.irb.hr)

By computing the relative (with respect to the 30 dbar surface) and absolute geostrophic currents and net transports from hydrographic data collected monthly to seasonally at six stations of the Po-Rovinj profile in the northern Adriatic, we demonstrate the existence of a descending current which usually appears in August along the Istrian coastal line and runs counter to the general Adriatic-wide cyclonic flow. We name it Istrian Coastal Countercurrent (ICCC). The current is found to be confined to the surface (of a 10 m depth) and coastal boundary (of a 10 km width) layers. Its mean relative speed is high, 7 cm/s (relative currents at the profile on average stay below 5 cm/s in winter and below 8 cm/s in summer), inducing a net geostrophic outflow near the Istrian coast. The ICCC was strong in 1968, 1977, 1983, 1984, 1988, 1989, 1991, 1992, 1996 and 1997, weak or absent in 1971, 1972, 1973, 1982, 1986, 1993, 1994 and 1995. Whenever the ICCC was well pronounced, a strong northerly flow was observed in the central part of the northern Adriatic profile, whereas a thick surface or subsurface layer of low density was found in the open waters off Rovinj. This points to a possible existence of a cyclonic gyre east of the Po delta and/or anticyclonic gyre off Rovinj. The existence of ICCC is confirmed by direct current measurements, which show that the descending coastal current was intense in 1977 and 1983, and that it did not develop in 1976, 1978 and 1987. The August intensity of the ICCC significantly correlates with the sea surface temperature (SST) recorded in preceding March in the northeastern Adriatic. Using a polynomial fit of the ICCC speed on the northeastern Adriatic SST a weak or non-existent ICCC is hindcasted for 1976 and 1987. It seems that a high intensity of ICCC coincides with oceanographic conditions which favour near anoxia or mucilage events, observed in 1988, 1989, 1991 and 1997.

PW1/W/03-A6

1200

## INTERNAL WAVES AND ACOUSTIC FIELDS IN THE SHELF ZONE OF SEA

Vadim V. NAVROTSKY, Alexander N. Rutenko (Pacific Oceanological Institute, 43 Baltiyskaya Str., Vladivostok, 690041, Russia, email: navr@online.vladivostok.ru)

Some results of experimental investigation of internal waves and their influence on the characteristics of acoustic fields in the shelf zone of the Japanese Sea are presented. In our field experiments we used continuous signals with sinusoidal frequency modulation in the range 306- 328 Hz. Simultaneous measurements of acoustic parameters and water temperature fluctuations at different levels were made with the help of a measuring system, placed at distance of 250 m from the emitter with the site depth of 38 m. It is shown, that intensities of acoustic signals with 4% difference of frequencies have rather different variations in time, sometimes in counterphase. The differences are maximum at levels, where the interference minimum is observed. Half-day tides cause 3 Hz displacements of the minimum in the interference structure of the measured acoustic field. The statistical analysis of temperature fluctuations at different levels was made. It was shown that in the range of short internal waves the most pronounced effects are due to resonant interactions of acoustic waves with sound velocity inhomogeneities, registered by temperature sensors. The main result of such interactions is redistribution of acoustic energy among normal modes with general flow of energy into higher modes and phase randomization.

PW1/E/01-A6

1220

## ANTHROPOGENIC DISCHARGES INTO THE MOZAMBIQUE CHANNEL

U.ASWATHANARAYANA (c/o Ministry for the Coordination of Environmental Affairs, C.P. 1947, Maputo, Mozambique. Email: anarayan@zebra.uem.mz)

Mozambique Channel receives two kinds of anthropogenic discharges:

(1) Discharges (accidental or deliberate) from about 200 ships (mostly tankers) that pass through the Mozambique Channel daily - no discharge data is available in this regard, and (2) anthropogenic discharges from the coast - these are studied along four principal coastal towns from south to north, namely, Maputo, Beira, Quelimane and Pemba.

In the case of Maputo and Beira, the industrial discharges into the sea are due to the port, oil installations, food and beverage processing, batteries, edible oils and soaps, textiles, fishing and canning, tourism, animal farms, etc. Municipal sewerage, with human faeces, is discharged into the sea untreated, with the consequence that the seawater is heavily contaminated with E.Coli ( $\times 1000/100$  mL). In the case of Quelimane and Pemba, the industrial discharges into the sea are minimal, but the biological pollution of the sea is serious, as a good part of the population defaecate in the mangroves or on the beach. The human faeces get washed into the sea at high tide, and end up in fish which people consume. If there are cholera pathogens in the human faeces, cholera epidemic results. The cholera epidemic caused by ENSO-induced flooding along the east coast of Africa, killed an estimated 5000 people last year.

Saturday 24 July PM

Presiding Chair: S.V. Durvasula, Kuwait Institute of Scientific Research, Kuwait

PW1/W/06-A6

1400

## STABILITY AND MORPHOLOGY OF THE COASTAL CONTOURS FROM SEDIMENTOLOGICAL LIFTING IN THE FORTALEZA-CE AREA, BRAZIL

Prof Agenor Cunha da Silva

This work was generated from studies required to the Directorate of Hydrography and Navigation of the Brazilian Navy by the National Union State Secretariat of the Ministry of the Treasury in order to analyse the evolution of coastal features in the municipalities of Fortaleza, Aquiraz, Caucaia and São Gonçalo do Amarante, Ceará State, Brazil, with views to determine the real mean high water line to charge taxes. The mean high water line was referred initially by the mean sea level in 1831, and it must be corrected because of the possible changes in that line. It includes granulometry and analysis of the sediments collected along the coast, between September 28 and October 02, 1993. The stability and contours of Northeastern and Southeastern beaches of Ceará, Brazil were researched. In addition, the intensity and evolution of the coastal process were examined in order to make a diagnosis, with the use of sedimentology, of areas where the contour mobility may imply loss of accuracy in cartographic works.

PW1/P/02-A6

1420

## THE FUTURE PROSPECTS OF OCEANOGRAPHIC RESEARCH IN THE MEDITERRANEAN AND RED SEAS BY THE SURROUNDING DEVELOPING COUNTRIES

S.H. SHARAF EL DIN, Oceanography Department, Faculty of Science Alexandria University

POEM is a multi-national co-operative research program initiated and carried out by scientists in both the regional oceanography and the potential of the eastern Mediterranean to provide a laboratory basin for global processes. In the past, some of the developing countries surrounding the eastern Mediterranean shared with a limited efforts in the various studies. More recently, several developing countries such as Egypt, Israel, Lebanon, Syria and Libya started to increase their scientific activities in the eastern Mediterranean. In Egypt, a lot of studies have been done on the management of the Egyptian Mediterranean coastal areas. Recently, study of the effect of some environmental factors on the distribution of the phytoplankton in the banias region on the Syrian coast has been taken place. In Lebanon, a model was constructed as a useful tool for the rehabilitation, protection and development of the Lebanese coast. Also, the status and solution of Beirut Bay wastewater problem was studied extensively. In Lybia, the marine science activities were devoted more recently to the fisheries, pollution and coastal zone management.

In the Red Sea area, most of the work carried out in Suez, Bay, was mainly pollution and coastal zone management. In Aquaba Gulf, most of the work done by a group of scientists from USA, Egypt and Israel. The project was mainly devoted to study the biological and environmental parameters in the Gulf. In the Red Sea, the research projects are still limited to the regional boundaries.

PW1/E/06-A6

1440

## CZM AND THE COASTAL SEA: THE NEED TO ASSESS COASTAL ZONE VULNERABILITY AND APPLY LONG TERM STRATEGIC MEASURES

A. N. BALCHAND (Department of Physical Oceanography, Cochin University of Science and Technology, Fine Arts Avenue, Cochin 682 016, India, email: oceans@md3.vsnl.net.in)

The interaction between the land and oceans has been recognized as an important surface process of short and long term time scales. The dynamic properties and functional attribute of the coastal zone are the results of cumulative global environmental change - sea level changes, landscape alterations, marine ecosystem changes, trends in sedimentary behavioral patterns, hydrological factors and so forth. Of immediate concern is the coastal zone vulnerability arising due to climate change, subsidence and recession of coastlines, mining activities, water abstraction and large changes in wetland management. Study subjects often chosen relates to areas at change and related population at risk, agricultural production at change and ecosystem losses. The sensitive tropical coastal regions (mostly in low lying lands) which are highly productive and densely populated are currently threatened by above stated changes. Thus the need to assess coastal zone vulnerability based on information gathered on the physical environment, geomorphological setup, evaluation of varying trends of both natural and anthropogenic influences is relevant. The evaluation methodology shall aim at assessing the extent of damage already inflicted to the region, the response pattern, the remedial measures adopted and thus help us to deduce better understanding on the development of the fragile coastal sea. A suitable database covering land water uses and practices, development of wetlands, their functions and resources along with risk estimation and hazard evaluation would lead to the right application of long term strategic measures.

PW1/E/07-A6

1500

## IMPACT OF RIVER DIVERSION IN SOUTHERN IRAQ ON THE HYDROBIOLOGY OF THE NORTHERN ARABIAN GULF

FAIZA AL-YAMANI Kuwait Institute for Scientific Research, P.O. Box 1638, Salmiyah-22017, Salmiyah, Kuwait.

The Arabian Gulf is a semi-enclosed body of water located in a climatically arid region with an average depth of 35 m, with a maximum depth of 120 m. Its only source of freshwater is seasonal and from the Shatt al-Arab in the north. High evaporation rates in excess of precipitation and river discharge result in high salinity (~42 psu). Frequent northwesterly winds mix the northern Gulf's shallow waters contributing to the resuspension of particulate matter and high turbidity from the silt-laden waters of the Shatt al-Arab. Freshwater enters the northern Gulf via the Shatt al-Arab, with an estimated annual discharge rate of 5 to 100 km<sup>3</sup>/yr. The Shatt al-Arab watershed and associated marshes are the main sources of nutrients that sustain a high productivity in the northern Gulf. Recently, Iraq completed its diversion of the Euphrates River to a man-made canal named the Third River which flows to the northwestern part of the Gulf. Additionally, more than 60% of the marshes in southern Iraq have been drained. Such developments as well as the ongoing Southeast Anatolia Project in Turkey, will exert a great impact, particularly in the northern Gulf. Comparison of recent data (1995-1998) with the earlier showed: a) a decrease in salinity in the northwestern Gulf to 25.60-33.00 psu, b) elevation of nutrients to higher ranges (6-15 mg-at/l nitrates, 0.4-0.9 mg-at/l phosphates, and 26-43 mg-at/l silicates). This is attributable to the impact of additional river runoff from the diversion. Additionally, higher turbidity levels (58-174 NTU), and higher phytoplankton biomass were recorded for the northern waters. Changes in the marine ecosystem resulting from alteration of flow regimes and water quality of the Shatt al-Arab waterway will probably have a major impact on the fishery resources of the northern Gulf. Especially the economically important species such as the shrimp-Metapenaeus affinis, the pomfret Pampus argenteus, and the suboor Tenualosa ilisha which are known to directly depend on freshwater inflow for spawning or nursery habitat. Additionally, indirect effects, operating through changes in the food web, may further impact population abundances, species diversity and imbalances amongst species.

PW1/W/01-A6

1520

## THE HEAT BUDGET OF A TIDAL BAY

SHIGALLA B. MAHONGO Tanzania Fisheries Research Institute P.O. Box 9750 Dar es Salaam Tanzania

Atmospheric, sea surface temperature and sea level data were collected for a 23-day period at Chwaka bay (Zanzibar Island) in 1996. The data were used to calculate the turbulent fluxes of heat and moisture from a bulk aerodynamic method. The net radiative (long-wave and short-wave) heat fluxes were computed from records of incoming and outgoing short-wave radiation, and net all-wave radiation. An independent method was used to calculate the advective heat flux, and results conformed with a qualitative analysis of net surface heat flux in relation to the tidal phase, and to the water temperature variability. The effect of water-sediment heat conduction was basically a net transfer of heat from sediments to inundating water layers. The heat budget of the bay involves a near balance between heating by solar radiation, and cooling by evaporation and advective exchange with the open ocean. Maximum net surface heating occurs at around noon, while maximum net surface cooling takes place immediately after sunset.





**MI01 Monday 19 – Wednesday 21 July****ATMOSPHERIC CHEMISTRY – CLIMATE INTERACTION, Part 1: AEROSOLS, CLOUDS AND CLIMATE (CACGP)**Location: Mechanical Engineering G33 LT  
Location of Posters: Old Gym**Monday 19 July AM**Presiding Chair: T. Iversen (Department of Geophysics, University of Oslo, Norway)  
Concurrent Poster Session**AEROSOLS****Introduction 0900****MI01/L/02-A1 Invited 0905****CLIMATE CHANGE AND RADIATIVE FORCING BY ANTHROPOGENIC AEROSOLS: A SUMMARY OF CURRENT UNDERSTANDING**

Joyce E. Penner (Department of Atmospheric, Oceanic and Space Sciences University of Michigan Ann Arbor, MI 48105, USA email: penner@umich.edu).

The Intergovernmental Panel on Climate Change (1996) published estimates for the direct and indirect forcing by anthropogenic sulfate, soot, and biomass aerosols which ranged from -0.2 Wm<sup>-2</sup> to -2.5 Wm<sup>-2</sup>. It is important to decrease the uncertainty associated with this range of forcing because if the forcing is as small as suggested by the lower limit and if the temperature change experienced in the last 100 years is mainly from the warming caused by greenhouse gases, then the climate should be relatively insensitive to greenhouse gas increases. On the other hand, if the forcing is as large as -2.5 Wm<sup>-2</sup>, then climate sensitivity to anthropogenic forcing is probably at the higher range of estimates and some of the observed increase in temperature must be associated with natural variability. Since the 1996 report, a number of advances and assessments of both the direct and indirect forcing by anthropogenic aerosols are available. This talk will summarise our current understanding of both the direct and indirect forcing and summarise current model capabilities to assess this forcing.

**MI01/W/12-A1 0945****COMPARISON OF THE VERTICAL DISTRIBUTIONS OF SULFUR SPECIES FROM MODELS PARTICIPATED IN THE COSAM EXERCISE WITH OBSERVATIONS**

Ulrike Lohmann (Dept. of Physics, Dalhousie University, Halifax, NS, B3H 3J5, Canada, email: Ulrike.Lohmann@Dal.Ca) Len Barrie, Richard Leaitch, Yuhong Yi (all at Atmospheric Environment Service, Downsview, ON, M3H 5T4, Canada) Kathy Law (Dept. of Chemistry, University of Cambridge, Lensfield Road, Cambridge, CB2 1EW, U.K.) and modellers

The comparison of large scale models simulating atmospheric sulfate aerosols (COSAM) was conducted to increase our understanding of sulfate aerosols and precursors. Earlier model comparisons (Rasch et al. 1999) focussed on wet deposition measurements and sulfate aerosol concentrations at the surface. It was found that different models simulated sulfate surface concentrations which agreed reasonably well with observations, but the column burden or the concentrations aloft were very different amongst different models. Thus, in the COSAM exercise, one aspect is the comparison of sulfate aerosol and precursor gases above the surface. Vertical profiles from observations are available from the NARE experiment, which took place in August/September 1993 off the coast of Nova Scotia, Canada and from EMEFSII, which took place in March/April 1990 in Ontario. Results from the participating models (global climate models and chemical transport models) will be presented in this talk.

**MI01/E/12-A1 1005****SIZE DISTRIBUTION AND COMPOSITION OF ATMOSPHERIC AEROSOL PARTICLES IN MARINE AND CONTINENTAL INFLUENCED AIR**

Sabine GRUBER, Sabine Matthias-Maser and Ruprecht Jaenicke (Institute for Atmospheric Physics, University of Mainz, Becherweg 21, 55099 Mainz, Germany; email: gruber@mail.uni-mainz.de)

The atmospheric aerosol is an external mixture of various particle types including minerals, sea salt, soot, biological particles and others. The composition as well as the concentration of the aerosol particles have a vast impact on the formation, microphysics and chemistry of clouds. For most numerical cloud simulations in marine air the particles are assumed to consist of sea salt only and hence to be 100 % water soluble. Recently it was shown that modelling marine clouds with a more realistic solubility of particles leads to noteworthy differences in the cloud droplet spectra. In this study, aerosol particles were collected size distributed on the island of Helgoland in the North Sea. The particles were investigated in a scanning electron microscope which was combined with an energy dispersive X-ray detector. Interpreting the morphology and elemental composition of each single particle, the particles were classified into different aerosol types. The size distributions for the various aerosol types were determined in the particle size range  $0.2 \mu\text{m} < \text{radius} < 2.2 \mu\text{m}$ , for the total and the biological aerosol even in the size range  $0.2 \mu\text{m} < \text{radius} < 41.6 \mu\text{m}$ . It turned out that in marine influenced air masses only half of the particles consisted of sea salt while 17 % were calcium sulphates and 9 % biological particles. The remaining 25 % of the particles consisted of soil dust, particles derived from combustion processes and others. It is well known that both the calcium sulphates and the biological particles have marine sources.

Calcium sulphate is produced by fractionated crystallisation of sea salt and biological particles like algae are spread into marine air by the bubble burst mechanism. Our measurements show that they are an important portion of the marine aerosol and therefore their existence should be taken into consideration when simulating marine scenarios.

**MI01/W/09-A1 1025****A SCHEME FOR MODELLING BLACK CARBON AND SULPHATE AEROSOLS IN GENERAL CIRCULATION MODELS**

Øyvind SELAND and Trond Iversen Department of Geophysics, University of Oslo P.O.Box 1022 Blindern, 0315 Oslo Norway

As a first step towards estimating the effects of aerosols on the earth's radiation budget, the spatial and seasonal distribution of the two aerosol components is calculated. The scheme is assigned to crudely take into account size distribution as a function of aerosol age. Aging is parameterised by coagulation processes, humidity processes and scavenging. In addition aging processes also describe the transition from elemental carbon with hydrophobic properties externally mixed with hygroscopic sulphate, to an internally mixed aerosol.

The scheme has been developed in a hemispheric transport model that uses analysed meteorological data from the ECMWF. This was done to be able to validate the scheme by comparing the results with measurements from the same time period. The turnover times calculated in the hemispheric model were 1.8 days for sulphur dioxide, 3.7 days for sulphate and 3.7 days for black carbon. Some sensitivity tests were performed as well, showing that the results were very sensitive to changes in the parameterisation of below-cloud scavenging. To obtain global distribution of the components the scheme is now included in the NCAR CCM3 General Circulation Model.

Results from the calculations will be presented, and compared with available measurements, with the main emphasis on the results from the CCM3. Both seasonal, latitudinal and vertical variations of particle concentrations will be discussed.

**MI01/L/06-A1****1110****THREE DIMENSIONAL MODELLING THE EVOLUTION OF THE DUST PARTICLE SIZE DISTRIBUTION DURING THE ACE-II FIELD CAMPAIGN**

Peter R. COLARCO, Irina N. Sokolik, and Owen B. Toon (all at Laboratory for Atmospheric and Space Physics, University of Colorado, Boulder, CO 80309-0392, USA, email: Peter.Colarco@Colorado.EDU)

The properties of mineral aerosols are highly variable in space and time, and are poorly understood. A major question is how the size distribution evolves as dust is transported downwind from its source region. The evolution of the size distribution is important for the assessment of direct radiative forcing by mineral dust and for satellite retrieval validations. We have incorporated an aerosol microphysical model into a three dimensional GCM to simulate dust emission and transport. Because the GCM is driven by assimilated meteorological fields, it can be used to simulate specific events and be tested against specific observations. Currently, the dust model includes an emission scheme to account for source strengths and locations, and a removal scheme to account for gravitational settling, dry deposition, and wet removal. We focus on the analysis of the time-dependent size distribution as Saharan dust is transported in the vertical and horizontal directions. The model is applied to the timeframe covered by the ACE-II experiment (mid-June through July, 1997). The model is able to reproduce dust optical depths and a plume shape in a good agreement with observations made by the AVHRR and TOMS instruments. The model results are also compared with observations made by ground based sun-photometers and other instruments from the ACE-II campaign. Future directions of this work are also discussed.

**MI01/E/04-A1****1130****MODELLING MINERAL DUST IN AN AGCM: PARAMETRIZATION AND RADIATIVE FORCING**

STEPHANIE WOODWARD and David L Roberts (Hadley Centre for Climate Prediction and Research, Meteorological Office, London Road, Bracknell, Berkshire, RG12 2SY, UK.)

Mineral dust aerosol is produced primarily through the action of wind on bare soil, the largest sources being in the major deserts. Small dust particles may be carried great distances and are found throughout the troposphere. The quantity of dust in the atmosphere may be large enough for it to have an appreciable effect on the earth's radiation balance, through both shortwave and longwave forcings.

A dust parametrization has been developed for the Hadley Centre climate model, in which dust is produced when the surface friction velocity exceeds a threshold. The magnitude of the dust flux depends on the friction velocity, air density, vegetation cover, soil moisture and particle size distribution. Dust is transported as six model tracers representing different particle size classes. Deposition processes include below-cloud washout, and dry deposition due to turbulent mixing and gravitational settling. The radiative properties of dust have been incorporated into the model's Edwards-Slingo radiation code.

Model integrations have been performed with the new scheme, to compare modelled dust distributions with observational data and to estimate radiative forcing. Partial cancellation occurs between shortwave and longwave forcings, and the global mean net top-of-atmosphere forcing is further reduced by spatial averaging over areas of opposite sign. There are still many uncertainties, particularly associated with dust production and radiative properties and the sensitivity of modelled dust amounts to many variables. However, it appears that the radiative forcing due to mineral dust may be appreciable, particularly on a regional scale.

**MI01/W/22-A1****1150****AN ILLUSTRATION OF THE TRANSPORT AND DEPOSITION OF MINERAL DUST ONTO THE EASTERN MEDITERRANEAN**

Nilgun Kubilay (Institute of Marine Sciences, Middle East Technical University, P.O. Box 28, Erdemli-ICEL, 33731, Turkey, email: kubilay@ims.metu.edu.tr) Slobodan Nickovic (University of Malta, Foundation for International Studies, ICoD, St Paul Street, Valletta, Malta, email: nicko@icod.org.mt) Francois Dulac (Centre des Faibles Radioactivites, CNRS-CEA, F91198, Gif-Sur-Yvette Cedex, France, email: dulac@lscce.saclay.cea.fr)

The analyses of aerosol samples and deposition (wet) measurements during August 1991 - December 1992 at Erdemli (36°N, 34°E) located on the Turkish coast of the Eastern Mediterranean has shown higher dust concentration and total deposition during transitional seasons (spring and autumn) compared to summer and winter seasons. The data, complemented by three-dimensional (3-D) air mass back trajectories and satellite observations suggest that North African and Middle East desert derived dust particles are transported to the region during transitional seasons. Transport events in the last part of March 1992 and early October 1992 are studied through combined analyses of ground based and satellite observations and modelling results. It is shown that dust transport constitutes a large fraction of the annual atmospheric deposition in the eastern Mediterranean, with two deposition events of short duration accounting up to 30 % of the total annual flux. Therefore, the dissolved and particulate species associated with dust could be extremely variable in the mixing layer during large deposition events and could easily be missed in a short -- term sampling program. The possible impact of large pulses on biological productivity of the sea also warrants consideration.

MI01/L/01-A1

1210

**COMPUTED SULPHATE AND NITRATE AEROSOL ATMOSPHERIC LOADING IN EUROPE**

Krzysztof Olendrzynski, Svetlana Tsyro, Jerzy Bartnicki, Jan Eiof Jonson, and E.Berge (Meteorological Synthesizing Centre-West of EMEP, Norwegian Meteorological Institute P.O.Box 34, Blindern, N-0313 Oslo, NORWAY)

Hazardous effects of atmospheric aerosols are numerous and appear on different time and space scales. The radiative forcing by aerosols is largest in industrial regions, but it can also have hemispheric and global effects. Estimations of radiative forcing rely primarily on aerosols concentration distribution calculated with chemical models and, thus, depend on the models adequate results. On the regional scale aerosols contribute to acidification and eutrophication of ecosystems, impaired visibility and adverse health effects. EMEP (Co-operative programme for monitoring and evaluation of the long range transmission of air pollutants in Europe) operates a 3-D Eulerian acid deposition model to compute concentration levels of nine sulphur and nitrogen components over Europe. The air concentrations and acidifying depositions derived from them when presented in a form of country-to-country budgets, provide a scientific basis for emission reduction negotiations under the UN Convention on Long-Range Transboundary air Pollution. The EMEP Eulerian model has twenty vertical layers (up to 100hPa) and horizontal resolution of ca. 50km x 50km. Input data include: official EMEP anthropogenic emissions of sulfur, nitrogen oxides and ammonia, as well as natural sulphur emissions; real-time meteorological data derived from a dedicated version of the Norwegian Weather Prediction Model (HIRLAM). No carbonaceous particles are included. The model has been applied to compute concentrations and column load of sulfate and nitrate aerosols in Europe in 1997. So far no information is given on the size distribution or number concentration. Neither photooxidation nor aerosol dynamics is accounted for. Both annual average mass concentration fields and column load of sulphate and nitrate aerosols are presented. The relative importance of sulphate and nitrate particles in the modelled aerosol burden in different European areas is also shown. Some examples are given of monthly/seasonal variation of aerosol loading in Europe. The computations have been compared with ...

Monday 19 July PM

Presiding Chairs: J.E. Penner (University of Michigan, USA)  
Frank Raes, (Environment Inst. Joint Research, Italy)

**AEROSOLS AND CLOUDS**

MI01/L/03-A1

Invited

1400

**EULERIAN AND LAGRANGIAN PROCESS STUDIES DURING ACE-2: DO THEY GIVE A CONSISTENT PICTURE OF ANTHROPOGENIC AEROSOL EVOLUTION WITHIN THE MARINE BOUNDARY LAYER.**

Frank Raes, Rita Van Dingenen, Commission of the European Communities, Environment Institute, 21020 Ispra (VA) Italy, Doug Johnson, Met. Research Flight Y24, Farnborough, Hampshire, UK, Colin O'Dowd, University of Sunderland Sunderland, UK.

The Aerosol Characterization Experiments of IGAC adopt both Eulerian and Lagrangian observation strategies. The latter is especially useful for process studies, as a single air parcel is identified and followed during its transport. Continuous observations at a fixed station will usually show a large variability which must mainly be ascribed to changes in the origin of the air masses. However, processes acting on these air masses upwind of the station, will also contribute to the observed variability. In this study we focus on measurements of sub-micron aerosol size distributions. On three occasions during ACE-2, an air parcel advecting within the MBL, was followed and sampled by aircraft. The observed changes in the size distribution during each of these Lagrangian experiments, reflected the importance of one process or another. Additionally, a station on the NE coast of Tenerife continuously characterized air masses coming from various areas in Europe, from N. America, as well as the clean Atlantic and Arctic. Given that air parcels with a longer residence time over the oceans undergo more processing, information can be obtained about the relative importance of several processes acting on the size distribution. Both observation strategies are consistent in their conclusion that, once the aerosol is some 24 hrs away from its continental source area, changes in its size distribution are mainly governed by meteorological factors, notably dilution by entrainment, and a modulation of sea salt accumulation mode by wind speed. Collision of aerosols with clouds and/or coalescence of cloud droplets, with subsequent re-evaporations, and aqueous phase chemistry are second in importance. Nucleation of new aerosol particles, and growth by condensation were unimportant during the ~ 30 hrs of each Lagrangian experiment, and were not observed at the station either. The station measurements, which include timescales of 5-10 days and more, support the idea that a steady state between entrainment, aqueous phase chemistry and coalescence/precipitation largely explains the size distribution of the clean MBL aerosol.

MI01/E/05-A1

1430

**MODELLING CLOUD PROCESSING OF AEROSOL DURING THE ACE-2 HILLCLOUD EXPERIMENT.**

MICHAEL J. FLYNN, Keith N. Bower and Thomas W. Choularton, Atmospheric Physics Research Group, Physics Department, University of Manchester Institute of Science and Technology, PO Box 88, Manchester, M60 1QD, UK.

The ACE-2 HILLCLOUD experiment used a hill cap cloud forming on the northern ridge of the island of Tenerife as a natural flow through reactor to study the response of cloud microphysics to the aerosol properties and gases in the airstream entering the cloud and to study the processing of aerosol and trace gases within the cloud.

A numerical model has been used to simulate the conditions observed during the field experiment, and to study the processes which may be taking place. The model incorporates gas phase chemistry of sulphur and nitrogen compounds upstream of the cloud, and the interaction of aerosol, precursor trace gases and oxidants within the cloud.

From this modelling study it can be concluded that in general in the remote environment the exchange of hydrochloric acid, nitric acid and ammonia between aerosol particles in the vicinity of cloud may be a very important mechanism in regulating the evolution of the aerosol spectrum.

Further a much more linear relationship between cloud droplet number and aerosol number was observed and predicted by the model than has been reported in the past. The implications of this for the indirect effect will be explored.

MI01/W/14-A1

1450

**NUMERICAL MODELLING OF THE MICROPHYSICAL AND RADIATIVE PROPERTIES OF A STRATOCUMULUS CLOUD STUDIED DURING ACE II**

S. GHOSH and P.R. Jonas (Dept. of Physics, UMIST, Manchester M60 1QD, U.K.)

The Aerosol Characterisation Experiment II was conducted from the 15 June to 23 July 1997 in the north-east Atlantic region. Although the air in the boundary layer originated from the Atlantic and the stratocumulus cloud was relatively 'clean', on some days observations indicate the possibility of advection of polluted continental air from Europe leading to some processing or modification of the aerosol and the cloud droplet spectrum. In this study we present results from an optimised three dimensional Large Eddy Simulation model (3D LES) which can distinguish between contaminated and clean clouds. We have also compared our model results with observations from the C130 aircraft for the 19th of July 1997 when the cloud was contaminated. The high resolution 3D runs yield a realistic cloud showing convective cellular organisation and the layer averaged liquid water content (LWC) profile agrees remarkably well with observations of the Johnson-Williams LWC. We have also calculated an optical depth map for this cloud covering a 10KmX2.5Km domain and we observe a great deal of variability in the optical depths and the mean and standard deviation of the modelled optical depths are in reasonable agreement with the limited observations available. Finally, we also performed 1D microphysical model runs (having a dynamical environment identical to the LES runs) with 0.1 ppb of HNO<sub>3</sub> since the maximum measured HNO<sub>3</sub> in the cloud samples are expected to be less than this value. We find that there is an increase of the droplet number concentration in the cloud interior of the 5 micron radius drops from 100/cm<sup>3</sup> to 125/cm<sup>3</sup>. The number densities did not change for larger drops and the largest droplet size that was obtained was 10 microns. The model was insensitive to changes in the acid concentration for values less than 0.1 ppb. The results obtained from this study are in accordance with the generally accepted fact that the droplet concentration in clouds that are formed in or pass over polluted air, is higher than in clouds formed in clean air and that these clouds have a correspondingly lower droplet size. Because of the rapid decrease in droplet encounter rates and collection efficiencies as the droplet size is reduced, formation of drops of precipitation size is likely to be inhibited in such clouds.

MI01/W/18-A1

1510

**ESTIMATING CLOUD DROPLET NUCLEATION FROM DIFFERENT AEROSOL COMPOUNDS IN A GCM**

Ulrike Lohmann (Dept. of Physics, Dalhousie University, Halifax, NS, B3H 3J5, Canada, email: Ulrike.Lohmann@Dal.Ca) Johann Feichter (Max Planck Institute for Meteorology, Bundesstr. 55, D-20146 Hamburg, Germany) Julian Wilson and Frank Raes (both at Environment Institute, Joint Research Centre, European Commission, 21020 Ispra (VA), Italy)

Cloud droplet nucleation depends on the hygroscopicity and size of the aerosols as well as on the maximum supersaturation. Lohmann et al. (1999) introduced a prognostic equation for the number of cloud droplets into the ECHAM GCM. For droplet nucleation they assumed a uniform monomodal aerosol size distribution for the marine and continental aerosol. However, the different aerosol species considered (sulfate, sea salt and carbonaceous aerosols) have different typical mode radii and different van't Hoff factors and, thus, grow differently with relative humidity and should be activated differentially. We will use Twomey's approach ( $N = c \text{ Smax}^{**k}$ ) to estimate the number of cloud droplets being nucleated and link  $c$  and  $k$  to our simulated aerosol size spectrum. The maximum supersaturation is obtained from the updraft velocity and again from information about the aerosol size spectrum. Results using this approach will be compared to observational data taken during ACE2.

MI01/W/04-A1

1640

**THE EFFECT OF AEROSOL AND CLOUD MICROPHYSICS ON THE ALBEDO OF MARINE STRATUS**

Mark COUTURE, Richard Leaitch, and Cathy Banic (Cloud Physics Research Division, Atmospheric Environment Service Downsview, Ontario M3H 5T4, Canada, Email: couture@armph3.tor.ec.gc.ca), Henry Leighton and Dean Gilbert (Department of Atmospheric and Oceanic Sciences, McGill University, Montreal, Quebec H3A 2K6), Ray Hoff and Kevin Strawbridge (Centre for Atmospheric Research Experiments, Atmospheric Environment Service, Egbert, Ontario L0L 1N0)

The Radiation, Aerosol and Cloud Experiment (RACE) was based in Greenwood, Nova Scotia, Canada and conducted in late August and early September of 1995. Two instrumented research aircraft were used to make observations of aerosols and low stratiform cloud over the Bay of Fundy and the Gulf of Maine. Four cases of optically thin clouds in air with different aerosol particle number concentrations at cloud base are compared. Measurements of visible cloud albedo exhibit a strong dependence on the measured optical depth, which, in turn, correlates with the measured optical extinctions in the clouds. Within each case, the in-cloud extinction varies predominantly with the liquid water content. From case-to-case, differences in the in-cloud extinction are predominantly related to the differences in the droplet number concentrations. A link from aerosol/CCN to cloud droplet number concentrations through optical depth is made. The cloud albedo increases by 25% for increases in the cloud-base aerosol number concentration from 80 to 265 cm<sup>-3</sup>. The observations are consistent with radiative transfer simulations of the cases.

MI01/E/03-A1

1700

**IN SITU CHARACTERIZATION OF OPTICALLY THIN MIDLATITUDE CIRRUS CLOUDS BELOW THE TROPopause**

Peter WENDLING, Franz Schröder, Ralf Meerkötter, Robert Baumann (all at Institut für Physik der Atmosphäre, DLR Oberpfaffenhofen, D-82234 Weßling, Germany, email: Peter.Wendling@dlr.de, Ralf.Meerkotter@dlr.de, Franz.Schroeder@dlr.de, Robert.Baumann@dlr.de), and Jean-Francois Gayet (Laboratoire de Meteorologie Physique, Université Blaise Pascal, 24 avenue des Landais, F-63177 Aubiere Cedex, France, email: gayet@opgc.univ-bpclermont.fr)

During the national CONTRAIL experiment in spring 1996 in situ characterization of upper tropospheric ice clouds including aerosols was performed with the german DLR research aircraft Falcon. The full instrumental detection range using both optical and nonoptical instrumental methods covered particle diameters from 0.01 - 800 µm (CN-counters: diameters > 10 nm; FSSP-300: 0.4 - 20 µm; FSSP-100ER: 5 - 100 µm; OAP-2DC: 20 - 800 µm; CVI(Counter Virtual Impactor): 5 - 80 µm; Hallett-Type Replicator; 3 - 100 µm). Since optically thin cirrus has obtained considerable interest due to increasing air traffic and its possible influence on the natural high level cloud cover we present a selected case of our measurements which has been analyzed with special emphasis on the characterization of small ice crystals and µm-sized hydrated aerosols. We interpret this case as a typical well documented example for a developing cirrus in an atmospheric environment which is influenced by emissions from air traffic. By use of computations with a doubling-adding radiative transfer model we determined the influence of the measured cirrus cloud including the hydrated aerosol on the radiation budget of the atmosphere.



**MI01/E/17-A1** **1720**

**A POSSIBLE LINK OF AEROSOL AND CLOUDS RADIATIONS TO ASIAN SUMMER MONSOON AND ITS IMPLICATIONS IN LONG RANGE FORECAST**

Toshiki IWASAKI (Geophysical Institute, Graduate School of Science, Tohoku University, Aoba-ku, Sendai, 980-8578, JAPAN, Email: iwasaki@wind.geophys.tohoku.ac.jp); Hiroto Kitagawa (Japan Meteorological Agency, Otemachi 1-3-4, Chiyodaku, 100-8122, JAPAN, Email: kitagawa@naps.kishou.go.jp)

1. Systematic errors of radiation budgets of JMA's global NWP model compared with satellite-derived TOA radiation, JMA's global NWP model considerably overpredicts absorbed solar radiation and outgoing long wave radiation over the continent though it predicts well their global means. Such errors are thought to come mainly from underprediction of clouds over the land and omission of aerosol effects in our model. Thus, we enhance model cloud over the land and introduce both parameterization schemes of direct and indirect effects of aerosols.
  2. Impacts of the modified parameterization scheme on forecasts of Asian summer monsoon. A series of one month forecast experiments for June, during which East Asian precipitation band migrates northward, has been performed to study systematic impacts of the modified parameterization scheme on Asian summer monsoon. The modified scheme reduces solar insolation over the land and suppresses heat low. As a result, the northward migration of East Asian fronts, the so-called Meiyu, Changma and Baiu, are considerably delayed. We can say that the model clouds and aerosols have significant impacts on forecast performance on Asian monsoon.
- Total optical thickness of cloud and aerosols even over the continents is not well known. We need intensive validation studies with observations to refine the cloud diagnostic or prognostic schemes and aerosol schemes.
3. Influence of other physics schemes on forecast performance of Asian summer monsoon. The monsoon formation is related to many diabatic processes. The control model has a systematic error of delay in the seasonal march of East Asian monsoon. The modified scheme further delays the seasonal march, although it improves model radiation budgets. Thus, we are studying the impacts of other physical processes on Asian summer monsoon, particularly of deep cumulus convections.

**MI01/W/05-A1** **1740**

**AN EXPERIMENTAL EVIDENCE OF THE INDIRECT AEROSOL EFFECT ON CLIMATE**

LOTHAR SCHÜLLER 1, Jean-Louis Brenguier 2, René Preusker 1, Jürgen Fischer 1 and Hanna Pawlowska 2, 1 Institut für Weltraumwissenschaften, Freie Universität Berlin, Fabeckstr. 69, 14195 Berlin, Germany, 2 Météo-France, (CNRM/GMEI), 42 av. Coriolis, 31057 Toulouse Cedex 01, France

The enhancement of the reflection of solar radiation as a result of light scattering at aerosol particles is referred to the direct effect of aerosols on climate, however, the indirect effect of aerosols on cloud microphysics and thus on reflected radiation leads to an overall cooling in the atmosphere, which is expected to be more important. The Twomey effect is the chain of processes: anthropogenic aerosol production, increased number of cloud condensation nuclei (CCN), smaller but more numerous cloud droplets and a larger ability to reflect solar radiation back to the sky. To reduce the large uncertainties in quantifying the overall effect on the global radiation budget (estimates range between 0 and  $-1.5 \text{ Wm}^{-2}$ ) more sophisticated observation techniques using radiance measurements from airborne instruments or satellites are required. In this study, we modified existing methods to derive cloud microphysical and optical properties from measurements in the visible and near infrared spectral range. The new approach is to focus on the cloud droplet concentration  $N_d$  rather than the cloud droplet radius as the most relevant parameter which determines the reflectivity of a cloud layer.  $N_d$  can be related directly to the changes in cloud microphysics, induced by an increase in cloud condensation nuclei (CCN), whereas the remotely sensed droplet radius is also dependent on the geometrical thickness of the cloud layer. Radiative transfer simulations of clouds with constant  $N_d$  and vertically variable droplet size has been performed to analyse measurements of the reflected radiation during the second Aerosol Characterisation Experiment (ACE 2) in 1997. The Twomey effect was clearly observed: a stratocumulus within a clean air-mass with low aerosol loading showed significant lower reflectivity than a stratocumulus of comparable vertical extension under a polluted environment. Coincidentally, the measured reflectance corresponds to the simulations calculated with lower res. higher droplet concentrations. The retrieved droplet concentrations agree with in situ measurements performed inside the cloud layers.

**Tuesday 20 July AM**

Presiding Chair: T. Novakov (LBNL, Berkely, USA)

**AEROSOLS AND RADIATION**

**MI01/E/07-A2** **Invited** **0930**

**AEROSOL SOLAR RADIATIVE FORCING OVER THE INDIAN OCEAN**

V. RAMANATHAN, W.C. Conant, Xu Li-Jones, I.A. Podgorny, K. Rajeev, and S.K. Satheesh (all at Scripps Institution of Oceanography, University of California, San Diego, 9500 Gilman Drive, La Jolla, California 92093-0021, USA, Email: vramanathan@ucsd.edu)

The first field phase of the Indian Ocean Experiment (INDOEX), which was conducted during January to March 1998, collected aerosol chemical, microphysical and column radiative properties from the surface, ship and from satellites. These data were synthesized to obtain the surface and the column aerosol solar radiative forcing on regional scales over the Arabian sea, Bay of Bengal and the equatorial Indian ocean. The aerosol solar radiative forcing is defined as the change in the solar radiative fluxes due to the presence of the aerosols. The synthesis is based on a detailed aerosol-radiation model that is consistent with the in-situ chemical data, vertical Lidar data and column spectral optical data. This model was used to obtain surface and top-of-the-atmosphere radiative forcing and separate the contribution to the forcing from sulfates, soot, mineral dust, sea salt and nitrates. Furthermore the model was also validated with satellite radiation budget data from CERES on board the TRMM satellite. This aerosol-radiation model was then used to develop bi-directional models for retrieving aerosol optical depths from the NOAA AVHRR satellite radiances. The retrieved optical depths were validated with ship and island sun-photometer optical depths over the Indian ocean. Lastly, the optical depths were combined with satellite radiation budget data and the aerosol-radiation model to obtain regional aerosol radiative forcing; these estimates are then compared with values determined directly from observations over selected locations.

It is shown that, during the north east monsoon period, significant amount of anthropogenic aerosol is transported from the sub-continent into the tropical Indian ocean, with aerosol visible optical depths ( $\tau_v$ ) ranging from about 0.3 in the Northern Arabian sea to values as high as 0.2 in the equatorial Indian ocean. Spatial gaps in the ITCZ are frequent enough that, aerosols are transported into the southern hemisphere tropical Indian ocean. The clear sky aerosol radiative forcing at the top-of-the-atmosphere is about  $-2 \text{ Wm}^{-2}$  per 0.1 increase in  $\tau_v$  and about a factor of three larger in magnitude at the surface. Soot and mineral dust aerosols are

the reason for the amplification of the forcing at the surface. The solar forcing values change in sign in the presence of clouds. The magnitude of the derived aerosol solar forcing values are separated into the contributions from the individual species and then compared with GCM predictions of the aerosol climate forcing.

**MI01/W/22-A2** **1000**

**IMPACT OF AEROSOLS ON THE SPECTRAL SOLAR IRRADIANCE AT THE SEA SURFACE DURING INDOEX**

Meywerk, J. (Scripps Institute of Oceanography, 9500 Gillman Dr., 230 La Jolla, CA 92037 USA, Email: jens@fiji.ucsd.edu)

During the First Field Phase (FFP) of the Indian Ocean Experiment (INDOEX) in February and March, 1998, the spectral global and direct beam irradiance have been measured between 350 and 1050 nm wavelengths using a 512 channel, fixed grating, photodiode array spectroradiometer. A detailed analysis of the instrument's reliability, the absolute calibration, and the corrections for deviation from the cosine response are presented. For most of the spectral region the total uncertainty is shown to be less than 2%. The changes in spectral and 400-700nm integrated irradiance are investigated for the global, direct, and diffuse portion of the solar spectrum reaching the ocean surface. For the aerosols in the Indian Ocean area the solar spectrum reaching the sea surface has been considerably modified. Comparing spectra from very clean regions south of the ITCZ with those measured within the range of influence of the Indian subcontinent show not only strongly decreasing direct beam irradiance accompanied with increasing diffuse irradiance, but also a remarkable spectral signature due to the existing aerosols. The direct beam spectral maximum is shifted to longer wavelengths due to the aerosol influence on the solar radiation - a combination of scattering and absorption of these aerosols. By comparing highly aerosol contaminated measurements with clean air radiative properties an anthropogenic climate forcing for these aerosols of  $-10 \text{ Wm}^{-2}$  was found for the given region and time period. These observed changes in the spectral solar irradiance together with decreased totally available solar energy will probably change the biomass production of the ocean.

**MI01/E/08-A2** **1020**

**GLOBAL DIRECT RADIATIVE FORCING DUE TO MULTICOMPONENT ANTHROPOGENIC AND NATURAL AEROSOLS**

Mark Z. JACOBSON (Dept. of Civil & Environmental Engineering, Terman M-13, Stanford University, Stanford, California 94305-4030, USA, Email: jacobson@ce.stanford.edu)

Results from the first global study of the solar plus infrared direct forcing due to the combination of all important anthropogenic and natural aerosol constituents in the atmosphere are discussed. Aerosol concentrations were constrained by observations to the greatest extent possible. In the presence of clouds, calculated tropopause forcings due to anthropogenic aerosols and all aerosols were  $-0.51 \pm 0.2$  and  $-1.6 \pm 0.5 \text{ W m}^{-2}$ , respectively. Natural chloride and its hydrated water in sea spray caused a net forcing of  $-0.62 \pm 0.3 \text{ W m}^{-2}$ , greater than that of any other natural aerosol constituent. Sodium, potassium, calcium, and magnesium caused positive forcing due to their interactions with solids.  $\text{SiO}_2(\text{s})$  was the dominant forcing component in soil particles. Clouds reduced the magnitude of forcing of all aerosol constituents. The treatment of elemental carbon as core material enhanced the magnitude of its positive forcing. The treatment of UV absorption by organic material slightly reduced the magnitude of its negative forcing. The inclusion of only a few aerosol constituents in a climate model will cause errors in climate model predictions.

**MI01/W/11-A2** **1100**

**A NEW PARAMETERIZATION SCHEME FOR AEROSOL OPTICAL PROPERTIES AND CCN CONCENTRATIONS FOR USE IN GCMs.**

Alf KIRKEVÅG, Trond Iversen, and Jon Egill Kristjansson (all at Department of Geophysics, University of Oslo, P.O. BOX 1022 - Blindern, 0315 Oslo, Norway)

The scheme which is outlined enables table interpolations to be carried out to yield the aerosol single scattering albedo, asymmetry factor, extinction coefficient and specific extinction coefficient. For supersaturated conditions, concentrations of cloud condensation nuclei (CCN) are estimated. Input parameters are: process attributed concentrations of BC and sulphate, ambient relative humidity or supersaturation, and a set of parameters determining the background aerosol size distribution and composition. The scheme is employed in a stand-alone version of the radiation module of the NCAR CCM3. Questions concerning CCN and the indirect effect will be addressed, but our main focus will be on direct effects from particulate sulphate and black carbon (BC), mixed internally and externally with the prescribed background aerosol.

Early results for hemispheric calculations for clear sky conditions in April show large regional differences. The direct forcing due to anthropogenic sulphate and fossil fuel BC ranges from  $-7 \text{ Wm}^{-2}$  (cooling) in eastern Europe (and  $-3 \text{ Wm}^{-2}$  in eastern USA), up to  $1.7 \text{ Wm}^{-2}$  (warming) near the large cities in western USA. Also areas (with high ground albedo) in North Africa, Asia and the Arctic experience some warming, up to  $0.5 \text{ Wm}^{-2}$ . The results, especially in the Arctic, are somewhat sensitive to the background aerosol distribution. The sensitivities to assumed aerosol and cloud vertical distribution, relative humidity, time of year, and to assumptions on the treatment of added sulphate, BC and OC, will also be examined.

**MI01/W/08-A2** **1120**

**DIRECT FORCING BY SULPHATE AEROSOLS IN CLOUDY SKIES**

ELEANOR HIGHWOOD (Department of Meteorology, University of Reading, UK)

Considerable uncertainty remains in the estimation of the direct climatic impact of aerosols. Reducing this uncertainty is a key aim of aerosol-climate studies. While much of the uncertainty arises from inadequate knowledge of the spatial and temporal distribution of aerosols, there is considerable variability in the methods of calculating radiative forcing itself. In particular, previous studies have disagreed on the importance of the direct radiative forcing in cloudy skies. Zenith angle dependence of radiative forcing is expected to be important where inhomogeneous cloud layers are present and this differs significantly between models, largely due to different treatment of the phase function. In this study the zenith angle dependency of aerosol forcing in two radiative transfer models is compared, initially for clear skies. The second part of the study uses simple representations of inhomogeneous cloud layers to investigate the contribution to aerosol radiative forcing from cloudy regions in each model.



**MI01/W/26-A2 1140****DETERMINATION OF THE AEROSOL SIZE DISTRIBUTION FROM SPECTRAL INTERPOLATED EXTINCTION COEFFICIENTS**

Ghislain FRANSENS (Belgian Institute for Space Astronomy, Email: ghislain.franssens@oma.be)

We propose a new method to determine the aerosol size distribution from aerosol spectral extinction measurements. It is applicable to spherical particles and is based on the Anomalous Diffraction Approximation. Our method solves the spectral extinction interpolation problem and solves the inversion problem as a by-product. The extinction interpolation uses a linear combination of carefully designed basis functions, each possessing the correct spectral behaviour of an extinction function. The expansion coefficients are obtained by minimising a fitting cost function, using a Generalized Reduced Gradient Method, with constraints. The method has been specifically designed so that it can be applied to sparse and noisy data. A number of numerical test examples and applications to real data will be shown.

**MI01/W/06-A2 1200****COMPARISON OF COMPUTED AND MEASURED OPTICAL PROPERTIES OF CONTINENTAL AEROSOLS IN WYOMING**

Ziguang Han, Derek C. MONTAGUE, and Jefferson R. Snider (all at Department of Atmospheric Science, Box 3038, University of Wyoming, Laramie, WY 82071-3038, USA, Email: montague@uwyo.edu)

Airborne observations of boundary layer (30 - 50 m agl) and free tropospheric aerosols (5400 m msl) were obtained using the Wyoming King Air, over the Green River Basin and Red Desert regions of southern Wyoming, USA, in late February and March, 1996. Light absorption and scattering extinction by aerosols were characterized using an aethalometer and a single wavelength (550 nm) nephelometer, respectively. Filter samples collected on board the aircraft, enabled the averaged mass loading and chemical composition of the aerosol to be determined, and hence its averaged refractive index to be estimated, for each flight. The refractive index values were used to carry out post-flight recalibrations of the measurements made with a Passive Cavity Aerosol Spectrometer Probe (PCASP) and a Forward Scattering Spectrometer Probe (FSSP), thereby allowing corrected particle size distributions and number densities to be determined, from which aerosol scattering extinction coefficients were computed, using Mie scattering theory, for comparison with the nephelometer data. In addition, combination of the scattering data with that for aerosol absorption, has allowed estimates of aerosol total extinction and single scattering albedo to be made, for both dry and wet aerosol. The scattering extinction coefficients have been examined in the context of both geographical location and altitude, as have correlations of the aerosol characteristic parameters with observed meteorological variables, local particulate sources, and measured trace gas mixing ratios. A summary of the results of these analyses will be presented.

**Tuesday 20 July PM**

Presiding Chairs: V. Ramanathan (Centre of Atmospheric Sciences, Scripps Institution of Oceanography, UCSD, USA)

D.L. Roberts (Hadley Centre for Climate Pred. And UK Meteorological Office, Berkshire, UK)

**AEROSOLS AND RADIATION****MI01/E/14-A2 Invited 1400****FUTURE SULPHATE AEROSOL DISTRIBUTIONS SIMULATED USING A CLIMATE MODEL**

Margaret J Woodage and DAVID L ROBERTS (Hadley Centre for Climate Prediction and Research, Meteorological Office, London Road, Bracknell, Berkshire, RG12 2SY, UK.)

The Hadley Centre climate model incorporates a fully-interactive sulphur cycle scheme which represents the emissions and large-scale advection of sulphur species, vertical transport by convection and boundary layer turbulence, and dry and wet deposition. Sulphur chemistry is parameterized using oxidant fields generated by a separate Lagrangian chemistry model (STOCHEM) as boundary conditions. The direct radiative forcing implied by the simulated sulphate aerosol distribution can be diagnosed using the model's radiation code, developed by Edwards and Slingo. In this study, the model will be used to investigate the impact of future changes in anthropogenic sulphur dioxide emissions, using recently devised emission scenarios. The sensitivity of the simulation to alterations in model parameterizations will also be explored.

**MI01/W/25-A2 1430****REGIONAL STUDIES OF RADIATIVE FORCING OF SAHARAN DUST USING TOMS AND ERBE DATA**

CHRISTINA HSU (Raytheon ITSS, Lanham, Maryland 20706, USA, email: hsu@wrabbit.gsfc.nasa.gov); jay herman (Code 916, NASA/Goddard, Greenbelt, Maryland, USA, email: herman@tparty.gsfc.nasa.gov)

Climate forcing due to tropospheric aerosols has gained increasing attention in recent years. In order to understand the role of aerosols such as Saharan dust in the radiative balance, we have combined measurements of dust loading derived over both land and ocean from TOMS (Total Ozone Mapping Spectrometer) with measurements from ERBE (Earth Radiation Budget Experiment) of the top-of-the-atmosphere (TOA) upward flux. In doing so, we've been able to estimate the effect of Saharan dust on the longwave and shortwave TOA fluxes. The changes in the TOA upward flux in response to the characteristics of aerosols will be discussed using these satellite measurements and radiative transfer model simulations. Since there is a significant change in the Saharan dust layer height from the winter to summer season, the observed effect of this altitude difference on the longwave TOA flux will also be addressed. Such studies are important in understanding the radiation budget on a regional scale.

**MI01/E/20-A2 1450****BLACK CARBON AEROSOL IN THE ATMOSPHERE IN BEIJING**

WANG GENGCHEN, Gu Zhifang, Kong Qinxin, Liu Guangren (Institute of Atmospheric Physics, Academia Sinica, Deshennmenwai Road, 100029, Beijing, China, email: wanggc@mim.cnc.ac.cn); Emilenko Alexander S. (Institute of Atmospheric Physics, Russian Academy of Sciences, 109017, Moscow, Zh-17 St. Pyzhevsky, 3, Russia)

Beijing, as one of the biggest cities in China, is seriously polluted at present time mainly by industrial emission and machine exhaust. The particulate carbon in the atmosphere is originated mainly by incomplete combustion of carbonic fuel and has a important effect on both air quality and physical, chemical and optical processes in the atmosphere. Concentration of the black carbon aerosol (BCA) and its variation characteristics in the atmosphere in Beijing are

discussed in this paper. Measurement results obtained for the last 3 years show a quite large variation of BCA concentration in the atmosphere in dependence on intensity of emission sources and the meteorological condition. In favourable conditions, 0.1 ug/m<sup>3</sup> of the BCA and 20 ug/m<sup>3</sup> of the total suspended particles (TSP) are observed as their background values, respectively, for Beijing city, while under some unfavourable meteorological conditions, especially in period of the later autumn and early winter when the city heating supply started, the daily average BCA is observed as high as 23 ug/m<sup>3</sup> in the atmosphere. In the most case of BCA diurnal variation, two peaks of the BCA concentration are observed, that are: maximum BCA concentration appears in the local time intervals of 7h - 10h and 20h - 24h. Variation behaviours for both TSP and BCA are quite consistent, that demonstrate the same sources of TSP and BCA for Beijing at present time.

**MI01/W/07-A2 1510****RADIATIVE FORCING OF VOLCANIC ERUPTIONS**

Claudia TIMMRECK and Hans-F. Graf, (Max-Planck-Institut fuer Meteorologie, Bundesstr.55 Hamburg, D-20146 Germany, email: timmreck@dkrz.de, graf@dkrz.de)

Major volcanic eruption have significant impact on stratospheric and tropospheric climate and circulation. Enhanced radiative heating caused by the aerosol absorption of solar and terrestrial radiation changed stratospheric temperature and circulation.

Using the stratospheric mesospheric version of the Hamburg climate model MA/ECHAM4, we performed interactive and non-interactive simulation with prognostic volcanic aerosol. The volcanic aerosol is described with the global sulfate mass (SO<sub>4</sub><sup>2-</sup>), while for the radiative calculation a mean volcanic size distribution is assumed with a mode radius  $r_m$  of 0.3  $\mu$ m and a standard deviation  $s$  of 1.5. For the current study, a sulfur cycle is coupled to the meteorological model, which takes into account the oxidation pathways of sulfur dioxide (SO<sub>2</sub>) and the removal processes of SO<sub>2</sub> and SO<sub>4</sub><sup>2-</sup> in the troposphere. Here model results for a Pinatubo like tropical and a major midlatitude eruption are presented. The climate effects of the two different volcanic disturbances will be discussed for the stratosphere and for the troposphere. The discussion includes the radiative forcing, the lifetime of the disturbance in the stratosphere and temperature effects in the lower troposphere. The model results will be compared to observations after the Mt. Pinatubo eruption (as example for a tropical volcano) and for the Laacher See (13.000 B.P) and the Katmai (1911) eruptions (midlatitude NH).

**MI01/W/20-A2 1640****THREE-DIMENSIONAL SIMULATION OF STRATOSPHERIC AEROSOL**

Claudia TIMMRECK, Johann Feichter and Hans-F. Graf, (Max-Planck-Institut fuer Meteorologie, Bundesstr. 55, Hamburg, D-20146 Germany, email: timmreck@dkrz.de, feichter@dkrz.de, graf@dkrz.de)

Stratospheric aerosol has various effects on the global climate system. It changes the chemical composition of the atmosphere due to heterogeneous reactions and disturbs the radiative balance.

Therefore, a sulfuric acid aerosol model has been implemented in the global climate model ECHAM4. This model treats the formation, the development and the transport of stratospheric sulfuric acid aerosol. The size distribution and the weight percentage of the aerosol is calculated dependent on the H<sub>2</sub>SO<sub>4</sub>/H<sub>2</sub>O-concentration, temperature and pressure in a size range between 3  $\cdot 10^{-4}$   $\mu$ m and 6.2  $\mu$ m. Homogeneous nucleation, condensation (evaporation), coagulation, water-vapor growth, sedimentation and sulfur chemistry are included. The microphysical model is combined with a tropospheric sulfur cycle. This sulfur cycle treats the natural and anthropogenic emissions, chemistry, dry and wet deposition and chemistry of DMS, SO<sub>2</sub> and SO<sub>4</sub><sup>2-</sup>. Globally and seasonally different SO<sub>2</sub>- and SO<sub>4</sub><sup>2-</sup>-sources for stratospheric aerosol can therefore taken into account.

Results of a multiyear simulation show that the stratospheric aerosol distribution is mainly determined by the aerosol flux from the troposphere. The formation of new particles through homogeneous nucleation takes place in the tropical lower stratosphere and upper troposphere and in polar spring. The aerosol surface area density and the aerosol mass concentration represent lower stratospheric background conditions quite well. Effective radius and aerosol mixing ratio agree with satellite and in situ measurements. The SO<sub>2</sub> and H<sub>2</sub>SO<sub>4</sub> concentrations are also in good agreement with observations.

**MI01/E/22-A2 1700****A MESOSCALE STUDY OF A DESERT PLUME OVER WEST AFRICA AND EASTERN ATLANTIC : RADIATIVE IMPACT**

Olivier CHOMETTE and Michel Legrand (Laboratoire d'Optique Atmosphérique, Université des Sciences et Technologies de Lille, 59655 Villeneuve d'Ascq, France, email: legrand@loa.univ-lille1.fr); Guy Cautenet and Fredric Pradelle (Laboratoire de Météorologie Physique, Université Blaise Pascal, 63170 Aubière, France, email: cotenet@opgc.univ-bpclermont.fr)

Desert dust is generated by wind erosion of the unprotected arid surfaces of the Saharan desert and its borders. About 0.7 GT (d'Almeida-1985) of Saharan dust is mobilized each year in this way. Then dust is transported over large distances, as far as America and Europe. At last it settles by gravitation (dry deposit) or after being scavenged by rain (wet deposit).

The spatial extension and the high frequency of occurrence of dust plumes is such that they have a significant effect on the global climate through their direct impact on the radiative budget of the Earth-Atmosphere system.

The simulation of mobilization, transport and deposition of dust, and of its radiative impact has been carried out. The model used is the CSU RAMS for the mesoscale transport, in association with a new physical dust emission scheme, a dry deposition module, and a radiative code. We present results for a case study which occurred at the beginning of May 1997. Dust was generated by sources located in the Western Sahara and transported westwards up to the Atlantic Ocean, beyond the Cape Verde Islands. The radiative impact is especially addressed in the presentation. Validations are made through remote sensing measurements acquired from the ground by sunphotometry and from space by satellite data (with both land and ocean coverages).

**MI01/W/19-A2 1720****PREDICTION OF AEROSOL OPTICAL PROPERTIES FROM PHYSICAL AND CHEMICAL MEASUREMENTS IN CANBERRA, AUSTRALIA**

YOSHITERU IINUMA and Gail P Box (both at Atmospheric Group, School of Physics, The University of New South Wales, Sydney, NSW, 2052, Australia, e-mail: iinuma@newt.phys.unsw.edu.au, gpb@newt.phys.unsw.edu.au) John Gras, Melita Keywood and Greg Ayers (all at CSIRO Atmospheric Research, PMB1, Aspendale, Vic, 3195, Australia, e-mail: john.gras@dar.csiro.au, mzk@dar.csiro.au, greg.ayers@dar.csiro.au)

Detailed information on the optical properties of aerosol particles is essential for assessing or predicting the effects of aerosol on air quality and visibility degradation. Successful prediction of aerosol refractive index using observed or modelled size-resolved chemical composition data is a key step towards the determination of extinction of light by aerosol particles. Properties of the winter aerosol in Canberra, Australia were measured during a field campaign in 1997 using a suite of instruments. These included a PMS ASASP-X laser size spectrometer for number concentration, nephelometers for the integrated scattering coefficients at 530 nm, a MOUDI sampler for chemical and mass size distributions and a TEOM mass balance for fine particle loadings (Daero < 2.5  $\mu\text{m}$ ). In this study we demonstrate the application of a thermodynamic equilibrium model and observed size-resolved composition for the estimation of mean aerosol refractive index and density. This data set allows a variety of tests of "closure" between predicted and observed aerosol optical and gravimetric properties that will be discussed.

**MI01/W/10-A2**

**1740**

**ATMOSPHERIC AEROSOL OPTICAL AND PHYSICAL PROPERTIES USING MULTIFILTER ROTATING SHADOWBAND RADIOMETER IN SYDNEY, AUSTRALIA**

Ghassan TAHA and Gail P. Box, (both at School of Physics, University of New South Wales, Sydney, Australia, 2052, email: gmt@newt.phys.unsw.edu.au, gpb@newt.phys.unsw.edu.au)

The aerosol optical depth of the atmosphere was obtained using ground-based Multifilter Rotating Shadowband Radiometer to monitor the global, diffuse and direct components of solar irradiance measurements. The columnar size distribution of aerosol particles was retrieved using Analytic Eigenfunction Theory. The correlation between the column and surface properties of aerosols, and the effect of humidity on the growth of aerosol particles are important for both aerosol modelling, and radiative forcing. For this purpose, the ambient optical depth was correlated with the scattering coefficient measured by an integrating nephelometer, and with the mass concentration of a PM10 TEOM. Local meteorological parameters were also investigated, in order to explain the aerosol variability, and its source, as well as giving some indication about its vertical distribution. Some results from this ongoing study in Sydney, including seasonal and diurnal variation of the aerosol will be presented, and discussed here.

**Wednesday 21 July AM**

Presiding Chair: W.R. Leaitch (Atmospheric. Env. Service (AES), Ontario, Canada)

**AEROSOLS, CLOUDS AND RADIATION**

**MI01/W/02-A3**

Invited

**0900**

**PROPERTIES AND DISTRIBUTION OF CARBONACEOUS AEROSOLS.**

T. NOVAKOV, T. Kirchstetter, C. Corrigan, Lawrence Berkeley National Laboratory, Berkeley CA 94720, USA

In contrast to sulfate and other inorganic aerosols our knowledge of sources, spatial and temporal concentrations, optical and nucleation properties of chemically complex carbonaceous aerosol component is largely inadequate and fragmentary. In this paper we present the results of our survey of existing measurements pertaining to carbonaceous aerosols performed over the past 20 years in various regions of the globe. Specifically, we examine the geographical and temporal distributions of reported mass concentrations of black (BC) and organic carbon (OC), the relative contributions of these and inorganic species to aerosol mass, supplemented by information on chemical and physical properties of these species. A simple compilation, however, of results from existing field measurements is not sufficient because the reported concentrations may be influenced by method and sampling dependent artifacts which, if unaccounted for, may either over- or underestimate the actual concentrations. Consequently, evaluation of uncertainties is important because these may be large enough to render some of the reported concentrations unacceptable for achieving either mass or radiative closure. In this work we are using the results of our laboratory and filed measurements to estimate the likely uncertainties in the reported data. The results to be presented should be useful in identifying global regions where useful data exists and regions where there is a severe lack of data.

**MI01/P/03-A3**

**0930**

**AN OBSERVATIONAL ASSESSMENT OF COOLING TREND IN SOUTH-EASTERN U.S.: ROLE OF SULFATE VERSUS CARBONACEOUS AEROSOLS**

V.K. Saxena (Cloud-Aerosol Interactions Lab (CAIL), North Carolina State University, Raleigh, NC 27695-8208, USA; email: saxenageos.ncsu.edu)

We have analysed the regional patterns of climate change in the south-eastern U.S. during the period 1949-94. The results indicate that a cooling trend, albeit very mild, is discernible during these 46 years. One of the explanations for such a trend may be found in the direct and indirect radiative forcing of both natural (such as Mount Pinatubo volcanic emissions) and anthropogenic aerosols (such as those transported from the Ohio River Valley) affecting the region. Using the data from Mount Mitchell, North Carolina (2,038 m masl, at 35°44' 05" N and 82°17' 15" W) for sulfates and soot, we have arrived at the following findings:

1. The sulfate concentrations were greater during 1993-97 when compared to those during 1986-89.
2. Cloud albedo retrieved from satellite data and calculated from surface observations does not indicate a monotonic increase with higher sulfate concentrations.
3. Based on the wintertime sulfate concentrations, the local direct forcing calculated for marine, continental and polluted urban air masses is -0.30, -0.44 and -0.70 W m<sup>-2</sup> respectively. Similar calculations based on the soot concentrations yielded +0.1 W m<sup>-2</sup> approximately for all the three air masses.
4. The direct and cloud-mediated radiative forcing effects due to sulfate aerosols are assessed to be -4.8 and -4.0 W m<sup>-2</sup>. These values far exceed the current model predictions.

**MI01/W/17-A3**

**0950**

**EFFECT OF ABSORBING AEROSOLS ON INDIRECT AEROSOL FORCING**

Catherine C. CHUANG (Lawrence Livermore National Laboratory, Livermore, CA 94550, USA, email: chuang1@llnl.gov) Joyce E. Penner (University of Michigan, 12455 Hayward St., Ann Arbor, MI 48105, email: penner@umich.edu) Keith E. Grant (Lawrence Livermore National Laboratory, Livermore, CA 94550, USA, email: keg@llnl.gov)

To properly evaluate the effects of aerosols on clouds and thereafter to estimate the magnitude of the indirect aerosol forcing, one must include the effect of absorbing aerosols on radiative properties of clouds. We have modeled this effect through modification of the refractive index for a droplet/soot mixture using the effective medium approximation together with the Maxwell

Garnett mixing rule. Given the refractive index for the droplet with embedded soot particles, we approximated the single scattering albedo of a drop using geometric optics. In practice, these approximations fail to be true for typical soot inclusions in water drops (volume fraction of soot within drop ~ 10<sup>-7</sup>) in the wavelength region > 2 micrometer. Fortunately, in this region absorption by water dominates that by soot, so that a smooth fit between the albedo predicted above and that from pure water provides a sufficiently accurate approximation.

These approximations have been incorporated into our global climate model for inclusion in the evaluation of the indirect forcing by absorbing aerosols. Results from this improved radiation code have shown lower indirect cloud forcing by carbonaceous aerosols than simulations without considering effect of absorbing aerosols on the single scattering albedo of clouds.

**MI01/W/16-A3**

**1010**

**GCM TESTS OF A NEW PARAMETERIZATION FOR CCN CONCENTRATIONS**

JÓN EGILL KRISTJÁNSSON, Alf Kirkevåg, Øyvind Seland and Trond Iversen Department of Geophysics, University of Oslo, P.O.Box 1022, 0315 Oslo, Norway

Recently Kirkevåg and Iversen developed a new parameterization scheme describing aerosol size distributions, subject to diffusion, coagulation and in-cloud oxidation, as functions of relative humidity. The scheme treats anthropogenic sulfuric and black carbon aerosols, in addition to a "background" consisting of various hygroscopic and hydrophobic particles. The parameterization scheme was designed for use in global models and consists of look-up tables of aerosol radiative properties in subsaturated air. Supersaturated conditions are also considered in which case the scheme provides concentrations of cloud condensation nuclei. We here present the first results from the implementation of this parameterization into a version of the global climate model NCAR CCM3, which carries prognostic cloud water. The release of precipitation in warm clouds is a function of the cloud droplet number concentration, which has separate prescribed values over land and over ocean. This represents our "control run" in the experiments that follow. We then replace the prescribed CCN by the output of the above parameterization scheme. The distribution of sulfuric and black carbon aerosols globally and in the vertical is obtained by running a life-cycle scheme recently developed by Seland and Iversen within the CCM3. The spatial distribution of background aerosols is based on literature estimates.

A number of sensitivity runs have been conducted with the model, as guidance for future model development. In these experiments we have e.g., looked at the sensitivity to the criteria for cloud formation. The simplest approach is to prescribe a "supersaturation threshold", which then determines the CCN concentration in a grid box, but alternative approaches are also considered.

We also investigate the sensitivity to assumptions on some aspects of the aerosols, such as spatial distribution, size distribution, and hygroscopicity. In some cases single-column model results are used as supplement to results from the full GCM simulations.

**MI01/L/04-3**

Invited

**1055**

**INSIGHTS INTO AEROSOL DISTRIBUTIONS AND RADIATIVE FORCING FROM ACLIMATE MODEL WITH ON-LINE SIZE-DISTRIBUTED AEROSOLS (NARCM)**

L.A. BARRIE, J.P. Blanchet, P. Chylek, R. Hoff, G.Lesins, S.L. Gong, M.Lazare, R. Leaitch, H. Leighton, H. Lin, U. Lohmann, N. McFarlane, N.O'Neill and A. Royer, K. von Salzen and L. Spack

A government/university effort in Canada is underway to put size-distributed aerosols into Canadian climate models (global and regional). It is intended that eventually a Canadian size-distributed aerosol modelling capability is developed by: (1) incorporating size-distributed aerosols processes in the models (2) simulating the spatial-temporal distributions of major aerosol types and checking with observations, (3) linking aerosols actively with clouds and atmospheric radiation, and (4) assessing the role of aerosols in climate processes. Currently, two natural aerosol types (sea salt and biogenic sulphur) as well as two anthropogenic aerosols (sulphate and black carbon) are modelled using a 12 size bin sectional model, off-line chemistry, an explicit cloud scheme, relative humidity dependent aerosol size and wet/dry aerosol removal processes. To date, steps (1) and (2) have been the focus of our effort. Next, we will begin to investigate the interplay between natural and anthropogenic aerosols in influencing the concentration and size distribution of atmospheric aerosols and hence their impact on direct and indirect radiative forcing. Highlights of the first two and a half years of this study are presented. In particular, the role of sea salt in influencing sulphate distributions will be discussed.

**MI01/E/13-A3**

**1125**

**STUDY ON THE CHARACTERISTICS OF AEROSOL OPTICAL DEPTH AND NUMERICAL SIMULATION OF AEROSOL RADIATIVE FORCING AND CLIMATE RESPONSE OVER CHINA**

LUO YUNFENG and Lu Daren (both at Institute of Atmospheric Physics, Chinese Academy of Sciences, Beijing, 100029, Email: lyf@linux2.iap.ac.cn) Zhou Xiuji and Li Weiliang (both at Chinese Acad. Met. Sci., Beijing, 100081)

Since pre-industrial times, the concentrations of tropospheric aerosols have been increasing obviously. Nowadays, with more attention to environment change and climate prediction, it is an urgent and important work to obtain aerosol's distribution, simulate its radiative forcing magnitude and finally study its climate response regionally and globally.

In this paper, by using the diurnal solar radiation and sunshine duration data of 47 solar observation stations in China from 1961-1990, as well as the TOMS version-7 ozone data, we retrieve the values of annual and monthly mean 0.75(m aerosol optical depth. Based on the results, we analyze the geographical distribution and temporal variation of aerosol optical depth in China. Then, we include aerosol radiative effect into the China Regional Climate Model (CRCM), and nest the CRCM into the NCAR CCM1 GenI

**MI01/P/02-A3**

**1145**

**STUDY OF OPTICAL AND PHYSICAL PROPERTIES OF HAZE AEROSOLS IN WINTER AT PUNE, INDIA**

P.C.S. DEVARA, P. E. Raj, R.S. Mahes Kumar and K.K. Dani (Indian Institute of Tropical Meteorology, Pune 411 008, India, email: devara@tropmet.ernet.in)

Atmospheric aerosols at Pune, a semi-arid station in India, exhibit unique features during winter months due to frequent low-level inversions and dust haze formations. Apart from the passage of air mass (rich in nuclei of continental origin) over the station, rapid fall in daily temperature, light surface winds, low relative humidity and incursion of aerosol particles due to combustion processes during these months make the study of aerosols more interesting and important. In order to investigate these distinct properties of aerosols, ground-based sunphotometer observations of direct solar radiation were carried out at the Indian Institute of Tropical

Meteorology (IITM), Pune (18°32'N, 73°51'E, 559 m AMSL), India on several cloud-free days during October 1998 - January 1999. These measurements obtained in different spectral bands were utilised to deduce columnar aerosol optical depth, size distribution and perceptible water vapour content. The aerosol optical depth was found to be large (more than double) on hazy days as compared to clear stable days. Size spectra of aerosols on hazy days show characteristic bimodal distribution with mode radii between about 0.1 and 1.0  $\mu\text{m}$ . Further increase in optical depths and drastic change in the size spectrum of aerosols were noticed during the occasions of smoke particles' emission from combustion processes in proximity to the experimental site and high water vapour content in the atmosphere. These aerosols during winter season at Pune reduce the solar radiation reaching the ground on cloud-free days and cause poor visibility. In this paper, we discuss the data retrieval procedures and explain the results in the light of transport of continental aerosol dust and trapping of surface-generated aerosols due to close-to-ground inversion during winter months at the observing station.

MI01/E/11-A3

1205

#### THE EVOLUTION OF AEROSOL PARTICLES IN A CLOUD-CAPPED MARINE BOUNDARY LAYER

SIMON R. OSBORNE, Douglas W. Johnson, Robert Wood (all at Meteorological Research Flight, Y46 Building, DERA Farnborough, Hampshire, GU14 0LX, UK, Email: sosborne@meto.gov.uk, dwjohnson@meto.gov.uk, robwood@meto.gov.uk)

Large uncertainties exist in the magnitude of the indirect forcing of aerosols on climate and so further measurements are required to elucidate the processes responsible for changes in the radiative properties of clouds. Parameterisations can then be developed for use in general circulation models.

Results presented show observations made upon the Meteorological Research Flight's C-130 aircraft during the second Aerosol Characterisation Experiment over the North Atlantic during June-July 1997. Measurements were made of the aerosol and cloud microphysics, the dynamic and thermodynamic characteristics, and trace gas chemistry within the marine boundary layer (BL) and lower free troposphere (FT) of a tagged column of air as it advected away from Portugal towards Tenerife. The aircraft followed the column of air over 3 back-to-back flights that covered a 29 h period of evolution.

Analysis shows that cloud processing of the aerosol was responsible for some of the modal changes in the aerosol size spectrum; an increase in the aerosol sulphate fraction and decrease in SO<sub>2</sub> substantiate this reasoning. However, the changes were complicated by entrainment of both polluted and clean aerosol from the FT, changes in the subsidence rate in the FT, and changes in the BL and cloud depths. The changes in the cloud microphysics were due to a combination of aerosol modification and BL dynamics.

MI01/P/01-A3

1225

#### GREENHOUSE WARMING VERSUS AEROSOL COOLING IN THE CONTEXT OF GLOBAL CLIMATE CHANGE

K.Ya. KONDRATYEV (Russian Academy of Sciences, Research Centre for Ecological Safety, 18 Korpusnaya St., 197110 St.Petersburg, Russia, email: nansen@online.ru)

I believe the time has come to reassess the situation in global climate studies from the viewpoint of priorities. Since it is doubtless true that global greenhouse warming may be compensated by aerosol cooling to a considerable extent, it is important to analyse the reliability of relevant estimates because the assumption of purely scattering aerosols is far from reality  $1/1$ . The results of complex CAENEX and GAAREX field programmes conducted in Russia have been considered in this context to demonstrate the significance of aerosol absorption. Also in this context, the case of Arctic haze deserves special attention. Another important aspect is the necessity to take into account the indirect aerosol impact on climate via changes in cloud optical properties. Since global climate modelling is still at an early stage of its development, the decisive role belongs to climate observations. The optimisation of the Global Climate Observing System (GCOS) with regard to combined use of conventional and satellite observations to solve climate dynamics problems in the context of global change is a must of current climate studies. Various aspects of this optimisation have been considered.

1. Kondratyev K.Ya. Climatic Effects of Aerosols and Clouds, Springer/Praxis, Chichester, 1999 (in print).

Monday 19 July AM

MI01/W/15-A1

Poster

0900-01

#### THE INVESTIGATION OF SPREADING OF AN AEROSOL CLOUDS IN ATMOSPHERE AND THEIR INFLUENCE ON THE CLIMATE

BIBILASHVILI, Tamar, Tbilisi State University, Email: sciteco@access.sanet.ge

In order to work out the models of aerosol spreading in the atmosphere and in the clouds the authors carried out the examinations of the formation and development of the artificial aerosol clouds formed by means of the explosion in the atmosphere. Experiments were carried out on the height of 3-6 km. The tension of the electric field, temperature humidity of the atmosphere have been registered by means of laboratory plane when flying through the artificial cloud. Geometrical sizes of the artificial cloud changed from 300-600m. Theoretical bases of modelling the spreading of aerosol clouds in the atmosphere have been worked out paralleled with it. Carried out numerical experiments and their comparison with the natural field experiments give the satisfactory result.

MI01/E/09-A1

Poster

0900-02

#### EFFECT OF CLOUD CONDENSATION NUCLEI ON THE OPTICAL PROPERTIES OF A LAYER CLOUD

Naomi KUBA, Kenichi Maruyama (both at Frontier Research System for Global Change, SEAVANS North BLDG. 7F 1-2-1 Shibaura Minato-ku Tokyo 105-6791, Japan, email: N.Kuba: kuba@frontier.esto.or.jp, K.Maruyama: maruyama@frontier.esto.jp), Hironobu Iwabuchi, Tadairo Hayasaka (both at Center for Atmospheric and Oceanic Studies, Tohoku University, email: H.Iwabuchi: buchi@caos-a.geophys.tohoku.ac.jp, T.Hayasaka: hayasaka@mail.cc.tohoku.ac.jp), and Takao Takeda (Institute for Hydrospheric-Atmospheric Sciences, Nagoya University, email: takeda@ihas.nagoya-u.ac.jp)

The influence of aerosol particles on the atmospheric radiative budget, especially the effect of cloud condensation nuclei (CCN) on the radiative properties of clouds, is one of the key issues to deeply understand and predict global climate change. The purpose of this paper is to quantitatively study the effect of CCN on the optical properties of a low-level layer cloud by numerically simulating. The vertical profile of the size distribution of cloud droplets, which form on the CCN and grow through condensation and coagulation processes is numerically simulated as accurately as possible. Our numerical model is an one-dimensional micro-physical model, in which the activation of CCN and the condensational growth of cloud

droplets in the layer near cloud base are computed in a Lagrangian framework to estimate the solution effect of CCN accurately and to avoid the artificial broadening of droplet size distribution. A special computational method is used for computing droplet size distribution in the middle and upper parts of a cloud, where the coagulation growth and sedimentation of droplets have a large influence on the change in droplet size distribution, to avoid the numerical diffusion of droplet size distribution. On the basis of the simulated vertical profile of the droplet size distribution, optical thickness, reflectivity, absorptivity and transmissivity of the cloud for short-wave radiation are computed by solving strictly radiative transfer equation, using a discrete ordinate method without any parameterization. It is widely understood that a cloud, which contains small cloud droplets in larger number concentration, has a tendency to show deeper optical thickness and larger reflectivity. In this paper, special attention is given to the sensitivity of cloud optical properties to the size distribution and constituents of the CCN and the velocity of an ascending air-current especially the number concentration of the activated CCN.

MI01/W/03-A1

Poster

0900-03

#### SIMULATING THE TRANSPORTATION OF SMOKE FROM A FOREST FIRE IN EASTERN, CANADA

H. Lin, W.R. Leitch, C.M. Banic, S.L. Gong, and L. Spacek (1). P. King, B. Stocks (2) Atmospheric Environment Service, 4905 Dufferin Street, Downsview, Ont. M3H 5T4, Canada, (1) Earth Sciences department, UQAM, Montreal, Que. H3C 3P8, Canada (2) Canadian Forest Service, 1219 Queen Street East, Sault Ste. Marie, Ont. P6A 5M7, Canada

Smoke originated from forest fires in Quebec, Canada (near 50N and 74W) was transported to the Canadian Maritime Provinces and Maine area on Aug. 22, 1995. Observations of the smoke plume were made at 44N and 66W, about 1000 km downwind of the source, in during the Radiation, Aerosol and Cloud Experiment (RACE 95). The measured aerosol properties include number concentration, size distribution, CCN concentration and major iron chemical composition was measured. The transport of the forest fire plume is studied using a Regional Climate Model coupled with a newly developed Canadian Aerosol Module (CAM). CAM is a size-segregated multi-component aerosol model simulating aerosol processes. It includes nucleation, condensation, coagulation, dry deposition and interaction with clouds as well as wet removal. The simulation has successfully been able to re-produce the observed transport pattern and vertical distribution of the smoke aerosol particles released from the location of the Quebec fires. We will present details of the simulation and comparison with the observations.

MI01/E/06-A1

Poster

0900-04

#### MODEL EVALUATION OF PARTICULATE CARBON IN MARINE AEROSOLS

Yulia LYUBOVITSEVA (Geophysical Center of RAS, 3, Molodezhnaya str, 117044 Moscow, Russia, email: lyubov@wdbc.rssi.ru)

Dimethylsulfide (DMS) is commonly recognized to be the major contributor to particulate nonseasalt sulfur. The conversion of DMS to sulfuric acid via the reaction with hydroxyl radical producing SO<sub>2</sub> and methylsulfonic acid (MSA). The subsequent transformation of sulfur dioxide is believed to produce additional sulfur containing cloud condensation nuclei. This path is well studied in contrast to the carbon path that was so far ignored as a producer of new aerosol particles. Meanwhile, some experiments indicate to the existence of the particulate carbon in the products of DMS destruction. This presentation reports on the evaluation of possible parameters of carbon containing aerosols that presumably form in the course of not yet well understood chemical and photochemical transformations of the oxidation products of DMS. The model used for the evaluation assumes that DMS is emitted by the ocean surface, then diffuses (turbulent diffusion is implied) in the atmosphere. The production of carbon containing precursors is supposed to be proportional to the rate of the DMS+OH process. Low volatile gaseous products are then assumed to nucleate (nonbarrier nucleation is considered) and to condense onto the surfaces of sea salt particles. An interplay of these two processes defines the concentration of newly born carbon containing aerosols. The latter is shown to be able to reach 10000 particles per cubic centimeter.

MI01/E/15-A1

Poster

0900-05

#### ORGANIC COMPOUNDS AND NONSEASALT SULFATE IN MARINE AEROSOL

Yulia LYUBOVITSEVA (Geophysical Center of RAS, 3, Molodezhnaya, 117044 Moscow, Russia, email: lyubov@wdbc.rssi.ru)

Main sources, size distributions of organic components (including MSA, its salts) and nonseasalt SO<sub>4</sub> are discussed on the basis of fractional analysis of IR absorption spectra of aerosol samples collected over different region of the Pacific and Atlantic oceans. Basic attention is given to the analysis of samples collected over remote region with high biological productivity where the oxidants of DMS emitted from sea water define considerably the chemical composition of submicron aerosols overoceans. Maximal presence of the organics is observed in aerosols collected over remote oceanic areas with high concentration of primary organics and phytoplankton whose activity is directly linked to vertical streams exerting intense water mixing. The fractional analysis of the IR spectra evidences in favour of heterogeneous condensation of DMS oxidants onto sea-salt particles. The presence of bands of other organic compounds (intense bands of CH<sub>2</sub>, CH<sub>3</sub> groups etc) pushes to the assumption on possible contribution to the particulate organics from two other sources: 1. organic hydrosol-aerosol transition and 2. Particles originated from slicks highly enriched with surface active hydrophobic organics like fatty acids, high alcohols etc. As a rule, in the particles collected over remote regions of the Pacific ocean low concentration of (NH<sub>4</sub>)<sub>2</sub>SO<sub>4</sub> are observed in contrast to highly polluted areas of the Atlantic ocean where the main component of the nonseasalt SO<sub>4</sub> is (NH<sub>4</sub>)<sub>2</sub>SO<sub>4</sub>.

MI01/W/01-A1

Poster

0900-06

#### ESTIMATING THE ANTHROPOGENICALLY INDUCED CHANGE IN GLOBAL AEROSOL NUMBER DISTRIBUTIONS.

Julian Wilson and Frank Raes, Environment Institute, European Commission

We have developed a simplified model of sulfate aerosol dynamics (Wilson et al, 1999) and coupled this to a model of the global black carbon aerosol cycle in an offline global transport model. The coupled model is able to describe the evolution of the size distributions of carbonaceous aerosols, pure sulfate aerosols and mixtures of the two. The model simulations for present day conditions show that the black carbon and mixed black carbon-sulfate aerosols predominate the estimated accumulation mode concentrations in the source regions while in remote regions the accumulation mode is primarily sulfate aerosol formed by gas to particle conversion and growth.

We will present both our present day and pre-industrial estimates of global aerosol number distributions, and investigate the sensitivity of these results.



**MI01/E/02-A1** Poster **0900-07**

**STUDY OF INTERCORRELATION BETWEEN THE CHEMICAL AND THE OPTICAL PROPERTIES OF THE AEROSOLS**

Veronique SOUFFLET, Karine Debout, Pascal Flament and Richard Santer (Laboratoire Interdisciplinaire en Sciences de l'Environnement, Université du Littoral Côte d'Opale, 30 Avenue Foch, BP 59, F-62930 WIMEREUX, e-mail: Veronique.Soufflet@loalil.univ-littoral.fr)

Simultaneous in-situ measurements of physico-chemical and optical properties of the aerosols were made during February and March 1998 in the North Littoral of France. The chemical characteristics were determined by the concentration and the size distribution of four major components: Organic carbon, Sulfate, Chloride and Nitrate, which are representative of 6 consecutive hours during the day. Parallel optical measurements of solar radiation extinction were performed at four wavelengths: 440, 670, 870 and 1020 nm, in order to follow the diurnal variation of the total aerosol optical thickness. Both maritime and urban aerosols were detected depending on the air mass backtrajectories. The intercorrelation between the two complementary types of information is studied. In particular, the relative contribution of each component in the optical signal is determined.

**MI01/E/01-A1** Poster **0900-08**

**RADIATIVE FORCING BY ANTHROPOGENIC SULFATE, NITRATE AND AMMONIUM AEROSOLS**

Joyce E. PENNER, (University of Michigan, 12455 Hayward St., Ann Arbor, MI 48105, e-mail: penner@umich.edu) Yan Feng (University of Michigan, 12455 Hayward St., Ann Arbor, MI 48105, e-mail: fengy@engin.umich.edu)

Climate forcing by anthropogenic aerosols has, in the past, been estimated in isolation of the volatile anthropogenic aerosol components nitrate and ammonium. For example, aerosol forcing by anthropogenic sulfate is typically estimated as the difference in reflected solar radiation at the top of the atmosphere with and without anthropogenic sulfate, assuming that all other aerosol components (except water) remain fixed. Alternatively, a fixed amount of ammonium has often been assumed to be associated with anthropogenic sulfate. Here, we investigate the possible changes in aerosol size distribution and forcing that result from the presence of the volatile aerosol components associated with ammonia and nitric acid in equilibrium with a specified distribution of sulfate. Accounting for the equilibrium distribution of volatile aerosols in general total forcing over that calculated from anthropogenic sulfate alone. This paper examines the forcing by anthropogenic sulfate, nitrate and ammonium and the effect of relative humidity on total forcing. We show the range of possible impacts from the major industrial and biomass burning areas associated with anthropogenic emissions.

**MI01/L/05-A1** Poster **0900-09**

**REGIONAL AEROSOL AND LONG RANGE TRANSPORT OVER THE PACIFIC OCEAN**

Clarke, A.D., Moore, K.G. and KAPUSTIN, V. N., School of Ocean and Earth Science and Technology, University of Hawaii, Honolulu, HI 96822

We have measured various aerosol types undergoing long range transport to the North and South Pacific during several recent experiments. These include dust events in the North Pacific and biomass burning in the South Pacific. Dust events from Asia were found to be several kilometers deep and reach down to the inversion near the Japan but after long range transport they tended to occur in thinner layers or "rivers" aloft and often mixed with submicrometer pollution aerosol. Ship measurements from Alaska to Samoa showed that the marine boundary layer (MBL) aerosol could also be significantly perturbed by pollution several thousand kilometers downwind of Asia. Here the MBL aerosol light scattering, light absorption and concentration all decreased as we approached the equator where a prompt transition to clean air was evident.

A climatological study in Hawaii (20N, 155W) is also underway with continuous optical depth measurements made at the surface and at Mauna Loa Observatory (MLO @ 3,400m). This has revealed that dust events observed at MLO show a much smaller perturbation to optical depth than detected at the surface. Some local vertical profiles indicate that much of the transported aerosol lies below 3,500m but above the trade wind inversion (about 1,600m) where it can be steadily entrained into the boundary layer. Other studies in the South Pacific reveal a layered combustion aerosol with a soot core and volatile coatings carried westward between 2-5km from South America. These had a low single scatter albedo of about 0.7-0.8 but lay above a clean Marine boundary layer with single scatter albedo near 1.0. The data suggest that regional aerosol characteristics above the MBL may be needed to interpret their radiative impact.

**MI01/W/21-A1** Poster **0900-10**

**LONG TERM VARIATION OF THE CHEMICAL COMPOSITION OF FINE AEROSOL PARTICLES IN HUNGARY**

Laszlo Bozo, Hungarian Meteorological Service, H-1675 Budapest, P.O.Box 39. HUNGARY e-mail: bozo@met.hu

Aerosol particles have been sampled in the central part of Hungary (K-pusztá) under regional background conditions since the late 70's. Samples are analysed for sulfate, nitrate, ammonium and metals. In 1996, two additional stations joined the programme (Nyirjes, NE of Hungary and Farkasfa SW of Hungary). Trace gas precursors (sulfur dioxide, nitrogen dioxide, nitric acid etc.) are also monitored at the stations.

Long term and seasonal variation of aerosol concentrations are presented in the paper. Regarding sulfate particles, the variation of atmospheric sulfur budget (sulfur dioxide and sulfate) over Hungary, and the country's role in the European sulfur budget is also evaluated for the period of 1980-1998.

**MI01/E/18-A1** Poster **0900-11**

**CHEMICAL ANALYSIS OF AEROSOL IN SEOUL DURING THE SPRING OF 1998**

Ha-Man Cho, Jae-Chon Choi, Young-Sin Chun, Ji-Young Kim and Ki-Joon Park (Meteorological Research Institute, Seoul, Korea, E-mail : hmcho@iris.metri.re.kr)

Intensive observation of aerosol has been conducted in Seoul during the spring (March to May) of 1998 in order to understand the chemical properties of aerosol in Seoul with putting special emphasis on the effect of Yellow sand. The measurement items were mass concentration of TSP/PM10 with the ion and heavy metal components and aerosol number density. The sampling of TSP/PM10 and the other observations have been carried out basically with the interval of about twice a week, however when the Yellow Sand occurred the observations were made every day. The chemical analysis of ion components was made by Ion Chromatograph

and that of heavy metals was made by Inductively Coupled Plasma.

The mean TSP mass concentration during the spring of 1998 was 98.9 $\mu$ g/m<sup>3</sup> with the maximum 264.8 $\mu$ g/m<sup>3</sup> and the minimum 23.9 $\mu$ g/m<sup>3</sup>. The major ion components in Seoul during spring were NO<sub>3</sub><sup>-</sup>, SO<sub>4</sub><sup>2-</sup> and NH<sub>4</sub><sup>+</sup> with the mean concentrations 9.7 $\mu$ g/m<sup>3</sup>, 8.3 $\mu$ g/m<sup>3</sup> and 4.2 $\mu$ g/m<sup>3</sup>, respectively. The ion concentration ratios of Yellow sand cases to the non-Yellow were 2.00, 1.61, 1.43 for Ca<sup>2+</sup>, Mg<sup>2+</sup>, SO<sub>4</sub><sup>2-</sup>, respectively, while were near 1.00 for F<sup>-</sup>, Cl<sup>-</sup>, Na<sup>+</sup>, NH<sub>4</sub><sup>+</sup>, showing that the high ratio of the ions particularly Ca<sup>2+</sup>, Mg<sup>2+</sup> were closely related with the Yellow Sand. The major heavy metals in TSP in Seoul during spring were revealed as Al, Ca and Fe with the mean concentrations 3.2 $\mu$ g/m<sup>3</sup>, 2.3 $\mu$ g/m<sup>3</sup> and 2.1 $\mu$ g/m<sup>3</sup>, respectively. In contrast with this, concentrations of some important pollutant heavy metals such as Pb, Cd, were 69.9ng/m<sup>3</sup> and 2.3ng/m<sup>3</sup>. The heavy metal concentration ratios of Yellow Sand cases to the non-Yellow were generally larger for Al, Ca and Fe with the ratio 3.30, 2.51, 2.65, showing that these high ratios of heavy metals were also have close correlation with the Yellow sand.

**MI01/E/10-A1** Poster **0900-12**

**ATMOSPHERIC CORRECTION ALGORITHM FOR CHINA COASTAL AREA**

WENYING SU and Beiyang Wu Lab for Middle Atmosphere and Global Atmospheric Observation Institute of Atmospheric Physics Beijing, 100029, China

Atmospheric correction is the key step to obtain the primary productivity of the ocean from the ocean color satellite since the atmosphere's contribution to the total radiance is about 70-80%. We devote our effort to establish an atmospheric correction model for the coastal area of China. The atmospheric radiative transfer model DISORT is used in combination with the aerosol model. First a Look Up Table (LUT) is calculated for case 1 water for various conditions. A clear and turbid water detection algorithm is developed to distinguish clear pixel from unclear pixel. Based on the LUT and the satellite observed total radiance the water-leaving radiance of clear pixel can be determined and the atmospheric correction factor. Then extrapolate this method to unclear pixel by using the atmospheric correction factor of adjacent clear pixel. Much of our concern are for the turbid water and try to correct our clear water algorithm for turbid water. The water-leaving radiances (or reflectances) of the coastal area of China are analyzed. Then the obtained results are compared with the outputs of the SeaWiFS Data Analysis System and the reasons for the difference are analyzed.

**MI01/W/13-A1** Poster **0900-13**

**THE EFFECTS OF THE SILVER IODIDE AEROSOLS INJECTION INTO A CUMULONIMBUS CLOUDS**

Mladjen CURIC and Dragana Vujovic (both at Institute of Meteorology, University of Belgrade, Belgrade, Yugoslavia, email: curic@rudjer.ff.bg.ac.yu) Biljana Music (Agricultural Faculty, Belgrade, Yugoslavia)

Hail suppression by seeding from the ground has been run in a large area of Yugoslavia since 1967. The primary purpose of the hail seeding is to reduce damage due to the hail. But, if we know seeding technology the increase in rainfall is logical to be occurred. In the area important amount of silver iodide is released in the atmosphere. The further behavior of this particles is analyzed by using numerical model of convective cloud. It is shown that silver iodide aerosols significantly influence the precipitation amount. Depending of the amount of aerosols the mean monthly precipitation may be increased by the 25%.

**MI01/C/JSV36/E/06-A1** Poster **0900-14**

**ANALYSIS OF THE EVOLUTION OF THE ASH CLOUD FROM THE DECEMBER 26, 1997 (BOXING DAY) DOME COLLAPSE OF SOUFRIERE HILLS VOLCANO, MONTSEERRAT USING GOES-8 IMAGERY**

Ms. Gari C. MAYBERRY, Michigan Technological University, Department of Geological Sciences, email: gcmayber@mtu.edu Dr. Bill I. Roseand Dr Gregg Bluth, Michigan Technological University, Department of Geological Sciences

There have been many serious incidents of aircraft encountering volcanic clouds in the past. By studying volcanic clouds we can monitor their paths, as well as learn more about their evolution, in an effort to mitigate the hazard they pose to aircraft.

The December 26, 1997 dome collapse of Soufriere Hills volcano, Montserrat resulted in a pyroclastic flow that descended the White River Valley ~4km and traveled across the sea an unknown distance. The slope failure and subsequent dome collapse occurred around 0700Z and lasted approximately 15 minutes and an associated volcanic ash cloud rose to an altitude of 47,000 ft. (14.3 km). The volcanic cloud was observed by the geostationary (GOES-8) satellite every 30 minutes, which resulted in a comprehensive record of its evolution. Seventeen images of the volcanic cloud, between 0715Z and 2345Z, were analyzed. The brightness temperature difference (BTD) between bands 4 (10.3-11.3 microns) and 5 (11.5-12.5 microns) of GOES-8 was used to distinguish the ash cloud from meteorological clouds. Ash clouds have a negative BTD while meteorological clouds have a positive BTD (Prata, GRL 16: 1293-1296, 1989). BTD data are used to map the volcanic cloud and retrieve basic data about the area of the cloud, mass of the fine ash particles (<10 microns radius), and the optical depth (Wen and Rose, JGR 99:5421-5431, 1994).

The volcanic cloud moved rapidly 20-28 km/hr to the south east until around 1145Z when it became more transparent and began to dissipate. The largest band 4 optical depth (~3) occurred at 0745Z, shortly after the eruption began, and rapidly decreased to about .3 less than 2 hours after the onset of the eruption. From about 0845Z to 1045Z the ash signal of the volcanic cloud was obscured by "masking", which was caused by a cloud of liquid water droplets with a positive BTD. The cloud with the positive BTD may have overlain or ...

MI02

Thursday 22 – Friday 23 July

**ATMOSPHERIC CHEMISTRY – CLIMATE INTERACTION, Part 2: TRACE GASES, AEROSOLS AND CLIMATE (ICAGP, IRC, ICCL, ICDM)**

Location: Mechanical Engineering, G29 LT

Thursday 22 July AM

Presiding Chair: Michael Prather (University of California, Irvine, USA)

**TROPOSPHERIC OZONE**

MI02/E/08-A4

0930

**SURFACE OZONE IN THE INDIAN REGION**

Shyam LAL, Manish Naja (Physical Research Laboratory Navrangpura, Ahmedabad 380 009, India)

Tropospheric ozone plays an important role in the radiative forcing due to its increasing abundance. However, the increase rates varies largely from place to place and at some of the locations mainly in Canada, it even shows declining trend. We have made measurements of surface ozone in different environments in India and also in the Indian ocean. Diurnal buildup of ozone is seen at sites where higher levels of NOx and other precursor gases are observed. Observations in the Indian ocean show sharp decrease in ozone mixing ratios from the coastal region to the open ocean. However, events of higher ozone levels are also seen in the open ocean due to transport of the polluted continental air. These results with emphasis on the measurements in the Indian ocean will be presented.

MI02/E/04-A4

0950

**VARIATIONS OF ATMOSPHERIC OZONE IN GEORGIA**

Jumber Kharchilava, Avtandil AMIRANASHVILI (both at the Institute of Geophysics of Georgian Academy of Sciences, 1, M. Aleksidze Str., Tbilisi 380093, Georgia, email: vazha@excite.com)

Measurements of atmospheric ozone (total ozone - TOZ, vertical distribution of ozone VDO, surface ozone concentration - SOC) began in Georgia in 1957 and are carried out also at present. It has been established, that TOZ, VDO, SOC variations depend on atmospheric processes, atmospheric pollution, local orography. A decreasing of TOZ during years has been revealed. It amounts to -0.3% per year in Abastumani and -0.2% per year in Tbilisi. Also an increase of SOC was detected for Tbilisi and rural locations, which is particularly high in the winter and amounts to 0.2% per year. Considering the fact, that the process of modern climate warming in Georgia manifests itself mainly in the considerable increase of the winter temperature, one may conclude, that the mentioned decrease of TOZ and increase of SOC contribute to a certain extent to this process.

MI02/E/01-A4

1010

**VERTICAL OZONE TRANSPORTS MEASURED AT A HIGH ALPINE SITE**

Michael STAUDINGER (Zentralanstalt f. Meteorologie und Geodynamik, Freisaalweg 16, A-5020 Salzburg, Austria, email: staudinger@zamg.ac.at)

Most ozone in the troposphere is photochemically produced. Still, a significant part is imported through stratospheric intrusions in particular synoptic patterns like tropopause foldings, cut-off lows or thunderstorms. These situations show a strong vertical gradient of the ozone concentration within the troposphere. Therefore high elevated mountain stations are perfect sites to monitor the daily variation of the ozone concentrations. Most of these episodes are very short term events, as the responsible synoptic patterns develop and cross the alps sometimes within less than a day. At the Sonnblick Observatory in the Austrian Alps (3105 m.a.s.l.) under clear sky conditions measurements in ten minute intervals of vertical thickness of the ozone column are taken with a Brewer spectrometer. The comparison of the dataset of the last 4 years with water vapour satellite imagery and vertical cross sections of radiosonde soundings over Europe show the corresponding vertical motions in the different parts of the troposphere in the investigated periods. Some of these events cover only small areas, partly larger fields of downward motions are involved.

MI02/E/10-A4

1100

**THE EFFECT OF CONVECTIVE TRANSPORT ON THE RADIATIVE FORCING FROM TROPOSPHERIC OZONE**

William COLLINS (email: wjcollins@meto.gov.uk); David Stevenson, Colin Johnson, Richard Derwent (Hadley Centre for Climate Prediction and Research, The Met. Office, Bracknell, RG12 2SZ, UK)

We have used a Lagrangian global tropospheric chemistry transport model with a Lagrangian convective transport scheme to investigate the effect of convection on tropospheric ozone. The strongest radiative impact of ozone is in the upper troposphere. We show that convective processes can efficiently transport surface emissions to the upper troposphere where, due to the cleaner environment, they are more effective at producing ozone. Our model also shows that the upper tropospheric oxidizing capacity is significantly enhanced by photolysis of carbonyl and hydroperoxide compounds that are transported from the surface up to this altitude by convection. Convection can also decrease upper tropospheric ozone by lifting up surface air with low ozone mixing ratios, this vertical redistribution of ozone has the effect of reducing its radiative forcing. We have used our model to investigate the importance of each of the effects mentioned and have calculated a value for the total change in ozone radiative forcing brought about by convection.

MI02/E/02-A4

1120

**IMPACT OF CONVECTION AND LIGHTNING NOX ON OZONE IN THE UPPER TROPOSPHERE AND ASSOCIATED RADIATIVE FORCING OF CLIMATE.**

Didier HAUGLUSTAIN (Service d'Aeronomie du CNRS, Universite de Paris 6, Paris, France, email: dh@aero.jussieu.fr); Guy Brasseur, Louisa Emmons (National Center for Atmospheric Research, Boulder, CO, email: brasseur@acd.ucar.edu)

Deep convection transports rapidly chemical species from the boundary layer to the middle and upper troposphere and, occasionally, to the lower stratosphere. Once aloft, the ozone precursors can be advected by synoptic scale transport and contribute to ozone

photochemical production on the global scale. Convective transport can also control the rapid photochemical balance of radicals and NOx in the upper troposphere by bringing fresh NO (from lightning, soil emissions, and combustion processes), and peroxides into this region. In addition to that, NOx production from lightning discharges can contribute substantially to the nitrogen budget in the mid- and upper-troposphere and therefore promote ozone formation. Climate changes have therefore the potential to affect the distribution of ozone in the upper troposphere through perturbations of convective and lightning activities. In this paper, we apply a global chemical transport model called MOZART to study the changes in ozone and its precursors associated with lightning activity and deep convection. In particular, we illustrate the essential role of lightning NOx in the formation of upper tropospheric ozone plumes in the tropics. The role of convection in the formation of ozone in the remote troposphere is also discussed. The radiative forcings associated with ozone changes and changes in methane photochemical lifetime are also calculated. The possibility of a significant positive climate feedback mechanism between convection and lightning activity and tropospheric ozone formation and associated radiative forcing of climate is discussed.

MI02/E/09-A4

1140

**AIRCRAFT NOX EMISSION, OZONE CHANGES AND THE TROPOPAUSE HEIGHT**

Beiyang WU (Guohui Li Lab for Middle Atmosphere and Global Atmospheric Observation, Institute of Atmospheric Physics, Beijing, 100029, China)

Using the NCAR/ACD 2D chemical transport model and NCAR/NCEP re-analyzed data, this paper studies the effects of the aircraft emission on local ozone. Two model runs were carried out: a) with aircraft NOx emission; b) without aircraft NOx emission. The results show that the aircraft emitted NOx is about 20-50% of the NOx at levels over mid-latitude from 8-15 km. The responding relative change in ozone mixing ratio is 0.4-0.6% (0.5-0.8ppb in mixing ratio) in January and 1-4% (1-3 ppb) in July. It shows those lower NOx emission height results in fewer changes in O3, but higher NOx emission height leads to larger changes in ozone. It also should be pointed out that lifting the emission height by 3 km in winter produces negative ozone change above 13 km. The tropopause height varies with season. The amplitude of the variation changes with latitude. At the equator, the 12 year average amplitude is about 0.5km while it increases to 3 km at 35N. The phase is reversed in the tropics and in the mid-high latitude. Therefore, effect of the aircraft emission of NOx on ozone could have opposite signs depending on the relative position of the emission source with the tropopause. Thanks are due to Dr. Guy Brasseur for the Socrates Model and many interesting discussions and Dr. Xuexi Tie for helpful suggestions.

MI02/W/02-A4

1200

**DYNAMICAL-CHEMICAL INTERACTIONS IN A 2D-CIRCULATION MODEL**

Axel GABRIEL, Gerhard Schmitz (Institut fuer Atmosphaerenphysik der Universitaet Rostock e.V., Schlostr.6, D-18225 Kuehlungsborn, Germany, email: gabriel@iap-kborn.de)

In this work we present the results of numerical experiments which are carried out with a dynamical-chemical 2D-circulation model to examine the climate effect of natural and anthropogenic induced atmospheric perturbations in an interactively coupled mode. The 2D-model was developed based on the 3D-GCM ECHAM3 and a complex photochemistry model. The model includes parameterizations of radiation, water cycle, clouds and boundary layer. One important feature of the 2D-model is a parameterization of the transient tropospheric eddy heat and momentum fluxes which describes the interactions between the zonally averaged dynamics and the eddy fluxes in a self consistent way. Stratospheric mixing processes are prescribed according to climatological data. The results give a realistic picture of the meridional mass circulation and the meridional distribution of trace gases. A cascade of model runs were carried out with and without natural and anthropogenic induced O3-perturbations and with different modes in the O3-induced radiative forcing, i.e. with the radiation being calculated with prescribed-undisturbed, with fixed-disturbed and with interactively-calculated ozone distributions. The results reveal the contributions of the 'direct' effects induced by the perturbations via the radiative forcing and the 'indirect' effects via additional changes in the heat fluxes, the meridional mass circulation and the transport processes. E.g. present and future NOx aircraft emissions lead to O3-perturbations of several percent in the upper troposphere which induce 'directly' temperature changes of several 0.1K as revealed by the fixed-disturbed mode and 'indirectly' additional changes in the temperature of about 1K and in the O3 mixing ratio of more than 10% as revealed by the interactively-calculated mode. The results of further sensitivity studies help to examine the feedback mechanisms of the dynamical-chemical interactions in connection with the radiation, the water cycle and the meridional mass circulation.

MI02/W/09-A4

1220

**GLOBAL SIMULATIONS OF TROPOSPHERIC CHEMISTRY-CLIMATE INTERACTIONS USING THE GISS GCM**

J. Lee GRENPELL, D. T. Shindell, D. Rind, D. Koch (NASA Goddard Institute for Space Studies &amp; Columbia University, New York, NY USA); C. Price (Tel Aviv University, Tel Aviv, Israel); M. Prather, O. J. Wild, L. (University of California, Irvine, CA USA); Mickle, D. Jacob (Harvard University, Cambridge, MA, USA)

Results are presented from multi-year integrations of the Goddard Institute for Space Studies (GISS) GCM with tropospheric chemistry. The resolution is 4x5 degrees in the horizontal and spans nine levels up to 10mb in the vertical. The chemistry scheme incorporates 9 dynamical tracers and 24 chemical species. The 'family' partitioning approach is adopted for NOx, HOx and Ox. N2O5 hydrolysis on sulphate aerosol is included. The 'fastj' photolysis scheme is incorporated. CO sources include anthropogenic and biomass burning input. NOx sources include aircraft, soil, fossil fuel, biomass burning, lightning and stratospheric input. The latter is also parameterized for ozone. Dry and wet depositions are coupled with the GCM's convection and circulation. Results focus upon the model's simulation of global tropospheric ozone and related chemical processes. Chemistry-climate interactions are presented from simulations with pre-industrial, present-day and doubled CO2 conditions.

Thursday 22 July PM

Presiding Chair: Hugh Coe (UMIST, Manchester, UK)

**TROPOSPHERIC TRACE GASES**

MI02/L/19-A4

1410

**MEASUREMENTS OF SHORT CHAIN ALKYL NITRATES IN AMBIENT AIR FROM MID AND HIGH LATITUDES AND FROM POLAR FIRN IN TWO HEMISPHERES**

H.P. McINTYRE, W.T. Sturges, S. Bauguutte, S.A. Penkett (School of Environmental Sciences, University of East Anglia, Norwich NR4 7TJ, UK, email: h.mcintyre@uea.ac.uk); E. Atlas, V. Stroud

(National Center for Atmospheric Research, Boulder, Colorado 80370, USA, email: atlas@acd.ucar.edu); J. Chapellaz (Laboratoire de Glaciologie et Géophysique de l'Environnement, CNRS, 54 rue Molière, Domaine Universitaire, BP96, 38402 Saint Martin d'Hères Cedex, FRANCE, email: jerome@glaciog.ujf-grenoble.fr); R. Mulvaney, A. Jones (British Antarctic Survey, High Cross, Madingley Road, Cambridge, CB3 0ET, UK, email: rmu@pcmail.nerc-bas.ac.uk)

The alkyl nitrates (RONO<sub>2</sub>) are a relatively stable component of odd nitrogen (NO<sub>y</sub>) formed in secondary reactions of hydrocarbons in the presence of NO<sub>x</sub> and are capable of transporting NO<sub>x</sub> long distances. They are therefore potentially significant in determining background ozone levels in the remote troposphere. Measurements of the C<sub>1</sub> and C<sub>2</sub> alkyl nitrates at Mace Head, Ireland provide information on their contribution to the total NO<sub>y</sub> budget of the well processed air reaching this site. Evidence for a high natural background was seen since similar levels were observed in oceanic and polluted airmasses.

Measurements of methyl nitrate and ethyl nitrate have also been made from ambient air from two sites in the Antarctic in order to assess their contribution to nitrogen chemistry in polar regions at different distances from the open ocean. Evidence for an oceanic source was again observed, as well as a diurnal cycle, which may relate to uptake in the snowpack. An historical trend of the tropospheric levels of the alkyl nitrates has also been made from air collected from increasing depths through the firm in the Arctic (Devon Island, Canada) and Antarctic (Dronning Maud Land, 1997 and Dome C, 1998). The historical record of methyl nitrate and ethyl nitrate in the firm appears to have been confused by local (marine) or in-situ production of the molecules. C<sub>4</sub>-C<sub>5</sub>- nitrates, however, appeared to follow a historical trend of increasing concentration since the late 1950s.

MI02/W/12-A4

1430

**TROPOSPHERIC ABUNDANCE AND GROWTH RATES OF RADIATIVELY-ACTIVE HALOCARBON TRACE GASES AND ESTIMATES OF GLOBAL EMISSIONS**

David E. ORAM, William T. Sturges, Stuart A. Penkett (School of Environmental Sciences, University of East Anglia, Norwich NR4 7TJ, UK, email: d.e.oram@uea.ac.uk); Paul J. Fraser (CSIRO/CRC for Southern Hemisphere Meteorology, Victoria, Australia)

As a result of the Montreal Protocol, the tropospheric growth rates of several ozone-depleting compounds such as CFCs have slowed considerably in recent years or even stopped. In contrast, the mixing ratios of CFC-replacements, such as HCFCs and HFCs, are increasing at rapid rates. Furthermore, a number long-lived perfluorinated compounds (PFCs and SF<sub>6</sub>) have been identified in the background atmosphere, whose concentrations have risen steadily over recent years. Concern arises as many of these trace gases are efficient absorbers of infrared in the 800-1200 cm<sup>-1</sup> region and are among the most potent greenhouse gases known, with GWPs typically 3 or 4 orders of magnitude higher than that of CO<sub>2</sub>. Measurements of a wide-range of halocarbons are being made at UEA by GC-MS, and data will be presented showing the changing atmospheric abundance of these compounds over the past 40-50 years, based on the analysis of the Cape Grim air archive, a unique series of air samples collected in Tasmania (41°S) since 1978, and from a preliminary analysis of firm air, dating back to the 1950s. The measurements will be compared with predicted concentrations derived using a 2-D global model, based on known industrial emission estimates. Where emissions are not known, the model will be used to derive an independent emission scenario based upon the measurements. Knowing the current atmospheric abundance and emission rates, the relative contributions to net radiative forcing will be discussed.

MI02/W/14-A4

1450

**VARIATIONS OF METHANE AND CARBON MONOXIDE TOTAL COLUMN AMOUNTS IN THE ATMOSPHERE FROM GROUND-BASED SPECTROSCOPIC MEASUREMENTS NEAR ST PETERSBURG**

M.V. MAKAROVA (St Petersburg State Univ., Russia); A.V. Poberovsky, Yu.M. Timofeev

Ground-based spectroscopic measurements of methane and carbon monoxide total column amounts in the atmosphere are performed by Solar IR Spectrometer near St. Petersburg. Time series of methane (1991-1998) and carbon monoxide (1995-1998) total column amounts measurements were analysed and the seasonal cycle of CH<sub>4</sub> and CO was revealed. The seasonal cycle of methane and carbon monoxide has maximum in February-March and minimum in July-September.

MI02/W/08-A4

1510

**A SLOWDOWN OF CO TOTAL COLUMN ANTHROPOGENIC INCREASE SINCE EARLY 1980S: IS IT A RESULT OF OH BUILD UP?**

Leonid YURGANOV (Department of Physics, University of Toronto, Toronto M5S 1A7, Canada, on leave from the Arctic and Antarctic Research Institute, St.-Petersburg, Russia, email: leonid@atmosph.physics.utoronto.ca); Evgeny Grechko, Anatoly Dzhola (both at Institute of Atmospheric Physics, Russian Academy of Sciences, Moscow 109017, Russia, email: egrechko@atm.phys.msu.ru)

Many of climate-active trace gases are removed from the troposphere in a reaction with tropospheric hydroxyl (OH). Meanwhile, present and future trends in hydroxyl concentration are not understood at all. The main sink for OH is its reaction with carbon monoxide (CO). Measurements of total column amounts of CO in Russia have been carried out since early 1970s. CO amount has been increasing with a rate of 1.5 % per year until 1983. After that considerable fluctuations were observed, but no trend was determined until now. Variations of CO sources and sinks should be studied to explain this slowdown. To determine an importance of changes in the CO sink a correlation between CO and total ozone was analyzed. A positive slope of 0.53 ppb CO in the troposphere per 1 Dobson Unit (DU) of total column amount of ozone was found for deseasonalized data (correlation coefficient 0.64). It is known that ozone total column currently declines in the northern mid latitudes with a rate of -1.3 DU per year. As a result, CO anthropogenic increase should be offset by -0.7 ppb per year. A hydroxyl build up after early 1980s due to more intense photochemical reactions initiated by increased UV was speculated to explain the CO behaviour. If it is the case, scenarios of long-term variations of trace gases, removed by OH, should be reevaluated in view of total ozone trends.

MI02/W/07-A4

1600

**MODELLING THE VARIATION OF DELTA 13C IN ATMOSPHERIC METHANE: PHASE ELLIPSES AND THE KINETIC ISOTOPE EFFECT**

W. ALLAN, M. R. Manning, A. J. Gomez, D. C. Lowe (National Institute of Water and Atmospheric Research, PO Box 14-901 Kilbirnie, Wellington, New Zealand, email: w.allan@niwa.cri.nz)

Methane is a climatically active gas. Its atmospheric oxidation rate and its consequent lifetime are therefore important factors in the link between atmospheric chemistry and climate. Using a plausible scenario for global methane source strengths and their isotopic ratios (delta

13C), we run the Max-Planck-Institute for Meteorology's TM2 3-D offline transport model with 1987 ECMWF wind fields to obtain a global set of time series for methane mixing ratio and delta 13C. Isotopic fractionation by OH oxidation of methane is incorporated into the model by including a kinetic isotope effect (KIE) of 5.4 permil. Plots of change in delta 13C versus change in mixing ratio (phase diagrams) are useful for interpreting results. These show that in the extra-tropical southern hemisphere methane oxidation is dominated by the local atmospheric OH sink. Particularly near Antarctica, the diagrams take the form of "phase ellipses". The major axes of these ellipses have tilts that are consistent with the input KIE of 5.4 permil.

Measurements at Baring Head, New Zealand, and Scott Base, Antarctica, show phase ellipses similar to those predicted by the model. However, the tilts of the ellipse major axes imply a KIE of about 13 permil. The reason for this is not obvious, but the result implies that our understanding of the atmospheric oxidation process is incomplete. We speculate on possible explanations of this anomalous KIE effect.

MI02/W/19-A4

1620

**REACTIVE TRACE GASES AND RADIATIVE FORCING**

D. STEVENSON (UK Met. Office, Room 153, London Rd, Bracknell, Berks, RG12 2SZ, UK, email: dstevenson@meto.gov.uk)

New calculations of the global distribution of tropospheric ozone, and its evolution over the period 1860-2050, simulated by the UKMO tropospheric chemistry-transport model, will be presented. The results include the effects of: (1) changing meteorology, as generated by a transient experiment using the fully coupled ocean-atmosphere Hadley Centre climate model; (2) changes in the magnitude and spatial distribution of anthropogenic emissions; and (3) observed stratospheric ozone depletion over the period 1979-1997, and its projected future recovery in the 21st century. The ozone fields for several snapshot years are used to calculate radiative forcings since pre-industrial times. Further sensitivity calculations reveal the contributions of changes in anthropogenic emissions of individual trace gases (NO<sub>x</sub>, CH<sub>4</sub>, CO, VOCs) to the ozone field, and hence the ozone radiative forcing. These experiments also show the roles played by these gases in changing oxidant fields (e.g. OH), allowing the impact on CH<sub>4</sub> and aerosol distributions to be estimated, raising the possibility of calculating Global Warming Potentials (GWPs) for reactive trace gases.

MI02/L/20-A4

1640

**CLIMATE FORCINGS FROM CHEMICAL PERTURBATIONS: ARE THEY DOMINATED BY THE PRIMARY NATURAL MODE OF CH<sub>4</sub>?**

Michael PRATHER, Oliver Wild (both at Earth System Science Dept, UC Irvine, CA 92697-3100 USA, email: mprather@uci.edu, oliver@halo.ps.uci.edu)

Chemical perturbations to the atmosphere that are driven by short-lived gases such as NO and CO are often believed to be short-lived since the gases themselves are highly reactive. Both numerical integrations of 3-D models and the mathematical decomposition of the chemistry-transport equations admit solutions of the form of eigenvectors for which the emission of NO or CO may excite the long-lived methane-like mode that decays with an e-fold of about 12 years. We look at how the integrated climate impact -- driven in this case by perturbations to the greenhouse gases ozone and methane -- is represented by this single mode rather than the larger, short-lived transient response of ozone.

Friday 23 July AM

Presiding Chair: Stuart Penkett (UEA, Norwich, UK)

STRATOSPHERIC OZONE

MI02/E/06-A5

0910

**ANALYSIS OF 6 YEAR OF SOUTHERN MID-LATITUDE MILLIMETER WAVE OZONE OBSERVATIONS: IMPROVED METHODOLOGY AND VALIDATION**

J.J. TSOU (GATS Inc., 11864 Canon Blvd., Newport News, VA 23606, USA, email: jj@gats-inc.com); B.C. Connor (NIWA, PB 50061, Omakau 9182, New Zealand, email:connor@kea.lauder.cri.nz); A. Parrish (619 IGRC, Univ. of Mass., Amherst, MA 01003, USA, email: parrish@fcrao1.phast.umass.edu)

A ground-based millimetre wave radiometer has been in daily operation at Lauder, New Zealand (45S, 169.7E) since November 1992 to monitor the middle atmospheric ozone continuously as a part of the international Network for the Detection of Stratospheric Change (NDSC). Due to the special observing conditions at this southern mid-latitude site, 3 refinements to the data processing and retrieval software were proposed: (1) corrections to the radiative transfer model to account for the local tropospheric climate; (2) corrections to observing elevation angles due to the settling of the foundation of the site; (3) usage of radiometric temperatures of calibration loads, instead of the physical temperatures, in the data calibrations and retrievals. The derivation of each of suggested improvements is discussed, and the effects on the overall retrieved ozone profiles were found to be less than 5%. The data from 1992 to 1998 were reprocessed, and the resulting ozone profiles were compared to other coincident ground-based or satellite overpass measurements. The comparison results will be presented here, and the quality of this data set will be evaluated.

MI02/W/04-A5

0930

**ON THE STATISTICS OF THE SOUTHERN OZONE HOLE**

Virginia SILBERGLEIT (Dep. de Física, Facultad de Ingeniería, Universidad de Buenos Aires, Av. Paseo Colon 850, 1063 Buenos Aires, Argentina, email: vsilber@tron.fi.uba.ar)

The thinning of the stratosphere ozone layer in the Antarctic region is studied by considering ground-based observations at Halley Bay Station. Gumbel's first distribution extreme values to evaluate the maximum depletion in the ozone layer are used. The present study shows the expected annual minimum values for the ozone layer density in the Southern Hemisphere.



**MI02/W/05-A5 0950****MEASUREMENTS OF STRATOSPHERIC OZONE AND CHLORINE MONOXIDE OVER NY-AALESUND, SPITSBERGEN, IN 1998 AND 1999**

U. KLEIN, B. Franke, K.F. Künzi, J. Langer, K. Lindner, I. Wohltmann (Institute for Environmental Physics University of Bremen, FB1 P.O. Box 330440, D-28334 Bremen, Germany, email: Ulf.Klein@Uni-Bremen.de)

Observations of stratospheric ozone and chlorine monoxide (ClO) are regularly being performed at the Arctic station of the Network for the detection of stratospheric change (NDSC), using a ground based millimetre wave radiometer. While ozone has been permanently monitored since 1994 at an observation rate of about 20 profiles per day, the strong and variable absorption of tropospheric water vapour and the necessity of day and night time observations are restricting ClO measurements. The location of the observation site, Ny-Ålesund (78.9 N, 11.9 E), enabled us to take data inside, outside and in the edge region of the polar vortex in 1998. We observed enhanced levels of stratospheric ClO from in the end of February 1998 of up to 1.0 ppbv in the vicinity of 20 km of altitude. A subsequent chemical ozone loss of approximately 15 ppb/day was observed in the same altitude range.

**MI02/W/06-A5 1010****A VERSATILE MM-WAVE RADIOMETER IN KIRUNA, SWEDEN**

Uwe RAFFALSKI, Åke Steen (both at Institute of Space Physics, Box 812, S-98128 Kiruna, Sweden, email: Uwe.Raffalski@irf.se); Gerd Hochschild (Institute of Meteorology and Climate Research, Research Center Karlsruhe, 76344 Eggenstein-Leopoldshafen, Germany, email: hochschild@imk.fzk.de)

The Swedish Institute of Space Physics in Kiruna (67.52 N, 20.26 W) is located inside or at the edge of the vortex throughout most of the winter period. The winter temperature and humidity provide extremely good conditions for the observation of the Polar stratosphere with both optical methods as well as mm-wave techniques. The institute started a mm-wave project in order to observe ozone at 203 GHz and chlorine monoxide at 204 GHz. The newly built instrument deploys a conventional Schottky receiver (cooled down to appr. 30 K) together with a broadband acousto-optical spectrometer with a total bandwidth of 1.0 GHz and an effective resolution of about 1.2 MHz. Besides monitoring the mentioned stratospheric trace gases in the altitude range of 18-65 km this radiometer will provide with ground truth data for satellite missions like the Swedish ODIN satellite (to be launched in September 1999), the American SAGE III satellite (to be launched in March 1999), or the European ENVISAT satellite planned for the year 2000. The radiometer is designed in a way that it can be pointed into any azimuth and elevation angle. This can be used to observe for instance ozone variation in the vicinity of lee waves due to the Norwegian mountain ridge and lee wave induced PSCs.

**MI02/W/15-A5 1100****DEVELOPMENT OF A STRATOSPHERIC NUDGING CTM**

H. AKIYOSHI, S. Sugata, H. Nakane (National Institute for Environmental Studies, Tsukuba, Ibaraki 305-0053, JAPAN, email: hakiyosi@nies.go.jp); Takigawa, T. Nagashima, M. Takahashi (Center for Climate System Research, University of Tokyo, Tokyo 153-8904, JAPAN, email: takigawa@ccsr.u-tokyo.ac.jp)

A stratospheric nudging CTM has been developed to study global ozone depletion and variations of atmospheric chemical constituents. Zonal and meridional wind and temperature of ECMWF data are inputted to the model every 12 hours, and nudged to model winds and temperature with the e-folding time of 1 day to avoid artificial oscillations of winds and temperature produced in the model. Photolysis rates of chemical constituents and vertical winds are calculated in the model. The model includes gas phase chemical reactions of O<sub>x</sub>, HO<sub>x</sub>, NO<sub>x</sub>, hydrocarbons, ClO<sub>x</sub>, and BrO<sub>x</sub>, and heterogeneous reactions on PSCs. The maximum height of the model is about 70km. The monthly mean wind and temperature of the CIRA data were used above 10 hPa levels where ECMWF data were not available. The results of a one-year simulation by the T10 version is shown.

**MI02/E/12-A5 1120****THREE-DIMENSIONAL CHEMICAL MODEL SIMULATIONS OF THE OZONE LAYER: 1979-2055**

John AUSTIN, Neal Butchart, Jeffrey Knight (Meteorological Office, London Road, Bracknell, Berkshire, RG12 2SZ, UK)

A comprehensive description of stratospheric chemistry is included in a state-of-the-art climate model, which has been extended to the middle mesosphere. The ozone concentration from the chemistry package is used in the model radiation scheme, thereby coupling the dynamical and chemical processes. Initial dynamical conditions are taken from a transient climate experiment. Simulations commence on 1 March on each of the years 1979, 1994-2014 (at 5 year intervals), and 2024-2054 (at 10 year intervals) and consist of a 4 month spin-up period, followed by a 1-year integration. The concentrations of the greenhouse gases (GHGs) are taken from the Intergovernmental Panel on Climate Change IS92a projection and halogen amounts evolve according to future expectations. The results for 1979/80 and 1994/95 are generally in good agreement with observations, indicating in the latter case a deep Antarctic ozone hole and some Arctic ozone loss. For the 1979 simulation only a very shallow ozone hole was simulated, in agreement with observations, although the low ozone persisted for longer than observed. As the GHGs increase, Arctic ozone continues to decrease, reaching a minimum in about the year 2010, about 10 years after the peak chlorine loading. In contrast, the Antarctic ozone hole is largest about 5 years earlier. In 2014, the Antarctic ozone hole reduces in size and depth but thereafter increases again, suggesting that in contrast to 2-D model projections the ozone hole will still be present in the second half of the next century due to the importance of chemistry-climate coupling processes.

**MI02/L/01-A5 1140****THE LONG-RANGE TRANSPORT OF AEROSOLS AND TRACE GASES OVER SOUTH AFRICA**

M.T. FREIMAN, S.J. Piketh, P.D. Tyson (Climatology Research Group, University of the Witwatersrand, Private Bag 3, WITS 2050, Johannesburg, South Africa); M.P. Mittermaier (South African Weather Bureau, Bethlehem, South Africa)

South Africa has one of the largest industrialised economies in the Southern Hemisphere and is the only industrialised regional power on the African continent. A large proportion of the industrial infrastructure, much of which is coal based, is concentrated in the Mpumalanga Highveld region. Air masses originating on the Highveld are transported southeastward and

eastward out of an initially anticyclonic circulation, exiting the subcontinent into the southwestern Indian Ocean at approximately 30°S. Prior to the final exiting of air masses off the subcontinent, regional- to subcontinental-scale recirculation of the air occurs. Alternatively, the air exits directly and recirculates off the African continent, returning inland after some time over the ocean.

The dispersion of pollutant emissions is a function of two components of motion, namely vertical mixing and horizontal movement. Pollutants may be transported thousands of kilometers under suitable conditions. Elevated absolutely stable layers occur throughout the troposphere over South Africa - at 850, 700, 500 and 350 hPa. These layers trap pollutants below their bases, inhibiting vertical dispersion and limiting transport to the horizontal. Consequently, only the depths of the atmosphere between these layers permit the ventilation of pollutants over a region. Such situations create obvious implications for local as well as regional transport of aerosols and trace gases.

The objective of the Aerosols, Recirculation and Rainfall Experiment (Dec-97, May/June-98 and Jan-99) was to examine the seasonal transport and recirculation of aerosol particles and cloud condensation nuclei over the eastern half of South Africa and investigate their possible influence on precipitation development over the region. Results indicate that, depending on the stability structure of the atmosphere and the prevailing circulation patterns, pollutants originating over the Highveld affect all the remote environments of South Africa.

**MI02/W/03-A5 1200****THE COUPLED CHEMISTRY-CLIMATE MODEL ECHAM4/CHEM: COMPARISON OF MODEL RESULTS WITH OBSERVATIONS**

Ralf HEIN, Martin Dameris, Volker Grewe, Ines Koehler, Michael Ponater, Christina Schnadt

The atmospheric general circulation model ECHAM4 has been coupled with the stratospheric and tropospheric chemistry module CHEM. Dynamical and chemical features resulting from an interactively coupled simulation (where concentrations of ozone, water vapour, methane, nitrous oxide, and CFCs calculated by the chemical model influence the radiative part of the GCM) are presented and compared with observational data. In particular, model calculated total ozone is shown to be in much better agreement with satellite-based observations than earlier model versions. Another outstanding result of the current model version is its capability to reproduce stratospheric warming in the Northern hemisphere.

**MI02/W/17-A5 1220****FUTURE DEVELOPMENT OF THE STRATOSPHERIC OZONE LAYER**

Christina SCHNADT, Martin Dameris (DLR Institut fuer Physik der Atmosphaere, Germany, email: christina.schnadt@dlr.de)

The coupled atmospheric general circulation and chemistry model ECHAM/CHEM is used to assess the future development of the stratospheric ozone layer. Several time-slice experiments have been conducted to compare possible future climate conditions with the present state of climate. In these simulations, abundance of greenhouse gases are assumed to increase according to the IS92a(IPCC) scenario, the atmospheric concentration of chlorofluorocarbons is specified following the restrictions of the Montreal Protocol (1987)/Copenhagen Amendment (1992). Special emphasis has been laid on the diagnosis of the dynamical and chemical features of the polar regions of both hemispheres in the respective winter and spring periods. First results indicate that the recovery of the ozone layer is delayed due to climate-chemistry interactions.

**MI02/E/03-A5 1240****A GENERAL CIRCULATION MODEL STUDY OF OZONE DECREASE AND ITS GLOBAL IMPACT**

Tatsuya NAGASHIMA, Masaaki Takahashi, Masayuki Takigawa (Center for Climate System Research, University of Tokyo, 4-6-1 Komaba, Meguro-Ku, Tokyo, Japan, email: tnagashi@ccsr.u-tokyo.ac.jp); Hideharu Akiyoshi (National Institute for Environmental Studies, 16-2 Onogawa, Tsukuba, Ibaraki, Japan, email: hakiyosi@nies.go.jp)

A fully coupled dynamical-chemical-radiative general circulation model has been used to study the evolution of ozone distribution and its global impact. Ozone distribution is calculated by continuity equation which takes account of advection, gaseous chemical reactions, photodissociation and heterogeneous reactions on the surface of PSC(Polar Stratospheric Cloud). The surface area of PSC is calculated from model-computed water vapor pressure, nitric acid vapor pressure and temperature. In this model, the radiative cooling and heating rates are calculated using the model-computed ozone distribution, which is the most significant feature of this model. A single year simulation shows the reasonable seasonal evolution of ozone distribution. The Antarctic springtime ozone decrease is also represented. It starts in late August and persists until early November with a minimum value of 250 Dobson units. The ozone decreases mainly occur in the lower stratosphere by chemical reactions of ClO<sub>x</sub>. Consequently the lower stratospheric temperature poleward of 60S decreases about 7K compared with the results of no-PSC calculation in late October. These features of ozone decrease are qualitatively similar to those of observed. The results of multi-year simulation using this model will also be shown.

Friday 23 July PM

Presiding Chair: John Austin (UK Meteorological Office)

**AEROSOLS****MI02/W/11-A5 1410****SULPHUR AS A POSSIBLE SOURCE FOR POLAR MESOSPHERIC CLOUDS**

Michael J. MILLS, Owen B. Toon, Gary E. Thomas (Lasp, University Of Colorado, Campus Box 392, Boulder, CO 80309-0392, USA); Susan Solomon (Noaa Aeronomy Lab, 325 Broadway, Boulder, CO 80303, USA)

A 2D microphysical model indicates that sulphuric acid derived from OCS, SO<sub>2</sub>, and volcanic sources reaches the mesopause, where it nucleates aerosol particles, which correspond well to observed polar mesospheric clouds. PMCs form in thin layers near 82 km altitude, and are thought to be composed of ice particles which nucleate on meteoritic dust. This study proposes sulphate aerosol as an alternative site for ice nucleation.

Stratospheric sulphate aerosol evaporates at the high temperatures present in the upper stratosphere, producing sulphuric acid and water vapor. At the very cold temperatures present at the summer mesopause, these gas-phase components nucleate to form new sulfate aerosol. Using observed temperatures from HRDI measurements, the model predicts the formation of aerosol in excess of 0.5 ppbv and 104/cm<sup>3</sup> during non-volcanic periods. These calculations increase dramatically following significant volcanic input. The maximum in aerosol

mass and concentration occurs between 75 and 85 km and poleward of 60° latitude, providing excellent correspondence to observed PMCs.

The model incorporates sulphur chemistry and microphysics into the Garcia-Solomon dynamical/chemical model, which covers altitudes from 2 to 112 km with 2 km resolution. Microphysical processes include classical binary homogeneous nucleation, coagulation, condensation, evaporation, sedimentation, and atmospheric transport.

**MI02/L/18-A5****1430****TRANSPORT OF AEROSOL PLUMES IN RIBBON LIKE STRUCTURES OVER SOUTHERN AFRICA**

S.J. PIKETH, M.T. Freiman, P.D. Tyson (Climatology Research Group, University of the Witwatersrand, Private Bag 3, WITS 2050, Johannesburg, South Africa); H.J. Annegarn (Group, Department of Geology, University of the Witwatersrand, Private Bag 3, WITS 2050, Johannesburg, South Africa); G. Helas (Max Planck Institute for Chemistry, Department of Biogeochemistry, Mainz, Germany)

Aerosol measurements have been taken during the Southern African Fire-Atmosphere Atmospheric Research Initiative (SAFARI-92), the Southern African Atmospheric Research Initiative (SAARI-94) and the Aerosol, Recirculation and Rainfall Experiment (ARREX-97/98), over southern Africa using a passive cavity spectrometer probe (model PCASP 100X; Particle measuring system Inc. (PMS) Boulder, Colorado). SAFARI-92 was conducted between September and October 1992 to investigate the role that biomass burning plays in contributing to the total atmospheric chemistry over southern Africa and the south central Atlantic ocean region. SAFARI-94 was a follow up experiment to SAFARI-92, to investigate the nature of the tropospheric chemistry in the absence of biomass burning and was undertaken in May 1994. The aim of ARREX (December 1997, May 1998 and January 1999) was to evaluate the recirculation of material over the subcontinent in both summer and winter and to characterise the nature of fine particulate matter acting as cloud condensation nuclei (CCN).

From the combined data sets, it has been possible to identify plumes of elevated aerosol concentrations over the entire southern African subcontinent. These layers occur in distinctive layers in the atmosphere at altitudes that correspond to the presence of absolutely stable layers. The spatial variability of the aerosol layers is determined by the large scale transport over the region. It is hypothesised that emissions from the Mpumalanga Highveld of South Africa feed a polluted layer of the atmosphere for a given period of time. The plume is eventually detached from the source of new pollutants and transported in a structured, highly stable manner over the subcontinent, in ribbon like structures. The ribbons of pollution persist in the atmosphere for days at a time and are transported for several thousand kilometres. There is considerable evidence that shows industrial pollutants impacting at remote sites in South Africa.

**MI02/W/01-A5****1450****ULTRA-FINE PARTICLE PRODUCTION IN RURAL AND MARINE AIR MASSES**

Hugh COE, Paul I. Williams, Keith, Martin W. Gallagher, Karl M. Beswick, Tom W. Choularton (All at Physics Department, University of Manchester Institute of Science and Technology, P.O. Box 88, Manchester M60 1QD, UK, email: hugh.coe@umist.ac.uk); Gordon McFiggans (at School of Environmental Sciences, University of East Anglia, Norwich NR4 7TJ, UK, email: g.mcfiggans@uea.ac.uk)

In past studies, the nucleation of new ultra fine particles has been observed in a wide variety of environments, but binary nucleation of sulphuric acid and water alone cannot explain the measurements. Breakdown products of biogenic hydrocarbons and photolabile iodine species have been postulated as precursors in coastal locations. Here we present results taken at a coastal location in the UK that in southerly and westerly wind directions samples air advected over agricultural farm land, whilst in northerly winds the site is exposed to polar maritime air, free from the influence of local sources from the inter-tidal zone.

There is some evidence of <5 nm particles existing in marine conditions, however, these particles do not appear to grow into the fine mode. Unlike other coastal observations, no dramatic increases in <5 nm diameter particles were observed and indicating that these phenomena are restricted to areas where substantial algal populations exist in the inter-tidal zone. In southerly and westerly winds substantial new particle production was observed, though not all of the time. These periods of production are compared with a parameterisation for sulphuric acid availability that accounts for both the oxidation of sulphur dioxide and loss to pre-existing surfaces. This correlation provides strong evidence for sulphuric acid driven nucleation, though other variables are clearly also important. The roles of humidity and temperature fluctuations in promoting the nucleation of particles were studied and there is also evidence for an unidentified night-time production mechanism.

**MI02/W/13-A5****1510****CONTRAST IN THE ULTRA - FINE MODAL BEHAVIOUR BETWEEN AN URBAN AND A COASTAL SITE**

Paul I. WILLIAMS, H. Coe, M. W. Gallagher, K. N. Bower, K. Beswick, T. W. Choularton (Physics Dept., UMIST, P. O. Box 88, Manchester, M60 1QD, Email Paul.I.Williams@umist.ac.uk); Gordon McFiggans (School of Environmental Sciences, University of East Anglia, Norwich, NR7 4JT, UK)

Many studies in recent years have concentrated on characterising and understanding the aerosol related processes of the rural and marine environments, and the impact they have on local and regional scales. However, more interest is being generated in probing the urban environment and associated urban plumes. As the investigations continue, it is clear from an aerosol point of view that most of the scientifically interesting behaviour occurs at the small end of the size distribution. This includes the high levels of ultra fine particle production (3 nm - 10 nm) and the secondary modification of accumulation mode aerosol (100 nm - 500 nm) by organics generated from motor vehicles. These facts are often swamped when only looking at PM10 levels as an indicator for urban pollution.

The preliminary results from two extensive field campaigns are presented here to contrast the modal behaviour from an urban and a coastal site. The urban measurements were taken from the city of Manchester in the North West of England and the coastal site is located in the South East of England at Weybourne, Norwich. Within the city there is always a concentration and hence production of ultra fine aerosol, whereas the coastal site concentration depends heavily on wind direction. The Urban measurements suggest that there are two mechanisms for production, one correlated with sulfur dioxide and sunlight and the other with motor vehicle exhausts. At the coastal site the number concentration of these nanometer particulates correlate well with predicated sulphuric acid production, although another damping process would appear to be acting.

**MI02/P/01-A5****1600****PRINCIPAL COMPONENT ANALYSIS OF NOX, SO2 AND SPM AT URBAN CITIES IN INDIA**

H.N. SRIVASTAVA (India Meteorological Department New Delhi- 1 10003, India, email: snb@imd.ernet.in)

Three megacities in India namely Bombay, Calcutta and Delhi and 7 major urban cities namely Ahmedabad, Hyderabad, Jaipur, Kanpur, Kochi, Madras and Nagpur are being monitored for suspended particulate matter (SPM), SO2 and NO, since 1978 through National Environmental Engineering Research Institute, Nagpur. In addition, ten Background Air pollution monitoring stations (BAPMON) are in operation in India since 1973-1974 by India Meteorological Department. Principal component analysis has shown that the first principal component explains more than 50% variance at all the stations. The relative loadings of SO2, NOX and SPM have been discussed in detail.

Data from Indian BAPMON stations were also analysed using the Principal Component Analysis by examining broadly the temporal and spatial distribution characteristics of the ions, from mineral and gaseous sources observed in rainwater samples. It was found that sulphates and nitrates are more homogeneously distributed and may, therefore, have gaseous precursors from the natural emissions. The anthropogenic impact of SO2 and NOX, results in relation to the urban climate have been discussed in detail using Principal Component Analysis.

**MI02/E/07-A5****1620****THE NUMERICAL STUDIES OF AEROSOLS SPREADING IN THE NEAR-BOUNDARY LAYER IN THE BAIKAL REGION**

Vladimir Makukhin, Vladimir POTEMKIM (both at Limnological Institute, Irkutsk, 664033 Russia, email: klimat@lin.irk.ru)

Experimental studies of the chemical composition of aerosols in snow cover around industrial sources in the Southern Baikal were carried out. Aerial distribution of mass concentration of main ions in aerosols for 1994-98 different seasons was investigated. It was established that calcium, sodium, and ammonium sulfates, having the total concentration 1.5-3 mg/kg cubic meter, were the predominant salts of aerosol soluble fraction. The main sources of air pollution for the coastline and aquatorium of the Southern Baikal are Baikalsk city and Slyudyanka city. The influence of anthropogenic source in Baikalsk city is traced by the sodium ion accumulation in snow cover. At present, this component may serve as a tracer to value scattering of the wastes of Baikalsk pulp and paper plant. For the first time, sampling of aerosols at the high-mountain station Mondy (the Eastern Sayan, elevation 2000 m above sea-level) and their chemical analysis were realised. Mondy may be considered as a station for monitoring of characteristics of the continental background aerosols. Mathematical modelling of transportation and turbulent diffusion of sulphur and nitrogen compounds, which takes into account chemical reactions, was fulfilled. A series of numerical experiments based on the data obtained during expeditional observations in Lake Baikal region was carried out to verify the mathematical models of atmospheric admixtures transportation. Correlation factors between computed and measured concentrations are equal 0.76 for sulphates and 0.84 for nitrates. Relative errors do not exceed 40% for sulphates and 50% for nitrates; mean square deviations of these errors are equal 25%. The highest deviations of computed concentrations from measured ones are connected with the influence of remote sources.

**MI02/W/20-A5****1640****THE DUAL APPROACH OF OBSERVATIONS AND NUMERICAL MODELLING**

Dr. David LARY (Tel Aviv Univ., Israel)

Issues such as ozone depletion, acid rain, and photochemical smog are all of considerable environmental importance. These issues are studied using the dual approach of observations and numerical modelling. In making balanced assessments of these issues it is vital to make the best use of all the information available to us, both theoretical and observational. This is a non-trivial task. The technique of 'data assimilation' is a powerful tool, which allows us to address this issue. It is revolutionising the way we can study atmospheric chemistry. Data assimilation allows us to simultaneously make good use of however many observations are available to us, our theoretical understanding, and any a priori information we have, within a mathematical framework. It even allows us to infer information about chemical constituents which are not observed. As we move into the new millennium it is a technique which is set to grow rapidly in importance.

**MI03****Wednesday 21 July****THUNDERSTORM CHARGE AND DISCHARGE PROCESSES (ICAE, ICCP)**

Location: Mechanical Engineering, G28 LRE  
Location of Posters: Old Gym

**Wednesday 21 July AM**

Presiding Chair: C.P.R. Saunders, Umist, Physics Department, Manchester, UK

**MI03-A3****Introduction****0950****MI03/W/06-A3****Oral and Poster****1000****PRELIMINARY RESULTS OF OBSERVATIONS OF ELECTRIC FIELD IN CONJUNCTION WITH OTHER METEOROLOGICAL VARIABLES AT THE SURFACE, UNDER A VARIETY OF METEOROLOGICAL CONDITIONS**

Aaron R. Bansemmer and William H. BEASLEY, School of Meteorology, University of Oklahoma, Norman, OK 73019 and Leon G. Byerley, Lightning Protection Technology, 2744 E. 5th St. Tucson, AZ 85716 U.S.A.

We have obtained a continuous series of observations of the vertical component of electric field at ground level at a remote site of the Oklahoma Mesonet. Thus, in conjunction with the electric-field data, we have comparable series of data on air temperature, wind speed and direction, relative humidity, pressure, rainfall rate, and solar radiation at the same site. The observations of electric field were obtained with a new, low-cost, low-power, low-maintenance electric-field mill especially designed for deployment at Oklahoma Mesonet stations. When deployed in significant numbers, these instruments will provide electric-field data at the surface in order to monitor the growth of thunderstorm charge overhead. During the first two

months of operation of a single field mill, we have observed the variations in electric field at the surface that occur during thunderstorms, during ice storms, and from day to day in fair weather. We have recorded frequent occurrences of the "sunrise effect" on mornings with appreciable solar insolation. The intensity of the effect appears to diminish with moderate or strong winds, suggesting that gentle surface fluxes, in the absence of significant winds, may contribute to the process. Other observations include diurnal variations in electric-field intensity, electric-field changes associated with the onset of measurable precipitation, and electric-field changes associated with changes in wind direction.

**MI03/E/04-A3****1020****SURFACE OBSERVATIONS OF POINT DISCHARGE CURRENT IN "RAIN" VERSUS "NO-RAIN" SITUATIONS**

S.S. KANDALGAONKAR, M.I.R. Tinmaker and G.K. Manohar Indian Institute of Tropical Meteorology N.C.L. Post Office, Dr. Homi Bhabha Road, Pashan, PUNE 411 008, INDIA e-mail : sskandal@tropmet.ernet.in

It is a well established fact that the point discharge current (PDC) through the sharp tips of raised earthed conductors and the topographic features of the earth's surface is established under the influence of high electric fields of the overhead thunderstorms. In thunderstorm activity, the reports of occurrence of precipitation associated with PDC are quite common. Measurements have shown that these precipitation elements are usually electrically charged bodies and normally deposit positive charge to the earth's surface (Williams and Heckman, 1993). A pertinent question that surrounds this situation is the interaction (scavenging and attachment) between the PDC ions and precipitation elements near the ground surface and its likely effect on pdc. It appears that little information on this intuitively appealing problem is available in the literature (price, 1993). In this study we describe the observed behaviour of pdc in "rain" and "no-rain" situations of many thunderstorms at pune (18°32'N, 73°51'E ; 559 m asl). Our sign convention of pdc is that the pdc signal received through the discharge needle is termed as positive when the surface potential gradient is positive and vice-versa. We present our results through one table giving average pdc for every half-a-kilo width of electric field in the range -7.0 to +6.5 k Vm<sup>-1</sup> during "rain" and "no-rain" situations. We also present scatter diagrams of one-minute interval values of pdc vs. electric field drawn over the "two" situations. Our results strongly suggest that PDC of both polarities in "rain" is reduced than that in "no-rain". The reduction for negative current was more obvious.

**MI03/E/03-A3****1040****SOME CHARACTERISTICS OF THUNDERSTORM ACTIVITY IN REGION KAKHETI OF GEORGIA**

Avtandil Amirashvili, VAZHA AMIRANASHVILI, Tengiz Gzirishvili (all at the Institute of Geophysics of Georgian Academy of Sciences, 1, M. Aleksidze Str., Tbilisi 380093, Georgia, email: vazha@excite.com) Zurab Chumburidze (Tbilisi State University, 1, Chavchavadze Ave., Tbilisi 380028, Georgia)

Investigation results of the thunderstorm activity of convective clouds in Kakheti (Eastern Georgia) are presented. Data of thunderstorm discharge observations by a network of thunderstorm registrators and electrostatic fluxmeters in summer months 1978-1984 were analysed. In particular, in the mentioned region the mean season intensity of the total number of intracloud and terrestrial lightning discharges amounts to 0.0017 disch. per minute per square km. The ratio of intracloud and terrestrial discharges equaled on the average to 2.2; during one thunderstorm day on the average 0.069-0.113 terrestrial discharges were detected per square km; the lightning discharge intensity was with a satisfactory precision proportional to the third power of the maximum radar cloud echo.

**MI03/E/05-A3****1120****INITIAL DEVELOPMENT OF PRECIPITATION AND ONSET OF CLOUD ELECTRIFICATION IN THUNDERSTORMS AT PUNE**

S.S. KANDALGAONKAR, M.I.R. Tinmaker and G.K. Manohar Indian Institute of Tropical Meteorology, Pune-411008, India N.C.L. Post Office, Dr. Homi Bhabha Road, Pashan, PUNE 411 008, INDIA

The understanding of the real-time sequence between the development of initial precipitation and onset of cloud electrification in the thunderstorms is very important. Such a study is interesting but intricate, because, unlike the other rain bearing clouds the growth of electrification and precipitation in the thunderstorms is so intense and rapid that these two phenomena appear to be simultaneously occurring. The purpose of this study was to examine the relationship between precipitation development and build-up of cloud electrification in thunderstorms. Using one-minute interval data on electric field and the records of rainfall measured at the ground surface, time sequence between initial registration of precipitation and electric field intensification in the neighbourhood of initial registration of precipitation was examined for a series of 14 thunderstorms of the year 1973 at pune (18°32'N, 73°51'E ; 559 m asl). The results of the study are presented in the form of one table and figure. The combined result of this study indicated in-cloud development of precipitation at least 3-7 minutes in advance of electric field intensification. Our result suggests that in most cases the precipitation development in thunderstorms is initiated well before the electric field begins to intensify. Our results appear to be in fair agreement with the results of earlier studies (dye et al., 1986 and 1989).

**MI03/W/05-A3****1140****NEW INSIGHT INTO THE PHYSICAL CHARACTERISTICS OF COMPACT INTRACLOUD DISCHARGES**

D. A. SMITH, P. E. Argo, K. B. Eack, A. R. Jacobson, R. S. Massey (Space and Atmospheric Science Group, MS D466, Los Alamos National Laboratory, Los Alamos, NM 87544, USA, Email: smithda@lanl.gov); W. Rison, P. R. Krehbiel, R. J. Thomas, K. C. Wiens, M. Brook (Geophysical Research Center, New Mexico Institute of Mining and Technology, Socorro, NM 87801, USA, Email: rison@arctic.nmt.edu)

Compact Intracloud Discharges (CIDs) are isolated electrical discharges that occur within intense regions of thunderstorms. We have recently begun to locate the events and characterize their unique physical properties using a number of research systems including the FORTE satellite, the Los Alamos National Laboratory Electric Field Change Sensing Array, and the New Mexico Tech Lightning Mapping System (LMS). Additionally we are employing data from meteorological radars to characterize CID source regions.

It has become clear that CIDs represent a distinct class of thunderstorm electrical discharge, and we are working to quantify physical characteristics that support this distinction. Among their remarkable characteristics are their efficiency at producing very powerful radio frequency radiation, their large characteristic current moments, and their spatial/temporal character. Our

most recent results indicate that RF emissions from CIDs are 20-30 dB stronger than radiation from other intracloud or cloud-to-ground lightning processes in the VHF. Current moments associated with the discharges are at least an order of magnitude greater than moments that occur in conjunction with other processes. Early results on the spatial/temporal character of CIDs indicated that the discharges most often occurred as singular, temporally isolated discharges. However, recent comparisons with the lightning mapping observations indicate that CIDs, when they occur, are followed within a few milliseconds or less by "normal" intracloud lightning flashes. The lightning mapping observations also indicate that VHF radiation from CIDs is not as well localized in space and/or time as the impulsive radiation events of normal lightning. The latter is consistent with the inference that CIDs develop at high speeds over a limited (500-1000 m) extent in the storm.

**MI03/E/01-A3****1200****EXPERTISE OF GROUND LIGHTNING IMPACT USING REMANENT MAGNETIZATION**

Violaine VERRIER and Pierre Rochette (CEREGE, BP80 13545 Aix en Provence Cdx 4, France; email: verrier@cerege.fr)

Most natural (rocks, soils, sediments, wood) or artificial non metallic materials (concrete, brick, plaster, plastic, glass) contain ferromagnetic microparticles carrying a "natural" remanent magnetization (NRM). This NRM, acquired in the weak geomagnetic field during cooling, deposition or solidification of the material, is much weaker than the isothermal remanent magnetization (IRM) acquired instantaneously by exposition to a strong magnetic field. In the environment, only lightning is able to generate a field strong enough to create a lightning induced IRM (LIRM). The LIRM is stable through time after the lightning impact provided that the material is coherent. This phenomenon is well known (e.g. Graham, 1961) but have never been developed for lightning expertise. We designed an original rock magnetic method to retrieve both the direction and intensity of the lightning peak field Bf from any material present in the impact vicinity (up to a few meters). The lightning fields recorded can vary between 10 and 100 mT. From the direction and the intensity of Bf the Ampere or Biot and Savart laws permit to estimate the lightning current geometry and its intensity. On a schoolyard tree struck by a lightning we were able to locate the impact point within a few centimeters, prove that it was a vertical positive current and estimate its peak value at 122 kA. Applications of this technique are numerous from the hazard assessment to the understanding of local magnetic anomalies from field magnetic survey which can be of lightning origin. A calibration of peak currents provided by lightning detection networks can be expected.

**MI03/L/02-A3****1220****ON THE ICE CRYSTAL-GRAUPEL COLLISION CHARGING MECHANISM OF THUNDERSTORM ELECTRIFICATION**

Peter BERDEKLIS and Roland List (both at Dept of Physics, University of Toronto, 60 St. George Street, Toronto, Ontario, Canada, M5S 1A7 email :peter@atmos.physcis.utoronto.ca, list@atmos.physcis.utoronto.ca)

The ice crystal-graupel collision charging mechanism was studied using a newly developed Triple Interaction Facility. The facility is the first to allow independent control of the solid, liquid and vapor phases of a simulated cloud.

As observed in previous studies, the sign and magnitude of the charge transferred during ice particle collisions was found to be a function of the temperature and effective liquid water content of the simulated cloud. However, the charge transfer was even more sensitive to the relative humidity (RH) at which the ice crystals were grown. Varying the RH from ice saturation to water saturation could change the sign of the charge transfer and vary the average magnitude by up to 30 fC per collision. At very high humidities charge transfers of up to -60 fC per collision were observed. Ice crystals grown near water saturation also exhibited a non-linear velocity dependence, with the greatest charge transfers occurring at 5 m s<sup>-1</sup>.

Analysis of the data indicates that a competition between two micro-physical charging mechanisms can provide a consistent physical model of the effect of RH. It will be shown that differences in the RH can explain quantitatively the discrepancies between the observations of previous investigators. A new conceptual model of thunderstorm electrification will also be presented.

**Wednesday 21 July PM**

Presiding Chair: C.P.R. Saunders, (UMIST, Physics Department, Manchester, UK)

**MI03/W/08-A3****Poster****1400-01****A STUDY ABOUT THE OCCURRENCE OF DAYS WITH HIGH ACTIVITY OF CLOUD-TO-GROUND LIGHTNING FLASHES IN THE SOUTHEASTERN BRAZIL IN THE YEARS 1992 TO 1994**

H. H. Faria, O. Pinto Jr., R. B. B. Gin and I. R. C. A. Pinto (all at the National Institute for Space research, INPE, CP 515, Sao Jose dos Campos 12201-970, Sao Paulo, Brazil, e-mail: heloisa@dge.inpe.br)

The occurrence of days with high activity of cloud-to-ground lightning flashes in the southeast of Brazil in the years 1992 to 1994 was investigated. The high activity days were arbitrarily defined as those with more than 20,000 cloud-to-ground flashes. The meteorological conditions and flash characteristics during these days were determined. The lightning data were obtained through a lightning location system (LPATS), and the flash characteristic studied were the polarity, the peak current intensity and the diurnal distribution. Of the 18 events found, 11 occurred in the transition period between the warm and cold seasons, and were associated with the presence of frontal systems organising the tropical convection, and intensifying the lightning activity. Considering the possible contamination of the positive cloud-to-ground flashes by intracloud flashes, only positive flashes with peak current larger than 15 kA were considered. The percentage of positive and negative lightning flashes varied from event to event, presenting average values of 30% and 70%, respectively. No dependence on the period of the year was found. The average peak current was approximately 30 kA for the positive and 40 kA for negative flashes. No dependence on the period of the year was found as well. The negative flashes located at lower latitudes presented higher average peak current than those located more to south higher latitudes, confirming recent studies for the same region. The same was not found for positive flashes. The diurnal distribution of positive and negative flashes presented the same behaviour, with a maximum activity around 18:00 LT. The average duration of the lightning activity during the events (considering 1000 or more flashes per hour) was 4 hours.



**MI03/W/10-A3** Poster **1400-02**

**THE INFLUENCE OF POSITION AND NUMBER OF ELECTRICAL DISCHARGES ON INITIATION AND INTENSIFICATION OF PRECIPITATION FOR CONVECTIVE CLOUDS**

ZLATKO VUKOVIC, 1286 Gryphon Mews Mississauga, L4W 3E5 ONT, Canada, Email: zlatko@armph3.tor.ec.gc.ca; Mladjen Curic, Institute of Meteorology, University of Belgrade, Belgrade, Yugoslavia, Email: curic@rudjer.ff.bg.ac.yu

A one-dimensional axial-symmetric time dependent model has been used to simulate the influence of electrical discharge (ed) on supercooled droplet spectra. The consequence of the lightning channel slope and the number of ed inside the same cloud volume were investigated through 15 different combinations of the initial cloud conditions at a temperature of -10c. The numerical results for a channel slope of 90 (vertical), 60, 45 and 30 degree and 1, 2 and 3 occurrences of ed showed the expected results. The amount of phase transformation of supercooled drops to frozen drop caused by ed shock waves and collisions between supercooled and frozen drops is more significant as the ed is more intensive (energy and number of ed), as the channel slope is closer to vertical position, initial cloud droplets are larger and electrical drop charges are higher. The results also demonstrate the potential of using the acoustic-electric coalescence model to study the microphysical transformations related to ed in convective clouds.

**MI03/W/07-A3** Poster **1400-03**

**THUNDERSTORM ELECTRIFICATION - COMPARISON BETWEEN DIFFERENT PARAMETERISATION SCHEMES OF NON-INDUCTIVE CHARGING**

RUMJANA MITZEVA(Dept. of Meteorology, Faculty of Physics, University o Sofia, Sofia-1164, Bulgaria, email: rumypm@phys.uni-sofia.bg)Atanas Manchev (Dept. of Meteorology, Faculty of Physics, University of Sofia, Sofia-1164,Bulgaria)Clive Saunders (UMIST,P.O.Box 88, Manchester M60, 1QD,UK, email: CPSAUS@mail1.mcc.ac.uk)

Two different sets of equations for non-inductive charge transfer during rebounding collisions between ice-crystals and a riming target, which may be used in numerical models of the development of thunderstorm electric field, will be presented. The first set of equations is derived using Takahashi 1978 and gives the magnitude and sign of charge transfer as a function of liquid water content and supercooling. The second set of equations is derived on the basis of modified laboratory data from Takahashi 1978 taking into account the results and discussion in Brooks and Saunders 1995 and in Brooks et al. 1997. The comparison between the results from the calculations of charge transfer at various cloud temperatures and rime accretion rates using both sets of proposed equations will be discussed.

**MI03/L/01-A3** Poster **1400-04**

**HIGH SENSITIVITY FIELD MILL**

Guiseppe DI STEFANO, Istituto Nazionale di Geofisica,

A simple physical principle, used for the first time at the 1933 by the Harnewell and Van Voorhis, allows building a sensitive and compact electrometer, suitable to measure the atmospheric electric field. Beginning from a mechanic sensor capable to generate a small current, through the electrostatic induction principle when it is placed into an electric field, has been developed a complex processing system, which utilizes the modern electronic methodology. The differential input allows using the instrument in an electromagnetically polluted environment; a high quality N-path filter and a lock-in detector allow obtaining a dc signal (with sign) by a passive integration process. The timing of the whole system operate in synchronous with only the signal of a quartz oscillator; this method is very elegant because it means that if we change the speed of motor the conditioning system keep a regular operation with its high performance. A built-in self-calibration system is periodically operated. This helps keeping the quality of measurements, and, when the instrument is used on a stratospheric balloon, allows to neglect the effect of the ions trapped on the non conductive parts of the field mill stator. During the periodic calibration a motored cover down the sensor and some sample voltage are applied on this shield. The value of the electric field induced by the shield is used to calibrate the instrument. The calibration also provides to recover and to control the effect of the bias current.

**MI03/W/02-A3** **1500**

**PARAMETERIZATION OF THE INTERACTION BETWEEN CUMULUS CONVECTION AND THE SUBCLOUD LAYER.**

Pier Siebesma, European Centre for Medium-Range Weather Forecasts, Shinfield Park, Reading, RG29AX, England. Email: siebesma@ecmwf.int. and Roel Neggers (Royal Netherlands Meteorological Institute, P.O. Box 201, De Bilt AE3730, the Netherlands. Email: neggers@knmi.nl

It is well known that the roots of cumulus convection reside in strong convective plumes that originate from the surface layer. Yet, in large scale weather and climate models it is still common practice to parameterize the dry boundary layer and the cloud layer separately. This results in unwanted overlaps between the schemes and double counting of the transport mechanisms. It also has the additional disadvantage that it requires extra boundary conditions for the convective fluxes at cloud base, which is usually referred to as the closure problem. To overcome these problems a mass flux parameterization is proposed and analysed for strong thermals in the convective boundary layer. Lower boundary conditions can be formulated using the surface layer similarity theory. By subsequently solving updraft equations for vertical velocity, temperature and moisture, this parameterization estimates the nonlocal convective transport of heat and moisture by strong thermals in the subcloud cloud layer that transform into cumulus updrafts in the cumulus cloud layer above the level of condensation (LCL). This way the closure problem is simply shifted to the surface layer and the interaction of cumulus convection with the subcloud layer is established in a natural way. The parameterization scheme is tested and developed using Large Eddy Simulation (LES) results and its impact is evaluated using the ECMWF model.

**MI03/W/01-A3** **1520**

**INITIAL RESULTS FROM A DEPLOYABLE 3-DIMENSIONAL LIGHTNING MAPPING SYSTEM**

William RISON, Paul Krehbiel, Ronald Thomas, Timothy Hamlin, Jeremiah Harlin (all at Geophysical Research Center, New Mexico Institute of Mining and Technology, Socorro, NM 87801 USA, email: rison@ee.nmt.edu)

A lightning mapping system based on Kennedy Space Center's real-time LDAR (Lightning Detection and Ranging) system has been developed that locates impulsive sources of RF radiation produced by lightning discharges. The system utilizes GPS timing at a number of

widely spaced locations to image lightning discharges in three spatial dimensions and time. The system was successfully deployed in two field programs in 1998 - in central Oklahoma during May and June and in central New Mexico during August and September. The RF sources clearly delineate charge layers. In Oklahoma we observe multiple horizontal charge layers, consistent with balloon measurements reported in the literature. We have observed several cases of "inverted" discharges taking place between a main positive charge and an upper negative charge. We also observe high-altitude (15-20 km) RF sources, which are spatially isolated from discharges in the maincloud (at altitudes below 15 km) and appear to occur in overshootingturrets. In New Mexico we observe a lower positive charge region associated with most negative cloud-to-ground discharges. We have located the RF sources from positive bi-polar (+BP) discharges (or compact intracloud discharges), and have found, in the dozen or so cases we have analyzed, that the +BP discharges are followed within a few milliseconds or less by "normal" intracloud lightning flashes.

**MI03/P/01-A3** **1600**

**SOME NEW RESULTS FROM A SIMPLE MODELLING OF THUNDERSTORM ELECTRIFICATION USING THE INDUCTIVE MECHANISM**

Staytcho KOLEV (National Institute of Meteorology and Hydrology, Blvd. Tsarigradsko Shaussee 66, 1784-Sofia, Bulgaria, email: stayko.kolev@aemeteo.bg)

Recent experimental studies in UMIST, have shown that the inductive process of graupel charging, proposed by Sir John Mason, is likely to be an active process of thunderstorm electrification in the later stages of storm development. In the present study are presented the results from modelling numerically the growth of the electric field for realistic thunderstorm conditions. The prepared parameterisation of the inductive charging process permit a wide range of cloud conditions to be examined. The results may be compared indirectly with the electric field growth in thunderstorm leading to the cloud discharges. Assuming that the pollution changes the number and the size of the cloud particles, we could to determinate the electric field variations in the cloud. It gives the necessary information in estimating the expected lightning activity. Using the typical accepted values of the cloud parameters, e.g. hail pellets of averaged radius  $R=0.2$  cm and density  $\rho=0.5$  g.cm<sup>-3</sup>, falling at velocity  $V=800$  cm.s<sup>-1</sup> through a cloud of ice crystals of radius  $r=50\mu$ m and concentration  $n_c = 105m^{-3}$ , with  $a=1$  (the fraction of cloud particles lying in the cylinder swept out by the hydrometeors which actually rebound from it) it has been shown the numerically obtained electric field growth depending on  $n_c$  and  $r$ . As it is expected the aerosols, involved by the polluted environmental, in cloud will modify the concentration of small cloud particles and using reasonable assumptions, it has been calculated the expected rates of growth of electric field in the these cases.

**MI03/W/03-A3** Oral and Poster **1620**

**OBSERVATIONS OF X RAYS AND ELECTRIC FIELD IN AND ABOVE THUNDERSTORMS**

Kenneth B. Eack (Los Alamos National Laboratory, Los Alamos, NM 87544, USA, email: keack@lanl.gov), William H. BEASLEY (School of Meteorology, University of Oklahoma, Norman, OK 73019, USA, email: wbeasley@ou.edu), W. David Rust (National Severe Storms Laboratory, 1313 Halley Circle, Norman, OK 73069, USA, email: drust@nsslgate.nssl.noaa.gov), Thomas C. Marshall and Maribeth Stolzenburg (Physics Department, University of Mississippi, University, MS 38677, USA, email: marshall@beauty1.phy.olemiss.edu)

Confirming the 1925 prediction by C.T.R. Wilson, we have observed the occurrence of bremsstrahlung x rays in thunderstorms, with durations on the order of seconds, in regions in which the electric field exceeded approximately two-thirds the breakdown field for electron runaway. We used balloon-borne x-ray detectors and electric-field meters to observe these quantities simultaneously as a function of height in and above thunderstorms. The x-ray observations are similar to those previously made from aircraft, but to the best of our knowledge, these are the only observations of x-ray intensity with simultaneous observations of electric field inside thunderstorms as a function of altitude. The duration of the x-ray events and the coincidence between reduction in the local electric field and reduction of x-ray intensity (to or nearly to background levels) led us to conclude that the mechanism for production of the observed x rays is driven by the large-scale thunderstorm electric field. The observations are consistent with a runaway electron model (electron multiplication) using estimates of the horizontal electric field and estimates of source distance based on the rate of change with height of the x-ray intensity. The observations are consistent with source distances of 100 m to 300 m from the balloon. Although physically plausible, this is certainly not the only possible explanation. Additional observations are needed not only to characterize the x-ray source better, but also to provide more information on the electric-field strength and vertical profile necessary for the production of the large numbers of energetic electrons thought to be responsible for the x-ray production observed.

**MI03/W/09-A3** **1640**

**RADIO EMISSIONS OF LIGHTNING: GLOBAL MAPS AND TIPP HEIGHT DETERMINATION**

R.S. ZUELSDORF (Institute of Geophysics and Planetary Physics, University of California, Los Angeles, 405 Hilgard Ave. Los Angeles, CA 90095, Email: rzuelsdo@igpp.ucla.edu) A. Jacobson (NIS-1, Los Alamos National Laboratory, Los Alamos, NM 87545) R.J. Strangeway, C.T. Russell (IGPP/UCLA)

From November 1997 throughout August 1998, the Los Alamos FORTE satellite was set to continuously detect lightning in two separate 22 MHz bands: one centered at 38 MHz and the other centered at 130 MHz. Triggering occurred when an RF transient exceeded the noise riding threshold by 20 dBm for 5 of the 8 1-MHz sub-bands in the 38 MHz centered sub-band. The resultant data have allowed for the production of world-wide maps indicating the rate of RF lightning detection. Initial maps indicated the detection of lightning generated RF transients over the equatorial oceans as well as over the continents. Heretofore lightning detecting satellites, which have had optical triggers, have indicated the vast majority of lightning occurs over land. Unfortunately these initial maps do not allow for the comparison of rates from one region to another since the background radiation from anthropogenic sources varies. Here we present maps showing the geographic variation of RF lightning detection from Northern Hemisphere winter, spring, and summer. We also provide maps where the threshold of detection is set to levels exceeding the highest level of global background noise, thus allowing for inter-region comparison. Such maps of the strongest lightning sources shows a strictly continental distribution. This suggests the most powerful of sources are continental. We also present maps of Trans-Ionospheric Pulse Pair (TIPP) detection. TIPP's consist of an initial pulse and a ground reflection, and have a relatively hard spectrum, the power in the 130 MHz band having at least 30% of the power in the 38 MHz band. Previous studies have shown TIPP's to be the most powerful of all satellite detected RF transients. Here we show that the global distribution of TIPP's is much more limited than all lightning generated RF emissions. Work with the Blackbeard instrument on board the ALEXIS satellite in conjunction with stations in the National Lightning Detection Network shows that TIPP heights can occur unusually high in the cloud. Here we present results indicating heights as great as 18 km.

**MI03/W/04-A3** Oral and Poster **1700**

**ELECTRIC-FIELD CHANGES CAUSED BY LIGHTNING, OBSERVED AT ALTITUDE IN AND ABOVE THUNDERSTORMS**

William H. BEASLEY (School of Meteorology, University of Oklahoma, Norman, OK 73019, USA, email: wbeasley@ou.edu) Kenneth B. Eack and David M. Suszcynsky (Los Alamos National Laboratory, Los Alamos, NM 87544, USA, email: keack@lanl.gov)

The atmospheric electrical phenomena known as sprites, elves, and jets have received considerable attention over the last five years. Observations of gamma emissions by the orbiting NGRO, our own observation of a burst of x-ray emissions, lasting about one second, at an altitude of 15km MSL, well above any significant accumulations of charge in a thunderstorm, and unaccompanied by any significant steady electric field, and, at about the same time, speculation in the literature that a quasi-static electric-field change caused by lightning might be the cause of discharges in the upper atmosphere above thunderstorms altogether led us to undertake a program to observe changes in electric field at altitude above thunderstorms, using balloon-borne instruments. We also made observations of x rays with sufficient time resolution to try to determine whether changes in electric field caused by lightning might be the cause of short-duration pulses in x-ray emissions such as those we had observed, as well as the cause of discharge phenomena above storms. During the summer and fall of 1998 we obtained a number of data sets of electric-field changes at altitude, some with accompanying x-ray data, but unfortunately nature did not cooperate with our attempts to get these data at the time of occurrence of sprites in the region. We present comparisons between the field changes as seen at altitude and correlated lightning data from the National Lightning Detection Network.

**MI05** **Monday 19 – Friday 23 July**

**WEATHER SYSTEMS – THEIR STRUCTURE, ORGANISATION AND INTERACTIONS (ICDM, ICCP, ICCL)**

Location: Mechanical Engineering G31 LT  
Location of Posters: Old Gym

**Monday 19 July AM**

Presiding Chair: H.C. Davies (ETH, Zurich, Switzerland)

**LARGE-SCALE ASPECTS**

**Introduction** **0900**

A.J.THORPE (Univ of Reading, UK)

**MI05/W/19-A1** **0910**

**INSIGHTS INTO OBSERVED STORM-TRACK BEHAVIOUR OBTAINED BY FEATURE TRACKING APPLIED TO THE ECMWF RE-ANALYSES**

Kevin I. HODGES (ESSC, University of Reading, Harry Pitt Building, 3 Earley Gate, Whiteknights, PO Box 238, Reading RG6 6AL, U.K., Email: kih@mail.nerc-essc.ac.uk); Brian Hoskins (Dept. of Meteorology, University of Reading, Whiteknights, PO Box 238, Reading RG6 6AL, U.K., Email: B.J.Hoskins@reading.ac.uk)

When the planetary scales are removed from meteorological fields it is possible to track individual features automatically, in a manner similar to that traditionally performed for surface low pressure centres. This procedure has been applied to a large number of fields on several levels from the ECMWF analyses for 1979 onwards. Diagnostics such as track density, feature strength, growth/decay rates and genesis regions have been produced as well as the traditional eulerian diagnostics.

It will be shown that the variables all show the two Northern Hemisphere winter storm-tracks but that they emphasise different aspects. For example 850mb cold and warm features both show a definite N Pacific track but with relatively weak features. The amplitudes are much larger on the upstram side of the N Atlantic storm-track. The cold features tend to originate over N America and the warm features over the subtropical ocean.

The procedure has also been performed on the data stratified by PNA and NAO indices, and interesting differences are apparent, particularly with respect to growth/decay rates.

If time permits some results of the inter-seasonal variation in the northern hemisphere and southern hemisphere will also be presented.

**MI05/W/42-A1** **0930**

**PRIMITIVE EQUATION MODELLING OF MOIST BAROCLINIC WAVES**

Dr Mazzino FANTINI (FISBAT-CNR, Email: M.Fantini@fisbat.bo.cnr.it)

A primitive equation model, in which latent heat release is represented by a small value of static stability for ascending air, is used to examine the early stages of nonlinear evolution of moist baroclinic waves. Results reveal an inconsistency of a previous quasi geostrophic study, and highlight the importance of the formulation of perturbation buoyancy, which is responsible for a temporary increase in growth rate. The perturbation buoyancy term can have a large effect on the dynamical fields even at small amplitude when it acts near the threshold of saturation, as it is shown by comparison of four alternative representations.

**MI05/E/19-A1** **0950**

**MOIST PROCESSES IN STORM-TRACKS AND LARGE-SCALE TEMPERATURE STRUCTURE**

Mike BLACKBURN (Centre for Global Atmospheric Modelling, University of Reading, PO Box 243, Earley Gate, Reading RG6 6BB, UK, email: M.Blackburn@rdg.ac.uk)

Moisture is a major contributor, through both its latent and radiative effects, to the distribution of heating and therefore of temperature in the extratropical troposphere. The latent heating occurs primarily in weather systems in the storm-tracks, whilst moisture transport in the weather systems helps to determine the distribution of moisture and therefore its radiative impact. Moisture thus plays a role in feedbacks between storm-track activity and the large scale structure of the extratropical atmosphere. Idealised experiments are performed to investigate these moist storm-track processes. The experiments build on the "dynamical core" framework, which excludes orography and land-sea contrasts and which includes only fixed or

linear diabatic and frictional effects, by adding a simple interactive moisture cycle and associated heating. Results focus on compensation between sensible and latent heat transports and on tropopause height. An aim is to understand systematic differences in large scale temperature structure and storm-track activity seen in climate simulations by GCMs which differ only in their dynamical formulation. The fact that dynamical processes alone appear unable to explain these differences points to the role of moisture in driving them.

**MI05/W/05-A1** **1010**

**THE MEAN DISTRIBUTION OF 500 HPA CYCLONE CHARACTERISTICS OVER THE SOUTHERN HEMISPHERE**

Murray Keable and Ian SIMMONDS (both at School of Earth Sciences, The University of Melbourne, Parkville, Victoria, 3052, Australia, email: ihs@met.unimelb.edu.au)

The 500 hPa level is understood to be an important 'steering' level for the development of weather systems. It follows that a deeper understanding of the behaviour of cyclonic systems at this mid-tropospheric level will aid in our interpretation of the development and evolution of their counterparts at the surface.

We present here the first comprehensive climatology of 'cyclones' at the 500 hPa over the Southern Hemisphere. This has been obtained by applying a state-of-the-art automatic cyclone tracking scheme to the 500 hPa analyses from the NCEP re-analysis set covering the period 1958-97. Overall, the climatological distribution of systems at 500 hPa bears great similarity to that at the surface and, in particular, both show high densities in the circumpolar trough region. A significant difference, however, is the high number of 500 hPa systems to be found over the Antarctic continent.

**MI05/E/26-A1** **1100**

**LOW FREQUENCY VARIABILITY IN A COUPLED ATMOSPHERE-SEA ICE MODEL**

G. Garric and I.N. JAMES (both at Dept of Meteorology, University of Reading, Box 243, Reading RG6 6BB, UK. E-mail: I.N.James@rdg.ac.uk)

A simplified global atmospheric circulation model is used to study the interactions between developing baroclinic waves and sea ice. A simple dynamical model of sea ice, in which the ice moves in response to the low level wind, leads to a prognostic equation for the lead fraction of the ice cover. At the same time, increasing lead fraction leads to enhanced heat fluxes into the atmosphere. The system gives rise to the possibility of strong feedback between the developing baroclinic wave and the distribution of sea ice, via an "anti-CISK" mechanism: divergence of the ice cover leads to enhanced low level heating while ice convergence leads to reduced low level heating. Even small changes in the ice fraction can lead to large changes in the low level heating. In turn, the changes of the low level heating modify the wind field and the development of the baroclinic wave.

Our parameterisation has relatively small impacts on the linear growth rates and structure of growing baroclinic waves. However, the effects on the non-linear phases of the lifecycles are more pronounced. In some circumstances, the feedback leads to pronounced large scale, low frequency fluctuations of the ice cover. These fluctuations may have spatial scales of several Rossby radii and periods of 50-100 days.

**MI05/E/30-A1** **1120**

**THE ATMOSPHERIC SIGNATURE OF THE NORTH ATLANTIC OSCILLATION**

Marten H. P. AMBAUM, (Dept of Meteorology, University of Reading, UK)

The North Atlantic Oscillation (NAO) is thought to be the major mode of variability in the North Atlantic storm track. It is associated with a dipolar anomaly pattern in the sea level pressure over the Atlantic with opposing centers of action over Iceland and over the Azores. The NAO also has a large impact on the Northern Hemisphere circulation, though the dominant mode of variability for the whole hemisphere has been identified recently as the so-called the Arctic Oscillation (AO). The sea level pressure pattern associated with the AO is more zonally symmetric and has a pronounced center of action over the Pacific. In the presentation, the relationship between the two modes of variability will be put forward. At the same time some comments on the physical interpretation of the two will be made. Evidence is shown that indicates that the NAO, as opposed to the AO, is the dominant physical mode of variability in the Northern Hemisphere midlatitude circulation.

**MI05/E/07-A1** **1140**

**THE STRUCTURAL ORGANIZATION OF ERRORS DURING S.H. BLOCKING**

MOZHENG Wei and Jorgen S. Frederiksen (CRC for Southern Hemisphere Meteorology CSIRO Atmospheric Research, PMB 1, Aspendale Victoria 3195, Australia email: mozheng.wei@dar.csiro.au)

The structures of randomly generated errors evolving in a barotropic tangent linear model, with time-dependent basic states taken from observations, is examined for cases of block development, in the Southern Hemisphere in 1989. The statistics of 100 evolved errors are studied for six day periods and compared with the growth and structures of fast growing finite-time normal modes (FTNMs). The amplification factors of most random errors are slightly less than those of the fastest growing FTNM for the same time-interval. During their evolution, the standard deviation of the error fields become concentrated in the regions of rapid dynamical development, particularly associated with developing and decaying blocks.

The probability distributions and the mean and standard deviations of pattern correlations between each of the 100 evolved error fields and the five fastest growing FTNMs have been calculated for the same time interval. The mean of the largest pattern correlation, taken over the five fastest growing FTNMs, increases with increasing time interval to a value close to 0.6 or larger after 6 days. FTNM 1 generally, but not always, gives the largest mean pattern correlation with error fields. Mean pattern correlations with fast growing FTNMs increase further when the time interval is increased beyond 6 days. The implications of our results for methods of ensemble prediction is discussed.

**MI05/E/16-A1** **1200**

**CONNECTION BETWEEN THE ATLANTIC AND PACIFIC STORM TRACK**

Ulrike BURKHARDT (Department of Meteorology, University of Reading, 2 Earley Gate, Whiteknights, Reading RG6 6BB, UK, Email: ulrike@met.reading.ac.uk)

The separation between the Atlantic and Pacific storm tracks is pronounced only at the lower levels. In the upper troposphere, there is very little break between the two storm tracks. The suggestion is that upper level disturbances cross North America, but the low level, more baroclinically active parts of the disturbances are blocked, mainly by the Rocky Mountains. The traversal upper level systems provide the seeds for the Atlantic storm track. In this way, there can be a coupling between the Pacific and Atlantic storm track. An analysis of this coupling in observational data and in simulations of a simplified global circulation model will be presented.

**Monday 19 July PM**

Presiding Chairs: B.J. Hoskins (University of Reading, UK),  
M.A. Shapiro (NCAR, Colorado, USA)

**LARGE SCALE ASPECTS**

**MI05/E/09-A1** **1400**

**ON THE EDDY ACCELERATION OF THE MEAN ZONAL FLOW IN THE ATMOSPHERE**

Arne M. BRATSETH (Dept. of geophysics, University of Oslo, 0315 Oslo, Norway, email: arne.bratseth@geofysikk.uio.no)

Data sets from a GCM and from the real atmosphere have been analysed in order to study the effect of eddies on the zonal mean zonal flow. For this purpose it is necessary to isolate the Coriolis torque of the mean meridional overturning. In order to avoid Stokes drift effects this is done by means of a transport circulation based on an advection-diffusion operator with transport characteristics as close as possible to the zonally averaged advective transport of the total data set. This transport circulation is direct almost everywhere, but very weak outside the tropics. The diffusivities show a complicated structure with minima near the jet maxima. Zonal accelerations due to other motions than the transport circulation are shown to be correlated to the diffusivities. It will be argued that this is to be expected on the basis of potential vorticity thinking. Weather systems which do not mix the air (for example steady waves) will not change the average PV-distribution, and will have no effect on the mean zonal flow. Strong accelerations of this flow are found when wave growth leads to irreversible wave breaking and mixing. These ideas are supported by an application of the circulation theorem which makes it possible to estimate the effect, and show that it is compatible with the analysed data

**MI05/E/04-A1** **1420**

**GREENLAND AND THE AMBIENT SYNOPTIC-SCALE FLOW**

Cornelia SCHWIERZ, Rene Fehlmann and Huw C. Davies (all at Institute for Atmospheric Science, ETH Zurich, Honggerberg HPP, CH-8093 Zurich, Switzerland, email: schwierz@atmos.univ.ethz.ch)

A study is undertaken of the influence of Greenland upon the synoptic-scale flow. The massifs has several distinctive features that can exert significant dynamical constraints upon the nature of the orographic modification of the ambient flow: (1) its high plateau (heights > 3000m) and steep lateral slopes connote a major nonlinear perturbation of incident airflow, (2) its delta-shape yields longitudinal scales that range from supra-synoptic in the north to meso-alpha further south (3) and its polar location places it somewhat north of the Atlantic storm track in a region with a low ambient tropopause and it also renders curvature effects significant.

In the present study we adopt two complementary approaches. First case studies of uniform incident flows and of an upper-level trough (PV anomaly) translating toward Greenland are performed using ECMWF analysis fields, and second a set of idealized simulations are undertaken with a modified version of the Europa Model (EM) of the German Weather Service (DWD). Together these approaches provide insight on key dynamical aspects of the synoptic-scale flow over and in the vicinity of Greenland.

**MI05/W/28-A1** **1440**

**AN INTERCOMPARISON OF TRACKING STATISTICS FOR ERAAND UNIFIED MODEL CLIMATOLOGY**

David ANDERSON. (Dept. of Meteorology, University of Reading, Earley Gate, PO Box 243, Reading, RG66BB) Brian Hoskins. (Dept. of Meteorology, University of Reading, Earley Gate, PO Box 243, Reading, RG66BB)

The success of a GCM can be judged by its ability to reproduce features and behaviour present in the atmosphere itself. The ECMWF ERA data set represents the best available estimate of the state of the atmosphere during the eighteen year period that it covers. The ability of the UK Met. Office Unified Model (UM) to reproduce mid-latitude variability is investigated by comparing data obtained using a tracking program developed by Dr. Kevin Hodges with similar data derived from the ERA data set. The version of the UM used is called HADAM3. It has produced an eighteen year simulation forced by prescribed sea surface temperatures.

Previous studies have focused on the comparison of the mean fields or the variability about this mean from an intrinsically Eulerian perspective. This study takes the more system orientated approach of tracking individual synoptic scale features throughout their lifetime and then compiling statistics to investigate the atmospheric variability. The results are complementary to the standard view of looking at the variability at a point. Also they allow further insight into the nature of this variability as it is possible to look at the contribution to the variance of the cyclonic and anticyclonic systems separately. Tracking results from a variety of diagnostics will be presented, including mean sea level pressure, meridional wind, geopotential and vorticity. The implications of these results will then discussed in terms of the ability of the UM to reproduce features observed in the ERA statistics.

**MI05/W/20-A1** **1500**

**A GCM INVESTIGATION INTO THE NATURE OF BAROCLINIC ADJUSTMENT**

Leon BARRY, George Craig and John Thurnburn (Department of Meteorology, University of Reading, Whiteknights, Reading, RG1 6BB, UK, email: swr97lb@met.rdg.ac.uk)

Spin down experiments have been conducted using an atmospheric general circulation model to determine the nature and timescale of adjustment to a baroclinic neutral state. The spin

down was obtained by turning off the radiative cooling of the atmosphere. The neutral state was characterised by narrower baroclinic zones with increased static stability but little reduction in maximum meridional temperature gradients. The adjustment was roughly exponential with a timescale of 15-20 days. A spin up experiment was also performed, where the radiation was turned back on in the adjusted state. The original climate was returned in a timescale of 5-10 days. This timescale is clearly shorter than the adjustment timescale, adding to the evidence that the mean state of the atmosphere cannot be said to be baroclinically adjusted.

**MI05/E/12-A1** **1550**

**THE ROLE OF FRONTOGENETIC AND FRONTOLYTIC CIRCULATIONS DURING THE DOWNSTREAM DEVELOPMENT OF BAROCLINIC WAVES**

Manfred KURZ, Deutscher Wetterdienst, Frankfurter Strasse 135, D-63067 Offenbach a.M., Germany, e-mail: istehr@dwd.400.de

The amplification of an unstable baroclinic wave is often followed by the intensification or new formation of waves in the upper current downstream of the first wave. With the aid of a typical example it will be demonstrated that during this process normally frontogenesis takes place ahead of the intensifying ridge or trough through which a solenoidally direct circulation across the frontal zone is released and an upper jet streak develops. The shear vorticity at the flanks of this jet streak is then advected downstream and contributes to the intensification of the next wave. Ahead of the jet streak the particles undergo a frontolytic effect in the wind field leading to a circulation in the opposite direction with an ascent of the colder air and a descent of the warmer air. As a result cold troughs and warm ridges develop, which are eventually cut off during their further development. The approach of such a cold trough towards a baroclinic zone in the lower troposphere can give rise to a coupling of waves and a strong cyclogenesis throughout the whole troposphere. On the other hand also a decoupling of waves with originally upright axes is possible during this kind of intensification process.

**MI05/E/15-A1** **1610**

**THE EFFECT OF MERIDIONAL STRAIN ON BAROCLINIC INSTABILITY**

S.HARE and I.N.James, (Department of Meteorology, University of Reading, U.K.)

Meridional overturning is found in the atmosphere in association with zonal acceleration at tropospheric jet entrance and exit regions. We suggest that such overturning will have an effect on the lifecycles of baroclinic waves, and, in particular, provides a mechanism for breaking the midlatitude baroclinic zone into relatively isolated storm tracks. The growth rates of normal modes of the linearised primitive equation model are reduced by up to 20% by realistic strengths of meridional overturning, and normal mode structures are also significantly affected.

Meridional circulations have a more dramatic effect on the non-linear stages of the lifecycle. A jet entrance type circulation leads to a reduction in maximum eddy energy of up to 80%, while a jet exit type circulation slightly increases the maximum eddy energy. Both types of circulation cause significant changes in eddy structure, particularly in the decay phases of the lifecycle. The calculations are being extended to allow the basic state to evolve, in order to represent the passage of evolving disturbances along the jet.

**MI05/E/06-A1** **1630**

**INTERACTION OF MESOSCALE TROPOPAUSE DEPRESSIONS WITH A WARM-CORE CYCLONE**

K.A.BROWNING, A.J.Thorpe, A. Montani, M. Griffiths, P.Panagi, E.M.Dicks, (Dept. of Meteorology, University of Reading, Reading, RG6 6BB, UK. email: k.a.browning@reading.ac.uk); D.Parsons, National Centre for Atmospheric Research, Boulder, Colorado, USA. email: parsons@atd.ucar.edu

This talk focuses on the coupling between the warm core of extratropical cyclone Lili and 2 pre-existing mesoscale tropopause depressions (TDs), ie downward intrusions of stratospheric air. The TDs approached the cyclone from widely separated sources after becoming cut off from different upper-level troughs upstream of it. Errors identified in model forecasts of cyclone Lili are attributed to analysis errors in the position of one of the TDs. Two methods are used to locate the analysis errors. Both are capable of being used in real time. The first is the identification via satellite imagery of an error in the Met Office model's water vapor analysis, and its translation into thermal and kinematic information via PV inversion. The second method, using singular vectors calculated from the ECMWF model, involves the identification of sensitive regions where any analysis error would be expected to grow rapidly. Forecast reruns made with the Met Office and ECMWF models after modifying the upper-level PV in the analysis showed some limited improvements.

**MI05/E/24-A1** **1650**

**AN EXTRATROPICAL CYCLONE'S PV-TOWER**

A. M. ROSSA\* (email: ros@sma.ch), H. Wernli (email: henry@atmos.univ.ethz.ch), and H. C. Davies (email: davies@atmos.univ.ethz.ch), Institute for Atmospheric Science, ETH Hnggerberg, CH-8093 Zurich, Switzerland \* current affiliation: Swiss Meteorological Institute, Krdhhlstrasse 58, CH-8044 Zurich, Switzerland

Mature extra-tropical cyclones are often associated with a troposphere-spanning column of anomalous Evidence of the modulating as opposed to the dominating influence of diabatic processes upon the cyclone's structure and strength is derived from consideration of: the tower's durable and ephemeral potential vorticity, the PV production along the warm front and sets of model simulations of the event that selectively suppress diabatic PV production.

**MI05/W/41-A1** **1710**

**OCCLUDED MID-LATITUDE CYCLONES**

J.E.MARTIN (Department of Atmospheric and Oceanic Sciences, University of Wisconsin-Madison, 1225 W. Dayton Street, Madison, Wisconsin, 53706 USA, Email: jon@meteor.wisc.edu)

Occluded mid-latitude cyclones are often characterized by a lower tropospheric thermal ridge that connects the sea-level pressure minimum to the peak of the surface warm sector. In an atmosphere in approximate thermal/gradient wind balance, such a thermal structure is associated with a characteristic tropopause-level potential vorticity (PV) distribution in which an isolated, low latitude high-PV feature is connected to the polar reservoir of PV by a thin filament of PV.

In this paper we employ output from a numerical simulation to investigate the evolution of such a "treble clef" tropopause PV distribution during the development of an observed occluded cyclone. It is found that at the tropopause the occlusion process involves the roll up and



breaking of a PV wave. The vector quantity,  $Q_{pv}$ , defined as the Lagrangian rate of change of the PV gradient on an isentropic surface, is employed to examine the kinematics of this wave breaking. Through appropriate partitioning of  $Q_{pv}$  it is shown that the vorticity at tropopause-level controls the cyclonic roll up of the low latitude portion of the "treble clef" (i.e. the PV wave crest). The total deformation field plays a dual role in the observed evolution. It serves to dilate the filament of high PV that connects the low latitude PV feature to the polar reservoir. Deformation also contributes to the wavebreaking by rotating the northern portion of the PV wave anticyclonically. The analysis sheds new light on the structural development of some occluded cyclones, emphasizing the distinct but complementary roles played by vorticity and deformation in the occlusion process. The results are considered in the light of recent idealized numerical experiments regarding the life cycles of extratropical cyclones.

**Tuesday 20 July AM**

Presiding Chairs: M.A. Shapiro (NCAR, Colorado, USA),  
K.A. Browning (The University of Reading, UK)

## EXTRA-TROPICAL CYCLONES

**MI05/W/43-A2**

**0930**

### MESOCYCLOGENESIS IN THE WEDDELL SEA AND THE ROSS SEA REGION OF ANTARCTICA

Thomas KLEIN (Meteorologisches Institut der Universitaet Bonn, Email: unf43e@rhrz.uni-bonn.de)

The Weddell Sea and the Ross Sea of Antarctica are favourable regions for mesocyclogenesis. The interaction of the katabatic wind system in these areas and the development of mesocyclonic vortices is investigated by means of numerical simulations. In contrast to the more homogeneous flow over the interior regions of Greenland and Antarctica, a more complex behaviour of the katabatic winds can be observed in the coastal areas, where the strongest topographical gradients are present. An intensification of the katabatic wind up to gale force can occur in large valleys near the coast, where the topographical structure leads to a channeling of the flow. Additionally, a quasi-permanent baroclinicity is present close to the coast, which can be intensified by the transport of cold air over the open water in association with katabatic surges. Several case studies using the mesoscale model NORLAM were performed in order to investigate the impact of the katabatic wind system on mesocyclogenesis in the Weddell Sea and Ross Sea areas of Antarctica. It is demonstrated that - in connection with suitable synoptical forcings - the katabatic wind system in these regions can trigger mesocyclonic developments by vortex stretching or/and by enhancing the baroclinicity near the surface.

**MI05/L/02-A2**

**0950**

### OBSERVATION OF A POLAR LOW ON THE ROSS ICE SHELF, ANTARCTICA

Michael Beles and Charles STEARNS (both at Space Science and Engineering Center, University of Wisconsin, 1225 West Dayton Street, Madison, Wisconsin 53706, USA)

Satellite images show the development of the comma shaped cloud system on the Ross Ice Shelf, Antarctica commonly called a polar low. The system passed over two United States Antarctic Program automatic weather stations (AWS) on the Ross Ice Shelf. The time variation of air pressure, air temperature, wind speed and wind direction provided a record for a sector of the polar low as the system passed over the two sites compared to nearby AWS sites whose records showed no evidence of the polar low. This polar low did not develop as a classical comma-type system, as is the case when polar lows develop over the open water. Data from the two AWS suggest that local sensible and latent heat fluxes as well as low level cyclonic vorticity contributed to the development of this polar low.

**MI05/W/18-A2**

**1010**

### CASE STUDY OF A QUASI-STATIONARY SYNOPTIC CYCLONE TO THE WEST OF THE ANTARCTIC PENINSULA AND RELATED MESO-SCALE DEVELOPMENTS

Charlotte HEARNSHAW (The Environment Centre, University of Leeds, Leeds, LS2 9JT); Doug Parker (The Environment Centre, University of Leeds, Leeds, LS2 9JT)

A case study of a synoptic cyclone which became quasi-stationary to the west of the Antarctic Peninsula shall be presented. As the fronts from this system crossed the peninsula from North West to South East satellite images showed meso-scale developments to the lee of the mountain barrier.

The dynamics of the processes which lead to these developments will be discussed with the aid of ECMWF operational analyses and data from the Antarctic First Regional Observing Study of the Troposphere (FROST) Special Observing Period 3 (SOP-3), January 1995. This data archive includes scatterometer measurements of surface winds, 1km resolution satellite images, Automatic Weather Station (AWS) data from the east side of the peninsula, data from manned stations on the west and surface pressure charts for the peninsula region prepared by the duty forecaster at Rothera.

**MI05/E/25-A2**

**1100**

### POTENTIAL VORTICITY AND SINGULAR-VECTOR PERSPECTIVES OF DOWNSTREAM BAROCLINIC DEVELOPMENT DURING THE NORTH PACIFIC EXPERIMENT (NORPEX)

Melvyn SHAPIRO (National Center for Atmospheric Research, Boulder CO, 80303, USA, email: mshapiro@etl.noaa.gov); Heini Wernli (Institute for Atmospheric Science, ETH, Zurich, Switzerland, email henry@atmos.unn.ethz.ch); and Rolf Langland and Ron Gelaro (Naval Research Laboratory, Monterey CA, 93943, USA, email: langland@nrlmry.navy.mil)

Simmons and Hoskins (1979) and Orlanski and Chang (1993) extended Rossby's (1949) concept of barotropic energy dispersion to idealized and observed downstream (upstream) baroclinic development. Operational analyses, enhanced with adaptive observations from NORPEX, reveal baroclinic wave packets initiated by cyclogenesis east of Japan. Downstream developing baroclinic disturbances from these packets led to destructive weather events over the western North America and rapidly deepening cyclones off the North-American Atlantic seaboard. Mid-Pacific lower-tropospheric upstream developments which phase with transient upper-level waves in the westerlies are identified. Analyses of tropopause potential vorticity (PV), and lower-tropospheric temperature and wind velocity from ECMWF analyses are used to describe the synoptic perspective of downstream (upstream) development for situations during NORPEX. Hovmöller diagrams for the latitudinal belt 35 to 55 N illustrate the longitude-versus-time evolution of the downstream (upstream) dispersion of tropopause potential vorticity anomalies and surface-based thermal anomalies for expanding baroclinic wave packets. Singular-vector calculations prepared from the NRL/NOGAPS global model identify both west-Pacific developments and their concurrent mid-Pacific downstream developments as observational targets for the reduction of analysis errors that limit 2 to 3 day forecast skill over western North America.

**MI05/E/14-A2**

**1120**

### UNDERSTANDING SINGULAR VECTOR EVOLUTION FROM A PV PERSPECTIVE

Michael C. MORGAN and Chih-Chieh Chen (both at Department of Atmospheric and Oceanic Sciences, 1225 W. Dayton Street, University of Wisconsin - Madison, Madison, Wisconsin 53706 USA, email: morgan@meteor.wisc.edu, chen@meteor.wisc.edu)

In this presentation, the basic mechanisms for development of SV's in a hierarchy of rather simple QG models (Eady, Green and Charney models) are discussed. The salient features of the singular development of these singular vectors are then identified and characterized by the SV's evolving PV distribution. Piecewise PV diagnostics are applied to interpret the SV evolution in terms of the evolution of the SV's interior PV and boundary potential temperature (BT) distributions. Decomposition of the SV's into modal structures (normal modes and continuous spectrum (CS) structures) reveals the role these modes play in the development. It will be shown that the modal decomposition of the SV's reveals that the continuous spectrum plays a detrimental (positive) role in the development for sufficiently long (short) waves. The structure of the CS is described and interpreted in terms of its PV and BT characteristics.

**MI05/E/27-A2**

**1140**

### IDEALIZED MIDLATITUDE CYCLONE DEVELOPMENT: SENSITIVITY TO SURFACE PARAMETERS

Jake BADGER, Brian Hoskins, Paul Valdes (Department of Meteorology, University of Reading, Earley Gate, PO Box 243, Reading, RG6 6BB, UK, E-mail: J.Badger@rdg.ac.uk); and Mike Blackburn (Centre of Global Atmospheric Modelling, Department of Meteorology, University of Reading, Earley Gate, PO Box 243, Reading, RG6 6BB, UK)

Experiments have been performed that explore the sensitivity of initial cyclone development to various profiles of fixed surface temperature, surface moisture and initial interior moisture, using the Reading Intermediate General Circulation Model. These experiments have shown that surface moisture, in conjunction with conditional instability, is crucial in determining system growth rates. How the ocean surface parameters are altered by the passage of weather systems will be shown by driving a mixed layer ocean model non-interactively using the atmosphere boundary layer fluxes. The importance of the feedback between the oceanic mixed layer and the atmospheric cyclone will be investigated by rerunning the life-cycle experiments with a fully coupled oceanic mixed layer. Implications for storm-track behaviour will be discussed.

**MI05/L/01-A2**

**1200**

### UPSTREAM DEVELOPMENT IN IDEALIZED BAROCLINIC WAVE EXPERIMENTS

Heini WERNLI (Institute for Atmospheric Science, ETH Zurich, Switzerland, email: henry@atmos.unn.ethz.ch); Melvyn A. Shapiro (National Center for Atmospheric Research, Boulder CO, 80303, USA, email: mshapiro@etl.noaa.gov); and Juerg Schmidli (Geography Institute, ETH Zurich, Switzerland, email: juerg@atmos.unn.ethz.ch)

An idealized dry primitive equation model on the  $f$ - $\sigma$ -plane is used to study upstream (and downstream) baroclinic wave development. The simulations are initiated with localized finite amplitude and vertically evanescent perturbations, specified either as upper-level potential vorticity or surface potential temperature anomalies. The nonlinear evolution of these nonmodal perturbations leads to the generation of large-scale upper-level induced primary and downstream surface cyclones, and of distinctively smaller, shallow and more slowly intensifying upstream systems. It is shown that in particular the genesis and evolution of upstream cyclones is highly sensitive to the scale of the initial perturbation. Narrow upper-level troughs (or zonally confined surface temperature anomalies) are favorable for upstream development, whereas no or only weak upstream activity occurs with broad planetary-scale troughs (or zonally extended surface temperature anomalies) as initial perturbations. It is proposed that this sensitivity property of upstream development is qualitatively related to the dispersion characteristics of surface edge waves. Consideration is also given to the vertical coupling of lower tropospheric upstream systems with transient upper-level waves.

**Tuesday 20 July PM**

Presiding Chairs: K.A Browning (The University of Reading, UK),  
P.Mascart (Laboratoire d'Aerologie, Toulouse, France)

## EXTRA-TROPICAL CYCLONES

**MI05/W/47-A2**

**1400**

### APPLICATION OF THE SPLITTING DIAGNOSTIC METHOD TO A RAPIDLY DEVELOPING CYCLONE

Qiu-shi CHEN (Byrd Polar Research Center, The Ohio State University, 1090, Carmack Rd., Columbus, OH 43210, USA, Email: qchen@polarmet1.mps.ohio-state.edu)

Sensitivity studies only reveal long-term, integrated effects and stop short of providing interpretations of how the evolution of the phenomenon is controlled by the step-by step interactions and feedbacks. The method of combining diagnostic and sensitivity studies together is a way for removing this shortcoming and for understanding the evolution of a phenomenon simulated in complex models. The traditional definition of the geostrophic wind cannot be used in the region near the equator because the Coriolis parameter is present in the denominator. Using the wind partitioning into the streamfunction and velocity potential, the geopotential field can be separated into a geostrophic part and an ageostrophic part. The horizontal pressure gradient force of the geostrophic geopotential is equal to the Coriolis force of the rotational wind. The ageostrophic part is the difference between the geopotential and its geostrophic part. An ageostrophic temperature is defined from the ageostrophic geopotential based on the hydrostatic equation. The vorticity and divergence equations are transformed into the inner part equations of streamfunction and velocity potential in a limited region (Chen et al. 1997, Mon. Wea. Rev., 143-167). These inner part equations are solved by a semi-implicit time splitting scheme with zero lateral boundary value, and the advection and heating terms are expressed by forcing terms. The solutions of the equations for each of splitting time steps can be separated into two parts. One is the solution of the homogeneous equations with the initial values, and it describes the geostrophic adjustment process from the initial values. The other is the solution of the inhomogeneous equations with the zero initial value, and in this solution, the ageostrophic geopotential and velocity potential are generated from the zero value by the advection-heating process. These two processes are interacted between two adjacent splitting time intervals. These interactions are the basic mechanism for the variations of the synoptic and mesoscale systems. The splitting diagnostic method is to use these interactions in diagnosis.

**MI05/E/21-A2 1420****MESOSCALE STRUCTURE OF CYCLONES IN THE NEW ZEALAND AREA**

Michael REVELL and Warren Gray (National Institute of Water and Atmospheric research, Wellington, New Zealand, email: m.revell@niwa.cri.nz); James McGregor (Research School of Earth Sciences, Victoria University of Wellington, Wellington, New Zealand, email: Jim.mcgregor@vuw.ac.nz)

Based on earlier classification work by Sinclair and Revell we have selected 4 cases of cyclogenesis (one from each of the major classes with contrasting frontal structures) that produced heavy rainfall, flooding and strong winds over northern New Zealand. The 4 cases consist of (a) an ex-tropical cyclone, (b) a convective storm, (c) a well organised intense front in a northwest-southeast trough, (d) a 'bomb' in the NE Tasman Sea. Calculations of potential vorticity (PV), system relative flow and trajectories derived from high resolution RAMS runs nested in ECMWF data will be used to explain some of the fine scale wind and rain patterns observed in high resolution satellite and radar output. Conceptual models will be presented showing how the differing synoptic-scale environments for the different classes, e.g the position of the major jet streams and PV anomalies relative to the storm, lead to contrasting frontal development.

**MI05/E/18-A2 1450****EXTRA-TROPICAL LIFE-CYCLE STUDIES OF COLD AIR CONVECTION IN HADAM3**

L. SHAFFREY (CGAM, Department of Meteorology, University of Reading, Reading, RG6 6BB, U.K., email: L.C.Shaffrey@reading.ac.uk); C. Jones (SMHI, Norrköping, Sweden, email: Colin.Jones@smhi.se)

In common with many AGCMs (Atmospheric Global Circulation Models), large amounts of convective activity can be seen in the wintertime storm tracks of the UKMO's atmospheric climate model, HadAM3. High resolution life-cycle studies of extra-tropical cyclones observed during FASTEX (Fronts and Atlantic Storm Track Experiment) are integrated and compared with UKMO analyses. This comparison reveals that there is too much convection occurring in the cold air behind the modelled extra-tropical cyclones.

A new non-local boundary layer scheme has been developed at the UKMO which should improve the representation of convective boundary layers in the model. The introduction of the new boundary layer scheme reduces the errors associated with the cold air convection, suggesting that some of these errors are due to a poor interaction between the boundary layer and the convection schemes.

**MI05/E/22-A2 1550****A PIECEWISE POTENTIAL VORTICITY DIAGNOSIS OF FRONTOGENESIS**

Michael C. MORGAN (Department of Atmospheric and Oceanic Sciences, 1225 W. Dayton Street, University of Wisconsin - Madison, Madison, Wisconsin 53706 USA, email: morganc@meteor.wisc.edu)

The technique of "piecewise" potential vorticity (PV) inversion is used to identify the non-divergent wind fields attributed to upper, middle, and the lower tropospheric PV anomalies in addition to the irrotational wind with the goal of diagnosing the respective wind field's frontogenetic potentialities. Frontogenesis is diagnosed using a piecewise separation of the Q-vector into parts associated with the partitioned wind field. Partitioned geostrophic Q-vectors are used to diagnose the vertical motion attributed to the upper, middle, and lower tropospheric PV anomalies.

Insight gained from this new diagnostic technique is demonstrated by examining surface and upper tropospheric frontogenesis associated with a particular case of extratropical marine cyclogenesis resulting from the interaction of an upper tropospheric shortwave trough with a surface thermal wave.

**MI05/W/13-A2 1610****FRONTOGENESIS AND FRONTAL COLLAPSE IN THE ADJUSTMENT OF NON-UNIFORM POTENTIAL TEMPERATURE GRADIENTS AND VERTICAL SHEARS OF HORIZONTAL WIND**

cZhe-Min TAN, (Department of Atmospheric Sciences Nanjing University Nanjing 210093 PR China)

In the atmosphere, a frontal-type discontinuity, e.g. see-breeze front and gust front can be formed with a few hours and have gravity current structure that limit the useful of balanced theory of front, e.g. the semi-geostrophic balanced mode. The geostrophic adjustment is one possible mechanism of frontogenesis when the deformation field is imposed. The frontal discontinuity was developed by the geostrophic adjustment. The frontogenesis and frontal collapse in the adjustment of non-uniform potential temperature gradients and vertical shear of horizontal wind under different initial conditions were discussed in detail. The initial unbalanced state play an important role in the time-scale of adjustment frontogenesis and frontal structure. Moreover, the role of diabatic heating on the frontogenesis by geostrophic adjustment were investigated by an approximate method.

**MI05/W/17-A2 1630****THE EVOLUTION OF A PASSIVE TRACER IN THE VICINITY OF AN ATMOSPHERIC FRONT AND ITS IMPLICATIONS FOR THE DEVELOPMENT OF NON-COINCIDENT FRONTS IN THE THERMAL AND TRACER FIELDS**

Douglas J. PARKER (The Environment Centre, University of Leeds, Leeds, LS2 9JT, UK)

Many observations have shown that a synoptic front is not generally an airmass boundary, and that there may be relative airflow through the frontal zone at different heights. Semigeostrophic theory allows for the description of frontal zones which are not airmass features: it will be shown how the evolution of such fronts allows trace properties of the air to be advected through the frontal zone, and thereby form fronts in the tracer field which are not coincident with the thermal front. These ideas will be used to suggest an explanation for the formation of forward-sloping cold fronts, and to describe the likely evolution of pollutants in a frontal environment.

**MI05/E/13-A2 1650****THE USE OF OBJECTIVE FRONTAL ANALYSIS TO CHARACTERIZE FRONTS IN THE NEW ZEALAND REGION**

Warren GRAY and Michael Revell (National Institute of Water and Atmosphere, PO Box 14 - 901, Wellington New Zealand, Email w.gray@niwa.cri.nz)

A simple objective method for the analysis of fronts in numerical model output, based on that of Hewson (1998), will be presented. This approach uses the Laplacian of the gradient of the temperature field to diagnose the location of fronts, and diagnostics of temperature advection to characterize the front. The role of this simple diagnostic in the synoptic weather systems program will be outlined - and its use in linking mesoscale model output to remotely-sensed observations of the weather associated with fronts. This research will lead to the development of conceptual models that will relate the model fields to the weather being experienced on the surface. A case study of a frontal system which lead to heavy rainfall, flooding, and strong winds will be presented. At various stages this front exhibited both forward and rearward sloping cold frontal systems (analogous to ana and kata fronts). Overlaying satellite imagery with model output and frontal analysis highlighted the cloud patterns associated with these particular examples. Diagnostics of potential vorticity highlighted an area of inertial instability. Analysis suggests that this area of instability was the consequence of diabatic heating resulting from latent heat release. Examples of radar-observed rainfall and wind fields will also be shown. Hewson, T. D. (1998) Objective fronts. Meteorol. Appl. 5, 37-65.

Wednesday 21 July AM

Presiding Chair: A. Joly (CNRM, Meteo, France)

**FASTEX-UPSTREAM****MI05/L/04-A3****0900****WHAT ARE THE MOST IMPORTANT ERRORS IN THE INITIAL CONDITIONS FOR NUMERICAL WEATHER FORECASTS ?**

C. SNYDER, (NCAR/MMM PO Box 3000 Boulder CO 80307 USA, Email: chriss@ucar.edu); T. Hamill (NCAR) and R. Morss (MIT)

From the perspective of numerical weather prediction, errors in initial conditions (or, the analysis) are important to the extent that they influence subsequent forecast errors. Owing to random errors in the observations and in models, this problem is inherently statistical; forecast uncertainty or expected forecast skill is quantified by the forecast covariance matrix. The leading eigenvector of that matrix is the structure that "explains" the largest fraction of forecast error variance, and the initial error that gives rise to that eigenvector (i.e., that is mapped onto the leading eigenvector by the forecast model) is the most important analysis error. We employ a simple quasi-geostrophic model and three-dimensional variational data assimilation scheme to produce Monte-Carlo simulations of analysis and forecast error statistics, from which we calculate the leading eigenvectors of the forecast error covariance matrix, and the analysis errors that give rise to them. The resulting initial errors have maximum amplitude aloft, near the tropopause, are deep with decay toward the surface, and have weak or nonexistent tilts in the vertical. These properties stand in contrast to those of the fastest growing errors (in, say, an energy norm), which are concentrated in the mid- to lower troposphere and have fine vertical structure and large vertical tilts. Although the optimal design of observing networks is a subtle question that itself depends on the statistics of short-range forecast errors, the results indicate that observations need not necessarily resolve fine vertical structure in the lower troposphere as has recently been speculated.

**MI05/W/14-A3****0920****SINGULAR VECTOR GROWTH FOR FASTEX CYCLONES**

Andrea MONTANI (ARPA-SMR, Viale Silvani 6, 40122 Bologna, Italy, Email: m1xukuej@sirio.cineca.it); Alan J. Thorpe (Dept. of Meteorology, Univ. of Reading, Reading RG6 6BB, UK, Email: swsthorp@reading.ac.uk)

Calculations of localised singular vectors (SVs) have been performed using the ECMWF/IFS forecasting model and the dynamical properties responsible for the SVs' growth have been investigated for cases of cyclogenesis during FASTEX. Theoretical results from earlier studies on fast-growing perturbations are examined and their applicability to events of SV growth related to real cases of cyclogenesis is assessed, gaining insight into the mechanisms by which SVs grow. Potential vorticity (PV) diagnostics are used to investigate the dynamical processes responsible for SV growth in terms of total energy and PV and SVs' growth rates are compared to those predicted by normal mode theory. The most dynamically active regions within a SV are looked for, by considering the independent evolution of perturbations initially confined either in the lower or in the upper troposphere. The part of SVs located below 500 hPa is found to play a major role in the interaction processes between the perturbation and the basic state fields and to be responsible for the SVs' development. The relative increase in terms of energy is related to the vertical propagation of the disturbance. In the early stages, SVs' growth rates well exceed those predicted by the Eady model, the non-normal nature of the perturbation being more evident. Then, the growth rates decrease, being closer (but still larger) than those predicted by normal theory. SVs also grow in terms of PV when their velocity components can interact with basic state PV horizontal gradients.

Perturbations initially confined at low levels can propagate vertically more efficiently than those localised above 500 hPa and the interaction with the upper-level basic state fields is much more effective. The extent to which balanced-flow theory, valid in idealised models of non-normal growth, can be applied during the evolution of SVs is also examined. If SVs are calculated with the total energy norm, their initial state is found to be out of balance, because of a lack of amplitude in the vorticity component, being about a factor 4 too small. During the evolution, SVs achieve a more balanced configuration. SVs, calculated with initial norms which are better approximation of the analysis error covariance metric, show no sign of imbalance also at initial time.

**MI05/W/46-A3****0940****THINKING AND SENSITIVITY TO INITIAL CONDITIONS: TO THE PRECURSORS OF A CYCLOGENESIS**

Philippe ARBOGAST, Joly. (G. Coriolis Toulouse Cedex France, Email: philippe.arbogasta@mateo.fr)

In the last few years, the theoretical study of cyclogenesis experienced a remarkable renewal. The new data required by 's concepts is provided by the observations collected during FASTEX field experiment. The aim of the presentation is to preexisting synoptic scale disturbances responsible for cyclogenesis using a new diagnostic tool: the manipulation initial conditions through quasi-geostrophic potential and its variational inversion. The QG perspective of the inversion, apparently not consistent with a primitive equation, turns out to be efficient in the modification of initial of a primitive equations model. technique is applied to demonstrate quantitatively various occurring between the key dynamical patterns involved the 17th Intensive Observations Period (IOP) of FASTEX. study reveals the unexpected importance of a low level whereas this case looked like a straightforward of the cyclone by an upper tropospheric disturbance. way this precursor influences, at a distance, the baroclinic where the new cyclone will form is studied quantitatively. is shown that this happens where the perturbation introduced the precursor favours barotropic energy conversion



**MI05/W/22-A3 1000****COMBINED USE OF SENSITIVITY INFORMATION AND OBSERVATIONS TO IMPROVE METEOROLOGICAL FORECAST**

Gwenaëlle HELLO (Meteo-France/CNRM/GMME, 42 Av Coriolis, 31057 Toulouse cedex, FRANCE. E-mail: Gwenaëlle.Hello@meteo.fr)

Progress in the area of the numerical prediction of weather events leads to a strange inconsistency: as the realism of the numerical modelling of very fine scale process such as regional winds, local events (fog, breeze) is increasing, the synoptic forecast of meteorological events of larger scales such as storms or cyclogenesis is still subject to major numerical forecast failures. Most part of it can be attributed to initial conditions errors. These errors are generally of little consequence, except in those situations that support large amplification of small perturbations. This underdetermination of the analysis state of the atmosphere can be due to the lack of observations and/or to the weakness of the assimilation scheme to use them properly.

The sensitivity fields (such as gradient fields, singular vectors) can be used in a pronostic way in order to identify in the initial conditions the geographical areas where analysis errors are likely to grow rapidly leading to a change inside the area of interest. This is used for example to determine the location of targeted observations. In this study, the sensitivity fields are used to perturb the analysis state in order to provide new initial conditions more consistent with the atmospheric flow. This is done using the available observations inside the sensitive area which are used to calibrate the amplitude of the "sensitive" perturbation.

The method and its application to real cases will be presented. The feasibility of the method in regard to operational applications as well as undergoing developments of it will also be discussed.

**MI05/W/21-A3 1100****ASSIMILATION OF OBSERVATIONS INSIDE SENSITIVE AREAS**

Alex DOERENBECHER (Meteo-France/CNRM/GMME, 42 Av Coriolis, 31057 TOULOUSE cedex, FRANCE E-mail: Alex.Doerenbecher@meteo.fr Gwenaëlle Hello and Thierry Bergot (same address)

Forecasts of rapid cyclogenesis events leads sometimes to predictability problems in Numerical Weather Prediction even at very short ranges. The study of such topics was one of the scientific objectives of the FASTEX field phase (Joly et al. 99). The concept of adaptive observations was tested in the experimental context of FASTEX. That means to make specific "targeted" observations inside geographical sensitive areas which had been numerically preprocessed (singular vectors and or gradient sensitivity fields). On the first hand, the current assimilation methods are not efficient enough to optimally take into account these observations, made inside sensitive areas. In cases of very weak predictability, the projection of the analysis error into the unstable subspace is detrimental for the forecast (Bergot et al. 99). On the other hand, adaptive observations is based on the only information available that is the definition of the area to sample. The challenge is then to sample efficiently this sensitive region. In order to achieve optimal sampling, the role and properties of data assimilation scheme employed cannot be neglected anymore. Extra observations, assimilation and the dynamical properties of the current trajectories must be linked together in a consistent global approach. The goal is to determine in advance where and how much extra data are required to maintain a good control of the unstable plane, knowing that a 3D-VAR or a 4D-VAR technique is employed. The theoretical approach needed will be outlined and some of the difficult or open points that it contains will be documented by diagnostic calculation performed on some FASTEX cases.

**MI05/W/44-A3 1120****DATA IMPACT EXPERIMENT OF FASTEX ADAPTIVE OBSERVATIONS**

T.BERGOT (Meteo-France, CNRM, 42 Av Coriolis, Toulouse, 31057, France, Email: Thierry.Bergot@meteo.fr); HELLO and Alex Doerenbecher (same address)

Of the main scientific objectives of FASTEX was to provide called adaptive observations, in area of strong sensitivity, order to control the development of forecast errors. The purpose this concept is to concentrate observations in that of the flow from where small analysis errors will amplify. Aircrafts equipped for GPS dropsondes (NOAA Gulfstream IV, hereafter GIV, and NCEP Learjet36, hereafter L36) tasked to sample these dynamically crucial areas (12 L36 flights and 8 GIV flights are studied here). main goal of this work is to investigate the efficiency of adaptive observations obtained in real time during FASTEX. model used for these tests is the ARPEGE/IFS model with a of T95C3.5 (3.5 stretching factor) and 27 vertical levels. the first step, the assimilation scheme used is an incremental 3Dvar, a T63 resolution for the increments. Most FASTEX adaptive observations a non-negligible impact on the short-range forecast (the impact defined as the difference between forecasts with and without observations). mean impact is about 9hPa for 36h forecasts (10.8hPa for the GIV7.8hPa for the L36), with a maximum of 28hPa. improvement of forecast quality is tested by comparing forecasts and without adaptive observations to verifying analyses. mixture of improvement and deterioration is obtained, for the 20 cases studied, the mean improvement is weak and has same order of magnitude as the analysis errors, but with a large spread. discriminating study of the cases shows that a strong improvement is when the guess is found a posteriori to be poor (i.e. when predictability is weak). these results prove that the adaptive observation technique, in real time during FASTEX, a large amplifying impact and could strongly influence forecasts. But also suggest that the current assimilation system, as 3Dvar, is not able to build efficient initial field (with no error in the most unstable directions for example). assimilation inaccuracies may hide the impact of observations, pointing out the lack of optimality of the assimilation system. results, using advanced assimilation method (4Dvar, control of the error on the unstable subspace), will also be presented, and will allow to discuss this point.

**MI05/W/45-A3 1140****FASTEX 4 D VAR RE-ANALYSIS**

G.DESROZIER (Meteo-France, CNRM, 42 Av Coriolis, Toulouse, 31057, France, Email: Gerald.Desroziers@meteo.fr)

An unique observation network has been settled during FASTEX in the Northern Atlantic ocean. This observation set was particularly based on high cadence radiosoundings performed by ships and dropsondes launched by planes. The dropsondes were made, for a part of them, in a far upstream domain, in order to observe precursors of subsequent cyclones. Additional vertical profiles were given by FASTEX ship soundings or by dropsondes in a "near" upstream area, observing cyclones at their developing stage. Finally, cyclones were sampled, at their mature stage, by high resolution dropsondes focussing on fine scale structures. We aim at producing a complete reanalysis of the FASTEX situations. A particular difficulty to handle the FASTEX observations is due to the fact that most of them are not synchronous with synoptic time. This problem is solved with a 4D-Var scheme, which allows the use of such asynoptic data. Such a 4D-Var analysis is under development at Meteo-France. A main feature

of the 4D-Var scheme developed at Meteo-France is the use of a stretched geometry for the reference trajectory, which provides a very high local resolution. The application of the 4D-Var scheme to the FASTEX data is found very encouraging, since it appears to handle this dataset consistently. There is also a clear impact of the FASTEX observations, which contain an information that is not given by the operational network. This is particularly true for high resolution dropsondes sampling the cyclones at their mature stage, and providing, through the use of 4D-Var, a description of the mesoscale structures of cyclones.

**MI05/W/29-A3 1200****SENSITIVITY OF DEEPENING CYCLONE WITH RESPECT TO THE SST IN THE FASTEX EXPERIMENT: APPLICATION TO THE IOP15**

Hervé GIORDANI (Meteo-France, CNRM, 42 Av Coriolis, Toulouse, 31057, France, Email: Giordani@meteo.fr); Guy Caniaux

Sensitivity of the cyclogenesis with respect to the SST is poorly known and the oceanic component of FASTEX experiment (1997) called CATCH contribute to answer towards this open question. Thanks to the operational and experimental data ships, optimal SST re-analyses were performed in the North Atlantic current region where the SST gradients reach  $5^{\circ}\text{C}/50\text{ km}$ . This paper presents the cyclogenesis development of the IOP15 (13-15 February 1997) because its strongest surface deepening occurs precisely when the cyclone crosses the SST front from the cold to the warm waters. In order to evaluate the impact of the surface differential heating on the frontogenesis and cyclogenesis, three atmospheric simulations were performed with the non hydrostatic model Meso-NH. The reference simulation was performed with the SST re-analysed and the other both are respectively carried out with constant SSTs of  $3^{\circ}\text{C}$  and  $15.6^{\circ}\text{C}$  over the domain. It appears that the reference simulation is 12 hPa lower,  $10^{\circ}\text{C}$  warmer and 5 g/kg moister in comparison with the cold SST simulation, and the low center trajectory is different in comparison with the warm SST simulation. Therefore spatial distribution of the surface turbulent fluxes will be presented and their impact on the atmospheric front intensity (vertical velocity, shear wind, precipitations, cold sector activity,) will be analysed for the three simulations.

**MI05/W/30-A3 1220****DETERMINATION OF THE THERMAL STRUCTURE AROUND THE TROPOPAUSE FROM TOVS OBSERVATIONS FOR 3 FASTEX IOPS**

N. FOURRIE (1), C. Claud (1), J. Donnadille(2), A. Joly(3), R. Armante(1) (1) CNRS/LMD/ARA, Ecole Polytechnique, F-91128 PALAISEAU Cedex (2) Laboratoire d'Aérodynamique, Observatoire Midi-Pyrénées, 14, avenue Edouard Belin, F-31400 Toulouse (3) METEO-FRANCE CNRM/GMME/RECYF, 42 av. G. Coriolis, F-31057 Toulouse Cedex 1

Among the numerous scientific objectives of the FASTEX campaign, an important issue concerns the genesis mechanism and more specifically the existence of preexisting upper level anomalies. Observations from the satellites of the TIROS-N series, equipped with the HIRS-2 (High Resolution Infrared Radiation Sounder) and MSU (Microwave Sounding Unit) radiometers, allow for the determination of the so-called Temperature of the Lower Stratosphere (TLS) as it has been defined in the 3I (Improved Initialization Inversion) approach to the inversion of the Radiative Transfer Equation and which represents the temperature around the tropopause. This parameter is determined at a spatial resolution of  $100 \times 100 \text{ km}^2$  which is a compromise between HIRS 2 and MSU spatial resolution. For 3 FASTEX IOPS (12, 17 and 18), TLS fields have been derived and will be discussed. TLS anomalies have been compared to other independent diagnostics : in particular, MSU channel 3 brightness temperatures, and 2PVU surface thermal fields computed with the ARPEGE model (Meteo-France). Such studies show the interest of such a variable for characterizing and following upper level structures (jets, potential vorticity cores).

In addition, recently, a new method for calculating TLS at HIRS 2 resolution (30 km) has been developed. We will therefore show the advantages of an increased spatial resolution for the diagnostic of altitude precursors.

Wednesday 21 July PM

Presiding Chair: J. Nielson-Gammon (Texas A&M University, Texas, USA)

**FASTEX-THEORY/MODELLING****MI05/E/23-A3 1400****SPLITTING WEATHER SYSTEMS: CYCLOGENESIS IN A COMPLEX SETTING SEEN IN FASTEX AND A CLIMATOLOGY OF NORTH-ATLANTIC CYCLONES**

Alain JOLY, Franck Ayrault, Christophe Baehr (Météo-France, CNRM/GMME/RECYF, Toulouse, France)

On several occasions during the two months of the FASTEX field experiment, the tendency for one well developed cyclone to split into two or even three new individual systems has been observed. One such case will be shown in some detail, and the other occurrence will be listed. From the point of view of predictability, this situation generates a maximum of uncertainty for the forecaster: which system will grow the most? Models often make different choices in these circumstances. This behaviour is also the characteristic feature of several "initiation" classes of the climatological study of cyclogenesis performed by one of us by an automatic classification procedure based on the tracking of all the cyclone events found in the ERA re-analysis. These classes show new lows forming in close proximity of older, larger ones. The environment is not a simple, 2D front or baroclinic zone, but a fully featured cyclone. It is possible, from this classification, to provide a sound statistical idea of the frequency and main characteristics of this behaviour. The possible mechanisms that can play a role in this problem will be reviewed finally.

**MI05/E/01-A3 1420****LOCAL ENERGETICS APPLIED TO FASTEX-CYCLONES**

Fred KUCHARSKI, Alan Thorpe (Department of Meteorology, University of Reading, Reading RG6 6BB, UK)

In this contribution the energetics viewpoint of cyclone development will be investigated. A local energy concept based on the extended exergy is applied to FASTEX-cyclones. The extended exergy has its roots in technical thermodynamics and characterizes the work availability of systems. When extended exergy is applied to the atmosphere it is a locally positive measure of deviations from a globally defined hydrostatic reference state and yields in combination with the kinetic energy a global conservation law for reversible-adiabatic processes. Because all scales of atmospheric motion are included in the deviations from the hydrostatic reference state, the extended exergy as well as the kinetic energy are decomposed into a mean part and a perturbation part. The perturbation part is interpreted here to mean the synoptic-scale disturbances while the mean part is defined as a zonal mean



extended exergy (e.g. over the longitudes covered by the cyclone) not resolving synoptic disturbances.

The importance of the different energy-production mechanisms in generating FASTEX-cyclones will be discussed. This provides a tool for classifying cyclones due to their generation mechanisms. The extent to which pre-existing diabatically-generated static-stability anomalies are important in determining the location and scale selection of some small-scale cyclones will be presented. This mechanism is additional to the classical one of baroclinic production and is proportional to vertical heat fluxes.

**MI05/W/07-A3****1440****DIAGNOSTIC STUDY OF AN UPPER-LEVEL FRONTGENESIS EVENT DURING FASTEX IOP16**

DONNADILLE (Laboratoire d'Aérogies, OMP, 14 Ave, Toulouse, 31400, France, Email: lamd@aero.obs.mip.fr); D. Lambert, J.-P. Cammas and P. Mascart (Laboratoire d'Aérogies UMR CNRS/UPS 5560), 14, Ave. E. Belin, F-31400 Toulouse. Email: donj@aero.obs-mip.fr

During FASTEX IOP 18 (Fronts and Atlantic Storm-Track EXperiment) an upper level frontogenesis develops as a Coherent Tropopause Disturbance (CTD) brings closer to the cyclonic shear side of the polar jet. This work, based on Arpege/IFS operational analyses, available every six hours, uses a new partitioning of the Q-vector into along- and cross-isohypse components (Jusem and Atlas, 1998). Using a quasigeostrophic omega equation we associate a vertical velocity to diagnose processes that appear to contribute to upper level frontogenesis such as confluence, horizontal shear in presence of thermal advection and curvature. Forcings having a key role on the transverse and direct ageostrophic circulation give way to a very deep tropopause fold. A meso-scale limited area model including a stratospheric passive tracer, transported by turbulence scheme, convection scheme and standard mass conserving and positive transport scheme. The stratospheric passive tracer is used to discuss the deep tropopause folding.

**MI05/W/37-A3****1500****REDUCED UPPER-TROPOSPHERIC POTENTIAL VORTICITY IN FASTEX INTENSIVE OBSERVING PERIOD ONE**

H.R. POMROY (Dept of Meteorology, Uni of Reading, UK Email: h.r.birkett@reading.ac.uk); A. J. Thorpe

Diabatic processes are recognised as an important secondary mechanism in cyclone genesis and development. Within the potential vorticity (PV) framework this is commonly thought of as adding a large positive PV anomaly at mid-levels. Theories of PV modification by latent heat release also imply a negative PV anomaly (Northern Hemisphere) at upper-levels. This phenomena of Reduced Upper-tropospheric PV (RUPV) will be looked at in a case study from the field programme FASTEX. The evolution of RUPV and its influence on the parent cyclone has been examined, and observational evidence from the experiment surveyed. The observations show that operational models do not have sufficient amplitude RUPV. The re-run forecasts with and without RUPV anomalies indicate that these anomalies can have significant dynamical effects on cyclone growth but that this depends on their location relative to downstream systems. Evidence from trajectory calculations shows that the evolution of RUPV is dependent on the structure of the air flow through the parent low.

**MI05/E/08-A3****1600****ANALYSIS OF THE STRUCTURES WITHIN A DEVELOPING CYCLONE**

N.M.ROBERTS and M.A.G.Dixon (Joint Centre for Mesoscale Meteorology UK Met Office and Dept of Meteorology) University of Reading, Reading, RG6 6BB, UK.

A wealth of information about the structure and development cyclones in the North Atlantic can now be gained from observations made during FASTEX experiment. Here, we concentrate mostly on the FASTEX case IOP16 of a rapidly deepening frontal wave cyclone. A combination of subjective and objective analysis techniques along with a synthesis of the available observations is used to identify structures within this system on a variety of scales. We examine how the overall system development is related to features such as multiple cloud heads associated with multiple cross-frontal circulations, convective rainbands and the low-level jet and infer some processes that may be responsible. Such a multi-scale observational study is essential if we wish to assess the performance of numerical models in representing these weather systems.

**MI05/W/27-A3****1620****DIAGNOSTIC AND IDEALIZED MODELLING STUDIES OF SLANTWISE CONVECTION**

R.S.DIXON and K.A.Browning (both at Department of Meteorology, University of Reading, Earley Gate, PO BOX 243, Reading RG6 6BB United Kingdom, Email: rdixon@met.rdg.ac.uk); G.J.Shutts (Meteorological Office, Bracknell)

A method of calculating the Slantwise Convective Available Potential Energy (SCAPE) in the UK Meteorological Office's Limited Area Model (LAM) is used to find situations where regions of the atmosphere may be slantwise unstable. By using an idealized model with a resolution fine enough to resolve slantwise convection well and with initial conditions based upon case studies from the LAM exhibiting an apparent existence of SCAPE in the model's atmosphere, we have attempted to assess whether slantwise convection actually occurs in these situations.

**MI05/W/25-A3****1640****SLANTWISE INSTABILITY IN THE CLOUD HEADS OF FASTEX CYCLONES**

Suzanne GRAY and Alan Thorpe (both at Department of Meteorology, University of Reading, Earley Gate, Reading RG6 6BB, UK, Email: S.L.Gray@rdg.ac.uk)

The issue of slantwise convective or symmetric instability must be considered separately from that of upright convective instability in mesoscale models. Slantwise instability may be released through slantwise ascent in the absence of upright instability. This is believed to occur in the cloud heads associated with some midlatitude cyclones. These distinctive features are often linked to the explosive deepening of cyclones into intense depressions with strong surface winds. The release of slantwise instability occurs over a greater horizontal extent than that of upright instability and, unlike upright convection, may potentially be explicitly resolved at mesoscale resolutions. The presence and release of slantwise instability in cloud heads associated with cyclones observed during FASTEX (the Fronts and Atlantic Storms Experiment, January and February 1997) has been investigated using data obtained from observations and simulations of the Unified Model at mesoscale resolutions. Values of SCAPE (Slantwise Convective Available Potential Energy) have been calculated for these three-dimensional systems. The interpretation of this quantity in terms of the release of instability will be discussed.

**MI05/E/20-A3****1700****MODELLING STUDIES OF MESOSCALE STRUCTURE OF A DEVELOPING CYCLONE**

H.W.LEAN, P.A.Clark and N.M.Roberts (Joint Centre for Mesoscale Meteorology UK Met Office, University of Reading, Reading, RG6 6BB, UK.)

The FASTEX experiment provides a unique observational dataset including several cases of rapidly developing systems. These data provide an excellent opportunity to compare mesoscale model representation of systems with the real atmosphere. We present results of running the UK Met Office Unified Model at 11km resolution for the FASTEX IOP16 case of a rapidly developing secondary cyclone with emphasis on the model representation of mesoscale structures in the system such as multiple cross front circulations. We will discuss how the model results shed light on the role of diabatic processes in generating this structure and the implications of the results for improving numerical weather prediction.

**Thursday 22 July AM**

Presiding Chair: A.J.Thorpe (The University of Reading, UK)

**FASTEX-MESOSCALE****MI05/W/35-A4****0930****WARM AND COLD FRONTS OBSERVED DURING FASTEX**

Roger M. WAKIMOTO and Brian Bosart (Department of Atmospheric Sciences, UCLA, Los Angeles, California, 90095-1565, USA, Email: roger@atmos.ucla.edu)

The finescale structure of warm and cold fronts collected using an airborne Doppler radar flown by the National Center for Atmospheric Research (NCAR) Electra during the Fronts and Atlantic Storm Track Experiment (FASTEX) is shown. Even though there have been numerous observational studies of fronts, few have documented the detailed three-dimensional structure of the cold front in general, and the warm front in particular. Most of the flight tracks for the cold front analyzed during FASTEX were flown in an elongated "box" pattern with the front centered within the box. The classical picture of a narrow cold frontal rainband associated with precipitation core and gap regions will be shown. The wind syntheses suggest that the strongest horizontal shears develop within the cores regions while weaker shear values are found within the gap regions. The updraft pattern provides a clearer picture of the vertical velocity/precipitation core than has been previously documented. The three updrafts are all located in the southeast corner of the core. Accordingly, these updrafts are located to the south of the locations of maximum reflectivity. This suggests that precipitation forms first in the southern section of the cores and is subsequently advected to the northeast before descending to the lowest levels. The flight pattern for the warm front was flown approximately perpendicular to the boundary. The unique aspect of this track was the distance flown by the Electra to the rear of the front (over 200 km) and the concurrent dropsondes deployed by the United Kingdom C-130. This flight pattern resulted in the construction of mean vertical cross sections that revealed the detailed kinematic and thermodynamic structure using the Doppler wind syntheses and the dropsonde data, respectively. In contrast to the cold front, the surface frontal boundary was not characterized by a ribbon of maximum vertical vorticity. Rather, an alternating pattern of anticyclonic and cyclonic vorticity maximum were noted. An assessment of the thermal wind balance of the wind field in the vicinity of the front will be shown.

**MI05/W/23-A4****0950****SIMULATION OF FASTEX IOP11 CLOUD SYSTEM COMPARISONS WITH OBSERVATIONS**

Jean-Pierre CHABOUREAU, Jean-Pierre Cammas, Isabelle Mallet\*, Patrick Mascart, (Laboratoire d'Aérogies, Université Paul Sabatier, 14 av. Belin, 31400 Toulouse, France) \*CNRM/MesoNH, Meteo-France, 42 av. Coriolis, 31057 Toulouse cedex 1, France)

The interaction between the baroclinic forcing and the diabatic processes in the development of extra-tropical cyclones has been recently highlighted during the "FASTEX cyclone" (Cammass et al 1999, Mallet et al. 1999). The role of such mechanisms and their interaction are investigated in a rather typical cyclone, Low 30 observed during IOP 11. Simulations with and without cloud processes have been done using Meso-NH, a non-hydrostatic mesoscale model with a very advanced set of cloud and hydrometeor schemes. Low 30 is also one of the well-documented FASTEX cases for which the survey involved the three instrumented aircrafts of the campaign. The extremely rich description of the simulated cloud system has been compared with in-situ observations and satellite retrievals (cloud classification from TOVS, water parameters from SSM/I). In addition, the brightness temperatures observed by Meteosat (in the so-called infrared and water vapor channels) have been compared with those simulated from Meso-NH. All these comparisons will be presented to validate the structure and the quality of the cloud fields simulated by Meso-NH, therefore to assess the confidence on their role on the development of Low 30.

**MI05/W/42-A4****1010****MULTISCALE BUDGETS OF MOMENTUM, HEAT AND MOISTURE WITHIN SECONDARY CYCLONE SAMPLED DURING FASTEX**

Y. LEMAITRE, (CETP/UVSQ, Email: lemaire@cetp.ipsl.fr); A. Protat and D. Bouniol, CETP/UVSQ.

Airborne Doppler radar and dropsonde data obtained in the multiscale sampling area of the FASTEX experiment are processed in order to get 3D circulations and cloud physics properties of cyclonic/frontal cloud systems including sub-structures. This work aims at studying the role of frontogenetic forcings, slantwise and upright convection in the observed cloudy and precipitating structure. It aims also at estimating the relative energetic importance of the various scales of motion involved in these cyclogenetic situations. To do so, budget analyses of momentum, heat and moisture are derived from the retrieved multiscale 3D dynamic and thermodynamic fields. These budgets are analysed in the light of prognostic and diagnostic equations. During the oral presentation, results from two extreme cases (frontal wave and explosive cyclogenesis) observed during Intensive Observing Periods 16 and 12 will be presented.

**MI05/E/29-A4****1100****SIMULATIONS OF FASTEX CLOUD SYSTEMS WITH THE ARPEGE MODEL**

Philippe LOPEZ (CRNM/GMME/RECYF, METEO-FRANCE, Toulouse, France, Email:lopez@cnrm.meteo.fr)

As part of the FASTEX-CSS Project, a series of 24-hour simulations of various cloud systems observed during the FASTEX campaign (Jan-Feb 1997) in the North Atlantic, have been

carried out with the ARPEGE model, developed at METEO-FRANCE. These simulations have been validated using all kind of available observational data, including multi-channel measurements from satellites (METEOSAT, DMS, NOAA), as well as airborne radar data collected during FASTEX. The sensitivity to both horizontal and vertical resolutions have been investigated, with a particular focus on their respective impact on the 3-D distribution of the diagnosed cloud fields. In parallel, a "simplified" large-scale condensation scheme with prognostic cloud condensate, designed for horizontal resolutions of typically 100 km, is being developed. This scheme should make it possible to assimilate cloud water in operational forecast models, and might also be profitable in global climate experiments. The tuning and validation of the cloud scheme will be performed utilizing a set of high resolution simulations from three different mesoscale models (HIRLAM, UKMO, and MesoNH).

**MI05/W/31-A4** **1120**

**RAINFALL FORECASTS DURING FASTEX USING HIRLAM**

Klara FINKELE and Peter Lynch (both at Met Eireann, Glasnevin Hill, Dublin 9, Ireland, Email: Klara.Finkele@met.ie, Peter.Lynch@met.ie)

FASTEX (Fronts and Atlantic Storm Track Experiment) took place in January and February of 1997. The main purpose of the experiment was to observe in detail the evolution of weather systems crossing the Atlantic using airborne Doppler radar and dropsonde observations as well as an enhanced coverage of conventional and ship observations. Two storms have been selected for simulation with HIRLAM (High Resolution Limited Area Model). HIRLAM is an operational forecast model for short range predictions. It is a hydrostatic model on a hybrid coordinate system with semi-Lagrangian advection scheme and a massflux scheme for convection. The selected cases are the intensive observation periods IOP11 and IOP16, which will also be used, for a model intercomparison study. IOP11 shows a deepening cyclone while crossing the Atlantic. IOP16 shows a fast moving and rapidly deepening cyclone. The simulation results are compared with satellite observations, cross sections derived from dropsonde data and surface rainfall observations over Ireland. Results are compared using a high resolution of 0.1 deg and the operational forecast resolution of 0.3 deg. The sensitivity of different convection parameterisation schemes is explored at these resolutions to the evolution of the storm and rainfall forecasts.

**MI05/L/03-A4** **1140**

**EFFECTS OF LATENT HEATING ON A FASTEX CYCLONE**

P. MASCART (1), I. Mallet (2), J.-P. Cammas (1), P. Bechtold (1), J.-P. Chaboureaud (1), J. Donnadille (1), D. Lambert (1) 1: Laboratoire d'Aerologie, CNRS/UPS, Toulouse, France 2: Meteo-France, CNRM/GMME, Toulouse, France

A set of numerical simulations is used to study the first development phase of a FASTEX cyclone (IOP17), a particularly well sampled frontal cyclone system developing on the trailing front of a primary large-scale baroclinic wave. The model is the Meso-NH non-hydrostatic model jointly developed by Meteo-France and Laboratoire d'Aerologie. The selected part of the life cycle of the cyclogenesis involves intense latent heating associated with warm frontogenesis and cloud head formation. Diagnostics tools are applied to the model outputs to show how the upper levels dynamics are modified by diabatic effects and how a positive feedback develops between the outflow jet aloft and the lower frontal circulation. Use is made of the results of a sensibility study that performs a non-latent heating run to propose a conceptual model of this positive interaction. It is suggested that such a positive feedback explains the near constant deepening rate of the cyclone while the baroclinic forcing associated with the upper level precursor decreases in this part of the life-cycle.

**Thursday 22 July PM**

Presiding Chair: C. Snyder (NCAR, Colorado, USA)

**MI05/W/41-A4** **Poster** **1400-01**

**SHORT-TERM WEATHER FORECAST OF BAROTROPIC ATMOSPHERE FOR THE CAUCASUS**

KHVEDELIDZE, (Tbilisi State University, Email: scitico@access.sanet.ge)

The autos carried out the numerical realization of the task, the short-term weather forecast of the atmospheric pressure of the barotropic atmosphere according to complete equations of hydrodynamics with due regard for the relief of the underlying surface for Caucasus. Inclusion of the relief effect with the preservation of the precise boundary conditions is realized by the measurement  $[x, y, \sigma = p/p_s, t]$  of coordinate system. The initial data are registered according to AT-850 chart while for every subsequent temporal step values of geopotential on the earth's surface are defined by means of the equations concerning 850mb of the surface. The forecasts were calculated for 24 and 48 hours, in the rectangular network field with the size of 26x22 knots while  $dt=10$  minutes and  $dL=3 \times 100000m$  As the average meaning of the relative mistake of the forecast was  $\sim 0.61$  and the coincidence of the sings was 0.55 so the given numerical model cloud be considered satisfactory.

**MI05/E/03-A4** **Poster** **1400-02**

**THE IMPACT OF EXTRA-TROPICAL CONVECTION ON THE STORM TRACKS OF HADAM3**

L. SHAFFREY (CGAM, Department of Meteorology, University of Reading, Reading, RG6 6BB, U.K., email: L.C.Shaffrey@reading.ac.uk); C. Jones (SMHI, Norrkoping, Sweden, email: Colin.Jones@smhi.se)

Storm tracks are regions where extra-tropical cyclones tend to grow and decay. Transient eddy variance measures can be used to determine the strength and location of the storm tracks. When transient eddy variances are used to compare the observed Northern Hemisphere storm tracks with those from a wintertime ensemble of integrations from the UKMO's atmospheric climate model, HadAM3, it becomes apparent that the lower to mid-tropospheric transient heat fluxes in the model are too weak. The weak transient eddy heat fluxes might be related to overactive extra-tropical convection in the wintertime storm tracks of HadAM3, as excessive lower tropospheric heating by convection in the cold air around the back of extra-tropical cyclones will equate to a reduction in the lower tropospheric transient eddy temperature variance.

A new non-local boundary layer scheme has been developed at the UKMO which should improve the representation of convective boundary layers in the model. Introducing the non-local boundary layer scheme into integrations of the HadAM3 reduces the amount of convection in the storm tracks. Associated with the reduction in convection is an increase in the lower to mid-tropospheric transient temperature variance of the model's storm tracks, even though there are no systematic increases in other measures of storm track strength. The results of these process studies are compared with longer integrations of HadAM3 with

and without the non-local boundary layer scheme, to determine the impact of the boundary layer and the convection schemes on the extra-tropical time-mean flow and the representation of the storm tracks in HadAM3.

**MI05/W/36-A4** **Poster** **1400-03**

**THE INFLUENCE OF SHEAR FRONTGENESIS ON THE DEVELOPMENT OF SECONDARY WAVE CYCLONES**

H. R. POMROY (Dept of Meteorology, Uni of Reading, UK Email: h.r.birkett@reading.ac.uk) J.-P. Chaboureaud, A. J. Thorpe

Previous work has shown that some of the secondary wave cyclones that occurred during the FASTEX field experiment developed whilst in a regime of strong vertical shear. This contradicts theoretical work using an Eady model that suggests in such situations the frontal waves have smaller growth rates than the front itself, and therefore cannot develop. This discrepancy motivates the use of a more complex model to simulate wave growth. Results of three-dimensional simulations of secondary wave development using a semi-geostrophic numerical model will be presented. The basic frontal state is two-dimensional and forced by an ambient along-front potential temperature gradient leading to shear frontogenesis. The growth of a "warm band" frontal wave instability has been calculated and will be presented.

**MI05/W/32-A4** **Poster** **1400-04**

**COLD AIR CYCLOGENESIS**

Abigail C. L. DEVESON and Keith A. Browning (Joint Centre For Mesoscale Meteorology, Department Of Meteorology, University of Reading, PO Box 243, Reading, RG6 6BB, UK, Email: a.c.l.deveson@reading.ac.uk); Tim D. Hewson (Joint Centre For Mesoscale Meteorology, UK Meteorological Office, Dept. Of Meteorology, University of Reading, PO Box 243, Reading, RG6 6BB, UK)

A method of categorising cyclones by the vertical motion associated with them has been developed as part of an attempt to establish an objective classification scheme for mid-latitude cyclones. Upper level troughs can be identified by a dipole of ascent and descent forced from upper levels (above 600mb) with ascent ahead of any tropopause depression and descent behind. A similar dipole can form, forced at lower levels (below 800mb), close to a low centre with a region of ascent located ahead of the low in the direction of its progression and descent behind. On using this vertical motion diagnostic to investigate FASTEX intensive observation periods (IOPs), two cases were found to be dominated by upper level forced vertical motion. Both IOPs involved cyclones forming at high latitudes, close to the ice edge and on the leading edge of a cold air outbreak. Further investigation revealed multiple cloud features associated with each cyclone. These took the form of shallow comma clouds which developed separately as the ascent maximum, associated with the upper level trough, was located overhead. Evidence showed a difference between the propagation speed of the cloud features and the upper level trough. It was noted that the cloud features grew and became organised only when the upper and lower level forced regions of ascent were in phase. The cloud features then become disorganised and convection within them was suppressed as the upper level trough overtook the cloud feature due to the trough's greater propagation speed. Both these cases of cyclogenesis showed large similarities to polar lows in their initial stages, prior to the development of frontal structures. Theories of polar low development have been applied to explain the development of the cloud features.

**MI05/W/26-A4** **Poster** **1400-05**

**SEA-LEVEL RISE IN THE SOUTHERN COAST OF BRAZIL APRIL 3-5, 1997**

Jaci Maria Bilhalva SARAIVA (Fundação Universidade do Rio Grande-FURG, Rio Grande-RS-Brazil, CEP 96.201-900, Email: dgejaci@super.furg.br); Cláudia Jaccondino de Campos (Universidade Federal de Pelotas-UFPel, Pelotas-RS-Brazil, CEP 96.010-900, Email: cjc Campos@ufpel.tche.br)

Due to the baroclinic waves position, the southern coast of South America is a source of cyclogenesis. The storms formed on the ocean in this region, when associated to an anticyclone on the continent, generate wind fetch of great extension on the ocean. These wind fetch generate strong waves in the coastal areas that in turn may cause a sea-level rise at the coast of Argentina, Uruguay, and south-southeastern of Brazil. Infrared GOES-8 satellite images and CPTEC (Centro de Pesquisas de Tempo e Clima - Brazil) 00 and 12 UTC Global Model fields were used as input to the Regional Atmospheric Modelling System (RAMS), to simulate the event observed between April 3-5, 1997, in the southern South America. That event consisted of a migratory polar anticyclone (1025 hPa) that reached the South American continent (45°S, 70°W). It generate a strong horizontal pressure gradient, due to deep marine storm (52°S, 43°W) having a centre of 985 hPa. The proximity of these two action centres generated SW winds of 20 m/s forming a wind fetch of approximately 2000 km. It caused a sea-level rise, along the Rio Grande do Sul state coast, presenting up to 3-m height waves.

**MI05/W/24-A4** **Poster** **1400-06**

**THE SIMULATION STUDIES OF THE INTERACTION OF THE MEI-YU FRONT AND SOUTH-EAST MONSOON FLOW**

Jing-Shan HONG (1) And Ben J-D Jou (2), (1)Central Weather Bureau, Taipei, Taiwan, (2) Atmospheric Science Department, National Taiwan University

During 5 intensive observing periods (IOPs) in MYEX98 (Mei-Yu heavy rainfall EXperiment in 1998), IOP4 (4 - 5 June 1998) and IOP5 (9 - 10 June 1998) were conducted due to the vital convective activities which lasted over one week in South China Sea. The heavy rainfall event was occurred as these convective systems are approaching to Taiwan. For example, the accumulated precipitation amount is up to 300 mm/day during IOP4. The convective activities are the interactions among southward movement of Mei-Yu front, the mid-level short wave trough, and the southwest flow associated the monsoon surge. The preliminary analysis also shows that Taiwan topography may pay important roles to modulate the interactions between the Mei-Yu front and the southwest flow when they are approaching Taiwan. Thus, for the purpose to improve the forecast of the heavy rainfall event around south Taiwan, it is necessary to further understand the structure and evolution of the Mei-Yu front near Taiwan, the mesoscale structure of the southwest flow and the role of the Taiwan topography on the evolution of the southwest flow. The proposal is a simulation study to investigate the issues mentioned above during MYEX98 IOP4 by using the Penn State/NCAR MM5 nonhydrostatic mesoscale model. The model initial condition will ingest the global upper air and surface observations (in FGGE format) from Central Weather Bureau and proceed with objective analysis which the firstguess is based on the ECMWF global analysis field with 0.5°x0.5 degree resolution. The high-resolution simulation (<10 km) will performed around Taiwan in nested grid system bounded in large domain so that can well represent the topographic effect and avoid the potential improper boundary condition from Tibetan plateau.

**MI05/W/08-A4** Poster **1400-07**

**COMPARING OBSERVED AND MODELLED AIR-SEA FLUXES DURING FASTEX**

D. Lambert (1), J. Donnadille (1), J.-P. Cammas (1), G. Caniaux (2) and P. Mascart (1). (1) Laboratoire d'Aérodynamique (UMR CNRS/UPS 5560), 14, Ave. E. Berlin, F-31400 Toulouse, (2) Météo-France/CNRM/GMGECE, 42, Ave. G. Coriolis F-31057 Toulouse Cedex.

The aim of the FASTEX/CATCH (Fronts and Atlantic Storm-Track Experiment / Couplage avec l'ATmosphère en Conditions Hivernales) experiment was to study the life cycle of cyclones evolving over the North Atlantic. In remote areas combining large fetch and strong winds, the interaction of the atmospheric boundary layer and its impact on cyclogenesis remain poorly documented. In this paper, FASTEX dropsonde data and CATCH surface flux measurements from some Intensive Observation Periods are used to validate the boundary layer characteristics modelled by the french Meso-NH (Météo-France/CNRS) mesoscale model. Results obtained with a standard scheme are compared with those of a more advanced package more suitable for high-wind conditions. The validated model results are finally combined with upper-air observations to discuss the impact of air-sea exchanges on cyclogenesis.

**MI05/E/02-A4** Poster **1400-08**

**THE STRUCTURE OF FLOWS IN FASTEX CYCLONES: AN OBSERVATIONAL ANALYSIS**

Mark A. G. DIXON, Keith A. Browning, Nigel M. Roberts (JCMM, Department of Meteorology, Reading University, Earley Gate, Berkshire, RG6 6BB, email: sws97mad@met.reading.ac.uk)

The FASTEX experiment provided an excellent opportunity to perform detailed analyses of the flow structure associated with extratropical cyclones. By combining data obtained using dropsondes and airborne Doppler radar, along with satellite imagery, coherent descriptions have been produced of the flows in rapidly evolving systems. Salient features include transverse slantwise circulations which lead to the formation of multiple cloud heads. Quantitative estimates of length-scales associated with the flows are presented, and possible mechanisms which lead to the analysed structure are considered.

**MI05/L/06-A4** Poster **1400-09**

**MODELLING STUDY OF SECONDARY CYCLOGENESIS DURING THE IOP12 OF FASTEX EXPERIMENT**

K. LAGOUVARDOS<sup>1</sup>, V. Kotroni<sup>1</sup>, Y. Lemaitre<sup>2</sup> and G. Kallos<sup>1(1)</sup> Laboratory of Meteorology, University of Athens, Panepistimioupolis Bldg. PHYS-V, 15784, Athens, Greece, E-mail: lagouvar@skiron.mg.uoa.gr (2)Centre d'Etude des Environnements Terrestre et Planétaires (CETP/IPSL/CNRS), Vélizy, France

In the frame of this work, the secondary cyclogenesis developed during the Intensive Observational Period (IOP) 12, of the FASTEX experiment, in the area south of Iceland, is studied. This system is analysed, using the mesoscale non-hydrostatic model CSU/RAMS (Colorado State University/Regional Atmospheric Modelling System). The two-way interactive nesting capabilities of RAMS model permit to resolve the different scales of motion taking into account the interaction among them. Model results are validated through comparisons with airborne observations collected in the Mesoscale Sampling Area of this experiment. Further, sensitivity tests are performed in order to assess the role of mechanisms such as surface fluxes and latent heat release, implicated in the development of this secondary cyclogenesis.

**MI05/W/09-A4** Poster **1400-10**

**SINGLE DOPPLER RADAR OBSERVATIONS OF MESOSCALE CIRCULATIONS IN TOGA-COARE MESOSCALE CONVECTIVE SYSTEMS**

Scott J. CARPENTER (Department of Atmospheric Science Colorado State University Fort Collins, CO 80523-1371); Dr. Colleen A. Leary (Atmospheric Science, Box 42101 Texas Tech University Lubbock, TX 79409-2101)

In order to obtain a better understanding of the vertical heating distribution of the mesoscale convective systems in the western Pacific warm pool region, the life cycle and morphology of these systems must first be better understood. This was one of the eight goals incorporated into the atmospheric component of the Tropical Ocean Global Atmosphere (TOGA) Coupled Ocean-Atmosphere Response Experiment (COARE) which was conducted from November 1992 to February 1993. This study focuses on obtaining a better understanding of the structure of the wind field within a mesoscale convective system using the single-Doppler radar data collected with the MIT Radar on board the R/V John Vickers.

The 24 December 1992 convective event consisted of several mesoscale convective systems advecting past the domain of the MIT Radar. This event occurred during a period just prior to a westerly wind burst phase of the intraseasonal oscillation (ISO). An analysis of the kinematics and convective and stratiform morphology of two of these systems, which occurred between 1000 UTC and 1800 UTC, will be described using results of a version of the Extended Velocity Azimuth Display (EVAD) method. The results will show that these particular mesoscale convective systems exhibited similar characteristics to the convective systems observed at middle latitudes in the central United States. The existence of front-to-rear system relative flow near the surface and aloft, rear-to-front system relative flow at middle levels near the radar bright band, and the general reflectivity structure of the convective, transition, and stratiform regions will be presented as examples of the kinematic and structural similarities. These similarities, if also observed in the multitude of other convective events during COARE, should help lead the modelling community to better parameterize warm pool convection and lead us to more successful simulations of the ocean-atmosphere interactions over time scales of months to years.

**MI05/W/16-A4** Poster **1400-11**

**LOW TEMPERATURE OCCURRENCE IN THE SOUTHERN BRAZIL DURING THE SUMMER**

Cláudia Jacondino DE CAMPOS (Universidade Federal de Pelotas-UFPEL, Pelotas-RS-Brazil, CEP 96.010-900, Email: cjc Campos@ufpel.tche.br); Jaci Maria Bilhalva Saraiva (Fundação Universidade do Rio Grande-FURG, Rio Grande-RS-Brazil, CEP 96.201-900, Email: dgejaci@super.furg.br)

Temperatures equal or lower than 15°C, in January and February, have a harmful effect in the reproductive phase of the rice crop, causing decrease in the productivity. The knowledge of synoptic situations associated to low temperatures, might establish actions that minimize the meteorological effects in this phase. In this work, surface synoptic charts, satellite images, surface data, and the Regional Atmospheric Modelling System (RAMS) were used to study the synoptic situation that caused temperatures lower than 15°C in Pelotas-RS, from February

13th to 16th, 1991. It was observed that the low temperatures were associated to a polar anticyclone formed in the region during the period studied.

**MI05/W/12-A4** Poster **1400-12**

**NUMERICAL STUDY OF HEAT AND MOISTURE EXCHANGE IN THE MORNING BOUNDARY LAYER**

Gergana GEROVA and Rumjana Mitzeva (both at the Department of Meteorology, Faculty of Physics, University of Sofia, J.Boucher,5, Sofia -1164,Bulgaria, email: rumypm@phys.uni-sofia.bg)

A one dimensional numerical model of the evolution of the morning convective boundary layer (CBL) for strong insolation and light wind will be presented. The basic assumption is that heat and moisture in the CBL are transported mainly by discrete convective elements - thermals. Governing equations for the vertical profile of horizontal-mean virtual potential temperature and specific humidity are derived by partitioning the CBL at each level and at each moment in two domains, one covered with thermals and the other occupied by downdrafts. The problem is closed by assuming that the thermals evolve as individual ones interacting with the environmental air by buoyancy and entrainment mechanisms.

The impact of the magnitude of the radiation heating, moisture and size distribution of thermals at the earth surface on the CBL characteristics will be studied and discussed. The comparison between model simulations and observations will be presented.

**MI05/W/03-A4** Poster **1400-13**

**SEASONALITY OF WIND AND GENERALIZED MONSOON SYSTEM**

LI Jianping Zeng Qingcun (State Key Laboratory of Numerical modelling for Atmospheric Sciences and Geophysical Fluid Dynamics (LASG), Institute of Atmospheric Physical, Chinese Academy of Sciences, Beijing 100080, China)

The rationality that the seasonality of wind presented by Zeng is used to study monsoon is theoretically investigated. It is proved that the seasonality of wind is proportional to the angle of wind shift, and the critical value of significantly seasonal variation for wind is obtained. Here indicates that monsoon regions are located in the regions of significant seasonality. Then generalized monsoon system is divided by the global wind for 1958-1997 from the NCEP/NCAR reanalysis data, and the vertical structure of generalized monsoon system is discussed. These results further verify that the seasonality of wind is an objective and qualitative index for studying monsoon and generalized monsoon system presented by Zeng is a reasonable and useful concept.

**MI05/E/11-A4** Poster **1400-14**

**WEATHER OSCILLATION WITH PERIOD 14 DAYS**

IVANOVA E.V. (Chemistry Department, Moscow State University, Russia); Ivanov V.V. (Institute of Marine Geology & Geophysics, Yuzhno-Sakhalinsk, Russia)

The spectra of air pressure, air temperature and sea level contain the broad bands close to the frequency 1/28 days, 1/14days, 1/7days. If the spectrum are calculated by time interval more than 4 years the each of these broad bands split into the group of lines. The main line is corresponded to the frequency 1/kTm.  $k = 1/2, 1, 2, 3, 4$ . The gap between the lines is equal to 1/Ts.  $Tm = 27.3$  days,  $Te = 365.25$  days. The number of lines inside the band close to the 10. The Moon rotation around the Earth evokes the bands. The splitting the narrow line into the group of lines is caused by the annual variations of the conditions at the Earth. Separate line has heterodyne frequency  $Wkn = 1/kTm + n/Ts$  ( $k = 1/2, 1, 2, \dots, n = 0, 1, 2, \dots$ ). The magnitudes of the spectral maxima varies from one year to another. The variation of parameters on time has a period 18.6 years. This is the period of variation of the angle between the axis of the Earth rotation and the Moon rotation round the Earth. This angle varies from 18 to 28 degree. The variation is illustrated by data for period from 1950 to 1990.

**Friday 23 July AM**

Presiding Chair: D.J.Parker (University of Leeds, Leeds, UK)

**MESOSCALE SYSTEMS**

**MI05/W/02-A5** **0900**

**WEAKLY-FORCED MOIST SLANTWISE CONVECTION: OBSERVATIONS AND SIMULATIONS**

John NIELSEN-GAMMON and Scott Overpeck (Texas A&M University, College Station, TX 77843-3150; email: n-g@tamu.edu)

The theory of conditional symmetric instability (CSI) has remained largely untested because most atmospheric cases studied to date have been strongly forced, either by frontogenesis or by synoptic scale vertical motion. We use the PSU/NCAR Mesoscale Model, version 5 (MM5) to simulate a well-observed case of slantwise convection in a weakly forced environment. The slantwise convection event was initiated by widespread convection over the Gulf Stream and adjacent Atlantic Ocean which evolved into bands with multiple layers of sloping ascent and descent. Observations include Doppler radar and rawinsondes launched at 90-minute frequency.

Numerical simulations are being undertaken at very high horizontal and vertical resolution in order to realistically simulate the event. Nudging to quality-controlled rawinsonde data is applied on outer grids to ensure the accuracy of the synoptic-scale pattern. Numerical output will be analyzed to determine the energetics of the instability, the sensitivity to the microphysical parameterizations, and the nature of along-line variability. Comparisons will be made to strongly-forced vertical motion in the presence of conditional symmetric instability and to along-line variability within squall lines. Results will be reported at the meeting.

**MI05/L/05-A5** **0920**

**CONVECTIVE DESTABILISATION BY A TROPOPAUSE FOLD DIAGNOSED USING POTENTIAL VORTICITY INVERSION**

Morwenna GRIFFITHS, Alan Thorpe and Keith Browning (Department of Meteorology, University of Reading, Reading, UK, email: m.griffiths@reading.ac.uk, a.j.thorpe@reading.ac.uk, k.a.browning@reading.ac.uk)

There is observational evidence to suggest that at the time tropopause folds in extra-tropical cyclones are descending into the mid troposphere there is frequently a destabilisation of the lower troposphere to moist convection. Here we consider the dynamical reasons for such a linkage using so-called potential vorticity (PV) attribution concepts. In particular a method is



described using PV inversion to find the wind shear attributable to the tropopause fold itself. This shear is used to quantify the tendency to generate regions of potential instability, ( $\xi_{em}$  i.e.) where the wet-bulb potential temperature decreases with height. The method is applied to a case of a modest tropopause fold ( $PV=2PVU$  down to 600mb) and it is found that the potential vorticity anomaly contained in the tropopause fold can contribute substantially to the instantaneous convective destabilisation. Indeed, at some locations, it can overcome a tendency to stabilise by the atmosphere without the fold. A climatology of extra-tropical cyclones, associated tropopause folds and regions of potential instability over the north Atlantic region will be shown and discussed.

#### MI05/W/15-A5 0940

##### RESPONSE OF THE AFRICAN EASTERLY JET TO MESOSCALE CONVECTION

BURTON, R.R & Parker, D. J., (The Environmental Centre, University of Leeds, Leeds, UK.)

The wind structure over west Africa in the Northern hemisphere summer months can be characterized by the low level (~600mb) African easterly jet (AEJ) and the high level (~200mb) tropical easterly jet (TEJ). Instabilities in the AEJ are thought to lead to the formation of African easterly waves (AEWs) with wavelengths of the order of 3000km; such waves have been extensively studied. The present investigation aims to broaden the spectrum of known wave behaviour by examining the response of the jets to an idealised squall-line - type forcing. In addition to AEWs, smaller scale waves propagate on the AEJ and TEJ and act to modify the environment of the storm. A hierarchy of numerical models has been implemented, using both idealised atmospheric profiles and radiosonde data taken over West Africa, to give a complete representation of the problem. The sensitivity of the forced waves to the jet structure (position, strength, related wind shear), and the upstream influence of the waves on the squall-line environment, will be presented.

#### MI05/E/28-A5 1000

##### BUSTER AND BERG WIND ON THE KWAZULU-NATAL COAST

M. P. DE VILLIERS (South African Weather Bureau, Private bag X97, Pretoria, South Africa, 0001, email: mpdev@cirrus.sawb.gov.za)

A Buster is a sudden strong south-westerly wind which occurs with the passage of a coastal low (Tyson 1965). The low is essentially a lee low, which owes its existence to the marked coastal escarpment and the migration of an offshore flow anticlockwise around the coast ahead of an approaching cold front and tends to reach its apex under the north-westerly flow from the interior ahead of eastward propagating west wind troughs (Hunter 1987). When the wind turns through north-westerly and remains moderate or stronger for a few hours, prior to the Buster, hot Berg winds (the local name for the Fohn-type wind) are experienced. These occur mainly in the latter part of the winter and the early summer (Tyson 1965). Such an event on the 12th October 1995, with temperatures over 40 C, is investigated. Aspects considered are:- propagation of the Buster from automatic weather stations along the coast; the UK Met. Office numerical model surface prognosis, which gave medium and short term warning of the development and progression of the low; low level divergence (calculated from the UK Met. office model grb data) in the 850-700 hPa layer where low level divergence was indicated, which is contrary to Dines compensation, but is consistent with the offshore flow at the level of the plateau; a potential temperature and wind vertical time section, which clearly indicated the displacement of moist subtropical air, under an inversion, by a trowel of warm subsided air, followed by a bulge of invading cooler Buster air and finally cold front air; and lastly a clear S-shaped leader front ahead of the cold front (Taljaard 1991, McInnes 1993).

#### MI05/E/05-A5 1020

##### RED SEA TROUGH: ITS DEVELOPMENT AND ROLE IN THE MEDITERRANEAN WEATHER

Simon KRICHAK (Dept. of Geophysics and Planetary Science, Tel Aviv University 69978 Ramat Aviv, Israel, e-mail: shimon@cyclone.tau.ac.il); Pinhas Alpert (Dept. of Geophysics and Planetary Science, Tel Aviv University, 69978 Ramat Aviv, Israel, e-mail: pinhas@cyclone.tau.ac.il)

Red Sea Trough (RST) cyclones are quite a typical element of the cool season weather conditions in the Eastern Mediterranean. Their development is characterized by meridional northward penetration of a subtropical trough along the Red Sea area. These cyclones are found during all periods of the cool season. During the winter months the axis of the upper tropospheric subtropical jet (STJ) is oriented to the central Europe. During the intermediate months of the cool season the axis of the average STJ ridge is oriented to the western part of north-Africa. During these periods the STJ wind maxima are frequently concentrated over the mountainous area of Red Sea. Analysis of the factors responsible for this process is performed. A low latitude, low resolution version of the MM4 PSU/NCAR model was used in a part of the simulations. Real data numerical simulations of the process of the RST cyclone development during the AlpeX 3-5 March 1982 period with different parameters included are performed. Results of the experiments are analysed by means of the factor separation approach. Contributions of four acting factors, - topography, surface latent and sensible heat fluxes and latent heat release due to cumulus convection and those of the synergistic interactions of the factors are analysed.

A separate set of the simulations of the RST is performed with the FSU Global Model. According to the model simulations the convective processes over the equatorial Africa play a major role in the developments. Also, the intensification of the upper tropospheric westerly winds due to the convection over the equatorial Africa stimulates the northward extension of the Red Sea trough which consequently diminishes the moisture influx for the tropical convection and therefore seems to serve as a negative feedback.

#### MI05/W/10-A5 1110

##### CLASSIFICATION OF THE POLAR MESOSCALE VORTEX DISTURBANCES OVER NORTH - EUROPEAN SEA BASIN

Victor LAGUN, E.I. Lutsenko (both at Arctic and Antarctic Research Institute, 38 Bering str., St.Petersburg, 199397, Russia; e-mail: lagun@aari.nw.ru)

Results of diagnosis of the wide range of different types of the mesoscale cyclonic cloud eddies in the polar atmosphere are presented. On the ground of the visual and infrared NOAA and METEOR satellite images for period of 1981-1995 the morphometric and genesis classifications of mesoscale disturbances, including polar low events, are made. According to shape and size morphometric parameters the mesoscale eddies are classified as coma, spiral and stripe ones. Due to genesis of eddies the secondary subsynoptic eddies, developing inside the extratropical cyclones, summer mesoscale eddies, polar lows and mesoscale vortex inside the anticyclonic areas are selected. For each type of eddies the frequency is calculated and the prevailed formation regions are determined. The analysis of synoptic conditions of mesoscale eddies development is presented based on the data from meteorological, aerological, hydrological and ice cover measurements. For the quantitative estimations of

mesoscale vortex parameters (boundary layer and free atmosphere energetics, sea-air energy exchange etc.) the multiyear NCAR/NCEP data set was used. The classification presented is compared with other modern known mesoscale and polar low studies results. The examples of analysis of the mesoscale eddies development under the extraordinary weather conditions over the Barentz and Kara Seas are discussed.

#### MI05/W/33-A5 1130

##### FORTE OBSERVATIONS OF GLOBAL THUNDERSTORM CHARACTERISTICS

Paul ARGO, David Smith, Abram Jacobson, and Steven Knox, (Los Alamos National Laboratory, Los Alamos, New Mexico, USA)

The FORTE satellite carries radio-frequency-receivers for the study of lightning. Although we observe emissions characteristic of the usual cloud to ground and intra-cloud lightning strokes, we also often observe very short (a few microseconds) wide band emissions that appear to come from very localized (hundreds of meters) regions within the thunderstorm. In fact, these impulsive emissions seem to predominate in the tropical regions.

Among the many interesting phenomena observed in the FORTE database is one we have termed "recurrent-emission storms." In fact, a majority of the RF events detected by the FORTE satellite are part of these recurrent-emission storms. We believe that the data is best described as emissions coming from a single storm which is radiating to FORTE recurrently during the overhead passage of the satellite (a single ground point is visible for approximately 15 minutes for a directly overhead passage). By using propagation effects on the pulse dispersion and the pulse separations measured for the trans-ionospheric pulse pairs (TIPPs) we can estimate the location of the recurrent emission centers.

As opposed to previous studies of satellite optical observations of lightning (and the optical systems carried on FORTE), we find that many of the cloud systems connected to these recurrent-emission storms appear (at somewhat reduced levels) over oceanic areas. This may be due to the specific discharge processes that could lead to such isolated impulsive events. Weather seasonal variations of the storm locations indicate a strong correlation with the Intertropical Convergence Zone boundaries. Using models of the TIPP separation dependence on source height, we have been able to map the height function of the observed discharges both geographically and seasonally, and will discuss these.

#### MI05/W/06-A5 1150

##### SENSITIVITY OF TRAJECTORY FORECASTING IN STRONG LOCAL WINDS TO WIND DATA FREQUENCY

Lazar LAZIC and Ivana Tosic (both at Department of Meteorology, University of Belgrade, P.O.Box 368, 11001 Belgrade, Serbia, Email: lazar@indy1.meteo.yu)

The Eta Model, with vertical coordinate which permits a step-like representation of mountains and quasi-horizontal coordinate surfaces (so-called eta coordinate), has shown to have excellent capabilities for simulation of mountain-induced phenomena. Trajectories are defined as the paths followed by air parcel with time. They are calculated from forecasted wind fields, with both horizontal and vertical wind components, derived from the Eta Model. Trajectories can be calculated forward and backward in time. Forward trajectories are calculated by specifying initial parcel locations and time and then tracing the parcels with increasing time to determine their final positions. Backward trajectories are calculated by specifying final parcel locations and time and then tracing the parcels with decreasing time to ascertain their origins. The realistic 48 h Eta Model based trajectories forecasted forward of the strong local bora and koshava winds in the winter season based on ECMWF (European Centre for Medium-Range Weather Forecasts) operational analyses i.e. real-time data for initial conditions and forecasts for boundary conditions, are presented. The model was run with  $0.25^\circ \times 0.25^\circ$  horizontal resolution (28 km x 28 km) and 16 layers in vertical. The maximum wind speed is predicted through tree-dimensional channels in the step eta mountain representations. In this paper sensitivity of forward trajectory forecasting to wind data frequency (every time step - 90 s - control case, 15 min, 30 min, 1 h, 3 h, 6 h and 12 h) are studied. Trajectories with wind data frequency of 15 min, 30 min and 1 h are accurate enough. Mean absolute error and mean relative error of parcel positions along trajectories show large values in case of 3 h, 6 h and 12 h wind data frequency. Trajectories calculated from the observed wind data (12 h data frequency) are not accurate.

#### MI05/W/11-A5 1210

##### ON THE SIMULATION OF THE SURFACE METEOROLOGICAL DIURNAL CYCLES BY ARTIFICIAL NEURAL NETWORKS TECHNIQUE

Oleg POKROVSKY (Main Geophysical Observatory, Karbyshev str.7, St.Petersburg, 194021, Russia phone:+7(812)247-64-43, fax:+7(812)247-86-61 e-mail: pokrov@main.mgo.rssi.ru)

The joint statistical distribution of principal meteorological variables (temperature and humidity of air, atmospheric precipitation, pressure, short-wave radiation, cloudiness) are investigated. Ten year length time series of one hour temporal resolution for several meteorological sites of Russian North -West Region are used. The data set of simultaneous observations (for all variables and stations) allows to reveal main features of joint diurnal distributions by means of known "min-max" fuzzy set approach. Known and novel interrelationships between various meteorological variables are reviewed. The revealed relationships between solar downward radiative fluxes and air temperature and humidity diurnal patterns allow to simulate all principal elements of surface energy exchange: longwave outgoing radiative fluxes in the atmosphere, soil heat fluxes, available, turbulent and latent heat fluxes. This approach could be considered as an alternative one to improve the simulation of surface meteorological, radiation and heat balance component diurnal cycles in most climate and weather models. Introduced stationary and transition modes for main meteorological variable diurnal patterns represent the background for simulation of all known weather phenomena. This modes are used also as a neural network's nodes for hidden layers. Implementation of neural networks (back propagation algorithm) allowed us to perform several modelling experiments. Observed and simulated diurnal pattern departures are explored. Intercomparison results, derived by proposed technique and conventional linear regression method, shows substantial modelling accuracy improvement due to nonlinear mapping advantage of artificial neural network. Problem of optimum network configuration (number of nodes in hidden layers) is discussed. Here number of nodes is equal to number of clusters. Another implementing direction is the diurnal cycle meteorological variable reconstruction. Our investigation show the ability of one hour diurnal pattern reconstruction with sufficient accuracy, based on 3-5 instantaneous meteorological observations. Adapted nonlinear mapping of one group variables (and its diurnal distributions) on another one allow to investigate the possibility of this approach application for diagnostic aims.

MI05/E/17-A5

1230

**ABL STRUCTURE AND EVOLUTION OF LOW PRESSURE SYSTEM DURING INDIAN SUMMER MONSOON**

C. A. BABU and Leena P, (Department of Atmospheric Sciences Cochin University of Science and Technology, Cochin - 682 016, INDIA)

The features of atmospheric boundary layer (ABL) in the coastal environment are examined during the presence of a monsoon depression in order to understand the influence of ABL structure on the formation of low pressure system during the Indian summer monsoon. The presence of such meso scale low pressure system enhances the activity of synoptic scale monsoon. The variations in fluxes of sensible heat, latent heat, water vapour and momentum that take place in the ABL and the thermodynamic structure of the atmosphere during the period from the formative stage to the dissipation stage over the vicinity of track of the system are studied. It is well known that the cyclones and depressions are regions of immense convection. CAPE and CINE are employed to evaluate the intensity of convective activity in association with the depression. The study is carried out using daily radiosonde and rawin data pertaining to the depression.

The day to day variation of ABL structure, characteristic features of fluxes and thermodynamic parameters during the evolution of the monsoon depression are discussed in detail. In addition, the variation in circulation above ABL due to the change in ABL structure during the presence of the depression is also discussed.

MI07

Tuesday 20 July

**ATMOSPHERIC SYNERGIES AND THEIR NUMERICAL SEPARATION**

Location: Chemical Engineering G35 LT

Tuesday 20 July AM

Presiding Chairs: Michael Fox-Rabinovich (NASA/GSFC, University of MD, MD,USA), Pinhas Alpert (Tel-Aviv University, Tel-Aviv, Israel)

**FACTOR SEPARATION 1**

MI07/W/01-A2

1100

**THE IMPACT OF SURFACE BOUNDARY FORCING ON SIMULATION OF THE 1988 SUMMER DROUGHT OVER THE U.S. MIDWEST USING FACTOR SEPARATION TECHNIQUE**

Uri STEIN and Michael Fox-Rabinovitz (Department of Meteorology, University of Maryland, College Park, MD, 20742-2425, USA)

The factor separation (FS) technique (Stein and Alpert 1993) has been utilized to evaluate quantitatively the impact of surface boundary forcings on simulation of the 1988 summer drought over the Midwestern part of the U.S. The four surface boundary forcings used are: (1) SST, (2) soil moisture, (3) snow cover, and (4) sea ice. The Goddard Earth Observing System (GEOS) GCM is used to simulate the 1988 U.S. drought. A series of sixteen simulations are performed with climatological and real 1988 surface boundary conditions.

The major single and mutual synergistic factors/impacts are analysed. The results show that SST and soil moisture are the major single pro-drought factors. The couple synergistic effect of SST and soil moisture is the major anti-drought factor. The triple synergistic impact of SST, soil moisture, and snow cover is the strongest pro-drought impact and is, therefore, the main contributor to the generation of the drought. The impact of the snow cover and sea ice anomalies for June 1988 on the drought is significant only when combined with the SST and soil moisture anomalies.

MI07/L/01-A2

1120

**ON THE IMPACT OF BIOGENIC EMISSIONS ON OZONE FORMATION IN THE MEDITERRANEAN AREA - A BEMA MODELLING STUDY**

P. THUNIS, C.Cuvelier, P.Grossi (all at Joint Research Centre, Environmental Institute, TP 051,1-21020 Ispra, Varese, Italy.)

The aim of this modelling study and to quantify the influence of biogenic volatile organic compound (BVOC) emissions on the formation of tropospheric ozone in the Burriana area (North of Valencia) on the east coast of Spain. The mesoscale modelling system used consists of the meteorology/transport module TVM and the two chemical reaction mechanisms LCC and RACM. The results of the model simulations are validated and compared with the data collected during the BEMA (Biogenic Emissions in the Mediterranean Area) field and air measurement campaign that took place in June 1997. The impact of the biogenic emissions is investigated on peak ozone values by performing simulations with and without biogenic emissions, while keeping anthropogenic emissions constant. The impact on ozone formation is also studied in combination with some anthropogenic emissions abatement strategies, i.e. when anthropogenic VOC emissions and/or Nox emissions are reduced. A factor separation technique is applied to isolate impact due to biogenic emissions from the overall impact due to biogenic and anthropogenic emissions together. The results indicate that the maximum impact of biogenic emissions on the formation of ozone represents at most 10 ppb O<sub>3</sub> while maximum ozone values are of the order of 100ppb. At different locations the maximum impact is reached at different times of the day depending on the arrival time of the sea breeze. It is also shown that this impact does not coincide in time with the maximum simulated ozone concentrations that are reached over the day. The Burriana area is characterised by large citrus plantations and amongst the various BVOC's emitted, the carbonyl species turned out to be the most efficient in producing ozone.

MI07/W/05-A2

1140

**SYNERGIES BETWEEN SURFACE HYDROLOGY AND ENERGY BALANCE FOR A VARYING CO<sub>2</sub> ENVIRONMENT**

Devdutta S. NIYOGI, Kiran Alapaty, Sethu Raman, Yongkang Xue (North Carolina State University, Raleigh, NC 27695-7236, USA); (University of Maryland, College Park, MD, USA, email: dev-niyogi@ncsu.edu. Telephone No: +001-919-513-2101 Fax No: +001-919-513-1441)

Soil Vegetation Atmosphere Transfer (SVAT) processes have a significant role in simulating planetary boundary layer interactions, mesoscale circulations, and regional climate. Two dominant components of the SVAT are CO<sub>2</sub> and soil moisture. Measurements suggest

increasing CO<sub>2</sub> would increase vegetation resistance inhibiting transpiration, while soil moisture availability initiates easier transpiration. Understanding the effects CO<sub>2</sub> and soil moisture exerts on surface energy will be hence both informative and critical.

Traditional techniques yield only lumped contribution providing a net effect. To explicitly quantify and extract the individual contribution due to each of the two variables: CO<sub>2</sub> and soil wetness, and their interactions, a designed experiment approach is adopted.

Variables considered in the design are: soil wetness, CO<sub>2</sub>, soil texture, and LAI Analysis of the synergies is performed using two different approaches: Fractional Factorial and Alpert's Factor Separation technique.

MI07/W/02-A2

1210

**INFLUENCE OF INITIAL AND LATERAL BOUNDARY CONDITIONS ON THE SIMULATION OF A HEAVY PRECIPITATION EVENT IN THE WESTERN MEDITERRANEAN**

V. HOMAR, C. Ramis, R. Romero and S. Alonso (all at Meteorology Group, Departament de Física, Universitat de les Illes Balears, 07071 Palma de Mallorca, Spain, email: dfscm0@ps.uib.es); P. Alpert (Department of Geophysics and Planetary Sciences, Tel-Aviv University, Tel-Aviv, Israel 69978, email: pinhas@cyclone.tau.ac.il)

A sensitivity study of the simulations of a heavy precipitation event in the Western Mediterranean to the initial and lateral boundary conditions, using the Hirlam mesoscale model, is presented. The study assesses the relative roles of these non-dynamical factors and their interaction as function of the simulation running period prior to the end of the event. That is, the simulations start at different times but end at the same time. For each running period a factor separation technique was applied, so four simulations were performed: a control experiment, a highly smoothed initial conditions experiment, a non-updated lateral boundary conditions experiment and a fourth one with highly smoothed initial fields and non-updated lateral boundary conditions. The analysis focuses on the effects of the considered factors on Potential Vorticity features and rainfall field.

MI07L/04-A2

1230

**AN AGEOSTROPHIC GEOPOTENTIAL AND A SPLITTING DIAGNOSTIC METHOD**

Qiu-shi CHEN, (Byrd Polar Research Center, The Ohio State University, 1090, Carmack Road, Columbus, OH 43210, USA, Email: qchen@polarmet1.mps.ohio-state.edu, Fax: 614-292-4697)

Numerical models provide a power tool for studying atmospheric motions caused by various individual factors. One of the most convenient ways is by performing sensitivity studies, which are conducted through the comparison of different simulations "with" and "without" a factor, respectively. However, these sensitivity studies only reveal long-term, integrated effects and stop short of providing interpretations of how the evolution of the phenomenon is controlled by the step-by-step interactions and feedbacks. The method of combining diagnostic and sensitivity studies together is a way for removing this shortcoming and for understanding the evolution of a phenomenon simulated in complex models.

The traditional definition of the geostrophic wind cannot be used in the region near the equator because the Coriolis parameter is present in the denominator. Using the wind partitioning into the streamfunction and velocity potential, the geopotential field can be separated into a geostrophic part and an ageostrophic part. The horizontal pressure gradient force of the geostrophic geopotential is equal to the Coriolis force of the rotational wind. The ageostrophic part is the difference between the geopotential and its geostrophic part. The ageostrophic characteristics of the atmospheric motion can be shown much more clearly and explicitly by the ageostrophic geopotential and velocity potential.

The vorticity and divergence equations of the streamfunction and velocity potential in a limited region (Chen et al. 1997, Mon. Wea. Rev., 143-167). These inner part equations are used instead of the primitive equations and they are solved by a semi-implicit time splitting scheme with zero lateral boundary value. In these equations, the advection and heating terms are expressed by forcing terms. The solutions of the equations for each of splitting step times can be separated into two parts. One is the solution of the homogenous equations with the initial values, and it describes the geostrophic adjustment process from the initial values. The other is the solution of the inhomogeneous equations with the zero initial value, and in this solution, the ageostrophic geopotential and velocity potential are generated from the zero value by the advection-heating process.

Tuesday 20 July PM

Presiding Chairs: C. Ramis or S.Alonso (Balearic Univ., Spain) A Berger (Univ. Catholique de Louvain, LLN, Belgium)

**FACTOR SEPARATION 2**

MI07/E/03-A2

1400

**SEA-LEVEL, VEGETATION AND THEIR SYNERGISM IN THE RESPONSE OF THE LLN CLIMATE MODEL TO ORBITAL FORCING OVER THE LAST GLACIAL-INTERGLACIAL CYCLE**

BERGER Andre, Dutrieux A., Loutre M.F. (Universite catholique de Louvain, Institut d'Astronomie et de Geophysique G. Lemaître, 2 Chemin du Cyclotron, B-1348 Louvain-la-Neuve, Belgium, email: berger@astr.ucl.ac.be)

Sensitivity experiments have been made over the last glacial-interglacial climatic cycle using the Louvain-la-Neuve 2-dimension Northern and Southern hemispheres climate model. The continental ice volume was simulated for the last 122 kyr in response to changes of both the insolation and CO<sub>2</sub> atmospheric concentration. The sensitivity of such a response to sea level changes and to the taiga-tundra - snow albedo feedback indicates that the 100-kyr cycle cannot be sustained if these processes are not taken into account. The factor separation technique was finally used to quantify the pure contribution of and the synergism between the sea-level-ice volume feedback and the high latitude forest-snow albedo feedback.

MI07/W/03-A2

1420

**ROLES OF ATLAS RANGE AND IBERIAN TOPOGRAPHY ON A HEAVY PRECIPITATION CASE IN THE WESTERN MEDITERRANEAN**

C. RAMIS, V. Homar, R. Romero and S. Alonso (all at Meteorology Group, Departament de Física, Universitat de les Illes Balears, 07071 Palma de Mallorca, Spain, email: dfscm0@ps.uib.es)

A convective case producing heavy precipitation in the Western Mediterranean region, characterised by pronounced upper levels forcing and main rainfall over the sea, is studied by means of a factor separation technique. On the day of the event (28 September 1994), more than 140 mm were recorded in coastal lands of eastern Spain, and 180 mm were estimated over the sea. Synoptically, the case combines warm and moist easterly advection at low levels, typically observed in torrential rainfall events of the region, with a less common strong upper

levels dynamical forcing. The influence of the topography on the rainfall field has been investigated through mesoscale numerical simulations with the Hirlam model. A complete simulation indicates that in addition to the lower levels forcing, a two-jets interaction is decisive for the triggering and driving of the convection during the event. A non-topographic simulation reveals that, although a significant part of the precipitation can be attributed to the dynamical forcing, nearly a half is forced by topography. With two additional simulations, the first including only the African topography and the second only the European one, the Atlas and Iberian peninsula individual effects, as well as their synergism, can be isolated. It is shown that the Atlas range induces an across-ridge pressure dipole, redistributing the precipitation over the Western Mediterranean. Iberian topography is responsible for notable local rainfall enhancements over the eastern coastal lands of Spain. The synergism between both topographic systems exhibits only weak effects.

**MI07/W/04-A2****1440****BIOSPHERIC INTERACTIONS IN TROPICAL AND MID-LATITUDINAL REGIMES**

Devdutta S. NIYOGI, Yongkang Xue\*, Sethu Raman (North Carolina State University, Raleigh, NC, USA); \*(University of Maryland, College Park, MD, USA)

Land Surface Processes are known to have a pivotal role in the manner in which climate forcing and climatic change can take place globally. In this study, we adopted the simplified version of the Simple Biospheric Model (SSiB) to study this feature in more details. What makes this study unique is that an attempt is made to delineate the synergistic interactions underway in the biospheric components, which provides an insight in the possible causality for the perceived climate change. Using SSiB, our aim is to compare the biospheric response in two different climate regimes: tropics and mid-latitude. The tropical and the mid-latitude scenarios are important as they represent a diverse landscape for regional climate simulations, in terms of both the hydrological and boundary layer feedback as well as the synoptic forcing. Using observations from two special field experiments: FIFE (for mid-latitude) and HAPEX-Sahel (for tropics), the SSiB model is integrated. For each of the two cases (FIFE and HAPEX-Sahel), 32 sets of simulations were performed with six varying factors (two-level variation). These factors were initial conditions of: surface albedo, soil wetness, stomatal (surface) resistance, vegetation cover, vapour pressure deficit, and ground temperature. The output analysed was the SSiB predicted evaporation, sensible heat flux, effective ground temperature, and the components of these output as resolved for bare ground, canopy and interception. Using these two-level interactions, direct synergism was extracted using a graphical analysis. This was further extended by performing 48 sets of simulations for the two cases, with three levels of variances in the input data. Through this analysis, explicit non-linear interactions were resolved for the biospheric variables. Results provide large details regarding the control mechanism for each of the surface characteristics. Overall it was concluded mid-latitude climate has larger interactive feedback while the tropical landscape was dominated by more stringent, non-interactive

**MI07/E/02-A2****1510****ROLE OF TROPICAL AREA MOIST DYNAMICS IN NOVEMBER 1-5, 1994 WEATHER**

Simon KRICHAK (Dept. of Geophysics and Planetary Science, Tel Aviv University 69978 Ramat Aviv, Israel, email: shiman@cyclone.tau.ac.il); Pinhas,Alpert (Dept. of Geophysics and Planetary Science, Tel Aviv University, 69978 Ramat Aviv, Israel, email: pinhas@cyclone.tau.ac.il)

Investigation of the role of moist dynamics in the atmospheric processes during the abnormally intensive stormy period of November 1-5, 1994 over the Mediterranean region is presented. Analysis focuses on the eastern Mediterranean area employing 96-hour model predictions over the Mediterranean region with the Florida State University (FSU) global spectral model. Sensitivity simulations differ only by prescribing the initial moisture fields in the selected regions located in the Arabian Sea, Red Sea, and over large areas in the low latitudes. The role of the moist effects in these regions in the Mediterranean large-scale atmospheric developments is considered as "factors" for the factor separation analysis. Synergistic interaction between the factors is analysed. Both the tropospheric trajectories and the model tests suggest that the heavy rains over the eastern Mediterranean were associated with unusually intensive propagation of air masses from the Arabian Sea region, which took place before and during the first 24 hours of the period. Air masses from the Arabian Sea participated also in the intensive developments in Italy and southern France on November 5, 1994.

**MI07/L/03-A2****1600****RADIATIVE DE-STABILISATION OF A STABLE SMOKE AEROSOL LAYER BY CLOUDS**

Joachim H. JOSEPH(1), Ilan Koren(1), Lorraine Remer(2) 1)Dept. of Geophysics And Planetary Sciences, TAU, Tel- Aviv 69978, Israel 2)Code 913, NASA Goddard SFC, Greenbelt, MD 20771, USA

The aged heavy smoke aerosol, covering extensive areas in Brazil during the biomass-burning season, may generate scattered clouds at its top. Factor analysis of the radiative fluxes divergence shows that the heating of the smoke layer is then largely due to synergism between the cloud and the aerosol. The clouds radiatively increase the local instability enough to lead to a positive feedback above and in the layer, increasing the depth of the latter as well as making the whole troposphere become thermo-dynamically unstable. The physical mechanism responsible will be described.

**MI07/L/02-A2****1620****EFFECT OF SEA-BREEZE ON AIR POLLUTION IN THE GREATER ATHENS AREA: ANALYSIS OF DIFFERENT EMISSION SCENARIOS**

P.GROSSI (1), P.Thunis (1), A.Martilli (2), A.Clappier (2). (1) Joint Research Centre, Environment Institute, TP051, 1-21020 Ispra (Varese), Italy, (2) (Swiss Federal Institute of Technology, CH-1015 Lausanne, Switzerland

The MEDCAPHOT-TRACE campaign, that took place in the Greater Athens Area from 20 August to 20 September 1994, has confirmed the role of sea-breeze circulation in photo-smog episodes already suggested by a number of experiments and numerical studies.

This work focuses on the study of the 14 September photo-smog event, associated with sea-breezes is investigated by isolated the effect of nighttime and daytime emissions on ozone levels. The same principle is then used to isolate the impact on ozone levels arising from the two main sources of emissions in the GAA: the industrial area around Elefsis and the Athens urban area. Finally the building up ozone from one day to another is investigated.

From this study, it comes out that ozone production in the Athens area is mainly a daily phenomenon. Indeed, the elevated values of photochemical pollutant (up to 130ppb at ground level) reached during summer time late afternoons on mountain slopes to the N and NE of the city are mainly related to the current day emissions. Nevertheless, the re-circulation of old pollutants can have an important impact on ozone levels in Athens downtown, but significantly in the Southern part of the Peninsula and over the sea, especially near Aigina Island.

**MI07/E/04-A2****1640****A NUMERICAL INVESTIGATION OF SYNERGISTIC CONTRIBUTIONS TO LEE CYCLOGENESIS**

Marina TSIDULKO and Pinhas Alpert (Department of Geophysics and Planetary Sciences), Raymond and Beverly Sackler (Faculty of Earth Sciences, Tel Aviv University, Israel, e-mail: marina@cyclone.tau.ac.il and pinhas@cyclone.tau.ac.il)

A number of simulations were carried out in order to investigate the roles of topography, lateral boundaries and upper-level dynamics during lee cyclogenesis. The PSU/NCAR mesoscale model (MM5) was employed (Grell et al, 1994). The well-studied ALPEX case of 3-6 March 1982 was chosen for experiments. In earlier numerical studies it was most surprisingly found that the lee cyclone was in the same location and almost with the same deepening in the simulations even without topography. It led to the conclusion that this case that earlier seemed to be the most 'classical' case of lee cyclogenesis is actually not caused by topography, and the topography only modifies its development. Two "no-topography" simulations with the same resolution (60-km) but with the different number of gridpoints in horizontal direction (31x46 and 58x73) were performed. It was found that topography/no topography simulations, usually applied by researchers for the mountain role estimation, should be carried out very carefully because of the significance of lateral boundaries and their hidden synergistic effect with the topography, which was shown to be of a considerable effect.

The factor separation method (Stein and Alpert, 1993) was applied to the dynamics of the process. Two factors were chosen for investigation - the upper-level PV advection (PV) and the mountains. The pure and synergistic contributions of the upper-level PV and topography were calculated. Their interactive effect was found to be strong and comparable to the pure PV advection contribution. Only the synergistic contribution produce the dipole structure oriented in agreement with theory and phase but becomes strongly cyclonic at the second phase of lee cyclogenesis development. Superposition of the pressure change patterns, produced by the two factors along with their interaction, has resulted in a strong deepening in the right location. Hence, the joint cyclogenetic action is proposed as an explanation

**MI07/E/01-A2****1700****THE FACTOR SEPARATION METHOD, ADVENTAGES AND PROBLEMS**

Pinhas ALPERT (Dept. of Geophysics and Planetary Science, Tel Aviv University 69978 Ramat Aviv, Israel, e-mail: pinhas@cyclone.tau.ac.il)

The factor separation method has been adopted by estimated 15-25 groups since it was introduced for atmospheric modelling in 1993 by Stein and Alpert (JAS, 1993). I will try to summarise the various applications with focus on new insights and findings directly related to the method.

Also, some questions/problems will be addressed. One example is the influence of the particular choice by the modeller of a particular set of factors on the final results. It was shown, for instance, by Alpert et al. (JAS, 1995) that if an important factor is for any reason being omitted, its contribution must show up with another factor that was chosen and the one which is the most synergistic with the factor that was omitted. Another problem to be discussed is the effect of the basic or control run choice on the results; I will show such an example from paleoclimate simulations by A. Berger. Can we choose any control case we wish? Or, are we allowed to choose unconventional factors like initial conditions and lateral boundary conditions; how can this be performed?

**PANEL DISCUSSION****1720**

A. Berger, (Louvain-La-Neuve, Belgium) C.Ramis, (Balearic Univ., Spain) U.Stein (Tel-Aviv Univ., Israel) P.Alpert, (Tel-Aviv Univ., Israel)

**MI08****Wednesday 21 – Thursday 22 July****RADIATION AND CLOUDS IN POLAR REGIONS (IRC, ICCP, ICPM)**

Location: Mechanical Engineering G34 LT

**Wednesday 21 July AM**

Presiding Chairs: K. Stamnes (Univ. of Alaska Fairbanks, USA), G.W. Paltridge (Univ of Tasmania, Australia)

**IMAS ASSOCIATION LECTURE****0830****RADIATION AND CLOUDS IN THE POLAR REGIONS**

Knut Stamnes and Garth Paltridge (Convenors)

**ARE POLAR CLOUDS SIGNIFICANT? OBSERVATIONAL EVIDENCE****Introduction****0930**

K.Stamnes and G.Paltridge

**MI08/E/05-A3****Invited****0940****POLAR CLOUDS AND THE BUDGETS OF HEAT AND MOISTURE AT HIGH LATITUDES - A REVIEW OF RECENT OBSERVATIONAL STUDIES**

Thomas P. CHARLOCK (NASA Langley Research Center, Mail Stop 420, Hampton, Virginia 23681, USA, email: t.p.charlock@larc.nasa.gov) and Takashi Yamanouchi (National Institute of Polar Research, B1-9-10 Kaga, Itabashi-ku, Tokyo 173, Japan, E-mail: yamanou@nipr.ac.jp)

This presentation gives a broad review of observational studies of clouds which have been reported by colleagues in the polar meteorology community. Recent advances have been enabled by the provision of large scale data sets, especially ISCCP D, TOVS Pathfinder, and Reanalyses; and through intensive measurements of ARM NSA, FIRE III, Syowa, and the remarkable SHEBA ice drift.

Analyses by NCEP/NCAR provide more accurate estimates for the atmospheric heat flux (largely by transient waves in the lower troposphere and by stationary waves at all levels) to



high latitudes. The new ISCCP D climatology (now spanning 9.7 years) reports more clouds and smaller optical depths than the earlier C version, but much of its seasonal variation has vanished. In the Arctic, ISCCP D clouds have a positive forcing to the surface. A surprisingly good match of the surface LW cloud forcing at SHEBA by ECMWF during the Arctic winter suggests that we may be approaching a satisfactory closure for the LW budget in the polar night. Polar clouds significantly contribute to the cooling of the atmosphere in NH and SH. Observations at Syowa and Amundsen-Scott in the Antarctic, and at FIRE III and SHEBA in the Arctic, do not find the "anomalous" SW absorption by clouds which has been reported by some researchers in lower latitudes. The active remote sensing at SHEBA (i.e., phase discrimination of water/ice by cloud lidar depolarization) is providing clues to puzzles such as the impact of pollution on IFN, the dessication of the Arctic atmosphere, and cloud/sea-ice feedback.

**MI08/L/03-A3** Invited **1010**

**ATMOSPHERIC PARTICLE CHARACTERISTICS AND RADIATIVE PROPERTIES OF CLOUDS: APPLICATION TO POLAR CLOUDS**

GAYET J P (Laboratoire de Meteorologie Physique, UPRESA/CNRS 6016 Universite Blaise Pascal, 24 avenue des Landais, 63 177 Aubi Cedex, France, e-mail : gayet@opgc.univ-bpclermont.fr

The communication highlights the role of the characteristics (size distribution, shape,) of condensed atmospheric particles on the radiative properties of cold clouds. Based on recent in situ observations of both ice particle size & shape and corresponding scattering phase function, experimental results show major differences with theoretical scattering phase functions used in cloud models which assume ice spheres or simple geometric shape of ice particles. Subsequent differences on derived optical and radiative parameters can result from radiative transfer models. Interpretation of the results suggests that neither the presence of interstitial particles nor the presence of black carbone condensation/ice nuclei inside the condensed particles significantly affect the scattering phase function. On the contrary, the shape and/or the surface roughness of the ice crystals can explain the reported differences. Furthermore, examples of observations realized in mixed stratiform clouds show thin layers of supercooled water droplets which occur preferentially near the cloud top whereas the scattering properties are dominated by ice particles in the lower cloud parts. These results highlight new potential insights, particularly for polar clouds which remain poorly documented, on both modelling of climate processes and methodologies of cloud remote sensing from satellite measurements.

**MI08/E/13-A3** **1100**

**CLOUDS OVER SEA ICE AND OPEN WATER IN THE SOUTHERN OCEAN: SOLAR TRANSMITTANCE AND CLOUD OPTICAL THICKNESS OBTAINED FROM SHIPBOARD RADIOMETERS**

Melanie FITZPATRICK (Geophysics Program, University of Washington, Seattle, WA, 98195-1650, USA, email: fitz@atmos.washington.edu) Stephen G. Warren (Department of Atmospheric Sciences, University of Washington, Seattle, WA 98195-1640, USA, email: sgw@atmos.washington.edu)

Atmospheric transmittance and surface shortwave cloud radiative forcing are determined for a springtime voyage of RSV Aurora Australis between Tasmania and East Antarctica, 47-69°S. Broadband solar irradiance was measured by two pyranometers on opposite sides of the ship. Visible irradiance is inferred from measurements by a quantum sensor. Surface albedo is obtained from hourly visual observations of fractional areas of ice types taken throughout the two-month voyage from September to November 1996, together with measured albedos of each type.

We define raw cloud transmittance (trc) as the ratio of the downward irradiance under cloud to that under clear sky at the same solar zenith angle. Clear sky is much more common over the sea ice. In the sea-ice zone trc under cloud is greater principally because of multiple reflections over the higher surface albedo. Transmittance through even the thinnest clouds was usually 20% less than that of clear sky, probably due to the threshold nature of the aerosol-to-cloud-droplet transition. The shortwave cloud radiative forcing at the surface is smaller over sea ice due to both the higher surface albedo and the less-frequent occurrence of clouds.

Cloud optical depth is calculated from a simple parameterization relating clear-sky and cloudy-sky downward fluxes to surface albedo, solar zenith angle, and cloud droplet number density derived by Wiscombe in 1973 for Arctic stratus clouds. Clouds over sea-ice and open water exhibit a similar range of optical depths. The values found are smaller to those found by Leontyeva and Stamnes over Barrow in the Arctic (0-100) and larger than those found by Mahesh, Walden and Warren over the South Pole (0-6).

Sensitivity of the parameterisation to cloud droplet number density is determined. Comparison with spectral measurements made at the same time on the same voyage enables evaluation of the model. In future work the analyses will be repeated for other voyages in different seasons and prior years for which the same instrumentation is available, to obtain representative seasonal values of cloud optical thickness and transmittance in the Southern Ocean and Antarctic sea-ice zone.

**MI08/E/07-A3** **1115**

**IN-SITU MEASUREMENTS OF CLOUDS IN THE COASTAL AREA OF ANTARCTICA**

Tom LACHLAN-COPE and Russ Ladkin (British Antarctic Survey, High Cross, Madingley Road, Cambridge, CB3 0ET. email: t.lachlan-cope@bas.ac.uk)

The British Antarctic Survey has developed a kite-borne cloud particle replicator and this has been used during the 1998/99 field season to take in-situ measurements of cloud particle size, phase and shape at a site at 75(S) and 76(W) in the coastal region of Antarctica. As well as the cloud measurements broadband radiometers were used to measure the surface radiation balance.

This paper reports the first results from this project and compares the results with measurements taken in previous field campaigns and with similar mid-latitude measurements. The difference between Antarctic clouds and mid-latitude clouds is emphasised as well as the difficulty in taking in-situ cloud measurements in Antarctica.

**MI08/W/19-A3** **1130**

**IS THE DETAILED PATTERN OF SNOW ACCUMULATION OVER ANTARCTICA PREDICTED BY GLOBAL MODELS?**

Tom LACHLAN-COPE, Russell Ladkin and Steven Leonard (British Antarctic Survey, High Cross, Madingley Road, Cambridge CB3 0ET. email: t.lachlan-cope@bas.ac.uk)

During the 1998/99 summer a series of 10m firm cores were taken in a traverse inland from the coast in the Bryan Coast area of Antarctica. The annual accumulation was determined from these cores using the Electrical Conductivity Method (ECM) in the field using a new portable ECM instrument developed for this project. The results give a detailed picture of how the

accumulation varies with height during 1997 and 1998. The results are compared with the annual precipitation, over the same period, given by the UK Met Office operational forecast model, the ECMWF operational model and a Lagrangian version of the UK Met. Office single column model.

A detailed comparison of the accumulation will show any gross errors in the parameterisation of clouds and precipitation processes in numerical models. Some thought is given to possible differences between the precipitation predicted and the accumulation measured, in particular the effect of blowing snow will be considered.

**MI08/W/12-A3** **1145**

**SUMMERTIME ARCTIC STRATUS CLOUDS: MICROPHYSICS AND MORPHOLOGY AS OBTAINED FROM IN-SITU MEASUREMENTS DURING REFLEX III**

ANDREAS REUTER (GKSS Research Centre, Institute for Atmospheric Physics, Max-Planck-Str., D-21502 Geesthacht, Germany, email: andreas.reuter@gkss.de)

During the field experiment REFLEX III (Radiation and Eddy Flux EXperiment), 17 flights through Arctic Stratus Clouds (ASC) over the pack ice in Fram Strait had been performed between June and August 1995. This field project is a cooperation between the Alfred-Wegener-Institute for Polar and Marine Research, AWI (Bremerhaven, Germany) and GKSS. Four PMS probes had been operated to cover the entire particle size range between 0.1 and 800 µm. The obtained large dataset was utilised to derive more characteristic features of ASC regarding layering, morphology, microphysical properties and liquid vs. mixed-phase nature.

One of the most striking results of REFLEX III is that classical single-layered ASC was only encountered in 30% of the cases while 35% of the cloud decks had been double-layered and the remaining 35% multi-layered ASC. For the single-layered ASC, average microphysical properties are in good agreement with literature. However, coherent cellular structures had been observed in some of these cases, illustrating inhomogeneity. Double-layered ASC was present on days when boundary layer temperatures had been relatively high. In these cases, the 0°C-isotherm was located at an average of 800 m (in comparison to 50 m for single-layer ASC).

Multi-layered ASC was always associated with frontal systems. These clouds showed a complex morphology and up to four separate cloud layers. Two third of them also contained ice particles. In all mixed-phase clouds, ice-enhancement could be observed with local ice particle concentrations up to 86 per litre for cloud top temperatures around -10°C.

Precipitation development, either drizzle or snow, occurred in 15 of the 17 cloud systems.

**Wednesday 21 July PM**

Presiding Chairs: K. Stamnes (Univ. of Alaska Fairbanks, USA), G.W. Patridge (Univ of Tasmania, Australia)

**ARE POLAR CLOUDS SIGNIFICANT? MODELLING EVIDENCE**

**MI08/E/03-A3** Invited **1400**

**A NUMERICAL MODEL OF THE CLOUD-TOPPED PLANETARY BOUNDARY-LAYER: INTERACTION BETWEEN AEROSOLS, CLOUDS AND RADIATION**

ANDREAS BOTT, Institut fuer Physik der Atmosphaere, Johannes Gutenberg Universitaet Mainz, D-55099 Mainz, Germany

In a numerical sensitivity study with the microphysical stratus model MISTRA the interaction between aerosols, clouds and the atmospheric radiation field is investigated. Model runs with different aerosol size distributions are presented. The numerical results show that the microphysical structure of the clouds is strongly affected by the physico-chemical properties of the aerosol particles. In situations with low aerosol number concentrations the clouds consist of few but large droplets. In contrast to this, model studies with high aerosol number concentrations yield many but relatively small cloud droplets.

The different droplet spectra have a direct influence on the radiative forcing of the clouds. In situations with many small droplets the reflectivity of the clouds is distinctly higher than in cases with few but large cloud droplets. The effective cloud droplet radii are larger in the model runs with few large cloud droplets than in the other cases. In all simulations the effective radii show a strong diurnal variation.

**MI08/W/15-A3** Invited **1430**

**SIMULATIONS OF MIXED-PHASE CLOUDS IN THE ARCTIC BOUNDARY LAYER**

J.Y. Harrington and P.Q. Olsson., A. SCHWEIGER, (University of Washington/Applied Physics Laboratory, 1013 NE 40th Street, Seattle, Wa. 98105 USA, e-mail: axel@apl.washington.edu Telephone No: 206-543-1312 Fax No: 206-543-3521)

Simulating clouds in the arctic regions poses challenges unlike those experienced in other geographic regions. Over the arctic pack ice, strong surface inversions and significant wind shears produce a complex turbulent environment. Cold temperatures ensure an active ice phase even during the summer months, which has a significant impact on cloud evolution and the boundary layer thermal and moisture structure. Frequent leads produce strong heat and moisture fluxes which can penetrate well into the overlying atmosphere. Additionally, air flowing off of the pack ice and over the marginal ice zone experiences extremely large heat fluxes which can produce a heavily cloud covered region composed largely of mixed-phase clouds.

Simulations of mixed-phase clouds that exist within the arctic boundary layer will be presented for two diverse situations. The first situation is that of mixed-phase stratus clouds positioned over the arctic ice pack during fall. The second situation is that of mixed-phase clouds produced during off-ice flow over the marginal ice zone. In each case, mixed-phase clouds have a strong impact on the evolution of the turbulent, thermal, and moisture budgets of the arctic boundary layer.

**MI08/E/12-A3** **1500**

**INTERACTION BETWEEN ARCTIC SEA ICE AND LOW-LEVEL CLOUDS IN A ONE-DIMENSIONAL MODEL**

Shouping WANG, Universities Space Research Association, USA

Arctic sea-ice processes influence global climate by modifying the surface albedo and regulating the thermohaline circulation of the global ocean. Arctic sea ice covers a large area and has an average albedo on the order of 0.7, compared with only 0.06 for the ocean surfaces. Thus, variability of sea ice coverage could considerably affect solar energy input into the Arctic Ocean in the summer season in the absence of clouds. In the mean time, coverage of the Arctic low-level clouds, with an albedo about 0.6, increases significantly from Spring to Summer. These clouds have a significant impact on the surface processes.

Recently, a year long SHEBA-FIRE field experiment was conducted aiming at understanding

the interaction among ocean, sea-ice, clouds and radiation. This study uses a one-dimensional PBL-sea ice coupled model combined with the SHEBA-FIRE data to study the interaction in a relative idealized scenario: given large-scale atmospheric and ocean dynamic forcing, how the clouds and sea ice interact each other in the spring-summer transition season.

The coupled model includes a atmospheric boundary layer model and a ocean-sea-ice model. The PBL is represented by a third-order turbulence closure model with a parameterization of clouds (liquid and ice phase), rain, snow and radiation. The sea-ice model is that of Elbert and Curry (1992) including sea ice, snow, leads, ponds and detailed parameterization of surface albedo. The two models are fully coupled through radiation and surface turbulent fluxes.

We first applied the PBL-only model forced by ECMWF large-scale advective tendencies to May, 1999 to simulate the evolution of PBL during SHEBA period. Compared with the field experiment data, the general feature of the PBL is represented. We then applied the model to the transition of May to June. In the one-month coupled simulation, cloud water path (including liquid and ice) increases with increasing ice and snow temperatures, and decreasing ice and snow thickness. The simulated cloud water path is significantly larger than those in ECMWF analysis. High level clouds have significant impact on the low-level clouds and sea ice, since existence of the clouds will reduce the cloud-top cooling in the boundary layer and thus reduce low-level clouds and turbulent fluxes. The leads seem to have weak influence on the coupled system since the ice-air temperature difference is not large enough. The research is going on, we will report more in the meeting.

#### MI08/W/05-A3 1515

##### AN ENHANCEMENTS OF A TWO-STREAM APPROXIMATION

Dietmar FRIESE (Alfred Wegener Institute, 27515 Bremerhaven, Germany, email: dfriese@awi-bremerhaven.de)

To study the interaction between radiation, cloud microphysics and dynamic processes, the experiment REFLEX III (Radiation and Eddy Flux Experiment) was conducted in summer 1995 in the European Arctic. Airborne mounted Eppley pyrometer and pyranometer as well as FSSP-100 probes are used to measure the short- and longwave irradiance and the particle size spectra of liquid water drops. The measurements consist of 400 vertical profiles as well as over 200 horizontal flight sections in arctic boundary layer clouds. With statistical methods we find a dependence not only between the radiation profiles and the liquid water path but also between radiation and the droplet size. Comparisons between two-stream models and measurement results of irradiance profiles in clouds show, that the best two-stream concept for shortwave radiation consist of the modified delta-Eddington approximation of Meador and Weaver [1980]. The back scattering function is parameterized with an analytic approximation of the Henyey-Greenstein backscatter function. The optimized value for the diffusivity-factor is a function of the liquid water path.

#### MI08/E/11-A3 1530

##### TURBULENT STRUCTURE OF SPRING ARCTIC BOUNDARY LAYER CLOUDS OBSERVED IN SHEBA-FIRE EXPERIMENT: A LARGE EDDY SIMULATION AND OBSERVATIONAL STUDY

Shouping WANG, Universities Space Research Association, USA, Qing Wang, Naval Postgraduate School, USA

This study focuses on the turbulent structure of the arctic cloud-topped boundary layer observed in SHEBA-FIRE experiment. The Flight 5 of C-130 presents a well-defined mixed-layer and predominately super-cooled liquid water clouds. With large-scale conditions obtained from the observations and ECMWF analysis, a LES model is used to simulate the turbulent structure. Turbulent fluxes are also obtained from high rate aircraft measurement. The simulated and observation-derived turbulence variables are compared well. Some sensitivity tests are performed to evaluate some external effects. The following results are interesting: 1. The presence of 2% leads has little impact on the overall cloud structure, although it indeed increases surface turbulent fluxes. This occurs because the surface temperature is not low enough (-7C) and sea ice-air temperature difference is not sufficiently large. 2. The turbulence is predominately driven by sensible heat flux (> 20 W/m<sup>2</sup>) since moisture flux is very small (several w/m<sup>2</sup>). Thus the latent heat contribution to the buoyancy flux is small, and thus cloud-top entrainment is primarily driven by radiative cooling, while evaporative cooling effect is significantly less. This is in contrast to the situation of subtropical marine boundary layer clouds where both radiative and evaporative cooling are very important in defining the entrainment. 3. Solar absorption by clouds reduces liquid water, although it does not decouple the cloud from the subcloud layer as in the subtropical marine boundary layer. 4. Existence of high clouds significantly increases downward longwave radiative flux so as to decrease the radiative cooling at the cloud top. Thus the turbulence intensity is significantly reduced.

#### REMOTE SENSING

#### MI08/L/06-A3 Invited 1605

##### A STUDY OF CLOUD MICROPHYSICAL PROPERTIES WITH USE OF VISIBLE, IR AND MICROWAVE IMAGERS

Teruyuki NAKAJIMA, Kazuaki Kawamoto, Shuichiro Katagiri, and Shunsuke Kuroda Center for Climate System Research, The University of Tokyo 4-6-1 Komaba, Meguro-ku, Tokyo 153-8904 TEL: +81-3-5453-3959; FAX: +81-3-5453-3964 e-mail: teruyuki@ccsr.u-tokyo.ac.jp

Possibility of retrieving cloud microphysical parameters, such as optical thickness and effective particle radius, will be discussed in this study. It is a big concern for cloud physics and cloud-aerosol interaction studies to depict the global distributions of these parameters. Our recent study found that combined use of wide spectral range radiances from visible to microwave wavelengths is useful for such retrievals. Especially, detection of effective particle radius for different cloud types, such as water and ice clouds, looks possible to be performed with multi-channel analyses. Global features of the water and ice cloud microphysics distributions, thus obtained, will be shown and discussed for understanding the cloud formation mechanism and strength of cloud-aerosol interaction.

#### MI08/W/14-A3 Invited 1635

##### SATELLITE CLOUD DETECTION AND CLASSIFICATION IN THE POLAR REGIONS

DAN LUBIN, (Scripps Institution of Oceanography, University of California, San Diego, 9500 Gilman Drive, La Jolla, California 92093-0221 USA, e-mail: dlubin@ucsd.edu. Telephone No: 619-534-6369 Fax No: 619-534-7452)

There are several well-known difficulties with polar cloud detection and classification using satellite imagery. These include (a) small shortwave radiance contrasts between high albedo surfaces and cloud tops, (b) small or negligible brightness temperature differences between low cloud tops and snow/ice surfaces, (c) large bi-directional reflectance effects at low sun elevations, and (d) smaller radiances in general over colder and darker scenes that are in the lower part of a given sensor's dynamic range. Several methods have been proposed in recent

years to manage these difficulties, and our ability to use satellite data for polar cloud detection and classification is improving. These methods include multispectral threshold techniques, Bayesian classifiers that use a balance between spectral and textural (grey level difference) features, the training of neural networks to recognize texture, and supplementing high resolution visible/mid-IR imagery with passive microwave data to classify the surface type underneath the cloud. This presentation will give an overview of these methods as applied primarily to AVHRR and similar polar-orbiting sensors. With the recent completion of the Surface Heat Budget of the Arctic (SHEBA) field program, new data sets exist that can provide objective validation and refinement of satellite cloud detection techniques.

#### MI08/L/05-A3 1705

##### RADIATIVE FORCING OF WINTERTIME POLAR CLOUDS: SENSITIVITY TO CLOUD PROPERTIES

J. M. INTRIERI, C. W. Fairall, and R. E. Moritz NOAA/Environmental Technology Laboratory 325 Broadway, R/E/ET2, Boulder, CO 80303 USA Tel: (303) 497-6594; Fax: (303) 497-5318 Email: jintrieri@etl.noaa.gov

The ETL's depolarization lidar, deployed in the Arctic for the year-long(1997-98) SHEBA experiment, provided unique measurements of the annual cycle of polar cloud occurrence and phase. These data, when combined with radiosonde and radiometer observations, provide more detailed information on cloud radiative forcing than previously possible. Results of radiative forcing with respect to the cloud temperature, cloud height, and cloud phase will be presented and discussed in terms of their relative importance and their respective impacts on the underlying surface.

#### MI08/W/11-A3 1720

##### ARCTIC CLOUDS FROM MULTIYEAR SATELLITE AND IN SITU CLIMATOLOGIES

Axel J. Schweiger, J. Key, J. Francis and R. Lindsey, University of Washington/APL, Seattle, WA 98105, USA

Previous comparisons of satellite climatologies of Arctic cloud properties and surface radiative fluxes showed large discrepancies between surface and satellite observations. In this paper we revisit this issue in light of new or reprocessed data sets. Recent progress in satellite retrievals is described, and a comparison of cloud parameters derived from the TOVS Polar Pathfinder Project, the AVHRR Polar Pathfinder Project, and the ISCCP D1 cloud product is presented. Satellite-derived cloud parameters and radiative fluxes are compared to surface observations from the Russian North Pole drifting stations and field experiments. The results show that significant problems remain in the reprocessed ISCCP-D1 data set with respect to retrieved cloud and surface parameters. Comparisons of surface observations with cloud information from the TOVS Path-P data set and the AVHRR Polar Pathfinder data set show promise. The TOVS Path-P data set properly captures the synoptic and annual variability of cloudiness in the central Arctic and appears suitable for a range of applications.

#### MI08/E/10-A3 1735

##### RETRIEVAL OF LOW AMOUNTS OF PRECIPITABLE WATER VAPOR USING MILLIMETER-WAVE RADIOMETRIC MEASUREMENTS

Paul RACETTE and Ed Kim NASA/GSFC, Mail Code 975 Microwave Sensors Branch Greenbelt, Maryland 20770 Phone: 301-614-5653 Fax: 301-614-5558 email: per@meneg.gsfc.nasa.gov Al Gasiewski, NOAA Environmental Technology Laboratory 325 Broadway MS R/E/ET1 Boulder, CO 80303 303-497-7275 Ed Westwater, and Yong Han CIRES 325 Broadway MS R/E/ET1 Boulder, CO 80303 303-497-6527 David Jones Numerical Weather Prediction Division Meteorological Office, London Rd, Bracknell, RG12 2SZ, UK Tel: +44 1344 854072, Fax: +44 1344 854412, email: dcjones@meto.gov.uk

The Atmospheric Radiation Measurement Program (ARM) operates a Microwave Radiometers (MWR) which measures downwelling radiation at 23.8 and 31.4 GHz. Measurements from this instrument are used to derive precipitable water vapor (PWV) and cloud liquid water. Retrievals of PWV using microwave radiometric measurements near the 22.231 GHz water vapor absorption line, like those made by the MWR, have been shown to be very accurate over a wide range of PWV values. However, when the amount of PWV falls below 10mm the accuracy of the derived estimates rapidly degrade; such conditions exist during the coldest driest days of the arctic winter. The degradation is attributed to the relatively weak response of the 22.235 GHz spectral line and limitations of the brightness temperature measurement accuracy. Numerical analysis based upon a set of model atmospheres has shown that improved retrieval accuracy under extremely dry conditions can be achieved by combining measurements near the 22.231 GHz line with those made near the much stronger 183.31 GHz water vapor line. An experiment is planned for 21 days during March 1999 at the North Slope of Alaska Cloud and Radiation Test (NSA/CART) site to investigate the utility and limitations of millimeter-wave radiometry during extremely dry conditions. Existing instrumentation at the NSA/CART site will be complemented by 24 additional radiometric measurement channels ranging from 20.6 GHz up to 340 GHz. These measurements will provide unique data under extremely dry conditions, as well as on millimeter wavelength spectra from liquid and ice clouds. A summary of the numerical analysis, an overview of the experiment, and preliminary results from the measurements will be presented.

#### MI08/L/04-A3 1750

##### ICE CLOUD SINGLE SCATTERING ASYMMETRY FACTOR FROM GLOBAL AVERAGED TRMM/VIRS BIDIRECTIONAL REFLECTANCE PATTERNS

YONG-X. HU Mail Stop 420, NASA LARC, Hampton, VA 23187, USA

The average single scattering asymmetry factor of non-spherical ice particles is significantly smaller than that of liquid water cloud droplets. The asymmetry factors differ for particles with different shapes, size parameters and aspect ratios. A simple method is developed here to compute the asymmetry factor from globally averaged bi-directional reflectance distribution functions (BRDFs) from TRMM/VIRS data. The cloud phase is determined from the combined visible, near-IR and IR window channels. Weighted mean radiance fields, with a strong weighting toward thin clouds, are investigated to uncover the cloud single scattering properties. Theoretical BRDFs are computed from different ice cloud phase functions with DISORT and are compared with the averaged VIRS BRDFs. The results show that the BRDF is very sensitive to the phase function, especially the asymmetry factor. The method is also applied to infer water cloud single scattering asymmetry factor and turns out to be reasonable. The ice cloud asymmetry factors derived in this study from the narrowband visible radiances, are applied to compute broadband radiances that are very close to the TRMM/CERES observations

Thursday 22 July AM

Presiding Chairs: K. Stamnes (Univ. of Alaska Fairbanks, USA),  
G.W. Paltridge (Univ of Tasmania, Australia)**SURFACE PROPERTIES AND CLIMATOLOGY OF POLAR REGIONS****MI08/E/09-A4** Invited **0830****SURFACE RADIATIVE PROPERTIES OF POLAR REGIONS**

STEPHEN G. WARREN (Department of Atmospheric Sciences, University of Washington, Seattle, WA 98195-1640, USA, email: sgw@atmos.washington.edu)

The spectral albedo of snow is sensitive to grain size and zenith angle in the near-infrared but not in the visible and UV. Radiative transfer modelling has proven successful in explaining the most accurate observations. The visible light penetrates deeply into the snow but eventually re-emerges upward from the surface. Essentially all of the absorbed radiation is in the near-IR, and this radiation is absorbed in the top few millimeters. The visible albedo is sensitive to small amounts of absorptive impurities. There is often sufficient soot in Arctic and midlatitude snow, but not in Antarctic snow, to reduce the spectrally-averaged albedo by 1-2%.

The albedo of growing snow-free sea ice depends on ice thickness and bubble content; for melting sea ice it depends on melt-pond coverage. Just a few millimeters of snow can dramatically raise the albedo of sea ice, especially in the near-infrared. The broadband solar albedo in the sea-ice zone varies from 0.07 for open water to 0.85 for snow-covered thick ice. The thermal infrared emissivity of snow and sea ice is very high, about 99%, but lower at large emission angles.

Snow is the most isotropic reflector of all natural surfaces on Earth, but still exhibits substantial anisotropy, which can be altered by natural forms of surface roughness. The BRDF is least variable in the near-nadir direction, and on central Greenland and the Antarctic Plateau the snow surface can be used as a calibration target for satellites. For near-nadir viewing, clouds also have little effect on reflected radiances over snow at visible and UV wavelengths, but they do cause an increase in near-infrared reflectance.

**MI08/W/06-A4** Invited **0900****POLAR CLOUDS: NOW YOU SEE THEM, NOW YOU DON'T**

FRANCIS, Jennifer (Institute of Marine and Coastal Sciences, Rutgers, 71 Dudley Road, New Brunswick NJ 08901-8521 USA. E-mail: francis@imcs.rutgers.edu Telephone No: 732 708 1217 Fax No: 732 872 3088)

Over many regions of the Earth, detecting and measuring clouds with satellite sensors is a challenge, but no where is it more difficult than in polar regions. Contributing to this problem are persistent surface-based temperature inversions, cold temperatures that approach sensor limits, months of continuous darkness, weak cloud-surface contrast, frequent non-black clouds, and diaphanous clear-air precipitation (diamond dust). In this presentation I will discuss existing and new techniques for detecting clouds and measuring some of their bulk properties under these difficult conditions.

**MI08/E/04-A4** **0930****PRELIMINARY RESULTS OF OBSERVATION OF LONGWAVE RADIATION AT DOME FUJI STATION, ANTARCTICA**

Naohiko HIRASAWA and Takashi Yamanouchi(both at National Institute of Polar Research, 1-9-10 Kaga, Itabashi-ku, Tokyo 173-8515, Japan, email: hira@nipr.ac.jp)

The observation of upward and downward longwave radiation was performed almost throughout a year in 1997 at Dome Fuji Station (77.3S and 39.7E), Antarctica. The station is located on the ridgeline of the continental ice sheet. This program was supported by the 38th Japanese Antarctic Research Expedition (JARE-38). Our presentation will focus on the relationship between downward longwave radiation ( $L_d$ ) and cloud amount based on surface observation in wintertime.

"Diamond dust" fell almost every day at Dome Fuji Station in wintertime. However cloud amount was generally small. For example, monthly mean cloud amount was 1.3 (21 days); This is the number of days of cloud amount < 1.5 in daily mean) in May and 3.0 (17 days) in July, respectively. Generally, clouds were not so thick as moon and stars lights do not directly penetrate. While the marked increases in the thick cloud amount were rare, those cases usually occurred under the influence of strong disturbances associated with blocking in the middle and high latitudes.

In our preliminary results,  $L_u$  (upward longwave radiation) is larger than  $L_d$  by about 15W/m<sup>2</sup> at the case of clear sky. On the other hand,  $L_d$  is larger than  $L_u$  at the thick cloud cases and  $L_d$  is comparable with  $L_u$  at the cases of cloud amount from 2 to 10. "10-" means overcast with thin. Interestingly,  $L_d$  is comparable with  $L_u$  at some cases of no cloud. This situation might be induced by spreading of extremely thin cloud or by warm air intrusion.

**MI08/E/02-A4** **0945****CLOUD LONGWAVE RADIATIVE FORCING IN ANTARCTICA**

J.C. KING and S.R. Leonard (both at British Antarctic Survey, Cambridge CB3 0ET, UK, email: j.c.king@bas.ac.uk)

We study the influence of clouds on downwelling longwave radiation at the snow surface ( $L_d$ ) over Antarctica during the winter (June-August) season using in-situ radiation measurements, cloud observations and data from the UK Meteorological Office global NWP model. At the South Pole, observations show that the mean  $L_d$  is about 81 W/m<sup>2</sup> under clear skies, rising to 130W/m<sup>2</sup> under fully overcast conditions. However, overcast conditions occur relatively infrequently here and the net cloud longwave radiative forcing is only about 10 W/m<sup>2</sup>. The NWP model gives a mean  $L_d$  of only 70 W/m<sup>2</sup> under clear skies and exhibits much weaker cloud radiative forcing than that observed. At Neumayer (a coastal station), observations indicate somewhat stronger cloud radiative forcing, and the NWP model and observations are in fair agreement. The parameterisations used for cloud physical and optical properties in the NWP model thus appear to work reasonably well in the relatively warm conditions that prevail around the coasts of Antarctica, but exhibit serious deficiencies when applied to the colder, drier environment of the Antarctic Plateau. Errors in the calculation of  $L_d$  contribute to a 2.5 degC cold bias in 3-day forecasts of South Pole surface temperature.

**MI08/W/02-A4** **1000****RADIATION CLIMATOLOGY OF THE GREENLAND ICE SHEET: SEASONAL AND INTERANNUAL VARIATIONS**

Konrad STEFFEN (University of Colorado, Cooperative Institute for Research in Environmental Sciences, Boulder CO 80309-0216, USA, email: koni@seace.colorado.edu)

The Greenland Climate Network (GC-Net) was established in spring 1994 with the emphasis to monitor climatological and glaciological parameters at various locations on the ice sheet over a time period of up to ten years. The objectives of the monitoring network are to assess daily, annual and interannual variability in accumulation rate, surface climatology and surface energy balance at selected locations on the ice sheet. Each instrument tower measures 32 parameters including temperature, humidity and wind profile at two levels, net radiation and shortwave radiation balance. The radiation is sampled at 15 s intervals and averaged over 60 minutes. All the other parameters are sampled every 10 minutes and averaged over 60 minutes. A total of 15 stations have been installed on the ice sheet by fall 1998. The data are continuously downloaded via the satellite link (ARGOS and GOES satellites). This project is part of the Program for Arctic Regional Climate Assessment (PARCA), more information can be found at <http://cires.colorado.edu/parca.html>

The seasonal and interannual variations of net radiation will be discussed. The net radiation balance for the dry snow area of the ice sheet is negative throughout the year with smallest values in spring and fall. Cloud parameterization based on longwave sky radiation is in good agreement with surface observation for low and middle level clouds. The cloud radiative signal is decreasing from 60 W m<sup>-2</sup> in summer to 25 W m<sup>-2</sup> in winter. Short-term surface temperature forcing in winter is mainly due to the turbulent mixing of heat from the top of the boundary layer, whereas radiative cloud forcing plays a secondary role.

**MI08/E/01-A4** **1015****CLOUD CLIMATOLOGY AT THE INTERIOR OF ANTARCTICA**

Takashi YAMANOUCHI and Naohiko Hirasawa (both at National Institute of Polar Research, 1-9-10 Kaga, Itabashi-ku, Tokyo 173-8515, Japan, email: yamanou@pmg.nipr.ac.jp)

Polar cloud climatology is an urgent issue to be solved for the study of global climate. Cloud radiative forcing is very special in the Antarctic. However, detection of clouds in the polar regions from satellite visible or infrared data involves many difficulties on account of the high albedo and low temperature of the snow and ice covered ground surface. Distribution of clouds over East Antarctica was derived using AVHRR split window channel data of NOAA satellite for thirteen months from January 1987 to January 1988. Brightness temperature differences of 11 and 12 mm for the indices of thin clouds, and the correlation of the brightness temperature difference and the brightness temperature itself was used for the cloud analyses. Annual mean cloud fraction ranged from 5 (tenth) to less than 1 according to the region, and seasonal variation of the area mean varied between 4 and 1.

Wintering observations were carried out at inland station Dome Fuji (77°S, 39°E, 3950 m a. s. l.) for three years, 1995 - 1997. From manual observation, monthly mean cloud amount ranged from 1.3 in May to 6.6 in December in 1997, normally smaller cloud amount in winter months. Though not in the same year, these results support the former AVHRR cloud climatology, qualitatively. Now, using a new data of ground surface measurements including radiative fluxes, cloud observation from AVHRR could be assessed. Clear sky precipitation (diamond dust), which we had occasionally, was a critical issue for the satellite detection.

**FORMATION AND ADVECTION OF CLOUDS****MI08/W/04-A4** Invited **1050****ANTARCTIC ICE CLOUDS AND SIMULATED GLOBAL CLIMATE**

David H. BROMWICH and Keith M. Hines (both at Byrd Polar Research Center, The Ohio State University, Columbus, OH 43210, USA, e-mail: bromwich@polarmet1.mps.ohio-state.edu) Dan Lubin (Scripps Institution of Oceanography, University of California, San Diego, La Jolla, CA 92093, USA, email: dlubin@ucsd.edu)

A sensitivity study with the NCAR CCM2 evaluates the local and global impact caused by changing the optical properties of clouds over the Antarctic continent. Runs are performed in which radiation interacts with 10 micrometer radius ice clouds rather than with the standard CCM2 water clouds. Experiments are carried out for perpetual January (summer) conditions with the diurnal cycle considered. Changes of the cloud radiative properties to those of ice clouds over Antarctica has significant impacts on regional climate during January including temperature increases throughout the Antarctic troposphere by 1-2 degrees. As a result of Antarctic warming the drainage flows at the surface and the meridional mass circulation are weakened. Similarly, the circumpolar trough weakens and moves northward. The simulated impacts of the Antarctic cloud radiative alteration are not confined to the Southern Hemisphere as the meridional mean mass flux, zonal wind and latent heat release exhibit statistically significant changes in the tropics and even extratropics of the Northern Hemisphere.

**MI08/L/01-A4** Invited **1120****CYCLONES AND CLOUD BANDS OVER THE EAST ANTARCTIC PLATEAU - INDICATIONS FROM THE FROST ANALYSIS SET**

MICHAEL POOK Antarctic CRC University of Tasmania GPO Box 252-80 Hobart Tasmania 7001 Email: M.J.Pook@utas.edu.au

The detection and tracking of cloud bands and associated cyclonic systems remains a difficult task over Antarctica and particularly, over the elevated plateau of East Antarctica. The problem becomes more acute during winter when the visible channels of AVHRR imagery lose effectiveness. Yet these cloud systems are responsible for a significant proportion of the precipitation falling over Antarctica. The First Regional Observing Study of the Antarctic Troposphere (FROST) which was conducted during the winter and spring of 1994 and in January of 1995 provided an opportunity to assemble comprehensive data sets for the region. The data obtained from this intensive collection effort were analysed at several centres around the world, including Hobart in Australia (Turner et al. 1996). The Hobart synoptic analysis program completed a set of MSLP, 1000-500 hPa thickness and 500 hPa contour fields for the region south of 50° S. Additionally, satellite imagery from the Defense Meteorological Satellite Program (DMSP) and AVHRR data were studied for evidence of the inland migration of cyclonic vortices. The imagery provides evidence of several vortices that moved southwards over East Antarctica during the latter part of July 1994 and appeared to decay over the high plateau. Other vortices were detected in the summer observing period, as well. Data from the network of automatic weather stations (AWS) over East Antarctica were combined with satellite imagery to infer the movement inland of these synoptic-scale and meso-scale systems. This investigation has identified broad-scale and synoptic-scale influences that contributed to the inland penetration of cyclones during the FROST Program. In particular,



atmospheric blocking in the South Pacific Ocean was found to exert a major influence on storm tracks in the Southern Ocean and the migration of lows across the Antarctic coast.

### MI08/W/18-A4 1150

#### ROLL CHARACTERISTICS AND MICROPHYSICS OF CLOUD STREETS IN ARCTIC COLD AIR OUTBREAKS DURING ARTIST

Andreas REUTER, Frank Albers, Uwe Maixner and Erhard Raschke (all GKSS Research Centre, Institute for Atmospheric Physics, Max-Planck-Str., D-21502 Geesthacht, Germany, email: andreas.reuter@gkss.de)

The objective of the EU-funded joint German-Italian-Finnish research project ARTIST (Arctic Radiation and Turbulence Interaction STudy) is the investigation of the Arctic wintertime boundary layer in the marginal ice zone of the Fram Strait. Among other things, airborne measurements of microphysics, turbulence and radiation of cloud streets in Arctic cold air outbreaks had been accomplished during the field phase of this project (March and April 1998). For microphysical measurements, several PMS probes and a Nevzorov TWC/LWC probe had been operated by GKSS.

The purpose of this contribution is twofold: First, it focuses on roll characteristics of the encountered cloud streets in Arctic cold air outbreaks. In this context, horizontal wavelengths of the circulation as well as aspect ratios are presented. It shows that in some of the cases the aspect ratio of the rolls stays constant while the wavelengths of the rolls are increasing further downstream in the outbreak. Here, the circulation is mainly limited by the boundary layer height. In some of the outbreaks, multiscale rolls with up to three consistent wavelengths had been observed.

The second focus of this work is the investigation of the microphysical properties of the cloud streets. Conditional sampling schemes have been applied to elaborate the variation of microphysical parameters across the cloud streets at certain distances from the ice edge. It reveals that the strongly increased liquid water content in the centre of the streets is primarily caused by a higher particle concentration since the particle diameter is only slightly increased. In addition, glaciation processes inside these convective clouds are investigated. For this purpose, particle habit detection schemes are applied to the OAP data to separate ice particles from water droplets, resulting in individual liquid- and ice particle size spectra. They illustrate the different particle growth processes inside mixed-phase convective systems. Generally, the upper third of the cloud was predominantly liquid, even at ambient temperatures around -20°C. These findings are corroborated by the Nevzorov probe data since this instrument allows the direct calculation of a separate liquid- and ice water content. Near cloud base, about 75% of the cloud water was frozen with a pronounced production of snow.

### MI08/W/01-A4 1205

#### SIMULATIONS OF AEROSOL ENTRAINMENT IN THE ARCTIC BOUNDARY LAYER

W. R. COTTON, H. Jiang, and G. Feingold (Colorado State University, Dept. of Atmospheric Science, Foothill Campus, Fort Collins, CO 80523, USA Email: cotton@atmos.colostate.edu)

Using RAMS developed at Colorado State University, we have performed large eddy simulations (LES) of the 18 May 1998 FIRE/SHEBA case. Because our previous simulations of Arctic stratus have revealed considerable sensitivity to the concentrations of cloud condensation nuclei (CCN) and ice-forming nuclei (IFN), we use this case to investigate the possible importance of entrainment of CCN from the overlying stable air on cloud microstructure and macrostructure.

The warm-cloud bin-resolving microphysics version of RAMS described by Feingold et al., (1998) is set up as an LES model with cyclic lateral boundaries, a rigid lid with a Rayleigh friction layer, and specified surface temperature of 266.0 K and surface roughness of 0.05 m. Simulations are done on a domain of 45 X 45 X 55 grid points with a 50 m grid spacing in the horizontal and 25 m grid spacing in the vertical. A time step of 2 sec is used in all integration.

The thermodynamic and CCN sounding data are taken from FIRE/SHEBA research Flight #5 (May 18, 1998) during the spring IOP. The CCN sounding is based on Hudson's CCN spectrometer data reported on his web page for a 0.2% supersaturation. The profile exhibits concentrations ranging from 40/cc below cloud base to a peak above the cloud in the base of the inversion of 250/cc, lowering to 160/cc at 700m.

After 2 hours of simulation we find that the cloud droplet concentration varies with height through the cloud layer with cloud base values being 50-60/cc and values near cloud top being as high as 200/cc. Sensitivity simulations with vertically-uniform values of CCN are being performed to examine the importance of entrainment of CCN to the radiative, microphysical, and dynamical structure of Arctic stratus.

### MI08/L/02-A4 1220

#### SIMULATION OF ARCTIC WEATHER WITH A SINGLE-COLUMN MODEL

Douglas G. C., Cara-Lyn Lappen, and David A. Randall (Colorado State University, Fort Collins, Colorado)

Among the various climate regimes of Earth the Arctic presents particular challenges. Complex feedback mechanisms of the ocean-ice-atmosphere system, in conjunction with the paucity of observational data, pose modelling difficulties not encountered elsewhere on the planet (Randall et al., 1998). In this study, we explore some of these issues by simulation of the Arctic environment with the Colorado State University (CSU) Single-Column Model (SCM), which is then compared with observational data gathered at the Surface Heat Budget of the Arctic (SHEBA) field project. Within the context of SHEBA, observational data were provided by both the Atmospheric Radiation Measurement (ARM) program, and the First ISCCP (International Satellite Cloud Climatology Program Regional Experiment (FIRE)). The CSU SCM has been used to simulate the observed sequence of weather events for the month of May at the SHEBA site. The results show periods of both agreement and disagreement with temperature and moisture sounding analyses provided by ECMWF, as well as the in-situ moisture and radiation measurements provided by SHEBA. Additionally, though not presented here, the SCM produced more precipitation than indicated by the ECMWF analyses. The most likely causes for the discrepancies in the SCM's performance are errors arising from the parameterizations of cloud characteristics and formation processes, and atmospheric radiative transfer inherited from the parent GCM. For example, deficiencies in the parameterizations of the radiation flux or cloud microphysical and optical properties, or cloud formation processes, or even the surface albedo could combine cumulatively to adversely affect the shortwave radiation received at the surface, which in turn will affect the evaluation of prognostic variables. Problems with the albedo prescription would almost certainly explain the large discrepancies between the observed and SCM-produced net surface shortwave fluxes leading to the warm bias noted at the surface. Though it would be difficult to detect the effects of changing a particular parameterization in a GCM given the complex interactions among its constituents, the SCM provides a means by which an individual parameterization made be studied in isolation. The preliminary results presented here are thus a first step in the challenge of using the SCM to individually identify, examine, and ultimately fine-tune the weaknesses of the myriad parameterizations found in GCMs.

### MI08/E/06-A4 1235

#### APPLICATION OF A FLEXIBLE, LONGWAVE RADIATIVE TRANSFER TOOL (FLRT) TO THE POLAR REGIONS

Jennifer DELAMERE and Knut Stamnes (both at Geophysical Institute, University of Alaska Fairbanks, Fairbanks, AK 99775 U.S.A., email: jen@land.gi.alaska.edu), Eli J. Mlawer and Shepard A. Clough (both at Atmospheric and Environmental Research, Inc., Cambridge, MA U.S.A.)

We apply a flexible, longwave radiative transfer tool (FLRT) to the study of the radiation and cloud environment in the polar regions. FLRT is used to create a correlated-k, multiple-scattering model across user-specified, spectral bandwidths. The method, which computes the gaseous optical depths required by the model, is based upon the rapid radiative transfer model RRTM (Mlawer et al., 1997), including the technique to handle absorption by multiple gases within a band. The combined contribution of gaseous absorption with absorption and scattering by cloud and/or aerosol particles are ported into the DISORT multiple-scattering algorithm. Using the newly-created radiative transfer model, we will present a study of the contribution of the mid-infrared spectral region to the near-surface cooling and longwave radiation budget at high latitudes. In particular, we will explore the influence of water vapor and clouds on the "Arctic Window", a spectral window (16 to 25 microns) that is infrequently observed in mid-latitudes.

Thursday 22 July PM

Presiding Chair: K. Stamnes (Univ. of Alaska, Fairbanks, USA),  
G.W. Paltridge (Univ of Tasmania, Australia)

### RESULTS FROM SHEBA, FIRE-3, BASE

#### MI08/L/11-A4 Invited 1400

#### OVERVIEW OF THE SHEBA AND FIRE-ACE CLOUD RESEARCH PROGRAMS

T. Uttal, R/E/ET6 Environmental Technology Laboratory 325 Broadway, Boulder, CO 80303, USA tel 01-303-497-6409 email: tuttal@etl.noaa.gov

The NSF Surface Heat Budget of the Arctic (SHEBA) and the NASA FIRE Arctic Cloud Experiment (ACE) were conducted North of Alaska over the permanent ice pack of the Beaufort and Chukchi Seas. SHEBA was a year long program which started in September of 1997 and ran continuously until September of 1998. This integrated ocean-ice-atmosphere research program had a state of the art array of instruments for remotely measuring cloud properties including radar, lidar, spectral and broad-band radiometers, and all sky imagers, as well as in-situ sensors flown on tethered balloons. The FIRE-ACE program provided satellite observations of clouds throughout the year, and in the Spring and Summer of 1998, conducted an extensive campaign during which aircraft instrumented within-situ and remote cloud microphysics and radiation sensors made more than 30 flights over the SHEBA ice station. These combined remote sensing and in-situ measurements are already providing a detailed look at previously unknown properties of Arctic clouds. Placed in context of the year long measurements and the equally detailed measurements of ice and ocean characteristics, it is expected that the SHEBA and FIRE-ACE results will significantly improve model parameterizations of Arctic clouds, validation of satellite methods for detecting Arctic cloud properties, and equally importantly, provide a solid observational data base for one full annual cycle of Arctic cloudiness.

#### MI08/L/08-A4 Invited 1430

#### ON THE CANADIAN RESEARCH CONDUCTED IN ASSOCIATION WITH THE BEAUFORT AND ARCTIC STORMS EXPERIMENT (BASE)

Ronald E. STEWART, David R. Hudak and Kit K. Szeto Atmospheric Environment Service 4905 Dufferin Street, Downsview, Ontario Canada M3H 5T4 E-mail: Ron.Stewart@ec.gc.ca

A number of high latitude storms were observed during the Beaufort and Arctic Storms Experiment (BASE), which was conducted from Sept 1 to Oct 15, 1994. Ensuing analysis studies have revealed a great deal about the nature of these cloud systems, and the results are now being applied towards climate model improvements). The objective of the Canadian effort within BASE was to better understand the nature of the cloud systems occurring over the southern Beaufort Sea and northern Mackenzie River basin during the autumn. A variety of situations were examined, including cyclonic storms, mesoscale vortices, and boundary layer alteration over varying surfaces. During the BASE period, more Arctic-origin storms occurred than is normal, but fewer were of a Pacific origin. These systems were observed by using a number of special measurements, including enhanced satellite data retrievals, additional soundings and surface observations, and special aircraft and Doppler radar observations. Analyses have included a study of the structure and evolution of a mesoscale vortex over the Beaufort Sea comparison of the broad classes of Pacific storm types studies of the Doppler radar information obtained at Inuvik and Tuktoyaktuk variational analysis of the dominant precipitation formation mechanisms and their associated mesoscale features; and a critical assessment of the International Satellite Cloud Climatology Project (ISCCP) products for Beaufort region cloud systems. High resolution cloud model simulations have also been carried out, and sublimational processes were found to be critical in replicating the observed fine-scale cloud and dynamic structures. In fact, ice phase processes such as sublimation are critical for determining the water budget of the systems, and small changes in initial water vapour content can translate into large effects on the water budgets as a consequence of these processes. These simulation results are now being used to assess the capabilities of climate models to account for such high latitude cloud systems.

#### MI08/W/03-A4 1500

#### IMPROVED IN SITU OBSERVATIONS OF MIXED PHASE CLOUDS DURING FIRE. ACE AND IMPLICATIONS ON RADIATIVE TRANSFER

R. Paul LAWSON and Tara L. Jensen, SPEC Incorporated, 5401 Western Ave., Suite B, Boulder, CO 80301, USA, email: plawson@specinc.com

Research conducted over the years for the First ISCCP Regional Experiment (FIRE) has led to major improvements in our understanding of the role of clouds in the global climate system. In the spring of 1998, FIRE conducted Phase III of the program in conjunction with the Surface Heat Budget of the Arctic Ocean (SHEBA). The goal of the FIRE Arctic Cloud Experiment (FIRE. ACE) was to study a variety of arctic cloud systems under spring and summer conditions.

A new instrument, the cloud particle imager (CPI), was deployed on the National Center for Atmospheric Research (NCAR) C-130 during FIRE. ACE in both May and July of 1998. The CPI records high-resolution (2.3 um) digital images of cloud particles "on the fly" as they pass through the instrument sample volume. The CPI makes it possible to study the detailed structure of ice crystals and discriminate them from water drops in clouds.

In this paper, we present an overview of data collected in various cloud types during the FIRE-ACE experiment, including all-water and mixed phase stratus, mixed-phase alto stratus and glaciated cirrus clouds. Particles Images, size distributions, liquid and ice water contents are presented. The results show that there is no discernible correlation between ice particle concentration and temperature. Clouds that were composed of nearly all water drops sometimes existed at temperatures as cold as -24 C, and relatively high concentrations of ice were sometimes observed at -4 C. Also, the clouds were sometimes very inhomogeneous on a spatial domain, transitioning from drizzle drops to rimed ice particles within a few kilometers. Implications on radiation and single column modelling will be discussed.

MI08/W/09-A4

1515

#### THE INFLUENCE OF THE MICROSTRUCTURE OF ARCTIC STRATUS CLOUDS ON SMALL SCALE FLUCTUATIONS IN SOLAR RADIATIVE FLUXES

Darrel BAUMGARDNER (Centro de Ciencias de la Atmosfera, Universidad Nacional Autonoma de Mexico, Ciudad Universitaria, 04510 Mexico DF, Mexico, email: darrel@servidor.unam.mx), Darnell Powers (Truman State College, Jefferson, Missouri)

Measurements of Arctic stratus clouds during the Surface Heat Budget of the Arctic Ocean (SHEBA) experiment in the spring and summer of 1998 show significant fluctuations in liquid water content, droplet number concentration and effective radius at length scales less than 100 m. These cloud microphysical parameters were measured with optical particle counters mounted on the NCAR C-130 research aircraft and the sample rates (the FSSP-100 at 10 Hz and PVM-100 at 250 Hz) provide information at length scales of 10 m and 0.4 m, respectively. These measurements were used in a one-dimensional, two stream radiative transfer model to evaluate how short wave radiative fluxes are affected by small scale variations in cloud properties. The results of this study show that 1) the variability in cloud microphysical properties and subsequent radiative fluxes increases as measurements are made at shorter spatial scales 2) there is greater sensitivity to changes in length scale as you go from thinner to thicker clouds and 3) the measured variability in down-welling short wave radiation, made with the airborne radiometers, is in good agreement with the 1D radiative transfer model. These results indicate that satellite measurements and global climate models may be missing smaller scale radiative effects that are climatically important.

MI08/W/13-A4

1530

#### OBSERVATIONS OF INTEGRATED WATER VAPOR AND CLOUD LIQUID WATER AT THE SHEBA ICE STATION WITH A DUAL-CHANNEL MICROWAVE RADIOMETER

James Liljegren (DOE Ames Laboratory, Ames, Iowa, USA, Email: liljegren@ameslab.gov)

In the Arctic water vapor and clouds influence the surface radiation balance to a greater extent than at lower latitudes. Because the integrated water vapor is often less than 5 mm, substantial radiative cooling occurs in the 20 micron infrared region whereas this region is normally opaque at lower latitudes having greater water vapor amounts. Thin, variable liquid water clouds also substantially affect the surface radiation balance. Integrated water vapor and cloud liquid water were measured continuously over a 12-month period at the SHEBA (Surface Heat Budget of the Arctic) ice station with a microwave water radiometer (MWR).

The MWR was among the suite of instruments deployed by the Atmospheric Radiation Measurement (ARM) Program of the U. S. Department of Energy. The radiometer was operated in a continuous elevation angle-scanning mode in order to permit calibration updates whenever the sky was clear. In addition, continuously scanning the sky between +/- 45 degrees about zenith at 5-degree intervals Permitted the time-varying spatial structure of water vapor and cloud liquid water to be observed. Comparison of the liquid water path derived from the microwave radiometer brightness temperatures with liquid water paths from the Gerber PVM probe aboard the NCAR C-130 generally exhibited good agreement.

Measurements of integrated water vapor exhibited good agreement with integrated water vapor derived from radiosondes: a slight bias of 0.2 mm was observed. Comparison of the measured radiometric brightness temperatures with model calculations based on the radiosondes was carried out in order to examine the model performance in the limit of low water vapor where the microwave signal is dominated by molecular oxygen.

MI08/W/08-A4

1545

#### SOLAR AND INFRARED RADIOMETRIC FLUXES IN THE ARCTIC ENVIRONMENT AS MEASURED FROM THE NCAR C-130 AIRCRAFT DURING FIRE-ACE

S.K. POPE, A. Bucholtz, B.C. Bush and F.P.J. Valero (Scripps Institution of Oceanography, University of California, San Diego 9500 Gilman Dr., 0242 La Jolla, CA 92093-0242 USA. E-mail: pope@arlu.ucsd.edu Telephone No: 619-534-9619 Fax No: 619-822-0517)

Airborne measurements of radiative fluxes in the Arctic environment during spring and summer conditions were recently carried out as part of FIRE-Arctic Cloud Experiment in conjunction with the SHEBA (Surface Heat Budget of the Arctic Ocean) field mission. Flux data were collected with a suite of radiometers with hemispherical fields-of-view mounted in zenith and nadir looking ports of the NCAR C-130 aircraft. Broadband fluxes were measured in the total solar bandpass, 0.224 to 3.91 microns, and in the infrared bandpass, 4.125 to 48.25 microns. Narrower bandpass measurements were made with a pair of instruments that have seven channels spanning the 400 nm to 700 nm wavelength range. Of this pair the uplooking one has a shadow arm which allows the measurement of the total, direct, and diffuse components. Flights were based out of Fairbanks, Alaska with multiple patterns flown in the vicinity of the SHEBA ship locked in the ice in the Arctic Ocean. Cloud conditions ranged from clear skies to broken to overcast stratus or cirrus clouds. Surface conditions varied from thick snow/ice with distinct leads in the spring to thin, fractured snow/ice in the summer. Results from these varied measurements will be discussed, including surface albedos, the flux signature due to leads, cloud reflectances, cloud transmittances, and cloud absorptances. Observations will be compared to model calculations.

MI08/W/16-A4

1600

#### SURFACE ENERGY BUDGETS AND CLOUD FORCING ON THE ARCTIC ICE CAP: ONE YEAR OF DATA FROM THE SHEBA EXPERIMENT

J. M. INTRIERI (Environmental Technology Laboratory, NOAA, Boulder, CO 80303, USA, email: jintrieri@etl.noaa.gov); C. W. FAIRALL (Environmental Technology Laboratory, NOAA, Boulder, CO 80303, USA, email: cfairall@etl.noaa.gov); T. Uttal (Environmental Technology Laboratory, NOAA, Boulder, CO 80303, USA, email: tuttall@etl.noaa.gov) P. O. G. Persson (Cooperative Institute for Research in Environmental Sciences, NOAA/ETL, Boulder, CO 80303, USA, email: opersson@etl.noaa.gov)

From November 1997 to October 1998 the Surface Heat Budget of the Arctic (SHEBA) engaged in a variety of atmospheric, ice, and oceanic measurements on the Arctic icecap as part of ice station SHEBA. The ice station was launched at 143 W and 75 N and ended at 166

W and 80 N. The measurements included eddy-correlation measurements of sensible and latent heat flux, upward and downward solar and IR fluxes, and snow/ice temperatures. Profiles of cloud information were obtained with an 8-mm-wavelength Doppler cloud radar and a 0.523 micron wavelength depolarization and backscatter lidar (dabul). We believe this is the first set of eddy-correlation heat flux, radiative fluxes, and comprehensive cloud data obtained over an entire annual cycle on the ice cap.

In this paper we will present simple statistics on the annual cycle of the components of the surface heat budget and cloud properties (fraction, thickness, ice vs water, etc). We will also provide a preliminary analysis of the annual cycle of cloud forcing of the surface heat budget.

MI08/L/09-A4

1615

#### ONE ANNUAL CYCLE OF CLOUD PROPERTIES DETECTED WITH LIDAR AND RADAR OVER THE SHEBA ICE CAMP

T. UTTAL, J. Intrieri, and B. Olson Environmental Technology Laboratory, NOAA, 325 Broadway, Boulder, CO 80303 USA email: jintrieri@etl.noaa.gov, tuttall@etl.noaa.gov, bolson@etl.noaa.gov

The NOAA/Environmental Technology Laboratory was funded by the National Science Foundation to operate a 35 GHz Doppler cloud radar and a dual-polarization lidar at the SHEBA ice camp to observe cloud properties. These two instruments in combination with surface radiometers provide a powerful mechanism for observing cloud properties, including cloud fraction, cloud thickness, number of layers, cloud phase, particle sizes, particle concentrations and optical depths. Some of the preliminary analysis on the variation of these cloud properties over one annual cycle will be presented. Using information from an identical radar operated by the Department of Energy in Barrow, Alaska, some comparisons will be made of these cloud statistics between the Coastal Arctic (Barrow) and the Arctic icepack (SHEBA ice station) sites.

Presiding Chairs: Arve Kylling, Norwegian Institute for Air Research, Norway  
Knut Stamnes, University of Alaska, Fairbanks, USA

### UV RADIATION

MI08/L/10-A4

Invited

1650

#### UV RADIATION IN THE ARCTIC

ELIZABETH C. WEATHERHEAD, University of Colorado at Boulder, email: betsy@srrb.noaa.gov

UV radiation has always been a significant environmental parameter in the Arctic. Recent changes in Arctic ozone levels have increased the natural UV levels significantly. Changes in ozone, including trends and brief episodes of extremely low ozone are most severe in the spring when biological systems are particularly susceptible to damage. However, assessing UV levels in the Arctic can be extremely difficult. Most primary production in the Arctic occurs under water, making standard measurements and satellite estimates only coarse indicators of biologically relevant levels. Terrestrial UV levels are dominated by low sun angles and high surface albedo, also making standard measurements and satellite estimates difficult to interpret. A number of important projects are currently underway to measure, model and estimate biologically relevant UV levels throughout the Arctic. Current understanding of Arctic ozone chemistry indicates that the Arctic will continue to experience elevated UV levels for at least the next few decades and may not recover to pre-1970 levels. Climate change is likely to slow Arctic recovery considerably. The impact of such a slow recovery in the Arctic is highly uncertain due to the sparsity of studies assessing UV effects in the Arctic. Current ozone and UV measurements will be reviewed and expectations for future will be summarized.

MI08/L/07-A4

Invited

1720

#### CLOUDS AS MODIFIERS OF UV SPECTRA AT THE GROUND

Dr. Gunter SECKMEYER, Fraunhofer Institute for environmental atmospheric research (IFU), Kreuzteckbahnstr. 19, D-82467 Garmisch-Partenkirchen, e-mail: seck@ifu.fhg.de

Clouds are known to be a major factor influencing UV irradiance at the ground. Usually clouds are attenuating the global irradiance, but there are also cases where the UV irradiance is enhanced due to reflection of radiation by clouds. It has been found that the attenuation of UV irradiance by clouds is not spectrally flat but is a function of wavelength. The radiation conditions under broken clouds can be even more complex. Broken clouds lead to wavelength dependent variations of UV irradiance mainly caused by Rayleigh scattering. An increasing temporal variability with increasing wavelength can be observed under broken cloud conditions. This will be demonstrated as case studies by a combination of measurements and models for cloudless skies.

MI08/E/08-A4

1750

#### A COMPARISON BETWEEN SATELLITE ESTIMATES AND OBSERVED ULTRAVIOLET (UV) IN THE ALASKAN ARCTIC

Renee TATUSKO, Barry Bodhaine, Ellsworth Dutton (NOAA/Climate Monitoring and Diagnostics Laboratory, 325 Broadway, R/E/CG1, Boulder, Colorado, U.S.A., 80303, email: rtatusko@cmdl.noaa.gov) Elizabeth Weatherhead (University of Colorado at Boulder, Cooperative Institute for Research in Environmental Sciences, Campus Box 449, Boulder, Colorado, U.S.A., 80309, email: betsy@srrb.noaa.gov) Knut Stamnes (University of Alaska at Fairbanks, Geophysical Institute, P.O. Box 757320, Fairbanks, Alaska, U.S.A. 99775-7320, email: knut@gi.alaska.edu) Jay Herman (NASA/Goddard Space Flight Center, Code 916, Greenbelt, Maryland, U.S.A. 20771, email: herman@tparty.gsfc.nasa.gov)

Decreases in ozone over the Arctic region have occurred over the last two decades, with record low levels recorded during the 1997 spring. Ozone depletion and increased UV radiation pose serious threats to the Arctic ecosystems and peoples. In 1997 and 1998, in response to a need for improved ground-based ultraviolet (UV) measurements in the Alaskan Arctic, NOAA's Climate Monitoring and Diagnostics Laboratory (CMDL) deployed narrowband spectral UV radiometers at Barrow, St. Paul, and Nome, which measure global solar UV irradiance in five UV-visible channels. These multichannel instruments show promise for long-term monitoring of UV-B, UV-A, and visible radiation levels as well as changes in the ozone level, cloud cover, and aerosols. Their ease in maintenance and lower cost, compared to a high-resolution spectroradiometer, make these instruments useful for deployment in the harsh Arctic environment. Estimates of UV exposure from satellite data are difficult to make in the Arctic region because of the complexity of atmospheric and environmental conditions. The main cause of difficulty arises from lack of knowledge of surface reflectivity in the presence of snow. A comparison between NASA's UV estimates based on satellite observations and ground-based measurements at the three sites in Alaska will be conducted. The results of this comparison as a function of temporal averaging, variable surface albedo, and cloudiness will be examined.



MI08/W/10-A4

1805

**DAILY AND MONTHLY UV DOSES AT A HIGH LATITUDE SITE AND THE EFFECT OF CLOUDS AND SURFACE ALBEDO**

Arve KYLLING (Norwegian Institute of Air Research, P.O. Box 100, 2007 Kjeller, Norway, e-mail: arve.kylling@nilu.no), Arne Dahlback (Department of Physics, University of Oslo, P.O. Box 1048, 0316 Oslo, Norway, e-mail: arne.dahlback@fys.uio.no) and Bernhard Mayer (National Center For Atmospheric Research (NCAR), P.O. Box 3000, Boulder, Co 80307, email: bmayer@ucar.edu)

At high latitudes the snowcover may significantly increase the surface UV radiation both for clear and cloudy situations. During 1997 in Tromsø, Norway, the direct and global irradiances were measured between 300 and 600 nm with a spectroradiometer. In addition a multichannel, moderate bandwidth filter instrument measured the ozone column, the cloud optical depth and the erythemally weighted irradiance. An inversion technique was developed to derive an effective regional spectral surface albedo from the measured direct and global irradiance spectra. At 320 nm the albedo varied between 0.57 (snowcover) and 0.08 (snowfree conditions). The derived albedo is used together with model simulations of the filter instrument irradiance to study the effect of a snow covered ground on daily and monthly UV doses both for clear and cloudy sky situations. The clouds are found to reduce the monthly doses by 20-40% compared to cloud free conditions. The snow increases the monthly UV doses by more than 20% compared to snowfree conditions.

MI09

Friday 23 July

**RADIATIVE PROPERTIES AND REMOTE SENSING OF AEROSOLS (IRC, ICACGP)**

Location: Mechanical Engineering G33 LT  
Location of Posters: Old Gym

Friday 23 July AM

Presiding Chairs: T. Nakajima (CCSR, Univ. of Tokyo, Japan)  
R.T. Pinker (Univ. of Maryland, USA)

**LARGE SCALE SATELLITE REMOTE SENSING OF AEROSOLS**

MI09/L/03-A5

Invited

0830

**REMOTE SENSING OF MINERAL DUST FROM SEAWIFS SPECTRAL MEASUREMENTS**

C. Moulin(1)(3), H.R. Gordon(1), V.F. Banzon(2), R.H. Evans(2) (1) Florida Department of Physics, University of Miami, Coral Gables, Florida, e-mail: moulin@fasol.physics.miami.edu. (2) Rosenstiel School of Marine and Atmospheric Science, University of Miami, Miami, Florida (3) Laboratoire des Sciences du Climat et de l'Environnement, CEA-CNRS, Gif-Sur-Yvette, France

Mineral dusts are a major component of the tropospheric aerosol in wide oceanic regions such as the tropical North Atlantic and the Mediterranean. Scientific interest for mineral dusts ranges from the assessment of their impact on the radiative budget of the Earth to the removal of their contribution to the signal measured by ocean color sensors. In both cases, large uncertainties remain because of the dust physical and optical properties. Indeed, mineral dusts are large and absorbing (mainly in the blue) particles with poorly known refractive index and size distribution, and their vertical distribution is highly variable. Here, we used spectral measurements of the sea-viewing wide-field-of-view sensor (SEAWIFS) to retrieve relevant information on mineral dust properties.

For several Atlantic and Mediterranean dust events, we extracted the reflectances at all available wavelengths (from 412 to 865 nm). Using radiative transfer computations, we tested the relevance of the spectral behavior of various mineral dust models. We show that for realistic refractive indices, only size distributions with two or three lognormal modes are able to reproduce the spectral variations of observed reflectances, i.e., almost constant between 670 and 865 nm, and decreasing from 555 to 412 nm. For these suitable models, we tested the impact of the vertical distribution of dust in the atmospheric column. We show that the standard assumption (an aerosol layer below a molecular layer) may lead to significant errors at shorter wavelengths (400-500 nm) when applied to a dust layer of few kilometers in height.

An important conclusion of the first part of this work is that the standard aerosol retrieval algorithm (based only on 765 and 865 nm bands) is not able to properly differentiate mineral dust from a sea-salt aerosol since the specific behavior of dust occurs at shorter wavelengths. This is particularly important for ocean color which requires a good accuracy in the blue. We then propose an improved mineral dust retrieval algorithm which uses all available bands and a relevant set of mineral dust models, including information on the altitude of the dust layer. Limitations of the method are shown in terms of in-water optical properties (e.g., case 2 waters). We applied this algorithm to SEAWIFS images and we discuss here the results for both retrieved optical depth and marine reflectances by comparison with SEAWIFS standard products.

MI09/L/02-A5

Invited

0855

**ESTIMATE OF THE AEROSOL PROPERTIES OVER THE OCEAN WITH POLDER**

Herman, M. (Laboratoire d'Optique Atmosphérique, Université de Lille 1. 59655 Villeneuve d'Ascq Cedex. France. e-mail: herman@loa.univ-lille1.fr); Deuzé J.L., G. Perry, A. Marchand, P. Goloub, and D. Tanré. (Laboratoire d'Optique Atmosphérique, Université de Lille 1. 59655 Villeneuve d'Ascq Cedex. France.)

The wide field of view imaging spectroradiometer POLDER (POLarisation and Directionality of the Earth's Reflectance) developed by CNES (Centre National d'Etudes Spatiales) and operated aboard the Japanese heliosynchronous platform ADEOS (Advanced Earth Observation Satellite) from October 30th 1996 till June 30th 1997, provided the first global systematic measurements of the spectral, directional and polarized characteristics of the solar radiation reflected by the Earth/atmosphere system. These original observational capabilities offer an opportunity to enhance the characterization of the aerosols. The inversion algorithms from which the aerosol parameters are derived, respectively over the ocean and over lands, are examined and examples of the outputs are presented. Special emphasis is given to the interest of directional and polarized measurements over the ocean.

MI09/E/06-A5

0920

**LONG-TERM MONITORING OF GLOBAL AEROSOL CHARACTERISTICS USING NOAA/AVHRR**

Akiko HIGURASHI (National Institute for Environmental Studies, 16-2 Onogawa, Tsukuba, Ibaraki 305-0053, Japan, e-mail: hakiko@nies.go.jp); Teruyuki Nakajima and Takayuki Usui (Center for

Climate System Research, University of Tokyo, 4-6-1 Komaba, Meguro-ku, Tokyo 153-8904, Japan, e-mail: teruyuki@ccsr.u-tokyo.ac.jp)

Aerosols are recognized to cause significant direct and indirect forcing on Earth's %fs climate. The evaluation of these effects, however, remains still highly uncertain for lack of our knowledge of aerosol characteristics on global and long-term scale.

We have developed the aerosol retrieval algorithm, which estimates aerosol optical thickness and !OgstrSN exponent using two channel radiance data of NOAA/AVHRR and have validated the results with ground-based observations. Retrieving !OgstrSN exponent addition to aerosol optical thickness has been shown to be very effective, as compared with past aerosol retrieval algorithm which obtains only aerosol optical thickness from one channel radiance assuming aerosol model, because it makes possible to distinguish the impact of human activities from that of natural aerosols represented by desert dust, and to estimate the number density of aerosol particles, which is very important to investigate the aerosol indirect effect.

We will report the global distribution of these parameters applying the algorithm to multi-year data sets of NOAA/AVHRR radiances. Preliminary analysis suggests increasing contribution of human emission of aerosols, especially off the east of Asia. Such long term analysis will indicate the natural and anthropogenic variabilities of aerosol properties.

MI09/E/02-A5

0937

**DUST FORCING OF CLIMATE INFERRED FROM CORRELATIONS BETWEEN TOMS AEROSOL INDEX AND ATMOSPHERIC MODEL ERRORS**

Pinhas ALPERT, I. Carmona(Dept. of Geophysics and Planetary Science, Tel Aviv University 69978 Ramat Aviv, Israel, e-mail: pinhas@cyclone.tau.ac.il) Jay Herman and Yoram Kaufman (NASA/GSFC, Greenbelt, MD20771)

Recently, Alpert et al (1998, Nature), suggested an indirect measure of the tropospheric temperature response to dust aerosols by using model updates, - roughly speaking model errors-of the NASA Goddard Earth Observing System (GEOS-1) data assimilation system. They have shown that these updates, which provide information about missing physical processes not included in the predictive model, have monthly mean patterns which bear a striking similarity to patterns of dust over the Atlantic.

This similarity in the number of dusty days was used to estimate the atmospheric response to dust. Here, the study is extended for all the major sub-tropical deserts over Africa and Asia using the Total Ozone Mapping Spectrometer (TOMS) aerosol index (AI) for dust recently derived by Herman et al (1997). It is shown that the TOMS dust is highly correlated with the model errors with a maximum at the altitude of about 580 hPa and for the month of June with average correlation coefficient of 0.69 reaching up to 0.8 for specific months. In contrast to the previous study where only dust over ocean was employed, here much higher dust concentrations are detected and the linear heating for weak dust becomes quickly saturated for AI above 1.5 then drops for very high AI exceeding about 3 in consistency with the theoretical predictions.

MI09/W/04-A5

0954

**LARGE SCALE ANALYSES OF CONVECTIVE CLOUD MICROSTRUCTURE FROM AVHRR DATA**

Daniel ROSENFELD (Atmospheric Science, The Hebrew University, Jerusalem, Israel, email: daniel@vms.huji.ac.il) Ron Drori (Atmospheric Science, The Hebrew University, Jerusalem, Israel, email: ron@cloud.es.huji.ac.il)

A method to infer from AVHRR data the precipitation properties of convective clouds has been developed recently by Rosenfeld and Lensky (BAMS, 11/1998). That method was developed for case studies. A new layer to this method had been added that enables us to implement it automatically over large areas. Various parameters, as defined by Rosenfeld and Lensky (1998) can be selected, in addition to newly defined parameters. One important parameter is the warmest temperature at which the effective radius of convective clouds exceeds the precipitation threshold of 15-micron (T15). An effective radius of 14 micron had been shown as a threshold for precipitating clouds (Rosenfeld and Gutman 1994). Reanalysis of the case over the Philippines had shown a rapid decrease of T15 for clouds moving from sea inland, becoming more microphysically continental. A much slower increase of T15 is observed on the downwind side of the islands, showing that the air can get polluted with CCN aerosols over land much faster than it becomes clean again over sea. Furthermore, a bulls-eye of drastically decreased T15 is evident over and downwind of Manila. This is a typical situation. Similar trends are generally observed in most AVHRR images taken at random.

Presiding Chair: R.T. Pinker (Dept. of Meteorology, Univ. of Maryland, USA)

**COLUMN CLOSURE EXPERIMENTS OF AEROSOLS**

MI09/W/14-A5

Invited

1030

**SATELLITE REMOTE SENSING OF AEROSOL PROPERTIES IN COLUMN CLOSURE EXPERIMENTS**

P. A. DURKEE, K. E. Nielsen (both at 1Naval Postgraduate School, Monterey, CA USA, Email: durkee@nps.navy.mil), P. B. Russell (NASA Ames Research Center, Moffett Field, CA USA), B. Schmid (Bay Area Environmental Research Institute, San Francisco, CA USA), J. M. Livingston (SRI International, Menlo Park, CA USA), D. Collins, R. C. Flagan, J. H. Seinfeld (all three at California Institute of Technology, Pasadena, CA USA), K. J. Noone, E. Öström (both at Stockholm University, Stockholm, Sweden), S. Gassó, D. Hegg (both at University of Washington, Seattle, WA USA), L. M. Russell (Princeton University, Princeton, NJ USA), T. S. Bates, and P. K. Quinn (both at NOAA PMEL, Seattle, WA USA)

Recent field programs designed to study aerosol properties have produced interesting contrasts across diverse regions of the globe. ACE-1 (Aerosol Characterization Experiment) observed conditions in the relatively unperturbed southern ocean near Tasmania in November-December 1995. The Tropospheric Aerosol Radiative Forcing Observational Experiment (TARFOX) observed aerosol transported of the North American coast over the Atlantic Ocean in July 1996. Most recently, ACE-2 measured the properties of aerosol from Europe and Northwestern Africa over the eastern North Atlantic Ocean in June-July 1997. The differences between these three regions are well observed by satellite remote sensing. The Advanced Very High Resolution Radiometer (AVHRR) aboard NOAA polar orbiting satellites measure radiance in five wavelength bands - two of which are sensitive to scattering by aerosol (Channel 1 - 0.63  $\mu$ m and Channel 2 - 0.86  $\mu$ m center wavelengths). Aerosol optical depth calculated for these first two channels of AVHRR and the radiance ratio of these channels can be used to parameterize size distribution properties. Retrieval of aerosol properties requires assumptions about the characteristics of aerosol number distributions, the absorption properties and vertical distribution of aerosol, surface reflectance, and others. This presentation will describe the array of airborne, surface, and shipboard data collected during field experiments that can be used to validate the satellite-based retrieval of aerosol



properties. Analysis of aerosol size distribution, aerosol optical depth, scattering and absorption characteristics will be used to test the assumptions in satellite retrieval algorithms.

**MI09/L/04-A5 1055**

**DERIVING AEROSOL RADIATIVE PROPERTIES FROM REMOTE SENSING SPECTRAL MEASUREMENTS**

John PORTER (Soest, University of Hawaii, 96822, Email: jporter@soest.hawaii.edu)

Satellites offer the possibility to derive aerosol properties over the whole earth. Unfortunately deriving these aerosol properties is not straight forward and typically requires an aerosol model. Here we use an existing aerosol model to develop algorithms to derive aerosol optical properties from multi-angle spectral measurements. The algorithms are applied to upwelling radiances collected from low flying aircraft during ACE1 and INDOEX. Comparisons are made with other measurements in order to test for closure.

**Introduction 1112**

**MI09/E/01-A5 Poster 1145-01**

**USE OF THE KERNEL COVARIANCE MATRIX TO PREDICT BEYOND THE MEASUREMENT RANGE**

Gail BOX (School of Physics, University of New South Wales, Sydney NSW 2052 Australia, email: gpb@newt.phys.unsw.edu.au)

The radiometers which are used to measure optical thicknesses usually make measurements in the range 0.38-1.05 microns. These measurements can be used to determine aerosol size distribution by inverting the integral equation connecting the optical thickness with the size distribution. However, it is known that more accurate inversions can be obtained if measurements over a wider wavelength range are available. Since the kernels of the integral equation are not independent of one another, there is the possibility of using the measurements made to predict measurement values beyond the instrument range.

We have applied a method based on the eigenvalues and eigenvectors of the kernel covariance matrix to predict measurements at wavelengths other than the measured ones, including beyond the range. The results look promising. Some of these results, including the effects of measurement errors, will be presented.

**MI09/E/03-A5 Poster 1145-02**

**THE OPTICAL PROPERTIES OF THE AEROSOLS IN THE COASTAL AREA OF CHINA**

Beiyang WU and Wenyang Su (Lab for Middle Atmosphere and Global Atmospheric Observation, Institute of Atmospheric Physics Beijing, 100029, China)

Aerosol climate effect is a currently concerned problem. International effort have been focused on it climate effect, and chemical compositions, especially in Asia region where the economic development has caused many environmental problems. Based on the observations in the last 20 years, the optical properties of aerosols in the coastal area of China is analyzed. The radiative effects is also simulated.

**MI09/E/04-A5 Poster 1145-03**

**SPECTRAL CHARACTERISTICS OF ASIAN DUST AEROSOL AROUND THE KOREAN PENINSULA AND JAPAN OBSERVED BY SEA WIDE FIELD-OF-VIEW SENSOR (SEAWIFS) IN 1998 SPRING**

Hajime FUKUSHIMA (School of High-Technology, Tokai University, Numazu, 410-0395 Japan, Email: hajime@fksh.fc.u-tokai.ac.jp) and Byung-Ju Sohn (Dept. of Earth Sciences, Seoul National University, Seoul, 151-742, Korea, Email: sohnbj@plaza.snu.ac.kr)

The study analyzes aerosol optical thickness and Angstrom exponent for different air mass observed by SeaWiFS, a satellite ocean color scanner, in the end of March to mid-April, 1998, when a couple of Asian dust (KOSA) event was observed by ground stations in Korea and Japan. The optical thickness and Angstrom exponent are derived from the near-infrared (666, 765, and 865 nm) band data, using SeaDAS, a NASA/GSFC-made SeaWiFS data processing software that assumes an appropriate pair of aerosol models chosen for every pixel out of 12 candidate aerosol model set. It is shown that Asian dust aerosol is well characterized by its relatively high optical thickness (0.6 or more at 865 nm) and low Angstrom exponent (about 0.3), in contrast to the clear-sky condition which typically shows low optical thickness (less than 0.1) and high Angstrom exponent. The size distribution obtained from a ground-level sky-radiance observation under KOSA-loaded air mass conducted in Anmyong-do, Korea, shows the dominance of larger particles (1-3 micro m in radius), explaining the low Angstrom exponent. Aerosol optical thickness at shorter wavelength region (443 and 555 nm bands) is also estimated for sampled area of 5 different scenes, assuming nominal or minimum water-reflectances. The results show that the Angstrom's law does not well approximate the spectral dependency of the Asian dust aerosol optical thickness, probably due to the absorption in shorter wavelength region. The study also discusses the applicability of the Asian dust aerosol model parameters proposed by the authors.

**MI09/E/05-A5 Poster 1145-04**

**LONG-TERM MONITORING OF URBAN AND MARITIME AEROSOL FEATURES WITH MULTI-WAVELENGTH SUNPHOTOMETERS**

Jinli LIU, Fang Li, Daren Lu (all at Institute of Atmospheric Physics, Chinese Academy of Sciences, Beijing 100029, CHINA, e-mail: jliu@linux2.iap.ac.cn, ludr@sun.ihep.ac.cn)

It is well recognized that the radiative forcing of atmospheric aerosols is a significant uncertainty to climate change prediction. Owing to the complexity of aerosol features and inevitable spatial and temporal variation, remote sensing of aerosol features by both space-borne and ground-based instruments is essential for understanding the function of aerosols in climate radiative forcing. Long-term monitoring of aerosol features at two ground stations are being made with multi-wavelength sun-photometers. The stations are one in Shanghai typical for urban area, and the other in a small island in East China Sea far from continent, typical for maritime atmosphere. The instrument is a ten-wavelength sun-photometer ranging from 400-1000nm. Observations are made for direct solar observation and zenith observation. From these observation, spectral optical depth can be derived at first. With some assumptions and combined with data of zenith observation, the knowledge of aerosol size distribution and single scattering albedo could be obtained. In this paper, results of observation at two sites will be presented and emphasized the difference of urban and maritime aerosols.

**MI09/E/09-A5 Poster 1145-05**

**SIMULATION AND OPTIMAL PARAMETRIZATION OF AEROSOL OPTICAL PROPERTIES**

Alexandr V. Vasilyev, Yuriy M. TIMOFEYEV (both at Research Institute of Physics, St.Petersburg State University, Ulyanovskaya 1, St.Petersburg-Petrodvorets, 198904 Russia, e-mail: tim@roll.phys.spbu.ru)

Statistical approach to modelling the atmospheric aerosol optical characteristics is presented. This approach is based on applying the different recent models of atmospheric aerosol and modelling the aerosol variability by the Monte-Carlo method. Examples of constructing the statistical models of vertical profiles of attenuation coefficients of stratospheric background aerosol are given. These models take into account an aerosol composition (sulfuric acid particles, meteoric dust, two-layer particles with meteoric dust core in sulfuric acid coat) and different correlations (between an aerosol concentration and temperature gradient, between a concentration of sulfuric acid aerosol and SO<sub>2</sub> content, etc.).

Different methods of parametrization of vertical and spectral distribution of aerosol attenuation coefficients applied in solving the atmospheric remote sensing problems are examined. Optimal parametrization method basing on the expansion of covariance matrix of aerosol attenuation coefficients in the eigenvectors is proposed. Number of the expansion terms necessary to achieve a preassigned approximation accuracies is determined. Results of estimating the accuracies of different parametrization methods through numerical experiments are given.

**MI09/E/10-A5 Poster 1145-06**

**SCIENTIFIC 'NUCLEAR WINTER' PICTURE AND BYRON'S APOCALYPTICAL CLAIRVOYANCE**

ANZOR GVELESIANI (Institute of Geophysics, Georgian Academy of Sciences, 1, M. Alexidze Str., Tbilisi 380093, Georgia, email: vazha@excite.com)

The materials of the numerical calculations of the "nuclear winter" model both of American and Soviet scientists represented on the Interantional Meeting (Tbilisi, 27th October, 1983) and other meteorological data and materials related to the global volcanic eruptions consequences manifesting themselves in the form of "year without summer" are analysed. The picture of the "year without summer" in detail described in Byron's famous poem "Darkness" and his journals written in a year after Tambora volcano eruption (April, 1815) almost identically coincides with the "nuclear winter" scenario obtained by the scientists. These results represent an interest in the light of the complex geophysical problems: climate change, volcanic eruptions consequences, climate effects of aerosols, "nuclear winter", etc.

**MI09/W/02-A5 Poster 1145-07**

**ATMOSPHERIC AEROSOL LOADING 1979 -1999**

R.G. GRAINGER and S.M. Wheaton (University of Canterbury, email: r.grainger@phys.canterbury.ac.nz)

This paper presents preliminary results on a project to create an history of aerosol loading in the atmosphere for use in quantifying the effect that aerosols have on the Earth's climate and ozone layer. The need for such a database because the modulation of climate by volcanic eruptions and other episodic events must be accounted for in efforts to detect trends associated with greenhouse gases or other anthropogenic climate forcing. The database is being constructed from measurements by the Advanced Very High Resolution Radiometer (AVHRR), the Stratospheric Aerosol and Gas Experiment (SAGE) I&II, the Cryogenic Limb Array Etalon Spectrometer (CLAES), the Halogen Occultation Experiment (HALOE), the High Resolution Doppler Imager (HRDI), the Improved Stratospheric and Mesospheric Sounder (ISAMS) and the Microwave Limb Sounder (MLS). These instruments offer a unique insight into volcanic clouds as they provide global observations of two of the largest eruptions this century, those of El Chichón and Mt Pinatubo, as well as several smaller eruptions. The database will contain aerosol properties of: composition, effective radius, surface area density, volume density, and multi-wavelength extinction.

**MI09/W/05-A5 Poster 1145-08**

**NUMERICAL CALCULATION OF THE SPECTRAL AEROSOL OPTICAL DEPTH USING DATA ON INTEGRAL IRRADIANCE OF THE DIRECT SOLAR RADIATION**

Vazha AMIRANASHVILI (Geophysics Institute of Georgian Academy of Sciences, 1. M. Aleksidze Str., Tbilisi 380093, Georgia, email: vazha@excite.com)

The determination of the wavelength dependence of the atmospheric aerosol optical depth represents one of important problems of atmospheric optics. A method for the numerical calculation of the spectral distribution of the aerosol optical depth is described in the work. This method is based on the solution of the non-linear integral equation of the radiation transfer, in which spectral aerosol optical depth is considered an unknown function. This equation belongs to s.c. ill posed problems and was solved in two stages. At the first stage the non-linear integral equation was reduced to a sequence of linear integral equations, while at the second stage the latter equations were solved using known methods of regularisation. A uniform convergence of the sequence of solutions of the linear equations to a solution of the non-linear equation is proved. Test calculations showed a good agreement with actual observational data on spectral aerosol optical depth.

**MI09/W/06-A5 Poster 1145-09**

**RELATIONSHIP BETWEEN OBSERVATIONAL INFORMATION AND EACH PARAMETER OF AEROSOL PROPERTIES**

Sonoyo MUKAI, Itaru Sano and Yasuhiko OKADA (Fac. of Sci. & Tech., Kinki University, Higashi-Osaka, Osaka 577-8502, JAPAN. E-mail: mukai@im.kindai.ac.jp)

This paper treats with inverse problems to estimate aerosol characteristics from the space borne data. The second generation of ocean color sensors, e.g. ADEOS/OCTS and POLDER, provide us with multi-spectral and Multi-directional measurements. Furthermore POLDER is the first sensor on board the satellite aimed to measure polarization by the Earth surface-atmosphere system, and performed multi-angle viewing of one target. Simply speaking, four kinds of observational information such as directional and spectral measurements of radiance and those of polarization are available to retrieve aerosol properties.

Aerosol models are described by the size, composition, concentration and shape. Our retrieval algorithm comes from an idea that aerosol properties over the ocean can be estimated in terms of multiple scattering behavior in the atmosphere-ocean system in the near infrared wavelengths. Here we focus on what kind of observational information is the key factor for retrieval of each parameter of aerosol characteristics. As a result effective aerosol retrieval is performed. Then the obtained aerosol models are applied for atmospheric correction of the ocean color data in the visible wavelengths.

**MI09/W/07-A5** Poster **1145-10**

**LIDAR AND SATELLITE STUDIES OF UPPER TROPOSPHERIC AEROSOL**

G.S. KENT and G.M. Hansen (both at Science and Technology Corporation, Hampton, Virginia 23666, USA, email: g.s.kent@larc.nasa.gov) and C.R. Trepte (Atmospheric Sciences Division, NASA Langley Research Center, Hampton, Virginia, USA)

The SAGE II satellite experiment has been used for several years to study the seasonal and global characteristics of upper tropospheric aerosols (for altitudes above 6 km). SAGE II data have been extensively validated for the stratosphere. Validation of similar measurements for the upper troposphere are made difficult by the presence of cloud, and few data intercomparisons have been made. Moreover, SAGE II data are inverted under the assumption of horizontal homogeneity, a condition that normally does not hold for the troposphere. We report recent measurements of upper tropospheric aerosols made using a ground based scanning lidar system. The objective of these measurements was to examine the possibility of obtaining (1) values for the aerosol extinction for direct comparison with the SAGE II measurements, and (2) information about the horizontal and vertical aerosol structure, in order to assess the implications for the SAGE II data inversion and validation. Preliminary data analysis indicates that accurate determination of the aerosol optical depth ( $\sim 0.01$ ) in the upper troposphere may be limited by the signal-to-noise ratio and the linearity of the lidar system. Analysis of the changes in backscattered signal intensity with direction and time show that measurement of the horizontal and vertical structure size is possible. An experimental case study showed aerosol layering with vertical and horizontal structure sizes of the order of 1 and 10 km respectively.

**MI09/W/09-A5** Poster **1145-11**

**A PRECISION FILTER RADIOMETER FOR AEROSOL OPTICAL DEPTH DETERMINATION**

CH. WEHRLI and C. Fröhlich (both at Physikalisches-Meteorologisches Observatorium Davos, Dorfstrasse 33, 7260 Davos Dorf, Switzerland)

We describe a newly developed Precision Filter Radiometer (PFR) for determination of aerosol optical depth at 4 wavelengths of 862, 500, 412 and 368nm. These instruments are used in a world wide-wide network being built up under the GAW program of WMO. They are radiometrically calibrated by source- and detector based methods in order to tie their sensitivities to traceable standards. Their stability is verified by periodic recalibrations. Exoatmospheric signal calibration values, needed to derive optical depth from irradiance measurements, are determined by Langley extrapolation from a high altitude station and, for one instrument, by a stratospheric balloon flight. First results on the internal consistency of calibrations and the accuracy of optical depths determination will be reported.

**MI09/W/10-A5** Poster **1145-12**

**DIRECT RETRIEVAL OF AEROSOL RADIATIVE FORCING IN THE SOLAR SPECTRAL REGION: EFFECT OF DIFFERENT PHASE FUNCTIONS**

TH. HEINEMANN and J. FISCHER Freie Universitaet Berlin Institut fuer Weltraumwissenschaften Fabbeckstrasse 69 14195 Berlin Germany

Aerosol radiative forcing is a key parameter for climate modelling. A global estimation of aerosol radiative effects from satellite sensor data will surely reduce the uncertainties in climate models. The largest direct climatic effect of aerosol is the backscattering of solar radiation to space. Common aerosol remote sensing methods using the backscattered radiation over known surface to estimate aerosol parameters like the optical depth and the aerosol size distribution. Since there is no method to get information about absorption by aerosol particles from nadir viewing sensors, the accuracy of aerosol optical depth retrieval is drastically reduced when absorbing aerosol are present. The change of upward radiative flux at top of atmosphere integrated over the solar spectrum can be derived from retrieved optical aerosol parameters with means of a radiative transfer model. On the other hand the change of upward flux can be derived directly from the measured radiance. The later method is much less sensitive to aerosol absorption. A method for the direct retrieval of upward radiative flux over open ocean water from measurements in the red and near infrared spectral region has been developed using the radiative transfer model MOMO. The retrieval scheme has been successfully applied to MOS-B data. The remaining problem is the unknown phase function. In this paper the effects of phase function change on the direct retrieval of upward flux are discussed. Radiative transfer simulations for 10 different aerosol types and aerosol optical depths between 0.0 and 0.5 were performed for 560 combinations of sun and viewing geometries which represent the whole range that can be observed from a polar orbiting satellite.

**MI09/W/11-A5** Poster **1145-13**

**STATISTICAL ANALYSIS OF PHASE MATRICES OF ATMOSPHERIC AEROSOLS**

Alex A. KOKHANOVSKY (Institute of Physics, 70 Skarina Avenue, Minsk 220072, Belarus e-mail: a.kokhanovsky@ieec.org)

Microphysical and chemical properties of the background atmospheric aerosol vary with space and time. However, changes in optical properties (e.g., phase matrices) at some observation geometries can be not so prominent. The task of this presentation is to study the variability of the elements of the phase matrix of atmospheric aerosols as functions of the scattering angle. The statistical ensemble of phase matrices was obtained with the Mie theory for effective radii of aerosol particles in the range 0.1-1.5 micrometers. The data obtained were used as an input for the correlation analysis of the statistical ensemble. Average values, coefficients of variance and skewness were calculated. It was found that phase matrices of the atmospheric aerosols only weakly depend on their microstructure at the scattering angle around 150 degrees, which can be used in satellite retrieval algorithms.

**MI09/W/12-A5** Poster **1145-14**

**POTENTIAL IMPACT OF DESERT-DUST CLOUD INTERACTIONS ON PRECIPITATION FORMING PROCESSES**

Rohen LAHAV (Atmospheric Sciences, The Hebrew University of Jerusalem, Israel Daniel ROSENFELD (Atmospheric Sciences, The Hebrew University of Jerusalem, Israel. e-mail:daniel@vms.huji.ac.il)

Microphysical measurements in convective clouds developing in a heavy dust storm over the eastern Mediterranean were made by remote sensing from satellite and in situ by cloud physics aircraft. Clouds forming in the desert dust had smaller droplets. The satellite inferred effective radius of cloud particles was much reduced in clouds developing in the dust, as compared to nearby clouds developing in visibly dust free air. The dust reduced the effective

radius to below the precipitation threshold of 15 micron.

Aircraft measurements were made in clouds forming in heavy dust. The dust reached the flight level of 3 km, from which the ground was completely obscuring by the dust. Vigorous convective elements, with base at 8C, reached temperature of -20C with more than 3 g/m<sup>3</sup> supercooled liquid water contents, with some dendrite crystals and graupel. No evidence for warm rain processes was evident.

These aircraft measurements corroborate the satellite inferences, and suggest that desert dust might be detrimental to precipitation forming processes. That raises the concern of a feedback mechanism for desertification: Dust causes clouds to precipitate less. The drier conditions lead to even more dust, closing the feedback loop.

**MI09/L/06-A5** Poster **1145-15**

**OBSERVATIONS OF THE GLOBAL DISTRIBUTION...**

Franklin MILLS (Division of Geological & Planetary Science, MS 170-25, California Institute of Technology, Pasadena, CA 91125, e-mail: FPM@mercuri.gps.caltech.edu)

Observations of the global distribution and composition of aerosol and cloud particles are needed to understand the radiative forcing effects of aerosols and their influence on global climatic change. Satellite measurements of aerosol distributions most commonly have been derived from visual and near-infrared measurements, such as those by the Stratospheric Aerosol and Gas Experiment (SAGE) and the Advanced Very High Resolution Radiometer (AVHRR). As shown by previous studies, the 750 - 3000 cm range also has potential for providing information on aerosol distributions and composition. Solar occultation spectra recorded by the Atmospheric Trace Molecule Spectroscopy (ATMOS) Fourier Transform Infrared (FTIR) spectrometer for this wavelength range have been examined to quantify the distribution of sulfate aerosols during the 1992, 1993, and 1994 ATLAS missions.

The ATMOS FTIR collected 4600 spectra during more than 300 occultations with excellent signal-to-noise at spectral resolution of 0.01 cm and vertical resolution of 2 - 4 km. These spectra were first processed to determine the vertical profiles of trace molecules for each occultation. Subsequently, the broad absorption features present in the 800 to 1400 cm spectra were examined to retrieve vertical profiles of sulfate aerosols in the lower stratosphere and upper troposphere. The aerosol distributions derived from our initial analyses are consistent with those published based on data from other instruments, such as the Cryogenic Limb Array Etalon Spectrometer (CLAES) on the Upper Atmosphere Research Satellite (UARS). The possible presence of water ice absorption features has been identified in some spectra, and further analysis of spectra collected at shorter wavelengths is in process to quantify the water ice distributions. Corrections for collision-induced absorption by O<sub>2</sub> and N<sub>2</sub> are also being implemented to increase the wavelength range that may be examined in search of aerosol absorption features.

**MI09/L/07-A5** Poster **1145-16**

**A SATELLITE STUDY OF THE LATITUDINAL VARIATION IN THE SMOKE INDIRECT EFFECT OVER TROPICAL SOUTH AMERICA**

J.Ramaprasad, L.Remer and Y.Kaufman, Code 913, Laboratory for, Atmospheres, NASA Goddard Space Flight Center, Greenbelt, MD 20771, USA

Analysis of several Advanced Very High resolution Radiometer (AVHRR) images over the Amazon Basin and Cerrado show that the effect of smoke on cloud drop sizes and cloud reflectances varies with latitude. The effect is strongest in the North and much weaker as we move South. Kaufman and Fraser (1997) suggested that this variation in the signal may be linked to variations in the precipitable water vapor in the atmosphere. We analyze model derived precipitable water vapor fields along with satellite signals of smoke optical thicknesses and cloud properties to examine the interactions between these variables. We find higher levels of precipitable water vapor as well as more uniform fields toward the north that could support the hypothesis. We also find that smoke optical thicknesses are negatively correlated with the water vapor levels. Interaction effects of smoke and precipitable water vapor on the magnitude of the indirect effect are to be examined.

**MI09/W/03-A5** Poster **1145-17**

**OPTICAL CHARACTERISTICS OF AEROSOLS DERIVED WITH TWO STATE OF THE ART SKY RADIOMETERS**

G. Pandithurai (Department of Meteorology, University of Maryland, College Park, MD, 20742, USA, email: pandi@atmos.umd.edu); Rachel T. PINKER (Department of Meteorology, University of Maryland, College Park, MD, 20742, USA, email: pinker@atmos.umd.edu); Brent Holben (Laboratory for Atmospheres, NASAGoddard Space Flight Center, Code 913, Greenbelt, MD, 20771, USA, email: brent@spamer.gsfc.nasa.gov); Tamio Takamura (Atmospheric Radiation Section, Sensor/Atmospheric Radiation Division, Center for Environmental remote sensing (CEReS), Chiba University, Chiba 263, Japan, email: takamura@rsirc.cr.chiba-u.ac.jp) Shi'ichi Kaneta (Atmospheric Radiation Section, Sensor/Atmospheric Radiation Division, Center for Environmental remote sensing (CEReS), Chiba University, Chiba 263, Japan, email: kaneta@rsirc.cr.chiba-u.ac.jp)

Progress has been made in developing instruments with capabilities to provide most of the needed information on optical properties of aerosols. This led to the establishment of coherent programs to characterize aerosol properties at numerous stations over the globe, of climatic importance (e.g., the AERONET program). The instrument selected for this effort is the automatic sun tracking photometer produced by CIMEL ELECTRONIQUE. In parallel, an observing network is being established in Asia, in support of remote sensing research related to observations to be made in the framework of the Japanese Global Imager (GLI) instrument on the Advanced Earth Observing Satellite (ADEOS) II mission, as sponsored by the National Space Development Agency of Japan (NASDA). The sun tracking photometer selected for this effort is the sky radiometer model POM-01L, produced by PREDE Inc. Results will be presented from an effort to intercompare the performance of these two radiometers at one midlatitude location. Use has been made of the SKYRAD.PACK code, as developed by T. Nakajima, to infer the various aerosol optical properties.

**MI09/W/13-A5** Poster **1145-18**

**NORTH ATLANTIC AEROSOL RADIATIVE IMPACTS BASED ON SATELLITE MEASUREMENTS AND AEROSOL INTENSIVE PROPERTIES FROM TARFOX AND ACE 2**

Robert W. BERGSTROM (Bay Area Environmental Research Institute, San Francisco, CA 94122 USA, email: bergstro@sky.arc.nasa.gov); Philip B. Russell (NASA Ames Research Center, Moffett Field, CA 94035-1000 USA, email: prussell@mail.arc.nasa.gov)

We estimate the impact of North Atlantic aerosols on the net shortwave flux at the tropopause by combining maps of satellite-derived aerosol optical depth (AOD) with model aerosol properties. We exclude African dust, primarily by restricting latitudes to 25-60 N. Aerosol properties were determined via column closure analyses in two recent experiments, TARFOX and ACE 2, as described by Russell et al. (this conference). The analyses use in situ measurements of aerosol composition and air- and ship-borne sunphotometer measurements



of AOD spectra. The resulting aerosol model yields computed flux sensitivities (dFlux/dAOD) that agree with measurements by airborne flux radiometers in TARFOX. It has a midvisible single-scattering albedo of 0.9, which is in the range obtained from in situ measurements of aerosol scattering and absorption in both TARFOX and ACE 2. Combining seasonal maps of AVHRR-derived midvisible AOD with the aerosol model yields maps of 24-hour average net radiative flux changes at the tropopause. For cloud-free conditions, results range from  $-9$  W/m<sup>2</sup> near the eastern US coastline in the summer to  $-1$  W/m<sup>2</sup> in the mid-Atlantic during winter; the regional annual average is  $-3.5$  W/m<sup>2</sup>. Using a non-absorbing aerosol model increases these values by about 30%. We estimate the effect of clouds using ISCCP cloud-fraction maps. Because ISCCP midlatitude North Atlantic cloud fractions are relatively large, they greatly reduce the computed aerosol-induced flux changes. For example, the regional annual average decreases from  $-3.5$  W/m<sup>2</sup> to  $-0.8$  W/m<sup>2</sup>. We compare results to previous model calculations for a variety of aerosol types.

**MI09/W/01-A5** Poster **1145-19**

#### VALIDATING ATMOSPHERIC CORRECTIONS TO SATELLITE OBSERVATIONS OF OCEAN COLOUR WITH MULTI-FILTER SOLAR PHOTOMETRY

J. DAVIES, B. Osborne, N. Santich and M. LYNCH (Remote Sensing and Satellite Research Group, School of Physical Sciences, Curtin University of Technology, GPO Box U1987, Perth, WA 6845, AUSTRALIA, email: jim@ra.clc.curtin.edu.au)

In October 1998 a Yankee Environmental Systems Multi-Filter Rotating Shadowband Radiometer (MFRSR-7) was installed at an offshore field station on Rottnest Island, some 18 km west of Fremantle in the Indian Ocean. The instrument was acquired primarily to provide validation data for atmospheric corrections applied to ocean colour data collected by the SeaWiFS satellite sensor. Under westerly flows, photometer measurements provide aerosol data on the maritime air mass through which SeaWiFS is viewing adjacent coastal waters. In this paper aerosol properties estimated from SeaWiFS channel radiances are validated against aerosol data products from the Rottnest Island MFRSR-7 solar photometer.

**MI09/E/06-A5** Poster **1145-20**

#### LONG-TERM MONITORING OF GLOBAL AEROSOL CHARACTERISTICS USING NOAA-AVHRR

Akiko HIGURASHI (National Institute for Environmental Studies, 16-2 Onogawa, Tsukuba, Ibaraki 305-0053, Japan, e-mail: hakiko@nies.go.jp); Teruyuki Nakajima and Takayuki Usui (Center for Climate System Research, University of Tokyo, 4-6-1 Komaba, Meguro-ku, Tokyo 153-8904, Japan, e-mail: teruyuki@ccsr.u-tokyo.ac.jp)

Aerosols are recognized to cause significant direct and indirect forcing on Earth's %fs climate. The evaluation of these effects, however, remains still highly uncertain for lack of our knowledge of aerosol characteristics on global and long-term scale.

We have developed the aerosol retrieval algorithm, which estimates aerosol optical thickness and !OgstrSN exponent using two channel radiance data of NOAA-AVHRR and have validated the results with ground-based observations. Retrieving !OgstrSN exponent addition to aerosol optical thickness has been shown to be very effective, as compared with past aerosol retrieval algorithm which obtains only aerosol optical thickness from one channel radiance assuming aerosol model, because it makes possible to distinguish the impact of human activities from that of natural aerosols represented by desert dust, and to estimate the number density of aerosol particles, which is very important to investigate the aerosol indirect effect.

We will report the global distribution of these parameters applying the algorithm to multi-year data sets of NOAA-AVHRR radiances. Preliminary analysis suggests increasing contribution of human emission of aerosols, especially off the east of Asia. Such long term analysis will indicate the natural and anthropogenic variabilities of aerosol properties.

**MI09/W/14-A5** Poster **1145-21**

#### SATELLITE REMOTE SENSING OF AEROSOL PROPERTIES IN COLUMN CLOSURE EXPERIMENTS

P. A. DURKEE, K. E. Nielsen (both at 1Naval Postgraduate School, Monterey, CA USA, Email: durkee@nps.navy.mil), P. B. Russell (NASA Ames Research Center, Moffett Field, CA USA), B. Schmid (Bay Area Environmental Research Institute, San Francisco, CA USA), J. M. Livingston (SRI International, Menlo Park, CA USA), D. Collins, R. C. Flagan, J. H. Seinfeld (all three at California Institute of Technology, Pasadena, CA USA), K. J. Noone, E. Öström (both at Stockholm University, Stockholm, Sweden), S. Gassó, D. Hegg (both at University of Washington, Seattle, WA USA), L. M. Russell (Princeton University, Princeton, NJ USA), T. S. Bates, and P. K. Quinn (both at NOAA PMEL, Seattle, WA USA)

Recent field programs designed to study aerosol properties have produced interesting contrasts across diverse regions of the globe. ACE-1 (Aerosol Characterization Experiment) observed conditions in the relatively unperturbed southern ocean near Tasmania in November-December 1995. The Tropospheric Aerosol Radiative Forcing Observational Experiment (TARFOX) observed aerosol transported to the North American coast over the Atlantic Ocean in July 1996. Most recently, ACE-2 measured the properties of aerosol from Europe and Northwestern Africa over the eastern North Atlantic Ocean in June-July 1997. The differences between these three regions are well observed by satellite remote sensing. The Advanced Very High Resolution Radiometer (AVHRR) aboard NOAA polar orbiting satellites measure radiance in five wavelength bands - two of which are sensitive to scattering by aerosol (Channel 1 - 0.63  $\mu$ m and Channel 2 - 0.86  $\mu$ m center wavelengths). Aerosol optical depth calculated for these first two channels of AVHRR and the radiance ratio of these channels can be used to parameterize size distribution properties. Retrieval of aerosol properties requires assumptions about the characteristics of aerosol number distributions, the absorption properties and vertical distribution of aerosol, surface reflectance, and others. This presentation will describe the array of airborne, surface, and shipboard data collected during field experiments that can be used to validate the satellite-based retrieval of aerosol properties. Analysis of aerosol size distribution, aerosol optical depth, scattering and absorption characteristics will be used to test the assumptions in satellite retrieval algorithms.

**MI09/L/01-A5** Poster **1145-22**

#### AEROSOL SIZE DISTRIBUTIONS, PROPERTIES AND VERTICAL PROFILES OVER THE PACIFIC: TOWARDS AN AEROSOL CLIMATOLOGY

CLARKE, A.D. and Kapustin, V. N., (Department of Oceanography, 1000 Pope Rd. Honolulu, HI 96822, USA, e-mail: tclarke@soest.hawaii.edu)

During the past decade we have participated in numerous ship and aircraft experiments throughout the Pacific. Measurements were made of size-distributions, physicochemistry, aerosol light scattering and absorption coefficients and other aerosol characteristics. Size distributions were obtained from 10 to 5,000nm dry particle diameter by using differential

mobility analyzers and optical particle counters. This often included thermal analysis up to 300C that revealed volatile (eg. sulfates) and refractory (eg. dust, soot, sea-salt components) in real time. Variations in the smaller sizes reveal processes related to the formation and processing of aerosol while the larger sizes reveal features that dominate aerosol radiative effects and optical depth. Vertical profiles and horizontal legs in the marine boundary layer and the free troposphere were obtained for diverse regions. These included regions of clean air as well as regions influenced by "layers" or "rivers" of continental aerosol at various altitudes above the MBL. Sources included dust, biomass burning, continental pollution as well as natural emissions including volcanic sulfates and sea-salt. Current work in progress is designed to link some of these features and their optical influence to meteorological and climatological regimes over the Pacific.

Friday 23 July PM

Presiding Chair: R.T. Pinker (Dept. of Meteorology, Univ. of Maryland, USA)

#### COLUMN CLOSURE EXPERIMENTS OF AEROSOLS (CONT.)

**MI09/W/15-A5** Invited **1500**

#### NORTH ATLANTIC AEROSOL PROPERTIES FOR RADIATIVE IMPACT ASSESSMENTS, DERIVED FROM COLUMN CLOSURE ANALYSES IN TARFOX AND ACE 2

Philip B. RUSSELL (NASA Ames Research Center, Moffett Field, CA 94035-1000 USA, email: prussell@mail.arc.nasa.gov); Robert W. Bergstrom and Beat Schmid (Bay Area Environmental Research Institute, San Francisco, CA 94122 USA, email: bergstro@sky.arc.nasa.gov, bschmid@mail.arc.nasa.gov); John M. Livingston (SRI International, Menlo Park, CA 94025 USA)

Aerosol effects on atmospheric radiative fluxes provide a forcing function that can change the climate in potentially significant ways. This aerosol radiative forcing is a major source of uncertainty in understanding the climate change of the past century and predicting future climate. To help reduce this uncertainty, the 1996 Tropospheric Aerosol Radiative Forcing Observational Experiment (TARFOX) and the 1997 Aerosol Characterization Experiment (ACE-2) measured the properties and radiative effects of aerosols over the Atlantic Ocean. Both experiments used remote and in situ measurements from aircraft and the surface, coordinated with overpasses by a variety of satellite radiometers. TARFOX focused on the urban-industrial haze plume flowing from the United States over the western Atlantic, whereas ACE-2 studied aerosols over the eastern Atlantic from both Europe and Africa. These aerosols often have a marked impact on satellite-measured radiances. However, accurate derivation of flux changes, or radiative forcing, from the satellite-measured radiances or retrieved aerosol optical depths (AODs) remains a difficult challenge. Here we summarize key initial results from TARFOX and ACE-2, with a focus on closure analyses that yield aerosol microphysical models for use in improved assessments of flux changes. We show how one such model gives computed radiative flux sensitivities (dF/dAOD) that agree with values measured in TARFOX and preliminary values computed for the polluted marine boundary layer in ACE-2. A companion paper (Bergstrom and Russell, this conference) uses the model to compute aerosol-induced flux changes over the North Atlantic from AVHRR-derived AOD fields.

**MI09/E/07-A5** **1525**

#### AEROSOL RADIATIVE CLOSURE EXPERIMENTS FROM TARFOX: A COMPARISON OF THE MEASURED RADIATIVE PROPERTIES AND RADIATIVE FORCING WITH THOSE USED IN GLOBAL CLIMATE MODELS.

James M. HAYWOOD and Peter N. Francis (Meteorological Research Flight, UK Met Office, DERA, Farnborough, Hants, GU14 0LX, UK. Email: jmhaywood@meto.gov.uk, pnfrancis@meto.gov.uk)

A primary aim of the Tropospheric Aerosol Radiative Forcing Observational Experiment (TARFOX) is to obtain closure in terms of the modelled and measured radiances and irradiances. This study presents results from such a closure experiment and compares them with those using size distributions and optical parameters from global modelling studies which estimate the direct radiative forcing of anthropogenic aerosol species.

Two methods for determining the size distribution of the aerosols are used. The first method uses that measured directly by the passive cavity aerosol spectrometer probe (PCASP-100X), and the second is derived from observations of the spectral radiances measured using the Scanning Airborne Filter Radiometer (SAFIRE). The results suggest that radiative closure can be obtained to within the experimental accuracy provided the aerosol size distribution is well determined. The PCASP-100X may significantly undersize aerosol particles as a consequence of the partially absorbing nature of the aerosols, and possibly due to partial drying of the aerosol within the instrument. A comparison of the measured radiative properties with those used in global calculations of the radiative forcing due to sulphate, organic and black carbon aerosols is also performed.

**MI09/W/08-A5** **1542**

#### MEASURED AND CALCULATED CLEAR-SKY RADIATION PROFILES USING DETAILED AIRCRAFT AND LIDAR AEROSOL DATA

Manfred WENDISCH, Andreas Keil, Ulla Wandinger, Dietrich Althausen, Heike Wex and Doerthe Mueller (all at Institute for Tropospheric Research, Permoserstr. 15, 04318 Leipzig, Germany, email: wendisch@tropos.de)

Results of a columnar closure type field experiment (LACE'98: Lindenberg Aerosol Characterization Experiment) are discussed. The campaign was performed south of Berlin in August 1998. The measurements mainly aimed at a comprehensive characterization of microphysical and chemical aerosol properties and an improved understanding of related radiative effects. Beside ground-based measurements, several aircraft and lidar systems were involved.

The aircraft measurements were combined with multiwavelength lidar observations in order to derive precise profile information as input for the radiative transfer calculations. The in-situ aircraft aerosol measurements include size distribution, concentration in different size ranges (>3nm, >10nm, >100nm particle diameter) volume scattering (three wavelength nephelometer) and absorption (photometer) coefficients as well as impactor samples. These data were used for an in-situ volume closure between the scattering and absorption coefficients calculated from the aerosol size distribution via Mie theory and those directly measured by nephelometer and photometer. The lidar measures backscatter coefficients at six wavelengths between 355 and 1064 nm as well as extinction coefficients at 355 and 532 nm. From these measurements, effective particle radius, volume, surface area, and number concentrations are derived. The lidar data are compared with those calculated from the aircraft size distribution measurements.

With the vertical profiles of aerosol microphysical properties as input radiative transfer calculations were performed. The results of the calculations are compared with airborne broadband solar and ultraviolet irradiance measurements and spectral (500-900 nm, 2.4 nm resolution) irradiance data measured simultaneously at the ground.



**MICROPHYSICAL AND RADIATIVE PROPERTIES OF AEROSOLS****MI09/L/05-A5** Invited **1620****AEROSOL OPTICAL PROPERTIES AND DIRECT SHORTWAVE RADIATIVE FORCING: DEPENDENCE ON SIZE AND COMPOSITION**

Stephen E. SCHWARTZ (Environmental Chemistry Division, Brookhaven National Laboratory, Upton NY 11973 USA, e-mail: ses@bnl.gov); John A. Ogren (NOAA Climate Monitoring and Diagnostics Laboratory, Boulder CO 80303 USA, email: jogren@cml.noaa.gov); Michael H. Bergin (Civil and Environmental Engineering and Earth and Atmospheric Sciences, Georgia Institute of Technology, Atlanta Georgia 30332 USA)

Direct shortwave radiative forcing of climate by an aerosol is the difference between top-of-atmosphere radiative flux in the presence of the aerosol and in its absence. The aerosol perturbation in radiative flux depends on the aerosol properties column extinction, the fraction of extinction that is scattered (single scattering albedo), and the angular distribution of light scattering, as well as the geophysical variables solar zenith angle, surface reflectance, and atmospheric transmittance above the aerosol. Aerosol optical properties depend on the size distribution of the aerosol (and shape, if non spherical) and real and imaginary components of index of refraction, which depend on composition. These properties are dependent on the source of the aerosol and its subsequent evolution in the atmosphere as modified by removal processes. Aerosol properties are thus not a constant but are variable, though they tend to be dominated by the most long-lived particles in the radius range 0.1 to 1  $\mu$ m, which happens to be the most efficient size range for light scattering. For hygroscopic aerosols (which include dominant ionic species sulfates and nitrates) size increases strongly with increasing relative humidity greatly enhancing light scattering and radiative forcing. Unfortunately, for a variety of historical and instrumental reasons, aerosol properties are commonly measured and reported at low relative humidity, leading to underestimate of light scattering and radiative forcing unless properly accounted for. This talk reports measurements of aerosol properties pertinent to shortwave forcing and their implications on estimates of this forcing.

**MI09/E/08-A5** Invited **1645****RETRIEVAL OF CLIMATE-RELEVANT AEROSOL PARAMETERS FROM TOP-OF-ATMOSPHERE (TOA) RADIANCE BY CLOSURES WITH GROUND-BASED SUN- AND SKY RADIANCE MEASUREMENTS**

Wolfgang von HOYNINGEN-HUENE, Torsten Schmidt, John P. Burrows (IUP University of Bremen FB1, BO-Box 330440, D-28334 Bremen, email: hoyning@gome5.physik.uni-bremen.de) Ana-Maria Silva (Dept. of Physics, University of Evora, P-7000 Evora, email: asilva@evuniv.uvora.pt) Bringfried Pflug (DLR, Institute for Space Sensor Technique Berlin, Bringfried.Pflug@dlr.de) Teruyuki Nakajima (CSR University of Tokyo, email: teruyuki@ccsr.u-tokyo.ac.jp)

The determination of realistic spectral features of the aerosol optical thickness from satellite data is one task to be solved for a determination of global aerosol data sets for different aerosol types and the observation of its variability in time and space. Comparisons between TOA radiances obtained a) by multi-channel satellite radiometers and b) by calculations from ground-based sun- and skyradiance measurements can be used for a validation of the aerosol parameters to be applied for the solution of the radiative transfer. Further they allow a determination of specific relationships between TOA-radiance and aerosol optical thickness for multi-channel sensors as OCTS/ADEOS or MOS-B/IRS-P3. This multi-channel approach reduces the errors in the determination of the Angstrom turbidity parameters compared with the commonly used 2 channel approaches. Examples from ACE-2 CLEARCOLUMN (clean marine conditions) and the forest fire events in South East Asia in October 1997 demonstrate the applicability of such an approach.

**MI09/W/16-A5** **1710****IMPACT OF CENTRAL AMERICAN FIRES ON THE RADIATIVE BUDGET OVER THE ARM CART SITE**

Xiang Li, Sundar Christopher, Joyce Chou and Ronald M. Welch (University of Alabama in Huntsville, Department of atmospheric science, Global Hydrology and Climate Center, Huntsville, AL 35899 USA, e-mail: xli@atmos.uah.edu)

Each year large amounts of biomass burning aerosols are released into the atmosphere, which influence the radiative energy budget of the earth-atmosphere system on both regional and global scales. During April and May 1998, large numbers of fires occurred over Central America, and the resultant smoke aerosols were observed to advect over North America. In this study, using both satellite and ground-based measurements, the radiative impact of biomass burning aerosols at both the top-of-the-atmosphere (TOA) and at the surface are investigated over the U.S. Southern Great Plains (SGP) Cloud and Radiation Testbed (CART) site in the Atmospheric Radiative Measurement (ARM) program in Oklahoma. With knowledge of optical thickness of biomass burning aerosols from sunphotometer measurements made at the ground, single scattering albedos of the aerosols are retrieved from NOAA-14 Advanced Very High Resolution Radiometer (AVHRR) visible imagery. Then, with these optical properties of aerosols, shortwave radiative fluxes at both the TOA and surface are calculated using a radiative transfer model. The calculated surface fluxes then are compared with the Baseline Surface Radiation Network (BSRN) ground-based measurements; the calculated TOA fluxes are compared with the Clouds and Earth's Radiant Energy System (CERES) S8 ERBE-like product from the Tropical Rainfall Measuring Mission (TRMM) platform. The radiative forcings of biomass burning aerosols are estimated at both the TOA and at the surface.

**MI09/L/01-A5** **1744****AEROSOL SIZE DISTRIBUTIONS, PROPERTIES AND VERTICAL PROFILES OVER THE PACIFIC: TOWARDS AN AEROSOL CLIMATOLOGY**

CLARKE, A.D. and Kapustin, V. N., (Department of Oceanography, 1000 Pope Rd, Honolulu, HI 96822, USA, Phone: 808-956-7777 FAX: 808-956-7112, e-mail: tclarke@soest.hawaii.edu)

During the past decade we have participated in numerous ship and aircraft experiments throughout the Pacific. Measurements were made of size-distributions, physicochemistry, aerosol light scattering and absorption coefficients and other aerosol characteristics. Size distributions were obtained from 10 to 5,000nm dry particle diameter by using differential mobility analyzers and optical particle counters. This often included thermal analysis up to 300C that revealed volatile (eg. sulfates) and refractory (eg. dust, soot, sea-salt components) in real time. Variations in the smaller sizes reveal processes related to the formation and processing of aerosol while the larger sizes reveal features that dominate aerosol radiative effects and optical depth. Vertical profiles and horizontal legs in the marine boundary layer and the free troposphere were obtained for diverse regions. These included regions of clean air as

well as regions influenced by "layers" or "rivers" of continental aerosol at various altitudes above the MBL. Sources included dust, biomass burning, continental pollution as well as natural emissions including volcanic sulfates and sea-salt. Current work in progress is designed to link some of these features and their optical influence to meteorological and climatological regimes over the Pacific.

**MC01****Monday 19 – Friday 23 July****IMPROVEMENTS AND INTERCOMPARISONS OF CLIMATE SYSTEM MODELS AND THEIR COMPONENT MODELS (ICCL)**  
Location: Howarth Building 203 LT**Monday 19 July AM**

Presiding Chairs: Peter Gleckler (Program for Climate Model Diagnosis and Intercomparison, PCMDI, Lawrence Livermore National Laboratory) and Jerry Potter (PCMDI, Lawrence Livermore National Laboratory)

**ATMOSPHERIC MODELLING AND INTERCOMPARISONS****AMIP Overview****MC01/L/01-A1** **0930****AN OVERVIEW AND UPDATE ON THE ATMOSPHERIC MODEL INTERCOMPARISONS PROJECT (AMIP)**

Peter GLECKLER (Program for Climate Model Diagnosis and Intercomparison (PCMDI), Lawrence Livermore National Laboratory, PO Box 808, Livermore, California, USA Email: gleckler1@llnl.gov)

AMIP is a standard experimental protocol for atmospheric general circulation models (AGCMs). It provides a community-based infrastructure in support of climate model diagnosis, validation, intercomparison, documentation and data access. The infrastructure that has been developed in support of AMIP enables a diverse community of scientists to analyze AGCMs in a systematic fashion, a process which serves to facilitate model improvement. Virtually the entire international climate modelling community has participated in this project since its inception in 1990. In this presentation an overview and status report of AMIP will be given.

**MC01/E/30-A1** Invited **0945****EVALUATING THE OVERALL PERFORMANCE OF AMIP MODELS**

Karl E. TAYLOR, Charles Doutriaux, and Peter J. Gleckler (all at the Program for Climate Model Diagnosis and Intercomparison, Lawrence Livermore National Laboratory, Livermore, CA 94550, U.S.A., email: ktaylor@pcmdi.llnl.gov)

Results from the Atmospheric Model Intercomparison Project (AMIP) are being archived in a common format and structure that facilitates efficient and comprehensive analysis of results. The procedure used to evaluate a single model's performance can be applied to all other models with little extra effort, resulting in an "economy of scale" which is one of the real benefits of model intercomparisons. Even with the advantages offered by a well organized and accessible data base, the enormous amount of model data produced by intercomparison projects like AMIP has made it difficult for comprehensive summaries of model results to be prepared. Recently, however, the Program for Climate Model Diagnosis and Intercomparison (PCMDI) has developed a capability, which continues to evolve, that can provide individual modelling groups with timely summaries of their model's performance. These summaries comprise both traditional plots showing how closely certain aspects of a simulation match observations and also innovative plots that can provide a more comprehensive statistical overview of model skill. These same diagnostic capabilities can be applied to monitor changes in the performance of models as they evolve. As an example, the performance of the most recent AMIP simulations (ca. 1998) will be compared to that of earlier simulations (ca. 1992).

**AMIP II Simulations****MC01/W/42-A1** **1015****THE CGAM CLIMATE MODEL EXPERIMENT FOR AMIP-II A**

O'Neill (1), W. A. Lahoz (1), J. Slingo (1), J. Cole (1), C. Jones (2) (1) CGAM, University of Reading, RG6 6BB, UK (2) Rossby Centre, SMHI, Sweden

As a contribution to the AMIP-II experiment, the Centre for Global Atmospheric Modelling (CGAM) has run a 17-year integration of a troposphere-stratosphere version of the UK Meteorological Office's Unified Model. The model has 58 levels in the vertical with a top at 0.08 hPa, and a horizontal resolution of 2.5 deg latitude by 3.75 deg longitude. The model contains the same parametrizations of physical processes (so-called HADAM3 physics) as the AMIP-II runs conducted by the Hadley Centre, with the additional feature that the CGAM version has a well-resolved stratosphere. Seasonally varying sources for trace gases were placed at the equatorial and polar tropopause in order to determine the large-scale circulation and mixing processes in the model. A detailed comparison of fields from this experiment will be made with ERA-15 analyses, focusing on the ability of the model to represent aspects of the seasonal evolution, and intraseasonal and interannual variability. Comparison of results with those obtained by the Hadley Centre will be made to determine the benefits of including a well-resolved stratosphere, particularly in the region of the tropopause. It is shown that the simulated atmospheric structure in the upper troposphere and lower stratosphere is sensitive to the number and location of model levels in the stratosphere.

**MC01/E/05-A1** **1030****CLIMATE VARIABILITY IN THE HADLEY CENTRE MODEL**

Henry BUCKLEY and Vicky Pope (both at Hadley Centre for Climate Prediction and Research, Met Office, London Rd., Bracknell, RG12 2SY, UK. Email: hbuckley@meto.gov.uk)

The aim of this study is to describe and validate the simulation of climate variability in the latest version of the Hadley Centre atmospheric climate model (HadAM3). Our model reproduces the mean climate well, and assessment of model variability provides an important and more stringent test of model performance. In climate variability studies a distinction is made between intrinsic variability (reflecting the internal chaotic behaviour of the system) and the systematic response to variable forcing. Ensemble runs provide a useful means of separating these components and studying them in isolation, and enable an estimate of the significance of

results based on single climate runs to be made. We have run an ensemble of six AMIP II integrations, which differ only in their initial atmospheric state; and a control run using climatological SSTs. We present a statistical analysis of the ensemble data, focusing on the spatial and seasonal dependence of the different components of variability, and validate our results against the ECMWF Reanalysis dataset.

**MC01/W/40-A1****1115****AMIP II SIMULATION OF NCC CLIMATE MODEL**

Zheng-Qing Ye Min Dong (National Climate Center, Beijing, 100081)

A 17-year integration in which the National Climate Center climate model is forced with observed monthly varying sea surface temperatures since 1979 is compared to reanalysis data and observed data. The results show that the model is able to reproduce the basic observed patterns of the pressure field and the properties of their seasonal pressure variations very well at sea level. The simulation can capture the Aleutian low, Icelandic low, Asian continent high in winter and their seasonal variations. On the other hand, the geopotential heights at 500 hPa and 300 hPa are quite well simulated. In winter, the troughs off the east coasts of Asia and North America, the trough over eastern Europe, the ridge over Russia and west coast of North America are simulated very well. In the wind fields, the simulation of jets and storm tracks is very similar to that of reanalysis data in both winter and summer. The location and amplitude of jets and storm tracks are in good agreement with the observed fields. In this paper, the atmospheric energy budget are also analyzed. Some striking results are given. Finally, the reasons for the differences between the simulation and observed data are also analyzed.

**MC01/E/13-A1****1130****SEASONAL PREDICTABILITY EXPERIMENTS BY JMA AGCM**

Shoji KUSUNOKI, Masato Sugi and Akio Kitoh (Climate Research Department, Meteorological Research Institute, Nagamine 1-1, Tsukuba, Ibaraki 305-0052, JAPAN, Email: skusunok@mri-jma.go.jp) Chiaki Kobayashi and Kiyoharu Takano (Climate and Marine Department, Japan Meteorological Agency, 1-3-4 Ootemachi, Chiyoda-ku, Tokyo 100-0004, JAPAN, Email: chiaki\_k@hq.kishou.go.jp)

A T63L30 resolution version of atmospheric general circulation model (AGCM) of the Japan Meteorological Agency (JMA) has been integrated for 4 months forced with the observed sea surface temperature (SST). The integrations were started from observed initial conditions of the European Centre for Medium-Range Weather Forecasts (ECMWF) Re-Analyses for all four seasons through the 15-years period of 1979-1993. Each ensemble consists of 9 members initiated from consecutive analyses 1 day apart. The skill of the ensemble simulations was evaluated over the extratropics and the tropics. The interannual variation of the boreal summer precipitation over India and Japan were not well simulated, while that over the Yangtze river valley in China exceeded the 95% significant level of correlation with observation.

**MC01/L/02-A1****1145****RESULTS FROM AMIP II: THE COLA GCM SIMULATION**

C. Adam Schlosser, L. Marx, V. Krishnamurthy, D. Straus, J. L. Kinter III, and J. Shukla

For the AMIP II experiment, an 18-year simulation of the global circulation was performed with the Center for Ocean-Land-Atmosphere (COLA) general circulation model (GCM) using prescribed sea-surface temperatures (1979-1996). We present a summary of the performance of the COLA GCM at simulating the monthly, seasonal, and annual variability of the global climate. Selected regional analyses of the simulation are also presented, and will focus on the performance of the model at reproducing the observed spatio-temporal patterns of regional climate phenomenon (e.g. the India monsoon). Where applicable, the analysis is presented in the context of model development and attempts to identify sources of optimal performance that result from recent changes in the COLA GCM parameterizations.

Monday 19 July PM

**Radiation Studies****MC01/W/31-A1****1400****OHMURAAMIP II SURFACE AND ATMOSPHERIC RADIATIVE FLUXES: SOME PRELIMINARY RESULTS**

Gerald L. POTTER, Justin J. Hnilo, Martin Wild and Atsumu

AMIP provided us with an unprecedented yet incomplete data source for climate model evaluation. In the process of preliminary model intercomparison, we found significant systematic errors in short-wave cloud radiative forcing. Unfortunately, insufficient models data was saved to properly diagnose any detail about the discrepancies between the models and the observational data. AMIP II is providing the scientific community with a much more complete data set critical to investigating the large discrepancies. The original errors in net cloud forcing will be discussed along with analysis of the latest results from AMIP II. In addition, implications of the errors as they relate to the controversial anomalous absorption of short wave radiation in the atmosphere by clouds will also be presented. From preliminary analysis, very little improvement in AMIP II cloud forcing has been detected thus indicating that more accurate calculation of solar absorption in the atmosphere continues to be an elusive goal. Part of the error in cloud forcing may be incomplete understanding of atmospheric absorption by clouds and water vapor. Fortunately, new surface data observations taken from updated versions of the Global Energy Balance Archive (GEBA) set has become available to compare with atmospheric model surface fluxes. This study is an extension of the work by Wild and Ohmura and will compare the atmospheric absorption from AMIP II with the new GEBA data.

**MC01/L/03-A1****1415****EVALUATION OF AMIP SIMULATIONS WITH TOVS/MSU**

John BATES, Climate Diagnostics Center, NOAA/ERL - R/E/CD1, 325 Broadway, Boulder, Colorado 80303, USA, email: bates@cdc.noaa.gov Coauthors: Richard Engelen, Graeme Stephens, and Darren Jackson

The longest, global observations of the 3-dimensional temperature and moisture structure of the atmosphere has been provided by the TIROS Operational Vertical Sounder (TOVS) suite of instruments on the NOAA polar-orbiting satellites. Since 1979, the High-resolution Infrared

Sounder (HIRS) and Microwave Sounding Unit (MSU) instruments have taken radiance observations of the mean layer temperature and moisture structure of the troposphere and lower stratosphere. Traditionally, these radiance observations are inverted to provide profiles of temperature and moisture. The inversion process, however, is ill-conditioned and conditioning the inversion requires a first-guess solution that creates complex and systematic errors in the retrieved profiles. The TOVS Radiance Pathfinder, in collaboration with this experimental subproject, has taken a different approach to producing climate products from the TOVS data. We are producing climate products from the raw radiance data and then comparing these observations with equivalent radiances computed from the AMIP-II simulations. In this presentation, the TOVS Radiance Pathfinder procedure will be outlined. This will include a discussion of instrument calibration and intercalibration, limb correction, and cloud detection and removal. The procedure for computing radiances from GCM simulations will also be outlined with particular emphasis on how to sample the GCM similar to how the NOAA satellites sample the earth. Initial results of comparisons between AMIP-II results from several modelling groups will be presented. A strategy for a 4-dimensional fingerprinting technique using the TOVS Radiance Pathfinder data and AMIP-II results will also be discussed.

**MC01/W/62-A1****1430****NOAA/NASA PATHFINDER LARGE SCALE HIGH RESOLUTION RADIATIVE FLUXES**

Rachel T. PINKER (Department of Meteorology, University of Maryland, College Park, MD 20742, USA, email: pinker@atmos.umd.edu) Banglin Zhang (Department of Meteorology, University of Maryland, College Park, MD 20742, USA, email: zhang@atmos.umd.edu) Istvan Laszlo (Department of Meteorology, University of Maryland, College Park, MD 20742, USA, email: laszlo@atmos.umd.edu)

Under the joint NOAA/NASA PATHFINDER activity, uniform, long term data sets from observations made from numerous satellites, are being prepared into homogeneous time series. Some of these data are processed into reduced resolution, multi-satellite, global coverage information, while others are available independently for each satellite from which the observations have been made (e.g., two from the United States (GOES), one European (METEOSAT), one Japanese (GMS), and several polar orbiting satellites). These observations are sampled at about 30 km, have temporal resolution of three hours, and are known as ISCCP DX data. The ISCCP DX data are of particular interest to scientists working on land-atmosphere interactions and hydrologic modelling due to their relatively high spatial resolution, representation of the diurnal cycle, and long term availability. They can also be considered as precursors to data streams anticipated under the EOS missions, such as the Clouds and the Earth's Radiant Energy System (CERES) and the Moderate Resolution Imaging Spectrometer Activity (MODIS). We will present an update as to the scope of radiative fluxes currently available under our PATHFINDER activity, as well as evaluation of the data, and efforts underway, to merge the information from the independent satellites.

**MC01/W/02-A1****1445****EVALUATION OF NCEP GDAS AND AMIP-II REANALYSIS RADIATIVE FLUXES WITH CERES/ERBE MEASUREMENTS**

Shi-Keng YANG 1, Yu-Tai Hou2, Ken Campana 3 and A. J. Miller 3. 1,RDC/Climate Prediction Center/NCEP/NOAA 2,GSC/Environmental Prediction Center/NCEP/NOAA 3,National Centers for Environmental Prediction/NOAA

The first 8 months measurements of TOA radiation fluxes from CERES/TRMM operation provides valuable information for evaluating the performance of NCEP Global Data Assimilation System (GDAS), which upgrades its shortwave radiative transfer parameterization during the same period. The upgrade was prompted from studying the earth radiation budget of NCEP/NCAR Reanalysis project, in which it was revealed that the global model excessively reflects solar radiation by 10%. Also the global insolation on the surface are more than 12% overestimated. Inadequacy in surface albedo was also found. A new parameterizations includes a shortwave radiative transfer code based on Chou (1992 and 1995), which contains multi bands in the ultra-violet, visible, and near infrared spectral regions is adopted for the improvement. The absorption and scattering by water vapor, ozone, CO<sub>2</sub>, O<sub>2</sub>, and those by clouds and aerosols are included. For preserving computational efficiency, Delta-Eddington approximation and two-stream adding scheme are used. The surface albedo scheme of Briegleb et al. (1986) with 14 surface types are implemented. Four components of the surface albedo in the direct and diffuse radiation in the UV-VIS, and near-IR regions are computed. The seasonal variations of the diffused components are derived from the clear sky ERBE data. The new parameterization was first subjected to a series of sensitivity tests, and later implemented for operational GDAS and NCEP/DOE AMIP-II Reanalysis. Evaluating of its accuracy, as well as its impacts on the dynamics, shows significant improvements in the radiative fluxes. Biases of the surface albedo over ocean and deserts are significantly eliminated as compared to Staylor's estimate using ERBE data (1990). Under-estimation of reflected shortwave at TOA is greatly reduced for most of the latitudes, except at the poles as compared to ERBE. The model forecast moisture is sensitive to the changes of the SW parameterization. Maximums are located near the surface for the control run, and are lifted to about 950mb for the experimental run. Temperature near the tropopause increases about 1.5 OC for the summer hemisphere, yet stays fairly constant near 500mb. In response to the warmer temperatures near the tropopause, the jetstreams are shifted pole-ward accordingly. Radiation fluxes from the operational NCEP GDAS are being inter-compared with CERES observations. The preliminary result from OLR shows that the new model substantially reduced the bias in the tropics. Global time series shows a significant reduction of TOA reflected solar flux by ~ 10 W/M<sup>2</sup>, which is a very fine improvement. Details of the model accuracy is to be further evaluated.

**MC01/W/22-A1****1500****COMPARISON ANALYSES OF GLOBAL SHORTWAVE RADIATION BUDGETS FROM REANALYSIS AND MULTIPLE SATELLITE PROJECTS**

Alexander TRISHCHENKO and Zhanqing Li Canada Center for Remote Sensing

Almost seven years of satellite global radiation budgets are available from ERBE (1985-1990), ScaRaB(1994-95) and CERES(1998) projects. They are compared to the product derived from the framework of NCAR/NCEP REANALYSIS project. The surface radiation budget (SRB) fields are estimated from satellite observations with comprehensive validation against surface measurements from several networks. Agreement and disagreement are analysed for different climatic regimes.

**MC01/W/33-A1****1515****IMPACT OF AN IMPROVED LONGWAVE RADIATION MODEL, RRTM, ON THE ENERGY BUDGET AND THERMODYNAMIC PROPERTIES OF THE NCAR COMMUNITY CLIMATE MODEL, CCM3**



M. J. Iacono, E. J. Mlawer, S. A. Clough Atmospheric and Environmental Research, Inc. Cambridge, Massachusetts, 02139

The effect of introducing a new longwave radiation parameterization, RRTM, on the energy budget and thermodynamic properties of the National Center for Atmospheric Research (NCAR) Community Climate Model, CCM3, will be presented. RRTM is a rapid and accurate k-distribution radiative transfer model that has been developed for the ARM program. Among the important features of RRTM are its connection to radiation measurements through comparison to the extensively validated line-by-line radiative transfer model, LBLRTM, and its use of an improved and validated water vapor continuum model. Comparisons between RRTM and the CCM3 longwave (LW) parameterization have been performed for a multi-year climatological SST simulation and a 15-year AMIP simulation using the full CCM3 climate model. RRTM produces an enhancement of LW absorption that is partly due to its use of the CKD\_2.3 water vapor continuum model. This reduces the clear sky global average outgoing longwave radiation (OLR) by 8-10 W/m<sup>2</sup> and reduces the total sky OLR by 2-4 W/m<sup>2</sup>. Downward surface LW fluxes are increased by as much as 8-10 W/m<sup>2</sup> at high latitudes. The LW tropospheric cooling rate is most significantly impacted at low and mid-latitudes. Greater cooling is noted in the upper troposphere, while less cooling is produced near the surface. This causes a general increase in temperature lapse rate that is shown to affect the thermodynamic properties of the climate model. In terms of computational cost, RRTM is competitive with the current CCM3 LW model while providing enhanced accuracy. RRTM is currently being tested for adoption as a new LW model for CCM4 and for the ECMWF weather forecast model.

### Sensitivity and Computational Studies

MC01/E/28-A1

1600

#### STORM TRACKS IN THE HADLEY CENTRE CLIMATE MODEL - SENSITIVITY TO RESOLUTION

Vicky POPE, Henry Buckley (Hadley Centre for Climate Prediction and Research, Met Office, London Rd., Bracknell, RG12 2SY, UK. Email: vdpope@meto.gov.uk)

The aim of this study is to diagnose and ultimately improve the representation of storm tracks in the Hadley Centre climate model. Most climate models have coarse resolution and can only represent storms very crudely. A likely way of improving the representation of storms is therefore to increase model resolution. We have a series of atmosphere only integrations of HadAM3 (the latest version of the Hadley Centre climate model) made for the AMIP II project which can be used to assess the model climatology and the impact of increasing resolution: Name latitude longitude no. of no. of resolution resolution levels integrations (deg) (deg) SRES 2.5 3.75 19 6 VRES 2.5 3.75 30 3 MRES 1.25 1.875 30 2 HRES 0.888 1.25 30 2 The standard model reproduces the broad climatology of observed storm tracks reasonably well. Increasing vertical resolution alone degrades agreement with climatology. Increasing horizontal resolution as well improves agreement. We use a range of diagnostics to assess the factors that influence these results; for example the relative importance of changes in the underlying background flow (such as a simple measure of baroclinicity) and more accurate representation of individual storms.

MC01/L/04-A1

1615

#### AN EXAMINATION OF THE SENSITIVITY OF A GCM TO A COUPLED AND UNCOUPLED MODE

Justin J. HNILO, James Boyle, Benjamin D. Santer and Gerald L. Potter (all at Program for Climate Model Diagnosis and Intercomparison, Lawrence Livermore National Lab, Livermore, CA, USA, Email: hniilo@pcmdi.llnl.gov) Allen S. Grossman (Atmospheric Sciences Division, Lawrence Livermore National Lab, Livermore, CA, USA, Email: grossman1@llnl.gov) Forcing Atmospheric General Circulation Models (AGCM) with prescribed Sea Surface Temperatures (SSTs) and sea ice in the hopes that the model will mimic observed atmospheric behavior is the emphasis of the Atmospheric Model Intercomparison Project (AMIP).

Results from participant modelling groups in AMIP I and II show that these prescribed boundary conditions appear to be sufficient in supplying enough information to an AGCM to allow it to reasonably represent recent atmospheric behavior. Some concerns have been raised about the use of prescribing SSTs in a model integration such as, the specified SSTs might alter the spatial and or the temporal variability of the simulation compared to a coupled run and presumably reality. This effect is expected to be most prominent in the mid to high latitudes. Our research herein directly addresses this issue by using the SSTs from the Coupled System Model (CSM) run which is a fully coupled Ocean-Atmosphere General Circulation Model (OAGCM) as boundary conditions to force the identical atmospheric component alone. Quantifiable differences between the two runs will be attributable in part to the use of prescribing SSTs (as a representation of the ocean) versus using a fully coupled (OAGCM) run. A simple and yet important question that we can quantify and answer is "Does the ocean component in this model act to diminish or enhance atmospheric variability when compared to a prescribed SST run and observations?". This research will highlight variables and regions of greatest magnitude and variability changes.

MC01/W/25-A1

1630

#### ELIMINATION OF COMPUTATIONAL SYSTEMATICAL ERRORS AND IMPROVEMENTS OF WEATHER AND CLIMATE SYSTEM MODELS IN RELATION WITH BAROCLINIC PRIMITIVE EQUATIONS

Qing ZHONG Institute of Atmospheric Physics, Chinese Academy of Sciences

Designing of a total energy conserving semi-implicit scheme for multiple-level baroclinic primitive equation remains unsolved for long. In this work, however, following an energy perfect conserving semi-implicit scheme of an ECMWF type sigma-coordinate primitive equation is recently successfully formulated, some real data experiments are conducted. Winter FGGE data test contrast between model of the new conserving scheme and that of an ECMWF type of global spectral semi-implicit scheme shows that RMS error of averaged forecast Height at 500mb can be improved clearly after the seventh integral day and the reduction can reach 40 percent to 60 percent within the tenth integral day and the thirtieth day. Further contrast test demonstrates that RMS error of monthly mean height in middle and low troposphere at the first, the second and even the third integral month also can be reduced largely and some well-known systematical defects can be improved greatly. More detailed analysis reveals that all these main positive contributions come from improvements of extra-long wave components. This indicates that a remarkable improvement of Model Climate Drift level can be achieved by the actual realizing of a conserving time-difference scheme which thereby eliminating a corresponding computational systematic error source/sink in the currently-used traditional type of weather and climate system models in relation with Baroclinic Primitive Equations.

MC01/W/59-A1

1645

#### HIGH PERFORMANCE PARALLEL COMPUTATION USING A REMOTE LINK LIBRARY IN A TCP/IP NETWORK FOR MODELLING

Ignatius KUNJUMON (Lecturer, School of Marine Sciences, Cochin University of Science and Technology, Lakeside campus, Cochin 682016, India; Email: atmos@md2.vsnl.net.in)

High performance computation can be achieved in a commonly available TCP/IP network. In this method multiple computers are taking part in the computation simultaneously and reducing the effective computation time. An example of a barotropic model is discussed in this paper in detail. First, the single processor program is converted to a parallel program. Then all time-consuming iterative functions have to be converted to remote library functions and be made available to the entire network, which is taking part in the computation. The main; controlling program running on one computer executes the model with the help of other computers. The effective computation time depends on the efficiency of the parallel algorithm, network communication speeds, and number of computers taking part in the computation. Since the speed of the network is increasing very fast compared to the speed of the CPU and TCP/IP networks are becoming more common, parallel computation in a TCP/IP network has greater application in high performance computation.

### Land Surface, Monsoon and Tropical Studies

MC01/E/37-A1

1700

#### VALIDATION OF MEAN BOUNDARY-LAYER STRUCTURE IN ATMOSPHERIC GLOBAL CLIMATE MODELS

J.R. GARRATT, L.D. Rotstajn & P.B. Krummel (all at CSIRO Atmospheric Research, Aspendale, Vic.3195, Australia)

Vertical resolution in atmospheric global climate models (GCMs) has increased significantly in recent years, so that significant vertical detail within the atmospheric boundary layer can now be resolved, allowing field observations to be used for validation of model boundary-layer structure and diurnal behaviour. To illustrate, we focus on diurnal and seasonal variations in the boundary layer simulated in the 18-level CSIRO GCM. Observations from six well-documented field experiments allow for detailed comparisons of boundary-layer structure at five locations - two over (Koorin and Wangara) and three south of (Southern Ocean Cloud (summer and winter) Experiments and Atmospheric Chemistry Experiment) the Australian continent, and one (First ISLSCP Field Experiment) over the USA. Comparisons are made in both day-to-day variability and in the monthly-averaged boundary-layer properties. Overall, the results are very encouraging, with features such as (1) capping inversions, and implied boundary-layer heights, (2) height and thickness of cloud layers, (3) early morning temperature and humidity inversions overland, (4) diurnal variation of screen temperature, friction velocity and boundary-layer height, and the absolute values of boundary-layer temperature and humidity well simulated at most locations. As well as strengths, we are also able to identify weaknesses, including (1) unrealistic temperature profiles in the convective boundary layer due to the use of a simple first-order sub-grid turbulence closure scheme, (2) failure to resolve thin regions near the top of both clear-sky and cloudy boundary layers where vertical gradients are large.

MC01/W/19-A1

1715

#### EVALUATION OF REVISED AMIP I SOIL MOISTURE SIMULATIONS

Alan ROBOCK, G. Srinivasan, Lifeng Luo Department of Environmental Sciences Rutgers - The State University of New Jersey 14 College Farm Road New Brunswick, NJ 08901-8551 USA Konstantin Y. Vinnikov, University of Maryland

Previously, we determined that AMIP I simulations were quite different from each other, especially in the tropics. Models with 15-cm field capacities did not capture the observed large high latitude values of soil moisture. In addition, none of the models properly simulated winter soil moisture variations in high latitudes, keeping soil moisture constant, while observations show that soil moisture varies in the winter as much as in other seasons. The observed interannual variations of soil moisture were not captured by any of the AMIP models. Several models had large soil moisture trends during the first year or two of the AMIP simulations, with potentially large impacts on global hydrological cycle trends and on other climate elements. This is because the simulations were begun without spinning up the soil moisture to the model climatology. The length of time it took for each to reach equilibrium depended on the particular parameterization. Although observed temporal autocorrelation time scales are about 2 months, some models had much longer time scales than that. In particular, the 3 parameterizations based on the Simple Biosphere Model (SiB) had trends in some regions for virtually the entire AMIP simulation period. Here we reexamine the simulations that have since been conducted with revised soil moisture schemes by a number of models, and compare them with those previously conducted with bucket models. We compare the simulations to observations in Russia, China, Mongolia, and Illinois, and determine if "improved" land surface schemes produce improved soil moisture simulations.

MC01/E/33-A1

1730

#### INCLUDING VEGETATION AND CO<sub>2</sub> AS INTERACTIVE ELEMENTS IN GCM SIMULATIONS

Peter COX, Chris Jones, Richard Betts (Hadley Centre for Climate Prediction and Research, Meteorological Office, London Road, Bracknell, Berkshire, RG12 2SY, UK, email: pmcox@meto.gov.uk) Ian Totterdell (Southampton Oceanography Centre, Empress Dock, Southampton SO14 3AZ, UK, email: I.Totterdell@soc.soton.ac.uk)

The land-atmosphere and ocean-atmosphere fluxes of carbon are known to be a strong function of climate, and the distribution and function of vegetation also varies directly in response to changes in atmospheric CO<sub>2</sub>. However, GCM simulations of climate change typically neglect feedbacks associated with vegetation and the carbon cycle, since they use prescribed CO<sub>2</sub> concentrations and vegetation fixed at current distributions. The Hadley Centre is developing a coupled climate-carbon cycle model by including representations of the land and ocean carbon cycles in its modelling framework. The ocean component, "HadOCC", treats the chemical processes involved with the dissolution and outgassing of CO<sub>2</sub>, and includes important marine biological processes through a 4-compartment model. The terrestrial component, "TRIFFID", calculates the areal coverage and leaf area index of each of 5 plant functional types based on the carbon balance of each and on competition amongst the types. Details of the submodels will be presented, along with early results from the fully coupled system.



MC01/E/08-A1

1745

**COMPARING SNOW SIMULATIONS FROM NCAR CCM3 COUPLED WITH TWO DIFFERENT LAND SURFACE PARAMETERIZATIONS: LSM AND BATS**

Zong-Liang YANG and Guo-Yue Niu Institute of Atmospheric Physics, University of Arizona, Tucson, AZ, 85721, USA (phone: 1-520-621-8922, fax: 1-520-621-6833, E-mail: zly@stratus.atmo.arizona.edu)

Three research questions remain to be addressed. First, are the current general circulation model (GCM) snow schemes adequately simulating the snow processes? Second, are the available global data sets and the model output variables adequate to assess the simulations of snow in GCMs? Third, what are the processes responsible for different snow simulations? The snow simulations from the National Center for Atmospheric Research (NCAR) Community Climate Model Version 3 (CCM3) coupled with the Land Surface Model (LSM) and the Biosphere-Atmosphere Transfer Scheme (BATS) are compared with each other and with global data sets from various sources including the National Oceanic and Atmospheric Administration satellite data and the Nimbus-7 Scanning Multichannel Microwave Radiometer data. For both North America and Eurasia, LSM-BATS produces less snow mass than BATS-CCM3 during the snow season (November-April). Some of these differences can be attributed to different simulated precipitation, surface air temperature and ground heat fluxes resulting from the fully-coupled land surface-atmosphere interactions. Therefore, it is unknown how the different model structures in LSM and BATS directly affect the snow simulations. To isolate this direct impact, an intercomparison of both land models is also made in off-line mode (i.e. uncoupled to the CCM3) using the long-term snow cover and meteorological data from a grassland catchment at the Valдай water-balance research site in Russia. This data set has been used in the Project for Intercomparison of Land-surface parameterization Schemes (PILPS) Phase 2(d) in which BATS participates. This paper presents results from the models in their original structure, and also investigates the impacts of using different parameterizations for snow density, albedo and snow cover areal extent. Like the on-line simulations, the off-line runs also reveal that LSM predicts less snow mass than BATS, mainly because of two reasons. First, the iterative surface energy balance in LSM tends to predict higher surface temperature and greater snow melt. Second, more vegetation is allowed to exist outside the snowpack which results in lower surface albedo and more solar energy for melting snow.

**Tuesday 20 July AM**

Presiding Chairs: Peter Gleckler (Program for Climate Model Diagnosis and Intercomparison (PCMDI), Lawrence Livermore National Laboratory) and Jerry Potter (PCMDI, Lawrence Livermore National Laboratory)

**ATMOSPHERIC MODELLING AND INTERCOMPARISONS Cont.****Land Surface, Monsoon and Tropical Studies**

MC01/W/32-A2

0930

**HIGH-RESOLUTION SIMULATIONS OF THE GLOBAL CLIMATE - VALIDATION OF MONSOON SYSTEMS OVER SOUTH AMERICA AND SOUTHWEST U.S.**

Andrea N. HAHMANN (Institute of Atmospheric Physics, University of Arizona, Tucson, AZ 85711, Email: hahmann@atmo.arizona.edu), Rong Fu and Robert E. Dickinson (both at Institute of Atmospheric Physics, University of Arizona, Tucson, AZ 85711).

Research over the past decade has demonstrated that sub-grid scale spatial heterogeneities in soil moisture, precipitation, and vegetation cover have substantial effects in determining surface evapotranspiration, runoff, and other surface properties coupled to atmospheric climate. Many of these processes occur on spatial scales too fine to be resolved by most current climate models. This paper will present the validation of a fine-mesh global model (CCM3/HRBATS) which explicitly includes spatial heterogeneities. Severe problems in the simulation of the hydrological cycle have been diagnosed with the standard model (CCM3) at T42 resolution for the main monsoonal regions of the Americas. Over South America, simulations at T42 resolution show that north of the equator, the model simulates a double peak where observations indicate a single peak, and south of the equator, the model has too pronounced a dry season. Over the Southwest U.S., while the simulation of wintertime precipitation appears to improve with increased resolution, the southwest summer monsoon of Arizona and Northern Mexico is consistently underrepresented. This presentation describes the validation of the hydrological cycle produced by the standard and fine-mesh models over the Amazon and Southwest U.S. regions.

MC01/W/60-A2

0945

**MONSOON AND VEGETATION INTERACTIONS-- A STUDY USING A COUPLED NCEP GCM/SSIB MODEL**

Yongkang XUE (Department of Geography, University of Maryland, College Park, MD 20742, USA Tel: 301-405-4050; fax: 301-314-9299, email: yxue@geog.umd.edu); H. H. Juang, M. Kanamitsu, S.Y. Hong (all at Development Division, NCEP, NOAA, Camp Springs, MD); M. Hansen (Department of Geography, University of Maryland); S. Nicholson (Department of Meteorology, Florida State University, Tallahassee, FL)

A coupled NCEP GCM/SSiB (Simplified Simple Biosphere Model) model has been developed to investigate the interactions between land surface processes and climate, in particular the interactions between land and monsoon system. The NCEP global model is a forecasting model that is also used for climate studies. A version with spectral triangular 62 truncation (T62) is used for this study. The corresponding gaussian grid for T62 is 192 by 94, roughly equivalent to 2 degrees in latitude and longitude. There are 28 unequally spaced sigma levels. About 8 levels are below 800 hpa. There are two soil layers in the original NCEP GCM, representing land surface processes. Using the original NCEP GCM and the NCEP GCM/SSiB, we have integrated the models for 4 months from May 1, 1987 to August 1, 1987, which is the boreal monsoon season. The most substantial differences between the NCEP GCM and the NCEP GCM/SSiB are the simulations in the African monsoon, the East Asian monsoon, and the Mexican monsoon. In the original NCEP GCM, the African monsoon is too weak, especially in July. The monsoon rainfall does not fully develop until August. With the coupled NCEP GCM/SSiB, the African monsoon rainfall in July is closer to the observations. In East Asia, the monsoon onset in May is too strong in the original NCEP GCM and the rainfall area approaches farther to the north; whereas the NCEP GCM/SSiB correctly simulates the monsoon's onset. In these experiments, the soil moisture and albedo are similar in the two models. Further experiments are also carried out to explore the impact of initial soil moistures and vegetation maps on the monsoon simulations. A newly developed global vegetation map (UMGEOG1) and a new soil moisture data are introduced to the NCEP GCM to specify land condition. This UMGEOG1 is developed at the Department of Geography, University of Maryland, and is based on the NOAA/NASA pathfinder AVHRR 1-km land data set. The classifications are derived using a decision tree classifier with training data derived from a global network of high resolution Landsat data. The land cover data sets are being validated with Landsat data as well as with regional data sets. The soil moisture data is developed at

NASA/GSFC by Sud's group. It is a part of the Global Soil Wetness Project. The SSiB has been driven offline by observed and assimilated meteorological data to produce 1987 soil moisture climatology. The impacts of these two data sets have been tested to compare with the original model simulations.

MC01/W/01-A2

1000

**EQUATORIAL CONVECTIVELY COUPLED WAVES IN AMIP II INTEGRATIONS WITH THE UK METEOROLOGICAL OFFICE UNIFIED MODEL**

Guiying YANG and Julia Slingo (both at Centre for Global Atmospheric Modelling, Department of Meteorology, University of Reading, Earley Gate, Reading, RG6 6BB, UK. Email: J.M.Slingo@reading.ac.uk)

Synoptic activity in the tropics is often associated with waves which can be related to the preferred equatorially-trapped modes of the atmospheric circulation based on shallow water theory (Wheeler and Kiladis 1998). Various modes (inertio-gravity, equatorial Rossby, mixed Rossby-gravity and Kelvin waves) can be detected, in many cases related to the active phase of the Madden-Julian Oscillation. That being the case, it is important that GCMs are able to represent these convectively-coupled equatorial waves. Global brightness temperature data (from the EU Project, 'Cloud archive User Service (CLAUS)') have been used to identify and characterise the equatorial waves based on time/space spectral analysis. The various modes noted above can be identified. The results have been used to evaluate the tropical variability in AMIP II simulations with the latest atmosphere-only version of the UK Meteorological Office model (HadAM3). The modulation of these waves by ENSO has also been studied.

MC01/E/06-A2

1015

**ASSESSING ATMOSPHERIC GENERAL CIRCULATION MODELS USING ANGULAR MOMENTUM DIAGNOSTICS**

David A. SALSTEIN and Richard D. Rosen (Atmospheric and Environmental Research, Inc., 840 Memorial Drive, Cambridge, MA 02139, USA, email: salstein@aer.com) Jean O. Dickey and Steven L. Marcus (Jet Propulsion Laboratory, California Institute of Technology, 4800 Oak Grove Drive, Pasadena, CA 91109, USA, email: jod@logos.jpl.nasa.gov)

Being subject to physical conservation laws, atmospheric angular momentum (AAM) has proved to be a robust index of global weather and climate fluctuations on a variety of timescales. Earlier, under the leadership of R. Hide, we examined mean, seasonal, and interannual fluctuations of AAM in the group of models that participated in the first Atmospheric Model Intercomparison Project. The annual cycle proved to be captured well by the AMIP-I models, although a tendency to underestimate the AAM peak in northern winter was noted. Interannual fluctuations in AAM were reasonably well simulated, as were the latitudinal anomalies associated with the El Niño/Southern Oscillation. The relative amplitudes of the 1982-83 and 1986-87 ENSO peaks in AAM, however, were not so well reproduced. Now the suite of AMIP-II models are becoming available, we can check if some of the shortcomings in the models' angular momentum series have been corrected. Given the extension of both model results and more recent analyses to higher levels, we will assess the AMIP-II model results for quasi-biennial and semiannual AAM signals that originate in the stratosphere. In addition, the longer AMIP-II period includes ENSO variability beyond that covered by AMIP-I, so that a larger number of ENSO-related AAM signals can be examined. Newly available from analysis systems and a number of AMIP-II models will be values of torques acting to exchange angular momentum between the atmosphere and other Earth components. Thus, we plan to assess how well AMIP-II models reproduce behavior in the relevant torques, due to friction and to pressure gradients across mountainous topography.

Presiding Chair: Michael Wehner (PCMDI, Lawrence Livermore National Laboratory)

**INTERCOMPARISON ACTIVITIES**

MC01/W/10-A2

1030

**THE DYNAMICAL CORE INTERCOMPARISON PROJECT**

Michael WEHNER, Program for Climate Model Diagnosis and Intercomparison Lawrence Livermore National Laboratory Livermore, CA 94550 USA  
email: mwehner@llnl.gov http://www-pcmdi.llnl.gov/dc

Researchers are invited to participate in The Dynamical Core Intercomparison Project. The aim of this intercomparison is to explore numerical methods for solutions of the hydrodynamic equations of motion on the sphere. In particular, the dynamics schemes of atmospheric general circulation models are targeted. The design of the experiment is intended to be minimally restrictive in order to foster a high degree of creativity. All types of numerical discretizations are encouraged. In the Dynamical Core Intercomparison Project, a prescribed forcing function replaces the detailed boundary layer turbulence, radiative and hydrological parameterizations of the typical atmospheric general circulation model. Only the equations for momentum and thermal energy are to be solved. No moisture equations are involved. Two differing forcing functions (Held-Suarez and Boer-Denis) have been published in the literature. It is requested that participating groups submit results for both forcing functions. Subgrid scale turbulent mixing and dissipation are intimately connected to the details of the numerical formulation. Hence, they are considered part of the model and left to the individual modelling groups to define. Furthermore, the simulated planet is smooth with no topography. Initial conditions are not provided. However, simulations should be run for an initial spinup period of a length chosen by the modelling group. Most of the standard output is defined as 90 day averages of zonal means using the results of 120 day segments of the integration. The first or last 30 days of each period should not be included in the averages supplied to the PCMDI in order to provide statistically independent 90-day samples. An additional request is made for a representative set of winds in order to calculate a kinetic energy spectrum. A small set of computational performance data is also requested to assess behavior of the various algorithms on different hardware. Results that have been submitted by the time of this presentation will be shown. A preliminary conclusion is that the middle atmosphere under the Held-Suarez forcing is far more sensitive to numerics and resolution than is the lower atmosphere.

MC01/W/51-A2

1045

**AN AQUA-PLANET TEST-BED FOR AGCMS**

Richard NEALE and Brian Hoskins (both at Department of Meteorology, University of Reading, PO BOX 243, Earley Gate, Reading RG6 6BB, UK, Email: R.B.Neale@reading.ac.uk)

It is proposed that aqua-planet runs of atmospheric GCMs for a set of specified idealised sea surface temperatures (SSTs) should be used as a standard test of the interaction of the physical parameterizations with each other and with the dynamics. Dynamical core tests have proved very useful in testing numerical formulation of models. Single column experiments are

valuable in developing parameterizations, but at present there is nothing between them and full GCM runs in which conclusions about how the parameterizations perform and interact are difficult to make. As an example, results will be shown from an aqua-planet version of the UKMO Unified Model (version HadAM2B) run with equinoctial solar forcing and idealised SSTs. Zonally symmetric SSTs test whether the model tends to have a single equatorial convective maximum or ITCZs off the equator and for what weak equatorial SST gradients the Hadley Cells disappear. Zonally asymmetric SSTs test the relative longitudinal location and magnitude of the convective maximum, the extent to which westerly tropical zonal flows are generated and to which the extratropical storm-tracks are organised.

**MC01/L/05-A2****1100****SNOW MODEL INTERCOMPARISONS**

Richard ESSERY (Hadley Centre, UK Meteorological Office), Eric Martin (Centre d'Etudes de la Neige, Météo-France), Hervé Douville (Centre National de Recherches Meteorologiques, Météo-France), Alberto Fernández (Instituto Nacional de Meteorología, Spain) and Eric Brun (Centre National de Recherches Meteorologiques, Météo-France)

Snow can greatly increase the albedo of a surface, reduce its roughness, insulate the underlying ground from the atmosphere and store or release large amounts of water. Models of snowpack processes are thus needed for a wide range of applications, from forecasting floods and avalanches to simulating long-term changes in climate, and many different models have been developed. To investigate the performance of snow models, the IAHS / ICSI working group on Snow and Climate is planning a snow model intercomparison project (SnowMIP), to be launched in 1999. A detailed comparison will be made between a wide range of snow models using data from several sites with different climates and characteristics. The aims of SnowMIP will be discussed, and results will be presented from a pilot study in which four models with a range of complexities were compared using observations made during two contrasting winters at a site in the French Alps. Experience gained in this study will be used to make recommendations for SnowMIP.

Presiding Chair: Jurgen Willebrand (Institut f. Meereskunde)

**OCEAN MODELLING AND INTERCOMPARISONS****MC01/W/52-A2**

Invited

**1135****MODELLING LARGE-SCALE OCEAN CIRCULATION: LESSONS FROM SENSITIVITY AND INTERCOMPARISON STUDIES**

Claus BOENING (Institut fuer Meereskunde, Kiel, Germany)

Understanding the relative impacts of resolution, parameterisations and numerics on the performance of ocean circulation models is still in its infancy. Some insight into the sensitivity to various model factors is provided by an increasing number of simulations for the North Atlantic, including dedicated model intercomparison studies such as in the DYNAMO project. While the simulation of seasonal to interannual (primarily wind-driven) variability is very robust, with little model-to-model differences or effects of parameterization schemes, simulation of the "mean" circulation and its response to low-frequency (decadal) variations in the surface buoyancy fluxes is extremely dependent on the representation of interior, often very small-scale processes: e.g., flows through sills and gaps, entrainment in downslope flows, interaction with topographic irregularities. It is obvious that ocean model development will benefit greatly from co-ordinated programmes of experimentation that systematically assess alternate model approaches; as part of these, ocean model intercomparisons are meaningful, if embedded in an exploration of the sensitivity to the representation of critical physical processes.

**MC01/E/24-A2**

Invited

**1155****A FORWARD-LOOKING RETROSPECTIVE OF OCEANIC CIRCULATION MODELLING**

Dale B. Haidvogel (Institute of Marine and Coastal Sciences, Rutgers University, 71 Dudley Road, New Brunswick, NJ 08901-8521; E-mail: dale@ahab.rutgers.edu)

The decade of the 1990's has witnessed significant improvements in the algorithmic variety, physical completeness, and realism of large-scale ocean circulation models. Factors related to these successes include the steady increase in spatial resolution made possible (largely) by enhanced computer performance, improved subgridscale parameterizations for (e.g.) eddy transports, and multiple classes of numerical models offering shared community development, regular user interaction, and ready availability of software and documentation via the World Wide Web. An increasing trend is the adaptation of ocean circulation models for studies of coupled physical/bio-geochemical interactions and the global climate system. Such coupled systems place further demands on the spatial resolution, numerical integrity, and sub-gridscale treatments of ocean models. Generalized coupling strategies, sophisticated parameterization schemes, and further gains in computer performance are all necessary ingredients for future progress in these inter-disciplinary areas. Also, given the relative lack of observational data (in particular, for the bio-geochemical variables), advanced forms of model/data fusion are essential. It is easy to show that continued improvement in computer power alone cannot meet these growing needs. One central issue that emerges instead is the interplay between spatial approximation and numerical resolution. Despite the overall simplicity of spatially structured, static grids, the inherent advantages of regionally enhanced resolution and adaptivity must in future spur the evolution of alternate approaches including finite element and block-structured grids, horizontally adaptive meshes, and various generalized adaptive vertical coordinates. Some initial progress in these areas is discussed.

**MC01/E/12-A2****1215****NUMERICAL SIMULATION OF THE NORTH ATLANTIC OCEAN AT 1/10 DEGREE**

Richard D. SMITH and Matthew E. Maltrud, Los Alamos National Laboratory B216, Los Alamos, NM 87545 Frank O. Bryan and Matthew W. Hecht National Center for Atmospheric Research P. O. Box 3000, Boulder, CO 80307

We present preliminary analysis of an 0.1 degree simulation of the North Atlantic Ocean using a level-coordinate ocean general circulation model forced with realistic winds covering the period 1985-1996. Results are compared to the North Atlantic sector of a global 0.28 degree simulation with similar surface forcing, and to a variety of satellite and in situ observations. The simulation shows substantial improvements in both the eddy variability and the time-mean circulation compared to previous eddy-permitting simulations with resolutions in the range of 1/2 to 1/6 degrees. The resolution is high enough that the first baroclinic Rossby radius is reasonably well-resolved at all latitudes, and the model appears to be capturing the bulk of the spectrum of mesoscale energy. The eddy kinetic energy constitutes 70% of the total basin-averaged kinetic energy. Model results agree well with observations of the magnitude and geographical distribution of eddy kinetic energy and sea-surface height variability, with the

wavenumber-frequency spectrum of surface height anomalies in the Gulf Stream, with estimates of the eddy length scale as a function of latitude, and with measurements of eddy kinetic energy as a function of depth in the eastern basin. The mean circulation also shows significant improvements compared to previous models, although there are notable discrepancies with observations in some areas. The Gulf Stream separates at Cape Hatteras, and its speed and cross-stream structure are in good agreement with current meter data, however, its path is somewhat too far south and its meander envelope too broad to the west of the New England Seamounts. The North Atlantic Current is remarkably well simulated in the model; it exhibits meanders and troughs in its time-mean path that agree with similar structures seen in float data, although the separation of this current in the region of the Northwest Corner is displaced somewhat too far to the northwest. The Azores Current appears in the simulation, perhaps for the first time in a basin-scale model, and its position, total transport, and eddy variability are consistent with observational estimates.

**MC01/E/16-A2****1230****INTERCOMPARISON OF FINITE DIFFERENCE AND FINITE ELEMENT MODELS IN THE NORTH ATLANTIC OCEAN**

Mohamed ISKANDARANI, Dale B. Haidvogel, Hernan Arango Institute of Marine and Coastal Sciences, Rutgers University, 71 Dudley Road, New Brunswick, NJ 08901-8521

We present an inter-model comparison between a newly developed ocean model based on the spectral element method, SEOM, and a finite-difference-based ocean model, SCRUM. The spectral element method can be briefly described as an h-p type finite element method characterized by rapid convergence rates, geometrically flexible unstructured grids, and dense computations at the element level leading to high scalability on parallel computers. In principle, the spectral element formalism offers attractive opportunities for high-resolution, regional ocean modelling; however, careful evaluation of this new technique in a basin-scale setting has been lacking. The present work is a first "validation" of SEOM simulation capabilities, using SCRUM as a reference. Both SEOM and SCRUM solve the hydrostatic primitive equations, account for the motion of the free surface, and are terrain-following. We summarize differences in the two models, and assess the relative merits of each within the context of the North Atlantic Ocean between 25 S and 75 N, using traditional measures of merit including Gulf Stream separation, water mass formation, and meridional overturning and heat flux. Novel methods of subgridscale mixing are identified as a key ingredient in the successful application of the new spectral element methods.

**Tuesday 20 July PM****MC01/W/41-A2****1400****EFFECTS OF LOCALLY ENHANCED VERTICAL DIFFUSIVITY OVER ROUGH BATHYMETRY ON THE WORLD OCEAN CIRCULATION**

Hiroyasu HASUMI and Nobuo Sugimoto (Center for Climate System Research, University of Tokyo, Tokyo 153-8904, Japan, e-mail: hasumi@ccsr.u-tokyo.ac.jp, nobuo@ccsr.u-tokyo.ac.jp)

Recent observations indicate that vertical diffusivity in the deep ocean is horizontally highly variable: it is much enhanced where the bottom topography is rough or steeply sloping, and it is as small as at the thermocline depths (about 0.1 CGS) elsewhere. Here we investigate effects of locally enhanced vertical diffusivity over rough bottom topography on the world ocean circulation by use of a coarse resolution (3 degree by 3 degree in horizontal) ocean general circulation model. Vertical diffusivity in the model is enhanced in the area where the standard deviation of the bottom depth, calculated from ETOPO5 data set, within a grid divided by the grid-averaged bottom depth is larger than a certain value. For comparison, a case without horizontal variations in vertical diffusivity is also made. Results show that there is significant difference in the three-dimensional structure of the deep circulation between the cases, especially in the Pacific. When the horizontal inhomogeneity in vertical diffusivity is taken into account, upwelling of deep water in the North Pacific is confined to the western half of the basin, where the bottom is rough. Accordingly, horizontal pattern of water transport differs qualitatively.

**MC01/L/06-A2****1415****USING NATURAL RADIOCARBON TO ASSESS THE EFFECTS OF NUMERICS ON BIOLOGICAL TRACERS**

Jean-Michel Campin (ASTR, Universite Catholique de Louvain, 2 Ch. du cyclotron, 1348 Louvain-la-Neuve, Belgium, email: campin@astr.ucl.ac.be) Anne Mouchet (LPAP, Universite de Liege, 5 av. de Coite, 4000 Liege, Belgium, email: mouchet@astro.ulg.ac.be)

The biological component of OCCMs often resorts to specific numerical treatment that are not shared by the dynamical component of the model (including active tracers, i.e., temperature and salinity). This choice is often made in order to satisfy particular requirements: off-line integration to save computer resources or positive advection scheme to avoid disastrous negative concentrations. The purpose of this study is to evaluate, in our OGCM, the impact of those numerical implementations used in the off-line carbon model, and thus to strengthen the validation of the second. The analysis concentrates on the simulated natural C14 distribution. C14 combines the advantages of an easy implementation, of a vertical distribution similar to that of several biogeochemical tracers and of a direct interpretation in terms of ventilation time scales. The results of several C14 equilibrium experiments obtained both on-line and off-line are presented. They address the effects of two different advection schemes: a low-dispersive one and the upwind scheme. In addition, two different convective adjustment schemes are tested, by enhanced vertical diffusivity and by vertical exchange of water. The convective adjustment effect is relatively small, whereas the upwind scheme induces significant differences, especially at intermediate depths, that are largely due to the vertical advection term. On the contrary the same modification in the transport scheme hardly has any effect on the salinity field. In order to reduce this effect on C14, a simple modification of the upwind scheme is proposed. Finally, the residual differences between the off-line and on-line models are discussed.

**MC01/L/07-A2****1430****ON THE ORIGIN AND PATHWAY OF THE SALINE INFLOW TO THE NORDIC SEAS**

L. NEW, S. Barnard (Southampton Oceanography Centre, Southampton SO14 3ZH, UK, email: A.New@soc.soton.ac.uk) P. Herrmann (Institut für Meereskunde, Düsternbrooker Weg 20, D-24105 Kiel, Germany) and J.-M. Molines (Laboratoire des Ecoulements Geophysiques et Industriel, 38041 Grenoble, France)

Three high-resolution (1/3 degree) ocean circulation models of the North Atlantic, differing in their description of the vertical coordinate, have been intercompared in the DYNAMO project. They are here used to elucidate the origins and pathways of the saline inflows into the Nordic



Seas, which may play a significant role in setting the depth of wintertime convection there, and in driving the Atlantic overturning circulation. In two of the models, Mediterranean Overflow Water (MOW) flows northwards, but only as far as the Porcupine Bank (53 N). In one of the models, the MOW also invades the Rockall Trough. However, none of the models allows the MOW into the Nordic Seas. Instead, they are unanimous in showing that the saline inputs to the Nordic Seas derive instead from near-surface water masses and result partly from branches of the North Atlantic Current (NAC), and partly from a poleward "Shelf Edge Current" (SEC) around the European continental slopes. The highest salinities are set and carried northwards by the SEC itself, which transports Eastern North Atlantic Water from the Bay of Biscay region. The high salinities on density surfaces appropriate to the MOW in the Nordic Seas result from the downward wintertime mixing of these saline inputs. The models also agree reasonably well with available observations. Overall, the intercomparison indicates the importance of the SEC in this process, and reveals the complexity of the current structures, which occur on scales too small to be resolved by typical climate models.

#### MC01/L/08-A2 1445

##### SENSITIVITY OF VENTILATION RATES AND RADIOCARBON UPTAKE TO SUBSURFACE MIXING PARAMETERISATION IN OCEAN MODELS

Matthew H. England, Centre for Environmental Modelling and Prediction (CEMAP) School of Mathematics The University of New South Wales Sydney NSW 2052 Australia

The sensitivity of ventilation time-scales and radiocarbon uptake to subgrid-scale mixing parameterisation is studied in a global ocean model. Seven experiments are examined that are identical in every manner apart from their representation of subgrid-scale mixing of tracers. The cases include (1) two runs with traditional Cartesian mixing (HOR), (2) a run with enhanced isopycnal mixing (ISO), and (3) four runs in which the effects of eddies on the mean ocean flow are parameterised following Gent and McWilliams (1990, GM). Horizontal, isopycnal, and isopycnal thickness diffusion coefficients are varied sequentially in the model runs. Of particular interest is the role of the tracer mixing schemes in influencing longer time-scale ventilation processes - centennial and beyond - such as deep water mass renewal and circulation. Simulated ventilation time-scales and  $^{14}\text{C}$  vary greatly between the three mixing schemes. The isopycnal mixing run exhibits the most rapid water mass renewal due to strong diffusion effects and excessive surface convective overturn, particularly in the Southern Ocean. In contrast, the GM cases show much more gradual renewal of deep and bottom waters, with limited vertical convection of surface waters and slower abyssal currents. Under GM, a background horizontal diffusion or altered isopycnal diffusion does not significantly change interior ocean ventilation rates. Reducing the GM isopycnal thickness diffusivity, on the other hand, significantly decreases the simulated deep water ventilation time-scales. In comparison with the HOR runs, deep and bottom water ventilation time-scales are reduced by about 30% in ISO, and increased by 30-40% under GM. Comparison is made between model simulated and observed  $^{14}\text{C}$ . The GM runs appear to be the least successful in the North Atlantic Ocean, exhibiting very gradual and only shallow water-mass renewal compared to observations. In the Pacific and Indian Oceans, the HOR and ISO runs are ventilated too rapidly due to strong convection and water-mass contribution from the Southern Ocean. In contrast, the GM runs simulate spuriously old and  $^{14}\text{C}$  depleted bottom and mid-depth water. Overall, none of the model cases reproduce global ocean ventilation rates over centennial time-scales. Higher horizontal resolution and a spatially-varying GM thickness diffusivity may be required before global models capture long time-scale ocean renewal processes with some degree of fidelity.

#### MC01/E/26-A2 1500

##### A MOMENTUM ADVECTION SCHEME FOR OCEAN MODELS WITH BOTTOM RELIEF, CONSERVING TOTAL MOMENTUM AND KINETIC ENERGY

Hiroshi ISHIZAKI and Tatsuo Motoi (both at Meteorological Research Institute, 1-1 Nagamine, Tsukuba 305-0052, Japan, email: hishizak@mri-jma.go.jp)

A finite-difference analogue of the nonlinear momentum advection for Arakawa's B-grid spacing was developed by Takano (1978) and Ohnishi (1978), which contained the concept of diagonally upward/downward mass and momentum fluxes along the bottom slope, and the generalized-Arakawa scheme for the horizontal advection, modified to be fit to arbitrary coastal shape. Here we reevaluate the scheme to put it to more practical use, by redefining it in a simple, generalized form and conferring its good performance through a comparison with a traditional scheme. Based on the definition of mass continuity for a momentum cell (U-cell) in terms of that for tracer cells (T-cell), the vertical and horizontal mass and momentum fluxes for U-cells are generalized on the arbitrary bottom relief in simple forms. Total momentum and kinetic energy are conserved in the advection process. A comparison of the present scheme with a traditional one embedded in an eddy-resolving ocean model indicates a less noisy state with a sharper western boundary current, permitting a longer time interval, in the former than in the latter. The present scheme shows better performance in the computational efficiency as well as in the reality of the simulated flow field than the traditional one does.

#### MC01/L/09-A2 1515

##### REGIONALIZATION OF CLIMATE MODEL RESULTS FOR THE NORTH SEA

Frank Kauker (AWI, Columbusstr. D-27568 Bremerhaven, Germany, EMAIL: fkauker@awi-bremerhaven.de)

A regional North Sea version of the Ocean General Circulation Model OPGC is used to investigate the variability of the North Sea and to downscale climate model results for the North Sea. In a hindcast experiment the model is forced with surface data from the ECMWF reanalysis in the period 1979 to 1993 to investigate the variability on two time-scales; the weekly to seasonal time-scales and the season to decade time-scales. The major modes of variability of the sea level elevation, the sea surface circulation, the sea surface temperature and the sea surface salinity are analyzed with the help of statistical tools as Empirical Orthogonal Functions, Associated Patterns, Canonical Correlation Analysis and Principal Oscillation Patterns. In the downscaling experiment possible changes of the mean state and the variability in the North Sea (and to some degree in the Greenland-Iceland-Norwegian Sea) are estimated in a doubled CO<sub>2</sub> climate.

## SEA-ICE MODELLING AND INTERCOMPARISONS

### MC01/L/10-A2 Invited 1550

#### SIMP RESULTS: INTERCOMPARISON OF SEA ICE DYNAMICS MODELS

Markus HARDER, Martin Kreyscher, Gregory M. Flato, Peter Lemke

The World Climate Research Programme (WCRP) has charged the Sea Ice - Ocean Modelling (SIOM) Panel to de-terminine an optimized sea ice model for use in coupled climate simulations. The intercomparison is performed in inter-national cooperation in the Sea Ice Model Intercomparison Project (SIMP) as a part of the WCRP Arctic Climate System Study (ACSYS). Phase I of SIMP investigated the performance of different sea ice dynamics schemes in a hierarchy of models with increasing complexity of sea ice rheology. All models were run on the same grid for the Arctic Ocean, were forced with the same boundary conditions, and use the same equations/parameterizations (such as thermodynamic ice growth/melt). Only the ice dynamics part differs. The model results are validated against a very large number of observations, such as IABP ice drift buoys, ice velocities and ice extent observed by satellites, ice thickness data measured by ULS on oceanographic moorings or submarines, and other sources. The intercomparison clearly shows that increasing the complexity of ice dynamics and especially sea ice rheology (associated with ice de-formation) significantly increases the performance of the simulation. Among the four models presently tested, the viscous-plastic rheology performed best, especially due to its representation of shear forces. It is planned to include other sea ice dynamics schemes in the intercomparison.

### MC01/E/32-A2 1620

#### SENSITIVITY OF A GLOBAL SEA ICE MODEL TO THE TREATMENT OF ICE THERMODYNAMICS

Thierry FICHEFET (Institut d'Astronomie et de Geophysique G. Lemaître, Université Catholique de Louvain, 1348 Louvain-la-Neuve, Belgium, email: fichefet@astr.ucl.ac.be) Miguel Angel Morales Maqueda (Department of Mathematics, Keele University, Keele, Staffordshire ST5 5BG, UK, email: maa21@cc.keele.ac.uk)

The sensitivity of a global thermodynamic-dynamic sea ice model coupled to a one-dimensional upper ocean model to degradations of the model physics is investigated. The study focuses on physical processes pertaining to (1) the vertical growth and decay of sea ice (thermal inertia of snow and ice, heat conduction, and snow cover), and (2) the lateral growth and decay of sea ice (leads and polynyas). A total of six sensitivity experiments have been performed. Each experiment consisted of removing a particular parameterization from the control run computer code. It appears that the thermal inertia of the snow-ice system is negligible in the Antarctic but not in the Arctic, where the total heat content of sea ice is chiefly dictated by internal storage of latent heat in brine pockets, sensible heat storage being of very minor consequence. It is also found that the inclusion of a prognostic snow layer and of a scheme of snow ice formation is important for sea ice modelling in the Southern Hemisphere. Furthermore, our results suggest that the thermodynamic effect of the subgrid-scale snow and ice thickness distributions and the existence of open water areas within the ice cover play a crucial role in determining the seasonal behavior of both ice packs. We can therefore conclude that all these processes should be represented in global climate models.

### MC01/E/19-A2 1635

#### INTERCOMPARISON OF THE MASS BALANCE OVER THE ANTARCTIC AND GREENLAND ICE SHEETS SIMULATED BY GCMs

W. M. CONNOLLEY (British Antarctic Survey, High Cross, Cambridge, CB3 0ET, UK; Email: wmc@bas.ac.uk) C. Genthon (LGGE CNRS, 54 Rue Molire, F-38402 Saint Martin d'Herès Cedex, FRANCE; Email: genthon@glaciog.ujf-grenoble.fr)

Accurate knowledge of the surface mass balance of Antarctica and Greenland is a key component of estimates of the contribution of the ice sheets to sea level rise. Because of the large and inhospitable areas involved, observational estimates are imprecise and it is natural to turn to GCMs which can, in theory, provide a more exact specification. GCMs, if we can believe them to be accurate, are also the best source for predictions of the contributions of the ice sheets to future sea level change. In this contribution we examine the precipitation and evaporation from GCMs of varying sophistication and compare their simulated mass balance to the most up-to-date observations. The best GCMs are found to be accurate (on a continental average) to within the degree of uncertainty in the observations and to perform as well as numerical weather prediction analyses such as ECMWF. However when the detailed pattern is examined there are possibilities for improvement in all GCMs. We examine the change in mass balance in a transient climate change experiment. Overall, the mass balance can be fitted quite well to temperature change. However, the relationship is not the same as for interannual variations in mass balance and temperature change representing internal variability in a control run for present-day conditions, and also there are significant regional variations. This may have implications for existing studies that have parametrized precipitation change by temperature change.

### MC01/W/12-A2 1650

#### ATMOSPHERE-SEA ICE-OCEAN INTERACTIONS IN A REGIONAL CLIMATE SYSTEM MODEL OF THE ANTARCTIC

David A. Bailey and Amanda H. LYNCH (both at PAOS/CIRES, CB 216, University of Colorado, Boulder, CO, 80309-0216, USA, email: bailey@cires.colorado.edu)

High-latitude interactions of local-scale processes in the atmosphere-ice-ocean system have effects on the local, Antarctic, and global climate. Phenomena including polynyas and leads are examples of such interactions which when combined have important impacts on larger scales. These smaller scale features can only be parameterized in global models, but can be explicitly simulated using high resolution, limited area climate system models. As such, the study of these interactions is well-suited to a regional modelling approach and is considered here using the Arctic Regional Climate System Model (ARCSyM). This model has been used for many simulations in the Arctic, and has now been implemented for the Antarctic. This work considers fine-resolution (25km) simulations in the Cosmonaut Sea region, with the eventual goal of elucidating the mechanisms involved in the formation and maintenance of the sensible heat polynya which is a regular occurrence in this area. This work will provide insight into the role of such polynyas in the atmospheric and oceanic circulations of the high southern latitudes.



**COUPLED OCEAN-ATMOSPHERE MODELLING AND INTERCOMPARISONS****MC01/W/18-A2** **1705****THE SEASONAL CYCLE IN COUPLED OCEAN-ATMOSPHERE GENERAL CIRCULATION MODELS**

Curt COVEY Lawrence Livermore National Laboratory Livermore, CA 94550, USA

We examine the seasonal cycle of near-surface air temperature in 17 coupled ocean-atmosphere general circulation models. Nine of the models use ad hoc flux adjustments to bring model simulations close to observations of the present-day climate. The seasonal cycle of zonal mean surface temperature is reasonably well-simulated with good intermodel agreement from about 40N-40S. Non-flux-adjusted models perform about as well as the flux-adjusted models for this diagnostic, though a detailed look at land vs. ocean responses shows better agreement with observations for the flux-adjusted models (as expected). Reasonable seasonal cycle simulation by the non-flux-adjusted models is an encouraging indication that GCMs may adequately simulate longer-term climate changes. There appears to be a weak positive relationship between climate sensitivity and seasonal cycle amplitude for the models in this study.

**MC01/L/11-A2** **Invited** **1725****THE NCAR CLIMATE SYSTEM MODEL**

Byron A. Boville (National Center for Atmospheric Research, Box 3000, Boulder CO 80307 USA, email: boville@ucar.edu)

The NCAR Climate System Model (CSM) is a physical climate model containing component models for the atmosphere, land surface, ocean, and sea ice. The CSM produces stable solutions for present (or pre-industrial) climate on multi-century time scales, without the need for flux corrections. Although the surface climate was stable, the initial version of the CSM had substantial deep ocean trends. This talk will summarize improvements in the model which have significantly reduced the deep ocean trends and added new capabilities which are used for climate change experiments. These improvements include an interactive sulphate aerosol model in the atmosphere and an asymmetric diffusion tensor in the ocean. Simulations from pre-industrial control simulations, and 20th and 21st century climate change experiments will be discussed.

**MC01/W/15-A2** **1740****BIOSPHERIC CARBON CYCLE RESPONSE TO GLOBAL WARMING**

Pierre FRIEDLINGSTEIN, Patrick Monfray and Philippe Ciais (LSCE, CE-Saclay, 91191, Gif/Yvette, France, email: pierre@lsce.saclay.cea.fr) Herve Letreut, Jean-Louis Dufresne (LMD, CNRS/UPMC, 75252 Paris Cedex 05, France)

The biospheric carbon cycle is directly linked to the climate system. CO<sub>2</sub> exchange between the atmosphere and the biosphere is controlled by atmospheric CO<sub>2</sub> and surface climate conditions. Elevated atmospheric CO<sub>2</sub> favors plant photosynthesis. Climate change, through changes in surface and soil temperature and humidity also affects the biospheric carbon storage. On the other hand, atmospheric CO<sub>2</sub> is controlled by anthropogenic emissions but also by land and ocean CO<sub>2</sub> fluxes. It is therefore crucial to estimate in the context of future climate what is the carbon cycle response to CO<sub>2</sub> increase and climatic change. In the context of the CMIP2 activity, several GCMs estimate the climate response to a 1% increase in the atmospheric CO<sub>2</sub> concentration. Here, we use CASA/SLAVE, a global model of the biospheric carbon cycle to estimate the biospheric response to this climate forcing. The model will be forced by atmospheric CO<sub>2</sub> and monthly means of surface temperature and precipitation field, available from the CMIP2 runs. The model needs to be initialized to steady state using constant climate, then it is run over the CMIP2 period. A preliminary study has been performed using the CMIP2 outputs from the LMD GCM. The biospheric response to the atmospheric CO<sub>2</sub> increase is an important biospheric carbon uptake, but the climate induced response, because of drying of the land surface, is a net release. However, the combined effect is a net biospheric sink.

**Wednesday 21 July AM**

Presiding Chair: Mojib Latif

**COUPLED OCEAN-ATMOSPHERE MODELLING AND INTERCOMPARISONS****MC01/E/11-A3** **0845****RELATIONSHIP BETWEEN THE ATLANTIC THERMOHALINE CIRCULATION AND THE DEEP CONVECTION ACTIVITY IN A GLOBAL COUPLED MODEL ?**

Yvonnick LE CLAINCHE (1), Pascale Braconnot (1), Olivier Marti (1) and Sylvie Joussaume (1) (1) Laboratoire des Sciences du Climat et de l'Environnement, UMR CEA-CNRS, CE Saclay, Orme des Merisiers, 91191 Gif sur Yvette, France, email: leclain@lsce.saclay.cea.fr

A 200 years simulation has been performed with the global IPSL ocean-atmosphere coupled model (Paris, France) in its low resolution version. No flux correction technique is used at the air-sea interface. The complete thermodynamic sea ice model developed at LODyC (Paris) has been included instead of the old diagnostic approach. It's the only major physical difference with a previous 150 years coupled simulation. We analyze the impact of the sea-ice model on the North Atlantic thermohaline circulation (THC), and relate the larger value produced in the new simulation (about 15 Sv) to the preservation of the deep convection in Greenland and Norwegian seas. Whereas this convection zone had disappeared with the simpler sea-ice representation, the variations of its intensity correlate well with the interdecadal variability of the THC in the last simulation. Furthermore, the mean value of the THC doubles around year 150, and then presents a very larger interannual variability. We'll discuss these important changes, and their links with the resumption of the convective activity in the Labrador sea, and also with the atmospheric forcing.

**MC01/W/64-A3** **0900****AN EXPLORATION OF THE NAO-RELATED TEMPERATURE VARIATIONS SIMULATED BY 17 GLOBAL COUPLED OCEAN-ATMOSPHERE MODELS**

PAVAN, Dr Valentina (CINECA, email: pavan@cineca.it)

This study investigates the North Atlantic surface temperature interannual variability simulated

by 17 state-of-the-art global coupled ocean-atmosphere climate models and compares model results with those obtained using Jones (1986) surface temperature data set for the period 1900-1994. The models are those participating in the Coupled Model Intercomparison Project (CMIP). Taking year-to-year differences in winter mean temperatures, interannual variations are separated from longer trends due both to interdecadal variability and to secular model drift. The ability of the models to reproduce the observed interannual variability associated with the North Atlantic Oscillation (NAO) is investigated using first area-average temperatures and then principal component analysis. Most of the models capture the anti-correlation between detrended temperatures over North-West Europe and North-West Atlantic. All the same, few of the models are able to capture the full NAO pattern that has nodes also over southern North America and the Arabian peninsula. For the non-drifting models, the leading principal component of the wintertime temperatures over the Atlantic well fits a red noise model but with a lag-1 correlation close to zero.

**MC01/W/26-A3** **0915****SENSITIVITY EXPERIMENTS WITH THE UCL'S COUPLED ATMOSPHERE-OCEAN GENERAL CIRCULATION MODEL**

Ch. PONCIN and Th. FICHEFET, Institut d'Astronomie et de Geophysique G. Lemaitre, Université catholique de Louvain, chemin du cyclotron 2, 1348 Louvain-la-Neuve, Belgium, email: poncin@astr.ucl.ac.be)

The UCL's coupled atmosphere-ocean general circulation model (AOGCM) is a coarse-resolution model, which does not include any flux correction. Its atmospheric component is an improved version of the atmospheric general circulation model (LMD5) built at the "Laboratoire de Meteorologie Dynamique" of the CNRS (Paris). The oceanic model (CLIO) is a free-surface, primitive-equation model developed at the UCL in Belgium. As many other AOGCMs without flux correction, this coupled model drifts away from realistic climatology. In order to improve the model behavior, a better understanding of its sensitivity to parameterizations is needed. Therefore, we have performed sensitivity experiments on atmospheric parameters in forced and coupled modes. The transition zone between cold and warm clouds acts upon the radiative fluxes around 45S and 45N. The precipitation rate of cold clouds regulates the efficiency of the thermal machine associated to the Hadley cell. Three approaches to the cloud overlapping along the vertical have been tested: maximum, random and max/random overlapping. The aim of all these sensitivity experiments is to analyze the model drift away from observed climatology and to choose the best parameters for scenario simulations.

**MC01/W/38-A3** **0930****LONG-TERM GLOBAL WARMING SCENARIOS COMPUTED WITH THE CLIMBER-2 MODEL**

Stefan RAHMSTORF and Andrey Ganopolski Potsdam Institute for Climate Impact Research, PO Box 60 12 03, D-14412 Potsdam, Germany, E-mail: Rahmstorf@PIK-Potsdam.de

We present a new, highly efficient coupled ocean-atmosphere-sea ice model of intermediate complexity, CLIMBER-2. In addition to showing model validation for the present and glacial climates we will discuss long-term global warming scenarios. Our simulations extend to the year 3000, beyond the expected peak of CO<sub>2</sub> concentrations. The Atlantic thermohaline ocean circulation declines strongly in all our scenarios over the next 50 years due to a thermal effect, consistent with other climate models. Changes in the hydrological cycle determine whether the circulation recovers or collapses in the long run. Both outcomes are possible within present uncertainty limits. In case of a collapse, a substantial long-lasting cooling over the North Atlantic and a drying of Europe is simulated.

**MC01/W/11-A3** **0945****MOBIDIC SIMULATED CLIMATE WITHIN PMIP**

Loutre M.F., Tulkens P., Crucifix M., Berger (Institut d'astro, email: loutre@astr.ucl.ac.be)

MoBidiC is a zonally averaged climate model. A quasi-geostrophic atmosphere model is coupled to a three-basin (latitude-depth) ocean-sea ice model. The main continental ice sheets are also represented. The atmospheric component of MoBidiC contains an interactive representation of the hydrological cycle based on meridional transport of moisture and zonal redistribution of precipitation. The sea-ice model enables to represent explicitly the climatic effect of ice formation and ablation and their consequences on the ocean circulation. The interconnected ocean basins allow this model to simulate the main thermohaline circulation processes. The six PMIP experiments were performed with MoBidiC. For the present day climate the 1950AD solar forcing and the present-day CO<sub>2</sub> atmospheric concentration (345 ppmv) forced the model. The SST and sea-ice were either prescribed or computed by the ocean model. For the 6-kyr experiment only the forcings (CO<sub>2</sub> and insolation) were modified compared to the control run. In the 21-kyr experiment the land surface features were adapted in addition to the modification of the forcings. Here we focus on the surface temperatures and precipitation patterns simulated for these experiments. Despite shortcomings in the representation of atmospheric dynamics and in the distribution of ocean salinity, the present-day simulated values are realistic. Moreover the comparison with the results of other models allows to point out the strong features of the model, systematic deviation or weaknesses.

**MC01/E/14-A3** **Invited** **1000****RESULTS FROM THE STOIC CGCM ASSESSMENT PROJECT**

Ken Sperber (Program for Climate Model Diagnosis and Intercomparison, LLNL, Livermore, CA, USA), Mike DAVEY and Matt Huddleston (both at The Meteorological Office, London Road, Bracknell, RG12 2SZ, UK, email: mkdavey@meto.gov.uk)

STOIC (Study of Tropical Oceans In CGCMs) is one of several projects set up by CLIVAR-NEG1 (now CLIVAR-WGSIP) to assess climate model behaviour on seasonal to interannual timescales. Monthly sea surface temperature, windstress and upper ocean vertically averaged temperature were collected from (at least) 20 year coupled GCM runs, for the tropics. This information from 24 models has been compared with observations, in terms of annual mean, seasonal cycle, and interannual variability. The models differ substantially in terms of resolution and coupling strategies: nevertheless, some common strengths and defects are apparent. For example, in the equatorial Atlantic, the mean zonal SST gradient in many models is opposite to that observed. Mean zonal winds in the equatorial Pacific tend to be too weak in the central Pacific, but too strong in the west Pacific. Model sea surface temperature anomalies in the Indian Ocean are generally positively correlated with anomalies in the Pacific, as observed.

MC01/L/12-A3 Invited 1020

## ENSIP: THE EL NIÑO SIMULATION INTERCOMPARISON PROJECT

M. Latif, Max-Planck-Institut fuer Meteorologie Bundesstrasse 55, D-20146 Hamburg, Germany and K. Sperber PCMDI, Lawrence Livermore National Laboratory P. O. Box 808, L-264, Livermore, Ca. 94551-9900, U. S. A.

An ensemble of twenty four coupled ocean-atmosphere models worldwide has been intercompared with respect to their performance in the tropical Pacific. The coupled models span a large portion of the parameter space and differ in many respects. The intercomparison includes TOGA-type models consisting of high-resolution tropical ocean models and coarse-resolution global atmosphere models, coarse-resolution global coupled models, and a few global coupled models with high resolution in the equatorial region in their ocean components. The comparison focusses on the tropical Pacific, and the performance of the annual mean state, the annual cycle and the interannual variability is investigated. The primary quantity analysed is sea surface temperature (SST). Additionally, the evolution of interannual heat content variations in the tropical Pacific and the relationship between the interannual SST variations in the equatorial Pacific to fluctuations in the strength of the Indian Summer Monsoon are investigated. The results can be summarised as follows: Almost all models (even those employing flux corrections) have still problems in simulating the SST climatology, although some improvements are found relative to earlier intercomparison studies. Only a few of the coupled models simulate the El Nino/Southern Oscillation (ENSO) in terms of equatorial SST anomalies realistically. In particular, many models overestimate the variability in the western equatorial Pacific. The evolution of interannual heat content variations is similar to that observed in almost all models, which indicates that equatorial wave dynamics is also important in coarse-resolution models. Finally, the majority of the models show a strong connection between ENSO and the strength of the Indian Summer Monsoon, which may be important to Monsoon predictions.

Presiding Chairs: Tom Phillips, Andy Pitman, and Ann Henderson-Sellers

## LANDSURFACE MODELLING AND INTERCOMPARISONS

MC01/E/31-A3 1100

## LAND-SURFACE EVALUATION: A MATURE AND SUCCESSFUL "MIP"

Ann HENDERSON-SELLERS (ANSTO, Lucas Heights, Sydney, NSW, Australia email: ahs@ansto.gov.au)

The first component of any intercomparison must be open to all who wish to participate and demands both high quality observational data and careful experimental design and quality control procedures. The second involves a smaller group of researchers and schemes with the specific goal of enhanced understanding. The two questions being posed by these two complementary activities are: a) does "your" scheme perform well enough to be part of international modelling efforts? and b) it is "understood" why your scheme performs the way it does? PILPS, the Project for Intercomparison of Land-surface Parameterization Schemes, one of the oldest "MIPs", serves the international modelling community in these two different and complementary ways: a) by providing open but quality controlled intercomparison opportunities as international benchmarks against which new and revised LSS can be validated; and b) by providing the tools and (more restricted) intercomparison frameworks by means of which the behaviour of LSS types can be analyzed and more fully understood. So far PILPS has completed seven full intercomparisons so that we estimate the resource commitment to date has been about \$7.5 million. The widespread international participation means that every intercomparison involves about one person year from each of 25 groups. Strategies for adding value to future land-surface intercomparisons include: multi-criteria optimization; higher order schemes and use of the CHASM-tool.

MC01/L/13-A3 1135

## VALIDATION STUDY OF THE CAPS MODEL LAND SURFACE SCHEME USING THE 1987 CABAUW/PILPS DATASET

S. Chang, D. Hahn, C.-H. Yang, and D. Norquist, Phillips Laboratory, Geophysics Directorate, Hanscom AFB, Mass. 01731 USA; M. Ek, NCEP/EMC/Mesoscale Modelling Branch, Suitland, MD 20746 USA

An updated complete and comprehensive description of the land surface parameterization scheme in the Coupled Atmosphere-Plant-Soil (CAPS) model is presented. The CAPS model has been in development at Oregon State University and Phillips Laboratory since 1981. The CAPS model was originally designed for a global atmospheric model, but it has also been used as a stand-alone model for a variety of applications. The land surface scheme in the CAPS model is one of the two dozen schemes that participated in the Project for Intercomparison of Land surface Parameterization Schemes (PILPS). Some unique features of the CAPS scheme are given in detail. A comprehensive dataset of one year (1987), including atmospheric forcing data and validation data from Cabauw, has been provided for PILPS by the Royal Netherlands Meteorological Institute. Using the Cabauw data, a validation study for the CAPS scheme has been carried out. The scheme's self-consistencies in terms of surface energy balance and water budget are discussed. Finally, the results of this validation study with emphasis on the performance of surface momentum and heat fluxes are presented.

MC01/E/10-A3 1150

## THE VALIDATION OF THE LAND-SURFACE PARAMETERIZATION SCHEME SWAP ON A REGIONAL SCALE

Yeugeniy Gusev and Olga NASONOVA (both at the Institute of Water Problems, Russian Academy of Sciences, Gubkina St.3, 117971 Moscow, Russia, e-mail: sowa@ipcom.ru)

The aim of this study was to evaluate the ability of the land-surface parameterization scheme SWAP to reproduce heat and water fluxes at the land surface at different scales varying from small catchments of areas 102 - 103 km<sup>2</sup> to a continental scale river basin (on the order of 106 km<sup>2</sup>) characterised by different natural conditions. The validation was carried out against streamflow data for the years 1979-1988 for 14 catchments situated within the Arkansas-Red River basin (USA) and for the whole basin. Forcing data and model parameters for 61 one degree grid cells composing the Arkansas-Red River basin, as well as streamflow data for the validation were provided by the organisers of the PILPS (Project for Intercomparison of Land-surface Parameterization Schemes) phase- 2(c) experiment. Runoff simulated by SWAP without any calibration for each grid cell was transformed into streamflow for different catchments and for the basin using the two-dimensional kinematic wave equation and routing model (provided by D. Lohmann, Princeton University, USA). Daily values of the calculated and observed (naturalized) streamflow were compared for 14 catchments and for the basin for 10-year period. For the whole basin the coefficient of correlation for daily values is 0.71, the relative deviation between mean annual calculated and observed streamflow is nearly 3%. For smaller catchments the errors in calculations increase with decrease in a catchment area (to

be exact, in the number of grid cells composing a catchment). That is in a good agreement with a theory of random errors. Analysis of the obtained results show that SWAP does not introduce systematic errors into the calculations and random errors mainly depend upon the number of grid cells, and accuracy of hydrometeorological data and land-surface characteristics.

MC01/W/29-A3 Invited 1205

## EVALUATION OF PILPS 2(D) HYDROLOGICAL SIMULATIONS AT VALDAI, RUSSIA

Alan ROBOCK, G. Srinivasan, Lifeng Luo Department of Environmental Sciences Rutgers - The State University of New Jersey 14 College Farm Road New Brunswick, NJ 08901-8551 USA Konstantin Y. Vinnikov, University of Maryland

The PILPS 2(d) experiment at Valdai, Russia offers a unique opportunity to evaluate land surface schemes in a climate with seasonal snow cover and seasonally frozen soil. Here we evaluate the 18-year simulations by the 21 schemes that participated in the experiment, in their ability to correctly partition the melting snow in the spring into runoff and infiltration. Using observed vertical profiles of soil temperature and soil moisture, we evaluate the relationship between infiltration and the frozen layer in the soil, and determine the dependence of this modeled relationship on the correct partitioning of snow meltwater. The large interannual variations allow us to provide new insights into the level of complexity necessary to correctly model this important aspect of land surface hydrology. We find that inaccurate snow simulations produce inaccurate timing of snow melt in some cases. In other cases, runoff is delayed and takes place over a longer time period than observed. Most models do not simulate soil temperature very well, but this does not seem to have a large effect on the accuracy of their runoff or soil moisture simulations. In collaboration with analyses by individual modelers, we identify parameterization decisions that produce both accurate and inaccurate simulations, and produce suggestions for the accurate modelling of cold season hydrology.

Wednesday 21 July PM

MC01/L/14-A3 1400

## ASSESSING SNOW SIMULATIONS OF LAND-SURFACE SCHEMES USED IN ATMOSPHERIC MODELS

A. Schlosser

A suite of 18-year, standalone simulations was performed by 21 land-surface schemes for a grassland catchment at Valdai, Russia (58N, 33E) for the PILPS Phase 2(d) experiment. The simulated water budgets of all the models are presented and compared against hydrologic observations made within the catchment. We focus our analysis on the models' representation and simulation of snow and frozen soil processes. Given the experimental framework, the model scatter of simulated snow is a result of differences in ablation. Scatter in ablation rates is primarily controlled by model disparity of energy available to the snowpack and how energy is distributed within the structure of the model (whether implicit or explicit). Factors such as the treatment fractional snow coverage, snow albedo, snow density, and vapor exchange all play a significant role.

MC01/E/04-A3 1415

## MODELLING SNOW COVER FORMATION AND SOIL FREEZING/THAWING PROCESSES IN THE LAND SURFACE PARAMETERIZATION SCHEME SWAP

Yeugeniy GUSEV and Olga Nasonova (both at the Institute of Water Problems, Russian Academy of Sciences, Gubkina St.3, 117971 Moscow, Russia, e-mail: sowa@ipcom.ru)

The land surface parameterization scheme SWAP (Soil Water-Atmosphere-Plants) includes physically based description of the heat and water transfer processes occurring not only during the warm period of a year, but also during the cold period. The latter represent snow formation processes (snow accumulation including solid and liquid fractions, snow evaporation and snowmelt), soil freezing and thawing, infiltration of liquid water into frozen soil, and surface runoff and drainage from frozen soil. The aim of this study was to validate the ability of SWAP to simulate the mentioned processes. The validation of the model was performed using a set of hydrometeorological data measured at a grassland catchment at the Valdai water balance station (Russia) during 18 years (1966-1983). Most of the data were provided by the organisers of the PILPS (Project for Intercomparison of Land-surface Parameterization Schemes) phase 2(d) experiment. The Valdai data set was chosen for the validation because the Valdai site is characterized by a clear seasonal course of hydrometeorological conditions, deep snow cover and seasonally frozen soil. Besides that, the Valdai water balance station has a unique hydrometeorological, soil and vegetation observations carried out during more than 30 years which are necessary for the model validation. On the base of comparison of the simulated and observed water balance components and different characteristics of snow cover formation we can conclude that the model SWAP parameterizes the cold season processes occurring in mid-latitude grassland quite reasonable.

MC01/W/05-A3 1430

## SENSITIVITY STUDIES OF MAPS/RUC LAND-SURFACE SCHEME USING PILPS 2(D) DATA

Tatiana G. SMIRNOVA (Cooperative Institute for Research in Environmental Sciences, Boulder, Colorado, USA, email: smirnova@fsl.noaa.gov) John M. Brown, and Stanley G. Benjamin (both NOAA Forecast Systems Laboratory, Boulder, Colorado, USA)

The Mesoscale Analysis and Prediction System (MAPS) is a four-dimensional data assimilation system (implemented operationally at NCEP as the Rapid Update Cycle or RUC) running in real time. The forecast component of MAPS includes a multilevel soil/vegetation/snow scheme for prediction of soil temperatures and volumetric water content, and also snow height and temperature in the cold season. Soil temperature, soil moisture and snow cover, as predicted by the soil/vegetation/snow model, are carried forward from the previous forecast to initialize the next forecast in the MAPS cycle. This continuous cycling allows the effects of abnormally wet or dry soil conditions to positively influence forecasts of the planetary boundary layer through surface fluxes. However, seemingly subtle aspects of the climatology of soil model, and especially the climatology of hydrological cycle components, such as soil moisture, root zone drainage, surface runoff and snow cover, can dramatically affect atmospheric predictions. Further, in the cold season the existence of frozen moisture in soil considerably changes the processes of heat and moisture transfer inside soil, and also affects all components of the hydrological cycle. This motivated us to further improve the soil/vegetation model by searching for ways of incorporating the effects of frozen soil physics into our soil model. In preparation for introducing the frozen-soil physics into the 3-d MAPS/RUC model, we performed extensive testing of this physics enhancement in a 1-d version of the MAPS land-surface model. These tests were performed for the PILPS 2(d)



experiment (Valdai) and also for other Russian stations. We will present results from the Valdai tests showing sensitivity to changes of soil properties with depth and to inclusion of effects of frozen soil.

### MC01/E/21-A3 1445

#### USING CHASM TO EXPLORE SURFACE ENERGY BALANCE COMPLEXITY IN GCM LAND SURFACE MODELS

Dr Carl DESBOROUGH (Macquarie University, email: cdesboro@penman.es.mq.edu.au)

A large number of land surface models (LSMs) have been designed for use in atmospheric general circulation models (GCMs) and GCM modellers therefore have a large number of options when selecting an LSM for their GCM. A framework within which sensitivity to LSM design can be tested is presented and a series of experiments carried out to investigate how general aspects of surface energy balance parameterisation affect land-atmosphere evaporation. Firstly, it is shown that a combination of surface energy balance complexity and aerodynamic parameterisation can be used to explain the gross simulation differences obtained in the Project for Intercomparison of Land-surface Parameterization Schemes (PILPS). Secondly, a simple surface energy balance parameterisation with a constant surface resistance is found to be as appropriate as more complex method for simulating annual, monthly and seasonally-averaged diurnal cycles of evaporation. However, complex aspects of surface energy balance parameterisation (canopy interception, bare ground evaporation and canopy resistance) are shown to contain substantial geographic and daily functionality that is not present in the simpler parameterisation.

### MC01/L/15-A3 1500

#### LAND SURFACE MODELLING AND CLIMATE VARIABILITY - BACK TO SIMPLICITY

NING ZENG and David Neelin, Dept. of Atmospheric Sciences and Inst. of Geophysics and Planetary Physics Univ. of California, Los Angeles

Land-surface modelling has gone over the last decade and half from the simple bucket model to sophisticated representations of the biosphere and surface energy and water cycle. Yet the models do not necessarily converge on their capability and confidence level in climate simulation. Using a land-surface model of intermediate complexity built on the PILPS experiences, we demonstrate the key aspects of a land-surface model relevant to climate simulation. Example will be shown for the amazon interannual climate and hydrological variability. A method using atmospheric reanalysis data and observed surface runoff to diagnose soil moisture variability will be highlighted as an important way for validating the models.

### MC01/E/18-A3 Invited 1535

#### STATUS REPORT ON PILPS PHASE 3: AMIP DIAGNOSTIC SUBPROJECT 12

Thomas J. PHILLIPS (Program for Climate Model Diagnosis and Intercomparison (PCMDI), Lawrence Livermore National Laboratory, PO Box 808, Livermore, California, USA, Email: phillips14@llnl.gov)

Phase 3 of the Project for Intercomparison of Landsurface Parameterization Schemes (PILPS) entails the diagnosis of diverse landsurface schemes that are designed to operate within atmospheric general circulation models (AGCMs). Because most of the world's AGCM groups have conducted climate simulations according to the standard protocol of the Atmospheric Model Intercomparison Project (AMIP), PILPS Phase 3 has functioned as an AMIP diagnostic subproject. The presentation will review the work of the subproject since 1992, including both the main findings of its first (AMIP I) phase and preliminary results from the recently initiated AMIP II intercomparison.

### MC01/E/09-A3 1550

#### LAND-SURFACE PARAMETERIZATIONS AND CLIMATE SIMULATIONS: PRELIMINARY RESULTS FROM AMIP II DIAGNOSTIC SUBPROJECT 12

HUQIANG ZHANG (Environment Division, Australian Nuclear Science and Technology Organisation, PMB 1, Menai, NSW 2234, Australia) Ann Henderson-Sellers (Environment Division, Australian Nuclear Science and Technology Organisation, PMB 1, Menai, NSW 2234, Australia)

Results from AMIP I diagnostic subproject 12 have shown large inter-model scatter in the surface energy and water partitions. Those large inconsistencies are identified to be partly responsible for the substantial differences in simulated continental climate. However, the analyses of AMIP I results were constrained by the fact that most AMIP I models employed bucket schemes and some models did not conserve energy and moisture. In the current study, we report some preliminary analyses of AMIP II results which became available in early 1999. We will focus on the quantitative assessment of the agreement among the models in simulating the surface energy partition (latent heat and sensible heat) and the surface water partition (evaporation, precipitation, runoff and others). Furthermore, how the differences in those two partitions affect the model simulation of ground temperature, soil moisture and snowpack is investigated. Following the model intercomparison of the aforementioned key surface variables, we then try to link the model performance with the land-surface schemes used in the models themselves. The aim is to understand how much the differences can be explained by the different behaviour of land-surface component in each model. For the models participating in AMIP I and/or PILPS projects, we will compare their performance with that seen in the previous studies. Finally, we will present some on-going activities in the joint AMIP/PILPS project. How to fully explore the AMIP II results to enhance our understanding of the role of land-surface in climate simulations will also be discussed.

### MC01/E/36-A3 1605

#### CHARACTERISING GCM LAND SURFACE SCHEMES TO UNDERSTAND THEIR RESPONSE TO CLIMATE CHANGE

Nicola GEDNEY and Peter Cox (both at Hadley Centre, UK Met Office), Herve Douville (Meteo-France), Jan Polcher (Laboratoire de Meteorologie Dynamique du CNRS, France), Paul Valdes (University of Reading, UK)

The impact of land surface representation on GCM simulations of climate change is analysed using 8 climate change experiments, carried out with 4 GCMs each utilising 2 different land surface schemes (LSS's). In the regions studied (Amazonia, the Sahel and Southern Europe) the simulations differ markedly in terms of their predicted changes in evapotranspiration and soil moisture. This is only partly as a result of differences in the predicted changes in precipitation and available energy. A simple "bucket model" characterisation of each LSS, demonstrates that the different hydrological sensitivities are also strongly dependent on properties of the LSS; most notably the runoff which occurs when evaporation is marginally

moisture stressed. This parameter varies significantly amongst the LSS's, and strongly influences both the soil moisture in the 1xCO2 control climate, and the sensitivity of evaporation and soil moisture to climate change. It is concluded that uncertainty in the predicted changes in surface hydrology are more dependent on such gross features of the runoff versus soil moisture curve, than on the detailed treatment of evapotranspiration.

### MC01/W/46-A3 1620

#### THE INFLUENCE OF TWO DIFFERENT LAND-SURFACE COUPLING TECHNIQUES IN THE MPI GCM

Jan-Peter SCHULZ (curr. aff.: Danish Meteorological Institute, Lyngbyvej 100, DK-2100 Copenhagen, Denmark, email: jps@dmi.dk) Lydia Dumenil (Max-Planck-Institut für Meteorologie, Bundesstrasse 55, D-20146 Hamburg, Germany, email: dumenil@dkrz.de) Jan Polcher (Laboratoire de Meteorologie Dynamique du CNRS, 4 pl. Jussieu, F-75252 Paris, France, email: jan.polcher@lmd.jussieu.fr)

Land surface processes have a significant impact on near surface climate phenomena. The component of an atmospheric general circulation model (GCM), that is responsible for the representation of land surface processes, is the land surface scheme (LSS), which essentially represents the land surface energy and moisture cycles. Various different LSSs have been developed for use in GCMs that utilize very different parameterizations of these physical processes and lead to differences in the simulated climates. In addition, the numerical coupling between land surface and atmosphere can also have a significant impact on the model simulation. The objective of PILPS phase 4 is to intercompare different LSSs which are coupled to the same atmosphere model. The focus is on assessing the impact of the different physical parameterizations on the simulated climate. In the present study, two versions of the ECHAM4 GCM are compared, one with semi-implicit coupling between land surface and atmosphere, the other one with implicit coupling. A global simulation was performed with both models, using the same initialization and climatological sea surface temperatures. The results show that the coupling technique has an important impact on the simulated surface climate and the water and energy cycles. These results are compared to an experiment with a third version of the ECHAM4 GCM, in which the SECHIBA land surface scheme is implemented in an implicit way. This allows one to estimate the relative importance of differences in land surface parameterizations and differences in surface-atmosphere coupling techniques.

### MC01/W/13-A3 1635

#### TESTING AGGREGATION RULES FOR SURFACE PARAMETERS USING REMOTELY SENSED LAND COVER DATA AND THE NCAR COMMUNITY CLIMATE MODEL (CCM3) COUPLED TO BATS

Eleanor J. BURKE, Muhammed Altaf Arain, Zong-Liang Yang, and W. James Shuttleworth (Department of Hydrology and Water Resources, The University of Arizona, Tucson AZ 85721, USA, email: eleanor@hwr.arizona.edu)

The land surface parameters required as input to a GCM grid box (typically a few degrees) are often set to be those of the dominant vegetation type within the grid box. This paper discusses the use and effect of aggregation rules for specifying effective values of these land cover parameters by taking into account the relative proportion of each land cover type within each individual grid box. Global land cover classification data at 1 km resolution were used to define Biosphere Atmosphere Transfer Scheme (BATS) specific aggregate (using aggregation rules) land cover parameters. Comparison of the values of the aggregate parameters and those defined using the dominant vegetation type (default parameters) shows significant differences in some regions, particularly in the semi-desert, and in forested regions, e.g. the Saharan desert and the tropical forest of South America. These two different sets of parameters were used as input data for two 10-year simulations of the NCAR CCM3 model coupled to the BATS land surface scheme. Statistical analyses comparing the results of the two model runs showed that the resulting differences are only significant in specific regions. For example, the sensible heat flux in the Saharan desert calculated for the aggregate run increased due to the marked increase in the minimum stomatal resistance and the decrease in fractional vegetation cover in the aggregate parameters over the default parameters. The modelled global precipitation and surface temperature fields were compared to observations: there is a general improvement in the performance of the aggregate run over the default run in areas where the differences between the aggregate and default run are significant. However, most of the difference between the modelled and observed fields is attributable to other model deficiencies. It can be concluded that the use of aggregation rules to derive land surface parameters results in significant changes in modelled climate and some improvements in the land surface diagnostics at the regional scale, however these are not as wide-spread or dramatic as the changes in vegetation parameters suggest.

### MC01/W/53-A3 1650

#### COMPARATIVE EVALUATION OF SIB2, BATS, AND BATS2 USING AMAZON FIELD DATA

Omer L. SEN, W. James Shuttleworth, and Zong-Liang Yang (All at Department of Hydrology and Water Resources, University of Arizona, Tucson, 85712, AZ, USA, Email: sen@hwr.arizona.edu)

Over the last decade, improved understanding of plant physiological processes has generated a major change in the way stomatal functioning is described in advanced land surface schemes. New versions of two widely-used, advanced land surface schemes, SiB and BATS, exist that reflect this change in understanding, but these two new models make different assumptions regarding the form of the humidity stress factor. The main goal of this study was to evaluate the new version of BATS, here called BATS2, using Amazon field data from the ABRACOS project, with emphasis on comparison against the original version of BATS and on comparison with SiB2. Evaluation of SiB2 using a 3-year time series of ABRACOS data revealed weaknesses not noticed in previous studies. Specifically, the model's description of early morning transpiration is poor with hourly-average forcing data and there is an unrealistic simulation of the yearly cycle in soil moisture status, with a resulting poor simulation of evaporation. Improved long-term simulation by SiB2 requires specification of a deeper rooting depth, this being a general feature required for all three models. In general, the original version of BATS gave good agreement with observations, but it showed excessive sensitivity to vapor pressure deficit in very dry atmospheres, and the value of minimum stomatal resistance specified by default was not optimal. Evaluation of BATS2 revealed that substantial changes are required in the parameters that determine stomatal behavior in the model for simultaneously realistic simulation of the net carbon uptake, nighttime respiration and transpiration. In general, all three models have weaknesses when describing the field data using their default parameters. However, if a few model parameters are modified in a plausible way, all three can give a good time-average simulation of measured exchanges, and there is little evidence of sensitivity to the different forms assumed for the humidity stress function.



MC01/W/54-A3 1705

**ENHANCING THE SIMPLIFIED BIOSPHERE MODEL (SSIB) TO ESTIMATE CARBON FLUXES OF TERRESTRIAL ECOSYSTEMS FOR REGIONAL CLIMATE STUDIES**

Xiwu Zhan, YONGKANG XUE (both at Department of Geography, University of Maryland, College Park, MD, USA, Tel: 301-405-4050; fax: 301-314-9299, email: yxue@geog.umd.edu), and G. James Collatz (Laboratory for Terrestrial Physics, NASA/GSFC, Greenbelt, MD, USA)

Increase in greenhouse gases, in particular CO<sub>2</sub>, has great impact on global climate change. It is desirable to accurately assess the CO<sub>2</sub> fluxes between the terrestrial ecosystems and the atmosphere in regional climate studies. The current version of the simplified biosphere model (SSIB) does not consider the photosynthetic activities of CO<sub>2</sub> assimilation of plants. The work in this paper is an enhancement of the SSIB model for the CO<sub>2</sub> flux modelling. The equations and parameters of the photosynthesis-stomatal conductance models developed by Collatz et al. for C3 or C4 plants are adopted for simulating the uptake or release of CO<sub>2</sub> by land surface ecosystems. These models have sound physiological basis and fine description to the interactive effects of environmental factors of plant photosynthesis and stomatal movement. However, the equations of these models are solved numerically with iterations, which consumes a great amount of computational time. In some cases, the iteration process may not be convergent and an appropriate solution may be difficult to obtain. In this study, a new procedure is developed to quasi-analytically solve the equations of these models. By using this procedure, appropriate solutions can be directly computed without iterations. When an appropriate solution of these models does not exist under some night time environmental conditions, the simple procedures are applied to simulate the processes because the land surface fluxes in these cases are not significant. The CO<sub>2</sub> release from soil surface is modeled with a soil respiration model similar to that of Porter et al's CASA model (the Carnegie, Ames, Stanford Approach). Off-line tests using the enhanced SSIB model are conducted to compare with measured CO<sub>2</sub> flux, latent heat and sensible fluxes.

Thursday 22 July AM

Presiding Chairs: Ray Arritt, Filippo Giorgi

**REGIONAL MODELLING AND INTERCOMPARISONS****Regional Model Intercomparisons**

MC01/L/16-A4 Invited 0930

**MODELLING EUROPEAN REGIONAL CLIMATE, UNDERSTANDING AND REDUCING ERRORS - THE MERCURE PROJECT**

Richard JONES (Hadley Centre for Climate Prediction and Research, UK Met. Office, London Road, Bracknell, RG12 2SZ, UK. Email: rgjones@meto.gov.uk)

MERCURE is a wide-ranging project whose main focus is on the improvement of simulation of European climate but which has implications for modelling regional and global climate generally. The main aim of the project is to improve regional climate models (RCMs) by understanding the source of errors and reducing them by improving the models' representation of physical processes (including increasing resolution). The focus will be on improving the simulation of surface air temperature and precipitation given their fundamental importance in assessing impacts of climate. Four main areas important for modelling regional climate are being focused on and results from these will be presented. 1) Improving the hydrological cycle in regional models via improved formulations of land-surface processes, radiation and precipitation physics. New aspects of the simulations will be validated by comparing with run-off, snow-pack and soil-moisture data. 2) Assessing the ability of regional models to reproduce observed precipitation frequency distributions (including the frequency of heavy events) as well as climatological means. 3) Further characterisation of errors in regional climate simulations nested in general circulation models (GCMs) derived from the GCM driving data. GCM errors which induce large-scale errors in the RCMs will be identified and GCM modellers will be encouraged to reduce them. 4) Providing a statistical-dynamical tool linking RCM and GCM simulations to extend the length of RCM integrations. The method will be able to reproduce the main features of long RCM simulations from large-scale driving data given shorter sets of both for calibration. This will allow the computation of statistical RCM scenarios for a wide range of GCM scenarios.

MC01/W/08-A4 0950

**PROJECT TO INTERCOMPARE REGIONAL CLIMATE SIMULATIONS**

RAYMOND W. ARRITT, William J. Gutowski, Jr., Eugene S. Takle and Zaitao Pan (all at Department of Agronomy, Iowa State University, Ames, Iowa 50011 USA, email: rwaritt@iastate.edu)

The Project to Intercompare Regional Climate Simulations (PIRCS) provides a common simulation framework for evaluating regional climate models. We describe the motivation and structure for the first PIRCS simulation experiment and present initial evaluations of the collective capabilities of participating models. Experiment 1 covers two periods of hydrologic extremes in the central United States: 15 May - 15 July 1988 (drought) and 1 June - 31 July 1993 (flood). For more details see the PIRCS Web site, <http://www.pircs.iastate.edu>. Initial results indicate that limited-area models forced by large-scale information at their lateral boundaries reproduce bulk temporal and spatial characteristics of observed fields. The 500 hPa height field's time average and temporal variability are generally well simulated by all participating models. Organized synoptic-scale precipitation systems are simulated deterministically, in that precipitation occurs close to the same time and location as observed (though amounts vary from the observations). Episodes of mesoscale and convective precipitation are represented in a more stochastic sense, with less precise agreement in temporal and spatial patterns. Simulated surface energy fluxes near the FIFE region show that inter-model differences in mid-day Bowen ratio tend to be closely associated with precipitation differences. Differences in daily maximum temperatures also are linked to Bowen ratio differences, while daily minimum temperatures show no clear link to Bowen ratio. Although some models have bias all reproduce the synoptic variability of observed daily maximum and minimum temperatures.

MC01/W/47-A4 1005

**A MODEL INTERCOMPARISON OVER THE BALTIC DRAINAGE BASIN**

Daniela JACOB (1), Xiaohua Yang (2), Werner Wergen (3), Burkhard Rockel (4), Nils Gustafsson (5), Roderick Smith (6) (1) Max-Planck-Institute for Meteorology, Bundesstr. 55, 20146 Hamburg, Germany (2) Danish Meteorological Institute, Lyngbyvej 100, 2100 Copenhagen, Denmark (3) Deutscher Wetterdienst, Frankfurter Str. 135, 63067 Offenbach, Germany (4) Forschungszentrum Geesthacht, Max-Planck-Strasse, 21494 Geesthacht, Germany (5) Swedish Meteorological and Hydrological Institute, Folkborgsvaegen 1, 60176 Norrköping, Sweden (6) Hadley Centre for Climate Prediction and Research, Bracknell, Berkshire, RG12 2SY, UK

Within the NEWBALTIC project, an EU-project under BALTEX, mainly concentrating on numerical studies of the energy and water cycle of the Baltic Region, a model intercomparison of regional atmospheric models has been carried out. This study points to differences in numerical modelling of the atmospheric water and energy cycles and it will discover uncertainties in model generated fields. The participating groups agreed on a common grid, identical initial and lateral boundary conditions and a validation strategy. The model intercomparison has been performed for a three months long period (1st August 1995 until 31st October 1995) over the entire Baltic Sea drainage basin. Within this period an intense data collection and analyses took place. Model results and a careful validation against observations will be presented.

MC01/E/34-A4 1020

**INTERCOMPARISON OF REGIONAL CLIMATE CHANGE SIMULATIONS FOR EUROPE**

Bennert MACHENHAUER, Martin Windelband, and Michael Botzet (all at Max Planck Institute for Meteorology, Bundesstr. 55, D-20146 Hamburg, Germany. emails: machenhauer / windelband / botzet@dkrz.de)

Time-slices of 10-30 years from present-day climate simulations and transient climate change experiments performed with two coupled atmosphere-ocean GCMs were used as boundary conditions for three 50 km resolution Regional Climate Models (RCMs) focusing on Europe. Simulated seasonal mean values of surface air temperature and precipitation in the present-day time-slices were validated against observed climatological data in nine sub-areas covering Europe. The relatively large number of large, statistical significant sub-area mean biases seems to be caused by: 1) systematic errors in the simulated general circulation, in particular in the cyclonic activity over Europe, 2) errors in the parameterization of certain physical processes, 3) errors in the sea surface temperatures determined by the coupled GCMs. In two doubling greenhouse gas climate change experiments we find statistically significant mean temperature increases for the whole European region. These are also large compared to the corresponding biases of the present-day climate simulations. However, the changes in sub-areas of the deviation from the European mean temperature as well as the sub-area changes of precipitation are only partly significant and are of the same order of magnitude or smaller than the corresponding biases. In many cases they are also significantly different in the two experiments. It is also found that due to interaction between the systematic model errors and effects of the radiative forcing the systematic errors cannot be assumed to cancel out when the changes are computed, i.e. when subtracting a control time-slice from a future scenario time-slice simulation.

MC01/E/23-A4 1035

**INTERCOMPARISON OF REGIONAL CLIMATE SIMULATIONS OF THE 1991 EAST ASIAN SUMMER MONSOON: SENSITIVITY TO LATERAL BOUNDARY CONDITIONS**

L. R. LEUNG (Pacific Northwest National Laboratory, P.O. Box 999, Richland, WA 99352, USA, email: ruby.leung@pnl.gov) W.-C. Wang, W. Gong (State University of New York at Albany, 100 Fuller Road, Albany, NY 12205, email: wang@climate.cesim.albany.edu) Z.-C. Zhao, and Y. Luo (National Climate Center, China Meteorological Administration, 46 Baishiqiao Road, Beijing 100081, China, email: zhaocz@sun.ihep.ac.cn)

To examine the sensitivity of different regional climate models to lateral boundary conditions (LBC), an intercomparison experiment has been performed where three regional climate models were driven by two sets of LBC from the ECMWF and NCEP/NCAR reanalyses to simulate an extreme flood event. Although the dynamical components of the models are almost identical, the physical parameterizations used to represent clouds, radiative transfer, turbulence transport, and surface processes are very different. Furthermore, some recent modifications have been applied to two of the models which render the simulations rather different from a previous intercomparison experiment reported using earlier versions of the models. The models were used to simulate the heavy precipitation during the 1991 summer which caused severe flooding over the Yangtze River in China. Comparison of the ECMWF and NCEP/NCAR reanalyses of the 1991 extreme flood case shows some large differences in the hydrological budgets represented. For example, the ECMWF reanalysis produced about 10% more net moisture advection into the study domain that centered over China. Consequently all regional climate simulations driven by the ECMWF reanalysis produced more precipitation than those driven by the NCEP/NCAR reanalysis. Analyses of the six regional simulations suggest that minor differences in the large scale LBC could be amplified by differences in the regional models because of the strong interactions among clouds, radiation, and surface processes.

**Regional Modelling and Hydrology**

MC01/W/44-A4 1110

**REGIONAL SIMULATIONS OF CALIFORNIA PRECIPITATION**

John ROADS (Scripps Institution of Oceanography, UCSD-0224, La Jolla, CA 92093, Email: jroads@ucsd.edu) Shyh Chen (Scripps Institution of Oceanography, UCSD-0224, La Jolla, CA 92093, Email: schen@ucsd.edu)

A global to regional modelling system, capable of making large-scale climate simulations and forecasts, and then downscaling these forecasts and simulations to regional scales is evaluated for California. Regional climate simulations of wet and dry winters compare well with available observations, especially in comparison to global simulations. While the global model paints a broad swath of precipitation across the western U.S., the regional model, forced by the large-scale background flow produced by the global model, more accurately simulates the increased precipitation over the Sierra Nevada and coastal regions. The regional model is especially advantageous for intense precipitation events at regional spatial scales. Although the regional simulations do not significantly alter the imposed large-scale features, they do significantly enhance the spatial as well as temporal variations of the hydrologic variables. Basically, downscaling by a regional model is a dynamically consistent method, which extends the usefulness of global climate forecasts. Still, current regional simulations are not perfect. Even higher resolution and further improvement in physical parameterizations are still needed.

MC01/W/17-A4 1125

**REGIONAL INTERPRETATION OF CLIMATE SCENARIOS FOR NORTHERN EUROPE; COUPLING OF AN ATMOSPHERIC MODEL, A 1.5-D REGIONAL OCEAN MODEL, LAKE MODELS AND HYDROLOGICAL MODELLING**

Markku RUMMUKAINEN, Anders Ullerstig, Jouni Räisänen, Björn Bringfelt, Anders Omstedt, Colin Jones, Ulrika Willén, Phil Graham and Ulf Hansson (Rossby Centre, Swedish Meteorological and Hydrological Institute, SE-61076 Norrköping, Sweden. Email: markku.rummukainen@smhi.se)

The climate of northern Europe is affected by numerous small-scale forcing features, or

phenomena that are characterized by large seasonal/spatial contrasts. Air masses arriving from the Oceans in the west and southwest first meet the Scandinavian mountains and thereafter traverse the landscape with numerous lakes as well as the Baltic Sea. The nature of the surface, including snow and ice modifies the surface climate. Variability in the regional topography also affects the strong seasonal transitions in climate via snow cover and in the hydrological budget in general. In order to construct a regional interpretation of the Nordic climate from global model results, it is necessary to improve the description of the small-scale forcing features. In the SWECCLIM regional climate modelling programme, this is addressed by coupling a model for the Baltic Sea and lake models into a climate version of a limited area weather forecast model HIRLAM. In addition, formulations from a hydrological model are imported to improve the modelling of soil moisture and point runoff. A description of the coupled model system, as well as results from 10-year downscaling integrations will be discussed, emphasizing the results for snow cover, lake ice cover and the Baltic Sea ice, as well as the hydrological budget. The simulations have been done with time slice data from the control and transient Hadley Centre HadCM2 integrations.

**MC01/W/28-A4** **1140**

**WATER AND ENERGY BALANCE OF THE BALTIC DRAINAGE BASIN**

Daniela JACOB Max-Planck-Institute for Meteorology, Bundesstr.55 20146 Hamburg, Germany

Within the BALTEx (BALTic sea EXperiment) project the hydrological and energetic budgets of the Baltic Sea drainage basin are under investigation with the aim to understand the water and energy cycles more completely. The budgets are influenced by meteorological phenomena on different time and space scales including the range from single episodes to multi year climate simulations. Extremes, interannual and decadal variabilities are of interest. The atmospheric regional climate model REMO has been used to study the water and energy budgets of the Baltic Sea drainage basin for a period of 21 months. Continuous simulations with two different physical parameterization packages and on two different horizontal resolutions have been carried out using analyses fields provided by the German Weather Service as initial and lateral boundary conditions. First results indicate that the annual cycle of the monthly total precipitation have a similar behaviour during the winter months but differences during the summer esp. over land. Furthermore the water balance over the Baltic Sea was positive (more precipitation than evaporation) during the first half of 1992 and during the period January to August 1993, while the signal during the second half of the year 1992 was not clear.

**MC01/P/01-A4** **1155**

**NUMERICAL SIMULATIONS ON IMPACTS OF THREE GORGES RESERVOIR ON SUMMER MONSOON RAINFALL OVER EAST ASIA**

ZONGCI ZHAO and Yong Luo (National Climate Center, Baishiqiaolu, No.46, Beijing, 100081, P.R. China E-mail: zhaozc@sun.ihep.ac.cn)

Three Gorges reservoir along the Yangtze River Valley of China is going to be reconstructed. The numerical simulations of Three Gorges reservoir have been conducted by using a regional climate model (RegCM2/EA) which was based on the NCAR RegCM2. The model has a domain of about 100-150E and 10-45N with a horizontal resolution of 60km x 60km and a vertical resolution of 23 layers. A sensitive experiment was designed a water body at around the Three Gorges region with 45 grid points and 50m or 100m of water depth to replace the vegetation of the present time. To compare the simulations of Three Gorges' reservoir run with the control run, it is found that the summer rainfall over some regions where are near the Three Gorges reservoir such as Southwest China, Yangtze-Huaihe River Valley and Hetao might be increased clearly. Impacts of the Three Gorges reservoir on Other variables have also been investigated in this research. The numerical experiments with the different areas and depths of this reservoir were also conducted.

**MC01/W/38-A4** **1210**

**SOIL WATER PARTITIONING AND ISSUES IN THE COUPLED HYDROSPHERE-ATMOSPHERE RESEARCH MODEL (CHARM)**

Lofgren, B. M.

Excessive boundary-layer cloudiness has been a problem within the Coupled Hydrosphere-Atmosphere Research Model (CHARM), a model of the Laurentian Great Lakes' regional climate system that uses the Regional Atmospheric Modelling System (RAMS) as the basis for its atmospheric component. This is in spite of a deficit of humidity in the lower boundary layer, in comparison to observations. Some of this problem stems from continued land surface evapotranspiration following the formation of fog. An altered formulation of evapotranspiration in the presence of fog helps to abate the resulting temperature and precipitation biases. A revised formulation of land surface runoff helps to remedy the problem of dry air in the lower boundary layer, without exacerbating the problem with stratus clouds.

Thursday 22 July PM

**Regional Applications and Scenario Generation**

**MC01/W/21-A4** **1400**

**THE ROLE OF REGIONAL CLIMATE MODELLING FOR THE IPCC THIRD ASSESSMENT REPORT**

Jens H. Christensen (Danish Met. Institute, Lyngbyvej 100, DK-2100 Copenhagen Ø, Denmark)

It is stated by the Intergovernmental Panel on Climate Change (IPCC) that the Third Assessment Report (TAR) - due in 2000/2001 - will be comprehensive and cover the complete range of scientific, technical, economic and social issues associated with the climate system and climate change, will be policy relevant but not policy prescriptive. Compared to the Second Assessment Report (SAR), TAR will emphasize the regional aspects of climate change, place additional emphasis on adaptation, provide a more quantitative treatment of uncertainties and clear exposition of different points of view. It will also describe advances and changes in the understanding since SAR. The major emphasis on regional aspects indicates a substantial change of attitude since the SAR. It reflects the strong development within impact related, economical and social sciences to assess the role of global change on the regional level, where adaptation and mitigation strategies have become relevant to the decision makers. Because of the focus on regional climate in TAR, regional climate modelling will be reviewed in its own chapter in TAR, reflecting the strong scientific investment in this field since the preparation of SAR. Here the role of regional climate modelling as seen from TAR will be reviewed.

**MC01/E/35-A4** **1415**

**A TWO-YEARS (1989-90) REGIONAL CLIMATE SIMULATION OVER EUROPE**

Clemente Gallardo (email: etnemelc@eucmos.sim.ucm.es), Manuel de CASTRO (email: mcastro@eucmax.sim.ucm.es), Juan A. Prego (email: japrego@eucmos.sim.ucm.es) (all at Department of Geophysics and Meteorology, University Complutense of Madrid, Spain) and Miguel A. Gaertner (Department of Applied Physics, Environmental Sciences Faculty, University of Castilla-La Mancha, Toledo, Spain, email: fige03@sis.ucm.es)

A comprehensive atmospheric regional climate model named PROMES, entirely developed at the Department of Geophysics and Meteorology of the Complutense University of Madrid (Spain), has been applied for the period from 1 October 1988 to 28 February 1991, in the framework of the MERCURE European intercomparison project. The model domain covers most of Europe and the Mediterranean basin with a horizontal resolution of 50x50 km<sup>2</sup> (cartesian coordinates). In the vertical 26 terrain-following sigma layers from surface up to 100 hPa level were considered. The model run was driven by ECMWF re-analysis (atmosphere and SST values) updated every 6 hours. Initial soil moisture fields were derived from climatological values. The used model version includes a sophisticated land-surface package (SECHIBA), a Fritsch and Chappell-type convective parameterization and a relaxation lateral boundary scheme. The simulated monthly averages of 2-m temperatures and precipitation are compared with CRU climatological data base in several subdomains defined according to the different climate regimes existing within the considered region. The seasonal cycle of temperature and precipitation is acceptably reproduced as well as the effects of topography. This shows that PROMES model is feasible to be applied to present and future climate studies.

**MC01/E/02-A4** **1430**

**WINTER SEASONAL PREDICTION OF TEMPORAL VARIABILITY OVER NORTH AMERICA - EXPERIMENTS WITH NESTED REGIONAL CLIMATE MODELS**

J. L. KINTER, M. J. Fennessy, E. Altschuler, and J. Shukla (Center for Ocean- Land-Atmosphere Studies, 4041 Powder Mill Road, Suite 302, Calverton, MD 20705 USA)

Several recent studies (Shukla, 1998; Fennessy and Shukla, 1999; Shukla et al. 1999; many others) have demonstrated spectacular success in simulating (hindcasting) and predicting the seasonal mean stationary wave pattern over the northern Pacific Ocean and North America in those winters when a large tropical sea surface temperature (SST) anomaly is present, i.e., El Niño or La Niña conditions. The anomalous stationary wave pattern includes the seasonal mean positions of the anomalous ridges and troughs over North America that are associated with departures from normal of the position and intensity of the jet stream and the location of the extratropical cyclones tracks. As a result, the seasonal mean anomalous surface air temperature and precipitation can be forecast in those winters when El Niño or La Niña conditions prevail. Such forecasts are shown in a companion paper (Fennessy et al. 1999) to be more accurate and potentially useful when made using nested regional climate models rather than global atmospheric general circulation models (AGCMs) only. We have examined the daily variability of temperature and precipitation in several winter cases simulated with the COLA R40 AGCM (C model) and with both an 80-km version of the National Centers for Environmental Prediction, Environmental Modelling Center Eta model (E model) and the MM5 regional model (M model), both for the North American region and both nested in the global COLA AGCM. The geographic distribution of the amplitude and frequency of precipitation events and the associated variations of temperature near the surface are quite well simulated in the E and M models, substantially better than in the C model simulations. Results documenting and quantifying the intraseasonal accuracy of these models will be shown.

**MC01/E/03-A4** **1445**

**ARCTIC WINTER SIMULATIONS WITH A REGIONAL CLIMATE MODEL**

Annette RINKE, Klaus Dethloff, Antje Weisheimer (all at Alfred Wegener Institute for Polar and Marine Research, Telegrafenberg A43, D-14473 Potsdam, Germany, e-mail: arinke@awi-potsdam.de) Jens H. Christensen (Danish Met. Institute, Lyngbyvej 100, DK-2100 Copenhagen Ø, Denmark)

Data analyses show that the circulation of the Arctic atmosphere undergoes large fluctuations about its monthly and annual means. A necessary prerequisite to correctly simulate climatic changes is that models are able to realistically represent this natural variability. The mean Arctic winter climatology and its interannual variation has been examined by regional climate simulations. The employed regional atmospheric climate model is called HIRHAM and includes the physical parameterization package of the GCM ECHAM. The simulations are performed at a horizontal resolution of 50 km and the model is forced at the lateral and lower boundaries by ECMWF analyses. An ensemble of winter simulations (December-February) of the six years 1990-1995) has been investigated in which the ensemble is large enough to represent a broad range of climatic conditions. It is shown that the dynamical aspects of the interannual variability can be adequately captured by the model simulations. To gain more insight into the spatial and temporal structures of the model's variability an empirical orthogonal function (EOF) analysis has been applied to determine the most significant structures in the fluctuations of the monthly mean dynamical fields. EOF 1 of the 500 hPa height field describes a regime with well-pronounced polar vortex and corresponds with the "Arctic Oscillation", whereas EOF 2 and 3 show wave structures. A pronounced interannual variability is noticed in the time series of the amplitudes of the EOFs.

**MC01/W/14-A4** **1155**

**HIGH RESOLUTION SIMULATION OF ARCTIC CRYOSPHERIC ANOMALIES**

A.H. LYNCH, R.I. Cullather, J.A. Maslanik and M.C. Serreze (all at CIRES, CB 216, University of Colorado, Boulder, CO 80309-0216, USA, tel: +1 303 492 5847, fax: +1 303 492 1149, email: manda@cires.colorado.edu)

Recent global climate modelling results highlight the Arctic as a region of particular importance in global climate change. Numerous observational studies have demonstrated the sensitivity of sea ice and snow to changes in regional climate and larger scale modes of atmospheric circulation. The goal of the current work is to identify the mechanisms responsible for recently observed trends and anomalies in the Arctic cryosphere, in an effort to elucidate the most important mechanisms involved, and hence determine the crucial processes missing from GCM simulations of the Arctic climate under conditions of change. A two-fold approach is being used. First, a rigorous testing of simulation skill and model behavior in a regional climate system model of the Arctic has been undertaken using an ensemble approach and highly constrained simulations. Second, analysis of observations and long simulations using a stand-alone sea ice model incorporating elastic-viscous-plastic rheology and multi-category ice thermodynamics have been undertaken to determine the modes of atmospheric variability in which the cryospheric anomalies occur, and whether the anomalies are reproducible in these modes.



**MC01/W/45-A4 1500****REGIONAL CLIMATE MODELLING RESEARCH AT CSIRO**

John L. and Jack J. Katzfey CSIRO Atmospheric Research, Melbourne, Australia

For some years CSIRO has had an active programme for modelling climate change using the Division of Atmospheric Research Limited Area Model (DARLAM) nested within the CSIRO spectral GCM. Recently we have extended our range of simulations to include other domains, to perform longer integrations, and to run at finer resolution. The presentation will describe the implementation of the model and its application to climate modelling over Australia, southeast Asia, New Zealand, South Africa and South America for model resolutions of 44 km to 125 km, as well as for the PIRCS experiments over USA. Particularly long nested simulations of 140-year duration for Australia at 125 km and 60 km resolution have been performed; for these the model is nested within the CSIRO GCM for transient increases of greenhouse gases according to the IS92a scenario. CSIRO has developed a new variable-resolution global GCM, which provides different opportunities for regional climate modelling than the one-way nested approach. The formulation of the new global model will be briefly described, and some results of simulations shown for present-day conditions.

**MC01/W/23-A4 1515****REGIONAL CLIMATE MODEL SENSITIVITY STUDIES FOR TROPICAL SOUTH AMERICA**

Anji SETH (National Center for Atmospheric Research, Boulder, CO, USA, email: seth@ucar.edu)

The prospects for seasonal prediction are good in the tropics, where sea surface temperature influences on regional climate anomalies are direct. Improved understanding of moisture transports, low level jets and other regional circulations which affect seasonal rainfall anomalies require higher resolution of topography, landuse and coastlines than most global models can provide. Results will be presented from seasonal integrations of the NCAR regional climate model (RegCM) over tropical South America. A number of simulations are performed, varying in duration from 1 to 4 months, for the anomalous seasons of 1982/83 and 1986/87. Time evolving atmospheric conditions are taken from NCEP Reanalyses to drive the lateral boundaries of the RegCM domain. Discussion will focus first on the sensitivity of the simulations to the parameterization of convection, and second, on the sensitivity of regional circulations and rainfall on choice of domain.

**Land Surface Processes in Regional Climate****MC01/W/30-A4 1615****EVALUATION OF REGIONAL PREDICTION MODELS USING REMOTELY SENSED DATA**

Ernesto H. Berbery (Department of Meteorology/CICS, University of Maryland, College Park, MD, 20742 USA, email: berbery@atmos.umd.edu) Rachel T. Pinker (Department of Meteorology, University of Maryland, College Park, MD, 20742 USA, email: pinker@atmos.umd.edu) Kenneth E. Mitchell (Environmental Modelling Center/NCEP/NOAA, Camp Springs, MD, USA, email: wd22km@sg121.wwb.noaa.gov)

The surface energy budgets from three operational mesoscale models and from the NCEP/NCAR Reanalysis are compared and evaluated against information derived from satellite observations. The three mesoscale models are: 1) the NCEP Eta model, 2) the Mesoscale Analysis and Prediction System (MAPS) model, and 3) the Global Environmental Multiscale (GEM) model. The objective is to evaluate the reliability of the surface energy budgets within the context and requirements of the GEWEX Continental -scale International Project (GCIP), which are aimed at the development and evaluation of coupled hydrologic/atmospheric models at resolutions appropriate to large scale continental basins. In particular, it is aimed to evaluate the land surface and atmospheric parameterizations from regional numerical weather prediction models and their associated Four Dimensional Data Assimilation Systems. Results will be presented on the biases found in all models in respect to "observed" surface radiative fluxes, and on the nature of energy partitioning between sensible and latent heat fluxes, in terms of the Bowen Ratio. Addressed will be plausible causes of the differences and needs for corrections.

**MC01/W/35-A4 1630****SURFACE CHARACTERISTICS FOR A REGIONAL CLIMATE MODEL BASED ON NEW HIGH-RESOLUTION DATA SETS**

J. H. CHRISTENSEN, O. B. Christensen (both at Danish Meteorological Institute, Lyngbyvej 100, DK-2100 Copenhagen Ø, Denmark, email: jhc@dmi.dk), S. Hagemann, and B. Machenhauer (both at MPI, Bundesstrasse 55, D-20146 Hamburg, Germany, email: hagemann@dkrz.de)

As a part of the MERCURE project, new satellite-based data sets have been used to improve the surface characteristics used by the regional climate model HIRHAM. Based on elevation and land use data sets in 1km resolution from the US Geological Survey, new fields of orography, vegetation ratio, roughness length, albedo, leaf area index and soil moisture capacity have been generated. Previous data sets were of a spatial resolution becoming inadequate for the resolution of present-day regional climate experiments aimed at in the MERCURE project. The algorithms used to construct the new parameter sets and differences to the earlier fields will be described, and the effects on simulations of the present climate will be presented. The latter is based on simulations in integration areas covering Europe with 25 and 50km resolution, respectively. Preliminary results show a better performance in summer in Southern Europe, as an excessive draught problem is diminished. The sensitivity to the particular changed fields will be investigated on the basis of a step-by-step change of these.

**MC01/E/27-A4 1645****USE OF AN ATMOSPHERIC RCM TO ESTIMATE THE CLIMATE RESPONSE TO DEFORESTATION OVER WESTERN MEDITERRANEAN**

Miguel A. Gaertner (Department of Applied Physics, Environmental Sciences Faculty, University of Castilla-La Mancha, Toledo, Spain, email: figeo03@sis.uclm.es), Juan A. PREGO (email: japrego@eucmos.sim.uclm.es), Clemente Gallardo (email: etnemelc@eucmos.sim.uclm.es) and Manuel de Castro (email: mcastro@eucmax.sim.uclm.es) (all at Department of Geophysics and Meteorology, University Complutense of Madrid, Spain)

A deforestation experiment has been performed over Western Mediterranean with PROMES atmospheric regional climate model, completely developed by the modelling group of the Universidad Complutense. SECHIBA land-surface package has been used to parameterize exchanges between soil-vegetation and atmosphere. Simulations have been done for year 1982, with lateral boundary conditions provided by ECMWF reanalysis. An ensemble technique, with partial reinitialization at the end of each cycle has been used, by allowing soil variables to evolve: the RCM has been run throughout seven iterations over 1982, for each

setup of experiment (control and deforestation). This procedure allows to measure the internal variability of RCM and enables us to express conclusions with statistical significance. The deforested area covers basically land zones with Mediterranean climate characteristics. For the present simulations, a 50x50 km uniform mesh has been used, with 25 vertical sigma layers of variable depth (more resolution near the soil). Significant changes in precipitation and evaporation are concentrated in late spring and summer, mainly over regions in the northern half of the domain, with weak Atlantic influence. No significant response is observed in autumn and winter over any region. The results are a good indication of the usefulness of regional climate models in sensitivity studies related to the interaction between mesoscale circulations and land surface processes.

**MC01/E/07-A4 1700****MODELLING OF THE SIBERIAN REGIONAL CLIMATE ON THE BASE OF ECSIB MODEL**

FOMENKO ALEXANDER ( Institute for Computational Mathematics and Mathematical Geophysics of SB RAS, Prospect ac. Lavrentieva, 6, Novosibirsk, 630090, Russia, email: foma@climate.sccc.ru ) Krupchatnikoff Vladimir (Institute for Computational Mathematics and Mathematical Geophysics of SB RAS, Prospect ac. Lavrentieva, 6, Novosibirsk, 630090, Russia, email: vkrup@ommfao1.sccc.ru )

The regional model of atmospheric dynamics is presented. The model is a component of global climatic model ECSib, has the increased spatial resolution and is designed for the reproduction of the climatic atmospheric characteristics on spatial scales not described by global model. In model the more detailed account of processes of interaction with the land surface is carried out. The surface and active layers of ground take into account presence of vegetative cover, layer of snow on the surface, processes of heat and moisture transfer in the soil layer, processes of melting of snow on the surface, receipt of moisture into the ground at the expense of large-scale and convective precipitations, interception of precipitations by vegetative cover, effects of moisture filtration. The some results of numerical modelling of Siberia climate are given. This work was supported by the INTAS 96-2074.

**MC01/L/18-A4 1715****THE PREDICTION OF THE REGIONAL NCEP ETA MODEL WITH DIFFERENT LAND SURFACE SCHEMES**

Yongkang XUE, Y. Ji (both at Department of Geography, University of Maryland, College Park, MD 20742,USA Tel: 301-405-4050; fax: 301-314-9299, email: yxue@geog.umd.edu); E. Roger, T. Black, Z. Janjic and K. Mitchell (all at Development Division, NCEP, NOAA, Camp Springs, MD, USA)

Previous studies show that a coupled Eta/SSiB model is able to realistically simulate different climate scenarios. In these experiments, the model is only integrated for 48 hours. The forecast for June 1988 and July 1993 are averaged, respectively, to obtain the regional climate. However, because the model is initialized every 24 hours in these studies, the prediction for some hydrological variables, such as runoff, is mainly determined by the initial conditions. To understand the regional climate predictability, we have developed the Eta/SiB model for long term prediction studies. Long term numerical integrations are carried out for June and July 1998, June and July 1993, and June 1988 to investigate the time scale of the predictability for the Eta model. Both the 1993 and 1998 spring season have strong ENSO events. The summer of 1988 is extremely dry. The Eta/SSiB has reasonably good simulations for 1998 and 1988. The results from the Eta/SSiB are compared with the current Eta model simulations (with different land surface scheme). The preliminary results show that adequate simulations of large scale circulation, i.e, the low level jet and 200mb wind fields, are the key in successful North American regional climate prediction. The results also show that land surface parameterizations have profound impact on these simulations.

Friday 23 July AM

Presiding Chairs: Ray Arritt and Filippo Giorgi

**REGIONAL MODELLING AND INTERCOMPARISONS (Cont.)****Implementing Regional Climate Models: Computational Methods and Parameterisations****MC01/W/06-A5 0830****REGIONAL CLIMATE SIMULATION WITH A VARIABLE RESOLUTION STRETCHED GRID GCM: THE 1988 U.S. SUMMER DROUGHT**

Michael FOX-RABINOVITZ and Uri Stein(both at Department of Meteorology/ESSIC,University of Maryland,College Park,MD 20742,USA, Email: foxrab@atmos.umd.edu, uristin@atmos.umd.edu) Lawrence Takacs and Ravi Govindaraju(both at General Sciences Corporation,6100 Chevy Chase Drive,Laurel,MD 20707,USA, Email: ltakacs@dao.gsfc.nasa.gov, ravi@dao.gsfc.nasa.gov) Max Suarez(code 913,NASA/Goddard Space Flight Center,Greenbelt, MD 20771,USA, Email: suarez@max.gsfc.nasa.gov)

The variable resolution stretched grid(SG) GCM based on the Goddard Earth Observing System (GEOS) GCM, has been developed and tested in a regional climate simulation mode. The GEOS SG-GCM is used for simulation of the 1988 summer drought over the U.S. Midwest. Within the stretched grid, the region of interest with a uniform ~60 km resolution is a rectangle over the U.S. Outside the region, the grid intervals increase or stretch with a constant stretching factor (as a geometric progression). The results of two-month simulation for the anomalous climate event of the U.S. drought of 1988, are validated against data analysis fields and diagnostics. The event has been chosen by the Project to Inter-compare Regional Climate Simulations(PIRCS). The efficient regional down-scaling as well as the positive impact of fine regional resolution, are obtained. More specifically, the precipitation, 500 hPa, and low-level jet patterns and characteristics are well represented in the simulation. The SG-concept appeared to be a promising candidate for regional and subregional climate studies and applications.

**MC01/E/15-A5 0845****DYNAMICS, STATISTICS AND PREDICTABILITY OF SIMPLE LIMITED-AREA FORECASTING MODELS**

Frederic CHOME (Institut Royal Meteorologique de Belgique, Section de Climatologie Dynamique, Av. Circulaire 3, B-1180 Bruxelles, Belgium, email: fchome@oma.be)

A canonical model describing the instability of plane wave solutions toward inhomogeneous long wave fluctuations emulating mesoscale atmospheric variability is used to analyze different strategies for building high-resolution models providing a more detailed description of a limited area of interest. The cases considered are : a regional fine grid model nested at regular time steps into a globally coarser one which evolves in time independently, and an autonomous continuous model with a variable mesh size. Comparative studies between a reference fine grid "perfect" model and the ones provided, successively, by a globally coarse



and the fine scale, limited-area ones are carried out. The statistical properties of the relevant fields are first analyzed, and an optimal size for which the deviations between the "perfect" model and the limited-area ones are minimized is identified. Predictability experiments, performed on statistical ensembles of close lying trajectories whose mean distance represents the uncertainty in the initial state of the system, reveals that the continuous variable-mesh model performs better than the nested limited-area one.

**MC01/W/49-A5****0900****VERIFICATION AND EVALUATION OF STORM TRACKS IN REGIONAL CLIMATE SIMULATIONS OVER AUSTRALIA**

J. Katzfey and J. L. McGregor CSIRO Atmospheric Research, Aspendale, Vic. Australia

Since much of the weather in midlatitudes is associated with the passage of cyclones and anticyclones, an accurate simulation of the climate of a region should not only capture the mean fields correctly, but also the daily variability associated with these weather systems. There are numerous measures which can quantify the location and intensity of weather systems. Two common techniques are either to track lows and highs, or to compute the standard deviation of the geopotential height or winds. In this study of regional climate model (RCM) simulations over Australia, an alternative technique is adopted: the jetstreams are verified using the mean kinetic energy, while the storm tracks are verified against the eddy kinetic energy. RCM simulations nested within ECMWF analyses are evaluated by this method, in addition to RCM simulations nested within the CSIRO GCM for present-day conditions. It is found that the RCM captures the location of the storm track very well, but underpredicts the intensity slightly at upper levels. Changes to the storm tracks under enhanced greenhouse conditions were then examined for simulations having transiently increasing CO<sub>2</sub> concentrations. Under these conditions, the upper level storm track intensifies and shifts equatorward. At low levels, the storm track tends to weaken, except in locations where the eddy growth rate increases, resulting in seasonally different changes.

**MC01/E/25-A5****0915****COMPARISON OF TWO MOIST CONVECTION SCHEMES IN A REGIONAL CLIMATE MODEL**

Daniel LUETHI (Swiss Federal Institute of Technology, LAPETH, Hoenggerberg HPP, CH-8093 Zurich, Switzerland, email: daniel.luethi@atmos.unn.ethz.ch) Christoph Schaer (Swiss Federal Institute of Technology, GI-ETH, Winterthurerstr. 190, CH- 8057 Zurich, Switzerland)

The representation of mid-latitude summertime precipitation is still one of the most challenging problems in regional climate modelling. This is presumably due to the increased role of moist convection and land surface processes and their interaction during this season. Therefore the parameterisation schemes for these processes contribute essentially to the performance of the model. The present study aims at investigating the influence of the change in the formulation of moist convection to summertime precipitation. The regional climate model used for this investigation is an adapted version of the operational mesoscale weather forecast model EM of the German weather service. The model is run at a resolution of 56 km and the model domain covers the simulation domain defined for the Project to Intercompare Regional Climate Simulations (PIRCS), i.e. essentially the continental US. The two 2-month PIRCS- periods (drought of 1988 and flooding of 1993) are simulated with this model setup using ECMWF-reanalysis data as initial and lateral boundary conditions. The convective schemes used in the model are the operational Tiedtke-scheme and the Emanuel-scheme. The simulations with both schemes are able to represent rather well the distribution of precipitation during the dry period and the overall increase of precipitation during the wet period. However, the amplitude of the precipitation maximum is underestimated with the Emanuel-scheme and its location is simulated too far north (Tiedtke-scheme) or northeast (Emanuel-scheme) by about 500 km. Further the sensitivity of the location and amplitude of the precipitation maxima to some tuning parameters of the Emanuel-scheme is investigated. For the interpretation of the results a detailed analysis of the water cycle as represented by the model is undertaken.

**MC01/E/17-A5****0930****IMPLEMENTATION OF BOUNDARY CONDITIONS IN NESTED REGIONAL CLIMATE MODELS**

Uri Stein and Michael FOX-RABINOVITZ (both at Department of Meteorology/ESSIC, University of Maryland, College Park, MD 20742 USA, Email: uristin@atmos.umd.edu, foxrab@atmos.umd.edu), Raymond W. Arritt (Department of Agronomy, Iowa State University, Ames, Iowa 50011 USA, email: rwarritt@iastate.edu)

Methodology for nesting regional climate models within larger-scale models has been explored using combined global and regional versions of the Goddard Earth Observing System (GEOS) GCM. This procedure allows controlled "twin" and "cousin" experiments to be performed in which the regional model numerics and physics are identical to those in the global model. These experiments have focused on the implementation of the lateral boundary buffer zone where information is transferred from the global model to the regional model. Particular attention is devoted to the effect of discontinuous temporal and spatial resolution. Among the results are that even when the regional model boundaries are updated every six hours the diurnal variation of the average domain-scale surface pressure in the regional model is greatly damped.

**MC01/W/34-A5****0945****THE STUDY OF CLIMATE DOWNSCALING WITH INTERACTIVE GENERAL CIRCULATION AND NONHYDROSTATIC REGIONAL MODELS**

Georgiy STENCHIKOV and Roni Avissar (both at Department of Environmental Sciences, Rutgers University, 14 College Farm Rd., New Brunswick, NJ 08901, email: gera@envsci.rutgers.edu) To study a climate downscaling we use the Colorado State University Regional Atmospheric Modelling System (RAMS) and the Goddard Institute for Space Studies General Circulation Model (GCM).

We conducted long-term nonhydrostatic calculations with RAMS in a mesoscale domain nested into the GCM grid. The climate and the climate response to CO<sub>2</sub> doubling calculated with the RAMS are compared with GCM output. The sensitivity of the calculated regional climate to resolution and size of the nested-grid domain are studied. The parameterized clouds and cloud radiative effects in GCM are compared with the RAMS cloud resolving calculations. The effects on the diurnal cycle of radiative heating, surface air temperature, water vapor mixing ratio, sensible and latent heat fluxes, convective activity, and precipitation are discussed.

**MC01/E/38-A5****1000****NESTING STRATEGIES FOR HIGH-RESOLUTION REGIONAL CLIMATE SIMULATIONS: SENSITIVITY EXPERIMENTS FOR THE ALPINE REGION**

Jan KLEINN, Christoph Frei, Christoph SchE4r (Institute of Geography, Swiss Federal Institute of Technology (ETH), Winterthurerstr. 190, 8057 Zurich, Switzerland) and Daniel LFCthi (Institute of Atmospheric Science, Swiss Federal Institute of Technology (ETH), ETH Hoenggerberg, 8093 Zurich, Switzerland)

Regional climate models constitute an attractive tool for downscaling the output from General Circulation Models and for conducting sensitivity and process studies. Our study examines the effect of several elements of the nesting strategy upon the results of high-resolution regional climate simulations over the area of the European Alps. Consideration is given to the effect of the boundary updating frequency, the benefit of two-fold nesting versus simple nesting, as well as the resolution of the driving fields. The effects are examined using month-long winter-time simulations driven by observed lateral boundary conditions from the ECMWF reanalysis. The simulated precipitation fields are evaluated against a meso-scale analysis derived from a unique high-resolution rain-gauge data set. The utilized regional climate model is a version of the operational forecast model of the German Weather Service and is used in resolutions of up to 14 km. The experiments reveal a strong sensitivity of the modeled precipitation upon the resolution of the lateral boundary fields, even when the model set-up is otherwise identical. It is demonstrated that the use of double nesting techniques is able to cope with the lack of (spatial and temporal) resolution in the lateral boundary fields. Furthermore, validation against the observational data base serves to demonstrate that increased resolution can substantially improve the mesoscale structure of the resulting precipitation fields.

Presiding Chair: Scott Denning

**ATMOSPHERIC TRACER TRANSPORT MODELLING AND INTERCOMPARISON****MC01/L/19-A5****1045****THE ATMOSPHERIC TRACER TRANSPORT MODEL INTERCOMPARISON PROJECT (TRANSCOM)**

Denning, S

The Atmospheric Tracer Transport Model Intercomparison Project (TransCom) was begun in 1993 to quantify and diagnose the uncertainty in inversion calculations of the global carbon budget. The specific objectives of the TransCom project are (1) quantify the degree of uncertainty in current carbon budget estimates that results from uncertainty in model transport; (2) identify the specific sources of uncertainties in the models; and (3) identify key areas to focus future transport model development and improvements in the global observing system that will reduce the uncertainty in carbon budget inversion calculations. More than a dozen modelling groups from around the world have participated in TransCom, representing dynamical cores used in most atmospheric chemistry codes as well. Initial experiments focused on the annual mean meridional structure of CO<sub>2</sub> arising from industrial combustion and the seasonal cycle produced by terrestrial vegetation. These experiments showed a surprising degree of differences among the models, especially aloft, and highlighted the effect of seasonal interactions between transport and emissions on annual mean gradients. A second experiment, simulated transport of sulfur hexafluoride, allowed "calibration" of the models against data and more detailed diagnosis of transport mechanisms. These results highlighted the importance of subgrid-scale vertical transport for large-scale horizontal spatial structure in the annual mean. A third phase of the study will quantify the sensitivity of the carbon budget to differences in transport among models, inversion methodology, and choice of observational data.

**MC01/L/20-A5**

Invited

**1115****INVERSION METHODOLOGY FOR TRANSCOM 3**

Peter RAYNER (CRC for Southern Hemisphere Meteorology Monash University Clayton, Victoria 3168 Australia email: pjr@vortex.shm.monash.edu.au), and Rachel Law (As P. Rayner, email: rml@vortex.shm.monash.edu.au)

This talk presents the underlying inversion methodology for the TransCom3 project. We briefly introduce the technique of synthesis inversion and demonstrate with an example the calculation of best estimates for CO<sub>2</sub> sources and their accompanying uncertainties. We show that the methodology is general enough to consider a range of inversion types such as prior constraints vs. unconstrained inversions or many unknowns vs. few. Finally, we show how the uncertainty in source estimates contributed by model-model differences can be compared with that due to uncertain and sparse concentration data.

**MC01/W/43-A5****1130****INTER-ANNUAL VARIATIONS OF CO<sub>2</sub> NET SURFACE FLUXES AS INFERRED BY INVERSE MODELLING OF ATMOSPHERIC CO<sub>2</sub> CONCENTRATIONS**

Philippe. BOUSQUET, P. Peylin and P. Ciais (Laboratoire des Sciences du Climat et de l'Environnement, Unité mixte de recherche CNRS-CEA, Orme des Merisiers, 91191 Gif sur Yvette cedex. Emails: bousquet@lscce.saclay.cea.fr, peylin@lscce.saclay.cea.fr, ciais@lscce.saclay.cea.fr)

A primary goal of developing the CO<sub>2</sub> atmospheric measurement network is to characterise better the sources and sinks of atmospheric CO<sub>2</sub>. Atmospheric transport models can be used to evaluate atmospheric measurements in terms of surface fluxes using inverse methodology. We present a Bayesian three dimensional inversion of atmospheric CO<sub>2</sub> measurements in order to infer monthly sources and sinks of CO<sub>2</sub> at a continental scale (continents and ocean basins) for the 1985-1995 decade. Solving this inverse problem requires 1) a data space representing monthly CO<sub>2</sub> measurements, here at 77 sites (surface, ships, planes), 2) a flux space describing a priori fluxes between carbon reservoirs, and 3) a 3-d transport model linking the flux space to the data space. The three components of the inversion are briefly described in this talk. Then we present and discuss the inter-annual net fluxes inferred by our inverse methodology for the 1985-1995 period. Finally, we describe a few tests showing the sensitivity of our standard solution to some parameters of the inversion: atmospheric network, transport model and a priori flux scenario. A special focus is put on the partition of the controversial CO<sub>2</sub> sink over the mid and high latitudes of the Northern hemisphere in the early 90's.

MC01/W/07-A5

1145

**A TIME DEPENDENT INVERSE CALCULATION OF THE CO2 BUDGET : WHAT CAN WE LEARN FROM THE SHORT TERM VARIABILITY ?**

P. Ciais, P. Peylin, P. Bousquet and M. Ramonet.

We will present a time dependent inversion of the atmospheric CO<sub>2</sub> budget. The inverse technique is of Bayesian type and uses monthly optimisation of the sources against monthly atmospheric measurements. Usually, inverse calculations are constrained by some estimate of the mean observed CO<sub>2</sub> concentration at many sites around the world. Short term variability is considered to be noise, and treated as such (gaussian errors on the data). However, at remote locations, far away from the direct continental and marine sources influence, the atmospheric transport on synoptic time-scales creates CO<sub>2</sub> variability whose monthly variance should relate to the sources strengths. We propose to make use of the information contained in the observed short term variability of CO<sub>2</sub> in the atmosphere, as an additional constraint on the surface fluxes. Mostly continuous records of atmospheric CO<sub>2</sub> can be used safely to serve this purpose. The presentation of our method and some illustration of its results will be given.

MC01/L/21-A5

1200

**ATMOSPHERIC CO2 INVERSION INTERCOMPARISON PROJECT (TRANSCOM 3)**

Gurney

Most of our understanding of the global carbon budget is derived from atmospheric observations of CO<sub>2</sub>. Hemispheric or regional fluxes may be calculated from atmospheric concentration measurements by a numerical procedure known as "inversion," which requires that atmospheric transport be accounted for using a chemical tracer model (CTM). Two such inversion calculations were presented at a recent international meeting. Songmiao Fan and colleagues at Princeton University found that most of the terrestrial uptake of atmospheric CO<sub>2</sub> is occurring in North America, and that this "sink" approximately balances fossil fuel emissions in the US. Working with the same atmospheric data but using a different CTM and inversion method, Peter Rayner and colleagues at the Australian CSIRO found that the sink is distributed much more widely, with North America accounting for only a small fraction. The Atmospheric Tracer Transport Model Intercomparison Project (TransCom) is a part of the IGBP Global Analysis, Interpretation, and Modelling (GAIM) initiative, whose objectives are (1) to quantify the degree of uncertainty in carbon budget inverse calculations that arises from CTM transport; (2) analyze the mechanisms by which the models differ; and (3) recommend and prioritize improvements to the observing and modelling systems to produce more robust carbon budget inversions in the future. We have previously analyzed the annual mean and seasonal structure of atmospheric CO<sub>2</sub> as simulated by leading CTMs (TransCom 1), and calibrated the transport properties of the models against a tracer of known distribution (SF<sub>6</sub>, TransCom 2). We now propose a third phase of the TransCom activity (TransCom 3), in which participants will perform a full carbon budget inversion using their models. To maximize participation among CTM groups around the world, we have structured the experimental protocol in such a way as to simplify the methods for those groups with limited resources, but allow for more detailed work by those who so choose. This experiment will compare inversion results across more than a dozen CTMs and across multiple inversion methods. The diagnostic output will help us understand why the models differ, how they can be improved, and how the CO<sub>2</sub> observing system can be optimized for more robust inversions.

MC01/W/39-A5

1215

**BIAS IN INVERSIONS OF ATMOSPHERIC TRANSPORT DUE TO COARSE RESOLUTION OF SOURCES**

Thomas Kaminski, Peter Rayner, and Martin Heimann

Models of atmospheric transport can be used to interpret spatio-temporal differences in the observed concentrations of a passive tracer such as CO<sub>2</sub> in terms of its sources and sinks. Inversion of the atmospheric transport is the systematic search for both a source/sink field that yields an optimal match between modeled and observed concentrations and, equally importantly, the uncertainties in this inferred source field. Since current observational networks are sparse, the inverse problem is underdetermined, i.e. there are many source configurations yielding the same modeled concentration at the observational sites. Hence, additional information about the source configurations is included in inversion studies by a combination of two strategies: - A few fixed source patterns are prescribed, whose unknown magnitudes are to be optimized, and - we require the optimal source field to be close to a prior estimate that reflects our knowledge of sources. The fewer patterns (and hence fewer unknowns) we use, the more the structure of these patterns is imposed on the optimal source field. Conventional approaches to the inverse problem necessitate one transport model per source pattern, i.e. the number of patterns is limited by the complexity of the transport model. With an adjoint approach, the computational cost is independent of the number of source patterns. Restricting the structure of the optimal source field by prescribing a few fixed patterns not only underestimates the uncertainties in the inferred source field but also causes a bias. The extent of this bias depends on the location of the stations, the atmospheric transport model, and the number and shape of the patterns. To explore this bias, the solution of the inverse problem has to be known. Hence, we generated "artificial observations" by running the atmospheric transport model TM2 for a prescribed CO<sub>2</sub> source field on the 8 by 10 degree model grid. Then we defined patterns by forming groups of 16 grid cells and performed an inversion on that coarser grid. Although this inversion was stabilized by inclusion of the (grouped) prescribed source field, the difference between the (grouped) prescribed source field and the optimal source field resulting from the inversion is large: In parts of Asia and South America this difference is about 100% of the prescribed source field itself. This difference is solely a result of the bias due to grouping gridpoints.

MC01/W/50-A5

1230

**TRACE GAS TRANSPORT USING THE CONFORMAL-CUBIC MODEL**

John L. McGregor and Eva A. Kowalczyk CSIRO Atmospheric Research, Melbourne, Australia

Transport of trace gases has been incorporated into the new CSIRO conformal-cubic model. This is a global grid-point primitive equations model with semi-Lagrangian numerics. The model has provision for stretching the grid to give high resolution over any selected region. The talk will show simulations for transport of CO<sub>2</sub> and radon, for both stretched and non-stretched grids. For these simulations the stretched grid has a resolution of about 75 km over Australia. Comparisons will be presented for simulations from the Division of Atmospheric Research Limited Area Model (DARLAM) run at a similar resolution, and for the concentrations of radon and CO<sub>2</sub> observed at Cape Grim.

**TERRESTRIAL ECOSYSTEM CARBON VEGETATION DYNAMICS: PIK/NPP AND VEMAP2 MODEL INTERCOMPARISONS**

Introduction

1400

T. Kittel and K. Hibbard

MC01/E/20-A5

Invited

1405

**HISTORICAL AND FUTURE SCENARIO CLIMATE DATASETS FOR THE CONTERMINOUS UNITED STATES AND ALASKA: MODEL INPUT DATA FOR VEMAP PHASE 2 T**

G.F. KITTEL, N.A. Rosenbloom, H.H. Fisher, D.S. Schimel (National Center for Atmospheric Research, Boulder, CO 80307, USA; lead author email: kittel@ucar.edu), J.A. Royle (USDI Fish and Wildlife Service, Laurel, MD 20708, USA), C. Daly (Oregon State University, Corvallis, OR 97331, USA), P.E. Thornton (Univ. of Montana, Missoula, MT 59812, USA), and VEMAP2 Participants.

The objective of Vegetation/Ecosystem Modelling and Analysis Project (VEMAP) Phase 2 is to evaluate time-dependent responses of 8 biogeochemical and dynamic global vegetation models to an array of historical and projected transient forcings, including those of climate and atmospheric CO<sub>2</sub> (see presentations by Thornton et al. and Bachelet et al.). Crucial to this goal was the development of a common climate database that provided (1) a "level playing field" for intercomparison of models and (2) a faithful representation of the domain's bioclimate permitting the evaluation of model historical- period simulations against observed ecological data. The result is a 0.5-degree latitude/longitude gridded historical climate input dataset for the conterminous U.S. (for 1895-1993) and Alaska (1922-1996) that meets the input requirements for the models. Variables included are monthly and daily

MC01/W/04-A5

Invited

1425

**PRELIMINARY RESULTS FROM VEGETATION DYNAMIC MODELS IN VEMAP PHASE 2: VEGETATION DISTRIBUTION AND ASSOCIATED C POOLS FROM 1895 TO 2100**

D. BACHELET (Dept of BioResource Engineering, Oregon State University, Corvallis, OR 97330, USA. Email: bachelet@fsl.orst.edu); J.M. Lenihan (Dept. of Botany, Oregon State University, Corvallis, OR 97331, USA). R.P. Neilson (PNW USFS, Corvallis, OR 97331, USA); R. Draprek (Dept. of Forest Science, Oregon State University, Corvallis, OR 97331, USA); and VEMAP2 participants

Predictions of potential vegetation distribution, natural fire frequency, carbon pools and fluxes are presented for DGVMs (Dynamic Global Vegetation Models) involved in the second phase of Vegetation/Ecosystem Modelling and Analysis Project (VEMAP). Results are preliminary since they represent a first attempt to link vegetation dynamics to biogeochemical cycling at a half-degree resolution for the coterminous USA. The models were run with historical (1895-1993) and predicted future climate (1994-2100), as provided by the National Center for Atmospheric Research (Boulder, CO, USA). The models were run with a detrended version of the historical meteorology files, at a constant CO<sub>2</sub> concentration, until C fluxes equilibrated (d(NEP)/dt close to 0). Models were then run with historical climate and an increasing CO<sub>2</sub> concentration from 295ppm in 1895 to 358ppm in 1993. From 1994, models were run either with a CO<sub>2</sub> concentration held constant at 359ppm or increasing to 1026ppm by year 2100. Results are presented with and without masking out cultivated areas in the coterminous USA. Crop growth was not simulated and a fixed fraction of each simulated cell was allocated to agriculture for the entire run. Results only concern the potential natural vegetation fraction of those cells. Results will focus more specifically on one of the DGVM, MC (Corvallis, USA), which was run with and without N limitation. Under the Hadley Climate Center future scenario, MC predicts a large expansion of forests into the Great Plains and into the dry interior west by the end of the 21st century. We will discuss competition between lifeforms as it relates to water and N limitation and affects vegetation dynamics. We will also address the issue of the representation of the CO<sub>2</sub> effect in each model and how it affects model response to climate change.

MC01/W/09-A5

Invited

1445

**PREDICTED NPP, NEE, AND CARBON STOCKS FOR HISTORIC (1895-1994) AND POTENTIAL FUTURE CLIMATE SCENARIOS OVER THE CONTIGUOUS UNITED STATES: AN INTERCOMPARISON OF TERRESTRIAL BIOGEOCHEMISTRY MODEL RESULTS FROM VEMAP PHASE II.**

Peter E. THORNTON, School of Forestry, University of Montana, Missoula, Montana 59812 USA. David S. Schimel, National Center for Atmospheric Research, P.O. Box 3000, Boulder, Colorado 80307-3000 USA, and Natural Resources Ecology Laboratory, Colorado State University, Fort Collins, Colorado 80523 USA, and VEMAP2 Participants.

Predictions of net primary production (NPP), net ecosystem exchange of carbon (NEE), and carbon stocks (vegetation and soil components treated separately) were carried out using three very distinct and well-established models of terrestrial biogeochemical processes (CENTURY, TEM, and BIOME-BGC), all of which used identical inputs for meteorological driving variables and other spatial data layers (described in companion presentation by Kittel). Simulations were performed over both an historical period for which there are observations of the meteorological driving variables (1895-1994), and a period of future climate conditions (1994-2100) derived from the results of a group of general circulation models (details covered by Kittel). All models were run to steady-state using a de-trended version of the historical meteorology files, at a constant CO<sub>2</sub> concentration. From this as a starting point, various scenarios were explored, including rising CO<sub>2</sub> with no trend in climate, observed trend in climate with constant CO<sub>2</sub>, and observed climate trend with rising CO<sub>2</sub>, in an effort to deconvolve the model responses to these co-occurring influences. Similar experiments were carried out over the period of predicted future climate. An additional set of experiments was performed to examine potential regional source-sink strengths under conditions of reforestation following agricultural land-clearance. These experiments involved the simulated removal of woody material at the steady-state and the monitoring of source-sink relationships as a new steady-state was approached. In addition to presenting a summary of the VEMAP Phase II results from these experiments, I will also discuss some implications of the steady-state experimental protocol and the sensitivity of model results to shared input data layers.

MC01/L/22-A5

Invited

1505

**RESULTS FROM THE POTSDAM 1995 MODEL INTERCOMPARISON OF TERRESTRIAL NET PRIMARY PRODUCTIVITY (NPP)**

Kathy A. HIBBARD, University of New Hampshire:IGBP/GAIM, Durham, NH 03824 USA; W. Cramer, Potsdam Institute for Climate Impact Research (PIK), Potsdam, Germany and "Potsdam '95" participants



Seventeen models of terrestrial biogeochemistry were compared with respect to total, regional, annual and seasonal fluxes of net primary productivity (NPP). The models differed widely in complexity and purpose, but could be grouped in three major categories: satellite-based models that use data from the NOAA/AVHRR sensor as their major input stream, models for seasonal fluxes that use a prescribed vegetation structure, and models that simulate vegetation structure and fluxes. Simulated annual NPP ranged from ca. 40-80 Pg C yr<sup>-1</sup>, however this range decreased considerably when two obvious outliers (which produced extreme results due to calibration problems connected with the comparison, were removed). The broad global pattern of NPP and the relationship of annual NPP to the major climatic variables coincided in many regions of the globe. Systematic biases due to the fundamental modelling strategy could not be found, but the inclusion of nutrient constraints seemed to produce lower values of annual NPP. The regional and global sensitivity of simulated water balance fluxes from diverse modelling strategies were clearly illustrated. Testing modelled sensitivity to the light environment was accomplished by decomposing NPP from those models that did not utilize remote sensing inputs into absorbed photosynthetically active radiation (APAR) and light use efficiency (LUE). A negative relationship between total APAR and LUE was observed when derived variables were compared to those from remotely sensed driven models, suggesting that the models may be unconsciously calibrated to achieve 'commonly accepted values' of NPP, while doing so with widely differing spatial and seasonal patterns. An analysis of the simulated net ecosystem productivity (NEP), using a three-dimensional atmospheric transport model and observed seasonal CO<sub>2</sub> observations from the flask sampling network suggested that uncertainties were larger in water limited systems of the southern hemisphere than elsewhere.

MC01/E/22-A5

1525

#### MODELLING THE EXCHANGES OF CO<sub>2</sub> BETWEEN LAND SURFACE AND ATMOSPHERE USING COUPLED VEGETATION - GENERAL CIRCULATION MODEL

Vladimir KRUPCHATNIKOFF (Institute Computational Mathematics and Mathematical Geophysics of SB RAS, Prospect ac. Lavrentieva,6, Novosibirsk, 630090, Russia, email: vkrup@ommaf1.sccc.ru ) Galin Vener and Lykossov Vassily (Institute for Numerical Mathematics of RAS, Gubkina Str., 8, Moscow, GSP-1, 117951, Russia, email: galin@inm.ras.ru, email: lykossov@inm.ras.ru)

Land surface processes have a strong impact on atmosphere climate phenomena. They determine surface sensible and latent heat fluxes, radiation budget and biochemical fluxes and therefore influence atmosphere and land parameters. It is therefore important to simulate surface processes in climate model as realistically as possible. Vegetation is important for hydrology of the atmosphere because it determines the rate CO<sub>2</sub> during photosynthesis and respiration and because of its effect on the latent heat flux. The most detailed parameterizations of vegetation are often found in the land surface models used with atmospheric models. It may be summarized as follows: effect of leaf area on the absorption of solar radiation at the surface; sensible and latent heat flux; biochemical fluxes; and the soil heat fluxes, which are important due to the effects of soil temperature on biochemical fluxes; soil hydrology. In this report I address the case of interaction between biosphere (vegetation patterns) and atmosphere. Required surface data for each grid cell derived from Olson et al.'s (1983), soil colors were taken from Dickinson et al. (1993), sand silt and clay data were derived from Webb et al.'s (1993), inland water data were derived from Cogly (1991). This dataset were used to carry out experiment, where the model was running in coupled mode. Five years present-day climate simulation have been performed. The current state of the atmosphere was simulated by Institute for Numerical Mathematics of RAS GCM, which is forced by the climatology of the annual cycle SST. In this report global patterns of photosynthesis, respiration and net fluxes CO<sub>2</sub> are presented.

Presiding Chair: James Orr

#### OCEAN CARBON CYCLE MODELLING INTERCOMPARISONS

MC01/W/56-A5

1600

#### THE OCEAN CARBON-CYCLE MODEL INTERCOMPARISON PROJECT (OCMIP): AN OVERVIEW

JAMES C. ORR (LSCE/CEA Saclay (IPSL), Bat. 709 L'Orme, F-91191 Gif-sur-Yvette, France, email: orr@cea.fr)

OCMIP is a coordinated model validation and intercomparison effort for global-scale, three-dimensional, ocean carbon-cycle models. Such models describe the transport and redistribution of carbon in the ocean by combining fundamental descriptions of ocean circulation and biogeochemistry. The long-term objectives of OCMIP are to improve the predictive capacity and accelerate development of these models. OCMIP began with four models in 1995 as a project of the Global, Analysis, Interpretation and Modelling Task Force (GAIM) of the International Geosphere-Biosphere Programme (IGBP). Studies within OCMIP have focused on (1) the distribution of oceanic carbon as well as (2) validation of model-predicted circulation (with C-14). The latter is a primary control of the former. For ocean carbon, emphasis has been on comparing and evaluating the state of the preindustrial distribution and how that has and will change as atmospheric CO<sub>2</sub> continues to increase. Models roughly agree concerning global uptake of anthropogenic CO<sub>2</sub> (on average 1.85 +/- 0.25 Pg C/year during the 1980's). Yet in the Southern Ocean, where uptake is largest, regional uptake differs by nearly a factor of two between models. Comparison of model and data-based estimates of anthropogenic CO<sub>2</sub> in the ocean suggests that most of the models overpredict storage in the Southern Ocean. These and other large differences between models have motivated a second phase of this project (OCMIP-2) during 1998-2000. Now being compared are 13 models from Europe, the U.S., Australia, and Japan. The focus remains on CO<sub>2</sub>, but in addition OCMIP-2 emphasizes new circulation tracers (e.g., CFC-11 and CFC-12), new biogeochemical tracers (e.g., oxygen), a common biogeochemical model, and improved ties to data-synthesis specialists from JGOFS and WOCE.

MC01/W/58-A5

Invited

1620

#### THE OCEAN'S ROLE IN INTERHEMISPHERIC CARBON TRANSPORT

Olivier AUMONT, James C. Orr, Patrick Monfray (LSCE/CEA Saclay (IPSL), Bat. 709 L'Orme, F-91191 Gif-sur-Yvette, France, email: aumont@lscce.saclay.cea.fr) Jorge L. Sarmiento and Richard Mumane (both at AOS Program, Princeton University, Princeton NJ 08544) Ernst Maier-Reimer (Max Planck Institute fuer Meteorologie, Hamburg, Germany), Wolfgang Ludwig (CFREM, Universite de Perpignan, F-66860 Perpignan, France), and Jean-Luc Probst (EOST, CGS, F-67084 Strasbourg, France)

Both atmospheric and oceanic observations have been used to imply that the preindustrial ocean transported significant carbon (up to 1 Pg C/yr) from the northern to the southern hemisphere. For further insight, we compared results from preindustrial carbon simulations performed with three different ocean models (from Princeton, MPI, and IPSL), who participated in the first phase of the Ocean Carbon-Cycle Model Intercomparison Project (OCMIP). Although regional patterns of the air-sea fluxes of CO<sub>2</sub> predicted by the three models differ significantly, predictions of interhemispheric transport are similar. Modeled global interhemispheric transport

of carbon during preindustrial time was near zero (<0.1 Pg C/year from north to south). Modeled southward transport in the Atlantic is compensated by northward transport in the Indian and Pacific Oceans. Thus our model estimates of interhemispheric transport of oceanic carbon disagree with larger estimates from previous observational studies. However, we further one mechanism by which to resolve this discrepancy, i.e., the "river effect". Rivers transport atmospheric carbon (from continental erosion and terrestrial photosynthesis) to the ocean, mostly in the northern hemisphere. Riverine carbon is subsequently transported within the ocean. We coupled the IPSL ocean carbon-cycle model to riverine carbon fluxes from the Global Erosion Model (GEM). We found that the river effect substantially alters interhemispheric carbon transport. Total southward interhemispheric transport is increased to 0.27--0.43 Pg C/yr, depending on the presumed lifetime of the riverine organic matter.

MC01/L/23-A5

1640

#### EVALUATION OF MODEL AND MEASUREMENT-BASED ANTHROPOGENIC CARBON TRACER DISTRIBUTIONS

C. L. Sabine, R. M. Key (both at Department of Geosciences, Princeton University, Princeton, New Jersey, 08544, USA, email: sabine@geo.princeton.edu, key@geo.princeton.edu) and J. Orr (Laboratoire des Sciences du Climat et de l'Environnement, CEA Saclay, Bat. 709 - Orme, F-91191 Gif-sur-Yvette Cedex, FRANCE, email: orr@lscce.saclay.cea.fr)

One component of the recently completed U.S. JGOFS field program was a global survey of CO<sub>2</sub> in the oceans. Inorganic carbon samples were collected and analyzed on nearly all of the U.S. WOCE one-time survey and NOAA/OACES cruises conducted during the past decade. The quality and quantity of these data will allow the first reliable global estimates of anthropogenic CO<sub>2</sub> inventories in the ocean. A parallel U.S. WOCE program, conducted on the same cruises, was the survey of radiocarbon in the world's oceans. One of the many uses of the C-14 data set is an examination of the distribution of bomb-produced C-14 in the oceans. These two anthropogenic carbon tracers have many similarities, however, there are also several significant differences (e.g. atmospheric history and equilibration times). This study will compare the distributions of anthropogenic CO<sub>2</sub> and bomb C-14 in the oceans. The observed trends will be compared to 3-D ocean GCM distributions during the second phase of OCMIP. Differences between the observed and model distributions will be evaluated by applying the data-based techniques for estimating the anthropogenic components to model derived properties. These estimates will then be compared to the anthropogenic distributions directly estimated in the model. Special attention will be given to potential sources of error in both the model and data-based estimates.

MC01/W/36-A5

1700

#### COMPARISON OF SIMULATIONS OF CFC-11 AND CFC-12 DURING OCMIP

J.-Cl. DUTAY (LSCE), J. Bullister (PMEL), J. C. Orr (LSCE), R. G. Najjar (PSU), M. Follows (MIT), R. Matear (CSIRO), S. Doney (NCAR), E. Maier-Reimer (MPI), Y. Yamanaka (IGCR), H. Drange (NERSC), A. Yool (SOC), J.-M. Campin (UCL), M.-F. Weirig (AWI), N. Gruber (Princeton), K. Caldeira (LLNL)

Thirteen groups are involved in the OCMIP2 project (Ocean Carbon Model Intercomparison Project - phase 2). These groups are running a variety of ocean carbon models. Chlorofluorocarbons (CFC's) have been chosen as the first tracers to be examined in detail as part of the project analysis. CFCs have increased rapidly in the atmosphere during the past 50 years. These gases dissolve in surface seawater and are subsequently carried into the interior of the ocean as passive tracers of ocean circulation and mixing processes. CFCs have been used to study a variety of physical processes in the ocean occurring on decadal time scales, including thermocline ventilation and the formation of intermediate and deep waters. In the OCMIP2 study, a common atmospheric CFC input history was used in the models. Results from model simulations of dissolved CFCs are compared to CFC measurements collected during recent major ocean observation programs (eg. AJAX, SAVE, WOCE). These comparisons provide a means of testing and evaluating each model's ability to realistically simulate the uptake and redistribution of gases in the ocean. Our analysis will focus in particular on the Southern Ocean, an important region where large uncertainties presently exist in the magnitude of the anthropogenic CO<sub>2</sub> sink.

MC01/W/55-A5

1715

#### OCEAN CARBON-CYCLE SIMULATIONS OF GLOBAL CHANGE AND INTERANNUAL VARIABILITY: FUTURE EMPHASIS FOR OCMIP

Patrick MONFRAY, Laurent Bopp, Corinne Le Quere, and James C. Orr (all at LSCE/CEA Saclay (IPSL), Unite Mixte CEA-CNRS, CEA Saclay, Bat. 709 L'Orme, F-91191 Gif-sur-Yvette, France, email: monfray@cea.fr)

The first two phases of the Ocean Carbon-Cycle Model Intercomparison Project (OCMIP), during 1995-1997 and 1998-2000, have used ocean carbon-cycle models with fixed ocean circulation, which thus do not consider effects due to climate change and interannual variability. Conversely, the third phase of OCMIP will focus on the effect of climate change on the ocean carbon cycle and marine biomass. The objective will be to study changes in marine biogeochemistry and the air-sea CO<sub>2</sub> flux under a warmer, more stratified ocean, where winds, evaporation, and precipitation are different. To validate the coupled carbon-climate ocean models that must be used for such a study, we will rely on simulations of interannual to interdecadal variability with the same models. Interannual variability of ocean carbon and marine biomass is driven by many of the same factors, such as changes in atmospheric fluxes of heat, water, and momentum, as well as changes in the delivery of macro- or micro-nutrients (e.g., N, P, Fe, CO<sub>2</sub>). Simulations of interannual variability will provide OCMIP with a pertinent, added dimension with which to evaluate ocean carbon-cycle models. Such comparison will lead to more reliable predictions from ocean models that will help shed light on the current controversy surrounding widely different estimates of the interannual variability of the air-sea CO<sub>2</sub> flux. With an aim towards model comparison, we will demonstrate what we have learned from making such simulations in one ocean carbon-climate model from IPSL.

MC01/E/01-A5

1730

#### INFLUENCE ON THE GLOBAL OCEAN CIRCULATION OF A PARAMETERIZATION OF DENSITY-DRIVEN DOWNSLOPING FLOW

Jean-Michel Campin and Hugues Goosse (Institut d'Astronomie et de Geophysique G. Lemaître, Université Catholique de Louvain, 2 ch. du cyclotron, 1348 Louvain-la-Neuve, Belgium, email: campin@astr.ucl.ac.be and hgs@astr.ucl.ac.be)

In the world ocean, high density water are found on the continental shelves, mainly near Antarctica, and are responsible for density driven, downsloping currents that influence the deep ocean water masses properties. This process is poorly represented in z-coordinate ocean models, especially in Ocean General Circulation Model (OGCM) with coarse resolution in both horizontal and vertical directions. Here we present a simple parameterization of



downsloping flow, designed for z-coordinate OGCM: at the shelf break, the downsloping current is evaluated from the horizontal density gradient between the two adjacent boxes, using a linear relation, and is assumed to go downward along the slope until it reaches a level of equal density. This parameterization has been implemented in an OGCM and two experiments, without and with this scheme, have been integrated until equilibrium, using annual mean forcing and restoring boundary conditions. The impact of this parameterization on the global ocean is dominated by the improvement of the Antarctic Bottom Water. This tends to reduce the intensity and depth of the North Atlantic Deep Water circulation and increases the density of the deep ocean. As a result of a higher exchange with the open ocean, the properties of continental shelf waters are also improved, with a marked reduction of the Antarctic shelves salinities. An additional simulation using a coupled ocean - sea ice model and a full seasonal forcing based on climatological fluxes, confirms the previous results, especially the improvement of the Antarctic shelves salinities.

**MC01/W/24-A5****1745****NUTRIENT, CARBON AND TRACER SIMULATIONS IN THE WORLD OCEAN: MODEL/DATA COMPARISON**

Marie-France WEIRIG (Alfred-Wegener-Institut, Columbusstrasse, D-27568 Bremerhaven, Germany, e-mail: mweirig@awi-bremerhaven.de), Reiner Schlitzer (Alfred-Wegener-Institut, Columbusstrasse, D-27568 Bremerhaven, Germany, e-mail: rschlitzer@awi-bremerhaven.de)

We present a large scale ocean circulation model that differs in several aspects from dynamical ocean models. While dynamical models calculate a time-varying ocean velocity field based on momentum equations and external forcing, the AWI-model uses a steady state three dimensional flow field representing the mean ocean circulation. Vertical particle fluxes of organic carbon, calcium carbonate and opal are formulated as functions of depth  $z$  ( $J(z) = a \cdot z^b$ );  $a$  and  $b$  are time-invariant parameters describing export flux and remineralization depth-scale, respectively.) The steady state circulation field as well as the biogeochemical parameters  $a$  and  $b$  are obtained by fitting the model to data of temperature, salinity and dissolved nutrients by means of the adjoint method. The resulting optimal model solution together with the standard OCMIP-2 gas exchange equations are implemented in order to simulate the distribution of different tracers in the ocean. Modeled nutrient, carbon and CFC distributions are shown and compared with recently collected data from the WOCE experiment. Deviations to measured concentrations are discussed and systematic model errors are analyzed. In general the calculated CFC concentrations reproduce the available data sets well. Comparing our modeled concentrations with the data of the AJAX1 section and the WOCE A16 section, we actually see the effects of intermediate, deep and bottom water currents, although there is a slight tendency to overestimate these concentrations. First results of carbon dioxide and helium simulations are also presented.

**MC06****Monday 19 July****SYMPOSIUM ON THE QUASI-BIENNIAL OSCILLATION (QBO) AND INTERNAL GRAVITY WAVES**

Location: Mechanical Engineering, G28 LRE

**Monday 19 July AM**

Presiding Chairs: I. Hirota (Kyoto University, Japan),  
M. Takahashi (University of Tokyo, Japan)

**Introduction****0930**

I. HIROTA

**MC06/E/02-A1****0940****LARGE-SCALE DYNAMICS AND THE EQUATORIAL QBO**

Peter HAYNES (Centre for Atmospheric Science, DAMTP, Silver Street, Cambridge, CB3 9EW, UK, email: phh@damtp.cam.ac.uk)

The dynamics of large-scale zonally symmetric circulations will be reviewed, focussing on implications for the QBO. The large-scale dynamics themselves have been argued to give a mechanism for determining the latitudinal scale of the QBO, irrespective of any scale set by, e.g. large-scale equatorial wave modes that might provide the necessary momentum fluxes. Simple model experiments have verified that this mechanism sets the latitudinal scale when the wave driving is provided by a homogeneous field of small-scale gravity waves. The relevance of the mechanism to the real QBO, where the wave forcing now appears to be provided by a broad spectrum of waves, including small-scale gravity waves and larger scale equatorial modes, will be discussed.

**MC06/W/05-A1****1020****OBSERVATIONS OF THE LINK BETWEEN THE QBO AND EXTRATROPICAL CIRCULATION ANOMALIES**

Mark P. BALDWIN (Northwest Research Associates, Bellevue, WA, USA)

Nearly 20 years ago Holton and Tan observed a link between the phase of the QBO and the strength of the northern winter polar vortex. They suggested that the QBO modified the zonal-mean wind in the subtropics, altering the wave guide for upward and equatorward propagating planetary waves. Observations continue to show that the wintertime Northern hemisphere stratospheric polar vortex is modulated by the phase of the equatorial QBO, and that wave propagation is affected in a manner consistent with the changes in the strength of the polar vortex. Modelling studies have confirmed this, and show consistently that QBO has global effects on the stratospheric circulation and distribution of constituents such as ozone. The high-latitude northern stratospheric vortex tends to be stronger during the winter, and sudden warmings are less likely when the QBO is in its west phase at 40 hPa. The effect of the phase of the QBO on the southern hemisphere circulation is similar in magnitude, but the seasonal timing and latitudinal location differ. The southern hemisphere polar vortex is much stronger, and is not easily penetrated by the weaker planetary-scale waves. During midwinter, any effect from the QBO is confined to midlatitudes, near the edge of the polar vortex. It is not until the time of the vortex breakdown (November) that the QBO affects the circulation over the polar cap. The difference between west and east phase composites of zonal-mean wind during November, at the time of the final warming in the southern hemisphere, are comparable to January in the northern hemisphere.

**MC06/C/JSM01/W/58-A1****1120****TEMPORAL AND SPATIAL STRUCTURES OF MID-LATITUDE QUASI-BIENNIAL OSCILLATION (QBO) IN THE LOWER STRATOSPHERE OBSERVED WITH OPERATIONAL RAWINSONDES DURING 1990-97**

Shin-Ya OGINO (Radio Atmospheric Science Center, Kyoto University, Gokasho, Uji, Kyoto 611-0011, Japan, email: ogino@kurasc.kyoto-u.ac.jp); Manabu D. Yamanaka (Graduate School of Science and Technology, Kobe University, Nada-ku, Kobe 657-8501, Japan, email: mdy@kobe-u.ac.jp)

Temporal and spatial (meridional and vertical) structures of quasi biennial oscillation (QBO) in the mid-latitude lower-stratosphere are investigated using operational rawinsonde data at about 400 stations over the world for 8 years (1990-97). In order to discuss inter-annual variations, mean seasonal variations and linear trends for the 8 years are subtracted from monthly mean temperature and zonal wind, and the obtained anomalies are smoothed by 12-month running average procedure. Oscillations of temperature and zonal wind anomaly fields in the lower stratosphere with a period of about 2 years accompanied by downward phase propagation with time are detected over the almost every stations located in the mid-latitude region (20-40degN/S), indicating that equatorial QBO-like structures also exist in the mid-latitude region, although in the zonal wind anomaly field vertically standing structures with somewhat longer period are dominated through troposphere and lower stratosphere and consequently the equatorial QBO-like signals are detected relatively weakly. Comparison between meridional gradient of temperature anomaly field and vertical gradient of zonal wind anomaly field shows that thermal wind relation is well satisfied. The phase of the mid-latitude temperature QBO is observed to be almost opposite to that of the equatorial QBO in the period during 1993-97, which is considered to be maintained by the mean meridional circulation. On the other hand, the out-of-phase relation is observed to be broken (the equatorial QBO shows a phase delay of about a half year to the mid-latitude QBO) during about 2 years after Mt. Pinatubo eruption in 1991.

**MC06/W/03-A1****1145****SPONTANEOUS QBO-LIKE OSCILLATIONS IN THE GFDL SKYHI MODEL**

Kevin HAMILTON (Geophysical Fluid Dynamics Laboratory/NOAA, P.O. Box 308, Princeton, New Jersey 08542, USA, email: kph@princeton.edu)

The tropical stratospheric mean flow in GFDL SKYHI troposphere-stratosphere-mesosphere general circulation model has been found to undergo a long-period oscillation when the model is run at sufficiently fine vertical and horizontal resolution. The boundary in resolution between oscillating behaviour and non-oscillating behaviour is around 250 km grid spacing in the horizontal and 1 km in the vertical. The mean flow oscillation is characterized by downward phase propagation, formation of strong shear zones and peak-to-peak amplitudes of ~50 m/s at the equator - all features in good agreement with the observed QBO. However, the period of the oscillation tends to be about half that of the real QBO. A number of experiments will be described which examined the sensitivity of the simulated mean flow oscillation to such factors as subgrid-scale diffusion, sea surface temperature, annual cycle forcing etc.

**Monday 19 July PM**

Presiding Chairs: K. Sato (Kyoto University, Japan),  
M.P. Baldwin (Northwest Research Associates, Bellevue, USA)

**MC06/W/04-A1****1400****NUMERICAL SIMULATIONS OF THE QBO USING GCM**

Masaaki TAKAHASHI, Tatsuya Nagashima (Center for Climate System Research, University of Tokyo, 4-6-1 Komaba, Meguro-Ku, Tokyo 153-8904, Japan, email: masaaki@cscs.u-tokyo.ac.jp, tnagashi@cscs.u-tokyo.ac.jp); Masanori Niwano (Grad. Sch. of Environmental Earth Sci., Hokkaido Univ., Sapporo 060-0810, Japan, email: niwano@ees.hokudai.ac.jp), Tepei Uetake, Fumio Hasebe (Department of Environment Sciences, Ibaraki University, Mito, Japan, email: uetake@env.sci.ibaraki.ac.jp, hasebe@mito.ipc.ibaraki.ac.jp)

A simulation of equatorial stratospheric QBO is performed. Reducing horizontal diffusion provides more gravity waves, which are related to noisier precipitation than that in normal general circulation models, to produce the QBO successfully. The period of the simulated QBO in T42 model is 800 days (27 months), which is almost the same as that observed. The amplitude of the zonal-wind oscillation is 20 m/s which is also comparable to the observed value.

Influence of a simulated QBO on the Northern hemisphere winter circulation in the higher latitudes is studied by analyzing output data in a T21 GCM. A comparison between the two phases of the QBO using composite analysis with five easterly and five westerly phase data is made. The zonally-averaged zonal wind composite exhibits a stratospheric dipole structure between high and middle latitudes, which has weaker (stronger) polar night jet during the easterly (westerly) phase of the equatorial QBO.

The ozone QBO is also simulated in a T21 GCM. Modified Chapman reactions of ozone photochemistry are included in the model, allowing the ozone to be fully interactive with the radiative and dynamical fields. The lower stratospheric ozone QBO over the equator is qualitatively similar to that observed, although the simulated amplitude of about 0.3 ppmv is less than that observed. The phase relationship between the equatorial upper and lower stratospheric ozone QBOs is successfully reproduced, although the phase of the modeled ozone QBO slightly precedes the observed phase in the upper stratosphere.

**MC06/E/01-A1****1440****SIMULATION OF A QBO-LIKE OSCILLATION WITH THE ECMWF MODEL**

Agathe UNTCH (ECMWF, Shinfield Park, Reading, RG2 9AX, UK, email: Agathe.Untch@ecmwf.int)

A realistic looking QBO-like oscillation in the zonal wind of the tropical stratosphere has been simulated in a climate integration with a version of the ECMWF model which resolves the atmosphere up to 0.1 hPa with 50 levels and has a vertical resolution of about 1.5 km in the stratosphere. Results from sensitivity studies of this simulated QBO-like oscillation to horizontal and vertical resolution and to different numerical advection schemes will be shown. Wave diagnostics and Eliassen-Palm diagnostics of wave-mean flow interaction will also be shown in an attempt to interpret the results.

**MC06/C/JSM01/E/22-A1****1505****MODELLING THE QBO AND SAO DRIVEN BY GRAVITY WAVES**

H. G. MAYR (NASA Goddard Space Flight Center, Greenbelt, MD; J. G. Mengel, Steven Myers and Associates Co., Vienna, VA; K. L. Chan, Hong Kong University of Science and Technology, Hong Kong, China); H. S. Porter (Furman University, Greenville, SC; C. A. Reddy, Formerly at Vikram Sarabhai Space Center, Trivandrum, India)

Our numerical spectral model, which incorporates Hines' Doppler spread parameterization (DSP) for small scale gravity waves (GW), can simulate the salient features of the QBO and SAO near the equator. The model has now been extended to describe phenomenologically the mean zonal circulation below 20 km, in part through tuning of the GW parameterization. To reproduce the upwelling at equatorial latitudes associated with the Brewer Dobson circulation that in part is modulated by the vertical component of the Coriolis force, the eddy diffusivity in the lower stratosphere had to be enhanced; and to compensate for that a larger GW source is required closer to the middle of the range recommended for the DSP. Through global scale momentum redistribution, the above development is conducive to extending the QBO and SAO to higher latitudes. Multi-year interannual oscillations are generated through wave filtering by the annual oscillation in the mean zonal circulation. In a 3D version of the model, GW momentum is absorbed and dissipated by tides and planetary waves. A somewhat larger GW source is then required to generate realistic QBO and SAO amplitudes.

MC06/C/JSM01/E/35-A1

1600

#### DYNAMICAL EFFECTS OF OZONE FEEDBACK ON THE EQUATORIAL QUASI-BIENNIAL OSCILLATION

Tepei UETAKE (Department of Environmental Sciences, Ibaraki University, Mito, 310-0056, Japan, email: uetake@env.sci.ibaraki.ac.jp); Fumio HASEBE (Department of Environmental Sciences, Ibaraki University, Mito, 310-0056, Japan, email: hasebe@mito.ipc.ibaraki.ac.jp); Masaaki TAKAHASHI (Center for Climate System Research, University of Tokyo, Tokyo, 153-9804, Japan, email: masaaki@ccsr.u-tokyo.ac.jp); Tatsuya NAGASHIMA (Center for Climate System Research, University of Tokyo, Tokyo, 153-9804, Japan, email: tnagashi@ccsr.u-tokyo.ac.jp)

An Ozone QBO is considered to be driven by the advection due to secondary mean meridional circulation coupled with zonal wind QBO. In this case, ozone and zonal wind QBO are in-phase relationship in the lower stratosphere. However, this is not agreement with observations. In experiment using a mechanistic model, a realistic ozone QBO is reproduced by adding the diabatic heating QBO due to solar absorption of ozone. So it is pointed out the importance of ozone feedback effect. Moreover, because the radiative ozone feedback changes vertical momentum flux through weakening secondary circulation, it affects zonal wind acceleration. In this study, we discuss the driving mechanism of ozone QBO and dynamical effect of ozone feedback, using a CCSRNIES AGCM which includes photochemical effect of a modified Chapman reaction. In dominant dynamical region, zonal-mean horizontal and vertical ozone fluxes are cancel out in zonally averaged ozone continuity equation over the equator. The ozone QBO is driven by eddy flux divergence. Long and short wave heatings are out-of-phase in the same height region. So we suggest that the ozone feedback effect weakens the secondary circulation and reduces the vertical momentum flux. Similarly, comparing each terms of zonally averaged zonal momentum equation, we conclude that the ozone feedback effect decreases the acceleration due to secondary circulation and produces opposite acceleration.

MC06/C/JSM01/W/43-A1

1625

#### MODULATION OF STRATOSPHERIC TRACE SPECIE TRANSPORT BY THE QBO: A THREE-DIMENSIONAL MODEL STUDY

Lori BRUHWILER (Climate Monitoring and Diagnostics Laboratory, R/E/CG1 325 Broadway, Boulder, CO 80303, USA, email: lbruhwiler@cmdl.noaa.gov); Kevin HAMILTON (Geophysical Fluid Dynamics Laboratory, Princeton Forrestal Campus, Rt.1, Princeton, NJ 08540, USA, email: kph@fdl.gov)

The equatorial stratospheric zonal wind and temperature quasi-biennial oscillation (QBO) has been observed for several decades and is well-documented. The response of stratospheric trace species, such as ozone, to the QBO-induced perturbations in stratospheric temperature and circulation have also been topics of intensive study, in particular with respect to tropical and extra-tropical interannual variability. Here, the results of a model simulation of ozone and other stratospheric trace species with a comprehensive general circulation model and a prescribed zonally symmetric QBO momentum source are presented. Use of this QBO parameterization results in a fairly realistic zonal wind and temperature QBO, which in turn result in realistic QBO responses of stratospheric trace constituents. The particular focus of this work will be on how the equatorial QBO modulates transport of trace species into and out of the tropics. In contrast to previous two-dimensional model studies, it is found that transport by eddies varies significantly with QBO phase.

MC06/W/01-A1

1650

#### QBO-INDUCED VARIATIONS IN ASCENT RATE INFERRED FROM TRACE GAS DATA IN THE TROPICAL LOWER STRATOSPHERE

Masanori NIWANO, Masato SHIOTANI (Division of Ocean and Atmospheric Sciences, Graduate School of Environmental Earth Science, Hokkaido University, Sapporo 060-0810, Japan, email: niwano@ees.hokudai.ac.jp)

Quasi-biennial oscillation (QBO)-induced variations in ascent rate in the lower stratosphere are investigated with use of the Halogen Occultation Experiment (HALOE) data from 1993 to 1998. The ascent rate is inferred from annually varying water vapor plus doubled methane ( $[H_2O]+2[CH_4]$ ) profiles in the 20-60 hPa layer within 15 degrees of the equator, where the ascent rate is assumed to be approximately comparable to the vertical advection velocity. The derived QBO components of the ascent rate exhibit maximum amplitudes over the equator. Those are about 0.15 to 0.2 mm/s at 20-50 hPa, which appear to be larger than those of the residual circulation derived radiatively. Above 40 hPa around 10 to 15 degrees in each hemisphere, the ascent rate QBO shows seasonality that enhanced anomalies occur in the winter hemisphere. Phase lags among the QBOs in ascent rate, temperature and ozone are also examined at the equator. It is found that descent anomalies precede positive anomalies of temperature and ozone by about 2-6 months, with its lag decreasing with height below 30 hPa, while some of works using coupled dynamical, radiative and photochemical system models have reported substantial in-phase relationship among the three. The larger lags between subsidence and ozone variations, seen in altitudes with the mixing barriers in the subtropics, may indicate relatively small diffusion in this region.

MC06/W/02-A1

1715

#### STEPS TOWARDS THE MODELLING OF THE QBO IN THE MIDDLE ATMOSPHERE GENERAL CIRCULATION MODEL ECHAM4

M.A. GIORGETTA (Max-Planck-Institute for Meteorology, Bundesstr. 55, 20146 Hamburg, Germany, email: giorgetta@dkrz.de)

The simulation of the QBO in a GCM is still a problem in current GCMs. This work aims at the simulation of this phenomenon in the middle atmosphere version of ECHAM4. This model is run with a triangular truncation T30, corresponding to a horizontal resolution of 3.8 degree. The model extends from the surface to 0.01 hPa. The standard version is run with 39 layers and

contains the Hines Doppler spread parameterization for a spectrum of gravity waves. The experimental design consists of various sensitivity experiments dealing with vertical resolution, momentum diffusion, deep convection, and gravity wave parameterization. The first three items concern resolved waves and hence the zonal wind forcing by EP-flux divergence. Experiments run with 69 and 88 layers are completed and show the forcing of westerly winds in the QBO domain at 30 hPa where easterlies dominate in the standard 39 layer version. These westerlies alternate with easterlies, but do not expose the observed downward propagation. Experiments with increased source strengths for gravity waves excited within the atmosphere allow to increase the amplitude of westerlies and easterlies, but may also deteriorate the SAO. Other experiments await completion.

MC07

Tuesday 20 – Wednesday 21 July

#### RADIATIVE FORCING AND CLIMATE CHANGE (IRC, ICCL)

Location: Mechanical Engineering, G29 LT

Location of Posters: Old Gym

Tuesday 20 July AM

Presiding Chair: V. Ramanathan (Scripps Institution of Oceanography, USA)

#### RADIATIVE FORCING / CLIMATE RESPONSE STUDIES IN GCMs

MC07/W/01-A2

Invited

0930

#### RADIATIVE FORCING OF CLIMATE CHANGE

M. RAMASWAMY (Geophysical Fluid Dynamics Laboratory, Princeton, New Jersey, 08542, USA)

The Earth's climate system has been influenced by a number of radiative agents over the past century. These include the forcings induced by anthropogenic changes in the concentrations of various radiatively-active gases and aerosols. While our knowledge of the various agents affecting the radiative balance of the climate system in a secular manner has evolved considerably in recent times, many uncertainties remain for several of the agents. We will review in particular the characteristics of the forcings due to the anthropogenic trace gases and aerosols, including the degree of spatial inhomogeneity of the respective forcings and strategies adopted for estimating them. We will also discuss some recent attempts that have used observations to explore the quantitative features of some of the important forcings. We will also examine the linkages between forcing and modeled climate response for some specific radiative agents.

MC07/W/02-A2

1015

#### A GCM STUDY OF CLIMATE SENSITIVITY AND CLIMATE FEEDBACKS

B. CHRISTIANSEN (Danish Meteorological Institute, Denmark, email: boc@dmu.dk)

The climate sensitivity factor  $\lambda = dT_s/dF$  measures the strength of the climate change  $dT_s$  to a prescribed radiative forcing  $dF$ . The value of  $\lambda$  reflects the strengths of the feedbacks in the climate system. Recently, climate model studies have questioned the usefulness of  $\lambda$  as a predictive tool: in addition to the strength of the forcing both its latitudinal variation and vertical partitioning influence the climate change. The nature of these complications will be studied by expanding the sensitivity factor in components representing the individual feedbacks. E.g., the change in the low outgoing flux at the TOA may be expressed as  $dF_{\lambda} = F_{\lambda} + (F_{\lambda}^C)(C T_s) + (F_{\lambda}^q)(q T_s)$ , where  $C T_s$  and  $q T_s$  represent the cloud and humidity feedback, respectively. The data for the analysis come from a series of GCM experiments with perturbations in ozone concentration, increased  $CO_2$ , and changed solar constant. Our results will be compared with empirical estimates. The approach could also be important for the inter-comparing of models.

MC07/E/01-A2

1035

#### CLIMATE RESPONSE AND RADIATIVE FORCING FROM ATMOSPHERIC OZONE CHANGES

Michael PONATER, Nicola Stuber, Robert Sausen (DLR-Institute for Atmospheric Physics, Oberpfaffenhofen, D-82230 Weßling, Germany, email: michael.ponater@dlr.de)

Based on experience from climate model experiments with either varying greenhouse gas concentrations or varying solar insolation, radiative forcing has been established as a reliable predictor of the associated climate impact. Likewise, the climate sensitivity parameter is usually found to be constant for a given model configuration, indicating a linear increase of surface temperature with increasing radiative forcing.

We have developed a method to calculate the adjusted radiative forcing (and the respective climate sensitivity) within the framework of the 3D climate model ECHAM4/MLO.  $CO_2$  increase experiments with this model system confirm the radiative forcing concept outlined above. However, in several experiments with respect to aircraft induced ozone changes a strong dependency of the climate sensitivity from horizontal structure, vertical structure, and amplitude of the ozone perturbation is apparent. The reasons for this failure of the radiative forcing concept is examined further by means of sensitivity experiments implying idealized patterns of atmospheric ozone concentration change.

MC07/W/04-A2

1115

#### THE RADIATIVE FORCING AND TEMPERATURE RESPONSE DUE TO STRATOSPHERIC WATER VAPOUR AND OZONE CHANGES SINCE 1979

P. M. de F. FORSTER, K. P. SHINE (Department of Meteorology, University of Reading, Reading, UK, RG6 6BB, email: piers@met.rdg.ac.uk)

There is observational evidence of substantial increases in stratospheric water vapour since 1980, from balloonsonde estimates and, over 1992-1996, from satellite measurements. This paper uses a fixed dynamical heating model and an Intermediate General Circulation model (IGCM) to assess the response of stratospheric temperatures to this water vapour change. It compares the effects of water vapour increases and ozone loss and finds that over the last two decades water vapour changes may have led to as much cooling, of the lower stratosphere, as ozone loss. Comparisons are also made between the stratospheric temperature response, calculated using the fixed dynamical heating approximation, to the temperature response in the IGCM.

MC07/E/05-A2

1135

## SIMULATION OF RADIATIVE FORCING DUE TO POLLUTION OF LYING SNOW

David L Roberts, Luke M. ROBINSON, Richard L H Essery\* (Hadley Centre for Climate Prediction and Research, Meteorological Office, London Road, Bracknell, Berkshire, RG12 2SY, UK.) (\* also at National Hydrology Research Institute, Environment Canada, 11 Innovation Boulevard, Saskatoon, Saskatchewan, S7N 3H5, Canada.)

It has sometimes been suggested, e.g. by Warren & Wiscombe (1980), that the contamination of lying snow by small concentrations of absorbing particles, especially black carbon particles, may depress the albedo of the snow surface enough to exert a significant warming effect on the climate. The present study is an attempt to assess the significance of this mechanism using the Hadley Centre atmospheric general circulation model. In order to do this, the normal (HadAM3) version of the model has been modified in two main ways. First, the existing snow surface albedo parameterization has been replaced with a more sophisticated scheme. This includes a parameterization of the darkening effect of black carbon particles, as well as a prognostic snow grain size variable which enables the simulation of the ageing of the snow cover. Secondly, the model has been adapted to include the transport and deposition of black carbon particles emitted during fossil fuel combustion and biomass burning. The black carbon deposited in snowfall or by dry deposition (onto an existing snowpack) is used to drive the snow albedo scheme. The resulting radiative forcing is evaluated by calling the radiation scheme twice, once with pure snow and once with polluted snow, and subtracting the radiative fluxes at the top of the atmosphere. The results of preliminary experiments suggest that the magnitude of the effect is not quite large enough to be significant on a global scale, but that it might be important on a regional scale, especially during boreal spring.

MC07/W/12-A2

1155

## A GCM STUDY OF RADIATIVE FORCING AND STRATOSPHERIC TEMPERATURE RESPONSE DUE TO PINATUBO AEROSOLS

S. RAMACHANDRAN (AOS Program, Princeton University, Princeton, New Jersey 08542, USA, email: snr@gfdl.gov); V. Ramaswamy, M.D. Schwarzkopf, S.M. Freidenreich (Geophysical Fluid Dynamics Laboratory, Princeton, New Jersey, 08542, USA)

Volcanic aerosols in the stratosphere produce significant transitory solar and infrared radiative perturbations, both at the top-of-the-atmosphere and at the surface. These, in turn, lead to thermodynamical and dynamical changes of the climate system. A spectral, latitude- and month-dependent set of aerosol optical parameters, derived from observations for two years following the Pinatubo eruption (June 1991 - May 1993), are employed in the GFDL SKYHI GCM to determine the associated changes in the radiative balance. Clear- and total-sky forcings, as well as the temporal evolution of the perturbations to the stratospheric heating rates, are analyzed. An ensemble of GCM integrations are performed using predicted clouds and climatologically varying SSTs, one set with and one without the aerosols ("control"), in order to study the evolution of the changes in stratospheric temperatures. These simulations are compared with results from a fixed dynamical heating calculation, and with the observed latitude-height stratospheric temperature changes. The statistical significance of the temperature changes and the relative roles of solar and longwave radiative effects will also be discussed.

MC07/E/04-A2

1215

## RADIATIVE FORCING OF CLIMATE BY LAND COVER CHANGE

Richard BETTS (Hadley Centre for Climate Prediction and Research, Meteorological Office, London Road, Bracknell, Berkshire, RG12 2SY, UK, email: rabetts@meto.gov.uk); Navin Ramankutty, Jonathan A. Foley (both at Climate, People and Environment Program (CPEP), Institute for Environmental Studies, University of Wisconsin, 1225 West Dayton Street, Madison, WI 53706, USA, email: nramanku@students.wisc.edu)

The Kyoto protocol includes afforestation and reforestation as possible means of reducing the radiative forcing of climate change through the uptake of atmospheric CO<sub>2</sub>. However, vegetation also affects the Earth's radiation budget through its impact on the surface albedo and cloud, so quantification of the net change in carbon fluxes may not provide a true reflection of the impact of forest cover changes on radiative forcing. Since a forest generally has a lower albedo than cultivated land, particularly when snow is lying, decreases in forest cover in mid- and high-latitudes may have provided a negative radiative forcing which partly opposes the positive forcing due to increased atmospheric greenhouse gas concentrations. This negative forcing may be reduced if forest cover in some regions is increased. This paper uses the HadAM3 General Circulation Model and a dataset of historical crop cover change to estimate the relative contributions of vegetation-related albedo and atmospheric CO<sub>2</sub> changes to radiative forcing relative to 1860, and discusses the implications of this for the use of afforestation and reforestation in reducing anthropogenic climate change.

Tuesday 20 July PM

Presiding Chairs: S.E. Schwartz (Brookhaven National Lab., USA)  
V. Ramaswamy (Geophysical Fluid Dynamics Lab, Princeton, USA)

## RADIATIVE FORCING AND GREENHOUSE GASES

MC07/E/02-A2

1400

## GCM STUDIES OF "RADIATIVE FORCING" BY WELL-MIXED GREENHOUSE GASES

William INGRAM, Stephanie Woodward (Hadley Centre for Climate Prediction and Research, Meteorological Office, London Road, Bracknell, Berks, RG12 2SY, UK)

We have compared in a GCM the impact of different well-mixed greenhouse gases, explicitly calculating the effects of their associated stratospheric temperature adjustment on their forcings as well as their effects on modelled climate. The qualitative differences between their forcings are as would be expected from the different spectral regions where they absorb. For CO<sub>2</sub>, stratospheric temperature adjustment seems to be reliably quantifiable as giving about a one-eighth reduction in the size of the forcing. Even allowing for this, we find our model more sensitive to the minor greenhouse gases than CO<sub>2</sub> by another 10-15%. We interpret this as due not to remaining inadequacy in our forcing estimates, but to different cloud feedbacks, ultimately attributable again to the different spectral regions where they absorb. Since modelled cloud feedbacks still vary considerably and cannot be considered reliable, this does not provide any good basis for increasing their "greenhouse warming potentials", but such uncertainties should be borne in mind when comparing the greenhouse effects of different gases.

MC07/W/08-A2

1420

## THE EFFECT OF UNCERTAINTIES IN RADIATIVE FORCING ON TEMPERATURE TREND PREDICTIONS

F. Forster, K. P. SHINE, Department of Meteorology, University of Reading, Reading, UK, RG6 6BB.

This paper firstly examines the range of uncertainty in our knowledge of the anthropogenic and natural radiative forcings since 1850. Then a Intermediate General Circulation Model (IGCM) is used to examine the likely effect of these forcings on the surface temperature and investigate the robustness of the radiative forcing concept for both idealistic and realistic changes in well-mixed greenhouse gases, ozone, aerosol and solar constant.

MC07/W/15-A2

1440

## GREENHOUSE FLUX INCREASES ASSOCIATED WITH INCREASES IN ATMOSPHERIC WATER VAPOUR

W.F.J. EVANS, E. Puckrin (Trent University, Peterborough, Ontario, Canada, K9J7B8)

Water vapour in the atmosphere is responsible for over half of the earth's greenhouse radiation, and therefore is potentially a major contributor to the problem of global warming if water increases. An increase in the amount of water vapour may have significant consequences on global climate change; hence, it is important to investigate the radiative impact of any increase, as well as the physical mechanism which is responsible for inducing changes in this gas. Recently, it has been noted that there may have been an increase by 5% in the water vapour amount in the atmosphere of the northern hemisphere during this century. The warming of the planet's surface by about 0.7°C over the last 100 years can account for only a 2% increase in the atmospheric water vapour amount, based on thermodynamic considerations. There is at present no widely accepted explanation for the cause of the additional 3% amount. However, a possible mechanism may be connected with the increase in tropospheric aerosol over the last 30 years. The combustion of fossil fuels may be responsible for increasing the number of condensation nuclei in the atmosphere on which tiny water droplets form, thereby enhancing the amount of water vapour in the atmosphere. The droplet sizes are typically 10 µm in diameter and they require condensation nuclei with smaller diameters which are commonly observed to exist in exhaust products. As well, over the last year there has been a significant increase in atmospheric water vapour due to the large El Niño which has now dissipated. It is essential to accurately quantify the increase in the greenhouse flux due to the greater abundance of water vapour; hence, we have used an accurate line-by-line radiative transfer code, FASCOD3, to model the radiative greenhouse flux associated with varying amounts of water vapour in the atmosphere. The calculations have been performed for three different scenarios of water vapour content; a 5% increase, a 10% increase, and a 20% increase in the tropospheric water vapour amount over a range of latitudes and seasons. The results show that the corresponding increase in the surface radiative forcing would range from 1.5 to 6.2 W/m<sup>2</sup>. A value of 1.5 W/m<sup>2</sup> represents a flux that is about half as large as the increase in the flux due to all the other greenhouse gases combined since the pre-industrial period. This flux increase may have contributed to the record warm year in 1998.

MC07/W/09-A2

1500

## THE ACCURACY OF LONGWAVE RADIATION CALCULATIONS FOR EARTH-ATMOSPHERE APPLICATIONS

Robert G. ELLINGSON (Department of Meteorology, University of Maryland, College Park, MD 20742, email: bobe@atmos.umd.edu)

The WCRP-sponsored Intercomparison of Radiation Codes used in Climate Models (ICRCCM) showed climatically important differences between different model calculations of radiative fluxes and heating rates when using the same atmospheric input - even for clear-sky conditions. Data from ARM have allowed much more stringent tests to be applied to detailed radiation models. The results show that conditions the downwelling clear-sky longwave radiation at the surface can be calculated to about 2 Watts per sq. m using line-by-line models - a reduction of the uncertainty by about a factor of 5. However, such accuracy is not generally supplied by radiation codes used in climate models. This paper summarizes the limitations of such models and summarizes areas needing additional research.

MC07/W/19-A2

Poster

1520-01

## UPDATED RADIATIVE FORCING ESTIMATES OF ATMOSPHERIC METHANE

Kamaljit SIHRA (University of Reading, 2 Earley Gate, Whiteknights, P.O. Box 239, Reading RG6 2AU, email: sws98ks@met.rdg.ac.uk); Keith Shine (University of Reading, UK)

Methane in the terrestrial atmosphere is an important greenhouse gas which has been steadily increasing since pre-industrial times. These increases have been shown to contribute 20% towards the radiative forcing from all well mixed greenhouse gases, in addition to causing increases in tropospheric ozone and stratospheric water vapour (IPCC, 1995). A previous investigation of the radiative forcing of methane as a function of concentration, by Myhre et al (1998) using the narrow band model (NBM) of Shine (1991), reveals differences of up to 20%, compared with IPCC (1995) estimates. The NBM is most accurate in the weak and strong limits for a Lorentz lineshape and this may not be appropriate for methane since the absorption for its present atmospheric abundance generally lies between these two limits. This paper tests the validity of the NBM for methane against the Voigt spectral lineshape and line-by-line calculations performed with the Oxford Reference Forward Model (RFM), an evolution of the GENLN2 line-by-line modelling program.

MC07/W/16-A2

1600

## A COMPARISON OF GCM MODELS WITH EXPERIMENTAL MEASUREMENTS OF SURFACE RADIATIVE FORCING BY GREENHOUSE GASES

W.F.J. EVANS, E. Puckrin (Environmental Resource Studies, Trent University, Peterborough, Ontario, K9J7B8, Canada)

Climate models predict that the emission of greenhouse gases into the atmosphere has altered the radiative energy balance at the earth's surface by several percent through increasing the greenhouse radiation from the atmosphere. With measurements at high spectral resolution, this increase can be quantitatively attributed to each of several anthropogenic gases. An energy flux imbalance of about 3 W/m<sup>2</sup> has been created by anthropogenic emissions of greenhouse gases of which we have measured over 1.0 W/m<sup>2</sup>. Calibrated radiance spectra of the greenhouse radiation from the atmosphere have been measured at ground level from Peterborough using an FTIR with a resolution of 0.1 wavenumbers. This long wave radiation consists of thermal emission from naturally occurring



gases such as CO<sub>2</sub>, H<sub>2</sub>O and O<sub>3</sub> as well as from many trace gases such as CH<sub>4</sub>, CFC11, CFC12, CFC22 and HNO<sub>3</sub>. The forcing radiative fluxes from CFC11, CFC12, CCl<sub>4</sub>, HNO<sub>3</sub>, CO<sub>2</sub>, CH<sub>4</sub> and O<sub>3</sub> have been quantitatively measured. The experimental fluxes are simulated well by the FASCOD3 radiation code. The greenhouse radiation fluxes from the various gases have been computed with the radiation code from the NCAR community model for the location and seasons of the measurements. Overall the agreement in most fluxes is good, providing increased confidence in the NCAR CCM. Similar comparisons of our experimental measurements with simulations using the column model from the Canadian GCM will be reported. Differences in the fluxes are over 50 % for CH<sub>4</sub> and N<sub>2</sub>O at mid latitudes in summer.

**MC07/W/22-A2****1620****RADIATIVE FORCINGS AND GLOBAL WARMING POTENTIALS OF WELL-MIXED GREENHOUSE GASES, CFCs, AND CFC REPLACEMENT COMPOUNDS**

Atul K. JAIN (Department of Atmospheric Sciences, University of Illinois, Urbana, Illinois, USA, email: jain@atmos.uiuc.edu); Bruce P. Briegleb (National Center for Atmospheric Research, Boulder, Colorado, USA); K. Minschwaner (Department of Physics, New Mexico Institute of Mining and Technology, Socorro, New Mexico, USA); Donald J. Wuebbles (Department of Atmospheric Sciences, University of Illinois, Urbana, Illinois, USA); M. D. Hurley (Ford Motor Company, Dearborn, Michigan, USA)

Using narrow-band and broad-band radiative transfer models for the global atmosphere, we evaluate the radiative forcing due to 39 greenhouse gases as a function of latitude and season. The gases examined include CO<sub>2</sub>, CH<sub>4</sub>, N<sub>2</sub>O, plus a number of chlorofluorocarbons (CFCs), hydrochlorofluorocarbons (HCFCs), hydrofluorocarbons (HFCs), hydrochlorocarbons, bromocarbons, iodocarbons, and fully fluorinated compounds. Latitudinal and seasonal variations are considered explicitly, using distributions of major greenhouse gases from a combination of atmospheric models and UARS measurements, and cloud statistics from the International Satellite Cloud Climatology Project (ISCCP). The model calculations are performed on a 5 deg. latitude grid from 82.5 deg S to 82.5 deg N. The determined radiative forcings are then used to derive Global Warming Potentials (GWPs) for each of the compounds. These results are compared with prior analyses. In addition, model analyses of the latitudinal and seasonal dependence of radiative forcing since pre-industrial time will be presented.

**MC07/W/13-A2****1640****RADIATIVE FORCING, GLOBAL WARMING POTENTIAL AND GLOBAL WARMING COMMITMENT CONCEPTS IN THE CLIMATE FORCING RADIATIVE FACTOR EFFECT ASSESSMENT**

Igor KAROL, V.A. Frolkis, A.A. Kiselev (all at Main Geophysical Observatory, 7 Karbyshev Str., St.Petersburg, 194021, Russia, email: karol@main.mgo.rssi.ru)

The Radiative Forcing (RF) and the Global Warming Potential (GWP) are widely used for the assessment of radiative effects of separate active substance content change in the atmosphere. The known advantages and deficiencies of these indices and of a concept of Global Warming Commitment (GWC) are discussed with account of the actual evolution of substance during the considered period, and by this it deviates from the GWP, being calculated by the same formula. A comparative analysis of RF and GWC of main Greenhouse Gases (GG) is carried out for their observed evolutions before 1995 and projected ones up to 2050 based on global photochemical models and on the known IPCC-92 scenarios. The GWCs of CH<sub>4</sub>, N<sub>2</sub>O and chlorofluorocarbons (CFCs) against CO<sub>2</sub> as a standard GG are different from relative RF and much more accurately reflect the real events in the above mentioned periods than the widely used RF of GG relative to RF of CO<sub>2</sub>, when the character of the GG content evolution during the time period considered is not accounted for.

**Wednesday 21 July AM**

Presiding Chairs: K. Shine (Dept. of Meteorology, Univ. of Reading, UK), I. Karol (Main Geophysical Observatory, St. Petersburg, Russia)

**AEROSOL FORCING AND OBSERVATIONS / MODELLING OF SOLAR RADIATION****MC07/W/05-A3**

Invited

**0830****SHORTWAVE RADIATIVE FORCING OF CLIMATE CHANGE BY ANTHROPOGENIC AEROSOLS: NARROWING THE UNCERTAINTIES**

Stephen E. SCHWARTZ (Environmental Chemistry Division, Brookhaven National Laboratory, Upton NY 11973 USA, email: ses@bnl.gov)

Tropospheric aerosols influence the shortwave reflectivity of the Earth by scattering and, to lesser extent, absorbing radiation (direct effect) and by increasing cloud reflectivity and perhaps lifetime (indirect effect). Increased aerosol loading over the industrial period is thought to exert a negative (cooling) radiative forcing that is comparable in global-average magnitude to the positive (warming) longwave forcing due to increased concentrations of greenhouse gases. However the aerosol forcing is highly uncertain, the greatest source of uncertainty in climate forcing over the industrial period. This uncertainty precludes confident assessment of net forcing over the industrial period and empirical inference of climate sensitivity to greenhouse forcing. Accurate description of the direct forcing requires knowledge of aerosol loading (column mass burden or optical depth) and the forcing per loading. Aerosol loading is highly variable because of nonuniform distribution of sources, short lifetime, sensitivity to relative humidity, and intermittent formation and removal processes as influenced by clouds and precipitation. Aerosol composition, size distribution and other microphysical and optical properties are also highly variable, leading to considerable variability in normalized forcing (forcing per mass burden or forcing per optical depth). Aerosol normalized forcing seems to be rather well modeled, at least for cloudfree sky, provided aerosol optical properties and surface reflectance are specified. The indirect forcing is more uncertain, as it is quite sensitive to perturbation in number concentration of cloud droplets. Because of correlations and feedbacks between aerosols and other climate variables, aerosol forcing must be represented "on-line" in climate models. This requires accurate representation of the source, evolution, and Removal processes governing aerosol mass loading, number, composition, microphysical properties, and geographical distribution, which in turn requires accurate and efficient means of representing aerosol processes in transport models and evaluation of the performance of these models. Future satellite measurements, especially satellite-borne Lidar, should greatly aid in model evaluation, but ground-based and in-situ measurements remain necessary, as do process research studies.

**MC07/W/07-A3****0915****FIELD MEASUREMENTS THAT MANIFEST THE FIRST AND SECOND TWOMEY EFFECTS**

James G. HUDSON, Seongsu Yum

The Twomey or Indirect Aerosol Effect comes about through changes in cloud microphysics due to anthropogenic cloud condensation nuclei (CCN). The primary Twomey effect is the increase in cloud droplet concentrations and decrease in cloud droplet sizes, which cause greater cloud albedo. The secondary effect is the inhibition of precipitation due to the smaller sizes of the cloud droplets, which results in greater cloud amounts, durations, and optical thicknesses. Here we present data from two field projects that clearly show that differences in cloud droplet concentrations, sizes, and precipitation are due to differences in CCN concentrations. In both the Small Cumulus microphysics Study (SCMS) on the East coast of Florida and the Atlantic Stratocumulus Transition Experiment (ASTEX) in the eastern Atlantic there are distinctly different clouds due to differences in CCN concentrations. Clouds formed in continental/anthropogenic air masses with high CCN concentrations are distinctly different from clouds formed in maritime air masses. Throughout these projects there are significant correlations between CCN and cloud droplet concentrations and anticorrelations between CCN and cloud droplet sizes; this is a manifestation of the First Twomey Effect. The anticorrelation between CCN and drizzle suggests the second Twomey effect. The finding of a threshold mean droplet size for the production of drizzle, which is usually exceeded in maritime clouds, which produce abundant drizzle, but seldom exceeded in continental clouds, which produce only small amounts of drizzle, seems to clearly manifest the second Twomey effect. The global significance of these results is bolstered by the consistent continental/maritime differences in CCN and cloud microphysics for the cumulus clouds of SCMS and the stratus clouds of ASTEX.

**MC07/W/20-A3****0935****EFFECTS OF RELATIVE HUMIDITY ON THE RADIATIVE FORCING DUE TO SULFATE AEROSOLS. CALCULATIONS WITH A REGIONAL HIGH RESOLUTION MODEL AND A GLOBAL MODEL**

Gunnar MYHRE (Department of Geophysics, University of Oslo, Norway, email: gunnar.myhre@geofysikk.uio.no)

The relative humidity has a non-linear effect on the radiative forcing of hygroscopic aerosols. The relative humidity varies within typical gridcells of global models. To investigate the impact of such variations we have used a chemistry transport model (CTM) with 50km horizontal resolution for a limited area and a global CTM to calculate sulfate distributions and the corresponding radiative forcing. Both CTMs use meteorological input data from numerical weather prediction models for the year 1996. The CTM and the radiative transfer calculations are performed in a consistent way, such that the humidity, clouds, and sulfate distributions are the same in both calculations. Optical properties of sulfate aerosols are the same as those used in a previous global radiative forcing calculation of sulfate. The effect of the relative humidity on the radiative forcing due to sulfate is much higher in the regional model, resolving more of the spatial variation in the humidity, than in the global model and previous global radiative forcing calculation. In addition to the large effect of spatial variation in the relative humidity on the radiative forcing due to sulphate also a large temporal effect is found.

**MC07/W/10-A3****0955****MEASURED AEROSOL ABSORPTION PROFILES AND THEIR INFLUENCE ON CLEAR-SKY AEROSOL FORCING**

Manfred WENDISCH, Andreas Keil (all at Institute for Tropospheric Research, Permoserstr. 15, 04318 Leipzig, Germany, email: wendisch@tropos.de)

Using a Particle/Soot Absorption Photometer (PSAP), airborne measurements of aerosol volume absorption coefficients were performed over a polluted rural area in Germany. Together with measurements of aerosol size distribution, aerosol composition and meteorological parameters a vertically resolved input for detailed one-dimensional radiative transfer calculations was obtained. A Mie mixing method was introduced in order to include the PSAP measurements in the calculations. Calculations were performed for three air masses with different levels of pollution and absorption which have been observed in December 1997. For the air mass with the highest absorption level and non-snow surface albedo conditions the aerosol forcing at the top of the atmosphere was -11.2 W m<sup>-2</sup> without including the measured aerosol absorption in the calculations and decreased to -9.6 W m<sup>-2</sup> when the Mie mixing method was applied. Assuming a snow covered ground the aerosol forcing for the same air mass changed from a cooling of -1.3 W m<sup>-2</sup> to a heating of +4.8 W m<sup>-2</sup>. For low levels of pollution (e.g. marine air masses) the inclusion of measured aerosol absorption in radiative transfer calculations had negligible influence. Additionally, vertical profiles of the black carbon volume fraction were obtained from the Mie mixing method. Typically, the black carbon fraction was largest near the ground and decreased rapidly in the free troposphere above temperature inversions. Furthermore, it was shown that unrealistic vertical profiles of black carbon volume fraction can be obtained if the mixing state of the particles is neglected and a size-independent mass absorption of black carbon (e.g. 10 m<sup>2</sup> g<sup>-1</sup>) is assumed.

**MC07/W/11-A3****1015****AEROSOL DIRECT RADIATIVE FORCING: A FIVE-YEAR CLIMATOLOGY AT THE ARM SGP CART SITE**

Qiang FU, G. Lesins, J. Higgins (All at the Department of Oceanography, Dalhousie University, Halifax, Nova Scotia B3H 4J1, Canada, Email: qfu@atm.dal.ca)

The aerosol direct radiative forcing at the ARM SGP CART site from the 1994-1998 has been analyzed using a radiation model with the input data collected at the ARM SGP central facility. The downward surface radiation measurements have been employed to validate the radiation model. We have discussed the uncertainties related to the surface albedo, aerosol composition and size distribution, and radiation model and measurements.

**MC07/W/14-A3****1055****VALIDATION OF SHORTWAVE SURFACE RADIATION BUDGET RETRIEVALS BASED ON ERBE, SCARAB AND CERES SATELLITE DATA.**

Alexander TRISHCHENKO, Zhanqing Li (Canada Center for Remote Sensing, Canada)

The surface radiation budget (SRB), one of the principal component of the earth's climatic system, is still fraught with uncertainties. For example, the estimates of global mean values of SRB vary from 142 Wm<sup>-2</sup> (42% of incoming solar flux) to 191Wm<sup>-2</sup> (55%). In this study we present the results of validation of algorithm for SRB retrieval developed by Li et al. (1993).

This algorithm is used in the NASA's Cloud and the Earth's Radiant Energy System (CERES) project. We tested this algorithm under variety of clear-sky and cloudy conditions for the satellite data from Earth Radiation Budget Experiment (ERBE), Scanner for Radiation Budget (ScaRaB) and CERES instruments. As ground truth we employed measurements from various radiation networks. They include data from the Atmospheric Radiation Measurement (ARM) in Oklahoma, the World Baseline Radiation Networks (BSRN), the radiation network of the Atmospheric Environment Service (AES) of Canada, etc. Surface albedo necessary to determine surface absorbed flux was derived either from measurements available, or from satellite-based estimation. Special emphasis is given to the SRB budget and effect of cloud radiative forcing in the polar regions over snow/ice covered surfaces.

MC07/W/17-A3

1115

#### HIGH RESOLUTION MODEL/MEASUREMENT VALIDATIONS OF DIRECT AND DIFFUSE FLUX IN THE SHORTWAVE

P.D. BROWN, S.A. Clough, E.J. Mlawer (Atmospheric & Environmental Research, Inc., USA); T.R. Shippert, Pacific Northwest National Laboratories, USA; F. Murray (University of Denver, USA); J. Michalsky, L. Harrison, P. Keidron (State University of New York at Albany, USA)

To assess and improve radiative transfer modelling capability in the shortwave, a Quality Measurement Experiment (QME) has been initiated in the solar regime as part of the DoE Atmospheric Radiation Measurement (ARM) Program. The objective of this closure experiment is to study direct and diffuse irradiance in the clear sky, focusing upon three components: (1) measurements of the direct and diffuse irradiance, (2) forward model calculations, including the solar source function, and (3) characterization of the atmospheric state in the radiating column. For this assessment, spectral irradiance measurements in the 2000-28600 cm<sup>-1</sup> regime, as measured by the Absolute Solar Transmittance Interferometer (ASTI) and the Rotating Shadowband Spectroradiometer (RSS), are used. The Line By Line Radiative Transfer Model (LBLRTM) is used to obtain layer optical depths, and the Code for High Resolution Accelerated Radiative Transfer with Scattering (CHARTS) is used for radiative transfer calculations in the scattering atmosphere. Results of this study are expected to make a contribution to the understanding of anomalous absorption reported in the shortwave. Of particular interest are issues associated with the line parameter database, water vapor continuum, collision induced continuum, solar source function, aerosol scattering, and surface albedo.

MC07/E/03-A3

1135

#### INSOLATION REGIME ON AND NEAR THE EARTH'S SURFACE

Tarzadin ULAANBAATAR (Department of Earth Sciences, National University of Mongolia, email: numelect@maginnet.mn)

The current scientific concept concerning theoretical description and calculation of the insolation regime on the earth surface in planetary-scale is faced with some uncertainties in consequence of atmospheric influences. In order to understand and overcome these disadvantages I decided to select the new insolation etalon measuring on the earth surface instead of familiar solar constant.

In this work a model which is created by author consists of three simple parameters: date, measuring time in hour, minute and second, and geographical latitude. Calculations based on the selected new etalon indicate that the insolation regime on the Earth's surface is in a good coincidence with the calculations of Detre, L., [1939], Monin, A. S., [1972], and data measured by Geophysical Observatory of National University of Mongolia. As results, the total insolation in different geographical latitudes or zonal amount of insolation in certain time interval, solar radiation weakening in atmosphere, reconstruction of insolation regime on the Earth's surface in geological past time are described. Furthermore, development of model drives to a new climate theory.

MC08

Wednesday 21 – Thursday 22 July

#### RADIATIVE EFFECTS OF WATER VAPOUR ON CLIMATE (IRC, ICCL)

Location: Chemical Engineering, G35 LT

Location of Posters: Old Gym

Wednesday 21 July AM

Presiding Chair: S.A. Clough (Atmos. and Env. Res., Inc., Cambridge, UK)  
Concurrent Poster Session

MC08/E/07-A3

0900

#### WATER VAPOUR AND RADIATION IN CLIMATE MODELS

Anthony SLINGO (Hadley Centre for Climate Prediction and Research, Meteorological Office, London Road, Bracknell, Berkshire RG12 2SY, UK, email: aslingo@meto.gov.uk)

Atmospheric water vapour exhibits a complex distribution in space and time, as a result of the many physical and dynamical processes which act on a water molecule from the moment it enters the atmosphere (mainly by evaporation from the oceans) to the time it leaves as precipitation reaching the surface. Water vapour is the most important greenhouse gas and a necessary ingredient for clouds, which also strongly influence radiative heating. The water vapour distribution thus provides a valuable tool for diagnosing the realism of these processes in climate models. Several new datasets have become available in the last few years from satellite instruments and re-analysis projects, which have been used to diagnose the relationship between the water vapour distribution and radiative heating. Studies of these data have often emphasized the importance of water vapour in the upper troposphere, but the role of water vapour at other levels should not be underestimated. This presentation will review some of the recent results in this field and highlight some of the strengths and weaknesses which have been found in climate model simulations, as well as in the observational data themselves. Some ways in which the weaknesses in both models and observations may be overcome will be discussed.

MC08/W/05-A3

0945

#### WATER VAPOR FEEDBACK ESTIMATES FROM GLOBAL CLIMATE MODELS AND CONSISTENCY WITH INDEPENDENT SATELLITE METHODOLOGIES

Franklin ROBERTSON (NASA Marshall Space Flight Center, Global Hydrology and Climate Center, 997 Explorer Blvd., Huntsville, AL 35806, USA, email: pete.robertson@msnfc.nasa.gov)

The fundamental role of water vapour in linking radiation, convection and dynamics has been widely studied and debated as a classical problem in climate dynamics. Water vapour feedback associated with climate change has been a subject of particularly intense debate since it is judged to be the most prominent feedback and the principal mechanism supporting claims of global warming scenarios. The present study uses a combination of space-based observations, radiation modelling, and the global climate models to estimate water vapour feedback associated with recent positive and negative phases of ENSO. ERBE and TOVS-based calculations which earlier suggested positive water vapour feedback based on the 1987/1989 warm/cold SST events are revisited in light of potential effects of undetected oceanic low clouds in biasing the top-of-atmosphere longwave clear-sky estimates somewhat low. Additional calculations of water vapour feedback from an algorithm based on the SSM/T2 are used for the period 1993 to the present.

Finally, simulations from the CCM3 and other climate models using observed SSTs are evaluated with the observed data sets to evaluate their ability to simulate longwave clear-sky feedback and its partitioned components of surface temperature and lapse rate feedback and water vapour feedback. The findings are discussed in the context of using short-term climate anomalies to understand feedback processes.

MC08/L/10-A3

1015

#### PHYSICAL PROCESSES AND FEEDBACKS OF THE GREENHOUSE EFFECT DUE TO WATER VAPOR: SOME NEW INSIGHTS

Zuohao Cao, Ronald E. Stewart and M. K. Yau (Climate Research Branch, Atmospheric Environment Service Downsview, Ontario, Canada) (Department of Atmospheric and Oceanic Sciences, McGill University, Montreal, Quebec, Canada)

This presentation is concerned with the greenhouse effect in the presence of water vapor. In particular, it is aiming at (1) gaining new physical insights by reformulating the expression of the greenhouse effect; (2) examining vertical, latitudinal, and seasonal variations of greenhouse trapping and causes of these variations by performing numerical simulations; and (3) assessing how the greenhouse trapping responds to a warmed atmosphere. It is shown that temperature differences between the surface and atmosphere determine not only the magnitudes but also the sign of the greenhouse effect. Positive (negative) values of this difference contribute to positive (negative) greenhouse trapping.

Numerical simulations using the radiation model MODTRAN with input data from both standard and ECMWF-reanalysis profiles have shown that over different latitudes and seasons the greenhouse trapping exhibits substantial vertical variations up to tropopause, and these variations are determined by the temperature contrast between the surface and atmosphere. Due to a low-level temperature inversion, there are negative contributions to the greenhouse effect at low levels of the troposphere during the winter over higher latitudes. It is also found that the northward decrease of the greenhouse trapping is attributed to the systematic variations of moisture and temperature. Strong seasonal variations of the greenhouse trapping, controlled by changes of atmospheric moisture contents, are characterized by the largest values in the summer over higher latitudes. Results also indicate that the feedback of greenhouse trapping is positive in a warmed atmosphere, although its magnitude varies with height and with season as a result of perturbations in atmospheric temperature and moisture profiles.

MC08/L/01-A3

Invited

1045

#### GROUND-BASED WATER VAPOR OBSERVATIONS: NEW TECHNIQUES, ACCURACY ISSUES AND IMPLICATIONS FOR SATELLITE OBSERVING BASED ON RESULTS FROM THE ATMOSPHERIC RADIATION MEASUREMENT (ARM) PROGRAM

H.E. REVERCOMB, D.C. Tobin, R.O. Knuteson, W.F. Feltz (University of Wisconsin-Madison, Space Science and Engineering Center, USA, email: hanks@ssc.wisc.edu); Dave Turner (Pacific Northwest National Laboratory, USA)

Understanding the uncertainties of water vapour observations is an important issue for the whole climate community. This issue is currently being addressed by the Atmospheric Radiation Measurement (ARM) Program of the US Department of Energy, that has established a National observing system for climate research. To support studies of radiative transfer, single-column models, clouds, and aerosols, the ARM Program has implemented new remote sensing technologies for measuring water vapour with frequent temporal sampling. These technologies are combined with more conventional techniques at several sites, the most extensive being at the Southern Great Plains (SGP) Central Facility in Oklahoma. The new profiling capabilities developed by ARM include one active and one passive approach that operate autonomously, day and night: (1) a Raman LIDAR system that samples as fast as once per minute with 39 m vertical resolution and with vertical coverage in the range 3-12 km (depending on averaging times and time of day), and (2) multiple Atmospheric Emitted Radiance Interferometer (AERI) systems that observe high spectral resolution downwelling IR radiance spectra every 8-10 minutes from which temperature and water vapour profiles are retrieved up to 3 km (combination with GOES retrievals gives coverage of the entire troposphere). Several two-channel microwave radiometers and GPS systems are also used to measure the total column water vapour. Questions about the consistency of sonde water vapour observations implied by ARM radiation measurements led to special Water Vapour Intensive Operating Periods (IOPs) conducted in 1996 and 1997 at the SGP Central Facility. The goal was to use the complement of ARM advanced instrumentation to better quantify measurement uncertainties and to find ways of improving the accuracy of water vapour observations (order 2% goal). Using dual sondes on the same balloon, these two IOPs graphically...

MC08/E/02-A3

1130

#### NEW WATER VAPOR MEASUREMENTS AND THEIR IMPACT ON THE ATMOSPHERIC RADIATIVE BUDGET

Cathy CLERBAUX (Service d'Aéronomie/CNRS, Paris, France, email: ccl1@aero.jussieu.fr); J. Tennyson (Department of Physics & Astronomy, University College London, UK); M. Carleer, R. Colin (Laboratoire de Chimie Physique Moléculaire, Université Libre de Bruxelles, Belgique); A.C. Vandaele (Institut d'Aéronomie Spatiale, Bruxelles, Belgium); A. Jenouvrier, M.F. Merienne (Groupe de spectroscopie Moléculaire Atmosphérique, Université de Reims, France); P. Bernath (Department of Chemistry, University of Waterloo, Canada); T. Clough (Atmospheric & Environmental Research, Cambridge MA, USA)

Accurate measurements of the water vapor absorption spectrum were recently obtained in the near-UV to near-IR region using a multi-reflection absorption cell coupled to Fourier transform interferometer Bruker IFS120M. The analysis of the spectra provides 1/3 more H<sub>2</sub>O absorption lines than available from the currently used spectroscopic databases. This water absorption dataset was used in a 1D radiative model in order to access its impact on the atmospheric radiative budget.

**MC08/W/01-A3** 1150**THE CURRENT SHORTWAVE SPECTROSCOPIC DATA BASE OF WATER VAPOR**

Prasad VARANASI (Institute for Terrestrial and Planetary Atmospheres, State University of New York, Stony Brook, NY 11794-5000, USA)

Absorption of solar radiation by atmospheric water vapor is a significant aspect of the climate models. The recent observation that the models underestimate the shortwave absorption considerably has brought the hitherto taken-for-granted extent of our knowledge of the shortwave absorption in water vapor bands under closer scrutiny. Our laboratory has, in collaboration with NASA's Ames Research Center and Science and Engineering Services Inc., performed extensive series of high-resolution measurements during the past year. High-resolution Fourier-transform spectroscopy and photoacoustic spectroscopy using a tuneable laser have been employed to make these measurements. Our recent data will be presented along with comparisons with the available spectroscopic databases.

**MC08/W/07-A3** 1210**AN ESTIMATE OF THE CONTRIBUTION OF UNKNOWN WEAK WATER VAPOUR LINES TO THE OPACITY OF THE ATMOSPHERE**

James Clarke, R C M LEARNER, Wenyi Zhong, Joanna D Haigh (all at Department of Physics, Imperial College, London SW7 2BZ, UK, email: r.learner@ic.ac.uk)

Thousands of unknown water vapour weak lines in the visible and near-infrared regions are deduced from extrapolations of experimental results. These extra lines are then included in the HITRAN database and used in line-by-line calculations of atmospheric opacity with standard atmospheric profiles. The effect of including the unknown weak lines will be compared with that of a continuum model.

**Wednesday 21 July PM**

Presiding Chair: A. Slingo (Meteorological Office, Bracknell, UK)

**MC08/W/08-A3** Invited 1400**OVERVIEW OF WATER PROPERTIES**

John BATES (Climate Diagnostics Center)

This overview presentation will begin by examining the current state of knowledge of the spectroscopic properties of water vapor. This will include a summary of what the current state of knowledge is and what observations and enhancements are necessary to improve our knowledge of water vapor radiative transfer. Particular emphasis will be given to recent observational results of the longwave rotational band of water vapor in cold, dry atmospheres. I will then present results of a recent comparison of radiation codes for retrieving upper tropospheric humidity conducted by the GEWEX Water Vapor Project. This will include a comparison of water vapor radiative transfer models including line-by-line models, narrow band models, and single band models. A discussion of the similarities and discrepancies between various models, their dependence on model physics, and implications for their use in climate models will be included.

The second part of this overview will examine how well the radiative properties of water vapor are represented in climate models. I will examine in detail the results from simulations from the NCAR CCM3 and the GFDL climate model. Particular emphasis will be given to the comparison of modelled versus observed water vapor and radiation changes during the extreme ENSO warm and cold events of the last 20 years. In addition, I will examine how well water vapor variability in the tropics is represented in AMIP simulations by comparing modeled versus observed water vapor radiance fields. Finally, I will explore a hypothesis regarding the role of water vapor cycling through deep tropical convection and water vapor-radiation feedbacks in the recent long-term climate stability and in rapid climate change of the past.

**MC08/E/08-A3** 1445**IMPACT OF A VALIDATED RADIATIVE TRANSFER SCHEME, RRTM, ON THE ECMWF MODEL CLIMATE AND 10-DAY FORECASTS**

J.-J. MORCRETTE (ECMWF, Shinfield Park, Reading Berkshire RG2 9AX, UK); S.A. Clough, E.J. Mlawer, M.J. Iacono (Atmospheric &amp; Environmental Research, Inc., 840 Memorial Drive, Cambridge MA 02139, USA)

Series of integrations with the ECMWF model including either the Rapid Radiative Transfer Model (Mlawer et al., 1997) or the operational longwave radiation scheme are used to study the response of the model to a better representation of the longwave radiation fluxes and cooling rates, as RRTM corrects a number of clear-sky systematic errors. In seasonal simulations, the impact of RRTM is a warming and drying of the lower troposphere and a cooling of the higher troposphere and stratosphere. Objective scores for 10-day forecasts show a minimum impact on anomaly correlation of geopotential at 1000 and 500 hPa, and a large and usually positive impact on the mean error of temperature at 850 and 200 hPa.

**MC08/W/06-A3** 1505**A NEW FORMULATION FOR THE WATER VAPOR CONTINUUM**

Eli J. MLAWER, Shepard A. Clough (Atmospheric and Environmental Research, Inc. Cambridge, MA, USA); David C. Tobin (University of Wisconsin, Madison, WI, USA)

A new formulation of the water vapor continuum, which is based on a conceptual framework that assumes that the continuum includes the effects of collision-induced transitions in addition to contributions from the wings of collisionally broadened allowed transitions, is presented. In previous versions of the CKD formulation, the allowed transitions were the sole source of the water vapor continuum. This new formulation, developed primarily as a result of recent detailed laboratory measurements of Tobin et al. (1996) and field observations obtained as part of the SHEBA under extremely dry conditions, produces a continuum that has higher-frequency features than in the previous formulation for both the self and foreign continua. The effect on model/measurement comparisons of applying the new continuum formulation in model calculations will be shown for the longwave and shortwave spectral regions.

**MC08/L/09-A3** Invited 1545**OUR KNOWLEDGE OF WATER VAPOR ABSORPTION: APPLICATION TO ATMOSPHERIC RADIATIVE TRANSFER WITH IMPLICATIONS FOR CLIMATE**

Shepard A. Clough, Eli J. Mlawer, Michael J. Iacono, Patrick D. Brown Atmospheric and Environmental Research, Inc. Cambridge, MA

Water vapor and its distribution in the atmosphere plays a central role in the radiative balance of the earth system. The distribution of water vapor is not only important for the calculation of surface and TOA fluxes, cooling rates and solar deposition, but for the proper treatment of cloud formation, a critical aspect of the earth's radiative system. In this paper we discuss the current state of our knowledge of water vapor absorption from the microwave to the ultraviolet including the effects of water vapor lines, the self and foreign broadened water vapor continuum (Clough et al., 1992).

The results of extensive atmospheric closure experiments for both the thermal region and the solar region will be presented. These studies have been carried out under the DoE ARM program and involve three critical components: (1) the measurement of atmospheric state; (2) spectral measurements of upwelling and downwelling radiance in the thermal region and direct and diffuse irradiance at the surface in the solar region; and (3) calculations with detailed radiative transfer models for direct spectral comparisons with the measurements. The assessment of errors from these studies and their anticipated effect on calculations for the global scale will be discussed, with particular emphasis on the upper troposphere.

The focus of this paper is on the importance of understanding and monitoring the global system, and GCM calculations for that system, from a spectral perspective and in that context improving our understanding of the role of water vapor.

Clough, S.A., M.J. Iacono, J.-L. Moncet (1992): Line-by-Line Calculation of Atmospheric Fluxes and Cooling Rates: Application to Water Vapor. *J. Geophys. Res.*, 97, 15761-15785.**MC08/L/12-A3** 1630**SATELLITE OBSERVATIONS OF CLOUDS AND UPPER TROPOSPHERIC HUMIDITY**

W. Paul MENZEL (NOAA/NESDIS, 1225 West Dayton St., Madison, Wisconsin 53706, USA, email: paul.menzel@ssec.wisc.edu); Donald P. Wylie (Space Science and Engineering Center, University of Wisconsin-Madison, 1225 West Dayton St., Madison, Wisconsin 53706, USA, Email: don.wylie@ssec.wisc.edu)

Global upper tropospheric transmissive cirrus cloud cover has been charted for the past ten years (June 1989 - Dec 1998) using NOAA polar orbiting HIRS multispectral infrared data. The HIRS carbon dioxide slicing approach has a higher sensitivity to semi-transparent cirrus clouds than visible and infrared window techniques; the threshold for detection appears to be at visible transmittances greater than 0.1. The global average cloud cover is found to be about 0.75. The effective cloud amount of the all semi-transparent clouds (visible transmittance < 0.6) ranges from 0.2 to 0.6 with an average value of about 0.5. Time trends of the ten year cloud record show indications of an increase of high clouds in the northern mid-latitudes (0.5% per year) but little change elsewhere. The seasonal cycle of cloud cover in the southern hemisphere becomes very noticeable in 1993. Upper tropospheric humidity (UTH), derived from the global HIRS water vapor sensitive radiances, and global model forward calculations are compared; biases of measured versus calculated water vapor sensitive radiances suggest a dry bias in the models. In addition, water vapor wind field divergences, derived from the geostationary satellites, are compared with the HIRS measured UTH and global cirrus coverage. There are close similarities, especially in the tropics, between areas of increased UTH and upper tropospheric wind divergence and high cloud amount. This suggests opportunities for improved model analysis as the relationship between clouds, ambient relative humidity fields, and large scale dynamics begins to emerge.

**MC08/W/03-A3** 1650**RADIATIVE EFFECT OF MOISTURE IN THE COMPUTATION OF CLEAR SKY OLR**

Man LI, C. WU, Siegfried Schubert (Data Assimilation Office, Code 910.3 Laboratory for Atmospheres NASA/Goddard Space Flight Center Greenbelt, Maryland 20771, USA, email: frmlw@indigoww.gsfc.nasa.gov); Ching I. Lin, Minghang Chen (General Sciences Corporation NASA/Goddard Space Flight Center Greenbelt, Maryland 20771, USA)

This study examines the water vapor effect on the computation of clear sky outgoing longwave radiation (CLR), broad band window radiance (win\_rad) and narrow band window radiance (nwin\_rad, center around 10.8 microns). The radiative calculations employ as input, atmospheric and surface data from ECMWF and NASA assimilated data. Results are compared with CERES-TRMM observations and ISCCP clear sky radiances. We found that most discrepancies in the computed CLR over land are due to differences in the surface skin temperatures in the two assimilated data sets, and most discrepancies over the oceans are due to differences in the moisture. Further analysis shows that the CLR is most sensitive to moisture between 200 and 500 hPa. In general, the sensitivity is largest in the upper levels and reduces with increasing distance from the top. The assimilation of TOVS moisture data in the NASA assimilation system results in a marked improvement in the CLR computation. Detailed discussion of the results will be presented in the conference. The focus will be on studies showing the sensitivity of CLR, win\_rad and nwin\_rad to the changes of the moisture in different layers of the atmosphere.

**Thursday 22 July AM**

Presiding Chair: J.D. Haigh (Space and Atmospheric Physics, Imperial College, UK)

**MC08/L/02-A4** Invited 0900**GLOBAL WATER VAPOR AND CLIMATE: A GEWEX PERSPECTIVE**

Graeme L. STEPHENS (Colorado State University, Dept of Atmospheric Science, Ft Collins, CO 8523-1371, USA)

Water vapor is the key greenhouse gas on Earth linking an assortment of complex and poorly understood processes that, through feedback, can significantly affect the response of the climate system to an imposed forcing. An approach to understanding the role of water vapor in determining such a response requires the integration of observations with models. The goal of the GEWEX Water Vapor Project (GvAP) is to provide a clear vision of the role of water vapor in the climate system. Part of the GvAP strategy is to establish an accurate and validated water vapor climatology on relevant space and time scales. This talk will review the critical issues relating to water vapor and climate and describe the steps GvAP is taking to address these issues.



MC08/L/14-A4

0945

## SPECTRAL RADIANCE AND IRRADIANCE, GPS, AND DIAL LIDAR MEASUREMENTS AT SURFACE AND MOUNTAIN TOP SITES IN HAWAII

John Porter, Shiv Sharma, Mike Bevis, Barry Lienert, Steve Businger, Duane Stevens, and Craig Motell (SOEST, University of Hawaii, 96822 USA). Email: jporter@soest.hawaii.edu

In order to measure the radiative effects of water vapor, clouds and aerosol one needs measurements above and below the layer of interest. Dual aircraft experiments have been used successfully to study cloud properties in this way. Here we describe the suite of measurements being set up in Hawaii at a surface site and at Haleakala (height ~3.3 km). The radiation measurements will include broad band and spectral (0.38-3  $\mu\text{m}$ ) diffuse and direct radiation. The GPS will measure integrated water vapor with ~1 mm accuracy. The radiation and GPS instruments will be at duplicated at both sites. A transportable DIAL lidar will be used to measure the vertical profile of water vapor at the surface site. By making long term differential measurements, the radiative effects of the layer can be characterized. Anticipated difficulties in these measurements and our proposed approach will be discussed.

MC08/W/02-A4

1005

## MEASUREMENTS OF INTEGRATED WATER VAPOR FROM MICROWAVE RADIOMETER, RADIOSONDES AND GLOBAL POSITIONING SYSTEM: IMPLICATIONS FOR RADIATIVE MODELLING

James LILJEGREN (DOE Ames Laboratory, Ames, Iowa, USA, email: liljegen@ameslab.gov); Barry Lesht (Argonne National Laboratory, Argonne, Illinois, USA, email: bmlsht@anl.gov); Teresa Van Hove and Christian Rocken (both at UCAR/GPS Science and Technology Group, Boulder, Colorado, USA, email: vanhove@ucar.edu, rocken@ucar.edu)

Measurements of integrated column water vapor from a microwave water radiometer (MWR) and a balloon-borne sounding system (BBSS) have been made continuously by the U. S. Department of Energy's Atmospheric Radiation Measurement (ARM) Program near Lamont, Oklahoma, USA since 1992, and at other sites in Oklahoma and Kansas since 1994.

The UCAR/GPS Science and Technology Group has continuously derived integrated column water vapor from global positioning system (GPS) receivers at these locations since 1995. An extensive comparison of integrated water vapor from these sensors for 1996 and 1997 have revealed a bias and increased variability between the MWR and both the BBSS and GPS during the summer months that are consistent from year to year and location to location. We have also observed substantial variations in the BBSS-MWR bias that correlate well with the radiosonde calibration lot number. Vaisala has recently developed a correction for their radiosonde relative humidity measurement.

This correction serves to increase the measured relative humidity. Because this correction depends on the age of the sonde (i.e. the difference between the time the sonde was calibrated and the time it was launched) it accounts for much of the lot-dependent variations we have observed. Because it corrects the relative humidity, the effect on the integrated water vapor is largest in the summer when the largest biases between MWR and BBSS are observed. For 1997 the correction changes the median BBSS-MWR difference during the summer from -1.1 to +0.4 mm of integrated water vapor, accompanied by a substantial reduction in the spread of the distribution of differences. However, during the winter the median difference increases from +0.05 to +0.45 mm due to the correction. Does the radiosonde correction over-correct the relative humidity measurement or ...

MC08/E/01-A4

Invited

1045

## RELATIVE HUMIDITY VARIABILITY AND THE WATER VAPOUR FEEDBACK

Richard P. ALLAN (Hadley Centre for Climate Prediction and Research, Meteorological Office, London Road, Bracknell, Berkshire RG12 2SY, UK, email: rpallan@meto.gov.uk)

The dependence of clear-sky outgoing longwave radiation (OLRc) on relative humidity (RH) and surface temperature (Ts) variations are examined using a simulation of the clear-sky greenhouse effect based on the European Centre for Medium Range Weather Forecasts Re-Analysis (ERA). There are two distinct regimes: polewards of about 40 degrees OLRc is determined primarily by temperature fluctuations while at lower latitudes humidity variations control the OLRc. The strongest sensitivity of OLRc to RH is experienced in the dry subtropical descending regions of low humidity. While OLRc is most sensitive to upper tropospheric RH, humidity variability is greatest at lower altitudes. Away from polar regions, RH fluctuations throughout the troposphere contribute significantly to interannual OLRc anomalies. In a global-mean sense over an interannual time-scale, the water vapour feedback in ERA appears to be similar to the positive feedback exhibited by assuming constant RH (dOLRc/dTs=2.3 Wm<sup>-2</sup>K<sup>-1</sup>). This result is dependent on the month chosen (July) and also the quality of ERA humidity. To validate the positive water vapour feedback depicted by climate models it is desirable to measure humidity changes globally throughout the troposphere in conjunction with significantly more than a decade of satellite radiation budget measurements.

MC08/W/04-A4

1130

## ASSESSING GCM PERFORMANCE USING A SPECTRAL LONGWAVE RADIATION DIAGNOSTIC PACKAGE

Eli J. MLAWER, Michael J. Iacono, Shepard A. Clough (Atmospheric and Environmental Research, Inc. Cambridge, MA, USA)

An important aspect of GCM evaluations has been the comparison of the spectrally integrated model fluxes with fluxes inferred from satellite-based radiance measurements from ERBE. While evaluations of the overall energy balance of this type are essential, they do not address the necessity that this energy be properly distributed across the longwave spectral region, evidence of the proper treatment in the model of the relevant physical processes. This paper presents the development<sup>a</sup> of and initial results from a longwave diagnostic package that has been coupled to a version of the NCAR Community Climate Model CCM3 using the accurate longwave radiation model RRTM. This longwave diagnostic package, employing the same physics and numerical approach as RRTM and run in parallel with RRTM in the GCM, models TOA spectral radiances for comparison with existing datasets. For the initial application, channel 12 of HIRS is used to assess the water vapor fields generated by the GCM. A series of simulations are performed for seasonal periods of interest from a 15-year AMIP simulation and the output spectral radiances are compared to measured values for a range of geographic areas.

Delamere, J.S., K. Stamnes, E.J. Mlawer, S.A. Clough, FLRT: Flexible, longwave radiative transfer in clear and cloudy atmospheres, poster presented at 9th Science Team Meeting of the Atmospheric Radiation Measurement (ARM) Program, San Antonio

MC08/E/04-A4

1150

## AIRBORNE MEASUREMENTS OF WATER VAPOUR RADIATIVE TRANSFER USING INTERFEROMETRY AND MICROWAVE RADIOMETRY

Jonathan TAYLOR (UK Meteorological Office, Remote Sensing Branch, Y70 Building, DERA, Farnborough, Hampshire GU14 0LX, UK, Email: jptaylor@meto.gov.uk)

The UK Meteorological Office, Meteorological Research Flight C130, is equipped with a thermal infra-red interferometer called ARIES which has the ability to measure in the zenith and nadir at a range of altitudes between 30 and 9000m over the wavelength range 3 to 16 microns. The in situ measurements of temperature and water vapour measured by the C130 have been used to initialise the GENLN2 line-by-line radiation code. Microwave radiometers flown on board the MRF C130 are used to give further guidance as to the accuracy of the input water vapour profiles. The predicted spectra from these model simulations are compared with the measurements from ARIES. The radiative properties of water vapour in the thermal infrared are important to understand both in terms of optimising the benefit from future space based interferometers for temperature sounding but also in the radiation balance of the atmosphere. In this paper the differences between observed and modelled spectra will be presented and a discussion of the possible causes of the discrepancies presented. This will include an analysis of the contribution of the water vapour continuum looking at data from mid-latitudes and the tropics.

MC08/E/03-A4

1210

## RADIATIVE PROPERTIES OF WATER VAPOR

Tarzadin ULAANBAATAR (Department of Earth Sciences, National University of Mongolia, email: numelect@magicnet.mn)

In this paper the understandings of the radiative properties of water vapor and its representation in climate model are described. Based on the thermal regimes (insolation and air temperature) on and near the Earth's surface is constructed a new climate model which is presented so-called World Climate Supercirculation as wishing by the Author.

According to author's studies and climate model the heating and cooling impacts of water vapor on the thermal regimes are existed two main feedback mechanisms (positive and negative) playing central role in World Water Supercycle and World Climate Supercirculation. The both impacts play main role for stabilization of the thermal regime in a certain level, existence of agreeable conditions of life and protection of biosphere from dangerous solar variabilities and external thermal hazards, as well for continuances of World Water Supercycle and World Climate Supercirculation. The radiative properties of water vapor are shown clearly in new climate model.

Wednesday 21 July AM

M

MC08/E/06-A3

Poster

0900-01

## THE NUMERICAL MODEL OF MESOMETEOROLOGICAL HUMIDITY PROCESSES

George GELADZE (Institute of Applied Mathematics, Tbilisi State University, 2, University Str., Tbilisi 380043, Georgia, email: Geladze@viam.hepi.edu.ge)

The two-dimensional non-stationary problem of a mesoscale boundary layer of atmosphere (MBLA) over thermal non-homogeneous underlying surface with regard to humidity processes is stated and solved. In the model humidity processes are taken into account by method, which includes an exclusion of the condensation/evaporation velocity from the equations of heat-transfer, water-vapor and liquid-water mixing ratio. The model was integrated numerically. The simulation of the full cycle (a generation, development and dissipation) of a stratus cloud and radiation fog on a thermodynamic background of MBLA is carried out. Time and space distributions of air velocity, temperature, pressure, water-vapor and liquid-water mixing ratio are obtained. The influence of geostrophical wind, relative humidity, temperature of the underlying surface, background temperature and atmospheric stratification is investigated. The moment of the cloud formation, maximum liquid-water mixing ratio level, height, lower and upper bounds of cloud and fog are determined. The latent heat of condensation contribution is estimated in the MBLA thermodynamics. The atmospheric stratification and relative humidity threshold significances are shown, at the beginning of the stream condensation process. The theoretical results are in a good agreement with experimental data.

MC08/E/05-A3

Poster

0900-02

## CHANGES IN THE STRATOSPHERIC HUMIDITY DISTRIBUTION CAUSED BY THE INCLUSION OF METHANE OXIDATION IN A 3D CLIMATE MODEL

Ralf Hein, Michael PONATER, Volker Grewe, Martin Dameris, Nicola Stuber (DLR-Institute for Atmospheric Physics, Oberpfaffenhofen, D-82230 Wessling, Germany, email: michael.ponater@dlr.de); Benedikt Steil (Max-Planck-Institute for Meteorology, PostBox 3060, D-55020 Mainz, Germany, email: steil@mpch-mainz.mpg.de)

Conventional 3D climate models (without interactive chemistry-climate interaction) do not include the stratospheric water vapour source due to methane oxidation. Hence, their ability to reproduce the observed humidity distribution in the lower stratosphere is inherently limited.

We present a comparison of the stratospheric water vapour distribution simulated by the atmospheric GCM ECHAM4 with and without coupling to a stratospheric chemistry module (CHEM). The inclusion of the chemical water vapour source indeed leads to a substantial enhancement of water vapour mixing ratio in the extratropical lower stratosphere. The humidity distribution produced by the coupled model system ECHAM4/CHEM is in closer agreement to observations. We point out the resulting differences in the stratospheric water vapour balance, radiative fluxes, and temperature. Respective changes of the radiative forcing to the troposphere/surface system are also discussed.

<b>MW01</b>	<b>Friday 23 July</b>
<b>INTERCOMPARISON OF TROPOSPHERE-STRATOSPHERE GCMs (ICMA, SPARC)</b>	
Location: Chemical Engineering, G35 LT	
Location of Posters: Old Gym	

**Friday 23 July AM**

Presiding Chair: Steven Pawson (NASA Universities Space Research Association, Greenbelt, USA)

<b>MW01/W/13-A5</b>	<b>Invited</b>	<b>0830</b>
<b>THE KINETIC ENERGY SPECTRUM OF HORIZONTAL MOTIONS IN MIDDLE-ATMOSPHERE GENERAL CIRCULATION MODELS</b>		

John N. KOSHYK (Dept. of Physics, University of Toronto, Toronto, Ontario M5S 1A7, Canada, email: koshyk@mam.physics.utoronto.ca)

Data from several middle-atmosphere general circulation models are used to calculate kinetic energy spectra as a function of total horizontal wave number,  $n$ . Tropospheric spectra show power-law behavior with slopes slightly shallower than  $-3$  for wave numbers  $n \rightarrow 10$  (horizontal wavelengths  $\sim 4000$  km), and are dominated by the rotational part of the flow. These spectra agree well with those calculated using data obtained from a global assimilation model and with the results of previous observational studies. Stratospheric spectra have larger amplitudes than tropospheric ones at planetary scales and smaller amplitudes at smaller scales. Mesospheric spectra are characterized by enhanced spectral amplitudes at all wave numbers compared to the stratosphere and spectral slopes in the wave number range  $n \rightarrow 10$  are generally shallower with values between  $-1$  and  $-2$ . Stratospheric and mesospheric spectra include significant contributions from both rotational and divergent parts of the flow for  $n \rightarrow 20$  in all models. These features appear to be independent of model resolution. The divergent part of the flow, presumably associated with naturally resolved inertia-gravity waves in the models, increases more rapidly with height above the lower stratosphere than the rotational part. The divergent part is fairly insensitive to season, whereas the rotational part changes considerably between January and July in the middle atmosphere region. Spectral amplitudes and vertical growth rates of both parts vary widely among models for a given season. The horizontal diffusion schemes used by the models are compared in an attempt to explain some of these differences.

<b>MW01/W/09-A5</b>	<b>Invited</b>	<b>0900</b>
---------------------	----------------	-------------

**SENSITIVITY OF MODEL SIMULATION OF THE MIDDLE ATMOSPHERIC CIRCULATION TO VERTICAL AND HORIZONTAL RESOLUTION**

Kevin HAMILTON (Geophysical Fluid Dynamics Lab/NOAA, P.O. Box 308, Princeton, New Jersey 08542, USA, Email: kph@princeton.edu)

This paper will begin with a brief review of earlier studies of the effects of model resolution on GCM simulations of the stratosphere and mesosphere. Then results of some recent simulations at very high resolution conducted with the GFDL SKYHI GCM will be discussed. These include one experiment with about 30 km horizontal grid spacing, and another with about 100 km horizontal resolution but roughly 400 m vertical level spacing (in the stratosphere). In general the simulated extratropical circulation is strongly dependent on horizontal resolution, while the tropical stratospheric circulation is much more dependent on vertical level spacing.

<b>MW01/W/05-A5</b>	<b>Invited</b>	<b>0930</b>
---------------------	----------------	-------------

**PARAMETERIZATION OF MEAN-FLOW FORCING DUE TO GRAVITY WAVES**

Joan ALEXANDER (Colorado Research Associates, 3380 Mitchell Lane, Boulder, CO 80301, USA Email: anlexander@colorado-research.com)

Gravity waves have characteristics that fill a broad spectrum, but have horizontal and vertical wavelengths that make them generally too small to be resolved in current GCMs or in data from the global meteorological observation network. Their global-scale effects are however important and must be parameterized. This parameterization problem has many variables, many unknowns, and too few constraints at present. Attempts to tune GCMs with existing gravity wave parameterizations typically lead to non-unique solutions and little insight into global wave properties. Some of the current approaches to the problem of parameterizing the effects of gravity waves in GCMs will be described and constraining data, where available, will be summarized. The talk will focus on the method of determining the force on the mean flow from a given source of gravity waves specified in the lower atmosphere.

<b>MW01/W/14-A5</b>	<b>Invited</b>	<b>1035</b>
---------------------	----------------	-------------

**VERTICALLY PROPAGATING WAVES AND THE MEAN FLOW IN THE EQUATORIAL LOWER STRATOSPHERE OF GRIPS AND OTHER GCMs**

Takeshi HORINOUCI (Department of Atmospheric Sciences, University of Washington, Seattle, WA 98195-1640, USA, Email: horinout@atmos.washington.edu)

Over the past two decades considerable effort has gone into simulating the quasi-biennial oscillation (QBO) in GCMs. Since the QBO affects the entire middle atmosphere, the ability to simulate the QBO is important for any GCM aimed at simulating the middle atmosphere. Recently a couple of GCMs succeeded in reproducing the QBO. Wave statistics of one of them, which was run by the author's group, are compared with those of the middle atmosphere version of the NCAR CCM3. The vertically propagating waves in the CCM carry much smaller momentum flux mainly because of its static cumulus convection. Resolution and cumulus parameterization seem to be the most important factors that affect the wave activities in the equatorial stratosphere. However, our understanding of the waves and wave forcing in GCMs is limited. We are currently collecting a new data set for GRIPS (GCM Reality Intercomparison Project for SPARC) in order to compare the vertically-propagating wave statistics of representative middle atmosphere GCMs. Analyses of dynamical and non-conservative terms will be made to improve our understanding of the causality of the difference between the models and provide a guideline on model settings. The results will be presented in the talk.

<b>MW01/W/01-A5</b>	<b>Invited</b>	<b>1105</b>
<b>PHYSICALLY-DERIVED DYNAMICAL CORES IN ATMOSPHERIC GENERAL CIRCULATION MODELS</b>		

Richard B. ROOD, Shian-Jiann Li (Code 910.3 NASA's Goddard Space Flight Center Greenbelt, MD 20771, USA)

The algorithm chosen to represent the advection in atmospheric models is often used as the primary attribute to classify the model. Meteorological models are generally classified as spectral or grid point, with the term grid point implying discretization using finite differences. These traditional approaches have a number of shortcomings that render them non-physical. That is, they provide approximate solutions to the conservation equations that do not obey the fundamental laws of physics. The most commonly discussed shortcomings are overshoots and undershoots which manifest themselves most overtly in the constituent continuity equation. For this reason many climate models have special algorithms to model water vapor advection.

This talk focuses on the development of an atmospheric general circulation model which uses a consistent physically-based advection algorithm in all aspects of the model formulation. The shallow-water model of Lin and Rood (QJRM, 1997) is generalized to three dimensions and combined with the physics parameterizations of NCAR's Community Climate Model. The scientific motivation for the development is to increase the integrity of the underlying fluid dynamics so that the physics terms can be more effectively isolated, examined, and improved. The expected benefits of the new model are discussed and results from the initial integrations will be presented.

<b>MW01/W/12-A5</b>	<b>Poster</b>	<b>1150-01</b>
---------------------	---------------	----------------

**THE STRATOSPHERE AND CLIMATE MODELLING**

W.A. LAHOZ (1), A. O'Neill (1), R. Swinbank (2), S. Pawson (2) and G. Roff (3) ((1) CGAM, University of Reading, RG6 6BB, UK; (2) DAO, NASA-GSFC, Greenbelt, Maryland, USA; (3) BMRC, Melbourne, Australia)

A number of AGCMs participating in both the AMIP-II and GRIPS projects have model levels extending to less than 1 hPa (models from UKMO, NCAR, CNRM and perhaps other institutions). Models such as those at UKMO and NCAR have been developed for use in climate and middle atmosphere studies. These models provide an ideal test-bed for controlled simulations of the stratospheric circulation.

The AMIP-II runs of these models will be compared with climatologies of the stratosphere produced from UKMO analyses, NCEP analyses and the ERA dataset to evaluate the AGCMs' performance in reproducing the mean climate and variability (e.g. stratospheric sudden warmings) of the stratosphere. This study forms the core of the AMIP-II Diagnostic Subproject #16 and addresses the question: "What elements are needed in AGCMs to provide an accurate representation of the stratosphere?"

<b>MW01/W/07-A5</b>	<b>Poster</b>	<b>1150-02</b>
---------------------	---------------	----------------

**CLIMATOLOGICAL STRUCTURES OF THE GRIPS MODELS: MEAN STATES AND FORCING**

Steven PAWSON (Universities Space Research Association, NASA GSFC, Code 910.3, Greenbelt MD 20771, USA)

The GCM-Reality Intercomparison Project for SPARC (GRIPS) is assessing and monitoring the performance of state-of-the-art general circulation models (GCMs). A wide variety of tasks have been initiated; these are designed to assess the ability of the GCMs to represent the current climatological structure of the troposphere and middle atmosphere, to compare their response to imposed forcing anomalies, and to estimate the certainty with which future climate perturbations can be predicted. This paper is concerned with assessments of the climatological states in the GCM simulations. Comparing the simulations with observational datasets reveals considerable discrepancies in the modelled fields. While it might be anticipated that certain types of biases in the model simulations might be related to the formulation of different aspects of the numerical package (dynamical schemes, cloud schemes, radiation transfer, inclusion of gravity wave drag), there is no clear relationship between these features. This paper attempts to draw a more comprehensive picture of the GCMs' performance than has previously been shown, by comparing the dominant forcing mechanisms in the models with observational estimates, and relating model deficiencies to the differences in the physical mechanisms in the GCMs.

<b>MW01/W/03-A5</b>	<b>Poster</b>	<b>1150-03</b>
---------------------	---------------	----------------

**TRACER TRANSPORT WITHIN THE TROPOSPHERE-STRATOSPHERE UNIFIED MODEL**

V. WEST and R. S. Harwood (Dept. of Meteorology, University of Edinburgh, JCMB, KB, Mayfield Road, Edinburgh, EH9 3JZ, Scotland. Email: vicky@met.ed.ac.uk)

Studies of atmospheric change, including the climatic effects of ozone depletion require the coupling of chemistry and general circulation models (GCMs). Such work requires that both the chemical and dynamical processes be accurately represented. As part of the UGMAP modelling effort we are currently involved in implementing coupled chemical-dynamical modelling in the Unified Model (UM). As a first step in this process, the ability of the GCM to reproduce known transport mechanisms in the stratosphere and near-tropopause regions is assessed with different configurations of the model.

The UM is run in troposphere-stratosphere mode and includes the simulation of several long-lived tracers such as H<sub>2</sub>O, CH<sub>4</sub>, O<sub>3</sub>, N<sub>2</sub>O and CFCs. Features such as the general stratospheric loading, the annual cycles in these tracers and the 'tape-recorder' effect in H<sub>2</sub>O are examined, and comparisons made to observational data.

<b>MW01/W/02-A5</b>	<b>Poster</b>	<b>1150-04</b>
---------------------	---------------	----------------

**A THEORETICAL ESTIMATION OF THE EVOLUTION OF THE STRATOSPHERE AT THE BEGINNING OF THE XXI CENTURY BY MEAN OF A COUPLED CLIMATE-CHEMISTRY MODEL**

Anne DE RUDDER, Franck Lefevre, Pascal Simon (CNRM, Météo-France, 42, avenue Coriolis, 31057 Toulouse, France, email: derudder@cnrm.meteo.fr); Hubert Teyssedre (Department of Chemistry, University of Cambridge, Lensfield Road, CB2 1EW Cambridge, UK, email: hubert@atm.ch.cam.ac.uk)

Within the next 15 or 20 years, the stratospheric content in gases emitted by the human activity is expected to change due to the increase in energy consumption and to the regulation imposed onto the production of chlorinated and brominated species. Most of these substances

having a double radiative and chemical role, the consequences of their evolution may be interestingly studied by mean of a model including both effects interactively. The 3-D global model used in this aim at Meteo-France includes an important aspect of this coupling, through the reciprocal dependence of dynamics and ozone chemistry. Two 6-year integrations of the model have been conducted, in source gases and SST conditions representative of Years 1995 and 2015 respectively. Stability and inter-annual variability of the model will be discussed, as well as its ability to reproduce the stratospheric dynamical regimes. Results corresponding to the present day atmosphere will be compared to observations. Calculated changes between the two dates will be analysed and discussed.

**MW01/E/02-A5** Poster **1150-05**

**EXAMINATION OF COLD BIAS IN THE POLAR WINTER STRATOSPHERE OF THE UKMO UNIFIED MODEL**

D.R. JACKSON, J. Austin (both at UK Meteorological Office, Bracknell, UK, email: drjackson@meto.gov.uk)

The stratospheric version of the UK Meteorological Office Unified Model (UM) is a state of the art troposphere – stratosphere GCM with 49 levels extending from the surface to 0.1 mb. Recent improvements have been made to the UM, including the incorporation of a more comprehensive and flexible radiation scheme, which can calculate heating rates from a wider range of atmospheric constituents, including CFCs. Results from a 20 year control run for 1995 conditions indicate the presence of a cold bias in wintertime zonal mean temperatures of up to around 5K in the region of PSC formation, and the cold model vortex persists longer than observed, particularly in the southern hemisphere. Consequently, simulations of stratospheric chemistry in this version of the UM could lead to potentially misleading results concerning predicted future ozone recovery rates. Here, possible reasons for the cold bias are examined. A comparison of model and observed planetary wave amplitudes is made and sensitivity tests of the model representation of radiative heating are carried out. In addition, tests of the representation of gravity wave drag are made. In the control run this is represented by an orographic gravity wave parametrization scheme up to the 20 mb level, and by Rayleigh friction above that level. When the level of switch - over is changed from 20 mb to 5 mb there is a clear impact on stratospheric temperatures, most strikingly in southern polar latitudes. In late southern winter, very low temperatures persist for approximately one month less than in the control run, and in early southern spring cold biases in daily polar minimum temperatures are significantly reduced.

**MW01/W/10-A5** Poster **1150-06**

**EUGCM EXPERIMENTS WITH A UNIFIED RADIATION SCHEME**

Wenyi ZHONG, Joanna D Haigh (both at Department of Physics, Imperial College, London SW7 2BZ, UK, email: w.zhong@ic.ac.uk); Warwick Norton (Department of Atmospheric, Oceanic and Planetary Physics, University of Oxford, UK, email: wan@atm.ox.ac.uk)

A unified radiation scheme has been developed which can be used throughout the troposphere and the middle atmosphere. It is based on the Morcrette (ECMWF) scheme but includes: - line-by-line precomputed LW transmission tables for CO<sub>2</sub> 15 micron band, O<sub>3</sub> 9.6 and 14 micron bands, H<sub>2</sub>O rotation band and 6.3 micron band; - an updated parametrization for the water vapour continuum throughout the infrared spectrum and for water vapour lines in the atmospheric window region and in the wings of the strong bands; - a representation of oxygen absorption in the Schumann-Runge bands and continuum and in the Herzberg continuum. Experiments have been carried out with several versions of the unified radiation scheme implemented in the EUGCM (the UGAMP troposphere-stratosphere-mesosphere model) to assess the impacts of the different improvements on model fields.

**Friday 23 July PM**

Presiding Chair: Lori Bruhwiler (NOAA CMDL, Boulder, USA)

**MW01/W/06-A5** Invited **1400**

**SELECTING METEOROLOGICAL INPUT FOR THE GLOBAL MODELLING INITIATIVE ASSESSMENTS**

Susan STRAHAN (General Sciences Corp., Code 910.3 NASA GSFC, Greenbelt, MD, 20771, USA, email: strahan@dao.gsfc.nasa.gov); Anne Douglass (Code 916 NASA GSFC, Greenbelt, MD, email: douglass@persephone.gsfc.nasa.gov); Michael Prather (University of California, Irvine, CA); Larry Coy (General Sciences Corp., Code 916 NASA GSFC, Greenbelt, MD); Tim Hall (Goddard Institute for Space Studies, New York City, NY); Phil Rasch (National Center for Atmospheric Research, Boulder, CO); Lynn Sparling (Raytheon STX, Code 916 NASA GSFC, Greenbelt, MD)

The Global Modelling Initiative (GMI) science team has developed a three dimensional chemistry and transport model (CTM) to evaluate the impact of the exhaust of supersonic aircraft on the stratosphere. An important goal of the GMI is to test modules for numerical transport, photochemical integration, and model dynamics within a common framework. This work is focussed on the dependence of the overall assessment on the wind and temperature fields used by the CTM. Three meteorological data sets for the stratosphere were available to GMI: the National Center for Atmospheric Research Community Climate Model (CCM2), the Goddard Earth Observing System Data Assimilation System (GEOS-DAS), and the Goddard Institute for Space Studies general circulation model (GISS-2). Objective criteria were established by the GMI team to evaluate which of these three data sets provided the best representation of trace gases in the stratosphere today. Tracer experiments were devised to test various aspects of model transport. Stratospheric measurements of long-lived trace gases were selected as a test of the CTM transport. This presentation describes the criteria used in grading the meteorological fields and the resulting choice of wind fields to be used in the GMI assessment. This type of objective model evaluation will lead to a higher level of confidence in these assessments. We suggest that the diagnostic tests shown here be used to augment traditional general circulation model evaluation methods.

**MW01/L/01-A5** Invited **1430**

**INTERCOMPARISON OF CLIMATE MODEL SIMULATIONS OF THE RESPONSE TO THE 1991 PINATUBO VOLCANIC ERUPTION**

Alan Robock, Georgiy L. Stenchikov Department of Environmental Sciences, Rutgers - The State University of New Jersey, 14 College Farm Road, New Brunswick, NJ 08901-8551, USA Phone: 732-932-9478, Fax: 732-932-8644 E-mail: robock@envsci.rutgers.edu

We have created a data set of aerosol distribution and properties needed for forcing climate model simulations of the effects of the June 1991 eruption of Mt. Pinatubo in the Philippines. Using data from SAGE II, UARS, balloons and lidar, we produced zonal-average, monthly-average loading and optical properties of the sulfate aerosols in the stratosphere from this eruption for 2 years from June 1991 through May 1993. This data set is available at any

vertical and spectral resolution for general circulation model (GCM) simulations, and, as leaders of the GRIPS Pinatubo simulation task, we encourage all GRIPS participants to conduct this experiment. If the models cannot actually calculate the radiative forcing from using the radiation scheme of the model, we will provide the radiative forcing calculated with the ECHAM4 model, which can be used to drive any GCM. A complete formulation of radiative forcing includes not only changes of net fluxes at the tropopause, but the vertical distribution of atmospheric heating rates and the change of downward thermal and net solar radiative fluxes at the surface.

As a pilot demonstration project, we present simulations we conducted of the climatic response to the 1991 Pinatubo eruption with 3 GCMs, Max Planck Institut ECHAM4, GFDL climate model, and GFDL SKYHI model. With ECHAM4, we simulated climate change for the two-year period following the eruption of Mount Pinatubo in the Philippines on June 15, 1991. We calculated statistical ensembles of GCM simulations with and without volcanic aerosols for 2 years after the eruption for three different sea surface temperatures (SSTs): climatological SST, El Niño-type SST of 1991-1993, and La Niña-type SST of 1984-1986. The temperature of the tropical lower stratosphere increased by 4 K because of aerosol absorption of terrestrial longwave and solar near-infrared radiation. The heating was larger than observed, because we did not account for quasi-biennial oscillation (QBO) cooling and ...

**MW01/W/04-A5** Invited **1500**

**ANTARCTIC OZONE DEPLETION STUDY USING A PHOTOCHEMICALLY COUPLED MIDDLE ATMOSPHERE MODEL**

Jean DE GRANDPRE, D.J. Chartrand, S.R. Beagley, J. C. McConnell (All authors in Earth and Atmospheric Sciences Department (EATS), York University, Toronto, Canada)

Middle Atmosphere Models (MAMs) coupled with photochemistry modules are powerful tools to study ozone trends and polar ozone depletion scenarios. These models represent a comprehensive approach allowing the inclusion of complex interactions between chemical, radiative and dynamical processes which is suitable to investigate long term ozone behaviour. However, there are also well known limitations to the capability of these models to reproduce the basic climatology of the middle atmosphere. For example, the understanding of the role played by gravity waves in such models is an important issue given its global impact on the strength and evolution of winter polar vortices. On the photochemical aspects, the basic representation of heterogeneous processes is also required to model an ozone climatology which is representative of the observed state in polar regions throughout the year. Nevertheless, with the development of parameterization schemes and heterogeneous photochemistry modules, such climate studies using MAMs can now be considered. In several cases, basic characteristics of the ozone annual and interannual behaviour can be reproduced with some success. The CMAM (Canadian MAM) has been used to investigate antarctic ozone hole scenarios. Results will show the capability of the model to represent the ozone hole evolution on a seasonal timescale. Studies on the potential impact of various forcing mechanisms involved will be addressed.

**MW01/W/11-A5** Invited **1550**

**FIRST RESULTS FROM THE RADIATION-INTERCOMPARISON PROJECT FOR GRIPS**

Ulrike LANGEMATZ (Institut fuer Meteorologie, Freie Universitaet Berlin, Carl-Heinrich-Becker-Weg 6-10, 12165 Berlin, Germany, email: lang@strat01.met.fu-berlin.de)

In order to assess the impact of the representation of radiation transfer in Climate-Middle-Atmosphere-models (CMAMs) on the models' climatology and variability, an offline intercomparison of radiative codes is being performed within GRIPS (GCM - Reality Intercomparison Project for SPARC). Using standardized input data, the calculated radiative fluxes and heating rates can be compared directly thus enabling an assessment of the performance of the radiation codes. Here, first results of this intercomparison will be presented. An important question is the sensitivity of the radiation schemes to uncertainties in the distributions of trace gases, especially ozone: are differences in heating rates most sensitive to uncertainties in the parametrizations or to the ozone distribution? This issue will be discussed using a sensitivity study performed with one of the participating radiative codes.

**MW01/E/01-A5** Invited **1620**

**THE IMPACT OF TWO DECADES OF OZONE CHANGE ON THE STRATOSPHERE**

Suzanne ROSIER, Keith Shine, Piers Forster (Department of Meteorology, University of Reading, Earley Gate, Whiteknights, Reading RG6 6BB, UK)

The 'Intermediate' General Circulation Model (IGCM) developed at Reading incorporates sufficient physical processes to reproduce fundamental features of Earth's climate, yet is simple enough to simulate many decades quickly. It is a global, 3-D spectral model spanning the troposphere and stratosphere. The Morcrette radiation scheme is employed and a satellite-based 3-D seasonally-varying ozone climatology is supplied.

Results are reported of using the IGCM to investigate the effect of the last two decades of ozone change on the stratospheric climate. Ozone scenarios representative of 1979 and 1997 were estimated by combining the climatology with monthly observations of the trend in total column ozone from 1979 to 1997, taken from the 1998 WMO Ozone Assessment. The model has been run to an equilibrium using each of these scenarios and the two simulations compared. Differences in the stratospheric temperature and wind structures are of particular interest. Early results indicate that, in the annual and zonal mean, the lower stratosphere has cooled by up to 2K in the Arctic and 3K in the Antarctic. The temperature changes are further examined using a 'Fixed Dynamical Heating' (FDH) version of the IGCM, in which contributions to the temperature tendency from the dynamics are held fixed at the 'control' (1979) values. Differences of the experiment (1997 ozone) from the control then more clearly differentiate the radiative and the dynamical response to the ozone change.

Also of interest is the potential positive feedback in which lower stratospheric ozone loss leads to a colder lower stratosphere, a more stable winter vortex and further ozone loss. Under such conditions it might be expected that stratospheric sudden warmings occur less frequently, exacerbating the ozone loss. Whilst the IGCM currently does not allow the investigation of climate-chemistry interactions, the frequency of occurrence of sudden warmings is examined under the 1979 and 1997 scenarios reported here. Early results indicate a reduction in the frequency of sudden warmings in the ozone-depleted 1997 scenario.

**MW01/E/03-A5** Invited **1650**

**GCM SIMULATIONS OF STRATOSPHERIC CLIMATE CHANGE FROM 1992 TO 2051**

Jeffrey KNIGHT, John Austin, Neal Butchart, Adam Scaife (Meteorological Office, London Road, Bracknell Bricks, RG12 2SZ, UK.)

Results are presented from two 60-year integrations of the troposphere-stratosphere configuration of the U.K. Meteorological Office's Unified Model with different initialisations both



representative of 1992 conditions. The Intergovernmental Panel on Climate Change scenario IS92a was used to specify changes in well-mixed Greenhouse Gas (GHGs) concentrations and sea surface temperatures (SSTs) and sea ice extents were taken from a separate coupled ocean-atmosphere experiment. Both integrations produced tropospheric warming and stratospheric cooling that increased with height, giving a trend in annual mean temperature of about -1.4 K per decade at 1.0 hPa. Trends from these integrations were in good agreement apart from in the polar winter stratosphere, where significant interannual variability arising from the sporadic occurrence of sudden stratospheric warmings prevented the identification of statistically significant trends. Even after decadal smoothing trends in the northern winter were still small compared to the variability resulting from changes in the flux of planetary wave activity from the troposphere. Unlike other studies, our use of results from two separate simulations shows the change in the frequency of warmings was due to internal variability and not the GHG or SST forcing. In the southern winter the higher wave flux from the troposphere caused increasing diurnal heating although this was offset by the trend in radiative cooling. Consequently the polar vortex became more stable, breaking-down about 10 days later by 2050. Changes in Polar Stratospheric Cloud amounts were also calculated from model temperatures, allowing the implications for future polar stratospheric ozone loss to be discussed.

**GENERAL DISCUSSION****1720****MW04****Monday 19 July****TIDAL SIMULATION IN GLOBAL MODELS (ICMA)**

Location: Mechanical Engineering, G29 LT

**Monday 19 July AM**

Presiding Chairs: K. Hamilton (Geophys. Fluid Dynamics Lab./NOAA, New Jersey, USA), C. McLandress (York University, Toronto, Canada)

**MW04/W/04-A1****0900****ATMOSPHERIC TIDES IN THE EQUATORIAL AND TROPICAL MESOSPHERE/LOWER THERMOSPHERE**

R. A. VINCENT, S. Kovalam, I. M. Reid (Department of Physics and Maths Physics, University of Adelaide, Adelaide 5005, Australia, email: rvincent@physics.adelaide.edu.au); D. C. Fritts, D. Riggin (Colorado Research Associates, Boulder, CO 80301, USA, email: dave@colorado-research.com); T. Tsuda, T. Nakamura (Radio Atmospheric Science Center, Kyoto University, Kyoto, Japan, email: tsuda@kurasc.kyoto-u.ac.jp)

Radar observations of winds in the Asia/Pacific equatorial and tropical MLT region are used to explore the tidal structure as a function of latitude and longitude. Stations include Adelaide (35S, 138E), Pontianak (0N, 109E), Christmas Island (2N, 157W) and Kauai (22N, 160W). GSWM-98 model results are used as a reference to compare with climatologies of the diurnal and semi-diurnal tides at these stations. It is shown that there are significant longitudinal variations in amplitude and phase, which suggest that non-migrating modes play a role in determining tidal structure. The long-term nature of the observations also allows interannual variability to be studied. A QBO-like modulation of diurnal tidal amplitudes is found in certain seasons.

**MW04/W/11-A1****0925****SEASONAL VARIATIONS OF THE SEMI-DIURNAL AND DIURNAL TIDES IN THE MLT: MULTI-YEAR MF RADAR OBSERVATIONS FROM 2-70N, AND THE GSWM.**

Alan MANSON, Chris Meek (Institute of Space and Atmospheric Studies, University of Sask., Canada, email: manson@dansas.usask.ca); Chris Hall (Auroral Observatory, University of Tromsø, Norway, email: chris.hall@phys.uio.no); Wayne Hocking, John MacDougall (Dept. of Physics and Astronomy, University of Western Ontario, Canada, email: whocking@danlon.physics.uwo.ca); Steve Franke (Space Science and Remote Sensing Laboratory, University of Illinois, USA, email: sfranke@uiwpls.ecce.uiuc.edu); Dennis Riggin, Dave Fritts (Colorado Research Associates, Boulder, USA, email: riggin@colorado-research.com); Bob Vincent (Dept. of Physics and Mathematical Physics, University of Adelaide, Australia, email: rvincent@physica.adelaide.edu.au); Maura Hagan (NCAR, Boulder, USA, email: hagan@ucar.edu); Mark Burrage (SPRL, University of Michigan, USA, email: burrage@hrdi.sprl.umich.edu)

Continuous observations of the wind field over 5-8 years have been made with 6 MF Radars: Xmas Is, 2N, Hawaii, 22N, Urbana, 40N, London, 43N, Saskatoon, 52N & Tromsø, 70N. 12-, 24-h tidal-wind oscillations are available from 75-95km. Comparisons with the GSWM, and the new GSWM-98, which are available for 3-month seasons are made. The new model includes an extended Gravity Wave stress scheme, and an updated background atmosphere. Monthly tidal profiles for each site, and latitudinal plots of amplitudes and phases at 80/90km are shown. For the Diurnal tide, the agreements between observations and the models are in general very good, both capturing the strong seasonal changes. These are the best agreements yet seen. In particular, the phases and wavelengths for the non winter months are now in excellent agreement. For the Semi-Diurnal tide, the strong transitions between clear solstitial states are less well captured by the GSWM. In particular the late summer/autumnal tidal maxima of mid-latitudes are observed to be larger than modelled. The new satellite 12-hr tidal data from HRDI(UARS) for mid latitudes shows useful agreement with radar observations. Finally, the longitudinal variations are shown for two other sites near 52N; amplitudes may vary considerably, but the wavelengths are remarkably similar. This is valuable information for comparisons using observations that are not global in longitude. Future plans for observations and for the GSWM are discussed.

**MW04/W/01-A1****0950****CLIMATOLOGY OF THE SEMIDIURNAL TIDE AT 52 N - 56 N FROM GROUND-BASED RADAR WIND MEASUREMENTS 1985 - 1995**

Ch. JACOBI, M. Lange (Institute for Meteorology, University of Leipzig, Germany, email: jacobi@rz.uni-leipzig.de); Yu.I. Portnyagin, T.V. Solovjova (Institute for Experimental Meteorology, Obninsk, Russia, email: portnyagin@iem.obninsk.ru); P. Hoffmann, W. Singer (Institute of Atmospheric Physics, Kühlungsborn, Germany, email: hoffmann@iap-kborn.de); A.N. Fahrudinova, R.A. Ishmuratov (Radiophysics Department, Kazan University, Russia, email: antonina.fahrudinova@ksu.ru); A.G. Beard, N.J. Mitchell (Department of Physics, University of Wales, Aberystwyth, U.K., email: beard@aber.ac.uk); H.G. Muller (Cranfield University, RMCS Shriveneham, U.K.); D. Kürschner (Institute for Geophysics and Geology, University of Leipzig, Germany); A.H. Manson, C.E. Meek (Institute of Space and Atmospheric Studies, University of Saskatchewan, Saskatoon, Canada, email: manson@dansas.usask.ca)

Long-term wind measurements carried out at 6 northern midlatitude sites (Saskatoon, Sheffield, Juliusruh, Collm, Obninsk, Kazan) are investigated to set up a climatology of the semi-diurnal tide in the mesopause region for the latitudinal range between 52 N and 56 N. Intercomparison of amplitudes and phases shows good agreement of the results from the different measuring systems. The phase gradients and the absolute phase positions are very similar for each of the measurements. The longitudinal variation of the semi-diurnal tidal amplitude is small in summer, but larger in winter. The possible influence of wave-tidal interaction in the stratosphere on the inter-annual variability of this difference is discussed.

**MW04/E/02-A1****1010****TIDAL SIGNATURES IN CRISTA 2 TEMPERATURE DATA**

Jens Oberheide, Michael Jarisch, Martin RIESE, Dirk Offermann (all at Department of Physics, Wuppertal University, Gauss Str. 20, D-42097 Wuppertal, Germany, email: jens@wpos2.physik.uni-wuppertal.de); William E. Ward (CRESTech/CRESS, 206 Petrie Bld., York University, 4700 Keele St., North York, Canada, M4J1P3, email: william@stpl.cress.yorku.ca)

Temperature data taken during the second CRISTA mission (Aug. 7-19, 1997) show strong tidal structures from high southern to high northern latitudes and from the lower stratosphere to the upper mesosphere. Zonal means of temperatures are analyzed with respect to migrating diurnal tides. For most part, the observations are in very good agreement with the predictions of the Global Scale Wave Model (GSWM). However, zonal temperature variations at southern mid-latitudes indicate that the tidal amplitude is not uniform at all longitudes. It will be shown that this variation is associated with a wavenumber 2 planetary wave.

**MW04/E/03-A1****1100****TIDAL OBSERVATIONS BY SATELLITE AND SIMULATIONS BY THE CANADIAN MIDDLE ATMOSPHERE MODEL**

Charles McLANDRESS (Department of Earth and Atmospheric Science, York University, Toronto M3J 1P3, Canada, email: mcland@stpl.cress.yorku.ca)

The first part of this presentation reviews satellite observations of atmospheric tides made by the Upper Atmosphere Research Satellite (UARS). These include direct wind measurements by the High Resolution Doppler Imager (HRDI) and the Wind Imaging Interferometer (WINDII), which together span the stratosphere, mesosphere and thermosphere from about 20 to 200 m. Stratospheric temperature data from the Microwave Limb Sounder (MLS) are also presented. The migrating diurnal tide at low latitudes is the focus of the discussion, although some semi-diurnal tidal results will be shown. Together these UARS observations have provided the first long term global dataset of tides in the middle atmosphere. One of the most striking results to have arisen from these observations is the presence of a strong semiannual variation in the amplitude of the propagating diurnal tide. Moreover, lower stratospheric wind measurements by HRDI reveal an intriguing correspondence between the mesospheric tidal amplitudes and the phase of the quasi-biennial oscillation (QBO) in the zonal mean winds in the tropics. The exact physical mechanism which causes the semiannual variation of the tide, however, is currently not understood. In the second part, numerical simulations of the migrating diurnal tide using the Canadian Middle Atmosphere Model (CMAM) are presented. The CMAM is a general circulation model extending from the earth's surface to approximately 100 km, which contains comprehensive physical parameterizations relevant to the different altitude regions of the atmosphere. The CMAM is found to generate a propagating diurnal tide which is in good qualitative agreement with the UARS observations. In particular it exhibits a strong semiannual amplitude signal in the mesosphere. Direct comparisons of the simulated tidal temperature fields with MLS observations in the stratosphere are also presented. We conclude the presentation with a brief examination of some of the possible mechanisms which may be responsible for causing the semiannual variation of the diurnal tide in CMAM: These include tropospheric heating, gravity wave drag and planetary wave-tidal interactions.

**MW04/C/JSM01/E/14-A1****1135****THE ROLE OF GRAVITY WAVES IN MODULATING ATMOSPHERIC TIDES**

H. G. MAYR (NASA Goddard Space Flight Center, Greenbelt, MD, USA); J. G. Mengel (Steven Myers and Associates Co., Vienna, VA, USA); K. L. Chan (Hong Kong University of Science and Technology, Hong Kong, China); H. S. Porter (Furman University, Greenville, SC)

We discuss results for the diurnal and semi-diurnal tides obtained from our 3-D, time dependent, numerical spectral model, which incorporates Hines' Doppler spread parameterization (DSP) of small scale gravity waves (GW). In the DSP, GW momentum (and energy) are conserved. As a consequence, the GW interaction produces strong nonlinear interactions between mean zonal circulation, tides, and planetary waves. The major conclusions are: (1) Since GW momentum is deposited in the altitude regime of increasing winds, the amplitude of the diurnal tide is amplified and its vertical wavelength is reduced between 80 and 120 km. Wave filtering by the zonal circulation (with peak velocities during solstice) causes the GW flux to peak during equinox, and this produces a large semiannual variation in the diurnal tide with peak amplitudes during equinox as observed on UARS. (2) The diurnal tide in turn filters out GW preferentially during equinox, so that the semi-diurnal tide at higher altitudes tends to be largest during solstice. (3) Under the influence of GW, the tides are modulated significantly by planetary waves, with periods between 2 and 30 days, which are generated preferentially during solstice in part due to baroclinic instability.

**Monday 19 July PM**

Presiding Chairs: K. Hamilton (Geophys. Fluid Dynamics Lab./NOAA, New Jersey, USA), C. McLandress (York University, Toronto, Canada)

**MW04/E/01-A1****1400****TIDAL SIMULATIONS WITH THE GLOBAL-SCALE WAVE MODEL (GSWM)**

J.M. FORBES (Department of Aerospace Engineering Sciences, Campus Box 429, University of Colorado, Boulder, CO 80309-0429, USA, email: forbes@zeke.colorado.edu); M.E. Hagan (High Altitude Observatory, National Center for Atmospheric Research, P.O. Box 3000, Boulder, CO, 80307, USA, email: hagan@ncar.ucar.edu)

The GSWM solves the coupled momentum, thermal energy, continuity and constitutive equations for linearized steady-state atmospheric perturbations on a sphere from the surface to the thermosphere (ca. 300 km). Given the frequency, zonal wavenumber and excitation of a particular oscillation, the height vs. latitude distribution of the atmospheric response is calculated. The model includes such processes as surface friction, mean winds and meridional gradients in scalar atmospheric parameters, parameterized radiative cooling, eddy and molecular diffusion and ion drag. The advantages and disadvantages of this type of global tidal simulation are reviewed, and examples of diurnal and semi-diurnal migrating and nonmigrating tides excited by various sources in the troposphere, stratosphere, mesosphere and thermosphere are discussed.

**MW04/W/06-A1 1425****TIDAL OSCILLATIONS SIMULATED BY THE GFDL SKYHI GENERAL CIRCULATION MODEL**

Kevin HAMILTON (Geophysical Fluid Dynamics Lab/NOAA, Princeton, New Jersey 08542, USA, Email: kph@princeton.edu)

The diurnal and semidiurnal tides as simulated in the GFDL SKYHI comprehensive general circulation model will be described. Aspects to be emphasized include the seasonal cycle, day-to-day variability, effects of subgrid-scale dissipation and interaction with other explicitly-resolved waves.

**MW04/W/08-A1 1450****SIMULATION OF THE TIDES IN THE EXTENDED UGAMP GCM**

W. NORTON (AOPP, University of Oxford, UK, email: wan@atm.ox.ac.uk)

A global circulation model which extends from the surface to approximately 128 km has been used to examine the simulation of the tides. From a three year integration, interannual variability of the diurnal, semi-diurnal, and non-migrating tides are examined. The heating distribution is also examined.

It is shown that large two-day wave activity reduces the amplitude of the diurnal tide around the solstice. The interaction of the tides with the two-day wave produces other waves including a wave-number 4, 16 hour wave. It is shown that the amplitude of the two-day wave is controlled by the mean structure of the summer mesosphere which is strongly influenced by the strength of parameterized gravity wave breaking. Hence the parameterized gravity wave breaking has a strong indirect influence on the simulation of the tides.

**MW04/W/05-A1 1545****TIDES IN THE MIDDLE ATMOSPHERE CIRCULATION MODEL AT KYUSHU UNIVERSITY**

Saburo MIYAHARA, Yasunobu Miyoshi (Department of Earth and Planetary Science, Kyushu University, Fukuoka 821-8581 Japan, e-mail: sbm@rossby.geo.kyushu-u.ac.jp, miyoshi@rossby.geo.kyushu-u.ac.jp)

The Middle Atmosphere Circulation Model at Kyushu University (MACMKU) is a three-dimensional general circulation model with a domain spanning from the ground to 150 km. The model's radiation processes have a diurnal cycle, so that tidal waves are generated. Heating sources which generate tidal waves in the model are reviewed at first. After that, model's ability to simulate the generated tidal waves is discussed. Output data of the MACMKU are analyzed to study behavior of tidal waves in the MLT region. It is shown that not only the migrating tides but also non-migrating tides exist in the model, and variability of amplitudes and phases of tides are larger for the non-migrating components than the migrating tides.

Only the zonal component of zonal mean momentum flux associated with tidal waves in the MLT region usually receive much attention in connection with zonal mean wind acceleration (deceleration). However, the present analysis shows that the meridional component of zonal mean momentum flux has large magnitude in the MLT region, and affects the geostrophic balance between the Coriolis force on the zonal mean zonal wind and the zonal mean meridional pressure gradient force.

**MW04/W/03-A1 1610****SIMULATION OF TIDES IN THE UK MET OFFICE UNIFIED MODEL**

Sophia OLIVER (Atmospheric Physics, Oxford University, Clarendon Rd., Oxford, OX1 3PU, UK, email: oliver@atm.ox.ac.uk)

The UK Met Office Unified Model version 4.0 is used to apply a mechanistic approach to the modelling of thermally forced tides in the middle atmosphere. The model has 36 vertical levels with the highest near 110km. Physics routines have been removed from the model set-up leaving only the dynamics core. The model is initialised with zonally symmetric background temperature and zonal wind fields, and is forced with specified westward-propagating heating fields in wavenumbers 1 and 2. This approach enables clear identification of features which are due to the tides and their interaction with each other and with the mean flow. A 54 level version of the unified model with Hadam 3 physics (extended from the 49 level model by Dave Stainforth) is also being used to calculate the tides and comparisons with the mechanistic approach are made.

**MW04/W/10-A1 1630****A MODEL STUDY OF UARS WIND, TEMPERATURE, AND AIRGLOW DATA: INTERANNUAL VARIABILITY OF TIDAL EFFECTS IN THE MLT REGION**

Marvin A. GELLER, Valery A. Yudin, Ling Wang (State University of New York at Stony Brook, Stony Brook, NY 11794, USA, email: mgeller@notes.cc.sunysb.edu)

The UARS wind, temperature, and airglow data have been analyzed using the Tuned Mechanistic Tidal Model (TMTM) approach and compared to the long-term tidal variability obtained from radar wind observations. The global coverage of the HRDI wind measurements in the stratosphere and MLT regions allows an estimate to be made for gravity wave effects on the zonal mean flow and the tides for the different stages of the strato-mesospheric QBO. Estimated values of the effective tidal dissipation derived from UARS tidal observations have been compared to the values of the eddy dissipation calculated with gravity wave parameterizations applied to the different years of UARS observations. The possible mechanisms for interannual tidal variability, including variability in the tidal forcing, dissipation, and propagation, have been simulated using the TMTM approach for 1992, 1993, and 1994 equinox conditions with prescribed zonal mean temperatures and winds (as constrained from HRDI/MLS UARS measurements). It is shown that the UARS observed interannual tidal variability simulated by the TMTM approach can induce the year-to-year variability of oxygen airglow emission rates in the equatorial MLT region.

**MW04/W/09-A1 1650****A MODEL STUDY OF UARS WIND, TEMPERATURE, AND AIRGLOW DATA: SEASONAL VARIABILITY OF TIDES AND GRAVITY WAVES IN THE MLT REGION**

Valery A. YUDIN, Marvin A. Geller, Ling Wang (State University of New York at Stony Brook, Stony Brook, NY 11794, USA, email: valery@dombai.uars.sunysb.edu)

The 1992-96 UARS wind, temperature, ozone and airglow data reveals a strong semiannual

variation in the mid-latitude and equatorial tidal fields. Several mechanisms have been suggested to interpret this semiannual variation of the diurnal tide: planetary wave-tidal interactions, variations of the effective tidal dissipation associated with gravity wave breaking, and possible changes in the tropospheric water vapor tidal forcing. A revised version of the Tuned Mechanistic Tidal Model (TMTM) utilizing UARS wind, temperature, and ozone data has been used to study the seasonal variability of the diurnal tide due to variations in the tidal forcing, background mean fields, and tidal dissipation. The tidal influence on the seasonal variation of the nighttime and daytime oxygen emissions have been simulated and compared to UARS observations. Several model case studies with prescribed zonal mean flow have been examined to show the solstice-equinox differences in the gravity wave and tidal fields for different local solar times. These have been compared to the wind and temperature structures observed by the HRDI and WINDII instruments.

**MW04/W/02-A1****1710****STRATOSPHERIC TIDES AND DATA ASSIMILATION**

R. SWINBANK (Universities Space Research Association, NASA Goddard Space Flight Center, Greenbelt, MD 20771, USA; email: swinbank@dao.gsfc.nasa.gov); R.L. Orris (Anne Arundel Community College, Arnold, MD, USA; email: rlorris@mail.aacc.cc.md.us); D.L. Wu (JPL, Caltech., Pasadena, CA 91109, USA; email: dwu@mls.jpl.nasa.gov)

In the upper stratosphere, the atmosphere exhibits significant diurnal and semi-diurnal tidal variations, with typical amplitude of about 2K in mid-latitudes. In this paper we examine how well the tidal variations in temperature are represented by the Goddard (GEOS-2) data assimilation system. We show that the GEOS-2 atmospheric model is quite successful at simulating the tidal temperature variations. However, the assimilation of satellite temperature soundings significantly damps the simulated tides. The reason is because the tides are not well-represented by the satellite retrievals used by the assimilation system (which have a typical tidal amplitude of around 1K). As a result of this study, we suggest improvements that should be made to the treatment of satellite soundings by the assimilation system.

**MW05****Tuesday 20 July****RADIATIVE PROCESSES IN THE MESOSPHERE AND LOWER THERMOSPHERE (ICMA, IRC)**

Location: Mechanical Engineering, G28 LRE

Location of Posters: Old Gym

**Tuesday 20 July AM**

Presiding Chairs: G.M. Shved (Atmospheric Physics Dept., St. Petersburg University, Russia), V.I. Fomichev (York University, Toronto, Canada)

**MW05/W/05-A2**

Invited

**0940****INFRARED RADIATIVE COOLING AND HEATING IN THE MESOSPHERE AND LOWER THERMOSPHERE AND ITS PARAMETERIZATION**

Victor I. FOMICHEV (Dept. of Earth and Atmospheric Science, York University, Toronto, Canada, email: victor@nimbus.yorku.ca)

The thermal regime of the middle atmosphere is determined to a great extent by infrared radiative cooling and heating processes. To account for these processes in numerical models of the atmosphere, parameterizations that are capable of quickly and accurately calculating infrared radiative cooling and heating rates are required. These parameterizations should also include NLTE effect and allow for feedbacks by ensuring that dependencies on all input parameters are accounted for. A review of the major mechanisms responsible for the infrared cooling/heating processes in the middle atmosphere as well as recently developed parameterizations will be presented.

**MW05/W/10-A2**

Invited

**1000****NON-LTE RADIATIVE AND CHEMICAL HEATING IN A TWO-DIMENSIONAL MODEL**

Xun ZHU (JHU/APL, 11100 Johns Hopkins Rd., Laurel MD 20723-6099, USA, email: xzhu@grant.jhuapl.edu)

The conversion of radiative energy into thermal energy that drives mesospheric circulation is critically dependent on the atomic oxygen distribution in two aspects. First, the deactivation of the CO<sub>2</sub> bending mode (15 micron band) by atomic oxygen increases the cooling rate around the mesopause region because it restores the CO<sub>2</sub> bending mode population closer to local thermodynamic equilibrium (LTE). Second, a longer photochemical timescale of atomic oxygen than its transport timescale above the mesopause produces a non-local chemical heating rate. Since the atomic oxygen distribution is determined collectively by both dynamics and photochemistry in the upper mesosphere and lower thermosphere (UMLT), a consistent evaluation of radiative and chemical heating balance requires a fully coupled model that produces a self-consistent picture of the temperature field, net radiative heating rate, and several chemical tracer distributions needed for the chemical heating rate calculations. The recently-developed JHU/APL fully-coupled 2-dimensional model is used to evaluate the energy balance in the UMLT region. Around 95 km, it is shown that the dynamically controlled atomic oxygen distribution produces a chemical heating rate with a latitudinal gradient that counters the gradient of the net radiative heating rate. The solar cycle effect of the Lyman alpha and Schumann-Runge continuum radiation on the energy balance in the UMLT region will also be examined.

**MW05/W/09-A2**

Invited

**1020****CARBON DIOXIDE AND ATOMIC OXYGEN IN THE LOWER THERMOSPHERE**

Klaus U. GROSSMANN (Dept. of Physics, University of Wuppertal, Germany, e-mail: gross@wpos2.physik.uni-wuppertal.de)

The Cryogenic Infrared Spectrometers and Telescopes for the Atmosphere (CRISTA) experiment took measurements of several infrared emissions in the lower thermosphere during two Shuttle flights in November 1994 and in August 1997. Among the recorded emissions are the 4.3 μm band of carbon dioxide and the atomic oxygen fine structure transition at about 63 μm. From the measured altitude distribution of the 4.3 μm band intensities the F densities are derived using a non-LTE model for the CO<sub>2</sub> emission during daylight. The atomic oxygen densities are calculated directly from the measured radiances using thermospheric temperatures from the CIRA model. The resulting data exhibit substantial

horizontal structures which are attributed to vertical movements in the lower thermosphere. The implications will be discussed.

**MW05/W/03-A2** Poster **1040-01**

**THE CO<sub>2</sub> NON-LTE PROBLEM TAKING ACCOUNT OF THE MULTIQUANTUM TRANSITIONS ON THE V<sub>2</sub>-MODE DURING CO<sub>2</sub>--O COLLISION**

V.P. OGIBALOV (Institute of Physics, St.Petersburg State University, St.Petersburg / Petrodvorets 198904, Russia, email: vpo@lmupa.phys.spbu.ru)

The strong anisotropy of the interaction potential during CO<sub>2</sub>--O collisions can result in transitions with the CO<sub>2</sub> state change of two- or more v<sub>2</sub>-quanta. The CO<sub>2</sub> non-LTE problem of the Earth atmosphere, taking account of these transitions, has been solved. The results have been compared with those obtained for the usually adopted one-v<sub>2</sub>-quantum transitions during the CO<sub>2</sub>--O collisions. Increasing up to tens of Kelvin degrees of vibrational temperatures of the CO<sub>2</sub> v<sub>2</sub>-mode manifold states in the lower thermosphere has been found, since in the case of multiquantum transitions these states can be excited by O from the ground state of the CO<sub>2</sub> molecule. Adopting multiquantum pathway results in a considerable increase of the 15 micron band limb radiance above 100 km as compared with the one-v<sub>2</sub>-quantum pathway case. The multiquantum transitions can result in the increase of cooling rate in the 15 micron CO<sub>2</sub> band up to 15--25 K/day at the altitudes of 125--130 km. Both these consequences are demonstrated to be caused mainly by increasing of populations of the 0200, 0220 and 1000 states of the principal isotope of CO<sub>2</sub>.

**MW05/W/06-A2** Poster **1040-02**

**HIERARCHY OF VIBRATIONAL STATE SETS FOR SOLUTION OF THE CO<sub>2</sub> NON-LTE PROBLEM**

V.P. OGIBALOV, G.M. Shved (Institute of Physics, St. Petersburg State University, St.Petersburg-Petrodvorets 198904, Russia, email: vpo@lmupa.phys.spbu.ru)

The set of 321 excited vibrational states belonging to 7 isotopes of the CO<sub>2</sub> molecule has been used to solve the CO<sub>2</sub> non-LTE problem of the Earth atmosphere. Employing the Feautrier technique and accelerated lambda iteration has provided computing the state populations to a high accuracy. Using the above set as a standard, the effect of reducing the quantity of involved states on the accuracy of evaluating state populations, cooling/heating rates in the CO<sub>2</sub> bands, and limb radiance in the both 4.3 and 15 micron CO<sub>2</sub> bands has been studied. Criteria for the selection of state sets have been proposed. Using the criteria, three sets for estimating populations of lower vibrational states to a specified accuracy have been recommended. In order of decreasing accuracy, those are the sets of 206 and 117 states, belonging to 7 CO<sub>2</sub> isotopes, and the set of 60 states, belonging to 5 isotopes.

**MW05/E/01-A2** **1115**

**EVIDENCE FOR NON-LTE EMISSIONS OF CO<sub>2</sub>, O<sub>3</sub>, H<sub>2</sub>O, AND NO<sub>2</sub> FROM UARS/CLAES**

David P. EDWARDS (National Center for Atmospheric Research, Boulder CO, USA, email: edwards@ucar.edu); Manuel Lopez Puertas (Instituto de Astrofísica de Andalucía/CSIC Granada, Spain, email: puertas@iaa.es)

We describe observations of non-local thermodynamic equilibrium (non-LTE) limb radiance using data taken by the Upper Atmosphere Research Satellite CLAES instrument. We have studied the relative radiance contributions from CO<sub>2</sub> and O<sub>3</sub> in the CLAES blocker 5 region at 10.83 microns, and have examined the correlation with solar zenith angle. The diurnal variation of the measured emission points to solar dependent mechanisms selectively populating molecular vibrational levels in CO<sub>2</sub> and O<sub>3</sub>. These processes are shown to affect the limb radiance for limb view tangent heights above about 40 km. The analysis shows good agreement between measured and calculated radiances and confirms our previous theoretical modelling of the non-LTE populations of these states.

There have been problems with the CLAES retrievals of H<sub>2</sub>O and NO<sub>2</sub> in the blocker 3 region at 6.2 microns. This has been primarily due to uncertainties in our understanding of the radiance measurements. We present results of a study examining the daytime non-LTE enhanced stratospheric emission from excited NO<sub>2</sub> states populated as a result of chemiluminescence and fluorescence processes. When examining the diurnal change in radiance, this must be considered alongside the photochemically driven change in NO<sub>2</sub> concentration. Emission from H<sub>2</sub>O shows a daytime enhancement in the mesosphere due to non-thermal collisions and solar absorption. We discuss the implications of these studies for the future measurements of the High Resolution Dynamics Limb Sounder (HIRDLS) due to be launched on the EOS-CHEM satellite in 2002.

**MW05/W/08-A2** **1130**

**EFFECT OF OZONE NON-THERMAL EMISSION ON THE COOLING RATE IN THE MIDDLE ATMOSPHERE**

Katerina KOUTOULAKI, Brian J. Kerridge (both at Rutherford Appleton Laboratory, Chilton, Didcot, Oxfordshire, OX11 0QX, UK, email: a.koutoulaki@rl.ac.uk); Manuel Lopez-Puertas, Francisco J. Martín (both at Instituto de Astrofísica de Andalucía (CSIC), Apdo. 3004, 18080 Granada, Spain, email: puertas@iaa.es)

Ozone thermal emission is the second most important source of infrared cooling in the middle atmosphere, due to emission at 9.6 microns. However, ozone is chemically pumped in the middle atmosphere by the recombination reaction: O + O<sub>2</sub> + M --> O<sub>3</sub>(v) + M This process leads to non-thermal emission from O<sub>3</sub>(v) that can potentially enhance the cooling rate, especially due to emission from ozone hot bands. The effect of this non-thermal emission on the ozone cooling rate will be investigated, between 10 mb and 0.1 mb. The vibrational populations used to calculate hot band cooling rates are those derived from the analysis of the Improved Stratospheric and Mesospheric Sounder (ISAMS) data (Koutoulaki, 1998). Furthermore, upper and lower limits on the above effect will be presented, consistent with the ISAMS data analysis. In this way, the importance of a) the nascent distribution from the recombination reaction and b) the collisional relaxation rates to the ozone cooling rate will be examined.

References: A. Koutoulaki, Study of ozone non-thermal IR emission using ISAMS observations, D.Phil thesis, University of Oxford, 1998.

**MW05/W/01-A2** **1145**

**ATOMIC OXYGEN PEAK HEIGHT AND PEAK DENSITY FROM GROUND BASED NIGHTGLOW MEASUREMENTS AT 23 S**

M. Stella, L. MELO, R.P. Lowe (The University of Western Ontario, Canada email: stella@danlon.physics.uwo.ca); Ian C. McDade (York University, Toronto, Canada

e-mail: mcdade@windh.yorku.ca); Hisao Takahashi (INPE, São Paulo, Brasil, e-mail: hisao@laser.inpe.br)

Atomic oxygen plays a fundamental role in the upper mesosphere-lower thermosphere (MLT) region. As a dominant minor constituent, it controls directly or indirectly many photochemical processes and plays an important role in the MLT energy budget through both heating and cooling processes. As its lifetime is relatively long atomic oxygen can also be used as a passive tracer of motions in the MLT. The inaccessibility of the MLT region to both balloons and satellites and the intrinsic sporadic nature of in situ rocket experiments make remote sensing of nightglow features one of the most useful techniques for obtaining information about atomic oxygen variability. However, it has generally been thought that ground-based measurements of the zenith integrated airglow intensities cannot provide useful information about vertical distributions of atomic oxygen. Here we demonstrate how ground-based measurements of selected airglow emission features may be used to determine the vertical distribution of atomic oxygen in the upper mesosphere and lower thermosphere. The technique is applied to ground-based measurements of the OI 557.7 nm green line, the O<sub>2</sub> Atmospheric (0-1) band and the OH Meinel (9-4) band emissions made at Cachoeira Paulista (230 S, 450 W), Brazil, between 1987 and 1994. The limits of validity of such technique are exploit using nightglow profiles measured by the WINDII experiment on board UARS satellite when both the satellite on board and the ground-based instruments were observing the same region.

**MW05/W/04-A2** **1200**

**IMPACTS OF MODIFIED SOLAR AND CHEMICAL HEATING ON THE CANADIAN MIDDLE ATMOSPHERE MODEL**

Chao FU, Victor Fomichev, Jean de Grandpre, John McConnell, Stephen Beagley (Department of Earth and Atmospheric Science, York University, 4700 Keele Street, North York, Ontario, M3J 1P3, Canada, email: chao@nimbus.yorku.ca)

The Canadian Middle Atmosphere Model (CMAM) is a GCM that extends from the surface to about 95 km with non-orographic gravity wave drag, solar and IR heating appropriate for the upper atmosphere. Also included is a comprehensive interactive chemical package that covers the region from 5-95 km. Recently, we have modified the heating parameterization above 50 km to allow explicitly for chemical heating. We have calculated the chemical heating rates associated with seven exothermic reactions involving odd-oxygen and odd-hydrogen families and adjusted the ozone heating to allow for the chemical potential energy; heating in the Schumann-Runge bands and continuum has been added. The addition of a more consistent heating scheme in the mesosphere and lower thermosphere results in several improvements in the model. For example, temperatures above the mesopause are increased. The diurnal variation of heating above mesopause is much more uniform than before and this has impacts on the circulation in this region and beyond. We will present results comparing the magnitude of the heating rates for the standard and new versions of the CMAM and also detail the impact on the circulation as measured against a standard climate run.

**MW05/W/07-A2** **1215**

**DERIVATION OF THE CO<sub>2</sub> VIBRATIONAL TEMPERATURES FROM THE LIMB RADIANCE MEASUREMENTS AND COMPARISON WITH MODEL PREDICTIONS**

Vladimir KOSTCOV, Vladimir Ogibalov, Yuri Timofeyev (Research Institute of Physics, St. Petersburg State University, Ulyanovskaya 1, St. Petersburg-Petrodvorets, 198904 Russia, email: vlad@troll.phys.spbu.ru)

The vibrational temperatures of the CO<sub>2</sub> state 01101 for the 626, 636, 628, and 627 CO<sub>2</sub> isotopes have been derived in the altitude range 60-130 km together with the kinetic temperature from the limb radiance spectra measured by the CRISTA instrument during 1994 mission. The measurement data inversion method did not involve an a priori information in the form of modelling of the processes driving non-LTE. The accuracy of the method has been estimated on the basis of error matrix calculations and numerical experiments. The selected for the analysis dataset included the vertical profiles of the kinetic and the vibrational temperatures for different atmospheric situations with latitudinal coverage 60S-60N and wide longitudinal coverage. On the basis of the derived kinetic temperature and pressure profiles the model vibrational temperatures for CO<sub>2</sub> have been calculated with certain assumptions caused by lacking of complete information on the atmospheric state during measurements. These model predictions have been compared with the vibrational temperature profiles retrieved from the CRISTA spectral data. The retrieval accuracy and the results of the comparison of derived and modeled profiles are discussed.

**MW05/E/03-A2** **1230**

**NATURAL POPULATION INVERSION FOR THE CO<sub>2</sub> VIBRATIONAL STATES IN THE EARTH'S ATMOSPHERE**

V.P. OGIBALOV, G.M. Shved (Institute of Physics, St.Petersburg State University, St.Petersburg-Petrodvorets 19890, Russia, email: vpo@lmupa.phys.spbu.ru)

The non-LTE problem of populations, n, for vibrational states of CO<sub>2</sub> molecules has been solved for the Earth's atmosphere in the daytime. The inversion of the 0001 level population with respect to the 1000 level population has been derived near the mesopause. The inversion occurs due to excitation of the 0001 level by two pumping mechanisms. The main mechanism is excitation due to solar radiation absorption in the CO<sub>2</sub> bands. The mechanism provides the peak values of ratio [n(0001)/n(1000)] up to about 1.2 in the 95--100 km layer. The second mechanism is an energy transfer from O(1D) produced during photodissociation of O<sub>2</sub>. This mechanism can significantly increase the above ratio. However, its contribution may not be estimated with a good validity, since the number of N<sub>2</sub> vibrational levels, exciting during the O(1D)--N<sub>2</sub> collisions, is unknown up to now. An utilization of the natural inversion for generation of the 10.4 micron laser emission is also discussed.



MW06

Wednesday 21 July

LOW FREQUENCY DYNAMICS IN THE MID-HIGH LATITUDES (ICMA)

Location: Law, 116 LR3

Wednesday 21 July AM

Presiding Chair: Chongyin Li (Institute of Atmospheric Physics, Beijing, China)

MW06/E/08-A3

0930

TOWARDS A FULL UNDERSTANDING OF THE WINTER STORM TRACKS

Mankin MAK (Department of Atmospheric Sciences University of Illinois, Urbana, Illinois, 61801, USA)

What have been learned from the dynamical studies of the winter storm-tracks in the past 20 years will be reviewed for the purpose of identifying what are relatively well established and why some aspects remain elusive. A recently completed analysis of the relative importance of several diabatic processes will also be reported. In conclusion, we will comment on some promising unresolved issues. We will begin by reviewing the observed characteristics of the normal winter storm-tracks and their interannual variability. Then we will review the early dynamical studies that aimed at accounting for the geographical locations of the two-winter storm tracks. The answer was sought by means of linear instability of a zonally inhomogeneous baroclinic flow, highlighting the pivotal role of the two pronounced localized jets in mid-latitudes. The central issue of maintenance of the winter storm-tracks has received considerable attention, but it proves to be somewhat elusive. Although most studies focussed on the dry dynamics per se, it is not certain whether or not condensational heating plays a role of first order importance in the storm-tracks dynamics. Some studies largely introduced the all-important localised jets in the form of an external forcing a priori. Their focus was to ascertain the extent to which the storm-tracks could be simulated under such condition. Another fundamentally different approach has been to analyse the storm-tracks as a linear forced stochastic response. The extent of success and limitation of these attempts will be reviewed. We will report a recent model analysis which is intended to delineate the impacts on the maintenance of the northern hemispheric winter storm tracks by the diabatic heating (radiative forcing, surface heat flux and self-induced condensational heating) in conjunction with orographic forcing. As the constituent eddies of the storm-tracks and the accompanying planetary localised jets are treated on equal footing as unknowns, the nature of their interdependence can be more clearly delineated.

MW06/E/07-A3

1000

MID-LATITUDE STORM-TRACKS SENSITIVITY STUDIES TO SST IN A GCM

Marie DREVILLON, Philippe Rogel, Laurent Terray (CERFACS, Climate Modelling and Global Change Team, 42 avenue G. Coriolis, 31057 Toulouse cedex 1, France, email: drevillo@cerfacs.fr)

This work aims at studying the coupled interaction between SST, storm-tracks activity and the mean flow characterized by the geopotential height at 500 hPa, and in particular at how SST anomalies and boundary layer processes may influence wave-mean flow interaction. This will be done through the following three points:

First mid-latitude storm-tracks are identified using the RMS of bandpass 2.2 to 6 day filtered geopotential height at 500 hPa, in NCEP reanalysis for the 1958-1998 period and ECMWF reanalysis for the 1979-1994 period, as well as in simulations of Meteo France ARPEGE-Climat GCM (T42). One of these simulations has a climatological and the other a month to month SST forcing. Storm-tracks variability is first addressed through an EOF analysis for each simulation and the reanalysis, which helps estimate the influence of interannual variability of sea surface temperature upon storm-tracks variability.

Second, in order to study coupled modes of variability, three two by two SVD analyses are performed on detrended datasets of SST, storm-tracks activity and geopotential height at 500 hPa. Periods with high and low covariance between those three fields are sorted out. These SVD computations are performed over monthly and winter averaged fields which allows a discussion of the results in terms of time scales ranging from intraseasonal to interannual.

Third, these results help determine sample situations with varying covariance between storm-tracks, forcing and background circulation, for which sensitivity experiments will be performed. Preliminary experiments testing the influence of SST anomalies are presented.

MW06/W/08-A3

1020

INTERANNUAL AND INTERDECADAL VARIATION OF NORTH PACIFIC WINTER-TIME BLOCKING

Tsing-Chang CHEN, Jin-ho Yoon (Department of Geological and Atmospheric Sciences, Iowa State University, Ames, IA 50011, USA, email: tmchen@iastate.edu)

We explore inter-annual and interdecadal variations in the occurrence frequency of North Pacific (NP) wintertime (December-February) blocking using the NCEP reanalysis data for the period 1958-1997. A systematic interannual variation of NP blocking occurrence frequency emerges. Blocking occurs more often during the La Nina winters than the El Nino winters. Furthermore, a clear interdecadal increasing trend of NP blocking stands out in the past four decades, while the winter mean location of NP blocks shifts eastward. The streamfunction budget (Laplace inverse transform of the vorticity equation) analysis is used to explain the dynamic cause of these interannual and interdecadal variations.

The dynamic processes (i.e. vorticity advection and stretching) maintaining the La Nina (El Nino) anomalous circulation spatially match (mismatch) with those maintaining (suppressing) blocking in such a way that blocking occurrence was facilitated (hindered) during the La Nina (El Nino) winter. For the interdecadal variation, centers of dynamic processes maintaining the anomalous circulation pattern shifted eastward over the past four decades. This shift also results in the eastward shift of dynamic processes maintaining the NP blocks. Since both the interannual and interdecadal anomalous circulation patterns are the atmospheres response to the tropical Pacific sea surface temperature (SST) change, the interannual and interdecadal variations in NP wintertime blockings are also the consequence of the tropical Pacific SST change.

MW06/W/07-A3

1100

A MODELLING OF THE RESPONSE OF ATMOSPHERIC CIRCULATION TO SST ANOMALIES IN THE WINTERTIME NORTH ATLANTIC

Nikolai A. DIANSKII, A. V. Glazunov (both at Institute of Numerical Mathematics RAS, ul. Gubkina 8, 117951, Moscow GSP-1, Russia, email: dinar@inn.ras.ru)

The interaction of atmosphere and ocean in the wintertime North Atlantic was studied. For this

purpose several numerical experiments with atmospheric general circulation model of INM RAS were carried out. In these experiments 360 month runs of the atmospheric model were performed in the perpetual January mode. In the first experiment a model of the upper mixed layer of ocean was coupled to the atmospheric model. It was shown that the spatial structures of leading empirical orthogonal functions (EOF) for interannual anomalies of H500 produced by the coupled model is closer to observations than these structures for the atmospheric model with the prescribed climatic SST. Two experiments were performed with prescribed stationary and alternative sign (with prescribed temporal evolution) SST anomalies in North Atlantic extracted from the results of the coupled model simulation. It was revealed that the stationary atmospheric response to SST anomaly may contain the global response along with the localized response. It was shown that the localized response of atmospheric model to the SST anomaly has baroclinic structure. This response can be identified as the response to the SST anomaly with prescribed temporal evolution by means of the method of singular value decomposition analysis. The global response has quasi-barotropic structure and is determined by the leading low-frequency EOFs. To reveal the temporal formations of localized and global response a Monte-Carlo numerical simulation was carried out.

MW06/E/03-A3

1120

BLOCKING OVER THE SOUTH PACIFIC: THE EXTRATROPICAL ROSSBY WAVE RESPONSE TO A MOVING DIVERGENCE FORCING IN THE TROPICS?

Michael REVELL, James Renwick (both at National Institute of Water and Atmospheric Research, Wellington, New Zealand, email: m.revell@niwa.cri.nz)

Atmospheric blocking events over the South Pacific are investigated using a 39 year record of 500 hPa height fields from the NCEP/NCAR reanalysis data set. The analysis extends earlier work using a 16 year record and confirms that the occurrence of blocking over the southeast Pacific is strongly modulated by the ENSO cycle during austral spring and summer. Comparison of results at 500 hPa with the 300 hPa meridional wind component showed that blocking events are associated with large-scale wave trains lying across the south Pacific from the region of Australia to southern South America. Similar wave trains are evident in both hemispheres in singular value decomposition analyses between 300 hPa meridional wind components and tropical Pacific outgoing longwave radiation (OLR) anomalies.

The hypothesis that the divergence associated with tropical OLR anomalies forces an extra-tropical wave response which results in enhanced blocking over the southeast Pacific was tested using a linearised, barotropic vorticity equation (BVE) model. Observed 300 hPa mean flow fields and divergence forcing which matched the anomalous OLR were used to drive the BVE model. The resulting pattern of meridional wind and stream function anomalies agrees closely with observations.

When the tropical OLR anomaly is given an eastward phase speed of 5 degrees per day, the extra-tropical response agrees even better with observations. This suggests that linear Rossby wave propagation provides an important link between anomalous convection in the tropics and the occurrence of blocking over the southeast Pacific Ocean.

MW06/W/01-A3

1140

EFFECT OF MIDLATITUDE SST ANOMALIES ON STORM TRACK POSITION AND AMPLITUDE - AN IDEALISED STUDY

David N. BRESCH (Massachusetts Institute of Technology, 77 Massachusetts Av, Cambridge, MA 02139, USA, email: bresch@mit.edu); Rene Fehlmann (Swiss Federal Institute of Technology, ETH Hoenggerberg, CH-8093 Zuerich, Switzerland, email: fehlmann@atmos.unmwn.ethz.ch); Huw C. Davies (Swiss Federal Institute of Technology, ETH Hoenggerberg, CH-8093 Zuerich, Switzerland, email: davies@atmos.unmwn.ethz.ch)

The contrasting properties of ocean and atmosphere render the coupled system of significant importance for the understanding of midlatitude climate variability. Indeed the linkage between oceanic and atmospheric fluctuations is an important component of the climate system, and has far-reaching practical implications, particularly in the realm of extended-range prediction of weather and climate. In this study, consideration is given to the effect of selected midlatitude SST anomalies on the atmospheric flow evolution in an idealised model setting, yielding insight on the (non-linear) interaction of ocean and atmosphere. A SVD analysis of observed coupled patterns of SST and storm track is both used to define the SST perturbations and for the purpose of model verification. An examination of the possible effect of the distinctive SST patterns formed the basis for a sequence of simulations with an idealised primitive equation model. The imposition of a dipole SST pattern leads to an intensification of the storm track and a concomitant strengthening of the (stationary) trough in the geopotential height field which bears some resemblance to the NAO dipole structure. While the anomalous atmospheric response does not perfectly project on the corresponding statistically derived coupled (SVD) patterns, particular features of the idealised model results do relate to the overall structure of the first coupled mode. This indicates that the SST dipole forces limited features of the whole coupled atmospheric patterns. Furthermore, the modelled atmospheric response is shown to be both non-linear and highly sensitive to the precise location of the SST anomaly.

MW06/E/06-A3

1200

THE DYNAMICS OF THE ANTARCTIC CIRCUMPOLAR WAVE

Peter G. BAINES (CSIRO Atmospheric Research, PMB No. 1, Aspendale, 3195, Australia)

The Antarctic Circumpolar Wave (ACW) is a large scale coupled atmosphere-ocean disturbance in the region of the Southern Ocean. Observations show that it consists of a zonal wave number two pattern in sea surface temperature, sea surface height, and sea ice extent from the Antarctic coast, with associated patterns of atmospheric sea level pressure and wind stress curl. It circles the globe with a period of approximately nine years, and a local period of about 4.5 years. It seems likely that the ACW has a significant effect on the climate (temperature and rainfall) of southern Australia, comparable with that of El Nino. A manifestation of this phenomenon has been observed in the CSIRO Mark 2 coupled model. A simple model that explores the dynamics of the ACW is presented. This consists of a baroclinic atmosphere and a two-layer ocean with the lower layer at rest, in which the atmosphere and ocean affect each other by wind stresses and heat fluxes. Perturbation equations describing the velocity and temperature fields in the atmospheric and oceanic layers show that unstable disturbances (implying positive feedback) can exist, with the most rapidly growing disturbances having properties consistent with those of the observations. The primary interaction exists between long barotropic Rossby waves in the atmosphere driving the ocean flow pattern by wind stress, and the ocean forcing the atmosphere by the effect of surface heat flux on the atmospheric vorticity. Growth times are of the order of 4 years for the inviscid case, and 22 years if viscosity and diffusion (with values equalling those in the CSIRO coupled model) are included.

**MW06/P/2-A3****1220****THE SEESAWING VARIATIONS BETWEEN THE TROPICAL AND SUBTROPICAL MONSOON IN EAST ASIA**

QingYun ZHANG (Institute of Atmospheric Physics, Chinese Academy of Sciences, Beijing 100029, China)

Based on the wind data at 200hPa and 850hPa level from the ECMWF datasets and Tbb data of Japan (JMA) Geostationary Meteorological Satellite (GMS) during 1980-1989, two convergence zones in East Asia, one over the South China Sea (called monsoon trough), the other over the Yangtze River Basin and Japan (called the MeiYu or Baiu front) were studied. There is the seesawing variation for the intensity between the two convergence zones. The tropical monsoon trough weakens and the MeiYu front strengthens; the MeiYu front weakens and the tropical monsoon trough strengthens. The westerly (easterly) wind anomalies at 850hPa during summer appear over the MeiYu front region, the MeiYu front intensifies (weakens); the westerly (easterly) wind anomalies at 850hPa during summer appear over the monsoon trough region, the monsoon trough intensifies (weakens).

The rainfall patterns in Eastern China during summer are greatly dependent on the intensity of the two convergence zones (the tropical monsoon trough and MeiYu front over East Asia). The study shows that when the MeiYu front over East Asia strengthened (weakened), the Rainfall over Yangtze River Valley is above (below) anomaly.

**Wednesday 21 July PM**

Presiding Chair: Carsten Segerlund Frederiksen (Bureau of Meteorology Research Center, Melbourne, Australia)

**MW06/P/04-A3****1400****DYNAMICAL MECHANISM OF INTRASEASONAL OSCILLATION IN THE MID-HIGH LATITUDES**

Li Chongyin (LASG, Institute of Atmospheric Physics, CAS, P.O. Box 2718, Beijing 100080, China, email: lcy@lasgsg4.iap.ac.cn)

The intraseasonal oscillation is also an important atmospheric system in the mid-high latitudes and obviously different in the structure and activity from that in the tropical atmosphere. The dynamical mechanism of intraseasonal oscillation in the mid-high latitudes has been studied from various angles. A comprehensive review will be given in this paper, it is shown that the dynamical mechanism of intraseasonal oscillation in the mid-high latitudes can be able to sum up several points as follows:

1. Low-frequency remote responses of the atmosphere to external forcings (the SSTa and so on).
2. The atmospheric circulation pattern caused by instability of basic flow in the atmosphere.
3. Non-linear interaction in the atmosphere, such as the resonant interaction of the waves and the modons.
4. Influences of tropical atmospheric anomalies, especially the convection activity in the tropics.

**MW06/W/05-A3****1430****INSTABILITY MECHANISMS AND LOW FREQUENCY ATMOSPHERIC DISTURBANCES**

Carsten S. FREDERIKSEN (Bureau of Meteorology Research Centre, GPO Box 1289K, Melbourne, Victoria 3001, Australia, email: C.Frederiksen@bom.gov.au); Jorgen S. Frederiksen (CSIOR Atmospheric Research, PB1, Mordialloc, Victoria 3195, Australia, email: Jorgen.Frederiksen@dar.csiro.au)

During the last decade or so, normal mode instability theory, generalized to analyse disturbances growing on three-dimensional flows has provided insights into many aspects of large-scale atmospheric dynamics. Early studies used barotropic or multi-level quasi-geostrophic models. Recently, an extension of the theory to the full primitive equations and including a Kuo-type cumulus convection parameterization has been successfully applied to studies of monsoon disturbances, intraseasonal oscillations, circulation anomalies associated with Australian Northwest Cloudband disturbances, and low frequency anomalies.

Here, we present an overview of three-dimensional instability theory and the role of eigenmodes and adjoint eigenmodes in the development of atmospheric disturbances, and review some of these recent studies. In particular, we focus on the roles of barotropic instability, baroclinic instability and convection in the formation and structures of intraseasonal oscillations, low frequency anomalies and teleconnections, Northern and Southern Hemisphere blocking and Australian Northwest Cloudband disturbances. We also discuss possible future development and application of the theory.

**MW06/W/02-A3****1500****PIECEWISE TENDENCY DIAGNOSIS OF INTRASEASONAL LOW FREQUENCY VARIABILITY**

Robert X. BLACK, Katherine J. Evans (School of Earth and Atmospheric Sciences, Georgia University of Technology, Atlanta, Georgia 30332-0340, USA, email: rxblack@voir.ias.gatech.edu)

A new diagnostic approach, piecewise tendency diagnosis (PTD), is employed to study the dynamics of intraseasonal low frequency variations occurring during Northern Hemisphere Winter. PTD extends piecewise potential vorticity inversion by first partitioning the local time tendency of quasi-geostrophic potential vorticity (QG PV) into an array of advective and nonconservative forcing terms. These forcing terms are then inverted separately to obtain the associated three-dimensional height tendency. The diagnostic is based upon the QG PV balance and conservation relations and is used to isolate individual mechanistic influences upon the atmospheric height tendency. This provides a quantitative methodology for assessing the contribution of individual dynamic and physical sources towards local height tendency. We extend PTD to include the effects of diabatic heating, ageostrophic forcings, and spherical geometry. In our study PTD is applied to study both the composite and individual case dynamics of the formation of persistent cyclonic circulation anomalies over the North Pacific. Our results indicate that the calculated height tendency patterns matches the observed tendency of the individual case and composite very well. In both situations, linear geostrophic advective terms provide the largest dynamic forcing. In particular, both the individual and composite cases develop largely from linear baroclinic processes, with spatial deformation processes providing a smaller first-order contribution. PTD analyses of the composite events provide results that are consistent with previous synoptic and diagnostic studies. For both the composite and case analyses, QG non-linear and non-QG advection terms played secondary but nonnegligible roles in intensification. The non-QG vertical advection of stratification anomalies generally opposes development, but is weak. The effect of diabatic heating was small in both cases, acting to intensify the low in the individual case and slow the development in the composite.

**MW06/W/03-A3****1520****MIDLATITUDE MESOPAUSE REGION WINDS AND THEIR CONNECTION WITH EUROPEAN AND ASIAN TROPOSPHERIC PARAMETERS**

Christoph JACOBI (Institute for Meteorology, University of Leipzig, Germany, email: jacobi@rz.uni-leipzig.de)

Comparison of long-term measurements of winter mesopause region zonal winds has shown a connection of northern hemisphere tropospheric parameters, as temperature and rainfall, and mesopause region dynamics. These are on one hand due to a connection of the stratospheric polar vortex and the North Atlantic Oscillation and on the other hand steered by a coupling of the lower stratosphere and the upper mesosphere/lower thermosphere region. The connection between European and Asian winter climatological parameters and the North Atlantic Oscillation leads to the fact, that the signal of Eurasian winter conditions can be found in the interannual variability of mesopause winds. Some of these winter tropospheric parameters influence the strength of the Indian monsoon in the following summer, and this leads to a correlation between winter mesopause winds and summer Indian rainfall, so that the midlatitude mesopause winter dynamics can be used as a precursory signal of the strength of the Indian monsoon.

**MW06/E/05-A3****1600****INTERPRETING LOW FREQUENCY MODES OF SOUTHERN HEMISPHERE ATMOSPHERIC VARIABILITY AS THE ROTATIONAL RESPONSE TO DIVERGENT FORCING**

Michael REVELL, John Kidson (both at National Institute of Water and Atmospheric research, Wellington, New Zealand, email: m.revell@niwa.cri.nz); George Kiladis (Aeronomy Lab, NOAA, Boulder, Colorado, USA, email: gkiladis@al.noaa.gov)

The principal, low frequency, modes of atmospheric circulation variability in the Southern Hemisphere have been calculated using a 39 year record of 200 hPa wind fields from the NCEP/NCAR reanalysis data set. Many of these modes show strong correlations with tropical convection as inferred from outgoing longwave radiation (OLR). We attempt to interpret these modes as the rotational response to a divergent forcing. For a range of mean states we use the linearised barotropic vorticity equation (BVE) to solve the CHI problem for the divergent wind that would generate these rotational modes. We find that several of these low frequency modes can be generated by forcing the BVE with fairly simple divergent wind fields that could be interpreted as resulting from anomalous convection. In particular we find divergence patterns that correspond well to the MJO and ENSO. These results are further evidence that linear Rossby wave propagation provides an important link between anomalous convection in the Tropics and the occurrence of low frequency circulation anomalies in mid-latitudes and vice-versa.

**MW06/W/06-A3****1620****MULTI-YEAR VARIABILITY IN A MIDLATITUDE OCEAN-ATMOSPHERE MODEL OF INTERMEDIATE COMPLEXITY**

Ernst VAN DER AVOIRD, Henk A. Dijkstra (both at the Institute for Marine and Atmospheric research Utrecht (IMAU), Princetonplein 5, 3584 CC Utrecht, The Netherlands, email: avoird@phys.uu.nl, h.a.dijkstra@phys.uu.nl)

The problem of interannual midlatitude climate variability is approached using dynamical systems theory applied to a quasi-geostrophic coupled ocean-atmosphere model of intermediate complexity. The model consists of a two-layer rectangular ocean basin underlying a two-layer zonal atmospheric channel. A constant depth mixed layer within the top layer of the ocean model with variable sea surface temperature determines the thermodynamic coupling. Simple parameterizations are proposed to represent the air-sea interaction which lead to non-local relations between SST-anomalies and the anomalous atmospheric flow pattern. The associated coupling parameters are estimated from data-analyses in the North Atlantic region. The stability of the mean flow consisting of the zonal atmospheric jet overlying the double gyre ocean circulation is investigated. Low frequency modes are found and described with the help of the perturbation structures at critical points in parameter space.

**MW06/W/04-A3****1640****THE IMPACT OF THE ANNUAL CYCLE UPON THE EXTRATROPICAL RESPONSE TO ANOMALOUS TROPICAL HEATING**

Matthew NEWMAN (NOAA-CIRES Climate Diagnostics Center, University of Colorado, Boulder, CO 80309, USA, email: men@cdc.noaa.gov); Prashant D. Sardeshmukh, Christopher R. Winkler (both at NOAA-CIRES Climate Diagnostics Center, University of Colorado, Boulder, CO 80309, USA, email: pds@cdc.noaa.gov, crw@cdc.noaa.gov)

The impact of the annual cycle in the zonally, meridionally, and vertically varying base state upon the extratropical response to anomalous heating is considered in the context of a linear baroclinic model. Using a diagnostic tool called the influence function, it is shown that the most sensitive areas of heating for producing a large local geopotential height response change from month to month. Over North America, this change is most dramatic in spring and fall. Also, as spring progresses, there is a marked increase in the sensitivity to smaller scale heating, particularly over the west Pacific.

These results suggest that the impact of the annual cycle must be taken into account in any complete theory of low-frequency variability. The impact is large enough to raise the possibility of significant interactions across time scales. In other words, it is possible for a steady forcing to produce an unsteady response, and equally, for an unsteady forcing to produce a seasonal-mean response. In such situations, particularly during the northern spring and fall seasons, investigating low-frequency anomalies as departures from 3-month seasonal climatologies may lead to confusion, and may not be useful.

A similar analysis is made in a linearized multi-level baroclinic model, showing the impact of the seasonally varying base state upon the North American response to MJO-like heating anomalies. Again, this impact is greatest during spring, but even during winter there are noticeable differences.

**MW06/P/1-A3****1700****THE RELATION BETWEEN THE PRECIPITATION OF SOUTHWEST CHINA (YUNNAN) IN MAY AND THE INTRASEASONAL OSCILLATION BEFORE MAY**

Xiao ZINU, Wen Min (Yunnan Meteorological Observatory, Kunming 650034, Yunnan, China)

Yunnan is in the south-west of China and influenced by the South Asia Monsoon. The precipitation in May reflects the time of the rainy season beginning in the area and it is very

important to agriculture there, based on black body temperature (TBB) data and Yunnan precipitation data, the relation between Yunnan precipitation in May and intraseasonal oscillation (30-60 days) over the equatorial Indian Ocean and the South Asian monsoon area before May is studied. The results revealed that the intensity of intraseasonal oscillation activities in winter over the equatorial Indian Ocean and the South Asian monsoon area has a close relation to the Yunnan precipitation in May. When the oscillation is stronger and the range of the activity extends eastward and northward obviously, the precipitation is more than usual; when the oscillation is weaker and it doesn't extend eastward and northward obviously, the precipitation is less than usual. Therefore, the amount of the precipitation of Yunnan in May is mainly influenced by south Asia monsoon. The precipitation of Yunnan in May is closely related to the intraseasonal oscillation activity over south Asia monsoon region in previous period. The intensity of the intraseasonal oscillation over the equatorial Indian Ocean in winter may be an important factor to forecast the precipitation of Yunnan in May and the beginning of Yunnan rainy season in next year.

**MW07****Thursday 22 July****GRAVITY WAVE SOURCES AND PARAMETRIZATION (ICMA, SCOSTEP/ PSMOS+EPIC, SPARC)**

Location: Mechanical Engineering, G28 LRE

**Thursday 22 July AM**

Presiding Chair: M. Joan Alexander, (Colorado Research Associates, Boulder, USA)

**MW07/W/15-A4**

Invited

**0830****OBSERVATIONS OF CONVECTIVELY GENERATED GRAVITY WAVES IN THE STRATOSPHERE**

Leonhard PFISTER (NASA/Ames Research Center Moffett Field, CA, 94035-1000 USA)

Gravity wave motions are an important driver of the stratospheric circulation. This arises from their ability to transport momentum through the atmosphere over long distances in the vertical. When the waves break, that momentum is deposited, effectively exerting a force that can drive the overall transport circulation. The location of the breaking region in the stratosphere depends on the gravity wave phase speed and amplitude, while the magnitude of the force depends on the gravity wave momentum flux. The amplitude, momentum flux, and phase speed spectra of topographically generated gravity waves are reasonably well known, with the phase speed spectrum being particularly simple (i.e., quasi-stationary). This is not true for convectively generated gravity waves, where one expects a much richer spectrum due to the transient nature of the convective forcing. In fact, a variety of techniques (satellite temperatures, radiosondes, aircraft, radar), which are sensitive to different portions of the spectrum of vertical scales, horizontal scales, and phase speeds have all detected strong gravity wave variance. Ultimately the goals are: (1) to produce a coherent picture of momentum flux as a function of phase speed and horizontal scale and (2) to link this spectrum quantitatively to mechanisms operating in convective systems and (on a synoptic scale), clusters of convective systems. This paper will review observations of convectively generated gravity waves and the role of various parts of the spectrum in the stratospheric momentum budget. The emphasis will be on mesoscale waves (up to 500 km horizontal wavelength) in the tropics as observed by aircraft, though the larger scales will be discussed as well. Among the new findings are: (1) clear observations of gravity waves in the tropics with vertical wavelengths at least marginally comparable to the ~10 km predicted by convective cloud models; (2) a case study showing the very short residence time of some convectively generated waves in the lower stratosphere; and (3) observations of inertia-gravity waves as seen in a horizontal view (as opposed to vertical profiles). These waves are seen to actually generate thin clouds near the tropopause, suggesting a role in the stratospheric water budget as well as the momentum budget.

**MW07/E/04-A4****0900****GRAVITY WAVE GENERATION IN A HIGH-RESOLUTION NUMERICAL MODEL OF DEEP TROPICAL CONVECTION**

Todd P. LANE, Michael J. Reeder (Centre for Dynamical Meteorology and Oceanography, Monash University, Australia and Cooperative Research Centre for Southern Hemisphere Meteorology, Australia)

Convective clouds are known to generate internal gravity waves. Indeed, such waves are thought to be important in adjusting the unsaturated environment of the cloud, and in shaping the mean flow in the middle atmosphere. However, the way in which convective clouds generate gravity waves is not well understood. The present study seeks to clarify the dynamics of wave generation using a high-resolution numerical model. The numerical calculations presented explicitly resolve both the mesoscale convective cloud cluster and the gravity waves generated. As the convective clouds evolve, they generate prominent gravity waves in both the troposphere and stratosphere. The source location is variable in time and space, but is related to the development of individual convective cells. The largest amplitude gravity waves are generated when the cloud tops reach the upper troposphere. The stratospheric momentum flux shows a distinct temporal cycle associated with the transient nature of the wave source. A new analysis technique is introduced in which the non-linear terms in the governing equations are taken as the forcing for linear gravity waves. The analysis shows that neither the shear nor the diabatic heating are the dominant mechanisms for wave generation. Instead, the wave source is most easily understood when viewed in a frame of reference moving with the level of neutral buoyancy, whereupon the source may be described as a vertically oriented, oscillating convective up-draught. This description is consistent with the properties of the modelled stratospheric waves.

**MW07/W/08-A4****0920****MOMENTUM TRANSPORT BY CONVECTIVELY GENERATED WAVES**

Carol ROADNIGHT, Stephen Mobbs (both at The Environment Centre, The University of Leeds, Leeds, LS2 9JT, UK, email: carol@lec.leeds.ac.uk)

Vertically propagating waves, excited by deep convective systems, can transport momentum to higher levels in the atmosphere and thus exert a significant acceleration, or deceleration, on the mean flow at levels of dissipation. The inclusion of this, apparently important, process in larger models has received much less attention than the related problem of momentum transport by orographically generated gravity waves.

A study of these convectively generated waves and their contribution to the vertical transport

of horizontal momentum will be presented using results from large-eddy simulations of the convective boundary layer and an overlying stable layer. A variety of idealised and realistic flow profiles are used to investigate the effects of convective intensity, wind shear and stability of the atmosphere on gravity wave generation and establish which conditions are associated with strong convective momentum transport.

**MW07/W/02-A4****0940****RADIOSONDE OBSERVATIONS AND MODELLING OF GRAVITY WAVES OVER THE TROPICAL INDIAN OCEAN AND THEIR EFFECTS IN THE STRATOSPHERE**

M. Joan ALEXANDER, Robert A. Vincent (Colorado Research Associates, 3380 Mitchell Lane, Boulder CO 80301, USA, email: alexand@colorado-research.com)

High resolution radioonde observations of temperature and winds from twice-daily launches over Cocos Island (12S, 97E) have been analyzed for information on gravity waves in the lower stratosphere. The observations span a six-year period 1992-1998. The results include measurements of the monthly-mean energy density and estimates of the momentum flux, as well as information on the intrinsic frequencies, horizontal and vertical wavelengths, and phase speeds of the waves. As in any data set, these observations will emphasize waves with certain properties while other waves may be present but go unobserved. These effects are taken into account in a corresponding model study of gravity wave propagation using the observed background stability and wind structure as model inputs. The results of the data analysis were used to constrain the model, and the model/data combination provide a unique tool for interpretation of these data and evaluation of the wave effects on the atmosphere. The model study shows that these data place strong constraints on many of the details of the source spectrum of gravity waves crossing the troposphere that includes interesting variations of the monthly-mean properties of the waves. A broad parameter space describing the wave sources was investigated and best agreement between modeled momentum flux and energy density time series were obtained with wave parameters similar to those determined independently from hodograph analyses of the data. The model is then further used to investigate the limitations of the observations for inferring wave effects on the mean flow.

**MW07/W/21-A4****1000****OBSERVATIONS OF GRAVITY WAVE GENERATION BY CONVECTION**

Tobias KERZENMACHER (The Environment Centre, University of Leeds, Leeds LS2 9JT, UK, email: Tobias@lec.leeds.ac.uk)

The parameterization of gravity wave drag due to convection is investigated using high resolution radioonde ascent data (~10 m) and radar data taken at mid-latitudes. In order to understand the physical processes behind wave generation by convection, the data are analyzed using a set of mathematical tools developed to detect gravity waves and convection in the data.

The importance of convection as a wave generation mechanism in the mid-latitudes is discussed based on the prevalence of simultaneous convection and gravity wave events in the data set. Furthermore inertial waves often develop after gravity wave events. These inertial waves may have a significant influence on the momentum budget. The occurrence of inertial waves has also been investigated and results will be presented.

**MW07/W/03-A4**

Invited

**1040****SHEAR EXCITATION OF INTERNAL WAVES, AND THEIR STABILITY**

B.R. SUTHERLAND (University of Alberta, 539 Central Academic Building, University of Alberta, Edmonton, AB T6G 2G1 Canada, email: bruce.sutherland@ualberta.ca)

Linear theory and the results of nonlinear numerical simulations have shown that strong coupling between radiating internal gravity waves and unstable stratified shear flow is anticipated if the stratification is sufficiently weak where the shear is strong and the stratification is sufficiently strong elsewhere. To examine these dynamics in the laboratory, experiments have been performed in a recirculating tank filled with salt-stratified water and driven near the surface by a Kovaszny pump to create a shear flow. The flow passes over a tall thin barrier spanning the width of the test-section of the tank, and the generation of internal waves from the mixing region in the lee of the barrier is observed. In the early stages of the flow development, internal waves are observed to couple with spanwise-coherent vortices that are shed in the wake of the barrier. Using a new technique, the amplitude of the excited waves is non-intrusively measured continuously in space and time. This analysis shows that large amplitude waves are generated when the mixing region is sufficiently weakly stratified and that these extract up to 7 percent of the momentum from the mean flow.

In experiments of uniformly stratified flow over the barrier, small amplitude internal waves are generated initially. Over time, however, the stratification in the mixing region becomes weaker and transient bursts of large amplitude internal waves are observed. Although the frequency spectrum of the internal waves excited by the turbulent mixing region can be broad in theory, they are observed to propagate typically at angles between 30 to 45 degrees to the vertical. A simple argument based on weakly nonlinear theory is proposed to help explain this phenomena. Specifically, it is proposed that an internal wave is unstable if the ratio of its maximum vertical displacement to its horizontal wavelength is greater than  $\sin(2\Theta)/(\pi \sqrt{8})$ , in which  $\Theta$  is the angle of the wave characteristics to the vertical. In particular, waves that propagate at very large or very small angles to the vertical are stable only if they are of infinitesimal amplitude. The predicted stability boundary is in excellent agreement with numerical simulations of horizontally periodic internal waves. However, horizontally compact waves are found to be stable at larger amplitudes than predicted if their angle of propagation to the vertical is moderately smaller than 45 degrees.

**MW07/W/14-A4****1110****GRAVITY WAVE EXCITATION BY SPATIALLY AND TEMPORALLY VARIABLE BODY FORCES IN A SPHERICAL GEOMETRY**

David C. FRITTS, Sharon L. Vadas (Colorado Research Associates, 3380 Mitchell Lane, Boulder, CO 80301, USA)

A spherical compressible model is used to study the radiation of large-scale gravity waves from sites of localized body forcing due to small-scale wave dissipation. This source can be viewed alternatively as the ageostrophic radiation of gravity waves accompanying geostrophic adjustment. In both cases, the radiated wave scales are imposed by the source geometry, with smaller horizontal scales suggesting more local effects at higher altitudes and larger horizontal scales implying more global responses. Because of the scales of such motions, there is a potential that they may play a role in momentum transport, induced circulations, and thermal and constituent responses well into the thermosphere.



MW07/W/04-A4

1130

**OBSERVATION OF STRATOSPHERIC INERTIA-GRAVITY WAVES ASSOCIATED TO AGEOSTROPHIC FLOW IN THE UPPER TROPOSPHERE**

Albert HERTZOG (Service d'Aeronomie du CNRS, BP3, F-91371 Verrieres-le-Buisson Cedex, France; email: albert.hertzog@aerov.jussieu.fr); Claude Souprayen (Department of Applied Mathematics and Theoretical Physics, University of Cambridge, Silver Street, Cambridge, CB3 9EW, England; email: c.souprayen@damtp.cam.ac.uk); Alain Hauchecorne (Service d'Aeronomie du CNRS, BP3, F-91371 Verrieres-le-Buisson Cedex, France; email: alain.hauchecorne@aerov.jussieu.fr)

Inertia-gravity waves are often observed in the mid-latitude lower stratosphere. Those low frequency waves, whose amplitude can reach several m/s, may induce important horizontal displacements of air parcels, and thus be involved in dispersion of tracers in the "surf zone" or at the vortex edge. Some recent observations of high amplitude inertia-gravity waves made in the south of France by Doppler Lidar will be presented. In order to determine the mechanism responsible for the generation of such waves, a 3D non-stationary ray tracing model has been developed. Backward trajectories of gravity wave packets have been simulated with atmospheric thermo-dynamical fields coming from the ECMWF T106 model and wave spectral parameters estimated on Lidar data. Those trajectories show retro-propagations to regions located in the upper troposphere and characterized by high baroclinic activity. Our results support the excitation of inertia-gravity waves by geostrophic adjustment.

MW07/E/05-A4

1150

**ENHANCED AND INHIBITED GRAVITY WAVE SPECTRA**

James A. WHITEWAY (Department of physics, University of Wales, Aberystwyth, SY23 3BZ, UK, email: jww@aber.ac.uk)

Meteorological balloon measurements were applied to investigate gravity wave activity in the upper troposphere and lower stratosphere above the Canadian High Arctic. These observations reveal that there are specific atmospheric conditions in which the spectrum of gravity waves is enhanced at all vertical wavelengths larger than 100 m; and that there are other distinct conditions in which the spectrum is inhibited. It will be shown that an enhancement in spectral magnitude in the lower stratosphere occurred only when tropospheric conditions were favourable for the generation and upward propagation of mountain waves. Otherwise, growth in spectral magnitude at the tropopause was inhibited and there was no response to the change in background atmospheric conditions between the troposphere and stratosphere. The enhanced spectra are consistent with the current gravity wave paradigm but the inhibited spectra are not so readily explained. Measurements will also be shown that demonstrate how large scale meteorological patterns influence the amount of gravity wave activity above the high Arctic. It was found that enhancements in wave activity were associated with the tropospheric jet stream and also the stratospheric polar vortex.

MW07/E/07-A4

1210

**TOPOGRAPHICALLY FORCED INTERNAL GRAVITY WAVES IN TIME DEPENDENT SHEAR WINDS**

Kwok-Aun TAN (School of Mathematics, University of New South Wales, Sydney, NSW 2052, Australia, email: K.Tan@unsw.edu.au); Stephen Eckermann (Code 7641.2, Naval Research Laboratory, Washington, DC 20375, USA, email: eckerman@map.nrl.navy.mil); Dave Broutman (School of Mathematics, University of New South Wales, Sydney, NSW 2052, Australia and Computational Physics, Inc., Fairfax, VA 22031, USA, email: D.Broutman@unsw.edu.au); Lance Leslie (School of Mathematics, University of New South Wales, Sydney, NSW 2052, Australia, email: L.Leslie@unsw.edu.au)

The flow of stable stratified air over topography generates internal gravity waves that can exert a drag on the atmosphere. The vertical propagation of these mountain waves can be affected by time-evolving shear flows in the atmosphere. In the present study, we investigate the effect of unsteady shears on mountain wave forcing and propagation. In particular, we consider shear flows that are transient and exhibit wind reversals. We use a non-hydrostatic numerical model that solves the non-linear, fully compressible Euler equations of the atmosphere using a split-time explicit scheme. The simulated mountain wave fields are compared to previous studies and predictions based on ray-tracing techniques. Mechanisms for unsteady mountain wave generation are discussed.

MW07/W/06-A4

1230

**EFFECT OF A WEAKLY DIRECTIONALLY SHEARED FLOW ON GRAVITY WAVE DRAG**

Maria Antonia VALENTE, Ian N. James (Department of Meteorology, University of Reading, PO Box 243, Earley Gate, RG6 6BB Reading, UK, email: antonia@met.reading.ac.uk, i.n.james@reading.ac.uk)

Several experiments were performed with a mesoscale 3D non-hydrostatic, non-linear model simulating a stably stratified directionally sheared flow over an isolated bell-shaped circular mountain. The wind turns monotonically with height from southerly at  $z=0$  to westerly at  $z=6$ km, maintaining the speed constant with height. Various mountain heights were tried, from  $h=10$ m to 3km, to obtain an extensive range of flow regimes, from linear flow to splitting flow, passing through breaking wave regimes (Froude number  $Fr$  varying in the range 13.2 to 0.44). Directional shear makes the flow more steady, but the surface drag magnitude is very similar to the drag for a uniform flow over the same mountain. The drag regimes are not significantly altered by the directional shear. In contrast, the vertical fluxes of horizontal momentum rotate with height following the wind turning and imposing an acceleration on the mean flow, even for linear regimes. The linear theory for a directionally sheared flow, stating that the momentum flux vector rotates with height in such a way that the acceleration is at right angles with the wind for each height, was tested for the different flow regimes. The simulations show that it is verified for linear flow regimes ( $Fr > 1$ ). The theory starts to fail for  $Fr$  near 1, but high drag regimes still have an acceleration vector turning as predicted by the theory. For low drag regimes, when the low level flow splits around the mountain, the theory is not valid. According to these results, directional shear effects should be included in parametrizations of GWD. The linear theory is adequate to parametrize linear drag regimes and could be useful for certain characteristics of high drag regimes. This theory is not useful for parametrizing flow splitting low drag regimes.

Presiding Chair: David C. Fritts (Colorado Research Associates, Boulder, USA)

MW07/E/03-A4

1400

**STRATOSPHERIC GRAVITY WAVES MEASURED FROM SPACE BY CRISTA: VERTICAL WAVELENGTHS, DAILY VARIATIONS AND SOURCES**

Peter PREUSSE (Department of Physics, Wuppertal University (BUGW); Gauss Str 20, D-42097 Wuppertal, Germany, email: preusse@wpos2.physik.uni-wuppertal.de); Stephen D. Eckermann (E. O. Hulburt Center for Space Research, Code 7641, NRL, Washington DC 20375-5352, USA, email: eckerman@ismap4.nrl.navy.mil); Martin Riese, Bernd Schaeler, Dirk Offermann (all three at Wuppertal University, Germany)

During shuttle missions STS-66 (November, 1994) and STS-85 (August, 1997) the CRISTA instrument measured around 14 days of temperature and constituent data with very high spatial resolution. Vertical profiles of Kalman-detrended temperatures and trace gases measured by CRISTA are analysed using a combination of MEM and harmonic analysis. The results are binned according to vertical wavelength. Zonal-mean values of gravity wave activity are calculated and compared to gravity wave variances inferred from other satellite data. Good agreement is found with the results obtained from the LIMS instrument (NIMBUS 7), as well as with radiance fluctuations recorded by the MLS instrument (UARS). The apparent discrepancies between LIMS and MLS are discussed. CRISTA variances reveal high spatial correlation between mountain ridges and observed wave patterns, most notably near the southern tip of South America, indicating that large-scale stratospheric mountain waves are present in these regions. In addition, strong gravity wave activity is observed at the equator and near the edge of the polar vortex. The findings will be compared to model simulations of global gravity wave activity during the mission days, obtained by coupling the NRL/MWFM and the GROGRAT model.

MW07/W/19-A4

Invited

1420

**GLOBAL MODELLING OF GRAVITY WAVES IN THE MIDDLE ATMOSPHERE: COMPARISONS WITH CRISTA DATA**

Stephen D. ECKERMANN, E. O. Hulburt (Center for Space Research, Code 7641.2, Naval Research Laboratory, Washington, DC 20375, USA); Peter Preusse, Bernd Schaeler, Dirk Offermann (Physics Department, University of Wuppertal, Germany)

Small-scale temperature variances in the middle atmosphere have been derived from data acquired by the CRISTA instrument. CRISTA flew on the CRISTA-SPAS satellite during shuttle missions STS-66 (3-14 November, 1994) and STS-85 (7-19 August, 1997) (see the presentation by Preusse et al.). Preliminary analysis indicates that much of this variance could be produced by gravity waves. We investigate this using two global gravity-wave models: the Naval Research Laboratory Mountain Wave Forecast Model (NRL/MWFM) and the Gravity Wave Regional or Global Ray Tracer (GROGRAT). We use the models in conjunction with assimilated global winds and temperatures for each mission day to generate global maps of gravity wave activity in the middle atmosphere. Specific bursts in stratospheric temperature variance observed during both CRISTA missions are also generated in the model runs. Enhanced variance near the southern tip of South America is produced in the simulations by long wavelength forced by flow over the Andes. Increased variance at the equator also arises due to effective transmission of non-zero phase speed waves into the middle atmosphere. We also show that effective interpretation of the data requires consideration of the spatial filtering characteristics of the measurement, supporting similar arguments by Alexander (1998) in reference to gravity waves inferred from the MLS instrument on the Upper Atmosphere Research Satellite.

MW07/E/08-A4

1450

**GRAVITY WAVE SOURCES INFERRED FROM SATELLITE TEMPERATURE DATA**

Charles McLANDRESS (Department of Earth and Atmospheric Science, York University, Toronto M3J 1P3, Canada, email: mccland@stpl.cress.yorku.ca); M. Joan Alexander (Colorado Research Associates, Boulder CO 80301, USA, email: alexand@colorado-research.com); Dong L. Wu (Jet Propulsion Laboratory, California Institute of Technology, Pasadena, CA 91109-8099, USA, email: dwu@mls.jpl.nasa.gov)

Gravity wave activity in the troposphere is inferred from high resolution temperature data from the Microwave Limb Sounder (MLS) on board the Upper Atmosphere Research Satellite. Global climatologies of temperature variance in the stratosphere are computed using six years of observations obtained from the instrument's limb-tracking and limb-scanning modes of operation. The summer hemisphere variances exhibit large spatial variations, with the maxima of both datasets located over the continental land masses at mid-latitudes and in the subtropics. The winter southern hemisphere is dominated by a region of large variance over the tip of South America. The variances for northern hemisphere winter are also located over the continents at high latitudes but the geographical positions of the individual maxima in the track and scan datasets differ more significantly.

A linear gravity wave ray model is used to interpret the observed temperature variances and determine whether information about the geographical distribution of gravity wave sources in the troposphere can be obtained. Realistic background wind and temperature fields which correspond to the MLS observing periods are used, and the model variances are filtered in a manner which qualitatively simulates the instrument's response to wavelike temperature perturbations. Source information is inferred by specifying a spatially-uniform spectrum of waves in the troposphere and comparing the simulated results in the stratosphere to the observations. Spectra representing both convectively- and orographically- generated gravity waves are tested. The model is able to reproduce the latitudinal variations of the observations, indicating that the MLS data yield little information about the latitudinal dependence of gravity wave sources. Longitudinal variations of the observations in the summer hemisphere, however, are most likely representative of variations in convective forcing since the model results exhibit much less variation in this direction. Simulations using the orographic spectrum exhibit large spatial variations as a result of critical level filtering by the background westerlies. This makes interpretation of the observed wintertime variances difficult. The large variances observed over the tip of South America, however, are most probably linked to orographic forcing since that is the only longitudinal sector containing any significant topography.

MW07/W/18-A4

1510

**GRAVITY WAVES EFFECTS ON 4.3 MM DATA APPLICATION TO HIRS DATA**

Gabriel CASTELAIN, Pierre Simoneau, Véronique Achard Onera (France)

Effect of gravity waves on atmospheric radiances in the 4,3 mm band of CO<sub>2</sub> was studied for satellite nadir observations. The SHARC-3 and FASCOD-3 codes (developed by Phillips Laboratory) were used to compute vibrational temperatures and radiances. In an other hand, NOAA-12 HIRS 16 and 17 data will be studied to attempt to detect gravity waves on the

Western Europe area. TOVS data are processed using AAPP software (EUMETSAT). Preliminary line by line computations show variations reaching more than 10 % discrepancy on radiances near 4.33 mm, for a gravity wave with a maximum temperature amplitude of 30 K at around 50 km of altitude. Taking into account the TOVS filters width, we can expect variations from 1 to 2 % on channel HIRS-16, and from 1 to 4 % on channel HIRS-17.

**MW07/W/17-A4** Invited **1530**

#### MOUNTAIN WAVES PARAMETERIZATION

F. LOTT (LMD-CNRS, Paris 6- case courrier 99, 4 Place Jussieu, 75252 Paris Cedex 05, France, email: flott@lmd.jussieu.fr)

The problem of the representation of subgrid-scale orography (SSO) in General Circulation Models (GCM) is presented. The presentation of a particular parameterization scheme is then given, it allows to represent non-linear low-level "blocked" flow drag and gravity waves drag. Its realism is evaluated with field data, its impact and its limitation are evaluated with different sets of GCM simulations.

**MW07/W/20-A4** **1620**

#### ANISOTROPY IN THE PARAMETERIZATION OF DRAG DUE TO FREELY PROPAGATING GRAVITY WAVES AND NEAR-SURFACE-FLOW DYNAMICS

John SCINocca, Norm McFarlane (Canadian Centre for Climate Modelling and Analysis Atmospheric Environment Service University of Victoria E-mail: john.scinocca@ec.gc.ca http://www.cccma.bc.ec.gc.ca)

A new orographic gravity-wave drag (GWD) parameterization is derived for implementation in the Canadian Climate Centre GCM. The new scheme is comprised of three principle components. The first component is a parameterization of the freely propagating gravity wave field forced by the unresolved topography (UT) in the GCM, and its interaction with the mean flow. Two waves are employed to represent the gravity-wave field launched by the UT in each GCM grid cell. The properties of each wave are derived from the linear-theory spectral density of horizontal momentum-flux for stratified flow over an elliptical obstacle (Phillips 1984). In this way, anisotropy in the gravity-wave field is represented by the direction and magnitude of momentum flux associated with each wave. The second component of the new scheme is a parameterization of drag associated with low-level wave breaking and downslope flows. The final component of the new scheme employs form drag to parameterize the drag resulting from near-surface-flow dynamics (e.g. blocking and lee-vortices). This drag is applied independently to the components of the low-level wind which are parallel and anti-parallel to two-dimensional ridge-like structure in the UT in each GCM grid cell. Consequently, in addition to retarding the flow, the form drag in the new scheme has the potential to deflect the flow along prominent unresolved topographic ridges. The Climate resulting from the implementation of the new scheme is compared with the climate obtained with the current GWD scheme (McFarlane 1987). The comparison indicates an improved tropospheric circulation with reduced anomalies from the observed climate.

**MW07/W/07-A4** **1640**

#### EFFECTS OF GRAVITY WAVE DRAG INDUCED BY CUMULUS CONVECTION ON ATMOSPHERIC GENERAL CIRCULATION

Hye-Young CHUN, Myung-Duk Song, Jeong-Woo Kim (Department of Atmospheric Sciences and Global Environment Laboratory, Yonsei University, Seoul, 120-749, Korea, email: chy@atmos.yonsei.ac.kr); Jong-Jin Baik (Department of Environment Sciences and Engineering, Kwangju Institute of Science and Technology, Kwangju, Korea, email: jjbaik@aromi.kjist.ac.kr)

Effects of gravity wave drag induced by cumulus convection on the zonally averaged fields and planetary waves are investigated using an atmospheric general circulation model, YONU AGCM ST15. Gravity wave drag induced by convection (GWDC) is parameterized based on the method proposed by Chun and Baik (1998, JAS). In this scheme, the stress at individual cloud top is calculated explicitly based on the linear theory of thermally induced internal gravity waves, and the vertical distribution of the stress is determined by a saturation hypothesis using a Richardson-number-dependent wave breaking formulation.

Two one-year integrations with and without GWDC parameterization for perpetual run in July are performed, and the last 90 day-averaged fields are used for analysis. The control simulation without GWDC parameterization reveals a systematic bias both in the zonally averaged temperature and wind. There is cold bias in the midlatitude-to-polar region of the Southern Hemisphere and polar region of the Northern Hemisphere and warm bias in the tropical lower stratosphere. Related to this temperature bias, polar jets are too strong compared with observations and no separation between the polar and subtropical jets is detected in the Southern Hemisphere. The simulation with GWDC parameterization shows that the magnitude of the stress on the cloud top is large near the Western Pacific and North Africa mainly by deep cumulus convection in the inter-tropical convergence zone. Even though the tendency of the zonal wind by GWDC is large in the regions of strong stress on the cloud top, the effects of GWDC in the zonally averaged wind and temperature are dominant in the midlatitude of the Southern Hemisphere. This is because GWDC activates the vertically propagating planetary waves in the westerly region and increases the southward transport of eddy momentum flux, hence reducing the westerly jet in the Southern Hemisphere. The stronger westerly bias in the Southern Hemisphere polar jets is alleviated by 7 m/s/day, and cold bias in the midlatitude-to-polar regions in the Southern Hemisphere and polar region in the Northern Hemisphere by 1 K.

**MW07/E/06-A4** **1700**

#### SENSITIVITY OF THE UKMO UNIFIED MODEL TO A PARAMETERIZED GRAVITY WAVE SPECTRUM

Adam A. SCAIFE (U.K. Meteorological Office, London Road, Bracknell, Berkshire, RG12 2SZ, UK, email: aascaife@meto.gov.uk); Christopher D. Warner (Centre for Atmospheric Science, D.A.M.T.P., University of Cambridge, Silver Street, Cambridge CB3 9EW, UK.); Neal Butchart, John Austin (U.K. Meteorological Office, London Road, Bracknell, Berkshire, RG12 2SZ, UK.)

The effects of non-orographic gravity waves are represented in the UKMO Unified Model using a simplified version of Warner and McIntyre's full power spectral model (Warner and McIntyre, 1996). The domain of the model is extended through the mesosphere to 1Pa to capture the effects of gravity wave breaking in the mesosphere. The launch height for the waves and the launch spectrum are both prescribed in this scheme. Multiannual integrations with a range of launch levels and launch spectra are used to investigate the sensitivity of the planetary scale flow to changes in the parameterized waves. Results are also compared to a control simulation where Rayleigh friction is used to moderate winds in the mesosphere. Significant effects on the model simulations are found in the tropical stratosphere at the level of the observed QBO and also in the polar night jet in the upper stratosphere. The effect on the model's cold polar bias will also be discussed.

**MW07/W/13-A4** **1720**

#### EIKONAL THEORY FOR THE SPECTRAL DISTRIBUTION AND TRANSFER OF ENERGY IN THE ATMOSPHERIC GRAVITY WAVEFIELD

Claude SOUPRAYEN (Department of Applied Mathematics and Theoretical Physics, DAMTP, University of Cambridge, Silver Street, UK, email: C.Souprayen@damp.cam.ac.uk); Albert Hertzog, Alain Hauchecorne (Serviced'Aeronomie du CNRS, Verrieres-Le-Buisson, FRANCE, email: A.Hertzog@aerov.jussieu.fr); Jacques Vanneste (Dept of Mathematics & Statistics, University of Edinburgh, UK, email: vanneste@maths.ed.ac.uk)

The parameterization of gravity waves in the atmosphere relies on an accurate description of the spectral distribution of their pseudo-energy and pseudo-momentum and of the transfer of such quantities toward the small dissipative scales. The weakly non-linear off-resonant interaction that could be responsible for the observed spectra is studied using an eikonal description for the wave action transport and ray-tracing techniques. The formation and maintenance of gravity wave spectra during the dispersive propagation of the wave field in realistic 3D "random" background wind and temperature fields is analysed; the commonly observed spectra are emerging from arbitrary wave sources distribution. In a simplified 1D stochastic model of the vertical propagation, it is shown that the transport (and the dissipation) is strongly related to the mean, the variance and the vertical correlation length of the vertical shear of horizontal wind. Deposition of pseudo-energy and pseudo-momentum results from the continuous spectral transfer toward and a removal by dissipation at small scales.

**MW07/W/05-A4** **1740**

#### PARAMETERIZATION OF THERMAL EFFECTS OF SATURATING GRAVITY WAVES

A.S. MEDVEDEV, G.P. Klaassen (York University, Toronto, Canada)

Breaking/saturating gravity waves (GWs) do not only provide drag on the mean flow due to their momentum deposition, but also affect the background thermally because of the associated energy flux divergence. We present a rigorous derivation of terms describing thermal effects of GWs on the mean flow. The parameterization is based on the corresponding energy cycle for wave/mean flow interactions, and on our recent non-linear theory of GW spectra. The combined effect of saturating GW is to produce both the differential heating/cooling by inducing a downward wave heat flux, and an irreversible wave energy loss into a heat. The former effect can also be represented as a thermodiffusion acting on the mean potential temperature, although there is no mean momentum diffusion counterpart exists. The parameterization requires the source GW spectrum as the only tunable parameter. Results of numerical simulations with the Canadian Middle Atmosphere Model will be shown, which demonstrate an important role of GW thermal effects in the strato- mesosphere.

**MW08** **Tuesday 20 July**

#### QUASI-DECADAL OSCILLATION (ICMA, SCOSTEP)

Location: Mechanical Engineering, G28 LRE

**Tuesday 20 July PM**

Presiding Chair: L.L. Hood (Univ. of Arizona, Tucson, USA)

**Introduction** **1400**

L.L. Hood (Univ. of Arizona, Tucson, USA)

**MW08/W/02-A2** **1405**

#### OBSERVATIONAL STUDIES OF THE QUASI-DECADAL OSCILLATION

Lon HOOD (Lunar and Planetary Laboratory, University of Arizona, Tucson, Arizona 85721, USA, email: lon@lpl.arizona.edu)

Previous studies have identified evidence for a quasi-decadal oscillation (QDO) of meteorological parameters and ozone in both the lower and the upper stratosphere. Here, we report a new statistical study of updated NCEP/NCAR reanalysis data and satellite-derived ozone data in order to investigate further the origin and characteristics of this oscillation. The analysis is limited to the period from 1979 to the present during which the data are highest in quality and upper stratospheric data are available. In the upper stratosphere, where photochemical and radiative forcing by solar UV flux variability is most direct, an in-phase QDO in ozone and temperature is present at low latitudes over nearly two 11-year cycles. An associated modulation of the mid-latitude zonal wind near the stratopause occurs during the early winter. In the lower stratosphere, geopotential heights exhibit a QDO with maximum amplitude near 30 mb and near 30 degrees latitude in each hemisphere. An associated modulation of column ozone and zonal wind is also present at low and middle latitudes, respectively. The derived characteristics of the stratospheric QDO represent important potential constraints on sun-climate models.

**MW08/E/03-A2** **1430**

#### THE INFLUENCE OF THE SUNSPOT CYCLE ON THE GLOBAL STRATOSPHERE

Harry VAN LOON (National Center for Atmospheric Research, P.O. Box 3000, Boulder, Colorado, USA); Karin Labitzke (Freie Universität Berlin, Carl-Heinrich-Becker-Weg 6-10, 12165 Berlin, Steglitz, Germany)

The NCEP/NCAR re-analyses of the global data have made it possible to examine the influence of the 11-year sunspot cycle on the stratosphere as high as the 10-hPa level (about 30 km above sea level). The correlations between the solar cycle and the 30-hPa heights on the Northern Hemisphere, using a 40-year data set from the Freie Universität Berlin, showed a strong signal which is repeated in the NCEP/NCAR data. The correlation pattern on the Southern Hemisphere is similar to the one on the Northern Hemisphere, not only at 30 hPa but at all the available levels in the stratosphere.

The largest correlations with the geopotential heights move poleward from winter to summer within each hemisphere, and the largest temperature correlations move from one summer hemisphere to the other. The first eigenvector in a principal component analysis of the 30-hPa heights in summer and in the annual mean has the same areal shape as the correlation between the solar cycle and the heights, and the time series of its amplitude is in phase with the 11-year solar cycle.

MW08/E/02-A2

1500

**THE QBO'S INFLUENCE ON THE SOLAR SIGNAL IN THE GLOBAL STRATOSPHERE DURING THE NORTHERN WINTER**

Karin LABITZKE (Freie Universität Berlin, Carl-Heinrich-Becker-Weg 6-10, 12165 Berlin, Steglitz, Germany); Harry van Loon (National Center for Atmospheric Research, P.O. Box 3000, Boulder, Colorado, USA)

The talk deals with correlations between the re-analyzed NCEP/NCAR, global stratospheric data below 10hPa and the 11-year solar cycle. In the northern summer the correlations with the temperatures and geopotential heights are strong and positive on the Northern Hemisphere and as far south as 30S, whereas they are weaker in the southern summer all over the earth. If, however, the northern winter data are stratified according to the phase of the QBO in the lower stratosphere, the correlations in the Arctic are large and positive in the west years, but only zero to 0.3 over the rest of the globe. In the east years, however, the arctic correlations are negative and to the south the correlations are positive and strong in the tropical and temperate latitudes of both hemispheres, as they are in the unstratified data during the other seasons. Qualitatively, this difference between east and west years stems from the fact that teleconnections in the stratosphere and the solar influence work in the same direction in the east years but oppose each other in the west years.

MW08/W/01-A2

1530

**SOLAR CYCLE VARIABILITY, OZONE, AND CLIMATE**

Drew SHINDELL, David Rind, Nambeth Balachandran (NASA Goddard Institute for Space Studies and Center for Climate Systems Research, Columbia University, 2880 Broadway, New York, NY, USA 10025); Judith Lean, Patrick Lonergan (Center for Space Research, Naval Research Laboratory, Washington DC, USA 20375); E.O. Hulburt (Space Science and Applications, Inc., 2880 Broadway, New York, NY, USA 10025)

Solar variability's capacity to influence climate, both on decadal and century time scales, is among the most controversial issues in global climate change. Previous modelling and observational studies have suggested a correlation between solar cycle variability and surface climate, but have failed to convince the community since the models could not reproduce observed quasi-decadal variations. In this study, we show how upper stratospheric ozone changes amplify observed, small 11-year solar cycle irradiance changes in the Goddard Institute for Space Studies (GISS) tropospheric/stratospheric general circulation model (GCM). Circulation changes initially induced in the stratosphere subsequently penetrate into the troposphere, affecting climate, demonstrating a dynamical coupling between the stratosphere and troposphere. The model reproduces observations, including the well-documented geopotential height variations, implying that observed 11-year oscillations are likely driven, at least partially, by solar variability.

MW08/W/04-A2

1630

**GLOBAL DYNAMICAL EFFECTS OF THE QBO**

Mark P. BALDWIN (Northwest Research Associates, Bellevue, WA, USA)

This talk will provide an overview of the dynamical effects of the equatorial quasi-biennial oscillation (QBO) on the extratropical circulation of the stratosphere. Observations show that the wintertime Northern hemisphere stratospheric polar vortex is modulated by the phase of the equatorial QBO. The high-latitude stratospheric vortex tends to be stronger during the winter, and sudden warmings are less likely when the QBO is in its west phase at 40 hPa. Modulation of the Southern hemisphere vortex is confined to middle latitudes at the edge of the polar vortex during May–October. The difference between west and east phase composites of zonal mean wind during November, at the time of the final warming in the southern hemisphere, are comparable to January in the northern hemisphere. Southern hemisphere effects are best seen using 25-hPa equatorial winds. Observations of effects from the QBO are supported theoretically by a mechanism involving modification of the wave guide for upward and equatorward propagating planetary waves. When the QBO is in its east phase, the wave guide in the northern hemisphere is narrower, and waves tend to be more focused toward the polar cap, where their convergence results in a deceleration of the zonal-mean wind. Studies with mechanistic 3-D models and GCMs confirm this mechanism. During winter in the northern hemisphere, the QBO appears to excite the Arctic Oscillation (AO), a deep, largely zonally symmetric mode which couples the stratosphere and the troposphere. AO anomalies are observed to propagate downward through the stratosphere and troposphere on a time scale of less than a month. This downward propagation may be a general mechanism for downward communication of stratospheric circulation anomalies associated with the QBO or other forcings.

MW08/E/01-A2

1700

**QUASI-DECADAL, QUASI-BIENNIAL, AND BIENNIAL OSCILLATION IN THE NORTHERN WINTER STRATOSPHERE**

C. MARQUARDT (Freie Universität Berlin, Institut für Meteorologie, Carl-Heinrich-Becker-Weg 6-10, 12165 Berlin, Germany, email: marq@strat01.met.fu-berlin.de)

The Quasi-Decadal (or Ten-to-Twelve Year) Oscillation (QDO, or TTO) was discovered as a modulation of the tropical Quasi-Biennial Oscillation's (QBO) influence on high latitude dynamics during northern hemisphere winter. Later on, statistical evidence was found that a global QDO has been in phase with the solar cycle for more than three decades irrespective of the state of the tropical QBO.

But the issue of a possible interaction between QBO and QDO during northern hemisphere winter has not yet been resolved. Instead, statistical evidence has been presented supporting both (1) a unique QBO effect in high latitudes (as proposed by Holton and Tan) as well as (2) a coupled QBO/QDO phenomenon (as proposed by Labitzke and Labitzke and van Loon). And recently, (3) an additional Biennial Oscillation (BO) has been found to dominate stratospheric frequency spectra at high latitude; the BO has been used as an argument against the reality of the QDO. Unfortunately, the physical cause of the extratropical BO is as uncertain as the origin of the QDO, and why the latter should be related to the solar cycle.

In this paper it is demonstrated that the extratropical BO can also be understood as a consequence of the interaction between annual cycle, tropical QBO and QDO. Contradictions between previously published statistical studies (Holton/Tan vs. a coupled QBO/QDO) will be resolved by showing that the development of wintertime dynamics follows a two stage process: During early and mid winter, a Holton/Tan-like oscillation dominates, but gets superseded by a Labitzke/van Loon-like behaviour propagating from upper levels into the mid and lower stratosphere during late winter.

MW08/W/06-A2

1730

**EFFECTS OF SOLAR CYCLE VARIABILITY ON THE LOWER STRATOSPHERE AND THE TROPOSPHERE**

Nambath K. BALACHANDRAN, David Rind, Patrick Lonergan, Drew T. Shindell (all at Goddard Institute for Space Studies, 2880 Broadway, New York, NY 10025, U.S.A., email: cdnkb@giss.nasa.gov)

The effects of solar irradiance variability on the lower stratosphere and the troposphere are investigated using observed and general circulation model (GCM) generated 30 mb and 100 mb geopotential heights. The annual and seasonal averages of the height differences between solar maximum and solar minimum conditions are evaluated. In the sub-tropics, observations indicate statistically highly significant increased geopotential heights during solar maximum, compared to solar minimum, in composite annual and seasonal averages. The model simulates this feature reasonably well, although the magnitude and statistical significance of the differences are often weaker than in observations, especially in summer. Both the observations and the model results show a strong di-pole pattern of height differences when the data are partitioned according to the phase of the QBO, with the pattern reversing itself with the change in the phase of the QBO. The solar effects on the lower atmosphere are interpreted as resulting from the effects of UV change on E-P flux divergence in the stratosphere and the associated circulation change below.



**HS3 Monday 19 – Tuesday 20 July****IMPACT OF LAND-USE CHANGE ON NUTRIENT LOADS FROM DIFFUSE SOURCES (ICWQ, ICCE, ICASVR)**

Location: Guild of Students, Council Chamber

**Monday 19 July AM**

Presiding Chair: Joop Steenvoorden, (DLO Winand Staring Centre, Institute for Integrated Land and Water Research, Wageningen University, NL)

**SMALL SCALE FIELD STUDIES OF LAND USE IMPACT ON WATER QUALITY****HS3/W/01-A1 0900****SIMPLIFIED CLASSIFICATION OF HYDROLOGICAL TERMINOLOGY FOR PHOSPHORUS TRANSFER**

Neil PREEDY (Institute of Grassland and Environmental Research, North Wyke, Okehampton, EX20 2SB, UK) Louise Heathwaite (Department of Geography, University of Sheffield S10 2TN, UK, email: a.l.heathwaite@sheffield.ac.uk) Phil Haygarth and Rachel Matthews (Institute of Grassland and Environmental Research, North Wyke, Okehampton, EX20 2SB, UK)

Understanding the importance of surface and subsurface hydrological pathways is critical to effectively manage diffuse transfers of phosphorus (P) from agricultural soils. However, limited understanding of the complexities inherent within the hydrological regime and unfamiliarity with hydrological terminology, can sometimes be a source of confusion for agronomists and soil scientists concerned with P transfer. Consistent use of terminology can help eliminate confusion and the use of ambiguous terms such as "runoff" and "leaching" that are commonly misused. The hydrological terms and processes defined here are identified at the spatial and temporal scales where they occur, and the potential of vertical and lateral water flows for P transfer, both over and through the soil, are discussed.

**HS3/W/02-A1 0925****COMPARISON OF NUTRIENT OUTPUTS FROM TWO LOWLAND WATERSHEDS WITH DIFFERENT AGRICULTURAL PRACTICES**

Kazimierz BANASIK (Department of Hydraulic Structures, Warsaw Agricultural University, ul. Nowoursynowska 166, 02-787 Warsaw, Poland, email: banasik@alpha.sggw.waw.pl) J. Kent Mitchell, Sharyl E. Walker (Department of Agricultural Engineering, University of Illinois at Urbana-Champaign, Urbana, Illinois 61801, USA) Elzbieta Rudzka (Environmental Protection Laboratory of the "Pronit" Factory, 26-600 Pionki, Poland)

Results of four-year water quality monitoring programmes carried out in two small, lowland agricultural watersheds with different agricultural practices, the Upper Little Vermilion River (ULVR) located in central Illinois and the Zagodzinka River located in central Poland, were analysed. Nitrate and orthophosphate concentrations and loads are presented and discussed in relation to meteorological conditions and hydrological responses of the watersheds. The watershed with intensive agricultural practices (ULVR) generates runoff with higher nutrient concentrations. Concentrations of the considered nutrients were, in the case of N-NO<sub>3</sub> about 7.6 times, and in the case of P-PO<sub>4</sub> about 2.3 times higher in the ULVR than in the Zagodzinka River.

**HS3/W/03-A1 0950****THE NITROGEN COMPOSITION OF STREAMS DRAINING GRASSLAND AND FORESTED CATCHMENTS: INFLUENCE OF AFFORESTATION ON THE NITROGEN CYCLE IN UPLAND ECOSYSTEMS**

P. J. CHAPMAN, A.C. Edwards (Macaulay Land Use Research Institute, Craigiebuckler, Aberdeen AB15 8QH, UK, email: p.chapman@mluri.sari.ac.uk) B. Reynolds (Institute of Terrestrial Ecology, Deiniol Road, Bangor, Gwynedd LL57 2UP, UK) C. NEAL (Institute of Hydrology, Wallingford, Oxfordshire OX10 8BB, UK)

The nitrogen (N) composition of streams draining three moorland and three plantation forest catchments in mid-Wales was investigated and compared. Samples of stream water were collected every four weeks over one year and analysed for total dissolved nitrogen (TDN), nitrate (NO<sub>3</sub>), ammonium (NH<sub>4</sub>), dissolved organic nitrogen (DON) and dissolved organic carbon (DOC). There was no significant difference in TDN concentrations between forested and moorland streams. However, NO<sub>3</sub> concentrations were significantly larger in the forested streams and DON and DOC concentrations were significantly larger in the moorland streams. Nitrate and DON also displayed contrasting seasonal patterns: NO<sub>3</sub> concentrations were largest in the winter, while the opposite was observed for DON and DOC. The results confirm conclusions from other studies that afforestation of upland semi-natural vegetation can promote nitrification within the soil system, which is reflected in a change in the TDN composition of stream water. The results also emphasize the need to consider both inorganic and organic forms of N in studies that assess the impact of land management strategies on N cycling in terrestrial and aquatic ecosystems.

**General Aspects of Nutrients in Waters****HSA3/W/05-A1 1015****LOSS OF NITROGEN THROUGH LEACHING AND RUNOFF FROM TWO POTATO LAND-USE SYSTEMS ON DIFFERENT SOILS**

U. C. SHARMA (ICAR Research Complex for NEH Region, Barapani, Meghalaya 793103, India)

Field experiments conducted for two years on three soils varying in texture, planted with potatoes grown by two methods of cultivation—terraced and bun (traditional method on hillslopes) revealed that nitrogen loss through leaching and runoff increased with increased application of nitrogen and was significantly influenced by the nature of the soil, the amount of rainfall received and the method of cultivation followed. The mean N loss was 14.2, 16.5 and 30.3 kg ha<sup>-1</sup> through leaching and 5.8, 5.5 and 4.0 kg ha<sup>-1</sup> through runoff in terraced and 7.1, 9.8 and 19.9 kg ha<sup>-1</sup> in leaching and 19.5, 19.4 and 33.7 kg ha<sup>-1</sup> in runoff in bun method from soils S1, S2 and S3, respectively. The NO<sub>3</sub>-N content of the soil was observed to be higher near the surface (0–20 cm) compared to lower depths (20–40 cm and 40–60 cm) in both methods of potato cultivation and it increased with increased application of nitrogen. Applied nitrogen increased the dry matter yield (tuber + shoots) of potato, and productivity was found higher in light textured soil.

**HSA3/W/05-A1 1110****NITRATE LOSSES UNDER VARIOUS CROPPING SYSTEMS**

J. Kent MITCHELL, Sharyl E. Walker, Michael C. Hirschi and Richard A. C. Cooke (Department of Agricultural Engineering, University of Illinois at Urbana-Champaign, 1304 West Pennsylvania Avenue, Room 332, Urbana, Illinois 61801, USA, email: j.k.m.@sugar.age.uiuc.edu)

The effectiveness of nitrogen management systems in reducing the movement of nitrate in surface and subsurface flow in the Little Vermilion River watershed is presented. Nitrate in subsurface tile flow have been monitored for six years from fields with various tillage and cropping management practices. Water samples have also been obtained along the mainstem of the watershed. Concentrations of nitrate differed little among specific sampling locations along the river, but they definitely followed a seasonal cycle. The pre-plant anhydrous-N application systems with average nitrogen application of 108 kg ha<sup>-1</sup> year<sup>-1</sup> had a mean concentration of nitrate-N of 16.8 mg l<sup>-1</sup> while the side-dress and manure application systems with average nitrogen application of 92 kg ha<sup>-1</sup> year<sup>-1</sup> had a mean concentration of nitrate-N of 10.2 mg l<sup>-1</sup>. The mean concentration of nitrate-N from a permanent meadow field was 1.0 mg l<sup>-1</sup>.

**Phosphorus in Waters****HS3/W/06-A1 1135****TRANSFER OF PHOSPHORUS FROM SMALL AGRICULTURAL BASINS WITH VARIABLE SOIL TYPES AND LAND USE**

P. J. A. WITHERS (ADAS Bridgets, Martyr Worthy, Winchester, Hampshire SO21 1AP, UK, email: paul\_withers@adas.co.uk) R. M. Dils (Environment Agency, National Centre for Ecotoxicology and Hazardous Substances, Evenlode House, Howbery Park, Wallingford, Oxfordshire OX10 8BD, UK) R. A. Hodgkinson (ADAS Boxworth, Boxworth, Cambridge, Cambridgeshire CB3 8NN, UK)

Three small rural basins in England with different soil types and farming systems were monitored from November 1994 to July 1998 to determine the amounts, forms, timing and pathways of diffuse phosphorus (P) transfer in land runoff. Annual loads of total phosphorus (TP) measured in two lowland and one upland basin ranged up to 4.2 and 1.4 kg ha<sup>-1</sup>, respectively and were heavily dependent on basin flow. In all three basins, most P was transported in particulate (PP) form during high flow rates in winter when stream biological activity is low. However, comparison of two monitoring programmes in one basin also indicated elevated loads of soluble P under lower intensity storms. Monitoring of individual field tile drains in the two lowland basins indicated that much of the P transfer was agriculturally derived. The amount of flow needed to generate P transfer was greater, and the concentration of P in the runoff under equivalent flows was lower, under upland grass than under arable or mixed arable/grass cropping.

**HS3/W/07-A1 1200****INVESTIGATIONS ON PHOSPHORUS LEACHING FROM SANDY SOIL**

T. TISCHNER (Institute of Freshwater Ecology and Inland Fisheries, Rudower Chaussee 6a, D-12484 Berlin, Germany, email: tischner@igb-berlin.de)

Investigations on phosphorus leaching were conducted at a field site with sandy soil. From soil sample analyses a linear relationship was found between total phosphorus (Pt) and the amount of water-soluble phosphorus (Pw). Regardless of soil depth and sampling point location only approximately 5% of Pt is water soluble. At a small test site at the border of the field, soil solution was extracted using ceramic- and nylon suction cups. The soil solutions showed that the concentration of total dissolved phosphorus (TDP) decreased significantly with depth. An averaged concentration of around 0.8 mg l<sup>-1</sup> was found at a depth of 30 cm, whereas at 180 cm about 0.1 mg l<sup>-1</sup> was observed. Phosphorus input to the groundwater is in the range of 0.1 kg ha<sup>-1</sup> year<sup>-1</sup>. At that site organic P forms are more important for phosphorus leaching than inorganic fractions. Since the start of investigations no more fertilizer has been applied at the small test site which has led to decreasing ionic strength in the topsoil (30 cm). In contrast, at a depth of 30 cm a continuous increase in the concentration of soluble phosphorus was observed. It is shown that this increase in the concentration of soluble P should be attributed to declining ionic strength and especially to declining Ca concentration. As a consequence changing land use from cultivation to fallow land may lead to enhanced mobilization of previously accumulated phosphorus.

**HS3/W/08-A1 1225****PHOSPHORUS TRANSPORT FROM DIFFUSE AGRICULTURAL SOURCES: SHALLOW SUBSURFACE PATHWAYS IN GRASSLAND SOILS**

R. M. DILS (Environment Agency, National Centre for Ecotoxicology and Hazardous Substances, Evenlode House, Howbery Park, Wallingford, Oxfordshire OX10 8BD, UK, email: r.dils@qub.ac.uk) A. L. Heathwaite (Department of Geography, University of Sheffield, Sheffield S10 2TN, UK)

Phosphorus (P) can be transferred from grassland soils along a number of surface and subsurface hydrological pathways. Currently, our understanding of subsurface transport mechanisms for P is limited. This research examines P transport in shallow subsurface pathways (matrix and macropore flow) under controlled laboratory conditions, and under true field conditions. Simulated rainfall experiments were performed on triplicate soil cores (0.01 m<sup>3</sup>) extracted in summer and winter from an intensively managed grazed grassland field. Matrix and macropore flow samples were collected in situ in this field. Despite the differences in sampling approach, the forms and amounts of P transported in matrix and macropore flow exhibited distinct similarities. In summer matrix flow, for example, total P (TP) concentrations ranged from 47–185 µg l<sup>-1</sup> in the field and from 76–163 µg l<sup>-1</sup> in leachate from cores, with soluble P constituting 65% and 61% of TP, respectively. These findings further current understanding of field-scale P transport processes.

**REGIONAL SCALE MONITORING STUDIES OF LAND USE IMPACT ON WATER QUALITY****General Aspects of Nutrients in Waters****HS3/W/09-A1 1400****NUTRIENT DISCHARGE BY GROUNDWATER AND RIVERS INTO LAKE BIWA, JAPAN**

Makoto TANIGUCHI (Department of Earth Sciences, Nara University of Education, Nara 630-8528, Japan, email: makoto@nara-edu.ac.jp) Norio Tase (Institute of Geoscience, University of Tsukuba, Ibaraki 305-8571, Japan)

Nutrient discharges not only by rivers but also by groundwater have been evaluated in Lake Biwa basin, Japan. In the eastern part of the basin, the densely populated urbanized areas and many agricultural fields have brought a large amount of nutrients such as NO<sub>3</sub><sup>-</sup>, SO<sub>4</sub><sup>2-</sup>, Cl<sup>-</sup> and Na<sup>+</sup> into Lake Biwa. The NO<sub>3</sub><sup>-</sup> concentration of the groundwater discharged from the lake bottom is three times larger than that of river water. A high concentration of Ca<sup>2+</sup> in three rivers and groundwater near those rivers was also found in the areas where the main geology consists of limestone. Land use, population, geology and groundwater flow systems are keys to understanding the nutrient discharge into the lake by rivers and groundwater.

**HS3/W/10-A1 1425****THE EFFECTS OF INTENSIVE DAIRY FARMING ON STREAM WATER QUALITY IN NEW ZEALAND**

Harvey J. E. RODDA (National Institute of Water and Atmospheric Research—NIWA, PO Box 11-115, Hamilton, New Zealand; now at Risk Management Solutions Ltd, 10 Eastcheap, London EC3M 1AJ, UK, email: harvey.rodda@riskinc.com) Robert J. Wilcock (NIWA, PO Box 11-115, Hamilton, New Zealand) Ude Shankar (NIWA, PO Box 8062, Christchurch, New Zealand) Bruce S. Thorold (AgResearch, Private Bag 3123, Hamilton, New Zealand)

This paper describes a three-year study on the effects of intensive dairy farming on the water quality of the Toenepi basin, near Hamilton in New Zealand's North Island. The study incorporated a detailed programme of water quality and flow monitoring, land use surveys, soil surveys, and stream ecology surveys. The monitoring not only generated a better understanding of the effects of intensive dairy farming on stream water quality, but also provided input and calibration data for a distributed basin-scale water quality model, which was set up to test the effects of a number of land-use change scenarios. The results of the monitoring programme showed higher levels of nutrients compared to other New Zealand streams, but sediment levels were not particularly high. The model scenario testing confirmed that any further intensification of land use could lead to stream nitrate-nitrogen concentrations above WHO guidelines.

**HS3/W/11-A1 1450****NUTRIENT CONCENTRATIONS AND FLUXES IN TRIBUTARIES TO THE SWAN-CANNING ESTUARY, WESTERN AUSTRALIA**

Norman E. PETERS (US Geological Survey, 3039 Amwiler Road, Suite 130, Atlanta, Georgia 30360, USA, email: nepeters@usgs.gov) Robert Donohue (Waters and Rivers Commission, Hyatt Centre, East Perth, Western Australia 6004, Australia)

In Western Australia, catchment nutrient availability on an areal basis is primarily controlled by the disposal of animal waste and the type and rate of fertilizer application, particularly in coastal areas. The coastal areas receive notably higher rainfall and have more intense horticulture and animal production than inland areas, and are undergoing rapid urbanization, particularly adjacent to the estuary. Also, the surficial aquifers on the coastal plain are generally sandy having a low nutrient retention capacity and rapidly transmit soluble and colloidal material through the subsurface. In the Swan-Canning basin, high air and soil temperatures and seasonally arid conditions cause rapid mineralization of nitrogen and phosphorus. The nutrients are subsequently available for transport during the onset of seasonal wet weather, which typically begins during the period from late April to June. In addition to the rapid mobility of nutrients in streamwater from agricultural areas during the wet season, drains in urban areas, which typically have high nutrient concentrations, also are an important source of nutrients as the drains flow directly to the estuary throughout the year.

**HS3/W/12-A1 1515****STUDIES OF EROSION AND SOIL LOSS IN THE SEMIARID NORTHEASTERN REGION OF BRAZIL**

Vajapeyam S. SRINIVASAN, José de Araújo Pereira and Carlos de Oliveira Galvão (Department of Civil Engineering, Centre for Sciences and Technology, Federal University of Paraíba, Campus II, Campina Grande 58100-970, Paraíba, Brazil, email: srinivas@reched.ufpb.br)

The effects of land clearing and some of the cultivation practices are analysed for a semiarid region in the northeast of Brazil, in terms of the runoff generated and the soil erosion caused. The data collected in an experimental basin with microbasins of about 0.5 ha in area and various erosion plots were utilized. The response of these micro-basins and plots to the events of rainfall as well as the influence of such factors as land cover, slope, etc. are presented. The most significant result is the ability of the native vegetation in preventing the soil erosion in spite of its sparse nature and fragility.

**HS3/W/13-A1 1615****CHANGE IN DISSOLVED LOADS AND BIOGEOCHEMICAL PROCESSES LINKED TO THE AIR TEMPERATURE FROM LOW MOUNTAINOUS TO SUB-ALPINE WATERSHEDS**

Tomohiro NARUOKA (Institute of Environmental Science, University of Tsukuba, 1-1-1 Tennodai, Tsukuba, Ibaraki 305-8572, Japan, email: lemieux@qb3.sonet.ne.jp) Shin'ichi Onodera (Department of Natural Environmental Sciences, Hiroshima University, 1-7-1, Kagamiyama, Higashi-hiroshima, Hiroshima 739-8521, Japan)

In order to clarify the effect of air temperature on biogeochemical processes in various environments, we confirmed the changes in dissolved load fluxes and biogeochemical processes with air temperature from low mountainous to sub-alpine watersheds in a part of Kanto mountains, west of Tokyo. The solute concentrations in spring water and soil water increased with a decrease in elevation. The organic acids concentrations in the surface soil showed not only seasonal variations but also variations depending on altitude change. This

result suggests that organic acids, produced by microorganisms in the surface soil, especially in the summer season cause the seasonal variations in the solute concentrations. Concentrations of organic acids were extremely low around the elevation of 1500 m where the soil temperature at a depth of 10 cm was below 15°C in summer. The relationship between solute concentrations and temperature was clear in the deeper soil. This result suggests that the variation in the reaction rate of chemical weathering is related to temperature.

**Nitrogen in Waters****HS3/W/14-A1 1640****NITRATE IN GROUNDWATER OF THE MIDWESTERN UNITED STATES: A REGIONAL INVESTIGATION ON RELATIONS TO LAND USE AND SOIL PROPERTIES**

Dana KOLPIN (US Geological Survey, 400 S. Clinton Street, Iowa City, Iowa 52244, USA, email: dwkolpin@usgs.gov) Michael Burkart (National Soil Tilth Laboratory, 2150 Pammel Drive, Ames, Iowa 50011, USA) Donald Goolsby (US Geological Survey, Box 2506, Denver Federal Center, Lakewood, Colorado 80225, USA)

The intense application of nitrogen-fertilizer to cropland in the midwestern United States has created concern about nitrate contamination of the region's aquifers. Since 1991, the US Geological Survey has used a network of 303 wells to investigate the regional distribution of nitrate in near-surface aquifers of the midwestern United States. Detailed land-use and soil data were compiled within a 2-km radius of 100 unconsolidated wells in the regional network to determine relations to nitrate concentrations in groundwater. For land use, the amount of irrigated land was directly related to nitrate concentrations in groundwater. For soils, the general water table depth and soil factors associated with rates of water movement were directly related to nitrate concentrations in groundwater.

**HS3/W/15-A1 1705****SOURCES OF NITRATE IN WATER FROM SPRINGS AND THE UPPER FLORIDAN AQUIFER, SUWANNEE RIVER BASIN, FLORIDA**

Brian G. KATZ (US Geological Survey, 227 N. Bronough Street, Suite 3015, Tallahassee, Florida 32301, USA, email: bkatz@usgs.gov) H. David Hornsby (Suwannee River Water Management District, 9225 County Road #49, Live Oak, Florida 32060, USA) Johnkarl F. Bohlke (US Geological Survey, 431 National Center, Reston, Virginia 20192, USA)

In the Suwannee River basin of northern Florida, nitrate-N concentrations are 1.5 to 20 mg l<sup>-1</sup> in waters of the karstic Upper Floridan aquifer and in springs that discharge into the middle reach of the Suwannee River. During 1996–1997, fertilizers and animal wastes from farming operations in Suwannee County contributed approximately 49% and 45% of the total N input, respectively. Values of d15N-NO<sub>3</sub> in spring waters range from 3.9‰ to 5.8‰, indicating that nitrate most likely originates from a mixture of inorganic (fertilizers) and organic (animal waste) sources. In Lafayette County, animal wastes from farming operations and fertilizers contributed approximately 53% and 39% of the total N input, respectively, but groundwater near dairy and poultry farms has d15N-NO<sub>3</sub> values of 11.0–12.1‰, indicative of an organic source of nitrate. Spring waters that discharge to the Suwannee River from Lafayette County have d15N-NO<sub>3</sub> values of 5.40–8.39‰, which are indicative of both organic and inorganic sources. Based on analyses of CFCs, the mean residence time of shallow groundwater and spring water ranges between 8–12 years and 12–25 years, respectively.

**MODELLING THE IMPACT OF LAND USE ON NUTRIENT BEHAVIOUR IN SMALL SCALE WATER QUALITY STUDIES****Nitrogen in Waters****HS3/W/16-A1 1730****RELATING POTENTIAL DENITRIFICATION RATES TO STREAMFLOW VARIABILITY**

Bente CLAUSEN (Department of Civil Engineering, University of Canterbury, Private Bag 4800, Christchurch, New Zealand; previously at: Department of Earth Sciences, Aarhus University, Denmark; email: b.clausen@civil.canterbury.ac.nz) Charles P. Pearson and Malcolm T. Downes (National Institute of Water and Atmospheric Research (NIWA), PO Box 8602, Christchurch, New Zealand)

Measurements of denitrification enzyme activity (DEA) were made in riparian zones within 27 subcatchments of a 114 km<sup>2</sup> catchment in Denmark during summer 1996, and the rates were related to the hydrological regime of the subcatchments. The hydrological regime was characterized spatially by the specific mean flow (QMEAN) and the baseflow index (BFI), which were almost linearly related. DEA was significantly higher in the top 50 cm soil samples compared with the samples taken from between 50 and 100 cm depth. DEA and BFI were found to be weakly related with higher DEA rates in upstream subcatchments with lower QMEAN and BFI (higher proportion of quickflow).

**Tuesday 20 July AM**

Presiding Chair: Dr. Chris Barnes, Department of Engineering, Australian National University, Canberra

**HS3/W/17-A2 0900****A SIMPLE MODELLING APPROACH TO IDENTIFY PROCESSES CONTROLLING STREAM NITRATE IN AN AGRICULTURAL CATCHMENT**

S. M. DUNN, P. Domburg, A. C. Edwards and R. C. Ferrier (Macaulay Land Use Research Institute, Craigiebuckler, Aberdeen AB15 8QH, UK, email: mi586@mluri.sari.ac)

The processes involved in nitrate generation at the catchment scale are highly complex. This paper investigates whether it is possible to use a modelling approach to derive a simplified set of processes that explain the temporal variability of stream nitrate. The approach is tested on an agricultural catchment where the majority of stream nitrate originates from diffuse runoff from the land. A simple nitrate transport model is combined with a hydrological model and different scenarios to describe potential nitrate leaching mechanisms are tested as drivers of the model. The resulting predictions of stream nitrate are compared with data from continuous sampling. The results suggest that in this catchment mineralization is a more important process in determining nitrate leaching than direct losses following fertilization of crops.

HS3/W/18-A2

0925

**MATHEMATICAL MODELLING FOR ESTIMATING THE SEASONAL CHANGES IN STREAMWATER NO<sub>3</sub>-N CONCENTRATION**

Takao TAMURA (Department of Civil Engineering, Takamatsu National College of Technology, 355 Chokushi-cho, Takamatsu City, Kagawa 761-8058, Japan, email: tamu@takamatsu-nct.ac.jp) Hiromu Yoshida and Michio Hashino (Department of Civil Engineering, The University of Tokushima, 2-1 Minami-jousanjima-cho, Tokushima City, Tokushima 770-8506, Japan)

A NO<sub>3</sub>-N runoff tank model was developed for describing seasonal changes of NO<sub>3</sub>-N concentration of streamwater in forested mountain basins. Three hydrochemical and biochemical processes, namely advection, solute exchange between mobile and immobile regions in the soil and nitrification are considered in the model. Three model types, Models A, B and C respectively, were applied to data obtained in a forested mountain basin in Japan. "Model C" which takes account of all three processes effectively described seasonal changes of NO<sub>3</sub>-N concentration in streamwater. However, "Model A" which represents only the advection process, and "Model B" which includes both advection and solute exchange processes, could not. It is suggested that it is necessary to take all three processes into consideration if any model is to be regarded as valid.

HS3/W/19-A2

0950

**MODELLING THE IMPACT OF LAND-USE CHANGE ON WATER QUALITY IN LOWLAND CATCHMENTS: THE ROLE OF DYNAMIC NITROGEN RESERVOIRS**

F. WORRALL (Department of Geological Sciences, South Road, Durham DH1 3LE, UK, email: fred.worrall@durham.ac.uk) T. P. Burt (Department of Geography, South Road, Durham DH1 3LE, UK)

The consequences of a decline in soil nitrogen following ploughing of permanent pasture are explored in terms of nitrate export at the catchment scale. The release and build up of reserves of organic nitrogen developed in grassland soils is modelled as a first-order kinetic decay and shows supply-limited hysteresis. In comparison with observed data, overestimates are achieved at times of maximum release of nitrogen reserves, implying that new sinks of nitrogen or the form of nitrogen release needs to be explored.

HS3/W/20-A2

1015

**MODELLING WATER AND NITROGEN BALANCE ON A CULTIVATED FIELD: A CHARACTERISTIC HILLSLOPE APPROACH**

Harri Koivusalo, Maija Paasonen-Kivekäs, Tuomo Karvonen and Pertti Vakkilainen (Laboratory of Water Resources, Helsinki University of Technology, PO Box 5200, FIN-02015 HUT, Finland, email: hkoivusa@ahiti.hut.fi)

The objective was to develop computational tools to simulate runoff generation and nitrogen leaching in agricultural areas under subsurface drainage. The hillslope was taken as a basic modelling unit corresponding to the scale where cultivation practices and the full range of hydrological processes occur. A quasi-two-dimensional model was used to describe water movement along a characteristic hillslope, which represented a typical cross-section of the fields. The nitrogen leaching with subsurface drainage flux and surface runoff was modelled using a simplified representation of the nitrogen cycle. The characteristic hillslope model was used together with measured runoff and water quality data to evaluate water and nitrogen balance during winter rye cultivation in southern Finland from 1995 to 1996. The results showed that most of the nitrogen was leached through subsurface drains, even if leaching with surface runoff may become important just after fertilizer applications.

HS3/W/21-A2

1110

**NITROGEN TRANSPORT VIA SURFACE AND SUBSURFACE FLOW IN AN AGRICULTURAL FIELD**

Maija Paasonen-KIVEKÄS, Harri Koivusalo, Tuomo Karvonen, Pertti Vakkilainen and Johanna Virtanen (Helsinki University of Technology, Laboratory of Water Resources, PO Box 5200, FIN-02015 HUT, Finland, email: mpaasone@ahiti.hut.fi)

Nitrogen in runoff waters and in soil was monitored in a clay field, in southern Finland. Subsurface drainage accounted for 51% of the total runoff (439 mm) and 79% of the total N losses (30 kg ha<sup>-1</sup>) in June 1994–December 1996. Nitrate nitrogen (NO<sub>3</sub>-N) formed 32–96% of the total N load. NO<sub>3</sub>-N in the subsurface drainage water rapidly increased from 2 to 60 mg l<sup>-1</sup> after the sequence of fertilization and rainfalls. NO<sub>3</sub>-N in the soil water indicated prominent preferential flow from the top layer into the tile drains. Total N in the runoff waters remained below 5 mg l<sup>-1</sup> during the snowmelt and below 10 mg l<sup>-1</sup> in the autumn. In these seasons, the determining factor in N transport was the high water volumes of surface runoff and subsurface drainage. The preferential flow paths are likely caused by both macropores and the drainage trench itself.

HS3/W/22-A2

1135

**IMPACT OF LAND-USE CHANGE ON NUTRIENT FLUXES IN A STRUCTURED CLAY-LOAM SOIL**

Lubomír LICHNER, Ivan Mészáro (Institute of Hydrology, Slovak Academy of Sciences, Racianska 75, PO Box 94, 830-08 Bratislava, Slovakia, email: lichner@uh.savba.sk) Peter F. Germann, Abdallah Mdaghri Alaoui (Institute of Geography, Bern University, Hallerstrasse 12, CH-3012 Bern, Switzerland) Miloslav Jřr (Institute of Hydrodynamics, Czech Academy of Sciences, Podbabská 13, 166-12 Prague 6, Czech Republic) Pavol Fa\_ko (Slovak Hydrometeorological Institute, Jeseniouva 17, 83-315 Bratislava, Slovakia)

Accepted management practices influence the distribution of surface-vented macropores and thus the nutrient fluxes in soil. Two ways to assess the impact of land-use change on nutrient fluxes in soils are presented: (a) estimating the bypassing ratio at the interface between the root zone and subsoil, and (b) monitoring the non-reactive tracer relative concentration vs depth distributions in the course of infiltration experiment. The 1993–1996 small-scale field experiments have shown that the bypassing ratio varied from 19 to 55% in a structured clay-loam soil. Impact of land use on the tracer relative concentration vs depth distributions was significant for small and medium cumulative infiltration (I = 40–54 mm) but not so significant for the bigger cumulative infiltration (I = 100–108 mm).

**MODELLING THE IMPACT OF LAND USE ON WATER QUALITY IN REGIONAL SCALE STUDIES****Nitrogen in Waters**

HS3/W/33-A2

1200

**A CONCEPTUAL MODEL FOR SIMULATION OF CATCHMENT SCALE NITRATE TRANSPORT**

Y. Van Herpe, P. A. Troch and L. Callewer (Laboratory of Hydrology and Water Management, University of Ghent, Coupour Links 653, B-9000 Ghent, Belgium, email: yves.vanherpe@rug.ac.be)

A conceptual catchment-scale model for simulating nitrate transport in rural watersheds is presented. The model consists of a hydrological part and a nitrate transport module. The latter comprises two functions: a production function controlling nitrate release from the unsaturated zone and a transfer function controlling the discharge of nitrate in the surface water. The production function simulates surface runoff and nitrate leaching towards the saturated zone in response to effective rainfall, duration of the leaching period and initial soil nitrate content of the leaching period. The transfer function defines a proportional relation between the catchment soil saturation deficit and the nitrate concentrations in the surface water. The model is found to be applicable for two different catchments under humid temperate climatic conditions.

HS3/W/24-A2

1225

**MODELLING NITROGEN TRANSPORT IN SWEDEN: INFLUENCE OF A NEW APPROACH TO RUNOFF RESPONSE**

Berit Arheimer and Sten BERGSTRÖM (Swedish Meteorological and Hydrological Institute, S 60176 Norrköping, Sweden, email: berit.arheimer@smhi.se)

The Swedish HBV-N model is aimed to be a decision-support tool to counteract eutrophication in the marine environment. It has recently been applied in several Swedish rivers for large-scale retention mapping, source apportionment, and optimization of measure allocation. The model proved to have difficulties in capturing the N dynamics of some rivers with low baseflow conditions and few lakes. The rigidity of the response function of the HBV model was questioned, and a new routine was developed. It was found out that the simple variability parameter for soil moisture in the hydrological HBV model also could be linked to percolation and recession coefficients, and thereby significantly improve low flow simulations. This resulted in rather modest impacts on the water discharge, but changed internal variables drastically, which improved N simulations of concentrations in rivers with unusual concentration patterns. The hydrological response function was found to be especially important when modelling low flow concentration dynamics which originate from diffuse pollution in catchments.

Tuesday 20 July PM

Presiding Chair: Dr Lubomir Lichner, Institute of Hydrology, Slovak Academy of Sciences, Bratislava

HS3/W/25-A2

1400

**FACTORS AFFECTING NITROGEN EXPORT FROM DIFFUSE SOURCES: A MODELLING STUDY IN THE ELBE BASIN**

Valentina KRYSANOVA, Dieter Gerten, Beate Klöcking, and Alfred Becker (Potsdam Institute for Climate Impact Research (PIK), PO Box 601203, D-14412 Potsdam, Germany, email: valen@pik-potsdam.de)

To investigate the factors affecting nitrogen export from diffuse agricultural sources of pollution, the model SWIM was applied in two mesoscale river basins located in the Elbe drainage area: the Stepenitz (gauge Wolfshagen, 575 km<sup>2</sup>) in the Pleistocene lowland subregion, and the Zschopau (gauge Lichtenwalde, 1504 km<sup>2</sup>) in the mountainous subregion. Significant parts of both basins are occupied by cropland, but they are different in relief and soil types. The modelling results show the pathways of nitrogen loss from different soils in cropland, and the influence of climate and agricultural practices (fertilization rates and timing, rotation schemes) on nitrogen export. The differences in nitrogen cycling for different soils and management practices revealed by the simulation provide a basis for further scenario evaluation and eventually for recommendations on improving agricultural practices.

HS3/W/26-A2

1425

**SCENARIO CALCULATIONS OF REGIONAL SUBSURFACE TRANSPORT OF PHOSPHORUS IN A SUB-BASIN OF THE SPREE RIVER NEAR BERLIN**

S. PUDENZ and G. Nützmann (Department of Ecohydrology, Institute of Freshwater and Fish Ecology, Rudower Chaussee 6a, D-12484 Berlin, Germany, email: step@igb-berlin.de)

The assessment of the potential eutrophication of surface waters in the northeastern lowlands of Germany depends on the phosphorus input from the basin. Therefore scenarios dealing with regional transport of phosphorus are helpful tools to calculate a prognosis for the diffuse loading of surface waters. In this study the compartment model MORPHO is applied to simulate the leaching of phosphorus in the unsaturated zone in a sub-basin of the Spree River near Berlin. The water soluble phosphorus content in the pore water indicates a strong relation between P leaching and water solubility of P. The calculated average mean annual TDP (total dissolved phosphorus) concentration of 187 mg l<sup>-1</sup> in a certain area of the sub-basin overestimates the mean annual measured concentration (112 mg TDP l<sup>-1</sup>) in drainage waters. However, the results of two scenarios averaged over the whole basin (0.56 and 1.39 kg TDP ha<sup>-1</sup> year<sup>-1</sup>) are of the same order of magnitude as values estimated in similar basins (0.25 and 1.15 kg TDP ha<sup>-1</sup> year<sup>-1</sup>). Finally the results indicate that managing agriculture without P fertilizing in the basin is not an efficient strategy to reduce P loading of drainage waters.

HS3/W/27-A2

1450

**EVALUATING STRATEGIES TO REDUCE NITRATE AND PHOSPHATE LOSS TO SURFACE WATER FROM AGRICULTURAL LAND ON JERSEY**

R. J. PARKINSON, J. E. Lott, M. P. Fuller (Department of Agriculture and Food Studies, Seale-Hayne Faculty, University of Plymouth, Newton Abbot, Devon TQ12 6NQ, UK, email: rparkinson@plymouth.ac.uk) L. Beattie (Department of Agriculture and Fisheries, PO Box 327, Howard Davis Farm, Trinity, Jersey JE4 8UF, UK)

Nitrate concentrations in reservoirs on the island of Jersey consistently exceed 11.3 mg l<sup>-1</sup> nitrate-nitrogen (NO<sub>3</sub>-N). In the 3.4 km<sup>2</sup> drainage basin of the Val de la Mare Reservoir



selected for this study, arable crops, predominantly early potatoes, in combination with a second crop, a cover crop or fallow, accounted for 53% of the total land use in both 1995 and 1996. Export coefficient modelling was used to calculate the total nitrogen delivered to the Val de la Mare reservoir annually. The model predicted that land allocated to early potatoes accounted for 86–87% of the total nitrogen lost to the reservoir from agricultural land during 1996 and 1997. Field trials were conducted during the 1997/98 winter drainage season to evaluate the effectiveness of various crop management strategies designed to limit nutrient losses from agricultural land within the drainage basin. Mean NO<sub>3</sub>-N and molybdate reactive phosphorus (MRP) concentration in soil water under a cauliflower/early potato crop during 1997/98 were 17.1 mg N l<sup>-1</sup> and 49.2 mg P l<sup>-1</sup> respectively, in comparison with 2.4 mg N l<sup>-1</sup> and 14.3 mg P l<sup>-1</sup> under ungrazed permanent grass.

**HS3/W/28-A2****1515**

#### THE IMPACT OF LAND USE CHANGES 1820–2020 ON WATER QUALITY AND QUANTITY IN SOUTHEAST MICHIGAN

Andrew J. BRENNER, Paul L. Richards (School of Natural Resources and Environment, University of Michigan, 430 E. University, Ann Arbor, Michigan, 48109-1115, USA) Mike Barlage and Peter Sousounis (Atmospheric, Oceanic and Space Sciences, Space Research Building, 2455 Hayward, University of Michigan, Ann Arbor, Michigan, 48109-2143, USA)

Since changes in land use and climate are impacting river systems around the world, there is a need to build models that enable integration of atmospheric and hydrologic models. This paper shows an adaptation to the soil curve number approach for continuous rainfall input, and the event mean concentration approach to simulate stream loading of total suspended solids, phosphorus (P) and Kjeldahl nitrogen. Simulated P loads were within 4.5% of measured values. Simulation using 1820, 1990 and predicted 2020 land covers showed that runoff has increased by 3.5 times since 1820, but will change little in the future. However, it appears that the large increases in pollutant loads that have occurred in the last 170 years will increase in the future. This emphasizes the need to implement non-point source pollution controls in the studied watershed.

#### General Aspects of Water Quality

**HS3/W/29-A2****1615**

#### SURFACE WATER POLLUTION FROM DIFFUSE AGRICULTURAL SOURCES AT A REGIONAL SCALE

Piet GROENENDIJK (DLO Winand Staring Centre, Institute for Integrated Land, Soil and Water Research, PO Box 125, 6700 AC Wageningen, The Netherlands, email: p.groenendijk@sc.dlo.nl) Paul Boers (Institute for Inland Water Management and Waste Water Treatment, PO Box 17, 8200 AA Lelystad, The Netherlands)

The approach used in the leaching models to assess the nutrient load on minor surface water systems at the regional scale in The Netherlands is presented. Regional spatially distributed patterns of soil type, land use and hydrology are schematized by a number of homogeneous subregions. In the model a sub-region is represented by a single vertical soil column. Lateral groundwater fluxes are used to compose a regional average discharge concentration. Results of the model approach are discussed for the study on the quantification of the nitrogen and phosphorus load on surface waters at a national scale, as has been conducted in the framework of the Fourth National Policy Document on Water Management in The Netherlands. The aim of the study was to analyse the impact of fertilizer management on N and P discharges to Dutch surface waters. It is concluded that hydrological insight into the system and an associated understanding of the relation between groundwater flow and the loading of surface water is of the utmost importance.

**HS3/W/30-A2****1640**

#### MODELLING SPATIAL AND TIME DEPENDENT NUTRIENT FLOW DYNAMICS BY DELINEATION OF VARIABLE CHEMICAL HYDROLOGICAL RESPONSE UNITS (VCRUS) WITH A GIS

Ulrike BENDE-MICHL (Department of Geography, Institute of Geoinformatics, Geohydrology and Modelling, Friedrich-Schiller University Jena, D-07743 Jena, Germany, email: c5ulbe@geogr.uni-jena.de)

Modelling hydrochemical contaminant catchment dynamics in heterogeneous basins is dealing with the detection and the quantification of spatially-distributed and time-variable impacts—known as nonpoint sources and the knowledge of their transformation and translocation into the output of the catchment. The concept of time and spatially variable chemical hydrological response units (VCRUs) through GIS analysis and the physically-based solute model WASMOD were linked to monitor the magnitude of export rates and dynamics of nutrients at the catchment outlet at different time and spatial scales. VCRUs are defined as areas having unique or similar hydrochemical dynamics related to physiographic catchment characteristics and to land-use strategies within a variable defined time sequence. Furthermore the time sequence was delineated according to the dominant hydrological pathways, the solute source and its determinant transformation process. The concept was applied to the 216 km<sup>2</sup> Broel River basin, Germany, which has been intensively mapped and digitized for GIS analysis. Data collection included water samples for dissolved solids, fertilizer application and catchment characteristics. Hydrological and chemical balances were modelled for different time series and the results were compared with the measured output at the gauging station. Modelling results showed a good fit during unique hydrological conditions whereas VCRUs were adapted to. Therefore the approach is validated to monitor and control land-use changes and its effects on the magnitude of nutrients losses at a basin-scale.

**HS3/W/31-A2****1705**

#### THE USE OF HIGH RESOLUTION DIGITAL TERRAIN MODELS TO REPRESENT WASH-OFF IN NATURAL AND MAN INFLUENCED ENVIRONMENTS

Paul QUINN (Water Resource Systems Research Laboratory, Department of Civil Engineering, University of Newcastle, Newcastle Upon Tyne NE1 7RU, UK, email: p.f.quinn@ncl.ac.uk) Steven Anthony (ADAS Research and Development, Wergs Road, Wolverhampton, WV6 8TQ, UK)

Modelling the wash-off of diffuse surface pollutant sources and sediment requires an accurate representation of flow pathways. The main problem of flow representation within models is one of scale. In reality processes that mobilize and transport pollution are highly localized and controlled by small-scale natural and manmade features. These features are essentially hydraulic structures that control the volume, direction and energy regime of the flow. However, at the larger scale, "hydrological" phenomena are used to represent the general flow accumulation of flow and pollutants. Recently, digital terrain maps (DTMs) have been used to depict flow paths, gradients and erosion indices (using grid resolution of 50–300 m in some

examples). There needs to be therefore, some form of simplification and some generalization of our flow assumptions. This poster paper seeks to investigate the scale problem by creating high resolution DTMs. In essence we are trying to create DTMs that are at a scale approaching "reality". This paper shows: the importance of local topography form on flow; the importance of manmade features controlling flow and the implication of grid resolution choice when modelling flow, erosion and sedimentation.

**HS3/W/32-A2****1730**

#### MODELS FOR EVALUATING WATER QUALITY AND BMP EFFECTIVENESS AT THE WATERSHED SCALE

Ray WHITTEMORE (National Council of the Paper Industry for Air and Stream Improvement—NCASI, Tufts University, PO Box 53015, Medford, Massachusetts 02153-0015, USA, email: rwhittemore@tufts.edu) George Ice (NCASI, Corvallis, Oregon, USA)

The Environment Protection Agency (EPA) and other water resource agencies have identified the need to develop watershed-scale assessments to evaluate progress in meeting the goals of the Clean Water Act. The forestry community has been a leader in developing these watershed evaluation techniques. While watershed-scale, monitoring, adaptive management assessments, and modelling combinations are all used effectively in the US, this paper emphasizes realistic modelling. Models can be used to test different alternatives and are not confounded by the weather or watershed variability associated with even well paired adjacent basins. Examples of watershed-scale models frequently used in forestry for assessing water quality response are DHSVM, BOISED, and BASINS2.0.

**HS4****Thursday 22 – Friday 23 July**

#### INTEGRATED METHODS OF CATCHMENT HYDROLOGY – TRACER, REMOTE SENSING AND NEW HYDROMETRIC TECHNIQUES (ICT, ICRSDT, ICSW, ICGW, ICSI, ICWQ)

Location: Guild of Students, Council Chamber

Location of Posters: Guild of Students, Room 46 & 47

**Thursday 22 July AM**

Presiding Chair: Chris Leibundgut (Institute of Hydrology, University of Freiburg, Germany)  
Concurrent Poster Session

**Introduction****0930**

LEIBUNDGUT Chris

**HS4/W/01-A4****0945**

#### A COMBINED TRACER-HYDROMETRIC APPROACH TO ASSESS THE EFFECT OF CATCHMENT SCALE ON WATER FLOW PATH, SOURCE AND AGE

Jeff McDONNELL (State University of New York, College of Environmental Science and Forestry, Syracuse, New York 13210, USA, email: jemcdonn@mailbox.syr.edu); Lindsay Rowe (Landcare Research, PO Box 69, Lincoln, New Zealand); Mike Stewart (IGNS, PO Box 31312, Lower Hutt, New Zealand)

The scaling of water source contributions to channel stormflow is not well understood. We collected rainfall–runoff data along with streamflow and rainfall d 180 information for four nested catchments in the Maimai watershed, South Island, New Zealand. The catchments ranged in size from 0.1 to 920 ha. Water source contributions and water age spectra were assessed for an 87 mm rainfall event using a new model by Stewart & Rowe (1999). We found that (a) the source contributions of new water increased with increasing catchment area for catchment scales above the representative elementary area of the system, and (b) water age (flow time) showed some increase with increasing catchment size (beyond the zero-order catchment scale), and peak water fraction increased linearly with catchment area. This work has implications for how we model stream water chemistry since it is affected by both the mixing of different catchment end members and contact time.

#### HYDROMETRIC APPROACHES

**HS4/W/02-A4****1015**

#### HYDROMETRIC APPROACHES TO GAIN A BETTER UNDERSTANDING OF SATURATION EXCESS OVERLAND FLOW

Gerd PESCHKE and Christoph Sambale (International Graduate School, Department of Environmental Sciences, Markt 23, D-02763 Zittau, Germany, email: peschke@ihi.htw-zittau.de)

This paper examines how hydrometric approaches can be used to obtain information about the spatial variability of runoff processes, especially saturation overland flow. This quick runoff component reflects the interaction between subsurface and surface flow and catchment features such as topography and soil properties, weather characteristics like rainfall intensity and amount, and antecedent soil moisture. We measured transects across the stream with both spatially integrated measurements and point measurements. This kind of experimental investigation provides data of a new quality and additional process knowledge needed for a better understanding of runoff production. With detailed mapping of the dominant runoff processes in combination with the most important influencing parameters, an improved construction of submodels becomes possible.

**HS4/W/03-A4****1045**

#### EFFECT OF A PERMEABLE BEDROCK ON RUNOFF GENERATION IN STEEP MOUNTAINOUS CATCHMENTS IN THE KANTO MOUNTAINS, JAPAN

Kunihide MIYAOKA (Faculty of Education, Bunkyo University, 3337 Minami-Ogishima, Koshigaya, Saitama 343, Japan, email: miyaoka@koshigaya.bunkyo.ac.jp); Shinichi Onodera (Faculty of Integrated Science, Hiroshima University, 1-7-1 Kagamiyama, Higashihiroshima, Hiroshima 739, Japan); Takashi Hirose (Faculty of Law and Literature, University of Ryukyus, 1 Senhara, Nishiharamachi, Chuto-gun, Okinawa 903-01, Japan)

We estimated the effect of the permeable bedrock on the runoff generation in two steep mountainous catchments west of Tokyo, using hydrological observation and hydrogeological surveys. Two small catchments, one underlain by granite bedrock, and the other with sedimentary bedrock were studied. Runoff decreased after the first peak in the granite

catchment, while it reached 5 times the initial peak value after 6 h in the sedimentary catchment. Runoff ratios were 12% in the granite catchment and 65% in the sedimentary rock catchment. Because the regolith layer is thinner in the sedimentary catchment than in the granite catchment, this observed secondary peak of runoff suggests the existence of significant flow-through fissures. Event water amounts in both catchments were estimated to be very low, using the natural tracers Cl<sup>-</sup> or d18O. These results indicate the contribution of pre-event water to storm runoff. The electrical sounding and infiltration experiments suggest that rainwater percolates into the fractured bedrock, mixes with soil water in the regolith, and discharges quickly in the sedimentary rock catchment.

HS4/W/04-A4

1105

#### QUANTITATIVE EVALUATION OF FOREST FLOOR EVAPORATION AND TRANSPIRATION REVEALED BY SOIL WATER CONTENT OBSERVATION IN HUMID TEMPERATE PINE FORESTS

Jun SHIMADA (Department of Earth Sciences, Faculty of Science, Kumamoto University, 2-39-1, Kurokami, Kumamoto 860-8555, Japan, email: j-shimada@sci.kumamoto-u.ac.jp); Takashi Yonesaka (196-11 Misono-cho, Yoichi machi, Hokkaido 046, Japan); Qi You Zhou (Doctoral Programme in Geoscience, University of Tsukuba, 1-1-1 Tennodai, Tsukuba 305-8571, Japan)

The combined monitoring of soil water content by soil heat conductivity probes and soil matrix potential by tensiometers was done at a Japanese red pine forest site during summer 1997. The total potential distribution during the study period revealed the existence of two separate zero flux planes at depths of 20 and 70 cm. The depth of the shallower zero flux plane was influenced by rainfall events, while the deeper zero flux plane was stable. The deeper zero flux plane was considered to be mainly influenced by the absorption of soil moisture through the root system of the Japanese red pine based on root depth distribution. The daily soil water content recorded by the soil heat conductivity probes was used to evaluate the day-to-day variations of soil water content at the monitored soil depth. The decreasing variations should be the influence of forest floor evaporation, or transpiration through root, or downward soil water infiltration to recharge the groundwater. The total potential distribution monitored by tensiometers can be used to separate those soil water reducing components by the direction of the soil water flow. The combination of the daily soil water content variations, and the soil water flux revealed by the total potential distribution, makes it possible to evaluate the quantitative separation of the forest floor evaporation and the transpiration.

HS4/W/05-A4

1225

#### WATER AND COMPONENT MASS BALANCES IN THE CATCHMENT OF LAKE STECHLIN

E. HOLZBECHER, G. Nützmann and G. Ginzel (Institute of Freshwater Ecology and Inland Fisheries, Department of Ecohydrology, Rudower Chaussee 6A, Building 21.2, D-12484 Berlin, Germany, email: holzbecher@igb-berlin.de)

Surface water and groundwater are hydraulically connected in the Lake Stechlin catchment. Therefore, there is an urgent need to study unsaturated and saturated flow and related major ion transport processes and exchange with the surface water to analyse the influence on the aquatic chemistry, especially on calcite precipitation in the lake. Based on long-term measured hydrological data, in an integrated approach a steady-state regional groundwater model was developed and fluid mass balances were calculated. Chemical analyses show higher concentrations of major components (Na<sup>+</sup>, K<sup>+</sup>, Ca<sup>2+</sup>, Mg<sup>2+</sup>, Fetot, Cl<sup>-</sup>, SO<sub>4</sub><sup>2-</sup>, NO<sub>3</sub><sup>-</sup>, HCO<sub>3</sub><sup>-</sup>) in groundwater than in lake water. Based on the computed subsurface water balance it can be deduced that groundwater has a strong influence on the composition of the surface water, especially for Ca<sup>2+</sup> and HCO<sub>3</sub><sup>-</sup>.

Thursday 22 July PM

Presiding Chairs: Gert Schultz (Univ. of Bochum, Germany) and Tadasji Tanaka (Univ. of Tsukuba, Japan)

#### REMOTE SENSING APPROACHES

HS4/W/06-A4

1400

#### SNOWMELT RUNOFF CONCEPTUALIZATION BASED ON TRACER AND SATELLITE DATA

Jaroslav MARTINEC (Alteinstrasse 10, CH-7270 Davos-Platz, Switzerland); Albert RANGO (USDA Hydrology Laboratory, BARC-West, Building 007, Room 104, Beltsville, Maryland 20705, USA, email: alrango@hydrolab.arsusda.gov)

As a result of thermonuclear test explosions in the atmosphere, tritium concentrations in precipitation in the sixties and seventies varied strongly from year to year as well as in the winter and summer half years. This paper illustrates how the contrasting tritium concentration in snow and in groundwater was used to develop a snowmelt runoff model (SRM). A new insight into the runoff mechanism and the role of the recession flow provided a concept of transforming the snowmelt into river flow on a daily basis. The adopted deterministic approach, without calibration of parameters, requires snow cover monitoring by satellites. While tritium tracing contributed to the model design, remote sensing enables the SRM model to be used around the world.

HS4/W/07-A4

1430

#### UNDERSTANDING HYDROLOGICAL PROCESSES IN CATCHMENTS USING REMOTELY SENSED TRACERS AND GEOGRAPHICAL INFORMATION SYSTEMS

Serwan M. J. BABAN (GRRU Group, Geography, School of Natural and Environmental Sciences, Coventry University, Priory Street, Coventry CV1 5FB, UK, email: s.baban@coventry.ac.uk)

Soil erosion and water degradation problems are currently major environmental problems. Attempting to solve them will require a clear understanding of the hydrological processes involved at the appropriate scale. Remote sensing techniques can provide information about areas prone to erosion and the subsequent sediment load in water bodies within a catchment area. This is usually based on the deduced spatial and temporal distribution of turbidity, suspended material and associated pollutants, acting as natural tracers. This paper explores the possible usage of remote sensing and geographical information systems (GIS) techniques in catchment studies. Remotely sensed tracer information is then used within a GIS framework to present a holistic approach that takes into consideration the causes as well as the effects of soil erosion and water degradation problems in hydrological catchments. This approach can easily be used to promote a clearer conceptual understanding of hydrological processes and to develop, monitor and simulate management strategies aiming at minimizing the magnitude of these problems within catchments.

HS4/W/08-A4

1450

#### APPLIED REMOTE SENSING FOR PARAMETERIZING SOLUTE TRANSPORT AND SEDIMENT MODELS IN THE ARSGISP PROJECT

Bettina MÜSCHEN, Wolfgang-Albert Flügel (Institute for Geography, Department of Geoinformatics, Hydrology and Modelling, Friedrich-Schiller-University of Jena, Löbdergraben 32, D-07743 Jena, Germany, email: arsgisp@geogr.uni-jena.de); Friedrich Quiel (Environmental and Natural Resources Information Systems, The Royal Institute of Technology, Brinellvägen 32, S-10044 Stockholm, Sweden); Giuliano Rodolfo (Dipartimento di Scienza del Suolo e Nutrizione della Pianta, Università di Firenze, Piazzale delle Cascine 15, I-50144 Firenze, Italy)

The EU project ARSGISP applies remote sensing techniques and GIS analyses to parameterize hydrological, erosion, and solute transport models. Activities of the first project stage are presented, emphasizing the common environmental problem of nutrient leaching within three representative European drainage basins located in Italy, Germany, and Sweden. Physically-based simulation models used by project partners are briefly described and the contribution of optical and radar remote sensing techniques for model parameterization is discussed. The scientific approach concentrates on deriving physical parameters characterizing soil and vegetation by means of land use/land cover classifications using Landsat TM, IRS-1C LISS, and ERS-2 SAR data. First results are quite promising: (a) agricultural crops and Mediterranean vegetation could be classified with optical and radar data, and (b) model parameters describing the distributed features of the test basins vegetation-soil-topography interface (VSTI) could be derived.

HS4/W/09-A4

1510

#### INTEGRATING TRACER WITH REMOTE SENSING TECHNIQUES FOR DETERMINING DISPERSION COEFFICIENTS OF THE DĂMBOVITA RIVER, ROMANIA

Mary-Jeanne ADLER, George Stancalie and Cristina Raducu (National Institute of Meteorology and Hydrology, Sos Bucuresti-Ploiesti 97, 71552 Bucharest, Romania, email: adler@meteo.inmh.ro)

Knowledge of dispersion coefficients in longitudinal, lateral and vertical flow directions is of utmost importance when evaluating the time-concentration distribution of pollutants at any point in a stream. Remotely sensed field data (from NOAA and teledetection) were used to identify the river sector for a dye tracing experiment. The main criteria were to locate a sector without significant anthropogenic influence and with similar hydraulic conditions. The sector selected for sampling was 2.5 km long. The longitudinal and three-dimensional dispersion coefficients were determined. The time-concentration curve for rhodamine dye obtained under different hydraulic conditions of flow (different stages) was measured on the Dâmbovita River. The stage was nearly constant for each experiment but different in each case, therefore it was possible to obtain information for different regimes. Additional information needed to make use of the one-dimensional and three-dimensional mathematical models of dispersion was obtained at the Malu cu Flori gauging station (continuous stage recording and stage-discharge curve). Finally, the experimental data were used to verify the mathematical dispersion model proposed for the Dâmbovita River.

HS4/W/10-A4

1530

#### APPLICATION DE LA THERMOGRAPHIE INFRAROUGE AEROPORTEE A L'ETUDE DE L'HETEROGENEITE D'UNE ZONE HUMIDE RIVERAINE D'UN COURS D'EAU

Hocine BENDJOURI, Celine Pinet (Laboratoire de Géologie Appliquée, Université Pierre et Marie Curie, 4 Place Jussieu, F-75252 Paris, France, email: bdj@biogeodis.jussieu.fr); Roger Guerin (Département de Géophysique Appliquée, Université Pierre et Marie Curie, Paris, France)

La compréhension du fonctionnement des zones humides riveraines du cours moyen des rivières passe par la reconstitution et la modélisation de la mise en place des alluvions qui leur servent de substrat. Sur les zones humides des vallées de l'Aube et de la Seine, une prospection thermique aéroportée a ainsi été mise en œuvre, dans le but de fournir des images dans le visible et le thermique lointain. Suite aux premiers résultats obtenus—distinction entre les zones d'eau libre et les zones d'eau stagnantes, localisation rapide et à grande échelle des anciens réseaux hydrographiques—un site test d'une superficie de 1 ha a été sélectionné sur un des axes de vol. Les mesures électromagnétiques et les sondages réalisés sur ce site ont révélés une concordance des résultats sur les sols vierges de toute pratique agricole. D'autres investigations géophysiques mais également géochimiques (traceurs), permettraient à l'avenir de définir les paramètres hydrauliques de cette zone humide.

#### TRACER APPROACHES

HS4/W/11-A4

1600

#### INTEGRATION OF TRACER INFORMATION INTO THE DEVELOPMENT OF A RAINFALL-RUNOFF MODEL

Stefan UHLENBROOK and Christian Leibundgut (Institute of Hydrology, University of Freiburg, Fahrenbergplatz, D-79098 Freiburg, Germany, email: uhlenbro@uni-freiburg.de)

A conceptual rainfall-runoff model has been developed for the mountainous Brugga basin (39.9 km<sup>2</sup>) situated in the Black Forest, south-western Germany. This model contains an extensive, physically realistic description of the runoff generation, considering seven unit types each with characteristic dominating runoff generation processes. The processes are conceptualized by different linear and non-linear reservoir concepts. Tracer concentrations (i.e. dissolved silica) are attributed to reservoir outflows, according to tracer hydrological investigations. A study period of 20 months showed a reasonable agreement between simulated and observed discharge. The simulated amounts of different runoff components also agreed well with calculations based on measurements of natural tracers. The tracer simulations were less accurate, whereas the general behaviour of the tracer concentrations and short time periods were modelled well.

HS4/W/12-A4

1630

#### ISOTOPE HYDROLOGICAL STUDY OF MEAN TRANSIT TIMES AND RELATED HYDROGEOLOGICAL CONDITIONS IN PYRENEAN EXPERIMENTAL BASINS (VALLCEBRE, CATALONIA)

Andreas HERRMANN, Susanne Bahls (Institute for Geography and Geocology, Technical University Braunschweig, Langer Kamp 19c, D-38106 Braunschweig, Germany, email: a.herrmann@tu-bs.de); Willibald Stichter (Institute for Hydrology, Research Centre for Environment and Health (GSF), Ingolstädter Landstr. 1, D-85764 Neuherberg, Germany); Francesc Gallart and Jerome Latron (CSIC Institute of Earth Sciences Jaume Almera, Lluís Sole Sabarís s/n, SP-08028 Barcelona, Spain)

Measurements of tritium and oxygen-18 concentrations in water samples from streams at low discharge, wells, and permanent springs are used to provide insight into hydrogeological conditions, storage properties, runoff formation, and flow partitioning of Pyrenean experimental basins 100 km north of Barcelona. Transit times as derived from tritium range between 8–11.5 years for wells, 8.5–13.0 years for streams, to 10.5–13.5 years for springs. These results are twice the usual values which suggests low permeability of the bedrock formations. Minimum groundwater reserves can be determined from low discharge and mean transit times, and groundwater plays an important role in flood generation. Tritium is still found to be a useful tracer provided that transit times are high enough and geological information is available.

HS4/W/13-A4

1650

#### HYDROLOGICAL PROCESSES IDENTIFICATION BY THE COMBINATION OF ENVIRONMENTAL TRACING WITH TIME DOMAIN REFLECTOMETRY MEASUREMENTS

C. JOERIN, A. Musy and F. Pointet (Soil and Water Management Institute, Swiss Federal Institute of Technology, CH-1015 Lausanne, Switzerland, email: christophe.joerin@dgr.epfl.ch)

This study begins with the application of environmental tracing in order to identify hydrological processes in the Haute-Mentue basin. The application of a three-component model, based on concentrations of silica and calcium demonstrates that the groundwater and soil water dominate streamflows. Mixing models identify volumes, but not water pathways. In this context, in order to specify which physical properties or mechanisms are responsible for the important contribution of subsurface flows, an experiment based on a time domain reflectometry system and additional measurements within the basin (piezometers and rainfall simulator) was conducted. The association of these experiments allows demonstrating that preferential flows are certainly responsible for the important contribution of soil water. Furthermore according field observations and a rainfall simulator experiment, it seems that macropores are at the origin of these preferential flows.

HS4/W/14-A4

1710

#### THE USE OF TRACER HYDROLOGICAL TIME PARAMETERS TO CALIBRATE BASEFLOW IN RAINFALL-RUNOFF MODELLING

Jens MEHLHORN and Christian Leibundgut (Institute of Hydrology, University of Freiburg, Fahrenbergplatz, D-79098 Freiburg, Germany, email: mehlnhorn@imbdec1.bau-vern.uni-karlsruhe.de)

This paper discusses the use of tracer time parameters to calibrate the baseflow time concentration in a conceptual rainfall-runoff model. A comparison showed that the modelling approaches in tracer hydrology and rainfall-runoff modelling were mathematically equivalent. Therefore, it was assumed that tracer time parameters were suitable to calibrate baseflow runoff models. It can be shown that this is possible if the mobile and immobile water volumes in the groundwater system are considered. In a case study, the tracer time parameter of baseflow was 920 days. This value indicates the age of all water in the groundwater system and has no influence on the shape of the hydrograph. Regression analyses led to a turnover time of the mobile water in the groundwater system of 340 days. Coupling the water age and turnover time made it possible to simulate the baseflow with more detail. The calculated baseflow reflects correctly the dynamics of the groundwater system and the age of the baseflow.

HS4/W/15-A4

1730

#### SEASONAL HYDROLOGY OF OXYGEN-18 IN THE ALLT A' MHCRAIDH, SCOTLAND: IMPLICATIONS FOR WATER MOVEMENT AND RESIDENCE TIMES

C. SOULSBY, R. Malcolm (Department of Geography, University of Aberdeen, Aberdeen AB24 2UF, UK, email: c.soulsby@abdn.ac.uk); R. C. Ferrier, R. C. Helliwell (Macaulay Land Use Research Institute, Aberdeen AB15 8QH, UK); A. Jenkins (Institute of Hydrology, Wallingford, Oxfordshire OX10 8BB, UK)

The seasonal variation of oxygen-18 has been observed in precipitation, groundwater and streamwater in the Allt a' Mharcraidh catchment, Cairngorm mountains, Scotland. Precipitation showed strong seasonal variation in its isotopic signature over the 1995–1998 study period. As anticipated, such variation was substantially damped in groundwater and surface water. Nevertheless,  $^{18}\text{O}$  proved a useful tracer, indicating the influence of spring snowmelt events and summer rainfall on stream waters. Detailed examination of the seasonal variation in  $\delta^{18}\text{O}$  levels in various catchment waters provided an insight into mixing processes and a first approximation of mean residence times. Preliminary estimates for the latter are <180 days for (inferred) near-surface soil water and storm runoff, 2.5 and >5 years for shallow and deeper groundwater respectively. These longer-term data sets demonstrate the ability of the catchment to effectively mix new precipitation with resident soil and groundwater over the hydrological year. This implies that the influence of groundwater on the hydrology and hydrochemistry upland catchments has been underestimated.

Friday 23 July AM

Presiding Chairs: C Soulsby (Univ. of Aberdeen, UK),  
Yucel Yurtsever (IAEA, Isotope Hydrology Section, Vienna)

### TRACER APPROACHES

HS4/W/16-A5

0900

#### INTEGRATION OF TRACER TECHNIQUES AND HYDROMETRIC APPROACHES IN CATCHMENT HYDROLOGY: RESEARCH ON HYDROLOGICAL PROCESSES IN THE KAWAKAMI EXPERIMENTAL BASIN, CENTRAL JAPAN

Tadashi TANAKA (Institute of Geoscience, University of Tsukuba, Ibaraki 305-8571, Japan, email: tadashi@atm.geo.tsukuba.ac.jp); Maki Tsujimura (Department of Environmental Earth Sciences, Aichi University of Education, Aichi 448-8542, Japan)

The Kawakami experimental basin, located in the mountain region of central Japan, has been monitored since 1985. Complex hydrological processes occurring in the forested mountain catchment were studied using both isotope and chemical tracers and hydrometric approaches. Tritium concentration data of soil water, groundwater, and stream water provided information on residence times of each as well as the mixing ratio of stream water with soil water and groundwater. Stable isotope data, such as deuterium and oxygen-18, showed the spatial characteristics of each stream water source. Additionally, hydrometric data including tensiometric and piezometric potentials revealed the physical dynamics of subsurface water in the catchment. All these data are necessary for consideration of flow mechanisms in the catchment, especially for stormflow and water quality studies.

HS4/W/17-A5

0930

#### WATER FLUXES THROUGH CLAY AND SANDY SOILS: INTEGRATION OF TRACING AND SOIL WATER DATA

Mary MOSUGU and Chris Bradley (School of Geography and Environmental Science, University of Birmingham, Edgbaston, Birmingham B15 2TT, UK, email: mem672@novell5.bham.ac.uk)

This paper considers infiltration studies in a cracking clay and a sandy loam soil at two sites in the UK. Changes in water potential during infiltration under natural and simulated rain events are determined using tensiometer nests within plots of 9 m<sup>2</sup>. An anionic tracer (Br<sup>-</sup>) was applied at a controlled rate, following which samples of soil water were collected at regular intervals from porous cup samplers within the two soil profiles. Br<sup>-</sup> concentrations were determined using HPLC ion chromatography. The results indicate substantial differences in timing and rate of infiltration and redistribution between the two soil types, and significant internal variability within the same soil. The results are analysed to assess seasonal changes in the nature and magnitude of water movement.

HS4/W/18-A5

0950

#### IN SITU EXPERIMENTS ON WATER INFILTRATION IN SAND DUNES TRACED BY TEMPERATURE

Changyuan TANG (Graduate School of Science and Technology, Chiba University, 1-33 Yayoi-cho, Inage-ku, Chiba 263, Japan, email: cytang@rsirc.cr.chiba-u.ac.jp); Shizuo Shindo (Centre for Environmental Remote Sensing, Chiba University, 1-33 Yayoi-cho, Inage-ku, Chiba 263, Japan); Yosuo Sakura and Isao Machida (Faculty of Sciences, Chiba University, 1-33 Yayoi-cho, Inage-ku, Chiba 263, Japan)

Knowledge of the mechanisms of water infiltration in sand dunes and wadis is the key to understanding the hydrological conditions in arid and semiarid regions. In order to trace infiltration processes in sand dunes, two sites were chosen in Al Ain, United Arab Emirates. An artificial rainfall infiltration experiment was conducted at one site. The other was left in its natural state. The variations in temperature between the sites were compared with soil water tension as well as soil water content at the same depths. Field observations showed that the temperature of the sand dune at the experimental site was more greatly affected by air temperature than that at the natural site, which means that the temperature distribution in the sand dune is closely related to the water content. The vertical distribution of temperature correlated well with the water movement in the sand dune, from which the average velocity of infiltration has been estimated as 3 cm h<sup>-1</sup>. The results showed that water infiltration in sand dunes is not continuous but stepped, and suggested the possibility of tracing water movement in sand dunes using temperature.

HS4/W/19-A5

1010

#### CONTRASTING RAINFALL-RUNOFF PROCESS BETWEEN GEOLOGY USING HYDROMETRIC AND TRACER APPROACHES IN STEEP, LARGE RELIEF MOUNTAINS

Maki TSUJIMURA (Department of Environmental Earth Sciences, Aichi University of Education, Kariya, Aichi 448-8542, Japan, email: mktsuji@aucecc.aichi-edu.ac.jp); Yuichi Onda, Jun'ichi Fujiwara (School of Agricultural Sciences, Nagoya University, Nagoya, Aichi 464-8601, Japan); Jun Ito (Department of Environmental Earth Sciences, Aichi University of Education, Kariya, Aichi 448-8542, Japan)

Hydrometric and tracer approaches have been applied to investigate the rainfall-runoff process in two headwater basins underlain by shale and granite. Four small basins were monitored; two in shale and two in granite. The rainfall peak was followed by the runoff peak in the shale basin, whereas peak runoff coincided with rainfall peak in the granite basin. Tensiometric data from hillslopes indicate that subsurface water percolated into the bedrock even during the rainstorm in the shale basin, whereas lateral saturated subsurface flow was often observed during heavy rainstorms in the granite basin. Considering the isotopic data from water, subsurface flow with relatively long residence times through the bedrock should be dominant so that the delayed runoff response was observed during the rainstorm in the shale basin, whereas lateral subsurface stormflow in the soil mantle should be dominant so that the quick response of runoff was observed during rainstorms in the granite basin.

HS4/W/20-A5

1030

#### USE OF ENVIRONMENTAL TRITIUM TO STUDY CATCHMENT DYNAMICS: CASE STUDY FROM THE DANUBE RIVER BASIN

Yucel YURTSEVER (Department of Nuclear Sciences and Applications, International Atomic Energy Agency (IAEA), Wagramer Strasse 5, PO Box 100, A-1400 Vienna, Austria, email: y.yurtsever@iaea.org)

Use of environmental isotopes, particularly, oxygen ( $^{18}\text{O}$ ) and hydrogen ( $^2\text{H}$  and  $^3\text{H}$ ) offers unique methodologies for investigations related to rainfall-runoff relationships and catchment dynamics. Using long-term tritium ( $^3\text{H}$ ) data in the Danube River, observed temporal variations in the river water have been simulated through a compartmental (mixing cell) modelling approach to estimate the fluxes of surface flow and groundwater to total river discharge and to characterise the transit time distribution of these component flows. The findings of this approach are compared to the results of an earlier simulation model based on the Artificial Neural Network (ANN) approach using the same long-term tritium data. The two approaches provide comparable results for the characteristics travel time of the water in the basin providing improved confidence for the results.

HS4/W/21-A5

1100

#### STUDY OF RAINFALL DISTRIBUTION AND GROUNDWATER FLOW USING THE CL- ION AND STABLE ISOTOPES ON A VOLCANIC ISLAND IN JAPAN

Isao MACHIDA (Graduate School of Science and Technology, Chiba University, 1-33 Yayoi-cho Inage-ku, Chiba 263-0022, Japan, email: isao@rsirc.cr.chiba-u.ac.jp); Shizuo Shindo (Centre of Environmental Remote Sensing, Chiba University, 1-33 Yayoi-cho Inage-ku, Chiba 263-0022, Japan)

Using the stable isotope and water quality method, we investigated groundwater movement in Hachijojima Island, a volcanic island located about 290 km south of Tokyo Bay, Japan. Rain samples for analyses of oxygen-18 and Cl<sup>-</sup> were collected by 20 evenly distributed precipitation collectors during a one-year period (April 1997–April 1998), with a sampling interval of 45 days. A hydrological survey was carried out, and more than 50 groundwater and surface water samples were also collected. We found: (a) Cl<sup>-</sup> in springs is a suitable tracer for groundwater study in this island; however, we could not estimate recharge area using oxygen-18 because the altitude effect (of precipitation isotope) is small; (b) Cl<sup>-</sup> concentration in springs and well water was more than 2 times higher than Cl<sup>-</sup> concentration of precipitation; we could



not calculate the recharge area, comparing Cl<sup>-</sup> concentration in precipitation with that in groundwater; (c) groundwater quality is classified into several groups, which reflect the different groundwater flow processes.

**HS4/W/22-A5****1120****FAN ISOTOPIC STUDY OF THE GROUNDWATER REGIME OF A SEEPAGE CALDERA LAKE DISTRICT, SOUTHERN JAPAN**

Masaya YASUHARA, Yoshihisa Kawanabe and Atsunao Marui (Hydrology Research Group, Geological Survey of Japan, 1-1-3 Higashi, Tsukuba, Ibaraki 305-8567, Japan, email: masaya@gsj.go.jp); Tadashi Kohno (Research Centre of Environmental Science and Technology, Nippon Bunri University, 1727 Ichiki, Ohita 870-0397, Japan); Yoshinori Satoh (Division of Social Studies, Joetsu University of Education, Joetsu, Niigata 943-8512, Japan)

The 233-m deep Lake Ikeda is a seepage caldera lake with no surface outflow or inflow. During February–March 1998 water samples were taken from lakes, rivers, wells, hot springs, and springs. They were analysed for dD, d18O, and Cl<sup>-</sup> concentration to determine the contribution of lake water to river discharge and down-gradient groundwater field. The results indicate that the influence of leakage from Lake Ikeda is confined to the area east-south of the lake, where a mixing of lake water, local rainwater, and sea water takes place. For certain rivers and springs, lake water contributes more than 80% of the discharge. Many of the wells and hot springs represent a 7–100% lake-water contribution. Leakage of lake water is most likely to occur through the southern caldera walls, where thick volcanic aquifers are hydraulically connected to Lake Ikeda. The study showed that leakage from Lake Ikeda was found to play a predominant role in the groundwater regime of the district.

**HS4/W/23-A5****1140****PRELIMINARY ANALYSIS OF BORON ISOTOPE RATIOS IN LEACHATE-CONTAMINATED GROUNDWATER**

Eduard HOEHN (Swiss Federal Institute of Water Science and Technology (EAWAG), CH-8600 Dübendorf, Switzerland, email: hoehn@eawag.ch)

Boron isotope ratios of municipal solid waste leachate and groundwater yielded values between -7.0 and 16.6‰. We feel that these ratios have the potential to be used as a tracer for the assessment of mixing of leachate-contaminated groundwater. The values were interpreted as a mixture of waters of a different origin. This interpretation is corroborated by independent findings from a hydrogeological site assessment.

**HS4/W/24-A5****1200****FLOW MODELLING, TRACER METHODS, AND HYDROMETRIC TESTS IN THE RIVER VAH BASIN, SLOVAK REPUBLIC**

Jozef HULLA, Emilia Bednarova and Danka Gramblíková (Department of Geotechnics, Slovak Technical University, Radlinského 11, 813-68 Bratislava, Slovak Republic, email: hulla@us.svf.stuba.sk)

Fifty-four reservoirs have been built in the basin of the River Vah, Slovak Republic, over various geological formations. The reservoirs are used for flood protection, drinking water supply and hydroelectric power. The grouting curtains were a serious problem during dam construction. Maximum seepage was estimated for the Liptovska Mara and Turcek dams and ranged between 0.060 and 0.070 m<sup>3</sup> s<sup>-1</sup>. The real seepage, and implications for the subsoil stability were questionable. Borehole tracer methods were used to address this problem. The results show that maximum real seepage was 0.030 m<sup>3</sup> s<sup>-1</sup>, and filtration velocities have never reached critical values for the filtration stability of fine fills in rock fissures or gravel pores.

**HS4/W/25-A5****1220****COMBINATION OF TRACER TECHNIQUES AND NUMERICAL SIMULATIONS TO EVALUATE THE GROUNDWATER CAPTURE ZONE**

Makoto TANIGUCHI (Department of Earth Sciences, Nara University of Education, Nara 630-8528, Japan, email: makoto@nata-edu.ac.jp); Kunimitsu Inouchi (Centre for Cooperative Research and Development, Ehime University, Matsuyama 790-8577, Japan); Norio Tase and Jun Shimada (Institute of Geoscience, University of Tsukuba, Ibaraki 305-8571, Japan)

The groundwater flow system and capture zone were evaluated using the combination of stable isotopes, continuous measurements of groundwater seepage rate, and numerical simulations by a 2-D unsaturated-saturated three-layer model. The inland effect of d18O of the precipitation was used as a tracer to detect the capture zone. The depth of the groundwater which discharges near the lake shore is estimated to be deeper than 100 m below the surface even though the clay layer exists from a depth of 10 to 20 m below the surface. The combination of tracer methods and numerical simulations enabled us to understand the groundwater flow system and the capture zone of the groundwater in the Lake Biwa basin.

**HS4/W/26-A5****1240****HYDROGRAPH SEPARATION USING SOLUTE CONCENTRATIONS AND TEMPERATURE AT THE PANOLA MOUNTAIN RESEARCH WATERSHED, GEORGIA, USA**

Norman E PETERS

Abstract not available at time of going to press

**Friday 23 July PM**

Presiding Chair: Jeff McDonell

(SUNY-ESF, College of Environmental Sciences and Forestry, USA)

**HIGHLY INTEGRATED APPROACHES****HS4/W/27-A5****1400****A CALL FOR HYDROLOGICAL MODELS BASED ON REMOTE SENSING, TRACERS AND OTHER MODERN HYDROMETRIC TECHNIQUES**

Gert A. SCHULTZ (Institute of Hydrology, Water Resources Management and Environmental Techniques, Ruhr University Bochum, D-44780 Bochum, Germany, email: gert.a.schultz@rz.ruhr-uni-bochum.de)

Modern hydrological models of the distributed system type subdivide the drainage basin into many area elements and do the computations of the vertical and lateral fluxes for each area element on the basis of digital maps, digital terrain models and remote sensing data. Although these more sophisticated models quite often provide a high accuracy as far as runoff volumes are concerned, they obviously do not represent the various flow components (surface, subsurface groundwater) correctly. Such knowledge was acquired only in recent times due to the successful application of tracer techniques. They show that subsurface flow, i.e. interflow and groundwater flow, plays a much more important and different role than usually assumed in hydrological models. In this paper close cooperation between hydrological modellers and tracer experts is postulated with the goal of producing new types of sophisticated hydrological models, in which the flows, particularly the subsurface flows, are simulated according to their true physical processes.

**HS4/W/28-A5****1430****RECENT TECHNIQUES IN LARGE ARID CATCHMENTS—WAYS TO OVERCOME MODEL CALIBRATION**

Jens LANGE, Christian Leibundgut (Institute of Hydrology, University of Freiburg, Fahnbergplatz, D-79098 Freiburg, Germany, email: jlange@uni-freiburg.de); Asher P. Schick (Department of Geography, The Hebrew University of Jerusalem, 91905 Jerusalem, Israel)

Advanced techniques were applied to determine the spatial distributed parameter values of a non-calibrated rainfall-runoff model in a large arid catchment. Channel dimensions and infiltration characteristics were determined by air-photo analysis and verified by careful fieldwork. A GPS device was used for positioning during field surveys and channel transmission losses were studied by artificial tracers. During one high intensity event (October 1991) rainfall radar yielded the spatial pattern of rainfall intensities, while during another (October 1979) the input rainfall was traced back by the model using a physically-based description of convective arid rainfall. Due to its physical basis, the model could combine different sources of information: basin characteristics determined by field surveys and remote sensing, results of existing experiments, and general scientific experience. Compared with calibrated conceptual models, this resulted in a higher flexibility facilitating applications to basins or events with poor data records, urgently needed for many parts of the arid zone.

**HS4/W/29-A5****1450****APPLICATION OF GIS-BASED DISTRIBUTED HYDROLOGICAL MODELLING FOR ESTIMATION OF WATER RESIDENCE TIMES IN THE SMALL SWISS PRE-ALPINE CATCHMENT RIETHOLZBACH**

Tomas VITVAR, Joachim Gurtz and Herbert Lang (Swiss Federal Institute of Technology (ETH), Department of Geography, Winterthurerstrasse 190, CH-8057 Zurich, Switzerland, email: vitvar@geo.unmw.ethz.ch)

A concept of water residence time distributions in the pre-alpine catchment Rietholzbach in northeastern Switzerland has been developed. The catchment covers an area of 3.18 km<sup>2</sup> and ranges from 680 to 960 m a.s.l. It is part of the Upper Freshwater Molasse overlaid by Quaternary deposits. The study combines runoff modelling with the use of the isotope 18O and consists of two parts. In the first part, runoff simulation over the period 1983–1997 was carried out using the model PREVAH-ETH. For the spatial data distribution, 100 m grid data were aggregated into hydrotopes by means of a GIS. An approach including the topographical index was integrated into the model, improving the simulation of runoff components. In the second part, the calculated groundwater recharge rates were used for the weighting of d 18O input functions. They served to estimate groundwater residence times at selected sites in the catchment over the period 1994–1997. The mean groundwater residence times range up to 2.5 years and depend on the mixing efficiency within the aquifers. The results form a contribution to the understanding of the water turnover processes in hilly pre-alpine basins with porous structures, as investigated using areal distributed hydrological modelling coupled with tracer techniques.

**HS4/W/30-A5****1510****HYDROGRAPH SEPARATION OF RUNOFF COMPONENTS BASED ON MEASURING HYDRAULIC STATE VARIABLES, TRACER EXPERIMENTS, AND WEIGHTING METHODS**

Markus WEILER, Simon Scherrer, Felix Naef and Paolo Burlando (Institute of Hydromechanics and Water Resources Management, Swiss Federal Institute of Technology Zurich, CH-8093 Zurich, Switzerland, email: weiler@ihw.baum.ethz.ch)

Hydrograph separation with natural tracers or isotopes has become a popular method to gain comprehensive insights into runoff processes. The mass balance approach, which uses the measured chemical signature of the rainfall as the signature of the event water, is generally used for this purpose. However, temporal variations in the composition of rainfall must be taken into account by an appropriate weighting technique that describes the time response of event water in a drainage basin. A conservative tracer was added to an artificially simulated intense rainfall event on a small-forested hillslope plot. A simple mass balance approach coupled with an appropriate weighting technique was used to separate the event and pre-event water fractions of the surface and subsurface flow. Runoff processes and their relation to mixing between event and pre-event water are identified for both flow paths by means of a detailed survey of both soil water changes and soil properties, as well as through a dye tracer experiment. The experiment demonstrates the importance of event water contributions to subsurface runoff by preferential flow.

**HS4/W/31-A5****1630****IMAGE ANALYSIS AND WATER TRACING METHODS FOR EXAMINING RUNOFF PATHWAYS, SOIL PROPERTIES AND RESIDENCE TIMES IN THE CONTINUOUS PERMAFROST ZONE**

William L. QUINTON and Philip Marsh (National Water Research Institute, Saskatoon, Saskatchewan, Canada S7N 3H5, email: bill.quinton@ec.gc.ca)

This paper integrates remote sensing and a tracer technique with existing information obtained from hydrometric measurements in order to improve the understanding of soil properties, runoff pathways and residence times on arctic tundra hillslopes in the continuous permafrost zone. Low altitude aerial photographs were analysed in order to quantify physical attributes of earth hummocks. These images were also used in a particle tracking procedure to determine the average tortuosity of inter-hummock channels. Image analysis was also conducted at a much smaller scale on thin sections extracted from soil cores to determine changes in physical properties with depth. Tracer experiments were repeated several times to determine the residence times for different saturated layer elevations. The subsurface drainage efficiency depends upon the physical attributes of the hummock cover, due to the influence of these attributes on the tortuosity of inter-hummock channels. The variations of the total and active porosity, and pore size with depth in the peat are important variables governing residence

times, due to their impact on the hydraulic conductivity. Average residence times increased from ~0.3–0.5 day to as high as ~38 days, as the saturated layer subsided into increasingly decomposed peat.

HS4/W/32-A5

1710

#### REQUIRED INTEGRATED APPROACH TO UNDERSTAND RUNOFF GENERATION AND FLOW-PATH DYNAMICS IN CATCHMENTS

Alfred BECKER, Andreas Güntner and Daniel Katzenmaier (Potsdam Institute for Climate Impact Research (PIK), PO Box 601203, D-14412 Potsdam, Germany, email: alfred.becker@pik-potsdam.de)

During the last 20 years, much has been learned about runoff generation processes and lateral flow along different pathways, especially at hillslope to small catchment scales. Nevertheless, this knowledge has only to a small extent contributed to modify model formulations/parameterizations describing runoff generation at the catchment scale. In this paper, we focus on a few examples where detailed field studies describe the essential elements of runoff generation and thus help to achieve a more realistic representation of the underlying mechanisms within process-oriented rainfall–runoff models.

FINAL DISCUSSION

1730

Thursday 22 July AM

HS4/L/01-A4

Poster

0930-01

#### STUDY OF THE INTERCONNECTION BETWEEN A LAKE AND SURROUNDING SPRINGS USING ENVIRONMENTAL TRACERS IN THE KUMAUN LESSER HIMALAYAS

Rm. P. Nachiappan and Bishm KUMAR (National Institute of Hydrology, Roorkee 247667, Uttar Pradesh, India, email: bk@nih.ernet.in)

The interconnection between Lake Nainital, located in the Kumaun Lesser Himalayas, and the springs issuing in the vicinity of the lake, was investigated using hydrochemistry. The lake water and most of the downstream springs have a high concentration of MgHCO<sub>3</sub>. Although, the downstream springs that issue in the Kailashan area southwest of the lake are dominated more by MgSO<sub>4</sub>, d 18O data confirmed the interconnection between the lake and the springs. The springs in the Balia ravine located south of the lake are also dominated by MgHCO<sub>3</sub>. However, the springs located in the area to the west of the lake are not hydrologically connected to the lake, as deduced from the stable isotope data. Based on the vertical profiles of the water chemistry and isotopic composition of the lake, we hypothesize that the leakage from the lake takes place from the epilimnion zone. The study highlights the usefulness of stable isotope data combined with water chemistry in identifying recharge sources.

HS4/L/02-A4

Poster

0930-02

#### MODIFIED QUANTITATIVE ESTIMATION MODEL OF EROSION AND DEGRADATION IN FOUR MOUNTAINOUS BASINS

Dimitrios A. Emmanouiloudis (Department of Forestry, Technological Educational Institute of Drama, Proastio 66100, Drama, Macedonia, Greece); Evangelos I. FILIPPIDIS (Department of Forestry and Natural Environment, AUT, 54006 Thessaloniki, Macedonia, Greece, email: efilippi@for.auth.gr)

This paper presents a new version of a well-known stochastic model to quantitatively assess drainage basin degradation in order to determine erosion in four torrential mountainous basins. This new three-dimensional version, combined with using geographical information systems for data processing, can provide a quantitative assessment of the degradation of any torrential basin in a very short time. Although this system was originally designed for these four particular basins, its flexibility enables it to be adapted for any torrential basin.

HS4/L/03-A4

Poster

0930-03

#### SPATIAL DELINEATION OF ZONES WITH THE SAME DOMINATING RUNOFF GENERATION PROCESSES

Eckhard RUTENBERG, Stefan Uhlenbrook and Chris Leibundgut (Institute of Hydrology, University of Freiburg, Fahrenbergplatz, D-79098 Freiburg, Germany, email: rutenb@uni-freiburg.de)

A spatial delineation of the dominating runoff generation processes, based on previous tracer experiments, was conducted in a mountainous area in the Black Forest in southwestern Germany. On saturated areas and boulder trains, rapid runoff is generated (Güntner et al., 1998; Mehlhorn, 1998). The area is dominated by periglacial drift cover on moderate to steep hillslopes, producing mainly delayed runoff (Leibundgut et al., 1998). Rainfall on hilly uplands and consolidated moraines results in slow runoff components (Lindenlaub, 1998). Characteristics of the drift cover and slope serve as main criteria for the differentiation of runoff generation processes. With the aid of a geographical information system, eight classes of spatial units with a characteristic runoff behaviour are defined.

HS5

Monday 19 – Wednesday 21 July

#### IMPACTS OF URBAN GROWTH ON SURFACE AND GROUNDWATER QUALITY (ICGW, ICWQ, ICSW, ICCE, IAH, IAWQ)

Location: Law, 303 LT

Location of Posters: Barber Institute, Concert Hall

Monday 19 July PM

Presiding Chair: Prof. B. Wilkinson (NERC Centre for Ecology & Hydrology, Wallingford, UK)

#### SURFACE WATER SESSIONS

Introduction

1400

Prof. J. B. ELLIS

#### Methodologies & Source Tracing

HS5/W/01-A1

1405

#### IDENTIFYING MAJOR SOURCES OF ORGANIC MICROPOLLUTANTS AND HEAVY METALS DURING FLOOD EVENTS IN A PARTLY URBANIZED HEADWATER CATCHMENT

Andreas KREIN, Reinhard Bierl (University of Trier, Department of Hydrology, D-54286 Trier, Germany, email: krein@uni-trier.de)

Since 1988 we have investigated flood events in a headwater catchment. Dissolved and particle-bound solids were analysed as well as particle characteristics. By surveying all the data, pollutant profiles and hydrograph patterns, different sources of pollutants can be identified and related to particular locations in the basin. The influence of main roads and sewer systems is obvious. Heavy metals are additionally mobilized from pore water during resuspension of sediments. There is also a clear tendency for a fast and distinct response of smaller polycyclic aromatic hydrocarbons (PAH) with higher solubility, which could be explained by a gradual enrichment of these partly mobile molecules at locations along the flow path. Patterns of PAH chemographs are further determined by chemical alteration and season. The maximum contents during flood events are controlled by pre-event climatic and hydrological conditions with storm intensity and duration controlling inputs of unpolluted material causing dilution. Experiments with artificial flood releases give some indications of in-channel source reactions.

HS5/W/02-A1

1425

#### SPATIAL VARIATION OF METALS IN BED SEDIMENTS OF AN URBAN DRAINAGE BASIN, HAWAII

Ross A. SUTHERLAND (University of Hawaii, Geomorphology Laboratory, Department of Geography, 2424 Maile Way, Honolulu, Hawaii 96822, USA, email: sutherland@hawaii.edu)

Fish from the Manoa Stream, Hawaii, have consistently shown the highest Pb concentrations and some of the highest Cu contents in nationwide surveys by the National Contaminant Biomonitoring Program (NCBP). To investigate the source(s) of these trace metals, a detailed systematic programme was instituted to collect bed sediment samples from 5.8 km of the Manoa Stream. Bed material <63 m was examined for a variety of elements; those reported here include Al, Cu, Ni, Pb and Zn. All statistical analyses and contaminant indices point to minor anthropogenic contamination for Cu and Zn; mineralogical control for Ni; and a very strong contamination signal for Pb. Maximum Pb concentrations (up to 1080 mg kg<sup>-1</sup>) were associated with anthropogenic material dumping in minor tributaries, storm sewer sediments and sediments in the "lower" section of the basin.

HS5/W/03-A1

1445

#### METALS IN SEDIMENTS OF SUSTAINABLE URBAN DRAINAGE STRUCTURES IN SCOTLAND

Kate HEAL (Institute of Ecology & Resource Management, University of Edinburgh, Darwin Building, King's Buildings, Mayfield Road, Edinburgh EH9 3JU, UK, email: kate.heal@ed.ac.uk)

Sustainable urban drainage solutions increasingly use structures, such as wetlands and ponds, to improve water quality. Previous studies have demonstrated the effectiveness of these structures in removing metals from runoff, but the fate of the captured contaminants has been neglected. Whilst organic contaminants and nutrients may biodegrade and be taken up by plants, metals are expected to accumulate in sediments. EDTA-extractable cadmium, chromium, copper, lead, nickel and zinc were measured in sediment sampled from three urban drainage structures (a wetland and two ponds receiving industrial and residential storm drainage) in Scotland, UK. Metal concentrations showed considerable variability within each structure, probably reflecting short-circuiting of flow. Zinc, chromium and cadmium concentrations were at very low levels at all sites, but copper, nickel and lead exceeded background concentrations for aquatic sediments. An index of metal contamination showed that the metal content of sediments increased with the age of the structure.

HS5/W/04-A1

1505

#### EVALUATION OF STREAM WATER QUALITY IN ATLANTA, GEORGIA, AND THE SURROUNDING REGION (USA)

Norman E. PETERS (US Geological Survey, 3039 Amwiler Rd, Atlanta, Georgia 30360-2824, USA, email: nepeters@usgs.gov); Stephen J. Kandell (Atlanta Regional Commission, 3715 Northside Pkwy, Atlanta, Georgia 30327, USA)

A water-quality index (WQI) was developed from historical data (1986–1995) for streams in the Atlanta Region and augmented with "new" and generally more comprehensive biweekly data on four small urban streams, representing an industrial area, a developed medium-density residential area and developing and developed low-density residential areas. Parameter WQIs were derived from percentile ranks of individual water-quality parameter values for each site by normalizing the constituent ranks for values from all sites in the area for a base period, i.e. 1990–1995. WQIs were developed primarily for nutrient-related parameters due to data availability. Site WQIs, which were computed by averaging the parameter WQIs, range from 0.2 (good quality) to 0.8 (poor quality), and increased downstream of known nutrient sources. Also, annual site WQI decreased from 1986 to 1995 at most long-term monitoring sites. Annual site WQI for individual parameters correlated with annual hydrological characteristics, particularly runoff, precipitation quantity, and water yield, reflecting the effect of dilution on parameter values. The WQIs of the four small urban streams were evaluated for the core-nutrient-related parameters, parameters for specific dissolved trace metal concentrations and sediment characteristics, and a species diversity index for the macro-invertebrate taxa. The site WQI for the core-nutrient-related parameters used in the retrospective analysis was, as expected, the worst for the industrial area and the best for the low-density residential areas. However, macro-invertebrate data indicate that although the species at the medium-density residential site were diverse, the taxa at the site were for species tolerant of degraded water quality. Furthermore, although a species-diversity index indicates no substantial difference between the two low-density residential areas, the number for macro-invertebrates for the developing area was much less than that for the developed area, consistent with observations of recent sediment problems probably associated with construction in the basin. However, sediment parameters were similar for the two sites suggesting that the routine biweekly measurements may not capture the short-term increases in sediment transport associated with rainstorms. The WQI technique is limited by the number and types of parameters included in it and therefore, should be used with caution.

HS5/W/05-A1

1525

#### WATER QUALITY AND ECOLOGY OF WATER BODIES IN URBAN TERRITORIES: ST. PETERSBURG AS A CASE STUDY

Sergei KONDRATYEV, Ludmila Efremova (Institute of Limnology, Sevastyanova 9, St. Petersburg, Russia, email: kond@lake.spb.org); Tatiana Gronskaia, Irina Varfolomeeva (State Hydrological Institute, 2 - liniya 23, St. Petersburg, Russia)

The ecological state of small water bodies located in large cities is the best indicator of the degree of environmental pollution within urban territories. This paper presents data and results on the ecological state of the water system of Lake Lakhinsky Razliv and its drainage basin located in the northwestern part of St. Petersburg, Russia. The research has evaluated the critical state of the urban water bodies, which are regarded as being in stages of ecological regress. The water bodies intercept, transform, and accumulate in their bottom sediments, the anthropogenically-derived pollutants coming in from the upper part of the drainage system. However it is considered that the water bodies still have not totally lost their possibility for self-purification.

Presiding Chair: N. E. Peters (US Geological Survey, Atlanta, USA)

### Identifying and Measuring Impacts

HS5/W/06-A1 1610

#### EVAPOTRANSPIRATION RATES IN URBAN AREAS

C. S. B. GRIMMOND (Climate and Meteorology Program, Department of Geography, Indiana University, Bloomington, Indiana 47405, USA, email: grimmon@indiana.edu); T. R. Oke (Atmospheric Science Program, Department of Geography, University of British Columbia, Vancouver, British Columbia, Canada)

For a significant number of urban hydrological issues, notably, water supply, water quality, groundwater recharge, saline intrusions, and flood runoff, knowledge of evapotranspiration (ET) rates is required. However, because little is known about the magnitude of urban ET rates and their spatial variability, broad assumptions have to be made in many applications. In this paper we present direct measurements of the magnitude and variability of ET rates using micrometeorological techniques (eddy correlation), in seven North American cities. The data demonstrate the importance of urban ET, and illustrate clear differences with land use. Simple relations between ET and measures of land cover are shown.

HS5/W/07-A1 1630

#### IMPACTS OF URBAN GROWTH ON SURFACE WATER AND GROUNDWATER QUALITY IN THE CITY OF DESSAU, GERMANY

U. RIEMANN (HGN Hydrogeologie GmbH, Rothenburgstraße 10-11, D-99734 Nordhausen, Germany, email: u.riemann@hgn-online.de)

From the mid 19th century, the city of Dessau (Germany) developed as an economic centre. The development of new residential and industrial areas changed the natural landscape having an adverse impact on the surface water, soil water and groundwater regimes. Between 1965 and 1990, public water supply, industry and agriculture pumped some 60 000 m<sup>3</sup> d<sup>-1</sup> groundwater out of the Dessau aquifer. As a result, groundwater levels fell by 2–3 m over large areas. Since 1990, extraction for drinking water supply, industry and agriculture has decreased from about 60 000 m<sup>3</sup> d<sup>-1</sup> to as little as about 5000 m<sup>3</sup> d<sup>-1</sup>. As a result of this, in some parts of the city groundwater levels are now only 0.5–1.0 m below the surface. The rising groundwater levels have caused flooding of existing buildings and structures over large areas. To minimize or prevent damage, extensive engineering studies and works have been carried out to keep the groundwater level as low as necessary. Extensive pollution of both groundwater and soil has been observed in a highly industrialized area at Dessau. Further impacts on groundwater quality are caused by gas stations, petrochemical production plants and related depots. The main pollutants are volatile organic compounds (VOCs), monocyclic aromatic hydrocarbons which include benzene, toluene, ethylbenzene and the three xylenes (m-, o- and p). Local contamination exceeds defined limit values for drinking water. A further problem is the concentration of heavy metals (arsenic, zinc, cadmium and nickel) in these areas.

HS5/W/08-A1 1650

#### DEVELOPMENT AND WATER QUALITY IN THE KAM TIN BASIN, HONG KONG

Mervyn PEART (Department of Geography, University of Hong Kong, Pokfulam Road, Hong Kong)

The economic development of Hong Kong has meant that some once rural areas have been transformed. Low-density housing, open storage and makeshift factories, in addition to agriculture have characterized them. This change in land use may have consequences for water quality especially as many areas are not connected to mains sewerage. In the Kam Tin basin, under baseflow conditions, water samples from the river in the developing lowland are characterized by much higher concentrations of calcium, magnesium, potassium, nitrate-nitrogen and dissolved phosphorus, than an undisturbed upland tributary. The Kam Tin River also has much greater suspended solids concentrations than the upland stream and significant amounts of floating debris and rubbish which is never seen in the upland tributary. More attention needs to be given to sewerage and waste disposal in the basin. Runoff pH appears little influenced by the acid rain input.

HS5/W/09-A1 1710

#### STORMWATER MANAGEMENT PROBLEMS IN A TROPICAL CITY - THE BELO HORIZONTE CASE STUDY

Nilo Oliveira NASCIMENTO, Márcio Benedito Baptista (Federal University of Minas Gerais, Av. Contorno, 842, Belo Horizonte, MG, 30110-060 Brazil, email: niloon@eh.ufmg.br); Luiz Augusto Kauark-Leite (SAFEGE, Consulting Engineers, 15/27, rue du Port, F-92007 Nanterre, France)

In developing countries urban stormwater management shows a set of particularities when compared to that of developed countries. These particularities are mostly related to the lack of adequate urban planning and regulation, operation and maintenance of drainage systems, economic, health, educational, demographic and social questions. In the present paper, these questions are analysed and discussed using the Brazilian city of Belo Horizonte as a case study. The role of stormwater master planning as an instrument to adequately handle the reported problems is a major conclusion of the paper.

HS5/W/10-A1 1730

#### AN INTEGRATED APPROACH TO THE MANAGEMENT OF WATER QUALITY IN A DEVELOPING SOUTH AFRICA

E. PRETORIUS (Department of Civil Engineering and Building, Technikon Free State, Private Bag X25305, Bloemfontein 9300, South Africa, email: ipretori@eng.tofs.ac.za); G. du T. de Villiers (Department of Geography, University of the Orange Free State, PO Box 339, Bloemfontein 9300, South Africa)

The majority of South Africans live in rapidly developing communities with inadequate or poorly functional services. Pollution from these developing communities has severe economic and health implications for downstream users and impacts on the natural functioning of river ecosystems. Water quality problems from developing communities arise where wastes produced in the community, reach the surface or groundwater resource, or where destruction of the riparian zone and river habitats occur. The key to sustainable management of pollution from developing communities lies in addressing the physical causes of water quality problems while the sustainability of these physical interventions rests on addressing the institutional and socio-economic factors contributing to the problem.

Tuesday 20 July AM

Presiding Chair: Prof. U. Shamir (Israel Institute of Technology, Haifa, Israel)

### Hydro-Ecology and Source Controls

HS5/W/11-A2 0900

#### NUTRIENT STORAGE IN URBAN WETLANDS

Tom Shatwell (Sinclair Knight Merz, 100 Christie Street, St Leonards, Sydney 2065, Australia); Ian CORDERY (School of Civil and Environmental Engineering, The University of New South Wales, Sydney 2052, Australia, email: i.cordery@unsw.edu.au)

A pond in Sydney's Centennial Park is fed by stormwater from a 120 ha catchment that has predominantly residential land use. Over a period of several months the pond inflow and outflow were monitored to observe flow rate, suspended solids and total phosphorus concentration. In all runoff events, the inflows were characterized by rapid increases in the concentration of both suspended solids and phosphorus. It appears that significant amounts of phosphorus and sediment accumulate in the pond during the small, more frequent rainfall events. In most small to medium size winter flood events, 60% of phosphorus and 80% of suspended sediments were deposited in the pond. The implication for use of ponds for stormwater treatment would appear to be that ponds can be effective in arresting the downstream movement of sediment, but may not significantly reduce the downstream movement of phosphorus.

HS5/W/12-A2 0920

#### THE USE OF CONSTRUCTED WETLANDS FOR REDUCING THE IMPACTS OF URBAN SURFACE RUNOFF ON RECEIVING WATER QUALITY

Michael REVITT, Brian Shutes and Lian Scholes (Urban Pollution Research Centre, Middlesex University, Bounds Green Road, London N11 2NQ, UK, email: m.revitt@mdx.ac.uk)

The design criteria for constructed wetlands for the treatment of urban runoff are described and particular attention is paid to pre- and post-treatment components, sizing considerations and the substrate structure. The pollutant removal performances of two constructed wetlands are discussed and the predicted maximum outflow pollutant concentrations are compared to existing water quality criteria. Suspended solids represent the main concern with higher outlet concentrations being discharged due to re-suspension processes. This problem highlights both the need for regular maintenance, particularly with respect to the emptying of sedimentation tanks, and the benefits of incorporating an overflow channel to reduce sediment mobilization during high flow conditions.

HS5/W/13-A2 0940

#### DESIGN CONSIDERATIONS FOR THE USE OF VEGETATIVE CONTROLS FOR THE TREATMENT OF HIGHWAY DISCHARGES

J. Bryan ELLIS (Urban Pollution Research Centre, Middlesex University, Bounds Green Road, London, N11 2NQ, UK, email: b.ellis@mdx.ac.uk)

The design of highway drainage in the UK has traditionally provided for the rapid removal of surface runoff from the carriageway with positive discharges being directly routed either to a roadside soak away system or to the nearest receiving water course. Such systems pay little attention to the potential pollution loads generated from rainfall-runoff events or their potential deleterious impacts upon receiving waters. Increasing regulatory agency concern over such discharges is leading to a review of such conventional drainage systems and an interest in the potential use of vegetative systems for the control and treatment of highway runoff quality. The paper identifies the range of pollutant removal efficiencies achieved by vegetative best management practice (BMP) controls and reviews available design procedures for grass-lined channels (swales) and constructed wetlands. Recommended design guidance for swales rarely specifically considers water quality criteria and usually results in over-design capacities; "over-the-edge" trough systems are preferred over conventional swale geometries. For wetland design, a multi-cell approach is recommended with sizing providing the critical control parameter in terms of performance efficiency and a quantitative comparison is given of hydraulic and kinetic sizing design approaches.

HS5/W/14-A2 1000

#### SUSTAINABLE MANAGEMENT OF CHRISTCHURCH'S WATERWAYS AND WETLANDS USING STORMWATER SOAKAGE DISPOSAL

Peter CALLANDER (Pattle Delamore Partners Ltd, PO Box 389, Christchurch, New Zealand, email: peter.callander@pdp.co.nz); Robert Watts and Tony Oliver (Christchurch City Council, PO Box 237, Christchurch, New Zealand)

The western margins of Christchurch City, New Zealand, are located on a large alluvial flood plain including areas of free draining gravel strata. In settings such as this, the disposal of stormwater via ground soakage will minimize the disruption that urban development causes to the hydrological cycle. The gravel strata also form part of a productive aquifer used (by wells) to provide the city water supply. The discharge of stormwater into a drinking water aquifer, rather than a surface aquatic environment, indicates that faecal coliforms are likely to be the main contaminant of concern, along with protection against chemical spillages. Removal of suspended sediments is also important to maintain the soakage capacity of the disposal system. An appropriate treatment and disposal system involves separate soakage of roof stormwater, reticulation of other stormwater using vegetated swales, and disposal via soil adsorption basins and rapid soakage overflow chambers. The location and shape of these components are designed with appropriate landscape and planting considerations to create an aesthetic enhancement to the urban environment.



**HS5/W/15-A2 1020****TOWARDS INTEGRATED STORMWATER-MELTWATER MANAGEMENT IN THE COASTAL PART OF NORWAY**

Sveinn T. THOROLFSSON (Department of Hydraulic and Environmental Engineering, The Norwegian University of Science and Technology, N-7034 Trondheim, Norway, email: sveinn.thorolfsson@bygg.ntnu.no); Magnar Sekse (The Municipality of Bergen, Division for Water Supply and Water Environment, Bergen City Hall, N-5002 Bergen, Norway)

New directions in urban runoff and water environmental management in the coastal part of Norway are being introduced. The goal is to manage the total urban runoff (wastewater and stormwater) so that environmental damage is avoided and the goals for the receiving water are achieved at reasonable cost. It is mostly based on the results from the research programme carried out in the Birkeland basin and the subcatchment Sandsli, in Bergen, since 1981, where use of the blue-green concept and the Sandsli-system has been successful. The green trend in urban stormwater management utilizes the capabilities of nature to store huge stormwater-meltwater volumes and to reduce the pollution content in the water. In the planning process, blue areas like lakes, rivers and brooks are to be kept in their natural condition.

Presiding Chair: Prof. I. Cordery (University of South Wales, Sydney, Australia)

**Management & Planning Approaches****HS5/W/16-A2 1100****IMPROVING DEGRADED URBAN WATER COURSES IN EASTERN SCOTLAND: A CASE STUDY**

Chris JEFFERIES (Wastewater Technology Centre, University of Abertay, Dundee, DD1 1HG, UK, email: c.jefferies@abertay-dundee.ac.uk); Anna Govier (ABB Power T&D Ltd., East Kingsway, Dundee, DD4 7RP, UK)

The outcome of a range of studies of the Lyne Burn in eastern Scotland is presented. This is a typical water course which has become degraded in the past from discharges directly related to urban influences. Changes include reduced low flows due to mining and at the same time increased washoff of pollutants from industry and sewerage, a major housing and commercial development and new highways. The drainage improvement actions and initiatives undertaken are also presented. Details of pollution causes and impacts are presented together with the changes in the water course quality mirroring the various initiatives. It is concluded that the index of stream classification has not changed and that a water course of this type can only be improved in the long term if source control measures are implemented in a wide range of areas and continual attention is paid to the causes of pollution.

**HS5/W/17-A2 1120****WATER-SENSITIVE URBAN PLANNING: THE CASE OF ISRAEL'S COASTAL AQUIFER**

Uri SHAMIR (Faculty of Civil Engineering, Technion - Israel Institute of Technology, Haifa 32000, Israel, email: shamir@tx.technion.ac.il); Naomi Carmon (Faculty of Architecture and Town Planning, Technion - Israel Institute of Technology, Haifa 32000, Israel)

Urban development above a phreatic aquifer can reduce substantially the amount of water that infiltrates and recharges the water resource. In Israel's coastal plain, the area of which is about 1900 km<sup>2</sup>, 650 km<sup>2</sup> are already urban, and another 625 km<sup>2</sup> are expected to be urbanized by 2020. This paper presents the motivation, methodology and results of estimating the present and expected future loss of recharge to the aquifer, as a consequence urban development above it. The paper ends with recommendations for implementing Water-Sensitive Urban Planning.

**HS5/W/18-A2 1140****STORMWATER MASTER PLANNING IN DEVELOPING TROPICAL COUNTRIES**

Luiz Augusto KAUARK-LEITE (SAFEGE, Consulting Engineers, 15/27, rue du Port, F-92007 Nanterre, France, email: luiz\_kauarkleite@safege.fr); Nilo Oliveira Nascimento and Márcio Benedito Baptista (Federal University of Minas Gerais, Av. Contorno, 842, 30110-060 Belo Horizonte, MG, Brazil)

In the present paper a methodology to design urban drainage master plans suited to cities located in tropical regions of developing countries is presented. The role of master planning in urban drainage and its objectives are reviewed and discussed. Fundamental methodological principles that should guide master planning are presented and a structure for its elaboration is suggested. A discussion is presented on the main actions and programmes that a master plan could lead to such as technical, institutional and legal initiatives.

**HS5/W/19-A2 1200****THE ALLOCATION OF RESOURCES TO STORMWATER POLLUTION CONTROL**

S. Brown, S. Shrestha and S. J. RILEY (School of Civic Engineering and Environment, University of Western Sydney Nepean, PO Box 10, Kingswood NSW 2747, Australia, email: s.riley@uws.edu.au)

Limited resources for ameliorating stormwater pollution in urban areas raises the issue of selecting and implementing appropriate methods of pollutant reduction. An effective stormwater management programme should consist of strategies that will achieve the goal at the minimum cost, thereby making the best use of limited available resources. This paper presents an optimization scheme that sizes various stormwater pollution control options. The options include a wide range of strategies, from street sweeping to constructed wetlands. The objective is to select the most effective strategies for limited funds. The non-linear problem is solved using LINGO, a non-linear problem solver. A heuristic method is used to select various possible options. The algorithm is applied to Plumpton Park in Blacktown, a suburb in Western Sydney, Australia.

**HS5/W/20-A2 1220****USE OF WEATHER RADAR FOR COMBINED CONTROL OF AN URBAN DRAINAGE SYSTEM AND A SEWAGE TREATMENT PLANT**

Markus QUIRMBACH, Gert A. Schultz (Institute for Hydrology, Water Management and Environmental Techniques, Ruhr-University Bochum, Universitätsstr. 150, D-44780 Bochum, Germany, email: markus.quirmbach@ruhr-uni-bochum.de); Torsten Frehmann (Institute for Urban Water Management, University of Essen, Universitätsstr. 15, D-45141 Essen, Germany)

In present practice, the design and operation of urban drainage systems, and the corresponding sewage treatment plants, are usually independent. In this paper an approach is presented, the aim of which is joint operation of an urban drainage system and the corresponding sewage treatment plant. This operation will be based on real-time flood forecasts, which are computed with the aid of radar rainfall measurements. The goal of this control is to minimize the combined negative effects of the hydraulic load (water quantity) and the pollution load (water quality) in the receiving waters during floods. In growing urban areas, higher imperviousness is the cause of increased flood peaks and volumes in the receiving water. In the test basin used, an industrial area with a high imperviousness strongly effects the control of the total system.

Tuesday 20 July PM

Presiding Chair: Prof. D. Lerner (University of Sheffield, UK)

**GROUND WATER SESSIONS****Introduction 1400**

Prof. D. LERNER

**National Perspectives****HS5/W/21-A2 1405****GROUNDWATER IN URBAN DEVELOPMENT—A REVIEW OF LINKAGES AND CONCERNS**

S. S. D. FOSTER (British Geological Survey, Keyworth, Nottingham, NG12 5GG, UK, email: s.foster@bgs.ac.uk); B. L. Morris and P. J. Chilton (British Geological Survey, Wallingford, Oxfordshire, OX10 8BB, UK)

Urban population growth in Asia and Latin America is occurring on a scale, and at a rate, unprecedented in human history. Many of the cities are sited on unconfined or semi-confined aquifers, depend on groundwater for much of their water-supply, and apply or dispose of most of their liquid effluents and solid residues to the ground. Urbanization causes radical changes in groundwater recharge, modifying existing mechanisms and introducing new ones. Concomitantly groundwater quality degradation is reported from a wide range of geographical locations, both within the urban area itself and in downstream alluvial aquifers. Its severity varies considerably with hydrogeological environment, development level and coverage of waterborne sewerage, but it is often the cause of increasing freshwater scarcity, escalating water-supply costs and a growing human-health hazard. As such it is an issue that urgently needs to be addressed.

**HS5/W/22-A2 1425****IMPACT OF GROUNDWATER ON URBAN DEVELOPMENT IN THE NETHERLANDS**

Frans VAN DE VEN (Delft University of Technology, Civil Engineering and Geosciences, Land and Water Management, Stevinweg 1, 2628 CN Delft, The Netherlands, and Institute for Inland Water Management and Wastewater Treatment (RIZA), PO Box 17, 8200 AA Lelystad, The Netherlands, e-mail: f.h.m.vdven@riza.rws.minvenw.nl); Michiel Rijsberman (Delft University of Technology, Civil Engineering and Geosciences, Land and Water Management, Stevinweg 1, 2628 CN Delft, The Netherlands, and, DHV Water BV, PO Box 484, 3800 AL Amersfoort, The Netherlands)

Although existing urban areas in the Netherlands suffer from groundwater nuisance, the groundwater system seems to be a neglected part of the urban water system. This also is the case in recent plans for new urban areas, which constitute a substantial growth of the total Dutch urban area. Groundwater related problems include hazards to public health, unwanted effects on the environment and economic attenuation. For these problems a number of causes and effect are identified. These include problems with groundwater quantity and quality, besides geological problems and organizational problems. The impact of groundwater on present Dutch urban development planning is too small, as groundwater related problems are not given proper attention.

**HS5/W/23-A2 1445****GROUNDWATER CONTAMINATION BY ORGANIC CHEMICALS IN INDUSTRIALIZING COUNTRIES: THE UNSEEN THREAT**

Oliver T. N. SILILO (Cape Water Programme, Environmentek, CSIR, PO Box 320, Stellenbosch 7599, South Africa, email: osililo@csir.co.za)

Industrialization brings with it a high production of wastes. Many of these are disposed of in the environment and can have a serious impact on groundwater. In developed, industrialized countries, hierarchical approaches to investigating contamination problems are generally well established. In many instances, individual organic chemicals have been identified as being critical in pollution plumes. On the other hand, in many industrializing countries, individual organic contaminants are rarely determined during groundwater pollution investigations. The reasons for this include low level of awareness, lack of analytical facilities and cost constraints. Three case studies are presented from the Western Cape, South Africa, where although organic contaminants were suspected, the investigation concentrated on inorganic contaminants. It is concluded that there is need for increased awareness of the potential impact of organic contaminants on groundwater and ultimately guidelines need to be developed for principal organic contaminants that should be analysed for at contaminated sites.

**HS5/W/24-A2 1505****PROBLEMS OF GROUNDWATER QUALITY RELATED TO THE URBAN ENVIRONMENT IN GREATER CAIRO**

Nahed E. EL ARABI (Nile Basin Dept., Research Institute for Groundwater, El Kanater El Khairia, Egypt)

Greater Cairo is faced with increases in population and unplanned extensions in urbanization. This has not been followed by an equal expansion in water supply and sanitary drainage, thus resulting in poor environmental conditions. Cairo covers 300 km<sup>2</sup> with intensive and varied urban land uses and encompasses the oldest industrial areas of Egypt, such as Shubra-Mostarad and Helwan. In addition, new industrial communities are located in the western desert fringe of Greater Cairo with many industrial areas located in zones of highly vulnerable groundwater. Pollution sources of industrial origin threatening groundwater occur in a wide variety of both large and small industrial areas. Moreover using sewage (waste) water for irrigation is reclaiming the desert fringes of Cairo. The adverse environmental impacts of unplanned urban expansion and industrial and agricultural activities could lead to deterioration in groundwater quality. This has dictated quick interventions based on groundwater quality monitoring systems designed to detect pollution sources and their spatial extension. This

paper presents groundwater quality indicators for domestic, agricultural and industrial pollution at representative sites within Greater Cairo.

**HS5/W/25-A2 1525**

**DETERIORATION OF GROUNDWATER QUALITY IN THE COASTAL PINGTUNG PLAIN, SOUTHERN TAIWAN**

Chung-Ho WANG (Institute of Earth Sciences, Academia Sinica, PO Box 1-55, Nankang, Taipei, Taiwan 11529, ROC, email: chwang@earth.sinica.edu.tw); Chung-Jung Chiang (Central Geological Survey, PO Box 968, Taipei, Taiwan 23557, ROC); Tsung-Ren Peng (Department of Soil and Environmental Sciences, National Chung Hsing University, Taichung, Taiwan 40227, ROC); Wen-Cheh Liu (Department of Horticulture, Taiwan Sugar Research Institute, Tainan, Taiwan 70123, ROC)

Population growth, urban expansion and economic development have persistently raised the demand for water supply and consequently, greatly increased the exploitation of groundwaters in the Pingtung Plain of southern Taiwan over past decades. Over-pumping of groundwaters due to booming freshwater aquaculture and agricultural activity has caused the groundwater level to fall and land to subside below sea level in some coastal areas. Isotopic and chemical groundwater analysis has verified the deterioration in coastal groundwater quality due to active seawater intrusion through the offshore outcrops of both unconfined and confined aquifers since 1980. The greatest extent of seawater encroachment has been estimated to be as far as 8.5 km inland with an affected area of about 104 km<sup>2</sup> for the deep confined aquifer in 1996. Remedial measures need to be immediately enforced to effectively restrain sea water encroachment and to alleviate groundwater salinization.

**HS5/W/26-A2 1545**

**GROUNDWATER QUALITY MANAGEMENT: POLLUTION PERSPECTIVES**

R. RAMESH (Institute for Ocean Management, Anna University, Chennai, India, email: auiomrr@md2.vsnl.net.in)

Water scarcity has been one of the most serious problems in Chennai, India for many years. In particular there has been a decline in both groundwater table level, and groundwater quality over recent years. This paper focuses on the distribution of major and trace elements in groundwater of the Chennai basin. It is seen that the concentration of major ions such as Na and Cl are predominantly influenced by anthropogenic activities, whereas natural processes control other major elements. The concentration of trace metals at a few wells along the waterways are high and in general there is a decrease in the relative concentration from summer to monsoon due to local precipitation and seepage which dilutes the concentration of trace metals and aids their migration. This study also highlights the impact on groundwater of urban growth in Chennai.

Presiding Chair: Dr. N. E. El Arabi  
(Research Institute for Groundwater, El Kanater El Kahairiya, Egypt)

**Modelling & Methods 1**

**HS5/W/27-A2 1635**

**MODELLING OF NITROGEN DYNAMICS IN THE SUB-SURFACE ENVIRONMENT**

A. Jake GUSMAN (URS Greiner Woodward Clyde, 2020 East First Street, Suite 400, Santa Ana, California 92705, USA, email: jake\_gusman@urscorp.com); Miguel A. Marino (Dept. of Land, Air, & Water Resources and Dept. of Civil & Environmental Engineering, University of California, One Shields Avenue, Davis, California 95616-8628, USA)

This paper presents a physically-based model (RISK-N) to simulate nitrogen cycling in soils, and nitrate transport and fate in soils and groundwater. The soil is separated into upper-root, lower-root, sub-drainfield, and intermediate vadose zones, each with uniform properties. Transport in each soil zone is modelled on the basis of complete mixing, by spatially averaging the related partial differential equation. Transport in the aquifer, however, is modelled using a two-dimensional advection-dispersion equation. Two example problems demonstrate and validate the use of the RISK-N model: (a) an irrigated and fertilized corn plot, and (b) a suburban area with septic tank systems and fertilized turfgrass.

**HS5/W/28-A2 1655**

**GROUNDWATER MODELLING IN URBAN AREAS AS A TOOL FOR LOCAL AUTHORITY MANAGEMENT: BARCELONA CASE STUDY (SPAIN)**

E. Vázquez-Suñé, X. SÁNCHEZ-VILA (Dept. Enginyeria del Terren, Universitat Politècnica de Catalunya, 08034 Barcelona, Spain, email: dsanchez@etseccpb.upc.es)

Urbanization poses some threats to both the availability and quality of groundwater resources in large cities worldwide, with corresponding significant social, environmental and economic implications. A good knowledge of urban hydrology requires a detailed quantitative analysis of water fluxes, but also of the quality of the resources. In any real case study one has to face at least three aspects: (a) process identification, (b) aquifer characterization and modelling, and (c) water resources management. This three-fold methodology has been applied to the city of Barcelona. The outcome is a groundwater model which among other things may become a management tool, as it allows definition, characterization and quantification of the potential risk to aquifers, as well as to urban structures, with all the implications for the population. This is an important step towards convincing city managers to consider groundwater as one of the topics to be taken into account in city planning.

**HS5/W/29-A2 1715**

**THE VULNERABILITY OF THE DUPI TILA AQUIFER OF DHAKA, BANGLADESH**

M. Kamrul Hasan, William BURGESS (Department of Geological Sciences, University College London, Gower St., London WC1E 6BT, UK, email: william.burgess@ucl.ac.uk); Jane Dottridge (Komet Clarice Bond, 129 Cumberland Road, Bristol BS1 6UY, UK)

Dhaka relies almost exclusively on groundwater for its water supply. Intensive abstraction from the Dupi Tila aquifer has led to induced recharge from rivers and enhanced vertical leakage from regions containing contaminated land. Low quality water has invaded the aquifer from a polluted stretch of river. Vertical hydrochemical profiles show that urban pollution has reached the upper levels of the aquifer within the city, but not the level of groundwater abstraction except in isolated cases. The aerobic environment of the aquifer may support the natural attenuation of contaminants. Contaminant transport modelling demonstrates that a general deterioration of groundwater quality is inevitable even if all sources of contamination are removed immediately. The model could be used to guide groundwater quality monitoring as

part of a protection policy for this strategically important aquifer. A programme of waste management should be based on factors identified as governing aquifer vulnerability.

**HS5/W/30-A2 1735**

**ECOLOGICAL INDICATORS AND INDICES OF SUSTAINABLE DEVELOPMENT**

Anna BELOUSOVA (Water Problems Institute, Russian Academy of Sciences, 3 Gubkina Str., Moscow 117971, Russia, email: anabel@eolss.msk.ru)

A system of ecological Pressure-State-Response (PSR) indicators has been developed. The first indicator, characterizing an impact in the PSR system, must take into account all time peculiarities of the impact on the underground hydrosphere. However, this will not help to fully assess the whole ecological situation in terms of groundwater in complex natural-anthropogenic conditions. Pressure indicators must be subdivided into Present (current) and Retarded (or delayed) Pressure Indicators. An additional indicator, the Foresight Indicator makes it possible to avoid confusion in assessing ecological consequences at present, with those in the near and remote future. State Indicators characterize changes in the hydrosphere under the impact of negative events (Present and Future State Indicators). Response Indicators characterize political, social and economical decisions. Index groups can characterize each of these indicators.

**Wednesday 21 July AM**

Presiding Chair: Prof. F. Van de Ven (Delft University of Technology, The Netherlands)

**Modelling and Methods 2**

**HS5/W/31-A3 0900**

**LOADINGS OF NON-AGRICULTURAL NITROGEN IN URBAN GROUNDWATER**

David N. LERNER (Groundwater Protection and Restoration Group, Civil and Structural Engineering, University of Sheffield, Mappin Street, Sheffield, S1 3JD, UK, email: d.n.lerner@shef.ac.uk); Yuesuo Yang (Environmental Engineering Centre, Queens University, Belfast, BT7 1NN, UK); Mike H. Barrett (Robens Centre for Public and Environmental Health, University of Surrey, Guildford, Surrey, GU2 5XH, UK); John H. Tellam (School of Earth Sciences, University of Birmingham, Edgbaston, Birmingham, B15 2TT, UK)

In the groundwater under Nottingham, nitrate concentrations are as high as they are in the surrounding rural groundwater. Fertilizer and agricultural practices are the main sources of rural nitrates, but are insignificant in the city environment. Urban sources of nitrogen in groundwater include leaking sewers, leaking water mains, landfills and industrial chemical spillages. We have recently completed a major field and modelling study of Nottingham to identify and quantify recharge sources and amounts, and loadings of solutes. A novel approach of combining a water balance with multiple solute balances provided the first estimates for a UK city. Sewers contribute about 13% of the nitrogen loading. The size of the nitrogen loading from leaking water mains is more important at about 36% of the total, because they provide over half the recharge in the urban area. The remaining 50% of the N loading includes parks, gardens, landfills and industrial spillages.

**HS5/W/32-A3 0920**

**GROUNDWATER PROTECTION INCORPORATED INTO LAND USE PLANNING: A STUDY FROM CEBU CITY, THE PHILIPPINES**

Ian HOLMAN, Robert Palmer (Soil Survey and Land Research Centre, Cranfield University, Silsoe, Bedfordshire, MK45 4DT, UK, email: i.holman@cranfield.ac.uk)

Municipal water suppliers to many Asian mega-cities rely on imports of surface water because recent rapid urban expansion threatens local groundwater quality. However, shallow groundwater resources beneath these cities are still utilized by private wells irrespective of health implications. If the quality of shallow resources is to be maintained, potentially polluting activities must be encouraged to locate in areas where groundwater is naturally protected. Groundwater vulnerability techniques are an appropriate, low cost management tool for defining both areas of natural protection and areas requiring strict land use controls. The UK vulnerability methodology, adapted for Philippine conditions, enables land to be zoned according to: soil and aquifer properties, depth to groundwater, and proximity to perennial rivers. The resulting 16 groundwater vulnerability zones have been simplified, for routine regulatory use, into a four-zone Development Constraint Map, which identifies the planning controls necessary to protect groundwater quality.

**HS5/W/33-A3 0940**

**AUTOPSY OF AN AQUIFER: A CASE STUDY OF AL HAYMA, YEMEN.**

Chris D HANDLEY (School of Oriental and African Studies, Russell Square, London WC1H 0XG, UK, email: chris@chrishandley.freeserve.co.uk)

Despite the absence of a unique solution, a combination of the following methods permits an assessment of "who stole the water?" from the main aquifer on which a city of 400 000 people depends: (a) the Penman-Monteith method for deriving crop and soil evaporation, (b) the US Soil Conservation Service curve number method for calculating runoff, and (c) groundwater flow modelling to match historical water level trends.

**HS5/W/34-A3 1000**

**SULPHATE ISOTOPE SIGNATURES IN BOREHOLE WATERS FROM THREE URBAN TRIASSIC SANDSTONE AQUIFERS, UK**

Anwen J. Hughes, John H. TELLAM, John W. Lloyd, Kim A. Stagg (Earth Sciences, Birmingham University, Birmingham B15 2TT, UK, email: j.h.tellam@bham.ac.uk); Simon H. Bottrell, Andrew P. Barker (Earth Sciences, Leeds University, Leeds LS2 9JT, UK); Michael H. Barrett (Robens Centre, Surrey University, Guildford, Surrey, GU2 5XH UK)

This paper outlines an investigation of the use of <sup>34</sup>S and <sup>18</sup>O data in provenancing sulphate in groundwaters of urban UK Triassic sandstone aquifers. The isotopic composition of potential S sources (precipitation, industrial acids, plating bath effluents, various building materials, public supply water, detergents, road salt, and geological materials) were determined. The isotopic data from pumped sampling in the Birmingham aquifer confirmed previous interpretations based on elemental concentrations, identifying natural and various anthropogenic sources. Detailed resolution of the anthropogenic sources was not possible, partly because of the common source of many man-made sulphur compounds in the aquifers studied (Triassic evaporites), and the mixed nature of the groundwater samples. However, the

isotope data set from Birmingham, Nottingham, and Liverpool all show that sulphide oxidation commonly occurs in the shallow subsurface: this has important implications for the attenuation of other pollutants. No sulphate reduction was apparent in any of the waters sampled from the three aquifers.

Presiding Chair: Dr. A. J. Gusman (URS Greiner Woodward Clyde, Santa Anna, USA)

### Process Studies

HS5/W/35-A3

1045

#### A STABLE CARBON ISOTOPE STUDY ON DIRECT PRECIPITATION RECHARGE TO THE AQUIFER IN THE CITY OF YAMAGATA, NORTHERN JAPAN

Masaya YASUHARA and Kohei Kazahaya (Hydrology Studies Group, Geological Survey of Japan, 1-1-3 Higashi, Tsukuba, Ibaraki 305-8567, Japan, email: masaya@gsj.go.jp); Hiroyuki Higuchi and Toshifumi Ueda (International Department, Kyowa Engineering Consultants Co. Ltd., 2-26-2 Sasazuka, Shibuya, Tokyo 151-0073, Japan)

A dynamic image of a shallow (<100 m below the surface) unconfined aquifer in the City of Yamagata, northern Japan has been obtained by  $\delta^{13}C$  and major element analyses of groundwater and river water. The chemical and isotopic composition of groundwater show significant variations across the study area, as a result of mixing, in varying proportions, of waters of different origin. A successive mixing of the infiltrated precipitation (direct precipitation recharge) with the infiltrated Mamiyasaki river water takes place beneath the downtown area of the city. Although about 70–80% of the surface has already been rendered impermeable, groundwater beneath the downtown area shows strong evidence of precipitation inputs. In the immediate area of the Mamiyasaki River, less than 10% of groundwater can be attributed to water of precipitation origin. With an increasing distance downslope, the infiltrated precipitation has an increasing influence on groundwater. A couple of kilometres away from the river, the results are indicative of a 40% precipitation contribution. This suggests that the direct precipitation recharge is still of great significance even in the highly urbanized areas like the City of Yamagata.

HS5/W/36-A3

1105

#### MONITORING SOLVENTS IN THE BIRMINGHAM AQUIFER (UK): 1987, 1998 AND ON TO THE NEXT MILLENNIUM

Lynda Taylor, Michael RIVETT (School of Earth Sciences, University of Birmingham, Edgbaston, Birmingham, B15 2TT, UK, email: m.o.rivett@bham.ac.uk)

Chlorinated solvents are exceedingly common groundwater contaminants in aquifers that underlie urban areas. A case study is presented of the Birmingham aquifer (UK) using data from two surveys of solvent occurrence conducted a decade apart (1987 and 1998). Active abstraction boreholes (mainly industrial-use) were used to obtain groundwater samples. The suitability of such boreholes to observe relevant contaminant hydrogeological processes and provide long-term monitoring is illustrated. Although the Birmingham data set is relatively sparse, interpretations may nevertheless be offered on solvent occurrence, persistence of solvent source zones, effects of changing groundwater abstraction, solvent attenuation in the aquifer and trends in solvent mass removal by groundwater abstraction. It is concluded that active abstraction boreholes may provide useful data on urban groundwater quality trends and their use in the next millennium should not be overlooked.

HS5/W/37-A3

1125

#### EVIDENCE FOR SEWAGE CONTAMINATION OF THE SHERWOOD SANDSTONE AQUIFER BENEATH LIVERPOOL, UK

Emily Whitehead, Kevin HISCOCK, Paul Dennis (School of Environmental Sciences, University of East Anglia, Norwich, NR4 7TJ, UK, email: k.hiscock@uea.ac.uk)

Urbanization of the Liverpool area in northwest England began in 1207 and the area was prosperous by the 1700s. As an area with a long history of urbanization, the objective of this study was to map the water quality of the underlying major Sherwood Sandstone aquifer with special attention to whether leaking sewers are contaminating the groundwater. The sewerage system in Liverpool has been extensive since the late nineteenth century, expanding along with the city. Twelve samples were collected from sites in Liverpool and analysed for several markers of sewage contamination, including the nitrogen isotope composition of dissolved nitrate, microbiological indicators, boron and major ions such as nitrate and potassium. The results showed saline intrusion and widespread contamination of the aquifer. The sewage "fingerprint" was positively identified and provides the first conclusive evidence for sewer-derived contamination of Liverpool's groundwater.

HS5/W/38-A3

1145

#### GROUNDWATER LEVEL EVOLUTION IN THE MILAN AREA: NATURAL AND HUMAN ISSUES

Tullia BONOMI (Dipartimento di Scienze dell' Ambiente e del Territorio, Università degli Studi Milano Bicocca, Milano, Via Emanueli 15, I-20126 Milano, Italy, email: bonomi@alpha.disat.unimi.it)

The history of groundwater level development in Milan province and in Milan city is analysed. It is very well recorded by piezometric data from a monitoring network of 284 wells, with a monthly frequency. In 1915 the water table depth, quite close to Milan city, was about 1 m below ground surface. The groundwater table has since fallen rapidly, with an historical minimum in the 1970s, some 40 m below ground surface. However, a rapid increase is now occurring and in recent years (1993–1997) the situation in Milan is getting worse. Many areas of the town's subsurface (parking, underground, houses, hospitals) are now flooded by groundwater. A study of the Milan hydrogeological system has been carried out to analyse the natural and human causes determining the groundwater level evolution. The historical sequences of all the different factors of the mass transfer, from the beginning of the century through to 1997, have been analysed to evaluate their synergistic relationships.

HS5/W/39-A3

1205

#### LOSS OF GROUNDWATER RESOURCES FOLLOWING MAJOR QUARRYING ACTIVITY IN URBAN AREAS: THE GALERIA-MAGLIANA QUARRY BASIN (ROME, ITALY)

Giuseppe Capelli, Renato Funicello, Daniela Iorio, Roberto SALVATI (Department of Geological Sciences, University of Rome TRE, L.go S. Leonardo Murialdo 1, I-00146 Roma, Italy, email: salvati@uniroma3.it)

In this paper we present the results of a study aimed to define the environmental impacts of quarry activities in the suburban belt of Rome. The hydrological and hydrogeological

modifications induced by the quarry activities receive particular attention and can be summarized as (a) disruptive groundwater lowering as a result of quarrying activity below groundwater level; (b) dewatering of large parts of the area as a consequence of quarry site back-filling with low permeability materials, morphological alteration and soil degradation, with consequent loss of environmental structure in large parts of the area; and (c) river system alteration or its complete disruption as a result of dispersed and unplanned site development. The study has been developed through a multidisciplinary approach using sedimentological, geomorphological and hydrogeological methods.

HS5/W/40-A3

1225

#### ASSESSMENT OF GROUNDWATER POLLUTION IN THE PATANCHERU INDUSTRIAL DEVELOPMENT AREA AND ITS ENVIRONS, MEDAK DISTRICT, ANDHRA PRADESH, INDIA

V. V. S. GURUNADHA RAO, K. Subrahmanyam, P. Yadaiah and R. L. Dhar (National Geophysical Research Institute, Hyderabad-500007, India, email: director@nngri.wiprobt.ems.vsnl.net.in)

A number of chemical and pharmaceutical industries have opened since 1978 in the Patancheru Industrial Development Area of Medak district, Andhra Pradesh, India. Both treated and untreated effluents from these industries are discharged to the Nakkavagu and Peddavagu streams and the former also receives effluents from an adjacent Industrial Development area. Groundwater level and water quality monitoring have been carried out on 30 observation wells over the last two years in Patancheru and its environs covering a 120 km<sup>2</sup> area, and a number of aquifer parameters were estimated at various pumping wells. Groundwater flow and mass transport models were prepared using visual MODFLOW software, allowing the extent of contaminant migration from Nakkavagu and other streams to be assessed for the last 20 years. The stream-aquifer interaction was found to be responsible for faster migration of contamination in the over exploited area around Nakkavagu in Arutla village.

Wednesday 21 July PM

Presiding Chair: Dr. K. Hiscock (University of East Anglia, Norwich, UK)

### Case Studies

HS5/W/41-A3

1400

#### IMPACT OF CHEMICAL GROUT INJECTION ON URBAN GROUNDWATER

Matthias EISWIRTH, Renke Ohlenbusch and Klaus Schnell (Department of Applied Geology, University of Karlsruhe, Kaiserstr. 12, D-76128 Karlsruhe, Germany, email: matthias.eiswirth@bio-geo.uni-karlsruhe.de)

In many urban areas, grout injections have been used to seal porous soil within the last decades. Silica hydrogels have been particularly applied in foundation engineering practice due to their wide applicability and economic advantages. For example in the City of Berlin between 1990 and 1995 about 100 000 m<sup>3</sup> of silicate gels were injected into porous aquifers. Therefore the environmental authority of Berlin insisted on detailed investigations of potential groundwater contamination risks. This paper presents the results of detailed investigations on an excavation site over a period of two years. Two main topics are the use of artificial and natural tracers as well as transport modelling to quantify potential changes in groundwater chemistry and to predict both longevity and toxicity of silica grouts.

HS5/W/42-A3

1420

#### THE IMPACT OF URBAN INDUSTRIAL GROWTH ON GROUNDWATER QUALITY IN VISAKHAPATNAM, INDIA

C. SUBBA RAO & N. V. Subba Rao (Department of Geophysics, Andhra University, Visakhapatnam-530003, India)

The process of urbanization and industrial expansion has been phenomenal in the port city of Visakhapatnam since 1940. In addition to the port, major industries such as shipyards, petroleum refineries, zinc smelter plants, fertilizer units, ceramics and polymers have started in the city heartland. Forty percent of the one million population lives in the industrial belt within which the quality of groundwater has become seriously polluted. Fifteen percent of the industrial well waters have recorded more than 3000  $\mu$ S level of conductivity and major ions have crossed the "safe" limits at many places. Toxic elements including lead, chromium, arsenic, zinc, cobalt have been traced in large amounts in the groundwaters of the industrial zones, with a zinc plant being identified as the worst offender followed by the port and polymer facilities. The extent of effluent contamination has been delineated using geo-electrical techniques.

HS5/W/43-A3

1440

#### MODELLING CONTAMINATION OF A DRINKING WATER SUPPLY WELL IN THE SABARMATI RIVER BED AQUIFER, AHMEDABAD, INDIA

V. V. S. GURUNADHA RAO (National Geophysical Research Institute, Hyderabad 500007, India, email: postmast@ngri.globemail.com); S. K. Gupta (Physical Research Laboratory, Ahmedabad 380009, India)

Drinking water supply wells in Ahmedabad city were constructed in the Sabarmati river bed aquifer using radial pipes; they are known as French Collector wells. Groundwater contamination from one of the French wells near Sabarmati railway bridge was noticed during 1992. The suspected pollution sources are Duff-nala of Shahibaug and two other sources from slum dwellings on either side of Sabarmati River. A combined groundwater flow, pathlines and mass transport model was constructed covering an area of 9 km<sup>2</sup> to analyse the capture zone of the French well under two different scenarios. Dry river bed condition was simulated under Scenario 1 and controlled flow in the river bed was simulated under Scenario 2. The groundwater velocity and migration of contaminant particles from sources was analysed in the pathline model. The computed pathlines and TDS concentration contours indicate likely migration of contaminant plumes from pollutant sources to the French well during 300 days under both scenarios. The modelling study emphasized the necessity of controlled release of surface water from the Dharoi reservoir to the Sabarmati riverbed throughout the year.

HS5/W/44-A3

1500

#### HAZARDS DUE TO MIGRATION OF SEPTIC TANK LEAKAGES IN PERI-URBAN SETTLEMENTS

H. K. Ramaraju, M. Venkatachallappa and G. RANGANNA (UGC-DSA Centre, Department of Mathematics, Bangalore University, 560 001 Bangalore, India, email: dsamath@blr.vsnl.net.in); C.



Sadashivaiah, N. Manamohan Rao (Department of Civil Engineering, Bangalore University, Janabharathi, 560 056 Bangalore, India)

Whilst it is widely accepted that a healthy environment is essential for human survival and sustainable development, two thirds of people living in developing countries still do not have adequate sanitation facilities. A field study carried out at three selected sites within the Bangalore peri-urban area has been undertaken to assess the contamination status of domestic well waters. The two-year study revealed that water quality of the domestic wells is deteriorating fast as partly indicated by very high nitrate levels. Thirteen wells out of 19 were found to be severely contaminated, five wells are marginally contaminated with only one well being considered fit for use. In some cases the nitrate level of the well waters has reached 495 mg l<sup>-1</sup> during summer months, which is far in excess of WHO stipulations. Based on two years of field data, certain measures are suggested for safe domestic waste disposal in the study areas in order to achieve a congenial groundwater environment and to provide long term protection for the health status of the local population.

Presiding Chair: Prof. M. Peart (University of Hong Kong)

### STORMWATER POSTER SESSION

HS5/W/45-A3 Poster 1545-01

#### THE URBAN GROWTH OF MOMBASA COASTAL TOWN AND ITS IMPLICATION FOR SURFACE AND GROUNDWATER RESOURCES

John Kioko MUSINGI, Shadrack Mulei Kithiia, Boniface Nzuve Wambua (Department of Geography, University of Nairobi, Box 30197, Nairobi, Kenya)

Mombasa is the second largest urban centre in Kenya after the city of Nairobi. The historical development of the town dates from the 15th century during the Arabian rule of the coastal strip. The town, which is about 500 km south east of Nairobi, is situated on Mombasa Island with an extension on the mainland. It has the largest harbour in eastern Africa with good sheltered harbour facilities at Kilindini port and is the gateway to the East and Central African region. The major industrial activity is associated with oil refining but the town is a major tourist destination due to its natural clean beaches. The city experiences acute water shortages due to increased demands from both industrial and population growth. This paper describes the historical and current growth of Mombasa town in terms of population and industrial activities as it affects water demand and use. The geology is examined as a means of quantifying groundwater resources and pollutant sources and the overall effects are examined in view of suggesting possible strategies to ensure continued urban growth without further environmental degradation impacts.

HS5/W/46-A3 Poster 1545-02

#### WATER RESOURCES UTILIZATION AND ITS INFLUENCE ON THE ECO-ENVIRONMENT IN THE ARID ZONE OF NORTHWEST CHINA

Wang GENGXU (Geology Department of Lanzhou University, and Lanzhou Institute of Glaciology and Geocryology, Chinese Academy of Sciences, Lanzhou, 730000, P. R. China, email: liusy@ns.lzb.ac.cn); Cheng Guodong (Lanzhou Institute of Glaciology and Geocryology, Chinese Academy of Sciences, Lanzhou, 730000, P. R. China)

Over the last 50 years exploitation of water and land resources in the arid northwest regions of China has been expanding to support the sustainable development of industrial and agricultural production. As a result river discharges have been drastically reduced (even dried-up), river courses shortened, and terminal lakes have contracted or dried-up. In the lower reaches of some inland river basins, desertification is rapidly developing at an annual rate of 3.5–6.9%. Economical and effective use of water resources and harmonization of eco-environment benefits with economic benefits are the only fundamental ways to achieve sustainable development of arid northwest China.

HS5/W/47-A3 Poster 1545-03

#### DYNAMICS AND QUALITY OF WATER RESOURCES IN THE NIGER DELTA

T. K. S. ABAM (Institute of Geosciences and Space Technology, Rivers State University of Science and Technology, P.M.B. 5080, Port-Harcourt, Nigeria)

The Niger Delta is a large and ecologically sensitive region, in which various water species (including surface and groundwater, saline and fresh waters) are in a dynamic equilibrium. Physical environmental attributes of these waters and the nature of their changes as well as the resultant adjustments in hydrodynamic and ecological boundaries are described. Groundwater over-abstraction in the urban coastal areas has resulted in increased aquifer salinity. The inland incursion of tidal waters has been strengthened by the reduction of fresh water discharge due to impoundment in upstream dams and reservoirs.

HS5/W/48-A3 Poster 1545-04

#### A MODEL OF THE FLOOD TRANSFORMATION IN THE AMUDARYA RIVER

Victor E. CHUB (The Main Administration of Hydrometeorology of Republic of Uzbekistan, 72, K. Makhsumov Str. 700052, Tashkent, Republic of Uzbekistan, email: uzhyet@hmc.tashkent.su); Sergey V. Myagkov (Department of Hydrological Forecast, Central Asian Regional Research Hydrometeorological Institute, 72, K.Makhsumov Str. 700052, Tashkent, Republic of Uzbekistan)

On the basis of modelling the flood transformation for a river with a deformed channel, a technique has been developed for short-range forecasting of the Amydarya River discharge. The model takes into account the relationship between the lag time of the flood peak and the water discharge as well as the deformational instability of the river channel. A description of the model and techniques of flow adjustment with a strongly deformed river channel and dynamic changes of the hydraulic bonds are presented.

HS5/W/49-A3 Poster 1545-05

#### CONTEMPORARY STATUS OF SURFACE WATER QUALITY OF THE ARAL SEA BASIN

E. I. CHEMBARISOV, E. I. Chemberisova (Institute of Water Problems, Uzbek Academy of Sciences, 700000, Uzbekistan, email: root@pwater.tashkent.su)

The problems of the Aral Sea desiccation and associated deterioration in ecology have now acquired a global importance. Estimates of ecological condition have been made using methods of systems and budget analysis, statistics and cartography. Surface water volume and quality in different regions of the Aral Sea basin have been determined together with optimum variants for irrigation systems. Means of decreasing the extent of river water pollution

and reducing the number of collector- drainage water discharges into rivers have been developed as well as principles for hydro-ecological zoning of territories.

Presiding Chair: Dr M. Rivett (University of Birmingham, Edgbaston, UK)

### GROUNDWATER POSTER SESSION

HS5/W/50-A3 Poster 1630-01

#### THE USE OF DRASTIC MODELLING INDICES FOR THE ASSESSMENT OF GROUNDWATER POLLUTION POTENTIAL

M. Chandra SEKHAR & K. Karuna Kumar (Water & Environment Division, Regional Engineering College, WARANGAL 506 004, India, email: mcs@recw.ernet.in)

The vulnerability of groundwater to pollution depends on various factors such as depth to water table, net recharge, aquifer media, soil media, topography, impact of vadose zone, hydraulic conductivity of the aquifer, cropping pattern etc. The Kakatiya canal area studied in this investigation was found to have polluted groundwater aquifers requiring immediate counter-measures and integrated management of pollution. However, some of the investigated factors, termed "DRASTIC" factors, constitute varying risks for pollution of the aquifer groundwaters. The vulnerability of groundwater pollution is estimated by giving suitable weights and rating to these "DRASTIC" factors which are determined from the collected seasonal study data.

HS5/W/51-A3 Poster 1630-02

#### IMPACT OF URBANIZATION ON THE KHASH AQUIFER, AN ARID REGION OF SOUTHEAST IRAN

E. KHAZAI (Department of Civil Engineering, University of Sistan and Baluchestan, Zahedan, Iran, email: khazai@hamoon.usb.ac.ir); M. G. Rigi (Sistan and Baluchestan Regional Water Authority, Zahedan, Iran)

This paper investigates both the quantitative and the qualitative impacts of urbanization on the Khash aquifer. The results indicate a general fall in the groundwater level and deterioration of groundwater quality. However, there are cases of improvement in the groundwater quality owing to reductions in evaporation effects.

HS5/W/52-A3 Poster 1630-03

#### URBAN IMPACTS ON GROUNDWATER QUALITY IN THE DELHI REGION

R. B. SINGH (Department of Geography, University of Delhi, Delhi 110 007, India)

In recent years, water supply and groundwater resources in India have become threatened following uncontrolled disposal of urban waste into water bodies, open waste dumping and poorly designed landfills. Within the urban fringe zones of Delhi, the contamination of groundwater by industrial and domestic effluents now presents serious challenges. Subsoil waters in the area through which effluents from major industries infiltrate, are already polluted more or less permanently. Wells in many residential areas are contaminated with nitrate, detergents and high salinity levels with the high content of fluoride also posing severe health hazards in surrounding regions.

HW1

Thursday 22 – Friday 23 July

GLOBAL DATA BASES (ICASVR, ICWQ, ICSW ICCE, WMO, IAHS/WMO JOINT WORKING GROUP, IGBP-BAHC)  
Location: Barber Institute, Concert Hall

Thursday 22 July AM

Presiding Chair: Charles Vörösmarty, (University of New Hampshire, USA)

### SUPPORT FOR SCIENCE

Overview 0845

Charles VÖRÖSMARTY

Keynote 0900

Wolfgang GRABS (WMO-Global Runoff, Data Centre, Germany)

SOUNDBITES 0930-1000

HW1/E/02-A4 0930

#### A REVIEW OF GLOBAL HYDROLOGIC DATA SETS IN RELATION TO THE GCOS/GTOS PLAN FOR TERRESTRIAL CLIMATE-RELATED OBSERVATIONS

JURATE LANDWEHR (USGS, 431 National Center, Reston VA 20192, USA; Email: jmlandwe@usgs.gov); Josef Cihlar (Canada Centre for Remote Sensing, 588 Booth Street, Ottawa, Ontario, Canada K1A 0Y7; Email: josef.cihlar@ccrs.nrcan.gc.ca)

TOPC (Terrestrial Observation Panel for Climate) is a joint activity of the Global Climate Observing System (GCOS) and the Global Terrestrial Observing System (GTOS), both of which are initiatives of WMO, UNEP, and ICSU. IOC of UNESCO also sponsors GCOS, and UNESCO and the FAO, GTOS. The purpose of GCOS is to provide a forum for the development of a comprehensive long-term global observing system to improve our capability to detect, predict and assess climate change. GTOS was established to provide policy makers, resource managers, and researchers data needed to detect, quantify, and give early warning of changes in the capacity of terrestrial ecosystems to support sustainable development and improvements in human welfare. TOPC has produced an analysis of data and actions needed to address these goals jointly. The GCOS/GTOS plan for terrestrial climate-related observations has been published and is available via the internet at [http://www.wmo.ch/web/gcos/pub/topv2\\_1.html](http://www.wmo.ch/web/gcos/pub/topv2_1.html). The TOPC plan not only identifies key hydrospheric, cryospheric and biospheric parameters but also compares their relative importance for their respective climate purposes and suggests methods and actions for obtaining this information. For example, for the hydrologic sector, the plan provides a detailed

rationale for the following variables: atmospheric water content near the surface (relative humidity), biogeochemical transport from land to oceans, discharge (runoff), evapotranspiration, ground water storage fluxes, precipitation, sediment load at large river mouths, snow cover area and snow water equivalent, soil moisture and surface water storage. TOPC is actively seeking to identify which data is available digitally to satisfy the above requirements. In this presentation, we will review which hydrologic data sources have been identified globally, and discuss the general availability and compatibility of this information, as well as gaps in the geographic or thematic coverage for the above variables.

#### HW1/L/-A4 0930

##### GLOBAL DATA SETS OF THE ISOTOPE HYDROLOGY SECTION OF THE INTERNATIONAL ATOMIC ENERGY AGENCY

ARAGUS-ARAGUS L

Abstract not available at time of going to press

#### HW1/L/09-A4 0930

##### GLOBAL DATA BASES IN SUPPORT OF THE NEWLY-CREATED IGBP WATER GROUP

Michel MEYBECK (UMR SISYPHE CNRS, Université de Paris VI, Place Jussieu, 75257 Paris FRANCE, e-mail: meybeck@biogeodis.jussieu.fr) Charles Vörösmarty (Institute for the Study of Earth, Oceans, and Space, University of New Hampshire, Durham NH 03824, USA, e-mail: charles.vorosmarty@unh.edu)

The terrestrial water cycle has played a central role in several of the individual Program Elements of the IGBP. In recognition of the key role that water plays in the Earth System, IGBP is now integrating its ongoing water-related activities through the newly-formed IGBP Water group. This group is carrying forward an analysis of Continental Aquatic Systems which are defined as all surface and subsurface waters participating in the hydrological cycle across the continents. The analysis focuses on understanding the past, contemporary, and future state of terrestrial water systems together with the biogeochemical constituents they store, transform, and transport to the coastal oceans. Central to this is an understanding of the role of humans in defining the status and use of these continental water resources. IGBP has developed different global data bases on river basins (IGBP-BAHC) and on the coastal zone (IGBP-LOICZ), including geo-referenced data sets for water discharge, chemical constituents, biophysical and socio-economic data depicting the world's drainage basins. The IGBP intends to launch an electronic River Archive Series to integrate existing data sets relevant to the analysis of drainage basin change at the global scale. These information resources are now being used to build a Typology of Global River Systems (TYGRIS-BAHC). The IGBP Water Group is also proposing to other organizations having such data repositories (e.g. WMO/GRDC, WHO/GEMS-Water, UNESCO/FRIEND) to construct a common data base on Globally-Significant Basins (GLOSIBA) which will combine both present-day basin attributes, long-term mean observations of river fluxes, and full time series over a minimum period of 20 years. The time series is intended to include water discharges, water chemistry, sediment discharge, and changing human pressure. The selection criteria for stations may combine basin size, length of record, and representativity of basins with regard to biophysical attributes and human impacts. Smaller pristine basins fully monitored over a long period may also be considered. The GLOSIBA is regarded as a data base common to all participating institutions with free on-line access.

#### HW1/L/0 -A4 0930

##### GLOBAL DATA SETS OF KEY GEOPHYSICAL PROPERTIES FOR ANALYSIS OF THE HYDROLOGICAL CYCLE

JENNE, R

Abstract not available at time of going to press

#### HW1/L/10-A4 0930

##### DATA FOR THE GLOBAL WATER AVAILABILITY AND USE MODEL WATERGAP

Petra DOELL and Joseph Alcamo (Center for Environmental Systems Research, University of Kassel, Kurt-Wolters-Str. 3, D-34109 Kassel, Germany, Tel. +49 561 804 3913, FAX +49 561 804 3176, e-mail: doell@usf.uni-kassel.de)

In order to assess the impact of global change on the problem of water scarcity, we are developing a global model of water availability and water use in drainage basins (spatial resolution 0.5° by 0.5°). Such a model is highly constrained by the availability of global data sets. Time series of gridded monthly climatic variables from 1901 to 1995 are provided by the Climate Research Unit at the University of East Anglia (New et al., 1998). These data sets are the first to allow a global-scale analysis of temporal variability of water availability, and, together with discharge data from the Global Runoff Center (Grabs et al., 1996), a calibration and validation of the model. A very important but highly uncertain parameter in runoff modeling is the water capacity of the soil, which was assigned using a WISE data set (Batjes, 1996) who derived it from the FAO Soil Map of the World and more than 4000 soil profiles. 85% of the global water consumption is used for irrigation. Based on international and national sources, we generated the first digital global map of irrigated areas, which shows the percentage of each 0.5° grid cell that is irrigated in the reference year 1995. This map enables us to compute cell-specific irrigation requirements. With respect to domestic and industrial water use, we need to rely on very heterogeneous values of national water uses. Efforts should be undertaken to encourage an improved and standardized collection of water use data by the individual countries.

#### OPEN DISCUSSION 1000

Eric WOOD (NASA, Univ of Princeton, USA)

#### APPLICATION TO IPCC AND OTHER POLICY INITIATIVES

##### Keynote 1100

Kenneth Strzpek (Univ of Colorado, USA)

#### SOUNDBITES 1130-1200

#### HW1/E/01-A4 1130

##### THE ARCSS DATA COORDINATION CENTER (ADCC) AT THE NATIONAL SNOW AND ICE DATA CENTER (NSIDC), USA: A DATA AND INFORMATION RESOURCE FOR ARCTIC HYDROLOGY AND CRYOSPHERIC STUDIES.

Matthew D. CROSS and Christopher K. McNeave (both at CIRES/NSIDC, University of Colorado, Campus Box 449, Boulder, CO, USA, 80309, email: mcross@kryos.colorado.edu)

The National Science Foundation's (NSF) Arctic System Science (ARCSS) Program is a multi-disciplinary approach to understanding polar processes for climate and global change. ARCSS is the only element of the U.S. Global Change Research Program specifically concerned with the arctic region. By focusing on understanding Arctic processes in great detail, investigators are better able to characterize global changes through the improvement of global scale models and other research tools. The ARCSS Data Coordination Center (ADCC) at the National Snow and Ice Data Center (NSIDC), USA, is funded by NSF to archive and disseminate data and information generated from the ARCSS program. Through this endeavor the ADCC strives to be a catalyst for system science and integration within ARCSS.

A major concern of the research community is the availability of reliable data for research. Working with ARCSS investigators, the ARCSS Committee and NSF, the ADCC is continually acquiring data and developing data products appropriate and useful for the research community. Integrating data and information from among the ARCSS ocean based, land based, ice core, paleoclimate and human dimension communities is a high priority at the ADCC. Many of the data sets available at the ADCC are directly applicable to hydrological studies within the Arctic (river runoff, land forms, vegetation cover, vegetation type, ice and snow accumulation, temperature, precipitation, etc.). We also work with other national and international data centers so as to provide optimum accessibility to data and information from the ARCSS archive.

The ADCC strives to provide the most contemporary means of data accessibility to the scientific community. The ARCSS home page (<http://arcss.colorado.edu/>) at the ADCC has become an important tool for data accessibility and integration within ARCSS. Data and information are also distributed on other media (CDROM's, disks, data catalogs, etc.) when appropriate. The ADCC also maintains a complete backup of the ARCSS archive to ensure data and information collected from the program are available on a long-term basis.

This paper summarizes the data and information currently available at the ADCC, and details the mechanisms by which investigators can access these data.

#### HW1/W/01-A4 1130

##### THE AVHRR POLAR PATHFINDER 1.25 KM DATA SET: HYDROLOGIC AND POLAR CLIMATE APPLICATIONS

Ted A. Scambos and Terry HARAN (both at National Snow and Ice Data Center, University of Colorado, Boulder CO 80309-0449, USA, email: haran@kryos.colorado.edu)

Visible and thermal infrared image data from the AVHRR sensor on the NOAA polar orbiting satellites have been archived at the National Snow and Ice Data Center since 1993, covering both polar regions at 1.1 km resolution. Now these data have been reprocessed to provide twice-daily composite images of albedo, surface temperature, cloud cover, and the calibrated separate channels, and once-daily sea ice motion vectors. The composite data, resampled to 1.25 km per grid cell, are designed to be used in conjunction with passive microwave data from the SSM/I Polar Pathfinder: the data are in an equal-area projection, the polar EASE-Grid, and the grid scale is an integer multiple (20) of the coarser (25 km) SSM/I grid. We intend to continue to archive the image data and generate products for at least one year after launch of the MODIS sensor on the EOS AM-1 platform.

The high resolution of the data also supports detailed regional studies; individual islands, small polynas, small ice caps, or river drainages may be monitored. Historical in situ data may be related to the regional pattern in the images. The data are especially useful in supporting field programs, allowing locally accurate field measurements to be extended to areas away from the field site. We will demonstrate some of these applications in selected regions of the northern hemisphere.

#### HW1/L/08-A4 1130

##### THE ANALYSIS OF LONG-TERM CHANGES OF SNOW COVER, CLIMATE AND HYDROLOGICAL PROCESSES IN THE NORTH OF RUSSIA - THE DATABASE GENERATION

L. Kitaev, A. Krenke, E. Barabanova, Institute of Geography, Russian Academy of Sciences, Russia, Moscow, 109017, Staromonetny per. 29, e-mail: climat@ipc.com.ru

A data base and analysis system defining long-term changes in the land surface hydrology of Northern Russia is presented. An observational period spans one hundred years, but in particular the most recent 30 years are targeted since these are most representative of contemporary conditions.

To analyse conjugate changes of land surface variables efficiently and with a sufficient degree of confidence, a special geoinformational technique was formulated. Historical in situ data and forcings encompassed surface-based snow cover, weather and other hydrological observations. The database with its information retrieval system permits searches over a full spectrum of quantitative and spatial identifiers.

To reveal the interaction between climatic and hydrological properties as well as temporal and spatial snow cover changes a special technique was developed. This study revealed that the character of snow cover distribution corresponds well to both air temperature and precipitation changes. Also, the spring flood snow component conforms well to the snow character. Snow cover thus plays an important role in linking both climatic and hydrological processes.

#### HW1/W/02-A4 1130

##### A LONG-TERM HYDROLOGIC DATA BASE FOR THE UNITED STATES

Thomas H. YORKE and Kenneth J. Lanfear (both of the U. S. Geological Survey, 12201 Sunrise Valley Drive, Reston, VA, 20192, USA; email: thyorke@usgs.gov; lanfear@usgs.gov)

The U. S. Geological Survey (USGS) recently completed an evaluation of the streamgaging network that it operates in the United States in cooperation with more than 800 other Federal, State, and local agencies. The evaluation focused on the major Federal goals of the network, which include measuring streamflow across state and national boundaries, determining river basin water budgets, providing data for flood mitigation and warning, determining water-quality trends, and documenting long-term changes to the hydrologic regime. A set of quantitative metrics was established to measure the extent to which each goal was achieved over time. The geospatial data base that was used for the analysis included: the locations of 18,000 streamgaging stations operated by the USGS; traces of 60,000 stream segments in the conterminous United States; boundaries of 329 major river basins and 2,100 small watersheds; boundaries of physiographic sections and ecoregions; locations of 3,000 flood forecasting points; and the locations of 15 million people at risk from riverine flooding.

The evaluation examined the effectiveness of the network in providing data for documenting long-term changes to the hydrologic regime. The results of the evaluation show that representative streams were being monitored in 76 percent of the ecoregions (areas with similar land use, land-surface form, potential natural vegetation, and soils) in 1996. Since 1976, however, there has been a decline in the number of representative streams in river basins and ecoregions throughout the conterminous United States. There also has been a decline in the number of stations with 30 or more years of record. In the 1990s, about 4 percent of the long-record stations were discontinued each year.

The USGS further refined the evaluation by analyzing the parts of the network that were represented by the USGS Benchmark station network and the USGS Hydro-Climatic Data Network. These networks consist of currently operated stations that have 30 or more years of record and represent watersheds that have little or no flow regulation and, thus, are suitable for the study of the relationships among climate, land use, and streamflow. A subset of stations that are part of these two special networks and that are spatially distributed within the major river basins, physiographic sections, and ecoregions of the United States have been identified as high priority long-term stations.

**HW1/L/10-A4****1130****LARGE-SCALE REGIONAL DATA SETS FOR ANALYSIS OF THE EASTERN PORTION OF NORTH AMERICA**

CONRAD, C

Abstract not available at time of going to print

**HW1/L/01-A4****RIVER MASS LOAD ESTIMATION FROM UK NATIONAL RIVER FLOW AND QUALITY DATABASES**

I.G. Littlewood, Institute of Hydrology, Centre for Ecology and Hydrology, Wallingford, Oxon, OX10 8BB, United Kingdom

Recent developments related to the need for, and systematic production of, river mass load estimates are outlined, with particular reference to the UK national river flow and quality databases. Selected details of the first effective merger of these two large databases for systematic river mass load estimation are given. Some results from recent work to derive time series of annual river mass loads discharged from the aggregated freshwater-monitored area of Great Britain are presented. Comments arising from this work are made which may be relevant to the management and use of other large river flow and water quality databases.

**OPEN DISCUSSION****1200**

Petra DOELL (Univ of Kassel, Germany)

Thursday 22 July PM

**COMPUTER-BASED TECHNOLOGIES****Keynote****1400**

Michael KEELER (ECologic, Inc, USA)

**SOUNDBITES****1430 - 1500****HW1/L/11-A4****1430****THE GLOBAL HYDROLOGICAL ARCHIVE AND ANALYSIS SYSTEM (GHAAS): HYDROGRAPHIC DATA SETS AVAILABLE ON-LINE**

Charles VÖRÖSMARTY, Balazs Fekete, Richard Lammers, Michael Routhier, and Pamela Green. (Institute for the Study of Earth, Oceans, and Space, University of New Hampshire, Durham NH 03824, USA, e-mail: charles.vorosmarty@unh.edu)

The Global Hydrological Archive and Analysis System (GHAAS) provides a computerized framework which supports a wide array of Earth Systems studies. The system is organized into individual modules that handle a variety of GIS-related functions in a hydrographic context. Modules include the Data Manager pre-processor, Data Analyzer to assemble model components, and River-GIS modeling tool for topologically-organized simulated river networks and drainage basin analysis.

The GHAAS initiative also encompasses the preparation and distribution of hydrometeorological data sets for wide distribution to the water sciences community. A brief synopsis of several of these data sets will be offered. Specific holdings include a gridded river network topology for potential river flow paths at 30-minute spatial resolution (STN-30p); climatologically-averaged station data for discharge co-registered to STN-30 (WMO/GRDC-UNH Composite); discharge and meteorological station time series in geographic coordinates (RivDIS v1.1; R-ArcticNET; R-HydroNET); and, gridded climate (R-HydroNET) and runoff fields (WMO/GRDC-UNH Composite; WBM-USA). All data are available free of charge and without restriction at <http://www.csrc.unh.edu/hydro/welcome.html>. Portions of the GHAAS data base are also made available through WWW sites and CD-ROMs maintained by the Oak Ridge National Laboratory NASA-DAAC (Oak Ridge, Tennessee USA), National Snow and Ice Data Center (Boulder, Colorado USA), and WMO Global Runoff Data Center (Koblenz GERMANY).

**HW1/L/07-A4****1430****UTILIZATION OF GLOBAL RIVER DISCHARGE DATA FOR THE VALIDATION OF LAND SURFACE MODELS THROUGH TOTAL INTEGRATING PATHWAYS (TRIP)**

Taikan OKI and Katumi Musiaka., Institute of Industrial Science, Univ. of Tokyo 7-22-1 Roppongi, Minato-ku, Tokyo 106-8558, Japan, e-mail: taikan@iis.u-tokyo.ac.jp

Land surface models (LSMs) are used within numerical atmospheric models to represent physical and biological processes at land surface. Calibration and validation of LSMs have been carried out mainly using observational data from enhanced observations of surface fluxes and physiological variables depicting the biosphere. However, these observations are limited both in space and time. In contrast, river discharge represents integrated runoff within the drainage area and it is the only direct measurement of areal mean hydrological response available on a large scale. Thus, river discharge has recently been used for validation of water balances calculated by LSMs.

To utilize river discharges for the validations of LSMs, three components are required. These are:

- digital information of river channel networks,
- a numerical model of river routing, and
- discharge data.

These together form a "digital river" for the validation of estimated water balances at the land surface. A 1deg. X 1deg. global mesh was used for validation of 11 LSMs in the Global Soil Wetness Project (GSWP). Under GSWP, the global soil moisture distribution for 1987 and 1988 was simulated in an offline mode. Even though observations and analyses from ISLSCP Initiative I CD-ROM were used as for forcing data, validation studies are necessary because LSMs may not simulate the water balance accurately.

A global river channel network, named Total Runoff Integrating Pathways (TRIP) was developed in 1deg. X 1deg. global mesh. A simple linear river routing model was prepared, as well. Even though river discharge data at only 20 gauging stations were available for 1987 and 1988 in the ISLSCP Initiative I CD-ROM, monthly river discharge data at 250 gauging stations in 150 river basins of the globe were collected and used for the validation of LSMs after error-checking.

As a result, river runoff information was found to be very effective for the validation of water cycling at the continental scale. Based on this study, it is clear that efforts to collect and prepare more comprehensive data sets of historical river discharge, as well as the promotion of international exchange of river discharge data in near real time, are highly recommended not only for the hydrological sciences but also for global climatological studies.

**HW1/E/03-A4****1430****DERIVATION OF GLOBAL GCM BOUNDARY CONDITIONS FROM 1 KM LAND USE SATELLITE DATA**

STEFAN HAGEMANN, Michael Botzet, Lydia Dumenil and Bennert Machenhauer; Max Planck Institute for Meteorology, Bundesstraße 55, D-20146 Hamburg, Germany, e-mail: Hagemann@dkrz.de

The coupling between atmosphere and biosphere is of particular importance over land surfaces from both the atmospheric and hydrological point of view. For adequate modelling of processes at the land surface boundary to the atmosphere an accurate representation of the land surface is necessary. The initial description of the land surface is a significant problem in global and regional climate modelling. The available datasets are particularly inaccurate in some regions of the world and up to now their spatial resolution was too coarse to fit the demands of high resolution limited area models. Remote sensing is a relatively new technique to measure land surface characteristics with a very fine spatial resolution which offers the possibility to create new datasets of land surface parameters.

At a resolution of 1 km a global distribution of major ecosystem types (according to Olson, 1994) was prepared by the U.S. Geological Survey which was derived from International Geosphere Biosphere Programme 1 km AVHRR data. From this global distribution a global dataset of land surface parameters is constructed by allocating parameters to the ecosystem types. These parameters are: background surface albedo, surface roughness length due to vegetation, fractional vegetation cover and leaf area index for the growing and dormancy season, forest ratio, plant-available soil water holding capacity, and volumetric wilting point. This global dataset is provided for the use in global and regional climate modelling.

**HW1/L/12-A4****1430****GEOINFORMATICS FOR WATER RESOURCES DATA MANAGEMENT IN HIMALAYAN INDIA**

R.B.SINGH

Abstract not available at time of going to press

**OPEN DISCUSSION****1500**

George LEAVESLEY (US Geological Survey, USA)

**DATA ACCESS POLICIES****Keynote****1600**

Arthur ASKEW (WMO Headquarters, Switzerland)

**SOUNDBITES****1630-1700****HW1/L/12-A4****1630****QUALITY INGREDIENTS FOR EFFECTIVE NETWORK DESIGN**

MARTIN P

Abstract not available at time of going to press

**HW1/L/06-A4****1630****A PLEA FOR INCREASED DATA COLLECTION**

IAN CORDERY (School of Civil and Environmental Engineering, The University of New South Wales, Sydney, 2052, Australia, email: i.cordery@unsw.edu.au)

It has been shown that for a fairly typical stream-flow data collection operation the value of the collected data can be about ten times the cost of collecting and archiving. Where data are not available planning and design exercises are dependent on intuitive approaches or (equally uncertain) importation of information from another region. Examples of the problems of using intuitive approaches and imported data will be given. Even greater problems occur for planners and regulators when there is a need to assess the current and likely future states of aquatic parameters which are currently only measured for research purposes, such as sediment and nutrient loads, and aquatic flora and fauna species diversity and population densities. Not only is little data available on many of these parameters but even less is known about their interrelationships and their interactions with parameters which are more likely to be measured. In the past changes to one aspect of the natural regime (eg to flow by construction of a reservoir, to chemical and biological properties by urbanisation or intensive farming) have, in some instances had dramatic effects on a range of other parameters. Sadly, most of these changes were not measured and in most cases it is not now possible to estimate what the former, natural conditions were. Currently efforts are being made to manage water extraction, land use changes and wastewater releases to ensure maintenance of "natural" conditions. But what were the natural conditions? What man-induced changes have occurred? Unless data collection is increased considerably, without the ever-present need for short-term economic justification, our ability to assess what changes are occurring and to maintain our living environment will continually diminish. We must collect more of the data we already collect, -at more locations and for longer-, and different types of data, -some of which may have no



apparent immediate usefulness. For example who, in the 1880s foresaw the value of collecting river salinity levels at the time when modern irrigation was just beginning?

**HW1/L/13-A4 1630**

**OVERVIEW OF ISCU DATA POLICIES**

F. WEBSTER

Abstract not available at time of going to press

**HW1/L/14-A4 1630**

**NASA HYDROLOGY DATA INITIATIVES AND DISTRIBUTION POLICIES**

E. WOOD

Abstract not available at time of going to press

**OPEN DISCUSSION 1700**

Ferris WEBSTER (Univ of Delaware, USA)

Friday 23 July AM

**SUMMARY REPORTS AND DISCUSSION**

**POSTER PRESENTATION 0845**

**SUPPORT FOR SCIENCE 1100**

**SUMMARY AND DISCUSSION**

Eric WOOD

**APPLICATION TO IPCC AND OTHER POLICY INITIATIVES 1130**

**SUMMARY AND DISCUSSION**

Petra DOELL

**COMPUTER-BASED TECHNOLOGIES 1200**

**SUMMARY AND DISCUSSION**

George LEAVESLEY

**DATA ACCESS POLICIES 1230**

**SUMMARY AND DISCUSSION**

Ferris WEBSTER

Friday 23 July PM

**OPEN DISCUSSION 1430**

**OPEN DISCUSSION 1600**

**FINAL SUMMARY 1715**

C. VÖRÖSMARTY

**HW5 Wednesday 21 July**

**INTERACTIONS BETWEEN SURFACE AND GROUNDWATER – QUANTITY AND QUALITY (ICGW, ICWQ, ICSW, ICT)**  
Location: Guild of Students Council Chamber

Wednesday 21 July AM

Presiding Chairs: E Sudicky (Dept. of Earth Sciences, University of Waterloo, Ontario, Canada) and J Turner (CSIRO Land and Water, PO Wembley, Australia)

**Introduction 0845**

E SUDICKY (Dept. of Earth Sciences, University of Waterloo, Ontario, Canada)

**HW5/W/01-A3 0900**

**COUPLING OF PARALLEL RIVER AND GROUNDWATER MODELS TO SIMULATE DYNAMIC GROUNDWATER BOUNDARY CONDITIONS**

Guy CARABIN (Laboratoires de Géologie de l'Ingénieur, d'Hydrogéologie et de Prospection éophysique (L.G.I.H.), University of Liège Bat. B19, B-4000 Liège, Belgium, email: carabin@lgih.ulg.ac.be), Alain Dassargues (L.G.I.H., University of Liège Bat. B19, B-4000 Liège, Belgium, email: adassarg@lgih.ulg.ac.be)

For groundwater modeling, interactions with the other parts of the water cycle (atmosphere, river and ocean) are usually taken into account with prescribed external input/output boundary fluxes. This is often considered as convenient in most of the studied cases when exchanges can 'a priori' be estimated. How could we take the interactions into account, when variations of water levels and solute concentrations in the river must also be computed. The proposed solution is based on a parallel run of the Groundwater Model (GWM) and the River Model

(RM). The exchanged water and solute mass fluxes through the contact interface are calculated by a junction on basis of the received results from each model at each time step. These calculations are made using a Fourier boundary conditions. As each model has its own time and space discretizations, the junction must organize the data exchanges, including various time and space interpolation schemes. The tests on a real case study, show the importance of these interactions on the computed groundwater quantity and quality in an alluvial aquifer where important pumping is made. The junction river-aquifer is being used in the scope of a research project entitled 'Integrated modeling of the hydrological cycle in relation to global climate changes', and it has already been used for the SALMON project (Sea Air Land Modeling Operational Network) designed to describe water and contaminant fluxes in a whole system (including marine, river, groundwater and atmospheric inputs) at regional scale.

**HW5/W/10-A3 0920**

**NUMERICAL SIMULATION OF GROUNDWATER - SURFACE WATER INTERACTION AND CONTAMINANT TRANSPORT AT A FRESHWATER COASTAL BARRIER BAR.**

Allan S. CROWE, Steven G. Shikaze and Carol J. Ptacek (National Water Research Institute, Canada Centre for Inland Waters, Box 5050, 867 Lakeshore Road, Burlington, Ontario, L7R 4A6, Canada)

Recent field work at Point Pelee, Ontario, Canada, has shown that the groundwater flow regime within the barrier bars is controlled by the width of the bar, the distribution and rate of recharge, and the seasonal fluctuations of the water levels in Lake Erie and the Point Pelee marsh. As a result, the flow system behaves in a complex, transient manner with seasonal reversals in the direction of flow in a portion of the barrier bar. Because of this complexity, a 2-D numerical model has been developed to simulate transient groundwater flow and contaminant transport in this environment, to aid in determining (1) the nature and extent of the hydraulic connection between the lake and the marsh, and (2) the potential for groundwater to transport septic-system derived contaminants to the marsh. The model presented here overcomes limitations with existing techniques, with respect to numerical accuracy, conceptual accuracy, and groundwater-wetlands boundaries. In our approach, the position of the water table (and shape of the groundwater domain) rises or falls in response to infiltration, evapotranspiration, and shorelines which can fluctuate both vertically and laterally in response to changes in the wetland or lake level fluctuations. Nodes and elements are added to or removed from a finite element mesh as a result of a rising or falling water table, respectively, thus maintaining accuracy with respect to the size and shape of the groundwater domain. Contaminant transport within the groundwater regime is simulated by either a particle tracking algorithm or by a standard Galerkin finite element solution to the advection dispersion equation.

**HW5/W/11-A3 0940**

**INTERACTION BETWEEN SHALLOW GROUNDWATERS AND SALINE SURFACE WATER IN A SEASONAL ESTUARY: THE SWAN RIVER SYSTEM**

J.V.TURNER, W.R. Linderfelt, L.R. Townley, G.A. Bartle, and G.D. Watson, CSIRO Land and Water, Centre for Groundwater Studies, Private Bag, PO Wembley WA 6014, Australia.

The Swan and Canning River system is a seasonally and tidally forced system which converges to form an estuary in contact with the Indian Ocean. The perception that the occurrence of nuisance algal blooms has increased in frequency in recent years has prompted the present investigation into the interaction of the shallow groundwater system with the Swan River. The principal aim is to determine the extent to which this interaction contributes nutrient delivery to the river system. It has been identified that groundwater interaction with the upper reaches of the Swan River occurs at three length scales. From the smallest scale upwards, these interactions are at the scale of the river-bed sediments (i.e. < 10m), at the scale over which tidal forcing of the river is transmitted into the adjacent aquifer (10's to several hundred meters) and at the regional or catchment scale (100's to 1000's m). Two dimensional groundwater flow modelling in plan covering the regional domain of the upper Swan River from the Causeway to Guildford shows that there is a net annual groundwater discharge to the Swan River of groundwater discharge of about 80,000 m<sup>3</sup>/day, or about 29 million m<sup>3</sup>/year. In 1996, the surface water flow entering the Swan River from the Avon was about 715 million m<sup>3</sup>, thus groundwater discharge contributed approximately 4% of the total river flow. Although this is a small percentage, nutrient concentrations, particularly ammonium, within the sediment pore fluids underlying the river are very high relative to concentrations in the river such that even low groundwater discharge rates introduce significant nutrient loadings to the river especially in summer when surface water inflow to the Swan River from the Avon effectively ceases. The nitrogen load to the Swan River derived from groundwater discharge is conservatively estimated at between 30 and 60 tonnes per year, meaning groundwater is one of the highest single inputs of nitrogen to the Swan River, contributing about 10% of the total nitrogen load entering this reach of the river. Seasonal and diurnal tidal forces increase the complexity of the system and may act to increase the presence and availability of groundwater-derived nutrients in the estuary system.

**HW5/W/12-A3 1040**

**SIMULATING HILLSLOPE HYDROLOGY AND INTERFLOW DYNAMICS FROM TEST SLOPES IN A MIDDLE MOUNTAIN CATCHMENT IN GERMANY**

Wolfgang-Albert FLÜGEL; Geographisches Institut, Universität Jena, Löbdergraben 32, D-07743 Jena, Germany, tel +49 - 3641 - 948 850; fax +49 -3641 948 852, e-mail: c5waf1@geogr.uni-jena.de

Between 1993 and 1996 detailed process studies of the dynamics of interflow were carried out on two test slopes within the catchment of the River Bröl (A = 216km<sup>2</sup>) located in the Rheinische Schiefergebirge, a middle mountain range characterized by gentle slopes and an oceanic type climate. Mean annual rainfall varies with elevation between 900 and 1200mm averaging to about 1070mm. Dominant land use is rangeland, coniferous, deciduous and mixed type of forest. The soils have greyish mottles above the impermeable bedrock indicating a distinct hydromorphic influence resulting from lateral interflow drainage. For simulating water balance and lateral interflow dynamics the HILLS-model developed by the USDA was applied and improved. HILLS is simulating unsaturated water fluxes by means of the RICHARDS equation and is routing interflow laterally using a kinematic wave approximation. The concept of the "Dynamic Storage" developed by the author was used to connect the hydrological dynamics observed in the valley floor with that of the contributing slopes. The concept makes use of the matrix potential and links the saturated groundwater aquifer with the overlying unsaturated soil zone. Both are intersecting with the footslope region on the one side and draining into the adjacent river on the other side. The following results can be presented so far: (1) Soil water dynamics in the unsaturated zone is not only influenced by the rainfall distribution but intensively from the interaction with the rooting vegetation; (2) understanding and simulating this dynamics must integrate plant physiological model in a much greater extend than it is done so far; (3) the HILLS-model is capable to simulate the hillslope drainage and interflow dynamics together with the groundwater fluctuations in the adjacent valley floor; (4) specific model extensions are necessary link the river system to the groundwater dynamics; (5) further research based on the HRU-concept is required to regionalize the approach to the catchment of the River Bröl.

HW5/E/05-A3

1100

**EPISODIC RISING IN NITRATE CONCENTRATION OF STREAMWATER BY PARTIAL WITHER OF PINE FOREST CATCHMENT IN TEMPERATE REGION IN JAPAN**

Naoko Tokuchi, Nobuhito Ohte, Asami Nakanishi, Masanori Katsuyama, and Yuko Asano (School of Agriculture, Kyoto University, Kyoto, 606-8502, Japan, email: nobu@bluemoon.kais.kyoto-u.ac.jp); Misuzu Hamada (Asia Air Survey Co. Ltd., Atsugi, 243, Japan)

The forest decline as an impact of environmental pollution is one of the major concerns not only of Japanese forestry community, but also for ordinary residents who utilise the water resources from forest catchments. The decline of pine forest has been extensively spread in the western part of Japan past thirty years, and environmental pollution has been considered as one of their important causes in addition to physiological and pathological conditions. The purpose of this study is to clarify the mechanism of changes in streamwater chemistry caused by episodic partial wither of pine forest. We focused on the disturbance of nitrogen dynamics in the scale from soil-profile to whole catchment. The intensive hydrochemical observations and in-situ lysimeter experiments at small head water catchment have been conducted since 1990. The partial (20% of the catchment area) wither of pine trees started in 1993, and continued until the fall of 1995. Before the wither events, the average nitrate concentration of streamwater was 0.04 meq/l, and much smaller than that of rainwater concentration. The cut-off of nitrate uptake by pine roots and nitrate supply with litters of dead trees brought about the three times higher nitrate concentration of subsurface groundwater and streamwater compared to those before the wither event. It was found that there was a remarkable two-year time lag between start of the event and the time when the concentration reached the highest level. The time lag and rising process of nitrate concentration can be explained by velocity of solute transport in unsaturated infiltration zone and mixing processes of soil water and saturated groundwater in riparian zone of catchment.

HW5/E/08-A3

1120

**UZBEKISTAN: INTERACTIONS BETWEEN SURFACE AND GROUNDWATER QUANTITY AND QUALITY**

Valentina Khaydarova (Institute of Water Problems, Uzbek Academy of Sciences, Uzbekistan, 700000, Tashkent, Ya. Kolas, 24B. Tel./Fax: +7 371 1391237) Lev POBEREJSKY (Association «Vodproject», Uzbekistan, 700000, Tashkent, Malyasov Street, 3, Tel.: +7 3712 340983, email: lena\_60@usa.net)

Uzbekistan, which is settled down in the drainage basins of Syrdarya and Amudarya rivers, takes actually the whole runoff of those rivers for the maintenance of the irrigated agriculture jointly with neighboring states. Groundwater is being formed by the filtration losses from watercourses and canals in the greater part of Uzbekistan, which is a plain. The portion of the surface runoff in the groundwater resources is equal to 78.7% or 669.7 m<sup>3</sup>/sek changing from 50% in the territory before mountains to 100% in the downstream area of Amudarya River. The damage of surface runoff by the groundwater exploitation is estimated for the planning of economic measures. Because of the difference in orographical conditions such damage in the Syrdarya basin is equal to 90% and it is equal to 77% in the Amudarya basin. The potential damage to surface runoff is equal to 646 m<sup>3</sup>/sek (85%) under the whole exploitation groundwater supplies. As a quantity the groundwater quality is the close correlation to the surface water quality. Mineral fertilizer, the poisonous chemical substances, pesticides pollutes the surface runoff, which enter to the water system jointly with the water return. Therefore the groundwater rapidly loses their drinking quality. For example, the whole groundwater supplies in Amudarya lower course are polluted so much as they present itself a risk for the human health. Under this cause the Aral-Amudarya area is announced officially as a zone of ecological disaster.

HW5/W/13-A3

1140

**QUALITY ASSESSMENT OF SURFACE AND SUBSURFACE WATER OF DAMODAR RIVER BASIN, INDIA**

ABHAY KUMAR SINGH and Syed I. Hasnain, School of Environmental Science, Jawaharlal Nehru University, New Delhi-110 067, INDIA, email: singhak@yahoo.com

Damodar is the main river of south Bihar and West Bengal and it runs through India's richest coal deposit belt. Damodar receives pollution load from various sources like domestic sewage, thermal power plants, steel plants, fertilizer factories and coal washeries. The water quality of Damodar river has swiftly deteriorated in recent years due to unplanned mining, urbanization and industrialization and it poses one of the major environmental problem that is drawing attention in recent years. As the increased mining activities and population in Damodar valley, so did the garbage, sewage and mining wastes which found their way directly into the Damodar river. This invited health hazards brought on basically by contaminated drinking water and also restrict its suitability for irrigation uses. The river Damodar constitutes the major source of water for south Bihar and Bengal and a large population and agriculture, especially in the lower valley are depend on the Damodar. Therefore regular monitoring and preservation of the quality of this river is a very important responsibility for everybody. In this paper the quality assessment of surface and subsurface water of Damodar river basin and its suitability for domestic and irrigation purpose will be presented. Besides that the source of dissolved ions and mechanism controlling water chemistry of Damodar river will also be discussed. Calcium and bicarbonate are the dominant cation and anion in surface water, while in subsurface water calcium is replaced by sodium in cationic abundance. The TDS content of subsurface water is two to three times higher than the surface water. The higher TDS of subsurface water may be due longer residence time, favoring acquisition of solutes through rock weathering. Gibbs variation diagram shows that chemistry of the Damodar river basin is mainly controlled by rock weathering. The higher concentration of sulphate and phosphate at some sampling sites indicate the impact of mining and anthropogenic activities on the water quality of the basin. Quality assessment study of Damodar river basin water shows that with few exceptions, subsurface water is suitable for drinking and domestic uses. Based on sodium adsorption ratio (SAR), residual sodium carbonate (RSC) and percent Na the surface water are fall within the excellent to good quality class and subsurface water within the good to permissible limit and it can be used for irrigation without any hazard. However the high %Na, RSC and SAR values at a few sites restrict its suitability for irrigation purpose. Ca-Na-HCO<sub>3</sub> is the dominant hydrochemical facies in surface water while Na-Ca-HCO<sub>3</sub> is the common hydrochemical facies in subsurface water.

Wednesday 21 July PM

Presiding Chairs: A Crowe (National Water Research Institute, Ontario, Canada)  
A Dassargues (LGIH, University of Liège, Belgium)

HW5/W/14-A3

1400

**DRAINAGE CONDITIONS IN IRRIGATED LANDS WITHIN A SEMIARID REGION: A CASE STUDY**

L. B. RODRÍGUEZ and C.A. Vionnet, Facultad de Ingeniería y Ciencias Hídricas, Universidad Nacional del Litoral, Casilla de Correo Nro. 217 - 3000 Santa Fe Argentina, email: leticia@fich1.unl.edu.ar

Usually the interaction between rivers and aquifers in semiarid regions is very intense and, under natural conditions, the exchange of water through the streambed follows the natural cycles induced by all the intervening processes. However, man's intervention can considerably alter the natural flow patterns. In this work we consider a semiarid area where land has been put into agricultural use, with pears and apples as the main crops. Due to the scanty precipitation, fruit production is only possible under irrigation with water diverted from the river that traverses the study area. On the other hand, the same river has been controlled for energy production, creating a conflict regarding water uses. Regulations exist to limit streamflows to allow the proper drainage of the irrigation fields. In spite of these regulations, the lowland portions of the study area, characterized by soils with poor drainage capacity, are still adversely affected during high surface water levels. Numerical modeling is being used to simulate the hydrodynamics of the surface water component, the groundwater component and their interaction. Computer simulations are instrumental in getting a better understanding of the system as a whole, and in particular, of the interrelationship between river, aquifer, and drainage system. Data collected during the past 2-3 years is used to calibrate the model to present conditions. The calibrated model is then used to explore different alternatives, among them pumping, to improve the drainage conditions in the area.

HW5/E/07-A3

1420

**PHYSICAL MODELING OF THE INFILTRATION PROCESS OF RIVERINE SURFACE WATER INTO THE GROUNDWATER**

Hubert HOLZMANN and Hans Peter Nachtnebel (Department of Water Management, Hydrology and Hydraulic Engineering, University of Natural Sciences BOKU, Muthgasse 18, A-1190 Vienna, Austria, email: holz@edv2.boku.ac.at)

At the IWHW hydraulic laboratory a model for assessing the infiltration process of ephemeral streamflow into the soil was constructed. The objectives of the experiment are twofold: First to provide estimates of the infiltration capacity as a function of the water level (head) of the surface (riverine) water and (saturated) groundwater and as a function of sediment component (hydraulic conductivity, particle distribution, clogging layer). Second to test the applicability of measurement equipment for field measurements in the laboratory.

This measurement tool includes tank lysimeters for collection of the infiltrated discharge. Two types of infiltration experiments were carried out, once under unsaturated condition with air entrapment. This reflects the situation of the beginning runoff event. Second the infiltration under saturated condition which can be observed after longer duration of runoff. This situation can be achieved in the experiment by filling the flume from the bottom of the soil layer. Due to these situations, the design of the tank lysimeters uses either simple filter material (fine sand) or a ceramic plate for water extraction.

The presentation will describe the model design, experiences with the observation devices and instrumentation and will give recommendations for the field experiment.

HW5/W/14-A3

1440

**228Ra/226Ra/232Ra AND 87Sr/86Sr ISOTOPE SYSTEMATICS FOR DETERMINING INTER-ACTIONS BETWEEN GROUND AND RIVER WATER**

Just EIKENBERG<sup>1</sup>, Guido Vezzu and Max Ruethi (Paul Scherrer Institute 5232 Villigen, Switzerland, e-mail: eikenberg@psi.ch), Aude Tricca (California Institute of Technology, Pasadena, CA 91125, USA, e-mail: tricca@gps.caltech.edu)

Ground and river waters of the Upper Rhine Valley (Alsace, France) were investigated for chemical composition of the major elements, Sr-isotopes and radionuclides from the U and Th series. In particular, the isotope ratios and concentrations of Ra and Sr were used as geochemical tracers to distinguish between different types of water and their interactions. The surface waters in the Rhine Valley can be described as strong mixtures between Ca-Na-HCO<sub>3</sub> rich plain ground-water and less mineralized river waters which have been migrated through crystalline (mainly granitic) basement rocks of the Voges mountains. Mixing of these waters yield positive correlations between bulk Sr, U, Ra and HCO<sub>3</sub>, indicating that carbonate rich sediments are the main source for U and (non-radiogenic) Sr in the plain aquifers. With increasing distance from the plain the 87Sr/86Sr ratios continuously increase from 0.708 to highly radiogenic ratios up to 0.725. For both end member types linear arrays between 226Ra and 224,228Ra can be observed, however, with different slopes. The almost constant (but different) 224Ra/226Ra and 228Ra/226Ra ratios in each end member type therefore indicate homogeneous U/Th isotopic composition in the corresponding source rocks which are in contact with the waters. Mixing ratios of non pure end-member waters were determined using three isotope diagrams (i.e. 224Ra/226Ra vs. 228Ra/226Ra) and the results obtained using the Ra isotope system are consistent to the data using isotopic Sr mixing relationships (i.e. 87Sr/86Sr vs. 1/Sr).

HW5/E/04-A3

1500

**USE OF SULFUR HEXAFLUORIDE, A CONSERVATIVE TRACER, TO INVESTIGATE GROUNDWATER/SURFACE WATER INTERACTIONS IN THE FLORIDA KEYS**

Jeffrey CHANTON, Kevin Dillon, William Burnett and Reide Corbett. (Department of Oceanography, Florida State University, Tallahassee, Florida 32306-4320, USA, email: jchanton@mailier.fsu.edu.), Lee Kump. (Department of Geoscience, Penn State University, University Park, PA 16802, USA.)

The Florida Keys has experienced rapid development. The main sewage disposal method is ground water injection through some 600 injection wells at 10-30m. Additionally there are some 24,000 septic tanks and an estimated 5,000 illegal cesspits which contribute to nutrient loading to the shallow groundwater aquifer. Both Florida Bay, which borders the Keys to the north, and the Key's reef tract to the south (ocean side of the Keys) have experienced significant environmental degradation of late including nuisance algal blooms, coral disease and seagrass die offs. We used SF<sub>6</sub> to test the hypothesis that water injected into septic tanks and 20-30m injection wells could rapidly migrate through the subsurface and reach surficial waters. We also conducted experiments to determine if non-conservative compounds (e.g. nitrate, phosphate) might be retarded by the carbonate framework relative to our inert tracer. Two types of experiments were conducted in differing limestone types. In Miami Oolite on Big Pine Key, where there is a shallow freshwater lens overlying a saline aquifer groundwater, transport rates were constrained to be between 0.11 to 1.87 m/hr. The second type of experiment took place on Key Largo where there is no freshwater aquifer and the matrix of the aquifer is solely the more porous Key Largo limestone. Here, groundwater transport rates were as great as 3.7 m/hr and were controlled by the Atlantic tide. SF<sub>6</sub> laden groundwater plumes moved back and forth due to tidal pumping. Our results indicate that wastewater injected into the Keys can travel rapidly and may reach marine surface waters within hours to days. There is evidence, however, that the limestone matrix retards phosphate, while allowing nitrate to pass with the wastewater.

**ASSESSMENT OF STREAM DEPLETION EFFECTS CAUSED BY GROUNDWATER ABSTRACTION**

Peter CALLANDER (Pattle Delamore Partners Ltd, P O Box 389, Christchurch, New Zealand, Email: peter.callander@pdp.co.nz) Dr Bruce Hunt (School of Engineering, University of Canterbury, Private Bag 4800, Christchurch, New Zealand)

In many areas of New Zealand the effect of groundwater abstractions on nearby surface waterways has historically been managed by defining arbitrary zones around streams and assuming that groundwater abstractions within this zone are equivalent to an abstraction direct from the surface water body.

However, since 1991 the focus of New Zealand's environmental legislation has been based on the "Resource Management Act" which requires an assessment of the actual effects arising from any groundwater abstraction. A consideration of these effects clearly demonstrates that in addition to the separation distance between a pumping well and a surface waterway, the duration and rate of groundwater pumping and the aquifer characteristics also have a key role in determining stream depletion rates.

Practical and accurate methods of calculating stream depletion rates have proved difficult for staff in regulatory agencies. The analytical solutions by Theis (1941) and Glover and Balmer (1954) are easy to apply but are considered to conservatively over-estimate stream depletion effects due to the assumption of a stream which fully penetrates the aquifer with perfect connection. Similarly the solution by Hantush (1965) is seen as requiring an unrealistic low permeability vertical layer along the stream edge.

Numerical modelling assessments undertaken by Spalding and Khaleel (1991) and Sophocleous et al. (1995) emphasise the uncertainty in the analytical methods described above. They identify streambed clogging and partial penetration of the stream as the key areas of inaccuracy. Whilst numerical models can most accurately quantify groundwater abstraction effects they are not practically accessible tools for many regulatory staff. Furthermore, the necessary site parameters for an accurate definition of the model parameters cannot be readily obtained.

As a practical alternative, Hunt (1998, in press) has derived a solution for unsteady flow from a well to a stream that only partially penetrates the aquifer and has a clogging layer around the wetted perimeter of the stream. A solution has also been derived for the draw-down at any point within the aquifer. This may be matched with field data from a pumping test with observation wells to obtain estimates for both aquifer and streambed leakage parameters. This is seen as a realistic representation of stream/aquifer interactions, which can be practically applied by regulatory staff.

**DIRECT MEASUREMENT OF GROUNDWATER EXCHANGE IN THE SWAN RIVER USING AN ELECTRONIC SEEPAGE METER**

David HERNE, CSIRO Land and Water, Private Bag, P.O. WEMBLEY WA 6014, Australia, email: David.Herne@per.clw.csiro.au

An instrument that measures the rate of groundwater exchange with surface water in the Swan River, Perth, Western Australia has been constructed by CSIRO Land and Water. The device, an electronic seepage meter, operates autonomously, measuring seepage rates at pre-defined intervals. The current prototype stores data on a notebook computer located nearby but a next-generation design incorporates onboard data processing and data logging.

In operation, a section of the riverbed is confined under a dome which is vented through an instrument package. The rate at which water flows through the instrument package, attached to the crown of the dome, is measured accurately and corresponds to seepage of water into the groundwater or conversely, into the river. Measuring the speed of water flowing through the instrument package gives a direct measure of groundwater seepage rates. Flow speed is measured by applying a short burst of heat to the water (about 1/3 of a second) and measuring the time it takes to travel through a tube inside the instrument package. The method is very sensitive and has currently permitted seepage rates as low as 2cm per day to be measured. All signals produced by sensors in the tube are measured by an electronics system built into the seepage meter, under the control of two microcontrollers. Separate power supplies for the electronics and heater are provided by sealed lead acid batteries housed on the seepage meter.

The seepage meter has returned rates of seepage of groundwater into the Swan River along a section of river bed at Garvey Park that agree strongly with model predictions made by this group.

**CALIBRATION OF MEASUREMENT TECHNIQUES FOR SUBMARINE GROUNDWATER DISCHARGE IN THE COASTAL ZONE**

William C BURNETT and Jeffrey P. Chanton (Department of Oceanography, Florida State University, Tallahassee, FL 32306-4320, USA, email: wburnett@mailier.fsu.edu; Makoto Taniguchi (Department of Earth Sciences, Nara University of Education, Nara 630-8528, Japan, email: makoto@nara-edu.ac.jp; Jaye E. Cable (Coastal Ecology Institute, Department of Oceanography, Louisiana State University, Baton Rouge, LA 70803, USA, email: jcable@unix1.sncc.lsu.edu

Quantitative estimates of submarine groundwater discharge (SGD) in the coastal zone have been made by a variety of approaches. Basically, the techniques fall into one of two groups: (1) hydrological; and (2) oceanographic. A standard hydrological approach is typically based on measurements made from monitor wells on land and flow is estimated via Darcy's Law. Coastal discharge may also be assessed using water balance considerations, assuming the data are sufficiently complete. A typical oceanographic approach has emphasized use of seepage meters, mini piezometers, and geochemical tracers - all measurements that are made within the coastal system itself. Thus, hydrogeologists (dry) and oceanographers (wet) tend to approach the same problem from different ends. Rarely are the methodologies combined.

Other measurement issues concern limits of detection as well as differences in spatial and temporal scales measured by various techniques. Certain types of tracers, for example, integrate over large time and space scales. Seepage meters, on the other hand, monitor only very small-scale processes. Yet seepage meters are essentially the only direct measurement of SGD available for use in the coastal zone and valuable information has been obtained by use of automated meters and/or use of multiple devices. The Scientific Committee on Oceanic Research (SCOR) and the Land-Ocean Interactions in the Coastal Zone (LOICZ) Project has recently formed a working group to evaluate the state of knowledge regarding groundwater flow into the coastal zone. The primary goal is to define more accurately and completely how submarine groundwater discharge (SGD) influences chemical and biological processes in the coastal ocean. An important shorter-term task has been set to examine questions relating to the measurement and sampling of SGD in the coastal zone. To this end, we are currently working on the design for an experiment to perform an intercalibration exercise using as many measurement techniques as possible. The results of our progress will be reported in this presentation.



**GA1.01 Friday 23 – Saturday 24 July**

**THE GEODYNAMO: THEORY, OBSERVATIONS AND MODELS (WITH DIV. V)**

Location: Muirhead Tower G08 LT  
Location of Posters: Muirhead Tower, Student Room (1st floor)

**Friday 23 July AM**

Presiding Chairs: Chris Jones (Exeter), Masaru Kono (Misasa)  
Concurrent Poster Session

**THEORY, EXPERIMENT, AND NEW TECHNIQUES**

**GA1.01/E/16-A5 0900**

**NON-AXISYMMETRIC MAGNETOHYDRODYNAMIC SHEAR LAYERS IN A ROTATING SPHERICAL SHELL**

Andrew SOWARD (School of Mathematical Sciences, University of Exeter, Exeter, EX4 4QE, UK, Email: A.M.Soward@exeter.ac.uk) Rainer Hollerbach (Department of Mathematics, University of Glasgow, Glasgow, G12 8QW, UK, Email: rainer@maths.gla.ac.uk)

Constant density electrically conducting fluid is confined to a rapidly rotating spherical shell and is permeated by an axisymmetric magnetic field of either dipole or quadrupole parity; the regions outside the shell are insulators. A prescribed non-axisymmetric body force drives slow steady non-axisymmetric motion. Linear solutions of the governing magnetohydrodynamic equations are derived in the small Ekman number limit analytically for values of the Elsasser number less than order unity and they are compared with new numerical results. The analysis extends Kleorin et al.'s (1997) study in the axisymmetric dipole case of the various shear layers on the equatorial tangent cylinder attached to the inner sphere. There are two new key results. Firstly, the quasi-geostrophic layers, which occur at small Elsasser number, have a new structure resulting from the asymmetry of the motion. Secondly, though at moderate Elsasser number the ageostrophic character of the Hartmann-Stewartson layer stumps attached to the equator of the inner sphere remains unchanged for asymmetric flow, motion is strongly suppressed by quadrupole magnetic fields with nonzero radial component at the equator.

**GA1.01/W/04-A5 0930**

**HELICITY AND ALPHA-EFFECT DUE TO COMPOSITIONAL PLUMES**

I.A. ELTAYEB (Department of Mathematics and Statistics, College of Science, SQU, Al-Khodh 123, Muscat, Sultanate of Oman)

The solidification of the heavy iron component of the fluid alloy occupying the outer core of the Earth is believed to occur in the neighbourhood of the inner core surface. The light component of the alloy released as a result of the solidification of the heavy component rises in the form of plumes to the upper reaches of the outer core. The flow giving rise to such plumes is discussed and its stability to infinitesimal perturbations is examined. In particular, the helicity and alpha-effect produced by the perturbations are investigated and their dependence on the rotation rate and the amplitude of the ambient magnetic field is examined in detail.

**GA1.01/W/21-A5 0945**

**TURBULENT TRANSPORT IN THE EARTH'S CORE**

Masaki MATSUSHIMA (Department of Earth Planetary Sciences, Tokyo Institute of Technology, Meguro-ku, Tokyo 152-8551, Japan, email: mmatsush@geo.titech.ac.jp) Takahiro Nakajima (Tono Geoscience Center, JNC, Gifu 509-5102, Japan, email: takahiro@tono.pnc.go.jp) Paul H Roberts (IGPP, UCLA, Los Angeles, CA 90095, USA, email: roberts@math.ucla.edu)

Fluid motions in the Earth's outer core are likely to be turbulent because of very small molecular diffusivities. Such small-scale motions are considered to be highly anisotropic, since they are strongly influenced by the Earth's rotation and the magnetic field. Large-scale fields are then transported by anisotropic turbulence. It is therefore important to understand the effect of such anisotropies on the geodynamo.

We have been examining anisotropic turbulence in the core by direct numerical simulation to understand the effect of the small-scale motions. We have found that the turbulent flux has a preferred direction, determined by the directions of the rotation axis, the imposed strong magnetic field and the gravitational force. The magnitude of turbulent flux is determined by the local values of the nondimensional parameters.

We here derive a transport equation for turbulent heat flux using a second order closure model. Then we compute the turbulent flux using the equation. It turns out that the turbulent flux thus estimated well approximates the one computed through direct numerical simulation.

**GA1.01/W/34-A5 1000**

**NUMERICAL MODELLING OF CONVECTIVE TURBULENCE IN THE EARTH'S CORE**

Emmanuel Dormy (I.P.G.P., 4 place jussieu, 75252 Paris Cedex 05, France, email: dormy@ipgp.jussieu.fr) Paul Roberts (I.G.P.P.-U.C.L.A., 405 Hilgard Avenue, Los Angeles Ca 90095-1567, USA, email: roberts@math.ucla.edu)

Direct numerical simulations of turbulence, including all scales of motion (from the largest to the Kolmogorov dissipation scale), are limited to Reynolds numbers too low to describe geophysically relevant situations. MHD convection in the Earth's core is turbulent despite the stabilizing tendency provided by the Earth's rotation and magnetic field. Rotational and magnetic effects however make small scale turbulence in the core highly anisotropic with respect to the directions of the angular velocity and magnetic field. Only recently could numerical simulations give a first insight into phenomena occurring in the core, implicit in those simulations were assumptions concerning the way that the small scale turbulent flow, which could not be numerically resolved, affected the large scale flow and field. The object of our work is to investigate numerically, on massively parallel computers, the behavior of the small scale motions in rapidly rotating MHD convective turbulence, to gain understanding of the nature of turbulent transport in the Earth's core and how it affects dynamo action that creates the Earth's magnetic field.

**GA1.01/W/26-A5 1015**

**ASYMPTOTIC BIFURCATION ANALYSIS FOR A NONLINEAR ALPHA- OMEGA- DYNAMO**

K. KUZANYAN (IZMIRAN, Solar-Terrestrial Dept., Troitsk, Moscow Region, 142092 Russia, email: kuzanyan@dnmtm.ru) M. Reshetnyak (United Institute of the Physics of the Earth, Moscow, Russia, 123810, email: rm@uipe.srcc.msu.ru) D. Sokoloff (Department of Physics, Moscow State University, Moscow, Russia, 119899, email: sokoloff@dds.srcc.msu.ru)

The generation of magnetic field in astrophysical bodies can be described by the induction equation. So far the solution of this equation grows exponentially with time and one may take into account the feedback of the magnetic field onto the flow. Usually the so-called alpha- and omega-quenching is considered as such feedback. The asymptotic analysis of this quenching at the threshold of generation of the magnetic field (in the vicinity of the critical dynamo number  $D$ ) can be an important source of information on the nature of the solution in general. On the example of Parker's migratory dynamo we perform bifurcation analysis of the equations for different types of alpha- and omega-quenching. We consider both the algebraic and dynamic quenching of the effects. The link between these forms in the limiting case of weak field is discussed. Our analysis shows that the relation between some factors of the quenching mechanism and the form of quenching controls the regime of bifurcation: the so-called soft (direct) and rigid (inverse) bifurcation scenarios may occur. Possible applications to the solar and geo-dynamos are considered.

**GA1.01/W/32-A5 1100**

**SHARP SOLUTIONS IN THE ANELASTIC MODEL OF GEODYNAMO**

Alexander ANUFRIEV, Geophysical Institute of BAS

Turbulent diffusivities of entropy and light constituent in the liquid Earth's core are usually supposed to be of order of magnetic diffusivity,  $\eta$ . Therefore dimensionless numbers associated with them are also of order of  $R_m = Vd/\eta$ , where  $d$  is a typical space scale of the core and  $V$  is its typical velocity. This number in the anelastic model we estimate using experimental data about superadiabatic heat flux. Its value obtained on this base is  $R_m \sim 10^3$ , which is well consistent with the results of computer simulations of Glatzmaier and Roberts (GR). Analysis of the equations of the anelastic model shows that together with smooth distribution of entropy, light constituent and magnetic field with space scale  $d$ , it has to exist disturbed sharp solutions, characterized by small space scale across the main flow of order of  $d/R_m^{1/2}$ . Though the amplitudes of these solutions are small, being of order of  $R_m^{-1/2}$  in comparison with smooth solutions, they play crucial role in the problem. In the equations for entropy and light constituent, they create large diffusional fluxes which is an essential feature of the GR solution. In the induction equation they create an  $\alpha$  effect for generation of magnetic field. Though value of this effect, formally estimated, is of order of  $R_m^{1/2}$ , it vanishes in the main approximation. Finally its value turns out to be of  $\sim 1$ . Estimations based on comparison of azimuthal and meridional magnetic fields in GR solutions support this conclusion. Estimations show that the Lorentz forces for sharp solutions are of order of the Arhimedean ones. They suppress the rise of sharp velocity, creating quenching for  $\alpha$  effect. We suppose that this is just the mechanism, restricting enhance of the magnetic field. Typical time values of sharp solutions are of order of  $(d^2/\eta) R_m^{1/2} \sim 2 \times 10^3$  years. It could be supposed that they are related to the secular variations of geomagnetic field. Together with the sharp solutions with small amplitudes, the sharp solutions with big amplitudes exist as well. In the distributions of entropy and light constituent these solutions typically arise on the core boundary, enhancing their fluxes into (out of) the core. In the solutions of magnetic field they can exit outside the boundaries as it can be observed from the figures of GR.

**GA1.01/W/22-A5 1115**

**WHAT THE CHARACTERISTIC AMPLITUDES DEPEND ON IN THE SOLUTION OF ANELASTIC GEODYNAMO MODEL?**

Alexander P. Anufriev (Geophys. Inst. Bulg. Acad. Sci., 1113 Sofia, Bulgaria, email: anufriev@geophys.bas.bg) Ivan Cupal (Geophys. Inst. Acad. Sci. Czech Rep., 141 31 Prague 4, Czech Republic, email: ic@ig.cas.cz)

Braginsky and Roberts (1995) presented energy and entropy balance equations which are applicable for 3D geodynamo model in anelastic approximation by Glatzmaier and Roberts (1997). These slightly modified equations allow us to discuss expected characteristic amplitudes in the solution of the model. We show that the whole energy balance of the dynamo does not participate in obtaining the characteristic amplitudes of the solution. The amplitudes are primarily influenced by the flux of light constituent and by the overadiabatic heat flux. On this basis we obtain the characteristic amplitudes of entropy, light constituent and velocity which are in good agreement with the solution by Glatzmaier and Roberts. The obtained characteristic amplitude of the magnetic field rather relates to the axisymmetric part of their solution. Our analysis also suggests suitable dimensionless units as a measure of individual quantities while solving the model.

**GA1.01/W/08-A5 1130**

**ARE THE GEODYNAMO PROCESSES INTRINSICALLY UNSTABLE ?**

Keke ZHANG, ( School of Mathematical Sciences, University of Exeter, EX4 4QE, UK), David Gubbins (School of Earth Sciences, University of Leeds, LS2 9JT )

Recent studies show a new picture of the geomagnetic field: both intensity and direction of the field suffer many substantial changes in the shorter time scales (Langereis et al, 1997). This paper attempts to shed light on the following related questions: Can the changes of the field affect the core dynamics significantly? Why can the geomagnetic field vary so rapidly and dramatically? Are the geodynamo processes intrinsically unstable? The subtlety of magneto hydrodynamics in the liquid core is investigated. It is found that the size of the magnetic Reynolds number in the core can change drastically in response to small fluctuations of the field, suggesting that the geodynamo processes are intrinsically unstable. Rapid variations in the geomagnetic field including collapses of the field may be a fundamental characteristic of the Earth's dynamo. The results may also explain why one encounters formidable difficulties in simulating geodynamo while there seems no such difficulties in the corresponding non-magnetic problem.

**GA1.01/W/13-A5 1145**

**A NEW APPROACH TO GEODYNAMO MODELS: CUBED SPHERICAL SHELL AND QUASI-UNIFORM GRIDS**

SHI-ZHUANG MA, (Institute of Geophysics, Chinese Academy of Sciences, Beijing 100101, China)K. Zhang and C. A. Jones (School of Mathematical Sciences, University of Exeter, UK)

It is becoming increasingly recognised that the computational inefficiency of the Legendre transform and its global nature are of major disadvantage to the spectral method on modern massively parallel computers. We use an algorithm that allows an efficient implementation on the parallel computers to develop a new numerical geodynamo model. The primary feature of the algorithm is to divide a spherical shell into the six identical "cubic" regions with quasi-uniform grids in which the coordinate singularities are eliminated. Furthermore, we use half-staggered mesh in the lateral direction and the standard staggered mesh in the radial direction. The centered Crank-Nicholson scheme is adopted for temporal evolution of the system. We can run the numerical model either with one single cube of the spherical shell with periodic boundary conditions or with the six coupled cubes as the whole spherical shell. We will report some preliminary results from our new model.

**GA1.01/W/35-A5 1200**

**SPHERICAL SPECTRAL ANALYSIS OF LINEARISED MHD MODELS FOR THE EARTH'S CORE**

David IVERS (School of Mathematics and Statistics, University of Sydney, NSW 2006, Australia; email: david@maths.usyd.edu.au) and Collin Phillips (Mathematics Learning Centre, University of Sydney, NSW 2006, Australia)

Linear stability models of the Earth's core complement and offer some advantages over fully-dynamical dynamo models. In particular they provide information about the time-behaviour and strength of the magnetic field, and allow investigation of parameter regimes inaccessible to time-stepping dynamical codes. The present model consists of the linearised rotating Boussinesq induction, momentum and heat equations for a uniformly-conducting spherical-shell fluid outer core with a conducting or non-conducting inner-core, non-conducting exterior and no-slip or stress-free boundary conditions. The basic state is steady and possibly three-dimensional, and may include both meridional and azimuthal velocity components. We use a vector and tensor spherical harmonics analysis of the equations, together with poloidal-toroidal representations of the velocity and magnetic fields. Vector spherical harmonics have been successfully used to solve laminar and mean-field dynamo problems with difficult interactions, such as the laminar induction term, anisotropic alpha-effects and anisotropic diffusion. Vector and tensor spherical harmonic representations produce concise systematic equations, which are readily coded into computer algebra programs to produce Bullard-Gellman type spectral equations or directly coded into numerical programs. A further advantage is that terms with the same structure, such as vector products and their curls, use precisely the same subroutines. This allows a large part of the code to be checked with simple analytical models such as free-decay. Both finite-differences and Chebychev collocation methods are used for the radial discretisation method. We have exploited the vector and tensor spherical harmonic approach to allow easy extension of numerical code to include a light component, the anelastic approximation and anisotropic diffusion.

**GA1.01/W/30-A5 1215**

**GEOPHYSICAL EXPERIMENTAL DYNAMO**

NATAF H.-C., D. Jault, Ph. Cardin and D. Brito L.G.I.T. (Observatoire de Grenoble, Université Joseph Fourier BP 53, 38041 Grenoble Cedex 9, France).

We are designing an experimental set-up to study the dynamics of a spherical cavity filled with liquid sodium in presence of both rotation and strong magnetic field. We have put this investigation under the umbrella of the French effort "Ampère" to build an homogeneous fluid dynamo. Such an experiment is interesting from the geophysical point of view because the physical properties (Prandtl number, magnetic Prandtl number) of liquid metals inside the inner cores of telluric planets are similar to the properties of liquid metals in the laboratories at the Earth's surface. We plan to begin with a prototype experiment. The liquid sodium is enclosed between two rotating spheres respectively of radius 10 cm and 30 cm. Fluid motion arises in response to the differential rotation of the inner sphere (200 revolutions per minute) with respect to the outer sphere (400 revolutions per minute). A permanent magnet (out of rare earth) is set inside the inner sphere. It yields a magnetic field of 0.2T. in the bulk of the fluid cavity. The dimensionless numbers of such experiment are: Magnetic Reynolds number  $Rm = UR/l = 18$ , Reynolds kinematic number  $Re = UR/\nu = 3.6 \cdot 10^6$ , Rossby number  $Ro = \tau W / l \nu = 1.7$  (rotation time over magnetic diffusion time), Elsasser number  $L = sB^2 / \rho \nu = 8$ , Ekman number  $E = \nu / W R^2 = 1.4 \cdot 10^{-7}$ . We will also be able to vary the rotation of the two spheres and to remove the inner magnet. Then, we hope to be able to advocate a larger experiment (a few cubic meters of liquid sodium) which would allow us to witness the dynamo effect. We can dream to record a lot of reversals because the magnetic diffusion time would be only 1 s.

Friday 23 July PM

Presiding Chairs: Seva Shapiro (Ekaterinburg), Ken Hoffman (San Luis Obispo)

**OBSERVATIONS: FROM REVERSALS TO JERKS**

**GA1.01/W/10-A5 1400**

**TEMPORAL ASPECTS OF A GEOMAGNETIC REVERSAL**

Kenneth A. HOFFMAN (Physics Department, Cal Poly State University, San Luis Obispo, CA 93407 USA, email: khoffman@calpoly.edu & Institut für Geophysik, ETH-Hönggerberg Zürich 8093, Switzerland)

Paleomagnetic studies of polarity transitions typically are concerned with the spatial character of the reversing field. We demonstrate that the distribution of virtual geomagnetic poles (VGPs) may be a reliable proxy regarding temporal aspects of the process as well. Our analysis of the VGPs contained in the select "MBD97" database for the Matuyama-Brunhes reversal reveals a global distribution of virtual poles so distinct that inferences concerning both the temporal nature as well as the energetics of the dynamo process can be drawn. The data clearly indicate the existence of four major groupings of virtual poles, suggesting that transitional fields in a state of quasi-equilibrium dominated the reversal process. Yet, while the VGP must cross the equator at least once during the polarity transition, a remarkable sparsity of low latitude poles in MBD97 is also observed. We propose that a formidable potential barrier exists between transitional field states where the VGP must change hemispheres. When this barrier is successfully surmounted VGP movement across the equator takes place at an apparently rapid rate of speed. That this stage of fast field change is a non-diffusive, driving process of

Earth's dynamo is an almost certain conclusion. Indeed, the process of frozen-in flux may largely dictate the configurational structure of directional behavior midway into a geomagnetic reversal.

**GA1.01/W/18-A5 1430**

**PALEOSECLAR VARIATION DURING BACK-TO-BACK GEOMAGNETIC REVERSALS FROM O'AHU, HAWAII, USA**

Emilio HERRERO-BERVERA (SOEST-HIGP 2525 Correa Rd. Honolulu, Hawaii, 96822, U.S.A., email: herrero@soest.hawaii.edu) Jean-Pierre Valet (Institut de Physique du Globe de Paris IGP 4, Place Jussieu, 75252 Paris CEDEX 05, France, email: valet@ipgp.jussieu.fr)

Paleomagnetic directions measured from 175 lava flows recorded in four volcanic sequences on the island of O'ahu (Hawaii) cover about 0.3 Ma of geomagnetic field changes and include detailed records of the successive Gilbert-Gauss (3.57 Ma) and Lower Mammoth reversals (3.33 Ma). The dominant pattern of the directional changes is the presence of large inclination variations with increasing amplitude and steep values during the transitional periods. The morphology of these recurring features during different transitions remind the characteristics of the zonal non-dipole field inferred from studies of paleosecular variation in the Pacific. These observations are consistent with transitional mechanisms yielding the emergence of non-dipole components with similar characteristics as during periods of stable polarity. Scatterers of transitional pole positions are not reproducible between parallel sections and thus appear to be linked to local eruptions rather than to long-lived states of the transitional fields.

**GA1.01/E/06-A5 1445**

**HEMISPHERICAL ASYMMETRY IN REVERSAL TRANSITION FIELDS**

Ji-Cheng Shao and Mike FULLER (HIGP-SOEST, U. Hawaii, Honolulu, Hawaii, 96822, USA, email: mfuller@soest.hawaii.edu)

The morphology of the Brunhes-Matuyama transition field has been obtained from inversion of the records from the Reversal Atlas of Athanassopoulou (Athanassopoulou, 1994) and those in the recent compilation of Love and Mazaud (1998). The method of inversion is standard with the exception that we use a Virtual Geomagnetic Pole constraint from Maxwell pole theory (Shao, 1998, Shao et al., 1999) in place of the more usual smoothest possible field on the core-mantle boundary. Analysis of the transitional field during the Brunhes-Matuyama reversal has revealed hemispherical asymmetry in its morphology. This result is robust in that it is found whether the all the records given in the Athanassopoulou Atlas (Athanassopoulou 1994), the small number of preferred data of Love and Mazaud (1997), or subsets obtained by elimination of different records from the Atlas, are used. The field model inverted from the Love-Mazaud data set was found to predict successfully records in the Atlas not used in the inversion. The low order asymmetry found is independent of the detailed alignment of the records. The changes which bring about the reversal appear to be dominated by strong radial field features which cross the equator close to the prime meridian, whereas there are no such features in the Pacific Hemisphere. The asymmetry is consistent with the predominance of VGP paths in the hemisphere centered on the prime meridian and with the clusters of poles in that hemisphere. The hemispherical asymmetry is similar to that seen in the present field and appears to be an important feature of the geodynamo suggesting that the processes which generate the field are more active in the hemisphere centered on the prime meridian.

**GA1.01/W/15-A5 1500**

**PHENOMENOLOGICAL MODELS OF THE REVERSING GEOMAGNETIC FIELD**

Jonathan M.G. GLEN (Berkeley Geochronology Center, 2455 Ridge Rd., Berkeley, CA 94709 USA, and Earth Sciences Department, University of California, Santa Cruz, CA, 95064, USA, email: jglen@bgc.org) and Lionel Hongre (Earth Sciences Department, University of California, Santa Cruz, CA, 95064, USA, email: lhongre@earthsci.ucsc.edu)

We present new results from a family of phenomenological models of the reversing geomagnetic field. The models, which are based in part on observations of the historic geomagnetic field, produce strongly confined virtual geomagnetic pole (VGP) paths quite similar to what is observed in records of the real field. This confinement is surprising given that the transitions consist of nondipole fields. We have found that simple models furnish useful guidelines for interpreting reversal records, and for building criteria for data selection. For example, they reveal that the duration of transitions largely depends on the site locality. As a result, a record with few transitional VGPs may contain valuable space-time information critical to constraining reversal models. In other words, the often-used criteria that accept only records that contain a certain number of intermediate poles could be a poor measure of whether a record is reliable or not. We also find that grouping similar transitional poles into a single pole may obscure information on the site-dependent rates of field change. In addition, the results suggest why existing data seemingly support arguments for both geographically confined and site-dependent VGP paths. The models also render significantly different VGP paths for some sites that are in close proximity; this may explain the existence of rapid jumps of VGPs in existing records. A comparison of our model results with the existing data will be given.

**GA1.01/W/25-A5 1515**

**INVERSION OF PALEOMAGNETIC DATA TO OBTAIN THE MEAN PALEOMAGNETIC FIELD FOR THE LAST 5 MA**

Masaru Kono (Institute for the Study of the Earth's Interior, Okayama University, Misasa, Tottori-ken 682-0193, Japan)

Description of the mean paleomagnetic field in terms of Gauss coefficients have already been derived from paleomagnetic data of the last 5 Ma by Kelly and Gubbins (GJ, 1997) and Johnson and Constable (GJ, 1997). However, it can be shown that they are not satisfactory because they neglect the fact that the mean of the field directions are affected not only by the means but also by the variances of the parameters (Gauss coefficients). Kono, Tanaka and Tsunakawa (JGR, 1999) presented the inversion of paleointensity data, which avoids this problem because data in this case are linearly related to model parameters. In their study, the inversion of data was carried out separately for the means and variances. In this study, I will present a new approach to the inversion of paleomagnetic data. Unlike Kono et al. (1999), we determine the means as well as the variances of the parameters at the same time. For this purpose, each single paleomagnetic datum is considered to be a sample drawn from the ensemble of models. The models have parameters which are samples of random variates normally distributed with unknown means and variances. The most plausible model parameters are determined by maximizing the likelihood function. This method was applied to paleomagnetic data from the last 5 Ma. The mean and fluctuation of the magnetic field thus determined will be discussed.

**GA1.01/W/19-A5 1600**

**ANGULAR DISPERSIONS OF FIELD AND VGP FROM THE MODELS OF PALEOMAGNETIC FIELD**

Hidefumi TANAKA (Faculty of Education, Kochi University, Kochi 780-8520, Japan, email: hidefumi@cc.kochi-u.ac.jp) Hideo Tsunakawa (Department of Earth & Planetary Sciences, Tokyo Institute of Technology, Ookayama, Meguro, Tokyo 152-8551, Japan, email: htsuna@geo.titech.ac.jp) Masaru Kono (Institute for Study of the Earth's Interior, Okayama University, Misasa, Tottori-ken, 682-01, Japan, email: mkono@geoph.s.u-tokyo.ac.jp)

Angular standard deviation (ASD) of paleomagnetic field shows clear variation to the latitude of the observation site; the higher the latitude, the smaller in field and the larger in VGP. Among the various models so far proposed to explain this feature, Constable and Parker (1988) first introduced a statistical model in which Gauss coefficients are zero mean random variables (except  $g_{10}$ ). Kono and his colleagues further developed a mathematical expressions of this model called a homogeneous background model (HBM), and pointed out that contribution of  $g_{21}$  (or  $h_{21}$ ) should be large to explain the latitude variation of ASD.

This study examines various statistical models of paleosecular variation (PSV) by a computer simulation in which random numbers are used to each Gauss coefficient. Importance of large variation in  $g_{21}$  (or  $h_{21}$ ) is so far ascertained, but we will also examine dependency of ASD on longitude of observation site. We will further apply the computer simulation to the models of time averaged paleomagnetic field which several authors studied by least squares methods. It is shown so far that the latitude variation of ASD is determined solely by how much variance is given to each Gauss coefficient as long as the model is close to an axial dipole field.

**GA1.01/W/17-A5 1615**

**SECCULAR VARIATION MODELS, TANGENTIAL GEOSTROPHY, AND LOCAL COMPUTATION OF THE PRESSURE AT THE TOP OF THE CORE**

Arnaud CHULLIAT, Gauthier Hulot (Institut de Physique du Globe de Paris, Laboratoire de Geomagnetisme, 4 place Jussieu, 75252 Paris cedex 05, France, email: chulliat@ipgp.jussieu.fr)

There are strong arguments for neglecting the horizontal component of the Lorentz force in the dynamical budget of the fluid at the top of the core. This tangentially geostrophic approximation reduces the degeneracy of the inverse problem for the determination of the flow from the secular variation data. It further makes it possible to compute the local value of the pressure at the CMB (Chulliat and Hulot, 1998). But these computations are quite sensitive to possible incompatibilities between the SV models and the tangentially geostrophic assumption. Furthermore, it is still not clear how close to tangential geostrophy the flow at the CMB actually is. In an attempt to address these difficulties, we have derived a new set of necessary conditions for the secular variation to be consistent with both the frozen-flux and the tangentially geostrophic assumptions. Following standard approaches developed for testing the frozen-flux approximation alone, we have computed SV models that : (a) satisfy these constraints, and (b) fit the SV data with the precision allowed by the present accuracy of the observations. Preliminary results show that the tangentially geostrophic approximation does not seem to be contradicted by the existing data. These new "geostrophic" SV models can also be used for computing the local pressure at the top of the core in a fully consistent way.

**GA1.01/W/33-A5 1630**

**GEOMAGNETIC SECULAR VARIATION FROM 1500**

Bondar Tatiana N, Burdelnaya Irina A and GOLOVKOV Vadim P (all at IZMIRAN, 142092 Troitsk, Moscow region, Russia, email: golovkov@izmiran.rssi.ru)

Global space-time model of the geomagnetic field has been produced for time interval 500 years from 1500. Navigational observations of the magnetic declinations as well as observations of the inclinations and the horizontal component of the geomagnetic field were used as a data set for analysis. A new algorithm for these data joint analysis was developed. It is based on the SH coefficient expansion into the Legendre polynomials to degree 3. Uniqueness of the solution was reached with usage of the modern SH model as a reference one. Adequacy of the model was tested with step by step increasing of the time interval under analysis from one to five hundred years. Main results of the model being the almost stable position of the magnetic poles and the latitudinal dependence of the westward drift are discussed.

**GA1.01/W/31-A5 1645**

**CHAOS IN THE SECULAR VARIATION OF THE RECENT GEOMAGNETIC FIELD**

DE SANTIS A. and Tozzi R. (both at the Istituto Nazionale di Geofisica, Roma, Italy, email: desantisag@ing750.ingrm.it), Barraclough D. (British Geological Survey, Edinburgh, UK, email: DRBAR@wpo.nerc.ac.uk)

A non-linear forecasting analysis has been applied to the secular variation of the three-component annual means of 14 observatories, unevenly distributed over the Earth's surface (12 in the northern and 2 in the southern hemisphere) and spanning the last 150 years. All results were in agreement, either in terms of possible evidence of chaos (against hypothesis of white or coloured noise), or in terms of the Kolmogorov entropy, confirming previous results obtained with only three European observatories. New tests and evidences are presented to support a non-linear chaotic behaviour underlying the observed secular variation of the recent geomagnetic field.

**GA1.01/W/29-A5 1700**

**A DESCRIPTION OF THE 1991 GEOMAGNETIC JERK**

Paola De Michelis (Istituto Nazionale di Geofisica, via di vigna Murata 605, 00143 Roma, Italy, email: demichelis@mart.ingrm.it) Lili Cafarella (Istituto Nazionale di Geofisica, via di vigna Murata 605, 00143 Roma, Italy, email: cafarella@ing750.ingrm.it) ANTONIO MELONI (Istituto Nazionale di Geofisica, via di vigna Murata 605, 00143 Roma, Italy, email: meloni@mart.ingrm.it)

The analysis of the temporal behaviour of the secular variation in the last fifteen years, carried out on 110 observatories widely distributed all over the world, clearly showed the existence of a jerk around 1990. A point of rapid change in the slope of the secular variation is almost always present in all examined magnetic observatory data. A complete quantitative description of this jerk is now shown. Contour plots of the distribution of the secular acceleration discontinuity for the three magnetic field components, which provide information on the worldwide intensity distribution of the jerk and contour plates of the jerk time occurrence distribution in the magnetic field component are shown and discussed. Finally, a spherical harmonic analysis is presented to reconfirm the internal nature of the jerk and to study the trend of the energy density spectrum as function of the order  $n$ .

**GA1.01/W/37-A5 1715**

**ON THE EXTERNAL NATURE OF JERKS IN GEOMAGNETIC SECULAR VARIATIONS**

Vsevolod Shapiro and Albina Akhmetzanova (Institute of Geophysics, 100 Amundsen str., Ekaterinburg, 620016, Russia. Fax: +7 3432 678872 Email: seva@maglab.mplik.ru)

Based on magnetic observatory data we have compiled annual total force isoporic maps for the secular variation foci of Northern hemisphere. In the course of analysis of these maps we have revealed short period variation - jerks of two types: variations observed at the phase of solar activity growth and changes of secular variation at the solar activity maximum. Jerks in other components of the field were occurred at the same phases of solar cycles too. The peculiarities of discovered jerks such as their global character, morphology of variation and the evident correlation with phases of solar activity leads us to conclusion about external nature of these variations. The parameters of investigated jerks are obviously specified by solar activity changes, its 11- and 22-years periodicities. The study has shown that during 1923-1995 (solar cycles 16-22) the jerks in the total force and north component of magnetic field similar to described were occurred both at the phases of solar activity growth and phases of its maxima. It is likely that another short-period changes in the structure of secular variation are induced by the solar activity. The obtained results made it possible to predict the behaviour of secular variations and to forecast jerks of revealed types during forthcoming solar activity cycles. The successful attempt of such prediction of the jerk on the period of maximum of the 22nd solar activity cycle was proved to be the case.

**Saturday 24 July AM**

Presiding Chairs: David Ivers (Sydney), Heitzler (Goddard)

**NUMERICAL SIMULATION OF DYNAMO**

**GA1.01/W/23-A6 0900**

**NUMERICAL MODELLING OF THE GEODYNAMO AND CORE-MANTLE COUPLING**

Jeremy BLOXHAM (Department of Earth & Planetary Sciences, Harvard University, Cambridge, MA 02138, USA. Email: Jeremy\_Bloxham@harvard.edu)

Of the various components of the Earth system, the most remote is the geodynamo operating in the Earth's core. The concomitant scarcity of observations is exacerbated not only by the complexity of the physics of the geodynamo but also by the inaccessibility of the dynamical regime of the core to direct numerical investigation. The almost vanishingly small role played by viscosity and the almost equally small, but nonetheless important, role played by inertia renders the system one that presents a great challenge to numerical studies. Nonetheless, significant progress has been made over the last few years in the development of numerical models of the geodynamo, though none of the models is free of approximations, some of which are, unfortunately, introduced more for numerical expediency than for sound geophysical reasons. Here we review this progress and comment on the effect of these approximations on the solutions.

An additional complicating factor is that the geodynamo cannot be considered in isolation from the rest of the Earth system. The transport of heat from the core - which drives the geodynamo - is controlled by the mantle, and the pattern of mantle convection imposes lateral variations in the heat flux from the core. We show that this thermal core-mantle coupling influences the pattern of magnetic field at the core-mantle boundary, and that the pattern of mantle convection inferred from seismic tomography gives rise to a certain observed features in the magnetic field.

**GA1.01/W/11-A6 0930**

**CONVECTION DRIVEN GEODYNAMO MODELS: REVERSAL MECHANISMS**

C.A.JONES and G.R.Sarson, School of Mathematical Sciences, University of Exeter, Exeter EX4 4QE, UK

Numerical models of convection driven geodynamos show reversals with many similarities to those of the actual geomagnetic field. Sarson and Jones (1998) analysed the nature of the solution in the core during one reversal process. The 2.5 dimensional model, which severely truncates the number of modes in the azimuthal direction was used in this investigation.

The reversal of the field was found to be strongly associated with changes in the axisymmetric component of the meridional circulation, driven by an instability of the buoyant convection located within the tangent cylinder. Analysis of the kinematic dynamo produced by a typical flow suggested that the drop in meridional circulation was sufficient to turn the dynamo from an essentially steady dipole into a reversing dipole, for the duration of the reduction in the meridional flow. Roberts (1972) first noted the role of meridional circulation in determining whether kinematic dynamo are steady or oscillatory.

In our more recent calculations, we have investigated more reversals and used more azimuthal modes, thus moving from 2.5 dimensional models to 3 dimensional modelling. The results of these new calculations, and comparison with palaeomagnetic data on reversals will be discussed.

**GA1.01/E/04-A6 0945**

**THE INFLUENCE OF DIFFERENT DRIVING MODES IN DYNAMO MODELS**

Carsten KUTZNER, Ulrich Christensen (Institute of Geophysics, University of Goettingen, Herzberger Landstrasse 180, 37075 Goettingen, Germany, e-mail: carsten@willi.uni-goephs.gwdg.de)

We use a 3-D numerical model of convection-driven dynamo in a spherical shell to study the influence of various sources of buoyancy on the magnetic field generation. In particular, we compare (1) fixed temperatures on both the inner and outer boundaries, (2) internal heat sources in the outer core or, equivalently, secular cooling, and (3) homogeneous sinks in the outer core with zero flux through the core-mantle boundary, which is meant to represent chemical convection. Both for fixed temperatures and for chemical convection we obtain strong dipole-dominated magnetic fields. The condition of internal heating or secular cooling leads to weaker fields with quadrupolar symmetry at lower Rayleigh number, changing to irregular field structures dominated by short wavelengths at higher Rayleigh number. Comparison with the geomagnetic field supports a predominantly compositional driving mechanism for the geodynamo.



**GA1.01/W/24-A6** **1000**

**THREE-DIMENSIONAL KINEMATIC DYNAMOS WITH THERMAL WIND FLOWS**

Graeme R. SARSON, (School of Mathematical Sciences, University of Exeter, Exeter EX4 4QE, UK. Email: rsarson@maths.ex.ac.uk)

Most three-dimensional kinematic dynamos studied to date have been chosen without reference to the magnetohydrodynamics applicable to the geodynamo; none of the simple cases in the literature are consistent with the magnetostrophic balance expected of the Earth's core. A simple flow is constructed which can be driven by the thermal-wind term present in the magnetostrophic regime. The kinematic dynamo action of this flow is investigated numerically, both via direct three-dimensional calculations, following the formalism of Bullard and Gellman, and via alpha-omega calculations, using the axisymmetric limit of Braginsky. The heat-source distribution necessary to drive this velocity is calculated; although in the present case artificial, this form allows comparisons with possible heat-distribution within the Earth, or in laboratory-scale experimental dynamos.

**GA1.01/W/06-A6** **1015**

**THE EFFECT OF INERTIA ON 2.5D HYDROMAGNETIC DYNAMOS**

Graeme MORRISON and Prof. D. R. Fearn (Both at Department of Mathematics, University of Glasgow, Glasgow, G12 8QW, Scotland. Email: gm@maths.gla.ac.uk)

This study examines the effect of inertia in a 2.5D dynamo which has been produced by reducing the azimuthal truncation and then suitably modifying an existing fully 3D dynamo model. Despite including only one non-zero azimuthal mode, this model is self-consistent and will run at significantly lower computational effort than a 3D model, making it perfect for investigating the effects of individual parameters. When the inertial term is included, its relative size is given by the Rossby number,  $Ro$ , which has a geophysical value of  $O(10^{-9})$ . This small value has resulted in the inertial term being neglected (i.e.  $Ro=0$ ) in previous 2.5D dynamo studies, although it is included in the 3D models of Glatzmaier and Roberts (GR) and Kuang and Bloxham (KB), and indeed most other 3D models. The (GR) dynamo models includes only the zonal, axisymmetric part of the inertial term with  $Ro$  of  $O(10^{-9})$ , while the (KB) model includes the full axisymmetric part of the inertial term, with  $Ro$  of  $O(10^{-5})$ . The choice of  $Ro$  may play a crucial role in determining the type of solution obtained, and the different solutions obtained by the (GR) and (KB) dynamos are perhaps due to the different choice of  $Ro$ . The full inertial term is already included in this 2.5D model, while a finitely conducting inner core, which is free to rotate about the vertical axis, has been incorporated to aid comparison with existing dynamo solutions. Both of the implemented changes have been rigorously tested and benchmarked against a well-established 2.5D code, which is itself capable of reproducing qualitatively the results of the Boussinesq (GR) model. Solutions are obtained for a tractable range of values of  $Ro$ . These are of interest in their own right, in addition to providing a useful complement to the more computationally intensive 3D studies.

**GA1.01/E/13-A6** **1100**

**FORCE BALANCES IN THE CORE AND GEODYNAMO SIMULATION**

Weijia KUANG (Space Geodesy Branch, Code 926, NASA Goddard Space Flight Center, Greenbelt, MD 20731, USA, email: Kuang@satfate.gsfc.nasa.gov)

One unavoidable issue in geodynamo simulation is the approximations on the force balances in the Earth's core, in particular the torque balance on the co-axial cylindrical surfaces across the fluid outer core. Due to the computational constraints, we are far from simulating the geodynamo with the parameters appropriate for the Earth's outer core. Several approximations have been applied on the torque balance in numerical modelling. We have examined extensively these approximations and the corresponding strong-field dynamo solutions with a model in which the solid inner core is electrically conducting and rotates subject to the Lorentz torque and (optionally) the viscous torque on the inner-core boundary (ICB). We found that the structures of the core flow and the magnetic field vary significantly when a strong viscous coupling (relative to that appropriate for the core) on the ICB is introduced. In particular, the thermal wind and the magnetic wind inside the tangent cylinder (the co-axial cylindrical surface tangent to the inner core at the equator) change greatly with the viscous coupling (provided that the inertia of the inner core is sufficiently small), thus altering the differential rotation of the inner core. We find also that torsional oscillations are also affected by the approximations: when a strong viscous coupling is retained, the torsional oscillations in the core are strongly damped by viscous dissipation inside the tangent cylinder; they almost disappear outside the tangent cylinder. To improve the force balance approximations, we introduce new asymptotic boundary conditions with which we are able to reduce significantly the strength of viscous coupling in modelling. We have implemented in our geodynamo model and examined the strong-field dynamo solutions for various parameters. We also examined the possibility of forecasting the geomagnetic field with the new model.

**GA1.01/E/02-A6** **1115**

**MAGNETOCONVECTION IN A RAPIDLY ROTATING ANNULUS**

Michael PROCTOR (DAMTP, University of Cambridge, Silver St. Cambridge CB3 9EW UK; email: mrep@damtp.cam.ac.uk) Chris Jones (Dept. of Mathematics, University of Exeter, Exeter EX4 4QE UK; email: CA.Jones@maths.exeter.ac.uk)

Recent numerical simulations of dynamo models in cartesian geometry have shown the importance of the separation that occurs in the strong-field regime between regions of high (zonal) field strength and corresponding long length scale motion, and relatively field free areas with short length scales. To model this process we adopt the annulus model of Busse, and impose a strong zonal magnetic field. The geometrical constraints on the motion mean that variations parallel to the angular velocity vector can be ignored; then the only (but important) contribution of the rotation is the so called beta-effect from the tilted boundaries. In the limit of rapid rotation and with appropriate magnitude of the field strength the zonal length scale is much shorter than the radial one, leading to the possibility of a mean-field theory for the effects of convection on the mean fields and flows. The resulting reduced system of equations is integrated numerically, so as to show the mechanism for the production of net mean flows, and the conditions for onset of self-sustained modulations in the zonal direction.

**GA1.01/W/14-A6** **1130**

**A NUMERICAL EXPERIMENT OF MAGNETOCONVECTION IN A ROTATING SPHERICAL SHELL FLUID**

Ataru SAKURABA, Masaru Kono (Department Of Earth And Planetary Physics, University Of Tokyo)

The dynamic interaction between magnetic field and fluid flow and the resulting deformation of convective rolls are investigated through a numerical experiment of magnetoconvection in an electrically conductive rotating spherical shell fluid to which a uniform magnetic field parallel to its spin axis is imposed. A uniform heat source in the sphere drives a time-independent thermal convection in which the maximum magnetic Reynolds number is 92. The Elsasser number measures the strength of the externally imposed magnetic field. In the course of the numerical experiment, the Elsasser number is increased discretely from 0.2 to 5.0 through several intermediate values.

An abrupt change of the mode of magnetoconvection occurred when the Elsasser number was about 0.5; the pattern of the fluid flow changed from geostrophic to magnetostrophic ones. At the same time, the induced magnetic energy jumped up to a higher level and the kinetic energy of the fluid also increased. The transition from geostrophic to magnetostrophic balances is responsible for the deformation of the anti-cyclonic convective rolls in which the fluid circulates in the opposite fashion to the rotation of the sphere so that the Coriolis force works inward. The lines of magnetic force in the equatorial plane are converged into the anti-cyclonic rolls due to the compensation flow of the Ekman pumping at the outer fluid-solid boundary. As the imposed magnetic field increases, the equatorial part of the anti-cyclonic roll expands because of the outward Lorentz force around there caused by the converged lines of magnetic force. The deformation of the convective rolls is a natural result of the effective thermal convection and the confinement of magnetic flux in the fluid shell. This study provides a basic idea to consider the dynamic structure in the Earth's outer core.

**GA1.01/E/15-A6** **1145**

**ROTATING MAGNETOCONVECTION IN VARIOUSLY STRATIFIED LAYERS IN DEPENDENCE ON BOUNDARY CONDITIONS**

J. BRESTENSKY, S. Sevcik, J. Simkanin, Dept of Geophysics, Faculty of Maths And Physics, Comenius University, Bratislava, Slovakia

Hydromagnetic instabilities, developing in the rapidly rotating horizontal fluid layer permeated by the azimuthal magnetic field linearly growing with the distance from the vertical rotation axis, are investigated for ranges of parameters (Elsasser, Roberts, Ekman number,) which can be roughly related to the Earth's core conditions. Both horizontal boundaries are thermally infinitely conducting and are either free or rigid ones with infinite or finite (Earthlike) electrical conductivities.

Cases of uniform and non-uniform stratification of the layer are considered with various widths of the upper stably stratified sublayer for the non-uniformly stratified layers. The lower sublayers are unstably stratified as in the Earth's core.

Frequencies of the instabilities, running in the azimuthal direction, are comparable to typical frequencies of the Geomagnetic Secular Variations only for order one values of Roberts number, the ratio of the times of ohmic and thermal diffusion. The question is, how the results for uniformly stratified layer are modified in various cases of the non-uniformly stratified layer. E.g. in uniformly stratified layer at stronger magnetic fields the finite electrical conductivity causes the development of MC waves, i.e. instabilities able to exist without the buoyancy. Furthermore, the rigid boundaries induce the marked competition of modes in viscous fluid. Moreover, the viscosity plays an important role in the dynamics of instabilities of greater azimuthal wave number.

**GA1.01/W/16-A6** **1200**

**MAGNETIC INSTABILITIES IN A SPHERICAL SHELL WITH FINITELY CONDUCTING INNER CORE**

FOTHERINGHAM, Paul, University of Glasgow

Continuing the work of Hollerbach and Jones(1993), in which they studied the weakly super-critical axisymmetric solutions of an alpha squared dynamo, I investigate the behaviour in the strongly super-critical regime. In particular, I will focus on the next symmetry breaking bifurcation in the sequence, which, for the alpha effect used by Hollerbach and Jones is to a fully non-axisymmetric solution. Given the possible importance of sub-critical instabilities in geomagnetic reversals, results confirming the nature of the bifurcations will be given.

**GA1.01/E/03-A6** **1215**

**INVERSION FOR FLUID FLOW AT THE CORE SURFACE -A TEST WITH RESULTS FROM DYNAMO MODELLING**

Steffen RAU, Ulrich Christensen, Johannes Wicht (Institute of Geophysics, University of Goettingen, Herzberger Landstrasse 180, 37075 Goettingen, Germany, e-mail: srau@willi.uni-geophys.gwdg.de)

Using the frozen flux approximation, secular variation data have been inverted for the horizontal flow  $v_h$  at the surface of the Earth's core. The non-uniqueness of the inversion problem must be removed by making additional assumptions for the velocity field. Here we invert the magnetic fields of 3-D numerical dynamo models for the near-surface velocity and compare the results with the actual velocity distribution. We find that the frozen-flux assumption is reasonably well satisfied at magnetic Reynolds numbers of order 100. Inversion schemes that employ only a regularisation condition (smooth flow), or that additionally assume purely toroidal flow, perform poorly in recovering the original velocity field. We find a decent correlation when using the assumption of tangentially geostrophic flow, even though a large fraction of the field  $v_h \cdot B_r$  is divergence-free, i.e., in the null-space of the inversion problem. The results justify cautious optimism concerning the retrieval of the long-wavelength part of flow near the top of the core.

**Friday 23 July AM**

Presiding Chairs: Chris Jones (Exeter); Masaru Kono (Misasa)

**GA1.01/E/09-A5** **Poster** **0900-01**

**THE MODEL OF ALPHA-QUENCHING IN GEODYNAMO**

A.Anufriev (Geophysical Institute, Bulgarian Acad. Sci., Bonchev str., bl. 3, 1113 Sofia, Bulgaria, email: anufriev@geophys.acad.bg); M.RESHETNYAK (United Institute of the Physics of the Earth, Moscow, Russia, 123810, emails: pavlov@upei-ras.scgis.ru and rm@upei.srcc.msu.su); D.Sokoloff (Department of Physics, Moscow State University, Moscow, Russia, 119899, email: sokoloff@dds.srcc.msu.su)

We believe that process of geomagnetic field generation can be described in terms of the mean-field dynamo theory. Usually, the equilibrium between the magnetic  $E_m$  and kinetic  $E_k$  energies is proposed: this is the case of the stars and the Galaxy. After the magnetic energy exceeds the state of equilibrium the quenching of the magnetic field starts. It corresponds to equilibrium of inertial and Lorentz terms in Navie-Stokes equation. So far the energy of the small scale motions is much smaller than the energy concerned with the large-scale kinetic energy, the alpha quenching is of the crucial importance. In the same time the observations of the geomagnetic field as well as its numerical simulations (Glatzmaier and Roberts, 1995) indicate that magnetic energy exceeds the kinetic energy more than three orders of magnitude. Thus, following the previous scenario the magnetic field had to suppress the flow motions and as a consequence to damp the process of the magnetic field reproduction. Here we propose the possible explanations of this phenomenon. Following the model alpha-quenching starts when the balance between the Coriolis and Lorentz forces in the Navie-Stokes equation is fulfilled. Then the ratio of  $E_k/E_m - Ro$ , where  $Ro$  is the Rossby number.

**GA1.01/W/02-A5** Poster **0900-02**

#### CURRENT LOOPS MODEL OF THE GEOMAGNETIC FIELD SOURCE

Vesvolod V. BOTVINOVSKY (Institute of Geophysics SB RAS, Koptyug av., 3, Novosibirsk 630090, Russia; e-mail: botvin@uiggm.nsc.ru)

We attempted to model the geomagnetic field by fields of several quasi-independent space-separated sources. Magnetic dipoles and current loops are used as sources of magnetic field. If we use single source located approximately in the Earth's center and four additional sources located under the world magnetic anomalies then the morphology of the simulated field is fitted in a good way to morphology of the real geomagnetic field. It allows to suppose the existence of relatively independent sources generating the main field (dipole form) and fields of the world anomalies (Canadian, Siberian, Brazilian and Antarctic).

It was found that using current loops with opposite current flows it is possible to create the model of quasi-symmetrical source of the main geomagnetic field. In order to attain the real tilt of geomagnetic axis and real asymmetry of intensity of the geomagnetic field it is enough to incline the loops at 1-2 degree to the equator plane and to shift the loops at 35 km apart from the Earth's center. These values are much less than that used in the model of displaced magnetic dipole.

**GA1.01/W/09-A5** Poster **0900-03**

#### MAGNETO-CONVECTION IN A ROTATING SPHERE OF LIQUID GALLIUM

D. BRITO, Nataf H.-C., B. Pascal and Ph. Cardin L.G.I.T., Observatoire de Grenoble, Université Joseph Fourier BP 53, 38041 Grenoble Cedex 9, France

Although numerous numerical studies are devoted to magneto-convection in a rotating sphere, there has been no experimental confirmation. We propose to study experimentally the magnetohydrodynamics of such a flow where Coriolis and Lorentz forces play an important role, as in the Earth's core.

We have built an experimental set-up where a 22 cm-diameter sphere is filled with liquid gallium and spun at up to 1000 revolutions per minute. Water is circulated at high flow rates in a cylinder inside the sphere, keeping the inner temperature constant and slightly above the melting point of gallium (29.8 °C). The device is located in a 2 m-side cabin in which air is kept at a higher temperature (up to 50 °C). This enables thermal convection to develop between the inner cylinder and the outer sphere. A 30 mT azimuthal magnetic field is created by a toric copper solenoid consisting in 360 loops being passed inside the inner cylinder and then along the outer sphere.

The Prandtl number is 0.027, the Ekman number is around 5.10<sup>-7</sup>, the Rayleigh number is expected to be a few times critical, and the Elsasser number is around 10-2. We expect convective velocities of a few millimeters per second, electrical potential differences of a few microvolts, and induced magnetic fields of the order of 20 mT.

We will measure convective velocities in opaque gallium using an ultrasonic Doppler velocimeter; prior velocity measurements obtained with this technique in a vortex of gallium will also be presented. Using platinum-constantan thermocouples, we plan to measure simultaneously the temperature fluctuations and the electrical potentials on the walls. We will also measure the induced magnetic field close to the outer surface of the sphere.

We will present a preliminary study of thermal convection in water as well as the first results of magneto-convection in gallium.

**GA1.01/W/27-A5** Poster **0900-04**

#### 2.5D-MODEL OF GEODYNAMO WITH RESOLVED EKMAN LAYER

Ivan Cupal and Pavel Hejda (Geophys. Inst. Acad. Sci. Czech Rep., 141 31 Prague 4, Czech Republic, email: ic@ig.cas.cz Maxim Reshetnyak (Inst. Phys. of the Earth, Russian Acad. Sci., Moscow, 123810 Russia, email: rm@upei.srcc.msu.ru)

The model is based on mean field approach (MFA), which has been applied by Jones et al. (1995). We decompose the quantities into axially symmetric and non-axisymmetric parts and in the azimuthal direction we take into account only several harmonics of the Fourier expansion (2.5 D approximation). In this approach mean values of non-axisymmetric magnetic field and velocity over azimuthal direction vanish. However, we resolve Ekman layer analytically and it enables to obtain solutions for Ekman numbers smaller than 0.000001. The numerical method is a special combined grid-spectral method which was successfully tested with a kinematic case. The first calculation of the model are performed without the inner core to be taken into account.

**GA1.01/W/20-A5** Poster **0900-05**

#### IS THE EARTH'S MAGNETIC FIELD POLARITY REVERSAL A SELF ORGANIZED CRITICAL PHENOMENON?

Paola DE MICHELIS (Istituto Nazionale di Geofisica, via di Vigna Murata 605, 00143 Roma, Italy, email: demichelis@martel.ingrm.it) Giuseppe Consolini (Istituto di Fisica dello Spazio Interplanetario, via del Cavaliere snc, 00133 Roma, Italy, email: giuseppe@sunago2.ifi.srm.cnr.it) Antonio Meloni (Istituto Nazionale di Geofisica, via di Vigna Murata 605, 00143 Roma, Italy, email: meloni@martel.ingrm.it)

The geomagnetic field property, best documented by paleomagnetism, is that the Earth's magnetic field has reversed its polarity hundred times in the Earth's history. It is generally considered that the polarity reversal intervals have an exponential distribution. Here, the geomagnetic polarity reversal record, for the past 165 Ma, is analyzed and a new approach to the study of the magnetic field time reversals, based on concepts coming from Self-Organized Criticality (SOC), is presented. More in detail, the occurrence of 1/f-noise (also called pink noise) in the Power Spectral Density (PSD), relative to geomagnetic field time reversals, and of a Zipf's law for the cumulative distribution of chrono duration are investigated. The obtained

results are compared with those coming from prototypical models of dynamical systems, exhibiting SOC, and discussed in the context of fluid motions acting within the Earth's outer liquid core.

**GA1.01/W/28-A5** Poster **0900-06**

#### NUMERICAL MODELLING OF FINITE AMPLITUDE CONVECTION IN RAPIDLY ROTATING SPHERICAL SHELLS. INTERACTIONS WITH THEORETICAL WORK AND EXPERIMENTAL DATAS

Dorny Emmanuel L.P.G.P., 4 place Jussieu, 75252 Paris cedex 05, FRANCE. Dominique Jault and Philippe Cardin L.G.I.T., U.J.F. Grenoble, 1381 rue de la piscine, Grenoble, FRANCE. C.N.R.S., FRANCE.

We present a numerical study of finite amplitude convection in rapidly rotating spherical shells with rigid boundary conditions. Solutions in a range of Taylor number ( $2\Omega a^2/\nu$ )<sup>2</sup> from 10<sup>7</sup> to 10<sup>12</sup> are discussed, great care is taken to make sure boundary layers are correctly resolved. Different kind of heatings and gravities are used. We study how the numerics compare with previously available experimental data. We discuss also the results expected from the Gallium experiment under development in Grenoble. Characteristics of the flow such as the critical mode, the phase velocity and its dependence on the Rayleigh number are investigated. Attention is given to the effects of the widely used centrifugal gravity. A comparison with the analytical (Soward 1977) description of finite amplitude convection and criticality of the bifurcation is performed with stress free boundary conditions.

**GA1.01/E/01-A5** Poster **0900-07**

#### THE EFFECT OF DIFFERENT ROTATIONS OF INNER CORE AND MANTLE ON GEOMAGNETIC FIELD

Bejo DUKA Faculty of Natural Sciences, Tirana, Albania

The existence of the difference between the angular velocities of Inner Core and Mantle is now an accepted fact (Glatzmaier and Roberts, 1996). Another interesting fact, drawn from seismological observations (Su Wei-jia and Dziewonski, 1995), is that the Inner Core has an axis of symmetry, which is tilted (about 10.5 degree) from the Earth's rotation axis. Supposing that the rotation of Inner Core is about its axis of symmetry, we modeled the motion of Outer liquid Core as the fluid flow inside a spherical shell where the inner and outer spheres rotate about different axes, with different angular velocities. Solving Navie-Stokes equations in spherical geometry, we found the velocity field. The presence of gravitational and magnetic field changes the hydrodynamic equations, but the gravitational field contributes only to the radial dependence of the pressure and does not influence the velocity field, while the Lorentz force is considered small and the velocity field is considered known from the solution of Navie-Stokes equations. Substituting the velocity field to the kinematic dynamo equation with known boundary conditions for the geomagnetic field, we discussed about the solution of the equation without claiming to find the exact solution.

**GA1.01/E/12-A5** Poster **0900-08**

#### A TIDE-DRIVEN DYNAMO - A PROPOSAL FOR A SYNTHESIS OF SEISMIC AND GEOMAGNETIC OBSERVATIONS, AND OF EARTH'S ROTATION ANOMALIES

Giovanni P. GREGORI (IFA-CNR, via Fosso del Cavaliere 100, 00133 Roma, Italy; e-mail: gregori@atmos.ifa.rm.cnr.it), Wen Jie Dong and Xiao Qing Gao (Lanzhou Institute of Plateau Atmospheric Physics, Academia Sinica, Lanzhou, Gansu Province, P. R. of China), and Fabrizio T. Gizzi (Istituto Internazionale di Studi Federiciani, Tito Scalco, Potenza, Italy)

Three kinds of objects exist in our galaxy: (1) stellar (all plasma), (2) cold (comets, meteorites, the Moon, ...) and (3) intermediate, i.e. having internal layers that can slide with respect to each other. Such last objects, when are subject to a tide, have an internal dynamo, a magnetic field, a magnetosphere, endogenous Joule's heating, volcanism, gas exhalation, and an atmosphere protected by their magnetosphere. II - The electric currents of the dynamo flow on the outermost possible internal layers, i.e. wherever they experience an abrupt step-like relative drop of the electrical conductivity. In the case of the Earth there are 3 such layers, i.e. ICB, CMB, ALB. III - Outward propagation of endogenous heat can hardly occur within such a bad thermal conductor as the Earth. It rather occurs by Hamilton's principle ("electric soldering iron mechanism"; cfr. Gregori, PEPI, 77, 39, 1993), thus feeding volcanoes. IV - The radii of the ICB, CMB and ALB can thus be computed either by seismology (during the last several tens years) or by geomagnetism (since ~1400 AD for ICB and CMB). The Earth appears to behave almost like a car-battery, recharging and discharging itself, solar modulated (for periods longer than solar cycle's) with a typical decay time of ~110 years. V - Such comparatively rapid internal transformations of state, imply: (i) large variations of the outer core pressure within an almost rigid mantle and lithosphere and a constant-radius Earth, and (ii) a time variation of the Earth moment of inertia, thus explaining the relation between the geomagnetic secular variation and the length of day (in progress). VI - Also lunar palaeomagnetism and -volcanism fit very well within such a model.

**GA1.01/W/36-A5** Poster **0900-09**

#### DYNAMICAL GEODYNAMO CODES ON A NETWORK

David IVERS, Les Farnell, Ron James and David Galloway (School of Mathematics and Statistics, University of Sydney, NSW 2006, Australia; email: david@maths.usyd.edu.au)

We report on the development of a low cost fully dynamical computer code to model the Earth's magnetic field. Various codes are being tested. The prototype geodynamo model underlying these codes consists of an electrically-conducting solid inner core, free to rotate about the geographic axis, and an electrically-conducting Boussinesq fluid outer core surrounded by a stationary insulating mantle. The convection is thermally driven by prescribed temperatures or heat fluxes at the inner and outer core boundaries. The magnetic, viscous and thermal diffusivities are uniform. The fields are governed by the magnetic induction, heat and momentum equations in a rapidly rotating frame with Coriolis, Lorentz, buoyancy and viscous forces, and may include inertia. The numerical methods use either spherical harmonics or Fourier expansions in colatitude and longitude, finite differences in time, and either finite differences or a Chebyshev tau method in radius. Fast Fourier and Gauss-Legendre methods are used to transform fields between physical and spectral spaces. Finite differences in radius allow efficient job-splitting across a distributed network of cpus for increased execution speed. Against this Chebyshev methods in radius offer greater accuracy for a given truncation level. Higher-order including maximal order finite-difference schemes are being explored for increased accuracy. The codes are implicit in the linear diffusion terms for stability, and explicit in the nonlinear terms for reduced cost. At present the message handling program PVM is used for job-splitting between CPUs. So far a finite-difference code for the magnetic induction and heat equations have been completed, including both laminar and mean field dynamo effects but with either a non-conducting inner-core or no inner-core at all. A Chebyshev-tau

code for the magnetic induction equation has also been completed. These codes have been tested on a 10-cpu network against known models, where either the exact solution or accurate numerical solutions are known. Currently a finite-difference code for the momentum equation is being developed and has been tested in the non-magnetic case. The fully-dynamical case is currently being tested.

**GA1.01/W/05-A5** Poster **0900-10**

**STRUCTURES OF THE MAGNETIC AND THE VELOCITY FIELDS WITHIN BOUNDARY LAYERS**

J. S. KATAYAMA, M. Matsushima, and Y. Honkura (all at Department of Earth and Planetary Sciences, Tokyo Institute of Technology, Meguro-ku, Tokyo 152-8551, Japan, Email:jsato@geo.titech.ac.jp)

We have been performing numerical simulations for an MHD dynamo model in a rotating spherical shell. We have investigated structures of the magnetic and the velocity fields under a condition that the Rayleigh number is slightly larger than the critical one for exciting a thermal convection. Columnar convection cells aligned in parallel to the rotation axis characterise the structure of velocity field. The structure of magnetic field is characterised by a strong toroidal field generated near the equatorial region close to the outer surface and by a poloidal field generated by convective columns.

We have so far examined these structures on stress-free boundary conditions. It has recently been pointed out, however, that the effect of boundary layers on dynamo action is of importance. We here impose rigid boundary conditions so as to resolve structures of these fields within thin boundary layers. The behaviour of the magnetic and the velocity fields is then studied for various non dimensional parameters.

**GA1.01/W/07-A5** Poster **0900-11**

**A NEW MODEL OF THE GEOMAGNETIC FIELD GENERATION**

Vladimir V. KUZNETSOV (Institute of Geophysics SB RAS, Koptyug av., 3, Novosibirsk 630090, Russia; e-mail: kuz@uigm.nsc.ru)

A new model of the generation of the magnetic field on the planets and satellites is suggested. The model is based on the "hot" Earth hypothesis and the idea of galvano- magnetic amplification of initial field. The initial field is generated by daily rotation of double electric layer (DEL) that arises on the boundary of inner and outer Earth's core (F-layer). The F-layer is the region of phase transition of extra-compressed gas (substance of inner core) to liquid (substance of outer core). The change of the "condensation" to "evaporation" leads to the change of DEL polarity and, as consequence, of the geomagnetic field polarity. It is a reversal of magnetic field. The model allows to explain the generation of magnetic field on the planet bodies in the beginning of their evolution while the inner core exists yet. Current contours generating the geomagnetic field like the double cylinder located in the F-layer close to the equator plane.

**GA1.01/L/01-A5** Poster **0900-12**

**ANISOTROPIC DIFFUSION AND THERMAL CONVECTION**

COLLIN PHILLIPS (Mathematics Learning Centre University of Sydney NSW 2006 Australia Email: collinp@scifac.usyd.edu.au) David Ivers (School of Mathematics and Statistics University of Sydney NSW 2006 Australia)

The current linear stability model allows investigation of anisotropic turbulent diffusion. Linear stability models in general compliment fully dynamical dynamo models. The present model incorporates the momentum and heat equations, for a fluid core with no slip boundary conditions. The fluid core consists of a basic state that is steady and axisymmetric.

The choice of representation, that being vector and tensor spherical harmonics, facilitates convenient production of the relevant spectral equations that are inaccessible using conventional methods. We utilise the close association and simple transformations to and from toroidal poloidal representations to impose solenoidal conditions. Though the transformation to toroidal poloidal conditions only occurs after the vector spherical harmonic analysis is used to produce spectral equations. The numerical code utilises the vector and tensor spherical harmonics directly in computing interaction terms and especially anisotropic diffusion.

The present model consists of thermal convection (with no magnetic basic state) with anisotropic turbulent diffusion influenced by the direction of rotation and gravitational forces independently.

We outline the methods and analysis for producing the relevant spectral equations and coding directly using vector spherical harmonics and present preliminary numerical results.

**GA1.01/E/08-A5** Poster **0900-13**

**CONCERNING A MODEL OF FORMATION OF TERRESTRIAL MAGNETISM**

RASULOV D.KH. Lange Institute of Hydrogeology and Engineering Geology, Tashkent, Uzbekistan, E-mail: root@ariel.tashkent.su

The work gives in detail a new piezoelectric model of terrestrial magnetism which permits all the main features of geomagnetism field to be explained from the unified positions. In accordance with the model, piezoelectric textures may be formed in the Earth's crust which is oriented along a direction close to the geographic parallels. The presence of mechanical strains in Earth's crust rocks caused by an action of terrestrial gravity is to lead to an emergence of a potential difference along the piezoelectric textures. As a result, an electric current runs along these directions forming a weak quasi-stable field, which direction is to be close to that of the geographic terrestrial axis. Electric charges of the liquid core rotated in this magnetic field are affected by a force acting in the normal direction to the rotation axis which causes electric polarization of the core. Namely, this rotation of the like electric charges of the core forms the main component of the geomagnetic field.

**GA1.01/W/12-A5** Poster **0900-14**

**EARTH'S MAGNETIC FIELD AND HOW IT REVERSES**

Richard. Eugene D

A comparison of the Geodynamo and the geomotor is presented. Various models of the Geomotor are given and the one utilizing relativity is emphasized. A comparison is made of the two theories. Then reversals are explained on the basis of a thermostatic action utilizing heat, relativity, and the size of the spherical electron cloud with the idea that all reversals during the Cenozoic Era could be explained by this theory.

**GA1.01/E/07-A5** Poster **0900-15**

**ON THE GEOMAGNETIC JERKS GENERATING PROCESSES**

Anahit SIMONYAN (Institute of Geophysics & Engineering Seismology, NAS RA, Leningradian 5, Giumry, 377515 Armenia, email: iges@shirak.am)

Examination of all the geomagnetic field secular variations data temporal series obtained elsewhere by magnetic observatories allows to develop the method of representing the dynamics of the Earth's magnetic field through the jerks. Jerks on the Earth's surface mean the discontinuities of the geomagnetic field elements annual mean values second time derivatives series while first time derivatives represent the straight line segments before and after the jerks epochs for the time intervals of a few decades. The geomagnetic field and its secular variations representative spatial models were obtained including the jerks as the "quintums" of field variability. The jerks characteristic timescales and temporal intervals under consideration permit us to neglect diffusion effect while obtain the jerks originating processes in the upper layers of the Earth's liquid core. Proceeding from the frozen-flux hypothesis the jerks originating movement systems on the top of the free stream are obtained. Depending on the investigating jerk morphological data that consist of rising and/or downflowing local foci of core liquid velocity field just beneath the core-mantle boundary.

**GA1.01/E/11-A5** Poster **0900-16**

**ROBUST MAXIMUM-LIKELIHOOD REGULARISED INVERSION FOR THE HISTORICAL CORE MAGNETIC FIELD**

M. WALKER and A. Jackson (School of Earth Sciences, University of Leeds, Leeds, LS2 9JT, UK. Email: M.Walker@earth.leeds.ac.uk ; A.Jackson@earth.leeds.ac.uk)

Traditionally models of the geomagnetic field have been constructed under the assumption that the data are contaminated with noise originating from a Gaussian distribution. Such a distribution would originate, for example, when a number of different, independent noise sources contribute and the Central Limit Theorem (CLT) is applicable. The resulting maximum likelihood inversion for the core field results in the data being fit under the 2-norm measure of misfit; perhaps an added attraction of the method is the low computational cost. Although intuitively appealing, the fact that the crustal field overwhelms all other sources of noise suggests that the conditions for the CLT to apply are not necessarily met.

There is a mounting body of evidence suggesting that the appropriate distribution of errors is better approximated by a double exponential, or Laplace, distribution. We apply a new maximum-likelihood method for modelling magnetic field survey data under a 1-norm measure of misfit. Despite some added computational complexity, modern computer power is sufficient that computational considerations are irrelevant. The technique is applied to geomagnetic data for the last century and comparisons will be presented between models constructed under Gaussian and Laplace distributions of error.

**GA1.02** **Monday 19 – Tuesday 20 July**

**ELECTROMAGNETIC INDUCTION STUDIES**

Location: Barber Institute, Lecture Theatre  
Location of Posters: Barber Institute, Corridor

**Monday 19 July AM**

Presiding Chair: M. Ingham Victoria University of Wellington, (New Zealand)  
Concurrent Poster Session

**ELECTROMAGNETIC INDUCTION STUDIES - THEORY AND TECHNIQUES**

**GA1.02/W/41-A1** **0830**

**ENVIROMT. A NEW RADIO/CONTROLLED SOURCE SYSTEM**

L.B Pedersen (Department of Earth Sciences/Geophysics, Uppsala University, Villavägen 16, 752 36 Uppsala, Sweden, email: lbp@geofys.uu.se) L. Dynesius, M. Bastani and M.Gharibi (Department of Earth Sciences/Geophysics, Uppsala University, Villavägen 16, 752 36 Uppsala, Sweden, email: ld@geofys.uu.se) and U. Matzander (Metronix, Neue Knochenhauerstr 5, D-38100 Braunschweig, Germany)

The design of new electromagnetic system using radio frequencies in the band 14 kHz to 500 kHz and two perpendicular horizontal magnetic dipole sources from 1 kHz and upwards has recently been completed by Uppsala University and Metronix company.

Two horizontal electric and three magnetic components are simultaneously measured in two bands 1-25 kHz or 10-500 kHz. In the first band there are numerous VLF transmitters present starting at ca 14 kHz. In the second band, in addition to the VLF transmitters, there are more than 20 transmitters present with a rather uniform distribution of azimuths, allowing for stable estimates of the full impedance tensor and the tipper vector. If only radio frequencies are used each site can be measured in just a few seconds. The system consists of three short magnetic sensors built into one small unit and 4 small steel electrodes connected to buffer amplifiers all of which are fed into a central analogue signal conditioner before being transferred to an advanced signal processor box with AD converters, GPS synchronisation, radio-communication modem between transmitter and receiver and a new dedicated software package for data playback and visualisation, and automatic 1-D inversion.

Each of the magnetic dipole sources have maximum magnetic moments of ca 4000 Am<sup>2</sup>, powered from ordinary car batteries, whereby the maximum transmitter receiver distance exceeds 1000 meters. Thus plane wave conditions prevail down to 200 meters depth of investigation.

**GA1.02/E/13-A1** **0845**

**ON THE STABILITY OF MAGNETOTELLURIC TRANSFER FUNCTIONS AND THE RELIABILITY OF THEIR VARIANCES**

Markus EISEL (GeoForschungsZentrum Potsdam, Telegrafenberg, 14473 Potsdam, Germany, email: eisel@gfz-potsdam.de) Gary D. Egbert (College of Oceanic and Atmospheric Sciences, Oregon State University, 104 Ocean. Admin. Bldg, Corvallis, OR 97331, email: egbert@oce.orst.edu)

Two years of continuous magnetotelluric (MT) time-series recordings from a two-station earthquake monitoring array were used to study the time stability of MT transfer functions (TFs), and the reliability of the estimation errors. A robust remote reference approach was used to calculate estimates of MT TFs in the band 2-3000 s for each day. No significant long



term variations could be detected, with typical deviations staying within a few percent of the long term averages. To assess reliability of the variance estimates we computed daily deviations from the median TF, divided by the respective variances. Distributions of these ratios show that the error variances are sometimes underestimated when standard (asymptotic) methods for computing error estimates are used. We also consider two variants on a jackknife approach to error bar calculation. With the first variant, the full robust TF estimation procedure is repeated using subsets of data (i.e., we omit a fixed fraction of the total set of data rather than single data entries.) This approach is very expensive in terms of computation time. With the second approach we estimate the data weights for the robust TF estimate once using all data, and then compute jackknife error bars for the weighted LS problem. We show that with this approach the error bars can be computed at essentially no cost; the result can be expressed in closed form. Both jackknife approaches yield more conservative variance estimates compared to the standard asymptotic approach. The first approach gives significantly more reliable variance estimates for periods from 10-100 s (where coherent noise contaminated TF estimates), provided the size of the omitted data fractions is large. At other periods where coherent noise does not affect the data, the smaller error bars computed by standard approaches more accurately reflect the variability in the TFs.

#### GA1.02/W/29-A1 0900

##### DC SENSITIVITY AND MT STATIC SHIFT

Klaus Spitzer (Joint Geoscientific Research Institute, Stilleweg 2, 30655 Hannover, Germany, email: klaus.spitzer@gga-hannover.de)

Magnetotelluric (MT) static shift is a non-inductive change or distortion of the MT apparent resistivity response that severely impairs the interpretation of MT data. Since MT static shift is a pure direct-current (DC) phenomenon, we can apply the DC sensitivity distribution to predict its behavior. Let us consider a four-point DC arrangement in Schlumberger configuration with current electrode spacing AB. Then negative sensitivities form two semi-spherical or bowl-shaped structures between current and potential electrodes. With the limit of AB toward infinity the semi-spheroids grow infinitely large leaving positive sensitivities only within a vertical dike structure between the potential electrodes. This arrangement represents the DC analog to the MT static shift case yielding horizontal current systems at the position of the potential electrodes or, in MT terms, of the telluric probes. Thus, the sign of static shift is due not only to the resistivity of the body but also to its location. For example, a conductive body between the telluric probes will decrease the MT apparent resistivity (positive sensitivity) whereas the same body being located aside from both probes yields an increase in apparent resistivity (negative sensitivity). 3D modelling clearly verifies this behavior. A field campaign was carried out in Unterfranken/Germany comprising MT, DC resistivity soundings, the vertical gradient method (VG) and borehole geophysics and serves as practical example. The DC resistivity data have been interpreted using 3D forward modelling to investigate the vicinity of the MT sites with respect to the static-shift problem. Finally, as a comparison undistorted results of the vertical gradient method are taken into account.

#### GA1.02/E/10-A1 0915

##### THE PHYSICS OF KEYHOLE IMAGING

Laszlo SZARKA (GGRI, H-9401 Sopron POB 5 and Universite Paris-Sud, F-91405 Orsay Cedex, Bat. 504, email: szarka@ggki.hu) and Michel Menvielle (CETP, F-94107 Saint Maur des Fosses and UPS, F-91405 Orsay Cedex, Bat. 504, email: michel.menvielle@cetp.ipsl.fr)

CSAMT analogue modelling results carried out in the Sopron modelling laboratory showed especially model-geometry connected anomalies over high-conductivity thin-sheet models, in a narrow period zone just at the end of the oscillating section of the sounding curves. Years later, full 3-D MT numerical modelling experiments confirmed the existence of such a phenomenon. We call these model geometry-connected images as keyhole images (Szarka and Menvielle 1999: Geophysical Prospecting, 47, 59-71). Recently, the analogue and numerical modelling results were completed by simple two-layer analytical derivation (Szarka, Menvielle and Spichak 1998: The keyhole imaging. Paper presented at the Sinaia EM induction workshop). By using analytical derivation it proved to be possible to predict keyhole images: the best keyhole images appear at periods where the response to a resistivity change at a certain depth has its maximum. In this paper further numerical modelling results are presented (both for conductive and resistive targets) and the full description of this interesting phenomenon, which might be useful in some field application in the future is given.

#### GA1.02/W/37-A1 0930

##### MODELLING THE ELECTRIC FIELD AT THE SEAFLOOR DUE TO A NON-UNIFORM IONOSPHERIC CURRENT

Risto PIRJOLA and Ari Viljanen (both at Finnish Meteorological Institute, Geophysical Research Division, P. O. Box 503, FIN-00101 Helsinki, Finland, email: risto.pirjola@fmi.fi)

The estimation of geomagnetically induced currents (GIC) and voltages on submarine cables requires the knowledge of the electric field produced at the seafloor during geomagnetic disturbances. In this paper we derive relations between the seafloor electric field and the surface magnetic field in the case of a non-uniform ionospheric source. The equations thus permit the calculation of the seafloor electric field, for example, in terms of observatory magnetic data. The relations can be expressed as inverse Fourier integrals over horizontal wave numbers or as spatial convolutions. It is important to note that the transfer functions and the convolution kernels between the seafloor electric and surface magnetic fields only depend on the properties of the seawater and of the basement below the seafloor. So, after they have once been determined they are applicable to all geomagnetic disturbance events. Corresponding relations also hold true for the seafloor magnetic field and the surface magnetic field.

#### GA1.02/E/18-A1 0945

##### PRESSURE DEPENDENCE OF ELECTRICAL CONDUCTIVITY OF MANTLE OLIVINE

Thomas J. SHANKLAND (Earth and Environmental Sciences Division, MS D443, Los Alamos National Laboratory, Los Alamos, NM 87545; Email: shankland@lanl.gov), Yousheng Xu (Bayerisches Geoinstitut, Universität Bayreuth, D-95440 Bayreuth, Germany, email: yousheng.xu@uni-bayreuth.de), A. G. Duba (L201, Lawrence Livermore National Laboratory, Livermore, CA 94551; Email: alduba@llnl.gov)

We report new measurements of electrical conductivity of olivine that were made in a multi-anvil press using solid buffers (usually Mo-MoO<sub>2</sub>) to control oxygen partial pressure. The temperature range was 950-1450°C and the pressure range was 4-10 GPa. When pressure effects are interpreted as activation volumes in the Arrhenius equation, they yield values of order  $0.5 \pm 0.85$  cm<sup>3</sup>/mole. In addition, we analysed older literature data, which produced a similar result but with larger variation. The common practice of assuming that the pressure

effect on electrical conductivity of olivine in Earth's upper mantle depends weakly on pressure has rested on uncertain grounds. These new observations suggest that at upper mantle conditions (depths of 80-200 km) neglecting pressure effects on conductivity is justified. A weak pressure effect also supports the small polaron (Fe<sup>3+</sup>) model as the dominant conduction mechanism, although the mainly positive activation volumes argue for a component of lattice deformation.

#### GA1.02/W/31-A1 1000

##### MAGNETIC MAPPING AND ELECTROMAGNETIC INDUCTION IN THE EARTH

ADRIAN HITCHMAN, Research School of Earth Sciences, Australian National University, Canberra ACT 0200, Australia; F.E.M. (Ted) Lilley, Research School of Earth Sciences, Australian National University, Canberra ACT 0200 Australia; Peter R. Milligan, Australian Geological Survey Organisation, GPO Box 378, Canberra ACT 2601, Australia

Time-varying magnetic fields arising from electromagnetic induction in Earth become part of the total magnetic field measured during magnetic mapping. The CICADA project is concerned with such induction effects, looking for ways to improve the resolution of the mapping and to exploit magnetic data for information on conductivity structure.

The CICADA project has four strands: \*Analysis of aeromagnetic crossover misfits for conductivity information. A Fourier technique has been used to reconstruct magnetic daily variations from crossover misfits. Comparison of these and base station variations allows spatial induction patterns to be mapped using aeromagnetic survey data.

\*Global Sq total-field curves. Type curves of the total-field quiet daily variation for the whole globe have been derived from an analysis by Campbell of observatory data from the International Year of the Quiet Sun. They show a pronounced latitudinal and seasonal dependence.

\*Total-field magnetic amphidromes. Near a conductivity contrast, at certain main field inclinations, total-field fluctuations of period less than one hour may be undetectable with a scalar magnetometer. Such locations are called "magnetic amphidromes".

\*Micropulsations and the coast effect. A line of three-component magnetometers, extending from onshore to the continental shelf, has been used to measure the coast effect at micropulsation periods. Such data provide valuable insight into the behaviour of the total field where aeromagnetic surveys are being conducted over the continental shelf, as is now common in Australia. (CICADA: Clarifying Induction Contributions to Aeromagnetic Data)

#### GA1.02/E/05-A1 1015

##### AN AEROMAGNETIC RISK MAP OF AUSTRALIA

CHARLES BARTON (Australian Geological Survey Organisation, GPO Box 378, Canberra ACT 2601, Australia, Email: cbarton@agso.gov.au)

Base station data are used to remove time-variations of the geomagnetic field from aeromagnetic surveys. The correction suffers from spatial non-uniformity of external fields and heterogeneity of the inductive response of the Earth's crust. The latter can be mapped using magnetometer arrays. An "aeromagnetic risk factor" is developed, based on the dispersion of Parkinson induction vectors, which is a measure how accurately a base station represents the time-varying field at a remote survey point. The aeromagnetic risk factor is frequency-dependent, with short-period values being representative of shallower and generally more heterogeneous conductivity structures. An "aeromagnetic risk map" for Australia for periods of 40-60 minutes has been prepared. Such maps indicated to aeromagnetic surveyors the spatial scale over which a single base station may, or may not, be useful.

Monday 19 July PM

Presiding Chair: J. Weaver (University of Victoria, Canada)  
Concurrent Poster Session

#### ELECTROMAGNETIC INDUCTION STUDIES - MODELLING

#### GA1.02/W/23-A1 1400

##### EM INDUCTION OVER A LARGE CONDUCTIVE BLOCK - A 3D NUMERICAL MODEL STUDY

A. K. Agarwal and H. W. Dosso (both at the Department of Physics and Astronomy, University of Victoria, B.C., Canada V8W 3P6, emails: numod@uvvm.uvic.ca and hdosso@uvic.ca)

Electromagnetic induction in a conductive cubic block of large dimensions (150km x 150km x 150km) over a wide range of periods ranging from .1 to 15000 s and for a uniform inducing field is investigated with the aid of a staggered grid finite-difference method. The 3.6 S/m conductive block is embedded in a uniform host of conductivity .000625 S/m and 600 km depth which is underlain by a uniform layer of conductivity 3.6 S/m. Responses are computed as induction arrows which are compared with corresponding 2D responses along a profile passing through the centre of the block.

The numerical results indicate that the in-phase induction arrows over a wide range of periods always point towards high current concentrations in the conductive block, whereas the quadrature arrows are found to be oppositely directed on either side of the interface so as to point either towards or away from each other. At shorter periods, the quadrature arrows near the interface point away from each other, and at longer periods they point towards each other. The period at which the transition of the quadrature arrow reversal takes place is the characteristic period (T<sub>c</sub>) of the model. It is known to be dependent on the model parameters. T<sub>c</sub> can be useful in identifying the horizontal dimension of the body if the resistivity of the host is known or visa versa. Similarly, the location of the quadrature arrow sign reversal can aid in delineating a conductive - resistive interface. Further, a comparison of 3D results with the corresponding 2D results along a profile passing through the centre of the block indicates that T<sub>c</sub> is at a lower period for 3D than for 2D, apparently due to the horizontal dimension of the block being the smaller in the 3D case. The 3D model responses at very short periods (< 5 s) along a central profile match very well with the 2D responses, but at longer periods (> 5 s) the difference increases rapidly with increasing period. Thus, the validity of a 2D assumption for a central profile over the conductive block is valid only at rather short periods.

#### GA1.02/W/30-A1 1415

##### ELECTROMAGNETIC MODELLING USING THE A-PHI FORMULATION

Eldad Haber (Dept of Earth and Ocean Sciences, University of British Columbia, Vancouver Canada, V6T- 1Z4, Email: haber@geop.ubc.ca); Uri Ascher (Dept of Computing Science, University of British Columbia, Vancouver Canada, V6T- 1Z4, Email: ascher@cs.ubc.ca); Doug Oldenburg (Dept of Earth and Ocean Sciences, University of British Columbia, Vancouver Canada, V6T- 1Z4, Email: doug@geop.ubc.ca);

Efficient modelling of quasi-static electromagnetic phenomena is a major obstacle in

recovering the earth's conductivity. There are two main difficulties in the modelling. First, the conductivity is highly discontinuous and therefore so too is the electric field. Second, Maxwell's equations in the quasi-static region tend to become singular in the case of very low frequency or very low conductivity goal is to overcome these obstacles by re-examining Maxwell's equations in the quasi-static region. First, we examine different formulations of the equations. Although it is possible to work with either: (1) a first order system involving E and H, (2) a second order system that involves E only, (3) a second order system involving H only, or (4) a second order system that involves the potentials A and phi, we show that it is better to work with either the A-phi or the H only-systems because these choices ensure smooth variables. Second we examine the A-phi and the H systems and show that the A-phi system can be reduced to a well-posed system, even in the low frequency or zero conductivity case. This is done by transforming the system into one which resembles the Stokes problem in fluid dynamics. We show that the magnetic potential A behaves like fluid velocity and the electric potential phi behaves like the fluid's pressure. Next, we show that a reliable discretization of the system that ensures physical solutions, can be obtained by using a mixed finite element method. This requires that the divergence-free condition is used as a constraint when solving the system. Finally, we discuss the solution of the system of algebraic equations which arise from this discretization. We show that it is possible to use efficient iterative methods that were developed for the Stokes problem to solve our system in a fast and reliable manner. Our code is tested on the magnetotelluric example.

**GA1.02/W/36-A1 1430**

**A PERTURBATION THEORY OF ELECTROMAGNETIC FIELD IN A THREE DIMENSIONAL INHOMOGENEOUS MANTLE WITH GRADUALLY LATERAL VARIATION**

Ma Shi-Zhuang (Institute of Geophysics, Chinese Academy of Sciences, Beijing, 100101, China, email: szma@mail.c-geos.ac.cn)

It is one of the classical problems in Earth's electromagnetism that continuation of the observational data of magnetic field into the conducting region. This paper built the coupling vector equations governing the poloidal, toroidal and potential fields in 3-D inhomogeneous conducting mantle. Considering the limitation on variable scale of inhomogeneities in global mantle from study of the Earth's deep interior, a perturbation theory of gradually lateral variation was presented. It is unnecessary that the 1-D spherical symmetric distribution of electric conductivity as zero-degree approximation. Serving as an example of solvability of the zero-degree approximation, it was demonstrated how the gradually lateral variation of electric conductivity effect on anti-diffusive problem of poloidal field in Earth's mantle.

**GA1.02/E/21-A1 1445**

**3-D INVERSION OF MT AND TENSOR CSMT DATA BASED ON QUASI-LINEAR METHOD**

Michael ZHDANOV and Gabor Hursan (both at the University of Utah, Department of Geology and Geophysics, Salt Lake City, UT 84112, USA, email: mzhdanov@mines.utah.edu Sheng Fang (Baker Atlas, 12021 Westheimer, Houston, TX 77042)

3-D electromagnetic (EM) inversion continues to be a challenging problem in electrical exploration. We have developed recently a new approach to the solution of this problem based on quasi-linear (QL) method of forward modelling (Zhdanov and Fang, 1996). This approach reduces the original nonlinear EM inverse problem to a set of linear inverse problems with respect to anomalous conductivity. The developed algorithm has been applied for interpretation of 3-D magnetotelluric (MT) survey conducted in the Minamikayabe area of Hokkaido, Japan, and for 3-D inversion of the tensor controlled source audio magnetotelluric (CSAMT) data collected over the Sulphur Springs thermal area, Valles Caldera.

**GA1.02/E/34-A1 1500**

**THREE DIMENSIONAL MT MODELLING FOR TOPOGRAPHY MODELS AND HIGH RESISTIVITY CONTRAST**

Elena FOMENKO (Geo-electromagnetic Research Institute RAS, Troitsk, BOX 30, Troitsk 142092, Moscow region, Russia, Email: igemi@pop.transit.ru) Toru Mogi (Department of Earth Resources Engineering, Department of Earth Resources Engineering, Graduate School of Engineering, Kyushu University 6-10-1 Hakozaki, Higashi-ku, Fukuoka, 812-8581, Japan Email: tmogi@mine.kyushu-u.ac.jp) Tatsuya Kajiwara (JMC Geothermal Engineering Co. Ltd, Takizawa, Iwate, 020-01, Japan)

We have searched 3D modelling scheme of 3D TM problems based on FEM methods (Mogi, Kajiwara, 1996) and the staggered grid finite difference formulation for electrical field (Fomenko, 1998).

The comparison was made for complex magnetotelluric 3D issues such as the island effect, volcano model and topographic distortion on the apparent resistivity and phase. These issues must deal with high conductivity contrast. We estimated that these effect is severe at some frequencies relating to the scale of the structure.

The numerical experiments show that 'natural' choice of continuous components of E, H fields, an appropriated choice good preconditioner of the system of linear equation and compensation of non-zero div J behavior played a principal role in obtaining solutions with high speed of accuracy and convergence. In case of absence this improvements it's problematic to obtain solution for high contrast problems with good accuracy at all.

**GA1.02/E/19-A1 1515**

**3-D ELECTROMAGNETIC AND MAGNETIC DATA INTEGRAL INVERSION**

P.S. MARTYSHKO, A.L. Rublev (Institute of Geophysics, Ural Branch of Russian Academy of Science, 620016, Ekaterinburg, Amundsen str. 100, Russia e-mail: pmart@igeoph.mplik.ru, fax: +7-3432-678872)

The interpretation of data obtained by EM methods involves considerable difficulties because in a general case the inverse problem is reduce to an operator equation of the first kind with an implicitly stipulated operator. The numerical solution of such equations requires considerable expenditures of computer time. We have obtained the new inverse problem equations of electromagnetic fields. There are the first generation equations with explicit operators. The primary field source can be arbitrary type. We've used representations of field functions through the values of the functions themselves and the derivatives at the boundary of the anomaly-forming object. The method for solving of 3-D nonlinear electromagnetic and magnetic inverse problem was divided (in the cases potential and monochromatic fields). It's based on the algorithm for solving explicit equations of the 3-D inverse problem. The algorithm was successfully tested on a number of model examples. We apply the Tikhonov regularization method to 3-D EMD inversion. We do AEM and/or magnetics data inversion by two-stage interpretation method:

- 1) approximation of the observed data with the fields of singular sources;
- 2) construction of equivalent objects with different physical parameters values.

As a result of interpretation we obtain the bodies stellate relative to some point with different

values of conductivity (permeability) which generated the same ( electrical or magnetic) field. We have studied the possibilities for solution uniqueness seeking on the based joint interpretation of different EMD (Airborne EM and magnetics data, charge method and so on). We have some examples with good results of interpretation.

**GA1.02/E/09-A1 1530**

**3D INVERSION OF MT DATA USING BAYESIAN STATISTICS**

Vjacheslav SPICHAK (Geophysical Research Centre, Moscow, Russia, e-mail: spichak@dol.ru) Michel Menviel (University Paris Sud, Orsay Cedex, France, e-mail: menviel@geol-u.psud.fr)

A Bayesian approach is used for inversion of MT-data in three-dimensional media. Complex three-dimensional structure is considered as composed from elementary homogeneous domains. The information available is determined in terms of the a priori probability law of the conductivity distribution.

The parameters to be found are the a posteriori conductivity values in the region of search. Thus, the solution of the inverse problem is reduced to the search for the a posteriori conductivity distribution by means of successive solution of the forward problem for the a priori values of the conductivities preset in the homogeneous domains. The solution of the forward problem is fulfilled using the program FDM3D. Iterative solution of the system of linear equations saves the time of calculations due to use of the previous results as good starting points for the next ones. The iteration process converges to the correct solution in the most cases in 15-20 iterations, which enables to solve the inverse problem in a reasonable time. Numerical experiments made using synthetic MT data indicate that the results of inversion are rather stable with respect to the a priori range of the conductivity palette in each domain of the region of search and to the a priori probability density function, however, they are very sensitive to increasing / decreasing of it's dimensions in comparison with those of the real target. An example of the ecological problem solution (detection of seawater invasion into a shallow coastal fresh water aquifer and mapping the boundaries of the salty water) by means of Bayesian inversion of synthetic AMT data is considered.

**Monday 19 July AM**

Presiding Chair: M. Ingham (Victoria University of Wellington, NZ)

**GA1.02/W/12-A1 Poster 1050-01**

**ERROR ANALYSIS OF THE SEVEN ROTATIONAL INVARIANTS OF THE MAGNETOTELLURIC IMPEDANCE TENSOR**

A. K. AGARWAL and J. T. Weaver (both at the School of Earth & Ocean Sciences, University of Victoria, Victoria, B.C., Canada, V8W 3P6, emails: numod@uvvm.uvic.ca and weaver@phys.uvic.ca)

In a previous presentation, the magnetotelluric tensor was characterized by seven independent rotational invariants each with its own physical interpretation associated with its numerical value becoming vanishingly small. In practice, the invariants will never vanish precisely because of noise in the measured data and because the idealized conditions under which the vanishing of the different invariants occur (such as two-dimensionality of the regional structure or real distortion of the complex tensor elements by a small-scale, near-surface, three-dimensional anomaly) are never more than approximately realized in nature. In this paper the analysis is taken a stage further by investigating the propagation of errors in the various invariants when Gaussian noise is added to synthetic data generated by a numerical model comprising a small conductive cube embedded in the surface of a layered earth and near a two-dimensional regional fault line. The effect of the noise on the seven invariants and their resulting stability is discussed, and conclusions are drawn about the general usefulness of the invariants in determining the regional direction of strike and in decomposing the tensor into its two-dimensional regional form.

**GA1.02/W/16-A1 Poster 1050-02**

**PERCOLATION THEORY WITH EMBEDDED NETWORKS - A MODEL FOR THE CONDUCTION MECHANISM IN THE MIDDLE CRUST.**

LABENDZ, Daniel

Electromagnetic deep sounding measurements often indicate a high conductive layer (HCL) in the middle crust (15-20 km) which very often exhibits an electrical anisotropy with respect to the two horizontal directions. A cause of the high conductivities has not been identified unambiguously but graphite or saline fluids are the major players. With the aid of mixing laws, percolation theory and an embedded 2D/3D network approach we model the heterogeneous rock matrix in order to determine the "electrical connectivity" of the highly conductive phase. An essential result is the electrical anisotropy, which indicates a deviation from the perfectly interconnected case.

We will present results of the dependence between connectivity and percolation probability as well as the embedding factor. It is not necessary to impose a fractal geometry on the model by incorporating embedded networks. However, in percolation experiments with large networks the resulting cluster at the percolation threshold has fractal geometry. Using magnetotelluric data containing anisotropy it becomes possible to calculate an indicator which can help to determine the cause of the high conductive layers. With the help of 3D networks the importance of vertical connectivity (conductivity) can be discussed.

**GA1.02/W/01-A1 Poster 1050-03**

**3D SOURCE EFFECTS ON MT AND GDS DATA**

PATRICIA MARTINELLI and Ana Osella Ciudad Universitaria - Pab. I - Departamento de Fisica - 1428 - Buenos Aires - Argentina

Usually, MT and GDS data are interpreted assuming a spatially uniform external magnetic field. This assumption has proved to work well in many cases, and its validity implies that the impedance tensor Z, and the tipper T, are independent of the unknown inductive field. Nevertheless, in some occasions, as for example in studies at high or low latitudes, this hypothesis fails, especially for hourly periods.

In previous works we proposed a 2D MT modelling method based on the application of Rayleigh scattering theory; later, the possibility of a 2D external field was introduced in the formulation. Here, we present the solution for general 3D inductive fields, and we give examples of the kind of distortions that such fields can produce on Z and T, and how these distortions can modify the final models obtained. In the last term, we propose a procedure to overcome the problem, using instead of Z and T other quantities that do not depend on the external field

GA1.02/W/03-A1 Poster 1050-04

**A NEW METHOD OF GEOELECTRICAL PROSPECTING BY VERTICAL ELECTRIC CURRENT SOUNDINGS**

V. MOGILATOV, Institute of Geophysics SB of RAS, Universitetsky Pr., 3, Novosibirsk, 630090, Russia, fax: 7-383-2333432, e-mail: VMogilat@uiggm.nsc.ru

Some advantages and problems of a new geoelectrical prospecting method, vertical electric current soundings (VECS) are discussed. This method is based on using a new source, circular electric dipole (CED). It is unique source for the electrical prospecting, which excite only TM (transverse magnetic) field. The source is installed in the following way. One of the transmitter poles is grounded in the central point. The other pole is uniformly grounded around with a radius determined by the depth of investigation desired. It can be defined as a noninductive source. The most interesting CED properties in the low frequency regime are as follows. CED has no magnetic field of its own. It is a pure TM exciter, which differs from a loop (only TE excitation) and from a line, which is both TE and TM exciter ("a line" here means a cable or insulated wire grounded at its end points). The normal magnetic field on the earth's surface (and above it) of a layered medium is absent (within the quasi-static approximation), and only a radial electric component exists. A CED field is at right angles to the loop field and has azimuthal symmetry. The CED field is always governed by a vertical medium structure (at the latter transient stage as well) rather than by the total longitudinal conductivity. An interesting result was obtained: in marine electrical prospecting a sea water layer will not play such a crucial role when a CED is used as in applying a loop or a line. In a medium with non-conducting basement the decay of the CED field is exponential. The transient process is more fast than in the case of a loop or a line. The CED can be also considered as a ground analogue of another known source, a vertical electric line. Besides, the CED a pure galvanic source that does not excite a long-term transient field. Thus it seems to be a new useful means to study IP processes. The author consider results of the initial field tests in the Ukraine (ore body) and in the Tartar republic (oil target).

GA1.02/E/36-A1 Poster 1050-05

**DIGITAL THREE-COMPONENT FLUX-GATE MAGNETOMETER FOR STUDIOS AND MEASUREMENTS OF ELECTROMAGNETIC INDUCTION (EMI) VARIATIONS**

An. P. NAUMOV (D.I. Mendeleev Institute for Metrology / VNIIM, St Petersburg, 198005, Russia, email: slovo@mail.line.ru) V.A. Prishepo and V.I. Sheremet (both at VNIIM, St Petersburg, 198005, Russia, email: hal@ont.vniim.spb.su)

This device, the digital three-component flux-gate magnetometer, was developed at Institute of Metrology for decision of problem of the coordinate determination of natural sources. This is source of EMI geovariations and sources of tectonic ULF magnetic impulses. The vector probe of magnetic field is a base of flux-gate magnetometer. Direct and inverse transducer form part of the probe described. As a direct transducer a new three-component flux-gate probe is used. As an inverse transducer there is used a system of three-component coil windings of which are placed on a cubic of ceramic. The inverse transducer cube is mechanically linked to a rectangular quartz prism normal to faces of which form a base coordinate system. Referencing the axes of the vector transducer for magnetic induction to the axes of the base coordinate system is effected using reference magnetic and optic measuring devices. The accuracy of flux-gate magnetometer - 5,0 nT, measurement range +/- 65.280 nT, a minor quantum 0,1 nT and range of frequency from 0 to 6 Hz.

GA1.02/E/40-A1 Poster 1050-06

**DYNAMIC ELECTROMAGNETIC DIAGNOSING OF ECOLOGICALLY DANGEROUS OBJECTS**

OLEG SAPUZHAK, Yaroslav Sapuzhak, Olena Neganova, Oleg Romanjuk (Carpathian Branch of Subbotin Institute of Geophysics NASU, 3b, Naukova str, 290601, Lviv, Ukraine, tel/fax +380 322 648563, email: olgs@carp.lviv.ua)

Methodology is developed for quick diagnosing of ecologically dangerous objects and for determining unstable energy active parts inside them. It is based on analysis of diurnal variations of electromagnetic parameters and includes the following stages: - analysis of existing geological and geophysical data on the object under investigation and static geoelectric modelling of its cut; - application of mathematical and physical modelling to study the geoelectric cut and determining the optimal schemes and parameters of field observations technique; - recording and analysis of diurnal variations parameters obtained by the methods of natural and artificial electromagnetic field; - processing and analysis of field observations data, designing the temporal and profile (or planar) characteristics of studied parameters; - complex interpretation of obtained data including determining the potentially dangerous energy active parts and their dynamic modelling, conclusions and recommendations. Active parts revealed may become the subject of more detailed and lasting planar and continuous observations. In its most part the methodology is based on methodological approaches, mathematical modelling software, equipment for physical modelling and high accuracy electromagnetic measurements originally developed in CBSIG NASU.

GA1.02/W/34-A1 Poster 1050-07

**PROPERTIES OF ROTATION INVARIANT MAGNETOTELLURIC IMPEDENCE TENSOR: A CASE STUDY FROM THE ARCHAEN PROTEROZOIC CONTACT OF THE SINGHBUH CRATON AND THE ADJOINING MOBILE BELTS**

K.K. ROY and S. Srivastava (both at Department of Geology and Geophysics, Indian Institute of Technology, Kharagpur - 721 302, India, Email: kkroy@gg.iitkgp.ernet.in) A.K. Singh (Department of Applied Earth Sciences, Delft University of Technology, Delft, The Netherlands)

Properties of the Magnetotelluric rotation invariant tensors (RITs) are studied on the field data collected from the Singhbuhm craton and the adjoining Proterozoic mobile belts. It is observed that the RIT apparent resistivities and phases viz., determinant, central and average can be used for 2D/3D modelling and plotting of pseudosections and surface plots. Two eigen values of the impedance tensor Z generate apparent resistivities computed from the two eigen values is equal to the determinant apparent resistivities. The arithmetic mean of the two phases obtained from two eigen values gives the determinant phase. Central apparent resistivity is equal to the average apparent resistivity plus the apparent resistivity obtained from the diagonal elements of the impedance tensor. Rotation invariant property exists in presence of noises in the MT field data. Rotation invariant plots show more consistent data with less error bar and statistical fluctuations. Models with RITs show more consistent results.

GA1.02/E/08-A1 Poster 1050-08

**IS THE MAGNETOTELLURIC IMPEDANCE TENSOR OR THE INDUCTION MATRIX A NORMAL PHYSICAL VALUE?**

VLADIMIR SHUMAN (Institute of Geophysics of the Ukrainian National Academy of Science, 252680, Palladina str. 32, Kiev, Ukraine, Email: earth@ighp.kiev.ua).

The concept of the tensor surface impedance and induction matrix in the theory of geoelectromagnetic methods is considered. It is a well-known fact that a wealth of experience in practical determinations of the impedance matrix or the induction matrix elements has shown the accuracy attained is much below the accuracy in measuring field variations and not always suit the geophysicists requirements. When identifying induction matrices, the scatter of values usually increases in comparison with impedance identifications. The correct formulation of the problem of MT-date processing and inversion is in these approximated model evidently difficult. Using the known results of Aboul-Atta and Boerner (1975), we have obtained accuracy local boundary conditions associating the normal and tangential components of electromagnetic field on closed discontinuity of media whose particular case are the approximated of Rytov-Leontovich. The horizontal gradient and geomagnetic depth sounding methods are special cases of the theory developed. The concept of the density of electromagnetic field helicity and its reflection in the structure of Maxwell's equations in an isotropic medium is analysed. This approach seems very likely to be more universal and better conforms with the logic of the date processing of MT-experiment and the problems of the monitoring of the dynamically process in comparison with the conventional conception of the tensor impedance or the induction matrix.

GA1.02/E/39-A1 Poster 1050-09

**MAGNETIC AND ELECTROMAGNETIC INDUCTION EFFECTS IN THE ANNUAL MEANS OF GEOMAGNETIC ELEMENTS**

Crisan DEMETRESCU, Venera Dobrica, Nadejda Ciocoiu (all at Institute of Geodynamics, 19-21 J.L. Calderon Str., R-70201, Bucharest, Romania, email: crisan@geodin.ro)

The solar-cycle-related (SC) variation in the annual means of the horizontal and vertical components of the geomagnetic field at European observatories, for sets of data between 1950-1995, is used to infer information on the magnetic and electric properties of the interior, characteristic to the observatory location, by identifying and analysing the magnetic induction component and respectively the electromagnetic induction component of the SC variation. The latter is further analysed in terms of response functions Q (internal/external) and W (vertical/horizontal) and mantle resistivity.

GA1.02/P/05-A1 Poster 1050-10

**INSTRUMENTATION FOR RECORDING AND ANALYSIS OF LOW LATITUDE PC3 GEOMAGNETIC PULSATIONS IN SOUTH-EAST AUSTRALIA EMPLOYING INDUCTION COIL MAGNETOMETER TECHNIQUE**

I. A. ANSARI (Department of Physics, Aligarh Muslim University, Aligarh (U.P.), Pin Code: 202 002, India)

Geomagnetic pulsations of Pc3 type are quasi-sinusoidal variations in the earth's magnetic field with a period range of 10-45 sec. The spatial and temporal variations in Pc3 wave polarisation and signal phase are vitally important since they provide evidence which can be directly related to wave generation mechanisms both inside and external to the magnetosphere and propagation modes inside the magnetosphere. An array of four low latitude induction coil magnetometer stations was established in south-east Australia to study the characteristics of low latitude Pc3 geomagnetic pulsation over a longitudinal range of 17 at  $L = 1.8$  and a latitudinal range of  $10^\circ$  over  $L = 1.8$  to 2.7. The geomagnetic north-south (X) and east-west (Y) components of variations in the 5-100 MHz band were recorded on slow speed frequency modulated analogue magnetic tape along with a 5 sec. time channel. Chronometers with an accuracy of 10 msec. per day were employed. Data were later digitised in the laboratory with a 5 sec. sample rate using the time channel pulses. The resulting X(t) and Y(t) time series were used to study dynamic spectra, polarisation ellipticity, major axis azimuth directions and the percentage of polarised wave power from the coherency matrix method. Interstation cross-spectral parameters were also studied. The recording and analysis instrumentation has been described.

Monday 19 July PM

Presiding Chair: M. Ingham (Victoria University of Wellington, NZ)

GA1.02/P/04-A1 Poster 1605-01

**ELECTROMAGNETIC INDUCTION IN THIN SHEETS BELONGING TO DIFFERENT SYSTEMS OF COORDINATES**

Attia A. ASHOUR (Math. Dept., Faculty of Science, Cairo University, Giza, Egypt, email: ashour@frcu.eun.eg) Moustafa S. Abou-Dina (Math. Dept., Faculty of Science, Cairo University, Giza, Egypt, email: msaboudina@frcu.eun.eg)

In electromagnetic induction problems in thin sheets if the boundaries involve natural surfaces in different coordinate systems, it will not be possible to use functions or harmonics belonging only to one system of coordinates. However, such problems involving mixed spherical, spheroidal and cylindrical boundaries can be treated using the relations between the different harmonics belonging to those systems which are found in the old literature (e.g. Copson (1936), Hobson (1955)...) and which have been collected by Smythe (1968). To illustrate this method, we solve the model problems of electromagnetic induction by a time varying magnetic field in: (1) A uniformly conducting spherical shell enclosed in a co-axial uniformly conducting infinite cylindrical shell. (2) A uniformly conducting spherical shell enclosing a perfectly conducting concentric oblate spheroidal shell.

References: 1- E.F. Copson, Theory of Functions, Oxford (1935), 2- E.W. Hobson, Spherical and Ellipsoidal Harmonics, Chelsea (1955), 3- W.R. Smythe, Static and Dynamic Electricity, 3rd ed., McGraw-Hill, Inc. (1968). See also references included therein.

GA1.02/W/26-A1 Poster 1605-02

**MODELLING THE INDUCTION LOG RESPONSES IN A 3D FORMATION WITH TILTED BOREHOLE AND INVADDED BEDS USING THE INTEGRAL EQUATION APPROACH**

Dmitry AVDEEV, Alexei Kuvshinov, Oleg Pankratov (all at Institute of Geoelectromagnetic Research, Russian Academy of Sciences, 142092 Troitsk, Moscow region, Russia, email: avdeev@gemri.msk.ru), and Gregory Newman (Sandia National Laboratories, Org. 6116, P.O. Box 5800, Albuquerque, NM 87185-0750, USA, email: ganewma@sandia.gov)



Three-dimensional (3D) frequency-domain solver, previously built for the magnetotelluric, controlled-source and airborne applications (Avdeev et al., 1996; 1997; 1998), is now developed for the induction logging problem. The solver calculates the responses in 3D models including a steeply, up to 90 degrees, tilted borehole and invaded beds, and accounts for displacement currents, induction polarization effects, anisotropy of the beds resistivities and cylindrical geometry of the borehole. The solver exploits the volume integral equation (IE) approach which has been originally presented in (Singer, 1995) as modified iterative dissipative method, and later generalized in (Pankratov et al. 1995, 1997). The IE approach is based on a Neumann (Born) series expansion, which is always convergent, even for extreme resistivity contrast.

For tilted boreholes in layered formations, there are no known analytical solutions. Therefore, our solution was first checked against the mode matching solutions (Chew et al., 1984; Liu, 1993) for vertical borehole models. Excellent agreements were obtained. Comparisons with staggered grid finite difference solution (Newman and Alumbaugh, 1995) were then conducted for a vertical and 45 degree tilted boreholes intersecting a horizontal bed boundary. These comparisons were again excellent, and demonstrate for the first time, verifiable induction log responses in the presence of tilted boreholes.

**GA1.02/E/28-A1 1605-03**

**EFFECTIVE INVERSION OF MT DATA OF THE TIEN SHAN TYPE**

Mark BERDICHEVSKY, Nina Golubtsova (both at Geological Department of Moscow State University, Moscow 119899, Russia, email: berd@geo.geol.msu.ru) Leonid Vanyan (Shirshov Institute of Oceanology, Moscow 117218, Russia, email: vanyan@geo.sio.rssi.ru)

MT-soundings carried out in the mountains of Kirghyz Tien Shan (Trapeznikov et al,1997) show that the crust of this region consists of four major elements: 1.heterogeneous sedimentary cover, 2.resistive upper crust, 3.heterogeneous conductive layer in the middle and lower crust, 4.subvertical conductive zones ( faults) crossing the upper crust. This geoelectrical structure is referred to as the structure of the Tien Shan type. Interpretation of MT-data of the Tien Shan type needs special approaches. So, we constructed a schematic 2D model of the Tien Shan type and tested different approaches to inversion of MT-data. On this basis an effective bimodal algorithm has been elaborated, being slightly affected by sub-surface inhomogeneities. It consists of three levels: 1)inversion of induction arrows, 2) inversion of TE phase curves, 3) inversion of TM apparent resistivity curves. The first level gives basic information on deep layers (particularly, on conductive layer in the middle and lower crust) and subvertical zones. The second and the third levels help to gain details of structures and evaluate the upper crust resistance. This algorithm opens the way to effective interpretation of MT-data in the joint Russian-Chinese project involved into the study of the Nothern Tien Shan.

**GA1.02/W/27-A1 Poster 1605-04**

**SCALE MODELLING OF THE FREQUENCY SEA-FLOOR CSEM SOUNDING IN PRESENCE OF 3D INHOMOGENITY**

Zalina Djatieva and Leonid Vanyan (both at Shirshov Institute of Oceanology, 36 Nakhimov Ave., 117851 Moscow RUSSIA, e-mail: djatieva@geo.sio.rssi.ru) Alexey Kuznetsov and Yury Popov (both at VNIIG Geophysics, 5 Kievskoe shosse, 143300 Naro-Fominsk RUSSIA)

One of the proper ways to solve the problem of analyzing a 3D inhomogeneity influence is to use a scale modelling. A scale modelling of the sea-floor frequency sounding was carried out in an electrolytic tank. The model consisted of three layers and included an underwater graben. Transmitter and receiver were placed parallel to each other. The dipole - dipole system was moved near the bottom across the graben. Electric field was measured at frequency band 0.63...8.0 MHz. According to the EM scaling these frequencies correspond to low frequencies used in practice.

An electric field magnitude strongly decreased when the dipole-dipole system was crossing a graben border. Unexpectedly attenuation curves inside 3D graben look like respective 1D curves. Probably this feature is due to the horizontal skin-effect attributed to the sea-floor frequency sounding. The presence of the graben results in a valuable shift of the apparent resistivity curve in comparison with the model without inhomogeneity (graben).

**GA1.02/L/04-A1 Poster 1605-05**

**MODELLING THE ELECTROMAGNETIC FIELDS IN A THREE-DIMENSIONAL SPHERICAL EARTH USING INTEGRAL EQUATION APPROACH**

Alexei KUVSHINOV, Dmitry Avdeev, Oleg Pankratov (all at Institute of Geoelectromagnetic Research, Russian Academy of Sciences, 142092 Troitsk, Moscow region, Russia, email: akuvsh@igemiras.msk.ru), and Sergei Golyshev (Institute of Terrestrial Magnetizm, Ionosphere and Radiowave Propagation, Russian Academy of Sciences, 142092 Troitsk, Moscow region, Russia, email: s.golyshev@mtu-net.ru)

We present numerical solution of Maxwell's equations in a spherical, full three-dimensional (3D) Earth's model allowing for an anisotropy of electrical conductivity. The solution exploits the volume integral equation (IE) approach which has been originally presented in (Singer, 1995) as modified iterative dissipative method, and later generalized in (Pankratov et al. 1995, 1997). The IE approach is based on a Neumann (Born) series expansion, which is always convergent, even for large conductivity contrast.

Our solution was first checked against the 3D Cartesian solution (Avdeev et al., 1997) for the models with an isotropic, and anisotropic, upper mantle local conductor that is embedded in radially symmetric section. The models are excited by Dst source. Very good agreements were obtained. Comparison with staggered grid finite difference solution (Uyeshima and Schultz, 1998) was then conducted for a model including surface and upper mantle conducting layers. The layers have hemispherical, longitude dependent, distributions of conductivity. This comparison was again very good.

**GA1.02/P/02-A1 Poster 1605-06**

**FINITE ELEMENT MODELLING OF MAGNETOTELLURIC FIELDS IN 2-D STRUCTURES WITH ARBITRARY ANISOTROPY**

YUGUO LI and Ulrich Schmucker (both at Institute of Geophysics, University of Göttingen, Herberberger Landstraße 180, 37075 Göttingen, Germany, email: yli@willi.uni-geophys.gwdg.de Josef Pek (Geophysical Institute, Academy of Sciences of the Czech Republic, Boční II/1401, 14131 Prague 4-Sporilov, Czech Republic, email: jpk@ig.cas.cz)

An algorithm for the numerical modelling of magnetotelluric fields in 2-D structures with arbitrary anisotropy is presented. Each anisotropic block is assigned a symmetric  $3 \times 3$  conductivity tensor. The problem leads to a coupled system of partial differential equations for the strike-parallel field components  $E_x$  and  $H_x$ , to be solved with the finite element (FE) method. The system of linear FE equations for the primary field components is solved by the

preconditioned conjugate gradient method. For the iterative solution, only the non-zero elements on and below the diagonal of the sparse coefficient matrix, arranged into a one dimensional array, are stored, which largely reduces the memory requirements of the solution. Subsequently, strike-perpendicular field components  $E_y$  and  $B_y$ , are evaluated numerically by the spline interpolation.

Our FE program has been tested by comparison with results from other methods, yielding satisfactory agreement. Three model types of anisotropy will be used to demonstrate their effect upon MT responses: horizontal, vertical and dipping anisotropy. They simulate the splitting of  $\rho_a$ -curves and tensor impedances with significant diagonal elements, as observed at many places.

**GA1.02/W/07-A1 Poster 1605-07**

**INVERSION OF CSEM DATA FROM FINITE-LENGTH LINE SOURCE EXCITING A 2D EARTH**

Xinyou Lu, Martyn Unsworth and John Booker, Geophysics Program, Box 351650, University of Washington, Seattle, WA 98195, USA, Email: xinyou@geophys.washington.edu

In practice, a real CSEM electrical source is composed of a length of grounded straight wire. Often, to improve signal-to-noise ratio, either a long grounded wire is used or receivers are close to the source for strong signals. The approximation of the infinitesimal dipole may not always valid. Therefore, the length of a long grounded wire source has to be considered. We have extended our CSAMT-RR1 inversion algorithm (Lu, et al., 1998) for data from electrical dipole to accommodate data from a finite-length line source. CSAMT-RR1 combines 2.5D EM finite-element forward modelling method developed by Unsworth et al. (1993) and the rapid relaxation inversion (RR1) of Smith and Booker (1991).

In order to invert data from a finite-length line source, we extend the 2.5D EM finite-element method for line source. The 2.5D EM finite-element method is flexible for various sources. The nature of the source is introduced by the primary field, which is defined as EM fields in wavenumber domain  $(k_x, y, z)$  for a simple conductivity structure, where  $x$  is defined as the strike direction.

The EM fields in domain  $(k_x, k_y, z)$  can be derived in closed form for 1D layered earth, then the required primary field can be computed readily. Once the primary field is given, the method can cope with any 2D model. We have investigated the effect on the EM fields, apparent resistivities and phases from the length of line source. The algorithm is tested on field data as well as theoretical models.

**GA1.02/E/07-A1 Poster 1605-08**

**BOUNDARY ELEMENT METHOD(BEM) AND 2D OR 3D GEOELECTRICAL STRUCTURE ANALYSIS**

Jiadong QIAN (Center for Analysis and Prediction, China Seismological Bureau, P. O. Box 166, 63 Fuxing Ave. Beijing ,100036 , China , email: jqdian@sdb.cdsi.ac.cn) Qingzhong Ma ( Department of Geology and geography, Lanzhou University , Lanzhou , 730000 , China) and Xianjin Mao (Seismological Bureau of Yunnan Province, Kunming, Yunnan Province, China)

Recent studies show that the effect of heterogeneous structure on the survey in geophysics , e.g. geoelectrical prospecting , should be taken into account more sufficiently . The previous methods with analytic solutions , however , could only be suitable for a few typically simplified patterns and numerical methods , such as Finite Element Method(FEM), Finite Difference Method(FDM) etc., usually demand huge amount calculations with inconveniences. This paper deals with the applications of Boundary Element Method(BEM) in the survey of apparent resistivity on the site with the 2D or 3D geoelectrical structure with better accuracy, more convenience and less computations than the previous ones. Furthermore, much more complicated cases in horizontally layered models with 2D or 3D heterogeneous bodies contained inside some of layers have been also dealt with in the paper with the treatment of the infinitely extended interfaces between adjacent layers . The special basic solutions in BEM have been taken to let the infinitely extended interfaces "disappeared", so that the integral equations only contain the term of integral along the boundaries of heterogeneous bodies without the demands for taking the integral along the infinitely extended interfaces into account. The method (BEM) and the approaches shown in this paper, have provided good tools for solving the problems in geoelectrical prospecting in which the effects of heterogeneous structures should be taken into account , and could give a good base either for forward problems or inverse ones in the same conditions. Some examples of the research on these aspects have been shown in this paper.

**GA1.02/W/25-A1 Poster 1605-09**

**MONTE-CARLO METHOD IMPLEMENTATION FOR DIRECT PROBLEMS OF INHOMOGENEOUS CONDUCTIVE MEDIUM ELECTROMAGNETIC SOUNDING**

Vladimir L. Saveliev, OLEG L. KROTOFF, Institute of Ionosphere, Almaty, Kazakstan

Using the transformation of Maxwell equations to integral form, the electromagnetic field disturbances was represented as the interference of virtual photons, scattered on the conductivity inhomogeneities. The FORTRAN code with flexible configuration options for simulation of virtual photons scattering have been created. The scheme with possibility to take into account the symmetry of the sources was considered. The results of calculations for simple models was compared with analytical solutions. The number of calculations was carried out for the various configurations of scattering objects. Also the efficient calculation algorithm for the mediums with piecewise-constant conductivity was created and implemented as FORTRAN code.

**GA1.02/E/20-A1 Poster 1605-10**

**NEURAL NETWORK BASED RECONSTRUCTION OF THE PARAMETERS OF 3D GEOELECTRIC STRUCTURES**

Vjacheslav SPICHAK (Geophysical Research Centre, Moscow, Russia, e-mail: spichak@do.ru) Kouichiro Fukuoka (OYO Co., Urawa, Japan, e-mail: fukuoka-kouichi@oyonet.oyo.co.jp) Toru Mogi (Kyushu University, Fukuoka, Japan, e-mail: tmogi@mine.kyushu-u.ac.jp) Irina Popova (Geoelectromagnetic Research Institute, Troitsk, Russia, e-mail: mpopov@isan.troitsk.ru)

Three-dimensional (3D) inverse problem of geoelectrics is solved by means of the Artificial Neural Network (ANN) approach. The properties of the supervised ANN are studied using the synthetic MT data base created for 3D conductivity model of the typical fault zone. Different groups of MT field components and their transformations as well as data compression ways are studied in order to find those which provide the best recognition abilities. The influence of the volume and structure of the training data pool (including the "gaps" and "no target" effects) on the recognition properties is estimated. Results of numerous ANN testings demonstrate that it possesses good interpolation and extrapolation abilities. The effect of noise is studied by means of mixing the synthetic MT data with 30%, 50% and 100% Gaussian noise. A special

noise treatment technique based on testing as well as teaching data pre-processing is suggested. A case history is considered. CSAMT data measured in the MINOU fault area (Kyushu Island, Japan) are interpreted by means of trained ANN in terms of 3D conductivity structure. The results of interpretation match the a priori geological information and the inversion of other geophysical data.

**GA1.02/E/15-A1** Poster **1605-11**

**PHYSICAL MODELLING NATURE ELECTROMAGNETIC FIELDS: MODERN STATE AND POSSIBILITY**

Kobzova Valentina, Ladanivsky Boris and Moroz Ivan ( all at Karpathian Branch of Subbotin Institute of Geophysics NASU, 3-b Naukova str., 290601 Lviv Ukraine, email: va@carp.lviv.ua )

Present report aims acquainting oneself with the state of modern physical modelling of electromagnetic fields in inhomogeneous media which are characteristic of real geoelectrical situations. Physical modelling method may be used when immediate observation, theoretical computation or mathematical modelling is impossible or very expensive. To realize this method the specific laboratory installations is necessary. They must answer complicated technical requirements due to which these installations are considered by restricted usage. The laboratory installation "Model" worked out in Ukraine contains electrolytic tank 5.0 x 5.0 x 0.7 m where one creates multi-layer inhomogeneous geoelectric section scale models. Variations both of natural electromagnetic field or man-made sources are simulated by harmonic plane-homogeneous or dipole field. Automatic measuring and recording of electromagnetic field provides interpreting programmes. Opportunities for this nontraditional method may be shown by obtained results. We have modelled electromagnetic fields anomalies generated by interfaces of continental and oceanic crust in subduction zones, deep electric signals arising before earthquakes in seismooactive zones, nonstationary heat fields, some 3D inhomogeneity and anisotropic media, some type of ionospheric sources, daily and bottom surface relief.

**GA1.02/E/23-A1** Poster **1605-12**

**QUASI-ANALYTICAL APPROXIMATIONS IN 3-D EM MODELLING**

Michael ZHDANOV and Gabor Hursan (both at the University of Utah, Department of Geology and Geophysics, Salt Lake City, UT 84112, USA, email: mzhdanov@mines.utah.edu ) Vladimir Dmitriev (Moscow State University, Moscow, 119899, Russia).

Quasi-linear (QL) approximation introduced by Zhdanov and Fang (1996) has been proved to be a powerful tool in 3-D EM forward modelling solution. It is based on an assumption that the anomalous electrical field within an inhomogeneous domain is linearly proportional to the normal field with some tensor coefficient called electrical reflectivity tensor. In this paper we introduce a new way to compute the QL approximation. It is based on a simple analytical formula for electrical reflectivity tensor calculation. This approach leads to construction of the quasi-analytical expressions for anomalous electromagnetic field for 3-D models. These solutions accelerate dramatically the forward EM modelling and make it practical an inversion over complicated 3-D inhomogeneous geoelectrical structures.

**GA1.02/E/36-A1** Poster **1605-13**

**THEORETICAL STATEMENT OF SEISMOELECTRICAL PROBLEM IN POROUS WATER-SATURATED MEDIA**

Boris S. SVETOV ( Geolectromagn. Res.Inst. RAS , Troitsk , Moscow reg., Russia, e-mail: svetov@geo.igemi.troitsk.ru), Valeriy P. Gubatenko ( State Techn. Univ., Saratov , Russia).

Rocks are porous water saturated media. As a result of electrolyte ions absorption double electric layers are appeared on the boundaries of solid and fluid phases. Under an influence of pressure gradient the fluid flow and electric current are occurred (an inverse electroosmosis). The current generates electric and magnetic fields. If a rock is in an alternating elastic field then such mechanism causes electromagnetic field generation. The interaction of elastic and electromagnetic fields in porous water-saturated medium may be described by complex self-consistent system of partial differential equations. The solution of the system is extremely severe. An approximate solution of the problem may be found by sequential solving of 4 subproblems: 1) Lamé equation for elastic field in the medium with effective parameters of Gassman. The result of the subproblem is a solid phase displacement  $U_s$ . 2) Averaged equations of fluidodynamics in porous fluidosaturated medium. Under known  $U_s$  a displacement of fluid phase  $U_f$  and pressure gradient  $\text{grad } P$  are found. 3) Averaged equations of electrokinetics. Convection electric current  $J_{ex}$  and electrokinetic coefficient  $Q$ , which connects the current with pressure gradient, are found. 4) Electrodynamic equations, in which the obtained convection current plays role of extrinsic current. The sources of this current and electric field are occurred in the areas where pressure gradients and petrophysical properties of medium (specific surface of porous space and permeability) are varied.

**GA1.02/E/37-A1** Poster **1605-14**

**ELECTROMAGNETIC SOUNDINGS IN POLARIZABLE MEDIA (RESULTS OF MODELLING)**

Vladimir V. Ageev and Boris S. SVETOV (both at Geoelectromagnetic Research Institute RAS, Troitsk, Moscow region, Russia, e-mail: svetov@geo.igemi.troitsk.ru ).

It is well known, that induced polarization (low frequency dispersion - LFD) of rocks influences on electromagnetic (EM) soundings results. Usually LFD is approximated by Cole-Cole formula with exponent  $C$ . The more  $C$  the faster IP process decays. Apparently the value of  $C$  is connected with the physico-chemical nature of IP process. It may be shown, that at some restrictions on polarizability  $C$  may be  $1 \leq C \leq 2$ . At these values IP decay becomes oscillating. Such processes may be observed in so named bianisotropic medium. The mathematical modelling of EM fields of electric and magnetic dipoles above conductive and polarizable sections was performed. It was established: 1) At transient soundings the greatest influence is observed in the late stage. 2) The IP influence on EM soundings depend on the type of source and receiver of the field. At galvanic excitation and reception of the field the IP influence is much more than at inductive ones. In the case and in the late stage IP process predominates at  $C \leq 3/2$ . Practically, in the case EM soundings are IP ones. 3) At inductive source electrodynamic process predominates at  $C \geq 1/2$ . In the case LFD of conductivity may lead to the increase of the depth of studies and of the resolution of the EM sounding. It corresponds to some degree to the experience of "high - resolution" electroprospecting. But in some cases IP distortions of EM sounding curves makes them non-interpretatable by standard present-day methods. In the form the problem of interpretation becomes nonunique. To make it unique it is necessary to perform and to interpret jointly different types of soundings.

**GA1.02/E/33-A1** Poster **1605-15**

**ON THE WAY OF TO THE EFFECTIVE SOLUTION OF TRANSIENT 3D MODELLING PROBLEM AND ITS APPLICATION TO GEOTHERMAL EXPLOURATION**

Elena Fomenko (Geoelectromagnetic Research Institute RAS, Troitsk, BOX 30, Troitsk 142092, Moscow region, Russia, Email: igemi@pop.transit.ru) Toru MOGI (Department of Earth Resources Engineering, Department of Earth Resources Engineering, Graduate School of Engineering, Kyushu University 6-10-1 Hakozaki, Higashi-ku, Fukuoka, 812-8581, Japan Email: tmogi@mine.kyushu-u.ac.jp) Tatsuya Kajiwara (JMC Geothermal Engineering Co. Ltd, Takizawa, Iwate, 020-01, Japan)

We have developed a new 3D modelling scheme of TEM data. The scheme based on the staggered grid finite difference formulation for electrical field (Newmann, 1995; Fomenko, 1998) with 'natural choice' continuous components of tangential electric field at the center of the edges and normal components of magnetic field at the center of each cell, opposite to well-known programs with discontinuous E-field at the face of the cells (Mackie and Madden, 1994; Smith, 1996; Weidelt, 1995). At first primary electrical field, excited by the electrical dipole source on the layered earth, is calculated. We introduced new kernels and extracted singularity analytically for halfspace kernel at all 3D grid in order to greatly accelerate the convergence of Fourier-Bessel integrals. Then secondary field, induced by the electrical charge accumulated at three-dimensional anomalous structures, is calculated in the frequency domain using BCGS-group methods. Due to 'natural choice' of components, all components of magnetic field are stably derived from derivatives of electrical field. At last transient vertical magnetic field is obtained from the Fourier transformation of the wide frequency range data.

**GA1.02/E/03-A1** Poster **1605-16**

**CONSERVATIVE MODELLING OF 3D ELECTROMAGNETIC FIELDS WITH NATURAL CHOICE CONTINUOUS COMPONENTS OF THE FIELDS FOR PERSONAL COMPUTERS**

Elena FOMENKO (Geoelectromagnetic Research Institute RAS, Troitsk, BOX 30, Troitsk 142092, Moscow region, Russia, Email: igemi@pop.transit.ru)

A new high effective 3D modelling scheme of MT data with conservation of electric current and magnetic flux is developed for personal computers. The scheme based on the staggered rectangular nonuniform grid finite difference (FD) formulation for the secondary electrical field with 'natural choice' continuous components of tangential electric field at the center of the edges and normal components of magnetic field at the center of face of each cell, opposite to well-known programs with discontinuous E-field at the face of the cells (Mackie and Madden, 1994; Smith, 1996; Weidelt, 1995). Due to 'natural choice' of E-field, all components of H-field are stably derived from curl E operation.

The speed of convergence of 13 band complex symmetrical system of linear equations was investigated for modern powerful BiCG methods. It is shown that good preconditioning of the matrix allows to decrease computation time in 10-20 times, especially for the low frequencies and high resistivity contrast, and greatly increase the accuracy of solution. The results are presented for Jacobi, SSOR and ILU preconditioners. During iterative process due to computer round-off errors Bi-CG vectors slightly lose orthogonality, it leads to appearance 'fictive currents' and greatly influences at the speed of convergence. The special module of correction of div-free current  $J$  was made similar to Smith's [1996] one, which allows greatly improve the speed of convergence and accuracy.

Due to effective combination good choice staggered grid, simple but effective preconditioner, support of div-free current  $J$  and powerful solvers program requires extremely small size of memory - 850 Kb/ 1000 nodes of the grid and allows obtain high accuracy for relative residual  $\|b - AX\|/\|b\| < 1.E-10$  within one-two hundreds iterations on the grids of medium dimensions - 30000 nodes. The obtained FD solution has the same accuracy as other FD and IE programs (Mackie, Wanameker, Weidelt et al) on the models of COMMEMI project and more fast speed of convergence than latter ones.

**GA1.02/E/38-A1** Poster **1605-17**

**MCMC INVERSION OF MT DATA IN 1-D SITUATIONS WITH PIECEWISE SMOOTH MODELS**

M. MENVIELLE (CETP, 4 Avenue de Neptune, F-94100 SAINT MAUR, FRANCE and Université Paris Sud, FRANCE), D. Marques, M. Roussignol (Université de Marne la Vallée, FRANCE) and M. Lavielle (Université Paris V, FRANCE)

In the Bayesian approach, the inverse problem solution can be obtained from a posteriori probability density function of the model parameters given the data and the a priori information. Stochastic algorithms based upon MCMC (Monte Carlo Markov Chain) methods have already been developed to solve the Bayesian inverse problems in MT 1-D situations with an a priori probability density function which favour smooth models. The domain under study is divided into a large number of thin horizontal homogeneous layers whose thickness is fixed, and the model parameters are the conductivity of each layer. For each layer, the a priori and a posteriori laws are digitised over a limited set of conductivity values.

We use the same approach with a modified a priori probability density function which favour piecewise smooth models. We present an application of this MCMC algorithm to the inversion of both synthetic and field magnetotelluric data.

**Tuesday 20 July AM**

Presiding Chair: M. Ingham (Victoria University of Wellington, NZ)

**GA1.02/E/30-A2** Poster **0930-01**

**PRELIMINARY RESULTS FROM AN MT-SURVEY AROUND IOANNINA AREA, NW GREECE**

G. BALASIS, N. Bogris, A. Abdulla and K. Eftaxias Solid Earth Physics Institute Panepistimiopolis, Zografos, Athens 15784, Greece

The magnetotelluric (MT) method is used towards the understanding of an eventual correlation, between the geoelectrical structure and the sensitivity of a region in recording Seismic Electric Signals. During the last years, MT measurements (frequency range 0.001-100 Hz) were made along a number of profiles, each one running approximately 20-30 km, that cross the Ioannina area in northwestern Greece. Mohr Circle Analysis as well as Groom-Bailey decomposition were applied to the full dataset defining dimensionality and strike. Preliminary results of modelling of the Ioannina electromagnetic response data using two-dimensional (2-D) inversion algorithms were also obtained.



**GA1.02/E/22-A2** Poster **0930-02**

**MAGNETOTELLURIC STUDIES OF THE KYRGYZ TIEN SHAN**

Vlad Batalev and Anatoly RYBIN (both at Scientific Station of the Institute for High Temperatures - Association, Russian Academy of Sciences, 720049, Bishkek, Kyrgyz Republic, E-mail: rybin@laurel.gdiric.ru)

Over a period of 15 years, magnetotelluric and magnetovariation measurements (more than 300 soundings of period range 0.1-1800 s and 10 long period sites) were collected along a series of long and short submeridional profiles across the Tien Shan interplate orogen in Kyrgyzstan.

Frequency analysis of the inhomogeneity and asymmetry MT parameters distribution and examination of Hilbert transform relationship had allowed to suggest a superposition of the regional 2D and local 3D electrical structures. After distortion impedance analysis and correction (static shift removing and Groom-Bailey decomposition) a 2D inversion was performed and revealed a highly conductive widespread zone at mid-low crustal depths (20-50 km) and narrow upper crustal conductor located near the regional fault systems.

One more interesting result was obtained at the Fergana range area. Extensive 2D modelling revealed a high resistivity (50000 Oh.m and more) structure along the Talas-Fergana deep fault. Estimated thickness is about 10 km, the length more than 150 km and the depth from 6-8 km to 40-50 km. Enigma consists of the object resistivity is essentially higher than is attributed to anyone of the high resistivity blocks for obtained geoelectrical model beneath the Kyrgyz Tien Shan.

Comparative analysis of electromagnetic images of mid and deep crust with velocity profiles from seismic tomography data had demonstrated a stable correlation of low resistivity with low velocity of seismic waves.

The fluid conception of the crustal electrical conductivity was suggested.

**GA1.02/W/28-A2** Poster **0930-03**

**INVERSION OF THE WEST CARPATHIANS GDS DATA FOR A THIN SHEET CONDUCTANCE**

V. Cerv(1), M. Menvielle(2,3), J. Pek(1), O. Praus(1) (1) Geophysical Institute, Acad.Sci. Czech Rep. Bocni II/1401, CZ-14131 Prague 4, CZECH REPUBLIC (2) Centre d'Etudes des Environnements Terrestres et Planetaires, CNRS/UVSQ, 4, Avenue de Neptune, F-91407 SAINT MAUR DES FOSSES CEDEX, FRANCE (3) Universite Paris Sud, F-91405 ORSAY CEDEX, FRANCE

Previous electromagnetic investigations carried out in the area of West Carpathians and the surrounding units, based on the distribution of the induction vectors and on available magnetotelluric data, evidence significant contrasts of the electrical conductivity in the middle and lower crust. The electromagnetic effects of the conductive asthenosphere at various depths on surface induction data is evaluated on the basis of the 3-D forward modelling and thin sheet approximation. For the modelling of the superficial layer an electromagnetic imaging program is used based on the thin sheet approximation. The sheet is digitised in homogeneous square cells, and a Markov chain is used to determine the a posteriori law of the conductance in each cell given the data and an a priori knowledge on the conductance. The obtained map of conductivity is presented and discussed in the tectonic framework of the region.

**GA1.02/W/19-A2** Poster **0930-04**

**A MAGNETOTELLURIC STUDY OF THE SEISMIC-ACTIVE REGION OF NORTHERN BOHEMIA**

Cerv V., Pek J. (both at Geophysical Institute AS, 141 31 Praha 4, Czech Republic, email: vcv@ig.cas.cz), De Santis A., Di Mauro D. (both at Istituto Nazionale di Geofisica, Rome, Italy, email: desantisag@ing750.ingrm.it), Manzella A., Volpi G. (both at C.N.R., International Institute for Geothermal Research, Pisa, Italy, email: adele\_m@irg.pi.cnr.it), Zaja A., Praticelli N. (both at Dip. Geologia, Paleontologia e Geofisica, Padua University, Padua, Italy, email: zaja@epidote.dmp.unipd.it)

A three-year Italian funded project allowed a cooperation between some Italian Institutions and the Geophysical Czech Institute with the objective of studying, from the electromagnetic point of view, the Northwest Bohemia (Czech Republic), a region interested by a peculiar seismicity characterised by micro-earthquake swarms occurring during apparently quiescent intervals between large macro-seismic swarms. During 1997, fifteen high-frequency magnetotelluric (MT) stations were installed in an area where 80% of the seismicity of the entire region has been recorded since 1986. This area showed a high electromagnetic noise, probably connected with the nearby industrial zone of Sokolov. 2D and 3D techniques were used to study and then model the MT characteristics. The results show a conductive structure in the depth range of 0.5 to 3 km that could be connected with the presence of the locally buried granitic massif. Models considering this shallow structure can explain most of the features found in the experimental data. The possibilities of detecting some conductive bodies connected to fracturation, thermometamorphism or paleofluids at the focal depth have been tested.

**GA1.02/W/13-A2** Poster **0930-05**

**ELECTROMAGNETIC STUDY OF CENTRAL ITALY**

De Santis A., Di Mauro D., (both at Istituto Nazionale di Geofisica, via di Vigna Murata, 605 00143 Rome, Italy; fax: +39065041181; email: desantisag@ing750.ingrm.it) Cerv V., Pek J. (both at Geophysical Institute AS, 141 31 Praha 4, Czech Republic; email: cv@ig.cas.cz)

During recent years Central Italy have been studied by means of a Magnetovariational technique. This research made it possible to propose 2-D models along several profiles of this area. In order to evaluate the effects of both the near surface sediments and the sea on our induction data, a novel conductance map of the investigated region is here presented and the contribution of the superficial layers is evaluated. Then a 3-D model is designed, whose the most evident feature is a deep conductive structure beneath the Apennines.

**GA1.02/L/03-A2** Poster **0930-06**

**SOME EXPERIMENTAL RESULTS OF "KOLA PROBE" PROJECT**

Fainberg, Ed., ABRAMOVA, L., Barsukov P., Vasilieva T., Kuksa Yu. Geoelectromagnetic Researches Inst. RAS. 142092 Troitsk, Moscow reg., box 30, Russia E-mail: abramova@geo.igemi.troitsk.ru

The experimental measurements were carried out at Kola Peninsula. The TEM-FAST system in one-loop configuration has been used in this experiment. The objective of the project was investigation of the induced polarization (IP) effect, estimation and monitoring of IP's parameters. Analysis of the field data allowed defining conclusions: Phase of the registered processes is opposite to a phase of inducing currents in the whole time-domain range; the amplitudes of the measured processes are proportional to cube of a loop size, while for

induction processes in near zone it should be proportional to a fourth degree of a loop size; magnetic susceptibility effects were not detected. Field data have been interpreted within the class of Cole-Cole models. Determined parameters of the models were used to construct synthetic sounding curves for the system with transmitter loop 4km\* 4 km and various configurations of receiving loops. Analysis of synthetic curves has shown that induced polarization processes can produce powerful negative signal in whole time-domain range. This work is supported by the Russian Foundation of Basic Researches, grant 97-05-64585.

**GA1.02/E/35-A2** Poster **0930-07**

**ANISOTROPY AND TERRAIN EFFECT ON MT DATA FROM TAURIDE TECTONIC BELT (SWTURKEY)**

Aysan GÜRER and O.Metin Ilkisik (both at University of Istanbul, Faculty of Engineering, Dept. of Geophysical Engineering, Avcilar Campus, Avcilar, 34850, Istanbul, Turkey, email: agurer@istanbul.edu.tr)

The Tauride belt has the most complicated geology among the six main tectonic belts of Anatolia. The collision tectonics between the African and Eurasian plates in Lower Miocene in the south lead to thickening in the crust and uplifting of the region. This resulted in development of Tauride mountain chain. The Hellenic subduction arc is one of the prominent tectonic events in the south of the region. The closure of Neo-Thethys Ocean in Late Cretaceous caused emplacement of the alloctonous units and formation thrust zones in western Taurides. These discontinuities are formed by late Miocene-Pliocene and Late Quaternary compression and Pliocene and Quaternary graben forming extension phases. The magnetotelluric (MT) studies were carried out in the western Tauride region in 1986, 1987 and 1997-1998 summers. A considerable anisotropy is observed in MT data from some certain sites that are located near to the strong terrain discontinuities. In some regions it is suspected that both of the topographic and tectonic discontinuities may contribute to the observed anisotropy together. It is important to separate the effects of the topography and subsurface tectonic structures on the MT responses especially in the regions where the geology is very complex. There are such MT sites on the 160 km long Elmalı profile in western Taurides. The terrain effect on the data from some selected sites along this profile will be removed by the distortion stripping off technique. As the result faults and 2D geological structures will appear more clearly on the MT sections by the separation of terrain and tectonic effects and deep relations of the fault and trust zones in the western Tauride belt that is situated in northern edge of Hellenic subduction zone will be explained more precisely.

**GA1.02/W/10-A2** Poster **0930-08**

**ANALYSIS OF DISTORTED GDS TRANSFERFUNCTIONS FROM THE PENNINIC ALPS OF EASTERN SWITZERLAND**

Marcus GURK (Groupe de Géomagnétisme, Institut de Géologie, Université de Neuchâtel, Rue Emile-Argand 11, CH 2007 Neuchâtel, email: marcus.gurk@geol.unine.ch)

We have carried out at least 64 MT and GDS soundings in the Alps of eastern Switzerland to get first information about the electrical conductivity distribution of this region. One of the main findings was an anomalous directional behaviour of the real induction arrows in the period range of T= 1-300 s on the mesozoic sediments (Bündnerschiefer). These sediments are situated between the Aar and Gotthard massifs to the North and the crystalline penninic nappes (Adula, Tambo and Suretta) to the South. Deep geoelectrical surveys in the Southern Alps revealed the existence of a substratum with high resistivity values (15 000 - 40 000 ohm). These values strongly suggest the existence of lateral conductivity contrasts of 1 to 10 000 and deep penetration depths of the electromagnetic field in the host medium from the mesozoic sediments. A particular geometry of the tectonic units in the investigation area leads to the assumption that telluric currents induced in remote areas and finally channelled in surface boundaries of the sediments are responsible for the anomalous directional behaviour of the induction arrows.

The analysis of the GDS transfer functions yields following conclusions: 1) a spatial decoupling of induction processes. 2) the mesozoic sediments in the investigation area are local conductive inhomogeneities. 3) a remote L shaped crustal conductive structure of regional extension with an azimuth of 45°N can cause the observed magnetic distortion of the GDS data

**GA1.02/E/14-A2** Poster **0930-09**

**CONDUCTIVITY OF EARTH CRUST AND UPPER MANTLE OF UKRAINE**

SERGEY KULIK, Tatjana Burakhovich (Institute of Geophysics of National Academy Science of the Ukrainian, Palladina str. 32, Kiev,252680, Ukraine, 252 Email: kulik@sabbo.net)

After a long time of studies by methods of magnetotelluric sounding and magnetovariation profiling a great amount of experimental material has been accumulated for construction a map of electro-conductivity of Earth crust and upper mantle using a technique of 2D and 3D modelling of magnetotelluric field. As a result, we received new data on electro-conductivity in different geological areas from procmbrrian crystalline Ukrainian Shield to alpine Ukrainian Carpathian Mountains. It's shown that contact between old East - European and more young West-European platforms is characterized by a series of high conductivity anomalies on depths of 20-30 km and width of anomalous areas of 50-60 km. In some cases, conductivity anomalies lie in the Earth Mantle on depths from 50 to 120 km with the resistance - 20 Ohm. A 600 km long anomaly is found on the Ukrainian Shield. In hercinian areas of Dnipro- Donec fault and Donbas electro-conductivity anomalies lie on depths from 10 to 20 km with the total longitudinal conductivity up to 10000 S. In Crimea's cimerids a conductor lies at the depth of 110 km and in the western Crimia an area of conductivity was discovered in the crust and upper mantle. Alpine Carpathian Mountains are characterized by the Carpathian conductivity anomaly at the depth of 12 km. It is possible to separate the nature of anomalous areas into two basic types. The first type consists of anomalous objects where increased conductivity is defined by the specific composition of ore elements in the Earth crust, like a possible presence of grafitisides or accumulation of ore elements. The second type consists of objects with increased conductivity and also anomalously high values of heat flow. A presence of highly mineralized fluids and anomalously high temperatures at big depths and consequently, partly melted rocks, caused by tectonical activation is probable there. In number of places horizontal size of areas of increased electro-conductivity is significantly bigger than size of heat flow anomalies. In other places spatial position of geo-electrical and heat flow anomalies coincides.

**GA1.02/W/38-A2** Poster **0930-10**

**CHARACTERIZATION OF THE TRANSITION ZONE BETWEEN SOUTH PORTUGUESE AND OSSA MORENA ZONES FROM MT DATA AND RHEOLOGICAL PROFILES**

Eugenio ALMEIDA, Fernando Santos, L. A. Mendes-Victor (Centro de Geofisica da Universidade de Lisboa, R. Escola Politécnica, 58, 1250 Lisboa, Portugal, email: dfams@fc.ul.pt) Jaume Pous, Alex Marcellou, Pilar Queralt (Departament de Geodinamica i Geofisica, Universitat de Barcelona, Marti Franques s/n, Barcelona, Spain, email: jaume@naturag.ub.es)



The transition between the South Portuguese Zone (SPZ) and the Ossa Morena Zone (OMZ) is made up of a major geosuture, which is indicated by the Beja-Acebuches ophiolite. Several geological data suggest that this suture is a result of an oblique collision, with a northward propagation, between SPZ and OMZ.

With the aim to characterize this transition zone Universities of Lisbon and Barcelona carried out a magnetotelluric survey. The 2D inversion model obtained, from 20 MT sites, revealed a large conductivity body (<10 Ohm m) with depth and thickness increasing from south to north. Considering heat flow values and seismic models, average rheological profiles were calculated for OMZ and SPZ. Average values of thickness and total strength of the lithosphere were estimated from those profiles. The observed distribution of seismic focal depths, in those zones, correlates well with depths suggested by the rheological profiles. A good correlation between soft layers and low electrical resistivity layers is also observed.

**GA1.02/W/15-A2** Poster **0930-11**

**A THREE-DIMENSIONAL MAGNETOTELLURIC INVESTIGATION OF THE VILARIÇA DEPRESSION (NE PORTUGAL)**

Fernando SANTOS, Liliãna Matos, Luís Mendes- Victor (Centro de Geofísica da Universidade de Lisboa, R. Escola Politécnica, 58, 1250 Lisboa, Portugal, email: dfams@fc.ul.pt ) António Mateus (Departamento de Geologia da Universidade de Lisboa) and Eugénio Almeida (Instituto Politécnico Tomar)

Magnetotelluric observations were carried out at 30 locations on the main tectonic depression associated with the Manteigas-Vilariça-Bragança fault, in northeast Portugal. The Vilariça Fault Zone (VFZ) is one of the major elements of the late Hercynian strike-slip network in the NW Iberia and the Vilariça depression (20 km long and 2-3 km wide). It is an example of intraplate neotectonic activity, since it is a pull-apart basin resulting from left-lateral strike-slip displacement of the VFZ during Quaternary times.

A three-dimensional magnetotelluric model of the studied zone was constructed based on the preliminary two-dimensional interpretation of three magnetotelluric profiles across the depression. The main tectonic structure represented by the segment of the Vilariça fault, oriented NNE-SSW, is well displayed in the model. The Quaternary sedimentary fill of the depression is expressed by low resistive bodies, surrounded by more resistive bodies, which are associated with metasedimentary formations which are overlying a high resistive gneissic basement.

**GA1.02/W/40-A2** Poster **0930-12**

**FIRST ELECTRIC FIELD OBSERVATIONS IN THE CAM-1 CABLE BETWEEN MADEIRA AND LISBON**

Fernando SANTOS, António Soares, Jorge Miranda, Luís Mendes-Victor (Centro de Geofísica da Universidade de Lisboa, R. Escola Politécnica, 58, 1250 Lisboa, email: dfams@fc.ul.pt) and the ISO-3D Group.

The voltage difference between the ends of the CAM-1 cable, a retired telephone cable between Madeira Island and Lisbon, has been monitored since November 1998. The cable is 1,100 km long and its end, near Lisbon (Portugal), is grounded to the ocean bottom. A previous analysis of the cable, carried out before the installation of the instrumentation, showed that the cable conditions have not significantly changed during the last year. Monitoring of the cable is being done at a sampling rate of 1 s but only the average values, taken over 30 s, are recorded. We present the first months data series, a preliminary analysis of the results and we discuss the possibilities open with the availability of this cable to regional scale studies. A new MT station in Porto Santo (Madeira) is foreseen to allow ocean transport and Earth electrical structure modelling.

**GA1.02/W/14-A2** Poster **0930-13**

**THE COMBINATION OF LARGE SCALE DC AND MAGNETOTELLURICS**

E. SCHNEIDER, J.B. STOLL (both: Institute of Geophysics, University of Goettingen, Herzberger Landstr. 180, 37075 Goettingen, Germany, email: edgar@geo.physik.uni-goettingen.de)

Layers of a high electrical conductivity are often found in the middle crust of central Europe. The MT-method is sensitive to high conductivities, so the top of such a layer can be resolved quite well whereas the bottom is hard to detect. In contrast, DC-sounding is sensitive to high resistivities. The combination of both methods can increase the resolution of the electrical parameters of the earth. Theoretical work about this combination was already done in the past, but field data is very rare. With a new generator/transmitter system the university of Goettingen can achieve a long scale field setup with transmitter-receiver distances of more than 50km. The poster presents measurements made in the Muenchberg gneissic massif, a crystalline nappe in the variscian part of southern Germany. The MT data reveals apparent resistivities lower than 1 Ohm\*m. Aim of the combined analysis is the resolution of a shallow layer of high conductivity.

**GA1.02/W/04-A2** Poster **0930-14**

**JOINT INTERPRETATION OF FOUR GEOPHYSICAL METHODS FOR THE DETERMINATION OF THE ELECTRIC RESISTIVITY IN THE UPPER CRUST**

Klaus Spitzer, Bernhard Fluche (Joint Geoscientific Research Institute, Stilleweg 2, D-30655 Hannover, Germany. Email: klaus.spitzer@gga-hannover.de, bfluche@gga-hannover.de) Wolfgang Storz (Hydrogeologie GmbH, P.O. Box 1330, D-04855 Torgau, Germany, Email: HGNTorgau@aol.com)

Within the framework of a research programme, field measurements with four different geophysical methods (well logging, DC geoelectric soundings, magnetotellurics (MT) and vertical gradient method) were carried out in the central part of Germany. The objective of this research program was to combine different geophysical methods for an integrated interpretation of the subsurface structures and to better understand the physics of the involved current systems.

On seven sites - five of them lay on a profile with a length of 50 km - magnetotelluric measurements have been carried out and were accompanied by DC soundings. At almost each site measurements with different electrode configurations have been performed. Additionally, at the central site also bore hole and vertical gradient measurements were conducted. One result of this project was to show the correlation between the DC sensitivities and the static shift in the MT measurements, another one to give an interpretation of the MT data with a reasonable resistivity model and the correction of the shifted MT data.

The distribution of the electric resistivity is investigated with electric and electromagnetic methods covering scale lengths varying over orders of magnitude. Borehole measurements yield information on the resistivity in close vicinity of the hole (metre range) whereas DC soundings penetrate into a depth of some hundred metres and MT measurements up to 100 km. In order to eliminate the static shift from the MT data the vertical gradient method was also applied. This method is similar to MT but the horizontal electric field components are replaced

by the vertical gradient of both horizontal magnetic field components obtained by measurements on the surface and in a bore hole. Since the conductance at this location is known then distorted MT data can be corrected.

**GA1.02/W/02-A2** Poster **0930-15**

**RESULTS OF MAGNETOTELLURIC MEASUREMENTS IN CENTRAL GERMANY AS A PART OF A JOINT INTERPRETATION**

Bernhard FLUCHE, Klaus Spitzer (Joint Geoscientific Research Institute, Stilleweg 2, D-30655 Hannover, Germany. Email: bfluche@gga-hannover.de, klaus.spitzer@gga-hannover.de) Wolfgang Storz (Hydrogeologie GmbH, P.O. Box 1330, D-04855 Torgau, Germany, Email: HGNTorgau@aol.com)

In 1996, magnetotelluric (MT) measurements were carried out in a region in the central part of Germany. These measurements were part of a campaign where different geophysical methods - borehole measurements, DC soundings and the vertical gradient method - were conducted besides MT. The area was located at the northern edge of the Central German Crystalline Zone. The geology of this region can be described by almost horizontally layered tertiary sediments with a slight dip from NW to SE. Underneath, these layers are followed by the zechstein base in approximately one km depth. In the northwestern part the measuring area is confined by the Rhoean mountains.

The MT measurements and DC soundings were carried out at five sites along a profile of 50 km length. The raw MT data seem to be rather uniform at all sites. After determining a nearly frequency-independent Swift angle of approximately 40 degrees a remarkable splitting of the apparent resistivity curves for both polarization modes is achieved. The direction of the Swift angle corresponds to the main geological strike. The splitting can either be explained by an anisotropic crust or by a rather simple 2D-resistivity model which matches most of the observed data in a wide period range. We prefer the latter explanation because of the geological situation of this region. While the phases could be explained well, discrepancies occurred in the fit of the resistivity curves. As a reason for this misfit we assume a static shift effect at least at one site. It is planned to find a procedure to eliminate this effect by using the results of the vertical gradient method and the DC sensitivities.

**GA1.02/E/04-A2** Poster **0930-16**

**MAGNETOTELLURIC STUDY OF THE TETHYAN SUTURE ZONE, ROMANIA**

Dumitru STANICA (Geological Institute of Romania, 78344 Caransebes Str.,1, Bucharest 32, Romania, Email: stanica@ns.igr.ro)

Magnetotelluric measurements have been carried out at 28 locations along a 320km west-east profile, crossing the Tethyan Suture Zone, which represents a complex tectonic unit constituted of ophiolitic and sedimentary formations, belonging to the Tethyan oceanic crust. The impedance tensor decomposition technique has been used to derive regional 2D resistivity and phase responses corresponding to the electromagnetic induction in orientation parallel and perpendicular to both the Tethyan suture and the major structural units. The model obtained by using 2D forward modelling (finite element method) reveals a large conductive zone (about 20km wide) to be associated with the Tethyan suture, placed between two blocks of continental crust: Inner Dacides (having a thickness of 22 - 25km), towards west, and Median Dacides (with a thickness of 28 - 30km), towards east.

**GA1.02/E/16-A2** Poster **0930-17**

**A DENSE MT PROFILE ACROSS THE IAPETUS SUTURE ZONE IN S.W. SCOTLAND**

S.TAUBER (1), O.Ritter (2), G.Dawes (1) and R.J.Banks (1), (1) Dept. of Geology and Geophysics, The Univ. of Edinburgh, UK, (2) GeoForschungsZentrum Potsdam, Germany

The resolution of MT is inherently limited by the attenuation of the electromagnetic fields. Nonetheless relatively thin vertical conductors associated with fault and shear zones have been detected in recent MT studies indicating the ability of the MT method to map zones of past or present zones of weakness in the earth crust. Previous MT profiles across the Iapetus Suture in southern Scotland and central Ireland have detected a highly conductive middle crust. The observations, limited in spatial density and frequency range, and of mixed quality, have been interpreted as indicating a quasi-continuous horizontal conductor at depths of 8-12 km, rising to less than 5 km at the inferred location of major faults and shear zones. A new MT profile with increased site density and frequency range crosses the suture zone in S.W. Scotland. The profile crosses a major fault, a ductile shear zone, and a number of outcrops of black shales which mark the base of thrust wedges, all created during the Caledonian orogeny and closure of the Iapetus ocean. In addition, the area is cut by later faults which have caused differential uplift of the Caledonian rocks along strike, affording "windows" to different structural levels. The principal cross-strike profile is supplemented by measurements on shorter parallel profiles and observations along the strike. 2-D inversion modelling suggests that high conductivity occurs in a number of thin vertical blocks (rather than a continuous layer) that correlate with the black shale outcrops.

**GA1.02/W/11-A2** Poster **0930-18**

**LONG OFFSET TENSOR APPARENT RESISTIVITY STUDIES OF THE TAUPO VOLCANIC ZONE, NEW ZEALAND**

H.M. BIBBY, T.G. Caldwell and G.F. Risk (Institute of Geological and Nuclear Sciences, PO Box 30-368, Lower Hutt, New Zealand. Email: h.bibby@gns.cri.nz)

The Taupo Volcanic Zone (TVZ) is the centre of rhyolite volcanism in New Zealand and is characterised by large-scale ignimbrite eruptions, numerous caldera centres and more than 20 active geothermal systems. Three long-offset multiple-source (tensor) bipole-dipole surveys, which together span the width of the TVZ, have been used to determine the resistivity structure down to depths of 5-8 km. These data have been interpreted using the constraints provided by extensive shallow (< 1 km) resistivity mapping made with the Schlumberger array.

The deep resistivity structure defines three distinct regions within the TVZ, with boundaries approximately parallel to the eastern margin. These zones appear to reflect the tectonic and hydrothermal processes that are occurring within the TVZ. The eastern zone of the TVZ is about 15 km wide and is characterised by highly conductive rocks (< 10 &#61527.m) that extend that extend from about 2 km to at least 3.5 km depth. The conductive nature of these rocks is believed to reflect clay minerals within volcanoclastics which have infilled a series of overlapping and coalescing calderas. About 70% of the geothermal discharge of the TVZ (4200 MW) occurs through this region. To the west of this zone lies the Taupo Fault Belt, beneath which resistivities are an order of magnitude higher (>300 &#61527.m) to depths of at least 7 km. In contrast to the eastern zone, the Taupo Fault Belt has low heat flux, high seismicity and is undergoing rapid tectonic extension. The third zone occurs at the west of the TVZ is conductive at depths below 500m, reflecting thick ignimbrite sheets whose low resistivity is believed to be caused by clay minerals produced by diagenetic alteration.

The resistivity observations support a model of convective heat transport in the TVZ. The thickness of high resistivity in the Taupo Fault Belt constrain the depth of the base of the convective zone that in turn represents the transition from brittle to ductile behaviour in the TVZ.

**GA1.02/E/31-A2** Poster **0930-19**

**A MAGNETOTELLURIC STUDY OF THE CENTRAL VOLCANIC REGION, NEW ZEALAND**

Malcolm INGHAM (Institute of Geophysics, Victoria University of Wellington, PO Box 600, Wellington, New Zealand, email: Malcolm.Ingham@vuw.ac.nz)

The Central Volcanic Region (CVR) of is a wedge-shaped area in the central North Island within which lie nearly all of New Zealand's active volcanoes and geothermal fields. Previous geophysical studies indicate that the CVR has a thin crust overlying a highly anomalous mantle. Earlier magnetotelluric soundings and bipole-dipole resistivity data have shown that within the eastern part of the CVR low resistivity exists at depths beneath about 1-2km. Little is known, however, of the deep resistivity structure of the region and how this relates to the extensive volcanic and geothermal features.

New broadband magnetotelluric soundings have been made on a transect of the CVR in the vicinity of Rotorua where the CVR has a width of about 75km. Initial indications are that the results confirm a sharp decrease in resistivity across the eastern boundary of the CVR but present a much more complex structural picture in the western part of the region.

**GA1.02/E/11-A2** Poster **0930-20**

**ELECTRICAL STRUCTURE OF THE HIKURANGI MARGIN, NEW ZEALAND**

Malcolm INGHAM (Institute of Geophysics, Victoria University of Wellington, PO Box 600, Wellington, New Zealand, email: Malcolm.Ingham@vuw.ac.nz) Kathy Whaler (Department of Geology & Geophysics, University of Edinburgh, Kings Buildings, West Mains Road, Edinburgh EH9 3JW, UK, email: kathy.whaler@ed.ac.uk) Don McKnight (Institute of Geological & Nuclear Sciences, PO Box 30368, Lower Hutt, New Zealand, email: d.mcknight@gns.cri.nz)

Broadband magnetotelluric soundings have been made at over 40 locations along and across the Hikurangi Margin on the east coast of the North Island of New Zealand. A 2D inversion of data from 19 sites along a 130km transect crossing the central southern part of the Margin shows a considerable variation in electrical resistivity structure. The onshore part of the Hikurangi forearc, comprising Cretaceous to Pliocene sediments is marked by a resistivity of less than 10 ohm-m down to a depth of about 5km. Further west exposed Mesozoic greywacke basement has a much higher resistivity. At the north-west end of the transect low resistivity to several kilometres depth corresponds to the Tertiary sediments of the Wanganui Basin. Beneath the eastern part of the transect there is no clear indication of a low resistivity zone associated with the top of the subducted plate at around 10-15km depth. Seismic refraction data from this part of the Margin similarly does not require a low velocity zone at the plate interface although amplitude modelling of seismic data from 100km further to the south-west does suggest the existence of such a feature. Data and results from both this transect and a second transect further to the south will be presented.

**GA1.02/W/21-A2** Poster **0930-21**

**THE COAST EFFECT IN GEOMAGNETIC PULSATIONS AT ANTARCTIC OBSERVATORY DUMONT D'URVILLE KLEIMENOVA N.G., KOZYREVA O.V., BITTERLY J., SCHOTT J.-J.**

The many years geomagnetic pulsations observations at Dumont d'Urville observatory show an unusual large enhancement of the vertical Z-component relating to the horizontal ones. This effect could be caused by induction ocean electric currents along coast line where this station is located. The frequency distribution of the geomagnetic transfer function for the daytime cusp pulsations has been analyzed. It was found that the value of this function is strongly and nonlinear depended on the pulsation frequency. The preliminary result showed some almost constant frequency maxima at about 2.0-2.5 MHz, 11-13 mHz, 20-25 mHz, 30-32 mHz, 38-42 mHz. The spectral distribution in frequency range 2-10 mHz may change from one event to another. The transfer function dependence on the geomagnetic activity, local time and season has been studied.

**GA1.02/E/01-A2** Poster **0930-22**

**A GEOMAGNETIC INDUCTION STUDY ACROSS THE EAST COAST OF AUSTRALIA, AND ITS RELEVANCE TO HIGH-RESOLUTION AEROMAGNETIC SURVEYS**

Peter R. MILLIGAN (Australian Geological Survey Organisation, GPO Box 378, Canberra, ACT 2601 Australia, email: Peter.Milligan@agso.gov.au) Adrian Hitchman (Research School of Earth Sciences, Australian National University, Canberra, ACT 0200 Australia, email Adrian@rse.ses.anu.edu.au) F.E.M. (Ted) Lilley (Research School of Earth Sciences, Australian National University, Canberra, ACT 0200 Australia, email: Ted.Lilley@anu.edu.au)

Geomagnetic variations measured close to a coastline usually show an enhanced vertical (Z) component. This is known as the "coast effect" (CE), and has been well documented by many studies at various continental margins for longer period variations (several minutes to many hours). The effect at micropulsation periods (a few seconds to several minutes) is relatively unknown.

At mid-latitudes, total field (F) variations, as measured by airborne surveys, also include influences from the CE, as Z variations provide a significant input to F. Most CE studies have not included information on F, which is important for accurate reduction of airborne magnetic survey data.

Time variations in three components of the geomagnetic field were recorded along a profile across the east coast of Australia, from the deep ocean to well inland. The instruments all used high-resolution ring-core fluxgate sensors, and sampled at 10 s or better. Z variations at long periods show the classical CE, although at short periods induction vectors at the coast point south, parallel to the coast. Close to the coast, induction at short periods may be complicated locally by a river and its estuary. F variations are more complex than Z, particularly at short periods - at the coastline, they are reduced in amplitude, but display a phase reversal and amplitude enhancement offshore.

**GA1.02/W/18-A2** Poster **0930-23**

**IMPLICATIONS OF DEEP RESISTIVITY STRUCTURE OF THE TAUPO VOLCANIC ZONE, NEW ZEALAND**

Y. Ogawa, S. Takakura, T. Uchida, N. Matsushima, T. Toshi, Y. Nishi (Geological Survey of Japan, Tsukuba, 305-8567, Japan, email: oga@gsj.go.jp) T.G. Caldwell, H. M. Bibby, S. L. Bennie (Institute of Geological and Nuclear Sciences, Lower Hutt, P.O. Box 30368, New Zealand)

We investigated the resistivity structure of the crust and upper mantle across the Taupo Volcanic Zone (TVZ) of North Island, New Zealand, which is a region of back-arc extension.

We had 16 wide-band (0.01-1800s) sites and 8 long period (20s -13,000s) sites along a 150km profile. Induction arrows and impedance decompositions support a regional strike of N45deg E. A deep resistivity model obtained after 2D inversions showed the followings. (1) The surface conductors down to 5km depth correspond to known caldera structure and active geothermal fields. (2) A deeper conductor (at 15km) was found beneath the Taupo Fault Belt (TFB), consistent with the seismic Moho depth and the seismic reflective layer offshore. This location also coincides with the area of concentrated extension inferred from recent GPS data. These suggest that the conductor is a magmatic melt. (3) Upper mantle beneath TVZ below 20km depth is relatively conductive. Consistency with a region of high seismic attenuation suggests a partial melting zone.

**GA1.02/L/AW2-A2** Poster **0930-24**

**SWELL: MAGNETOTELLURIC INVESTIGATION OF THE HAWAII HOT-SPOT**

ANTONY WHITE and Graham Heinson (School of Earth Sciences, Flinders University, GPO Box 2100, Adelaide 5001, Australia, email: antony.white@flinders.edu.au, graham.heinson@flinders.edu.au) Steven Constable (Scripps Institution of Oceanography, La Jolla, CA 92093-0225, USA, email: sconstable@ucsd.edu)

From April to December 1997, 8 ocean floor magnetotelluric sites and 8 hydrophone sites were occupied in a joint MT/seismic study of the Hawaii Swell. The MT objective of the experiment was to image melt accumulation beneath the 1000 km wide, 1 km high area of the swell. MT and geomagnetic depth sounding estimates over periods of 600-100,000 seconds were obtained.

The ocean floor electric field was remarkably uniform across all sites; this is a common feature seen in ocean floor MT experiments. In conjunction with land magnetic field variations measured on Hawaii this produces a 1-D inversion showing uniform conductivity of 10 ohm-m to great depth beneath Hawaii itself. In general, the MT data range from >100 ohm-m at short periods to 10 ohm-m at long periods and show effects due to the Hawaiian Islands and their associated bathymetry. A 2-D inversion which includes bathymetry suggests that a molten layer (< 20 ohm-m) rises beneath the island chain by about 50 km vertically and over a lateral scale of 400 km.

**GA1.02/L/AW1-A2** Poster **0930-25**

**SWAGGIE: SOUTHERN WATERS OF AUSTRALIA GEOELECTRIC AND GEOMAGNETIC INDUCTION EXPERIMENT**

ANTONY WHITE and Graham Heinson (School of Earth Sciences, Flinders University, GPO Box 2100, Adelaide 5001, Australia, email: antony.white@flinders.edu.au, graham.heinson@flinders.edu.au) Steven Constable (Scripps Institution of Oceanography, La Jolla, CA 92093-0225, USA, email: sconstable@ucsd.edu) Peter Milligan (Australian Geological Survey Organisation, GPO Box 378, Canberra, ACT 2601, Australia, email: pmilliga@agso.gov.au) Ted Lilley (Research School of Earth Sciences, Australian National University, Canberra, ACT 0200, Australia, email: Ted.Lilley@anu.edu.au)

In April-May 1998, 53 magnetotelluric (MT) and magnetometer sites were occupied to study the crustal structure of the southern margin of Australia. Of these, 23 were land sites on Eyre Peninsula, South Australia, 18 were long period (40-100,000 seconds) marine MT sites and 12 were short period (0.1-1000 seconds) shallow marine MT sites. The marine instrument array stretched from the coastline, across the continental shelf, and into the deep ocean. It thus extended the investigation of the Eyre Peninsula Anomaly (EPA), a major linear electrical conductivity structure, of 3,000-10,000 Siemens total conductance, which has previously been mapped from the coastline to about 500 km inland. The marine data show that the EPA can be traced to the edge of the continental shelf, confirming it as a continuous crustal feature associated with major regional tectonic faulting.

High frequency MT results were dominated by the oceanic swell whose EM signal was several orders of magnitude larger than that induced by ionospheric activity. This signal was also evident in towed magnetometer and self potential (SP) data. 500 km of this latter data revealed a strong marine SP anomaly of up to 200 mV. There is little correlation of the SP and magnetic data, suggesting a non-ferrous source. It is possible that the SP signal is associated with graphite mineralisation within a mylonite zone evident in southern Eyre Peninsula, but not directly coincident with the conductivity anomaly.

**GA1.02/L/01-A2** Poster **0930-26**

**GEOELECTROMAGNETIC INVESTIGATION AT SEYMOUR ISLAND, ANTARCTICA**

M. Mamanf (1), D.Trad (2), B.Castiglione (3) (1)Univ. Nac. de La Rioja; CONICET, Ortiz de Ocampo 1700. La Rioja. (2)CONICET, Mendoza, Argentina (3)Univ. Nac. de La Rioja y Univ. Nac.de Cuyo, Argentina.

In order to investigate the near surface conductive layers at Seymour island, next to Antarctic peninsula, four magnetotelluric soundings were carried out (Mara 1,2,3 y 4) in 1996. Three soundings were performed on the central plateau and the fourth next to the coast. Electromagnetic recordings in the range of periods from 0.0025 s to 250 s were obtained in each location, aparted 1400 m each other. Recorded data in one place (Mara3) were found to be noise contaminated, due to the proximity of Base. A robust program was used for processing and the three soundings on the plateau were principally used for the interpretation. All sites show a similar results: on the plateau 1D modellings give an estimation for the depth of permafrost's bottom of 170 m with 53 - 98 ohmm. Toward the coast the permafrost becomes thinner and more conductive. The sub permafrost has a thickness of 300 m with a resistivity less of 3 ohmm. An average thickness of 5 km for the sedimentary cover was estimated at the plateau with a resistivity less of 10 ohmm and constituted by Tertiary and upper Cretacic formations in agreement with previous MT soundings (Fournier et al 1980).

**GA1.02/E/27-A2** Poster **0930-27**

**GEO-ELECTRICAL STRUCTURE UP TO LOWER MANTLE DEPTHS BENEATH INDIAN REGION DERIVED FROM 27-DAY VARIATION AND ITS HARMONICS**

E. CHANDRASEKHAR (Indian Institute of Geomagnetism, Dr. Nanabhoj Moos Road, Colaba, Mumbai - 400 005, India, e-mail: esekhar@iig.iigm.res.in)

C-response function estimates have been determined by Z:H method, utilizing two years of continuous records of geomagnetic data, recorded during 1975-77, at a chain of 13 stations, encompassing Himalayan collision boundary, confined to 75 E longitude band, extending from equatorial to polar regions. This unique latitudinal distribution of stations has facilitated to test statistically, the validity of P<sub>1</sub>N<sub>0</sub> assumption of the inducing field. With the combined analysis of Sq and 27-day variation and its harmonics, an integrated conductivity-depth profile is obtained, involving all stations. The derived conductivity profile has shown that the internal structure of the Earth beneath the Indian region could be viewed as a stack of inhomogeneous layers from surface up to a depth of 1200 km. In the depth range of about 850 km, the



presence of "mid-mantle conductor" is observed, compatible with the other regional and global models. The tectonic interpretation of the derived conductivity-depth profile and its correlation with seismic wave velocity profile is discussed. Statistically reliable C-response estimates at individual sites are obtained only for 6 stations, situated in mid-latitude region. Single site response estimates have revealed that at stations north of Himalayan boundary, the obtained depth estimates are rather low, compared with those, obtained at stations situated south of Himalayan boundary. It is still not clear, whether Himalayan collision boundary can be treated as a major discontinuous boundary, even at lower mantle depths. The average depth of perfect substitute conductor in Indian region, at stations free from lateral heterogeneities is found to be 1200 (+/-200)km with an average conductivity of 0.7 (+/-0.3)S/m.

**GA1.02/W/20-A2** Poster **0930-28**

#### ELECTRICAL CONDUCTIVITY STRUCTURE BENEATH THE BAY OF BENGAL

E. JOHN JOSEPH (Geological Survey of Japan, 1-1-3, Higashi, Tsukuba-shi, 305-8567 Japan, email: john@gsj.go.jp) H. Toh (Ocean Research Institute, University of Tokyo, Tokyo, 164 Japan) H. Utada (Earthquake Research Institute, University of Tokyo, Tokyo, Japan) R.V. Iyengar (Indian Institute of Geomagnetism, Colaba, Mumbai, India) J. Segawa (School of Marine Science and Technology, Tokai University, Japan)

Seafloor magnetometer array experiments were conducted in the Bay of Bengal to delineate the subsurface conductivity structure in the close vicinity of the 85 degree East Ridge and Ninety East Ridge (NER), and also to study the upper mantle conductivity structure of the Bay of Bengal. The experiments were conducted in three phases. Array 1991 consisted of five seafloor stations across the 85 degree East Ridge along 14 degree North latitude with a land reference station at Selam (SLM). Array 1992 also consisted of five seafloor stations across the 85 degree East Ridge along 12 degree North latitude. Here we used the data from Annamalai Nagar Magnetic Observatory (ANN) as land reference data. Array 1995 consisted of four seafloor stations across the NER along 9 degree North latitude with land reference station at Tirunelveli (TIR). OBM-S4 magnetometers were used for seafloor measurements. Geomagnetic Depth Sounding (GDS) method was used to investigate the subsurface lateral conductivity contrasts. Vertical gradient sounding (VGS) and horizontal spatial gradient (HSG) methods were used to delineate the depth-resistivity structure of the oceanic crust and upper mantle of the Bay of Bengal. The observed seafloor 3-component magnetic field variations show that the Electromagnetic induction process in the Bay of Bengal may be 3-dimensional. We made an attempt to solve this 3-D problem numerically and followed two approaches, namely (1) thin-sheet modelling and (2) 3-D forward modelling. Thin-sheet and 3-D forward model calculations jointly show that the observed induction arrows could be explained in terms of near surface features such as deep-sea fans of the Bay of Bengal, the 85 degree East Ridge and the sea water column above the seafloor stations. VGS and HSG responses provided depth-resistivity profile as a resistive oceanic crust and upper mantle followed by a very low resistive zone at a depth of 250-450 km. This depth-range fairly agrees with the seismic low velocity zone of the northeastern Indian Ocean, derived from seismic tomography. Thus we propose an electrical conductivity structure for oceanic crust and upper mantle of the Bay of Bengal.

**GA1.02/E/06-A2** Poster **0930-29**

#### CRUSTAL STRUCTURE IN THE KOYANA REGION OF WESTERN MAHARASHTRA, INDIA, USING MAGNETOTELLURIC STUDIES

C.K. RAO, S.G. Gokarn (Indian Institute of Geomagnetism, Colaba, Mumbai, email: kamesh@iig.res.in); Yasuo Ogawa (Geological Survey of Japan, Tsukuba, Japan, email: oga@gsj.go.jp)

Magnetotelluric studies were conducted along East-West profile in seismically active Koyana region of western Maharashtra passing through Guhagar-Karad-Vite. The survey region is covered by Deccan flood basalts. The impedances were decomposed and the strike angle estimated to be North three degrees East, which coincides with the strike direction of Western ghats in the survey region. The interpretation of the data shows the thickness of the Deccan flood basalts varies considerably along the profile. The thickness varies from 900 m at the western end of the profile to 200 m at the centre of the profile (edge of Western ghats). Towards eastern side the thickness varies from 2000 m to 600 m. The basement shows step like feature on entire profile. A conductive body of 20 ohm-m observed at the station 10 to a depth of about 3 km, beyond which sensitivity analysis failed to show the depth extent. This conductive body is understood to be a fault present in the region. Mid-crustal conductor is not seen in this region due to noise in the period range 1-10 sec. Lithosphere-asthenosphere boundary is observed at some of the stations at a depth of 100 km.

**GA1.02/W/32-A2** Poster **0930-30**

#### MAGNETOTELLURIC TRAVERSE ACROSS THE ARCHAEOAN PROTEROZOIC CONTACT IN SUKINDA COLLISION ZONE, EASTERN INDIA

K.K. ROY and S. Srivastava (both at Department of Geology and Geophysics, Indian Institute of Technology, Kharagpur - 721 302, India, Email: kkroy@gg.iitkgp.ernet.in) A.K. Singh (Department of Applied Earth Sciences, Delft University of Technology, Delft, The Netherlands)

Magnetotelluric survey was conducted across the low grade granite green stone belt of Archaean Singhbhum craton and Proterozoic high grade granulite terrain of Eastern ghats. 2-D RRI algorithm was used for interpretation of MT data. Use of rotation invariant parameters viz., determinant, central and average viz., apparent, resistivities and phases. The detailed study shows the faults located just north of the Sukinda collision zone could be detected and mapped by the parameters with minimum static shift effect viz., all the phases, the parameters generated out of magnetic transfer functions, magnetic components, twist and shear etc. RRI model gives 130km as the depth of the electrical lithosphere - asthenosphere boundary. The signatures for the vertical faults extended upto 12 to 15kms from the surface. Pseudo - 3D surface plots of apparent resistivities and phases show the signature of the Archaean - Proterozoic contact. Qualitative interpretation has a big role to play in Magnetotellurics. Most of the MT parameters totaling 30 have some role to play in MT data interpretation. They are non trivial. Since, rotation invariant parameters should be used for modelling and interpretation.

**GA1.02/E/0A2** Poster **0930-31**

#### ELECTROMAGNETIC INDUCTION EFFECTS IN GEOMAGNETIC FIELD VARIATIONS AT EQUATORIAL LATITUDES IN INDIA

R.G.RASTOGI, Department of Physics, Gujarat University and Physical Research Laboratory, Ahmedabad 380 009, India, e-mail: parvs@prl.ernet.in

The paper describes the abnormally large induction effects in the daily, seasonal and solar cycle variations of geomagnetic field at low latitude Indian stations. The frequency

dependence of the inductance effect is discussed from the observations of geomagnetic D, H and Z fields during counter electrojet. Solar flares, sudden storm commencements and other geophysical events. Various suggestions given by earlier workers are examined in the light of new observations.

**GA1.02/E/3A2** Poster **0930-32**

#### ELECTRICAL CONDUCTANCE MAP OF INDIA

T. HARINARAYANA and K. Naganjaneyulu (National Geophysical Research Institute, Hyderabad - 500 007, India, tel +91-40-7170141, fax +91-40-7171564, email: postmast@csngri.res.nic.in)

Electrical conductance is one of the important parameters in the interpretation of electrical and electromagnetic data. Study of the distribution of conductance parameter in a region helps to understand the subsurface geoelectrical structure. Based on the results obtained from about 500 shallow electrical resistivity soundings, 200 deep resistivity and magnetotelluric soundings and also the geological sections derived from a few deep seismic soundings and deep boreholes, an attempt has been made here for the first time to construct the regional electrical conductance map of India. Since the data is widely distributed more emphasis is given on the data from sedimentary basins, conducting regions such as rift zones, Alluvium covered areas etc. and the present study is limited to upper crustal depths. The map thus prepared shows a good correlation with major geological features. The regions in Arunachal Pradesh, Assam and Cambay region in western part show comparatively high conductance values of the order of 2000-4000 Siemens. The results of these studies are compared with other regional maps of India and discussed.

**GA1.02/W/24-A2** Poster **0930-33**

#### MAGNETOTELLURIC SURVEY OF TAIWAN

Chow-Son Chen (Institute of Geophysics, National Central University, Taiwan. Email: chusen@sal.gep.ncu.edu.tw)

The Island of Taiwan is located in the active boundary between the Philippine Sea plate and the Eurasian plate. The relative plate velocity between the Philippine Sea plate and Eurasian plate is at about 7.1 cm per year in the direction of about N50°W. While the Philippine Sea plate is subducting northwestward from the Ryukyu Trench in the northeast of Taiwan, the Eurasian plate is subducting beneath the Philippine Sea plate along Manila Trench in the south of Taiwan. Although this overall plate configuration in the vicinity of Taiwan has been well defined by seismicity, the composition and nature of the crust, which are closely correlated to the electrical structures, are basically unknown. The magnetotelluric investigation (MT) was undertaken during the recent three years with more than 50 soundings uniformly covering the Island of Taiwan. The Occam<sub>1</sub>s inversion, which produces a model that is maximally smooth in resistivity structure, was used to produce a 1D model for each sounding data. The organized 3D plot indicates that the resistivities variations observed to be closely correlated to the change of the surface geology of Taiwan down, at best, to a shallow depth of the upper 20 km. Beneath this depth, there exists a regional zone of sharply-decreasing electrical resistivity. The appearance of the low resistivity zone at depth about 20 km underneath Taiwan is both very interesting and significant. Based on the temperature estimates and some drill holes, it is probably caused by a structural zone with densely interconnected fluid phase. One possibility for the origin of such fluids is through dehydration of the crust, which has previously been invoked as an explanation for the common occurrence of low resistivities in the continental crust. In other words, the recent Taiwan Orogeny has formed an evident decollement structure in which the upper zone above the depth of 20 km exhibits entirely independent structural style from the lower one. MT observations seem to support the model of thin-skinned Taiwan orogeny.

**GA1.02/W/08-A2** Poster **0930-34**

#### UNDERSTANDING OF SEISMOTECTONICS THROUGH A WINDOW OF CRUSTAL CONDUCTIVITY

Y Fujinawa 1, N Kawakami2, J Inoue 2, Y Honkura3 1: Nat. Res. Inst. Earth Science and Disaster Prevention 2: Geothermal Energy Research and Development Co., Ltd. 3: Tokyo Institute of Technology

Wideband (0.002-20,000Hz) magnetotelluric measurements (MT) observations have been conducted along three traverses in the central Tohoku district of the northeastern Japan arc at 78 observation sites in order to image the conductivity profile. The experiment is expected to provide an example of more reasonable interpretation of seismo-tectonics in the crust based on results of conductivity measurement. Analysis is performed to obtain reasonable 2-D models using the MT impedance tensor corrected for the effects of the subsurface 3D conductivity heterogeneity. Smooth two-dimensional georesistivity models were obtained by applying the Generalized Rapid Relaxation Inversion (GRR) algorithm to the corrected impedance tensors assuming NS direction as the regional 2D structural strike, which is inferred from the tensor decomposition procedure, and is in general agreement with the strike of geological units. The whole crust is seen to be homogeneous in conductivity without enhanced conductivity in the lower crust where the resistivity is relatively high in agreement with results in the northern part of the Tohoku district, but in contrary to the stable continental crust. The northernmost cross section is more complex possibly because of the presence of Quaternary volcanoes and an active geothermal source area in the vicinity. The resistivity profiles delineate clearly two clear near surface conductive anomalies in the fracture zone between the Dewa Hill and Central Basin Range and in the Kitakami, Abukuma river regions of Quaternary or Tertiary sediment as well as several smaller resistivity anomalies. Conductors or their boundaries in the crust in the west of the Sekiryu Mountain Range generally correlate well with mapped faults or pre-Tertiary tectonic lines and seismicity. And several buried fault are suggested from the earthquake hypocenter and conductivity distribution. The conductivity distributions, seismic velocity and active fault are combined to interpret the seismo-tectonics and geologic regime associated with the subduction processes.

**GA1.02/W/22-A2** Poster **0930-35**

#### CONSTRAINTS ON THE ELECTRICAL CONDUCTIVITY BENEATH THE JAPAN SEA BY MT RESPONSE OF THE JAPAN SEA CABLE (JASC)

Tadanori GOTO (Aichi University of Education, Kariya, Japan), Hisayoshi Shimizu, Hisashi Utada (University of Tokyo, Tokyo, Japan), Yoshikazu Tanaka (Kyoto University, Kumamoto, Japan), Kiyofumi Yumoto (Kyushu University, Fukuoka, Japan), Valerian Nikiforov (Pacific Oceanographic Institute, Vladivostok, Russia), Nick Palshin, Renat Renat Medzhitov, and Leonid Vanyan (Shirshov Institute of Oceanology, Moscow, Russia)

Electrical potential difference between Nakhodka (Russia) and Naoetsu (Japan) has been observed by using the Japan Sea Cable (JASC) since 1996. Our aim in this study is to estimate MT response by using the JASC potential data, and to constrain the conductivity structures



beneath the Japan sea and the West Pacific region. MT response was obtained from the observed JASC voltage for the frequency range from 300 to 30,000 seconds. Magnetic data from several observatories were used for testing the inhomogeneity of the source field. Three-dimensional forward modelling, using a code by Mackie et al. (1993), was carried out to examine how each structure is constrained by the observed JASC MT response. Obtained implications are as follows: The high conductance of the upper mantle (the depth range of 100 - 400km) beneath the Japan sea is well constrained by the JASC MT response. The JASC MT response is also sensitive to the conductivity of the crust. The crustal effect is recognized such as 'static shift'. The conductivity of the lithosphere beneath the Japan sea affects the JASC MT response, although it is smaller than the effects of the upper mantle and the crust.

**GA1.02/W/05-A2 Poster 0930-36**

**PRELIMINARY RESULTS FROM AN EM INDUCTION STUDY IN THE PACIFIC USING SUBMARINE CABLE ELECTRIC FIELD DATA**

Takao KOYAMA, Hisayoshi Shimizu, Hisashi Utada (Earthquake Research Institute, University of Tokyo, Yayoi 1-1-1, Bunkyo-ku, 113-0032, Japan, Email: tkoyama@eri.u-tokyo.ac.jp , shimizu@enkumi.eri.u-tokyo.ac.jp , utada@utada-sun.eri.u-tokyo.ac.jp ) and Alan D. Chave (Woods Hole Oceanographic Institution, Woods Hole, MA 02543, USA, Email: alan@whoi.edu )

This paper reports first results of an EM induction study over the entire North Pacific region to elucidate the electrical conductivity structure in the deep mantle. Geoelectric field data measured by using submarine cables in the region that have been retired from telecommunications service are analyzed for this purpose. Geomagnetic data are obtained from standard observatory sources for Honolulu, Guam, Kakioka and so on. The electric potential measurements in the Pacific were initiated over the past decade by the independent efforts of US and Japanese research groups, and the data have now been merged to make a comprehensive dataset. The network of submarine cables consists of HAW-1, HAW-2, and HAW-3 (extending from California to Hawaii), TPC-1 (connecting Hawaii to Midway, Midway to Guam, Guam to Philippines, and Guam to Ninomiya, Japan), TPC-2 (connecting Hawaii to Guam and Guam to Okinawa), COMPAC (connecting Hawaii to Fiji), OKINAWA (connecting Okinawa and Ninomiya). By using these datasets, we can estimate MT responses and try to obtain a model of semi-global conductivity structure beneath the Pacific. A "semi-global model" means that we may have to take sphericity of the earth and the source field configuration into consideration because of the size of area of interest This talk will present preliminary results toward this goal.

**GA1.02/L/05-A2 Poster 0930-37**

**MAGNETOTELLURIC MEASUREMENTS ACROSS THE BACKBONE RANGES OF NORTHEAST JAPAN ARC**

Y. Ogawa (Geological Survey of Japan, Tsukuba, 305-8567, Japan, email:oga@gsj.go.jp)T. Goto (Aichi Univ. Educ., Kariya, Japan) M. Mishina (Tohoku U., Sendai, Japan) M. Uyeshima (ERI, Univ. Tokyo, Tokyo, Japan)T. Kasaya, M. Ichiki, N. Oshiman (DPRI, Kyoto Univ., Uji, Japan)S. Sakanaka (AVL, Kyoto Univ., Kumamoto, Japan )Y. Takahashi, T. Nishitani (Akita Univ., Akita, Japan)Y. Takahashi, Y. Honkura (Tokyo Institute of Technology, Tokyo, Japan) H. Satoh(Hokkaido Univ., Sapporo, Japan)H. Murakami(Kochi Univ., Kochi, Japan)

Wideband magnetotelluric(MT) measurements were conducted across the backbone range of Northeast Japan, which is a typical subduction system. The objective of the study is to reveal the deep structure of the active faults which run on both side of the mountain ranges. We had 15 MT sites along a 45km profile which goes across the mountain ranges. We used simultaneously 5 sets of 5 component MT systems and 5 sets of telluric-only systems. Preliminary two-dimensional inversion results using TM mode revealed the deep sub-vertical conductors corresponding to the active faults, which were recently imaged by the reflection seismic data on the same profile. These conductors imply fractured zones of the active faults. The whole profile is also underlain by lower crustal conductor at around 20km depth. The sub-vertical conductors may be linked to the deep conductor.

**GA1.02/E/17-A2 Poster 0930-38**

**THIN-SHEET MODELLING OF THE MAGNETOTELLURIC FIELD IN THE TIEN SHAN AREA**

Leonid VANYAN (Shirshov Institute of Oceanology, Moscow117218, Russia email: vanyan@geo.sio.rssi.ru), Xiangru Kong (Institute of Geophysics, CAS,100101 Beijing, China, email: xrkong@mail.cgeos.ac.cn), Mark Berdichevsky and Anastasia Kazurova (both at Geological Department of Moscow State University, Moscow 119899, Russia, email: berd@geo.geol.msu.su)

Eastern Tien Shan mountains belong to China while the Western Tien Shan occupies Kirgystan territory. Geophysicists of the Institute of Geophysics (Beijing), Shirshov Institute of Oceanology (Moscow) and Moscow State University started a joint Project for uniting the magnetotelluric data obtained in Russia and China and further developing the deep conductivity model of the Tien Shan area. Interest in this region is due to four circumstances: 1. High heat flow values, 2. Very thick crust (up to 60km), 3. Cenozoic activation (25-30 millions of years ago), 4. Existence of a conductive layer in the deep crust which is supposed to be caused by fluids released at the dehydration process initiated by temperature increase. Interpretation of united MT-data demands separation of deep and surficial effects. To this end, authors compiled a map of sedimentary basin conductance and constructed a model with the inhomogeneous thin sheet (sediments) underlain by a deep layered structure ( the Earth's crust and upper mantle). The thin-sheet technique of quasi-3D modelling shows that the Chu, Tarim and Junggar basins surrounding Tien Shan mountains cause strong electromagnetic anomalies, which distort MT-curves and induction arrows. The results of the modelling serve as a basis for correcting magnetotelluric and magnetovariation data. This work was partly supported by the Russian Basic Research Foundation (Projects 96-05-10037 and 99-05-64187).

**GA1.02/E/25-A2 Poster 0930-39**

**MT MEASUREMENTS IN THE NORTHERN TIENSHAN MOUNTAINS AND JUNGGAR BASIN, WESTERN XINJIANG AUTONOMOUS REGION**

Guozhe ZHAO, Yan Zhan, Ji Tang, Junmeng Zhao and Guangwen Jin Institute of Geology, Seismological of China, Beijing 100029, China, email: zhaogz@public.bta.net.cn

MT data have recently been obtained at 61 sites along a profile about 700km long and oriented approximately N-S in the western Xinjiang autonomous region. The profile stretches from the middle of the Tianshan mountains in the south, through the Junggar basin, ending in the Artai Mountains at the north end. Impedance tensor decomposition and RRI 2-D inversion are used for data interpretation. The electrical structure of the crust and lithosphere beneath the profile can be divided into three units, from south to north: (1) the Tianshan fold system; (2)the Northern Tianshan-Junggar fold system and (3)the Artai fold system. The Bolokenu-

Arqikekuduke fault, Erqisi fault belt and Darbute fault are found to be lithospheric faults. A contour plot of the conductive layer near the surface can be compared with sediments that have the greatest thickness of about 10km, in the southern part of the Junggar basin. There are some low resistivity blocks in the crust of the northern part of the Junggar basin at a depth of about 15-20km with about 20 km thickness. No conductive layer in the crust was found in the Tianshan mountains and Artai mountains. The thickness of the lithosphere for the three units is about 160km, 120km and 160-180km, respectively. The above results are supported by seismic data observed along same profile.

**GA1.02/E/29-A2 Poster 0930-40**

**TECTONIC SETTING AND CRUSTAL RESISTIVITY STRUCTURE IN THE INDONESIA ISLAND ARC**

Toru MOGI (Department of Earth Resources Eng., Kyushu University, Fukuoka 812-8581, Japan, email: tmogi@mine.kyushu-u.ac.jp) Djedi S. Widarto and Edy M. Arsadi (both at RD Ctr for Geotechnology-LIPI, Jalan Sangkuriang, Bandung 40135, Indonesia, email: widarto@bdg.centrin.net.id) Yoshikazu Tanaka (Aso Volcanological Laboratory, Kyoto University, Choyo-son, Aso-gun, Kumamoto Pref., 869-1400, Japan, email: tanaka@aso.vgs.kyoto-u.ac.jp) Susumu Nishimura (Kyoto Institute of Natural History, Yoshida-Kawaramachi, Sakyo-ku, Kyoto 606-8305, Japan, email: S\_nishimura@pop07.odn.ne.jp)

A magnetotelluric survey has been made at three areas, where the plate is subducting in different style, such as normal subduction, oblique subduction and collision, in the Indonesia island arc. Style of volcanic and geothermal activities are reflected by these tectonic setting. In a normal subduction area, central Java, high resistivity zone which referred to old marine sediment was seen in fore arc side and low resistivity zone reflected high temperature lower crust was appeared in back arc side. As for oblique subduction area, southern Sumatra island, remarkable low resistivity zone reaching to the deeper depth was found along the transcurrent fault zone (Great Sumatra Fault) which is moving by dragging of the oblique subduction, and where some pull-apart basins were formed. The Australian continent plate is colliding at the eastern Sunda arc of Flores area. The upper crust of the Flores area is relatively high in resistivity beneath the recent volcanic front. From these result, we have characterized crustal structure based on the resistivity structure.

**GA1.02/E/26-A2 Poster 0930-41**

**ANOMALOUS DIRECTIONAL BEHAVIOUR OF INDUCTION ARROWS ABOVE THE FAULTS OF RED RIVER IN VIETNAM.**

TRUONG QUANG HAO. Institute of Geophysics Hanoi, Box 411, Buedien, Boho Hanoi Vietnam, email: tqhao@igp.ncst.ac.vn).

The analysis of transient geomagnetic variation events recorded by a simultaneously operated chains of magnetometers across the Red river from SAPA,XUANGIAO to PHORANG, YENBAI, PHUTHUY and from HOABINH to HUATRAM,PHUTHUY and BACGIANG indicated an interesting feature:A reversal sign of the vertical field fluctuations is located at the faults of Red River. The induction vectors for short period events of geomagnetic variations at two sides of the faults show an anti paralleled direction. This fact points the existence of high electrical conductivity in the faults with high seismicity zone. The estimation of geoelectrical parameters as longitudinal conductivity and the depth of location of this high conductivity were made(G=1/1000.000.000 S.m , h= 20 Km). A subsequent magnetometer array is suggested in order to study the region of high conductivity in detail for mapping of subsurface structures for regional tectonic studies.

**GA1.02/L/02-A2 Poster 0930-42**

**AN INTERPRETATION OF MT DATA OVER THE BENUE TROUGH, NIGERIA**

E.A.ARIYIBI, :Department of Physics,Obafemi Awolowo University, Ile-Ife ,Nigeria.

Magnetotelluric(MT) measurements were performed simultaneously at three sites spaced at about 100km from each other in the Middle Benue trough.The three sites are: Lafia(8.50 N,8.50 E) ,Makurdi (7.75N,8.50E) and Otuorkpo(7.25N,8.25S). Night and day events were selected from the data and processed before analysis.Induction vectors and rho\*vs Z\* curves were obtained and used to model and understand the subsurface structure at the middle of Trough. The induction vectors at Lafia(LAF) point to the Chain lineament and at akurdi(MAR) to the Charcot lineament ,which according to aeromagnetic result trend in NE-SW direction.These lineaments mark the structural boundary of the trough.The induction vectors at Otuorkpo (OTU) point to a narrow fault zone within the trough. The rho\* vs Z\* curve suggest the presence of a crustal conductor at the middle of the trough. An earth model is derived from results of several 2D models which compared favourably with observed field data.

**GA1.02/W/35-A2 Poster 0930-43**

**MAGNETOTELLURIC STUDIES OF THE CALDAS NOVAS GEOTHERMAL AREA, BRAZIL**

PATRICIA P. DE LUGAO, Geosignal/Baker Hughes, USA, email: lugao@geosignal.com; Sergio L. Fontes, Observatorio Nacional/CNPq, Brazil, email: sergio@on.br; Emanuele F. Laterra, Observatorio Nacional/CNPq, Brazil, email: laterra@on.br

A magnetotelluric (MT) survey was conducted in the Caldas Novas geothermal area located in the state of Goi'as, central part of Brazil. The region of Caldas Novas is a popular tourist spot due to its hot water springs. The purpose of this MT survey was to provide more information on the geoelectrical structure of this important geothermal reservoir. The area of the Serra de Caldas is located on the NE border of the Paran'va Basin, over the Canastra Arch in the SE portion of the state of Goi'as. It is constituted by an anticline that is supported by quartzites that resisted erosion and that belong to a sequence of upper Precambrian metasediments. The lithology does not follow stratigraphic layering, but superposition imposed by the tectonic movement (Ribeiro et al., 1994). From a tectonic point of view, the Serra de Caldas has an elliptical shape with 15 and 9 kilometers in diameter, with the major axis coinciding with the N10W direction (Campos et al., 1980) bounded by fracture zones with trend NW-SE. Most geothermal waters occur within this region (Anjos et al., 1994). Data were acquired along two profiles crossing the Serra de Caldas with a total of 25 MT stations. Frequencies of acquisition were in the range from 0.008 to 176 Hz. Spacing between stations were usually around 5 km. Apparent resistivity and phase data from the transverse electric (TE) and transverse magnetic (TM) modes are consistent for both profiles. Very high (100,000's ohm-m) apparent resistivity values in the TM mode indicate either distortion caused by 3-D resistive structures or by topography of the mountains. Two-dimensional (2-D) inversion and three-dimensional (3-D) modelling suggests a basin-like model with very high resistivity block structures associated with concentric faulting below the Serra de Caldas and extending to depths of approximately 20 km. This model is in good agreement with gravity data and the available geological information in that area. The high resistivity associated to the depression in the MT model can be interpreted as caused by the low permeability quartzites which form the Serra de Caldas.

**GA1.02/W/39-A2** Poster **0930-44**

**IMAGING THE ONSET OF ANDEAN DEFORMATION IN THE NORTHERN SIERRAS PAMPEANAS ARGENTINA**

M. CRISTINA POMPOSIELLO (CIRGEO, Ramirez de Velasco 847,1414 Buenos Aires, Argentina, email: cpmposi@mail.retina.ar) John Booker and Shenghui Li (both at Geophysics Program, University of Washington, Seattle WA 98195 USA, email: booker@geophys.washington.edu and shenghui@geophys.washington.edu) Alicia Favetto and Ana Osella (both at Dpto. de Fisica, Univ. Buenos Aires, Ciudad Universitaria, Pabellon I, 1428 Buenos Aires, Argentina, e-mail: favetto@df.uba.ar and osella@df.uba.ar) Claudia Sainato (Catedra de Fisica, Fac.Agronomia, Univ. Buenos Aires, Av. San Martin 4453, 1417 Buenos Aires, Argentina, email: csainato@ciudad.com.ar)

The Sierras Pampeanas (SP) of Argentina are a region of active thick-skinned deformation between stable cratonic South America and the Andes. The Tucuman Plain (TP) lies just east of the most easterly active faults (which dip west). In October 1998, we collected 18 wideband magnetotelluric sites along two east-west transects of the TP. The northern transect coincides with industry seismic reflection data reprocessed to image structure to almost 40 km. The southern transect crosses an large, low temperature geothermal reservoir. For the northern line, we conclude: (1) There is essentially no distortion of deep electrical structure information by the highly uniform near-surface. (2) Beginning at 10 km and perhaps extending to the Moho, the lower crust beneath the TP has very low resistivity (below 1 Ohm-m). (3) To the east, the top of the low resistivity dips steeply eastward to the Moho and continues in weaker form horizontally under the resistive cratonic crust. This dip is essentially orthogonal to the dominant dip of seismically imaged active faults at the same location. The southern line is more difficult to interpret with very conductive shallow structure probably associated with geothermal alteration that strongly distorts the electromagnetic fields.

**GA1.02/W/06-A2** Poster **0930-45**

**MAGNETOTELLURIC INVESTIGATION OF THE DAMARA BELT IN NAMIBIA**

O. Ritter, P. Ritter, V. Haak (GeoForschungsZentrum Potsdam, Telegrafenberg, D-14473 Potsdam, Germany, email: oritter@gfz-potsdam.de)

Within the framework of an integrated geophysical and geological project we recorded broadband magnetotelluric and GDS data along a 33-site profile in NW Namibia. Preliminary interpretation of the impedances and induction arrows indicates three conductive features associated with different period ranges: (1) numerous small scale structures in a generally resistive upper crust which is typical for the granites and metasediments of the Damara belt, (2) two interconnected subvertical conductors in the middle crust and (3) the influence of the South Atlantic in a distance of approximately 150 km. To examine this complex conductivity structure we compare electric and magnetic decomposition methods and discuss modelling results. The geometry of two near-vertical conductivity anomalies connected by a subhorizontal conductor in the mid crust is consistent with the distribution of shearzones produced by ramp tectonics during the late stages of the Panafrican Damara orogeny. The high conductivity is likely due to graphite in shearzones, as suggested by the discovery of graphite-rich mylonitic marbles along the SW extension of the Waterberg Fault, which correlates with the southern conductivity anomaly.

Results from the crystalline of Sweden are compared with coincident VES measurements over a narrow 200 meter wide valley near Stockholm. Both methods define the resistive boundaries of the valley and a small, shallow resistive block in the middle of the valley. Results from a waste dump site in the Netherlands, where a number of geophysical techniques have been applied to trace the leakage of conducting fluids in the form of plumes, show good agreement with standard VES and TEM measurements. 2-D inverse models give a very clear indication of the lateral extension of the plume.

**GA1.02/W/33-A2** Poster **0930-46**

**STUDIES OF THE MAGNETOTELLURIC SOURCE EFFECT DUE TO AURORAL CURRENTS**

Ari VIILJANEN, Risto Pirjola and Olaf Amm (Finnish Meteorological Institute, Geophysical Research Division, P.O.B. 503, FIN-000101 Helsinki, Finland, email: ari.viljanen@fmi.fi)

We apply the complex image method to calculating the electromagnetic field at the earth's surface during typical high-latitude geomagnetic disturbances. We use realistic three-dimensional models of ionospheric currents determined using ground-based data. A special attention is paid to attempts to reduce the source field distortion in magnetotellurics.

**PANEL DISCUSSION** **1700**

MARCUS EISEL (University of Potsdam), JOSEF PEK (Geophysical Institute, Prague), T. HARINARAYANA (NGRI, Hyderabad), CRISTINA POMPOSIELLA (CIRgeo, Buenos Aires), ANTHONY WHITE (Flinders University), MICHEAL ZHOANOV (University of Utah)

**GA1.04** **Thursday 22 – Saturday 24 July**

**PALEOMAGNETISM: CONTRIBUTIONS TO TECTONICS**

Location: Barber Institute, LT  
Location of Posters: Barber Institute (Corridor)

**Thursday 22 July AM**

Concurrent Poster Session

**GA1.04/W/31-A4** Invited **0900**

**PALAEOGEOGRAPHY AND GEODYNAMIC EVOLUTION OF PALAEOZOIC TERRANES IN THE CALEDONIAN-APPALACHIAN OROGEN**

Conall MAC NIOCAILL (Dept. of Earth Sciences, University of Oxford, Parks Road, OX1 3PR, UK, email: conallm@earth.ox.ac.uk); Ben van der Pluijm and Rob Van der Voo (Dept. of Geological Sciences, The University of Michigan, Ann Arbor, MI 48109-1063, USA, email: vdpluijm@umich.edu; voo@umich.edu)

Since J. Tuzo Wilson's, now classic, demonstration of a proto-Atlantic (or Iapetus) ocean the Caledonian-Appalachian orogen has been a key area in the construction of Palaeozoic palaeogeographic models. The latitudinal positions of the main palaeocontinents involved in the orogeny (Laurentia, Baltica, Avalonia and, later, Gondwana) are now relatively well

established, with the northward convergence of Baltica and Avalonia, with respect to an equatorial Laurentia, during the Ordovician leading to a final closure of the Iapetus ocean in the Silurian. In recent years, however, there has been considerable debate as to the relative longitudinal positions of these palaeocontinents, with some workers advocating a shared Middle-Ordovician tectonic history between Laurentia and the South America margin of Gondwana. Similarly, the palaeogeography and origin of several of the accreted terranes that are now found along the orogen has been the subject of much discussion. Recent work, which combines palaeomagnetic, faunal and geochronologic data, has produced an internally consistent history of terrane migration and accretion in the Northern Appalachians, involving the presence of arcs along the Laurentian and Avalonian margins, and possible intra-oceanic arcs or seamount complexes within the Iapetus Ocean in the Ordovician. However, the picture is less clear when it comes to the origin and accretion of other Ordovician terranes, such as the Precordilleran Terrane of South America. Recent palaeomagnetic data have confirmed a Laurentian origin for the Precordilleran Terrane in the Early Cambrian but the precise mechanism of its Middle Ordovician transfer to the South American margin of Gondwana remains in dispute.

**GA1.04/W/06-A4** **0930**

**A NEW INITIATIVE FOR PALAEOMAGNETIC WORK IN THE TASMAN FOLD BELT**

Mark A. LACKIE (Department of Earth and Planetary Sciences, Macquarie University NSW, Australia 2109, email: mlackie@laurel.ocs.mq.edu.au); Phillip W. SCHMIDT (CSIRO Exploration and Mining, North Ryde NSW, Australia 1670, email: p.schmidt@syd.dem.csiro.au); David A. Clark (CSIRO Exploration and Mining, North Ryde NSW, Australia 1670, email: d.clark@syd.dem.csiro.au)

Despite much effort Gondwana's early Palaeozoic apparent polar wander path remains ill-defined particularly for the Siluro-Ordovician segment. Rocks of this age in the Tasman Fold Belt cover a wide range of lithologies but most do not appear to contain grains of optimum stability to allow the pole path to be unambiguously defined. In our continuing effort to address this problem we have begun a study of volcanics and mineralisation/alteration systems in central-western NSW and northern Queensland. Normally it might be expected that the problems with structure and age control of mineralised/altered rocks are insurmountable, however, the systems we have targeted are well dated, they cover a broad geographical area and the structures of the parent rocks are well known. Given the magnitude of the problem we feel this approach is justified. Often haematite accompanies the alteration and it is the palaeomagnetic signature of this mineral that we particularly seek. So far sampling has been undertaken at deposits in western and central-western NSW. Pilot samples were collected from fresh and altered rocks of the Late Silurian Wondalga Granodiorite, the Late Ordovician Gidginbung Volcanics at Temora and gabbroic diorites and monzonoidorites of the Early Silurian Wallundry Suite. As well, samples were collected from the Late Ordovician Tethenhall Monzoniorite and Tallwood Monzonite and their associated hornfels, usually within the Forest Reefs Volcanics. In areas of no outcrop samples were taken from oriented drill core. The results obtained from preliminary measurements taken on the above samples will be discussed.

**GA1.04/W/01-A4** **0950**

**TECTONIC ROTATIONS IN THE CALEDONIAN-APPALACHIAN OROGEN DEDUCED FROM PALAEOMAGNETIC REMANENCE**

Mark SMETHURST and Trond Torsvik (Geological Survey of Norway, Leiv Eirikssons vei 39, N-7040 Trondheim, Norway, email: mark.smethurst@ngu.no)

Palaeomagnetic remanence has been used extensively in orogenic belts to determine the former latitudinal positions of terranes and to construct detailed palaeogeographies of former oceanic tracts. Less attention has been paid to the information offered by palaeomagnetic remanence on the paleo-orientation of terranes. Rotation of terranes was an important part of the late stage tectonic development of the Caledonian-Appalachian orogen; rotated terranes have been recognised at intervals along the full length of the orogen. We assembled palaeomagnetic data from Britain and Ireland (Caledonides) and Newfoundland (NE Appalachians) to map the extent and timing of tectonic rotations associated with the final closure of Iapetus. Special attention was paid to links between the complex pattern of Silurian rotations recognised in the Irish Caledonides and the equally complex pattern of rotations recognised in Silurian rocks of the Appalachians in Newfoundland. The palaeomagnetic record carried by Silurian volcanics and sediments in Newfoundland is complicated by magnetic anisotropy. A study of the anisotropy in the two rock types will accompany the history of tectonic rotations.

**GA1.04/W/40-A4** **1010**

**REMAGNETIZATION AND OROGENIC FLUIDS: TESTING THE HYPOTHESIS IN THE CENTRAL APPALACHIANS**

R. Douglas ELMORE (University of Oklahoma, USA)

The migration of orogenic fluids is a popular, although largely untested hypothesis invoked to explain widespread chemical remagnetization in sedimentary rocks. Preliminary paleomagnetic and geochemical studies in the central Appalachians indicate that a relationship between orogenic fluids and remagnetization is not straightforward. For this study, samples were collected for fold tests from Paleozoic units in the Valley and Ridge province in West Virginia. Samples from the Devonian Helderberg Fm. contain a synfolding late Paleozoic magnetization with the best grouping at ~60% unfolding ( $D = 155/ I = -4$ ). Rock magnetic studies indicate that the magnetization, interpreted to be a CRM based on high unblocking temperatures and moderate burial depths, resides in magnetite. Samples from the overlying Oriskany sandstone on the same fold contain a similar synfolding magnetization (~55% unfolding;  $D = 171/ I = 5$ ) in magnetite, although it is weaker and the decay not as linear. Fold tests on these units from a second fold produced similar results. Similarly, a fold in the Ordovician Trenton Fm. also contains a synfolding magnetization with best grouping at 25% unfolding ( $D = 163/ I = 5$ ). However, the fluid histories of the Oriskany and the two limestone units differ significantly. Stable isotope and fluid inclusion data from veins indicate that low salinity (7 to 15 wt.% NaCl equiv.), high temperature (155 to 225°C minimum) fluids migrated through the Oriskany. In contrast to the results from the Oriskany, fluids in the Helderberg and the Trenton were restricted to 'in-situ' high-salinity, low temperature brines. This is consistent with previous diagenetic studies which indicate that most of the Helderberg in West Virginia was only subjected to burial diagenetic processes with only localized alteration by warm exotic fluids. Although the results from the Oriskany are consistent with remagnetization by orogenic fluids, the connection is more difficult to make in the Helderberg and Trenton which do not contain evidence for such fluids.

**GA1.04/W/30-A4** **1100**

**PALAEOGEOGRAPHY AND GEODYNAMIC EVOLUTION OF PALAEOZOIC TERRANES IN THE VARISCAN AND ALPINE FOLDBELTS**



TAIT J, Schätz, M., Zwing, A., and Bachtadse, (V. Inst. f. Allg. Angew. Geophysik, Ludwig-Maximilians-Universität München, Theresienstr. 41, 80333 München)

Early and pre-Variscan terranes in Europe, particularly in southern realms, have undergone multiple deformational phases making determination of the pre-collisional plate configuration difficult. Nevertheless, recent geological, palaeogeographical and palaeomagnetic findings have led to significant improvements in our understanding of the Palaeozoic orogenic events. Palaeomagnetic studies of several different Palaeozoic sequences in central and southern Europe demonstrate that the so-called "Armorican Microplate" was in fact an assemblage of (semi)autonomous terranes or microblocks, which are now separated by major tectonic discontinuities. The term 'Armorican Terrane Assemblage' (ATA) is now used to refer to these Palaeozoic elements. They had similar drift histories during the Palaeozoic, and the Rheic Ocean separating Avalonia from the ATA closed in Late Silurian/Early Devonian times. The situation for the southern margin of the ATA, especially sections which are belong to the Alpine realm, is complex and the palaeogeography of the various terranes remains unclear due to the strong Alpine overprint and deformation. Recent palaeomagnetic data from the eastern and southern Alps point to a more independent history of these units, which is in accordance with their general faunal and lithofacial records. These Alpine terranes rifted from the northern margin of Gondwana in Ordovician times, and drifted northwards

**GA1.04/W/18-A4 1120**

**PALEOMAGNETIC AND ROCK MAGNETIC RESULTS FROM A LATE DEVONIAN INTRUSIVE COMPLEX (FRANKENSTEIN GABBRO, ODENWALD, GERMANY)**

A. ZWING, V. Bachtadse, H. Soffel (Institut für Geophysik, Ludwig-Maximilians-Universität München, Theresienstr. 41, 80333 München, Germany. email: azwing@magbakt.geophysik.uni-muenchen.de)

Paleomagnetic results from late Devonian and Carboniferous rocks in the internal part of the European Variscides (Massif Central, Vosges, Black Forest, Odenwald and Spessart) indicate large scale rotations and disagree with the systematic deviation of paleodeclinations as a function of the overall structural trend, which has been observed in the Iberian, Armorican and Bohemian Massifs. In this context the paleomagnetic and rock magnetic properties of the Frankenstein Gabbro (Odenwald, Germany) were studied in detail. The Frankenstein intrusive complex was subjected to rapid cooling in late Devonian times ( $363 \pm 7$  Ma) and not reheated above 200°C (Kirsch, 1988) since then. A magmatic layering, indicating the orientation of the paleohorizontal was observed in the field and in the orientation of the AMS-ellipsoids. During stepwise thermal and alternating field (AF) experiments three components (A,B,C) of magnetisation could be identified. Component A is parallel to the present day geomagnetic field in the study area and the result of a recent VRM. Component B reflects presumably a magnetic overprint of Permo-Carboniferous age. Component C has been identified in 124 samples from 22 sites. The resulting overall site mean based on stable endpoints and remagnetisation circle intersections (Dec=198°/Inc=40°; VGP: 15°S/9°W) is interpreted to be of primary origin. This is supported by a positive baked contact test and a positive reversal test. Component C is predominantly characterised by unblocking temperatures of 580°C and in few samples over 600°C, indicating magnetite and hematite as the carriers of the characteristic remanent magnetisation. The study of polished sections revealed two types of hematite and suggest primary hematite lamellae in ilmenite and secondary hematite overgrowth as carriers of Component C and Component B, respectively. Comparing the resulting paleopole position to the reference Apparent Polar Wander Path for stable Europe indicates 20° anticlockwise rotations of the region studied. This is significantly less than published by Edel (1991) based on palaeomagnetic data for the Odenwald, Spessart, Black Forest and the Vosges.

**GA1.04/W/16-A4 1140**

**THE ROTATIONS OF THE VARISCAN BELT DURING THE CARBONIFEROUS COLLISION**

Jean-Bernard Edel (EOST-Institut de Physique du Globe, 5 rue Descartes, 67084 Strasbourg Cedex, France, email: Jean-Bernard.Edel@eost.u-strasbg.fr)

Paleomagnetic investigations carried out on the Paleozoic outcrops of the European Variscides, demonstrate that at least 90% of the Visean volcanites and plutonites have undergone magnetic overprinting during Carboniferous to Jurassic times. In general, sediments contain only young overprints. Thanks to the overprinting phenomenon, a nearly continuous paleomagnetic record, interpretable in terms of geotectonic evolution, was obtained for each massif. After 340 Ma, which is the age of most of the investigated units, the geotectonic evolutions of the Armorican Massif, Central Massif, Vosges, Black Forest, Odenwald, Spessart, Bohemian Massif and Sudetes were nearly the same: - From 340 Ma up to 330-328 Ma, the presently striking SW-NE Variscides were oriented SE-NW (Cn-Cp magnetic components; mean VGPs: 16°S/46°E to 31°S/50°E) and likely underwent a N-S drift along the margin of Baltica; - A prominent compression phase (the Sudetic phase), probably resulting from blocking of the eastern Variscides against the south-western margin of Baltica, marked the end of the drift and led to uplift, folding, wrenching and magnetic overprinting (Cp overprints). Primary Cp components were recorded in syn-tectonic dykes dated around 330 Ma; - The compression became strong enough to give rise to a 70-80° clockwise rotation (Cp-B) that closed the Lizard-Giessen oceanic basin; - After the closure, the convergence continued and high pressure metamorphism was recorded along the Saxothuringian - Rhenohercynian boundary. During the relaxation that followed the rotation, large-scale post-tectonic overprinting (B directions, mean VGP: 10°N/124°E) in relation with low-grade metamorphism affected all outcrops of the internal Variscides. - In the time range 320-303 Ma, still under pushing of Gondwana, the whole Variscides east of the Iberian-Armorican arc, rotated clockwise by 40-50° (B-A1). The Rhenohercynian zone was thrust over the Caledonian Brabant block. After acquisition of the primary and secondary A1 magnetizations (mean VGP: 32°N/153°E), the clockwise rotations continued, up to the end of the Alleghanian convergence in the Middle Permian (270 Ma); - In the Latest Carboniferous- Early Permian (300-270 Ma)...

**GA1.04/L/07-A4 1200**

**PALEOMAGNETISM AND PALAEOGEOGRAPHY OF THE BARRANDIAN TERRANE IN THE BOHEMIAN MASSIF: ASPECTS OF INTERPRETATION**

MIROSLAV KRS, Otakar Man and Petr Pruner (Institute of Geology, Academy of Sciences, Rozvojov 135, 165 02 Prague 6 - Lysolaje, Czech Republic. email: inst@gli.cas.cz)

Paleomagnetic data inferred for the Variscan and pre-Variscan formations of the Bohemian Massif (BM) were interpreted in terms of tectonics and palaeogeography. The evaluation of the data from the BM was preceded by the study of the effect of the Trans-European Suture Zone (TESZ) on the dispersion of the European palaeomagnetic pole positions during the Variscan episode. Horizontal palaeotectonic rotations are well documented for Variscan and pre-Variscan rock complexes in the so far studied Barrandian and Moravian Zone terranes within the BM. Magnitudes of horizontal palaeotectonic rotations in the BM affected by the Variscan tectonism are notably similar to those in the Western Carpathians affected by Alpine tectonism. Senses of the rotations are, however, different with clockwise rotations prevailing in the BM

and counterclockwise rotations prevailing in the Western Carpathians. To guarantee a critical evaluation, the BM data were recalculated into the form of palaeolatitudes and palaeomagnetic declinations for a single reference point in the Barrandian area and interpreted in the context of all-European data recalculated for the same reference point. The study of tectonics and palaeogeography of Cambrian to Devonian rock formations in the Barrandian area, which is considered as a peri-Gondwanide terrane with affinities to Armorica, may serve as a case history of study of a terrane incorporated into a stable lithospheric plate, with some new aspects of interpretation of the palaeotectonic rotations. Here, the Barrandian terrane became a part of the European Plate as a component of emerging Pangea supercontinent in the final phase of the Variscan orogeny.

**GA1.04/W/31-A4 1220**

**MOSCOVIAN PALEOMAGNETIC POLE FROM THE EDJELEH FOLD (SAHARAN CRATON, ALGERIA)**

Mohamed. El-Messaoud, DERDER, Boualem Bayou, Hamou Djellit and Mohamed Amenna (CRAAG, BP 63, 16340 Bouzareah, Algiers, Algeria, email: mderder@hotmail.com); Bernard Henry (Géomagnétisme et Paléomagnétisme, IGP and CNRS, 4 avenue de Neptune, 94107 Saint-Maur cedex, France, email: henry@ipgp.jussieu.fr)

Numerous paleomagnetic studies of Paleozoic formations have been conducted in the Illizi basin. Although these studies have led to the determination of new African Upper Paleozoic paleomagnetic poles, no paleomagnetic tests can be performed. Therefore a new study was carried out in a Moscovian (310 Ma) formation located in the Edjeleh anticline, the only area where important dips can be observed in the Upper Paleozoic series of the Illizi basin. The paleomagnetic results are similar to previous ones performed in neighboring areas, and show the existence of three magnetization components. The first one is better grouped in geographic coordinates and its corresponding paleomagnetic pole is close to Tertiary to Quaternary African poles. This component is then a Cenozoic remagnetization. The second one is slightly better grouped in geographic coordinates, but the fold test is inconclusive because all specimens are from the same limb of the fold. The paleomagnetic pole in stratigraphic coordinates is close to the previous African Permian remagnetization poles. The third component, determined by both remagnetization circles analysis and well defined ChRMs is defined by D=134.8°, I=34.2°, k=96, a95=6.9° and D=133.7°, I=32.7°, k=254, a95=4.2°, respectively before and after dip correction. The optimal value during a progressive unfolding is obtained for an approximately total unfolding, and the fold test is positive and significant. The corresponding paleomagnetic pole is 25.6°S, 59.5°E, K= 381, A95= 2.9°. Our positive fold test "validates" thus the previous Upper Paleozoic poles from the Saharan platform.

Thursday 22 July PM

**GA1.04/W/21-A4 1400**

**AUTUNIAN PALEOMAGNETIC POLE FROM THE MEZARIF BASIN (ALGERIA)**

N. MERABET, A. Kherroubi and S. Maouche (CRAAG, BP 63, 16340 Bouzareah, Algiers, Algeria, email: merabetn@hotmail.com); B. Henry (Paléomagnétisme et Géomagnétisme, CNRS and IGP, 4 av. Neptune, 94107, Saint-Maur cedex, France, email: henry@ipgp.jussieu.fr)

During the last decade, a substantial number of Permo-Carboniferous poles had been determined in the Algerian Saharan basins. These poles improved the definition of the Permo-Carboniferous segment of the African Apparent Polar Wander Path. However, the knowledge of more precise kinematics evolution of this continent, which will clarify the Pangea configuration during late Paleozoic times, requires more investigations. For this purpose, a paleomagnetic study had been carried out in the Autunian series of Nekheila (Mezarif basin, Algeria), which is situated in the northern part of the stable West-African craton. A total of 122 specimens containing hematite and collected at seven (07) sites had been subjected to successive thermal cleaning steps. Visualization of orthogonal diagrams showed, after the destruction of a weak viscous component at low temperature, the existence of a dominant ChRM. The ChRM mean direction obtained, after dip correction, is defined by D=131.5°, I=18.4°, k=56, a95=7.1°. The associated paleomagnetic pole is situated at 28.0°S and 55.3° E, and is very close to that (29.1° S and 57.8° E) of the Autunian lower unit of the neighboring Abadla formation. It is also close to the Stephano-Autunian one (33.8° S and 61.4° E) of the lower Tiguertourine formations belonging to the stable Eastern Saharan craton. Thus our new datum confirms the reliability of Paleozoic paleomagnetic data obtained these last years in the Algerian Saharan craton. It improves also the precision of the mean African Autunian paleomagnetic pole and represents thus a new contribution for a better comprehension of the geodynamic evolution during the Paleozoic times.

**GA1.04/W/22-A4 1420**

**NEW PALEOMAGNETIC CONSTRAINTS ON THE DATING OF THE ABADLA REDBEDS (ALGERIA)**

H. BOUABDALLAH, N. Merabet, and S. Maouche (CRAAG, BP 63, 16340 Bouzareah, Algiers, Algeria, email: h.bouabdallah@lancaster.ac.uk); B. Henry (Paléomagnétisme et Géomagnétisme, CNRS and IGP, 4 avenue de Neptune, 94107 Saint-Maur cedex, France, email: henry@ipgp.jussieu.fr).

The 2000 m thick Abadla redbeds formation (31.2°N, 2.7°W) consists of two units; a lower unit whose Autunian age is well established by the presence of characteristic microflora fossils, and an azoic and undated upper unit whose age could be either Permian or Triassic (Doubinger et Fabre, 1981, Pollen et Spores 25, 91-116). This last undated unit yields a paleomagnetic pole (Morel et al., 1981, Earth Planet. Sci. Lett. 55, 65-74) considered as a reference for the African Apparent Polar Wander Path (APWP). Our new paleomagnetic data (magnetic direction: N = 11, D = 130.1°, I = 13.0°, k = 138, a95 = 3.6° and pole: 29.1°S, 57.8°E, A95 = 2.0°) were obtained from the better dated Autunian levels of the lower unit, and its primary origin is indicated by the stratigraphic variation of the magnetic direction. This new pole should thus take the place of the previous one in the definition of the Autunian part of the African APWP and help, along with other data from the Saharan Craton, to tightly constrain the Middle Carboniferous – Autunian segment of this APWP. This new pole is very close to Morel et al.'s, determined from the unfossiliferous upper unit of the Abadla formation, therefore giving an Autunian age for this upper unit. Consequently, the subsidence of the Abadla basin and the deposition of the whole succession occurred during a period of less than 20-25 Myr. The accumulation rate of the sediments in the Abadla basin (100 m/Myr) is much higher than those of the other parts of the Sahara (e.g. Illizi basin, 10 m/Myr).

**GA1.04/W/32-A4 1440**

**NEW PRELIMINARY PALEOMAGNETIC DATA FROM LATEST PROTEROZOIC - EARLY PALEOZOIC ROCKS FROM THE RIO DE LA PLATA CRATON**

Augusto E. RAPALINI (Lab. Paleomagnetismo D.A. Valencio, Depto. Cs. Geológicas, Univ. Buenos



Aires, Pub. 2, C. Universitaria, 1428, Buenos Aires, Argentina, email: rapalini@gl.fcen.uba.ar); Carlos W. RAPELA (Centro de Investigaciones Geológicas, Univ. Nacional de La Plata, Calle 1 N°644, 1900, La Plata, Argentina, email: crapela@cig.museo.unlp.edu.ar)

The global paleogeographic evolution in the Late Proterozoic has apparently been governed by the breaking up of Rodinia and the later assembly of Gondwana, H. although details of this evolution are not well known. In particular, Western Gondwana was apparently formed by the coalescence of several independent cratons by the end of the Proterozoic. One of these is The Rio de La Plata craton (RP) in southeast South America. In order to better determine its paleogeographic evolution and the kinematics of Gondwana assembly, a new preliminary paleomagnetic study was carried out on Late Proterozoic - Early Paleozoic rocks exposed at Sierra de Los Barrios (province of Buenos Aires, Argentina). Cores were drilled from: 1) subhorizontal purple claystones correlative to the Las Aguilas Fm or Balcarce Fm (Vendian - Cambrian?, 5 sites, 36 samples) and 2) basaltic to gabbroic sills (K/Ar 498-450 Ma, 3 sites, 26 samples). Preliminary results after both AF and thermal demagnetization indicate high remanence stability in the samples from both units. A preliminary paleomagnetic pole obtained from the mean characteristic remanence carried by hematite in the claystones is consistent with a recently obtained pole for the RP from magmatic rocks of 550-565 Ma in Uruguay, suggesting a similar age for the claystones. These poles fall near the beginning of the APWP for the already assembled Gondwana, confirming that RP was already part of Gondwana at those times. The mean geomagnetic pole from the sills, although probably not averaging PSV, suggests high paleolatitudes. This can be interpreted easier assuming a Late Ordovician age, although other alternatives are explored.

GA1.04/L/07-A4

1500

#### SOME PALEOMAGNETIC CONSTRAINTS ON THE ANDEAN UPLIFT OF THE EASTERN PRECORDILLERA OF ARGENTINA

AUGUSTO E. RAPALINI (Laboratorio de Paleomagnetismo Daniel Valencio, Depto. Cs. Geológicas, FCEyN, Universidad de Buenos Aires, Pabellón 2, Ciudad Universitaria, 1428, Buenos Aires, Argentina, email: rapalini@gl.fcen.uba.ar) Osvaldo Bordonaro (CRICYT, CC 131, 5500, Mendoza, Argentina)

Paleomagnetic sampling was done on several carbonatic units (limestones to dolomites) of Middle Cambrian to Arenig age at 23 sites (140 samples) from 5 localities in the Eastern Precordillera (EP) of San Juan province (Argentina). Standard AF and thermal demagnetization indicated two different magnetic behaviours. Samples from 2 localities showed a single, posttectonic component attributed to Recent viscous or chemical remagnetization. Samples from the remaining localities showed two components: a low unblocking temperature (350°C) magnetization coincident with that found at the previous localities and a high temperature one (up to 550°C). The latter was also found to be post-folding (post-Devonian, in situ mean direction: Dec: 272.6°, Inc: 68.9°, A95: 8.9°, N=11). This is not consistent with any expected direction for the study area since the Carboniferous. It is inferred that these rocks underwent substantial tectonic displacement since this magnetization was recorded. Comparison of their magnetic characteristics with those of similar Early Ordovician limestones in the Central Precordillera and the San Rafael Block, that were remagnetized in the Permian, suggests that the same process affected the carbonatic rocks in the EP and, therefore, the age of the component is likely to be Permian. Restoration of the in situ mean direction to the expected one for a Permian remagnetization can be obtained by a 40° ccw rotation around an inclined axis of 30° Az and plunging 30° to the NE. This supports a model suggesting that the EP behaved as a series of rigid blocks during the Andean orogeny and was mainly uplifted by displacement along a major East dipping N to NE backthrust that marks its western boundary.

GA1.04/W/26-A4

1520

#### PALEOMAGNETIC CONSTRAINTS ON AGE OF DEFORMATION OF THE "SAMFRAU" BELT, SOUTHWEST GONDWANA BOUNDARY, ARGENTINA, DURING THE LATE PALEOZOIC

Renata N. TOMEZZOLI (CONICET-Universidad de Buenos Aires, now at S.U.N.Y. Binghamton, Department of Geological Sciences, Binghamton, NY 13902-6000; email: rtomezz@binghamton.edu), William MacDonald (S.U.N.Y. at Binghamton, Department of Geological Sciences, Binghamton, NY 13902-6000; email: wdmacdon@binghamton.edu)

Following the paleomagnetic study of the Sierras Australes thrust and fold belt (Tomezzoli 1997), we have extended our studies westward, in rocks of similar late Paleozoic ages. This zone constitutes the "Sam Frau geosyncline" of Du Toit (1927). The current studies involve rocks from Mendoza and La Pampa Province. The previous paleomagnetic study in Sierra de la Ventana yielded two paleomagnetic poles, one syntectonic in the Lower Permian and one pre-tectonic in the Lower Upper Permian. The objectives of the current work are: regional comparisons; improving the APWP of the late Paleozoic - early Mesozoic of South America; location of the top of the Kiaman; determination of the Permian - Triassic boundary; establishing the age of the deformation by region to evaluate time - transgressive migration; exploration of AMS signatures to evaluate regional deformation; and a better understanding of the assembly, deformation, and fragmentation of Gondwana / Pangea. References: Du Toit, A., 1927. A geological comparison of South America with South Africa, Carnegie Institute of Washington Publications. 381, 1-157. Washington. Tomezzoli, R.N., 1997. Geología y Paleomagnetismo en el ámbito de las Sierras Australes de la provincia de Buenos Aires. Tesis doctoral, Universidad de Buenos Aires, inédita, 306 p.

GA1.04/E/11-A4

1610

#### PALEOMAGNETIC RESULTS FROM THE MID-PROTEROZOIC RICHTERSFLYA SUPERGROUP OF QUEEN MAUD LAND, ANTARCTICA - THE KALAHARI CRATON-GRUNEHOGNA PROVINCE CONNECTION

D.L. JONES & M.P. Bates (both at University of Zimbabwe, Harare, Zimbabwe) G.Hodgkinson & B.Cornier (both at University of the Witwatersrand, Johannesburg, S. Africa) & C.McA.Powell (University of Western Australia, Perth, Australia)

The Umkondo Group of Zimbabwe (UGZ) includes dolerites, part of the Umkondo Igneous Event (UIE), widespread throughout southern Africa. The dolerites are reliably dated at 1100 Ma with a well established paleomagnetic (UIE) pole at 65 N and 36 E (alpha-95 = 6 deg). Paleomagnetic results are reported from 54 sites in the Richtersflya Supergroup (RSG) of Queen Maud Land (QML). Sites are mostly in igneous rocks intruded into unconsolidated RSG sediments but include 4 sites in sediments & one in lavas. Published results for the RSG suggest an age also close to 1100 Ma. Extensive af & thermal demagnetization of samples reveals a mean remanence direction of D = 234, I = -4 with k = 25 & alpha-95 = 4 deg giving a pole at 232 E, 8 S. Paleomagnetic & rock magnetic results suggest this remanence is held in single domain grains of magnetite and hematite (sediments only) and, notwithstanding a regional low-grade metamorphism, that it is primary. Rotation of QML into its familiar Gondwana position results in a difference of only 6 deg between the mean poles for the UIE & RSG providing strong support for the view that the UGZ & the RSG are contemporaneous

& that the Kalahari craton & Grunehogna Province of QML were in close proximity 1100 Ma ago.

GA1.04/E/15-A4

1630

#### PALEOMAGNETISM OF THE 1.73 GA URUGUAYAN DIKE SWARM, RIO DE LA PLATA CRATON: IMPLICATIONS FOR A MESOPROTEROZOIC SUPERCONTINENT

Manoel S. D'AGRELLA-FILHO and Igor I. Gil Pacca (Instituto Astronômico e Geofísico, Universidade de São Paulo, São Paulo, SP, 3386, 01060-970, Brazil, email: dagrella@iag.usp.br)

The Uruguayan dike swarm intrudes country rocks of the Rio de La Plata Craton that were deformed and metamorphosed to high grade during the 2200-1900 Ma Transamazonian orogeny. 40Ar/39Ar plateau ages for igneous hornblende (1727±10 Ma) and biotite (1725±10 Ma) are taken as the best estimate for the emplacement of the Uruguayan swarm.

AF and thermal demagnetization on 78 samples collected from 19 mafic dykes revealed a multicomponent behavior. The most representative component (Dm=9.5°; Im=-34.9°; K=16.6; a95=9.0°; N=17) includes both polarities, and is displayed by the majority of the dykes. Rock-magnetic experiments suggest that this component is carried by Ti-poor titanomagnetites, most of them in single domain/pseudo single domain structures.

The corresponding Uruguayan dikes (UD) pole (337.0°E; 74.4°N) does not agree with a pole of similar age from the Richtersveld Subprovince nor with poles from the Kaapvaal Craton, in a pre-Atlantic configuration of South America and Africa. However, if the Rio de La Plata Craton is rotated 109° counterclockwise around an Euler pole at 250.5°E; 23.1°S, the UD pole falls on the 1750-1700 Ma time interval of the Laurentia apparent polar Wander path. In this reconstruction, the eastern border of the Rio de La Plata Craton fits to the southwestern border of Laurentia (North America in its present position). The northern border of the Rio de La Plata Craton, in a proposed supercontinent reconstruction, fits to East-Antarctica.

GA1.04/E/16-A4

1650

#### PRELIMINARY PALEOMAGNETIC RESULTS OF A SEDIMENTARY SEQUENCE FROM THE MESOPROTEROZOIC AGUAPEI GROUP, AMAZONIA CRATON

Manoel S. D'Agrella-Filho and Igor I. Gil PACCA (Instituto Astronômico e Geofísico, Universidade de São Paulo, São Paulo, SP, 3386, 01060-970, Brazil, email: dagrella@iag.usp.br)

The Aguapei basin from Central-Western Brazil (Amazonia Craton) has been interpreted as a NNW/SSE aulacogen associated with the development of the marginal WNW-trending Susnas Belt. They are geographically separated by the Paragua Block. Recent Proterozoic reconstructions of supercontinents have considered the Susnas belt as an exposition of the Grenville belt produced during the Laurentia-Amazonia collision at the end of the Mesoproterozoic (1300-950 Ma).

Paleomagnetic results of sedimentary samples collected from 10 nearly horizontal stratigraphic levels from the Aguapei Group and of samples from a basic dike cutting these sediments are presented. Alternating field and thermal demagnetizations of these rocks yielded a northern (southern) direction with moderate to steep negative (positive) inclination. Magnetization is carried by magnetite in the dike samples and by hematite in the sediments. No radiometric dating is yet available to constrain the age of this direction. Although not far from the present geomagnetic field, its corresponding pole is compared with other Grenvillian poles in the configurations proposed for the Mesoproterozoic Rodinia supercontinent.

GA1.04/P/02-A4

1710

#### PALEOMAGNETIC AND ROCK MAGNETIC STUDY OF A DEEPLY EXPOSED PRECAMBRIAN METAMORPHIC TERRANE: THE CHARNOCKITE BELT OF SOUTH INDIA

S. BASU MALLIK, G Bandyopadhyay and A.K. Das (Department of Geological Sciences, Jadavpur University, Calcutta -700 032, India) J.D.A Piper (Geomagnetism Laboratory, Department of Earth Sciences, University of Liverpool, Liverpool L69 7ZE, U.K.)

The Archaean-Early Proterozoic craton of South India is bounded by a broad E-W zone from Mangalore in the West to Madras in the east dominated by granulites and charnockites uplifted from depths of 25-35km and cooled at ~2600Ma. To the north Precambrian terranes are dominated by Archaean supracrustal belts in gneissic granulites and granite. The boundary zone grades from granulite to upper greenschist facies. We have sampled the central and eastern sectors of this transitional belt. Intensities and susceptibilities of magnetisation are strong in the granulite and charnockite facies and comparable to younger basaltic rocks. They therefore provide a strong contributing source to deep crustal magnetic anomalies. Thermomagnetic determinations and thermal demagnetisation show remanence carried mostly by low-Ti magnetite. Titaniferous hematite occurs rarely in the granulite facies and pyrrhotite is present in the lower grade terranes. Hysteresis, KLT and KHT studies show dominantly multidomain magnetite although most samples have stable remanence probably because domains are pinned by shape effects. Anisotropy of susceptibility is low in comparison with many metamorphic rocks with little preferential fabric. This accords with the dominantly-static metamorphism producing charnockite facies. In the centre of the belt a NNW-SSE shallow axis is defined by the uplift magnetisations. With other early Proterozoic paleomagnetic results from the Indian Shield data show that it occupied a low latitude location probably rotating anticlockwise at ~2600Ma and moving into high latitudes before moving back to low latitudes by ~2400Ma.

GA1.04/P/03-A4

1730

#### PALEOMAGNETIC INVESTIGATION OF THE CAMEROON VOLCANIC LINE

R-U. Llibangoh and I. G. PACCA (Unit for Geophysical and Volcanological Research, B.P. 370 Buea, Cameroon)

Paleomagnetic investigation of samples collected from the Cameroon Volcanic Line has presented six new paleomagnetic poles for the African continent at 243.6° E, 84.6°N, a95 = 6.8°; 224.3° E, 81.2° N, a95 = 8.4°; 176.1° E, 82.0°N, a95 = 8.5°; 164.3° E, 86.4° N, a95 = 3.4°; 169.4° E, 82.6° N, a95 = 4.6° and 174.7° E, 72.8° N, a95 = 9.5° belonging to rocks which have been dated by the K-Ar method at 0.4 - 0.9 Ma, 2.6 Ma, 6.5 - 11 Ma, 12 - 17 Ma, 20 - 24 Ma and 28 - 31 Ma respectively. The results are in general agreement with other paleomagnetic poles from Oligocene to Recent formations in Africa.

The first three poles for rocks formed between 0.4 and 11 Ma are not significantly different from the present geographic pole. Together with other African poles for the same period suggesting very little movement of the African continent relative to the pole since 11 Ma. The other three poles for rocks dated between 12 and 31 Ma are significantly different from the present geographic pole showing a 5° polar deviation from the present pole in the Miocene and 13° in the Middle Oligocene.

An apparent polar wander path constructed using a compilation of paleomagnetic results from Africa including the newly determined poles shows that the African continent on the average, has been drifting approximately northwards. Using this idea and the available

geochronological data for the oldest rocks in the volcanic centres along the line a NE-SW migration of its volcanism has been proposed.

Friday 23 July AM

GA1.04/E/12-A5

0900

**PALEOMAGNETISM AND MAGNETIC TEXTURE OF OPHIOLITE FROM THE POLAR URALS**

Natalia LUBNINA (Department of Dynamic Geology, Geological Faculty, Moscow State University, Vorobyevy Gory, Moscow, Russia, email: lub@dynamo.geol.msu.ru); Alexey Didenko (Institute Physics of the Earth RAS, Moscow, Russia)

The Urals is a Hercynian nappe-fold structure, which resulted from the collision between the East-European and Kazakhstan-Siberian continents. We have chosen the Polar segment of the Urals (Voikar-Synya ophiolite massif) as the main object to study the history of its development. Petrographic study of gabbro and diabase from that ophiolite massif has allowed to type of the magnetic texture and orientation of major axes of magnetic susceptibility ellipsoid. Anisotropy of magnetic susceptibility of the main part of cumulative gabbros and gabbro-norites samples does not exceed 1-2%. No reference direction of main axes of ellipsoids of magnetic susceptibility is observed. Magnetic texture of these rocks was formed under hydrostatic compression, that is indicative of primary cumulative nature of the observed layering. Oblate fabric of the most part of dyke swarm reflects a magma flow during intruding. Big and average axes of ellipsoids of magnetic susceptibility lie in planes of the dykes stretch and have Fisher's distribution on the sphere. Average direction of big axes reflects a directions of basaltic magmas intruding. According to paleomagnetic data from ophiolites of the Polar Urals, paleoceanic basin was located at 8-14°N in the interval 420-490 Ma, the spreading zone striked in the NNW direction. The present Northern margin of the Siberia bordered the paleoceanic from the East. Paleomagnetic data from the sequences of continental slope and rise (the Lemva zone) suggest its position near the East-European Continent at 47°3.9'N in Upper Cambrian-Early Ordovician. During Ordovician the Lemva zone suffered clockwise rotation for about 50° relatively East-European Continent.

GA1.04/L/03-A5

0920

**WHERE WAS TUVA TERRAIN IN ORDOVICIAN?**

KAZANSKY A.Yu. (Institute of Geology UIGGM SB RAS, Academic Kopt'ug ave. 3, Novosibirsk, 630090, Russia, Email: kaz@uiggm.nsc.ru); Sennikov N.V. (Institute of Petroleum Geology, Academic Kopt'ug ave. 3, Novosibirsk, 630090, Russia, Email: sennikov@uiggm.nsc.ru); Mikhailov N.E., Kungurtsev L.V. (Institute of Geology UIGGM SB RAS, Academic Kopt'ug ave. 3, Novosibirsk, 630090, Russia, Email: kaz@uiggm.nsc.ru)

Tuva terrain the modern part of the southern margin of Siberian Craton is the object of unclear tectonic history. Some different scenarios are proposed to explain the uncertainties of geological history of this region (Sengor et al, 1993, Mossakovsky et al, 1993, Berzin, Dobretsov, 1993, and many others). This work was performed to clarify the relative position of Tuva on the base of paleomagnetic and biostratigraphical data. Paleomagnetic data were obtained from two locations in Ordovician sedimentary sequence in Uyk depression of Tuva trough (52N, 93E) which is well dated by different groups of fauna (Vladimirkaya, 1960). Sampling was performed so that the main fauna horizons fall stratigraphically just between the strata which was sampled paleomagnetically. Thermal demagnetization resulted in following ChRM directions: D=42, I=-8, a95=12 (location 1) and D=40, I=-19, a95=9 (location 2), which show both polarities successfully pass fold test and is quite close to previous data (Pavlov et al., 1997). The ChRM directions obtained show sufficient differences with reference directions from Siberian APWP (Smethurst et al, 1998). On the base on sedimentological and paleontological data (trilobites, brahiopods, conodonts, etc.) it is appeared that Tuva fauna association was developed in an individual basin, different from Altai-Salair shelf basins surrounding Siberian continent during Ordovician time. So one of the possible continents where Tuva sedimentary basin with inherent fauna association can be developed is Gondwanaland. If we accept the southern position of Tuva terrain in Ordovician, paleomagnetic data appears to be in a good agreement with paleontological and geological data. Moreover the connection between Tuva and Gondwanaland faunas still remains [Yolkina et al., 1996] in Silurian-Early Devonian and available paleomagnetic data [Pavlov et al., 1997] reinterpreted with southern position of Tuva is in a good agreement with the tectonic history of Gondwanaland during Silurian (Zhao, 1996). However, we realize that the final decision about the position of Tuva terrain is still ambiguous without additional data on palaeomagnetism, tectonics and paleobiogeography.

GA1.04/E/03-A5

0940

**THE LATE VARISCAN HORIZONTAL DEFORMATIONS OF FERGANA SECTOR OF TIEN SHAN BY PALEOMAGNETIC DATA**

Yu. S. RZHEVSKY (St.Petersburg State University, 14th Line 29, V.O.,199178, St.Petersburg, Russia, email: yurkov@icape.nw.ru )

The natural remanent magnetisation of the Middle and Late Carboniferous formations has been investigated. With employment diagrams of Zijderveld results of thermal demagnetising a samples of rocks (15-20 from the each point of selection) has revealed two NRM-components (prefolding and postfolding). Incline average of prefolding component display a Functional dependence from strike of rocks. Variations in trend of prefolding remanent magnetisation vectors are co-ordinated with geological data on postfolding rotation of structures in Fergana sector on South Tien Shan on angles from 30 to 90 degrees against of movement hand. Late Variscan horizontal deformations are associated with the formation of horizontal flexure-Fergana sigmoid and its further complication at the expense of movements along the Talas-Fergana Fault and the adjacent fractures.

GA1.04/E/07-A5

1000

**THE MIDDLE CARBONIFEROUS PALEOMAGNETISM OF HISSAR RIDGE AND IT'S SOUTH WESTERN BRANCHES (SOUTH TIEN SHAN), AND IT EMPLOYMENT FOR INVESTIGATE THE PROCESSES OF FOLDING**

Yu. S. RZHEVSKY (St.Petersburg State University, 14th Line 29, V.O.,199178, St.Petersburg, Russia, email: yurkov@icape.nw.ru )

Around 300 oriented samples of sandstones and siltstones (Middle Carboniferous) selected from different regions of Hissar ridge and it's South - Western branches has been investigated by paleomagnetic methods. The methods of investigate are simple: thermal cleaning and revealing the NRM-components with help of the Zijderveld's diagrams. Thus, NRM of investigated rocks contains, generally, the Early Permian postfolding component, which selected with small errors A95 <= 10 degrees). Prefolding component have little size and doesn't selected. Results of this investigate has been used for Alpine folding processes. The

are group Alpine large anticlines at the South-Western branches of Hissar ridge. The Middle Carboniferous rock forming the cores of structures indicated upper. The Mesozoic and Cenozoic rocks contains limbs of this folds and lies on Paleozoic rocks by steep angles (80-90 degrees).The Paleozoic rocks outcropped at cores of anticlines had been subjected only vertical movements by paleomagnetic data, and it's incline near contact with Mesozoic rocks (has steep incline) doesn't exceed 10-15 degrees. Thus, investigate structures are typical stamp folds.

GA1.04/W/24-A5

1100

**PALEOMAGNETISM OF DEVONIAN SEQUENCES IN VIETNAM**

N T K THOA, L T P Lan and V H Nam (Institute of Geophysics, Box 411 Buudien Boho Hanoi, Vietnam, email: thoa@igp.ncst.ac.vn)

Devonian sequences exposed widely in Northern and Central parts of Vietnam. 198 oriented samples were taken from 27 sites on limestones and basalts. Paleomagnetic treatments were carried out at the Institut für Allgemeine und Angewandte Geophysik in Munich, Germany. During detailed stepwise thermal and alternating field demagnetisation experiments two components of magnetisation (A and B) to be identified in basalts: components A is characterised by unblocking temperatures up to 300°C and shows direction which is not significantly different to the direction of the local present day geomagnetic field. The component B characterised by maximum unblocking temperature of 580°C, indicating magnetite as the carrier of characteristic remanent magnetisation. In limestones samples: A component is similar with viscous component and removed at 150°C, B component characterised by unblocking temperatures of 580°C. The resulting overall site mean direction, based on stable endpoints, (D= 16602, I=-3208, a95= 6.4, k= 29.3, N=24 sites), is interpreted to be of primary origin. This is supported by presence of normal and reversed direction of magnetisation in two kind of rocks. The second group of site of limestones yield B component with unblocking temperature at 650°C and high saturation field with direction (D=29007, I=-6507, a95=10.4, k=45.6, N=3). Comparison of magnetic hysteresis parameters of both groups shows value of Mrs/Ms and Hcr/Hc generally lie in the pseudo-single domain. At the same time for second group with the presence of hematite, wide range of Hcr/Hc and "wasp-waisted" hysteresis loop were observed. Devonian paleomagnetic data together with Cambrian and Ordovician data from region appear to support the former southern paleolatitudes of the terrain, based on paleontological, stratigraphic and structural relationships.

GA1.04/W/12-A5

1120

**NEW EARLY PALEOZOIC PALEOMAGNETIC RESULTS FROM THE NORTH CHINA BLOCK AND IMPLICATIONS FOR GONDWANA**

Zhenyu YANG (Institute of Geomechanics, CAGS, Beijing, China; Kobe University, Japan. Email: zzyang@kobe-u.ac.jp); Baochun Huang (Institute of Geophysics, CAS, Beijing, China); Yo-ichiro Otofujii (Department of Earth Sciences, Kobe University, Japan); Zhiming Sun and Xinghua Ma (Institute of Geomechanics, CAGS, Beijing, China)

In the last five years, we have sampled the Cambrian-Ordovician in 14 sections (28 oriented block and 1900 oriented core samples covered over 222 sites) from Henan, Shanxi, Shaanxi, Hebei and Ningxia provinces of the North China Block (NCB). The samples were measured using the CTF, 2G magnetometers at the paleomagnetic laboratories in China, France and Japan. All samples were demagnetized stepwise using thermal, AF or a composite of thermal and AF methods. Multiphase and heavy secondary remagnetization have been revealed. The characteristic remanent magnetization (ChRM) for six periods between Cambrian and Ordovician is isolated only from 400 samples. They are directed to the NW (up) and SE (down) and form two antipodal clusters after tilt correction, which differs from those of the Permian and Mesozoic. Reliability of these ChRM directions is ascertained through positive fold and reversal tests, and also a good correlation of magnetic polarity pattern in the Cambrian/Ordovician boundary and lowest Ordovician across over different continents. The latter constrains the definition of early Paleozoic polarity for the NCB. New APWP between the Cambrian and Ordovician indicates that the NCB was located in the Southern Hemisphere around 15° in latitude during Cambrian-Ordovician time. Large motion of the NCB occurred at a period between the Early and Middle Cambrian: CCW rotation of 22.3°7.0° and northward motion of 7.2° 6.8°. Comparing Cambrian-Ordovician APW paths between North China and Gondwana, we suggest that the NCB was part of Gondwana during the Cambrian and lowest Ordovician, and started BREAKING away from Gondwana in the lower Ordovician.

GA1.04/W/28-A5

1140

**NEW PALEOZOIC PALEOMAGNETIC RESULTS FROM THE ALASHAN/HEXI CORRIDOR TERRANE AND THEIR TECTONIC IMPLICATIONS**

Baochun Huang (Institute of Geophysics, CAS, Beijing, China, email: bchuang@mail.c-geos.ac.cn); Yo-ichiro Otofujii and Zhenyu Yang (Department of Earth Sciences, Kobe University, Japan)

The relationship between the Alashan/Hexi Corridor (AHC) terrane and the stable North China Block (NCB), which is defined as the eastern part of the NCB beyond the Helanshan fold belt, is an unresolved problem for geologists and paleomagnetists who are interested in the Paleozoic paleogeography of the NCB. In the past three years, we sampled 566 oriented core samples over 69 sites from the eastern part of the AHC, northwest China. The sampled rocks are spanning from the Middle Cambrian to Carboniferous, and are largely composed of limestone, oolitic limestone, redbed, and quartz-sandstone. All the samples were progressively demagnetized using thermal, alternating field (AF) or a hybrid thermal and AF methods. Through the detailed magnetic component and rock magnetic analysis, characteristic directions and secondary remagnetizations were separated. The primary origin of the characteristic directions is ascertained by positive fold and reversal tests. The Silurian and Devonian results from three sampling sections show good consistency, indicating that our results may exclude the local rotation and represent for autochthonous terrane. Comparing our results with those from the stable NCB, the AHC terrane would have been the western extension of the NCB since the Ordovician, Silurian, Devonian, and Carboniferous results from the AHC terrane may therefore be used to supply the paleomagnetic database of the NCB. Our new Carboniferous poles are distinct with the coeval ones for Inner Mongolia, Outer Mongolia, South China, Tarim and Eurasia at 95% confidence level, suggesting that these blocks were separated in Carboniferous time.

Friday 23 July PM

GA1.04/E/14-A5

1400

**MAGNETIC FABRIC IN RELATION TO THRUST SHEET STRUCTURE OF THE EASTERNMOST RHENOHERCYNIAN**



Frantisek HROUDA (AGICO Inc., CZ-621 00 Brno, Czech Republic, Email: agico@agico.cz); Jiri OTAVA (Czech Geological Survey, CZ-602 00 Brno, Czech Republic, Email: otava@cgu.cz)

The easternmost Rhenohercynian is mostly represented by flysch-like Lower Carboniferous sedimentary rocks characterized by weak anchimetamorphism to weak epimetamorphism and structures ranging from sedimentary structures, through fracture and slaty cleavage, to metamorphic schistosity. The AMS is characterized by low degree of AMS, oblate magnetic fabric, and magnetic foliation parallel to the bedding in the formations with conspicuous sedimentary structures. In formations with spaced cleavage, the degree of AMS is higher, the magnetic fabric is on transition between linear and planar, the magnetic fabric is parallel to bedding, but the magnetic lineation is parallel to the bedding/cleavage intersection line. In the formations with slaty cleavage, the degree of AMS is high, the magnetic fabric is clearly oblate, the magnetic foliation is parallel to the cleavage and the magnetic lineation is parallel to the bedding/cleavage intersection lines. In Silesian metamorphic rocks, occurring to the west, the magnetic fabric shows very similar orientation to that of the Rhenohercynian, thus indicating incorporation of these crystalline complexes into the Rhenohercynian thrust sheet structure.

GA1.04/W/36-A5

1430

#### MAGNETIC ANISOTROPY AND PALAEOMAGNETISM OF PLIO-PLEISTOCENE SEDIMENTS FROM THE ADRIATIC MARGIN OF THE NORTHERN APENNINES (ITALY)

Leonardo SAGNOTTI and Aldo WINKLER (Istituto Nazionale di Geofisica, Via di Vigna Murata 605, 00143 Roma, Italy, email: sagnotti@marie.ingrm.it)

The study of the magnetic anisotropy and palaeomagnetism of the Plio-Pleistocene sediments that crop out along the Adriatic margin of the central-northern Apennines (Italy) provides an opportunity to extend to the external front of the belt the analyses that were previously conducted in the central and northern Apennines and to push the geodynamic reconstruction for the region to the last few million years. Standard palaeomagnetic cores were drilled in 27 sites, distributed in the region between the towns of Ancona and Pescara, in marine fine-grained sediments of early Pliocene to early Pleistocene age. The anisotropy of magnetic susceptibility (AMS) of the studied sediments indicates a prevalent sedimentary-compactional magnetic fabric with variable overprint of the tectonic strain. The integration of the AMS data with the results from previous studies on the present-day stress field and the AMS of older sediments in the Apenninic belt allows the evaluation of the spatial-temporal evolution of the strain pattern in the area since the early Pliocene. The new palaeomagnetic data, on the other hand, provide constraints on the dynamic and the timing of the oroclinal processes that were previously recognized for the northern Apennines.

GA1.04/L/01-A5

1450

#### MAGNETIC FABRICS OF ORDOVICIAN AND SILURIAN GREYWACKES FROM NW ENGLAND AND SW SCOTLAND

W.H. OWENS (School of Earth Sciences, University of Birmingham, Edgbaston, Birmingham B15 2TT, UK, email: w.h.owens@bham.ac.uk)

The challenge, always, for magnetic fabric analysis is to provide reliable information that is not easily obtainable by other methods of geological enquiry. A critical review is attempted here of progress in attaining this goal, in the context of work on greywackes from the Lake District and the Southern Uplands.

These rocks lie within the Caledonian fold-belt and their magnetic fabrics, in many cases, clearly reflect that tectonic framework. The magnetic fabric we now see, however, results from a superposition of the effects of many processes, sedimentary, pre-lithification and diagenetic, as well as tectonic. As a sensitive grain fabric technique, magnetic methods might be expected to provide information on, say, current flow direction in sedimentary deposition, quantitative measures of deformation through grain reorientation, or more general, subtle indicators of processes acting. The key to such application, however, is the identification of cause and effect, the confident attribution of a fabric to a process. In complex situations, as here, a first step is to identify end-member cases, where one process either acts alone or dominates all others. Criteria can then be established to characterise the style of magnetic fabrics associated with that regime. Only when a causal link is certain can quantitative interpretation, based on empirical correlation or, ideally, an understanding of how a fabric has developed, be applied. In other cases, where multiple causes are suspected, caution is necessary.

GA1.04/W/32-A5

1510

#### MAGNETIC FABRIC AND FLOW DIRECTIONS IN SURGES AND ASSOCIATED PIROCLASTIC LOW DEPOSITS FROM THE NORTHERN PUNA ( 22.5° S-66.6° W ), ARGENTINA

Silvia Singer, Juan F. VILAS and Rubén Somoza ( Laboratorio de Paleomagnetismo Daniel Valencio, Departamento de Ciencias Geológicas, Universidad de Buenos Aires, Argentina, email: singer@gl.fcen.uba.ar) Beatriz Coira (Instituto de Geología y Minería, Universidad Nacional de Jujuy, Argentina)

A study of magnetic fabric, supported by field evidences, microscopic observations and paleomagnetic data was carried out on Upper Miocene piroclastic deposits from the Northern Puna ( Central Andes of Argentina) in order to determine their flow directions. These deposits are formed by subhorizontal ignimbritic sequences associated at their bases with friable surges. These contain similar phenocryst assemblages with biotite as the main paramagnetic mineral and titanomagnetite as the predominant ferromagnetic mineral.

Both the surges and ignimbrite deposits show bulk susceptibilities that vary between 100 and 200 mSI although the ignimbrites have larger values due to these are richer in titanomagnetite, as shown by polished thin sections, NRM and saturated remanent magnetisation data.

Both kinds of deposit show low to moderate degrees of anisotropy, oblate magnetic fabrics with subhorizontal foliation planes. In spite of these similarities different magnetic fabrics are found between the ignimbrites and their associated surges. These results will be discussed.

GA1.04/L/02-A5

1600

#### ALPINE TECTONIC OVERPRINT OF THE MAGNETIC FABRIC IN THE VARISCAN GRANITES OF THE WEST CARPATHIANS

Frantisek HROUDA (AGICO Inc., CZ-621 00 Brno, Czech Republic, Email: agico@agico.cz); Marian Putis (Petrology Dept., Komenský University, SK-862 00 Bratislava, Slovakia, Email: putis@fns.uniba.sk); Dagmar Gregorova (Geophysical Institute, Slovak Acad. Sci., SK-800 00 Bratislava, Slovakia, Email: geofdage@savba.sk)

The Central West Carpathians of Slovakia, unlike the Alps and other mountain chains, do not create a continuous mountain range, but crop out as the so-called Core Mountains within the mostly unfolded Intracarpation Palaeogene and Neogene. The granitic rocks, which are Late Palaeozoic (mostly Carboniferous) in age, occur in the central areas of the Core Mountains,

being associated with Early Palaeozoic metamorphic rocks and covered by Permo-Triassic to Middle Cretaceous sedimentary rocks. The granites are mostly weakly magnetic and correspond to the S type granites. The magnetic fabric in the sedimentary rocks covering the granites can be classified as partially up to entirely deformational in origin. The magnetic fabric patterns in the granites are very similar to those in sedimentary rocks in the region of the Veporic unit because of their common ductile deformation. Consequently, the magnetic fabric in granites does not represent the intrusive magmatic fabric associated with the granite emplacement, but the deformational fabric associated with early-Cretaceous motion of the nappes and mid-Cretaceous strike-slip tectonics of the Central West Carpathians. In the Tatric Core Mountains where mid- to late-Cretaceous/early-Tertiary deformation occurred in unmetamorphic to anchimetamorphic environment the granitic bodies suffered cataclasis and together with metamorphic mantle sometimes preserve pre-Alpine mesoscopic and magnetic fabrics, which differ between the Core Mountains.

GA1.04/W/39-A5

1620

#### MAGNETIC FABRICS OF SOFT-SEDIMENT FOLDED STRATA WITHIN A NEOGENE ACCRETIONARY COMPLEX, MIURA GROUP, CENTRAL JAPAN

EMILIO HERRERO-BERVERA (SOEST-HIGP 2525 Correa Rd., Honolulu, HI, USA, email: herrero@soest.hawaii.edu) Toshiya Kanamatsu (JAMSTEC, 2-15 Natsushima-Cho, Yokosuka 237, JAPAN, email: toshiyak@jamstec.go.jp) Asahiko Taira (ORI, University of Tokyo, 1-15-1 Minami-dai Nakano-ku, Tokyo 164, JAPAN, email: ataira@ori.u-tokyo.ac.jp)

The anisotropy of magnetic susceptibility (AMS) has been utilized for distinguishing various processes in deformation of sediments in which visible grain-scale deformation can scarcely be recognized. We have applied the AMS method on the middle Miocene-Pleistocene sedimentary sequence in the Boso and Miura Peninsulas, central Japan, which is associated with abundant synsedimentary deformation structures of folding and faulting generated in accretionary tectonics. The patterns of variation in AMS were compared to the stage of the deformation in order to understand the evolution of magnetic fabric from undeformed to deformed forms. The lineation growth and anisotropy decrease in magnetic fabrics are recognized with progress of deformation. The direction of lineation (alignment of the maximum susceptibility (K<sub>max</sub>) direction) develops perpendicularly to the compressive stress. The development of such features is clearly recognized within the hinge zone of a ductile soft-sediment fold structure. The pattern of the shape parameters and susceptibility axes indicates that the growth of lineation occurs prior to the formation of a great circle distribution of the minimum susceptibility (K<sub>min</sub>) direction. This suggests that the early fabric development in sediment under a highly compressive stress regime is dominated by the grain rotation.

GA1.04/W/02-A5

1640

#### PALAEOMAGNETIC ROTATIONS OBSERVED ON EARLY MIOCENE DYKES FROM THE INTERNAL ZONE OF THE BETIC CORDILLERAS (SOUTHERN SPAIN)

Manuel CALVO (Dep. Física, E.P.S., Universidad de Burgos, 09006 Burgos, Spain, Email: mcalvo@ubu.es); José María Tubía and Julia Cuevas (Dep. de Geodinámica, Fac. de Ciencias, Universidad del País Vasco, Bilbao, Spain, Email: gpccuuj@lg.ehu.es)

Palaeomagnetic data from the Internal Zones of the Betic Cordilleras are relatively scarce. In this study we present preliminary palaeomagnetic results obtained on rocks belonging to an Early Miocene (22-23 Ma) dyke swarm which intrudes Maláguide and Alpujárride units in the central and western parts of the Internal Zone of the Betic Cordilleras. The aims of this study were to ascertain if relative perpendicular orientations (N-S and E-W) shown by different dyke families are of primary or secondary origin and to find out if palaeomagnetic rotations can be detected in this area.

Palaeomagnetic studies were carried out on rocks belonging to seven different sites. In addition, susceptibility-versus-temperature curves and AMS were determined. Intensities of magnetisation were found to be low, remanence being carried by pyrrhotite and magnetite. Six out of seven sites offer reliable results, though dispersion is in some cases relatively high. Mean palaeomagnetic directions show both normal and reversed polarities, and strongly clockwise rotated palaeodeclinations (approx. 90-140°) are observed in all cases. As both dyke families show similar rotations, independently of their original direction, their relative perpendicular orientation seems to be of primary, intrusive origin. These rotations are in accordance with other block rotations observed in the Internal and External Betics, although their magnitudes are much stronger.

Saturday 24 July AM

GA1.04/L/04-A6

0900

#### PALEOMAGNETISM OF CARBONATES AND PB/ZN MINERALIZATION IN SOUTHERN FRANCE

M.T. LEWCHUK, H. Rouvier, B. Henry and M. Le Goff (IGP, Lab. de Géomagnétisme et Paléomagnétisme, 4 ave. du Neptune, 94107 St. Maur Cedex, France, email: mlewchuk@aol.com); D. Leach, USGS Mineral Resource Program, US Geological Survey, Mail Stop 973, Box 25046 Denver Federal Center, Denver, CO 80225

A temporal relationship between orogenesis, large scale crustal fluid migration, dolomitization, hydrocarbon localization and MVT mineralization has been inferred from geochemistry, paleomagnetism and isotopic dating in several orogenic belts and adjacent basins throughout the world. We are examining the applicability of this model for MVT mineralized carbonates from several locations in the structurally complex Cévennes region of southern France. Clay alteration dates have been used to infer an Early Jurassic age for this mineralization, although there may be conflicting geological evidence.

We isolated a single polarity, northerly, steep downward remanent magnetization during demagnetization at all locations. After partial untilting, the direction is close to the Eocene reference pole for the European Apparent Polar Wander Path. There is geological, geochemical and paleomagnetic evidence to suggest that this is the age of the magnetization. Since this magnetization is much younger than either the clay ages or maximum burial for the area the magnetization must therefore be related to fluid movement. This paleomagnetic evidence for Eocene fluid flow argues that the Cévennes district conforms to the orogenically-driven fluid-flow model for other MVT districts. The MVT mineralization is probably the product of crustal fluid migration during Pyrenean orogenesis, a process similar to virtually all other MVT deposits worldwide.

GA1.04/E/02-A6

0920

#### TERTIARY ANTICLOCKWISE ROTATIONS IN THE SW ALPINE REALM

Pierre ROCHETTE Frédéric Kechra, Didier Vandamme, and Frédéric Ollagnier (CEREGE, BP80 13545 Aix en Provence Cdx 4, France; email: rochette@cerge.fr)



Liassic to Cretaceous marls and limestones of the European margin in SE France show a widespread remagnetization with normal polarity, carried by magnetite. This remagnetization is usually pre-folding and have a Tertiary inclination. A study of 12 sites in the Cévennes region, folded during the Pyrenean phase around 40 Ma shows no rotation with respect to Tertiary stable Europe and may point to a syntectonic remagnetization, linked to Pyrenean orogenic fluids, during the 5 Ma period of largely dominant normal polarity spanning Chrons 16-18N. In the Provencal area perfectly similar paleomagnetic behavior is observed but mean declination points toward a  $15 \pm 10$  degree anticlockwise rotation during Tertiary. Alternatively no rotation is implied if remagnetization occurred during Cretaceous long normal but inclination does not match. However, primary magnetizations in Paleogene sediments as well as in the 30 Ma Estérel intrusion confirms the anticlockwise rotation.

The Provencal area is surrounded to the N and W by areas showing no rotation in similar remagnetized sediments, to the S and E by the Corsica-Sardinia block and the internal alpine zones, all showing large (>30) anticlockwise rotations since 30 Ma. Therefore the Provencal area may have been partially dragged during the possibly synchronous rotation of the Apulian-Corsican-Sardinian "block", limited by dextral strike slip movement on the Penninic front and rifting in the Provencal basin. Alternatively the different rotations observed are independent and the Provencal rotation corresponds to a lateral escape during the indentation of the Apulian block into the European plate. New data from Corsica helping to understand its suturing to Apulia will be presented.

**GA1.04/W/10-A6**

**0940**

**STRUCTURAL RECONSTRUCTION AT AN INTERMEDIATE STAGE OF FOLDING USING REMAGNETIZATION DIRECTION**

B. HENRY and M. Le Goff (Paléomagnétisme et Géomagnétisme, CNRS and IPGP, 4 avenue de Neptune, 94107 Saint-Maur cedex, France, email: henry@ipgp.jussieu.fr); H. Rouvier (Laboratoire de Géologie Appliquée, Univ. P. et M. Curie, 4 place Jussieu, 75252 Paris cedex 05, France)

In the Cévennes area (Southwestern border of the French Massif Central), a widespread remagnetization, related to fluid migration during Eo-Oligocene times, has been pointed out (Rouvier et al., 1995). This magnetic overprint has been acquired between two phases of deformation. In two areas, several neighboring sites has been studied.

In the Durfort - Grande Vernissière area, the overprint orientation reveals that a large block underwent an important clockwise rotation since the remagnetization. The low temperature component, likely carried by goethite, shows for some of the sites also a clockwise rotation, but of smaller amplitude.

The Montagne de La Fage is presently the southern limb of an anticline, with increasing dip towards the South. According to the levels, the remagnetization shows different orientation, mainly around a vertical plane perpendicular to the main fold axis. Assuming rotation around an horizontal axis, the geometry of the main structure has been reconstructed for the time of the magnetic overprint acquisition, replacing the obtained paleomagnetic directions in coincidence with the mean orientation of the remagnetization.

H. ROUVIER, B. HENRY et M. LE GOFF, 1995. Regional remagnetization and Mesozoic levels containing "Mississippi Valley Type" deposits: the southern border of the French Massif Central. XXI UGGI Gener. Assemb., Boulder, Colorado.

**GA1.04/W/20-A6**

**1000**

**PALEOLATITUDES FOR IBERIA FROM THE MIDDLE TO THE LATE JURASSIC**

Maria Luisa OSETE and Cristina Osete (Dep Geofísica, Facultad Ciencias Físicas, Complutense University, Madrid 28040, Spain, email: mlosete@eucmax.sim.ucm.es); Juan José Villalafán (Escuela Universitaria Politécnica, Burgos University, Spain); Paola Romana Gialanella (Dept. of Earth Science, Univ of Naples "FedericoII", Italy); Friedrich Heller (Institut für Geophysik, ETH, Zurich, Switzerland)

New palaeomagnetic data are reported from 11 well dated sedimentary sections from the Betic Cordillera (southern Spain) and the Iberian Range (Central Spain) that allow to calculate the palaeolatitude of the Iberian Plate from the lower Toarcian to the Tithonian. In the investigated rocks (marly and red nodular limestones) at least two magnetic components were observed. A low-temperature component of normal polarity and maximum unblocking temperature of about 400-450°C which has been interpreted as a secondary Cretaceous or Tertiary remagnetization. And a higher-temperature component (the ChRM) that was isolated from 450 up to 550-575°C. The ChRM, considered as the original Jurassic magnetization, exhibited both normal and reversed polarities. Directions pass the fold test and the reversal test. High palaeolatitudes (close to the present palaeolatitude of Iberia) were observed from the lower toarcian sites and lower palaeolatitudes have been obtained from upper Jurassic sites. Results have been transferred and compared with the two proposed APW paths for the North-American plate.

**GA1.04/W/13-A6**

**1100**

**PALEOMAGNETISM IN NORTH-WESTERN BULGARIA : WIDESPREAD REMAGNETIZATION AND TECTONICS**

B. HENRY (Paléomagnétisme et Géomagnétisme, UMR 7577 CNRS and IPGP, 4 avenue de Neptune, 94107 Saint-Maur cedex, France, email: henry@ipgp.jussieu.fr); N. Jordanova and D. Jordanova (Geophysical Institute, Bulgarian Academy of Sciences, Acad. G. Bonchev Str., block 3, 1113 Sofia, Bulgaria, email: vaneidi@geophys.bas.bg); D. Dimov (Sofia University "St Kliment Ohridski", 15 Tzar Osvoboditel Bld., 1000 Sofia, Bulgaria, email: dimo@gea.uni-sofia.bg); F. Bergerat (Département de Géotectonique, ESA 7072 CNRS, B 129, Univ. P. et M. Curie, 4 place Jussieu, 75252 Paris cedex 05, France, email: bergerat@lgs.jussieu.fr)

Paleomagnetism of Mesozoic formations, mainly Lower Triassic red sandstones and Middle-Upper Triassic carbonates, have been studied in the Moesian platform, the Stara Planina and the Prebalkan. Directions of the primary magnetization, mostly obtained in the red sandstones, are in good agreement with the Triassic data from stable Europe. There is therefore no important local rotations in these sites. In the carbonated rocks, the ChRM is of normal polarity. Positive fold test has been obtained in two sites, but progressive unfolding using all the sites points out a synfolding magnetization. Conglomerate test shows that these rocks are remagnetized. The application of the method of Surmont et al. (1990) and Shipunov (1997) using small circles intersection shows that, according to the sites, this remagnetization is refolding or synfolding. The paleomagnetic pole of this magnetic overprint corresponds to about a Lower to Middle Eocene age, and the beginning of the main folding is at the end of the Middle Eocene. This implies that this area was locally affected by moderate folding before the main deformation. This remagnetization could be related to fluid migration during the preliminary stages of the main orogeny.

**GA1.04/W/27-A6**

**1140**

**PALEOMAGNETIC EVIDENCE FOR OPENING OF THE GULF OF EDREMIT, NW TURKEY**

N.ORBAY (1), M.Sanver (2), Y.Yilmaz (3), T.Isseven (2), F.Özçep (1), C.Tapirdamaz (2), M..Hisarlı (1) (1- University of Istanbul, Faculty of Engineering, Department of Geophysics, 34850, Istanbul

TURKEY, 2- ITU, Faculty of Mines, Department of Geophysics, Istanbul TURKEY, 3- Istanbul Technical University Faculty of Mines, Department of Geology, email: norbay@istanbul.edu.tr , Istanbul TURKEY)

The aim of this paleomagnetic study is to clear out the controversy, which has been created due to the different tectonic interpretations proposed on the Gulf of Edremit. For this purpose, the paleomagnetic techniques were applied to 479 samples. They are collected from 52 Neogene volcanic rocks obtained from the northern part of the Gulf of Edremit (Biga Peninsula) and around of the towns of Ayvalik, Dikili and Bergama. The remanent magnetization directions, obtained from the Lower-Middle Miocene and the Upper Miocene rock samples display, 200 clockwise and 250 counter-clockwise rotations, respectively. The remanent magnetization directions of the Lower-Middle Miocene samples, collected from the southern part of the Gulf of Edremit and the Foça area also show 190 and 300 clockwise rotations. The coeval rocks from the Bergama area, on the other hand, display 300 counter-clockwise rotation. The difference in sense of rotations from different locations of the Northwestern Anatolia may be interpreted as a result of the opening of the Gulf of Edremit during the N-S extensional regime. The different inclination angles, measured from the rocks of the western part of the studied area essentially reflect the inclined block movements, which are created by the listric normal faults during the development of the present E-W garben systems.

**GA1.04/P/01-A6**

**1200**

**PALEOMAGNETIC RESULTS ON THE MAIN VOLCANIC OCCURRENCES FROM BAHARIYA OASES, WESTERN DESERT, EGYPT**

SALAH A. MOUSA (Geophysics Dept., Fac. Of Sci., Ain Shams Univ., Cairo, Egypt.) Mohamed H. Abdel Razek (Egyptian Geological Survey, Cairo, Egypt ) Karam S. Farag (Geophysics Dept., Fac. Of Sci., Ain Shams Univ., Cairo,Egypt.)

A paleomagnetic investigation has been carried out for 44 independently oriented hand blocks (comprising 336 specimens) collected from seven reasonably spaced basaltic volcanic exposures, distributed within and outer Bahariya depression. After AF and/or thermal demagnetisations, all specimens reveal stable components of magnetisations probably of TRM origin residing mainly in magnetite and ilmenite grains. A tentative correlation of these lava extrusions, on the basis of polarity of magnetisation, has been suggested. Two distinct populations of paleomagnetic pole positions of the encountered occurrences are computed from their stable remanence orientations. Basalt Hill and El-Bahr basaltic exposures represent the first group of paleopoles which are  $78.25^{\circ}$  S/ $34.3^{\circ}$  E and  $78.90^{\circ}$  S/ $21.7^{\circ}$  E respectively, while the basaltic exposures of El-Hefhuf, Mandisha/El-Aguz and Maesera represent the second group of paleopoles which are  $56.2^{\circ}$  S/ $10.8^{\circ}$  E ,  $58.9^{\circ}$  S/ $19.4^{\circ}$  E and  $50.6^{\circ}$  S/ $14.8^{\circ}$  E respectively. On the other hand, west El-Tebniya basaltic exposure shows a paleopole,  $36.7^{\circ}$  S/ $349.5^{\circ}$  E, intermediate between the two groups. This may indicate that the Bahariya Oases were subjected to two main alternative episodes of volcanicity. This activity is considered to be intimately related with the late Tertiary (pre-Miocene to lower Miocene) epirogenic movements in Egypt. The present reliable Tertiary results represent a good contribution to the Egyptian paleomagnetic database.

Saturday 24 July PM

**GA1.04/E/04-A6**

**1400**

**PALEOMAGNETISM OF SE ASIA: CONTRIBUTIONS TO CENOZOIC TECTONICS**

Mike FULLER and Gina Frost (HIGP-SOEST, University of Hawaii, Honolulu, Hawaii, 96822, USA, email: mfuller@soest.hawaii.edu)

SE Asia lies at the intersection of the Euroasian, Indian-Australian and Philippine Sea Plates and as such is an area of active tectonics. The paleomagnetism of the region remains incompletely established, but major patterns are emerging. A region in the north including Myanmar and Thailand exhibits a history of Cenozoic clockwise (CW) rotation and southerly motion. To the south in Peninsular Malaysia, Borneo, Celebes Sea and much of the Philippines counterclockwise (CCW) rotations predominate with little change in latitude. The Mesozoic basement of Palawan, which lies to the northeast of Borneo between the South China and Sulu Seas, is an exception having moved southward. Ophiolites obducted on to this basement appear to have moved northward and rotated counterclockwise. The timing and magnitudes of these rotations have not yet been satisfactorily established, but constraints on some are evident. For example, the CCW rotation of Borneo can be demonstrated to have consisted of some 40 to 50° between approximately 25 and 10 Ma and an additional similar amount between 25 and 80 Ma. The CCW rotation of Peninsular Malaysia is some 40°, but the absence of a Tertiary section on the peninsula leaves the timing of the rotation poorly constrained as post-60 Ma. The CW rotation in Myanmar and Thailand is interpreted as a response to the Indian-Eurasian collision. The southward motion of Palawan is readily interpreted as a consequence of South China Sea spreading. The rotation of Borneo follows from the convergence between the Indian-Australian plate and Eurasia which has given rise to the accretionary wedge of northwest Borneo. The timing of the rotation of Peninsular Malaysia and its tectonic explanation remain unclear, but will likely be resolved by results from Sumatra. In this area of complicated Cenozoic tectonics paleomagnetism is helping to establish tectonic history, but many of the results remain controversial.

**GA1.04/W/17-A6**

**1420**

**EARLY TRIASSIC PALEOMAGNETIC POLE FROM THE KOREAN PENINSULA**

Koji UNO (Division of Environmental Science, Graduate School of Science and Technology, Kobe University, Kobe 657-8501, Japan, Email: unokoji@kobe-u.ac.jp)

Greenish sandstones in the Early Triassic Nogam Formation were collected for paleomagnetic study at 23 sites in the Ryeongnam Block, Korean Peninsula. A remanent magnetization component with low unblocking temperatures by 650C is obtained from 15 sites, while reliable remanent magnetization component with high unblocking temperatures of 670-690C is isolated from 7 sites. Paleomagnetic directions of the low temperature component before tilt correction are close to that of the present Earth's geomagnetic field. The directions yield a negative fold test at the 95% confidence level, indicating a recent remagnetization. Paleomagnetic directions of the high temperature component from 7 sites significantly cluster after tilt correction (from  $k=36.1$  to  $k=120.8$ ). The fold test is positive at the 95% confidence level.

The tilt-corrected mean direction of the Nogam Formation ( $D=347.1$ ,  $I=23.8$  with  $a95=5.5$ ) is regarded as a characteristic direction of the Ryeongnam Block in the Early Triassic time. The mean direction is of primary origin because of the folding age of Middle Triassic. Paleomagnetic pole calculated from primary directions of the Nogam Formation ( $62.5N$ ,  $336.8E$  with  $A95=4.7$ ) shows good agreement with the coeval pole for the North China Block. The paleomagnetic evidence suggests that the Ryeongnam Block has been a part of the North China Block at least since the Early Triassic time.

GA1.04/W/11-A6

1440

**SOUTHWARD DISPLACEMENT AND DIFFERENTIAL CLOCKWISE ROTATION OF INDOCHINA: PALEOMAGNETIC EVIDENCE FROM MIDDLE CRETACEOUS RED SANDSTONES IN NORTHWESTERN YUNNAN, CHINA**

Ken SATO, Yuyan Liu, Zhicheng Zhu, Zhenyu Yang and Yo-ichiro Otofujii, (Department of Earth and Planetary Sciences, Faculty of Science, Kobe University, Kobe 657-8501, Japan  
email: ken@shidahara1.planet.kobe-u.ac.jp)

Paleomagnetic samples from middle Cretaceous redbeds were collected at 20 sites around Yunlong (25.8 N, 99.4 E), northwestern part of Yunnan province, in the northern part of the Indochina block. After stepwise thermal demagnetization, high temperature component magnetization with unblocking temperature of about 675 C is isolated. Positive fold test at the 99% confidence limit shows that the high temperature component magnetization is primary for the middle Cretaceous Nanxin Formation. A tilt-corrected formation mean direction is  $D = 40.2$ ,  $I = 49.9$  with  $a95 = 3.9$ , corresponding to a paleopole at 54.6 N, 171.8 E with  $A95 = 4.4$ . Comparison with previously reported Cretaceous paleomagnetic directions indicates that the Yunlong area has been subjected to southward displacement by 11.9, 7.5 (corresponding to 1300, 800km) with respect to the stable Yangtze craton since Cretaceous time as well as clockwise rotation through 36.3, 13.6. The amount of latitudinal displacement observed in this study is compatible with the previously observed southward displacement of the Indochina block, whereas variable amount of clockwise rotation is observed throughout the Indochina block. This study elucidates that the Yunlong area in the Simao Terrane is a northernmost part of the southward translating Indochina block. We conclude that Indochina was squeezed out from Asian continent due to collision of India accompanied with internal differential clockwise rotation.

GA1.04/L/05-A6

1500

**PALEOMAGNETIC DATA OF UPPER JURASSIC-LOWER CRETACEOUS ROCKS IN CENTRAL PATAGONIA: EVIDENCE FOR TECTONIC ROTATIONS**

Silvana Geuna, Ruben Somoza and Haroldo VIZAN (Departamento de Ciencias Geológicas, FCEyN, Universidad de Buenos Aires, email: sgeuna@gl.fcen.uba.ar); Eduardo Figari (YPF S.A.); Carlos Rinaldi (Instituto Antártico Argentino)

We report preliminary paleomagnetic data from a widespread distribution of sites of Upper Jurassic to lowermost Cretaceous volcanic and sedimentary rocks in the Cañadón Asfalto basin, central Patagonia. Monocomponent and multicomponent magnetizations were observed during both thermal and AF demagnetization procedures. Some sites show the presence of both normal and reverse polarities, while only one polarity is observed in others. The resulting time-averaged paleomagnetic vector of each site was compared with the expected Late Jurassic-Early Cretaceous paleofield for South America. Despite problems with the accurate definition of the APWP of this continent, the paleodeclinations of the studied rocks suggest the widespread occurrence of vertical axis rotations. In contrast, the unconformable overlying Cretaceous rocks in the region do not show paleomagnetic evidence of vertical axis rotations. This indicates that most tectonic rotations detected in rocks of the Cañadón Asfalto basin are coeval with, and perhaps closely related to the opening of the South Atlantic Ocean.

GA1.04/W/15-A6

1520

**PALEOMAGNETISM ON MESOZOIC SEDIMENTS FROM SOUTHERN SIERRA MADRE ORIENTAL. EVIDENCE FOR POST CRETACEOUS DIFFERENTIAL TECTONIC BLOCK ROTATIONS.**

Juan José VILLALÁIN (Dpto. de Física, E. Politécnica Superior, Universidad de Burgos, 09006-Burgos, Spain, email: villa@ubu.es); Daniel Rey (Dpto. de Geociencias Marinas, Universidad de Vigo, 36200-Vigo, Spain); V. Carlos Ruiz & M. Luisa Osete (Dpto. Geofísica, Univ. Complutense, 28040-Madrid, Spain); Cecilia Caballero (Instituto de Geofísica, UNAM, 04510, México DF, México)

This paper reports on Upper Triassic to Upper Cretaceous rocks from the southern Sierra Madre Oriental. This chain has traditionally been interpreted as a Laramide fold belt, related to an upper Cretaceous-lower Tertiary orogenic event. The 22 sites investigated are representative of the variety of lithologies and ages that crop out in the Guayacocotla antiform. The structure of the NRM shows several common features in despite of their geographical distance, age disparity and lithological variety of the sampling sites. Their main palaeomagnetic characteristic is the presence of a stable reversed polarity component that generally unblocks between 450 and 500°C. The majority of the fold test results indicate that this component is a post-folding overprint, although there are a few cases indicating the contrary. Consequently we have concluded that the NRM of the investigated samples is dominated by a pervasive overprint that has affected rocks of different age and lithology distributed over a large area of the southern section of the western Sierra Madre in Mexico. This remagnetisation event was first suggested by Böhnell et al. (1990). Comparison of the overprint directions with the lower Tertiary North American expected direction indicates two important features: 1) The inclination of the overprint is consistent with the expected lower Tertiary directions for North America. 2) The palaeodeclination values indicate the existence of differential anticlockwise palaeomagnetic rotations in a very consistent distribution.

GA1.04/W/33-A6

1540

**TECTONIC CENOZOIC EVOLUTION OF THE CENTRAL ANDES (28°-40° LAT. S) ON BASIS OF PALEOMAGNETIC AND GEOCHEMICAL DATES**

GUILLERMO H. Ré (Lab. D. Valencio - UBA - Cdad. Universitaria, P.2, 1428 Bs.As., Argentina; email: indio@gl.fcen.uba.ar); Juan F. Vilas (CONICET - Lab. D. Valencio - UBA - Cdad. Universitaria, P.2, 1428 Bs.As., Argentina; email: vilas@gl.fcen.uba.ar)

The region understood between the 28° and the 40° S is characterized to present two clearly different subduction styles. Flat-slab subduction occurs among 28° and 33° S and normal subduction to the south of the 34°. In the north sector, it was carried out magnetostratigraphic studies in six localities. Additionally, paleomagnetic information corresponding to other eight localities was compiled. In the south sector it was carried out paleomagnetic and geochemical studies in fourteen localities, and the available geochronological information was compiled for the same ones. As a consequence of the obtained results it arises that the north sector presents a highly compressive tectonic, for events of different duration, at least from the 18 Ma.

On the other hand, in the south sector it was determined the existence of a group of distensives events and compressive that affected the district from the 20 Ma. These results might indicate that as a consequence of the reduction in the Nazca plate subduction angle (effective from the 10 Ma.) distensives events in the south sector that could be related with the compressive events that occurred in the north with equivalent time. This relationship may indicate the existence of a tensional field that would act as element of compensation of the cortical stress induced by the different subduction's regimens.

GA1.04/E/17-A4

Poster

0930-01

**MAGNETIC SUSCEPTIBILITY AND PARTIAL ANHYSTERETIC REMANENCE ANISOTROPIES IN THE MAGNETITE-BEARING GRANITE PLUTON OF TOURAO, NE BRAZIL**

Ricardo TRINDADE (Instituto Astronômico e Geofísico, Universidade de São Paulo, 3386, 01060-970, Brazil, email: rtrindad@iag.usp.br) Maria Irene B Raposo (Laboratório de Anisotropias Magnéticas, Instituto de Geociências, USP, São Paulo-SP, Brazil) Marcio Ernesto (Instituto Astronômico e Geofísico, Universidade de São Paulo-SP, 3386, 01060-970, Brazil)

The Tourao granite (Serido belt, NE Brazil) was emplaced along a set of NE and E-trending dextral strike-slip shear zones. Rock magnetism revealed that magnetite is the unique ferromagnetic mineral in these rocks. Anisotropy of low-field magnetic susceptibility (AMS) was measured in 83 sites and showed a strong scatter for 20% of the sites. Anisotropy of partial anhysteretic remanence (pAAR) was determined for 29 sites in the 0-50 mT (pAAR0-50) and 19 sites in the 50-90 mT (pAAR50-90) windows to isolate the fabric contribution of the remanence bearing fine- and coarse-grained magnetites. The pAAR0-50 is related to coarse-grained early crystallized magnetites while the pAAR50-90 is interpreted as due to fine needle-shaped magnetites hosted in biotites. Although the intrusive body does not show any imprint of solid-state deformation, magnetic fabrics were able to record discrete kinematic events that affected the pluton. The AMS and pAAR0-50 fabrics for most sites seems to be correlated to the early NNE-trending magmatic fabric, whereas pAAR50-90 gives a new fabric probably related to late partitioning of strain along E-trending magmatic shear zones. The former fabrics are probably related to the NE-trending shear zones stress field and were partially overprinted by the E-trending fabric recorded by pAAR50-90 suggesting that the set of E-trending structures is slightly younger than the major NE-trending shear zones.

GA1.04/W/07-A4

Poster

0930-02

**A CASE OF THERMAL ENHANCEMENT OF ANISOTROPY OF THE MAGNETIC SUSCEPTIBILITY IN THE NATURE**

Silvia Singer, Juan VILAS, Claudia Prezzi and Ruben Somoza (Departamento de Geología, Facultad de Ciencias Exactas y Naturales, Universidad de Buenos Aires, e-mail: somoza@gl.fcen.uba.ar)

As part of a paleomagnetic study in northern Chile we sampled sedimentary rocks in both the limbs of a kilometer-scale, north-south trending syncline. Additional samples from posttectonic dikes of andesite were taken in the eastern limb.

Most samples of sedimentary rocks from the eastern limb show a posttectonic magnetic component of reverse polarity, with magnetite as the main carrier. The same component is observed in the dikes, suggesting that the posttectonic component founded in the sedimentary rocks of this limb is related to the volcanism. In contrast, all the samples from the western limb show a pre-tectonic, normal-polarity magnetic component carried by hematite.

On the other hand, the sedimentary rocks of the eastern limb show a well defined, parallel-to-stratification magnetic foliation, whereas the magnetic susceptibility axes from sedimentary rocks of the western limb show a random distribution. However, these latter show a good clustering after thermal treatment, with the laboratory-induced magnetic foliation being parallel to the stratification. This suggests that the well-defined, natural magnetic fabric observed in the eastern limb is due to enhancement of the anisotropy of the magnetic susceptibility by heating during the volcanic activity.

GA1.04/L/06-A4

Poster

0930-03

**PRELIMINARY PALAEOMAGNETIC DATA FROM PRECAMBRIAN, CAMBRIAN AND LATE ORDOVICIAN/EARLY SILURIAN ROCKS AROUND NUNEATON (MIDLAND PLATFORM OF THE UK)**

VIZAN H.(1); Tommaso M.(1), Carney J.(2), Clarke P.(1), Turner P.(1) and Mullen R.(1). School of Earth Sciences, University of Birmingham, Edgbaston, Birmingham B 15 2TT. (2) British Geological Survey, Keyworth, Nottingham NG12 5GG.

A collaborative study by the British Geological Survey and the University of Birmingham is being carried out on Precambrian (~603 Ma), Cambrian (?530-540 Ma) and late Ordovician/early Silurian (442 +/- 3 Ma) rocks around Nuneaton. The Precambrian rocks consist of crystal tuffs and a variety of tuffaceous lithologies, intruded by basaltic andesites and a granophyric diorite stock. These rocks display an increasing red colour and spheroidal weathering as the unconformity is approached and are overlain by red, lithic-rich granulestones and sandstones basal to the Lower Cambrian Hartshill Sandstone Formation. All of these rocks are in turn intruded by late Ordovician/early Silurian (Ashgill to Llandovery) lamprophyres. Preliminary palaeomagnetic data suggest that each of these three ages of rocks show a different characteristic remanent magnetization (ChRM). The mean ChRM in the Precambrian rocks pass a contact test and differ substantially from those previously published. In-situ, its steep inclination ( $I=+76$ ,  $Dec=123$ ) is quite close to that recorded in Precambrian rocks of the Church Stretton area (75 km to the west of Nuneaton). The mean ChRM in the Cambrian strata has a shallow inclination ( $I=-2$ ,  $Dec=170$ ) and, in-situ, is close to that recorded for various other parts of the UK during the Carboniferous. The mean ChRM of the Upper Ordovician dykes, in-situ, has an intermediate inclination ( $I=-41$ ,  $Dec=160$ ) between the other values. In order to determine the origin of these different magnetizations, we conducted follow-up palaeomagnetic studies and geological observation, including strain testing of rocks using anisotropy of magnetic susceptibility and tilt testing the ChRM.

GA1.04/E/10-A4

Poster

0930-04

**IS THE PLATE MOVEMENT RANDOM?**

Vsevolod N.VADKOVSKY (Department of Geology, Moscow State University, 119899 Vorobeyevy gory, Moscow, Russia, email: vad@dynamo.geol.msu.ru)

On the face of it would seem that the plate movement is deterministic process at least latest 300 my (Cox, Hart,1985). Do any estimates of random wandering of lithospheric plates exist? The characteristic of random (brownian) wandering of the particle is a root-mean displacement  $z$  which depends from time as square root:  $z=\sqrt{2^*D^*t}$ , where  $D$  - diffusion coefficient (or mobility) of particle in the environment. This Einstein relation is the true for brownian wandering on a sphere surface too (Mardia,1972), but the displacement is an angle distance  $f$  between the start-point and point in any time. The analog of the root-mean displacement on a sphere is  $v=1-\cos(f)$  (Fisher, 1953). There are analysed non-smoothed data of time-series of apparent palaeomagnetic pole positions for different plates on different time intervals. It has been found that non-smoothed palaeomagnetic data on Baltic shield for the period from 2850 to 600 my interval (Elming,1993) and the same data on East-European plate for the period from 430 to 34 my interval (Khramov,1991) correspond to brownian behaviour due to its  $v(t)$  dependences. The Global Palaeomagnetic Database (McElhinny, Lock,1995) was used for study of joint motion of the plates ensemble. The time period under study (2800 my - 0) was divide on non-



overlap intervals of different length (10,20,50,100..my). The empiric latitude and longitude distributions of palaeoposition of all continents were calculated for every temporal-window. This distributions were compared with theoretical distributions. The comparison of this distributions leads to the conclusion that plate motions has brownian type. Maybe somebody very exactly knows trajectory of a plate in the past, but nobody knows it in the future ... In what direction will propagate Red sea rift?

**GA1.04/W/08-A4** Poster **0930-05**

**PALAEOMAGNETISM OF THE LOWER PALAEOZOIC VOLCANICS OF THE KACZAWA COMPLEX: EVIDENCE FOR VARISCAN MOBILISM IN THE POLISH SUDETES**

Marek LEWANDOWSKI (Institute of Geophysics, Polish Academy of Sciences, Ks. Janusza 64, 01-452 Warsaw, Poland, email: lemar@igf.edu.pl); Ryszard Kryza (University of Wrocław, Institute of Geological Sciences, Cybulskiego 30, 50-205 Wrocław, Poland, email: rkryza@ing.uni.wroc.pl), Niels Abrahamsen (Department of Earth Sciences, Aarhus University, Finlandsgade 8, DK-8200 Aarhus N, Denmark; email: Abraham@geo.aau.dk)

Palaeomagnetic studies on Lower Palaeozoic metavolcanics from the Kaczawa Mts (West Sudetes, NE part of the Bohemian Massif) are reported. The rocks under study represent mostly bimodal within-plate volcanics with a U-Pb multigrain zircon age of 511±39 Ma, successively metamorphosed under blueschist and greenschist facies conditions. Samples for palaeomagnetic and mineralogic studies comprised some 140 oriented hand samples and cores, collected from 13 sites on area of 200 km<sup>2</sup>. The stable ChRMs are all of post-folding origin and may be divided into three groups: A, B, and C, according to their orientation. Group A show NNE declination with moderate down-dip inclination, which probably represents an Alpine overprint. Group B shows W-to-SSW declination with shallow inclination, and is interpreted as acquired during a clockwise rotation of the Kaczawa unit during the Variscan orogeny. Group C display northern declination and a very steep inclination, similar to the remanence reported earlier from the Ordovician of Armorica. Lack of similarity of remanence C with known Phanerozoic palaeomagnetic directions from Baltica may indicate a possible separation of the Kaczawa Unit from Baltica at the time when this remanence was acquired. A resulting high latitude position of the Kaczawa Unit during the post-folding remagnetization, as suggested by the Group C, poses again a question upon the age and evolution of the Kaczawa structure, and a possible role of Caledonian movements within the area of Variscides.

**GA1.04/W/09-A4** Poster **0930-06**

**KINEMATIC RELATIONS BETWEEN MAGNETIC (AMS, AARM) AND TECTONIC FABRICS IN THE SHEAR ZONE (NIEMCZA FAULT ZONE, SUDETES FORELAND, SW POLAND)**

Tomasz WERNER (Institute of Geophysics, Polish Academy of Sciences, ul. Ks. Janusza 64, 01-452 Warszawa, Poland, Email: twerner@igf.edu.pl)

Anisotropy of magnetic susceptibility (AMS) and anisotropy of anhysteretic remanence (AARM) studies were performed for 22 sites with mylonites, gneisses, black shales, gabbros, serpentinite and granitoids within and in the vicinity of the Niemcza Fault Zone located in the Sudetic foreland in SW Poland. Some previous petrographic, structural and micro-tectonic studies in sites within the zone support the process of mylonitization of the Sowie Mountains gneisses in the strike-slip regional-scale sinistral shear zone developed along the eastern margin of the Sowie Mountains block.

Magnetic foliation (AMS kmin and AARM kmin axes) are in general closely correlated with tectonic foliation planes as well as magnetic (Kmax) with tectonic lineation on sample and site scale. Those relations were used as the kinematic indicators of non-coaxial deformation with a dominant sinistral shear component within the area.

The regional variability of the magnetic fabric (both direction and anisotropy parameters) was researched to test the postulated Sowie Mountains gneissic origin of the Niemcza zone mylonites. The relation of the magnetic fabric of late-tectonic gabbro, serpentinite and granitic bodies within the Niemcza zone with those of mylonites was also evaluated

**GA1.04/E/09-A4** Poster **0930-07**

**MAGNETIC FABRIC OF MESOPROTEROZOIC DIKE SWARMS FROM THE ILHÉUS, OLIVENÇA AND ITAJU DO COLÔNIA REGIONS, SE BAHIA STATE, BRAZIL**

Maria Irene B. RAPOSO (Lab. de Anisotropias Magnéticas, Instituto de Geociências, Universidade de São Paulo, São Paulo, SP, 11348, 05422-970, Brazil, Email: irene@usp.br); Manoel S. D'Agrella-Filho (Instituto Astronômico e Geofísico, Universidade de São Paulo, São Paulo, SP, 3386, 01060-970, Brazil, Email: dagrella@iag.usp.br)

The anisotropy of low-field magnetic susceptibility (AMS) was employed in the Ilhéus (IL), Olivença (OL) and Itaju do Colônia (IT) dike swarms from the São Francisco Craton, to investigate the magnetic fabric of these dikes and to provide information on their mode of emplacement. Most dikes (69) show a normal fabric, i.e., K1-K2 parallel to the dike wall, representing magma flow within the dikes. In 7 dikes it was found an intermediate fabric, i.e., K1-K3 parallel to the dike wall, which can be interpreted as resulting from the vertical compaction of a static magma column with the minimum stress along the dike direction. In 10 dikes an inverse fabric (K1 perpendicular to dike plane) was found. This fabric is not related to an exchange of K1 and K3 axis since hysteresis parameters indicate magnetic grains in the PSD-MD state for all studied dikes. Anisotropy of anhysteretic remanence (AAR) performed in dikes with inverse fabric suggests that this fabric was acquired after dike emplacement. The normal fabric shows, generally, steep K1 inclinations (>40°) for the IT dikes, suggesting that they were fed by inclined up to vertical flow. The opposite is observed for the IL-dikes where shallow K1 (<20°) inclinations predominate suggesting distant magma source. However, the OL-dikes have both steep and shallow K1 inclinations. These data suggest that if a single magma source fed the 3 swarms it was probably close to Itaju do Colônia area. Our data could also suggest another source close to the Olivença area.

**GA1.04/E/06-A4** Poster **0930-08**

**THE PROBLEMS OF PALEOMAGNETIC RECONSTRUCTION OF THE EAST-EUROPEAN CONTINENT IN ORDOVICIAN**

Ideya SVYAZHINA and Zifa Mezenina (Institute of Geophysics, Urals Branch of RAS, Amundsen Str., 100, Ekaterinburg, 620016, Russia, email: gloukhikh@geoph.mplik.ru); Valerian Bachtade and Jenny Tait (Institute fuer Allg. und Angew. Geophysik Ludwig-Maximilians-Universität Muenchen, Theresienstrasse 41, 80333 Muenchen, Germany, email: jenny@magnbakt.geophysik.uni-muenchen.de)

Shelf and slope deposits of the eastern edge of East-European continent were sampled within the structures of Southern, Middle and Northern Urals. According to the data received by the authors and other investigators, the continent in Early Ordovician was situated approximately between N 50 and S 200. Later in Middle and Late Ordovician it moved to the North (on modern geographical coordinates) and at the end of the period it was situated in equator-side zones of the Northern and Southern hemispheres.

According to the data received for Baltica (T.H.Torsvik and others) the East-European continent was also situated in Southern hemisphere in more high latitudes - between S 300 and S 600. During Ordovician it moved firstly to the South in Arenig-Llanvirn and later - to the North. As to polarity in Ordovician there are no differences in this problem. In Early Ordovician the polarity is supposed to be reverse and in Late - the normal one.

**GA1.04/E/13-A4** Poster **0930-09**

**PRELIMINARY PALEOMAGNETIC STUDY ON PALAEOZOIC SEDIMENTARY ROCKS FROM NORTHERN VIETNAM**

N T K THOA (Institute of Geophysics Box 411 Buidien Boho, Hanoi Vietnam, email: thoa@igp.ncst.ac.vn)

Northern Vietnam is belonging to the South China block. Many tectonists believe that this block together with Southeast Asia were formerly part of Gonwanaland during early Paleozoic time. The late Proterozoic, Cambrian and Ordovician sedimentary sequences, exposed along Song Ma suture in Northern Vietnam. For preliminary paleomagnetic study, 340 oriented samples from 35 sites were collected by using a portable gasoline-powered drill. Paleomagnetic treatments were carried out at the Institut für Allgemeine und Angewandte Geophysik in Munich, Germany. Samples were submitted to standard stepwise alternating field and thermal demagnetization. The principal component analysis showed that only a half part of samples yields useful paleomagnetic data. These samples were taken from limestones, sandstones and siltstones sequences. Additional magnetic measurements on IRM, Hc, Hcr, Mrs, Ms, Ist, Tc and hysteresis loops seem to confirm the content of primary mineral in these rocks (goethite and magnetite in limestones, hematite in sandstones and siltstones). The reversal test, fold test and conglomerate test were positive. The observed mean directions for paleozoic age of samples in North of Vietnam are follow: for Early Cambrian: D= 1807 I= -1002; for Midl Cambrian: D= 35504, I=-1409; for Late Cambrian: D= 18408, I= -1405, for Early Ordovic: D= 20400, I= -1706. Local paleotectonic reconstruction of region is calculated as well as the comparison of these data with the expected directions for a reference point in Northern Vietnam (j = 220N, I = 1050E). These results appear to support the former southern paleolatitudes of these terranes, based on paleontological, stratigraphic, and structural relationships.

**GA1.04/W/34-A4** Poster **0930-10**

**PALEOMAGNETIC RECONSTRUCTION OF THE EARLY PALAEOZOIC METAIGNEOUS COMPLEX FROM THE WEST SUDETES (KARKONOSZE - IZERA MASSIF, SW POLAND) BASED ON THE MAGNETIC FABRIC STUDY**

Maria JELENSKA, Tomasz Werner, Magdalena Kadzialko-Hofmök (all at Institute of Geophysics, Polish Academy of Sciences, ul. Ks. Janusza 64, 01-452 Warszawa, Poland, Email: bogna@igf.edu.pl) and Stanislaw Mazur (Institute of Geological Sciences, University of Wrocław, Pl. M. Borna 9, 50-205 Wrocław, Poland, Email: smazur@ing.uni.wroc.pl)

The southern and eastern margins of the Karkonosze-Izera massif in the Sudetes (northern Bohemian Massif) expose a nappe pile overthrust towards the NW onto the pre-Variscan continental basement of the Saxothuringian basin. The tectonically uppermost in the nappe pile is the Leszczyniec unit, composed of metaigneous Early Palaeozoic metabasites and gneisses. The isotopic age of protholith is about 500 Ma. The rocks underwent heterogeneous deformation accompanied by mostly epidote-amphibolite grade metamorphism of probably Late Devonian to Early Carboniferous age. Paleomagnetic studies revealed several components of NRM of steep and intermediate normal inclinations and scattered declinations. Among them some Carboniferous remagnetizations were recognised. However, the paleopoles calculated for other palaeomagnetic directions lie far from the reference APWPs for Baltica or for terranes derived from Gondwana. Therefore, in situ palaeomagnetic directions were corrected to remove effects of superimposed tectonic evolution. Since the magnetic fabric (AMS) for Leszczyniec unit is characterised by approximately N-S trending almost vertical foliation planes, the rotation that brought Kmin axes close to the horizontal E-W attitude was performed. The same correction applied to NRM components rotated them towards the Early Palaeozoic segment of the APWP for Baltica.

**GA1.04/W/35-A4** Poster **0930-11**

**VARISCAN REMAGNETIZATION AND TECTONIC ROTATIONS IN THE HOLY CROSS MOUNTAINS AND ARDENNES : PRELIMINARY CONCLUSIONS**

Rafał SZANIAWSKI and Marek Lewandowski (Institute of Geophysics, P.A.S., Ks. Janusza 64, 01-772 Warszawa, Poland, email: rafsz@igf.edu.pl); Olivier Averbuch, Jean-Louis Masy and Juliette Lamarche (Sédimentologie et Géodynamique, U.F.R., Lille 1, Villeneuve d'Ascq, France, e-mail: Olivier.Averbuch@univ-lille1.fr)

Comparative palaeomagnetic studies have been undertaken on the Palaeozoic rocks of the Holy Cross Mts. (HCM, Poland) and Ardennes-Boullonnais (AB, northern France), aiming to point out differences and similarities in tectonic evolution during Variscan diastrophic cycle. HCM and AB are situated in the eastern and central segment of the northern Variscides, respectively. In both regions Devonian clastics and carbonates were analysed, concentrating mainly on the localities situated in the central and western branch of French Ardennes, places so far not investigated palaeomagnetically by previous teams. Main carrier of NRM in the early Devonian redbeds was hematite, while secondary magnetite and/or hematite dominate in the mid-upper Devonian carbonates. NRM display single to multicompartment structure. All components identified so far are of secondary origin and were acquired at various stages of tectonic development thus remanence acquisition is most probably related to (syn)orogenic Variscan movements. Reversed polarity is dominating except for Radkowiec (southern unit of HCM) where normal polarity is observed. Common feature for the calculated VGPs in HCM and AB is their noticeable Northwest deviation from APWP for Baltica, a magnitude of the deviation varying from place to place. This is indicative for akin clockwise rotations in the distant parts of the Variscan fold belt, represented by structural units developed under different geotectonic setting.

**GA1.04/W/19-A4** Poster **0930-12**

**YUKON-TANANA TERRANE: BACKSTOP FOR THE ACCRETED NORTH AMERICAN CORDILLERAN TERRANES**

SYMONS, D.T.A., McCausland, P.J.A. (Earth Sciences, University of Windsor, Windsor, Ontario, Canada, N9B 3P4, ph: 519-253-3000, ext. 2493, e-mail: dsymons@uwindsor.ca); Hart, C.J.R. (Yukon Geology Program, Whitehorse, YT, Canada, Y1A2C6)

The Yukon-Tanana Terrane (YTT) underlies much of northern British Columbia, the Yukon and Alaska where it abuts against the North American craton. It is an enigmatic polymetamorphosed Phanerozoic terrane of either postulated far-travelled accreted or pericratonic origin. Preliminary paleomagnetic analysis of specimens collected by helicopter from 21 sites in the 190 +/- 5 Ma Jurassic Big Creek batholith (~500 km<sup>2</sup>), a coarse-grained quartz-hornblende synite to monzonite pluton, and from 16 sites in the ~82 Ma Seymour



Creek stock (~4 km<sup>2</sup>), a granodiorite pluton, yields poles at 147°E, 68°N (dp=6°, dm=7°) and 195°E, 59°N (dp=11°, dm=11°), respectively. Al-in-hornblende geothermobarometry indicates Big Creek was emplaced at ~6 kbar, with uplift soon after intrusion, and Seymour Creek at ~3 kbar so that it froze on intrusion into the Big Creek batholith to provide a contact test in addition. Comparison of the YTT apparent polar wander path (APWP) segment given by these poles to the craton's APWP indicates that the YTT was formed alongside the craton with ~30° of subsequent counterclockwise rotation but no relative translation. This indicates that the YTT was formed next to the cratonic margin and that the accreted terranes impacted against it.

depositional data is tilt corrected and separated into different time blocks characteristic of directional changes. A positive test of rotation is defined by clockwise/anticlockwise drift with time of normal declination in syn-depositional data and no drift in the post depositional data. Finally the data is assembled on a tectonic map of the area to infer the rotations with reference to present day tectonic elements to signify its application.

**GA1.04/E/08-A4** Poster **0930-13**

**GA1.04/W/37-A4** Poster **0930-17**

**GEODYNAMIC MODEL FOR THE CENTRAL SECTOR OF ALPINE-HIMALAYA FOLD-BELT FOR RECENT TIME BASED ON PALAEOMAGNETIC DATA ANALYSIS**

**PALAEOMAGNETIC INVESTIGATION OF NEOTECTONIC CRUSTAL DEFORMATION IN CENTRAL-WEST TURKEY TURGAY ISSEVEN**

Yu. S. RZHEVSKY (St.Petersburg State University, 14th Line 29, V.O., 199178, St.Petersburg, Russia, email: yurkov@cape.nw.ru )

John PIPER (Istanbul Technical University, Mining Faculty, Department of Geophysics, 80626 Maslak, ISTANBUL, Turkey); Orhan Tatar (Geomagnetism Laboratory, Department of Earth Sciences, University of Liverpool, LIVERPOOL L69 3BX, U.K.); Halil Gursoy (Department of Geology, Cumhuriyet University, 58140 SIVAS, Turkey.)

The conception offered is developed on the basis of the long-standing experience of palaeomagnetic data using in geodynamic investigations of the study region (Rzhevsky, 1964-1997). This conception uses the curves of migration of the instantaneous poles of rotation and synchronous curves of instantaneous rotation velocities for the different blocks of the Earth crust (Afgano-Tajik depression, North, Central, and Southeast Pamir, etc.). These curves are produced on the basis of palaeomagnetic data analysis for the recent time. Complex analysis of these curves allows us to make up the palaeogeographic reconstructions of the blocks for different time moments. Analysis of the palaeogeographic reconstructions obtained allows us to reconstruct the geodynamics of any part of the study area at any moment of recent time. Moreover, the model constructed lets to predict the character of geodynamic processes for any part of the studied area. Computer program, based on this model, may be used for evaluating of seismic potential of any area.

Present day Turkey is the site of collision between the Eurasian and Afro-Arabian Plates where a collage of accretionary belts comprising the Anatolian Block is being extruded laterally by tectonic escape. A widespread distribution of young volcanic rocks in this region provides a record of tectonic rotation during the Neotectonic Phase since termination of collision in Miocene times. Anticlockwise rotation averages about 30° in the eastern part of the Anatolian Block but increases to ~50 ° across the Ecmis Fault Zone, a major intracrustal strike slip belt cutting the south eastern sector of the Anatolian Block. This anticlockwise rotation is observed in young volcanic units attributed to the Quaternary and implies that rotation is a late feature of tectonic development of this region. In the Cappadocian ignimbrite province (~12-2 Ma) in the south of the block comparable anticlockwise rotations are observed in the oldest and youngest units. This shows that rotation associated with escape has only occurred late in the Neotectonic history presumably when strain release by crustal thickening consequent upon the continental collision could no longer be sustained. The rotations in Eocene volcanic units emplaced during the pre-collisional Palaeotectonic Phase are not markedly different from rotations found in much younger rocks and confirm that significant rotation has only characterised the last stage of the Neotectonic history. In northern Turkey the same ~30° anticlockwise rotation is observed in Eocene units on either side of the North Anatolian Fault Zone and indicates that this east-west lineament has been established as an intracontinental transform only at a late stage of the Neotectonic history. This general anticlockwise rotation is however, not uniform across Anatolia. Towards the southern margin of the Block it diminishes to near zero whilst in the north it changes westwards from anticlockwise to clockwise. Also towards the Aegean the strike slip regime gives way to an extensional province. In the vicinity of this transition in the Kutahya region clockwise rotations are observed in Miocene lavas and anticlockwise rotation in Pliocene rocks. Collectively these results show that the Anatolian Block is not a plate sensu stricto but is deforming in a distributed and differential manner. In the south west it is being extruded into...

**GA1.04/W/05-A4** Poster **0930-14**

**GA1.04/L/01-A4** Poster **0930-18**

**USING ROCK AND PALEOMAGNETIC METHODS TO ORIENT DRILL CORE: EXAMPLES FROM THE WESTERN CANADA SEDIMENTARY BASIN**

**OPENING HISTORY OF POWELL BASIN, ANTARCTIC PENINSULA**

Cioppa, M.T., SYMONS, D.T.A., (Earth Sciences, University of Windsor, Windsor, Ontario, Canada, N9B 3P4, ph: 519-253-3000, ext. 2502, email: mcioppa@uwindsor.ca), Lewchuk, M.T., (Institut de Physique du Globe, Paris, France), Gillen, K.P (Vox Terrae International, Calgary, AB)

EAGLES, G (University of Leeds, School of Earth Sciences Woodhouse Lane, Leeds, LS2 9JT UK); Roy A. Livermore (British Antarctic Survey, High Cross, Madingley Road, Cambridge, CB3 0ET, UK)

Oriented core provides information on various directional properties in a reservoir, i.e. fracture orientation, anisotropy of permeability, and in-situ stress tensors. Paleomagnetism may be used to restore core to its in-situ position. The viscous remanent magnetization (VRM) method aligns the VRM to either the Earth's present or dipole-averaged magnetic field. However, in six dolomite hydrocarbon reservoir studies in the Western Canada Sedimentary Basin (WCSB), this technique worked wholly in only one, partially in three, but not at all in two reservoirs. The method failed due to the lack of a VRM and/or the presence of a drilling induced remanence (DIRM) that is correlated to pyrrhotite. Thus, alternative paleomagnetic methods of orientation were needed. In all six studies the characteristic remanent magnetization (ChRM) had a steep inclination, usually reversed, that was used to orient drill cores. In case 1 three sampled cores were drilled at very different angles, and the angle between the core and the ChRM inclination provided a unique solution to the true ChRM orientation. It could then be dated by using the reference apparent polar wander path (rAPWP). In case 2 the paleolatitude small circle determined from the ChRM intersected the rAPWP only once, thus dating its ChRM. In case 3, the presence of a high temperature component was suggested by remagnetization circles from the ChRM to a shallow inclination. Geochemical and petrologic data suggested that the host Mississippian carbonates were either unaltered or early diagenetic in origin. Assuming that the high temperature component was Mississippian resulted in a Late Cretaceous age for the ChRM. In all three cases, the known ChRM direction could then be used to orient the cores.

The opening history of Powell basin, located at the northernmost Antarctic Peninsula, is modelled with constraint from its marginal and regional geology and newly-gridded magnetic data over the basin itself. Opening began with rifting of Mesozoic continental crust and breakup volcanism. This was followed by creation of oceanic crust at a slow spreading ridge oriented along N20W as a response to N55W relative plate motion of South America with respect to Antarctica during the Eocene and Oligocene. Models of the seafloor spreading anomalies suggest that the spreading phase of opening occurred between 32.1Ma and 23.3Ma. Microplate motions on the evolving Powell Basin's margins are assessed and presented using gridded magnetic data.

**GA1.04/W/03-A4** Poster **0930-15**

**GA1.05** Friday 23 – Saturday 24 July

**PALAEOMAGNETIC ORIENTATION OF DRILL CORE IN THE WESTERN CANADA SEDIMENTARY BASIN: RESULTS FROM A WORST CASE SCENARIO**

**ROCK MAGNETISM: METHODS AND APPROACHES IN ROCK MAGNETISM (SESSION A) AND MAGNETIC PROPERTIES AS ENVIRONMENTAL PROXY PARAMETERS (SESSION B)**

M.T. LEWCHUK (IPGP, Lab. de Géomagnétisme et Paléomagnétisme, 4 ave. du Neptune, 94107 St. Maur Cedex, France, email: mlewchuk@aol.com) D.T.A. Symons, I. S. Al Aasm (Dept. Earth Sci., Univ. Windsor, Windsor, Ontario, Canada, N9B 3P4) and K. P. Gillen, (Vox Terrae International, 40, 820-9a Street N.W. Calgary, Alberta, Canada, T2N 1V1)

Location: Muirhead Tower 112 LR2  
Location of Posters: Student Room (1st Floor)

Paleomagnetic analysis on drill cores is often done with the aid of external orienting tools such as well logs and fracture/bedding patterns to orient the core. Alternatively the orientation can be obtained by rotating the remanent magnetization data about the azimuth of the core axis until the viscous remanence is aligned with the present Earth's magnetic field direction. We present paleomagnetic data from the Western Canada Sedimentary Basin for which there were no external references for core orientation and the viscous magnetization was absent or unstable. Further, the core was broken up and had been extensively handled so that even the true up direction was uncertain for several pieces. We used the inclination of the characteristic remanence magnetization (ChRM) to determine the uphole direction assuming a single polarity component. We then generated a mean core magnetization angle (CMA), defined as the specimen ChRM inclination with respect to the core azimuth, for three cores drilled in different directions (vertical, inclined and horizontal). Plotted as small circles around the borehole azimuth, the three CMA's intersected at a best fit point that defined a Laramide age for the magnetization. We interpret this as a remagnetization related to hydrocarbon migration which agrees well with several other studies of similar rock sequences in the region. Thus, despite a worst case scenario for paleomagnetic analysis we were able to conduct a complete study on these cores, providing both core orientation and age of magnetization.

**Friday 23 July AM**

Presiding Chairs: K Fabian (University of Bremen, Bremen, Germany)  
J King (University of Botswana, Dept. of Physics, Gaborone, Botswana)  
Concurrent Poster Session

**METHODS AND APPROACHES IN ROCK MAGNETISM**

**GA1.04/E/05-A4** Poster **0930-16**

**GA1.05/W/38-A5** **0830**

**A TEST OF ROTATION FOR MAGNETOSTRATIGRAPHIC DATA**

**GRAIN-SIZE DEPENDENCE OF LOW-TEMPERATURE MEMORY IN MAGNETITE: POTENTIAL FOR GRANULOMETRY**

S. J. SANGODE Wadia (Institute of Himalayan Geology Dehradun 248 001, INDIA)

David J. Dunlop (University of Toronto at Mississauga, Mississauga, Ont., Canada L5L 1C6; email: dunlop@physics.utoronto.ca) Ozden Ozdemir (same address) Masayuki Torii (Biosphere-Geosphere System Science, Okayama University of Science, 1-1 Ridai-cho, Okayama 700-0005, Japan; email: torii@big.ous.ac.jp)

Determination of vertical axis rotations of a tectonic block in an orogenically active terrain from magnetostratigraphic data pertains to several doubts. Some of the important problems in the conventional handling of such data are highlighted and a test of rotation is suggested to express the quality of data for such studies. Magnetic polarity stratigraphy provides sequential information on the palaeomagnetic directions of a given site over a stipulated time. Several authors used such data as a composite time to deduce vertical axis rotation of the site representing tectonic block. Here mean D and I (by PCA) are analyzed for a demagnetization spectrum of viscous component for post-depositional rotation and that of primary component for syn-depositional rotations over a red-bed sequence of Siwalik molasse dating 4 to 0.78 Ma. While the post depositional data is used compositely to test of reversal and fold test, the syn-

We have measured the changes in saturation remanence (SIRM), produced either at 10 K or at 300 K, in 10-K intervals during zero-field warming-cooling or cooling-warming cycles between these endpoint temperatures. The first experiment is often used as a means of detecting magnetic minerals in rocks and soils by their characteristic remanence transitions (e.g., the magnetite Verwey transition around Tv = 120 K). The second experiment is the basis of low-temperature de-magnetization (LTD), a paleomagnetic cleaning technique. Neither has been seriously explored as a method of grain size determination in suites of rocks, sediments or soils with common mineralogy, but we find there is definite granulometric potential in both experiments. Our samples are natural crushed magnetites separated into narrow grain-size fractions with mean sizes of 0.6, 1, 3, 6, 9, 14, 20, 110 and 135 micrometers. Both unannealed and annealed samples were tested. A small fraction of low-temperature SIRM survives heating across the Verwey transition (first memory) with a very small recovery of the lost remanence in the second crossing of Tv during re-cooling (second memory). The transition is more sharply expressed in annealed samples, but un-annealed samples have larger first and second memories. Both memories increase steadily with decreasing grain size. Room-temperature

SIRM behaves in a comparable way except that most of the remanence loss and subsequent recovery occurs gradually between 300 K and the isotropic temperature,  $T_i = 130$  K, rather than sharply at  $T_v$ . The second memory is much larger than for 10 K SIRM. Both memories increase in a general way with decreasing grain size, but the size dependencies are monotonic only in the range 1-20 micrometers.

**GA1.05/E/12-A5 0850**

**XRD AND SEM ANALYSIS OF EXTRACTED MAGNETIC MINERALS IN RIVER SEDIMENTS AND IN BURNED TROPICAL SOILS**

SATRIA BIJAKSANA (Department of Physics, Bandung Institute of Technology, Jalan Ganesa 10, Bandung 40132, INDONESIA, email: fisika@bdg.centrin.net.id) Eleonora Agustine (Applied Geophysics Graduate Program, Bandung Institute of Technology, Jalan Ganesa 10, Bandung 40132, INDONESIA, email: E.Agustine@hotmail.com); Ian Yulianti (Department of Physics, Bandung Institute of Technology, Jalan Ganesa 10, Bandung 40132, INDONESIA, email: Ianyuli@hotmail.com); Dini Fitriani (Department of Physics, Bandung Institute of Technology, Jalan Ganesa 10, Bandung 40132, INDONESIA)

Changes in environmental condition often reflect in changes in magnetic mineralogy and granulometry. We have studied magnetic mineralogy and granulometry of extracted magnetic grains from river sediments and burned tropical soils using X-ray diffraction (XRD) and scanning electron microscopy (SEM) methods. Magnetic grains were extracted using a bar magnet. The river sediments were taken along the Cikapundung River in West Java. The river originated from the relatively pristine Juanda national park, runs through Bandung, the city inhabited by three million people. Samples were taken from locations along the river to see whether pollution or other anthropogenic impacts can be identified through mineralogical, and visual and compound analysis of extracted magnetic grains. Results show that the shape of magnetic grains extracted from the river somewhat change during transportation processes while change in Fe/Ti ratio indicates new sources of magnetic grain. The river's morphology also plays a role in retaining certain forms of magnetic grains. Meanwhile, the tropical soils were analyzed to see the impact of burning on magnetic grains contained in the soils. Samples taken from Juanda National Park were burned for 4 hours, 12 hours, 24 hours, and 10 days to simulate forest fires. Natural, unburned, soils were also used for comparison. Results show that the Fe/Ti ratio does not change until the soils were burned for 12 hours after which the ratio does not vary with burning time. In some cases, burning also changes the texture of the grains. For both river sediments and tropical soils, magnetite is the main magnetic mineral.

**GA1.05/W/08-A5 0910**

**COERCIVITY OF MULTIDOMAIN MAGNETITE AT LOW TEMPERATURES**

Ozden OZDEMIR (University of Toronto at Mississauga, Mississauga, Ontario L5L 1C6, Canada, email: ozdemir@physics.utoronto.ca), David J. Dunlop (same address) Masayuki Torii (Biosphere-Geosphere System Science, Okayama University of Science, 1-1 Ridai-cho, Okayama 700-0005, Japan)

Hysteresis measurements were made on mm-size natural single crystals of magnetite at a series of 16 temperatures from 300 K to 10 K using a MPMS2 SQUID magnetometer. The coercive force  $H_c$  decreased gradually with cooling to the isotropic temperature, where the first magnetocrystalline anisotropy constant  $K_1$  becomes zero. The crystallographic phase transition  $T_v$  is marked by a discontinuous increase in  $H_c$  at 119 K, where the cubic [001] hard direction suddenly becomes the monoclinic easy direction of magnetization. In crossing the Verwey transition, the coercive force increased more than two orders of magnitude, from 0.2 Oe to 24 Oe, which is more than an order of magnitude higher than  $H_c$  at 300 K. Between  $T_v$  and 10 K,  $H_c$  remained almost constant. As the crystal warmed from 10 K,  $H_c$  retraced the cooling curve, peaking just below  $T_v$ , and then decreased dramatically to 0.2 Oe in recrossing the Verwey transition. The abrupt changes in  $H_c$  in crossing  $T_v$  are mainly a result of large increases in  $K_1$ , magnetostriction and magnetoelastic constants due to the switching of the easy directions of magnetization at  $T_v$ . Another factor controlling  $H_c$  below  $T_v$  is the presence of monoclinic twin boundaries, which interact strongly with the domain walls and tend to act as wall pinning sites.

**GA1.05/W/12-A5 0930**

**EFFECT OF MANETITE OXIDATION ON THE HOPKINSON PEAK**

J.G. KING (Dept. of Physics, P/bag 0022, Gaborone, Botswana, email: kingjg@noka.ub.bw)

To determine if magnetic particles in a rock sample are capable of storing paleomagnetic field faithfully over a long time period (geological time), one need to know their characteristics. Such characteristics include, the type of mineral, its particle size, shape and oxidation state. Since paleomagnetic useful particle sizes for the natural remanent magnetisation major carrier mineral (magnetite) is in the micron to sub-micron range, it is not possible to use ordinary microscopes for viewing these particles. Even with high resolution specialised microscopes, it is not an easy task to identify these particles. Since there is no direct easy method of identifying magnetite particle characteristics from a rock sample, it is often necessary to infer these from indirect measurements such as hysteresis loop parameters. In this study an attempt was used to characterise magnetite particles using the Hopkinson peak. The main interest was to find if the Hopkinson peak characteristics could be used to infer the nature of magnetite particle oxidation state. The results show that apart from its use in determining particle size of magnetite samples, the Hopkinson peak can be used successfully to infer their oxidation state.

**GA1.05/W/04-A5 0950**

**THREE-DIMENSIONAL MICROMAGNETIC MODELLING OF RANDOMLY ORIENTED SINGLE-DOMAIN AND PSEUDO-SINGLE-DOMAIN MAGNETITE (0.03-0.3 MICRON)**

K. FUKUMA (Japan Marine Sci. Tech. Center, Yokosuka 237-0061, Japan, email: fukuma@jamstec.go.jp) and D. J. Dunlop (Univ. Toronto, Mississauga L5L 1C6, Canada)

Three-dimensional micromagnetic structures were obtained for magnetite cubes with <100> edges in a size range from 0.03 to 0.3 micron. We employed the Metropolis algorithm (Monte Carlo method) to find equilibrium micromagnetic structures starting from initially uniformly magnetized states. Directions of initial magnetizations were chosen randomly to simulate a randomly oriented assemblage. Small grains (< 0.07 micron) exhibit single-domain structures parallel to a magnetic easy axis <111> irrespective of initial magnetization directions. Vortex structures represent pseudo-single domain grains above the single-domain threshold size. Axes of the vortices are parallel to <100> in the transitional size range, but become randomly oriented with increasing grain size. Neither lamellar domain structures nor multiple vortex structures were found for grains less than 0.03 micron. Reduced magnetization decreased gradually in a relatively narrow grain size range (0.07-0.15 micron) down to ~-0.1 with increasing grain size. Such a grain-size variation of magnetization depends on vortex structures inside a single grain and the randomness of grain magnetization directions in an assemblage.

**GA1.05/E/11-A5 1040**

**MICROWAVE MAGNETIZATION**

DEREK WALTON (Dept. of Physics and Astronomy, McMaster University, Hamilton, Ont., L8S 4M1, Canada)

Microwave magnetization and demagnetization of ceramics has been shown to reduce any alteration effects to unobservable levels because the microwave energy is, essentially, only absorbed by the magnetic grains. In order for this to occur the microwave frequency must be high enough to generate spin waves, and the microwave magnetic field must exceed a threshold. Failure to satisfy these conditions doomed early attempts to use microwaves for magnetization to failure. If the conditions are satisfied the permeability of the magnetic grains becomes extremely high with the result that virtually all the energy is absorbed by the magnetic grains: for instance with the latest version of our apparatus at the University of Liverpool, a small sample of pottery, occupying 1/500 of the volume of a microwave cavity, and containing on the order of 0.1% magnetite, absorbed over 90% of the incident power. In order to achieve these efficiencies stringent conditions must be met, and these conditions will be discussed. The efficiency of the process is also strongly frequency dependent, which to a large extent determines whether or not the process will work. The reasons for this will be discussed in some detail.

**GA1.05/W/02-A5 1100**

**A TEST OF THE THELLIER LAWS OF PARTIAL TRM FOR MULTIDOMAIN GRAINS OF MAGNETITE**

David J. DUNLOP (University of Toronto at Mississauga, Mississauga Road North, Mississauga, Ontario, Canada L5L 1C6; email: dunlop@physics.utoronto.ca) Ozden Ozdemir (same address)

We have carried out Thellier double-heating experiments (simulated paleointensity determination) and stepwise thermal demagnetizations of individual partial TRM's for large grains of magnetite, in the size range 125-150 micrometers. The results allowed us to test to what extent the three Thellier laws of single-domain partial TRM apply to multidomain grains. The law of reciprocity, or equality of blocking and unblocking temperatures, was strongly violated. From the first steps of the Thellier experiment, unblocking temperatures of pTRM's were lower than their blocking temperatures, producing a sagging, convex-down curve on an NRM-pTRM plot. This non-linearity has serious consequences for paleointensity determination, leading to paleofield estimates that are high by as much as a factor 2. The law of independence of adjacent pTRM's was also violated. We tested adjacent pairs, pTRM ( $T_c$ ,  $T_i$ ) and pTRM ( $T_i$ ,  $T_o$ ), with  $T_i = 300, 400, 500,$  and  $564^\circ\text{C}$ . For the lower-T pTRM of each pair, the pTRM intensity depended on initial state, as reported previously by Vinogradov and Markov (1989) and McClelland et al. (1996). For consistency, a thermally cooled initial state was used in thermal demagnetization experiments. Adjacent pTRM's are definitely not independent in their thermal demagnetization. At the boundary temperature  $T_i$  between them, 20-23% of the lower pTRM remains undemagnetized, while 8-15% of the higher pTRM has already been erased. The overlap of unblocking temperatures is not confined to a small range near  $T_i$ , but extends practically all the way from  $T_o$  to  $T_c$ . Therefore there is no temperature range where "primary" and "overprint" pTRM's of multidomain grains could be cleanly separated by thermal demagnetization. Surprisingly, the law of additivity of pTRM's was obeyed to within 2-3% for three of the pTRM pairs and to within 6% for the  $T_i = 564^\circ\text{C}$  pair. The additivity holds throughout the unblocking process: the sum of thermal demagnetization curves of pairs of adjacent pTRM's almost exactly matches the total TRM demagnetization curve, over the whole range from  $T_o$  to just below  $T_c$ .

**GA1.05/W/11-A5 1120**

**ON THE ACQUISITION OF WEAK-FIELD THERMOREMANENT MAGNETIZATION IN MULTIDOMAIN PARTICLES**

Karl FABIAN (FB Geowissenschaften, University of Bremen, Germany, email: karl.fabian@uni-bremen.de)

At present there exist several physical descriptions of multidomain (MD) thermoremanent magnetization (TRM). Each of them has its own merits and drawbacks. While up to now all hysteretic models of TRM acquisition assume a sharply defined blocking process after which the magnetization structure remains unchanged during cooling, the kinematic theories are physically justified only by a vague analogy between spin glasses and MD particles. A recent proposal to use renormalization group theory for the description of MD TRM acquisition seems to join both of the above disadvantages. Yet it offers a new physical approach to understand fluctuation processes in the vicinity of the Curie temperature. Using thermodynamic arguments, here it will be shown from first principles that the equilibrium weak-field TRM is at all temperatures proportional to the external field. Physically based phenomenological arguments further extend this result to obtain a kinematic equation for TRM which substantiates the result of Shcherbakov et al. (1993) and at the same time restrict its validity to weak-field TRM. The presented results together with the new work on hysteretic and renormalization theories give hope that a physically based phenomenological model of weak-field TRM is within reach for rock magnetists.

**GA1.05/E/20-A5 1140**

**TO THE THEORY OF MD PTRM**

V.P. SHCHERBAKOV (Geophysical Observatory Borok, Borok, 152742, Russia, email: shcherb@borok.adm.yar.ru)

Let  $pTRM_a(T_1, T_2)$  be the pTRM acquired when the upper temperature  $T_1$  is reached by cooling from  $T_c$  and  $pTRM_b(T_1, T_2)$  be the pTRM acquired by heating to  $T_1$  from room temperature  $T_r$ . Let tail of  $pTRM_a(T_1, T_2)$  is the rest of  $pTRM_a(T_1, T_2)$  after it was partially thermodemagnetized by heating to  $T_1$ . As was shown experimentally by Shcherbakova et al., a relationship  $pTRM_a(T_1, T_2) = pTRM_b(T_1, T_2) + \text{tail of } pTRM_a(T_1, T_2)$  (1) exists for the MD grains between these three variables. An aim of this report is to present a simple phenomenological scheme to explain this regularity based on the thermofluctuational MD Neel's model. This model was chosen particularly because of requirement that any theory of MD TRM should include thermofluctuational elements to account for the linear dependence of value of TRM on  $H$  in weak fields. To show the idea note let the equation (1) may be interpreted by such a way that the remanence carriers, which constitute tail of  $pTRM_a(T_1, T_2)$ , do not participate in creation of  $pTRM_b(T_1, T_2)$ . In terms of unblocking temperatures  $T_{ub}$  appearance of the tail may be understood as a result of increase of  $T_{ub}$  above  $T_1$  due to irreversible variations of the domain structure during thermal treatment. Increase of  $T_{ub}$  leads to failure of the same grains to acquire  $pTRM_b(T_1, T_1)$ . Apparently, these simple arguments lead to the desired decomposition of  $pTRM_a(T_1, T_r)$  into two parts.



**GA1.05/E/19-A5 1200****PROPERTIES OF PARTIAL THERMOREMANENT MAGNETIZATION IN PSD AND MD MAGNETITE GRAINS**

V.V. SHCHERBAKOVA, V.P. Shcherbakov (Geophysical Observatory 'Borok', Russian Academy of Sciences, Russia, email: shcherb@borok.adm.yar.ru), F.Heider (GeoForschungsZentrum, PB 3.3, Telegrafenberg, 14473 Potsdam, Germany)

An experimental study was carried out to investigate the thermal demagnetization properties of pTRM(T<sub>1</sub>,T<sub>2</sub>) imparted in different temperature intervals (T<sub>1</sub>,T<sub>2</sub>). Fifteen igneous rock samples and five synthetic specimens containing crushed and hydrothermally grown magnetite of different grain sizes were studied. The domain structures (DS) of the samples cover the range from SD to MD grains. Two different kinds of pTRM were considered: 1.) pTRMa(T<sub>1</sub>,T<sub>2</sub>) acquired when the upper temperature T<sub>1</sub> is reached by cooling from the Curie temperature T<sub>c</sub> and 2.) pTRMb(T<sub>1</sub>,T<sub>2</sub>) acquired by heating to T<sub>1</sub> from room temperature. As was shown previously, the intensity of TRM(T<sub>1</sub>,T<sub>2</sub>) depends on the thermal pre-history of the sample, e.g. pTRMb(T<sub>1</sub>,T<sub>2</sub>) is not equal to pTRMa(T<sub>1</sub>,T<sub>2</sub>). Furthermore, any pTRM(T<sub>1</sub>,T<sub>2</sub>) has a tail that is not removed by thermal demagnetization to T<sub>1</sub>. The properties of pTRM(T<sub>1</sub>,T<sub>2</sub>) depend strongly on the temperature interval (T<sub>1</sub>,T<sub>2</sub>). Half of the natural samples under consideration have MD or PSD properties for the low-temperature pTRMs and typical SD-PSD behavior for the high-temperature pTRMs. A linear relation was found for MD samples where pTRMa(T<sub>1</sub>,T<sub>2</sub>)/pTRMb(T<sub>1</sub>,T<sub>2</sub>) = (intensity of the tail of pTRMa(T<sub>1</sub>,T<sub>2</sub>) after thermal demagnetization at T<sub>1</sub>). This relationship implies that the remanence carriers, which constitute the tail of pTRMa, do not contribute to pTRMb. The relative value of the tail is suggested as an independent means to evaluate the DS of a sample. The deviation in the Arai-Nagata plot from a straight line is proportional to the normalised value of the tail of pTRM(300,T<sub>r</sub>), where T<sub>r</sub> is room temperature. The presence and intensity of such a tail can be used as a test for suitability of a sample for paleointensity determinations with the Thellier method.

**GA1.05/E/21-A5 1220****ROLE OF MAGNETOSTATIC INTERACTIONS IN ACQUISITION OF TRM AND VRM IN AN ENSEMBLE OF SD GRAINS**

V.P. SHCHERBAKOV and N.K. Sycheva (Geophysical Observatory Borok, Borok, 152742, Russia, email: shcherb@borok.adm.yar.ru), B.E. Lamash (Far East State University, Suhanova 8, Vladivostok 690600, Russia)

A direct numerical calculations of susceptibility  $k$  of small number  $N=(2-20)$  interacting uniaxial SD grains, randomly dispersed over space, are carried out using the Boltzmann's distribution. The results of the calculations were averaged over 10000 randomly chosen configurations. For moderate interactions (the volume concentration  $c=(0.5-2)\%$ ) the dependence  $k(N)$  shows saturation. As expected the interactions lead to decrease of  $k$  in comparison with the susceptibility of non-interacting ensemble but the decrease does not exceed 20%. Hence for the practical purposes it is admissible to neglect the magnetostatic interactions when  $k$  of SD grains is considered. As a consequence, TRM depends on the interactions through increase of the blocking temperatures  $T_b$  mainly but not due to change of  $k(c)$ . Limit value of VRM only slightly depends on the interactions but they drastically change the spectrum of relaxation time  $T_r$ . This leads to quasilogarithmic increase of VRM with time  $t$  even for the ensemble of non-interacting SD grains

**Friday 23 July PM**

Presiding Chairs: Ö Özdemir (University of Toronto, Canada)  
K Fabian (University of Bremen, Bremen, Germany)

**METHODS AND APPROACHES IN ROCK MAGNETISM****GA1.05/E/02-A5 1400****THE NEW THEORY OF THE RESIDUAL MAGNETISM OF MAGNETITE BEARING ROCKS**

Vladislav GERNIK (Russian Geological Research Institute, Sredny pr. 74, 199106 St. Petersburg, Russia, email: gernik@mail.dux.ru)

This theory comprises the following theses:

1. Residual magnetization (RM) of magnetite is generated by the inclusions of ferrimagnetic minerals represented, mainly, by hemoilmenites or magnesioferrites. Inclusions-free magnetite matrix can not to acquire RM.

2. These inclusions, as a rule, are consisted of products (phases) of solid solution decay. On the contact of the each magnetic phase with magnetite matrix exchange interaction appears. This process induces exchange anisotropy, which creates the space energetic barrier in a magnetite grain. The barrier prevents retrieving of magnetite domain boundaries into position corresponding to demagnetized state. Thus, in RM of a magnetite grain the magnetization of the phases of inclusions appears, but matrix plays role of powerful amplifier of their weak magnetic moment. 3. Hence, the state of residual magnetization of magnetite is determined by the properties of the solid solution, namely: - by the number of the products of its decay and by their magnetic interaction between one another; - by the relaxation time of decay-homogenization process of solid solution and by its tolerance to the temperature changes.

All these theses have been proved experimentally and repeatedly tested. The new theory explains really all the known effects: the physical essence of the Rayleigh law, the cause of the offence of the Thellier laws, mechanism of self-reverse thermoremanence, origin of multi-component NRM, and the cases of chaotic diversity of its directions, which can not be removed with magnetic cleaning, etc.

**GA1.05/W/37-A5 1420****JUXTAPOSED AND SUPERIMPOSED REMANENT MAGNETIZATIONS IN TWO FORMATIONS OF THE TINDOUF BASIN (ALGERIA)**

H. BOUABDALLAH, N. Merabet, and S. Maouche (CRAAG, BP 63, 16340 Bouzaréah, Algiers, Algeria, email: h.bouabdallah@lancaster.ac.uk). B. Henry (Paléomagnétisme et Géomagnétisme, CNRS and IPGP, 4 avenue de Neptune, 94107 Saint-Maur cedex, France, email: henry@ipgp.jussieu.fr).

Two paleomagnetic studies in the West African Craton have been carried out in the Tindouf basin, in the Merkala red sandstones of the lower Stephanian age and in the Reouiana red sandstones of Namurian age. During thermal treatment, after elimination of a weak viscous magnetization A, two components B and C are clearly separated. B is isolated between 200-250°C and 550-580°C, and C at higher temperatures until 670°C. Rockmagnetic studies pointed out the presence of hematite and probably of magnetite.

On the one hand, the components B and C are well defined, with nice clustering and should represent a nice example of juxtaposed magnetizations. On the other hand, the angle between

the mean directions of B and C appears remarkably constant, in value and in orientation, from one site to another. A strong relation exists therefore between B and C. B component is interpreted as resulting from the superimposition of the component C with an unknown component. To determine this component D, the intersection of great circles containing B and C directions has been studied. At Merkala, the component D has been obtained, and is a Permian overprint (paleomagnetic pole at 38.9°S and 60.0°E). At Reouiana, the best intersection unfortunately corresponds to component C, which is therefore better grouped than D. At Merkala, component C allows a lower Stephanian paleomagnetic pole to be defined: 32.4°S, 56.6°E. The Namurian pole determined with C at Reouiana is situated at 28.4°S, 56.9°E.

**GA1.05/E/07-A5 1440****NATURE OF NATURAL REMANENT MAGNETISATION OF LOWER CRETACEOUS RED-BEDS OF AFGANAL-TADJIK DEPRESSION (SOUTH TIEN-SHAN)**

Yu. S. RZHEVSKY (St.Petersburg State University, 14th Line 29, V.O., 199178, St.Petersburg, Russia, email: yurkov@icape.nw.ru )

Natural remnant magnetisation of the rocks studied has chemical character, that is magnetic moments of the particles distributed in the rock have been oriented and fixed by the ancient magnetic field when the particles reach the same size. However, the other process affects the remnant magnetisation as well. This process appears as partial diagenetic transformation of hematite into maghemite, which lead to reversal magnetisation (in relation to original hematite) due to negative unidirect magnetic anisotropy. In the rocks studied this additional process lead to partial self-reversal remnant magnetising, and in some cases produces the full self-reversing of the magnetisation.

**GA1.05/W/05-A5 1500****SECONDARILY ACQUIRED MAGNETIZATION OF CRETACEOUS GRANITIC ROCKS IN KITAKAMI MASSIF OF NORTHEAST JAPAN**

Yo-ichiro OTOFUJI, Koji Uno, Takahiro Higashi, Tomomichi Ichikawa, and Tuyoshi Ueno (Department of Earth and Planetary Sciences, Faculty of Science, Kobe University, Kobe 657, Japan email: otofuji@kobe-u.ac.jp; unokoji@kobe-u.ac.jp)

Cretaceous granitic rocks of the Kitakami massif, whose K-Ar ages range between 107 and 120 Ma, are categorised into two types on the basis of paleomagnetic directions; (A) westerly direction with shallow inclination which is sub-parallel to the paleomagnetic direction of the Paleogene Heizaki volcanics and (B) northwesterly direction with moderate inclination which is sub-parallel to the paleomagnetic direction of the Early Miocene times for northeast Japan. Thermal demagnetization of the composite IRM shows that magnetite is carrier for hard and medium components in coercivity of both types. Alternating field demagnetization shows that Type A is characterised by low coercivity (less than 10 mT in MDF) whereas Type B reveals high median destructive field larger than 20 mT. Microscopic observation indicates that fairly large and euhedral magnetite occurs in neighbouring to biotites in Type A. In Type B, small grains of magnetites (less than 10 mm) are observed within alternating parts of hornblende where original green colour is bleached and becomes pale green. Studies by a scanning electron microscope equipped with a energy-dispersive analytical system show that a magnetite in Type A contains a small amount of Ti (the Fe/Ti ratio is 51.8) whereas a magnetite in Type B is free from Ti. The energy-dispersive analysis also shows that the bleached area in Type B reflects enrichment of Mg due to release of Fe. The pure magnetites within the bleached areas of Type B are originated from released Fe in hornblende, implying the secondary products. We conclude that origin of the remnant magnetization of Type B is CRM which is acquired by secondarily originated magnetites during alteration of rocks at about 20 to 30 Ma. Type A preserves primary magnetization, although its coercivity is low.

**GA1.05/E/16-A5 1520****SIMULTANEOUS REMAGNETIZATION AND PB ISOTOPE RESETTING IN THE BAMBUÍ CARBONATES (BRAZIL)**

Manoel S. D'AGRELLA-FILHO and Ricardo L.F. Trindade (Instituto Astronomico e Geofisico, Universidade de Sao Paulo (USP), SP, 3386, 01060-970, Brazil, email: dagrella@iag.usp.br, Marly Babinski (Instituto de Geociencias, USP, Sao Paulo, SP, Brazil) William R. Van Schmus (Department of Geology, University of Kansas, Lawrence, KS, USA)

Paleomagnetism, rock magnetism, U-Pb and Pb isotopic data on carbonates from the southern São Francisco basin support a close connection between a pervasive remagnetization and the resetting of the isotopic system of these rocks at 530-500 Ma, during the final stages of the Brasiliano/Pan-African orogeny. The post-depositional origin of the magnetization directions is strengthened by the following: (a) the rock magnetic properties, such as wasp-waisted hysteresis loops, anomalously high hysteresis ratios and contradictory Lowrie-Fuller and Cisowski tests, are typical of remagnetized carbonates; (b) thermomagnetic analysis and scanning electron microscopy suggest authigenic magnetite as the main magnetic carrier, and (c) paleomagnetic poles from carbonate sequences and adjacent Brasiliano metamorphic rocks are similar and coincide with high quality Gondwanan paleomagnetic poles for the 530-500 Ma interval. Most Pb-Pb and U-Pb ages from the carbonates coincides with ages of metamorphic rocks from marginal fold belts. In addition, undeformed carbonates containing radiogenic crustal Pb with an isotopic signature of the Archean/Paleoproterozoic basement suggest Pb incorporation through fluids which promoted the resetting of the isotopic system and the severe remagnetization in the carbonates. The similarity between paleomagnetic and isotopic results from the Bambuí and the 1000 km far Salitre carbonates implies a large scale event that simultaneously affected the whole basin.

**GA1.05/W/09-A5 1540****INTERPRETATION OF MAGNETIC PROPERTIES OF ESTONIAN CARBONATE ROCKS USING FACTOR ANALYSIS**

Alla SHOGENOVA (Institute of Geology at Tallinn Technical University, 7 Estonia Avenue, Tallinn, EE10143, Estonia, email: alla@gi.ee)

Magnetic susceptibility ( $k$ ) and saturation isothermal remanent magnetization (SIRM) were studied together with bulk and grain density and chemical composition of Estonian Lower Palaeozoic carbonate rocks. Magnetic properties were analyzed on some 700 samples of argillaceous to varying degree limestones and dolomites of different genesis. The total database was subdivided into 6 data sets from Lower Ordovician up to Silurian age. To analyze together 17 parameters the R-mode factor analysis was applied. It permitted to determine the two principal factors controlling the alteration of magnetic properties and of two studied iron forms FeO and Fe<sub>2</sub>O<sub>3</sub>. These factors are clay content and dolomitization. In the non-dolomitized carbonate formations magnetic susceptibility increases with increasing clay content, including both iron forms and in the rocks, which included impurities of iron oxides (Fe<sub>2</sub>O<sub>3</sub>). In the Lower and Middle Ordovician data sets with samples from widespread



dolomite layers, dolomitization is the first principal factor. It caused increase in magnetic susceptibility and both iron forms in Middle Ordovician dolomite layer and increase in FeO in Lower Ordovician layer. In the Middle Ordovician dolomites from the fracture zone dolomitization caused increase in k and both iron forms. In Silurian rocks clay content is the more important factor in rise of magnetic susceptibility and both iron forms. Dolomitization caused there less increase in k, and this is connected with increase in FeO. In Upper Ordovician sequence both clay content and dolomitization control increase in Fe<sub>2</sub>O<sub>3</sub>, but more influence were made there by clay content, which also controls alteration in SIRM in most of Ordovician rocks. Application of factor analysis helped in interpretation of magnetic properties and processes caused their alteration.

**GA1.05/W/06-A5**

**1630**

**AGE DEPENDENCY OF MAGNETIC PROPERTIES IN OCEAN FLOOR BASALT**

Juergen MATZKA and Nikolai Petersen (Inst. f. Pure a. Appl. Geophysics, University Munich, Theresienstr. 41, 80333 Muenchen, Germany, email: matzka@rockmag.geophysik.uni-muenchen.de), Thomas Kunzmann (Inst. f. Mineralogy a. Petrography, University Munich, Theresienstr. 41, 80333 München, Germany, email: kunzmann@petro1.min.uni-muenchen.de)

Due to the gradual low temperature oxidation of titanomagnetites in ocean floor basalts, a corresponding age dependency of magnetic properties arises. This process, reflected for example by an increase in Curie temperature, is regarded as a two step process: rapid oxidation in the first 10 to 20 Ma and a slower oxidation rate thereafter. Coinciding with the transition from step one to two, a minimum is observed in both NRM intensity and amplitudes of the marine magnetic anomalies.

A rock magnetic study on a set of ocean floor basalts covering an age span from 0 Ma to more than 100 Ma, reveals also an age dependency of magnetic hysteresis properties. At room temperature, parameters reflecting magnetic hardness (e.g. coercivity) show an increase with age to a maximum at ca. 10 Ma and a decrease for older samples. For the samples younger than 10 Ma hysteresis parameters show distinctive differences depending upon whether they were measured at room temperature or at liquid nitrogen temperature. For samples about 10 Ma old, ratios of Hcr/Hc and Mrs/Ms approach extreme values typical for SD particles and the NRM is very stable against AF-demagnetization. It is, however, unlikely that this is a grain-size related phenomenon. The susceptibility normalised on saturation magnetization reaches a minimum for these same samples. These samples exhibit Neel's P-type characteristics in their thermomagnetic curves with a maximal saturation magnetization at around 100°C. All together, we will discuss a number of particular magnetic properties coinciding with the above mentioned minimum in NRM intensity, which seems to be of a rather intrinsic than paleofield related origin.

**GA1.05/W/14-A5**

**1650**

**REMANENCE ACQUISITION OF OCEANIC GABBROS FROM HOLE 735B**

H.-U. WORM (BGR, Hannover, Germany), J. Gee, E. Kikawa & ODP Leg 176 Scientific Party

The vertical structure of the sources of marine magnetic anomalies have remained poorly known ever since the recognition that the oceanic crust records reversals of the geomagnetic field. Inferences on the magnetization of lower crustal rocks from studies of dredged rocks are ambiguous because these surficial samples have been subjected to varying degrees of seawater alteration that may have significantly affected the magnetic properties. To date, ODP Hole 735B constitutes by far the deepest penetration into plutonic basement and thus arguably provides the best available information on the magnetization of oceanic gabbros. The high average NRM intensities of ~2.5 A/m, together with a large Q-Factor of 13.4 and high stability during af and thermal demagnetization suggests that gabbros constitute a significant source for lineated marine magnetic anomalies. The gabbros from Hole 735B may be considered to be typical for the lower crust generated at slowly spreading ridges, however, the observation that stable inclinations scatter by more than 10° within meter distances does not fit the model of a slowly cooling deep crust. Possible explanations are: (a) a fraction of the magnetite grains was formed below Tc and thus carry a CRM, (b) stress and strain deflected the NRM, (c) late intrusions reheated the gabbros locally, (d) magnetic anisotropy affected the primary TRM acquisition. (c) can probably be ruled out based on the petrographic description. (b) can hardly be investigated by experiment. Laboratory measurements of continuous thermal demagnetization, pTRM acquisition, AMS, and TRM anisotropy suggest that the NRM is a primary TRM that was strongly affected by anisotropy. TRMs acquired parallel kmax and kmin can vary in intensity by a factor of 3. Another question of interest is, up to which temperature a primary TRM can survive a subsequent polarity reversal. For that purpose thermoviscous measurements were also conducted with a 2G SQUID magnetometer equipped with a non-magnetic furnace inside.

**GA1.05/E/14-A5**

**1710**

**MUD-FILLED CAVITIES IN SPELEOTHEM SAMPLES FROM TRENGGALEK, EAST JAVA AND REMANENCE ACQUISITION**

SATRIA BIJAKSANA (Department of Physics, Bandung Institute of Technology, Jalan Ganesa 10, Bandung 40132, INDONESIA, email: fisika@bdg.centrin.net.id) Siti Zulaikah (Department of Physics, Bandung Institute of Technology Jalan Ganesa 10, Bandung 40132, INDONESIA)

Giving their continuous accumulation and relatively precise orientation, speleothems (such as stalagmites, stalagmites and flowstones) occasionally might be valuable for paleomagnetic studies especially for the Holocene. Low content of magnetic minerals, however, results in very low magnetic intensity requiring a very sensitive magnetic magnetometer to measure. While measuring anisotropy of magnetic susceptibility (AMS) of two stalagmites from a cave complex in Trenggalek, East Java, we find that the susceptibility of the samples varies greatly from one sample to another. Variations in both magnetic susceptibility and anisotropy apparently depend on the presence of small mud-filled cavities of about 2-5 mm in diameter. During occasional flooding, muds might be trapped inside the minute holes in the uneven surface of the stalagmites. Muds taken from the vicinity of the stalagmites is indeed rich in magnetic minerals. The presence of these mud-filled cavities, on one hand, will enhance the sample's magnetic intensity. On the other hand, they will mask the remanence carried by finer magnetic grains embedded in the calcite or aragonite matrix. If this so, instead of averaging the secular variation over longer period of time, the remanence in one stalagmite sample represents a rather implusive record of the Earth's magnetic field. Study on the stability of magnetic remanence in samples with such cavities is underway.

**GA1.05/W/13-A5**

**1730**

**EFFECTS OF ALTERNATING FIELD DEMAGNETIZATION ON ANISOTROPY OF MAGNETIC SUSCEPTIBILITY - A CASE STUDY ON MARINE SEDIMENTS**

Hirokuni ODA (Marine Geology Department, Geological Survey of Japan, Higashi 1-1-3, Tsukuba, Ibaraki 305-8567, Japan, email: hoda@gsj.go.jp), Abdelaziz L. Abdeldayem (Institute of Geoscience, University of Tsukuba, Tsukuba 305-8571, Japan, email: dayem@gsj.go.jp)

Potter and Stephenson (1988, 1990a, b) have shown that static AFD shift the directions of AMS principal axes and increase the degree of anisotropy by using synthetic samples and basalts bearing magnetite. It is generally believed that the tumbling AFD would not impress the anisotropy and even in some cases (e.g. Park et al., 1988) it was recommended to be used to eliminate stress induced anisotropies. To our knowledge, no such experiments have been yet carried out in detail on natural samples. In this study, we demonstrate that tumbling AFD increases the lineation, changes the shape parameter, and changes the directions of principal axes of natural sediment samples.

Paleomagnetic cube samples were taken from a 3.5m-long siliceous sediment core from Bransfield Basin close to Antarctic Peninsula. According to the low-temperature magnetic phase transition and hysteresis analysis, the samples comprises mainly of multi-domain magnetite. The static AFD was confirmed to impress the anisotropy on AMS of the specimens. The daughter samples were AF demagnetized with a 3-axes tumbling system. With increasing tumbling AF, AMS shows gradual increase in average susceptibility up to 2% of the original values; Kmax and Kmin increases particularly resulting in increase of lineation, decrease of foliation and change in shape parameter from oblate to prolate. The concentration of principal axes increases with increasing AF, then minimum and intermediate axes interchange for the samples from 0.5-1.0m depth above 60 mT AFD. These lines of evidence suggest that not only static AFD but also tumbling AFD should be avoided before measurement of AMS particularly for sediments.

**Saturday 24 July AM**

Presiding Chairs: A P Roberts (University of Southampton, School of Ocean and Earth Science, Southampton, UK) and M Torii (Okayama University of Science, Okayama, Japan) Concurrent Poster Session

**MAGNETIC PROPERTIES AS ENVIRONMENTAL PROXY PARAMETERS**

**GA1.05/W/36-A6**

**0830**

**SIMULATION OF MRS/MS AND HCR/Hc VALUES (DAY PLOT) FOR MIXTURES OF SUPERPARAMAGNETIC, SINGLE-DOMAIN, MULTIDOMAIN AND PSD GRAINS**

David J. Dunlop (University of Toronto at Mississauga, Mississauga, Ont., Canada L5L 1C6; email: dunlop@physics.utoronto.ca)

A plot of saturation remanence ratio Mrs/Ms versus coercivity ratio Hcr/Hc was proposed by Day et al. (1977) as a method of discriminating domain state (single-domain, SD; pseudo-single domain, PSD; multidomain, MD) and by implication, grain size. For Day et al.'s sized titanomagnetite grains, values of the two ratios trend along a single approximately hyperbolic curve for all four compositions (x = 0, 0.2, 0.4, 0.6). There is a monotonic trend with grain size, the finer grains approaching SD values and the coarser grains approaching MD values. However, different compositions trend along different sections of the hyperbola, and my data for annealed and unannealed magnetites show that different internal stress levels also shift points along the master curve. In order to use the Day plot to determine grain size, mineral composition and state of internal stress must be independently known. Data from suites of oceanic rocks (Dunlop, 1981; Gee and Kent, 1999) and continental limestones (Channell and McCabe, 1994) show that there is in fact no single master curve. Jackson (1990) proposed that the different trends for remagnetized and unremagnetized limestones result from mixtures of superparamagnetic (SP) and SD grains in the first case and SD-MD mixtures in the second case. Gee and Kent likewise propose SP-SD and SD-MD mixtures as the cause of different trends in suites of submarine titanomagnetites. Tauxe et al. (1996) numerically modelled SP-SD mixtures and were able to fit the trends displayed by submarine basaltic glasses. However, until the present study there has been no first-principles theoretical treatment of the parameters Mrs, Hcr, Hc and their correlation in the Day plot for SP, SD, PSD, and MD grains, and their mixtures. The results indicate that MD grains have a separate trend that intersects the curve for SD-MD mixtures at a large angle. SP-SD mixtures generate a variety of trends, all lying well above the MD or SD-MD trends. A simple SD-MD mixture ...

**GA1.05/E/13-A6**

**0850**

**CAN WE MATHEMATICALLY UNMIX NATURAL MAGNETIC MIXTURES?**

Roy THOMPSON (Geology and Geophysics Dept., University of Edinburgh, email: eph08@holyrood.ed.ac.uk)

Natural materials such as soil, lake gyttja, marine clay and atmospheric dust are complex mixtures. Using hysteretic or laboratory-imparted remanence measurements as basic magnetopetrological data we wish to model these natural mixtures as linear combinations of known reference minerals. Extremely good mathematical fits (r<sup>2</sup> > 0.99) can be generated from constrained regression or optimisation algorithms. Approaches to assessing the quality (skill) of such fits will be described. The magnetic properties of magnetite have been well known since the work of Parry (1965). Recently we have been able to characterise the properties of bacterial magnetosome chains, making them easy to recognise and to include in unmixing calculations. A key remaining question concerns the magnetic properties of additional end-members, not included in our models. Despite much laboratory and theoretical work, in recent decades, on the thermo-remanence properties of titanomagnetites and titanohaematites, the range of their hysteresis properties, in the natural environment, appears to remain surprisingly poorly known.

**GA1.05/E/01-A6**

**0910**

**A NEW TECHNIQUE FOR CHARACTERIZING THE MAGNETIC PROPERTIES OF NATURAL SAMPLES**

Christopher R. Pike (Dept. of Geology, University of California, Davis, California, 95616 USA) Andrew P. ROBERTS (School of Ocean and Earth Sciences, Southampton Oceanography Centre, University of Southampton, Southampton, UK) Kenneth L. Verosub (Dept. of Geology, University of California, Davis)

Environmental magnetic studies are commonly conducted on samples with mixtures of magnetic minerals and/or grain sizes. Such measurements are often ambiguous because they represent the composite response of all magnetic grains in the sample. Overcoming this ambiguity represents one of the most important challenges for environmental magnetism. We have developed a new method for studying the magnetic properties of natural samples using a class of partial hysteresis curves known as first order reversal curves (FORCs). These curves are transformed into contour plots (FORC diagrams) which look similar to Preisach diagrams, but which are not model-dependent. The shape and location of features on a FORC diagram can be used to obtain a qualitative estimate of the magnetic grain size distribution in a sample. FORC diagrams can be used to detect the presence of superparamagnetic grains and non-single-domain behaviour that result from domain wall nucleation and annihilation, as well as the effects of magnetic interactions. We have calibrated the FORC technique with well-characterised samples and our interpretations are consistent with FORC distributions obtained

from theoretical models. Preliminary results indicate that it is possible to characterise a wide range of natural samples and to clearly identify and discriminate between the different components that contribute to wasp-waisted hysteresis loops.

**GA1.05/L/01-A6****0930****A NEW METHOD FOR THE CHARACTERIZATION OF MAGNETIC GRAIN SIZE DISTRIBUTIONS**

Horst-Ulrich Worm (Federal Institute for Geosciences &amp; Natural Resources, Hannover, Germany)

Measuring the frequency dependence of susceptibility ( $\chi_{fd}$ ) is the commonly applied method for detecting superparamagnetic (SP) grains in rocks and soils. However, this method fails if the concentration of ferrimagnetic minerals is so low that their susceptibility contribution to the bulk susceptibility is comparable to the para- or diamagnetic contribution. Therefore, alternative methods have been explored using measurements of remanent magnetizations that were acquired at various time constants. As test specimens served a variety of natural and synthetic samples containing distinct grain size distributions of SP, stable single domain (SSD), multidomain (MD) magnetite, titanomagnetite, hematite and pyrrhotite grains, respectively. ARM acquisition and AF demagnetizations were performed in the frequency range 50 to 640 Hz. The results, however, are nearly frequency-independent. Differences are only noticeable for samples with the highest  $\chi_{fd}$ . Much more revealing proved to be a second method where IRMs were acquired in time spans of 0.01 s and 10 s, respectively. Depending on the field intensity the IRM ratios can be as large as  $> 10$  for SP samples. The IRM intensities of SSD grains also increase significantly with field exposure time, and the ratio is smallest for MD grains. Viscous decay following IRM acquisition is pronounced for SP grains while it is at least an order of magnitude smaller for SSD and MD grains.

**GA1.05/W/30-A6****0950****THE VERWEY TRANSITION AS A REMARKABLY SENSITIVE INDICATOR OF MINOR AMOUNT OF MAGNETITE IN SEDIMENTS**

M. Torii (Fac. Info., Okayama Univ. Sci., Okayama 700-0005, Japan, email: torii@big.ous.ac.jp), C.-S. Horng (Inst. Earth Sci., P.O. Box 1-55, Taipei, Taiwan, email: cshorng@earth.sinica.edu.tw)

Magnetic mineralogy in sediments is generally complex. Not only magnetite and hematite, but also iron sulfides, such as greigite and pyrrhotite, have been increasingly reported from sediments. We should also be careful with goethite and other iron hydroxides. However, the presence of magnetite is still critical to understand magnetic property of samples. Magnetite has larger magnetization compare to the other minerals. Magnetite can survive as a detrital, chemical or biogenic particle in most sediments. It is thus crucial to detect magnetite in a target sample even if the concentration is very low. We found complex magnetic mineralogy having magnetite, pyrrhotite, and greigite in the marine sediment from Southwest Taiwan (Horng et al., 1998). Such a situation makes the NRM records very complicated. The characteristic remanent component was only revealed with applying thermal demagnetization of the moderate temperature, which corresponds to the decomposing temperature of greigite. We determined magnetic mineralogy first with an X-ray diffractometry. For the X-ray method, however, we have to separate significant amount of the magnetic minerals from the sediment of one kg or more. We also applied a low-temperature method using an MPMS. The sample for MPMS is only a scoop of about 10 mg from the sample for NRM measurement. We found the Verwey transition is very sensitive to suggest the presence of minor amount of magnetite.

**GA1.05/W/35-A6****1010****MICROWAVE INDUCED SYNTHESIS OF MAGNETIC CRYSTALS**

C. PETERS and A. G. Whittaker, (Department of Chemistry, University of Edinburgh, King's Buildings, West Mains Road, Edinburgh, EH9 3JJ, Scotland)

The growth and characterisation of synthetic magnetic crystals are important for attempting to identify magnetic components within natural, soils, sediments and rocks. A new technique using microwave radiation is currently being developed to synthesise magnetic crystals. Microwaves allow rapid, uniform heating of solutions under either pressure or reflux conditions. The overall size of the crystals can be controlled by the length of time the radiation is applied. Crystal morphology may be controlled by face-blocking agents e.g. the presence of phosphate ions yield needle-shaped particles. The resulting magnetic mineralogy of the crystals is dependent on the initial reactants. Microwave-hydrolysed ferric ions produce haematite, for example, whereas mixed ferric and ferrous ions initially yield goethite and ultimately magnetite. Under optimum conditions the microwave technique allows the direct synthesis of magnetite crystals. The resulting synthetic magnetic crystals are characterised using x-ray diffraction and scanning electron microscopy, in addition to magnetic studies.

**GA1.05/W/42-A6****1100****MAGNETIC CHARACTERISTICS OF TREE NEEDLES AND HUMAN LUNG SPECIMEN AS AN INDICATOR OF ANTHROPOGENIC DUST IMMISSION**

Viktor HOFFMANN, Mathis Knab, Carsten Leven (Institut fuer Geologie und Palaeontologie, Arbeitsbereich Geophysik, Universitaet Tuebingen; Sigwartstrasse 10, 72076 Tuebingen, Germany; email: viktor.hoffmann@uni-tuebingen.de). Manfred Wildner (Bavarian Public Health Research Center, University of Munich, School of Medicine, Tegernseer Landstrasse 243, 81549 Muenchen, Germany; email: wil@ibe.med.uni-muenchen.de)

Emission and deposition of aerosols and dusts often containing highly toxic substances can reduce significantly the quality of the environment and seriously affect human health. Forest decline e. g. in northern Bohemia or southern Poland is a consequence of the acid rain and the partly extremely high content of heavy metals in the soil. High rates of allergies or diseases of the respiratory system (e. g. lung cancer) are caused by polluted air or the uptake of potentially contaminated food or water. Since the pilot studies of Oldfield et al. (1985) we know that magnetic parameters can be used successfully for the discrimination of geogenic and anthropogenic aerosols and dusts. Here we present results of our investigations concerning the magnetic signature of the following sample sets: fir tree and spruce needles were collected in various areas with different states of lmission including so-called clean-air areas without any local industrial emissions. Further on, pilot studies were done on human lung specimen. Hysteresis and backfield data as well as IRM-acquisition curves were measured by using the micromag (Geophysics group in Tuebingen and Physics Department, Univ. of Toronto, D. Dunlop). In general, we obtain a clear magnetic signal, which is dominated by a soft magnetic, maybe magnetite-like phase in various grain sizes. In addition, the magnetic signature of highly magnetic single spherules of various sources (grain-size 20-100 microns) was determined in order to be able to compare the magnetic signal on the emission as well as on the immission side. In this way, the reconstruction of the transport paths and the sources of toxic aerosols seem to be possible just by using magnetic proxies.

**GA1.05/E/10-A6****1115****SOURCES OF FERRIMAGNETIC MINERALS IN CEMENT DUSTS**

Beata Goluchowska (Institute of Biology and Environment Conservation, University of Opole, ul Kominka 4, 45-035 Opole, Poland, email: beska@uni.opole.pl) Zygmunt STRZYSCZCZ (Institute of Environmental Engineering, Polish Academy of Sciences, ul. M. Skłodowskiej-Curie 34, 41-819Zabrze, Poland, email: zygmunt@ipis.zabrze.pl)

Former studies have shown a wide variation in magnetic susceptibility of cement dusts (90 - 1620  $\times 10^{-8} \text{m}^3 \text{kg}^{-1}$ ). It was because of additives using in clinker production and during a cement grinding. Still open is a question if any new ferrimagnetic minerals can be forming during the cement production as a result of mineralogical changes in existing iron compounds. The laboratory experiment based on firing of raw materials and additives in the same proportion in a presence of different amount of carbon monoxide proved that mineral changes leading to increase of magnetic susceptibility during the cement production are possible. Except a temperature the crucial factor in this process is CO content. The magnetic susceptibility of agglomerate obtain in presence of 1 % Co was 4  $\times 10^{-8} \text{m}^3 \text{kg}^{-1}$ . Increase of CO content to 10 % caused an increase of magnetic susceptibility to 245  $\times 10^{-8} \text{m}^3 \text{kg}^{-1}$ . In presence of 30 % CO the magnetic susceptibility increased to 330  $\times 10^{-8} \text{m}^3 \text{kg}^{-1}$  and ferrimagnetic forms made 73 % of total iron. During the firing in atmospheric air only 1 - 2 % of total iron were present in ferrimagnetic form. These data suggest that a wide variation of magnetic susceptibility in cement dusts can be not only a result of additives but also as a result of occurring new ferrimagnetic minerals during a process of cement production.

**GA1.05/W/21-A6****1130****CHANGES OF MAGNETIC PARAMETERS OF POWER-PLANT FLY ASHES UNDER CONDITIONS OF DIFFERENT SOIL ENVIRONMENTS**

Ales KAPICKA, Eduard Petrovsky and Neli Jordanova (Geophysical Institute, Acad.Sci., Prague 4, Czech Republic, email: kapicka@ig.cas.cz), Sergej Ustjak (Research Inst. of Crop Production, Chomutov, Czech Republic)

Areas of high and low levels of contamination due to atmospheric deposition of fly ashes from coal-burning power plant were determined on the basis of magnetic susceptibility mapping. Investigation of soil depth profiles showed that anthropogenic ferrimagnetic minerals are concentrated in the depth between 5 and 10 cm. Magnetic parameters of contaminated soil layers as well as fly ashes collected from power plant were studied in detail (thermomagnetic curves, frequency dependent susceptibility, hysteresis parameters). In order to examine magnetic stability of fly ashes, samples were exposed to soil extracts for periods of 1 to 8 weeks. Soil extracts from typical soils around the power plant with pH=5.0 and pH=7.0 and distilled water as a control medium were used in experiments. Our results show that nonstoichiometric (maghemitised) phase dominates the ferrimagnetic fraction (about 10 vol%) of fresh fly ashes, with Tc typically of 630 deg.C. This phase could be identified only in the most polluted soil samples from close neighbourhood of the source. However, it seems to be quite unstable and upon exposure to soil extract it transforms to stable magnetite phase with Tc = 580 deg.C. At the same time irreversible changes of k, Js, Jrs and Hcr were observed in dependence of increasing time exposition to soil extracts. Stable magnetite was also identified as a main ferrimagnetic phase in most of the contaminated soil layers around the power plant.

**GA1.05/W/24-A6****1145****MONITORING OF HEAVY METALS POLLUTION FROM COPPER-SMELTING PLANT: APPLYING MAGNETIC METHOD**

Alla NULMAN, Rimma Kopteva and Alexandr Rytsk (Institute of Geophysics, UD RAS, Amundsen str.100, 620016 Yekaterinburg, Russia, email: nulm@igeoph.mplik.ru)

Considerable number of data about links between magnetic properties and quantities of various pollution in different environmental components has been obtained already. That allows magnetic proxy in the monitoring systems to be included. Some results of such a work for heavy metals aerogenic polluted zone by Middle Ural Copper-Smelting Plant (MUCP) is presented here. That zone contains several towns and a part of Yekaterinburg's drinking pond catchment, while the relief is rather intricate and the weather is quite variable. Therefore the thick monitoring network is necessary. But the cost of spectrochemical analysis is very high and that is just the case a magnetic proxy would be useful.

For working up the magnetic monitoring method a snow cover has been utilised as a natural accumulating plane. During 3 years 53 samples have been collected from 20 sites in the zone of influence of MUCP (the effect of another heavy metals sources was excluded). The samples have been selected and melted by different methods. The magnetic properties of the samples (solutions and solid fractions) have been studied. For 20 samples collected in 1998 the quantity of 10 heavy metals have been determined by usage of spectrochemical analysis. The quantities of Cu, Pb, Zn, As, Cd and the values of differential magnetic moments (dM/dH) of snow samples solid fractions obtained by standard methods of hydrometeorological service has been found to be correlated. Calibration curves for calculation of heavy metals quantities in snow samples from dM/dH are shown here.

**GA1.05/W/26-A6****1200****COMPARATIVE MAGNETIC MEASUREMENTS ON POLLUTED AND UNPOLLUTED SOILS FROM BUENOS AIRES PROVINCE (ARGENTINA)**

Ana M. SINITO (CONICET-IFAS, Universidad Nacional del Centro, Pinto 399, 7000-Tandil, Argentina, email: asinito@ifas.exa.unicen.edu.ar) Marcos A. Chaparro and Claudia S. G. Gogorza (IFAS, Universidad Nacional del Centro, Pinto 399, 7000-Tandil, Argentina, email: cgogorza@ifas.exa.unicen.edu.ar)

Magnetic measurements of soils exposed to pollution became one auxiliary tool of estimating contamination. In this study, magnetic properties of recent soils from Buenos Aires Province (Argentina), with special attention on magnetic enhancement on soils/superficial layers, are presented. "In situ" susceptibility measurements on unpolluted and polluted (by metallurgical dust) sites were carried out. Hand samples coming from these sites were studied in laboratory. Results of susceptibility (K) at two different frequencies, Isothermal Remanent Magnetization (IRM), Saturation Isothermal Remanent Magnetization (SIRM), coercivity of remanence (Bcr), S ratio and relationship between SIRM and K are complemented with studies of changes of susceptibility with temperature (heating and cooling curves). These studies contribute to the knowledge of magnetic mineral composition, grain size, characteristics of the main carriers, concentration of heavy metals, etc. The comparison of the results between polluted and unpolluted soils shows significant differences, which are analysed.



GA1.05/E/05-A6

1215

**SEASONAL CHANGES OF MAGNETIC SUSCEPTIBILITY IN SEDIMENTS FROM ZYWIECLAKE (SOUTH POLAND)**

Tadeusz MAGIERA, Zygmunt Strzyszczyk, Maciej Kostecki (Institute of Environmental Engineering, Polish Academy of Sciences, ul. M. Skłodowskiej-Curie 34, 41-819Zabrze, Poland, email: magiera@ipis.zabrze.pl), Friedrich Heller (Institute of Geophysics, ETH Honggerberg, CH-8093, Switzerland, email: frieder@mag.ig.erdw.ethz.ch)

Lake Zywiec is a man-made lake constructed in 1965 on the river Sola in the Beskid Mountains (South Poland). The lake is the largest one in a flood control reservoir system known as Sola Cascade. Its area is about 10 km<sup>2</sup> and the average depth is 6.3 m. In May and in September 1970, separated by a big flood event in July, the lake was sampled twice for rock magnetic, chemical and granulometric studies. Low field specific magnetic susceptibility of very recent lake sediments is generally low (6 - 30 x10<sup>-8</sup>m<sup>3</sup>kg<sup>-1</sup>). The spatial variation of the susceptibility is rather low but higher values (27 - 30 x10<sup>-8</sup>m<sup>3</sup>kg<sup>-1</sup>) are observed near the eastern shore of the main basin of the lake. A susceptibility anomaly is observed in the most eastern part of the lake where the susceptibility rapidly increases to 70 x10<sup>-8</sup>m<sup>3</sup>kg<sup>-1</sup>. In 85 % of the September samples, susceptibility decreases by 10 - 40 % compared to the value measured in the May samples. In September 1970 the spatial variation of susceptibility was lower (15 - 25 x10<sup>-8</sup>m<sup>3</sup>kg<sup>-1</sup>) than in May with the only exception of the eastern lake anomaly where susceptibility increased by about 40 % above the May value. Granulometric studies showed that the average grain size varies between 2.7 and 2.9 μm near the dam at the northern edge of the lake and 120 μm at the southern edge near the town of Zywiec. In the September samples, grain size varies stronger. The maximal grain size increases to 340 μm especially in southern and eastern lake parts and muddy areas were enlarged as a result of the big summer flood in July 1970. Seasonal changes are also observed in the total Fe content and some heavy metals. A general decrease in Zn, Pb, Cd, Cu and Cr content during the summer season was observed in the whole lake. The content of other metals such as Mn and Ni increased in samples taken in September.

GA1.05/W/23-A6

1230

**ROCK MAGNETIC PARAMETERS EXPRESSION OF SEDIMENTOLOGICAL AND DIAGENETIC CONTROLS OF CONTAMINANTS IN AN STUARINE-LIKE ENVIRONMENT**

Daniel REY, Belen Rubio, M Nombela & F Vilas (Dpto. Geociencias Marinas, Universidad de Vigo, 36200 Vigo, Spain. email: danirey@uvigo.es)

This paper will presents the results of a preliminary study intended to investigate the application of environmental magnetism techniques in the study of the relationships between contaminant distribution, mobility and spatial variations in sediment character and diagenetic processes in stuarine-like deposits. Its interest relies in presenting a multidisciplinary analysis integrating rock magnetic, sedimentological and diagenetic parameters with contaminant profiles. The study is based in three 90 cm long gravity cores collected in July 1997 at three locations within the inner (1), middle (2) and outer (3) parts of the Ria de Pontevedra in NW Spain. The cores were cut into 3 cm slices in preparation for a range of textural, mineralogical, geochemical, and rock magnetic analyses.

The grain size, mineralogical and magnetic evidence suggests that sediment in the Ria is derived from two main sources: (a) terrestrial and (b) marine. At the Core 1 site terrestrial sediment is dominant, while at sites 2 and 3 marine derived sediment assumes greater importance. Susceptibility is very low in Core 1 as a result of the finer and clay-rich nature of the terrestrial-derived sediments, that have a greater capacity to transport and sorb contaminants after reduction of original oxides during early diagenesis. Cores 2 and 3 were different from Core 1. They showed a two orders of magnitude higher susceptibility values in the top 10-20 cm. This indicates that these sediments experience a higher rate of organic matter oxidation than in Core 1, and the sediments overall are less anoxic and higher in authigenic iron oxyhydroxides and iron silicate phases.

**Saturday 24 July PM**

Presiding Chairs: A P Roberts (University of Southampton, School of Ocean and Earth Science, Southampton, UK) M Torii (Okayama University of Science, Okayama, Japan)

**MAGNETIC PROPERTIES AS ENVIRONMENTAL PROXY PARAMETERS**

GA1.05/W/34-A6

1430

**A LATE QUATERNARY ROCK MAGNETIC RECORD OF CLIMATIC AND OCEANIC CHANGE; TANNER BASIN, CALIFORNIA BORDERLAND**

Franz HEIDER (GeoForschungsZentrum, PB 3.3, Telegrafenberg, 14473 Potsdam, Germany), Ingrid Hendy and James P. Kennett (Dept. of Geological Sciences, UC Santa Barbara, CA, USA), Juliane M. Bock and Jürgen Matzka (Institut für Allgemeine und Angewandte Geophysik, Ludwig-Maximilians-Universität, Theresienstr. 41, 80333 München, Germany)

A high-resolution record of rock magnetic properties and oxygen isotopes was determined from marine isotope stage 6 to the Holocene (130 Ka to P.D.) for hemipelagic sediments (ODP Leg 167) from Tanner Basin. The sedimentation is 12 cm/kyr and sample spacing is 10 cm. Anhyseteric remanent magnetization (ARM) is taken as a measure for the concentration of magnetic minerals. The quantity of magnetic material increased during transitions from warm to cool periods, and resulted from increased shelf erosion during lower sea levels. During interglacials and inter-stadials a reduction in the quantity of magnetic material in the sediment occurred, decreasing magnetic susceptibility. This resulted from dilution of the magnetic fraction due to increased biogenic deposition during these warm intervals. The ratio of ARM to ARM after 15 mT AF demagnetization is used as a coercivity indicator. The magnetic properties of these sediments are largely determined by two climatically controlled fluxes of magnetic material. Large and magnetically softer hematite grains were deposited during times of decreasing sea level when the concentration of magnetic particles was elevated. Small magnetite grains (< 2 μm) control the magnetic properties during transgressing and high sea levels, when detrital hemo-ilmenite was low. The ARM ratio leads the delta18O curve by 0.8 m. This offset between the coercivity parameter and intervals of climatic change represents evidence for autigenic growth of magnetite grains near the Fe-redox boundary. Authigenic growth of magnetite is associated with rapid climate events as recorded by planktonic foraminiferal assemblage shifts. These relations may have resulted from changes in oxygen concentrations in intermediate waters.

GA1.05/W/29-A6

1445

**ORGANIC CARBON FLUX CONTROLS THE MORPHOLOGY OF MAGNETOFOSSILS IN MARINE SEDIMENTS**

Toshitsugu YAMAZAKI and Hodaka Kawahata (Geological Survey of Japan, Tsukuba 305-8567, Japan, email: yamazaki@gsj.go.jp)

Magnetotactic bacteria produce chains of magnetite crystals within a cell. Bacterial magnetites have characteristic morphologies and sizes under strict biological control. The morphologies of bacterial magnetites (hexagonal prism, octahedron, and teardrop shapes) appear to be species specific, but factors that control the morphology have not been understood. We examined morphologies of fossil bacterial magnetites (magnetofossils) preserved in deep-sea sediments and its relation to organic carbon fluxes (Corg). Magnetofossil morphology was determined under a TEM on magnetic extracts from Pacific deep-sea surface sediments at 13 sites obtained by box-corer or multiple corer. At 8 of 13 sites, Corg fluxes were determined from particulates collected by sediment traps moored for about 1 yr. Isotropic crystals dominate magnetofossils in sediments in a relatively oxidized condition (lower Corg flux), whereas proportion of anisotropic crystals increases in a more reduced condition (higher Corg flux). Geographically, the isotropic-dominant region corresponds to the low primary productivity province. Our finding has important implications for iomineralization processes, and demonstrates the potential of magnetofossil morphology as a paleoenvironmental indicator.

GA1.05/W/19-A6

1500

**MAGNETIC STUDY OF CORE MD972151 FROM SOUTHWESTERN SOUTH CHINA SEA AND ITS PALEO-ENVIRONMENT IMPLICATIONS**

T.Q. Lee (Inst Earth Sci., Acad. Sinica, Taipei, Taiwan; e-mail: tqlee@earth.sinica.edu.tw).

This study will present paleomagnetic and rock magnetic results of core MD972151 taken from Southwestern South China Sea during IMAGES III-IPHIS Cruise in 1997. Paleomagnetic secular variation pattern indicated a reversed polarity event appeared at depth between 21.7 and 23.8 meters. It is recognized as the Blake event of about 130 ka in age. Results of the oxygen isotope dating and many well established time series of other proxies proposed that the boundary of stage 5-6 is located at about 21.5 m. These assignments are in very good consistency. In addition, a short event is also found at the bottom of the core. It is tentatively assigned to an excursion of intensity low which has an age interval of about 150-160 ka reported by Valet et al. (1993). Thus, the core MD972151 is thought to provide records for the last 160 ka.

To study the environment changes, several magnetic parameters are used, such as magnetic susceptibility, NRM, ARM, SIRM, soft and hard components of SIRM, S-ratio etc. Relative high peak values and quick variations were found at the depths below 21.5 m for all the studied magnetic proxies. This phenomenon suggests that a very important event of environment change should have happened at the time during the boundary of stage 5-6. The sediments of the core studied major came from its surrounding area, such as southeast Indochina peninsula at the western part, Sunda Shelf, Indonesia and Borneo at the southern part. From magnetic patterns, it is thought that some of the source areas might have stopped to supply sediments to the area studied since of about 120 ka. In addition, hard component of SIRM is found to vary at the opposite sense relative to those of the other proxies, such as UK'37 SST and carbonate abundance etc. Abundance of magnetic minerals correspond to contribute the hard component of SIRM, such as hematite, is thus considered to be one of the important proxies for paleo-environment change studies at least at the area studied.

GA1.05/W/01-A6

1515

**MAGNETIC SIGNATURE OF BRIEF INTERSTADIAL EVENTS IN LAKE BIWA DURING THE PAST 40 KYRS**

AKIRA HAYASHIDA (Doshisha University, Kyo-Tanabe, Kyoto 610-0321, Japan; email: ahay@doshisha.ac.jp), Y. Kuniko (Kyoto University), M. Ali (Geological Survey of Pakistan), M. Torii (Okayama University of Science), K. Yamada, H. Fukusawa (Tokyo Metropolitan University), H. Kitagawa (International Research Center for Japanese Studies), K. Takemura (Kyoto University)

Lake Biwa, situated in the central part of Japan, is a sedimentary basin that can provide continuous record of past environments since the Middle Pleistocene. Although the paleoclimatological data from previous core samples are correlated to major glacial and interglacial cycles during the last 430 kyrs, high-resolution studies on both paleomagnetism and paleoenvironment have not yet been attained. In 1995, seven piston cores of 10-15 m long were obtained at three localities in the northern part of Lake Biwa. Detailed studies of tephrochronology and AMS radiocarbon dating showed that two piston cores of about 15 m long, which were recovered on the margin of the deep depression, cover the time period of the last 40 kyrs. The total organic carbon content (TOC) data from this site show increased value in the post-glacial period, and also mimic millennial-scale climatic variations during the glacial period. Magnetic mineral concentration, represented by ARM or SIRM intensities, shows a remarkable correlation with the TOC data. In particular, the ARM variation from 40 to 30 kyrs BP is well correlated to the Dansgaard-Oeschger cycles recorded in Greenland ice cores. We interpret that flux of fine grained magnetite and organic carbon were both increased during interstadial periods, probably associated with greater precipitation. It is thus suggested that there were rapid changes in climate around Lake Biwa in response to the instability of the glacial climate. of AMS particularly for sediments.

GA1.05/E/08-A6

1545

**MAGNETIC STUDIES OF MEXICAN LAKE SEDIMENTS AND SOILS**

John D.J. BRAISBY (Geology and Geophysics Dept., University of Edinburgh), Roy Thompson (Geology and Geophysics Dept., University of Edinburgh, Sarah E. Metcalfe (Geography Dept., University of Edinburgh)

Magnetic techniques provide useful methods for the detection of environmental and climatic change as recorded in lake-sediment sequences. Lake-sediments can contain complex mixtures of magnetic minerals derived from a range of sources. We have explored a variety of parsimonious unmixing algorithms that can be used to identify the magnetic components. These include unmixing in terms of (1) catchment materials, (2) type horizons, (3) reference magnetic minerals and (4) combinations of (1), (2) and (3). Perturbation analyses are used to explore the propagation of errors through the models. At Babicora lake in northernmost Mexico clear variations in magnetic concentration closely parallel changes in diatom abundance. These reflect climatic changes associated with switches in the season of precipitation from summer to winter. Magnetic measurements also pick out 16 distinct, and yet previously unrecognised, horizons from the last 61,300 years.



GA1.05/E/17-A6

1630

**CONTRASTING MAGNETIC PROPERTIES FROM TWO LOESS/PALEOSOL SECTIONS IN GANSU PROVINCE, WEST CHINA**

Toshiaki Mishima (Division of Earth and Planetary Sciences, Kyoto University, Kitashirakawa-Oiwakemachi, Sakyo, Kyoto 606-8502, Japan, email: mishima@kobe-u.ac.jp), M. Torii, H. Fukusawa, S. Tsukamoto, K. Ohi, T. Sasaki, Y. Ono, X.-M. Fang, B.-T. Pan, J.-J. Li

Loess/paleosol samples were taken from the two sections in the western part of the Chinese Loess Plateau: the Beiyuan section, Linxia City and the Shajinping section, Lanzhou City. Although the distance between these two localities is less than 100 km, contrasting magnetic properties are observed.

The magnetic properties of the Beiyuan section is controlled by the following two magnetic components. The background component does not change in mineralogy, grain size distribution and concentration throughout the loess/paleosol sequences. Amount of the enhanced component increases at paleosols, which results in enhancement of magnetic susceptibility. Grain size distribution of the enhanced component does not change with the degree of enhancement. On the contrary, the background component is identical to that of the Shajinping section where no enhanced component was found. The identical background component can be considered as of pristine loess in the western part of the Loess Plateau. Soil formation process may not always included enhanced production of magnetic particles.

GA1.05/W/32-A6

1645

**VARIABLY OXIDIZED MAGNETITE OF LOESS AND PALEOSOL FROM NORTHEAST CHINA**

K. FUKUMA (Japan Marine Sci. Tech. Center, Yokosuka 237-0061, Japan, email: fukuma@jamstec.go.jp), M. Torii (Okayama Univ. Sci., Okayama 700-0005, Japan), H. Fukusawa (Tokyo Metro. Univ., Hachioji 192-0397, JAPAN), Y.-H. Yin (Liaoning Normal Univ., Dalian 116029, China), and Y. Yasuda (International Research Center for Japanese Studies, Kyoto 610-1192, JAPAN)

Magnetic susceptibility variations of loess-paleosol sequences from the Chinese Loess Plateau provide excellent records of paleoclimate change for the last 2.5 m.y. Susceptibility is believed to be enhanced during pedogenesis and usually regarded as a proxy of precipitation. However, there is still no consensus on how precipitation induces such a susceptibility enhancement. We collected loess, Holocene and S1 paleosol samples from northeast China. The susceptibility and hysteresis properties are similar to those of Luochuan in the Chinese Loess Plateau. Temperature dependence of isothermal remanent magnetization imparted at 5 K were measured continuously using the RSO mode in which temperature is gradually changed with vibrating a sample. Three types of behaviors were observed for samples from northeast China; Holocene black paleosols exhibit distinct Verwey transitions near 115K, loess samples show gradual magnetization changes in a temperature range from 90 to 120K, but no transition is observed for S1 paleosols. These low temperature behaviors reflect different oxidation states of magnetite. The distinct Verwey transition points to non- or only slightly oxidized magnetite, the suppressed Verwey transition to partly oxidized magnetite, and the extinct Verwey transition to highly or completely oxidized magnetite (maghemite). Partly oxidized magnetite has been thought to be responsible to the susceptibility enhancement. Our low-temperature results suggest that non- or only slightly oxidized magnetite is primarily formed in soil layers and subsequently oxidized.

GA1.05/W/22-A6

1700

**MAGNETIC MINERALOGY OF SANDS FROM TAKLIMAKAN DESERT, WESTERN CHINA: IMPLICATION FOR SOURCE OF CHINESE LOESS**

M. Torii (Okayama Univ. Sci., Okayama 700-0005, Japan, email: torii@big.ous.ac.jp), T.-Q. Lee (Inst. Earth Sci., Taipei, Taiwan), H. Oda and T. Yamazaki (Geol. Surv. Japan, Tsukuba, Japan), N. Ishikawa (Kyoto Univ., Kyoto, Japan), and K. Fukuma (JAMSTEC, Yokosuka, Japan)

Surface sand samples collected across the Taklimakan Desert in the Tarim Basin, Xinjiang Uygur Autonomous Region, western China were examined with a rock magnetic method to elucidate magnetic mineralogy. We collected 19 samples along a route spanning about 1200 km in 1997. Magnetic mineralogy was determined based on high-temperature and low-temperature magnetic phase transitions. All samples clearly show the Verwey transition. The Curie temperature of 580°C is also observed without exception. Some samples show minor Curie temperature at about 300°C. Combined with the low-temperature analysis, we suggest coexistence of minor amount of titanomagnetite together with stoichiometric magnetite. Magnetic grain size suggested by the hysteresis parameters ranges from PSD to MD. It is now well established that the magnetic minerals in the Chinese loess/paleosol are either magnetite or maghemite. And even in the pristine loess, magnetite is oxidized to maghemite to some extent. However the magnetic mineral of the Taklimakan Desert samples shows the distinctive Verwey transition with relatively larger grain size. These lines of evidence suggest that either the desert sands of Taklimakan was not major source of the Chinese loess, or the magnetic minerals in the loess were substantially changed from its aeolian origin even in the pristine loess.

GA1.05/W/17-A6

1715

**PALAEOLIMATIC SIGNIFICANCE OF MAGNETIC CHARACTERISTICS ALONG TWO LOESS/PALAEOSOL PROFILES FROM BULGARIA**

JORDANOVA, DIANA (1) and J. Hus(2) (1) Geophysical Institute, Bulg. Acad. Sci., Acad.G. Bonchev Str., bl.3, 1113 Sofia, Bulgaria, email: vanedi@geophys.bas.bg (2) Centre de Physique du Globe, 5640 Dourbes, Belgium

Magnetic susceptibility variations along the two loess/paleosol profiles in Bulgaria (profile Korfen with thickness of 34m and profile Viatovo with thickness of 26m) are used together with the ratio of susceptibility to saturation magnetization ( $X/J_s$ ) for palaeoenvironmental reconstructions and correlation with the global 18O record (ODP 677 core). The two susceptibility records show clear distinction between loess and palaeosol horizons similar to the situation observed in China. Laterally separated at about 120km sampling sites, the shape of the two-susceptibility records match in details. The one significant difference is the relative maximum susceptibility enhancement of the palaeosol horizons, which is an expression of peculiarities in the local environmental and soil-forming factors. On the basis of the proposed correlation between susceptibility variations and 18O record, a correction of the existing stratigraphy of the upper part of the loess complex in NE Bulgaria is proposed.

GA1.05/W/33-A6

1730

**EVOLUTION OF MAGNETIC MINERALOGY IN QUATERNARY SOIL CHRONOSEQUENCES FROM THE CENTRE OF THE IBERIAN PLATE**

Mari Fe Bógalo (Dpto. de Física, Universidad de Burgos, 09001, Burgos, Spain, email: mfbogalo@ubu.es); María Luisa Osete (Dpto. de Geofísica, Universidad Complutense, 28040 Madrid, Spain, email: mlosete@eucmax.sim.ucm.es); Friedrich Heller (Institut für Geophysik, ETH Hönggerberg, CH-8093, Zurich, Switzerland, email: frieder@mag.ig.erdw.ethz.ch); Alfredo Pérez-González (Dpto. de Geodinámica, Universidad Complutense, 28040 Madrid, Spain, email: alfredog@eucmax.sim.ucm.es)

Soil profiles from three systems of river terraces of Plio-Pleistocene to Holocene age in the centre of the Iberian plate have been investigated. Specifically, a study of the behaviour of magnetic parameters as a function of depth of each profile and age of the terraces has been carried out in several of the soil profiles. Magnetic-mineralogical properties are shown to be different in the distinct soil horizons (enhanced surface horizon, stable B and C horizon) of each profile, and also their pattern of variation with age has been established. Fine grained magnetite and/or maghemite are the dominant magnetic minerals in the enhanced surface horizon. In the stable B horizon the high contribution of goethite and hematite is proved by IRM measurements at different fields and temperatures and by "wasp-waisted" hysteresis loops. The contribution of different minerals in superparamagnetic state at room temperature is qualitatively determined. The behaviour with age of most magnetic soil parameters suggests a reduced activity of the pedogenic processes in the centre of the Iberian Peninsula during Early to Middle Pleistocene.

Friday 23 July AM

Presiding Chairs: A P Roberts (University of Southampton, School of Ocean and Earth Science, Southampton, UK) M Torii (Okayama University of Science, Okayama, Japan)

**MAGNETIC PROPERTIES AS ENVIRONMENTAL PROXY PARAMETERS**

GA1.05/E/15-A5

Poster

0900-01

**ROCK MAGNETIC RECORDS FROM ITALIAN LAKE SEDIMENTS, PART 1: LAGO DI MEZZANO, CENTRAL ITALY**

Ute BRANDT, Norbert R. Nowaczyk, and Jörg F.W. Negendank (GeoForschungsZentrum Potsdam, Telegrafenberg, D-14474 Potsdam, Germany, email: brandt@gfz.potsdam.de) Antje Ramrath (Dept. of Geography, University of Western Australia, Nedlands, WA6907, Australia)

Detailed rock magnetic and sedimentological investigations were carried out on two sediment cores recovered from Lago di Mezzano, central Italy, yielding a continuous record of climate change for the last 31 ka. IRM acquisition experiments, hysteresis loop and backfield as well as thermomagnetic measurements revealed magnetite in the pseudo-single to multi-domain range as the main carrier of the remanence. Sedimentological investigation comprise dry density, total organic carbon, total sulphur and loss on ignition. All parameters investigated reflect the climatic controlled changes in the composition of the sediment due to the transition from the late Pleistocene to the Holocene. The variations in the concentration dependent parameters k, ARM and SIRM are linked to the increase/decrease of minerogenic influx, whereas the grain-size dependent parameters like ARM/SIRM, SIRM/k, kARM/k and the F-Factor reflect the dissolution of the fine grained magnetite fraction linked to a varying content of organic material. An apparent enrichment of high coercivity minerals during intervals of high organic productivity, documented in the S-ratio and the MDFARM, is interpreted as a result of dissolution and dilution processes.

GA1.05/E/09-A5

Poster

0900-02

**ROCK MAGNETIC RECORDS FROM ITALIAN LAKE SEDIMENTS, PART 2: LAGO GRANDE DI MONTICCHIO, SOUTHERN ITALY**

Ute BRANDT, Norbert R. Nowaczyk, Achim Brauer, Jens Mingram and Jörg F.W. Negendank (GeoForschungsZentrum Potsdam, Telegrafenberg, D-14474 Potsdam, Germany, email: brandt@gfz.potsdam.de)

A 65 m long sediment core from the crater lake of Lago Grande di Monticchio revealed a rock magnetic and sedimentary record of climatic change in the time interval from 20 to 105 kyr. Detailed rock magnetic investigations comprise magnetic susceptibility (k), ARM and IRM acquisition, hysteresis loops and backfield as well as thermomagnetic measurements. Sedimentological investigation includes dry density, total carbon, total sulphur and loss on ignition. Magnetite in the pseudo-single domain was identified as the main remanence carrier. Variations in the concentration dependent parameters k, ARM and SIRM are controlled by an increase/decrease of minerogenic influx due to climatic change as well as by an authigenic carbonate production and a varying organic productivity within the sediment profile. The variations in the content of organic material also controls the S-Ratio and the MDFARM, suggesting, that there is an increase of high coercivity minerals during intervals of decreased minerogenic influx. In contrast, there is no relation between the variations in the grain size parameters ARM/SIRM, SIRM/k and kARM/k and the composition of the sediment as determined dry density and total organic carbon content.

GA1.05/W/27-A5

Poster

0900-03

**ROCK-MAGNETIC PROPERTIES OF PLEISTOCENE-HOLOCENE SEDIMENTS FROM CUITZEO LAKE, CENTRAL MEXICO**

Israde-Alcantara, I. (1), Urrutia-Fucugauchi, J. (2) & Garduño-monroy, V.H. (1) (1) Departamento de Geología, Universidad Michoacana de San Nicolás Hidalgo, Morelia, Mexico and (2) Instituto de Geofísica, UNAM, Coyoacan 04510 D.F., Mexico)

Results of a paleoenvironmental study of the Pleistocene-Holocene sedimentary sequence of Cuitzeo Lake are reported. The lake, located in the Michoacan volcanic highland, has a tectono-volcanic origin and forms part of the extensive lake system that developed in central Mexico during the Late Quaternary. This study is based on samples taken from a 27 meters long core drilled in the central sector of the lake. Preliminary chronological control is based on nine AMS radiocarbon dates for the shallow section of the core down to 9.1 m (42,000 yr BP). Results show that Cuitzeo Lake underwent several climatic and environmental changes, with more humid phases during the Late Pleistocene than during the Holocene. Sediment chemistry and diatom records suggest that before 50,000 yr BP the lake was a fresh water eutrophic system. There is evidence for two fairly humid intervals around 50,000 and 100,000 yr. From 42,400 yr to present, the lake experienced episodes of aridity and intense erosion, becoming a shallow alkaline saline water body. There is a hiatus between 8,830 and 17,605 yr BP, which correlates with intense volcanic activity. From 2,000 yr BP to present, there is a

tendency to arid conditions, with Cuitzeo Lake becoming shallow, with saline and turbid waters. magnetic susceptibility shows an apparent cyclicity, with peaks every 3 m for the complete core, which may correlate with periods of increased detrital input. Spectral analysis of the susceptibility and NRM intensity records show evidence for several characteristic periods.

**GA1.05/W/28-A5** Poster **0900-04**

**LATE QUATERNARY ENVIRONMENTAL CHANGE IN SONORAN DESERT, MEXICO**

Beatriz ORTEGA and Margarita Caballero (Instituto de Geofísica, Universidad Nacional A. de Mexico, 04510 DF, email: bortegea@tonatiuh.igeofcu.unam.mx) Socorro Lozano (Instituto de Geología, Universidad Nacional A. de Mexico, 04510 DF)

The research on climatic change during Late Quaternary has been scarce in the Mexican portions of Sonoran desert, particularly in Baja California, mainly due to the fact that the fossil record is poorly preserved in many stratigraphic sequences of this area. We have carried out a number of experiments in sediments collected in a 9.5 m long core, in a playa lake from Baja California (San Felipe), to characterise the magnetic fraction in terms of magnetic mineralogy, concentration of magnetic grains and grain-size distribution, and combined these data with palynological, organic content and particle size distribution data as a first approach to reconstruct the environmental history of the area. The sequence spans the last 70 kyr. Results from mineral magnetic analyses (including room- and low-temperature X and Xfd%, ARM, SIRM, Curie temperatures, hysteresis parameters and S ratios), and the other proxies analysed show highly contrasting environmental conditions between the glacial and the late glacial-Holocene. Very low magnetic concentrations are characteristic in late glacial. Pollen record is only present in the full glacial, between 40 and 15 kyr B.P. Arboreal and lacustrine elements indicate moist conditions and the presence of a steady lake. The late glacial-Holocene sediments display a 5-fold increment in the magnetic concentration parameters, in the abundance of finer SD and SPM magnetic grains, and in sedimentation rate. These changes are interpreted as an increment of erosion that cut through the mantle soil and rocks in the catchment. The onset of the present arid conditions is around 4 kyr B.P.

**GA1.05/-A5** Poster **0900-05**

**PALEOCLIMATIC AND DEPOSITIONAL CONTROLS OF LATE PLEISTOCENE LOESS/PALAEOSOL SEQUENCES FROM SIBERIA**

Galina MATASOVA, Alex Kazansky and Valentina Zykina (UIGGM, Siberian Division, Russian Acad. Sci., Akad. Koptug ave. 3, 630090 Novosibirsk, Russia, email: galina@ig.cas.cz), Neli Jordanova, Eduard Petrovsky and Ales Kapicka (Geophysical Institute, Acad. Sci. Czech Rep., Bocni II/1401, 141 31 Prague 4, Czech Republic, email: neli@ig.cas.cz)

Two loess/palaeosol sections in Southwestern Siberia (Bachat and Kurtak) have been studied magnetically. Rock-magnetic properties, as well as anisotropy of magnetic susceptibility were investigated in detail. The results obtained up to now suggest combination of "Alaskan" and "Chinese" models of deposition. While for one site, magnetic susceptibility distinguished well between loess and palaeosol layers, the other site expressed practically constant susceptibility values for the whole profile. However, in the latter case, frequency-dependent susceptibility suggests enhancement of pedogenesis in palaeosol layers. Studies of anisotropy of magnetic susceptibility reveal well-defined sedimentary magnetic fabric for both sections. Different mechanisms of loess deposition (pure aeolian in Bachat and aeolian/colluvial/alluvial features for Kurtak) is reflected well by AMS pattern. The two sections showed also different magnetic-phase composition. While for the Bachat section only one type of thermomagnetic curves was found, the Kurtak one contains different minerals in loess and palaeosol layers. Magnetic properties of samples from the two sections will be discussed in terms of paleoclimatic and depositional conditions.

**GA1.05/W/20-A5** Poster **0900-06**

**MINERAL MAGNETISM AND ARCHAEOLOGY AT GALSON ON THE ISLE OF LEWIS, SCOTLAND**

C. PETERS(1), M.J. Church(2) and G. Coles(2) (1) Department of Chemistry, University of Edinburgh (2) Department of Archaeology, University of Edinburgh

Coastal erosion is cutting a section through a complex later prehistoric archaeological site at Galson. 168 samples from individual features e.g. middens and hearths, and also from several continuously sampled vertical profiles were collected from the site. A range of mineral magnetic measurements, including susceptibilities and laboratory induced remanent magnetisations, have been carried out on the samples. The strong magnetic signal of the hearth material can be traced in selected floors and middens giving an indication of the anthropogenic use within the dwellings. The magnetic data also highlight differences between visually similar soils. The variation of susceptibility with temperature, measured at 2cm intervals in a vertical profile through a hearth in one of the dwellings, has revealed two distinct magnetic mineralogies, with varying domain states, possibly reflecting different fuel sources.

**GA1.05/W/38-A5** Poster **0900-07**

**THE MAGNETIC METHOD FOR SEARCHING OBJECTS**

Victor Zemtsov (Institute of Geology, Karelian, Research Centre RAS, Pushkinskaya St., 11, Petrozavodsk 185610, RUSSIA, email: Klubukov@post.krc.karelia.ru, in the Subject: zem)

The method proposed can be used to search for various objects in geophysics and geology, for cosmic (the Moon, the Mars etc.) and archaeological investigations, for estimation of the quality of manufactured articles and measurement of low temperatures (T) in technology. The objects of search can be isotropic and anisotropic, solid, liquid and gaseous, re-covered by unconsolidated sediments, by water and can have various T. The method is especially indispensable for the study of planets that have no global magnetic field and for the analysis of atmospheric oxygen. The method comprises periodical pressing of permanent magnet to an object at frequency (f), measurement of altitude of inductive impulse (Emax), the calculation of mass of the magnetic (c) in the object from the correlation: (c)=b (Emax /f), where b is the constant obtained on an object with the known mass of magnetic. According to the last invention, an united geometric system of sensors consisting of n-pair identical sensors is composed. In each pair, the clearance of the first permanent magnet is oriented in the direction of searching and that of the second magnet at the right angle to it. Besides, the method can be used to estimate the magnetization (I) of the object, its I-anisotropy and the optimal direction of search. The system of sensors can be enlarged by adding a T-sensor. A paramagnetic standard is brought at frequency f into the clearance of the T-sensor. One should know the T-object to be able to accurately determine the mass of the T-dependent magnetic. The system can have one more f-sensor used to measure f in working sensors. Searching may be completely automated.

**GA1.05/W/25-A5** Poster **0900-08**

**ORIGIN AND DISTRIBUTION OF MAGNETIC PARTICULATE MATTER ON TREE LEAVES IN THE URBAN ENVIRONMENT**

Juergen MATZKA (Inst. f. Allg. u. Ang. Geophysik, Universität München, Theresienstr. 41, 80333 München, Germany, email: matzka@rockmag.geophysik.uni-muenchen.de), Barbara A. Maher (School of Environmental Sciences, University of East Anglia, Norwich NR4 7TJ, UK, email: B.Maher@uea.ac.uk)

Our study on the distribution of magnetic particles in the urban atmosphere is based on measurements of the IRM(300 mT) of tree leaves collected in Norwich and in a coastal location in Norfolk, UK. The leaves provide an almost non-magnetic surface on which particulate matter can settle. Known anthropogenic sources of magnetic particles in the atmosphere are the combustion of fossil fuel in cars or power stations. For each sample, the IRM(300 mT) was normalised on the leaf area.

All birch leaves are characterised by very similar remanence coercivity spectra typical for PSD magnetite. Therefore, we assume a very homogenous magnetomineralogy for all our samples and a proportionality between the IRM and the amount of remanence carrying particles. Most of the particles can be removed by washing the leaves, indicating that the particles are in fact adhering to the leaf surface. In nature, rain was found to remove the particles to some extent, too, therefore wet deposition could be excluded. The IRM is strongly dependent on the sampling location's distance to road traffic. In general, IRM values are maximal nearby roads and decrease significantly within a few tens of meters. The signal is also dependent on the slope of the road, or in other words, on the fuel consumption of the traffic. This identifies automotive combustion to be the source of the particles. Individual trees show significant maxima in IRM proximal to streets, indicating the trees' ability to remove particulate matter from the atmosphere.

**GA1.05/W/41-A5** Poster **0900-09**

**MAGNETIC SIGNATURE OF ROADSIDE SOILS AND SPECIMEN OF POTENTIAL EMISSION SOURCES OF VEHICLES**

Carsten LEVEN, Mathis Knab, Viktor Hoffmann (Institut fuer Geologie und Palaeontologie, Arbeitsbereich Geophysik, Universitaet Tuebingen; Sigwartstrasse 10, 72076 Tuebingen, Germany; email: viktor.hoffmann@uni-tuebingen.de)

Emissions of vehicles represent a significant contribution to environmental pollution along roads and highways. Amongst toxic gases (NOx, CO, CO2, ...), solid components such as soot particles from the exhaust system, abrasion products from the brakes, smaller parts and particles from the car body as well as abrasion products from the asphalt are emitted in the environment and accumulated in soils or sediments or transported to surface and ground water. In this study the magnetic signature of roadside soils and of potential pollutants from the vehicles has been investigated in more detail. A series of magnetic measurements have been performed on a large sample set depending on distance from the highway and depth from the soil surface: susceptibility, hysteresis and backfield curves, thermo-magnetic runs (J(s) and J) from -200 C to Curie temperatures, IRM acquisition and ARM. In addition, X-ray and microscopic observations were done on selected samples. A magnetite-like phase was found to be the dominating ferrimagnetic phase in the soil as well as in the emission products from the vehicles. In closer distances to the asphalt, many spherical magnetite particles with sizes of 10-150 microns were observed showing skeleton and dendritic structures, which are an indicator of a rapid cooling process. We believe that abrasion products from the braking system and from the asphalt could represent the main sources of the ferrimagnetic particles of anthropogenic origin in roadside soils and sediments. Therefore the distribution and the magnetic signal from these phases can be used as an excellent magnetic proxy for the detection and mapping of areas which are affected or contaminated by vehicle emissions.

**Saturday 24 July AM**

Presiding Chair: Ö Özdemir (University of Toronto, Mississauga, Canada)

**METHODS AND APPROACHES IN ROCK MAGNETISM**

**GA1.05/W/03-A6** Poster **0900-01**

**AN EXPERIMENTAL STUDY OF ORIENTATIONAL MAGNETIC ANISOTROPY IN MAGNETITE-BEARING ARTIFICIAL SEDIMENTS**

Andrei A. KOSTEROV and Vladimir A. Shashkanov (Earth Physics Department, Institute of Physics, Saint-Petersburg University, 198904, Saint-Petersburg, Russia; email: kosterov@snoopy.phys.spbu.ru)

Oriental magnetic anisotropy of sediments arises from an alignment of magnetic grains during deposition in an external field. Albeit weak in small fields, orientational anisotropy has some potential to provide insight into the intrinsic structure of ferrimagnetic grains contained in a sediment, being sensitive, in particular, to their intrinsic magnetic anisotropy. We present the results of an experimental study of field dependence of orientational magnetic anisotropy carried out on magnetite-bearing artificial sediments deposited in horizontal magnetic fields ranging from 0 to 4.8 mT, and in vertical fields up to 4 mT. Oriental magnetic anisotropy was defined as the ratio of anhysteretic remanences (ARM) acquired parallel and orthogonally to the sedimentation field respectively. Obtained experimental results may be summarized as follows:

1. For the sediments produced in horizontal field orientational anisotropy approached saturation values of about four in the maximum sedimentation field.
2. Shape of angular dependences of ARM direction suggests that the ferrimagnetic phase of studied sediments is mostly represented by uniaxial grains.
3. Sediments deposited in vertical magnetic field reveal rather surprising result: grains' alignment suppresses vertical anisotropy (which is due to the sediment compaction) but fails to induce orientational anisotropy even in the strongest sedimentation field used.

**GA1.05/W/39-A6** Poster **0900-02**

**AN EXPERIMENTAL STUDY OF DRM INCLINATION ERRORS IN ARTIFICIAL SEDIMENTS DEPOSITED IN LARGE-SQUARE VESSELS**

Andrei A. KOSTEROV, Vladimir A. Shashkanov, Igor V. Samsonov and Elena V. Isupova (Earth Physics Department, Institute of Physics, Saint-Petersburg University, 198904, Saint-Petersburg, Russia; email: kosterov@snoopy.phys.spbu.ru)

Inclination error is a feature commonly observed in the laboratory experiments modelling the acquisition of detrital remanent magnetization (DRM). Such observations raised a problem of the possible occurrence of inclination errors in nature as well, and also prompted the search for the methods to correct them. To investigate in detail the origin of inclination errors occurring in laboratory redeposition experiments, we have prepared artificial sediments using large-square vessels (25 cm vs. 20 cm, height 25 cm). Slurry was deposited in the laboratory magnetic field (Ho = 54 μT, j = 72 degrees) with the horizontal component parallel to the long wall of a vessel. Study of surface distribution of DRM and of magnetic anisotropy of such large-

square sediments has shown that these quantities are essentially but regularly scattered over the sediments' area. Vessel walls appear to disturb the DRM acquisition even at the center of vessel. At the same time, we obtained a clear correlation between inclination errors and magnetic anisotropy. This yielded an experimental material for a throughout check of proposed earlier [Shashkanov et al., 1989] method of correction of inclination errors making use of sediment's magnetic anisotropy.

**GA1.05/W/40-A6 Poster 0900-03**

**STABILITY OF ORIENTATIONAL MAGNETIC ANISOTROPY OF ARTIFICIAL SEDIMENTS AGAINST HEATING**

Vladimir A. Shashkanov, Andrei A. KOSTEROV, Andrei A. Bachurin and Sergei I. Morshchikhin (Earth Physics Department, Institute of Physics, Saint-Petersburg University, 198904, Saint-Petersburg, Russia; email: kosterov@snoopy.phys.spbu.ru)

The orientational magnetic anisotropy is acquired in sediments during deposition through the alignment of ferrimagnetic grains in an ambient magnetic field. However, its magnitude depends not only on the sedimentation field intensity, but also on the grains' intrinsic anisotropy. So far the magnetic anisotropy has been considered as a very stable element of a magnetic state of natural samples, often even more stable than the natural remanent magnetization. The stability of orientational magnetic anisotropy to heatings has been studied for the artificial sediments, deposited in the magnetic fields ranging from 0 to 5 mT. The most striking result is that for strongly anisotropic sediments anisotropy factor (defined as the ratio of ARMs acquired parallel and orthogonally to the sedimentation field respectively) while initially approaching 4.5 - 4.7, decreases drastically with heating, reaching values about 1.6 - 1.8 after heating to 620°C. Possible mechanisms explaining this phenomenon are discussed.

**GA1.05/E/06-A6 Poster 0900-04**

**TEMPORAL CHANGE OF ROCK MAGNETISM DURING 1991-1995 ERUPTION AT UNZEN**

Naoko UENO (Natural Science Laboratory, Toyo University, Asakashi, Saitama 351-8510, Japan, email: ueno@hakusrv.toyo.ac.jp)

Twenty-five samples of dacitic lavas including bombs and pyroclastics from Mt.Unzen erupted during 1991-1995 were studied on the temporal change of rock magnetic properties during eruption. The ten samples were studied as pilot. The work included intensity measurement by the Thelliers' method, hysteresis analysis by vibrating sample magnetometer. In progress of time in eruption, natural remanent magnetization increased, initial susceptibility decreased, Curie temperature increased, coercive force and remanent coercive force increased, ratio of remanent saturation magnetization to saturation magnetization increased. Temperature dependence of hysteresis parameters was measured both during descent and ascent. The other fifteen samples collected by S. Nakada throughout the eruption are studied to find the correlation with other temporal petrological characters such as effusion pulsation, Fe-Ti oxide temperature and chemical composition of Fe-Ti oxide minerals reported by Nakada and Motomura (1999).

**GA1.05/E/04-A6 Poster 0900-05**

**ACTIVATION ENERGY OF THE VISCOSITY MAGNETIZATION PROCESSES IN ROCKS**

V.A.Bol'shakov (Geographical Department, Moscow State University, 119899, Moscow, Russia, email: pasha@nbz.ru)

The author proposed the original approach for calculation of temperature-time parameters for T-cleaning of a viscous magnetization. This approach is based on the experimental evaluation of the activation energy (Ea) of the magnetic viscosity. Ea knowing for the concrete samples make it possible to carry out T-cleaning in the most gently manner. In this case primary remanence would be affected in the least degree. The author developed some methods for Ea determination. They consist in measurement of the viscous magnetization curve displacement after a little changing of temperature. Anisotropy changes and conversion of some magnetic particles in super-paramagnetic phase after a little temperature increase were neglected from the beginning. However, the recent investigations of loess-soil samples have shown that such neglects lead to mistakes in Ea measurements. The methods of minimizing such mistakes were proposed.

**GA1.05/W/07-A6 Poster 0900-06**

**ANISOTROPY RESULTS OF IGIMBRITES FROM THE TRANSMEXICAN VOLCANIC BELT**

A.M. SOLER-ARECHALDE, Caballero-Miranda, C., Rebolledo-Vieyra, M., Bautista A., and Urrutia-Fucugauchi, J. (Laboratorio de Paleomagnetismo y Geofísica Nuclear, Instituto de Geofísica, UNAM., Circuito Institutos s/n, 04510, Coyoacán, México, D.F., México. tel (5) 6 22 41 13, email: anesoler@tonatiuh.igefocunam.mx)

Preliminary results of a study of anisotropy of magnetic susceptibility of ignimbrite units from four calderas in the TMVB, are presented. Amealco, Huichapan, Zitacuaro volcanic complex and the Las Americas Formation within the central sector of the TMVB were selected for this project. Detailed sampling was performed on several profiles of 3 to 8 mts high each (one sample every 10 cms) and at different distances from the ignimbrite source. Anisotropy parameters were employed to analyse and characterise the distinct flow conditions over the profile. In a similar way, these parameters were compared for different distances from the source and on different sources. The magnetic fabrics was compared with observed flow directions and used to determine these directions in the absence of other indicators.

**GA1.05/W/16-A6 Poster 0900-07**

**MAGNETIC SUSCEPTIBILITY ANISOTROPY OF THE CANTERA IGIMBRITE, SAN LUIS POTOSI VOLCANIC FIELD, MEXICO**

Torres-Hernández J. Ramón. (Instituto de Geología de la UASLP and UACyP, UNAM), C. I. Caballero-Miranda and L. Alva-Valdivia (both at Instituto Geofísica, UNAM, Coyoacán D.F. 04510, México; email: cecilia@tonatiuh.igefocunam.mx; lalva@tonatiuh.igefocunam.mx)

Magnetic Susceptibility Anisotropy (AMS) results from 168 specimens from 8 sites (5 sites with 25 specimens average each and 2 with 8), from La Cantera Ignimbrite, belonging to the San Luis Potosi Volcanic field, are presented. These results together with gravimetry data, geomorphologic analysis and available traditional geological indicators, are used in order to determine whether a linear or a central flow origin of the ignimbritic flow. The AMS results were measured with the JR5 instrument, structural corrected and computed with principal components statistics. AMS ellipsoids are mainly oblate with minimum susceptibility axes nearly vertical and maximum susceptibility axis near the horizontal, sometimes showing a very

good imbrication. Flow direction may be inferred quite well in half of the sites. In the other sites other sort of data has to be used in order to determine the flow direction with confidence. Presently available results suggest a central flow origin, which may correspond to a caldera according with gravimetric and geomorphologic analyses

**GA1.05/W/10-A6 Poster 0900-08**

**A METHOD OF PALEOMAGNETIC DETERMINATIONS USING THE CHARACTERISTICS OF MAGNETIC ANISOTROPY OF ROCKS**

Juliya B. ROSANOVA and Vladimir A. Shashkanov (Earth Physics Department, Institute of Physics, Saint-Petersburg University, 198904, Saint-Petersburg, Russia; email: rosa@geo.phys.spbu.ru)

Theoretical possibility of subdivision of rocks' magnetic anisotropy into components in accord with their physical nature and detection of a paleomagnetic component, i.e. the component caused by primary remanent magnetization and therefore making possible paleomagnetic determinations, has been investigated. Magnetic torque method was used to measure magnetic anisotropy. The magnetic torque curves of samples has been interpreted in two ways: (1) by direct determination of the standard paleomagnetic direction (J, D) and (2) with method of spherical harmonic analysis of the energy of magnetic anisotropy. Results of experimental and theoretical studies of the magnetic anisotropy for a representative collection of igneous rocks have shown that the latter method is more stable with respect to the rocks' inhomogeneity.

**GA1.05/W/15-A6 Poster 0900-09**

**PHYSICAL MODELLING OF MAGNETIC ANISOTROPY OF ROCKS AND A POSSIBILITY OF PALAEOMAGNETIC DETERMINATIONS USING MAGNETIC ANISOTROPY**

Pavel V. DUBROVIN and Vladimir A. Shashkanov (Earth Physics Department, Institute of Physics, Saint-Petersburg University, 198904, Saint-Petersburg, Russia; email: packo@geo.phys.spbu.ru)

Being the integral part of magnetic state of rocks, magnetic anisotropy is generally more stable than their natural remanent magnetization (NRM) both in time and with respect to various physical factors altering NRM. Taking into account that remanence acquisition often leads to the formation of a respective component of anisotropy (paleo-informative component), one can assert that magnetic anisotropy itself contains palaeomagnetic information. Generally, magnetic anisotropy of rocks may have more than one component but these latter can be almost always considered as uniaxial. Therefore a palaeomagnetic determination using magnetic anisotropy should be a throughout investigation of magnetic anisotropy of the rock, with the ultimate goal of subdividing the anisotropy into uniaxial components and detecting a palaeomagnetic component which is due to primary magnetization. The magnetic anisotropy has been investigated using the magnetic torque method, which had been previously applied only to studies of magnetocrystalline anisotropy on single crystal ferromagnetics and for mineralogical analysis. A technique of measuring and interpretation of the torque curves has been developed that make it possible to determine the orientations of magnetic axes for the rock samples. This technique has been tested on the several model samples prepared to mimic both "pure" uniaxial (one easy axis - one hard plane or one easy plane - one hard axis) and biaxial (two different uniaxial components) magnetic anisotropy. Palaeomagnetic investigations of series of natural igneous rocks samples have been carried out with the developed method.

**GA1.05/W/18-A6 Poster 0900-10**

**THE METHOD FOR DETERMINING THE MAGNETIZATION ANISOTROPY OF VARIOUS MAGNETICS OF ROCKS**

Victor ZEMTSOV (Institute of Geology, Karelian Research Centre RAS, Pushkinskaya St., 11, Petrozavodsk 185610, RUSSIA, email: Klabukov@post.krc.karelia.ru, in the Subject: zem)

The orientation of particles in rock is not the result of chance accumulation. The origin of rocks determines the process of orientation. There are mechanical, physical and chemical orientating factors. As a result, plane and axial fabrics are formed in rocks. If in a sample there are two fabrics one of which is secondary, then magnetization (I) anisotropy tensors can be determined separately by the method proposed. Calculations and experiments show that an individual magnetic fabric is characterised by the I-anisotropy tensor over a wide range of magnetic fields (H) and temperatures (T). Ferromagnetics have different ranges in which spontaneous magnetization exists, and are magnetized to saturation in different fields (Hs), too. Paramagnetics and diamagnetics have the linear dependence I(H,T). In fields H>Hs the I-tensor of ferromagnetic fabrics turns into a sphere. The I-anisotropy parameters of the "nonmagnetic" fabrics of rocks can be determined by choosing optimum H and T. The effect of another magnetic fabric can be minimised in the same manner. The major axis of the I-anisotropy tensor of the fabric of interest can be determined as the direction of maximum growth of the magnetization vector by its derivative dI/dH or dI/dT in the three-dimensional coordinate system of the sample. The method proposed can be used to reveal the superposed rock fabrics, to make paleomagnetic data more reliable and to obtain the anisotropy parameters of paramagnetic and diamagnetic rocks. 1. GA 5.11, GA 1.052. Contribution of Rock Magnetism (Petrophysics) to Anomaly Interpretation, Rock Magnetism: Methods and Approaches in Rock Magnetism





**IMAGING RIOMETERS, RADARS, AND D-REGION CHEMICAL MODELS**

Location: Gisbert Kapp Building, NG15 LR1  
Location of Posters: Gisbert Kapp, Coffee Room

Monday 19 July AM

Presiding Chair: Esa Turunen  
Concurrent Poster Session

GA2.01/E/07-A1

Invited

0900

**MIDDLE AND UPPER ATMOSPHERE OBSERVATIONS AT POKER FLAT WITH RADIO AND OPTICAL TECHNIQUES INCLUDING 16X16 IMAGING RIOMETER**

Y. MURAYAMA, H. Mori, K. Kato, S. Kainuma, K. Igarashi (Communications Research Laboratory, Koganei, Tokyo 184-8795 JAPAN, email: murayama@crl.go.jp); Hans Nielsen, Tom Hallinan (Geophysical Institute, University of Alaska Fairbanks, Fairbanks, AK 99775-7320 USA)

A program of comprehensive middle and upper atmosphere observation at Poker Flat, Alaska, is being promoted and proceeding by Communications Research Lab. (CRL) of Ministry of Posts and Telecommunications of Japan, in cooperation with Geophysical Institute of Univ. of Alaska Fairbanks (GI/UAF). The comprehensive observation stage starts in 1998-1999, deploying the 16x16 imaging riometer (1995-), an MF radar (Oct. 1998-), two Fabry-Perot interferometers (1998-), two airglow imagers (to be in 1999), and a millimeter-wave radiometer (Jan. 1999-), for ionospheric, neutral dynamics, and chemical observations covering strato-meso-/thermospheric heights. CNA and luminosity images by the imaging riometer and the GI all sky camera (ASC), respectively, with both time resolution of 2 sec are compared for a discrete aurora on 20 March 1996, which suggests that CNA variation shows delay (const. ~10 sec) perhaps causing changes of CNA and ASC arc shapes. CNA data and energy data of the DMSP spacecraft show that the power law does not seem satisfactory for their temporal/spatial correlation. Also CNA and other data such as winds will be compared.

GA2.01/W/03-A1

Invited

0925

**RECENT RESULTS FROM IMAGING RIOMETER MEASUREMENTS COVERING A WIDE LATITUDE AND LONGITUDE RANGE**

Allan WEATHERWAX, Ted Rosenberg (both at Institute for Physical Science and Technology, University of Maryland, College Park, MD 20742-2431 USA, email: allanw@ipst.umd.edu)

The University of Maryland operates imaging riometers in both polar regions for the purpose of studying the spatial and temporal structures of ionospheric disturbances over a wide range of locations from near the plasmapause to the magnetic pole. This presentation will focus on a few topics of recent interest. Included will be a study of the occurrence and nature of short-duration (~ a few minutes), intense (to10 dB) absorption spikes observed around the dusk meridian and near the plasmapause (L ~ 4-5). These events are accompanied by weak ionospheric current flow, as manifested by small variation of the local magnetic field. This suggests that the absorption may be caused by the precipitation of very energetic electrons depositing most of their energy in or below the lower D region. We will also describe the features of very weak (typically < 0.2-0.3 dB) absorption variations observed deep in the polar cap (> 85 degrees magnetic latitude).

GA2.01/E/05-A1

0950

**A PECULIAR FEATURE OF RADIO WAVE ABSORPTION IN THE CUSP-LATITUDE DURING NORTHWARD IMF: A CASE STUDY**

Masanori NISHINO (Solar-Terrestrial Environment Laboratory, Nagoya University, Toyokawa, Aichi, 442-8507, Japan, email: nishino@stelab.nagoya-u.ac.jp); Nozomu Nishitani (Solar-Terrestrial Environment Laboratory, Nagoya University, Toyokawa, Aichi, 442-8507, Japan, email: nishitani@stelab.nagoya-u.ac.jp); Nattuo Sato, Hisao Yamagishi (National Institute of Polar Research, Itabashi-ku, Tokyo 173-8515, Japan, (email: nsato@nipr.ac.jp, yamagishi@nipr.ac.jp); Mark Lester (University of Leicester, University Road, Leicester, LRI 7RH, UK, e-mail: le@ion.le.ac.uk); Jan A Holtet (The University of Oslo, Blindern, Oslo, Norway)

An example of daytime radio wave absorption at 30 MHz observed by the imaging riometer (IRIS) at Ny-Alesund(76.1 invariant latitude), Svalbard in the cusp-latitude is presented. The absorption was observed during about 3.5 hours in the magnetic noon sector on February 28, 1996. The absorption intensity first increased up to 0.6 dB in the prenoon (near 10 MLT) with the increase of the IMF north-south component (Bz), thereafter varied within 0.6 dB intensity during subsequent weak northward and moderate southward IMF. A peculiar feature during the northward IMF is an intensity fluctuation of the absorption observed in the southern part of the IRIS field of view at: The fluctuating absorption showed a 'rectified response' to an abrupt change of the clock angle defined by the IMF north-south and east-west (By) components. The turning of the rectified response is approximately 45 degrees on the clock angle in the northward-dawnward plane. The plasma convection observed simultaneously by the Finnish HF radar showed antisunward drift associated with the abrupt IMF southward excursion, and immediately changed to a sunward drift associated with the subsequent IMF northward return. The magnetic X-component obtained by the ground magnetometer showed positive and negative deflections synchronized with abrupt IMF changes. The particle data from DMSP satellite identified the cusp crossing near Ny-Alesund and represented no precipitation of energetic electrons attributable to the observed absorption. These results indicate that the cusp-latitude absorption observed during the northward IMF is related to E-region electron heating by horizontal electric fields which is driven by the high-latitude magnetic merging at the dayside magnetopause and penetrate into the cusp-ionosphere through the magnetic field lines.

GA2.01/E/08-A1

1005

**DETECTION OF FIELD-ALIGNED CURRENTS AND PARTICLE PRECIPITATION ASSOCIATED WITH SMALL-SCALE HIGH-LATITUDE CONVECTION DISTURBANCES**

P. STAUNING (Solar-Terrestrial Physics Division, Danish Meteorological Institute, Lyngbyvej 100, DK-2100 Copenhagen, Denmark, email: pst@dmu.dk)

Small-scale disturbances like "twin convection vortices", "travelling convection vortices", "ionospheric FTE or PTE signatures", or simply "magnetic impulses" constitute a host of events that link processes in the outer magnetospheric regions to features in the high-latitude ionosphere. These features are observable from ground by radar methods like incoherent scatter radars or HF coherent radars or through the associated magnetic disturbances detectable from the existing array of magnetometer stations. The coupling between the outer

magnetosphere and the high-latitude ionosphere is mainly accomplished through field-aligned current systems which are spatially more localized and temporally more transient than the more steady region 1 and 2 field-aligned currents. Hence they are difficult to detect by space-based observations. However, the combination of the mapping of these transient events from their ionospheric signatures detectable from ground and the high-precision magnetic measurements from Xrsted and other satellites provides a possible tool to resolve such events. In addition to the geomagnetic effects of currents and convection we have investigated the signatures in high-energy electron precipitation and related radiowave absorption features associated with such transient disturbances.

GA2.01/E/03-A1

1040

**OPTICAL AURORAL FORMS AND RIOMETRIC IMAGING**

P. H. STOKER, A. Wilson (Space Science Unit, Potchefstroom University for CHE, Potchefstroom 2520, South Africa, email: fskphs@puknet.puk.ac.za, burt.wilson@za.pwcglobal.com)

Digitized allsky images of auroral optical emissions, recorded by a low light level TV system at the new SANAE 4 antarctic base on Vesleskarvet (71x40'S, 2x51'W, L = 4.1), have been mapped onto the angular sensitivity functions of the 64-beam riometer. The two-dimensional spatial and temporal characteristics of discrete auroral forms and of riometric imagery of cosmic radiowave absorptions are examined and intercompared with better resolution than previously (J. Geophys. Res. 102, 7439, 1997). The tendency is confirmed that cosmic radio noise appears to be more strongly absorbed in regions adjacent to discrete auroral arcs than in the arc regions themselves. Furthermore, temporal changes in absorption appear to be delayed up to tens of seconds relative to changes in luminosity. The significance of these results are explored. The long delay times suggest that the observed differences in spatial and temporal characteristics should be of magnetospheric rather than ionospheric origin.

GA2.01/W/07-A1

1055

**THE MORPHOLOGY OF AURORAL OPTICAL EMISSIONS, RIOMETER ABSORPTION AND RADAR BACKSCATTER: A CASE STUDY**

M. J. KOSCH, E. Nielsen, M. Rietveld, T. Hagfors (Max Planck Institut für Aeronomie, 37191 Katlenburg-Lindau, Germany, email: kosch@linmpi.mpg.de), F. Honary, N. Stamatiou (Communications Research Centre, University of Lancaster, UK)

During the night of 9 November 1998 simultaneous recordings were made in a common field of view of auroral optical emissions by the Digital All-Sky Imager (DASI), riometer absorption patterns by the multi-beam Imaging Riometer for Ionospheric Studies (IRIS), coherent-backscatter by the Scandinavian Twin Auroral Radar Experiment (STARE) and incoherent-backscatter by the European Incoherent SCATter radar facility (EISCAT). In the period 15 - 24 UT there was strong substorm activity with Kp = 5+ - 7- and sigma-Kp = 46 for the day. DASI makes recordings of auroral optical emissions at 557.7 nm, for an assumed height of 100 km, within the area 67.6-72.6 deg. North and 13.5-26.0 deg. East. The images give estimates of the precipitating patterns of soft electrons. IRIS makes recordings of cosmic radio noise absorption at 38.2 MHz, for an assumed height of 90 km, within the area of 67.8-70.2 deg. North and 17.75-23.75 deg. East. The images give estimates of the precipitating patterns of hard electrons. STARE measures the Doppler shift and backscatter intensity at 140 MHz, for an assumed height of 105 km, within the same area as DASI. EISCAT, located at 69.6 deg. North and 19.2 deg. East, can measure various ionospheric parameters such as electron density and temperature and ion velocity and temperature. In this case recordings were made along the local magnetic field line in the altitude range 87-587 km. The interaction of the various parameters will be discussed.

GA2.01/E/01-A1

Invited

1110

**INTERHEMISPHERIC CONJUGACY OF THE AURORAL POLEWARD EXPANSION OBSERVED USING AN IMAGING RIOMETER NETWORK AND HF RADARS**

Hisao YAMAGISHI (National Institute of Polar Research, Kaga 1 chome, Itabashi-ku, Tokyo 173-8515, Japan, email: yamagishi@nipr.ac.jp); Peter Stauning (Danish Meteorological Institute, Lyngbyvej 100, DK-2100 Copenhagen O, Denmark, email: pst@dmu.min.dk); Masanori Nishino (Solar Terrestrial Environment Laboratory, Nagoya University, 3-13, Honohara, Toyokawa 442-8507, Japan, email: nishino@stelab.nagoya-u.ac.jp); Liu Ruiyuan (Polar Research Institute of China, 451 Shangchuan road, Pudong, Shanghai 200129, China, email: uap@mail.pric.cn)

Auroral poleward expansion is a strong manifestation of the substorm expansion phase, and it can be observed by a riometer network as multiple-step progress of the absorption region into the polar cap (Stauning, 1995). Interhemispheric conjugacy of this phenomena was studied with a network of imaging riometers from east Greenland to Svalbard and in their conjugate region in Antarctica. We have analyzed the data from Danmarkshavn in East Greenland, Ny-Alesund and Longyearbyen in Svalbard, and Chinese Zhongshan Station in antarctica in the period of 1997-1998. For the poleward expanding CNA events observed in the northern hemisphere, more than half of them were observed simultaneously at Zhongshan Station. Local time dependence of the conjugate point latitude is discussed, making use of the longitudinal extent of the network. Poleward expansion sometimes show easterly, or westerly deflection as observed by the imaging riometers, and this feature is discussed in connection with the IMF By variations. The area of this imaging riometer network is covered by SuperDARN HF radars. The radar echo usually disappears when the poleward expansion takes place due to enhanced D-region absorption and/or reflection of the transmitted signal by sporadic auroral E-region. It is therefore difficult to know the electric field inside the poleward expansion from the radar data. However, the area of the echo disappearance can tell about the spatial extent of the absorption region, and this is directly compared with the absorption observed by the riometers.

GA2.01/W/06-A1

1135

**A COMPARISON OF RIOMETER AND HF RADAR RESPONSES TO SUBSTORM-ASSOCIATED ENHANCED PARTICLE PRECIPITATION**

Jonathan K. GAULD, T.K. Yeoman (Department of Physics and Astronomy, Leicester University, Leicester. LE1 7RH, UK); F.Honary (Lancaster Communications Research Centre, Engineering Department, Lancaster University, Lancaster, LA1 4YR, UK)

The common occurrence of an HF radar signal loss during strong auroral precipitation at the substorm expansion phase onset is examined, using radar data from the CUTLASS SuperDARN HF radar, and supported by riometer data from IRIS at Kilpisjärvi, within the CUTLASS field of view. The mechanism or mechanisms which could cause a radar signal loss are analysed from a theoretical standpoint, employing ray tracing techniques, and in relation to radar elevation angle data measured by the interferometer array, which has then been used as a constraint in producing models of the radar propagation. The implications of the results for both the electrodynamics of the ionosphere-magnetosphere system during the substorm

expansion phase and for radar operational constraints during this key dynamical process are discussed.

**GA2.01/W/01-A1 1150**

**THE TEMPORAL FINE STRUCTURE OF NIGHT-TIME AURORAL ABSORPTION INVESTIGATED BY A WAVLET METHOD**

Aarne RANTA (Sodankylä Geophysical Observatory, 99600 Sodankylä, Finland, email: Aarne.Ranta@sgo.fi); John K. Hargreaves (Engineering Department, University of Lancaster, Lancaster LA1 4YR, UK, email: j.hargreaves@lancaster.ac.uk); James D. Annan (Proudman Oceanographic Laboratory, Bidston Observatory, Birkenhead L43 7RA, UK, email: jdan@mail.nerc-bidston)

The onset of a substorm is often characterised by a burst of Pi2 magnetic pulsations. Another common feature is the occurrence of a short-duration spike event in auroral absorption monitored using a riometer. A wavelet approach, which can identify how the various periodicities develop during the event, has been applied to absorption spikes in the night sector, using observations from the imaging riometer at Kilpisjärvi (L=5.9) at 1 second resolution. It is found that the spike events, though only lasting for about 2 minutes, often show a fine structure with periodicity in the range 20-40 seconds. Some events are compared with the magnetic pulsations observed simultaneously at the same site.

**GA2.01/E/11-A1 1205**

**STUDY OF SUBSTORM ACTIVITY FROM COMBINED IRIS, EISCAT AND DASI OBSERVATIONS**

C.F. DEL POZO, F. Honary, N. Stamatiou (Ionosphere and Radio Propagation, Communications Res. Centre, Lancaster University, UK); M. Kosch (Max-Planck Institute für Aeronomie, Katlenburg-Lindau, Germany)

A number of simultaneous observations of substorm activity by the IRIS, EISCAT, and DASI systems is presented. The spatial extent and structure, as well as the temporal evolution of the localised 2-D absorption signatures, and their correspondence with digital all-sky optical measurements, during the various phases of substorm activity are discussed. EISCAT observations provide high-resolution time-series and altitude profiles of the various physical parameters defining the state of the ionosphere above Tromsø (electron density, electron and ion temperatures, electric field, etc.) and allow the estimation of the electron precipitation spectrum as well as the height and width of the absorption layer. These features are studied from the point of view of the precipitation spectrum in the 1 to 400 keV energy range and the related phenomena in the D and E regions. The systematic analysis of the concurrency of auroral absorption and optical signatures allows the characterisation of cases when soft and hard precipitation may correspond to either the same or two different populations. The differential time of arrival between the higher and lower energy components of the precipitation at the late growth and onset phases is also studied.

**GA2.01/E/12-A1 1220**

**SIMULTANEOUS IRIS/EISCAT OBSERVATIONS OF CME EVENT ON 10 JANUARY 1997**

C.F. DEL POZO, F. Honary, H. Tao (Ionosphere and Radio Propagation, Communications Res. Centre, Lancaster University, UK); I. McCrea (EISCAT group, Rutherford Appleton Laboratory, Didcot, UK)

Simultaneous observations of the Coronal Mass Ejection event on 10 January 1997 by the IRIS and EISCAT systems are presented. The effects of this event on the lower ionosphere are investigated, namely the spatial extent and dynamics of the absorption patches, the changes in altitude and width of the absorption layer, and the evolution of the electron precipitation spectrum. These features are correlated and contrasted with the observations by a number of satellites at various locations in the interplanetary medium, the tail and inner magnetosphere.

This CME event was relatively weak with very low proton fluxes at energies > 1.6 MeV measured by the satellites. The flux of energetic electrons with energies greater than 400 keV measured by a number of geostationary and GPS satellites was also weak. The corresponding series of electron injections are clearly seen in the IRIS and EISCAT data. In particular those at 04:40 UT and 07:00 UT and subsequent injections over the period with IMF Bz < 0 associated with the first pressure pulse at ~ 01:00 UT, but not the enhancement fluxes near 11:00 UT reported by the satellites. EISCAT measurements show that the precipitation fluxes are generally too low to produce ionisation above the radar sensitivity level (> 5.109 el/m<sup>3</sup>). Only between 04:00 UT and 10:00 UT ionisation reach low enough to produce absorption in a narrow layer with variable height above 75 km, for precipitating electrons with energies smaller than 400 keV. Maximum absorption occurs around 04:40 UT and 07:00 UT, the precipitation spectrum normally extends up to 150 keV with the exception of a 30 min hardening at about 07:00 UT (up to 350 keV).

**Monday 19 July PM**

Presiding Chair: Peter Stauning (Danish Meteorological Institute, Copenhagen, Denmark)

**GA2.01/W/09-A1 1400**

**GUISDAP - PART OF THE EISCAT SVALBARD RADAR SOFTWARE PACKAGE**

Markku LEHTINEN, Juha Pirttilä (both at Sodankylä Geophysical Observatory, 99600 Sodankylä, Finland, email: markku.lehtinen@sgo.fi, juha.pirttila@sgo.fi); Asko Huuskonen (Finnish Meteorological Institute, 00100 Helsinki, Finland, email: asko.huuskonen@fmi.fi); Pekka HIITOLA (Department of Physical Sciences, Oulu University, 90570 Oulu, Finland Email: Pekka.Hiitola@oulu.fi)

In 1986 was first GUISDAP (Grand Unified Incoherent Scatter Radar Data Analysis Package ver 1.0) demonstration in EISCAT Workshop in Sweden. After that some new version of GUISDAP were launched, but all of those were based purely on MATLAB scripts so-called m-files. In 1995 Finnish GUISDAP group started to create next generation GUISDAP program. First step was assess weaknesses of old version and after define new one. All time-consuming parts of GUISDAP had to be translate into C++ and other parts keep in same or almost same than into old versions. This programming period takes about three years. And nowadays EISCAT community has a new generation data analysis package. This talk compare some old data analysis programs and GUISDAP 2 and show some reasons of those differences.

**GA2.01/W/04-A1 Invited 1415**

**EISCAT OBSERVATIONS AND IMPLICATIONS CONCERNING MINOR SPECIES**

Martin FRIEDRICH (Department of Communications and Wave Propagation, Technical University Graz, A-8010 Graz, Austria, e-mail: friedrich@inw.tu-graz.ac.at)

The ionosphere at auroral latitudes has been monitored for more than a solar cycle by the European incoherent scatter radar EISCAT; this instrument has probably yielded more data on electron density from one location than any other instrument. In addition there were about 100 rocket soundings from near the location of the EISCAT measurements which provide extensions to lower densities and altitudes. This impressive body of data allows to study the behaviour of the ionosphere not only for disturbed conditions - which are really "normal" at these latitudes - but also for undisturbed situations which are thus comparable to the conditions prevailing outside the auroral zone. The combined database will be used to investigate the solar controlled behaviour, the impact of solar activity and season, but also to study these variations at times of disturbances, primarily expressed in terms of locally measured riometer absorption. Tests will be presented in which the observed riometer values are contrasted to corresponding simulations. Of the neutral minor species which have a bearing on the lower ionosphere, nitric oxide and atomic oxygen are the most prominent. "Reasonable" limiting values will be derived for these species based on suitably averaged undisturbed electron density profiles. Finally an attempt will be shown in which the effective electron recombination rate from empirical data will be contrasted to theory.

**GA2.01/E/06-A1 Invited 1440**

**ELECTRON DENSITY VARIATIONS IN THE POLAR D REGION FROM IN SITU MEASUREMENTS**

A.D. DANILOV (Institute of Applied Geophysics, Rostokinskaya 9, Moscow 129 128, Russia, email: hciag@sunny.aha.ru)

A dataset of more than 500 in situ (probe method) measurements of the electron concentration in the D region on board M100B meteorological rockets at Heiss Island (Arctic) and Molodzhnaya station (Antarctic) is considered. Dependencies on season, solar zenith angle and magnetic activity are studied. Some asymmetry of the hemispheres is found. It is shown that the electron concentration behavior at Heiss Island depends on whether the station is in the sub-auroral zone, auroral oval or polar cap.

**GA2.01/W/10-A1 1505**

**RAPID CHANGES IN BACKSCATTER RANGE IN QUIET MAGNETIC CONDITIONS**

Erhard MRAVLAG (Space Physics Research Institute, University of Natal, Durban 4041, South Africa, email: mravlag@scifs1.und.ac.za)

Extremely rapid changes in backscatter range have been observed at the SHARE radar at SANAE. These changes usually tend to follow the pattern of diurnal changes in backscatter range, ie. usually away from the radar site in the morning and towards the radar site in the evening. This is not always true, however. The changes generally occur in magnetically quiet conditions, with |B| < 10nT and B\_z small. Similar patterns were seen in the data recorded at Halley.

**GA2.01/E/09-A1 Invited 1540**

**THE POTENTIAL OF COMBINED INCOHERENT SCATTER RADAR, MST RADAR AND IMAGING RIOMETER OBSERVATIONS ON SVALBARD**

Juergen ROETTGER (Max-Planck-Institut fuer Aeronomie, D-37191 Katlenburg-Lindau, Germany, email: roettger@limpi.mpg.de)

The middle atmosphere in high latitudes is the merging region of forcing from below and above. Gravity waves, created in the troposphere propagate to mesospheric altitudes, where they deposit energy and momentum. Electric fields and particles penetrate into the lower thermosphere and mesosphere, where they significantly influence the ionization structure. The combination of the EISCAT Svalbard Radar (ESR), the SOUSY-Svalbard-Radar (SSR) and the Imaging Riometer System (IRIS), all collocated near Longyearbyen, can excellently be used to study this merging region. Polar Mesosphere Summer Echoes (PMSE), detected with the SSR MST radar, are phenomena which reflect ionization structures, gravity waves and turbulence. The PMSE, thus, are most proper tracers of some dominant phenomena occurring in the merging region. We will discuss the potential of studies of PMSE, detected by the SSR, combined with observations of electron density profiles (and conceivably PMSE) measured with the ESR. The horizontal structure of ionization content, measured with IRIS, should be compared with the occurrence and structure of PMSE. Such combined studies will be exclusively valuable in the magnetospheric cusp region, which is passing over Svalbard. The orography of the Svalbard archipelago comprises an effective source region of mountain waves, which can propagate into the middle atmosphere. Their effect on mesosphere dynamics can be studied with PMSE observations. Finally we will debate the plausibility whether PMSE and their environment could affect the ionization structure measured with the ESR and IRIS.

**GA2.01/W/11-A1 Invited 1605**

**VARIATIONS OF MESOSPHERIC ION AND NEUTRAL COMPOSITION AS DEDUCED FROM IMAGING RIOMETER DATA**

ESA TURUNEN, Thomas Ulich Sodankylä Geophysical Observatory, Tahtelantie 112, FIN-99600 Sodankylä, Finland; Pekka Verronen, Erkki Kyrola, Finnish Meteorological Institute, Geophysical Research, PO Box 503, FIN-00101 Helsinki, Finland

Using recent detailed ion chemistry models it is in principle possible to estimate the effect of precipitating high energy particles on the ion and neutral composition, if the spectrum of the precipitating particles is known. However, in practice the variations in concentrations of the constituents are not only determined by local processes, but to a large extent also governed by horizontal transport. Since imaging riometers can map both spatial and temporal variations of the ionization produced by precipitating particles, we would expect this data to be extremely useful as constraints in model studies of the effects of precipitation. An attempt is made to combine a detailed ion chemistry model, with coupled neutral chemistry, and data provided by imaging riometer, in order to study the spatial effects of local ionization enhancements.

**GA2.01/W/08-A1 Invited 1640**

**ELECTRICAL EFFECTS ON THE MESOSPHERE AND LOWER IONOSPHERE FROM THUNDERSTORMS**

Prof. Robert H.HOLZWORTH (University of Washington, USA)

The effects on the ionosphere and magnetosphere caused by ordinary cloud-to-ground (CG) lightning include conductivity enhancement, heating and plasma wave stimulation. These effects, have been observed directly from rockets and satellites in the mesosphere and ionosphere, give us a statistical picture of the electromagnetic energy input to the ionosphere



which is significant up to 2000 km from the point of the lightning. Individual case studies of CG and now even IC (intracloud) lightning provide evidence that orientation and dynamics of the lightning events within the clouds can have significant control over the resulting ionospheric waveform of the lightning pulse. Direct lightning related phenomena such as Red Sprites can also have a dramatic electromagnetic effect on the mesosphere and ionosphere. In this talk I will review the recent research on lightning, thunderstorms and related high altitude phenomena such as red sprites, as they affect the mesosphere and lower ionosphere.

**GA2.01/W/05-A1 1705**

**THE APPLICATION OF IMAGING RIOMETERS FOR DETECTION OF THIN METALLIC-ION LAYERS**

B.J. WATKINS (Geophysical Institute, University of Alaska Fairbanks D.F.Bede US Military Academy, West Point, NY, USA); T.J. Rosenberg, A.T. Weatherwax (University of Maryland at College Park, USA); P. Stauning (Danish Meteorological Institute, Copenhagen, Denmark)

The incoherent-scatter radar at Sondrestrom, Greenland has been used to study the morphology and occurrence of thin metallic-ion layers that occur in the lower ionosphere at altitudes from about 90 to 110km; these result from the accumulation of metals from meteor ablation. The structures are frequently limited in spatial extent and move horizontally in response to electric fields and neutral winds. We report on efforts to use the co-located imaging riometer at the radar site to detect the presence, spatial extent, and motion of metallic-ion layers. The levels of cosmic noise absorption are typically about 0.1 dB and therefore the detection of these structures is limited to geomagnetically quiet periods in the absence of auroral ionospheric structures. Imaging riometer data, in conjunction with a number of radar-observed layer events, will be presented.

Monday 19 July AM

**GA2.01/W/02-A1 Poster 0900-01**

**ARTIFICIAL PERIODIC INHOMOGENEITIES AND A MODEL OF THE D-REGION**

V.V. BELIKOVICH, E.A. Benediktov, V.N. Bubukina, V.D. Vyakhirev (Radiophysical Research Institute, Nizhny Novgorod, Russia, email: belik@nirfi.sci-nnov.ru)

New studies of the D-region using API technique were carried out by means of SURA heating facility (56.13 N, 46.1E) in August 1996. The heating of the ionosphere was conducted by extraordinary mode with a frequency of 4.7 MHz and effective radiated power 60-100 MW beamed vertically upwards during 3 s followed by off period of 12 s. In pause the impulses having duration of 20 mks and a repetition frequency of 40 Hz were radiated. The quadratures of the scattered signals were recorded with a height resolution of 1.2 km and were encoded by 10-digit analogue-digital converter. The height dependencies of the relaxation time and the amplitude of the scattered signal are obtained. They are compared with the model of the API formation. The once are constructed on the basis of the balance of ionization using one negative ion model. The diffusion redistribution of plasma is slower at the D-region heights and more quick processes as attachment and detachment of electrons dominate. The main physical cause of API formation at the D-region heights is the temperature dependence of the rate of the electron attachment to the oxygen molecules in three bodies collisions. The model is in agreement with factual data well. Our studies show that the model profiles of the API amplitude and the relaxation time are sensitive to atmospheric density and to the atomic oxygen concentration. It seems upper boundary of the API in the D-region to depend on increase of the atomic oxygen concentration and can be an indicator of this process. It is a new method of the middle atmosphere study. The work is supported by RFBR-DFG under grant 96-05-00074.

**GA2.01/E/13-A1 Poster 0900-02**

**HIGH-ENERGY ELECTRON PRECIPITATION AND FIELD-ALIGNED CURRENTS IN THE CUSP REGION MEASURED FROM XRSTED SATELLITE AND CORRELATED GROUND-BASED OBSERVATIONS OF IONOSPHERIC CONVECTION AND ABSORPTION**

TINA CHRISTENSEN, Peter Stauning, Freddy Christiansen, Torsten Neubert, Vladimir Papitashvili, Jian-Guo Wu (all at Danish Meteorological Institute, Lyngbyvej 100, DK-2100, Copenhagen, Denmark, email: tic@dmi.dk)

The cusp region located at approximately 77-80 degrees invariant latitude close to local noon at the dayside of the polar cap is threaded by field-aligned currents arising from interactions of the solar wind with the outermost reaches of the Earth's magnetosphere. The field-aligned current systems can be detected through high-precision geomagnetic measurements from the Xrsted satellite. These currents affect the high-latitude ionospheric convection, which may be defined from ground magnetometer array observations augmented by incoherent scatter radar measurements. The cusp region also marks the high-latitude boundary of the high-energy electron precipitation from the trapped radiation population in the inner magnetosphere. The Xrsted charged particle (CPD) electron precipitation, while the effects of the precipitation into the upper atmosphere are detectable from ground through radio wave absorption measurements (e.g., by imaging riometers). This presentation will focus on the correlation of satellite-based and ground-based detection of current systems and high-energy electron precipitation in the cusp region. Particular attention will be given to the detection of the relative location of the field-aligned currents with respect to the boundaries of the trapped and precipitated radiation in vicinity of the cusp/cleft region.

**GA2.01/E/04-A1 Poster 0900-03**

**QUIET DAY CURVES RECORDED WITH 46 AND 64 ANTENNAE IN A 64-BEAM IMAGING RIOMETER ARRAY**

A. WILSON, P. H. Stoker (Space Science Unit, Potchefstroom University for CHE, Potchefstroom 2520, South Africa, email: burt.wilson@za.pwglobal.com, fskphs@puknet.puk.ac.za)

Since April 1997, a 64-beam 38.2 MHz imaging riometer has been in operation at SANAE 4. To test the operation of the riometer a 408 MHz continuum map of the radio sky brightness (Haslam et al. 1982) was digitized and was convolved with the directivity of the eight beams in a central north-south row of the riometer antenna array. These estimated diurnal variabilities are compared with the quiet day curves (QDC's) obtained from cosmic radio noise recordings by the eight beams concerned.

After functioning for several months a severe storm damaged 18 of the 64 crossed dipole antennae. The damaged antennae were removed from the array and their inputs were terminated at the Butler matrix, resulting in a change in the angular sensitivities of the 64 beams. The peaks of the 64 QDC's of the array operating with 46 antennae appeared to be a

little flatter than those recorded by the original array of 64 antennae, indicating an increase by several degrees of the -3 dB beam width of 13x of the near vertical beams. Furthermore, the signals strengths recorded in the directions of the 64 beams were reduced by about 46/64.

**GA2.01/E/02-A1 Poster 0900-04**

**DAYTIME RIOMETRIC ABSORPTIONS DURING GEOMAGNETICALLY QUIET PERIODS**

WILSON, P. H. Stoker (Space Science Unit, Potchefstroom University for CHE, Potchefstroom 2520, South Africa, email: burt.wilson@za.pwglobal.com, fskphs@puknet.puk.ac.za)

On 16 May, 1997 from 1400 - 1630 UT and on 12 September, 1997 from 1200-1530 UT absorptions with maxima of about 1 dB have been observed by the 64 beam imaging riometer at SANAE 4 (71x40'S, 2x51'W, L = 4.1). Kp was around 2 for most of both days and increased to, respectively, 4- and 3x during the events. At SANAE 4 the local K-indices did not show any increase during the events from the low values of these days. The Bz component of the interplanetary magnetic field turned negative shortly before the start of these absorptions and returned positive again by the end of the absorptions. The solar wind velocities were moderate. The latitude angles of the flows were at zero degrees during the events, and at positive angles before and after. The geomagnetic field was active during the days preceding these events. Electrons trapped in the magnetosphere may have been accelerated to relativistic energies during preceding days. This is supported by the increases in intensity of several orders in magnitude of electrons with energy greater than 2 MeV as recorded by the GEOS geostationary satellite. Presumably these electrons were precipitated at SANAE 4 when Bz turned negative, expedited by SANAE 4's location at the southern edge of the South Atlantic Radiation Anomaly.

**GA2.07 Monday 19 – Tuesday 20 July**

**IONOSPHERIC IMPACT ON MAGNETOSPHERIC-IONOSPHERIC (M-I) COUPLING (WITH DIV. 2 AND 3)**

Location: Gisbert Kapp E203 LT1  
Location of Posters: Gisbert Kapp, Coffee Room

Monday 19 July AM

Presiding Chairs: J.J.Sojka, Utah State University (USA)  
A. Yau, University of Calgary Department of Physics and Astronomy (USA)

**Introduction 0830**

**GA2.07/W/28-A1 Invited 0830**

**OBSERVATIONS OF IONOSPHERIC ION OUTFLOWS AND CAUSAL PHENOMENA IN THE LOW-ALTITUDE CUSP/CLEFT BY POLAR**

M. Hirahara (Dept. Physics, Rikkyo Univ., Toshima-ku, Tokyo 171-8501, Japan, E-mail: hirahara@se.rikkyo.ac.jp), J. L. Horwitz (CSPAR, UAH, Huntsville, AL 35899, USA, E-mail: horwitzj@cspar.uah.edu), T. E. Moore (Interplanetary Physics Branch Laboratory for Extraterrestrial Physics, NASA-GSFC, Greenbelt, MD 20771, USA, E-mail: Thomas.E.Moore@GSFC.NASA.gov), J. S. Pickett, A. M. Persoon, D. A. Gurnett, C. A. Kletzing, and J. D. Scudder (all at Dept. of Physics and Astronomy, Univ. of Iowa, Iowa City, IA 52242, USA, E-mail: pickett@iowave.physics.uiowa.edu; persoon@iowave.physics.uiowa.edu; gurnett@iowave.physics.uiowa.edu; cak@space-theory.physics.uiowa.edu; email: jds@space-theory.physics.uiowa.edu), X. Liu and C. T. Russell (both at IGPP, UCLA, Los Angeles, CA 90024-1567, USA, E-mail: xliu@igpp.ucla.edu; crussell@igpp.ucla.edu)

Characteristics of upflowing ionospheric ions (UFIs), plasma waves, precipitating solar wind components, and field-aligned currents (FACs) in the cusp/cleft at low altitudes are presented on the basis of the observational results by the thermal ion dynamics experiment (TIDE), the multichannel analyzer of the plasma wave instrument (PWI-MCA), the charged particle instrument (Hydra), and the magnetic field experiment (MFE) on board the POLAR satellite. We mainly focus on cusp/cleft conics and the other crucial phenomena causing transverse ion acceleration (TIA) in the topside ionosphere. Energy and pitch angle distributions of the conics observed by TIDE and their spatial distributions show that the TIA is a dominant process in the cusp/cleft to effectively supply ionospheric ions into the polar magnetosphere. Some of these outflowing ionospheric ions could be observed in the magnetotail after further acceleration, which we reported as cold ion flows observed in the lobe/mantle regions by the Geotail spacecraft. The energies and cone angles of the conics and their variations are different between H+ and O+. Namely, the energies and cone angles of O+ are generally larger than those of H+, and their latitudinal variations are slower for O+ than for H+. These features imply that acceleration rates of the ionospheric ions would be dependent on locations (altitude and latitude) and that they could be different between H+ and O+. It is also likely that the convection effect appears differently in fast H+ and slow O+ ions. Comparisons with the observational results by PWI, Hydra, and MFE support these ideas and bring further insights: The spatial distribution of the TIA in the cusp/cleft is latitudinally wide (>1 deg.); small-scale intense FACs are embedded in the larger-scale FAC system typically seen in the cusp/cleft and accompanied by broadband electrostatic plasma waves at low frequencies close to gyrofrequencies of H+ and O+ in the 5300-km altitude cusp/cleft. It is also noteworthy that multiple TIA regions are repeatedly observed during some of the cusp/cleft crossings and also well correlated with repetitive appearances of the plasma wave enhancements and the small-scale FACs.

**GA2.07/W/16-A1 Invited 0855**

**IONOSPHERIC OUTFLOW AS A LOAD IN MAGNETOSPHERIC ENERGY TRANSFER PROCESSES**

R. Lundin, Swedish Institute of Space Physics, Kiruna, Sweden

The outflow of ionospheric plasma is a direct consequence of the solar wind interaction with the terrestrial magnetosphere. However, unlike the direct solar wind interaction with the ionosphere for the planet Mars, the interaction with the Earth is indirect and coupled to the magnetospheric boundary layers and the magnetotail by field-aligned currents. The intrinsic magnetic field of the Earth serves as a guidance for the currents/charged particles as well as the waves, feeding energy into and heating the ionospheric plasma, subsequently leading to escape. The escape regions may therefore be rather localized, confined to small-scale or large-scale depletion regions.

The outflow, or excavation, of the ionospheric plasma occurs predominantly over the auroral region, but extends also into the polar cap. During large magnetospheric disturbances this erosion may also extend to subauroral latitudes.



It will be argued here that the heating/acceleration of ionospheric plasma, and the corresponding outflow, may be considered a loading of field-aligned and transverse currents in the ionosphere in such a way that plasma escape occurs for both upward and downward currents. The most efficient heating/acceleration appears to occur inside density cavities, effectively replenishing plasma at the edges of the cavities.

EISCAT radar and approximately 80 % events are associated with either increased ion or electron temperatures. Thereby it is the strictly reason to believe that the auroral thermal wave is an important source of the upflows auroral beams in the ionospheric F-region.

**GA2.07/W/13-A1 0920**

**THERMAL ION HEATING AND OUTFLOW OBSERVED BY AKEBONO SATELLITE BETWEEN 1989 AND 1999**

Shigeto Watanabe and M. Yamada (Department of Earth and Planetary Science, Hokkaido University, Sapporo, Japan, Email: shw@pspace.sci.hokudai.ac.jp) T. Abe (The Institute of Space and Astronautical Sciences, Sagami-hara, Japan) E. Sagawa (Communications Research Laboratory, Koganei, Japan) A.W. Yau (University of Calgary, Calgary, Canada)

The data obtained by the suprathermal ion mass spectrometer (SMS) on Akebono during 10 years were analyzed to investigate the spatial and temporal distributions and the physical processes of thermal ion heating and outflow in the topside polar ionosphere. Akebono was launched on February 1989 from Kagoshima space center of the Institute of Space and Astronautical Science and continues to observe the polar ionosphere. An escape of polar ionospheric ions is important to a loss process of the earth's atmosphere as well as a source of magnetospheric plasma. The escape rate of 5-50 tons/day was already estimated on the basis of rocket and satellite observations. The data showed the ion outflow, transverse ion energization (TIE), and ion conics at altitude below 10000km. The energy and pitch angle distributions of conics and their spatial variations verified that the TIE is a dominant process in the cusp/cleft to effectively supply ionospheric ions into the magnetosphere. The TIE occurred near the polar cap boundary and correlated with both low frequency wave activity and upward field aligned currents in the cusp/cleft region.

**GA2.07/W/11-A1 0940**

**AN INVESTIGATION OF THE IONOSPHERIC CONTRIBUTION TO MAGNETOSPHERIC PLASMA USING THE AKEBONO SUPRATHERMAL MASS SPECTROMETER (SMS) DATA SET: FIRST RESULTS**

Donovan, E. F., G. G. Arkos, A. W. Yau, and C. M. Cully

The importance of the ionosphere as a source of magnetospheric plasma (relative to the solar wind) has become evident in recent studies. The Suprathermal Mass Spectrometer (SMS) has been in continuous operation onboard the Akebono (EXOS-D) spacecraft since 1989. It regularly measures the distribution functions of H<sup>+</sup>, He<sup>+</sup> and O<sup>+</sup> ions in the satellite spin plane, at altitudes between one and two Earth radii above the auroral and polar ionosphere. This data has been used in studies of ion outflow, ion heating and the polar wind and is well suited for a comprehensive study of the ionospheric contribution to magnetospheric plasma. As a first step in this study, we have implemented a model of ion motion in the electric and magnetic fields in the Earth's magnetosphere. The field model is a combination of the IGRF and Tsyanenko (1987, 1989) magnetic field models and the Weimer electric potential model (Weimer, GRL, 1986). Particle trajectories are calculated by considering the guiding center drift in the direction perpendicular to the magnetic field and solving the equation of motion in the noninertial reference frame parallel to the magnetic field as described in Northrop (1963). In this paper, we outline aspects of the SMS data set relevant to this study. As well, we use information from distribution functions obtained by the instrument as initial conditions for particle trajectory tracings in the model fields. Finally, we discuss the results of these tracings with regard to the ionospheric contribution of ions to the magnetotail plasma.

**GA2.07/W/14-A1 1000**

**ON A MECHANISM OF CONTROL OF SMALL SCALE AURORAL ACCELERATION BY IONOSPHERIC CONDUCTIVITY**

E. V. MISHIN (Max-Planck-Institut für Aeronomie, e-mail: mishin@linmpi.mpg.de)

Satellite and ground observations of auroral acceleration events, including auroral displays, particle acceleration, and accompanied electromagnetic phenomena, have revealed the significant seasonal and local time variation. This points out the dependence of the acceleration mechanism(s) upon the ambient ionospheric conductivity in that most intense acceleration events favor low ambient conductivity. These results are probably the most convincing arguments in favor of an active role that the ionosphere plays in magnetospheric-ionospheric coupling.

Mishin and Banaszekiewicz [GRL, 25, 4309, 1998] have addressed the statistical results from Freja and Viking on the preference for the midnight to early morning period of the diverging electric field shocks, upward electron beams, and O<sup>+</sup> conics in terms of the stratification instability of the plasma convection. Its development is favored by low ambient conductivity. In the region of downward Birkeland current and mainly equatorward convection electric field, this instability results in formation of diverging electric field shocks and average downward parallel electric field. In the present work, it is taken into consideration that in the region of upward Birkeland current and mainly poleward convection electric field generation of converging electric field shocks and upward parallel electric field is favored. Therefore, the statistical results on downward electron acceleration and upward ion acceleration can qualitatively be understood in terms of the convection stratification instability.

**GA2.07/W/22-A1 1020**

**AURORAL THERMAL WAVE AS A SOURCE OF AURORAL ION UPFLOWS IN THE IONOSPHERIC F-REGION**

G. O. ZHIZHKO, V.G. Vlasov (both at Department of Mathematics, Irkutsk State Technical University, Lermontov 83, Irkutsk, 664074, Russia, e-mail: zhizhko@math.istu.irk.ru)

An auroral thermal wave is the phenomenon results from the collective interaction of the auroral electron beams with the F-region ionospheric plasma. The auroral electron beams, which is a course of the auroral arcs, are stabilized by the large-scale inhomogeneity of the plasma density at their path from the acceleration region up to the E-region of the ionosphere. The collective dissipation of the electron beam energy is possible only in the area of the small plasma density gradients in the F2-region maximum. Because of the electron beam energy is dissipated at the area with the small spatial size ( $\sim 10-100$  km), there are intensive plasma heating in this area (electron and ion temperature can reach 8000 K and 6000 K correspondingly). This heating results in ion upflows with the velocity around 1000 cm s<sup>-1</sup> and density  $10^{14}$  cm<sup>-2</sup> s<sup>-1</sup>. The similar flows are repeatedly observed by the

**GA2.07/W/25-A1 1100**

**INTERACTION OF THE DYNAMIC IONOSPHERE WITH ALFVÉN WAVES**

ROBERT L. LYSACK and Yan Song, (University of Minnesota, 116 Church Street SE, Minneapolis, MN 55455, USA)

The field-aligned currents and the resulting precipitation associated with the propagation of shear Alfvén waves can produce narrow-scale structuring of the ionospheric conductivity and the production of secondary Alfvén waves at the conductivity gradients. These interactions can give rise to a positive feedback interaction, leading to strong, localized enhancement of the ionospheric conductivity. This feedback interaction is particularly effective when coupled with the dynamics of Alfvén waves above the ionosphere, where the sharp gradient of the Alfvén speed gives rise to a resonant cavity with frequencies in the 1 Hz range. The development of this conductivity and current structure may play an important role in the coupling of the ionosphere and magnetosphere, particularly during magnetospheric substorms, and can lead to the formation of narrow-scale auroral arcs. Numerical simulation of the dynamics of this feedback interaction will be presented.

**GA2.07/W/12-A1 1120**

**MAGNETOSPHERE-IONOSPHERE STRUCTURING CAUSED BY IONOSPHERIC ALFVÉN WAVE GENERATION**

J. J. Sojka and L. Zhu Center for Atmospheric and Space Sciences Utah State University Logan, UT 84322-4405

The conventional methods of carrying out M-I coupling are often no more than simple cases of a magnetospheric system driving an ionosphere load. Often even the load, the integrated Hall and Pedersen conductivity, is held fixed. However, even in the case where the Hall and Pedersen conductivities change at each time step, the M-I scheme still does not include the complete physics of M-I coupling. When an ionospheric conductivity changes in time, an "Alfvén wave" is generated. Such an Alfvén wave would exist in the presence of magnetospheric Alfvén waves as well as its reflected Alfvén wave from the ionospheric load. It is the Alfvén wave being generated in the ionosphere, along with the reflected Alfvén waves, that we argue are responsible for auroral structuring and even possibly the orientation of large scale features such as the Harang discontinuity. The M-I coupling MHD modelling work of Zhu et al. for both polar cap and auroral arcs is presented to highlight the significant role played by the ionosphere in M-I coupling. Emphasis is placed on the conditions under which an unstructured magnetospheric source reads to highly structured ionospheric auroral forms. The characteristic scales of these forms are shown to be commensurate with observed scale sizes of large scale auroral arcs. Observations from both ground and satellite instrumentation are presented in support of our suggestion.

**GA2.07/W/07-A1 1140**

**FRAYING OF THE IONOSPHERIC RESPONSE OF A FLUX TRANSFER EVENT DUE TO CONDUCTIVITY STRUCTURES**

HANS NILSSON (Swedish Institute of Space Physics, Box 812, 981 28 Kiruna, Sweden, email: hans.nilsson@irf.se); Alan Rodger (British Antarctic Survey, High Cross, Madingley Road, Cambridge CB3 0ET, UK, email: A.Rodger@bas.ac.uk)

The time constant of the inductive circuit coupling the source at the magnetopause to the load (the ionosphere) is to first approximation only dependent on the distance between source and load and the Pedersen conductance of the ionosphere. In the cusp region, the field line geometry is relatively simple and the connection between source and load very direct. The aim of this talk is to examine to what extent conductivity structures (pre-existing or caused by spatial variations in the cusp particle precipitation) will affect the ionospheric (and therefore also magnetospheric) response to a flux transfer event.

If separate field-aligned currents are set up feeding energy into regions with different conductance, these regions will respond differently. Regions with low conductance will respond fast whereas regions with high conductance will respond slower. If the response is slow, the inductive circuit will seldom be in steady state, the rotation of the electric field inside the current loop connecting the source with the load will be non-zero and consequently there will be a slippage of the magnetospheric field lines. This will cause a fraying of the response to a flux transfer event, with different flows and different magnetopause mapping for different regions in the ionosphere. An alternative scenario is that instead of field-aligned currents setting up on the borders of conductivity structures a polarization charge build-up will keep the Pedersen current constant. The result is still a slower response to a flux transfer event in a region with higher conductance.

Furthermore, the non-zero curl of the electric field resulting from the long ionospheric response time may explain a number of "meso-scale" phenomena observed by satellites such as overlapping magnetosheath injections.

**GA2.07/E/05-A1 1200**

**HF POWERFUL WAVE IMPACT ON MAGNETOSPHERIC-IONOSPHERIC COUPLING OBSERVED DURING TROMSOE HEATING CAMPAIGN OF FEBRUARY 1996**

Nataly Blagoveshchenskaya, Victor KORNIENKO, Renata Lukianova, Oleg Troshichev (all at Arctic and Antarctic Research Institute, 38 Bering Str., St.Petersburg, 199397, Russia, email: vikkom@aari.nv.ru), Asgeir Brekke (Auroral Observatory, University of Tromsø, N-9037, Tromsø, Norway, email: asgeir@phys.uit.no), Mike Kosch, Michael Rietveld (both at Max-Planck-Institut fuer Aeronomie, 37189 Katlenburg-Lindau, Germany, email: kosch@linax1.mpae.gwdg.de).

The complex study of the geophysical and radiophysical processes during the Heating campaign on 15-17 February, 1996, in the nocturnal auroral ionosphere has been carried out. The following instruments were involved in the study: IMAGE magnetometer network, HF Doppler multichannel equipment, Tromsø Dynasonde, EISCAT UHF radar, all-sky imager (DASI), and satellite data sets. The features of the processes imply the modification of the M-I coupling associated with the HF Heater action: (1) local ionospheric currents redistribution during heating cycles; (2) local field-aligned current modification; (3) possibly the Alfvén wave excitation; (4) triggering of particle precipitation; (5) possibly field-aligned current sheet

development disturbance. As key parameters in geophysical conditions for the observed phenomena we outline: (1) the HF Heater affected on the current carrying E-layer; (2) the ionospheric modification (the HF pumping) was in the closest vicinity of field-aligned current sheet (indicated by the discrete auroral arc). The inferred scenario is the following: the HF Heater produces the ionospheric modification in the E-layer, artificial field-aligned irregularities are excited; ionospheric current system are locally changed; conditions for field-aligned currents shortening are changed; field-aligned potential change leads to electron precipitation; the auroral arc development changed.

**GA2.07/W/23-A1 1220**

**AN INVESTIGATION OF THE TIME SCALE OF THE CONVECTION RESPONSE IN THE IONOSPHERE TO IMF VARIATIONS AT THE MAGNETOPAUSE**

Yan Song and Robert L. Lysak (both at School of Physics and Astronomy, University of Minnesota, 116 Church St. SE, Minneapolis, MN 55455, USA, e-mail: yan@aurora.space.umn.edu & bob@aurora.space.umn.edu)

The response time of ionosphere convection to IMF transients depends on (1) the intrinsic parameters of the magnetosphere-ionosphere system; and (2) the external forcing by the solar wind. For a given electric field and/or a current, the ionospheric response is caused by the drag force due to the collisions between the ions, electron and the neutrals.

The characteristic times of the ions, electrons and neutrals at different ionospheric altitudes to a given electric field and/or a given current are investigated numerically by solving the eigenvalue problem of a set of equations for the ions, the electrons and the neutrals. The response at different altitudes is coupled by the passage of Alfvén waves.

The time scales of the ionospheric response to an electromagnetic perturbation in the form of MHD waves and in the form of convection are different. The time scale of the response of the ionospheric reconfigures to a sudden IMF change is usually not the Alfvén travel time. We will report results from a numerical model of the ionospheric response time to the different driving forces.

**Monday 19 July PM**

Presiding Chairs: A Yau (University of Calgary, Alberta Canada)  
J.J. Sojka (Utah State University Logan, (USA)

**GA2.07/L/01-A1 Invited 1400**

**AURORAL FIELD-ALIGNED CURRENT DESTABILIZATION IN THE IONOSPHERE**

Supriya B. Ganguli and V. V. Garishchaka

Our research has shown that multimoment, multispecies generalized fluid models with appropriate parameterization of important plasma instabilities via anomalous transport coefficients are a promising vehicle to study the effects of auroral field-aligned current destabilization in the ionosphere. Our simulation results show that the presence of field-aligned currents in the ionosphere generate field-aligned current driven instabilities that alter ionospheric flow into the magnetosphere by producing plasma density cavities and energization processes. Recent observations indicate that the field-aligned flows often have transverse structures. A structured flow can generate spatial gradient driven instabilities that can result in cross-field transport in addition to plasma energization. Our 3D, multifluid, multispecies model solves the continuity, momentum and energy equations in dipole magnetic field and allows self-consistent treatment of the cross-field transport. We have shown that the low-frequency D'Angelo instability, driven by the transverse inhomogeneity in the magnetic field-aligned ion flow, can be excited for the typical parameters in this region. The instability generates cross-field transport, which significantly modifies the field-aligned ionospheric outflow. In the non-linear stage of the instability, V-shaped potential structures with magnitude ~1kV are formed. The simulation results will quantify ionospheric outflow, provide insight into the dynamical evolution of D'Angelo instability in the auroral region, its effects on ionospheric outflow and formation of 3D potential structures. The results will be compared with recent observations.

**GA2.07/W/26-A1 Invited 1425**

**IONOSPHERIC MASS LOADING OF THE MAGNETOSPHERE DURING MAGNETIC STORMS**

Ioannis A DAGLIS (National Observatory of Athens, Institute of Ionospheric and Space Research, 15236 Penteli, Greece)

A variety of observations in the inner magnetosphere have shown that the terrestrial plasma (singly charged oxygen in particular) is an important part of the energetic ion population. In particular, measurements have demonstrated that during intense magnetic storms, the abundance of ionospheric oxygen increases dramatically. The result is a rapid intensification of the ring current and an ionospheric dominance in the inner magnetosphere around storm maximum. The mass loading of the magnetosphere and the compositional change in favor of oxygen affect, among other processes, the decay of the ring current through the species- and energy-dependent charge exchange and wave-particle scattering loss. We will present relevant observations and modelling results, and will discuss the importance of the ionospheric mass loading in terms of its consequences for magnetic storm dynamics.

**GA2.07/W/18-A1 1450**

**NEW ALFVEN WAVE GENERATION MECHANISM ASSOCIATED WITH MAGNETOSONIC WAVE INCIDENCE**

P. NENOVSKI, Geophysical Institute, Bulgarian Academy of Science, Sofia, Bulgaria

The well-known mechanism of Alfvén wave resonances by magnetosonic waves usually takes places at regions with steep gradients, plasma sheet boundaries, plasmopause, etc. The Alfvén resonances are however observable also on field lines where such resonance conditions cannot be matched. An alternative mechanism of Alfvén wave generation should be responsible for such resonances. An Alfvén wave generation mechanism of ionospheric origin is suggested. The initial incident disturbance is again a magnetosonic wave. We demonstrate a non-resonant Alfvén wave generation mechanism due to polarization effects of the low-altitude ionosphere on the incident magnetosonic wave. Owing to polarization effects through the ionosphere-atmosphere system the magnetosonic wave dissipation process yields a non-zero amplitude Alfvén-type wave transmitted in the magnetosphere. This new Alfvén wave generation ionosphere mechanism emerges however under specific conditions. The mechanism is most effective under condition  $SH = (SP + Am)^{0.5}$ . Here SH, SP correspond to

the Hall and Pedersen conductances in the low-ionosphere part and Am is proportional to  $(k^2)/V_{ph,hor}$  (k is the horizontal wavenumber of the incident magnetosonic wave,  $V_{ph,hor}$  the horizontal phase velocity, and l the Hall region thickness). Hence, only magnetosonic waves with appropriate wave characteristics are able to initiate an Alfvén

**GA2.07/W/27-A1 1510**

**GEOMAGNETIC HISTORY AFTER A SUBSTORM: THE NEUTRAL WIND DYNAMO EFFECT**

ANASUYA L. ARULIAH, Alan D. Aylward, Ingo C.F. Mueller-Wodarg (all at Atmospheric Physics Laboratory, University College London,67-73, Riding House St., London W1P 7PP, England; e-mail: anasuya@apg.ph.ucl.ac.uk)

The Neutral Wind Dynamo is known to be a significant source of electric fields at low- and mid-latitudes, thus creating the Sq current system. At high-latitudes the magnetospheric dynamo is so much larger that the neutral wind dynamo is generally ignored. However, there are certain conditions when this is not the case. These occur when Bz is small resulting in weak ionospheric convection, whilst the neutral convection is strong. The strong neutral convection may exist for two reasons, either owing to the pressure gradient or a residual high-speed flow left over from a previously active condition that has quickly become quiet. A particular example is the recovery stage of a substorm. Model simulations, using the UCL-Sheffield-SEL CTIP model, are compared with FPI average wind speeds to investigate the significance of the neutral wind dynamo in this circumstance. Individual periods are also examined where simultaneous observations are made by the EISCAT radars at Tromsø and Longyearbyen together with FPIs at Kiruna and Longyearbyen. These provide measurements over a large region extending from the polar cap to the auroral oval.

**GA2.07/W/30-A1 1530**

**SOME NEW FEATURES OF HIGH-ALTITUDE CURRENT SYSTEM POSSIBLY GENERATED BY IONOSPHERIC NEUTRAL WIND**

Toshihiko IYEMORI (Graduate School of Science, Kyoto University, Kyoto 606-8512, Japan, email: iyemori@kugi.kyoto-u.ac.jp) Masahisa Sugiura(Research Institute of Science and Technology, Tokai University, Tokyo 151-0063, Japan: email: sugiura@jspan.kugi.kyoto-u.ac.jp) Ryoichi Nakashima (Sony Co., 1-7-4, Tokyo 108-0075, Japan, email: rnaaka@shiba.sony.co.jp) James A. Slavin (Code 696, Goddard Space Flight Center, Greenbelt, MD20771, U.S.A., email: slavin@lepias.gsfc.nasa.gov)

Using the magnetic field data from DE(Dynamics Explorer)-1 and -2, we have investigated the electric current structure over the ionosphere including the mid-latitude field-aligned currents. Firstly, we deduced the magnetic fields of external origin by subtracting a model field from the observed field, and then averaged the field data in each latitude-longitude mesh. From the DE-2 (low-altitude satellite) data, we found four vortices of horizontal magnetic field centered around (4MLT, 40N), (20MLT,40N), (4MLT,40S), and (20MLT,40S), which suggest the existence of midlatitude field-aligned currents connected to an inner magnetospheric transverse current. Another new feature, observed with the DE-1 (high-altitude satellite) magnetometer, is the altitude dependence of the disturbance field over the polar cap, which appears to indicate horizontal currents flowing at high-altitudes of several thousand km in the dusk-to-dawn or dawn-to-dusk direction. We discuss the characteristics of these newly found current systems and their generation mechanism.

**GA2.07/W//06-A1 1610**

**STATISTICAL CHARACTERISTICS OF THE MID-LATITUDE TROUGHS (LIT) AND LOW-LATITUDE SUBTROUGHS IN HE+ IONS DENSITY ON SEASON, LOCAL TIME AND MAGNETIC ACTIVITY**

Larissa SIDOROVA and Alexander Karpachev (Institute of Terrestrial Magnetism, Ionosphere and Radiowave Propagation Russian Academy of Sciences, Troitsk, Moscow region, 142092, Russia, e-mail: golovkov@izmiran.rssi.ru)

Quantitative characteristics of the mid-latitude troughs (LIT) and the low-latitude subtroughs in He+ of the topside ionosphere (~1100 km) were obtained by statistical analysis of "ISS-b" satellite data set (~1100 orbits, F10.7~180). The trough occurrence probability variations on local time, season and magnetic activity have rather unexpected character. So, for a nighttime the LIT's occurrence probability is maximal in vernal equinox, by other hand, this probability in winter conditions, having being comparative with summer's one, is about 50% only. For a daytime the LITs, contrary to expectation, are rather frequent (~30%) in summer and occasionally in winter (5-10%). However the low-latitude subtrough characteristics have got more "correct" character. So, the subtroughs are more frequent in winter nighttime (30%). For a daytime the most of subtroughs are observed in summer only (~7-12%). The occurrence probability for the both troughs depends poorly on the magnetic activity. Their diurnal probability variations have the pre- and post-midnight maximums. It is shown that these ones are determined by the corresponding [He+] variations. The obtained results suggest the revision of the LIT's formation mechanism. It is shown, particularly, that the summer daytime LITs are formed by the competition between "winter bulge" in [He+] and polar wind. It is found also the strong [O+] effect on the [He+] behaviour. This influence is determined by the dynamics of the H+, He+ and O+ flows and increases with the latitude growth.

**GA2.07/W/02-A1 1630**

**A MODEL STUDY OF THE MAIN IONOSPHERIC TROUGH AND PLASMAPAUSE RELATIONSHIP**

A.V.Tashchilin and E.B.Romanova (both at Institute of Solar-Terrestrial Physics, Russian Academy of Science, 664033, Irkutsk, POBox 4026, Russia, e-mail: avt@iszf.irk.ru )

The main ionospheric trough (MIT) is a distinguishing structural feature of the subauroral ionospheric F2-layer. If the latitude range, in which MIT is located, is mapped along geomagnetic field lines into the equatorial plane, then the resulting set of values of the parameter L will also show an abrupt decrease in electron density which is called the plasmopause (PP). It was established that the formation of PP and MIT is dramatically affected by the magnetospheric convection electric field which leads to a spatial redistribution of thermal plasma in the ionospheric F-region and near the plane of the geomagnetic equator. This inevitably brings up the questions: Are these structures brought about by the operation of some general mechanism, and do other physical factors influence the observed characteristic properties of MIT and PP. In an effort to investigate the formation process of MIT and PP under quiet and disturbed conditions, a model has been developed for thermal plasma evolution at

heights over 150 km, applicable at middle, auroral and polar latitudes. The model calculates the density distributions of the O<sup>+</sup>, H<sup>+</sup> and M<sup>+</sup> ions and electrons, their temperatures, as well as charged particle and heat fluxes through a numerical integration of the magnetohydrodynamic equations of thermal plasma transport and the kinetic equation of photoelectron transport along the entire drifting dipole plasma tube, including both the northern and southern hemispheres. The model takes into account the production of ions as a result of photoionization and impact ionization by magnetospheric electrons, as well as the processes of interaction of charged particles with the thermosphere. We present and discuss the calculated latitudinal density and temperature profiles of charged particles in the subauroral F2-region, in the topside ionosphere, and in the geomagnetic equatorial plane, corresponding to 00, 06, 12 and 18 MLT for quiet conditions and during a disturbance such as a magnetic storm.

GA2.07/W/29-A1

1650

#### THE PERSISTENCE OF HIGH-LATITUDE CONVECTIVE FLOWS THROUGH NORTHWARD IMF TURNINGS AS EVIDENCE OF THE IONOSPHERIC DYNAMO

J. MICHAEL RUOHONIEMI and Raymond A. Greenwald (both at Johns Hopkins University, Applied Physics Laboratory, Johns Hopkins Rd., Laurel, MD, 20723, USA, email:mike\_ruohoniemi@jhuapl.edu)

Convection in the magnetosphere is most often discussed in terms of the coupling of energy and momentum from the solar wind to the magnetosphere with the ionosphere acting as a more-or-less passive load. However, energy stored in the ionosphere-thermosphere system can be released through dynamo action resulting in an ionospheric driver for magnetospheric convection. One manifestation of this mechanism is the neutral flywheel effect, which, upon a change in the solar wind-magnetosphere coupling conditions, causes the pre-existing convective flows to exert an influence in the ensuing period. We have identified one particularly clear example of the neutral flywheel effect in SuperDARN HF radar observations of high-latitude convection, namely, the persistence of flows after IMF turnings from southward to northward at latitudes which are generally sub-auroral for IMF northward conditions. The coverage afforded by the combined radar fields of view approaches  $\sim$  of the entire global convection pattern and the temporal resolution is usually 2 minutes. The convection is seen to evolve from an expanded pattern characteristic of Bz- to a contracted pattern characteristic of Bz+ with a gradual ( $\sim$  tens of minutes) decay of velocity within the latitude interval that effectively loses its source for convection in the solar wind-magnetosphere coupling. We present several examples of this phenomenon and discuss the dependencies of the time constants that characterize the decay of convection. These can be interpreted in terms of the effectiveness of the ionospheric dynamo for driving magnetospheric convection.

GA2.07/W/15-A1

1710

#### THE RELATIONSHIP BETWEEN SUPERDARN DOPPLER VELOCITIES AND GROUND MAGNETOMETER DATA

C.L. Waters, M.D. Sciffer, I.S. Dunlop, F.W. Menk, F. Fenrich, and J.C. Samson

Doppler oscillations at ultra low frequencies (ULF) in HF signals that encounter the ionosphere have been observed and studied since the 1960s. Only recently has a suitably sophisticated theoretical treatment been developed to model these effects [Sutcliffe and Poole, 1989]. This model concerned Doppler oscillations in HF ionospheric propagation due to the shear Alfvén ULF wave mode. In this paper we extend the treatment to include both the shear Alfvén and fast mode ULF wave modes in the ionosphere. Given relevant ionospheric parameters and the ULF wave characteristics obtained from ground based magnetometers, the model predicts the associated Doppler oscillations as a function of altitude. These results are discussed within the context of SuperDARN Doppler data and ULF magnetometer data.

GA2.07/W/10-A1

1730

#### OBSERVATIONS OF ULF FIELD LINE OSCILLATIONS IN THE IONOSPHERE AND ON THE GROUND AT HIGH LATITUDES

Fred W. MENK (Department of Physics, CRC for Satellite Systems, University of Newcastle, Callaghan, NSW, 2308, Australia, email: hyspuls3@cc.newcastle.edu.au) Tim K. Yeoman, Darren M. Wright and Mark Lester (all at Department of Physics and Astronomy, Leicester University, Leicester, LE1 7RH, UK, email: dmw7@ion.le.ac.uk)

We examine an interval where Pc5 field line oscillations were recorded with the same frequency across the entire IMAGE and SAMNET magnetometer arrays, spanning 51 to 76 degrees latitude, and simultaneously in the high latitude ionosphere with the CUTLASS HF radar and an HF Doppler sounder experiment. A signature was also observed with a nearby imaging riometer. The event was triggered by a solar wind pressure pulse. This seems to have produced global mode oscillations in the magnetospheric cavity which coupled to field line resonances near the last closed field lines. The scale size and three-dimensional velocity vectors in the ionosphere are also determined.

Tuesday 20 July AM

Presiding Chairs: A Yau (University of Calgary, Alberta Canada)  
J.J. Sojka (Utah State University Logan, USA)

GA2.07/W/17-A2

Poster

0930-01

#### GLOBAL APPEARANCE OF THE MHD SIGNALS INCIDENT TO THE HIGH-LATITUDE IONOSPHERE IN THE IONOSPHERE

Shigeru Fujita (Meteorological College, Kashiwa, Chiba, 277-0852, Japan, Email: sfujita@typhoon.mc-jma.ac.jp, Masahiro Itonaga, Department of Education, University of Yamaguchi, Yoshida, Yamaguchi, 753-8513, Japan, email: itonaga@po.cc.yamaguchi-u.ac.jp, Yutaka Ogawa, Kashiwa, Chiba, 277-0852, Japan, email: yogawa@tsunami.mc-jma.ac.jp.)

Pi2 and PR1 are associated with the field-aligned current injected to the high-latitude ionosphere. Traditional theory on horizontal spread (transmission) of the ionospheric electric field has not considered the magnetosphere-ionosphere coupling. Therefore, we study again theoretically the horizontal spread of the ionospheric electric field.

There are two possible mechanisms of the horizontal spread. One is the Earth-ionosphere waveguide transmission that was first suggested by Kikuchi and Araki (1979). Another is the instantaneous spread of the ionospheric electric field within the ionosphere. Theoretical consideration revealed that the latter is effective in horizontal spread of the Pi2 and PR1 signals.

GA2.07/W/08-A2

Poster

0930-02

#### STIMULATION OF THE KELVIN-HELMHOLTZ INSTABILITY IN THREE DIMENSIONS

Kristi KELLER and Robert Lysak (both at School of Physics and Astronomy, University of Minnesota, 116 Church St., Minneapolis, MN 55455, e-mail: kellerk@aurora.space.umn.edu)

The Kelvin-Helmholtz instability is a mechanism for transport at the magnetopause. The results from a compressible three-dimensional MHD simulation that is coupled to the ionosphere through the boundary conditions will be presented. We will examine the effect of time changing conductivities on the Kelvin-Helmholtz instability and current generation at the ionosphere. We will also explore how hemispheric asymmetries change the evolution of the Kelvin-Helmholtz instability. We will explore the relation between the formation of curl and spirals in the aurora with the Kelvin-Helmholtz instability and ionospheric boundary conditions. We will also examine the effect of ionospheric conductivity on field line resonance.

GA2.07/W/09-A2

Poster

0930-03

#### SEPARATION OF THE DIFFERENT TYPES OF THE [HE+] TROUGHS IN THE TOPSIDE IONOSPHERE

Larissa SIDOROVA and Alexander Karpachev (Institute of Terrestrial Magnetism, Ionosphere and Radiowave Propagation Russian Academy of Sciences, Troitsk, Moscow region, 142092, Russia, e-mail: golovkov@izmiran.troitsk.ru)

Mid-latitude light ion trough (LIT) and low-latitude subtrough characteristics, permitting to divide troughs precisely, are detected by the system analysis of the large "ISS-b" satellite data set. It is shown, particularly, that the LITs are more often observed in nighttime than in daytime and just a little more often - in winter than in summer. LITs locate close and rather equatorwards to the internal plasmapause during whole day. LITs together with internal plasmapause shift to the equator during geomagnetic activity increasing. More high-latitude LITs, connected with external plasmapause, are sometimes observed in summer day period. The subtroughs are observed in the wide belt of the invariant latitudes of  $\sim$ 25-55° practically independently from geomagnetic activity. In summer condition the subtroughs are usually detected in evening, in winter condition - after midnight. Averaged subtrough occurrence probability is higher in the Southern Hemisphere than in the Northern one. In general, the subtrough occurrence probability is less than that of LITs, but more than expected one. The subtrough characteristics and an appearance region have got complicated season-diurnal variations and depend on a hemisphere. All these variations determine an asymmetry of the Northern and Southern Hemispheres in inhomogeneous structure of the topside ionosphere.

GA2.07/E/02-A2

Poster

0930-04

#### ASYMMETRY EFFECT IN CHANGES OF PLASMA DENSITY AND TEMPERATURE AT THE MAIN IONOSPHERIC TROUGH LATITUDES IN CONJUGATE HEMISPHERES

STEPANOV A.E. Zikrach E.K., Khalipov V.L., Plotnikov I.Ya., Shestakova L.V. (Institute of Cosmophysical Research and Aeronomy, 677891 Yakutsk, Russia, email: ikfia@sci.yakutia.ru) Afonin V.V. (Space Research Institute, 117810 Moscow, Russia, email: vafonin@esoc1.bitnet)

On data of the "Cosmos-900" satellite the variations of electron density (Ne) and temperature (Te) at latitudes of a main ionospheric trough in conjugate hemispheres in different conditions of geomagnetic activity are investigated. The measurements are analysed during an equinox, when the conditions of light exposure are identical in both hemispheres. It is revealed that in quiet geomagnetic conditions the magnitude of Te in a minimum of a trough in northern hemisphere is higher, than in southern. The appropriate significance of Ne in northern hemisphere, on the contrary, is lower than Ne in a southern hemisphere. During geomagnetic disturbances the character of modifications of Ne and Te in a minimum of a trough in both hemispheres varies on opposite. The physical explanation of the observable phenomenon is offered.

GA2.07/E/04-A2

Poster

0930-05

#### NIGHTTIME VARIATIONS OF THE IONIZATION IN F REGION

Bienvenido LAZO, Amada Toledo Ricardo Dmaz, Alexander Calzadilla Departamento de Geofísica Espacial, IGA/CITMA, Calle 212 No 2906, La Lisa, C.P. 11600, C. de La Habana, Rep. de Cuba

Experimental evidences of nighttime seasonal anomaly in ionospheric observations of ground-based vertical sounding and Faraday rotation carried out in Havana (23.0 N; 82.5 W), are given. Favoring conditions for mechanisms of interhemispheric coupling to explain the enhancement of ionization during winter nighttime are subject to discussion. The results of physical modelling of the interhemispheric coupling in the American sector (L=1.5) during low solar activity, are shown. The anomalous behavior of NmF2 in connection with solar activity was analyzed. It was established that seasonal anomaly is manifested only in night conditions for R12 values ranging from 5 and 16, i.e., in low solar activity conditions, favored by plasma fluxes directed in the winter season from the Southern to Northern hemisphere. For values of the R12 parameter larger than 35 thermospheric composition changes dominate and ion-drag effectivity increases, which benefits the existence of winter foF2 values larger than those of the summer, in day conditions. The space distribution of the anomalous behaviour, both diurnal and nocturnal, of the electronic concentration was also studied and established. At the height of 250 Km, the electronic concentration displays an anomalous nocturnal behaviour for the studied five levels of solar activity, i.e., the winter values of foF2 are larger than those of the summer, which could suggest that the interhemispheric coupling through the protonosphere is the main physical mechanism responsible of the winter night-time anomaly for heights lower than hmF2 in a wider range of solar activity.

GA2.07/W/20-A2

Poster

0930-06

#### FIELD-ALIGNED CURRENT PATTERN ON THE IONOSPHERIC DATA

Alla M. LYATSKAYA (Institute of Physics, University of St.-Petersburg, St.-Petersburg 198904, Russia; e-mail: lyatsk@snoopy.phys.spbu.ru)

The small-scale spatial structure of the field-aligned current (FAC) is known always present at high latitudes. Instantaneous FAC pattern occurred during substorm has constructed from ionospheric parameters obtained by means of ground-based observations. Such construction of the FAC structure by means of ionospheric data is confirmed by results of the carried out study of the connection between the time-spatial structures of the field-aligned current and the ionospheric blanketing frequency fBEs for both positive and negative IMF Bz and By components during quiet and active magnetic activity: 1) a coincidence of the regions of the upward and downward FAC with the regions of enhancements and decreases of fBEs; 2) the observed dawn-dusk asymmetry in the behavior of fBEs with the increase of the magnetic activity; 3) the existence of the sharp latitude gradient of the fBEs near midnight what may be



connected with the narrow sheet of the upward field-aligned current in the Harang discontinuity region; 4) the opposite behavior for  $B_y < 0$  and  $B_y > 0$ . Field-aligned current pattern over the sheets of high conductivity was obtained by means of the numerical modelling with taking into account the coupling with the ionospheric layers, and magnetosphere.

**GA2.07/W/24-A2** Poster **0930-07**

**HF WAVES AS A TOOL TO DIAGNOSE IONOSPHERIC-MAGNETOSPHERIC COUPLING IN THE MAIN IONOSPHERIC TROUGH**

H. Rothkaehl Space Research Centre PAS, Bartycka 18A, 00-716 Warsaw, Poland

The region of the main ionospheric trough acts like a lens focusing a variety of instabilities and disturbances from different re-gions of the Earth's environment. The theoretical approach and the satellite measurements at the vicinity of the plasmopause at the top-side ionosphere as well as more recent trough data derived from analysis of HF radio spectrometer located on the board of Magion-3 satellite confirmed that ionospheric trough and plasmopause lay very close to each other. The aim of this paper is present the evolution of plasmopause position and the minimum of the trough during strong geomagnetic disturbances and to analyse the physical mechanism responsible for the generation broad band HF emission over ionospheric trough area.

**GA2.07/W/21-A2** Poster **0930-08**

**HIGH LATITUDE GEOMAGNETIC VARIATION REFERENCE FIELD MODELS FOR 20-22 SOLAR ACTIVITY CYCLES**

Vladimir Papitashvili (Space Physics Research Laboratory, University of Michigan, Ann Arbor, MI 48109, USA, email: papita@umich.edu) Boris BELOV (Institute of Terrestrial Magnetism, Ionosphere and Radio Wave Propagation, IZMIRAN, Troitsk, Moscow Region, 142092, Russia, email: bbelov@adonis.iasnet.ru) Natalia Papitashvili (Raytheon STX and NSSDC, NASA/Goddard Space Flight Center, Greenbelt, MD 20771, USA, email: natasha@nssdca.gsfc.nasa.gov)

We present a newly obtained set of linear regression models of the ground magnetic response on 1-nT changes in the corresponding interplanetary magnetic field (IMF) components for the 20-22 solar activity cycles (from 1965 to 1997). These models are obtained over both the northern and southern polar regions and for different seasons of a year (summer, winter, and equinox). Data from 116 magnetic observatories were collected and quality controlled. The hourly means of the IMF and ground geomagnetic field components are analyzed utilizing the linear "black box" approach. The spherical harmonic analysis is applied to obtain a set of harmonic coefficients capable of modelling the ground geomagnetic responses on changing IMF conditions for any time instance between 1965 and 1997. The new set of models is compared with similar models obtained during the development of IZMIRAN Electrodynamic Model for two solar activity maximums (1968-1969 and 1979-1983). It shown that generally there are little differences in the models harmonic coefficients through the solar activity cycles. This allows us to apply the obtained results beyond of the studied interval. Validation of the new linear regression models against magnetic observatory data is also presented and discussed.

**GA2.07/W/31-A2** Poster **0930-09**

**A MECHANISM OF ANTICORRELATION IN OCCURRENCE OF ULF ELECTROMAGNETIC NOISE RESONANCE STRUCTURE AND PC 1 OBSERVATIONS WITH THE SOLAR ACTIVITY CYCLE**

V. Y. Trakhtengerts, A. G. DEMEKHOV (both at: Institute of Applied Physics, Nizhny Novgorod, Russia; email: andrei@appl.sci-nnov.ru) P. P. Belyaev, S. V. Polyakov, E. N. Ermakova, and S. V. Isaev (all at: Radiophysical Research Institute, Nizhny Novgorod, Russia)

The observed anticorrelation between the 11-year solar activity cycle and occurrence of Pc-1 geomagnetic pulsations as well as the resonance structure of the electromagnetic noise spectrum (RSS) in frequency range 0.1-10 Hz is explained based on the role of ionospheric Alfvén resonator (IAR) in formation of both phenomena. The reflection coefficient R of Alfvén waves from IAR determines the threshold of the ion cyclotron instability (CI) which is the cause of Pc-1 pulsations. At the same time the quality of IAR, which varies synchronously with R, controls the RSS modulation depth. It is shown that the decrease of |R| maximum value during the maximum phase of the solar activity cycle remarkably increases the CI threshold and sharply decreases the modulation depth of RSS, thus decreasing the occurrence probability of both phenomena.

**GA2.07/E/01-A2** Poster **0930-10**

**LONG-TIME TRENDS IN F2-LAYER OF SUBAURORAL IONOSPHERE**

Smirnov V.F., Kobyakova S.E.(Institute of Cosmophysical Research and Aeronomy, 677891 Yakutsk, Russia, email: ikfia@sci.yakutia.ru)

On data of vertical sounding on an Yakutsk station are considered long-time variation of F2-layer parameters for period 1956-1995. Statistical analysis of time series of midday and midnight values of foF2 and h'F parameters is conducted with the purpose of determination maximum and minimum values of subauroral ionosphere parameters, their cyclical, annual and seasonal variations, parameter variability on different phases of a solar cycles. Is shown that for the last three cycle of solar activity there is a tendency of growth average values of height of a F-layer, increasing tendency of maximum values of critical frequencies of a F-layer within a maxima of solar activity and decreasing of critical frequencies within a minimum of activity. It is shown the close connection of height growth of a F-layer with growth of average value temperatures in near-earth atmospheric layer for winter conditions.

**REPORTER REVIEWS**

Location: Gisbert Kapp, E203 LT1

Presiding Chair: M. Lockwood

**SESSION 1**

**GA3.01/W/04-A2**

**0830**

**THE MAGNETOPAUSE AND ITS BOUNDARY LAYERS**

T.G. ONSAGER

The magnetopause and its boundary layers have a critical role in controlling the coupling between the solar wind and the magnetosphere/ionosphere/thermosphere system. The magnetosheath boundary layer, the low latitude boundary layer, the cusp, and the mantle all are controlled directly by the processes occurring in the magnetopause as driven by the solar wind/magnetosheath conditions. An emphasis over the past two years has been on the properties of the magnetopause and its boundary layers at high latitudes and on the flanks of the magnetosphere. New satellite observations have provided many insights on the plasma transport processes in these regions, including reconnection and non-reconnection related mechanisms, and on the dependence of these processes on the orientation of the interplanetary magnetic field. Numerical simulations have given new results on the large-scale properties of the magnetopause and transport across it, as well as on the small-scale processes occurring within the magnetopause. Recent progress on magnetopause studies will be reviewed, and future directions of this research will be discussed.

**GA3.01/W/01-A2**

**0915**

**REPORTER REVIEW: DYNAMICS OF THE GEOMAGNETIC TAIL**

T. I. PULKKINEN (Finnish Meteorological Institute, Helsinki, Finland)

The ISTP program that became fully operational in 1996 has now continued measurements through the solar minimum to the rising solar activity period. A substantial data set covering solar, solar wind, magnetospheric, and ionospheric observations now has been collected and partially analyzed. The past two years have brought the solar community together with the magnetospheric and ionospheric communities in an unprecedented manner with several analyses that have followed the detailed sequence of events from solar events to near-Earth geomagnetic activity. Simultaneously, a vast amount of new results have been obtained about the detailed structure of the magnetotail and its dynamics during geomagnetically active events. Recent results of the analysis of the Solar-Terrestrial chain of events especially from the magnetotail point of view are reviewed.

Presiding Chair: G. Atkinson

**SESSION 2**

**GA3.01/W/02-A2**

**1030**

**THE INNER MAGNETOSPHERE**

J. U. KOZYRA (Space Physics Research Lab, University of Michigan, 2455 Hayward, Ann Arbor, Michigan 48109-2143 USA, email: jukozyra@engin.umich.edu)

The physics of the inner magnetosphere is key to our understanding of magnetic storm development and recovery. It is also the region where radiation belts are created and linger and thermal plasmas of ionospheric origin reach their highest densities in the magnetosphere. The perturbations to the inner magnetospheric plasmas and fields, associated with elevated magnetic activity, have served as a focal point for investigations into the dynamics of this region and its coupling to the solar wind, magnetotail and ionosphere. Intense interest exists in understanding: (1) the role of composition, importance of variations in the source populations, and impact of non-adiabatic processes and structured electric fields in the ring current development and decay, (2) the acceleration mechanisms, solar wind drivers and source populations for the radiation belts, (3) the electrodynamic and energetic processes that structure the thermal plasma, possibly preconditioning the inner magnetosphere and impacting storm development, and (4) the redistribution of energy by interactions between different plasma populations. All of these processes play a role in the global energy balance and its variation among storms with different characteristics and different solar wind drivers. A review of current research on these and other issues relevant to our developing understanding of inner magnetospheric physics will be presented.

**GA3.01/E/03-A2**

**1115**

**LARGE-SCALE FIELDS AND FLOWS IN THE IONOSPHERE-MAGNETOSPHERE SYSTEM**

R. A. WOLF (Rice University MS 108, P. O. Box 1892, Houston, TX 77251 U.S.A.)

An attempt will be made to review the progress of the last several years, refining our understanding of large-scale plasma flow, electric currents, and electromagnetic fields in the Earth's magnetosphere-ionosphere system. Geotail observations of the inner and middle plasma sheet have clarified crucial aspects of the substorm problem. Energetic neutral atom images of the inner magnetosphere, mainly from the Polar spacecraft, have begun to provide useful information on the injection of the ring current. Knowledge of the electric-field coupling between the inner and middle magnetosphere has improved as a result of careful analysis of older data from the CRRES spacecraft and incoherent-backscatter radars. On the theoretical side, global MHD models have continued to proliferate and to serve with increasingly effectiveness both as data-analysis tools and as sources of theoretical ideas. The connection between basic research and the effort to achieve improved space-weather forecasts continues to strengthen and to motivate areas of research. For years, many theorists have expressed the philosophical view that proper quantitative representation of the large-scale behavior of the entire magnetosphere-ionosphere system will require synthesis of theories and models that utilize different formalisms and operate on different regions and scales; in the last few years, modest but significant practical steps have been taken in the direction of theoretical synthesis.

Tuesday 20 July PM  
 Presiding Chair: M. Lockwood

**SESSION 3**

**GA3.01/W/05-A2** 1315

**REPORTER REVIEW ON LARGE-SCALE MORPHOLOGY OF THE MAGNETOSPHERE**

Patrick T. NEWELL (Johns Hopkins University Applied Physics Laboratory, 11100 Johns Hopkins Rd., Laurel, MD 20723, USA)

A review of developments over the last two years in the area of large-scale morphology of the magnetosphere will be given. The emphasis is on plasma and auroral structure on the largest scales.

**GA3.01/W/03-A2** 1400

**WAVE PARTICLE INTERACTIONS**

Yoshiharu OMURA (RASC, Kyoto University, Uji, Kyoto 611-0011, Japan, Email: omura@kurasc.kyoto-u.ac.jp)

Roles in wave growth/damping, particle heating and diffusion, and mesoscale phenomena such as magnetic reconnections through anomalous resistivity. Recent spacecraft observations have been yielding coordinated high-quality wave and particle data with finer resolution than those of the previous observations, making it possible to compare the observations with theory and simulations quantitatively. Computer simulations based on particle, hybrid and Vlasov codes have been performed to clarify nonlinear wave-particle interaction that are absent in MHD or multi-fluid description. Nonlinear ion dynamics have been followed self-consistently by hybrid codes in realistic open and nonuniform systems. With such simulations, the signatures of ions at different regions of the magnetosphere have been clarified. Much work still needs to be done in two and three-dimensional configurations, where different types of instabilities and processes compete or couple with each other. High-energy electrons can carry information concerning acceleration and heating processes occurring at a distant location along the magnetic field. However, the high energy electrons are also subject to strong wave-particle interactions and thus to nonlinear processes, whose evolution in space and time cannot be described by quasi-linear theory or simple simulations in a uniform system. Many more studies are necessary, along with more powerful computational capabilities, in order to clarify nonlinear electron dynamics in realistic nonuniform systems.

**GA3.01/LL/01-A2** 1445

**ACTIVE AND LABORATORY EXPERIMENTS**

P.A. BERNHARDT

Abstract not available at the time of going to press

Presiding Chair: G. Atkinson

**SESSION 4**

**GA3.01/E/02-A2** 1600

**REPORTER REVIEW ON ULF WAVES**

Kazue TAKAHASHI (Johns Hopkins University Applied Physics Laboratory, Laurel, MD 20723-6099, e-mail: kazue.takahashi@jhuapl.edu)

This review covers ULF waves throughout the magnetosphere, their morphology, excitation, propagation, damping and detection. Much attention will be given to the recent multipoint observations and numerical simulations of global propagation of ULF waves.

**GA3.01/E/01-A2** 1645

**MAGNETOSPHERES OF OTHER PLANETS**

Vytis M. VASYLIUNAS (Max-Planck-Institut fuer Aeronomie, D-37191 Katlenburg-Lindau, Germany, e-mail: vasyliunas@linmpi.mpg.de)

Planets with well-defined magnetospheres include, in addition to Earth, Mercury, Jupiter, Saturn, Uranus, and Neptune. Most attention continues to be devoted to the magnetosphere of Jupiter, where data from the Galileo orbiter have possible systematic, extended-time-scale studies of the configuration and dynamics of the magnetosphere and have also revealed a great variety of different interactions between the magnetosphere and the moons of Jupiter, including the magnetosphere-within-magnetosphere case of Ganymede. Speculations about similarities or differences between the magnetospheres of Earth and of Jupiter can now, with the availability of orbiter data from both, rest on a firmer ground. Second in the amount of attention is the magnetosphere of Saturn, with the Cassini/Huygens orbiter/probe mission now on the way to the planet.

**GA3.06** Tuesday 20 – Wednesday 21 July

**AURORA PROCESSES: MAGNETOSPHERE, IONOSPHERE – THERMOSPHERE COUPLING, ARCS AND MICROPROCESSES (WITH DIV. II)**

Location: Gisbert Kapp NG15 LR1  
 Location of Posters: Gisbert Kapp Coffee Room

Tuesday 20 July AM

Presiding Chair: R.J Strangeway (IGPP/UCLA, Los Angeles, California, USA)  
 Concurrent Poster Session

**AURORAL PROCESSES AND MIT COUPLING - 1**

**GA3.06/W/19-A2** Invited 0930

**WHAT OBSERVATIONS BY THE FAST SATELLITE REVEAL ABOUT AURORAL MIT COUPLING**

Charles W. Carlson (Space Sciences Lab, University of California at Berkeley, Berkeley CA 94720, USA, email: cwc@ssl.berkeley.edu)

The FAST satellite observes auroral processes relevant to MIT coupling on scales ranging from micro- to macroscale. The largest scale is organized around the major field-aligned current systems that connect the magnetosphere and ionosphere in the auroral zone. Magnetic field-aligned potential drops arise in both upward and downward current systems. Precipitating electrons carrying upward current deposit energy into the ionosphere, causing ionization and heating. In downward current regions, upward accelerated electrons and heated ions are a source of new populations of particles for the magnetosphere. Microphysical processes associated with the parallel potential drops are responsible for intense heating and outflow of ionospheric ions, and these processes also accelerate escaping ionospheric electrons to energies of hundreds of eV. These parallel potential drops also decouple the magnetospheric and ionospheric flows in localized regions.

**GA3.06/P/02-A2** Invited 1000

**THE FREJA PERSPECTIVE ON THE AURORAL CURRENT CIRCUIT**

GVRAN MARKLUND and Tomas Karlsson, Alfvin Laboratory, The Royal Institute of Technology, SE10044 Stockholm, Sweden e-mail: marklund@plasma.kth.se

The recent discovery that particle acceleration to keV-energies is a common feature not only on auroral field lines in the upward current region but also on 2black auroral field lines2 in the return current region makes it necessary to consider the entire auroral current circuit for understanding the auroral phenomenon. Assuming a current generator that drives the auroral currents, particle acceleration is necessary to maintain the current at times and regions of low plasma density. The altitude distribution and intensity of the acceleration region will thus depend strongly on the local ambient plasma conditions, and thus vary with local time, season and magnetic activity level. A lowering of the acceleration region and increase in acceleration energies are features characteristic of nighttime and wintertime plasma conditions. Although much information has been obtained by various spacecraft at different altitudes on auroral electric field, current, particle and plasma characteristics, the results need to be combined in order to obtain a coherent picture on how the acceleration region is influenced by season, local time and activity level within the upward and downward current region. An effort of this kind has been initiated using relevant data from the Viking, Polar, Freja and FAST satellites supplemented by results from other satellites reported on in the literature. First results of this study will be reported.

**GA3.06/L/06-A2** 1050

**FIELD-ALIGNED CURRENTS AS SEEN BY THE POLAR AND INTERBALL-2 DURING 11 JANUARY 1997 EVENT**

A.Z. Bochev 1, Guan Le 2, V.G. Petrov 3, D.L. Danov 1, Y.I. Feldstein 3, P.T. Newell 4 1 Solar - Terrestrial Influences Laboratory, BAS, Sofia, Bulgaria 2 Institute of Geophysics and Planetary Physics, Los Angeles, USA 3 Institute of Earth's Magnetism and Radiowave Propagation (IZMIRAN), Moscow, Russia 4 Applied Physics Laboratory, The John Hopkins University, Laurel, USA

In this talk field-aligned currents (FAC) in the north auroral magnetosphere during the CME geomagnetic storm on January 11,1997 are examined by using data mainly from magnetic field experiments on board of INTERBALL-2 and POLAR satellites. During the event from 0300 to 0600 UT, the spacecrafts crossed the dusk side from low to high latitudes in the altitudinal range 12000 to 40000 km. FAC structures were identified for sure on both magnetograms. The measurements permitted to monitor two unusual FAC systems separated from each other. The equatorward system was a remarkable demonstration of intense oscillating fields during steady IMF Bz >>0, immediately after the end of the most dramatic compression of the magnetosphere. In contrast the poleward system appeared as irregular structures probably controlled by a strong unsteady IMF By. Correlations with double-theta aurora are discussed also.

**GA3.06/W/42-A2** 1110

**POLAR OBSERVATIONS OF INTENSE ELECTRIC FIELDS AND POYNTING FLUX NEAR THE PLASMA SHEET-TAIL LOBE BOUNDARY AT HIGH ALTITUDE**

A. KEILING, J.R. Wygant, C. Cattell, M. Johnson (School of Physics and Astronomy, University of Minnesota, Minneapolis, MN, USA, email: wygant@ham.space.umn.edu) M. Temerin, F.S. Mozer (Space Sciences Laboratory, University of California, Berkeley, CA, USA) C.A. Kletzing, J.D. Scudder (Department of Physics and Astronomy, University of Iowa, IA, USA) W. Peterson (Lockheed-Martin Palo Alto Laboratories, Palo Alto, CA, USA) C.T. Russell (IGPP, University of California, Los Angeles, CA, USA) G. Parks, M. Brittacher (Geophysics Program, University of Washington, USA) W. Lotko (Dartmouth College, Thayer School of Engineering, Hanover, NH, USA)

In this talk, we present measurements from the Polar spacecraft of intense electric field structures near the outer boundary of the plasma sheet, at altitudes of 4-6 Re near local midnight. The electric field variations have maximum values exceeding 100 mV/m and are typically polarised approximately normal to the plasma sheet boundary. The electric field structures vary over time scales (in the spacecraft frame) ranging from 0.1 to 30 seconds. They are associated with strong magnetic field fluctuations. The Poynting flux measured at these altitudes is about 1-2 ergs/cm2s and is directed along the magnetic field towards the ionosphere. If the measured Poynting flux is mapped to ionospheric altitudes along converging magnetic field lines, the resulting energy flux can exceed 100 ergs/cm2s. Simultaneous UVI

images of aurora demonstrate that these structures occur during periods when the Polar spacecraft is magnetically conjugate (to within a one-degree-mapping accuracy) to intense auroral structures. The electron energy flux (averaged over a spatial resolution of 0.5 degrees) deposited in the ionosphere due to electron beams as estimated from UVI images is 20-30 ergs/cm<sup>2</sup>s. Thus, there is strong evidence that these electric field structures provide sufficient Poynting flux to power the acceleration of auroral electrons (as well as the energisation of up-flowing ions and joule heating of the ionosphere). The E/B ratios are about 4000-10000 km/s which is consistent with Alfvénic variations, but is an order of magnitude larger than those expected for the typical values of the height integrated conductivity of the ionosphere. Minimum variance analysis...

**GA3.06/W/26-A2 1130**

**AUREOL-3 SATELLITE OBSERVATIONS OF MULTIPLE INVERTED-V STRUCTURES AND HOT PLASMA STRATIFICATION THEORY**

M. V. STEPANOVA, O. Luizar (both at Universidad de Santiago de Chile, Ecuador 3493, Casilla 307, Santiago, Chile, email: mstepano@lauca.usach.cl, oluizar@lauca.usach.cl), E. E. Antonova, (Skobel'syn Institute of Nuclear Physics, Moscow State University, Moscow 119899, Russia, email: antonova@taspd.npi.msu.su), J. M. Bosqued, (Centre d'Etude Spatiale des Rayonnements, CNRS/UPS, BP 4346, 31029 Toulouse, France, email: Jean-Michel.Bosqued@cesr.fr), and R. A. Kovrazhkin (Space Research Institute, Academy of Sciences of Russia, Profsoyuznaya 84/32, Moscow 117810, Russia, email: kovrazhkin@romance.iki.rssi.ru)

During the analysis of multiple inverted-V structure formation using AUREOL-3 satellite data, cases of formation of one, two, three and four structures are identified. This corresponds to the longitudinal stratification of the upward field-aligned current into extended in latitudinal direction multiple current sheets. This number is compared with the predicted by a hot plasma stratification theory. The theory is based on the suggestions, that plasma in the center of plasma sheet is in magnetostatic equilibrium, and plasma sheet ion motion is unmagnetized for the spatial scales in which the structures are formed. The solution of the magnetosphere-ionosphere interaction problem shows that upward field-aligned current may split into separate sheets. This number is determined by a parameter which depends on current density, current band width, hot magnetospheric ion temperature, and height-integrated Pedersen conductivity. It was found that in the majority of cases, the theory predicts well the number of observed structures.

**GA3.06/W/01-A2 Invited 1150**

**THE AURORAL ACCELERATION REGION IN GLOBAL MHD SIMULATIONS**

Joachim RAEDER (Institute of Geophysics and Planetary Physics, University of California, 405 Hilgard Ave, Los Angeles, CA 90095, USA, email: jraeder@igpp.ucla.edu)

The auroral acceleration region provides the interface between magnetospheric and ionospheric dynamics. Thus, any realistic global model of the magnetosphere - ionosphere system must include the acceleration region to some degree. For obvious reasons it is impossible to model the acceleration region down to microscales, or even mesoscales; therefore parameterizations of the microphysics in the auroral regions must be used. However, although the acceleration region is not treated with ab-initio calculations of the acceleration processes, global modelling is well suited to study the effects of different parameterizations on the global magnetospheric dynamics. Because the parameterizations used in the global model embody our current understanding of the acceleration processes, the global model provides a means to test their validity. We present several case studies in which we compare the model predictions with in-situ observations and discuss what the model can tell us about the auroral acceleration processes.

**GA3.06/W/03-A2 1220**

**PHASE-SPACE MAPPING SIMULATIONS OF STORMTIME DIFFUSE AURORAL (PLASMASHEET) ELECTRONS IN STRONG PITCH-ANGLE DIFFUSION**

Margaret W Chen (Space & Environment Technology Center, The Aerospace Corporation, M2-260, P. O. Box 92957, Los Angeles, CA 90009, USA, e-mail: mchen@aero.org) Michael SCHULZ (Lockheed Martin Advanced Technology Center, O/H1-11, B/255, 3251 Hanover Street, Palo Alto, CA 94304, USA, e-mail: schulz@agena.spasoci.com)

Strong pitch-angle diffusion so thoroughly randomises the first two adiabatic invariants of charged-particle motion that it conserves a phase-space volume  $\Lambda$ , equal to the cube of the particle momentum  $p$  times the occupied flux-tube volume per unit magnetic flux. We trace drift shells of plasmashet electrons with representative values of  $\Lambda$  in a magnetic field model that consists of a dipole field plus a uniform southward field. Using the simulated drift shell results, we map phase-space densities from the neutral line according to Liouville's theorem (modified by attenuation due to particle precipitation) and compute corresponding rates of energy deposition into the auroral ionosphere along the trajectories and at the energies corresponding to the conservation of  $\Lambda$ . In the past we have applied a time-independent Størn-Volland electric-field model with a 25-kV cross-tail potential drop to represent quiescent conditions. Our quiet-time simulation results show a paucity of precipitating energy flux in the afternoon sector, in qualitative agreement with the "darkness" of POLAR/PIXIE X-ray images of the diffuse aurora in that sector. In this work we apply a larger (storm-associated) cross-tail magnetospheric electric field enhanced by impulses to represent substorm effects. We compute the energy deposition rate and characteristic energy of the precipitating electron spectrum as functions of magnetic latitude and local time during a model storm for indirect comparison with observational data on precipitation-induced ionospheric conductivities and with spectral characteristics of X rays detected by PIXIE.

**Tuesday 20 July PM**

Presiding Chair: Goran Marklund (Alfvén Laboratory, The Royal Institute of Technology, Stockholm, Sweden)

**AURORAL PROCESSES AND MIT COUPLING - 2**

**GA3.06/W/15-A2 Invited 1400**

**AURORAL ARCS AND AURORAL STRUCTURES PRODUCED BY SHEAR ALFVEN FIELD LINE RESONANCES**

John C. SAMSON, R. Rankin, and I. Voronkov (all at Department of Physics, University of Alberta, Edmonton, Alberta, Canada T6G 2J1, email: samson@space.ualberta.ca) V. Tikhonchuk (P. N. Lebedev Physics Institute, Russian Academy of Sciences, Moscow 117924, Russia)

Abundant experimental evidence now indicates that ULF (1-5 mHz), shear Alfvén field line resonances produce some types of auroral arcs. Dispersive effects in the FLR, including electron inertia, can lead to parallel electric fields, and acceleration of electrons to form auroral arcs with

overall latitudinal scale sizes of about 10 km, with 1 km scale discrete arcs embedded in the larger structure. Non-linear effects, including ponderomotive forces in the FLR, can lead to density cavity formation in the acceleration region, and an even more rapid onset of dispersive effects. In this talk, we will review observations, computational models, and recent non-linear theories of these FLRs and address the issue of magnetosphere ionosphere coupling through FLRs.

**GA3.06/W/27-A2 1430**

**DEVELOPMENT OF SMALL-SCALE STRUCTURES IN AURORAL ARCS**

Robert L. LYSAK (University of Minnesota, 116 Church Street SE, Minneapolis, MN 55455, USA)

Auroral currents and fields form on scales from 100 km to scales less than 1 km, the scale of individual auroral arcs. The formation of structure on such a variety of scales is examined through a model of auroral currents and fields involving the propagation of Alfvén waves along auroral field lines. Large-scale parallel electric fields can be involved in the larger scale structures, and can lead to decoupling of the magnetosphere and ionosphere on scales less than a few tens of kilometers. Smaller scale Alfvénic structures can be formed from non-linear effects, the interactions of Alfvén waves with perpendicular gradients in the density, or through ionospheric feedback. The roles of these phenomena in producing the spectrum of scales observed in auroral structures will be examined.

**GA3.06/E/01-A2 1450**

**FIELD LINE RESONANCE INTERFERENCE MODEL FOR MULTIPLE AURORAL ARC GENERATION**

Wladislav LYATSKY (Polar Geophysical Institute, Apatity, 184200, Russia, email: lyatsky@pgi-ksc.murmansk.su) R. D. Elphinstone, Q. Pao, and L. L. Cogger (all at Institute for Space Research, University of Calgary, Calgary, Alberta, Canada T2N 1N4, email: rob@hobbes.phys.ucalgary.ca)

A simple model for the generation of poleward moving multiple auroral structures in the nighttime ionosphere is described. The model is based upon the premise that field line resonance oscillations are responsible for auroral arc generation. The auroral structures are considered to be a result of interference between Alfvén field line resonance oscillations on different L shells. Because of the dependence of the Alfvén resonance frequency on L shell, any two neighbouring L shells which oscillated initially with the same phase, after some time appear to be in opposite phase. That results in the appearance of counter-directed electric fields at these L shells and a large field-aligned current between them, which can produce the electron acceleration along the magnetic field and be responsible for auroral arc generation. The out of phasing between the oscillating L shells begins first at low latitudes and then propagates poleward producing poleward moving auroral arcs. The field line resonance interference model explains periodic behavior in such auroral activity having frequencies in the Pc5 range. The poleward propagation of the auroral arcs in this model is a result of the poleward propagation of interference maxima rather than any real plasma or wave propagation.

**GA3.06/W/35-A2 1510**

**PARALLEL ELECTRIC FIELD GENERATION BY AN ALFVEN WAVE IN A MIRROR FIELD**

Tadas K. NAKAMURA (Fukui Prefectural University, Fukui 910-1195, Japan, e-mail: tadas@fpu.ac.jp)

In a simple classical picture, the parallel (to B field) electric field of Alfvén waves is negligibly small. This is because the high mobility of electrons enables this small electric field to cause enough field aligned current in the MHD scale. On the other hand, there are models that predict the existence of parallel electric field in a static limit. For example, the model by Knight (PSS, 1973) suggests that a finite parallel electric field is required to create a finite field aligned current in a mirror field. To solve this contradiction, it is proposed in this paper that an Alfvén wave must have a parallel electric field due to the mirror effect. In a converging magnetic field, mobility of electrons is restricted by the mirror force and a parallel electric field must exist to carry a field aligned current associated with Alfvén waves. The parallel electric field created by this mechanism can be much larger than that of a kinetic or inertial Alfvén wave.

**GA3.06/E/07-A2 Invited 1550**

**IONOSPHERIC ION OUTFLOWS AND THEIR EFFECTS ON THE MAGNETOSPHERE**

Andrew W. Yau (Department of Physics and Astronomy, University of Calgary, Calgary, Alberta, Canada T2N1N4; and Herzberg Institute of Astrophysics, Dominion Astrophysical Observatory, Victoria, BC, Canada V8X4M6, e-mail: yau@space.phys.ucalgary.ca)

A number of ion flow and energisation processes contribute to the outflow of ionospheric ions to the magnetosphere. These include bulk ion flows such as the polar wind and auroral bulk upflows, and energisation processes such as upflowing ion beams, conics, and transversely accelerated ions. The overall rate of ion outflows is strongly dependent on magnetic and solar activity, and sometimes exceed  $3 \times 10^{26}$  O<sup>+</sup> ions/sec and  $1 \times 10^{26}$  H<sup>+</sup> ions/sec. We will review observations of ion outflow processes from both recent and earlier satellites, and discuss their morphological characteristics. In addition, we will assess their relative contributions to the overall outflow, and their effects on the composition and dynamics of the magnetosphere.

**GA3.06/W/22-A2 1620**

**DOWNWARD ION ACCELERATION IN THE LARGE-SCALE DOWNWARD CURRENT REGION**

D M KLUMPAR, M H Boehm (Lockheed Martin, Advanced Technology Center, Space Physics Laboratory, Palo Alto, CA 94304; e-mail: klump@sierra.spasoci.com); C W Carlson, J P McFadden, M A Terner (University of California at Berkeley, Space Sciences Laboratory, Berkeley, CA 94720); and R J Strangeway (University of California at Los Angeles, Institute of Geophysics and Planetary Physics, Los Angeles, CA 90095)

Using ion spectrometers on the FAST Auroral Snapshot Explorer we have observed striking field-aligned ion precipitation features imbedded in the auroral plasmashet precipitation. The identification and cataloguing of dozens of events along with the detailed examination of specific events reveal the following characteristics. The ion precipitation structures occur within the large-scale downward current region and are frequently found in the pre-midnight MLT sector. In this MLT sector they are located well equatorward of the discrete aurora commonly associated with electron inverted-Vs and upward moving ion beams. Ion mass spectrometer measurements reveal that the ions are dominantly hydrogen. This new class of ion precipitation feature has a very characteristic energy-time profile. Individual events are narrowly confined in latitude (typically < 1 degree), and display a latitude profile similar to



electron inverted-Vs. The flux versus energy spectral distributions are peaked, with the peak energy first rising and then falling with increasing latitude. Peak characteristic energies often reach 1 keV. The phase space density distributions are ring-like, with an ionospheric loss cone, as would be expected for a population that has been accelerated downward into a converging magnetic field. The downward ion beams are easily distinguished from the more energetic precipitating plasmasheet ions observed on the same or adjacent flux tubes, and carry an order of magnitude or more greater differential energy flux. The observations are consistent with the downward acceleration of ions through a quasi-static, downward-directed, parallel potential structure lying above the satellite. It is likely that the quasi-static potentials that are commonly observed at FAST to be accelerating electrons upward can, at times, move to a location above the FAST orbit producing these downward moving ion beams.

**GA3.06/W/37-A2 1640**

**PONDEROMOTIVE UPWARD ACCELERATION OF IONS UNDER THE ACTION OF ULF WAVES OVER THE POLAR REGIONS**

R. LUNDIN, (Swedish Institute of Space Physics, Kiruna, Sweden) A. Guglielmi, (Institute of Physics of the Earth, Moscow, Russia)

A ponderomotive theory, describing the acceleration of magnetospheric ions along geomagnetic field lines, is developed and compared with Viking and Freja satellite observations. The theory is in agreement with observations of ULF electric field fluctuations correlating with the upward escape of ions. Attention is here focused on the non-resonant acceleration of the polar wind and the resonant acceleration of a small admixture of heavy ions under the action of Alfvén and ion cyclotron waves. We show that the critical point of supersonic transition shifts toward the Earth under the ponderomotive action of waves, and the velocity, as well as the acceleration of the flow at this point increase as the wave amplitude increases. The asymptotic behavior of the flow is also modified substantially under the action of waves. In particular high amplitude Alfvén waves results in field aligned small-scale plasma density depletions observed by polar orbiting satellites. We show that the gain in energy of heavy ions under favourable conditions increases as the power of one of the wave amplitude ( $\propto E$ ) despite the fact that the ponderomotive force (magnetic moment "pumping") is proportional to the power of two of the wave amplitude ( $\propto E^2$ ).

**GA3.06/E/11-A2 1700**

**HIGH- AND LOW-ALTITUDE OBSERVATIONS OF ADIABATIC PARAMETERS ASSOCIATED WITH AURORAL ELECTRON ACCELERATION**

Kazuo SHIOKAWA (Solar-Terrestrial Environment Laboratory, Nagoya University, 3-13, Honohara, Toyokawa, Aichi 442-8507, Japan, email: shiokawa@stelab.nagoya-u.ac.jp) W. Baumjohann and G. Haerendel (Max-Planck-Institut fuer extraterrestrische Physik, 85740 Garching, Germany, Email: bj@mpe-garching.mpg.de) H. Fukunishi (Faculty of Science, Tohoku University, Sendai 980-0845, Japan, Email: fuku@pat.geophys.tohoku.ac.jp)

Electron density and temperature, adiabatic thermal current, and field-aligned conductivity have been estimated on the basis of observations by the DMSP satellites above the auroral oval and from measurement by the AMPTE/IRM satellite in the near-Earth plasma sheet. We found that the estimated densities are comparable between these two satellites, while the temperatures obtained from an accelerated Maxwellian fitting procedure used on the DMSP spectra are lower by a factor of 2-3 than those measured by IRM in the near-Earth plasma sheet. The DMSP data show that a large field-aligned potential difference, which accelerates auroral electrons downward, is formed in the region with low field-aligned conductivity. The AMPTE/IRM data show that the field-aligned conductivity decreases with increasing Xgsm-distance, increasing AE index, and after earthward high-speed flow passage. We suggest from these results that large field-aligned potential difference tend to be formed in higher latitudes of the auroral oval (which is connected to larger Xgsm-distances), during high magnetic activity, and in the newly dipolarized magnetic field region after the flow passage.

**GA3.06/W/29-A2 1720**

**ON THE MASS DEPENDENCE OF TRANSVERSE ION ACCELERATION BY BROAD-BAND EXTREMELY LOW FREQUENCY WAVES**

E MÖBIUS, E J Lund, K A Lynch (all at Space Science Center, Morse Hall, University of New Hampshire, Durham, NH 03824 USA; email: Eric.Lund@unh.edu, Eberhard.Moebius@unh.edu, Kristina.Lynch@unh.edu), D M Klumpar (Lockheed Martin Advanced Technology Center, 3251 Hanover St., Palo Alto, CA 94304 USA; email: klump@teams.spasci.com), R E Ergun, C W Carlson (both at Space Sciences Laboratory, University of California, Berkeley, CA 94720 USA; email: ree@ssl.berkeley.edu, cwc@ssl.berkeley.edu)

Recent data from the Fast Auroral Snapshot Explorer (FAST) and other satellites indicate that broad-band extremely low frequency (BBELF) waves account for the majority of the transverse ion acceleration in the aurora. These waves tend to accelerate ions of different masses to approximately the same energy. We analyse selected events from the FAST data set to assess the mass dependence, or lack thereof, of transverse ion acceleration by BBELF waves. We also examine the spectral shapes of the BBELF emissions in order to estimate heating rates for each ion species. The data will be compared with a simple model of transverse ion acceleration [Gorney et al., J. Geophys. Res. 90, 4205, 1985] in order to assess the roles that parallel electric fields and spectral shapes play in transverse ion acceleration.

**GA3.06/W/23-A2 1740**

**IONOSPHERIC SHEAR FLOW SITUATIONS OBSERVED BY THE MIRACLE NETWORK, AND THE CONCEPT OF HARANG DISCONTINUITY**

Olaf AMM, P. Janhunen, H. J. Opgenoorth #, T. I. Pulkkinen, and A. Viljanen (Finnish Meteorological Institute, Geophysical Research, P.O. Box 503, FIN - 00101 Helsinki, Finland, email: Olaf.Amm@fmi.fi, Pekka.Janhunen@fmi.fi, Hermann.Opgenoorth@fmi.fi, Tuija.Pulkkinen@fmi.fi, Ari.Viljanen@fmi.fi) ; (# also at: Swedish Institute of Space Physics, Uppsala Division, S - 75591 Uppsala, Sweden)

Ionospheric shear flow situations regularly occur at the edges of the ionospheric potential cells, one of the most prominent leading to the transition from positive to negative values of the H ground magnetic disturbance component in auroral latitudes around magnetic midnight, named as Harang discontinuity. We present observations of such shear flow situations made by the MIRACLE network in northern Fennoscandia. The network comprises an array of magnetometers and all sky cameras, as well as the STARE coherent scatter radar pair. Thus it provides two-dimensional data of the ground magnetic and ionospheric electric field (or, equivalently, electron flow velocities), and of the optical activity. Some of the most interesting shear flow situations are processed with the 'method of characteristics' to obtain distributions of ionospheric conductances, true ionospheric currents, and field-aligned currents (FACs). Our discussion focuses on the differences in the physical state of the ionosphere between shear

flow regions that are governed by upward and downward FACs, respectively, and their different roles in the global magnetospheric current systems. Based on our observations, we point out that what is defined as the Harang discontinuity in the ground magnetic variation field can be caused by currents flowing in topologically different regions of the ionospheric potential cells, depending on the degree of activity. Therefore, a refined definition of terms is introduced to clearly distinguish the different shear flow situations. We show that shear flow situations in the auroral ionosphere are typically connected with ionospheric conductance minima, with the conductance increasing from the shear flow zone to the south. Hence, two latitudinally separated layers of FACs of the same sign.

**Wednesday 21 July AM**

Presiding Chair: Gang Lu (NCAR High Altitude Observatory, Boulder, CO, USA)

**AURORAL PROCESSES AND MIT COUPLING - 3**

**GA3.06/W/40-A3 Invited 0830**

**PLASMA WAVE EFFECTS ON AURORAL MIT COUPLING**

Raymond POTTELETTE

One of the main challenges of the space plasma community consists in the requirement to understand interacting global and microscopic nonlinear processes on a hierarchy of scales. Due to the high sampling and telemetry rates implemented on recent rocket and satellite experiments, and the subsequent development of new experimental techniques (such as wave-wave and wave-particle correlators), it has become possible to determine the role of transient non-linear structures - associated with large amplitude waves - in the basic microscopic processes taking place in the variety of plasmas characterizing the MIT coupling. We will show some observations performed in space plasmas related to the formation of non-linear coherent structures (solitons, cavitons). The main emphasis will be put on recent theoretical developments which focus on the relevance of these structures with regard to turbulence, generation of radiation, and particle acceleration.

**GA3.06/P/01-A3 0900**

**DEVELOPMENT OF CURRENT DRIVEN INSTABILITIES AND RELATION TO AURORAL PRECIPITATIONS: OBSERVATIONS FROM INTERBALL-2**

Sylviane PERRAUT, Alain Roux, Patrick Robert, Claude de Villedary (CETP/UVSQ, 10- 12 Av. de l'Europe 78140 VILLIZY, France) Jean André Sauvaud, Daniel Popescu (CESR/CNRS, 9 Av. du Colonel Roche -31400 Toulouse, France) Nicolas Dubouloz (CETP/CNRS, 4 Av. Neptune, 94107 Saint-Maur-des-Fossés, France) François Lefeuvre (LPCE, 3A Av. de la Recherche Scientifique, 45071 ORLEANS Cedex-2) Mikhail Moglevskii (IKI, MOSCOW, Russia)

Electromagnetic fluctuations in the frequency range just below the proton gyrofrequency are commonly observed when the INTERBALL-2 s/c crosses the boundary between the polar cap and the auroral region, as well in the night and morning sectors. We study the main characteristics of these fluctuations: polarization, direction of propagation, E/B ratios... It leads to identify these waves as current driven instabilities which result from the differential velocity between ions and electrons in presence of a parallel electric field which develops at these boundaries. It will be shown that these waves which are driven unstable by electron drift provide energy to ions, thereby ensuring a collisionless dissipation of the current. It is suggested that this collisionless dissipation controls the development of larger scale processes such as surface waves at magnetospheric boundaries and interchanges/ballooning instabilities at substorms.

**GA3.06/W/20-A3 0920**

**THE POLARIZATION, FREQUENCY STRUCTURE AND BANDWIDTH OF AURORAL KILOMETRIC RADIATION**

R. J. STRANGEWAY (Institute of Geophysics and Planetary Physics, University of California, Los Angeles, CA 90095, USA, Email: strange@igpp.ucla.edu), P. L. Pritchett (Department of Physics and Astronomy, University of California, Los Angeles, CA 90095, USA, Email: pritchet@physics.ucla.edu), R. E. Ergun, C. W. Carlson, J. P. McFadden, and G. T. Delory (all at: Space Sciences Laboratory, University of California, Berkeley, CA 94720, USA)

The FAST spacecraft is able to make detailed observations of Auroral Kilometric Radiation (AKR), both inside and outside of the source region. These observations indicate that within the source region AKR can occur below the local cold electron gyro-frequency. Furthermore, the wave electric fields are polarised perpendicularly to the ambient magnetic field near the low frequency cut-off. The wave magnetic field is found to be polarised parallel to the ambient magnetic field. This polarisation is consistent with perpendicularly propagating X-mode waves, which together with the observation of a cut-off below the cold electron gyro-frequency indicates that the accelerated and mirroring auroral electrons are the primary energy source for AKR. This type of distribution is referred to as a "horseshoe" distribution. This electron population is being continuously re-energised by the parallel electric field in the auroral acceleration, and we might expect strong emission intensities for AKR, without invoking multiple transitions of the source region. Analysis of the waveforms acquired within the source region indicate a packet-like structure. This may be a signature of the reformation of the distribution. In addition, both inside and outside of the source region rapidly falling tones are observed roughly 50% of the time. These falling tones may be caused by ion beam modifications of the plasma density within the source region. The bandwidths of the emissions are usually ~ 200 Hz, both inside and outside of the source region. This bandwidth may be narrower than that expected from simple linear instability analysis, and propagation effects could be controlling the width of the emitted spectrum. However, we have yet to observe the very narrow tones that would indicate the presence of a feedback oscillator in the AKR source region.

**GA3.06/W/14-A3 0940**

**THE BURSTY NATURE OF CYCLOTRON MASER EMISSIONS IN A DRIVEN MODEL OF THE AKR SOURCE CAVITY**

P L PRITCHETT (Department of Physics and Astronomy, University of California, Los Angeles, CA 90095-1547, USA, email: pritchet@physics.ucla.edu), R J Strangeway (Institute of Geophysics and Planetary Physics, University of California, Los Angeles, CA 90095-1567, USA, email: strange@igpp.ucla.edu), C W Carlson, R E Ergun, J P McFadden, and G T Delory (all at Space Sciences Laboratory, University of California, Berkeley, CA 94720-7450, USA)

The Fast Auroral Snapshot (FAST) satellite has made observations in the AKR source region with orders of magnitude higher time and frequency resolution than previous missions. Wave observations within the source region often showed highly structured spectra, and the particle distributions revealed clear signs of free energy associated with the primary inverted-V

electrons. We present the results of high resolution 2-D particle-in-cell simulations of the cyclotron maser emission process driven by a down going distribution of energetic magnetospheric electrons in the auroral cavity. The relative roles of the inherent bandwidth of the maser instability process and of the magnetic field inhomogeneity in determining the emission spectrum are contrasted, and the possible influence of transverse density variations on the emission process will be examined.

**GA3.06/E/10-A3 1000**

**FINITE AMPLITUDE ELECTROSTATIC ION-CYCLOTRON WAVES IN AURORAL BEAM PLASMA SYSTEM**

R. V. REDDY and G. S. Lakhina (both at Indian Institute of Geomagnetism, Dr. Nanabhoj Moos Road, Colaba, Mumbai - 400 005, India, email: vreddy@iig.igm.res.in)

The low frequency finite amplitude electrostatic ion-cyclotron modes in a magnetised auroral beam-plasma system is studied. The dispersion relation is solved numerically and the growth rates and the real frequencies are calculated for the auroral plasma parameters. The non-linear evolution equation is derived using the reductive perturbation method. The numerical solutions of the non-linear evolution equation are obtained and the essential features of the waveform are compared with the observed waveform. Implications of these results for the generation of parallel electric fields in the auroral region are discussed.

**GA3.06/E/02-A3 1020**

**PLASMA INSTABILITIES IN AURORAL REGION**

A.A.Shaikh( C.U.Shah Science College,Ashram Road,Ahmedabad-3800014,India) A.C.Das(Physical Research Laboratory,Navrangpura,Ahmedabad-380009,India, email: acd@prl.ernet.in)

A plasma instability mechanism seeded by steep density and temperature gradients in a weakly ionized magnetoplasma is proposed with a view to understand some type of density irregularities in the auroral region of ionospheric plasma. Gradients are associated with auroral processes namely precipitated charged particles which are to be believed due to the transfer of solar wind energy into the magnetosphere. It is shown that the growth of proposed instability depends on collision between charged particle with neutrals as well as the ratio of density and temperature scale lengths. We have also studied the effects of recombination and loss process in our model. The potential candidacy of our results is set forth to explain some characteristics of echo received from auroral region. Furthermore, the model is supported by the electron density and temperature gradient measured with EISCAT in the auroral region.

**GA3.06/W/05-A3 Invited 1100**

**ESTIMATES OF ENERGY TRANSFER BETWEEN THE MAGNETOSPHERE AND THE UPPER ATMOSPHERE USING THE AMIE PROCEDURE**

Arthur D. RICHMOND and G. Lu (NCAR High Altitude Observatory, P.O. Box 3000, Boulder, CO 80302-3000, USA, email: richmond@ucar.edu)

Electromagnetic energy transfer between the magnetosphere and the upper atmosphere can be described either as a deposition of heat and kinetic energy into the upper atmosphere, or as a divergence of a Poynting flux that can be defined in a number of different ways. We use the Assimilative Mapping of Ionospheric Electrodynamics (AMIE) procedure to estimate the large-scale energy transfer during disturbed periods, and we use AMIE inputs to the NCAR Thermosphere-Ionosphere-Electrodynamics General Circulation Model to evaluate how thermospheric winds influence the energy transfer calculations.

**GA3.06/L/08-A3 1130**

**INVESTIGATION OF AURORAL COUPLING BY CONJUGATE HEMISPHERE OBSERVATIONS.**

S. B. Mende, H. U. Frey, Space Sciences Laboratory, University of California, Berkeley, CA 94720, email: mende@ssl.berkeley.edu J. H. Doolittle, Lockheed-Martin Palo Alto Research Laboratories, Palo Alto, CA 94304 J. A. Cummock, Dept. of Physics, Univ. Texas Dallas, Richardson, TX, 75083.

The conjugate behavior of auroral processes is examined from optical observations from the large area array of ground based Automatic Geophysical Observatories (AGO-s) and simultaneous ultra-violet imaging data from the POLAR UVI experiment. The ground based optical data is available from the Austral winter (April-August) periods from 1996 to 1998. The ground-based stations provide a detailed view of the aurora, which is sometimes difficult to compare with the much larger scale global view seen from the POLAR satellite. The observations show that substorm expansions occur in conjugate pairs, however the onset regions are usually displaced to a small extent in latitude and often substantially more in longitude. Conjugate behavior of transpolar arcs was also studied. Current understanding of transpolar arcs would predict that arcs located in the dawn side on one hemisphere would have their conjugate counterparts on the opposite, dusk side on the other hemisphere. Although this situation is often observed, there are cases when a transpolar arc has a counter part in the conjugate hemisphere located on the same side of the noon midnight meridian. It should be noted that in our observations the conditions of the two conjugate ionospheres are quite different. Ground based optical images are always taken while the ionosphere is dark and there is no solar illumination on the atmosphere while the satellite images are mostly taken when the atmosphere/ionosphere is illuminated by the sun consequently having high conductivity.

**GA3.06/W/06-A3 1150**

**POLAR CAP AURORAL ARCS OBSERVED FROM SCOTT BASE, ANTARCTICA**

B. J. FRASER, I. M. Wright, and F. W. Menk (Physics Department, CRC for Satellite Systems, University of Newcastle, NSW, 2308, Australia, email: physpuls20@cc.newcastle.edu.au, phbjf@cc.newcastle.edu.au, physpuls3@cc.newcastle.edu.au)

The morphology and movement of auroral arcs observed at Scott Base, Antarctica by a dual wavelength allsky image intensified imager have been related to conditions prevailing in the upstream solar wind and interplanetary magnetic field (IMF). The wavelengths observed in the red 630 nm emissions and the blue 427.8 nm emissions correspond to electron reactions with atomic oxygen and nitrogen in the upper atmosphere, respectively. Data have been collected over three observation seasons, in the 1996, 1997, and 1998 Austral winters, mainly during quiet magnetic conditions, with 1998 data from more active times. Observations from a fixed ground station are necessarily limited in extent, and modulated by viewing conditions, which means the examples examined are selected because definitive features are apparent. The useable field of view is about 500 km in diameter, which is only a small part of the polar cap. The polar cap arcs discussed are mostly relatively small-scale local

events that are in some cases aligned with the cusp or the sun direction. The intensity and structure of arcs vary during their lifetime. Average lifetime is some tens of minutes, and occasionally longer than 1 hour. Wave-like intensity variations can propagate along the arcs. The relationship of the motion and other properties of these arcs to ionospheric plasma convection, solar wind and IMF conditions and the open/closed field line boundary will be discussed for a number of events.

**GA3.06/W/08-A3 1210**

**STATISTIC CHARACTERISTICS OF THE AURORA OBSERVED AT ZHONGSHAN STATION, ANTARCTICA**

Liu RUIYUAN (Polar Research Institute of China, 451 Jinqiao Rd, Shanghai 200129, China, email: pric@stn.sh.cn) Hu Hongqiao (Department of Space Physics, Wuhan University, Wuhan 430072, China, email: pric@stn.sh.cn)

Statistic analysis has been done with the auroral observation taking from an all-sky TV camera for the years of 1995 and 1997 at Zhongshan Station of Antarctica, which is located at 69.4S, 76.4E.

The invariant latitude of this station is 74.5S (L=13.9), and the dayside auroras are observable there during mid-winter. The diurnal variation of the aurora occurrence has two peaks. One peak locates in postnoon sector (1400-1800MLT), and the other in midnight (2200-0300MLT). It is shown that there are often gaps between dayside auroras and nightside auroras. Four types of aurora have been examined. They are corona aurora, band aurora, active surge and transpolar aurora arc. The corona aurora mainly occurs in postnoon and midnight sectors. The band aurora mainly occurs in postnoon sector, equatorward side of evening and equatorward of midnight. But the active surge mainly occurs in midnight and the transpolar arc in midnight too. It is revealed that 75% of aurora belongs to the band in postnoon sector and 52% belongs to the active surge in midnight sector. The relationship between the aurora occurrence and the geomagnetic activity is also studied by considering the conditions of  $Kp <= 1$ ,  $1 < Kp <= 2$  and  $Kp > 2$  respectively. It is quantitatively shown that the occurrence and luminosity of aurora are positively correlated with Kp index. On geomagnetic quiet days the postnoon aurora is mainly a week band one with a pole ward movement. On disturbance days there is corona aurora as well in postnoon sector and active surge is dominant in midnight although the band aurora and transpolar arc sometimes occur.

**Wednesday 21 July PM**

Presiding Chair: David Rees (CASS, Utah State University, Utah, USA)

**AURORAL PROCESSES AND MIT COUPLING - 4**

**GA3.06/W/34-A3 Invited 1400**

**AURORAL PROCESSES STUDIED BY ALIS**

Ake STEEN, Urban Brandstrom and Bjorn Gustavsson (Swedish Institute of Space Physics, Kiruna Sweden), Takehiko Aso and Masaki Ejiri (National Institute of Polar Research, Tokyo, Japan), Mikhail Pudovkin and Oleg Kornilov (University of St. Petersburg, St. Petersburg, Russia)

The optical aurora clearly illustrates the complexity of the MIT interaction processes. Three-dimensional (3-D) tomographic imaging of the optical auroral signal has a considerable potential for investigations of several of the MIT interaction processes. ALIS (Auroral Large Imaging System) is a multi-station (six stations currently) imaging system in the Kiruna-region using high-performance CCD-imaging (3-D), remote Internet operation, and in the future AI-operations. The presentation is mainly concentrating on the study of the development of auroral vortices using several of the methods available in ALIS and also in co-ordination with other measurements. Auroral vorticity is a characteristic auroral feature occurring on almost all scale sizes. Using ALIS auroral vorticity can be investigated from a few hundred metres up to a few hundred kilometres at the same time. ALIS 3-D imaging is carried out in individual auroral emissions, e.g. N2+ 427.8 nm and OI 846.6 nm. An example of the methods used is the technique of spectroscopic ratios. Spectroscopic ratio images can be used to study the 2-D temporal development of the energy characteristics of the precipitating particles, e.g. during the development of an auroral vortex structure.

**GA3.06/E/06-A3 1430**

**RECENT OBSERVATIONS OF MOMENTUM COUPLING IN THE HIGH LATITUDE THERMOSPHERE AND IONOSPHERE BY DOPPLER IMAGING SYSTEMS.**

David REES (CASS, Utah State Univ. Utah State University, Logan, UT 84322-4405, USA, email: walnut1@easynet.co.uk)

Within the Polar Cap and Auroral Oval, magnetospheric electric fields generate a large and highly variable, inflow of momentum for the thermosphere through momentum coupling from the rapidly-motion of ionospheric plasma to the neutral gas via ion drag. Two Doppler Imaging Systems, located, respectively, at Kiruna, Northern Sweden, and in Svalbard, have provided a series of graphic illustrations of the development of complex thermospheric flow patterns during a series of geomagnetic disturbances during the past two years of increasing solar activity.

**GA3.06/W/18-A3 Invited 1450**

**HOW WELL CAN EMPIRICAL MODELS PREDICT IONOSPHERIC STORMS**

Timothy FULLER-ROWELL, M.V. Codrescu, (both at NOAA Space Environment Center and CIRES, University of Colorado, Boulder, CO 80303, USA, email: tjfr@sec.noaa.gov; mcodrescu@sec.noaa.gov); E.A. Araujo-Pradere (Inst. de Geofisica, UNAM, Ciudad Universitaria, Coyoacan 04510, Mexico DF, email: earaujo@sec.noaa.gov)

Recent understanding of the physical processes responsible for ionospheric changes during a geomagnetic storm has led to the possibility of capturing part of the response in an empirical model. The model simulates the expected change in neutral composition during the evolution of an event by integrating the auroral power injected into the atmosphere over the previous 30 hours, weighted by a filter. The model is particularly well suited to the storm-time response in summer, when no feature boundaries are expected. In winter, where sharp discontinuities are expected, the empirical model is less accurate.

**GA3.06/W/25-A3 1520**

**RESPONSE OF THE AURORAL AND POLAR THERMOSPHERE TO GEOMAGNETIC FORCING**

M. J. KOSCH, K. Cierpka, M. Rietveld, T. Hagfors and K. Schlegel (Max Planck Institut für Aeronomie, 37191 Katlenburg-Lindau, Germany, email: kosch@linmpi.mpg.de), D. Rees (Utah State University, USA)

The upper atmosphere above ~ 80 km altitude consists of over 99% neutral gas (generally termed the thermosphere). The remainder is ionised, comprising the embedded ionosphere. At high latitudes the ionosphere is strongly controlled by the magnetospheric convection electric field which responds strongly to geomagnetic disturbances such as substorms and associated auroral events. Through ion-neutral collision processes, the dynamics, thermodynamics and composition of the high-latitude thermosphere can also be strongly influenced by geomagnetic disturbances. For example, increasing geomagnetic activity is accompanied by enhanced convection electric fields, which accelerate the ions, and auroral precipitation, which increases ionospheric Pedersen conductivity. The result of increased ion density, combined with their higher velocities, imparts increased momentum to the neutral gas by collisions (ion drag). The neutral gas may be accelerated to velocities of many 100s of m/s, whilst enhanced Joule heating increases both ion and neutral temperatures. Conversely, a strong horizontal neutral wind may change the ionospheric composition by driving ions up or down the magnetic field lines into a region of different recombination rates. It is clear that the ionosphere and thermosphere are closely coupled. Past work from models, satellite observations and ground-based instruments will be reviewed with emphasis on the effect of geomagnetic forcing on the thermosphere. A powerful experimental combination for thermospheric studies is the incoherent-backscatter radar co-located with a ground-based optical interferometer. The radar and the interferometer can measure velocities and temperatures of the ions and neutrals, respectively. Examples from northern Scandinavia from the EISCAT radar and the Skibotn Fabry-Perot interferometer will be discussed.

**GA3.06/W/28-A3 1540**

**MIRACLE OBSERVATIONS OF MAGNETIC AND ELECTRIC FIELD VARIATIONS NEAR AURORAL ARCS**

K. KAURISTIE, A. Viljanen, P. Janhunen, A. Pajunpaa, M.T. Syrjasuo, T.I. Pulkkinen, H.J. Opgenoorth, and P. Eglitis (all at Finnish Meteorological Institute, Geophysical Research, P.O.Box 503, FIN-00101 Helsinki, Finland, email: kirsti.kauristie@fmi.fi)

Auroral arcs can be classified to different categories according to the distribution of the electric field and ionospheric currents near the arc. For example, a narrow region of intensified horizontal electric field can be observed either equatorward (evening sector) or poleward (morning sector) of the arc. We assess the generality of these findings using data of years 1997-1999 recorded by the Scandinavian MIRACLE network which is a two-dimensional array of magnetometers, ionospheric radars, and allsky cameras. The distribution of ionospheric Hall currents is estimated with equivalent current vectors derived from ground-based magnetic field data. Reliability of the vectors especially in the vicinity of the arcs where the conductivity gradient is large is tested with the radar observations. Long-term recordings provide us the possibility to get a view on how the arcs distribute in magnetic local time: Do they appear preferentially in the evening sector of the oval, like some arc theories predict?

**GA3.06/W/10-A3 1620**

**OPTICAL OBSERVATIONS OF TOPSIDE MOLECULAR NITROGEN IONS IN THE POLAR CAP: ALTITUDE PROFILES OF THE VIBRATIONAL AND ROTATIONAL DISTRIBUTIONS**

G. J. ROMICK, J. H. Yee, M.F. Morgan, D. Morrison (JHU/APL, Laurel, MD. 20723)

The Ballistic Missile Defense Organization's (BMDO) Midcourse Space Experiment (MSX) obtained optical observations of molecular ions at very high altitudes above the northern polar cap. MSX's Ultraviolet and Visible Imagers and Spectrographic Imagers (UVISI) instrument shows the presence of molecular nitrogen ions over the high latitude northern polar region (geomagnetic latitude 75° - 85°N, 12-06 MLT) at altitudes above 900 km on Nov.7, 1997 and only to 700 km on Nov.8, 1997. The contiguous wavelength coverage of UVISI allows us to unambiguously identify the N2+ First Negative Bands over a range of wavelengths from 330 to 471 nm. Transitions from the v = 0, 1, and 2 vibrational levels are identified in the observed spectrum. In addition, transitions from the v = 2, 3, 4, and 5 vibrational levels of the Meinel bands were also observed. The source must be solar resonance fluorescence of upward moving molecular nitrogen ions associated with the general morning-side polar ion outflow. If the source were particle impact excitation other emissions such as the N2 1st and 2nd Positive Bands and the atomic oxygen line at 557.7 nm would have been observed. The recorded spectra show the N2+ 1st Negative Bands with an integrated band intensity of 2.5 kR. This implies an N2+ number density of about 1x 10<sup>3</sup> ions/cm<sup>3</sup> at 900 km. In order to understand the energy associated with these ions and possibly differentiate between ambient and energetic ions, the altitude profiles of the relative populations of the vibrational states of N2+ 1st Negative and Meinel bands as well as the effective rotational temperatures will be presented.

**GA3.06/E/12-A3 1640**

**GEOMAGNETIC VARIATIONS AT EQUATORIAL AND AURORAL LOCATIONS, AND THEIR INTER-RELATIONSHIP DURING STORM AND SUBSTORM CONDITIONS**

Girija RAJARAM, T. Arun, A.N. Hanchinal (Indian Institute of Geomagnetism, Colaba, Mumbai-400 005, India, email: girija@iig.iigm.res.in, tarun@iig.iigm.res.in, arun@iig.iigm.res.in), Jacques Vassal (Observatoire de St.Maur 4 avenue de Neptune 94107, St.Maur-Cedex, email: jacques.vassal@cetp.ipsl.fr), M.Salam Ndiath (Observatoire ORSTOM, B.P. 50, M'BOUR, Senegal)

This work is an attempt to understand the elusive problem of electromagnetic coupling between the high and low latitudes of Earth, markedly during disturbed conditions. The stations selected are the French low-latitude location M'BOUR (geog.14.4N, 343.05E; geom.21.3N, 55E), and the Indian Antarctic location MAITRI (geog.70S, 12E; geom.66.8S, 56.3E), which lie more or less on the same flux tube. Any electromagnetic coupling between the two is thus sought to be understood in terms of field-aligned behaviour.

Selected magnetic storms of 1994 are chosen, and the X,Y,Z variations at the two stations are examined for substorm intervals. Power spectrum analysis is carried out for the two locations with frequency filters which select the Pi2 signal(6.66-25mHz) and the Ps6 signal(1-2mHz), both being typical features of the Substorm.

Preliminary analysis of the ssc storm of 28 May '94, and the gc storm of 2 April '94 indicate that while geomagnetic variations at these two locations can show positive, negative or even no correlation, depending on the phase of the storm, the typical frequencies associated with the Pi2 and the Ps6 pulsations show up strongly at both high and low latitudes during substorms. The implications of these are being understood by examining more storm cases during 1994.

**GA3.06/W/17-A3 1700**

**POLAR ARCS AND LARGE-SCALE CONVECTION**

A. E. LEVITIN, S. A. Golyshev, Y. I. Feldstein, Isaev N. V.(Institute of Terrestrial Magnetism, Ionosphere and Radio Wave Propagation, Troitsk, Moscow Region, 142092, Russia, email: Igmrova@izmiran.troitsk.ru) Marklund G., Blomberg L. (Alfvén Laboratory, Royal Institute of Technology, S-100 44 Stockholm S-100 44, Sweden, email: marklund@plasma.kth.se)

The influence of the polar arc appearance on the spatial convection pattern in the high latitude ionosphere, were analysed. Particular events of the polar arcs appearance were considered using Viking and DMSP data. The IZMEM model, which accepts variations of the interplanetary magnetic field and the solar wind parameters as input parameters (Feldstein and Levitin, J. Geomagn. Geoelectr., 38, 1143-1182, 1986) were used as a background model of the electric field and current systems. The currents connected with the polar arcs were put over the background distribution of the electric field and currents. The high latitude ionosphere conductivity variations were taken into account based on DMSP satellites data. The spatial-temporal distributions of the convection before and after the polar arcs appearance are presented. They show that polar arcs which appear in the polar cap have weakly influence on the large-scale convection system. The connected with polar arcs spatial scales and amplitudes of disturbances of the electric and magnetic fields and electric currents have been calculated.

**GA3.06/L/05-A3 1720**

**VELOCITIES OF AURORAL FORMS AND PROCESSES IN THE MAGNETOSPHERE**

Oleg KORNILOV, Mikhail Pudovkin (both at Institute of Physics, St.Petersburg State University, St. Petersburg, Petrodvorets, 198904, Russia, Email: mikhail.pudovkin@pobox.spbu.ru, pudovkin@snoopy.phys.spbu.ru)

Well known, that registration of aurora by video cameras allow us to receive a lot of new data about processes in the magnetosphere. In particular, velocities of moving auroral forms provides an unique information about electric fields, field-aligned currents, plasma instabilities etc. For these purposes algorithm of full automatic velocity calculation was proposed. Application of this routine to real auroral video data allowed us to determinate system of field-aligned currents that drifts westwards with a speed of some kilometers per second.

**GA3.06/L/09-A3 1740**

**INTERPRETATION OF AURORAL ARC DYNAMICS BASED ON MODEL OF MAGNETIC RECONNECTION IN THE MAGNETOTAIL**

Yulia BOGDANOVA and Vladimir Semenov (both at Institute of Physics, St.Petersburg State University, St.Petersburg, 198904, Russia, Email: julia@geo.phys.spbu.ru, sem@snoopy.phys.spbu.ru) Richard Rijnbeek and Maria Buchan (both at Space Science Centre, University of Sussex, Brighton, BN1 9QH, UK, Email: R.P.Rijnbeek@sussex.ac.uk, M.J.Buchan@sussex.ac.uk)

We present new results to predict the motion of nightside auroral arcs during the expansion phase of a magnetospheric substorm. The model is based on the hypothesis that reconnection in the magnetotail plays a central role in substorm development. We suppose that auroral arcs are interpreted as the ionospheric manifestation of upward field-aligned currents, induced by Alfvén waves generated during reconnection pulse in the vicinity of an X-line in the magnetotail current sheet. The non-uniform plasma medium leads to dispersion of the waves, and in this case manifestation of magnetotail reconnection could correspond to both poleward and equatorward moving auroral arcs. Furthermore, we show that the morphology and location of the arcs depend on the dissipative electric field in the diffusion region, the plasma density distribution in the magnetotail, and the position of the X-line. Dynamics of auroral arcs deduced from our model is in a good agreement with experimental data.

**Tuesday 20 July AM**

Presiding Chair: R.J.Strangeway (IGPP/ULLA, USA)

**GA3.06/E/03-A2 Poster 0930-01**

**MODEL STUDY OF IONOSPHERIC ELECTRODYNAMICS OF AURORAL SUBSTORMS**

Lie ZHU, Jan Sojka, Robert Schunk, Mike Bowline (Center for Atmospheric and Space Sciences, Utah State University, Logan, UT 84322-4405, U.S.A., email: zhu@cc.usu.edu)

In the ionosphere, the theoretical models have been developed to an extent that the 3-D global as well as small-scale ionospheric features of substorms can be simulated within the model capability. But the inconsistency among available global time-varying magnetospheric drivers for the ionospheric models, especially the global convection and precipitation, or/and the coarse spatial and temporal resolutions of these drivers have been restricting the global ionospheric models from producing the observed small-scale auroral structures and dynamical features of substorms in the ionosphere. In this work, we used a set of magnetospheric drivers produced from a theoretical M-I coupling model as the inputs for the USU Time-Dependent Ionospheric Model (TDIM) to study the ionospheric electrodynamics during a representative substorm. The features of these theoretical magnetospheric drivers include the sharp convection reversals, the narrow precipitation channels, the self-consistency between convection and precipitation, and the high spatial and temporal resolutions. The simulation results revealed many interesting dynamical and small-scale features of the ionospheric electrodynamics during substorms. Specifically, the results showed that there were both electron and ion hot spots associated with the auroral substorm in the ionosphere, but these two spots were spatially separated. The temporal and 3-D spatial features of plasma structures in these hot spots were examined and the underlying physics will be discussed in this presentation.

**GA3.06/L/02-A2 Poster 0930-02**

**AURORAL DENSITY CAVITIES AND ASSOCIATED ENERGETIC ION BEAMS**

H L COLLIN and W K Peterson (Lockheed Martin ATC, Space Physics Laboratory) P D Craven (NASAMarshall Space Flight Center) M Andre (University of Umea SWEDEN) C A Kletzing (University of Iowa) T E Moore (NASA Goddard Space Flight Center)

Inverted V regions associated with ion beams and a field aligned potential drop are regions of reduced plasma density, density cavities. The nature of ion and electron acceleration process is strongly limited by details of the local ion velocity space distribution. In particular it is important to know the relative contribution of the thermal core and higher energy ion beams and if there are other significant plasma components in these cavities. POLAR/TIDE measures ions with energies below 300eV and estimates the thermal ion density in the cavities. Comparison with the POLAR/TIMAS measurements of high energy ion beams it is evident that



the thermal plasma is much lower inside the cavities than in adjacent regions and suggests that the contribution of the high energy part of the beams makes up at substantial part of the total density. In the archetypal auroral ion beam which has been accelerated through a field aligned potential all ions have roughly the same drift speed. Although heated by wave-particle interactions they are still relatively cool. It is therefore surprising that POLAR/TIMAS commonly sees ion beams which have a narrowly field aligned component extending down to tens of eV and persist through regions. The presence of such a low energy ion component is also supported by the simultaneous POLAR/TIDE observations.

**GA3.06/L/03-A2** Poster **0930-03**

**THE RELATIVE LOCATION OF AURORAL ION BEAMS AND FIELD ALIGNED CURRENTS**

H L COLLIN (Lockheed Martin ATC, Space Physics Laboratory) W J Peria (University of California, Berkeley) W K Peterson (Lockheed Martin ATC, Space Physics Laboratory) P J Chi and C T Russell (IGPP University of California Los Angeles)

It is well established that, statistically, energetic ion beams occur in the same region of the auroral zone as do upward field-aligned currents. However, there have been few studies investigating the details of their spatial relationship in individual events. Upflowing energetic ion beams are detected by the POLAR ion mass spectrometer in the southern auroral zone near perigee. In order to identify field-aligned current sheets we have adapted an automatic algorithm first developed for use with the FAST dataset. We will present the initial results of a survey of the spatial relationship of ion beams and current in a large number of auroral zone transits.

**GA3.06/E/04-A2** Poster **0930-04**

**OCCURRENCE OF O-SHAPED POTENTIALS OVER AURORAL OVAL**

Pekka JANHUNEN (Finnish Meteorological Institute, Geophysical Research, POB 503, FIN-00101, Helsinki, Finland, email: Pekka.Janhunen@fmi.fi)  
Annika Olsson (Swedish Institute of Space Physics, Uppsala Division, S-75591 Uppsala, Sweden, email: ao@irfu.se)

Over stable auroral arcs, the absence of convergent perpendicular electric fields and energetic oxygen beams in POLAR satellite data at 25000-30000 km altitude has suggested that the potential pattern above stable arcs is O-shaped rather than U-shaped. This means that there is no net potential drop between the ionosphere and the magnetosphere, although there are parallel electric fields and the low-altitude electron spectra are of the inverted-V type. An O-shaped geometry can produce peaked "accelerated" electron spectra by filtering out the lower energy part of the magnetospheric thermal electron flux. A negative O-shaped potential well is supposed to be an ion and electron cavity, because it repels electrons and increases the speed of ions within itself.

We review our most recent findings about the O-shaped potential. Especially, we present a large statistical Freja satellite study (about 1700 km altitude) of more than 80 inverted-V events on different MLT sectors. In this study we determine the field-aligned current density and the apparent source plasma density, temperature and the peak potential for each data point. From the relationship between the peak potential and the field-aligned current density on different MLT sectors we can infer something about the occurrence frequency of O-shaped potentials as a function of MLT.

**GA3.06/W/21-A2** Poster **0930-05**

**THE STATISTICAL X RAY AURORA AS OBSERVED BY PIXIE**

S.M.PETRINEC, J.Mobilia, D.L.Chenette, W.L.Imhof

The Polar Ionospheric X ray Imaging Experiment (PIXIE) on board the NASA/GGS POLAR spacecraft has been making global observations of X rays from the Earth's auroral regions since March, 1996. PIXIE remotely senses the bremsstrahlung produced by the loss of multi-keV electrons from the magnetosphere into the ionosphere. In this study we examine more than two years of X ray observations of the northern auroral region from the PIXIE instrument. Emitted X ray flux is estimated from the PIXIE observations, which allows us to produce synoptic auroral maps representing the precipitation of energetic electrons as a function of geomagnetic activity as determined by various indices. Effects on the average and median auroral X ray flux are also examined as a function of solar wind parameters, including IMF clock angle.

**GA3.06/E/05-A2** Poster **0930-06**

**AURORAL SUBSTORM AS SEEN IN INTERBALL-2 UV IMAGES**

Wladislav LYATSKY (Polar Geophysical Institute, Apatity, 184200, Russia, email: lyatsky@pgi-ksc.murmansk.su) and Leroy L. Cogger (Institute for Space Research, University of Calgary, Calgary, Alberta, Canada T2N 1N4, email: cogger@phys.ucalgary.ca)

The study of substorms from Interball UV measurements and ground-based magnetometer arrays, shows that a specific phase of a substorm is often observed between the expansive and recovery phases when the substorm stops in its progressing but the energy release remains to be very large, and it can be thought to be a result of a directly driven activity as was suggested earlier by Akasofu [1980]. A real recovery phase is observed in the end of this period. Interball UV images show also that the formation of a bright auroral border at the poleward edge of the auroral bulge seems to be the most remarkable and significant feature of all substorms observed. When reaching some latitude after the beginning of a substorm, this poleward auroral border can stop and remain there during a long time. Sometimes this border occupies a wide interval of local time forming an inner auroral ring described earlier by Elphinstone et al.[1995] as the double oval structure. Interball UV images show that the auroral distribution in the region occupied by auroral substorm forms often bubble or petal-like structures which seem to be growing from a bright protuberant region on the equatorward boundary of the auroral oval. Earlier the similar bubble-like structure of aurora during substorms as seen from Viking UV images was demonstrated by Lyatsky et al. [1998].

**GA3.06/L/04-A2** Poster **0930-07**

**TIME AND SPACE CORRELATIONS BETWEEN PULSATING AURORA AND VLF CHORUS**

Iliia KORNILOV (Polar Geophysical Institute, Apatity, Murmansk region, 184200, Russia, Email: kornilov@pgi.kolasc.net.ru)

On the base of all-sky TV and VLF data aurora-chorus correlations for the different intervals of local time and geomagnetic positions of the recording stations have been studied. It was found that time interval about 22h.- 08h.LT can be separated into three intervals with the different pulsations characteristics. During the interval 20h.-02h.LT typical optical and VLF

pulsations have a periods about 5-10 sec, VLF being represented by pulsating hiss. Correlation analyses reveals anticorrelation between optical and VLF pulsations, and anticorrelating auroral pulsations lead VLF for about 0.5-1.5 sec. Later, about 02h.-05h.LT high frequency component with periods about 0.5-2sec. Appears in aurora pulsations, though strong traces of previous periods of 5-10 seconds are still exist. Chorus elements are also became obvious in VLF emissions. Aurora - VLF correlation is positive, with time delays concentrating preferably around zero. Time interval of the late morning hours (05h.-08h.LT) corresponds to auroral pulsations in the form of week, low brightness fast flashers with a periods about 0.3-1sec., VLF emissions are intensive chorus. Integrated correlation function shows two maxima in delays distribution. VLF lead aurora for 2 seconds and aurora lead VLF for 1.5 sec., and these time delays between aurora and VLF are very well defined. The fact may denote that in the late morning hours aurora and VLF pulsations generating magnetosphere system involves in some global-scale self-synchronization. Study of pulsating aurora and chorus correlations for the different areas of TV screen has revealed, that independently on the position of the maximum of pulsating aurora intensity, the best correlation is achieved for the northern stations (L=5.9) at the south and for the southern station (L=5.2) preferably at the north. These data may point out the position of plasmopause.

**GA3.06/W/12-A2** Poster **0930-08**

**OBSERVATIONS OF DAYSIDE AURORAL PULSATATIONS BY THE INTERBALL UV IMAGER AND EISCAT RADAR**

Alexander KOZLOVSKY (Dept. of Physical Sciences, University of Oulu, P.O. Box 3000, FIN-90401 Oulu, Finland, email: kozlovsky@skynet.oulu.fi), Jorma Kangas (Sodankyla Geophysical Observatory, FIN-99600 Sodankyla, Finland, email: Jorma.Kangas@sgo.fi), Leroy Cogger (Dept. of Physics and Astronomy, The University of Calgary, Calgary, Alberta, Canada, email: cogger@phys.ucalgary.ca) Antti Oikarinen, and Ritva Kuula (both at Dept. of Physical Sciences, University of Oulu, Oulu, Finland)

10 min pulsations in dayside Interball UV auroral measurements and in the magnetic and electric fields variations were studied. The pulsations were observed on 12 February 1997, during quiet geomagnetic conditions and stable IMF Bz = 2nT. Interball UV imager showed 10 min period pulsations of the dayside auroral arc brightness. Corresponding pulsations occurred in the northward electric field over Tromso as measured by EISCAT radar. However, the northward electric field variations over Tromso were in better agreement with the northward magnetic field variations at Svalbard (about 8 degrees northward from Tromso) than with those at Tromso. We believe that this phenomenon is due to inhomogeneous ionospheric conductivity in the vicinity of terminator.

At the Svalbard magnetometer network, northward propagation of the phase of pulsations was observed with a velocity of about 3 km/s, but there was not any visible phase delay along the geomagnetic parallel (Hopen Island - Jan Mayen). Observed pulsations are discussed in terms of magnetic field line resonance oscillations.

**GA3.06/W/13-A2** Poster **0930-09**

**CROSS-SECTION OF AN AURORAL ARC INFERRED FROM EISCAT RADAR MEASUREMENTS**

Alexander KOZLOVSKY, Timo Lakkala (both at Dept. of Physical Sciences, University of Oulu, P.O. Box 3000, FIN-90401 Oulu, Finland, email: kozlovsky@skynet.oulu.fi) Jorma Kangas (Sodankyla Geophysical Observatory, FIN-99600 Sodankyla, Finland, email: Jorma.Kangas@sgo.fi), Antti Oikarinen, and Ritva Kuula (both at Dept. of Physical Sciences, University of Oulu, Oulu, Finland)

Variations of the electric field and ionospheric plasma parameters were measured by the EISCAT incoherent scatter radar during 10 cases of auroral arcs passing through the radar beam. Optical observations of the arc brightness allowed us to separate temporal and east-west spatial variations and to derive a picture of electric fields, currents, electron precipitation, plasma density, electron and ion temperatures across the arc.

The following results are discussed in the light of existing theories of auroral arc formation:  
a) relationship between the auroral precipitation characteristics (energy flux and electron energy) and field-aligned current;  
b) difference between the velocity of the arc and plasma convection velocity,  
c) influence of the electric field and electron precipitation on the electron temperature in E and F regions.

**GA3.06/W/11-A2** Poster **0930-10**

**HIGH-ALTITUDE AURORAL CAVITIES AND THEIR GROUND SIGNATURES**

MÄKELÄ, J.S., P. Janhunen, H. Laakso, and A. Viljanen (Finnish Meteorological Institute, PO Box 503, 00101 Helsinki, Finland. email: Jakke.Makela@fmi.fi. JM also at Physics Department, University of Helsinki, Finland)

We present observations of large-scale plasma cavities at 1 RE and above 4 RE made by the POLAR satellite. We compare the results to ground data from the IMAGE magnetometer chain and EISCAT radar, where applicable. We note that a large-scale cavity with well-defined boundaries can be identified at high altitudes under a wide variety of geomagnetic conditions. There is smaller-scale fine structure within these cavities that can be highly variable. We compare our findings to ground data at the POLAR footprint. No specific ground signature is found to correspond exclusively to the high-altitude cavity.

**GA3.06/W/16-A2** Poster **0930-11**

**DYNAMICS OF AURORAL ELECTRON ACCELERATION REGION AS REVEALED BY AURORAL HISS**

E.E. Titova, A.G. YAHNIN (Polar Geophysical Institute, Apatity, Russia, email: titova@pgi.kolasc.net.ru), F. Jiricek, J. Smilauer, P. Triska (Institute of Atmospheric Physics, Prague, Czech Republic, email: fji@ufa.cas.cz) M.M. Mogilevsky, T.V. Romantsova, A.A. Rusanov (Institute of Space Research, Moscow, Russia, email: mogilevsky@romance.iki.rssi.ru) Smith (Geophysical Institute, University of Alaska, Fairbanks, Alaska, USA, email: bblw@geewiz.gi.alaska.edu)

The Interball-2 satellite auroral hiss observations performed during November-December 1996 were compared with simultaneous observations of auroras. Auroral data were obtained from the ground-based observations on Kola peninsula and Svalbard. Auroral dynamics was used as indicator of the temporal and spatial behavior of the acceleration region. Main attention is paid to strong variations of auroral hiss intensity and frequency at latitudes poleward of the auroral oval, and their relation to auroral dynamics. The temporal intensifications of the hiss, which were observed well poleward from the auroral oval, correlate with both substorm onset and week intensification of a single aurora arc. The auroral hiss cutoff frequency likely depends on distance between auroras and satellite. The cutoff frequency of auroral hiss decreases when the distance between satellite footprint and auroras

decreases and vice versa. Thus the variations of intensity and cut-off frequency of auroral hiss observed by the satellite poleward of auroral oval are close related with both temporal and spatial dynamics of auroral electron acceleration region. Applicability of auroral hiss characteristics for diagnostic of acceleration region is discussed.

**GA3.06/L/07-A2** Poster **0930-12**

**STUDY OF THE MORPHOLOGY OF LARGE SCALE INVERTED-V STRUCTURES**

Oswaldo LUIZAR (Departamento de Física, Universidad Nacional de San Antonio Abad del Cusco, Peru, email: oluizr@inti.unsaac.edu.pe) Marina Stepanova (Departamento de Física, Universidad de Santiago de Chile, email: mstepano@lauca.usach.cl) Jean Michel Bosqued (Centre d'Etude Spatiale des Rayonnements, CNRS/UPS, France) Elizaveta Antonova (Skobel'syn Institute of Nuclear Physics, Moscow State University, Russia) Rostislav Kovrazhkin (Space Research Institute, Academy of Sciences of Russia)

The present work reports the morphological study of multiple inverted-V structures performed in base of the AUREOL-3 satellite data. The upward field-aligned current obtained by integrating of the precipitating electron fluxes often stratifies latitudinally forming multiple large-scale current sheets. Observed events have been classified considering the level of stratification, latitudinal asymmetry of individual current sheet, and increasing (or decreasing) of the current maxima with latitude. It was found that all events show latitudinal asymmetry. The correlation study between the event morphology and the geomagnetic activity shows that the level of stratification increases with the AE-index, and that the mean slope of the structure's asymmetry is determined by the AO-index. The performed classification and the established dependencies can be useful for the development of the field aligned current generation theories.

**GA3.06/E/13-A2** Poster **0930-13**

**IONOSPHERIC CONDITIONS DURING BRIGHTENINGS OF THE POLEWARD BORDER OF THE DIFFUSE AURORAL BAND**

ARJA PAJUNP, Mikko Syrjäso, Pekka Janhunen, Kirsti Kauristie, Ari Viljanen, and Tuija Pulkkinen (all at Finnish Meteorological Institute, Geophysical Research, P.O. Box 503, FIN-00101 Helsinki, Finland, email: arja.pajunpaa@fmi.fi) Erling Nielsen (Max Planck-Institute für Aeronomie, D-37191 Katlenburg-Lindau, Germany, email: nielsen@mirage.mpae.gwdg.de)

During geomagnetically moderate and intense periods there are usually two or three substorm sequences associated with the westward electrojet. We will discuss the brightenings of the poleward border of the diffuse auroral band, which are seen in the vicinity of the latest substorms near the magnetic midnight or morning side. We consider their temporal and spatial occurrence with respect to the substorm expansion phase.

We use data of MIRACLE, which consists of the IMAGE magnetometer network, five all-sky auroral CCD cameras, and the STARE radar system. Events to be investigated are selected based on the magnetometer and all-sky data. Ionospheric equivalent currents are described by IMAGE, and the electric field and the plasma convection are determined by STARE. With the use of available satellite data, we obtain information of conditions in the solar wind and the magnetotail.

**GA3.06/W/32-A2** Poster **0930-14**

**SIMULTANEOUS MEASUREMENTS OF AURORAL FINE STRUCTURE WITH RADARS, PHOTOMETERS, ALL-SKY CAMERAS AND TV-CAMERAS**

J. JUSSILA, H. Holma and K. Kaila (Department of Physical Sciences, University of Oulu, P.O. Box 3000, FIN-90401 Oulu, Finland, email: Jouni.Jussila@oulu.fi)

In November 1998 an Finnish EISCAT measurement campaign was organized. During this EISCAT was supported with versatile ground-based instrumentation. High resolution optical equipment were installed in line at Tromsø, Kilpisjärvi and Karesuvanto in northern Scandinavia. They included two wide-field-of-view real-speed TV-cameras and three photometers. The Tromsø area was also covered with all-sky cameras at Kilpisjärvi (Finnish Meteorological Institute) and Skibotten (Max-Planck-Institut für Extraterrestrische Physik).

In evening 18.11.1998 an auroral substorm occurred at about 2000 UT. Substorm was mainly located north of Tromsø. During the substorms break-up discrete auroral structure passed by the EISCAT radar beam and were clearly observed with optical equipment.

This paper deals with the results of movement of the auroral arc measured by different instruments.

**GA3.06/W/09-A2** Poster **0930-15**

**UNUSUAL AURORAL STRUCTURES OVER THE KOLA PENINSULA**

S.CHERNOUSS, A.Yahnin, A.Roldugin (Polar Geophysical Institute, Apatity, Russia, email: SergeyChernouss@hotmail.com)

Unusual space wave structures in the auroral luminosity (or nightglow) were observed by low light level TV camera from Lovozero station at the Kola Peninsula January 10, 1997 during about one hour in auroral disturbed day. Complete description of the pattern is done in the report and presents by the TV recordings. The periodical luminosity wave structure looks like auroral gravity waves pattern described before by K.Henriksen and M.Taylor (Gravity Wave Studies at Polar Latitudes, in "The Electromagnetic Coupling in the Polar Clefts and Cusps", NATO ASI Series, 1988, p.421.) but have other space and temporal scales and features. The question is a nature and source of the periodical luminosity structures event. Have they an auroral source or atmospheric one connected with thermospheric disturbances after the rocket launch from Plesetsk launch station several hours before the event. Both ideas are under consideration.

**GA3.06/W/31-A2** Poster **0930-16**

**AURORAL ACTIVATIONS OVER KOLA PENINSULA AND X-RAYS MEASURED BY POLAR/PIXIE, ON FEBRUARY 9, 1997**

G.STARKOV1, L.Lazutin1, J.Stadsnes2, J.Bronstad2, I.Kornilov1, T. Kornilova1, L.Borovkov1, N. Ostgaard2, E.Thorsen2, S. Chernouss1 1)Polar Geophysical Institute, Academia, Apatity, Murmansk Region, 184200, Russia, email: lazutin@pgi.kolasc.net.ru 2)Department of Physics, University of Bergen, Allegt. 55, N-5007, Bergen, Norway, email: Johan.Stadsnes@fi.uib.no

During substorm onsets and intensifications acceleration and precipitation into the atmosphere of charged particles occur in a wide energy range from hundreds of eV to several MeV. Some types of active aurora are related to the enhancement of the low energy electrons alone, whereas other types are also accompanied by the increase of the electron flux with energy more than 20 keV. We have analysed four hours of continuous auroral activity on February 9, 1997, registered by TV cameras on the Kola peninsula and the X-ray imager PIXIE on the

POLAR satellite to study visual aurora and X-ray aurora relation and to find different types of auroral activations. Comparison shows that aurora and enhanced X-rays in the midnight sector are observed in general within the same latitudinal boundaries. The main difference is related to the duration of the emission: aurora was observed continuously over Kola peninsula, whereas X-rays were recorded with considerable interruptions. Auroral activations can be divided into three groups by positive, moderate and negative correlation with the X-ray increases. X-rays have been recorded in three out of four substorm onsets with poleward expansion during the initial equatorial arc brightening and several first activations of the poleward expansion. One intense auroral activation with fast southward expansion was also accompanied by X-ray enhancement. Moderate cases include brightening of auroral arcs moving equatorward and active auroral forms in the evening sector. Auroral arcs observed between the substorm intensifications and active auroral forms occurring after first 10-15 minutes of substorm onset and expansion are not accompanied by X-rays enhancement.

**GA3.06/W/30-A2** Poster **0930-17**

**IMPULSIVE CURRENT VORTICES IN THE EVENING SIDE IONOSPHERE**

A. AIKIO (Department of Physical Sciences, University of Oulu, FIN-90570 Oulu, Finland, e-mail: Anita.Aikio@oulu.fi), M. Persson, A. Olsson (both at Swedish Institute of Space Research, Uppsala Division, S-75590 Uppsala, Sweden), M. Lester (Radio and Space Plasma Physics, Department of Physics and Astronomy, University of Leicester, Leicester LE1 7RH, UK)

Short duration (1-2 min) impulsive events in the evening side ionosphere are studied. These events appear as intense short-lived spikes in magnetograms and when differential equivalent current vectors are examined, it appears that they are small-scale current vortices in the ionosphere. Since the vortices are associated with simultaneous bursts of short-period broadband magnetic pulsations (PiBs) it is likely that field-aligned currents accompany these vortices. Two time periods have been selected for a further analysis, the other one is measured by the EISCAT radar and the other by the CUTLASS radar. Relations to auroral features, magnetospheric convection and solar wind will be discussed.

**GA3.06/W/39-A2** Poster **0930-18**

**LOWER IONOSPHERIC RADIO EMISSION AND THE ROLE OF MESOSCALE DENSITY STRUCTURE**

A T WEATHERWAX, P H Yoon, and T. J. Rosenberg (Institute for Physical Science and Technology, University of Maryland, College Park, MD 20742 USA, email: allanw@ipst.umd.edu)

Recent observational and theoretical works on the medium-frequency (1-4 MHz) narrow-band auroral radio waves detected at the ground level, known as auroral roars, have revealed the importance of the mesoscale density cavity structure. Here the F-region density structure is modelled on the basis of measured density structure at the times of roar emissions. In this paper, the excitation of the Z-mode waves at 2 and 3 times the local electron cyclotron frequency inside a model density cavity is investigated, and the subsequent propagation of the Z-mode is studied together with the convective cyclotron growth/damping property as well as collisional damping. It is shown that, in order for the excited Z-mode waves to remain trapped inside the density cavity and continue to grow, the density cavity must be "deep enough." The linear mode conversion of Z-mode to O-mode is also studied by means of simple ray tracing technique, and the mode-converted O-mode rays are also followed to the ground. It is found that the Z-mode waves maintain sufficiently high wave intensities despite the cyclotron and collisional damping, owing to the spontaneously emitted Z-mode waves by the energetic electrons. It is also shown that the linear mode conversion of Z to O mode through the Ellis radio window is possible under broad circumstances, which include the initial wave normal angle and the source height.

**GA3.06/W/38-A2** Poster **0930-19**

**AKR FINE FREQUENCY STRUCTURE AS A MESO-MICROSCALE COUPLING PROCESS**

P H YOON (Institute for Physical Science and Technology, University of Maryland, College Park, MD 20742 USA, email: yoonp@ipst.umd.edu) A T Weatherwax (Institute for Physical Science and Technology, University of Maryland, College Park, MD 20742 USA, email: allanw@ipst.umd.edu)

A theory for the fine frequency structure (< 1 kHz) associated with auroral kilometric radiation (AKR) is presented. It is based upon a realistic model of electron distribution function inside the AKR source region, which is constructed on the basis of mesoscale constraints such as dipole magnetic field strength and parallel potential drop. The growth rate of the X-mode is determined from the local microscopic electron cyclotron maser instability calculation. The resulting normalised bandwidth associated with the X-mode instability growth rate is of the order 0.0001 to 0.001, which may naturally account for the AKR fine frequency structure. The results are quite different from those obtained in many previous calculations and simulations of AKR which relied on simple model electron distribution functions. The convective growth and saturation of individual wave packets can be discussed on the basis of quasi-linear theory combined with the ray trajectory calculations. The numerical results will also be discussed.

**GA3.06/W/04-A2** Poster **0930-20**

**X-MODE RADIATION IN THE HOT NON-MAXWELLIAN AND INHOMOGENEOUS PLASMA**

Alexey KUZNETSOV and Valerii Vlasov (both at Department of Mathematics, Irkutsk State Technical University, Lermontov str. 83, Irkutsk, Russia, email: vlasov@math.istu.irk.ru)

According to recent observations, the auroral kilometric radiation (AKR) is generated in small-scale sources where the propagation of electromagnetic waves is determined mainly by the hot component of plasma. Another feature of these cavities is the presence of sharp plasma density gradients. The dispersion equation for the case when electrons have a ring-like distribution is obtained. To take into account the plasma and magnetic field inhomogeneities, we use Hamiltonian equations. It is shown that inhomogeneities limit the time, during which the wave can be in resonance with particles in the positive slope region. This effect has to be taken into account when determining the amplification rate of the waves in the AKR source.

**GA3.06/W/07-A2** Poster **0930-21**

**FRACTAL STRUCTURE OF AURORAL IMAGES AND SELF-ORGANISED CRITICALITY**

KOZELOV B.V. (Polar Geophysical Institute, Apatity, Russia, email: kozelov@pgi.kolasc.net.ru) Jussila J. (University of Oulu, Oulu, Finland)

Auroral phenomena display the processes in the magnetospheric plasma. The spatial structure of aurora may be described by fractal geometry. We use the box-counting procedure to obtain fractal dimension of isoline as a function of intensity on digitised TV image. This



procedure has been applied to long set of images during substorm. Last decade the conception of self-organised criticality (SOC) as a manner of plasma existence in the magnetic field becomes very popular one. We compare the dynamics of fractal characteristics of auroral images with some features of clusters in the SOC model. The possible connections are discussed.

**GA3.06/W/41-A2** Poster **0930-22**

**STATISTICAL HI-LATITUDE SURVEY OF THE RATIO OF THE WAVE TO STATIC CURRENT POWER USING E/B RATIOS AND A MODEL HI-LATITUDE IONOSPHERE**

J.P.KEADY (Geoloc Coporation, 1601 N.Kent St., Suite 1102, Arlington Virginia 22209 USA, email: keady@geoloccorp.com)

Magnetic field lines are the communication link between the ionosphere and the magnetosphere. Energy deposition by plasma (Alfvén) waves and static currents into and out of the ionosphere is an important consideration in modelling ionospheric and magnetospheric coupling, and are dependent on the ability to distinguish temporal and spatial signals in satellite E and B data. The following statistical study uses derived E/B ratios for transmitted, reflected, absorbed low frequency Alfvén waves and static currents, and a realistic electron density profile for the D,E,F regions (from Geoloc's physics based ionospheric model) to interpret the ratio of wave to current power entering the high latitude regions as a function of various Kp ranges, IMF orientations, seasons and scale sizes.

**GA3.06/W/33-A2** Poster **0930-23**

**IMF BZ ASSOCIATED VARIATIONS OF THE EQUATORIAL ELECTROJET**

Lilia SIZOVA (Institute of terrestrial magnetism, ionosphere and radiowave propagation; 142092, Troitsk, Moscow region, Russia; email: sizov@izmiran.rssi.ru) Mikhail Pudovkin (St. Petersburg State University; 198904, Petrodvorets, Russia; email: pudovkin@snoopy.spbu.ru)

Interaction between solar wind, magnetosphere and equatorial ionosphere has been analysed. For this purpose the daytime characteristics of the equatorial F2 ionospheric layer observed during magnetic storms, and the H-component of the geomagnetic field variations at magnetic equator have been compared with the IMF Bz. The electric field produced by the cusp aligned currents is supposed to cause observed disturbances of the equatorial ionosphere and additional magnetic variations at magnetic equator. Decrease of the H-component (counterelectrojet effect) associated with the appearance of the westward electric field is produced by the field-aligned currents of the zone II. An additional increase of the H-component are associated with the appearance in the day side ionosphere of an eastward electric field produced there by the field-aligned currents of the zone I.

**GA3.06/W/24-A2** Poster **0930-24**

**QUANTITATIVE PARAMETERS OF AURORA-SOUNDS AND OF RELATED ACTIVE ARC**

E. TIMOFEEV, A. Roldugin, V. Kosolapenko (Polar Geophysical Institute of the Kola Science Center of the Russian Academy of Sciences, Murmansk, Russia) M. Syrjasuo, T. Tuomi (Finnish Meteorological Institute, Helsinki, Finland) H. Holme, K. Kaila (Physical Department of the University of Oulu, Finland)

A set of ground-based geophysical data is analyzed for Feb.9, 1997 event when being outdoors three PGI scientists have heard a noisy-like aurora-sound during about one minute when extremely bright rayed arc passed the Lovozero observatory zenith. The set includes data of two TV cameras, scanning photometer, VLF-emissions and ground-based magnetometer recordings at the Kola peninsula, the Tromso, Kiruna and Kilpisjärvi scanning photometer recordings, color Abisko all-sky camera film and variations of the low atmospheric currents recorded in the Sodankyla meteorological observatory. According to the witnesses the sounding rayed arc had red (pink) color at its lower edge and was accompanied by a luminosity streamer propagating down from the edge to non-usually low altitudes so that the luminosity was even visible at the background of the hills surrounding the observatory. The following quantitative parameters of the active arc and of the related sounds are estimated: the Lovozero luminosity intensity was more than 100 kR, the Tromso luminosity time derivative was more than 100 kR/s, velocity of the polarward expansion was the same at the both meridians at distance more than about 500 km and equal to about 5.7 km/s, frequencies of the aurora sounds covered range from about 1 to 5 kHz. The sound phenomenon was not accompanied by any considerable variations of the low atmospheric currents at least by recordings made in Sodankyla at distance of about 300 km from the Lovozero observatory. The results are discussed in terms of a nonlinear transformation of the natural electromagnetic waves and in the light of the contemporary theories of the electro-hydrodynamics of the low atmosphere.

**GA3.07** **Wednesday 21 – Saturday 24 July**

**FORESHOCK, BOW SHOCK, MAGNETOSHEATH, MAGNETOPAUSE, CUSP: STRUCTURE, TRANSIENTS AND WAVES (WITH DIV. II,IV)**

Location: Gisbert Kapp E203 LT1  
Location of Posters: Gisbert Kapp, Coffee Room

**Wednesday 21 July AM**

Presiding Chair: D. G. Sibeck (University of California, Berkeley USA)  
Concurrent Poster Session

**GA3.07/P/01-A3** **0900**

**IMF SCALE LENGTHS AND PREDICTABILITY**

MICHAEL R. COLLIER, J. A. Slavkin, A. Szabo and R. P. Lepping (Laboratory for Extraterrestrial Physics, NASA/GSFC, Greenbelt, Maryland 20771, U.S.A.), Kokubun (Solar-Terrestrial Environment Laboratory, Nagoya University, 3-13 Honohara, Toyokawa, Aichi 442, Japan)

We discuss the results of a systematic study using simultaneous data from three spacecraft, WIND, IMP 8 and Geotail, to examine the properties of magnetic field structures in the typical solar wind. This represents a continuation of the work described in Collier et al. [1998]. Time periods were selected when the plane formed by the three spacecraft included the GSE x-direction so that, in the case of planar structures, the two adjacent spacecraft pairs would determine the same structure angles. Consequently, if effects such as the motion of the Earth relative to the interplanetary structures and deviations in the solar wind direction from GSE x-axis alignment are taken into account, differences in the measured structure angle between

the two spacecraft pairs may be used to deduce structure curvature. Current results indicate typical radii of curvature of ~150-200 RE. This leads to the conclusion that there are two important IMF scale lengths relevant to predictability: (1) the (well-established) scale length over which correlations observed by two spacecraft decay along a given IMF structure, on the order of a few tens of Earth radii and (2) the scale length over which two spacecraft are unlikely to even observe the same structure because of structure curvature, on the order of a hundred Earth radii.

**GA3.07/W/70-A3** **0930**

**CORRELATIVE STUDIES OF THE SOLAR WIND MAGNETIC FIELD AT TWO NEAR-EARTH SPACECRAFT:IMP8 AND ISEE1**

Zerefsan KAYMAZ (Istanbul Technical University, Faculty of Aeronautics and Astronautics, Maslak, 80626, Istanbul, Turkey, Email: zerefsan@itu.edu.tr) David Sibeck (John Hpkins University, Applied Physics, 11100 John Hopkins Road, Laurel, Maryland, 20723, US, Email: sibeck@s1pxv9.jhuapl.edu)

Interplanetary magnetic field (IMF) at two near- Earth spacecraft are compared for the purposes of space weather program. For the magnetospheric studies, both spacecraft are often used as solar wind monitor of the IMF. Previous correlative studies with one spacecraft at the liberation point and the other near-Earth showed that the correlations were highly variable. Among the factors suggested that might effects the correlation are the spacecraft separation, IMF direction and variance, foreshock region, and solar wind parameters. In the present study, despite both the spacecraft are near-Earth orbiting, the correlations still show great variability. We search for parameters that effect the correlation between these two spacecraft. We find that in addition to the distance between spacecraft, foreshock region plays an important role in determining the degree of correlation. The correlation is found to be better if both spacecraft are outside the foreshock region and close to each other. While in the foreshock region, determined by the upstream waves in the magnetic field signature, our initial results show that the distance to the bow shock is important. The upstream waves are large and have high frequencies when spacecraft is close to the bow shock. The larger the amplitude of the waves the lower the correlation is found. While increasing IMF strength and variance result in lower correlation, no clear correlation is found with the solar wind velocity. These results suggest that one should be cautioned while using either of these spacecraft and be aware of the conditions under which they can be used.

**GA3.07/E/23-A3** **1000**

**HOT FLOW ANOMALIES REVISITED**

Steven J. SCHWARTZ (CESR/CNRS, BP 4346, 9 Avenue du Colonel Roche, 31028 Toulouse Cedex 4, France, email: Steve.Schwartz@cesr.fr; permanent address: Astronomy Unit, Queen Mary and Westfield College, London E1 4NS, UK, email: S.J.Schwartz@qmw.ac.uk) Goetz Paschmann (MPI fuer Extraterreische Physik, Postfach 1603, D-85740 Garching,Germany, email: gep@mpe.mpg.de) Malcolm Dunlop (Space and Atmospheric Physics, Imperial College, South Kensington, London SW7 2AZ, UK, email: m.dunlop@ic.ac.uk) Andrew Fazakerley (Mullard Space Science Laboratory, Holmbury St. Mary, Dorking, Surrey RH5 6NT, UK, email: anf@mssl.ucl.ac.uk) Michelle Thomsen (Space and Atmospheric Sciences (NIS-1), Los Alamos National Laboratory, Mail Stop D466, Los Alamos, NM 87545, USA, email: mthomsen@lanl.gov)

Hot Flow Anomalies (HFA) are events near the Earth's bow shock characterised by extremely hot ion temperatures and flow deceleration/deflections greatly in excess of those found in the nearby magnetosheath. Observations and numerical simulations suggest they are the result of an interaction between interplanetary tangential discontinuities and the bow shock. We have put together all studied examples to investigate the statistics of the underlying discontinuities and other aspects. These suggest that HFA formation is favoured by orientations perpendicular to the solar wind flow (resulting in long connection times). We also use multi-spacecraft techniques both to investigate the undisturbed interplanetary discontinuity, which in at least one case is a rotational discontinuity, and to investigate in detail the relative motions of the internal structures.

**GA3.07/W/39-A3** **1100**

**SMALL SCALE SOLAR WIND ION FLUX AND IMF CORRELATED STRUCTURES IN THE EARTH'S FORESHOCK REGION: INTERBALL-1 OBSERVATIONS**

Pavel EIGES, Georgy Zastenker, Mihail Nozdachev (Space Research Institute, Profsovnaya str. 84/32, Moscow, 117810, Russia, Email: eiges@iki.rssi.ru)

The foreshock phenomenon is an important part of solar wind-magnetosphere interaction. In our work long series (up to several hours) of high time resolution (up to 16 Hz) measurements of solar wind plasma and IMF made onboard INTERBALL-1 were used to study large and fast fluctuations in the Earth's foreshock region. Several types of fluctuations in the foreshock have been selected in consequence of statistical analysis. Comparison analysis was also applied in order to establish unique characteristics of each type. High positive correlation (correlation coefficient is about 0.7-0.8) between plasma and magnetic field ULF (3-30 mHz) variations during all the time of foreshock observations was found. Existence of such correlation is supposed as a typical foreshock feature. Many events of simultaneous nearly harmonic oscillations of solar wind ion flux and IMF magnitude with periods 1-3 seconds and duration of wave-packet up to 20 seconds were observed and case study of them was performed.

**GA3.07/E/10-A3** **1130**

**STATISTICAL BOW SHOCK MODELS: COMPARISON WITH NEW OBSERVATIONS**

J. SAFRANKOVA, Z. Nemecek, M. Borak (Faculty of Mathematics and Physics, Charles University, Prague, Czech Republic, Email: jana.safrankova@mff.cuni.cz)

During the time interval from August 1995 to August 1997, the MAGION-4 satellite (INTERBALL-1's subsatellite) observed more than 850 bow shock crossings. Due to the high inclination and temporal evolution of its elliptical orbit, the MAGION-4 data set covers mainly two latitudes - near the equatorial plane and around the  $\zeta_{GSE} = \pm 10 R_{ES}$ . Both outbound and inbound crossings are spread from the subsolar region to the  $\zeta_{GSE} \approx \pm 10 R_{ES}$  and occurred under various upstream conditions: the solar wind dynamic pressure varied from 1 to 12 nPa and  $Alfv_{nic}$  Mach number from 4 to 50. GEOTAIL bow shock crossings measured in the same time interval covered the equatorial plane near the terminator. These new data set provides an opportunity to test empirical models describing the bow shock position. We have tested influence of the solar wind and IMF fluctuations, solar wind aberration, and Mach number with motivation to find a direction for further development of models.



Wednesday 23 July PM

Presiding Chair: D. G. Sibeck (University of California, Berkeley USA)

**GA3.07/W/48-A3 1400**

**ON BOW SHOCK SURFACE WAVES NEAR SOLAR MINIMUM**

R. L. KESSEL, NASA GSFC, Greenbelt, MD 20771, USA

Earth's bow shock represents the outermost boundary between that region of geospace which is influenced by Earth's magnetic field and the undisturbed interplanetary medium streaming from the Sun. This boundary is important because it is here that the streaming solar wind is slowed, heated, and partially deflected around the Earth's magnetosphere. From solar wind observations, we know there exist rotational and tangential discontinuities, current sheets, magnetic holes and clouds, many of which eventually impact the Earth's magnetosphere with first contact at the bow shock. There are also any number of small scale structures, inhomogeneities, or perturbations present in the solar wind which hit the bow shock. As solar wind structures or changes in the solar wind impinge on the bow shock, it moves in response. In this presentation we investigate under what conditions waves can form on the surface of the bow shock due to structures in the solar wind. We use Geotail data near solar minimum (1995-1997); concentrating on bow shock flank crossings because it is here that more motion and wave activity is expected - the nose is more tightly locked into place while the flanks can flap in the breeze. High speed solar wind streams are dominant during the descending phase of the solar cycle because the polar coronal holes producing the fast solar wind, reach their maximum latitudinal extent near sunspot minimum, confining the slow solar wind to a narrow equatorial belt. We correlate the high speed streams to times of large numbers of bow shock crossings with bow shock normals significantly different from model normals. We also explore increased fluxes of energetic electrons using SAMPEX data which have also been correlated with high speed streams. If the structures in the solar wind are responsible for exciting the magnetosphere, waves on the bow shock may be the first signal.

**GA3.07/W/09-A3 1430**

**UNUSUAL SHAPE AND MOTIONS OF EARTH'S BOW SHOCK**

ADAM SZABO (Laboratory for Extraterrestrial Physics, NASA Goddard SFC, Greenbelt, Maryland, 20771, USA, email: Adam.Szabo@gfsc.nasa.gov)

Multi-point observations of Earth's bow shock by WIND, IMP 8, Interball, and Geotail reveal unusual motions and/or distortions in the shock surface. The results of non-linear least squares, Rankine-Hugoniot fittings carried out for observations at each spacecraft will be presented. It has been established that the bow shock moves significantly even during relatively calm solar wind conditions without any apparent trigger disturbance. In particular, one set of observations, when IMP 8 and Geotail crossed the bow shock within a few Re of each other and nearly simultaneously, indicate highly distorted bow shock shapes as both spacecraft encounter it multiple times. Possible physical sources of these distorted bow shock motions will be discussed.

Thursday 22 July AM

Presiding Chair: D. G. Sibeck (University of California, Berkeley USA)  
Concurrent Poster Session

**GA3.07/W/11-A4 0930**

**SYNOPTIC MAPS OF EARTH'S MAGNETOSHEATH**

J. D. RICHARDSON, K. I. Paularena, M. A. Kolpak, (M.I.T., Center for Space Research, Cambridge, MA, USA, 02139) and G. L. Siscoe (Center for Space Physics, Boston University, Boston, MA 02215).

We present results of a study of Earth's magnetosheath using data from 1977-1984 and 1994-1998. IMP 8 crosses the sheath twice every 12 days, and ISEE 1, ISEE 3, and WIND serve as upstream solar wind monitors. We transform coordinate systems to produce maps of plasma parameters in the magnetosheath. Previous work showed a dawn-dusk temperature and density asymmetry near solar maximum that was not present during solar minimum. We look at an additional five years of data to investigate this effect. The average plasma parameters are compared with those predicted by gasdynamic models. We also show that a poleward circulation is present in the plasma mantle and describe the properties of this region. Comparisons are made with published synoptic maps of the magnetic field in the magnetosheath and magnetotail.

**GA3.07/E/08-A4 1000**

**SOLAR-WIND/MAGNETOSPHERE COUPLING: SPECULATIONS ABOUT THE ROLE OF THE MAGNETOSHEATH**

Joseph E. BOROVSKY and John T. Gosling (both at Space and Atmospheric Sciences Group, Los Alamos National Laboratory, Los Alamos, NM 87545, USA, email: jborovsky@lanl.gov)

Any coupling of the solar wind to the Earth's magnetosphere is mediated by the magnetosheath, which interposes. The known correlations between the solar wind and the magnetosphere are reviewed: these include (1) electrodynamic coupling wherein vBz of the solar wind is correlated with power outputs and substorm occurrences in the magnetosphere-ionosphere system and (2) mass coupling wherein the densities and velocities of the solar-wind plasma are correlated with the densities and temperatures of the hot magnetospheric plasma. Following the review, we will discuss these couplings in light of the changes that occur to the solar wind within the magnetosheath.

**GA3.07/W/72-A4 1030**

**MODELLING THE LARGE-SCALE DYNAMICS OF THE MAGNETOSPHERIC BOUNDARY USING GLOBAL MHD SIMULATIONS**

Jean Berchem (Institute of Geophysics and Planetary Physics, University of California, Los Angeles, California 90095-1567, USA, Email: jberchem@igpp.ucla.edu)

Understanding the large-scale dynamics of the magnetospheric boundary is an important step in assessing the global transport of plasma and energy through the geospace environment. In this talk we review the results from several case studies of the dynamics of the magnetospheric boundary based on three-dimensional magnetohydrodynamic (MHD) simulations of the solar wind-magnetosphere-ionosphere system. In these studies, interplanetary magnetic field (IMF) and plasma parameters upstream of the bow shock served as input to the global simulations; results reveal the large-scale response of the magnetospheric boundary including the dynamics of the magnetospheric cusp. The case studies presented encompass both typical and severe solar wind conditions, as well as

different orientations of the IMF and upstream activities. After reviewing global configurations of the dayside magnetosphere for generic solar wind inputs to the simulations, we discuss the results from simulations that use real input from solar wind monitors. In particular, we use the comparison of the local data streams from the simulations with time series measured by spacecraft crossing the magnetospheric boundary to reconstruct the global geometry and dynamics of the magnetospheric boundary during the events.

**GA3.07/E/15-A4 1130**

**POTENTIAL PROBLEMS IN THE INTERPRETATION AND TESTING OF LARGE SCALE MHD SIMULATIONS**

T. D. ARBER (Mathematical Institute, University of St. Andrews, St. Andrews, Fife KY16 9SS, Scotland, UK, email: tda@dcs.st-and.ac.uk)

Over recent years there has been a rapid growth in the use of large scale numerical simulations to solve problems in MHD. This has been due not just to the increase in computing power but also to the sheer number of different codes which are now available.

This paper presents a review of problems which can occur in such simulations and the tests which should be performed in order to avoid them. These potential problems should be well known to numerical specialists. However, large codes are now often being used as 'black box' research tools by scientist whose primary interest is not in numerical techniques. This paper is intended to clarify the problems one can expect when performing these simulations. At the simplest level this involves tests such as checking energy conservation and convergence. Following on from this are more complex and subtle issues which vary from potential problems with conservative codes (which guarantee exact conservation of total energy) to how one can be sure that the scheme converges to the correct physical solution.

**GA3.07/W/13-A4 1200**

**WIND SURVEY OF MIXED MAGNETOSHEATH-PLASMA SHEET ION REGION EARTHWARD OF XGSE = -20 RE: IMPLICATIONS FOR PLASMA TRANSFER**

Tai PHAN (Space Sciences Lab, University of California, Berkeley, CA, 94720, USA, email: phan@ssl.berkeley.edu) and Masaki Fujimoto (Earth and Planetary Sciences, Tokyo Institute of Technology, 2-12-1 Ookayama, Meguro 152, Tokyo, Japan, email: fujimoto@geo.itech.ac.jp)

We have surveyed more than 20 WIND spacecraft perigee passes to investigate the occurrence of regions of mixed low-energy magnetosheath and high-energy plasma sheet ion populations and its possible dependence on the IMF. We found that at low magnetic latitudes, the mixed region is generally confined to the magnetopause and a thin boundary layer, which is simply the low-latitude boundary layer (LLBL) with its typical tailward plasma flow. At higher magnetic latitudes, however, we have found at least two examples of the mixed ion region deeper inside the magneto-sphere. In one case, which occurred during the first perigee pass of WIND's new high-inclination (45o) petal orbit, on Nov. 27, 1998, an extended region of mixed ions was detected. This region is located between the lobe and the hot plasma sheet, and occurred during an extended period of northward IMF. The two ion populations in the mixed region are remarkably similar (in temperature) to the distributions detected in the magnetosheath and plasma sheet proper, respectively. But in contrast to the LLBL distributions, the plasma in this mixed region is nearly stagnant. The electron distributions in the mixed ion region consist only of a single population with energy between those of the magnetosheath and the plasma sheet proper. Electron pitch angle information reveals that the entire mixed region is on closed field lines, unlike the LLBL. However, the absence of high-energy plasma sheet electrons in this region may suggest that the region was once on open field lines. The exact path of plasma entry to form the mixed region cannot be discern with single-point observations. But it is possible to rule out the mantle as a source for the plasma seen in this region. A possible path is along the boundary between the lobe/mantle and the plasma sheet. In essence, our survey raises the possibility of a latitude dependence of plasma transfer across the flank magnetopause. Finally, comparisons will be made with a Geotail survey of the mixed region in the -35 RE < Xgse < 0 RE range.

Thursday 22 July PM

Presiding Chair: D. G. Sibeck (University of California, Berkeley USA)

**GA3.07/E/05-A4 1400**

**ORIGINS OF ENERGETIC IONS IN CEP EVENTS AND THEIR IMPLICATIONS**

Jiasheng CHEN and Theodore A. Fritz (both at Center for Space Physics, Boston University, 725 Commonwealth Avenue, Boston, MA 02215 USA, http://buspace.bu.edu/EPG/jiasheng/chen.html, email: chen@buasta.bu.edu)

A new magnetospheric phenomenon called a cusp energetic particle (CEP) event has been discovered by the POLAR spacecraft in 1996 [Chen et al., GRL, 24, p.1447, 1997]. The events were detected in the dayside polar cusp near the apogee of POLAR and could last for hours, in which the measured helium ions had energies up to 8 MeV [Chen et al., JGR, 103, p.89, 1998]. A fundamental question is where do the cusp MeV ions come from? It was found that all of these events were associated with a dramatic decrease in the magnitude of the local magnetic field, and that the charge state distribution of these ions was indicative of their source being recently the solar wind. Furthermore, the simultaneous observations indicated that the ion fluxes in the CEP events were higher than that in both the upstream and the downstream from the bow shock. Therefore, bow shock acceleration cannot explain the measured ion flux in the CEP events. We have determined the power spectra of the local magnetic field turbulence calculated over the CEP event periods for fluctuations in the ultra-low frequency (ULF) ranges, corresponding to periods of about 0.33-500 seconds. It is found that the integrated power of the turbulent spectra over the ULF ranges is correlated with the intensity of the MeV helium flux. These results provide the first direct observation evidence that the high-altitude dayside cusp is a new acceleration region of the magnetosphere.

**GA3.07/L/03-A4 1430**

**ELECTRIC FIELDS AND ULF/ELF PLASMA WAVES IN THE CUSP OBSERVED WITH THE POLAR AND FAST SPACECRAFT**

R. Pfaff (Laboratory for Extraterrestrial Physics, NASA/Goddard Space 46 light Center Greenbelt, MD 20771), C. Carlson, R. Ergun, F. Mozer, J.McFadden (all at Space Sciences Laboratory, University of California, Berkeley, CA), R. Strangeway (IGPP, Univ. of Calif., Los Angeles, CA)

Both the FAST and Polar spacecraft have encountered the Earth's cusp on numerous occasions during their first years in orbit. Intense quasi-DC electric field structures and distinct plasma waves are consistent features of these cusp encounters which are identified primarily by their localized keV dispersed ion "injections". In the Polar electric field data set at altitudes of 5-7 RE, intense (5-10 mV/m, rms), localized ULF electric field structures are a consistent

feature of these cusp encounters. Distinct magnetic field perturbations, evident in the Polar magnetometer data, are also commonly associated with these cusp encounters, and reveal evidence for Alfvén-C8nic wave structures and field-aligned and filamentary currents. By analyzing simultaneous measurements of the electric and the magnetic field components of the ULF plasma waves, we address the energy flow associated with the wave fields and provide important information concerning the source region of the waves. The FAST data, near 4000 km, also reveals intense ULF electric field turbulence but also several wave modes associated with localized acceleration processes have been identified thus far include: intense (>100 mV/m rms) ULF/ELF waves, emissions observed near the lower hybrid frequency and associated ion Bernstein modes. We examine several cusp encounters in detail in order to study the complex relation of the waves with the DC electric fields, ambient plasma density, and the cusp energetic particle populations, and relate these to larger scale driving processes.

**Friday 23 July AM**

Presiding Chair: D. G. Sibeck (University of California, Berkeley (USA))  
Concurrent Poster Session

**GA3.07/W/71-A5 0900**

**ULF WAVES IN THE MAGNETOSHEATH**

Richard E. Denton (Department of Physics and Astronomy, 6127 Wilder Lab, Dartmouth College, Hanover, NH 03755-3528, USA, email: Richard.denton@dartmouth.edu)

The magnetosheath is both a conduit into the magnetosphere for upstream waves and a source region for new waves. Alfvén and ion cyclotron waves are commonly observed just downstream of the bowshock. Velocity anisotropies generated at the bowshock and within the magnetosheath proper drive mirror and ion cyclotron waves; these waves can be significantly modified as they approach the magnetopause where the plasma beta decreases. The mirror modes can pile up in front of the magnetopause, thus acquiring a finite phase velocity relative to the flow. Waves previously identified as slow mode waves have now been shown to be best identified as the mirror mode (it is possible that there is some coupling between the two). Kinetic Alfvén waves may also exist in the vicinity of the magnetopause. Waves recently identified as the quasi-parallel mirror mode (with wave vector roughly parallel to the background magnetic field) probably consist of a mixture of conventional mirror mode (quasi-perpendicular wave vector) and Alfvén waves. Quasi-parallel shock conditions (interplanetary magnetic field roughly parallel to the shock normal) lead to high beta large amplitude fluctuations, the properties of which are only now beginning to be examined.

**GA3.07/W/10-A5 0930**

**CAVITIES, WAVEGUIDES AND OTHER BEASTS: THE GLOBAL ULF RESPONSE OF THE MAGNETOSPHERE**

W. ALLAN (National Institute of Water and Atmospheric Research, PO Box 14-901 Kilbirnie, Wellington, New Zealand, email: w.allan@niwa.cri.nz)

Virtually all the energy in the magnetosphere comes from outside. Some of this energy arrives by direct solar heating, but most of it comes from the solar wind through the magnetopause and the magnetospheric cusps.

Hydromagnetic waves, or ultra-low-frequency (ULF) waves, are basic modes of the magnetospheric system. Changes in the energy distribution of the magnetosphere must be accompanied by ULF waves to transmit the changes. The waves can therefore be used as diagnostics of the changing magnetosphere.

In the last two or three decades, a zoo of strange creatures has appeared in the literature. These beasts include field line resonances, global or cavity modes, flank waveguide modes, tail waveguide modes, and waveguide modes energized by over-reflection at the magnetopause.

I will conduct a relaxed tour of this zoo, giving a qualitative description of the animals' interesting features, and briefly discussing the observations that have called them into existence.

**GA3.07/W/32-A5 1000**

**EXCITATION OF MAGNETOSPHERIC WAVEGUIDE MODES BY MAGNETOSHEATH FLOWS**

I.R. MANN (Dept. of Physics, University of York, Heslington, York, YO10 5DD, U.K., email: ian@aurora.york.ac.uk) A.N. Wright, K.J. Mills, and V.M. Nakariakov (Mathematical Institute, University of St. Andrews, St. Andrews, Fife, Scotland, KY16 9SS, U.K., email andy@dcs.st-and.ac.uk, katie@dcs.st-and.ac.uk, valery@dcs.st-and.ac.uk)

Using a model incorporating a realistic free magnetopause boundary we show how the compressional fast mode oscillations excited by the solar wind and supported by the Earth's magnetosphere have characteristics which are strongly local time dependent. In regions of low magnetosheath flow speed, such as near local noon, the magnetosphere acts as a leaky cavity. Only at magnetosheath locations where the flow speed is sufficiently fast can modes become perfectly reflected at the magnetopause so that solar wind energy becomes trapped in the magnetosphere. Importantly, for faster flow speed conditions, magnetosheath flows can energise the magnetosphere through the development of magnetopause Kelvin-Helmholtz shear flow instabilities. The mechanism by which these magnetospheric waveguide modes are excited can be understood in terms of the over-reflection of waveguide modes at the magnetopause, over-reflection being more prevalent on the flanks where the magnetosheath flow speed is high. Field line resonances (FLRs), are believed to be driven by these waveguide modes. Our model for the interaction of MHD waves in the magnetosheath and in the magnetosphere can explain both the observed local time dependence of FLR wave power, and the observed correlation between high solar wind speeds and Pc5 wave power. Moreover, the over-reflection mechanism can excite a waveguide mode spectrum displaying preferred azimuthal wavenumbers. This provides an explanation for the observation that FLRs are driven with a particular azimuthal wave number. Finally, we show how a waveguide bounded by a free magnetopause supports quarter-wavelength modes which have lower frequencies than the standard (magnetopause velocity node) half-wavelength modes. This boundary condition may have more success in producing waveguide eigenmodes possessing the millihertz eigenfrequencies required to drive the FLRs which are observed at these frequencies by HF radars and ground-based magnetometers.

**GA3.07/L/05-A5 1100**

**WAVE ENERGY TRANSFER IN COUNTERSTREAMING MHD MEDIA - ACTIVE BOUNDARIES OR NEGATIVE ENERGY WAVES**

A. D. M. WALKER University of Natal, Durban

The plasmas in the magnetosheath and magnetosphere are in relative motion. This allows an MHD wave, incident on the magnetopause, to be amplified or attenuated by exchanging energy with the background flow. Conventional treatments of this problem use a definition of the wave energy in which energy is conserved at the boundary. An amplified reflected wave then leads to the requirement of a transmitted wave carrying negative energy. Such an approach, while producing correct results, assumes harmonic waves and obscures the nature and location of the energy interchange. The proper definition of energy density and flux in a moving plasma will be discussed and related to the group velocity. The mechanism of energy exchange between streaming plasma and wave is through the work done by the Maxwell and Reynolds stresses on the gradient of velocity at the boundary. The location of the energy exchange can be identified as the active boundary, with no need to invoke ideas of negative energy. The relationship between the two approaches will be critically discussed.

**GA3.07/W/38-A5 1130**

**WHY IS THERE A TERRESTRIAL MAGNETOPAUSE?**

Katharine J. Mills, ANDREW N. WRIGHT, Michael R. Ruderman, and Aaron W. Longbottom (all at Mathematical Institute, University of St. Andrews, St. Andrews, Fife KY16 9SS, Scotland, U.K., email: andy@dcs.st-and.ac.uk)

The existence of the terrestrial magnetopause is extremely well established observationally, but its stability is understood theoretically to a limited extent. Indeed, normal mode stability calculations show that a typical magnetopause should be Kelvin-Helmholtz unstable. Field line tension introduces a threshold for instability, and nonlinear effects may saturate the instability. Nevertheless, there should be plenty of occasions when the magnetopause can be expected to blow itself up, but this is never seen in data. Why? We suggest the answer can be found in a more detailed classification of stability: Absolute instabilities grow exponentially at every point in space. Convective instabilities can be interpreted as a wavepacket that grows but also propagates rapidly enough that the amplitude at a fixed point does not grow exponentially but tends to zero at a large enough time. Our preliminary calculations indicate that the magnetopause is onlyconvectively unstable. As a result, disturbances on the flanks will propagate into the tail as they grow and not lead to the disruption of the flank magnetopause (which will have the appearance of a "stable" boundary).

**Friday 23 July PM**

Presiding Chair: D. G. Sibeck (University of California, Berkeley (USA))

**GA3.07W/23-A5 1400**

**MODELS OF FLUID FLOWS IN THE HIGH ALTITUDE CUSP**

P.J. Cargill and M.G.G.T. Taylor (ImperialCollege, London, SW7 2BZ), UK, email:p.cargill@ic.ac.uk

A new model for the interaction of a supersonic magnetosheath flow with the high altitude cusp is proposed. Archival and recent observations have suggested that the cusp is a region of indentation, where solar wind plasma is found Earthward of the nominal magnetopause position. It is proposed that a supersonic solar wind flow interacts with such an indentation by being first accelerated through an expansion fan, and then decelerated by a shock. For most realistic parameters the shock cannot originate from the deepest part of the cusp, but must be detached. The rarefaction of the magnetosheath plasma leads to a rather shallow cusp (< 1 Re),and also implies that the cusp becomes less indented the more tailward it is located. Models will also be presented where a magnetosheath magnetic field is present.

**GA3.07/E/07-A5 1430**

**CONSTITUTION OF DAYSIDE FIELD-ALIGNED CURRENT SYSTEMS**

Masakazu WATANABE (National Institute of Polar Research, 1-9-10 Kaga, Itabashi-ku, Tokyo 173-8515, Japan, email: maskaz@nipr.ac.jp)

Morphology of dayside field-aligned current (FAC) systems is a classic but still stimulating topic because of its importance in magnetospheric physics. This paper provides characteristics of large-scale dayside FACs revealed by DMSP F7 observations, in particular, intensity balance between currents flowing into and away from the ionosphere. It is well known that dayside FACs are controlled by the interplanetary magnetic field (IMF). We deal with two specific IMF conditions: (1) Bz<0nT and |By|>4nT (strong By case), and (2) |By|<1.5nT and -0.5nT<Bz<1.5nT (extremely quiet magnetosphere). For periods of strong IMF By (IMF condition 1), By-dependent FACs are found in cusp/mantle regions, with the intensity of the poleward mantle current either counterbalancing or exceeding the intensity of the equatorward cusp current. This suggests that in addition to the coupling of the mantle and cusp currents themselves, another coupling exists in the magnetosphere. By comparing the current intensities of prenoon and postnoon region 1 currents, we infer that the extra part of the mantle current is connected with the boundary layer region 1 current located downstream of the By-dependent midday ionospheric convection. In contrast, FAC systems that persist even under the extremely quiet magnetosphere (IMF condition 2) are the prenoon/postnoon region 1 currents and the counter region 0 currents poleward of and adjacent to region 1. Both currents are collocated with boundary layer particles with their current intensities evenly balanced. This implies that the basic mode of the dayside FAC systems consists of the coupling of region 0 and region 1 in the magnetospheric boundary region(s).

**Saturday 24 July AM**

Presiding Chair: D. G. Sibeck (University of California, Berkeley)  
Concurrent Poster Session

**GA3.07/E/18-A6 0900**

**IONOSPHERIC TURBULENCE OBSERVED WITH SUPERDARN RADARS, AND RELATIONSHIP TO THE DAYSIDE PROCESSES**

Raphael ANDRE, Mike Pinnock and Alan Rodger (Upper Atmospheric Division, British Antarctic Survey, High Cross, Madingley Road, Cambridge CB3 0ET, United Kingdom) Jean-Paul Villain (LPCE/CNRS, 3A, Av. de la Recherche Scientifique, 45071 Orleans cedex 2, France) Christian Hanuise (LSEET/CNRS, Université de Toulon, BP 132, 83957 La Garde, France)

The SuperDARN radars use ionospheric irregularities (15 meters scale length) as tracers of

the plasma motion, and derive the average line of sight velocity from a complex autocorrelation function (ACF) obtained by the emission of a multipulse sequence. The characteristics of the associated velocity spectrum (spectral width, shape, ...) are directly linked to the properties of the ionospheric turbulence and of the larger-scale electric field projected from the magnetosphere.

These ACFs can be used to describe both micro-scale and macro-scale processes in the ionosphere, which can be linked to magnetospheric processes. A statistical survey of these characteristics over the whole polar ionosphere shows their relationship to magnetospheric processes such as that associated with soft electron precipitation.

The dayside observations show some characteristic features, spatially localized, which give useful information on the solar wind-magnetosphere-ionosphere coupling. In this talk, we describe the ACFs characteristics associated with particular plasma regimes comment on them in some case studies of the dayside ionosphere.

**GA3.07/W/30-A6 0930**

**OBSERVING THE GLOBAL STRUCTURE OF SUDDEN IMPULSE AND TRAVELING VORTEX EVENTS USING GROUND-BASED MAGNETOMETERS AND THE ASSIMILATIVE MAPPING OF IONOSPHERIC ELECTRODYNAMICS TECHNIQUE**

AARON RIDLEY (Southwest Research Institute, San Antonio, TX 78228-0510, USA, email: ridley@zed.space.swri.edu)

Magnetic impulsive events (MIEs) have been observed at high and mid-latitude magnetometer stations for a number of years. With the availability of global data sets, an understanding of the global characteristics of MIEs is developing. We present a study of two different types of MIEs: sudden impulse events and traveling vortex events. The assimilative mapping of ionospheric electrodynamics technique is used to invert the ground-based magnetometer data to show the global electric potential pattern for the different types of events. It is shown that while all traveling vortex events differ in some respect, they all occur at cusp latitudes, have a latitudinal width of approximately 10 degrees, and typically originate in the prenoon sector. The differences in the traveling vortices include direction of travel, speed, and number of vortices. No solar wind or interplanetary magnetic field driver has been verified for these type of events. The sudden impulse events are manifested as a reversed convection pattern superposed upon the already existing large-scale convection pattern. The superposed pattern lasts for 2-5 minutes, and are shown to follow a rapid change in the solar wind dynamic pressure.

**GA3.07/W/24-A6 1000**

**GROUND OBSERVATIONS OF CUSP ASSOCIATED FLOWS AND TRANSIENTS: RECENT RESULTS FROM THE MACCS MAGNETOMETER ARRAY**

David MURR and W. J. Hughes (Center for Space Physics, Boston University, Boston, MA 02215, USA, email: murr@bu.edu) Mark Engebretson (Augsburg College, Minneapolis, MN 55454, USA, email: engebret@augsborg.edu)

Combining the MACCS array with magnetometers from CANOPUS, Greenland, and the MAGIC chains provides a unique opportunity to investigate cusp related flows. The combined network provides a large field of view, 10 hours in local time by 20 degrees in latitude, and a high time resolution of 20 seconds. We have used this array to study the dynamic nature of ionospheric flows as they are driven by the IMF and solar wind. By correlating the IMF and ground magnetograms we find that the ionosphere responds to IMF changes with time scales longer than approximately 15 minutes with a delay of several minutes. These driven flows are punctuated by transients (such as traveling convection vortices) as the ionosphere-magnetosphere system responds to discontinuities in the IMF and solar wind. Using data from solar wind monitors we have identified separate categories of ionospheric transients that appear to be in response to specific types of changes in the IMF and solar wind.

**GA3.07/W/69-A6 1100**

**RECENT RESULTS FROM RADAR OBSERVATIONS OF PULSED IONOSPHERIC FLOWS IN THE DAYSIDE AURORAL ZONE**

T. K. YEOMAN, S. W. H. Cowley, M. Lester, S. E. Milan, D. A. Neudegg, and G. Provan (Department of Physics and Astronomy, University of Leicester, University Road, Leicester, LE1 7RH, U.K.)

The use of special high temporal and spatial resolution scan modes run on the SuperDARN HF radars has provided a wealth of new experimental information about the ionospheric footprint of the cusp. Coordinated experiments with the Equator-S satellite have led to the first convincing simultaneous observations in space and from the ground of the effects of individual pulses of transient reconnection at the magnetopause. The dynamics of such pulsed antisunward ionospheric flows induced on newly opened field lines, and the resulting plasma flows in the return flow on closed field lines have been characterised. The influence of the IMF By component on these pulsed ionospheric flows has been investigated, on both a case study and a statistical basis, as has the latitude, MLT extent and seasonal variation. Comparisons have been possible between radar and optical data, and have shown a very close relationship between the radar backscatter and cusp precipitation. These new observations directly confirm many theoretical predictions of the spatial and temporal development of ionospheric flows in response to transient magnetopause reconnection.

**GA3.07/W/01-A6 1130**

**MULTI-INSTRUMENT GROUND AND SATELLITE OBSERVATIONS OF DYNAMICAL FEATURES IN THE CUSP/CLEFT AURORAL IONOSPHERE**

J. Moen (Air Force Research Laboratory/ VSB (Space), Hanscom AFB, MA-01731-3010, USA. On sabbatical leave from Arctic Geophysics, University Courses on Svalbard, N-9170 Longyearbyen, Norway, Email: jmoen@unis.no)

The complex chain of mechanisms involved in the transfer of solar wind energy, momentum and particles into magnetosphere-ionosphere system manifests itself in the aurora as a rich spectrum of activities. Systematic work on cusp/cleft auroral morphology, however, has provided us a rather comprehensive description of one particular class of activity. That is the poleward moving forms near magnetic noon of which location and motion pattern are strongly regulated by the IMF orientation. Since it was first suggested in the mid-eighties it has been an ongoing debate on whether or not this event class actually is a footprint of pulsed magnetopause reconnection. Ambiguity problems pertain mainly due to the suffer of a limited longitudinal coverage of optical observations. Multi-instrument data from Svalbard and Greenland will be presented to illustrate the IMF By effect on the occurrence probability of poleward moving auroral transients on either side of noon, the IMF By effect on the cusp location, and the relationship between moving auroral forms and excitation of polar cap flow.

**GA3.07/W/25-A3 Poster 0900-01**

**FIELD-ALIGNED CURRENTS BETWEEN BOW SHOCK AND MAGNETOPAUSE**

Igor ALEXEEV (Institute of Nuclear Physics, Moscow State University, Russia, 119899, email: alexeev@dec1.npi.msu.su)

The bow shock and magnetopause are two current surfaces where perpendicular to magnetic field current density is large. The magnetic field jump is a main marker of these surfaces. The bow shock currents system and the tangential to bow shock electric field rigid connected with IMF direction. In opposite magnetopause currents determined by mutual orientation of the geomagnetic dipole and IMF vector. Electric field tangential to magnetopause and magnetopause currents differ for southward and northward IMF. As consequence of this difference the field-aligned currents between bow shock and magnetopause generated. These field-aligned currents was calculated as function of IMF direction. The possibility of the experimental discovery of these currents was discussed.

**GA3.07/W/49-A3 Poster 0900-02**

**COMPOSITION OF MAGNETOSHEATH TURBULENCE**

I. BATES (e-mail: bates@acse.sheffield.ac.uk), M.A. Balikhin, H.St.C.K. Alleyne (all three at:Department of Automatic Control and SystemsEngineering, University of Sheffield, Mappin Street, Sheffield, S1 3JD, UK.), M. Dunlop (Department of Physics, Imperial College of Science, Technology and Medicine, UK.)

The dynamics of turbulence in the magnetosheath is complicated and often there is more than one wave mode observed at the same frequency. The determination of the wave propagation directions at this frequency by standard application of minimum variance analysis is impossible. A method was developed to filter wave data both in frequency and wave number domains to allow the separation of the wave modes. This enables the propagation direction for each separate wave to be determined by minimum variance analysis. Thus the wave mode for each of the observed waves can be determined. Such a technique was applied to the magnetic field data obtained by AMPTE-UKS and AMPTE-IRM satellites in the terrestrial magnetosheath. The wave mode composition of the turbulence for a number of magnetosheath observations have been determined. The results are compared with previous findings based on dimensionless ratios and with the theory of plasma instabilities in the magnetosheath. It is shown that the mirror waves in the turbulence are present to a lesser degree than suggested by the previous findings based on dimensionless ratios.

**GA3.07/E/06-A3 Poster 0900-03**

**ON THE SPATIAL STRUCTURE OF MIRROR MODE FLUCTUATIONS IN THE DAYSIDE MAGNETOSHEATH**

G. ERDOS and M. Tatraylay (both at KFKI Research Institute for Particle and Nuclear Physics, 1525 Budapest P.O. Box 49, Hungary, email: erdos@rmki.kfi.hu)

Magnetohydrodynamic waves generated by the mirror instability are analyzed in this presentation based on magnetic field data collected aboard ISEE-1 and ISEE-2 in the terrestrial magnetosheath. In many cases the time profiles of quasi-periodic mirror mode oscillations are practically the same as observed by the two satellites. However, in the special case discussed here ISEE-1 and ISEE-2 detected long lasting antiphased irregular fluctuations of periods 20 - 50 s close to the magnetopause in spite of the small distance (700 - 800 km) between them. This unique observation helped us to impose some constraints on the geometrical characteristics of the instability, in particular on the longitudinal and lateral size of the structures. Further, the event was associated with multiple quasi-perpendicular bow shock and magnetopause crossings suggesting that the variations of interplanetary parameters might have contributed to the development of the instability.

**GA3.07/W/41-A3 Poster 0900-04**

**UNUSUAL MAGNETOSHEATH PROPERTIES OBSERVED BY ISEE ON OCTOBER 30-31, 1978**

C J FARRUGIA (Space Science Center, University of New Hampshire, NH 03824, USA, Email: farrugia@monet.sr.unh.edu), D Vogl, H K Biernat, S Muehlbacher (all at Space Research Institute, Austrian Academy of Sciences, A-8042, Graz, Austria), R J Fitzenreiter, K W Ogilvie (both at NASA Goddard Space Flight Center, Greenbelt, MD 20771, USA), N V Erkaev (Institute of Computational Modelling, Russian Academy of Sciences, 660036 Krasnoyarsk 36, Russia), G Le, C T Russell (both at Institute of Geophysics and Planetary Physics, University of California, Los Angeles, CA 90024, USA)

We examine a long crossing of the dawnside magnetosheath made by ISEE 2 on October 30-31, 1978, focussing on proton temperature anisotropies but discussing also electron data from the nearby ISEE 1 spacecraft. The observations show a number of unusual features among which are the following. The magnetosheath is mirror stable throughout. No left hand polarized ion cyclotron waves are excited. We find no relation between the proton temperature anisotropies and the proton beta parallel to the magnetic field, and only a weak relation with the proton beta perpendicular to the magnetic field. Following Hau et al. [1993], we study double-polytropic relations. Though polytropic relations fit the data best, the proton thermal behaviour may nonetheless be approximated by an isothermal law.

**GA3.07/E/14-A3 Poster 0900-05**

**TRANSIENT DENSITY EVENTS IN THE MAGNETOSHEATH AND PLASMA IMPULSIVE PENETRATION IN THE DAYSIDE MAGNETOSPHERE**

Daniel HUBERT (Departement de Recherche spatiale, Observatoire de Paris, 92195 Meudon CEDEX, France) Christopher T. Russell (Institute of Geophysics and Planetary Physics, University of California, Los Angeles)

This study uses ISEE-3 observations at the L1 Lagrangian point and ISEE 1-2 observations in the subsolar magnetosheath along an outbound crossing. Thanks to fortunate occurrence a same phenomenon is successively observed in the solar wind, in the inner magnetosheath and in the dayside magnetosphere near the magnetopause. First we discuss the formation of transient density events (TDE) in the inner magnetosheath which are related to rotational discontinuities in the solar wind. The duration of the TDE varies from tens of seconds to about a minute. The density of the TDE in the magnetosheath can exceed background level by a factor of 40%, while the modulus magnetic field in the TDE is only 30% of the field in the surrounding regions. Then we discuss the interaction of the TDE's with the magnetopause. It is shown that this interaction can be analyzed in terms of impulsive penetration of a plasma element. Thanks to the high time resolution of the electron density and magnetic field data, the filamentary structure of the element of plasma observed in the magnetosphere is analyzed.



**GA3.07/W/36-A3** Poster **0900-06**

**THE MAGNETIC FIELD STRUCTURE IN THE MAGNETOSHEATH**

V.V. Kalegaev; Institute of Nuclear Physics, Moscow State University, 119899 Moscow, Russia

The magnetic field structure in the magnetosheath is considered using new dynamic model of supersonic solar wind - Earth's magnetosphere coupling. The magnetopause and bow shock are assumed to be represented as paraboloids of revolution. The supersonic solar wind flow past the parabolic magnetopause is calculated, taking into account changing of the magnetopause and bow shock location and flaring due to solar wind variations. Magnetosphere is presented by the paraboloid model. The condition of magnetic field continuity was held on the magnetopause. The MHD equations in the magnetosheath, where the ohmic conducting solar wind plasma flow past the magnetosphere, are solved analytically as a singularly perturbed system with two independent small parameters, which are inversely proportional to Mach-Alfvén and magnetic Reynolds numbers.

It is found that the magnetic field enhancement on the bow shock is determined by plasma compression. Taking into account plasma conductivity near the magnetopause allows us to describe the magnetic field and energy transport into the magnetosphere and estimate the reconnection efficiency, potential difference across the polar cap, energy input rate into the magnetosphere by IMF and solar wind parameters. For the typical magnetosheath conditions, magnetopause thickness is about of 100 times less than stand-off distance. The magnetic field near the magnetopause is formed due to mutual diffusion of the magnetospheric magnetic field in the solar wind and IMF into the magnetosphere. It allows us to explain the difference between magnetic field structures near the magnetopause for the cases of high and low magnetic shears. The magnetic field and plasma flow in the magnetosheath are calculated and compared with those measured by AMPTE/IRM satellite during magnetosheath passes on 24 October 1985 (low magnetic shear) and 28 August 1984 (high magnetic shear).

**GA3.07/W/55-A3** Poster **0900-07**

**MAGNETOHYDRODYNAMIC MODELLING OF THE SOLAR CORONA FOR SPACE - WEATHER APPLICATIONS**

LINKER

Abstract not available at the time of going to press

**GA3.07/W/26-A3** Poster **0900-08**

**A TWO-DIMENSIONAL NUMERICAL STUDY OF STRUCTURE WITHIN QUASI PERPENDICULAR COLLISIONLESS SHOCKS**

ROBERT LOWE and David Burgess (both at Astronomy Unit, Queen Mary and Westfield College, Mile End Road, London E1 4NS, UK email: R.Lowe@qmw.ac.uk)

Two-dimensional hybrid simulations of quasi perpendicular collisionless shocks reveal structure in the magnetic field along the shock front. This structure manifests itself as ripples of magnetic field moving along the shock ramp. The ripples are particularly pronounced in the component of magnetic field perpendicular to the shock front. A physical mechanism for the production of this structure has yet to be satisfactorily determined. We present the results of a numerical study of these ripples using a two-dimensional implementation of the CAM-CL scheme. Our results show that the ripples have a dispersion relation which would be consistent with the presence of MHD-like modes. We investigate how instabilities at the shock front may drive the ripples. In particular, we look at processes driven by downstream waves. We also examine the possibility of trapping MHD-like modes within the shock ramp. Collisionless shocks are observed to be a source of relativistic electrons, although the exact acceleration mechanism remains poorly understood. One-dimensional simulations show that shock drift acceleration is insufficient unless the shock is nearly perpendicular. We examine how ripples might provide additional acceleration by reflecting electrons within the shock structure.

**GA3.07/E/16-A3** Poster **0900-09**

**PROPAGATION AND EVOLUTION OF SOLAR WIND DISCONTINUITIES THROUGH THE MAGNETOSHEATH**

Z. NEMECEK, J. Safrankova (Faculty of Mathematics and Physics, Charles University, Prague, Czech Republic, Email: zdenek.nemec@mf.cuni.cz) G. N. Zastenker (Space Research Institute, Moscow, Russia) K. I. Paularena (MIT, Cambridge, USA)

Abrupt changes of the solar wind dynamic pressure and the IMF magnitude or direction are a dominant factor controlling the magnetospheric dynamics. However, all discontinuities should pass the magnetosheath before they reach the magnetopause. The steady magnetosheath flow can be described by the gasdynamic model but the problem of the propagation of transient phenomena through the magnetosheath is very complicated. In quasisteady state, it should involve the spatial profile of magnetosheath parameters as well as the changing magnetopause geometry and magnetosheath thickness but the transformation of the discontinuities at the bow shock makes the investigation even more difficult.

Our study is based on the simultaneous measurements of the INTERBALL-1 and MAGION-4 satellites in the magnetosheath supported by the WIND data monitoring of the solar wind and IMF. The data from other spacecraft (GEOTAIL, IMP-8) are used whenever available. We have chosen disturbed solar wind intervals, often connected with the magnetic clouds, and traced the propagation of distinct features through the magnetosheath.

**GA3.07/E/04-A3** Poster **0900-10**

**POLAR OBSERVATIONS OF ELECTRIC AND MAGNETIC FIELD BOW SHOCK STRUCTURE**

J. A. NEWBURY, C. T. Russell (both at the Inst. of Geophysics and Planetary Physics, University of California Los Angeles, 405 Hilgard Ave., Los Angeles, CA 90095-1567 USA; email: newbury@igpp.ucla.edu and crussell@igpp.ucla.edu), M. Gedalin (at Dept. of Physics, Ben-Gurion University, Beer-Sheva, 84105 Israel), A. J. Hull and F. S. Mozer (both at Space Sciences Laboratory, Univ. of California Berkeley, Berkeley, CA 94720 USA), and J. Wygant (School of Physics and Astronomy, Univ. of Minnesota, Minneapolis, MN 55455 USA).

On May 4, 1998 the dynamic pressure of the solar wind was great enough to push the magnetosphere in to the point where the POLAR spacecraft observed six crossings of the Earth's bow shock (GSE coordinates: X ~ 6 RE, Y ~ 0 RE, Z ~ 6 RE). This provided the opportunity to examine the structure of both the electric and magnetic fields in collisionless shocks with very high magnetosonic Mach number (4.8 - 9.1), with high plasma beta (2.1 - 4.8), and with quasi-parallel and quasi-perpendicular orientation of the upstream magnetic

field to the shock normal (20 - 66 degrees). Large-scale electric field structure is observed when the convective E-field is oriented within the spin axis of POLAR (where measurements from POLAR's Electric Field Instrument are most accurate). Integrating the electric field across the shock ramp and assuming that the ramp thickness is in the range of 0.2 - 0.6 ion inertial lengths, the cross-shock potential is roughly estimated to be in the range of 2000 - 6000 V. This is on par with the ~3 keV change in kinetic energy of an ion across this shock (as expected from the Rankine-Hugoniot shock jump relations). When the convective electric field is primarily out of the spin plane, the large electric field fluctuations were examined (amplitudes up to 50 mV/m and frequencies of 1 - 20 Hz). The orientation and polarization of these fluctuations are analyzed with respect to the magnetic shock profile and the implications of these observations on shock heating are explored.

**GA3.07/W/02-A3** Poster **0900-11**

**MIRROR INSTABILITY WITH FINITE ELECTRON TEMPERATURE EFFECTS**

O.POKHOTELOV, (Institute of Physics of the Earth, Moscow, Russia, Email: pokh@uipe-ras.scgis.ru); M. Balikhin and H. Alleyne (both ACSE, The University of Sheffield, Mappin Street, Sheffield, UK, Email: m.balikhin@sheffield.ac.uk, H.Alleyne@sheffield.ac.uk)

A theory of mirror instability accounting for the finite electron temperature effects is developed. Using the standard approach to the analysis of this instability we have derived an expression for the growth rate and analyzed the modifications of the instability due to the presence of finite electron temperature and arbitrary electron anisotropy. In comparison with earlier analyses which were limited to isotropic electron distributions, consideration of the general case of arbitrary electron anisotropy allows the application of the results obtained to various regions such as the terrestrial magnetosheath or ring current. In the particular case of isotropic electron distribution comparison with the previous results have been made. It is shown that the earlier analysis is inadequate, because some important resonance terms have been overlooked. This led to the incorrect expression for the growth rate of the mirror instability in a finite electron temperature plasma.

**GA3.07/W/34-A3** Poster **0900-12**

**CALCULATIONS OF PLASMA FLOW IN THE DAYSIDE MAGNETOSHEATH BASED ON THE BOUNDED ANISOTROPY MODEL**

A.A SAMSONOV and M.I.PUDOVKIN

Experimental data show existence of the proton temperature anisotropy in the dayside magnetosheath. The adiabatic MHD model for an anisotropic plasma is known as the CGL equations. But exploitations of the CGL equations for the magnetosheath modelling overestimate the temperature anisotropy values. To improve this situation the CGL model has been developed into the bounded anisotropy model. The last model takes into account the proton pitch-angle diffusion resulting from a plasma instability growth. We calculate a 3D MHD flow around a sphere based on the bounded anisotropy model and compare the results with experimental data. We conclude that the model can describe the observed anisotropy values. Also we compare results of the isotropic and anisotropic models. The calculated magnetosheath width is bigger for the anisotropic model.

**GA3.07/E/21-A3** Poster **0900-13**

**THE KINETIC MIRROR MODE: POLARISATION AND PROPERTIES**

Steven J. SCHWARTZ\* and Christian Mazelle (CESR/CNRS, BP 4346, 9 Avenue du Colonel Roche, 31028 Toulouse Cedex 4, France, email: Steve.Schwartz@cesr.fr; \*permanent address: Astronomy Unit, Queen Mary and Westfield College, London E1 4NS, UK, email: S.J.Schwartz@qmw.ac.uk)

According to anisotropic MHD theory, the mirror mode is a non-propagating fluctuation with magnetic field magnitude and plasma density in anti-phase. The mode, derived in MHD theory from the magnetosonic branch, can grow in regions of perpendicular temperature anisotropies, especially in regions of high plasma beta such as the Earth's magnetosheath. More recently, kinetic aspects have been highlighted which reveal the curious role of the "resonant" particles and the co-existence of the mirror mode with the low frequency magnetosonic modes. All of this work, however, suggests that the mode is polarised in the traditional coplanar magnetosonic sense, i.e., that the fluctuations in magnetic field lie in the plane defined by the wavevector and background field. In numerical simulations, and in spacecraft data, however, a non-coplanar component is seen during the nonlinear phase. We show that such a non-coplanar component can, in fact, be present even in linear kinetic treatments, though it is not clear whether this component is responsible for that seen in the simulations. We explore other aspects of the mirror mode characteristics for such non-coplanar cases.

**GA3.07/W/65-A3** Poster **0900-14**

**FORESHOCK PRECONDITIONING**

D. G. SIBECK (JHU/APL, Laurel, MD 20723 USA, Email: david.sibeck@jhuapl.edu); T. D. Phan and R. P. Lin (both at Space Science Laboratory, UCB, Berkeley, CA, email: phan@ssl.berkeley.edu)

Kinetic processes within the foreshock can greatly modify the incoming solar wind shortly prior to the time when it encounters the bow shock and the magnetosphere, perhaps resulting in pressure pulses or hot flow anomalies. The multipoint observations provided by the ISTP program allow us to better determine the extent of this preconditioning. We begin by presenting a case study of simultaneous Wind, Geotail, Interball-1, and IMP-8 foreshock observations on April 19, 1996 which indicate that bursts of backstreaming ions in the foreshock can create diamagnetic cavities in the solar wind in which densities and magnetic field strengths are depressed by a factor of two. The multispacecraft observations allow us to demonstrate that the dimensions of these cavities are smaller than those of the magnetospheric obstacle, and to demonstrate that the extent of the diamagnetic effect decreases with distance from the bow shock. We then present the results of a survey of Wind perigee passes designed to determine the dependence of the diamagnetic effect on solar wind conditions and spacecraft distance from the bow shock.

**GA3.07/W/29-A3** Poster **0900-15**

**INTERBALL TAIL OBSERVATIONS OF HOT FLOW ANOMALIES**

Oleg Vaisberg Alexander Skalsky, Valery Smirnov, and Levon Avnanov (Space Research Institute, 84/32, Moscow, 117810 Russia, email: olegv@iki.rssi.ru) James Burch, J.Hunter Waite, Jr. (Southwest Research Institute, San Antonio, TX 78228, USA, email: jburch@hal.space.swri.edu)

Several Hot Flow Anomalies in front of the bow shock were identified in 1996 in the data of fast 3-D ion measurements of the SCA-1 ion spectrometer on the Interball Tail Probe. We use

ion and magnetic data to analyze the structure of these HFAs and the magnetic conditions favorable to their development. We also use WIND data to tentatively identify interplanetary discontinuities responsible for these HFAs. We report two new findings compared to previous investigation of HFAs with AMPTE and ISEE spacecraft. One is distinct double structure of HFAs in the solar wind with the trailing (sunward) part being more isotropized. Another is a clear evidence of two ion components within HFA: modified solar wind beam and non-gyrotropic reflected ion beam(s). We present detailed development of interaction of two ion components within HFAs and the magnetic structures within these HFAs. A number of very strong flow anomalies within the magnetosheath, including ones quite close to the magnetopause, are identified. We present evidence that these flow anomalies, apparently associated with the propagation of interplanetary discontinuities through the magnetosheath, lead to the development of wave motions of the magnetopause.

**GA3.07/W/05-A3** Poster **0900-16**

**TURBULENCE GENERATION UPSTREAM OF A QUASIPERPENDICULAR SUPERCRITICAL BOW SHOCK**

S. Walker, M. Balikhin University of Sheffield, UK (University of Sheffield, ACSE, Mappin Street, Sheffield, S1 3JD UK. Email: simon.walker@sheffield.ac.uk); M. N. Nozdrachev, KI, Moscow, Russia

Nonlinear dynamics of the magnetic field turbulence observed upstream of a quasiperpendicular, supercritical bow shock by AMPTE-IRM and Interball are studied using high order spectral analysis techniques. Such an analysis provides evidence in favour of the generation of this turbulence by the internal macrodynamics of the shock front itself, rather than plasma micro instabilities.

**GA3.07/W/21-A3** Poster **0900-17**

**MAGNETOSHEATH STRUCTURE JUST UPSTREAM OF THE MAGNETOPAUSE: DUAL SPACECRAFT ANALYSIS**

T. I. WOODWARD and M. W. Dunlop Space and Atmospheric Physics, Imperial College, London SW7 2BZ, England, UK S. J. Schwartz Astronomy Unit, Queen Mary and Westfield College, London, England, UK. A. N. Fazakerley, Mullard Space Science Laboratory, Holmbury St. Mary, Dorking, Surrey, UK N. Sckopke Max-Planck-Institut für Extraterrestrische Physik, Garching, Germany.

It is well known that the flow of the magnetised solar wind over the Earth's magnetosphere establishes an intricate system of upstream wave-fronts and shocks. In the framework of MHD theory, the bow shock is formed by the fast mode, while physical conditions for the Alfvén and slow mode waves to stand in the flow behind the bow shock (but upstream of the magnetopause) exist. It is the purpose of the current study to use data from the dual spacecraft AMPTE IRM/UKS mission to identify and analyse the motion and structure of low frequency, wave-like structures recorded in the data from regions upstream, but adjacent to, the magnetopause. Evidence for a plasma depletion layer, slow/Alfvén mode standing front, as well as mirror mode-like compressional structures in the local noon region has been reported previously. Here we find evidence for variation in composition between the noon and dawn-side regions and further investigate structural features by inter-comparison of the dual spacecraft data. These wave structures are discussed in the context of the local magnetosheath flow and magnetic field conditions and their occurrence in local time.

**GA3.07/W/64-A3** Poster **0900-18**

**INTERACTIONS OF DISCONTINUITIES WITH THE BOW SHOCK**

XIAOXIN ZHANG(Center for space science and applied research,Chinese academy of sciences, P.O.Box 8701,Beijing 100080, email: zhangxx@center.casar.ac.cn and Yu Lin (Physics department,Auburn University, Auburn, AL 36849, email: ylin@physics.auburn.edu)

Recent theoretical studies have shown that the interaction of a solar wind discontinuity with the bow shock will produce a more complicated structure in the magnetosheath than that by a simple convection. We are searching for the observational evidences for such an interaction. In this study, we investigate the response of the plasma and magnetic field in the magnetosheath to the variations in the interplanetary magnetic field(IMF) direction. The correlation of the magnetosheath observations with the solar wind plasma and the IMF is studied by using magnetosheath data from ISEE-1, ISEE-2 and IRM and the solar wind data from ISEE-3 and IMP-8. We use the solar wind and the IMF measurements as input to the gasdynamic convected field model, as implemented in a new space weather forecast model, and get the relatively accurate timeshift from the solar wind monitor to the magnetosheath and also obtain the prediction properties of the plasma and magnetic field in the magnetosheath. Comparing the magnetosheath observations and predictions with the solar wind and IMF can discern the effects of the variation of the IMF direction on the plasma and magnetic field properties in this process from a simple convection process.

Thursday 22 July AM

**GA3.07/W/31-A4** Poster **0930-01**

**THE PARABOLIC MAGNETOPAUSE FORM AND LOCATION VERSUS SOLAR WIND PRESSURE AND IMF**

I.I. Alexeev, V.V. Kalgaeav, Yu.G. Lyutov ; Institute of Nuclear Physics, Moscow State University, 119899 Moscow, Russia

The new parabolic approximation of the magnetopause is presented using magnetopause crossings data set. The main aim of this study is to provide a more "realistic" magnetopause for the paraboloid model of the magnetosphere which form and location depends on the IMF and solar wind dynamic pressure. This approach allows us to carry out the pressure balance on the magnetopause and provides more accurate calculations of the magnetospheric magnetic field in the framework of paraboloid model. The magnetopause subsolar distance and tail flaring identifying completely the parabolic magnetopause are obtained using crossings of ISEE, Prognoz, Explorer and IMP series satellites. The average values of these parameters are calculated separately for positive and negative Bz component of IMF. It was shown that magnetopause subsolar distance is larger and flaring is smaller for a positive Bz than those for negative one. The dependence of the magnetopause subsolar distance normalized to the average solar wind dynamic pressure on IMF Bz is found. It is less sensitive to positive IMF Bz variation than negative ones. The paraboloid model of the magnetosphere is presented in the form taking into account the magnetopause shape dependence on Bz IMF direction.

**GA3.07/E/11-A4** Poster **0930-02**

**INTERACTION BETWEEN THE MAGNETOSHEATH AND MAGNETOSPHERIC PLASMAS AT THE DAYSIDE MAGNETOPAUSE**

Elena BELENKAYA (Institute of Nuclear Physics, Moscow State University, Moscow, 119899, Russia, Email: Elena@dec1.npi.msu.u)

The structure of the magnetopause is one of the extensively studied questions in the recent years. Investigation of motions of the two sorts of collisionless plasma (magnetosheath and magnetospheric) with frozen-in strong magnetic fields allow to construct a self-consistent model. Low-latitude dayside magnetopause is a double-current layer. For southward IMF, both currents flow from noon to dusk. This is a metastable configuration, in which reconnection may occur. For northward IMF, the current created by the magnetosheath ions is directed to dusk, and the current generated by the magnetospheric ions is directed to dawn. A mechanism of a double-current layer generation at the dayside low-latitude magnetopause is connected with the difference of plasma parameters and magnetic fields in the magnetosheath and magnetosphere. The direction of charged particles gyration at the magnetopause is such that the magnetic field generated by each boundary current creates diamagnetic effect.

**GA3.07/W/56-A4** Poster **0930-03**

**STATISTICAL STUDY OF MAGNETOPAUSE AND IT'S BOUNDARY LAYERS. INTERBALL-1 OBSERVATIONS.**

N.L.BORODKOVA (Space Research Institute Russian Academy of Sciences, Moscow, Russia, Email: nbor@afed.iki.rssi.ru), D.G.Sibeck (Johns Hopkins University Applied Physics Lab., Email: david.sibeck@jhuapl.edu), S.A.Romanov (Space Research Institute Russian Academy of Sciences, Moscow,Russia, Email: sroman@mx.iki.rssi.ru),J.-A.Sauvauud (Centre d'Etude Spatiale des Rayonnements, Toulouse, France, Email: sauvauud@cesr.cnrs.fr)

Magnetopause and its boundary layers play an important role in the transport of magnetosheath mass, momentum and energy into the magnetosphere. Interball-1 spacecraft crossed the magnetopause and boundary layers in a wide range of local times and latitudes. In this paper magnetopause results obtained from electron and magnetic field measurements from Interball-1 during 1995-1998 are reviewed. INTERBALL-1 observations have revealed the existence of very extensive low-latitude boundary layer(LLBL) at the flanks of the magnetopause. The dependence of LLBL encounter on IMF direction is presented. Electron measurements indicate that LLBL is located inside closed magnetospheric field lines.

**GA3.07/E/24-A4** Poster **0930-04**

**SIGNATURES OF MAGNETOTAL RECONNECTION DERIVED BY NUMERICAL SIMULATIONS AND VERIFIED IN SPACE**

JOERG BUECHNER, B. Nikutowski (Max-Planck-Institut fuer Aeronomie, Max-Planck-Str. 2, D-37191 Katlenburg-Lindau, Germany); W. Baumjohann, G. Haerendel (Max-Planck-Institut fuer extraterrestrische Physik, D-85740 Garching, Germany); H.-U. Auster, K.-H. Fornacon (Technische Universitaet Braunschweig, Braunschweig, Germany); E. Georgescu(ISS, Bucharest, Romania)

We present EQUATOR-S magnetic field observations of low-latitude dayside reconnection signatures between December 1997 and February 1998. All clear cut reconnection cases were obtained during periods of large magnetic field shear angles between the ambient solar wind (magnetosheath) and magnetospheric fields. At the same time when the reconnection signatures were found the observations additionally show strong magnetic field excursions in the current direction. We interpret this field behavior in terms of three-dimensional kinetic reconnection. We illustrate the latter by results of kinetic plasma simulations of magnetopause reconnection and compare observations and simulation results in an appropriate magnetopause normal coordinate system.

**GA3.07/E/13-A4** Poster **0930-05**

**A FIRST APPROACH TO THE DYNAMICS OF THE SOLAR WIND MAGNETOSPHERE INTERACTION**

Ricardo Dmaza, Bienvenido Lazo, Alexander CALZADILLA and Ricardo Mansilla Departamento de Geofísica Espacial, IGA/CITMA, Calle 212 No 2906, La Lisa, C.P. 11600, C. de La Habana, Rep. de Cuba. \*Universidad de la Habana, Facultad de Matemática, San Lazaro esq. 29

In this work, we study the predictability of the time evolution of the magnetic activity index Dst, using the methods of the theory of non linear dynamics. The Lyapunov exponents and the correlation dimension were estimated for different sets of Dst data corresponding to the years 1978, 1979, 1980, 1985, 1986, 1995 and 1996; as well as their variation with the embedding dimension. We also performed calculations of autocorrelation functions, probability distributions, and IFS clumpiness tests. Evidences were found of the presence of sensitive dependence of initial conditions, as well as a complicated dynamics of high dimensionality and tough prediction.

**GA3.07/W/60-A4** Poster **0930-06**

**3D ANN DAYSIDE MAGNETOPAUSE MODEL: APPLICATION FOR SUB-SOLAR POINT AND CUSP DYNAMICS**

A.V. DMITRIEV and A.V. Suvorova (Institute of Nuclear Physics, Moscow State University, 119899, Moscow, Russia, email: dalex@srdlan.npi.msu.u)

The code of 3D Artificial Neural Network Model of Dayside Magnetopause is used to describe the dynamics of subsolar point and cusp region under different solar wind and interplanetary magnetic field conditions. The dependence of the subsolar point location on the dynamic pressure and IMF Bz- and By- components is expressed in the form of modified logistic function which permits to describe three different regimes of magnetopause formation controlled by IMF Bz-component. The dynamics of the cusp region extension in longitudes and latitudes is presented. Effects of "dimple" formation in the region of the subsolar point and the cusp disappearance under strong negative Bz (<-10nT) are described.



**GA3.07/W/22-A4** Poster **0930-07**

**DUAL SPACECRAFT VERIFICATION OF MAGNETOPAUSE MOTION DETERMINED BY METHODS BASED ON SINGLE SPACECRAFT DATA**

M. W. DUNLOP Space and Atmospheric Physics, Imperial College, London SW7 2BZ, England T. M. Bauer and N. Scokopke Max-Planck-Institute für Extraterrestrische Physik, Garching, Germany. A. V. Khrabrov and B. U. O. Sonnerup Thayer School of Engineering, Dartmouth College, Hanover, NH 03755, USA A. N. Fazakerley, Mullard Space Science Laboratory, Holmbury St. Mary, Dorking, Surrey, UK.

We attempt to validate results from multi-instrument, single spacecraft, methods for the determination of magnetopause speed and orientation by use of dual spacecraft data, including position and timing. Among these methods, which utilise measured plasma velocity and magnetic field, time series data, are: (1) the determination of the deHoffmann-Teller frame velocity, giving, in combination with the boundary (MVA) normal, the magnetopause speed along the normal, (2) Minimum-Faraday-Residue analysis, which yields both the magnetopause normal and speed and (3) for tangential discontinuities, use of the average measured plasma velocity in combination with the boundary normal to yield magnetopause speed. These techniques rely on certain assumptions, whose validity can be tested, concerning boundary structure and stationarity, and therefore can differ in result. They determine most closely the local properties sampled by a particular spacecraft. The results of such analysis can be verified by comparison with timings of boundary crossings between two or more closely separated spacecraft. We undertake such validation using a range of crossings taken from the AMPTE UKS/IRM data set, which exhibit different boundary characteristics and occur for different spacecraft configurations with respect to the boundary. If the spacecraft separation is small, the local conditions measured by each spacecraft are likely to be similar. But timing differences are then typically small, so that the analysis becomes sensitive to both data calibration effects and to uncertainties in relative spacecraft position and timing. If the spacecraft separation is large, the spacecraft may sample different magnetopause properties, but analysis and measurement errors are then less significant, unless the spacecraft separation vector is nearly perpendicular to the boundary normal. Our results indicate that, under favourable conditions, the aforementioned single spacecraft methods yield magnetopause velocities that agree well with those derived from dual-spacecraft time shifts.

**GA3.07/W/63-A4** Poster **0930-08**

**PROPERTIES OF THE DAWN-SIDE MAGNETOPAUSE AND ADJACENT MAGNETOSHEATH OBSERVED BY EQUATOR-S**

M. W. DUNLOP, E. A. Lucek, P. J. Cargill and A. Balogh, Space and Atmospheric Physics Group, Imperial College, London SW7 2BZ, England. G. Haerendel, W. Baumjohann, E. Georgescu and H. U. Auster Max-Planck-Institute für extraterrestrische Physik, Garching, Germany. Institute of Space Sciences, Bucharest, Romania. K.-H. Fornacon Institut für Geophysik und Meteorologie, TUB, Braunschweig, Germany.

A large number (more than 100) of magnetopause crossings in the low latitude, morning sector of the magnetosphere were observed by the German, Equator-S satellite between December 1997 and the end of March 1998. We review briefly the magnetopause locations, as observed in the magnetometer data (MAM experiment), and relate them to both solar wind and geomagnetic conditions, as well as routinely comparing the magnetospheric field to geomagnetic field models. The apogee of the spacecraft, at a height of 67,000 km, allowed long duration coverage (between 6:00 and 10:40 LT) of the magnetopause and adjacent magnetosheath for medium to high pressure solar wind conditions. Both crossing position and boundary normals compare well to predicted magnetopause location and orientation, but suggest a blunter magnetopause shape than in current magnetopause models. Little evidence is found for large deviations in local boundary normals, as would occur for a wavy boundary. This is consistent with the additional observation of a well ordered, draped magnetosheath field, typically under conditions of high magnetic shear at the magnetopause. The orbit of Equator-S was particularly suited to sample magnetosheath waves. During twelve of the orbits where the spacecraft crossed into the magnetosheath, intervals of intense compressional signatures, suggestive of mirror-mode structures, were observed, often immediately adjacent to the magnetopause. By contrast, no evidence for ion cyclotron waves in the magnetosheath has been found, suggesting the absence of a plasma depletion layer, extending into this dawn-side region. Spectral analysis of the mirror mode structures shows a characteristically shaped shoulder, well defined in the power spectral density, at about 0.05 Hz. The main features of the spectrum appear to be stable, despite significant changes in the temporal distribution and shape of the structures. We discuss the occurrence and characteristics of the observed mirror structures and the crossings associated with them.

**GA3.07/W/28-A4** Poster **0930-09**

**STATISTICAL STUDY OF THE FLANK LLBL LOCATION AND PROPERTIES UNDER DIFFERENT IMF CONDITIONS. INTERBALL-TAIL OBSERVATIONS.**

Andrei FEDOROV, Elena Budnick (both at Space Research Institute, 34/82, Profsovnazna st., Moscow, Russia, email: af@afed.iki.rssi.ru), Jean-Andre Sauvaud, Helene Renault-Stenuit (both at CESR-CNES, 9, avenue de Colonel-Roche, Toulouse, France, email: sauvaud@cesr.cnes.fr)

The Low Latitude Boundary Layer (LLBL) is one of the important plasma and energy transition region between magnetosheath and magnetosphere. The characteristics of LLBL strongly depend on IMF direction and of magnetosheath plasma conditions, however the coupling processes remain unclear. Interball-Tail Probe was surveying the LLBL regions during 1995-1998. Four types of LLBL-type plasma were distinguished for this study. Every pass was divided in several zones according to different plasma regimes. Spacecraft position was projected along model field lines onto XY GSM plane and normalized to average magnetopause position. About fifty boundary layer crossings were investigated. It is shown that different LLBL regimes appear at the magnetospheric flanks depending on IMF direction. Based on this statistical study some assumptions on LLBL formation are presented. The evidence of appearance of ionospheric ions at the plasmashet edge of LLBL is presented and discussed.

**GA3.07/W/61-A4** Poster **0930-10**

**ORDERING OF ELECTRON ANISOTROPY IN THE LOW-LATITUDE BOUNDARY LAYER**

Mike Hapgood and Mike Lockwood, (CLRC Rutherford Appleton Laboratory, Chilton, Didcot, Oxfordshire, OX11 0QX, UK, Email: M.Hapgood@rl.ac.uk)

Enhanced fluxes of 100 eV to 1 keV electrons parallel and anti-parallel to the magnetic field are observed during most crossings of the low-latitude boundary layer (LLBL). We show that these "counter-streaming electrons" are well-ordered by the magnetopause transition parameter of Hapgood and Bryant (1992), which also orders other independent quantities such as the magnetic field and ion bulk velocity. These results will be discussed in the context of a reconnection model of the LLBL.

**GA3.07/W/54-A4** Poster **0930-11**

**TWO DIMENSIONAL STRUCTURES IN THE MAGNETOPAUSE RECOVERED FROM SINGLE-SPACECRAFT DATA**

L.-N. Hau (Institute of Space Science, National Central University, Chung-Li, Taiwan 320, email: lhau@jupiter.nccu.edu.tw); Q. Hu and B.U.Ö. SONNERUP, (both at Thayer School of Engineering, Dartmouth College, Hanover NH 03755, USA, e-mail: qiang.hu@dartmouth.edu, sonnerup@dartmouth.edu)

A technique for recovering magnetic field maps that describe two-dimensional, coherent field structures observed in space is documented, benchmarked, and applied to magnetopause crossings by the spacecraft AMPTE in which the basic observed signatures were those associated with a tangential discontinuity. The calculations consist of the numerical solution of the plane Grad-Shafranov equation, using as initial values magnetic field and plasma data collected by a single spacecraft along a straight-line trajectory, produced when structures are convected past it. The integration proceeds in small spatial steps in both directions away from the trajectory. The method offers a substantial field of view of the region surrounding the trajectory, within which the map accuracy is a few percent. For the magnetopause events examined, it is found that the simple tangential-discontinuity structure is modified by embedded strings of magnetic islands, separated by X-type nulls in the transverse field. These configurations are a manifestation of the tearing mode, after it has reached its saturated state. Two or more islands contained within larger islands are observed, indicating that, during the active phase of the tearing mode, the reconnection rate was not the same at all X points. The possibility exists that one dominating X point produces a pair of narrow channels of open flux, connecting the magnetosphere to the magnetosheath. Even without such open flux, the presence of the islands should allow flow of plasma along magnetic fieldlines, from the outermost (magnetosheath) to the innermost (magnetosphere) parts of the magnetopause current layer, thus facilitating the overall plasma transport across the layer.

**GA3.07/W/52-A4** Poster **0930-12**

**OBSERVATIONAL STUDY OF MODE CONVERSION OF LOW FREQUENCY MHD WAVES AT THE MAGNETOPAUSE: DEPENDENCE ON MAGNETIC ROTATION**

Jay R. JOHNSON and C. Z. Cheng (Princeton University, Plasma Physics Laboratory, Princeton, NJ 08543, Email: jrj@pppl.gov, fcheng@pppl.gov)

At the magnetopause, large amplitude, low frequency, transverse MHD waves are nearly always observed. These waves are likely the result of mode conversion of compressional MHD waves observed in the magnetosheath. Mode conversion readily occurs at the magnetopause because there is a steep gradient in Alfvén velocity [Johnson and Cheng, Geophys. Res. Lett., 24, 1423, (1997)]. A number of observational features support this scenario: a dramatic change in polarization is typically observed from longitudinal in the magnetosheath to transverse at the magnetopause, an increase in wave amplitude at the magnetopause, a change in Poynting flux from cross-field in the magnetosheath to field-aligned at the magnetopause, and a steepening in the wave power spectrum at the magnetopause. In this paper, we explore the dependence of the mode conversion process as a function of magnetic shear. In particular, we shall compare relative wave amplitudes in the magnetosheath and magnetopause; wave polarizations; and spectral slope as functions of magnetic rotation across the magnetopause boundary. The results of this data survey will be compared with theoretical predictions, and implications for transport processes at the magnetopause will be discussed.

**GA3.07/W/18-A4** Poster **0930-13**

**ANALYTICAL MAGNETOSHEATH-MAGNETOSPHERE INTERACTION MODEL WITH EMPIRICALLY DETERMINED FREE PARAMETERS**

Esa J. Kallio and HANNU E. J. KOSKINEN\* (Finnish Meteorological Institute, Geophysical Research, P.O.Box 503, FIN-00101 Helsinki, Finland; e-mail: Esa.Kallio@fmi.fi; \*also at University of Helsinki, Department of Physics)

We describe a new analytical model for studies of solar wind-magnetosphere interaction. Our aim has been to develop a computationally simple model with a small number of free parameters that can be varied to give the best possible fit to one or more satellite observations of the upstream plasma flow and the estimated position of the magnetopause. The magnetic field in the magnetosheath is derived from an analytical model of the plasma flow assuming that the magnetic field is frozen into the flow. The magnetosheath flow is parameterized by a small number of constants. The internal magnetic field model consists of dipole and ring current contributions with a variable dipole tilt. The field is confined inside a parabolic magnetopause. The subsolar point and the width of the parabola can be varied according to observationally or theoretically derived shape of the magnetopause. We can simulate the interconnection of the external and internal fields by letting the two regions overlap within a boundary layer of variable thickness. Although the model does not describe the local physics of the interconnection, it can be used to investigate, e.g., the favorable regions for reconnection under arbitrary direction of the upstream magnetic field after it has passed the bow shock and become wrapped around the magnetopause. The advantages of the model are its numerical simplicity and its adjustability to actual observations. We illustrate the effects of variation of the model parameters using observations of solar wind magnetosphere interaction.

**GA3.07/W/06-A4** Poster **0930-14**

**CHARACTERISTICS OF FTES OBSERVED BY GEOTAIL AND INTERBALL SPACECRAFT**

G.I.Korotova(1),D.G.Sibeck(2),S.Kokubun(3),K.Kudela(4),T.Mukai(5),V.P.Petrov(1), J.Safrankova(6),B.Styazkin(1),K.Takahashi(2) 1.IZMIRAN,Troitsk,Moscow Region,Russia, 2.JHU/APL,Laurel,MD,USA 3.STEL,Toyokawa,Japan; 4.IEF in Cosice,Slovakia; 5.ISAS in Sagamihara,Japan; 6.KEFV MFF UK,Prague,Czech Republic

We present results from case and statistical studies of FTES,observed by the Geotail and Interball spacecraft on the dayside and flank magnetopause. Magnetic field data acquired with Geotail constitute the main data base in this study. We used classical classification scheme and created data base that covers period from 1992 to 1997 and includes more than 1000 FTES with their characteristics and values and orientation of ambient magnetic field in the magnetosheath and magnetosphere. We study FTE occurrence and recurrence patterns as a function of latitude,local time and solar wind parameters. The equatorial events show a marked tendency to occur for southward IMF orientation,consistent with the merging interpretation. We compare the characteristics of the events with recent numerical simulations of bursty merging at a patch, along a single x-line, and along multiple x-lines.



**GA3.07/E/25-A4** Poster **0930-15**

**ANALYSIS OF THE PRESSURE BALANCE EQUATION ALONG THE MAGNETOPAUSE UNDER DIFFERENT CONDITIONS IN INTERPLANETARY MEDIUM**

S.N.KUZNETSOV and B.Yu.Yushkov (both at Skobel'syn Institute of Nuclear Physics, Lomonosov Moscow State University, 119899, Moscow, Russia, e-mail: kuznets@srdlan.npi.msu.ru)

Analysis of the available data set, containing numerous intersections of the magnetopause by different satellites over more than 30 years leads to the conclusion, that the form of the magnetopause should be approximated by a more complicated surface than those of the 2 order (ellipsoid, paraboloid). The form of this surface is not only a function of pressure but also of the Bz IMF component. We used real data for calculation of the pressure balance equation under different conditions in interplanetary medium and for comparison with model values. Results of this comparison are discussed.

**GA3.07/W/35-A4** Poster **0930-16**

**RECONNECTION PROCESSES ON LOW LATITUDE DAYSIDE MAGNETOPAUSE AND HIGH LATITUDE GEOPHYSICAL PHENOMENA DURING 24 JULY, 1996 EVENT**

Tamara Kuznetsova (IZMIRAN, Russian Academy of Sciences), Troitsk, Moscow region, 142092, Russia, email: tvkuz@izmiran.rssi.ru David SIBECK (APL/Johns Hopkins University), Rd., Laurel, MD 20723, USA, email: david.sibeck@jhuapl.edu

The IMF and the magnetosphere are strongly coupled by the magnetic field lines connecting boundary layers of the magnetosphere with the auroral ionosphere. We present our analysis of earlier reported event of dayside magnetopause deformation (24 July, 1996) detected by Interball-1 based on multi-instrument observations. Magnetosphere had a quiet state before event (DMSP F13). Parameters of the solar wind had not sharp changes before and during the event. Study of the geomagnetic data of the stations that allow to determine a sign of the IMF structure shows that sector structure changed sharply (from  $B_x > 0$ ,  $B_y < 0$  to  $B_x < 0$ ,  $B_y > 0$ ), data in the solar wind (Wind, IMP-8) confirm this changes and show Bz change (to  $B_z > 0$ ). Constructed current system DP4 depending from a sign of  $B_y$  IMF explains observed regularities in geomagnetic variations in the cusp and cap and dawn-dusk asymmetry in the Polar UVI images. Reconnection with  $B_y > 0$  IMF on the magnetopause leads to the dawnward convection of magnetic force lines on the dayside boundary of the polar cap concentrating at the cusp. This leads to field-aligned currents and transverse magnetic disturbances under the cusp that are seen at vector diagrams of the relevant stations. Current system DP3 depending from sign of Bz IMF explains additional regularities in the geomagnetic variations. Calculated orientations of reconnection line, intensities of  $E_y$  and  $E_z$  electric fields on the low latitude magnetopause caused by IMF orientation changes projecting on the polar ionosphere explain geomagnetic variations in the cusp and cap, strong electric fields observed by incoherent scatter radar, movements of the low latitude boundary layer at Interball-1.

**GA3.07/E/12-A4** Poster **0930-17**

**RECONNECTION CONFIGURATION AT THE MAGNETOPAUSE BOUNDARY LAYER**

Zhenxing LIU, Tao Chen, and Chao Shen (all at Center for Space Science and Applied Research, Chinese Academy of Sciences, Beijing 100080, China, e-mail: liu@sun20.cssar.ac.cn) Zuyin Pu (Department of Geophysics, Peking University, Beijing 100871, China, email: pzy@pku.edu.cn)

We have investigated the reconnection configuration in the subsolar region of dayside magnetopause boundary layer and high latitude boundary layer (HLBL) by using two-dimensional compressible MHD model. It is supposed that the local and transient magnetic reconnection in the subsolar region can be caused by the impact and sudden stop of a single directional transverse shear flow. It is found that the state of a flow and its lasting period play an important role in reconnection processes. When the inflow is a sheared one, magnetic reconnection always occurs in the magnetopause region. If the impact switches off, the system changes drastically, many kinds of reconnection configurations and fluid vortices are generated in the current sheet region. It is pointed that the sudden stop of external flow impact may be an important triggering mechanism of energy transformation and magnetic reconnection in the plasma boundary layer.

We have also studied the transient reconnection processes caused by the field-aligned shear flow at the high latitude boundary layer for different interplanetary magnetic field. A model of global reconnection configurations for IMF BZ=0 and IMF BZ is northward are proposed. We supposed that the flux transfer events might occur in the HLBL region when IMF is northward.

**GA3.07/W/16-A4** Poster **0930-18**

**TRANSMISSION OF MAGNETOHYDRODYNAMIC WAVES THROUGH THE ROTATIONAL DISCONTINUITY AT THE EARTH'S MAGNETOPAUSE**

A.A. Lubchich (Polar Geophysical Institute, Apatity, Russia; E-mail: lubchich@pgi.kolasc.net.ru)

Reflection and transmission of small amplitude magnetohydrodynamic (MHD) waves of solar-wind origin through the Earth's open magnetopause are studied. The open magnetopause with a nonzero normal component of magnetic field is assumed to be a rotational discontinuity. Transmission of MHD waves through the rotational discontinuity has been considered earlier. For instance, L.C.Lee (Planet. Space Sci., V.30, 1127, 1982) has studied the transmission of Alfvén waves for a rotational discontinuity in which the magnetic field rotates by 180° across the boundary. Y.C.Kwok and L.C.Lee (J. Geophys. Res., V.89, 10697, 1984) have studied the transmission of any of the incident waves for any rotational discontinuity. However, correctness of the results obtained in the last paper (for example, existing of the very high amplification regions and non-zero amplitude of transmission entropy wave for the case of an incident non-entropy wave) is doubtful. We performed the more accurate consideration and got different results. We also found that for any incident wave, there is one reflected wave (usually, it is a fast magnetosonic wave, but under some specific conditions it can be a slow magnetosonic wave) and five transmitted waves (one fast magnetosonic wave, two slow magnetosonic waves, one Alfvén wave and one entropy wave). The transmitted entropy wave appears only in the case of the incident entropy wave. Dependence of the transmission and reflection coefficients on the type of incident wave, the incident angle (all possible angles are included in the consideration), the orientation and strength of the ambient magnetic field is studied. In contrast to the result of Kwok and Lee, it is found that maximal amplitude of the emanating waves differs only by factor 1.5 in comparison with amplitude of the incident waves.

**GA3.07/L/04-A4** Poster **0930-19**

**SIMULATION AND VERIFICATION OF THE SELF ORGANIZATION IN THE MAGNETOPAUSE KELVIN HELMHOLTZ INSTABILITY**

Akira Miura (Department of Earth and Planetary Physics, University of Tokyo, Hongo 7-3-1, Bunkyo-ku, Tokyo 113-0033, Japan, email: miura@sunep1.geophys.u-tokyo.ac.jp)

It is shown by using two-dimensional MHD simulations that the successive pairings of vortices occurring in the nonlinear stage of the Kelvin-Helmholtz instability is a self-organization process, in which the small-scale vortices excited by the instability near the dayside magnetopause evolve into global-scale vortices in the tail of the magnetosphere. The self-organization arises because of the inverse cascade. The total kinetic energy remains almost constant, but the enstrophy decreases rapidly owing to the selective dissipation by the numerical viscosity during the self-organization. Both the kinetic energy, the enstrophy, and the magnetic energy form power law spectra in the wavenumber space in the well developed nonlinear stage. A current eddy is associated with each flow vortex. The simulation results are tested against observations of the magnetopause oscillation. The linear relationships obtained by the simulations between the period of the magnetopause oscillation and the distance along the magnetopause from the subsolar point are in good agreement with the observed period vs. distance relationship. The comparison of the simulation results and the observations gives a thickness of the velocity shear layer near the subsolar point, which is slightly larger than the thickness of the magnetopause.

**GA3.07/W/57-A4** Poster **0930-20**

**CRITERIA FOR FIELD-ALIGNED CURRENT-CARRYING SURFACE WAVES GROWTH AT RECONNECTION**

P. NENOVSKI Geophysical Institute, Bulgarian Academy of Sciences, Sofia, Bulgaria

A surface wave model of field-aligned current (FAC) generation at reconnection has been suggested. The FAC associated with the surface waves flows along the separatrices which divide the unperturbed inflow region from the outflow. These separatrices confine the reconnection region of finite conductivity where the surface wave generation process is initiated. A simple model of velocity dependent conductivity is introduced and an associated reactive-diffusive equation scheme is constructed. The solution found yields the magnitude of the field-aligned currents depending on three parameters - the magnetic Reynolds number, the Mach number and the magnetic field-plasma density ratio. The associated solution has a periodicity trend of relaxation of the perpendicular current which feeds the FAC. When this current evolves to its final state the surface wave FAC process stops. The region of parameters under which the surface waves are marginally stable is examined. Consideration is made for magnetopause conditions.

**GA3.07/L/01-A4** Poster **0930-21**

**USE OF HIGH CHARGE STATE ION COMPOSITION AS A TRACER FOR SOLAR WIND ENTRY INTO THE MAGNETOSPHERE**

C.H., M. Grande and B. Kellett, S. Hefti and T. H. Zurbuchen, G. Gloeckler J.F. Fennell, B. Wilken and T. Fritz

Using data from Polar and ACE during the 1-3 May 1998 CME event we present a comparison of high charge state ion composition measurements from Polar in the magnetosphere with ACE near L1. The solar wind frozen-in charge state distribution for Fe ions was observed to undergo several abrupt changes during this period with the average charge state varying between +4 and +15. These abrupt changes have been used to demonstrate the connectivity between the observations at L1 and those made in the LBL/Cusp region. They indicate direct entry of solar wind material during periods of southward IMF and provide some evidence for prompt entry of these ions into the plasma sheet though not in this case to below geostationary altitude. Having demonstrated that magnetospheric observations of high charge state ions provide a good means of tracing solar wind entry, we use a statistical survey of these measurements taken by Polar over a three-year period, to investigate the entry and transport of solar wind material in the magnetosphere as a function of location and geomagnetic conditions.

Friday 23 July AM

**GA3.07/W/66-A5** Poster **0900-01**

**DIRECT DETERMINATION OF CUSP CURRENT SYSTEMS USING SUPERDARN RADAR AND GROUND MAGNETOMETER DATA - A LINK TO THEORY ON CUSP CURRENT ORIGIN**

Olaf AMM (Finnish Meteorological Institute, Geophysical Research, P.O. Box 503, FIN - 00101 Helsinki, Finland, email: Olaf.Amm@fmi.fi); M. J. Engebretson (Augsburg College, 2211 Riverside Avenue, Minneapolis, MN 55454, USA, email: engebret@augsborg.edu), R. A. Greenwald (Johns Hopkins University, Applied Physics Laboratory, Johns Hopkins Road, Laurel, Maryland 20723-6099, USA, email: ray\_greenwald@jhuapl.edu), H. Luehr (Geoforschungszentrum Potsdam, Telegrafenberg, D-14473 Potsdam, Germany, email: hluehr@gfz-potsdam.de), and T. Moretto (Danish Space Research Institute, Juliane Maries Vej 30, DK-2100 Copenhagen, Denmark, email: moretto@dsri.dk)

We analyse an ionospheric 'enhanced convection event' in the cusp on November 13, 1996, at 1900 UT, using data of the SuperDARN radar, of the IMAGE, Greenland, MACCS and CANOPUS magnetometer arrays, and from other magnetometer stations. The event occurs about 20 minutes after a transition of the IMF By component from positive to negative and an according reconfiguration of the ionospheric electric potential pattern. The data allows a two-dimensional instantaneous view of the event in terms of the ionospheric electric and ground magnetic field. The 'method of characteristics' is used to obtain distributions of ionospheric conductances, true ionospheric currents, and field-aligned currents (FACs) for the interval under study. Our results show that the region of enhanced convection observed by the radar corresponds to an area of low conductances, ranging only slightly above the UV conductance values. However, due to the strongly enhanced electric field, it is governed by enhanced westward flowing Hall and southward flowing Pedersen currents. At the northern and southern borders of the enhanced convection region, sheets of downward and upward FACs are observed, respectively, with magnitudes around 1 A/sqkm. We call this situation an 'inversed Cowling channel' since the resulting current system is similar to a Cowling channel, but the roles of the electric field and the conductance in producing the enhancement of the current are reversed. The geometry of the current system resembles the earlier introduced DPY current system. With our results, we test alternative theories on cusp current origin that lead to different predictions of the relative location of the cusp current system with respect to the open / closed fieldline boundary. The location of this boundary is inferred from DMSP satellite data.

**GA3.07/L/06-A5** Poster **0900-02**

**HIGH ENERGETIC PARTICLES AS A CAUSE OF VLF PLASMA WAVES MEASURED ONBOARD MAGION 4 IN THE OUTER POLAR CUSP**

J.Blecki1, K.Kudela6, J.Slominski1, R.Wronowski1, Z.Nemecek4, J.Safrankowa4, S.Savin2, J.A.Sauvaud5, P.Triska3. 1 Space Research Centre PAS 00-716 Warsaw, Bartycka 18A, Poland, 2 Space Research Institute RAS, Moscow, Russia, 3 Institute of Atmospheric Physics ASC, Prague, Czech Republic, 4 Charles University, Prague, Czech Republic, 5 CESR, Toulouse, France 6 Institute of Experimental Physics, Slovak Academy of Sciences, Kosice, Slovak Republic. email: jblecki@cbk.waw.pl/

The satellite Interball Tail probe and Magion-4 -its subsatellite with their orbits with apogee about 30 RE and an inclination of 650 crossed the polar cusps many times at different altitudes. In this presentation we discuss results of measurements of the spectra of magnetic field fluctuations in the frequency range 30-2000Hz registered onboard Magion-4 and onboard Interball 1 in frequency range 0.1-200Hz. Presented in this paper results of wave measurements in the polar cusps shown, that in this region the wave are a good indicator of the dynamic processes. The most characteristic features of the wave spectra are the broad band emissions and maxima at the lower hybrid, electron cyclotron frequency and sometimes its harmonics. These waves correlate with strong fluxes of the high energetic electrons often observed within the polar cusp by Interball and Magion 4 satellites. The mechanism of the generation of the VLF waves by high energetic electrons will be briefly discussed.

**GA3.07/W/04-A5** Poster **0900-03**

**EXTERIOR CUSP STRUCTURE UNDER DIFFERENT IMF CONDITIONS: THE EVIDENCE FOR THE OPEN MAGNETOSPHERIC TOPOLOGY**

Andrei Fedorov, Elena BUDNICK (both at Space Research Institute, 34/82, Profsovnaja st., Moscow, Russia, email: af@afed.iki.rssi.ru), Eduard Dubinin (Max-Planck Institute fur Aeronomie, Katlenburg-Lindau, Germany, email: dubinin@helene.mpae.gwdg.de), Paul Song (Space Physics Research Laboratory, The University of Michigan, USA, email: pson@sprl.umich.edu), Jean-Andre Sauvaud (CESR-CNES, 9, avenue de Colonel-Roche, Toulouse, France, e-mail: sauvaud@cesr.cnes.fr)

We present observations of plasma flow in the exterior cusp in the vicinity of the magnetopause made onboard the Interball-Tail satellite for different directions of IMF. Under southward IMF three types of ion distribution function are observed in the magnetospheric parts of magnetic field lines (torus-like, pancake and D-shaped). They display a gradually decreasing ion entry along 'old' reconnected magnetic field lines. Under northward IMF D-shaped distributions with varying cutoff velocity parallel to the magnetic field are observed. Such distributions are typical for particles injected along recently reconnected magnetic field lines. We also present results of a simulation that uses the Toffoletto-Hill model of the open magnetosphere to trace the particles from the magnetosheath to magnetospheric locations of Interball. The simulation successfully reproduces the main features of measured distribution functions. Study of plasma behavior shows that the entry of magnetosheath plasma into the magnetosphere can be described in terms of reconnection leading to open topology of field lines near the exterior cusp.

**GA3.07/W/17-A5** Poster **0900-04**

**A SEMI-QUALITATIVE MODEL OF REGION 0 CUSP CURRENTS AND MOVING ARCS**

Galperin Yuri, Space Research Institute of RAS

A simple model of cusp Region 0 FA currents is suggested. It is based on the well known GVBT formula (Grad, 1964; Vasyliunas, 1972; Bostrom, 1975; Tversky, 1982) applied to the region of enhanced plasma pressure within the outer cusp plasma flux tubes as observed by the INTERBALL-1 and MAGION-4 closely-spaced satellites. A pair of Region 0 FA currents with the proper sign is generated at the sides of the outer cusp. A wave-like pressure variation in the outer cusp moving downward with about ion sound velocity will distort the Region 0 current pattern in a way that can lead to a double-sheet FAC formation and excitation of a transient poleward moving arc. The available data on the plasma pressure and magnetic field gradients at the outer cusp edges do not allow to calculate the FAC densities from the GVBT formula. So for quantitative comparisons of this simple model with experimental data we must await the CLUSTER-2 multi-point measurements.

**GA3.07/W/08-A5** Poster **0900-05**

**THE MAGNETOSPHERIC MAGNETIC FIELD IN THE HIGH-ALTITUDE CUSP REGION. THE COMPARISON OF INTERBALL-TAIL MEASUREMENTS AND TSYGANENKO96 MODEL**

Alexander Grigoriev, Andrei FEDOROV, Elena Budnick, Mikhail Nozdachev, (Space Research Institute, 34/82, Profsovnaja st., Moscow, Russia, email: af@afed.iki.rssi.ru), Nickolai Tsyganenko (Raytheon STX Corporation NASA/Goddard Space Flight Center, Greenbelt, Maryland, USA)

It is well-known, that Tsyganenko96 model fails to describe the topology of magnetic field in the exterior cusp region. Recent observations of Polar spacecraft allowed to adjust the model at the middle altitudes. We performed the comparison of T96 model and Interball measurements in the cusp region adjacent to the magnetopause. The observations show the significant deviation of model from real magnetic field. The attempt to find an additional current responsible for this deviation was made.

**GA3.07/W//62-A5** Poster **0900-06**

**FLOWS AND CURRENTS OBSERVED IN AND NEAR THE CUSP BY POLAR AND MACCS**

W.J. HUGHES, K.A. Walker, and D.L. Murr (Center for Space Physics, Boston University, Boston, MA 02215, USA; e-mail: hughes@bu.edu), N. Maynard (Mission Research Corporation, Nashua, NH, USA), W.K. Peterson (Lockheed Martin Space Physics Laboratory, Palo Alto, CA, USA), J.D. Scudder (Department of Physics, University of Iowa, Iowa City, IA, USA)

Flows in and around the magnetospheric cusp, as observed in the ionosphere, respond quickly to changes in the solar wind and IMF, presumably in response to changes in the location and rate of magnetic reconnection as well as to changes in the size and shape of the magnetopause. These changes also manifest themselves in observations made in the high altitude cusp by, for example, POLAR. We correlate observations made in and near the cusp by the field and plasma instruments on the POLAR spacecraft with IMF and solar wind observations, and with ionospheric convection flows deduced from magnetometer observations made around the foot of the POLAR field line. The fast, irregular, very rapidly varying flows observed at POLAR altitudes in the cusp completely mask any signature of the slower flows seen in the ionosphere. But the plasma signatures observed by POLAR vary in step with the changes in convection flow seen in the ionosphere and with IMF changes.

**GA3.07/W/15-A5** Poster **0900-07**

**CHARGED PARTICLES TRAPPING IN THE REGION OF LOCAL MAGNETIC FIELD MINIMUM IN THE EXTERIOR CUSP**

Igor Kirpichev, Andrei Fedorov, Elena BUDNICK, Volt Lutsenko (Space Research Institute, 34/82, Profsovnaja st., Moscow, Russia, email: af@afed.iki.rssi.ru), Jean-Andre Sauvaud (CESR-CNES, 9, avenue de Colonel-Roche, Toulouse, France, email: sauvaud@cesr.cnes.fr)

The models of magnetospheric magnetic field predict a local field minimum along the field lines passing through the exterior cusp near the magnetopause. The bouncing motion of quasi-trapped particles should thus be observed in this region. The Interball-Tail spacecraft was crossing this region during 1995 - 1998. To identify trapping region we investigated the pitch-angle anisotropy of suprathermal ions and electrons in the energy range, 10 - 25 keV and of high-energy electrons (30 - 300 keV). The intensification of 90 degrees pitch-angle population is observed in the region predicted by Tsyganenko96 model. We discuss the possible origin of observed particles and the dependence of their appearance on the cusp configuration.

**GA3.07/W/27-A5** Poster **0900-08**

**THE MORPHOLOGY OF UP-GOING O+ IONS IN RELATION TO INJECTED H+ IONS IN THE MID-ALTITUDE CUSP**

IAN KRAUKLIS, Alan Johnstone, Mullard space science laboratory, Department of space and climate physics, University college London, Dorking, England. Bill Peterson, Lockheed-Martin Palo Alto res. lab. CA 94304, USA.

A common observation by the Polar/TIMAS instrument during cusp crossings is the close association of the energy of the up-going ionospheric O+ with the injected H+ populations. We present a survey of 14 cusp crossings where the interplanetary magnetic field (IMF) was south. A common feature is the rapid acceleration of the O+ co-incident with the onset of the injected H+ population. The average kinetic energy ratio, O+/H+, is approximately 5. There was no significant difference in this ratio for cusp crossings with the IMF northward. No time lag was observed between variations in the energy of the H+ and O+ populations. In the polar cap the parallel component of the bulk velocity of the H+ exceeded the O+ velocity by approximately 30 km/s. The rapid acceleration is inconsistent with centrifugal acceleration mechanism, resulting from convecting field lines, being responsible for the motion of the O+. However the observed velocity difference is consistent with a two stream instability.

**GA3.07/W/68-A5** Poster **0900-09**

**DETERMINATION OF FIELD-ALIGNED CURRENT STRUCTURE ALONG SPACECRAFT TRAJECTORY WITH REGARD FOR EDGE EFFECTS OF CURRENT SHEETS**

R.Yu. LUKIANOVA and O.A. Troshichev (Arctic and Antarctic Research Institute, St.Petersburg, Bering str. 38, Russia, email: renata@geophys.spb.su) Yu.I. Galperin and N.V. Jorjio (Institute of Space Research, Moscow, Profsovnaja 108, Russia email: ygalperin@iki.rssi.ru)

Numerical method of determination of the field-aligned current patterns taking into account both, zonal and meridional, components of magnetic disturbances observed along the spacecraft trajectory has been developed. While the zonal component of magnetic field testifies to number and latitude location of the field-aligned current sheets, the meridional component is evidence of edges of the current sheets. The last circumstance is important for the day-time cusp region where Region 1 FAC are terminated in the vicinity of noon meridian whereas the current sheets located poleward of Region 1 (i.e. cusp currents) are evidently confined to limited MLT sector. Method of model simulation has been used to derive general regularities in latitudinal variation of zonal and meridional components in cases of one, two, three and four longitudinally limited current sheets, two-dimensional equation for vector magnetic potential being solved numerically in spherical coordinates. Latitudinal variations observed by spacecraft are compared with model ones and parameters of the current model are so designed that both curves match best. The optimal current sheet parameters providing similarity of observed and model variations for zonal and meridional components are determined by method of gradient descent in solving of equations for local minimums for each parameter. Magnetic field perturbations observed by AUREOL-3 spacecraft in the day-time region in vicinity of noon meridian have been used as experimental basis. The current patterns consisting with observed features of magnetic perturbations for IMF conditions Bz0 and By<0 involves the following main structures: sheet of upward current at latitudes 70-75 deg., sheet of downward current at latitudes 78-80 deg., and the third current sheet at latitudes above 80 deg. First two sheets are extended from dusk and terminated near the noon meridian, the third sheet consists of downward current in the pastnoon sector and upward current in the prenoon sector. These current sheets can be identified as FAC Region 2, Region 1, and Region 0 (cusp), correspondently. It implies availability of only one additional current sheet poleward of Region 1 under condition of northward IMF.

**GA3.07/E/03-A5** Poster **0900-10**

**THE EXTERIOR CUSP: TWO-POINT OBSERVATIONS**

J. MERKA, Z. Nemecek, J. Safrankova, O. Santolik, L. Prech (Faculty of Mathematics and Physics, Charles University, Prague, Czech Republic, Email: merka@aurora.troja.mff.cuni.cz) S. Savin, A. Skalsky (Space Research Institute, Moscow, Russia)

The cusp is a part of the Earth's magnetosphere, where geomagnetic field lines are directly interconnected with IMF. Since the IMF lines are draped around the magnetopause and blown tailward with the magnetosheath flow, a permanent reconnection took place at the cusp-magnetosheath boundary. Reconnection produces accelerated plasma populations which excite different kinds of plasma waves. As a result, the region adjacent to the magnetopause is highly turbulent and occupied by the heated magnetosheath-like plasma with a low-drift velocity. This region is called turbulent boundary layer, stagnation region or exterior cusp in different papers and it seems to be a proper source of the cusp precipitation. We have used two closely spaced (INTERBALL-1 and MAGION-4) satellites orbiting in the mentioned region with motivation to determine its structure under different upstream conditions monitored by WIND. The topology of the exterior cusp is determined by a direction of the magnetosheath magnetic field just above the cusp. The plasma entry shifts tailward when the magnetosheath magnetic field turns northward and the amount of the plasma entering the exterior cusp is controlled by the magnetosheath fluctuations.

**GA3.07/W/07-A5** Poster **0900-11**

**A SIMPLE MODEL OF PLASMA MANTLE PARTICLE DISTRIBUTIONS DURING PERIODS OF HIGH-LATITUDE RECONNECTION WITH A COMPARISON TO GEOTAIL OBSERVATIONS**

R. T. Mist, and C. J. Owen, Rosalind Mist, Astronomy Unit, Queen Mary and Westfield College, London E1 4NS, E-mail: R.T.Mist@qmw.ac.uk



Hirahara et al. (1997) have previously reported observations of double ion beams close to the magnetopause in the geomagnetic tail. These observations were interpreted as evidence for the occurrence of high-latitude reconnection poleward of the cusp. We test this conclusion by presenting a simple, time-dependent model of the structure of the lobe magnetopause and plasma mantle during the switch from southward IMF/dayside reconnection to northward IMF/high-latitude reconnection. In particular, we address the motion of the plasma entering the magnetosphere from the magnetosheath, along field lines that may have been opened as a result of either subsolar or high-latitude reconnection, or both. We use the model to make predictions of the velocity distributions of these particles within the entry layer just inside the magnetopause. We compare these results to the observations made by Geotail close to the distant tail magnetopause, and show that the model successfully predicts the bulk velocities and densities of the observed plasma populations. Hence, on the basis of this model, the observed double ion beams do indeed appear consistent with the occurrence of high-latitude reconnection.

**GA3.07/L/02-A5** Poster **0900-12**

**DC AND WAVE ELECTRIC FIELDS AND OTHER PLASMA PARAMETERS OBSERVED ON TWSOUNDING ROCKETS IN THE DARK CUSP DURING IMF BZ NORTH AND SOUTH CONDITIONS**

R. F. Pfaff, S. Bounds, M. Acu=D2a (all at NASA Goddard Space Flight Center, Greenbelt, MD), N. C. Maynard (Mission Research Corporation, Nashua, NH), J. Moen (UNIS, Longyearbyen, Norway), A. Egeland, J. Holtet, K. Maseide, P. E. Sandholt (all at University of Oslo, Norway), F. Soraas (University of Bergen, Norway), J. Sharber (Southwest Research Institute, San Antonio, TX), M. Coplan, J. Moore (both at Univ. of Maryland, College Park, MD), W. Burke, D. Hardy, P. Ning, E. Weber ( ), J. Clemmons (M. Lockwood, M. Grande), A. Van Eiken ( ), M. Lester, S. Milan ( )

Two Black Brant IX sounding rockets were launched into the dark, dayside cusp near magnetic noon on December 2 and 3, 1997, from Ny Alesund, Spitzbergen at 79 degrees N reaching altitudes of approx. 450 km. Real-time ground-based and Wind IMF data were used to determine the launch conditions. The first launch, with Bz north conditions, crossed into and back out of an open field region with merging poleward of the projected trajectory. The second flight, into Bz south conditions, was timed to coincide with an enhancement in the merging rate from a increase in the negative Bz, while the DMSP F13 satellite was situated slightly to the north of the rocket trajectory. Each payload returned DC electric and magnetic fields, plasma waves, energetic particles, photometer data, and thermal plasma data. Data from both flights will be shown, with an emphasis on the DC electric field results. In particular, the data gathered on December 2, 1997 will be used to discuss ionospheric signatures of merging and the open/closed character of the the cusp/low latitude boundary layer. In contrast, the data gathered on December 3, 1997 shows evidence of pulsed electric field structures which will be examined in the context of cusp plasma entry recesses. Both data sets returned a rich variety of plasma waves, as well as optical emissions and thermal plasma data.

**GA3.07/W/46-A5** Poster **0900-13**

**WAVES OBSERVED IN THE OUTER CUSP AND THEIR SIGNIFICANCE IN CUSP PROCESSES**

J. S. PICKETT, J. D. Menietti, W. S. Kurth, D. A. Gurnett, and J. D. Scudder (all at: Department of Physics and Astronomy, The University of Iowa, Iowa City, IA 52242, email: pickett@uiowa.edu) S. Savin and S. Romanov (Space Research Institute, Russian Academy of Sciences, Profsoyuznaya 84/32, GSP-7, Moscow, 117810, Russia, email: ssavin@iki.rssi.ru)

A multitude of waves (ULF-VLF) have recently been observed by the Polar and Interball-1 satellites in the turbulent outer cusp region at 7-9 Re. Although many of these waves have been observed previously, we are gaining more insight into them due to the sophisticated instrumentation contained on both spacecraft. Most of the advances have come through the simultaneous capture of six components (three electric, three magnetic) of the waveform in the time domain at high resolution. From this, we have discovered that many of the broadband wave features observed in the past in the frequency domain are actually a numerical artifact of Fourier transformation of pulse-type and nonsinusoidal waveforms. Many of these waveforms have been associated with structures and nonlinear wave packets, rather than classical wave trains. We will discuss the potential of these structures to heat and accelerate particles in the cusp, and comment on their existence in this turbulent area of the cusp. We will also discuss the significance of more typical types of waveforms and Poynting vector distributions observed in the outer cusp, such as those associated with short bursts of whistler mode waves and of electron cyclotron harmonic waves. Examples of the different waveforms will be presented along with the discussion of their significance in the outer cusp.

**GA3.07/E/02-A5** Poster **0900-14**

**PENETRATION OF THE MAGNETOSHEATH-LIKE PLASMA INTO LOBES**

L. PRECH, J. Safrankova, Z. Nemecek, O. Santolik (Charles University, Prague, Czech Republic, Email: lubomir.prech@mff.cuni.cz) D. G. Sibeck (JHU, APL, Laurel, Maryland, USA)

Magnetospheric lobes are bounded by the plasma sheet and high-latitude magnetopause. Satellites orbiting in this region generally measure a low plasma density but sometimes the cavities filled with the magnetosheath-like plasma are encountered. As a rule, the frequency of their occurrence rises in the vicinity of the magnetopause suggesting their magnetosheath origin. A lot of phenomena have been proposed to explain such observations: flux ropes connecting the magnetosheath with ionosphere, surface magnetopause waves of large amplitudes, detached plasma vortices, etc.

Two point observations of the closely spaced INTERBALL-1 and MAGION-4 spacecraft allow us to determine the motion and spatial extent of the observed plasma structures. We have used both statistical approach and case studies to determine a probability of different sources of these events.

**GA3.07/W/59-A5** Poster **0900-15**

**OBSERVATIONS OF THE TIME-VARYING CUSP BY POLAR**

J. RAE, M. Lester (at Leicester University, Leicester, LE1 7RH, U.K.), M. Grande (at Rutherford Appleton Laboratory, Chilton, Didcot, Oxon, U.K.), T. A. Fritz (at Boston University, Boston, Massachusetts, U.S.A.), J. Scudder (at University of Iowa, Iowa City, U.S.A.), C.T. Russell (at University of California, Los Angeles, U.S.A.)

We present a multi-instrument study of the signatures associated with the cusp observed by the Polar satellite. Particle fluxes in the 1-50 keV range are found to pulse on a time-scale of between 12 and 20 minutes, while also pulsing on a shorter time-scale of 2-4 minutes. These pulsed particle populations on cusp field lines are dominated by He++ ions (of solar wind origin). Closed field line populations are of higher energy (50-200 keV), and dominated by protons. Dispersed ion fluxes are observed close to the boundary between open and closed

flux. The pulse-within-a-pulse observations are discussed in terms of possible flux transfer events occurring at the magnetopause.

**GA3.07/W/33-A5** Poster **0900-16**

**HF-VLF PLASMA EMISSION DETECTED IN THE CUSP REGION AT IONOSPHERIC ALTITUDE**

H. Rothkaehl (1), J. Blecki (1), K. Stasiewicz (2), A. Eriksson (2). (1) Space Research Centre PAS, Bartycka 18A, 00-716 Warsaw, Poland (2) Swedish Institute for Space Physics, Uppsala, Sweden

Despite the long history of the observations and theoretical approach to the topside ionosphere at day-side sector still our knowledge in question about instability in cusp area during strong geomagnetic disturbances is not sufficient. HF waves measurements performed in the cusp area on board the ionospheric altitude orbiting satellite Freja reveal the existence of two types of emission: whistler mode waves and Langmuir emissions. The HF and VLF emissions restricted to the cusp region, provide a spatial picture of generation instability in cusp region during strong geomagnetic disturbances. The aim of this paper is presented nature of waves excited during recovery phase of geomagnetic storm in the cusp area.

**GA3.07/W/74-A5** Poster **0900-17**

**FACTORS CONTROLLING THE LOCATION OF THE POLAR CUSP: DIPOLE TILT, IMF ORIENTATION AND SOLAR WIND PRESSURE**

C. T. RUSSELL, X-W. Zhou and Guan Le (All at Institute of Geophysics and Planetary Physics, University of California, Los Angeles, CA, USA, email: ctrussell@igpp.ucla.edu) S. Fuselier (Lockheed Martin, Palo Alto, CA, USA); J. Scudder (University of Iowa, Iowa City, IA, USA)

Nearly 500 crossings of the polar cusp by the POLAR spacecraft at high altitudes over the northern polar cap have been used to examine the statistical behavior of the location of the polar cusp. The tilt of the polar cusp toward the sun moves the invariant latitude of the cusp poleward by 1 degree for every 14 degrees of tilt. Southward IMF causes the cusp foot points to move equatorward but northward IMF has almost no effect on the latitude of the cusp. The cusp also thickens in invariant latitude as the IMF becomes increasingly northward. The eastwest component of the IMF causes the local time of the cusp to move away from local noon inferring that the reconnection site has moved away from the subsolar point, much as foreseen by Crooker and Luhmann. Increasing solar wind pressure thickens the cusp in latitude and widens it in longitude. These results are consistent with those seen by the DMSP satellite when allowance is made for the hourly averaged IMF data used in their work.

**GA3.07/E/09-A5** Poster **0900-18**

**TWO-POINT STUDY OF PLASMA STRUCTURES IN THE NEAR-EARTH MAGNETOTAIL**

O. SANTOLIK, J. Safrankova, Z. Nemecek (Faculty of Mathematics and Physics, Charles University, Prague, Czech Republic, Email: Ondrej.santolik@mff.cuni.cz) A. Fedorov, A. Skalsky (Space Research Institute, Moscow, Russia) J.-A. Sauvaud (CESR, CNRS/University of Toulouse, France)

The data of the INTERBALL project allow to study the motion of plasma structures observed in the near-Earth magnetotail at distances up to 30 Earth's radii and in the wide range of latitudes. Near the boundaries of the magnetotail lobes, the INTERBALL 1 - MAGION 4 satellite pair sporadically encountered plasma structures with temperatures from several hundreds eV to several keV. They move with velocities ranging from several km/s to several tens of km/s and their size is comparable with the Earth's radius. Our statistical study shows that their occurrence rates and positions depend on the external conditions. We discuss possible sources of these plasma structures.

**GA3.07/L/09-A5** Poster **0900-19**

**THE FINGERPRINT OF COLLISIONLESS RECONNECTION**

J. D. SCUDDER and P. Puhl-Quinn (Department of Physics and Astronomy, University of Iowa, Iowa City, Iowa, USA, email: jack-scudder@uiowa.edu) F. S. Mozer (Department of Physics, SSL, UC Berkeley, Berkeley, CA, USA, email: fmozer@sunsport.ssl.berkeley.edu) N.C. Maynard (Mission Research Corp., Nashua, NH, USA, email: nmaynard@mrcnh.com) C. T. Russell (IGPP, Department of Earth and Space Science, UCLA, Los Angeles, CA, USA, email: ctrussell@igpp.ucla.edu)

A protracted 4 hour immersion of the GGS-Polar spacecraft in the current carrying region of the cusp magnetopause during a distended northward IMF pass on May 29, 1996 has been analyzed to demonstrate with hitherto unseen precision the following necessary fingerprints of collisionless magnetic reconnection: 1) non-zero tangential electric field measured in the required geometry of the normals of the rotational discontinuities; 2) 44 quantitatively successful Walen test for Alfvénic structures on both sides of the diffusion region; 3) a protracted interval of large (10mV/m) parallel electric fields measured with three axis electric field measurements with the preponderance of signal from long spin plane antennae; 4) parallel electric current density measured by direct cancellation of numerically integrated electron and ion fluxes; 5) regions of systematically positive  $J(\text{parallel})E(\text{parallel})$  required for field erosion; 6) non-gyrotropy sensed in the electron distribution function and the pressure tensor; 7) detection of all the relevant scales predicted from the collisionless Generalized Ohm's law have been observed including: electron beta modified ion inertial lengths and electron inertial length scales; 8) firm lower bounds of the scales for the electron pressure divergence parallel and perpendicular to B and electrical current density are organized by the observed strength of field erosion; 9) independent cross checks on the scales perpendicular to the magnetic field of the currents from Ampere's equation and the measured currents and the Generalized Ohm's law; 10) ambipolar electric field identified observationally as supporting the parallel electric field; 11) super Alfvénic mach number electron flow sheets observed in agreement with simulations near the separatrix; 12) inflow speeds are sub Alfvénic while reconnected tubes moving at nearly Alfvén mach number unity. A three dimensional pictorial overview of the four hour period will be shown to be consistent with the layer being an example of quasi-stationary, anti-parallel collisionless reconnection with very weak or non-existent guide field and that the spacecraft was on both sides of the separatrix as evidenced by the signs of the Walen proportionality constants and penetrated the region of flux erosion.

**GA3.07/W/20-A5** Poster **0900-20**

**COMPARISON OF THE CUSP/CLEFT DPY CURRENTS OBTAINED FROM THE ØRSTED SATELLITE AND FROM GROUND-BASED INSTRUMENTS**

Peter STAUNING, Freddy Christiansen, Tina Christensen, Vladimir Papitashvili\*, and Ole Rasmussen (all at Danish Meteorological Institute, Lyngbyvej 100, DK-2100, Copenhagen, Denmark, email: ps@dmu.dk; \*also at SPRL, University of Michigan)

The DPY current system associated with the azimuthal component of the interplanetary



magnetic field (IMF) is located in the cusp/cleft region, at approximately 75-80 degrees invariant latitude at the dayside of the polar cap. It appears that the DPY currents comprise the oppositely directed field-aligned current sheets bordering the cusp/cleft region. These currents close in the ionosphere through the horizontal, north-south-directed Pedersen currents, while the potential structure imposed by these currents drives the transverse, east-west-directed convection flows and associated Hall currents. The Hall currents are detectable from ground through their magnetic effects. During the intervals of northward or weak southward IMF these currents appear to be located in the cusp region, while during the strongly southward IMF conditions they appear to progress into the polar cap. The presentation will focus on the correlation of the satellite-based detection of the field-aligned currents, located inside and poleward of the cusp region, and the ground-based detection of the ionospheric DPY currents. These systems, in turn, will be correlated with the strength and direction of the interplanetary magnetic field and other solar wind parameters.

**GA3.07/W/51-A5** Poster **0900-21**

#### SPATIAL AND TEMPORAL STRUCTURES IN THE CUSP

K.J. TRATTNER, S.A. Fuselier, W.K. Peterson, D. Klumpar, M. Boehm (Lockheed Martin ATC, 3251 Hanover Str., B255, H1-11, Palo Alto, CA 94304, USA, e-mail: trattner@mojave.spasci.com), N. Dubouloz (Ctr. d'Etude des Environ. Terrestre et Planetaire, Saint-Maur Cedex, France), J.-A. Sauvaud (Ctr.d'Etude Spatiale des Rayonnements, Toulouse, France), Y. Galperin, D. Chugunin (Space Research Institute IKI, Russian Federation)

Single point measurements of downward precipitating ions in the cusp suffer from the ambiguity of distinguishing between temporal and spatial effects. Therefore, combined observations from ISTEP satellites, e.g. Polar, Fast and Interball together with upstream information from Wind or IMP-8, provide an unprecedented opportunity to examine plasma entry into the magnetosphere and structural properties of the cusp to resolve this fundamental ambiguity.

We have identified a series of magnetic conjunctions and close encounters of polar orbiting satellites to investigate cusp features including flux variations and sudden changes in the energy of cusp precipitating ions. Such variations and changes are generally interpreted as signatures of variations in the reconnection rate and/or changes in the de Hoffman-Teller velocity at the magnetopause. They are expected to be temporal features which move poleward with convecting field lines. However, our analysis showed that series of cusp features observed at one satellite are remarkable similar to cusp features observed up to 1.5 hours later by a second satellite, suggesting that these features are the result of spatial structures and not temporal variation in reconnection parameters.

Saturday 24 July AM

**GA3.07/W/53-A6** Poster **0900-01**

#### MODEL STUDY OF IONOSPHERIC CONDUCTIVITY DISCONTINUITY EFFECT ON OBSERVED LATITUDINAL POSITIONS OF TRAVELLING CONVECTION VORTICES

Leonid BENKEVICH (Polar Geophysical Institute, Apatity, 184200, Russia, email:Ben@PGL.KolaSC.Net.RU W. Lyatsky (Institute for Space Research, University of Calgary, Calgary, AB T2N 1N4 Canada, email: Lyatsky@Phys.Ucalgary.CA)

Our aim was to model the ground magnetic effect of mesoscale high latitude ionospheric travelling convection vortices (TCVs). We took into account secondary interhemispheric field aligned currents that emerge if there are some conductivity discontinuities, e.g. at the terminator line. We have developed two models, analytical and numeric ones, each permitting calculation of the equivalent ionospheric current systems resulted from some incident magnetospheric currents. While the analytical model only allows constant though different conductivity magnitudes on either side of the discontinuity line and point current sources to be specified, the numeric one lets obtaining the equivalent currents under any arbitrary distributions of both the conductivity and the incident field-aligned currents. A good conformity is observed between the outcomes from both of the models under the same boundary and initial conditions. Results of modelling under the ionospheric conductivity conditions close to the real ones are shown. The experiments on either model give evidence for the fact that despite high-latitude incident current position (conceivably in the cusp/cleft region) the resulting vortex focus may be located at lower latitudes of 75°-80°, namely, on the terminator line. As an application, our work suggests the explanation why the TCVs are observed in so low latitudes that it is in contradiction with the magnetopause-surface-wave theories of their origin. This work has been supported by the RFBR grant 97-05-65894.

**GA3.07/W/67-A6** Poster **0900-02**

#### HIGH-TIME RESOLUTION SUPERDARN RADAR OBSERVATIONS OF THE DAYSIDE CONVECTION RESPONSE TO CHANGES IN IMF

G.CHISHAM and M.Pinnock (British Antarctic Survey, Cambridge, UK) A.D.M.Walker (Department of Physics, University of Natal, Durban, South Africa)

We present data from two of the southern hemisphere SuperDARN radars describing the high-latitude ionosphere's response to a change in the IMF By direction during a period of steady IMF Bz southward. Data from the WIND and GEOTAIL spacecraft describe the solar wind while the FAST satellite provides a snapshot of the convection reversal boundary region in the radars' field-of-view. Data from the northern hemisphere SuperDARN radars provide a conjugate view of the event. The radars were operating in a special mode which gave high time resolution data (30 s) on 3 beams with a full scan every 3 minutes. The location of the radars in the noon time sector gave a detailed observation of the change in the ionospheric convection pattern as IMF By changed from negative to positive. In particular the development of the westward edge of the afternoon convection cell is observed in the radars' field-of-view. Detailed study of the phase velocity of the changes in the ionospheric convection pattern will be presented. The plasma flow burst behaviour around the event is also studied and found to confirm the results of previous work which shows such bursts originating well equatorward of the convection reversal boundary. The observations are examined in the context of current ideas about the mapping of the magnetopause merging line to the ionosphere and the causes of plasma flow bursts.

**GA3.07/W/14-A6** Poster **0900-03**

#### INVESTIGATIONS OF IMF BY DRIVEN CONVECTION AND CONVECTION REVERSAL BOUNDARY TURBULENCE

C. R. Clauer, J. B. Baker, C. P. T. Groth, D. L. DeZeeuw T. I. Gombosi (all at Space Physics Research Laboratory, University of Michigan, Ann Arbor, MI 48109-2143, USA, email: rclauer@umich.edu); K. G. Powell (Department of Aerospace Engineering, University of Michigan, Ann Arbor, MI 48109, USA, email: ken\_powell@umich.edu) A. J. Ridley (Southwest Research Institute, 6220 Culebra Rd., San Antonio, TX 78238-5166, USA, email: ridley@worf.space.swri.edu)

Dayside ionospheric convection patterns have been investigated using high latitude measurements by incoherent scatter radar and arrays of magnetometers. Particular focus has been placed on conditions where the interplanetary magnetic field (IMF) By component is large compared to the Bz component. During these conditions, a convection pattern develops which shows asymmetry between dawn and dusk, and between the northern and southern polar regions. The convection cells observed in the ionosphere under such conditions generally show 2 cells (a dusk cell and a dawn cell), with one banana shaped cell and another more round shaped cell. As the value of IMF By increases, the shear across the convection reversal boundary in the banana shaped cell increases and sometimes becomes very turbulent. The turbulence which develops at the convection reversal boundary appear in the ionospheric plasma convection as a series of traveling convection vortices centered on the boundary. We believe these waves to be generated through a Kelvin-Helmholtz instability initiated at the shear near the inner edge of the magnetospheric boundary layer. We report here on these observations and the relationship between the ionospheric convection and magnetospheric convection. This relationship is investigated using an advanced adaptive-grid MHD simulation code which enables us to resolve phenomena across 9 orders of magnitude. Thus, it is possible to investigate the magnetospheric configuration for IMF By conditions and to obtain the mapping from the outer dayside magnetosphere to the ionosphere. While the MHD simulation cannot resolve the Kelvin-Helmholtz instability, it does show, in three dimensions, the large scale convection and locations of strong velocity shear.

**GA3.07/L/01-A6** Poster **0900-04**

#### IONOSPHERIC FOOTPRINT OF THE MAGNEOPAUSE MERGING LINE AS PREDICTED BY THE ANTI-PARALLEL MERGING HYPOTHESIS

I J Coleman, M Pinnock and A S Rodger

The anti-parallel merging hypothesis holds that reconnection takes place on the dayside magnetopause where the solar and geomagnetic fields are oppositely directed. We have mapped the predicted merging regions to the ionosphere (using the Tsyganenko 96 magnetic field model). We will present the resulting shape, width and latitude of the ionospheric dayside merging region in both hemispheres, showing its seasonal and diurnal dependence as well as its conditioning by the IMF clock angle and other solar wind parameters. These predictions have implications for the conjugate electric fields in the northern and southern cusps, as measured by the SuperDARN HF radars for example. The relationship to cusp definitions derived from satellite data will also be examined. We will show to what extent this data supports the anti-parallel hypothesis.

**GA3.07/W/12-A6** Poster **0900-05**

#### DAYSIDE TRANSIENT PRECIPITATION STRUCTURES DURING CONDITIONS OF LARGE NEGATIVE BY AND POSITIVE BZ

O DE LA BEAUJARDIERE, (Air Force Research Laboratory, Hanscom Air Force Base, MA 01731, USA, Email: odelabe@plh.af.mil); M Ruohoniemi (Applied Physics Laboratory, Laurel, MD 20723, USA, Email: mike.ruohoniemi@jhuapl.edu; T Mukai (ISAS, Sagami-hara, Japan, Email: mukai@jtl.isas.ac.jp)

The Sondrestrom Incoherent Scatter Radar, the Goose Bay SuperDARN Radar and the Akebono Satellite observed weak auroral features associated with plasma velocity increase and oppositely oriented field-aligned currents (FAC), around 1400 MLT, on January 27, 1992. The observations took place during stable solar wind conditions (Bz = + 5 nT, By = - 20 nT). The Sondrestrom Radar saw repeated quasi-periodic (20 min.) instances of auroral arcs that emanated close to a 75 degree invariant latitude boundary and that appeared to drift equatorward. The apparent equatorward motion is unexpected at this local time. The Sondrestrom as well as the Goose Bay radar data show that increases in poleward plasma velocity and vorticity were associated with these arc structures. A close Akebono satellite overpass of the Sondrestrom Radar showed that these soft arcs were within the Low Latitude Boundary Layer, were associated with a narrow FAC pair, and were near the region-1 region-2 FAC boundary. The data are consistent with elongated weak arcs that are slightly inclined with respect to the L shell direction and that drift westward (toward dusk). For this IMF, merging is expected in the northern hemisphere dawn flank and in the southern hemisphere dusk flank. We advance the hypothesis that the observed arc structures are the conjugate footprint of southern hemisphere newly-merged magnetic field lines.

**GA3.07/W/47-A6** Poster **0900-06**

#### HYDROMAGNETIC EMISSIONS OF INTERPLANETARY PLASMA AND DIAGNOSTICS OF GEOEFFECTIVE STREAMS OF SOLAR WIND

B. V. Dovbnya, E. T. Matveyeva, V. F. Ruban, R. V. Shchepetnov (Geophysical observatory Borok of United Institute of Physics of the Earth RAS, 152742, Russia, email: dov@borok.adm.yar.ru) V. A. Parkhomov (Irkutsk State Economic Academy, Irkutsk, 664003, Russia)

A new type of hydromagnetic emissions of varying frequency in a range 0.5-4.0 Hz is discovered and investigated at latitudes of dayside polar cusp. On a totality of features it is possible to make a conclusion the appearance of this phenomenon is connected with the flare streams. According to morphological features the emissions are divided on two groups - "singlets" characterized by one frequent band of emission and "doublets" - with two bands of emission. A ratio of central frequencies at "doublets" is as a rule 1:2. Typical amplitudes of emission is about 10 nT with several times prevalence of a signal in a H-component. The comparison with parameters of a solar wind has shown that the emission arises at increased velocity and proton density (no less than a threshold value) of a solar wind that indicates the threshold character of their excitation. The modulation of emission frequency strictly follows a change in proton concentration in a solar wind. The bottom band in "doublets" is presumably excited by helium ions. Various hypotheses of physical mechanisms of discovered emissions are considered. According to established relations between emission parameters and parameters of a solar wind the technique of hydromagnetic diagnostics of the main characteristics of a solar wind such as density and its variations, breaks and waves, inhomogeneities and ion composition is suggested on the basis of the ground observational data under extreme conditions in the outer space. The recommendations for system of emission observation for continuous tracking of interplanetary medium state are presented.

**GA3.07/L/07-A6** Poster **0900-07**

#### UPSTREAM WAVES AS AN ENERGY SOURCE OF NARROWBAND PC 3 WAVES OBSERVED IN THE POLAR CAP REGION

Hiroshi Fukunishi "\$B!"(JAtsushi Shono "\$B!"(JMitsuteru Sato (Department of Geophysics, Graduate School of Science, Tohoku University, Sendai 980-8578, Japan, email: fuku@pat.geophysics.tohoku.ac.jp) L. J. Lanzerotti and C. G. MacLennan (Bell Laboratories, Lucent Technologies, Murray Hill, NJ 07974, USA, email: ljl@bell-labs.com)

Automatic Geophysical Observatories (AGOs) are the first large-scale network of stations in Antarctica and cover the region mapped to the cusp, cleft, LLLBL, plasma mantle and magnetotail lobe. At present this network consists of six sites, P1 - P6, located from 70 to 87 degree magnetic latitude. ULF waves are observed by search coil and fluxgate magnetometers installed at these AGO sites. Using the ULF data obtained from the AGO network and South Pole station at 74 degree magnetic latitude, we have investigated the spectral characteristics of Pc 3 waves in the frequency range of 0.02 - 0.1 Hz and the dependences of Pc 3 activity on IMF. It is found that the occurrence probability of Pc 3 waves with a narrowband structure is very high at these latitudes, and that the frequencies of Pc 3 spectral peaks coincide with the expected frequencies of upstream waves calculated by the relation given by Russell et al.(1983),  $f$  (mHz) =  $5.81 \times B$  (nT) where B is the magnitude of the interplanetary magnetic field. This result suggests that these Pc 3 waves are originated from upstream waves. It is also found that Pc 3 waves occur both in small and large cone angle conditions of IMF. This fact indicates that upstream waves can penetrate into the magnetosphere not only across the subsolar magnetopause but also across the flankside magnetopause.

**GA3.07/E/01-A6** Poster **0900-08**

**AN INCREASE OF THE PC1 WAVE ACTIVITY PRIOR TO THE MAGNETIC SUDDEN IMPULSES SI**

Anatoly Guglielmi (United Institute of the Physics of the Earth, Moscow, Russia, email: gugl@scgis.fisgeos.iitp.ru) Jorma KANGAS and Johannes Kultima (both at Sodankylä Geophysical Observatory, FIN-99600, Finland, email: jorma.kangas@sgo.fi) Alexander Potapov (Institute of Solar-Terrestrial Physics, Irkutsk, Russia, email: potapov@iszf.irk.ru)

The occurrence of Pc1 magnetic pulsations prior to the magnetic sudden impulses SI has been studied statistically by using midlatitude ground based observations. Totally, 11 years of Pc1 data and 280 SI events were analysed. It has been discovered that there is a tendency for an increase in Pc1 activity as the time gets closer to the SI. The phenomenon is interpreted as an impact of the upstream regions of the interplanetary shocks on the magnetosphere.

**GA3.07/W/03-A6** Poster **0900-09**

**SUPER-DARN RADAR OBSERVATION OF FLOW BURSTS IN THE CUSP IONOSPHERE CAUSED BY SOLAR WIND DYNAMIC PRESSURE PULSE**

Takashi KIKUCHI, Kumiko Hashimoto (Communications Research Laboratory, Koganei, Tokyo 184, Japan, e-mail: kikuchi@crl.go.jp), Mike Pinnock, Alan Rodger (British Antarctic Survey, UK), Masukazu Watanabe (NIPR, Japan), Jean-Paul Villain (CNRS, France), Mike Ruohoniemi (JHU/APL, USA)

Super DARN radar observed an abrupt increase in the ionospheric plasma flow velocity around the cusp when an impulsive ground magnetic increase (Si) was recorded at 1350 UT, July 16, 1995. WIND measured an abrupt increase in the solar wind plasma density; the dynamic pressure increased from 9.8 to 12.2 nPa under conditions of  $B_y = -10$  nT and  $B_z = -10$  nT. The plasma flow at the cusp was north-eastward with a speed of 600 m/s before the Si, while an intensified flow region appeared at the equatorward border of the cusp with a speed of 1200 m/s at the arrival of the pressure pulse. There occurred another impulsive cusp flow burst due to the pressure pulse on April 21, 1997. Radar scattering with high flow speed (up to 1000 m/s) abruptly occurred at 1634 UT in a spot region around the cusp where no scattering was observed before the arrival of the pressure pulse. The scatter region expanded poleward and azimuthally with keeping high flow speed. These observations suggest that the dayside reconnection was intensified by the abrupt increase in the solar wind dynamic pressure during Bz<0.

**GA3.07/E/17-A6** Poster **0900-10**

**LATITUDINAL DEPENDENCE FOR THE AZIMUTH PROPAGATION VELOCITY OF GEOMAGNETIC SUDDEN IMPULSES**

G.A. Makarov, S.I. SOLOVYEV, and D.G. Baishev (all at: Institute of Cosmophysical Research and Aeronomy, 677891 Yakutsk, Russia, Email: g.a.makarov@sci.yakutia.ru) M.J. Engebretson and J. Posch (both at: Department of Physics, Augsburg College, Minneapolis, MN 55454, USA, email: engebret@augsborg.edu) W.J. Hughes (Boston University, Center for Space Physics, Boston, MA 02215, USA, email: hughes@buasta.bu.edu) K. Yumoto (Kyushu University 33, Fukuoka 812-81, Japan, email: yumoto@geo.kyushu-u.ac.jp) V.A. Pilipenko (Institute of Physics of the Earth, 123810 Moscow, Russia; email: pilip@iophys.msk.ru)

Propagation of the geomagnetic sudden impulse (SI) in the high-latitude regions of the Earth has been studied by using ground-based magnetic station data. SI in the winter period caused by sharp decreases of the solar wind plasma density which are accompanied by abrupt changes of the IMF By and Bz components have been considered.

It is obtained that SIs are propagated from the dayside to the nightside of the polar cap with the velocities of 5-40 km/s. The latitude-dependence of the azimuth SI propagation velocity is found: the velocity decreases as geomagnetic latitude from 65 deg to 78 deg increases.

**GA3.07/W/19-A6** Poster **0900-11**

**A STATISTICAL STUDY OF THE OCCURRENCE RATES AND REPETITION FREQUENCIES OF PULSED IONOSPHERIC FLOWS IN THE DAYSIDE AURORAL ZONE**

K. A. MCWILLIAMS, T. K. Yeoman, G. Provan (Department of Physics and Astronomy, University of Leicester, University Road, Leicester, LE1 7RH, U.K. )

A study has been performed on the occurrence of pulsed ionospheric flows (PIFs) as detected by the SuperDARN HF radars. These flows have been suggested as being created at the ionospheric footprint of newly-reconnected field lines, during episodes of magnetic flux transfer into the terrestrial magnetosphere (flux transfer events or FTEs). Two years of both high-time resolution and normal scan data have been analysed in order to perform a statistical study of the occurrence rate and repetition frequency of the PIFs. These statistical results obtained from ionospheric flows are compared to occurrence rates and repetition frequencies of FTEs derived from in situ spacecraft data.

**GA3.07/W/42-A6** Poster **0900-12**

**POST-NOON TWO-MINUTE PERIOD PULSATING AURORA AND THEIR RELATIONSHIP TO THE DAYSIDE CONVECTION PATTERN**

S E MILAN, T K Yeoman, M Lester (All at Department of Physics and Astronomy, Leicester University, Leicester LE1 7RH, UK. Email: Steve.Milan@ion.le.ac.uk) J Moen (UNIS, P.O.Box 156, N-9170 Longyearbyen, Norway) P E Sandholt (Department of Physics, University of Oslo, P.O.Box 1048 Blindern, N-0316 Oslo, Norway)

Poleward-moving auroral forms in the vicinity of the cusp region are generally assumed to be the optical signature of flux transfer events. Another class of quasi-continuous, short-period (1-2 minutes) wave-like auroral emission has been identified, closely co-located with the convection reversal boundary in the post-noon sector, which is otherwise similar in appearance to cusp aurora. It is suggested that such auroral emissions are associated with ULF magnetohydrodynamic wave activity, which is observed simultaneously by ground magnetometer stations. This association with ULF wave activity is strengthened by the observation of several harmonic frequencies in the pulsation spectrum, each an overtone of the fundamental standing wave.

**GA3.07/W/37-A6** Poster **0900-13**

**MAGNETOPAUSE PROCESSES AND ASSOCIATED POLAR IONOSPHERIC FLOWS OBSERVED BY EQUATOR-S AND SUPERDARN**

Neudegg D.A. (1), U. Auster(4), W. Baumjohann(2), Cowley S.W.H.(1), J. Büchner (3),M.J. Engebretson (6),K.-H. Fornacon(4), E. Georgescu (2,5),R. Greenwald(8), G. Haerendel(2), Lester M.(1), Milan S.(1), B. Nikutowski (3), J. Sigwarth(10),G. Sofko(9),P. Stauning(7) and Yeoman T.K.(1) (1) Dept. Physics and Astronomy, University of Leicester, UK(2) Max-Planck Institut für Extraterrestrische Physik, Garching, Germany (3) Max-Planck Institut für Aeronomie, Katlenburg-Lindau, Germany (4) Technische Universität von Braunschweig, Braunschweig, Germany (5) ISS, Bucharest, Romania (6) Augsburg College, Minneapolis, USA (7) Danish Meteorological Institute, Copenhagen, Denmark(8) Applied Physics Lab, Maryland, USA (9) University of Saskatchewan, Saskatoon, Canada (10)University of Iowa, USA

Using the Equator-S spacecraft and SuperDARN HF radars, observations have been made of processes at the magnetopause and associated flows in the polar ionosphere. The magnetopause processes include interactions with the IMF and solar wind such as transient reconnection/merging (FTEs) and pressure pulse effects. Appropriate geomagnetic field mappings to the fields of view of SuperDARN radars were performed to observe the effects preserved transmitted by FACs to the polar ionosphere. Cases of 'pulsed ionospheric flows' (PIFs) observed with a range of instrumentation and associated with different magnetopause processes will be presented. The strong correlation between reconnection/merging and the observationally established ionospheric 'flow channel events' (FCEs) will be shown.

**GA3.07/E/19-A6** Poster **0900-14**

**COUPLING BETWEEN MAGNETIC IMPULSE EVENTS AND P11 NOISE BURSTS AT CUSP LATITUDES**

Viacheslav PILIPENKO, Sergey Shalimov (Institute of the Physics of the Earth, Moscow, Russia; e-mail: vpilipenko@uipe-ras.scgis.ru) Mark Engebretson (Augsburg College, Minneapolis, MN55454, USA; e-mail: engebret@augsborg.edu)

The estimated densities of local field-aligned currents related to nighttime substorm onset or magnetic impulse events at cusp latitudes may exceed the threshold for the excitation of high-frequency turbulence in the topside ionosphere. The evolution of an ion-acoustic instability is shown to lead to quasi-oscillations around the saturation level. Consequent variations in anomalous conductivity will result in pulsed electron precipitation and noise generation in the P11 band. This proposed mechanism gives a natural interpretation to the experimentally observed coupling between localized magnetic disturbances, electron precipitation/acceleration, and bursts of high-frequency ULF noise. The alternative interpretations based on mechanisms of ion-cyclotron instability stimulation and ionospheric Alfvén resonator excitation can be applied only under specific plasma conditions. Several seemingly uncoupled geophysical phenomena (long period magnetic impulses, electron precipitation/acceleration, bursts of auroral brightness, and splashes of intensity of high-frequency ULF waves) find a natural interpretation as related consequences of the mechanism proposed.

**GA3.07/W/50-A6** Poster **0900-15**

**ON THE ORIGIN AND PROPAGATION MECHANISMS OF CUSP REGION PC3 PULSATIONS**

Pavlo PONOMARENKO, Brian J Fraser, Sean T Ables, and Fred W Menk (all in Department of Physics, CRC for Satellite Systems, University of Newcastle, Callaghan, NSW, 2308 Australia, Email: phpp@alinga.newcastle.edu.au), Ray J Morris (Australian Antarctic Division, Channel Hwy, Kingston, TAS, 7050 Australia); Liu Ruiyuan (Polar Research Institute of China, Shanghai 200129, China)

Ground-based investigations of pulsation activity at the magnetospheric cusp region have shown two pronounced spectral component in Pc5 and Pc3 ranges. The first peak is believed to be a signature of field line resonances, but the second one is more puzzling. Several mechanisms have been proposed including Kelvin-Helmholtz and ion-cyclotron instabilities as well as particle precipitation. In an attempt to solve the problem, we have assumed that different generation and propagation mechanisms could produce different seasonal and diurnal dependencies. The generation mechanisms can be identified through their relationship to the interplanetary magnetic field and plasma parameters. Also, the polarization structure and spatial coherency on the ground should depend on the propagation mode. Relative contributions of the different mechanisms can be found by comparison between data obtained from regions lying poleward and equatorward of the cusp. We investigated the statistical characteristics of Pc3 pulsations using induction magnetometer data from Antarctic cusp stations Davis (Australia) and Zhong Shan (PRC). Data from other Australian Antarctic stations, Casey (polar cap) and Mawson (auroral region), were used for comparative studies. Analysis suggests that the principal generation mechanism is the ion-cyclotron instability of solar wind protons upstream of the bow shock. The main mode seems to be a compressional wave propagating isotropically through the magnetosphere, but other mechanisms may give substantial contribution around local magnetic noon.

**GA3.07/W/40-A6** Poster **0900-16**

**ARE PULSED IONOSPHERIC CUSP FLOWS DRIVEN BY SOLAR WIND ALFVEN WAVES?**

P. PRIKRYL (Communications Research Centre, P.O.Box 11490, Station "H", Ottawa, ON K2H 8S2,Canada, email: prikryl@canrc.dgcr.crc.ca); G. Provan, K.A. McWilliams and T.K. Yeoman (Department of Physics and Astronomy University of Leicester, Leicester LE1 7RH, UK, email: gp3@ion.le.ac.uk)

Ionospheric signatures of flux transfer events (FTEs) in the cusp footprint have been observed by the CUTLASS SuperDARN radar in high resolution modes. The ionospheric flow in the cusp footprint, which is believed to be a consequence of magnetic reconnection at the dayside magnetopause, was pulsed with periods from a few to several minutes. Here the quasiperiodic FTE signatures are correlated with Alfvénic fluctuations that were observed by ISTP satellites in solar wind. It is concluded that on these occasions the FTEs may be driven by Alfvén waves



coupling to the dayside magnetosphere. Case studies will be presented in which the dawn-dusk component of the Alfvén wave electric field appears to modulate the reconnection rate as evidenced by the radar observations of the ionospheric cusp flows. In addition, the multifrequency MHD waves generated in the magnetosheath through the interaction between the solar wind Alfvén waves and the bow shock may excite field line resonances (FLRs) deeper in the magnetosphere. In this composite picture, the inter-FTE periodicity may be influenced by the FLR period on the last closed field line that is subsequently reconnected with the IMF.

**GA3.07/E/20-A6** Poster **0900-17**

**WHERE ARE THE IONOSPHERIC SIGNATURES OF POST-TERMINATOR FLUX TRANSFER EVENTS?**

A S RODGER, M Pinnock, G Chisham and I J Coleman British Antarctic Survey, Madingley Road Cambridge CB3 0ET, UK (email: A.Rodger@bas.ac.uk)

Flux transfer events (FTEs) are arguably the most important process by which energy is transferred from the magnetosheath into the magnetosphere. The manifestation of FTEs in the ionosphere near magnetic noon has been extensively reported over the last decade in terms of plasma velocity transients, optical auroral forms and magnetometer perturbations, though as yet no unified theory is forthcoming, and several key questions remain.

Perhaps what is more puzzling is the fact that FTEs at the magnetopause show little magnetic local time dependence along the magnetopause from -04 to 20 MLT. To date there have been few reports of ionospheric signatures of FTEs well away from noon. In this paper, we will address the physics of why the ionospheric signatures of near-terminator reconnection have not yet been clearly identified. The critical physics involves both the current carrying capacity of the magnetosphere and the local Alfvén speed. The extent to which the magnetosphere and ionosphere become decoupled will be discussed. Furthermore we will consider the relationship between the ionospheric location of these reconnection events with respect to the convection reversal boundary, a feature that is often, but erroneously taken to be the ionospheric signature of the polar cap. We will support our hypotheses using data from rockets, satellites and a variety of ground-based instrumentation.

**GA3.07/W/58-A6** Poster **0900-18**

**THE ONSET TIME OF MAGNETIC RECONNECTION**

Simon Shepherd, Raymond A. GREENWALD, and J. Michael Ruohoniemi (all at Johns Hopkins University, Applied Physics Laboratory, Johns Hopkins Rd., Laurel, MD, 20723, USA, email: Simon.Shepherd@jhuapl.edu)

One of the most important processes in space plasma physics is that of magnetic reconnection. It is important because this process is generally thought to be responsible for the transfer of mass, energy, and momentum from the solar wind to the Earth's dayside magnetosphere. While the precise nature of the reconnection process is still unknown, one topic that may be attacked with existing sets of satellite and ground-based data is the growth time of the reconnection process. Recently, Ruohoniemi and Greenwald [1998] have shown that enhancements in ionospheric convection in response to a southward turning of the IMF are observed at all local times within two minutes of the time that they are first observed near the noon meridian. In their study, they did not attempt to identify the time that the southward directed IMF actually impacted the magnetopause. In the present study, we have attempted to resolve this issue by using data from the Geotail spacecraft when it was located in the subsolar magnetosheath within a few Re of the dayside magnetopause. Under these conditions, the delay time between the observation of an IMF transition at Geotail and its impact on the magnetopause will typically be less than one minute. There will be an additional delay of 2 minutes for the magnetic signature of the freshly reconnected field line to propagate to the ionosphere. Any delay beyond these three minutes must correspond to the growth time of the reconnection process. In our study, we have found typical delay times of 10-12 minutes indicating that the growth time of the reconnection process at the magnetopause is ~7-9 minutes.

**GA3.07/W/43-A6** Poster **0900-19**

**SOLAR WIND TANGENTIAL DISCONTINUITIES: TRIGGERS FOR IMPULSIVE GROUND MAGNETIC SIGNATURES?**

R. J. SITAR and C. R. Clauer (both at Space Physics Research Laboratory, The University of Michigan, 2455 Hayward, Ann Arbor, MI 48109, USA, email: sitar@umich.edu, rclauer@umich.edu)

Magnetic impulse events (MIEs) have been associated with impulsive deformations of the magnetopause produced by sudden changes in the solar wind dynamic pressure. Other observations suggest that MIEs can be produced in the absence of pressure changes when there is a sudden change in the IMF orientation. Using data from the IMP 8 satellite, we have identified 121 IMF orientation changes which occur during intervals of steady solar wind dynamic pressure. The relationship between IMF orientation changes and MIEs are studied using Greenland magnetometer data. Preliminary analysis shows that the occurrence of MIEs produced by IMF orientation changes exhibits a weak dependence on the orientation of the motional electric field on both sides of the current sheet responsible for the orientation change. The motional electric field has also been shown to contribute to the production of hot flow anomalies (HFAs), suggesting that HFAs might play an intermediary role in MIE production.

**GA3.07/W/44-A6** Poster **0900-20**

**THE MORPHOLOGY AND DYNAMICS OF MAGNETIC IMPULSE EVENTS: SHIRE IMAGING RIOMETER RESULTS**

M.B.Terkildsen, B.J.Fraser, and F.W.MENK, (Physics Department, CRC for Satellite Systems, University of Newcastle, NSW, 2308, Australia, email: phmbt@alinga.newcastle.edu.au) T.J.Rosenberg (IPST, University of Maryland, College Park, MD 20742, USA) R.J.Morris (Australian Antarctic Division, Kingston, TAS, Australia)

The SHIRE imaging riometer at Australia's Davis Antarctic station is located under the magnetospheric cusp region and is being used to study the morphology and dynamics of regions of enhanced electron density in the high-latitude ionosphere. Those regions of enhanced density associated with magnetic impulse events (MIEs) are being specifically investigated. MIEs are a possible ionospheric signature of magnetic reconnection (FTEs) on the dayside magnetopause. MIEs commonly appear as a bipolar spike in the geomagnetic field at the ground at high latitudes, most often with an associated patch of enhanced electron density detectable with a riometer. The imaging riometer enables a 2-dimensional spatial "image" to be made of the electron density structures associated with such impulsive events. The dynamics and morphology of a large number of impulse events, detected using a co-located fluxgate magnetometer, have been studied in this way and the results provide some insight into MIE generation and propagation mechanisms. Of particular interest is the ionospheric motion of MIEs in the vicinity of the southern polar cusp region.

**GA3.07/L/08-A6** Poster **0900-21**

**DAYSIDE AURORAL TRANSIENT EVENTS OBSERVED BY POLAR ULTRAVIOLET IMAGERY.=20**

V.G. Vorobjev, O.I. Yagodkina (Polar Geophysical Institute, Apatity, Murmansk region, Russia), D. Sibeck (Applied Physics Laboratory, Johns Hopkins University, Laurel, Maryland)

We have analyzed morphological features of dayside auroral transient events (ATE) using images acquired from the ultraviolet imager (UVI) on board the Polar satellite. The UVI data set used for the investigation covers a time of about 5 winter months, from Dec. 3, 1996 to Feb. 28, 1997 and from Oct. 19 to Dec. 23 in 1997. During period under investigation we found 31 cases of the auroral transient events in the pre noon sector while only 12 events of auroral transients were registered in the after noon sector. Pre noon ATEs generally appear as the bright "spot" of auroral luminosity in 09-11 MLT sector at the latitudes about 740 CGL. Bright aurorae then quickly shifted westward and the poleward part of the bright spot contained the discrete aurorae moved poleward as well. Afternoon ATEs usually appear like a sudden intensification of aurorae in the 13-16 MLT sector at 750-760 CGL. Bright band of luminosity quickly extended eastward achieving in 15-20 min the longitude of 20-21 MLT at 700-720 CGL. Global features of auroral luminosity evolution during 5 SSC events have been investigated as well. We have analyzed the interplanetary medium conditions during the pre noon ATEs, the after noon ATEs and the SSCs registrations. In the paper the comparative characteristics both of morphological features of three auroral phenomena and the interplanetary magnetic field and solar wind plasma changes associated with different auroral events are presented.

**GA3.07/W/45-A6** Poster **0900-22**

**THE MAGNETOPAUSE DYNAMICS ACCORDING OF INTERBALL-1/MAGION-4 DATA AND ITS CONNECTION WITH GEOMAGNETIC DISTURBANCES**

Alexander ZAITZEV (Institute of Terrestrial Magnetism, Ionosphere and Radio Wave Propagation, Troitsk, Moscow Region, 142092, RUSSIA, e-mail: zaitzev@izmiran.rssi.ru) Nadya Nikolaeva, Georgii Zastenker (both of Space Research Institute RAN, Profsovnaya 84, GSP-7, Moscow, 117810, RUSSIA, e-mail: nikolae@vml.iki.rssi.ru) Jana Safrankova, Zdenek Nemecek (both of Charles University, Y Holesovickach 2, 180 00 Praha 8 - Troja, Czech Republic, e-mail: Jana.Safrankova@mff.cuni.cz)

The INTERBALL-1/MAGION-4 data base was analyzed to find the events of multiple magnetopause crossings. It was chosen the crossings near the X-Y plane after dawn-dusk meridian. Each case was analyzed and the relative amplitude and periodicity of magnetopause motion was estimated and summarized as a regular pattern of magnetopause dynamics. Further analyses was pointed toward the search of the connection between magnetopause motion and geomagnetic disturbances. Ground-based geomagnetic data from high latitude stations was used to infer the state of magnetosphere. It was suggested that large-scale magnetopause movements correlate with the level of geomagnetic disturbances. The connection of such processes might be considered in favor of a boundary layer model for magnetospheric substorms.

**GA3.08** Saturday 24 – Monday 26 July

**MAGNETOTAIL DYNAMICS AND RELATIONSHIP TO HIGH-LATITUDE IONOSPHERIC PHENOMENA**

Location: School of Education G33 LT (Saturday Only)

Location: Gisbert Kapp E203 LT1 (Monday)

Location of Posters: Gisbert Kapp, Coffee Room

**Saturday 24 July AM**

Presiding Chair: T. Nagai, (Tokyo Institute of Technology, Japan)

**GA3.08/W/21-A6** **0900**

**THE RESPONSE OF THE MAGNETOSPHERE TO AN INTERPLANETARY SHOCK: THE MAGNETOSPHERIC COMPRESSION ON SEPTEMBER 24, 1998**

C. T. RUSSELL, P. Chi, Guan Le, J. Raeder and R. J. Strangeway (All at Institute of Geophysics and Planetary Physics, University of California, Los Angeles, CA 90095-1567, USA, email: crussell@igpp.ucla.edu); H. J. Singer (Space Environment Center, NOAA, Boulder, CO, USA); H. Kawano (Kyushu University, Fukuoka, Japan); T. E. Moore (Goddard Space Flight Center, Greenbelt, MD, USA); W. K. Peterson (Lockheed Martin, Palo Alto, CA, USA)

At approximately 2344 UT on September 24, 1998 the nose of the magnetosphere was suddenly compressed by a strong interplanetary shock wave. As evidenced by successive compressions of the magnetic field at GOES 10, POLAR and GOES 8, the compressional wave moved rapidly through the magnetosphere. At POLAR the compression caused the magnetopause to move closer to the spacecraft, causing rapid cross field flows and altering the location of the conjugate point in the ionosphere. The pre-existing flows were heated locally only slightly by betatron acceleration because the flows were mainly field aligned. Waves also did not lead to much heating because they were small in amplitude. Centrifugal heating may have been a more important local process. Some of the observed change in the plasma observed at POLAR was associated with the motion of the non-uniform polar cap outflow across POLAR. Snapshots of the polar cap by FAST confirm that the outward polar cap flows are non-uniform at this time but also show that strong heating is present and subsequently is very important in determining the outflow of plasma. Ground station recordings, synchronized with GPS signals, enable the disturbance to be followed through the magnetosphere from high latitudes to low. This event teaches us much about how the ionosphere is coupled to the magnetosphere and demonstrates the symbiosis of ground based, ionospheric and magnetospheric observations with modelling in magnetospheric studies.

**GA3.08/W/09-A6** **0920**

**POLAR IONOSPHERIC OUTFLOW RESPONSE TO SOLAR WIND CONDITIONS AT 2-9 RE**

Moore, T.E. and B.L. GILES (both at NASA Goddard Space Flight Center, Greenbelt, MD 20771 USA, Email: thomas.e.moore@gsfc.nasa.gov), M.O. Chandler (NASA Marshall Space Flight Center, Huntsville, AL 35812 USA), M.R. Collier (NASA Goddard Space Flight Center, Greenbelt, MD 20771 USA), H.L. Collin (Lockheed Martin Advanced Technology Center, Palo Alto, CA, 94304 USA), R. Fitzenreiter (NASA Goddard Space Flight Center, Greenbelt, MD 20771 USA), W.K. Peterson (Lockheed Martin Advanced Technology Center, Palo Alto, CA, 94304 USA), C.J. Pollock (Southwest



Research Institute, San Antonio, TX 78228 USA), C.T. Russell and R.J. Strangeway (both at University of California, Los Angeles, CA 90024 USA)

We report observations of direct ionospheric plasma outflow response to the incidence of an interplanetary shock and associated coronal mass ejection upon the earth's magnetosphere. Data from the WIND spacecraft, 185 RE upstream of Earth, document the passage of an interplanetary shock at 23:20 UT on 24 Sept. 1998, traveling at 860 km/s. The polar cap plasma environment sampled by the POLAR spacecraft changed abruptly at 23:45 UT, reflecting a displacement of the previously remote plasma mantle to the vicinity of the spacecraft, as the shock propagated through the polar magnetosphere. At about 02:00 UT, POLAR reentered the lobe and polar wind, finding it had changed to a colder, slower, and denser outflow dominated by O<sup>+</sup> plasma. The O<sup>+</sup>-dominated outflow continued as the spacecraft passed through the northern cleft at ~4.5 RE and then the southern cleft at 1.8 RE (geocentric). Such a direct response of the ionosphere to solar wind pressure disturbances is of potential significance to the dynamics of the magnetotail.

**GA3.08/W/17-A6 0940**

**CENTRIFUGAL ACCELERATION OF IONS OBSERVED ON POLAR SPACECRAFT NEAR 9 RE OVER POLAR CAP UPON ARRIVAL OF CME-DRIVEN SHOCK**

John B. CLADIS, Harry L. Collin, and William K. Peterson (all at Lockheed Martin Advanced Tech. Center, 3251 Hanover Street, B 255, Palo Alto, CA 94304, USA, email: cladis@spasci.com) Thomas E. Moore (NASA Goddard SFC, Code 692, Bldg. 2, Greenbelt, MD 20771-1000, USA, email: thomas.e.moore@gsfc.gov) Christopher T. Russell (Inst. of Geophysics and Planetary Physics, UCLA, Los Angeles, CA 90095-1567, USA, email: crussell@igpp.ucla.edu)

A shock driven by a coronal mass ejection struck the magnetosphere about 2344 UT on September 24, 1998. The POLAR spacecraft was near apogee over the northern polar cap, at (X,Y,Z)GSM = (-2.3803, -2.7148, 8.1450) in RE. During the following 144 s, from 2345:18 UT to 2347:42 UT, (i) the magnetic field measured on-board with the UCLA magnetometer increased sharply from 126.16 nT to 182.00 nT; (ii) the field components changed from (BX,BY,BZ)GSM = (84.91, 32.55, -87.45) to (151.11, 50.655, -87.867); (iii) the full rotation of B was 19.870; and (iv) the velocity components of both the H<sup>+</sup> and O<sup>+</sup> ions increased by about 75 km/s antiparallel to B. We suggest the ions were flung along -B by the "motion" of the magnetic field, according to the centrifugal-acceleration process first described by Cladis [GRL, 13, 893, 1986]. A parallel-velocity increase of 35 km/s was computed by integrating the term  $dV/dt = vE-d\theta/dt$ , using the local values of  $vE$  (the drift velocity) implied by the ion-velocity components perpendicular to the magnetic field and the measured values of  $\dot{\theta} = B(t)/B(t)$ . The higher acceleration of the ions was confirmed by a computer simulation of the process along the ion paths.

**GA3.08/W/13-A6 0940**

**FAST OBSERVATIONS DURING THE SEPTEMBER 24TH AND 25TH 1998 MAGNETIC STORM**

R. J. STRANGEWAY, C. T. Russell (both at: Institute of Geophysics and Planetary Physics, University of California, Los Angeles, CA 90095, USA, Email: strange@igpp.ucla.edu), D. M. Klumppar (Lockheed Martin Advanced Technology Center, 3251 Hanover St., Palo Alto, CA 94304, USA), C. W. Carlson, J. P. McFadden, R. E. Ergun (all at: Space Sciences Laboratory, University of California, Berkeley, CA 94720, USA), T. E. Moore (NASA Goddard Space Flight Center, Greenbelt, MD 20771, USA), and W. K. Peterson (Lockheed Martin Advanced Technology Center, 3251 Hanover St., Palo Alto, CA 94304, USA)

During September 24th and 25th 1998 the FAST spacecraft acquired data over the Northern Polar Cap in the noon-midnight local time sector. This allowed for detailed observations of the dayside cusp at ~ 4000 km altitude. The spacecraft was therefore ideally suited for monitoring the outflow of ionospheric plasma which was also observed at the higher altitude POLAR spacecraft. The interval around the Sudden Impulse (SI) at 23:45 UT on September 24th is characterized by enhanced field-aligned currents in the cusp region. Because the FAST orbital period is ~ 135 minutes, we can provide snapshots of the cusp region, and FAST passes through the cusp at ~ 00:10 UT on September 25th, some 35 minutes after the SI. The field-aligned currents at this time are significantly larger than on the previous orbit. Large fluxes of 100 eV oxygen ions are also observed to be flowing out of the ionosphere, with decreasing energy for increasing latitude. These ions form a conic in pitch angle, consistent with the "pressure cooker" model of ion acceleration, where transverse heating overcomes a downward electric field. As already noted the field-aligned currents are weaker on the previous orbit, and a weaker oxygen conic is also observed. This suggests that the main effect of the increased solar wind dynamic pressure is to enhance already existing ion outflow through an increase in the field-aligned currents and the associated parallel electric fields and ion heating in the cusp ionosphere.

**GA3.08/W/05-A6 1040**

**THE RESPONSE OF THE MAGNETOSPHERE TO AN INTERPLANETARY SHOCK: GROUND-BASED OBSERVATIONS OF THE SUDDEN IMPULSE ON SEPTEMBER 24, 1998**

P. Chi, Guan Le, J. Raeder, C. T. RUSSELL and E. Zesta (All at Institute of Geophysics and Planetary Physics, University of California, Los Angeles, CA, USA, email: pchi@igpp.ucla.edu); K. Yumoto, H. Kawano and K. Kitamura (All at Kyushu University, Fukuoka, Japan); V. Angelopoulos (University of California, Berkeley, CA, USA); M. Moldwin (Florida Institute of Technology, FL, USA)

The strong interplanetary shock wave that intersected the front of the magnetosphere at about 2344 UT on Sept. 24, 1998, launched a compression of the magnetosphere that was followed around the globe by a new generation of magnetometers with rapid sampling and precise GPS-synchronized timing. Magnetometers of these chains included those in the Circum Pacific Magnetometer Network, those in the IGPP/LANL array, those in the MEASURE array and those in the MACCS array. The event exhibited all the classical signatures of an SI including the preliminary decrease before the main increase in the H-component. The ability to model this event and its induced ionospheric currents using an MHD code allows us to compare the compression as it is seen in the magnetosphere with the response of the ionospheric currents.

**GA3.08/W/02-A6 Invited 1100**

**RECENT ADVANCES IN MAPPING MAGNETOTAIL BOUNDARIES USING SUPERDARN HF RADARS**

Mervyn P. FREEMAN (British Antarctic Survey, High Cross, Madingley Road, Cambridge, CB3 0ET, U.K., email: M.P.Freeman@bas.ac.uk)

We review and discuss recent publications which have shown how HF radars can remotely sense magnetotail boundaries and thereby measure how these boundaries respond to changes in the IMF and to substorms. Specifically, we present the following: (1) Evidence for

a relationship between the boundary plasma sheet/central plasma sheet (bps/cps) interface in the magnetotail and the equatorward edge of HF radar backscatter from the ionosphere or a latitudinal gradient in the Doppler spectral width of the backscatter. (2) Examples using this empirical relationship to track both rapid (of order 1 min) and slow (of order 1 h) changes in the ionospheric projection of the bps/cps interface. (3) Comparison of the time-varying location of the bps/cps interface observed in these examples with that predicted by a magnetic reconnection-based magnetospheric model using concurrent solar wind observations.

**GA3.08/W/25-A6 1130**

**ELECTRON PRECIPITATION AS A FUNCTION OF MAGNETOTAIL STRETCHING**

THOMAS SOTIRELIS and Patrick T. Newell, The Johns Hopkins University Applied Physics Laboratory, Laurel, Maryland, 20723

A model for the differential energy flux of precipitating electrons from 32 eV to 30 keV is presented. The model spectra are keyed to the degree of magnetotail stretching as inferred from the precipitation itself. The result is less smeared and more flexible than previous work because a given portion of the oval—such as from the structured/unstructured boundary to the poleward edge of the oval—is averaged only with the appropriate precipitation. Data from twelve years and eight DMSP spacecraft are used. Extensive variations in the energy flux, average energy, and spatial extent of the precipitation are seen for different degrees of magnetotail stretching.

**GA3.08/W/31-A6 1150**

**AURORAL PRECIPITATION BOUNDARIES AND THE MAGNETOSPHERIC TAIL ENERGETICS FOR VARIOUS LEVEL OF THE MAGNETIC ACTIVITY**

YA. I. FELDSTEIN, L. I. Gromova (Institute of Terrestrial Magnetism, Ionosphere and Radio Wave Propagation, Troitsk, Moscow Region, 142092, Russia, email: Igmromova@izmiran.troitsk.ru) B. V. Rezhnev, G. V. Starkov, V. G. Vorobjev (Polar Geophysical Institute, Apatity, Murmansk region, 184200, Russia, email: vorobjev@pgi.kolasc.net.ru)

luminosity structure allow to suggest physically substantiated method of the plasma regimes boundaries identification (Newell et al., 1996; Feldstein and Galperin, 1996). The interrelationship between these high-latitude plasma regimes in the nightside to dawnside sectors and plasma domains of the distant magnetosphere has been demonstrated. DMSP satellites data have been used for statistical investigation of the plasma regimes boundaries dynamics depending on the magnetic activity level. Boundaries determining the polar cap location (b6) and characteristic break of latitudinal variation of the electron energy (b2e) have been used to define the magnetic flux dynamics and to calculate the magnetic energy in the magnetospheric tail during the transition period from the quiet conditions to the very disturbed ones. P. Newell, Y. Feldstein, Y. Galperin, C.-I. Meng, JGR, 101,A5,10737-10748, 1996; Y. Feldstein, Y. Galperin, Cosmic Research, 34, N3, 209-227, 1996.

**GA3.08/W/22-A6 1210**

**ENERGETIC IONS FROM THE POLAR SATELLITE AS TRACERS FOR PLASMA SHEET CONDITIONS**

P. K. Toivanen, D. N. Baker, W. K. Peterson (LASP, University of Colorado at Boulder, Boulder, CO, USA, Email: petri.toivanen@lasp.colorado.edu) T. I. Pulkkinen (Finnish Meteorological Institute, Helsinki, Finland)

Observations from the POLAR satellite obtained by the Toroidal Imaging Mass-Angle Spectrograph (TIMAS) and by the MICS sensor of the Charge and Mass Magnetospheric Ion Composition experiment (CMMICE) frequently show multiple peaked distributions in energetic H<sup>+</sup> and O<sup>+</sup> ions (12–120 keV) in the dusk side magnetosphere. These ions are on open drift paths and thus drift from the tail plasma sheet to the dusk side geostationary region. Our earlier results suggest that, under certain geomagnetic conditions, these observations can be used to determine remotely characteristics of the plasma sheet over a large portion of the tail. In this study, we mainly address the large-scale electric field, which is responsible for the acceleration of these ions during their drift from the plasma sheet. To trace back the observed distributions, we use an ionospheric electric field model mapped to the plasma sheet together with a modified version of the T89 model in our drift model. These traced-back distributions are then linked to GEOTAIL observations, which show frequently pristine field-aligned O<sup>+</sup> beams on energy range up to a few keV originating from the ionosphere. Thus our final aim is to form a coherent picture of O<sup>+</sup> flow from the ionosphere to the plasma sheet and of consequent earthward transport and related acceleration of O<sup>+</sup> ions.

**Saturday 26 July PM**

Presiding Chair: Mark Lester, (University of Leicester, UK)

**GA3.08/W/29-A6 Invited 1400**

**OBSERVATIONS PERTAINING TO THE LOCATION OF THE SUBSTORM ONSET INSTABILITY**

L. A. FRANK, J. B. Sigwarth and W. R. Paterson (All at: Department of Physics and Astronomy, The University of Iowa, Iowa City, IA, USA, email: frank@iowasp.physics.uiowa.edu) S. Kokubun (Solar-Terrestrial Environment Laboratory, Nagoya University, 3-13 Honohara, Toyokawa, Aichi 442, Japan)

Recent observations of the initially brightened auroral arc at substorm onset provide considerable evidence that the instability is located at geocentric radial distances in the range of about 6 to 12 Re. These findings are based upon unique, high-resolution images from a camera for visible wavelengths on board the Polar spacecraft. The location of the onset instability is particularly important for theoretical analysis and modelling of magnetospheric substorms in that the plasma and magnetic field parameters are significantly different at the above radial distances compared to those for radial distances in the range of 20 to 30 Re which are used for several current theory efforts. Simultaneous measurements of plasmas and magnetic fields at the relevant radial distances in the equatorial magnetotail are used to search for the position of the onset instability. It is found that the onset instability is initially confined to a narrow range of longitudes (local time) and rapidly expands in longitude and to greater radial distances.

**GA3.08/E/01-A6 1430**

**COMPARISON OF AURORAL ARCS OBSERVED WITH POLAR/VIS MEDIUM-RESOLUTION CAMERA AND FINNISH ALL-SKY CAMERAS AND THEIR MAPPING TO THE MAGNETOTAIL**

T. I. PULKKINEN, K. Kauristie, and M. T. Syrjasuo (Finnish Meteorological Institute, PO Box 503, FIN-00101 Helsinki, Finland, tel. 358-9-19294654, fax 358-9-19294603, e-mail: tuija.pulkkinen@fmi.fi) D. N. Baker, N. E. Turner (Laboratory for Atmospheric and Space Physics, University of Colorado, Boulder, CO 80309-0590) L. A. Frank and J.B. Sigwarth (Department of Physics and Astronomy, University of Iowa, Iowa City, IA 52242) T. Mukai, Institute of Space and Astronautical Science, Sagami-hara, Japan) S. Kokubun (Solar Terrestrial Environment Laboratory, Nagoya University, Toyokawa, Japan) L. Zelenyi (Space Research Institute, Moscow, Russia)

The POLAR/VIS medium-resolution camera can resolve auroral arcs to a scale of a few km. The camera observations show individual arcs embedded within a diffuse band of luminosity, allowing for detailed examination of the auroral breakups and their relation to other substorm onset-associated processes. Observations from the POLAR/VIS medium-resolution camera, Earth camera, Finnish all-sky camera network, and ISTP spacecraft are utilized to examine details of auroral arc breakups and their mapping to the magnetotail during several substorm events in late 1997 and early 1998. In particular, an isolated substorm of about 400-nT intensity occurred on Dec 17, 1997, after almost 20 hours of quiescence. The POLAR/VIS medium resolution camera observed two intensifications in the auroras at 2051 UT and at 2221 UT. The all-sky camera data from Kilpisjärvi showed that auroral activity intensified at 2050 UT, the auroras moved equatorward between 2140 and 2230 UT, after which a strong breakup and poleward motion of auroras followed. Magnetic field modelling techniques are utilized to obtain an accurate mapping between the auroral observations and the magnetotail substorm signatures as observed by GEOTAIL and INTERBALL Tail Probe, both in the nightside magnetotail. The results are used to discuss the processes prior to the global instability onset and their association to the processes creating auroral breakups.

**GA3.08/W/03-A6 1450**

**THE EXPLOSIVE PHASE OF THE SUBSTORM**

John C. SAMSON, R. Rankin, and I. Voronkov (all at Department of Physics, University of Alberta, Edmonton, Alberta, Canada T6G 2J1, email: samson@space.ualberta.ca)

The explosive phase of the substorm, with time scales of 10s of second to minutes, follows the initial brightening of an arc on field lines threading the inner edge of the plasma sheet. Optical data from the Canadian CANOPUS array indicate that the initial brightening is followed within 10s of seconds by enhanced cross tail currents in the inner plasmasheet, and then by dipolarization. Lobe flux reconnection begins within three minutes of the initial arc brightening, indicating an extremely dynamic process with Alfvénic time scales. We argue that the Alfvénic time scales indicate that the explosive phase requires a nonlinear instability. We discuss a hybrid model in which the explosive phase is triggered by shear flow ballooning followed by tearing and reconnection. Ultimately, lobe flux reconnection begins at about 25-30 RE down the magnetotail.

**GA3.08/W/19-A6 1520**

**SHARE RADAR OBSERVATIONS OF INTENSE FLOW BURSTS IN THE MAGNETOTAIL**

A. D. M. WALKER and J P S Rash (University of Natal, Durban) K B Baker (The Johns Hopkins University Applied Physics Laboratory) M Pinnock and J R Dudeney (British Antarctic Survey)

Observations are presented of a very unusual event on March 10 1997. At this time, the solar wind conditions were extremely quiet. On the night side the SHARE and Halley radars observed a succession of flow bursts in the ionosphere with velocities exceeding 2 km per s. The poster presents a variety of observations including data from satellites in the solar wind, low altitude satellites passing over the radar field of view, and ground based instrumentation from unmanned ground instruments under the field of view in Antarctica. The event shows some of the characteristics of a substorm, but occurs in the absence of any external driving mechanism. It may be that this is an observation of a fundamental mode of magnetospheric oscillation, uncontaminated by external driving mechanisms.

**GA3.08/W/32-A6 Invited 1600**

**HF RADAR OBSERVATIONS OF IONOSPHERIC CONVECTION IN THE NIGHTSIDE AURORAL ZONE DURING SUBSTORMS**

T. K. Yeoman (Department of Physics and Astronomy, University of Leicester, University Road, Leicester, LE1 7RH, U.K. )

High time resolution data from HF radars reveal short-lived convection signatures in the auroral ionosphere during the three phases of the magnetospheric substorm. For example, transient modulations of the electrojet currents during the substorm expansion phase have reported in data from HF radars. The features typically show an interval of suppressed electric field, characterised by large equivalent currents deduced from ground magnetometers, presumably as a consequence of enhanced ionospheric conductivity due to energetic particle precipitation. Following this an enhanced electric field causes a vortical flow. Ground magnetometer data has suggested that the flow vortices propagate azimuthally at up to 6 km s<sup>-1</sup>, and are typically characterised by equatorward flow enhancements of order 600 m s<sup>-1</sup>. Recent data from high time resolution HF scans parallel to the L-shell have provided direct measurements of the azimuthal propagation and plasma velocity during such impulsive convection features. The features are not usually accompanied by Pi2 pulsations and in one case study there is some evidence from Geotail spacecraft data of a relationship a dawnward perturbation and dipolarisation of the magnetic field and dawnward plasma flow in the magnetotail, perhaps related to bursty bulk flows. The possible implications of these observations for the substorm process will be discussed.

**GA3.08/W/07-A6 1630**

**CUTLASS HF RADAR OBSERVATIONS OF HIGH LATITUDE AZIMUTHALLY PROPAGATING CONVECTION FEATURES DURING MAGNETOSPHERIC SUBSTORMS**

J.A. WILD and T.K. Yeoman (both at Radio & Space Plasma Physics Group, Dept. of Physics and Astronomy, Leicester University, University Road, Leicester, UK, LE1 7RH. Email: jaw11@ion.le.ac.uk)

Previous observations have identified transient high latitude convection features in the substorm electrojets associated with the expansion phase which were inferred to propagate azimuthally from ground magnetometer data. In addition, during the substorm recovery phase,

high time resolution radar modes have been used to study omega bands propagating in an eastward direction. The high time resolution and multi-point nature of the observations leads to a refinement of the previous models of omega band structure. This study combines new data from the CUTLASS radars with observations from the IMAGE, SAMNET, NIPR and Greenland magnetometer networks and the STARE VHF radar in order to look at the zonal flows within the CUTLASS radar field of view. Intervals have been identified in which regions of pulsed flow propagating eastwards are observed directly by the radar and also demonstrate characteristic magnetic behaviour. By directly combining measurements of magnetic field strength and line of sight velocity it is possible to estimate the height integrated ionospheric conductivities at several points within the fields of view of the radars. The continuous nature of the multi-instrumental observations allows the study of the occurrence of azimuthally propagating convection features with respect to substorm phase as well as yielding information regarding the bulk properties and structure of the features themselves.

**GA3.08/E/09-A6 1650**

**THE ELECTRICAL COUPLING OF MAGNETOSPHERIC FLOW VORTEXES AND FLOW CHANNELS TO THE RESISTIVE IONOSPHERE**

John W. Bonnell and Joseph E. BOROVSKY (both at Space and Atmospheric Sciences Group, Los Alamos National Laboratory, Los Alamos, NM 87545, USA, email: jborovsky@lanl.gov)

Owing to their polarization electric fields, flows in the magnetosphere drive field-aligned currents that electrically couple to the ionosphere. The details of d.c. current systems driven by flow vortexes in the magnetosphere are examined. It is found that the current systems driven by positive (angular velocity antiparallel to B) and negative (angular velocity parallel to B) vortexes differ greatly. Positive vortexes drive stronger current systems, dissipate more power, and spread across B whereas negative vortexes drive weaker currents, dissipate less power, and do not spread across B. The signatures above the ionosphere of the two types of vortexes also differ. The details of d.c. current systems driven by flow channels in the magnetosphere are examined. A flow channel in the magnetosphere will exhibit an asymmetry when it couples to the ionosphere; this asymmetric coupling is explored. Extrapolating these studies to flow turbulence in the plasma sheet, predictions are made about the statistics of electric-field divergence at low altitudes and flow vorticity at high altitudes.

**GA3.08/W/26-A6 1710**

**PLASMA SHEET VARIATIONS DURING SUBSTORM ACTIVITY: OBSERVATIONS ON 17TH MAY 1996**

J.STOREY, M. Lester (Both at Radio & Space Plasma Physics Group, University of Leicester, Leicester, United Kingdom) T. A. Fritz (Dept. of Astronomy, Boston University, Boston, USA) C. T. Russell (Institute of Geophysics and Planetary Physics / UCLA, Los Angeles, USA) M. Brittner (University of Washington Geophysics Program, Seattle, USA) J. B. Blake (The Aerospace Corporation, Los Angeles, USA) J. Scudder (Department of Physics & Astronomy, University of Iowa, Iowa City, USA)

This presentation details the initial results obtained from a study of an interval of substorm activity observed in the high-latitude plasma sheet by the Polar spacecraft, during a pass over the Scandinavian sector on 17th May 1996. The study makes use of the CAMMICE and MFE instruments on board the Polar spacecraft, specifically to investigate any substorm related plasma flows and associated magnetic field variations. Other Polar instruments from which data have been used include two other particle instruments, Hydra and CEPPAD, and the Ultra-Violet Imager (UVI), which provides images of the auroral zone throughout the interval and hence shows ground signatures of the plasma flows observed in situ. Other instrumentation includes the WIND magnetometer and the IMAGE and SAMNET magnetometer chains. These instruments provide background data sets that are used to confirm the presence of substorm activity and give the timing of the onset of any such activity. The particle instruments observe PSBL signatures twice during this interval. The first entry into the PSBL is due to a slight re-configuration of the field geometry caused by pseudobreakups occurring at 20:48 and 21:00 UT. The continuing growth phase causes the tail field lines to become more tail-like resulting in the spacecraft exiting the plasma sheet, before the expansion phase onset results in the spacecraft observing CPS ions at 21:45UT.

**GA3.08/E/08-A6 Invited 1730**

**ON THE ROLE OF RESONANCES IN THE TRANSPORT IN THE MAGNETOSPHERE**

ENNIO R. SANCHEZ, SRI International, 333 Ravenswood Ave., Menlo Park, CA 94025

The Sun-Earth connection produces magnetospheric boundaries, cavities, and waveguides where ULF resonances and instabilities can be excited. A combination of simultaneous measurements from high-, low-, and ground-altitude instruments has been used to identify how ULF resonances influence transport in the magnetosphere and onset and evolution of substorms. Intervals were selected for which ISTP spacecraft were appropriately positioned in conjugate positions to ground-based magnetometer and radar chains. Spectral analysis of the observations for the first time establishes a direct relationship between Pc-5 pulsations measured on the ground and the periodicity of dipolarizations and particle injections at geosynchronous altitude, discrete westward electrojet intensifications, plasma and magnetic field oscillations of the plasma sheet and lobes, plasma and magnetic field oscillations in the magnetosheath, and plasma density, convection, and magnetic field pulsations in the plasma sheet. These observations strongly suggest a coupling of resonant cavity modes, which involve energy transfer from compressional oscillations propagating from the outer magnetosphere into the near-Earth closed field lines, with other wave modes in different parts of the magnetosphere. Those modes include waveguide modes originated in the high-latitude open field line regions of the magnetosphere, and waveguide modes in the low-latitude closed field line regions of the magnetosphere encompassed by the low-latitude boundary layers and the plasma sheet. The coupled response of different magnetospheric regions to solar wind input defines a measure of coherence of the magnetosphere-ionosphere system. The coherence of the system defines a correlation between periodicities in reconnection and bursty plasma transport in the magnetotail and periodicities in magnetic flux buildup and particle injection in the near-Earth region.



Monday 26 July AM

Presiding Chair: Larry Lyons, (UCLA, Department of Atmospheric Sciences, Los Angeles, USA)  
Concurrent Poster Session

**GA3.08/W/12-B1** Invited **0930**

**THE GLOBAL IONOSPHERIC CONVECTION RESPONSE TO CHANGES IN THE SOLAR WIND AND INTERPLANETARY MAGNETIC FIELD ORIENTATION**

AARON RIDLEY (Southwest Research Institute, San Antonio, TX 78228-0510, USA, email: ridley@zed.space.swri.edu)

It has been shown that the ionospheric convection is closely coupled to the interplanetary magnetic field (IMF) orientation and more loosely coupled to the solar wind speed and density. Most studies of the convection have investigated the statistical steady state conditions. Recently, a number of studies have focused on the how the convection changes in response to IMF reorientations. The first studies of this kind showed localized observations of how the convection changed with time. More recently, studies have focused upon how the global convection changes. One result of the global studies is that the global convection pattern is shown to change as a whole, instead of the change in convection spreading slowly over the polar cap. Examples of such simultaneous changes are shown to occur for both IMF orientation changes and sudden changes in the dynamic pressure of the solar wind. We present arguments on the interpretation of the convection data, showing the simultaneous change in convection in the noon, dawn, and dusk sectors. We present ground-based magnetometer data to verify these arguments. In addition, we discuss the ramifications of these observations on the dynamics of the magnetosphere-ionosphere system.

**GA3.08/E/03-B1** **1000**

**DYNAMICS OF HIGH-LATITUDE IONOSPHERIC CONVECTION AND CURRENT SYSTEM FOLLOWING A SUDDEN SOUTHWARD TURNING OF THE IMF**

Nozomu NISHITANI and Tadahiko Ogawa (Solar-Terrestrial Environment Laboratory, Nagoya University, 3-13 Honohara, Toyokawa, Aichi 442-8507, Japan, e-mail: nisitani@stelab.nagoya-u.ac.jp) Natsuo Sato and Hisao Yamagishi (National Institute of Polar Research, 1-9-10 Kaga, Itabashi, Tokyo 173-8515, Japan) Mike Pinnock (British Antarctic Survey, High Cross, Madingley Road, Cambridge CB3 0ET, England) Jean-Paul Villain (LPCE/CNRS, 3A Av. de la Recherche Scientifique, 45071 Orléans Cedex 2, France) George Sofko (Department of Physics & Engineering Physics, University of Saskatchewan, 116 Science Place, Saskatoon, SK., S7N 5E2 Canada)

One example of the global dynamics of ionospheric convection and current system has been studied by using the SuperDARN radar network and high-latitude magnetograms when the IMF changed stepwise from northward to strongly southward. There were two-step changes in the ionospheric flow pattern. The first change of the convection pattern can be characterized by a sudden formation of a large flow vortex in the afternoon sector. This change propagated from the noon sector to the evening sector within 2 to 4 minutes. The second change, which occurred twenty minutes later, can be characterized by a sudden antisunward shift of the flow vortex. The ionospheric current system observed by the high-latitude magnetograms showed gradual formation of the DP2 current system. The formation began simultaneously with the first response of the convection flow and completed a few minutes after the second response. Distortion of the DP2 current system, that is, antisunward shift of the center of the two vortices, occurred simultaneously with the second response of the ionospheric convection pattern. From these observations, we speculate that the first response is associated with the propagation of magnetosonic waves, and that the second response is due to the configuration change of the magnetosphere after the solar wind discontinuity arrived in the magnetotail region.

**GA3.08/W/27-B1** Invited **1040**

**ION AND ELECTRON HEATING IN MAGNETIC RECONNECTION**

M. Hoshino (The University of Tokyo, Tokyo, 113-0033 Japan, email: hoshino@geophys.s.u-tokyo.ac.jp)

The origin of hot and dense plasma in the Earth's plasma sheet has been a long-standing problem. Observations have established that the ion temperature is the order of several keV, and the ion temperature in the plasma sheet is always about several times larger than the electron temperature. Many microscopic and macroscopic plasma processes are thought to be involved in the plasma heating: magnetic reconnection plays an important role on energy conversion process from magnetic into kinetic energy, and provides the preferential plasma heating of ions. Current-driven instabilities around the plasma sheet boundary layer are believed to be substantial for the electron heating. Strong turbulence of waves in the plasma sheet is probably important for understanding the hot plasmas as well. These effects are undoubtedly important for various stages of magnetotail evolution associated with magnetic reconnection. We have started to investigate the self-consistent plasma heating and acceleration processes in association with the kinetic magnetic reconnection by using a three-dimensional, electromagnetic, particle-in-cell simulation, in which both the current-driven instabilities and the collisionless reconnection process are described. We have studied where and when ions and electrons gain their energy during reconnection evolution. The results are discussed in terms of the GEOTAIL observations.

**GA3.08/E/02-B1** **1110**

**SIGNATURES OF MAGNETOTAIL VARIABILITY IN THE AURORAL ZONE**

VAHE PEROOLIAN, Maha Ashour-Abdalla (Both at UCLA-IGPP, Box 951567, Los Angeles, CA 90095-1567, USA, e-mail: vahe@igpp.ucla.edu) Lev M. Zelenyi (Space Research Institute, Academy of Sciences, Moscow, Russia, e-mail: lzelenyi@iki.rssi.ru)

We use a self-consistent, large-scale kinetic model to investigate the formation of the magnetotail and the auroral manifestations of the complicated temporal dynamics that occur there during quiet periods. In our model, the magnetotail's current is calculated by following ion trajectories in a magnetic field that is made up of ion currents calculated at the previous time step. The model takes into account both the local inductive and global dawn-dusk electric fields. We find that the magnetotail is quite variable: magnetic islands are formed, then decay and merge. This process appears to be quasi-periodic, and results from the cycles of loss and replenishment that current-carrying particles undergo in the current sheet; these cycles are themselves caused by the rapid and non-adiabatic energization of ions in the vicinity of the x-lines that form in the model. Ion inertia determines the characteristic time scale for this periodicity, which is on the order of 5 - 10 minutes. The magnitude of the dawn-dusk electric field also influences the time scale. In our model, ion acceleration near the temporally variable location of the x-line stimulates the formation of quasi-periodic, velocity-dispersed ion structures in the ion precipitation profile. Many polar-orbiting spacecraft have observed structures such as these. We will compare our results with these observations.

**GA3.08/W/33-B1** **1130**

**WIND OBSERVATIONS OF THE NEAR-EARTH PLASMA SHEET: SOLAR WIND AND GEOMAGNETIC ACTIVITY DEPENDENCE**

M. OIEROSET, T. D. Phan, L. Chan, and R. P. Lin (Space Sciences Laboratory, University of California, Berkeley, CA 94720, E-mail: oieroset@ssl.berkeley.edu)

We have studied 20 WIND perigee passes through the plasma sheet earthward of 24 Re. The plasma sheet observations are sorted according to region, interplanetary magnetic field values, solar wind plasma parameters, and Kp values, in an attempt to increase our understanding for the causes of the variations in the plasma sheet plasma parameters. Preliminary results indicate a cold and dense plasma sheet for low Kp values while the plasma sheet gradually becomes heated and less dense with increasing Kp. Our findings are also in agreement with GEOTAIL observations by Terasawa et al. (GRL, 24, 935-938, 1997), showing a cold and dense plasma sheet for northward IMF when the IMF is averaged over several hours prior to the plasma sheet observations. We also survey the interrelationship between the thermal and flow parameters in the plasma sheet in order to investigate the structure and dynamics of the plasma sheet.

**GA3.08/E/12-B1** **1150**

**IS THE MHD APPROACH VALID IN THE DISTANT PLASMA SHEET?**

Oleg TROSHICHEV (Arctic and Antarctic Research Institute, St.Petersburg, 199397, Russia, email: olegtro@aari.nw.ru); Elizabeth Antonova (Scobeltin Institute of Nuclear Physics, Moscow State University, Moscow, 119899, Russia, email antonova@orearm.msk.ru); Yohsuke Kamide (Solar Terrestrial Environment Laboratory, Nagoya University, Toyokawa, Aichi, 442, Japan, email: kamide@stelab.nagoya-u.ac.jp)

Measurements of the magnetic field and low energy plasma by the GEOTAIL spacecraft were utilized to study correspondence between the plasma velocity and magnetic oscillations in the distant plasma sheet at X = -(79-200) RE. A total of 14 extremely quiet days from available GEOTAIL data in 1993-1994 (12-s averages of the magnetic field and plasma parameters) were chosen for the analysis, identification of the plasma sheet and estimation of the magnetic activity being realized according to Troshichev et al. [JGR, in press]. Case study of behavior of magnetic field and plasma velocity shows that correspondence between the changes in these parameters often is not carried out. The Fourier analysis also sometimes shows striking discrepancy in the frequent spectra for magnetic and plasma parameters when powerful oscillations of plasma velocity (usually VY or/and VZ components) in range 3-8 min occurs against the almost calm magnetic field and vice versa. These results suggest that MHD approach is often violated in the distant plasma sheet even under the extremely quiet conditions.

**GA3.08/W/24-B1** **1210**

**OBSERVATION OF PROLONGED, STEADY RECONNECTION IN THE MAGNETOTAIL BY THE GEOTAIL SPACECRAFT**

R. T. Mist and C. J. OWEN (Astronomy Unit, Queen Mary and Westfield College, London, UK), T. Mukai (Institute of Space and Astronautical Science, Sagamihara, Japan), S. Kokubun (Solar Terrestrial Environment Laboratory, Nagoya University, Toyokawa, Japan)

It is relatively unusual for conditions in the distant tail to allow a spacecraft to remain in the central plasma sheet continuously for a prolonged period. However, on October 27, 1994, when the Geotail spacecraft was situated in the deep tail (X=-170 RE, Y=20 RE and Z=0 RE), the spacecraft crossed from the north to the south lobe, and spent about 4 hours continuously in the plasma sheet. The magnetic field and plasma moment data throughout this period are consistent with the plasma sheet being formed by quasi-steady reconnection. The level of geomagnetic activity during this period is steady and moderate, with no obvious enhancements due to substorms. We analyse the two-dimensional ion distributions from the LEP instrument during this interval, and study the plasma populations in the north and south lobes, the PSBL and the plasma sheet. We compare these observed distributions with the predictions of reconnection models based on the balance of magnetic field and plasma stresses at the central, cross-tail current sheet. In these models, the plasma sheet population is formed by both heating and acceleration of the inflowing lobe plasma during its interaction with the current sheet. We show that the observed ion distributions are consistent with the expectations of these reconnection models.

Monday 26 July PM

Presiding Chairs: M. Hoshino, (University of Tokyo, Japan)  
M. Fujimoto, (Tokyo Int. Tech, Tokyo, Japan)

**GA3.08/W/14-B1** Invited **1400**

**THE EARTH'S DYNAMIC MAGNETOTAIL**

A. Nishida (Institute of Space and Astronautical Science, Sagamihara, 229-8510, Japan, email: nishida@gtl.isas.ac.jp)

Following the first comprehensive study of the magnetotail conducted with the IMP 1 satellite, Ness [1969] reviewed the latest findings on the physics of the Earth's magnetotail. It is impressive that most of the fundamental concepts were already established in that review. At the end of the paper he listed outstanding problems which future studies should be directed to resolve. In the present paper we shall summarize the advances made in the physics of the magnetotail with reference to the problems he listed, and discuss the remaining issues. Answers to the problems he enumerated as (1) to (6) are given in the following. (1) The formation of the magnetotail is due to magnetic reconnection on the magnetopause. (2) Coherent, well-ordered tail exists at least to the distance of 200 Re and there is no indications of filamentation. (3) The merging across the neutral sheet is impulsive at the near-Earth neutral line. (4) Accelerations both in the magnetotail and in the solar flare are governed by magnetic reconnection. (5) Accelerations occur at the slow-mode shock and in the neutral sheet including the vicinity of the neutral sheet. (6) Electron islands events correspond to plasmoids and plasma-sheet boundary layer. Remaining important issues include (1) mixing of plasma-sheet and magnetosheath plasmas in the LLLB, (2) paucity of the slow-mode shock identification, and (3) trigger of the near-Earth reconnection.

**GA3.08/W/16-B1** **1430**

**AURORAL POLEWARD BOUNDARY INTENSIFICATIONS: A FUNDAMENTAL MAGNETOSPHERIC DISTURBANCE COUPLING BURSTY PLASMA SHEET FLOWS TO THE AURORAL IONOSPHERE**

L. R. Lyons (Department of Atmospheric Sciences, UCLA, Los Angeles, CA 90095-1565, USA, email: larry@atmos.ucla.edu); G. T. Blanchard (Department of Chemistry & Physics University of



Southeastern Louisiana SLU 10878, Hammond, LA 70402-0878, USA); T. Nagai (Department of Earth and Planetary Sciences, Tokyo Institute of Technology, Tokyo 152, Japan); T. Yamamoto, T. Mukai, A. Nishida (All at: Institute of Space and Astronautical Science, Sagami-hara 229, Japan); J. C. Samson (Department of Physics, University of Alberta, Edmonton, Alberta, T6G 2E9, Canada); S. Kokubun (Solar-Terrestrial Environment Laboratory, Nagoya University, Toyokawa 442, Japan)

Poleward boundary intensifications are nightside geomagnetic disturbances that have an auroral signature that moves equatorward from the poleward boundary of the auroral zone. They occur repetitively, and they appear to be the most intense auroral disturbance at times other than the expansion phase of substorms. They connect to the magnetotail via upward field-aligned currents that are sufficiently intense that a field-aligned potential drop is required. We have used data from nightside conjunctions of the GEOTAIL spacecraft in the magnetotail with the CANOPUS ground-based array in central Canada. During periods with identifiable poleward boundary intensifications, we find that the plasma sheet has considerable structure and bursty flow activity. During periods without such intensifications, the plasma sheet is far more stable with little flows. This is consistent with the intensifications being the result of the mapping to the ionosphere of the electric fields that give rise to bursty flows within the plasma sheet. Two different types of plasma sheet disturbance have been found to be associated with the poleward boundary intensifications. The first is fows that result from Speiser motion of particles in a localized region of thin current sheet. The second, seen preferentially in the near-Earth plasma sheet, consists of energy dispersed ion structures that culminate in bursts of low energy ions and isotropic low-energy electrons. Both are associated with localized regions of enhanced dawn-to-dusk electric fields.

**GA3.08/W/23-B1 1450**

**CHARACTERISTICS OF AURORAL POLEWARD BOUNDARY INTENSIFICATIONS**

Efthya Zesta (Department of Atmospheric Sciences, UCLA, Los Angeles, CA 90095-1565, USA, email: ezesta@atmos.ucla.edu); Larry R. Lyons (Department of Atmospheric Sciences, UCLA, Los Angeles, CA 90095-1565, USA); John C. Samson (Department of Physics, University of Alberta, Edmonton, Alberta, T6G 2E9, Canada); Erick Donovan (Department of Physics and Astronomy, University of Calgary, Calgary, Alberta, T2N 1N4, Canada)

Poleward Boundary Intensifications (PBIs) of the aurora are a frequently occurring auroral-zone disturbance. They consist of auroral enhancements that move equatorward from near the magnetic separatrix and are associated with ground magnetic disturbances of 20-100 nT and P12 pulsations. They are a phenomenon distinct from substorms, occurring both during substorm and non-substorm periods, and are often observed both during enhanced convection intervals and during quiet times. We used meridional scanning photometer data from the CANOPUS stations during the winter of 1996-1997 to identify a number of periods with PBI events. We investigate both the occurrence characteristics and the correlation of PBIs with the IMF direction and magnitude. We find that PBIs are statistically a dusk-to-midnight region phenomenon and are therefore associated with the upward region 1 field-aligned currents. We find that only half of our identified events are associated with substorms. The non-substorm associated PBIs are found to have a clear preference for a radial IMF. However, the radial IMF is a necessary but not sufficient condition for the occurrence of PBI events in the nightside aurora. We also examine all-sky-imager data from the CANOPUS station of Gillam at the time of our PBI events and determine the possible correlation of PBI events, identified in the meridional scanning photometer data, with short-lived, north-south aligned auroral arcs and with equatorward moving east-west aligned auroral arcs.

**GA3.08/W/28-B1 1510**

**LOCAL INTENSIFICATION OF THE TAIL CURRENT AND ASSOCIATED OCCURRENCE OF MAGNETIC RECONNECTION IN THE MAGNETOTAIL**

T. MUKAI, Y. Asano, I. Shinohara, and Y. Saito (Institute of Space and Astronautical Science, Yoshinodai, Sagami-hara 229-8510, Japan, email: mukai@stp.isas.ac.jp); T. Nagai (Department of Earth and Planetary Sciences, Tokyo Institute of Technology, Tokyo 152-8551, Japan, email: nagai@geo.titech.ac.jp)

Recent GEOTAIL observations have clearly demonstrated a crucial role of magnetic reconnection in substorms. There are well-known growth phase signatures in the magnetotail, such as increasing pressure and configuration change to the tail-like magnetic field, representing enhancement of the tail current and thinning of the current sheet. However, these signatures are seen over a wide range of distances down the tail and are not enough to explain a certain location where the reconnection is first initiated. Fortunately we have found a substorm event in which the GEOTAIL spacecraft stayed in the current sheet at a distance of ~17 Re and could clearly observe temporal evolution of the tail current intensification and associated occurrence of magnetic reconnection there. Following the gradual increase in the growth phase, the tail current density increased sharply a few minutes before the onset. The tailward fast flows and increasing plasma temperatures were also observed to start in association with the intensification of the current density. These signatures can be interpreted as the initial occurrence of magnetic reconnection associated with local thinning of the current sheet (because the case is very rare). As time proceeds, the current sheet further thins and the current density is further intensified. This sequence evolves explosively through a few steps in several minutes, expanding the active region.

**GA3.08/W/34-B1 Invited 1550**

**THE HALL TERM EFFECTS IN MAGNETIC RECONNECTION**

Dr Masaki Fujimoto Dept. Earth Planet. Sci., Tokyo Inst. Tech

Geotail observations have shown that there are strong field-aligned currents (FACs) that are very likely to be the Hall current generated in magnetotail reconnection. 2D Hall MHD simulations do show that the FACs due to the Hall term are significant and should not be neglected in considering coupling to the ionosphere. These lead us to make 3D Hall MHD simulations of magnetic reconnection to study the three-dimensional structure of the generated FACs. Details of the results, especially in comparison with those obtained by MHD models, will be discussed.

**GA3.08/W/11-B1 1620**

**SIMULATIONS SHOWING GENERATION OF FILAMENTARY FIELD-ALIGNED CURRENTS ABOVE THE AURORAL IONOSPHERE**

Daniel W. Swift (Geophysical Institute, University of Alaska, Fairbanks, AK 99775-7320, USA, email: swift@gi.alaska.edu) Yu Lin (Physics Department, 206 Allison Laboratory, Auburn University, Auburn, AL 36849-5311, USA, email ylin@physics.auburn.edu)

A two-dimensional hybrid code is used to simulate the midnight meridian plane of the magnetosphere. The simulation domain extends from the Earth's ionosphere to 35 Earth radii

in the antisunward direction and to 11 Earth radii along the polar axes. The simulation is driven by a dawn-to-dusk electric field imposed at the boundaries. The sequence of events follows those associated with the growth and expansive phases of the substorm. Momentum exchange between the plasma being accelerated Earthward in the neutral sheet and the magnetic field results in a stretching of the magnetic field lines and thinning of the plasma sheet. A pair of field-aligned currents develops connecting the inner edge of the plasma sheet to the auroral ionosphere, with the downward current equatorward of the upward current. The breaking of the inward plasma flow drives these currents. Next follows the apparent dipolarization. "Dipolarization" is carried outward by plasma rebounding off the dipole field. Ion-ion two streaming instabilities are excited behind the expanding dipolarization front. The effect of these instabilities is propagated Earthward along magnetic field lines by shear Alfvén waves. These are seen as field-aligned current filaments above the auroral ionosphere. We take the upward field-aligned current filaments as proxies for auroral arcs.

**GA3.08/W/15-B1 1640**

**STUDY OF THREE-DIMENSIONAL HYBRID SIMULATION OF MAGNETOTAIL RECONNECTION**

MASAO NAKAMURA (Solar-Terrestrial Environment Laboratory, Nagoya University, Honohara 3-13, Toyokawa, Aichi 442-8507, Japan, Email: nakamura@stelab.nagoya-u.ac.jp) and Masaki Fujimoto (Department of Earth and Planetary Sciences, Tokyo Institute of Technology, Ookayama 2-12-1, Meguro, Tokyo 152, Japan)

The three-dimensional structure of magnetic reconnection in a thin current sheet (thickness comparable to the relevant ion inertia length), which models the near-Earth tail current sheet just before substorm onsets, are studied by means of 3-D hybrid simulations (ion particle, charge neutralizing massless electron fluid). Magnetic reconnection is initiated by fixing a localized anomalous resistivity in the plasma sheet and generates fast plasma flows in the Earth-tail direction as a result of its explosive growth. On the other hand, the thin plasma sheet is unstable to the tail Kelvin-Helmholtz (K-H) instability, which kinks plasma sheet in the cross-tail plane. For the small resistivity cases, the tail K-H instability is well generated before the explosive growth of reconnection starts. While the kink structure of the plasma sheet modifies the plasma flow, the essential features, such as the dawn-dusk asymmetry of plasma flows and field configuration, still remains unchanged from the large resistivity case where the explosive growth starts before the influence of the tail K-H instability is visible.

**GA3.08/E/04-B1 1700**

**SIGNATURES OF MAGNETOTAIL RECONNECTION DERIVED BY NUMERICAL SIMULATIONS AND VERIFIED IN SPACE**

JOERG BUECHNER AND B. Nikutowski (Max-Planck- Institut fuer Aeronomie, Max-Planck-Str. 2, D-37191 Katlenburg-Lindau, Germany)

The true physics behind magnetic reconnection is still an open question. On the other hand large scale topological considerations have shown that reconnection must take place in the Earth's magnetotail. The magnetotail is, therefore, an appropriate site to test reconnection models. We have developed a kinetic model of three-dimensional reconnection and derived its signatures by kinetic plasma simulations. Here we present current results of numerical plasma simulations of specific signatures of collisionless reconnection through thin current sheets. We illustrate some of them in the context of ISTP spacecraft measurements of INTERBALL-1 and GEOTAIL.

**GA3.08/W/20-B1 1720**

**A TAIL CROSSING AT 200 RE--GEOTAIL/HEP-LD OBSERVATION**

B. Wilken, Q.G. Zong ( both at Max-Planck-Institut fuer Aeronomie, D-37191 Katlenburg-Lindau, Germany, Email: wilken@limpi.mpg.de) T. Doke (Advanced Research Center for Science and Engineering, Waseda university, Tokyo, Japan) S. Kokubun (Solar-Terrestrial Environment Laboratory, Nagoya University, Toyokawa, Japan)

In April 1994 Geotail was travelling on a deep tail trajectory. Sustained moderate geoactivity was driven by the passage of a corotating interaction region (CIR) which started on 3 April and continued until 20 April. On 17 April a CME impinged on the magnetosphere and caused a major magnetic storm. Geotail observed the CME in the dusk magnetosheath/magnetosphere interface at a GSE position (-200,30,-5 Re). Shortly after the CME Geotail started the dusk-to-dawn tail passage. The general level of activity in the magnetotail was found to be very low which corresponded to rather quiet conditions in the geosynchronous orbit and on the ground. However, quasi-periodic low intensity energetic particle bursts embedded in plasmoid-like structures passed Geotail. In the absence of corresponding near-Earth disturbances it is suggested that the regular structures in the deep tail resulted from large amplitude Alfvén wave in the solar wind.

**GA3.08/E/07-B1 1740**

**NUMERICAL SIMULATION OF PLASMOID DYNAMICS**

B P PANDEY, G.S.Lakhina and M.Roy (Indian Institute of Geomagnetism, Bombay 400 005, India, email: pandey@iig.iigm.res.in, lakhina@iig.iigm.res.in)

The plasmoid dynamics has been studied by a 2-D magnetohydrodynamic simulation code for a magnetotail configuration which takes into account the flaring of the tail. The plasmoid formation and its subsequent motion down the tail is followed for a few hundreds of Alfvén time. Simultaneously, the spatial and temporal evolution of density, pressure, temperature and magnetic field is studied. The results are compared with the Geotail observations.

**Monday 26 July AM**

Presiding Chair: T. Nagai, Tokyo Int. Tech, Japan

**GA3.08/W/06-B1 Poster 0900-01**

**THE RESPONSE OF THE MAGNETOSPHERE TO AN INTERPLANETARY SHOCK: GLOBAL SIMULATIONS OF THE SEPTEMBER 24, 1998 SUDDEN IMPULSE EVENT**

J RAEDER, C T Russell (both at: Institute of Geophysics and Planetary Physics, University of California, 405 Hilgard Ave, Los Angeles, CA 90095, USA, email: jraeder@igpp.ucla.edu)

A very strong interplanetary shock was observed by the Wind spacecraft on September 24, 1998, 2221 UT. The resulting sudden impulse (SI) was observed by several magnetospheric spacecraft, as well as by ground magnetometers. This event gives us a unique opportunity to

study the response of the magnetosphere using our global magnetosphere - ionosphere model, and to compare our results in detail with the observations. Besides providing an assessment of the accuracy and robustness of our model for such an event, we will also present a more complete picture of the magnetospheric response as the observations alone could provide. In particular, we will discuss the propagation of the SI initiated waves through the magnetosphere, SI modifications to the current systems, and the causes of the ground magnetic perturbations.

**GA3.08/W/04-B1** Poster **0900-02**

**TAIL PLASMA FLOWS AND ELECTROJET ACTIVITY**

Tsugunobu Nagai (Earth and Planetary Sciences, Tokyo Institute of Technology, Tokyo 152-8551, Japan, email: nagai@geo.titech.ac.jp) Tuija I. Pulkkinen (Finnish Meteorological Institute, P.O.Box 503 FIN-00101 Helsinki, Finland, email tuija.pulkkinen@fmi.fi) Peter Stauning, Danish Meteorological Institute, Lyngbyvej 100, DK-2100 Copenhagen, Denmark, email pst@dmi.dk) Toshifumi Mukai (Institute of Space and Astronautical Science, Sagami-hara 229-8510, Japan, email: mukai@gt.lisas.ac.jp) Susumu Kokubun (Solar-Terrestrial Environment Laboratory, Nagoya University, Toyokawa 442-8507, Japan, email: kokubun@stelab.nagoya-u.ac.jp)

The spacecraft Geotail observes tailward/earthward convection plasma flows in the plasma sheet at radial distances of 10-30 Re in association with substorm activity. The ground magnetometer chains in Scandinavia and Greenland monitor electrojet activity, and the central latitude of the westward electrojet can be determined. In this paper, we examine the relationship between tail plasma flows and ground electrojet activity. Tailward plasma flows observed at 20-30 Re are usually associated with westward electrojets at magnetic latitudes of 64-68 degrees, whereas earthward plasma flows observed around 30 Re are often associated with the westward electrojet near 70 degrees. Unusual tailward plasma flows inside 20 Re are related with the westward electrojet near 60 degrees. We present several event studies and statistical results.

**GA3.08/E/10-B1** Poster **0900-03**

**SUBSTORM ACTIVITY AS A SELF-ORGANIZED CRITICAL PHENOMENON**

Vadim M.URITSKY, Mikhail I.Pudovkin (Department of Geophysics, St.Petersburg State University, Petrodvorets, St.Petersburg 198904, Russia, Emails: uritsky@snoopy.phys.spbu.ru, pudovkin@snoopy.phys.spbu.ru)

The effect of self-organized criticality (SOC) is proposed as an internal mechanism of generation of 1/f<sup>b</sup>-like fluctuations in Earth's magnetosphere. It was suggested that localized in space current instabilities developing in the magnetospheric tail at the initial substorm phase can be considered as the SOC avalanches - dynamic clusters, superposition of which leads to the 1/f<sup>b</sup> fluctuations of macroscopic characteristics of the system. Using sandpile model of SOC, numerical investigation of both spatially localized and global disturbances of magnetospheric current layer was carried out. The dependence of model's sensitivity on the accumulated internal energy was shown to be similar to that characterizing natural geomagnetic activity. The power spectrum of sandpile model fluctuations controlled by real solar wind parameters reproduces all distinctive features of the AE fluctuations spectrum, including presence of two frequency ranges with different spectral slopes, that provides an important evidence for our hypothesis. Furthermore, quantitative and qualitative conformity between disturbed dynamics of self-organized critical state of the model and the main phases of real magnetospheric substorm development is demonstrated.

The results obtained suggest that the application of the theory of SOC and cellular automaton technique creates a new promising approach for modelling substorm activity. This approach seems to be adequate for the describing of fractal stochastic features of geomagnetic variations which are difficult to interpret on the base of traditional methods.

**GA3.08/W/30-B1** Poster **0900-04**

**ONE-DIMENSIONAL KINETIC MODEL OF THE PLASMA SHEET EVOLUTION DURING A SUBSTORM ACTIVATION**

V.I.Domrin and A.P.Kropotkin, Skobel'syn Institute of Nuclear Physics, Moscow State University, Moscow, 119899, Russia

A one-dimensional simulation model is constructed for analysis of the plasma sheet (current sheet, CS) evolution in the near-Earth tail region where an intense CS thinning is known to occur during a substorm activation. Dynamics of the hot plasma in the plasma sheet and of the ambient cold plasma is examined on the kinetic equation basis; a macroparticle code is used for ions to solve the equations while electrons are considered as a massless cold background. Self-consistent electromagnetic fields are calculated as numerical solutions of the Maxwell equations. The plasma sheet evolution takes place under action of an MHD disturbance that is applied on the boundary of the simulation box. That disturbance is assumed to be a consequence of fast tearing process occurring further in the magnetotail.

In the course of the simulated evolution, the electric field of the disturbance penetrates down to the central plane of the CS. That results in acceleration of ions in the CS; accelerated ions then escape CS along the field lines. Eventually the initial CS becomes replaced by an anisotropic one. The current is now carried by initially cold ions which are brought into CS by convection from the tail lobes. Magnetic field "annihilation" is a consequence: electromagnetic energy brought to CS from both sides, is transformed into energy of accelerated ions.

**GA3.08/W/01-B1** Poster **0900-05**

**GENERAL ANALYTICAL THEORY OF SELF-CONSISTENT QUASIADIABATIC CURRENT SHEETS**

Zeleniy Lev (Space Research Institute, Russian academy of sciences, 117810, Moscow, Russia, Email: lzeleniy@iki.rssi.ru); Sitnov Mikhail and MALOVA HELMI (Skobel'syn Institute of Nuclear Physics, 117899, Moscow, Russia, email: stn@dec1.npi.msu.su, mlv@dec1.npi.msu.su)

The basics of unified analytical theory of the structure of self-consistent quasiadiabatic current sheets created by the impinging ion streams are presented. The problem is considered neglecting the jumps of the invariant I<sub>z</sub> of nonmagnetized ions. Nonlocal analogue of the Grad-Shafranov equation for the sources of arbitrary anisotropy is obtained and solved numerically. The universal solutions corresponding to the regimes of strong and weak anisotropies are investigated. Resulting self-consistent current is a sum of the drift cyclotron current and the magnetization currents flowing in the opposite directions. The maximum thickness of the current sheet is achieved in a case of weak anisotropy and equals to the thermal gyroradius of ions outside the sheet. In a case of strong anisotropy the sheet is compressed to minimal thickness. The effects of real nonadiabaticity are considered when the quasiadiabatic approximation is violated. Jumps of quasiadiabatic invariant I<sub>z</sub> result in the gradual suppression of anisotropy and smearing of the current sheet. Influence of electron component creates an additional layer

which also effectively broaden the current structure. We also discuss the relevant experimental data from ISEE and modern ISTP spacecraft (Geotail, INTERBALL) about the structure of the current sheets in the distant and near Earth parts of the tail.

**GA3.08/W/10-B1** Poster **0900-06**

**EVIDENCES OF UNMAGNETIZED ELECTRON MOTION WITHIN THE PLASMA SHEET AND ITS POSSIBLE CAUSES**

Marina STEPANOVA (Universidad de Santiago de Chile, Ecuador 3493, Casilla 307, Santiago, Chile, email: mstepano@lauca.usach.cl), Elizavieta Antonova, Ilya Ovchinnikov, Mickail Teltzov, Elena Vikhrev, (all at Skobel'syn Institute of Nuclear Physics, Moscow State University, Moscow 119899, Russia, email: antonova@taspd.npi.msu.su)

We present the results of experimental and theoretical investigation of unmagnetized stochastic motion of electrons and plasma mixing within the plasma sheet. Analysis of electron temperature distributions within the plasma sheet has been made using Intercosmos-Bulgaria-1300 polar orbiting satellite. It was shown, that the temperature, which has been obtained taking into consideration the acceleration of precipitating electrons by field-aligned potential drop, is nearly constant in the meridional direction within upward field-aligned current region and their values do not change for different orbits during a quiet geomagnetic time. Analysis of spatial fluctuations of precipitating electron fluxes at a fixed electron energy has shown, that fluctuation spectra of primary electrons have a power dependence and is close to the spectra of electric field fluctuations observed within the plasma sheet. The results of observations are interpreted as the consequence of stochastic plasma sheet particle motion and intensive plasma sheet plasma mixing. The role of different processes in such stochasticization is analyzed. For the majority of plasma sheet ions, their Larmor radius can be comparable with the radius of curvature of magnetic field line which can be the source of stochasticization. But, in case of electrons such mechanism can be effective only for particles with quite high energy or in the regions of extremely low B<sub>z</sub>. Therefore, it is suggested that the main source of observed electron stochasticization and one of the powerful source of ion stochasticization is their motion in the inhomogeneous electric fields with characteristic scales comparable with particle Larmor radius. Chaotization of particle trajectories may be the part of stochasticization process. Particle motion in the homogeneous magnetic field and regular inhomogeneous electric field having sinusoidal distribution in one direction and homogeneous distribution in perpendicular direction is analyzed as an example of a chaotic motion.

**GA3.08/W/08-B1** Poster **0900-07**

**APPLICATION OF AN INVERSION METHOD BASED ON MID-LATITUDE MAGNETIC DATA TO ESTIMATIONS OF MEANINGS OF PARAMETERS OF THE GEOMAGNETIC TAIL AND THE IONOSPHERE**

Vagina L.I.

On the basis of an inversion method based on mid-latitude magnetic data during the development of 71 substorms we have calculated characteristic temporary and spatial substorm current systems parameters: characteristic times of current increase and decrease, maximal current values, characteristic spatial sizes. The received characteristics were used to find the values of the constants for the homogeneous differential equation of the second order with constant factors. Using the received constants we have made estimations of meanings of parameters of the geomagnetic tail and the ionosphere. The meanings of estimated parameters have appeared within the limits of typical meanings of parameters of a geomagnetic tail and ionosphere, received other methods.

**GA3.08/E/06-B1** Poster **0900-08**

**PECULIARITY OF GEOMAGNETIC FIELD ON GEOSTATIONARY ORBIT, CONSEQUENCE FOR STATIONARY CONVENTION**

KUZNETSOV S.N. (Skobel'syn Institute of Nuclear Physics, Lomonosov Moscow State University, 119899, Moscow, Russia, e-mail: kuznets@srldan.npi.msu.su)

Analysis of GOES data on geomagnetic field during 1993-94 years shown that in time intervals near equinox we observe stationary increasing of the magnetic field near local midnight. This effect was not observed in solstice intervals. We proposed that this effect is projecting to midnight range of unreally position of field-align currents. This effect may be connected with asymmetry in precipitation of cosmic ray electrons in magnetic lines of a plasma tail. The range of quasidipolar field near midnight may be foundation of tetha-strap in an aurora.

**GA3.08/E/05-B1** Poster **0900-09**

**ON THE KELVIN-HELMHOLTZ HYDROMAGNETIC INSTABILITY**

ANZOR GVELESIANI (Institute of Geophysics, Georgian Academy of Sciences, 1, M. Alexidze Str., Tbilisi 380093, Georgia, email: vazha@excite.com)

An analytical magnetohydrodynamic model of tangential discontinuity stability in the Earth's magnetosphere plasma sheath, magnetopause and plasma and neutral sheets is suggested. The general discussion relations for multilayer plasma flows of plane and cylindrical configuration are received. It is shown the role of the plasma compressibility and geometric parameters - thickness and curvature of layers boundaries - on the Kelvin-Helmholtz hydromagnetic instability. The compressibility of plasma results in destabilisation of plasma layers motion. It is found the parameter (product respectively the relations of plasma densities and magnetic fields squares of the neighbouring layers) from the value of each (more or less than 1) defines the effect of the geometry both of tangential discontinuity surface on the cylindrical and plane form of incompressible plasmatic jets.

**GA3.10** **Saturday 24 July**

**THE MAGNETOSPHERE AND IONOSPHERE UNDER NORTHWARD IMF (WITH DIV. II) (IGA)**

Location: Muirhead Tower, 424 LR5  
Location of Posters: Muirhead Tower, 422 LR4

**Saturday 24 July AM**

Presiding Chairs: O. Troshichev (Arctic and Antarctic Research Institute, St. Petersburg, Russia), A. Egeland (University of Oslo, Blindern, Norway)

**GA3.10/E/05-A6** **Invited** **0830**

**SUN-ALIGNED AURORAL ARCS IN THE HIGH-LATITUDE MORNING SECTOR UNDER NORTHWARD IMF**

Kazuho SHIOKAWA (Solar-Terrestrial Environment Laboratory, Nagoya University, 3-13, Honohara, Toyokawa, Aichi 442-8507, Japan, Email: shiokawa@stelab.nagoya-u.ac.jp)

Sun-aligned arcs are often observed in the high-latitude morning sector under the northward IMF conditions. On the basis of 6 year ground observation of the arcs at two Canadian stations (84MLAT and 78MLAT), we show characteristics of the arc appearance and motions. We found that most arcs for which we can define the direction of the motion move poleward with a typical velocity of 500 m/s. The arcs tend to move poleward repeatedly with a period of several minutes. Most of such events occur around the end of substorm-like magnetic activity, suggesting that the source of the moving arcs is related to the plasma sheet particles. Satellite observation shows that periodically-moving arcs occur during when both IMF Bz and By are positive or near zero. These arcs are caused by accelerated electron precipitation and are located around the boundary of the large-scale sunward flowing region at lower latitudes and the antisunward flowing region at higher latitudes. These results suggest that the arcs are connected to the boundary region between the plasma sheet and the low-latitude boundary layer in the morningside tail flank. From these observational facts, we discuss the source mechanism of the arcs, including pressure gradient force and flow shear in the tail flank.

**GA3.10/W/07-A6** **Invited** **0855**

**THE POLAR CAP IONOSPHERE DURING PERIODS OF IMF BZ NORTHWARD ORIENTATIONS**

C. E. VALLADARES (Institute for Scientific Research, Boston College, Chestnut Hill, MA 02167; email: cesar@dl5000.bc.edu)

When the IMF is directed northward, the ionospheric convection within the polar cap is more variable than during times of IMF southward. Measurements of the plasma convection during times of Bz north have shown the existence of sunward flows within the polar cap and the formation of three or four cells. These properties of the plasma convection are able to sustain the development of Sun-aligned and transpolar auroras practically at any location inside the polar cap. Another region of the polar cap, which seems to be strongly controlled by the IMF Bz, is the ionospheric cusp. When Bz points north, the footpoints of the merging region are displaced poleward and sometimes exist as two regions displaced in latitude by few degrees, each associated with field aligned currents. These facts point to the idea that reconnection may occur simultaneously on open and closed field lines. Particles impinging the cusp region show reversed ion dispersion and reversed convection. The IMF By component may also dictate the type of display seen at the ionospheric cusp. The ratio of By and Bz, under Bz positive conditions, may control the amount of closed/open field lines being reconnected. This paper reviews current measurements of the ionospheric cusp at darkness and the theoretical implications derived from joint optical and radio measurements.

**GA3.10/W/20-A6** **0920**

**MIDDAY AURORA AND DPY CONVECTION CURRENT FOR NORTHWARD IMF**

Per Even Sandholt and Alv EGELAND (both at Department of Physics, University of Oslo, P. O.Box. 1048, Blindern 0316, Oslo, Norway, e-mail: p.e.sandholt@fys.uio.no)

We report a characteristic bifurcation of the aurora in the midday sector in association with northward turnings of the interplanetary magnetic field (IMF), leading to the coexistence of latitudinally separated forms, called types 1 and 2. The northernmost form (type 2), generally located north of the observation site at 75 deg MLAT, is characterized by a brightening sequence during intervals of nonzero IMF By. The auroral observations are discussed in relation to the DPY convection current obtained from the IMAGE magnetometer chain. The type 2 auroral activity and its associated convection current are interpreted as ionospheric signatures of reconnection between the IMF and the terrestrial lobe field at the high-latitude magnetopause.

**GA3.10/W/23-A6** **0935**

**FLOWS AND CURRENTS NEAR THE CUSP UNDER NORTHWARD IMF CONDITIONS**

D.L. MURR and W.J. Hughes (Center for Space Physics, Boston University, Boston MA 02215, USA; e-mail: murr@bu.edu)

Arrays of magnetometers provide a means of monitoring the high latitude ionospheric currents, and hence flows, over extended regions. We make use of magnetometer arrays in North America and Greenland to study flows during times of northward IMF and during transitions from southward to northward conditions. These combined magnetometer arrays provide a coverage of over 10 hours in MLT allowing us to monitor flows around noon continuously for several hours. We find that flows change from predominantly antisunward to predominantly sunward when the northward component of the IMF becomes larger than about 2 nT. The transition from one flow pattern to another is rapid, taking only a few minutes to completely change. From the portion of the ionosphere we are able to image, we see little evidence for convection patterns with more than two cells, but patterns do evolve very quickly.

**GA3.10/W/03-A6** **0950**

**PARTICLE AND ELECTRIC FIELD MORPHOLOGIES FOR PERIODS OF BZ LARGE AND NORTHWARD**

M.S. GUSSENHOVEN, D.H. Brautigam (Air Force Research Laboratory, Hanscom AFB, MA 01731) C.Y. Huang (Institute for Scientific Research, Boston College, Newton, MA 02159) F.J. Rich (Air Force Research Laboratory, Hanscom AFB, MA 01731)

A study is made of cases for which the Bz component of the interplanetary magnetic field (IMF) is large and positive for periods greater than 24 hours. The cases span Solar Cycle 23. Patterns of convection, of ion density and of precipitating auroral ions and electrons are determined for each case using data from the DMSP topside thermal plasma monitor and auroral particle detectors. Variations in the patterns are related to previous magnetospheric activity, solar wind kinetic energy, season, and solar cycle position. To this end, the patterns are also compared to statistical models for similar IMF and solar wind conditions for which persistence of conditions for 24 hours was not a requirement. They are also compared to magnetic cloud periods during which Bz slowly rotates from south to north (or vice versa), but typically stays in one configuration for less than 6 hours. Additional information on magnetospheric conditions is obtained from the CRRES data for several cases near solar maximum. WIND data provides information on low energy electrons and ions in the solar wind after before and during solar minimum.

**GA3.10/W/19-A6** **1005**

**MULTI-INSTRUMENT OBSERVATIONS OF THE DAYSIDE POLAR IONOSPHERE UNDER STEADY NORTHWARD IMF**

S.E. PRYSE and A.M. Smith (Department of Physics, University of Wales Aberystwyth, Ceredigion, SY23 3BZ, U.K. Email: sep@aber.ac.uk, ams93@aber.ac.uk)

Results are presented from a multi-instrument case study of the polar dayside ionosphere under steady northward IMF. Optical emissions reveal Type 2 signatures, characteristic of lobe reconnection. The sunward plasma flow on lobe cells is identified by HF radar measurements. Downstream of the reconnection footprint, the reverse ion energy dispersion is seen in satellite particle data. Its effect is also evident in a tomographic image as a gradient in the altitude of the F-region ionisation peak, with altitude increasing with decreasing latitude. A steep latitudinal electron density gradient in the tomographic image, separating polar structure from the ionisation at lower latitudes, is interpreted as the adiabatic polar-cap boundary. Supporting evidence for the plasma structure is provided by electron density and temperature measured by the EISCAT Svalbard Radar.

**GA3.10/W/13-A6** **Invited** **1050**

**IONOSPHERIC CONVECTION AND FIELD-ALIGNED CURRENTS DURING NORTHWARD IMF**

L. G. Blomberg (Alfvén Laboratory, Royal Institute of Technology, Stockholm, Sweden, email: blomberg@plasma.kth.se), J. A. Cumnock (Alfvén Laboratory, Royal Institute of Technology, Stockholm, Sweden and William B. Hanson Center for Space Science, University of Texas at Dallas, Richardson, TX, USA)

The high-latitude ionosphere acts as a projection screen for electrodynamic processes in the magnetosphere. The interaction is particularly intriguing for northward IMF where the large-scale convection pattern may contain two, three, or four cells, and where polar current systems (NBZ currents) may occur in addition to the regular region 1 and region 2 currents. We review the current understanding of large-scale ionospheric convection and field-aligned currents during northward IMF. Results from applying the KTH convection model to northward IMF situations are shown, for events with a stable transpolar arc as well as for events where a transpolar arc is moving across the polar region. Recent data from the polar-orbiting Swedish microsatellite Astrid-2 are discussed.

**GA3.10/E/04-A6** **Invited** **1115**

**DAYSIDE FIELD-ALIGNED CURRENT SYSTEMS UNDER NORTHWARD IMF BZ**

Shin-ichi OHTANI (The Johns Hopkins University Applied Physics Laboratory, Johns Hopkins Road, Laurel, MD 20723-6099, USA, Email: ohtani@jhuapl.edu), Tomoyuki HIGUCHI (The Institute of Statistical Mathematics, 4-6-7 Minami-Azabu, Minato-ku, Tokyo 106, Japan, Email: higuchi@ism.ac.jp)

The objective of the present paper is to report new attempts to study field-aligned currents (FACs) under northward IMF as well as to review recent studies. One of the major restrictions of investigating FACs with satellite magnetic field data has been that we have to count on visual examination of data plots. We recently developed an automatic procedure to identify FAC systems and applied it to the entire set of the DMSP-F7 magnetometer data, which consists of about 35,000 auroral zone crossings. In this paper we will focus on two interesting features of dayside FACs which we found to be related to the northward IMF orientation. One is the 4-sheet FAC structure. The associated polar distribution of FACs can be interpreted in terms of ionospheric convection, in which the existence of the lobe convection is essential. The preference of the event occurrence for northward IMF Bz also suggests that the field line merging between the IMF and the lobe magnetic field plays an important role. The other phenomenon to be reported is the disappearance of dayside FACs. Events are observed predominantly in the winter hemisphere, indicating that ionospheric conductance is important. By comparing FAC patterns in the summer hemisphere, we address the role of the ionosphere in the generation of FACs under northward IMF Bz.

**GA3.10/W/25-A6** **1140**

**PATTERNS OF ELECTRIC POTENTIALS AND FIELD ALIGNED CURRENTS FOR NORTHWARD IMF DERIVED FROM SATELLITE MEASUREMENTS**

Daniel WEIMER (Mission Research Corporation, 1 Tara Blvd., Nashua, NH, 03033, USA, email: dweimermrn.com)

Results of empirical modelling of both the electric potentials and field aligned currents under conditions of northward IMF will be shown. Previous publications had shown that two-dimensional maps of the electric potential over the polar caps can be derived from measurements of the electric potential along multiple satellite passes, by using a least-error fit of spherical harmonic coefficients. By applying the same technique to satellite magnetic field measurements, new maps of field aligned currents have been obtained. The new method uses a "magnetic potential", which is obtained by rotating the measured magnetic field perturbations by 90 degrees and then integrating along the satellite path. Maps of this magnetic potential are then obtained from many combined passes by the spherical harmonic technique. The field-aligned current density is then calculated from the Laplacian of the magnetic potential, which will be shown to be equivalent to the curl of the two-dimensional perturbation vector field. Maps that are derived with this technique show unprecedented detail. How the electric potential and field aligned current patterns evolve as the IMF orientation changes from +Y to purely northward and then to -Y will be shown and discussed.



**GA3.10/W/18-A6 1155**

**HIGH-LATITUDE IONOSPHERIC CONVECTION AND FIELD-ALIGNED CURRENTS DETECTED FROM GROUND MAGNETOMETERS AND FROM THE ØRSTED SATELLITE DURING NORTHWARD IMF CONDITIONS**

Freddy CHRISTIANSEN, Vladimir Papitashvili\*, Ole Rasmussen and Peter Stauning (all at Danish Meteorological Institute, Vindbyvej 100, DK-2100, Copenhagen, Denmark, email: fch@dmi.dk, \*also at SPRL, University of Michigan)

During southward interplanetary magnetic field (IMF) conditions the high-latitude ionospheric convection patterns usually display a large-scale, twin vortex system with the antisunward convection across the center of the polar cap and the sunward return flow at lower latitudes. However, during the northward IMF (NBZ) conditions, the antisunward convection almost ceases and is replaced by the sunward flow at the dayside portion of the near-pole region, while the two-cell system remains at lower latitudes forming a complicated convection pattern of three or more vortices. The NBZ convection pattern is generally associated with the Region 0 field-aligned current system in the central polar cap. These currents are possibly generated through high-latitude merging processes. We will focus on selected cases during NBZ conditions as defined by the IMF data obtained from IMP 8 and ACE spacecraft observations. The high-latitude ionospheric convection will be described from high-latitude ground magnetometer data, while the field-aligned current systems will be derived from high-precision geomagnetic measurements made by the Ørsted satellite.

**GA3.10/W/06-A6 1210**

**INSTANTANEOUS GLOBAL PATTERNS OF HIGH-LATITUDE CONVECTION DURING NORTHWARD IMF**

J. Michael RUOHONIEMI and Raymond A. Greenwald (both at Johns Hopkins University, Applied Physics Laboratory, Johns Hopkins Rd., Laurel, MD, 20723, USA, email: mike\_ruohoniemi@jhuapl.edu)

The nature of high-latitude convection for northward IMF conditions remains a somewhat unsettled problem. Although recent experimental results have tended to favor the multi-cell over the distorted two-cell model, these have been limited by the continuing difficulty of obtaining truly global-scale images of the instantaneous high-latitude convection pattern. The role of the azimuthal IMF component in ordering convection during northward IMF is also not clear. To date, the most complete portrayals of convection for northward IMF are due to large statistical studies.

With the SuperDARN network of HF radars in the northern hemisphere, it is possible, at times, to measure convection velocities over nearly the entire pattern with a temporal resolution of 2 minutes. In earlier work involving common-volume measurements with one pair of SuperDARN radars an example of a single reverse dayside convection cell was shown (Greenwald et al. [1995]). Using a new technique to combine the line-of-sight velocity data from all six radars into a best-fit estimate of the global pattern, we have examined several periods of northward IMF. These demonstrate the prevailing morphology of the pattern for northward IMF (multi-cell) and its great variability. Comparison with statistical convection models indicate that, even when these express the appropriate multi-cell morphology, they usually significantly underestimate the magnitude of the flows. We attempt to characterize the emergence of multi-cell convection in terms of IMF and other factors and interpret the patterns within the context of solar wind-magnetosphere coupling processes.

**GA3.10/W/26-A6 1225**

**SUNWARD CONVECTION AND GLOBAL MAGNETOSPHERIC OSCILLATIONS DRIVEN BY LOBE RECONNECTION DURING AN EXTENDED PERIOD OF NORTHWARDS IMF T.K.**

Yeoman (Radio and Space Plasma Physics Group, Dept. of Physics and Astronomy, Leicester University, University Road, Leicester, LE1 7RH, U.K., email: yxo@ion.le.ac.uk) I.R. MANN (Dept. of Physics, University of York, Heslington, York, YO10 5DD, U.K., email: ian@aurora.york.ac.uk) G. Chisham and M.P. Freeman (British Antarctic Survey, High Cross, Madingley Road, Cambridge, CB3 0ET, U.K., email: gchi@pcmail.nerc-bas.ac.uk, mpf@pcmail.nerc-bas.ac.uk) J.A. Wanliss (Dept. of Physics, University of Alberta, Edmonton, Alberta, T6G 2J1, Canada, email: wanliss@space.ualberta.ca)

We present observations from an interval of 11 hours of almost continuously northward IMF which suggest that lobe reconnection may have provided a powerful internal source for global magnetospheric oscillations. The interval is between around 2200 UT on the 19th, and 0900 UT on the 20th, March 1995. From 0400 UT, the SuperDARN Finland radar records good backscatter from high latitudes, and shows a well developed high latitude convection pattern consistent with clockwise flow driven by lobe reconnection under By positive conditions in the northern hemisphere. At around 0900 UT, the Finland radar again observes velocities consistent with continuing lobe stirring, however between the two radar observations the spectral widths suggest that the polar cap has contracted. The radar also detects intervals of convection consistent with four cell convection between these two times. Coincident observations from the IMAGE magnetometer array show the existence of two wave packets of discrete spectrum Pc5 waves, between 0300-0500 UT and 0600-0800 UT, having dominant period of around 512s and 430s respectively. Complex demodulation analysis reveals clear field line resonances (FLRs) in both cases, the first at 73 and the second at 75 degrees geomagnetic. The waves provide an excellent closed field line diagnostic which also show the polar cap to be strongly contracted at this time, the IMAGE estimates of the last closed field line being consistent with those inferred from the Finland radar spectral widths. Whether the northwards motion of the FLR is caused by contraction of the polar cap, or occurs due to local time changes in magnetic geometry is not clear. Unfortunately, the southern hemisphere radar at Halley has insufficient backscatter at polar cap latitudes to confirm whether or not the sunward convection which would be required to generate new closed flux and hence to contract the polar cap was occurring in the southern hemisphere during this interval. Interestingly, however, between 0300-0500 UT and at lower latitudes, the Halley radar does observe ULF wave activity coherent with and of the same period as the waves seen by IMAGE around 6 hours of local time away in the opposite hemisphere. The same wave packet was also seen near the equatorial plane on the dawn flank by Geotail. This shows the ULF waves to be truly global in nature. Since the solar wind speed is relatively slow, and the ram pressure relatively constant, we believe that the waves were not driven directly by the solar wind. Our observations suggest that lobe reconnection may have been responsible and that it may provide a powerful internal source for global magnetospheric oscillations.

**GA3.10/W/24-A6 Invited 1400**

**TOPOLOGY OF MAGNETOSPHERE AND IONOSPHERE COUPLING**

Patrick NEWELL (Johns Hopkins University Applied Physics Laboratory, 11100 Johns Hopkins Rd., Laurel, MD 20723)

The polar cap (and hence the magnetosphere) for northward IMF can be open and simply connected, open and not simply connected (theta aurora), or closed. Examples of all three states can be found, although by far the most common is open and simply connected (a region void of precipitation around the magnetic pole). This is because northward IMF intervals normally include brief southward IMF fluctuations, and dayside merging can open flux much more quickly (about 10\*\*5 Wb/s) than it subsequently drains during quiet times (about 7 x 10\*\*3 Wb/s in our estimate). Examples of these various states of the magnetosphere/ionosphere configuration will be given, along with the conditions under which they occur.

**GA3.10/E/01-A6 Invited 1425**

**MAGNETOSPHERE-IONOSPHERE COUPLING AND THETA-AURORA FORMATION**

Elizaveta E. ANTONOVA (Skobel'syn Institute of Nuclear Physics, Moscow State University, Moscow, 119899, Russia; email: antonova@orearm.msk.ru, antonova@tasdp.npi.msu.ru)

The analysis of the experimental observations of the magnetosphere and the ionosphere under northward IMF conditions give the possibility to develop the theoretical approach to the magnetosphere-ionosphere coupling and theta-aurora formation. The theory consider the observed reconnection phenomena as the consequence of inner magnetosphere current dynamics.

Generation of electric field including large-scale dawn-dusk electric field is explained like the consequence of the existence of hot plasma pressure gradients in the magnetosphere producing large-scale field-aligned currents in the regions where magnetic field lines are closed and bulk plasma velocity is much lower than Alfvén and sound velocity. The existence of plasma sheet developed turbulence is taken into account. The theory give the possibility to explain the plasma sheet bifurcation under northward IMF conditions, the formation of NBZ current system, the change of the electric field direction from dawn-dusk to dusk dawn in the center of polar cap (and corresponding change of plasma flow from antisunward to sunward).

**GA3.10/W/04-A6 Invited 1450**

**ALMOST STATIC PLASMA SHEET IN GEOMAGNETICALLY QUIET TIMES**

A. NISHIDA and T. Mukai (both at Institute of Space and Astronautical Science, Sagami-hara, 229-8510, Japan, email: nishida@gtl.isas.ac.jp, mukai@gtl.isas.ac.jp); S. Kokubun (Solar Terrestrial Environment Laboratory, Toyokawa, 442-8507, Japan)

During geomagnetically quiet intervals, there are times when the flow velocity is very low ( $|V_x| < 100 \text{ km/s}$ ) in the distant plasma sheet. We shall call them as almost static plasma sheet. This paper studies characteristics of such cases in combination with those of PSBL and more normal (in terms of flow speeds) plasma sheet that were observed in close succession over a period of 12 hours at  $x = -112 \text{ Re}$ .  $B_z$  was positive and  $|B_y|$  was much less than  $B_z$  in the almost static plasma sheet studied here. It is found that all the plasma sheet data points, including both very low speed and normal speed cases, satisfied the same temperature-velocity and density-velocity relations which are very well defined. In this sense the almost static plasma sheet is not an anomaly. Ion temperature that corresponds to zero flow velocity is about 300 eV. The temperature-velocity and density-velocity relations for the PSBL are clearly different from these and are almost orthogonal; that is, while in the lobe/PSBL density increases with  $|V_x|$  it decreases with  $|V_x|$  in the plasma sheet. In these correlation diagrams the points representing the almost static plasma sheet are located at the intersection between the lobe/PSBL and the plasma-sheet curves. This observation is discussed in the light of the statistical results on the structure and dynamics of the magnetotail in geomagnetically quiet times.

**GA3.10/W/16-A6 Invited 1515**

**THE MAGNETOSPHERE UNDER NORTHWARD IMF: MODELS AND SIMULATIONS**

Joachim RAEDER (Institute of Geophysics and Planetary Physics, University of California, 405 Hilgard Ave, Los Angeles, CA 90095, USA, email: jraeder@igpp.ucla.edu)

Substantial progress has been made over the past several years in modelling the magnetosphere under northward IMF conditions. Models have become capable of using measured solar wind and IMF data as input, thus enabling the direct comparison of model results with in-situ measurements of the magnetosphere, to the effect that model results are now much more reliable as in the past. We will review the modelling efforts of the past several years and discuss what the models can say about the reconnection geometry, tail structure, and magnetospheric and ionospheric convection under northward IMF. In particular we will address the still controversial issue of whether or not the magnetosphere can attain a closed topology during quiet times and/or northward IMF.

**GA3.10/E/09-A6 1600**

**GLOBAL MHD SIMULATIONS OF THE SOLAR WIND-MAGNETOSPHERE COUPLING FOR NORTHWARD IMF**

P. SONG, D. L. DeZeeuw, T. I. Gombosi, C. P. T. Groth, and K. G. Powell (The University of Michigan, Ann Arbor, MI, USA, e-mail: psong@umich.edu)

We present a series of global MHD simulations for northward IMF conditions. We investigate the effect of the solar wind velocity, density, and IMF strength on the length of the magnetotail. We will also investigate the global magnetic field configuration, ionospheric and magnetospheric plasma convection patterns and current systems for steady-state northward IMF conditions.

**GA3.10/W/02-A6 1615**

**MAGNETopause CURRENT SYSTEMS AND TRANSPORT FOR ZERO IMF**

B.U.Ö. SONNERUP (Thayer School of Engineering, Dartmouth College, Hanover NH 03755, USA, email: sonnerup@dartmouth.edu) W.W. White, K.D. Siebert, N.C. Maynard, and D.R. Weimer (Mission Research Corp., Nashua NH 03062, USA, email: bwwhite@mrcnh.com, ksiebert@mrcnh.com, nmaynard@mrcnh.com, dweimer@mrcnh.com) G.L. Siscoe and G.M. Erickson (Center for Space Physics, Boston University, Boston MA 02543, USA, email: siscoe@buasta.bu.edu, erickson@buasta.bu.edu)

A numerical MHD-based simulation code is used to investigate the morphology and dynamical role of those global magnetospheric current systems that remain in the limit of vanishing interplanetary magnetic field (IMF). In this limit, reconnection does not occur on the magnetopause so that magnetospheric convection is driven exclusively by viscous/diffusive transport. The remaining current systems include the classical Chapman-Ferraro currents, the geotail currents and the Region 1 currents, all of which thread the magnetopause/low-latitude boundary layer (MP/LLBL) region. In particular, the Region 1 currents connect the LLBL to the high-latitude ionospheres, where they serve to maintain the standard two-cell polar-cap convection system. The associated polar-cap potentials, found in the simulations, agree well with values derived from observations when the IMF is weak. A simple analytical model of flows and fields in the equatorial MP/LLBL region has been developed. It describes density, velocity and magnetic-field variations across these layers and permits estimation of the effective, numerically produced, MP/LLBL transport coefficients associated with the code. Results indicate resistive and viscous diffusion coefficients that are in fortuitous agreement with estimates derived from in-situ observations of the LLBL.

**GA3.10/W/01-A6 1630**

**LOW ENERGY IONS OBSERVED BY POLAR/TIDE FOR NORTHWARD IMF NEAR SOLAR MINIMUM**

H. A. Elliott and R. H. COMFORT ( both at The University of Alabama in Huntsville, CSPAR, TH S101, Huntsville, AL 35899, Email: comfotr@cspar.uah.edu) M. O. Chandler and P. D. Craven (both at NASA/Marshall Space Flight Center, Space Science Laboratory, ES83, Redstone Arsenal, Alabama, AL 35812) T. E. Moore (NASA/Goddard Space Flight Center, Laboratory for Extraterrestrial Physics, Greenbelt, MD 20771)

This study examines characteristics of low energy ions near the polar cap boundary and within the polar cap in relationship to convection velocities. Since convection has been shown to be related to IMF conditions, cases during northward IMF conditions will be contrasted with southward IMF cases. The primary source data for this study comes from the Thermal Ion Dynamics Experiment (TIDE) on the Polar satellite early in the Polar mission near solar minimum. TIDE can measure 3-D velocities and covers the low energy range 0-450 eV, with mass discrimination. The Polar orbit has apogee near 9 RE geocentric over the northern polar region and perigee near 2 RE over the southern polar cap. IMF conditions will be obtained from observations by Wind or IMP-8. Convection near the polar cap boundary is of particular interest since the convection there is often highly structured, and convection reversals may be associated with O<sup>+</sup> outflow. Cleft ion fountain studies have shown that O<sup>+</sup> flows out of the cleft and convects poleward as it falls into the polar cap. In addition to characterizing ion properties at both high and low altitudes for northward IMF for solar minimum, this study examines the density structures of O<sup>+</sup> in relationship to the convection velocities and location within the polar cap. Initial analysis of TIDE data has shown that the O<sup>+</sup> density can maximize poleward of a convection reversal that is found in the cleft region. The density then decreases across the polar cap. In the nightside auroral region, Transverse Ion Acceleration events have been shown to be co-located with convection reversals. Examining such relationships can provide insight into understanding the consequences of the 3-D flow on the density and temperature structures of O<sup>+</sup> ions in the polar cap, and transport of O<sup>+</sup> across the polar cap.

**GA3.10/E/02-A6 1645**

**THE COUPLING MODE BETWEEN KELVIN-HELMHOLTZ AND RESISTIVE INSTABILITIES IN COMPRESSIBLE PLASMAS**

Chen SHEN (Center for Space Science and Applied Research, Chinese Academy of Sciences, Beijing 100080, China, e-mail: sc@center.cssar.ac.cn); Zhenxing Liu (Center for Space Science and Applied Research, Chinese Academy of Sciences, Beijing 100080, China, e-mail: liu@center.cssar.ac.cn)

We have investigated the coupling mode between K-H and resistive instabilities using a compressible MHD simulation method. It is found that, in compressible plasmas, the coupling mode can take place in a limited range of ambient shear flow velocity, beyond which the coupling mode is stabilized. The flow shear can significantly enhance the growth of the coupling mode. Only in a limited range of plasma beta, could the coupling mode occur. Through comparing the observation characteristics of the magnetic reconnection at Earth's magnetopause with the results here, we deduce that the coupling mode between K-H and resistive instabilities can appear at Earth's magnetopause, especially at the high latitude boundary layer when the IMF is northward.

**GA3.10/L/01-A6 Poster 1700-01**

**THE RELATION OF HIGH-LATITUDE AURORAL ARCS TO THE PARTICLE PRECIPITATION REGIONS IN THE MORNING SECTOR**

V.L.ZVEREV and V.G.Vorobjev (Polar Geophysical Institute, Academy, Murmansk region, 184200 Russia, Email: zverev@pgi.kolasc.net.ru)

Ground-based observations of high-latitude auroral arcs in the 05-09 MLT sector by the all-sky camera at Vostok station (-83.3MLAT, MLT=UT-1) and simultaneous DMSP F6-F9 particle precipitation measurements have been examined. DMSP F6-F9 satellites have been processed by a neural-network-based automated identification algorithm (Newell et al., 1991) designed to indicate the source of precipitation. A total of 17 simultaneous events in 1985-1990 were analysed. The IMF Bz component was northward during these events. It was found that during these events in the regions of high-latitude Sun-aligned arcs the plasma mantle particle signatures have been observed. In most cases the locations of polar arcs are consistent with the particle definition of the poleward edge of the plasma mantle. The regions with the high-latitude Sun-aligned arcs were not separated from the main auroral oval by the particle precipitation typical for the polar cap. Some dusk-dawn asymmetry of particle precipitation boundaries locations during satellite passes was observed. P.T.Newell, S.Wing, C-L.Meng and V.Sigillito. The auroral oval position, structure, and intensity of precipitation from 1984 onward: an automated on-line data base. J.Geophys.Res. VOL.96, NO A4, 5877-5882, 1991.

**GA3.10/E/10-A6 Poster 1700-02**

**THE STRUCTURE OF PLASMA CONVECTION IN THE HIGH-LATITUDE IONOSPHERE FOR NORTHWARD IMF**

N.V.ISAEV. Institute of Terrestrial Magnetism Ionosphere and Radio Wave Propagation , 142092 Troitsk, Moscow Region, Russia.

The results of the DC- electric field examination depending on the IMF based on measurements onboard the "Interkosmos-Bulgaria-1300" satellite are presented. It is shown that for a strong values of Bz (IMF)>0 and different directions of By (IMF) the electric field in the polar ionosphere is abruptly inhomogeneous - local increases of the electric field values up to 120 mV/m in the dayside and nightside auroral region. Besides, at strong Bz > 0 in the polar cap occur 2-3 vortex convective systems of definitely non-stationary character with convection velocity direction determined by the sign of By IMF. Empirical high-latitude electric field models have been constructed. Distribution of the potential in the polar ionosphere (global convection of the ionospheric plasma) for small values of Bz IMF and Kp index was calculated and formed on the basis of statistical data from satellites. It is obtained that large-scale convective cell (Bz<0) or two cells (Bz>0) can appear in the polar cap region, the direction of plasma rotation is determined by sign By IMF. The effect of the convection electric field penetration into the region of main ionospheric trough (MIT) is determined for the different directions of IMF and geomagnetic activities. It is concluded that the IMF structure is in general determined by a direction and intensity of electric field. The density inhomogeneity in the region of MIT develops as a result of gradient-drift instability.

**GA3.10/W/10-A6 Poster 1700-03**

**GLOBAL OBSERVATIONS OF TRANSPOLAR ARC EVENTS**

J. A. CUMNOCK (Alfvén Laboratory, Royal Institute of Technology, Stockholm, Sweden and William B. Hanson Center for Space Science, University of Texas at Dallas, Richardson, TX, USA; email: cumnock@plasma.kth.se), L. G. Blomberg (Alfvén Laboratory, Royal Institute of Technology, Stockholm, Sweden), R. Coley (William B. Hanson Center for Space Science, University of Texas at Dallas, Richardson, TX, USA), J. F. Spann (NASA Marshall Space Flight Center, Huntsville, AL, USA), F. J. Rich (Phillips Laboratory, Hanscom AFB, MA, USA)

It has been observed that the most stable theta aurora configuration (i.e., a transpolar arc extending along the noon-midnight meridian and attached to the auroral oval on both the day and nightsides) evolves from an expanded dawn or dusk side of the auroral oval. The transpolar arc evolves from the dusk (dawn) side of the auroral oval when the IMF is northward and By changes from positive to negative (negative to positive). The expanded dawn and/or dusk sides of the auroral oval map to an expansion of the plasma sheet in the magnetosphere. How the transpolar arc maps to the magnetosphere once it has separated from the auroral oval is not yet clear. While these transpolar arcs are normally associated with northward IMF, they can persist for as long as 30 minutes after the IMF turns southward. Preliminary analysis of the ionospheric signatures of this evolution are shown. The global UV patterns of interest are identified utilizing POLAR UVI data. Precipitating particles and the resulting density enhancements measured by the DMSP satellite are examined. Field aligned currents and plasma drifts are generated with the KTH convection model.

**GA3.10/W/15-A6 Poster 1700-04**

**CONVECTION FLOW IN THE NORTHERN HEMISPHERE DURING INTERVALS OF POSITIVE IMF BZ AS OBSERVED BY THE SUPERDARN RADARS.**

G. PROVAN and T. K. Yeoman (Department of Physics and Astronomy, University of Leicester, Leicester LE1 7RH, UK.)

Super Dual Auroral Radar Network (SuperDARN) is a global network of HF radars which provide information on the high-latitude ionosphere in the Northern and Southern hemispheres, obtaining the E x B drift of ionospheric plasma by scattering radio waves off F region irregularities. By merging the line-of-sight velocities observed by several pairs of SuperDARN radars, it has been possible to study the ionospheric convection flow over a large area of the high-latitude ionosphere. A number of cases studies have been performed on the effect of a northward Bz component of the Interplanetary Magnetic Field (IMF), as measured by the WIND satellite, on the convective flow of plasma in the high-latitude Northern hemisphere ionosphere as observed by the SuperDARN radars. The dynamics of the convection patterns and their relationship to the location and motion of the polar cap boundary are investigated.

**GA3.10/W/05-A6 Poster 1700-05**

**CONVECTION SYSTEMS FOR GROUND STATE OF MAGNETOSPHERE**

R. LUKIANOVA (Arctic and Antarctic Research Institute, Bering st., St.Petersburg, Russia, email: renata@geophys.spb.su)

Convection systems generated by different patterns of the ground state field-aligned currents taking place in periods of geomagnetic quiescence are calculated by method of numerical simulation. Method of calculation implies solution of the boundary problem for elliptic system of partial differential equations on the spherical surface, the electrodynamic connection between the hemispheres and realistic assumptions about the current systems and the ionospheric conductivities. The convection systems have been examined in a way that is consistent with Region 0, 1, 2 currents. It is shown that the main feature of the ground state convection in the polar ionosphere are convection cells attached to day-time cusp region. The convection cells are reduced to form smaller-scale structures at local times extending from dayside to nightside. Calculation have been carried out for equinox and solstice in both hemispheres to show seasonal effects.

**GA3.10/W/08-A6 Poster 1700-06**

**HIGH LATITUDE IONOSPHERIC CONVECTION AND FIELD-ALIGNED CURRENTS DURING NORTHWARD IMF: GLOBAL PATTERNS AND THEIR DYNAMICS**

AARON RIDLEY (Southwest Research Institute, San Antonio, TX 78228-0510, USA, email: ridley@zed.space.swri.edu) Vladimir Papitashvili (Space Physics Research Laboratory, University of Michigan, Ann Arbor, MI 48109, USA, email: papita@umich.edu)

The IZMIRAN Electrodynamic Model (IZMEM) was recently re-calibrated against experimental observations made by five DMSP satellites between 1993 and 1996. We utilized the combined IZMEM/DMSP ionospheric electrostatic potentials (e.g., <http://www.sprl.umich.edu/MIST>) for systematic study of the ionospheric convection and field-aligned current dynamics in the dark and sunlit ionospheres during changing northward IMF conditions. The cross-polar potential differences and changes in the convection pattern are studied as a function of the IMF Bz and

various By over the both northern and southern polar regions. We test the predictive capabilities of this model by comparing the modeled potential and field aligned current patterns to results derived from the AMIE (assimilative mapping of ionospheric electrodynamics) technique. In order to determine how the models compare, we have run both during periods of dynamic, northward, IMF. It is found that when the IMF is low-pass-filtered, both the IZMEM model and the AMIE technique show similar behavior as the convection evolves during IMF changes and that changes occur almost simultaneously over the entire polar cap. It is further found that while the behavior is similar, the base patterns can be significantly different. This is explained in terms of the viscous interaction pattern.

**GA3.10/W/17-A6** Poster **1700-07**

#### HIGH-LATITUDE IONOSPHERIC CONVECTION FOR NORTHWARD IMF

L. A. DREMUKHINA, Ya. I. Feldstein, A. E. Levitin (Institute of Terrestrial Magnetism, Ionosphere and Radio Wave Propagation, Troitsk, Moscow Region, 142092, Russia, email: lgromova@izmiran.troitsk.ru)

The complexity of ionospheric convection patterns for northward IMF makes difficult to understand the behavior of plasma at high latitudes. Every empirical model of high latitude ionospheric convection (developed from satellites or radar observations, or utilizing the ground magnetograms inversion technique) is based on some definitions, "a priori" determining differences in convection over the polar region for particular IMF strength and direction as well as for various solar wind parameters. In this study we carry out comparisons of the basic convection patterns developed during northward IMF with the satellite and radar data. The presentation will focus on reasons how the multi-vortex convection patterns can be obtained for northward IMF from satellite passes. When only the satellite observations are taken into account in drawing the near-orbit pattern, the localized multi-vortex system can easily be produced. However, that kind of drawing can be disputed from the analysis of the global convection patterns modeled for particular situation in the IMF during the satellite pass.

**GA3.10/E/07-A6** Poster **1700-08**

#### THE IMF DEPENDENCE OF HIGH-LATITUDE FIELD-ALIGNED CURRENTS AS ESTIMATED FROM MAGNETIC SATELLITE DATA

Nils OLSEN, Therese Moretto and Eigil Friis-Christensen (Danish Space Research Institute, Juliane Maries Vej 30, DK-2100 Copenhagen, e-mail: nio@dssi.dk)

We have estimated high-latitude field-aligned currents from data of high-precision low-altitude satellites like MAGSAT and Oersted. After subtraction of a main field model, the data were divided according to season and the direction of the y- and z-component of the IMF, and averaged on a grid (2 deg geomagn. lat. / 1 hour MLT). The radial component of the current density was estimated from the averaged horizontal magnetic field of the four neighboring grid-cells. We present average field-aligned current patterns for nine different directions of the IMF and for different seasons, and compare our results with those obtained from magnetic ground-based data.

**GA3.10/W/12-A6** Poster **1700-09**

#### AIR FORCE STATISTICAL AURORAL MODELS (AFSAM)

D.H. BRAUTIGAM (Air Force Research Laboratory, Hanscom AFB, MA 01731, USA, email: brautigam@ph.af.mil)

Since 1985, the Air Force Research Laboratory (AFRL) has created a series of statistical auroral models based on electrostatic analyzer data (electron and ion flux) from the Defense Meteorological Satellite Program (DMSP) satellites. A set of hemispheric auroral maps are constructed over a wide range of auroral activities, parameterized both by Kp and by interplanetary conditions. Of particular relevance to this session are the maps which are parameterized according to the z-component of the interplanetary magnetic field (Bz) and solar wind speed (Vsw) [Brautigam, et al., JGR, 96, 1991]. Individual maps are created by compiling the raw data into average spectra over a spatial grid defined by corrected geomagnetic latitude and local time coordinates. From these average spectra, a number of average quantities are derived, including integral number flux, integral energy flux, Hall and Pedersen conductivities, and average energy. Analytical fits to these average quantities have been recently completed, with the goal of making the models more accessible to ionospheric modelers. Sample maps constructed from the analytical fits will be presented to compare and contrast the Bz north with the Bz south cases.

**GA3.10/E/06-A6** Poster **1700-10**

#### SEASONAL EFFECTS IN MODELLED IONOSONDE DRIFTS AT CASEY, ANTARCTICA

P. R. Smith(1),(2), P. L. DYSON(2), and R. J. Morris(3): (1)Dept. of Electronic Engineering, LaTrobe University, Bundoora, VIC 3083, Australia (2)Dept. of Physics, LaTrobe University, Bundoora, VIC 3083, Australia (3)Australian Antarctic Division, Channel Hwy, Kingston, TAS 7050, Australia

A digital ionosonde located at Casey, Antarctica (at -81° CGL), in the southern polar cap, has collected four years of F-region plasma drift measurements. This large data-set was used to create linear regression models of the plasma flow, parameterized by the direction and strength of the Interplanetary Magnetic Field (IMF) in the By-Bz plane. The drift is primarily influenced by the IMF Y and Z components, but separate models created for summer and winter show there exists a definite seasonal effect. The summer hemisphere convection pattern is predicted to include a lobe cell circulating on open field lines, embedded within one of the merging cells. The drift vectors at Casey's latitude are consistent with convection patterns derived from DMSP satellite data, with a larger, rounder dusk cell for -By (for southern hemisphere), but more evenly sized cells for +By. The Casey model is also consistent with patterns from the Weimer 96 (W96) electric potential model generated for dipole tilts of  $\pm 15^\circ$ . The W96 model is used to track the movement of convection cell centers with season and illustrates, for example, that in summer the dusk cell center passes poleward of Casey for a large -By component while in winter it does not. An effect analogous to the seasonal one should also be caused by the direction of the IMF X component, which is frequently overlooked. Using equinox data only to negate seasonal effects, drifts associated with negative Bx are very similar in appearance to summer, and likewise for positive Bx and winter.

**GA3.10/E/08-A6** Poster **1700-11**

#### THE MAGNETOSPHERE AND IONOSPHERE UNDER NORTHWARD IMF ION ENERGY DISPERSION EVENTS IN THE CUSP/CLEFT AND MANTLE: GENERAL DISPERSION SIGNATURE

Marina GONCHAROVA, W.Lyatsky, and V.Krivilov (Polar Geophysical Institute, Apatity, Russia); David G.Sibeck (APL/JHU, Laurel, Maryland, USA)

From the DMSP F7 satellite measurements for September, October and November 1984, the general dispersion signature of precipitating ions (the signature responsible for the average energy decline with changing latitude) are investigated in the 08 - 14 MLT sector under quiet IMF Bz/By conditions just above the boundary of the most sharp growth of the 100 eV electron flux with increasing latitude. Total of 112 polar cap crossings were considered. The meridian component of the dispersion-forming velocity and the probable injection source latitude inferred from the general dispersion pattern measurements are studied as functions of IMF Bz/By, immediate and 30 minute forestalling, solar wind velocity, solar wind electric field, 3-hr Kp index and magnetic local time (MLT). The poleward dispersion-forming velocities are found to drop with increasing IMF Bz southward and to rise with IMF Bz northward though the equatorward energy declines were also present by this polarity. The results obtained in the cusp/cleft would suggest the presence of the Axford-Hines mechanism activity footprint under IMF Bz<0 and would be in favor of 4-vortex convection system in the cusp/cleft and mantle under IMF Bz>0. The likelihood of the dispersion-forming velocity patterns at lower and higher altitudes with the expected convection patterns of Axford-Hines and Dungey type respectively imply the convection flow input is dominating when shaping the general dispersion signature. So far, the counterstreaming general dispersion signatures under Bz>0 included into analysis can be understood as a result of a joint activity of both convection types.

**GA3.10/W/11-A6** Poster **1700-12**

#### PLASMA ENTRY INTO THE MAGNETOSPHERE UNDER NORTHWARD IMF CONDITIONS DURING THE RECOVERY FROM STRONG CME-DRIVEN COMPRESSION

HANNU E. J. KOSKINEN\*, Anssi M. Malkki, Tuija I. Pulkkinen, Esa J. Kallio (Finnish Meteorological Institute, Geophysical Research, P.O.Box 503, FIN-00101 Helsinki, Finland, e-mail: Hannu.Koskinen@fmi.fi; \*also at University of Helsinki, Department of Physics) William K. Peterson (Lockheed Martin Space Physics Laboratory, Palo Alto, CA 94304, USA) Ingrid Sandahl (Swedish Institute of Space Physics, P.O. Box 812, S- 98128, Kiruna, Sweden) Kile B. Baker (The Johns Hopkins University, Applied Physics Laboratory, Laurel, MD 20723- 6099, USA)

The solar wind plasma entry into the magnetosphere under northward IMF conditions is a more difficult process to describe than the entry during southward IMF because subsolar reconnection process cannot be invoked. We investigate the entry process starting from observations of several impulsive dispersion ramps of magnetosheath protons observed by the Interball-2 satellite on January 11, 1997, when the magnetosphere was recovering from strong compression caused by the plasma cloud of a coronal mass ejection event. These dispersion ramps were observed in the evening sector at high magnetic latitudes over a wide local time sector. One of the ramps was detected also by the Polar satellite at higher altitude when its ground track crossed the track of Interball-2 in close temporal conjugacy. The ions were observed in a region of sunward convection. A remarkable feature of the observations was that the spacecraft data indicate substantially higher ion drift speed than a reasonable ionospheric convection speed during northward IMF, a discrepancy confirmed by simultaneous SuperDARN observations. In addition to data analysis we examine the process using a phenomenological model for the solar wind-magnetosphere interaction, which includes 3D models both for the magnetosheath and for the magnetosphere.

**GA3.10/W/09-A6** Poster **1700-13**

#### FAST EARTHWARD PLASMA FLOWS OBSERVED IN THE MID/DISTANT TAIL UNDER QUIET CONDITIONS: RELATION TO SUBSTORMS

Oleg TROSHICHEV (Arctic and Antarctic Research Institute, 199397, St.Petersburg, email: olegtro@aaari.nw.ru) Susumu Kokubun, Yoshuke Kamide (Solar Terrestrial Environment Laboratory, Nagoya University, Toyokawa, Aichi, 442, Japan) Toshifumi Mukai and Tatsundo Yamamoto (Institute of Space and Astronautical Sciences, Sagamihara, Kanagawa 229, Japan)

Abstract. Measurements of the magnetic field and low energy plasma by the GEOTAIL spacecraft have been used to study fast earthward plasma flows in the distant (130-200 Re) and middle (40-80 Re) tail and their relation to substorms. Results of the analysis show that high-speed earthward ion flows are often observed in the mid/distant tail under conditions of low magnetic activity (AE<100 nT), when IMF BZ component is northward or oscillates about zero. The considerable part of the fast earthward flows (29% in the distant tail and 53% in the middle tail) seems to be precursor of the substorm onsets on the Earth. These flows occur at closed magnetic field lines. The cause and effect relations between fast earthward plasma flows in the distant tail and substorm activity suggest that neutral line can form at distances far beyond 100 Re in quiet conditions.

**GA3.10/W/22-A6** Poster **1700-14**

#### GEOMAGNETIC RESPONSE TO MULTIPLE SOLAR WIND PRESSURE VARIATIONS DURING NORTHWARD INTERPLANETARY MAGNETIC FIELD CONDITIONS

Patrizia FRANCIA, Umberto Villante (both at Dipartimento di Fisica, Universita' de L'Aquila, L'Aquila, Italy; Email: patrizia.francia@aquila.infn.it), Stefania Lepidi (Istituto Nazionale di Geofisica, Roma, Italy; Email: stefania.lepidi@aquila.infn.it) and Alan J. Lazarus (Center for Space Research, MIT, Cambridge, USA; Email: ajl@space.mit.edu)

A study of the geomagnetic field response to a series of consecutive solar wind pressure variations has been performed during interplanetary events characterized by stable northward magnetic field conditions. The geomagnetic field H component well responds to the solar wind pressure changes on a time scale of few minutes. The amplitude of the geomagnetic field response is found to be different at different local times, showing greater values around local noon and midnight.

**GA3.10/E/03-A6** Poster **1700-15**

#### TURBULENT PLASMA SHEET DURING NORTHWARD INTERPLANETARY MAGNETIC FIELD CONDITIONS

Elizaveta E. Antonova and Ilya L. Ovchinnikov (both at Skobeltsyn Institute of Nuclear Physics, Moscow State University, Moscow, 119899, Russia; email: antonova@tasdp.npi.msu.ru)

The theory of plasma sheet with medium scale developed turbulence predicted the existence in the plasma sheet of quasi-diffusion transport and the meaning of later obtained on the base



of ISEE data diffusion coefficient. Its application to the case of northward IMF orientation give the possibility to model the processes of plasma sheet bifurcation and theta-aurora formation. The input parameters in the quasi-3-dimensional plasma sheet model are electric field distribution at the ionospheric level and magnetic field model. Empirical electric field models and Tsyganenko magnetic field models were used for the obtaining of plasma sheet configuration under northward IMF conditions. The model plasma sheet has the bulge region in its center. The decrease of electric field in the bulge region due to particle drift and electric charge accumulation on the bulge borders lead to the bulge growth. The change of the electric field direction.

**GA3.10/W/14-A6** Poster **1700-16**

**AN EFFECT OF NORTHWARD IMF ON PLASMA DYNAMICS IN GEOSYNCHRONOUS ORBIT**

Nataliya A. VLASOVA, Elmar N. Sosnovets, Michail V. Teltsov, Nickolay N. Pavlov (Skobeltzyn Institute of Nuclear Physics, Moscow State University, Moscow, 119899, Russia, email: vlasova@taspd.npi.msu.su)

According to theoretical conceptions and available experimental data, a number of specific features arises under the northward IMF ( $B_z > 0$ ) in the magnetospheric electric field, field-aligned current, aurora and distributions of precipitating particles. What is about experimental results for the  $B_z > 0$  conditions, the most of these were obtained from the low-altitude polar spacecraft, geophysical rockets and high-latitude ground stations. In this paper we present our data from geosynchronous satellite for 1992-1994. The study concerns dynamics of plasmas of 0.1-12 keV energy.

During the northward IMF, the following features of the measured plasma were observed:  
 - in electrons: softening of the plasmashet spectra, decreasing of intensity and disappearance of the diurnal variation;- in ions: formation of an intensive flux of ions of 5 keV through 12 keV energy in the night sector and disappearance of the diurnal variation;- recovery of all measured parameters after the IMF reorientation to  $B_z < 0$ .

It is shown that at least qualitatively the reported effects can be explained in the frame of a model of "closed" magnetosphere under the northward IMF. The work has been supported by the RFBR grant 97-02-16870.

**GA3.10/W/21-A6** Poster **1700-17**

**COLD, DENSE BOUNDARY OF MAGNETOSHEATH ORIGIN OBSERVED BY GEOTAIL IN THE FAR-TAIL PLASMA SHEET**

R. T. MIST and C. J. Owen (Astronomy Unit, Queen Mary and Westfield College, London, UK), T. Mukai (Institute of Space and Astronautical Science, Sagami-hara, Japan), S. Kokubun (Solar Terrestrial Environment Laboratory, Nagoya University, Toyokawa, Japan)

On September 25, 1994 the Geotail spacecraft was located close to the flank of the distant magnetotail ( $X = -170$  RE,  $Y = 24$  RE and  $Z = -2$  RE). During a 4 hour interval (13 - 17 UT) the spacecraft encountered both north and south lobes and the plasma sheet region before finally exiting into the magnetosheath. Within the plasma sheet, two different regimes were observed a fast flowing and slow flowing region. The slow flowing region is less dense and cooler than the fast flowing region. The properties of neither of these regions are consistent with simple reconnection models. Distributions taken from the LEP instrument show that the fast flowing region contains two populations. The first of these is similar in character to that observed in the slow flowing region. The second of these has similar characteristics to the magnetosheath. However, the peak flux of this population is about one half of the magnetosheath flux, and the bulk velocity is slightly lower than the sheath velocity. This suggests that a fraction of the magnetosheath population has crossed the magnetopause, losing energy in the process. We also note that the observed  $B_z$  in the plasma sheet/MSBL region is northward throughout, and is also very strongly northward at times. This suggests that the plasma sheet may well be on closed field lines. Hence we suggest that this may be evidence for magnetosheath plasma penetration into the plasma sheet across a closed magnetopause.

**GA3.10/L/02-A6** Poster **1700-18**

**INTERPLANETARY CONDITIONS IN ASSOCIATION WITH PROLONGED GEOMAGNETIC CALM INTERVALS**

G.K. RANGARAJAN Observatorio Nacional Rua General Bruce 586 Sao Cristovao Rio de Janeiro Brazil e-mail: ranga@dgel.on.br

From the 3-hourly index  $K_p$  of geomagnetic activity, we identify several intervals (at least four-day long sequences) when the magnetospheric conditions are considered very calm (as represented by  $K_p = 0$  or 1). We examine 16 solar wind and IMF parameters in the vicinity of such intervals using the method of Principal Component Analysis to highlight the stability/variability of the solar wind and IMF. In addition, we also study the IMF/solar wind control of quiet / disturbed magnetospheric conditions using sequences when  $K_p = 0-1$  or  $K_p = 4-9$  occurred at least for 8 consecutive intervals. The results are evaluated in terms of the variability of IMF and the contribution of the north-south component of the Interplanetary Magnetic Field.

**GA4.01** **Tuesday 20 July**

**CYCLE 23 SOLAR EVENTS AND HELIOSPHERIC CONSEQUENCES**

Location: School of Education, G33 LT  
 Location of Posters: School of Education, Conference Room

**Tuesday 20 July AM**

Presiding Chair: R.M. Skoug (Los Alamos National Laboratory, USA)

**GA4.01/W/17-A2** Invited **0900**

**EARLY LIFE OF CORONAL MASS EJECTIONS**

N. GOPALSWAMY (NASA Goddard Space Flight Center, Bldg 26, Room G-1, Code 682.3, Greenbelt, MD 20771, USA, e-mail: gopals@fugee.gsfc.nasa.gov)

There are a number of dedicated solar instruments at present -- both ground based and spaceborne -- that provide new information on coronal mass ejections (CMEs). Phenomena such as coronal dimming, coronal Moreton waves, shocks and coronal arcade formations have now become closely associated with CMEs and have provided several new insights into the CME

process. Recent advances in our understanding of the near-surface manifestations of CMEs will be reviewed with particular emphasis on X-ray, EUV and radio observations from SOHO, Yohkoh, Wind/WAVES and Nobeyama Radioheliograph. Relationship between CMEs and other transient phenomena such as flares, prominence eruptions and shock waves will be discussed.

**GA4.01/W/18-A2** **0930**

**CMES AND GEOACTIVITY IN SOLAR CYCLE 23**

David F. WEBB, ISR, Boston College, 140 Commonwealth Ave., Chestnut Hill, MA02467-3862, USA, email: webb@phf.af.mil

CMEs are important for space weather because they cause the largest geomagnetic storms and often drive interplanetary shocks, a key source of energetic particle events. During the rise of the present solar cycle, observations at the Sun using Yohkoh, SOHO, TRACE, radio and other data of CMEs and new kinds of related phenomena such as halo-like CMEs and EUV surface waves have provided insight into the source regions and development of CMEs. Halo CMEs observed by LASCO since 1996 suggest the launch of geoeffective disturbances toward Earth. This has been confirmed by good correspondences found between halo CMEs with associated solar surface activity within about 30 degrees of sun center and shocks, magnetic clouds and geomagnetic storms at Earth 3-5 days later. I will discuss some common aspects of the recent Sun-Earth connection events and what they tell us about the structure of CMEs and their geoeffectiveness.

**GA4.01/E/05-A2** **0950**

**SOLAR ACTIVE FILAMENTS AS SOURCES OF THE NEAR EARTH DISTURBANCES**

K.G.Ivanov and E.PROMASHETS Institute of Terrestrial Magnetism, Ionosphere and Radio Wave Propagation of Russian Academy of Sciences (IZMIRAN), Troitsk, Moscow Region, 142092 Russia, email: romash@izmiran.rssi.ru

The long-standing idea on the solar active filaments as sources of the near Earth geomagnetic disturbances (M.Valdmeier, 1946, Kkiepenheuer, 1947) and its modern generalization (K.Ivanov, 1998) were applied to use the contemporary presentation of the active filament and prominence data in the Solar-Geophysical Data (Active Dark Filament (ADF), Arch Filament System (AFS), Disappearing Solar Filaments (DSF) and so on). The three examples of the near Earth interplanetary disturbances on Jan 1997, May 1997, and Jan 1998 generated by ADF and AFS will be considered.

**GA4.01/E/03-A2** Invited **1010**

**RECENT OBSERVATIONS OF CORONAL MASS EJECTIONS**

O. C. St. CYR (CPI/NRL, Code 682, NASA-Goddard, Greenbelt, MD 20771, USA, email: cst@sdac.nascom.nasa.gov)

We will review some new understandings and new questions concerning coronal mass ejections (CMEs) that have appeared with the onset of solar Cycle 23. White-light observations of CMEs have been obtained by groundbased and spacebased telescopes for almost 30 years. Literally thousands of CMEs have been identified and measured in data from Skylab, Solwind, SMM, MLSO, and SOHO observations. Many CMEs (both individually and in statistical studies) have been compared to other observations of solar, interplanetary, and planetary phenomena. From this, there is general agreement on the basic properties of CMEs: (1) their rate varies by a factor of ~10x in phase with other solar activity signatures; (2) the location of their appearance is somewhat variable during the solar cycle, with many (if not most) CMEs arising from pre-existing coronal structures; (3) the apparent size and speed distributions are asymmetric, with average width being ~50 degrees and average speed being ~400 km/s, both values as measured projected onto the plane-of-the-sky; (4) CMEs are commonly associated with the destabilization and eruption of other magnetic structures on the Sun (prominences and active regions); (5) CMEs are the primary cause of severe geomagnetic storms.

But there remain basic outstanding questions concerning CMEs: What is their true three-dimensional structure? What is the sequence of physical processes that leads to a CME, and can the launch of a CME be predicted? How are CMEs accommodated into the solar wind flow? Are there reliable signatures of Earthward-directed CMEs that are available by groundbased methods?

**GA4.01/W/11-A2** **1100**

**FLUX ROPE MODELLING OF ICMEs OBSERVED AT MULTIPLE SPACECRAFT OVER VARIABLE SEPARATIONS**

T. Mulligan and C. T. RUSSELL (both at Institute of Geophysics and Planetary Physics and the Department of Earth and Space Sciences, University of California Los Angeles, USA, e-mail: tamitha@igpp.ucla.edu) B.J. Anderson (Applied Physics Laboratory, John Hopkins University, Laurel MD, USA) M.H. Acuna and R.P. Lepping (both at Goddard Space Flight Center, National Aeronautics and Space Administration, Greenbelt MD, USA) J.T. Gosling (Los Alamos National Laboratory, Los Alamos, NM, USA) J.G. Luhmann (Space Science Laboratory, University of California Berkeley, USA)

Measurements of the interplanetary magnetic field with NEAR have been compared with those of the WIND spacecraft during the near simultaneous passage of ICMEs over a variety of separations.

Non-force-free magnetic rope models, fit to the observations using the downhill simplex inversion technique, show that when the azimuthal separation of the observations is of the order of 0.05 AU or less, the geometry and orientation of the ropes are similar at the two locations when allowance is made for expansion of the structure. This is not surprising as the typical radius of an ICME flux rope is on the order of 0.05 AU. Unexpectedly, near simultaneous ICME observations occur even when the separation is much greater than the size of an individual rope. Thus either the same rope has become very twisted and extends over a wide range of longitudes or multiple ropes are ejected from the sun simultaneously over a wide range of longitudes. As the azimuthal separation increases the angular difference of the rope orientations increases, yet the overall appearance of the ropes and their helicity remain the same.

GA4.01/E/04-A2

1120

REMOTE RADIO TRACKING OF CORONAL AND INTERPLANETARY SHOCKS

M. J. REINER (Raytheon ITSS, Code 690.2, NASA/GSFC, Greenbelt, MD, 20771, USA, e-mail: reiner@urap.gsfc.nasa.gov)

Type II radio emissions observed by the WAVES experiment on the Wind spacecraft are generated by shocks that originate in the corona or interplanetary medium. These shocks may originate from blast waves associated with solar flares and/or from coronal mass ejections (CMEs) in the interplanetary medium. Type II radio emissions provide a means of remotely tracking shocks (and CMEs) from the solar corona out to 1 AU and beyond. When the observed radio intensity is displayed as a function of inverse frequency (1/f) versus time, the frequency-drifting kilometric type II radio emissions are organized along straight lines that converge to the CME liftoff time. The slopes of the lines vary as the ratio of the shock speed to the square root of the plasma density, normalized to 1 AU. Thus this method of analysis inherently reveals the dynamics of the CME in the interplanetary medium. When in-situ measurements of the shock are also made, we can determine unequivocally whether the type II emissions occurred at the fundamental or harmonic of the local plasma frequency in the upstream or downstream regions of the CME-driven shock. At high frequencies (1-14 MHz), corresponding to heliocentric distances within the field of view of the LASCO coronagraph, the frequency track of the type II radio emissions deviates from a straight line on the 1/f versus time dynamic spectra due to the complex behavior of the coronal density. Using coronal density models, derived from white light observations, we establish the relationship between the ground-based metric and space-based hectometric type II radio emissions and the LASCO CME. We find that in some cases, two temporally separated shocks are required to explain the coronal (high frequency) radio observations. One shock is generated by the CME and the other may be from the blast wave associated with the flare.

GA4.01/W/09-A2

1140

EISCAT MEASUREMENTS OF THE SOLAR WIND VELOCITY AND THE ASSOCIATED LEVEL OF INTERPLANETARY SCINTILLATION

A. FALLOWS, A. R. BREEN, P. J. MORAN, C. A. VARLEY, and P. J. S. WILLIAMS (University of Wales, Aberystwyth, UK)

Interplanetary Scintillation (IPS) in the radio signals from sources of small angular diameter is an indication of plasma irregularities in the solar wind. Previous measurements of the level of interplanetary scintillation have been of limited value without simultaneous measurements of solar wind velocity, and scattering per unit volume along the line of sight. Using the spaced antennas of EISCAT to measure IPS, and deriving the boundaries of fast- and slow-streams in the solar wind from optical measurements of the corona, comparison can be made between the level of scintillation and the presence of fast- and slow-streams along the line of sight. Especially interesting are those occasions when an interaction region occurs along the line of sight. Near such interaction regions it is expected there will be a deceleration of the fast stream, an acceleration of the slow stream, and an increase in the level of turbulence. EISCAT IPS measurements can provide evidence for each of these characteristics and follow their development with time as the interaction region moves outward from the Sun.

GA4.01/E/09-A2

1200

CORONAL SOURCES, 3D-STRUCTURE AND EVOLUTION OF CIRs DURING THE ONSET OF A NEW SOLAR CYCLE: SOHO, WIND AND ULYSSES OBSERVATIONS

Arik POSNER, Volker Bothmer, May-Britt Kallenrode, Horst Kunow, Reinhold Mueller-Mellin (all at Extraterrestrische Physik, IEAP, Univ. Kiel, Leibnizstr. 11, 24118 Kiel, Germany, email: posner@kernphysik.uni-kiel.de) Barbara J. Thompson and Adam Szabo (both at NASA Goddard Space Flight Center, Greenbelt, MD, USA, email: thompson@eitv3.nascom.nasa.gov) Robert J. Forsyth (Space & Atmospheric Physics, The Blackett Laboratory, Imperial College, Prince Consort Road, London SW7 2BZ, U.K., email: r.forsyth@ic.ac.uk) John T. Gosling (Los Alamos National Laboratory, NM, USA, email: jgosling@lanl.gov) Bernd Heber (MPAE, Max-Planck-Str. 2, 37191 Katlenburg-Lindau, Germany, email: bheber@linmpi.mpg.de) Alan J. Lazarus (Massachusetts Institute of Technology, Cambridge, MA, USA, email: ajl@space.mit.edu) R. J. Marsden, T. R. Sanderson (ESA/ESTEC, Noordwijk, Netherlands, email: rms@esa.esa.nl)

During the solar minimum in late 1996 the tilt of the magnetic dipole axis was low. The near Earth spacecraft SOHO and Wind detected recurrent energetic particle enhancements and CIR-associated features in the solar wind. EUV observations revealed the presence of warps in the polar coronal hole boundaries. Ballistical backmapping from 1 AU indicated that two extensions from the north polar coronal hole towards the heliographic equator coincided in heliolongitude with the in situ CIRs. At that time the Ulysses spacecraft, in a polar orbit about the Sun, was in a favorable position for a correlative study, at mid-northern heliolatitudes heading southward. For the first time since the northern polar pass, in September 1996 and at 32 deg N Ulysses dipped into the band of slower wind. As a consequence Ulysses encountered a recurrent series of CIRs. Estimations of the corresponding coronal source longitude for the CIR at Ulysses outside 4 AU coincided with one of the in-ecliptic CIRs. This study focuses on the 3D-structure of the CIRs including their sources, as well as on temporal effects from restructuring of the corona during the onset of the new solar cycle.

GA4.01/E/15-A2

1220

LONG-TERM MAGNETIC EVOLUTION OF AN ACTIVE REGION AND ITS FLARE & CME PRODUCTIVITY

Lidia VAN DRIEL-GESZTELYI (Observatoire de Paris, DASOP/LPSH, F-92195 Meudon Cedex, France, Email: lvandrie@mesioq.obspm.fr), Cristina H. Mandrini (IAFE-CONICET, CC.67, Suc.28, 1428 Buenos Aires, Argentina, Email: mandrini@iafe.uba.ar), Barbara Thompson (NASA/Goddard SFC, Greenbelt, MD 20771, USA, Email: thompson@eitv3.nascom.nasa.gov), Simon Plunkett (USRA, Naval Research Laboratory, Washington, DC 20375, USA, email: plunkett@kreutz.nascom.nasa.gov), Salvatore Orlando (ESA Solar System Division, Space Science Dept., ESTEC, Noordwijk, The Netherlands, Email: orlando@so.estec.esa.nl), Pascal Demoulin and Guillaume Aulanier (both at Observatoire de Paris, DASOP/LPSH, F-92195 Meudon Cedex, France, email: demoulin@obspm.fr and aulanier@obspm.fr)

Using SOHO/MDI full-disc magnetic maps, we follow the magnetic evolution of a solar active region for several months in the period of July-November 1996. We extrapolate the photospheric magnetic fields in the linear force-free approximation and match the modelled field lines with the soft X-ray loops observed with the Yohkoh/SXT in order to diagnose the coronal magnetic shear. We find that while the turbulent motions diffuse the flux, the differential rotation, and possibly twisted flux emergence, increase the magnetic shear. Flares are observed during the first three rotations, while CME events (observed by SOHO/EIT and LASCO) originate from this AR from its emergence throughout its decay. We analyse the flares and look for related CME events. We find that the early CMEs are related to flare events, while the late CMEs are not. The late CMEs occur when the magnetic shear, after accumulating for

four rotations, reaches a high level and saturates. We propose that the AR gets rid of excess shear and helicity through CME activity.

Tuesday 20 July PM

Presiding Chair: N. Gopalswamy (NASA GSFC, Catholic University of America, USA) Concurrent Poster Session

GA4.01/E/02-A2

1400

CHANGES IN THE HELIOSPHERIC MAGNETIC FIELD IN THIS SOLAR CYCLE: ULYSSES OBSERVATIONS

SMITH

When solar cycle 23 began in May, 1996, the Ulysses spacecraft was at 38=83 heliolatitude and a heliocentric distance of 3.7 AU and headed toward the equator and 5.3 AU which were reached in Dec.1997. Ulysses is now at 30=83 S headed for the south pole so that the spacecraft has been at relatively low latitudes and large distances during this entire interval. Since the beginning of the new cycle, we have sought evidence of changes in the HMF indicating the onset of solar activity leading to the next maximum. Three indicators of the onset have been identified: an abrupt increase in field magnitude in mid-1997 followed by a second increase in early 1998, (2) evidence of an increase in the inclination of the Heliospheric Current Sheet and (3) the reappearance and gradual increase in the numbers of Coronal Mass Ejections and Magnetic Clouds. The relative abruptness of these changes can be taken advantage of to seek corresponding changes in the sun and solar magnetic field. We have continued to monitor changes in the field during the march to solar maximum. The Ulysses results will be presented and compared with simultaneous changes in other indicators of solar activity at the sun and throughout the heliosphere including the onset and evolution of cosmic ray modulation.

GA4.01/W/13-A2

Invited

1420

MAGNETIC FIELD STRUCTURE OF TRANSIENTS AT ULYSSES: THEIR RELATIONSHIP TO CORONAL STRUCTURE AND CMES

R. J. FORSYTH and A. Balogh (The Blackett Laboratory, Imperial College, London SW7 2BZ, UK, email: r.forsyth@ic.ac.uk), E. J. Smith (Jet Propulsion Laboratory, Pasadena, CA 91109, USA), J. T. Gosling (Los Alamos National Laboratory, Los Alamos, NM 87545, USA)

In the course of its polar orbit around the Sun, the Ulysses spacecraft has encountered a large number of transient events in the solar wind which are the interplanetary consequence of coronal mass ejections or CMEs. In particular, since mid-1997, the number of transient events detected at Ulysses has been increasing as would be expected with the rise in solar activity. In this paper we focus on the magnetic field signatures of these events, discussing in particular whether or not they exhibit magnetic cloud signatures such as smooth rotations of the field direction and enhanced magnetic field strength with low variability. We make particular mention of transient events at Ulysses where a possible solar counterpart event has been identified in images from the Yohkoh or SOHO spacecraft and discuss the relationship between the heliospheric and coronal signatures.

GA4.01/W/05-A2

Invited

1450

ELECTRON CHARACTERISTICS OF CORONAL MASS EJECTIONS IN THE SOLAR WIND

R. M. SKOUG, W. C. Feldman, J. T. Gosling, and D. J. McComas (all at Los Alamos National Laboratory, MS D466, Los Alamos, NM, 87544, USA, email: rskoug@lanl.gov)

The solar wind plasma instrument (SWEPAM) on the ACE spacecraft, which has been in a halo orbit about the L1 point since December, 1997, has detected counterstreaming halo electrons (~100- 1370 eV) during approximately 20% of observations when the spacecraft was not connected to the Earth's bow shock. Counterstreaming electrons indicate that the spacecraft is on closed magnetic field lines, and thus indicate the presence of coronal mass ejections (CMEs) in the solar wind. This large fraction of closed field lines represents a rate of 2-4 CME events per month, and may be due in part to the high sensitivity of SWEPAM in this energy range. In this paper, we present characteristics of the electron distributions observed by SWEPAM during CMEs in the solar wind, including the presence of open or disconnected field lines (unidirectional electron flow), the electron pitch angle distributions, and the relative contributions of the core and halo electron populations. We find an anti-correlation between the ratio of halo to core density and the total electron density, as has been reported by other studies. However, we find that this behavior is not unique to CME events. Rather, the halo density contributes more to the total density during low density periods, regardless of the magnetic topology. We also investigate electron temperatures within CME events, including core and halo temperature contributions, temperature anisotropies, and variations with electron density.

GA4.01/W/04-A2

1520

INTERPLANETARY DISTURBANCES DURING THE ASCENDING PHASE OF THE SOLAR CYCLE 23

Takashi WATANABE (Department of Environmental Sciences, Ibaraki University, Mito 310-8512, Japan, e-mail: watanabe@env.sci.ibaraki.ac.jp); Masayoshi Kojima and Munetoshi Tokumaru (Solar-Terrestrial Environment Laboratory, Nagoya University, Toyokawa 442, Japan)

We examine three-dimensional propagation properties of CME-associated interplanetary disturbances observed in the ascending phase of the Solar Cycle 23 (1997-1998). Data sources are solar wind data obtained by spacecraft and IPS (interplanetary scintillation) observations. Interplanetary consequences of halo CMEs are found to have similar configurations; broad interplanetary disturbances with the local minimum of the propagation speed along the heliospheric current sheet, which was running near the ecliptic plane. This makes a clear contrast with interplanetary disturbances observed in the maximum solar activity phase, which are tend to be confined within the hemisphere where the relevant solar events take place. A correlative study between edge-on CME and geomagnetic data suggests that CME-associated interplanetary disturbances have a broad azimuthal extent during the ascending phase of the solar activity.

GA4.01/E/08-A2

1600

SPACE ENVIRONMENTAL CONDITIONS DURING APRIL-MAY 1998: PROTOTYPICAL SOLAR MAXIMUM EVENTS?

D.N. BAKER (Laboratory for Atmospheric and Space Physics, University of Colorado, Cam-pus Box 590, Boulder, Colorado, 80309-0590, USA, e-mail: baker@lynx.colorado.edu); J.H. Allen (NOAA, PO

Box 3000, Boulder, CO 80303); J.B. Blake (The Aerospace Corporation, MS 259, Los Angeles, CA 90009); S.G. Kanekal (Goddard Space Flight Center, Greenbelt, MD 20771); G.D. Reeves (Los Alamos National Laboratory, MS D-436, Los Alamos, NM 87545)

The space environment in April and May of 1998 is examined in detail. Evidence is found of highly disturbed solar, solar wind, and geomagnetic conditions in late April and early May. The combination of coronal mass ejections, solar flares, and high speed solar wind streams led to a powerful sequence of solar wind drivers of terrestrial magnetospheric processes. The result of the compounding solar wind disturbances was to produce a deep, powerful, and long-lasting enhancement of the highly relativistic electron (HRE) population throughout the outer terrestrial radiation zone. A new radiation belt feature was produced at  $L=2.2(\pm 0.2)$  on 4 May and the subsequent HREs persisted at high intensities for the subsequent 2-3 weeks. The high-energy electron fluence levels at geostationary orbit were the highest in May 1998 that had been seen for the preceding two years. The April-May 1998 period provided a fascinating set of Sun-Earth connection events and in many ways may be considered a prototype of what may be expected frequently during the upcoming solar maximum period (2000-2002).

**GA4.01/W/07-A2** Invited **1620**  
**GEOSPACE REACTION TO BOTH SOLAR MINIMUM AND SOLAR MAXIMUM-DRIVEN EVENTS**

Nicola J. FOX (JHU/Applied Physics Laboratory, 1100 Johns Hopkins Road, Laurel, MD 20723; and NASA/Goddard Space Flight Center, Code 696, Greenbelt, MD 20771; email: nicola.fox@gsfc.nasa.gov)

The major focus of the Sun-Earth Connection program, and the ISTP program itself, is to study the physical processes that link the Sun and the Earth, specifically, to understand the transfer of energy from the Sun to the Earth and the response of the Earth's coupled magnetosphere-ionosphere-atmosphere system to this energy transfer. The variability in the energy transfer is of special interest. Two of the predominant time scales for solar variability are the solar cycle and transient events, the most prevalent of the latter being coronal mass ejections (CMEs). Dominant terrestrial reactions include magnetic storms or the ring current energization, substorms with ionospheric current enhancements, high energy radiation belt enhancements, energy deposition into the atmosphere to produce the aurora, joule heating, enhanced plasma circulation in the ionosphere and plasmoid release down the tail. During the first 10 months of 1997, the satellite and ground facilities of the ISTP "observatory" tracked a number of solar-minimum type eruptions from the Sun, through interplanetary space, to the Earth. From November 1997, however, the events became more characteristic of solar maximum, particularly early in May 1998, when a series of three CMEs impacted the Earth in a few days. In this paper, observations from a variety of ISTP spacecraft, ground facilities and theory programs will be presented, together with supporting data from collaborating missions. We will compare the early ISTP events with those which have happened more recently, driven by a more active Sun. Thus we will look at a number of quantitative relationships as a function of the portion of the solar cycle from solar minimum, when the events are well spaced apart, to the more active phase of the solar cycle, when multiple events may be affecting in much more complex ways the terrestrial response.

**GA4.01/W/03-A2** **1650**  
**HALO CMES AND THEIR ASSOCIATED GEOMAGNETIC ACTIVITY**

Hildner Ernest. St. Cyr, Herlihy, Balch, NRL folk. NOAA Space Environment Center, 325, Broadway, Boulder, Colorado 80303, USA. E-mail: ehildner@sec.noaa.gov.

Starting January 1997, the whitelight coronagraphs of the LASCO instrument aboard the SOHO spacecraft began to see occasional coronal brightenings over a large fraction of all position angles around the sun, as projected in the plane of the sky (as seen from Earth). Because coronal mass ejections (CMEs) seen at the limb of the Sun usually appear to sweep a constant solid angle as they propagate outward, these brightenings surrounding the coronagraph's occulting disk – so-called 'halo CMEs' - were interpreted as CMEs propagating radially from the Sun nearly toward or away from Earth, becoming visible when they grew to subtend angles at SOHO larger than the coronagraph's occulting disk. With their greater than ambient density, often greater than ambient speed, and embedded out-of- the ecliptic magnetic field, it is to be expected that CMEs hitting Earth are likely to cause geomagnetic activity. In this paper, we report the results of our search for associations between halo CMEs and subsequent geomagnetic activity. We find that approximately 90 percent of severe geomagnetic storms were preceded by halo CMEs thought to be traveling Earthward. But only two-thirds of Earthward-directed halo CMEs preceded severe geomagnetic storms. Because the geomagnetic field was so quiet during the minimum between solar cycles 22 and 23, the association between each, rare, halo CME and the rare, subsequent geomagnetic activity is usually clear. Our results tend to confirm both the interpretation that coronal brightenings surrounding the coronagraph's occulting disk arise from CMEs headed Earthward and the expectation that an ejection from the Sun usually, if not always, increases geomagnetic activity when it hits Earth.

**GA4.01/W/08-A2** **1710**  
**HELIOSPHERIC X-RAY EMISSION ASSOCIATED WITH CHARGE TRANSFER OF THE SOLAR WIND WITH INTERSTELLAR NEUTRALS**

Thomas E. CRAVENS (Dept. of Physics and Astronomy, University of Kansas, Lawrence, KS, 66045, USA, email: cravens@kuplas.phsx.ukans.edu)

X-ray emission has been observed from many objects throughout the solar system including the Sun, the Moon, the Earth, Jupiter, and comets. The discovery of X-rays from comet Hyakutake (Lisse et al., 1996), and later from a number of other comets, was surprising. One proposed emission mechanism that can explain most features of the observed emission is the charge transfer of heavy solar wind ions with cometary neutrals (Cravens, 1997). Highly stripped heavy ( $Z > 2$ ) solar wind ions charge transfer with neutrals leaving the product ions with one more electron but still highly stripped and usually in an excited state. The solar wind ions then emit x-ray or extreme ultraviolet photons. Many different heavy ion species are present in the solar wind, reflecting the composition and the charge state distribution of ions in the solar corona. Soft X-rays should be emitted throughout the heliosphere due to the charge transfer of solar wind ions with interstellar neutral H and He atoms which are able to flow past the heliopause. The estimated total soft X-ray luminosity is about 10000 TW. These X-rays are emitted from the entire sky and are responsible for just a part of the soft X-ray background emission observed by the Einstein Observatory or ROSAT. However, unlike the part of the x-ray background coming from hot interstellar gas, the heliospheric x-ray emission should exhibit spatial and temporal variations that are associated with variations in the solar flux and composition. Of course, these solar wind variations reflect the changing conditions in the solar corona. The x-rays emitted from comets due to the charge transfer mechanism should also exhibit temporal variations due to solar wind variations. The expected morphology of the heliospheric x-ray emission will be discussed.

**GA4.01/E/01-A2** **1730**

**GLOBAL MHD SIMULATION OF A SPACE WEATHER EVENT: CME FORMATION, INTERPLANETARY PROPAGATION AND INTERACTION WITH THE MAGNETOSPHERE**

C. P. T. Groth, D. L. DeZeeuw, T. I. Gombosi, and K. G. Powell (The University of Michigan, Ann Arbor, MI, USA, e-mail: groth@umich.edu)

The numerical simulation of the complete time history of a space weather event, including the onset and initiation of a coronal mass ejection (CME) at the solar surface, the propagation of the CME and magnetic cloud from the solar corona into interplanetary space, and subsequent interaction of the disturbance with the terrestrial magnetosphere, is considered using a three-dimensional global magnetohydrodynamic (MHD) model. In the model, the solar wind and magnetospheric plasma flow is prescribed by solving the equations of ideal MHD using a parallel adaptive mesh refinement (AMR) upwind finite-volume scheme. The initial state of the corona and solar wind is described by assuming that the inner solar corona is a large rotating reservoir of hot plasma with an embedded magnetic field field represented by a tilted dipole and octupole. A value of 5/3 is used for the plasma specific heat ratio and a parameterized volumetric heating function is used to produce a solar wind, having both fast and slow streams. The CME is initiated by a localized isothermal density enhancement at the solar surface and the interaction of the CME with the magnetosphere is included as part of the computation. Results of the simulation will be described. This will include a discussion of the structure and evolution of the CME and its geo-effectiveness as measured in terms of its ability to drive geomagnetic activity.

Presiding Chair: R. Harrison (Rutherford Appleton Laboratory, Didcot, UK)

**GA4.01/W/10-A2** Poster **1400-01**

**DETECTION OF SOLAR LARGE-SCALE SHINING CHAINS AND THEIR RELATION TO CMES**

Iliia CHERTOK (IZMIRAN, Russian Academy of Sciences, Troitsk, Moscow Region, 142092, Russia, e-mail: ichertok@izmiran.troitsk.ru)

An analysis of modified heliograms in the microwave (Nobeyama Radioheliograph), soft X-ray (Yohkoh/SXT), EUV (SOHO/EIT, TRACE), and other ranges has revealed a novel phenomenon of the large-scale solar activity: relatively weak extended shining chains with characteristic sizes comparable with the solar disk diameter. It turns out that rather often bright elements and points are not scattered chaotically through the solar disk, but are aligned at definite structures forming large-scale chains (and threads) of various (sometimes very puzzled) configurations.

The long-living chains exist and keep their general form during many days, can coincide with sharp boundaries of coronal holes and outline footpoint lines of some large X-ray arcades. The transient chains with a characteristic time scales from several hours to one day appear to be closely associated with coronal mass ejections (CMEs) and to outline the large-scale structures involved in the processes of a CME and post-eruption energy release in the corona. The features of the chains mean that some large-scale structures shine as a result of energy release associated either with the long-term evolution of the large-scale magnetic fields or with disturbances identified with CME events. It is probable, that the detected chains and threads Light separatrixes separating different interacting large-scale magnetic flux systems in the complex solar magnetosphere.

**GA4.01/W/12-A2** Poster **1400-02**

**ANALYSES OF CME ONSET STUDIES USING EUV SPECTROSCOPY**

Richard HARRISON, Rutherford Appleton laboratory, Space Science Department, Chilton, Didcot, Oxfordshire, OX11 0QX, UK, email: r.harrison@rl.ac.uk

We present selected results from the SOHO multi-instrument campaigns to study coronal mass ejection (CME) onsets which make use of SOHO-CDS extreme ultraviolet data to derive plasma diagnostics in the CME onset region. For some events, we consider the low and high coronal response as well as the passage of the CME in interplanetary space. The relevance of these observations to established CME models is discussed.

**GA4.01/W/19-A2** Poster **1400-03**

**EVOLUTION OF THE MAGNETIC STRUCTURE OF SEVERAL ACTIVE GROUPS IN CYCLE 23 AND HELIOSPHERIC EVENTS**

BORIS IOSHPA and Vladimir Obridko (both at IZMIRAN, Troitsk, Moscow Region, 142092, Russia, Email: iosHPA@izmiran.troitsk.ru)

Magnetic field observations in active groups during 1986-88, carried out with a magnetograph at IZMIRAN, and magnetic maps from some other observatories have been used to analyze evolution of the magnetic structure in the photosphere, corona, and interplanetary space. The results are compared with the X-ray and EUV spacecraft data on structural variations and with CME occurrences.

**GA4.01/W/01-A2** Poster **1400-04**

**THE EARLY STAGES OF CORONAL MASS EJECTIONS AS OBSERVED BY SOHO/EIT**

B.J. THOMPSON, NASA Goddard Space Flight Center, Greenbelt, MD, USAO.C. St. Cyr, Computational Physics, Inc., USA H.S. Hudson, SPRC/ISAS, Japan S.P. Plunkett, USRA, Naval Research Lab, USA J.B. Gurman, NASA Goddard Space Flight Center, USA

As with all data collected with new instrumentation, a great deal of information can be extracted. Usually, there is more information than is deemed tractable, and the number of events required to form a "statistical" sample remarkably increases. After more than two years of operation, the EUV Imaging Telescope (EIT) on SoHo has observed several hundred CME's. These are being assembled into a catalogue of CME's, and are categorized according to their manifestation in the inner corona. By distinguishing between the variety of eruptions spanning the range of EUV signatures, information can be derived from the comparison and contrast of compatible events.

**GA4.01/E/06-A2** Poster **1400-05**

**MODELLING OF DYNAMICAL SPECTRA PRODUCED BY TYPE II RADIO BURST**

ROMASHETS E.P. and IVANOV K.G., Institute of Terrestrial Magnetism, Ionosphere and Radio Wave Propagation of Russian Academy of Sciences (IZMIRAN), Troitsk, Moscow Region, 142092 Russia, email: romash@izmiran.rssi.ru



It was shown earlier that disturbed HCS can reflect, deflect radio waves. In this work the attempt to model such situations was made and typical pictures for two different cases - when HCS was near ecliptic plane and far below or above it. The method used for calculation - to add all radio waves came from shock on its way from the Sun, taking into account their phases, time lags, amplitudes etc. We assumed that shock had speed 900 km/s, angular size 30°30'. The results can clarify why sometimes strong shocks seen from interplanetary observations were not accompanied by type II bursts and related questions.

**GA4.01/W/02-A2** Poster **1400-06**

**CORONAL MASS EJECTIONS ASSOCIATED WITH INTERPLANETARY DISTURBANCES OBSERVED WITH IPS**

S. BRAVO and A. Carrillo (Instituto de Geofísica, UNAM, Coyoacan DF, 04510, Mexico, email: sbravo@tonatiuh.igeofcu.unam.mx)

We compare the observations of large-scale interplanetary disturbances by means of interplanetary scintillation (IPS) and the coronal mass ejections (CMEs) recorded during a 6 month period. We obtain that coronal mass ejections are more frequent than large-scale interplanetary disturbances by a factor of about 6, that is, only 1/6 of the CMEs had an associated interplanetary disturbance. We analyse the CME characteristics in order to find out which of them determine the capability of a CME to importantly disturb the interplanetary medium.

**GA4.01/W/06-A2** Poster **1400-07**

**MULTI-SPACECRAFT OBSERVATIONS OF INTERPLANETARY TRANSIENT SHOCKS**

Americo GONZALES-ESPARZA and Miguel Yunez (both at Instituto de Geofísica, UNAM, Ciudad Universitaria, Mexico D.F. 04510, MEXICO, Email: americog@fis-esp.igeofcu.unam.mx)

We study multi-point observations of transient shock waves by different spacecraft: Helios 1 and 2, IMP, and Voyager 1 and 2, during 1976 and 1977 (ascending phase of solar sunspot cycle 21). We discuss some properties of the propagation of transient shocks in the interplanetary medium, in particular with respect to the magnetic sector structure.

**GA4.01/W/14-A2** Poster **1400-08**

**THE GROUND LEVEL SOLAR COSMIC RAY ENHANCEMENT OBSERVATION BY ALMA-ATA NEUTRON MONITOR IN SOLAR CYCLE 23**

O.N. KRYAKUNOVA, V.M.Aushev , E.A.Dryn

There are adduced experimental data of the last GLE events observed by high-mountain neutron monitor at Alma-Ata. The amplitudes and time of maximum of enhancements are shown. The analysis of the solar sources of these events and comparison with another data were carried out.

**GA4.01/E/07-A2** Poster **1400-09**

**ON THE PREDICTION OF THE MAXIMUM AMPLITUDE AND TIME OF RISE FOR THE 23D SOLAR CYCLE**

GALAL, A.A. (National Research Institute Of Astronomy And Geophysics, Helwan, Almarsad Street, Cairo, Egypt, email: salahmm@frcu.eun.eg); Hamid,R.H.(National Research Institute Of Astronomy And Geophysics, Helwan,Almarsad Street, Cairo, Egypt, email: salahmm@frcu.eun.eg)

The maximum amplitude and the time of rise for the cycle 23 have been predicted using spotless-event technique as precursor. This technique have been successfully used for the prediction of the mentioned parameters for the cycle 22. It is based upon the count of lengths and durations of spotless events during an interval of one year before and after the preceding minimum of the coming cycle.

The results obtained indicate that the cycle 23 is expected to be of moderate strength and its maximum sunspot relative number will be 147 +/- 17.11. The predicted time of rise of the cycle under examination is found to be 3.55 +/- 1.26 years.

Comparison of the present results with those obtained by geomagnetic precursors illustrates the sensitivity of spotless event technique to the geomagnetic activity of solar origin.

**GA4.02** Thursday 22 July

**CMEs, ERUPTIONS AND FLARES: ONSETS AND RELATIONSHIPS (WITH SCOSTEP)**

Location: Gisbert Kapp NG15 LR1

Location of Posters: Gisbert Kapp Coffee Room

Thursday 22 July AM

Presiding Chairs: Brigitte Schmieder (Observatoire de Paris, France)

D. Webb (Boston College, Hanscom AFB, MA, USA)

Concurrent Poster Session

**GA4.02-A4** Introduction **0845**

SCHMIEDER, B (Observatoire de Paris)

**GA4.02/W/30-A4** Invited **0900**

**LASCO AND EIT OBSERVATIONS OF CORONAL MASS EJECTIONS**

Kenneth DERE (Naval Research Laboratory, Washington DC 20375-5320, email: dere@halcyon.nrl.navy.mil)

Observations of the Sun with the LASCO and EIT experiments on LASCO have provided a new and unique basis for studying coronal mass ejection (CME) physics. The EIT and LASCO together allow imaging of CMES from their initiation at the base of the corona through a distance of 30 solar radii. CMEs are often associated with magnetic neutral lines in association with emerging or decaying flux regions, flares and eruptive prominences. Their original extent can often span nearly the entire solar disk. However, the characteristics of the region giving rise to CMEs are still not clear. The appearance of many CMES indicates that they consist of

helical magnetic flux ropes such as the magnetic clouds observed near the Earth. Observations of halo CMEs directed toward the Earth have proven to be a good predictor of geomagnetic storms caused by CMEs.

**GA4.02/W/14-A4** Invited **0925**

**INITIATION OF CME EVENTS: THE ROLE OF MAGNETIC SHEAR AND HELICITY**

Lidia VAN DRIEL-GESZTELYI, Brigitte Schmieder Pascal Demoulin and Guillaume Aulanier (all at Observatoire de Paris, DASOP/LPSH, F-92195 Meudon Cedex, France, Email: lvandrie@mesioq.obspm.fr, schmieder@obspm.fr, demoulin@obspm.fr and aulanier@obspm.fr), Cristina H. Mandrini and Marcelo Lopez (both at IAFE-CONICET, CC.67, Suc.28, 1428 Buenos Aires, Argentina, Email: mandrini@iafe.uba.ar and lopez@iafe.uba.ar)

Recent multiwavelength observations (using SOHO, Yohkoh and ground-based data) as well as theoretical developments indicate the importance of highly sheared and/or twisted magnetic configurations in solar active regions (ARs) in the initiation of coronal mass ejections (CMEs). Through multiwavelength analysis of three representative events we make an attempt provide constraints for CME models. The first two events to be presented (25 Oct. 1994 and 14 Oct. 1995) start with the expansion of a sigmoids, which are associated with highly twisted magnetic flux tubes. Such events can be linked to highly twisted interplanetary magnetic clouds. Then, we show the importance of magnetic shear in a CME source region. A filament disarption brusque (DB) associated with a multiple CME event was observed on 25/26 September 1996. We show that both the DB and the CME occurred when the non-potentiality (magnetic shear) of the magnetic fields in the AR reached a high (threshold) level. We propose that highly twisted and sheared magnetic configurations located in a complex (multipolar) magnetic environment are good candidates for being source regions of CMEs.

**GA4.02/W/16-A4** Invited **0945**

**THE RELATIONSHIP BETWEEN PROMINENCE ERUPTIONS AND CORONAL MASS EJECTIONS**

George SIMNETT (School of Physics and Space Research, University of Birmingham, B15 2TT, UK, Email: gms@star.sr.bham.ac.uk)

The SOHO observations with LASCO and EIT present an ideal opportunity to study the relationship between prominence eruptions and coronal mass ejections (CME). High-cadence measurements of prominence eruptions are demonstrating that the prominence eruption is not generally the cause of the associated CME, but that it is more probable that the destabilisation of the CME in fact releases the constraints on the prominence, causing it to erupt. We report here observations of associated CMEs and prominence eruptions covering the period of SOHO operations from mid-January, 1996 to mid-December, 1998. In addition to the causality, we find that in general the projected speed of the prominence eruption matches fairly closely the projected speed of the associated CME. Furthermore, the prominence eruption is generally simply one facet of the coronal transient activity, of which there are often several other discrete parts. The prominence eruption is also generally offset in heliolatitude from the centre of the CME. The relationship of these finding with current theoretical models is discussed.

**GA4.02/W/13-A4** **1005**

**CHANGES OF PHOTOSPHERIC AND CORONAL MAGNETIC FIELDS ASSOCIATED WITH LDES**

X P ZHAO and J T Hoeksema (Hansen Experimental Physics Laboratory HEPL B204, Stanford University, Stanford, CA 94305-4085, USA, email: xpzhao@solar.stanford.edu)

Large-scale, long-duration soft X-ray eruptive events (LDEs) often originate in large-scale multipolar photospheric magnetic field regions. They involve reconfigurations of large-scale coronal magnetic field, such as the change in pre-existing coronal hole boundary, the formation of coronal loop arcades, and the occasional occurrence of "transient coronal holes". This work examines changes of the large-scale photospheric magnetic field before and after the four LDEs analyzed by Webb et al. (JGR, 102, 24161, 1997) to see if the changes are associated with differential rotation or emerging flux. We use a methodology developed recently for constructing a proxy of the instantaneous global photospheric magnetic field and for modelling change of large-scale coronal structures observed on time scale of a day or less to compute the large-scale coronal field before and after the LDEs. Our goal is to see how the coronal field reconfiguration relates to the change of the photospheric magnetic field.

**GA4.02/W/05-A4** Invited **1020**

**FLARES, RECONNECTION AND MERGING OF HELICAL MAGNETIC STRUCTURES**

G. S. CHIO and C. Z. CHENG (Princeton Plasma Physics Laboratory, Princeton University, Princeton, NJ 08543)

Based on the theoretical model that flaring events are associated with magnetic energy release which takes place via magnetic reconnection processes we have demonstrated in numerical 2-1/2D MHD simulations that flaring events can occur in a bipolar magnetic arcade due to energy supply (or drainage) through the photosphere. The energy supply (or drainage) processes are through the fieldline footpoint motion (shearing, converging and diverging) and/or flux emergence. We will demonstrate the Poynting flux distributions in the photosphere of these processes and discuss how these energy exchange processes can affect the flaring events. We will also demonstrate how homologous flares successively take place in a magnetic arcade at the same place with a short time interval on the order of one day. Accompanying the homologous flare events are successive generation and merging of magnetic islands. With continuing supply of energy through the photosphere new magnetic island can created below a previously existing upper island, and this new island can rise faster and merge with the upper island very quickly to form a bigger island because they have same helicity. The combined island will continue to rise with a faster speed than the original upper island. As this process is being repeated, several impulsive events of magnetic energy release take place and the growing magnetic island is eventually driven away from the sun. Different types of footpoint motion can produce different Poynting flux distributions in the photosphere and the time interval between flaring events is accordingly varied.

**GA4.02/W/07-A4** Invited **1100**

**RECENT STUDIES OF YOHKOH/SXT CME-RELATED STRUCTURES, AT SXR AND EUV WAVELENGTHS**

STERLING, Alphonse C, Institute of Space and Astronautical Science

Although Coronal Mass Ejections (CMEs) were originally identified as white-light phenomena, they have since been extensively studied at other wavelengths from space-borne telescopes. In recent years, observations with the Soft X-ray Telescope (SXT) on the Yohkoh satellite have furthered our knowledge of these features at soft X-ray (SXR) wavelengths. Images from SXT prior to and after CME eruption hint at the nature of the magnetic structures that undergo expulsion. Frequently, the preflare SXR structures take the form of S-shaped features, often referred to as "sigmoids," which may indicate sheared magnetic fields. A powerful tool used in these studies is analysis of SXR "dimming" regions, in which the intensity of the corona near the eruption site drops precipitously near the time of the CME ejection. Analysis of these regions can give information on the temperature and mass of the ejected SXR material associated with the CME. There are also extensive contemporaneous studies of CMEs at EUV wavelengths obtained from, e.g., the EIT instrument on SOHO. In this presentation we review recent work on CME observations from SXT, and comparisons between the SXT CMEs and corresponding (or closely related) features seen at EUV wavelengths.

**GA4.02/W/09-A4** Invited **1125**

**WHAT CAN WE LEARN ABOUT RECONNECTION FROM CME OBSERVATIONS?**

Terry FORBES and Jun Lin (both at EOS Institute, University of New Hampshire, Durham, NH 03824, USA, Email: terry.forbes@unh.edu)

Recent, and continuing, improvements in X-ray telescopes and coronagraphs should make it possible to use observations of CMEs to answer several outstanding questions concerning the nature of magnetic reconnection in the solar corona. The detection of cusp features at the top of "post"-CME/flare loops by the Solar X-Ray Telescope (SXT) on Yohkoh is thought to be associated with the lower tip of a reconnecting current sheet, while the occasional detection of Y-shaped structures by the SOHO coronagraph on LASCO is thought to be associated with the upper tip of the same current sheet. It should be possible, at least in principle, to combine such measurements to determine the evolution of the current sheet, which is thought to be created by a CME. Here we show how the variation in the length of the current sheet with time allows a direct determination of the rate of magnetic reconnection and can also provide information on the nature of the reconnection dynamics.

**GA4.02/W/15-A4** **1145**

**STATISTICAL ANALYSIS OF CMES AND THEIR SOFT X-RAY SIGNITURES**

Shinichi WATARI (Communications Research Laboratory, 4-2-1 Nukuioka, Koganei, Tokyo 184-8795, JAPAN, email: watari@crl.go.jp) Takashi Watanabe (Ibaraki University, 2-1-1 Bunkyo, Mito, Ibaraki 310-8512, JAPAN, email: watanabe@env.sci.ibaraki.ac.jp)

Mark III K-coronameter (MK3) at the High Altitude Observatory (HAO)/Mauna Loa observatory covers the solar corona from 1.1 Rs to 2.4 Rs. Its field of view overlaps with that of the soft X-ray telescope (SXT) on board Yohkoh. It is possible to compare CMEs observed by the MK3 with soft X-ray observations directly. We examined the CMEs observed by both the MK3 and the SXT statistically. Almost half of the CMEs did not show any drastic soft X-ray activities. The soft X-ray activities were equally observed under the CME span and near footpoint of CMEs. Soft X-ray arcades were usually formed associated with the CMEs.

**GA4.02/W/01-A4** **1200**

**X-RAY PLASMA EJECTIONS ASSOCIATED WITH SOLAR FLARES**

Masamitsu OHYAMA and Kazunari Shibata (National Astronomical Observatory, Japan, E-mail: ohyama@solar.mtk.nao.ac.jp)

Yohkoh discovered X-ray plasma (plasmoid) ejections in many impulsive and LDE flares. We analysed 39 limb flares between October 1991 and December 1994 which were observed with soft and hard X-ray telescopes, and found that X-ray plasma were ejected in 27 flares (about 70 %). This result indicates that X-ray plasma ejection is a general phenomenon associated with a solar flare. Moreover, we found that X-ray plasma started to be ejected before a maximum peak of hard X-ray emission. Next, we analysed an X-ray plasma ejection just before the onset of the hard X-ray emission quantitatively in detail. The X-ray ejecta formed after its footpoint brightened long before the impulsive phase. Before the impulsive phase the X-ray ejecta was already heated to about 10 MK and its electron density was already an order of magnitude larger than the typical density of the active-region corona. From these observational results we propose that the ejected plasma was supplied by the chromospheric evaporation caused by the preflare heating.

**GA4.02/W/08-A4** **1215**

**DYNAMICS OF SEVERAL EVENTS OBSERVED BY SXT AND TRACE**

R.D. BENTLEY Mullard Space Science Laboratory, Holmbury St. Mary, Dorking, Surrey RH5 6NT, UK

Significant changes in emission in the corona observed by SXT. Where available, supporting data from SoHO and ground-based observatories have been used. Observations made by TRACE at several wavelengths have been compared with data taken by the Yohkoh SXT instrument for a number of events. The good time cadence afforded by both instruments allow the dynamics of the solar atmosphere to be studied over a wide range of temperatures and heights. Where possible, active regions have been followed over a period of hours or days in order to try to track the evolution of structures that subsequently disrupt. The changes in the morphology region that result from such disruptions are discussed, particularly where they result in a for some of the events.

Presiding Chairs: B. Schmieder (Observatoire de Paris, France)  
T. Forbes (Space Science Center/EOS, Univ of New Hampshire, Durham USA)

**GA4.02/W/02-A4** Invited **1500**

**UNDERSTANDING CMEs AND THEIR SOURCE REGIONS**

DAVID F. WEBB (ISR, Boston College, Chestnut Hill, MA 02467-3862, USA, email: webb@plh.af.mil)

CMEs are an important aspect of coronal and interplanetary dynamics. They can eject large amounts of mass and magnetic fields into the heliosphere, which can drive large geomagnetic storms, and interplanetary shocks a key source of energetic particles. However, our knowledge of the origins and early development of CMEs at the Sun is limited. CMEs are most frequently associated with erupting prominences and long-enduring X-ray arcades, but sometimes with little or no observed surface activity. I will review some of the well-determined coronal properties of CMEs and what we know about their source regions, including recent studies using Yohkoh, SOHO and radio data. One exciting, new type of observation is of halo-like CMEs, which suggest the launch of a geoeffective disturbance toward Earth. Besides their utility for forecasting the arrival at Earth of magnetic clouds and geomagnetic storms, halo CMEs are important for understanding the source regions and internal structure of CMEs since we can view and measure their characteristics along their central axes. I discuss some common aspects of the source regions of CMEs and what the recent ISTP-era events can tell us about the structure of CMEs.

**GA4.02/W/34-A4** Invited **1525**

**THE CME AND PROMINENCE ERUPTION OF JUNE 2, 1998**

S.P. PLUNKETT (1), A. Vourlidis (2), S. Simberova (3) (1) Universities Space Research Association, Naval Research Laboratory, Washington, DC 20375, USA. (2) Naval Research Laboratory, Washington, DC 20375, USA. (3) Astronomical Institute, Czech Academy of Sciences, 251 65 Ondrejov, Czech Republic.

Coronal mass ejections (CMEs) are frequently associated with erupting prominences near the solar surface. A spectacular eruption of the southern polar crown prominence was observed on June 2, 1998, accompanied by a CME that was well-observed by the LASCO coronagraphs on SOHO. The prominence was observed in its quiescent state and was followed throughout its eruption by the SOHO EIT and later by LASCO. Ground-based H-alpha observations of the prominence were obtained at the Ondrejov Observatory in the Czech Republic. A great deal of fine structure was observed within the prominence as it erupted. The CME contained a helical structure that is consistent with the ejection of a magnetic flux rope from the Sun. Similar structures have been observed by LASCO in many other CMEs. The relationship of the flux rope to other structures in the CME is often not clear. In this event, the flux rope clearly lies above the prominence, and it can be observed from the onset of the CME in the low corona all the way out to the edge of the LASCO field of view. We will discuss the relationship of the structures observed within the CME with the structure of the streamer and prominence before the eruption, and the dynamical evolution of the CME and prominence as it propagates outward from the Sun.

**GA4.02/W/29-A4** **1545**

**CME ONSET OBSERVED IN FE XII AND HE II**

Delann'ee C., Delaboudini'ere J.-P. (Institut d'Astrophysique Spatiale, Universit'e Paris XI, bat 121, 91405 ORSAY, France, E-mail: delannee@medoc-ias.u-psud.fr) Lamy P. (Laboratoire d'Astronomie Spatiale, Traverse du Siphon, Les Trois Lucs, 13012 Marseille, France, E-mail: lamy@astrsp-mrs.fr)

The Extreme ultra-violet Imaging Telescope provide observations of the whole solar disc in the chromospheric He and in the low coronal Fe in the chromospheric line, the ejections of the prominences are well observed. In the coronal line, propagations of cavities above the limb or of dimmings of the solar surface are observed. We compared the events seen in He and in Fe to the coronal mass ejections observed with the Large Angle and Spectrometric Coronagraph C2 in white light emitted in a region and at a time which can be related to the underlying events. We found that the He events are very difficult to compare to the CMEs. They evolve on only two image in average. So we can suspect that we miss the most chromospheric event using a 17 minutes cadence between two images. In Fe the cavities and dimmings are related in the most of the cases to CMEs. They are emitted above active regions or prominences. Active regions produced faster (300 km s<sup>-1</sup>) CMEs than prominences did (100km s<sup>-1</sup>).

**GA4.02/E/01-A4** **1600**

**MAGNETIC STRUCTURE AND DYNAMICS OF CME IN DEPENDENCE ON THE ONSET CONDITIONS DURING THEIR DETACHEMENT - PLASMA SIMULATION RESULTS**

JOERG BUECHNER (Max-Planck- Institut fuer Aeronomie, Max-Planck-Str. 2, D-37191 Katlenburg-Lindau, Germany)

We present results of plasma simulations of formation and evolution of the CME configurations. The CME formation is discussed in terms of three-dimensional kinetic reconnection. In particular we have investigated the influence of the magnetic field shear at the onset on the further evolution of magnetic fields and plasma inside CME's.

Presiding Chair: G. Simnet (Univ of Birmingham, UK)

**GA4.02/W/32-A4** **1635**

**CME INITIATION: MODELS AND OBSERVATIONS**

WU, Dr S.T (The University of Alabama in Huntsville)

We use three types of observed coronal mass ejection (CME) events together with numerical magnetohydrodynamic simulation to illustrate three distinct CME initiation processes: (1) emerging flux, (2) photospheric shear motion and (3) plasma flow. Category (1) can be interpreted as the erupted filament disrupting a streamer to produce a CME, (06/07 Jan 1997). Category (2) is the case in which the photospheric shear motion disrupts the streamer when the filament is lifted up. In this case, we observed the CME first, followed by filament eruption (25/26 Sept 1996). Category (3) is entirely different from the previous two, this event (04/05 Oct. 1995) does not show any relation with the filament/flux-rope. Overall, we suggest the first two categories are flux-rope driven because the energy source, which propels the CME, is stored in the flux-rope and the third category is driven by plasma flow. It exhibits wave type characteristics and is the fastest (~600 km s<sup>-1</sup>) among the three events. Both observations and numerical MHD simulation will be presented to sustain our claims.

GA4.02/W/10-A4

1650

**A STUDY OF THE EFFECTS OF EMERGING ACTIVE REGIONS ON THE LARGE-SCALE CORONAL MAGNETIC FIELD: POSSIBLE IMPLICATIONS FOR CMES**

J.G. Luhmann and Y. Li (Space Sciences Laboratory, University of California, Berkeley, CA 94720, USA, email: jgluhman@ssl.berkeley.edu) J.T. Hoeksema and X-P. Zhao (Stanford University, Stanford, CA 94305, USA, email: todd@quake.stanford.edu)

We use simple potential field source surface representations of the large-scale coronal magnetic field and emerging active regions to investigate the global consequences of localized flux emergence. In our "experiments", we approximate the before and after states of coronal magnetic fields in response to the appearance of bipolar active regions in different locations with respect to large scale features such as the helmet streamer belt and coronal holes. These tell us about the sensitivity of the global field to the localized fields, giving insight about those particular scenarios that are subject to drastic reconfigurations or large open flux increases (possible signatures of major CMEs). While this approach does not simulate the detailed physical behavior and properties of the evolving system like global MHD models, it provides possible guidance for space weather forecasts as well as for future, more rigorous CME modelling efforts.

GA4.02/W/03-A4

1705

**INVESTIGATING THE RELATIONSHIP BETWEEN EIT WAVES AND THE ONSET OF SOLAR FLARES**

D.A. Biesecker (SM&A Corporation), B.J. Thompson (NASA/GSFC), S.P. Plunkett (USRA - NRL)

The mechanism or mechanisms, which trigger the initiation of a solar flare, are unknown. Here we investigate the occurrence of solar flares as the result of a passing disturbance, such as an EIT wave observed with the EIT instrument onboard the SOHO spacecraft. While not all flares are triggered by such a mechanism, it is possible that some flares are. Many authors have attempted to look for evidence of flare initiation as a result of another, earlier event. There is no evidence that sympathetic events occur frequently. There is some evidence, though not conclusive, that sometimes flares occur as a result of some sympathetic event. If it can be shown that EIT waves can cause a solar flare to be triggered, the mechanism of flare initiation can be investigated. We consider EIT waves as a potential source of sympathetic events since it has been suggested that EIT waves are a coronal counterpart to Moreton waves. A common idea is that flare initiation begins in the corona, so EIT waves interact with potential flare initiation sites. We investigate the possibility that EIT waves trigger flares with a statistical comparison of the flare occurrence rate in the time that EIT waves traverse the solar disk to the flare occurrence rate in intervals preceding EIT wave events.

GA4.02/W/28-A4

1720

**VARIATION OF IONIC CHARGE STATES BETWEEN DIFFERENT SOLAR ENERGETIC PARTICLE EVENTS AS OBSERVED WITH ACE SEPICA**

E Möbius, M A Popecki, L M Kistler, A B Galvin, D. Heitzler, D. Morris, C. Siren (Dept. of Physics and Inst. for the Study of Earth, Oceans and Space, University of New Hampshire, Durham, NH 03824, email: Eberhard.Moebius@unh.edu); B Klecker, A Bogdanov, D Hovestadt, (Max-Planck-Institut für extraterrestrische Physik, Postfach 1603, D-85740 Garching, Germany)

With the ULEZEQ instrument on ISEE-3 the ionic charge states of Fe and Si ions measured during Fe and 3He rich solar events had been found to be substantially higher than during strong gradual events, which have a composition that resembles more closely that of the solar corona. This seemed to indicate a split into two different groups of source populations for the energetic particles with highly different temperatures. However, the results for small impulsive events had to be averaged over the entire observation period of about one year.

With its much larger geometric factor the SEPICA instrument on ACE allows for the first time to obtain direct charge state measurements for individual small events. The charge states of C, O, Ne, Mg, Si and Fe have been determined for a variety of solar energetic particle events. Except for C, which is already close to fully ionized for all events, there is a trend towards higher charge states for the small events that carry signatures of impulsive events. For events that show Fe charge states of about 20 all elements up to Mg and sometimes Si appear almost fully ionized. However, solar events are also observed that produce intermediate charge states. All elements seem to be affected in a similar way for individual events. Different from earlier reports the observed charge states appear to be compatible with single temperature ranges for any individual event. Possible correlations of the observed charge state variations with the presence or absence of CMEs during the events and with variations in the elemental composition will be discussed. It is puzzling that events with substantial deviations from coronal abundances accelerate almost fully stripped ions, which do not lend themselves easily to fractionation processes based on mass and charge.

GA4.02/W/18-A4

1735

**CORONAL MASS EJECTION EXPANSION AND ITS IMPLICATIONS DERIVED FROM CHARGE STATE DATA**

Simon Hefti, Thomas Zurbuchen, Len Fisk, Nathan Schwadron, and George Gloeckler (all at Univ. of Michigan, College of Engineering, Dep of Atmospheric, Oceanic and Space Sciences, 2455 Hayward Street, Ann Arbor, MI 48109-2143, USA, Email: hefti@umich.edu)

The Coronal Mass Ejection (CME) passing the Advanced Composition Explorer (ACE) in May 1998 shows a very interesting composition, particularly of minor ion charge states. Not only are unusual ions like O<sup>3+</sup> observed during this CME, but high and low charged ions are measured simultaneously (Gloeckler et al. 1998). This challenges theories of solar-wind like expansion of CMEs. We use the charge composition of He, O, and Fe, measured with the SWICS instrument on ACE together with a simple model of an expanding and cooling cloud to reconstruct the temperature history of the CME. We will discuss the implications of this data for the origin, expansion and size of CMEs.

GA4.02/W/11-A4

1750

**SOLAR LARGE-SCALE SHINING CHAINS: TWO CME-ASSOCIATED EVENTS**

Iliia CHERTOK (IZMIRAN, Russian Academy of Sciences, Troitsk, Moscow Region, 142092, Russia, e-mail: ichtertok@izmiran.troitsk.ru)

Transient large-scale shining chains and threads, associated with the near-the-limb coronal mass ejections (CMEs) of 22 August 1996 and 2 June 1998, are analyzed by the SOHO/EIT, Yohkoh/SXT, and some other imaging data. It is found that a pronounced evolution of the chains and threads in the EUV, soft X-ray and other ranges can occur during many hours both before and after a CME on a considerable part of the visible disk but especially near the place

of a CME eruption. It is difficult to ascertain the relation between chains and CMEs unambiguously. However, such a relation seems to be plausible because both the phenomena ultimately are consequences of the evolution of large-scale magnetic fields and have often a global character. It is reasonable to assume that the chains preceding CMEs display energy release resulting from Evolving large-scale magnetic structures at the stage when development of these structures is approaching to a CME eruption. On the other hand, the chains following CMEs can result from the post-eruption energy release when magnetic fields in an extended region of the corona, strongly disturbed by a CME eruption, relaxes to its initial state via magnetic reconnection in large-scale coronal current sheets.

Thursday 22 July AM

Presiding Chair: Brigitte Schmieder (Observatoire de Paris, France)

GA4.02/E/03-A4

Poster

0900-01

**SOLAR FLARES IN MAGNETIC INTERACTING ACTIVE REGIONS**

L. GABRIELA BAGALA' (Max Planck Institut fuer Extraterrestrische Physik, Postfach 1603, D-85740 Garching, Germany, Email: gbagala@mpe.mpg.de), C.H. Mandrini, M.G. Rovira (both at Instituto de Astronomía y Física del Espacio, IAFE, CC.67, Suc.28, 1428 Buenos Aires, Argentina) and P. De'moulin (Observatoire de Paris, DASOP, URA2080 (CNRS), 92195 Meudon Cedex, France)

We present in this poster a study of the active region (AR) 7031, where several flares occurred between January 26 and February 2, 1992. We analyse in detail the three largest flares observed on January 30, 1992, using H alpha and soft X-ray data (SXT, on board Yohkoh). Two of these flares are homologous and occurred in the northern part of the AR; while the third one, the most extended and intense in H alpha, was located towards the South. During its transit across the disc this region interacted with another one (AR 7038) located at the South, as indicated by the recurrent brightening in soft X-rays of an interconnecting loop.

Using a linear force extrapolation of the photospheric magnetic field, we compute the locations of regions of rapid change in field-line linkage, called Quasi-Separatrix Layers (QSLs), as we have done in previous works (see e.g. Demoulin et al. 1997, A&A 325, 317). QSLs are the likely places where the magnetic field can reconnect. The comparison between the position of flare brightenings and QSLs, let us conclude that these flares occurred due to magnetic reconnection driven by the interaction of different structures in the same AR. Although these interactions could be traced in the topology computed from a magnetogram obtained at the time of the third flare, the energy release switched on or off in one site or the other of the AR following the photospheric field evolution.

We also find field lines connecting AR 7031 and AR 7038, having footpoints at the QSLs computed when magnetograms belonging to both ARs are combined. This indicates that the evolution of the photospheric field in one AR induces energy release at the QSL common to both regions.

GA4.02/E/07-A4

Poster

0900-02

**MEASUREMENTS OF SOLAR WIND VELOCITY OVER A WIDE RANGE OF HELIOCENTRIC DISTANCES**

A.R. BREEN, R.A. Fallows, P.J. Moran, P.J.S. Williams University of Wales, Aberystwyth, Wales, E.U. M. Guruhakurta Goddard Space Flight Laboratory, Greenbelt, Maryland, U.S.A. M. Kojima STELab, Nagoya University, Japan A. Ananthkrishnan Tata Institute for Fundamental Research, India

Measurements of Interplanetary Scintillation provide information on solar wind velocity over a wide range of distances from the Sun. Observations made at high radio frequencies can probe the solar wind close to the Sun, while observations at lower frequencies provide information on the solar wind at greater heliocentric distances. These observations are of particular value in extending the profile of coronal velocities measured by spacecraft instruments out into the interplanetary medium.

In this paper we discuss the results of a series of co-ordinated observations Interplanetary Scintillation observations made at 327 and 931 MHz in August 1998 and a second series of observations involving coronal observations from SPARTAN-201 and interplanetary scintillation measurements at 931 MHz, made in October-November 1998. We also hope to report initial results from co-ordinated interplanetary scintillation measurements at 931 and 1400 MHz, made in May 1999. Taken together, these measurements provide solar wind velocities from inside 2 solar radii to beyond 100 solar radii.

GA4.02/E/10-A4

Poster

0900-03

**H-ALPHA SOLAR TELESCOPE FOR ARGENTINA**

M.G. ROVIRA (Instituto de Astronomía y Física del Espacio, IAFE, CC 67 Suc. 28, 1428, Buenos Aires, Argentina), L.G. Bagala (Max Planck Institut fuer extraterrestrische Physik, Postfach 1603, D-85740 Garching, Germany), O.H. Bauer (Max Planck Institut fuer extraterrestrische Physik, Postfach 1603, D-85740 Garching, Germany), R. Fernandez (Instituto de Astronomía y Física del Espacio, IAFE, CC 67 Suc. 28, 1428, Buenos Aires, Argentina), C. Francile (Observatorio Astronomico Felix Aguilar (OAFa), Avda. Benavidez 8175 Oeste, 5413 Chimbos, San Juan, Argentina), G. Haerendel (Max Planck Institut fuer extraterrestrische Physik, Postfach 1603, D-85740 Garching, Germany) and E. Rieger (Max Planck Institut fuer extraterrestrische Physik, Postfach 1603, D-85740 Garching, Germany)

The release of a large amount of energy in sheared magnetic fields and the subsequent acceleration of charged particles is a common phenomenon in the universe. Since in the Sun flares, eruptive prominences and coronal mass ejection's are the direct results of impulsive releases and particle acceleration and can be resolved spatially, its observation is of crucial importance in the understanding of these phenomena. In order to study the evolution of solar flares with high spatial (1.5 arcsec) and temporal (up to 2sec) resolution from ground, a solar telescope in H-alpha (6563 Å) has been set up at the OAFa mountain astronomical observatory in EL Leoncito, San Juan, Argentina. HASTA (H-alpha Solar Telescope for Argentina) is a 110 mm refractor with a focal length of 165 cm, a tunable (+- 1Å) Lyot-Filter with a bandwidth of 0.3 Å and a PC-controlled CCD-camera with a resolution of 1280x1024 pixels. In patrol mode the camera takes an image every 30-sec. It is analysed and if a flare is detected the camera switches into high-speed mode. In this mode it takes and stores full frame images every 2 sec or sub-frame images (in the region where the flare is developed) up to 0.3 sec. The Hard Disk capacity allows two hours of high-speed recording. HASTA started operations on May 1998 and in this work we are describing the first results. HASTA complements three other solar instruments which have been or will be installed in the near future in EL Leoncito: MICA, a mirror coronagraph to observe the solar corona above the limb from 1.1 to 2 solar radii, a submillimeter radio-telescope for measurements up to Far Infrared, and a high resolution spectrograph. Combining the observations of these four instruments new insights into the active Sun phenomena can be expected.

GA4.02/E/09-A4

Poster

0900-04

**EFFECT OF MASS VELOCITY AND AMPIBOLAR DIFFUSION IN THE C AND SI LINE PROFILES OF SOLAR PROMINENCES**



M. ROVIRA (Instituto de Astronomia y Fisica del Espacio, IAFE, CC.67, Suc. 28, 1428, Buenos Aires, Argentina), J.M. Fontenla (771 West Dahlia Street, Louisville, CO 80027, USA), A. Costa (Instituto de Astronomia y Fisica del Espacio, IAFE, CC.67, Suc. 28, 1428, Buenos Aires, Argentina) and S. Patsourakos (Institut d'Astrophysique Spatiale, Unite Mixte Paris XI-CNRS, Batiment 121, 91405 ORSAY CEDEX, France

We developed a numerical code to solve the ionisation equilibrium equation for a given atom and a given atmosphere. The population for the different stages of ionisation, the source function and the optical depth can be obtained for different intensities and configurations of the flux mass. The line profiles are deduced in order to obtain patterns that can be compared with observations. Although this method can be applied to any atom and any atmosphere, in this case, we restrict ourselves to the C and Si atoms and to the thread prominences model developed in a previous paper. In this work we show that solving the ionisation equilibrium equations for the C and Si atoms significant differences in the line profiles are observed while the intensity and configuration of the flux mass are varied.

**GA4.02/E/08-A4 Poster 0900-05**

**FIRST COMBINED OBSERVATIONS IN THE GERMAN-ARGENTINIAN SOLAR OBSERVATORY**

G. STENBORG (Max Planck Institut fuer Aeronomie, Max-Planck-Str. 2, D-37191, Katlenburg-Lindau, Germany), L.G. Bagala (Max Planck Institut fuer extraterrestrische Physik, Postfach 1603, D-85740 Garching, Germany), R. Fernandez (Instituto de Astronomia y Fisica del Espacio, IAFE, CC 67 Suc. 28, 1428, Buenos Aires, Argentina), O. Bauer (Max Planck Institut fuer extraterrestrische Physik, Postfach 1603, D-85740 Garching, Germany), M. Rovira (Instituto de Astronomia y Fisica del Espacio, IAFE, CC 67, Suc.28, 1428, Buenos Aires, Argentina) and R. Schwenn (Max Planck Institut fuer Aeronomie, Max-Planck-Str. 2, D-37191, Katlenburg-Lindau, Germany).

The SOHO era revealed that mass ejections from the sun include not only hot coronal plasma but also cold prominence material. The role of solar activity (flares or filament eruptions) is not yet well understood. Furthermore, if the cold material pushes the hot one or if the hot one drags the cold one is still an unresolved question. Thus, crucial information about the onset of a coronal mass ejection (both in space and time) can be obtained by combining coronagraphic observations of the emission line corona and H alpha images of the sun disk at a high cadence as well as insight about the relation between prominences and coronal mass ejections can be provided. In the recently inaugurated German-Argentinian Solar-Observatory at El Leoncito, San Juan, Argentina, an H alpha telescope (HASTA) and a mirror coronagraph (MICA) daily image the solar disk and the inner solar corona. MICA is essentially similar to LASCO-C1 on board SOHO. Since its installation in August 1997 it has been imaging the inner corona with high temporal and spatial resolution in two spectral ranges: the well known green (~1.8 MK) and red (~1.0 MK) coronal lines at 5303 A and 6374 A respectively. Its field-of-view ranges from 1.05 to 2.0 solar radii above the sun center. Thus, it is ideally suited to observe the hot material and reveal the fast processes that occur in the coronal plasma. HASTA started operations on May 1998. It is a 110-mm refractor with a focal length of 165 cm, a tunable (+-1A) Lyot-Filter with a bandwidth of 0.3 A and a 1280\*1024 CCD array. In patrol mode the camera takes images every 30-sec. In high-speed mode full frames can be taken every 2-sec and partial frame images every 0.3 sec.. We present observations as taken by both telescopes. Emphasis is put on future applications.

**GA4.02/E/02-A4 Poster 0900-06**

**MULTIINSTRUMENT OBSERVATIONS OF 3HE AND 4HE FLUX SPECTRA IN IMPULSIVE SOLAR ENERGETIC PARTICLE EVENTS WITH ACE/SEPICA AND SOHO/HSTOF**

A.T. BOGDANOV(1), E. Moebius(2), B. Klecker(1), M. Hilchenbach(3), D.Hovestadt(1),L.M. Kistler(2), M.A. Popecki(2), E.J. Lund(2), D. Heitzler(2), A.B. Galvin(2) (1) Max-Planck-Institut fuer extraterrestrische Physik, Garching, D-85740, Germany, Email: atb@mpe.mpg.de (2) Space Science Center, University of New Hampshire, Durham, NH, 03824, USA (3) Max-Planck-Institut fuer Aeronomie, Katlenburg-Lindau, D-37189, Germany

We investigate the energy dependence of the 3He/4He ratio during a number of impulsive solar energetic particle events observed between September 1997 and December 1998. The data of two instruments with complementary energy ranges, the Solar Energetic Particle Ionic Charge Analyzer (SEPICA) on ACE and the time-of-flight mass spectrometer HSTOF on SOHO are used to cover the energy range from ~ 0.1 to 3.5 MeV/nuc. The observed monotonous increase of the 3He/4He ratio with energy which for the events with extremely high 3He abundances ranges between ~ 0.1 at the lower energy end and ~ 1 at the upper end confirms the trend known from previous ISEE observations and extends their energy range to lower values. We discuss the observational data on the background of existing theoretical work on selection and acceleration mechanisms in impulsive flares.

**GA4.02/E/05-A4 Poster 0900-07**

**MODELLING OF SHOCK WAVE SURFACE EVOLUTION AHEAD OF TOROIDAL MAGNETIC CLOUD ON IYS WAY FROM THE SUN TO THE EARTH'S ORBIT**

E.ROMASHETS Institute of Terrestrial Magnetism, Ionosphere and Radio Wave Propagation of Russian Academy of Sciences (IZMIRAN), Troitsk, Moscow Region, 142092 Russia, email: omash@izmiran.rssi.ru

Fast magnetic clouds may create bow shocks in front of them, which in turn produce type II radio bursts in interplanetary space. We consider here isolated toroidal magnetic cloud evolving (expanding) on its way from the Sun. The position and shape of the shock surface determines the frequency depth and duration of radio emission at given frequency, and intensity. Fluctuations and inhomogeneities of ambient solar wind will also lead to broadening of emission lines and will cause changes of the cloud's shape and velocity even slow MHD speed the bow shock will disappear and there is no emission. We will show preliminary results of modelling of the evolution of toroidal magnetic cloud and associated shock on the basis of approach developed in Romashets (1996) and will use them for interpretation of radio busts of January 1997 and May 1997, observed by WIND and ULYSSES wave instruments.

**GA4.02/E/13-A4 Poster 0900-08**

**THE RECONNECTION POWER AND RATE IN THE COURSE OF EACH OF THE TWO ACTIVE PHASES OF TYPE-LDE LARGE SOLAR FLARES**

V. MISHIN (Institute of Solar-Terrestrial Physics,P.O.Box 4026, Irkutsk, 664033, Russia, email: mishin@iszf.irk.ru) C.-G. Falthammar (The Royal Institute of Technology, The Alfvén Laboratory, Stockholm, Sweden, email falthammar@plasma.kth.se) A. Altyntsev (Institute of Solar-Terrestrial Physics, P.O.Box 4026, Irkutsk, 664033, Russia, email: altyntsev@iszf.irk.ru)

The time dependent values of open magnetic flux Psi in the flare-producing region were determined by Mishin et al., a, for three large flares of LDE type, 3B class. Two active phases

are noticed for each of the flares, one during Psi growth, and next when Psi was fast decreasing. In this paper, estimates are made of the Poynting flux to the flare region from the outside and of the reconnection power and rate for each of the two active phases of each flare. In the CSHKP model, these two phases are produced by the reconnection in the closed and open parts of the magnetosphere, respectively. It is concluded from the calculated results that the reconnection power and rate of the open magnetic flux exceed those for the first active phase, as it was found in the case of magnetospheric substorms,

**GA4.02/E/06-A4 Poster 0900-09**

**TWO ACTIVE PHASES OF LARGE SOLAR FLARES OF LDE TYPE**

V. MISHIN and A. Altyntsev (both at Institute of Solar-Terrestrial Physics,P.O.Box 4026, Irkutsk, 664033, Russia, email: mishin@iszf.irk.ru) C.-G. Falthammar (The Alfvén Laboratory, Stockholm, Sweden, email: falthammar@plasma.kth.se)

Before Yohkoh, solar flares were classified into two types, such as LDE vs impulsive or eruptive vs confined, or two ribbons vs compact, etc. Yohkoh, however, revealed that both these types could be considered as the events, which are usually accompanied by eruptions of plasmoids or plasma jets (the unified model of flares, Shibata, 1996). In the present paper, Shibata's model is supplemented by H-alpha data on three large, class 3B, flares of LDE type: flare 1, 12.10.81 (Kurokawa, 1989), flare 2, 5.10.70 (Banin, 1982), and flare 3, 27.06.81 (Yazev, 1985). The known phase of two ribbons separation was observed in each of above flares, which is interpreted as the eruptive phase in the CSHKP model. According to this model, the area St inside the outer boundaries of two ribbons, measured at the end of the flare, was taken by us to be approximately equal to the largest (total) area during the flare, crossed by the open magnetic flux Psi, whose reconnection creates the flare eruptive phase. Further, for an arbitrary time t, we calculated the values of Psi as a product B cross S3, where B=250 Gauss is the accepted characteristic value, and S3=S2, with S2 being the area inside the outer boundaries of two flare ribbons measured at time t. The plot of Psi, obtained by such a way for flare 1, clearly shows two phases of Psi variation: Psi was growing during impulsive phase, 0607-0626 UT, and only after it, the phase of a fast decrease of Psi, which corresponds to the separation of two ribbons, was observed. These two phases both are active: the brightness and areas of the ribbons are comparable in both phases, and the hard X-ray intensity starts to increase at 0614 UT and peaks around 0626 UT. Thus, two active phases are noticed for flare 1, the first of which has no signatures of eruption. Similar conclusions were drawn from the data for flares 2 and 3, although these data are less complete.

**GA4.02/E/12-A4 Poster 0900-10**

**GEOMAGNETIC SUPERSTORMS AND THEIR SOLAR AND INTERPLANETARY SOURCES**

Dmitri I. PONYAVIN (Institute of Physics, University of St.Petersburg, 198904, Russia, e-mail: ponyavin@snoopy.phys.spbu.ru)

Geomagnetic activity variations recorded in St.Petersburg from 1841 to 1999 have been analysed. Statistics of major geomagnetic storms (superstorms) show a significant semiannual and dual-peak variation during a course of solar activity cycle. Superstorms occur in close association with recurrent streams of the solar wind. The role of interplanetary conditions and magnetic fields on the Sun, its organisation and evolution in appearing such phenomena was discussed.

**GA4.02/L/02-A4 Poster 0900-11**

**THE MECHANISM OF PLASMA JET EJECTION FROM THE SUN.**

I.M Podgorny (1) and A.I. Podgorny (2) (1) Institute for Astronomy RAN, Moscow, 109 017, Russia. (2) Lebedev Physical Institute RAN, Moscow, 117 924, Russia.

The dynamics of vertical current sheet creation and plasma jet ejection are numerically simulated in resistive MHD approximation. Plasma compression and anisotropy of the thermal conductivity are taken into account. A solar flare appears prior to the jet ejection which has been observed by Yohkoh. Fast electron precipitation and Pedersen currents produce local chromospheric evaporation. After that a powerful post flare loop appears. The strong plasma fluxes meet at the loop top, and induce an upward plasma jet. As a result of jet motion across the magnetic field a current sheet is created. The reconnection in the current sheet gives rise to electron heating and soft x-rays radiation. The results of computation are compared with observed data.

**GA4.02/L/03-A4 Poster 0900-12**

**INVESTIGATION OF ENERGY ACCUMULATION IN CORONA FOR ACTIVE REGION OF FLARE ON MAY 30 1991**

A.I. Podgorny Lebedev Physical Institute RAN, Moscow, 117 924, Russia,

The possibility of magnetic energy accumulation at current sheet creation in corona for the active region AR NOAA 6654 which produced the flare May 30 1991 was investigated. The field of 4 main spots which were situated almost on the same line in the photosphere was approximated by field of 4 magnetic dipoles placed vertical under the photosphere. MHD equations were solved in the corona for magnetic disturbances corresponded to changing dipole moments and/or dipole motion. The numerical code PERESVET was developed which permitted to solve compressible MHD equations with dissipative terms and anisotropy of thermoconductivity. Absolutely implicit difference scheme was used. Calculations were done for large scale numerical region which contains all active region but have rough step and small scale region with fine steps but uncertainty of field setting on non-photospheric boundary. Comparing this calculations helped to separate the physical effect. Calculations for small scale region showed the possibility of current sheet creation which inclined on rather large angle to the photosphere which give possibility for CME appearance. Calculations for large scale region showed that for moving up two central dipoles or increasing their moments the current sheet was very weak. Decrease of two external dipoles caused the current sheet creation. Current sheet may be inclined to photosphere or be practically parallel to it depending on disturbance

**GA4.02/W/04-A4 Poster 0900-13**

**SOFT X-RAY JETS AND THEIR RELATIONSHIP TO QUASI-STEADY CORONAL MAGNETIC STRUCTURES**

Yoshimichi Nkagawa and Takashi WATANABE (Department of Environmental Sciences, Ibaraki University, Mito 310-8512, Japan, e-mail: nakagawa@env.sci.ibaraki.ac.jp)

Among coronal disturbances observed by Yohko SXT, soft X-ray jets are interesting

phenomena both from the observational and theoretical aspects. We study well-observed examples of large-scale soft X-ray jets through the comparison between Yohkoh SXT images and coronal magnetic configurations, which are inferred from photospheric magnetic observations (Kitt Peak) by using a potential field model. It is found that, for several events, jets were formed along the field line of long-lived (for 2-3 solar rotations) coronal field. According to the present study, the following scenario of the jet phenomenon will be proposed. (1) The magnetic configurations of the coronal region including the jet are predominantly governed by quasi-steady magnetic structures, which are well approximated by the potential model. (2) The emerging flux makes reconnection with the steady pre-existing magnetic field structures. (3) The soft X-ray jet is formed along the pre-existing field line.

**GA4.20/W/05-A4** Poster **0900-14**

**FLARES, RECONNECTION AND MERGING OF HELICAL MAGNETIC STRUCTURES**

G. S. CHIO and C. Z. CHENG (Princeton Plasma Physics Laboratory, Princeton University, Princeton, NJ 08543)

Based on the theoretical model that flaring events are associated with magnetic energy release which takes place via magnetic reconnection processes we have demonstrated in numerical 2-1/2D MHD simulations that flaring events can occur in a bipolar magnetic arcade due to energy supply (or drainage) through the photosphere. The energy supply (or drainage) processes are through the fieldline footpoint motion (shearing, converging and diverging) and/or flux emergence. We will demonstrate the Poynting flux distributions in the photosphere of these processes and discuss how these energy exchange processes can affect the flaring events. We will also demonstrate how homologous flares successively take place in a magnetic arcade at the same place with a short time interval on the order of one day. Accompanying the homologous flare events are successive generation and merging of magnetic islands. With continuing supply of energy through the photosphere new magnetic island can be created below a previously existing upper island, and this new island can rise faster and merge with the upper island very quickly to form a bigger island because they have same helicity. The combined island will continue to rise with a faster speed than the original upper island. As this process is being repeated, several impulsive events of magnetic energy release take place and the growing magnetic island is eventually driven away from the sun. Different types of footpoint motion can produce different Poynting flux distributions in the photosphere and the time interval between flaring events is accordingly varied.

**GA4.02/W/06-A4** Poster **0900-15**

**DISSIPATIVE CME PROCESSES**

I.S. VESELOVSKY (Institute of Nuclear Physics, Moscow State University, Moscow 119899, Russia, email: veselov@dec1.npi.msu.su)

An attempt is undertaken to estimate the relative importance of dissipative MHD and kinetic plasma processes during CME initiation and evolution processes. Dimensionless parameter analysis is performed of the mass, momentum and energy conservation laws together with material and Maxwell equations. The complexity and the large diversity of real situations are explained by the nonlocal and nonlinear multi-scale nature of the CME phenomena. In addition to the ideal MHD processes, the heat conduction, viscosity and finite electrical conductivity are essential in different proportions for different eruptive events. Strong anisotropy is introduced by the magnetic fields in the transport processes. Higher order kinetic deviations (accelerated particles, nonthermal radiation etc.) are playing a comparable role in a bulk sense from case to case. A crucial role in the conditions that lead to plasma ejection belongs not only to the evolution of the photospheric fields. Electric currents and a free magnetic energy of the corona are also important and rather independent reservoirs of the dynamic plasma self-organisation.

**GA4.02/W/17-A4** Poster **0900-16**

**ENERGY EVOLUTION OF CMES**

JUN Lin and Terry G. Forbes (both at EOS Institute, University of New Hampshire, Durham, NH 03824, USA, email: jun.lin@unh.edu)

To model the energy evolution of a CME we use a two-dimensional flux-rod model, which drives the ejection by means of a catastrophic loss of mechanical equilibrium. Reconnection plays an essential role because without it the CME cannot escape into interplanetary space. In the model the initial energy release is independent of the reconnection process, but after a few minutes reconnection becomes increasingly important. Assuming that the flows into the reconnection region are less than the local Alfvén speed, we show that the model generates a power output which closely resembles the so-called "light-curves" of Long Duration Events (LDE) associated with CMES.

**GA4.02/W/19-A4** Poster **0900-17**

**PROTON ENERGY SPECTRUM AND SOURCE NATURE OF THE LARGE SOLAR EVENT OF SEPTEMBER 29, 1989**

E.V. Vashenyuk 1, L.I. MIROSHNICHENKO(2), and A.O. Vdovichev(1) 1) Polar Geophysical Institute, Apatity, Murmansk Region, 184200, RUSSIA; 2) Instituto de Geofísica, UNAM, 04510, Mexico, D.F., MEXICO; Permanent address: IZMIRAN, Troitsk, Moscow Region, 142092, RUSSIA

Ground Level Enhancement (GLE) of solar cosmic rays on September 29, 1989 is studied. The event was remarkable for a number of unusual features. Among them were the double-peak increases observed at some neutron monitor (NM) stations and complicated behaviour of the proton energy spectrum and anisotropy. Two component structures of the proton intensity-time profiles in the event has been demonstrated. The first (prompt) component had a short duration and very hard energy spectrum. The second (delayed) component, being ejected from the Sun ~1 h later, was dominated by a particle population with the soft energy spectrum and gradual profiles. An existence of two different sources of particle acceleration separated in time and possibly in space during the event has been suggested. The properties of the prompt component give some evidences for its source is linked with a magnetic reconnection process in the trailing part of the ascending coronal transient. Parameters of the magnetic field and plasma in the source have been estimated by fitting observed proton spectrum to the calculated one in a computational model with a fast acceleration mechanism at the first stage of the event. Optimization procedure gave the following set of parameters:  $B = 91$  G;  $n = 1.2 \cdot 10^7$  cm<sup>-3</sup>;  $L = 109$  cm ( $B$ ,  $n$  and  $L$  are magnetic field intensity, plasma density at the acceleration site and linear dimension of the current sheet, respectively). Such values of  $B$  and  $n$  are characteristic for the trailing part of coronal transient (behind of an eruptive filament) at the coronal heights of several tenth of solar radius, and the value of  $L$  is of order of filament length.

**GA4.02/W/20-A4** Poster **0900-18**

**A STUDY OF PLASMA WAVES IN CMES AND THE SEARCH OF THE SOURCES OF ION ACOUSTIC WAVES IN THE SOLAR WIND**

NAIGUO Lin, P. J. Kellogg (School of Physics and Astronomy, University of Minnesota, Minneapolis, Minnesota, USA) R. J. MacDowall (NASA/Goddard Space Flight Center, Greenbelt, Maryland, USA) J. T. Gosling, D. J. McComas (Los Alamos National Laboratory, Los Alamos, New Mexico, USA) R. J. Forsyth, A. Balogh (Imperial College of Science and Technology, London, UK)

In order to study the occurrence and properties of plasma waves associated with coronal mass ejections (CMEs), a number of CMEs observed by the Ulysses spacecraft in a large range of heliographic latitudes are examined. Four wave modes are observed within the CMEs: (1) Electric waves at a few kHz, which are interpreted as Doppler shifted ion acoustic waves (IAW). They are observed within the CME structures, where the proton temperature becomes low and thus the electron to proton temperature ratio is larger than one. The ratio varies significantly. A comparison of the intensities of IAW to the  $T_e/T_i$  ratios may provide information on the damping rate of the waves. A survey of IAW intensity in the solar wind in a several year period, which include CME intervals, will be presented to examine the occurrence and intensities of IAW from different solar wind sources. The relation between the IAW intensity and the electron heat flux will also be discussed. (2) Electromagnetic whistler waves. They are observed in regions where the solar wind plasma is turbulent (near interplanetary shocks or during periods of increasing solar wind velocity). (3) Electric waves near the electron plasma frequency, which are probably generated by streaming electrons within the CME structure. (4) Electric fluctuations below the local electron cyclotron frequency are observed during periods of decreasing solar wind velocity, which is also a characteristic of an expanding CME.

**GA4.02/W/21-A4** Poster **0900-19**

**MULTIPLE PARTICLE ACCELERATION AT THE SUN DURING LARGE EXTENSION AND LONG DURATION GAMMA RAY EVENTS**

R. Pérez Enriquez(1) and L.I. MIROSHNICHENKO (2) Instituto de Geofísica UNAM, México, D. F., 04510, MEXICO; (1) Campus UNAM, Juriquilla, Querétaro; (2) Permanent address: IZMIRAN, Troitsk, Moscow Region, 142092, RUSSIA

Gamma ray lines (GRL) from the event of September 29, 1989 originated at solar longitudes of 25-30 degrees from the flare site. Although a CME-driven shock has been proposed as the most plausible mechanism to account for the accelerated particles responsible for the gamma rays, no generally accepted explanation exists at present. On the other hand, in 1991, at least three long duration GRL events (June 4, 11, and 15) were observed at several satellites. Likewise, none of the models put forward to explain these events are convincing. For example, the prolonged particle acceleration during the late stage of the flare of June 15, 1991 can explain many of the peculiar features of this kind of events, especially the accompanying microwave emission; however, it cannot account for the fact that this emission, at least in this particular event, is oscillating in nature. In our opinion, this kind of event should be considered in the framework of a new concept of multiple particle acceleration in the extended coronal structures. In this paper, we make a comparison of the situations involving these peculiar events and find reasons to suspect that a possible mechanism might involve the collapse of a large loop filled with stochastically accelerated particles. As a result of the collapse, a CME and a shock might be produced in the corona, and a precipitation of a fraction of the accelerated particle population into the chromosphere might occur. The interaction of these particles with the chromospheric material outside an active region would produce an extended long lasting GRL event; escaping particle population forms a long duration SPE in space.

**GA4.02/W/22-A4** Poster **0900-20**

**EUV OBSERVATIONS OF THE DECEMBER 17 1998 CME ONSET**

Dr Richard A. HARRISON Rutherford Appleton Laboratory

Extreme ultraviolet observations of the solar eastern limb on December 17, 1998, revealed an extremely active Sun with a complex, active loop system occupying much of the limb, including a prominence in the south. The activity included a significant eruption, which was subsequently seen in coronagraph data. The onset of this event is considered in detail and the relevance of established mass ejection models discussed.

**GA4.02/W/23-A4** Poster **0900-21**

**MHD FLOWS SUPPORTING THE STATIONARY STRUCTURE OF 3D MAGNETIC NULLS AND THRESHOLD TO THE COLLAPSE**

Vyacheslav.S. TITOV and Gunnar Hornig (both at Theoretische Physik IV, Fakultät fuer Physik und Astronomie, Ruhr-Universität Bochum, D-44780 Bochum, Germany, Emails:st@tp4.ruhr-uni-bochum.de, gh@tp4.ruhr-uni-bochum.de)

The exact solutions of resistive magnetohydrodynamic equations describing stationary incompressible flows near a three-dimensional null point of magnetic field are found. It is shown that the magnetic null-point configuration with locally non-potential structure may be supported generally by a stationary non-potential flow of stagnation type if the current density does not exceed some critical value. This critical value coincides with the threshold one, which separates the topologically different cases of skewed improper and spiral nulls (see Parnell et al., 1995).

The obtained results imply that stationary MHD flows may support generally only the skewed improper null configuration but not the spiral one, while the latter is probably realised only in collapse-like non-stationary flows as (for instance) found by Bulanov and Olshanskoy (1984). The topological structure of the obtained solutions is studied in terms of the relative location of the one-dimensional and two-dimensional invariant manifolds (so called spine line and fan plane, in notations of Priest and Titov, 1995) of magnetic and velocity fields. The implication of these solutions for three-dimensional magnetic reconnection problem in active phenomena like solar flares and magnetospheric substorms is also considered.

**GA4.02/W/24-A4** Poster **0900-22**

**THE 24-25 DECEMBER 1996 MAGNETIC CLOUD AND ITS ASSOCIATED RECONNECTION LAYER**

C J FARRUGIA (Space Science Center, University of New Hampshire, NH 03824, USA, Email: farrugia@monet.sr.unh.edu), V S Semenov, I Kubyshekin (both at Institute of Physics, State University of St Petersburg, St Petersburg 198904, Russia), H K Biernat (Space Research Institute, Austrian Academy of Sciences, A-8042, Graz, Austria), R B Torbert, L Janoo (both at Space Science Center, University of New Hampshire, NH 03824, USA), J D Scudder (Department of Physics and Astronomy, University of Iowa, Iowa City IA 52240, IO, USA), K W Ogilvie, L F Burlaga and R P Lepping (all at NASA Goddard Space Flight Center, Greenbelt MD 20771, USA)



A two-hour-long pressure balanced structure preceded the magnetic cloud observed by WIND on December 24-25, 1996. Not only does the magnetic field decrease to very low values; there are also perturbations in all solar wind parameters. Stress balance analysis is satisfied across the structure. Studying the configuration further, we show that the data may consistently be interpreted in terms of disturbances from a reconnection site close to the Sun which have been transported, with varying delay times, to 1 AU. The distance to the reconnection site is estimated.

**GA4.02/W/25-A4** Poster **0900-23**

**LASCO HA OBSERVATIONS OF THE SOLAR CORONA 19-22 JUNE 1998**

MICHAEL D. ANDREWS (Raytheon ITSS, 4500 Forbes Blvd., Lanham, MD 20706, USA, Email: andrews@louis14.nrl.navy.mil) Angelos Vourlidas (Center for Earth Observing and Space Research Institute for Computational Science and Information, George Mason Univ. Fairfax, VA 22030, USA) Russell A. Howard (E. O. Hulburt Center for Space Research, Naval Research Laboratory, Code 7660, Washington DC 20375, USA)

On 19-22 June 1998, the LASCO team performed a special observation sequence using all three coronagraphs to search for Ha emission. Several Coronal Mass Ejections were observed. A C1 line-scan recorded at 01:05UT on 22 June 1998 recorded Ha emission that saturated the detector at line-center. This emission corresponded to the eruption of a prominence observed by the Nobeyama Radioheliograph at 17 GHz. There is no significant Ha emission associated with the leading edge of any of the several CMEs. One of the events does show fine scale Ha structure in C2. Due to the significant CME motion, the analysis of this emission is difficult. We will present a quantitative estimate of the Ha emission observed in the C2 field of view. The only Ha emission observed by the C3 coronagraph is from the interstellar source RINGC 2174. There is no evidence of coronal Ha emission in the C3 data. LASCO is the Large Angle Spectroscopic Coronagraph which is one of the instruments on the Solar and Heliospheric Observatory (SOHO) which is a mission of international cooperation between NASA and ESA. The LASCO experiment was developed by a consortium of institutions from four countries: E. O. Hulburt Center for Space Research, Naval Research Laboratory, Washington, DC; Laboratoire d'Astronomie Spatiale, Marseille, France; Max-Planck-Institut für Aeronomie, Lindau, Germany; and Space Research Group, School of Physics and Space Research, University of Birmingham, Birmingham, UK

**GA4.02/W/27-A4** Poster **0900-24**

**SOLAR SOURCES OF HIGH-VELOCITY STREAMS IN THE SOLAR WIND**

Mikhail I. PUDOVKIN, Svetlana P. Bogdanova, Svetlana A. Zaitseva (Institute of Physics, St. Petersburg University, St. Petersburg 198904, Russia, e-mail: pudovkin@snoopy.phys.spbu.ru)

Orientation of the magnetic field frozen in the plasma of high-velocity streams to the solar wind correlate with the direction of the large-scale solar magnetic field at the regions of associated solar flares. This result convincingly confirms the supposition that sources of those streams are located within the flare regions. The time taken by the stream to propagate from the Sun to the Earth is shown to depend on the location and duration of the corresponding flares and on the mutual orientation of the magnetic fields within the stream body and within the background solar wind.

**GA4.02/W/31-A4** Poster **0900-25**

**DOES THE CYCLIC VARIATION OF CME VELOCITIES EXIST?**

E.V.IVANOV, V.N.Obridko, and E.V.Nepomnyashchaya (IZMIRAN, Troitsk, Moscow Region, 142092, Russia, Email: solter@izmiran.troitsk.ru)

The cyclic variation of the annual mean CME velocities has been studied for the time interval of 1979-1989. The annual mean CME velocity displays a growth at the maximum and decrease at the minimum of the cycle and a secondary peak at the minimum of the cycle. It is shown that CME velocities and widths are mainly determined by the large-scale magnetic field system with a characteristic size of cells of about 40 degrees. The secondary peak of the annual mean CME velocity is due to a significant contribution of high-speed CMEs with a width of ~100 degrees at the minimum of the cycle, which means another large-scale magnetic field system with the size of cells of ~90-100 degrees.

**GA4.02/W/33-A4** Poster **0900-26**

**ARE CMES MAGNETICALLY DRIVEN?**

P. SUBRAMANIAN (GMU/NRL), A. Vourlidas (GMU/NRL), K. P. Dere (NRL), R. A. Howard (NRL)

It is commonly assumed that Coronal Mass Ejections from the Sun are magnetically driven. We address this question with data from the LASCO coronagraphs aboard the SOHO spacecraft. These observations provide fairly direct measurements of the kinetic and gravitational energy of CMEs. We determine the kinetic and gravitational energies and their evolution for several helical CMEs. We estimate the evolution of the magnetic energy based on the conservation of magnetic flux and observations of magnetic clouds near the Earth. From the magnitude and variation of these three forms of energy, we examine the energetics of CMEs from the perspective that they are driven through their internal magnetic energy.

**GA4.02/W/35-A4** Poster **0900-27**

**THE SOLITARY STRUCTURES IN OVERDENSE IONOSPHERIC PLASMA**

A.V. KOCHETOV and B.A. Mironov (both at Institute of Applied Physics, N.Novgorod, Russia, e-mail: kochetov@appl.sci-nnov.ru) G.I.Terina and V.N.Bubukina (both at Radiophysical Research Institute, N.Novgorod, Russia, e-mail: ter@nirfi.sci-nnov.ru)

The results of the modelling of non-linear dynamic effects arising in the ionospheric plasma under the action of the powerful radio waves are presented. Numerical solutions of non-linear Schrodinger equation in the linearly inhomogeneous plasma layer excited by the heating radio wave were obtained. The processes of the formation of the solitary structures of the electric field and disturbances of plasma density and processes of their relaxation for different values of density gradient and the amplitude of the heating wave were analysed. The spatial evolution of the electric field and disturbances of the plasma density and time dependencies of the reflected signal were obtained. With the heater turn-on the penetration of the solitary structure into the overdense plasma takes place which increases under the heating power increase and the decrease of the plasma density gradient. The decreasing of the scale of the spatial soliton structure, the periodic and chaotic solitons generation during the heater time is observed. When the heater is turned off, the solitons continue to travel into the overdense plasma for some time, increasing in the amplitude, until they reach the turning point. Then they reflect and propagate into the underdense plasma, decreasing in the amplitude, and disappear. The

obtained results allow to interpret the appearance of the scattered signal after the heater turn-off - "aftereffect plasma signal" (AEPS). The Education Department of Russia (grant N 97-0-5.3-113) supported this work.

**GA4.05**

**Monday 19 July**

**NEW INSIGHTS ON CORONAL HEATING AND SOLAR WIND ACCELERATION**

Location: School of Education, G33 LT

**Monday 19 July AM**

Presiding Chair: E. Leer (Univ. of Oslo, Norway)

**GA4.05/L/02-A1**

Invited

**0830**

**THE CHROMOSPHERE/TRANSITION-REGION/CORONA/SOLAR-WIND SYSTEM: AN OVERVIEW**

Thomas E. HOLZER (High Altitude Observatory, National Center for Atmospheric Research, P.O. Box 3000, Boulder, CO 80307-3000, USA, Email: holzer@ucar.edu)

It has become clear in recent years that a satisfactory understanding of solar wind acceleration requires consideration of the coupled system comprising the upper chromosphere, transition region, corona, and wind. The need to consider the chromosphere and transition region arises to some extent from the energy lost through heat transport from the corona to the chromosphere, but more importantly from the effect this heat transport has on the location of the transition region and thereby on the coronal base pressure. In addition, the processes controlling the abundance of helium in the corona (which may play a significant role in solar wind acceleration) are operative primarily in the upper chromosphere and transition region. Finally, it is possible that a significant fraction of the energy flux required to heat the corona and drive the solar wind is generated in the chromosphere and transported through the transition into the corona.

A number of recent studies have elucidated the effects on wind acceleration of simply parameterized energy transport and dissipation (as well as helium diffusion) in the chromosphere-corona system, and there have also been useful hydromagnetic simulations of the propagation and dissipation of large amplitude waves in the corona and solar wind. The time has now come, however, to carry out realistic simulations in the chromosphere-corona-wind system of specific processes that may be important in the transport and dissipation of energy, as well as in the diffusion of helium. With the advent of significantly improved observational information now available from such sources as the SOHO and TRACE missions, the results of such simulations could be thoughtfully compared with observations to reveal which physical processes are important in coronal heating and solar wind acceleration.

**GA4.05/W/02-A1**

Invited

**0910**

**CORONAL HEATING; WHAT HAVE WE LEARNED FROM SOHO?**

John L. KOHL (Harvard Smithsonian Center for Astrophysics, 60 Garden Street, Cambridge, MA 02138, USA, email: jkohl@cfa.harvard.edu)

Observations and analyses of data from the Solar and Heliospheric Observatory (SOHO) have revealed significant new information about the physical processes that deposit energy and momentum into the solar corona. The Michelson Doppler Imager has made detailed measurements of magnetic flux emergence and cancellation in network sites which are potential source regions for energy release. The Coronal Diagnostics Spectrometer and the Solar Ultraviolet Measurements of Emitted Radiation (SUMER) instrument have produced evidence that the electron temperature in coronal holes is lower than previously believed, but this result must be reconciled with higher "freezing in" temperatures derived from "in situ" observations. SUMER measurements of spectral line profiles near the base of coronal holes indicate that ion temperatures increase with mass-per-charge. Measurements of coronal holes up to 3 solar radii with the Ultraviolet Coronagraph Spectrometer find anisotropic velocity distributions with hydrogen speeds, perpendicular to the magnetic field, corresponding to temperatures that are much higher than those of the electrons, OVI perpendicular speeds corresponding to temperatures about 100 times that of hydrogen, and outflow speeds for hydrogen and O VI becoming supersonic within 2 solar radii with higher outflow speeds for the OVI. This presentation will review the latest results related to coronal heating from SOHO.

**GA4.05/W/04-A1**

**0950**

**THE ENERGY BALANCE ANALYSIS IN THE SOLAR WIND FORMATION REGION**

S.I. MOLOYKH, V.A. Kovalenko

Solar corona observations in the white light and in separate coronal lines have been used in analyzing the energy balance of the solar wind formation region within heliocentric distances 1.02-1.5 solar radii. It is shown that losses through emission in different coronal lines have a significant influence on the energy balance of the solar wind formation region. An analysis of observed coronal line profiles suggests the conclusion that the energy flux input to the solar wind formation region is constant. It is shown that the flow divergence in the solar wind formation region determines the parts of energy going into solar wind acceleration and lost due to emission in different coronal lines. An increase in flow divergence is accompanied by an increase in energy flux going into solar wind acceleration, and by a decrease in energy emitted in coronal lines. On the base of solar wind model it is shown that magnetic field configuration determines the flow divergence and consequently affects energy balance. It is concluded that the main part of the energy flux which input to the solar wind formation region is the Alfvén wave energy flux.

**GA4.05/W/07-A1**

**1000**

**ELECTRON PROPERTIES CLOSE TO THE SUN FROM IN SITU CHARGE STATE DATA AND ELECTRON DISTRIBUTION FUNCTIONS**

T. H. ZURBUCHEN, S. Hefti, L. A. Fisk, G. Gloeckler\*, and N. A. Schwadron, (Department of Atmospheric, Oceanic, and Space Sciences, University of Michigan, Ann Arbor, MI, USA, 48109-2143, email: thomasz@umich.edu); D. Larson, and R. P. Lin, (Space Research Laboratory, University of California, Berkeley, CA 94720, USA) \*G. Gloeckler also at Department of Physics and ISTP, University of Maryland, College Park, Maryland, USA, 20742

The ionic charge state of minor ions is a reliable tracer for electrons close to the Sun. The charge state can be determined in its frozen-in state at 1 AU by the SWICS experiment on



ACE. The suprathermal portions of electron distribution functions are also expected to provide information on the low corona. These distribution functions are independently measured by the WIND 3DP instrument.

The combination of these data provides a powerful set of constraints on models describing the radial dependence and the character of electron distribution functions close to the Sun. We will focus on the non-thermal properties of electrons in the solar vicinity and their effect on the freeze-in process of the ionic charge state of minor ions.

GA4.05/E/02-A1

1010

#### CO-ORDINATED INTERPLANETARY SCINTILLATION AND OPTICAL MEASUREMENTS OF THE ACCELERATION PROFILE OF THE SLOW SOLAR WIND

A.R. BREEN, R.A. Fallows, P.J. Moran, P.J.S. Williams Prifysgol Cymru, Aberystwyth, Wales, E.U.; R. Schwenn, N. Srivastava Max-Planck Institut fuer Aeronomie, Katlenburg-Lindau, Germany, E.U.

The slow solar wind is substantially denser and more variable than the fast wind. Interplanetary scintillation measurements suggest that the slow wind has reached its 'cruising' velocity by ~30 solar radii from the Sun, while optical measurements of the drift velocity of large-scale irregularities suggest acceleration out to 25-35 solar radii. In this paper we compare the results of near-simultaneous IPS and optical measurements of slow wind velocity from EISCAT and LASCO, at heliographic distances between 2 and 50 solar radii. The effective fields of view of the two instruments overlap, allowing direct comparisons of velocities derived from the two techniques. We also hope to present the initial results of co-ordinated dual-frequency IPS observations (931 and 1400 MHz, covering ~10-50 solar radii) and optical measurements made in May 1999 using EISCAT, the MERLIN system and LASCO

GA4.05/W/05-A1

Invited

1050

#### PROPAGATION AND DAMPING OF WAVES IN THE CORONA

Joseph V HOLLWEG (University of New Hampshire, USA, email: joe.hollweg@unh.edu)

In 1968, Hartle and Sturrock showed that a model electron-driven solar wind resulted in flow speeds at 1AU which were too slow and proton temperatures at 1AU which were much too low, especially when compared to the high-speed solar wind streams which were essentially discovered during the Skylab era. Moreover, it was soon realized that heavy ions in the solar wind were flowing faster than the protons and hotter than the protons roughly in proportion to their masses; heavy ions like iron were recognized to have temperatures at 1AU which were well in excess of the typical coronal electron temperatures. Clearly the protons and heavy ions were being heated and accelerated by some "non-thermal" source. In 1969 the discovery of ubiquitous low-frequency Alfvén waves in the solar wind by Belcher, Davis, and Smith began three decades of work on the roles of waves in the solar wind. The waves were recognized to exert a wave pressure on the wind, and dissipation could lead to heating. The heavy ions were soon realized to require higher-frequency cyclotron-resonant waves. Descriptions for these effects in a multi-ion solar wind were available by the early 1980's, but various models failed in detail, mainly because they emphasized the effects of the waves in interplanetary space, but not in the corona itself. In fact an early study of resonant proton heating in the corona predicted coronal proton temperatures which were at the time regarded as too high, but which have been verified more recently by the remarkable UVCS/SOHO observations. The UVCS data now strongly suggest that resonant heating of protons and ions by waves is the dominant process heating coronal holes, and providing the thermal energy which is converted into flow energy. We will discuss some of the basic physics of the resonant heating and acceleration of coronal protons and ions, emphasizing the kinetic physics, and showing how it can account in principle for the basic UVCS observations. However, we will point out that there are basic questions concerning the wave source, and thus the origin and evolution of the power spectrum, knowledge of which is essential for calculating the resonances.

GA4.05/W/06-A1

Invited

1130

#### CORONAL HEATING IN MAGNETICALLY OPEN AND CLOSED REGIONS: SIMILARITIES AND DIFFERENCES

Prof. E.R. PRIEST and Dr. R.W. WALSH

Energy release in Stellar Coronae remains one of the main unanswered astrophysical questions. In the case of the Sun, it appears beyond doubt that the solar magnetic field as well as the turbulent motions of the photosphere play the most vital roles in this heating problem. In this review the authors outline possible coronal heating mechanisms applicable to both open and closed magnetic structures. The dissipation of wave motions, sites of magnetic reconnection and magnetohydrodynamic turbulence are all possible candidates for providing the necessary coronal energy deposition.

For example, wave heating theories for coronal hole regions along with the associated concepts for polar plume activity will be discussed. On the other hand, the evidence for magnetic reconnection within the corona from theoretical modelling as well as from SOHO observations is compelling. The important contribution made by coronal bright points will be summarised with examples from coordinated TRACE/MDI studies. Scaling laws for discrete energy release from both statistical models and EIT/SXT observations will be reviewed as well as the plasma dynamics, time variability and possible observational signatures of random, localised heating episodes within active region and large scale X-ray loops.

GA4.05/E/01-A1

1210

#### SURFACE WAVE INDUCED MAGNETIC RECONNECTION IN THE SOLAR CORONA

B. P. PANDEY (Indian Institute of Geomagnetism, Bombay 400 005, India, email: pandey@iig.iigm.res.in); G.S.Lakhina (Indian Institute of Geomagnetism, Bombay 400 005, India, email: pandey@iig.iigm.res.in); C Uberoi (Indian Institute of Science, Bangalore 560 012, India, email: cuberoi@iisc.ernet.in)

The low-frequency surface wave induced magnetic reconnection may be a possible candidate for the coronal heating and emission of jets and surges on the Sun. We demonstrate that the lifetime and scale lengths of the coronal plasmoid ejection compares favourably with the analytical results of surface wave induced tearing of the current sheet.

GA4.05/W/01-A1

1220

#### SAND-PILE MODEL OF CORONAL HEATING BY MICRO FLARES: EFFECT OF THE FORCING

O.V. Podladchikova, B. LEFEBVRE, V. Krasnoselskikh (LPCE/CNRS, 3A av. de la Recherche Scientifique, 45071 Orleans, France)

We model coronal heating of the quiet corona by means of micro flares in the framework of a

"sand-pile" model. There exist such models of self-organised criticality applied in this context [1,2]. Here, we are interested in examining the dependence of characteristics of energy dissipation upon the statistical characteristics of the magnetic fields sources (forcing). The dissipation process is assumed to take place when the characteristic current density exceeds some threshold. This corresponds to the formation of multiple reconnection sites with small-scale current layers. It is shown how does energy dissipation is influenced by probabilistic as well as deterministic forcing terms.

Monday 19 July PM

Presiding Chair: E. Leer (Univ. of Oslo, Norway)

GA4.05/L/01-A1

Invited

1400

#### THE SOLAR WIND

W.I. AXFORD and J.F. Mckenzie (Max Planck Institut fur Aeronomie, 37191 Katlenburg-Lindau, Germany)

In order to model the solar wind it is first necessary to understand that only the fast wind can be regarded as being time-stationary and that the slow wind is mainly an assembly of filamentary structures each carrying a non-stationary wind with an individual history and varying connection to the Sun. The fast wind is heated and accelerated by relatively high frequency waves which are emitted from the chromospheric network with an unknown spectrum and which ultimately damp mainly by cyclotron absorption. The latter has a characteristic effect on the behaviour of the plasma, notably in the ion temperature anisotropy and the heating and acceleration of minor ions. Furthermore it is essential that the correct geometry be used. It is also necessary eventually to match the solar wind solution to the source of the wind in the network: this is not simple because the source of energy probably lies in microflare activity which is inherently time-dependent and inhomogeneous. We describe a model of the fast wind which satisfies these requirements and also appears to be in good agreement with observations. Our approach is iterative in that we must first assume a heating function associated with wave damping, then calculate the corresponding wave pressure gradient and finally to determine the wave spectrum from a suitable wave transport equation assuming that the waves are Alfvénic. We also assume that wave-particle interactions determine the effective particle mean free path rather than Coulomb interactions and hence that ion heat conduction and viscosity do not play an important role. It is inevitable on the basis of a model of this type that the corona is very hot, the plasma accelerates rapidly within the first few solar radii and the minor species have temperatures per atomic mass unit which exceed the proton temperature and accordingly are accelerated more rapidly. There appears to be little room for any FIP effect apart perhaps from helium. The ion charge distributions must be determined by a high energy tail in the electron energy distribution and do not reflect the coronal temperature of the core electron.

GA4.05/E/03-A1

1440

#### PRIMARY FLOWS, THE SOLAR WIND AND THE CORONA

Swadesh MAHAJAN (Institute for Fusion Studies, The Univ. of Texas, Austin, TX 78712; email: mahajan@peaches.ph.utexas.edu); Ricard Miklaszewski (Institute of Plasma Physics and Laser Microfusion, 00-908 Warsaw, Str. Henry 23, P.O. Box 49, Poland; email: rysiek@ifpilm.waw.pl); Kommuna Nikol'skaya (Institute of Terrestrial Magnetism, Ionosphere and Radio Wave Propagation (IZMIRAN), Troitsk of Moscow Region, 142092 Russia; email: hellab@izmiran.troitsk.ru); Nana Shatashvili (Plasma Physics Department, Tbilisi State University, Tbilisi 380028, Georgia; email: lkh@cosmr.acnet.ge)

Based on the conjectured existence of primary solar emanations (flows from the solar surface), a model for the Origin of the Fast Solar Wind, and the creation and primary heating of the coronal structures is developed. In this model the directed velocity fields are fully treated. Preliminary results reproduce many of the salient observational features both for the SW and for the structures which comprise the solar corona (for the quiescent Sun). We also derive the flux constraints on the primary emanations if they are to be the primary source which provides, on a continuous basis, much of the required material and energy. It is co-primacy accorded to the flows which is the distinguishing component of our model. The strong interaction between the fluid and the magnetic aspects of the plasma results in opening new avenues to explore the solar atmosphere. For example, we find that it is possible to have a fast varying (spatially) velocity field with a relatively smooth magnetic field. The viscous dissipation of this velocity field, then, provides the primary, uniform heating for the coronal structures.

GA4.05/L/03-A1

Invited

1450

#### AN MHD MODEL OF TWO REGIMES OF THE POLAR SOLAR WIND ACCELERATION

Dr. Yuri PISANKO, Institute of Applied Geophysics, Rostokinskaya st.9, Moscow 129128, Russia; tel.: 007095-1813312; fax: 007095-1877513; Email: geophys@ns.wmc.rssi.ru

Remote observations of the polar corona on board of the SOHO have detected two different regimes of the rapid polar solar wind acceleration on the first few solar radii above the solar surface (presentations at the 5th SOHO Workshop by Kohl et al. and by Brueckner et al.). An attempt is made to propose an MHD model to describe both regimes taking into account the rotation of the magnetized Sun as an expansion under the inverted Rossby number. The model (Habbal & Tsinganos, 1983, JGR, 88, 1965) of the steady isothermal solar wind with momentum deposition allowing a continuous (Parker's) solution as well as solutions with shock discontinuities is used as zero-order approximation (absence of rotation). The rotation induced effects, i.e. the double electric layer in the polar corona and the system of field-aligned electric currents above the double layer creating the additional pressure gradient and hence the additional polar solar wind acceleration are taken into account in the first-order approximation (slow rotation). In the framework of this model 1) the empirical polar solar wind acceleration curve derived from H I Ly alpha emission line intensity measurements from the SOHO UVCS (Kohl et al.) is successfully simulated when a continuous (Parker's) solution is used as zero-order approximation; 2) SOHO LASCO observations of high (terminal) polar solar wind velocities close to the solar surface (Brueckner et al.) are successfully simulated when a discontinuous solution with shock transition (and momentum deposition) is used as zero-order approximation.

GA4.05/W/03-A1

Invited

1500

#### THOUGHTS ON THE FUTURE OF THE SOLAR WIND THEORY

L. OFMAN (Raytheon ITSS/NASA GSFC, Mail Code 682, Greenbelt, MD 20771, USA)

Solar wind has been studied theoretically for more than forty years since Parker's first paper in 1958. The theory of the solar wind is driven mostly by space based in-situ and remote sensing observations. The theoretical study of the solar wind is important for the understanding of the conditions of the interplanetary environment (i.e., space weather). This computationally

challenging problem parallels somewhat the advances in computational technology. I will review some of the current solar wind models. These models can produce the gross properties (velocity, density, and temperature) of the solar wind with reasonable accuracy. However, this is usually achieved by an ad-hoc heating function and momentum addition incorporated into the MHD equations. Some of the major unresolved issues in solar wind theory are: the exact mechanism that leads to the heating and the accelerations of the fast solar wind; the mechanism that leads to the uneven flow of the slow solar wind and the transition to the fast flow; the 3D structure of the solar wind; and the excess heating and acceleration of the minor ions. The wealth of recently obtained observations of the solar wind are placing stringent constraints on solar wind models. In addition to the solar wind velocity the models must match the energy input, the mass flux, the density the temperature the magnetic field at the Sun and near Earth, and the unresolved 'turbulent' velocities. SOHO observations suggest that the source of the solar wind energy and momentum is in the form of waves, with low-frequency MHD waves and high-frequency ion-cyclotron waves as the major candidates. The development of a global 3D solar wind model that incorporates the self-consistent heating due to waves, and more realistic energy equation that includes collisional and collisionless transport is needed. The ability of such a model to reproduce the observed solar wind is the ultimate test that will allow to rule-out or support various wave-heating and acceleration models.

**GA4.05/L/04-A1** Invited **1615**

**FUTURE WORK ON CORONAL HEATING AND SOLAR WIND ACCELERATION, OBSERVATIONS**

Hardi PETER, High Altitude Observatory / NCAR, Email: hpeter@ucar.edu

The space-based observatories SOHO and TRACE have shown some very interesting results on the structure and dynamics of the Sun and its atmosphere, e.g. the extremely high ion temperatures or the enormous variability in the corona. But one question is still open to debate: how to use these data to distinguish between different types of physical heating processes, as e.g. absorption of high-frequency Alfvén-waves or reconnection events? It is of importance to ask this question also of future space-missions, as the Solar Probe or the Solar Orbiter. What can they really contribute to this problem? To what extent will they yield the possibility to measure e.g. high-frequency waves or the change of the magnetic field during reconnection events? Will they enable us to decide if the heating of the closed and open corona and the acceleration of the wind is due to a single or a multiple process? And is it possible to address one of the most interesting questions, namely why the Sun converts just that amount of energy flux into solar wind acceleration that we observe? As the corona and most probably its heating is controlled by the magnetic field, the strength and the direction of the latter one has to be measured in the corona and also in the underlying photosphere in order to study the connection between these two regimes. The up-coming Solar-B mission will enable one to study the photospheric magnetic field with increased spatial and temporal resolution. The development of a large mirror coronagraph combined with IR-polarimetry for measuring the coronal magnetic field is on its way. Finally the interaction with the stellar community should be intensified to take advantage of the study of different types of stars.

**DISCUSSION** **1700**

**GA4.09** **Saturday 24 July**

**TURBULENCE AND SOLITARY STRUCTURES IN SPACE PLASMAS: THEORY, EXPERIMENT AND ANALYSIS (WITH DIV. III)**

Location: Hills 212 LT  
Location of Posters: Old Gym

**Saturday 24 July AM**

Presiding Chair: C. Stasiewicz (Swedish Inst. of Space Physics, Sweden)

**GA4.09-A6** Introduction **0830**

KRASNIOSELSKIKH, V (LPCE/CNRS, Orléans)

**GA4.09/L/02-A6** **0840**

**ALFVENIC STRUCTURES IN THE MAGNETOSPHERE AND THEIR ROLE IN ION AND ELECTRON ENERGIZATION**

K. STASIEWICZ and Y. Khotyaintsev (Swedish Institute of Space Physics, Uppsala Division, SE-75591 Uppsala, Sweden, email: ks@irfu.se)

Alfvénic structures or nonlinear waves associated with large density depletions at small perpendicular scales are commonly observed in the magnetosphere. At lower altitudes (<3000 km) they have characteristics of shear Alfvén waves with transverse scale and dispersion related to the inertial electron length. At larger distances, in hot magnetospheric plasma, the Alfvénic structures exhibit kinetic and compressional properties. On the basis of measurements obtained on Freja satellite we show that the Alfvénic structures play important role in the electron and ion acceleration and in the formation of magnetospheric plasma cavities. The ion energization is shown to be related to chaotization of orbits and breaking of adiabaticity caused by strong perpendicular electric field gradients within the Alfvénic structures. The electron acceleration is related to the parallel electric field, and ponderomotive effects of the electric field can cause cavitation of ionospheric plasma! ried by inertial Alfvén waves.

**GA4.09/W/15-A6** **0900**

**SOLITARY STRUCTURES, TURBULENCE AND QUASISINUSOIDAL WAVEFORMS OBSERVED IN THE CUSP AT 7-9 RE**

J. S. PICKETT, J. D. Menietti, R. M. Braunger, E. B. Bogusch, W. S. Kurth, D. A. Gurnett and J. D. Scudder (all at Department of Physics and Astronomy, The University of Iowa, Iowa City, IA 52242, USA, email: pickett@uiowa.edu) B. T. Tsurutani (Jet Propulsion Laboratory, 4800 Oak Grove Drive, Pasadena, CA 92209, email: btsurutani@jplsp.jpl.nasa.gov)

Two of the waveform receivers who are a part of the Plasma Wave Instrument (PWI) on the Polar spacecraft have captured various waveforms in the cusp at radial distances of 7-9 Re. Both waveform receivers simultaneously sample three orthogonal electric field and three orthogonal magnetic field components (two in the spin plane and one along the spin axis) in the

time domain. The Low Frequency Waveform Receiver (LFWR) records the waveforms incident in the 0.1 to 25 Hz range. In normal mode the LFWR samples at 100 Hz for 2.56 s every 28 s. The High Frequency Waveform Receiver (HFWR) records waveforms in the 0.2 to 25 kHz range. In high telemetry rate mode (data formatted into a digital data stream and telemetered directly to the ground), the HFWR samples at 71.43 kHz for 0.45 s every 9.2 s. These PWI waveform receivers obtain typical sinusoidal waveforms, e.g. low frequency equatorial waves and high frequency chorus, hiss and whistlers, throughout each orbit, which can be analysed in a straightforward manner using FFTs. Many of the waveforms obtained in the cusp do not lend themselves to this type of analysis since they appear as pulses, wave packet bursts, quasi-sinusoidal wave trains and turbulence. We have analysed these data in the time domain by transforming them to a B-field-aligned coordinate system. Other methods, such as wavelet analysis, are being used to obtain further information about these waveforms. Examples of the various waveforms and the results of analyses of will be presented. The role that these waves could play in particle acceleration and heating, if any, will be discussed briefly.

**GA4.09/W/11-A6** **0920**

**NONLINEAR PLASMA WAVES IN THE POLAR CAP BOUNDARY LAYER**

Bruce TSURUTANI, J.K. Arballo, L.D. Zhang, D. Croley, (all at Jet Propulsion Laboratory, California Institute of Technology, Pasadena, CA 91109, email: tsurutani@jplsp.jpl.nasa.gov) Jolene Pickett and Donald A. Gurnett, (University of Iowa, Dept of Physics & Astronomy, Iowa City, IA 52242)

We show examples of solitary/nonlinear electric and magnetic plasma wave structures in the POLAR plasma wave data in regions called the Polar Cap Boundary Layer (PCBL). The wave mixture is a form of plasma turbulence and is related to enhanced low energy ions. We discuss the detailed feature of these waves, their global distribution and their possible interplanetary (WIND) control.

**GA4.09/W/07-A6** Invited **0940**

**FAST SOLITARY STRUCTURES**

R. E. ERGUN, C. W. Carlson, J. P. McFadden, L. Muschietti, (Space Sciences Laboratory, University of California, Berkeley, CA.)

Large-amplitude, spatially coherent, plasma structures known as "fast solitary structures" or "electron phase space holes" have been observed in several regions of the magnetosphere including the auroral zone, plasma sheet boundary layer, and bow shock. There has been rapid theoretical progress in understanding these structures. Solitary structures can develop from bidirectional electron beams. Once developed, the one-dimensional properties, parallel to the magnetic field, can be adequately described by analytical treatment as BGK structures. Finally, there is evidence that the structures dissipate by radiating whistler waves. There remains, however, much work to do.

The origin of the bidirectional electron beams, the development of two- or three-dimensional structures, and the observed periodicity at the ion cyclotron frequency are not well understood, nor is the relationship of the structures to parallel electric fields. We show detailed observations from the FAST satellite that suggest that the solitary waves arise from a nonlinear process that starts with an ion-cyclotron drift instability. This model can explain many of the observed properties electron solitary structures in the auroral zone including the perpendicular scale size, the periodicity, and the development of the bidirectional electron beam.

**GA4.09/W/02-A6** **1000**

**FAST SATELLITE MEASUREMENTS OF ION HOLE SOLITARY WAVE VELOCITIES USING PARTICLE OBSERVATIONS**

J. P. MCFADDEN, C. W. Carlson, R. E. Ergun (all at Space Sciences Laboratory, University of California, Berkeley, CA 94720, USA, Email: mcfadden@ssl.berkeley.edu, cwc@ssl.berkeley.edu, ree@ssl.berkeley.edu)

Ion hole solitary waves are bipolar parallel electric field structures that are associated with up-going auroral ion beams. Recent measurements by the FAST satellite show the largest amplitude solitary waves can produce a measurable energy shift in the electron spectral peak. From the inferred potentials, which can exceed 100 Volts, the solitary waves are determined to be moving at 100-1000 km/s, and have scale sizes of a few kilometers (~10 Debye lengths). Measurements using separated dipole antennas support the high velocity for these structures. These observations contrast sharply with Viking reports of low velocity (5-50 km/s), small size (~100 m), small potential (~1 volt) solitary waves, as inferred from signal delays in separated Langmuir current probes. FAST records similar signals in its Langmuir current probes, however these signals are not caused by a decrease in density within the solitary waves. The current signals appear to be caused by the solitary wave electric field reducing the spacecraft photoelectron current to the probes, which produces a delay given by the wave half-period rather than a delay related to the solitary wave velocity.

**GA4.09/E/13-A6** Invited **1020**

**MODULATIONAL INTERACTION OF THE LOWER HYBRID WAVES WITH ELF DENSITY PERTURBATIONS IN THE AURORAL IONOSPHERE: ION ACOUSTIC AND KINETIC ALFVEN MODES**

V. D. SHAPIRO Physics Department, University of California San Diego, La Jolla CA 92093/0319 USA

It is well known that the auroral ionosphere is a place of very strong lower hybrid wave activity, most probably excited by the fluxes of the precipitated energetic electrons. In the paper a system of equations describing the coupling and modulational interaction of the lower hybrid waves with the extremely low frequency (ELF) density perturbations is constructed and analysed. Two versions of density perturbations in the form of either ion acoustic or kinetic Alfvén waves are considered. In the coupling mechanism density perturbations are sustained by Reynolds stresses of the lower hybrid waves, while trapping of these waves into density depletions results in the proper modulation of wave intensity. The modulational instability driven by the coupling has been investigated, and thresholds in the lower hybrid wave energy have been calculated for both types of coupling and compared with observations. The nonlinear evolution of the modulational instability leads to the formation of the magnetic field aligned cavitons of the lower hybrid waves. In the case of ion acoustic cavitons a quasi-stationary structure, similar to those observed in the auroral ionosphere, can be formed. This structure is supported by a balance between the pumping of energy into lower hybrid waves by energetic electrons and energy dissipation due to Landau damping and transverse ion acceleration. In the case of Alfvén waves a stationary envelope soliton is formed with the transverse size comparable to the electron skin depth. Lower hybrid oscillations, much shorter in wavelength, are trapped inside the density profile associated with such a structure.

GA4.09/E/02-A6 Invited 1100

## NONLINEAR PROPAGATION OF DISPERSIVE ALFVEN WAVES IN SPACE PLASMAS.

P. K. Shukla Fakultät für Physik und Astronomie, Ruhr-Universität Bochum, D-44780 Bochum, Germany

There is a growing interest in understanding the properties of linear and non-linear dispersive Alfvén waves in magnetized plasmas. Attention has then been focused on inertial and kinetic Alfvén waves, with applications in the Earth's ionosphere and magnetosphere as well as in solar and laboratory plasmas. Our objective here is to discuss some linear and nonlinear mechanisms for generating dispersive Alfvén waves in a magnetoplasma. When the amplitudes of dispersive Alfvén waves are sufficiently large, they interact nonlinearly with themselves and also with the background plasma, thereby producing many interesting non-linear effects, such as the ponderomotive force driven density cavitation/refraction, and charged particle acceleration, energy cascading within the Alfvén wave spectra, formation of coherent non-linear structures (envelope Alfvénic shocks, dark and bright Alfvén solitons, as well as solitary Alfvén vortices), and routes to chaos. Here, we describe the physics of the various non-linear processes involving finite amplitude dispersive Alfvén waves, and present details of important non-linear models that could account for the salient features of some coherent non-linear structures. Possible applications of our investigation to space and laboratory plasmas are pointed out.

GA4.09/E/08-A6 Invited 1120

## NONLINEAR ALFVEN WAVES IN SPACE PLASMAS: THEORY AND OBSERVATIONS

Oleg POKHOTILOV (Institute of Physics of the Earth, 123810 Moscow, Russia, Email: pokh@uipe-ras.scgis.ru)

In recent years new experimental results have pointed out the importance of large amplitude small-scale phenomena in auroral ionosphere and magnetosphere. We present a review of the modern theories of large amplitude non-linear inertial and kinetic Alfvén waves in space plasmas. A special attention is paid to the study of the Alfvén solitary wave structures. High time resolution measurements performed by recent satellite missions in ionospheric and magnetospheric plasma provide strong evidence that a large number of auroral forms are related to solitary electromagnetic structures of similar sizes. It is shown that some of the observed electromagnetic structures can be described in terms of non-linear theory of large amplitude inertial Alfvén waves. The stationary solutions of these equations in the form of a solitary dipole vortex and vortex streets are discussed. The examples of numerical simulation are presented. Such structures can exist in the space as well as in the laboratory plasmas. The generalisation of this theory to the case of relativistic electron-positron plasma is also reviewed. It is shown that the solitary structures in this case can be described by the similar equations which have the stationary solutions in the form, analogous to those in electron-ion plasmas. The deep physical similarity of magnetospheric processes and those in astrophysical plasmas is pointed out.

GA4.09/W/05-A6 Invited 1140

## CAVITATION OF LOWER-HYBRID WAVES IN THE EARTH'S IONOSPHERE

H. L. PECSELI (Physics Department, University of Oslo, Norway, Email: hanspe@fys.uio.no), S. H. Kjus (Swedish Institute of Space Physics, Box 812, S-981 28 Kiruna, Sweden, email: solveig.kjus@irf.se), B. Lybekk (Physics Department, University of Oslo, Norway, email: blybekk@fys.uio.no), J. Trulsen (Institute for Theoretical Astrophysics, University of Oslo, Norway, email: jtrulsen@astro.uio.no), A. Eriksson (Swedish Institute of Space Physics, Uppsala, Sweden, email: aie@irfu.se)

Lower hybrid wave cavities detected by the FREJA satellite are analysed. Based on simple statistical arguments by use of signals from two density probes, it is possible to obtain rather general results concerning the individual shapes of these cavities. In particular it is demonstrated that a cylindrically symmetric Gaussian density depletion seems to give a very good fit for a vast majority of cases. The validity of this model is shown to give a great simplification in the interpretation of the data. As a result, a number of well-defined characteristics are obtained which have to be accommodated within an ultimate theory describing the observed wave phenomena. Methods for obtaining the velocity distribution of the cavities are also outlined. The statistical distributions of regions of occurrence, peak density perturbations, and cavity widths are presented, together with distributions of the lower-hybrid wave amplitudes associated with the cavities. Scenarios for the formation of the lower-hybrid wave cavities are discussed.

GA4.09/W/10-A6 1200

## PARTICLE SIMULATIONS OF SOLITARY WAVES IN THE AURORAL REGION

T. Miyake, Y. Omura, and H. Matsumoto (all at Radio Atmospheric Science Center, Kyoto University, Gokasho, Uji, Japan, e-mail: miyake@kurasc.kyoto-u.ac.jp, omura@kurasc.kyoto-u.ac.jp, matsumoto@kurasc.kyoto-u.ac.jp)

We perform two-dimensional electrostatic particle simulations of electron beam instabilities using parameters characteristic of the auroral region. Counter-streaming electron beams interact strongly to form large electrostatic potentials trapping the beam electrons. The potentials coalesce with each other to form electrostatic solitary waves (ESW) which have been observed by recent spacecraft in various regions of the magnetosphere. The nonlinear trapping of the electron beams leads to formation of electron holes in the velocity phase space. We study two cases with different thermal velocity of the electron beams, i.e., cold and warm electron beams. In the case of cold beams, we find two-dimensional potentials are formed under a relatively strong magnetic field corresponding to the electron cyclotron frequency equal to the electron plasma frequency. These two-dimensional potentials, however, are diffused by ions, and disappear with the time scale of the plasma oscillation period of ions. On the other hand, in the case of warm beams, one-dimensional potentials elongated in the direction perpendicular to the magnetic field at the saturation phase of the beam instability. As time goes on, these one-dimensional potentials are modulated with the ion gyroradius in the perpendicular direction, leading to formation of two-dimensional structures which are stable for more than 26 plasma oscillation periods of ions.

GA4.09/W/13-A6 1220

## ON THE DEVELOPMENT OF ION ACOUSTIC AND ION CYCLOTRON INTERMITTENCY IN THE AURORAL ACCELERATION REGION

Dr Abdelhaq M. Hamza

We analyze a simple model of ion fluctuations (ion acoustic and ion cyclotron fluctuations)

driven by an electron current which leads to intermittent fluctuations when the linear growth rate exceeds the wave packet dispersion rate. The fluctuation amplitude  $\delta\phi/T\phi$  can be much larger than the order  $\delta m_{\perp}(e)/m_{\perp}(i)$  level predicted by quasilinear theory or Manheimer's theory. Although the ion motion is linear, intermittency is produced by the strong nonlinear electron response, which causes the electron momentum input to the ion fluctuations to be spatially localized. We treat the one-dimensional case because it is especially simple from an intuitive and analytical point of view, but it is readily apparent that the effect occurs in a three dimensional magnetised plasma.

Saturday 24 July PM

Presiding Chair: V. Krasnoselskikh (LPCE/CNCS, Orleans, France)  
Concurrent Poster Session

GA4.09/W/16-A6 Invited 1400

## SELF-ORGANIZED CRITICALITY-A RATIONAL APPROACH TO TURBULENCE AND COMPLEXITY IN SPACE PLASMA PROCESSES

Chang, Prof Tom

Observations indicate that space plasma processes are generally multiscale, sporadic and localized. Examples include the intermittent nature of the magnetotail, the distribution of double layers in the auroral acceleration region, the fast electron holes and associated wave-particle interactions, the strongly interacting lower hybrid turbulence, solar flares and related disturbances. We suggest that most of these processes can be viewed as driven dissipative systems near "self-organized criticality (SOC)". Self-consistent simulations, cellular automata calculations, scaling laws, and power-law distributions, as well as renormalization group invariant arguments will be provided to demonstrate the plausibility of such a suggestion.

GA4.09/W/08-A6 Invited 1420

## ON TURBULENT RELAXATION OF A COLLISIONLESS PLASMA

Tadas K. NAKAMURA (Fukui Prefectural University, Fukui 910-1195, Japan, email: tadas@fpu.ac.jp)

Relaxation process of a collisionless plasma by a turbulent field is examined based on statistical theory. Essential mechanism of the relaxation process is similar to the "violent relaxation" of stars in a galaxy, which has been proposed by Lynden-Bell [1]. In the present paper, a method using H-function developed by Tremaine et al. [2] is applied. Correcting the flaws of their method, it has been shown that the most probable distribution function is a Maxwellian distribution when the phase space volume is mixed well by the turbulent field. This result explains "Langmuir's paradox"; the reason why the Maxwellian distribution is so commonly found in collisionless plasmas. [1] Lynden-Bell, 1967, MNRAS, v136, p101. [2] Tremaine et al., 1986, MNRAS, v219, p285.

GA4.09/W/01-A6 Invited 1440

## ADVANCED STATISTICAL METHODS FOR ANALYZING SPACE PLASMA MEASUREMENTS

W. WERNIK and M. Grzesiak (both at Space Research Center, Polish Academy of Sciences, ul. Bartycka 18a, 00-716 Warsaw, Poland, email: aww@cbk.waw.pl)

Space plasma is a highly dynamic and irregular medium. Large amplitude fluctuations in the velocity, magnetic field, and density occur over wide range of spatial and temporal scales, suggesting the importance of non-linear processes. Linear analysis techniques, such as auto- and cross-spectra, and correlations, are obviously of limited value when non-linear processes dominate. In recent years sophisticated methods have been developed for detecting and quantifying non-linear systems. Some of those methods are briefly described and illustrated with examples using both synthetic and real data. Methods for testing for nonlinearities in seemingly stochastic data are described. Deeper insight into the physics of non-linear processes provides the wavelet transform. The main advantage of using the wavelet transform is that it preserves the information about local features (e.g. singularities) of the signal and allows its reconstruction only over a given range of scales (frequencies). This property is of particular importance in studying turbulence, which often shows coherent structures apparently related to non-linear processes. The structure function approach commonly used in describing and modelling the intermittent behaviour of turbulence is compared with the wavelet-based modulus maxima method. There are convincing arguments that strong turbulence can be decomposed into coherent structures, and random, stochastic fluctuations. Methods and criteria of such decomposition are presented and discussed. Some concepts developed in the context of dynamic systems, such as the system dimension, Lyapunov exponents, are briefly described. Importance of testing for the significance of the results is emphasised and illustrated.

GA4.09/E/06-A6 1500

## A WAVELET ANALYSIS OF FIELD-ALIGNED ANISOTROPY IN MHD TURBULENCE

Tim HORNBURY (Astronomy Unit, Queen Mary and Westfield College, London, email: t.hornbury@qmw.ac.uk) Andre Balogh (The Blackett Laboratory, Imperial College, London)

We present a novel wavelet method of measuring the field-aligned anisotropy of MHD turbulence using single spacecraft observations. Using this method it is possible to calculate the anisotropy of power levels, spectral indices and intermittency. We show how these results can be related to the terms of the two-point correlation tensor of MHD turbulence, and can place limits on the three dimensional structure (for example, "slab" or "2D") of the fluctuations.

GA4.09/E/12-A6 1520

## VERY LOW AMPLITUDE FLUCTUATIONS WITHIN CO-ROTATING TRAILING EDGES

Elizabeth Lucek (The Blackett Laboratory, Imperial College, London, email: e.lucek@ic.ac.uk) TIM HORNBURY (Astronomy Unit, Queen Mary and Westfield College, London, email: t.hornbury@qmw.ac.uk) Andre Balogh (The Blackett Laboratory, Imperial College, London) David McComas (Los Alamos National Laboratory, Los Alamos)

Ulysses magnetic field and bulk plasma observations within the trailing edges of high speed streams at mid-latitudes revealed the presence of an unusual population of very low amplitude fluctuations with a broadband  $1/f$  magnetic field power spectrum on scales of minutes to hours. These fluctuations are unlike those in high or low speed streams nearby and often have very low cross helicity levels on hourly scales. This population was present in only some rotations, but has been observed in both Northern and Southern hemispheres. We present these observations, along with the results of a search for similar populations in data from Pioneer 10



and 11 and Helios 1 and 2, between 0.3 and 5 AU at low latitudes. The possible origins of this population (solar or local dynamics) are discussed.

**GA4.09/W/03-A6** Invited **1600**

**INTERMITTENCY OF TURBULENCE IN SPACE PLASMA**

Vincenzo CARBONE, Pierluigi Veltri, Luca Sorriso-Valvo Dipartimento di Fisica Universita' della Calabria 87036 Rende (CS), Italy Roberto Bruno Istituto di Fisica dello Spazio, Area di Ricerca di Tor Vergata, Roma, Italy

We present a review of a decade of satellite observations of turbulence in the Solar Wind plasma. Particular emphasis is done on the properties of intermittency of the turbulence, say the departure from a gaussian of the probability distribution functions of both velocity and magnetic fluctuations. The possibility of modelling the non-linear energy cascade taking into account intermittency is also presented.

**GA4.09/W/12-A6** Invited **1620**

**DISSIPATIVE PROCESSES IN COLLISIONLESS PLASMAS AND COHERENT ELECTROSTATIC NONLINEAR WAVES**

MANGENEY A.Despa, Observatoire de Paris-Meudon, 5 Place Jules-Janssen, 92195 Meudon Cedex.

A number of observations made in the collision less plasmas of the earth environment suggest that in many cases the dissipation of large scale "MHD" perturbations occurs through the deformation of the distribution functions (formation of beams, holes, etc.) and the corresponding excitation of plasma waves. One of the striking results obtained in the recent years is that these waves are basically electrostatic and coherent, in the form of solitary structures or modulated wave packets. The details of these waveforms appear to depend of the region of observation, (which determine the plasma regime and the properties of the large-scale fluctuations). In this paper we shall first review the available observational evidence; then we shall discuss the relevant theoretical interpretations and numerical simulations that have been put forward to explain these observations.

**GA4.09/E/10-A6** **1640**

**THE ALFVEN RATIO TEST RE-EXAMINED**

Jack D. SCUDDER (Department of Physics and Astronomy, University of Iowa, Iowa City, Iowa, 52240, USA, email: jack-scudder@uiowa.edu)

From their earliest detection Alfvén wave trains and rotational discontinuities have failed the Walén test for the proportionality between the vectorial changes of the magnetic field. The Alfvén ratio is defined to be the multiplicative factor times the Walén proportionality factor that relates observed field and plasma flow velocity changes. For interplanetary examples this ratio falls between 0.5-0.8 and is systematically low against the value of 1 predicted by Walén. A similar deficit is recorded at Alfvén wave structures standing at the magnetopause. This paper will explain the essentials of this discrepancy with a realistic model Alfvén, showing that the cause of this systematically smaller Alfvén ratio is the mistaken presumption (even for wavetrains dominated by long wavelength power) that the center of mass of the plasma can follow the torsioning of the magnetic field exactly. A much better theoretical and observational test for these structures is the electron fluid velocity that can more agilely follow the torsioning magnetic field. A model and observational tests from the Polar spacecraft will be illustrated that recovers the systematically smaller Alfvén ratio for ions, while obtaining the correct Walén ratio for the electrons. Simulations of interplanetary wavetrains recover the small Alfvén ratio, demonstrating the cause. Explicit techniques for correcting ion measurements short of measuring the electron flow velocity will be illustrated with the model and data. Interesting insights into the observed frequency (wavenumber) dependence of the Alfvén ratio are recovered by this approach by exhibiting the full relationship between the ion flow vector's spatial profile in the wave and that of the magnetic field, demonstrating that it is not of the Walén form.

**GA4.09/E/01-A6** **1700**

**FLOW TURBULENCE IN THE EARTH'S PLASMA SHEET: WHAT IS GOING ON?**

Joseph E. BOROVSKY, Herbert O. Funsten, Elena Neagu, and Richard C. Elphic (all at Space and Atmospheric Sciences Group, Los Alamos National Laboratory, Los Alamos, NM 87545, USA, email: jborovsky@lanl.gov)

The turbulent bulk flows observed by the ISEE-2 spacecraft in the Earth's plasma sheet are examined. It is argued that these bulk flows are owed to an MHD flow turbulence rather than to an Alfvén-wave turbulence. The role of magnetosphere-ionosphere coupling on the magnetospheric flow turbulence is examined theoretically. This coupling acts to (1) lower the turbulent Reynolds number of the plasma sheet, (2) introduce a time-delayed viscosity to the plasma sheet flows, (3) preferentially damp out magnetospheric vortices with angular velocities that are antiparallel to B, and (4) transfer vorticity to larger spatial scales. It is argued that a "viscoelastic-fluid turbulence" description has some validity for the Earth's plasma sheet coupled to the dissipative ionosphere.

**GA4.09/W/14-A6** **1720**

**MAGNETIC DEPRESSIONS IN THE SOLAR WIND**

Markus FRAENZ and David Burgess, Astronomy Unit, Queen Mary & Westfield College, London, E1 4NS, UK. email: m.fraenz@qmw.ac.uk

Magnetic depressions in the solar wind occur on a wide range of temporal scales, starting with magnetic holes with a duration of several seconds extending to larger scale structures of more than 30 minutes duration. Usually these depressions are bound by tangential discontinuities and stabilised by anisotropic proton distributions. Using data of the Ulysses magnetometer instrument we investigate which instability mechanisms can cause the observed structures. On the other hand the high occurrence rate of depressions leads to an asymmetry in the field distribution towards low values of |B|. This asymmetry can be expressed in the skewness of the distribution as a time dependent parameter. We investigate how this parameter depends on solar wind type and how it relates to the observed skewness in the plasma beta distribution. Finally we discuss whether the field asymmetry is a specific signature of instabilities or other non-linear processes leading to field energy loss like e.g. energy cascading.

**GA4.09/E/04-A6** **1740**

**NONLINEAR SOLITARY ROSSBY VORTICES IN THE EARTH'S IONOSPHERE**

Tamaz KALADZE (I.Vekua Institute of Applied Mathematics, Tbilisi State University, 2 University str., Tbilisi, 380043, Georgia, E-mail: kaladze@viam.hepi.edu.ge)

The influence of the interaction between inductive current and the spatially inhomogeneous terrestrial magnetic field on the possibility of the formation of non-linear solitary Rossby vortices in the different slightly ionized D, E and F layers of the Earth's ionosphere is considered. It is shown that such interaction manifests itself only in the E and F layers and leads to the new effects and properties of the Rossby waves. The magnetised Rossby waves and solitary vortices are found in the E layer. The real natural mechanism which can lead to the inversion of propagation direction of free, noncaptured by flows, Rossby waves is indicated. The spatial inhomogeneity of the geomagnetic field causes opposite to the Coriolis force vorticity and in consequence weakens the vortical structures in the E layer. As regards the F layer, acting like viscosity the so-called induction inhibition stipulates the final damping of Rossby waves and solitary vortices. The corresponding rate of damping is defined. Thus, the longlived structures mainly exist in the D layer of the ionosphere in the form of solitary dipole Rossby vortices. Along with two-dimensional structures the three-dimensional pancake and cylindrical Rossby vortices of finite heights are constructed as well in the approximation of incompressible ionosphere. The corresponding original non-linear equations describing the dynamics of vortical formations are obtained.

**Saturday 24 July PM**

Presiding Chairs: V. Krasnoselskikh (LPCE/CNRS, Orleans, France)

**TURBULENCE AND SOLITARY STRUCTURES IN SPACE PLASMAS**

**GA4.09/P/01-A6** Poster **1600-01**

**STRONG VORTICAL (SOLITARY) TURBULENCE OF THE MIDDLE ATMOSPHERE**

George D.ABURJANIA, Vachtang Jandiere (Insitute of Applied Mathematics Tbilisi State University str., 2 380043, Tdilisi-43, Georgia, Email: aburj@viam.hepi.edu.ge/dtapha.keta.ge)

On the basis of the available data from observations and experiments, we can assume that before natural extraordinary phenomena and during influence, the processes in the atmosphere develop according to the following scenario. Source of extraordinary influence exits atmospheric-pressure disturbances (Acoustic-gravity (AG) waves), over region of it's location by vertical pulsed action on air. AG waves propagate vertically almost without damping to the height of E-layer and give rise to collective motion in the form of nonlinear strongly localized AG vortices (solitons) structures. It was found that the energy of AG vortices becomes negative I the E-layer of stratified atmosphere. For the energetic standpoint, this layer is the most appropriate for the formation of these structures; hence they are self-sustaining (like autosolitons) due to dissipative processes. Vortex structures contain trapped particles and mixing in an atmosphere can cause strong fluctuations of medium density and an increase heat and particle transfer. Accordingly, strong turbulence state in atmosphere is excited. We assume turbulence to be gas of ensembl randomly distributed weakly interacted similar vortices, composing the ground state. We determine density fluctuation spectrum and estimate turbulent diffusion coefficient.

**GA4.09/W/04-A6** Poster **1600-02**

**ON THE NATURE OF THE STRONG TURBULENCE OVER CUSP/CLEFT**

S. Savin, S. Klimov, M. Nozrdachev, S. Romanov, Yu. Yermolaev, V. Romanov (all Space Research Inst., Russian Academy of Sciences, Profsoyuznaya 84/32, GSP-7, Moscow, 117810, Russia, E-mail savin@iki.rssi.ru), J.BLECKI, J. Juchniewicz, R. Wronowski (all Space Research Center, Polish Academy of Sciences, Warsaw, Poland), J. Buechner, B. Nikutowski (Max-Planck Inst. Aeronomie, Lindau, Germany), A. Otto (Geophys. Inst., U. Alaska, Fairbanks, USA), C. T. Russell (IGPP, UCLA, USA), K. Stasiewicz (Inst. Space Physics, Uppsala, Sweden), P. Triska (Inst. Atmospheric Physics, Praha, Czechia)

Interball-1 high latitude data have shown that just outside magnetopause main current sheet (MP) and at its boundary the turbulent boundary layer (TBL) exists with the average RMS maximum about 25 nT and the occurrence rate 83%. The compressible and non-compressible magnetic spectra comparison, electric to magnetic field amplitude ratios and the wave polarization have shown that the dominant waves/structures in TBL are consistent with the Alfvén non-linear vortices (ANV). The trapped particle existence displays the strong non-linearity of the ANV, their characteristic scales are in the range 100-10000 km. The Interball-1 data shows that TBL is registered not only at high latitudes but also at low latitudes in the disturbed conditions; Polar data confirms that in the cusp vicinity. The ANV produce 'magnetic bubbles' with highly reduced magnetic field and heated plasma inside, average ion heating reaches 200-400 eV (i.e. 1.5- 3 times). Part of these 'bubbles' are transported inside MP, they constitute a mechanism of plasma penetration into the cusp/cleft. The geometrically TBL above the outer cusp could be presented as the spot of 6 Re with characteristic amplitude maximum of 37 nT. In the geomagnetic tail the TBL is seen along the mantle/LLBL boundary down to X<sub>s</sub> = - 20 RE that might provide the direct solar wind plasma penetration into the near Earth tail via its flanks. We briefly compare AVN with time dependent 2D MHD and 3D kinetic modeling.

**GA4.09/W/06-A6** Poster **1600-03**

**THE SOLITARY STRUCTURES IN OVERDENSE IONOSPHERIC PLASMA**

A.V. Kochetov and B.A. Mironov (both at Institute of Applied Physics, N.Novgorod, Russia, e-mail: kochetov@appl.sci-nnov.ru) G.I.TERINA and V.N.Bubukina (both at Radiophysical Research Institute, N.Novgorod, Russia, e-mail: ter@nirfi.sci-nnov.ru)

The results of the modelling of nonlinear dynamic effects arising in the ionospheric plasma under the action of the powerful radio waves are presented. Numerical solutions of nonlinear Schrodinger equation in the linearly inhomogeneous plasma layer excited by the heating radio wave were obtained. The processes of the formation of the solitary structures of the electric field and disturbances of plasma density and processes of their relaxation for different values of density gradient and the amplitude of the heating wave were analyzed. The spatial evolution of the electric field and disturbances of the plasma density and time dependencies of the reflected signal were obtained. With the heater turn-on the penetration of the solitary structure into the overdense plasma takes place which increases under the heating power increase and the decrease of the plasma density gradient. The decreasing of the scale of the spatial soliton structure, the periodic and chaotic solitons generation during the heater time are observed. When the heater is turned off, the solitons continue to travel into the overdense plasma for some time, increasing in the amplitude, until they reach the turning point. Then they reflect and

propagate into the underdense plasma, decreasing in the amplitude, and disappear. The obtained results allow to interpret the appearance of the scattered signal after the heater turn-off - "aftereffect plasma signal" (AEPS). This work was supported by the Education Department of Russia (grant N 97-0-5.3-113).

**GA4.09/W/09-A6** Poster **1600-04**

**THE PERIODIC GENERATION OF CAVITON FORMATIONS IN MODIFIED IONOSPHERIC PLASMA**

G.I.TERINA (Radiophysical Research Institute, Nizhny Novgorod, Russia, e-mail: ter@nirfi.sci-nnov.ru)

Results of experimental study of periodic variations of a "caviton" signal amplitude scattered by caviton formations in sounding of the artificial ionospheric turbulence by probing radio pulses of both ordinary and extraordinary polarization are presented. The experimental data were obtained at "Zimenki" and "Sura" heating facilities. The probing transmitter radiated radio pulses with a duration of 50 nks in the frequency range 5.50-5.87 MHz. The heating transmitter operated in range 4.5 MHz - 4.8 MHz ( under sounding by X mode pulses) and 5.5 MHz -5.8 MHz ( for O mode pulses). "Caviton" signal (CS) appeared when the heating transmitter was turned on, decreasing then in amplitude. The time dependencies of CS in the main are series of maxima. CS period was changed from a few milliseconds up to several seconds and increased with the decrease of the heating power, the increase of difference of heating and probing reflection heights and during the anomaly attenuation time. The decrease of CS period was observed with the approach of CS scattering height to the reflection height of the probing wave. CS amplitude decreased with CS period increase. At times the periodic and chaotic travel of CS maximum to smaller heights was observed with the velocity of the order and greater the ion sound velocity. The obtained results allow to study the peculiarities of periodic generation of caviton formations, arising in the ionospheric plasma under the action of powerful radio waves. This work was supported by the Education Department of Russia (grant N 97-0-5.3-113).

**GA4.09/E/11-A6** Poster **1600-05**

**STRUCTURE AND SOURCES OF LONG-PERIOD OSCILLATIONS NEAR HIGH-SPEED FLOWS OF SOLAR WIND**

Mikhail Pudovkin (Department of geophysics, The Institute of Physics, St.Petersburg State University, Petrodvorets 198904, Russia, email: pudovkin@snoopy.phys.spbu.ru); Olga KHABAROVA(Department of Solar-Terrestrial Physics, The Institute of Terrestrial Magnetism, Ionosphere and Radiowaves Propagation, Russia 142092, Moscow region, Troitsk; email: MARYL@izmiran.troitsk.ru)

A little studied phenomenon of a rise of steady long-period magnetohydrodynamic space plasma oscillations near high-speed flows of solar wind is considered in details. These oscillations with period from minutestill hours can be observed nearby both flows from solar flares (having shock wave ahead of main body of the flow) and recurrent flows (distinguished by a smooth profile of parameters increase). The identical structure of such oscillations does not speak about the unified mechanism of generation. The mechanism of the oscillations swing is different in each particular case. The calculations show that the long-period oscillations before flows from solar flares can be explained by a) ion-cyclotron instability of protons reflected from the shock wave, having speed large, than speed of ambient plasma and resonance inducing with MHD-waves (such instability gives periods about minutes for waves running along the magnetic field and about hours for practically perpendicular propagating waves) b) instability produced by reflection of cosmic rays from the shock wave (the wave, swayed by this way have maximum amplitude at perpendicular propagation and periods of oscillations from minutes till hours).

The oscillations inside the body of flare's flow can be considered as a result of Alfvén wave passage through front of strong shock wave. The oscillations near recurrent flows can explain by gradient instability. The various periods of oscillations are corresponded to various component of plasma gradients.

The recurrent flows are registered after interception of the sector boundary more often. It can result in wrong treatment of the cause of considered oscillations appearance. I.e. the oscillations can be attribute of the current layer which generate MHD-waves at magnetic reconnection. An experimental material that illustrates above-mentioned mechanisms is selected.

**GA4.09/L/01-A6** Poster **1600-06**

**ELECTRON ACCELERATION BY ALFVEN WAVES: FREJA AND SOUNDING ROCKET OBSERVATIONS**

Y. KHOTYAYNTSEV, K. Stasiewicz, M. Berthomier Swedish Institute of Space Physics, Uppsala Division, S-75591 Sweden e-mail: yuri@irfu.se M. Ivchenko Alfvén Lab, Royal Institute of Technology, Stockholm, S-10044 Sweden

Alfvén waves with frequencies of several Hz are usually observed in the auroral zone. In the low-beta ionospheric plasma Alfvén waves are in the inertial mode. Field aligned electron populations with egergies 50-5000 Ev streaming through cold background plasma are observed in spatially localized regions with perpendicular to the magnetic field size in order of electron inertial length. Using observations from Freja and sounding rockets we show that electron acceleration is most likely caused by parallel electric field of the inertial Alfvén wave.

**GA4.09/E/03-A6** Poster **1600-07**

**THE SOLUTION OF THE VORTEX NONLINEAR EQUATION FOR THE SOLAR WIND PLASMA NEAR THE EARTH'S MAGNETOSPHERE**

ARCHIL KHANTADZE (Tbilisi State University, 1, Chavchavadze Ave., Tbilisi 380028, Georgia, email: vazha@excite.com); Anzor Gvelesiani, Zurab Ioseliani (both at Institute of Geophysics, Georgian Academy of Sciences, 1, M. Alexidze Str., Tbilisi 380093, Georgia, email: vazha@excite.com)

An analytically not enough investigated problem of the non linear waves generation process - solitons and systems of vortical configurations – in inhomogeneous hydromagnetic field of the solar plasma flow streamlined the day-side of the Earth's magnetosphere is considered in detail.

Using typical values of magnetosheath parameters numerical calculations of the solitary vortical waves are carried out.

**GA4.09/E/05-A6** Poster **1600-08**

**ON PLANETARY NONLINEAR SOLITARY VORTICES IN THE MESOSPHERE**

Anzor Gvelesiani (Georgian Academy of Sciences, Institute of Geophysics, 1 Alexidze Str., Tbilisi 380093, Georgia), Tamaz KALADZE (I. Vekua Institute of Applied Mathematics, Tbilisi State

University, 2 University str., Tbilisi 380043, Georgia, E-mail: kaladze@viam.hepi.edu.ge)

The theory of nonlinear solitary dipole Rossby vortices for explanation of vortical perturbations in fields of wind's velocity and atmosphere's temperature (Energy Budget Campaign, 1980) observed at different heights of atmosphere is supposed. The corresponding calculations of parameters of spatially localized perturbations moving during the 1 week along parallel towards the East with the velocity of 10 m/s and transverse size of 1000 km are carried out. The comparison of numerical calculations by means of supposed theoretical model for nonlinear solitary dipole vortices with characteristics of observed longwave perturbation in the mesosphere (at heights of 80 km) shows the satisfactory agreement.

**GA4.09/L/03-A6** Poster **1600-09**

**ENERGETIC PARTIAL NONLINEAR...**

DORMAN

Abstract not available at time of going to press

**GA4.09/L/04-A6** Poster **1600-10**

**ON THE INFLUENCE OF ENERGETIC PARTIAL...**

DORMAN

Abstract not available at time of going to press

**GA4.09/L/05-A6** Poster **1600-11**

**MODEL OF SPACE TURBULENT**

KHUTOROVA

Abstract not available at time of going to press

**GA4.09/L/06-A6** Poster **1600-12**

**ION-ACOUSTIC SOLITONS AND DOUBLE LAYERS IN A TWO-ELECTRON TEMPERATURE PLASMA**

S.G.TAGARE (Department of Mathematics and Statistics, University of Hyderabad, Hyderabad 500046, India., email: sgtsm@uohyd.ernet.in)

It is found that two-electron temperature plasma with isothermal par electrons and cold ions admits both compressive and rarefactive solitons par as well as compressive and rarefactive double layers (depending on the par concentration of low-temperature electrons). We have derived K-Dv par equation and K-dV type equations with cubic and fourth order par nonlinearity at the critical density of low-temperature isothermal par electrons to discuss the properties of ion-acoustic solitons intwo-electron temperature plasma. In the vicinity of the critical electron density of low-temperature isothermal electrons we have derived K-dV type equation with mixed nonlinearity and solution of this equatioun will have both compressive and rarefactive double layers for those values of critical electron density of low-temperature

**GA4.10** Thursday 22 – Friday 23 July

**PLANETARY ATMOSPHERES, IONOSPHERES, MAGNETOSPHERES AND SOLAR WIND INTERACTIONS (WITH DIV. II, III) (IAGA)**

Location: School of Education, G33 LT

Thursday 22 July AM

Presiding Chairs: H. Shinagawa (Solar Terrestrial Environment Lab., Nagoya Univ., Japan), A. Nagy (Dept. of Atmospheric, Ocean and Space Science, Univ of Michigan, USA)

**MARS PRESENT AND FUTURE. UPPER ATMOSPHERES AND THEIR INTERACTIONS WITH THE SOLAR WIND**

**GA4.10/W/14-A4** Invited **0900**

**THE MARS THERMOSPHERE: GLOBAL MGS ACCELEROMETER MEASUREMENTS**

G.M. KEATING, R.H. Tolson, S.N. Noll, T.J. Schellenberg, R.L. Stephens, M.S. Bradford, D.T. Baird (all at George Washington University/NASA Langley, Hampton, VA, USA), S.W. Bougher (University of Arizona, Tuscon, AZ, USA) and J.L. Hollingsworth (NASA Ames, Mountain View, CA, USA)

An accelerometer experiment aboard the Mars Global Surveyor has provided insitu measurements of nearly 1000 vertical structures of the Mars thermosphere, compared to only 3 previously (Viking 1, Viking 2, Pathfinder). These measurements of vertical and latitudinal variations in density, temperature and pressure have been obtained in the afternoon in both the Northern and Southern Hemispheres between 110 and 170 km. The accelerometer experiment along with lower atmosphere measurements, has allowed us to establish the linkage between processes in the upper and lower atmosphere as well as linkage with topography. Unexpected results include: (1) enormous thermospheric responses in the Northern Hemisphere to regional dust storms in the Southern Hemisphere, (2) stationary (apparently topographically forced) planetary waves in the thermosphere which rotate with the planet creating factor of 2 variations with longitude, and (3) thermospheric densities persistently much higher than indicated in GCM's. The physical processes possibly responsible for these phenomena are discussed.

**GA4.10/W/13-A4** Invited **0930**

**SOLAR WIND INTERACTION WITH MARTIAN CRUSTAL MAGNETIC ANOMALIES**

D. L. MITCHELL, R. P. Lin, M. OIEROSET (Space Sciences Laboratory, Univ. of Calif., Berkeley), D. Crider, C. Law, P. Walker, P. Cloutier (Rice Univ., Houston, TX), and M. H. Acuna (NASA-GSFC, Greenbelt, MD)

While aerobraking beneath the ionosphere, the Magnetometer/Electron Reflectometer (MAG/ER) experiment onboard the Mars Global Surveyor spacecraft has detected numerous magnetic anomalies in the martian crust, many of which exceed 100 nT at spacecraft orbital altitudes of ~110-170 km. Despite these strong local anomalies, the global dipole moment is less than 2 x 10<sup>21</sup> G-cm<sup>3</sup> and cannot contribute significantly to the effective size of the

obstacle presented by Mars to the solar wind. Consequently, the solar wind interaction with Mars is similar to that at Venus and at an active comet, that is, primarily an ionospheric-atmospheric interaction. During a typical periaapsis pass, a distinct boundary is observed at ~300-500 km altitude where the flux of 0.1-1.0 keV electrons drops abruptly by about an order of magnitude. This is accompanied by a dramatic change in the electron energy spectrum: above the boundary, the spectrum is characteristic of the solar wind, while below the boundary, the spectrum is dominated by ionospheric photoelectrons. The photoelectron spectrum extends to ~1 keV and exhibits an Auger peak at ~500 eV, which is produced by K-shell ionization of atmospheric oxygen. This electron boundary marks the location where the solar wind is deflected around the ionospheric obstacle, resulting in a horizontal magnetic field that inhibits vertical transport and mixing of the solar wind and ionospheric plasmas. Occasionally, the spacecraft passed over a strong crustal magnetic anomaly while inside the ionosphere, resulting in a significant vertical field component. During this time, both the solar wind and photoelectron energy distributions are observed simultaneously. Photoelectrons travel upward along the magnetic field lines and out into the solar wind, while solar wind electrons precipitate downward into the atmosphere. This observation indicates that the crustal magnetic field is connected into the solar wind, providing a conduit for the exchange of ionospheric and solar wind plasmas.

**GA4.10/W/12-A4 0950**

**STRUCTURE OF THE IONOSPHERES OF VENUS AND MARS**

Andrew F. NAGY (Dept. Atmospheric, Oceanic and Space Sci., U. of Michigan, Ann Arbor, Mi., 48109, U.S.A., Email: anagy@umich.edu)

The ionospheres of the two terrestrial planets Venus and Mars are believed to have significant similarities. The composition and structure of the neutral upper atmospheres of both planets are CO<sub>2</sub> dominated and their temperatures are in the 200 to 300 K range. A great deal of direct information is available about the ionosphere of Venus, mainly from measurements obtained by instruments carried aboard the Pioneer Venus Orbiter. On the other hand, the only direct ionospheric data from Mars are the two vertical profiles obtained by the retarding potential analyzer carried aboard the Viking landers. A large number of one and multidimensional models have been developed to describe the ionospheric structure of both planets. The Venus models were reasonably well constrained by the measurements, while the Mars calculations were guided to a degree by analogies to Venus. In this talk the observational data base and the relevant model results are summarized and critically reviewed.

**GA4.10/E/05-A4 1005**

**STRUCTURE AND DYNAMICS OF THE MARTIAN IONOSPHERE**

Hiroyuki SHINAGAWA (Solar-Terrestrial Environment Laboratory, Nagoya University, Toyokawa 442-8507, Japan, email: sinagawa@stelab.nagoya-u.ac.jp)

The Mars Global Surveyor found that the surface magnetic field is likely to be smaller than about 5 nT, indicating that the solar wind interaction with Mars is similar to the solar wind-Venus interaction. This fact also suggests that the Martian ionosphere is filled with the solar wind-induced magnetic field, and that the magnetic field lines are transported downward in most of the dayside ionosphere. On the other hand, relatively large O<sub>2</sub><sup>+</sup> density in the topside ionosphere observed by the Viking spacecraft suggests that the ionospheric plasma should be transported upward. The observed electron density profiles of Mars also appear to be significantly different from those of Venus. Similarities and differences between the Martian ionosphere and the Venus ionosphere will be discussed based on our ionospheric MHD model of Mars. A few possible scenarios of structure and dynamics of the Martian ionosphere will be presented.

**GA4.10/L/05-A4 1040**

**VARIABILITY OF THE MARS THERMOSPHERE : MGS TRENDS AND MODEL INTERPRETATION**

S. W. BOUGHER (Lunar and Planetary Laboratory, University of Arizona, Tucson, AZ 85721; email: sbougher@lpl.arizona.edu); G. M. KEATING (George Washington University, NASA Langley, Hampton, VA 23681); J. R. MURPHY (New Mexico State University, Las Cruces, NM 88003); J. L. HOLLINGSWORTH (NASA Ames Research Center, Moffett Field, CA 94035)

Mars Global Surveyor (MGS) recently obtained coordinated lower-atmosphere (thermal and/or dust) measurements and simultaneous upper atmosphere accelerometer data (densities, scale heights, temperatures) yielding the first quantitative glimpse of the lower atmosphere processes driving Mars thermospheric variations during low to mildly dusty conditions and during a regional dust storm event [Keating et al. 1998]. In particular, measurements from the z-axis accelerometer (ACC) aboard MGS have provided to date more than ~1000 vertical structures of the Mars thermospheric density and derived temperature and pressure, as compared to only 3 previous in-situ profiles. These data have been obtained over two distinct Mars seasons spanning solar minimum to moderate conditions: (Phase I) 7-months approaching perihelion from southern Spring to early Summer (L<sub>s</sub> = 180 to 300), and (Phase II) 4.5-months near aphelion from northern Spring to early Summer (L<sub>s</sub> = 30 to 95). The sampling coverage (170 km to as low as 110 km over most latitudes, limited local times, and selected longitudes) has provided solar and seasonally driven variations to be monitored in the Mars thermosphere as a function of latitude, longitude, local time and altitude. Also, "deep atmosphere weather" patterns are visible at thermospheric heights, and may be composed of both stationary (fixed to surface features) and traveling planetary waves. Finally, the Noachis regional dust storm of late-1997 illustrated a global atmospheric expansion (contraction) with the onset (decay) of the storm consistent with lower atmosphere heating (cooling) and dust. Initial model studies have been conducted to simulate the Mars thermosphere variations and the lower atmosphere coupling observed by MGS measurements [Bougher et al. 1998]. The Mars Thermospheric General Circulation Model (MTGCM) (70-300 km) and the NASA Ames Mars General Circulation Model (MGCM) (0-90 km) have been crudely coupled for this purpose. Early simulations suggest that the mean solar cycle, seasonal-orbital, latitude, and diurnal variations of the Mars lower thermosphere (aerobraking altitudes) are generally reproduced. However, observed day-to-day variations over 100 to 130 km (especially longitude fixed variations) are not well modeled, owing to missing dynamical processes. Also, simulations have thus far not been able to reproduce the rapid thermal expansion or the global response of the Mars atmosphere to the Noachis event. An improved coupling scheme is needed linking the MGCM and MTGCM to address these "deep atmosphere weather" features.

**GA4.10/L/02-A4 1055**

**NEW ORBIT PLAN OF PLANET-B(NOZOMI) AND EFFECTS ON MARTIAN UPPER ATMOSPHERE STUDY**

K. TSURUDA, H. Hayakawa, and I. Nakatani (The Institute of Space and Astronautical Science, 3-1-1, Yoshino-dai, Sagami-hara, Kanagawa 229-8510, Japan)

Japanese Mars orbiter Nozomi(Planet-B) was launched on July 4th, 1998. The main scientific objective of Nozomi is to study the interaction of Martian ionosphere with the solar wind. For this purpose, the Nozomi spacecraft carries 14 scientific instruments and takes an elliptical orbit of low periaapsis altitude(150 km) and relatively large apoapsis distance of 15 Mars radii. The low periaapsis altitude is chosen to study the structure and dynamics of the ionosphere under the strong interaction with the solar wind and large apoapsis distance is employed to study the Martian tail region where the escaping ionospheric ions will be detected. Nozomi was supposed to arrive at Mars on October 11, 1999, but unfortunately one of the valve in the engine module did not open completely during its departure from the Earth orbit on December 20, 1999 and Nozomi had to use more propellant to compensate the shortage of the thrust. As this result, it becomes difficult for Nozomi to be captured in the planned Mars orbit in 1999. ISAS decided to take another orbit scenario for Nozomi. According to the new orbit plan, Nozomi takes three rotations around the sun, twice Earth swing bys and arrives at Mars in December 2003. The propellant budget is sufficient for this new orbit scenario and originally planned orbit at Mars can be accomplished. Effects of this delayed arrival at Mars on Mars upper atmosphere study and possible sciences during Nozomi's long cruising in the interplanetary space will be discussed.

**GA4.10/L/03-A4 1110**

**SOLAR WIND VARIABILITY OF THE MARTIAN HOT OXYGEN CORONA: DETECTION CAPABILITY OF PLANET-B**

Helmut LAMMER (Institute of Space Research, Austrian Academy of Sciences, Elisabethstrasse 20, A-8010 Graz, Austria, Email: helmut.lammer@oeaw.ac.at); Willibald Stumptner and Siegfried J. Bauer (both at Institute for Space Research, austrian Academy of Sciences and Institute of Meteorology and Geophysics, University of Graz, Halbaerthgasse 1, A-8010 Graz, Austria, Email: willibald.stumptner@oeaw.ac.at).

The Japanese Planet-B spacecraft will have the possibility to detect for the first time in-situ with the neutral mass spectrometer the suggested hot oxygen corona on Mars, if the corona number density is at least in the order of 10000 [cm<sup>-3</sup>]. Since the most important mechanism for the production of the hot oxygen atoms in the Martian exosphere is electron dissociative recombination of ionospheric molecular oxygen ions, we investigated the solar wind variability of this production mechanism. Results from the Viking and Mars Global Surveyor missions have been used for this study. The resulting influence of the corona number density distribution was calculated with a Monte Carlo technique.

The Monte Carlo technique is used to simulate the atomic diffusion process in the Martian atmosphere by simulating the collision probability, particle direction and energy loss after collisions with random numbers. Our results show that the detection capability of the hot oxygen corona by Planet-B requires periods of high solar activity, which should occur during the Planet-B measurement phase. However, in-situ-measurements of the hot oxygen number density would be important for adjusting atmospheric escape models, which is significant for evolution studies of the Martian atmosphere.

**GA4.10/W/24-A4 1125**

**STUDIES OF THE SOLAR WIND - MARTIAN ATMOSPHERE INTERACTION BY ESA'S MARS EXPRESS**

R. LUNDIN, S. Barabash and O. Norberg (Swedish Institute of Space Physics, Kiruna, Sweden)

Lacking a strong intrinsic magnetic field the planet Mars is continuously subject to atmospheric scavenging by the direct impact of solar wind plasma on the topside atmosphere. This scavenging process is known to be significant, depleting the present atmosphere at a rate corresponding to a total depletion in about 108 years. A possible source of replenishment, maintaining the existing atmosphere, may be subsurface deposits of volatiles. This also raises the question about the higher abundance of volatiles that existed in the past. Is the main reason for loss of the martian atmosphere and hydrosphere indeed due to the solar wind interaction? One important science objective of the ESA Mars-Express mission is to study the solar wind interaction with the martian atmosphere using a partly new measurement technique - energetic neutral atom (ENA) imaging. Combined with measurements of the ionospheric plasma outflow, the ENA technique will make it possible to study the outflow locally (plasma) as well as globally (ENA imaging). A determination of the net outflow of energetic neutrals from the martian upper atmosphere will also be provided by the ENA-technique. Altogether, the objective is to provide a much improved quantitative measure of the loss from the martian atmosphere.

**GA4.10/L/01-A4 1145**

**NUMERICAL SIMULATION OF MASS LOADING EFFECTS ON THE SOLAR WIND INTERACTING WITH THE MARS ATMOSPHERE**

Yu Yi (Department of Astronomy and Space Science, Chungnam National University, Daejeon, South Korea, E-mail: euyiyu@hanbat.chungnam.ac.kr), Jhoon Kim (Korea Aerospace Research Institute, Daejeon, South Korea, Email: jkim@viva.kari.ac.kr), Eojin Kim and Yong Ha Kim (both at Department of Astronomy and Space Science, Chungnam National University, Daejeon, South Korea, E-mails: ejkim@astro6.chungnam.ac.kr, yhkim@hanbat.chungnam.ac.kr).

A three-dimensional compressible magnetohydrodynamic simulation of solar wind interaction with the Martian atmosphere was carried out to investigate the influence of pick up ion mass loading on the global structure of Mars magnetosphere. The code used for a simulation of comet interacting with solar wind [Yi et al. 1996] was modified for this purpose. It was assumed that the neutral atmosphere consists of mainly oxygen atoms and carbon dioxide molecules, whose radial distribution profiles were modeled with a spherical symmetry. It was also assumed that the neutrals ionized by solar EUV contribute for mass loading on the solar wind. The simulation was able to produce the similar features of the interaction of solar wind with the Venus atmosphere such as the bow shock, the magnetopause and the magnetic tail boundary even though those values are weaker. The results were compared with results from pure gas dynamic simulations with and without the mass loading. The plasma and field measurements of NOZOMI, which is expected to arrive at Mars on October 1999, were predicted based on this simulation.

**GA4.10/P/03-A4 1200**

**EFFECTS OF MAGNETIC FIELD ON THE NIGHTSIDE IONOSPHERE OF MARS: SOLAR WIND - MARS INTERACTION**

S. A. HAIDER (Physical Research Laboratory, Ahmedabad 380 009, India, email: haider@prl.ernet.in; S. P. Seth (Bhavan's R. A. College of Science, Ahmedabad 380 001, India); Anil Bhardwaj (Space Physics Laboratory, Vikram Sarabhai Space Centre, Trivandrum 650 022, India).

Among the planets of solar system, our knowledge of magnetic field on Mars are not enough.



From the available data of magnetic field measurements onboard Mariner 4, Mars 2, 3, 5 and Phobos 2, several workers have reported that Mars has weak intrinsic magnetic field. Others have indicated that the Martian magnetic field is associated with interplanetary magnetic field. Recently, the Mars Global surveyor spacecraft has obtained magnetic field and plasma observations above 100 km. This observation suggests that solar wind interaction with Mars is in many ways similar to that of Venus, that is, primarily ionospheric-atmospheric interaction. To understand the solar wind - Mars interaction and its dynamical effect on the night-time ionosphere, a theoretical model has been developed to study ion and electron densities. In this model the production rates of  $N_2^+$ ,  $O_2^+$ ,  $O^+$  and  $CO_2^+$  in the nightside ionosphere of Mars are calculated using analytical yield spectrum approach due to ion transport from the dayside by analogy to Venus where horizontal plasma transport was found to be an important source of nightside ionosphere in absence of intrinsic magnetic field of the planet. Later these production rates were used in continuity and momentum equations for the calculation of ion and electron densities. In this model the magnetic field in the ionosphere is assumed purely induced and horizontal. It is found that the ion loss due to horizontal plasma motion in presence of induced magnetic field is an important process for all ions above 150 km. Below this altitude the ionosphere of Mars is controlled by chemical equilibrium condition.

**GA4.10/W/10-A4** 1215

#### MULTI-FLUID MHD STUDIES OF THE SOLAR WIND INTERACTION WITH MARS

Yifan LIU, A. F.Nagy, T. I. Gombosi, C. P. T. Groth, D. L. DeZeeuw and K. G. Powell (University of Michigan, Ann Arbor, MI., USA; e-mail: anagy@umich.edu)

The interaction of the solar wind with non magnetic planets, such as Mars and Venus, involves their ionospheres. Single fluid MHD models, which incorporate some of the important mass-loading processes, have been useful in reproducing a variety of the observed features at these planets, such as the location of the bow shock, for example, but they do have obvious limitations. In our continuing, step-by-step, effort to develop appropriate and comprehensive models to study all of the interaction processes, we are developing a multi-fluid MHD model, based on the so called BATS-R-US (Block Adaptive-Tree Solar-wind Roe-type Upwind Scheme) numerical code. Our present model is a two-fluid one, which considers hydrogen and atomic or molecular oxygen ions, separately. We have used this model to study the interaction processes at Mars. We present results for mass- loaded simulation studies; we have paid special attention to the fluxes of oxygen ions in the tail, in order to be able to make comparisons with observations.

**Thursday 22 July PM**

Presiding Chairs: A. Nagy (Dept. of Atmospheric, Ocean and Space Science, Univ of Michigan, USA), T.I. Gombosi (Univ. of Michigan, USA)

**UPPER ATMOSPHERES AND THEIR INTERACTIONS WITH THE SOLAR WIND. DUST AND NEUTRAL GAS INTERACTION WITH PLASMAS**

**GA4.10/W/33-A4** Invited 1400

#### HOW THE SOLAR WIND INTERACTION WITH WEAKLY MAGNETIZED PLANETS CAN AFFECT ATMOSPHERE EVOLUTION: WHAT WE KNOW AND DON'T KNOW

J.G. LUHMANN (Space Sciences Laboratory, University of California, Berkeley, CA 94720, USA, email: jgluhman@ssl.berkeley.edu); R.E. Johnson (Department of Engineering Physics, University of Virginia, Charlottesville, VA 22901, USA, email: rej@virginia.edu); S.H. Brecht (Bay Area Research, Orinda, CA 94563, USA, email: brecht@hooked.com)

We review current understanding of the processes by which planets like Mars and Venus may have lost substantial amounts of atmosphere because they had weak internal magnetic fields throughout much of their early history. These processes include atmospheric ion pickup, sputtering by the pickup ions, and charge exchange with solar wind ions, which have occurred in addition to photochemically mediated escape, impact erosion, and hydrodynamic escape. A major challenge confronting atmosphere evolution modelling is the lack of unambiguous constraints on many of the assumed conditions and parameters involved. We suggest work that can be done, including measurements, that would help us to narrow the range of possible evolutionary scenarios for such planetary atmospheres, and lead to a better evaluation of the solar wind's role.

**GA4.10/L/06-A4** Invited 1430

#### EFFECTS OF PLASMA MIXING PROCESSES ON THE SOLAR WIND INTERACTION WITH NON-MAGNETIZED PLANETS

T. TANAKA (Communications Research Laboratory, Koganei-shi, Tokyo 184-8795, Japan, email: tanaka@crl.go.jp)

The solar wind interaction with the ionosphere of non-magnetized planets is numerically simulated in the framework of 3-D magnetohydrodynamics (MHD) with a two-component plasma. In cases 1 and 2, solar extreme ultraviolet (EUV) flux values is set so the peak ionospheric plasma pressure is below and above the incident solar wind dynamic pressure. While the formation of the bow shock and the magnetic barrier in the upstream region is seen in both cases, a clear formation of the ionopause is seen only in case 2.

In case 1, the interplanetary magnetic field (IMF) penetrates from the magnetosheath to the dayside ionosphere so as to adjust the ionospheric total pressure. Penetrating IMF affects the vertical motion of the ionospheric plasma. However, formation process of the ionotail is little affected by the penetrating IMF. In both cases 1 and 2, partial penetration of the IMF occurs from the magnetic barrier to the terminator ionosphere. The penetrated magnetic field emerges in the ionohole on the nightside. This nonideal MHD process characterized by the penetration of flowing magnetized plasma into non-magnetized plasma plays a principal role in the mixing interaction between the solar wind and the planetary ionosphere.

**GA4.10/W/30-A4** 1450

#### WIND ENHANCED ESCAPE, ION PICKUP AND THE EVOLUTION OF WATER ON MARS

R. E. HARTLE and H. G. Mayr (NASA-Goddard Space Flight Center, Greenbelt, MD Email: hartle@carioca.gsfc.nasa.gov)

Preferential loss of hydrogen over deuterium from Mars has produced a deuterium rich atmosphere possessing a D/H ratio 5.2 times that of terrestrial water. Rayleigh fractionation is applied, constrained by the deuterium enrichment factor, to determine the magnitudes of ancient and present water reservoirs on the planet. The dominant loss mechanisms of H and D from the current atmosphere are thought to be thermal escape and solar wind ion pickup of the neutral and ion forms of these constituents, respectively. During an earlier Martian epoch, only thermal escape was significant because Mars had a terrestrial sized magnetosphere that

protected the atmosphere from solar wind scavenging processes. The magnitudes of present and ancient water reservoirs are estimated when thermal escape is considered alone and subsequently when the effects of ion pickup are added. The escape fluxes of H and D are significantly increased above the respective Jeans fluxes when the effects of thermospheric winds and planetary rotation are accounted for at the exobase. Such wind enhanced escape also increases as the mass of an escaping constituent increases; thus, the increase in the escape flux of D is greater than that of H. When the fractionation process is also constrained by the D/H ratio observed in hydrous minerals of SNC meteorites, an ancient crustal reservoir of Martian water is derived, tens of meters in global-equivalent depth, considerably exceeding that obtained with no winds. The reservoir becomes even larger when ion pickup processes are added.

**GA4.10/W/04-A4** 1505

#### 2D HYBRID SIMULATIONS OF THE SOLAR WIND INTERACTION WITH MERCURY

M.HOPCROFT, S.C.Chapman (University of Warwick, Coventry, UK)

The results of an investigation into the interaction of the super-magnetosonic solar wind flow around Mercury, and the planet as a field and plasma source are presented. We wish to identify the key processes of energy momentum transfer that results in the global magnetospheric structure observed. Mercury is of particular interest as the typical gyroradius of its pick-up ions is slightly larger than the planet itself, and so of the order of the characteristic scale of the magnetosphere.

The investigation was conducted by means of 2D hybrid numerical simulations which represent spatial coordinates in two dimensions whilst resolving three dimensional fields, velocities and bulk plasma vector variables. The hybrid scheme represents ion velocity distributions with computational particles advanced via the Lorentz force law, and the electrons via fluid equations where the inertial term has been neglected, the plasma is quasineutral. The source region consists of an inner dense core and an outer halo, to represent thermal and particle sputtered populations respectively. We examine the relative importance of these regions and the effect of including the planets' intrinsic magnetic field.

**GA4.10/W/29-A4** 1520

#### MAGNETOHYDRODYNAMIC SIMULATIONS OF THE VARIABILITY OF THE MARS BOW SHOCK

Eojin KIM, Yu Yi, and Yong Ha Kim (all at Department of Astronomy and Space Science, Chungnam National University, Daejeon, South Korea, e-mail: ejkim@astro6.chungnam.ac.kr, euyiyu@hanbat.chungnam.ac.kr, yhkim@hanbat.chungnam.ac.kr), Jhoon Kim (Korea Aerospace Research Institute, Daejeon, South Korea, Email: jkim@viva.kari.re.kr )

To investigate the variability of the Mars bow shock, a three-dimensional numerical magnetohydrodynamic simulations of solar wind interaction with Martian atmosphere were performed. In this calculation, a neutral atmospheric model was assumed as a source of mass loading ions. Only photoionization due to solar radiation was provided as an ionization mechanism. The neutral atmosphere was modeled with the oxygen and carbon dioxide cloud. The simulation produced the global features of the interaction of solar wind with the atmosphere of unmagnetized planet such as the weak bow shock and the magnetic barrier. The influences of different values of solar wind parameters such as density, velocity and the interplanetary magnetic field were considered to study the changes of Martian global structure due to those variations. In addition, several Martian atmospheric neutral oxygen density distribution profile models were tested. The best-fit parameters of solar wind and the variables of the neutral density distribution model were found to match the bow shock positions distances observed by the previous Mars exploration spacecraft.

**GA4.10/W/22-A4** 1600

#### GENERATION AND TRANSPORT OF DUSTY PLASMAS IN THE ENVIRONMENT OF OUTER PLANETS

Mihaly HORANYI (Laboratory for Atmospheric and Space Physics, University of Colorado, Boulder, CO 80309-0392)

During the Voyager, Ulysses and Galileo missions we learned to appreciate the importance of electromagnetic effects on charged dust in the Solar System. Planetary rings are examples where the orbital evolution of small dust grains can be strongly coupled to the plasma environment.

There are many exciting phenomena associated with the interaction of magnetospheric fields and plasmas with the embedded dust grains. Lorentz resonances, gyrophase-drifts due to compositional and/or plasma density and/or plasma temperature gradients, transport due to charge or magnetic field fluctuations, shadow resonance and the coupling between radiation pressure and electrodynamic forces, for example, might all contribute to shaping the fine dust distribution in planetary rings. The dust becomes an integral component of the magnetosphere since it acts as a source/sink of the plasma. The produced low energy photo and secondary electrons or the sputtered off ions might significantly alter the magnetospheric plasma distribution, for example. Though many of these processes are now recognized, dusty planetary magnetospheres still hold surprises.

In this talk I will summarize our understanding of dusty plasma generation and transport at Jupiter and show that similar effects are also expected to shape the fine dust distribution in the magnetosphere of Saturn.

**GA4.10/W/21-A4** 1620

#### LOW LATITUDE JOVIAN X-RAY EMISSION FROM SCATTERING AND FLUORESCENCE OF SOLAR X-RAYS

Ahilleas N. MAURELLIS (Atmospheric Photophysics Group, FOM-Institute, AMOLF, Amsterdam, The Netherlands, email: ahilleas@amolf.nl) Thomas E. CRAVENS (Dept. of Physics and Astronomy, University of Kansas, Lawrence, KS, 66045, USA, email: cravens@kupas.phsx.ukans.edu); G. R. Gladstone and J. H. Waite, Jr. (Dept. of Space Science, SWRI, San Antonio, TX, USA)

X-ray emission from Jupiter's equatorial region has recently been observed (Waite et al., 1997). X-ray emission from Jupiter's auroral region was previously observed by the Einstein and ROSAT X-ray observatories (Metzger et al., 1983; Waite et al., 1994). Both the estimated total auroral X-ray power and the total low-latitude X-ray power are on the order of 1 GW. The X-rays emitted from Jupiter are primarily "soft" X-rays with energies of up to a few hundred eV. One mechanism proposed for the auroral emission is heavy (mainly sulfur and oxygen) ion precipitation followed by line emission from highly excited, high charge state ions (Waite et al., 1994; Cravens et al., 1995). Waite et al. (1997) further suggested that the X-ray emission at low latitudes may also be explained by heavy ion precipitation, although the ions would originate in this case in the inner magnetosphere of Jupiter rather than in the middle magnetosphere. In this paper we explore alternative mechanisms for the observed low-latitude

X-ray emission related to scattering of solar X-rays photons: (1) scattering by H<sub>2</sub> molecules, (2) fluorescent carbon K-shell scattering. (The carbon atoms are contained in the methane molecules located below the homopause). Our preliminary intensity estimates are about a factor of 10 less than the observed low-latitude intensities but many uncertainties are present in the calculations and are now being re-examined. Observations have shown that jovian X-ray emission is: (1) at a maximum in the subsolar region; (2) correlated in time with total solar X-ray emission (Gladstone et al. 1998), both of which are expected in a situation where solar photon scattering and fluorescence mechanisms are complementary to that of heavy ion precipitation in the production of equatorial X-ray emission.

**GA4.10/W/32-A4 1635**

**AURORAL AND SATELLITE FOOTPRINT EMISSIONS AT JUPITER AND SATURN**

J.H. WAITE, Jr., T. Majeed, G.R. Gladstone (all at SwRI, San Antonio TX 78228, USA, e-mail: hunter@kronos.space.swri.edu); J.T. Clarke (University of Michigan, Ann Arbor MI 48109, USA); J. Comerney (GSFC, Greenbelt MD 20771, USA); D. Grodent, J.-C. Gerard (both at University de Liege, B-4000 Liege, Belgium); S. Bolton (JPL, 4800 Oak Grove Dr., Pasadena CA 91109, USA); B. Mauk (APL, Laurel MD 20723, USA); R. Walker (UCLA, Los Angeles CA 90095, USA)

Two events have dramatically increased our ability to observe auroral emissions from the outer planets. The first was the detection, in 1988, of strong near-IR emissions from H<sub>3</sub><sup>+</sup> in Jupiter's auroral zone, which provided a sensitive means of probing the auroral ionospheres of the outer planets with ground-based telescopes. The second event was the deployment in 1990 of the Hubble Space Telescope, whose instruments have acquired increasingly high-resolution data on the FUV auroras of Jupiter and Saturn. Observations of FUV emissions with HST and of H<sub>3</sub><sup>+</sup> emissions from the ground have, in particular, led to significant advances in our knowledge of the jovian aurora, which, because of its brightness, has been the primary target of outer planet auroral observations. Spectroscopic data on H<sub>3</sub><sup>+</sup> emissions in the near-IR regime and on H<sub>2</sub> band emissions at FUV wavelengths have yielded important new inputs for models of the thermal structure of Jupiter's auroral atmosphere, while imaging of the H<sub>3</sub><sup>+</sup> and FUV auroras has provided a detailed picture of the morphology of the auroral emissions, revealing their probable local-time and System III dependencies and responsiveness to solar wind as well as corotational influences. Emissions associated with the footprints of Io and Ganymede have also been identified. We review recent observations of jovian H<sub>3</sub><sup>+</sup> and FUV emissions and discuss their implications for our understanding of jovian aeronomy and of magnetosphere-ionosphere coupling in the Jupiter system. We conclude with a comparative look at Saturn's FUV aurora.

**GA4.10/W/28-A4 1655**

**INTERACTION OF FLUX TUBE ELECTRONS WITH IO'S ATMOSPHERE**

Marykutty MICHAEL and Anil Bhardwaj (Space Physics Laboratory, Vikram Sarabhai Space Centre, Trivandrum 695022, India, email: spl\_vssc@vssc.org)

During its flyby in December 1995 Galileo passed within 1000 km of Io through its wake region. The Galileo plasma analyzers revealed the presence of a dense ionosphere of density 40000 electrons per cc. The energetic particle detector observed an intense, bi-directional, magnetic field-aligned beam of electrons of energy greater than 15 keV. These electrons may mirror and return in the vicinity of Io and may impact its atmosphere. A Monte Carlo model has been constructed to study the interaction of these high energy electrons with the neutral species present in the Io's atmosphere. The intensities of neutral O and S ultraviolet emissions resulting from the energetic electron impact on the atmospheric gases of Io are calculated and will be compared with the observed intensities particularly from the Hubble Space Telescope. Implications of the model for the ionization of the Io's atmosphere will also be discussed.

**GA4.10/W/19-A4 1710**

**THE INTERACTION OF IO AND EUROPA WITH JUPITER'S MAGNETOSPHERE**

Arvydas J. KLIORE, Aseel Anabtawi (Jet Propulsion Laboratory, California Institute of Technology, Pasadena, CA 91109, USA, e-mail: akliore@jpl.nasa.gov); Tamas Gombosi (Space Physics Research Laboratory, University of Michigan, Ann Arbor, MI 48109, USA, e-mail: tamas@umich.edu)

The Galileo orbiter has provided radio occultation measurements of the electron density profiles of the plasma surrounding Io and Europa. There have been six occultations of Io, providing twelve electron density profiles at various locations relative to the ram direction of the impinging particles of the Jupiter magnetosphere on Io, and eight profiles on Europa. The two satellites were found to have very different plasma environments, with Io having a proper ionosphere produced on top of an endogenous SO<sub>2</sub> atmosphere by magnetospheric particle precipitation and solar EUV, while Europa has a tenuous plasma environment produced by the same mechanisms from an oxygen atmosphere itself also produced by sputtering of water ice from its surface by impinging magnetospheric particles. In both cases the observed electron density profiles are highly asymmetrical, with a compressed profile on the ram side, and an extended one on the wake side. The presence of several measurements for each satellite at different ram-to-wake directions provided data for estimating an approximate distribution of ionization from the ram direction to the wake direction, which were compared with the results of MHD simulations.

**GA4.10/W/27-A4 1725**

**CARBON EMISSIONS IN COMETS: PREDICTION FOR ROSETTA**

Anil BHARDWAJ (Space Physics Laboratory, Vikram Sarabhai Space Centre, Trivandrum 695022, India, email: spl\_vssc@vssc.org); S.A. Haider (Physical Research Laboratory, Ahmedabad 380009, India)

Several emissions of carbon atoms in neutral (Cl 156.7 nm, 165.7 nm, 193.1 nm) and ionized (CII133.5 nm) forms have been observed in comets. These emissions can be produced by various mechanisms, like, resonant scattering of solar radiation by carbon atom/ion, solar photon and electron impact dissociative excitation of major carbon containing species (viz., CO and CO<sub>2</sub>), electron impact excitation of C. The knowledge about the relative contribution from each of these mechanisms provide unique information regarding the physical and chemical processes occurring in the cometary coma. The Cl 193.1 nm emission is unique in the sense that it arises from a transition in carbon atom that leaves the C in the metastable 1D state: suggesting that a large fraction of carbon in cometary coma reside in the metastable form. A coupled chemistry-transport model in conjunction with an efficient emission production code is used to study the chemistry of C(1D) atoms and the production of Cl 193.1 nm emission in the coma of comet P/Wirtanen: the target of the ROSETTA mission. The model calculations and predicted intensity of the Cl 193.1 nm emission will be presented and its implications for the carbon budget will be discussed.

**THE OUTER PLANETS MAGNETOSPHERE**

**GA4.10/E/02-A5 Invited 0900**

**THE DYNAMICS OF JUPITER'S MAGNETOSPHERE**

Vytis M. VASYLIUNAS (Max-Planck-Institut fuer Aeronomie, D-37191 Katlenburg-Lindau, Germany, e-mail: vasyliunas@linmpi.mpg.de)

Plasma in the magnetosphere of Jupiter is predominantly injected deep within the magnetosphere and lost by outward transport. This simple fact implies the existence of most of the important processes of Jovian magnetospheric dynamics without by itself specifying their properties: plasma transport by interchange motions within the closed magnetic field region, reconnection of the magnetic field in the magnetodisc, ultimate loss of plasma down the magnetotail must all occur, but their driving mechanisms as well as their spatial and temporal scales remain largely uncertain or even unknown. I review the evolution of our ideas on these processes, the impact of observations from Galileo, and recent developments particularly concerning internal or external drivers and possible analogies to the magnetosphere of Earth.

**GA4.10/W/15-A5 0930**

**LOCAL TIME ASSYMETRIES IN THE MAGNETOSPHERE OF JUPITER**

KRISHAN K. KHURANA (Institute of Geophysics and Planetary Physics, UCLA, Los Angeles, CA 90095, USA)

We have used magnetic field data from the Real Time Science (RTS) mode of Galileo (resolution of 24 sec. or better) and the very low-resolution data from the Memory Read Out (MRO) of the MAG instrument (resolution 32 minutes) to study the configuration of Jupiter's magnetosphere. We show that in the middle magnetosphere (radial distance between 40 and 90 R<sub>J</sub>), the field line sweepback is larger in the dawn magnetosphere compared to its value in the midnight and dusk sectors. We will show that these differences correspond to much larger radial currents in the dawn sector compared to their value in the midnight sector of the magnetosphere. By using current continuity, we will calculate the field-aligned current strengths and identify their sources in the magnetosphere.

Observations of the current sheet structure show that the current sheet crossing times are less delayed in the midnight and dusk sectors compared to the delays observed in the dawn sector. We will show that the current sheet is warped mainly by the effect of the solar wind flow on the magnetotail and not by the action of centrifugal forces on the plasma. We will present a new model of the structure of the current sheet that can predict the current sheet crossings with an accuracy of ~ 15 degrees in longitude. Finally, we show that the current sheet is much more disordered in the mid-night and dusk sectors compared to a relatively organized current sheet encountered in the dawn sector. Sources responsible for this asymmetry will be explored.

**GA4.10/E/06-A5 Invited 0945**

**MAGNETIC RECONNECTION IN THE JOVIAN MAGNETOSPHERE**

Raymond J. WALKER (Institute of Geophysics and Planetary Physics, University of California at Los Angeles, Los Angeles CA, 90095-1567, USA, email: rwalker@igpp.ucla.edu)

Magnetic reconnection is widely thought to be responsible for driving flows within the Earth's magnetosphere. In this paper we will consider the effects of magnetic reconnection within Jupiter's magnetosphere. Plasmas rotate with the planet throughout much of Jupiter's magnetosphere. However, the oppositely directed magnetic field in the Jovian magnetic tail is expected eventually to reconnect across the current sheet, allowing plasma produced near Jupiter to escape tailward. We will use observations from the Galileo spacecraft and global magnetohydrodynamic simulations to investigate the conditions under which reconnection becomes important at Jupiter. Reconnection between the interplanetary magnetic field (IMF) and the Earth's magnetic field at the dayside magnetopause is followed by reconnection within the magnetotail. At Jupiter our simulations indicate that reconnection caused by inertial effects can occur in the magnetotail even when there is no dayside reconnection. We will investigate the effects of the IMF on the reconnection in Jupiter's magnetotail. Initial calculations indicate that for northward IMF the tail neutral line moves toward Jupiter and drives stronger flows than without an IMF.

**GA4.10/W/02-A5 1005**

**COMPARISON OF THE AZIMUTHAL FIELD COMPONENTS MEASURED DURING FLY-BYS OF JUPITER: PIONEER, VOYAGER AND ULYSSES OBSERVATIONS**

E.J.BUNCE and S.W.H.Cowley (Department of Physics and Astronomy, Leicester University, UK)

Distortions of the jovian magnetic field out of meridian planes result from magnetospheric interactions with both the solar wind and the planetary ionosphere, each giving different dependencies on distance and local time. Here we will compare fly-by data from the Pioneer, Voyager and Ulysses spacecraft, as well as data from the Galileo orbiter as it becomes available, to examine the spatial variability of the azimuthal field component produced by these distortions, and to consider the implications for large-scale jovian magnetospheric dynamics. In the case of the azimuthal field perturbation which is due to magnetosphere-ionosphere coupling, the data will also be used to make an estimate of the effective value of the Pederson conductivity of Jupiter's ionosphere. This estimate requires use of magnetic models to map field lines between the spacecraft and the ionosphere.

**GA4.10/W/08-A5 1020**

**JOVIAN CURRENT SHEET STRESS BALANCE AND MASS DENSITY**

C. T. RUSSELL, K. K. Khurana and M. G. Kivelson (All at Institute of Geophysics and Planetary Physics, University of California, Los Angeles, CA 90095-1567, USA, email: crussell@igpp.ucla.edu); D. E. Huddleston (Hughes Space and Communications Company, El Segundo, CA, USA); J. A. Ansher, D. A. Gurnett and W. S. Kurth (All at University of Iowa, Iowa City, IA, USA); D. J. Williams (Johns Hopkins University, Applied Physics Laboratory, Laurel, MD, USA)

In the middle magnetosphere the magnetic and plasma pressure forces dominate the forces associated with rotation and the magnetosphere remains quasi dipolar. Beyond about 24 R<sub>J</sub> in the Galileo epoch, the magnetosphere becomes disk-like with a thin central current and stretched lobes above and below at all local times. Estimates of the balance of forces indicate that this is the region where the centrifugal force dominates over the particle forces. We can use the magnetic measurements to estimate these various forces under simplifying assumptions and from those estimates deduce a value for the 'cold' mass of the magnetodisc

plasma. Herein we compare those estimates with the density deduced from the electron plasma frequency found from the plasma wave measurements and compare plasma pressure estimates with those observed.

**GA4.10/W/26-A5 1035**

**PLASMA SHEET DYNAMICS IN THE JOVIAN MAGNETOTAIL: EVIDENCE FOR SUBSTORM-LIKE PROCESSES**

J. WOCH, N. Krupp, S. Livi and B. Wilken (all at: Max-Planck-Institut für Aeronomie, D-37191 Katlenburg-Lindau, Germany, email: woch@linmpi.mpg.de); K.K. Khurana and M.G. Kivelson (both at: Institute of Geophysics and Planetary Physics, University of California Los Angeles, CA, USA) A. Roux and S. Perraut (both at: Centre d'Etude des Environnements Terrestre et Planétaires, Vélizy, France) P. Loarn (CESR, Université Paul Sabatier, Toulouse, France) A. Lagg and D.J. Williams (both at: The Johns Hopkins University Applied Physics Laboratory, Laurel, MD, USA)

During Galileo's orbit G2 in 1996 the Energetic Particles Detector (EPD) onboard the spacecraft detected a number of particle bursts with large radial/antisunward anisotropies in the distant Jovian magnetotail [Krupp et al., 1998]. The bursts were embedded in predominantly corotating plasma. They showed a tendency to reoccur every 2 to 3 days. In this letter we focus on a detailed analysis of one of the bursts. Prior to the onset of the burst particle fluxes at low energies increase over several hours. The end of this plasma loading phase coincides with the detection of a flux rope like signature in the magnetic field evidenced by a bipolar excursion of the north-south component together with a strong core field. After the passage of the flux rope the plasma sheet has thinned considerably. At the boundary of the thin plasma sheet and in the lobe regimes strong wave emissions in the 100 Hz range are detected. Accelerated/heated ion beams first from the Jovian direction later from the tail direction are seen at the plasma sheet and lobe interfaces. The event is tentatively interpreted as a substorm-like process, where the magnetotail is internally driven unstable by mass-loading of magnetic flux tubes.

**GA4.10/W/03-A5 Invited 1110**

**TRANSPORT OF ENERGETIC CHARGED PARTICLES IN JUPITER'S MAGNETOSPHERE**

B. H. MAUK (The Johns Hopkins University Applied Physics Laboratory, 11100 Johns Hopkins Road, Laurel, Maryland 20723-6099; 240-228-6023; Fax: 240-228-6670; email: Barry.Mauk@jhuapl.edu)

The magnetospheres of Jupiter and Earth are representative of two extremes in the behaviors of the space plasma environments surrounding magnetized planets. Earth's magnetosphere is extremely dynamic because it is powered by its strong interactions with the highly variable interplanetary/solar wind environment. It is no surprise, then, that the transport of energetic particles within the Earth's magnetosphere is associated largely with dynamic "storm" and "substorm" processes that are caused by the solar wind interactions. Jupiter's magnetosphere, in contrast, is powered predominantly by the "rock-steady" planetary rotations. The processes that give rise to dynamics within Jupiter's magnetosphere are largely unknown, and the predominant mechanisms that cause the transport of energetic particles and other plasmas with Jupiter's magnetosphere are not established. During the Voyager era, researchers focused much attention on the so-called interchange instability as a cause of transport within the inner magnetosphere. Signatures of transport within the more distant magnetospheric regions included the so-called magnetospheric wind. More recently, new transport signatures have been identified that appear to have some similarities to Earth-magnetospheric dynamic events. There are speculations about possible roles for the interplanetary environment in either powering or stimulating some of the transport. Here we review the history and the status of our understanding the transport of energetic particles within the Jovian magnetosphere. Recent findings from the Galileo spacecraft are emphasized.

**GA4.10/W/01-A5 1130**

**PROPERTIES OF GANYMEDE'S MAGNETOSPHERE AS REVEALED BY ENERGETIC PARTICLE OBSERVATIONS**

D. J. WILLIAMS, B. Mauk, and R. W. McEntire (Johns Hopkins Applied Physics Laboratory, Laurel, MD 20723, USA)

Abstract energetic particle observations made during the Galileo satellite's close encounters with Jupiter's moon Ganymede provide a measure of many characteristics of Ganymede's magnetosphere, a magnetosphere larger than that of Mercury. Changes in energetic ion anisotropy signatures, caused by Jupiter's corotating magnetic field, show that Ganymede's magnetosphere significantly slows down the ambient nearly-corotating Jovian plasma. The data further indicate that this convection slow-down apparently extends at least several Jupiter radii away from Ganymede along Jovian field lines connected to the moon. The locations of these anisotropy signature changes occur at the locations of magnetometer and plasma wave magnetopause identifications that match surprisingly well the predictions of a simple model comprised of an intrinsic dipole field superimposed on Jupiter's ambient field. Loss cones measured throughout Ganymede's magnetosphere provide a quantitative estimate of the moon's surface magnetic field along the sub-satellite track that agrees well with model field predictions and provides verification of Ganymede's intrinsic magnetic field. On Jovian field lines connected to Ganymede, electrons are trapped between the moon and a near-Jupiter mirror point for several bounces as they convect across Ganymede's magnetosphere. This unique geometry allows a measurement of the amount of electron pitch angle scattering occurring in a single bounce between the Ganymede and near-Jupiter mirror points. The energy-dependent pitch angle diffusion coefficient and scattering lifetimes have been extracted from these observations. The consistency of these results from encounter to encounter demonstrates the stability of these processes, at least over the several month interval between encounters. Evidence for loss cone signatures established one Jovian rotation (~10 hours) earlier indicates that the entire Jovian L-shell region traversed by Ganymede provides an electron scattering environment similar to that measured on Jupiter-Ganymede field lines. Measurements from Galileo's last close encounter with Ganymede show electron pitch angle distributions characteristic of particles trapped on closed magnetic field lines in a distorted magnetospheric configuration. Thus with its distorted magnetic field and apparent radiation belt, Ganymede takes its place as a unique member of the solar system family of magnetospheres.

**GA4.10/W/16-A5 1145**

**ENERGETIC HEAVY IONS IN JUPITER'S MAGNETOSPHERE**

N. MURPHY (Jet Propulsion Laboratory, 4800 Oak Grove Dr., Pasadena, CA 91109, USA) C.M.S. Cohen and E.C. Stone (California Institute of Technology, 1201 E. California Blvd., Pasadena CA 91125)

The Galileo spacecraft penetrates deeply into the Jovian magnetosphere on each of its orbits, thus allowing a far more extensive survey of inner and middle magnetospheric processes than

previously available. The spacecraft carries a suite of magnetospheric instruments, with the Heavy Ion Counter (HIC) providing information about the fluxes of energetic heavy ions in the energy range of 6 to 200 MeV/amu, and species from carbon through iron.

Ions in the HIC energy range provide useful diagnostics of many magnetospheric processes, including particle transport and absorption by moons. We will examine the variability of ion fluxes and pitch angle distributions over the HIC energy range between 9 and 20 R<sub>J</sub>, in an attempt the shed light on the complex nature of Jupiter's magnetosphere. In particular we will examine the effects of Europa on the local particle distributions and estimate the rate of inward radial diffusion.

**GA4.10/W/25-A5 1200**

**AURORAS ON THE OUTER PLANETS**

Anil BHARDWAJ (Space Physics Laboratory, Vikram Sarabhai Space Centre, Trivandrum 695022, India, e-mail: spl\_vssc@vssc.org); G. Randall Gladstone (Southwest Research Institute, San Antonio, TX 78238, USA, email: randy@whistler.space.swri.edu)

Auroras are emissions occurring at high latitudes of a planet resulting from the precipitation of energetic charged particles from the planets magnetosphere. Auroral emissions from the outer planets have been observed from ground, Earth-orbiting satellites, flyby spacecraft, and orbiter-based instruments at X-ray, UV, visible, IR, and radio wavelengths. The UV, visible, and IR auroras are atmospheric emissions, produced or initiated when ambient atmospheric species are excited by the precipitating particles, whileradio and X-ray auroras are beam emissions, produced by the precipitating species themselves. The emissions at different wavelengths provide unique and complimentary information, accessible to remote sensing, about the key physical processes operating in the atmospheric and magnetospheric regions where they originate. This paper will discuss our current understanding of the auroral emissions on Jupiter, Saturn, Uranus, and Neptune as revealed by through multi-spectral observations and supplemented by plasma measurements. A qualitative picture of the energetics and morphology of the aurora on the outer planets will be presented.

**GA4.10/W/35-A5 1215**

**THE ENERGY BALANCE IN SATURN'S MAGNETOSPHERE**

J. D. RICHARDSON (M.I.T., Center for Space Research, 37-655, Cambridge, MA, USA, 02139)

Recent observational and modelling work shows that Saturn's inner magnetosphere is dominated by neutrals. We review recent HST observations and the implications of these observations. Then we extend this work by looking at the energy balance for the plasma. Energy is lost via radiation and gained via ionization of neutrals, with coulomb collisions also important. Observations show that both electron and ion temperatures decrease towards Saturn, suggesting that the ion temperatures are driven by the pickup process. This study discusses how well "neutral theory" predicts observed temperatures and where additional energy source and losses are needed and speculates on what these might be.

**GA4.10/W/18-A5 1230**

**ION DISTRIBUTIONS IN SATURN'S MAGNETOSPHERE NEAR TITAN**

S. A. LEDVINA, T. E. CRAVENS (University of Kansas, Department of Physics and Astronomy, Lawrence, KS 66045, USA, email: cravens@kuplas.phsx.ukans.edu); K. Kecskemeti (KFKI Research Institute for Particle and Nuclear Physics, H-1525 Budapest, Hungary)

Titan possesses an extensive atmosphere consisting of mainly molecular nitrogen and methane. These neutrals are ionized by photoionization and electron impact ionization forming an extensive ionosphere. At the time of the Voyager encounter Titan was found to be within Saturn's magnetosphere. Saturn's magnetospheric plasma impinges on Titan with a flow speed of about 120 km / s. The plasma analyzer on the Voyager 1 spacecraft detected H<sup>+</sup> and N<sup>+</sup> ions in the near-Titan wake with temperatures of about 200 eV and 2.9 keV, respectively [Hartle et al., 1982]. These ions will have gyroradii comparable to Titan's size [Luhmann et al., 1996], which has interesting consequences for the plasma interaction with that body. We numerically determine the trajectories of several thousand ions in the vicinity of Titan using for the required electric and magnetic fields the output from a three-dimensional MHD model of Titan. The MHD model is an improved version of the earlier model [Ledvina and Cravens, 1998], and includes ionospheric processes such as ion production, ion-neutral friction and dissociative recombination. We have calculated velocity space distributions of both pick-up and ambient ions using the numerically determined ion trajectories. These results are statistically analyzed to provide insight into the external plasma interaction with that satellite as well as to make predictions for the Cassini Orbiter particle experiments.

Friday 23 July PM

Presiding Chairs: K. Khurana (Univ. of California, Los Angeles, USA), R. Walker (Univ. of California, Los Angeles, USA)

**MAGNETOSPHERE MOON INTERACTIONS. WAVES AND INSTABILITIES**

**GA4.10/W/17-A5 Invited 1400**

**PLASMAS NEAR THE GALILEAN MOONS**

W. R. PATERSON and L. A. Frank (Both at: Department of Physics and Astronomy, The University of Iowa, Iowa City, IA, USA, email: paterson@iowasp.physics.uiowa.edu)

The Galilean moons offer unique and exciting environments for studies of plasma processes. Measurements from the Galileo plasma instrumentation (PLS) reveal features of the interactions that occur as magnetospheric plasmas encounter each of the major satellites. Io's wake is found to have a dense ionosphere threaded with beams of electrons, and the flanks of the interaction region exhibit pickup hydrogen and other ions. Europa's contribution to the plasmas of the torus can now be quantified because pickup from its atmosphere and the entrainment of ions from the ionosphere are directly measured. The interaction at Ganymede is seen to be complex with a significant energy flux of electrons into the polar regions, an outflow of protons, and a system of currents carried by electron beams. Observations near Callisto show the presence of ions sputtered from the surface. In this presentation we review the observations and discuss recent results.

**GA4.10/E/04-A5 1420**

**POPULATING JUPITER'S MIDDLE AND OUTER MAGNETOSPHERE FROM THE IO TORUS**

R.L. RICHARD (Institute of Geophysics and Planetary Physics, University of California at Los



Angeles, Los Angeles, CA 90095 USA); R.J. WALKER (Institute of Geophysics and Planetary Physics, University of California at Los Angeles, Los Angeles, CA 90095 USA); M. Ashour-Abdalla (Institute of Geophysics and Planetary Physics and Department of Physics and Astronomy, University of California at Los Angeles, Los Angeles, CA 90095 USA); T. Ogino (Solar Terrestrial Environment Laboratory, Nagoya University, Toyokawa, Japan)

Jupiter's magnetosphere is thought to be populated by plasma whose ultimate source is the volcanically active moon Io. We have calculated the trajectories of ions from this inner magnetospheric source in electric and magnetic fields from global magnetohydrodynamic (MHD) simulations of the magnetosphere and its interaction with the solar wind. The MHD simulations show how the properties of Jupiter's magnetosphere depend on interplanetary magnetic field (IMF) conditions and the Io source. The ion trajectories allow us to evaluate the importance of physics not included in the MHD model such as non-adiabatic particle motion. We investigate how these ions populate the system by launching heavy ions from the inner magnetosphere and following them until they leave the simulation system, strike the inner boundary of the simulation or become trapped.

**GA4.10/W/06-A5 1435**  
**ENERGETIC ELECTRON BEAMS AND TRAPPED ELECTRONS AT IO**

D J WILLIAMS1, R. M. Thorne2 and B. Mauk1 (Johns Hopkins University Applied Physics Laboratory Laurel, MD 20723-6099, USA), 2(University of California, Los Angeles Department of Atmospheric Sciences Los Angeles, CA 90095-1565, USA)

We present results from a continuing study of the magnetic field-aligned energetic electron beams and accompanying trapped electron distributions discovered during the Galileo satellite's passage through Io's cold, dense, low-speed wake on 7 December 1995 (Williams et al., 1996). A companion paper by Thorne et al. (1998) presents an analysis and explanation of the evolution of the electron pitch angle distributions measured on approach to Io and describes the resulting energetic electron flow paths and adiabatically "forbidden" regions expected to exist around Io. In Io's wake only bi-directional, field-aligned electron beams are seen--no ion beams are observed. At energies >~15 keV, the measured beams represent an energy flow of ~0.03 ergs cm<sup>-2</sup> s<sup>-1</sup> and if they penetrate Jupiter's atmosphere, can provide an energy deposition of ~15 ergs cm<sup>-2</sup> s<sup>-1</sup> at the foot of the Io flux tube. This is sufficient to stimulate observable aurora in Jupiter's atmosphere. Extrapolating the measured spectra to lower energies yields much higher values (eg. ~10<sup>4</sup> ergs cm<sup>-2</sup> s<sup>-1</sup> at 0.25 keV). The angular width of the measured trapped-like electron distributions is independent of energy and varies across Io's wake in a manner consistent with the measured magnetic field variation. We conclude that these electrons are trapped in Io's magnetic field configuration. The narrowness of the beams and the simultaneous existence of an apparently unaccelerated trapped electron population provide evidence that the source region for the beams is close to Jupiter. A deconvolution of the detector response to the beams gives a beam angular half-width of ~6°, placing the formation of the beams at an altitude of ~0.6 - 0.7 RJ. The slight energy dependence of the beam width provides a rough upper limit estimate of <~1.8 (10)8 cm-3 for Io's neutral SO2 atmosphere in the flyby region. No proposed acceleration mechanism operating close to Io (neither double layers nor Fermi acceleration via propagating Alfvén waves) is able to reproduce measured beam characteristics.

**GA4.10/W/11-A5 Invited 1450**  
**SOURCES AND TRANSPORT OF PLASMA IN THE IO TORUS**

Frans CRARY (Laboratory for Atmospheric and Space Physics, University of Colorado, Boulder, USA)

The Io torus is generated by the escape of neutral gases from Io, and their subsequent ionization; the structure of the torus is determined by (among other things) this source and the processes which transport away from the source. This presentation will review the existing theories and observations of the logenic plasma source and of the transport processes, and then describe results of recent analysis of observations made by the Galileo spacecraft. Measurements made during the Dec. 1995 encounter with Io allow estimates of Io's neutral exosphere and place limits on the near-Io plasma production rates. Plasma observations made in the Io torus indicate that the abundance of oxygen ions increases with distance from Io. This had previously been suggested to explain Voyager ultraviolet spectra, and may indicate a source of oxygen from Europa. Finally, the Galileo spacecraft observed a number of events associated with plasma transport. Some of these events are in good agreement with theoretical descriptions of flux tube interchange. Other events have a more complex structure, and measurements of inward flow velocities show that they are associated with transport.

**GA4.10/W/31-A5 1510**  
**PLASMA INTERACTIONS WITH THE GALILEAN MOONS OF JUPITER**

Margaret KIVELSON (Department of Earth and Space Sciences and Institute of Geophysics and Planetary Physics, University of California, Los Angeles, CA 90095-1567, USA, email: mkivelson@igpp.ucla.edu)

Half way into its fourth year in orbit around Jupiter, Galileo has acquired data on several passes by Jupiter's three outer Galilean moons and on one pass by Io. The diversity of observed signatures is astonishing. At Europa and Callisto, the data support the concept of conducting layers not far below the surface, a conclusion that has led to reconsideration of the ways in which the outer icy layers of these moons have cooled. There is evidence that the structure of the Alfvén wings at Ganymede and Europa is consistent with theoretical proposals of Neubauer (1998). Our proposal that the field-aligned currents carried in the Alfvén wings are intense enough to produce signatures in Jupiter's ionosphere are supported by Hubble images recently acquired by Clarke and co-workers. In the wakes of both of these bodies, ion pickup dominates part of the ULF power spectra and can be used to estimate the pickup rate of heavy ions. Ganymede's mini-magnetosphere has revealed a remarkable complexity of structure both in particle distributions and in field fluctuations. The opportunity to investigate an approximately steady state magnetosphere allows us to test our ideas of convection and reconnection. It remains perplexing, and we will review the issues that remain unresolved but may be

**GA4.10/E/07-A5 Invited 1525**  
**THE MAGNETOSPHERE OF SATURN AND ITS INTERACTION WITH TITAN**

T. I. GOMBOSI, D. L. DeZeeuw, C. P. T. Groth, K. C. Hansen, K. Kabin, and K. G. Powell (The University of Michigan, Ann Arbor, MI, USA e-mail: tamas@umich.edu)

This talk will briefly review our pre-Cassini understanding of the Saturnian magnetosphere and its interaction with Titan. We will also present the results of a new multiscale MHD simulation of the Saturnian plasma environment. The simulation explores the magnetohydrodynamic coupling between Saturn and Titan, as well as the influence of the IMF and planetary rotation on the large-scale features of the Kronian magnetosphere.

**GA4.10/W/20-A5 1545**

**ION PICKUP AND ASYMMETRIES IN EUROPA'S WAKE**

M. VOLWERK, M.G. Kivelson and K.K. Khurana

The plasma pick up near Europa [Kivelson et al., 1998, submitted to JGR] gives rise to strong wave activity at frequencies  $f < 0.4$  Hz in the geometrical wake region, which is defined as the region behind Europa of width  $2 R_e$  (Europa radii) perpendicular to the plasma flow. In the E11 and E15 flybys we can identify a region of left-handed polarized waves, with strong coherence between the two components perpendicular to the background magnetic field, at a frequency near 0.2 Hz. This is consistent with ion cyclotron waves generated by the ring current distribution of the freshly picked up ions near Europa. The frequency matches the gyrofrequency of a singly charged, 32 AMU mass ion (S or O<sub>2</sub>). The wave activity gets transformed into local ion density cf. Huddleston et al. [JGR 103, 19887, 1998]. The activity during the E4 flyby seems more difficult to explain by pick-up processes. There is an asymmetry in the wave activity and the crossing of the Alfvén wing created by Europa. This asymmetry could be caused by the magnetic induction effect of the moon embedded in Jupiter's time varying magnetic field. It seems to agree with the model by Neubauer [preprint, 1998], describing the offset of the Alfvén wings due to induction effects.

**GA4.10/W/34-A5 Invited 1620**

**PLASMA WAVES IN THE OUTER PLANET MAGNETOSPHERES**

W. S. Kurth, D. A. Gurnett (Dept. of Physics and Astronomy, University of Iowa, Iowa City, IA, 52242, Email: william-kurth@uiowa.edu), A. Roux (CETP/UVSQ, Velizy, France), S. J. Bolton (Jet Propulsion Laboratory, Pasadena, CA 91109).

Based on Voyager observations at Jupiter, Saturn, Uranus, and Neptune, one finds a number of similarities in the plasma wave spectra in the outer planet magnetospheres and these are shared in many respects with those in the terrestrial magnetosphere, as well. This result is profound, given the dramatic differences in size, heliospheric distance, dipole and rotation axes orientations, and internal sources of plasma across these five planetary magnetospheres. In this short review we address such similarities and use recently obtained Galileo observations to update the situation at Jupiter and suggest the types of advances that are possible with the arrival of Cassini at Saturn in 2004.

**GA4.10/E/03-A5 1640**

**PARTICLE ACCELERATION BY MAGNETIC RECONNECTION IN THE JOVIAN MAGNETODISC**

Joerg BUECHNER (Max-Planck- Institut fuer Aeronomie, Max-Planck-Str. 2, D-37191 Katlenburg-Lindau, Germany)

Current Galileo investigations have shown that in the course of substorm-like dynamic events plasmoid-like structures are formed in the Jovian magnetotail (cf. Woch, Krupp, et al., this meeting). We present results of calculations of particle acceleration by magnetic reconnection processes, demonstrating similarities and differences of reconnection related particle acceleration in the magnetotails of the Earth and Jupiter. For example, in contrast to the Earth tail the specifics of the Jovian magnetodisc field structure and strength allows also the immediate acceleration of electrons to high energies.

**GA4.10/W/05-A5 1655**

**MIRROR MODE STRUCTURES AT THE GALILEO FLYBY**

C. T. RUSSELL, R. J. Strangeway, M. G. Kivelson and K. K. Khurana (All at Institute of Geophysics and Planetary Physics, University of California, Los Angeles, CA 90095-1567, USA, email: ctrussell@igpp.ucla.edu); D. E. Huddleston (Hughes Space and Communications Company, El Segundo, CA, USA); X. Blanco-Cano (University of Mexico, D.F., Mexico); L. A. Frank, W. Paterson, D. A. Gurnett and W. S. Kurth (All at University of Iowa, Iowa City, IA, USA)

As Galileo passed through the wake of Io it encountered a number of magnetic depressions that have been interpreted to be the result of the mirror mode instability. Herein we examine the magnetic signatures of these structures and simultaneous measurements of the electron density and temperature. These structures have phase fronts that propagate at large angles to the magnetic field and scale sizes of several ion gyro radii. The density enhancements that accompany the magnetic field depressions range up to 200% of the background density. The spread in normal directions suggests that the depressions are cylindrical and not sheet-like.

**GA4.10/W/09 A5 1710**

**ASPECTS OF THE OUTER JOVIAN CURRENT SHEET AS DETERMINED FROM PARTICLE SIMULATIONS**

L YIN, P L PRITCHETT, and F V Coroniti (all at Department of Physics and Astronomy, University of California, Los Angeles, CA 90095-1547, USA, email: ylin@physics.ucla.edu, pritchet@physics.ucla.edu), L A Frank and W R Paterson (both at Department of Physics and Astronomy, The University of Iowa, Iowa City, IA 52242, USA)

The Galileo spacecraft has made extended observations of the middle and outer Jovian magnetosphere, including the outer current sheet region in the Jovian tail. We examine the electromagnetic behavior of the current sheet by means of self-consistent, 2-D particle-in-cell simulations. A cold plasma source, representing plasma transported outward from Io, is injected into a rapidly rotating dipole-like field configuration. We investigate the temporal variability of the plasma sheet near and outside of the Alfvén point with the aim of determining how a centrifugally slung plasma may break the magnetic field topology and escape into some sort of steady or turbulent outflow. We observe substantial ion heating and formation of non-Maxwellian velocity distributions in regions where super-Alfvénic outflow and fast-shock-like layers form.

**GA4.10/W/23-A5 1725**

**MAGNETIC SOUNDING OF THE CONDUCTIVITY STRUCTURE OF GALILEAN MOONS USING MULTIPLE FREQUENCIES OF JUPITER'S FIELD**

C. ZIMMER, K. K. Khurana, M. G. Kivelson (Institute of Geophysics and Planetary Physics, University of California Los Angeles, USA)

Evidence from Galileo measurements for a secondary magnetic field produced by Europa and Callisto as a response to the primary time-varying field of Jupiter implies the presence of conducting media close to the moon's surfaces. To first order, the magnetic signatures at both

moons are consistent with the inductive response of a perfectly conducting spherical shell. For finite conductivities, the secondary field is both reduced in amplitude and delayed. An analytical expression can be obtained for a layered spherically symmetric model of the moon's interior (Srivastava [1966]). Assuming from the Galileo data that the amplitude of the secondary field at the synodic period is 80% or more of the perfect conductor response, we find that the required conductivities must be at least of the order of 0.1 S/m. This is most probably an indication for salty oceans lying beneath the visible rigid ice crust. If the conductivities are comparable to that of oceans on Earth, they must be at least a few km thick. Due to the concentration of currents close to the "meridian" plane perpendicular to the main direction of the time-varying primary field, the oceans need not be global to produce the observed induction effect. Further constraints on the characteristics of the conducting regions can be obtained by taking into account the other frequencies contained in the primary field, particularly at the orbital periods of the moons. The amplitudes at different frequencies are a function of the tilt and offset of the Jovian dipole, the eccentricity and inclination of the moon's orbit, and

**GA4.10/W/07-A5 1740**

**OBLIQUE ION CYCLOTRON WAVES IN THE NEAR-IO TORUS**

X. BLANCO-CANO (Universidad Nacional Autonoma de Mexico, D.F., Mexico, email: xbc@fis-esp.igofcu.unam.mx), C. T. Russell, D. E. Huddleston, R. J. Strangeway, M. G. Kivelson, K. K. Khurana (University of California, Los Angeles, CA, USA)

Ion cyclotron waves were identified in the Galileo magnetic field data in the near-lo torus. These waves are generated by pickup ion instabilities. To zeroth order they grow at the sulfur dioxide gyrofrequency, are left-hand polarized and propagate along the magnetic field. A more detailed study reveals that the waves grow over a finite bandwidth, propagate at an angle to the field and are elliptically polarized. In this work we perform a kinetic dispersion analysis and show that the growth rate of oblique cyclotron modes can be significant in the multicomponent plasma near Io. We find that variations in the sulfur dioxide pickup ion density may lead to the observed bandwidth of frequencies.

**GA5.01 Monday 19 July**

**GEOMAGNETIC OBSERVATORIES AND REPEAT SURVEYS: INSTRUMENTATION, PRACTICE AND ANALYSIS (WITH CDC)**

Location: Muirhead Tower 424 LR5  
Location of Posters: Muirhead Tower 422 LR4

**Monday 19 July AM**

Presiding Chairs: R C Coles ( Surv., Ontario, Canada) and Arthur W Green (US Geol. Surv, Denver, USA)  
Concurrent Poster Session

**Introduction 0830**

J.L. RASSON (Royal Met. Inst, Belgium)

**GA5.01/W/05-A1 0835**

**GEOMAGNETIC OBSERVATORIES AND REPEATED STATIONS IN JAPAN**

Satoru TSUNOMURA and Takaji Kurihara (both at Kakioka Magnetic observatory, Japan Meteorological Agency, Kakioka 595, Yasato machi, Niihari-gun, Ibaraki-ken 315-0116, Japan, email: stsunomu@mri-jma.go.jp), Arata Sengoku and Yoshiharu Nagaya (both at Maritime Safety Agency, Hydrographic Department, 5-3-1 Tukiji, Chuo-ku, Tokyo 104-0045, Japan, email: asengoku@cue.jhd.go.jp), Shouchi Matsumura (Geographical Survey Institute, 1 Kitasato, Tsukuba, Ibaraki-ken, 305-0811, Japan, email: matsumura@gsi-mc.go.jp), Masahisa Sugiura (Research Institute of Science and Technology, Tokai University, 2-28 Tomiyaga, Shibuya-ku, Tokyo 151-0063, Japan, email: sugiura@jspan.kugi.kyoto-u.ac.jp), Toyohisa Kamei (WDC-C2 for Geomagnetism, Graduate School of Science, Kyoto University, Sakyo-ku, Kyoto 606-8502, Japan, email: toyo@kugi.kyoto-u.ac.jp)

For historical reasons, three government institutions, the Japan Meteorological Agency (JMA), the Geographical Survey Institute (GSI), and the Maritime Safety Agency, share the responsibilities of routine geomagnetic observations in Japan. The Kakioka Observatory, which is under JMA, is responsible for the long-term precision observations at Kakioka, Memambetsu and Kanoya, and for the tests of magnetic instruments. The GSI, an agency responsible for the production of magnetic charts on land, conducts repeat magnetic surveys at over 100 stations in Japan and operates magnetic observatories at Kanozan and Mizusawa as reference points for the repeat stations. Since 1996, the GSI has been operating continuous magnetic observation system at 11 field stations. The responsibilities of the Maritime Safety Agency include the production of marine magnetic charts, the conduct of shipboard magnetic observations over the oceans near Japan, and the operation of the magnetic observatory at Hattijo as the reference point for their magnetic surveys. The magnetic observatories mentioned above are equipped with a fluxgate magnetometer and a proton precession magnetometer for variation measurements and with a magnetic theodolite and a proton precession magnetometer for absolute measurements. In addition, the Kakioka Observatory conducts variation measurements with a high sensitivity, high time resolution fluxgate magnetometer and additional Overhauser type proton precession magnetometers. In this paper, characteristics of the instruments used by the three agencies are described. Discussions also refer to the increasing difficulties faced by these agencies concerning the operation and maintenance of the magnetic observatories and repeat stations.

**GA5.01/E/12-A1 0905**

**GEOMAGNETIC D, H AND Z RECORDINGS AT EQUATORIAL OBSERVATORIES**

R.G.RASTOGI, (Department of Physics, Gujarat University and Physical Research Laboratory, Ahmedabad 380 009 India, email: parvs@prl.ernet.in)

Classically the most important component of geomagnetic field at equatorial stations is considered to be the horizontal field H. The other components D and Z are comparatively ignored and some ambiguities have occurred in the publication of these data. Some new results related to the quiet and disturbed time observations are discussed and a need to improve the sensitivity of D and Z records are discussed. Importance of the operation of regular observatories in Sri Lanka, Central Africa, Brazil and Vietnam are stressed.

**GA5.01/W/03-A1 0920**

**EXPERIENCE OF ABSOLUTE BASELINE CONTROL OF MAGNETIC RECORDING INSTRUMENTS AT TERRA NOVA BAY OBSERVATORY, ANTARCTICA**

Lili CAFARELLA, Antonio Meloni, Paolo Palangio and Achille Zirizzotti (Istituto Nazionale di Geofisica, via di Vigna Murata 605, 00143, Rome, Italy, email: cafarella@ing750.ingrm.it)

The magnetic observatory at the Italian Base Terra Nova Bay in Antarctica (Lat. 74.695° S, Long. 164.124° E, Mag. Lat. 77.32° S (IGRF 1990)) started its operations in 1986/87. During the years, the obtained data were used for studies on secular variation, seasonal effects on geomagnetic daily variation, solar cycle influence on magnetic activity, pulsation studies and data reduction during magnetic surveys. Geomagnetic observatory instruments are installed on solid rock and include two proton precession magnetometers for digital recording of total intensity F and two recording systems, using fluxgate magnetometers for monitoring time variations of H, D and Z. Absolute measurements are made independently using a DI fluxgate theodolite magnetometer; they are input to a mathematical procedure in order to determine baseline values for the relative fluxgate measurements. Absolute magnetic measurements are also made continuously by means of an independent fluxgate vectorial magnetometer that was operating automatically since summer 1997/98 and was checked against the other two magnetometers. Baselines computation results for all magnetic elements show the very high stability of this new instrument.

**GA5.01/E/03-A1 0935**

**A PARTLY MANNED GEOMAGNETIC OBSERVATORY DEPLOYED IN ANTARCTICA PROVIDES A RELIABLE, STABLE TIMELY DATA SET**

J. Miquel TORTA (Observatori de l'Ebre, CSIC, 43520 Roquetes, Tarragona, Spain, email: ebre.jmtorta@readysoft.es) John C. Riddick, Chris Turbit (both at British Geological Survey, email: jcr@wpo.nerc.ac.uk) Alberto Castejon and Alicia Garcia (both at Programa Nacional de Investigacion en la Antartida, email: castejon@pna.es)

During the 1996-1997 Austral summer survey a new geomagnetic observatory was deployed at the Spanish Antarctic Station, Juan Carlos I (Livingston Island, South Shetland islands). The main instrument is an Overhauser magnetometer deployed at the centre of a pair of dual axis Helmholtz coils, in a deltaD/deltaI configuration. For the absolute measurements of D and I a D/I-fluxgate theodolite is used. The site is only manned during the summer, but the variometer is left recording throughout the rest of the year. It is designed for low power consumption, with an embedded PC as the main processor unit, including three RS232 ports allowing automatic measurements from the proton precession magnetometer, regular time synchronisations from a GPS and serial transmission of data. An internal flash memory disk offers a secure medium for storing up to one year of vector data. Power supply is guaranteed by a combination of solar cells and wind generators which charge a battery rack.

This system has revealed itself to be very reliable, providing uninterrupted 24V DC for two years now. For the real time access to the data, there exist three possibilities which have been checked during the last survey: using either METEOSAT or GOES Data Collection Systems, or by retrieving them by modem through INMARSAT. Stability is another of the abilities of the system since, apart of a slight drift in I observed during the first survey, H and Z baselines are kept within 5 nT since then, and D baseline within 1'.

**GA5.01/W/18-A1 0950**

**QUALITY ASSURANCE OF CHAMBON LA FORET GEOMAGNETIC DATA BY INTER-COMPARISON OF MAGNETOMETERS**

MIOARA MANDEA ALEXANDRESCU and Jean-Louis Le Mouél (Institut de Physique du Globe de Paris, 4 Place Jussieu, 75252 Paris Cedex 05, France, email: mioara@ipgp.jussieu.fr, lemouel@ipgp.jussieu.fr)

In Chambon la Forêt observatory three magnetometer systems are running: VFO, TSA and 390. Each one includes a triaxial variometer in the variometer building and an Overhauser magnetometer measuring the absolute total field intensity: two of the three Overhauser are in the variometer building, the third in the absolute house (from summer 1996 onwards). This installation gives us the ability to check continuously the differences of the total field intensity between the variometer building and the absolute house. Any change in these differences could mean either a problem with one of the magnetometers or the presence of a localised interfering magnetic field. In this paper we present results from this inter-comparison of data for the 1996 - 1998 period. Two kinds of perturbations can appear. These disturbances, very different in form and amplitude, are presented and their causes are discussed. We stress the importance of such inter-comparisons in assuring the highest quality of magnetic observatory data.

**GA5.01/E/21-A1 1005**

**THE MAGNETIC OBSERVATORY OF FÚQUENE, COLOMBIA: NEW INSTRUMENTATION**

ARIAS WILLIAM and Quintero Wilson. ( Instituto Geográfico "Agustín Codazzi". Carrera 30 No. 40-51, Santa Fe de Bogotá, Colombia. Phone 57 1 368 7441. fax 57 1 368 0991; 57 1 368 1040. email: wjarias@igac.gov.co

Fuquene Observatory is situated on a small island about 100 km from Santa Fe de Bogotá, and was purpose built for magnetic work. Now is also installed a meteorological station, a seismological station and strong motion station. The Observatory is operated by the Geophysical Section of the Instituto Geográfico "Agustín Codazzi". Continuous geomagnetic measurements began in 1954.

As a result of a project of updating the geomagnetic network, the Instituto Geográfico "Agustín Codazzi" installed a Digital Magnetic Observatory in September 1995, close to the analogue three components Ruska Variometer, installed in 1954.

The digital system of three components fluxgate magnetometer (GEOMAG) measure the D, H, and Z components of the geomagnetic field.

Absolute observation has been carried out using a classical Askania magnetometer for H and D. For total intensity (F) it is used a Geometric PPM. I values are calculated from the H and F measurements. Two QHM are also used for the precise determination of horizontal intensity. In December 1998, the Askania Magnetometer was replaced by a Diflux - Theodolite (FLM1/B fluxgate magnetometer electronics) with a resolution of 0.1 nT, manufactured by the Royal Meteorological Institute of Belgium. In 1999 with the co-operation of this Institute, it will replace the analogue variometer for a digital variometer and also the old Ruska magnetometer used in field work for a Diflux.

The result of comparisons of magnetic data recorded in both, the analogue and digital Observatory of Fuquene will be presented in this paper.

**GA5.01/E/08-A1** Invited **1045**

**ON THE ACCURACY OF MAGNETIC SCALAR MEASUREMENTS WITH MODERN OPTICALLY PUMPED MAGNETOMETRES.**

E. B. ALEXANDROV, S.I.Vavilov (State Optical Institute, St.Petersburg 199034, Russia).F

The problems of accuracy of the magnetic-field scalar measurements (mainly in observatory environment) are reviewed. Nowadays, three types of optically pumped atomic resonance magnetometers are considered to be most accurate: the potassium narrow-line Mx-magnetometer and two combined systems – the alkali-helium Mz-magnetometer and tandem combinations of different Mx-Mz-type magnetometers. A common feature of all these instruments is their good baseline stability - not worse than 0.05 nT. This was directly confirmed by long-term comparison of a Cs-He combined magnetometer with a Cs-K tandem magnetometer. The expected long-term stability of the tandem-type magnetometers with one of its constituent being a narrow line potassium Mz-magnetometer is better than 0.01 nT. Other characteristics of the instruments (short-term resolution, response time, expected absolute accuracy and others) are analysed and compared.

**GA5.01/E/29-A1** **1100**

**BI-COMPONENT MAGNETOMETER-VARIOMETER BASED ON SCALAR CAESIUM SENSORS**

An. P. NAUMOV, ( D.I.Mendeleyev Institute for Metrology / VNIIM, St Petersburg, 198005, Russia, email: slovo@mail.line.ru ) Yu. V. Tarbeyev and I.S. Chasiev ( both at VNIIM, St Petersburg, 198005, Russia, email: hal@ont.vniim.spb.su )

The magnetometer-variometer (MV) consisting of a scalar fast-acting optical pumped caesium sensor inside of quartz astatic coil-system has been developed. This device was developed for decision of problem of the exact measurements of ULF Earth's magnetic field variations in active tectonic regions. (The vector of source magnetic moment of ULF signals has direction along of geomagnetic field vector). All construction of device contains two parts: MVa and MVb. The MVa measures of the Z component of Earth's field and consists of a quick response Cs sensor (of Sx type) and quartz coil-system (along of magnetic meridian). The MVb measures of the total intensity of Earth's field, he consists of a quick response optical pumped Cs sensor too (of Szx type) and disposed side by side. High sensitivity of the MV (resolution - 0.01 nT) assures precision measurements and magnetic location of geovariation sources. Measurement cycles 0.2-1.0 seconds, the accuracy of the field measurement is not worse than 0.5 nT.

**GA5.01/E/13-A1** **1115**

**A NEW TANDEM SCALAR MAGNETOMETER BASED ON POTASSIUM-39 4-QUANTUM TRANSITION**

E.B.Alexandrov, M .V. Balabas, A. K .VERSHOVSKII. (S.I.Vavilov State Optical Institute, St.Petersburg 199034, Russia.)

A new tandem-type quantum magnetometer is described. As any tandem magnetometer it consists of a fast-response self-oscillating unit and a high precision low-speed Mz unit. Unlike the Bender's prototype our tandem comprises a single atomic cell with a mixture of potassium and cesium at certain proportion. Cesium vapor is used in the self-oscillating unit. Its output signal after frequency doubling is slightly shifted to match the narrow potassium resonance, which provides the high accuracy of the instrument. The special frequency shifting scheme using 32-bit synthesizer was designed. As a reference potassium resonance line the four-quantum resonance  $m=-2 \leftarrow m=+2$  is chosen. The four-quantum resonance has an advantage of perfect frequency linearity with magnetic field strength and the highest resolving power. The output resolution of the magnetometer is about  $1 \text{ pT}/(\text{Hz})^{1/2}$  while its absolute accuracy is expected to be of the order of 10 pT.

**GA5.01/E/14-A1** **1130**

**THE LONG TERM STABILITY OF THE USGS DELTA I - DELTA D (DIDD) SYSTEMS**

LEROY W. PANKRATZ( US Geological Survey, PO Box 25046, MS968, Denver Federal Center, Denver, Colorado, USA,80225-0046, email: pankratz@ghmail.cr.usgs.gov) Edward A. Sauter( U S Geological Survey, PO Box 25046, MS968, Denver Federal Center, Denver, Colorado, USA,80225-0046, email: esauter@ghmail.cr.usgs.gov)

The US Geological Survey presently operates thirteen geomagnetic observatories throughout the continental United States, Alaska, Guam, Hawaii and Puerto Rico. In addition we have international co-operative agreements with Brazil, Hungary, India and South Korea operating geomagnetic observatories. All of these observatories are equipped with Fluxgate Magnetometers, Geometrics or GEM Systems Proton Magnetometers and Synergetics Data Collection Platforms. In addition most of these observatories provide weekly absolute calibrations provided by Diflux Magnetometers and supplemented with DIDD's. This paper will attempt to address and analyse the long-term stability of the DIDD's employed at many of the United States observatories.

The method of analysis will include comparison of the baseline differences derived from the Diflux observations and those generated from the DIDD. In order to proceed we have made the reasonable assumption that the fluxgate magnetometer can be considered stable over a minimum two-hour period. Thus the Diflux derived baselines can be compared to the two DIDD observations which most surely flank those of the Diflux. Therefore the DIDD baseline can be extrapolated between these two points and a difference derived. It has been determined that in all three elements H, D and Z the differences vary by no more than +/- 1.25 nT during any thirty day period. Long term data comparisons including temperatures will be presented.

**GA5.01/W/16-A1** **1145**

**STABILITY OF DELTA "I" - DELTA "D" (DIDD) QUASI-ABSOLUTE SYSTEM**

Laszlo HEGYMEGI, Alpar Kormendi, Andras Csontos, Balazs Heilig (Eotvos Lorand Geophysical Institute, Budapest, Columbus utca 17-23, H-1145, Hungary, email: hegymegi@elgi.hu)

Geomagnetic recording systems are generally relative instruments, their baseline is changing with time. The baseline has to be determined regularly with an absolute instrument. It would be an ideal solution if we could use absolute instrument for recording the field variation. There were several attempts in the past to realise this idea but because of several disadvantages of the constructed instruments these efforts did not prove to be very successful. Some years ago in co-operation of Eotvos Lorand Geophysical Institute (ELGI), U.S. Geological Survey (USGS) and GEM Systems a new quasi-absolute system (DIDD) was developed which consists of a small size spherical coil system and an overhauser proton magnetometer. The system performs a complete set of measurements in every two seconds and provides the absolute value of the field vector F, the declination D and Inclination I. The stability of the data

measured depends mostly on the mechanical stability of the coil system.

To verify the stability of the new DIDD system working in Tihany Observatory of ELGI, declination and inclination absolute measurements were carried out by two declination-inclination theodolite (DIM) twice every week. The result of this investigation is presented in this paper.

**GA5.01/W/08-A1** **1200**

**NEW DESIGN IN LINEAR FLUXGATE SENSORS**

Otto NIELSEN(Institute for Automation, Technical University of Denmark, DK-2800 Lyngby, Denmark, email: ovn@iauu.dtu.dk); Ole RASMUSSEN(Danish Meteorological Institute, Lyngbyvej 100, DK-2100 Copenhagen, Denmark, email: or@dmu.dk)

Based on the experiences from the ORSTED satellite magnetometer a new linear fluxgate sensor has been developed. The sensor core is made from an amorphous metal alloy with has been given a special heat treatment to minimise the magnetostriction and the noise. The mechanical parts of the sensor are made from glass and quartz to minimise thermal drift. Preliminary results will be presented showing noise figures lower than 20 pT RMS and offset drifts as low as 5 nT over a temperature range of 80°C.

**GA5.01/E/06-A1** **1215**

**MORE ABOUT THE MAGNETOMETERS NOISE**

Rikhard Berkman and Valery KOREPANOV (Lviv Centre of Institute of Space Research, 5-A Naukova str., 290601, Lviv, Ukraine, email: vakor@isr.lviv.ua)

The modern requirements of magnetic surveys data quality need to lower as much as possible the magnetometers noise level (NL). By this, all zero line instabilities are kept in mind as NL: from very long time fluctuations (1 year and more) to some Hertz and more.

Two types of magnetometers are examined as the most widespread ones: search-coils and flux-gates. For each type the semi-empirical expression allowing to estimate the theoretically lowest possible NL is derived. The most important parameter determining NL - sensor length - is singled out. Then using the NL criterion the recommendations as to the proper choice of flux-gate or search-coil magnetometers are given if it is necessary to study the magnetic fluctuations in the intermediate frequency band where both types seem to be equally efficient. For search-coils magnetometers a new calculating method using so called generalised parameters is proposed. It is shown that using this method an optimal combination of search-coil magnetometer is achieved for given limitations. Some practical examples confirm good matching of calculated and obtained NL parameters. The physical nature of the flux-gate sensor noise is investigated more in details and main factors contributing to its NL are discussed. For extremely low frequency, the deviation of magnetic noise distribution from the normal law is shown, and lower than 1/f slope of the NL dependence from the frequency is confirmed. The optimal parameters of the core material for flux-gate sensor are discussed and the special influence of Curie temperature of such alloys is illustrated. Some other peculiarities of flux-gate sensor construction are discussed which can essentially improve the magnetometer parameters. Their practical level for recently developed magnetometers is reported.

**GA5.01/P/02-A1** **1230**

**MAGNETIC MODEL FOR A NOT STEEL-FREE THEODOLITE**

V. AUSTER MAGSON GmbH, Rudower Chaussee 6, 12489 Berlin

In the geodetic practice, for example in the forestry, also at present theodolites in connection with a sensitive compass are used. Therefore we carried out experiments with a "DI-Flux" equipment, consisting of a theodolite ELTA 50 (ZEISS) and a full scale flux - gate magnetometer (MAGSON). Using POISSON's equations for the magnetic deviation we calculated a model for the magnetic disturbance on the sensors place. Basing on this we developed a method, which gives an automatic adjustment to magnetic north as zero point for the measurement of the horizontal angle.

**Monday 19 July PM**

Presiding Chairs: Ole Rasmussen, (Danish Met. Inst)  
L.M. Barreto (Observatorio Nacional, Brasil)  
Concurrent Poster Session

**GA5.01/E/04-A1** Invited **1400**

**SOLAR ECLIPSES MAGNETIC EFFECTS, A REVIEW**

A. Orozco and E. HERNANDEZ (Instituto de Geofisica, Ciudad Universitaria, 04510, Mexico, D.F., Mexico; Adolfo (tonatihu.igeofcu.unam.mx; Esteban (tonatihu.igeofcu.unam.mx).

The magnetic effects of solar eclipses have been measured since the beginning of this century. In the first time it was concluded that the source of this effects was at an atmospheric layer above 100 km and the model in general only took into account the total shadow area. The confirmation of the existence of the ionosphere gave a new push to this study, using ionosondes to monitor the changes in electrical conductivity and free electron content during the totality of the eclipse phenomena. Anyway, there was a lack of qualitative and quantitative explanation of some of the main aspects of this effect. Particularly an asymmetry of the peak effect respect to the optical totality and the apparent existence of magnetic effects outside the general path of the eclipse.

In this paper we present an overview of these stages of the problem and a qualitative model that explains the principal characteristics of the phenomena.

**GA5.01/W/21-A1** **1415**

**FIELD AND OSERVATORIES MAGNETO-TELLURIC WIDE AREA NETWORK**

Eugene KOPYTENKO, Yury Kopytenko, Andrej Radilov (SPbF IZMIRAN, Muchnoj per.2, Box 188, St.Petersburg, Russia, email: ek@eak.izmi.ras.spb.ru)

SPbF IZMIRAN is continued its developing in the field of high sensitive magnetometric system. On the base of MVC-2DS, multipurpose magnetotelluric station, it was build Wide Area Network for monitoring quick running processes both in magnetic and telluric fields, and in a third (three component) geophysical channel in quasi real time. System consist of Remote Station equipped with high sensitive torsion type magnetometer, 24-bit resolution Analogue to Digital Converter driven by GPS controlled clock, remote PC running under LINUX (UNIX clone OS) and Laboratory's Server. Data are buffered at remote PC. Server collects it and transmits it to the computers wich are included into the list of recipients.



**GA5.01/E/16-A1 1430**

**MAGNETOMETER FOR FIELD SURVEYS: TESTS AND FIRST RESULTS**

Hans-Joachim LINTHE (GFZ Potsdam, Adolf-Schmidt-Observatory, Lindenstr. 7, D-14823 Niemege, Germany, email: linthe@gfz-potsdam.de) Valery Korepanov and Leonid Rakhlin (Lviv Centre of Institute of Space Research, 5-A Naukova str., 290601 Lviv, Ukraine, email: vakor@isr.lviv.ua)

The repeat surveys are one of the most difficult tasks if high quality results of magnetic investigation have to be obtained. First of all it is because the field magnetometer for this work has to combine high quality of the observatory instrument with good temperature stability and convenience of rapid installation in operative position.

To facilitate these works a fully autonomous magnetic station LEMI-008 was developed. Its main advantages are:

- wide measurement range (up to 100 000 nT);
- wide operating temperature range (-5 (+40) C);
- GPS synchronization and coordinates determination;
- flush-type internal memory;
- low weight and power consumption.

The latest modernization was made with the sensor suspension: all system is fixed in fully hermetized housing with gimbals using the needle balance. It is firmly blocked during transportation and quickly released after installation. The developed tests of the magnetometer were executed: temporal and thermal drifts determination, tilt compensation ratio study, multiple switching on and off influence etc. and their results are reported. First results of field measurements are presented and the estimation of their quality is made.

**GA5.01/E/07-A1 1445**

**GEOMAGNETIC SUPER-REPEAT STATIONS**

Charles BARTON and Andrew Lewis (Australian Geological Survey Organisation, GPO Box 378, Canberra ACT 2601, Australia, email: cbarton@agso.gov.au)

Experience in Australia has demonstrated that frequent (annual) occupations of a relatively small number of well-placed magnetic repeat stations is more cost-effective than five-yearly occupations of many stations. The main advantage of this "Super-Repeat Station" strategy is improved ability to track and predict the secular variation. Other advantages are better and quicker identification of bad data, more flexibility in avoiding magnetically disturbed observing conditions, easier schedules for field parties, steady-state annual funding demands, and reduced costs.

**GA5.01/E/26-A1 1500**

**COMPARATIVE ANALYSIS OF DIFFERENT PROCEDURES FOR THE EXTRACTION OF THE DIURNAL VARIATION**

MANUEL CATALÁN, Antonio Pazos (Geophysic Department, Royal Naval Observatory, San Fernando 11100, Cádiz, Spain)

During one month (August) in the summertime of 1995, 1996 and 1997, an marine geophysical campaign has been carrying out at the Spanish Exclusive Economic Zone (ZEE) at the Balear Sea (West Mediterranean), as a collaboration between the Spanish Defence Ministry, and the Spanish Oceanographic Institute (IEO).

For different reasons, at 1995 we were not able to have a reference magnetic station at a close area, so to correct the diurnal variation data we were obliged to use a reference station (San Pablo-Toledo observatory) that, on average, is 600 km. away from the working zone.

This fact, usually, is corrected affecting the reference station data by a scale factor, once have been corrected by time difference. This correction does not take into account possible scattered effects.

We have developed a procedure based on the Transfer Function concept result from the analysis, at frequency domain, of one-month magnetic registers obtained from 1996 campaign using two reference stations:

- The same one we used at 1995, that is San Pablo-Toledo
- Another nearby site of the surveyed zone, situated on a hill of Mahon Naval Station (Minorca, Balearic Island).

In this job we compare classical methods with this procedure, using magnetic registers of 1997 campaign.

Result shows that errors are in the same order for this procedure and classical methods. Nevertheless, a better behaviour could be obtained using our method during quiet days.

**GA5.01/E/24-A1 1515**

**IMPROVEMENTS IN REPEAT STATION NETWORKS FOR DEVELOPING COUNTRIES**

Luiz Muniz BARRETO (Observatorio Nacional, Rua General Bruce, 586.-20921-400 Rio de Janeiro, RJ, Brasil, email: barreto@on.br)

To understand the geomagnetic field behaviour we need to know its changes in space and time. To achieve a global coverage of space variations it would be necessary a dense network of observing stations. Besides this, a complete knowledge of time changes requires that, in each of these stations would be installed instruments to cover the whole time geomagnetic spectrum. These requirements are impossible to be achieved. A feasible solution was adopted: a possible network of magnetic observatories where all time changes are recorded, and a supplementary network of repeat stations where punctual values are obtained.

We must understand that the results and objectives of both kinds of stations are different. About 40 years ago, geomagnetic data from specific satellites have improved our data collection but, in spite of this modern method, we cannot neglect good ground level data, for many reasons (anomalies, observing continuity, for instance). In general, we could say that a desired complete coverage of the geomagnetic field could be obtained from a global network of geomagnetic observatories, economical and logist reasons inhibit the existence of an adequately dense network. The actual geographic distribution of permanent geomagnetic stations shows that, besides the great gaps of the oceans, seas and remote regions, the area covered by Developing Countries (DC) has a poor density of such stations. Notwithstanding the limited output from repeat station networks, they are useful to prepare magnetic charts and to study secular variation, mainly in large area countries. It is essential that they could produce good data with adequate periodicity and continuity. A scrutiny of the actual conditions of DC repeat stations shows technical and economical problems, as well as a bad use of the results. In order to improve the situation some procedures must be made. They include a priority to place the observing points, taking into account local peculiarities such as special geomagnetic patterns (EEJ, SAGA, regions with high values of the secular variation, for instance), besides a reduction of the time in field work by using modern instruments and procedures. Some trials were made in Latin-America with reasonable results.

**GA5.01/E/25-A1 1530**

**SECULAR VARIATION CHARTS OBTAINED FROM MAGNETIC REPEAT STATION NETWORK IN VIETNAM**

H D CHAU, T Q Hao, V T Son (Hanoi Institute of Geophysics, Box 411 Buudien Boho Hanoi Vietnam, email: chau@igp.ncst.ac.vn)

Geomagnetic secular variation charts were constructed from the absolute measurements of the geomagnetic field carrying out at the repeat stations network in Vietnam for epochs 1991.5 and 1997.5. The calculation of charts was based on the absolute data from 56 magnetic repeat stations, sparsely distributed all over the territory of Vietnam.

The results are given in the form of several tables (magnetic secular variation of the field elements in the various stations for period from 1991 - 1997). The magnetic secular variation charts for 7 elements X, Y, Z, T, H, D, I were calculated using the analytical method of approximation of magnetic secular variation field following a second degree polynomial. The characteristics of magnetic secular variation field of every element were shown. Secular variation of total magnetic field and its components in Vietnam are varied in the following intervals:

- 18 nT/year < dT < 31 nT/year;
- 8 nT/year < dH < 20 nT/year;
- 56 nT/year < dZ < 78 nT/year;
- 0.5 'year < dD < 3.0 'year;
- 3.8 'year < dI < 6.7 'year;
- 6 nT/year < dX < 18 nT/year;
- 6 nT/year < dY < 35 nT/year.

These results were compared with the IGRF Secular Variation Model.

**GA5.01/W/19-A1 1600**

**COMPARISON BETWEEN TWO PERIODS OF DETAILED GEOMAGNETIC SURVEYS CARRIED OUT IN ISRAEL**

Boris SHIRMAN (Survey of Israel, Lincoln str. 1, 65220 Tel-Aviv, Israel, email: rd\_soi@hotmail.com)

Geomagnetic anomaly component maps of Israel made in two surveys in 1983-1985 and 1993-1995 are presented. Maps of total field, horizontal and vertical components and declination were constructed based on absolute measurements at 140 and at 130 points during the first and second surveys respectively. Site locations and geographic azimuth were determined using GPS and GIRO instruments. Geomagnetic measurements were performed by a total field proton magnetometer (ELSEC-770) and declination-inclination magnetometer (ELSEC-810) with an accuracy of 1 nT and 10", respectively. All measurements were brought to base lines of the Amatsia and Bar-Giora observatories in 1984 and 1991. The anomaly field was calculated as residual between the averaged measurements and IGRF-1995 (7th generation). All components of the residual field were gridded using the Kriging method.

The main features of the maps may be described briefly as follows. The central area of the country is dominated by the large Hebron anomaly which peaks about 200 nT in the H-component against a background of about -100 nT. Several intense anomalies of 150-200 nT are observed in the southern part of the Negev desert. In the northern part of the country, the positive Carmel anomaly, which peaks at about 200 nT in the total field, stands out. A special feature of the D-component anomaly map is a positive anomaly extending along the Mediterranean coast that is not observed in the total field maps.

These features are typical for both surveys. The distribution of the differences between the surveys are presented as residual maps. These differences are defined as random distribution of the field with ± 20 nT amplitude. This quantity increases at anomaly locations. The main reason for such differences is an inconsistency between the measured points at two periods. The residual maps give an accuracy estimate of the map construction.

**GA5.01/P/04-A1 1615**

**MAGNETIC SURVEY FOR EL - QUSEIR - EGYPT.**

FATHY MOHAMED AHMED, National Research Institute of Astronomy and Geophysics, Helwan Cairo, Egypt. Fax: 002 - 02 -5548020)

Observations were made for the area northwest of El Quseir Egypt by two proton magnetometers, one for the base station and the other one for the Survey. Total magnetic Intensity anomaly map was made for the area. It shows that the basement Complex of the area has 12 step faulting systems, 4 horsts, 6 grabens took place from 13 normal faults.

**GA5.01/E/10-A1 1630**

**COMBINATION OF EUROPEAN REPEAT STATION SURVEYS**

Monika KORTE and Volker Haak (GeoForschungsZentrum Potsdam, Telegrafenberg, D-14473 Potsdam, Germany, email: monika@gfz-potsdam.de)

Geomagnetic repeat station surveys should provide a good basis for a detailed investigation of the spatial distribution of secular variation and detection of its possible anomalies.

Our aim was to carry out such an investigation on a continental scale by combining repeat station data of several European countries. Such a combination shows good results when calculating a smoothed model of large-scale secular variation but fails when trying to model anomalies. There are two main reasons for this. In some countries there have only been magnetic ground vector surveys, which are neither repeated in short enough time spans nor do they offer the desired accuracy. Even repeat station surveys sometimes seem to lack accuracy. If the data are not carefully corrected for external influences, the errors in the measured absolute values can reach the values of annual secular variation.

**GA5.01/E/05-A1 1645**

**AN OVERVIEW OF COMPASS ROSE SURVEYS IN THE UNITED STATES**

BERARDUCCI A.M., (U.S. GEOLOGICAL SURVEY, GOLDEN, COLORADO, USA)

The U.S. Geological Survey, Geomagnetism Group has considerable experience performing magnetic surveys of compass calibration pads (compass roses). The Group also provides consultation on compass rose construction and calibration training to companies who do their own surveys. Few private survey firms are capable of doing these surveys. The FAA (Federal Aviation Administration) provides specific guidelines for compass roses. In this paper, the variety of instruments and techniques used in performing compass rose surveys and techniques used in data reduction are described. In doing these surveys, geomagnetism programs can provide a valuable service to commercial and military aviation communities. Income generated from compass rose surveys can be a significant source of income for a geomagnetism program.

**GA5.01/W/04-A1 1700**

**A VECTOR MAGNETOMETER FOR QUASI-ABSOLUTE MEASUREMENT OF THE GEOMAGNETIC FIELD AT SEA**

Toby D G CLARK and Chris W Turbitt (British Geological Survey, West Mains Rd., Edinburgh, EH9 3LA, Scotland, UK; e-mail: t.clark@bgs.ac.uk)

A vector magnetometer is being developed to measure the strength and direction of the geomagnetic field at sea from a sailing vessel. Its purpose is to make geomagnetic measurements during a voyage to circumnavigate the Atlantic to mark the 300th anniversary of Edmond Halley's voyages in the "Paramore" and his chart of the Earth's magnetic field. The instrument consists of a tri-axial full-field fluxgate magnetometer, supplied by the Danish Meteorological Institute, mounted on a rigid frame together with the four antennas of an Ashtech 3DF GPS Attitude Determination Unit (ADU). The ADU is capable of measuring the attitude of the frame (and hence magnetometer) in pitch, roll and true heading with an accuracy of 0.2 degrees at a rate of 2Hz. A proton magnetometer will also be incorporated to provide absolute measurements of the magnetic field intensity. The calibration of the instrument will be described, and we will also discuss its application in making repeat station measurements at sea.

**GA5.01/E/02-A1 1715**

**TIME SERIES ANALYSIS BY NI SIGNAL PROCESSING SUITE**

Alpar KORMENDI (Geofizikai Observatorium, H-8237 Tihany, Kossuth L. u. 91, Hungary, email: alpar2@mail.mataw.hu)

The high computing power of contemporary PCs and advanced data processing software made possible to analyse large data sets in a laboratory or at home. National Instruments (US) offers several toolkits for sophisticated data analysis. Paper demonstrates the use of Joint Time Frequency Analysis (JTFA) to reveal periodical components in long time series and how to remove (or select) the detected components by digital filters designed (DFD) on the "a priori" knowledge of the frequency spectra. Daily and hourly means of the geomagnetic variations recorded from the beginning of the century have been analysed for selected observatories of the northern and southern hemisphere. Some results were surprising at least for the author.

**GA5.01/E/19-A1 1730**

**VIDEO OF MAGNETIC REPEAT STATION SURVEY WORK IN AUSTRALIA, 1937**

Dudley Parkinson (68 Risdon Road, Newtown, TAS 7008, Australia) and CHARLES BARTON (Australian Geological Survey Organisation, GPO Box 378, Canberra, ACT 2601, Australia, Email: cbarton@agso.gov.au)

This video is a 20 minute extract from a film made by photojournalist Jim Fitzpatrick in 1937 showing a magnetic repeat station occupation carried out by Wilfred C. Parkinson. Parkinson was employed by the Department of Terrestrial Magnetism, Carnegie Institution of Washington. The survey work, which extended to Papua New Guinea and many Pacific islands, was undertaken during three years away from his duties as officer-in-charge of the Watheroo Magnetic Observatory in Western Australia. A modern commentary has been added by Parkinson's son (the first author) to explain the methods and instruments being used.

**Monday 19 July AM**

Presiding Chair: J.L. Rasson (Royal Met. Inst, Belgium)

**GA5.01/E/28-A1 Poster 0900-01**

**THE ALGERIAN REPEAT STATION NETWORK**

A. ABTOUT, F. Anad and N. Akacem (C.R.A.A.G., Algerian Research Center of Astronomy, Astrophysics and geophysics, B.P. 63 Bouzareah, Algiers, Algeria, e mail: geoph@ist.cerist.dz)

Several maps of the element of the geomagnetic field in Algeria are presented. They were carried out from the magnetic repeat station network of 1989- 1993 and 1997. The maps include inclination, declination, vertical, horizontal and total intensities and their corresponding secular variations.

The algerian geomagnetic repeat station network consists of 35 stations chosen to give a fairly uniform distribution throughout the country. All magnetic data were reduced to the Tamanrasset Observatory.

Maps obtained display a regular evolution of the terrestrial magnetic field. In addition, magnetic anomalies at the Hoggar shield and the Sud atlasique flexure are observed. Finally, we present a comparison between these maps and those obtained from the IGRF values.

**GA5.01/P/01-A1 Poster 0900-02**

**MAGNETIC SURVEY FOR ARAB REPUBLIC OF EGYPT**

FATHY MOHAMED AHMED (National Research Institute of Astronomy and Geophysics Helwan, Cairo, Egypt, Fax 002 - 02 - 5548020)

Observations were made for Arab republic of Egypt for the Geomagnetic field elements Vertical, Horizontal , Declination , and total force. 10000points of observations were observed along all accessible roads of Egypt. The magnetic Daily recordi Tfgs of Misallat observatory were used to eliminate. the daily variations to reduce the field observationsto the datum. Contour maps were made for the Geomagnetic field of Egypt.

**GA5.01/L/01-A1 Poster 0900-03**

**REPEAT SURVEYS AND ITS RESULTS IN CUBAN ARCHIPELAGO**

Rosa ALVAREZ (Institute of Geophysics and Astronomy, Science, Technology and Environmental Minister, 212 N. 2906 e/ 29 y 31, La Lisa, Havana, Cuba)

This is a recount of the magnetic survey repetition and others vectorial surveys in the territory of the Cuban Archipelago where the first repeat station net was established since 1965 and the last in 1999. Part of the work was the evaluation and selection of the repeat net station of first and second order according to geographical localization, effect of the regional and local Sq variation and results.

The elaboration of the data permitted to establish the behavior of the secular variation in the period under analysis. It is very important the adequate knowledge of the minimum and maximum values of the variation's period for the region with a purpose to determinate the

frequency of the repetition survey.

The obtained data were used in the determination of the secular variation and evaluation of the regional magnetic models for 1965-1999.

**GA5.01/L/02-A1 Poster 0900-04**

**INVESTIGATION OF THE GEOMAGNETIC FIELD ON THE TERRITORY OF THE CZECH REPUBLIC FOR 1995.5 AND ITS SECULAR VARIATION**

Pavel Hejda and Josef Horacek (both at Geophysical Institut AS CR, Bocni II/1401, 141 31 Prague, Czech Republic, email: ph@ig.cas.cz)

The measurements of geomagnetic field on the territory of the Czech Republic cover continuous observations at the Geomagnetic observatory Budkov, measurements at 7 repeat stations (carried out about every two years) and magnetic survey. A recent stage of magnetic surveying activity was started in the fifties by setting up a fundamental network of the first order consisting of 199 points. The network was re-occupied in 1976-78 and 1994-1996. The last magnetic survey was carried out by a flux gate theodolite for measurements of declination and inclination and by a proton precession magnetometer for the total intensity. The azimuth was determined by the Sun observations.

All values were reduced to the epoch 1995.5. With regard to rather long period of the measurements (more than 2 years) the temporal and spatial changes of the secular variation had to be taken into consideration when reducing data. The main problem was how to estimate the unknown secular variation at the individual points. As the Central Europe is covered by a quite dense net of geomagnetic observatories, we have used their annual means together with the repeat stations data for creating a regional model of secular variation. Nevertheless, this process was not free of complications, because our study revealed large discrepancies in some observatory data. A plausible solution was found after more detailed analysis and with help of IGRF secular variation model.

**GA5.01/W/11-A1 Poster 0900-05**

**A MODEL OF GRID MAGNETIC ANGLE FOR GREAT BRITAIN**

SUSAN MACMILLAN and Jim Carrigan (British Geological Survey, Murchison House, West Mains Road, Edinburgh EH9 3LA, UK. email: S.Macmillan@bgs.ac.uk, J.Carrigan@bgs.ac.uk)

Using declination data from observatories and repeat stations, a model of grid magnetic angle (the angle between grid north and magnetic north in the horizontal plane) for the period 1999 to 2002 is derived for Great Britain. We describe the reduction to magnetic quiet level of the raw data, the derivation of a regional secular-variation model and reduction of data to epoch, and the final computation of grid magnetic angle. The resulting model is used in a service to provide magnetic information to the Ordnance Survey, the national mapping agency.

**GA5.01/E/09-A1 Poster 0900-06**

**THIN STRUCTURE OF SECULAR VARIATION OF GEOMAGNETIC FIELD IN EUROPE**

Valentyn MAKSYMCHUK (Carpathian Branch of Subbotin Institute of Geophysics NASU, 3b, Naukova Str, Lviv, 290601, UA, email: valentyn@carp.lviv.ua)

To analyze secular variation on the territory of Europe, average annual values of X, Y, Z - components of geomagnetic field on the European network of magnetic observatories in 1950-1993 have been used. During the time interval in question there existed in Europe two focuses of SV: European, with the epicenter in Southern Europe, and Arctic, with the epicenter in the north of Europe. Dynamics and kinematics of these focuses had the crucial influence on the structure of the field SV. Both focuses had low intensity (20-40 nT/year). It looks like the European focus appeared in Southern Europe (in the region of the Balkans) in the fifties in the result of transfer of the Caspian focus. Velocity of its drift during this period made up approximately 2 grade/year. The Arctic focus of SV emerges in the region of Scandinavia in the seventies. It drifted south, its speed of transfer in separate attained 15 grade/year. In 1980-1990 SV focus remained steady in Central Europe, approximately in the vicinity of European SV focus in the sixties. Analysis of annual maps of SV convincingly demonstrates that there were 2 SV focuses in Europe at that time. By the end of the eighties Arctic focus finally disappeared, and European SV focus still existed on the territory of Central Europe. Calculations of SV centers depth were performed. Despite of the differences in SV field morphology and intensity, drift velocities, the depth of their sources turned to be rather close and were within 3500-4500 km, corresponding to the liquid part of the Earth's core.

**GA5.01/E/18-A1 Poster 0900-07**

**GEOMAGNETIC SURVEY OF ESTONIA**

H. NEVANLINNA (Finnish Meteorological Institute, P.O.Box 503, FI-00101 Helsinki, Finland, email: heikki.nevanlinna@fmi.fi) K. Pajunpää (Finnish Meteorological Institute, Nurmijärvi Geophysical Observatory, FI-05100 Röykkä, Finland, email: kari.pajunpaa@fmi.fi) L. Kreen (Estonian Air Navigation Services, Lennujaam 2, EE-0011 Tallinn, Estonia, email: lauri@eans.ee)

During summer 1998 geomagnetic field components were measured at 11 sites in Estonia. One of the aim of the project was to re-measure declination at airport reference point (ARP) that have not been done since the Soviet era in Estonia. By collecting all the declination data available in the Soviet geomagnetic maps in the 70's, a reconstruction of the distribution of declination in Estonia was carried out and a preliminary declination chart (1: 500 000) of Estonia for 1998.0 was published [1]. The plan is to make in the near future a more detailed geomagnetic survey (say in 30 km x 30 km grid) of Estonia by using a movable DI-flux together with the proton magnetometer.

[1]. Nevanlinna, H., Sallinen, T. and Kork, M., 1998. Geomagnetic declination chart of Estonia 1998.0. Finn. Met. Inst. - Geophys. Publ. 45.

**GA5.01/E/23-A1 Poster 0900-08**

**CERTIFICATION OF AIRCRAFT COMPASS CALIBRATION BASES: A JOB FOR GEOMAGNETIC OBSERVATORY PEOPLE**

JEAN L. RASSON, (Institut Royal Meteorologique, Centre de Physique du Globe, B-5670 Dourbes Belgique)

An airport should have a special area where the magnetic compasses of aircraft can be checked and calibrated. This area (the Compass Base) should be surveyed for establishing its magnetic cleanliness and for measuring the Magnetic Declination on it. This very specialised task is easily accomplished by geomagnetic observatory staff using the standard absolute instrumentation. We review the procedures and requirements for Compass Base surveying. An example at the Brussels International Airport is presented.

**GA5.01/E/32-A1** Poster **0900-09**

**THE MAGNETIC REPEAT STATION SURVEYS IN SWEDEN**

Kjell Borg and Gerhard SCHWARZ (Geological Survey of Sweden, Box 670, S-75128 Uppsala, Sweden, email: gerhard@sgu.se)

In recognising the need for more systematic magnetic observations a net of sites was established in Sweden in the 1920s that were almost evenly distributed over the country and intended to serve as repeat stations for future re-occupations. In 1930 the net consisted of 86 stations. A number of them were installed in remote areas and the effort in surveying these sites periodically was very large. Therefore, this extended net of observational points was reduced to only 10 sites in the early 1950s. The remaining sites were then revisited every other year until today.

We will present here the procedures for measuring secular magnetic variations and their development in time. The derived normal magnetic field will be compared in space and time with other available magnetic reference fields. We will outline future perspectives and strategies for secular magnetic variation measurements in Sweden and compare them with ordinary magnetic observatory recordings.

**GA5.01/E/31-A1** Poster **0900-10**

**GLOBAL DP2 CURRENT SYSTEM OBSERVED IN CIRCUM-PAN PACIFIC MAGNETMETER NETWORK**

Hiroshi TACHIHARA, Manabu Shinohara, Hideaki Kawano, Kiyohumi Yumoto (all at Dept. of Earth and Planetary Sciences, Kyushu University, Fukuoka, 812-8581 Japan, Email: tachi@geo.kyushu-u.ac.jp), Yasuo Kitamura (Tohoku Institute of Technology, Sendai, 982-8577 Japan) and CPMN Group

We have started geomagnetic observations at seven stations in the magnetic equator (IMLAT= 0-1.55) as the Circum-pan Pacific Magnetometer Network (CPMN). These stations are located along the magnetic equator and scattered at the places in local time of midday to midnight. We can expect the detailed analysis of local time variation of the equatorial electrojet from this global observation arrangement. Moreover, these observations can reveal the details and local time dependence of disturbance energy transfer in the earth ionosphere, from the auroral to the equatorial region in company with other global observations in mid- to high-latitudes. We present the analysis of DP2 current system observed in the magnetic storm time on August 26, 1998 by using the magnetic data from these CPMN network.

Our newly established equatorial observations are at Ancon (Peru ; MLAT=1.55 ; MLT midnight in UT = 4.80), Guadalupe (Peru ; MLAT=-0.02 ; MLT= 4.74), Canete (Peru ; MLAT=0.78 ; MLT= 4.77), Yap (Micronesia ; MLAT=0.45 ; MLT= 15.13), Davao (Philippines ; MLAT=-1.35 ; MLT= 15.88), Cebu (Philippines ; MLAT=0.73 ; MLT= 15.96) and Bac Lieu (Vietnam ; MLAT=0.85 ; MLT= 17.02). These stations are located quite near to the magnetic equator. We examined the global DP2 current system in the magnetic storm time on August 26, 1998 by using these equatorial data as well as other CPMN data. It is well known that global DP2 current system consists of twin-vortex currents in dawn and dusk sides and the global eastward current in the dayside and nightside equatorial regions. Our analysis revealed the strong eastward current in the dayside equatorial region and, however, variation of currents in the nightside equatorial region. We will present several analysis of global DP2 current system focused to the equatorial currents.

**GA5.01/W/13-A1** Poster **0900-11**

**USE OF GEOMAGNETIC INDUCTION VECTORS TO CONTROL MAGNETOMETER DATA QUALITY**

Ari VILJANEN (Finnish Meteorological Institute, Geophysical Research Division, P.O.B. 503, FIN-00101 Helsinki, Finland, email: ari.viljanen@fmi.fi)

Geomagnetic induction vectors are used in scientific investigations to locate highly-conducting anomalies in the earth. Another application is found in a long-term control of magnetometer data quality. This is based on the time-independence of the induction vectors, because the earth's structure does not vary. Consequently, changes in vectors indicate instrumental problems, man-made noise or, mostly at high latitudes, the source effect due to non-uniform ionospheric currents. The latter is a natural phenomenon to be distinguished from the first ones. This presentation illustrates the use of induction vectors to control the IMAGE magnetometer data recorded in Fennoscandia and Svalbard, where the source effect also plays a significant role.

**Monday 19 July PM**

Presiding Chair: Hegymegi Laszlo (Elgi, Hungary)

**GA5.01/P/03-A1** Poster **1300-01**

**MISALLAT OBSERVATORY GEOMAGNETIC DATA FOR THE YEAR 1995 AND ITS INTERPRETATION**

FATHY MOHAMED AHMED (National Research Institute of Astronomy and Geophysics, Helwan , Cairo , Egypt. Fax : 002 - 02 - 5548020)

The Observations for the geomagnetic field elements of Misallat Observatory Egypt (Lat. 29° 30. 9' N , Long. 30° 53.5'E) were measured for the year 1995 by Fluxgate magnetometer , Vector magnetometer, Askania Pivot Declinometer , BMZ , QHM , proton magnetometer , and Automatic Observatory - 8200. Computer Programmes were prepared and used to interpret the data. The Interpretations of the data are Very well I shown on very good figures.

**GA5.01/E/11-A1** Poster **1300-02**

**AUTOMATED COMPUTATION OF ABSOLUTE OBSERVATIONS FOR OBSERVATORIES AND REPEAT SURVEYS**

BERARDUCCI, A.M., (U.S. Geological Survey, Golden, Colorado,USA) Worthington, E.W., (Geophysical Institute, University of Alaska, Fairbanks, Alaska,USA)

The USGS is using a spreadsheet program for computing DI-Flux absolute measurements. The program is primarily used at Observatories and Repeat Stations, though it has applications wherever DI-Flux observations are made. The program computes absolute values, baseline values, baseline averages and standard deviations. Macros are used to output each set of observations, a summary of baselines and historical graphs of baselines. Use of the program allows for electronic transfer of results to the main office immediately after the data has been entered. It has also helped reduce computation errors and has automated compilation of absolute and calibration files.

**GA5.01/W/01-A1** Poster **1300-03**

**CONTROL METHODS FOR GEOMAGNETIC FIELD MEASUREMENTS BASED ON PROTON PRECESSION SIGNAL PROCESSING**

Olga DEKUSAR, Alex Denisov, Vladimir Sapunov, Dmitriy Savelyev, Serg Kiselev (Ural State Technical University, Quantum Magnetometry Laboratory, Mira St., 19, Ekaterinburg, 620002, RUSSIA, email: sva@dpt.ustu.ru)

This report proposes technical methods, which can be useful for measurement of the geomagnetic field in the observatory and fieldwork. The use of proton precession signal processing allows to improve not only sensitivity of proton magnetometers but also analysis of the magnetic variations.

To control of proton magnetometer accuracy, the QMLab offers to use a quality measurement criterion (QMC) based on time analysis of proton precession signal periods. The QMC can be determined in units of magnetic fields (nT) in single reading. This criterion is equal to a standard deviation of continuous measurements at stable geomagnetic fields. The QMC is not susceptible to geomagnetic variation and takes into account real conditions (proton signal value, noise, magnetic gradient, etc). A self-adapting cut of proton signals by signal statistic analysis is useful to suppress harmful pulses (lightning, microphone effect, malfunction, etc). In this case, the QMC outputs a real measurement accuracy also. The methods are field-tested and are introduced in the QMLab Overhauser magnetometer POS-1. In this report, the algorithm and background of signals processing are submitted.

It is discussed a background of algorithm and signal precession treatment to measure of geomagnetic field rate in single reading. Thus, a proton magnetometer can operate us a new device namely a speed magnetometer. Sensitivity was evaluated about 0.01 nT/sec for Overhauser's speed magnetometer at 3 sec sampling rate. This method may be useful at rather slow measurements.

**GA5.01/W/12-A1** Poster **1300-04**

**A NEW GENERATION OF U.S. MAGNETIC OBSERVATORY DATA ACQUISITION SYSTEMS**

D.C. HERZOG (USGS, Box 25046 MS 966, Denver Federal Center, Denver, Colorado, 80225-0046 USA, email: herzog@ghmail.cr.usgs.gov)

The U.S. Geological Survey's (USGS) Geomagnetism program is undergoing a major modification in the data acquisition systems (DAS) used at its network of 13 magnetic observatories. The correct data collection platforms (DCP) are nearly two decades old and lack sufficient capabilities to perform the functions required for today's observatory operations, including: the collection and storage of 1-second data; orderly shutdown & start up in the event of power failures; and dedicated access to the Internet. The new generation of DAS will use commercial, off-the-shelf personal computers (PC's) with multi-user, multi-tasking operating systems (OS) for observatory operations including: 1-second data recording and storage; numerical filtering; GPS time synchronization; satellite data transmissions; on-site data access, display, and diagnostics; ftp and e-mail operations; and remote system administration from the data collection & processing center located in Golden Colorado.

**GA5.01/W/17-A1** Poster **1300-05**

**ABOUT THE METHOD OF SPIKES FILTERING IN DIGITAL RECORDS**

Gianibelli Julio C., CABASSI, Iris R., and KHON,Jaqueline (Dep. of Geomagnetism and Aeronomy, Faculty of Astronomical and Geophysical Sciences, La Plata University, Paseo del Bosque s/n, 1900 La Plata, Argentina, email: jcg@fcaglp.fcaglp.unlp.edu.ar, rosy@fcaglp.fcaglp.unlp.edu.ar, jkhon@fcaglp.fcaglp.unlp.edu.ar )

Normally, the geomagnetic variations are masked by a noise mixing forming random spikes in the digital records. Three types of filters are analysed: the observations comparison method, the window-filter based on the median determination, and the FFT filter by means of a low-pass window. The application of these methods allow us to establish important characteristics using the median filter method for the Q-days or minimum magnetic activity. Thus, insulated spikes or, sometimes, consecutive apikes are present on the temporal sampling of the system. When the density of spikes is high in the digital records, the FFT and low-pass filters help us for the variation determination. Examples with Trelew magnetic observatory data are showed.

**GA5.01/W/15-A1** Poster **1300-06**

**RESULTS OF THE INTERCOMPARISON OF THE DI-FLUX THEODOLITES AT GEOPHYSICAL OBSERVATORY "KLYUCHI", NOVOSIBIRSK, RUSSIA**

S.Y. KHOMUTOV, O.I. Fedotova, V.V. Kuznetsov, A.F. Pavlov, N.N. Semakov (Institute of Geophysics SB RAS, Koptyug av., 3, Novosibirsk 630090, Russia; email: hom@uiggm.nsc.ru)

DI-flux system for absolute magnetic measurements is developed at Geophysical observatory "Klyuchi" (Novosibirsk, Russia). It includes a standard theodolite 3T2KP with resolution of 2" (precision system) or theodolite 4T30P with resolution of 30" (field system), manufactured on PO "UOMZ" (Ekaterinburg, Russia), fluxgate sensor mounted on the telescope and electronic null indicator. All magnetic units of the theodolites were replaced on non-magnetic ones. The results of the intercomparison of the absolute D and I measurements using two precision systems, one field system and theodolite Theo 020 are presented. Theo 020 is used at the observatory for the magnetic field monitoring and it is considered as a reference for comparison.

**GA5.01/W/07-A1** Poster **1300-07**

**THE DIGITAL VARIATION STATION FOR MAGNETIC OBSERVATIONS**

S.Y. KHOMUTOV, A.N. Fedorov, V.V. Kuznetsov, (Institute of Geophysics SB RAS, Koptyug av., 3, Novosibirsk 630090, Russia; email: hom@uiggm.nsc.ru), V.K. Palamarchuk (Okeangeologia, St.-Petersburg, Russia), A.I. Zhelevsky (Institute of Automation and Electrometry SB RAS, Novosibirsk 630090, Russia)

The operating sample of vector digital magnetometer with the synchronous registration, was devised by us. The Earth's magnetic field components are registered simultaneously by two identical measuring systems separated by up to 800 m and controlled by common PC. Zeeman effect is used to register the magnetic field in sensors. The sensors are fixed in the Helmholtz coils. The PC programs appended, ensure automatic data registration and process. Dynamic range of field absolute measurements: from 20 000 to 100 000 nT. Resolution is equal to 0.01 nT for the accumulating time 0.2 sec. Stability of the field absolute values averaged per one day is equal to 0.1 nT. This magnetometer was field tested as the part of the station for the magneto-telluric sounding and also as registrar of the magnetic field components on the airplane.



**GA5.01/E/17-A1 Poster 1300-08**

**SODANKYLÄ POLAR YEAR OBSERVATORY 1882-1883**

H. NEVANLINNA (Finnish Meteorological Institute, P.O.Box 503, FI-00101 Helsinki, Finland, email: heikki.nevanlinna@fmi.fi), J. Kultima (University of Oulu, Sodankylä Geophysical Observatory, FI-99600, Finland, email: johannes.kultima@sgo.fi)

Sodankylä was one of the 11 stations that were in operation during the First International Polar Year 1882-1883. In this poster we demonstrate results of magnetic observations carried out in Sodankylä (September 1, 1882 - August 31, 1883) in a similar manner that is the usual practice for modern geomagnetic observatory data. The magnetic field during the Polar Year period 1882-1883 was very disturbed. One of the greatest (eighth strongest according to the aa-statistics 1844-1998) magnetic storm occurred on November 20th, 1882. The motivation to publish and analyse more than 100-year old geomagnetic data arises from the fact that the quality of the data collected at Sodankylä is good for e.g. analysis of the time behaviour of the geomagnetic activity. The data, about 28 500 hourly readings of the declination (D), horizontal (H), and vertical component (Z) of the geomagnetic field is now in electronic form and will be distributed to the World Data Centers. The quality and homogeneity of magnetic observations of D and H is good but Z is less reliable. Similar data analysis of geomagnetic data from other geomagnetic observatories (like Helsinki 1844-1910) has been successful in reconstructing geomagnetic activity index series for the 19th century (the data is available through internet: <http://www.geo.fmi.fi/pub/data/Helsinki/>). Such analyses, as well the utilisation of Sodankylä Polar Year data presented here, promote the construction of long time series of geomagnetic activity that are important in studies of e.g. space climate.

**GA5.01/W/10-A1 Poster 1300-09**

**A DESCRIPTION OF A NEW GEOMAGNETIC OBSERVATORY IN UPPSALA, SWEDEN**

Birna OLAFSDOTTIR (Geological Survey of Sweden, Box 670, SE-751 28 UPPSALA, Sweden, email: birna@sgu.se)

Lovö Geomagnetic Observatory in Stockholm, which is Sweden's main geomagnetic observatory, will be closed down in a few years because of a ring road project with years of tunnelling work close to the observatory. Also the Lovö Observatory is contaminated by noise from the Stockholm underground trains. A new observatory, which will succeed Lovö, has been built 68 km north of the old observatory, in the vicinity of Uppsala. The guidelines used when choosing the new observatory site and the design and technical details of the observatory will be shown. The main problems in getting short and long-term stability and continuous registrations will be revealed.

**GA5.01/E/15-A1 Poster 1300-10**

**HIGH-SENSITIVE MAGNETIC CLEANLINESS STUDY - PROCEDURE DEVELOPMENT AND TEST RESULTS**

Kari PAJUNPAA (Finnish Meteorological Institute, Nurmijärvi Geophysical Observatory, FI-05100 Ryykkö, Finland, email: kari.pajunpaa@fmi.fi) Viktor Tarassov and Valery Korepanov (Lviv Centre of Institute of Space Research, 5-A Naukova str., 290601 Lviv, Ukraine, email: vakor@isr.lviv.ua)

Nurmijärvi magnetic observatory has well-known calibrating facilities allowing to verify practically all parameters of Earth's field magnetometers. Last year taking into account very favourable surroundings it was completed by a new magnetic cleanliness measuring system which was built in order to solve very important tasks: magnetic cleanliness study and discovered magnetic moments compensation. One of the first system applications is to serve to European and especially local satellite instruments manufacturers.

An existing reference coil system and electronics for magnetometer calibrations were utilised as basic components for the new equipment. A non-magnetic rotating table and a sensing three-components flux-gate magnetometer were installed additionally in the coil system center and corresponding interactive software was written for fast and accurate measurements. A low-frequency (1-10 Hz) demagnetising facilities are available and their higher frequency (50 Hz) development is under construction. Tested bodies with dimensions of about half a meter and weight till 30 kg can be brought inside the coil system. The software is based on LINUX operating system and allows to choose operation modes of rotating table and reference coil system in dependence of the test procedure progress and to compensate automatically Earth's magnetic field variations. Parameters and operational features of the system as well as first measurement results will be presented.

**GA5.01/E/01-A1 Poster 1300-11**

**THE DELTA I - DELTA D (DIDD) QUASI-ABSOLUTE COIL SYSTEM. IT'S HISTORY, EVOLUTION AND FUTURE**

LEROY W. PANKRATZ, (US Geological Survey, PO Box 25046, Mail Stop 968, Denver Federal Center, Denver, Colorado, USA, 80225-0046, email: pankratz@ghnail.cr.usgs.gov), Alpar Kormendi, (Eotvos Lorand Geophysical Institute, Budapest, Hungary, email: alpar2@mail.mtatv.hu)

Standard geomagnetic recording systems in use today are relative instruments; the absolute baseline of which changes with time. The absolute baseline of the variation instrument requires regular calibration with an independent, true absolute instrument. Several attempts in the past 35 years have been made to develop a quasi-absolute instrument. However, due to cumbersome control and recording systems these concepts were soon abandoned. In order to achieve near absolute stability an absolute instrument has been adapted to measure field variations. The proton precession magnetometer, which is a scalar instrument, is used to measure the components of the Earth's Geomagnetic Field by applying momentary, sequential deflection fields in mutually orthogonal coils. In the case of the classical proton precession magnetometer, the sampling rate is relatively low, resulting in a time difference between the measurement of individual components which can produce measurement errors especially during rapid variations in the field. Another problem which was the difficulty of producing homogeneous fields in a large volume occupied by the sensor of proton precession magnetometer. An inhomogeneous field yields a rapid signal decay, providing an inaccurate measurement. In order to accommodate the rather large sensors available years ago, in a homogeneous volume required large Helmholtz coils. These early coils were in excess of 70 cm in diameter. The resulting coil system was expensive, less stable and required a large pier and shelter.

Recent attempts have concentrated on much smaller spherical coils and the overhauser proton magnetometer. In addition, advances in electronic and computer circuitry have allowed rapid switching of coil bias currents and acquisition and preprocessing of the data.

**GA5.01/L/04-A1 Poster 1300-12**

**NETWORKED AUTOMATIC DATA PROCESSING AT IRKUTSK GEOMAGNETIC OBSERVATORY**

Victor Egorov, Stanislav Nechaev, and Alexander POTAPOV (all at Institute of Solar-Terrestrial Physics, P.O.B. 4026, Irkutsk, 664033 Russia, e-mail: potapov@iszf.irk.ru)

Irkutsk magnetic observatory has a 113-year history. First measurements were taken here in 1886. Irkutsk observatory changed from an analog to digital form of recording, starting in January 1996. At present a three axis quartz variometer with digital output (one minute values of three components) is used as a sensor. It is connected to the observatory local network consisting of four computers. The net provides data acquisition and preliminary processing including on a routine basis, as well as data transmission through a telephone line under remote control to the Institute of Solar-Terrestrial Physics (ISTP) 30 km from the observatory. The information collector at ISTP has access to the local Institute's network and the global Internet. From the observatory to ISTP, the data are transferred automatically once every three hours (an one-hour regime is available). Once a day the data are sent to the INTERMAGNET geomagnetic information node in Edinburgh via e-mail (automatic transmission is under development). The three-hour preliminary K index and one-hour local magnetic variation amplitude are estimated in the automatic mode and disseminated through the local net to users. Data quality control is provided by weekly absolute measurements using the scalar magnetometer and declinometer/inclinometer system. Error analysis and hardware control help to ensure data quality.

**GA5.01/E/30-A1 Poster 1300-13**

**RESULTS OF DIFLUX INTERCOMPARISONS AT THE 8TH WORKSHOP ON GEOMAGNETIC OBSERVATORY INSTRUMENTS, DATA ACQUISITION AND PROCESSING IN VASSOURAS, BRASIL, SEPTEMBER 1998**

JEAN L. RASSON, (Institut Royal Meteorologique, Centre de Physique du Globe, B-5670 Dourbes Belgique Ronaldo Marins Carvalho, Observatorio Nacional, Rua General Bruce 586, 20921-400 Rio de Janeiro, RJ Brasil)

An extensive inter-comparison of geomagnetic observatory instrumentation took place during the "8th Workshop on Geomagnetic Observatory Instruments, Data Acquisition and Processing" in Vassouras, Brasil, during September 1998. In total 15 Diffluges of various makes from 3 continents (Zeiss 020, Zeiss 010, Bartington, Ruska, Sokkisha) were inter-compared using the observatory INTERMAGNET digital fluxgate variometer baseline and proton precession magnetometer. The results for the Diffluges are presented. This inter-comparison allows us to make a global appreciation on the observation accuracy currently achieved.

**GA5.01/W/06-A1 Poster 1300-14**

**NEW PROCESSOR OVERHAUSER SENSORS INTENDED FOR OBSERVATORIES AND FIELDWORK**

Vladimir SAPUNOV, Dmitriy Saveliev, Alex Denisov, Sergey Kiselev, Olga Dekusar (Ural State Technical University, Quantum Magnetometry Laboratory, Mira St., 19, Ekaterinburg, 620002, RUSSIA, email: sva@dpt.ustu.ru)

The QMLab develops Overhauser cycling magnetometers of total and components geomagnetic field that are based on unique stable working substances, computer methods of calculation and sensors optimisation, digital processing methods of proton free precession signal. Examples of these techniques are presented, paying particular attention to the new processor Overhauser sensor POS-1 in which novelties are applied in most extent.

The sensor small-size head (working volume is only Dia30x70 mm) offers smaller Braunbeck's coil size up to 20 cm at measurement of the geomagnetic field components by proton precession methods. Highest signal to noise ratio of our sensor OS-2 (it is used the DNP-ampoule A-54/30) allows to measure geomagnetic components up to 0.03 nT sensitivity and up to 1 nT absolute accuracy (G. Dgirov, Kazakhstan; V. Pak, St-Peterburg). The field-cycling Overhauser and proton standard sensors are analogous with each other but FC-Overhauser mode ensures the best property (rms up to 0.01 nT, accuracy 0.1-1 nT, drift less 0.05 nT/year). In particular, there is simple opportunity to improve of proton existing magnetometers by Overhauser's sensors.

**GA5.06 Wednesday 21 July**

**PRODUCTION AND USE OF GEOMAGNETIC INDICES (IGA)  
Location: Muirhead Tower, 112 LR2**

**Wednesday 21 July AM**

Presiding Chair: H.-J. Linthe (GFZ Potsdam, Niemeck, Germany)

**GA5.06/E/01-A3 0900**

**ON LINE DATA AVAILABILITY: THE EXPERIENCE OF THE ISGI PUBLICATION OFFICE**

J. PARIS (CETP, 4 Avenue de Neptune, F-94107 Saint Maur des Fosses Cedex, FRANCE) and M. MENVIELLE (CETP and Universite Paris Sud, FRANCE)

A software for routine derivation and dissemination of quick-look values of K derived planetary geomagnetic indices am and aa is run by the ISGI Publication Office since the end of 1996. The minute values are automatically got from 15 observatories on a daily basis through data transfer facilities like ftp procedure or e-mail. Our experience shows that:

1. a delay on the order of two weeks is necessary to get the data allowing the derivation of longitude sector indices, such as those provided in the frame of the Oersted program;
2. the on line data availability allows a routine derivation of quick-look planetary indices at day D+2;
3. shortening the delay of dissemination of quick-look planetary indices requires to reduce the number of observatories and to get directly the data from the observatory.

**GA5.06/E/02-A3 0920**

**PRODUCTION AND DISTRIBUTION OF THE KP AND DERIVED INDICES - CONTINUATION OF A TRADITION**

Hans-Joachim LINTHE (GFZ Potsdam, Adolf-Schmidt-Observatory, Lindenstr. 7, D-14823 Niemeck, Germany, email: linthe@gfz-potsdam.de)

Scientific applications require continuous series of geomagnetic activity indices. Besides of long-term series more and more the near real-time derivation becomes important. The global geomagnetic indices Kp, ap, Cp extend back to January 1932 and are now provided twice a month on a routine basis. At the beginning of the year 1997 the tradition of these indices was

taken over from the Institute of Geophysics of the University Goettingen to the Adolf-Schmidt-Observatory Niemegk. The indices are calculated under full consideration of the method approved by the IAGA. The current stage of the production will be presented. The indices are calculated halfmonthly and distributed per e-mail, FTP and presented on WWW. It should be discussed the question of increasing the frequency of the production and distribution.

**GA5.06/W/01-A3 0940**

**DERIVATION OF NEAR REALTIME DST INDEX**

Toyohisa KAMEI (WDC-C2 for Geomagnetism, Graduate School of Science, Kyoto University, Sakyo-ku, Kyoto 606-8502, Japan, email: toyo@kugi.kyoto-u.ac.jp); Masahisa Sugiura (Research Institute of Science and Technology, Tokai University, 2-28 Tomigaya, Shibuya-ku, Tokyo 151-0063, Japan, email: sugiura@jspan.kugi.kyoto-u.ac.jp)

Responding to the growing demands for quicker availability of the Dst index, we have started derivation of Near Real-time (Quick-look, QL-) Dst index. In the past the Dst indices were made available in two steps. In the first step, a Provisional Index is derived as soon as the necessary (provisional) data are received from the contributing observatories, and is disseminated by post or by other means. The Provisional Index is meant for uses for diagnostic purposes only. The second is a final index of high quality suitable for scientific analyses, which is derived and distributed annually. Now we have added one more version for quick-look monitoring purposes. This version is derived by data transfer through the INTERMAGNET system and having cooperation from the contributing stations. It is derived using estimated baselines and simplified Sq models. It is updated with a time delay of 3 hours to 3 days and is made available through WWW of WDC-C2 for Geomagnetism, Kyoto (http://swdcd.kugi.kyoto-u.ac.jp). However, the user is strongly advised to use the QL-Dst index only for monitoring purposes. The unchecked, uncalibrated data directly sent from the stations are used, and these data contain spikes, errors and missing values. For scientific analyses we advise to use the final Dst index or at least the provisional Dst index. The user for forecasting should be aware that the QL-Dst index is updated from time to time, and should use the latest version. Update information is provided separately from the WWW services.

**GA5.06/W/09-A3 1000**

**CHARACTERISTICS OF THE INDIVIDUAL AE STATIONS WITH RESPECT TO THEIR CONTRIBUTION TO THE AE INDICES**

Toyohisa KAMEI and Tohru Araki (both at WDC-C2 for Geomagnetism, Graduate School of Science, Kyoto University, Sakyo-ku, Kyoto 606-8502, Japan, email: toyo@kugi.kyoto-u.ac.jp); Masahisa Sugiura (Research Institute of Science and Technology, Tokai University, 2-28 Tomigaya, Shibuya-ku, Tokyo 151-0063, Japan, email: sugiura@jspan.kugi.kyoto-u.ac.jp)

The AE indices are derived using data from 12 stations along the auroral zone. Since 1996 one of these stations, i.e. Cape Wellen (CWE), has stopped operation due to power failure. We have analyzed the contributions of individual stations to the AE indices in order to delineate the effect of the loss of CWE. This station is situated at a latitude (invariant latitude 62 degrees) somewhat lower than the other AE stations; for this reason the station has been thought to be of less importance than the other stations. By our analysis we conclude that CWE indeed does not contribute to AE Under quiet and moderately disturbed conditions (AL > -500nT or AE < 100nT), but it can significantly contribute to both AL and AU under disturbed conditions (-500nT < AL or AE > 100nT). As the CWE record saturates at -2000nT, this station has failed in the past to demonstrate its potential importance during disturbed periods. Since it appears very difficult to re-open the CWE station, an effort is being made to open a replacement station near Pebek in Siberia to fill in the large gap between Tixie and Barrow. For this replacement station, we plan on installing a magnetometer with a wider dynamic range than with the CWE instrument. However, our attempt to create this new AE station is encountering great difficulties because of local political and economical situations. Through this analysis we conclude that we should increase AE stations at invariant latitude 62-63 degrees to obtain improved AE indices for disturbed periods.

**GA5.06/E/04-A3 1020**

**THE ISGI WWW HOMEPAGE**

J. Paris, C. Vernin (CETP, 4 Avenue de Neptune, F-94107 SAINT MAUR DES FOSSES CEDEX, FRANCE) and M. MENVIELLE (CETP and Universite Paris Sud, FRANCE)

The ISGI Publication Office has recently established a WWW homepage at the following address: <http://www.cetp.ipsl.fr/~isgi/homepag1.htm>

The ISGI WWW site aims at providing simple and efficient access to geomagnetic indices, either directly or through mirror links to the WWW sites of the ISGI Collaborating Institutes (GFZ Potsdam, Germany; WDC-C2 for Geomagnetism, Kyoto, Japan; Observatori de l'Ebre, Roquetes, Spain). The information and data series available at the ISGI WWW site are:

- information on ISGI;
- information on indices derivation and availability;
- provisional and definitive values of AU, AE, AL, aa (Kpa), am (Kpm), Kp, and Dst indices as monthly tables or ASCII files (hourly values for AU, AE, AL, and Dst; 3-hour values for the K-derived indices);
- definitive list of ssc;
- quick-look, provisional, and definitive values of K-derived longitude sector activity indices
- quick-look values of aa (Kpa) and am (Kpm) indices, for the current month and the two previous ones;
- musical diagrams (as postscript files) for aa and am indices;
- ISGI Monthly Bulletins for the current year and the two previous ones;
- selected papers about new advances in indices derivation

**GA5.06/W/07-A3 1100**

**WHEN DO THE GEOMAGNETIC AA AND AP INDICES DISAGREE?**

Helen E. COFFEY and Edward H. Erwin (both at Solar-Terrestrial Physics Division, NOAA National Geophysical Data Center, World Data Center A for Solar-Terrestrial Physics, 325 Broadway, Boulder, CO 80303 USA, email: hcoffey@ngdc.noaa.gov)

The next geomagnetic cycle has been predicted using the long term aa index database. Current real time predictions use the Ap index. Unfortunately, the aa and Ap index do not always agree. The correlation is at the 0.8 level, even though the two aa stations are included in the Ap index. We investigate the differences between these indices, looking for trends at different levels of activity, different solar cycle periods, different times of the day, different Bz orientations, etc. Plots are presented to display these results.

**GA5.06/W/03-A3 1120**

**SOLAR CYCLE CHANGES IN THE STATISTICAL PROPERTIES OF MAGNETIC INDICES**

Robert L. MCPHERRON (Inst. of Geophys. and Planet. Phys. and Dept. of Earth and Space Sci., University of California, Los Angeles, CA 90095-1567, e-mail: rmcphe@ucla.edu)

The most frequently used indices include Kp, AE, PC and Dst. These indices were originally defined as simple measures of the strength of different current systems that produce the disturbances collectively known as geomagnetic activity. Kp is a measure of bay disturbances by subauroral and midlatitude stations, AE, or more precisely, AU and AL, respectively measure the strength of the eastward and westward auroral electrojets with auroral zone stations. PC utilizes a single polar cap station to measure the strength of the sheet current that returns current from the electrojets across the polar cap. Finally, Dst measures the strength of the ring current with equatorial stations. Since geomagnetic activity is driven by the solar wind these indices are highly correlated with each other and with a variety of solar wind coupling functions. Furthermore, because the properties of the solar wind depend on the Sun the indices all exhibit correlations with indices of solar activity such as the sunspot number. In this paper we investigate the properties of these indices and their interrelations as a function of the solar cycle. We expect that the indices will exhibit semi-annual variations, 27-day recurrence and diurnal variations, and that these change systematically with the solar cycle. Our initial results are surprising. For example, AL weakens towards solar max while AU strengthens such that AE shows almost no variation. Also, Kp displays a clear semi-annual variation while the AE index does not. These results suggest that there are systematic effects in the indices that cause them to behave in unexpected ways. We will illustrate other properties of the indices and attempt to explain their behavior in terms of physical processes and the methods of derivation. We conclude with recommendations for improvements in the indices.

**GA5.06/W/08-A4 1140**

**SEARCH FOR QUIET, REGULAR, AND DISTURBED DAYS DEFINITION**

Severino L. G. DUTRA and Nalin B. Trivedi (Instituto Nacional de Pesquisas Espaciais-INPE, C.P. 515, São José dos Campos, SP, 12201-970, Brazil, e-mail: dutra@dge.inpe.br, trivedi@inpe.dge.br); Jose M. DA COSTA (Universidade de Taubaté-UNITAU, Taubaté, SP, 12020-270, Brazil, e-mail: dacosta@dge.inpe.br)

The studies of the Sq geomagnetic field day-to-day variability are based on the concept of "quiet" geomagnetic time. Presently, the most accepted method for Sq determination uses the average of field values from a selection of five geomagnetic quietest days for each month. These five quiet days are selected within few days after a month is over by the International Service of Geomagnetic Indices and announced to the geophysical community. However chosen quiet days are not necessarily very quiet and its selection is difficult during the period of high solar activity. This work presents a method that enables the best determination for geomagnetic quiet, regular neither quiet nor disturbed) and disturbed days. It uses geomagnetic indices directly related with the solar activity.

**Wednesday 21 July PM**

Presiding Chair: M. Menville (CETM, Saint Maur, France)

**GA5.06/E/05-A3 Invited 1400**

**POLAR CAP (PC) MAGNETIC ACTIVITY INDEX: REVIEW AND NEW DIRECTIONS**

O. A. TROSHICHEV and R. Yu. Lukianova (both at Arctic and Antarctic Research Institute, 38 Bering St., St. Petersburg, 199397, Russia, email: olegtro@ari.nw.ru); V. O. Papitashvili\* and P. Stauning (both at Danish Meteorological Institute, Lyngbyvej 100, DK-2100, Copenhagen, Denmark, email: vp@dmu.dk; \*also at SPRL, University of Michigan)

The PC index has been proposed as index characterizing magnetic activity in the polar cap related to the interplanetary magnetic field penetrating into the magnetosphere. The PC index is derived on the base of two near-pole stations, Thule in the Northern Hemisphere and Vostok in the Southern Hemisphere, because of ionospheric conductivities are quite different in the winter and summer polar caps. In this presentation, we focus on a study of the PC indices derived from a number of near-pole stations, such as Vostok, Thule, Savissivik and Nord, all stations being located above 80 degrees of invariant latitude. These independent indices are compared with the cross-polar electric field derived from the convection patterns obtained from a network of the polar cap stations. Ground magnetic variations are also compared with high-precision magnetic measurements on board the Danish Oersted satellite. These results can be utilized for investigations of dynamics of the high-latitude plasma convection, as well as for validation of the new 1-minute PC index. The major motivation of this study is to provide such an index that could be regarded as a measure of the convection electric field generated in the polar ionosphere by the solar wind-magnetosphere coupling and value of the corresponding transpolar current.

**GA5.06/W/04-A3 1440**

**REAL-TIME MONITOR OF GEOMAGNETIC FIELD IN THE NEAR-POLE REGIONS FOR THE SPACE WEATHER FORECAST**

Tsutomu NAGATSUMA (Hiraiso Solar Terrestrial Research Center, CRL, 3601 Isozaki, Hitachinaka 311-1202, JAPAN, Email: tnagatsu@crl.go.jp), K. Hayashi (Department of Earth and Planetary Science, University of Tokyo, 3-1 Hongo 3chome, Bunkyo-ku, Tokyo 113, Japan), H. Ishibashi, T. Obara, and M. Kunitake (both at Hiraiso Solar Terrestrial Research Center, CRL, 3601 Isozaki, Hitachinaka 311-1202, JAPAN)

Solar wind electric field that penetrates into the magnetosphere is a driving force of magnetospheric disturbances. The magnetic activity in the near-pole regions is controlled by this electric field. The PC index proposed by Troshichev et al. (1988) is based on this idea. Therefore, it is expected that the magnetic activity in the near-pole regions and PC index is a useful for the nowcast and forecast of magnetospheric disturbances. Now the data from Vostok, southern near-pole region are being collected in real time based on the INTERMAGNET project. We plan to collect the data from Eureka (Canada), northern near-pole region in real time and produce an index for the space weather forecast using the same method of PC index. In this paper, the possibility of PC index as nowcast and forecast of magnetospheric disturbances and the similarity and difference between the index produced from Eureka data and PC index produced from Thule data.

**GA5.06/E/03-A3 1500**

**DYNAMICS OF THE AURORAL ELECTROJETS IN TERMS OF DP-1 AND DP-2 VARIATIONS**

Vladimir SHELOMENTSEV (Institute of Solar-Terrestrial Physics, 664033, P.O.Box 4026, Irkutsk, Russia, email: vshel@iszf.irk.ru)



A study of the geomagnetic disturbances is defined in many respects by the diagnostics of the substorm phases and amplitude. Along this line, a relationship of the auroral indices AE with the geomagnetic variations DP-1 and DP-2 is investigated based on a determination of the appropriate polar cap indices PC1 and PC2 (with a high temporal resolution in 1.5 min). A good correlation between AE and PC1, PC2 testifies about an opportunity to diagnose AE on the polar cap data, and to evaluate the contributions of the variations DP-1 and DP-2 into an instant value of the AE-index. Such contributions were estimated using the multiple regression analysis. A notion about the two-component westward auroral electrojet (controlled by both of the dawn-dusk electric field and the conductivity) is a point at issue. Results are discussed also in terms of driven and loading/unloading processes in the magnetosphere. This study is supported by the RFBR grants 95-05-14385, 98-05-65120.

**GA5.06/W/05-A3 1520**

**FEASIBILITY AND VARIABILITY OF HIGHER-TIME RESOLUTION "KP-LIKE" GEOMAGNETIC INDICES**

D. DELLA ROSE, J. J. Sojka, R. W. Schunk, and L. Zhu (Center for Atmospheric and Space Sciences, Utah State University, Logan, Utah 84322-4405, e-mail: sls0r@cc.usu.edu)

Historically, the 3-hour Kp index has widely been used as a measure of geomagnetic activity for ionospheric studies. Specifically, it is the index used to determine the geomagnetic dependence of statistical auroral patterns as well as convection electric field patterns. Its pseudo anti-logarithm, the ap index, is similarly used in statistical models of the neutral atmosphere and neutral wind. Geomagnetic activity is, however, known to act on time scales significantly shorter than three hours, e.g., the auroral electrojet index (AE) shows rapid changes on time scales of minutes. The question then arises as to whether it is reasonable to consider higher-time resolution "Kp-like" indices? If so, is it then true that such higher-time resolution indices are good proxies for the temporal behavior of ionospheric drivers? We have already partially addressed these issues by driving the Utah State Time-Dependent Ionospheric Model (TDIM) with higher-time resolution "Kp like" indices. We now continue the work by examining the contribution of geomagnetic indices in ionospheric modelling versus other factors such as the IMF dynamics. We will also use ionospheric observations, such as auroral imagery, to compare against the results of our higher-time resolution TDIM simulations. These same high-latitude observations will also be contrasted with results derived from other existing geomagnetic indices, such as the PC index. In so doing, we attempt to identify the effectiveness of short-term geomagnetic variability on the ionosphere, and thus better understand the temporal variability spectrum relevant to the ionosphere.

**GA5.06/E/06-A3 1600**

**USE OF KP INDEX IN THE FORECAST OF SOLAR ACTIVITY**

G.K. RANGARAJAN and L.M. Barreto (Observatorio Nacional Dept. of Geophysics Rua General Bruce 586 Sao Cristovao Rio de Janeiro Brasil e-mail: ranga@dge1.on.br)

It is now well established that geomagnetic activity in the declining phase of a solar cycle is a useful precursor of the amplitude of the solar activity in the next cycle. In the present analysis, we show that the FREQUENCY of OCCURRENCE of Kp index with values (0 - 1) representing geomagnetic calm and with values (4 - 7) representing moderate magnetic disturbances, typically associated with high speed solar wind streams responsible for recurrent geomagnetic storms in the declining phase is linearly related with the sunspot maximum of the next cycle. Highest correlations are obtained when the frequencies are averaged over three years preceding the solar minimum epoch. In addition, we show that the frequency of occurrence of consecutive 4 or 6 intervals of Kp index with the same magnitude (0 - 1) or (4 - 5) are also equally reliable as predictors of the ensuing solar maximum. We find that the rate of increase of sunspot number to the solar maximum and its subsequent rate of decline can also be predicted reliably using the occurrence frequencies of Kp index with magnitude (0-1) or (4-5). Based on the observations for the past six solar cycles we expect the coming solar maximum to be associated with an annual mean sunspot number of about 140 with a rate of increase of 34 per year to the maximum epoch followed by a decline at the rate of 25 per year.

**GA5.06/W/02-A3 1620**

**PREDICTION OF THE AMPLITUDE OF SUNSPOT CYCLE 23**

Rajmal JAIN

A few prediction methods to forecast the solar activity have been developed using the "precursor" techniques and are found to be successful. On the basis of geomagnetic activity aa indices during the descending phase of the preceding cycle, we have established an expression which predicts the maximum annual mean sunspot number in cycle 23 to be 166.2. This indicates that cycle 23 would be a highly active and historic cycle. The average geomagnetic activity aa index during the ascending phase of cycle 23 would be about 24.9, comparable to 22.2 and 24.8 in cycles 21 and 22 respectively. This further indicates that during the ascending phase of cycle 23 energetic two-ribbon flares will be produced so as to give rise to strong proton events.

**GA5.06/W/06-A3 1640**

**THE UTILITY OF THE AP INDICES TO DETERMINE THE NOCTURNAL REFERENCE LEVEL FOR THE SURVEYS DATA CORRECTIONS**

GIANIBELLI Julio C., and CABASSI, Iris R. (Dep. of Geomagnetism and Aeronomy, Faculty of Astronomical and Geophysical Sciences, La Plata University, Paseo del Bosque s/n, 1900 La Plata, Argentina, email: jcg@fcaglp.fcaglp.unlp.edu.ar, rosy@fcaglp.fcaglp.unlp.edu.ar)

The minimum magnetic activity level to correct the surveys by diurnal variation, using low and middle latitude observatories, is analysed through ap index. The relationships between the minor magnetic activity over the monthly Q-days five and the solar cycle in the period 1932-1998 is studied. An example with digital data of the total intensity on pre-selected intervals over the period 1993-1998 of Trelew magnetic observatory is presented. An evolution model and analytic prediction of the Nocturnal Reference Level are showed.

**GA5.09 Tuesday 20 July**

**NEAR-EARTH MAGNETIC REFERENCE FIELD MODELS**

Location: Muirhead Tower, 424 LR5

Location of Posters: Muirhead Tower, 422 LR4

**Tuesday 20 July AM**

Presiding Chair: T.J. Sabaka (GSFC/NASA, Greenbelt, USA), J.M. Torta

**GA5.09/W/10-A2 0930**

**AN ESTIMATE OF THE ERROR OF THE IGRF/DGRF FIELDS 1900-1995**

Frank LOWES (Physics Department, University of Newcastle, NEWCASTLE UPON TYNE NE1 7RU, UK, email: f.j.lowes@ncl.ac.uk)

The IGRF coefficients inevitably differ from the correct values. Estimating the uncertainty of numerical models is difficult, but, mainly by comparing some IGRF and DGRF models with ones produced later, I have tried to produce realistic estimates of the coefficient accuracies. For simplicity the errors are summarized in terms of the root-mean-square vector error in the corresponding field at the Earth's surface. (What is averaged is the square of the length of the expected vector difference between the model and true vector fields, and the average is taken over the Earth's surface.) The rms errors suggested vary from a few hundred to a few nanotesla. Here it is assumed that the IGRF is trying to model the (low-pass filtered) field due to all (long-period) internal sources - it is meant for users interested in the field outside the Earth, not for core-field theoreticians. So far we have rounded the main-field coefficients to 1 nT; this in itself contributes a root-mean-square error of about 9 nT. If we do in fact get a succession of global magnetic field satellites in the future, we should be able to achieve consistently higher accuracy, and perhaps should reconsider the rounding level. Similarly, so far we have truncated the spherical harmonic series at n=10. gain, with consistently better data, some extension could be justified.

**GA5.09/W/02-A2 0950**

**A MODEL OF GEOMAGNETIC FIELD AT EPOCH 2000.5**

Miora Manda ALEXANDRESCU and Benoit Langlais (Institut de Physique du Globe de Paris 4 Place Jussieu 75252 Paris Cedex 05, France, email: mioara, email: langlais@ipgp.jussieu.fr)

Earth's deep interior studies are heavily dependent on the Earth's main field and its secular variation models. An important aspect in modelling is the good distribution of available data over the globe and acquired over long periods of time. Satellite data provide the best geographic coverage, but - for the moment - are unlikely to be available except after possibly long intervals of time (about 20 years between MAGSAT and OERSTED). Then, at the present date, to build a main field model at epoch 2000.5 we only have access to surface data (when OERSTED data will be available the situation will be completely different). Indeed, a dataset as large as possible adjusted to 1997.5 is used to model the geomagnetic field for this epoch (80 Gauss coefficients for the main field and 3 for the external field). In order to extrapolate this model to the epoch 2000.5 a secular variation model is applied. In doing so we pay attention to the distribution of geomagnetic observatories and continuity of time-series. The data are extrapolated from 1997.5 to 2000.5 and in this way it is possible to get annual means from the same observatories over a 35-year period. This dataset is then used to compute secular variation models for each year, which permit us to extrapolate the main field model from 1997.5 to 2000.5. The paper presents the data (with comments on distribution and quality), the inversion and extrapolation methods, and the obtained models.

**GA5.09/W/06-A2 1010**

**A MODEL OF RECENT AND FUTURE SECULAR VARIATION**

Susan MACMILLAN (British Geological Survey, Murchison House, West Mains Road, Edinburgh EH9 3LA, UK, email: S.Macmillan@bgs.ac.uk)

In connection with the current IGRF revision, a series of models of the secular variation for the period 1990 to 2005 was needed. I describe how secular-variation records at magnetic observatories and repeat stations are extended to 2005 using linear prediction filters and linear regression respectively, and how the models are produced.

**GA5.09/W/09-A2 1030**

**ADJUSTING SHC COEFFICIENTS TO N = 15 FOR EPOCH 2000.**

Joseph CAIN and David Mozzoni (both at Geophysical Fluid Dynamics Institute/FSU, Tallahassee FL 32306-4360, USA, e-mail: cain@geomag.gfdi.fsu.edu and cyric@leyla.gfdi.fsu.edu)

Most reference models of the internal geomagnetic potential function have attempted to define the "main" internal field by limiting the analyses to spherical harmonic degrees up to n = 13 of the potential function without the use of higher terms. Such models contain intrinsic "aliasing" errors in practice in spite of theory that properly orthogonalized analyses should be error free. Though small due to the relatively low power of higher degree contributions at satellite altitude, there is no need to add yet another error source to those already extant from electrical currents below, within, and above the volume of measurement considering modern computer resources. Models presented herein utilize high degree terms previously derived from LEO Magsat data (to n = 60), updating those that can be improved with the higher altitude data provided by Ørsted and Astrid-2, and holding higher terms fixed. Major anomalies are automatically incorporated in the analyses and little harm is done by including small noise contributions in the "bland" areas. This technique allows adjustments of the main field contributions to terms in the transition region, 14 < n < 17 where though diminishingly less important, the changing main field nevertheless can be determined. The satellite data themselves are utilized in conjunction with secular change estimates obtained from surface observatory hourly values.

The external field contributions are handled by techniques developed for POGO and Magsat and employ surface variational data as well as ad hoc techniques to incorporate variations that are due to broad scale magnetospheric effects (Dst) as well as those that are more dependent on magnetic local time and magnetic latitude (e.g. Sq). The resultant models can be used as a "reference" with the user making the decision as to truncation level, or identification of degrees believed to be "crustal" compared to "core." They also have the advantage of providing those interested in ionospheric and magnetospheric studies the confidence that most significant internal crustal noise has already been removed.



**GA5.09/W/03-A2 1110**

**AN IGRF 2000 CANDIDATE MODEL BASED UPON OERSTED SATELLITE DATA**

T.J. SABAKA (Raytheon ITSS Corp., Lanham, MD 20706, USA, email: sabaka@linus.gsfc.nasa.gov; Oersted Main Field Working Group)

The Danish satellite Oersted, launched in January 1999, is to provide the best sampling of the geomagnetic field for main field modelling purposes since the Magsat mission of 1980. An IGRF 2000 candidate model, derived from this high-precision vector data set and supplemental observatory measurements, will be presented.

**GA5.09/W/08-A2 1130**

**CANDIDATE MODELS FOR IGRF 2000-2005**

BONDAR Tatiana N and Golovkov Vadim P (both at IZMIRAN, 142092 Troitsk, Moscow region, Russia, email: golovkov@izmiran.rssi.ru)

Candidate model for the IGRF2000.0 and the corresponding model for the secular variation 2000.0-2005.0 are presented. Forecast of the field changes for a few years is uncertain due to stochastic nature of both external and internal variations. We tried to decrease as much the forecast uncertainty using a few independent algorithms and comparing the forecast results. These algorithms are as follows:

- 1 IZMST (Golovkov et al., 1997) was taken as a basic ones. The time functions of this model were extrapolated with parametric method till epochs 2000.0 and 2005.0.
  - 2 A new generation of IZMST was developed with a new set of natural orthogonal components. These new NOC's were derived from a few observatories which annual means series were extrapolated by hand.
  - 3 By hand extrapolations of annual means series from whole observatories on the globe were used as the data set for independent SH analysis for both epochs.
- Comparison of modeled field shows a rather good agreement over whole globe except two regions. Largest declinations of the models take place over East Pacific and Indian Oceans. Arguments in favour of the second algorithm are presented, but definite conclusion can be done after analysis of data from coming Oersted mission.

**GA5.09/E/01-A2 1150**

**POTENTIAL EFFECTS OF INDUCED MAGNETISATION IN A SPHEROIDAL SHELL**

Andrew Jackson (School of Earth Sciences, Leeds University, Leeds LS2 9JT, UK, Email: jackson@earth.leeds.ac.uk), Vincent LESUR (School of Earth Sciences, Leeds University, Leeds LS2 9JT, UK, Email: lesur@earth.leeds.ac.uk) and Denis Winch (Department of Applied Maths, University of Sydney, Sydney NSW 2006, Australia).

Runcorn in 1975 established that, in a linear approximation, a spherical shell of constant susceptibility which is magnetised by an internal magnetic field does not generate any external field. He applied this result with great success in explaining the very small external field of the moon. The situation on the earth may be different because of its larger flattening. We analyse the external field generated by a shell of constant susceptibility and defined by two oblate spheroids when it is magnetised by an internal magnetic field of arbitrary complexity. An exact calculation takes into account the magnetic field of the crust itself, generating fields which depend on the square of the susceptibility; we call these the non-linear terms. We find an analytical expression for such a crustal field, expressed in an oblate spheroidal coordinate system, that take into account both the effects due to the flattening of the earth and the non-linear effects. In the limit case of the spherical shell, the basis becomes the usual spherical system of coordinates and by Runcorn's theorem, only the non-linear terms can produce an external field. For each spherical harmonic degree, the crustal field coefficient is a small portion of the internal magnetic field coefficient. Therefore the crustal field is weak and dominated by the long wave-lengths. In the case of an oblate spheroidal shell, the flattening of the earth introduces a linear term. However, the external field which is generated is still dominated by the non-linear effects.

**GA5.09/W/13-A2 1210**

**HIGH LATITUDE GEOMAGNETIC VARIATION REFERENCE FIELD MODELS FOR 20-22 SOLAR ACTIVITY CYCLES**

Vladimir PAPITASHVILI (Space Physics Research Laboratory, University of Michigan, Ann Arbor, MI 48109, USA, email: papita@umich.edu); Boris BELOV (Institute of Terrestrial Magnetism, Ionosphere and Radio Wave Propagation, IZMIRAN, Troitsk, Moscow Region, 142092, Russia, email: bbelov@adonis.ijsnet.ru); Natalia Papitashvili (Raytheon STX and NSSDC, NASA/Goddard Space Flight Center, Greenbelt, MD 20771, USA, email: natasha@nssdc.gsfc.nasa.gov)

We present a newly obtained set of linear regression models of the ground magnetic response on 1-nT changes in the corresponding interplanetary magnetic field (IMF) components for the 20-22 solar activity cycles (from 1965 to 1997). These models are obtained over both the northern and southern polar regions and for different seasons of a year (summer, winter, and equinox). Data from 116 magnetic observatories were collected and quality controlled. The hourly means of the IMF and ground geomagnetic field components are analyzed utilizing the linear "black box" approach. The spherical harmonic analysis is applied to obtain a set of harmonic coefficients capable of modelling the ground geomagnetic responses on changing IMF conditions for any time instance between 1965 and 1997. The new set of models is compared with similar models obtained during the development of IZMIRAN Electrodynamic Model for two solar activity maximums (1968-1969 and 1979-1983). It shows that generally there are little differences in the models harmonic coefficients through the solar activity cycles. This allows us to apply the obtained results beyond of the studied interval. Validation of the new linear regression models against magnetic observatory data is also presented and discussed.

**GA5.09/P/01-A2 1230**

**A REMARK ON THE VERTICAL MAGNETIC FIELD NEAR THE GEOMAGNETIC POLES IN SUMMER**

Naoshi FUKUSHIMA (Dept. of Earth and Planetary Physics, University of Tokyo, Tokyo 113-0033 Japan, email: fukushima@nipr.ac.jp)

For improving the Near-Earth Reference Field Model it will be necessary to pay special attention to a remarkable decrease in the magnitude of vertical geomagnetic field  $z$  in the summer polar regions centring the northern or southern magnetic poles, which amounts even to several tens of nT. This peculiar phenomenon was known since the Second International Polar Year 1932-1933, through an extensive analysis of world data by Vestine et al. compiled

in the Carnegie Institution of Washington Publication No. 580 (1947). With the aid of the data during IGY and succeeding years, Mansurov and Mansurova (1971) demonstrated that the same kind of  $z$ -decrease was observed also at Vostok, magnetic south pole station in the Antarctica. It is worth noting here that the geomagnetic anomaly maps by Langel and Estes (Figs. 1b and 2b on pages 2497-8 in JGR 90 [1985] for the calculated difference of  $z$ -values at 500 km level from their model based on the Magsat data) show the greatest negative anomaly over Vostok, because they used the Magsat data during the austral summer. Since the peculiar decrease in the geomagnetic  $z$ -field near the magnetic poles is observed only in local summer seasons, it will be practical to prepare in advance a correction for this summer phenomenon, in order to discuss real magnetic anomalies of inner origin in the polar regions.

**Tuesday 20 July PM**

Presiding Chairs: T.J. Sabaka (GSFC/NASA, Greenbelt, USA), J.M. Torta

**GA5.09/W/07-A2 Poster 1400-01**

**THE EARTH'S MAGNETIC FIELD IN THE 18TH AND 19TH CENTURIES FROM FRENCH ARCHIVAL DATA**

Mioara Manda ALEXANDRESCU (Institut de Physique du Globe de Paris, 4 Place Jussieu, 75252 Paris Cedex 05, France, email: mioara@ipgp.jussieu.fr), Andrew Jackson (Leeds University, Leeds LS2 9JT, UK email: A.Jackson@earth.leeds.ac.uk), Anne Murray (London, UK)

We aim to show how our database (on which models of the historical magnetic field are based) has been improved by exploiting archive records available in the Paris libraries (Archives Nationales and Bibliotheque Nationale). One of the most accurate sources for studying the past behaviour of the Earth's magnetic field is the series of declination measurements taken over the last few hundred years by land observers or by mariners on voyages of trade, plundering and exploration. These data exist in the original ships' logs or as compilations held by hydrographic institutions in order to make charts of declination for the use of shipping. The data in the Paris archives exist in both forms, but we report on the use of some very large compilations which we have discovered. After correcting for differences in the reference longitude used when the measurements were recorded, the measurements were checked by comparing them with estimates calculated from Bloxham and Jackson's model ufm2. The number of useful measurements recovered in this way is of the order of 60000, covering the late 18th and early 19th centuries, although there is likely to be some duplication. Some studies on the statistics of the compiled data are presented, and we discuss how they can be integrated with the existing dataset.

**GA5.09/W/05-A2 Poster 1400-02**

**SPHERICAL CAP HARMONIC ANALYSIS OF GEOMAGNETIC VARIATIONS OVER JAPAN**

Golovkov Vadim P., FILIPPOV Sergey V., Burdelnaya Irina A. (all at IZMIRAN, 142092, Troitsk, Moscow region, Russia, e-mail: golovkov@izmiran.rssi.ru), Fujiwara Satoshi (Mizusawa Geodetic Observatory Geographical Survey Institute, Kitasato-1, Tsukuba, Ibaraki 305, Japan, e-mail: fujiwara@gsi-mc.go.jp), Tanabe Tadashi (Geography and Crustal Dynamics Research Center Geographical Survey Institute, itasato-1, Tsukuba, Ibaraki 305-0811, Japan, e-mail: tanabe@gsi-mc.go.jp).

The space-time model ROM - FAR EAST70/95 has been described by Golovkov et al. (1997). In this model Natural Orthogonal Components (NOC) are used for modelling temporary functions and rectangular Legendre polynomials are used as spatial functions describing geomagnetic field variations. The model covers the area of the Japanese Islands and, partially, surrounding seas. Data from Japanese magnetic observatories and the first class repeat station network were used. For filling empty (no data) areas (the seas) the global models were used. Now new model of this region - CAP-NOC-JAPAN70/95 - is presented. This model also use the NOC analysis for separating temporal variations, but the spherical cap harmonic analysis (Haines, 1985) is used to describe the spatial distribution of geomagnetic variations. Both two models cover almost the same area (the Japanese Islands and surrounding seas) and use the same data set for analysis (Japanese repeat station and observatory data). Results of modelling and the comparison of these regional models over the small region as well as comparisons with global model IZMST are presented. The methodical questions of regional modelling as well as accuracy of obtained models are discussed.

**GA5.09/W/04-A2 Poster 1400-03**

**A NEW RESULT OF THE WESTWARD DRIFT IN THE GEOMAGNETIC FIELD**

Wen-Yao XU AND Zi-Gang Wei (Institute of Geophysics, Chinese Academy of Sciences, Beijing 100101, China, email: wyxu@mail.c-geos.ac.cn)

A technique of correlation analysis of moving random patterns is used to the non-dipole part of the Earth's magnetic field in order to study its westward drift. The technique considers the overall features of the pattern instead of some special contour lines or the focus. The results show that the Asia Anomaly drifts westward at an average speed of 0.07 degree per year during 1900-2000. The time variation of the drift speed indicates three periods of the westward drift. During 1900-1930 the Asia anomaly steadily drifted westward at a speed of 0.1 degree per year, then the drift turned to northwest, and finally the drift almost stopped after 1980. The other large-scale magnetic anomalies also show their own characteristics in westward drifts.

**GA5.09/W/01-A2 Poster 1400-04**

**REGIONAL MODELS OF GEOMAGNETIC FIELD CHANGES OVER CANADA**

BURDELNAYA Irina A., Golovkov Vadim P. (both at IZMIRAN, 142092, Troitsk, Moscow region, Russia, email: golovkov@izmiran.rssi.ru), Newitt Larri R. (Geological Survey of Canada, 1 Observatory Cres, Ottawa, Canada, K1A 0Y3).

Regional space-time models of the geomagnetic field have been produced by a variety of techniques for describing temporal and spatial variations. The Canadian Geomagnetic Reference Field for 1995 (CGRF95) has been described by Haines and Newitt (1997). Cosine functions were used to express the time variations and spherical CAP harmonics to describe the spatial distribution. The ROM-Canada has been described by Golovkov et al. (1997). A new high precision regional space-time of the geomagnetic field model over Canada, CAP+NOC(71/95), has been created. The model uses the methods of both the NOC analysis, which separates temporal variations, and the CAP analysis (Haines, 1985), which models the spatial distribution over the Canadian region. The three models use ordinary observatory annual means and Canadian repeat station data. Results are presented which

show comparisons of these regional models over the same region as well as comparisons with global models IGRF, IZMST. The comparisons are of interest for modelling the magnetic field over a portion of the globe.

**GA5.09/W/11-A2** Poster **1400-05**

**REDUCTION OF GEOMAGNETIC DAILY VARIATION EFFECTS IN SATELLITE DATA USED FOR MAGNETIC FIELD MODELLING**

Peter R SUTCLIFFE and Pieter B Kotzé (Hermanus Magnetic Observatory, P O Box 32, Hermanus 7200, South Africa; E-mail: psutclif@csir.co.za and pkotze@csir.co.za)

A regional geomagnetic daily variation model is developed using magnetic observatory data and artificial neural network (ANN) techniques. Input variables considered in the daily variation model are geomagnetic latitude, season, sunspot number, and degree of geomagnetic activity. Spherical harmonic analysis techniques are then used to extend the validity of this ground-based model to satellite altitudes. This extended model is then used to correct for the effects of the geomagnetic daily variation in satellite data used for geomagnetic main field and anomaly modelling. Results demonstrating the effects of correcting for the daily variation in satellite data over southern Africa are shown.

**GA5.11** **Wednesday 21 July**

**CONTRIBUTION OF ROCK MAGNETISM (PETROPHYSICS) TO ANOMALY INTERPRETATION (WITH DIV. 1)**

Location: Barber Institute, LT  
Location of Posters: Barber Institute, Corridor

**Wednesday 21 July AM**

Presiding Chairs: S.A. McEnroe (Geological Survey of Norway, Norway); J.V. Korhonen (Geological Survey of Finland, Finland)

**Introduction** **0900**

S.A. McENROE, J. KORHONEN

**GA5.11/W/02-A3** **0910**

**ORIGIN OF MAGNETIC ANOMALIES OF LOWER CRUSTAL ROCKS**

Gunther KLETETSCHKA, Patrick Taylor, Mike Purucker, and Peter Wasilewski (all at codes 921/690, GSFC/NASA, Greenbelt, USA, email: gunther@denali.gsfc.nasa.gov); Dhananjay Ravat (Department of Geology 4324, SIUC, Carbondale, 62901, USA)

Remanent and induced magnetization must both be considered when attempting to explain the source of crustal magnetic anomalies. Magnetite, hematite, or pyrrhotite are the responsible minerals. For magnetite, remanent and induced magnetizations are of the same order of magnitude. Hematite and pyrrhotite have negligible induced magnetization. The remanent magnetization of hematite is of the same order as both the remanent and the induced magnetization of magnetite. The remanent magnetization of pyrrhotite is in the same range or larger than the remanent magnetization of magnetite. Samples of hematite and magnetite bearing rocks were collected along a traverse from background into the supposed source of the significant crustal magnetic anomaly which occupied a 50-100 kilometer region in central Labrador. Induced magnetization of the rocks did not change in any significant way along the traverse including the boundary from background to the apparent source of the magnetic anomaly. However, the remanent magnetization changes significantly and can account for the crustal magnetization signature in this region. These field data together with the magnetic property studies of the collected samples and the known properties of the important magnetic minerals indicate that magnetic anomaly modelling cannot be realistic without the consideration of the remanent and the induced magnetization. Considering this conclusion we are using the Kursk iron ore region as a test case. The Kursk region has voluminous amounts of geologic and geophysical data, rock magnetic data and multilevel magnetometer data, including satellite data. Consequently we will attempt to model magnetization source(s) using remanent and induced magnetic signatures constrained by geologic and geophysical data.

**GA5.11/W/01-A3** Invited **0930**

**TITANOHEMATITE AS THE CARRIER IN REMANENCE-DOMINATED MAGNETIC ANOMALIES: ROCK MAGNETIC AND PETROGRAPHIC STUDIES OF THE RUSSELL BELT MICROCLINE SILLIMANITE GNEISS, ADIRONDACKS, NEW YORK, USA**

Laurie L. BROWN (Department of Geosciences, University of Massachusetts, Amherst, MA 01003, USA, email: lbrown@geo.umass.edu); Suzanne A. McEnroe (Norges Geologiske Undersokelse, Trondheim, Norway, email: Suzanne.McEnroe@ngu.no)

A large (2240 nT) negative aeromagnetic anomaly over microcline-sillimanite-quartz gneisses in the Russell belt, northwest Adirondack Mountains, New York was first investigated by Balseley and Buddington some 40 years ago. Anomaly lows are closely related to surface outcrops known to contain metamorphic hematite. The granulite-facies metamorphism here dates from the Ottawa phase (1100-1000 Ma) of the Grenville Orogeny. It is obvious from the anomaly that there is a strong remanence contribution to the aeromagnetic signal. Samples from six sites in the Russell belt have been collected, providing 36 oriented cores for rock magnetic and petrographic studies. The gneisses contain up to 3% iron oxides, predominantly titanohematite, occurring as both ilmenohematite and hemoilmenite, as well as nearly pure hematite. Microprobe data indicates the range of compositions of titanohematite to be from 78 to 99% Fe<sub>2</sub>O<sub>3</sub> end member. Rare grains of pseudo-single domain end member magnetite have been observed. Bulk susceptibility measurements yield a bimodal distribution with over 70% of the samples having values less than 9x10<sup>-4</sup> SI, and a median value for all samples of 4.2 x 10<sup>-4</sup> SI. NRM intensities are strong, with a mean of 3.6 A/m, and average directions of declination 290 and inclination -65. Not surprisingly, the Koenigsberger ratios (Q values) are high, ranging from 0.4 to 562, with a mean Q for all samples of 170. Progressive thermal demagnetizations show very little loss of magnetization until 600 C; generally 90 to 95% of the original remanence remains at this temperature. Low temperature measurements of remanence reveal both Verway and Morin transitions in some samples, as well as only Morin transitions in other samples. Hysteresis properties show considerable variation, with the ratio of coercivity of remanence to saturation coercivity varying from 1 to 18, although 75% of the samples have ratios of 3.2 or less. The ratio of saturation magnetization to remanent magnetization varies from 0.131 to 0.739 with a mean of 0.407. Hysteresis curves are typically wasp-waisted or "hummingbird" in shape. Wasp-waisted loops retain their distinctive shape up

to 575C and by 600C have reverted to lozen-shapes. Original hummingbird loops retain their shapes above 600C.

All rock magnetic and petrologic data indicate that titanohematite is the predominant oxide present in any grain size, from MD to SD. Although the high NRM intensities are not easily explained with small amount of titanohematite present, it is the primary carrier of remanence. Titanohematite may be an important phase in aeromagnetic studies and could be contributing to deep crustal anomalies.

**GA5.11/E/01-A3** **0950**

**PETROPHYSICAL DATA FOR MAGNETIC AND GRAVITY ANOMALY INTERPRETATION**

Juha V. KORHONEN (Geological Survey of Finland, P.O. Box 96, FIN-02151 ESPOO, Finland, Email: juha.geofys@gsf.fi) and Michael Purucker (Geodynamics Branch and Raytheon ITSS, Goddard Space Flt Ct Greenbelt, MD 20771, Email: urucker@geomag.gsfc.nasa.gov)

The usefulness of regional, continental, and global scale magnetic and gravity data will be considerably increased when combined with petrophysical information. Using petrophysics the anomalies can be associated with definite geological formations and lithologies an separated into shallow and deep seated sources. Correlation between density and magnetic properties establishes to what extent the magnetic and gravity anomalies are caused by the same sources. Defining the magnetization and density from petrophysical information leaves more freedom to interpret other source parameters. An attempt was made to collect meta-information on petrophysical data sets. A questionnaire was sent to 110 organizations or persons. 14 responses were received, totalling 468 000, 513 000, 279 000 and 12 600 measurements of bulk density, magnetic susceptibility, intensity of remanence and direction of remanence respectively in 8 countries. The received metadata information is available at the address <http://www.gsf.fi/> where references to data owners are given. Most of the current data is clustered on the Fennoscandian shield which has an average data density of 30 measurements of susceptibility and bulk density values per 100 sq km. Combined with geological data this information allows estimation of average upper crustal magnetization for interpretation of Kiruna, Gulf of Finland and Baltic MAGSAT magnetic anomalies and corresponding magnetic provinces in more near surface studies. For the most part, there is little petrophysical control on the 60 magnetic anomalies observed at satellite altitude. Based on the published literature, we feel that more petrophysical data must exist at geological institutions around the world. To accumulate this information, the questionnaire will remain open and the WWW metadatabase will be updated upon receipt of new information.

**GA5.11/W/04-A3** Invited **1010**

**THE CALCULATION OF MAGNETIC COMPONENTS AND MOMENTS FROM TMI: A CASE STUDY FROM THE TUCKERS IGNEOUS COMPLEX, QLD**

Phillip W. SCHMIDT (CSIRO Exploration and Mining, North Ryde NSW, Australia 1670, email: p.schmidt@syd.dem.csiro.au); David A. Clark (CSIRO Exploration and Mining, North Ryde NSW, Australia 1670, email: d.clark@syd.dem.csiro.au)

This paper re-examines some largely forgotten methods that are eminently adaptable to modern computing environments. The methods were originally formulated before the advent of electronic computers and do not appear to have been fully developed, or given the attention they deserve. Components of anomalies can be derived from total magnetic intensity (TMI) observations, or indeed, any other component irrespective of its direction. For large anomalies which distort the local field so it can no longer be treated as a potential field an iterative method enables estimates to converge on accurate solutions. Furthermore, for an isolated anomaly integrals of first order moments of the components yield information such as the direction and magnitude of the total anomalous magnetic moment of the source.

Examples of the application of the methods are derived from a survey over the Tuckers Range area of north Queensland. This survey was chosen because the magnetic properties of the lithologies giving rise to the magnetic anomalies have been thoroughly studied. The selected areas contain many anomalies showing effects of magnetic remanence of reverse polarity. The results of the methods used herein agree well with those expected from the measured magnetic properties and magnetic modelling.

**GA5.11/W/07-A3** Invited **1100**

**MAGNETIC PROPERTIES AND MAGNETIC SIGNATURES OF PORPHYRY-RELATED GOLD AND COPPER-GOLD DEPOSITS IN EASTERN AUSTRALIA**

David A. CLARK (CSIRO Exploration and Mining, PO Box 136, North Ryde, NSW 1670, Australia, email: d.clark@syd.dem.csiro.au)

Intrusive igneous rocks that are genetically associated with Au and Cu-Au deposits have certain features in common: they are derived from high temperature melts that have undergone substantial fractional crystallisation, and they are almost invariably oxidised. Substantial metasomatised aureoles, often with remanence-dominated magnetisations, are commonly developed around the mineralising intrusions. Fractional crystallisation within oxidised suites produces strong magnetisation contrasts. Zoned magnetic signatures are associated with larger plutons and complex signatures, indicative of multiple nested intrusions of varying composition, are also commonly associated with deposits. Hydrothermal alteration substantially modifies the magnetic properties of the various intrusive phases and the host rocks. Magnetic signatures of alteration can provide a guide to mineralised centres within the system. Magnetic signatures of intrusive-related (Cu)-Au deposits depend strongly on the geological setting, but in a relatively predictable way. This allows magnetic exploration models to be developed from geological models of the magmatic and hydrothermal evolution of gold-bearing porphyry systems. Case studies of the magnetic petrophysics, magnetic petrology and magnetic signatures of several porphyry-related (Cu)-Au deposits from eastern Australia illustrate these generalisations.

**GA5.11/W/05-A3** **1120**

**INTERPRETING THE AEROMAGNETIC SIGNATURE OF ILMENITE DEPOSITS IN ROGALAND, NORWAY: THE IMPORTANCE OF PETROPHYSICAL MEASUREMENTS AND ROCK-MAGNETIC PROPERTIES**

Suzanne A. MCENROE (Norges Geologiske Undersokelse, Trondheim, Norway, email: suzanne.mcenroe@ngu.no)

Petrophysics, rock-magnetic properties and magnetic petrology are required for accurate geological interpretation of magnetic surveys. Exploration for the titanium minerals ilmenite and rutile, which is a strategic mineral, will continue well into the next century. With the possibility that synthetic rutile can be produced from ilmenite, accurate methods for ilmenite exploration are become increasingly important. Igneous and metamorphic ilmenite deposits and hemo-ilmenite rich rocks commonly have remanence-influenced or -dominated aeromagnetic anomalies. Allard Lake, Canada; Adirondacks Mtns, USA and Rogaland,



Norway are such examples. Understanding the parameters which control the magnetic signatures of ilmenite deposits greatly enhances exploration. To further this aim, a large petrophysical data set and detailed rock-magnetic measurements have been made by Norwegian Geological Survey for ilmenite deposits and associated rocks in the Rogaland region of Norway. In addition, the magnetic characteristics of the surrounding anorthosite body and the coeval mafic intrusions were examined.

Bulk magnetic measurements of the NRM and susceptibility show a wide range of values, and yield Koenigsberger ratios (Q values) from >1 to >> 100. Samples with low Q values are generally from mafic intrusions which have near end-member ilmenite with minor or no hematite lamellae and abundant coexisting magnetite. These magnetites have a wide range of microtextures produced by exsolution and oxidation-exsolution. Samples with high Q values are harder to interpret, but very important because they come from intrusions rich in ilmenite or hosting ilmenite ores. The hosting anorthosite body has Q values up to 150. Actively mined and historic ilmenite deposits in the Rogaland region all contain ilmenite with abundant {0001} hematite exsolution lamellae. Historic, ilmenite deposits have Q values up to 30. Samples taken from the Tellnes deposit, one of the world's largest active ilmenite mines, have Q values up to 12. "Pure ilmenite" dikes have Q values up to 58. To identify the magnetic phases responsible for the high Q values, detailed rock-magnetic measurements, optical identification and microprobe analyses were used. Verwey and Morin transitions, hysteresis properties were measured and combined with thermal and AF demagnetization spectra. The sources for the high Q values were: 1) ilmenite-hematite, 2) ilmenite-hematite and/or magnetite-ilmenite exsolution in pyroxenes, 3) fine inclusions in plagioclase. These measurements further enabled us to interpret the airborne magnetic data and to explore for further ilmenite reserves.

**GA5.11/L/01-A3** Invited **1140**

#### MAGNETIC SIGNATURES OF IMPACT STRUCTURES - THE ROLE OF PETROPHYSICS

Lauri J. Pesonen and Juha V. KORHONEN (both at Geological Survey of Finland, P.O. Box 96, FIN-02151 Espoo, Finland, Email: lauri.pesonen@gsf.fi, juha.korhonen@gsf.fi)

The magnetic methods provide four types of data of terrestrial meteorite impact structures. First, they have led to new discoveries of impact craters (e.g., Suvasvesi, Finland). Second, they provide additional (to gravity, seismics, etc.) estimates of morphometric parameters of impact structures. Third, magnetic modellings, coupled with paleomagnetic data of the impact rocks, have led to estimates of the age of impact events (e.g., Siljan, Sweden). Fourth, the polarity reversals in the impact rocks have provided further constraints for the age of impact events (e.g., Chixculub, Mexico). However, the applications of magnetic data of impact structures is often hampered by the lack of petrophysical data of the rocks from the structures. Here we outline the known magnetic signatures of terrestrial impact structures with emphasis on the role of petrophysical data of impactites and target rocks in constraining the magnetic modellings and the datings.

The magnetic anomalies of impact structures are generally subdued due to impact induced decrease in susceptibility and NRM of host rocks. Peak anomalies can occur in places where impact melt is present (e.g., Lappajärvi, Finland). Impact breccias and suevites often have relatively strong remanent magnetisation (high Q-values) due to impact induced TRM (e.g., Ries, Germany). In some cases the NRM of the breccias is randomized causing the weak magnetic anomaly relief. In a few instances a SRM (shock remanent magnetization) has been isolated in impact rocks (e.g., Slate Islands, Canada). The magnetic signatures of the complex structures are broader and relatively less pronounced than for simple structures due to smaller depth to diameter ratio. The complex structures may also show a broad central anomaly (positive or negative) due to central uplift of the target basement.

**GA5.11/W/06-A3** **1200**

#### GEOPHYSICAL INDICATIONS OF MAGMATIC AND TECTONIC ACTIVITY IN THE NORTHERN PART OF BARENTS SEA

Andrew ZAYONCHEK, Vladimir Glebovsky, Evgeniy Korago, Sergei Maschenkov, Evgeiny Mysatov, Mihail Zykov (all Russian Research Institute for Geology and Mineral Resources of the World Ocean, 1, Angliyskiy Pr., St. Petersburg, 190121, Russia, E-mail: andrew@vniio.nw.ru)

In accordance with existing geological information the major magmatic activity in the northern part of Barents Sea occurred during Jurassic-Cretaceous times. Joint analysis of geophysical data and geological observations on Franz Josef Land revealed the evident relationship between potential fields anomalies and known magmatic occurrences. It was found that main igneous sources correspond to the high intensity magnetic anomalies. This allowed to develop the geophysical criterion's for contouring igneous structures and apply them to the adjacent sea areas were direct geological is poor. In our study we have used the regional gravity, magnetic anomaly and seismic reflection data. Structural interpretation was based on the various geophysical maps: gravity Free-air, Bouguer anomalies and their transformations (vertical and horizontal gradients, local and regional anomalies), bathymetry and magnetic anomalies. Additional information was obtained from the calculations of depths to magnetic sources performed by Werner deconvolution technique. To study the magmatic occurrences we used detailed magnetic anomaly maps, based on the 1x1 km grids. The presented study allowed to clarify the position of general tectonically and magmatically active zones in the region. In some areas the main directions of the faults related to the magmatic activity (which previously were seen in the seismic data) were revealed.

Wednesday 21 July PM

Presiding Chairs: S.A. McEnroe (Geological Survey of Norway, Trondheim, Norway), J.V. Korhonen (Geological Survey of Finland, Finland)

**GA5.11/E/01-A3** Poster **1430-01**

#### PETROPHYSICAL DATA FOR MAGNETIC AND GRAVITY ANOMALY INTERPRETATION

Juha V. KORHONEN (Geological Survey of Finland, P.O. Box 96, FIN-02151 ESPOO, Finland, Email: juha.geofys@gsf.fi) and Michael Purucker (Geodynamics Branch and Raytheon ITSS, Goddard Space Flt Ctr Greenbelt, MD 20771, Email: urucker@geomag.gsfc.nasa.gov)

The usefulness of regional, continental, and global scale magnetic and gravity data will be considerably increased when combined with petrophysical information. Using petrophysics the anomalies can be associated with definite geological formations and lithologies an separated into shallow and deep seated sources. Correlation between density and magnetic properties establishes to what extent the magnetic and gravity anomalies are caused by the same sources. Defining the magnetization and density from petrophysical information leaves more freedom to interpret other source parameters. An attempt was made to collect meta-information on petrophysical data sets. A questionnaire was sent to 110 organizations or persons. 14 responses were received, totalling 468 000, 513 000, 279 000 and 12 600 measurements of bulk density, magnetic susceptibility, intensity of remanence and direction of remanence respectively in 8 countries. The received metadata information is available at the address <http://www.gsf.fi/> where references to data owners are given. Most of the current data is clustered on the Fennoscandian shield which has an average data density of 30 measurements of susceptibility and bulk density values per 100 sq km. Combined with

geological data this information allows estimation of average upper crustal magnetization for interpretation of Kiruna, Gulf of Finland and Baltic MAGSAT magnetic anomalies and corresponding magnetic provinces in more near surface studies. For the most part, there is little petrophysical control on the 60 magnetic anomalies observed at satellite altitude. Based on the published literature, we feel that more petrophysical data must exist at geological institutions around the world. To accumulate this information, the questionnaire will remain open and the WWW metadatabase will be updated upon receipt of new information.

**GA5.11/W/03-A3** Poster **1430-02**

#### ORIGIN OF MAGNETIC ANOMALIES OF LOWER CRUSTAL ROCKS

Gunther KLETETSCHKA, Patrick Taylor, Mike Purucker, and Peter Wasilewski (all at codes 921/690, GSFC/NASA, Greenbelt, USA, email: gunther@denali.gsfc.nasa.gov); Dhananjay Ravat (Department of Geology 4324, SIUC, Carbondale, 62901, USA)

Remanent and induced magnetization must both be considered when attempting to explain the source of crustal magnetic anomalies. Magnetite, hematite, or pyrrhotite are the responsible minerals. For magnetite, remanent and induced magnetizations are of the same order of magnitude. Hematite and pyrrhotite have negligible induced magnetization. The remanent magnetization of hematite is of the same order as both the remanent and the induced magnetization of magnetite. The remanent magnetization of pyrrhotite is in the same range or larger than the remanent magnetization of magnetite. Samples of hematite and magnetite bearing rocks were collected along a traverse from background into the supposed source of the significant crustal magnetic anomaly which occupied a 50-100 kilometer region in central Labrador. Induced magnetization of the rocks did not change in any significant way along the traverse including the boundary from background to the apparent source of the magnetic anomaly. However, the remanent magnetization changes significantly and can account for the crustal magnetization signature in this region. These field data together with the magnetic property studies of the collected samples and the known properties of the important magnetic minerals indicate that magnetic anomaly modelling cannot be realistic without the consideration of the remanent and the induced magnetization. Considering this conclusion we are using the Kursk iron ore region as a test case. The Kursk region has voluminous amounts of geologic and geophysical data, rock magnetic data and multilevel magnetometer data, including satellite data. Consequently we will attempt to model magnetization source(s) using remanent and induced magnetic signatures constrained by geologic and geophysical data.

**GA5.11/L/02-A3** Poster **1430-03**

#### MAGNETIC PETROPHYSICAL STUDY IN THE HAMERSLEY PROVINCE, WESTERN AUSTRALIA AND ITS APPLICATION IN AEROMAGNETIC INTERPRETATION - I: MAGNETIC PETROPHYSICS

Wanwu GUO, Zhengxiang Li, Michael C. Dentith and Christopher McA. Powell (Tectonics Special Research Centre, Department of Geology and Geophysics, The University of Western Australia, Nedlands, Perth, WA 6907, Australia, Email: wguo@geol.uwa.edu.au)

The Hamersley Province is situated in the northwest of Western Australia. It contains extensive banded-iron formations (BIFs) and large iron deposits. Such a type of BIF-derived iron deposit, which mainly consists of hematite/martite and goethite, dominates the world's iron-ore reserves and outputs. A few magnetic petrophysical and palaeomagnetic studies have been conducted in the Hamersley Province, but sampling in these previous studies was not systematic. Therefore, to properly interpret aeromagnetic data in the Province, it was necessary for us to undertake a systematic magnetic petrophysical investigation. This paper presents the main magnetic petrophysical results. Applications of these results in aeromagnetic interpretation in the Province will be presented in the next paper.

Five hundred and seventy-three oriented samples from natural exposures and eleven industrial drill cores were collected from the Province. Bulk susceptibility, anisotropy of magnetic susceptibility (AMS) and natural remanent magnetisation (NRM) of all the samples were measured. More than 1000 data sets of each of the three parameters were obtained. Five out of the six BIF units (Marra Mamba, Bruno's Band, Dales Gorge, Weeli Wolli, and Boolgeeda) all show a similar logarithmic bimodal distribution in mean bulk susceptibility (MBS), which means that there are two major susceptibility groups for each unit. However, the MBS of Joffre BIFs exhibits a logarithmic normal distribution. The Weeli Wolli, Joffre, Dales Gorge and Bruno's Band BIFs have the highest MBS. The Boolgeeda BIF has intermediate MBS, but it is still higher than that of iron ores and other non-BIF units. The Marra Mamba BIF has the lowest MBS, which is even lower than the iron ores. Iron ores have intermediate MBS. Brockman martite-hematite ores have slightly higher MBS than Marra Mamba martite-goethite ores. Other non-BIF units generally have low MBS. The Dales Gorge, Joffre and Weeli Wolli BIFs have high AMS with well-developed bedding-parallel or sub-bedding-parallel magnetic foliation. Some hematite ores, the Boolgeeda BIF and the Mt. McGrath hematite conglomerate have low AMS with recognisable sub-bedding-parallel magnetic foliation. The intensively weathered Marra Mamba BIF and other non-BIF units are generally isotropic. The in-situ NRM directions of all the BIF units are random in terms of magnetic interpretation. This is likely...

**GA5.11/L/03-A3** Poster **1430-04**

#### MAGNETIC PETROPHYSICAL STUDY IN THE HAMERSLEY PROVINCE, WESTERN AUSTRALIA AND ITS APPLICATION IN AEROMAGNETIC INTERPRETATION - II: AEROMAGNETIC INTERPRETATION

Wanwu GUO, Michael C. Dentith, Zhengxiang Li and Christopher McA. Powell (Tectonics Special Research Centre, Department of Geology and Geophysics, The University of Western Australia, Nedlands, Perth, WA 6907, Australia, Email: wguo@geol.uwa.edu.au)

Banded-iron formations (BIFs) are very special in magnetic interpretations. BIFs usually produce strong magnetic anomalies, from which geophysicists can easily approach the objective area. On the other hand, it remains problematic how to accurately determine which portion of an anomaly may be produced by high-grade ores, often having lower magnetism than BIFs, from the huge magnetic 'sea' dominated by the BIF's contribution. In the Hamersley Province, only a few magnetic petrophysical studies directly target magnetic anomalies of BIFs, ores and other units, but sampling in these previous studies was not systematic and modelling was relatively simplified and not linked to the iron ore deposits. Therefore, a systematic magnetic petrophysical investigation especially designed for magnetic anomaly interpretations was needed in the Province and recently completed. The previous paper reported the main magnetic petrophysical results of this investigation. This paper presents the applications of these magnetic petrophysical results to aeromagnetic interpretations in the Province.

Different from other rocks, BIFs are characterised magnetically by high susceptibility, significant anisotropy of magnetic susceptibility (AMS), intensive natural remanent magnetism (NRM) and strong self-demagnetisation effects. These factors make the features of a BIF-related magnetic anomaly very complicated. In this paper, these effects are systematically analysed and illustrated by our theoretical models. One synthetic example and two practical examples considering these effects are also given.



The first example shows a synthetic ground magnetic profile over the West Angelas deposit. The result indicates that the total magnetic response is dominated by ...

**GA5.11/L/04-A3** Poster (Invited) **1430-05**

**GEOLOGICAL INTERPRETATION OF SYSTEMATIC AEROMAGNETIC AND PETROPHYSICAL DATA FROM FINNISH LAPLAND, THE NORTHERN FENNOSCANDIAN SHIELD**

Meri-Liisa AIRO, Geological Survey of Finland, PO BOX 96, FIN-02151 Espoo, Finland, fax: +358-205 50 12, Email: meri-liisa.airo@gsf.fi

A synthesis for the tectonic history of the Precambrian high-grade gneiss and granitoid area in southeastern Finnish Lapland was derived from integrated studies of regional geophysical data sets. The tectonic imprints in the aeromagnetic, gravity and digital elevation data were evaluated by incorporating systematic petrophysical data into the interpretation. The investigations aimed to explain the relationship between magnetic signatures and geology, particularly in terms of magnetic petrology. The results show that the present aeromagnetic character of southeastern Finnish Lapland was mainly produced during two major deformational events. The same weakness zones that were created due to the fragmentation of the Archaean crust during the continental rifting period at 2.5-2.1 Ga ago, were kinematically reactivated during the Svecofennian deformation at 1.9-1.8 Ga ago. These weakness zones emerge as crustal scale fracture and shear zones in the regional aeromagnetic and gravity data. They separate the more coherent crustal blocks, which are characterized by typical magnetic anomaly patterns and trends and Bouguer-anomaly levels. The high-resolution aeromagnetic data reveal variation in composition and petrofabrics of the anomaly sources. There are signs that crustal stress is still released along the same weakness zones during the postglacial time, but part of the large scale bedrock structures in southeastern Lapland may originate from the late Archaean. The Archaean structures are hard to recognize since they were later obscured by the Palaeoproterozoic tectonics.

**GA5.11/W/02-A3** Poster **1430-06**

**ANALYSIS AND INTERPRETATION OF GEOLOGICAL, ETROPHYSICAL AND GEOPHYSICAL DATA FOR THE KRAKA PHOLIOLITE ON THE SOUTH URALS**

Natalia FEDOROVA, Kirill Ivanov (Institute of Geophysics, 100 Amundsenstr., Yekaterinburg, 620016, Russia, email: eva@maglab.mplik.ru)

Kraka massives and surrounding continent-slope and volcanic complexes are not typical for the western paleocontinental sector of the Urals. It was main argument for idea that Kraka hyperbasite complex with environments are allochthon package overthrust to the West from a zone of a Main Uralian Fault on a distance no less than 20 km. Petrological and geochemical researches of hyperbasites are conducted, and stratigraphy and tectonic of surrounding complexes are also studied. The interpretation of gravity and magnetic fields are carried out and alternative variants of cross-sections are constructed. The results of study showed that massives have the flat position. The greatest depth of hyperbasite complex under the Middle Kraka is 3.5 km while the depth for sources of the South and the North massives are 2.0 km. In the Kraka region the autochthon, paraautochthon and four allochthones are allocated and the plates initially occupying probably more eastern and/or deeper positions were disposed in higher structural level at the final package of tectonic plates. Our data allows to assume that the whole package was folded just after overthrusting, i.e. at Early Carboniferous. In Triassic the region undergone post-collision extension, during which system of large normal faults was generated and metamorphic complexes of the Uraltau anticlinorium were uplifted to the surface. Investigations are being done in framework of "Europrobe".

**GA5.11/W/09-A3** Poster (Invited) **1430-07**

**FAULT GOUGE AS A SOURCE OF THE GEOMAGNETIC FIELD ANOMALY**

Dr. Norihiro NAKAMURA (The Tohoku University Museum)

Regional static anomaly for geomagnetic field are often observed along active faults. Previous studies interpreted the anomaly as placing the high susceptible dyke-like body along faults. Here we propose the alternative physical source for this anomaly. In brittle fault zones, the circulating fluid can chemically alter the magnetic properties of rocks. But, few theoretical relation between magnetic properties and chemical reactions in magnetic bodies has not been considered yet. In the light of irreversible thermodynamics, a new model for susceptibility change of rocks associated with chemical potential change induced by chemical reaction of magnetic bodies is proposed. The model indicates that the change in magnetic susceptibility is attributed by the negative change in chemical potential of rocks. In the hydration process with fluid-rock boundary, the chemical potential of rocks decreases as that process proceeds. Thus, it is expected that fault gouge zones show the high value in magnetic susceptibility rather than the surrounding wall rocks, because gouge zone with a high specific surface area can react with fluid easily. The comparison of our model with the natural data along the Nojima earthquake fault gives a good correlation that fault gouge has a two-order-of-magnitude higher value in bulk magnetic susceptibility (magnetic source was a ferrimagnetic goethite) than the wall rock. Because of this unusual magnetic properties of fault gouge, the rock-magnetic study affords us an interesting key to analyze the ferrimagnetic mineral localization in fault zones and the physical candidate of the geomagnetic field anomaly along faults. This study may lead to more realistic physical model needed in our understanding of the electromagnetic properties of faulted zones.

**GA5.11/W/08-A4** Poster (Invited) **1430-08**

**USING TEXTURAL MEASURES OF AEROMAGNETIC DATA TO INFER LITHOLOGY**

Mark GETTINGS (U.S. Geological Survey, Geologic Division, Suite 355, 520 N. Park Ave., Tucson, AZ 85719, USA, email: mgetting@swfo.arizona.edu)

Aeromagnetic data of high spatial resolution contains information related to the distribution of magnetic sources at many scales. This information can be quantified by textural measures (such as number of peaks and troughs or roughness and relative amplitudes) and can be used to help identify the lithology of the source rocks both where exposed and beneath cover. Data processing proceeds by calculating the desired textural measures in a moving window on the original flight-line data (not low-pass filtered, gridded data). Using flight-line data utilizes the full information content but introduces a directional bias in the result because of wide flight-line spacing. Two robust measures that have been used are Euclidean length per km and number of peaks and troughs per km within the window. Window width is selected to be about the same length as the minimum characteristic length of geological features of interest; the textural measures will detect all features of larger characteristic lengths. Each textural measure value then forms a data point at the center of its window. A grid of each textural measure is then computed. The textural measure grids are then combined using fuzzy logic to produce a new grid of categories (e.g. many peaks and troughs and large amplitude versus few peaks and troughs and large amplitude) which can then be correlated with the geology in areas of exposed rocks. This procedure has been applied to an aeromagnetic dataset flown

at 250-m line spacing, 250-m terrain clearance, and an along-line spacing of approximately 9m between data points in the Santa Cruz Valley and Santa Rita Mountains area of southeastern Arizona. The results show that the textural measures can be followed beneath cover for shallow and intermediate depths of both alluvial and magnetic volcanic cover.

**GA5.11/E/02-A3** Poster **1430-09**

**DENSITY AND MAGNETIC PROPERTIES OF CRYSTALLINE ROCKS OF THE RUSSIAN PART OF THE FENNOSCANDIAN SHIELD**

Anatoli Tchepik (North-West Regional Geological Centre, 24/1 Odoevsky street, St.Petersburg, 199155, Russia, Email: root@geol.spb.su); Lioudmila JDANOVA (State company "Mineral", 6 Veselnaya street, St.Petersburg, 196106 Russia, Email: frank@DF3136.spb.edu); Larisa Galitshanina (Geological Institute of the Kola Sci. Centre of Russian Academy of Sciences, Apatity, 184200, Russia); Nikolai Philippov, Gennady Muradymov, Anton Radchenko (State company "Mineral", 6 Veselnaya street, St.Petersburg, 196106 Russia, Email: frank@DF3136.spb.edu)

Published earlier petrophysical material, as: "The Petro-magnetic and Petro-density maps of geological formations of the eastern Baltic Shield at a scale of 1:1 000 000 (editor N.Dortman, 1977) and other compilations (L.Galitshanina, et al. 1988, V.Tyuremnov et al.1982, I.Azbel et.al. 1993) do not enable to use petrophysical properties for detailed geological interpretation on PC. The project "The Geological and Geophysical Maps of the Russian part of Fennoscandian Shield 1:1 mill." started in Russia in 1997. It includes collecting information of density and magnetic properties of crystalline rocks and construction of petrophysical Database (Paradox on PC). The responsible organizations are North-West Regional Geological Centre, Petersburg Geophysical Expedition (before November 1998) and State Company "Mineral" (since November 1998). Petrophysical properties will be compared with digital geological data and used for interpretation of the gravity and magnetic anomalies of the Shield. This project will fill a gap in the petrophysical information available for modern, computer-based methods using magnetic and gravity maps. Authors present the Petrophysical maps for different areas of the Russian part of Fennoscandian Shield: published earlier and based on digital petrophysical Database.

**GA5.11/E/03-A3** Poster **1430-10**

**DIFFERENT VIEWS OF BEDROCK IN PETROPHYSICAL DATA SETS**

Heikki Saavuori and Juha V. KORHONEN (both at Geological Survey of Finland, P.O. Box 96, FIN-02151 ESPOO, FINLAND, Email: heikki.saavuori@gsf.fi, juha.korhonen@gsf.fi); Rein Vaher (Geological Institute of Tallinn, 7 Estonia Ave., EE-00011, Tallinn, Estonia, Email: rein@prgeol.gi.ee)

The Geological Survey of Finland started petrophysical measurements for magnetic and gravity anomaly interpretation in 1954. The first petrophysical data base was established in 1971. The current PARADOX application PETROBASE 2.0 represents the fifth generation. The data consists of magnetic properties and bulk density measured from 250 700 samples, corresponding to an average data density of 74 samples per 100 sqkm in the level of whole country. The set is spatially inhomogenous, however, because of varying exposure of bedrock in different parts of the country and differing sampling techniques. Hand specimens (131,000 samples) taken from exposures, represent 3 per cent of bedrock at high local topographic level. A subset of this, the dyke samples (8000 specimens), represents more middle and lower crustal properties than the upper crust. Resampled cores (111,600 specimens) were originally drilled for mineral prospecting and stratigraphical studies and are partly of local nature, partly well representative in formational level. Boulders of local glacial till (8100 samples) represent approximately 50 per cent of the bedrock of the source area. These boulders are typically transported less than 500 m from its source in Northern Finland. The Estonian data set (3000 samples) was drilled from Precambrian basement through Phanerozoic sediments and the sites were selected by geophysical maps. The anomaly distribution partly affected this sampling. The different sources give us a different view of petrophysical characteristics. Overall regional properties can be obtained by properly weighting the data. A study is going on how to do this using regional geophysical information. The poster displays the new petrophysical maps of Finland and results from comparison of petrophysical properties in different types of sample sets.

**GA5.12** **Tuesday 20 July**

**WORLD MAGNETIC ANOMALY FIELD MAPS DERIVED FROM MARINE, AIRBORNE AND SATELLITE DATA**  
Location: Muirhead Tower 112 LR2  
Location of Posters: Student Room (1st Floor)

**Tuesday 20 July AM**

Presiding Chairs: T. Ishihara (Geological Survey of Japan, Japan)  
J. Arkani-Hamed (Univ of McGill, Quebec, Canada)

**GA5.12/E/04-A2** **0930**

**MAGNETIC SURVEYING AT THE EASTERN SPANISH COAST. THE EXCLUSIVE ECONOMIC ZONE PROJECT (ZEEE)**

M.CATALAN (J.Martin,J.A.Marin,and R. Alvarez (Geophysics Department, Royal Naval Observatory, San Fernando, Spain); M.Pardo,J.Rico (Hydrographic Institute Spanish Navy, S/N, 11007 Cadiz, Spain); P.Herranz, J.L.Sanz, C.Palomo and J.Acosta (Spanish Oceanographic Institute, Avda. Del Brasil 31, 28020 Madrid, Spain)

The Exclusive Economic Zone project is an ambitious multi-disciplinary study, that started in 1995, as a collaboration of the Spanish Defence Ministry with the Spanish Oceanography Institute (IEO), acting as co-ordinators, the Hydrographic Institute of the Navy (IHM) and the IEO.

Several Spanish Institutions are involved in it. Its aim is to obtain additional information related with classical geophysical disciplines like gravimetry, geomagnetism, or bathymetry, etc, that could allow a deeper knowledge of the Spanish Exclusive Economic Zone. As marine acquisition platform it is being used the Spanish Research Vessel HESPERIDES. Along 1995,1996 and 1997 summertime (August), activities were concentrated at the Spanish Gulf of Valencia and Balearic Sea area. The geomagnetic side of the project is a responsibility of the Geophysics Department of the Spanish Royal Naval Observatory at San Fernando. In this marine survey, several magnetic instruments were involved: One classical marine proton magnetometer and an Overhauser effect marine magnetometer. As fixed reference station we installed a magnetometer at Minorca Island (Balearic Island). The aim of this project, in the geomagnetism aspects, is to conform not only a spatial database but also a series of Total Field and Magnetic anomalies series of charts to be edited as a collaboration between the IHM

and the IEO. We will present in this Communication, the details of this project, in the geomagnetic aspect, some results obtained in the 1995-97 period at the Valencia gulf and Balearic Sea, and the present and next future activities at the Canaries Islands Zone.

**GA5.12/W/01-A2****0950****MAGNETIC ANOMALIES IN THE NORTH PACIFIC**

Nobuhiro ISEZAKI (Department of Earth Sciences, Chiba University, 1-33, Inageku, Chiba, 263-8522, JAPAN, Email: nisezaki@earth.s.chiba-u.ac.jp) Takemi Ishihara (Marine Geology Department, Geological Survey of Japan, 1-1-3, Higashi, Tsukuba, 305-8567, JAPAN, Email: tishi@gsj.go.jp)

The geological and geophysical atlas for the Pacific (GAPA) has been under the press for long time. This atlas will contain the magnetic anomaly map of the Pacific using the magnetic data provided by the NGDC (National Geophysical Data Center) of NOAA (WDC-1) in 1985. We will show survey tracks, the magnetic anomaly contour and profile maps in the Pacific. We will present a new map using additional recent NGDC data as well. Through the program for compiling and publication of the geological/geophysical data of world oceans under the auspices of the International Oceanographic Commission (IOC) of UNESCO, mainly entrusted by the Soviet Union, firstly the Atlas for the Indian Ocean was published in 1975 and for the Atlantic Ocean later in 1990. The atlas for the Pacific Ocean was scheduled to publish in 1994, however, the great change was occurred in Soviet Union in 1991 and this program was suspended hereafter. One of the authors (Isezaki) presented the magnetic anomaly map in the Pacific Ocean based on the data obtained before 1985 provided by the NGDC. Recently we got data from NGDC from 1958 till 1993 and made a new magnetic anomaly map in the north Pacific because there are not enough data to make a contour map in the south Pacific. In the NGDC data, there are about 15,278,670 data in the North Pacific Ocean in which the oldest was measured in 1958. The characteristics of magnetic anomaly pattern in the North Pacific Ocean are the lineation distribution. There are two magnetic bights in the NW and NE corners of the North Pacific Ocean, which are clearly presented in the coloured map. We will present the track line map and the result of statistics of data used as well.

**GA5.12/L/01-A2****1010****RESULTS OF RUSSIAN MAGNETIC SURVEYS IN THE ARCTIC AND ATLANTIC OCEANS**

GLEBOVSKY V.YU, Maschenkov S.P. (both at VNIIOkeangeologia, 1. Angliysky pr., 190121, St.-Petersburg, Russia, Email: gleb@vniio.nw.ru), Merkuriev S.A., Sochevanova N.A. (both at Institute of Terrestrial Magnetism, Ionosphere and Radiowave Propagation, St.-Petersburg Filial, 2, Muchnoy per., 191023, St.-Petersburg, Russia, Email: sam@NF1480.spb.edu).

The Arctic and North Atlantic oceans are the main regions for regular magnetic investigations were carried out by various Russian agencies. The Deep Arctic ocean and Russian Arctic shelf are covered by aeromagnetic surveys. The total length of aeromagnetic profiles in the Arctic region is about 2,000,000 line km. All magnetic anomaly profile data were digitized combined, totally reprocessed and loaded into the coherent magnetic data base. The new magnetic compilation in the Arctic Ocean is much more detailed than those developed by GSC-Atlantic (Verhoef et al., 1996).

The most part of Greenland-Norwegian and Reykjanes (between Iceland and Charlie-Gibbs FZ) Regions are covered by marine magnetic surveys. Two additional marine magnetic datasets collected within 200 km wide swaths of the Canary-Bahamas and Angola-Brazil Geotransects (CBG and ABG). Marine magnetic data are mostly in a digital, partly in an analog form. The most part of magnetic anomaly data in the North Atlantic and within ABG are not available yet for the geoscience community.

Existing computer generated colour shaded relief maps, examples of not published initial anomaly magnetic profile data, and schemes of marine and airborne tracklines for all mentioned above regions of the Arctic and Atlantic oceans are presented.

Being reprocessed and compiled with magnetic data have been collected by western countries the Russian data would provide significant additional information for geological and tectonic interpretation.

**GA5.12/W/02-A2****1100****ADMAP - A DIGITAL MAGNETIC ANOMALY MAP AND DATABASE FOR ANTARCTICA**

P.MORRIS (British Antarctic Survey, High Cross, Madingley Road, Cambridge CB3 0ET, UK, email: pmor@bas.ac.uk) R.B von Frese (Dept. of Geological Sciences & Byrd Polar Research Center, The Ohio State University, Columbus, OH 43210, USA, email: vonfrese@osu.edu)

With encouragement from IAGA and SCAR a working group of scientists from eight countries, including representatives of nearly all with major magnetic activities in the Antarctic, met in Cambridge in September 1995 to consider the establishment of a digital database of magnetic data and the production of a magnetic anomaly map of the continent. It was agreed to create a database and digital grid for the region south of 60degS. This would involve the integration of all available ground, airborne and marine surveys with satellite data being used, where appropriate, to link separated surveys and infill blank regions. Given the distribution of the existing datasets and the regional interests of the various research groups involved, the study area was divided into three equal sectors in which the data could be compiled separately. The three datasets could then be brought together to form a complete set for the whole continent. Since that date the members of the working group have been active with two further meetings being held, in Italy and the United States, to discuss the progress of the work and present related research findings. The compilation is now reasonably well advanced with two of the sectors being essentially complete. It is hoped that the complete grid and database will be available in the year 2000. We shall describe some of the practical problems, which have had to be overcome during this work and report on the latest situation.

**GA5.12/E/10-A2****1120****AEROMAGNETIC ANOMALY MAPPING AND THE GEOLOGIC ARCHITECTURE OF CENTRAL GONDWANA**

Colin REEVES and B.K. Sahu (International Institute for Aerospace Survey and Earth Sciences (ITC), Kanaalweg 3, 2628 EB Delft, The Netherlands. E-mail: reeves@itc.nl)

Most of the world's Precambrian geology is hidden by younger cover formations. Mapping the magnetic anomalies arising from the hidden igneous and metamorphic terrane provides a unique window on the unseen crystalline geology. In the Precambrian terranes of central Gondwana (Africa, Antarctica, Madagascar, India, Sri Lanka) many hundreds of individual aeromagnetic surveys have already been compiled to give continental-scale syntheses of magnetic anomaly patterns that are now continuous over many large areas. While problems still surround the free publication of many of these data sets, many outline interpretations have been published and may be augmented where the magnetic data can be accessed. We have digitally assembled and elaborated these interpretations for the fragments of central Gondwana using the Cambridge 'Atlas' PC software. This has made possible the refining and defining in

terms of absolute Euler rotation poles a defensible, tight re-assembly for central Gondwana. The result is presented as a map that shows a number of circular or highly rounded Archean nuclei around which the terranes created or reworked during the Proterozoic show structures that are largely concentric. Outcrop data and radiometric dating can be used by those having access to these and other data to verify and refine our geometric model that is available digitally. During the Phanerozoic, the extensive Karoo-Gondwana rifting (late Carboniferous to earliest Jurassic), supercontinent fragmentation (mid-to-late Jurassic) and renewed rifting in the Tertiary all appear to have, for the most part, avoided the Archean nuclei but followed instead the grain of the Proterozoic terranes.

**GA5.12/E/08-A2****1140****A DECADE OF MAGNETIC COMPILATIONS: FROM MICRO TO MACRO**

FAIRHEAD, J. D., Green, C. M. and Mushayandebvu, M. F. (GETECH, School of Earth Sciences, University of Leeds, Leeds, LS2 9JT, UK, email: jdf@getech.leeds.ac.uk)

Magnetic data compilations over the last decade have ranged in size from countrywide to continental scale and are now rapidly becoming global. Academics and explorationists to provide important insights into earth structure and geological processes at varying scales and resolutions are using them. These compilation projects, initiated by GETECH in 1989, have preserved historic data that otherwise might have been irretrievably lost and would not have been possible without the generous financial support of both the oil and mineral industries and the foresight and encouragement of national organisations. Innovative techniques have been developed to recover data and reprocess them into consistent, merged grid and profile databases. The presentation reviews a decade of magnetic compilations carried out by GETECH, often in association with other groups, for Africa, South America, Eastern Europe, FSU, China, Middle East and South East Asia, and illustrates the variable data types, problems and solutions. The importance of quality control, recognising resolution limitations as well as accurately recording survey technical specifications helps to preserve the long-term usability of these data sets. Availability of such data for academic research is encouraged, albeit within a legal framework proprietary data owners, governments and sponsors externally impose that on GETECH. The volume and spatial distribution of the compiled magnetic (and gravity) datasets that now exist allows their use in studies directed at earth evolution in new interactive ways, within a plate tectonic environment, using specially designed computer visualisation software. Such software besides identifying the inadequacies of current global plate tectonic model parameters does allow the investigation of the pre-drift structure and configuration of continents and their subsequent evolution and deformation.

**GA5.12/W/07-A2****1200****GRADIENT GEOMAGNETIC SURVEYS AT STRATOSPHERIC ALTITUDES: THEIR STRENGTHS, PECULIARITIES AND INTERPRETATION**

Yu Tsvetkov (IZMIRAN, Troitsk, Moscow Region, 142092, Russia) M PURUCKER (Geodynamics Branch, Goddard Space Flight Ct, Greenbelt, MD20771 USA, email: purucker@geomag.gsfc.nasa.gov) N Rotanova (IZMIRAN, Troitsk, Moscow Region, 142092, Russia)

The measurement of gradients of the geomagnetic field by stratospheric balloons along continental-scale transects offers a new perspective on the geomagnetic field complex. The proper interpretation of these surveys requires an understanding of the peculiarities of both the survey technique and the ability to separate the multiple sources of the geomagnetic field. The measurement devices are three scalar proton-precession magnetometers separated along a 4-km vertical line at equal distances. We will show that this measurement configuration is optimised for the extraction of remanent and induced magnetic signals from the entire thickness of the crust. The peculiarities of the technique that should be understood by an interpreter are 1) deviations of the measurement axes from a vertical line because of stratospheric winds, 2) rotations about the vertical axes, 3) vertical pendulum oscillations, and 4) day-night altitude differences. We will discuss these peculiarities, the errors they introduce into the measurements, and their alleviation. These gradiometer measurements provide a view of a range of wavelengths intermediate between those sensed by aeromagnetic surveys on the one hand and satellite magnetic surveys on the other hand.

**GA5.12/W/08-A2****1220****ACCESS TO AIRBORNE AND MARINE DATA THROUGH THE IAGA WG-V9 WEB SITE**

S. J. MCLEAN and C. A. Williams, National Geophysical Data Center, 325 Broadway, Boulder, CO USA 80303

At the 8th Scientific Assembly of IAGA in Uppsala, Sweden, the World Data Center-A in Boulder, Colorado agreed to develop and host the web site for Division V Working Group 9 Magnetic Anomalies (Land And Sea). The purpose of the web site is to provide access to data and information pertaining to the development of the world magnetic anomaly map. The status of the web site (at URL <http://www.ngdc.noaa.gov/IAGA/wg9/>) will be explained and possible directions for the future explored. The goal of the Working Group is to provide access to publicly available grids and metadata with information on related restricted higher resolution. We will demonstrate a pilot system to access magnetic grids via the WWW. The ESRI Spatial Data Engine (SDE) and Oracle database are the heart of the data access. If large file size presents a data transfer problem, we offer an alternate off-line data distribution method using CD-R or DVD-R.

**Tuesday 20 July PM**

Presiding Chairs J. Arkani-Hamed (Univ of McGill, Quebec, Canada)  
T Ishihara (Geological Survey of Japan, Japan)

**GA5.12/E/01-A2****1400****ON USING DOWNWARD FIELD CONTINUATION TO DETERMINE WORLD MAGNETIC ANOMALY MAPS**

Wigor A. WEBERS, GeoForschungsZentrum Potsdam, Telegrafenberg, D- 14473 Potsdam, Germany

The spatial wavelengths of the internal magnetic field sources are differently represented in the SHA terms when SHA field models of different concentric reference spheres as the Earth=92s surface and the satellite altitude are compared. This reflects the different physical content of both field data sets and can be evaluated by downward field continuation.

The mathematical reason is that both the SHA field models are infinite power series expansions of different convergence quality. In practically treating them they were truncated at a definite index N and used as finite partial sums. This does not remove the mathematical background, which explains that upward and downward field continuations are inverse ill-posed problems.

Referring SHA field models of concentric reference surfaces to each other only by the ratio of the radii is therefore an approximation that can be restrictedly used only because of increasing errors. As a consequence this shows that global ground-based and satellite anomaly fields significantly differ. Applying the downward field continuation procedure WIGCONT



demonstrates the problem and enables to combine both anomaly maps.

**GA5.12/W/04-A2 1420**

**APPLICATION OF THE 3D FILTERING FOR THE DERIVATION OF MAGNETIC ANOMALY MAPS FROM THE MEASUREMENTS OF SATELLITES**

Károly KIS (Geophysics Department, Loránt Eötvös University, Ludovika tér 2, 1083 Budapest, Hungary, email: kisk@ludens.elte.hu Géza Wittmann (MOL Rt, Hungarian Oil & Gas Co., Exploration, Field Development and Reservoir Engineering, Batthyány u. 45, 1039 Budapest, Hungary, email: gwittman@mol.hu)

Derivation of magnetic anomaly maps from the measurements of satellites is regarded as a problem of interpolation. The presented procedures were applied for the scalar and vector data of the Magsat. The processed anomaly maps are derived for the European region. The first phase of the data processing includes the correction of effect of the external and induced magnetic fields; separation of the data into dawn and dusk parts; and selection of the data according to the planetary Kp index. In the second phase of the data processing Gaussian low-pass and band-pass; and Laplacian low-pass and band-pass filterings are applied for the solution of the interpolation problem. The data are interpolated for the surface of a sphere of radius 6771-km. The interpolation procedures are designed in spatial frequency domain and implemented in space domain. The derived anomaly maps are compared to the regional geological structure of the European region.

**GA5.12/W/06-A2 1440**

**HOW CAN GLOBAL SPHERICAL HARMONICS ASSIST IN MAP CONSTRUCTIONS?**

Joseph CAIN and David Mozzoni (both at Geophysical Fluid Dynamics Institute/FSU, Tallahassee FL 32306-4360,USA, Email: cain@geomag.gfdi.fsu.edu and cyric@leyla.gfdi.fsu.edu)

We here compare maps constructed from band-passed global geomagnetic anomaly models with those computed from other authors who processed data residuals beyond a scale size represented by SHC to  $n = 13$ . The more recently constructed maps appear to be smoother than those previously. It is shown that while most features seen at satellite altitude are amply described using up to  $n = 40$ , the few strong anomalies require terms of the order of  $n = 60$  even though surface projections show noise patterns in the "bland" regions. This technique, or any other, does not resolve the problem of separating the contributions from the main field in the size range corresponding to  $3 < n < 15$ .

Obtaining near surface observations that are consistent in accuracy and especially in level that can be incorporated in global modelling at high degree is yet a problem. We recommend that international agreements to draw a "standard" global geomagnetic map be approached cautiously so "users" of such standard maps are clearly aware of the limitations. Further, because regional maps will continue to be made by near surface data, that any such to be considered part of a "standard" either be adjusted to the levels that can be determined from global satellite results, or that level differences are part of the data for each map. Producers of future near-surface surveys should be advised that maps produced from such surveys would be much more valuable if there were adequate information to determine the absolute level at some specific universal time so as to aid in integrating with global models. It would also be valuable to perform sample resurveys of some areas where small-scale maps are available to provide such data, or the map levels readjusted.

**GA5.12/W/03-A2 1500**

**USE OF MAGNETIC SATELLITE DATA IN LARGE SCALE AEROMAGNETIC AND MARINE COMPILATIONS**

K A WHALER (Department of Geology and Geophysics, University of Edinburgh, West Mains Road, Edinburgh EH9 3JW, Scotland, e-mail: kathy.whaler@ed.ac.uk); D Ravat, Department of Geology, Southern Illinois University at Carbondale, Carbondale, IL 62901-4324, USA

Satellite data are most useful in large-scale compilations of near surface magnetic anomaly data when they are downward continued to the same level as the survey data. Most previous methods have either only been able to downward continue over continental scale areas, or have not preserved the resolution of the satellite data. We present the results of applying the conjugate gradient algorithm to downward-continue global three-component satellite anomaly datasets. The shortest wavelengths present in the satellite data agree well with the longer wavelengths present in surveys with high altitude, long tie lines. Examples will be shown using data from the former Earth Physics Branch of the Geological Survey of Canada, where the anomalies agree both in pattern and amplitude. Individual small-scale surveys can then be 'draped' onto such models, providing the intermediate wavelength control not present in the surveys, which otherwise causes levelling problems in large-scale compilations. The advantages and some of the problems in this type of an approach will be discussed.

**GA5.12/E/07-A2 1520**

**TOWARD THE WORLD MAGNETIC ANOMALY MAP: METHODS AND EXAMPLES OF MERGING REGIONAL-SCALE NEAR SURFACE AND SATELLITE-ALTITUDE MAGNETIC DATA**

D. RAVAT (Dept. of Geology, Southern Illinois University at Carbondale, Carbondale, IL 62901-4324, U.S.A., email: ravat@geo.siu.edu) M. Purucker (Raytheon-STX/Geodynamics Branch Code 921, NASA-GSFC, Greenbelt, MD 20771, U.S.A., email: purucker@geomag.gsfc.nasa.gov) K. Whaler (Dept. of Geology & Geophysics, Grant Institute, West Mains Road, Edinburgh, EH9 3JW, Scotland, U.K., email: whaler@mail.glg.ed.ac.uk) M. Pilkington (Geological Survey of Canada, 615 Booth Street, Ottawa, Ontario, CANADA K1A 0E9, email: pilkington@gsc.NRCan.gc.ca)

Many previous regional-scale comparisons of near-surface and satellite-altitude magnetic anomaly data used methods and procedures that assumed that either the field at one of the altitudes was accurate or analytical rectangular co-ordinate continuation methods were adequate. These assumptions were partly incorrect and led to imprecise results that showed that the two sources of data were not compatible. We have developed a methodology in which we invert both the sources of the data to a common set of spherical-co-ordinate equivalent sources. Our results show that the near-surface and satellite-altitude fields are highly compatible over all regions we have analysed so far (Canada, the U.S., and parts of Antarctica). For these regions, the spatial correlation coefficients between the observed and the inverted fields are around or above 0.90. Rigorous wavenumber-domain comparisons indicate also the high correspondence between the fields at the relevant wavenumbers (~500-3000 km). Our results show that, in general, long wavelengths (>1000 km) in near-surface compilations are less accurate than those in satellite data and vice versa for short wavelengths (<500 km), as might be expected intuitively. Thus, the approaches that utilise and benefit from the individual strengths of these data, such as our approach, should be more suitable for the preparation of the world magnetic anomaly data.

**GA5.12/W/05-A2 Poster 1600-01**

**A NEW MAGNETIC ANOMALY MAP OF THE CENTRAL SECTOR OF EAST ANTARCTICA**

ALEXANDER V. GOLYNSKYI & V. N. Masolov 2 VNIIOkeangeologia, 1 Angliysky Ave., 190121, St. Petersburg, Russia. (email: sasha@gus1.vniio.nw.ru) 2 PMGRE, 24, Pobeda St., 189510, Lomonosov, Russia.

Aeromagnetic and marine observations in the central sector of East Antarctica and adjacent seas of Indian ocean have been compiled in a new database as a part of the initiative to produce a new magnetic anomaly map of Antarctica (ADMAG). Extensive regional magnetic flights by Russian expeditions commenced in 1955 has resulted in over 260 000 line kilometres of data collected with line-spacings of about 5 km, 20 km and 50 km. The aeromagnetic and marine data used in the compilation consists of a combination of digitally recorded data and data digitised from published and unpublished profile maps. These were edited to remove high-frequency errors before network adjustment was carried out. Data for each individual survey were projected and gridded by using either a 1.5-km or 5 km grid interval. Surveys using line spacings of 50 km or more were initially gridded at a coarser interval, then regridded. In the final compilation step the surveys were merged together using Geological Survey of Canada grid stitching program and gridded at intervals of 5 km. The most advantageous result of this compilation is the shaded-relief map, which show one of the most complete and coherent perspectives to date of the region's magnetic character. In combination with other types of data, this information promises to shed new light on the structure, processes and tectonic evolution of the ice-covered Antarctic continent and surrounding ocean. It will be a valuable tool for structural and tectonic correlations between fragments of Gondwana, and as such will be a key element of the proposed World Magnetic Anomaly Map. The magnetic anomalies correlate with many of the study area's structural features. On continent interpretation of magnetic data allowed to better define the boundaries between the Archean stable blocks and the Proterozoic mobile belts, and to trace these boundaries beneath the ice sheet. In sedimentary basins these data provided an important source of information about the depth and tectonic nature of the basement and thickness of sedimentary cover.

**GA5.12/E/05-A2 Poster 1600-02**

**AEROMAGNETIC MAP OF THE RUSSIAN PART OF THE FENNOSCANDIAN SHIELD 1:2.5 MILL**

Anatoli Tchepik (North-West Regional Geological Centre, 24/1 Odoevsky street, St.Petersburg, 199155, Russia, Email: root@geol.spb.su Lioudmila JDANOVA (State company "Mineral", 6 Veselnaya street, St.Petersburg, 196106 Russia, Email: frank@DF3136.spb.edu)

The project "The Geological and Geophysical Maps of the Russian part of Fennoscandian Shield 1:1 mill." started in Russia in 1997. It includes the construction the digital model of Aeromagnetic Map in a scale 1:1mill. On the base the authors of this abstract are making the matrix (1x1 km. grid). The responsible organisations are northwest Regional Geological Centre, Petersburg Geophysical Expedition (before November 1998) and State Company "Mineral" (since November 1998). At the same time, in 1997 the Geological Surveys of Finland, Norway and Sweden together with the Northwest Regional Geological Centre, Russia have started the compiling of digital geological and geophysical maps in a scale of 1 : 1 mill. The Geological Survey of Finland (GTK) co-ordinates the work, that is planned to be completed by the end of 2000. A preliminary map of the Russian part has been included into the preliminary versions of common Aeromagnetic Map of the whole Fennoscandian Shield: a preliminary version (0.3) of the Magnetic map in a scale of 1:2 mill has been compiled in August 1997 and presented at the 8th Scientific meeting of IAGA in Uppsala and at the Crustal Model Workshop in Espoo (Korhonen et al. 1997); a preliminary version (0.5) of the Magnetic map in a scale 1 : 4 mill. has been compiled in November 1998 and presented at the 3th workshop Svekalapko in Repino (Russia). The authors present a new version of the Aeromagnetic Map of the Russian part of the Fennoscandian Shield with additional aeromagnetic data for Northern and Western parts. The checking of magnetic map level has been done by a measuring tie line.

**GA5.12/E/06-2 Poster 1600-03**

**MAGNETIC DGRF-65 ANOMALY MAP OF THE FENNOSCANDIAN SHIELD 1:4 MILL**

Juha V. KORHONEN (Geological Survey of Finland, P.O. Box 96, FIN-02151 ESPOO, Finland, Email: juha.geofys@gsf.fi), Sven Aaro (Geological Survey of Sweden, P.O.Box 670, 75128 Uppsala, Sweden, Email: sven.aaro@sgu.se), Jan Reidar Skilbrei (Norges geologiske undersøkelse, Postboks 3006 Lade, 7002 Trondheim, Email: jan.skilbrei@ngu.no), Anatoli Tchepik (Northwest Regional Geophysical Centre, 24/1 Odoevsky Street, 199155 St Petersburg, Russia, Email: root@geol.spb.su, Lioudmila Jdanova (State Company "Mineral", Veselnaya Street 6, 196106 StPetersburg, Russia, Email: frank@DF3136.spb.edu)

In 1997 the Geological Surveys of Finland, Norway and Sweden and the Petersburg Geophysical Expedition started to compile a magnetic DGRF-65 anomaly map in a scale of 1:1 mill on a 1 km x 1 km grid. The purpose was to support studies of crustal structure and evolution in the Fennoscandian Shield and to contribute to the world aeromagnetic map. The participating countries will provide the data of their territory as 1 km x 1-km subgrids after making reductions to DGRF-65 anomaly level. Most of the data originates from airborne surveys; ground and seaborne information will patch gaps. Consistent anomaly levels will be ensured by long tie lines. Available petrophysical data (270 000 measurements of induced and remnant magnetisation) will be used to compile magnetic characteristics of major geological formations and to further calculate a 5 km x 5 km geologically weighted magnetisation grid. The aim is to interpret the depth extent of major surficial geological formations, and to identify previously unknown magnetic anomaly sources at depth. A preliminary magnetic anomaly map on a scale of 1:4 mill on a 2 km x 2 km grid and examples of petrophysical correlation of anomalies are at display.

**GA5.12/L/03-A2 Poster 1600-04**

**AEROMAGNETIC TIE LINE SURVEY OF FINLAND 1998**

Juha V. KORHONEN, Maija Kurimo and Toivo Korja (all at Geological Survey of Finland, P.O. Box 96, FIN-02151 ESPOO, Finland Email: juha.korhonen@gsf.fi)

The first national aerogeophysical mapping programme of Finland was carried out in 1951-72 and covered 418,000 sqkm. In 1968-69 the relative magnetic intensities were tied to absolute values by tie lines, which were separated by 40 km from each other and were referenced to both Finnish magnetic observatories. Comparison with modern absolute magnetic surveys indicates a standard error less than 20 nT. The second national programme was started in 1972. The altitude was 40 m and track separations were 200 m. Eighty per cent of the Finnish land area was covered by 1998. The daily magnetic variation was corrected by one base station, which was located in the survey area. The measurements were reduced to absolute total intensity 1965.0 referencing the base station to magnetic observatories in



Nurmij\_SB'S\_(Bvi and Sodankyl. The accuracy of this procedure depends on the best homogeneity of magnetic field variation observed during each survey. The main source of error is nonlinear spatial change in total field, which can be corrected by denser net of magnetic base stations only. Comparisons with repeated measurements indicate, that the standard error of absolute level is better than five nT in a 25-year span. In 1998 the SVEKALAPKO BEAR experiment and IMAGE project in Fennoscandia (66 stations together) offered an opportunity to estimate spatial distribution of nonlinear drift in six weeks time and to use the network as base stations for tie lines, which were flown at 40 m altitude and with 100 km track separations. The aim was to use results in checking survey qualities, in future reduction of aeromagnetic measurements, in compilation of a Fennoscandian aeromagnetic map 1:1 mill and in interpretation of lithospheric magnetic sources. On display are the reduction procedure, results of comparison with elder magnetic measurements and the newest version of the aeromagnetic DGRF-65 anomaly map of Finland.

**GA5.12/E/03-A2** Poster **1600-05**

**THE SWEDISH TIE-LINE PROJECT OF 1998: AN AIRBORNE MAGNETIC AND RADIOMETRIC RE-SURVEY**

Soren Bystrom, Anders H. Linden and Gerhard SCHWARZ (Geological Survey of Sweden, Box 670, S-75128 Uppsala, Sweden, email: gerhard@sgu.se) Maija Kurimo and Juha V. Korhonen (Geological Survey of Finland, Box 96, FIN-02151 Espoo)

The first airborne geophysical measurements were done in Sweden about 40 years ago and today large parts of the country are surveyed by magnetic and radiometric measurements as well as partly by VLF-mappings. But, the huge amount of individual data sets taken over a longer period causes some problems in data treatment. When combining data sets that were measured in different years levelling errors may occur, both with the radiometric as well as with the magnetic data. Therefore, the Geological Survey of Sweden was doing an airborne magnetic as well as radiometric re-survey on a large scale all over Sweden, called the tie-line project. The project aims on compiling new magnetic and radiometric maps that consider all available airborne data. The airborne survey was flown by GTK of Finland during the summer of 1998. The distance between flight lines was about 18 km. At the same time the magnetotelluric array of the BEAR group of EUROPROBE's SVEKALAPKO project was in operation. Further information on the time varying magnetic field was provided by the IMAGE network, as well as by three to five total field moving base stations.

This scheme of fixed and moving base stations resulted in a distance between a ground station and the airplane not exceeding about 100 km. It allows to remove the time varying external magnetic field with better accuracy than in previous surveys. We will show maps compiled from the newly obtained magnetic and radiometric data. We will outline also strategies for further data treatment, e.g., fitting in airborne magnetic data from previous surveys into the newly obtained data, as well as considering the bias caused by electrical high conductivity zones.

**GA5.12/L/02-A2** Poster **1600-06**

**CONSISTENT GEOMAGNETIC IMAGES WITHIN THE LOW DANUBE AREA. MAGLODAN PROJECT**

Lucian Besutiu and Georgeta Besutiu (Geological Institute of Romania, 78344 Bucharest 32, sector 1, 1, Caransebes str., fax: +401 224.0404; e-mail: besutiu@igr.sfos.ro ), Inna Pashkevich and Mikhail Orlyuk (Institute of Geophysics Kiev, 32, Palladin av., Ukraine, Marian Ivan (University of Bucharest, 1, Traian Vuia str., Romania), Vasile Neaga (Institute of Geophysics and Geology Chisinau, 3, Academiei str., Republic of Moldova)

MAGneticLowDANube project represents the first step in a joint venture between the Geological Institute of Romania, Institute of Geophysics Kiev and Institute of Geophysics and Geology Chisinau in an attempt to join the national geomagnetic maps of Romania, Ukraine and Republic of Moldova. Based on a common international magnetic reference network, a consistent data set of absolute values of the total intensity scalar of the geomagnetic field was obtained for the whole Low Danube area. Total intensity scalar and geomagnetic anomaly maps were constructed. Horizontal gradient maps have been performed to check up the quality of the joining operation. Various local models of the reference field were used to achieve geomagnetic anomaly images. Regional and local effects are presented and discussed.

**GA5.12/E/02-A2** Poster **1600-07**

**STRUCTURAL STUDY OF SEDIMENTARY BASIN USING AEROMAGNETIC DATA. CASE STUDY: THE TIN-SERIRINE SEDIMENTARY BASIN, HOGGAR ALGERIA.**

Haydar BAKER (Departement de Geophysique, IST, USTHB, El-Alya, Alger, Algeria, email: djeddi@ccr.jussieu.fr) NasrEddine Bourenas (CREM, El-Biar, Alger, Algeria) Mohamed Hamoudi (Departement de Geophysique, IST, USTHB, El-Alya, Alger, Algeria, email: hamoudi@ipgp.jussieu.fr)

The Tin-Seririne basin is situated in the SW of the Hoggar region in Algeria. It forms the continuity of the Ti-Merso-lullmeden basin in the north of Nigeria. It is situated between the latitudes 8=B0 & 23=B0 and longitudes 20=B0 & 23=B0.

The interpretation of the magnetic anomalies and the results obtained from four regional gravimetric profiles suggest that the region has been subjected to intensive tectonic activities. Three principal fault systems have been differentiated in this work, namely the NS, the NNE-SSW and the NNW-SSE.

The NS fault system, which is essentially composed of three faults (along the latitudes 6=B015', 6=B050' & 7=B030' respectively) is considered to be the one responsible for the formation of the Tin-Seririne sedimentary basin during the late phase of the Pan-African orogenesis. The first phase of sinking is thought to have occurred along the seventh latitude, while the second phase is considered to have been associated with two important faults of the NNE-SSW system.

However, based on detailed geophysical and geological studies, a geodynamic model is given with six zones of distinctive geological characteristics.

**GA5.12/P/01-A2** Poster **1600-08**

**ROLE OF AEROMAGNETICS IN THE DELINEATION OF THE GROSS STRUCTURAL FRAMEWORK OF GABAL MEATIQ AREA, CENTRAL EASTERN DESERT, EGYPT**

Ahmed A. Amar, Said I. Rabie and Magdy A. GOUDA (all at Exploration Division, Nuclear Materials Authority, P.O.Box 530 Maadi, Cairo, Egypt) Nasser M. Abu-Ashour ( Geophysics Dept., Faculty of Science, Ain Shams Univ., Cairo, Egypt)

The delineation of the regional structure framework of Gabal Meatiq Area, Central Eastern Desert, Egypt, at the deep-seated and the near-surface levels, was achieved through the

integrated application of some geophysical interpretation techniques to the aeromagnetic survey data reduced to the north magnetic pole (RTP) of the earth.

Two main average interfaces at depths 1.1 and 2.2 kms below measuring level were calculated through the application of the two-dimensional power spectrum. Isolation of the magnetic anomalies was conducted using filtering combined with analytical downward continuation at the two assigned interfaces. In addition, the magnitudes of the normalised total and horizontal magnetic vectors (gradients) of the field intensity were calculated at the two stated interfaces. Moreover, variations of the horizontal phase angle were calculated at the two fixed interfaces.

The information obtained from all the methods of interpretation were integrated to construct two interpreted magnetic basement structural maps at the two designated levels. These two maps show the gross structural framework of the area under study. The major delineated magnetic structural elements affecting the basement complex at the two appointed interfaces are faults and folds in the form of upfaulted blocks or anticlines and down-thrown blocks or synclines as well as dykes. Statistical trend analysis was executed, principally, for the defining the trend directions of the interpreted magnetic structural lineaments using the successive overlap technique.

**GA5.12/W/09-A2** Poster **1600-09**

**AN AEROMAGNETIC SYNTHESIS OF THE ARABIAN SHIELD: GEOLOGICAL IMPLICATIONS**

FAWZIA ASPIRANE HADDADJ, Pierre Nehlig, Antonin Genna, Philippe Bernard, Jean-Marc Miehé (BRGM, 3 Ave. C. Guillemin, B. P. 6009, 45060, Orléans cedex 02, France) and Abdallah Ahmed Showail (DMMR, USGS mission, P.O box 1488 Jeddah, 21431, Saudi Arabia)

In the frame of a global reevaluation of the geology and metallogeny of the Arabian shield, a compilation of all the aeromagnetic surveys covering western Saudi Arabia has been completed (655000km2). Ten aeromagnetic surveys, carried out from 1962 to 1983, stored on magnetic tapes, realised at different terrain clearance (150 m, 300 m and 500 m) and different line spacing (800 m, 500 m and 2000 m) have been compiled in a 1 km elementary squared grid at an altitude of 300 m. In order to interpret the magnetic anomalies in terms of geological structures a reduction to the pole to replace the magnetic anomalies at the top of the sources has been achieved. A vertical gradient has been computed in order to underline the short wavelength anomalies which are associated to shallow sources such as the basaltic dykes due to the opening of the red sea. The resulting maps show magnetic anomalies, which are well correlated with geological features, which are constrained in terms of structures, lithology and geochronology. They shed new light on the accretion, the pan African tectonics and the intimate relationship between the N-S Nabitah belt and the NW SE Nadj faults system.

**GA5.12/E/09-A2** Poster **1600-10**

**THE INTERPRETATION OF GRAVITY AND MAGNETIC ANOMALIES OF RUDAN AREA**

Naser H. GUYA (Institute of Geophysics, Tehran University, P. O. Box 14155-6466, Tehran, I. R. Iran, email: nhzguya@chamran.ut.ac.ir)

Using magnetic and gravity data from a relatively small area close to Makran subduction zone in south-east Iran, we are trying to understand the complex geology of this area and say something about the plate tectonics of this part of the world. It has been suggested that the Iranian plateau has been compressed in south and south-west by the Arabian plate, and in south-east by the subduction of oceanic plate along Makran belt. This paper investigates the causes of observed anomalies and their relation to the tectonics of the area. The observed magnetic anomalies are mostly deep seated and show a north-south lineation. The gravity map also shows this lineation and a good correlation with magnetic data. We suggest that the north-east tectonic forces have stopped at the Sabzevaran fault and therefore the folding of basement in an east-west direction has occurred.

**GA6.01** Friday 23 – Saturday 24 July

**LONG AND SHORT TERM VARIABILITY IN SUN'S HISTORY AND GLOBAL CHANGE (WITH DIV. IV)**

Location: Gisbert Kapp, NG15 LR1  
Location of Posters: Gisbert Kapp, Coffee Room

Friday 23 July AM

Presiding Chair: W. Schröder (Geophysical Institute, Bremen, Germany)  
Concurrent Poster Session

**Introduction** **0830**

H. MORITZ

**GA6.01/W/08-A5** **0835**

**EVOLUTION OF THE CONCEPT OF MAGNETOTAIL RECONNECTION AS A SOURCE OF ENERGY FOR MAGNETOSPHERIC SUBSTORMS**

Gordon ROSTOKER (Department of Physics, University of Alberta, Edmonton, Alberta, Canada T6G 2J1, email: rostoker@space.ualberta.ca)

Not long after the 1961 suggestion by J. Dungey that energy transfer from the solar wind to the magnetosphere was modulated by the direction of the interplanetary magnetic field with respect to the dayside terrestrial magnetic field, it became clear that large scale enhancements of auroral and geomagnetic activity (termed magnetospheric substorms) were associated with frontside magnetic field merging and subsequent reconnection behind the earth in the magnetotail. Since the mid 1960's, the concept of neutral line formation in the magnetotail has been an integral part of most attempts to explain the most spectacular and explosive part of substorm development, the expansive phase. In this paper, I shall trace the evolution of neutral line models of substorm activity from both the observational and theoretical points of view. It will become clear from this presentation that a universally acceptable framework in which substorm activity can be understood has not yet materialized, and major changes in the dominant paradigm for understanding substorm activity have occurred from time to time even in the 1990's.

**GA6.01/E/03-A5 0900**

**EDMOND HALLEY AND THE EARTH'S MAGNETIC FIELD**

Alan COOK (Selwyn College, Cambridge, CB3 9DQ, UK, e-mail: ahc13@cam.ac.uk)

Three hundred years ago, at the end of June 1699, Edmond Halley returned from his first cruise to measure the magnetic declination around the Atlantic. In the middle of September, he sailed on his second cruise of nearly a year. The cruises, and the printed chart derived from them, set the course of geomagnetic studies for a century and more. Halley had first observed the magnetic declination as a schoolboy. He had proposed a model of the interior of the Earth to account for the westerly drift. In 1716 he showed that the patterns of aurorae matched those of the circumpolar geomagnetic field. So he posed three questions to which answers are only now appearing, the structure of the main field, the cause of the westerly drift, and the interaction of the solar wind with the geomagnetic field.

Halley stood on the shoulders of predecessors, of Petrus Peregrinus in the 13th century, William Gilbert in 1600, Gellibrand and Athanasius Kirchner early in the 17th century. His fundamental understanding of the geophysical implications of the nature of the field were his own. His successors, such as Sabine, improved and extended charts of the geomagnetic field. Halley realised that the large scale anomalies of the field must have deep lying sources, but a formal treatment had to wait for C F Gauss. Halley's ideas about the field and aurorae have been justified after three centuries by dynamo theory and by the discovery that the upper atmosphere is a plasma with its geometry controlled by the main geomagnetic field.

**GA6.01/E/10-A5 0930**

**HALF A CENTURY OF GEOMAGNETISM**

Atia A. ASHOUR (Math. Dept., Faculty of Science, Cairo University, Giza, Egypt, e-mail: ashour@frcu.eun.eg)

The author reviews his work over more than 50 years in theoretical modelling of electromagnetic induction in the earth and ionosphere; and how this work was influenced by the pioneers Sidney Chapman, Albert Price, Vincent Ferraro and others.

**GA6.01/E/20-A5 1030**

**CAN SOLAR SEISMOLOGY ILLUMINATE TERRESTRIAL CLIMATIC CHANGES?**

G.R. ISAAK (School of Physics and Astronomy, University of Birmingham, Birmingham, B15 2TT, U.K.)

Solar oscillations have now been monitored for over twenty years, a complete magnetic cycle. The completeness, quantity and quality of the acquired data has steadily improved and the resultant power spectra show a rich discrete and a continuum spectrum due to convective noise. The discrete spectrum is due to acoustic eigenmodes of the Sun and can be characterised by eigenfrequencies, amplitudes, splittings, line-widths and shapes: the acoustic analogue of the term values of an atom. The eigenfrequencies can now be measured to accuracies of a few parts per million and provide a superb probe of the interior of our Sun. Amplitudes and the other parameters are measured to only a modest precision. The eigenfrequencies and amplitudes are found to vary appreciably over the solar cycle, closely correlated with the solar irradiance. It would seem that the eigenfrequencies, at least, provide an excellent and readily measured proxy of the solar irradiance and, therefore, information on changes of the dominant term controlling the Earth's climate.

**GA6.01/W/02-A5 1055**

**THE EFFECT OF SOLAR VARIABILITY ON CLIMATE**

Sofia SABATINO (Department of Astronomy, Yale University, P.O. Box 208101, New Haven, CT 06520, USA, email: sofia@astro.yale.edu)

Because the Sun supplies nearly the totality of the energetic input (photons and particles) in the Earth's environment, it is clear that any significant variation of the solar input should affect global change in general, and climate in particular. Here I will only address the effects of radiation. Variability of the total irradiance on timescales up to the activity cycle has been well determined, and understood. Its direct climate consequences are negligible. The larger fractional variability of the EUV-UV radiation affects the structure of the upper atmosphere of the Earth, in well-documented ways, but the energy content of radiation in this wavelength range is very small. It has been suggested that these variations may trigger processes, which indirectly cause climate change. It is fair to say, however, that none of the processes proposed to accomplish this has received wide acceptance. Finally, for timescales of several decades to centuries, direct measurements do not exist except for crude features, such as sunspot number. At the same time, various paleoclimatic data suggest the existence of a strong solar component. We propose in this paper the existence of a solar variability mechanism related to changes of the internal solar structure caused by the variable magnetic field due to the dynamo process. We present proxy data that support this view, and suggest additional work required to better understand the properties of this mechanism, and its implications for climate change.

**GA6.01/E/02-A5 1120**

**RESPONSE OF THE LLN MODEL TO THE ASTRONOMICAL FORCING OVER THE QUATERNARY AND THE NEXT 130 THOUSANDS YEARS**

A. BERGER, M.F. Loutre, X.S. Li (UCL, Institut d'Astronomie et de Géophysique G. Lemaître 2 Chemin du Cyclotron, B-1348 Louvain-la-Neuve, Belgium)

The LLN 2-D climate model has been used to reconstruct the long-term climatic variations over the Quaternary Ice Age. An atmospheric CO2 concentration decreasing linearly from 320 ppmv at 3 Myr BP (Late Pliocene) to 200 ppmv at the Last Glacial Maximum was used to force the model in addition to the insolation. Under such condition, the model simulates the intensification of glaciation around 2.75 Myr BP, the late Pliocene-early Pleistocene 41-kyr cycle, the emergence of the 100-kyr cycle around 900 kyr BP, and the glacial-interglacial cycles of the last 600 kyr. The hypothesis was put forward that during the Late Pliocene (in an ice-free - warm world) ice sheets can only develop during times of sufficiently low summer insolation. This occurs during large eccentricity times when climatic precession and obliquity combine to obtain such low values, leading to the 41-kyr period between 3 and 1 Myr BP. On the contrary in a glacial world, ice sheets persist most of the time except when insolation is very high in polar latitudes, requiring large eccentricity again, but leading this time to interglacial and finally to the 100-kyr period of the last 1 Myr. Using a reconstructed CO2 concentration over the last 600 kyr from a regression based upon SPECMAP, it has been shown that stage 11 and stage 1 request a high CO2 to reach the interglacial level. The insolation profile at both stages and modelling results tend to show that stage 11 might be a better analogue for our future climate than the Eem. Although the insolation changes alone act as a pacemaker for the glacial-interglacial cycles, CO2 changes help to better reproduce past

climatic changes and, in particular, the air temperature and the southern extend of the ice sheets. Using the calculated insolation and a few scenarios for CO2, the climate of the next 130 kyr has been simulated. It shows that an interglacial will most probably last particularly long (50 kyr). This conclusion is reinforced if we take into account the possible intensification of the greenhouse effect, which might result from man's activities over the next centuries.

**GA6.01/W/14-A5 1145**

**SOLAR VARIABILITY AND POSSIBLE RESPONSES IN THE TERRESTRIAL SYSTEM: THE EFFECTS OF SOLAR WIND VARIATIONS ON EARTH'S RATE OF ROTATION**

Nils-Axel MOERNER (Paleogeophysics & Geodynamics, Sweden, e-mail: morner@pog.su.se)

The solar wind is known to interact with the Earth's own geomagnetic field which effects the Earth's shielding of incoming cosmic ray, measured by the in-fall of 10Be and the atmospheric production of 14C. The solar wind is also known to vary with the sunspot cycles. During the Spörer, Maunder and Dalton main sunspot minima, the solar wind decreased which weakened the shielding so that the 14C production increased like the in-fall of 10Be (less clear). A correlations has previously been observed between sunspot activity and variations in the Earth's rate of rotation. Because of a rough correlation with periods of cold climate - "Little Ice Ages" - in NW Europe, it has been proposed that solar irradiance (luminosity) decreased at the same time and that there exists a solar-terrestrial climate linkage. However, I have been able to show that the Medieval warm period and the cold periods 1440-1460, 1687-1703 and 1808-1821 in NW Europe were all driven by changes in the distribution in the North Atlantic of warm surface water from the SW and cold arctic water from the N. These changes were driven by variations in the Earth's rate of rotation (in a feed-back coupling system). This affected the oceanic circulation so that the a major current like the Gulf Stream sent less warm equatorial water along its northern branch towards NW Europe at the same time as Arctic water penetrated further south. This led to severe cold periods in the NW European region. In southern Europe and northern Africa the same periods were characterized by increased heat. This means that these periods represent changed distribution of the terrestrial energy. And this was driven by increased rate of rotation. In this scenario, we do not need to call for hypothetical large-scale variations in solar irradiance; only an influence of the solar wind variability on Earth's rate of rotation.

**GA6.01/E/01-A5 1210**

**THE EARTH'S MIDDLE ATMOSPHERE AND THE SUN'S INTERIOR**

Michael E. McINTYRE (Centre for Atmospheric Science at the Dept. of Applied Mathematics and Theoretical Physics, Cambridge CB3 9EW, UK, email: mem@damp.cam.ac.uk)

The atmosphere used to be thought of using classical ideas about turbulence that looked back to analogies with gas kinetic theory, involving among other things an assumption that departures from spatial homogeneity are weak. This led to problematic notions like 'negative eddy viscosity'. However, today's understanding of the global-scale atmospheric circulation, especially that of the middle atmosphere, recognizes --- as essential, leading-order features --- the strong spatial inhomogeneity of atmospheric turbulence together with the crucial role of wave propagation and wave breaking. The latter involves a phase-coherent interaction between the waves and (highly inhomogeneous) turbulence --- not pre-existing turbulence, but turbulence that owes its existence to the arrival of the waves, as with the familiar example of ocean-beach gravity waves. This description applies to all the wave types involved, from internal gravity to Rossby or potential-vorticity waves, provided that the term 'wave breaking' is interpreted in a suitable way, consistent with the fundamentals of wave-mean interaction theory. The chirality of Rossby waves, tied to the sense of the Earth's rotation, results in an angular momentum transport that is intrinsically one-signed and therefore ratchet-like, producing via Coriolis effects an inexorable 'gyroscopic pumping' of air systematically poleward that dominates, for instance, the global-scale transport of chlorofluorocarbons and other long-lived greenhouse gases in the stratosphere. Some of the same considerations apply to the fluid dynamics of the Sun's stably stratified radiative interior. Together with recent helioseismic data they are forcing us to a novel conclusion: the Sun not merely can, but must, have in its radiative interior a poloidal magnetic field that is strong enough to reshape, drastically, the circulation and differential rotation in the interior. This has far-reaching consequences for understanding solar spindown history and internal variability, and for performing helioseismic inversions.

**GA6.01/L/01-A5 1240**

**NORTHERN LIGHTS RESEARCH IN SCANDINAVIA UP TO THE 19TH CENTURY**

A. EGELAND, Department of Physics, University of Oslo, Norway, email: alv.egeland@fys.uio.no

Because northern lights could be observed directly without scientific aids, it has stirred man's imagination, curiosity and fear as long as the Earth has been inhabited. The scientific name aurora was suggested 400 years after the Vikings have named this phenomenon Northern Lights. It is described in vivid details in the Norwegian chronicle Kongespeilet from around year 1200.

A close connection between aurora and the magnetic field was discovered by Hiorter and Celsius around 1730. They also strongly stressed the importance of accurate observations. Thus, already around 1750 it was suggested that the Northern lights formed a ring 10 to 20 degrees off the geographic pole. The first auroral atlas was published by Barhow in 1751.

In the period 1880 to year 1900 a number of ideas and theories of lasting importance in the field of auroral and plasma physics were advanced.

Friday 23 July PM

**GA6.01/P/03-A5 1400**

**CHANGE-POINT DETECTION IN GEOPHYSICAL TIME SERIES**

Raymond SNEYERS, Institut royal météorologique de Belgique avenue Circulaire, 3, B-1180 Bruxelles, Belgium Email: rsneyers@oma.be.

Besides the search for periodicities and autocorrelation, the statistical problem of change-point detection in geophysical time series is raised both for verifying homogeneity of data and for characterising the natural instability of the evolution of geophysical phenomena. In this paper, the used methodology is fully justified at the theoretical point of view and an illustration is given by the example of the Global NH air and sea-surface temperature for annual and seasonal averages. Conclusions are derived from results in connection with the physics of the general atmospheric circulation.

**GA6.01/W/11-A5 1425****TRANSIENT CLIMATE SIMULATION FORCED BY CHANGES IN SOLAR IRRADIANCE OVER THE LAST THREE CENTURIES**

Cedric BERTRAND and Jean-Pascal van Ypersele (both at Institut d'Astronomie et de Géophysique G. Lemaître, Université catholique de Louvain, 2 chemin du cyclotron, 1348 Louvain-la-Neuve, Belgium, email: cedric@astr.ucl.ac.be)

Numerical experiments have been carried out with a two-dimensional sectorially-averaged global climate model in order to assess the potential impact of solar variability on the Earth's surface temperature from 1700 to now. In the absence of a full physical theory able to explain the origin of the observed total solar irradiance variations, four different total solar irradiance reconstructions have been used. A total solar irradiance change due to the photospheric effects incorporated in the Willson and Hudson (1988) parameterization, the reconstructed solar total irradiance variations from the solar models of Hoyt and Schatten (1993) and Lean et al. (1995), and the Reid's (1997) historical reconstruction.

Our results indicate that the modelled global warming due to the four inferred total solar irradiance reconstructions is insufficient to reproduce the observed 20th century warming. Nevertheless, our simulated surface temperature response to the changes in The Sun's radiant energy output suggests that the Gleissberg cycle solar forcing should not be neglected in explaining the century-scale climate variations.

Finally, spectral analysis seems to point out that the 10- to 12-year oscillations found in the recorded Northern Hemisphere temperature variations from 1700 could be unrelated to the solar forcing. Such a result could indicate that the eleven-year period which is frequently found in climate data might be unrelated to oscillations in the atmosphere or oceans, internal to the climate system.

**GA6.01/E/13-A5 1440****CLIMATE VARIABILITY RELATED TO THE DOUBLE SOLAR CYCLE**

Cornelius J.E. SCHUURMANS (Institute of Marine and Atmospheric Research, Utrecht University, P.O. Box 80.005, 3508 TA Utrecht, The Netherlands)

Winter temperatures in The Netherlands over the period 1634- 1977 (344 years) were, on average, found to be lower and more variable during odd solar cycles than during even solar cycles (Schuurmans, 1978). The two solar cycles which passed since this result was published confirmed this behaviour. Further analysis showed that also summer temperatures show a tendency to be slightly lower (and less variable) in odd, as compared to even solar cycles. Climate variations of this type can be explained in terms of decadal changes of the atmospheric circulation over the Atlantic- European area. Indeed, over the last 140 years the North Atlantic Oscillation (NAO) has varied on this time scale. Since the solar- climatic relation exists over more than 350 years, the question arises if the NAO- variability on this time scale possibly could be induced by solar activity?

**GA6.01/W/18-A5 1455****CONSTRAINTS ON SUN-INDUCED CLIMATIC CHANGES OVER THE LAST 100 YEARS**

Willie SOON, Sallie Baliunas (both at Harvard-Smithsonian Center for Astrophysics, 60 Garden Street, Cambridge, MA 02138, USA, email: wsoon.sballiunas@cfa.harvard.edu); Eric Posmentier (Science Division, Long Island University, Brooklyn, NY 11201, USA, email: eposment@titan.liunat.edu)

Recent progress in monitoring the climate and the solar output, as well as modelling of the physical processes involved, is leading to improved understanding of the influence of solar variability on terrestrial climate change. We will present constraints on the solar total irradiance change on timescales of decades to centuries based on results from direct observations of the Sun and solar-type stars as well as modelling efforts. We will discuss another possible coupling mechanism through the interaction of the solar ultraviolet irradiance with stratospheric ozone and upper atmospheric clouds. We will also discuss the possible role of solar and cosmic ray charged particles in producing terrestrial climate change on timescales of months to years.

**GA6.01/E/15-A5 1510****PATTERNS OF SOLAR PROTON EVENTS OVER FOUR SOLAR CYCLES**

D.F. SMART and M.A. Shea (both at Air Force Research Laboratory, VSB5, 29 Randolph Road, Hanscom AFB, Bedford, MA 01731-3010, U.S.A., email: smart@plh.af.mil)

We now have a solar proton event database for more than four solar cycles. A statistical study of the events having more than 10 particles/(sqcm-sec-ster) above 10 MeV indicates that the number of events as a function of time over the solar cycle exhibits a skewed Gaussian curve similar to the smoothed sunspot number. This result is somewhat surprising considering the extreme differences in the occurrence of these events for each individual solar cycle. Other results show a surprising consistency in the number of events per solar cycle recorded at Earth. In addition approximately 15% of the events each solar cycle contain relativistic solar protons. The solar proton events during the first two years of the 23rd solar cycle will be discussed in context with the events of the previous four solar cycles.

**GA6.01/W/03-A5 1525****DESCEND TO AND ASCEND FROM THE MAUNDER MINIMUM**

K. MURSULA (Department of Physical Sciences, University of Oulu, P.O. Box 3000, FIN-90401 Oulu, Finland, email: Kalevi.Mursula@oulu.fi), and I. Usoskin (Ioffe Physical Technical Institute, St. Petersburg, Russia)

We study the properties of solar cycles around the Maunder Minimum (MM) using the recently proposed group sunspot numbers (Hoyt and Schatten, Sol. Phys., 181, 1998) and the delayed component method. The method can be used to study the regularity of the solar cycle using a 2- or 3- dimensional presentation. The new sunspot group numbers cover a few cycles even before MM. We find that the last three cycles before the MM have a very different behaviour. The last cycle before MM is rather strong and has a regular 2-dimensional shape. The descend to MM undergoes very rapidly. Interestingly, the first cycle (SC -4) after MM is very regular despite its extremely low amplitude. This suggests that regular processes with approximately 11-year cycle can proceed in the Sun even during the great minima such as the Maunder Minimum.

**GA6.01/E/14-A5 1600****SOLAR AND TERRESTRIAL SIGNALS IN THE PRECIPITATION AND TEMPERATURE IN ITALY FROM 1867 TO 1996**

M. Brunetti (1), S. Cecchini (2), M. Maugeri (3), T. NANNI (1) (1) Istituto FISBAT-CNR – via Gobetti, 101 – 40129 Bologna; (2) Istituto TESRE-CNR – via Gobetti, 101 – 40129 Bologna; (2) Istituto di Fisica Generale Applicata – via Brera, 28 – I20121 Milano

We investigate the variability of annual and seasonal precipitations and temperatures in Italy during the last 150 years and their association with changes in solar (geomagnetic indexes, sunspots and aurorae) and terrestrial (NAO, SOI) time series. Significant correlations and common periodicities are discussed.

**GA6.01/E/11-A5 1615****A MAGNETIC STORM - SIMULTANEOUSLY REGISTERED AT TWO SITES IN 1741**

Olof BECKMAN (Dept of Materials Science, Uppsala University, Box 534, S-75121 Uppsala, Sweden, email: Olof.Beckman@angstrom.uu.se)

The daily variation in the magnetic declination was observed by George Graham in London in 1722. However, the connection between the aurora and sudden displacements of a magnetic needle was first observed by the Swedish astronomers Anders Celsius and Olof Hiorter in 1741. The aurora was known to occur high up in the atmosphere. In March 1741 Celsius wrote a letter to Graham asking him to observe the magnetic needle in order to find out if disturbances might occur simultaneously in two so widely situated sites as London and Uppsala. Already on April 5th, 1741, such an event appeared, resulting in the very first documented simultaneous observation. Grahams data as well as Celsius's notes will be presented. The two recordings from London and Uppsala are quite similar in size (60 to 80 minutes of arc) and duration. The time difference between the events amounts to around 1 hour and 12 mins, which equals the difference in local solar time. Neither Celsius nor Hiorter have commented on this fact, however, which is remarkable since Celsius was very interested in time differences for longitude determination, an important problem of the time. Probably Celsius did not comment on this because he considered the aurora to be a terrestrial phenomenon. Celsius determined the longitude difference between Uppsala and other sites such as Tornea, København and Isle de Bourbon (Réunion) by help of eclipses of the moon and the Jupiter satellites. When Celsius visited Graham in 1735, they observed a total eclipse of the moon. At Uppsala Hiorter calculated the difference in longitude between Uppsala and Graham's garden in London to be 1 hour 11 mins and 50 secs. For longitude determination, one had to rely upon an event outside the earth (not the aurora).

**GA6.01/L/02-A5 1630****HISTORICAL NOTES ON GEOMAGNETIC MEASUREMENTS IN AND AROUND ICELAND**

Leo KRISTJANSSON and Thorsteinn Saemundsson (both at Geophysics Division, Science Institute, University of Iceland, Dunhaga 3, 107 Reykjavik, Iceland, email: leo@raunvis.hi.is. and halo@raunvis.hi.is)

Records of the use of a compass in Iceland reach at least as far back as the mid-17th century. Geodetic and hydrographic surveys using magnetic north as reference are known from about 1720. A source of disturbance in the geomagnetic field which is more serious in Iceland than in most other countries, is the strong magnetization of the bedrock which consists mostly of basalt lavas with little sediment cover. This and other problems of geomagnetic observations in the area, as well as the origin of the field, were discussed at length in publications by P. Lywenyrn of Denmark who made many determinations of declination and some of inclination off the coast of Iceland in 1786. Daily magnetic variations in Iceland were studied in some detail by V. Lottin who participated in P. Gaimard's 1836 expedition on the corvette 'La Recherche': a temporary observatory was erected in Reykjavik where declination values were recorded at 15 min - 1 hr intervals during 10-28 Aug simultaneously with measurements in European observatories. French expeditions also carried out declination measurements in the seas around Iceland, at various times during the 19th century.

Continuous recordings of the geomagnetic field were made by Th. Thorkelsson in Iceland during much of the 1932-33 International Polar Year and again for four months in 1937. An observatory established by Th. Sigurgeirsson at Leirvogur near Reykjavik has operated continuously since 1957. Located in the auroral zone and bridging the gap between continents, this observatory has played an important role in the international network of observatories.

Some of the key methods and concepts employed in paleomagnetic research originated in the studies on reserved and transitional remanence directions in Icelandic Tertiary lava sequences which were conducted by J. Hospers, Th. Sigurgeirsson and others during the 1950s.

**GA6.01/E/21-A5 1645****LONG-TERM VARIATION OF SUNSPOT LATITUDES**

Pentti J. PULKKINEN (Dept. of Physics, P.O.Box 0, FIN-00014, University of Helsinki, Finland, email: pentti.pulkkinen@helsinki.fi), John Brooke (Manchester Computing, University of Manchester, Oxford Road, Manchester, M13 9PL, United Kingdom; and Department of Mathematics, University of Manchester, Oxford Road, Manchester, M13 9PL, United Kingdom), Jaan Pelt (Tartu Astrophysical Observatory, Toravere 1-6, Tartu 202444, Estonia; and Astronomy Division, University of Oulu, P.O.Box 333, FIN-90571 Oulu, Finland), Ilkka Tuominen (Astronomy Division, University of Oulu, P.O.Box 333, FIN-90571 Oulu, Finland)

This work is based on a study(1), in which we use the whole time range of modern sunspot measurements (1853-1996), thus covering sunspot cycles 10 to 22. The data are combined with measurements by Carrington and Sporer and the Greenwich Photoheliographic Results. We first point out that the sunspot latitude is a measure of cyclic activity; the more active cycle the higher is the mean cyclic latitude per hemisphere. Further, if we calculate the global "centre of mass" of sunspots, we find variation over long period of time. The amplitude of this variation is 1.3 degrees and the period 34 000 days, or 93 years. Although we use the word "period", only the future measurements will confirm whether this variation is really systematic. This period of 93 years is of similar length than some other long-term periods found in sunspot data (Gleissberg cycle, north-south asymmetry variations by Verma(2) and Olivier & Ballester(3), or cycle length variation by Lassen & Friis-Christensen(4)). A possible explanation for this 93-year variation could be a mixed parity mode in which a quadrupolar component of the solar magnetic field is oscillating with this period. This phenomenon could also produce the observed asymmetry variations



## REMARKS ON LIFE AND WORK OF JULIUS BARTELS

Hannelore and KARL-HEINZ BERNHARDT (Platz der Vereinten Nationen 3, D-10249 Berlin, Germany)

J. Bartels (1899-1964), who was president of IAGA (1954-57) and, later, vice-president of IUGG (1957-63), worked at the beginning of his academic career at the university of Berlin and at the forestry college of Eberswalde from 1927 to 1944. Bartels' activities during this period of his life as well as his relation to the Prussian Academy of Sciences are characterized based on archival records. Also most of his significant contributions to mathematical statistics in meteorology and geophysics, which are considered in some details as an important part of his versatile lifework, have been written in this time.

Following the doctor thesis (Göttingen, 1923), Bartels started in the fields of statistics with the study of cyclic variations of meteorological and geomagnetic parameters which are superimposed by strong non-cyclic components. The application of the synchronization method in this connection required to eliminate carefully the selection or curvature effect, which had often been misinterpreted formerly. Further, Bartels improved the methods of periodogram analysis and the statistical testing of their results on the basis of the contemporary theory of probability. Special attention was paid by him to problems of statistical testing in case of auto-correlated data as connected with the phenomena of persistence and quasi-persistence in meteorological and geophysical time series. Finally, he introduced special Monte Carlo like methods, as the shaking test, to test the significance and the reliability of phenomena observed in time series. His rigorous criticism and the numerous remarks to avoid misleading conclusions from incorrect statistical data interpretation should be considered as exemplary also nowadays.

## THE NAGYCEK GEOPHYSICAL OBSERVATORY AND ITS LONG DATA SERIES

Antal Ádám, Pál BENCZE and József Vero (Geodetic and Geophysical Research Institute, Hungarian Academy of Sciences, H-9401 Sopron, P.O.B. 5, Hungary, email: bencze@ggki.hu)

The Nagycenk Geophysical Observatory devoted to the study of the electromagnetic field of the Earth was opened in 1957. The favourable location of the Observatory due to the thick sedimentary overlay and undisturbed conditions enabled the achievement of long series of earth current, geomagnetic, atmospheric electric and ionospheric data. These long data series make possible the study of long period variations, or trends attributable to the change of the environment. In case of the earth current data e.g. the establishment of the attenuation of the pulsations during the solar cycles, regarding the geomagnetic data the study of the main field was possible. Furthermore considering atmospheric electricity, the long-term change of the charge transfer between the atmosphere and the Earth could be investigated, while the ionospheric measurements enabled the study of changes in the state of the lower ionosphere due to several solar activity effects.

## CLIMATE EVOLUTION, AND MANKINGS ACTIVE AND PASSIVE ROLE AND RECORD THEY SYNERGISM BETWEEN EXACT SCIENCES AND HUMANISTIC DISCIPLINES

MICHELE COLACINO, Giovanni P. Gregori (both at IFA-CNR, via Fosso del Cavaliere 100, 00133 Roma, Italy, email: gregori@atmos.ifa.rm.cnr.it) and Wilfried Schroder (Hechelstrasse 8, 28777 Bremen-Roenebeck, Germany)

'History of Science' can be conceived according to 5 viewpoints: (1) dealing with the life of scholars who made science; (2) dealing with the impact of environment on mankind; (3) dealing with the impact of mankind on environment; (4) dealing with the history of ideas; and (5) dealing with the availability of observational records (either instrumental or proxy) got by means of the measuring instrument 'mankind'. The leading part of human civilisation was developed during the last several 104 years within the belt encompassing Sahara and Sahel, the Mediterranean, Middle East, Mesopotamia, the Indus Valley, and the Silk Road. Such an entire area dramatically suffered by the profound desertification, and the anthropic factor is seriously suspected of being severely co-responsible for it. For example, if we want to understand the future consequence of an eventual deforestation of the Amazon basin, perhaps we should first understand the crucial role of mankind in Sahara's desertification. Using mankind as a proxy datum, however, implies assessing the anthropological aspect of its time-varying understanding of the environment. Hence, such an investigation requires an effective synergism between exact sciences and humanistic disciplines. The present subdivision of Earth's sciences into standard disciplines appears a substantial obstacle towards such a general cultural implementation. The present frontier ought to be rather concerned with extended interdisciplinary scenarios, with large team work, and with far-looking brain-storming.

## CURRENT RESEARCH OF SOLAR-TERRESTRIAL PHYSICS IN EGYPT

M. A. Mosalam SHALTOU, National Research Institute of Astronomy and Geophysics (NRIAG), Helwan - Cairo - Egypt, Phone (202)2630833 ; Fax (202)5548020 E-mail: mamshaltout@frcu.eun.eg

Solar-Terrestrial physics in Egypt start since more than sixty years ago, when Dr. Hurst, Director of Helwan Observatory, studied the influence of sunspots on Nile flooding. Starting from 1970 the effect of dark filament disappearance on the solar disk on the Geomagnetic components recorded at El-Messallat Geomagnetic Observatory in Egypt was studied. From world-wide Solar-Geophysical data many researches are carried out about the effect of solar flares in Geomagnetic storms and Sudden Ionosphere Disturbance at NRIAG. Also, the influence of sunspots, faculae, and solar constant in the climatic change and the Nile flooding for long periods by using the computers in time series analysis to obtain on short and long-term periodicities in solar activity and Nile flooding was performed. The current of research is about: 1-The influence of ultraviolet solar radiation EUV on the Ozone layer of Earth, 2-The periodicities in the Solar wind and its correlation with Geomagnetic storms, 3-The effect of solar proton flares on Radio communications, near satellites Orbits, high-latitudes electric grids, Ionosphere electric currents, and Polar Cap absorption. Also, there are some studies about Solar activity and its influence on trees rings and C14 abundance in the earth's atmosphere since thousands years. The variability of Solar constant measured from ground stations and artificial satellites and its influence on the earth's atmosphere was studied. The correlation between the old solar activity and the Nile flooding in the ancient Egypt and the periods of rising and falling of the civilization of the ancient Egyptians through seven thousands years was restudied on the base of long data of Nile flooding and C14 abundance. Most of the research published in National Scientific Journals, but some of them published in International Journals of Geophysics, Space Science, Solar and Astro-physics.

## SOFT X-RAY VARIABILITY OF THE SUN FROM YOHKOH OBSERVATIONS

Hirohisa HARA (National Astronomical Observatory, 2-21-1 Osawa, Mitaka, Tokyo 181-8588, Japan, Email: hara@solar.mtk.nao.ac.jp)

Coronal activities from the maximum phase of cycle 22 to the rising phase of cycle 23 are presented from the Yohkoh soft X-ray observations. The variation of solar X-ray flux is investigated for two coronal components; active regions and the other dark features consisting of quiet regions and coronal holes. The X-ray flux from active regions is strongly dependent on the size of active regions and changes with the 11-year solar magnetic activity cycle in phase. We find that the X-ray flux from the other dark features also changes with the activity cycle, and that there is a strong correlation between the X-ray flux from the coronal dark features and the corresponding photospheric magnetic flux outside active regions. These show that the solar corona is heated in conjunction with the magnetic field, and there is no possibility of being due to the acoustic heating. The whole-sun X-ray flux does not monotonically decrease. Rather, there is a period of enhancement with about a one-year interval in the whole-sun X-ray flux. The activity appears as bright clusters in the butterfly diagram of the soft X-ray intensity and corresponds to the emergence of complexes of activity in the sunspot zones. We also find an intermittent activity with a time scale of about a year in the high-latitude regions.

## THEORY OF THE SOLAR DYNAMO

Paul ROBERTS (Institute of Geophysics and Planetary Physics, UCLA, Los Angeles, CA 90095, USA, email: roberts@math.ucla)

The overshoot layer (OSL) at the base of the solar convection zone (SCZ) is often seen as the probable seat of the solar dynamo, and specific models have been proposed. These are hard to evaluate, since turbulence in the SCZ effectively masks the OSL from observation and interpretation. The role of turbulence above the OSL is poorly understood. What is its inductive effect? Does it assist or impede the OSL dynamo? The small length scales of the turbulence make it impossible to answer these questions by simulating the entire SCZ numerically, and two alternatives have been investigated. First, mean field electro-dynamics has been generalized to turbulent magnetoconvection (mean field MHD). Contentious issues have arisen, such as the quenching of the (effect by the mean field, but mean field models of the solar dynamo model have been constructed that have also aimed simultaneously to simulate the differential rotation that has been inferred helioseismically. Second, direct numerical simulations (DNS) of field and flow in small test volumes situated at different latitudes and depths in the SCZ have been performed. These not only provide a useful picture of the character of turbulence in the SCZ but also supply information about turbulent transport coefficients that is valuable to mean field theories. These and related issues will be described in this presentation.

## THE INSTABILITY OF SOLAR MAGNETIC FIELDS

T. D. ARBER (Mathematical Institute, University of St. Andrews, St. Andrews, Fife KY16 9SS, Scotland, UK, email: tda@dcs.st-and.ac.uk)

Of all the physical processes active in the solar corona those which result from unstable magnetic field structures have the capacity to be the most abrupt and dramatic. It has been postulated that they could be responsible for triggering both two ribbon and simple loop flares. Considerable progress has been made over recent years in the magnetohydrodynamic (MHD) theory of such instabilities. While such theories at present only deal with simplified geometries and idealised physics they are none the less beginning to show some degree of correlation with observable features of the corona. This paper presents an overview of the current state of our understanding of such MHD instabilities, including a brief discussion of the nature of the magnetic field topology expected, how it may have evolved and why it suddenly becomes unstable.

Numerical simulations are now reaching a sufficient level of accuracy to be able to predict the observational signatures which should be present if simple flare loops are indeed caused by large scale MHD instabilities. These observational signatures are summarised and compared with those of transient brightening loops. The use of three dimensional simulations to fill the gap between theories of MHD instabilities and large scale observable properties is still in its infancy. Recent work is however encouraging and the paper ends with a sketch of the way forward in trying to determine whether MHD instabilities are indeed a major cause of solar flares.

## REVIEW OF THE TWO DECADE LONG SPACE-BORNE IRRADIANCE MEASUREMENTS

Judit PAP (Department of Physics and Astronomy, University of California, Los Angeles, 405 Hilgard Ave., Los Angeles, CA 90095-1562, USA)

Solar irradiance (both bolometric and at various wavelengths) have been measured for two decades from several space platforms. Analyses based on these measurements have established conclusively that solar irradiance varies on various time scales: from minutes to the eleven year solar cycle. Although the overall pattern of the long-term irradiance variations is similar at various wavelengths, being higher during high solar activity conditions, remarkable differences exist between the magnitude and shape of the observed changes. These differences result from the different physical conditions in the solar atmosphere where the irradiances are emitted. In this paper we review the results of the two decade long space-borne measurements of solar irradiance integrated over the entire spectrum, hence total irradiance, and from EUV to the infrared portions of the solar spectrum. New techniques in solar irradiance modelling are also demonstrated to better understand the potential climate impact of solar variability over decades to centuries.

## THE CLIMATIC INFLUENCE OF THE SUN AS A VARIABLE STAR

Edward HANNA (Department of Meteorology, University of Reading, Earley Gate, PO Box 243, Reading, Berkshire, RG6 6BB, UK)

Recent satellite observations have shown that solar output is intrinsically variable on many

spatial and temporal scales. The so-called "solar constant" (a misnomer) actually varies on the decadal timescale by ~0.1%, with substantially larger variations at ultraviolet wavelengths. Quasi-periodic secular changes several times greater drive interaction of the solar wind and cosmic rays with Earth's magnetosphere and ionosphere. Such effects may modulate stratospheric ozone and global climate, including cloud cover, planetary waves and atmospheric circulation patterns. Here I critically examine the historical solar and climatic records, and find much circumstantial evidence to support the hypothesis that our Sun, as a variable star, has a discernible influence on Earth's climate. Using stellar analogues from the broader astronomical scene, I argue that the Maunder Minimum and other well-documented solar anomalies in the historical record represent the Sun's natural and unremitting evolution between active (cycling) and quiet (non-cycling) phases. Some intriguing statistical evidence suggests that long-term (>11-year) solar activity cannot be overlooked as a potential cause of an appreciable part of twentieth-century global warming, and might in particular explain the latter's hiatus or even slight reversal between 1940-70. On this basis, I provide a forecast of future global temperature on the basis of projected solar activity. The role of the Sun should definitely be included in any consideration of Earth's continually changing climate, which is subject to natural as well as anthropogenic influences. The problem is that some of the former, including solar forcing, remain poorly defined in global climatic models.

**GA6.01/W/12-A6 1020**

**INTENSIFICATION OF THE GLOBAL UPPER OCEAN TEMPERATURE RESPONSE TO CHANGING SOLAR IRRADIANCE BY POSITIVE FEEDBACKS FROM WATER VAPOR AND CLOUDS**

Warren B. WHITE, Michael D. Dettinger, and Daniel R. Cayan

**Abstract.** Global-average upper ocean temperature fluctuated in fixed phase with changing solar irradiance on decadal timescales over the past 100 years, but its amplitude was 50 to 100% larger than expected from the Stefan-Boltzmann radiation balance (White et al., 1997, 1998). The latter yields a temperature sensitivity for the Earth of 0.3°K per Watt m<sup>-2</sup> of changing surface radiative forcing. Examination of the global patterns of upper ocean temperature response indicates that the Earth's temperature does not respond passively to changing solar irradiance; rather, natural variability on decadal timescales is either excited by or brought into phase with the solar signal. This has the potential for intensifying Earth's temperature response as simulated already in Earth climate system model experiments (e.g., Rind, 1998). We have combined analyses of upper ocean temperatures, atmospheric moisture content and clouds from SIO, COADS, NCEP, and TOVS, finding the warm upper ocean temperature response to peak solar irradiance associated with increased global tropospheric moisture content and decreased global cloud cover. The surface radiative forcing associated with these internal responses will be presented, used to quantitatively assess Earth's net temperature sensitivity to changing solar irradiance on decadal timescales.

**GA6.01/W/07-A6 1100**

**THE SOLAR NEUTRINO PROBLEM**

L. PATERNO' (Istituto di Astronomia, Università di Catania, Città Universitaria, 95125 Catania, Italy, Email: lpaterno@alpha4.ct.astro.it)

Helioseismology has demonstrated that the standard solar model is accurate within 0.5%, therefore the solar neutrino problem, namely the huge discrepancy between predicted and measured neutrino fluxes, can hardly be attributed to a wrong modelling of the solar interior. It is shown that unordered changes in the properties of the physical processes operating in the Sun's interior are needed for reducing the predicted neutrino flux to the observed one. However, such changes produce dramatic changes in the internal stratification of the Sun, which are incompatible with the very accurate results of helioseismic data inversions. Non standard neutrino properties, which require massive neutrinos, have been proposed as a suitable solution for the observed neutrino deficit. The solution relies upon the change of neutrino flavour in the path from the solar core to the Earth, which renders the emitted electron neutrino undetectable by the experiments. Various possibilities, such as vacuum oscillations, MSW resonant transition in the matter and spin-flip, are discussed in the framework of the results of the neutrino experiments presently in operation. The potentialities of the future neutrino experiments are also discussed.

**GA6.01/L/01-A6 1130**

**SOLAR NEUTRONS**

J.F. VALDES-GALICIA (Instituto de Geofísica, UNAM, 04510, Mexico, D.F., MEXICO)

Observations of neutrons from solar flares are providing important new information on particle acceleration in solar flares and on the flare process itself. They are produced directly by nuclear interactions of the flare-accelerated protons and heavier ions with ambient gas in the solar atmosphere. Thus they yield the most direct information available on different aspects of the flare region. Neutrons were first observed from the flare of 21 June 1980 and since then a number of solar neutron events were detected with instruments on board satellites and also with ground based cosmic ray neutron monitors. I will briefly review the rich variety of neutron emission that has been observed from solar flares over the past two decades. I then will discuss what we have learned from these observations and how solar neutrons can be considered as a manifestation of the Solar Variability. Finally I will discuss some recent work to understand the transport of high energy neutrons in the Earth's atmosphere.

**GA6.01/W/13-A6 1150**

**THE EXTENDED CORONA AND SOLAR WIND**

G. NOCI

The observations with the instruments on board the SOHO spacecraft have greatly increased our knowledge of the solar corona. They have concerned the morphology as well as the space distribution of physical parameters, such as densities, temperatures, element abundances, outflow velocity. The SOHO findings, with particular attention given to the data from the Ultraviolet Coronagraph Spectrometer, are discussed, focussing on the problem of the coronal expansion. They are compared with the results from the Ulysses spacecraft.

**GA6.01/W/19-A6 1210**

**VARIABILITY OF THE SOLAR WIND AND ITS COMPOSITION**

R. VON STEIGER and J. Geiss (International Space Science Institute, Bern, Switzerland); G. Gloeckler (Dept. of AOSS, Univ. of Michigan, Ann Arbor, USA, and Dept. of Physics, Univ. of Maryland, College Park, USA)

The solar wind seems to be a continuous and ubiquitous phenomenon. Ancient solar wind can be found as inclusions in meteorites and in the lunar regolith. On historical time scales it can be inferred from the existence of comet tails. During the last few decades the solar wind has been observed by in situ spacecraft and its variations were measured on time scales from a solar cycle down to minutes.

The composition of the solar wind provides us with a nearly unaltered sample of the material that constituted the protosolar nebula. Moreover, it is a powerful diagnostic tool for decoding the solar wind origin and acceleration: The charge states of heavy elements are indicative of the coronal temperature and its profile, whereas the elemental abundances probe the conditions and the processes in the chromosphere and lower transition region.

The Solar Wind Ion Composition Spectrometer (SWICS) on the Ulysses mission has now given us routine measurements of the abundances of 8–10 elements in up to 30 charge states at nearly all heliographic latitudes over the past 8 years. This data set provides the baseline solar wind composition and its variability during the time of decreasing and minimum solar activity. We will present an overview of the implications on the source regions of the solar wind and the processes active at these sites as inferred from the composition.

**GA6.01/W/06-A6 1235**

**NEW IDEAS AND TRADITIONAL VIEWS IN EARTH SCIENCES FROM MIDDLE AGE TO RENAISSANCE**

Giancarlo SCALERA (Istituto Nazionale di Geofisica, via di Vigna Murata 605, 00143 - Roma, Italy)

The different degree of tolerance and/or intolerance about a series of basic earth science topics at the passage from middle age to modern age has been examined. Starting from the first scholastic criticisms to the Aristotelian system, which were needed because of the incompatibility of the infinity of the time compared to the Biblical Genesis, an attitude to extend the criticisms to other aspect of the Greek science diffuses among the intellectual class of the time. The discussion about the motions of the planet Earth and the Copernican heliocentrism, which initially was held also in presence of open mind Vatican hierarchies, suffers an involution towards sometime dramatic upshot after the conclusion of the Council of Trento. Both the earth mobility and the findings of marine fossils on the top of mountains were in contradiction with the biblical myth, but a less conflictual story of relations with the exponent of the dogmatic view was reserved to people which refuse to explain the marine fossils on the heights a...

**GA6.01/W/16-A6 1250**

**SOME HISTORICAL NOTES ON THE SOLAR-TERRESTRIAL PHYSICS IN THE UNIVERSITY OF ISTANBUL (INCL. THE WORKS OF GLEISSBERG AND OTHERS)**

Ferhat ÖZÇEP (1), Naci ORBAY (1), Hüseyin MENTEŞE (2) and Adnan OKTEN (2) (1-University of Istanbul, Faculty of Engineering, Department of Geophysical Engineering, Division of Earth's Physics, 34850, Istanbul TURKEY, E mail: ferozcep@istanbul.edu.tr; 2- University of Istanbul, Faculty of Science, Department of Astronomy and Space Sciences)

In the University of Istanbul, the studies on the solar-terrestrial physics can be investigated in two parts. One of these is the studies in the Astronomy Department. Second one is in Geophysical Department. The first geophysical and astronomical department for educational and scientific purposes was established in Istanbul Darülfünunu (University of Istanbul) by Fatih Gökmen in 1926 as "the Institute of Astronomy and Geophysics". In the same year, first geophysical lecture was given as a " Lesson of Meteorology and Geophysics" at the same Institute. University of Istanbul was reorganized in 1933. By this year, Prof. Dr. Freunlich, he was the director of Einstein Institute (Berlin, Potsdam) and Astrophysical Observatory of Berlin, invited for the reorganization of the Department of Astronomy. Later, to assist to himself, Dr. Gleissberg was invited to the Department of Astronomy in 1934. Dr. Gleissberg initiated an expanded program of sunspot observation and continued his researches at the Astronomy Department up to his departure in 1958. Today, solar photospheric observations are still continued as well as chromospheric observations in the same Department. During Gleissberg term as director of the Department, six students completed their PhD works on the subject of the lifetime and perspective foreshortening of sunspot groups, relative number (or Wolf number) curves of sunspot cycles, and the latitudinal distribution of sunspot groups under his supervision. The most important contribution to the sunspot research of the Gleissberg is to show the existence of secondary cycle of about eighty years duration within the long term sunspot records. Today, this long-period is known as the Gleissberg Cycle in the literature. By the 1952, Geophysical Institute of University of Istanbul was strongly reestablished in Faculty of Science by the contributions of Prof. I. Özdoğan, M. Fouche, Coulomb and J. Barthels in this time. At the same department, by the 1960, Ionospheric Research Center was established and the Center began the ionospheric Data. In the same year, Prof. Dr. Rikitake was invited to the Department for educational and scientific aims. He had one Ph.D. student and he gave "Seismology", "Physics of Earth's Interior" and "Physics of Upper Atmosphere" Lectures in 1960-1961 Semester.

**Friday 23 July AM**

Presiding Chair: W. Schröder (Geophysical Institute, Bremen, Germany)

**GA6.02/E/18-A5 Poster 0900-01**

**JOHANN VON LAMONT - FIRST YEARS OF GEOMAGNETIC RESEARCH IN MUNICH, 1836 - 1845**

Martin BEBLO and Heinrich Soffel (both at Geophysical Observatory Fuerstenfeldbruck, University of Munich, Ludwigshoehe 8, D-82256 Fuerstenfeldbruck, Germany, Email: magnetic@fur.observatory.uni-muenchen.de).

Johann von Lamont started with sporadic geomagnetic observations in Munich in 1836. Since 6 o'clock in the morning on August 1st, 1840, he run regular observations with variometers built by Gauss and Meyerstein in Goettingen. In May and June 1841 Lamont replaced the Gauss variometers (suspended magnets with a weight of 25 lb - 11.4 kg) by instruments of his own design using very small and light magnets. These instruments improved significantly accuracy and sensitivity of geomagnetic measurements and made geomagnetic surveys possible. Some years later Lamont developed his travel modiolite and distributed 45 instruments of this type for scientific work worldwide. His instruments became international standard for geomagnetic instruments for more than 50 years.

**GA6.01/E/18-A5 Poster 0900-02**

**JOHANN VON LAMONT - FIRST REGIONAL MAGNETIC SURVEYS 1850 - 1858**

Martin BEBLO and Heinrich Soffel (both at Geophysical Observatory Fuerstenfeldbruck, University of Munich, Ludwigshoehe 8, D-82256 Fuerstenfeldbruck, Germany, Email: magnetic@fur.observatory.uni-muenchen.de).

In the 1850s Johann von Lamont started to make regional magnetic surveys at about 250 points in the kingdom of Bavaria. Probably no other country in the world was equipped with such an early and dense survey net. Lamont extended his survey into many European countries and documented the results in voluminous maps, 1856 for France, Spain and Portugal and 1858 for northern Germany, Belgium, Holland and Denmark. His central European maps with isolines of the geomagnetic elements are parts of the classical literature. Many of Lamont's reference points can still be used today.

**GA6.01/L/05-A5** Poster **0900-03**

**AN ADJOINT METHOD OF CALCULATION OF ENERGETIC SOLAR-PARTICLE-EVENT EFFECTS ON THE EARTH'S ATMOSPHERE**

K. O'Brien, Northern Arizona University, Flagstaff, AZ 86011, USA; Herbert H. Sauer, CIRES, University of Colorado, Boulder, Co 80303, USA, NOAA Space Environment Center, Boulder, CO 80303, USA

High-energy solar particles, produced in association with solar flares and coronal mass ejections, occasionally bombard the earth's atmosphere, resulting in radiation intensities additional to the already-present cosmic-ray dose rates. Access of these particles to the earth's vicinity during times of geomagnetic disturbance are not adequately described by using static geomagnetic field models. These solar fluxes are also often distributed non-uniformly in space, so that fluxes measured by satellites obtained at great distances from the earth and which sample large volumes of space around the earth cannot be used to predict fluxes locally at the earth's surface. We present here a method which uses the ground-level neutron monitor counting rates as adjoint sources of the flux in the atmosphere immediately above them to obtain solar-particle dose rates as a function of position over the earth's surface. We have applied this approach to the large September 29-30, 1989 event (GLE 42) to obtain the magnitude and distribution of the dose rates from an atypically large event. This approach could easily be adapted to the calculation of other atmospheric quantities of interest, such as ionization and energetic primary and secondary particle fluxes.

**GA6.01/P/13-A5** Poster **0900-04**

**RELATIONS BETWEEN SOLAR, GEOMAGNETIC AND CLIMATE VARIABILITY**

Václav Bucha (Geophysical Institute, Czech Academy of Sciences, 141 31 Praha 4 Spriřilov, Bocni II, Czech Republic, email: bucha@ig.cas.cz)

Historical records of long and short-term solar variability and climate contribute to the study of cyclic changes which were observed both in solar and geomagnetic activity and temperature as well as in 14C and have a similar trend. It is shown that the external geomagnetic forcing has a strong effect also on short-term meteorological processes. This justifies our suggesting a hypothesis for explaining Sun-weather relations. Several very similar cycles are clearly detectable not only in yearly but also in daily variations of both solar and atmospheric variability. A composite curve was suggested roughly representing basic cycles of geomagnetic and solar activity, temperature and 14C during the past millennia as well as their possible trend for the next centuries.

**GA6.01/E/23-A5** Poster **0900-05**

**THE ORIGIN OF THE METEOROLOGICAL OBSERVATIONS IN ROME**

M. COLACINO (Istituto di Fisica dell'Atmosfera, CNR, Via del Fosso del Cavaliere, 100 - 00133 Roma, Italy, email: colacino@atmos.ifa.rm.cnr.it)

As it is well known the origin of the Meteorology as science based on the observations and measurements dates back to the second half of XVII century. In that period many pupils of Galileo, pursued, in the frame of the "Accademia del Cimento", the setting up of different meteorological instruments. They began to use thermometers, barometers, hygrometers in order to study the physical properties and motions of the atmosphere. Being aware that the atmosphere must be studied not only locally, but at larger scale, they sustained the creation of a meteorological network that was sponsored by Granduke of Tuscany and realised in 1656. The network collected data for about ten years: after more or less a century its heritage was assumed by the "Meteorological Societas Palatina" created by Prince Carl Theodor in 1780. This Society was aimed to diffuse the meteorology in Europe and this goal was pursued by creating a network, which included more than 30 stations covering all the Continent. In Italy were involved the observatories of Bologna, Padova, Roma and Chioggia where some meteorological observations were already carried out. The official series of measurements dates in Rome from 1782, year in which the network began its activity, in the observatory of "Collegio Romano" that was managed by Jesuits. In the present work after a short recall of different meteorological data series collected in Rome, the history of "Collegio Romano" station from the origin till the end of XIX century is presented, stressing the role that this institution had in promoting the meteorology in Italy.

**GA6.01/E/22-A5** Poster **0900-06**

**THE UNPUBLISHED CORRESPONDENCE BETWEEN NOBILE AND EREDIA DURING THE PREPARATORY PHASE OF THE ARCTIC EXPEDITION OF 1928**

M. COLACINO (Istituto di Fisica dell'Atmosfera, CNR, Via del Fosso del Cavaliere, 100 - 00133 Roma, Italy, email: colacino@atmos.ifa.rm.cnr.it); O. FERRANTE, M.R. VALENSISE (Segreteria Antartica, CNR, Viale Marx, 15 - 00137 Roma, Italy, Tel: +39 06 86090308)

The 70th anniversary of the Nobile expedition with the Dirigibile Italia has been celebrated in 1998. The expedition was characterised also for the scientific objectives and involved scientists and geophysicists well known as Finn Malgram (Sverige), Aldo Pontremoli (Italy), Francesco Behounek (Cecoslovacchia). The history of the expedition is well known, but new insights could be brought by the examination of a very important archive, not yet examined, composed by more than 3000 documents and presented for the first time during the above said celebration. The preliminary work, now under development, consists in a catalogation and a first interpretation of the documents. Among them particularly interesting is the correspondence between Nobile and Professor Eredia, who had been charged to study the meteorological aspects of the travel in order to cross the Alps in the course Milano-Friederichshafen and to give a description of the climatology of the Svalbard islands from which the Dirigibile Italia should start to reach the Pole. In addition Eredia was requested of a specific advice in order to cross the Carso, that was believed dangerous not only for the meteorological conditions, but also for the lacking of meteorological data and information. The rich correspondence (16 letters) is important not only as unpublished documents, but gives a detailed picture of the care paid in preparing the expedition and represents an useful reference in order to analyse the development of the meteorology in Italy after the first world war.

**GA6.01/E/04-A5** Poster **0900-07**

**WITHIN- AND AMONG-SOLAR-CYCLE (S) VARIATIONS AND HUMAN MORPHOLOGY, PHYSIOLOGY AND PATHOLOGY**

G. CORNELISSEN, R.B. Sothorn, L. Gheonjian, T. Paatashvili, Y. Watanabe, T. Breus, F. Halberg (Univ. of Minnesota, Minneapolis, MN 55455, USA; e-mail: halbe001@maroon.tc.umn.edu); Wilfried Schroeder (Hechelstrasse 8, D-28777 Bremen-Roennebeck, Germany)

An increase in myocardial infarctions (MI) after magnetic storms, among other effects of interest to space life science, was validated on 85,819 cases added to those reviewed by Dubrov and Gamburtsev. But even dense or long samples show that the solar cycle number and stage may lead to different associations. Heart rate measured automatically around the clock every -half-hour over 11 years was positively correlated with Wolf's numbers (WN) during the ascending (r=0.535; P=0.001) but not during the descending stage (r=0.078; P=0.556). Heart rate, self-measured up to 6 times a day for 31 years, was positively correlated with WN during the descending stage of one solar cycle (Jan 1970-Dec 1975: r=-0.398; P=0.001) and negatively during the next 2 descending stages (Jan 1982-Dec 1985: r=-0.427; P=0.002 and Aug 1991-Jul 1996: r=-0.450; P<0.001). A remove-and-replace approach (with 7-day components in solar wind present or absent) also revealed solar amplification of about 7-day cycles in heart rate, a result in keeping with more prominent about-weekly variations in mortality from MI in Tbilisi, Georgia, during high vs. low solar activity. For each biological rhythm, notably when desynchronized from the obvious socio-ecologic light-dark and temperature cycles of the habitat niche, a more remote as well as proximal physical match or near-match should be sought and vice versa. Consistent relations found over several solar activity cycles in heart rate variability (gauged by the standard deviation), mood and blood pressure, vs. WN or Kp, may be informative. Physical and physiological series should then be aligned, to gauge by cross-spectral coherence, superposed epochs and remove-and-replace approaches, life's past and/or present interactions with environments near and far, via feedsidewards (multiple interactions), revealing biological associations with two "master" switches, helio-geomagnetics and light, as they behave over several solar cycles.

**GA6.01/P/04-A5** Poster **0900-08**

**HISTORICAL SOLAR ECLIPSE**

Holger Filling, Geophysical Station, Hechelstrasse 8 D-28777 Bremen

Extracts from historical sources relating to solar activity and eclipses are presented here so as to give an idea of studies and observations during the last decades.

**GA6.01/E/19-A5** Poster **0900-09**

**THE CLIMATE CHANGE IN PAST 600 YEARS AND ITS RELATION WITH SOLAR ACTIVITY**

Xiaoping GAO (Lanzhou Institute of Plateau Atmospheric Physics, Chinese Academy of Sciences, Lanzhou 730000, P.R.China, email: xgao@lzu.edu.cn) Giovanni P. Gregori (Istituto di Fisica dell'Atmosfera, CNR, Rome 00133, Italy, email: gregori@atmos.ifa.rm.cnr.it)

The solar-terrestrial relationship is always the hot topic in geoscience. There are two ways in which the sun can influence the Earth environment. One is from up to down (by radiation process), another is from down to up (by geodynamo process). In this paper the focus is on the latter one. The geomagnetic model for past 600 years was used for computing the variation of geomagnetic field. There were two abrupt changes in geomagnetic field, which related to the solar activity. The climate on the Earth also experienced two low temperature periods in the same time. It suggests that solar activity, geomagnetic field change and climate change are related in some way. We know that the climate can be influenced by heat flux coming from the Earth. And Joule heat is produced by geodynamo and is varying in time. It is possible that the geothermal releasing is the key to solar-terrestrial relationship.

**GA6.01/P/07-A5** Poster **0900-10**

**DOES THE 155-DAY PERIODICITY OF THE SUNSPOT AREA FLUCTUATIONS DURING THE PERIODS OF THE MAXIMUM OF THE 11-YEAR CYCLES REALLY EXIST?**

Ryszarda Getko, Astronomical Institute, University of Wrocław 51-622 Wrocław, Kopernika 11

The problem discussed in this article concerns the issue of the short-term periodicities of the daily sunspot area fluctuations from July 1923 to September 1933. For these data the correlational analysis indicates negative correlation for the periodicity of 155 ± 10 days but the spectral analysis indicates a statistically significant peak in this time interval. Thus, in this paper, a new method of the diagnosis of an echo effect in spectrum (MDE) was proposed. On the basis of this method it was stated that the 155-day periodicity is a harmonics of the periodicities from the interval of [400, 500] days. The comparison of autocorrelation functions for the fluctuations of Sunspot areas of the one rotation time interval on the both hemispheres, separately for the whole solar cycle 16 and for the maximum period of this cycle, shows no differences, especially in the interval of [120, 180] days, what proves against the thesis of the existence of strong positive fluctuations of the 155 ± 10-day interval in the maximum period of the solar cycle 16.

**GA6.01/E/05-A5** Poster **0900-11**

**CHRONOASTROBIOLOGY- AND CHRONOBIOASTRONAUTICS-AGENDA INVOLVING MONITORING THE BIOSPHERE AND COSMOS: THE BIOCOS PROJECT**

Franz HALBERG, Germaine Cornelissen, Othild Schwartzkopff (University of Minnesota, 420 Washington Ave. SE, Minneapolis, MN 55455, USA; e-mail: halbe001@maroon.tc.umn.edu); Wilfried Schroeder (Hechelstrasse 8, D-28777 Bremen-Roennebeck, Germany)

A statistically highly significant -9-hour lead of about-daily (circadian) rhythmic murine hepatic RNA formation before DNA synthesis corresponds to a lesser statistically significant lead of RNA over DNA contents of Euglena. Both leads support, before our DNA world, an RNA-world wherein RNA could replicate itself. In a broader comparative physiological context, these sequences may provide evolutionary information. Changes in relative prominence of about-weekly (circaseptan) vs. circadian rhythms during the development of individuals and species, features of adaptive integration, may differ between sites of life's origins. On the ocean floor, without daily alternating light with darkness, geomagnetic disturbance may prevail: it has a circaseptan component, noted as a broad band by Vernova, demonstrated by us as a narrow spectral band around 6.7 days, confirmed by physicists, quantified by circaseptan-to-circadian amplitude ratios. On the earth's surface, circadian rhythms are prominent. Immediately after birth the circaseptan amplitude is larger in humans, pigs, rats, crayfish and some short series on Euglena. Acetabularia, E. coli and cyanobacteria require further study, but their circadians predominate in currently too-short series. Half-yearly changes in nocturnally circulating



melatonin point to a corresponding helio- and/or geomagnetic signature as a second "master" switch complementing yearly changes in light and temperature. About 10.5- and about 21-yearly changes in human morphology, physiology and pathology are at least numerically associated with solar activity cycles as documented by data covering up to 112 years of neonatal weight, height, and circumference of head, chest and abdomen, revealing in the same babies numerical associations of one variable with 10.5- and another with 21-year cycles. From monitoring for chronobiology blood pressure and heart rate as gauges of biosphere effects from solar activity variation, critical information may be obtained for risk reduction in chronobiology and vice versa.

**GA6.01/E/12-A5** Poster **0900-12**

**PRELIMINARY ANALYSIS ON SOLAR ACTIVITY AND PRECIPITATION IN YANGZI RIVER BASIN**

HAN YAN-BEN (Beijing Astronomical Observatory, Chinese Academy of Sciences, Beijing 100012, P.R. China, email: hyb@class1.bao.ac.cn) Zhao Juan (Department of Astronomy, Beijing Normal University, Beijing 100875, P.R. China)

In 1998, the serious anomalous precipitation appeared in some regions in China. The precipitation caused the serious flood in some ones of the regions. The data that the precipitation of the observational stations in the regions in recent 100 years and more have been analyzed. The preliminary result shows that the solar activity affected the rainfall in the regions. The study of the relationship between precipitation and solar activity will be helpful for the prediction of precipitation in the regions possibly.

**GA6.01/P/09-A5** Poster **0900-13**

**HELMHOLTZ AND THE AGE OF THE SUN'S HEAT**

Herbert Hörz (Leibniz-Sozietät, Hirtshulzstr 13, 12621 Berlin, Germany, email: Herbert.Hoerz@t-online.de)

In the second half of the nineteenth century in connection with Darwin's theory of evolution scientists discussed the age of the sun's heat. In 1854 Hermann von Helmholtz (1821-1894) in a lecture about new insights in physics defended the hypothesis of Kant-Laplace about the evolution of the planetary system. He explained the shrinking of the sun as the source of heat generating. His theory was fifty years the foundation of cosmogonic thinking about the sun's heat. In his lecture in 1871 about the evolution of planetary system Helmholtz spoke about the beginning and the end of the energy of the sun as the source of living systems on the earth. William Thomson (1824 - 1907), the later Lord Kelvin, gradually switched from the meteoric theory to the position of Helmholtz. How Helmholtz was able to found such a long-living theory? Four reasons are described. Firstly his position of the universality of natural laws and secondly he was thoroughly convinced that the conservation of energy is such a law. Thirdly he was an evolutionary thinker in the tradition of Kants hypothesis and fourthly the new insights in physics with the spectroscopical methods showed him the truth of his general philosophical position about laws. Discoveries in nuclear physics in our century brought cosmogony to new theories on the sun's heat.

**GA6.01/W/15-A5** Poster **0900-14**

**MATHEMATICAL MODEL OF SOLAR ACTIVITY TAKING INTO ACCOUNT NON-LINEAR PROCESSES IN SUNSPOT FORMATION**

Lev Tsurulnik, Tamara KUZNETSOVA, Viktor Oraevsky (all at IZMIRAN, Troitsk, Moscow region, 142092, Russia, email: tsurul@izmiran.rssi.ru)

A method of nonlinear spectral analysis (called the method of global minimum: MGM) has been used to find periodicities in annual Wolf sunspot numbers (W) during the period 1700-1997. The study harmonics with time-varying phase and amplitude allows to detect time intervals of development of nonlinear processes in sunspot formation. An additional new and important result, manifested by MGM is a non-stationary behavior of some of the harmonics during the studied period. The powerest spectral triplet at period T=204 yr. testifies to the existence of the slowest non-stationary processes in sunspot formation during the studied interval. Time behavior of the triplet shows depressions in long term solar activity during periods known as Dalton's and Gnevishhev's minima in solar physics. Our analysis excludes interpreting such cycle anomaly as Maunder minimum in terms of stochastic behavior and demonstrates that solar activity is not discontinuously changed at the end of the period: these changes are connected with decline and rise phases of the over long non-stationary triplet. The second power spectral peak at T=82 yr. is a non-stationary doublet, period of which coincides with period T=80 yr. found by Gleisberg in Schove's set of polar aurora for 16 centuries. The calculated model confirms our previous conclusion concerning a non-stationary triplet at T=37.8 yr. that we associate with period T= 36-37 yr. found by Bricekner in historical sets of hydrometeorological phenomena from 1700 and by Clough in drought data in Europe from 1200. This period was discussed in the solar physics (solar or not). We for the first time derived it in sunspot data and consequently showed it's solar origin. These results demonstrate long term synchronous variations in solar and terrestrial phenomena. Long and short term variability in the solar and terrestrial phenomena are discussed.

**GA6.01/W/05-A5** Poster **0900-15**

**HIERARCHY OF CYCLIC CHANGES IN SUNSPOT ACTIVITY**

Alexander V. MORDVINOV, Georgy V. Kuklin (Institute of Solar-Terrestrial Physics, Russian Academy of Sciences, P.O. Box 4026, Irkutsk, 664033, Russia, email: avm@iszf.irk.ru)

Energetic and phase wavelet analyses were applied to study cyclic behaviour of sunspot activity. Energetic wavelet spectra of both the relative sunspot numbers and numbers of sunspot groups clearly show the cyclic mode, which varies its amplitude and period at about 11-yr timescale. Long-term changes are also seen in the spectra at about 50-100 yr timescale. Phase wavelet spectra of sunspot indices clearly show cyclic structure even if amplitudes of temporal changes are small. It is remarkable that the phase spectra resemble a picture of period doubling intrinsic for a fractal process. Phase wavelet spectra and the skeleton of zero-phase lines show fork-like structures of period-doubling bifurcations at various timescales. Separate 11-yr cycles are combined in pairs to make up complete magnetic cycles.

The phase spectra show three different regimes in solar activity behaviour. Regime of low activity for 1645-1715 known as the Maunder Minimum was changed to more-or-less regular cyclic variations with irregular amplitude alternation from even cycle to the odd one for 1745-1855. Since 1855 the cyclic mode of solar activity has been established with regular amplitude alternation according to the Gnevishhev-Ohl rule: every odd cycle exceeds the previous even cycle in amplitude. According to this scheme, if the amplitude of coming cycle 23 turn out to be lower than that of the preceding cycle, this might imply that a new regime of solar dynamo begins to operate.

**GA6.01/P/02-A5** Poster **0900-16**

**THE FIRST PHOTOGRAPHICAL RECORD OF TERRESTRIAL MAGNETIC PULSATIONS IN 1896 BY M. ESCHENHAGEN AND THE REGISTRATION OF A PASSING ELECTRICAL CIRCULATING CURRENT**

Wilfried SCHRÖDER and Karl Heinrich WIEDERKEHR

As pulsations and circulating currents are caused by the activity of the sun, I'd like to begin with a short survey of the way to the recognition about solar influences on terrestrial magnetism, particularly about the hypotheses of Balfour Stewart and the two treatises of Arthur Schuster about the daily variations. In meteorology and geomagnetism photographic self-registering apparatuses were already early developed in Greenwich and Kew. E. Mascart and M. Eschenhagen continued this line. With the help of his "Feinregistriergerät" (quick-run magnetograph) Eschenhagen could record pulsations for the first time more precisely. Through short-time simultaneous observations suggested by him the course of a terrestrial magnetic disturbance could be pursued. This disturbance was identified by A. Schmidt in 1899 as a moving circulating current in the upper strata of the atmosphere.

**GA6.01/P/01-A5** Poster **0900-17**

**A NOTE ON THE SUGGESTED VARIABILITY OF THE LENGTH OF THE SOLAR CYCLE DURING RECENT CENTURIES AND SOME CONSEQUENCES**

Wilfried Schröder and Hans-Jürgen Treder, Geophysical Station, Hechelstrasse 8, D-28777 Bremen Germany

It is shown that there exists neither physical explanation nor plausible mechanism which could initiate or support any variability in the length of the solar cycle. Furthermore, any suggestions concerning a relationship with terrestrial climate are questionable and without any supporting physical evidence.

**GA6.01/P/10-A5** Poster **0900-18**

**THE EVALUATION OF THE SOLAR ACTIVE REGION NO. 6555 DURING MARCH 1991**

M. A. Mosalam Shaltout, National Research Institute of Astronomy and Geophysics, Helwan, Cairo, Egypt. Phone: (202) 2630833; Fax (202) 5548020 E-mail: mawshaltout@frcu.eun.eg

In 22 March 1991 during the declining phase of solar cycle 22, a very high energetic solar flare was released at UT 22h 47m from NOAA/SESC active region No. 6555. The proton flux of particles had energies > 10 Mev was 43,000 particle flux units (pfu), measured by GOES space craft. It is the highest measured one during the solar cycles 21 and 22. The flare was associated by microwave great burst of level 36,000 sfu on 10 cm wavelength, and type II meter radio burst. The data used have been obtained from "Solar - Geophysical Data" Prompt Reports No. 560 and 561, and comprehensive reports No. 561 and 591, published by NOAA, Boulder, Colorado, USA.

One of our method for forecasting the high energetic solar proton flares depend on increasing of the ratio of microwave flux on two wavelengths emitted from the solar disk. The Air Weather Services Sagamore Mill (SGMR) observations are selected. The solar microwave flux adjusted to 1 Astronomical Unit, and Calibrated to bursts. The ratio of 2695 MHz flux to 8800 MHz flux, and the ratio of 4995 MHz flux to 8800 MHz flux are represented for March 1991. The spectral type of the great outstanding microwave bursts associated with the high energetic solar proton flare of 22 March was determined using the solar radio emissions measured at frequencies 80000, 35000 and 7000 MHz of Nobeyama station (NOBE), and the solar radio emissions measured at frequencies 15400, 8800, 4995, 2695, 1415, 610, 410, and 245 MHz of Learmonth station.

**GA6.01/P/12-A5** Poster **0900-19**

**SOLAR ULTRAVIOLET RADIATION AND ITS INFLUENCE ON THE OZONE LAYER**

M. A. Mosalam Shaltout and A. Okasha, National Research Institute of Astronomy and Geophysics, Helwan, Cairo, Egypt, Fax: (202) 5548020, Phone (202)2630833 E-mail: mamshaltout @ frcu.eun.eg

It is confirmed that the method of Health and Schlesinger for the core to wing ratio of Mg II h and k lines at 280 nm in solar emission was a good measure for the relative temporal variation of UV fluxes in the range 170 - 295 nm and chromospheric UV and EUV fluxes at shorter wavelengths.

Short and long-term variability of the Ultraviolet Solar Radiation is very important factor for the variations in the earth's stratospheric ozone. Measurements of the solar ultraviolet radiation in Mg II h and k lines band were performed by the artificial satellites Nimbus 7 and NOAA 9, and the daily data of Mg II center to wing ratio for the period from November 1978 to December 1988 were published in the comprehensive reports of Solar - Geophysics Data Edited by NOAA, Boulder, Colorado, USA. Also the concentration of ozone in the stratosphere of the Earth's atmosphere observed by Nimbus 7 from November, 1979 to December, 1992. Power spectra analysis of the solar UV radiation and ozone concentration show periodicity close to 27 days (period of the sun rotation) and the period of revolution of Earth in ecliptic orbit around the sun (solar year). Other periodicities similar to 13 days and 6 months are clear in the power spectra diagram.

**GA6.01/P/08-A5** Poster **0900-20**

**POWER SPECTRA ANALYSIS FOR INTERPLANETARY HIGH ENERGETIC CHARGED PARTICLES MEASURED BY GOES FROM JANUARY 1987 TO JUNE 1998**

M. A. Mosalam Shaltout and S. El-Genedi, National Research Institute of Astronomy and Geophysics, Helwan, Cairo, Egypt, Phone: (202) 2630833; Fax (202) 5548020 E-mail: mamshaltout@frcu.eun.eg

The proton fluence in the interplanetary medium is measured by GOES of NASA at three different energetic levels as > 10MeV, > 100MeV, and > 1000MeV. The data for the period (January 1987-June1998) are published in "Solar - Geophysical Data", of NOAA, Boulder, Colorado, USA. The data are provided merely as a tool to distinguish when events occur. Where, during the period of January 1987 - June 1998 more than seventy solar proton events affecting the earth environment are recorded by the GOES Space Craft at Geosynchronous orbit, for energies > 10 MeV. Also, in 22 March 1991 during the declining phase of solar cycle 22, a very high energetic solar proton flare was released at UT 22h 47m from NOAA/SESC active region No. 6555. The proton flux of particles had energies > 10 MeV was 43,000 particle flux units (pfu), measured by GOES space craft. It is the highest measured one during the solar cycle 21 and 22. The power spectra analysis are applied on the time series of the daily proton fluence measured by GOES for the period (January 1987 - June 1998) for the three energetic levels. The results show a variability in the proton fluence as short and long-term periodicities close to the periodicities of the solar activity.

**GA6.01/W/10-A5** Poster **0900-21**

**QUASI-BI-DECADAL CLIMATE OSCILLATIONS RELATED TO SOLAR ACTIVITY**

Zhongwei YAN (Institute of Atmospheric Physics, Beijing 100029, China email: yzw@ast590.tea.ac.cn)

Climate variations of decadal time-scales behave variously in different regions, thus forming the complexity of global change. This study tried to recognize the mentioned scale signals that are of global significance. The Morlet wavelet method was applied to global 5 longitude X 5 latitude grid monthly temperature series. In the global mean case of the last 100 years, besides the 4-5-year variations, the bi-decadal ones showed strong power. Although they might not be dominant everywhere, these two signals were of global significance. If the short scale signal could be conventionally related to ENSO, the bi-decadal one remained less known. It was noted that the bi-decadal oscillations decayed since the 1960s. The precipitation in northern China of the last 100 years were also analyzed. Besides the strong interannual fluctuations, the quasi-bi-decadal variations were of strong power. They also decayed suddenly since the 1960s, when a long-term dry phase began in northern China. The temperature difference between southern and northern China has the similar spectra with a prominent peak around the bi-decadal scale. At this time-scale, the larger the temperature difference, the more the regional precipitation, thus performing some climatological 'front' effect. Similar oscillations also existed in northern America, where the higher the temperature, the less the precipitation. This regional relation seemed broken since the 1960s, when the quasi-bi-decadal signal decayed and a long-term warming and wetting trend occurred. The reason for the prevalence of the quasi-bi-decadal oscillations in climate remained unsolved. It was interesting that the same time-scale variations existed in the sunspots' umbra/penumbra ratios and more interesting that they decayed during the late half of this century.

**GA6.01/P/11-A5** Poster **0900-22**

**LONG-TERM UPPER ATMOSPHERIC COOLING AND SUBSIDENCE TOOK PLACE AT LEAST DURING ALL THROUGH 20TH CENTURY**

SHEFOV

Abstract not available at the time of going to press

**GA6.01/E/09-A5** Poster **0900-23**

**EFFICIENCY FACTORS IN THE SOLAR-TROPOSPHERIC RELATIONS**

Andras LUDMANY and Tunde Baranyi (both at Heliophysical Observatory, H-4010 Debrecen P.O.Box 30. Hungary, email: ludmany@tigris.klte.hu)

Two basic paradigms of solar-tropospheric relations are reviewed and compared in the report. They are based on different energy transfer mechanisms: the irradiance and the solar corpuscular radiation. It used to be widely accepted for a long time that the solar impact affects the troposphere through irradiance variations. It turned out, however, that under certain circumstances the impact of the particle flux variations may be more efficient than that of the irradiance. The efforts of the Debrecen Observatory are devoted to study both paradigms in a parallel and comparative way, both approaches need long-term datasets. On one hand the irradiance studies are supported by our sunspot catalogues, the Debrecen Photoheliograph Data which is a catalogue of sunspot positions and areas (like the Greenwich Photoheliograph Results), and a new, ambitious project in preparative state, the Historical Solar Image Database, which will contain full disc white light images of the Sun for every day since the beginning of the regular observations, the present contribution provides the first report about it to the solar-terrestrial community. On the other hand the paradigm of corpuscular impacts is also investigated by using long-term datasets of the surface temperatures and the aa-index. These latter studies revealed several previously unknown regularities in the terrestrial responses to the incoming solar effects, they are mainly of vectorial nature which is a clear signature of corpuscular influence. The atmospheric response depends on 1) the polarity of the main solar magnetic dipole field (22-yr modulation), 2) the mutual attitudes of the Sun-Earth axes (semiannual fluctuation), 3) the solar origin of the plasma flow (polar or equatorial), and 4) the terrestrial hemisphere (eastern or western). It is not appropriate to treat any of these paradigms in an exclusive way, we provide their brief comparison in order to overview their relevance.

**GA7.01** **Saturday 24 July**

**EQUATORIAL GEOMAGNETISM AND AERONOMY IN DEVELOPING COUNTRIES**

Location: Gisbert Kapp NG16 LR2

**Saturday 24 July AM**

Presiding Chairs: B.R. Arora (Indian Institute of Geomagnetism, Mumbai, India)  
C.A. Onwumechili (Emeritus Scientist, Nigeria, Maryland, USA)

**GA7.01/E/10-A6** Invited **0900**

**ACTUAL STATUS OF GEOMAGNETISM IN DEVELOPING COUNTRIES**

Luiz Muniz Barreto Observatorio Nacional. Rua General Bruce,586. 20921-400, Rio de Janeiro,RJ. Brasil e-mail : barreto@on.br

Besides its mathematical and physical approaches, Geomagnetism is substantially a natural science. Its results and conclusions must be made after methodic enquiries to the Nature : observations are essential. Geomagnetic phenomenon embraces our planet and a great region around it. For this reason, among some important requirements for good observed data, two conditions must be considered first : an homogeneous and adequate distribution of permanent observing stations, and a continuous operation for a very long time. Both conditions are difficult to be accomplished, because we must keep in mind that about 70% of the terrestrial surface is covered by oceans and seas, and in the remaining 30% the situation is not satisfactory, mainly for cultural and economical reasons, because a great part of land area is represented by the Developing Countries (DC). However, there are in DC areas some important geomagnetic field patterns, such as the EEJ and the SAGA, typically scientific questions, that need to be addressed. Despite the clear evidence of the importance of DC for Geomagnetism, there are many problems to be solved. To install new stations with modern instruments is only a part of a satisfactory solution. It is necessary to train observers, to improve local scientific research and, above all, to convince local authorities about the importance of our Science. Some fruitful examples could be given, for instance the African

French speaking countries, Latin-America, India, China, Vietnam. In all these examples the presence of an international cooperation has been a source of the success.

**GA7.01/P/04-A6** **0930**

**EVIDENCES OF SEVERAL CURRENT SYSTEMS GENERATING THE MAGNETIC FIELD SUPERPOSED ON QUIET DAYS EQUATORWARD OF THE SQ FOCUS**

C. Agodi ONWUMECHILI (4813 Lackawanna Street, College Park, Maryland 20740, USA, email: agodi onwumechili@yahoo.com)

The horizontal magnetic field, SPMF(H), superposed on the monthly mean Sq(H) to compose the diurnal profile of Sq(H) on a given quiet day, has been found to be complex. Its diurnal pattern varies from day to day and can be different at two stations on the same longitude. However, the pattern is normally very similar at all the stations in the equatorial electrojet (EEJ) zone and very similar at all the stations in the worldwide part of Sq (WSq) zone outside the influence of the EEJ. The 9 possible categories of SPMF in the EEJ zone vis-a-vis the WSq zone to be expected if the intensities of EEJ and WSq vary independently have all been found. Only one category occurs preferentially. In particular, variations of the intensities of the EEJ and WSq current systems in phase and in antiphase respectively are found to occur with equal frequency. These independent variations of the EEJ and WSq current systems explain the lack of correlation between the Sq(H) in EEJ and WSq zones. The particular types of SPMF that cause abnormal phase quiet days (APQDS) in the EEJ zone and in the WSq zone respectively are also found. In the EEJ zone it is generated by a current system resembling the counter equatorial electrojet (CEJ) current system but in the WSq zone it is generated by the single vortex current (SVC) system.

**GA7.01/P/03-A6** **0945**

**CORRELATIONS OF SQ HOURLY AMPLITUDES AND THEIR IMPLICATIONS FOR LOW LATITUDE IONOSPHERIC CURRENTS**

C. Agodi ONWUMECHILI (4813 Lackawanna Street, College Park, Maryland 20740, USA, email: agodi-onwumechili@yahoo.com)

The investigation of the correlation of DH at all local time hours of the day has given a lot more information on the correlation of the ionospheric current intensities and their changes than is obtainable from daily ranges. It is found that the correlation coefficients of all pairs of stations in night-time are positive, very high and independent of the distance separating the two stations. It is explained that the small-amplitude variations at night being correlated arise from magnetospheric sources even on very quiet days. The correlation coefficients at two stations (called E stations) in the equatorial electrojet (EEJ) zone or at two stations (called L stations) in the worldwide part of Sq (WSq) zone outside the influence of the EEJ are positive, very high and remain fairly steady at all hours of the day. This is because each pair of stations is under the same current systems. The correlation of L-L pair of stations in daytime decreases with the distance separating the stations because the ionospheric parameters that determine ionospheric current intensity and its changes are different at the two stations. The correlation coefficients of E-L pairs of stations fall drastically from very high values at night-time to very low and often insignificant values in daytime. This is principally due to the differences in the ionospheric parameters that determine the current intensities of the EEJ and WSq current systems in the different environments of the two stations. However, there is evidence that the counter equatorial electrojet (CEJ) current system occasionally modulating the EEJ current system and the single vortex current (SVC) system occasionally modulating the WSq current system make their minor contributions.

**GA7.01/P/01-A6** **1000**

**REGIONAL SQ VARIABILITIES TO BE STUDIED AT INDIVIDUAL OBSERVATORIES**

Naoshi FUKUSHIMA (Dept. of Earth and Planetary Physics, University of Tokyo, Tokyo 113-0033 Japan. email: fukusima@npr.ac.jp)

A general seasonal tendency of the geomagnetic Sq-field is to show a maximum intensity in local summer (June-July in the northern hemisphere) and a minimum in local winter over the world. However, we find some regional modifications of the Sq intensity observed on the ground throughout the year; for example:

- (1) The Sq intensity is usually strongest in the end of August in the western Pacific countries in the northern hemisphere;
- (2) At some Indian stations the Sq intensity is maximum in September;
- (3) At Argentine stations the Sq maximum is seen at both vernal and autumnal equinoxes, and so forth.

These interesting regional features of the geomagnetic Sq-field must be studied extensively in the near future, with international cooperation in data exchange and analysis. It is hoped also that some more examples of the regional dependence of the Sq-field will be found to contribute eventually to the understanding of the air motion and the resulting electric current in the ionospheric region.

**GA7.01/W/06-A6** **1015**

**STUDY OF GEOMAGNETIC VARIATIONS AT EQUATORIAL STATIONS SITUATED ON TWO CLOSELY SEPARATED LONGITUDINAL PROFILES**

NALIN B. TRIVEDI, Severino L. G. Dutra ( Instituto Nacional de Pesquisas Espaciais-INPE , C.P.-515, São Jose dos Campos, SP 12201-970, Brazil, email: trivedi@dge.inpe.br ); José M. Da Costa ( Universidade de Taubate-UNITAU, SP 12020-270, Brazil, email: dacosta@dge.inpe.br )

During September and October 1994 we had recorded geomagnetic daily variations at several stations near the magnetic equator on 45° West meridian (three stations ) and on 60° West meridian ( six stations ). The equatorial electrojet (EEJ) and counter electrojet (CEJ) characteristics were studied using H, D and Z data for 10 quiet days (Ap less or equal to 6) of the above mentioned period. The results of the analysis regarding longitudinal differences in the daily range in H and ionospheric current system associated with the equatorial counter electrojet (CEJ) are presented and discussed.

**GA7.01/E/02-A6** **1100**

**OVERVIEW ON EQUATORIAL GEOMAGNETISM (INVITED TALK)**

R.G.RASTOGI, Department of Physics, Gujarat University and Physical Research Laboratory, Ahmedabad 380 009, India e-mail: parvs@prl.ernet.in

The discovery of equatorial electrojet immediately led to the two important features of the ionosphere (1) equatorial sporadic E layer (2) Equatorial ionization anomaly. Later it was found the Spread F is also related to the special features of the equatorial electric field. The long



series of HF Ionospheric Drift observations at Thumba led to the first time a close relation between the electrojet field and the Interplanetary Magnetic Field. Today the new results of equatorial geomagnetic storm effects are redefining the global magnetic disturbance phenomenon. The paper would define the role of electrojet in ionosphere, space physics and in the solar wind magnetospheric relationships. It is a rewarding opportunity for developing countries to contribute significantly to global science through electrojet studies.

**GA7.01/E/06-A6**

**1130**

**CEJ RELATED EQUIVALENT CURRENT SYSTEM: A CASE STUDY ALONG INDIAN SECTOR**

BALDEV R. ARORA and S.K. Bhardwaj (Indian Institute of Geomagnetism, Colaba, Mumbai 400 005, India, email: bra@iig.iigm.res.in)

The method of Principal Component Analysis (PCA) is applied to geomagnetic daily variations in H and D along the Indo-Russian chain of stations to establish spatial-temporal structures of the source currents on normal and counter electrojet days. It is found that first two principal components (PCs) are able to describe the characteristics of CEJ related field variations within and outside the equatorial belt. The first PC depicts the well-known latitudinal behaviour of Sq variations. Second PC describes the salient perturbations at low and middle latitudes accompanying the large negative excursion in H field at equatorial stations. When the perturbation in H and D components are combined, the nature of deduced flow path of source current favours superposition of additional current system caused by some global tidal modes in the dynamo region. The CEJ related current system, marked by intense westward current flow in equatorial belt, is shown to close its path by forming a clockwise loop extending up to mid-latitudes, with a well defined focus around 10 (degree) dip latitude. Their comparison with numerically simulated current system, due to various tidal modes, emphasize the significance of semidiurnal symmetric tidal modes in the generation of CEJ events.

**GA7.01/E/11-A6**

**1145**

**GROUND-BASED DD DIURNAL VARIATIONS IN THE EQUATORIAL ELECTROJET INFLUENCE AREA IN AFRICAN**

VAFI DOUMOUYA (Universite de Cocody, UFR-SSMT, BP 582, Abidjan 22, Ivory Coast, email: doumouv@syfed.ci.refet.org) Jacques Vassal (CETP, 4, Avenue de Neptune, 94107 Saint-Maur, France, email: jacques.vassal@cetp.ipsl.fr) Yves Cohen (IPGP, Laboratoire de Geomagnetisme, 4, place Jussieu, 75252 Paris Cedex 05, email: cohen@ipgp.jussieu.fr); Michel Menvielle (Physique de la terre, Bat.504, Universite Paris Sud, 91405 Orsay Cedex, France).

During the International Equatorial Electrojet Year (IEEY), the DH, DZ and DD daily variations of the geomagnetic field have been recorded in a network of ten stations across the dip-equator, along the 50W meridian in West-Africa. For a former experiment in Central Africa, these same variations were recorded from 1968 to 1970. In this paper, we describe and make an attempt to interpret the DD variations as observed during these two experiments.

The DD diurnal pattern is characterized by a very strong day to day variability. But some days, it presents a fairly regular structure in the northernmost and southernmost stations. In the light of the data from the Central African experiment, we have shown that DD displays four distinct zones with opposite signs: a positive northern area and a negative southern area in the morning; a negative northern area and a positive southern area in the evening. This structure has been interpreted as related to a meridional current system which converges in the morning and diverges in the evening. As this current system seems to be close to the dip-equator, we analyze and discuss its likely origins and relations with the equatorial electrojet.

**GA7.01/E/08-A6**

**1200**

**VARIATIONS OF THE LUNAR GEOMAGNETIC TIDE IN THE INDIAN REGION**

R.J. Stening (School of Physics, University of New South Wales, Sydney 2052, Australia, e-mail: R.Stening@unsw.edu.au) and R.G. Rastogi (Physical Research Laboratory, Ahmedabad 380 009, India, e-mail: parvs@prl.ernet.in)

Hourly magnetic field values from several observatories in the Indian region have been analysed for lunar tides using up to ten years of data. The average form of the seasonal variation of the lunar geomagnetic tide is described and also year-to-year changes are shown in the phase of the tide and in the position of the current system focus (when there is one).

**GA7.01/E/13-A6**

**1215**

**ANOMALOUS BEHAVIOUR OF SQ CURRENT SYSTEM ALONG 75 (DEGREE) E MERIDIAN**

S.K. Bhardwaj and BALDEV R. ARORA (both at Indian Institute of Geomagnetism, Colaba, Mumbai - 400 005, INDIA, email: bra@iig.iigm.res.in)

Analysis of Sq variation along the Indo-Russian chain of observatories has shown disappearance of the northern hemispheric 'Sq Vortex' during winter months. In order to understand the possible source and whether this anomalous feature persists in southern hemisphere, the Sq behaviour at a few stations in southern hemisphere are examined through the method of Principal Component Analysis (PCA). It is seen that Sq(H) at mid-latitude stations, confined between longitude slice of 25-90 (degree) E, exhibits markedly different diurnal pattern than those recorded at comparable latitudes outside this longitudinal belt. PCA of Sq(D) variations also indicates the presence of two distinct patterns, one corresponding to regular Sq and the other associated with second component which has similar waveform both in northern and southern hemispheres. This component, indicative of the presence of strong inter-hemispheric currents, undergoes much stronger seasonal variability than the first component. It is deduced that the magnetic effects associated with these currents tend to dominate the weak wintertime Sq dynamo effects, accounting for the disappearance of Sq vortex in the northern hemisphere. This longitudinal sector is also marked by an anomalous pattern in vertical component of Earth's main magnetic field. The contours of isolines, instead of following the circle of latitudes, tend to align north-south in this longitudinal belt in the southern hemisphere. A possible effect of this main field anomaly on the dynamo mechanism is discussed, among other feasible factors, as a possible source of the peculiar behaviour of Sq along this longitude sector.

**GA7.01/W/05-A6**

**1230**

**THE SIGNATURE OF THE 18.6 YEARS MN LUNAR TIDAL EFFECT OVER HUANCAYO EQUATORIAL MAGNETIC OBSERVATORY**

GIANIBELLI, Julio C. Dep. of Geomagnetism and Aeronomy, Faculty of Astronomical and Geophysical Sciences, La Plata University, Paseo del Bosque s/n, 1900 La Plata, Argentina, email: jcg@fcaglp.fcaglp.unlp.edu.ar

The lunar wave of 18.6 year on the monthly mean values of the geomagnetic elements recorded during 70 years at Huancayo magnetic observatory is determined. It is supposed that this very long term signal is important on the modulation of aeronomic effect. The methodology used is the non-linear Maximum Entropy Method (MEM) with a switch of 90% in all the error predictor filter (fpe) longitudes.#

**Saturday 24 July PM**

Presiding Chairs: L.B. Barreto (Observatorio, Nacional, Brasil)  
N.B. Trivedi (Instituto Nacional de Pesquisas Espaciais, Brazil)

**GA7.01/W/08-A6**

**1400**

**MAGNETIC REPEAT STATION NETWORK IN VIETNAM ( FROM J = 80N TO J = 230N)**

N T K THOA, H D Chau and N V Giang (Institute of Geophysics, Box 411 Buidien Boho Hanoi Vietnam, email: thoa@igp.ncst.ac.vn) Daniel Gilbert (Institut de Physique du Globe de Paris, 4 place Jussieu 75252 Paris Cedex 05, France)

During the years 1990-1991 and 1997 in the frame of the project of cooperation between Hanoi Institute of Geophysics and Institute of Earth's Physics in Paris, the absolute measurements of total intensity of geomagnetic field (T) with its components in 56 points, distributed sparsely all over the territory of Vietnam (from j = 80N to j = 230N) were carried out. With the instruments having a high degree of precision as proton magnetometer ELSEC for the measurement of total intensity of geomagnetic field (T), magnetic theodolite FLUXGATE for the measurement of declination (D), inclination (I), and from it, calculate the horizontal (H) and vertical components (Z). Repeat measurements at 56 points in 1997 were carried out with the same degree of precision. The error of measuring and reducing is 1' for D, 9 nT for H and T and 4.5 nT for Z. The precise methods were used to correct time variation \*T with the attention to strong influence of Equatorial Electrojet, in order to reduce the measured values to the epoch 1991.5 and 1997.5 (00h of July 1st, 1991 and 1997). The values of measurements of geomagnetic field in the territory of Vietnam for two epoch are follow: 1991.5 1997.5 41100 nT £ T £ 45700 nT 41 200 nT £ T £ 46 000 nT 38300 nT £ H £ 41300 nT 38 200 nT £ H £ 41 300 nT 0nT £ Z £ 24000 nT, 500nT £ Z £ 25 500 nT 0o £ I £ 35o, 0o £ I £ 34.5o -1.2 o £ D £ 0o -1.2 o £ D £ 0o 1. GA 7.01 2. Equatorial Geomagnetism and Aeronomy in Developing Country 3. N T K THOA Institute of Geophysics, Box 411 Buidien Boho Hanoi, Vietnam, email: thoa@igp.ncst.ac.vn , tel: 84 48 352380, Fax: 84 48 364 696 4. O 5. No 6. No 7. N V Giang and Daniel Gilbert : No, N T K THOA and H D Chau : YES

**GA7.01/E/12-A6**

**1415**

**INTENSE SOLAR FLARE EFFECTS AND STORM SUDDEN COMMENCEMENTS IN THE INDIAN CHAIN OF OBSERVATORIES**

R.G.Rastogi (Physical Research Laboratory, Ahmedabad 380 009 India, email: parvs@prl.ernet.in) B.M.PATHAN and D.R.K.Rao(both at Indian Institute of Geomagnetism Colaba, Mumbai 400 005, India, email: bmpathan@iig.iigm.res.in)

With the close network of thirteen magnetic observatories along the Indian longitudinal sector from 0 deg to 70 deg dip latitudes, it has been possible to identify the Sfe and SSC at the same local time.

First, the direction of Sfe vector is found to be identical with the pre-flare Sq vector suggesting that the meridional currents causing changes in declination flow in the same altitude range as that of Sq current at low and middle latitudes. The daily variations at low latitudes are not due to the field line currents as these high altitude currents would not be affected by the solar flares. Extraordinarily large electro- magnetic induction effects are observed in the vertical component at the equatorial stations. The latitudinal profile of SSC in H during nighttime shows a small decrease in amplitude at stations near the magnetic equator. These observations are explained as due to the concentration of the low latitude induced currents in the conducting layers inside the earth around the Palk Strait between India and Sri Lanka forming an intense band current flowing westward.

**GA7.01/W/04-A6**

**1430**

**EQUATORIAL ENHANCEMENT OF STORM TIME PC5-6 GEOMAGNETIC PULSATIONS**

Pathan B.M., N.G.Kleimenova, O.V.Kozyreva, D.R.K. Rao and R.L.Asinkar

The geomagnetic Pc5-6 range (1-4 mHz) pulsations during several magnetic storms have been analyzed using ground observations at array of 5 Indian stations from 0.8ø to 25ø dip latitude and two pairs of low-latitudes (~20ø) - near equator (~4-5ø) stations, located at ~4 hours to the West and East from this profile. The pulsations were occurred as separate wave packets and characterized by similar spectra at all stations with two dominate bands of frequencies: ~1.5-2.0 mHz and ~2.5-4.0 mHz. Very strong daytime equatorial enhancement of the waves intensity has been noted. The higher enhancement was observed in the noon-afternoon times and the same is reduced to the morning and evening times. The polarization of both frequency bands at the equator is noticed to be almost linear, mainly along the H-direction. The amplitude in the D-component of the pulsations is found to decrease as one approaches the dip equator. The mechanism of day time equatorial enhancement of long period geomagnetic pulsations obviously is connected with the influence of the Cowling conductivity effects in the vicinity of the dip equator.

**GA7.01/E/05-A6**

**1445**

**A METHOD FOR REDUCTION OF MAGNETIC MEASUREMENTS IN THE AREA OF INFLUENCE OF EQUATORIAL ELECTROJET**

H D CHAU (Hanoi Institute of Geophysics, Box 411 Buidien Boho Hanoi Vietnam, email: chau@igp.ncst.ac.vn)

Magnetic repeat station network in Vietnam has just been built from 1990 -1991. The measurements of the geomagnetic field were carried out in 1991 and 1997. The errors of absolute measurements are 1' for D, 9 nT for H and T and 4.5 nT for Z. When reduce the data measured into a certain epoch, the authors have to overcome the difficulties follow: The territory of Vietnam is elongated from 8 dgr.N to 23 dgr.N latitudes and Southern Vietnam lies under the influence of Equatorial Electrojet, so diurnal geomagnetic variation in this region is very complicated. For correcting and reducing to an epoch, the data of a station which is near to the observatory, one can use directly the variation data of this observatory. But when the station is far from the observatory, one will commit big errors. The errors of reducing from variations can be very big, especially if the measurements are carrying out at maximum and minimum of solar activity. We managed to resolve this problem, using the magnetic variation data recorded in 4 magnetic observatories distributed sparsely over the territory of Vietnam: Chapa (22 dgr.21'N, 103 dgr.50'E), Phu Thuy (21 dgr.02'N, 105 dgr.57'E), Da Lat (11 dgr.57'N, 108 dgr.29'E), Bac Lieu (09 dgr.17'N, 105 dgr. 44'E). The Bac Lieu observatory is lied just under the band of Equatorial Electrojet, and Da Lat observatory at its edge. The station data are corrected according to the observatory magnetograms and reduced to the midnight base.



On the hypothesis that the amplitude of the diurnal magnetic variation between two observatories (for example Phu Thuy and Da Lat) change linearly with the latitude, one can calculate the this amplitude in a point between two observatories by interpolation. This hypothesis was very carefully checked by the measurement data for many years. This method has given the precisions enough for the elaboration of the magnetic charts in Vietnam.

**GA7.01/W/02-A6 1500**

**LOW LATITUDE IONOSPHERE- MAGNETIC STUDIES DURING STRONG MAGNETIC STORM OF MARCH 13,1989, BASED ON OBSERVATIONS IN PHUTHUY, VIETNAM**

T Q Hao, N T K THOA, P V Tri ( Institute of Geophysics, Box 411 Buidien Boho Hanoi, Vietnam, email: tha@igp.ncst.ac.vn), N G Kleimenova (Institute of Physics of the Earth, Bolshaya Gruzinskaia 10, D-242, Moscow, Russia)

Strong magnetic storm of March 13-14,1989 started at 01.27 UT with  $K_p=9$ , maximal value of  $Dst = - 578$  nT,  $A_p = 246$ . The comparison between ionospheric and magnetic records at the observatory Phuthuy, Vietnam ( $j = 21002$ ,  $l = 105057$ ) showed that in the main phase of storm (11UT 13.03.1989 - 06UT 14.03.1989) the sudden fluctuations of  $h'F$  occurred simultaneously but in the antiphase with the magnetic disturbances. The increase of  $h'F$  from  $\sim 240$  km at 14 UT 13.03.1989 to  $\sim 450$  km at 15 UT 13.03.1989, the strong decrease of the frequency of F layer in the correlation with magnetic activity confirm the appearance of additional source in the ionosphere during the night time at low latitude.

**GA7.01/W/01-A6 1515**

**PC3-5 STUDY OF GEOMAGNETIC MICROPULSATIONS AT VERY LOW LATITUDE, IN BRAZIL**

Ademilson ZANANDREA , Severino L G Dutra and Nalin B Trivedi (all at Instituto Nacional de Pesquisas Espaciais-INPE, São José dos Campos, SP, 12201-970, Brasil, e-mail: ademil@dge.inpe.br); José M Da Costa (Universidade de Taubaté-UNITAU, Taubaté, SP, 12020-270 and at Instituto Nacional de Pesquisas Espaciais-INPE, São José dos Campos, SP, 12201-970, Brasil, e-mail: dacosta@dge.inpe.br); K Yumoto, T Kitamura, M Shinohara and H Tachihara (Kyushu University,Fukuoka 812, JAPAN, e-mail: yumoto@geo.kyushu-u.ac.jp)

This present study is aimed at the understanding of source mechanisms and propagation modes of Pc3-5 micropulsations at very low and equatorial latitudes. It used simultaneous data measured with a chain of 10 geomagnetic stations in Brazil using high sensitive fluxgate magnetometers. Multiple tapered spectral estimation method based on Fast Fourier Transforms (FFT) was used to obtain micropulsation power spectra, polarization parameters and phases. It was observed an increase on the occurrence of highly polarized Pc3-5 pulsations, reaching maxima close to local noon (14:00 and 15:00 UT) in the stations nearest to the magnetic equator. The dynamic spectra showed the occurrence of 81 simultaneous events of Pc3-4 pulsations with high degree of polarization, mainly during daytime. The diurnal events showed increases in the polarized power density of 3,2 times for pulsations observed at stations close to the magnetic equator in comparison to the more distant ones. The phase of the pulsations observed at station close of the magnetic equator showed a delay of  $48^\circ$  and  $62^\circ$  in relation to the most distant one. This effects is clearly related to the increase of ionospheric conductivity and equatorial electrojet intensity. The amplitude of north-south component is much larger than the west-east one (poloidal mode oscillation). This result could be an evidence that field line resonance mechanism does not explain Pc3-5 micropulsations observed at very low and equatorial latitudes. The propagation of compressional waves may excite the trapped compressional mode or the compressional global mode. The resulting phenomenon, field lines forced oscillations in the plasmasphere, may be a possible source mechanism for Pc3-4 pulsations at very low latitudes.

**GA7.01/W/07-A6 1530**

**ULF FIELD GEOMAGNETIC OBSERVATIONS ASSOCIATED WITH ELECTRICAL ATMOSPHERIC STORMS IN BRAZIL**

José M DA COSTA (Universidade de Taubaté-UNITAU, Taubaté, SP, 12020-270 and Instituto Nacional de Pesquisas Espaciais-INPE, São José dos Campos, SP, 12201-970, Brasil; e-mail: dacosta@inpe.dge.br); Severino L G Dutra, Nalin B Trivedi, Ademilson Zanandrea and Nelson Arai (all at Instituto Nacional de Pesquisas Espaciais-INPE, São José dos Campos, SP, 12201-970, Brasil; e-mail: dutra@inpe.dge.br); José R S Souza (Universidade Federal do Pará - UFPA, Belém, PA, Brasil)

An experiment to verify the influence of atmospheric electrical storms on ULF geomagnetic micropulsations parameters was conducted at low latitude stations as Belém ( $1.4^\circ S$ ,  $48.4^\circ W$ ), Cuiabá ( $15^\circ S$ ,  $56^\circ W$ ) and Cachoeira Paulista ( $22.7^\circ S$ ,  $45^\circ W$ ), in Brazil. The geomagnetic field was monitored with high sensitive low noise fluxgate magnetometers in the DC-1Hz frequency range. The thunderstorm sensors could detect atmospheric electrical activity within a radius of 180km from the station. The local atmospheric electrical activity was also confirmed by the analysis of a sequence of satellite cloud cover data. The data analysis shows increases on the amplitudes of some Pc3 and Pc4 micropulsations events in association with electrical thunderstorms.

**GA7.01/W/03-A6 1615**

**PLASMA DIAGNOSTIC EXPERIMENTS ON BOARD THE BRAZILIAN SCIENTIFIC APPLICATIONS SATELLITES SACI-1 AND SACI-2P**

MURALIKRISHNA, M.A. Abdu, S. Domingos, J.A.C.F. Neri (all at Instituto Nacional de Pesquisas Espaciais - INPE/MCT, C.P. 515, 12201-970, São José dos Campos - SP, Brazil, email: murali@dae.inpe.br) and Koh-Ichiro Oyama (Institute of Space and Astronautical Science, 3-1-1, Yoshinodai, Sagamihara 229-850, Japan, email: oyama@bochan.ted.isas.jp)

A set of three plasma diagnostic experiments, are proposed to be launched on board the two Brazilian Scientific Applications Satellites SACI-1 and SACI-2 to investigate the phenomenon of ionospheric plasma bubbles, known to exist in the ionospheric region over a wide range of latitudes. While the micro satellite SACI-1 is going to be put in a near polar (98 degree inclination) orbit SACI-2 is going to be put in a low inclination orbit. Their launches are presently scheduled for this year, SACI-1 being programmed for launch in the middle of this year. The two plasma diagnostic packages will be practically identical in functioning but will be different in the mechanical mounting of the sensors on board. It is intended to make measurements of the density, temperature and spectral distribution of the irregularities, of the plasma using (1) a High Frequency Capacitance Probe for measuring the plasma density, (2) a fixed-bias Langmuir Probe for measuring the electron density profile and the spectral distribution of plasma irregularities, and (3) an Electron Temperature Probe for measuring the kinetic temperature of the ionospheric electrons. In the High Frequency Capacitance Probe a metallic sensor in the form of a sphere of about 60mm diameter, mounted at the extremity of one of the solar panels is used as a capacitance element in the tank circuit of a "Clapp" type oscillator. In the fixed bias Langmuir Probe a metallic sensor, similar to that used in the HFC

experiment, is mounted at the extremity of another solar panel and the sensor potential is selected using telecommands. In the Electron Temperature Probe two semicircular metallic sensors in the form of a circular disc, mounted at the extremity of a third solar panel is used to determine the kinetic temperature of the ionospheric electrons. The experiment details along with details of the data acquisition system, on board processing of the LP ac data etc. are presented here.

**GA7.01/E/04-A6 1630**

**DEVELOPMENT OF A FABRY-PEROT INTERFEROMETER TO STUDY THE THERMOSPHERIC DYNAMICS OF THE UPPER ATMOSPHERE**

G.K.Mukherjee Indian Institute of Geomagnetism Colaba, Mumbai 400 005 India e-mail:gkm@iig.iigm.res.in

A pressure scanning Fabry-Perot Interferometer has been fabricated under AICPITS programme sponsored by DST, Govt.of India. The interferometer has been installed at a low latitude station, Kolhapur ( $16.8$  deg N,  $74.2$  deg E, dip latitude  $10.6$  deg N) in India. The high resolution spectrometer consists of a pair of etalons of  $150$  mm in diameter( IC Opt sys,UK) and is used to monitor temperature and horizontal winds in the thermosphere from the Doppler broadening and shift of the peak of [OI]  $630.0$  nm emission line in the night airglow. This is the largest aperture interferometer operating in the country.

Salient features of the spectrometer and preliminary data obtained are presented here.

**GA7.01/E/07-A6 1645**

**COORDINATION OF GROUND BASED AND ROCKET BORNE STUDIES OF EQUATORIAL ELECTROJET**

R.G.RASTOGI, H.Chandra, H.S.S.Sinha and Som Sharma Physical Research Laboratory, Ahmedabad 380 009, India, e-mail: parvs@prl.ernet.in

The discovery of the longitudinal variation of equatorial electrojet current strength from IGY data still remains a unsolved problem. The second problem to be solved is the association of electrojet with Sq. A study has been made to coordinate the ground based magnetic data, vertical incident ionospheric data and the rocket borne current profile data in Indian and American longitudes. The longitudinal inequality is sufficiently reduced when the ground data are calibrated with rocket data. It is concluded that many of the longitudinal variations of equatorial geomagnetism and aeronomy are due to corresponding variation of the horizontal electric field in the equatorial E region of the ionosphere.

**GA7.01/E/14-A6 1700**

**EQUATORIAL F2 PEAK ENHANCEMENTS AND THE BRAZILIAN F3 STRATIFICATIONS**

E. Sambou (UCAD Dept de physique, Dakar-Fann, Senegal); R. Fleury (FT/CNET DMR/TSI, 22307 Lannion Cedex,France); P.M. VILA (CETP/CNRS StMaur-des-Fosses 94107, France)

We compare the Brazilian F3 phenomenon of 1995 ionograms (Fortaleza,  $4.5^\circ$  South mag. latitude) interpreted by Balan et al.(1998), with the morning crest and dome events documented from the 1993-94 West African ionosonde series (Sambou et al., 1998). Although the two features have much in common, a new scrutiny of their morphologies and physical conditions shows clear distinctions. We bring about auxiliary results to help discussing the respective mesoscale dynamics acting in the two longitude sectors, quite different despite their geographic vicinity.

G1

Wednesday 21 July

**POSITIONING (SECTION 1)**

Location: Law 303 LT

Location of Posters: Poynting Physics, Old Gym

Wednesday 21 July AM

Presiding Chairs: F.K. Brunner (TU Graz, Austria),  
C. Boucher (IGN, Paris, France)

G1/L/05-A3

0830

**GEODESY SECTION 1, POSITIONING: SECRETARY'S REPORT**

Yehuda BOCK (Scripps Institution of Oceanography, La Jolla, CA 92093-0225, USA, e-mail: ybock@ucsd.edu)

The section has sponsored 5 special study groups during this last 4-year period (1996-1999) dealing with important topics and issues in geodetic positioning:

- SSG 1.154: Quality Issues in Real-Time GPS Positioning, Chris Rizos (Australia),
- SSG 1.155: Active GPS Networks Hiromichi Tsuji (Japan),
- SSG 1.156: Advanced GPS Analysis for Precise Positioning, Geoffrey Blewitt (United Kingdom),
- SSG 1.157: GPS Ambiguity Resolution and Validation, Paul J. de Jonge (The Netherlands)
- SSG 1.158: GPS Antenna and Site Effects, Jan M. Johansson (Sweden)
- SSG 1.159: Use of GPS Positioning for Atmospheric Monitoring, Michael Bevis (USA)

We summarize briefly the major findings of these groups and discuss positioning issues for consideration in the next 4-year period, in particular, new developments and applications with an enhanced Global Positioning System.

G1/L/06-A3

0850

**REPORT OF THE IAG COMMISSION 10 ON GLOBAL AND REGIONAL GEODETIC NETWORKS**

Claude BOUCHER (IGN/LAREG, 2 Avenue Pasteur B.P. 68, 94160 Saint-Mandé, France, email: bock@ign.fr)

This presentation provides a summary of the report on the activities of the IAG Commission 10 on Global and Regional Geodetic Networks (GRGN) for the period 1996-1999. This includes a survey of the activities of its working groups and subcommissions, as well as the works achieved by participating countries. Some views for the future contributions of GRGN are then presented, with a particular focus on three topics: the developing use of ITRF, GPS versus other systems and the development of a global vertical datum.

G1/E/49-A3

0910

**REALIZATION OF A TERRESTRIAL REFERENCE FRAME FOR LARGE-SCALE GPS NETWORKS**

Detlef ANGERMANN, Juergen Klotz, Christoph Reigber (GeoForschungsZentrum Potsdam, Telegrafenberg C2, 14473 Potsdam, email: dang@gfz-potsdam.de)

The GFZ Potsdam established GPS networks for geodynamic studies in South America (SAGA), Central Asia (CATS) and South-East Asia (GEODYSSSEA), in cooperation with various organizations in the host countries, as well as in Europe and North America. This presentation concentrates on the datum definition of these networks.

The GPS data of the large-scale networks were processed simultaneously with data of the IGS station network using the GFZ software EPOS. The mean station coordinate residuals between our global network solutions and the ITRF96 coordinates are 1cm horizontally and 1-2 cm vertically. With respect to a regional reference frame the mean station coordinates residuals are in the range of 2-5 mm horizontally and below 1 cm for the height. For the interpretation of our network results we focus on regional tectonics and relative plate motions. To achieve this goal we define the datum of the station velocities in a regional frame. We present results for the datum definition of the SAGA and CATS network.

G1/E/46-A3

0930

**THE EUROPEAN REFERENCE SYSTEM COMING OF AGE**

J. Adam, W. Augath, C. Boucher, C. Bruyninx, P. Dunkley, E. GUBLER, W. Gurtner, H. Hornik, H. van der Marel, W. Schlüter, H. Seeger, M. Vermeer, J.B. Zielinski (members of the EUREF-Technical Working Group)

Ten years ago, the advantages of GPS technology were recognised and a first GPS campaign covering the western part of Europe was organised in order to establish a uniform European Reference Frame (EUREF). Through successive GPS campaigns, the network has been extended towards eastern parts of Europe and various countries have undertaken densification campaigns. This International co-operation within Europe has resulted in the establishment of a high accuracy, 3 dimensional geodetic network with links to global and national reference systems.

Strategies and guidelines have been developed for network densification, observation procedures, data flow and data analysis. This has resulted in today's permanent GPS network comprising in excess of 75 stations, a data handling service and supported by 12 analysis Centres. The results show an accurate and consistent network (+/- 3mm in the horizontal component, +/- 6mm in the height component).

Since 1995, emphasis has been placed on the height component, resulting in an extended and improved adjustment of the United European Levelling Network (UJELN) and the establishment of the European Vertical GPS Reference Network (EUVN). Today, the EUREF Network contributes towards multi-disciplinary activities such as the estimation of meteorological parameters and links to tide gauges.

G1/E/38-A3

0950

**A NATIONAL NETWORK OF CONTINUOUSLY OPERATING GPS RECEIVERS (COGRS) FOR THE UK**

Alan DODSON, Richard Bingley, Leighton Symons, Nigel Penna (IESSG, University of Nottingham, Nottingham, NG7 2RD, UK, email: alan.dodson@nottingham.ac.uk)

A national network of COGRs can provide a temporal and spatial density of continuous GPS data which can greatly expand the potential use of IGS data. For example, flood defence monitoring on a national scale can be related to the mean sea level monitoring carried out on

a global scale.

Similarly, the use of data from a national network, supplemented with data from the IGS global network, will permit detailed studies of tropospheric and ionospheric activity. The potential of COGRs has already been recognised by four UK government organisations, namely the Environment Agency (EA), the Meteorological Office (MO), the Ministry of Agriculture Fisheries and Food (MAFF) and the Proudman Oceanographic Laboratory (POL). By the end of 1998, a national network of thirteen COGRs was effectively in place in the UK. These thirteen COGRs will be supplemented by the Ordnance Survey of Great Britain, who have recently announced the establishment of a number of COGRs as active survey reference stations. In order to optimise the use of COGR data by the environmental community, the IESSG is in the process of establishing a national centre responsible for the transfer, archiving, processing and analysis of data from all COGRs in the UK, which could include about thirty stations by mid 1999. This presentation intends to discuss how the national data archive will be structured at the IESSG and illustrate preliminary results from a number of UK government funded projects.

G1/L/23-A3

1010

**QUALITY CONTROL ISSUES IN REAL-TIME GPS POSITIONING**

Chris RIZOS, Shaowei Han (both at School of Geomatic Engineering, The University of New South Wales, Sydney NSW 2052, Australia, email: c.rizos@unsw.edu.au, s.han@unsw.edu.au)

Real-time carrier phase-based GPS positioning techniques are now increasingly used for many surveying and precise navigation applications on land, at sea and in the air. Quality control (QC) issues are becoming more important for all applications. QC has been addressed at different stages of the GPS positioning process, for example, data collection, data processing and data display. In this paper, the quality control procedures or methodologies for the following critical operations are discussed:

- Measurement quality control for single receiver data, concerned with issues such as failed satellites, ionospheric scintillation, multipath and cycle slips.
- Quality assurance for data communication and data transmission delay.
- Quality control of the position modelling procedure, related to systematic error mitigation and stochastic modelling.
- Ambiguity resolution and validation procedures.
- Additional constraints for particular applications.

As examples, the proposed quality control procedures implemented in the Singaporean multi-base station network and the GPS-based volcano deformation monitoring system in Indonesia are described and future or unresolved considerations are outlined.

G1/L/17-A3

1100

**ARE GPS DATA NORMALLY DISTRIBUTED?**

Christian TIBERIUS (Delft Univ. of Technology, The Netherlands, email: c.c.j.m.tiberius@geo.tudelft.nl); Kai Borre (Aalborg Univ., Denmark, email: borre@kom.auc.dk)

In precise relative GPS positioning, like in many geodetic applications, the data are routinely processed using a least-squares algorithm, either in batch or in recursion mode as a Kalman filter implementation. The least-squares principle requires the specification of a functional relation between observations. The full probability density function of the observed data is not needed for estimating the parameters. This function, however, is needed to interpret the precision of the estimators. Next, a statistical testing procedure for integrity monitoring to spot outliers and cycle slips in the data does rely directly on the probability distribution. And thirdly, also making probabilistic inferences for resolution of the ambiguities requires knowledge of the probability density function of the data. In this contribution we will analyse the probability distribution of GPS data. The analysis is based on the least-squares residuals, as a time-series at 1-second rate, per channel (satellite), per epoch and per observation type, from a coordinates and ambiguities constrained solution. We consider data from several state of the art geodetic receivers, used in different experiments like a zero baseline and an ordinary baseline in the field. Statistical tests known from literature are used to indicate and quantify by the level of significance, whether the normal probability density function is a reasonable model for the distribution of GPS code and phase data. The preliminary conclusion is that fortunately, this seems to be the case indeed, although the conclusion's validity may be restricted to certain circumstances. In addition the findings will be supported by some graphical analysis.

G1/W/42-A3

1120

**ON THE ACCURACY AND RELIABILITY OF NEAR REAL-TIME GPS PHASE OBSERVATION AMBIGUITIES**

Hansjoerg KUTTERER (University of Karlsruhe, Geodetic Institute, Englerstrasse 7, D-76128 Karlsruhe, Germany, email: kutterer@gik.uni-karlsruhe.de)

During the past decade the integer fixing of the GPS carrier phase ambiguities has been studied in a variety of papers. The available techniques are more or less sophisticated regarding the selection of the possible solutions contained in the ambiguity search space and, consistently, of the reduction of the observation epochs necessary for the unique solution. As incorrect solutions may occur, it is indispensable to study their impact on the coordinate estimates and accuracies. Thus, quality issues concerning the ambiguity resolution techniques are both of practical and theoretical interest.

The paper focuses on the theoretical aspects of the near real-time case with short baseline lengths. The float ambiguity solution is restudied giving new insight in the composition of the ambiguity search space. In addition, an approach is outlined for describing the accuracy of the ambiguities regarding their integer nature. Finally, reliability aspects are considered taking possibly incorrect ambiguity solutions into account.

G1/L/07-A3

1140

**APPLICATION OF GEODESY TO ENGINEERING - NEW TRENDS**

O. Univ.-Prof. Dr.-Ing. Heribert KAHMEN (University of Technology Vienna, Institute of Geodesy and Geophysics, Dept. of Applied and Engineering Geodesy, Gusshausstrasse 27, 29/E128/3, A-1040 Vienna, email: Heribert.Kahmen@tuwien.ac.at)

Rapid developments in engineering have greatly changed both instrumentation and methodology in engineering geodesy. To document the body of knowledge in this field and to encourage new developments, IAG Spec. Com. 4 was established. To accomplish these objectives working groups did research work in areas of current interest. This paper presents some highlights of the activities.

Multi sensor systems have become an emerging trend in mapping applications because they allow a task-oriented implementation of geodetic concepts at the measurement level. To fulfill the need for up-to-date inventory and georeferenced data along transportation routes two developments are of especial interest: Digital imaging and precise navigation with respect to geodetic reference systems.

Concepts for new structures-bridges, towers, buildings - break barriers of scale in span or height. Technically, the lateral and vertical deflections and the dangerous vibrations must be studied. Therefore, another topic dealt with the development of georeferenced measurement systems and the investigation of the mathematical and physical models of the kinematic systems. Another challenging topic was: Traffic and guidance control and autonomous vehicle navigation. Digital maps are a key technology all traffic information and navigation systems. In the future an information service provider for accurate complete up-to-date and in time available information with precise geometrical attributes will be of great interest.

### G1/L/11-A3 1200

#### RE-WEIGHTING OF GPS BASELINES FOR VERTICAL DEFORMATIONS ANALYSIS

Henk DE HEUS, Marcel Martens, Hans van der Marel (Delft University of Technology, Thijsseweg 11, 2629 JA Delft, The Netherlands, email: H.M.deHeus@geo.tudelft.nl)

In the Netherlands GPS is used to monitor subsidence caused by extraction of natural gas. GPS campaigns are organised on a yearly basis. Each campaign consists of GPS observations on 30 to 60 points, using typically 5 dual frequency GPS receivers. The duration of a session is between one and two hours, but as every point is observed several times, up to 56 sessions have been observed for each campaign. The area is about 75 by 60km, resulting in an average baseline length of 10 km. The GPS data is processed using a stepwise - iterative - approach. First the GPS data is processed session by session. Then the sessions are combined, using their full co-variance matrix in a network adjustment. The network adjustment is used to estimate the proper variance of the GPS observations. This involves removal of outliers using statistical procedures, estimation of variance components, re-scaling and reprocessing of the GPS sessions. The best results are obtained using L1 and L2 phase data with an ionospheric constraint determined from the network adjustment, and using distinct weighting factors for the horizontal and vertical components. The precision of the heights after the network adjustment is on the average 6 mm for individual campaigns. This has been confirmed by independent levelings.

### G1/E/62-A3 1220

#### STOCHASTIC MODELLING OF THE IONOSPHERE FOR FAST GPS AMBIGUITY RESOLUTION

Dennis ODJIK (Department of Mathematical Geodesy and Positioning, Delft, University of Technology, Thijsseweg 11, 2629 JA Delft, The Netherlands, email: D.Odijk@geo.tudelft.nl)

Integer carrier phase ambiguity resolution is the key to precise GPS positioning. For baselines with a length up to 100km the errors due to the ionosphere are a limit for the ability to resolve the integer ambiguities within the shortest observation time span. One can of course estimate the ionospheric delays, but due to the extra unknowns in the model the shortening of the time span will be limited. On the other hand very short time spans can be reached by not estimating the delays at all, but only if the ionospheric delays in the data are within certain bounds. In this contribution the effect is investigated of a priori weighting of the ionosphere on integer ambiguity resolution with LAMBDA. Stochastic modelling of the ionosphere can mathematically be regarded as the addition of pseudo observations to the model of GPS observation equations, together with a variance matrix in which the uncertainty of the ionospheric delays is modelled. Note on the one hand that if "infinite" weights are used for these ionospheric pseudo observables, we get the model in which no ionospheric delays are estimated. On the other hand if these observables are not weighted at all, the model in which the ionospheric delays are estimated is obtained. Stochastic modelling in a way interpolates between these two "extreme" models and for a medium-length baseline it will be shown that with this technique it is possible to get the correct integer ambiguities within a shorter time span than with the model in which the ionospheric delays are considered as completely unknown.

## Wednesday 21 July PM

Presiding Chairs : Y. Bock (SCRIPPS, San Diego, USA),  
F.K. Brunner (TU Graz Austria)

### G1/W/37-A3 1400

#### FINAL REPORT BY SSG 1.158: GPS ANTENNA AND SITE EFFECTS

Jan JOHANSSON (Onsala Space Observatory, Chalmers University of Technology, SE-49392 Onsala, Sweden, email: jmj@oso.chalmers.se)

The improvement in precision obtained in GPS observations over recent years has revealed some problems related to the local conditions at the GPS site. In order to further improve precision investigations of site dependent effects and GSP antennas are required. The objectives for Special study group 1:158 were to provide information and recommendations regarding: the characteristics of different GPS based on measurements in anechoic chambers, field experiments, and numerical evaluation; the influence of electromagnetic scattering (including multipath) on the antenna characteristics; the effects of using different types of antennas in the same network; design and testing of new GPS antennas; elimination of radio interference; monumentation and establishment of permanent stations including construction of pillars and monitoring of their long-term stability; glassfiber radomes used to protect permanently installed antennas; the influence of snow, rain, and local atmospheric conditions. Here, we review some of the problems associated with site-specific errors and present recommendations on how to eliminate or minimize these effects.

### G1/E/34-A3 1420

#### THE IMPACT OF GPS ANTENNA PHASE CENTER VARIATION ON HEIGHT ACCURACY

Chun-Sung CHEN (Department of Civil Engineering, National Chiao Tung University, Hsinchu 30050, Taiwan, R.O.C., email: ccs@cc.nctu.edu.tw); Yi-Jau Chen (Department of Civil Engineering, National Chiao Tung University, Hsinchu 30050, Taiwan, R.O.C.)

The precise point of a station whose position is being measured using GPS surveying is generally assumed to be the phase center of the GPS antenna. However, the phase center of a GPS antenna is neither a physical point nor a stable point. For any given GPS antenna, the phase center is varied according to the direction of the signal from a satellite. Therefore, the variation of the GPS antenna phase center is very complicated. Besides, the phase center variations are antenna-type-dependent. This effect has to be carefully modified when different types of antennas are used simultaneously. Ignoring these phase center variations can lead to serious (up to 10 cm) vertical errors that are independent on the baseline length. Even if the same types of antennas are used, the main effect is a scale factor up to about 0.015ppm. In this study, the antenna phase center drifts and variations using GPS data will be estimated. The results of GPS height measurements with phase center corrections and no corrections will be compared. Besides, a feasible method to calibrate antenna phase center and a correction model is suggested.

### G1/W/28-A3 1440

#### MITIGATING MULTIPATH ERROR USING SEMIPARAMETRIC MODELS FOR HIGH PRECISION POSITIONING

Minghai JIA, Maria Tsakiri, Mike Stewart (all at School of Spatial Sciences, Curtin University of Technology, GPO Box U 1987 Perth WA 6845, Australia, email: jia@vesta.curtin.edu.au)

Multipath delay is a dominant error source of the double differential GPS observation data in short distance GPS models. Although important progresses to feature and mitigate the impact of the multipath errors on the positioning results, more practicable methods need to be developed.

A major obstacle to mitigate the multipath errors is how to model those errors. Since the multipath errors results from the mixture of many reflected signals, it is very difficult to model those error with the existing parametric methods. We have developed a semiparametric model to model and mitigate those error. Semiparametric model is a new mathematical tool developed in the last decade. In the semiparametric model, the multipath errors can be considered as a complicated function without caring the parameters and the pattern of the function. Using penalised least squares principle, the function and other parameters, such as site coordinates, can be estimated simultaneously. Trial results have shown that the multipath errors can be efficiently estimated and can be reduced to the level of the receiver noise.

### G1/E/58-A3 1500

#### THE IMPACT OF THE ATMOSPHERE ON WADGPS

Stefan SCHAER, Markus Rothacher (both at Astronomical Institute, University of Berne, Sidlerstrasse 5, CH-3012 Berne, Switzerland, email: stefan.schaer@aiub.unibe.ch); Urs Wild, Adrian Wiget (both at Federal Office of Topography, Seftigenstrasse 264, CH-3084 Wabern, Switzerland, email: urs.wild@lt.admin.ch)

The Swiss Federal Office of Topography is currently building up the Automated GPS Network for Switzerland, called AGNES. This GPS network will serve various purposes, like national surveying, engineering surveying, navigation, meteorology, and research. For Wide-Area Differential GPS (WADGPS), in particular precise real-time positioning using the GPS phase data of one or more reference stations of the AGNES network, one may expect that atmospheric refraction plays the crucial role, since the reference stations may be rather widely separated in Switzerland, typically by 50-100 kilometers. In the time period of the next solar maximum, the ionospheric refraction will probably be the most crucial error source, in particular for resolving the initial phase ambiguities, which is mandatory when aiming at accuracies on the centimeter-level. Nowadays, global and regional total electron content (TEC) maps, like those produced by the Center for Orbit Determination in Europe (CODE), are available and may be used to model the mean ionospheric refraction. However, on time scales of few minutes, ambiguity resolution usually suffers from short-term ionospheric fluctuations which are not accounted for by such TEC maps. Significant height differences with respect to the nearest reference stations may also occur, especially in mountainous areas like Switzerland. This implies that mismodeled tropospheric refraction may cause biases too. Therefore, we will monitor ionospheric as well as tropospheric biases, study their impact on WADGPS results, and investigate whether it is possible to extract atmospheric information from the AGNES network for correcting the data of mobile GPS receivers in (near) real time.

### G1/W/24-A3 1520

#### IMPROVING THE MODELLING OF ATMOSPHERIC DELAY USING METEOROLOGICAL DATA ASSIMILATION MODELS

D. S. MacMILLAN (NVI, Inc./Goddard Space Flight Center, Greenbelt, MD 20771, USA, email: dsm@leo.gsfc.nasa.gov); C. Ma (NASA Goddard Space Flight Center, Greenbelt, MD 20771, USA)

We have investigated using meteorological data assimilation models to correct tropospheric delay models in space geodetic analysis. We considered two sources of modelling error: the mapping function that gives the elevation dependence of the delay and the gradient model that describes the azimuthally asymmetric part of the delay. From analysis of radiosonde profile raytracings, the uncertainty of the site vertical due to current mapping functions is about 5-9 mm for the hydrostatic and about 3-4 mm for the wet assuming a wet delay of 10 cm. To more accurately determine the mapping function and its short-term variation, it is necessary to have information about the atmospheric profile above a site. We have therefore determined site-dependent mapping functions by raytracing atmospheric profiles derived by interpolation of gridded global data assimilation data. The hydrostatic mapping functions were then applied in the analysis of VLBI data. On tests with VLBI data from 20 CONT94 R&D experiments (January 1994), the baseline length repeatabilities were improved by about 0.2 ppb from 0.7 ppb. Raytracing of atmospheric data is not always practical, for example, in the analysis of daily GPS data from hundreds of sites. We consider site-dependent seasonal models derived from the assimilation model data and various approximations to full raytracing of atmospheric profiles.

Unmodeled atmospheric refractivity asymmetries can produce large errors in geodetic analysis. Typically gradient estimates from VLBI data, which typically have rms variations of about 45 mm at a 5 deg elevation angle, are correlated with gradients computed from data assimilation models with correlation coefficients of about 0.5-0.6. We investigate the use of the assimilation model gradients as an a priori estimate in the geodetic analysis.

### G1/L/03-A3 1540

#### ACHIEVEMENTS, TRENDS AND RESEARCH OPPORTUNITIES IN POSITIONING

Fritz K. BRUNNER, (Engineering Surveying and Metrology, Technical University of Graz, Steyrergasse 30, A-8010 Graz, Austria, email: brunner@aig.tu-graz.ac.at)

Currently Positioning is concerned with the scientific aspects of the following topics: measurement and analysis of regional and global geodetic networks, satellite and inertial positioning and applications of geodesy in engineering. Tremendous advances of GPS surveying have occurred especially in precision and applicability. Furthermore, GPS measurements have shown the potential to be used as a remote sensing tool of atmospheric parameters.

Traditionally the research in Positioning has been driven by the needs of National Survey Organisations and the geodetic community. However, it appears that the availability of better hardware and the nearly unlimited computational capabilities of today, allow the development of new geodetic methods for novel applications. Geodetic GPS arrays are already the backbone of crustal motion studies, development of new survey systems, deformation monitoring systems, and remote sensing systems of water vapour and electron content in the atmosphere. Fusion of data from GPS and other sensors will allow the development of new monitoring and positional control systems for engineering applications. A scenario for the future of Positioning and associated research opportunities will be discussed.



**G1/E/48-A3** Poster **1620-01****EFFECTS OF AURORAL IONOSPHERIC DISTURBANCES ON DGPS POSITIONING ACCURACIES**

Susan SKONE (Department of Geomatics Engineering, University of Calgary, 2500 University Dr. NW, Calgary, Alberta T2N 1N4, Canada, email: sksone@ensu.ucalgary.ca); M. Elizabeth Cannon (Department of Geomatics Engineering, University of Calgary, 2500 University Dr. NW, Calgary, Alberta T2N 1N4, Canada, email: cannon@ensu.ucalgary.ca)

GPS satellite signals must travel through the dispersive ionosphere prior to being received at the Earth's surface, causing ranging/positioning errors dependent on both the given signal frequency and ionosphere electron content. This effect is the single largest source of GPS positioning error (up to tens of metres), outside of Selective Availability (errors intentionally imposed by the U.S. military). Ionosphere range errors may be mitigated through the use of differential GPS (DGPS) positioning algorithms, where range corrections are calculated at reference stations and transmitted to remote users. Accuracies of such differential techniques depend on the spatial decorrelation of ionospheric TEC, which can be significant in regions characterized by geomagnetic storm and substorm events, such as the auroral zone. These effects are expected to increase in the next few years, approaching solar maximum, with corresponding degradations in DGPS positioning accuracies. In this paper the spatial decorrelation of ionospheric range delay errors, and corresponding effects on DGPS positioning accuracies, are investigated during several recent geomagnetic substorm events at high latitudes. These events are representative of intense effects at solar maximum. Periods of auroral disturbances are identified from ground-based and space-borne magnetometer measurements and ultraviolet images. GPS observations are provided by the Natural Resources Canada wide area network, allowing extensive coverage of the auroral region.

**G1/W/01-A3** Poster **1620-02****IONOSPHERIC CALIBRATION CONSIDERING THE SATELLITE AND RECEIVER L1/L2 DIFFERENTIAL DELAY EFFECT ON SINGLE FREQUENCY GPS USERS**

Cajun XU (School of Geo-Science & Surveying Engineering, Wuhan Technical University of Surveying and Mapping, 129 Luoyu Road, Wuhan, 430079, China, email: cjxu@hpb1.wtsum.edu.cn); Yong-qi Chen (Dept. of Land Surveying & Geo-Informatics, The Hong Kong Polytechnic University, Hung Hom, Kowloon, Hong Kong, email: lsyqchen@polyu.edu.hk); Jingsong Huang (Engineering Research Center for Satellite Positioning System, Wuhan Technical University of Surveying and Mapping, 129 Luoyu Road, Wuhan, 430079, China, email: huang@public.wh.hb.cn)

Since the ionosphere acts as a dispersive medium to GPS signals, dual-frequency(L1 at 1575.42MHz,L2 at 1227.60MHz) GPS receivers can eliminate(albeit to the first order) ionospheric delay through a linear combination of the L1 and L2 observations. However, this option is not available to single-frequency GPS receiver users. This kind of users needs an ionospheric model or ionospheric delay from GPS dual-frequency receiver at reference station in order to eliminate the ionospheric delay from the single-frequency measurement. However, both the satellite and receiver differential delay biases introduce error in the measurement of TEC or ionospheric delay (Coco et al., 1991, E. Sardon et al., 1994, Wilson, 1994, L.-S. Lin et al., 1996). They may result in an error of 9 TECU and 30 TECU respectively (Wilson et al., 1994). Without calibrating for this satellite and receiver differential delay, it is impossible to obtain precise TEC and ionospheric delay estimation from GPS measurements. Considering this factor, the satellite-plus-receiver (SPR) differential delays and ionospheric delay in real time at the DGPS universal reference stations in Hong Kong area are calculated, and they are applied to single-frequency GPS measurements in mobile stations. These mobile stations are used to gather GPS raw data, their distances to the DGPS universal reference stations are about 10km to 37km, the span time of gathering GPS data are about one hour to two hours. The results of ionospheric calibration considering SPR differential delay effects on single-frequency GPS positioning are discussed in the paper.

**G1/W/04-A3** Poster **1620-03****THE IMPACT OF RADOMES ON GPS HEIGHT ESTIMATES**

Klaus KANIUTH, Klaus Stuber (Deutsches Geodätisches Forschungsinstitut, Marstallplatz 8, D-80539 Muenchen, Germany, email: kaniuth@dgfi.badw.de)

GPS height estimates are sensitive to a number of modelling and processing strategy variations. These include the adjustment cut-off angle setting, the troposphere prediction model in combination with the applied mapping function and the selected antenna phase center variation model. In addition, during the past few years some time series of GPS position determinations showed significant jumps in the height estimates of up to several centimeters as a consequence of setting up or dismantling an antenna radome.

In order to contribute to the understanding of the interaction between protective radomes and the height estimation, we analyze in this paper the data set of a dedicated experiment as well as data collected by some permanently operating GPS stations. The analysis comprises several modern geodetic receiver/antenna systems and radomes either supplied by the manufacturers or individually designed by scientific institutions.

**G1/W/07-A3** Poster **1620-04****GPS AT TIDE GAUGES: IS MULTIPATH DUE TO WATER SURFACES A CONCERN?**

Volker Janssen, Chris Rizos, Shaowei Han (School of Geomatic Engineering, The University of New South Wales, Sydney, AUSTRALIA)

A geodetic application receiving increased attention these days is the use of the GPS technology to survey tide gauge benchmarks in support of studies relating to sea level change. While such an application can be addressed using "conventional" GPS Geodesy techniques, whereby dedicated survey campaigns are carried out to collect epoch data subsequently processed using scientific GPS software, proposals have been made to install permanent GPS receivers at the tide gauge sites themselves. However, rather than monitor the tide gauge benchmark itself (which is generally located some distance from the tide gauge sensor), it has been suggested that the GPS antenna be installed right next to the tide gauge sensor. In such a configuration the antenna is often surrounded by the water surface. This paper presents the results of a study on how a GPS receiver, equipped with choke ring antenna, is affected by reflected signals from the water surface. Such multipath affects may need to be accounted for if ultra precise height estimates are to be obtained using the GPS technology.

**G1/W/13-A3** Poster **1620-05****AMBIGUITY RESOLUTION FOR PRECISE GPS/GLONASS POSITIONING**

Jinling WANG, Mike Stewart, Maria Tsakiri, Troy Forward (School of Spatial Sciences, Curtin University of Technology, GPO Box, U1987 Perth, WA 6845, Australia, email: Wang@vesta.curtin.edu.au)

When processing GLONASS or GPS/GLONASS carrier phases, the standard double-differencing (DD) procedure cannot cancel receiver clock errors due to the multiple frequencies of the GLONASS carrier phases. Consequently, the resulting normal matrix becomes singular. To deal with this problem, some methods have been proposed in the literature. These methods, however, rely on the use of pseudo-ranges. As contaminated by multi-path and hardware delays, biases in the pseudo-ranges are significant and may result in unreliable ambiguity resolution. This paper will address some critical issues in GPS/GLONASS ambiguity resolution. Firstly, both existing mathematical and stochastic modelling methods are critically reviewed and feasible modelling methods are identified. Secondly, a new approach for GPS/GLONASS ambiguity resolution is presented. Thirdly, a quality control procedure for GPS/GLONASS ambiguity resolution is discussed. Testing results of ambiguity resolution for GLONASS and combined GPS/GLONASS positioning will be demonstrated.

**G1/W/16-A3** Poster **1620-06****THE GIL NETWORK OF CONTINUOUS GPS MONITORING IN ISRAEL FOR GEODETIC AND GEOPHYSICAL APPLICATIONS**

Shimon WDOWINSKI (Department of Geophysics and Planetary Sciences, Tel Aviv University, Ramat Aviv, Israel, email: shimon@geol.tau.ac.il); Yehuda Bock (Institute for Geophysics and Planetary Physics, Scripps Institution of Oceanography, University of California, San Diego, USA, email: ybock@ucsd.edu); Yosef Forrai, Yosef Melzer (both at Survey of Israel, 1 Lincoln St, Tel Aviv, Israel, email: forrai@soi.gov.il, melzer@soi.gov.il); Gideon Baer, Dov Levitte (both at Geological Survey of Israel, 30 Malchai Israel St, Jerusalem, Israel, email: baer@mail.gsi.gov.il)

GIL (GPS in Israel) is a network of 10 continuous GPS stations, in which 7 stations are operating and the additional 3 stations will be operative before 8/2000. The network is built, maintained, and operated by researchers from Tel Aviv University, Scripps Institution of Oceanography, the Survey of Israel and the Geological Survey of Israel and is funded by the Israel Space Agency and by the Survey of Israel. It provides a reference network for precise GPS measurements in Israel and serves basic and applied research, including (1) monitoring plate motion and crustal deformation across the Dead Sea Fault, and (2) mapping atmospheric water vapor content. Preliminary results from 18 months of continuous GPS measurements reveal that the current displacement rate between Tel Aviv and Katerin (Golan) is 2.34±0.9 mm/yr, reflecting interseismic deformation across the Dead Sea Fault due to 5-6 mm/yr of relative motion between the Sinai and Arabian plates. Further collection, processing and analysis of the GIL network data can verify the preliminary results in a higher confidence level and will provide a detailed description of the current deformation pattern along the Dead Sea Fault.

**G1/W/18-A3** Poster **1620-07****SYSTEMATIC EFFECTS IN GPS DOUBLE DIFFERENCE PHASE RESIDUALS**

Juan MOIRANO (Facultad de Ciencias Astronomicas y Geofisicas, Universidad Nacional de La Plata, Paseo del Bosques s/n, 1900 La Plata, Argentina, email: jmoirano@fcalp.fcalp.edu.ar); Klaus Kaniuth (Deutsches Geodätisches Forschungsinstitut, Marstallplatz 8, D- 80539 Muenchen, Germany, email: kaniuth@dgfi.badw.de)

Compared to the precision resulting from the least squares adjustment or from solution repeatabilities the accuracy of GPS positioning estimates may be worse by up to one order of magnitude. This degradation is due to modelling errors which will not show up in the adjustment results as long as network geometry, processing strategy and models remain unchanged. However, systematic structures in the adjustment residuals may be indicators of modelling errors and may help identifying the responsible error sources. Therefore, this paper analyzes a large number of double difference phase residuals series resulting from adjustments using the Bernese GPS software 4.0. The analysis comprises most of the presently available geodetic receiver and antenna systems and data sets acquired in regional and local networks in Europe and South America. Particular emphasis is put on identifying tropospheric refraction asymmetries, mapping function errors as well as phase center variation model discrepancies.

**G1/W/21-A3** Poster **1620-08****THE AUTOMATED GPS NETWORK FOR SWITZERLAND (AGNES)**

Urs WILD, René Hug, Thomas Signer, Adrian Wiget (Swiss Federal Office of Topography (S+T), Seftigenstrasse 264, CH-3084 Wabern, email: urs.wild@lt.admin.ch)

The Swiss Federal Office of Topography (S+T) is establishing a network of permanent GPS track-ing stations in Switzerland, named the Automated GPS Network for Switzerland (AGNES). The main goals of AGNES are:

- Reference for national and engineering surveys
- Reference for differential navigation applications
- Research (geodynamics, atmosphere)

Currently 9 stations are already operating and the network will be densified according to the needs for real-time kinematic (RTK) applications using an adapted WADGPS approach for phase observations.

The poster outlines the general concept of AGNES, describes the station hard- and software and gives first results of the daily geodetic processing (including the estimation of troposphere parameters) as well as of the first field tests for RTK applications using GSM mobile phones.

**G1/W/23-A3** Poster **1620-09****PRECISION GPS/GLONASS GEODETIC ANTENNA CALIBRATIONS**

Thomas A. CLARK (Laboratory for Terrestrial Physics, NASA/GSFC, Greenbelt MD 20771 USA, email: clark@tomcat.gsfc.nasa.gov); Bruce R. Schupler (AlliedSignal Technical Services Corp., Lanham, MD 20706, USA, email: schuplb@thorin.atsc.allied.com)

For a number of years, we have used the microwave anechoic chamber at GSFC for a series of calibrations of antenna parameters which impact the accuracy of GPS geodetic observations. These include the geometric location of the antenna's phase center, amplitude and polarization responses, and the effects of objects in the vicinity of the antenna. Last year, the indoor antenna range was completely refurbished with new microwave instrumentation, data acquisition system, and a more stable antenna positioner. We report on measurements

made with the new antenna range and compare them to our earlier published results. The new capabilities have allowed us to extend the frequency coverage to span the entire 1.2-1.6 GHz band used by GPS and GLONASS. We report on the measured phase center variations of standard "DM" geodetic choke ring antennas (designed by JPL and used at many permanent IGS GPS stations) over the full ~40 MHz bandwidth of L1 and L2 GPS and GLONASS signals, and at the possible new L3 frequencies. Our earlier presentations included measurements designed to understand effects of "real world" conductive and dielectric objects in the near-field of the antenna such as mechanical mounting fixtures, protective radomes, and the antenna's mounting pier. We report on new measurements of these effects that our new anechoic chamber capabilities have allowed us to emulate.

**G1/W/25-A3** Poster **1620-10**

**A SOLUTION OF THE ON-THE-FLY DUAL-AMBIGUITY-PROBLEM FOR LONG BASELINES**

Stefan LEINEN (Institute of Physical Geodesy, Petersenstr. 13, 64287 Darmstadt, Germany, email: stl@ipgs.ipg.verm.tu-darmstadt.de)

Kinematic applications of GPS, aiming at highest accuracy, require a reliable ambiguity resolution On-the-Fly. In case of long baselines (25 km and more) the ionosphere free linear combination of phases has to be applied to remove the major error effect, namely the ionospheric refraction. Before this the dual-ambiguity-problem has to be solved completely. By a complete solution of the dual-ambiguity problem the determination of the ambiguities of both the L1- and L2-phases is meant. In case of long baselines this is usually done in two steps: at first the correct set of wide lane ambiguities is identified by some kind of search algorithm. Keeping these wide lane ambiguities fixed the common approach is to resolve the narrow lane ambiguities in the second step. This step is the critical and limiting aspect of this approach due to large residual error effects in the observable compared to wavelength. In this presentation a discussion of this narrow lane problem and the inherent error effects will be given. A mathematical model revealing the drawback of this narrow lane method compared to other phase linear combinations will be presented. This leads to an alternative strategy with solving for the ambiguity of a phase linear combination better suited than the narrow lane. Additionally the superiority of the new method will be shown by results of various experiments and real data evaluations.

**G1/W/27-A3** Poster **1620-11**

**IONOSPHERE-INDUCED-RAY-PATH BENDING EFFECTS IN PRECISION SATELLITE POSITIONING SYSTEMS**

Victor H. RIOS (Laboratorio de Técnicas Satelitales, Instituto de Física, UNT, Avenida Independencia 1800 (4000), San Miguel de Tucumán, Argentina); Norbert Jakowski (DLR/DFD Remote Sensing Station, Neustrelitz, Germany)

In precise satellite-based positioning systems, propagation errors represent a major factor in the measurement accuracy. Due to the dispersive properties of the ionosphere, first order effects may easily be eliminated with dual frequency receivers. The aim of this paper is to discuss refraction-induced errors due to ray path bending. Although relatively small, such errors may play a certain role in geodetic applications particularly since they are not completely compensated by linear difference methods commonly used. Numerical ray-tracing methods were used to determine the excess path length as a function of both, geometrical - as well as medium-describing parameters. The analysis takes into account a large number of samples covering a wide range of variability in geometry and ionospheric behaviour. The derived quasi-empirical formulas for estimating the excess path length need only a few parameters. The results are discussed in relation to their possible use in satellite navigation systems such as NNSS, DORIS, and GPS over Argentina.

**G1/W/29-A3** Poster **1620-12**

**PRECISE REAL TIME POSITIONING IN REGIONAL GPS REFERENCE STATION NETWORKS UNDER THE INFLUENCE OF INCREASING IONOSPHERIC ACTIVITIES**

Stefan WILLGALIS (Institut fuer Erdmessung, University of Hannover, 30165 Hannover, Schneiderberg 50, Germany, email: willgalis@mbox.ife.uni-hannover.de); Cord-Hinrich Jahn (Landesvermessung + Geobasisinformation Niedersachsen, 30659 Hannover, Podbielskistr. 331, Germany, email: jahn@lgn-3.h.uu.net.de)

Within the research project HPPS II a network of DGPS reference stations with an average spacing between 40 and 60 km is being set up in Lower Saxony. Carrier phase based precise differential (PDGPS) corrections are provided in real time. Targeting the 1 cm accuracy, this reference network is built to satisfy the precise positioning needs for land and cadastral surveys as well as for precision navigation in various applications. Critical for precise real time positioning are ionospheric disturbances. The upcoming maximum of solar cycle 23 predicted for 2000/2001 will make this situation even worse. Depending on the distance from the nearest reference station, the positioning accuracy will be degraded, and ambiguity fixing in real time will be impeded - if not impossible. To minimize the ionospheric error, as well as other distance dependent errors, the reference stations are interlinked, i.e. the differential corrections are exchanged, coefficients for network correction are computed, and transmitted to the user. Results of measurements in the Lower Saxony test network, which show the influence of ionospheric activities, will be presented. Solutions derived from standard differential corrections will be compared with positioning results obtained from network corrections.

**G1/W/30-A3** Poster **1620-13**

**THE DESIGN AND APPLICATION OF DATA PROCESSING AND SOFTWARE FOR THE GPS AUTOMATIC MONITORING SYSTEM FOR DAM DEFORMATION**

Jingnan LIU, Shaoquan Xu, Zhenghang Li, Kongzhe Chen, Weiping Jiang, Liwen Dai (School of Geoscience and Surveying Engineering, Wuhan Technical University of Surveying and Mapping, 129 Luoyu Road, Wuhan 430079, China, email: jnliu@wtusm.edu.cn)

This article expounds a general method of designing GPS automatic monitoring system for the external deformation of concrete dam in hydroelectric power stations, especially the design scheme of automatic data acquisition, processing, management, analyzing and relevant systemic software. It introduces an important example of the application of this scheme: in one of the crucial branches of Yangtse River - Qingjiang River in Hubei Province - a GPS automatic monitoring system for external dam deformation has been established in the Geheyan reservoir there. After 18 months of continuous operation, especially during the period of the unusual flood in Yangtse River in 1998, it is testified that this design scheme can meet the request of technical specification for dam deformation monitoring. With this scheme, the availability can reach 99.95%, and the reliability can reach 96%. The accuracy for determination of horizontal deformation is higher than  $\pm 1$ mm, and the accuracy for determination of vertical deformation is higher than  $\pm 1.5$ mm, based on 2 hours of GPS static monitoring data. The response time of automatic data processing and analyzing is less than

10 min. This GPS automatic monitoring system for dam deformation has played a key role in the unusual flood of Yangtse River in 1998. Under its continuous real time monitoring, sluice level of Geheyan was 4 meters higher than prescriptive water level and the external dam deformation reached 16mm, which is still within the security limitation after examination. Thus it insured the sequent over-water-level sluice in Geheyan reservoir and the success of staggering the overlap of the two flood peaks in the Qingjiang River and in Yangtse River.

**G1/W/31-A3** Poster **1620-14**

**TROPOSPHERIC EFFECTS IN GPS SURVEILING EXPERIENCE**

Domenico Sguerso, Paolo ZATELLI (Dpt. Ingegneria Civile e Ambientale, Università degli Studi di Trento Via Mesiano 77, 38050 Trento, Italy, email: domenico.sguerso@ing.unitt.it, paolo.zatelli@ing.unitt.it)

A cinematic GPS campaign applied to navigation for environmental monitoring has been carried out to investigate air quality and meteorological variable sampling by airborne surveying. Several flights at different altitudes over the Trento city in Val d'Adige (Italy) are performed. The different survey steps are described, from instrumentation installation to GPS data collection and processing. The emphasis is on the detection and the recovering from significant tropospheric, multipath and phase centre variation effects.

**G1/W/32-A3** Poster **1620-15**

**VARIABILITY OF GPS ERRORS ON-SITE - INVESTIGATIONS OF ANTENNA PCV AND MULTIPATH TOWARDS A STATION CALIBRATION**

Volker BOEDER, Falko Menge, Guenter Seeber (Institut fuer Erdmessung, Universitaet Hannover, Schneiderberg 50, D-30167 Hannover, Germany, e-mail: boeder@mbox.ife.uni-hannover.de); Gerhard Wuebbena, Martin Schmitz (Geo++ GmbH, Steinriede 8, D-30827 Garbsen, Germany, e-mail: geopp@ibm.net)

The Institut fuer Erdmessung (IfE) and the Geo++ company extensively carry out research in the field of GPS antenna calibration. With the improving GPS precision the whole error budget 'on-site' demands increased attention, especially to antenna behavior and to multipath. One task is the absolute calibration (here done in the field) of the phase center variations (PCV) of the used antenna types. These results must be site-independent in order to have a model as precise as possible for a certain antenna type, which hence can be used everywhere. With the knowledge of PCV the next task is the verification and determination of multipath effects and its variability on 'on-site' observables and coordinates, which might be input for an adequate station dependent model. Since the results should be precise, consistent, reliable and be fast attainable, an automation is desirable. Therefore, the use of a robot is currently implemented for the field work. In this poster, several investigations and results concerning the variability of site dependent errors and steps towards a station calibration are presented.

**G1/W/33-A3** Poster **1620-16**

**DEFORMATION MONITORING USING SINGLE-EPOCH GPS DATA**

Mike STEWART (School of Spatial Sciences, Curtin University of Technology, GPO Box U 1987, Perth WA 6845, Australia, email: stewart@vesta.curtin.edu.au); Maria Tsakiri (School of Spatial Sciences, Curtin University of Technology, GPO Box U 1987, Perth WA 6845, Australia, email: tsakiri@vesta.curtin.edu.au)

Precise measurement of displacements of large structures is one of the most important activities in engineering surveying as results can indicate subtle damage that could be of concern to public safety. The use of permanent GPS positioning arrays can provide continuous and timely monitoring of deformations of multiple points but with a prohibitive cost for implementation if many localised points must be monitored. Instead, it is desirable to conduct episodic occupations of the points of interest whilst retaining many of the advantages of continuous monitoring. In practice, episodic monitoring using kinematic GPS techniques can be undertaken for a fraction of the expense of running a typical permanent antenna array but at the cost of a loss of the information and precision which may be obtained from permanent local arrays. This paper explores the resolution of single epoch GPS data for the episodic monitoring of large, slowly moving structures. Single epoch GPS data are supplemented by knowledge of the a priori location of the monitoring points and the mode of deformation to aid ambiguity resolution, solution quality and reliability. Data from an episodic GPS deformation monitoring regime on the North Dandalup dam in Western Australia is analysed. Since 1995, some 60 points have been monitored using GPS and conventional surveying techniques. The time interval between surveys has been approximately three months. Results using single epoch GPS carrier phase data are presented and compared with results from the conventional surveys.

**G1/W/35-A3** Poster **1620-17**

**PLANNING OF KINEMATIC GPS INCLUDING REALISTIC OBSTACLES DESCRIPTION**

Domenico SGUERSON, Paolo Zatelli (Dpt. Ingegneria Civile e Ambientale, Università degli Studi di Trento Via Mesiano 77, 38050 Trento, Italy, email: domenico.sguerso@ing.unitt.it, paolo.zatelli@ing.unitt.it)

A good planning is a key factor for the success of a GPS survey. A realistic forecast of the DOP requires to take into account the obstacles that can hide part of the sky. This is specially true in a mountainous region (natural obstacle) and in the urban area (artifact obstacle). In practice it is relatively easy to take into account the various obstacle in the planning of a static survey, but it is more difficult to do the same for a kinematic survey. In the present work an automatic procedure for the planning of a kinematic survey has been realized with a dedicated procedure inside a GIS. The realized procedure is interfaced with the almanac, a DHM for the planning in M.A. and a cartographic data base for the planning in urban areas (still in project) and computes the DOP with the standard algorithm for the points in a given trajectory.

**G1/W/40-A3** Poster **1620-18**

**RTK GPS POSITIONING USING MULTIPLE REFERENCE STATIONS**

Jinglin WANG, Mike Stewart (School of Spatial Sciences, Curtin University of Technology, GPO Box, U1987 Perth, WA 6845 Australia, email: Wang@vesta.curtin.edu.au)

Real-time kinematic (RTK) GPS positioning techniques have been widely used in surveying and navigation. In RTK GPS positioning, both measurement bias elimination and integer ambiguity resolution are critical issues. For short-range kinematic positioning, differencing GPS measurements collected from both roving and reference receivers can virtually cancel many measurement biases, such as satellite orbital bias, ionospheric and tropospheric biases,

and thus, integer carrier phase ambiguities can be easily identified. For long-range kinematic positioning, however, integer ambiguities become increasingly difficult to resolve as the residual biases in the differenced measurements are significant. To efficiently reduce the magnitude of residual biases, a RTK positioning strategy using multiple reference stations has been developed. Basic idea behind this positioning strategy is combining the measurements from precisely determined multiple reference stations to estimate and then correct the measurement biases.

Following a critical review of the existing methods, this paper will present a new approach to RTK positioning using multiple reference stations. An advantage of this proposed approach is that it fully exploits the intrinsic relationship between reference stations and thus, has an optimal performance in practical applications. Some preliminary results will be presented.

**G1/E/01-A3** Poster **1620-19**

#### PHASE CENTRE VARIATIONS IN HIGH PRECISION KINEMATIC GPS SURVEYS

Fritz K. BRUNNER, H. Hartinger, A. Wieser (Engineering Surveying and Metrology, Technical University of Graz, Steyergasse 30, A-8020 Graz, Austria, email: brunner@aug.tu-graz.ac.at)

For high precision kinematic GPS applications the phase centre variations (pcv) have to be taken into account. In general the pcv values depend on the horizontal and vertical angle-of-arrival of the signal with respect to the antenna, however, they are assumed to be equal for the same antenna type. In kinematic applications the orientation of the rover antenna in relation to the reference antenna may change and thus the pcv differences need to be considered. We present an experimental field set-up to verify whether two antennas have the same pcv and to measure the azimuthal pcv variations of antennas having different orientations. The pcv values are determined as single differences using a special GPS sensor system which allows the elimination of the receiver clock errors. The results of the experimental determination of the azimuthal pcv of several antenna types shall be presented.

**G1/E/06-A3** Poster **1620-20**

#### MITIGATION OF SIGNAL DIFFRACTION EFFECTS ON PRECISE GPS-POSITIONING

Lambert WANNINGER, Volker Frevert, Steffen Wildt (Geodetic Institute, Dresden University of Technology, D-01062 Dresden, Germany, email: Lambert.Wanninger@mailbox.tu-dresden.de)

GPS signal diffraction is a common error source in precise GPS positioning if obstructions exist above the antenna horizon. It occurs whenever the direct signal is obstructed but nevertheless a diffracted signal is received and processed. The longer propagation time of the diffracted signal causes carrier phase errors of up to several cm. A common characteristic of all diffracted signals is their weaker signal power as compared to the corresponding direct signal.

We have tested several weighting and selection algorithms for mitigation of signal diffraction effects on GPS data processing, i.e. on ambiguity resolution and on coordinate estimation. They are based either on the observed signal power level (e.g. the SIGMA-Delta weighting algorithm suggested by Brunner et al. 1998) or on the estimated observation residuals. The ability to automatically detect diffraction effects and to process the observation data accordingly significantly improves ambiguity resolution and GPS position accuracy.

**G1/E/08-A3** Poster **1620-21**

#### RAPID GPS AMBIGUITY RESOLUTION OVER MEDIUM RANGE DISTANCES

Paul DE JONGE, Yehuda Bock (both at Scripps Institution of Oceanography, University of California, San Diego, La Jolla, CA 92093-0225, USA, email: deJonge@lox.ucsd.edu)

Resolving the phase ambiguities is the key to fast high precision GPS positioning. The main factor preventing a successful estimation of the integer ambiguities, is the delay experienced by the signal while traveling through the ionosphere; more specifically, it is the difference in delay at the two end points of the baseline that is important. Some factors that may influence the size of the ionospheric delay are: geographical location, orientation of the baseline, diurnal cycle, 11-yearly sun spot cycle, and the length of the baseline.

In this contribution we show how different circumstances influence the ambiguity resolution for a number of baselines in Southern California with lengths of up to 100 km. The analysis was done using the MIT/SIO GPS processing software (GAMIT). The existing algorithm to form orthogonal observables from the phase observables and ionospheric pseudo-observables was extended to include also pseudorange observables to enable instantaneous positioning. For the integer estimation of the ambiguities, the Least-squares AMBiguity Decorrelation Adjustment method (LAMBDA) was implemented.

**G1/E/09-A3** Poster **1620-22**

#### PRECISE POSITIONING WITH THE USE OF JPS LEGASY GPS/GLONASS RECEIVERS AT THE REMOTE SITES OF RUSSIA

Javad ASHJAEE, Viktor Iodis, Andrey Maiorov, Konstantin Saliy, Pavel Tolkachev (all at Javad Positioning Systems, 1731 Technology Drive, San Jose, CA 95110, email: javad@javad.com); Gleb Demianov, Vladimir Kaftan, Viktor Kashaev, Nikolay Makarenko, Vladimir Zubinsky (all at Central Research Institute of Geodesy, Aerial Surveying and Cartography, Onezhskaya 26, 125413 Moscow, Russia)

Several JPS Legacy receivers were installed at the remote Russian sites Ekaterinburg, Yakutsk, Magadan and Petropavlovsk-Kamchatsky situated in Ural, Siberia and Far Eastern regions. GPS/Glonass observations were performed during the latest part of the IGEX98 field campaign in severe climate conditions. The observation points covered the large part of Russian territory which enabled to improve the homogeneity and global distribution of the IGEX98 stations. Some practical and instrumentation recommendations were made. The coordinate determination results are also discussed.

**G1/E/10-A3** Poster **1620-23**

#### THE ANTENNA CALIBRATION OF THE FINNISH PERMANENT GPS NETWORK (FINNREF)

Antti Kulkilahti, Hannu KOIVULA, Markku Poutanen (Finnish Geodetic Institute, P.O.Box 15, 02431 Masala, Finland, email: hannu.koivula@fgi.fi, markku.poutanen@fgi.fi)

The Finnish permanent GPS network (FinnRef) was established mainly to study the crustal deformations in Finland by the Finnish Geodetic Institute (FGI). One big unmodelled error source is the antenna phase centre variation. It contains of two components: phase centre offset and antenna phase centre variation (PCV). The purpose of this study was to determine the zenith angle dependent PCV and the vertical phase centre offset of nine stations of the FinnRef using the field calibration method. During summer 1998 FGI performed a test campaign and an actual field campaign to calibrate 9/12 antennas of the FinnRef. Data

processing the Bernese GPS software 4.0 was used. We describe both the test campaign and the field calibration campaign and show the results of the calibration.

**G1/E/16-A3** Poster **1620-24**

#### COMPARISON OF INDEPENDENTLY DERIVED ATMOSPHERIC PARAMETERS

Dirk BEHREND, Antonio Rius (both at Institut d'Estudis Espacials de Catalunya, Edif. Nexus-204, Gran Capita 2-4, 08034 Barcelona, Spain, email: behrend@ieec.fc.es); Lubomir P. Gradinarsky, Ruediger Haas, Jan M. Johansson (all at Onsala Space Observatory (OSO), Chalmers University of Technology, SE-439 92 Onsala, Sweden, email: geo@oso.chalmers.se); Stephen J. Keihm (Mail Stop 246-101, Jet Propulsion Laboratory, 4800 Oak Grove Drive, Pasadena, CA 91109, USA, email: Stephen.J.Keihm@jpl.nasa.gov)

Atmospheric parameters can be estimated using different space geodetic and remote sensing techniques. The stations Madrid (Spain) and Onsala (Sweden) have collocated equipment for space geodetic measurements using Very Long Baseline Interferometry (VLBI) and the Global Positioning System (GPS) and are equipped additionally with Water Vapor Radiometers (WVR).

Observations using these three micro wave techniques are affected by the atmospheric propagation delay of radio waves. Simultaneous observations with the three techniques allow the comparison of atmospheric parameters derived from each of the techniques. We will present a comparison of zenith wet delay and horizontal North and East gradients for simultaneous observation epochs for Onsala and Madrid. The GPS data will be analyzed using different software packages (GIPSY, GAMIT, Bernese). The results will be intercompared and compared to the results of other techniques. Apart from this an additional comparison with meteorological models will provide an independent check of the parameter retrieval.

**G1/E/19-A3** Poster **1620-25**

#### INTEGER AMBIGUITY SEARCH IN THE COORDINATE AND AMBIGUITY DOMAINS USING CONDITIONED ADJUSTMENT

Guochang XU (National Survey and Cadastre - Denmark Rentemestervej 8, DK-2400 Copenhagen NV, Denmark)

An integer ambiguity search method based on conditioned adjustment theory is proposed in this paper. This method has been implemented in a GPS software KSGSoft (Kinematic/Static GPS Software, developed in GFZ Potsdam) and used for extensive real data processing of EU project AGMASC0. The search can be carried out in coordinate domain or in ambiguity domain or in both domains by using this technique. The most published least squares ambiguity search methods are a special case of this algorithm, if only ambiguity search domain is selected and without considering the uncertainty of ambiguity. A general criterion for ambiguity searching is then obtained to ensure an optimal search result. Detailed formulas are derived and their usages are outlined.

**G1/E/20-A3** Poster **1620-26**

#### PRECISE REAL-TIME POSITIONING IN WADGPS NETWORKS

Günther RETSCHER (Department of Applied and Engineering Geodesy, Vienna University of Technology, Gusshausstrasse 27-29 E128/3, A - 1040 Wien, AUSTRIA, email: gretsch@pop.tuwien.ac.at); C H Jason Chao (Department of Land Surveying and Geo-Informatics, The Hong Kong Polytechnic University, Hung Hom, Kowloon, HONG KONG, e-mail: Ischchao@polyu.edu.hk)

Local DGPS services have been established all over the world for many different kind of applications. However, the main disadvantage of Local Area DGPS Systems (LADGPS) is that position accuracy of a user degrades as the reference-to-user separation increases. Therefore Wide Area DGPS Systems (WADGPS) are being developed to overcome the main drawbacks of LADGPS. The spatial decorrelation of the error sources, i.e. the atmospheric propagation and satellite orbit errors, are the main causes for the degradation of position accuracy. The combination of the measurements of several reference stations can be used to model these error components separately. To achieve position accuracies better than 5 m (95 %) the satellite orbits have to be determined with an accuracy of the order of 10 m using pseudorange data from three different reference stations and atmospheric models need to be estimated. For real-time positioning the orbit and atmospheric models need to be predicted ahead.

The covered area of the LADGPS system is also limited by the perceived range of the used HF/MF radio systems. Satellite based DGPS systems became both commercially and technically feasible with the introduction of broadcasting via geostationary satellites at the start of the decade; available services are e.g. Fugro OmniStar and Racal LandStar. A annual subscription service charge for the receiving of corrections has to be paid. Most users are completely satisfied with code DGPS services for horizontal positioning. However, for special applications and for vertical positioning accuracies on the decimetre or few centimetre level are required. Therefore real-time kinematic positioning with carrier phases and OTF (on-the-fly) ambiguity resolution strategies have to be applied.

**G1/E/40-A3** Poster **1620-27**

#### EXTRACTING IONOSPHERIC INFORMATION USING GPS MEASUREMENTS

Claudio Brunini (Facultad de Ciencias Astronómicas y Geofísicas, Universidad Nacional de La Plata, Buenos Aires, Argentina, email: claudio@fcaglp.fcaglp.unlp.edu.ar); María Andrea Van Zele (Facultad de Ciencias Exactas y Naturales, Universidad de Buenos Aires y CONICET, Buenos Aires, Argentina, email: avanzele@tango.gl.fcen.uba.ar); Amalia Meza (Facultad de Ciencias Astronómicas y Geofísicas, Universidad Nacional de La Plata, Buenos Aires, Argentina, email: ameza@fcaglp.fcaglp.unlp.edu.ar); Mauricio GENDE (Facultad de Ciencias Astronómicas y Geofísicas, Universidad Nacional de La Plata y CONICET, Buenos Aires, Argentina, email: mgende@fcaglp.fcaglp.unlp.edu.ar)

Signals from GPS satellites received at the surface of the earth have passed through the terrestrial atmosphere and are therefore affected by refraction in the ionosphere and the lower neutral atmosphere. In Geodesy and in Astrometry these refraction effects are typically seen as a nuisance and are removed from the measurements using appropriate models. The complementary point of view is that the refraction effects in GPS measurements contain useful information accumulated by passing through the atmosphere. In this scenario, the ionospheric and tropospheric delay are seen as remotely sensed data related to atmospheric parameters, with the possibility to recover some or all of these parameters through proper data analysis.

The main goal of this kind of ionosphere research is to make use the capability of these observations to continuously and routinely ionosphere monitoring at global scale. In particular, we will focus in the estimation of parameters describing the distribution of free electrons in the ionosphere and their changes along time. We describe the algorithms used to produce ionospheric global maps automatically. We analyse the GPS observations collected in some years by around forty earth stations globally distributed and we discuss the correlation between some estimators obtained from the ionospheric model and the geomagnetic and solar activity.



**G1/E/44-A3** Poster **1620-28**

**FAST AMBIGUITY RESOLUTION USING THE GPSEQ SOFTWARE**

Joco Francisco Galera MONICO, Wagner Carrupt Machado (both at Department of Cartography, Sao Paulo State University UNESP, Presidente Prudente, CEP 19060-900, BR, email: galera@prudente.unesp.br)

GPSeq is a software under development at the Department of Cartography, FCT/UNESP, to process GPS data. At the present stage, it allows to process GPS baselines taking into account single frequency data only. A recursive processing algorithm with outliers detection was applied. The double differences of phase and pseudorange are the basic observables. For ambiguity resolution, the LAMBDA method, developed at the Delft University of Technology, is used. It is intended that in the future the software can also allow the processing of double difference receiver data, using broadcast or IGS predicted orbits. At such a case, instantaneous ambiguity resolution is possible. Some experiments were carried out using GPSeq. GPS data files collected in Brazil, forming baselines of up to 10 km were processed. The results have shown that the ambiguities can be solved within four minutes period of data collection at 15 seconds sample rate. In this paper, a brief description of the software is presented, together with the description of the several tests carried out. Additionally, the quality control approach used to evaluate the results is presented, as well as the future plans to upgrade the software

**G1/E/59-A3** Poster **1620-29**

**USING GPS OBSERVATIONS TO DETERMINE VERTICAL REFRACTION IN ZENITHAL OBSERVATIONS**

Jorge PINTO, Helena Ribeiro (Instituto Português De Cartografia E Cadastro, Rua Artilharia 1, nº 107, 1070 Lisboa, Portugal, email: jtpinto@ipcc.pt, lenarib@ipcc.pt)

The great precision and accuracy that nowadays is ensured by the GPS technique provide an interesting mean to estimate the vertical refraction in classical theodolite ground to ground vertical observations, which is the limiting factor of using simultaneous and reciprocal zenithal distances observations, as a tool to determine geoidal undulations height differences. The authors conceive and realize some experiences that shows the possibility to evaluate, with enough precision, the refraction angle in both stations and so, to estimate the existing geoidal height difference between the both stations. This experiences were made in Geobase, Estremoz, which is a precise geodetic test network facility, existing in South Portugal, near the Spanish border. The test facility provide distances that ranges between some hundreds meters to 15 kilometers. Due to terrain constraints, lack of time and also financial problems only a short number of sides were observed, but the experiences made were quite impressive, leaving no need to perform more to validate the method. The range can easily be, with the appropriate instrumentation, widened to greater distances, than the 15 kilometer provided by Geobase. Actually, as greater the distance and the height difference between the stations, as smaller the relative error in the vertical angle refraction determination.

**G1/L/10-A3** Poster **1620-30**

**PROGRESS IN TRIAL STUDY ON RAINFALL ESTIMATION BY GPS TECHNOLOGY**

Li YANXING, Hu Xinkang, Wang Min (First Crustal Deformation Monitoring Center, China Seismological Bureau, Tianjin, 300180, P.R. China, email: dzjl@shell.tjvan.net.cn); Xu Baoxiang, He Ping, Yang Hongmei (Chinese Meteorological Scientific Research Institute, Beijing, P.R. China)

In the paper, a new model for atmospheric refraction delay, a Tm calculation model and a model for calculating the precipitation of atmospheric column height have been established by the authors. Cooperated with Chinese Meteorological Scientific Research Institute, storm observation test by GPS technology was carried out on three meteorological stations in South China from May to June dai 998. The test results indicate that the precipitation value calculated from GPS data is very close. In the value calculated from the data observed by meteorological sounding; The highperiod precipitation calculated from GPS data is highly interrelated to the actual rainfall process; For a heavy rainfall, the precipitation generally has an increasing process before the rainfall and a decreasing process when the rainfall is ended; Before the occurrence of a sudden storm, the precipitation is often to increase abruptly by a big margin; Before a heavy storm, there is a very obvious developing period lasting for a rather long time.

**G1/L/18-A3** Poster **1620-31**

**OPTIMAL INTERPOLATION OF IONOSPHERIC DELAY FOR A VIRTUAL GPS STATION**

Inseong Song, H. VAN DER MAREL (Delft University of Technology, Thijsseweg 11, 2629 JA Delft, The Netherlands, email: H.vanderMarel@geo.tudelft.nl)

In the Netherlands a network of five permanent GPS receivers is operated. The data from the permanent stations is sent every hour to a computing centre, from where the data can be downloaded using an a flexible World Wide Web interface. A new feature is the so-called virtual GPS station. In this innovative approach the network of GPS stations is used to generate data for a non-existing receiver at a location selected by the user. The purpose of the virtual station is to let the user benefit from all the advantages of a network approach, including reduced observation times, without changing the processing from the user point of view. In order to compute virtual station data, atmospheric delays must be computed at the virtual station. This is done by an optimal least squares interpolation method. The method has been tested on the slant ionospheric delays computed from dual frequency GPS phase measurements from the network of reference stations. The interpolation routine is able to handle double differenced ionospheric delays, or the appropriate estimable functions in case of undifferenced processing.

**G1/W/02-A3** Poster **1620-32**

**TRANSFORMATION OF THE CLASSIC TRIANGULATION IN POLAND INTO EUREF REFERENCE SYSTEM**

L. JAWORSKI, J.B. Zieliński (Space Research Centre, Polish Academy of Sciences, 00-716 Warsaw, Poland, email: leszek@cbk.waw.pl); S.Gelo (National Office of Geodesy and Cartography, Warsaw, Poland)

The classic triangulation network in Poland has been constructed over many decades, using data from different sources and different measurement campaigns. Number of solutions was produced, among them the solution which was part of the unified eastern block geodetic network adjustment. All these solutions are compared with the modern GPS solution named POLREF, which is part of the European Reference Frame EUREF. It allowed assessing the quality of old solutions and after transformation to include large part of the old network in the modernised network. No important errors were found in old solutions but some weak

segments of the network could be identified. The comparison with the last classic solution gives the scaling factor equal to 0.9999997 and the average deformation on the level of 10 cm.

**G1/W/03-A3** Poster **1620-33**

**INVESTIGATION OF SITE DISPLACEMENTS DUE TO TIDAL LOADING EFFECTS FOR GPS ARRAY IN TAIWAN**

Chia-Chyang CHANG (Department of Surveying and Mapping Engineering, Chung Cheng Institute of Technology, Tahsi, Taoyuan 335, Taiwan, email: ccchang@cc04.ccit.edu.tw)

High precision GPS measurements are always required for many scientific applications, such as the establishment of national geodetic control networks, geodetic observations for the monitoring of crustal movement, deformation monitoring of main engineering structures, and the determination of global sea level changes. It is also essential to develop some strategies and techniques for GPS observation and data processing, in order to effectively enhance the accuracy of coordinates based on GPS measurements. One of the GPS error sources, based on the effects of tidal loading, can theoretically cause significant site displacements during the GPS observation. The effects of tidal loading, thus, have to be investigated if a higher level of GPS positioning accuracy is expected. It can be achieved through the use of a set of model tested with GPS data and defined for the tidal loading corrections.

Site displacements caused by the tidal loading effects, in terms of the polar tides and atmospheric pressure loading, are practically investigated in this paper in order to realise their influence on GPS positioning. These tidal loading models, also used by the IERS, have been tested with the auxiliary data required and the GPS data collected at the GPS tracking stations in Taiwan. The results show that the polar tides can reach the average displacements of 8 mm in height and 2 mm in plan coordinates over a time scale of one year. Moreover, the variations of vertical displacements caused by the atmospheric pressure loading can be as large as 10 mm for data observed in different seasons, and up to 25 mm for data collected at different sites in Taiwan area.

**G1/W/05-A3** Poster **1620-34**

**CHTRF98: THE FIRST RE-OBSERVATION OF THE SWISS GPS CONTROL NETWORK**

Adrian WIGET, Elmar Brockmann, Dieter Schneider, Thomas Signer (Swiss Federal Office of Topography, Seftigenstr. 264, CH-3084 Wabern, email: adrian.wiget@lt.admin.ch)

Between 1988 and 1994 the Federal Office of Topography established a new GPS-based control network called LV95. This high-precision network, integrated in EUREF, consists of 104 main points and approx. 60 densification points. It realizes the reference frame (CHTRF95) for the new national geodetic reference system CHTRS95. The nationwide accuracies (1 sigma) of the coordinates relative to the SLR station Zimmerwald are better than 1 cm for the horizontal and 3 cm for the vertical components. However, modern high-precision geodetic networks are no longer static. The concept for the determination of a kinematic model for CHTRS95 (called CHTKM95) includes permanent measurements of the Automated GPS Network for Switzerland (AGNES) as well as periodic re-observations of LV95. In 1998 this network (plus some additional reference points in neighbouring countries) were re-observed for the first time using the 9 permanent AGNES stations and 14 mobile GPS receivers. The measurements were collected in a total of 15 night sessions and were processed with the Bernese GPS Software 4.1. Results of a kinematic analysis of the two sets of coordinates (CHTRF95 and CHTRF98), partly bridging a timespan of ten years, will be pre-sented. Further goals of the re-observation were: to determine a new set of coordinates (CHTRF98), thus improving the reliability of the existing CHTRF95 coordinates (in particular the ellipsoidal heights) to check the stability of the LV95 points and to verify the quality of the monumentations to combine LV95 with the AGNES and the EUREF permanent networks to improve the connections with modern GPS networks in neighbouring countries to provide a more homogeneous and more precise reference for future kinematic studies at the earliest time possible.

**G1/W/08-A3** Poster **1620-35**

**THE USE OF GPS TO ESTABLISH A ZERO-ORDER GEODETIC DATUM IN MALAYSIA**

Zarina AHMAD-BERGER, Chris Rizos, A. H. W. Kearsley (at School of Geomatic Engineering, The University of New South Wales, Sydney, AUSTRALIA, email: z8635633@student.unsw.edu.au, c.rizos@unsw.edu.au, w.kearsley@unsw.edu.au); Peter Morgan (at School of Computing, University of Canberra, Canberra, AUSTRALIA, email: pjm@mawson.canberra.edu.au)

Over the last decade, precision GPS positioning has been used to strengthen the Malaysian geodetic datum. Several problems have been identified with the existing geodetic framework. For example, there is no homogeneous adjustment of the current levelling network. Also, the use of the existing tide gauge network as the basis for the vertical datum needs revisiting, and the Malaysian geodetic network needs to be transformed to an ITRS-based datum. Such "problems" have several consequences. For example how does one deal with the apparent sea surface slope between the east and west coast of the Peninsular Malaysia? Should the geodetic network be considered a one-off activity, or be subject to regular "maintenance" and be a dynamic datum? Such matters have an important impact on the allocation of material and human resources to Geodesy in countries such as Malaysia, which may not be able to justify the same level of investment as countries which are more prone to earthquake and other such natural hazards which can be monitored by geodetic observations.

At the heart of modern geodesy is the reconciliation of GPS Geodesy, a powerful technique for the definition of modern geometric datums, and gravimetric geodesy, which is required to transform GPS heights into orthometric heights and to define the vertical reference surface in a physically meaningful manner. The Department of Mapping and Surveying Malaysia (DSMM) in late 1998 established a permanent network of approximately 12 GPS stations throughout Malaysia. This paper considers what roles such a network could play in defining and maintaining the precise Geodetic Network, supporting mean sea level/tide gauge studies as well as providing the means of integrating the conventional levelling networks with gravimetric geoid models. In particular, the issue of how DSMM GPS processing may be meaningfully integrated with regional and global GPS networks using the "ITRF densification via SINEX files" approach will be addressed.

**G1/W/09-A3** Poster **1620-36**

**THE DETERMINATION OF COASTLINE VARIATION WITH GPS**

Cláudia Pereira KRUEGER (Graduate Program in Geodetic Sciences, Federal University of Paraná, Centro Politécnico, CP. 19001, Curitiba, Paraná, Brazil, 82531-990, email: ckruieger@cce.ufpr.br); Carlos Roberto Soares (at Marine Studies Center, Federal University of Paraná, Avenida Beira-Mar s/n, CP 43, Pontal do Sul, Paraná, Brazil, 83255-000, email: soaresc@aica.cem.ufpr.br)

At the Paraná state coast can be observed many areas (like Mel island and Pontal do Sul resort) where the coastline is changing in response to progradation or retreat processes.

These variations can be detected by different alternatives: aerial photographs, satellite imagery, surveying with theodolites, levels and total stations and actually with GPS. The GPS has a simple application, continue availability and independence of weather conditions, becoming an attractive practice. Since 1996 GPS has been used in the monitoring of some areas of the Paraná coastline, with the kinematic positioning. Initially the raw data was collected with Ashtech Z-XII receiver and post-processed with GEONAP-K software. Actually is being applied the GNRT-K software, which permits results in real time with high precision. The overlay of preliminary results allows the detection of the progradation and retreat areas, and the rates of these processes, which have variations from centimetric to metric level.

**G1/W/10-A3** Poster **1620-37**

**IMPROVEMENTS IN INSTRUMENTATION, PERFORMANCE AND POSITIONING OF THE SLR TRACKING STATION AT SAN FERNANDO, SPAIN**

Isabel VIGO-AGUIAR, Jose M. Ferrandiz (Dpt. Applied Mathematics, EPS, University of Alicante, E-03080-San Vicente, Alicante, Spain); Carmelo Belza, Jorge Garate, Jose Martin Davila, Manuel Quijano (Real Instituto Y Observatorio de la Armada, 11110- San Fernando. Cadiz. Spain); Dave Rowlands (Space Geodesy Branch, Code 926, NASA Goddard Space Flight Center, Greenbelt, Maryland 20771, USA)

The Royal Astronomical Observatory (RAO) of the Spanish Navy at San Fernando is strategically located near the Gibraltar Strait, by the boundary between the Eurasia and African tectonic plates. A satellite laser ranging (SLR) station, a Global Positioning System (GPS) station and a set of atomic clocks are co-located at this site. While routinely contributes to laser ranging to several satellites as well as the international time service, the San Fernando SLR station is engaged in an improvement process. We have made a complete overhaul of its electronics and its optics, enabling routine tracking of LAGEOS at about 200 successful LAGEOS night passes per year, while at the same time doubled the number of successful night passes for lower orbit satellites. With the substitution of the old dome for a new one, we are now in the process of improving the quality of the measurements. We have reduced the pulse width to 50 psecs. Currently we are in the process of installing a Single Photon Avalanche Diode (SPAD), we have already got, for the reception system. We are building a new calibration system, we have rebuilt some parts of the station control software, and we are investigating the time counter behaviour. On the other hand, we are automating the focusing and trying to smooth the telescope movements with a new control system. We hope that this work enable our station to get high quality performances. At the same time, better determinations of the site position have been obtained using the NASA software GEODYN. We obtain the solutions by fitting 10-day arc data from LAGEOS I in terms of normal points from the global SLR tracking network. Past determinations of the station coordinates with respect to ITRF had root-mean-square(RMS) values on the order of as large as 6 centimeters, hindering a representative contribution to the determination of satellite orbits and plate motions, as well as related geodetic studies. Now combining 3 months of data between March and May 1998, we derived a San Fernando station position with RMS below 3 centimeters. It is expected that more data will yield further and better adjustments of the station position.

**G1/W/12-A3** Poster **1620-38**

**POSITION CHANGES DUE TO RECENT CRUSTAL DEFORMATIONS ALONG THE CARIBBEAN - SOUTH AMERICAN PLATE BOUNDARY DERIVED FROM THE CASA GPS PROJECT**

Klaus KANIUTH, Hermann Drewes, Klaus Stuber, Herbert Tremel (Deutsches Geodaetisches Forschungsinstitut, Marstallplatz 8, D-80539 Muenchen, Germany, email: kaniuth@dgfi.badw.de); Napoleón Hernández (Servicio Autónomo de Geografía y Cartografía Nacional, Edif. Camejo, Esq. Camejo CSB, Piso 2, oficio 216, Caracas 1010, Venezuela, email: hernandez.sagecan@conicic.ve); Melvin Hoyer and Eugen Wildermann (La Universidad del Zulia, Apartado Postal 10311, Maracaibo, Venezuela, email: mhoyer@europa.ica.luz.ve); Hans-Gert Kahle and Alain Geiger (Eidgenössische Technische Hochschule, HPV G 52, CH-8093 Zuerich, Switzerland, email: kahle@geod.ethz.ch)

The Central And South America (CASA) GPS project aims at monitoring crustal deformations in the tectonically complex area of interaction of the Caribbean, Cocos, Nazca and South American plates. Since its initialization in 1988 several GPS campaigns were performed by various institutions, unfortunately not always covering the whole area simultaneously. This paper concentrates on presenting the latest estimates of deformations along the Caribbean - South American plate boundary as covered by the Venezuelan part of the project. The Venezuelan network has been regularly observed from early 1993 on. The eastern part suffered from an earthquake of magnitude 6.9 in July 1997 and a subsequent seismic activity culminating in another earthquake of magnitude 4.5 in December 1998. Our analysis comprises GPS data collected up to spring 1999 and provides estimates of linear horizontal velocities as well as discontinuous displacements in a global reference frame. The processing strategy for deriving velocities is outlined and the accuracy and reliability of the results is discussed.

**G1/W/17-A3** Poster **1620-39**

**SIMULATED ANNEALING - OPTIMISATION METHOD FOR GPS SURVEYING NETWORKS**

Hussain SALEH, Peter Dare (Applied Geodesy Research Unit, School of Surveying, University of East London, Longbridge Road, Dagenham, Essex, RM8 2AS, UK, email: Hussain2@uel.ac.uk)

For Global Positioning System (GPS) epoch surveys,  $m$  receivers ( $m > 1$ ) are placed in a sequential manner on the  $n$  ground points whose coordinates are required. If  $n > m$ , as is usually the case in epoch surveys, then receivers will have to move between points to ensure that all points have been visited. When  $m$  receivers are observing simultaneously, this defines a session. When  $n > m$ , more than one session will be required to connect the points together to form a network. The list of sessions required to form the network is known as the schedule. Determining the best order of the sessions (i.e., determining the cheapest schedule) is not a trivial task and this paper describes an analytical approach to determining the optimal schedule given a list of sessions and the cost of moving receivers between points.

The approach is based upon the development of a Simulated Annealing (SA) heuristic technique for the optimisation of the scheduling of GPS receivers and gives examples of its application. In the design of GPS surveying networks there are difficulties in establishing good schedules for the network observation. The optimal schedule can be determined for relatively small networks using exact methods. Generally, however, solving large networks to optimality requires impracticable computing time. To avoid this, the SA technique provides near-optimal solutions for large networks within an acceptable amount of computational time when parameter values for the SA algorithm are correctly chosen.

Currently, an experienced surveyor in GPS surveying performs this task manually. In this research, the problem has been formulated as a Combinatorial Optimisation Problem (COP) and solved by making use of the SA algorithm. This technique enables the surveyor to generate an observation schedule for the whole network in an efficient manner. The developed SA algorithm is found to be very effective for solving schedule design problems and has been coded in Visual C++ under Windows NT. Computational results indicate that the SA heuristic technique, which has been validated using real data, consistently provides significantly better

GPS receiver schedules than those established manually. The speed of the SA technique enables near-optimal solutions to be produced in a real-time environment.

**G1/W/27-A3** Poster **1620-40**

**A DETAILED MODELLING OF THE SOLAR RADIATION PRESSURE ACTING ON ERS SATELLITES**

F. VESPE (Agenzia Spaziale Italiana-Centro di Geodesia Spaziale -Matera, Italy); R. Devoti, V. Luceri (Telespazio-Centro di Geodesia Spaziale -Matera, Italy)

In the last few years the weakening and deflection of the solar radiation through the atmosphere has been deeply investigated. An empirical model based on star light observations is proposed that combines both the geometric and physical effects of the penumbra transitions. The weakening and deflection of the solar radiation caused by the atmosphere are treated using the observed atmospheric data for the extinction and deflection of the star light that are usually collected during an astro-photometric calibration. These data are used to formulate the empirical relationship between the atmosphere's extinction and deflection and the height measured from the Earth's surface.

This model can be useful in enhancing the orbit modelization of Earth satellites of complex shape such as ERS-1 and ERS-2. A validation of the model is performed analysing the orbital residuals of both ERS satellites using SLR and PRARE data during the eclipses transitions.

**G1/W/22-A3** Poster **1620-41**

**OCEAN-LOADING DEFORMATIONS DERIVED FROM GPS OBSERVATIONS**

M.S. SCHENEWERK (NOAA, SSMC3 1315 East-West Highway Silver Spring, MD 20910, USA, email: mark@tony.grdl.noaa.gov); T.M. van Dam, O. Francis (Observatoire Royal de Belgique, Avenue Circulaire, 3 B-1180 Bruxelles Belgium, email: tonie@oma.be)

The proliferation of continuously operating GPS tracking sites and improvements in estimating the vertical component of a site's position from GPS measurements presents a unique opportunity to directly observe the effects of ocean tidal loading. The long, continuous record from these permanent sites permits the coherent accumulation of observations with respect to the driving tidal forces. Techniques like this defeat atmospheric, geometrical, and multipathing effects which can have a comparable magnitude, but do not have the same periods as the ocean-loading signals.

A project is underway to estimate ocean-loading effects at selected sites in North America. Agreement with a priori estimates of height variation generated from existing models is excellent. This presentation will describe the technique used, results and the feasibility of extending this processing globally. The significance of these results for local, regional, and global GPS data processing will be discussed.

**G1/W/26-A3** Poster **1620-42**

**REALIZATION OF THE VERTICAL REFERENCE SYSTEM IN VENEZUELA**

Hermann DREWES, Wolfgang Bosch, Klaus Kaniuth (all at Deutsches Geodaetisches Forschungsinstitut, Marstallplatz 8, D-80539 Muenchen, Germany, email: drewes@dgfi.badw-muenchen.de); Napoleón Hernández (Servicio Autónomo de Geografía y Cartografía Nacional, Av. Este 6, C.S.B., Edif. Camejo, Piso 2, Caracas 1010, Venezuela, email: hernandez.sagecan@conicic.ve); Melvin Hoyer, Eugen Wildermann (both at Escuela de Ingeniería Geodesica, La Universidad del Zulia, Maracaibo, Venezuela, email: mhoyer@luz.ve)

The height reference system of Venezuela is defined by the La Guaira tide gauge in the central part of the caribbean coast. The mean sea-level at this site during the epoch of definition was considered to coincide with the geoid. Recent models of sea surface topography as derived from Topex/Poseidon altimetry present a quite heterogeneous pattern along the Venezuelan coast-line. Long-term tide gauge records at La Guaira, at Carupano (about 400 km east of La Guaira), and at Amuay (about 400 km west of La Guaira) show a quite different behaviour of sea-level changes ranging from -2 mm/a decrease to +2 mm/a increase. The ellipsoidal heights of those three tide gauges (Amuay, La Guaira, and Carupano) have been determined repeatedly over six years by precise GPS observations.

They are reduced by the (quasi-) geoid heights from different models and compared with the sea surface topography from satellite altimetry. The differences are analyzed in order to define a height reference system which refers to the (quasi-) geoid instead of the zero mark of the tide gauge. The height variations are discussed with regard to eventual recent crustal movements.

**G1/W/34-A3** Poster **1620-43**

**THE ESTABLISHMENT AND MAINTENANCE OF THE TWD97 GEODETIC REFERENCE FRAME**

Ming YANG, Ching-Liang Tseng, Jyh-Yih Yu (all at Department of Surveying Engineering, National Cheng Kung University, Tainan 701, Taiwan, email: myang@mail.ncku.edu.tw)

Taiwan is located in an active seismic region on the boundary of the Eurasian plate and the Philippine plate. Severe crustal movements at rates of greater than 5 centimeters per year have been recorded in the area. For the time period from 1995 to 1998, the Global Positioning System (GPS) had been used to establish a geodetic reference frame in Taiwan, the Taiwan Datum 1997 (TWD97), which includes 8 GPS permanent tracking stations and 726 1st- and 2nd-order control points. TWD97 has the following major properties in its establishment and future maintenance: (1) connection with the International Terrestrial Reference Frame (ITRF); (2) incorporation of velocity field models in various regions. In order to retain the required accuracy for the control network, remeasurements of selected points are scheduled, depending on the associated velocity fields of different regions.

**G1/W/38-A3** Poster **1620-44**

**TESTS FOR THE MAINTENANCE OF FUNDAMENTAL GPS NETWORKS IN TAIWAN**

Chia-Chyang CHANG (Department of Surveying and Mapping Engineering, Chung Cheng Institute of Technology, Tahsi, Taoyuan 335, Taiwan, email: ccchang@cc04.ccit.edu.tw); Hung-Chih Chen (Lands Survey Bureau, Taiwan Provincial Government, Taichung 400, Taiwan, email: ccandrew@mail.lsb.tpg.gov.tw)

The "new" type of national reference system, consisting of one set of 3-D coordinates accurately defined in the ITRF for those well-distributed GPS control stations in the fundamental networks, has become possible to effectively carry on the maintaining work. The fundamental GPS networks composed of 8 permanent GPS tracking stations, 105 first-order, and 621 second-order GPS control stations in Taiwan area had been established during 1993 to 1997. As the facts that Taiwan is located at the fringes of two different tectonic plates, and



many geodetic observations have shown the significant crustal deformation of up to 3-8 cm/yr at most of the monitoring sites in this area, it is particularly required to carry on the maintenance for the GPS control stations in Taiwan.

This paper is aimed at investigating some of the related effects on the maintenance of the fundamental GPS networks, in order to provide one set of 3-D coordinates with the reliable accuracy. The results based on the simulation tests are analysed and discussed for the following topics: (1) Coordinate variations of the GPS tracking stations related to the update of the ITRF; (2) Coordinate variations of the first- and second-order GPS control stations estimated using velocity fields decided by the GPS tracking stations; (3) The effective period of maintenance required to provide high quality of coordinates for the GPS control stations; (4) The optimal operation procedure designed for re-occupying or re-building the GPS control stations whose sites or coordinate accuracies were found to be damaged or assessed to be degraded.

**G1/W/39-A3** Poster **1620-45**

#### ON THE USE OF LOW COST INERTIAL SYSTEMS IN AIRBORNE SURVEYING

Sérgio CUNHA (Electric Eng. Dpt., Porto University, Portugal, email: sergio@fe.up.pt); Phillip Tomé, Telmo Cunha, Luisa Bastos (Astronomical Obs., Porto University, Portugal, email: phillip@oa.fc.up.pt, telmo@oa.fc.up.pt, lcbastos@oa.fc.up.pt)

Geodetic airborne surveys such as gravimetry and altimetry require the determination of precise aircraft position and attitude. The first can be most successfully obtained using carrier phase differential GPS, reaching decimetre level accuracy. By integration with low cost inertial units, precise attitude and robust position measurements can be achieved. The combined use of these two sensors can, however, be also employed to estimate the gravity anomaly. The methodology to compute position, attitude and gravity anomaly from a system based on a low cost inertial device and two GPS receivers (with access to GPS reference station data) is focused. The presented approach is supported by data selected from an extensive airborne gravimetric and altimetric survey that took place in the Azorean area in 1997. The correlation between sensor errors and the resulting position, attitude and gravity anomaly estimation errors is discussed.

**G1/W/41-A3** Poster **1620-46**

#### THE VERTICAL REFERENCE SYSTEM OF ARGENTINA

Klaus KANIUTH, Wolfgang Bosch, Hermann Drewes (all at Deutsches Geodaetisches Forschungsinstitut, Marstallplatz 8, D-80539 Muenchen, Germany, email: kaniuth@dgfi.badw-muenchen.de); Claudio Brunini, Juan Moirano, Maria Paula Natali (all at Facultad de Ciencias Astronomicas y Geofisicas, Universidad La Plata, La Plata, Argentina, email: claudio@fcaglp.fcaglp.edu.ar)

The classical height reference system of Argentina is defined by the fundamental station at Tandil which was determined in the forties by a precise spirit levelling to the 120 km distant tide gauge at Mar del Plata. The mean sea level at Mar del Plata averaged over a few months at that time was considered to coincide with the geoid. Recent models of sea surface topography derived from Topex/Poseidon altimeter data show not only the deviations of the mean sea surface from the geoid but also a significant sea surface variability with dominant annual oscillation.

The ellipsoidal heights of the fundamental station Tandil as well as of the Mar del Plata tide gauge were determined in December 1998 and repeatedly in 1999 by precise GPS observations. They are reduced by height anomalies in order to obtain the corresponding normal heights. The results are compared with the sea surface heights resulting from satellite altimetry in order to detect systematic effects.

**G1/W/43-A3** Poster **1620-47**

#### NATIONAL PREPARATION FOR THE USE OF THE GLOBAL REFERENCE FRAME

Martin LIDBERG (Geodetic Research Division, National Land Survey, 801 82 Gavle, Sweden, email: martin.lidberg@lm.se)

The paper describes the project RIX95 from a technical point of view. The aim of the project is preparation for the use of the Global Reference Frame (WGS84/ITRF/EUREF89), increase accessibility of the national network, and connect numerous local geodetic networks (with an extension of some 10th of km) to the National and Global Reference Frames. To do so, a new network is established including all points in the national horizontal network, and principal points in regional networks. A number of points in the first order levelling network are also included. The new network is also connected to the 21 permanent GPS stations in the SWEPOS network, where the Global Reference Frame has been realised.

The origin of the project is the wish to take advantage of the possibility for increased efficiency in surveying, coming from the rapid development in satellite geodesy. The high accuracy over long distances, the new infrastructure with continuously operating reference stations, the efforts towards real time cm level positioning services can be mentioned as some examples. The most interesting subjects in the project from a scientific point of view are the method for densification of a geodetic network from the SWEPOS stations, the handling of several coordinate systems, and strategies for future reference networks.

**G1/W/44-A3** Poster **1620-48**

#### USE OF OBJECT-ORIENTED PROGRAMMING IN PARTICLE ACCELERATOR ALIGNMENT

Catherine M. Le COCQ (Stanford Linear Accelerator Center, Stanford University, P.O. Box 4349, MS21, Stanford, CA 94309, USA, email: lecocq@slac.stanford.edu)

Aligning particle accelerator components presents specific characteristics that force data treatment programs to be very modular, extensible and feature-rich. Spending the time and effort to design a software framework, both efficient and open, has proven to be well worth the investment in the long run.

The history of LEGO, the latest geodetic adjustment package in use at Stanford Linear Accelerator Center (SLAC), is a good illustration of how certain concepts of object-oriented programming (OOP) can be used to make a product flexible and portable. Started as a simple C program designed to handle laser tracker observations, LEGO has evolved into a multi-instrument, multi-platform, and multi-model C++ package. It has been successfully used for different tasks such as final adjustment of the B-Factory storage ring integrating laser tracker, theodolite and precise level observations simultaneously, feasibility test of a high resolution digital camera and simulation of a two-story network in the National Ignition Facility project.

The first part of this paper describes how LEGO benefits from OOP design. An overview of the different C++ object definitions involved (called "classes") demonstrates how portability is achieved. The description of the relationship between the classes highlights one of the strengths of OOP: data hiding. This is the key for safe and quick implementations within

various environments. Other OOP concepts such as encapsulation, base classes and virtual functions are detailed. They have been introduced during the adaptation of LEGO to the new types of measurements and treatments needed for faster and better quality surveys in particle accelerator centers. The second part of this paper starts from the analysis of the limitations of the existing package. It then proposes an object-architecture for the next generation of SLAC alignment package under study for the Next Linear Collider project.

**G1/E/03-A3** Poster **1620-49**

#### LINK OF BRAZILIAN VERTICAL DATUM TO SIRGAS NETWORK

Silvio R.C. DE FREITAS (Graduate Program in Geodesy, Department of Geomatics, University of Paraná, 81531-990, Curitiba, Brazil, email: sfreitas@cce.ufpr.br); Juiclei Cordini (Department of Civil Engineering, University of Santa Catarina, 88040-900, Florianópolis, Brazil, email: cordini@mbox1.ufsc.br); Eduardo Marone (Centro de Estudos do Mar, University of Paraná, 83255-000 - Pontal do Sul, Brazil, email: maroned@cce.ufpr.br)

The present activities of the SIRGAS project in South America are mainly directed to the connection of the different national height systems in a coherent continental network linked to the South American geodetic geocentric frame. This frame is one of the most recent and precise realizations of ITRF in the world. The WG III of SIRGAS established some recommendations related to the steps for this purpose. The definition of the geocentric position of the different national vertical Datum was pointed as a fundamental step for the intended connection. The Graduate Program in Geodesy, University of Paraná, established a 315 km long continental profile of observation in Southern Brazil with three stations, devising to establish the geocentric position of the Brazilian vertical Datum, placed at the Imbituba harbour. The first station was located at Imbituba itself, being the second one 50 km away from the sea (in the city of Blumenau), and the third one 80 km inland (in Curitiba - SIRGAS station). In each one of them dual-frequency GPS receivers were installed, plus a gravimeter for observation of gravity tide, and air pressure and temperature sensors. Two IGS stations were also used (Santiago and Brazilia). The results of these observations considering the GPS data processing, using fiducial techniques and the dynamical effects coming from gravity tides, meteorological and ocean indirect effects, are discussed in the presentation.

**G1/E/04-A3** Poster **1620-50**

#### PRESENT-DAY TECTONICS IN WESTERN TURKEY BASED ON GPS OBSERVATIONS

Yüksel ALTINER, Hermann Seeger (both at Bundesamt für Kartographie und Geodäsie, Frankfurt, Germany, email: seeger@igs.ifag.de); Mustafa Ocak, Ali Türker (both at General Command of Mapping, Ankara, Turkey); Mustafa Ergüdü, Müjgan Salk (both at the University of the 9th September, Izmir)

For the determination of the complex movements in the western part of the Anatolian plate in 1992 a GPS network of 35 stations around the rivers Gediz and Büyük Menderes was established. In this network from 1992 to 1997 four GPS-campaigns were carried out. For the processing of these data the Bernese Software was used. The magnitude of the horizontal velocities relative to the SLR station Yigilca (north of the North Anatolian Fault Zone) varies from 1 cm/yr to 3 cm/yr, increasing from east to west. The stations in the eastern part move in east-west direction while those in the western part turn to the west-south. The results of a deformation analysis based on the analytical surface deformation theory indicate that the western part of the investigation area (Gediz Graben System) may be characterized as compression and the southern part as extension (Büyük Menderes Graben System). Both regions are separated from each other by a region of very small deformation.

**G1/E/07-A3** Poster **1620-51**

#### A NATION-WIDE GPS GEODETIC NETWORK IN CHINA

Ziqing WEI, Duan Wuxing (both at Xian Research Institute of Surveying and Mapping, 1 Yanta mid-road, Xian, Shaanxi 710054, P.R.China, email: ziqingw@public.xa.sn.cn)

A nation-wide GPS geodetic network has been set up in China. Its primary purposes are threefold: first, to control and strengthen the astro-geodetic network; second, to refine the geoid in this region; third, to establish the regional geocentric coordinate system. The whole network was subdivided into the first order network and the second order one; both are nation-wide and laid out in the form of overall continuous network. The station spacings is about 700 km for the first order network and 150-200 km for the second order network. The first order network was observed from May 1991 to April 1992 using MINI-MAC 2816 receivers, with the data processing conducted in 1994. It was shown that the accuracy of baseline components reaches 0.03 ppm and the accuracy of geocentric coordinates ranges from 0.3 to 0.5 metres. For the second order network the field operation was carried out between 1992 and 1997 mainly employing Ashtech Z12 receivers, and the data processing was performed in 1998 by means of the GAMIT software developed by MIT and SIO. It was exhibited that the accuracy of geocentric coordinates is better than 0.1 metres, and the accuracy of baseline components is mostly at the 0.02 ppm level.

**G1/E/13-A3** Poster **1620-53**

#### INFLUENCE OF GPS SATELLITE ORBITS' QUALITY ON POSITIONING PRECISION

A. KRANKOWSKI (Institute of Geodesy, Olsztyn University of Agriculture and Technology, 10-957 Olsztyn, POLAND, e-mail: kand@moskit.art.olsztyn.pl)

In the paper, results of analysis of the influence of the CODE orbits' quality on positioning precision were presented. The following orbits were taken into account:

- final orbits
- 1-day orbits, accessible with 3 days delay,
- rapid orbit, accessible with 16 hours delay,
- predicted orbits (24 and 48 hours prediction).

Using mentioned above orbits the repeatability of the following vectors were monitored: Lamkowko-Borowa Gora, Lamkowko-Borowiec, Lamkowko-Metsahovi, Lamkowko-Matera. Results were referred to those obtained using IGS final orbits. As results of investigations the following conclusions can be stated:

1. Very good agreement between final IGS and CODE orbits permits to use both in geodynamic investigations.
2. One-day and rapid orbits can be used for high precision engineering works (postprocessing).
3. Orbits predicted one day ahead can be used for precise real time positioning.

**G1/E/14-A3** Poster **1620-54**

#### SWEPOS - DESIGN, APPLICATIONS AND FUTURE DEVELOPMENT

Gunnar Hedling, Bo JONSSON (National Land Survey of Sweden S-80182 G E4vle, Sweden, email: gunnar.hedling@lm.se, bo.jonsson@lm.se)



The presentation describes the design of the Swedish network of GNSS reference stations, SWEPOS and the goals for the network. SWEPOS consists of 21 stations and has been in operation since 1993, during the latest 1 BD year as a real time network. Each station hosts two high-precision dual frequency PS-receivers and on some stations combined GPS/GLONASS dual/single-frequency receivers are also installed. GPS-data is transmitted once a second from the stations to the control centre to be forwarded to real-time distributors and stored for post-processing applications. The data flow, experiences from the operation and statistics for the data availability and data quality are shown. The purpose of SWEPOS is to provide data both for scientific applications, e. g. studies of crustal movements and production applications, e. g. surveying and navigation. A summary of the SWEPOS applications today is given in the presentation. SWEPOS is also a national realisation of the Global Reference Frame. An overview of development activities for integrity monitoring of RTK-data and new applications where the network is used is also presented. Onsala Space Observatory, Teracom and the National Land Survey are working together in the Ciceron project to develop a RTK service with centimetre accuracy, covering the whole Sweden. In another project SWEPOS data is going to be used to compute the atmospheric water vapour content over Sweden.

**G1/E/15-A3** Poster **1620-55**

#### THE CATALAN GPS PERMANENT NETWORK

Julià TALAYA, Miquel Àngel Ortiz, Ernest Bosch, Carme Parareda (Institut Cartogràfic de Catalunya, Parc de Montjuïc, Barcelona 08038, Spain, email: talaya@icc.es)

Since 1992 the Institut Cartogràfic de Catalunya is deploying a network of GPS permanent stations for covering an area of 30000 square km. At present the network consists in 8 stations equipped with dual frequency receivers and four of them with meteorological measurement systems. The data collected by the stations is of public domain and can be accessed via ftp (ftp.icc.es). The GPS stations are also used for generating and monitoring code corrections (RASANT system) that are transmitted via RDS (Radio Data System, a subcarrier of commercial FM transmissions). We are working on the broadcasting of phase observations from the stations via DAB (Digital Radio System, the new digital radio standard) that will allow RTK positioning all over Catalunya. Future developments will include the transmission of the data observed by the receivers in real time to the ICC headquarters using VSAT platforms (Very Small Aperture Terminal, a satellite based communications technique).

This network is used by the scientific community to monitor the crustal deformation of the Pyrenees area, some of the stations belongs to the IGS and EUREF networks and the stations that collect meteorological information are used by different scientific groups for computing water vapour contents of the atmosphere.

**G1/E/18-A3** Poster **1620-56**

#### THE DEVELOPMENT AND IMPLEMENTATION OF NEW ZEALAND GEODETIC DATUM 2000

Don GRANT, Graeme Blick, Merrin Pearse (all at Land Information New Zealand, PO Box 5501, Wellington, New Zealand, email: dgrant@linz.govt.nz); John Beavan (Institute of Geological and Nuclear Sciences, PO Box 30368, Lower Hutt, New Zealand, email: john.beavan@gns.cri.nz); Peter Morgan (University of Canberra, PO Box 1, Belconnen, ACT 2616, Australia, email: peterm@ise.canberra.edu.au)

There has been clear evidence in recent years that New Zealand Geodetic Datum 1949 is inadequate for some current and emerging applications. A new geocentric datum, New Zealand Geodetic Datum 2000 (NZGD2000), designed and built during 1998, is realised through ITRF96 and uses the GRS80 ellipsoid. Coordinates for 29 primary 1st Order 2000 network stations, were generated at an epoch of 1996 using data from 5 repeat GPS surveys made between 1992 and 1998. Data from these and other repeat surveys are used to generate a velocity model to account for crustal deformation across New Zealand, primarily due effects of plate tectonics. The velocity model has been used to generate coordinates at epoch 2000.0 (the reference date for the new datum of 1 January 2000) for the 1996 dataset. The velocity model will also be used to ensure that Land Information New Zealand can generate epoch 2000 coordinates from observations made at other times and to allow other specialised users to generate up-to-date coordinates for times other than the reference epoch. As the geodetic network is densified, new marks will be incorporated into the new datum. The new datum will be implemented in conjunction with the implementation of the New Zealand Survey and Title Automation Programme, Landonline. A description of the new datum, its design, and implementation will be presented.

**G1/E/21-A3** Poster **1620-57**

#### DENSIFICATION OF THE EUREF NETWORK IN FINLAND

Matti OLLIKAINEN, Hannu Koivula, Markku Poutanen (Finnish Geodetic Institute, Geodeetinrinne 2, FIN-02430 Masala, Finland, email: FinnRef@fgi.fi)

During the years 1996 and 1997 the FGI measured a GPS network of 100 points over Finland in order to densify the network of EUREF points. The network was measured using the 12 permanent GPS stations of the FGI as initial points. Four of these stations belong to the network of permanent EUREF stations.

The main part of the observation sites were First-Order triangulation points, however, in order to connect the GPS network to the national height system (N60), some tide gauge sites as well as precise levelling benchmarks were included in the network. The observations were processed in ITRF96 (Epoch:1997.0). Finally, the coordinates were transformed to ETRF89 (Epoch 1997.0).

The GPS solution of the network was performed using the Bernese v. 4.0 software. In the final adjustment the RMS values of the coordinates, which were computed according to the discrepancies between different observation sessions, were  $\pm 2$ mm,  $\pm 2$ mm,  $\pm 6$ mm in North, in East and in Up component, respectively.

The 7-parameter transformation parameters were solved between EUREF-FIN coordinates and terrestrial systems (e.g. ED50, DE87). The residuals of the solutions show the deformation of the old triangulation network. The largest residuals were more than 2 meters. The densification of the network was continued in 1998 when 190 points, located in the Southern part of the country, were connected to the network observed in 1996-97. The new points were observed in order to improve the availability of the EUREF points for further GPS determinations.

**G1/E/22-A3** Poster **1620-58**

#### GEODYNAMICAL RESEARCH IN THE VENEZUELAN ANDES: NEW RESULTS OF LAST ANALYSIS OF THE APARTADEROS-SIERRA-NEVADA-GEOTRAVERSE

Klaus LINKWITZ (University of Stuttgart, Stuttgart, Germany); Heinz Saler (Fachhochschule Karlsruhe, Karlsruhe, Germany)

Induced by a co-operation since 1970 of partners in Venezuela and Germany below, sponsored by the Volkswagen-Foundation, Hannover, the project Apartaderos Sierra Nevada Geotraverse could start in 1980 and ended intermediately in 1995 with a final analysis and evaluation of different -including earlier field campaigns between 1970 and 1993. Objective of the project were precise geodetically orientated investigations within a selected part of the Bocono Fault about 50 km. East of the town of Merida, not very far from the Pico Bolivar (5100 m). The very unusual topographical environment, the crystal clear air in the dry weather period between December and March (the Astro-Observatory of Merida lies directly in the traverse), the apparent visibility of the Bocono Fault, and a comparatively easy accessibility give this region the character of an open air laboratory not readily found elsewhere. The other, also extraordinary characteristic of the investigations is the fact, that all field campaigns unto 1987 still used the classical geodetic methods of triangulation and trilateration, complemented intensively by astronomical and gravimetric observations. However, the campaigns 1991 and 1993 used also differential GPS and were (minor) part of the large international project CASA DOS extending far in to the Caribbean Sea and its islands. Consequently, the analysis and evaluation had to develop and use an extended model, combining the heterogeneous classical geodetic observables and the new GPS observables. As a result of the extended and complex analysis a number of thesis about the kinematic properties of the Fault in the area of investigation can be formulated of which some are contrary to original expectations and therefore surprising. This is dealt with in detail in the paper processed in ITRF96 (Epoch: 1997.0). Finally, the coordinates were transformed to ETRF89 (Epoch 1997.0).

The GPS solution of the network was performed using the Bernese v. 4.0 software. In the final adjustment the RMS values of the coordinates, which were computed according to the discrepancies between different observation sessions, were  $\pm 2$  mm,  $\pm 2$  mm  $\pm 6$  mm, in North, in East and in Up component, respectively. The 7-parameter transformation parameters were solved between EUREF-FIN coordinates and terrestrial systems (e.g. ED50, ED87). The residuals of the solutions show the deformation of the old triangulation network. The largest residuals were more than 2 metres.

The densification of the network was continued in 1998 when 190 points, located in the southern part of the country, were connected to the network observed in 1996-97. The new points were observed in order to improve the availability of the EUREF points for further GPS determinations.

**G1/E/25-A3** Poster **1620-59**

#### THE NEW STANDARD BASELINES MEASURED BY THE FGI

Jorma JOKELA (Finnish Geodetic Institute, Geodeetinrinne 2, FIN-02430 Masala, Finland; email: Jorma.Jokela@fgi.fi)

The Finnish Geodetic Institute is one of the National Standard Laboratories in Finland, being responsible (among other things) for length standards in geodetic applications. In 1998 we measured two new Vaisala baselines in very special places: One of them is indoors under the main building of the Helsinki University of Technology. The other is an old calibration baseline, not originally planned for interferometric measurements, near Chengdu in China. We present results and experiences of these and other recent projects. In addition to white light interferometry, we have used high precision EDM instruments, like Kern Mekometer ME5000, in our metrological projects.

At the new baselines the Vaisala baseline benchmarks and the equipment for calibration measurements are on the same observation pillars, contrary to general standard baseline design. We discuss the advantages and possible drawbacks of the new system, especially in the stability control and projection measurements needed to combine the interferometric and other geodetic measurements.

**G1/E/26-A3** Poster **1620-60**

#### APPLICATION OF REAL-TIME KINEMATIC GPS TECHNOLOGY TO MANNED MODELS SHIPHANDLING SIMULATION USING VIRTUAL PORT PRESENTATION

Janusz BOGUSZ, Lech Kujawa, Jerzy B. Rogowski (all at Institute of Geodesy and Geodetic Astronomy, Warsaw University of Technology, 00-661 Warszawa, POLAND, email: jb@gik.pw.edu.pl); Mirosław Korcz (Gdynia Maritime Academy, POLAND); Wojciech Leszczyński (Institute of Meteorology and Water Management, Warsaw, POLAND); Marcin Szoucha (Topographic Service of Polish Army General Staff, Warsaw, POLAND)

This paper presents an application of RTK methods for simulation and monitoring ships' slow speed manoeuvres while manoeuvring in the harbour as well as on approaching to the quay. It describes results of tests, which were performed using manned models of Ferry and VLLC in Ship Handling Research and Training Centre in Iawa, Poland. Trimble and Ashtech RTK systems were used and compared with kinematic method and DGPS in real time based on mobile telephones for reference data transmission. The paper discusses the successful implementation of RTK method for the simulation of ship manoeuvres in virtual port.

**G1/E/27-A3** Poster **1620-61**

#### DETECTION OF SUBCENTIMETRE DEFORMATIONS WITH GPS

H. Hartinger, Fritz K. BRUNNER (Engineering Surveying and Metrology, Technical University of Graz, Steyrergasse 30, A-8020 Graz, Austria, email: hartinger@aig.tu-graz.ac.at)

Frequently, the capability of deformation monitoring systems based on conventional surveying instruments is decreased by weather effects which prevent line-of-sight measurements. GPS observations are not restricted to the line-of-sight, however, presently the attainable accuracy of GPS measurements is not as high as that of the conventional deformation monitoring systems. The final goal of this research project is a subcentimetre, near realtime GPS deformation monitoring system which is generally applicable. Each station consists of a choking antenna, a GPS receiver and a data transmission unit. The measurements of all stations are simultaneously transmitted to a control station which stores and processes the original GPS data. The most difficult research area for achieving subcentimetre accuracy in local GPS deformation monitoring systems are systematic errors, mainly multipath. This difficulty is even amplified in near realtime systems because of the low frequency characteristics of multipath. This poster reports about the development of the GPS hardware and software of a monitoring system which performs at a 3 to 5 mm accuracy range. Several strategies have been investigated for the reduction of systematic errors and the results shall be presented. In a first practical application the GPS system was used to monitor the motions of a landslide area. The results show that an accuracy of 2 mm in position is achievable for a time resolution of 3 minutes using the appropriately filtered raw GPS data.

**G1/E/28-A3** Poster **1620-62**

#### EVALUATION OF THE HIGH PRECISION GPS POINT POSITIONING USING GPS DATA FROM BRAZIL

Joco Francisco Galera MONICO (Department of Cartography, Sao Paulo State University UNESP, Presidente Prudente, CEP 19060-900, BR, e-mail: galera@prudente.unesp.br)

Point positioning is generally referred to the estimation of station/receiver parameters by the use of the pseudorange data, constraining the satellite parameters to the values given in the navigation message. The quality of the results is affected by the Selective Availability (SA), which degrades the orbits and clocks of the satellites and by the quality of the observable (pseudorange), which precision is of the order of 1 m. In the high precision point positioning, besides the pseudorange observable, the carrier phase one is also included in the processing. Additionally, in order to eliminate the effects of SA, one has to use precise ephemerides, which are obtained in a post-processing approach. Additionally to the satellite orbits, the precise ephemerides also provide the corrections to the satellite clocks. Results documented in the GPS literature refer to daily precision of the order of few millimeter in the horizontal components and centimeter in the vertical.

GIPSY-OASIS II software, developed at Jet Propulsion Laboratory, provides means of performing high precision point positioning. In order to evaluate the quality of the results of this approach in Brazil, data from the Brazilian continuous GPS network (RBMC) was processed using this software. The results of this strategy besides being compared to those obtained from the network approach, they were analyzed using the concept of repeatability. Preliminary results agree with the quality claimed in the literature. The basic fundamentals of the precise point positioning approach and the description of the GPS data used, together to the quality control applied will be the main topics of this paper.

**G1/E/29-A3** Poster **1620-63**

**CONNECTION OF THE COLOMBIAN VERTICAL DATUM TO THE GEOCENTRIC REFERENCE SYSTEM**

Laura SANCHEZ, William Martinez, Juan Florez (all at Instituto Geografico Agustin Codazzi, Carrera 30, No. 48-51, Santafe de Bogota, Colombia, email: lsanchez@igac.gov.co); Hermann Drewes, Klaus Kaniuth, Herbert Tremel (all at Deutsches Geodatisches Forschungsinstitut, Marstallplatz 8, D-80539 Muenchen, Germany, email: drewes@dgfi.badw.de)

The classical Colombian vertical datum is defined by the Buenaventura tide gauge at the Pacific coast. The mean sea level at this tide gauge is assumed to coincide with the geoid. All the official Colombian height values derived by spirit levelling refer to this datum. Recent comparisons of ellipsoidal heights derived from GPS observations and corrected by geoid undulations (regional geoid for Colombia based on EGM 96 with local refinements), show a systematic offset of about 2 meters.

To verify this discrepancy, the ellipsoidal height of the Buenaventura tide gauge was determined by a dedicated GPS survey and corrected by the sea surface topography as derived from satellite altimetry. The geoid height obtained in this way is compared with that of the regional geoid for Colombia and allows some estimates of a systematic offset in EGM 96. To control the offset, two other tide gauges at Tumaco (south of Buenaventura) and Cartagena (Caribbean coast) are observed in the same way and confirm the results.

**G1/E/30-A3** Poster **1620-64**

**IMPROVEMENT OF PRECISE AND RELIABLE KINEMATIC GPS POSITIONING IN REAL-TIME OVER LONG DISTANCES**

Rock SANTERRE (Centre de recherche en geomatique, Universiti Laval, Ste-Foy, Quebec, G1K 7P4, Canada, email: Rock.Santerre@scg.ulaval.ca); Claude St-Pierre (VIASAT Gio-Technologie, Montrial, Quebec, H2S 1Z2, Canada, email: cstpiere@viasat.qc.ca)

This research project, which is part of the Canadian GEOID (Geomatics for Informed Decisions) Network of Centres of Excellence, is dedicated to the improvement of the methodology and the algorithms to achieve more precise and more reliable kinematic GPS positioning (which implies more reliable and efficient phase ambiguity resolution) over distances even longer than 75 km: for the support, but not exclusively, of bathymetric surveys in real-time. This research will lead to added-value for the customized software already developed for the Canadian Coast Guard (CCG) and this will consequently further support the modernization and the cost-effectiveness of bathymetric operations. To reach these goals, different research avenues will be considered. The main avenues are: 1) GPS relative positioning with multiple reference stations, 2) the improvement of ionospheric modelling, 3) the use of precise real-time orbits, 4) the integration of Glonass observations and 5) radio-communication management (which includes the problem of time latency).

In this presentation, first results related to the interpolation of relative ionospheric delays will be presented. Ionospheric information is extracted from the reference stations - about 125 km apart in our case, along the St. Lawrence river. It is shown that this significantly improves the success rate of ambiguity resolution of phase observations collected by a GPS receiver onboard a survey ship navigating midway between two reference stations.

**G1/E/31-A3** Poster **1620-65**

**STATUS AND DEVELOPMENT OF THE EUROPEAN HEIGHT SYSTEMS**

J. Adam, W. Augath, F. Brouwer, G. Engelhardt, W. Gurtner, B. G. Harsson, J. IHDE, D. Ineichen, H. Lang, J. Luthardt, M. Sacher, W. Schlüter, T. Springer, G. Wöppelmann (members and associated members of the EUREF-Technical Working Group)

After a break of ten years, the work on the United European Levelling Network (UELN) resumed in 1994 under the name UELN-95. The objectives of the UELN-95 project being to establish a unified vertical datum for Europe at the one decimeter level with the simultaneous enlargement of UELN as far as possible to include Central and Eastern European countries. More than 3000 nodal points were adjusted, constraint-free, in geopotential numbers linked to the reference point of UELN-73 (gauge Amsterdam). The new heights in the system UELN-95/98 are available for more than 20 participating countries.

The European Vertical GPS Reference Network (EUVN) is designed to contribute to the UELN project along with the connection of European tide gauge benchmarks as contribution to monitoring absolute sea level variations, the establishment of fiducial points for the European geoid determination. The EUVN includes 195 points all over Europe. At every EUVN point, three-dimensional coordinates in ETRS89 and levelling heights primary in the system of the UELN-95 have to be derived. The GPS computations are finalised, though some levelling connections still have to be realised. At the tide gauge stations of EUVN additional sea level observations have to be included.

The height systems will be developed as a combination of GPS permanent observations, levelling, and geoid information under consideration of well-known vertical movements towards a European kinematic height reference system.

**G1/E/33-A3** Poster **1620-66**

**EFFECTS OF IMPLEMENTATION OF GEOCENTRIC DATUM UPON INTEGRAL DEVELOPMENT OF GEOMATIC ENGINEERING**

LU ZHIPING, Li Hui, Li Baoli (Department of Geodesy, Zhengzhou Institute of Surveying and Mapping, Zhengzhou 450052, China)

Since 1993, National Geodetic Coordinate System 1980 has been put into effect in China as the datum of mapping and other engineering applications in order to gradually substitute Beijing Geodetic Coordinate System 1954. However, the regional reference coordinate system is only an outcome of traditional Geodesy. In the age of modern geodetic surveying, the implemented reference datum should facilitate various uses and coincide with international geodetic datum under the global integration circumstance. Along with the progress in science and technology and the change of user's needs in datum, the regional reference datum is bound to be substituted by kinematic, continuing and highly accurate geocentric datum. This is the inevitable of the integral development of geomatic engineering.

The paper expresses that it is inevitable development to implement geocentric datum in China by analyzing requirements of user's in geomatic engineering, development of geodesy and investigating international trends on adoption of datum. The implementation of National Geodetic Coordinate System 1980 at present maybe well result in that all Chinese geoinformation don't refer to a single, homogeneous, geodetic datum. So it is necessary to implement geocentric datum in China as soon as possible.

**G1/E/35-A3** Poster **1620-67**

**USING ON-LINE ATMOSPHERE MODELS AND PRECISE PREDICTED ORBITS FOR RTK-GPS POSITIONING IN THE SATVB REFERENCE STATION NETWORK**

Helmut TITZ, Johannes Boehm (both at Department of Advanced Geodesy, University of Technology Vienna, Gusshausstr. 27-29, A-1040 Vienna, Austria, email: htitz@luna.tuwien.ac.at)

In August 1997 the BEWAG, a local power supply company in Austria, established in cooperation with the Department of Advanced Geodesy in Vienna a network of 4 permanent GPS reference stations called the SATVB network (Satellitenvermessung Burgenland). The reference stations are interconnected by means of a wide area token ring network which allows for the computation of atmospheric models and correction parameters for distance dependent errors in realtime. Mobile rover stations making use of the correction models are able to do a faster and more reliable ambiguity resolution. Future extensions will also make use of precise predicted orbits (IGP) transmitted to the rovers over the air link.

In addition to the realtime measurements all GPS observations are recorded in RINEX format. This observation data has been processed at a daily basis since January 1998. The resulting time series allow for investigations concerning the ionospheric and tropospheric behaviour as well as for multipath effects. Comparisons between realtime and postprocessing solutions are possible.

**G1/E/36-A3** Poster **1620-68**

**SPECTRAL ANALYSIS FOR TRANSFORMATION PARAMETERS DETERMINATION: THE COLOMBIAN CASE**

Laura Sanchez, William MARTINEZ, Juan Florez. (Instituto Geografico Agustin Codazzi, Carrera 30 No. 48-51, Santafe de Bogota, Colombia, email: lsanchez@igac.gov.co)

The new Colombian reference frame MAGNA (Marco Geocentrico de Referencia Nacional) has been established by the Instituto Geografico Agustm Codazzi (IGAC) as the realization of the SIRGAS datum in Colombia. MAGNA has replaced the old classical network defined on Bogota Datum to which all of the cartographic surveys made in the country have been tied.

In order to make consistent the current cartography with the GPS technique, IGAC computed some sets of transformation parameters using the Bursa-Wolf method, Molodenskiy-Badekas formulae and Helmert transformation. However, they can not take account local deformations of the old frame.

To determine both, systematic and aleatory changes between the Colombian frames, IGAC has proposed a solution that involves spectral techniques. In this way, it is possible to evaluate different sources of deformation, e.g. geometrical weaknesses in the old network, the non-rigorous adjustment, crustal deformations and the poor definition of a geoid model before the 90s.

**G1/E/37-A3** Poster **1620-69**

**FLIGHT STATE MONITORING OF AN AIRBORNE REMOTE SENSING SYSTEM BY USING GPS**

G. XU (National Survey and Cadastre, Rentemestervej 8, DK-2400, Copenhagen, Denmark); L. Bastos (Astronomical Observatorium, Monte da Virgem, 4430 V.N.Gaia, Portugal); R. Forsberg, L. Timmen (GeoForschungsZentrum Potsdam, Telegrafenberg A17, D-14473 Potsdam)

Using GPS for flight state monitoring of an airborne remote sensing system has been carried out in Europe within the EU project AGMASCO. About two Months of kinematic GPS flight data and static data have been collected in four campaigns during the past of three years. Several GPS softwares have been used for the extensive real data processing. In this paper, the general scenario of the campaigns is briefly outlined. The strategies and principle of the data processing are discussed and detailed given. The multiple static reference data are used for kinematic positioning to strengthen the geometric stabilities. Static results are used as conditions for reducing the unknown number and modifying the ambiguity resolution in the kinematic positioning. Multiple kinematic GPS data are evaluated simultaneously for flight state monitoring. Constraints of known distances between antennas fixed on the airplane are introduced into the data processing. Results, precision estimation and comparison are outlined.

**G1/E/39-A3** Poster **1620-70**

**A NEW ADAPTIVELY ROBUST FILRTERING FOR KINEMATIC GEODETTIC POSITIONING**

Yuanxi YANG Xi'an (Research Institute of Surveying and Mapping, No.1 Mid-Yanta Road, 710054 Xi'an, P.R. China)

The Kalman filter has been applied extensively in the area of kinematic geodetic positioning. The reliability of the linear filtering results, however, will degrade when the kinematic model noise is not accurately modeled in filtering or the measurement noises at any measurement epoch are not normally distributed. A new adaptively robust filtering is proposed based on the robust M (Maximum likelihood type) estimation. It consists in weighting the influence of the updated parameters in accordance with the magnitude of discrepancy between the updated parameters and the robust estimates obtained from the kinematic measurements and in weighting individual measurement at discrete epoch. The new procedure is different from functional model error compensation, it changes the variance matrix or equivalently changes the weight matrix of the predicted parameters to cover the model errors. A general estimator for adaptively robust filter is developed, which includes the estimators of classical Kalman filter, adaptive Kalman filter, robust filter, sequential least squares (LS) adjustment and robust sequential adjustment. The procedure can not only resist the influence of outlying kinematic model errors, but also control the effects of measurement outliers. In addition to the robustizing properties, feasibility in implementation of the new filter is achieved through the equivalent



weights of the measurements and the predicted state parameters. A numerical example is given to demonstrate the ideas involved.

**G1/E/41-A3** Poster **1620-71**

#### THE COLOMBIAN NATIONAL GEOCENTRIC REFERENCE FRAME

Laura SANCHEZ (Instituto Geografico Agustin Codazzi, Carrera 30, No. 48-51, Santafe de Bogota, Colombia, email: lsanchez@igac.gov.co); Herbert Tremel, Hermann Dreses (both at Deutsches Geodätisches Forschungsinstitut, Marstallplatz 8, D-80539 Muenchen, Germany, email: mailer@dgfi.badw.de)

The Colombian National Geocentric Reference Frame (Marco Geocentrico de Referencia Nacional, MAGNA) is realized by a GPS base network of 60 stations covering the entire country. The network includes the five Colombian stations of the South American Geocentric Reference System (SIRGAS) and 16 points of the Central and South American (CASA) geodynamics network. It was observed by three GPS campaigns in 1994, 1995 and 1997.

The results presented here are based on a data processing using the Bernese software version 4.0. In a first step, "free network" adjustments of the partial (annual) networks were done using the IGS precise orbits. The internal precision estimated from daily repeatabilities is in the centimeter-level. In the second step, the partial networks are transformed to the SIRGAS stations providing the geocentric orientation. The position accuracy is estimated to be in the order of a few centimeters.

For an external quality check, the MAGNA coordinates are compared with the SIRGAS and the CASA coordinates. Some discrepancies are explained by recent crustal movements, which are very large in this area. A soon repetitive observation of the MAGNA network is necessary to determine the corresponding station velocities.

**G1/E/42-A3** Poster **1620-72**

#### LONG BASELINE OF KINEMATIC GPS

Andy EVANS, Gethin Roberts, Vidal Ashkenazi (IESSG, University of Nottingham, Nottingham, NG7 2RD, UK, email: isxaje@isn1.ieessg.nottingham.ac.uk)

It is well established that static GPS surveying using the carrier wave of the GPS code signal can achieve relative positions at a resolution of a few millimetres suitable for geodetic work. Past developments to improve geodetic positioning solutions in terms of reliability and speed of results has allowed techniques to emerge for the positioning of moving receivers with solutions approaching geodetic accuracies. There are two important areas of consideration when positioning with the carrier wave, these are ambiguity resolution and the modelling of observation errors. On-the-fly (OTF) kinematic GPS is a method specific to carrier wave relative positioning. Over short baselines (<10 kilometres) millimetric accuracies are achievable and thus a viable method for numerous engineering applications. Due to the short baseline constraint observation errors between receivers are negligible and so effective ambiguity resolution is the primary factor. As the baseline length increases so the accuracy degrades as observation errors have greater effect. The focus of this work is to examine methods for increasing the workable baseline length whilst maintaining short baseline accuracy and quick ambiguity resolution. The areas of investigation are the use of multiple reference stations (MRS) to improve the ambiguity resolution process and the modelling of observation errors in the received signals.

**G1/E/43-A3** Poster **1620-73**

#### ATMOSPHERIC LOADING EFFECTS IN GPS VERTICAL TIME SERIES

Marijke Brondeel, Tonie M. van Dam (Royal Observatory of Belgium, Ringlaan 3, B-1180 Brussel, Belgium, email: Marijke.Brondeel@oma.be, Tonie.vanDam@oma.be); Mark SCHENEWERK (NOAA, SSMC3, 1315 East-West Highway, Silver Spring, MD, 20910, U.S.A., email: mark@ness.grdl.noaa.gov)

Atmospheric pressure loading is known to generate noise in GPS vertical time series. Even weekly solutions of GPS determined vertical coordinates are correlated with atmospheric loading in more than 70% of the stations investigated. A recent investigation of these effects indicates they are larger than previously observed. First, we investigate the reason for the larger signal by comparing solutions using the different meteorological data sets (ECMWF, NCEP Reanalysis, and NMC). Second, we present an analysis of the loading effect in one year of GPS heights from 1) Europe (CODE daily solutions), 2) Globally (CODE weekly solutions and 3) Globally (JPL daily solutions). Preliminary results indicate that the loading effects are more significant in the global solutions, presumably due to the fact that for smaller networks the loading is coherent over the station spacing in the network. Furthermore, we compare the Two Coefficient Correlation Equation Method with the Convolution Method for calculating the atmospheric loading effects. Finally we will consider the effects of the loading on GPS orbit determination by calculating orbits with and without pressure loading corrections for one month of GPS data.

**G1/E/45-A3** Poster **1620-74**

#### THE INTEGRATION OF BRAZILIAN GEODETIC SYSTEM INTO TERRESTRIAL REFERENCE SYSTEMS

Sonia Maria Alves COSTA (Department of Geodesy, IBGE, Av. Brasil 15671, Parada de Lucas, Rio de Janeiro, RJ, Brazil, 21241-000, email: soniamaria@ibge.gov.br); Marcelo Carvalho dos Santos (Graduate Program in Geodetic Sciences, Federal University of Parana, CP. 19001, Curitiba, Pr, Brazil, 82531-990, email: mcsantos@geoc.ufpr.br); Camil Gemael (Graduate Program in Geodetic Sciences, Federal University of Parana, CP. 19001, Curitiba, Pr, Brazil, 82531-990, email: cgemael@geoc.ufpr.br)

The motivation for the work described here is on the integration between geodetic reference systems. To begin with, a global and simultaneous adjustment of the Brazilian geodetic network into South American Geocentric Reference System (SIRGAS) was carried out. SIRGAS is considered as the most accurate realisation of ITRF in South America. It is an example of regional network integration based on ITRF/IGS products. In this adjustment, GPS and classical networks are combined on a simultaneous adjustment using Helmert Blocking technique and three-dimensional modelling.

As a second step, these results are integrated into ITRF's versions. The establishment of the Brazilian Network for Continuous Monitoring of GPS (RBMC), with 9 stations in operation since 1997 (the same ones occupied during the SIRGAS campaign), has provided all information for the integration of Brazilian geodetic system into ITRF. The intention is to estimate a velocity field for the RBMC stations, as well as to compare between GPS results and the global plate motion model recommended by the IAG, namely the NNR-NUVEL-1A. For the estimation of velocity field, 4 epochs of GPS data comprising 15 days will be processed with software Bernese version 4.0.

**G1/E/47-A3** Poster **1620-75**

#### PRELIMINARY RESULTS OF THE GPS BUOYS DATA PROCESSING IN THE NORTH WESTERN MEDITERRANEAN SEA

M. MARTINEZ-GARCIA (Dept. Applied Mathematics and Telematics, Universitat Politècnica de Catalunya, c/ Jordi Girona 1-3, 08034 Barcelona, Spain, e-mail: marina@mat.upc.es); J.J. Martinex-Benjamin (Dept. Applied Physics, Universitat Politècnica de Catalunya, c/ Jordi Girona 1-3, 08034 Barcelona, Spain, e-mail: benjamin@grace.upc.es); G.L.H. Kruizinga (Satellite Geodesy and Geodynamics Systems Group, Jet Propulsion Laboratory, Caltech, Pasadena, California, U.S.A., e-mail: Gerhard.Kruizinga@jpl.nasa.gov)

Preliminary results are presented on GPS buoy positioning in the North Western Mediterranean Sea in support of the absolute range altimeter calibration for the US/French altimeter satellite TOPEX/POSEIDON.

The experiment was conducted in March 1999 off the coast near Begur Cape (Catalonia, Spain). The objective is to compare the sea level derived from GPS buoys and TOPEX/POSEIDON and to calibrate the satellite altimeter system. The experiment consisted out of two reference GPS stations on shore and two GPS buoys underneath the TOPEX/POSEIDON ground track. Local tide gauge measurements were used to correct GPS buoy heights to estimate the Mean Sea Surface height along the TOPEX/POSEIDON and ERS-1/2 ground tracks. An analysis of the different techniques and software used in the GPS data processing will be presented.

**G1/E/51-A3** Poster **1620-76**

#### PROSPECTIVE USE OF WIDE AREA AUGMENTATIONS IN THE SOUTHERN HEMISPHERE

Marcio Aquino, Vidal Ashkenazi, Terry MOORE (IESSG, University of Nottingham, Nottingham, NG7 2RD, UK, email: marcio.aquino@nottingham.ac.uk)

The footprint of the Inmarsat 3 series of satellites enables the transmission of augmentation corrections, provided by EGNOS and WAAS, to southern hemisphere regions such as Africa and South America. The integrity and availability functions of both EGNOS and WAAS will be valid worldwide, regardless of the location of the service area where they have been derived, but the same does not apply to the WAD (Wide Area Differential) function. The latter includes orbital and the atmospheric corrections that will best correlate to the area where the corresponding ground network is placed. A regional WADGPS system has been developed at the University of Nottingham, which may overcome this drawback and complement either of the existing augmentation services with regard to the provision of WAD corrections. The "orbit relaxation" technique, in conjunction with improved atmospheric models, form the background for the proposed system. This technique is simpler and less costly to implement than alternative methods of orbit improvement, such as the dynamical orbit determination. Generation of WAD corrections and their application by the user, within the context of the new approach, have been evaluated as part of the project. Initial results of this study were presented at the IAG-97 scientific assembly, primarily relating to tests carried out with simulated data. This paper presents the latest outcome of the investigations. Further validation tests with simulated data were performed and were followed by real data tests. The presentation concentrates on extensive processing of data collected at a Brazilian permanent GPS tracking network. Results are presented and discussed, with a special view to a possible application of the system in Brazil.

**G1/E/52-A3** Poster **1620-77**

#### COORDINATE TRANSFORMATIONS FROM WGS84 TO THE MAPPING DATUM IN IRELAND

Chris HILL, Vidal Ashkenazi, Richard Bingley, Wu Chen, Terry Moore (IESSG, University of Nottingham, Nottingham, NG7 2RD, UK, email: chris.hill@nottingham.ac.uk)

This paper describes two recent projects carried out by the IESSG under a joint contract to the Ordnance Survey of Ireland and the Ordnance Survey of Northern Ireland. The first project was on the design, computation and implementation of a Zero Order GPS based ETRF89 Reference Framework for the whole of Ireland, and its Densification. The methodology used and the results obtained were presented to and accepted by the EUREF Technical Working Group in 1996. The second project established a transformation between the mapping datum (Ireland 1975) and the new GPS-based coordinate reference system. The project investigated three different coordinate transformations. Each was assessed against a series of criteria, such as transformation accuracy, invertibility/reversibility, conformality, extensibility, and uniqueness. Based on this analysis, two dedicated transformation methods were identified to transform coordinates from Ireland 1975 to ETRF89, and vice-versa. This paper briefly outlines the principles and algorithms for the three transformation methods, and the steps taken to evaluate each method against the required criteria.

**G1/E/53-A3** Poster **1620-78**

#### STUDY OF REFRACTION VARIATION OBSERVATION USING VIDEO THEODOLITS

Ismail Kabashi, Günther RETSCHER (both at Department of Applied and Engineering Geodesy, Vienna University of Technology, Gusshausstrasse 27-29 E128/3, A-1040 Wien, AUSTRIA, email: ikabashi@pop.tuwien.ac.at, gretsch@pop.tuwien.ac.at)

Optical observations over long distances are significantly affected by the refraction of the signal. In a research study at our department the observation of refraction variations with video theodolits is currently being analysed. In this paper the results of a series of test measurements will be presented. Thereby observations with the video theodolite are taken between two buildings of the Vienna University of Technology over an about 400 to 500 m long distance at changing weather conditions. The angles are observed with sampling rates of up to 10 Hz, i.e. 10 observations per seconds. In comparison this baseline is also observed with GPS.

**G1/E/54-A3** Poster **1620-79**

#### TRANSFORMATION BETWEEN GEODETIC SYSTEMS WITH RESIDUAL MODELLING

Marcelo Carvalho dos SANTOS (Universidade Federal do Parana, Departamento de Geometria, C.P.19001, Curitiba, Pr, Brazil, CEP: 82531-990, email: mcsantos@geoc.ufpr.br); Moises Ferreira Costa (Universidade Federal do Parana, Departamento de Geometria, C.P.19001, Curitiba, Pr, Brazil, CEP: 82531-990, email: mfcosta@geoc.ufpr.br)

A methodology intended to allow transformation between geodetic systems in which the distortions of the networks are taken into account is described and tested. Typically, only a similarity transformation is used, resulting in 7 parameters that portray the relationship between the systems. In our approach, the distortions are accounted for by treating the residual field (entries of the residual vector) as a mathematical surface. Therefore, besides the 7 parameters,



corrections are applied for each and every coordinate allowing a point-to-point transformation. The methodology was tested for transforming between two realisations of the Brazilian Geodetic System (BGS). Only a part of the BGS was used, in an area covering the State of Parana. A comparison between the application of the 7 parameters transformation only with the referred methodology (7 parameters transformation plus residual modelling) has shown an 84% improvement when applying the methodology. In this study, the residual field was approximated by a fourth order polynomial.

**G1/E/56-A3** Poster **1620-80**

#### REAL TIME GPS MONITORING OF RIVER LEVELS

Terry MOORE, Gethin Roberts, Kefei Zhang (IESSG, University of Nottingham, Nottingham NG7 2RD, UK, email: terry.moore@nottingham.ac.uk), Vidal Ashkenazi, Mark Dumville (Nottingham Scientific Ltd, University Park, Nottingham, NG7 2RD, UK), Gareth Close (Science Systems (Space) Ltd, Bristol, UK); Roger Moore (Institute of Hydrology, Wallingford, UK)

This paper presents current progress of the project "River Level Monitoring Using GPS Heighting (RiGHt)" conducted at the University of Nottingham in partnership with Science Systems (Space) Ltd and the Institute of Hydrology, awarded by the British National Space Centre (BNSC), under the UK Government's Space Foresight Programme. The aim of the project is to demonstrate how space technologies may be used to address the problem of continuously monitoring river heights at any point in the world, from a remote platform. This paper presents a space-based real-time river level monitoring system using kinematic GPS, satellite communication and GIS techniques. A GPS receiver is mounted on a river buoy together with other sensors for water quality sampling and attitude determination of the buoy. Communication satellites are used for the datalink between the buoy and the GPS reference stations. The system architecture, configuration and instrumentation of such a comprehensive river level monitoring system are described, and operation and applications of such a buoy are discussed. Field trials have been conducted using both a buoy simulator and a prototype integrated positioning system onboard a buoy. Preliminary results show that a consistent millimetre precision of the RTK GPS water level measurements can be achieved. The continuing investigation will also be described, with the aim of developing a reliable and practical system. The ultimate goal is to remotely monitor river levels in real-time, in a cost-effective manner and with high precision.

**G1/E/57-A3** Poster **1620-81**

#### DEVELOPMENT AND MAINTENANCE OF GEOCENTRIC REFERENCE FRAME IN THE CZECH REPUBLIC AND ITS USE FOR MODERNIZATION OF TERRESTRIAL GEODETIC CONTROL

Jan Kostecky, Jaroslav SIMEK (Research Institute of Geodesy, Topography and Cartography, Geodetic Observatory Pecny, 251 65 Ondrejov 244, CZ, email: gope@asu.cas.cz)

Starting with November 1991, the EUREF reference frame was established with the help of BKG Frankfurt am Main and a little later densified by a sequence of EUREF post-campaigns performed by the Czech National Geodetic Agencies in 1992-1994, to the present density 1 point/400 km sq. The geodetic frame, formed in this way, was used together with existing S-42/83 for an essential modernization of the obsolete civilian system S-JTSK for its new version S-JTSK/95. In addition to it so called "Basic Geodynamical Network" which integrates precise GPS, levelling and gravity measurements, was established in 1996 and since that time has been periodically re-measured several times. Research Institute of Geodesy is also taking an active part in further development of EUREF by operating in Local Analysis Center of EUREF Permanent Network, EUVN pre-processing and analysis center and by continual evolution of time series of observations of a number of European permanent GPS stations. Methods used for merging different EUREF post-campaigns in the Czech Republic and procedures related to creating new civilian system S-JTSK/95 are described in more detail as well as some results stemming from new projects. An outlook is attached describing present activities towards further densification of the EUREF frame and integration of horizontal and vertical geodetic control.

**G1/E/60-A3** Poster **1620-82**

#### GEOIDAL GEOPOTENTIAL AND WORLD HEIGHT SYSTEM

Working Group Global Geodesy Topics: Satellite Altimetry Applications (WG GGT): Milan Bursa (Astronomical Institute, Academy of Sciences of the Czech Republic, Prague, CR, email: bursa@ig.cas.cz); Jan Kouba (Geodetic Survey Division, Natural Resources Canada, Ottawa, Canada, email: kouba@geod.enr.ca); Muneendra KUMAR, Scott A.True (National Image and Mapping Agency, St.Louis, MO 63118-3399 USA, email: KumarM@nima.mil, TrueS@nima.mil); Achim Muller (Federal Armed Forces, Geographic Office, Euskirchen, Fed.Rep. of Germany, email: amil-geo@t-online.de); Karel Radej, Viliam Vatr, Marie Vojtiskova (Topographical Service of the Army of the Czech Republic, Topographical Institute VTOPIÚ, Dobruška, CR, email: vatr@vtopu.army.cz, vojtskova@vtopu.army.cz)

The geoidal potential value of  $W_0 = 62\,636\,855.6 \pm 0.5\text{m}^2\text{s}^{-2}$ , determined from 1993-1998 TOPEX/POSEIDON altimeter data, can be adopted for the practical definition and realization of the World Height System. The  $W_0$  - value can also uniquely define the geoidal surface. The  $W_0$  - value is required for a number of applications, including the General Relativity in precise time keeping and time definitions. Furthermore, the  $W_0$  value provides a scale parameter for the Earth that is independent of the tidal reference system. All of the above considerations make the geoidal potential  $W_0$  ideally suited for official adoption as one of the fundamental constants, replacing the currently adopted semi-major axis  $a$  of the mean Earth ellipsoid. Vertical shifts of the Local Vertical Datum (LVD) origins can easily be determined with respect to the World Height System (defined by  $W_0$ ), using the recent EGM96 gravity model and ellipsoidal height observations (e.g. GPS) at leveling points. Using this methodology the LVD vertical displacements for the NAVD88(North American Vertical Datum 88), NAP (Normal Amsterdam Peil), AHD (Australian Height Datum), KHD (Kronstadt Height Datum), and N60 (Finnish Height Datum) were determined with respect to the proposed World Height System as follows: -59.1 cm, -14.9 cm, +38.3 cm, -15.5 cm and -2.2 cm, respectively.

**G1/L/01-A3** Poster **1620-83**

#### GPS PRECISE POINT POSITIONING (PPP): REPEATABILITY EXPERIMENTS

Paulo C.L. SEGANTINE (Sao Carlos Engineering School, Univ. of Sao Paulo, Brazil, email: seganta@st.eesc.sc.usp.br); S. Wichayangkoon (Dept. of Civil Engineering, Faculty of Engineering, Thammasa Univ., Thailand, email: wichay@spatial.maine.edu)

Since the establishment of IGS with the multi-international cooperation in 1993, the accuracy of IGS products has been improved dramatically, particular the GPS orbits and clock information. JPL as one of IGS Analysis Centers has recently launched automated service for analyzing single station observations using the GIPSY-OASIS II software. JPL orbits are at the same accuracy, or slightly better than JPLs. However, JPL clock information is better than that

of IGS. JPL Auto service uses its information for Precise Point Position (PPP) analysis. PPP provides solutions as centimeter level for dual-frequency observation. PPP has been proven to be computationally efficient since the engagement to a network is avoided, in addition to base satellite and base receiver. The result of the analysed position is free of network distortion and is in the OTRF96 reference frame rather than a relative position.

This analysis experiments with repeatability of different length of observation data in PPP. The accuracy of PPP depends upon given approximate position as well as observation length. GPS observation data with 1-, 2-, 3-, 4-, 8-, 12-, and 24-hour length is tested. The accuracy of 1cm seems to be stabilized after x hours of observation. Sub-centimeter accuracy absolute positioning is obtained for more than 12-hour data.

**G1/L/02-A3** Poster **1620-84**

#### GPS - AN IMPORTANT TECHNOLOGY IN CARTOGRAPHIC BASES GEOCODING

Paulo C.L. SEGANTINE, Maurício Roberto Veronez, Eliana Ederle Dias Chaves, Reginaldo Macedônio da Silva (São Carlos Engineering School, EESC/USP, Department of Transportation, Post office box 359, CEP 13560-250, São Carlos, São Paulo, Brazil, email: seganta@st.eesc.sc.usp.br)

Nowadays, with the progress of the computer science, some activities began to appear in a preoccupating way. It is the case of the establishment of a Geographic Information System - GIS without the necessary attention with the cartographic base quality. It is essential in case of GIS for the manipulation of spatial data. The quality of a cartographic base is directly related with the scale and with the reference system of the map. The geocoding of a cartographic base is only possible using coordinates transformation parameters. This paper has the intention to show the importance of the use of the GPS system in the cartographic base geocoding through a study of case through two simulations. In the first one it was considered that the study area is not associated to any reference system, that is, just related with a local topographical system. In the second one, the base is geocoded in UTM system (Hayford) and through a transformation Afin this base also went compatible with the local topographical system. In both simulations, the validity of the proposals methodologies was tested in function of 15 controls points distributed in the whole study area and very identifiable in the land and in the map.

**G1/L/04-A3** Poster **1620-85**

#### EFFECTS OF SOFTWARE-NOISE AND REFERENCE-NETWORK-NOISE ON GPS-RESULTS, SHOWN FOR AN EXTENDED GPS NETWORK IN ANTARCTICA

W. NIEMEIER, H. Salbach (Technical University Braunschweig, Pockelstraße 4, D-38106 Braunschweig, Germany); R. Dietrich, R. Dach, J. Perlt (Technical University Dresden, Germany); H.W. Schenke, T. Schöne (Alfred-Wegener Institut, Bremerhaven, Germany); G. Seiber, F. Menge, C. Völsken (University Hannover, Germany); K. Lindner, M. Mayer (University Karlsruhe, Germany)

In 1995 and 1998 large-scale GPS - Campaigns could be realized for the Atlantic Sector of Antarctica, a region of special interest for geosciences. This Antarctic network was tied into the ITRF-IERS terrestrial reference frame by including several well-spread ITRF stations in the southern hemisphere into the processing of the data and embedded into the IGS by using precise IGS-orbits. The campaigns were coordinated by the Scientific Committee of Antarctic Research (SCAR) and were only possible by extensive international support and participation. Each group had processed the data separately, applying its own software package, using its own selection of fiducial stations and defining its own strategy to determine the solution. In this paper the following items will be pointed out: Basics for the establishment of this network to serve for various scientific activities.

**G1/L/08-A3** Poster **1620-86**

#### MEDIUM-RANGE GPS POSITIONING TECHNIQUES AND THEIR APPLICATIONS

Shaowei HAN, Chris Rizos (School of Geomatic Engineering, The University of New South Wales, Sydney NSW 2052, Australia, email: s.han@unsw.edu.au, c.rizos@unsw.edu.au)

Continuously operating GPS networks are increasingly being established to support surveying, mapping, or navigation applications, often with reference receiver separations of the order of 100 or more kilometres. Carrier phase-based, medium-range GPS kinematic positioning can potentially provide centimetre accuracy trajectories even when the separation between the mobile receiver and reference receiver(s) is many tens of kilometres. Such a technique is based on a linear combination functional model, formed from the single-differenced functional equation for baselines from the mobile receiver to three or more reference receivers. The orbit bias and ionospheric delay can be eliminated, and, in addition, the tropospheric delay, multipath and observation noise can be significantly reduced. In this paper, further test results are described for the following scenarios:

- 1 Medium-range, single-epoch GPS positioning using state-of-the-art GPS receivers.
  - 2 Medium-range, rapid static positioning for geodetic network densification using low-cost, single-frequency GPS receivers.
  - 3 Establishment of a high precision, high density geodetic network using low-cost, single-frequency GPS receivers, for example, to determine the spatial characteristics of crustal deformation across an area of interest.
- Three examples: (a) the single-epoch GPS kinematic positioning experiment, (b) the Taiwan geodetic network densification, and (c) the Indonesian GPS-based volcano monitoring network, are described, and further comments are given with regard to future implementation scenarios.

**G1/L/09-A3** Poster **1640-87**

#### A GEODETIC NETWORK FOR MONITORING CHANGES IN REGIONAL GROUND LEVEL IN THE THAMES ESTUARY AND GREATER LONDON

Richard BINGLEY, Simon Booth, Nigel Penna, Vidal Ashkenazi (IESSG, University of Nottingham, Nottingham, NG7 2RD, UK, email: richard.bingley@nottingham.ac.uk)

Small ground movements can have major strategic or economic significance in certain regions of the world, for example in low lying river estuaries and coastal regions susceptible to flooding. One such region where small ground movements are exhibited is the Thames Estuary and Greater London, warranting the construction of tidal defences, such as the Thames Barrier.

In 1996, the UK Environment Agency initiated a project involving the IESSG and the British Geological Survey. The objective was to develop a generic strategy for monitoring changes in regional ground level using GPS and the ITRS, and providing an interpretation of such changes in terms of local and regional geology. The strategy developed is based around the use of a small number of continuously operating GPS receivers, acting as reference stations for a dense network of monitoring stations, observed using episodic GPS measurements. The strategy has been tested in the Thames Estuary and Greater London region, and the presentation will give details of the establishment of the monitoring network and the results from the first two years of measurements.

**G1/L/12-A3** Poster **1620-88**

**MODELLING AND CORRECTION OF GPS/GLONASS OBSERVATION DATA USING TIME SERIES METHODS FOR IMPROVING SURVEYING PRECISION**

Minghai JIA, Maria Tsakiri, Mike Stewart (all at School of Spatial Sciences, Curtin University of Technology, GPO Box U 1987 Perth WA 6845, Australia, email: jia@vesta.curtin.edu.au)

Since the observation data from GPS/GLONASS are contaminated by multiple complicated error sources, the GPS/GLONASS observation errors rarely subject to a normal distribution. Even specific techniques to reduce the observation errors, such as diverse differential methods, have been widely used, there still exist some patterns in the observation errors in some circumstances such as the multipath delay errors in the monitoring of open pit walls and the residual ionospheric refraction errors in the processing of the long baselines. In this study, time series methods have been used for the modelling and correction of diverse GPS/GLONASS observation data including the non-differences and the diverse differences of pseudorange and carrier phase data as well as their different frequency combinations. The developed procedure has been merged into the GPS/GLONASS software developed by Curtin University of Technology.

Trial results for the data sets from different circumstances have shown that the developed procedure can build reliable models for the data sets. An ARMA (1, 2, 0) model, for example, to all visible satellite is applicable for a specific non-difference carrier phase data set at a sampling rate of 1Hz. Using the developed procedure, some errors such as the multipath delay errors and the residual ionospheric refraction errors can be largely modelled and corrected, and also, the slips of one to two cycles in GPS observation data been detected and corrected. Improvement of the modelling rate is expected for perfecting the developed procedure.

**G1/L/13-A3** Poster **1620-89**

**REAL TIME POSITIONING BY DIFFERENTIAL GPS IN THE WESTERN MEDITERRANEAN SEA**

S. KAHLOUCHE, A. Zeggai, A. Ayouz, S. Touam, H. Abbas, S. Benahmed Daho (Geodetic Laboratory, National Centre of Spatial Techniques, CNTS BP 13, Arzew 31200, Algeria); H. Mouheb (Office National de Signalisation Maritime, 9 Bd Amirouche, Algiers 16000, Algeria)

The setting up of the three DGPS emitting stations (Oran, Algiers and Jijel) for maritime applications in the south basin of the western Mediterranean sea needed a choice of site implantation for the optimal covering of the Algerian coast.

The geodetic configuration, initially based on the ADOS (African Doppler Survey) network with a metric accuracy, was carried out by the establishment, in the WGS84 system of a precise absolute network determined from the TYRGEONET (Tyrrhenian Geodetic Network) network established for regional geodynamical studies in the western Mediterranean. The GPS observing campaigns, using the Ashtech Z-12 receivers, are processed with PRISM software and provided a centimetre accuracy of the stations.

The use of the emitting stations (range of 800 Km) permit, from the differential corrections elaborated, a real time positioning (every 0.6 s) with a metric (2 m) accuracy. The maritime applications in the local reference system (Nord Sahara) needs the determination of the transformation parameters from the establishment of a coastal network.

**G1/L/14-A3** Poster **1620-90**

**THE NEW NATIONAL HEIGHT SYSTEM (LHN95) OF SWITZERLAND**

A. Schlatter, U. MARTI (both Federal Office of Topography, Seftigenstrasse 264, CH-3084 Wabern, Switzerland, email: Andreas.Schlatter@t.admin.ch, Urs.Marti@t.admin.ch)

The existing old height system of Switzerland (LN02) consists of purely levelled heights without considering gravity measurements. This causes difficulties in the application of modern techniques such as GPS for height determination in mountainous areas and in the data exchange with neighbouring countries. Therefore, a new rigorous height system LHN95, based on geopotential numbers and the corresponding geoid, is being determined at the Federal Office of Topography (L+T) in collaboration with the Federal Institute of Technology at Zurich. LHN95 not only serves as the new National Height Network but it also fulfills the demands of large engineering projects. LHN95 is treated as a kinematic network with respect to the Alpine uplift which reaches amounts of up to 1.5 mm/year. The corresponding relative vertical movements are determined by repeated observations of the first and second order levelling lines. For LHN95, it was decided to use ortho-metric heights. This implies the use of the geoid as the reference because it has a smooth surface and can be interpolated easier than the quasigeoid.

First results can now be presented from these extensive computations. Of special interest is the information obtained on recent vertical movements in Switzerland resulting from a dense network of repeated measurements. From the comparison of LHN95, the new geoid for Switzerland (GEOID98, Marti) and the repeated observations of the new satellite-based national control survey (LV95), informative conclusions may be drawn concerning the possibilities of absolute height determination in Alpine regions with height differences of over 2000 m.

- Software Noise: The effect of different software packages and strategies on the results of the GPS data processing
- Reference network noise: The effect of a different number of fiducials and differences in their stochastics on the resulting coordinates.

**G1/L/15-A3** Poster **1640-91**

**SATELLITE GEODESY ON CURVED MANIFOLDS**

SCHWARZE

A consistent model for satellite geodetic observations is developed within the framework of general relativity at post-Newtonian level. The theoretical model consists of three parts. The first part considers the motion of some satellite vehicle, the second the propagation of electromagnetic waves and the third the definition of observable quantities.

The satellite vehicle, the electromagnetic wave and the observer are considered to move on a curved four-dimensional manifold of pseudo-Riemann type. The impact of the relativistic model on the geodetic adjustment process is considered by the simulation of several satellite based positioning scenarios involving several differencing techniques (single-, double- and triple-differences).

**G1/L/19-A3** Poster **1640-92**

**FUTURE DIRECTIONS OF THE NATIONAL CORS SYSTEM**

WESTON

The National Geodetic Survey (NGS) continues to enhance the continuously operating reference station (CORS) system, thereby improving people's ability to use Global Positioning System (GPS) data for positioning points with cm-level accuracy throughout the United States

and its territories. People also use CORS data to develop geographic information systems, to monitor crustal deformation, to determine the distribution of water vapor in the atmosphere, to support remote sensing applications, and to monitor the distribution of free electrons in the ionosphere. To enhance the CORS system, NGS is steadily increasing its spatial coverage by adding an average of 3 new CORS sites per month. (In December 1998, the system contained 145 sites.) In addition, NGS plans to regularly upgrade its user-friendly CORS information server, making CORS data and related information (descriptive text, site positions and velocities, GPS ephemerides, selected meteorological data etc.) more readily accessible via the Internet. Also the agency is:

- generating digital models of: antenna-phase-center variation, crustal motion, total electron content in the ionosphere, and geoid heights;
- supporting research to develop a reduced multipath GPS antenna;
- investigating the possibility of providing nationwide digital maps of pertinent meteorological data to enable more rigorous GPS processing;
- striving to produce and provide accurate GPS ephemerides and digital models more rapidly so that the users can determine accurate point positions in a timely manner.

Moreover, NGS is continuing to study how enhancements to the CORS system impact positioning accuracy and its dependence on the distance to the nearest CORS site and the duration of an observing session.

**G1/L/20-A3** Poster **1640-93**

**A NEW QUALITY CRITERION FOR GPS MEASUREMENTS**

Kerstin WIENHOLZ (TU Berlin, Str. d. 17. Juni 135, D-10623 Berlin, Germany, email: wienholz@inge3.bv.tu-berlin.de)

The GPS signal can be disturbed by cycle slips, multipath and refraction effects. These factors can influence the ambiguity fixing. The resulting coordinates are therefore affected by the accuracy and reliability of the determination of ambiguities. Especially for networks with longer baselines the computation of ambiguities is still an unresolved problem. Today, the average user has no other choice than to trust the results of the GPS phase measurements. The only available additional information (besides coordinates) is restricted to the P-DOP value, which represents the quality of the geometrical configuration of satellites.

This study introduces a supplementary criterion based on further sources of disturbance. For this we need a trustworthy preprocessing of GPS data to obtain cycle slips and a new method for the ambiguity fixing. The necessary parameterization of the observation equations is being presented. This parameterization contains also an elimination of several unknowns. Using the resulting quality factor the user can decide between a longer observation time or stopping the measurements. This is especially important in GPS realtime measurements because the observer gets coordinates and their quality estimate at the same time. In the future, a broader range of the radio transmission of the information from the base station to the rover will make realtime phase observations within larger areas possible. Than the demonstrated method can become an important part of the realtime processing.

**G1/L/21-A3** Poster **1640-94**

**THE UNIFICATION OF GLOBAL VERTICAL DATUMS**

KEARSLY

Since at least the mid-1970's, a unified global vertical reference system has been the desire of many geodesists, and the subject of successive IAG Special Study Groups. These have been formed to study, inter alia, "methods for the determination of a unique global vertical reference surface", and "strategies for developing and implementing a World Vertical Datum". With the advent of GPS, other space-based techniques, and the development of the ITRF and regional GPS super-control networks, we now have the means to link vertical datums geometrically. Some campaigns have had as their specific aim the strengthening of the regional vertical datum (e. g., EUVN; NAVD). However, for most of these networks the vertical component has been of secondary, if any, interest - their primary intent was to provide control for GPS surveys, superior geodetic infra-structure for regional GIS's (e.g., APRGP97), or a means of tracking horizontal deformation (e. g., GEODYSSSEA). Nevertheless, it is possible to make use of these latter campaigns, as they provide an invaluable source of vertical data. We now also have with the production of superior global geopotential models (e. g., EGM96), a globally recognised physical reference surface. We thus have the capacity to bring to a full realisation the goals of those earlier Study Groups. In this presentation I will be proposing a strategy which, by involving national and regional authorities, national vertical datums can be tied into the regional GPS super-control networks and, indirectly or directly, onto the ITRF. The properties desired of such tie points will be proposed, and the problems associated with such ties, (e. g., distortions in a national vertical datum) foreshadowed, with possible solutions proposed.

**G1/L/22-A3** Poster **1640-95**

**THE SINGAPOREAN GPS REFERENCE RECEIVER NETWORK: AN "OPEN AIR" LABORATORY FOR INNOVATIVE HIGH PRECISION GPS TECHNIQUES**

Chris RIZOS, Shaowei Han (both at School of Geomatic Engineering, The University of New South Wales, Sydney, Australia, email: c.rizos@unsw.edu.au, s.han@unsw.edu.au); Pong Chai Goh, Tam Khoon Tor (both at School of Civil & Structural Engineering Nanyang Technological University, Singapore, email: cpcgoh@ntu.edu.sg, cpcgoh@ntu.edu.sg)

Continuously operating GPS networks have been used for many years to address two types of positioning applications. The first, perhaps the best known application, is in support of geodetic goals such as the determination of crustal motion on a variety of spatial scales - from the measurement of the broad kinematics of tectonic plates to deformation monitoring of local areas. Currently, hundreds of permanent GPS stations around the world are now formally part of the global network known as the International GPS Service (IGS). The second class of applications that have traditionally been addressed by continuously operating GPS receiver networks are those that require real-time, differential GPS (DGPS) services over many hundreds of kilometres, to determine coordinates to accuracies of the order of a few metres. The DGPS corrections to pseudo-range data are determined at groups of permanent GPS stations which service wide continental or oceanic regions, using a positioning technique generally referred to as Wide Area DGPS.

The population of continuously operating GPS receivers is growing. Some are being established to address a single application, while others are designed for multi-functional use. In some countries permanent GPS stations are intended to support local surveying users. However, the GPS reference receivers, because of their high cost, often cannot be established in a dense enough configuration to satisfy all user requirements. For example, GPS surveying typically requires receiver separations of less than 30km (and even <20km for OTF-kinematic and rapid static positioning techniques). In this paper, several new static and kinematic GPS techniques for user positioning which are optimised for GPS baseline lengths of the order of 50-100km are described, and the role of the Singaporean GPS reference receiver network in the development and testing of such techniques is highlighted.

One implementation is a form of "densification" of a network of dual-frequency GPS receivers



in which a permanent array of single-frequency GPS receivers is deployed to increase the basic network spatial resolution. Such an implementation would benefit deformation monitoring applications. Another implementation is analogous to the "rapid static" GPS surveying technique, but using a network of base receivers. An enhanced (single-epoch) OTF-kinematic technique suitable for real-time positioning applications is also described. What makes the Singaporean network unusual is that the permanent GPS reference receivers are linked by high speed datalinks to a single control station in a manner analogous to the WADGPS systems, simplifying testing and simulating a real-time operational environment for such techniques.

**G1/L/25-A3** Poster **1640-96**

**TRANSFORMATION OF WGS84 CO-ORDINATES IN LOCAL DATUM USING GPS BASELINES**

A. ZEGGAI, S. Touam, B. Ghezali, N. Nabel (Geodetic Laboratory, National Centre of Spatial Techniques, BP 13 Arzew, 31200, Algeria)

The co-ordinates transformation models between geodetic reference systems (Bursa-Wolf, Molodensky-Badekas, Veis) are generally the most used to compute the transformation parameters if both systems are identical. The accuracy obtained depends on the accuracy of the co-ordinates used.

In the case of Algeria, the parameter computation remains altered by the total absence of information of the geoid undulation above astro-geodetic ellipsoid (Clarke 1880 A). The planimetric solution proposed from the computation of the geodetic baselines (azimuth, geoidic length) can give better results if we consider azimuthal correction and scale Variation bei between both lengths (in both systems). This problem is particularly important for geodetic and cadastral works in the south region of ALGERIA (Sahara) where the geodetic data are not sufficiently available (GPS and National bench marks, spirit levelling, etc). An experimental network based on GPS baselines measurements with bifrequency receivers, was observed in the south west of ALGERIA (Oran - Bechar). The accuracy given from preliminary results is about 2 to 3 cm for short baselines 2 to 15 kilometres) and metric for long baselines (500 kilometres).

**G1/L/26-A3** Poster **1640-97**

**GPS SATELLITE ORBIT PERTURBATIONS DUE TO THE SOLAR WIND: INITIAL RESULTS**

Marek ZIEBART, Peter Dare (both at Applied Geodesy Research Unit, School of Surveying, University of East London, Longbridge Road, Dagenham, Essex RM8 2AS, UK, email: marek@uel.ac.uk, peter@uel.ac.uk)

Orbit representation customarily uses time-tagged position and velocity vectors. These are determined by solving the satellite's second order differential equation of motion. The non-gravitational forces modelled include solar radiation pressure (SRP). Empirical scaling factors for the SRP models are usually applied to compensate for modelling errors. Accelerations due to the solar wind, have previously not been modelled. Most of the solar wind is deflected away from the Earth at 6-10 earth radii, whereas at the magnetic poles particles from the solar wind spiral down to lower altitudes. This flux may act as a perturbing acceleration to the GPS orbit. Variations in the SRP scaling factors are considered. Time-tagged scaling factor data is used to compute a fourier series for each satellite. This data is used to map the satellite ground tracks, colour graduated with the SRP scaling factor. An algorithm is also developed to compute the orientation of the satellites' solar panels with respect to a simplified model of the Earth's magnetic field. There appears to be a correlation between the satellite attitude and the magnitude of the SRP scaling factors which may be due to the flux of the solar wind particles in the magnetic field interacting with the satellite. Orbit analysis is carried out using GIPSY-OASIS II.

**G1/C/G5/E/05-A3** Poster **1620-98**

**ON THE PERMANENT EARTH TIDES**

Wenke SUN, Lars E. Sjöberg (both at Royal Institute of Technology, Department of Geodesy and Photogrammetry, S-10044 Stockholm, Sweden, e-mail: sunw@geomatics.kth.se)

The tidal deformation caused by the luni-solar potential includes not only a periodic part, but also a time-independent part, called the permanent tide. How to deal with the tidal correction in gravimetric observations, especially the treatment of the permanent tide, has been discussed for a long time (e.g. Honkasalo 1959; Heikkinen 1979; Ekman 1989), since some practical and physical problems exist anyhow. To avoid the problems, Ekman (1979) and Groten (1980) proposed that the permanent tidal attraction of the Moon and the Sun are eliminated, but the permanent tidal deformation of the Earth is maintained. This is called zero gravity and the geoid associated with it is the zero geoid. This concept was accepted in a resolution of IAG in 1983. As to the crust deformation, Poutanen et al. (1996) suggested that coordinates should be reduced to the zero crust, i.e. the crust that includes the effect of the permanent tide. This research shows that horizontal components of the permanent earth tides, which have never been considered up to now, is also important in GPS positioning and geoid determination. Since the tide-generating potential can be expanded into harmonics and divided into two parts: geodetic coefficients and the group of harmonic waves, the permanent earth tides can be easily obtained by multiplying the amplitude of the zero-frequency wavelength by the corresponding geoid geodetic coefficient. Results show that the vertical permanent crust change reaches -12 cm at the poles and 6 cm at the equator. The horizontal permanent crust displacement and geoid deflection also reach as much as 2.5 cm and 8.9 cm, respectively. According to the solution of IAG (1983), the permanent vertical components are kept in GPS positioning and geoid computation. Thus, it is natural to include the horizontal components correspondingly.

**G1/C/G5/E/09-A3** Poster **1620-99**

**THE METHOD OF IMITATING BLOCK MOTION IN ESTABLISHING REGIONAL GEODEIC DATUM**

Lu ZHIPING (Department of Geodesy, Zhengzhou Institute of Surveying and Mapping, Zhengzhou, 450052, P.R.China); Liu Jingnan (Wuhan Technical University of Surveying and Mapping, 39 Luoyu Road, Wuhan, 430070, P.R.China)

The high-density and high-precision GPS geodetic network in China, called the scientific engineering "China Crustal Movement Observation Network", is carrying out since 1998, which is the occasion of establishing Chinese practical regional kinematic geodetic datum. In order to make practical application convenient, we define kinematic datum parameters (e.g., rotation of block), which is similar to static datum parameters (e.g. ellipsoid and orientation parameters). And the added parameters are corresponding to a certain block, not corresponding to a point such as velocity parameters in ITRF. So a group of kinematic parameters can be resolved using multi-point observed data in the same block. In practice, the

coordinates change so slow that they would not affect engineering application such as digital mapping for 20-30years. But once considered, the time dependency of the datum established in this method can ensure the continuity of datums in different periods and make relative positions unchanged within the block.

The concrete processes of the method are as follows: First, dividing the tectonic blocks which can be reflected by observed data. This will refer to geological and geomorphic models, but completely determined by the precision and time-scale of observed data. Second, resolving the motion parameters of each block by the combined adjustment. The concrete types of motion models led into adjustment model are determined through model tests before the adjustment.

**G1/C/G5/E/04-A3** Poster **1620-100**

**VELOCITY FIELD ESTIMATION FOR GEODEIC NETWORKS USING METHOD MODIFIED KALMAN FILTERS**

Wu CHEN, Cahit Tagi Celik, Richard Bingley, Vidal Ashkenazi (IESSG, University of Nottingham, Nottingham, NG7 2RD, UK, email: wu.chen@nottingham.ac.uk)

The use of permanent GPS networks has been expanding rapidly over recent years, providing great opportunities for geodynamics research. With long-term observations, horizontal and vertical movements on the Earth can be precisely measured and used to form coordinate time series. Kalman filtering techniques can then be used as an efficient way to estimate station velocities from these coordinate time series. However, any short-term local motion (eg due to an earthquake) or inconsistencies in the coordinate time series (eg due to GPS equipment changes) can contaminate the velocity estimates for a significant period when using a conventional Kalman filter. In order to overcome this problem, two types of modified Kalman filter have been developed and implemented. The first tries to reduce the velocity estimate error by modifying the covariance matrices, and the second uses an adaptive filter to estimate the local movement separately.

The performance of these two modified Kalman filters has been tested using a real/simulated data set, based on the effect of the 22 November 1995 earthquake on a geodetic network in the East Mediterranean. The presentation will give details of the modified Kalman filters and will compare their performance, based on the results obtained using the real/simulated data set.

**G1/C/G5/E/02-A3** Poster **1620-101**

**REVIEW OF THE REALIZATIONS OF THE INTERNATIONAL TERRESTRIAL REFERENCE SYSTEM AND CURRENT RESULTS**

Zuheir ALTAMIMI, Claude Boucher, Patrick Sillard (all at IGN/ENSG/LAREG, 6-8 Avenue Blaise Pascal, 77455 Marne-la-Vallée, France, email: altamimi@ensg.ign.fr)

Since the creation of the IERS in 1988, the International Terrestrial Reference System (ITRS) is realized nearly yearly through the International Terrestrial Reference Frame (ITRF). A review of these realizations are presented in this paper, focused on their quality as well as the progress achieved to improve the ITRF implementation. Specific attention is given to the most recent ITRS realizations, namely ITRF96 and ITRF97 which represent the "starting point" of new generation of ITRF solutions based on more rigorous physical and statistical combination modelling. The most current results and analysis of ITRF are presented in this paper.

**G1/C/G5/E/15-A3** Poster **1620-102**

**IGS REALIZATIONS OF ITRF, AN UPDATE**

R. FERLAND, D. Hutchison, Y. Mireault (all at 615 Booth Street, Ottawa, Ontario, Canada, K1A 0E9, e-mail: ferland@geod.nrcan.gc.ca, hutch@geod.nrcan.gc.ca, mireault@geod.nrcan.gc.ca)

The objectives of the International GPS Service (IGS) realization of the International Terrestrial Reference Frame (ITRF) are to provide an accurate, consistent and unique set of station coordinates, velocities and Earth Orientation Parameters (EOP). The consistency is ensured by simultaneously combining the station coordinates and EOP using their variance-covariance information. The Analysis Centers (AC) compute a new solution every week containing station coordinates and daily EOP. The Global Network Associates Analysis Centers (GNAAC) combine these AC solutions. The final results are based on a unique combination of the GNAAC weekly solutions. The IGS realization of ITRF is accomplished by aligning the solutions to a carefully selected set of 47 reference frame stations. There are currently more than 180 stations in the network with an objective of 200 to 250 well distributed stations. Over 3 years of weekly solutions have been combined. Weekly geocenter estimates are extracted. The formal sigma weekly time series on the geocenter indicates a gradual improvement in the solutions. The geocenter Z component shows an annual period with amplitude of about 25 mm. The RMS residuals at the reference frame stations are 3-4 mm horizontally and 9-10 mm vertically. A spectral analysis of the residuals shows the presence of a small annual and/or semi annual period at some stations mainly in the vertical component. EOP comparisons will also be analyzed.

**G1/C/G5/W/18-A3** Poster **1620-103**

**INVESTIGATION OF A GPS PROCESSING STRATEGY FOR THE AFRICAN CONTINENT**

Cara LINDSAY, Peter Dare (both at Applied Geodetic Research Unit, School of Surveying, University of East London, Longbridge Road, Dagenham, Essex, RM8 2AS, UK, Email: c.l.wilson@uel.ac.uk)

Processing of GPS data is increasingly being adapted to benefit crustal dynamic applications, however, the results depend on the processing strategy adopted. The key objective of this paper is the establishment of an analytical procedure to study the plate kinematics of the African continent. This enables the rates of displacement to be determined to a precision of millimetres between reference points. Data will be drawn from a globally distributed network of high precision receivers maintained by the International GPS Service (IGS). The IGS data used covers a three year period, where weekly solutions are computed using the GIPSY-OASIS II suite of programs. The flexibility, yet complexity of the software lends itself well to this project. Three primary vectors that span the African plate have been selected. This set of vectors has been computed using varying strategies. Different models are used to distinguish the most effective method for gaining significant results. These include modelling for the wet tropospheric delay, phase centre variation and resolving for integer ambiguities. Additional IGS stations are included in the processing to tie the overall solution into the International Terrestrial Reference Frame. These span the Eurasian and Arabian plates, including stable SLR and VLBI sites. Limited crustal dynamic work has been carried out on the African continent, thus reducing the agreement or disagreement with other global plate motion models, e.g. NUVEL 1A and the work by M.B.Heflin. Comparison of results from the different strategies gives an initial understanding of the components that need to be considered for the African continent.



G1/E/17-A3 Poster 1620-104

## AN EXTENDED WEIGHT MODEL FOR GPS PHASE OBSERVATIONS

Andreas Wieser, Fritz K. BRUNNER (Engineering Surveying and Metrology, Technical University of Graz, Steyregasse 30, A-8020 Graz, Austria, email: wieser@aig.tu-graz.ac.at)

The accuracy of GPS based point determinations in small scale engineering applications is mainly limited by multipath and signal diffraction. Often the observation sites are determined by positional requirements rather than by ideal observation conditions, which increases the probability of obstructions and signal distortions. In order to improve satellite geometry and reduce the required observation time, low elevation data is included in the processing, but this increases noise and systematic errors. Thus careful weighting of the phase observations is needed. The measured carrier-to-noise-power-density ratio (C/N0) has proven to be an excellent tool for the estimation of the random errors of the phase observables. Due to the strong correlation between the satellite elevation and the C/N0, a template function can be determined to derive the expected C/N0 for a certain elevation angle and receiver-antenna combination. The difference (Delta) between the C/N0 observation and the template value is an indicator for systematic signal distortion, which is also shown a posteriori by the residuals of the phase data. In this paper an extended weighting model is presented, which combines the information inherent in C/N0, Delta and the residuals in order to take random errors and diffraction effects properly into account. A comparison of the proposed method with equal weighting and elevation dependent weighting shows a significant reduction of the signal distortion influence on baselines up to a few kilometers. Consequently, accuracy and ambiguity resolution are improved and the required observation time can be minimized.

G1/C/G2/E/02-A3 Poster 1620-105

## DATA PROCESSING AND ACCURACY ANALYSIS OF THE SECOND-ORDER GPS NETWORK IN CHINA

ZHA MING and Xu Bilin (Xi'an Technical Division of Surveying and Mapping, 36 Xiyinglu, Xi'an, Shaanxi 710054, P.R.China) Duan Wuxing and Tang Yingzhe (Xi'an Research Institute of Surveying and Mapping, 1 Zhongduan, Yantalu, Xi'an, Shaanxi 710054, P.R.China)

The nationwide GPS geodetic network comprised the first-order and the second-order network in China has been established. It will play an important role in strengthening an astro-geodetic network, refining a geoid and realizing a regional geodetic terrestrial reference frame. The first-order network involving 44 stations was measured during the period from late May 1991 to early May 1992. Based on the first-order network, the field survey of the second-order network including 534 stations was performed in 1992, 1993, 1994, 1995 and 1997. Now the data processing of the second-order network has been completed. Fiducial Point Technology has been used for the data processing. The coordinates of a regional distributed set of IGS tracking stations are constrained weightily to force the second-order network refers to ITRF96. GAMIT GPS analysis software was used for baseline processing. The software VECADJ was developed to make the network adjustment. According to the accuracy analysis of the adjustment results, it has been shown that the absolute positional accuracy is better than 0.1m and the relative positional accuracy is better than 0.1ppm.

G1/C/G5/E/26-A3 Poster 1620-106

## SOME ERROR SOURCES IN HIGH PRECESSION INTERFEROMETRIC AND ELECTRONIC DISTANCE MEASUREMENTS

Yuriy GALKIN (Department of Physics, Moscow State Forestry University, Mytischki-5, Moscow reg., 141005, Russia, email: galkin@mglu.ac.ru)

It is shown that, besides anomalous refractivity, the non-linearity of the dispersive behavior of the refractive index of air, particularly near the absorption lines of the atmospheric components, affects measured lengths as a systematic error. This is particularly important for interferometry in metrology and very high accuracy laser EDM. The magnitude of the error depends on the specific device and measurement conditions. The results of computer simulations are presented.

G2 Tuesday 20 July

## ADVANCED SPACE TECHNOLOGY (SECTION 2)

Location: Law Building, 303 LT  
Location of Posters: Old Gym

Tuesday 20 July AM

Presiding Chair: P.Willis (Inst. Geogr. National)

G2/L/01-A2 0930

## SPACE GEODETIC TECHNIQUES

Reiner Rummel (IAPG, Techn.Univ.Munich, Arcisstrasse 21, D-80290 Muenchen, Germany, email: rummel@step.iapg.verm.tu-muenchen.de)

Again the past four years brought about considerable advances in space geodesy. GPS applications were extended to atmospheric sounding, continuous tracking of LEO's, earth rotation time series with high resolution. Precise orbits for GLONASS satellites will come soon and IGS plays a prominent role on all of the above. CSTG established services for VLBI and laser ranging very similar to that for GPS. VLBI and satellite laser ranging are still progressing in terms of efficiency, automation, precision and reliability, as do the tracking systems DORIS and PRARE. A further milestone is the prospect of a series of dedicated gravity field missions. They will change the face of geodesy and its role in Earth sciences. There remains the big challenge of really combining geodetic space techniques so as to form one integrated "instrument" encompassing our planet.

G2/L/02-A2 0945

## HIGHLIGHTS OF RECENT DEVELOPMENTS IN THE INTERNATIONAL GPS SERVICE AND PERSPECTIVES FOR FUTURE DIRECTIONS

R. Neilan (1), Ch. Reigber(2), T. Springer(3), G. Beutler(3), J. Kouba(4) 1. IGS Central Bureau, Jet Propulsion Laboratory/Caltech Pasadena, CA, USA 2. GeoForschungsZentrum Potsdam, Germany 3. Astronomical Institute University of Bern, Switzerland 4. Natural Resources of Canada, Ottawa, Canada

In December 1998, the IGS Governing Board officially changed the name of this IAG service from 'International GPS Service for Geodynamics' to simply the 'International GPS Service'. This change of name reflects the fact that today the IGS supports numerous scientific projects outside the traditional geodetic and geodynamic disciplines. A number of IGS projects and working groups have been established, each concentrating on a particular science application, such as the ionosphere, atmosphere, reference frame, precise time transfer, etc. These activities are enabled and stimulated by the IGS and directly contribute to the continuing development of the service. The IGS is currently poised to respond to evolving user requirements that focus on timeliness and reliability of data and products, particularly in support of a slate of Low Earth Orbiter missions over the next decade. Perspectives on the future of the IGS will be developed based on current directions as well as anticipated external influences, such as GPS satellite modernization, GLONASS, availability of global communications, and plans for the European GALILEO (Global Navigation Satellite System - GNSS). We will address development of user friendly interfaces and IGS product tutorials.

G2/L/03-A2 1000

## THE CONTRIBUTION OF THE WEGENER PROJECT TO AN INTEGRATED MONITORING OF THE EARTH SYSTEM

Susanna Zerbini (email: zerbini@astbo1.bo.cnr.it), Hans-Peter Plag and Bernd Richter

The Special Commission 6 of IAG Section II, the WEGENER Project, has promoted the development of scientific space-geodetic activities in the Mediterranean and European area for the last fifteen years and has contributed to the establishment of geodetic networks designed particularly for Earth science research. The WEGENER Project has three main objectives: 1) to study the three-dimensional deformations and gravity along the African-Eurasian plate boundaries and in the adjacent deformation zones in order to contribute to a better understanding of the associated geodynamical processes; 2) to monitor the three-dimensional deformations in a large region centered around Fennoscandia in order to determine the magnitude and extent of the present-day postglacial rebound in that area, thereby extending our knowledge about the viscoelastic properties of the Earth; 3) to investigate height and sea-level variations in order to identify and separate the processes contributing to these variations. However, WEGENER activities include contributing to improvements of the measurement techniques, testing of new technological means, proposals for new missions and providing syntheses of observable quantities and inversion of the observations for geodynamically relevant parameters.

The WEGENER Project is conscious of the importance of contributing to the implementation of the principle of sustainable development and, in this context, is now trying to develop an effort, at European scale, which addresses the need to realize an integrated multi-purpose network for the acquisition and availability of long-term, continuous, high-quality spatial and in situ measurements. WEGENER intends to specifically contribute, among other objectives, to the definition of a high-precision network of permanent GPS stations in the European area, to the availability of the data collected by the stations for scientific exploitation and to lay the basis for the realization of an infrastructure where the different partners involved in the establishment and operation of permanent space-geodetic networks can meet, plan and organize the activities in a coherent, cost-effective manner. Such a network would also provide a significant contribution to the detection and understanding of climate change, to assess impacts at global, regional and local scale and would provide fundamental observations to validate models.

G2/L/04-A2 1015

## DEDICATED GRAVITY FIELD MISSIONS

Karl Heinz ILK (Institute of Theoretical Geodesy, University of Bonn, Nussallee 17, D-53115 Bonn, Germany, email: ilk@theor.geod.uni-bonn.de)

The investigation of the Earth's gravity field will enter a new era at the turn of the millennium. After three decades of careful preparation of various spaceborne gravity field mission concepts there are excellent chances to realize all three of them. These three mission concepts are high-low SST, low-low SST and SGG. CHAMP and GRACE will be launched in the years 2000 and 2001 with an overlapping mission period of two years. These two missions will provide the gravity field of the Earth with unattained accuracy and an eventual time dependency at least of the long-wavelength part of the gravity field. ESA's satellite gravity gradiometry mission concept GOCE has an excellent chance to become the first Earth Explorer mission. It is a dedicated high resolution gravity field mission concept and will open a completely new range of spatial scales of the earth's gravitational field spectrum down to 100km wavelength. Careful investigations have shown that the characteristics of the three mission concepts are rather complementary than competitive. Together with complementary geophysical data, satellite gravity data represent a "new frontiere" in studies of the system Earth.

G2/L/05-A2 1100

## SAR INTERFEROMETRY TECHNOLOGY

ROLAND KLEES (Department of Geodetic Engineering, Delft University of Technology, Thijsseweg 11, 2629 JA Delft, The Netherlands, email: kleees@geo.tudelft.nl)

The main objective of the SSG 2.160 SAR Interferometry Technology was (1) to make significant contributions to the development of SAR Interferometry (InSAR) as a technique for topographic mapping and surface change detection and (2) to promote the implementation of InSAR into geodetic and geodynamic work. This has led to the following major research topics of the SSG: (1) data processing strategies, (2) quality description and validation, (3) applications in Earth sciences, (4) limitations to InSAR.

We will give a review of the SSG-research according to the classification mentioned before: ad (1) phase unwrapping strategies, filter techniques, ad (2) nature of noise, coherence estimation, comparison with GPS and levelling, ad (3) detection of tectonic deformations, post- and co-seismic deformation measurements, volcano monitoring, glacier and ice sheet monitoring, monitoring of local subsidence due to anthropogenic activities, and atmospheric tomography for operational meteorology; ad (4) decorrelation and atmospheric disturbances in SAR interferograms. The presentation will finish with an outlook on future work in the field of InSAR.

G2/L/06-A2 1115

## SPACE BORNE ATMOSPHERIC GNSS SOUNDINGS

Christian Rocken, COSMIC and GST Programs, UCAR 3300 Mitchell Lane Boulder, CO 80301, USA, E-mail: rocken@ucar.edu

The international research community has achieved significant progress in space borne atmospheric limb sounding with GPS. Most high-quality data from the GPS/MET proof-of-

concept mission have been analyzed, archived, and made available to the research community. Statistical validation of these results confirmed the high theoretically expected equivalent temperature accuracy of approximately 1 K from near the surface to 40 km. It was further demonstrated that accurate water vapor profiles can be retrieved when ancillary temperature data are available. The occultation sounding data have also been used for the measurement of accurate (~ 10 meters) geopotential heights and for the study of gravity waves. Perhaps the most important meteorological result from GPS/MET was that the agreement with numerical weather prediction (NWP) models is noticeably better in data dense than in data poor regions. This means that occultation data assimilated into NWP models should improve the weather forecast. In the ionosphere the data were used for electron density profiling. Comparison with the global ionosonde network showed ~15% rms agreement in the critical plasma frequency foF2. Techniques for tomographic analysis of the occultation data in combination with ground based observations have been developed. Two space missions carrying Jet Propulsion Laboratory-developed GPS occultation receivers have been launched in early 1999, and at least 6 more missions with limb sounding receivers have been funded and are scheduled for launch in the next 3 years. The goals of these missions ranges from limb sounding technology improvement to demonstrating the impact of this technology on weather prediction, space weather prediction, and climate monitoring. This presentation will highlight key limb sounding results obtained during the last 4 years and describe the scientific goals of planned future missions.

**G2/L/07-A2 1130**

**PRECISE ORBITS USING MULTIPLE SPACE TECHNIQUES**

SCHARROO

Abstract unavailable at the time of going to press

**G2/L/08-A2 1145**

**CSTG DEVELOPMENT IN THE TIME PERIOD 1995-1999**

Gerhard BEUTLER (Astronomical Institute, University of Bern, Sidlerstrasse 5, CH-3012 Bern, Switzerland, email: beutler@aiub.unibe.ch) Hermann Drewes (Deutsches Geodaetisches Forschungsinstitut, Marstallplatz 8, D-80539 Munich, Germany, e-mail: mailer@dgfi.badw-muenchen.de)

International Coordination of Space Techniques for Geodesy and Geodynamics (CSTG) is Commission VIII of the International Association of Geodesy (IAG) and Sub-Commission 2.B of the Commission for Space Research (COSPAR).

According to its charter, CSTG has to develop links between various groups engaged in the field of space geodesy and geodynamics by various techniques, to coordinate the work of these groups, elaborate and propose projects implying international cooperation, follow their progress, and report on their advancement and results.

In the time period 1995 to 1999 CSTG the commission's structure was considerably changed through the creation of two new services, the ILRS (International Laser Ranging Service) and the IVS (International VLBI Service) as successors of the the SLR/LLR subcommission and the VLBI subcommission of CSTG. CSTG was also the lead organization of the first global GLONASS tracking and analysis experiment, the IGEX-98. Four issues of the CSTG Bulletin fully document the work performed by the Commission in this time period.

We highlight the essential developments within CSTG of the past four year period and we address the future of the Commission in view of the changes that took place in the time period 1995-1999.

**G2/L/09-A2 1200**

**FROM THE VLBI SUBCOMMISSION TO THE IVS: SCIENTIFIC HIGHLIGHTS AND PERSPECTIVES**

W. SCHLUETER (Bundesamt fuer Kartographie und Geodaesie, Wettzell, Germany, email: schluer@wettzell.ifag.de), N. Vandenberg (Goddard Space Flight Center/NVI, Inc., Greenbelt, Maryland, USA, email: nrv@gemini.gsfc.nasa.gov), J. Campbell (Geodetic Institute University of Bonn, Bonn, Germany, email:campbell@sn\_geod\_1\_geod.uni-bonn.de), T. Clark (Goddard Space Flight Center, Greenbelt, Maryland, USA, email: clark@tomcat.gsfc.nasa.gov)

The International VLBI Service for Geodesy and Astrometry (IVS) was established over the last two years under the leadership of the International Association of Geodesy (IAG) Commission VIII, the International Coordination of Space Techniques for Geodesy and Geodynamics (CSTG).

The IVS was the third service to be established, following the International GPS Service (IGS) and the International Laser Ranging Service (ILRS). The objectives of IVS are:

- to intensify the international cooperation of the responsible agencies,
- to encourage new contributions from the international community,
- to provide an international umbrella for all participating groups, and
- to ensure the world wide service for provision of the required products from the VLBI technique for the terrestrial and celestial reference frames and the Earth orientation parameters needed for research and applications.

This paper summarizes the events leading up to the establishment of the IVS, points out its components and structure, and gives current information on the scientific perspectives and highlights of the IVS.

**G2/L/10-A2 1215**

**FROM THE SLR/LLR SUBCOMMISSION TO THE ILRS: HIGHLIGHTS...**

DEGNAN

Abstract unavailable at the time of going to press.

**G2/L/11-A2 1230**

**THE DEVELOPMENT OF THE ISGN: STATUS AND PERSPECTIVES**

DREWES

Abstract unavailable at the time of going to press.

**HIGHLIGHTS OF SPACE GEODESY**

**G2/L/11-A2 1400**

**THE IGEX-98: HIGHLIGHTS AND PERSPECTIVES**

WILLIS

Abstract unavailable at the time of going to press

**G2/W/02-A2 1415**

**INTEGRATED EARTH OBSERVATION MODEL**

SCHWARZE, Volker (Stuttgart University Department of Geodetic Science email: schwarze@gis.uni-stuttgart.de)

Geodetic space techniques like Very Long Baseline Interferometry or Lunar Laser Ranging as well as satellite based systems give deep insight into the system behaviour of the Earth. To use the full physical and geometrical information of the geodetic sensors all types of observations have to be combined within a consistent physical, geometrical and stochastic model.

The physical model is developed consistently within the framework of general relativity at post-Newtonian order. This part contains the motion of extended bodies as well as the description of the physical properties of the Earth.

The geometrical part contains the definition and connecting of geodetic coordinate systems as well as the definition of observable quantities on a curved four-dimensional manifold of pseudo-Riemann type.

The combination of heterogenous observations leads to the problem that the components of their variance-covariance matrix has to be determined from an adjustment procedure. Several estimators to fulfil additional optimization conditions are given and extensively discussed.

**G2/W/07-A2 1430**

**CONTRIBUTIONS OF LASER RANGING TO THE GOALS OF SPACE GEODESY**

Richard EANES (Center for Space Research, University of Texas at Austin, 3925 W. Braker Lane, Suite 200, Austin, TX 78759-5321, USA, email: eanes@csr.utexas.edu)

Laser ranging to artificial satellites and to the Moon is one of the primary techniques of space geodesy. The principle advantages of laser ranging (LR) are: 1) the effects of the earth's atmosphere and ionosphere can be modeled to few mm accuracy; 2) delays in the ground segment can be calibrated to few mm accuracy; 3) the delay at the target can be modeled to few mm accuracy; 4) appropriate targets are available from low-Earth orbit (LEO) to the moon, 5) the LEO targets provide a link of the crust-fixed TRF to the origin of the local inertial frame located at the Earth's center of mass. The LR technique's major weaknesses are its high cost per station (relative to GPS) and its vulnerability to weather. These disadvantages have kept the number of LR observatories low and have resulted in less than optimum spatial and temporal distribution of observations, but the strengths of the LR more than compensate and ensure that the technique will continue to be a significant component in the Integrated Global Geodetic Observing System. Laser ranging has contributed to several broad areas of geodynamics research including: determination of the mean gravitational field of the Earth (including GM) and its temporal variations due to redistribution of mass in the atmosphere, hydrosphere, and cryosphere; determination of motions of crust-fixed observatories relative to the center of mass of the planet; orbit determination of and calibration of altimetric satellites; and tidal and non-tidal variations of earth orientation parameters. While presenting the contributions of laser ranging to geodynamics research I will highlight the complementary contributions of the other space geodesy techniques that were required for success.

The future of laser ranging looks bright. The establishment of the International Laser Ranging Service (ILRS) was completed in September 1998 and should rapidly lead to improved coordination of the network of laser ranging observatories, increased cooperation among the analysis community, and more effective promotion of ideas for new satellite missions and new scientific applications of the technique. Remotely operated satellite laser ranging systems have already been successfully deployed and the design of advanced systems with nearly complete automation is well underway and should significantly lower the cost of LR. Two new systems with dual lunar and satellite laser ranging capability are currently operating in engineering status, and several excellent mobile stations are available for deployment to areas that will improve the geographic distribution of the technique. These advances ensure that laser ranging will play an important role in the integrated space geodesy measurement system of the future.

**G2/W/10-A2 1445**

**ICESAT PRECISION ORBIT DETERMINATION**

Hyung-Jin RIM, Charles Webb, and Bob E. Schutz (Center for Space Research, University of Texas at Austin, Austin, TX 78712, USA, email: rim@csr.utexas.edu)

The Ice, Cloud and land Elevation Satellite (ICESat) is scheduled for launch on July 2001 as a part of the NASA Earth Science Enterprise missions. The Geoscience Laser Altimeter System (GLAS) will be carried on the ICESat to measure ice-sheet topography and associated temporal changes, as well as cloud and atmospheric properties. To accomplish the ICESat science objectives, the position of the GLAS instrument in space should be determined with an accuracy of 5 cm and 20 cm in radial and horizontal components, respectively. This knowledge will be acquired by the Precision Orbit Determination (POD) activities using the data collected by the GPS receiver on ICESat and the ground-based satellite laser ranging (SLR) data.

The predicted radial orbit errors at the ICESat orbit (600 km altitude) based on recent gravity models, such as JGM-3 and EGM-96, are 15-20 cm, which exceeds the 5 cm requirement. Gravity model improvement effort for the ICESat mission (gravity tuning) will be carried out during the Verification Phase (first 90-120 days from launch) using the collected GPS and the SLR data. Since the scheduled launch date of the ICESat is near the next solar maximum, the drag model errors will be the limiting factor for a successful gravity tuning and for the ICESat POD.

The results of an in-depth simulation study to assess the ICESat POD accuracy are summarized in this paper. Effects of the drag model errors on the gravity tuning and the POD are examined. Experiments on how to minimize the effect of drag model errors are summarized.

**G2/W/05-A2** 1500**ADVANCED SPACE TECHNOLOGIES FOR GEODESY OF THE MOON: SELENODETTIC MISSIONS IN SELENE AND SELENE2**

Kosuke HEKI, H. Hanada, T. Tsubokawa, N. Kawano and M. Ooe (National Astronomical Observatory, 2-12 Hoshigakoa, Mizusawa, Iwate 023-0861, Japan, email: heki@miz.nao.ac.jp) N.Namiki (Kyushu University, Fukuoka, Japan) T.Iwata (National Space Development Agency, Japan)

SELENE, the Japanese lunar explorer to be launched in 2003 July, involves three missions of lunar geodesy, VRAD, RSAT and LALT (laser altimetry). Two radio transmitters on board the lunar orbiter and lander (VRAD) are used as radio sources for differential VLBI from the Earth. Its combination with conventional R&RR measurements enables three dimensional measurement of the satellite position and lunar gravitational acceleration. The relay satellite at a high eccentric orbit (RSAT) relays Doppler signals from the main orbiter to perform first direct gravimetry of the lunar farside. Feasibility study has started for the next project SELENE2 toward the launch in ~2006. There we are proposing a selenodetic mission aimed at the lunar rotational dynamics, "In-situ Lunar Orientation Measurement (ILOM)"; a small optical telescope is deployed near the lunar pole, fixed toward the celestial pole, star positions (accurate to <math>\lt;0.1''</math>) are recorded with a CCD camera. Year-long star trajectories are analysed to determine amplitudes and phases of major components of forced librations of the Moon, as well as to detect its free librations.

**G2/C/G5/W/23-A2** 1515**CORE: ACCURACY OF VLBI UT1 AND POLAR MOTION**

D S MacMillan (NVI, Inc./Goddard Space Flight Center, Greenbelt, MD 20771, USA, email: dsm@leo.gsfc.nasa.gov) C. Ma and T. A. Clark (both at NASA Goddard Space Flight Center, Greenbelt, MD 20771, USA)

VLBI is one of the most important techniques measuring Earth orientation parameters (EOP). Measurements of EOP can provide constraints on geophysical models of the solid Earth, the atmosphere, and the oceans. Recognizing the importance of EOP measurements, the international VLBI community is engaged in a program to make continuous EOP measurements beginning in 2001, ramping up from four 24-hour sessions per week during 1999. This campaign is called CORE (Continuous Observations of the Rotating Earth). One of the principal problems with high precision VLBI measurements is determining its accuracy. In the CORE program, EOP measurements will be made with several networks, each operating on a different day. It is therefore important to determine whether there are systematic differences between EOP derived from different networks. The basic test for accuracy is to examine the differences between simultaneous measurements of EOP from independent VLBI measurements. From the history of VLBI sessions from 1980 to the present, there are about 300 such simultaneous sessions. These comparisons imply that the formal EOP errors should be increased by a factor of 1.5-2.0. The EOP precision of these measurements varies over a wide range (by about a factor of ten compared to current precision) so that it is difficult to determine whether the differences are due to random or systematic errors. To determine current accuracy and to prepare for the CORE program, we have run a series of VLBI experiments that are either simultaneous (CORE-A) with the weekly NEOS network or on adjacent days (CORE-B). These experiments began in 1997 and continue to the present time. Analysis of 70 simultaneous experiments again indicates that the formal errors are too small by a factor of 1.5-2.0. However, there are large systematic differences between the networks, which are much larger than the expected average differences. The cause of these differences is under active investigation.

**G2/W/13-A2** 1530**ESTIMATION OF TROPOSPHERIC DELAY FROM VLBI DATA**

Oleg TITOV (Astronomical Institute of Saint-Petersburg University, Bibliotechnaya sq., 2, Petrodvoretz, Saint-Petersburg, 198904, Russia, email: oleg\_titov@usa.net)

Temporal instability of troposphere leads to loss of accuracy at VLBI data adjustment. Conventionally, all scientists wish to reduce an influence of troposphere on more important geodetic and geodynamic parameters (station coordinates, polar motion, length-of-day, etc.). Nevertheless, it is possible to estimate the variations of troposphere delays directly from VLBI data. Least squares collocation technique allows to obtain time series with temporal resolution up to 3-5 minutes for any VLBI station. Special covariance function based on theoretical consideration and large set of measurements has been used as a priori information. Results of adjustment of two-weeks VLBI experiment CONT94 are presented. All calculations made using OCCAM software. Comparison of the time series with independent measurements by WVR (water vapor radiometry) made at the Onsala Space Observatory (Sweden) shows that VLBI has a strong potential for the problem solution. It allows to reduce a costs for WVR equipment installation and service.

**G2/E/02-A2** 1545**SATELLITE GRAVITY GRADIOMETRY WITH GRACE ?**

Wolfgang KELLER (Geodetic Institute, University Stuttgart, Geschwister-Scholl-Str. 24/D, 70174 Stuttgart, GERMANY, email: wolfgang.keller@gis.uni-stuttgart.de)

The GRACE mission will be a satellite-to-satellite-tracking (SST) mission. Compared to SST, a satellite-gravity-gradient (SGG) mission is expected to provide a higher resolution. The paper presents a simulation study about the accuracy of artificially generated gravity gradients, which can be derived from GRACE range-rate data. It will be shown that the accuracy is comparable to the accuracy of planned SGG missions, provided the GPS derived satellite positions and velocities have a sufficient quality. Two independent methods for the recovery of the gravity field from artificial SGG data are investigated. Both methods give almost identical resolutions

**G2/L/10-A2** 1630**FROM THE SLR/LLR SUBCOMMISSION TO THE ILRS: SCIENTIFIC HIGHLIGHTS AND PERSPECTIVES**

Michael Pearlman John DEGNAN, Carey Noll, and Erricos Pavlis, Van Husson, Scott Wetzel, Peter J. Dunn and Mark H. Torrence

With the endorsement of the IERS and the CSTG in April, 1998, the International Laser Ranging Service (ILRS) was created to support geodetic, geophysical, and lunar research activities and to provide the IERS with timely, high quality products important to the maintenance of an accurate International Terrestrial Reference Frame (ITRF). Patterned in part after the highly successful International GPS Service (IGS), the ILRS is responsible for the development of the standards and specifications necessary for product consistency and

the encouragement of international adherence to its conventions. The ILRS, which started officially on November 1, 1998, collects, merges, analyzes, archives and distributes satellite and lunar laser ranging data to satisfy a variety of scientific, engineering, and operational needs and encourages the application of new technologies to enhance the quality, quantity, timeliness, and cost effectiveness of its data products. The ILRS is organized into permanent components: (1) a Governing Board, (2) a Central Bureau, (3) Tracking Stations and Subnetworks, (4) Operations Centers, (5) Global and Regional Data Centers, and (6) Analysis, Lunar Analysis, and Associate Analysis Centers. The Governing Board, with broad representation from the international SLR and LLR community, sets policy and defines the service philosophy while the Central Bureau oversees and coordinates the daily service activities. In addition, the Governing Board has established four standing working groups: (1) Missions, (2) networks and Engineering, (3) Data Formats and Procedures, and (4) Analysis. These Working Groups draw operational and technical expertise freely from the SLR community in order to better exploit current capabilities and challenge the ILRS membership to keep pace with evolving user needs. The ILRS currently tracks 25 retroreflector-equipped satellites and the Moon and is conducting four specialized campaigns in support of specific scientific or engineering studies.

**G2/W/01-A2** Poster 1630-01**SPACE GEODETIC EXPERIMENTS BETWEEN COLLOCATED STATIONS**

Taizoh YOSHINO, H. Kunitomi, F. Katsuo, J. Amagai, K. Sebata, M. Furuya, T. Otsubo, Y. Takahashi, and H. Kiuchi (Communications Research Laboratory, 4-2-1 Nukui-kita, Koganei, Tokyo 184-8795, Japan, e-mail: yosh@crl.go.jp) T. Kondo, R. Ichikawa, and Y. Koyama (Kashima Space Research Center, Communications Research Laboratory, 893-1 Hirai, Kashima, Ibaraki 314-0012, Japan)

Modern geodetic observations are performed using the several space techniques. Each technique has strength and weakness. In Japan, a geodetic observing network around Tokyo (the Key Stone Project) is working regularly for a study of crustal deformation. The network consists of four collocated stations, which has VLBI, SLR and GPS facilities. Intercomparison of the geodetic results are performed using these independent techniques. To compare the global position and its time variations of the stations, the K-4 type VLBI system (256Mbps recording) is transported to Wettzell stations in 1999 which is also an ideal collocated station. SLR and GPS data is exchangeable. The results from the experiments between collocated station will not only contribute the terrestrial reference frame, but will help to understand the systematic error sources which is invisible from an observation using only one technique.

**G2/W/12-A2** Poster 1630-02**GLOBAL COORDINATES OF VLBI/SLR/GPS COLLOCATED KEYSTONE STATIONS - INITIAL RESULTS**

Toshimichi OTSUBO (NERC Satellite Laser Ranging Group, Monks Wood, Abbots Ripton, Huntingdon PE17 2LS, UK, email: t.otsubo@ite.ac.uk, on leave from Communications Research Laboratory, Japan) Yasuhiro Koyama and Ryuchi Ichikawa (both at Kashima Space Research Center, 893-1 Hirai, Kashima, Ibaraki 314-0012, Japan, email: koyama@crl.go.jp and richt@crl.go.jp)

The Communications Research Laboratory, Japan, has developed four geodetic stations around Tokyo utilizing the space geodetic technologies - VLBI, SLR and GPS. They have been worked as the VLBI regular measurement of the regional crustal deformation since 1994, and they can now act as the collocation between the independent three technologies. We derived the global station co-ordinates in ITRF96. In the VLBI analysis, the position of the four Keystone antennae were connected, through a series of tie experiments, to the Kashima 34m antenna whose co-ordinates are listed in ITRF96. In the precise SLR global orbit determination, only the Keystone station co-ordinates were solved for, while the other global stations were fixed to ITRF96. For GPS, the co-ordinates of Keystone and some others were freely estimated, whilst constraining some IGS points to ITRF96. An initial analysis showed that the SLR and GPS co-ordinates agreed with the VLBI co-ordinates within +/- 3 cm in the horizontal components and within +/- 4 cm in the vertical components, after the correction of local ties.

**G2/E/06-A2** Poster 1630-03**COLLOCATION EXPERIMENTS AT CERGA**

Joelle NICOLAS, P. Exertier, P. Bonnefond, C. Berger, Y. Boudon, J.J. Walch (1) E.Calais (2), J. Hinderer (3), J.F. Crétau (4), C. Boucher (5), J. Haase (6) (1) Observatoire de la Côte d'Azur - CERGA, av. Copernic - F06130 Grasse (2) CNRS-Geosciences Azur, F-06560 Sophia-Antipolis (3) EOST, r Descartes, F-67000 Strasbourg (4) CNES, av. E. Belin, F-31401 Toulouse (5) IGN-LAREP, ENSG, F-77455 Marnes-La-Vallée (6) ACRI - rte du Pin Montard - BP234, F-06904 Sophia-Antipolis

Since more than 20 years, the French geodynamics site located near Grasse, France has participated to the tracking of many geodynamic, geodetic, and oceanographic satellites. The Satellite- and Lunar Laser Ranging stations (SLR fixed and mobile, and LLR) are the main systems, but special efforts have been made during the 90's to combine different space geodetic and gravimetric techniques such as : GPS, DORIS, GLONASS, Laser, VLBI, and absolute gravimetry. The aim was to search for systematics and unstabilities in the measurements and the positioning in order to improve the accuracy of different tracking systems. In this poster, the purpose is to summarize the results of different collocation experiments. We present a cross-analysis of laser measurements made on geodetic satellites (especially Lageos 1 and 2) and on the GPS and GLONASS constellations. Methods of data comparison are proposed as well as techniques for orbit quality control. Correlations between the laser residuals computed for different orbits and instruments (SLR and LLR) are shown to provide some evidences of the objective quality of the stations, and their positioning. Then a comparison between the absolute positioning resulting from the different techniques (SLR, GPS, DORIS, and g measurements) is presented.

**G2/W/04-A2** Poster 1630-04**LUMPED COEFFICIENTS - A MEANS FOR ORBIT SENSITIVITY ANALYSIS**

CH. SCHAEFER and E.W. Grafarend (Geodetic Institute of the University of Stuttgart, Geschwister-Scholl-Strasse 24/D, D-70174 Stuttgart, Germany)

A possible concept for an orbit sensitivity analysis will be presented, based on the concept of lumped coefficients and Fourier- / frequency investigations of the satellite's orbit data. The method will be set up taking into account the needs and mission specifics of the German satellite mission CHAMP, which is due to be launched in autumn 1999 for the determination of the Earth's gravitational field, besides other goals. The main aim of the presented analysis is to get an idea on the sensitivity of the mission layout with respect to gravitational field determination and thus to reduce the number of relevant unknowns to be estimated from the tracking data.



**G2/W/11-A2** Poster **1630-05****THERMAL FORCE EFFECTS ON SATELLITES**

Jânia DUHA (Departamento de Geomática, Universidade Federal do Paraná, UFPR, Curitiba, Brasil, email: jduha@geoc.ufpr.br) Germano B. Afonso (Departamento de Física, Universidade Federal do Paraná, UFPR, Curitiba, Brasil, email: afonso@fisica.ufpr.br)

The precision of satellite orbit determination has continually increased, in the past years, because of the improved tracking technologies and increasing density of high-quality tracking stations. Subtle dynamical effects of non-gravitational origin become apparent, and as a result, a considerable effort has been devoted to the analysis of non-gravitational perturbations. A satellite heated up by a thermal energy source (sun, earth, etc.) have one hemisphere preferentially heated over the other. After a characteristic time the thermal radiation is re-emitted by the satellite's surface. The photons emitted by the hotter hemisphere carries away more momentum than the ones emitted by the colder hemisphere, so that the satellite is subjected to a thermal thrust.

In this work, we propose an improved thermal model that presents the total thermal effect as the sum of the summer-winter and the "generalized" day-night effects. We show that a unified model (J. Duha, M. Sc. Degree, 1996) may take into account the sin  $q'$  term for the day-night force component (longitudinal) and the cos  $q'$  term (where  $q'$  is the co-latitude of the thermal energy source) for the summer-winter force component (latitudinal). These terms yields from temperature variations on the satellite's surface due to its movement around the thermal energy source and allow to the simultaneous application of these two effects resulting in a unified total thermal effect. Thus, the total thermal force has two components: the summer-winter force, in the satellite spin axis direction ( $z$ ), and the generalized day-night force, in the satellite equatorial plane ( $x,y$ ).

We calculate the along-track accelerations for a test-satellite (parameters based on the LAGEOS satellite data) obtaining an averaged along-track acceleration equal to  $-3.46 \times 10^{-13}$  m s $^{-2}$ , for the day-night effect, and  $-2.85 \times 10^{-12}$  m s $^{-2}$ , for the summer-winter effect. That leads to a residual orbit decay of nearly 1.08 mm d $^{-1}$ .

Finally, we analyze the behavior of the averaged radial and along-track accelerations, and the thermal lag angle, as a function of the satellite altitude, and show the "selective law" (J. Duha, M. Sc. Degree, 1996) that control the satellite orbit decay, and associate the maximum thermal effect to the radius and altitude of the satellite.

**G2/L/12-A2** Poster **1630-06****GLONASS ORBIT COMPARISONS FROM THE IGEX FIELD EXPERIMENT**

Robert WEBER, Elisabeth Fragner (both at Department of Advanced Geodesy, University of Technology Vienna, Gusshausstr. 27-29, A-1040 Vienna, Austria, email: rweber@luna.tuwien.ac.at)

In September 1998 the IGEX (International Glonass Experiment) field campaign has been started in order to set up a global Glonass observation network and to determine Glonass orbits in the ITRF with a quality of about one meter or even better. IGEX is an international project sponsored by CSTG (Coordination of Space Techniques for Geodesy and Geodynamics), IGS (Int. GPS Service), ION (Institute of Navigation) and the IERS (Int. Earth Rotation Service).

In January 1999 the IGEX steering committee decided, that the field campaign will be prolonged at least till end of April 1999. Besides that, the first author has been appointed to act as IGEX Data Analyses Coordinator, responsible e.g. for orbit comparisons and the documentation of the orbit processing methodologies in use. This presentation characterizes the current status of the IGEX campaign, summarizes results of the orbit comparisons obtained so far and discusses strategies for the combination of the orbit submissions.

**G2/E/22-A2** Poster **1630-07****A SINGLE FREQUENCY IONOSPHERIC CORRECTION FOR GPS**

Yuriy GALKIN, Victor Kharchenko, Daniil Zakharov (all at Department of Physics, Moscow State Forestry University, Mytitschi-5, Mosciv reg., 141005, Russia, email: galkin@mgul.ac.ru)

It is shown that the non-linearity of the dispersive form of the refractive index of the medium affects a propagating radio signal in a complicated manner. This effect depends on the signal form and the dispersive properties of the medium. Computer simulations demonstrate that the GPS signal and the dispersive properties of the ionosphere allow to determine a new parameter in the received signal that is a function of the total electron content in the propagation path of the radio wave.

**G2/E/16-A2** Poster **1630-08****CORRECTION OF THE WATER VAPOUR ABSORPTION LINE EFFECT FOR EDM WITH INFRARED EMITTING DIODES**

Yuriy GALKIN (Department of Physics, Moscow State Forestry University, Mytitschi-5, Moscow reg., 141005, Russia) Ruben Tatevian (Department of Metrology and Standardisation, Central Research Institute of Geodesy, Air-Survey and Cartography, 26 Onezhskaya Street, Moscow, 125413, Russia) Lev Blank (Scientific Research Centre "Geodynamics", 4 Gorokhovskii side-street, Moscow, 103064, Russia)

The theory of the anomalous refraction and the spectral absorption effects are shown for wideband emission and amplitude modulated signal as in used by electronic distance meters with emitting diodes in near infrared spectral region. Software is being developed for correction of 6714 water vapour absorption lines (taken from HITRAN, between 750 and 1000 nm) on EDM with a Gaussian emitted spectrum. This correction has already been estimated for many conditions and found to reach magnitudes of several ppm of distance on occasions.

**G2/W/06-A2** Poster **1630-09****AUTOMATION OF THE VLBI DATA ANALYSIS USING A KNOWLEDGE-BASED SYSTEM**

Wolfgang SCHWEGMANN and Harald Schuh (both at: Deutsches Geodätisches Forschungsinstitut (DGFI), Marstallplatz 8, 80539 München, Germany, email: schwegmann@dgfi.badw.de)

VLBI is an extremely precise modern space geodetic technique for monitoring the Earth rotation and for the realization of the global reference system. However, there is still a delay of at least one week between the time of observation and the availability of results and the data analysis requires a lot of manual operations. An important contribution to the acceleration of the VLBI procedure is a faster and semiautomatic data analysis, which is in particular needed in view of the increasing amount of VLBI data to be processed in the next years. Most of the tasks in the VLBI data analysis are very complex and their automation requires typical knowledge-based techniques. A concept for the automation of one of the most widely used VLBI software packages the MarkIII Data Analysis System was already presented. Now, an

intelligent assistant for support and guidance of the analyst is being developed using the workbench BABYLON, which is based on methods of artificial intelligence. First the knowledge acquisition has to be carried out. Then the concept and design of the knowledge-based system has to be completed by the formalization and the representation of the knowledge using rules, objects, etc. Additionally an explanation-component is going to be developed as a part of the system to check its decisions. This component can also be used as a teaching-system for less experienced analysts. This would be very helpful, because there is a shortage of qualified experts and the analyst's training takes a long time. Examples will be given about the current status of the project, e.g. it will be shown how knowledge-based methods can be used to automate the final selection of parameters in the VLBI data analysis.

**G2/W/14-A2** Poster **1630-10****VLBI DATA ANALYSIS WITH A FULL VARIANCE-COVARIANCE MATRIX**

Harald SCHUH and Volker Tesmer (both at: Deutsches Geodätisches Forschungsinstitut (DGFI), Marstallplatz 8, 80539 München, Germany, email: schuh@dgfi.badw.de)

The complete model of least squares adjustment contains the full variance-covariance matrix. Its diagonal elements can be computed from the a priori errors of the observables; the off-diagonal elements can be derived from the a priori errors and from the correlation coefficients between each pair of observables. However, in all present standard VLBI solutions, only the variances of the observed time delays are introduced, whereas no a priori correlations between the observables of a VLBI-session are taken into account, i.e. the covariances are set to zero. The causes of such correlations will be pointed out: They are in particular due to imperfections of the models used in VLBI data analysis. The determination of empiric correlation coefficients has shown that they depend on the geometry of the network and on the time of the observations, i.e. are relatively high for temporally close observations. There are also other reasons for correlations, e.g. observations of the same radio source may be correlated due to systematic influences of the source position and of the source structure. In a first attempt, the correlation coefficients determined empirically will be entered into the VLBI data analysis. The results will be compared with those of an uncorrelated approach. The OCCAM 3.4 VLBI software, which is used by several international VLBI groups, was modified for that purpose by introducing the full variance-covariance matrix, and was applied for the investigations.

**G2/E/08-A2** Poster **1630-11****THE COMPARISON OF VLBI AND GPS STATION MOVEMENTS AND THEIR VARIATIONS LONGER THAN ONE MONTH**

Yukio TAKAHASHI, Hitoshi Kiuchi, Akihiro Kaneko, Yasuhiro Koyama, Noriyuki Kurihara, Mamoru Sekido, Tetsuro Kondo, Ryuichi Ichikawa, Taizoh Yoshino, Jun Amagai, Masato Furuya and Kouichi Sebata (Communications Research Laboratory, 4-2-1 Nukui-kita-machi, Koganei, Tokyo 184-8795, Japan, Email: takahashi@crl.go.jp)

We compared the station movements obtained by VLBI and GPS data in the domestic observation network. CRL constructed the KSP (the Crustal Deformation Monitoring System for Tokyo Metropolitan Area) with 4 stations which have VLBI, SLR and GPS facilities. In the KSP, the daily VLBI observations started since January, 1995. There are some GPS stations of GSI located near KSP stations. The KSP is a good test bench for comparing the results of VLBI, GPS and SLR. The current reliability of VLBI was almost the same as that of GPS. The dispersions of measurements in one-day experiments were about 2 mm and 10 mm for horizontal and vertical movements, respectively. The variations longer than one month for the station movements measured by both VLBI in KSP and GPS were 0.5-1 mm and 2-5 mm for horizontal and vertical movements, respectively. However, their variations of VLBI data were different from those of GPS data. The station velocities obtained by VLBI data in KSP agreed well with those by GPS data.

**G2/E/01-A2** Poster **1630-12****ATMOSPHERIC GRADIENT EFFECTS ON THE COMPACT VLBI NETWORK AROUND THE TOKYO METROPOLITAN AREA**

Tetsuro KONDO, R. Ichikawa, Y. Koyama, M. Sekido, and N. Kurihara (Kashima Space Research Center, Communications Research Laboratory, 893-1 Hirai, Kashima, Ibaraki 314-0012, Japan, e-mail: kondo@crl.go.jp) T. Yoshino, J. Amagai, and K. Sebata (Communications Research Laboratory, 4-2-1 Nukui-kita, Koganei, Tokyo 184-8795, Japan)

Regular measurements on the compact VLBI network consisting of the four stations (Kashima, Koganei, Miura, and Tateyama; the longest distance between any two stations is about 135 km) around the Tokyo metropolitan area shows a good repeatability such as a 2-mm level in baseline length.

However the repeatability tends to be degraded in summertime. A correlation analysis between measured baseline lengths and surface meteorological data was made and it was suggested that an apparent position change of Kashima occurred according to the change of weather condition. Considering from the location of the station and the general characteristics of weather condition in Japan, this apparent position change is supposed to be caused by the atmospheric gradient, in particular by the wet component. We evaluate the effect of atmospheric gradient on the baseline length measurements quantitatively. Results will be presented at the meeting.

**G2/E/04-A2** Poster **1630-13****RAPID UT1-UTC ESTIMATION USING REAL-TIME VLBI TECHNIQUE.**

Yasuhiro KOYAMA, Tetsuro Kondo (both at Kashima Space Research Center, Communications Research Laboratory, 893-1, Kashima, Ibaraki 314-0012 JAPAN, email: koyama@crl.go.jp, kondo@crl.go.jp), Jun Amagai, and Kouichi Sebata (both at Communications Research Laboratory, 4-2-1 Nukui-kita, Koganei 184-8795 JAPAN, e-mail: amagai@crl.go.jp, seba@crl.go.jp)

Communications Research Laboratory has established four space geodetic observation sites in and around Tokyo, Japan under the Key Stone Project. Regular geodetic VLBI experiments are currently performed every two days with the duration about 24 hours by using four 11m antennas. The observed data are transferred to a correlator system over high speed ATM network and data from four VLBI stations are processed in real-time. The data analysis procedures are fully automated and the results are generated immediately after each experiment. Usually, the data are analyzed to estimate precise positions of the VLBI sites, but we successfully demonstrated the capability of the data for estimating UT1-UTC by fixing a priori site positions. The uncertainties of the estimated UT1-UTC are typically 0.1 msec. The accuracy of the estimation can be improved by expanding the baseline lengths between observation sites and we are currently investigating a possibility to connect existing VLBI sites by a high speed communication link.

**G2/E/10-A2** Poster **1630-14****WORLDWIDE FREQUENCY AND TIME COMPARISONS USING GPS CARRIER PHASE**

G. PETIT, C. Thomas and Z. JIANG (Bureau International des Poids et Mesures Pavillon de Breteuil, 92312 Sevres CEDEX, France, email: gpetit@bipm.fr, cthomas@bipm.fr, zjiang@bipm.fr)

Recently-developed frequency standards state an accuracy well below  $1 \times 10^{-14}$ , so comparing their frequency over a sufficiently short interval is a challenge for existing time and frequency transfer techniques. In this aim, we study the use of carrier phase and code measurements from Ashtech Z12-T receivers, a version of the usual geodetic Z12 which has been specially modified to meet the stability requirements of time and frequency comparisons. Over baselines of a few meters, it has been shown that the relative frequency stability between two independent systems is below  $1 \times 10^{-16}$  for averaging durations of half a day. We have carried out frequency comparisons between hydrogen masers over baselines ranging from a few kilometres to several thousand kilometres.

For these experiments, the Z12T data have been included in a larger set of measurements from a geodetic GPS data base maintained by the International GPS Service for Geodynamics (IGS). We study the impact of different processing strategies, regarding the treatment of troposphere and ambiguity parameters and the characteristics of the session processed, on the frequency comparison between remote hydrogen masers. In order to be used also for time transfer, these receivers should be calibrated to obtain the true values of the hardware delays and their variation with the environment. We discuss preliminary results of an exercise of absolute calibration of the Ashtech Z12-T receiver carried out using a GPS signal simulator.

**G2/W/09-A2** Poster **1630-15****TEMPORAL VARIATIONS OF OCEAN TIDAL TERMS IN UT1-UTC**

Oleg TITOV (Astronomical Institute of Saint-Petersburg University, Bibliotchnaya sq., 2, Petrodvorets, Saint-Petersburg, 198904, Russia, email: oleg\_titov@usa.net)

Global redistribution of mass water causes a variations in Universal Time. VLBI technique allows to detect and estimate the corresponding oceanic tides with periods near 12 and 24 hours. Usually, scientists obtain the estimates using global set of VLBI data. Possibility of the tides variations from year to year is considered in this paper. About 500 VLBI experiments (NEOS-A, CONT'96, etc.) from 1991 till 1998 year were analyzed. All reductional calculations have been made using OCCAM software. Least squares collocation method (LSCM) provides us the time series of UT1-UTC variations with high temporal resolution (one point for 3-5 minutes). The full number of points exceeds 100.000. Therefore the standard deviation of yearly estimates is reasonable. Variations of UT1-UTC obtained using the LSCM are in a good agreement with ones recommended by IERS Conventions. Estimates of main tidal terms in UT1-UTC independently for every year as well as for full set of data are presented. It is shown that the yearly estimates are slightly differ from each other. The various reasons of the effect are discussed.

**G2/E/35-A2** Poster **1630-16****EARTH ROTATION PARAMETERS AND TERRESTRIAL REFERENCE FRAME REALIZATION FROM LAGEOS-1 AND LAGEOS-2 1983-1998 SLR DATA ANALYSIS**

Sergei RUDENKO (Main Astronomical Observatory, National Academy of Sciences of Ukraine, Golosiiv, Kiev 252022, Ukraine, email: rudenko@mao.kiev.ua)

A homogeneous series of the Earth rotation parameters and a realization of the Terrestrial Reference Frame have been derived by the joint processing of Lageos-1 and Lageos-2 SLR data acquired by the global network of stations since September 1, 1983 until December 15, 1998. Lageos-1 data consists of 939,134 normal points obtained by 109 stations and Lageos-2 data represents 370,861 normal points acquired by 72 stations. The data analysis has been performed using KIEV-GEODYNAMICS 5.2 software which basically follows the IERS Conventions (1996). Among the estimated parameters are: satellite orbital elements - at 15-day orbital arcs, Earth rotation parameters (Xp, Yp pole coordinates, UT-UTC) - at 3-day arcs, geocentric cartesian coordinates of 109 stations and velocities of 65 stations located at 42 sites at the whole 15-year span. The formal errors of station coordinates and velocities are 0.1-1 cm and 0.2-5 mm/y, respectively, for the majority of stations. The formal errors of ERP are 0.19 and 0.17 mas for Xp and Yp pole coordinates and 0.015 ms for UT. The derived station coordinates and velocities have been compared with ITRF96, and the ERP values were compared with EOP(IERS)C04 series. Our solution SSC(GAOUA)99L01 has 89 common stations with ITRF96. The coordinates of many stations given by our solution are at a few cm level in agreement with ITRF96. The transformation parameters between two these solutions are presented. Discussion on the residuals in the coordinates and velocities of some stations given by two these solutions is also given in the paper.

**G2/C/G5/L/13-A2** Poster **1630-17****ON COMPUTATION OF DAILY AND SUBDAILY SLR EOP SERIES**

Zinovy MALKIN (Institute of Applied Astronomy RAS, nab. Kutuzova 10, St.Petersburg 191187, Russia, e-mail: malkin@quasar.ipa.nw.ru)

In spite of GPS provides determination of EOP with impressive accuracy and operativity, SLR EOP results are very important for combined IERS solutions for improvement of systematic accuracy of the final IERS products. Unfortunately, EOP series produced by SLR analysis centers are not so unified as GPS products which makes difficult their comparison and combination. In the paper possible ways of computation of daily EOP series from the SLR observations are discussed and attempt to choose optimal strategy have been made. The main problems with computation of daily EOP series are discussed. These are densification of SLR EOP series without loss of accuracy (from usual 3-5 days to daily solution), computation strictly daily series (for 0h every day instead of more or less accident fraction of day depending on distribution of observations) and computation of UT series from LOD one.

Special strategy is proposed to improve accuracy of operational solution. As results of operative determination of EOP depend on initial value of EOP, this effect was investigated in various ways. To eliminate it in routine operative computation special iterate procedure have been developed. In particular, it requires accurate short-time prediction of EOP. Improved method of EOP prediction is advanced. Proposed strategy have being used in routine daily EOP computation in the IAA and shows good density (one day), accuracy (0.2-0.3 mas for Pole coordinates and 0.02-0.003 ms for LOD) and operativity about 2 days (if sufficient number of observations are present) of EOP results.

A possibility to get more dense SLR EOP series (12 and 6 hours) was investigated. Unfortunately, accuracy of these determination evidently is not sufficient to make substantial contribution to research of high-frequency variations of the Earth's rotation. Nevertheless, combination of SLR and VLBI observations for this purpose seems interesting.

**G2/W/03-A2** Poster **1630-18****GEOID AND SEA LEVEL OF THE NORTH ATLANTIC REGION FROM MULTI MISSION AND MULTI CHANNEL REMOTE SENSING DATA**

P. Knudsen, O. B. ANDERSEN, T. Knudsen, O. Leeuwenburgh (all at National Survey and Cadastre, Copenhagen NV, Denmark, email: pk@kms.dk) A. A. Nielsen, K. B. Hilger (both at IMM, Technical University of Denmark, Lyngby, Denmark) C. C. Tscherning, N. K. Højerslev, G. Moreaux (all at University of Copenhagen, Geophysical Department, Copenhagen OE, Denmark); E. Buch, V. Hues (both at Danish Meteorological Institute, Copenhagen, Denmark).

The interdisciplinary project GEOSONAR (funded by the Danish Earth observation programme) analyses multi-disciplinary contributions to sea level and its variations on different time scales. This includes geodetic, oceanographic and meteorological effects on sea level, focussed in the North Atlantic and particularly the North Sea.

In addition to traditional geodetic remote sensing techniques, such as altimetry, this project also involves the use of multi-channel scanning radiometers data, in the visible and infrared wavelengths. Data have been obtained from the Sea-viewing Wide Field-of-view Sensor (SeaWiFS), as well as from the NOAA advanced very high resolution radiometer (AVHRR), and the ERS along track scanning radiometer (ATSR).

The project and initial results are presented. One of these results is a new enhanced cloud removal technique for SeaWiFS data. This technique is based on maximum auto-correlation factors analysis (MAF). Extracting geodetic and oceanographic signal from these merged multi-channel data sources is non-trivial, however, the MAF analysis tool has also proven to valuable in the interpretation of the data.

**G2/W/15-A2** Poster **1630-19****THE IGES CROSS OVER ADJUSTMENT WITH A NEW SOFTWARE FOR THE SST IN THE MEDITERRANEAN SEA**

A. Piatti and G. VENUTI (both at DIAR Politecnico di Milano - Facolta' di Como - p.le Gerbetto, 6 - Como - email: giove@ipmtf4.topo.polimi.it)

Having in mind to determine the Mediterranean stationary SST from the radar altimetric observations an ad hoc procedure was built up. After a trackwise collocation filtering on the repeat mission data from both T/P and ERS1/2 to determine the stationary SST from the fully corrected altimetric observations, a local cross-over adjustment is needed to model the residual radial orbital error and the tidal error. The main characteristics of the proposed cross-over adjustment are: the possibility to merge data from different satellite missions and to allow a stepwise adjustment in which a set of tracks is capt fixed, playing the role of reference system. We will present the main feature implemented to search the cross-over positions and to fix the rank defect of the adjustment model. As a result we will show the stationary SST obtained by applying this procedure to T/P and ERS1/2 data in the Mediterranean area.

**G2/W/16-A2** Poster **1630-20****IMPROVED TIDE MODEL FROM TOPEX/POSEIDON AND GEOSAT ALTIMETRY OVER SHALLOW SEAS**

Xiaoli DENG and Dingbo Chao (School of Geo-science of Engineering Surveying, Wuhan Technical University of Surveying and Mapping, 39 Luoyu Road, Wuhan 430070, P. R. China, email: dxl@ultra2.wtusm.edu.cn)

TOPEX/POSEIDON (T/P) data and Geosat ERM data have been used to extract errors in major diurnal and semidiurnal tidal constituents of the CSR3.0 model over the Western Pacific. Due to spatial complexity of tides in shallow seas, the coarse bin technique, which is necessary to overcome tidal aliasing problems in altimetry, does not be performed to avoid considerable distortion of the tidal signal. Using the harmonic analysis, this has been done here from over 4.5 years of T/P data along the ground track and Geosat ERM data at crossover locations with both ascending and descending track data. Comparison of simulated tides to the CSR3.0 model shows that more accurate information about tides in shallow water can be obtained from along-track T/P data, and that tides at crossover locations can be improved from both ascending-track and descending-track of Geosat data which have a shorter data record than T/P. They both contribute to the local region studied where resolution is more important than regular spacing.

**G2/E/05-A2** Poster **1630-21****GPS-ALTIMETRY TESTS - MEASURING GPS SIGNAL REFLECTED FROM THE SEA SURFACE**

P. Knudsen, H. Olsen, G. Xu National Survey and Cadastre - Denmark (KMS) Rentemestervej 8, DK-2400 Copenhagen NV, Denmark

Several so-called GPS-altimetry tests have been carried out at the National Survey and Cadastre - Denmark (KMS) for measuring the GPS signal reflected from the sea surface. The purpose of such tests is to see if it is possible to use downward GPS antenna to receive the reflected GPS signal for applications such as sea surface or ice sheet topography determination. Usually, in satellite altimetry or airborne altimetry, profiles of footprints over the sea surface are measured, however, by using GPS-altimetry, every measured profile of footprints has a bandwidth. So that such GPS-altimetry can be used for sea surface or ice sheet topography coverage. This paper describes the details and the intention of our tests. An upward antenna and a downward antenna are used, one for positioning the antenna platform and the other for the reflection surface measurement. Results of the GPS data analysis are given. Theoretical basis is discussed and outlined.

**G2/W/08-A2** Poster **1630-22****SIMULATION OF GOCE ORBIT DETERMINATION AND GRAVITY FIELD RECOVERY**

J. VAN DEN IJSSEL, R. Koop and P. Visser (Delft Institute for Earth-Oriented Space Research, Delft, The Netherlands, email: jose.vandenijsel@lr.tudelft.nl) A. Selig, P. Hoyng and M. Smit (SRON, Utrecht, The Netherlands) N. Sneeuw, J. Mueller and R. Rummel (IAPG, Muenchen, Germany)

The Gravity field and steady-state Ocean Circulation Explorer (GOCE) is one of 4 ESA candidate missions in the Earth Explorer Mission program. Its main mission objective is a high-resolution, high-accuracy and homogeneous determination of the static Earth's global gravity field. To this aim GOCE will be equipped with a gradiometer providing Satellite Gravity Gradiometry (SGG) measurements, a GPS/GLONASS (GRAS) receiver providing Satellite-to-Satellite Tracking (STT) measurements and a Drag Free Control (DFC) to compensate non-conservative forces. The gravity field recovery of the GOCE mission will be based on both SST and SGG measurements. The gradiometer is particularly sensitive to the medium and high frequency gravity field information and the GRAS receiver will be used for the long and

medium wavelengths. In the framework of the preparations for this mission and parallel to the phase A development a simulator facility is being developed. The main purpose of this simulator is to show how all system aspects of the satellite affect both the SGG and SST measurement accuracy and hence the final achievable gravity field recovery accuracy. To this end orbit recovery simulations are conducted to determine realistic values for the achievable orbit accuracy in the presence of error sources like e.g. measurement noise, dynamic modelling errors for the gravity and tides model and tropospheric correction errors. Furthermore, software is developed for the least-squares estimation of geopotential coefficients from SGG and SST data from GOCE. The procedure is based on an iterative, semi-analytical approach with a block-diagonal normal matrix. Recent progress in the development of the simulator will be shown.

**G2/E/01-A2** Poster **1630-23**

#### GENERALIZED SPHERICAL HARMONIC ANALYSIS OF SATELLITE GRADIOMETRY

Zhang CHUANDING and Wu Xiaoping (Department of Geodesy, Zhengzhou Institute of Surveying and Mapping, 66 Longhai Road, Zhengzhou 450052 Henan, P. R. OF CHINA)

This paper mainly focuses on the generalized spherical harmonic series representation of satellite gradiometry and on the generalized spherical harmonic analysis of satellite gradiometry. Using the form of generalized spherical harmonics, the combination of several components of satellite gradiometry can be represented as in series of generalized spherical harmonics, which are several subset of larger group of orthogonal functions: the D-functions. If the observations are preprocessed by averaging to form a constant radius, equiangular grid, we can easily obtain good formulae for high degree and order global spherical harmonic analysis from D-functions as eigenfunctions. This paper secondary aims to the realization of D-functions or d-functions. d-functions are homogeneous polynomial and are given explicitly by Wigners formula, but it is too complexly to compute. By using the relations of d-functions (third index  $m=0,1,2$ ) and the  $k$  ( $k=0,1,2$ ) order derivatives of Legendre functions, a new recursive methods for calculations of d-functions (third index  $m=0,1,2$ ) is presented. We conclude if we view upon the data set as being a set of observations distributed in some way in three dimensional space, a regular, global of observations in geocentric cartesian system or in local geocentric spherical coordinate system is more convenient for recovery of spherical harmonic coefficients, and if we consider the data set as a times series, the observations given in subsequent points along a satellite orbit, the observations in geocentric cartesian system or in orbital coordinate system is more convenient for computation of spherical harmonic coefficients.

**G2/E/11-A2** Poster **1630-24**

#### RECENT RESULTS IN THE SIMULATION OF THE GRAVITY FIELD MISSION GOCE

Juergen MUELLER, Helmut Oberndorfer and Nico Sneeuw (Institut fuer Astronomische und Physikalische Geodaesie, Technische Universitaet Muenchen, D-80290 Muenchen, Germany, email: jxm@alpha.fesg.tu-muenchen.de); Martijn Smit (Space Research Organisation Netherlands, NL-3584 CA Utrecht, NL) Radboud Koop and Pieter Visser (Delft Institute for Earth Oriented Space Research, Delft University of Technology, NL-2629 JA Delft, NL)

GOCE (Gravity Field and Steady-State Ocean Circulation Explorer) is one of the dedicated gravity field missions of the next years. Its main objective is the determination of the Earth's gravity field with high spatial resolution and with high homogeneous accuracy by applying: Satellite-to-Satellite Tracking (SST) in high-low mode for the orbit determination and for the retrieval of the long-wavelength part of the gravity field, and Satellite Gravity Gradiometry (SGG) for the derivation of the medium/short-wavelength parts. For a realistic simulation, the various errors (e.g. misalignments, drag coupling or S/C rotation) as well as the interactions between the sensors/actuators (e.g. for attitude control) have to be considered and their effect on the scientific end-products (e.g. spherical harmonics, geoid heights or gravity anomalies) has to be investigated. The simulation is performed by different techniques using different mathematical tool boxes whose results are compared. Our preliminary results show that the aspired accuracy level of  $10^{-3}$  Eotvoes/sqrt(Hz) can be achieved which enables to derive a gravity field up to degree and order 250.

**G2/E/09-A2** Poster **1630-25**

#### A NEW TECHNIQUE FOR ENHANCEMENT OF SAR INTERFEROMETRIC IMAGES IN VOLCANIC AREAS

Libero Bertucco and Giuseppe Nunnari, (Dipartimento Elettrico, Elettronico e Sistemistico, Università di Catania, Viale A. Doria, 6, 95125, Catania, Italy, email: gnunnari@dees.unict.it) Pierre Briole Institut de Physique du Globe, 4, Place Jussieu, 75252, Paris, France, e-mail: briole@sismo15.ippg.jussieu.fr Jean-Luc Froger UMR 6524, OPGC-CRV, 5, Rue Kessler, 63000, Clermont-Ferrand, France, e-mail: froger@opgc.univ-bpclermont.fr Giuseppe PUGLISI (Istituto Internazionale di Vulcanologia, Consiglio Nazionale delle Ricerche Piazza Roma, 2, 95123, Catania, Italy, tel. +95 448084, fax +95 436801, email: geo@iiv.ct.cnr.it)

Synthetic Aperture Radar (SAR) is a high-resolution imagery system for remote sensing. We propose a new technique for enhancement of wrapped interferometric SAR images. The aim of filtering is to reduce the noise in wrapped images before unwrapping step. The reasons of this work rise from the need to have low-noisy images for the parameters inversion of ground deformation sources. The volcanic areas represent a good test site because the SAR images relevant to these areas often show breaks in the continuities in the SAR interferometric phase. There are many sources of these phenomena; for instance, the typical cone-shape of the relief that give rise to large lay-over or shadow phenomena or the juxtaposition of fresh lava and vegetated areas having large difference in coherence give small scale breaks. The images examined to validate the proposed algorithm are differential interferometric images acquired from ERS-1 and ERS-2 satellite systems. The technique, called MPSF (Median Phase Shift Filter) is essentially based on two steps. First step is a particular median filtering based on phase shift; second step is based on the analysis of the neighborhood of every pixel of the image. The results obtained on test-images shown a appreciable improvement of the processed images.

**G2/L/14-A2** Poster **1630-26**

#### CRUSTAL DEFORMATION MONITORING OF VOLCANOES IN JAPAN USING L-BAND SAR INTERFEROMETRY

MURAKAMI

Abstract unavailable at the time of going to Press

**G2/L/11-A2** Poster **1630-27**

#### THE DEVELOPMENT OF THE ISGN: STATUS AND PERSPECTIVES

Hermann DREWES, John Bosworth, Tom Herring

The Working Group on the establishment of an International Space Geodetic Network (ISGN) was created during the IAG Scientific Assembly in Rio de Janeiro in a joint meeting of CSTG, IERS and IGS. Its installation was an outcome of the previous Working Group on the IUGG Fundamental Reference and Calibration Network (FRCN). The main objectives of the ISGN WG were: - to define the criteria for including a station into the ISGN, and - to install a better cooperation between the individual techniques. The criteria defined by the ISGN WG include the sites criteria, the analysis criteria, and the IERS requirements. They were presented to and accepted by the CSTG Executive Committee and the IERS Directing Board in April 1998. In the next step, all those stations of the existing space geodetic sites were selected, which fulfill these criteria. They are the candidates for the new ISGN to be installed in the next months.

**G2/L/15-A2** Poster **1630-28**

#### HORIZONTAL SITE DISPLACEMENT DUE TO ATMOSPHERIC LOADING

Tadahiro SATO, Yuki Hatanaka and Shin'ichi Miyazaki, Seiichi Shimada

Atmospheric mass loads the Earth and deforms its surface. Temporal variations of atmospheric mass distribution lead to site displacement. Atmospheric loading effect is large in high latitude, at inland area and in winter season. Vertical component of atmospheric loading effect is more than 5cm in an extreme case, while horizontal component is less than 5mm. However, thanks to improvement of GPS positioning accuracy, horizontal site displacement is detectable in some GPS stations.

Horizontal site displacement due to atmospheric loading is computed by convolving Green's function with global surface pressure values estimated by Japan Meteorological Agency. Computed horizontal displacement has correlation with horizontal gradient of surface pressure distribution; sites move toward high pressure. Comparison between theoretically computed horizontal site displacement and GPS results will be discussed.

**G3** **Friday 23 July**

#### DETERMINATION OF THE GRAVITY FIELD (SECTION 3)

Location: Law Building 303 LT  
Locations of Posters: Old Gym

**Friday 23 July AM**

Presiding Chairs: M.G. Sideris (Univ. Calgary, Canada),  
R. Forsberg (KMS, Copenhagen, Denmark)

#### IAG SECTION 3 REPORTS

##### Business Section

**REPORT OF IAG SECTION 3** **0830**

R. Forsberg

**REPORT OF THE INTERNATIONAL GRAVITY COMMISSION** **0845**

I. Marson

**REPORT OF THE INTERNATIONAL GEOID COMMISSION** **0905**

H. Sunkel

**G3/L/06-A5** **0925**

#### AN ATTEMPT TO ASSESS DIGITAL TERRAIN MODELS - REPORT OF SSG 3.163

D. ARABELOS (Department of Geodesy and Surveying, Aristotle University of Thessaloniki, Univ. Box 474, GR-540 06, email: arab@eng.auth.gr)

One of the main tasks of the SSG 3.163 was the assessment of the global digital terrain models. Apart of comparisons with high resolution data from national data-banks, an intercomparison of the 5' global DTMs ETOPO5, TBASE and JGP95E, showed considerable differences between them. The standard deviation of these differences globally is about 100 m with min. and max. values ranging from -3.8 to 4.7 km. An attempt was made to estimate the errors in the different types of topographic reductions due to the errors of the above mentioned DTMs. The results showed that the influence was smaller in the case of the RTM reductions. A plot of the standard deviation of the topography versus the standard deviation of the gravity computed from EGM96, showed that in different areas of the earth there are serious errors due to the low quality of the topography or/and of gravity.

**G3/E/42-A5** **0940**

#### FROM AIRBORNE GRAVIMETRY TO AIRBORNE GEOID MAPPING - REPORT OF SSG3.164

Wei MING

This paper summarizes some of the works done in the Special Study Group 3.164 "Airborne Gravimetry Instrumentation and Methods" over the last four years but it does not give a comprehensive overview of all activities. During the last four to five years, major advances in implementing airborne gravimetry as a production system have been made. The LaCoste & Romberg S-model gravimeter has been successfully used for airborne gravimetry by several groups. The inertial scalar gravimetry using inertial system in conjunction with DGPS has also reached a production level. The airborne gravity data over Greenland and parts of the Arctic and Antarctic has been used for determination of earth gravity model EGM96. The local geoid determination using airborne gravity data has achieved excellent results. All these progress shows that the roll of airborne gravimetry in geodesy, particularly in geoid determination, becomes more important.

After the review of the progress in airborne gravimetry, the paper discusses the different



techniques for airborne gravimetry. The concept and algorithm to determine geoid, especially the regional or local geoid, using the airborne gravity data combined with other gravity data are also described in the paper. This opens a new subject - airborne geoid mapping, defined as determining geoid using airborne gravimetry data. Test results show that the local geoid determined by airborne gravity data has achieved an accuracy of 5 cm of the geoid undulation. Some critical issues in airborne gravimetry and airborne geoid mapping are also included as conclusions.

### G3/E/45-A5 0955

#### GLOBAL GRAVITY FIELD DETERMINATION AND EVALUATION - REPORT OF SSG3.165

Dr. Nikolaos K. PAVLIS ( Phone: (301)-441-4121 Raytheon STX Corporation FAX: (301)-441-2432 7701 Greenbelt Road Suite 400 Greenbelt, MD 20770 e-mail: npavlis@geodesy2.gsfc.nasa.gov USA

This presentation will review some of the work performed by members of the Special Study Group (SSG 3.165), and by other interested colleagues, which addressed the goals identified in the SSG's program of activities. A major effort of SSG members and other interested parties involved the development and evaluation of contemporary global geo-potential models such as EGM96, TEG-3, and GRIM4-C4. The evaluation of EGM96 in particular was greatly enhanced through numerous tests that were performed by an international group of investigators, working under the auspices of IGeS. A significant effort was made to collect and systematically archive data and information that can be used to evaluate global geo-potential models. GPS-determined heights and levelling data constitute the bulk of this test database. The current status of this database will be reviewed, and the need for such independent test data in areas void of such information will be emphasised. The prospects of geo-potential mapping satellite missions such as CHAMP, GRACE and GOCE intensified the work related to the determination of the gravitational field and its temporal variations, from satellite-to-satellite tracking and satellite gradiometry approaches.

### G3/W/05-A5 1010

#### REGIONAL LAND AND MARINE GEOID MODELLING - REPORT OF SSG3.167

I.N. TZIAVOS (Department of Geodesy and Surveying, Aristotle Univ. of Thessaloniki, Univ. Box 440, 54006 Thessaloniki, Greece, Email: tziavos@eng.auth.gr)

This paper summarizes the activities and achievements of the IAG Special Study Group (SSG) 3.167: "Regional Land and Marine Geoid Modelling", which was established by the XXIIth General Assembly of IAG held in Boulder, Colorado, USA, July 3-14, 1995. The objectives of the SSG3.167 reflects the duality between past and future and it consolidates what it has already been achieved, and works towards addressing open and new questions. The current state of knowledge in regional geoid modelling refers to: (a) theoretical models related to BVP (e.g., how to include terrain and non-linear effects); (b) data reductions and data preparations; (c) modelling procedures for land and marine geoids; (d) accurate regional-scale marine geoid solution and their contribution to sea surface topography and other related oceanographic studies; and (e) validation procedures regarding the quality of the geoid product. Looking to open issues we could mention: (a) new efficient ways of working with heterogeneous data; (b) the impact of GPS - heights not only to validation procedures but also to common adjustments with geoid heights; (c) the study of compatibility of neighbouring datums through geoid determination; (d) the contribution of oceanography to synthetic geoid modelling; and (e) new solutions of the global BVP, which can lead to better theoretical geoid models. In terms of applications, and in the frame of the above mentioned main tasks, considerable work has been carried out in regional land and marine geoid modelling applying successfully efficient spectral and stochastic algorithms, as well as several new alternatives, and using large amounts of terrestrial and airborne gravity data, satellite altimetry data from recent and most accurate missions, and new global reference models.

### G3/W/44-A5 1025

#### PROGRESS REPORT FOR IAG SSG3.177: SYNTHETIC MODELLING OF THE EARTH'S GRAVITY FIELD

W.E. FEATHERSTONE (School of Spatial Sciences, Curtin University of Technology, GPO Box U1987, Perth, WA, 6845, Australia, email: wfeather@cc.curtin.edu.au)

In 1997, the IAG created an out-of-cycle special study group concerning the construction of a synthetic model of the Earth's gravity field. This group aims to develop the theoretical basis and computational methods for the production of a synthetic, yet realistic, model of the Earth's gravity field. Such a model is not currently available to the physical geodetic community and geodetic researchers have to rely on analytical error estimates, often based on observed data. Importantly, many of the discrepancies between the various gravity field theories are at the limit prescribed by the current data availability. A synthetic gravity model will thus give an independent validation of the procedures used. This paper will give an overview of the aims and objectives of the Group, review what progress has been made in constructing a synthetic Earth gravity model, and summarise some of the current approaches being explored by the members of the Group. (The Group's web-page is located at <http://www.cage.curtin.edu.au/~will/iagssg3177.html>)

### GRAVITY FIELD DETERMINATION 1

### G3/W/39-A5 1100

#### THE 1999 GFZ PRE-CHAMP HIGH RESOLUTION GRAVITY MODEL

Th. GRUBER, Ch. Reigber, P. Schwintzer (GeoForschungsZentrum Potsdam / GFZ, Division 1, Telegrafenberg A17, D-14473 Potsdam, Germany, e-mail: gruber@gfz-potsdam.de)

In preparation of the CHAMP gravity and magnetic field satellite mission, a completely new satellite-only gravity field solution named GRIM5 was recently computed by GFZ and GRGS. Based on the full variance-covariance matrix of this solution and terrestrial and altimetry derived surface gravity data, a new high resolution global gravity field model up to degree and order 359 was computed. The solution was calculated by a rigorous combination of full variance-covariance matrices from the satellite-only model and the land and ocean surface gravity data with block-diagonal structured variance-covariance matrices from the high resolution terrestrial and altimetric gravity information provided by the U.S. National Imagery and Mapping Agency (NIMA). For this new solution the spherical harmonic degree and order for the full variance-covariance matrices was extended to 120, compared to degree 100 for previous GFZ solutions and degree 70 for the EGM96 model. It can be shown with this new model, that due to the extension of the full normal equation system the quality of the final model could be increased significantly for this frequency range. Quality parameters for such investigations were derived from the internal error parameters from the least squares solution and from comparisons with external independent gravity and geoid information. The new high resolution combination model represents a major improvement towards a series of new gravity

models with unprecedented accuracy and resolution from the CHAMP and GRACE gravity field missions. With these missions long and medium wavelengths will be dominated by satellite data, while short wavelengths still will be determined solely from surface data. Therefore the presented combination technique can be extended also to the computation of high resolution CHAMP and GRACE based gravity models.

### G3/W/42-A5 1120

#### THE REGIONAL GEOPOTENTIAL MODEL TO DEGREE AND ORDER 720 IN CHINA

Yang Lu H.T.Hsu F.Z.Jiang Institute of Geodesy and Geophysics, Chinese Academy of Sciences, email: luyang@asch.whigg.ac.cn

For the time being, the spherical harmonic expansion is a powerful method describing local and global gravity field in frequency domain yet. In principle, the resolution of gravity field and its precision expressed by spherical harmonic model are proportional to degree and order of model explaining. For this reason a higher degree geopotential model is advantageous for us. It is possible to develop a regional model to degree and order 720 although that seems more difficult for global model in terms of the precision and density of gravity data over global area. Following the tailored method, we have developed an ultra regional geopotential model to degree and order 720 suitable to China. The gravity anomalies from new model have a mean square error (6.4 mgal). The modeled geoid undulations have a mean square error (0.67m in China land, but both mean square errors of gravity anomaly and geoid undulation are the same as one from reference model EGM96 in global area without China.

### G3/W/02-A5 1140

#### COMPARISON AND EVALUATION OF THE NEW RUSSIAN GLOBAL GEOPOTENTIAL MODEL TO 360 DEGREE

P. MEDVEDEV, (Geophysical Center, Russian Academy of Sciences, Molodezhnaya 3, 117296, Moscow, Russia, email: pmedv@wcb.rssi.ru); G. Demianov (Central Research Institute of Geodesy, Air Surveying and Cartography, Federal Service of Geodesy and Cartography of Russia, 26, Onezhskaya, 125413 Moscow, Russia, e-mail: gleb@space.ru)

New Russian global geopotential model created with use the detailed gravity data, satellite tracking and altimetry data. The test data that we used for model evaluations include geoid undulations (or height anomalies) determined from GPS positioning and level observations, geoid undulations from EGG96 (Denker et al.), global geopotential models EGM96, GPM98A (Wenzel, 1998), global marine gravity field from russian GEOIK altimetry data and from GEOSAT, ERS-1, TOPEX (P.Medvedev et al., 1998; Sandwell et al. 1997; Andersen et al., 1998). Future problems geoid determinations discussed.

### G3/E/05-A5 1200

#### GRAVITY AND MACRO-MODEL TUNING FOR THE GEOSAT FOLLOW-ON SPACECRAFT

Frank G. LEMOINE (email: fleoine@olympus.gsfc.nasa.gov), David D. Rowlands, Gregory C. Marr (NASA Goddard Space Flight Center, Greenbelt, MD 20771 U.S.A.); Nikita P. Zelensky, Scott B. Lutcke, Christopher M. Cox (Raytheon ITSS, 7701 Greenbelt Rd., Greenbelt MD 20770 U.S.A.)

The US Navy's GEOSAT Follow-On spacecraft was launched on February 10, 1998 and the primary objective of the mission was to map the oceans using a radar altimeter. The spacecraft tracking complement consisted of GPS receivers, a laser retroreflector and Doppler beacons. Since the GPS receivers have not yet returned reliable data, the only means of providing high-quality precise orbits has been through satellite laser ranging (SLR). The spacecraft has been tracked by the international satellite laser ranging network since April 22, 1998, and an average of 7.4 passes per day have been obtained from US and participating foreign stations. Since the predicted radial orbit error due to the gravity field is two to three cm, the largest contributor to the high SLR residuals (7-10 cm RMS for five day arcs) is the mismodelling of the non-conservative forces, not withstanding the development of a three-dimensional eight-panel model and an analytical attitude model for the GFO spacecraft. The SLR residuals show a clear correlation with beta-prime (solar elevation) angle, peaking in mid-August 1998 when the beta-prime angle reached -80 to -90 degrees.

In this paper we discuss the tuning of the non-conservative force model, for GFO and report the subsequent addition of the GFO tracking data to the Earth gravity model solutions.

### G3/L/22-A5 1220

#### THE NRL AIRBORNE GEOPHYSICS PROGRAM

John M. BROZENA, Vicki A. Childers, Naval Research Laboratory, Code 7420, 4555 Overlook Ave. SW, Washington DC, USA 20375-5350. Email: vicki@qr.nrl.navy.mil

In this talk we provide an overview of recent efforts under the Naval Research Laboratory (NRL) aerogeophysics program that includes large area gravity and magnetics surveying, noise reduction efforts in aerogravity, measurements of ocean surface and the geoid, and possibly gravity gradiometry. NRL, in conjunction with the University of Texas Institute for Geophysics and the University of Oslo, has been conducting a long-range, large-area aerogeophysical survey over the Arctic Ocean. The goal of this survey is to provide insight into the tectonic history of the region and to make continuous measurements of gravity, magnetics, and the geoid across the region. Over the course of five field seasons, aerogravity and magnetics were measured over a region that encompasses the southern Canada Basin, the Chukchi Plateau, the Alpha Ridge, and a portion of the Mendeleev Ridge out to the 1800 meridian. Last summer, our survey extended to the Eurasian Basin, from east of the Alpha Ridge to the Svalbard continental slope, an area entirely contained within the ?hole? over the pole in the ERS-1/2 gravity data. This summer we return to Svalbard to extend the survey eastwards. There is the possibility that the Lockheed Martin gravity gradiometer will be installed in the aircraft for this mission, with our goal being to merge the long wavelength gravity information from the scalar measurements with the shorter wavelength gravity measurement from gradiometry to enhance the resolution of the aerogravity measurement.

Recently, our work has focused on developing new techniques for noise reduction in our aerogravity data. We have improved our determination of aircraft vertical positioning in several ways: GPS position solutions are corrected for jumps and spikes, are ?lever arm? corrected to translate the GPS antenna location to the gravimeter, and we now compute and compare accelerations determined from GPS, radar, and a combination of radar plus the acceleration of a gravimetrically derived geoid surface. We have enhanced the gravimeter measurement by improving the offlevel correction, averaging the two gravimeter measurements, and refining the lowpass filter for each particular survey. These developments have provided a substantial reduction in measurement error. Last summer...

Friday 23 July PM

Presiding Chairs: W. Featherstone (Curtin Univ. of Technology),  
R. Forsberg (KMS, Copenhagen, Denmark)**GRAVITY FIELD DETERMINATION 2****G3/L/8-A5****1400****GEOID MODELLING IN COASTAL REGIONS USING AIRBORNE AND SATELLITE DATA: CASE STUDY IN THE AZORES**

M. J. FERNANDES (email: mjfernan@oa.fc.up.pt); L. Bastos (email: lcbastos@oa.fc.up.pt) Observatório Astronómico, Faculdade de Ciências, Universidade do Porto, Monte da Virgem, 4430 Vila Nova de Gaia, Portugal, R. Forsberg, (email: rf@kms.min.dk); A. Olesen (email: avo@kms.min.dk), National Survey and Cadastre, Rentemestervej 8, DK 2400, Copenhagen NV, Denmark F. Leite (Departamento de Matemática Aplicada, F. C. T. , Universidade de Coimbra, Apartado 3008, 3000 Coimbra, Portugal, email: cb@mat.uc.pt)

Airborne altimetry and gravimetry can play an important role in regional geoid mapping, particularly in coastal zones where satellite altimetry shows limited accuracy. This study is concerned with the determination of a high resolution regional geoid in the area surrounding the Azores Islands, integrating multi-sensor airborne and marine observations with satellite and land data.

In the scope of the MAST III project AGMASCO several airborne gravimetry/altimetry campaigns have been performed. The usefulness of airborne measurements to complement satellite and marine data in coastal regions, bridging the gap between land areas and the open ocean, has been proved.

The airborne and marine data used in this study have been collected in one those campaigns, which took place in the Azores region, in October 1997. This area shows very high gradients in the sea bottom topography as well as in the islands altimetry, with corresponding large variations in the gravity field.

Airborne, marine and land gravimetry, together with altimeter derived gravity anomalies, have been merged in a combined geoid solution. In this computation an improved bathymetric and altimetric model has been used. The final geoid solution has been validated using airborne and satellite altimetry and tide gauge data.

Model accuracy and improvement over existing global and local models is accessed and presented.

**G3/W/33-A5****1420****ASSESSMENT OF THE GLOBAL LAND ONE-KILOMETER BASE ELEVATION DEM**

Allen M. HITTELMAN, David A. Hastings, Paula K. Dunbar (NOAA's National Geophysical Data Center, 325 Broadway, Boulder, CO 80303, USA, email: amh@ngdc.noaa.gov)

The Global Land One-kilometer Base Elevation (GLOBE) digital elevation model (DEM) is the most thoroughly designed, reviewed and documented global digital elevation dataset to date. GLOBE was developed by an international group of specialists, cooperating with the Committee on Earth Observation Satellites (CEOS) Working Group on Information Systems and Services (WGISS), International Geosphere-Biosphere Programme's Data and Information System (IGBP-DIS), and ISPRS Working Group IV/6.

GLOBE's initial objective was to populate a two-dimensional latitude-longitude 30 arc-second grid with the best available data that could be distributed with minimal restrictions. In addition, a completely unrestricted version of GLOBE was envisaged. The final DEM has been assembled using 11 original sources (raster and vector source data), some of which had more than one form of post-source processing. A total of 18 combinations of source/lineage were used in GLOBE.

The quality review of the GLOBE Version 1.0 DEM included (1) viewing source imagery with various color palettes in NGDC's GeoVu public domain browse and visualization utility and the GRASS GIS; (2) viewing slope, aspect, and shaded relief images of each source data set; (3) principal components analysis of all available sources for a given area; (4) histogram analysis for each source data set; and (5) statistical comparisons between sources.

**G3/W/56-A5****1440****RECENT ADVANCES IN THE ACQUISITION AND USE OF TERRAIN DATA FOR GEOID MODELLING OVER THE UNITED STATES**

Dr Dru SMITH

In recent years, the accuracy requirements for high resolution geoid models have reached the centimeter level. In order to attempt such accuracy, extremely detailed models of the terrain, free from systematic errors, must be used for computing the gravitational signal induced by topography. At the United States National Geodetic Survey, new efforts have been made to incorporate a 30 meter horizontal resolution digital elevation model (DEM, from the U.S. Geological Survey) into geoid computation procedures. This data, unlike previously available DEM's, has consistency in data collection, datum registration, and shows internal consistency with heights recorded at gravity measurement sites. Initial tests indicate that large systematic errors in previously used 3 arcsecond DEM data have induced geoid errors exceeding 10 cm, spread over 100 km or more. These systematic errors do not seem to exist in the new 30 meter data. The computer power needed to store and process the data is substantial: to completely describe the western half of the United States with this DEM requires 32 Gb. Acquisition of new data was only the first step. Recent investigations into methods for computing Helmert gravity anomalies indicate that the rigor with which the gravity signal induced by the terrain is computed must be increased. This new rigor removes many previous assumptions and replaces them with new techniques. This includes the use of spherical coordinates, sloped-tops for terrain prisms, attention to datum biases, and properly accounting for the terrain of the entire globe. While these new steps remove systematic errors that can exceed 10 mGals, there is a trade off for computational time that is being carefully weighed to find the most practical solution.

**G3/W/11-A5****1500****GRAVITY FIELD AND GEOID FOR JAPAN**

Yuki KUROISHI (Space Geodesy Laboratory, Geographical Survey Institute, 1 Kitasato, Tsukuba, Ibaraki 305-0811, Japan, email: yuki@gsi-mc.go.jp)

The Japanese islands are located in a trench and island arc region and the topography/bathymetry is very rugged. The gravity field and geoid, therefore, are complicatedly undulated.

A newer version of gravimetric geoid model, JGEOID98, was determined in a remove-restore manner by one-dimensional FFT realization of Stokes integration of residual Faye anomalies with reference to EGM96 global geopotential model. Gravity data were prepared only from surface gravity observation. Over the original geoid model, JGEOID93, several improvements

of data quality were applied: replacement of reference model OSU91A by EGM96, removal of possible offset errors in network-adjusted ship gravity data, removal of Stokes kernel approximation (from 2-D FFT to 1-D FFT), and widening of ship gravity coverage.

When compared with nation-wide GPS/leveling geoidal undulations, JGEOID98 shows significant improvement of 30% in short wavelength over JGEOID93 after best-fit planes removed. Though the comparison was made only on land where both models share completely the same gravity data, improvement of data quality and coverage at sea yields the geoid improvement even on land.

Gravity data at sea seems to have some systematic errors in long wavelength. The adjustment method for ship data significantly improves inter-consistency, but has weakness in anchoring absolute values of gravity. In order to assess the data at sea, discussion will be developed with several models of gravity from satellite altimetry in this region.

**G3/E/42-A5****1520****THE GWR DUAL SPHERE SUPERCONDUCTING GRAVIMETER C029 AT FRANKFURT A.M. AND WETTZELL - FIRST RESULTS AND CALIBRATION**

Martina Harnisch, Guenter Harnisch, Ilona Nowak, Bernd RICHTER, Peter Wolf (Bundesamt fuer Kartographie und Geodäsie, Richard-Strauss-Allee 11, D-60598 Frankfurt am Main, Germany, email: richter@ifag.de)

The GWR dual spheres superconducting gravimeter enables enhanced reliability of the data and better drift monitoring to achieve a high resolution and reliability in monitoring temporal gravity variations. The dual sphere system is equivalent to two single instruments, but the technical expenditure and the costs are considerably reduced. By differencing the signals of both systems even micro steps can be detected. For test phase of 83 days the gravimeter C029 was installed in the basement of a BKG building in Frankfurt a.M. / Germany. Despite of unfavourable environmental conditions five small offsets between 0.1 and 1.5 microgal occurred, which reliably were detected by the differential signal. The linear drift of both systems was in the order of + 30 and + 40 microgal/year with a small but significant exponential initial drift. At the end of October 1998 the C029 has been moved to Wettzell / Germany. Contrary to the results achieved in Frankfurt a.M., a very large initial drift occurred, different in sign and amplitude for the both systems. Whereas the upper system reached stability after about 2 weeks the decay process of the lower system is going on over more than 10 weeks. The noise of the gravity output (tide filter) is in the order of 0.1 microgal. No steps were observed in the first ten weeks of operation. - The scale factors of both systems of the C029 has been estimated by the acceleration method and by comparisons with absolute gravity measurements. The stability of the scale factors may be checked by comparison of the two gravity signal.

**OVERVIEW OF POSTER SESSION BY CHAIRMAN****1540****Global Gravity****G3/L/05-A5**

Poster

**1610-01****THE KMS99 GLOBAL ALTIMETRIC MARINE GRAVITY FIELD**

O. Andersen, P. Knudsen, (both at National Survey and Cadastre, Copenhagen NV, Denmark, email: oa@kms.dk, pk@kms.dk)

The KMS99 altimetric derived global marine gravity field is the latest version of gravity fields derived from ERS-1 and GEOSAT geodetic mission. This presentation describes the new gravity field and the improvements over the older KMS global marine gravity fields as described by Andersen and Knudsen (JGR, 97, ERS special issue) . The present resolution of the KMS gravity field is 1/30 degree corresponding to 2 minutes or 4 km at the Equator. In order to improve the capability of the gravity field to map short spatial wavelength in the gravity field, it has been necessary to investigate if data with a higher along track sampling than the present 1Hz data can be used. For the KMS99 gravity field the possibility of using reinterpolated 2 Hz along track observations have been carried out. Some of the other improvements that have been introduced in the new version of the gravity field is the use of repeat track altimetry to improve the spatial resolution at high latitude. Similarly, investigation of a better screening of the raw data have been carried out to improved the gravity field in especially coastal regions.

**G3/E/27-A5**

Poster

**1610-02****THE GRIM5 GLOBAL GEOPOTENTIAL MODELS**

Jean-Michel LEMOINE, R. Biancale, G. Balmino, J.C. Marty, B. Moynot (CNES/GRGS, Toulouse, France), F. Barlier, Y. Boudon, P. Exertier, O. Laurain (OCA/CERGA, Grasse, France); P. Schwintzer, Ch. Reigber, A. Bode, Z. Kang, F.H. Massmann, H. Meixner, J.C. Raimondo, S. Zhu (Geoforschungszentrum Potsdam, Div. 1, Potsdam, Germany)

The final models of the first version of GRIM5 Earth global gravity models are described on poster : GRIM5-S1, satellite only model based on the analysis of perturbations of 15 well tracked (since 1985) geodetic satellite and GRIM5-C1, combined with gravity and altimetry data through 30' mean surfaces, including the list of used data, characteristics of fields, an analysis of orbit performances, comparisons with data and former models, variance-covariance analysis.

**G3/E/28-A5**

Poster

**1610-03****RUSSIAN MODEL OF THE EARTH'S GRAVITY FIELD (GAO-98)**

G.V. DEMIANOV, B.V. Brovar, A.V. Kryukova, A.N. Majorov, N.G. Nazarova, N.N. Pashina, V.A. Taranov (Central research institute of geodesy, air surveying and cartography, Federal Service of Geodesy and Cartography of Russia, 26, Onezhskaya, 125413 Moscow, Russia, e-mail: gleb@space.ru)

Through the research and operations executed, the global Earth gravity field model GAO-98 of ZNIGAik, Moscow, with the resolution level corresponding to the geopotential expansion into spherical harmonics up to 360th degree has been developed. The main parameters of the model developed are a set of mean anomalies for 30'x30' - blocks covering the whole surface of Earth and a set of spherical harmonics up to 360th degree resulted from the expansion of the geopotential. The said model is destined mainly for a highly accurate quasigeoidal heights determination which will significantly improve the efficiency of implementing GPS/GLONASS satellite equipment's into the routine geodetic operations of the Federal Service of Geodesy and Cartography of Russia. Presentation of the EGF model GAO-98 in form of mean gravity anomalies for 30'x30' -blocks allows to make gravity data compatible with the global EGF parameters which contributes to detection and rejection of systematic errors of detailed gravity surveys.

The accuracy of absolute quasigeoidal heights by use of the model developed is for most



regions of Russia  $M = 20-25$  cm, and that for relative heights at the distance 200-300 km of  $m = 3-4$  cm. These data of a priori accuracy estimation are confirmed by the results of precise GPS-measurements along the traverse Moscow-Sankt Petersburg on a high-precision levelling line.

**G3/E/07-A5** Poster **1610-04**

**THE 1998 TO 1999 GEOS-3 TRACKING CAMPAIGN: ANALYSIS AND RESULTS**

F. G. LEMOINE (NASA Goddard Space Flight Center, Greenbelt, MD 20771 U.S.A., email: flemoine@olympus.gsfc.nasa.gov)

The GEOS-3 spacecraft was launched by NASA on April 23, 1975. The payload of the gravity-gradient stabilized spacecraft consisted of a radar altimeter, Doppler beacons, and a laser retroreflector. The GEOS-3 satellite-to-satellite tracking (SST) Doppler data and the satellite laser ranging (SLR) data have been an integral and valuable part of gravity model solutions developed at the Goddard Space Flight Center from GEM 9 through EGM96. GEOS-3 is located in a unique orbit at 850 km altitude and 115 degrees inclination. The data included in these solutions were acquired from 1975 through 1980. Since 1980, the SLR system precision has improved from 8 to 10 cm in 1980 to the subcm level for the best stations in the 1990's. The ILRS (International laser ranging service) initiated a new tracking campaign for this spacecraft in October 1998, and through January 1999, some 850 passes and 10,000 normal points were acquired. The quality of the "new" data obtained during this tracking campaign is assessed, and the impact of these "new" data on Earth gravity model solutions is evaluated.

**G3/E/40-A5** Poster **1610-05**

**NUMERICAL SIMULATION OF THE GRAVITY FIELD RESTITUTION WITH THE CHAMP MISSION**

Sylvain LOYER, F. Perosanz, A. Bolland, R. Biancale (CNES/GRGS, Toulouse, France)

One of the main mission of the German satellite CHAMP that will be launched in December 1999 is the mapping of the global Earth gravity field as well as his temporal variations. The satellite will fly at a very low altitude (from 470 to 270 km) with a tracking system consisting of a GPS receiver (JPL-USA) and a Laser Retro Reflector. The non-gravitational accelerations will be measured by a very sensitive STAR accelerometer (ONERA/CNES-France). In order to assess the Earth gravity field recovery capability we have performed numerical simulations. One month of data of the three cited-above instruments including realistic noises and errors have been processed. We present the results of this numerical simulation in term of gravity field recovery as well as orbit precision and accelerometer calibration parameters restitution.

**G3/L/40-A5** Poster **1610-06**

**ESTIMATION AND EVALUATION TO THE DIFFERENCE BETWEEN THE NORMAL GRAVITY FIELDS FROM PHYSICAL GEODESY AND GEOPHYSICS**

LI FEI and Chongbing Liu (both at Department of Geodesy, Wuhan Tech. Univ. of Surveying and Mapping, Wuhan, 430079, P.R.China, email: fl@dms.wtusm.edu.cn)

As we have known that the gravity anomaly used in physical geodesy means the difference between the observed gravity on the geoid and the normal(theoretical) gravity on the spheroid. Usually, the gravity anomaly is an important boundary value in determining the earth's figure and external gravity field. However, if the gravity anomaly is used to inverse the interior density anomaly relative to some theoretical density mode such as PREM from geophysics, there will exist two problems: one is caused by un-identity of the normal density, and the other by inconsistency of reference boundary surfaces and vertical deviation. Although such problems could be neglected in traditional gravity inversion, the errors covered by them are worth being taken into account in nowadays researches such as cm-order geoid and high resolution of gravity inversion. Therefore, the difference between the normal(theoretical) gravities corresponding respectively to normal spheroid and PREM mode is analyzed and compared from the original definition of the gravity anomaly. Then the errors in gravity anomaly caused by inconsistency of the reference boundary surfaces and vertical deviation are estimated. At last, the indetermination in inversion using gravity anomaly is summarized and evaluated, and a suggestion that gravity disturbance should be used directly is proposed.

**Satellite Altimetry and Sea-level**

**G3/W/30-A5** Poster **1610-07**

**THE KMS GRAVITY FIELD: ACCURACY ANALYSES AND IMPROVEMENTS**

O. ANDERSEN, P. Knudsen (National Survey and Cadastre, Copenhagen NV, Denmark, email: oa@kms.dk, pk@kms.dk); R. V. Sailor, M.L. Driscoll, J.A. Shorter (Litton-TASC, Reading, MA, USA, email: rvsailor@tasc.com); D. Manning and R. Trimmer, (National Imagery and Mapping Agency, St Louis, USA, email: ManningD@nima.mil, TrimmerR@nima.mil)

The KMS global marine gravity field is based on 50 million 1 Hz radar altimetric observations from the ERS-1 and GEOSAT geodetic missions. The resolution of the KMS98 gravity field is 1/30 degree corresponding to 2 minutes (equivalent to 4 km at the Equator). Using 1 Hz altimetric data, the track to track distance (average 4 km) is shorter than the along track distance of 6-7 km between observations.

In an effort to improve the mapping of especially short wavelength gravity features, the 1 Hz along track spaced data was replaced with 2 or 3 Hz values computed from the raw 10 Hz observations. Averaging, least squares collocation, and the use of an equalizer function (inverse of the alpha-beta on board GEOSAT filter) have been tested.

Detailed investigations at NIMA and TASC, focused on the accuracy evaluation of the gravity field. Extensive comparisons with in-situ observations along with analyses of power spectral densities, and frequency content will be presented. One of the investigations has shown the existence of some discontinuities and outliers in the present KMS gravity field, especially close to the coast. Finally, recent improvements in the KMS global marine gravity field are presented. One of these being collocation interpolation of the geoid anomalies using a spatial varying covariance function that models local sea level variability.

**G3/W/22-A5** Poster **1610-08**

**SEA SURFACE TOPOGRAPHY ESTIMATION BY A GENERALISED MULTIPLE INPUT-OUTPUT METHOD**

V.D. ANDRITSANOS (Department of Geodesy and Surveying, Aristotle University of Thessaloniki, 540 06 Thessaloniki, Greece, e-mail: bandrit@edessa.topo.auth.gr), M.G. Sideris (Department of Geomatics Engineering, The University of Calgary, 2500 University Drive N.W., Calgary, Alberta, T2N 1N4, Canada, e-mail: sideris@acs.ucalgary.ca) and I.N. Tziavos (Department of Geodesy and Surveying, Aristotle University of Thessaloniki, 540 06 Thessaloniki, Greece, e-mail: tziavos@olimpia.topo.auth.gr)

The generalised theory of multiple input-output systems is briefly presented, with emphasis on the signal properties used. In addition, the theory of individual un-correlated systems is compared with the generalised form and the advantages and disadvantages of each technique are pointed out. The proper use of the data sets in each case is also discussed. The FFT application makes this method very efficient in combining large heterogeneous data sets. Additionally, data errors can be propagated into the results.

An application to the computation of Sea Surface Topography (SST) is presented using pure altimetric data derived from various satellite missions and shipborne gravity measurements. The assumptions related to the data noise are given, and comments are made on the noise spectrum determination. Finally, some comparisons with existing SST models are performed. Preliminary results have shown that the expected accuracy of this technique is at the level of a few to several centimetres.

**G3/W/08-A5** Poster **1610-09**

**DERIVED FROM THE 3RD GPS-CAMPAIGN 1997.4 OF THE BALTIC SEA LEVEL PROJECT**

Alireza AZMOUDEH-ARDALAN and Erik W. Grafarend (Geodetic Institute, University of Stuttgart, Geschwister-Scholl Str. 24D, 70174 Stuttgart, Germany, Tel: +49 711 121 4086, Fax: +49 711 121 3285, email: ardalan@gis.uni-stuttgart.de)

An analysis of the Fundamental Geodetic Parameter based upon the 3rd GPS-Campaign 1997.4 of the Baltic Sea Level Project is performed. The computation is referred to the following method: (1) Cartesian co-ordinates of GPS positioned gauge stations are transformed into spheroidal co-ordinates. (2) The spherical harmonic expansion of the EGM 96 Geopotential Model (F.G. Lemoine et al, Nasa/TP-1998-206861, Goddard Space Flight Center, Greenbelt/Maryland 20771/1998) is transformed to the spheroidal harmonic expansion of the external gravity field of the Earth. (3) The orthometric heights of the GPS positioned gauge stations are used to obtain the spheroidal free-air reduction in order to convert the geopotential data at the GPS positioned gauge stations into potential values closest to Mean Sea Level. The best estimate in the Tide Free Reference System has been documented.

**G3/W/03-A5** Poster **1610-10**

**TIME VARIATIONS OF BASED ON THE GPS OBSERVATIONS OF BALTIC SEA LEVEL PROJECTS**

ALIREZA AZMOUDEH-ARDALAN and Erik W. Grafarend (Geodetic Institute, University of Stuttgart, Geschwister-Scholl Str. 24D, 70174 Stuttgart, Germany, Tel : +49 711 121 4086, Fax: +49 711 121 3285, email: ardalan@gis.uni-stuttgart.de)

Based on GPS observations of the Baltic Sea Level Projects, First, Second, and Third Campaigns time variations of fundamental geodetic parameter is computed. The calculations are based on spheroidal eigenvalue eigenvector expansion of the external gravity potential field of the Earth. Cartesian GPS coordinates are first transformed into spheroidal coordinates. The spheroidal harmonic coefficients are supplied by conversion of geopotential model EGM96 into spheroidal harmonic coefficients using the numerical transformation method. Orthometric heights of the GPS stations are used to determine spheroidal free-air potential reduction for the calculated potential values at the GPS stations to reduce them into mean-sea-level or geoid's surface. Our best estimate for gauge value in tide free reference of geoid system corresponds to for the first campaign 1990.8, for the second campaign 1993.44, and for the third campaign 1997.4. The computations indicate a raise of in the value of .

**G3/L/18-A5** Poster **1610-11**

**IMPROVED TIDE MODEL FROM TOPEX/POSEIDON AND GEOSAT ALTIMETRY OVER SHALLOW SEAS**

Xiaoli Deng and Dingbo Chao (School of Geo-science and Engineering, Surveying, Wuhan Technical University of Surveying and Mapping, 39 Luoyu, Road, Wuhan 430070, P. R. China, email: dxl@ultra2.wtusm.edu.cn)

TOPEX/POSEIDON (T/P) data and Geosat ERM data have been used to extract errors in major diurnal and semidiurnal tidal constituents of the CSR3.0 model over the Western Pacific. Due to spatial complexity of tides in shallow seas, the coarse bin technique, which is necessary to overcome tidal aliasing problems in altimetry, does not be simply performed to avoid considerable distortion of the tidal signal. Using the harmonic analysis, this has been done here from over 4.5 years of T/P data and Geosat ERM data, in which the T/P simulation is done along the ground track. Comparison of simulated tides with the CSR3.0 model shows that more accurate information about tides in shallow water can be obtained from along-track T/P data. The tides can be improved by combination of T/P and Geosat ERM data. They both contribute to the local region studied where resolution is more important than regular spacing.

**G3/L/10-A5** Poster **1610-12**

**IMPROVEMENT OF THE REGIONAL GRAVITY MODEL FOR CHINA AND ITS ADJACENT SEA BY COMBINING THE GRAVITY AND SATELLITE ALTIMETRY DATA**

H.T.Hsu Yang Lu (Institute of Geodesy and Geophysics, Chinese Academy of Sciences, Wuhan 430077, P.R.China, Email: luyang@asch.whigg.ac.cn)

We study and develop the tailored method to improve the regional gravity model by using joint data of gravity and satellite altimetry, and obtain the improved local solution of the so-called altimetry-gravity fixed problem. By using the stack of four years (1992-1996) Topex/Poseidon and ERS-1 satellite altimetry data and the gravity anomalies (30'x30') of China land, we derive the geoid undulations of China and its adjacent sea. Then according to the tailored method mentioned above, we achieve a regional gravity model (IGG-LS) to degree and order 360 for China and its adjacent sea. To detect the actual external precision of the model, we compare geoid undulations and gravity anomalies computed from the model with their measurement values. The results obtained show: the gravity anomalies (30'x30') from model IGG-LS in China land (versus their actual measurement values) have a mean square error (8.7mgal, the model geoid undulations in China land (versus the GPS measurement results) have a mean square error (0.70m, the model geoid undulations of China-adjacent sea (versus the geoid undulations of satellite altimetry) have a mean square error (0.13m. As to the global model OSU91A, the corresponding mean square errors will be (23.7 mgal, (1.54m, (0.60m, respectively. In addition, for model IGG93, which is obtained from the tailored method with gravity data in China land only, the corresponding mean square errors are (8.8mgal, (0.71m, (0.58m, respectively. So IGG-LS model provides a considerably perfect representation of the gravity field feature in China and its adjacent sea. The regional gravity model can greatly improve the fitness of the global one in the local area. It can be computed from the different kinds of data and their combinations.



**G3/W/15-A5** Poster **1610-13**

**THE KMS99 GLOBAL HIGH RESOLUTION MEAN SEA SURFACE**

P. KNUDSEN and O. Andersen (National Survey and Cadastre, Copenhagen NV, Denmark, email: pk@kms.dk, oa@kms.dk)

Satellite altimetry from the GEOSAT and the ERS-1 geodetic missions provide altimeter data with a very dense coverage. Hence, the heights of the sea surface may be recovered very detailed from these geodetic missions. On the other hand, satellite altimetry from the 35 days repeat cycle mission of the two ERS satellites and, especially, from the 10 days repeat cycle TOPEX/POSEIDON satellite mission provide repeated height observations, so that the mean sea surface heights along the ground tracks can be recovered very accurately. In this presentation a new and revised version of the KMS global high resolution mean sea surface (1/15 by 1/15 degree) is presented. The new KMS99 multi mission high resolution mean sea surface, has been derived from five different satellite missions using almost twice as many data as for the previous mean sea surface. Similarly, the resolution has been enhanced from 1/8 degree to 1/15 degree, and several steps in derivation of the mean sea surface has been improved.

**G3/L/11-A5** Poster **1610-14**

**COMPUTING MARINE GRAVITY ANOMALIES VIA LAPLACE'S EQUATIONS IN SPHERICAL COORDINATE FROM SATELLITE ALTIMETRY**

Jiancheng Li; Dingbo Chao. (School of Geoscience and Surveying Engineering, Wuhan Technical University of Surveying and Mapping, 129 Luoyu Road, Wuhan 430079, China, email: jcli@wtusm.edu.cn, dbchao@wtusm.edu.cn)

Using Laplace's equation in planar coordinate, the gravity anomaly can be calculated from deflections of the vertical. In practice, the vertical deflection grids are formed in spherical coordinate. The errors will be caused due to transforming spherical coordinate into planar one in a local Cartesian coordinate system. To avoid this drawback, the formula for converting deflections of the vertical to gravity anomaly is derived based on the Laplace's equation in spherical coordinate. Its representation in frequency domain using FFT techniques is also given. With EGM96 model as the reference gravity field, the gravity anomalies over the China seas and their neighbours are implemented using deflections of the vertical derived from altimeter data according to this principle. The comparison of this procedure with that in planar coordinate is also discussed in this presentation.

**G3/W/52-A5** Poster **1610-15**

**AN INTEGRATED SATELLITE ALTIMETRY, GRAVITY AND GEODESY DATA BASE, DATA PROCESSING AND REGIONAL MARINE GRAVITY FIELD MODELLING**

P. MEDVEDEV, D.Pleshacov, (Geophysical Center, Russian Academy of Sciences, Molodezhnaya 3, 117296, Moscow, Russia, email: pmedv@wcb.rssi.ru); A. Bulychev, (Lomonosov MSU, Geology Faculty, Geophysical Department, Moscow, Russia)

The integrated database of satellite altimetry data and supplementary gravity and geodesy information which is necessary for geodesy, geophysics, geology and oceanography applications was created in Geophysical Center of RAS. The satellite altimetry data sets of the Russian GEOIK geodetic satellites and GEOSAT and TOPEX/POSEIDON data are used for marine gravity modelling North Atlantic region, Baltic and Okhotsk sea. The results of these investigations are presented. Comparisons with gravity measurements and resolution of satellite altimetry data are discussed. New approach to processing the altimetric measurements for closed seas and some unsolved problems are discussing also. The work was supported by Russian Basic Research Foundation.

**G3/W/07-A5** Poster **1610-16**

**HIGH-RESOLUTION GRAVITY ANOMALIES FROM ALTIMETRY IN COASTAL AREAS**

Matthias RENTSCH, Michael Anzenhofer and Alexander Braun, (GeoForschungsZentrum Potsdam(GFZ), Division 1, Section 1.2, c/o DLR Oberpfaffenhofen, D-82234 Wessling, e-mail: rentsch@gfz-potsdam.de)

The generation of high-resolution marine gravity maps based on satellite altimetry is well known and was refined in the recent years by several groups. Although the processing can be improved and slightly better results can be expected, the main focus in the future should be on regional applications, also including airborne altimetry.

The standard altimeter geophysical data records are provided as 1-Hz measurements and are mainly flagged as 'invalid' in shallow water areas and near coastlines. The problem can be solved by using waveform data with a higher resolution, e.g. 20-Hz measurements for ERS-1 and ERS-2. Using retracking algorithms, these waveform data are processed individually and can be interpolated at different time stamps. However, new problems arise by using such data, e.g. a higher noise level and the absence of convenient corrections like ocean tide and wet tropospheric path delay.

This presentation reflects the state-of-the-art of high-resolution marine gravity processing in coastal areas based on conventional altimeter data. Additionally, the new results using the retracked altimeter waveforms at different sampling rates demonstrate the gain in resolution and accuracy of satellite-derived gravity anomalies.

**G3/L/21-A5** Poster **1610-17**

**HIGH RESOLUTION MEAN SEA SURFACE HEIGHT AND MARINE GRAVITY ANOMALIES FROM SATELLITE ALTIMETER DATA**

Y M WANG (Raytheon ITSS , Greenbelt, MD 20770, USA Email: wang@geodesy2.gsfc.nasa.gov)

The availability of high spatial resolution altimetry from the ERS-1 and Geosat missions in combination with the high-precision TOPEX/POSEIDON data has allowed significant advances to be made in computing marine-based geodetic quantities. We have computed the mean sea surface height and the gravity anomalies over the oceans on a 2' x 2' grid using satellite altimeter data from these three missions. In order to reduce the long and medium wavelength errors in the altimeter data (Geosat and ERS-1 data) a crossover adjustment is performed in a 2 degree latitude bands. The mean sea surface height is forced in the TOPEX reference frame by fitting the altimeter data to the 3-year TOPEX/POSEIDON mean tracks. The mean sea surface heights are computed on a 2' x 2' global grid using least squares collocation. Gravity anomalies are then computed using the mean sea surface height-implied geoid undulation in the inverse Stokes formula. A 1-dimensional FFT is used to speed up the evaluation of the global numerical integration. The accuracy of the mean sea surface and the marine gravity anomalies are provided at every 2' cell. The comparisons between the mean sea surface heights will be shown. Comparisons between ship gravity data and the gravity anomalies from the altimetry will also be presented.

**G3/E/43-A5** Poster **1610-18**

**ON THE ADVANCES OF MARINE GRAVITY ANOMALY MODELS DETERMINED FROM GEOSAT, ERS-1 AND TOPEX/POSEIDON SATELLITE RADAR ALTIMETRY**

Yuchan YI (Department of Civil and Environmental Engineering and Geodetic Science, The Ohio State University, 470 Hitchcock Hall, 2070 Neil Avenue, Columbus, OH 43210-1275, USA, Email: yi.3@osu.edu); C.K. Shum and Hong-Zeng Tseng (both at The Ohio State University, USA); Michael Anzenhofer and Matthias Rentsch (both at GeoForschungsZentrum Potsdam, Germany); Cheinway Hwang (National Chiao Tung University, Taiwan)

Using an estimation procedure based on the gravity signal properties, the marine gravity field is determined from reprocessed satellite radar altimeter data in selected areas. These areas include the South China Sea region and regions off coast California. The specific improvements in these altimeter measurements include more accurate orbital, geophysical and media corrections for inferring sea surface heights, and studies on retracked altimeter measurements near coastal regions. The dense data of Geosat Geodetic Mission and ERS-1 Geodetic Phase are included as the sea surface height slopes along ground tracks. And the sparse but more accurate time-averaged sea surface height data from TOPEX/POSEIDON and ERS-1's 35-day repeat phase are combined to obtain the gravity anomaly predictions along with accuracy estimates. The accuracy of the resulting gravity anomaly model and other state-of-the-art models is assessed by the comparison with ship gravity profile data.

**Airborne Gravimetry**

**G3/E/12-A5** Poster **1610-19**

**SPECTRAL ANALYSIS AND POST-FILTERING OF AIRBORNE GRAVITY DATA**

A.M. BRUTON, K.P. Schwarz, C.L. Glennie (Department of Geomatics Engineering, The University of Calgary, 2500 University Drive, N.W. Calgary, Alberta, Canada T2N 1N4)

A major challenge in airborne gravity is the task of simultaneously increasing the accuracy and resolution of airborne gravity data to meet the needs of geodetic and geophysical applications. This implies the need for a thorough understanding of the subsystem errors and a means of removing them. This paper will treat these problems using filtering methods in post-mission. In June of 1998 three flights were undertaken which tested a LCR gravimeter and a strapdown INS gravity side by side. Data from this test will be used in this paper because it provides a unique opportunity to study the responses of both the LCR gravimeter and strapdown INS systems to the same environmental conditions. Comparisons between systems and with shipborne gravity data will be used to do this characterization.

The paper has three objectives. The first is to characterize the errors currently coming from each of the component systems in the frequency domain. One way to remove these subsystem errors is by post-filtering the data.

The second objective is to use the common data set to compare and evaluate several methods of post-processing. These methods include filtering using an adaptive filter, a modified wave filter and the traditional method that uses a lowpass filter. The frequency response (phase and amplitude) of each of these is also studied and its importance made clear.

Finally, a proposal is made for ways to describe the quality of airborne gravity results. This includes discussions of both the spatial resolution and the accuracy that result from each of the filtering methods treated in this paper.

**G3/L/04-A5** Poster **1610-20**

**AIRBORNE GRAVITY SURVEY OF THE POLAR SEA NORTH OF GREENLAND**

Rene FORSBERG, Arne V. Olesen, K. Keller (Geodynamics Dept., KMS, Rentemestervej 8, DK-2400 Copenhagen NV, Denmark, email: rf@kms.dk)

An airborne gravity survey was carried out north of Greenland in 1998, covering the Lincoln and Wandel Sea shelf areas of the Arctic Ocean. Measurements were done with a Twin-Otter, using a Lacoste and Romberg model S gravimeter, multiple GPS receivers, a laser altimeter and custom-made data logger and INS unit. Flight conditions were generally good and a high accuracy has been obtained in processing of the data, as indicated by 2 mgal r.m.s. cross-overs after bias adjustment, and independent comparisons to shipborne and ice surface gravity measurements. Our results show that with careful processing the need for cross-over adjustment of airborne gravity measurements can be virtually eliminated.

The paper will present the survey, processing methods and evaluation of results. Our measurements represent a contribution to the Arctic Gravity Project, an international effort to compile a grid of all available and releasable gravity data for the Arctic region, in support a.o. of the upcoming satellite gravity field missions.

**G3/W/17-A5** Poster **1610-21**

**AIRBORNE VECTOR GRAVIMETRY USING INS/GPS - RESULTS**

Christopher JEKELI, Jay Kwon (Department of Civil and Environmental Engineering and Geodetic Science, Ohio State University, 2070 Neil Ave., Columbus, OH 43210, USA, e-mail: jekeli.1@osu.edu); and Jin Wang (Center for Mapping, Ohio State University, Columbus, OH 43210, USA).

A number of recent airborne flights of an inertial navigation system (INS) integrated with the Global Positioning System (GPS) provided opportunities to test different algorithms for vector gravimetry, that is, the determination of the total gravity vector at aircraft altitude. The principle behind vector gravimetry is that INS senses only specific (action) forces, while the total trajectory, as determined from GPS, is due to both action and kinematic forces, where gravitation belongs to the latter. Therefore, the difference between accelerations derived from INS and GPS, in a generic sense, provides information about the gravitational field. Two algorithms were considered. The first compares positions determined from INS accelerations to GPS positions; the second compares accelerations determined from GPS positions to INS accelerations. Repeat tracks from one test flight showed internal consistency better than 8 mgal (rms) in the horizontal component not affected by high dynamics. For the second flight, a comparison to truth data, comprising ground deflections of the vertical, showed differences of about 5-6 mgal (rms). The vertical component was determined to an accuracy of about 4-5 mgal. The resolution for each component was about 10 km. The paper presents details of the algorithm comparisons and analyzes the significant sources of error.

**G3/L/15-A5** Poster **1610-22**

**GRAVITY MEASUREMENT USING A HELICOPTER-BORNE NEW GRAVIMETER**

Jiro SEGAWA (School of Marine Science and Technology, Tokai University, 3-20 -1 Orido, Shimizu, Shizuoka 424-8610 Japan, email: jsegawa@scc.u-tokai.ac.jp); Hiroshi Hasegawa (Aero Asahi Corporation, 43rd Fl. Sunshine 60 Bldg., 1-1, Higashi-Ikebukuro 3-chome, Toshima-ku, Tokyo 170-0013 Japan); Takemi Ishihara (Geological Survey Japan, 1-3 Higashi 1-chome, Tsukuba-shi, Ibaraki-ken 305-0046 Japan); Sadaomi Sakuma (Tokimec Inc. 3-1 Takakuko, Nasumachi, Nasu-gun, Tochigi 325-0001 Japan)

Development of the airborne gravimeter started five years ago using a converted sea-gravimeter and a fixed-wing plane. Although this experiment taught us valuable things about the techniques and problems on airgravimetry, it proved to be a failure. In the course of the last study we changed the policy so that we use a helicopter as a gravimeter platform. The helicopter is able to adjust its speed in case of take-off and landing, and besides, when a detailed survey is necessary to enhance resolution, the helicopter can move as slowly as a motorcar while keeping a stable flight. As for the real time positioning, it has become possible to use the marine DGPS supporting stations maintained by Maritime Safety Agency Japan since last year. These stations are for ship's use, and enable the cruising ships to make positioning with the accuracy of 1 m in real time. We planned to utilize these stations, not from sea but from air. Our objective is to develop a helicopter-borne gravimetry system came from the necessity to fill in the gravity blanks in the land/sea bordered areas. We believe a deliberate operation of the helicopter gravimeter would be the only means by which the land-to-sea gravity gap could be filled. Our system is composed of a servo accelerometer sensor, a stabilized platform, an optical-fibre gyro to control the stabilized platform, a data processor and a controller, a GPS receiver and a receiver for the land-based DGPS supporting stations. The drift rate of the gravity sensor is a few mgal/month. The real time DGPS positioning was successful and we could get the positions of the helicopter within the error of two to three meters. For the exact correction for the effect of the helicopter motion an interferometric GPS positioning is necessary. This is done by post processings. We have made measurements from a heliport in the suburbs of Tokyo over to Ibaraki Prefecture and the neighboring seas. We will report the results from these measurements.

### Surface Gravimetry

**G3/E/21-A5** Poster **1610-23**

#### PLAN OF A G.I.S. TO ARCHIVE AND MANAGE PHYSICAL GEODESY DATA IN ANTARCTICA

Alessandro CAPRA and Stefano Gandolfi (DISTART Dept., University of Bologna, Viale Risorgimento 2, 40136 Bologna, Italy, email: alessandro.capra@mail.ing.unibo.it)

Within the activities of WGGGI (Working Group on Geodesy and Geographic Information) of SCAR (Scientific Committee on Antarctic Research) a "Physical Geodesy" project was planned for the period 1998-2000. Till today a geoid map of Antarctica was produced by AUSLIG (Australia) showing the geoid-ellipsoid separation between GRS80 and OSU89A. Researchers from different countries tried to compute new local and regional high-resolution geoid, but the goal of the project is the collection and the analysis of data useful to a development of a new high resolution geoid for the most part of Antarctica. A first phase of information and extensive data collection, related to geodesy, topography, bathymetry and gravity, was activated in collaboration with Institutions and Specialist Group (BEDMAP, ADGRAV, ADMAP, RAMP. The different set of data and their size need for a specific Data Base Management System; moreover the data representation in spatial and time ranges is important. A preliminary plan of a G.I.S. for a correct data archiving and management and for his utilisation for a successive geoid computation is presented.

**G3/L/09-A5** Poster **1610-24**

#### A STUDY OF GROUNDWATER VARIATIONS BY MEANS OF MICROGRAVITY MEASUREMENTS, ABSOLUTE GRAVITY MEASUREMENTS AND LEVELING SURVEYS IN BEPPU AREA, JAPAN

Yoichi Fukuda (Department of Geophysics, Graduate School of Science, Kyoto University, KitashirakawaOiwakecho, Sakyo-ku, Kyoto 606-8502, Japan, email: fukuda@kugi.kyoto-u.ac.jp) Hideo Mawatari, Yuki Yusa (both at Beppu Geothermal Research Laboratory Graduate School of Science, Kyoto University, Noguchibaru, Beppu 874-0903, Japan email: mawatari@bp.vgs.kyoto-u.ac.jp, yusa@bp.vgs.kyoto-u.ac.jp), and Shuhei Okubo (Earthquake Research Institute, University of Tokyo, 1-1-1 Yayoi, Bunkyo-ku, Tokyo 113-0032, Japan, email: okubo@eri.u-tokyo.ac.jp)

It is obvious that the groundwater variations cause gravity changes at surface and gravity observations conversely give us important information about the hydrological characteristics in the area concerned. The groundwater level observations in the Beppu geothermal system, which is one of the largest geothermal systems in Japan, have been conducted over a long period to study the characteristics of the hot water flow or other purposes. It has already been known that the peak-to-peak amplitude of annual groundwater level variations are very large and it sometimes reaches more than 10 meters. In order to detect the gravity changes associate with the groundwater variations in Beppu area, we conducted repeat precise gravity measurements, absolute gravity measurements and leveling survey. Using a LaCoste & Romberg gravimeter (G-534), 40 microgravity surveys were made from February 1993 to January 1998, at 11 survey marks in the Beppu area. The absolute gravity measurements were conducted in June 1995 and in September 1997. The leveling surveys were conducted 7 times from June 1995 to January 1998 to monitor the vertical movements of the area concerned. The result of the gravity measurements shows that some tens micro gals of gravity changes were observed during the period, while no significant vertical displacement was observed by the leveling surveys. This means that all the gravity changes were due to the actual mass changes associated with the groundwater variations. To investigate the characteristics of the groundwater variations and/or the relation between the variations and the gravity changes, we employed Principal Component Analysis (PCA). The results of PCA shows that; (1) the 1st and the 2nd components explain almost 90 % of the variations, (2) the 1st component reflects the groundwater level of the shallow unconfined aquifer, the level to which the amount of rainfall directly relate, and (3) the spatial pattern of the 2nd component is possibly explained by the movements of the deeper groundwater.

**G3/W/20-A5** Poster **1610-25**

#### COMPILING AND DOCUMENTING GRAVITY DATABASES

Allen M. HITTELMAN and David T. Dater (NOAA's National Geophysical Data Center, 325 Broadway, Boulder, CO 80303, USA, email: amh@ngdc.noaa.gov)

The 1999 2-volume edition of the Gravity CD from the National Geophysical Data Center (NGDC) has recently been released. This compilation contains a wealth of gravity measurements contributed by many national and international academic and government organizations, including: regional land and marine surveys, absolute measurements, regional and global gridded data sets, and correlative data (e.g., geoids and global relief). Approximately, 70 percent of the data are observed values; another 30 percent represent grids and other summary data sets.

Access software on the CD simplifies data and documentation extraction and browsing. To support end-user validation of the data: point distribution plots illustrate coverage (as .PCX and .GIF images); histogram distribution plots have been prepared for each parameter within each data set; and, a data dictionary presents standardized terminology to facilitate comparison of different data sets. The document contains HTML, Postscript, Word, and WordPerfect files that summarize source information, a printout of first ten records, and maximum and minimum values of each field. Instead of following the traditional approach of making all data sets fit into

a fixed common format, NGDC employees a standard format description, preserving fields unique to a specific data collection and allowing access to the data without concern for formats.

**G3/E/19-A5** Poster **1610-26**

#### BOUGUER ANOMALY MAP OF THE FENNOSCANDIAN SHIELD 1:4 MILL

Juha V. KORHONEN and Seppo Elo (Geological Survey of Finland, P.O.Box 96, FIN-02151 Espoo, Finland, Email: juha.korhonen@gsf.fi, seppo.elo@gsf.fi); Jussi K...riainen (Finnish Geodetic Institute, Geodeetinrinne 2, 02430 Masala, Kirkkonummi, Finland, Email: jussi.kaarainen@fgi.fi); Sven Aaro (Geological Survey of Sweden, P.O.Box 670, 75128 Uppsala, Sweden, Email: sven.aaro@sgu.se); Lars ?ke Haller (Lantm...teriverket, 801 82 G...vle, Uppsala), Jan Reidar Skilbrei (Norges geologiske undersøkelse, Postboks 3006 Lade, 7002 Trondheim, Email: jan.skilbrei@ngu.no); Dag Solheim (Statens kartverk, NO-3500 H...nefoss, Norway, Email: dagso@gdiv.statkart.no); Anatoli Tchepik (Northwest Regional Geological Centre, 24/1 Odoevsky Street, 199155 St Petersburg, Russia, Email: root@geol.spb.su); Anatoli Kulnich (Petersburg Geophysical Expedition, 195009 St Petersburg, Russia); Lioudmila Idanova (State Company "Mineral", Veselnaya Street 6, 196106 St Petersburg, Russia, Email: frank@DF3136.spb.edu)

In 1998 the Geological Surveys of Finland, Norway and Sweden, the Petersburg Geophysical Expedition, the Finnish Geodetic Institute, the National Land Survey of Sweden and the Norwegian Mapping Authority started to compile a Bouguer anomaly map on a scale of 1:1 mill on a 2.5 km x 2.5 km grid to support compilation of a geological map of the Fennoscandian Shield. The participating countries provide the data of their territories as grids of Bouguer anomalies (Bouguer density 2670 kg/cum) in Gauss-Krueger projection (central meridian 21 deg E) and in WGS-84 datum. The reduction principles of the original data have been described, e.g. in the explanation of the Bouguer anomaly map of Finland 1:1 mill (K...riainen, J., J. M...kinen, 1997. The 1979-1996 gravity survey and results of the gravity survey of Finland 1945-1996. Publ. Finn. Geod. Inst. no. 125). A preliminary Bouguer anomaly map on a scale of 1:4 mill on a 5 km x 5 km grid, compiled in 1999, and examples of its geological correlation by petrophysics are represented.

**G3/E/01-A5** Poster **1610-27**

#### PRECISE GRAVITY MEASUREMENTS IN AZORES ISLANDS

Clara LAZARO (Centro de Geodesia, Instituto de Investigacao Cientifica Tropical, Rua da Junqueira 534, 1300 Lisboa, Portugal, Email: cgeod@iict.pt J. Pereira Osorio (Observatorio Astronomico "Prof. Manuel de Barros", Faculdade de Ciencias, Universidade do Porto, Portugal); Luisa Bastos (Observatorio Astronomico "Prof. Manuel de Barros", Faculdade de Ciencias, Universidade do Porto, Portugal) Jaakko Makinen (Geodeettinen Laitos, Masala, Finland) Gunter Hein (IfEN, University FAF Munich, Germany)

The Azores Archipelago is a region of well-known seismic and volcanic activity. It has been the object of scientific interest since it is located in the junction of three main tectonic plates: Eurasian, North American and African. Nine islands, two of them lying in the North American plate and the others in the so-called Azores microplate, form the archipelago.

The gravimetric surveys started in 1992 with the establishment of two absolute gravity stations, Flores and Faial, and relative measurements in all of the nine islands. These gravity measurements were intended to complement the GPS data obtained, since 1988, in the TANGO (TransAtlantic Network for Geodynamics and Oceanography) project. Therefore, the relative stations include all the GPS sites and other stations of geophysical, seismological and geodetic interest. Later, in 1994, a new absolute gravity station was established in S. Miguel Island and the Faial station was reobserved. The three absolute stations were reobserved in 1997. The absolute measurements have been made using the JILAg-5 gravimeter, belonging to the Finnish Geodetic Institute (FGI). A total of 114 relative gravity stations were measured by using LaCoste & Romberg gravimeters in three campaigns - 1992, 1994 and 1997.

In the paper, it is intended to present details of the three gravity surveys, the methods used for data processing and the results derived so far.

**G3/W/09-A5** Poster **1610-28**

#### GRAVIMETRY IN SOUTH-WESTERN CHINA

H.LI, S.A.SUN, D.Z.Liu, C.F.Xing, G.Y.Fu, Y.J.Zhang, A.M.Xiang, X.E.Lei (Institute of Seismology, CSB)

As the part work of the Crustal Movement Observation Network of hina (CMONOC), gravity surveys in south-western China had been carried out during the September to December of 1998 by employing three LaCoste and Romberg gravimeters. The gravimetry connected 5 permanent stations and 14 base stations of CMONOC through about 80 connecting stations which comprised of absolute gravity stations, national gravity stations, local gravity stations, local GPS stations, high level levelling stations and some temporary stations. This paper will firstly introduce the network and the observations. Secondly, the adjustment of the measurements will be described.

At the last part, we will discuss the precision and its reliability.

**G3/W/23-A5** Poster **1610-29**

#### GRAVITY CHANGES IN WEST YUNNAN OBSERVED BY RELATIVE GRAVIMETRY

H. LI, S.A.SUN, M.Y.JIA, C.F.Xing, A.M.Xiang (Institute of Seismology, CSB)

Since 1985, gravity surveys at the local gravity network in the Western Yunnan Earthquake Prediction Experiment Area (WYEPEA) have been carried out 2-3 times a year by the Institute of Seismology, Chinese Seismological Bureau (ISCSB), and the Yunnan Provincial Seismological Bureau (YPSB), employing LaCoste and Romberg (LCR) relative gravity meters. The network comprises several absolute gravity stations and more than 130 field gravity stations. Until now 32 observance campaigns were performed. This paper firstly introduced the network and the observations, which include absolute and relative gravimetry. Secondly, the adjustment of the measurements was described, and the gravity changes displayed by contour map were given. The results show that the precision of the network is estimated to 0.07-0.1ms<sup>-2</sup>\*10<sup>-6</sup>(0.01ms<sup>-2</sup>\*10<sup>-6</sup>~1gal\*10<sup>-6</sup>). It means that the network can detect the gravity changes with the scale of about 0.2ms<sup>-2</sup>\*10<sup>-6</sup>. At the last part, we discussed the relationship between the earthquake preparation especially for Lijiang earthquake (Ms7.0, 1996) and gravity changes.

**G3/W/24-A5** Poster **1610-30**

#### ADJUSTMENT OF SEA GRAVITY CRUISES USING ALTIMETRY DATA

SARRAILH Michel (BGI/CNES); Jiancheng Li (School of Geoscience and Surveying Engineering, Wuhan Technical University of Surveying and Mapping, 129 Luoyu Road, Wuhan 430079, China 430079 China)



Sea gravity often suffers, for the oldest ones, from biases and shifts, observed at crossovers. They can be adjusted between themselves, but the gravity information, derived from altimetric geodetic missions, can be used as a reference and offers an alternative way. Benefits and problems resulting from this last method are discussed.

**G3/E/30-A5** Poster **1610-31**

#### PROPOSED GRAVITY BASE NETWORK OF IRAN

Mehdi NAJAFI-ALAMDARI (Surveying Eng. Dept., Faculty of Civil Eng., 1346 Valiasr Ave., Mirdamad intersection, Technical University of K.N. Toosi, E-mail: mmajalm@dpi.net.ir, Fax #: +9821 877 9476, Tehran, Iran); M. Mashhadi-Hossain-Ali, Y. Hatam-Chavari, F. Tavakkoli (National Cartographic Center (NCC) of Iran, Mearaaad Str., P.O. Box 13185- 1684, Fax #: +9821 600-1971, Tehran, Iran).

A gravity base network comprising of 19 points is proposed for Iran. For fast accessibility by relative instruments (gravimeters), the points will be located at airports. Absolute gravity will be measured at 9 of these points (absolute points). Six of these will make a calibration line, extending from extreme North-West to extreme South-East end of the country. The remaining 10 points, uniformly distributed throughout the country, will be connected to the absolute points by precise relative measurements.

Based on the 5 æGal accuracy of the Canadian gravimeter CG-3M and the assumed 3 æGal accuracy of a modern absolute gravimeter, pre-analysis of five different designs (networks) have been carried out. In the pre-analysis, the nine absolute points were considered known with limited observational weights and no correlations. The residual gravimeter drift was assumed linear in time within an interval no longer than 8 hours. Individual gravimeter readings were assumed uncorrelated, while mathematical correlations between reading differences (relative measurements) were assessed. Relative measurement accuracies were taken to be proportional to the time of measurement with the constant of proportionality to be determined by an adjustment.

Redundancy numbers and internal reliability at 90% probability level were evaluated for each design to study the robustness of each design against gross errors. Individual potential maximum undetectable gross errors were then displayed to show the potential maximum deformation of the networks. The optimum network design was chosen for which the achievable accuracy is the best, and redundancy numbers, all larger than 0.5, are uniformly distributed throughout the network. Even for the optimum design, gross errors up to 25 æGal may remain undetected, but the maximum potential distortion caused by this error would not exceed the sought accuracy of 5 æGal. In this design, unknown points are linked to at least three known points and every observational link is the line of flight, fore and back, with a relative gravity measurement.

Observations in the optimum network are to be carried out in two steps: 1) the relative measurements between absolute points are made to determine the scale factor and the accuracy of the gravimeter; 2) the relative observations between known unknown and unknown-unknown pairs of points are carried out. To test for outliers among the observational mis-closures, the estimated accuracy of the instrument is used.

**G3/E/11-A5** Poster **1610-32**

#### UNIGRACE - A EUROPEAN PROJECT FOR THE UNIFICATION OF GRAVITY SYSTEMS IN CENTRAL AND EASTERN EUROPE

E. REINHART, B. Richter, H. Wilmes (Bundesamt fuer Kartographie und Geodaesie, Richard-Strauss-Allee 11, 60598 Frankfurt am Main, D, e-mail: reinhart@ifag.de) J. Sledzinski (WUT, Warsaw, Poland) I. Marson (DINMA, Univ. de Trieste, Italy) E. Erker (D. Ruess, BEV, Vienna, Austria) J. Makinen (Finn. Geod. Inst., Masala, Finland)

In the EC-funded project UNIGRACE, partner institutions from 12 countries in Central and Eastern Europe co-operate with the aim of unifying the gravity systems in the countries involved. Benefit is expected for metrology, mapping, surveying and navigation, height determination, sea level variation studies, geophysical research, geological exploration and mining. Five European groups from Austria, Finland, Germany, Italy and Poland carry out absolute gravity measurements on 17 reference stations at two epochs. They are supported by the partners in the hosting countries Bulgaria, Croatia, Czech Republic, Hungary, Romania, Slovakia and Slovenia who are responsible for the station selection and preparation and who determine the connections to the national gravity networks. This will build up a unified gravimetric reference in the countries involved and will enable to transform all gravity data available to the common reference. The first project phase 1998 was carried out with the reconnaissance and site preparation. The sites have been selected in each participating country emphasis to geological stability; in countries with access to the sea tide gauge sites have been added to the network in order to contribute to sea level variation studies. In the second half of 1998 absolute gravity measurements have been carried out at most of the selected sites including inter-comparisons at the reference sites Wettzell (Germany) and Josefowslaw (Poland) for all absolute gravimeters used in the project. In 1999 special emphasis is put on the relative gravity measurements on calibration lines in the networks. In the year 2000 a second absolute gravity campaign will follow to verify the stability of stations and instrumentation.

**G3/E/22-A5** Poster **1610-33**

#### GEODYNAMIC INTERPRETATIONS OF HEIGHT CHANGES (DERIVED BY PRECISE LEVELLING) BY GRAVIMETRIC METHODS

Diethard Ruess, Norbert HOEGGERL (Federal Office of Metrology and Surveying, Schiffamtsgasse 1-3, A-1025 Wien, Austria, email: diethard.ruess@univie.ac.at); Bruno Meurers (Institute of Meteorology and Geophysics, University of Vienna, Hohe Warte 38, A-1190 Wien, Austria, email: bruno.meurers@univie.ac.at); Ewald Brueckl (Institute of theoretical Geodesy and Geophysics, Technical University of Vienna, Gusshausstrasse 25-29, A-1040 Wien, Austria, email: ebrueckl@luna.tuwien.ac.at)

Repeated precise levellings in Austria show recent height changes of the crust. The uplift of 1-2 mm/y may be an isostatic rebound effect but may also be caused by active tectonic movements. The periadriatic line in the south of Austria, a collision zone between the Eurasian and the African plate is of great interest for some more investigations about the recent seismicity in this area. Therefore several geodynamic GPS projects are running in the surrounding area. Furthermore a combination of repeated measurements in precise levelling and absolute gravity is an important method for analysing geodynamic processes. A common project founded by the Austrian Foundation of Scientific Research was started in 1995 to establish a network of precise levelling sites across the periadriatic line in the Karawanks combined with 4 absolute gravity stations. Short precise relative gravity profiles along the precise levelling lines near the absolute stations monitor their stability. The used absolute gravimeter JILAg-6 was upgraded to the technical standard of the FG5 absolute meters before the field observations were started. Absolute measurements at background stations and at international reference stations guarantee the results of the absolute gravity observations. Attention was directed to the precision of the instruments used and to the selection of the measuring points. An overview of the project, its tasks and first results of the observations that have been made so far are presented.

**G3/W/24-A5** Poster **1610-34**

#### ADJUSTMENT OF SEA GRAVITY CRUISES USING ALTIMETRY DATA

Michel SARRAILH, BGI/CNES, 18av.E.Belin 31401 Toulouse, Cedex 4, France, email: michel.sarrailh@cnes.fr

Sea gravity often suffers, for the oldest ones, from biases and shifts, observed at crossovers. They can be adjusted between themselves, but the gravity information, derived from altimetric geodetic missions, can be used as a reference and offers an alternative way. Benefits and problems resulting from this last method are discussed.

**G3/W/28-A5** Poster **1610-35**

#### SEA SURFACE GRAVITY MEASUREMENTS WITH INTERFEROMETRY GPS POSITIONINGS

Mikio SATOMURA (Faculty of Science, Shizuoka University, Oya, Shizuoka 422-8529, Japan, E-mail: satomura@sci.shizuoka.ac.jp); Jiro Segawa (Faculty of Marine Science and Technology, Tokai University, Ordo, Shimizu, Shizuoka 424-0902, Japan, E-mail: jsegawa@scc.u-tokai.ac.jp); Junji Tanimoto (Faculty of Science, Shizuoka University, Oya, Shizuoka 422-8529, Japan) Yuichi Imanishi, Chieko Kuramoto, Kin-ichiro Koizumi (Ocean Research Institute, University of Tokyo, Minamidai, Nakano-ku, Tokyo 164-0014, Japan)

One of the most serious error sources of gravity obtained on the sea surface is inaccurate estimation of the Eotvos corrections due to inaccurate positionings.

Gravity measurements were carried out by a NIPR-ORI gravimeter as well as interferometry GPS measurements with three antennas in the KH-96-1 cruise of Hakuho-maru on the Pacific Ocean, south off central Japan. Eotvos corrections for the gravity data obtained were performed by using four kinds of positioning data; 1) a single antenna position data of single positioning GPS, 2) a single antenna position data of interferometry GPS, 3) center of the three antennas of interferometry GPS, and 4) gravity sensor position from interferometry GPS. Velocities were calculated from their positions and a digital filter was applied to their EW component as well as gravity data.

Two gravity values at each cross point were compared each other in order to study the precision of gravity values obtained. As a result, gravity values based on interferometry GPS positionings were much more precise than those based on single positionings, while precisions of three kinds of gravity values based on a single antenna position, center of the three antennas and gravity sensor position were approximately equivalent.

**G3/W/10-A5** Poster **1610-36**

#### ENVIRONMENTAL EFFECTS ON GRAVITY MEASUREMENTS IN THE CITY OF HANNOVER, GERMANY

Karin SCHMIDT (Institut fuer Erdmessung, Universitaet Hannover, Schneiderberg 50, 30167 Hannover, Germany, email: schmidt@ife.uni-hannover.de)

For the interpretation of gravity observations to detect horizontal or vertical crustal movements, seismic activities or simply to define high precise gravity values in a gravity reference network, the measurements should have an accuracy of 0.01-0.1 µm/s.

Since march 1998 the Institut fuer Erdmessung (IfE), University of Hannover, carries out a measurement project to analyse the variations of gravity which are caused by environmental effects with combination of relative and absolute measurements as well as earth tide recordings. Within the frame of the measurement project a micro gravity network consisting of 4 gravity stations was established. The gravity values of the 4 stations are monitored with weekly relative gravity observations between the stations with 2 or 3 LaCoste&Romberg modell-G gravimeters. The center of the network is located in a cellar of the IfE, since thirteen years the station was regularly occupied by the absolute gravimeter JILAG-3 of the IfE. During the measurement campaign absolute gravity determinations were carried out regularly in the cellar, also an earth tide registration was established. Additionally precipitation data, ground water data as well as global, regional and lokal air pressure data were collected. First results of the analysis concerning the correlation of precipitation, ground water an gravity values of the network will be presented.

**G3/E/26-A5** Poster **1610-37**

#### IS AN EVERY ABSOLUTE GRAVIMETER A PRIMARY STANDARD?

S. SVITLOV, G. Sidorenko, V. Bondarenko, Yu. Lokshin (State Scientific Industrial Association "Metrology", Ukraine, email: svet@online.kharkiv.com); A. Sas-Uhrynowski, A. Sas, L. Siporski, E. Zanymonski (Institute of Geodesy and Cartography, Warsaw, Poland, email: zgf@igik.edu.pl)

In this presentation some problems of legal metrology concerning gravimetry will be outlined. What is a primary gravity standard? To answer this question, an absolute gravimeter is considered any time at the head of the hierarchy scheme. But starting from the Sakuma-type device, every new generation absolute gravimeter discovers a systematic error of a previous one. At different gravity stations a difference between different type gravimeters (say, free-fall and rise-and-fall) can reach up to +/- 0.05 mGal that may be caused by unrecognized site-dependent systematic errors of the gravimeters. In this case we consider a gravity network adjusted using both various absolute and relative gravity determinations to be a primary group gravity standard. The New Polish Reference Gravity Network includes 10 absolute gravity stations which are occupied by the FG5-107 (USA), FG5-101 (Germany), JILAg-5 (Finland) and ZZG (Poland) absolute gravimeters. Relative connections are made with the La Coste & Romberg and Scintrex CG3 gravimeters. The combined adjustment of those stations is resulted in standard error of order 0.01 mGal. We have then 'calibrated' the Ukrainian (GP-05 type) and Polish (PBGm-97) transportable absolute gravimeters at the Polish Reference Gravity Network (Primary Standard). Standard error of an each gravimeter is estimated to be about 0.03 mGal that is a satisfactory value for a secondary standard. Hence, upgrading of a gravity system (creation of the 1st an 2nd order gravity networks) could be made using those secondary standards. Advantages to use an absolute gravimeter as a secondary standard and future plans to develop and unify Polish and Ukrainian gravity networks will be discussed.

**G3/E/24-A5** Poster **1610-38**

#### NEW ABSOLUTE GRAVITY DETERMINATIONS IN UKRAINE

S. SVITLOV (Kharkov State Research Institute of Metrology, Ukraine, email: svet@online.kharkiv.com)

Status of the Ukrainian absolute gravimetry will be outlined. Having got only few relative gravity stations of the former Soviet Union's gravity system, the modern Ukrainian gravity network lacks of absolute gravity sites. Furthermore, due to some reasons Ukraine did not join a current project called UNIGRACE (Unification of Gravity System in Central and Eastern Europe). Fortunately, in 1991-1993 it was performed a lot of repeated measurements at the gravity stations "Kharkov" (Ukraine) and "Borowa Gora" (Poland) with an Ukrainian rise-and-



fall absolute gravimeter, the GP-05. Later, in 1995-1997, this last station was re-visited by the FG5-101 (Germany), FG5-107 (USA), JILAg-5 (Finland) and ZZG (Poland) absolute gravimeters. Those results are scattered up to  $\pm 0.016$  mGal about the FG5-101's value and give a possibility to compare the GP-05 gravimeter with others. Since the FG5-101 gravimeter is essentially involved in the international comparison campaigns as well as into the UNIGRACE project, we compare our GP-05 gravimeter just with the FG5-101 one. In such a way, a systematic error of the GP-05 gravimeter of order  $(+0.08 \pm 0.012)$  mGal was found. Being too large at first sight, this error is consistent with those shown by anotherise-and-fall gravimeters, the JAEGER/BIPM and GSI, during the ICAG94 comparison. Taking this systematic error into account, we have transferred the FG5-101's absolute gravity value from Borowa Gora to Kharkov. Hence, for the first time the new Ukrainian absolute gravity station connected with the international gravity network is established. Further we plan to develop the Ukrainian gravity network using the station "Kharkov" as a reference one. Comparing with older known gravity values obtained at Kharkov from adjusted relative determinations, the new one is lower up to 0.05 mGal. Possible interpretations of this difference will be given.

**G3/E/25-A5** Poster **1610-39**

#### REDUCING EFFECT OF VIBRATIONS ON ABSOLUTE GRAVITY MEASUREMENTS

S. SVITLOV (Kharkov State Research Institute of Metrology, Ukraine, e-mail: svet@online.kharkiv.com)

Observed non-tidal gravity variations comprise various environmental effects (polar motion, re-distribution of atmospheric, hydrologic and oceanic masses, etc.) that are a matter of separate interests. Another disturbing effects occurring everywhere are external and internal vibrations. Ambient seismic noise reduces short-term resolution of gravity measurements. Being site-dependent, systematic errors due to gravimeter/floor recoil effect can considerably distort shallowspaced gravity results. That is why the modeled environmental effects must include influence of both ambient and internal vibrations on absolute gravity measurements. To solve these problems, theory of an absolute gravimeter analysis in the frequency domain is developed. Obtained exact and approximated frequency responses are useful tool to investigate gravimeters' errors caused by any vibrations. Firstly, the developed approach is used to design an anti-vibration system for an absolute gravimeter basing on invariance principle. Vibration accelerations are independently detected by the high-sensitive piezo-electric accelerometer and then further transformed into correction following the frequency response of a rise-and-fall absolute gravimeter developed at Kharkov. As a result, standard uncertainty is reduced over 3 times. Secondly, frequency responses are applied to investigate a systematic error caused by coherent vibrations when the drop length and starting interval in an absolute gravimeter are varied. Assuming parameters of the FG5 absolute gravimeter in real measurement conditions, it is theoretically shown that unrecognised systematic errors order 0.01 mGal can be detected. It will also be shown that results of various related experiments could be easily explained using the proposed absolute gravimeter frequency response technique.

**G3/E/15-A5** Poster **1610-40**

#### NEW GENERATION NAOM ABSOLUTE GRAVIMETER

T. TSUBOKAWA, H. Hanada and S. Tsuruta (National Astronomical Observatory, Mizusawa, Japan, email: tsubo@miz.nao.ac.jp); S. SVITLOV (Kharkov State Research Institute of Metrology, Ukraine, email: svet@online.kharkiv.com)

The National Astronomical Observatory, Mizusawa (NAOM), Japan, has developed a new generation transportable free-fall absolute gravimeter. The main features of the gravimeter are as follows: digital acquisition of a fringe signal, data processing algorithm based on a second difference method, simple dropping mechanism called "Silent Drop", automatic correction of the calculated gravity values using independent recording of ground vibration. A fringe signal is digitized with the high-speed waveform digitizer (digitization rate is 200 MHz) order to avoid possible errors due to analogue processing of the signal. A second difference method allows to calculate only the equally spaced in time fringe phases and then to reconstruct the fall distances intervals rather than to continuously process the signal. Performed theoretical uncertain analysis shows an achievable submicrogal resolution level in an absolute gravity value that is proven by simulation experiments when a stable function generator is used instead of real fringe signal. The "Silent Drop" uses three hybrid elements composed of a stacked piezo-translator and a mechanical expansion amplification system; this mechanism operates at high vacuum and produces as small as possible vibration disturbances. Ground vibrations during free fall are simultaneously recorded with a seismometer and then processed using a special algorithm in order to follow the frequency response of the absolute gravimeter. Developed gravimeter has to be used to monitor long-term absolute gravity variations at the NAOM and the Esashi gravity station.

**G3/E/16-A5** Poster **1610-41**

#### MEASUREMENTS OF FREE FALL ACCELERATION AT SITE A OF THE GRAVITY MICRONETWORK OF THE BUREAU INTERNATIONAL DES POIDS ET MESURES (SEVRES)

Leonid F.VITUSHKIN and Jean-Marie Chartier (Bureau International des Poids et Mesures, Pavillon de Breteuil, 92312 Sèvres Cedex, France, email: lfvitushkin@bipm.fr; jmchartier@bipm.fr)

The results of regular measurements of  $g$  made since October 1997 at site A at the Bureau International des Poids et Mesures are presented. Site A is used as a reference site for the International Comparisons of Absolute Gravimeters, which are held at the BIPM approximately every four years. The measurements were carried out using an absolute gravimeter FG5-108 belonging to the BIPM. They were generally performed on two days per week (usually during the weekends). Twenty-four sets of measurements were made on each day (one set per hour); each set comprised 150 or 200 drops with a time interval between drops of 10 s or 20 s. The data was processed using commercial software from "Micro-g Solutions, Inc."

**G3/W/04-A5** Poster **1610-42**

#### ADJUSTING OF SHIPBORN GRAVITY DATA WITHIN CANARY- BAHAMAS GEOTRANSECT (23-29 N) AND IN THE WESTERN RUSSIAN ARCTIC SHELF.

Andrew ZAYONCHEK (All Russian Research Institute for Geology and Mineral Resources of the World Ocean, 1 Angliysky Pr., St. Petersburg, 190121, E-mail: andrew@vniio.nw.ru)

The adjustment procedure of shipborn gravity data was developed to create coherent gravity database. Results of recent high quality data were used as reference information for adjusting of historical observations of worse quality. Cross-over analysis of overlapped data sets obtained in the different cruises allows the systematic errors to be distinguished. This errors were divided for a few components connected both with incorrect definition of zero drift for single profiles and groups of profiles, and levelling problems. In order to identify and remove these errors, new software has been developed. It allows to adjust the data in interactive regime. This means that the individual solution could be found for each single profiles and

cruise. As a results of processing, after removing of systematic errors, the final standard deviations of RMS of definition of gravity anomaly field within studied areas were reduced from previously estimated as 3,5 mGal to 1,2 -1,5 mGal. This allows to calculate more detailed 7x7 km grids and produce the accurate comprehensive free-air gravity anomaly maps with 5 mGal contour interval.

**G3/W/38-A5** Poster **1610-43**

#### ON THE COMPENSATION OF SYSTEMATIC ERRORS IN MARINE GRAVITY MEASUREMENTS

GUAN ZHENG, Huang Motao, Zhai Guojun, Ouyang Yongzhong(all at Tianjin Institute of Hydrographic Surveying and Charting, Tianjin, 300061, China, email: nvsurvey@public.tjuc.com.cn)

Based on an analysis of the sources of errors in marine gravity measurements, an error model, firstly, is constructed mathematically which can characterise the change of the systematic errors and with which a new crossover adjustment model is presented in this paper. Then a new method of compensating the systematic errors is suggested, i. e. the self-calibrating adjustment. Some questions involved in solving the adjustment problem, such as the rank deficiency, the choice of error model, the weighting of additional parameters and the test of significance of compensation efficiency, etc., are discussed in detail. Finally, a practical survey data set is used as a case study to prove the efficiency and reliability of the compensation method.

**DEM**

**G3/W/48-A5** Poster **1610-44**

#### AN INDEPENDENT GLOBAL ASSESSMENT OF THE QUALITY OF CURRENT GLOBAL DIGITAL ELEVATION MODELS

BERRY, P.A.M., Hoogerboord, J.E. & Pinnock, R.A. (Geomatics Unit, De Montfort University, Leicester LE1 9BH, UK)

Within the last few years, a number of Global Digital Elevation Models (GDEMs) have been created with a spatial resolution of five arc minutes or better. These GDEMs present global estimates of land orthometric heights derived from a compendium of ground truth datasets of varying and often unknown accuracy. Intercomparison of the various models in the public domain reveals differences in some regions, generally due to upgrading of the height data in particular regions as more precise information becomes available. However, to obtain an accuracy estimate of these models requires comparison with an independent dataset. The generation of a near global set of orthometric height data wholly derived from ERS-1 and ERS-2 radar altimetry has now enabled an assessment of the quality of public domain GDEMs. This paper presents the results from this comprehensive comparison with several GDEMs including GLOBE, TerrainBase and JGP95E, including the identification of common error 'signatures' where erroneous ground truth datasets have been incorporated into successive DEMs.

**G3/W/12-A5** Poster **1610-45**

#### NATURAL LAND TARGETS FOR ALTIMETER SIGMA0 CALIBRATION.

BERRY, P.A.M., Pinnock, R.A. & Hoogerboord, J.E. (Geomatics Unit, De Montfort University, Leicester LE1 9BH, UK)

A global evaluation of the earth's land surface characteristics using ERS-1 and ERS-2 radar altimeter data has revealed several land sites where the surface characteristics and aridity permit accurate modelling of the spatial variation of sigma0 over areas of hundreds of square kilometers, by using an expert system to filter and interpret the individual altimeter waveform shapes. This paper presents results from ERS-1, ERS-2 and TOPEX data over these calibration sites, to provide an assessment of the precision to which sigma0 can be measured over land and hence illustrate the potential of land calibration. In addition, variations in TOPEX sigma0 measurements are quantified using those calibration sites for which TOPEX waveforms are available.

**G3/W/47-A5** Poster **1610-46**

#### COMPARISON AND VALIDATION OF DTM'S IN THE SAME AREA

L. Biagi (Politecnico di Milano, IGes, Facoltà di Ingegneria di Como, P.le Gerbetto 6, 22100, Como, Italy, Email: ludo@gemini.como.polimi.it) M. A. BROVELLI (Politecnico di Milano, DIAR, P.zza Leonardo da Vinci 32, 20133, Milano, Email: maria@ipmtf4.topo.polimi.it), A. Monti Guarnieri (Politecnico di Milano, Facoltà di Ingegneria di Como, P.le Gerbetto 6, 22100, Como, Italy, Email: monti@elet.polimi.it)

In the scientific community there is a demand for very dense and accurate DTM's. This is true for geodetic (i.e. the RTC computation), for geophysical (inversion of the gravity field, determination of the seismic risk) and environmental (hydrological analyses) applications. At the same time there is today the availability of big amount of data provided by satellite techniques (i.e. SAR observations) which can be used to integrate the conventional DTM's. In this framework we can individuate two main aims. The first one consists in the statistical analysis, validation and classification of the available DTM's, in order to point out possible inconsistencies, blunders or outliers in the data. Secondly we present methods for consistently merging different data. In the present work some proposals in this direction are shown and are applied to significant examples belonging to Italian DTM's files.

**G3/W/01-A5** Poster **1610-47**

#### AN EVALUATION OF TECHNIQUES FOR DIGITAL ELEVATION MODEL CORRECTION USING SATELLITE ALTIMETER DATA

DOWSON, M., Berry, P.A.M & Hoogerboord, J.E. (Geomatics Unit, De Montfort University, Leicester LE1 9BH, UK)

The identification of regional errors in Global Digital Elevation Models (GDEMs) using a near global set of orthometric heights derived from ERS-1 and ERS-2 altimetry data has confirmed that significant deficiencies currently exist in these models due to limitations in the source datasets. This paper presents initial results from a study exploring the use and limitations of altimeter data in quantifying and correcting these errors. Validation of the altimeter derived dataset by comparison with accurate regional DEMs has enabled a quality graded height set to be produced; the highest quality data have been used to examine the nature of the common error signatures detected in GDEMs and, where possible, to improve the data over these areas using a variety of techniques including crossover analysis, warping, and integration of ground truth and altimeter derived heights.

**Gravity Field Modelling and Theory****G3/E/33-A5** Poster **1610-48****OPTIMUM POINT MODEL OF GRAVITY FIELD OF THE EARTH COMPILED ON THE BASIS OF ABSOLUTE VALUES OF GRAVITY**

Stoyan AVDEV and Simeon Kostyanov (University of Mining &amp; Geology, Sofia - 1100, Bulgaria, e-mail: skost@staff.mgu.bg)

An optimum point model of the global gravity field has been compiled on the basis of data for absolute values of gravity. It has been composed of point masses. Optimum parameters of the masses have been determined by the least squares method. This model is univalent and stable for the set of data used and provides the best description of the field with the least number of parameters of its sources. It approximates the used absolute values of the gravity with a mean squared error about 40 mGal, and only for data in the USA territory - 30 mGal. The field of the optimum point model is similar to the field of the rotary ellipsoid (the normal gravity field), and the other anomalies - to the free air anomalies. An advantage of the point model of the global field of the Earth in comparison to the ellipsoidal one is its flexibility and higher precision for information processing and its application in geophysics and geodesy.

**G3/E/31-A5** Poster **1610-49****ERROR COVARIANCE FUNCTIONS FOR MARINE GRAVITY DATA IN THE EUROPEAN SEAS**

Dirk BEHREND (Institut d'Estudis Espacials de Catalunya, Edif. Nexus-204, Gran Capita 2-4, 08034 Barcelona, Spain, email: behrend@ieec.fr.es)

Various tasks in gravity field modelling depend on the availability of suitable error information. A proper description of the error behaviour is provided by error (covariance) functions. These are employed e.g. in geoid determination when using spectral combination or collocation techniques. This presentation deals with the computation of error covariance functions of gridded gravity anomalies in different regions of the European Seas, being done by the author when he was with the Institut fuer Erdmessung, University of Hannover, Germany. To this end cross-over adjusted sea gravity data sets (cruises) were predicted cruise-wise onto a common 1°x1.5' grid. As a certain number of grid cells is covered more than once, this "over determination" can be used to derive the looked-for error functions. The experimental functions thus obtained can be fitted to an exponential model, which show the following features: (1) The correlation length is almost identical for all functions (about 14 km). (2) The error standard deviations range between 2 mGal and 8 mGal.

**G3/W/51-A5** Poster **1610-50****DETERMINING PARAMETERS OF A COVARIANCE FUNCTION BY ANALYTICAL RULES**

Shaofeng BIAN (Institute of geodesy and geophysics, Chinese academy of sciences Xudong Road 54, 430077 Wuhan China)

Two analytic rules for determining the parameter of a covariance function are described in the paper. One is formulated from the analytic implication of collocation in the Hilbert space. Another is formulated from the equivalence between B-splines and Gaussian functions. Preliminary numerical examples are attached to illustrate the availability of the two rules. The investigation indicates that the two rules provide a good alternative for the usually adopted covariance function fitting in practice.

**G3/W/54-A5** Poster **1610-51****SELECTION OF THE DEGREE OF GEOPOTENTIAL MODEL AND INTEGRATION RADIUS FOR GRAVIMETRIC GEOID COMPUTATION**

W.E. FEATHERSTONE (School of Spatial Sciences, Curtin University of Technology, GPO Box U1987, Perth, WA, 6845, Australia, email: ffeather@cc.curtin.edu.au); J.D. Evans (Department of Mathematics, The University of Wales, Aberystwyth, Ceredigion, SY23 3BZ, UK, email: joe@aber.ac.uk); P. Vanicek (Department of Geodesy and Geomatics Engineering, University of New Brunswick, PO Box 4400, Fredericton, NB, E3B 5A3, Canada, email: vanicek@unb.ca)

In regional gravimetric geoid determination, it has become customary to combine the complete expansion of a recent global geopotential model with terrestrial gravity anomalies via Stokesian integration over a region of arbitrary extent. This contribution derives a more objective means with which to select an optimal combination of the spherical harmonic degree of a global geopotential model and the integration area, which is taken to be a spherical cap. This approach is based upon the criterion that the error in the approximated geoid height is minimised. However, this approach ultimately depends upon the error degree variance of the global geopotential model and the degree and error degree variances of the terrestrial gravity data, which are not accurately known. Therefore, both published and postulated values of these quantities have been utilised in order to estimate the optimal combination of the degree of the global geopotential model and spherical cap radius. The optimal combination of these two variable parameters derived here broadly agrees with empirical results from gravimetric geoid computations made by other authors.

**G3/C/G6/W/02-A5** Poster **1610-52****GEOLOGICAL REFINEMENT OF THE GEOID**

Gottfried GERSTBACH (Inst. of Geodesy &amp; Geophysics, TU Vienna, email: ggerstb@terra.tuwien.ac.at)

To get a centimetric geoid in alpine or tectonic areas, geology is a limiting factor. Several geoid projects show that usual terrain correction requires very narrow point spacing (1-2km gravimetry, 5km astro). Surface rock density data (2D) improve the geoid by 20%, subsurface data (3D) by 40-60%. This is demonstrated by examples in Austria (tectonic basin and Limestone Alps). For full 3D modelling of the geological subfloor a special program was developed, based on density regions and vertical prism gridding. A 2\_D method (inclined layers) is used, if only rough geological data exist. Hence, aiming to a geoid of ±2cm/100km, astropoints of 10km spacing are sufficient. Together with the expected automation by CCD, this procedure is efficient even in very rugged terrain. At large networks the geoid error increases very slowly (±3cm/1000km).

**G3/W/43-A5** Poster **1610-53****USING A SYNTHETIC EARTH GRAVITY MODEL TO ASSESS THE PERFORMANCE OF MODIFIED KERNELS IN GRAVIMETRIC GEOID COMPUTATIONS**

Simon HOLMES (School of Spatial Sciences, Curtin University of Technology, GPO Box U1987, Perth 6845, Australia, tel: +61 8 94873838, fax: +61 8 9266 2703, email: holmes@vesta.curtin.edu.au) Will Featherstone (tel: +61 8 9266 2734, fax: +61 8 9266 2703, email: Featherstone\_WE@cc.curtin.edu.au)

A Synthetic Earth Gravity Model (SEGM), designed to generate matching sets of gravimetric and geometric quantities from first principles, can provide an independent means of testing the processing and interpretation of gravimetric data. In the current study, a preliminary SEGM based on spherical harmonics was used to assess the extent to which various modifications to the traditional Stokes kernel are able to reduce the truncation error in gravimetric geoid heights. This error results from the Stokesian integration of gravity anomalies over a spherical cap rather than over the entire Earth as the derivation of Stokes's integral requires. Some kernels also perform the auxiliary function of partially filtering low frequency errors from terrestrial gravity data. To test each kernel, self-consistent grids of synthetic gravity anomalies and geoid heights were computed from hypothetical geopotential coefficients used in a standard spherical harmonic series. Coefficients up to degree 1800 were sourced from the existing geopotential model GPM98B. Model coefficients from degree 1800 were then scaled and 'recycled' as hypothetical coefficients for the higher degrees. FFT software was used to convolve the synthetic anomalies with various kernels using spherical caps of different sizes. The resulting grids of geoid heights were then compared with the 'control' grid generated from the synthetic model. The modified kernels were found to improve upon the traditional Stokes kernel.

**G3/E/32-A5** Poster **1610-54****APPLICATION OF ASTRONOMIC TIME-LATITUDE RESIDUALS IN GEOSCIENCE**

Hu HUI, Wang Rui, Mao Jirong Yunnan (Observatory, Academia Sinica, Kunming, 650011 China)

Yunnan is a seismic active region. After the earthquake of Ms 6.1 occurred in Luquan County, Yunnan Province on April 18, 1985, we analysed in detail the relationship between the major earthquakes and the astronomical time-latitude residuals (ATLR) of Yunnan Observatory. It was found that there appear the anomalies of the ATLR before earthquakes which happened in and around Yunnan. Afterwards based on the studies the anomalous characters and laws of the ATLR of Yunnan Observatory were summarized before earthquake, and provided better warning information for a few major earthquakes. ATLR are the rest parts after drawing the Earth Orientation Parameters from the observations of time and latitude. They are quantities relating to the changes in the local geophysical field, including the plumb line variation (PLV). The PLV before the earthquakes due to the motion of the groundmass in a seismic region during the pregnancy of earthquakes may be the main reason of the anomaly. Recently the comparison analyse of the PLV at Yunnan has been made using the observations of the gravimetric network there and the ATLR of Yunnan Observatory by Li Zhengxin and Hu Hui et al.. The results of PLV at Yunnan from the two different techniques are in good accordance at interannual time scales, especially its south-north component. It once again confirms that the anomaly of ATLR is true. The anomaly reflects the PLV, instead of atmospheric refraction or meteorological effects. Therefore it is also used for monitoring the change in the gravity field around the Observatory.

**G3/W/18-A5** Poster **1610-55****TOPOGRAPHIC MASS MODELLING IN THE VIEW OF THE ONE CENTIMETER GEOID**

Michael KUHN (Geodetic Institute, University of Karlsruhe Englerstrasse 7 D-76128 Karlsruhe Germany, Phone: ++49-721-6082723, Fax: ++49-721-694552 e-mail: kuhn@gik.uni-karlsruhe.de)

In the framework of determining the earth's gravity field the geoid as a particular equipotential surface plays a central role. In providing orthometric heights the geoid is the reference surface for this height system and therefore an exact knowledge is necessary for converting GPS-Heights in orthometric heights. But if we want an exact description of the geoid, with respect to a reference ellipsoid, we end up by the well known Stokes Problem and for the solution we need a sufficiently good knowledge of the topographic masses. Here a simple modelling of the topographic masses with a constant density is not sufficient for providing a geoid in the view of an one centimeter accuracy. This paper intends to give an insight in different possibilities to model the topographic and also the isostatic masses. Numerical results will be illustrated for theoretical examples and the area of Baden-Wuerttemberg in Germany.

**G3/W/50-A5** Poster **1610-56****A STUDY OF NUMERICAL STABILITY AND ACCURACY OF BASIS FUNCTIONS IN THE EXPANSION OF GEOPOTENTIAL MODEL TO VERY HIGH DEGREE AND ORDER**

JIANCHENG LI Dingbo Chao (School of Geoscience and Surveying Engineering, Wuhan Technical University of Surveying and Mapping, 129 Luoyu Road, Wuhan 430079, China, email: jcli@wtusm.edu.cn, dbchao@wtusm.edu.cn)

Some new geopotential models to higher degree and order more than 360 by spherical harmonic expansion increasingly improve the description of refined structure of Earth's gravity field, however their aliasing errors of geopotential coefficients still exist. The aliasing effects are caused by sampling of surface gravity data, methods of spherical harmonics expansion and accuracy of spherical harmonic functions etc.. The fact that the numerical instability of high degree associated Legendre functions is a main factor, which limited to their accuracy. This paper will concentrate on investigation of the numerical stability and accuracy as well as their behaviour of associated Legendre functions. An accurate algorithm for computing high degree associated Legendre functions are proposed. Some numerical results of spherical harmonic coefficients to higher degree have been compared between new accurate basis functions and those calculated by historic algorithm.

**G3/W/31-A5** Poster **1610-57****LOCAL GRAVIMETRIC SOLUTIONS FROM SATELLITE GRAVITY GRADIOMETRY DATA: A COMPARISON STUDY**

ZHICAI LUO, Yongqi Chen (Department of Land Surveying and Geo-Informatics, The Hong Kong Polytechnic University, Hung Hum, Kowloon, Hong Kong. Email: lsclu@polyu.edu.hk) and Jinsheng Ning (Wuhan Technical University of Surveying and Mapping, Luoyu Road 129, Wuhan 430079, P.R.China. Email: jnsning@dns.wtusm.edu.cn)

For the determination of the earth's gravity field a large amount of gradiometry data is available from satellite gravity gradiometry in the near future. In local gravity field approximation three methods to deal with the downward continuation of gradiometry data are studied in the



paper, including least squares collocation in frequency domain, planar approximation method and spectral combination method with optimum integral kernel function. At first, the principles and corresponding mathematical models of above methods are discussed respectively, and then their advantages and disadvantages are analyzed theoretically. It's pointed out that some advanced numerical techniques and computational strategies should be considered carefully to overcome the spectral leakage and computational instability. Finally, numerical simulation results are given to demonstrate the effectiveness of the methods proposed in the paper. These methods can be applied not only to process the downward continuation problem of satellite gravity gradiometry data, but also to refine the local gravity field by combining gradiometry data, terrestrial gravity anomaly, satellite altimetry data and etc..

**Key Words** satellite gravity gradiometry, downward continuation, least squares collocation in frequency domain, planar approximation method, spectral combination method.

**G3/E/20-A5** Poster **1610-58**

**A NEED TO CHANGE GRAVITY DATA REDUCTION PROCEDURE FOR TOPOGRAPHIC CORRECTION**

D.V. SUBBA Rao (National Geophysical Research Institute, Hyderabad 500 007, India.)

In regional gravity studies, applying correction for topographic mass up to sea level and in prospecting, reducing data to local base have introduced additional anomaly in Bouguer gravity in form of negative bias in case of former and have changed nature of anomaly in case of later due to improper correction for topographic mass. This is based on the observation that gravity effect of local topography only is present while that of regional topography is represented by zero values in free air gravity

**G3/L/14-A5** Poster **1610-59**

**SPHERICAL EARTH TERRAIN CORRECTION MODELS**

Douglas ROBERTSON (NOAA Table Mountain Gravity Observatory, 8600 North 39th Street, Longmont, CO 80503, USA, and CIREs, Campus Box 216, University of Colorado, Boulder, CO 80309, USA, e-mail: doug@tmgo.colorado.edu)

Analytic models that use terrain data to generate terrain corrections typically assume flat-topped rectangular Cartesian prisms on a flat-Earth model. To investigate the accuracy of such models, and to investigate more rigorous ways to implement Helmert's second method of condensation, we have developed a model that uses numerical quadrature techniques to calculate the gravitational attraction of topographic masses and condensed masses on a spherical Earth with non-Cartesian prisms and more realistic prism top shapes. One of the main problems with the numerical techniques involves the  $r=0$  singularity in the region close to the observing station, which is dealt with using polynomial extrapolation. This model could be modified in a straightforward manner to make use of terrestrial density variation data if such data were available. Preliminary tests indicate that with a 30x30 arcsecond terrain grid the largest errors arise from the assumption of flat prism tops. In rough terrain, such as in the Rocky Mountains, these errors are of the order of tens of milligals. Most of this error is concentrated in the central prism and the next "ring" of 30x30 prisms. Errors arising from the flat-Earth assumption are much smaller. Comparison with 3x3 arcsecond data indicate that a bilinear-top prism model will produce agreement between the 3x3 and the 30x30 arcsecond grids at the level of better than one milligal.

**G3/E/06-A5** Poster **1610-60**

**GRAVITY SHIELDING: MYTH OR REALITY?**

Lev SAVROV (Sternberg Astronomical Institute, Moscow University, Universitetsky av.13, 119899 Moscow, Russia, email: savrov@sai.msu.ru)

M. Allais used the solid paraconic pendulum to detect the gravity effect during solar eclipses in 1954 and 1959. G. Jeverdan in 1961 and M. Denis in 1991 used the classic Foucault pendulum for the same aim. All of them observed the change of direction of the oscillation plane of pendulum during the phase of eclipse. These results are doubted mostly because the pendula were not isolated from the atmosphere. Author took part in international expeditions for total solar eclipses at Rostov (USSR, 1961), Bielomorsk (USSR, 1990), Mexico-City (Mexico, 1991), Pato Branco (Brazil, 1994), and tried to detect the gravity effects by paraconic pendula of his own constructions. All devices were placed in thermostatic vacuum chambers, and had remote control start-stop mechanisms, photoelectrical registration sensors, computing data acquisition systems. The increase of velocity of pendulum oscillation plane during solar eclipses was taken place in direction of Foucault effect with the value of order of Foucault effect. The analysis of data showed that all types of abnormal effects are inside of instrumental, measuring, and computational errors.

**G3/L/20-A5** Poster **1610-61**

**ON THE BEHAVIOUR OF THE ITERATIVE SOLUTION OF THE SCALAR FREE BOUNDARY VALUE PROBLEM ON A SPHERE AND AN ELLIPSOID**

Kurt Seitz, Geodetic Institute, University of Karlsruhe, Englerstrasse 7, D-76128 Karlsruhe (Germany) Phone: ++49-721-608-6576, Fax: ++49-721-608-6808, e-mail: seitz@gik.uni-karlsruhe.de

One way to solve for the earth's gravity potential  $W$  in the mass-free space outside the boundary surface  $S$  is to formulate a boundary value problem. If we assume the horizontal position of all boundary points  $P$  to be known the vertical position of  $P$  and  $W$  remain as unknown functions and we have to deal with the scalar free boundary value problem (bvp). In a first step the nonlinear boundary conditions are linearized with respect to suitably chosen approximations of the unknowns. In this context the normal potential  $w$  and the telluroid  $s$  is introduced. In the second step the linear reduced boundary conditions have to be (downward) continued from  $s$  to a reference surface which shows a rotational symmetry with respect to the earth's mean rotational axis. Here we consider a sphere and the surface of an ellipsoid of revolution. After the analytical continuation of the evaluation operator, the boundary condition can be split in two parts. The main component is covered by the isotropic term which corresponds to the Stokes-problem. The second part consists of the ellipsoidal and topographical components which are functionals of the disturbing potential which we solve for. Therefore an iterative solution strategy is appropriate. To model the ellipsoidal and topographical terms mostly ellipsoidal corrections in linear approximations are applied. In this paper we are dealing with ellipsoidal and topographical corrections in a second order approximation. In the third step the resulting isotropic problems have to be solved iteratively. The main topic of this contribution is to show the results of numerical studies, where the numerical behaviour of the iterative procedure is intensively studied. In case of the continuation onto the ellipsoid the procedure of the iterated harmonic analysis is convergent, but in case of the sphere divergence is observed.

**G3/L/01-A5** Poster **1610-62**

**A COMPARISON OF DOWNWARD CONTINUATION TECHNIQUES OF TERRESTRIAL GRAVITY ANOMALIES**

Michael SIDERIS (Department of Geomatics Engineering, University of Calgary, Calgary, Alberta T2N 1N4, Canada, email: siederis@ucalgary.ca); Petr Vanicek and Jianliang Huang (both at Department of Geodesy and Geomatics Engineering, University of New Brunswick, Fredericton, N.B. E3B 5A3, Canada, email: vanicek@unb.ca)

There are two fundamental downward continuation techniques of gravity for the determination of geoid used in geodetic practice:

- (1) the discrete Poisson downward continuation which represents a discrete form of Fredholm's integral equation of the first kind; and
- (2) the analytical downward continuation based on the Taylor expansion of the gravity anomaly

In this paper, we compare these two methods numerically, using point and 5' by 5' mean values of Helmert gravity anomalies from the area of the Canadian Rocky Mountains. The techniques are compared in terms of accuracy and computational efficiency and stability. Results are given both in the gravity and in the geoid space. For the downward continuation of point values, the "downward continuation correction" amounts to several tens of mGal (approximately between -25 and 65 mGal), with the mean and standard deviation of the order of 1 and 5 mGal, respectively. The corresponding values in the geoid space vary from -0.03 m to 0.80 m, with the mean of 0.43 m. For the downward continuation of mean anomalies, the values range from approximately -45 to 102 mGal, with a mean is 1 mGal and standard deviation of 8 mGal. The corresponding values in the geoid space are between -0.03 m and 0.93 m, with a mean of 0.48 m.

**G3/E/17-A5** Poster **1610-63**

**REGIONAL GRAVITATIONAL MODELS DERIVED BY MEANS OF THE SNAP METHOD**

V.N. STRAKHOV (United Institute of Physics of the Earth, Russ. Acad. Of Sciences, Moscow, Russia); U. SCHAEFER (Bundesamt fuer Kartographie und Geodaesie, Aussenstelle Potsdam, Michendorfer Chaussee 23, 14473 Potsdam, Germany, email: ufer@potsdam.ifag.de); A.V. Strakhov (Computing Center of the Russ. Acad. of Sciences, Moscow, Russia)

A number of regional analytical models of the Earth's gravitational field for Central Europe has been developed on the basis of Strakhov's new analytical approximation (SNAP) method. The models are equivalent to spherical harmonic expansions of degree and order  $N=36, 48, 72, 180, 360, 720$  and 1080. These models have been derived as stable approximate solutions of strongly underdetermined systems of linear algebraic equations with up to about two million of unknowns using several thousands of original gravity data from the BGI gravity data base (i.e. point observations). The quality of the SNAP models has been evaluated by means of independent control data sets and by comparing them to other analytical models, as e.g. the EGM96. One of the outstanding results is that the SNAP models are nearly free of bias and provide a significant better RMS fit than the EGM96 not only in the original data set used to derive these SNAP models but also in the control data sets. The control points are randomly distributed over an test area of 700000 square kilometers, covering Germany and adjacent areas. Below is given -as an example- the mean deviation and the RMS for the SNAP#13 ( $N=360$ ) model in the 4000 original and 424 control points: (-0.023 +/- 6.909) mgal; (+0.212 +/- 7.573) mgal and for the EGM96 ( $N=360$ ) model: (-5.941 +/- 18.822) mgal; (-3.095 +/- 10.982) mgal, respectively.

**G3/E/13-A5** Poster **1610-64**

**EFFECT OF ANOMALOUS TOPOGRAPHICAL DENSITY ON HELMERT GRAVITY**

Marc VERONNEAU (Geodetic Survey Division, Dept. of Natural Resources, 615 Booth Street, Ottawa, Ontario, Canada, K1A 0E9, email: marc@geod.nrcan.gc.ca)

For the computation of a gravimetric geoid model, it is customary to use an average topographical density of 2.67 g/cm<sup>3</sup> when reducing the masses above the geoid. However, the lateral variations of density have to be taken into account for a high accuracy geoid model. Martinec (1993) demonstrated that anomalous density could contribute at the decimetre level in the Helmert approach. His work focused on the direct topographical effect and the primary indirect topographical effect, but he did not consider the implicit part of the density in the downward continuation. The anomalous density could contribute metres to the geoid model when the downward contribution is taken into consideration in the Helmert approach. However, the large effect of the anomalous density is not present in the current geoid models (with average crustal density) because the downward continuation and the condensed terrain effect have not been considered in the formulation. These two terms approximately cancel each other. A theoretical investigation of these effects is conducted on an earth model without atmosphere. The model omits the atmospheric effect, ellipsoidal corrections, the secondary indirect effects and the centrifugal force. This simplified model allows a better understanding of the behaviour of the topographical density without being cumbersome by a series of terms, which are negligible or not related to the topographical density. Therefore, a heterogeneous sphere, with topography on its surface, could represent the earth. In addition, the ellipsoidal earth model, which usually represents the normal field, is replaced by a homogeneous sphere, which has the same radius and mass as the earth without the atmosphere.

**G3/E/03-A5** Poster **1610-65**

**EXPLORING THE DETAILED STRUCTURE OF THE LOCAL EARTH'S GRAVITY FIELD USING FRACTAL AND FOURIER POWER SPECTRUM TECHNIQUES**

Kefe ZHANG (IESSG, University of Nottingham, Nottingham, NG7 2RD, UK, Email: kefei.zhang@nottingham.ac.uk); Will Featherstone (School of Spatial Sciences, Curtin University of Technology, GPO Box U1987, Perth, WA 6845, Australia, Email: Featherstone\_WE@cc.curtin.edu.au)

As one of the world's oldest continents, Australia has experienced a complicated geological history and thus has a distinctive landscape and an extensively weathered topography. As such, the gravity field of Australia behaves differently to that in other countries. This paper investigates the features of the Australian gravity field for both surfaces and profiles. The methods used are a simple statistical comparison, Fourier power spectrum analysis and the Hurst fractal technique. Fourier spectral analysis and the fractal geometry method offer a new paradigm for understanding detailed structure and features of the Earth's gravity field. Three test areas (the Hamersley Ranges, Central Australia and the Snowy Mountains), that represent extreme features of the Australian gravity field, have been selected. From these, it is shown that the gravity field of Australia is not always correlated with the terrain and the topography often contains longer wavelength features than the gravity anomalies. It is demonstrated that the simple statistical analysis and Fourier power spectral methods are the most informative tools for measuring the smoothness of the gravity field. Using these, it is shown that none of the free-air, Bouguer or (Airy-Heiskanen) topographic-isostatic gravity anomalies is consistently the smoothest type in Australia. Sometimes, the Bouguer anomaly is more variable than the free-air anomaly and thus should not necessarily be used for gravity field gridding in Australia.



**Geoid****G3/W/55-A5** **1610-66****ASTROGEOIDETIC GEOID COMPUTATION FOR AUSTRIA USING SEISMIC MOHO DEPTHS**

Hussein ABD-ELMOTAAL (Civil Engineering Department, Faculty of Engineering, Minia University, Minia 61111, Egypt, email: hamotaal@frcu.eun.eg); Norbert Kuehtreiber (Section of Physical Geodesy, Institute of Theoretical Geodesy, Graz University of Technology, Steyrergasse 30, A-8010 Graz, Austria, email: kueh@phgg.tu-graz.ac.at)

The depths of the Mohorovicic discontinuity (Moho depths) derived by seismic observations are available for this study for an area covering the central part of Europe. The computation of the terrain reduction is carried out using those pre-estimated seismic Moho depths. The TC-program (originally written by Forsberg, 1984) has been modified to compute the effect of the compensating masses on the gravity anomalies, geoid undulations and deflection components using the digital Moho models. Both fine (11.25" x 18.75") and coarse (90" x 150") digital height and seismic Moho models are available for this investigation. An astrogeoidetic geoid for Austria has been computed using the seismic Moho depths, representing the compensating masses, by the least-squares collocation technique. For the sake of comparison, an another astrogeoidetic geoid for Austria has been computed using the Airy-Heiskanen isostatic model for generating the compensating masses. A wide comparison between both geoids is carried out.

**G3/E/44-A5** **Poster** **1610-67****DENSIFYING GEOID INFORMATION IN VENEZUELA BY GPS DENSE POINTWISE DETERMINATION OF GEOID UNDULATIONS IN VENEZUELA THROUGH GPS**

G. ACUÑA, M. Hoyer, E. Wildermann (Laboratorio de Geodesia Física y Satelital, Escuela de Ingeniería Geodésica, Universidad del Zulia, Maracaibo, Venezuela; email: mhoyer@luz.ve); J. Hernández (Servicio Autónomo de Geografía y Cartografía Nacional, Caracas, Venezuela)

The Zulia University (LUZ) and the National Cartographic Administration (DCN) planned and measured a GPS campaign in Venezuela (about one million Km<sup>2</sup>) with the aim to obtain dense geoid undulations in the country.

Venezuela, as most countries in South American, are working very intensive in their geoid determination. The information, for this target, obtained by a single observational procedure is not enough. Data from different sources have to be combined like gravimetric data, digital height information, GPS observations and geopotential models. As part of a national combined geoid project the GPS derived undulations in many stations of the country can help to increase the available information.

80 Bench Marks with mean separation of 50 Km were occupied in a 14 days observations campaign using 5 dual frequency receivers and the GPS permanent station (IGS-Maracaibo). In this first part of the GPS project was covered the half of the country, from its western limit to the central region. A second and last part of GPS observations is planned for the first half of 1999. The density of the points allows a uniform data concentration over the country with a high resolution for geoid calculations.

The specifications of the measurement campaign satisfied the high requirements of the height determination by GPS. The adopted procedure can be applied in similar projects. The processing by Bernese software tried to obtain highest quality for the results. The  $\pm 1$  cm rms. for the GPS derived ellipsoidal heights and the same level of precision in the orthometric heights of the Bench Marks used allowed to obtain the geoid undulations with equivalent quality. A later combination with different type of data by collocation is planned. Finally, the comparison with EGM 96 geopotential model showed discrepancies up to 2 m confirming the urgent need of a regional geoid determination in the country.

**G3/E/14-A5** **Poster** **1610-68****ASTROGEOIDETIC GEOID DETERMINATION IN TURKEY**

Osman ALP (General Command of Mapping TR-06100, Ankara, Turkey, Tel : +90 312 3638550/2223 Fax : +90 312 3201495 Email: oalp@hkg.mil.tr)

Astrogeoidetic deflections in ED50 at 200 astronomic points scattered throughout Turkey are utilized. The points at which astrogeoidetic deflections are known are on the topographical surface, and the horizontal variation of the astrogeoidetic deflections are nonlinear due to rough topography and large distances between the points. Hence, Helmert's astronomic leveling is extended to the astrogravimetric leveling considering both the gravimetric correction due to the non-linearity and the orthometric correction in order to project the astronomic point onto the geoid. In order to compute the gravimetric correction, gravimetric geoidal heights and gravimetric deflections of the vertical at points are interpolated using bicubic splines from 3'x 3' gridded file of Turkish Geoid-1991 (TG-91). To compute the orthometric correction, observed gravities and orthometric heights at points are used in the well-known orthometric correction formula. Two networks consisting of geoidal height differences resulted from Helmert's astronomic leveling and astrogravimetric leveling respectively are adjusted separately. The rms of ( 1.13 m for the difference between two geoids indicates the benefits of astrogravimetric leveling.

**G3/E/18-A5** **Poster** **1610-69****LAST DEVELOPMENTS IN ESTIMATING THE ITALIAN QUASI-GEOID AND FUTURE PERSPECTIVES**

Riccardo BARZAGHI, Alessandra Borghi, Giovanna Sona, Vincenza Tornatore (DIAR-Politecnico di Milano, Piazza Leonardo da Vinci 32, 20133 Milano, Italy)

New data and the last global geopotential model EGM96 made it possible to estimate an improved quasi-geoid for the Italian area. The remove-restore procedure was applied to get the final solution. The last geopotential model EGM96 was used to represent the low frequency component of the geopotential field. This improved the gravity residuals statistics with respect to OSU91A, especially in the area surrounding the Corsica island. A careful validation of the DTM used in the computation and density information led to a more refined RTC component, which is crucial in an area such as Italy. A windowed collocation solution was tuned and used to obtain the residual quasi-geoid component from gravity residuals. Comparisons of the new solution with GPS/leveling data were also computed and discussed. Finally, a new remove-restore procedure was proposed and tested in a small area in Central Italy.

**G3/L/19-A5** **Poster** **1610-70****THE NEW IGES SOFTWARE FOR RTC**

L. Biagi (Politecnico di Milano, IGES, Facoltà di Ingegneria di Como, P.le Gerbetto 6, 22100, Como, Italy, Email: ludo@gemini.como.polimi.it), C. Sciarretta (Telespazio SpA, Space Geodesy Center, Matera, Italy, Email: cecilia@asi.it)

At present, very dense DTM's are available in some regions as well as information on surface density. It is well known that the software usually used in RTC computation goes by two alternative methods: numerical integration by prisms or FFT integration. The first approach involves long computation time, particularly for dense DTM's; the second one, faster, involves significant approximations in areas where topography is rough. In the framework of a cooperation between IGeS and ASI-CGS a new formulation for RTC has been studied and implemented; particularly, we have tried to develop a method based on approximations which are acceptable in the majority of cases and numerically fast. Besides, we are studying a possible approach for a correct modelling of surface density variations in RTC computation. In this work the proposed algorithms and the results obtained are shown.

**G3/W/26-A5** **Poster** **1610-71****THE CONTINUOUS EFFORTS TOWARD A 10' RESOLUTION GEOID FOR SOUTH AMERICA**

Denizar BLITZKOW (Sub-Commission for the Geoid in South America, Escola Politécnica da Universidade de São Paulo, Caixa postal 61548, - 05424-970 São Paulo - SP - Brazil, E-mail: dblitz@usp.br); Maria Cristina B. Lobianco (IBGE-DEGED, Av. Brasil, 15671, - 21241-051 Rio de Janeiro - RJ - Brazil, E-mail: lobianco@ibge.gov.br); J. Derek Fairhead (University of Leeds, Earth Science Department, Leeds UK, LS2 9JT, E-mail: jdf@geotech.leeds.ac.uk)

In the last few years, as a result of the Sub-Commission for the Geoid in South America (SCGSA) establishment and due to the facilities offered by the GPS to derive geometric height, many efforts have been carried out in the different countries of South America, in order to improve the geoid (quasi-geoid) computations. A great validation process of the gravity data in many countries such as: Brazil, Uruguay, Argentina, Colombia and Chile has improved many of the gravity surveys. GPS observations carried out on bench marks of the geometric levelling have been facilitated by the SIRGAS (Geocentric Reference System for South America) project and are contributing for testing the gravimetric determination of the quasi-geoid. The Digital Terrain Model (DTM) has been improved considerably in Brazil and Argentina; Chile has been planning a big effort in the same direction as well. The objective is to generate a DTM grid of 3' resolution (DTM3) for the south-american continent. Gravity surveys carried out in the north of Brazil, in the Amazonas region, contributed for a better acknowledgement of the gravity field, at least along the rivers. Local and national geoid computations gained much more importance recently. The Second Geoid School, organized in Rio de Janeiro just after the IAG Scientific Assembly and supported by IGeS (International Geoid Service), has had a strong influence in the efforts for geoid computations in different countries. Numerical integration of the modified Stokes integral and the application of FFT are techniques much used up to now in South America with the objective of a 10' resolution quasi-geoid.

**G3/P/06-A5** **Poster** **1610-72****GRAVIMETRIC GEOID DETERMINATION. A CASE STUDY: ALGERIA**

Mustapha BOUZIANE, Madani Aarizou (Laboratory of Geodesy, National Centre of Spatial Techniques, BP 13 Arzew 31200, Algeria)

Orthometric height differences obtained from a combination of global positioning system (GPS) ellipsoidal height differences and gravimetric geoid predictions have the potential of replacing costly and time-consuming spirit levelling, especially in remote unsurveyed areas like the south of Algeria. This paper provides numerical examples for the computation of the geoid heights by the solution of Stokes's Boundary Value Problem (e.g. using planar approximation, analytical kernel spectrum and rigorous one dimensional spherical evaluation). In order to obtain such a geoid, high resolution point or mean gravity field data and topographic information are needed as well as a good spherical harmonic reference model. A detailed geoid has been computed in the area covering Algeria  $20^{\circ} \leq j \leq 37^{\circ}$ ,  $-7^{\circ} \leq l \leq 10^{\circ}$  where  $j$  is the latitude and  $l$  is the longitude) using a gravity data file of 12000 gravity points, not homogeneously distributed. The gravimetric data used are on a grid with various spacing from 5 to 15 arc seconds and are predicted using collocation. The spherical harmonic coefficient set OSU91 completed to degree 360 was used for the calculation of the global solution. The Residual Terrain Model (RTM) method based on Bouguer plates was used. Involving a 1km Digital Terrain Model, the topographic effects were computed and subtracted from the free air anomalies in order to smooth the locally varying gravity field. The usual Remove-Restore method is used in order to smooth the gravity data which were used to compute the residual geoid using spherical Fast Fourier Transform (Forsberg and Tscherning 1994). Numerical computations were done using FFT techniques, where 50% of zero padding was used. The largest changes between the quasi-geoid and geoid were notified in the north where the heights vary between 1000 and 3500 m. Differences are from few centimetres to few metres. The solution presented in the following is suffering from the lack of gravity data both in Algeria and the neighbouring countries.

**G3/E/38-A5** **Poster** **1610-73****THE EFFECT OF HIGH BATHYMETRIC MODEL ON GEOID COMPUTATION**

J.C. CATALAO (Faculdade de Ciências de Lisboa, Escola Politécnica 58, 1250-102 Lisboa, Portugal email: mjoao@fc.ul.pt); M. J. Sevilla (Instituto de Astronomía y Geodesia, Universidad Complutense, 28040 Madrid, Spain email: maast01@sis.ucm.es)

The effect of a new detailed regional terrain model on geoid computation has been studied. A new detailed bathymetric model around Azores Islands has been constructed based on new ocean depth information obtained from echo soundings during ship surveys. These bathymetric data were merged with high precision height data on land producing a new terrain model (AZDTM98) with 1'x1' resolution on sea and 20'x20' on land. Global digital terrain models ETOPO5U and JPG-95E were compared with AZDTM98 model. Sea and land gravity data covering the area were merged with satellite derived gravity anomalies for geoid computation. Least squares collocation was used for geoid estimation according to the remove-restore technique using EGM96 geopotential model and RTM method. Three geoid solutions were obtained from AZDTM98, ETOPO5U and JPG-95E models and compared with 12 GPS stations on land and with ERS-1 and ERS-2 altimetric data on sea.

**G3/W/45-A5** **Poster** **1610-74****ANALYSIS OF GRAVITY MEASUREMENTS FOR NEW HEIGHT SYSTEM IN TAIWAN**

Ruey-Gang CHANG (Department of Civil Engineering, Ming Hsing Institute of Technology, Hsingfong, Hsinchu 304, Taiwan, email: fukwo100@ms16.hinet.net); Chia-Chyang Chang (Department of Surveying and Mapping Engineering, Chung Cheng Institute of Technology, Tahsi, Taoyuan 335, Taiwan, email: ccchang@cc04.ccit.edu.tw)

The high precision absolute gravity measurements have been carried out by four times at selected sites in Taiwan area since 1991. These results have been analysed and investigated to realise the variations of the gravity values. It has been found that the absolute gravity values

are varied with the crustal vertical movement in this area. The sites measured by absolute gravimeter are assessed and to be selected as the base stations for a dense gravity network proposed for Taiwan area. This fundamental gravity network will be incorporated with the new national height system, consisting of the first-order levelling network and measured by precise levelling, GPS, and relative gravity. The measurements for the establishment of this new national height system will be carried on in 1999 and 2000, and expected to provide detailed information for all the geodetic and engineering applications.

**G3/P/05-A5** Poster **1610-75**

#### GRAVIMETRY DATA VALIDATION IN ALGERIA

S. A. BENAHDW DAHO, S. Kahlouche, B. Chemaa (National Centre of Spatial Techniques Geodetic Laboratory - B.P 13 Arzew - 31200 - ALGERIA)

A Method for validation of gravity measurements is applied on a small zone in Algeria using the Least Squares Collocation (LSC) method and Gravsoft software of the Copenhagen University. The gravity data, provided by the Bureau Gravimétrique International (B.G.I.), and consisting of 12472 gravity measurements covering the region were analysed and validated. The validation has been applied systematically to predict free air gravity anomalies reduced from the effect of the spherical harmonic coefficient set OSU91A. The detected gross errors represents 1.18 % of the land data. This work shows the non homogeneity of data used and their insufficient accuracy.

**G3/P/04-A5** Poster **1610-76**

#### THE NEW GRAVIMETRIC GEOID IN ALGERIA

S. A. BENAHMED DAHO, S. Kahlouche (National Centre of Spatial Techniques, Geodetic Laboratory - Po. Box 13 Arzew- 31200 - ALGERIA)

A new gravimetric determination of the geoid over Algeria has been made using the following data types :a) a global geopotential model, namely the OSU91A spherical harmonic coefficients set, b) a set of 12325 validated point free air gravity anomalies covering the region, and c) a 1000x1000 meters digital terrain model for the north of Algeria and the ETOPO5U for the rest of the area.

The method used for the computations is the remove-restore technique in connection with the Fast Collocation which allows to obtain the solution over the entire area in one step only. The input data were gridded gravity anomalies. The terrain correction was applied to the data and the corresponding indirect effect was taken into account.

The result final is a quasi geoid grid in  $20^{\circ} \leq j \leq 37^{\circ}$ ,  $-7^{\circ} \leq l \leq 10^{\circ}$  with a grid mesh of  $5' \times 5'$ . Unfortunately, the precise data type GPS/levelling is not available in Algeria. This will certainly help to make an independent verification of the precision of the geoid.

**G3/P/02-A5** Poster **1610-77**

#### GEOPOTENTIAL MODELS COMPARISON IN THE REGION OF ALGERIA

S. A. BENAHMED DAHO, S. Kahlouche, B. Chemaa (National Centre of Spatial Techniques Geodetic Laboratory - B.P 13 Arzew- 31200 - ALGERIA)

The choice of the best geopotential model to reduce geodetic data is one of the critical step in computing the geoid. In this work, an analysis was carried out to define the geopotential model which fits best the gravity field in Algeria.

Global geopotential solutions which are used in the comparison are as follows: GPM2 and OSU91A. The test of the fit of these high order geopotential models to the gravity field in Algeria is based on using the point gravity data supplied by the Bureau Gravimétrique International (B.G.I.). The comparisons were made at all gravity points by calculation of the residual gravity anomalies (i. e. observed data minus model).

The result of this test comparison shows that the OSU91A model describes the geoid most closely in Algeria. The OSU91A model is able to recover gravity anomalies over 43% of the Algerian territory to within 5 mgal and over 71 % of the country to within 10 mgal.

**G3/L/07-A5** Poster **1610-78**

#### GRAVIMETRIC GEOID DETERMINATION USING LAND AND SEA POINT GRAVITIES FOR DEFINING VERTICAL DATUM

E. ÖMÜR DEMIRKOL (General Command of Mapping, TR -06100, Ankara, Turkey Tel : 0 312 3638550/2210 Fax : 0 312 3201495, Email: odemirkol@hgk.mil.tr)

Determination of high accurate geoid has become an area of interest to many scientists and is attracting still more of them. Especially utilisation of space based techniques has significantly improved the importance of geoid which was once regarded as a pure theoretical topic. The practical use of satellite techniques such as GPS, SLR and VLBI necessitates a conversion from ellipsoidal height to orthometric height. The conversion is accounted by the difference between these heights which simply corresponds to geoidal height.

Among the techniques to determine geoid is the remove-restore which is also applied in this study. Gravity anomaly and geoidal height are split into three parts, corresponding respectively to long, medium and short wavelength effects of gravity field. In this study, 1762 land and 161 marine point gravities within the area with latitudes 36 - 37 and longitudes 30 - 31 are used. Long wavelength effects are calculated separately by geopotential models OSU91A and EGM96, while short wavelengths are obtained through RTM and isostatic gravity reductions utilising topography available at  $15'' \times 20''$ ,  $5' \times 5'$  and  $15' \times 15'$  grid nodes. Least squares collocation and Fast Fourier Transform are applied for the computation of medium wavelength effect. Additionally, 4 GPS/levelling geoidal heights available for this area are utilised to increase the accuracy of geoid. Totally, 12 geoids are determined by combination of geopotential models, gravimetric reductions and prediction methods. The geoids differ from each other due to the differences in global models, gravimetric reductions and prediction methods. Inclusion of GPS/levelling geoidal heights has contributed significantly to obtain a more accurate geoid. Additionally, an attempt is carried out in order to define the vertical datum at Antalya tide gauge station, via using the GPS ellipsoidal height, geometric levelling height difference, tide gauge data and geoidal heights.

**G3/W/49-A5** Poster **1610-79**

#### THE NEW GRAVIMETRIC GEOID OF AUSTRALIA: TERRESTRIAL DATA TREATMENT AND COMPUTATIONS USING THE 1D-FFT AND A DETERMINISTICALLY MODIFIED KERNEL

W.E. FEATHERSTONE (School of Spatial Sciences, Curtin University of Technology, GPO Box U1987, Perth, WA, 6845, Australia, email: feather@cc.curtin.edu.au); J.F. Kirby (School of Spatial Sciences, Curtin University of Technology, GPO Box U1987, Perth, WA, 6845, Australia, email: jfk@vesta.curtin.edu.au); A.H.W. Kearsley (School of Geomatic Engineering, The University of

New South Wales, Sydney, NSW, 2052, Australia, email: W.Kearsley@unsw.edu.au); J.R. Gilliland (School of Geoinformatics, Planning and Building, University of South Australia, Adelaide, SA, 5000, email: John.Gilliland@unisa.edu.au) G.M. Johnston (Geodesy Section, Australian Surveying and Land Information Group, PO Box 2, Belconnen, ACT, 2616, Australia, email: GaryJohnston@auslig.gov.au) K.F. Zhang (IESSG, The University of Nottingham, Nottingham, NG7 2RD, UK, email: kefei.zhang@nottingham.ac.uk) R. Forsberg (Geodynamics Department, NMG, Rentemestervej 8, DK-2400 Copenhagen NV Denmark, email: rf@kms.dk) M.G. Sideris (Department of Geomatics Engineering, The University of Calgary, 2500 University Drive NW, Calgary, Alberta, T2N 1N4, Canada, email: sideris@acs.ucalgary.ca)

A new gravimetric determination of the Australian geoid has been made, based on a spectral implementation of the appropriate integrals in physical geodesy. This geoid solution has been termed AUSGeoid98 and is available free-of-charge from the Australian Surveying and Land Information Group (<http://www.auslig.gov.au/geodesy/geoid.htm>). AUSGeoid98 combines the EGM96 global geopotential model, the 1996 release of the Australian gravity data-base, a 250m resolution digital elevation model, and a set of marine gravity anomalies derived from several satellite altimeter missions combined with ship-track data via least squares collocation. The residual gravimetric geoid undulations were computed on a regular two-minute grid using the one-dimensional fast Fourier transform technique, which has been adapted to include a deterministically modified Stokes kernel over a spherical cap. This approach was necessary since the use of the whole Australian data area in conjunction with an unmodified Stokes kernel gives considerably worse agreements with Global Positioning System (GPS) and Australian Height Datum (AHD) heights over the continent. This is most probably due to one or both of errors in the gravity data or systematic distortions in the AHD.

**G3/W/14-A5** Poster **1610-80**

#### A PRELIMINARY GEOID MODEL FOR TIERRA DEL FUEGO (ARGENTINA)

Graciela FONT (Facultad de Ciencias Astronomicas y Geofisicas, Universidad Nacional de La Plata, Paseo del Bosque s/n, 1900 La Plata, email: graciela@fcaglp.fcaglp.unlp.edu.ar); Claudia Tocho (Facultad de Ciencias Astronomicas y Geofisicas, Universidad Nacional de La Plata, Paseo del Bosque s/n, 1900 La Plata, Argentina, email: ctocho@fcaglp.fcaglp.unlp.edu.ar)

A preliminary geoid model has been computed for Tierra del Fuego province in the south of Argentina ( $52^{\circ}30' S - 55^{\circ}30' S$ ;  $64^{\circ}30' W - 69^{\circ} W$ ). Since there are not orthometric heights in the island, orthometric heights were generated from ellipsoidal heights and the undulations of the Geopotential Model EGM96, in a tide - free system. Digital Terrain Model ( $3' \times 3'$ ) from the University of Leeds was used to take into account the topography. Geoid undulations were determined using the remove - restore technique. The Gravimetric Network of the Tierra del Fuego Island, was established from a series of summer surveys by the Departamento de Gravimetria de la Facultad de Ciencias Astronomicas y Geofisicas. Gravity stations were determined on the existing Geodetic Network, additional stations, separated by 5 to 8 Km, were also measured in order to have a better coverage. The gravity values in the north of the island were referred to the pendular value of Rio Grande. It was determined by the Observatorio Astronomico de La Plata in 1940 using a pendulum instrument (Askania). The remainder values, at the south, were referred to the pendular value of Rio Grande and Ushuaia, both values are referred to the Pilar Fundamental de La Plata  $g = 979751.6$  mgals. All gravity values have been adjusted to IGSN71. Disturbing and anomaly gravity maps are also presented showing the characteristics of the area. Both of them are referred to WGS - 84.

**G3/W/41-A5** Poster **1610-81**

#### ASTROGEOIDETIC CCD MEASUREMENTS FOR CENTIMETRIC GEOID MONITORING

Gottfried GERSTBACH (Inst.of Geodesy & Geophysics, TU Vienna, email: ggerstb@terra.tuwien.ac.at)

Geoid solutions of cm level need narrow point spacings of 5-10km (astro) or 1-3km (gravimetry). Because of high astrogeoid economy the effort is minimized by automatic measurement of vertical deflections with small CCD instruments. Geological data improve the geoid further by 50%. Hence, many countries may reach cm geoid accuracies within the next decade. Results of two CCD projects at the TU Vienna are shown. Transportable instruments yield accuracies of  $\pm 0.4''$  within 1 hour of star observations: a) Servo-theodolites with CCD cameras; b) Prism astrolabe (Ni2) with CCD line or array; c) Zenith tubes ( $\pm 1m$ ) with cooled CCD array. Presently the methods b, c are semiautomatic. Some problems concern CCD sensors, mounting stability and PC control. Automatic measurement will be possible in 2000, supported by dGPS navigation ( $\pm 1m$ ). Contrast tuning may enable daylight observations in 2005. Therefore CCD astrogeodesy fits the demand of precise GPS, terrestrial surveys and Integrated Geodesy on a cm-geoid level.

**G3/W/25-A5** Poster **1610-82**

#### GPS/LEVELLING TRAVERSES FOR TESTING GRAVIMETRIC QUASIGEOID SOLUTIONS IN EASTERN ANDALUSIA (SPAIN)

Antonio J. GIL (Dept. Ing. Cartografica, Geodesica y Fotogrametria, Escuela Politecnica Superior, Universidad de Jaen, Virgen de la Cabeza, 2, 23071 Jaen, Spain, email: ajgil@ujaen.es) Gracia Rodriguez-Caderot and M.Clara de Lacy (Dept. Astronomia y Geodesia, Fac. CC. Matematicas, Universidad Complutense de Madrid, 28040 Madrid, Spain) L. Biagi (Facolta di Ingeg.di Como, Politecnico di Milano, Italy)

To test the accuracy of some gravimetric quasigeoid solutions computed in a test area located in the south of Spain two GPS traverses have been established with benchmarks belonging to the First Order Spanish Levelling Network in the east of Andalusia. The GPS constellation was tracked during 4 hours observed session windows over baselines ranging from 3 to 85 km. The equipment used consisted of 3 Leica SR399 and 1 Leica 9500 dual frequency carrier phase GPS receivers. Bernese 4.0 with precise ephemerides was used to process the GPS observations and NETGPS for the adjustment of the network. A statistical study of GPS results is presented. GPS/levelling geoid undulations have been compared with the values provided by Fast Fourier Transform and Fast Collocation methods. The mean values of the standard deviation of the discrepancies after a four parameter datum shift amount to 4 cm.

**G3/W/13-A5** Poster **1610-83**

#### PRELIMINARY GEOID DETERMINATION IN THE CENTRAL PART OF THE ETHIOPIAN RIFT VALLEY

Addisu HUNEGNAW (Department of Geodesy and photogrammetry, Royal Institute of Technology, S-100 44 Stockholm, Sweden)

The central part of the Ethiopian Rift Valley is characterized by a complex near surface geology, and the existence of a number of different intrusive centers. The determination of the geoid may help further study of the geology and structural features in this area. Geoid solutions were carried out in the central part Ethiopian Rift Valley. These local geoid



predictions were based on terrestrial gravity data, height data, using as a reference the new EGM96 geopotential model. The irregularly distributed gravity data derived by land survey were gridded on 8' x11' geographical grid and in this form were used in the numerical tests. Combining the Stokes' kernel modification techniques and high degree reference gravity field techniques did the geoid computations. A total terrain correction directly on the geoid was applied following a new method by Sjöberg (1994, 1995 and 1996a, b). The atmospheric effect was also treated differently from the classical method adopted by the International Association of Geodesy (IAG) adopting a new method by Sjöberg (1998). The computed geoid heights were compared with 4 GPS/levelling stations within and above the rift valley an area characterised by rough topography, along a trigonometric levelling line. The results show that the differences between control and predicted geoid heights have a standard error of 83cm. Using a regression model to the geoid predictions corresponding to the GPS/levelling values, we find an improvement from 83 cm to 74 cm.

**G3/W/06-A5** Poster **1610-84**

**DIFFERENT GRAVITY DATA SOURCES FOR LATVIA GEOID STUDIES**

J.KAMINSKIS (State Land Service of Latvia, 11.Novembra krastmala 31, LV-1050 Riga, Latvia, email: kaminski@main.rsrf.rtu.lv)

To follow up the growing need for accurate and common vertical reference network in our country the fitting of geoids has been made to find an effective technique that satisfies national needs for "quick" reference surface. As a starting point of using geoid for practical application the NKG89 should be mentioned. Later the Baltic '96 geoid has become available, too. Global European geoid solution EGG97 has been tested locally. The regional and irregularly distributed differences of the EGG97 to the local geoid are found. Basically our geoid solutions are evaluated using different gravity data sets by GRAVSOFTE package. In 1998 the new gravity reference network is started to create in addition to our 12 000 gravity points originally from the 1960's. We would like to complete gravity reference network and continue gravity measurements to verify and improve Latvia gravity data base. For that purpose we are going to use our new gravimeter Scintrex CG-3.

For the maintenance of the Latvia geodetic reference system and needs of the surveying the local geoid has been authorised by national geodetic commune for the official use.

**G3/E/41-A5** Poster **1610-85**

**FOUR-COUNTRY ASTROGEOIDIC GEOID IN CENTRAL EUROPE**

Norbert KUEHTREIBER (Physical Geodesy, Technical University Graz, Steyrergasse 30, A-8010 Graz, Austria, email: kueh@phgg.tu-graz.ac.at); Bernhard Hofmann-Wellenhof (Positioning & Navigation, Technical University Graz, Steyrergasse 30, A-8010 Graz, Austria, email: howe@tu-graz.ac.at); Drazen Svehla and Kresimir Colic (Faculty of Geodesy, University of Zagreb, Kacicева 26, HR-41000 Zagreb, Croatia, email: dsvehla@public.srce.hr and kcolic@public.srce.hr); Gyula Toth and Jozsef Adam (both at Department of Geodesy, Technical University of Budapest, Muegyetem rkp. 3.1.61, H-1111 Budapest, Hungary, email: gytoth@epito.bme.hu and jadam@epito.bme.hu)

In 1998, Austria has presented a recomputed Austrian astrogeoidic geoid at the "Second Continental Workshop on the Geoid in Europe" in Budapest. The impact for this recomputation was the input data set which has been improved not so much with respect to additional deflections of the vertical but more with respect to the refinement of the digital terrain model, additional orthometric heights and the inclusion of GPS points.

During the Budapest and further addressed at the Second International Symposium Geodynamics of the Alps-Adria Area at Dubrovnik, the idea evolved to extend the geoid computation over Hungary, Croatia, and Slovenia. From the theoretical point of view, the datum problem is most challenging since each of the four countries uses its own local datum. After unifying the input data in one common frame, the computation of the astrogeoidic geoid using either the collocation method or a free network adjustment is straightforward.

**G3/E/34-A5** Poster **1610-86**

**AUSTRIAN GEOID2000 - MOST RECENT RESULTS**

Norbert KUEHTREIBER (Physical Geodesy, Technical University Graz, Steyrergasse 30, A-8010 Graz, Austria, email: kueh@phgg.tu-graz.ac.at)

At the last General Assembly of the IUGG in Boulder the recomputation of the Austrian Geoid under the project title GEOID2000 was announced. The new computation of the Austrian geoid was initiated with the objective to obtain a relative accuracy of at least 0.5 ppm throughout the country. As far as Austria is concerned, the data input consists of a 50 x 50 m digital terrain model, some 30 000 gravity data, about 800 deflections of the vertical, and GPS-derived points. From the neighbouring countries, gravity and height information is available in different quality and density. Most recent results achieved by different approaches and data combination techniques (least squares collocation method, the integration method using Fast Fourier Transform) are presented.

**G3/W/27-A5** Poster **1610-87**

**HIGH RESOLUTION REGIONAL GEOID DETERMINATION IN TARIM BASIN AND HAINAN ISLAND OF CHINA**

JIANCHENG LI, Jinsheng Ning, Jingnan Liu, Dingbo Chao (School of Geoscience and Surveying Engineering, Wuhan Technical University of Surveying and Mapping, 129 Luoyu Road, Wuhan 430079, China, email: jcli@wtusm.edu.cn)

Two regional geoids with high resolution in Tarim Basin and Hainan Island, located in far west China and south China, respectively, have been determined. The geopotential models WDM94 and EGM96 are considered as the alternative reference field. The 2.5'x2.5' gridded free air gravity anomaly are formed using topographic-isostatic anomaly for alternative methods of smoothing and interpolating of the gravity field in computation of the geoid. The input data include 102,719 point gravity observations in Tarim Basin, and 1817 ones in Hainan Island, and a 0.5'x0.5' Digital Terrain Model for both geoid computations. The determination of geoid and quasi-geoid are based on a strict evaluation of both Stokes integral and Molodenskii series solution using Faye anomalies. The 1D convolution is commonly adopted for more effective evaluation of Stokes integral and Molodenskii series solution to determine the geoid and/or quasi-geoid. The geoid is then fitted to the one from GPS/Leveling data with 8 B order GPS points in Tarim and 87 C order ones in Hainan to yield a so called GPS-gravimetric geoid, and both a smoothed geoid and a smoothed quasi-geoid are finally determined in the two areas. The standard deviations of differences between the geoid height and height anomaly and the GPS/Leveling are  $\pm 0.63m$  and  $\pm 0.70m$  in Tarim and  $\pm 0.30m$  and  $\pm 0.29m$  in Hainan. The standard deviations of residuals after fitting of geoid and quasi-geoid to GPS/Leveling points are better than  $\pm 0.33m$  and  $\pm 0.32m$  in Tarim and  $\pm 0.13m$  and  $\pm 0.14m$  in Hainan, respectively.

**G3/W/29-A5** Poster **1610-88**

**IMPROVEMENT OF THE QUASIGEOID MODEL IN POLAND BY GPS AND LEVELLING DATA**

A.LYSZKOWICZ

The experience with comparison of the GPS/levelling data against high resolution quasigeoid model Quasi97b in Poland have shown discrepancies. This circumstance opens the possibility to develop an empirical corrector surface which relates the quasigeoid model to the reference system of GPS and levelling data. This paper presents the results of modelling such corrector surface.

**G3/W/53-A5** Poster **1610-89**

**THE FINAL SOLUTION OF THE SWISS GEOID CHGE098**

Urs MARTI (Federal Office of Topography, Seftigenstr. 264, CH-3084 Wabern, Switzerland, email: urs.marti@lt.admin.ch)

In the last few years the geoid and quasigeoid of Switzerland was developed in a joint project of the Federal Institute of Technology (ETH Zurich) and the Federal Office of Topography (L+T, SWISSTOPO). In summer 1998 the final solution CHGE098 was calculated and was declared as the official geoid for Switzerland in October 1998. The geoid is now available to the public and can be interpolated on-line via our www-Site (www.swisstopo.ch). It forms the reference surface of the new orthometric national height system of Switzerland (LHN95).

The method used for the determination of the geoid and quasigeoid was a least squares collocation. As input about 600 deflections of the vertical and about 80 GPS/levelling stations could be included. The gravity data were used only for the downward continuation to sea level of the other observations. The remove/restore process was performed with a 25 meter DTM, a 5 km model of the Moho-depth and some other density information. The accuracy of CHGE098 is in the order of 3 cm in the flatter areas and about 5 cm in the Alps over the whole country. This could be verified by a comparison with the European quasigeoid EGG97 and with the comparison of GPS/levelling measurements which were not included in the adjustment process.

The poster shows the final solution of the geoid, the comparison with GPS/levelling measurements, the comparison with the solutions of neighbouring countries and presents the software as now available to the public.

**G3/W/34-A5** Poster **1610-90**

**TOWARDS A PRECISE QUASI-GEOID MODEL FOR SOUTHERN AFRICA**

Charles MERRY (Department of Geomatics, University of Cape Town, Private Bag, Rondebosch, 7701, South Africa; e-mail: cmerry@engfac.uct.ac.za)

The quasi-geoid plays a crucial role in transforming GPS-derived heights to normal heights. This paper describes a pilot study to determine quasi-geoidal heights from gravity data, for southern Africa. The global EGM96 model is used to define the long-wavelength components, and the convolution approach is used for the detailed quasi-geoid structure, for a selected test area. The result is compared to a quasi-geoid determined from a combination of GPS and precise levelling, yielding an RMS agreement of 6cm. Proposals are made for the extension of this technique to the rest of southern Africa.

**G3/E/04-A5** Poster **1610-91**

**COMPARISON BETWEEN GEOIDAL MODELS IN ARGENTINA**

María Cristina PACINO (IFIR – UNR, Av. Pellegrini 250, 2000, Rosario, Argentina, E-mail: mpacino@fceia.unr.edu.ar); Claudia Tocho and Graciela Font (both at FCAGLP, Paseo del Bosque s/n, 1900, La Plata, Argentina, E-mail: graciela@fcaglp.fcaglp.unlp.edu.ar); Denizar Blitzkow (EPUSP, Sao Paulo, Brazil, E-mail: dblitzko@usp.br); New geoid models were calculated for Argentina under the umbrella of the SCGSA (Sub Commission for the Geoid in South America).

Preliminary models have been computed performing the numerical integration of the modified Stoke's formula with several resolutions (30'x30', 20'x20', 10'x10'). Recently, a new geoidal model was developed using FFT methods on a 10'x10' grid. All the models use the same local gravity data, topographic information and the EGM-96 geopotential model for the global field. Comparisons between all the calculated models and with GPS/levelling measurements are described in the paper.

**G3/W/46-A5** Poster **1610-92**

**THE IMPROVEMENT OF THE GEOID MODEL OF LITHUANIA**

Eimuntas PARSELIUNAS (Department of Geodesy and Cadastre, Vilnius Gediminas Technical University, Sauletekio al. 11, 2040 Vilnius, Lithuania, email: eimis@ap.vtu.lt); Rene Forsberg (National Survey and Cadastre, Rentemestervej 8, Copenhagen, Denmark, email: rf@dk)

The geoid model for Lithuania territory was calculated by the Geoid Determination Working Group of the Nordic Countries Geodetic Commission three times: in 1994, 1996 and 1998. The main efforts were directed for collecting the gravity data and for determination of the most reliable benchmarks set. Gravity data of the terrain, Baltic Sea and Kursiu lagoon, totally about 12000 points, and DTM with agrid of 1 km have been prepared. The average density of the gravity data is 1 point per 5 sq km. The sources of the gravity data were the gravimetric maps at the scale of 1:200000 and catalogues of the gravity points. The gravity data used are of the period of 1954-1974. Also the some data from the surrounding areas were involved, totally about 3000 points.

The accuracy of ellipsoidal heights ensures the Lithuanian GPS Network, which consists of zero, first and second order stations, totally 1078 points. The Zero Order GPS Network covering the territories of Estonia, Latvia and Lithuania was established in 1992, during the international EUREF BAL'92 GPS campaign. The First Order GPS Network was designed and observed in 1992-1993 by the Geodetic Institute, Vilnius Technical University. The Second Order GPS Network was measured and adjusted in 1994-1996 by Geodetic Institute as well. Density of Lithuanian National GPS Network is 1 station per 60 sq km. According to the software for the adjustment of the GPS networks the accuracy of the ellipsoidal heights of the stations of the state GPS network is 2-5 mm. But these parameters do not reflect the real co-ordinating accuracy. More realistic accuracy was calculated from the differences of the double co-ordinating. In this case the 20 mm accuracy of the ellipsoidal heights was determined. The GPS network was a base for the positioning the benchmarks of the first and second order levelling lines. Totally it was co-ordinated 120 benchmarks, from which 70 most reliable were chosen for the geoid fitting. The GRAVSOFTE software package was used for calculations. The geoid model of Lithuania fit at the 3 cm level was obtained.



**G3/L/13-A5** Poster **1610-93**

**A PRELIMINARY RESULTS OF WEST JAVA AND ITS SURROUNDINGS AREA GEOID DETERMINATION BASED ON GETECH'S GRAVITY DATABASE**

Kosasih PRIJATNA and J. Kahar (Department of Geodetic Engineering, Institute of Technology Bandung, Jl. Ganesa 10, Bandung, Indonesia, email : prijatna@gd.itb.ac.id)

The need of a detailed geoid in Indonesian region is mainly related to the increase of GPS heighting application. An existing formal gravimetric geoid of this region was derived in 1981 with a precision of about 4 meters. In this case, the subject of gravimetric geoid determination as derived earlier needs to be reconsidered.

Now a days, the gravity data covering Indonesian archipelago and its surroundings are available. Based on the so called South East Asia Gravity Project, GETECH (University of Leeds) processed and compiled all types of gravity data in the region into a unified data set. The GETECH's derived gravity product is in the form of 5'x5' grid of free-air, Bouguer, and isostatic anomalies. Recently, there is also new geopotential model available, i.e. EGM96.

This paper will present preliminary results of detailed gravimetric geoid determination in the Indonesian region by combining gravity data and geopotential model. In this case, the use of Molodenski's approach will be studied. Here, the area of West Java and its surroundings will be used as case study area. Several conclusions and recommendations will be made for future work.

**G3/E/39-A5** Poster **1610-94**

**A PRECISE GEOIDAL MODEL FOR SANTA FE (ARGENTINA)**

Rubén RODRÍGUEZ (Geomática Argentina S.A., Julio A. Roca 584, 1067 Buenos Aires, Argentina, E-mail: geomatic@server1.startel.com.ar); María Cristina Pacino (IFIR – UNR, Av. Pellegrini 250, 2000, Rosario, Argentina, E-mail: mpacino@fceia.unr.edu.ar)

Santa Fe province (Argentina) is located westwards the Paraná river, between 28° and 34° South latitudes and between 59° and 63° West longitudes. It has an area of 133.000 Km<sup>2</sup> and the altitudes range between 10 and 125 meters. Marcovich, Lebedinsky & Asociados, by contact with the Servicio de Catastro e Información Territorial (Cadastral office of Santa Fe Province) measured a precise geodetic net with 120 stations, 100 of which had orthometric heights values. With this data and the ellipsoidal height, we obtained the N value and then a geoidal chart was constructed for the province. The chart was compared with values from OSU 91A and EGM 96 geopotential models up to different grades. It was also compared with the 20'x20' geoidal model for Argentina and a -0.4 meters average deviation was obtained. Undulations differences (DN) were also calculated with respect to a fixed data point. The average deviation with respect to the referred models reach a few centimeters.

**G3/E/02-A5** Poster **1610-95**

**TOWARDS A BETTER GEOID MODEL FOR COLOMBIA**

Laura Sanchez, William MARTINEZ and Juan Florez. (Instituto Geografico Agustin Codazzi, Carrera 30 No. 48 51, Santafe de Bogota, Colombia. E-mail: lsanchez@igac.gov.co)

A new high-resolution geoid, GEOCOL99, has been computed for Colombia and its adjacent marine areas. The EGM96 geopotential model was combined with 10 x 10 mean gravity anomalies and 5 x 5 topographic grids. The remove-restore technique was used for the computation of terrain effects by Helmerts condensation reduction. The contribution of the local gravity data to the geoid was computed by using the FFT method.

Satellite altimetry derived geoid heights and marine gravity anomalies have been combined to determine a detailed gravity field over marine areas using spectral analysis.

The relative precision of the new Colombian geoid was also evaluated through error propagation analysis by FFT. Its values show that the new geoid achieves better agreement than GEOCOL98 with the GPS/leveling data.

**G3/E/08-A5** Poster **1610-96**

**DIFFERENT APPROACHES TO PRECISE QUASIGEOID MODELLING – CASE STUDY FOR THE CZECH REPUBLIC**

Jaroslav SIMEK (Research Institute of Geodesy, Topography and Cartography - Geodetic Observatory Pecny, 251 65 Ondrejov 244,CZ, email: gope@asu.cas.cz) Ivan Pesek (Czech Technical University, Faculty of Civil Engineering, Department of Advanced Geodesy, Thakurova 7, 160 00 Praha 6,CZ, email: pesek@fsv.cvut.cz)

After a detailed evaluation of terrestrial gravity anomalies coming from different sources, high resolution gravimetric quasigeoids (1'x1.5') are modelled on parts of EGM96 and EGG97 global/regional models for the territory of the Czech Republic using 1D spherical FFT. The results are further stepwise evaluated by other data types (GPS/levelling, vertical deflections) and after that these data are incorporated into least squares processing to produce a combined model based on heterogeneous data. In addition, the combined solution is compared with the model based on point masses.

**G3/W/19-A5** Poster **1610-97**

**GRAVIMETRIC GEOID FOR ARGENTINA USING FFT**

Claudia Tocho (Facultad de Ciencias Astronomicas y Geofisicas,UNLP, Argentina, email: ctocho@fcaglp.fcaglp.unlp.edu.ar); Graciela Font (Facultad de Ciencias Astronomicas y Geofisicas, UNLP, Argentina, email: graciela@fcaglp.fcaglp.unlp.edu.ar); Maria Cristina Pacino (Instituto de Física de Rosario, UNR, Argentina, email: mpacino@fceia.unr.edu.ar); Denizar Blitzkow (Escola Politecnica da Universidade de Sao Paulo, Brazil, email: dblitzko@usp.br)

A new gravimetric geoid has been computed for the whole Argentina,between the limits 22°S to about 55°S for latitudes and 55°W to 76°W for longitudes. The geoid was generated combining the EGM96 global geopotential model with a 10'x10' mean gravity anomaly grid and a 3'x 3' Digital Terrain Model for South America. Geoid undulations have been determined using the classical remove - restore technique. The contribution of the reduced gravity data to the geoid was computed by the spherical 1D - FFT technique, which allows the evaluation of the discrete spherical Stokes integral without any approximation, parallel to parallel. To demonstrate the performance of the gravimetric geoid, comparison between the undulations derived from gravimetric information and GPS points established on the geometric leveling network are presented.

**G3/W/40-A5** Poster **1610-98**

**IMPROVING OF REGIONAL GEOID MODELLING IN TAIWAN**

GWO-CHYANG TSUEI (Department of Civil Engineering, National I-LAN Institute of Technology, No. 1, Shen Lung Road, I-LAN 260, Taiwan, email: gctstuei@mail.ilanitech.edu.tw)

With the rapid expansion applications of GPS positioning and the improvement of positioning accuracy, there is a demanding need for an unified gravimetric geoid of high accuracy. We have seen in the past the necessity of a geoid with metre accuracy changed to a geoid in the cm level accuracy. Especially in the case of determining orthometric heights from GPS-derived ellipsoidal heights.

A new 3' X 3' high resolutions geoid model has been computed for the Taiwan area, using remove-restore technique by 1D Fast Fourier Transform method. The computations was carried out by using EGM96 geopotential model, 3' X 3' terrestrial gravity data, and 0.5' X 0.5' terrain model of Taiwan. The terrain effects on the geoid computation due to the second method of Helmert's condensation and residual terrain model were studied. And the effect of different topographic representations is investigated. Using the mass prism topographic model and the mass line topographic model. The differences between GPS/Levelling and gravimetric geoid undulations in Mean, RMS, Min, and Max. values are 4, 8, -12, 19 cm for Helmert geoid, and 7, 11, -12, 19 cm for RTM geoid. By fitting four parameter model to the geoid prediction, yield geoid fits of about 4 cm for both Helmert and RTM geoids. The relative accuracy achieved was of the order of 0.4 to 0.8 ppm for a mean baseline of 100 km.

**G4**

**Wednesday 21 July**

**GENERAL THEORY AND METHODOLOGY (IAG, SECTION 4)**

Location: Poynting Physics S06 LT

Location of Posters: Old Gym

**Wednesday 21 July AM**

Presiding Chair: P. Holota (Research Inst. of Geodesy, Topography and Cartography, Czech Republic)

**BUSINESS MEETING OF SECTION 4**

**Introduction**

**0830**

P. HOLOTA (Research Inst. of Geodesy, Topography and Cartography, Czech Republic)

The President of the section, the President of special commission 1 and the Chairman of individual special study groups (i.e. SSG4.168, 4.169, 4.170, 4.171, 4.176) will present their reports.

Presiding Chair: E.W. Graferend (Dept. of Geodesy and Geo Informatics, Stuttgart Univ.)

**G4/W/14-A3**

**1045**

**BIASES AND ACCURACY OF, AND AN ALTERNATIVE TO DISCRETE NONLINEAR FILTERS**

Peiliang XU (Disaster Prevention Research Institute, Kyoto University at Uji, Kyoto 611-0011, Japan, email: pxu@rcep.dpri.kyoto-u.ac.jp)

The purposes of this paper are to discuss the biases and accuracy of the extended Kalman filter (EKF) and a second order nonlinear filter (SONF) from the point of view of a frequentist, which are, otherwise, often derived by applying the relevant conditional quantities to the linear Kalman algorithm under the Bayesian framework. The EKF and the SONF are biased, though the SONF has been derived with hope to improve first order filters. Unfortunately, the biases of the SONF may be magnified further, because the second order terms of the relevant Bayesian conditional quantities have never been properly used to derive the SONF from the frequentist point of view. The variance-covariance matrix of the SONF given in the literature is proven to be incorrect up to the second order approximation, and the correct one is derived in this paper. Finally, also from the point of view of a frequentist, an alternative, almost unbiased SONF is proposed, if the randomness of partials is neglected.

**G4/E/10-A3**

**1105**

**A WAVELET APPROACH TO NON-STATIONARY COLLOCATION**

Wolfgang KELLER (Geodetic Institute, University Stuttgart, Geschwister-Scholl-Str. 24/D, 70174 Stuttgart, GERMANY, email: wolfgang.keller@gis.uni-stuttgart.de)

Collocation is based on the assumption of stationarity. Typical data types, as for instance gravity data, are not stationary: Due to the regionally varying measurement techniques the variance of the data is also regionally varying. The paper extends collocation to the non-stationary case. The resulting Wiener-Kolmogorov equations are not longer of convolution type. Since the data-noise variance is regionwise constant, the covariance functions can be modeled by wavelets. This leads to wavelet-Galerkin equations for the solution of the non-stationary Wiener-Kolmogorov equations. These equations can efficiently be solved by a preconditioning using the sparse structure of the Galerkin matrix.

**G4/W/06-A3**

**1125**

**CONVOLUTION OPERATORS IN GEODESY COMPUTED BY WAVELET TRANSFORM**

Battista BENCIOLETTI, Paolo Zatelli (Dpt. Ingegneria Civile e Ambientale, Università degli Studi di Trento Via Mesiano, 77, 38050 Trento, Italy, email: battista.benciolelli@ing.unitn.it, paolo.zatelli@ing.unitn.it)

Several convolution operators, including Stokes and terrain correction, are suitable for the application of numerical methods based on multiresolution techniques, namely the wavelet transform. This is related to the behaviour of the implied kernels that are smooth far from the origin (in fact the traditional partition into "inner zone effect" computed with a fine data grid and "far zone effect" computed with a coarse data grid is an ante-litteram multiresolution technique). We investigate both the implementation problem and the general performance of the evaluation of the operators, taking into account the special structure of the wavelet transform of convolution kernels.

**G4/W/11-A3 1145****A GENERAL LEAST-SQUARES SOLUTION OF THE GEODETIC BOUNDARY VALUE PROBLEM**

Martin VAN GELDEREN (Delft Institute for Earth-Oriented Space Research, Delft University of Technology, Thijsseweg 11, 2929 JA, Delft, The Netherlands, email: gelderen@geo.tudelft.nl); Reiner Rummel (Institut fuer Astronomische und Physikalische Geodaesie, Technische Universitaet Muenchen, Arcisstrasse 21, D-80333 Muenchen, Germany, email: rummel@iagp.step.verm.tu-muenchen.de)

The geodetic boundary value problem in the spherical, constant radius approximation can be easily formulated as a least-squares adjustment problem. Assuming a continuous and homogeneous data coverage closed expressions for the solution can be found for many combinations of observation types; all integral operators of Stokes' type. Under some restrictions, a general solution for arbitrary data types can be found. Specialisations to many common gbvps are also given with their solution both in the frequency and in the space domain. Weighting of the observations is possible as long as the weights are uniform in the entire domain.

**G4/W/03-A3 1205****A THEOREM OF INSENSITIVITY OF THE COLLOCATION SOLUTION TO VARIATIONS OF THE METRIC OF THE INTERPOLATION SPACE**

F. Sansó (DIAR, Politecnico di Milano, Facolta' di Como, p.le Gerbetto 6, 22100 Como, email: fsanso@ipmtf4.topo.polimi.it); C.C.Tcherning (Dep. of geophysics; University of Copenhagen, Julian Maries vej 30, Copenhagen, email: cct@gfy.ku.dk); G. VENUTI (DIAR, Politecnico di Milano, Facolta' di Como, p.le Gerbetto 6, 22100 Como, email: giove@ipmtf4.topo.polimi.it)

The collocation approach to the estimation of a field from observed functionals, is known, by examples and simulations, to display a not very strong dependence from the choice of the specific reproducing kernel-covariance function. In fact the situation is similar to the case of the dependence of least square parameters on the weight of observations. The paper, after recalling the basic theory according to the deterministic and stochastic interpretation, shows that the variation of the sought solution is infinitesimal with both, the variation of the metric of the interpolation space, going to zero, and the quantity of information carried by the observations on the specific functional of the field that we want to predict, going to 100%. The combined effect of the two gives an infinitesimal of the second order, namely a theorem of "insensitivity" of the solution to the metric of the interpolation space. Different simulations show the action of this particular effect.

**G4/W/20-A3 1225****BOUNDARY VALUE PROBLEMS FOR AN ELLIPSOIDAL BOUNDARY**

HECK Bernard (Geodetic Institute, University of Karlsruhe, Germany)

Boundary value problems for ellipsoidal surfaces result quite naturally from various set-ups of the Geodetic Boundary Value Problem (GBVP) by neglecting the topographic terms in the boundary conditions or by having continued the boundary data analytically from the earth's topographical surface to the chosen earth ellipsoid. The boundary operators resulting in this way from the fixed, scalar free and vectorial free versions of the GBVP are compared with other forms of the boundary conditions published in literature. Further alternatives of boundary conditions for ellipsoidal boundary value problems result from choosing different curvilinear coordinate systems. Thus, another comparison of boundary conditions refers to the choice of elliptical, geodetic and polar co-ordinates. The respective forms are derived up to second order terms in the flattening, presupposing a normal field of Somigliana-Pizzetti type. Finally, closed analytical solutions for first order approximations of the boundary conditions are developed, based on an ellipsoidal boundary.

**Wednesday 21 July PM**

Presiding Chairs: B. Heck (Geodetic Institute, Univ. of Karlsruhe, Germany), Ch. Jekeli (Dept. of Civ. and Env.Eng. and Geodetic Science, Ohio State Univ. Columbus, USA)

**G4/W/17-A3 1400****VERTICAL DEFLECTIONS, THE HORIZONTAL BOUNDARY VALUE PROBLEM AND THE COMPLETION OF THE MEISSL DIAGRAM**

Erik W. GRAFAREND (Geodetic Institute, Stuttgart University Geschwister-Scholl-Str. 24D, D-70174 Stuttgart, Germany, email: grafarend@gis.uni-stuttgart.de)

If vertical deflections are given on a geodetic reference figure, e.g. a sphere of reference, then as a linear horizontal operator (LHO) they define a special horizontal boundary value problem (hor BVP). The external hor BVP is solved in the space of vector-valued spherical harmonics. Special reference is made to G.G. Stokes (Transactions of the Cambridge Philosophical Society 8 (1849) 163-164, formulae (40), (41)). The solution of the external hor BVP completes the vertical Meissl diagram by its horizontal constituents. In particular, it can be used to relate vertical deflections in the space outside the geodetic reference figure, e.g. or (the level ellipsoid of revolution of Somigliana-Pizzetti type), with those vertical deflections on the geodetic reference figure. As an inverse first linear integral equation it solves by regularization the downward continuation of vertical deflections.

**G4/W/12-A3 1420****A COMBINED PANEL CLUSTERING AND FAST MULTIPOLE METHOD FOR THE SOLUTION OF THE SCALAR MOLODENSKY PROBLEM**

Martin VAN GELDEREN, Roland Klees (Delft Institute for Earth-Oriented Space Research, Faculty of Civil Engineering and Geosciences, Delft University of Technology, Thijsseweg 11, 2629 JA Delft, The Netherlands, e-mail: klees@geo.tudelft.nl)

When standard boundary element methods are used in order to solve the scalar Molodensky problem we have to deal with large dense linear systems of equations. We propose a combination of panel clustering and fast multi-pole method, which allow to set up and solve the linear system of equations in a number of operations that grows almost proportional to the number of unknowns. The method is based on an approximation of the kernel function of the integral operator by a degenerate kernel in the farfield, which is provided by a multipole expansion of the kernel function. We present numerical results for the scalar Molodensky problem, which is the basis of today's global gravity field solutions. Moreover, we compare the solution with classical boundary element methods, which proves the superiority of our approach.

**G4/E/16-A3 1440****NUMERICAL REALIZATION OF THE NEW ITERATION PROCEDURE FOR RECOVERING THE POTENTIAL SPHERICAL HARMONIC COEFFICIENTS**

Margarita PETROVSKAYA and Andrey Vershkov (both at Main Astronomical Observatory of Russian Academy of Sciences, Pulkovskoe Shosse 65, Pulkovo, St. Petersburg, 196140, Russia, email: petrovsk@gao.spb.ru) Nikolaos K. Pavlis (Raytheon STX Corporation, 7701 Greenbelt Road Suite 400, Greenbelt, MD 20770, USA, email: npavlis@geodesy2.gsfc.nasa.gov)

The application of the standard iteration procedure for recovering the spherical harmonic coefficients  $C_{nm}$  of the earth's potential (used in particular by Pellinen, Rapp and Cruz, Petrovskaya) reveals the "exotic" behavior of the found  $C_{nm}$ , as a consequence of the unbounded increment of the iteration coefficients with increasing the degree  $n$ . The new iteration procedure recently proposed by Petrovskaya is more appropriate for evaluating high degree potential coefficients. In the present paper this procedure is numerically realized for recovering  $C_{nm}$  on the base of the global gravity data which were used for constructing EGM96 geopotential model. The results of computations of the potential coefficients by means of both the old and new iteration procedures are presented in figures and tables. Their comparative characteristics and the asymptotic behavior of  $C_{nm}$  with growing  $n$  are studied.

**G4/W/02-A3 1500****ON THE DETERMINATION OF SCALE EXPONENTS IN ENERGY SPECTRA AND STRUCTURE FUNCTIONS WITH WAVELETS AND THEIR APPLICATION TO CCD-CAMERA DATA**

Stefan BETH, Willi Freeden (Geomathematics Group, University of Kaiserslautern, P.O. Box 3049, D-67653 Kaiserslautern, GER, email: beth@mathematik.uni-kl.de); Norbert Casott, Dierk Deussen, Bertold Witte (Geodetic Institute, University of Bonn, Nussallee 17, D-53115 Bonn, GER)

Wavelets are selfsimilar functions, more explicitly, the dilated and translated versions look similar to corresponding mother wavelet. Hence they can be used to characterise the fractal and multifractal properties of functions in terms of scaling exponents in structure functions and energy spectra. In general, the determination of scaling exponents requires a sufficient number of realizations of an experiment under the same conditions. Often this is not possible such that stationarity and ergodicity are assumed. Stationarity allows the time series analysis of single points and ergodicity causes independence of the direction and place. Under these conditions the energy spectra of a time series is easily constructed by the Fourier transform, which in general does not lead to a smooth result, but to a mean variation around the expected scaling behaviour. Therefore filter techniques are applied to smooth the characteristic regions of the spectra. In recent years it could be shown that the same effect can be gained by a wavelet based energy spectra. In particular, the computation can be summarized to one working step. In the same way it was proven that wavelet based structure functions of positive order behave like structure functions of positive order as usually defined via differences. Moreover, the wavelet based structure functions can also be defined for negative orders, which supplements the multifractal theory. For both methods a good coincidence is proven for the application on wind velocity data and in addition the problem of the evaluation of CCD-Camera data concerning refraction effects in the surface layer.

**G4/W/19-A3 1520****HARMONIC SPHERICAL SPLINES WITH LOCALLY SUPPORTED KERNELS**

Guilhem MOREAUX (University of Copenhagen, Department of Geophysics, Juliane Maries Vej 30, 2100 Copenhagen O, Denmark, email: gm@gfy.ku.dk)

Harmonic spherical spline is a very flexible method in gravity field modelling, which permits the use of data of different kinds and with different noise-characteristics. The method has however the drawback that one needs to solve a symmetric positive definite (SPD) system which (1) involves as many equations as the number of data and parameters (2) is full due to the harmonicity of the reproducing kernels. Therefore, for large data sets, both direct and iterative methods give heavy computation burden. Meanwhile, because for a great number of harmonic kernels there exists angles of separation beyond which the kernel values, i.e. the matrix entries, are negligible small, Moreaux and al. (1998) proposed three techniques to approximate any harmonic kernel on the sphere by locally supported strictly positive definite functions in order to get sparse SPD approximations of the full SPD matrices. In this talk, we apply the first technique developed in Moreaux and al. (1998) to gravity field modelling in both cases of differentiation (gravity gradients from gravity) and integration (geoid and gravity from gravity gradients) and compare the results with the ones obtained by the full kernels. After that, some numerical results about the use of these sparse matrices as preconditioners of the full systems for the conjugate gradient method are given. Moreaux G, Tscherning CC, Sanso F (1998) Approximation of harmonic covariance functions on the sphere by non harmonic locally supported ones. Submitted to J Geod.

**G4/E/18-A3 1540****IMPROVED ANALYTICAL APPROXIMATIONS OF THE EARTH'S POTENTIAL FIELDS**

V.N. Strakhov (United Institute of Physics of the Earth, Russ. Acad. of Sciences, Moscow, Russia); U. SCHAEFFER (Bundesamt fuer Kartographie und Geodaesie, Aussenstelle Potsdam, Michendorfer Chaussee 23, 14473 Potsdam, Germany, email: ufer@gpotsdam.ifag.de); A.V. Strakhov (Computing Center of the Russ. Acad. of Sciences, Moscow, Russia)

One of the burning problems in gravimetry and magnetics is to derive linear analytical models of the Earth's potential anomaly fields with high spatial resolution that are consistent with the observations of various potential field elements at the Earth's surface and in outer space. For modelling the anomalous potential on a global, regional or local scale it is meaningful to apply linear approximations since they allow to find other field elements (e.g. higher derivatives) by means of elementary operations. From a methodological point of view it is essential to make direct use of observations at the physical surface of the Earth and/or from outer space without any reductions to a certain reference surface. In that case the problem to find out linear analytical approximations may be reduced to the problem of solving huge systems of linear algebraic equations. The matrix of the respective equation system is full and the number of unknowns may reach the order of  $10^7$  to  $10^8$ . These equation systems can be generated by means of three main approaches: 1) simply equating the analytical approximations with the observed data; 2) using the least square method (in the frame of given base functions, e.g. spherical or spheroidal functions); 3) using linear integral representations and variational principles (generalized Backus-Gilbert method). In the first approach one normally get systems with rectangular matrices with  $N>M$  for global and  $N<M$  for regional and local approximations ( $N$  equations;  $M$  unknowns). For the second and third approach one obtains systems with symmetric positive semi-definite matrices. We present main constructional ideas ensuring to receive stable solutions of the problem. One of them is perfectly new in numerical linear algebra: to reduce huge systems to 1 equation with 1 unknown.

Presiding Chairs: B. Heck (Geodetic Institute, Univ. of Karlsruhe, Germany),  
Ch. Jekeli (Dept. of Civil and Environmental Eng. and Geodetic Science,  
Ohio State Univ. Columbus, USA)

**Introduction 1600**

P. HOLOTA (Research Institute of Geodesy, Topography and Cartography, ZDIBY, PRAHA)

**G4/W/21-A3 Poster 1620-01**

**THE IMPACT OF UNCERTAINTIES OF THE STOCHASTIC MODEL ON THE RESULTS OF LEAST SQUARES ADJUSTMENTS**

Hansjoerg KUTTERER (Geodetic Institute, University of Karlsruhe, Germany)

In common adjustment problems both the functional and the stochastic model are considered to be free of errors. If the adjustment results have to be interpreted in a wider context, the development of a proper perturbation theory for the mathematical model and the quantities derived by means of least squares adjustments is indispensable. The paper studies the impact of uncertainties of the stochastic model on some characteristic results of least squares adjustments like the estimated values of the parameters and their variance-covariance matrix. Linearizations are used regarding rigorous error bound. To efficiently treat the uncertainty aspect, interval mathematics proves to be a useful tool.

**G4/E/13-A3 Poster 1620-02**

**OPTIMAL DESIGN OF THE REFERENCE AND OBSERVATIONS WEIGHTS IN GEODETIC NETWORKS FROM CRITERION MATRIX**

Jose Luis VACAFLOR (Instituto de Geodesia, Facultad de Ciencias Exactas y Tecnologia, Universidad Nacional de Tucuman, Avenida Independencia 1800, (4000) San Miguel de Tucuman, Argentina, email: vacaflor@arnet.com.ar)

An efficient strategy based in the least square solution (LESS) of the Gauss-Markov model (GMM), is developed in order to find the optimal Datum definition - by means of an appropriate set of constraints - of a geodetic network, in such way that: any improvement in the weights of the observations will produce a Dispersion Matrix of the estimated parameters close to the given Criterion Matrix. Finally, a geodetic network is processed in detail as a numerical example.

**G4/E/09-A3 Poster 1620-03**

**THE EFFICIENCY OF OPTIMIZED WEIGHTS FROM CRITERION MATRICES**

Nardo Geronimo Lopez Ferneti, Jose Luis VACAFLOR (both at Instituto de Geodesia, Facultad de Ciencias Exactas y Tecnologia, Universidad Nacional de Tucuman, Avenida Independencia 1800, (4000) San Miguel de Tucuman, Argentina, email: geosupe@herrera.unt.edu.ar, vacaflor@arnet.com.ar)

Once the Datum, the configuration of the geodetic net together with its criterion matrix is decided, then: taking into account the characteristics of the available instruments for measurements and the alternative ways for conformation of a stochastic model, we endeavor to obtain a real solution which matches as closely as possible to the previous one, proving the potentiality of the notion of "sensitivity". The theoretical concepts and the designed methodology are shown in detail on a geodetic network.

**G4/W/16-A3 Poster 1620-04**

**SEPARABILITY OF LINEAR MODELS AND ITS APPLICATIONS IN GEODESY**

Jinling WANG (School of Spatial Sciences, Curtin University of Technology, GPO Box, U1987, Perth, WA 6845, Australia, email: Wang@vesta.curtin.edu.au)

Geodesists, like other scientists, are sometimes confronted with the problem of selecting one best model from two or more competing linear models. For example, in GPS and GLONASS carrier phase integer ambiguity resolution, the identification of the most likely integer ambiguity combination from numerous potential combinations can be considered as a process of model selection. In practice, the model selection is commonly performed using a search criterion based on the minimisation of the quadratic form of the least squares residuals. Intuitively, the best model is associated with the minimum quadratic form. Before the best model is employed in data processing, however, it is important to test whether or not the best model is statistically better than the second best model as defined by the second minimum quadratic form of the residuals. To this end, rigorous statistical tests have recently been developed, called model discrimination tests. Like other statistical tests, the power of the model discrimination tests depends on the significance level used in the tests, the stochastic model of observations and the geometry of compared models. Following Baarda's reliability theory, separability of compared linear models is introduced. Applications of the concept of separability in GPS/GLONASS ambiguity resolution and the outlier detection and identification will be presented to determine a derived flood frequency curve.

**G4/W/01-A3 Poster 1620-05**

**ROBUST ESTIMATORS FOR NETWORK ADJUSTMENT**

Entela KANANI, Alessandro CAROSIO (both at Institute of Geodesy and Photogrammetry, Swiss Federal Institute of Technology, CH-8093 Zurich, Switzerland, email: kanani@geod.ethz.ch); Fridolin Wicki (Vermessungsamt der Kanton Aargau, Frey-Herossestrasse 12, CH-5000 Aarau, Switzerland, email: fridolin.wicki@ag.ch)

Most parameters in geodesy are determined by statistical estimator procedures. The method most commonly employed is that of Least Squares - an optimal estimator for normal distributed measurements. In practical evaluation, however, there often occur many observations which do not conform to the expected normal distribution. The classical compensation method of Least Squares is extremely sensitive and quickly leads to unusable results when significant deviations from the normal distribution are present. Robust estimators are currently of considerable interest therefore, and our research is directed at establishing and developing new procedures based on robust estimators for geodetic applications such as: compensation of geodetic networks and linear geodetic transformations. An optimal estimator which bounds the influence of standardised residuals has been developed for the evaluation of geodetic networks. The chosen estimator is a Maximum Likelihood-estimator of Schweppe-type and has an objective function similar to the Least Square Method. When no outliers are present (normal distributed measurements) this estimator gives the same results as the method of Least Squares, when this is not the case, the algorithm limits the influence of the standardised residuals (instead of the residuals as in P. Huber estimator, for example). This has the effect of providing an upper limit to the influence of a spurious observation (e.g. an gross error) on the unknown parameters also in cases of small redundancy (leverage points). The limiting value is determined by the standard deviation of a residual multiplying a constant

c. Furthermore, our attention has been directed towards high breakdown estimators and their implementation for the determination of unknown parameters in the linear geodetic transformations. Although this group of estimators is generally associated with a large amount of calculation time, their implementation for the analysis of deformation measurements can be of considerable value. The number of parameters to be estimated in a linear transformation is limited (4, 6, 7 and so on), which restricts the calculation time to manageable proportions. A high breakdown estimator (Least Median of Squares) has been investigated further. The results have shown that inserting a robust estimator...

**G4/P/04-A3 Poster 1620-06**

**THE LP ESTIMATION OF THE SCALE PARAMETER AND THE ACCURACY EVALUATION**

Shinjian ZHOU (Dept. of Surveying Engineering, East China Institute of Geology, Linchuan City, Jiangxi Province, China, email: zsj@ecgi.jx.cn)

Abstract not available at time of going to press.

**G4/P/05-A3 Poster 1620-07**

**THE UNIQUENESS AND UNBIASEDNESS OF THE LP ESTIMATION**

Shijian ZHOU, Deyan Zang (Dept. of Surveying Engineering, East China Institute of Geology, Linchuan City, Jiangxi Province, P.R. of China, email: zsj@ecgi.jx.cn); Yongqi Chen and Conrad Tang (Dept. of Land Surveying and Geo- Informatics, The Hong Kong Polytechnic University, Hong Kong, email: yqchen@polyu.edu.hk)

It is well known that the LP estimation can be applied in the processing of the observational data with the outliers distributed, but the statistical properties of the Lp have less discussed, thus it's not convenient to employ for us. This paper aimed at this problem, the uniqueness of the Lp estimation has first obtained when  $p > 1$  and the error distribution is symmetrical population. Basing on a symmetrical and the objective function is an even function, the robust estimation is an unbiased estimation that has first been proved if it is calculated by iterative weight Least Squares with an antisymmetrical estimation as starting points, so that the Least absolute Sum has also unbiasedness as a special case of the robust estimation. The results ensure that the Lp estimation has the optimal statistical properties also and can be employed widely.

**G4/P/07-A3 Poster 1620-08**

**BIASED ESTIMATION FOR PARAMETER ADJUSTMENT WITH CONSTRAINTS**

Gui QINGMING, Zhang Jianjun (both at Zhengzhou Institute of Surveying and Mapping, No.66 Longhai Road, Zhengzhou 450052, Henan, P.R. China)

The parameter estimation problem in parameter adjustment model with constraints is considered when some multicollinearities occur among the columns of the design matrix. We propose a class of restricted biased estimators by grafting the unrestricted biased estimation philosophy into the restricted least squares (RLS) estimator, and establish some important statistical properties. Many well known unrestricted biased estimators (e.g. shrinkage least squares estimator, ridge estimator, principal component estimator etc.) are extended to parameter adjustment model with constraints. A numerical example is presented to illustrate that these restricted biased estimators are superior to the RLS estimator in sense of the reduced MSE.

**G4/E/05-A3 Poster 1620-09**

**RELIABILITY OF GPS OBSERVATIONS USING A WEIGHTED IONOSPHERE**

Kees DE JONG (Delft University of Technology, Department of Mathematical Geodesy and Positioning, Thijsseweg 11, 2629 JA Delft, The Netherlands, e-mail: k.dejong@geo.tudelft.nl)

The theory and application of statistical quality control is well-established in surveying and geodesy. Internal reliability, as represented by the Minimal Detectable Bias (MDB), describes the size of biases (model errors) that can just be detected using appropriate test statistics. For GPS these biases are assumed to consist of outliers in the pseudo range and (integer) cycle slips in the carrier observations. The MDBs can be computed without actual data. Therefore, MDBs provide an important design tool when setting up a GPS measurement scenario. Recently, analytic expressions for the MDBs of GPS pseudo range and carrier single-difference observations were derived and published. These expressions, however, apply to short baselines only, i.e., baselines for which the ionospheric effects at both ends are fully correlated. For longer baselines, residual ionospheric effects should be taken into account. In the research described here general analytic expressions have been derived using an ionospheric variance matrix, which allow for a weighting of the ionosphere. The presented expressions differ depending on the observation scenario considered (static receivers, one static and one moving receiver, both receivers moving).

**G4/E/12-A3 Poster 1620-10**

**A COMBINED ADJUSTMENT OF ASTRO-GEODETIC NETWORK AND GPS GEODETIC NETWORK IN CHINA**

Ziqing WEI (Xian Research Institute of Surveying and Mapping, 1 Yanta mid-road, Xian, Shaanxi 710054, P.R.China, email: ziqingw@public.xa.sn.cn)

A combined adjustment of the whole astro-geodetic network and the nation-wide first-order GPS geodetic network was carried out in China in recent years, which embraces 48,519 astro-geodetic points and 40 first-order GPS points evenly distributed over the entire country and involves 311,986 directions, 467 taped or EDM distances and extension sides, 1,693 traverse sides, and 942 Laplace azimuths. The adjustment was undertaken on the reference ellipsoid in the geocentric datum, whose origin, orientation and scale are totally defined by three-dimensional coordinates of GPS points referred to the ITRF91. The results show that, on the average, the standard errors for the length and bearings are 4.0 ppm and 0.59" respectively for 10-20 km sides, and 1.48 ppm and 0.31" respectively for 21-35 km sides. The absolute accuracy of horizontal coordinates of a point relative to the defined datum is at the submetre level. Hence, as a consequence of adjustment, the accuracy and homogeneity of the astro-geodetic network has been significantly improved; the regional geocentric coordinate system has been established with 1m accuracy.



**G4/E/02-A3** Poster **1620-11****RESEARCH ON THE COMBINATION OF LOCAL GPS AND TERRESTRIAL OBSERVATIONS**

Zha MING, Ouyang Guichong (Xi'an Technical Division of Surveying and Mapping, 36 Xiyinglu, Xi'an, Shaanxi 710054, P.R.China)

With the development of GPS and traditional surveying techniques, the combined use of GPS and traditional surveying techniques might be the optimal choice in many cases. Because GPS surveying yields three-dimensional vectors, the three-dimensional geodetic model is the most natural model to be used. This paper proposes the method of combined three-dimensional adjustment of local GPS and terrestrial observations. Deflection components of the vertical are used to make up for the lack of astronomic latitudes and longitudes, the first-order atmospheric vertical refraction effect is deleted by using the vertical angles at each end of the line. It is preferable that the coordinates of GPS stations are introduced into the adjustment as weighted parameters reflecting the accuracy of the GPS geodetic network. Based on the model, the three-dimensional adjustment software CPSTGD has been developed. According to combined adjustment results of several local GPS and terrestrial networks, it has been shown that the method is theoretically perfect and practically effective.

**G4/W/07-A3** Poster **1620-12****ON THE LOCATION OF ABNORMAL DATA IN MARINE SURVEYING**

Huang Motaoy, Zhai Guojun, Wang Rui Ouyang Yongzhong, Guan ZHENG (all at Tianjin Institute of Hydrographic Surveying and Charting, Tianjin, 300061, China, email: nvsurvey@public.tjuc.com.cn )

Based on an analysis of the characteristic of marine surveying, two robust methods for detecting the abnormal data in marine measurements are proposed in this paper. One is called the statistical hypothesis test based on sample quantile. The other is called the interpolation comparison test based on robust M-estimation by iterative weight determination. Some questions involved in the implement of the suggested methods are discussed in detail. Compared to the existing methods, the two new methods have more strong capacity of locating abnormal data. A synthetic study and an actual numerical example for multibeam soundings are given to test the performance of the methods. The results have illustrated the effectiveness of the methods in the detection and identification of multiple blunders. The use of the new methods will play an important role in improving the quality and reliability of marine measurements in our country.

**G4/E/17-A3** Poster **1620-13****REGIONAL GRAVITY FIELD RECOVERY FROM FUTURE SATELLITE MISSIONS USING MULTI-SCALE APPROXIMATION**

Juergen KUSCHE, Stephan Rudolph (Institute of Theoretical Geodesy, University of Bonn, Nussallee 17, 53115 Bonn, Germany, email: kusche@uni-bonn.de)

The task of the envisaged SST/SGG-missions like CHAMP, SAGE, GRACE, and GOCE is the computation of a global gravitational field with high resolution and precision and - if possible - with repetition in time. Global approaches are aimed at the recovery of spherical harmonic coefficients. The spherical harmonics provide a "natural" multiresolution of the field, but they do not possess any localising properties in space. Therefore it is not possible to focus the analysis of satellite mission data to regions of special interest, i.e. for the study of time-dependent phenomena. On the other hand, regional approaches have been developed to recover gravity anomalies or point masses. They provide good space-localization, but lack in scale decomposition properties. This means, phenomena on different length scales are not clearly separable. To overcome these difficulties, wavelet and filtering techniques have been proposed recently. In our study, wavelet and filtered copies of base functions are combined to form a multi-scale version of the classical approximation in a Hilbert space. A rigorous theoretical analysis is performed. Special emphasis is laid on the topic of regularisation, which is always a crucial point in regional approaches. Next, parameter choice strategies for "designing" a suitable base function system are considered. Finally a two-scale approximation scheme is constructed suitable to a low-low SST gravity field mission and a simulation experiment using GRACE mission parameters is performed. First results are encouraging.

**G4/E/11-A3** Poster **1620-14****THE USE OF WAVELETS FOR THE ANALYSIS AND DE-NOISING OF KINEMATIC GEODETIC MEASUREMENTS**

A.M. BRUTON, J. Skaloud, K.P. Schwarz (Department of Geomatics Engineering, The University of Calgary, 2500 University Drive, N.W. Calgary, Alberta, Canada T2N 1N4)

The objective of this paper is to discuss and demonstrate the use of wavelets for improving the performance of geodetic measurement systems. More specifically, wavelets are used as a tool for analyzing and de-noising the errors that are inherent in such systems. Because the Wavelet Transform provides a time-scale representation of a signal, it offers the ability to both analyse the error characteristics of a system at different resolutions and to localize them in time. These features are the key components used for analysing and de-noising the measurements in kinematic geodetic systems.

Examples are drawn from research projects being carried out at the University of Calgary. These use real data and include discussions of GPS and INS measurement systems. Issues such as practical implementation, observed error characteristics (under varying vehicle dynamics) and accuracy improvements are treated. First results indicate that these tools can be used to significantly improve the performance of a navigation grade INS. In this case, it is observed that the noise is self-similar over several decades of frequencies (i.e. has the same characteristics in more than one frequency band). A model for the noise is developed using a frequency band in which vehicle dynamics are not present and then used to de-noise the bands that do contain dynamics. This results in an improvement of 20% over traditional techniques.

**G4/E/15-A3** Poster **1620-15****WAVELET ANALYSIS OF SSH DERIVED FROM ERS-2 ALTIMETER DATA NEAR CHINA SEA**

Hanjiang WEN, H.Suenkel (Institute of Theoretical Geodesy, Steyrergasse 30, TU-Graz, A-8010 Graz, Austria)

A small area near China sea was used to study the sea surface height derived from ERS-2 altimeter data. Firstly, continuous wavelet transform was used to get the scalogram of SSH along satellite ground tracks about 4000km in length, from which one can see that the energy of SSH is mainly concentrated on the wavelength between 1000km and 1200km. Secondly, the orthogonal discrete wavelet transform was applied to get the multiresolution analysis of SSH, from which, the information contained in SSH was divided into different parts with

respect to different scales, variations of the information between successive scales can be seen. We also got the wavelet variances at different scales of the SSH.

**G4/P/03-A3** Poster **1620-16****THE WAVELET ARITHMETICS OF THE G1 -TERM IN MOLODENSKY'S BOUNDARY VALUE PROBLEM**

Yu JINHAI, Peng Fuqing (both in Institute of Zhengzhou Measuring and Mapping, 450052, Zhengzhou, Henan, P.R. China)

Molodensky's boundary value problem cannot be directly used in actual works because of the complexity in computing singular integrals, although Molodensky, Brovar, Moritz, Holota and many other scholars have made great contributions to it. In this paper, following the Brovar's series solution, we strictly prove the existence of strongly singular integral G1 - term in the sense of Cauchy principal value at first, and then discuss its arithmetics with help of wavelet method where a compact scaling function is chosen. The obtained results illustrate that the key step lies in resolutions of the kernel function, which are independent on the terrains and the gravity anomaly and can be computed in advance. The computation results in an area of 20km x 20km with step length 200m also illustrate that the wavelet arithmetics are much superior to FFT which only fits to convolution integral. Particularly, the obtained wavelet arithmetics satisfy the requirements in large scale computation of singular integrals in physical geodesy.

**G4/P/02-A3** Poster **1620-17****APPLICATION OF THE WAVELET TRANSFORM FOR CLOCK BREAKS DETECTION IN THE VLBI OBSERVATIONS**

TAIBI H., Ghezali B., Kahlouche S. (Geodetic Laboratory, National Centre of Spatial Techniques, BP 13 ARZEW, 31200, Algeria)

The method of clock breaks detection developed in the National Centre of Spatial Techniques is based on the concept of multi-resolutions (time - frequency) using wavelet analysis. The object of this method is to identify the clock breaks which are translated into great coefficients with high frequency of the associated wavelet. The used observations in the processing are constituted by an IRIS-A program session including 518 observations and comprising three primary stations and a secondary (mobile) station.

In the processing of the VLBI data, the behaviour of each clock is a linear model, consequently the residues after adjustment of parameters have to be randomly distributed around a straight line. The deviations between the clocks can be determined only if one of the clocks (the most stable) is chosen as a reference. The signal to analyse is represented by a cloud of points constituting the residues of VLBI observation as a function of time.

The detection criterion of the clock breaks rests on the analysis of the residues regularity : the clock break, which is a systematisme, is translated by the presence of a very great coefficient with high frequency of the associated wavelet. In the regions where the signal is very regular, the coefficients of the associated wavelet of high frequencies are very small while an abrupt discontinuity of the signal makes "explode" the coefficient of the associated wavelet. The results obtained with this method are identical to these obtained by the manual method.

**G4/W/22-A3** **1620-18****THE GEOID TAKING THE FLATTENING OF THE ELLIPSOID INTO ACCOUNT**

Z.L. Fei, M.G. SIDERIS (Department of Geomatics Engineering, University of Calgary, 2500 University Drive NW, Calgary, Alberta, Canada, T2N 1N4, email: sideris@ucalgary.ca)

Geoid undulations are typically being computed by Stokes's formula. They can be called spherical undulations because the flattening of the ellipsoid is neglected in the computation. We are proposing a new method for computing the ellipsoidal geoid, which consists of two parts: the Stokes solution No (spherical geoid undulation) and the ellipsoidal correction N1. The ellipsoidal correction N1 is expressed as a sum of two closed integral formulas, integrating gravity anomaly data  $\gamma_g$  and spherical geoidal undulation data No. The kernel functions have the same degree of singularity at the origin as the original Stokes function. The relative geoidal undulation error is  $O(e^4)$ , which can be neglected for most practical purposes.

This method is especially suited for the computation of ellipsoidal corrections in areas where spherical geoid undulations are available. It avoids some of the approximations employed in other methods available in the geodetic literature and it also uses simpler integration kernels. In this paper, besides the theoretical equations, we give a numerical computation of N1 in some areas in Canada where we have both gravity anomaly data  $\gamma_g$  and spherical geoidal undulation data No.

**G4/E/21-A3** Poster **1620-19****SIMPLIFICATION OF TRANSFORMATIONS BETWEEN THE ELLIPSOIDAL AND SPHERICAL SPECTRA OF THE GEOPOTENTIAL**

Margarita PETROVSKAYA (Main Astronomical Observatory of Russian Academy of Sciences, Pulkovskoe Shosse 65, Pulkovo, St. Petersburg, 196140, Russia, email: petrovsk@gao.spb.ru)

When constructing the geopotential models OSU91 and EGM96 Jekeli's ellipsoidal harmonic approach was successfully applied for recovering the spherical harmonic potential coefficients  $C_{snm}$  from the surface gravity anomaly. In the present paper the transformation formulas between  $C_{snm}$  and the ellipsoidal harmonic potential coefficients  $C_{enm}$ , derived from gravity data at the ellipsoid surface, are modified. The original relations between them contain hypergeometric series which converge very slowly for large values of n and m. Now such a series is transformed to a product of simple binomial factors, depending on the ellipsoid eccentricity, and a very quickly convergent hypergeometric series. As a result, the numerical procedures for evaluating the coefficients  $C_{snm}$  from  $C_{enm}$  will be essentially simplified while constructing the earth's potential models. The above transformations are also used for deriving a boundary relation which connects  $C_{enm}$ , expressed in terms of  $C_{snm}$ , and the gravity anomaly at the ellipsoid surface. It will allow to apply the least squares collocation procedure in a simultaneous treatment of satellite and gravity data at the ellipsoidal harmonic approach.

**G4/E/23-A3** Poster **1620-20****FUZZY SET THEORY AND GEOSPATIAL DATA MANAGEMENT: A FOCUS ON BOUNDARY VALUE PROBLEM**

E.A. SHYLLON, J.B. Olaleye, V.O.S. Olunloyo (Geoinformatics Laboratory, Faculty of Engineering, University of Lagos, Lagos, Nigeria)

To deal with unmanageable complexity of Geospatial data at all levels, Geospatial data Managers resorted to the use of statistical averages and probability theory. In spite of its wide

usage, the probability theory is not capable of capturing uncertainty in boundary values (data element "which is" or "which is not" within).

Fuzzy set theory exploits the tolerance for uncertainty, imprecision and partial truth of various types to achieve tractability, low solution cost and better rapport with reality. It provides a strict mathematical environment in which vague conceptual phenomena are rigorously studied. The membership grade functions of the fuzzy subsets are constructed to define the boundary values. This is an interval between [0,1]. It is easy to formulate for soft computing. The primary aim of this paper is to explain and develop computational methods that produce acceptable solution to boundary value problem.

**G4/W/08-A3** Poster **1620-21**

**SPECTRAL DECOMPOSITION OF THE GRAVITY ACCELERATION VECTOR AND GRAVITY GRADIENT TENSOR**

Gilles METRIS (CERGA, Observatoire de la Côte d'Azur, Av. N. Copernic, 06130 Grasse, France, email: metris@obs-azur.fr)

In satellite geodesy, many measurements (e.g. satellite altitude, radial velocity, components of the gradient of acceleration) have more simple expressions in the satellite orbital frame. This has motivated a large effort in the last years to (1) derive the expressions of the variations of position, velocity, acceleration, gradient of acceleration due to the gravity potential, in that frame, and (2) to compute their spectral decomposition using simplified theories of satellite motion. This is used to efficiently analyze the expected performances of satellite to satellite tracking or satellite gravity gradiometry missions.

We propose an alternative method to obtain the spectral decomposition, in the orbital frame, of the gravity acceleration vector and gravity gradient tensor components. We use the relation between spherical harmonics and rectangular coordinates to directly (i.e. without derivatives with respect to spherical coordinates) express the successive derivatives of the gravity potential with respect to body fixed rectangular coordinates. Then, the classical rules of tensor transformation by rotations are applied to convert the components into the orbital frame. Finally, we use a Kaula like development to express these components as functions of orbital elements. They are decomposed in sums of periodic functions using a linear theory of the satellite motion. We have used this new method in the study of the French space mission MICROSCOPE, which aims at testing the equivalence principle by means of accelerometric measurements.

**G4/P/01-A3** Poster **1620-22**

**THE SENSITIVITY OF THE REDUCED DYNAMICS TO THE EARTH'S GRAVITY MODEL IN THE ORBITOGRAPHY OF LEO SATELLITES WITH GPS: THE POSAT - 1 CASE STUDY**

Isabel OSÓRIO, J. Pereira Osório (both at Faculty of Sciences, University of Porto, Monte da Virgem, 4430 Vila Nova de Gaia, Portugal, email: iposorio@oa.fc.up.pt, posorio@oa.fc.up.pt); J.M. Rebordão (INETI / LAER - Aerospace Laboratory, Estrada do Paço do Lumiar, 1699 Lisboa Codex, Portugal, email: jmr@laerineti.pt)

Codephases and Doppler measurements from a TRIMBLE TANS II receiver are available on board of the Portuguese micro-satellite PoSAT - 1. Due to the big amount of geometrical information contained in the GPS measurements and, also, due to the cadency of these observations (0.5s) a reduced dynamical model is used as the satellite orbit propagator in a Kalman filter, where the observations are the codephases smoothed by Doppler measurements.

As PoSAT -1 is a polar LEO satellite, at an altitude of 710 km, the effect on its orbit of the nonspherical gravity field has a meaningful value. There are not any specific gravity field model advised for this satellite. So, in this work, different Earth gravity models were used and the differences in the positions were plotted. The state variables used to describe the satellite motion are modified Poincaré variables. Indeed these variables are a quasi-canonical set of variables and, by this reason, a semi-analytical process for the orbit propagation was used. In this paper the algorithms developed are described and the results are presented.

**G4/W/15-A3** Poster **1620-23**

**AERODYNAMIC FORCE ENHANCEMENTS FOR THE ERS SATELLITES**

P. MOORE, S. Carnochan, R.J. Walmsley (Aston Geodesy Group, Division of Civil Engineering, Aston University, Birmingham, B4 7ET, UK, email: moorep@aston.ac.uk)

Accuracy of orbit determinations for altimetric satellites such as ERS-1 are now approaching that achieved for the higher satellite TOPEX/Poseidon. Much of this improvement is due to gravity field enhancement specific to the ERS orbit. For example ERS-1 crossover rms residuals of 8.9cm, 8.4cm and 7.6cm have been obtained for the first multidisciplinary, geodetic and second multidisciplinary phases respectively. These are close to the 7cm obtained with TOPEX. However, the ERS-1 residuals reflect the decrease in solar activity from 1993-6 and thus reveal imperfections in the underlying thermospheric model. In this study we propose a methodology for enhancing the DTM94 thermospheric model through ERS-1 along track accelerations. Comparisons of the original and enhanced models will be presented.

**G4/W/13-A3** Poster **1620-24**

**ANATOMIZING THE GRAVITATIONAL LOAD LOVE NUMBERS**

Ming FANG, Bradford H. Hager (Dept. Earth Atmospheric & Planetary Sci., MIT, Cambridge, MA 02139, USA, email: fang@chandler.mit.edu)

Recent estimates (Wahr, 1998) indicates that the gravitational signals of post-glacial rebound and contemporary surface mass redistribution will be prominent in the high precision data to be collected by the Gravity Recovery And Climate Experiment (GRACE) mission. Contributions of the solid Earth to these signals are traditionally modelled by calculating the surface response as a function of rheological parameters within the mantle. This approach fails to provide a clear picture of how the surface responses relates to the perturbations in the interior. In this paper, we present an integral relation which directly links the gravitational load Love number,  $kn$ , to the displacement field in the core, lower, and upper mantle. For a laterally homogeneous Earth, this relation can be reduced to a simple radial integral allowing us to infer ("anatomize") the contributions of each individual layer to  $kn$ . We demonstrate by numerical modelling the application of our new method to the interpretation of the rate of change of gravity at a variety of spatial frequencies.

**G4/W/09-A3** Poster **1620-25**

**GLOBAL TREND OF THE EARTH'S PRINCIPAL AXES AND MOMENTS OF INERTIA: CANONICAL FORM OF SOLUTION**

Alexander N. MARCHENKO, Oleg A. Abrikosov (both at Faculty of Geodesy, State University 'Lviv Polytechnic', S. Bandera St. 12, 290646 Lviv, Ukraine, email: march@polynet.lviv.ua)

Evolution of the Earth's dynamical figure was formulated as the time-dependent eigenvalues-eigenvectors problem in the canonical form and based on the special standardisation of the time-dependent quadratic form of the 2nd degree gravity potential  $U(t)$ . A remarkable separation of the 2nd degree harmonic coefficients was applied: 1) second degree variance of these coefficients, representing the invariant quantitative characteristic of  $U(t)$ ; 2) standardized harmonic coefficients of the 2nd degree, describing the qualitative characteristics of  $U(t)$  of this quadrupole's potential. As a result, the non-linear functional dependencies between the standardised harmonic coefficients were found.

The non-linear hyperbolic model for harmonic coefficients was constructed especially for avoiding infinite values of  $U(t)$  when time  $t$  tends to infinity. This model restores the properties of the well known linear model exactly at the neighbourhood of an adopted reference epoch and provides the limited potential  $U(t)$  at the ends of infinite time interval. So, the linear model is nothing else but the boundary case of the hyperbolic one. The trigonometric form of the hyperbolic model leads to the consideration of the potential  $U(t)$  as  $U(w)$  ( $w$  corresponds one-to-one to  $t$ ) within the closed finite interval for  $w$ . These theoretical investigations and temporal variations of 5 harmonic coefficients according to EGM96 gravity model and special additional conditions lead to the evaluation of the global trend of the Earth's principal axes, moments of inertia and global density distribution within the whole infinite time interval that becomes possible in contrast to the standard linear model.

**G4/W/10-A3** Poster **1620-26**

**THE DIFFERENCE BETWEEN COMPRESSIBLE WAVE AND DILATABLE WAVE AND THE MODIFIED BRANDT'S ELASTIC THEORY**

Xu LIU, Zhu Yanqing (Both at Shanghai Seismological Bureau, Shanghai 200062, China, email: xliu@sbsn.net)

Based on the discontinuity, a model of mass bi-spring is suggested. The model together with some experiments approve that there can be a great difference of wave velocity between compressible wave and dilatible wave. Within  $1/4$  of wavelength, the pure compressible or dilatible wave can be tested. A new concept, elastic cementing coefficient ECC, is put forward. ECC can comparatively represent the degree of cementation. When the geotechnical relations between primary wave velocity and engineering parameters are studied, primary wave should be thought of as compression or dilatation respectively. The Brandt's elastic theory for porous granular media is modified by a term in that its volume modulus is identical to that of Biot-Geertsma's theory. A new way to calculate the skeleton elastic wave velocity is suggested. Some effect of physical parameters on elastic wave velocity are discussed. Key words: Elastic wave, geotechnical engineering, the skeleton of soils.

**G4/C/G5/W/01-A3** Poster **1620-27**

**DEFORMATIONS OF A NUMERICAL EARTH MODEL (NEM) DUE TO A) SURFACE LOADS, B) INTERNAL DISLOCATIONS**

M. ABOLGHASEM, J. Engels, E.W Graferand (Geodetic Institute, University of Stuttgart, Germany)

This is the result of an attempt to compute the displacement field of a Numerical Earth Model (NEM) under the application of a deformation source. A NEM, compared to the present analytical models, is more flexible to account for:

- (1) lateral, in addition to radial, heterogeneity, which is not expected to be negligible in the near-field displacements of a dislocation source
  - (2) internal discontinuities
  - (3) input of geodetically observed displacements as boundary conditions.
- The paper presents the deformations of a NEM under a) surface loads, b) internal dislocation source, and concludes with a comparison of the results with those obtained from analytical models.

**G4/C/G5/W/04-A3** Poster **1620-28**

**CONTEMPORARY KINEMATICS OF THE PHYSICAL SURFACE OF THE EARTH: SURFACE STRAIN AND SURFACE VORTICITY DEDUCED FROM VLBI DATA**

B. VOOSOGHI, E. W. Grafarend (Geodetic Institute, University of Stuttgart, Stuttgart, Germany)

The Global patterns of surface strain and surface vorticity (surface rotation) are derived from a data set of VLBI velocities. In contrast to a strain and surface-vorticity analysis with respect to a reference surface of the earth, here focus is on surface strain and surface vorticity with respect to the physical surface of the Earth (topographic surface) via a finite element triangulation.

**G4/E/03-A3** Poster **1620-29**

**A GLOBAL TOPOGRAPHIC-ISOSTATIC GEOID BASED ON A LOADING THEORY**

Wenke SUN, Lars E. Sjöberg (both at Royal Institute of Technology, Department of Geodesy and Photogrammetry, S-10044 Stockholm, Sweden, e-mail: sunw@geomatics.kth.se)

This new global topographic-isostatic model originates from a completely new idea - the geoid undulation is the response of an elastic earth to the topographic mass load. Assuming the topography as a condensed surface mass load, expressions are derived for calculating the vertical displacement, potential and equipotential surface changes, based on the load theory proposed in Sun and Sjöberg (1998). The modeled geoid is composed of three parts: loading potential, surface displacement and mass redistribution. The surface displacement and mass redistribution of the earth compensate to some extent the topography. In practical calculations the Getech's Global Digital Terrain Model (DTM5) is adopted. Using the load Love numbers and Green's functions obtained from the PREM earth model, the vertical displacements and equipotential surface changes are calculated and discussed for the following depths: earth's surface,  $d=36$  km and the core-mantle boundary. Numerical results show that the displacements at depth 36 km and the earth's surface have the same distribution pattern and magnitude, while the vertical movement of the core-mantle boundary appears much smoother and smaller. The modeled geoid undulations at the earth's surface caused by the topographic mass load vary between -352 and +555 m. Comparing the modeled and observed geoid undulations shows that there are strong positive correlations between them, but a compensation only by elastic deformations is not sufficient to explain the observed undulations because of the big difference in magnitude between the two geoids. More geodynamic effects should be considered to better explain the long-wavelength geoid features.

**G4/E/01-A3** Poster **1620-30**

**INVERSE PROBLEMS IN ISOSTASY: THE CASE OF VENING MEINESZ**

Hussein ABD-ELMOTAAL (Civil Engineering Department, Faculty of Engineering, Minia University, Minia 61111, Egypt, email: hamotaal@frcu.edu.eg)

Inverse problems in isostasy will consist in making the isostatic anomalies to be zero under a certain isostatic hypothesis. In case of the Vening Meinesz isostatic hypothesis, the density contrast is constant, while the Moho depth (depth of the Mohorovicic discontinuity) is variable. Hence, the inverse Vening Meinesz isostatic problem aims to determine a suitable variable Moho depth for a prescribed constant density contrast. The main idea is easy but the theoretical analysis is somewhat difficult. Moreover, the practical determination of the variable Moho depths based on the inverse Vening Meinesz problem is a laborious and time consuming task. The formulas used for computing the inverse Vening Meinesz Moho depths are derived. The computational tricks essentially needed for computing the inverse Vening Meinesz Moho depths are described. The Moho depths for a test area are computed based on the inverse Vening Meinesz isostatic problem. The resulted inverse Vening Meinesz Moho depths are compared with Moho depths obtained from seismic profiles. The comparison shows a good agreement between both sets of Moho depths.

**G4/E/08-A3** Poster **1620-31**

#### GEOID AND CRUSTAL STRUCTURE IN ARGENTINA

María Cristina PACINO (IFIR - UNR, Av. Pellegrini 250, 2000, Rosario, Argentina, email: mpacino@fceia.unr.edu.ar)

Land uplift, according to isostatic concept, is a process through which the uppermost zone of the Earth deforms towards equilibrium. Isostatic theories (Airy's, Pratt's, Vening-Minesz's) have been very helpful in interpreting the Earth's gravity field since any land uplift causes changes in the gravity field due to mass redistribution inside the Earth. Besides gravity change, the geoid rises together with the Earth's surface. The Argentina geoidal chart - computed using the Stoke's integral algorithm- as well as several geopotential models (JGM-3, OSU-91A, EGM-96) show geoid undulations which softly remains the topography reaching almost 50 meters beneath the Central Andes. A geophysical interpretation of this geoidal undulations is presented here. It will be shown that geoidal heights may be only partially justified at crustal levels.

**G4/E/07-A3** Poster **1620-32**

#### ON COSMOLOGICAL ORIGIN OF CERTAIN GEODETIC FEATURES OF THE EARTH

A.O. ADEKUGBE-JOSEPH (Center for Fundamental Study, P.O.Box 22415 University of Ibadan P.O., Ibadan, Oyo State, Nigeria, email: nigeria@netbox.com)

The angle 66.5 degrees of inclination to the ecliptic of earth's rotational axis (rotational slanting of the earth), has been predicted accurately, and the ratio of polar diameter to equatorial diameter (polar flattening of the earth), of 0.997 has been recalculated exactly, within a new cosmological model.

An instantaneous rate of increase of earth's radius of 0.108cm/yr, as well as instantaneous relative drift rate of 0.108y cm/yr. of two points with longitudinal separation of  $\gamma$  degrees along the equator, have been calculated as consequences of the expansion of the earth with the universe in the new model. A remarkable agreement of the predicted rate of increase of earth's radius of 0.108cm/yr, earth's rotational slanting of 66.5 degrees and earth's polar flattening of 0.997 is shown.

The slight westward deflection in the north and eastward deflection in the south of continental plates have also been explained as local consequence of the new cosmological model. These numbers as well as the westward deflection in the north and eastward deflection in the south of continental plates are increasing, but discernible changes occur in time scales of between 10 million and billion years only.

**G5** Thursday 22 July

#### GEODYNAMICS (SECTION 5)

Location: Law Building, 303LT

Location of Posters: Old Gym

Thursday 22 July AM

Presiding Chair: B. Richter (Bundesamt fuer Kartographie und Geodaesie, Frankfurt, Germany)

#### PLANETARY DYNAMICS, INTERNATIONAL STUDY OF REGIONAL DEFORMATIONS

**G5/W/15-A4** **0930**

#### DEGREE-ONE ELASTIC DEFORMATION OF THE EARTH

GREFF-LEFFTZ Marianne (Institut de Physique du Globe de Paris, 4 place Jussieu, 75005 Paris, France) Legros Hilaire (E.O.S.T., 5 rue R. Descartes, 67084 Strasbourg, France)

The degree one deformations of the Earth, in a reference frame related to the centre of mass of the planet, are computed using a theoretical approach (Love numbers formalism) at short time-scale, where the Earth has an elastic behavior. The translations at each interface of the incompressible layers of the Earth's model (especially at the surface, at the Core-Mantle boundary (CMB) and at the Inner Core boundary (ICB)) are computed when the excitation source is the atmospheric pressure or a magnetic pressure acting at the CMB and at the ICB. The effects of external and internal tangential tractions are also investigated. The total force, resulting from the excitation sources, in a geographic frame (centred at the centre of mass) has to be equal to zero, in order to conserve the centre of mass of the Earth. This involves a relation between the different forcing mechanisms: we obtain a Consistency Relation, i.e., a special condition that the degree-one valid solutions have to obey (Farrell, 1972). As geophysical application, we have computed the degree-one deformation induced by atmospheric loading. To conclude, we note that in using the degree one Love numbers, it is necessary to be carefully about the definition of the Love numbers and the chosen reference frame, especially its origin, that is whether it is related to the mass centre of the deformed Earth or the undeformed Earth and whether it is related to the centre of figure or the surface of the planet (for geodetic measurements, the stations are located at the Earth's surface).

**G5/W/11-A4** **0945**

#### OCEAN LOADING TIDES IN GPS AND RAPID VARIATIONS OF THE FRAME ORIGIN

H-G. SCHERNECK, J.M. Johansson (both at Chalmers, Onsala Space Observatory, SE-43992 Onsala, Sweden, e-mail: hgs@oso.chalmers.se); F.H. Webb (Jet Propulsion Laboratory, Pasadena, CA 91190, e-mail fhw@dunsinane.jpl.nasa.gov)

Increasing precision and long record lengths from observations of GPS satellites in precise point-positioning mode make possible the retrieval of sub-mm oscillations in the three spatial components. We determine co-tidal oscillations at a number of stations operating for the IGS. Due to limitations in the orbit ephemerides and the daily processing scheme we are at present able to only retrieve tides due to principal lunar terms. Using extremely continental stations like Irkutsk (Siberia), we can clearly demonstrate that geocentre tides (movements of the centre of the solid earth counterbalancing the mass centre of the ocean tide) are not contained in the range between the satellite and the station, most probably because they were not included in the generation of the orbit data. We conclude that the physical geocentre is only weakly constraining the translation components of the orbit alternatively the frame origin, and that models for geocentre tides are not needed at present. We end by suggesting to SLR groups to attempt a similar project in order to resolve whether this technique has a higher sensitivity.

**G5/L/05-A4** **1000**

#### ABOUT TIDAL ANGULAR MOMENTUM BUDGET OF THE OCEAN

DE VIRON O, Dehant V, Van Hoolst T,

The effect of the ocean on the Earth's rotation in the diurnal time scale is mostly related with the oceanic tides. This effect can be computed by using the angular momentum budget equation of the ocean-Earth system: the tidal angular momentum change of the ocean is equal to the angular momentum change of the Earth related to the tidal forcing. This effect can also be evaluated by computing the interaction torque between the Earth and the ocean. The two methods, as presently developed, give quite different results due to a non-equivalence that can be shown analytically. This problem will be investigated.

**G5/E/29-A4** **1015**

#### GEODYNAMICS FROM MEAN ORBITAL MOTION OF GEODETIC SATELLITES: LAGEOS, LAGEOS-2, AND STARLETTE

Pierre EXERTIER, S. Bruinsma, G. Métris, Y. Boudon and F. Barlier, (Observatoire de la Côte d'Azur - CERGA - GRGS, avenue Copernic, F-06130 Grasse, France)

The secular and long periodic perturbing forces acting on the orbit of an artificial satellite have been modelled and included in a semi-analytical theory of the mean orbital motion. Gravitational and non-gravitational forces have been averaged using analytical transformations and numerical quadratures, respectively. As non-gravitational modelling is the first source of problems arising in the determination of geodynamical parameters, special attention has been given on this question. Resulting averaged equations of motion are integrated numerically allowing to exhibit long periodic signals in the classical mean orbital elements. Observed mean orbital elements of Lageos (18 years), Lageos-2 (6 years) and Starlette (14 years) have been carefully computed from Satellite Laser Ranging (SLR) measurements which have been first reduced by classical orbit fits on short arcs. The results of our long arc solutions using the three orbits exhibit geodynamical coefficients at different frequencies ranging from seasonal (6 months, 1 year) effects to long period and secular ones. Values of coefficients are compared to geophysical processes like atmosphere mass redistribution, ocean and solid tides, anelasticity and post-glacial rebound. Finally, inputs are proposed in order to homogenize satellite orbit contributions which actually use different processes and units and provide geodynamical parameters that are not directly comparable.

**G5/W/25-A4** **1100**

#### LOW DEGREE GRAVITATIONAL CHANGES FROM EARTH ROTATIONAL VARIATIONS

J.L CHEN, C.R. Wilson, B.D. Tapley, and R.J Eanes, (Center for Space Research, University of Texas at Austin, Dept of Geological Sciences, University of Texas at NASA Headquarters, Washington D.C Email: chen@csr.utexas.edu)

We estimate the 2 degree gravitational variations (C21, S21, C20) using Earth rotational changes, caused mass redistribution and movement within the Earth system. These rotation changes are accurately measured by space geodetic techniques. Wind and oceanic current effects are removed from the earth rotation series using atmospheric and oceanic circulation data-assimilating models. The results are compared with Lageos satellite laser ranging (SLR) determinations, and also with geophysical contributions estimated from the atmospheric surface pressure, continental water storage, and non-steric sea level change. Our conjecture is that using Earth rotational changes to infer long wavelength gravitational variations has the potential to be more accurate than satellite-based techniques in some case. Consistent with this we find that C21 and S21 variations from this study are in better agreement with geophysical observations than Lageos SLR determinations of C21 and S21, especially at intraseasonal scales. However, the earth rotation-derived estimate of C20 variation is probably less accurate than the Lageos-derived result, due to the large atmospheric wind contribution to LOD variation which must be removed, and the natural sensitivity of Lageos to C20 changes, via precession of the satellite node.

#### ROTATIONAL DYNAMICS

Introduction **1115**

V. Dehant (Royal Observatory of Belgium, Bruxelles)

**G5/W/13-A4** Poster **1115-01**

#### OCEAN LOADING TIDES IN VLBI AND PERTURBATIONS OF EARTH ORIENTATION PARAMETERS

R. HAAS, H-G. Scherneck (both at Chalmers, Onsala Space Observatory, SE-439 92 Onsala, Sweden, e-mail: haas@oso.chalmers.se)

A greater fraction of geodetic VLBI stations are located sufficiently close to the coast for being significantly affected by ocean tide loading. We show the impact of horizontal displacements particularly on the estimation of earth orientation parameters in sparse global networks. We can show that local problems like differences between models of the tides in the Gulf of Maine



cause effects exceeding 0.2 mas in for instance the CORE project devised for monitoring earth rotation during the coming years. In order to test and improve existing ocean tide loading models we use the VLBI network to estimate amplitude and phase parameters of loading tides for a variety of stations and tide constituents in the diurnal and semidiurnal bands for both vertical and horizontal displacement components. The estimation succeeds with typical standard deviations of 0.2 to 0.5 mm.

**G5/E/13-A4** Poster **1115-02**

#### MODULATION OF WAVES OF ATMOSPHERE TIDES

Tadeusz CHOJNICKI (Space Research Centre, Polish Academy of Sciences, Bartycka 18A, 00-716 Warsaw, Poland, email: tch@cbk.waw.pl)

Seasonal modulation of Earth tide waves has now been investigated for several years, however, the origin of this modulation is unclear. Much indirect evidence points to Earth atmosphere as the source generating modulation of Earth tide waves. Therefore our Warsaw research group undertook a study of atmosphere tides, based on previous 10-year air pressure observations conducted at over a dozen of stations throughout Poland's territory. In this work we present the results concerning one aspect of the observations, namely the seasonal modulation of waves of atmosphere tides. The methods used were similar with those used previously for calculation of the seasonal modulation of Earth tides: for analysis the observations were collected in groups embracing the same months from different years. The results for greater waves are given, and conclusions and suggestions are made concerning the relationship between modulation of Earth tides and the Earth atmosphere.

**G5/E/45-A4** Poster **1115-03**

#### ATMOSPHERIC TIDES AND THEIR DISTRIBUTION IN THE AREA OF POLAND

Janusz BOGUSZ (Institute of Geodesy and Geodetic Astronomy, Warsaw University of Technology, 00-661 Warszawa, POLAND, e-mail: jb@gik.pw.edu.pl)

Growing accuracy of tidal measurements (actually below 0.1  $\mu$ Gal) makes us to consider many of environmental parameters which affect these observations. The biggest of them is the ocean indirect effect, nowadays very well known and many times presented. This paper deals with the distribution of the tides of the atmosphere in time and space and their influence to the gravimetric tidal measurements. The ocean tides, observed by rise and fall of the water twice a day on most open ocean coast have been known from time immemorial. Obviously atmospheric tides cannot be measured in this way, as atmosphere does not have such a boundary layer. We assumed that the changes showed by barometer indication system are accompanied by daily changes of mass distribution of the air. So the analysis was done upon 10-years of observations of the pressure changes on several Polish stations of the Institute of Meteorology and Water Management. Paper presents the results of such computing: dimension of the tidal parameters (amplitude and phase shift) for particular tidal components, investigation of seasonal properties of considered phenomenon and distribution of the atmospheric tides in the area of Poland. Additionally the size of atmospheric indirect effect is exhibits.

**G5/E/21-A4** Poster **1115-04**

#### DIURNAL AND SEMIDIURNAL LOAD GREEN FUNCTIONS TO A POINT LOAD

Shuhei OKUBO, Daijiro Tsuji, and Masato Furuya (Earthquake Research Institute, University of Tokyo, Yayoi 1-1-1, Bunkyo-ku, Tokyo 113-0032, Japan, email: okubo@eri.u-tokyo.ac.jp)

Load Green functions (gravity/tilt/strain etc) were first presented by Farrell (1972) assuming quasi-static response of the earth. They are now routinely used to correct for the effects of oceanic loading on continuous measurements of gravity, tilt, strains and so on. Recalling that the oceanic loading has specific periods and that the load Love numbers are dependent on the loading frequency, the Green functions themselves must have frequency dependence. We will present representative Green function for diurnal and semidiurnal frequency for the PREM earth model. We also include the effect of anelasticity when computing the Green functions. These functions will serve for the better correction of oceanic tide against the earth tide registration.

**G5/E/30-A4** Poster **1115-05**

#### THE ELASTIC CHARACTERISTIC PARAMETER OF EARTH TIDE AND ITS ABNORMAL VARIATION

Yanbin ZHANG, Jun Jiang, and Shengle Li (Institute of Seismology, China Seismological Bureau, Wuhan, 430071, China)

According to the definition of Love number in tidal theory, Love Number can be used to describe the earth's deformation and it is also a parameter indicated the elasticity. The change of Love Number will be caused by an elastic variation of the earth medium. In this paper, Love Number that is a tidal parameter is regarded as a characteristic parameter in the kinds of tidal precursory observation. Based on tidal theory, we discuss the uniform and synthetic method for tidal data processing and Love Number inversion using actual tidal data included tidal linear strain, plane strain, volumetric strain, tilt, gravity and water level, etc.. The anomalous evolution of Love Number is studied by the physical and deformational properties of Love Number.

This paper intends to analyze synthetically a physical property of the crust using tidal observations. We regarded Love Number that can describe both micro deformation and elasticity of the crust in tidal observation as a physical and mechanical parameter. Research a seismic mechanical process and its precursory abnormality of a region based on the variation of Love Number. In this paper, a feasible way and method to synthetically calculate the second-step Love Number on the earth's surface is discussed and determined by tidal theory. Love Number  $h_2$  in the boundary region of Sichuan and Yunnan province is practically calculated using tidal observations, and the precursory anomalous variation of Lijiang earthquake ( $M_s=7.0$ , Feb. 9, 1996) is analyzed. The result shows that large-scale Love Number anomaly in the Sichuan-Yunnan region began from 1994. The anomaly moves from south to southeast, north and northwest in the region, and the epicenter is an anomalous empty. Finally, the anomalous area was concentrated to Lijiang and Yongsheng located northwestern Sichuan-Yunnan region on December 1995, and the epicenter area in future is drawn out clearly.

**G5/L/02-A4** Poster **1115-06**

#### EFFECT OF ROTATION AND ELLIPTICITY ON EARTH TIDES AND FORCED NUTATIONS

Vladimir GORBUNOV (Vavilov State Optical Institute, Birzhevaya 12, St.-Petersburg, 199034, Russia, E-mail: gorbunov@neva.spb.ru); Polina Serebryanaya (SPbF IZMIRAN, Muchnoi per.2, St.Petersburg, 191023, Russia, Email: gorbunov@neva.spb.ru)

We present the results of numerical computations of the frequencies of normal modes, body tides and forced nutations of rotating, elliptical and oceanless earth model. Our numerical procedure is direct integration of linearized equations of motion by using expansions in vector spherical harmonics. This approach that has been already used by numerous authors (M.Smith, J.Wahr, V.DeHant,...) allows a simultaneous computation of the Earth's deformational and rotational tidal response which systematically includes the effects of rotation and elliptical material stratification. The motivation for the present work is the hope that more accurate implementation of this method can remove some discrepancies in modelling earth tides, nutations and near diurnal free wobble. The scheme we use to convert vector equations with boundary conditions into an equivalent set of ordinary differential equations over radius is considerably modified. Among other things it does not require the ellipticity to be small.

Rotation and ellipticity can be modeled either together or separately. It is interesting to note the existence of nutational normal mode with a period slightly larger than 1 day duration in the case of rotating but spherically symmetric Earth. This mode involves the rotation of the solid inner core with respect to the outer core and mantle and it is caused by coupling between them due to only elastogravitational deformation. We have found that the spectrum of internal oscillations in a stably stratified fluid core (modified PREM) radically contrasts with that of core without rotation. Eigenperiods of core low-degree modes with increasing undertone numbers accumulate towards a limiting value. Work on numerical solutions for the forced motion is currently underway.

**G5/W/05-A4** Poster **1115-07**

#### FREE OSCILLATION OF THE EARTH'S INNER CORE IN THE EARTH'S NONEQUILIBRIUM COVER FIELD

Sergey Pasyuk, Sternberg Astronomical Institute, Moscow State University, Universitetskii prospect 13, 119899, Moscow, Russia. Email: pasyuk@sai.msu.ru

This paper has paid special attention to nonequilibrium Earth cover influence on the free oscillation of the Earth's inner core. Oscillations are considered in any direction which may be not polar. The additional mass tensor for this task was obtained. Earth's nonequilibrium cover field corrections in the periods are proportional to Earth's rotation corrections. Periods have splitting at the nonequilibrium Earth's cover field and it (and its amplitudes) are very like as splitting periods which were obtained by D.E.Smylie[14]. Therefore new Smylie's splitting periods interpretation as the splitting periods in the nonequilibrium Earth's cover field is proposed.

**G5/W/24-A4** Poster **1115-08**

#### ROTATION OF THE EARTH'S INNER CORE IN THE EARTH'S NONEQUILIBRIUM COVER FIELD

Sergey Pasyuk, Sternberg Astronomical Institute, Moscow State University, Universitetskii prospect 13, 119899, Moscow, Russia. Email: pasyuk@sai.msu.ru

This paper has paid special attention to non-equilibrium Earth cover influence on the Earth's inner core rotation. Part of the mutual gravitational potential function of the Earth's non-equilibrium cover and Earth's inner core which depends on Earth's inner core Euler angles have been obtained. The Earth's inner core rotation parameters were calculated for Earth's external core absence case. It was shown that non-equilibrium Earth's cover field could be dissymmetrical velocity field source. It is important result for geomagnetic field generation problems. It was shown that non-equilibrium Earth's field has to take in to account rotation theories, which include ellipticity as the first power. One can use this potential function which was obtained in this paper.

**G5/E/46-A4** Poster **1115-09**

#### LUNAR INTERIOR AND FREE CORE NUTATION OF THE MOON

Natasha PETROVA, Alexander Gusev, Viktor Bashkov (Dpt. of Astronomy and GRG, Kazan University, Kremlevskaja Str., 18, Kazan, 420008, Russia, E-mail: petrova@astro.ksu.ras.ru)

The interdisciplinary approach to lunar investigations: traditional astronomical observations, laser and seismic ranging, spacecraft experiments (Apollo 1969, Galileo 1989-1991, Clementine 1994, Lunar Prospector 1997) - gives an essential progress in our knowledge about deep lunar interior. Many modern observational data, such as the noticeable free librations in the presence of great dissipation, involve the appropriate consideration of active lunar internal stratigraphy, including elliptical liquid core (of 220 to 500-km) and rigid or viscose mantle. Certain discovery of free lunar librations and large rotational dissipation from LLR analyses propose the existence of a small lunar core. The instable thermodynamical processes at lunar CMB, arising under differential core-mantle rotation, lead to lower dissipation factor  $Q=26.5$  of the Moon. The presence of fluid core with a turbulent or convective layer at CMB appears to be the plausible source not only for great dissipations, but also for exciting and supporting of free librations. The dissipative energy at CMB, converted in heat, creates instable thermal layer leading of the upwelling mantle plumes. Top of the plumes in early Moon were conserved in form of mascons in the lunar continental crust (up to 100-km). Then the specific surface characteristics should be observed. These are such phenomena as the pluto-like bodies ("mascons"), as specific fluctuations of thermal, gravitational fields, as the Moho uplifts and as topographic features --- such as the plume at the thick Russian plate of the Earth is manifested itself. The plume trace on the surface should be manifested in the form of "warm spot" and of arched lineament chain, if the crust moved through the top of plume. In the frame of the two-layer model of the Moon (rigid mantle and elliptical liquid core) Chandler mode with period  $P_{(CW)}=74.06$ -yr and Free Core Nutation  $P_{(FCN)}=6.782$ -yr are calculated. It is calculated that prograde super-rotation of lunar core relative the mantle is roughly to  $2.4 \times 10^{-4}$  yr.

**G5/E/25-A4** Poster **1115-10**

#### VARIATION OF THE EARTH ROTATION DERIVED FROM TIMED OBSERVATIONS OF ECLIPSES IN ANCIENT CHINA

HAN Yan-Ben (Beijing Astronomical Observatory, Chinese Academy of Sciences, Beijing 100012, P.R. China, email: hyb@class1.bao.ac.cn); Zhang Pei-yu (Purple Mountain Astronomical Observatory, Chinese Academy of Sciences, Nanjing 210008, P.R. China)

Some ancient observations, such as the observations and records of solar and lunar eclipses in ancient times, are useful to the study of secular variation of the Earth's rotation in recent about 30 centuries. The relationship between the variation of the rotation and ancient observations is set up through the use of different time scale. In China, the history of observations and records of ancient solar and lunar eclipses is very long and the rich observations are preserved in ancient books. The authors made the textual research again for Chinese ancient timed observations of over 80 solar and lunar eclipses are analyzed in the

study. A  $\Delta T$  series, which can describe the secular variation of the Earth's rotation, is derived from the ancient observations of the eclipses. The variation of the length of the day is about 1.5 millisecond per century according to the result.

**G5/E/24-A4** Poster **1115-11**

**POSSIBLE CONTRIBUTION OF JAPANESE TIMED RECORDS OF SYZGY IN HISTORY FOR STUDY OF THE EARTH'S ROTATION VARIATION**

HAN Yan-Ben (Beijing Astronomical Observatory, Chinese Academy of Sciences, Beijing 100012, P.R. China, email: hyb@class1.bao.ac.cn)

Records of observed time of some ancient astronomical phenomena in local time scale, such as the local apparent solar time of eclipses and syzygy, can be used in the study of the variation of the Earth's rotation. There are some records of syzygy in Japan in the period of 19th-20th century. In this paper, the observations of syzygy and the possibility that the data are used in the study is investigated. The initial result showed that the observations will be significant for the study of the variation of the Earth's rotation in the period.

**G5/E/20-A4** Poster **1115-12**

**LENGTH OF DAYLIGHT**

Tarzadin ULAANBAATAR (Department of Earth Sciences, National University of Mongolia, email: numelect@maginet.mn)

For the study of time-dependent phenomena a best way of controlling opportunities of motions in the Earth's system is that mathematical understanding of the nature of length of daylight by daily and yearly motions of the Earth themselves. Otherwise, to describe more realistic and detailed simulations of the length of daylight we must not driven to the astronomical calculations, but it needs only for comparison.

Length of day is a whole hierarchy of complexity. However, if we can know it by step to step this hierarchy will clear in front of us, i. e. after final calculations the remains or biases between the model result and observation of the length of daylight indicate the irregular time change connecting the impacts of external objects and Earth's interior or man-made. Without this manner we can not select the self-supporting and impacting phenomena on the length of day, as well as study of time-dependent phenomena is very difficult.

In this matter the equation of length of daylight model including three simple parameters: number of day from winter solstice, measuring time in hour, minute, second, and geographical latitude as well model results, daily and yearly changes of sun's altitude, times of sunrise and sunset, directions of sun's location in space are described.

Utilization of the model in space-time study of time-dependent phenomena, and climate is presented.

**G5/L/03-A4** Poster **1115-13**

**ESTIMATION OF REAL ACCURACY OF EOP PREDICTION**

Zinovy MALKIN (Institute of Applied Astronomy RAS, nab. Kutuzova 10, St. Petersburg 191187, Russia, e-mail: malkin@quasar.ipa.nw.ru)

Many authors propose various methods for improvement accuracy of prediction of EOP. For comparison of various methods they compute rms residuals between predicted and observed values of EOP using preceded several years IERS series. However, such estimation of accuracy of prediction doesn't reflect real errors of predicted values of EOP because they depend not only on method used for prediction but also on initial EOP series used as fiducial for the computation of predicted values.

Real EOP prediction needed for practice have being made using operative EOP values with accuracy worse than accuracy of final EOP series that usually used for test investigations of accuracy of prediction. To estimate real accuracy of prediction by various methods used in practice of EOP services special tests have been performed.

The first test is intended to estimate real accuracy of EOP prediction on preliminary testing stage. For this purpose fiducial EOP series used for computation of prediction and further comparison of predicted and observed EOP values was artificially disturbed in such a way that it could imitate real errors of operative EOP as compared with final ones. Results of this test show that error of predicted value may be several time large than inputed error for some methods of prediction.

For estimation of real accuracy of prediction all predictions made by IERS Subbureau for Rapid Service and Prediction and in the IAA EOP Service beginning from March 1998 were analyzed. Results show that errors of prediction are practically the same for both centers but differ substantially from published values.

Supplement criteria was used for estimation accuracy of prediction. Usually rms residuals used as only criteria. However it seems interesting to know also maximum error of prediction to allow user to have "guaranteed" accuracy which may be useful for practical needs. So, these maximum errors was obtained for predictions computed in the IERS and IAA and was found that they are about 2-3 times large than rms errors.

**G5/L/04-A4** **1115-14**

**REPORT OF THE WG ON NON-RIGID EARTH NUTATION THEORY DEHANT V. ET AL., (ROYAL OBSERVATORY OF BELGIUM, BRUXELLES)**

The WG on 'Non-rigid Earth nutation theory' has been created 6 years ago and is at the end of its term. We present here the report of the activities of this WG. These activities are mainly meetings and email exchanges with discussions over particular points of interest for nutations of a non-rigid Earth. We have worked on 6 levels: (1) seismic models used, (2) Earth's transfer function, (3) nutations for a rigid Earth, (4) convolution between the Earth's transfer function and the nutations for a rigid Earth, (5) atmospheric and oceanic effects on nutations, (6) comparison of the theoretical nutations with the observations.

**FUNDAMENTAL CONSTANTS**

**Introduction** **1130**

E. Groten (IPG, Darmstadt Institute of Technology, Germany)

**G5/L/07-A4** Poster **1130-01**

**REPORT OF SC 3 ON FUNDAMENTAL CONSTANTS**

Erwin Groten (IPG, Darmstadt Institute of Technology, Darmstadt D-64287, Germany, email: groten@ipgs.ipg.verm.tu-darmstadt.de)

The report summarises the activities of Special Commission 3 during the interval 1995-1999. Current best values as well as official values of Fundamental Constants are reviewed and considered in detail. Research on the related topics is reflected for the interval 1995 to 1999. The values were reconciled with those which are to be published in the forthcoming IERS conventions 1999. Changes of related parameters with time are also taken into account. The results represent those values which found general agreement of members of Special Commissions 3 and the international scientific community.

**G5/P/02-A4** Poster **1130-02**

**REFRACTIVE INDICES OF LIGHT, INFRARED AND RADIO WAVES IN THE ATMOSPHERE**

JEAN M. RÜEGGER (School of Geomatic Engineering, University of New South Wales, Sydney NSW 2052, Australia, email: J.Rueger@unsw.edu.au); Philip E. Ciddor (National Measurement Laboratory, CSIRO, P.O. Box 218, Lindfield NSW 2070, Australia, e-mail: pec@dap.csiro.au); Michael G. Cotton (Institute of Telecommunications Sciences, NTIA/ITS.S3, 325 Broadway, Boulder CO 80303, USA, e-mail: mcotton@ntia.its.bldrdoc.gov); Yuri S. Galkin, Ecological Laboratory, Dept of Physics, Moscow State University of Forestry MGUL, Mytischy-1, Moscow Region 141001, Russia, e-mail: galkin@mgul.ac.ru); Reginald J. Hill (R/E/ET6, NOAA, US Department of Commerce, 325 Broadway, Boulder Colorado 80303, USA, e-mail: rhill@etl.noaa.gov); Hirokazu Matsumoto, Quantum Metrology Division, National Research Laboratory of Metrology (NRLM), 1-4, Umezono I-Chome, Tsukuba Ibaraki 305, Japan, e-mail: hiro&nrlm.go.jp); Ruben A. Tatevian, Dept of Metrology and Standardisation, General Research Institute of Geodesy, Air-Survey and Cartography, Onezskaya 26, Moscow 125413, Russia)

This ad-hoc working group of the IAG Special Commission (SC3) has carefully reviewed the progress in the measurement and modelling of the refractive index of air. For light and near infrared waves, a closed simple formula is proposed for electronic distance measurement (EDM) to 1 ppm precision or worse. For EDM of higher precision, a computer routine is proposed that uses the full Lorentz-Lorenz relationship, the new temperature scale of 1990, the BIPM density equations and the recently revised water vapour refractivity. The group notes that the perceived accuracy of any continuum formula is invalidated by anomalous refractivity near absorption lines. Further work on the effect of absorption lines on the phase and group refractive indices of air is strongly recommended as are new absolute measurements of the refractivity of the constituent gases of the atmosphere (incl. water vapour) at non-laboratory conditions.

**G5/L/01-A4** **1145**

**GEODYNAMICS OF S.E. ASIA: RESULTS OF THE SULAWESI 1998 GPS CAMPAIGN**

W.J.F. SIMONS, D. van Loon, B.A.C. Ambrosius (DEOS, TU Delft, The Netherlands); J. Kahar, H.Z. Abidin, D.A. Sarsito (ITB, Bandung, Indonesia); S. Haji Abu (DSMM, Kuala Lumpur, Malaysia); P. Morgan (University of Canberra, Australia)

In November 1998, concurrently with the third GPS campaign of the international GEODYSSSEA (GEODYNAMICS of South and South-East Asia) project, a dense geodetic network in Sulawesi, Indonesia was re-measured with GPS. The network is situated in a tectonic complex region near the triple junction of the Eurasian, the Philippine and the Indo-Australian tectonic plates. The GPS campaign included second and third repeat measurements for densification sites of the GEODYSSSEA network in this region, and also a re-measurement of a Palu-Koro fault transect in Sulawesi. The acquired data, together with data from IGS stations in the same region, have been processed at DEOS, using the JPL GPSY-II software, while the DEOS 3D-Motion software was used for the network deformation analysis. The station coordinates were analyzed together with those of the previous Sulawesi campaigns and the GEODYSSSEA campaigns of 1994 and 1996. Our kinematic model for the present motions was further validated and improved, and contains both steady state velocity and non-linear displacements. The tectonic block and fault motions are compared with previous results and are geophysically interpreted, and provide detailed new information for this region.

**G5/E/39-A4** **1200**

**BACKARC SPREADING OF THE MARIANA TROUGH AS OBSERVED BY GPS OBSERVATIONS**

T. KATO, S. Nakao, Y. Kotake, H. Takiguchi (Earthquake Research Institute, University of Tokyo, 1-1 Yayoi 1, Bunkyo-ku, Tokyo 113-0032, Japan, email: teru@eri.u-tokyo.ac.jp); A. Kurashima (Faculty of Science, Ibaraki University, 2-1-1 Bunkyo-cho, Mito, Ibaraki 310-0056, Japan); T. Matsumura (Shimabara Earthquake and Volcano Observatory, Kyushu University, 2-5643-29, Shinzan, Shimabara, Nagasaki 855-0843, Japan); J. Beavan (Institute of Geological and Nuclear Sciences, P O Box30-368, Lower Hutt, New Zealand); J. T. Camacho (Emergency Management Office, Saipan, CNMI)

The Mariana trough is one of rapidly spreading backarcs in the world. The magnetic lineation data at spreading center suggests about 30mm/yr spreading in the recent geological age. In order to estimate its instantaneous spreading rates, we have conducted GPS observations in the Northern Mariana Islands. The first observation was done in 1992 and 1994. Succeeding to these first occupations, the second observation was conducted in January to February 1998. The sites that we reoccupied are Guam (AAFB), Saipan (MPLC and SPNA), Anatahan, Guguan, Pagan, and Agrihan islands from south to north. We used 1994 and 1998 data to estimate backarc spreading rates, except Agrihan where no observation data was available in 1994. For baseline analysis, first, we estimated the motion of the Philippine Sea plate relative to Eurasia based on otherwise obtained GPS data. Then the displacement of Guam (GUAM) IGS site relative to the Philippine Sea plate was estimated. The results suggest of about 57.8mm/yr eastward motion relative to the Philippine Sea plate. Then, the rates of displacements of the Northern Mariana Islands; Saipan, Anatahan, Guguan, Pagan; were estimated assuming that AAFB site has the same velocity as GUAM IGS site. The results show that the displacement rates are, from south to north, 46.5mm/yr in Saipan, 40.5mm/yr in Anatahan, 28.9mm/yr in Guguan, and 27.7mm/yr in Pagan. The average of five islands is 40.3mm/yr, which is more than 30% larger than the geological rates from magnetic lineation data. This might suggest that the spreading has accelerated in the recent years, or, the spreading rate is not uniform between the Mariana trench and the Mariana trough. Moreover, the rate is decreasing from south to north and the direction of motion is not uniform but has component of north-south spreading. The Euler pole of the Mariana block is located nearby the northern end of the block. The third observations that will be done in February 1999 may provide us with more accurate results as well as new results in Agrihan.



G5/E/36-A4

1215

**AN INTERDISCIPLINARY APPROACH TO STUDYING SEISMIC HAZARD THROUGHOUT GREECE**

Paul CRUDDACE, Paul Cross (Department of Geomatic Engineering, University College London, London, WC1E 6BT, UK. Email: paul.cruddace@ge.ucl.ac.uk, paul.cross@ge.ucl.ac.uk); George Veis, Haris Billiris, Dimitris Paradissis, Jordan Galanis (email: veis@survey.ntua.gr, billiris@central.ntua.gr, dempar@central.ntua.gr, jorgalan@survey.ntua.gr); Barry Parsons, Philip England (email: barry.parsons@earth.ox.ac.uk, philip.england@earth.ox.ac.uk); Helene Lyon-Caen, Peire Briole (lyoncaen@ipgp.jussieu.fr, briole@ipgp.jussieu.fr); Boudewijn Ambrosius (email: b.a.c.ambrosius@lr.tudelft.nl); Hans-Gert Kahle, Marc Cocard, Peter Yannick (email: kahle@geod.ethz.ch, cocard@geod.ethz.ch, ypeter@geod.ethz.ch); George Stavrakakis (email: g.stavr@egeledos.gein.noa.gr); Peter Clarke (email: peter.clarke@newcastle.ac.uk); Mikael Lilje (email: mikael.lilje@lm.se)

This paper describes and reviews the progress of a European Commission FP4 (Climate and Natural Hazards) funded project entitled GPS Seismic Hazard in Greece (SING), in which a major international interdisciplinary consortium is investigating and comparing strain derived using both geodetic and seismic methods. The specific objectives of SING are to assess strain accumulation throughout Greece, to identify areas of high seismic hazard, to develop new and more efficient operational and computational methods for GPS, and to improve our understanding of the relationships between geodetic strain, seismic catalogues and geological data. New GPS networks have been installed in regions of significant hazard and some initial computations have been carried out. To date a primary result of SING is the integration of 33 historical geodetic data sets to provide a national strain map. This gives the first full picture of geodetic strain in Greece and provides the basis for the setting up of the new geodetic networks.

**THE AFRICA-EURASIA PLATE BOUNDARY**

Introduction

1230

M. Feissel (Institut Geographique National, Mame la Vallee, France)

G5/W/03-A4

Poster

1230-01

**USING GPS OBSERVATIONS FOR STUDYING THE DYNAMICS OF THE AZORES-GIBRALTAR REGION**

Luisa Bastos, Jose Osorio and Paulo Baptista (Astronomical Observatory, University of Porto, Portugal); Gunter Hein (IEN, University FAF Munich, Germany); Ron Noomen (DEOS, TU Delft, The Netherlands); Rui FERNANDES (DMI, University of Beira Interior, Portugal, email: rmanuel@noe.ubi.pt)

The western part of the Eurasian/African plate boundary meet the Mid Atlantic Ridge at the Azores triple junction. Different models for the structure and behaviour of this section of that plate boundary have been proposed but a definite solution has not yet been found. We have used GPS observations, from stations located in three different plates, acquired during several campaigns realised since 1988, and combined them with data from the IGS stations, in order to obtain a velocity field for our stations in a global reference frame (ITRF96). From this velocity field, we have derived strain parameters. We compare the results obtained for the motion of our stations with the results proposed in global and regional tectonic models (based on geophysical and geological data). We show that, for the most part of the stations, the magnitude and direction of the displacements is in good agreement with some of those models. We also interpret the computed strain parameters for some of the sub-networks under analysis, in the frame of the proposed geodynamic models for those regions.

G5/W/19-A4

Poster

1230-02

**GROUND DEFORMATION MONITORING IN THE CENTRAL SECTOR OF BETIC CORDILLERA (SPAIN) FROM GEODETIC TECHNIQUES: STATUS REPORT**

Antonio J. GIL, A.M. Ruiz, E. Mata, M. J. Borque, M.A. Caro (Dept. Ing. Cartografica, Geodesica y Fotogrametria, E.P.S. de Jaen, Universidad de Jaen, Virgen de la Cabeza, 2, 23071 Jaen, Spain, e-mail: agil@ujaen.es); Gracia Rodriguez-Caderot, M. Clara de Lacy (Dpto. Astronomia y Geodesia, Fac. C.C. Matematicas, Universidad Complutense, 28040 Madrid, Spain); Mario Ruiz (I.G.N., Divina Pastora, 7, 18012 Granada, Spain); Mattia Crespi (Universita di Roma La Sapienza, via Eudossiana 18, 00184 Roma, Italy)

The aim of this research is the application of geodetic techniques to the central sector of Betic Cordillera, the most important region in Iberian Peninsula from Active Tectonics point of view, to detect microdisplacements to be correlated with the seismicity in the area. Seismicity in this area is tied to a regional comprehensive strain in NW-SE direction along the convergence zone between African and EuroAsian plates. None the less numerous faults in all directions present normal vertical movements, which are not congruent with that compression. Ground movements related to geophysical phenomena are generally subdivided into horizontal and vertical deformations. In order to find the former in the area, a local triangulation and trilateration network measured by means of high-precision geodetic instrument has been established. With the purpose to detect vertical movements, a series of high-precision levelling profiles have been observed. A regional network observed by GPS has been measured so as to find both of them. This paper describes the status of this research project, which started in October 1998, to determine ground deformations in the central sector of Betic Cordillera.

G5/W/20-A4

Poster

1230-03

**DISPLACEMENT FIELD OF THE CENTRAL MEDITERRANEAN AREA: RESULTS AFTER EIGHT YEARS OF THE TYRGEONET PROJECT**

Marco ANZIDEI, Giuseppe Casula, Federica Riguzzi (Istituto Nazionale di Geofisica, via di Vigna Murata 605, 00143 Roma, Italy, email: riguzzi@ing750.ingrm.it); Paolo Baldi (Dipartimento di Fisica, Universita' di Bologna, viale B. Pichat 8, 40100 Bologna, Italy, email: baldi@ibogf.f.d.unibo.it); Alessandro Galvani, Arianna Pesci (Italian Space Agency Fellowships at Istituto Nazionale di Geofisica, via di Vigna Murata 605, 00143 Roma, Italy, email: galvani@ing750.ingrm.it); Antonio Zanutta (DISTART, Universita' di Bologna, p.le Risorgimento 2, 40100 Bologna, Italy)

The TYRGEONET (TYRrhenian GEOdetic NETwork) project started to work in 1991 with the aim to study the crustal deformations of the Italian and surrounding regions by analyzing repeated non-permanent GPS surveys. At present, we dispose of GPS data coming from six large campaigns performed in 1991, 1994, 1995, 1996, 1997 and 1998, involving each time more than 15 sites of the TYRGEONET. Each campaign lasted more than six DOYS to achieve a good redundancy of observations. GPS data processing was performed by the Bernese v. 4.0 software obtaining one network solution per DOY. All the baselines and the

covariance matrices pertaining to each campaign were jointly adjusted obtaining one network solution (coordinates and error ellipsoids) per year into the ITRF96 reference system. The significance of the coordinate differences of each sites were evaluated by computing the 2D displacement vectors and the corresponding error ellipses on the local tangent plane. The displacement pattern of the analyzed area displays interesting features both for the sites whose trends were previously known and for those not yet investigated by GPS.

G5/P/03-A4

Poster

1230-04

**GEODYNAMICAL STUDY OF THE NORTH OF ALGERIA BY GPS : THE ALGERIAN GEODYNAMICAL NETWORK (ALGEONET)**

S. KAHLLOUCHE, S. Touam, B. Gourine, B. Ghezali, H.Taibi (Geodetic Laboratory, National Centre of Spatial Techniques, BP 13 ARZEW- 31200 - ALGERIA); H. Mouzaia, A.Khalifoun (National Institute of Cartography, BP 430 Hussein Dey, ALGIERS, ALGERIA); A. About (Research Centre in Astronomy, Astrophysics and Geophysics, BP 15-16 Bouzareah, Algiers, Algeria).

The western Mediterranean, particularly the north African region, is characterised by an important geodynamical activity due essentially to the collision between the Eurasian and African plates and gave place to some earthquakes of strong intensities (El Asnam 1980).

Since 1998, the National Centre of Spatial Techniques (CNTS), with the collaboration of the National Institute of Cartography (INC) and the Research Centre in Astronomy, Astrophysics and Geophysics (CRAAG) have set up the ALGEONET (Algerian Geodynamical Network) project with the aim of a geodynamical surveillance of the Northern Algerian Country. The network, composed of eight stations selected for their situation on stable blocks with a geodynamical criteria, is located in the Tellian Atlas, the Saharian Atlas and Northern Sahara. As two stations of the network (Arzew and Algiers) are included in the TYRGEONET (Tyrrhenian Geodetic Network) project since 1995, both ALGEONET and TYRGEONET GPS observations campaigns were performed during the simultaneous period (June 1998) using the Ashtech Z-12 receivers. The processing of the data collected during 6 days were performed with the Bernese 4.0 Software. The final solution was obtained by the adjustment of the daily GPS baselines with regard to the fixed station Arzew. In the north of Algeria, for determining the slow geodynamical movements (5mm/year), as provided by global models, observations have to be performed over a long period.

G5/E/27-A4

Poster

1230-05

**GRAVIMETRIC STUDY OF THE ALGIERS SEISMIC ZONE**

A. ABTOUT, A.K. Yelles Chaouche and S. bourouis (Both at C.R.A.A.G., Algerian Research Center of Astronomy, Astrophysics and Geophysics, B.P. 63, Bouzareah, Algiers, Algeria, e-mail: geoph@cerist.ist.dz)

During the last centuries, the Algiers region (northcentral part of Algeria) has experienced several major earthquakes (02/01/1365 ; 10/03/1673 ; 03/02/1716 ; 02/01/1867, 29/01/1989 ;04/09/1996) causing huge damages to the capital and other important towns of the Mitidja basin. Until now, a little is known about the active faults which generate this strong activity. In the Algiers region, gravimetric data collected are issue from: the Lagrula's measurements, the gravimetric survey on the Algiers massif, 171 stations of the Chenoua's massif survey and the BGI data bank.

The Bouguer's anomaly map displays near the cost E-W positive anomalies which reach values of 90 mgals due to effect of the oceanic nature. Towards the south, the Bouguer anomalies decrease (5 mgal/km) and become negative with a value of -40 mgal. Data analysis display two major tectonic features: one corresponding to the Sahel anticline which has previously triggered several major earthquakes. The second tectonic feature with an orientation NNW-SSW crosscut the Mitidja basin in two parts. This later major fault was never revealed by geological investigations. Orientation of the faults agree with the compression NNW-SSE stress regime which characterizes the northern region of Algeria.

G5/E/48-A4

Poster

1230-06

**MONITORING RECENT CRUSTAL MOVEMENTS IN SINAI, GULF OF AQABA AND GULF OF SUEZ, EGYPT**

S.MAHMOUD, H.Khalil and T.Kebeasy (National Research Institute of Astronomy and Geophysics, Helwan, Cairo, Egypt, email: salahmm@frcu.eun.eg); H.Koivula, (Finnish Geodetic Institute, Masala, Finland)

Recent seismic activity has been observed in regions of Sinai, Gulf of Aqaba and Gulf of Suez. For monitoring the recent crustal movements in Sinai and around the Gulf of Suez a regional GPS network consists of 11 geodetic points was established early 1994.

The initial geodetic measurements were performed in 1994 and repeated in 1995, 1996, 1997 and 1998 using Trimble 4000 SSE/SSI receivers. A Co-Seismic displacements of 16 cm was determined 20 km southwest the epicenter of the 22, November 1995 earthquake in the Aqaba Gulf using GPS observation. This study is initiated for more better understanding of the seismotectonics in and around these regions. The analysis of these measurements together with the frequency and intensity of seismic activity may leads for more understanding the earthquake activities and geodynamics of these regions.

G5/E/41-A4

Poster

1230-07

**GPS MEASUREMENTS AROUND NASSER LAKE FOR MONITORING CRUSTAL DEFORMATION, ASWAN, EGYPT.**

A.Tealeb, K. SAKR, H.Khalil, S..Mahmoud, A.S.Mohamed.(National Research Institute of Astronomy and Geophysics, Helwan, Cairo, Egypt. e-mail: kamalms@frcu.eun.eg)

A program for monitoring recent crustal movements has been started as far as early 1983 after the occurrence of an earthquake in 1981 with magnitude 5.6. This earthquake occurred 70 km south of the Aswan High Dam which consider the main project in Egypt. The epicenter of the earthquake located on the active zone of Kalabsha fault. Local geodetic networks were established to cover the area of active faults at northwestern part of Nasser Lake. For monitoring regional crustal movements for Nasser Lake area, GPS network from 11 stations was established around the northern part of the Lake in 1997 with baseline lengths from 12 to 87 km. This network was measured three times with Trimble Receivers 4000SSE and 4000SSI. Analysis of GPS data shows that, the range of displacement of geodetic points for horizontal component between 0.03 - 15mm.

G5/E/23-A4

Poster

1230-08

**SEISMIC HAZARD ASSESSMENT IN THE MARMARA SEA REGION**

Namk Yaln, Semih ERGINTAV, Mustafa Aktar (T\_B TAK, MRC, ESRI, Istanbul, Turkey, email: Semih@Mam.Gov.Tr); Emin Ayhan, Onur Lenk (General Command Of Mapping, Ankara,



Turkey); Aykut Barka, Haluk Eyido (Istanbul Technical University, Istanbul, Turkey); Cemil Gorbuz, Onur Gorkan (Bo Aziđl University, Koeri, Istanbul, Turkey); Robert Reilinger, Nafi Toksoz (Massachusetts Institute Of Technology, Erl, USA)

The Marmara Sea region which accommodates 30% of Turkey's population, including the Istanbul area, and 40% of all national industrial activity is bisected by three major strands of the North Anatolian Fault (NAF). During the historical period, the North Anatolian Fault Zone (NAFZ) has been responsible for creating number of large earthquakes. Recent GPS studies indicate that ~20 mm/yr slip is accommodated by the NAF system in this region which is significantly higher than the rates obtained from the previous geological and seismological studies. For this reason, a multidisciplinary project has been initiated with contributions from different organizations and universities. The main goal of the project is to monitor strain accumulation and release along the strands of the NAF in the Marmara Sea region. To achieve this goal, 10 continuous GPS stations have been installed around the Marmara Sea. Using the GAMIT/GLOBK software and precise IGS orbits, we automatically process the daily observations from this continuous network and publishing the results immediately on the World Wide Web. Periodically, a denser network of approximately 40 GPS sites is occupied by mobile GPS receivers. This combined continuous and survey style GPS study provides the dense temporal and spatial resolution necessary for estimating interseismic strain accumulation, coseismic slip and postseismic relaxation. Additional studies (e.g. detailed mapping of active faults, monitoring earthquakes with denser seismic network and detailed bathymetric survey), have also been undertaken. We will present an overview of the project and discuss the preliminary results.

**G5/E/11-A4** Poster **1230-09**

**MONITORING OF THE FAULT ZONE BETWEEN THE AFRICAN AND THE EURASIAN PLATE (PERIADRIATIC LINEAMENT) IN THE SOUTHERN REGION OF AUSTRIA**

Norbert HOEGGERL, Diethard Ruess (both at Federal Office of Metrology and Surveying, Schiffamtsgasse 1-3, A-1025 Wien, Austria, email: diethard.ruess@univie.ac.at)

The Periadriatic lineament from the Seisa Zone (Italy) to the Pannonic Lowland (Hungary) is one part of the collision zone between the African tectonic plate and the Eurasian tectonic plate. The activity of this lineament is documented by different earthquakes during the last centuries (Villach/Austria 1348, Friaul/Italy 1976, Bovec/Slovenia 1998, a.o.). To monitor possible displacements of the earth's surface along the Periadriatic lineament, different control networks were established in this part of southern Austria: control points measured by GPS-technology were tied to a network of different levelling lines. These different networks contain control points situated north and south of the fault zone. The control points are spread over an area of about 20x50km. In addition to the geodetic control network, 4 absolute gravity points were established. The local stability of these absolute gravity points will be monitored by micro-gravimetric measurements and precise levellings. The combination of the geodetic and the gravimetric networks offers the possibility to investigate and jointly interpret changes of the earth's surface and of the earth's interior. Results derived from the comparison of repeated levelling measurements (periods 1952, 1964, 1976, 1987 and 1997) across the Periadriatic lineament show significant height changes. The correlation of these height changes with the earthquakes 1976 and 1998 will be presented.

**G5/E/19-A4** Poster **1230-10**

**ON THE RECENT VERTICAL CRUSTAL MOTIONS IN UZBEKISTAN**

A.R.YARMUKHAMEDOV, D.A.Tashkhojaev, L.P.Yun (Institute of Seismology, Khurshid str.3, 700128 Tashkent, Uzbekistan, email: root@seismo.tashkent.su)

A new map of the recent vertical motions (RVCM) of the territory of Uzbekistan (scale-1:2500000) was constructed in 1997 on the basis of new geodetic data (to 1994 inclusive). Analysis of this map and large-scale map of some test-grounds and cities shows that RVCM include platform and orogenous areas of Uzbekistan. About 70% of the territory of Uzbekistan are involved in the rise. Distinct geostructural differentiation of RVCM is outlined in some structures. The most part of the geological structures in the platform areas is involved in the rise and intensity of their vertical motions increases from east to west and north-west. Intensive ascending motions (from 6 to 10 mm/year) include both the positive and negative (under 6 mm/year) geostructures. Tectonic activity is typical for the structures adjacent to the Aral Sea (10-14 mm/year). The connection between RVCM and seismicity indicates the sign-alternating motion of tectonic nature. One of the main features of RVCM is their differentiation caused by engagement of the border parts of the blocks. Destruction of the engagement zones leads to the stress drop in some regions but does not change the regional motions. It follows from the above stated that slow and quick (seismic) motions are intercommunicated manifestation of the continuous processes of stress accumulation and discharging in the earth's crust. Three main directions for the zones of the high-gradient motion change are outlined. Intersections of the zones are connected with earthquake sources, cracked zones and engineering-geological processes.

**G5/E/43-A4** Poster **1230-11**

**THE GEOPHYSICAL AND GEOLOGO-GEODETTIC STUDIES OF THE RECENT CRUSTAL MOTIONS ON THE TAVAKSAI TEST-GROUNDS IN UZBEKISTAN**

K.N.ABDULLABEKOV, A.R.Yarmukhamedov, S.Kh.Maksudov (Institute of seismology, Khurshid str.3, 700128 Tashkent, Uzbekistan, email: root@seismo.tashkent.su)

The geomagnetic, geologo-geodetic and radiometric studies have been carried out on the gedyndamic test-grounds of Uzbekistan and in particular on the Tashkent test-grounds since 1968 to determine strong earthquake precursors and their spatial and temporal features. In geologo-tectonic respect the region under investigation is located in the zone of the regional Karzhantau and Tavaksai faults intersection. The north side of the Karzhantau fault is a rise of the same name, the south one is Chirchik depression. In 1992-1995 10 cycles of the high-precise repeated levelling, length measurement between special triangulations (20 sides) and 8 cycles of geomagnetic and radiometric observations were being carried out. The results obtained show that there are some anomalous changes of the geomagnetic field (T), recent vertical (h) and horizontal (L) crustal motion, gamma-activity in the geological structures of the Tavaksai test-grounds. Spatial and temporal variations of the T and h values have the following tendencies: anomalous changes of the geomagnetic field (T) of small amplitude (1-5 nT) on the right side of the Tavaksai fault do not correlate with the geodetic data; considerable changes of the T value (10-15 nT) which are in a good agreement with the geodetic data are registered directly in the Tavaksai fault zone; anomalous trend of the recent crustal motions (direction, intensity) and geophysical parameters forestalling seismic event becomes apparent in different geotectonic structures of the fault.

**G5/E/34-A4** Poster **1230-12**

**CORRELATION BETWEEN RECENT STRUCTURES AND RECENT GPS MOTIONS WITHIN THE CENTRAL TIEN SHAN (KYRGYZSTAN AND KAZAKHSTAN)**

Yuriy Trapeznikov, Alexander Zubovich, Vitaly Bragin and Alexander MIKOLAICHUK (International Research Center - Geodynamic Proving Ground in Bishkek, 720049, Bishkek-49, Kyrgyzstan, email: mav@laurel.gdirc.ru)

East-west trending ranges alternating with subparallel sedimentary basins are the main structural units of the Central Tien Shan. The ranges are characterized by block and fold deformation of pre-Paleogene erosion surfaces which are uplifted to elevations of 5-7 km. In the sedimentary depressions this structural surface is lowered to 3-4.5 km below sea level. The maximum thickness of Cenozoic deposits reaches 5-5.5 km. Within this region a GPS network was installed, presently including 240 sites. Regular measurements have been conducted for six years. The whole system of ranges and depressions shortens in the sublatitudinal direction relatively to the Kazakh platform. The velocity of motion decreases to the north, varying from 11 - 12 mm/yr at the Kokshaal range to 0 - 1 mm/yr at the Zailii range. At the meridional section, the Tien Shan ranges bound depressions by right and left-striking reverse-slip faults. The observed horizontal motion gradient field does not comply with these major faults. The structure of vertical motion modern field also does not comply with major morphostructural units of the Central Tien Shan.

**Thursday 22 July PM**

Presiding Chair: V. Dehant (Royal Observatory of Belgium, Bruxelles, Belgium)

**REGIONAL AND GLOBAL DEFORMATIONS**

**G5/L/06-A4** **1400**

**CRUSTAL DEFORMATION MONITORING OF VOLCANOES IN JAPAN USING L-BAND SAR INTERFEROMETRY**

Makoto MURAKAMI, Satoshi Fujiwara, Shinzaburo Ozawa, Hiroyuki Nakagawa And Mikio Tobita (Geographical Survey Institute, Kitasato-1, Tsukuba-Shi, Ibaraki-Ken, 305 Japan, Tel : +81-298-64-6925, Fax: +81-298-64-2955, E-mail: mccoyp@gsi-mc.go.jp)

Since 1994 we have been conducting studies to apply interferometric L-band SAR (InSAR) for the detection of crustal deformations. L-band InSAR is particularly useful for monitoring of crustal deformations associated with volcanic activities. We observed crustal deformations caused by inflation of magma source of Mt. Mihara of Izu-Oshima Island as well as subsidence of the volcano's caldera. The pattern of crustal deformation is in good agreement with predicted by an inflation model. We also detected the volcanic crustal deformation of Mt. Iwate which has been active since March 1998. The spatial pattern of the detected deformation by InSAR strongly suggests an existence of an inflation source about 8 km below the ground surface. Our experiences show that in some applications the InSAR data plays a key role to understand physical process of volcanic activities. We also carried out a repeatability study over Izu-peninsula where coverage of JERS-1 data is fine and crustal deformations are persistent. We processed many scenes and compared them. We found to model water vapor distribution is difficult without additional information. Water vapor effects sometimes show a correlation with topography but it is not always consistent. A pragmatic way to eliminate this effect is to perform temporal averaging for multiple interferograms obtained at different epochs. After this averaging the precision of measurement of crustal deformation using JERS-1 SAR is estimated better than 1 cm. In this paper we will review our experiences using L-band InSAR for volcanic studies and discuss advantages and limitations of the technology. Although JERS-1 ceased to operate on October 12, 1998, there are enormous amount of existing data taken by JERS-1 available and we can detect unknown crustal deformations from them. Another good news is a next generation L-band SAR sensor onboard ALOS is to be launched in 2002.

**GEODETTIC INSTRUMENTATION AND MEASUREMENTS**

**Introduction** **1415**

B. Richter (Bundesamt fuer Kartographie und Geodaesie, Frankfurt, Germany)

**G5/E/37-A4** Poster **1415-01**

**ABSOLUTE CALIBRATION OF SUPERCONDUCTING GRAVIMETERS - A COMPRISON OF METHODS**

Bernd RICHTER, Ilona Nowak, Herbert Wilmes (all (Bundesamt fuer Kartographie und Geodaesie, Frankfurt a.M., Germany, email: richter@ifag.de)

Stationary superconducting gravimeters can be calibrated by parallel observations with other gravimeter types during phases of relatively strong (tidal) gravity changes or by applying known artificially induced accelerations to the gravimeter sensor. Repeated parallel observation with an absolute gravimeter have two advantages: (1) the improved determination and verification of the gravity factor and (2) the survey of drift behaviour respectively the determination of drift factors. Artificial accelerations can be applied to the superconducting gravimeter by the Frankfurt calibration system. Periodic vertical movements of the gravimeters with varying period lengths and amplitudes exert known accelerations which are used to determine the calibration factors and instrument characteristics of the superconducting gravimeter. New developments have been made to increase the vertical basis and to improve the precision of the interactive feedback and registration system. The results of the different methods will be compared and analysed in relation to systematic effects.

**G5/E/38-A4** Poster **1415-02**

**SIMPLIFIED SUPERCONDUCTING GRAVIMETERS FOR OPERATION AT REMOTE LOCATION**

Bernd RICHTER (Bundesamt fuer Kartographie und Geodaesie, Frankfurt a.M., Germany, email: richter@ifag.de); Eric W. Brinton, Richard C. Reineman, R. J. Warburton (all GWR Instruments, Inc., 6264 Ferris Square, Suite D, San Diego, CA, USA, email: warburton@gwrinstruments.com)

Except for two dense clusters of Superconducting Gravimeters (SGs) in Europe and Japan, the worldwide distribution remains sparse. This is both due to the difficulty and expense associated with supplying liquid helium needed for cooling the gravimeter, and by the need for highly trained technicians to operate the gravimeter. In this paper, we report progress toward a SG system that is easy to deploy and operate at remote sites, requires no helium replenishing, and which can be operated remotely via modem. In recent work, we describe the development of an ultra long holdtime dewar where all boiled off helium gas from the dewar is

re-condensed. Developments have been started for a system that uses only 2 kW of power and methods will be discussed to avoid helium loss during power failures. This system is designed to be serviced and maintained by local personnel. Setting up, initializing, and operating a SG requires a technician with specialized skills which currently are learned over a period of several years working with SGs. Progress is made to simplifying these procedures so they can be performed via computer modem by either users or GWR personnel operating from their home base. These improvements and simplified operation will enable users to operate SGs at many new sites of geophysical interest.

**G5/W/08-A4** Poster **1415-03**

**GRAVITY OBSERVATIONS AT THE GEODYNAMIC OBSERVATORY MOXA, GERMANY**

Corinna KRONER and Thomas Jahr (both at Institute for Geosciences, FSU Jena, Burgweg 11, 07749 Jena, Germany, e-mail: kroner@geo.uni-jena.de)

In the scope of the expansion of the seismological observatory Moxa (Thuringia, Germany) into a geodynamic broadband-observatory the continuous monitoring of temporal gravity changes started last year.

In order to determine first tidal parameters for Moxa station and to get to know the station noise in the period range from a couple of minutes up to several days, a LCR earth tide and a LCR-D gravity meter recorded simultaneously for some months. These recordings were basically done in preparation of the monitoring with a superconducting gravimeter at the observatory starting in 1999. Results obtained from these first gravity observations esp. with regard to station noise and environmental influences are presented.

**G5/W/17-A4** Poster **1415-04**

**HIGH PRECISION TIDAL MODELLING AT THE GRAVIMETRIC STATION OF BRASIMONE (ITALY).**

Giuseppe CASULA (Istituto Nazionale di Geofisica, Roma, c/o Department of Physics - Sector Geophysics Univ. Of Bologna, V.le C.B. Pichat n.8 40137 Bologna, Italy, E-Mail: casula@ibogfs.df.unibo.it); Paolo Baldi (Department of Physics Univ. Of Bologna, V.le C.B. Pichat n.8 40137 Bologna, Italy, E-Mail: baldi@ibogfs.df.unibo.it).

A superconducting gravimeter GWR number T015 was installed in the ENEA research center of Brasimone, in the Italian Apennines between Bologna and Florence (44° 07' N 11° 07' E 890m H). The instrument was involved in the Global Geodynamics Project in July 1996 and is actually recording continuously the local acceleration of gravity.

The gravimeter is continuously calibrated by means of a moving mass system with a precision of 0.3% or better; the calibration factors computed with the mass experiments were verified by means of an intercomparison campaign with the absolute gravimeter FG5-205 of IPG of Strasbourg, in October 1997. The results of the two calibration methods are in good agreement and the calibration constant of the SG gravimeter has been improved by a factor 2 by means of absolute gravimetry.

Several months of data records were collected and sent to the ICET (International Center of Earth Tides), the data were elaborated with the aid of Eterna-Preterna Softwares to compute amplitudes, gravimetric factors and phases of the Tamura 1987 tidal catalogue. The effect of the barometric pressure on gravity was computed and the resulting barometric pressure admittance, about -0.32 microgal/mbar, is in agreement with the physical models, and was used to eliminate barometric pressure noise from data.

**G5/P/06-A4** Poster **1415-05**

**OBSERVATIONS OF THE EARTH TIDE VARIATIONS IN SOUTH KOREA**

Uk HAN (Dept. of Environmental Sciences, Korea Military Academy, Seoul, 139-799, Korea, email jiguogong@chollian.net); Jung Hwan Park (Dept. of Earth Sciences & Engineering, AIMST, Seoul, 139-799, Korea)

Earth tide observations were taken at KMA observatory in South Korea by LaCoste-Romberg ET gravimeter for determining the gravimetric factor (d) and analysing the tidal components from September 2 to 16, 1997. Meter drifts were corrected by regression and then denoised by thresholding wavelet, a data processing tool. The mean value of d is 1.2 and the mean phase lag of k(M2, S2) and AK(K1, O1) is  $0.07 \pm 0.03^\circ$  and  $0.08 \pm 0.07^\circ$  by analysing the observed earth tides. For yielding measurements of gravity accurate to about 0.01 mgal, the Earth tide observations are required by ET meter. The tidal variations are due to the planet's distance and zenith angle. With the exception of Earth-Moon and Earth-Sun mechanism, the possible causes of tidal variations are tectonical, meteorological and hydrological perturbations. The long period and broad observations are required for determining the state of gravimetric factor and tidal constituents in Korea.

**G5/E/32-A4** Poster **1415-06**

**DEVELOPMENTS OF MULTICOMPONENT LASER STRAINMETER SYSTEMS AND THEIR USE IN SEISMOLOGY AND GEODYNAMICS**

Mstislav N. DUBROV and Rostislav F. Matveev (both at Institute of radioengineering and electronics, Russian Academy of Sciences, ac. Vvedensky sq., 1, Fryazino, Moscow region, 141120 Russia, email: mnd139@ire216.msk.su)

Our recent progress in laser interferometry developments brings forward the new approach to instrumental geophysics and terrestrial observations. The number of tensor components which characterise the deforming earth surface can be obtained by means of the novel laser strainmeters. The original scheme of multicomponent laser instrument with spatially distanced arms has been analysed. We obtained the forms of seismic wave responses for arbitrary laser strainmeter length and orientation. Seismic and strain signals have been investigated by two separately located laser strainmeters at Moscow region. The distance between the instruments is about of 100 km, the analysed frequency band is  $10^{**}(-6)...120$  Hz. The analogue and digital records and the results of their spectral analysis have been obtained. The comparison of seismic waves parameters has been done for simultaneous records by pendulum seismometers and 2-component laser strainmeter. The experimental prototype of jamproof laser strainmeter has been tested, and its resolution of 1 nm has been proved on the basis up to 150 m. The quantitative relation between atmospheric pressure variations and earth strain oscillations has been investigated in the wide frequency range. We have obtained the values of strain/pressure ratios for the laser strainmeters. Specific features of the strain-pressure interactions have been revealed. The problems of laser strainmeter's practical application in the global geodynamic reference frame are analysed.

**G5/E/28-A4** Poster **1415-07**

**THE LONG WATER TUBE TIDAL INSTRUMENT IN KSIASZ GEOPHYSICAL STATION**

Marek KACZOROWSKI Space Research Centre, (Polish Academy of Sciences, Bartycka 18A, 00-716 Warsaw, Poland, email: marekk@cbk.waw.pl)

In 1997 Comity of Scientific Investigations accepted to realisation project "Installation of the long water tube tidal instrument in Ksiaz geophysical station". Since April 1997 initial works were made. Natural geological and morphological conditions are very suitable there to carry out tidal observations. During 25 years the tidal observations are permanently realised in Ksiaz station by use of the quartz horizontal pendulums. Relationship between old tidal observations gather in Ksiaz station and recent one obtained with use long water tube make a good change to initial new investigations of earlier series of tidal observations. In case of the long water tube we have in practise instrument without drift. Comparison of the observations of two different instruments allowed us to determine drift of quartz horizontal pendulums. We can expect that long water tube instrument help use to improved accuracy of determination the long period and systematic variations of vertical line as well as yearly and half yearly modulations of daily and half daily tidal waves. Absent of drift in water tube instrument make a special occasion to initialisation new investigations like investigations of secular variations of the world gravity field, modern crust movement and tectonic of the Sudet mountain. Transitionally, a new instrument will weave monitoring process occurred in global ocean which caused generation of the long period and systematic variations of vertical and tidal waves modulation. The mention variations in the ocean are generated by global hothouse effect being fundamental ecological problem. The installation works of long water tube are leading parallel in underground of Ksiaz station as well as in optic laboratory of Space Research Centre of Polish Academy of Sciences.

**G5/E/31-A4** **1430**

**THE SEA SURFACE OF THE BALTIC =96 A RESULT FROM THE BALTIC SEA LEVEL PROJECT (IAG SSC 8.1)**

Markku POUTANEN and Juhani Kakkuri (Finnish Geodetic Institute, Geodeetinrinne 2, FIN-02430 Masala, Finland email: Markku.Poutanen@fgi.fi)

We describe the final results of the Baltic Sea Level (BSL) 97 GPS campaign and the combination of three successive BSL campaigns. Because the last campaign was made simultaneously with the EUVN (European Vertical Reference Network) GPS campaign, we were able to obtain a well-defined connection between the two networks. Moreover, combining tide gauge data and gravimetric precise geoid NKG96, we recomputed the sea surface topography (SST) of the Baltic Sea with a greater accuracy than before. We compare this with the more detailed SST obtained from the satellite altimetry. In satellite altimetry we use a Gradient method which we describe in the paper. We also discuss the future of the Baltic Sea Level project.

**G5/W/09-A4** **1445**

**PRELIMINARY STUDY OF BLOCK ROTATION MODEL IN NORTH CHINA AREA BY USING GPS MEASUREMENTS**

Caijun XU, Jingnan Liu, Dingbo Chao, and Ting Chen (School of Geo-science and Surveying Engineering, Wuhan Technical University of Surveying and Mapping, 129 Luoyu Road, Wuhan, 430079, China, email: cju@hpb1.wtustm.edu.cn); Jusheng Xu (Institute of Seismology, State Seismological Bureau, Xiaohongshan, Wuhan, 430071, China)

North China as a lithospheric dynamics subregion is located in the middle part of eastern China. It is characterized by more intense activity of lithospheric dynamics in comparison with Northeast China and South China. Two parts of North China region separated by Taihang Mts. The eastern part is basin, it may be further divided into Jizhong block, Jilu block, and Luliao block from west to east, and their boundaries are Changdong fault and Yilu fault respectively. The western part may be divided into two blocks by Ordos's fault; they are Ordos block and Taihang block.

Repeated GPS surveys in North China provide a direct measurement of current crustal motions. GPS surveys have been carried out in the region in 1992, 1995, and 1996 respectively, the GPS velocity field are estimated and they are used to estimate that North China sub-plate and intra-block rotation motions. The rotation rate of North China sub-plate by GPS measurements is good fitting the ratio of fault slip to fault spacing from Neogene in this area. The current rotation pattern of Ordos block, Taihang block and North China Plain block indicate decreasing actions toward western boundary of Ordos block from south to north by Qinghai-Tibet plateau uplifting and extending. It is also associated with the collision of India, Pacific with Eurasia.

**KINEMATICAL STUDY OF CRUSTAL DEFORMATIONS**

**G5/E/06-A4** Poster **1500-01**

**A REVIEW OF PLATE TECTONIC MOTIONS IN SOUTHEAST ASIA**

Sobar SUTISNA and Parluhutan Manurung (both at Center for Basicdata Survey, National Coordination Agency for Surveying and Mapping, P.O.Box 46/CBI, Cibinong 16911, INDONESIA, email: sobar@cbn.net.id)

This paper is aimed at reviewing and discussing the major tectonic activities of the current plate motions existing in the Southeast Asia. The study based on literature of various publication of research activities, of which mostly are carried out by geophysicists. Publications of regional studies with geodetic measurements are also discussed based on GPS observation started from the past ten years ago.

This review concluded that in terms geodynamics, Southeast Asia is considered as a young region, active and very complicated where continental collision, subduction, continental-island arc collision and junction of four plates are occur. This region accounts for a substantial number of earthquakes and also severe and catastrophic in where 500 million people are living. This area are indeed an excellent field laboratory for studying plate tectonic motions. Some GPS geodynamic monitoring results in the region from some years ago are also highlighted and discussed.



**G5/W/02-A4** Poster **1502-02****SPATIAL AND TEMPORAL VARIATIONS OF CRUSTAL STRAIN IN THE TAIWAN AREA**

Shui-Beih YU, Long-Chen Kuo and Chin-Hsiang Yen (Institute of Earth Sciences, Academia Sinica, P.O. Box 1-55, Nankang, Taipei, Taiwan, R.O.C., email: eayusb@ccvax.sinica.edu.tw)

The "Taiwan GPS Network" is composed of 131 annually surveyed mobile stations and 9 continuously recording permanent stations. The mobile stations have been surveyed 7-8 times from 1990 to 1997, while the permanent stations have been in operation since November 1991. The changes of baseline length are utilized to study the spatial and temporal variations of crustal strain in the Taiwan area. The entire network is divided into 78 subnets. Then the average strain rates and their annual variations for each of the subnets are estimated. Dramatic compressive strain rates are observed in the Longitudinal Valley of eastern Taiwan and near the Chukou fault of southwestern Taiwan. The extremely high strain rates in the Longitudinal Valley area are mainly caused by the aseismic slip on the Longitudinal Valley fault. In contrast, the crustal strain is likely to be accumulating in the vicinity of Chukou fault and gives rise to a possibility of generating major earthquakes. The western Coastal Plain and central Taiwan show slight to moderate contractions, while the southern Central Range, northern Taiwan and Ilan Plain reveal significant extensional deformation. Except the strain rates of very few subnets have been disturbed by the occurrence of the nearby moderate earthquakes, the temporal variations of crustal strain are generally quite uniform during the past few years.

**G5/E/33-A4** Poster **1504-03****TIME SERIES OF INTERPLATE COUPLING IN THE TOKAI REGION, CENTRAL JAPAN, DEDUCED FROM EDM RANGING AND LEVELING DATA IN 1978-1997.**

Fumiaki KIMATA (School of Science, Nagoya University, Nagoya, 464-8602 JPN, email: kimata@seis.nagoya-u.ac.jp). Kazuro Hiragata (Graduate School of Science, Nagoya University, Nagoya, 464-8602 JPN, email: hirahara@eps.nagoya-u.ac.jp); Naoyuki Fujii (School of Science, Nagoya University, Nagoya, 464-8602 JPN, email: fujii@seis.nagoya-u.ac.jp).

To clear the time series of interplate coupling of the Eurasian Plate and the Philippine Sea Plate under the Tokai region, southwest Japan, authors discuss the EDM and leveling data observed seasonally or yearly in the period 1978-1997. Discussing the EDM rangings on two baselines clear that contraction of line lengths are repeated acceleration and reduction of the contraction with a frequency of four to five years. For example, contractions show  $5.4 \times 10^{-7}/\text{yr}$  and  $4.2 \times 10^{-7}/\text{yr}$  in 1983-1987 and deduced to  $0.9 \times 10^{-7}/\text{yr}$  and  $0.0 \times 10^{-7}/\text{yr}$  in the next period of 1987-1991. Episodic vertical movements are also deduced from the yearly leveling by Geographical Survey Institute. When the contractions of line lengths are accelerated, the subsidence on the west coast of Suruga Bay is extended to the westward in this region. Contrary subsidences are observed only in the eastern part of the west coast in the period of deduced contraction. The inversion analysis based on baseline length changes and vertical movements shows back slip vectors of 3-4 cm/yr toward northwest under the Tokai region throughout the observation period, and vectors of 10 cm/yr in 1983-1987, which is the period of acceleration of contraction and tilting. It is suggested that interplate coupling is episodic with time in the Tokai region.

**G5/W/21-A4** Poster **1506-04****INVESTIGATING THE EFFECT OF MW 6.2 EARTHQUAKE IN TAIWAN WITH GPS OBSERVATIONS**

Jenn-Taur LEE (Department of Surveying and Mapping Engineering, Chung Cheng Institute of Technology, Tahsi, Taoyuan, Taiwan 33509, email: jtlee@cct.edu.tw)

The biggest earthquake for last thirty-four years occurred on July of 1998 in the southern portion of Taiwan. In 1906, there was a MW 7.1 earthquake appeared around the same area. Since Taiwan is located at the collision belt between Eurasia plate and Philippine sea plate, the collision and oppression happened frequently between these two plates. The conducted stress does obviously move towards the western parts of Taiwan and the energy may release at the active fault along the western coast of Taiwan.

A set of GPS observations was obtained from the Taiwan's GPS network project to study the effect of the MW 6.2 earthquake in Taiwan. The GPS raw data measured with TurboRogue SNR-8000 come from five GPS continuous stations in the Taiwan GPS network, FLNM, KDNM, PKGM, TMAM, and YMSM. These GPS measurements were linearly combined to the ionosphere free form and the double-differencing technique associated with the relaxing satellite orbit was used to do the estimation task. Moreover, the phase ambiguity resolved with the wide-lane approach. Since the PKGM station is not far away from the origin of earthquake, the position variation of PKGM is about 2, 3, and 20 cm along the north, east, and upper directions, respectively. The length between PKGM and the others are shorten about 5 cm which is similar to the average normal field velocity per year of Taiwan island. In addition, the movement direction of each baseline is approximately to the PKGM station in which may explain the outcome from the oppression of the collision belt.

**G5/P/04-A4** Poster **1508-05****PREDICTION OF MODERN CRUSTAL MOVEMENTS IN THE AREAS OF NUCLEAR POWER PLANT**

V.N. Morozov, V.N. Tatarinov, A.A. Lopanthuk (Geophysical Center, Russian Academy of Sciences, Molodzhzhayna, 3, Moscow, II 7296, Russia)

It is well known that the deformations features of geological environment can serve as precursors of seismic events. Complex geophysical and geodetic monitoring allows us to estimate speeds and directions of modern geodynamic horizontal movements, to connect them with periods of preparation of possible seismic events, and to make conclusions about conditions of geological environment in zones of abnormal deformations in the areas where ecologically dangerous nuclear-fuel cycle objects are located.

In 1995-96 three series of GPS-observations were conducted on geodynamic sites in the area of Kalinin and Novovoronezh Power Plant. As a result of this work, the technique of GPS-observations was elaborated, initial coordinates and lengths of basic vectors between reference points were obtained and preliminary data on features of modern geodynamic movements in the areas where nuclear power plants are located were received.

The data were correlated with data obtained by regional observation stations located on the East-European platform, thus allowing us to obtain the relative error of basic vectors length definition equal - 1.10-6.

**G5/W/14-A4** Poster **1510-06****INVERSE ANALYSIS OF GPS MONITORING DATA IN SUZHOU, CHINA**

Jicang WU, Dajie Liu, and Congwei Hu (Surveying Department, Tongji University, Shanghai, 200092, China, email: jcwu@ceiliang.tongji.edu.cn)

In this paper, four campaigns of GPS monitoring data (distance changes, and height changes) since 1996 have been used to determine the local crust deformation model by Bayesian inversion method. The geological investigation data, and seismic activities of the main geological faults in this area have been used as the prior information in the inverse analysis. According to the GPS monitoring data, this area has suffered the significant subsidence caused by extracting underground water. Our inversion results show that the ground subsidence caused by human has a significant affect on the movements of the main geological faults in this area.

**G5/W/27-A4** Poster **1512-07****THE ESTIMATION OF CRUSTAL DEFORMATION IN SHANXI AREA, CHINA, FROM THE 1995 AND 1996 GPS OBSERVATIONS**

Q.W. LIU and Y.Q. Chen (both at Department of Land Surveying & Geo-Informatics, The Hong Kong Polytechnic University, Hunghom, Kowloon, Hong Kong, email: lsqwu@polyu.edu.hk); Y.X. Li (The First Crustal Deformation Monitoring Center, State Seismological Bureau of China, Yihaoqiao, Hedong District, Tianjin 300180, China, email: dzjl@shell.tjvan.net.cn)

Two years of GPS data is analysed to detect crustal deformation in the Shanxi area, one of the most seismological active area in China. A rigorous statistical iterative approach based on the classical F (Fisher) test is applied to solve the datum problem. The multi-epoch simultaneous estimation model, is employed to construct a regional displacement rate field. Furthermore, the displacement-strain relationship with some special modelling considerations is used to build the regional strain field. Although more substantial geophysical conclusions require more detailed observations, the estimated displacement pattern and strain pattern are generally coherent with the features of the main tectonic structures identified for this area. Some important regional deformation information has been found in this study.

**G5/W/10-A4** Poster **1514-08****DIFFERENCES BETWEEN VERTICAL DATUMS, POSTGLACIAL REBOUND EFFECT AND HORIZONTAL MOVEMENTS IN THE SOUTHERN PART OF BALTIC REGION DETERMINED FROM BSL GPS CAMPAIGNS PERFORMED IN 1993 AND 1997**

Ryszard ZDUNEK, Janusz B. Zieliński (Space Research Centre of the Polish Academy of Sciences, ul. Bartycka 18A, 00-716 Warszawa, Poland)

In a frame of Baltic Sea Level Project three GPS Campaigns were performed up till now. The first campaign in 1990 was organized rather for testing purposes. The second one was made in 1993 and the third (from May 21 to May 29, 1997) coincided with the European Vertical GPS Reference Network (EUVN). This paper presents some results obtained from these measurements. For studies of main goals of the project (e.g. unification of vertical datums and their time variability for the countries around the Baltic Sea, determination of mean sea level and sea surface topography of the Baltic Sea, study of the effect of sea floor topography and monitoring the postglacial rebound of Fennoscandia) 29 stations were selected from the whole network which were identical in last two GPS BSL campaigns. Coordinates of these stations were computed using Bernese Software ver. 4 with vector constructions which minimized known systematic effects like e.g. mixing different types of antennas and receivers. Taking into account obtained accuracy of station coordinates (ab. 1mm in horizontal and 3mm in height component) and the additional data from precise levelling and tide gauge readings collected during GPS campaigns in 1993 and 1997 we determined the differences between national vertical datums existing in Baltic countries and postglacial rebound effect as well as horizontal movements of stations especially in southern part of Baltic region.

**G5/W/07-A4** Poster **1516-09****GEODYNAMIC OF THE EAST SUDETEN (BORDER AREA OF THE CZECH REPUBLIC AND POLAND)**

Vladimír SCHENK, Zdeňka Schenková and Pavel Kottbauer (all at Institute of Rock Structure and Mechanics, Academy of Sciences, CZ-182 09 Praha 8, The Czech Republic, email: schenk@irms.cas.cz); Stefan Cacoň, Bernard Kontny and Jaros\_aw Bosy (all at Department of Geodesy and Photogrammetry, Agricultural University, PL-50-357 Wrocław, Poland, email: cacon@kgf.ar.wroc.pl)

The structural geological block Sudeten builds the north-east part of the Bohemian Massif. Occurrences of earthquakes, neovolcanic intrusions, CO<sub>2</sub> mineral water sources, monitoring of geodetic deformations give evidences on an existence of the recent mobility on its tectonic elements. In 1997 the existing Polish and Czech regional GPS geodynamic networks joined into one SUDETEN network. Its length is approximately 150 km in the NW-SE direction and approximately 80 km in the perpendicular direction. The GPS points, in a form of concrete blocks with a base of 40x40 cm and height between 40 and 120 cm, were built on places of hard rock outcrops and/or very stable structures. Moreover, in the area of the SUDETEN network three permanent and three local seismic stations with start-stop registrations and one local seismic array operate. In 1997 and 1998 two simultaneous GPS campaigns on Czech and Polish points were performed. The main goal of the present geodynamic investigations of the Sudeten area, realised under the Polish and Czech research projects, is an identification of recent mobile active zones, a motion potential classification of particular geological blocks and a verification of a possible mobile activity of significant equatorial faults. Applied methodology allowed the accuracy in GPS points determination to be increased. RMS errors calculated for individual points were obtained lower than 2 millimetres. The results of this investigations and preliminary interpretation of the GPS monitoring verified by seismic observations are presented in the paper.

**G5/E/12-A4** Poster **1518-10****ON MONITORING THE FINNISH PERMANENT GPS NETWORK - FINNREF**

Hannu KOIVULA and Markku Poutanen (Finnish Geodetic Institute, P.O.Box 15, FIN-02431 Masala, Finland email: Hannu.Koivula@fgi.fi)

The Finnish GPS network FinnRef has been operating since 1994. The full deployment of 12 stations was reached in October, 1996. All stations are equipped with Ashtech Z-12 receivers with Dorne Margolin antennas (except Mets=E4hovi, which is equipped with a Turbo Rogue). The network is used as reference when the GPS network has been densified. Data are processed using Bernese 4.0 Software. From daily solutions the normal equations are saved



and used later to produce weekly and monthly solutions and their time series. We will show the latest status and the performance of the network and show three years time series, the effect of the Finnish winter on them, and how they are and will be used for studying and monitoring the post-glacial rebound.

**G5/E/17-A4** Poster **1520-11**

**ACHIEVEMENTS OF THE LONG TERM COOPERATION IN GEODESY AND GEODYNAMICS OF SIXTEEN CEI (CENTRAL EUROPEAN INITIATIVE) COUNTRIES. FUTURE PLANS**

Janusz SLEDZINSKI (Warsaw University of Technology, Institute of Geodesy and Geodetic Astronomy, 00-661 Warsaw, Poland, Pl. Politechniki 1, e-mail: sledzinski@gik.pw.edu.pl Chairman and International Coordinator of the CEI WGST Section C "Geodesy" Chairman of the IAG Subcommittee "Geodetic and Geodynamic Programmes of the CEI")

The paper includes concise information on some recent geodetic and geodynamic projects that are realised in international co-operation of the Central European countries in the frame of the scientific programme of the CEI WGST Section C "Geodesy". The main achievements of the first phase of the international European geodynamic project CERGOP (Central Europe Regional Geodynamics Project) are outlined. The general objectives of another CEI project UNIGRACE (Unification of Gravity Systems in Central and Eastern Europe) and the results of the 1998 campaign of absolute gravity measurements are pointed out. The programmes of activities of the Section C Working Group on Satellite Navigation Systems and actions realised by the Working Group on University Education Standards are summarized. Some cooperation links between CEI WGST Section C and European Geophysical Society (EGS) and International Association of Geodesy (IAG) are mentioned.

**G5/E/10-A4** Poster **1522-12**

**VERTICAL MOVEMENT AT SLR STATIONS**

R. KOLENKIEWICZ and D. E. Smith (Laboratory for Terrestrial Physics, NASA GSFC Code 920, Greenbelt, MD 20771, USA e-mail: ronk@ltpmail.gsfc.nasa.gov); P. J. Dunn and M. H. Torrence (Raytheon Corp., 7701 Greenbelt Rd., Greenbelt, MD 20770, USA)

The twenty year record of vertical position at SLR stations tracking the LAGEOS I satellite contains signals with periods between hours and years, as well as the long-term effects of crustal movements or post-glacial rebound. Improved temporal sampling from the second satellite in the LAGEOS constellation enables us to separate geophysical from instrumental effects better than was possible with LAGEOS I data alone, as well as to eliminate the effect of orbit error. A growing number of SLR instruments of constantly improving accuracy have been tracking a number of lower geodetic satellite, in particular, Starlet, and these observations also reveal a variety of features in station position motion. Crustal movements which affect vertical control at a station include the Earth's tidal response to the sun and the moon, and strong sensitivity to this variation enables the SLR network to define accurate global parameters, as well as to indicate any geographical dependence. We also find that atmospheric pressure loading produces millimeter level displacements with a signal which depends on the regional pressure, and the effects of ocean tidal loading also appear at some stations. This facilitates the use of the Global Laser Tracking Network's geocentric reference frame to connect regional and local positioning networks monitoring sea level change.

**G5/E/18-A4** **1525-13**

**INTERANNUAL VARIATIONS OF THE VERTICAL AND THEIR POSSIBLE INTERPRETATION**

Zheng-xin LI (Shanghai Observatory, Chinese Academy of Sciences, 80 Nandan Road, Shanghai, 200030, China, email: lzx@center.shao.ac.cn)

Base on the results of plumb line variation (PLV) measured by the gravimetry and astrometry techniques at two different locations ( Jozefoslaw of Poland and the Yunnan province of China), the studies of the interannual variations of the plumb line (vertical) is concluded in the paper. It is clear now that other than the tidal variations of the plumb line, which have already been corrected now in the studies, there are also detectable non-tidal PLV in these two regions, of which the interannual component is in the order of 0.01"-0.02", and one can use either of the two techniques to measure it in practice. Base on the discoveries of the correlationship between the interannual PLV, detected at a certain regions over the world, and the other geodynamical quantities, some possible interpretation is also given in the paper.

**DYNAMICAL STUDY OF CRUSTAL DEFORMATIONS**

**G5/W/22-A4** Poster **1540-01**

**GRAVIMETRIC AND TOPOGRAPHIC FEATURES ACROSS SUBDUCTION ZONES**

P. HARABAGLIA,(Universit' della Basilicata, Centro di Geodinamica, via Anzio s.n, Potenza 85100 Italy Tel no. 39971-474-413 Email: hp245sci@unibas.it); C. Ciorciari, C. Doglioni

We derive the average gravimetric and topographic features of world-wide subductions by stacking of profiles across subduction zones, after an appropriate multiple cross-correlation. The averaged profiles we obtain for each subduction can be grouped in two different categories depending on the orientation of the subduction. In the first there are subductions dipping W-ward or NW-ward; in the second there are those E-ward, NE-ward or NNE-ward. In a hot-spot reference frame, the lithosphere has an average delay of about 2 cm/yr with respect to the underlying upper mantle; this in turn can be as a relative eastward mantle flow. The first group of subductions would contrast this flow, while the second would be oriented flow-ward.

**G5/W/16-A4** Poster **1542-02**

**PLUMB LINE VARIATION CALCULATED FROM RELATIVE GRAVIMETRY**

H. LI, G. Y.Fu (Institute of Seismology, CSB), Z.X.Li(Shanghai Observatory, Chinese Academy of Science)

32 and 46 campaigns of gravity surveys at the local gravity networks in the Western Yunnan Earthquake Prediction Experiment Area (since 1985) and the north China(since 1987) have been performed by using LaCoste and Romberg relative gravity meters, respectively. This paper firstly gave the gravity changes displayed by contour map. Then the plumb line variations were derived from the gravity changes with the Vening-Meinesz formula for Xiaguan and Beijing point which located at the central part of the network, respectively. The results displayed the long term changes and some periodic changes with the scale of about several 0.01". Spectrum analyses show that the amplitudes of interannual changes are about 0.02". These results are consistent with the that derived from the astronomical observance, especially for the that of Xiaguan derived from the gravimetry to that of Kunming derived from the astronomical observance.

**G5/E/42-A4** Poster **1544-03**

**INTERANNUAL VARIATIONS OF THE VERTICAL AT YUNNAN BY ASTROMETRY AND GRAVIMETRY TECHNIQUES**

Zheng-xin LI (Shanghai Observatory, Chinese Academy of Sciences, 80 Nandan Road, Shanghai, 200030, China, email: lzx@center.shao.ac.cn); Hui Li and Guang-yu Fu (Institute of Seismology, SSB, Xiao Hongshan, Wuhan, 430071, China, email: lihui@public.wh.hb.cn); Hui Hu (Yunnan Observatory, Chinese Academy of Sciences, Kunming, 65011, China, email: huhui@public.km.yn.cn)

A determination of the plumb line variation (PLV) during 1985-1997 at the Yunnan province of China has been made recently in using the observations of the gravimetric network there. The purpose of this study is to compare the PLV results, obtained from gravimetry technique, with the time and latitude residuals at the same period derived from the observations of photoelectric astrolab at Yunnan Observatory. The interannual variation of the PLV obtained from the gravimetric technique are in a good accordance with the correspondent component in the time and latitude residuals derived from the astrometric observations. This fact shows once again the evidence with which one may recognize the reality of the interannual variations of the plumb line(vertical) at Yunnan, of which the amplitudes are in the order of 0.02", and also the ability of the two techniques in measuring them in practice.

**G5/E/47-A4** Poster **1546-04**

**THREE DIMENSIONAL ISOSTATIC STUDY OF TAGUS ABYSSAL PLAIN AND AMPERE SEAMOUNT**

Alexandra CARVALHO (Centro de Geofísica da Universidade de Lisboa, R. Escola PolitÁcnica, 58, 1250 Lisboa, Portugal, email: adias@fc.ul.pt); J.M. Miranda (Centro de Geofísica da Universidade de Lisboa e Departamento de Física da Faculdade de Ciências da Universidade de Lisboa, R. Escola PolitÁcnica, 58, 1250 Lisboa, Portugal, email: jmiranda@fc.ul.pt)

The isostatic equilibrium of the Western Iberian Margin has been already analysed from ship gravity compilation and Seasat gravity data. However, no clear results was obtain, even in what concerns the main geological features of the area. Being so, a new gravity compilation over the West Iberian Margin was performed and together with TOPEX-ERS-1 data we study the isostatic compensation of Tagus Abyssal Plain and Ampere Seamount, in North Atlantic Ocean, on a spectral domain, in a 3D approach. Results were compared with studies made by seismology.

We conclude that Tagus Abyssal Plain shows evidence for a local compensation scheme with a crystal thickness of 105 km and that Ampere Seamount is not isostatically compensated.

**G5/E/46-A4** Poster **1548-05**

**ELASTIC THICKNESS OF THE LITHOSPHERE AT THE AZORES PLATEAU. A SPECTRAL ANALYSIS APPROACH**

Alexandra CARVALHO (Centro de Geofísica da Universidade de Lisboa, R. Escola Politécnica 58, 1250 Lisboa, Portugal, email: adias@fc.ul.pt); Joaquim Luis (Universidade do Algarve, UCEH, Campus de Gambelas, 8000 faro, Portugal, email: jluis@mozart.sj.ualg.pt); J.M. Miranda (CGUL, R. Escola Politécnica 58, 1250 Lisboa, Portugal, email: jmiranda@fc.ul.pt)

The azores plateau is a zone of anomalously shallow topography with an approximately triangular form defined by the Mid-Atlantic Ridge (MAR) axis between 40 and 37°30'N in the West, the East Azores Fracture Zone (EAFZ) in the South and a line running WNW-ESE from the MAR to the Western limit of Gloria fault and is often interpreted as the morphological signature of the third arm of the Azores Triple Junction.

A study performed in 1996 account for a regional compensation scheme of the Azores Plateau and a lack of local compensation in topographic high and deep lows, reinforcing the conclusion that the Terceira Axis constitutes a zone of intense intraplate volcanism, but where there is no gravity evidence for the existence of a spreading axis.

Here we present a isostatic study based on a spectral approach, using a free air anomaly map and a bathymetric data shipboard gravity data. These data allowed to compute the admittance, which carries information on the rheology of the lithosphere, and to compare it to theoretical estimates of some isostatic models. Results were compared to available magnetic, gravity and seismic information.

**G5/W/26-A4** Poster **1550-06**

**GEO-DYNAMIC MEASUREMENTS OF COOPERATION BETWEEN CHINA AND SPAIN IN LANZAROTE ISLAND SPAIN**

Jun JIANG (Institute of Seismology, China Seismological Bureau, Wuhan 430071, P. R. China, email: JiangJun@public.wh.hb.cn); R. Vieira (Institute of Astronomy and Geodesy CSIC-UCM, Madrid, Spain, email: vieira@iagmat1.mat.ucm.es); Weixin Cai and Shiling Tan (both at Institute of Seismology, China Seismological Bureau, Wuhan 430071, P. R. China); J. Arnos and E. Velez (both at Institute of Astronomy and Geodesy CSIC-UCM, Madrid, Spain)

The geo-dynamic measurements of the cooperative project between China and Spain in Lanzarote Island of Spain were started in 1991, after the recommendation of United Nations to dedicate the last decade of the century to investigation and possible prevention of natural disasters. The objective is to obtain the tidal tilt and strain models as well as to study the non-tidal tilt and strain variations that can be produced by local tectonic movements. These variations can be studied by continuous observation of surface deformation with tilt and strain techniques (Vieira et al., 1995). It was convenient to include between the objectives of our researches. It was not only the traditional results of tidal observations but also the investigation of those phenomena of geodetic origin that can disturb the tidal parameters or at least produce signals in the recordings of very sensitive instruments use in tidal research (Vieira, 1997). There have been three periods of the cooperation between China and Spain since 1991. We have installed seventeen geo-dynamic sensors in Lanzarote to take the cooperative researches in fields of tidal measurements, volcanic monitoring and possible prevention of natural disasters. In this paper, we will mainly introduce the results of the geo-dynamic measurements in Timanfaya from 1996 to 1998, that is the third period of the cooperation between China and Spain. There are nine geo-dynamic sensors included the tilt-meter (water tube and vertical pendulum), horizontal extensometer, air temperature thermometer, rock temperature thermometer and underground high temperature thermometer running in Timanfaya laboratory for tidal measurements and geo-dynamic researches. The sensitivities of the instruments in Timanfaya were changed into a lower than the instrumentation for tidal measurements on May of 1998 because the environmental influence is so stronger that is too difficult for the tidal measurement, and also they are completely settled for a volcanic activities monitoring and investigation. For the above purpose, here we make some new methods and use them to do the data analysis besides the tidal analysis. In this paper, the geo-dynamic instruments installed in Timanfaya are introduced briefly. Three different filter and spectrum models are applied to the data processing. The spectrum features from the models are investigated and compared. The environmental influence for the geo-dynamic measurements is estimated. The features of ground deformation in Timanfaya is investigated and discussed.

Finally, we also put forward some proposals and applied ways to study the dynamic process of volcanic activities with tidal measurement and geo-dynamic researches.

**G5/E/03-A4**                      **Poster**                      **1552-07**

**TIDAL EFFECTS ON DETERMINING A POINT AT THE BOTTOM OF THE SEA BY COMBINING GPS AND SONAR OBSERVATIONS**

Wenke SUN and Lars E. Sjöberg (both at Royal Institute of Technology, Department of Geodesy and Photogrammetry, S-10044 Stockholm, Sweden, e-mail: sunw@geomatics.kth.se)

This paper treats three kinds of Earth tides: crust tide, equipotential surface point (ocean depth) tide and geoid tide, which are closely related with an observation scheme to determine a point at the bottom of the sea by combining GPS and Sonar observations. The relations between the Earth tides and the tidal effects on GPS and ocean depth observations are discussed. The corresponding mathematical expressions are derived and numerical calculations are performed to demonstrate the tidal effects on GPS and Sonar observations. The maximum vertical tidal effects are estimated to reach 102.9 cm for the geoid tide and 48.0 cm for the crust tide, while the maximum horizontal tidal effects are as much as 410.5 cm and 26.6 cm for geoid tide and crust tide, respectively. Theoretical results imply a very interesting conclusion, namely, in a local area, the static position of a point at the bottom of the sea can be obtained by the dynamic observations via a platform on the sea without any tidal correction. Actually, the tidal effects cancel each other in the mentioned observation scheme. It therefore indicates that the observation scheme is free of tidal effects. Furthermore, we learnt that the divergence caused by any error source on ocean surface is canceled and does not affect the final results. Therefore, to determine the position of a point at the bottom of the sea, we need not consider any tidal effects.

**G5/E/07-A4**                      **Poster**                      **1554-08**

**STUDY OF TRANSFER FUNCTIONS BETWEEN AIR PRESSURE AND OBSERVED EARTH TIDE AT CURITIBA TIDAL STATION, BRAZIL**

Sílvia Helena S. SCHWAB (Graduate Program in Geodetic Sciences, Federal University of Parana, C.P.19001, Curitiba, Pr, Brazil, CEP - 81531-990, email: silviass@geoc.ufpr.br) Sílvio Rogério Correia de Freitas (Graduate Program in Geodetic Sciences, Federal University of Parana, C.P.19011, Curitiba, Pr, Brazil, CEP - 82531-990, email: sfreitas@cce.ufpr.br) Wladimir Shukowsky (Astronomical and Geophysical Institute, São Paulo University, SP, Brazil, email: wladimir@iag.usp.br)

The influence of air pressure on gravity tide is theme of on-going research due to the increasing precision in observations. For this purpose it is important to study its influence in the different frequency bands of the tidal spectrum. Curitiba Tidal Station has been used as reference station since 80's for South American determinations of earth tide parameters but the local and regional air pressure influence patterns have not been studied until now. As a consequence, usually in data processing, standard values have been adopted to correct its influence on tidal gravity measurements. This work presents the study of the Curitiba station air pressure admittance in each tidal band, based on an observation series performed with the GEO 783 gravity meter. Comparisons of the obtained transfer functions of fortnightly blocks have been made as a way to generate a set of values which were compared with the usual pattern.

**G5/E/08-A4**                      **Poster**                      **1556-09**

**A DISCUSSION ABOUT GRAVITY PARAMETERS AT CURITIBA STATION**

Silvio Rogerio Correia DE FREITAS (Graduate Program in Geodetic Federal University of Parana, C.P. 19011, Curitiba, Brazil 82531-990, Email: sfreitas@cce.ufpr.br); Silvia Helena Soares Schwab (Graduate Program in Geodetic Sci Federal University of Parana, C.P 19001, Curitiba, Brazil email: silviass@geoc.ufpr.br); Marta Silvia Maria Mantovani (Astronomical and Geophysical Ins Paulo University, SP, Brazil, Email: marta@iag.usp.br); Wladimir shukowsky (Astronomical and Geophysical Institute, Sao University, SP, Brazil Email: wladimir@iag.usp.br)

The tidal gravity factors at Curitiba Tidal Station, Brazil, determined in 1982/84. This determination was performed based month long series of observations with the Geo783 gravity calibrated at Brussels station. Besides this series of observations gravity meters were used around the same period to check main parameters.

The determined tidal parameters were considered as reference normalisation of other gravity meters used in the tidal observations in America. Considerations about the adequacy of the tidal factor Brussels Fundamental Station and observations with other gravity calibrated on other basis which operated in Curitiba Tidal Station indicate the need of discussion about the redefinition of tide in Curitiba.

A discussion is proposed in this presentation, taking into account the comparison of gravity tides residuals and ocean load at the station.

**G5/E/44-A4**                      **Poster**                      **1558-10**

**TIME-DEPENDENT PHENOMENA MONITORED BY ONE-HOUR GPS OBSERVATIONS**

Janusz BOGUSZ, Mariusz Figurski and Micha Kruczyk (Institute of Geodesy and Geodetic Astronomy, Warsaw University of Technology, 00-661 Warszawa, POLAND, e-mail: jb@gik.pw.edu.pl)

From December 1998 Observatory in Jęzefosaw has started permanent GPS observations with one-hour sampling rate. WUT EUREF Local Analysis Centre plans to begin from 1st of January 1999 one-hour GPS data processing using BERESE v. 4.0 software and Hewlett Packard J200 machine. There would be tested simultaneously two methods of computing:

1. Processing of one-hour observations with the aim to explore local geodynamical changes based on part of EUREF network.
  2. Analysis of possibility of generating ionosphere and troposphere parameters in quasi-real time.
- We hope that acquired solutions would help us to create new possibilities of researching of local and fast changeable geodynamical processes. This paper will present preliminary results of such processing and analytical methods implemented to solve all involved problems.

# Contents - abstracts week B

<b>U</b>	UL3	B.1	<b>V</b>	VS2	B.167	<b>H</b>	HS1	B.301		
	UL4	B.1		VS3	B.173		HS2	B.306		
	U6	B.1	<b>S</b>	ST3	B.177		HW2	B.309		
	U7	B.2					ST4	B.192	HW3	B.312
	U8	B.7				ST5	B.211	HW4	B.315	
<b>IA</b>	JSP23	B.13	<b>P</b>	P11	B.227	<b>A</b>	GA1.03	B.319		
	JSM24	B.32					P13	B.236	GA1.07	B.324
	JSP25	B.36					P15	B.242	GA1.15	B.326
	JSM26	B.52					P16	B.245	GA2.02	B.328
	JSA27	B.60	<b>M</b>	MC02	B.249		GA2.03	B.335		
	JSG28	B.62					MC03	B.254	GA3.02	B.338
	JSV29	B.68					MC04	B.255	GA3.03	B.339
	JSV30	B.70					MC05	B.258	GA3.04	B.346
	JSS31	B.76					MC09	B.259	GA3.05	B.349
	JSM32	B.80					MC10	B.262	GA3.08	B.357
	JWS33	B.82				MC11	B.264	GA3.09	B.364	
	JWA34	B.89				MI04/MI10	B.268	GA4.03	B.370	
	JSA35	B.91				MI06	B.282	GA4.04	B.374	
	JSV36	B.93				MI11	B.288	GA4.06	B.377	
	JSA37	B.102	MI12	B.291	GA4.08	B.381				
	JSP39	B.105	MW02	B.294	GA5.08	B.382				
	JSA40	B.113	MW03	B.296	GA6.02	B.387				
	JSM41	B.117	<b>G</b>	G6	B.393	<b>INDEX</b>	Alphabetical listing of authors	I.1		
	JSS42	B.126								
	JSM43	B.134								
JSS44	B.136									
JSA45	B.146									
JSS46	B.150									
JSV47	B.153									
JSA48	B.158									
JSP49	B.161									

**Please Note:**  
Abstracts are divided into the equivalent of two published volumes for weeks A & B



## UNION LECTURE 3

## VOLCANIC HAZARDS, CITIES AND PUBLIC AWARENESS

Franco Barberi

## UNION LECTURE 4

## VARIABILITY OF WEATHER AND CLIMATE

Brian Hoskins, UK

The variability of weather and climate on time-scales from weeks to seasons will be discussed. The extent to which it is predictable is as yet largely unknown, though any such predictive power could have important consequences. It will be argued that the natural variability is now the key to progress on discussions of anthropogenic climate change. In one view it provides the noise against which the signal has to be determined. Alternatively, the most important regional anthropogenic climate change may be expected to occur through a biasing of the probability distribution of the modes of natural variability. In this talk it will be stressed that the system whose variability is being considered is increasingly being extended from the physical atmosphere-ocean system to include more of the geosphere-biosphere system and that simultaneous consideration of the human dimension is also becoming increasingly important.

## U6

Tuesday 27 July

## VOLCANISMS – MECHANISMS AND CONSEQUENCIES

Location: Great Hall

Tuesday 27 July AM

## OPENING REMARKS

1000

Wally Johnson

## U6/W/03-B2

Invited

1005

## SEISMIC TOMOGRAPHY OF IGNEOUS SYSTEMS

Bernard CHOUET (U.S. Geological Survey, 345 Middlefield Road, Menlo Park, California 94025, USA, email: chouet@chouet.wr.usgs.gov)

High-resolution tomography based on iterative inversions of travel-time data from local earthquakes has been used to image the internal structures of a few volcanoes at scales ranging from 0.5 to 2 km.

In southern Hawaii, high-velocity bodies in the upper 9 km of the crust beneath the summits and rift zones of Mauna Loa and Kilauea Volcanoes are interpreted as solidified gabbro-ultramafic cumulates from which surface volcanism is derived. Embedded in the high-velocity body beneath the Kilauea Caldera region is a low P-wave velocity body roughly the size of the caldera and which extends through the upper 4 km of the crust. The velocity contrast between this body and the surrounding structure is about 10%. Associated with the low P-wave velocity structure is a zone with anomalously high ratios of P- to S-wave velocities, which is consistent with a hot volume which may contain a small fraction of melt.

The most prominent feature observed in the velocity structure of Redoubt Volcano, Alaska, is a relative low-velocity near-vertical, pipe-like structure approximately 1 km in diameter that extends from 1 to 6 km beneath sea level. This feature aligns axially with the seismicity and is interpreted as a highly fractured and altered zone encompassing a magma conduit. No large low-velocity body suggestive of a magma chamber is resolved in the upper 7-8 km of the crust. Results at Mount Etna, Sicily, show a near-vertical low-velocity zone extending beneath the central crater to a depth of 10 km. This low-velocity region coincides with a band of steeply-dipping seismicity and is interpreted as a zone of crustal weakness through which magma migrates to the surface. A high-velocity body beneath the southeast flank of Etna is interpreted as a remnant mafic intrusion. This structural feature influences both volcanism and east flank slope stability and faulting.

## U6/W/04-B2

Invited

1035

## FLOOD BASALTS, PLUMES, AND PLATE TECTONICS

Millard F. COFFIN (Institute for Geophysics, The University of Texas at Austin, 4412 Spicewood, Springs Road, Building 600, Austin, TX 78759-8500, USA, email: mikec@ig.utexas.edu); Olav Eldholm (Department of Geology, University of Oslo, PO Box 1047, Blindern, N-0316 Oslo, Norway, email: olav.eldholm@geologi.uio.no); James W. Head III (Department of Geological Sciences, Brown University, Box 1846, Providence, RI 02912, USA, email: James\_Head\_III@brown.edu)

Large igneous provinces (LIPs) result from voluminous mafic magmatism. On Earth, LIPs originate from the mantle via mass and energy transfer which acts both independently of, and in conjunction with, seafloor spreading processes manifested along the mid-oceanic ridge system. Not readily explained by plate tectonic theory, the massive magmatism is most commonly attributed to mantle plumes. Most LIPs form in extensional tectonic settings, suggesting a relationship with thinned lithosphere. The post-150 Ma LIP record reveals both many events and large melt volumes from 135-85 Ma, and a distinct decline since 50 Ma. These trends may reflect variations in mantle circulation and have links to global environmental change. In contrast to Earth, other terrestrial planets of the solar system show no significant evidence of plate tectonics: the dominant form of mass and energy transfer from planetary interiors is apparently plumes. On the Moon, ascending basaltic magma collected in reservoirs at the base of the thick anorthositic crust, and when the reservoirs became overpressurized, dikes propagated to the surface. Titanic Martian shield volcanoes formed on stable lithosphere over hot spots lasting a billion years or more. Impact cratering studies on Venus suggest rapid, planet-wide volcanic resurfacing at about 300 Ma, an event that resembles mantle overturn events proposed for Earth. Such an event has implications for episodic and catastrophic LIPs throughout the history of the planets.

## U6/E/06-B2

Invited

1105

## EXPLOSIVE VOLCANISM: CAUSES AND CONSEQUENCES

R.S.J. SPARKS (Department of Earth Sciences, University of Bristol, Bristol, BS8 1RJ, UK, Email: steve.sparks@bris.ac.uk)

Progress in understanding explosive volcanism has been prodigious in the last two decades as a consequence of detailed documentation of several major eruptions, the increasing sophistication of numerical models and the application of laboratory experiments. The eruptions of Mount St Helens (1980-86), Mount Pinatubo (1991) and the Soufriere Hills Volcano, Montserrat (1995-1998) have provided comprehensive case histories in which geochemical, geophysical, petrological and remote sensing techniques have been combined with geological studies to provide quantitative information and constraints from the magma chamber to the stratosphere on explosive processes. The rapid increase in computer power has enabled a number of research groups to develop numerical models of explosive flows which are increasingly realistic in terms of simulating natural complexity and conditions. Incorporation of non-equilibrium effects, strong rheological changes, compressible flow dynamics, better degassing models and fragmentation criteria are examples of features of the new generation of computer models. New insights including understanding changes and discontinuities in discharge rate, stability of eruptive discharges into the atmosphere and transitions between effusive and explosive eruptions. Major results include the recognition that strong non-linearities and feedback processes cause pulsations, sudden transitions in eruptive style and, in some cases, multiple states for exactly the same conditions, making explosive activity at a certain level inherently unpredictable. Laboratory experiments have also had an important role. Shock tube experiments, using both analogue and natural materials, show the complexities of two-phase flows, giving new insights into fragmentation mechanisms. Some features of explosive flows, for example strong spatial heterogeneity, are still beyond the reach of numerical calculations. Future developments are likely to involve application of geophysical and remote sensing techniques to make direct measurements of explosive flow properties.

## U6/W/07-B2

Invited

1135

## MELTING, STORAGE AND MOVEMENT OF MAGMA

Jon DAVIDSON (Dept. of Earth and Space Sciences, UCLA, Los Angeles, CA 90095, USA, email: davidson@ess.ucla.edu)

Understanding processes of magma generation and differentiation remains an elusive yet critical goal in Earth Sciences. On the one hand, inferences about magma sources and mantle-crust fluxes or mantle reservoir characteristics and their evolution are largely based on incompatible trace element and isotope characteristics of mafic magmas. On the other hand, the nature of high-level differentiation processes, magma chamber or otherwise, and the timescales of operation are important controls on the volcanological behavior of magma systems, such as eruption magnitudes and frequencies. One approach in addressing such problems is "from the bottom up". Theoretical calculations of melt compositions are currently quite sophisticated. These calculations are able to incorporate empirical data collated from experiments – such as in the MELTS algorithm – and take into account elemental exchange effects during transport, which initially is assumed to be relatively slow (chromatographic porous flow). The alternative approach is more "top down", taking as its basis real data collected from magmatic rocks and their component minerals and glasses, and associated volatiles. Of the methodologies used to invert such data to constraining processes and sources U-series geochronology (to constrain differentiation timescales) and crystal isotope stratigraphy/ melt inclusion studies (to constrain differentiation pathways) have proved particularly fruitful. It is clear that differentiation may profoundly modify many of the geochemical characteristics of primary magmas thus creating a potential mismatch between the actual data characterizing a magma system, and the assumed source characteristics which form the basis of "bottom up" approaches. Nevertheless, an integration of perspectives is conceivable and should be pursued in our efforts to employ magmatic rocks as probes of crust and mantle processes through time.

## PANEL DISCUSSION

1205

W. Johnson, Chair

Tuesday 23 July PM

## U6/E/02-B2

1400

## OZONE DEPLETION: THE ROLES OF CHLOROFLUOROCARBONS AND VOLCANOES

Susan SOLOMON (Aeronomy Laboratory, 325 Broadway, Boulder, CO 80303 USA, email: solomon@al.noaa.gov)

Early theories of ozone depletion by chlorofluorocarbons were based upon understanding of gas-phase photochemistry. Ozone depletion was first observed in the Antarctic, and was quickly shown to be driven by heterogeneous chemistry involving chlorine compounds and polar stratospheric clouds. Significant ozone changes have also been observed in the Arctic and at mid-latitudes. Some aspects of ozone depletion are clearly related to gas-phase reactions, while others are coupled to heterogeneous reactions. Volcanoes play a major role in modulating the abundances of polar stratospheric clouds and of mid-latitude stratospheric aerosols. It will be shown that short-term (interannual) and longer-term (decadal) changes in volcanic aerosols very likely contributed along with trends in anthropogenic chlorine and bromine in triggering the ozone losses observed at mid-latitudes and in polar regions in the early 1980s. However, this chemistry is linked to the chlorine abundance, so that volcanoes are not a mechanism for ozone loss independent of human emissions of chlorofluorocarbons. The timing and magnitude of future ozone losses are likely to be strongly dependent upon volcanic aerosol variations as well as on future chlorine and bromine loading, so that the recovery of the ozone layer in the 21st century will very likely be modulated by volcanic activity, as it has been in the 20th.

## U6/W/10-B2

1430

## GASES OF PLANET EARTH: MANTLE ORIGINS AND ATMOSPHERIC IMPLICATIONS

Bernard MARTY (Centre de Recherches Pétrographiques et Géochimiques et Ecole Nationale Supérieure de Géologie, BP 20, 54501 Vandoeuvre Cedex France, Email: bmarty@crpg.cnrs-nancy.fr)

Most of volatiles (water, carbon dioxide, nitrogen, halogens, rare gases) present at the Earth's surface were contributed early during accretionary processes. Since then, volcanism is supplying gases in proportions roughly proportional to its activity rate. Part of these volatiles are recycled back into the mantle, so that each species has its own geochemical cycle. Some are cycled between the mantle and the surface with time constants lower than the age of the Earth (e.g., C, S), so that it is possible to derive a mean residence time at the surface. For

others (e.g., nitrogen, rare gases), the flux from the mantle to the surface exceeds the return flux, allowing primitive isotope heterogeneities between the surface and the deep Earth to survive. Since the mantle is chemically heterogeneous, it is possible to characterise mantle sources of lavas and corresponding tectonic settings by analysing the isotope composition of some of these elements. Helium provides a sensitive provenance tracer since its isotopic composition in volcanic rocks and gases varies over an order of magnitude between arc-type, and plume-type volcanisms. Rare gases allow also to derive quantitative fluxes of major volatiles (e.g., carbon dioxide), and to model their geochemical history. Volatile isotope geochemistry has recently allowed to demonstrate that major LIP provinces are linked with the development of plumes originating below the convective mantle feeding mid-ocean ridge volcanism. Since the emission of CFB and related felsic volcanism occurs in a limited interval of time, it is likely that such gigantic volcanism has had noticeable climatic impact. The case of the Afar-Ethiopian plume province (CFB and ignimbrite emissions at 30 Ma) will be discussed in this context.

**U6/W/12-B2** Invited **1500**

#### REMOTE SENSING: NEW WAYS TO LOOK AT VOLCANOES AND THEIR GASES

Peter FRANCIS (Earth Sciences, Open University, Milton Keynes, MK76AA, UK;  
email: P.W.Francis@open.ac.uk)

Increasing world population, urbanization and the technical complexity of society combine to increase the risks presented by volcanic eruptions, exemplified by the hazards to aircraft encountering ash clouds. Developments in remote sensing have provided new ways of both monitoring and to some extent mitigating such hazards, while minimizing risks to volcanologists. Satellite remote sensing provides a powerful volcanological tool because its synoptic coverage makes even the most remote volcanoes accessible; and because sensors working in different parts of the electromagnetic spectrum provide complementary information. Geostationary and polar orbiting platforms are used to measure the heights of ash columns; to assess ash burdens; and to track the dispersion of eruption clouds on an hemispheric scale. The Total Ozone Mapping Spectrometer (TOMS) provides a unique method of measuring sulphur dioxide injected into the atmosphere, while other instruments measure conversion of this gas to stratospheric aerosols which affect global radiation budgets. Infrared sensors are used to measure radiant thermal energy budgets of volcanoes and lavas, and form the basis of automated eruption detection and monitoring systems. Synthetic Aperture Radar satellites provide both high quality topographic data, and a method for detecting ground deformation at a scale of centimetres related to magma movements. Hitherto, observations have been made using sensors designed for purposes ranging from meteorology to agriculture. Future satellites will carry instruments specifically designed for volcanological applications.

New ground based optical remote sensing techniques provide a safer approach to conventional direct chemical sampling of volcanic gases. Open-path Fourier Transform Spectroscopy (FTIR) techniques have been successfully used to study plume gases at several volcanoes, and have the potential for automated monitoring. Applications of LIDAR techniques promise further refinements to studies of gas composition, evolution of plume chemistry, and aerosol formation.

**U6/W/09-B2** Invited **1530**

#### THE NEW EXPERIMENTAL VOLCANOLOGY

Donald B DINGWELL (Bayerisches Geoinstitut, Universitaet Bayreuth, D-95440 Bayreuth, Germany,  
Email: don.dingwell@uni-bayreuth.de)

Recent advances in laboratory-based investigations have now made possible a host of experiments on volcanic materials undergoing volcanic processes that may be collectively termed the "new experimental volcanology". The most distinct aspect of this branch of experimental geosciences; and that which makes it almost unique in the "solid" earth sciences, is that experiments are possible in real-time. Thus a key achievement of the past few years has been the enablement of precise experimental control and monitoring of real-time laboratory experiments on natural magmas at the conditions extant in volcanoes. The relevant experimental parameters of temperature, pressure and stress can be measured on extremely short timescales during processes of parameter variation such as decompression and in the context of the textural development of the magma such as crystallisation and vesiculation. The pre-experiment and post-experiment, magma and the experimental volcanic products, respectively, can be analysed using micro- and macro- physical and chemical methods. The resulting documentation of sample evolution yields a very complete comparative picture of the consequences of eruptive processes such as decompression, ascent, vesiculation, crystallisation, foaming and fragmentation on the volcanic materials investigated. The detailed comparison of the products of experimental volcanology with natural volcanic products is also a feature of experiments conducted on natural magmas that cannot be adequately achieved using analogous materials. The salient features of recent experimental work in this field, together with an outlook for future developments, will be presented.

**PANEL DISCUSSION** **1600**

D. Hilton and F. Prata, Co-Chairs

**U7**

**Monday 26 July**

#### INTEGRATED GLOBAL MONITORING NETWORKS

Location: Great Hall

Location of Posters: Old Gym

**Monday 26 July AM**

Presiding Chair: C.N.K. Mooers, (University of Miami, Florida ,USA)

Concurrent Poster Session

**Introduction** **0830**

C.N.K.MOOERS

**U7/W/09-B1** Invited **0835**

#### GLOBAL MONITORING OF THE OCEAN

John WOODS (Huxley School of Environment, Imperial College, London SW7 2BP,  
email: j.woods@ic.ac.uk)

The Global Ocean Observing System (GOOS) was launched by the IOC at the Second World Climate Conference in 1992. That stimulated a proposal for a Global Climate Observing System, with the GOOS providing the ocean observations. Thus integration of global monitoring for climate has been on the agenda for a decade. However the customer base for GOOS is much broader than climate. It includes organisations in both the public and private sector that have responsibility for monitoring and predicting the ocean environment at particular locations. This multi-faceted business already totals billions of Euros per annum and is growing rapidly. The case for global monitoring is that these service providers will be able to improve their products if their operations are set in a global context. That will be achieved by providing each local operational area with information about the open ocean boundary conditions derived from analysis of a global model supported by a global network of observations. The first steps are being taken at a number of centres around the world to link operational global models to operational local high resolution models. Rapid progress has been made during the 1990s in developing ocean and ocean-atmosphere models, and as predicted the Teraflops computers needed to run them are now available. These are being supported by global observations from the World Ocean Observing System and from ongoing global observations of opportunity, notably satellites, drifters and XBTs. The field phase of the World Ocean Circulation Experiment (successfully completed in 1997) provided invaluable experience with novel observing systems, and others not available for WOCE are now being tested, notably acoustic remote sensing and long-range autonomous subsurface. The cost of these observing systems is falling rapidly. The next step is to undertake a number of pre-operational trials involving the integration of observing networks and models at global and local scales. Such trials are being promoted by EuroGOOS and other regional organisations. Their success will depend on the active involvement of the oceanographic research community, who will gain long term benefits from the provision of global observations on a consistent basis year after year.

**U7/E/05-B1** Invited **0900**

#### MASS TRANSPORT IN GLOBAL GEOPHYSICAL FLUIDS

B. F. CHAO (Space Geodesy Branch, NASA's Goddard Space Flight Center, Greenbelt, Maryland 20771, USA; email: chao@denali.gsfc.nasa.gov)

Mass transports occurring in the atmosphere-hydrosphere-solid Earth-core system (the "global geophysical fluids") are important geophysical phenomena. They occur on all temporal and spatial scales. Examples include air mass and ocean circulations, tides, hydrological water redistribution, mantle processes such as post-glacial rebound, earthquakes and tectonic motions, and core geodynamo activities. With only a few exceptions on the Earth surface, the temporal history and spatial pattern of such mass transport are often not amenable to direct observations. Space geodesy techniques, however, have the capability of monitoring certain direct consequences of the mass transport, including Earth's rotation variations, gravitational field variations, and the geocenter motion. These techniques include the very-long-baseline interferometry, satellite laser ranging and Doppler tracking, and the Global Positioning System, all entail global observational networks. While considerable advances have been made in observing and understanding of the dynamics of Earth's rotation, only the lowest-degree gravitational variations have been observed and limited knowledge of geocenter motion obtained. New space missions, projects and initiatives promise to further improve the measurements and hence our knowledge about the global mass transports. The latter contributes to our understanding and modeling capability of the geophysical processes that produce and regulate the mass transports, as well as the solid Earth's response to such changes in constraining the modeling of Earth's mechanical properties.

**U7/E/08-B1** Invited **0925**

#### GLOBAL INTEGRATED GEODETIC AND GEODYNAMIC OBSERVING SYSTEM

Reiner RUMMEL (IAPG, Techn.Univ.Muenchen, Arcisstrasse 21, D-80333 Muenchen, Germany,  
email: rummel@step.iapg.verm.tu-muenchen.de)

In a very successful effort the international geodetic community succeeded to realize a terrestrial and celestial reference frame with greatest precision. Modern kinematic monitoring space techniques such as satellite altimetry (ocean and ice), interferometric SAR, or ground based GPS together with terrestrial techniques such as tide gauges or leveling provide a global picture of temporal changes of the Earth's land surface, its ice cover and of the oceans, provided these techniques are rigidly tied to one global terrestrial reference frame. Observation of the variations of Earth rotation adds information to the observing system of the integrated effect of any change in angular momentum of the Earth's system components. The third component, the Earth's gravity field, is currently least well determined, but the situation will change soon with the upcoming satellite missions CHAMP, GRACE and GOCE. Then the complete observing system, comprising geo-kinematics, Earth rotation and gravity, will increase significantly our understanding of surface ocean circulation (and consequently add insight to ocean mass transport), sea level rise, ice flux and mass budget, land surface motion and stresses, and off-sets between and biases of height systems.

**U7/L/01-B1** Invited **0950**

**INTERMAGNET - THE MODERN GLOBAL DIGITAL MAGNETIC OBSERVATORY NETWORK, IN A MULTI-DISCIPLINARY CONTEXT**

Richard COLES (Geological Survey of Canada, Geomagnetic Laboratory, 7 Observatory Crescent, Ottawa K1A 0Y3, Canada, email: coles@geolab.nrcan.gc.ca

In the INTERMAGNET program, high-quality geomagnetic data from a world-wide network of observatories are sent in near-real-time via satellite and electronic connections, such as Internet, to collection and dissemination centres known as Geomagnetic Information Nodes (GIN). Currently, more than 70 observatories from over 30 institutes in 25 countries are participating in INTERMAGNET, with six GINs operating in North America, Europe and Asia. Each year, new participants are joining INTERMAGNET. The INTERMAGNET data are fundamental to much geophysical and space science research, particularly concerning our near-earth environment and deep-earth (core-mantle) studies. A survey of the world's observatories has shown that many are already co-located with stations belonging to other monitoring networks. Further, the survey showed an overwhelmingly positive response to the idea of accepting additional co-located monitoring systems and to the concepts of increased synergy in operations and data management.

**U7/E/07-B1** Invited **1045**

**SELECTED GROUND-BASED OBSERVATIONS OF THE UPPER ATMOSPHERE AND IONOSPHERE**

Jurgen ROETTGER (Max-Planck-Institut für Aeronomie Katlenburg-Lindau, Germany); Shoichiro Fukao (Radio Atmospheric Science Center Kyoto University, Uji, Kyoto, Japan)

We will present selected ground-based observations of the upper atmosphere and the ionosphere which are performed in polar, middle and equatorial latitudes. We will concentrate this summary on observations by radar and supporting instrumentation. Of particular importance are studies of the coupling of the lower atmosphere with the upper atmosphere, which is primarily occurring in equatorial latitudes by convective processes and upwelling. Effects of the solar wind on the magnetosphere are linked down into the ionosphere, which is the dominating coupling mechanism in polar regions. Latitudinal coupling between high and low latitudes is of eminent importance and it needs to be considered how these low and high latitude phenomena develop and interact in the middle and upper atmosphere. On the global scale the dynamical coupling in vertical direction is dominantly by gravity waves generated in the troposphere, which propagate upwards and deposit their energy and momentum in the middle and upper atmosphere. A brief summary of the coupling phenomena in the polar and equatorial ionosphere and upper atmosphere will be given and examples of observations will be discussed, which are obtained by radar systems. This is partially done in a globally coordinated manner. We will also highlight certain international programs, campaigns and projects, which had been performed or are underway for these studies of the global response and development of atmospheric processes.

**U7/P/01-B1** Invited **1110**

**REVIVING HYDROLOGICAL NETWORKS**

John C. RODDA (IAHS, Institute of Hydrology, Wallingford, Oxon OX10 8BB, UK, email: 106201.1774@compuserve.com)

With a rapidly rising global demand for water, the increasing havoc wrought by floods and the growing degradation of the aquatic environment by pollution, it might be assumed that the capture and management of water data of all types would be a top priority. But this is not the case. National hydrological networks and those providing most of the other types of water data are generally degrading over much of the world. Many nations are now less able to assess their water resources than 30 years ago, largely because of reducing government support for these activities. And this is happening when the threat of climate change should be placing a new premium on hydrological data. Then from the scientific point of view, there is the problem that modelling capabilities have outrun the capacity to capture data, while remotely sensed data is not yet the expected panacea for the ills of ground-based data acquisition systems. There are, however, a number of initiatives underway which are designed to redress this situation, both nationally and internationally. International data centres have been established, while certain international programmes cater for scientific cooperation in large scale field experiments. Others give support hydrological networks in developing countries. Fresh ideas are being developed which are likely to provide additional help. Will integration with global monitoring networks add a further stimulus?

**U7/E/01-B1** Invited **1135**

**AT THE CROSS-ROADS OF TIME, SPACE, ACCURACY AND URGENCY: MONITORING OF LARGE AREA LAND EVAPORATION**

Massimo MENENTI(1), Z.B. Su, G. Roerink, H. Pelgrum, B.v.d. Hurk(2) and B.J. Choudhury(3) The Winand Staring Centre (SC-DLO), P.O.B.125, 6700 AC Wageningen, The Netherlands; (1) Universite Louis Pasteur e-mail: menenti@sepia.u-strasbg.fr (2)Royal Netherlands Meteorological Service (3) Laboratory for Hydrospheric Processes.

The loss of water from water and land to the atmosphere is the focus of research and applications in a diverse context. Precise answers to theoretical and practical issues are scarce, notwithstanding significant efforts over a long period of time. The paper attempts to explain this situation in terms of the diverse spatial and temporal scales involved, of the accuracy of observations and of the demanding requirements of science and application. The feasibility of accurate observations of potential, maximum and actual evaporation is discussed first. Observational concepts to measure actual evaporation are briefly reviewed to explain the interest of space- and airborne measurements to understand and model the evaporation of heterogeneous land surfaces. This is illustrated with examples of application of the Surface Energy Balance Index (SEBI) at local and large spatial scales. Radiative and PBL forcing can be considered constant when dealing with small areas. Under these conditions use of remote measurements to estimate actual evaporation through the heat balance of the land surface is feasible. Spatial and temporal variability of radiative and PBL forcing must be taken into account in the large-area case. In the example shown this was done using data sets produced through four dimensional data assimilation. Finally, modeling of land evaporation is revisited in view of the ESA Land Surface Processes and Interactions Mission.

**U7/L/06-B1** Invited **1200**

**A NEW INTEGRATED APPROACH TO THE WORLD WEATHER WATCH GLOBAL OBSERVING SYSTEM**

Robert LANDIS (email: landis@www.wmo.ch)

The World Weather Watch (WWW) was established over 35 years ago with the Global Observing System (GOS) as one of its major components. It has evolved as the major worldwide infrastructure supporting meteorological requirements for observations and processed data for most all nations and territories of the world. The initial objective of the WWW/GOS was to provide those observations needed in support of Numerical Weather Prediction for time scales out to about 48 hours. Since that time it has grown in scope to parallel the developments of NWP in both the shorter time scales as well as time scales of medium range (i.e. 10 days) and beyond. To meet the requirements of both finer spatial resolution and longer time scales (seasonal to interannual) a new integrated approach to the GOS has been initiated. This approach involves integration from several aspects: (1) the co-ordinated observing of the atmosphere, hydrosphere, lithosphere, and cryosphere; (2) the combination of In Situ and remote sensed observations, particularly from space based platforms; (3) the use of observing tools provided for a multitude of purposes including research, long-term monitoring, and operations; and (4) the co-ordinated effort of individual scientists, institutions, agencies, and national governments. Initial efforts are already underway that include a new composite upper air observing system and co-operative observing schemes for voluntary ships and data buoys. Major key elements needed to assure success for such a large integrated approach include the ability to utilise new complex data assimilation techniques and a mechanism for dialogue among those participating in the Integrated Global Observing Strategy.

**Monday 26 July PM**

Presiding Chair: H.P. Plag, (Geodetic Institute/Norwegian Mapping Authority, Norway)

**U7/L/04-B1** Invited **1400**

**GLOBAL MONITORING OF RADIATIVE EFFECTS OF AEROSOLS**

Teruyuki NAKAJIMA: (Center for Climate System Research, University of Tokyo, 4-6-1 Komaba, Meguro-ku, Tokyo 153-8904, Japan TEL: +81-3-5453-3959; FAX: +81-3-5453-3964; e-mail: teruyuki@ccsr.u-tokyo.ac.jp)

The methodology for global monitoring of radiative effects of aerosols will be discussed in this paper. Satellite remote sensing of aerosol optical parameters is useful for finding the aerosol amount and species on global scale. Optical thickness and single scattering albedo can be estimated by the aid of such satellite retrievals and a global circulation modeling. Ground-based measurements of solar irradiance and sky radiance are another important component for providing a useful information for aerosol radiative effects. Validation of satellite-retrieved values of aerosol optical thickness and single scattering albedo is indispensable to maintain the quality of the global monitoring. Ideas and real data processing with NOAA-AVHRR and ADEOS/OCTS will be presented.

**U7/W/17-B1** Invited **1425**

**TOWARD OPERATIONAL OCEANOGRAPHY AND CLIMATE PREDICTION**

Neville SMITH (Bureau of Meteorology Research Centre, Melbourne Vic. 3001, Australia, email: N.Smith@BoM.GOV.AU)

Oceanography is gradually evolving from an era characterized by research, experimentation and discovery, into one where routine applications and valued services are an accepted component. Through analogy with meteorology, we think of this as the transition from scientific research to operational oceanography. In reality it is simply a natural evolution whereby application and exploitation follow research and development. The development of predictive skill is usually the paradigm adopted for operational activities - the notion that foreknowledge of the ocean state, or of climate conditions, can be used to benefit industry, commerce and other sectors of our society. However in oceanography, and particularly in climate, it is not only the ability to forecast that is valued, but also the ability to integrate, extrapolate and interpolate information for nowcasts and hindcasts. As a young field, oceanography relied on the careful analysis and interpretation of data gathered specifically for research. For the future, data will be gathered for many different uses, both research and applied, and analysis and interpretation will more often than not rely on processed fields from models and data assimilation. In this paper we will concentrate on the processing and predictive elements of the global ocean and climate systems. The term "intelligence gathering" is often used in the non-scientific world to describe the process of collecting data and knowledge on a subject. It is also an apt term in the present context since it is impossible to build skilful analysis, assimilation and model systems without adequate knowledge of the ocean and climate. This "intelligence" comes not only in the form of data but also in the form of parameterizations used for ocean state estimation and for unresolved model scales. This implies that the development of assimilation and prediction systems will forever depend upon data and improved understanding (science). For oceanography and climate, the TOGA and WOCE initiatives have delivered the advances necessary to make this step and it is the responsibility of the present community to ensure proper advantage is taken of their legacy.

**U7/E/06-B1** Invited **1450**

**GLOBAL OCEAN OBSERVATIONS FOR CLIMATE STUDY**

Dean ROEMMICH (Scripps Institution of Oceanography, University of California San Diego, La Jolla, CA, 92093-0230, USA, email: droemmich@ucsd.edu)

The need for global climate-relevant observations in the ocean has been recognized for many years. Observations are required to reveal the evolving state of the climate system, for improved understanding of processes controlling climate variability, and for data assimilation and forecast model initialization. The WOCE hydrographic survey, the TOGA/WOCE thermal network and the TAO array provide modern examples of observations with great value. Until now, however, the lack of appropriate technologies has placed systematic global observing systems beyond reach. The needs for data greatly exceeded the practical capabilities. Revolutionary advances in technology during the past 5 years have finally brought the required observing systems within reach. Rapid progress in development of in situ instrumentation has been spurred on in part by parallel advances in satellite measurements of the sea surface. Altimetric sea level, surface temperature and scatterometer winds are of higher quality and greater community value than could be imagined a few years ago. While in situ networks cannot match the resolving power of satellite systems, they provide essential information for interpretation and calibration of surface measurements. There is now a near-consensus in the oceanographic community on the components of a global observing system. Major enabling technological advances include:



Development of cost effective mooring technologies for the TAO array. Development of the autonomous profiling float. A global array of temperature and salinity profilers is now practical and has been proposed (the Argo network). Improvements in meteorological sensors and their incorporation into systems with potential for broad deployment. The capability exists to make measurements of air-sea fluxes of momentum, heat and freshwater with the accuracy needed for climate research. These developments have greatly elevated the achievable value of an ocean observing system for climate. Additional elements of an integrated observing system include time-series measurements at special locations, measurements in boundary currents and selective deep-ocean hydrography. The remaining challenges are for implementation of the global systems by international consortia, for efficient design of the additional measurements, and for flexibility to accommodate new technologies and sampling strategies.

**U7/L/02-B1** Invited **1515**

#### GLOBAL GEOPHYSICAL NETWORKS AND THE CORE-MANTLE COUPLING

Yozo HAMANO, (Dept. Earth & Planetary Physics, Univ. of Tokyo, Bunkyo-ku, Tokyo, 113-0033, JAPAN); Hisashi Utada, (Earthquake Research Institute, Univ. of Tokyo, Bunkyo-ku, Tokyo, 113-0033, JAPAN)

Ocean Hemisphere Project (OHP) Network consists of seismic, geomagnetic and geodetic networks covering the wide area of the Pacific Ocean. One of the purposes of the joint observations by the geophysical networks is to investigate the nature of the core-mantle coupling through the core-mantle boundary. Causes of the lower mantle heterogeneity and the surface motion of the outer fluid core are the main targets for the purpose. Global networks are inherent for investigating the dynamics of the earth's deep interior, but most of the observatories are distributed on land, and the observatories in and around the Pacific ocean are scarce. In order to cover the Pacific Ocean, sea floor observatories are necessary as well as the observatories on islands. For long-period (more than several years) sea floor measurements, power source and data recovery are main difficulties. We have been developed the long-term geomagnetic observation apparatus and made a preliminary observation at sea floor in 1998. The long-term deployment is planned within this year (1999). The apparatus measures three components of the geomagnetic field by the fluxgate sensors, the total force of the geomagnetic field by the Overhauser proton magnetometer, two components of the horizontal electric field, and two components of the tilt of the apparatus, and is equipped with long-life Li-battery power sources, a recording system, and a ultra-sonic communication system for data transfer. In order to elucidate the cause of the heterogeneity (temperature or chemical) of the lower mantle (D" layer and hot plumes), we need to obtain the information on the electrical conductivity of the heterogeneity in addition to the seismic observation. Since the Electro-magnetic sounding from the surface cannot clarify the lower mantle structure, we need to identify the Electro-magnetic signals from the core surface. Decay of the signals through the lower mantle can be used to obtain the conductivity structure of the lower mantle. However, at present, identified geomagnetic field variations of core origin are limited to belong to several tens of years, because of 1) the comparable order of the external and the internal geomagnetic signal at the period range of 1-10 years, and 2) the nonhomogeneous distribution of the geomagnetic observatories on the earth's surface.

**U7/W/10-B1** Invited **1610**

#### THE NEW GENERATION GLOBAL SEISMIC NETWORK: CONTRIBUTIONS TO THE STUDY OF DEEP EARTH STRUCTURE

Barbara ROMANOWICZ (Seismological Laboratory, University of California, Berkeley, CA, 94720, USA, email: barbara@seismo.berkeley.edu)

Through complementary efforts of about a dozen countries, coordinated within the Federation of Digital Seismic Networks (FDSN), there now exists a global network of over 200 state-of-the-art, high dynamic range, broadband seismic stations, developed over the last 15 years. These stations contribute to an ever growing global database suitable for a large number of seismological studies on topics ranging from deep earth structure (from the upper mantle down to the inner core) to detailed studies of the rupture process of large earthquakes, and including many regional fine scale studies as well. The individual data archives are generally accessible on-line over the internet and are currently being linked into a "seamless" database. Recently, efforts have also focused on the establishment of permanent ocean bottom observatories to complement the land-based network and fill gaps in the global distribution of stations. These efforts are being coordinated on the international scale within the International Ocean Network (ION).

The high quality global broadband seismic dataset has in particular led to improved resolution of deep mantle structure, which we illustrate through examples of work in our laboratory on global waveform elastic and anelastic mantle tomography as well as forward modelling of complex structure at the base of the earth's mantle.

**U7/W/06-B1** Invited **1635**

#### MITIGATING THE HAZARD OF VOLCANIC CLOUDS USING SATELLITE REMOTE SENSING

W I ROSE (Geological Engineering and Sciences, Michigan Technological University, Houghton, MI 49931, e-mail: raman@mtu.edu) AJ Krueger (NASAGoddard Space Flight Center, Greenbelt, MD 20771)

Satellite remote sensing is providing a unique and increasingly comprehensive portrait of explosive volcanism, by its ability to map and quantify volcano/atmosphere interactions. Data collected by meteorological satellite detectors (TOMS, AVHRR, GOES) designed for other purposes provide an archive record of earth's volcanism which is being interpreted by scientists. Because these detectors are able to map the position of volcanic clouds and because of the well demonstrated near-real-time use of satellite data for weather forecasting, the goal of using satellite data to mitigate hazards to aircraft from volcanic clouds is being seriously explored. Timing is a key issue. Jet pilots need to get information about the 3 D position of volcanic clouds near them that is as current as possible. One stated goal is to get information communicated within 5 minutes, a period during which a jet may travel ~70-80 km. Satellite volcanic cloud detectors must be uniquely sensitive to volcanic clouds, and need to be able to detect volcanic clouds anywhere with high temporal and adequate spatial resolution. The global responsibility for this hazard must be regionally shared so that the people close to the hazard know immediately. Successful mitigation will require that: 1. Satellite detectors must be positioned more favorably and the way their data are used to map and measure volcanic clouds must be improved. 2. An unprecedented cooperative effort between scientists, agencies and countries must be developed and IUGG could play a valuable role. 3. Challenging scientific/technical communications to regional centers must be completed. A new initiative by NASA, called VOLCAM, is planned to attempt the above. New detectors specifically designed for volcanic clouds will be placed on geostationary satellites. Data will be collected every 15 minutes and analyzed and communicated within 5 minutes. A 2 year demonstration period is planned for 2002-2004.

**U7/L/07-B1** Invited **1700**

#### TOWARDS GLOBAL, GEODETIC, REAL TIME MONITORING OF VOLCANOES

Timothy H. DIXON (RSMAS, University of Miami, 4600 Rickenbacker Cswy., Miami, FL33149-1098, USA, email: tdixon@rsmas.miami.edu); C. Meertens, (UNAVCO, A. Newman, Northwestern University, S. Stein, Northwestern University and UNAVCO)

Geodetic measurements of ground deformation are an important tool for monitoring volcanoes, predicting eruptions, and investigating magma dynamics at depth. Two recent technological advances make it possible to develop a cost-effective global volcano monitoring system that includes geodesy. First, new phase-tracking single frequency Global Positioning System (GPS) receivers can provide the required high-precision, high-rate data at dramatically lower cost than previously possible. These systems can be deployed in large numbers, making possible continuous, high spatial and temporal resolution "imaging" of magmatic sources. Second, new VSAT satellite communications make it possible to return data from remote areas in essentially real time, without reliance on ground-based communication, at low cost, using small, rugged, low power systems. This communications infrastructure can be used for any data type, in any area. We believe it will revolutionize autonomous monitoring of remote regions, which until now has suffered from lack of a cost-effective space-based approach. We have performed limited tests of key parts of both systems. This paper will present the result of those tests, as well as cost comparisons with other real-time and near-real-time data delivery systems.

**U7/L/01-B1** Invited **1725**

#### MEASUREMENTS FOR EARTH SYSTEM SCIENCE

Francis BRETHERTON, (University of Wisconsin-Madison, Space Science and Engineering Center, 1225 West Dayton St, Madison, WI 53706 U.S.A); E-mail: fbretberton@ssc.wisc.edu Phone: (1) (608) 262-7497 Fax: (1) (608) 262-5974

Driven by concerns over human influences on the global environment, renewed attention is being given to the functioning of Earth as an complete system. A new discipline is emerging, devoted to understanding the interactions between the component parts which have been the foci of customary areas of specialization. Quantitative modeling can assist a synthesis, but structuring, organizing, and sustaining appropriate long-term measurements is a continuing challenge. There will be no single global observing system, but interoperating networks sharing information dedicated to common standards of quality measurements for critical variables. Great progress has been made, but it is essential to demonstrate sufficient utility to the public and their governments to assure continued support. New modes of collaboration are needed among scientists and end users of this information. New measures of scientific achievement must reward those contributing to this common understanding. Still broader horizons are needed to allocate scarce resources in an effective manner.

**PANEL DISCUSSION** Invited **1750**

H-P Plag, (Norwegian Mapping Agency), Y Fukao (Univ of Tokyo), C.N.K Mooers, (Univ of Miami)

**Monday 24 July AM**

Presiding Chair: Y. Fukao, (University of Tokyo, Japan)

#### INTEGRATED GLOBAL MODELING NETWORKS

**U7/W/07-B1** Poster **0830-01**

#### THE INTERNATIONAL SPACE GEODETIC AND GRAVIMETRIC NETWORK (ISGN)

Hermann DREWES (Deutsches Geodaet. Forschungsinstitut, Marstallplatz 8, D-80539 Muenchen, Germany, email: drewes@dgfi.badw-muenchen.de); Gerhard Beutler (Astronomisches Institut, Universitaet Bern, Sidlerstr. 5, CH-3012 Bern, Switzerland, email: beutler@aiub.unibe.ch); John Bosworth (NASA, Goddard Space Flight Center, Code 920.1, Greenbelt MD 20771, USA, email: jmb@tppmail.gsfc.nasa.gov); Claude Boucher (Institut Geographique National, 6-8 Avenue Blaise Pascal, Cite Descartes, F-77845 Champs-sur-Marne, France, email: boucher@ensg.ign.fr); Tom Herring (Mass. Institute of Technology, Dept. of Earth, Atmospheric and Planetary Sciences, Cambridge MA 02139, USA, email: tah@mtglas.mit.edu); Ivan Mueller (Ohio State University, 4361 Shire Creek St., Hilliard OH 43026, USA, email: mueller@mps.ohio-state.edu)

The ISGN is an integrated global monitoring network of space geodetic observatories. It is jointly installed by the IAG Commission VIII on Coordination of Space Techniques for Geodesy and Geodynamics (CSTG) and the International Earth Rotation Service (IERS). The observatories being included in the network have to fulfill certain criteria which were set up by a CSTG/IERS Working Group in order to guarantee an effective operation and optimum scientific benefit. The scientific objectives of the ISGN are discussed and the criteria for the inclusion of stations into the network are summarized. A list of included stations is presented and the role of observatories or groups of observatories, respectively, with respect to the scientific objectives is characterized. The future scientific impact of the ISGN and its status in the international services is discussed.

**U7/W/12-B1** Poster **0830-02**

#### DATA ASSIMILATION IN THE MERIDIAN NETWORK

Jian-Shan GUO (Center for Space Science and Applied Research, Chinese Academy of Sciences, P.O.Box 8701, Beijing 100080, P.R.China, Email: guojs@center.casar.ac.cn); Hong Zheng, She-ping Shao, Nana Liu (idem)

Meridian Network is a regional network for collection, processing, and dissemination of data for Meridian Chain-a project that has been approved by Chinese government. The Meridian Chain is a ground-based observatory chain equipped with multi-instruments (radio, optical and geomagnetic). The Meridian Network consists of data base; high performance computer system and a communication platform covering five main nodes along about 120°E meridian from Mohe (122°E, 53°N) to Zhongshan (76°E, 69°S) and being able to connect with worldwide data centers. We discuss the key topics - data assimilation in view of physical process, model studies and design of network topology of the Meridian Network. The considerations here would be validate for integrated global monitoring network. The data assimilation is a data processing procedure fully taking advantages of different type of observations. The main points would be: State estimation is a procedure making use of optimally constrained weighted least-squares method to estimate the values of a physical (electrodynamic and/or dynamic) parameter with error values to form a pattern (state) over the interested region or global by fitting to a set of direct and indirect observations took within so short period that the physical process could be considered as steady-state. The state shows the physical characteristics of the region for the instant of time, and can also be converted from other fitted parameter state in the light of physical law. The error pattern on the region provides the basis for network topology design

Physical process could be illustrated by a series of states for individual instant of time. The carefully chosen state could be considered as initial or boundary conditions or coefficient model for driving physical model or solving a set of physical equations to obtain the evaluation of the process numerically or analytically. The set of physical equations could also be solved by moment method with time point match function - a series of fitted states at different instant of time, to obtain a point fitted process.

**U7/W/03-B1** Poster **0830-03**

#### THE SCIENTIFIC AND TECHNOLOGICAL OBJECTIVES OF THE INTEGRATED GEOPHYSICAL MONITORING NETWORK IN RUSSIA

Oleg Starovoi (Geophysical Survey, Russian Academy of Sciences, 189 Lenin str., Obninsk, Kaluga region, 249020 RUSSIA, e-mail: ostar@gssas.ru); Suria Tatevian (Institute of Astronomy RAN, 48 Pyatnitskaya str., Moscow 109017, RUSSIA, e-mail: statev@inasan.rssi.ru); Alexander ZAITZEV (Institute of Terrestrial Magnetism, Ionosphere and Radio Wave Propagation, Troitsk, Moscow Region, 142092, RUSSIA, e-mail: zaitzev@izmiran.rssi.ru)

Rapid advances in global geophysics based on the recent technological achievements in computers, telecommunications and space observations. In this paper we consider the idea of integrated geophysical monitoring network which include seismic, magnetic and geodetic instruments. Such an idea has a new chance for realization in the coming decade due to achievements referred to above. This idea is based on the scientific and technological objectives. First, taking into account that transition between mantle and core is the key factor for understanding of the internal dynamics of the Earth, we believe that all available observations regarding the internal structure of the Earth ( seismic, magnetic, gravity, and rotational) should be gathered in order to derive a coherent model, able to fit all types of data. Geomagnetic and gravitational fields variations have sources in the crust and correlate with seismic activity. External disturbances take place due to solar activity which trails also observed in geophysical fields. Second, technological objectives are evident if we take into account that the volume of seismic-magnetic-geodetic digital data is in proportion as 100-10-1. So it is the way to save the funding if we'll use the same basic links of the INTERNET for data transfer to the analyses centers. A real situation with the existing Russian geophysical stations is considered and a project of upgrading of the integrated network for the geophysical monitoring is discussed.

**U7/E/09-B1** Poster **0830-04**

#### GLOBAL MONITORING OF CLIMATE VARIABILITY VIA THE SCHUMANN RESONANCE

Colin PRICE (Department of Geophysics and Planetary Sciences, Tel Aviv University, Ramat Aviv 69978, Israel, email: cprice@flash.tau.ac.il); Earle Williams (Parsons Laboratory, Massachusetts Institute of Technology, Cambridge, MA 02139, USA, email: earlew@juliet.ll.mit.edu)

The earth's surface and the ionosphere at an altitude of 60-100km result in the earth-ionospheric waveguide that allows for the propagation of electromagnetic waves over great distances. Waves in the extremely low frequency (ELF: 1-100 Hz) range can propagate with little attenuation in the atmosphere and therefore travel a few times around the earth before decaying. In the atmosphere the main natural source of these waves is from lightning discharges. Since the ELF waves from each lightning discharge travel around the globe a few times before decaying, we can theoretically sit at a single location and monitor changes in global lightning activity. Furthermore, due to the physical structure of the earth-ionosphere waveguide, certain resonance frequencies occur at 8, 14, 20, 26 ...Hertz known as the Schumann resonance. By monitoring the amplitude of these resonant modes continuously, we are able to monitor changes in lightning activity around the planet on hourly, daily, monthly, annual and interannual timescales. Such monitoring stations now exist at a few locations around the globe, and are providing a cheap, reliable way of monitoring the global climate system. Lightning activity is directly related to microphysical processes that occur in deep convective clouds. The strength of updrafts, the amount of convective rainfall, the production of nitrogen oxides, and the location of flash floods are all associated with the lightning activity in these storms. Since the majority of the earth's lightning activity occurs in the tropics, we propose that ground-based measurements of the Schumann resonance are a way of monitoring changes in the tropical hydrological cycle. In addition, the authors have previously shown strong connections between the globally integrated ELF lightning signals and global climate parameters such as surface temperature and upper tropospheric water vapour. It may therefore be extremely useful to include in future integrated global monitoring networks parameters related to atmospheric electricity.

**U7/E/04-B1** Poster **0830-05**

#### TYPIFICATION OF NATURAL AND CULTURAL BIOGEOCOENOSES LOCATIONS FOR HYDROLOGIC AND INTEGRATED MONITORING NETWORKS DESIGN (ARAL AND CASPIAN BASINS CASE STUDY)

Vijay P.Singh, Dr.Sci., Prof. (Louisiana State University, Civil and Environmental Engineering Department, 3502 CEBA Building, Baton Rouge, LA 70803-6405 USA, email: cesing@unix1.sncc.lsu.edu); Nina M. NOVIKOVA, Dr.Geogr.Sci. (Water Problems Institute, email: novikova@novikova.msk.ru); Yeugeny M. Gusev, Dr.Biol.Sci. (Water Problems Institute, email: sowa@ipcom.ru); Valentina A.Khaydarova, Ph.D (Water Problems Institute, email: akalashnikov@usaid.gov); Natalia V.PENKOVA, Ph.D (State Hydrological Institute, Water email: george@tetris.dux.ru)

Within the spatial domain of scientific design and exploitation of integrated (ground and space-based) monitoring networks the different level geoecosystems structure investigations are under consideration. The emphasis to the problem of compatibility of hydrologic and ecologic geosystems parameters in space-geometric and "matter" ("substance") aspects is given. The results of comparison analyses of some geographical (the comparative-descriptive) and relatively rigorous formal methods of biogeocoenoses locations typification in mountain, piedmont and lowland parts of the regions examined are presented: - identification of hydrologic conditions with the help of plants-indicators using ground and space data; - detailing the cartographic images and technique for mapping the homogeneous geophysical and geobotanic "fields" with due regard for geostructural features of the regions and for peculiarities of topologically connected channel networks; - dependence of the geochemical landscape types on exposition and steepness of watersheds slopes; - methods of "mono-systems" (vertical) articulation of the landscapes at inadequate water consumption by irrigated crops assessment.

**U7/C/U1/E/05-B1** Poster **0830-06**

#### AN ENVIRONMENTAL MONITORING NETWORK AND DATABASE FOR MOZAMBIQUE

U.ASWATHANARAYANA ( c/o Ministry for the Coordination of Environmental Affairs, C.P. 1947, Maputo, Mozambique ; Email: anarayan@zebra.uem.mz)

Presently, biological pollution due to human wastes constitutes the main environmental problem for Mozambique. Pollution due to industries, and the use of fertilizers and pesticides is currently limited to particular pockets, but this situation is changing rapidly. An environmental monitoring network and database have been designed to address the emerging situation in Mozambique. The monitoring process involves the following : (i) Identification of the various sources of pollution of drinking water, soils, sediments, air and biota, (ii) Modelling the pathways of pollutants to man and risk analysis of the pollutants, (iii) Ways and means of monitoring the pollutants ( in technical and regulatory terms, cooperation with industries and communities and with neighbouring countries) and (iv) Cost-benefit analysis of the various pollution mitigation measures. The chemical analyses will be performed in the central laboratory in Maputo ( being equipped with ICP-AES, GC-MS-MS, GC-ECD, etc.) in cooperation with five field units equipped with portable instruments for the analysis of waters, soils and biota. To facilitate decision-making and implementation, databases are being organised, (i) sector-wise ( such as, chemical and metallurgical industries, food and beverage processing, textiles, transport, tourism, habitation and sanitation, waste disposal, etc.) for the country as a whole, (ii) ecosystem-wise ( e.g. Coastal Resources Management), and (iii) area-wise (town-wise and province-wise). The data will be disseminated through the Mercure satellite station located in Maputo.

**U7/L/03-B1** Poster **0830-07**

#### AUTOMATIC GREENHOUSE GASES MONITORING, DATA DISSEMINATION SYSTEM AND ANALYSIS SUPPORT TOOL FOR GLOBAL ENVIRONMENTAL RESEARCH

Y.Fujinuma, M.Hashimoto, M.KATSUMOTO (National Institute for Environmental Studies Center for Global Environmental Research 16-2 Onogawa, Tsukuba-shi, Ibaraki-ken 305-0053, Japan FAX/+81-298-508-2645 (contact person Masayuki Katsumoto e-mail: katsumoto.masayuki@nies.go.jp)

CGER-NIES has carried out several Greenhouse gases monitoring studies in East-Asia: by two ground-based stations at remote sites of Japanese-Archipelago, by chartered airplane over Siberian wetland and forest, and by ship-of-opportunity over Pacific Ocean. To analyze these data, the evaluation of the air mass attained at the sampling points is indispensable. In this presentation, the automatic monitoring system at remote sites, "Analysis Support System for " , developed at CGER/NIES, will be introduced. In the latter, the ECMWF data, Japanese meteorological data, etc., have been used. Also the trajectory analysis of air mass attained at Hateruma and Cape Ochi-ishi monitoring stations, located at south-west and north-east extreme of Japanese archipelago, will be discussed. Keywords: Global Environmental Monitoring, Air Mass Evaluation, Trajectory, Greenhouse gases.

**U7/C/U3/W/11-B1** Poster **0830-08**

#### ON MECHANISMS OF THE EARTH CLIMATE AND ECOSYSTEM VARIATIONS

Vadim V. NAVROTSKY (Pacific Oceanological Institute, 43 Baltiyskaya Str., Vladivostok, 690041 Russia, email: navr@online.vladivostok.ru)

The notions of Climate Change and Climate Variability are discussed. It is shown that generally used parameters for detecting and analysing Global Climate variations are inadequate to description of real climate regime shifts. A more precise definition of the notion 'Climate Change' is given, and a scheme of climatic informational system is proposed, based on the specific spatio-temporal net of observations, averaging and analysis. It is generally recognized that climate regime shifts are connected to ecosystem changes. There are many published results showing rather high correlations between global climate characteristics and productivity of the specific widely separated populations, although in many cases the local conditions for the populations are very different. Our approach to the explanation of such high correlations is based on the experiments and theory of coherent oscillations in biological systems, excited by extremely weak electromagnetic signals. Electric vibrations in the 100 to 1000 billion Hz region, associated with metastable states with very high dipole moments in biological membranes, lead to the specific oscillatory biochemical reactions and to macroscopic oscillations in the 10 to 100 Hz region, which directly influence functioning, productivity and state of organisms, as well as their collective behaviour. Electromagnetic fluctuations on the Earth are influenced by many external processes, such as solar activity, cosmic rays, tilt of the Earth rotation axis, precession of the equinoxes, changes in eccentricity of the orbit, motions inside the Earth etc. Evidently, these processes influence also climatic changes, and careful analysis of their cyclicity and periods of biological fluctuations gives an explanation to many climate-ecosystem correspondances even without taking into account many fold casual interactions between climate conditions and living matter on the Earth.

**U7/W/05-B1** Poster **0830-09**

#### MULTI-CRITERIA OPTIMIZATION APPROACH FOR OPTIMAL LOCATION AND EQUIPMENT OF REGIONAL METEOROLOGICAL NETWORK SITES

Oleg POKROVSKY, Vladimir Kondratyuk (Main Geophysical Observatory, Karbyshev str.7, St.Petersburg, 194021, Russia, e-mail: pokrov@main.mgo.rssi.ru)

Ground-based observational network efficiency is described by criteria set, which could be distributed into three groups : informational, economical and instrumental ones. First group is linked with such characteristics as a meteorological field accuracy representation, its spatial resolution, list of measured parameters et al. Economical criteria includes: total expenditures, e.g. measurement costs and expected gain of potential meteorological information users. Measurement precessions, systematic and stochastic error components, list of observed parameters, instrument costs are among instrumental criteria. Multi-criteria optimization model of observational networks has been proposed and considered as a mathematical problem of Boolean programming. Three types of optimization problem are discussed: 1) maximization of information content (Shannon information measure is used); 2) minimization of observational sites under some guaranteed value of inferred information content.; 3) minimization of total expenditures. Some application examples are considered. This approach is developed with respect to any set interrelated meteorological parameters. So corresponding results are fair for any complex observing sites. Results of numerical optimization for several Russian regional networks (North-West region, Kamchatka peninsula and Far East region) allow to formulate some recommendation for optimal observing site set (its composition and configuration), by its ordering, accordingly to information content contributions. The obtained conclusions also show how to find out the compromise between informational and economic criteria, having near values for some of considered sites. This approach allow us to determine the regional observational network providing the lowest optimal interpolation error level with respect to any other choices. Its other advantage is capability to consult optimal instrument selection for each meteorological site equipment. This method could be used for other ground-based networks : hydrological, oceanological and sea-coastal ones. Next step is to generalize the proposed approach for global networks.



**U7/E/02-B1** Poster **0830-10**

**REPEAT MERIDIONAL SURVEY OF THE WESTERN PACIFIC SURFACE CURRENT BY AN ADCP ON A COMMERCIAL SHIP**

Arata KANEKO, Zhu Yuan, Noriaki Gohda, Masazumi Arai and Hideo Nakajima (Faculty of Engineering, Hiroshima University, Higashi-Hiroshima 739-8527, Japan, email: akaneko@ipc.hiroshima-u.ac.jp); Hong Zheng (Japan Science and Technology Corporation/Hiroshima University, Higashi-Hiroshima 739-8527, Japan, email: hzheng@ocean.hiroshima-u.ac.jp); Takahige Sugimoto (Ocean Research Institute, University of Tokyo, 1-15-1 Minamidai, Nakano-ku, Tokyo 164-8639, Japan, email: sugimoto@ori.u-tokyo.ac.jp)

The western Pacific is one of the most important regions considering global climate research. Poleward transport of warm water by the Kuroshio may be part of the coupling mechanism between tropical and subtropical ocean at the decadal scale. An ADCP program, which has started since January 1997, aims at measuring ocean surface currents in the western Pacific on a almost monthly basis, intending to run over 10 years. A huge mineral transport ship, the "First Jupiter" (83,658 t in weight and 289 m in length), equipped with a shipboard RDI-BB 150 kHz ADCP, operates mainly between Japan and Australia. During regular cruises, the ship crossing of the Kuroshio south of Japan leads by about five days the crossing of the North Equatorial Current off Philippines, in the source region of the Kuroshio. Time-series of both currents contribute to monitor the western part of the Pacific Subtropical Gyre. The meridional distribution of the annual mean zonal transport for upper 220 m is determined from the 1997 data. The Rossby waves of first baroclinic mode are also caught with the westward propagation at 6N and 25 N by analysing the anomaly from the annual mean data

**U7/W/02-B1** Poster **0830-11**

**AN INTEGRATED SYSTEM FOR OBSERVING, MODELING AND PREDICTING OCEAN TIDES**

C. Le PROVOST (email: Christian.Le-Provost@cnes.fr); F. Lefevre (email: Fabien.Lefevre@cnes.fr); F. Lyard (email: Florent.Lyard@cnes.fr); F. Ponchaut (email: ponchaut@cnes.fr); and P. Techine (email: Philippe.Techine@cnes.fr); (all at LEGOS/GRGS, UMR5566 CNES-CNRS-UPS, 14 Avenue E. Belin, 31400 Toulouse, France)

Tides are the major contributor to the high frequency variability of the sea level. They have been observed by traditional tide gauge techniques since more than a century, but along the coasts and on islands. During the sixties, deep sea tide gauge technology developed, allowing to measure tides offshore. But only a few hundreds of sites have been visited. Since the advent of high precision satellite altimetry, it is now possible to observe tides over almost the whole ocean, with however unusual time sampling, and particular space sampling. The mid-nineties have seen a major step in our ability to precisely describe ocean tides, through hydrodynamic modelling, satellite data analysis, and data assimilation in these models. The aim of this talk is to present an integrated approach based on a finite element hydrodynamic model, analysis of sea level data from in situ networks and satellite altimetry, and a methodology for assimilation of these data. This approach has been successfully applied to the determination of the deep ocean tides by assimilating satellite data. We have more recently applied the same approach but focusing on the assimilation of in situ data in order to improve our tidal solution in shallow waters and along the coasts. This system has been used also to evaluate the quality of the in situ data sets accumulated since the beginning of the century, and estimate their representativeness of the local or more global characteristics of the tides. The model/assimilation technique can help also to study the impact of a given observation on the local and global quality of the product issued from this system

**U7/W/14-B1** Poster **0830-12**

**SONEL: TOWARDS A NATIONAL INTEGRATED COASTAL SEA-LEVEL MONITORING SYSTEM**

Serge Allain (1): 13 rue du Chatellier, BP 426, 29275 Brest, France), Claude Boucher (2): IGN/LAREG, 6-8 Avenue Blaise Pascal, 77455 Marne-la-Vallée, France), Loïc Daniel (3): IGN/ENSG, 6-8 Avenue Blaise Pascal, 77455 Marne-la-Vallée, France), Bernard Simon (1) et Guy WOPPELMANN (1)

SONEL stands for "Système d'Observation du Niveau des Eaux Littorales". The project is developed by both French agencies: IGN (Institut Géographique National) and SHOM (Service Hydrographique et Océanographique de la Marine). The motivation is to ensure the maximum efficiency in existing services related to sea and land surface level measurements and to get a greater benefit from those through synergy and cooperation. The primary goal of SONEL is to provide a service to support, through geodetic and tide gauge data products, research activities on long term sea level variations related to climate change. SONEL aims to be the natural interface with international organizations and projects: GLOSS, Med-GLOSS, EOSS... The concept of SONEL is based upon the idea of getting more from several mono-thematic permanent observing networks (either geodetic or sea-level oriented), this will come from integrating them in an efficient data collection and dissemination scheme and combining their measurements in order to provide specific products. This synergy is indeed the only way to get a clear and unambiguous sea-level signal among other things.

After a quick description of SONEL and its main components our presentation will focus on the data management aspects. We will present the precise scheme of the data management system, its objectives and specifications. Some technological data processing and computer systems aspects will be developed. In conclusion, we will present the status of the project, its first realizations and the upcoming actions.

**U7/W/04-B1** Poster **0830-13**

**THE GLOBAL SEA LEVEL OBSERVING SYSTEM (GLOSS)**

Philip L.WOODWORTH (Permanent Service for Mean Sea Level, Proudman Oceanographic Laboratory, Bidston Observatory, Birkenhead L43 7RA, UK, email: plw@pol.ac.uk)

The Global Sea Level Observing System (GLOSS) is an Intergovernmental Oceanographic Commission (IOC) coordinated programme for the establishment of a global network of tide gauges, and associated geodetic devices, for application to climate, oceanographic and coastal sea level research. GLOSS can be considered a component of the Global Ocean Observing System (GOOS), and particularly as a major contributor to its Climate and Coastal Modules. During 1996-97, GLOSS objectives were extensively re-assessed by the GLOSS Group of Experts, resulting in a new Implementation Plan for the programme approved by the IOC Assembly in July 1997. The Plan defines a GLOSS Core Network (GCN) of around 280 gauges distributed worldwide, designed to provide an approximately evenly-distributed sampling of global coastal sea level variations; a GLOSS Long Term Trends (LTT) set of gauge sites (some, but not all, of which are in the GCN) for monitoring long term trends and accelerations in global sea level, these will be priority sites for GPS and DORIS receiver installations to monitor vertical land movements; a GLOSS altimeter calibration (ALT) set, mostly islands, to provide an ongoing facility for mission intercalibrations; and a GLOSS ocean circulation (OC) set, including in particular gauge pairs at straits and in polar area, complementing altimetric coverage of the open deep ocean. The Implementation Plan has

also outlined updated mechanisms for global tide gauge data flow. These are intended to make sea level data more accessible to the community. GLOSS activities now include a large number of regional projects and products, and a range of international training courses and materials. Manuals are available on 'How to Operate a Tide Gauge', and a manual on 'How to Operate GPS at Gauge Sites' is planned for 1999. The present manuals are also available in CD-ROM form. GLOSS has newsletters on the web and in conventional paper form.

**U7/W/01-B1** Poster **0830-14**

**TOWARDS MULTIPARAMETER NETWORKS FOR THE NEXT CENTURY**

Genevieve ROULT, Jean-Paul Montagner, Jean-Francois Karczewski and Eleonore Stutzmann (Departement de Sismologie, Institut de Physique du Globe, 4 place Jussieu, 75252 PARIS-Cedex 05, France)

The design of the future networks cannot be separated from the scientific issues which scientists are faced to, nor from the new technology tools that are to be developed for the next century. The trilogy, science, scientist and instrument must be well balanced in order to make implementation of the network achievable. Since most of the scientific issues are multiscale for spatial scales as well as for temporal scales, we present the general design of the network which should enable to address these scientific issues. They must be able to explore different scales of heterogeneities from global scale to local scale. We review the different technological developments which are presently explored, and which prefigure what will be the future geophysical networks. The technical developments carried out by various French scientific programs (GEOSCOPE, OPTIMISM, SOFM) will be presented as an illustration. The concept of multiparameter station is defined and it is demonstrated the great scientific interest in installing different kinds of sensors at the same place in a seismic station. Every seismic station will have to be transformed into a multiparameter geophysical station. It is also necessary to cover the oceanic desert by a dense network of geophysical observatories which can fulfill the scientific requirements of the whole geoscientist community.

The recent progresses made by Japanese, French and US groups show that the technical challenge of installing permanent geophysical ocean bottom observatories (coined GOBOs) is not out of reach. Therefore, the new generation network will have to be composed of multiparameter continental or oceanic stations including at least broadband seismometers, microbarometers, microthermometers, and eventually other sensors (electromagnetic sensors, strainmeters, GPS, ...). The design of the complete chain of acquisition, from the sensor to the distribution of data, will imply to integrate all the technical progresses made in micromechanics, electronics, computers, space science, and telecommunication systems. Finally, the new generation of geophysical networks must be able to provide scientific data at all scales, from the global scale to the local scale.

**U7/W/13-B1** Poster **0830-15**

**OCEAN HEMISPHERE NETWORK PROJECT DATA CENTER**

Shingo WATADA and Yoshio Fukao (both at Earthquake Research Institute, University of Tokyo, 1-1-1 Yayoi Bunkyo-ku, Tokyo 113-0032, Japan, email: watada@eri.u-tokyo.ac.jp); Seiji Tsuboi (Department of Geosciences, National Defense Academy, Yokosuka 238-8686, Japan, email: tsuboi@cc.nda.ac.jp)

The Ocean Hemisphere network Project (OHP) is to establish a network that comprises of a wide range of geophysical sensors on islands and the ocean floor in the western Pacific and its peripheral continents. For example, broad band seismic, GPS, geo-electromagnetic, and superconducting gravimeter networks have been operating on land. Ocean bottom seismometers and hydrophones are attached to retired ocean bottom cables, borehole drilling for broadband seismometry on the ocean floor is expected soon, and voltage measurements between the two ends of retired ocean bottom cables already started. All these data are, or will be, available through the OHP Data Center (<http://ohpdmcc.eri.u-tokyo.jp>). The data center facilitates the data exchange between other data centers and data distribution to every researcher in a standardized format. The former POSEIDON seismic network is being upgraded with new data loggers and STS-1 seismometers. OHP seismic waveform data, including accelerograms and hydrophone data from the TPC-1 ocean bottom cable, and broadband data from the CMG-3T network of the Earthquake Research Institute in central Japan area, are distributed in the SEED format. As a data exchange, seismic event waveform data archived by IRIS are also available from the data center. The data center also collects software packages developed by the members of OHP. A package to compute synthetic seismograms using the Direct Solution Method is downloadable from the home page.

**U7/W/16-B1** Poster **0830-16**

**THE GLOBAL SEISMOGRAPHIC NETWORK**

Jonathan BERGER, IGPP, SIO, (University of California San Diego, 9500); Gilman Dr. La Jolla CA 920393-0225, email: jberger@ucsd.edu); Rhett Butler, (IRIS, 1200 New York Ave, NW, Washington DC, 20005, Email: rhett@iris.edu) Charles R. (Hutt, U.S. Geological Survey Seismological Laboratory, Building 10002), Kirtland AFB-East, Albuquerque, NM 87115, email: hutt@asl.cr.usgs.gov

We describe the genesis and development of the Global Seismographic Network, a collection of about 125 geophysical observatories with common management, funding, instrumentation standards, and data distribution. Organized and managed by the Incorporated Research Institutions for Seismology (IRIS), stations of the network are operated and maintained by the USGS and by the University of California San Diego. Stable long-term funding is provided by the U.S. National Science Foundation and by the U. S. Geological Survey. Each station of the network is organized with the following key elements: 1. A formal agreement with a local host organization which covers the establishment and long-term operation; 2. Observatory facilities required to support instrumentation; 3. Local operational personnel; 4. Data collection, archiving, and distribution mechanisms; 5. Internet connectivity at most stations. The current GSN represents over 15 years of development and an investment of over 80M USD. We describe some of the practical problems encountered in the execution of this enterprise and a few of the lessons learned. While the principal purpose of these observatories is seismological, they can easily be equipped with a variety of other geophysical instrumentation. With sites on all continents and many oceanic islands, the GSN offers valuable opportunities for other global geophysical monitoring programs to utilize these facilities and their associated logistic support.



**U7/E/03-B1** Poster **0830-17**

**CONTRIBUTION FOR THE MONITORING OF THE SW PORTUGUESE MARGIN: CRUSTAL THINNING ALONG IAM5**

Alexandra AFILHADO (at CGUL, R. Escola Politécnica 58, 1250 Lx, Portugal, email: ammg@fc.ul.pt; also at ISEL, R. Conselheiro Emídio Navarro, Lx, Portugal); Dina Vales (IM, R. C. Aeroporto, Lx, Portugal, email: dina.vales@meteo.pt); Alfred Hirn (IPGP, P. Jussieu, Paris, France, email: hirn@ipgp.jussieu.fr); A. Gonzalez (DCCT, CICESE, Ensenada, B.C. México, mindundi@cicese.cicese.mx); Luis Matias and L. Mendes-Victor (both at CGUL and DFFCUL, email: lmvictor@fc.ul.pt)

In order to complement the understanding of the Geodynamic processes that generate rifted margins, many deep crustal seismic surveys have been performed in the last few years. OBSs as well as land seismic stations (LSS) are usually included in the surveying, providing very helpful information on the deep crust and upper mantle velocity structure. The Tagus Abyssal Plain (TAP), SW offshore of Portugal, cannot be closed in most Pangea reconstructions. The nature of the crust as well as the amount of thinning is still debated, mainly due to a poorly constrained crustal structure related to a lack of data. Both OBSs and LSS wide-angle seismic information were collected during Iberian Atlantic Margins (IAM) fieldwork along the line IAM5 crossing the TAP up to the continental margin. The modeling of the data sets were performed by two steps: (1) separately modeling of LSS data and OBS data; (2) modeling simultaneously both data sets, using the former P-wave crustal velocity models as initial models. This procedure allows us to better constrain the convergence of both models and it also quantitatively evaluates the reliability of non reversed wide-angle data modeling to study the thinning at continental margins. New seismic data on the TAP is being collected under the scope of Big Source of Earthquakes and Tsunamis (BIGSETS) project. The deployment of OBSs is also programmed and will be an important contribution for the network design in order to assure an adequate monitoring of this region.

**U7/W/11-B1** Poster **0830-18**

**SOME ASPECTS OF USING OBJECT-ORIENTED TECHNIQUE FOR DISTRIBUTED SEISMIC DATA PROCESSING**

Osadchuk, A (Institute of Geophysics NASU, Palladin 252680, Ukraine, Tel: 380 44 414 90 90, Email: osadchuk@adam.kiev.ua)

Modern seismic is faced with a problem of simplifying methods of searching and acquiring seismic records from different data sources. The fact is that the data is stored in different formats on separate servers which use different access procedures. Using of object-oriented modular tools can help to solve this task, by means of attracting independent developers for writing access methods to each information block. Under centralized control should be only the basic set of classes that define the main information structures and their interrelations. As an example of such set of classes one can take FISSURES classes, proposed by IRIS. Further development of seismic data processing instruments will include adding and modification of classes responsible for the work with specified information format. Author demonstrate realization of object-oriented technique on the example of Java-based platform independent client's program that visualize multi-ray seismic records and can be upgrade (without rebuilding) to support any seismic data format.

The next question under discussion is distribution data processing tasks between servers and clients programs and choosing of appropriate software solutions for each of them.

**U7/W/18-B1** Poster **0830-19**

**DATA COLLECTION FROM THE GLOBAL SEISMOGRAPHIC NETWORK**

Robert WOODWARD (United States Geological Survey, Albuquerque Seismological Laboratory, Bldg. 10002, Kirtland AFB-E, Albuquerque, NM 87115-5000, USA, e-mail: woodward@aslr.cr.usgs.gov); J. Peter Davis (Institute of Geophysics and Planetary Physics, Scripps Institution of Oceanography, University of California, San Diego, La Jolla, CA, 92093-0225, USA, e-mail: pdavis@ucsd.edu); Tim Ahern (Incorporated Research Institutions for Seismology, Data Management Center, 1408 NE 45th Street, Seattle, WA, 98105, USA, e-mail: tim@iris.washington.edu)

The Global Seismographic Network (GSN) comprises roughly 125 seismographic stations distributed around the Earth. Data are used for a variety of purposes, including studies of Earth structure, seismic hazard, and monitoring of the comprehensive test ban treaty. Each station site is comprised of a suite of sensors, including three-component very-broad-band-response seismometers, high frequency seismometers, and in some instances strong-motion seismometers and meteorological instrumentation. Typical stations generate 10 megabytes of data per day, with some sites generating 30 to 40 Mb of data per day. Data are retrieved by two Data Collection Centers using a variety of methods, including mailing of tapes, Internet links, telephone dial-up, satellite links, and Inmarsat telephone connections. Data from a number of the stations are available in near-real-time. At the Data Collection Centers the data are subjected to quality control review, data problems are identified and flagged and/or repaired, and the data are reformatted to a standardized distribution format. All data are then forwarded to key data centers around the world, including the Incorporated Research Institutions for Seismology (IRIS) Data Management Center (DMC) in Seattle, Washington, USA. From the IRIS DMC all GSN data are available to the entire geophysical community. Key issues in the collection and distribution of the GSN data are the standardized format, open data access policies, and highest possible quality standards. The increasing emphasis on retrieval of data in near-real-time, combined with the availability of all digital data ever collected by the GSN and its (digital) predecessor networks, allows studies at multiple time- and spatial-scales

**U7/L/10-B1** Poster **0830-20**

**CABLE-CONNECTED OCEAN BOTTOM OBSERVATION NETWORKS IN JAPAN**

Katsuyoshi KAWAGUCHI, Hajimu Kinoshita, Kenji Hirata and Ryouichi Iwase (Japan Marine Science and Technology Center 2-15, Natsushima-cho, Yokosuka 237-0061, Japan)

Real-time scientific measurements at deep seafloor are getting very important to make clear scientific phenomena in earth. Ocean bottom observatories utilizing submarine cables have been very attractive for the geo-scientific studies and natural hazards (such as earthquakes and tsunamis). The developments of observatories are accelerated by the demand for the arrangement of seismic observation network around the Japan islands and retirement of coaxial submarine cables for overseas telecommunications. JAMSTEC has designed submarine cable connected seismic observatory and helped deployment and data transmission to Japan Meteorological Agency (JMA) database, which is accessible to other institutions and universities. The point of the end of 1998, two of seven sets of deep seafloor observatories deployed around the Japan islands are designed by JAMSTEC and a new observatory is under construction. The telecommunication submarine cable systems on world seafloor are innovated optical fiber cable system and coaxial cable system is to be closed its service. Some of the demission submarine cable system was donated from international telegram and telephone company in Japan (KDD) to universities coalition for scientific

reutilization. Nine research institutes in Japan are joining and planning to carry out a project to construct complex scientific observatory using demission submarine cable for studying deep sea environmental changes around the Philippine Sea plate. This is a foremost complex observatory which will install to demission telecommunication cable and the project is named VENUS (Versatile Eco-monitoring Network by Undersea-cable System) project.

These types of cable connected ocean bottom observatories will be a powerful tool for precise natural hazards observation and geo scientific studies.

**U8**

**Wednesday 28 July**

**GEOPHYSICAL ASPECTS OF THE COMPREHENSIVE TEST BAN TREATY**

Location: Great Hall  
Location of Posters: Old Gym

**Wednesday 28 July AM**

Presiding Chair: A. Dainty

**Introduction** **0850**

HUSEBYE, DAINTY

**U8/P/02-B3** Invited **0900**

**A BRIEF HISTORY OF SEISMOLOGY AND TEST BAN VERIFICATION**

P.D. MARSHALL & A. DOUGLAS (AWE Blacknest, Brimpton, Reading RG7 4RS, UK, email: alan@blacknest.gov.uk)

In the beginning the only method that seismologists could suggest for distinguishing between earthquakes and underground explosions was first motion. For explosions the first motion of P should everywhere be away from the source; for earthquakes there should be somewhere where motion is towards the source. In practice the method is difficult to apply principally because first motion could not be used confidently at low signal-to-noise ratios. Complexity of P seismograms then looked to be capable of identifying at least 90% of earthquakes from observations at teleseismic distances. The short-period P signals from explosions (as observed at arrays) were always it seemed simple - a single wavelet followed by a low amplitude coda - whereas the signals from shallow earthquakes often had amplitudes 30s after onset, as large as or larger than direct P. With time this apparent clear separation became blurred. The most robust criterion for distinguishing between earthquakes and explosions is the so-called mb/Ms, criterion: for a given Ms/mb, is Much larger for explosions than for earthquakes, but again as with all criteria there are difficulties in its application. Now after 40 years of research the basis of most identification criteria is understood and these criteria can be combined to answer the question: are the observations from a given seismic disturbance compatible with an earthquake source? If not then the disturbance could precipitate a demand for an on-site inspection to look for evidence of a possible nuclear test.

The paper describes some of the main advances in test ban seismology since 1958 and how these advances influenced the negotiations for a treaty banning all nuclear tests and eventually led to the signing of the Comprehensive Test Ban Treaty in September 1996.

**U8/W/11-B3** Invited **0925**

**THE INTERNATIONAL DATA CENTRE OF THE PREPARATORY COMMISSION FOR THE COMPREHENSIVE NUCLEAR-TEST-BAN TREATY ORGANIZATION PROVISIONAL TECHNICAL SECRETARIAT**

Rashad M. KEBEASY (CTBTO, Provisional Technical Secretariat, Vienna, International Centre, P.O. Box 1250, Vienna, A-1400 Austria, email: rkebeasy@ctbto.org)

According to the Comprehensive Nuclear-Test-Ban Treaty (CTBT), the International Data Centre (IDC), of the Comprehensive Nuclear-Test-Ban Treaty Organization (CTBTO) Preparatory Commission has the function to receive, collect, automatically process, interactively analyze, report on, and archive seismic, hydroacoustic, infrasound and radionuclide data from the 337 stations and laboratories of the International Monitoring System (IMS). Its function is also to carry out, at no cost to States Parties, special studies, technical assistance and technical analysis of IMS or other data if requested by the organization or State Party. Moreover, the IDC has to progressively enhance its technical capabilities and provide standard IDC products with no prejudice to final judgements.

The plan for progressive commissioning of the IDC in Vienna, Austria continues according to the schedule established by the Preparatory Commission. A number of major milestones have been achieved since the start of the IDC establishment in 1997. Following to this plan more than 60 highly qualified staff members have already been hired. Most computer hardware and commercial software required for installation, testing and validation of software releases from the prototype International Data Center (pIDC) in Arlington, Virginia have been procured. A high speed telecommunication link between the IDC in Vienna and the pIDC in Arlington has been established to support transition and installation of the various releases as well as transmitting data for real-time testing of the software. A US \$70 million contract was signed last September for turnkey services including the design, manufacture, delivery, installation, operation and maintenance of a complex Global Communication Infrastructure (GC) to ensure the swift and secure transport of data between the IDC and over 500 IMS facilities and National Data Centres of the Treaty Signatory States.

Already the IDC is demonstrating its potential as testing continues using the second release of applications software delivered from the pIDC. This system provides the capability to process and analyze realtime data from a network of about 100 "volunteer" stations, with the ability to expand and improve as the IMS network grows and experience is gathered.

**U8/E/08-B3** Invited **0940**

**THE INFRA-SOUND SEGMENT OF CTBTO'S INTERNATIONAL MONITORING SYSTEM**

Douglas CHRISTIE (Provisional Technical Secretariat, Comprehensive Nuclear-Test-Ban Treaty Organization, Vienna International Centre, P.O. Box 1250, A-1400 Vienna, Austria, email: Dchristie@ctbto.org)

The infrasound component of the International Monitoring System (IMS) for Comprehensive Nuclear-Test-Ban Treaty verification will consist of 60 array stations distributed as uniformly as possible over the surface of the globe. This network of high sensitivity stations will be capable of detecting and locating all nuclear explosions in the atmosphere with yields of 1 kt or more. In many parts of the world, the detection threshold will be significantly less than 1 kt. The infrasound monitoring system will be far larger and more sensitive than any other

previously operated infrasound network. High-resolution data from this network will provide an unprecedented opportunity for the study of a wide range of geophysical phenomena in the atmosphere. In addition to infrasound from nuclear explosions, the network will detect acoustic and non-acoustic waves generated by large chemical explosions, volcanic eruptions, severe storm activity, tornadoes, the aurora, air flow over mountains, supersonic aircraft, meteors, earthquakes, and a variety of sources associated with the space industry. Data from the network will be especially important for studies of the frequency of occurrence and size distribution of meteors and studies of the dynamical behaviour of the upper atmosphere. All significant volcanic explosions will be detected by the IMS infrasound network. The data will therefore be of interest to the aviation community since prompt notice of volcanic activity can be used to reduce the hazards associated with volcanic ash clouds.

**U8/W/08-B3** Invited **1005**

**GLOBAL RADIONUCLIDE SURVEILLANCE THE SENSITIVE NOSE OF THE CTBTO VERIFICATION SYSTEM**

Lars-Erik De GEER (Provisional Technical Secretariat, Vienna International Centre, P.O.Box 1250, Vienna, A1400, Austria, Email: ledg@ctbto.org)

The Comprehensive Nuclear-Test-Ban Treaty Organization (CTBTO) verification system employs four different techniques, three of which are basically listening to and analysing the continuous sound in the three terrestrial environments, the underground, the oceans and the atmosphere. The fourth technique, the collection and analysis of airborne radionuclides, is mainly focused on the atmosphere, but it can also catch information from the other two environments if the circumstances are right. And, that is very important, for a cheater to try to avoid being heard by the "sound" system he/she has inevitably to create those circumstances and increase the risk of putting radioactive odours into the atmosphere which can be smelled by the CTBTO radionuclide system. The Treaty defines a total of 80 stations worldwide for the collection of atmospheric aerosols, half of which will also be collecting samples of noble gases, especially focusing on xenon isotopes. All aerosol samples will be collected during 24 hours, allowed to let co-collected and disturbing radon daughters to decay for up to 24 hours and then they will be counted for another 24 hours. The xenon samples need no decay period and the technique employed might well even work on shorter cycles (like 6 hours) although the reporting time is only requested to be 24 hours by the Treaty.

The results in the form of energy spectra will be sent daily to the IDC in Vienna where they will immediately be subject to an automatic analysis and then interactively checked by an analyst. To minimise the human interaction time great efforts are put into developing effective software capable of finding all existing nuclides with a minimum of false detections of nuclides which are not present.

The current status of the network and the analysing software employed by the CTBTO/IDC in Vienna will be described.

**U8/L/02-B3** **1030**

**COSMOS 1809 SATELLITE MEASUREMENTS OF VLF EMISSIONS IN NEAR EARTH SPACE ASSOCIATED WITH UNDERGROUND NUCLEAR TESTS**

Vlaimir KOSTIN and Yury Romanovsky (both at Fedorov Institute of Applied Geophysics, Rostokinskaya 9, Moscow, 129128, Russia, email: hciag@sunny.aha.ru); Yakov Sobolev (Institute of Terrestrial Magnetism, Ionosphere and Radiowave Propagation, Troitsk, Moscow Region, 142092, Russia, email: ymich@izmiran.rssi.ru)

During 1987-1991 years COSMOS 1809 satellite (the orbit parameters: H= 950km, inclination-82°) carried out in near Earth space measurements of VLF emissions (f=70Hz-20kHz) associated with underground nuclear tests (UNT) of USA, France and former Soviet Union. Ten UNT events were observed at different distances from test ranges. Electromagnetic impulse of UNT has been revealed only one time when the satellite crossed L-tube projected immediately at a test range. Anomalies of whistler propagation were registered during 5-10 hours within the region of 2000 km from UNT point. This effect is proposed to be caused by the ionosphere disturbances due to acoustic waves after an explosion. Relaxation processes after UNT with power of 100 kt were appeared in near Earth space over UNT ranges as an increase of VLF noises in 2-3 times during 2-3 days. To clarify and indicate VLF signatures of UNT the database of VLF appearances of different man-made effects on near Earth space was prepared and analyzed. It is concluded that VLF emissions associated with UNT can be additional mean to monitor environmental effects caused by nuclear tests.

**U8/E/03-B3** Invited **1110**

**T-WAVE STATIONS FOR THE CTBT: A GLOBAL PERSPECTIVE**

Emile A. OKAL, (Department of Geological Sciences, Northwestern University, Evanston, IL 60208, USA)

As part of its monitoring efforts, the CTBT mandates the deployment of a network of "T wave stations", i.e., seismic stations located in the immediate vicinity of a shoreline and detecting the seismic waves resulting from the conversion of acoustic "T" waves. We review the mechanisms by which the seismic/acoustic and acoustic/seismic conversions take place, and give a perspective on the principal milestones in the use of seismically recorded T waves in the geophysical exploration of the Pacific Ocean over the past 40 years.

The application of simple models of reflection and refraction at the water/rock interface, as well as more involved modeling based on finite element applications, and the comparison with actual records, indicate that the optimal conditions for an efficient conversion require steep slopes as found on coral reefs, or at the heads of fresh basalt flows, similar to the Hawaiian "palis". The conversion can result in a shadow zone for converted-P, in which case the arrival can take the form of an S wave, or of a surface wave guided in the surficial layers.

In the environment of the Pacific Ocean, T waves have led to the discovery of several underwater volcanoes (Macdonald -- from acoustic records; and Hollister -- from seismic records), and to the recognition of various forms of their activity depending on the particular spectral characteristics of the phase. In addition, because of their capability to transmit energy at very high [seismic] frequencies over distances limited only by the size of the oceanic basin, T waves have been used to investigate such diverse problems as the tomographic mapping of the source of large earthquakes (Antarctic event of 25 March 1998), or the mechanical structure of subducting slabs (from such deep earthquakes as the 1994 Bolivia and 1990 Sakhalin events).

Finally, regarding the detection of explosive sources in the ocean, we will discuss seismic records of T waves from such sources as local seismic refraction experiments in Polynesia, a crustal refraction study in Mexican waters, marine seismics off the coast of California, and the presumed firing of ICB test missiles from submarines (all recorded in the Central Pacific).

**U8/E/10-B3** **1135**

**THE SEISMOLOGICAL SEGMENT OF THE CTBT MONITORING SYSTEM**

Robert NORTH (Center for Monitoring Research, 1300 North 17th Street, Suite 1450, Arlington, Virginia 22209, USA, email: north@cmr.gov)

The majority of the recording stations of the International Monitoring System are seismic. Digital data from 171 sites, of which 37 are arrays with apertures of up to 60km, will be received at the International Data Centre (IDC). Here they will be automatically processed and the results reviewed by experienced analysts. The techniques and procedures for processing and analysis are the culmination of many decades of research and algorithm development, and the corresponding software in many cases represents the first routine and automatic application of many such developments in an operational global seismic monitoring system. Examples include maximum likelihood estimation of magnitudes, a variety of event characterization measurements, and the association of hydroacoustic and infrasonic observations with seismic events.

A prototype IDC has been operating continuously at the Center for Monitoring Research since 1995, and the software that has been progressively developed and exhaustively tested there forms the basis of the CTBT IDC system. With continuous data from only 35 stations, the prototype IDC has achieved lower overall global detection thresholds than existing centres and provided an extensive data base of new parameters that is being used as the basis for further improvements. The seismic processing and analysis system will be briefly described and a summary provided of some of the more significant results to date.

**U8/E/09-B3** Invited **1155**

**CONSTRUCTION AND CALIBRATION OF A COMBINED P AND S MODEL OF THE CRUST AND UPPER MANTLE BENEATH CENTRAL AND SOUTHERN ASIA**

M Barmin, E R ENGDAHL, A Levshin, P Molnar, M Ritzwoller, A Villasenor (ph. 1 303 535 4853; e-mail: engdahl@lemond.colorado.edu, University of Colorado at Boulder, Boulder, CO 80309-0390 USA); W Mooney (U. S. Geological Survey, Menlo Park, CA 94025 USA); W Spakman, J Trampert (Utrecht University, Utrecht, The Netherlands); C Thurber (University of Wisconsin, Madison, Madison, WI 53706 USA)

Our aim is to combine the complementary features of global and regional scale body and surface wave tomography to produce a new model of P and S wave structure of the crust and upper mantle beneath Central and Southern Asia. The purpose of the model will be to improve location capabilities in the region of study under realistic regional monitoring conditions. The goal is to provide a uniform lateral resolution of 100 - 200 km across the entire region of study. To accomplish this goal we utilize the following recently published data: for S velocities in the crust and upper mantle we use long-period surface wave phase velocities and regional and continental scale group velocity measurements at intermediate periods; for P velocities in the mantle we use teleseismic and regional P-wave measurements; finally we use a priori information about the crust to regularize the inversions. To ensure its accuracy and usefulness, we validate and calibrate the model with empirical travel times, including those from Ground Truth data bases. We present information about how 3D structures in the crust and upper mantle affect travel times and ray paths and how these effects are manifested in biasing event locations under a variety of regional monitoring scenarios, in particular where data coverage is governed by the proximity of International Monitoring System (IMS) stations.

**U8/E/06-B3** **1215**

**RECOGNIZING CHEMICAL EXPLOSION SITES AND LOCATING EARTHQUAKES TIED TO AUTOMATED ENVELOPE ANALYSIS OF LOCAL NETWORK RECORDS**

Eystein S. HUSEBYE (IFJ, UoBergen, Allegaten 41,N-5007, Norway, email: eystein.husebye@ifj.uib.no) Yura V. Fedorenko (IFJ and Inst. North Industrial Ecology Problems RAS, Fersman Str. 14, Apatity, 184200 Murmansk Reg., Russia)

In monitoring local seismicity we are faced with 2 major problems namely that of properly identifying numerous chemical explosions and also locating accurately earthquakes. Preferably this should be done in an automated manner which is not feasible if tied to high-frequency network recordings. An alternative to conventional analysis is to replace the original complex waveforms with corresponding smooth envelope traces which are convenient for automated analysis. Chemical explosions are characterized by stationary envelope waveforms in time and space for individual mines. stationary. demonstrate how we utilized these features in combination with an artificial neural net (ANN) scheme for teaching the computer to recognize new explosion recordings from a specific site. In case of a single 3-comp. station recording we used the 9 different complex covariance elements in a multitude of frequency bands as diagnostic features. We are attempting to adapt the same procedure to non-stationary earthquake recordings. The new strategy here aims at utilizing waveform information from former earthquake recordings serving as a basis for construction of an automatic event locator. The basic idea is to 'backproject' individual station records to a fixed distance (100km) and compare waveforms using the ANN scheme. The distances providing the best fits are then used for epicenter locations. This approach is in principle similar to synthetic seismogram analysis but modelling is empirical and not physical - energy propagation in stratified media is complex. Both the explosion and earthquake location concepts have been extensively tested on Norwegian network recordings of very many local events with excellent results.

**Wednesday 28 July PM**

Presiding Chair: E.S Husebye (IFJ, UoBergen, Allegaten 41,N-5007, Norway.)

**U8/W/01-B3** Invited **1400**

**OUTSTANDING ISSUES IN CTBT MONITORING. HOW CAN GEOPHYSICISTS CONTRIBUTE TO THE TREATY VERIFICATION SYSTEM?**

K. L. MCLAUGHLIN (Center for Monitoring Research, SAIC, Suite 1450, 1300 N. 17th. St. Arlington, VA, 22209, 703-247-1826, email: scatter@cmr.gov)

Calibration of each network (seismic, hydroacoustic, infrasound, and radionuclide) remains a major task before their full monitoring potentials can be realized. This talk will highlight how geophysics can make significant contributions to this international effort. Regional travel-time calibration is required to provide location uncertainties for small continental events better than 1000 square km. This ambitious goal requires maximum use of high quality seismic arrays and regionalized travel time tables. Most small events will be detected by only three primary plus one or two regional auxiliary stations. The Prototype International Data Center (PIDC) currently uses regionalized corrections to IASPEI Pn, Pg, Sn, and Lg tables for North America and Fennoscandia. Corrections are specified for source-specific locations on a lat-lon grid. Major effort remains to coordinate construction of such corrections for the entire Earth. Corrections must be independently validated against well recorded or ground truth events. In



addition, empirical azimuth and slowness corrections are estimated for each station and array since all stations and arrays show some significant azimuth and slowness anomalies. Calibration of seismic surface waves remains another future area. Detection and identification of long-period Rayleigh (LR) waves is based on a worldwide group velocity grid. Further refinement of the grid is required to lower LR thresholds. Infrasound is the least mature of the monitoring technologies. It is well known that infrasound propagation is strongly affected by 3D atmospheric winds and temperature profiles. Less well understood is whether useful propagation can be predicted from atmospheric models and how often the models must be updated. The hydroacoustic network will include 4 high frequency island seismic stations, to register acoustic energy converted to seismic energy. Researchers have yet to provide a predictive model for this conversion process.

**U8/W/03-B3****1425****STATUS OF THE IMPLEMENTATION OF THE INTERNATIONAL MONITORING SYSTEM FOR THE CTBT**

Peter BASHAM, Sergio Barrientos, Alberto Veloso, Martin Lawrence and Joachim Schulze (International Monitoring System Division, CTBTO Provisional Technical Secretariat, Vienna, email: pbasham@ctbto.org)

The implementation of the International Monitoring System (IMS) began with the establishment of the CTBTO Provisional Technical Secretariat (PTS) in Vienna in March 1997, although a critical mass of staff were not in place until late 1997. This presentation will describe the status of the stations of the IMS: 321 seismic, hydroacoustic, infrasound, and radionuclide stations identified in the Treaty that need to be established around the globe. The annual budgets for the IMS Division of the PTS for 1997, 1998 and 1999 are \$US9.8, 25.9 and 35.6 million, respectively, representing a total capital investment in stations of \$US57.5 million. This is approximately 40% of the total capital investment required to complete the IMS networks. Seismic is the most mature technology of the IMS, with about 85 primary and auxiliary stations currently sending data to the International Data Centre (IDC) in Vienna. By the end of 1999, these networks should be about 70% complete. Three hydroacoustic stations are currently sending data to the IDC, although they will require significant upgrades to meet specifications; this network will be about 70% complete at the end of 1999. Only one infrasound station existed at a Treaty location at the beginning of IMS developments; this network will be about 30% complete at the end of 1999. Although there are many pre-existing radionuclide stations monitoring atmospheric radioactivity, very few meet the IMS specifications; this network will also be about 30% complete at the end of 1999. This presentation will give the status of these networks as of July 1999, and a plan for completing the networks prior to entry-into-force of the Treaty.

**U8/W/04-B3****1450****OPTIMIZED THRESHOLD MONITORING**

Tormod KVÆRNA, Frode Ringdal, Johannes Schweitzer, and Lyla Taylor (all at NORSAR, P.O. Box 51, N-2007 Kjeller, Norway, email: tormod@norsar.no)

In order to enhance the automatic monitoring capability for the Novaya Zemlya (NZ) nuclear test site, we have derived a set of optimized processing parameters for the arrays SPITS, ARCES, FINES, and NORES. From analysis of the tuning events we have derived values for beamforming steering delays, filter bands, STA lengths, phase travel-times and amplitude-magnitude relationships for each array. By using these parameters for Threshold Monitoring (TM) of the NZ testing area, we obtain a monitoring capability varying between mb 2.0 and 2.5 during normal noise conditions.

The advantage of using a network, rather than a single station or array, for monitoring purposes becomes particularly evident during intervals with high global seismic activity (aftershock sequences), high seismic noise levels (wind, water waves, ice cracks) or station outages. For example, for the time period November-December 1997, all time intervals with network magnitude thresholds exceeding mb 2.5 were manually analyzed, and we found that all these threshold peaks could be explained by teleseismic, regional, or local signals from events outside the NZ testing area. We could therefore conclude at the 90% confidence level that no seismic event of magnitude exceeding 2.5 occurred at the Novaya Zemlya test site during this two-month time interval.

**U8/W/06-B3****1505****MONITORING THE COMPLIANCE WITH THE CTBT FROM THE PERSPECTIVE OF THE GERMAN NATIONAL DATA CENTER (NDC)**

Manfred HENGER (Federal Institute for Geosciences and Natural Resources, Stilleweg 2, 30655 Hannover, Germany, Email: henger@sdac.hannover.bgr.de)

National data centers (NDCs) are important elements of the international monitoring system (IMS), however, their functions are nowhere defined in the CTB treaty text. In general, NDCs are responsible for the operation and maintenance of participating national IMS stations, act as communication hubs, technical point of contact for the Vienna International Data Center (IDC), and have to provide expertise to national authorities. Since the CTBT was opened for signature, and even before, there were several cases where the German NDC was confronted with the problem of event identification. On the basis of IMS data and IDC products available at that stage this was a rather challenging task. The various problems encountered will be presented for selected questionable events. It can be shown that data from seismic networks operated for other purposes than CTBT monitoring considerably improved seismic event location and facilitated identification. However, there are a number of reasons that may prevent or make it impossible for an NDC to use data from other national networks, such as a lack of communication facilities, limited availability of events due to recording of seismic signals in triggered mode, lack of knowledge about seismic stations operated by a country, impossibility of timely data access, format problems, a lack of calibration data, and others. These difficulties could be solved with existing technical means without significant cost. Moreover, it is recommended that irrespective of the dedication of seismic stations and networks, the operation, as well as procedures of data retrieval and data archiving, should be standardized as much as possible for the sake of solving both scientific and politically motivated seismological issues.

**U8/E/11-B3****1520****FOCAL MECHANISMS OF LOW-MAGNITUDE EARTHQUAKES FROM HIGH-FREQUENCY P AND S OBSERVATIONS: AN EXAMPLE USING SOURCES IN THE BARENTS SEA REGION**

David BOWERS and Alan Douglas (AWE Blacknest, Brimpton, Reading RG7 4RS, UK. Email: bowers@blacknest.gov.uk)

At long range earthquakes have successfully been identified by demonstrating that the observed seismograms are consistent with the radiation pattern expected from a double couple. For seismograms from small disturbances recorded at regional distances the effect of the path is so dominant that the radiation pattern can rarely, if ever, be inferred. We present evidence that paths across the Barents Sea, from northwest Russia and the Kara Sea, to Spitsbergen (SPITS) show weak P and S attenuation, allowing clear P and S to be observed at frequencies above 15 Hz at distances of at least 1200 km from small (3.3 mb) disturbances. As a result of the efficient propagation of P and S in the Barents/Kara sea region, clear three-component P and S seismograms were recorded at SPITS, KEV (Kevo, Finland) and AMD (Amderma, Kola, Russia) from the 16 August 1997 3.3 mb seismic disturbance in the Kara Sea. The S waves recorded at these three-component stations, and the P waves recorded by the Scandinavian arrays HFS (Hagfors, Sweden) and NORES (Norway), are consistent with a double couple.

**U8/W/13-B3**

Invited

**1600****GLOBAL ENVIRONMENTAL MONITORING AND THE CTBTO INTERNATIONAL MONITORING SYSTEM**

DR. John A. ORCUTT, (Cecil & Ida Green Institute of Geophysics and Planetary Physics (0225), Scripps Institution of Oceanography, La Jolla, CA 92093, email: jorcutt@igpp.ucsd.edu)

The International Monitoring System for the Comprehensive Test Ban Treaty presents many opportunities for enhanced monitoring of the environment on a global basis. In many cases, the increases in capability are incremental (e.g. seismology) while in other areas (e.g. Infrasound), the enhancement of capability is fundamental. I will discuss each of the four elements of the IMS: Seismology, Hydroacoustics, Infrasound, and Radionuclides. In each case, the augmentation of present capabilities will be noted and the requirements for the instrumentation will be compared with current standards. Potential environmental monitoring tasks for each of these capabilities, including capabilities resulting from synergies between technologies, will be explored. In many cases, limitations on the full utilization of the installed instrumentation will be seen to arise from political rather than technical issues.

**U8/W/07-B3****1625****MULTIMODAL DISTRIBUTION OF SEISMIC PHASE ARRIVAL TIMES FOR AUTOMATIC LOCATION OF REGIONAL SOURCES**

Vladimir PINSKY, (Seismology Division, Geophysical Institute of Israel, P.O. Box 2286, Holon 58122, Israel, tel: 972-3-5576050; e-mail: vlad@iprg.energy.gov.il)

Adoption of the CTBT regime leads to increased sensitivity of regional seismic networks and an expansion of the event flow. Automation of location thus becomes a crucial issue. Recently, several research groups concentrated on the possibility of using envelopes of the pre-filtered network seismograms for automatic location of event epicenters and provided simple and robust solutions. Our approach, tested with Israel Seismic Network (ISN) recordings, is based on inversion of characteristic time points:  $T_p$  and  $T_s$  - local maximums of the envelopes, related to P and S phases. For local ISN events the corresponding travel times were measured to be close to:  $T_p(R)=2.5+R/6.4$  sec.,  $T_s(R)=3.5+R/3.6$  sec., where R is distance in kilometers. The bottleneck of the whole approach is automatic recognition of the phases from seismograms or envelopes which is provided by a logic based on choosing the specific threshold levels and time windows [1]. However, misidentification of the phases frequently occurs. We overcome this problem by introducing the statistics  $tp(R)$  and  $ts(R)$ , both having 2-modal (multi-Gaussian) distributions concentrated at  $T_p(R)$  and  $T_s(R)$ . Vector statistic  $dT$  of differences of the measurements for all pairs of the network stations we represent as scalar statistic  $dt$ , described by the multi-Gaussian density function. Epicenter location is provided by maximization of the corresponding likelihood function through a grid search. As a result of the preliminary study of a set of more than 120 local earthquakes and quarry blasts, ML-1.5-2.5, we obtained an accuracy of approximately < 6 km for epicenter estimation for both types of events. The procedure was also successfully tested on a set of calibration quarry blasts with precisely known coordinates and ignition time. The algorithm can be considered as a first step, providing constrained time windows for P and S on-sets on the seismograms. Further improvement of results is achieved by estimating P and S wave arrival times within the time windows specified above, using the well-known maximum likelihood algorithm [2] with following application of the standard location procedure

**U8/W/02-B3**

Poster

**1640-01****COUPLING OF SEISMIC WAVES TO T-WAVES VIA SEAFLOOR SCATTERING**

Catherine de GROOT-HEDLIN (IGPP, SIO, University of California at San Diego, 92093-0225, CA, USA, email: cdh@eos.ucsd.edu) John Orcutt (IGPP, SIO, University of California at San Diego, 92093-0225, email: jorcutt@igpp.ucsd.edu)

One of the challenges of monitoring the ocean basins for nuclear explosions at sea is in discriminating between hydroacoustic signals from nuclear tests and those excited by earthquakes occurring below the seafloor. T-phase excited by earthquakes can be classified into 2 types: abyssal T-phases which are generated near earthquake epicenters at depths well below the SOFAR channel, and "slope-generated" T-phases which are excited at shallow depths at continental margins or ocean islands at some distance from the epicenter. In this study, we demonstrate that both types of arrivals are consistent with scattering from a rough seafloor. We show that abyssal T-phases result from scattering into high order, bottom-interacting acoustic modes, while the "slope-generated" T-phases are modelled as low order acoustic modes generated at shallow depths which cease interaction with the bottom as they propagate seaward to the deeper ocean. The synthesized T-phase coda exhibit characteristics also observed in hydroacoustic recordings of T-waves: the abyssal T-phase coda is nearly symmetric and typically peaks at frequencies of 10-20Hz, whereas the slope-generated T-phase coda usually peaks at 4-8Hz and has a shape which is strongly influenced by near-source bathymetry. Furthermore, the modelling correctly predicts that abyssal T-waves are attenuated more severely by bathymetric interactions along the propagation path than the "slope-generated" T-phases. We compare hydroacoustic recordings of T-waves from earthquakes in the Pacific basin with results from synthetic modelling of T-phases, and contrast these with recordings of the 1995-1996 French nuclear tests in the islands of the Tuamotu archipelago.



**U8/W/05-B3** Poster **1643-02**

**ANALYTIC AND NUMERICAL STUDIES OF NATURAL SOURCES OF ATMOSPHERIC INFRASOUND: MICROBAROMS AND MOUNTAIN INFRASOUND**

David C. FRITTS, Steve Arendt, and Gregory S. Poulos, (Colorado Research Associates, 3380 Mitchell Lane, Boulder, CO 80301 USA)

We have used analytic and numerical techniques to assess the mechanisms responsible for infrasound radiation from ocean storms and mountain topography. Microbaroms arise from interactions among ocean surface waves having frequencies of a few seconds (wavelengths of ~ 100 m) and approximately equal and opposite wavenumbers. Contributions to microbarom radiation come from monopole, dipole, and quadrupole terms in the resonance equations. Mountain infrasound arises from flow intermittency over and around mountain obstacles on scales of ~ 10 km and comprises exclusively dipole and quadrupole radiation. Also discussed will be the manner in which infrasound radiation frequencies are selected.

**U8/L/01-B3** Poster **1646-03**

**COLLECTION OF GROUND TRUTH INFORMATION FOR THE CALIBRATION OF THE CTBT INTERNATIONAL MONITORING SYSTEM**

Istvan BONDAR and Petr Firbas (both at CTBTO, IDC, Vienna Int'l Centre, P.O.Box 1200, A-1400 Vienna, Austria, emails: Istvan.Bondar@idc.ctbto.org, Petr.Firbas@ctbto.org)

Although there is a general agreement that location calibration is necessary to improve locations provided by international agencies, no such attempt has so far been made on a global scale. The On-Site Inspection provision of the Comprehensive Nuclear-Test-Ban Treaty (CTBT) limits the inspection area to 1000 sq km. In order to achieve a corresponding location accuracy with the relatively sparse and largely teleseismic CTBT International Monitoring System network a detailed location calibration is required.

The prototype International Data Centre (pIDC) has started and the CTBTO IDC is taking over a program of seismic location calibration program that includes the collection, categorisation and validation of "ground truth" events from a variety of sources as well as the development and operational testing of both empirical and model based corrections. The collection of ground truth events requires broad international co-operation between scientific as well as governmental institutions. The events belonging to different ground truth categories (GT0, GT2, GT5, GT10 and GT25) are used to derive and validate corrections in both time and slowness domain. The scientific community may benefit from preparation of the ground truth database. Technical information on the selection procedures and categorisation of calibration and ground truth events will be given.

**U8/W/12-B3** Poster **1649-04**

**MONITORING ACTIVITY OF THE IDC**

CHERNOBAY, I (CTBTO, Provisional Technical Secretariat, Vienna International Centre, Vienna, Austria, Email: ichernobay@ctbto)

The commissioning plan for the International Data Center (IDC) of the Preparatory Commission for the Comprehensive Nuclear-Test-Ban Treaty Organization Provisional Technical Secretariat consists of seven phases. The IDC is currently at its fourth stage. To perform its functions, the IDC receives monitoring capabilities from its prototype (pIDC) in Arlington, Virginia (USA). The transition of these functions will take place in a series of four technically progressive software releases. Release 1 of the IDC application software was under operation in Vienna since May 15 till December 1998 and provided to the IDC initial limited operational capability. Realtime data from about 60 stations of the International Monitoring System were flowing through the pIDC to the IDC via a high capacity T1 link. Automatic data acquisition and automatic processing continued 24 hours per day and 7 days per week to assess the capability and robustness of the software. Standard Event Lists (SELS) were automatically produced daily. The IDC's analysis staff reviewed and corrected one data day per week of seismic, hydroacoustic and infrasound data, and almost all of the radionuclide spectra. At this stage, automatic processing of the waveform data was based on the data from primary stations and used only one network processing pipeline ~ 2 hours behind realtime. No data from auxiliary stations were involved in producing the Standard Event Lists. With this limited capability, the IDC succeeded in locating the 100 tons calibration chemical explosion in Kazakhstan (August 22).

Starting in the middle of December 1998, the IDC is under preparation for the installation and operation of Release 2 Application Software. With this Release, the IDC will be running automatic data processing based on three consecutive network processing pipelines (2, 6 and 12 hours behind real time). The first one will use data from primary stations only while the second and third pipelines will also incorporate data from auxiliary stations. In May 1999, the IDC is expected to distribute Reviewed Event Bulletins, ramping up from one day per week in May to seven days per week in a few months.

**U8/E/02-B3** Poster **1652-05**

**SEISMIC ANALYSIS AT THE UK NDC**

David BOOTH, Russ Evans, and Aoife O'Mongain (British Geological Survey, West Mains Road, Edinburgh EH9 3LA, UK, email: d.booth@bgs.ac.uk)

The UK has chosen to set up a National Data Centre for the purpose of monitoring the Comprehensive Test Ban Treaty (CTBT), using data recorded by the International Monitoring System, and transmitted by the International Data Centre, of the CTBT Organisation. The British Geological Survey accepted responsibility for the establishment and operation of the UK NDC in January 1998. Since then, the BGS has been developing systems to receive the IDC data and present it in a form suitable for its scientists to analyse and interpret. Initially, the UK NDC is concentrating on the analysis and interpretation of seismic data. The seismic analysis system makes use of the flexibility of the Geotool software developed by Coyne and Henson, which has proved to be very versatile and has allowed the development of a system which is being customised for the analysis requirements of the UK NDC. Assessments of various seismic events are presented, to illustrate the capability of the system.

**U8/W/10-B3** Poster **1655-06**

**SLOWNESS CORRECTIONS- ONE WAY TO IMPROVE THE IDC PRODUCTS**

Johannes SCHWEITZER (NORSAR, P.O.Box 51, N-2007 Kjeller, Norway)

The first step to identify and locate a seismic event is the association of observed onsets belonging to the same event. During this process the challenge is to define only real events but to associate as much as possible of all detected phase.

One advantage of the data processing at the IDC is the extensive measurement of all relevant

parameters of the detected phases. Well defined slowness (i.e. ray parameter, or apparent velocity and backazimuth) measurements are very useful for associating seismic onsets. For events only defined by a small number of observations, slowness measurements are also helpful for locating these events. Therefore such data are used during all steps at the IDC to produce the final bulletins. The observed slowness parameters measured with small aperture arrays, which are mostly used in the IMS as primary stations, show a relatively large scatter. However, one can derive mean slowness deviations, which show a relatively stable and array specific pattern, a result of differences between Earth models and the local and regional structure around these arrays. In this contribution, different approaches will be presented to estimate an easily implementable set of slowness corrections.

**U8/E/07-B3** Poster **1658-07**

**COMPLEXITY OF TELESEISMIC P WAVES FROM THE CASPIAN SEA EARTHQUAKE OF 29 OCTOBER 1995**

C. B. SNOWDEN (Dept of Geology and Geophysics, Grant Institute, West Mains Rd., Edinburgh, EH9 3JW, UK, email: conor.snowden@glg.ed.ac.uk); A. Douglas and D. Bowers (AWE Blacknest, Brimpton, Reading, RG7 4RS, UK)

Both the source radiation pattern and earth structure contribute to the complexity of observed teleseismic short-period (SP) seismograms. Modelling shows that the amplitude of a S-to-P conversion, at a boundary below the source, can be larger than the geometric phases P, pP and sP. SP array seismograms from the Caspian Sea earthquake (mb=5.8) of 29 October 1995 (06:27 UT) appear to show a large phase (bP) after P, which if pP, suggests a source depth of about 30 km (REB pIDC). A simple SP S-wave recording in the UK indicates a simple near-receiver structure and low attenuating path, suggesting that the observed complexity is related to the source region (radiation pattern and/or structure).

We show that the interpretation of bP as pP is inconsistent with a double couple at a depth of 30 km. On broadband seismograms bP is weak and P, Pp and sP are clear, suggesting a source depth of 68 km. Further, we demonstrate that the SP phase bP can be modelled as a S-to-P conversion at a boundary approximately 100 km below the source. Reliable depth estimates are important in the monitoring of the CTBT and this shows the usefulness of teleseismic records even if regional data is not available.

**U8/E/01-B3** Poster **1701-08**

**P-WAVE AMPLITUDES OBSERVED FROM EXPLOSIONS AND EARTHQUAKES AND THE DISTRIBUTION OF REGIONS OF HIGH ATTENUATION IN THE EARTH**

A. DOUGLAS, D. Bowers and J.B. Young (AWE Blacknest, Brimpton, Reading RG7 4RS, UK, Email: alan@blacknest.gov.uk)

The body-wave magnitude (mb) of a seismic disturbance is estimated from the individual station magnitudes; the station magnitudes being estimated from SP P seismograms. Station magnitudes are usually widely scattered. Such scatter is due to both source and path effects. Body-wave magnitude plays an important role in test ban verification and thus has been the subject of detailed study principally to estimate and allow for path effects and so improve estimates of source size. The path effects however, reveal something of the distribution of attenuating regions in the earth. The association of high attenuation with orogenic regions is well-established. However, the attenuating zones must have a patchy distribution because for example, some stations in orogenic regions that lie on paths that are highly attenuating for P, record PcP that shows little evidence of attenuation. The paper draws together amplitude observations from explosions at most of the sites where underground tests have been carried out, to determine the distribution of the attenuating regions.

**U8/E/04-B3** Poster **1704-09**

**LOW-FREQUENCY SPECTRAL CLASSIFICATION FOR CONTROLLED QUARRY BLASTS RECORDED BY ISRAEL SEISMIC NETWORK AND SINGLE BB STATION EIL**

Yefim GITTERMAN (Seismology Division, The Geophysical Institute of Israel, P.O.B. 2286, 58122 Holon, Israel, email: yefim@iprg.energy.gov.il)

Based on numerous observations of quarry blasts, it was found that spectral modulation analysis at low (0.5-10 Hz) frequencies is more effective for event classification than at high frequencies (10-50 Hz) and it is better to reveal and analyze the modulation using usual smoothed spectral curves for several stations at different azimuths. The observed source features - the first spectral null f1 (at low frequencies) and the main maximum fm (at high frequencies) - are explained by the physical phenomenon of interference of seismic waves from inter-shots with millisecond delays and not by source (space or time) finiteness. For a regular blast pattern the feature are connected with delays, t, and number of delays, n, by the simple linear interference theory: f1=1/(nt), fm=1/t. Any random variation of a delay time or charge per delay, or any other non-regularity of a last pattern, will destroy the spectral modulation features, most significantly at high frequencies. For controlled regular quarry blasts (t=40 msec, n=5) in the Negev with Ground Truth Information of class GT10, an outstanding first spectral null was observed at short-period network stations and the EIL BB station, corresponding well to the theoretical value of f1. The main maximum spectral modulation feature (fm=25 Hz) could not be found, even at the BB records, owing to the steep descend of spectra after 10 Hz associated with the regional crustal structure of widespread unconsolidated sediments absorbing intensively high frequencies. All three components of the BB EIL showed the same spectral modulation pattern and the spectra average corresponds well with the network stations average. Application of the new-developed discriminants - energy ratio (1-3 Hz)/(6-8 Hz) and spectral semblance (1-12 Hz) (measuring spectral curves coherency) - to network stations and single BB (3C) recordings showed surprisingly similar results related to the explosion population.

**U8/W/15-B3** Poster **1707-10**

**RECENT NUCLEAR TESTS RECORDED BY THE ISRAEL NETWORK AND BB STATIONS**

Yefim GITTERMAN, Vladimir Pinsky, Rami Hofstetter (Seismology Division, Geophysical Institute of Israel, P.O. Box 2286, Holon 58122, Israel, e-mail: yefim@iprg.energy.gov.il)

We analyzed observations of Israel Seismic Network (ISN) and Broad Band (BB) stations of the recent nuclear tests conducted by India and Pakistan. Only the test on 28.05.98 (NEIC mb=4.8, r=26 deg.) triggered the short-period ISN stations. Two tests (11.05.98, mb=5.2, r=32deg. and 28.05.98) triggered the EIL BB station (80 Hz data), and signals of the weakest test (30.05.98, mb=4.6, r=25 deg.) were revealed in the continuous BB 20 Hz data after heavy band-pass filtering in different ranges. Detectability of the BB stations, EIL, MRN and JER, was investigated for the three known detectors of STA/LTA, Murdock-Hutt (MH) and Adaptive Optimal Detector (AOD) algorithms, using 20 Hz continuous records. The EIL station, installed in a 100 m long tunnel, is the quietest (spectral density of noise ~ 3 nm<sup>2</sup>/Hz at 1 Hz), where the Indian test was reliably detected by all the three detectors. The first Pakistan test was

detected by AOD and MH at all the stations within 0.5-5 Hz band, but STA/LTA failed for the JER station. The smallest Pakistan test was masked by coda of a local event and was hardly detected by STA/LTA, but was reliably extracted by AOD and MH for all the stations. Spectra of a P-waves portion (~17 sec) at vertical components of the ISN stations for the test on 28.05.98 showed a pronounced coherent spectral null at 1.7 Hz, which could be interpreted in terms of interference of P and pP phases. The relatively high null frequency corresponds to the reported shallow source depth of a few hundreds meters. Two new-developed multi-channel spectral discriminants (energy ratio and semblance) were applied to the P-wave spectra for a set of events including the three tests and several close Pakistani earthquakes. The two discriminants were calculated for a sub-set of the short-period ISN stations, and for the three components of the BB EIL station. The both estimates (multi- and single station) correspond well to the results obtained before for Kazakh and Chinese events - nuclear tests demonstrate lower values of energy ratio (0.6-1Hz)/(1-3Hz) and spectral semblance (0.6-2Hz) than earthquakes.

**U8/E/05-B3** Poster **1710-11**

**YIELD ESTIMATION OF PAKISTAN NUCLEAR EXPLOSION OF MAY 28, 1998 BY ILPA SEISMOGRAMS**

Abdolrahim JAVAHERIAN and Ahmad Sadidkhai (both at Institute of Geophysics, Tehran University, P. O. Box 14155-6466, Tehran, I. R. Iran, email: javaheri@chamran.ut.ac.ir)

Seismic measurements are recognized as a valuable source for use in monitoring underground nuclear tests. Their uses include detection, yield estimation and discrimination of nuclear explosions. In order to investigate seismic yield one has to obtain relationships between seismic parameters and yield of underground nuclear explosions.

In the present research, we estimated the yield of Pakistan nuclear explosion of May 28, 1998 by two methods. In the first approach, the magnitude of surface waves (in the frequency domain) using the maximum amplitude spectrum of the vertical component of Rayleigh waves recorded at ILPA (Iranian Long Period Array) have been considered. In the second approach, the amplitude of P wave (with a period of 1 s) recorded at ILPA have been employed. The yield of this explosion have been estimated for 4 possible media which may surround the test site. These media were granite, salt rock, tuff and alluvium.

**U8/W/16-B3** Poster **1713-12**

**MONITORING OF THE INDIAN AND PAKISTANI NUCLEAR TESTS**

Tormod KVÆRNA, Frode Ringdal, Johannes Schweitzer, and Lyla Taylor (all at NORARSAR, P.O. Box 51, N-2007 Kjeller, Norway, email: tormod@norsar.no)

Monitoring of possible testing areas is one of the main applications of the Threshold Monitoring (TM) method. Recently, both India and Pakistan conducted underground nuclear tests, and, in particular, the Pakistani explosions provided a very interesting scenario for testing of the method. Firstly, the two events on May 28, 1998 (Explosion 1) and May 30, 1998 (Explosion 2) were located about one degree apart, and it is interesting to investigate the performance of the TM method for Explosion 2 when monitoring the target area for Explosion 1. Secondly, the origin time of Explosion 2 was about 38 minutes after the origin time of an mb 5.5 earthquake in Afghanistan, and the explosion signals were mixed with the coda and aftershocks from this earthquake. The earthquake was located 9-10 degrees away from the explosion sites. Our results demonstrate that the TM method can be effective at teleseismic distances. Using data from European and Australian arrays, the Pakistani test area can be monitored down to a magnitude of 3.0 during background noise conditions. The benefit of using a network for monitoring becomes particularly apparent during the earthquake sequence located as close as 10 degrees from the target region, where the TM method suppressed the aftershock signals by up to 0.5 mb units.

**U8/P/01-B3** Poster **1716-13**

**SEISMOLOGICAL CONSTRAINTS IN DETECTION OF UNDERGROUND NUCLEAR EXPLOSIONS**

H.N. SRIVASTAVA (India Meteorological Department New Delhi- 110003, India, e-mail: snb@imd.emet.in)

The Pokhran underground nuclear explosion of 17th May, 1974(M5.0) in Rajasthan, India, produced a seismogram exactly similar to near earthquake at about 600 km away through SP Benioff seismograph showing typical Pn, P\*, Pg and Sn, S\* and S phases at Delhi observatory. However, the S phases became less discernible at larger epicentral distances from the source as expected. The yield of the explosion estimated from Wood Anderson Seismometers agreed with the estimates of US Geological Survey. Since then, several stations have been upgraded through digital seismographs including broadband type. A question arises whether in case of multiple nuclear explosions at short intervals as reported in India and Pakistan during May, 1998, the seismological methods would be able to provide a realistic estimate of the yield even if location problem is resolved by using only P wave arrival time for the first explosion. Techniques of analysis for such exigencies have been proposed for discussion.





**JSP23** Friday 23 – Tuesday 27 July**GEOPHYSICAL HAZARDS AND RISKS: PREDICTABILITY, MITIGATION, AND WARNING SYSTEMS (IAPSO, IASPEI, IAVCEI, IAHS, IAMAS, IAG, IAGA, IUGG TSUNAMI COMMISSION, ILP)**Location: Poynting Physics S02 LT  
Location of Posters: Bridge Poynting/Watson

Friday 23 July AM

Presiding Chair: T BEER (CSIRO Atmospheric Research, Aspendale, Australia)  
Concurrent Poster Session**HAZARD AND RISK ASSESSMENT, RISK MITIGATION AND MANAGEMENT****JSP23/C/U5/P/01-A5** Invited **0830****ATMOSPHERIC HAZARDS ASSOCIATED WITH THE EL NINO/SOUTHERN OSCILLATION PHENOMENA: A SYNTHESIS**

Madhav L KHANDÉKAR (Consultant, Baird &amp; Associates, Ottawa, Ontario, CANADA, L3R 7Z5)

The ENSO phenomenon – spreading of warm water from the equatorial central Pacific to the equatorial South American coast and associated global weather anomalies – is now identified as the strongest signal in the global climate system after the annual cycle. The term El Niño refers to the spreading of anomalously warm water off the coast of Ecuador and Peru and associated weather anomalies over the west coasts of the Americas. The Southern Oscillation is the atmospheric counterpart of El Niño and refers to the slowly varying atmospheric pressure differential over the eastern and western regions of the tropical Pacific. The two phenomena together are now popularly known by the acronym ENSO (El Niño/Southern Oscillation). The appearance of warm water off the coast of South America and associated changes in the regional weather patterns were known to Peruvian fishermen for over 400 years. The landmark papers of Jacob Bjerknes in the Nineteen Sixties provided a physical link between ENSO and weather anomalies over the entire equatorial Indo-Pacific basin. Several studies inspired by Bjerknes' landmark papers and reported in the last twenty-five years have documented a link between ENSO and global weather anomalies.

This paper provides an overview of global weather anomalies and associated atmospheric hazards in the context of the ENSO phenomena. The paper further presents several examples of atmospheric hazards associated with extreme weather events and their relationship to the various phases of ENSO. The importance of monitoring various phases of the ENSO phenomena through suitable atmospheric and oceanic indices will be discussed in the context of long-range weather forecasting.

**JSP23/W/04-A5** **0910****ENSO AND 'ENSO-LIKE' IMPACTS ON INTERANNUAL TO SECULAR TIME SCALES**

Robert J. ALLAN (CSIRO Atmospheric Research, Aspendale, Victoria 3195, Australia, email: rob.allan@dar.csiro.au); Ian N. Smith (CSIRO Atmospheric Research, Aspendale, Victoria 3195, Australia, email: ins@dar.csiro.au).

Efforts to improve our understanding of the various types of natural variability inherent in the global climate system have included a growing focus on the El Niño Southern Oscillation (ENSO) phenomenon and lower frequency 'ENSO-like' decadal to secular scale fluctuations. Signal detection analyses applied to global historical sea surface temperature and mean sea level pressure anomalies, reveal significant climatic signals operating on quasi-biennial, inter-annual, decadal multi-decadal and secular time scales. The ENSO signal is seen to consist of quasi-biennial (QB) and lower frequency (LF) components that interact to produce important modulations of the phenomenon. 'Protracted' El Niño and La Niña episodes are found to be a consequence of the 'phasing' of quasi-decadal and inter-decadal 'ENSO-like' signals with the QB and LF ENSO components. Further climatic modulations are provided by 'ENSO-like' phenomena operating on multi-decadal time scales. The secular trend, reflecting the observed global warming signal, reveals neutral to slightly 'La Niña-like' conditions in the Pacific sector. The impact of the above climatic signals can be seen in the patterns of correlation with global precipitation and mean surface land temperatures. Significant contributions to rainfall and land temperature variability are evident, not just in known 'ENSO-sensitive' regions. In addition, El Niño and La Niña episodes on inter-annual time scales can be both synchronous and asynchronous with 'El Niño-like' and 'La Niña-like' signals on various decadal to multi-decadal time scales, resulting in the range of fluctuations seen in many rainfall and temperature impacts over time.

**JSP23/L/01/A5** **0930****HAZARD AND RISK MITIGATION BY IMPROVING THE CULTURE OF SOCIETY AND OF THE DECISION MAKERS**

FABRIZIO FERRUCCI and Giovanni P. Gregori

Hazard and risk management requires a precise preliminary assessment of their respective formal definition, sources and causes. The natural environment, likewise demography, territory use, and energy consumption, are not steady in time. They rather experience a continuous transformation or evolution. Every so-called natural catastrophe is a strict need by natural reality. Neither it makes sense to search for a forerunner (that in a strict sense can be given, at most, only with some relevant error bar, that makes a forecast of little practical help). Moreover, a prevision is often useless in terms of concrete reduction of causalities and/or damages. The entire problem rather emphasises per se the great need for improving the consciousness of the specific characteristics of every type of natural catastrophe, and of the ways by which its consequences can be prevented or minimised. A forgotten aspect of human history is concerned with the epoch when mankind got the consciousness of space orientation, and much later also of absolute time. Similarly to this, at present there is a great need for educating both society and decision makers about the correct cultural approach to Nature, to environmental knowledge, and to territory management. All this appears the unique concrete viable approach for solving the threaten by the progressively stronger impact of mankind on environment, a factor that is closely and unavoidably related to the same progress of civilisation. Several case histories will be specifically discussed.

**JSP23/W/31-A5** **0950****FLOOD EVENTS IN THE RHINE RIVER BASIN: GENESIS, INFLUENCES AND MITIGATION**

Markus DISSE (German Federal Institute of Hydrology, P.O. Box 309, D-56003 Koblenz, Germany, Email: disse@bafg.de); Heinz Engel (German Federal Institute of Hydrology, P.O. Box 309, D-56003 Koblenz, Germany)

The catchment of the river Rhine can be distinguished in 4 main subcatchments: the alpine region with the river Aare as the main tributary and downstream the lower mountain regions of the tributaries Neckar, Main and Moselle. These four basins clearly generate different hydrographs. Due to the geographical circumstances, the average discharge maximum shifts from summer towards winter downstream the Rhine. However, spatial and temporal precipitation patterns have a strong influence on the individual flood. The particular genesis of recent and historical floods will be discussed. Besides the climatological causes a brief overview of the manmade alterations to the river system itself (Rhine and tributaries) and to the linked catchments are given and their effect will be indicated. However, up to now the influence of land surface and river training measures on flood conditions in the Rhine basin has not exactly been quantified. Therefore, the Dutch-German project LAHOR has been established within the framework of the EU-project IRMA (INTERREG II C Rhine Maas Activities). The results of this project may give efficient advice for the "Action Plan on Flood Defence" of the International Commission for the Protection of the Rhine (ICPR), which is briefly introduced. In this plan a multidisciplinary approach to mitigate floods is suggested that can yield to synergic effects between flood prevention, water management, regional planning, agriculture, forestry and ecological demands.

**JSP23/E/37-A5** **1010****THE SUVA EARTHQUAKE RISK MANAGEMENT SCENARIO PILOT PROJECT (SERMP) - MITIGATION OF EARTHQUAKE AND TSUNAMI RISKS FOR THE CITY OF SUVA, FIJI**

Jack RYNN (Centre for Earthquake Research in Australia, PO Box 276, Indooroopilly, Brisbane, Queensland 4068, Australia, email: sally.brown@uq.net.au); Poasa Raveo (Department of Regional Development and Multi-Ethnic Affairs, Government of the Republic of Fiji, PO Box 2219, Government Buildings, Suva, Fiji); Atu Kalounaira (South Pacific Disaster Reduction Management Office, c/o UNDP, Private Mail Bag, Suva, Fiji, email: atu@sopac.com.org)

The 1953 Suva earthquake (ML 5.6) and associated tsunami is a stark reminder of the vulnerability of the City of Suva to such natural hazards. Through the UN IDNDR program, per the 1994 "Yokohama Statement", the Government of the Republic of Fiji took the challenge to counter mitigation strategies. SERMP was a co-operative effort of the Government, UNDP-UNDHA and international consultants. A specific methodology was developed to address definitive project components of hazard, vulnerability and risk assessments, mitigation measures, response planning, public awareness, policy support and dissemination of findings. Wide-ranging outcomes for both earthquake and tsunami, of risk assessments, loss estimations, disaster planning, risk management and tsunami warning, with 90 recommendations, were documented as an "information resource." These were implemented as "practical applications" in building codes, GIS, land use planning, disaster plans, training, emergency management and community education. A Sub-Regional Seminar and exercise "SUVEQ 97" were conducted. SERMP also demonstrated mitigation measures to decision makers in all Pacific Island Countries.

**JSP23/W/19-A5** **1050****THE AUSTRALIAN ENVIRONMENTAL RISK MANAGEMENT FRAMEWORK**

Tom BEER (CSIRO Atmospheric Research, Aspendale, 3195, Australia, email: Tom.Beer@dar.csiro.au)

Environmental risk management deals with impacts on the environment, as well as with impacts on organisations that disturb the environment. Management options are based on a measure of the risk, which is obtained through an analysis of both the likelihood and the consequences of the impact. Many of the concepts, and much of the terminology, of environmental risk assessment have arisen from its use by the US EPA as an objective tool that provides information on which to base environmental decisions. A key step in the United States was to maintain a clear separation between risk treatment and risk assessment. Risk treatment is an activity undertaken by decision-makers and managers, whereas risk assessment is an activity undertaken by technicians. Many workers have argued that one cannot maintain such a clear distinction and a conference of the Australian Academy of Science developed an Environmental Risk Management framework. Australia has been reluctant to embrace the US-inspired clear distinction between risk treatment and risk assessment. Australia has, instead, combined risk assessment (envisaged as a combination of risk analysis and risk evaluation) and risk treatment within a generic risk management framework that has been incorporated into the Australian/New Zealand Standard on Risk Management, AS/NZS 4360. This presentation synthesises the Australian Risk Management and Environmental Risk Management frameworks.

**JSP23/W/02-A5** **1110****CAUSE-EFFECT MODELS OF LARGE LANDSLIDES**

Ewald P. BRUECKL (Vienna University of Technology, Gusshausstrasse 27-29, A-1040 Vienna, Austria, email: ebrueckl@luna.tuwien.ac.at)

Within the scope of IDNDR cause-effect models of large landslides are being developed to estimate potential danger. This work is based on structural exploration of the landslides mainly by seismic methods. Information about the status of deformation is got by comparison of the actual topography with a reconstruction of the original topography, GPS and SAR interferometry. Geological and geomorphological evidence, as well as relevant information from other geoscientific disciplines, is included. The Finite Element method is used to model the initial phase of a mass movement. Later on this modelling will be extended to the quasi-stationary creep phase and the transition from creeping to rapid sliding. Three large landslides within the crystalline rocks of the Eastern Alps have been investigated since 1997. The largest one is the Koefels landslide with a total volume of 3.9 km<sup>3</sup> and a potential energy release of 5<sub>10</sub><sup>16</sup> Joule. Refraction and reflection multi-component seismic techniques were applied successfully to resolve structure and elastic parameters of the landslide masses. For the modelling of the initial phase of the landslides by the Finite Element method a strain softening behaviour of the rock mass has been assumed. The development of softened or fractured zones according to the structures obtained by the seismic measurement was simulated.

**JSP23/L/04-A5 1130**

**PSEUDOSCIENCE U.N. DOCUMENT: GEOMAGNETIC FORECASTING OF EARTHQUAKES AND METEOROLOGICAL DISASTERS**

Wallace H. CAMPBELL (World Data Center A for Solar-Terrestrial Physics, NGDC / NOAA, 325 Broadway, Boulder, CO 80303-3328, USA, e-mail: whc@ngdc.noaa.gov)

The United Nations recently published a "Manual on the Forecasting of Natural Disasters: Geomagnetic Methods" (1998) by Chinese and U.N. authors that stretches the imagination with prediction of earthquakes and Meteorological disasters. A careful reading of this document reveals an illusionary approach to the subject with no valid supporting evidence of prediction capability. The "mathematical" section simply copied well-known formulae that provided no scientific details of any physics connecting changes in geomagnetic recordings and subsequent localized disastrous earthquakes or meteorological events. The presented data indicated that 82.3 % of the recorded earthquakes did not correspond well to predictions. The authors ignored the recommendations and testing suggestions of a 1996 international London meeting, Assessment of Schemes for Earthquake Prediction. The manual provides clear and reliable evidence of the improper use of public funds for building hopes of disaster relief with projects totally lacking in scientific merit.

**JSP23/W/26-A5 1150**

**25 SECONDS FOR BUCHAREST**

Friedemann WENZEL, Mihnea C. Oncescu, Michael Baur and Frank Fiedrich (University of Karlsruhe, 76128 Karlsruhe, Germany, email: fwenzel@pwiw1.physik.uni-karlsruhe.de); Constantin Ionescu (National Institute for Earth Physics, P.O. Box MG-2, 76900 Bucharest, Romania, email: viorel@infp.ifa.ro)

The Romanian capital Bucharest faces a significant earthquake hazard with a 50% chance for an event in excess of 7.6 moment magnitude every 50 years. Within the last 60 years Romania experienced 4 strong Vrancea earthquakes: Nov. 10, 1940 (Mw = 7.7, 160 km deep); March 4, 1977 (Mw = 7.5, 100 km deep); Aug. 30, 1986 (Mw = 7.2, 140 km deep); May 30, 1990 (Mw = 6.9, 80 km deep). The 1977 event had catastrophic character with 35 high-rise buildings collapsed and 1500 casualties, the majority of them in Bucharest. A group of civil engineers and seismologists from the National Institute of Earth Physics (NIEP) in Romania and Karlsruhe University in Germany propose an Early Warning System (EWS) for the capital city of Bucharest. The group studied the seismological boundary conditions of an EWS for the Romanian capital of Bucharest. The earthquakes threatening the capital are intermediate deep events with magnitudes close to Mw = 8.0 at an almost fixed epicentral distance of about 150 km. The travel-time difference between the destructive S-wave arriving in Bucharest and the epicentral P-wave is always greater than 25 s, which represents the maximum possible warning time. Moreover source mechanisms are extremely stable for larger and smaller events so that a projection of the level of ground motion to be expected in Bucharest can be based on the amplitude of the epicentral P-wave rather than on cumbersome determination of magnitude and depth. This feature allows the design of a simple, robust and fast EWS. With 25 s, a system with the largest warning time after the Seismic Alarm System for Mexico City could be established. Even this small time window can provide opportunities to automatically trigger measures such as, shutdown computers; re-route electrical power; shutdown airport operations; shutdown manufacturing and high-energy facilities; stop trains; shutdown gas distribution; alert hospital operating rooms; open fire station doors; start emergency generators; stop elevators in a safe position; issue audio alarms; maintain safe-state in nuclear facilities. The value of an EWS can be judged on the basis of an application specific cost-benefit analysis, but simple considerations suggest that it will be cost-efficient.

**JSP23/E/31-A5 1210**

**GLOBAL VOLCANIC SIMULATOR: ERUPTION FORECASTING AND URBAN PLANNING OF DENSELY POPULATED AREAS**

Flavio DOBRAN (Global Volcanic and Environmental Systems Simulation, 32-50, 34 Street, Long Island City, New York 11106, Email: dobran@idt.net)

A Global Volcanic Simulator consists of physico-mathematical models of the volcano that are effectively implemented for solution on distributed or parallel computers. Such a simulator can be used to forecast future eruptions and for studying their effects on people and infrastructures for the purpose of mitigating eruption consequences. Current simulator for Vesuvius models magma reservoir volume, temperature, and pressure changes, variable rates of magma supply into the chamber, and varying elastic, plastic, and heat transfer characteristics of magma reservoir surroundings. Different types of magma ascent models allow for time-varying and non-isothermal simulations, including magma flow regime changes and melting of conduit walls. These models have been used to forecast that a plinian or subplinian eruption of Vesuvius will occur within the next 100 years and that the pyroclastic flows from column collapses can destroy the surrounding territory in several minutes. The simulator is also being employed to study the effects of different eruption scenarios on the territory and how this territory can be protected by engineering intervention measures. Computer simulations of possible eruptions of Vesuvius are also being utilised to sensitise the population of the area. A useful simulator requires reliable geological and geophysical data of the volcano's internal structure, whereas the verification and validation of complex physical models on computers presents both computational and physical modeling challenges that are described in: Dobran, F., Theory of Structured Multiphase Mixtures, Springer Verlag, New York, 1991; Dobran F., Global Volcanic Simulation of Vesuvius, Giardini, Pisa, 1993; Dobran, F., Etna: Magma and Lava Flow Modeling and Volcanic System Definition Aimed at Hazard Assessment, Topografia Massarola Offset, 1995.

Friday 23 July PM

Presiding Chair: Prof. Dr.F Wenzel (Universitaet Fridericiana Karlsruhe, Germany)

**JSP23/E/20-A5 1400**

**EXTRATROPICAL EVOLUTION OF TROPICAL CYCLONES AS AN UNEXPLORED HAZARD IN MIDDLE AND HIGHER LATITUDES**

Jenni L. EVANS (Department of Meteorology The Pennsylvania State University University Park PA 16802, USA.)

A recent climatology of extreme rainfall incidence in the northeast United States (including New England) reveals that the passage of a tropical cyclone is the cause of major rainfall events every 2-3 years over most of this region. Locations such as Boston and Cape Cod are particularly susceptible, with individual events resulting in twice their monthly rainfall due to a single tropical cyclone passage every 5-6 years. At the time that these tropical cyclones are delivering such copious rainfalls, they are typically undergoing complex structural changes that are poorly understood.

The lifecycle of the tropical cyclone through to a hybrid or truly extratropical cyclone and the associated rainfall evolution will be elucidated here and a theoretical underpinning provided.

**JSP23/C/U5/E/14-A5 1420**

**NATURAL DISASTERS: A POSTGRADUATE PROGRAM AT UNIVERSITY OF KARLSRUHE**

Jens MEHLHORN, Frank Fiedrich and Fritz Gehbauer (Institute for Construction Equipment and Construction Management, University of Karlsruhe, Am Fasanengarten, 76126 Karlsruhe, Germany, email: mehlhorn@imbdec1.bau-verm.uni-karlsruhe.de)

According to the United Nations the annual financial loss as a result of natural disasters increased from 50 billion to 360 billion US-dollar during the last 35 years. This fact presents a tremendous challenge to politics, society, and the scientific community. Disaster related research has to be increased. On the basis of fundamental research new knowledge will be created and used to develop practical tools for hazard and risk assessment. More effective measures for reducing this risk can be taken and the performance of emergency response can be improved. These steps towards a better understanding of disaster causes and effects and improved disaster management have been demanded since the UN-decade IDNDR (International Decade for Natural Disaster Reduction) started in 1991. The Postgraduate Program Natural Disasters has to be seen in this context. A total of 15 institutes of different fields work together in this project involving five departments of the university. The research projects include topics like Modelling of Hazard and Risk, Development of Disaster Scenarios, Mitigation Aspects and Economic Consequences of Natural Disasters. During the first period the activities concentrate on floods, earthquakes, strong rainfalls and land-slides. Natural sciences like physics, hydrology, meteorology and geosciences give a contribution to the basic understanding of the disaster process. Mathematics and computer sciences are used for complex models, for modelling fuzzy and imprecise information and for forecasts. With the help of economics the risk can be quantified and evaluated. In addition the institutes dealing with engineering aspects develop measures and tools for risk mitigation.

**JSP23/C/U5/W/13-A5 1440**

**WORLD MAP OF NATURAL HAZARDS – A DEPICTION OF THE GLOBAL DISTRIBUTION OF SIGNIFICANT HAZARDS AND THEIR INTENSITY**

G. Berz, S. Ehrlicher, T. Loster, E. Rauch, A. Siebert, J. Schimetschek, J. SCHMIEDER, A. Smolka and A. Wirtz (Munich Re, Geoscience Research Group, D-80791 Munich, Germany, Tel. 0049-89-3891-5291, Fax: 0049-89-3891-5696, E-mail: info@munichre.com)

For over 25 years now Munich Re's Geoscience Research Group has been looking at natural hazards throughout the world. Twenty years ago it summarised the overall results of its work in the first edition of the World Map of Natural Hazards. The map represents a unique source of information for numerous insurance companies, engineering offices, planning authorities, geoscientists, schools and interested lay people world-wide. For the recently released third edition all the basic data was for the first time captured and analysed using Munich Re's geographical information system (GIS). The resulting maps were created using digital cartography. Four auxiliary maps have supplemented the new edition. The earthquake and windstorm zones contained in the previous editions have been updated, refined and augmented. There are also details of other significant natural hazards like severe rainfall, storm surges, hail and lightning. A particularly interesting innovation is the auxiliary map on climate change. It deals on the one hand with the effects of El Niño, which generated so much interest and concern internationally in 1997/98 and was responsible for numerous natural catastrophes. Even more important are the effects that are to be expected from the emerging phenomenon of global warming, which will be accompanied by more frequent and more dramatic natural catastrophes in many parts of the world and will lead to a distinct long-term deterioration in the risk situation. The accompanying publication provides a detailed catalogue of historic natural catastrophes that have occurred in countries all over the world, grouped by continent and listed chronologically with additional information on the number of deaths and the economic losses.

**JSP23/C/U5/W/11-A5 1500**

**ASSESSMENT OF HYDROLOGICAL HAZARDS OF VOLCANIC ALLUVIAL FANS**

Kazuo OKUNISHI (Disaster Prevention Research Institute, Kyoto University); Gokanoshō Uji, (611-0011 Japan, Email: okunishi@slope.dpri.kyoto-u.ac.jp); Hiroshi Suwa (Disaster Prevention Research Institute, Kyoto University, Gokanoshō Uji, 611-0011 Japan, Email: suwa@slope.dpri.kyoto-u.ac.jp)

Alluvial fans on the foot of volcanoes have high hazard potential because of frequent inundation of debris flows and floods accompanying marked topographic changes. However, the social needs for the development of such lands are ever increasing, because of their high demand for recreational and touring sites. Assessment of hazard potential and regulation of land use are thus urgent problems. We propose fundamental principles for the assessment of hazard potential on the basis of a case study carried out at the Kikkakezawa Fan on the southern foot of Mt. Yatsugatake, central Japan. Existing villages are located below a major spring zone in the alluvial fan, which is fed by the groundwater in the volcanic body. Construction of a new road stimulated land developments along it and further upstream. It has been found that the debris-flow deposits had covered the fan in three geologically distinct ages. The ages of the deposits of new-age and middle-age debris flows are estimated on the basis of aerial photographs and a field investigation to assess their recurrence interval. The three kinds of debris flows are characterized by relative height from the current stream bed and by the area of deposition. Since the hazard assessment is needed for any part of the fan for any time span of the planned land use, it is advisable to define and assess the hazard potential of a fan from which the risk is calculated taking account of the location in the fan, and the time-span and the mode of the planned land use.

**JSP23/E/54-A5 1520**

**THE ADVANTAGES OF HOLONIC DESIGN FOR WARNING AND ALARM SYSTEMS**

Gary GIBSON (Seismology Research Centre, 2 Park Drive, Bundoora, Victoria 3083, Australia, email: gary@seis.com.au)

Warning and alarm systems are near real-time monitoring systems. They may be adversely affected by the events they are seeking to detect, such as a communication failure caused by an earthquake. Holonic systems were developed in manufacturing engineering, and require that each system element involves both task performing and decision making. A holon is an intelligent system element, either human or computer based, that is normally in communication with other holons. A holon is AUTONOMOUS (it can perform tasks alone if communications fail) and COOPERATIVE (overall results are enhanced when holons help each other, and it monitors the health of neighbouring holons, providing an immediate alarm if a failure is detected, and may attempt to compensate for any loss of function). Holonic systems are designed so that no elements or communication links are critical. It must



be accepted that any particular component will fail, and the system must be designed to cope with this. The Internet is a system designed to continue in operation after individual components have failed. An holistic system is one, which self-organises and evolves to dynamically optimise survivability, adaptability, flexibility, efficiency and effectiveness. Earthquake and tsunami warning and alarm systems are ideally suited to holistic design. They use "Event Oriented Seismology", requiring minimal data flow. Each seismograph may be event triggered, may record continuously and only transmit selected waveform segments on request, and/or may transmit minimal continuous data to facilitate event detection. They respond to requests or issue messages to other holons in the system. Communication can vary from the Internet, to slow digital radio links, or even dial-up telephone. A system is holistic if each element sends and receives information to and from other elements, but continues to function autonomously when communications fail. Any system failure should be immediately reported by one or more system elements. Holonic systems may be very economical because they only perform the tasks that are required. Compared with continuously tele-metered data from non-holonic digitisers, there is a dramatic reduction in total data flow, and usually in operating cost, with enhanced reliability and flexibility.

**JSP23/C/U5/W/08-A5****1600****URBAN LOCAL EARTHQUAKE DISASTER RISK INDEX**

Yang TING (Geophysics Institute, China Seismological Bureau. Now at Shanghai Seismological Bureau, No.87, Lanxi Rd, Shanghai, China, 200062. Email: tyang@263.net); Zhu Yuanqing (Shanghai Seismological Bureau, No.87, Lanxi Rd, Shanghai, China, 200062)

In many modern cities, especially megacities with low seismicity, there exist a lot of hidden disadvantages, except for the frequency of historical earthquake and ground shaking level, that may amplify the influence of earthquakes and cause a catastrophe to them. The Urban Local Earthquake Disaster Risk Index (ULEDRI), which is firstly presented by authors, will highlight those disadvantages with an easily understandable form for city decision-makers, planners, organizations and individuals. ULEDRI is a variation of EDRI, which is a new approach that can directly compare the relative overall earthquake disaster of megacities worldwide, and describe the relative contributions of various factors to that overall risk. Unlike EDRI, whose study unit is the greater metropolitan area, ULEDRI uses the local area of an urban, e.g. administrative district, postal area, as its unit of study. What's more, depended on the demand of users, ULEDRI's study unit can be a larger one (e.g. every administrative district of city), or a smaller one (e.g. several blocks). As a result of this difference between EDRI and ULEDRI, the objectives, uses and developing approach of ULEDRI will differ distinctly from those of EDRI. ULEDRI involves a large amount of knowledge about earthquake disaster of a wide range of disciplines, and the factors that contribute to overall ULEDRI of a city include those of geophysics, geology, engineering, residents, socio-economics, culture and so on. ULEDRI has the following potential uses. First, this kind of index can serve as a simple tool to directly compare the relative overall earthquake disaster risk of different local area of a city, so the decision-makers and administrators can find where the most dangerous local area is when an earthquake affects the city. Second, through disaggregated ULEDRI, the users can find the reason why a local region has a high overall ULEDRI, and which factor is the most important one that causes this. For city planner and disaster manager, the information will be significant in urban function planning and disaster mitigation. Third, any organization and individual will be able to refer to the index in allocating resources and increasing awareness of disaster. As a sample, ULEDRI of Shanghai, which is based on several districts, has been constructed, and its feasibility and potential application have also assessed.

**JSP23/C/U5/E/16-A5****1620****THE GSHAP WORLD MAP OF SEISMIC HAZARD**

D. GIARDINI (ETH, 8093 Zurich, Switzerland, email: giardini@seismo.ifg.ethz.ch); G. Grunthal (GFZ, Potsdam, Germany); H. Gupta (NGRI, Hyderabad, India); D. Mayer-Rosa and S. Sellami (ETH, Zurich, Switzerland); K. Shedlock (USGS, Boulder, USA); P. Zhang (SSB, Beijing, China); T. Annaka (Tokyo Electric Power Services, Japan); M. G.-Ashatiany (IIEES, Tehran, Iran); K. Atakan (Bergen University, Norway); S. Balassanian (NSSP, Yerevan, Armenia); P. Basham (CTBTO, Vienna, Austria); C. Dimate (Ingeominas, Bogota, Colombia); M. Erdik (Kandilli Obs., Istanbul, Turkey); M. Garcia (CSIC, Barcelona, Spain); Giesecke (CERESIS, Lima, Peru); K. McCue (AGSO, Canberra, Australia); R. McGuire (Risk Engineering, Boulder, USA); R. Musson (BGS, Edinburgh, UK); S. Riad (Assiut University, Cairo, Egypt); D. Slejko (OGS, Trieste, Italy); V. Ulomov (JIPF, Moscow, Russia)

The Working Groups of the GSHAP regions: Central-North America, Central-Northern Europe, Eastern Asia, Northern Eurasia, Ibero-Maghreb, Adria, the working Groups of the projects: PILOTO, CAUCAS, RELEMR, SESAME, PAIGH-IDRC, EU-QSEZ-CIRPAN.

The Global Seismic Hazard Assessment Program (GSHAP) was launched in 1992 by ILP and ICSU and endorsed as a demonstration program by the UN/IDNDR. The GSHAP promoted a regionally co-ordinated, homogeneous approach to seismic hazard evaluation. Regional activities were concluded in 1992-98; the results have now been compiled in a uniform set of databases and in a world map of seismic hazard expressed in PGA. Support for the GSHAP implementation was provided by ING, Roma, by national and regional institutions, by IASPEI, UNESCO, ICSU, ILP, IDNDR, EU, NATO, INTAS and IGCP. All GSHAP materials (regional report, maps, datasets) can be retrieved on the GSHAP web site at <http://seismo.ethz.ch/GSHAP/>. The GSHAP world map of seismic hazard will be presented for the first time at the IUGG assembly and will be available for distribution at the assembly.

**JSP23/E/33-A5****1640****RISK ASSESSMENT AND MANAGEMENT IN RUSSIA**

Shakhramanjan M.A.(1), Nigmatov G.M.(1), Larionov VI (1), FROLOVA N.I.(2), Suchzhev S.P.(3), Ugarov A.N.(3) Agency on Monitoring and Forecast of Emergency Situations, Ministry of Emergency Situation of Russian Federation (2)Seismological Center of IGE, Russian Academy of Sciences (3) Extreme Situations Research Center

At present in Russia the new technologies and procedures of natural and technological disasters monitoring and forecast of their consequences are elaborated and implemented. they are the following: procedure for individual seismic risk and losses assessment and identification of effective response scenarios; technology of operative zonation of the territories according to the rate of forest fires and flooding hazards; procedure of complex risk assessment and mapping with taking into account different natural and technological hazards; technology od estimation of buildings and structures' stability and earthquake resistance with the help of mobile diagnostic complexes; technology of operative monitoring of the territories with the use of remote sensing. All the technologies and procedures are realised on the basis of modern geographical information systems (GIS). The main blocks of the special GIS is described. The examples of individual seismic risk computations for different earthquake prone areas and cities of the Russian Federation, as well as for other countries are given. The influence of secondary engineering geological processes (landslides and liquefaction) is considered. The procedure of acceptable seismic risk level estimation is proposed. The examples of complex risk estimations are also given for the areas where different natural hazards (earthquakes, volcanic hazard, tsunami, flooding, hurricanes and storms, avalanches,

forest fires) are possible. The preventive measures plans and measures for reduction the risks from separate hazards are proposed. The maps of operative zonation of the territories according to the rate of forest fires and flooding hazards are presented for some regions of Russia and other countries. The application of the obtained results to disaster management practice may increase significantly the efficiency of measures aimed at risk reduction for population in urban areas.

**JSP23/E/39-A5****1700****EARTHQUAKE RISK ASSESSMENTS AND PRACTICAL APPLICATIONS FOR EARTHQUAKE MITIGATION STRATEGIES IN AUSTRALIA**

Jack RYNN (Centre for Earthquake Research in Australia, PO Box 276, Indooroopilly, Brisbane, Queensland 4068, Australia, email: sally.brown@uq.net.au)

In response to the United Nations IDNDR program, the Australian IDNDR Co-ordination Committee of Emergency Management Australia facilitated the earthquake zonation mapping of urban areas in Australia as one of its initial projects. The catalyst for this was the devastating 28 December 1989 Newcastle earthquake. A specific methodology was developed which has been expanded to address the national requirements for earthquake mitigation strategies. This involves a multidisciplinary approach integrating, both quantitatively and qualitatively, earth science, engineering, socio-economic, humanitarian, disaster planning, emergency management and community aspects. The results are compiled as an "information resource" in terms of hazard and vulnerability assessments and the integrated risk assessments, earthquake scenarios, potential ground motions and possible damage situations relative to the built and natural environments and the community. The outcomes are translated into practical applications to address awareness and preparedness for earthquake codes,

**JSP23/W/11-A5****1720****HYDRODYNAMIC SIMULATION EXTREME STORM SURGES IN AZOV AND CASPIAN SEAS**

Olga TIKHONOVA, Sergei Popov, Guennady Safronov, Oleg Zilberstein (State Oceanographic Institute, Kropotkinski per. 6, 119838, Moscow, Russia, email: oleg@soins.msk.ru)

Problems of storm surges description and prediction are very important because surges often lead to loss of human life and bring substantial damages to national economies. Thus for prevention their fatal consequences it is necessary to forecast storm surges according to available operative meteorological information and to calculate the storm surges characteristics. Besides of that, each extreme storm surge case is very important for determination of long return period characteristics of sea level and currents for hydrodynamic support hydro-technical engineering and marine shelf oil and gas exploration. Design and installation of stationary shelf oil platforms require information about vertical structure of currents. These characteristics are obtained by the 3D hydrodynamic model simulation. In this paper a non-linear 2D and 3D hydrodynamic models were applied for calculation of some extreme storm surges in Azov and Caspian Seas (including the catastrophic cases). The regime of sea level variations was investigated.

GIS mapping, education and training, loss reduction, disaster planning and emergency management. Such projects have been undertaken in the urban areas of Sydney, Southeast Queensland, Newcastle and Melbourne. Particular effort is directed towards real-time simulated earthquake exercises in co-operation with emergency services authorities. Collaboration with several international organisations and other risk projects in Australia is continuing. Although Australia is a moderate seismicity active interplate regime, the record of albeit "rare" earthquake disasters pointedly attests to the need for mitigation strategies.

**JSP23/E/40-A5****1740****TOWARDS REAL-TIME MONITORING OF LAVA EFFUSION RATES DURING VOLCANIC ERUPTIONS**

Andrew HARRIS and Luke Flynn (HIGP/SOEST, University of Hawaii, 2525 Correa Road, Honolulu, HI 96822, USA, email: harris@kahana.pgd.hawaii.edu)

Determining volumetric effusion rates for lava flows is an important but challenging task. Effusion rates are a major consideration in considering the potential threat posed by a lava flow. For channel-fed flows, higher effusion rates produce flows that are longer, more rapidly moving, voluminous, and aerially extensive than those with low effusion rates. High effusion rate flows thus have greater potential to inflict damage on distant communities with less advance warning. To calculate effusion rates we use satellite-derived (TM and AVHRR) thermal data in a heat balance. High spatial resolution TM data are collected infrequently, but allow high precision. Using TM data for active flows at Kilauea, Hawaii, we obtain effusion rates of  $1.76 \pm 0.57$  and  $0.78 \pm 0.27$  cubic meters per second on 23 July and 11 October 1991, respectively. These rates compare with field measurements of  $1.36 \pm 0.14$  and  $0.89 \pm 0.09$ . Using lower spatial resolution weather satellite (AVHRR) data collected at higher spatial resolution (>1 image per day), we obtain similar but more poorly constrained effusion rates. However, comparison with ground-based and TM data for eruptions at Kilauea, Krafla and Etna show that the AVHRR-derived time series reliably show waxing and waning phases of effusive eruptions with high temporal precision.

All of our systems are automated, and with direction reception of TM and AVHRR at the University of Hawaii we anticipate providing a web-based real-time lava flow monitoring tool. This will display current effusion rate time series, up-dated within minutes of satellite overpass at-least once every 6 hours for AVHRR, once every 8 days for TM. This system will be similar to our GOES-based real-time hot spot monitoring site at <http://volcano1.pgd.hawaii.edu>.

**Saturday 24 July AM**

Presiding Chair: A Ansal (Istanbul Technical University, Istanbul, Turkey)  
Concurrent Poster Session

**SEISMIC RISK MAPS AND SCENARIOS: TOOLS FOR THE PROTECTION AGAINST EARTHQUAKES****JSP23/W/17-A6****0830****THE LONG AND WIDING ROAD FROM EARTHQUAKES TO DAMAGE**

A. Ansal (Istanbul Technical University, Faculty of Civil Engineering, Maslak, Istanbul 80620, Turkey, tel: (90)-212-285 3702, fax: (90)-212-2856006, e-mail: ansal@itu.edu.tr); D. SLEJKO (Osservatorio Geofisico Sperimentale, P.O.Box 2011, 34016 Trieste, Italy, tel: (39)-40-2140248, fax: (39)-40-327307, e-mail: dslejko@ogs.trieste.it)

The impact of destructive earthquakes has two faces: one in the short term and the other in the long term. The first is given by the number of victims, damaged structures and direct economic losses. The second is given by the negative influence on the social structure in the



## INTER-ASSOCIATION

following years. Although the direct economic losses can be absorbed by the country, especially with international support, in most cases the social structure suffers permanent damages. The recent earthquakes of Northridge and Kobe have shown the long term problems caused respectively to the insurance companies and private inhabitants. This is one of the reasons why in seismically active countries (e. g.: Italy), a general private insurance against natural calamities is now being implemented. The knowledge on seismic risk is, therefore, fundamental for loss reduction. Seismic hazard maps at national level are the basic tool for defining the national seismic zonation which is relevant for planning adequately new settlements and constructing properly new buildings. The choice of the hazard parameter to consider for zonation is critical when the description of the whole contents of the seismic excitation is desired. However, these maps are only valid at large scales and local effects are not taken into consideration. Seismic risk maps at national scale are strategic for planning the policy for retrofitting old buildings in the presence of limited investments: their definition in a quantitative manner remains mainly a research topic for the difficulty of quantifying properly the ingredients. Risk scenarios at regional to local scale are very popular in recent years as they have the potential to limit earthquake victims and structural damage when a dangerous event is presumed to take place. In fact, based on the information and analysis concerning earthquake resistance capacity of existing buildings and structures, strengthening and retrofitting programmes can be optimised. The good knowledge ...

**JSP23/E/34-A6**

**0850**

### DETERMINISTIC VS. PROBABILISTIC EARTHQUAKE HAZARDS AND RISKS

Robin K. MCGUIRE (Risk Engineering, Inc., 4155 Darley Ave, Suite A, Boulder, Colorado, 80403, USA, email: mcguire@riskeng.com)

Deterministic vs. probabilistic approaches to assessing earthquake hazards and risks have differences, advantages, and disadvantages that often preclude the use of one over the other. Factors that influence the choice include the decision to be made (i.e. the purpose of the hazard or risk assessment), the seismic environment (whether the location is in a high, moderate, or low seismic risk region), and the scope of the assessment (a single-site risk, a multi-site risk, or risk to a region).

Decisions coming from earthquake assessments include selection of design or retrofit criteria and levels, financial planning for earthquake losses, and planning for emergency response and long-term recovery. The more quantitative the decision to be made, the more appropriate is probabilistic hazard and risk assessment.

For high seismic regions (e.g. California or Japan) where the largest earthquakes occur every 100-300 years), a deterministic scenario for the largest event will allow details to be examined such as ground motion effects caused by rupture propagation. In low seismic regions, extreme deterministic scenarios will have probabilities of occurrence that are too low to be useful for most decision purposes.

Specific site analyses generally require a probabilistic approach. Multiple-site analyses (e.g. for a portfolio of exposed or insured properties, or a lifeline) often require a probabilistic analysis because of multiple variables and complexities of the system, and a deterministic check can be misleading. Regional assessments often benefit most from deterministic models.

**JSP23/C/ST3/E/21-A6**

**0910**

### METHODOLOGICAL CONSIDERATIONS OF PROBABILISTIC SEISMIC HAZARD MAPPING

R.M.W. MUSSON (British Geological Survey, West Mains Road, Edinburgh, EH9 3LA, UK, Email: R.Musson@bgs.ac.uk)

The study of seismic hazard is perhaps the most practically oriented aspect of earthquake seismology. As such, it should not be treated in an idealised or academic manner, but with regard to the needs of the consumers of the final product. This has important consequences when it comes to the topic of probabilistic seismic hazard maps. Who are these for? Historically, early studies of probabilistic seismic hazard tended to be done for engineers for specific design requirements. Consequently, there has been a tendency to treat seismic hazard maps as a sort of pan-national study for engineers, who can identify the design requirements for any site by picking them from the map. A dissenting point of view argues that seismic hazard maps are by their very nature too generalised to be used in this way; that such maps provide a first indication of relative hazard and should not be a substitute for site studies. There are, therefore, a number of interesting and important methodological questions to be asked: what are the practical differences in undertaking a seismic hazard map from calculating hazard for a site? Should probabilistic seismic hazard maps have the same degree of conservatism as site studies? How can seismologists meet the needs of different audiences? An engineer may think in terms of ground acceleration, but this parameter probably means little to people in other professions who still need access to seismic hazard data, but in a form they can understand. These are questions that need to be addressed directly; one should not leave them to be answered by default.

**JSP23/E/03-A6**

**0930**

### EARTHQUAKE SCENARIOS FOR SWITZERLAND

FAEH, D., Bay, F., Giardini, D., Kind, F., Mayer-Rosa, D., Sellami, S. (Swiss Seismological Service, ETH Zurich); Lang, K., Bachmann, H., Wenk, T. (Institute of Structural Engineering, ETH Zurich); Noack, T., Huggenberger, P. (Institute of Geology, University of Basel)

The goal of our project is to develop a method for the estimation of expected damage from earthquakes. The presentation is giving an overview of the state of the project, which includes, the modelling and mapping of ground motion on a regional scale for the area of Switzerland, and on a local scale for the Basel area, the classification of the vulnerability of buildings to earthquake ground motion for some target areas, and the realization of scenarios. We will present the deterministic seismic hazard in form of scenario ground motion maps. This can be done on a regional scale or on a local (microzonation) scale. On the regional scale the scenario ground motion maps should include significant earthquakes in a regional sense. Maps will then display ground motion with different probabilities of occurrence in different locations. On a local scale, ground motion scenario maps are most appropriately computed for single possible earthquakes, and these maps can be combined with a vulnerability assessment of existing structures. In this combination the scenario maps include the level and duration of shaking. Furthermore they make it possible to identify localities where ground is likely to fail through liquefaction or landslides, and they enable us to pinpoint structures that are likely to be severely damaged and to find weak links in life-line structures. Such studies can be done with different levels of detail. The project will contribute to the necessary seismic upgrading of existing buildings, as well as to reliable earthquake resistant design of new structures, to the education of the general public, the emergency planning and it will serve as a reminder that there is a large difference between what is expected from probabilistic maps and what is a possible event.

**JSP23/E/08-A6**

**0950**

### REGIONAL AND LOCAL SEISMIC HAZARD ASSESSMENT

A. MARCELLINI, R. Daminelli, G. Franceschina e M.Pagani (Istituto di Ricerca sul Rischio Sismico, CNR, via Bassini 15, 20133 Milano, Italy, e-mail: marcel@irrs.mi.cnr.it)

Site effects can produce, at a local scale, abrupt changes of the ground motion as also instability phenomena such as landslides and soil liquefaction; microzonation studies are the scientific response for the evaluation and mitigation of this kind of phenomena. Seismic microzonation generally produces on a municipal scale Landuse planning criteria and defines seismic actions for engineering purposes. Seismic codes instead, are issued on the basis of Seismic Hazard studies, that is, seismic actions and seismic zonation are a direct consequence of a probabilistic seismic hazard, generally assessed considering a 474 yr R.P. In other words seismic actions assessment is biased by the inefficiency of seismic hazard evaluation procedure to account properly of parameters controlling the ground motion, mainly due to the limited number of factors used in the attenuation laws. It should be pointed out that till now this limits appears unavoidable due to the scarcity of strong motion recordings. Microzonation investigation can overcome these limitations, but only if the reference input motion is properly assessed by adopting the same level and the same criteria of protection used to issue seismic codes at national level. The case study here presented refers to a zonation and microzonation investigation performed in the Forlì provincia (Emilia-Romagna) for the purposes of seismic prescriptions to be issued both at regional and local level and we will main focus on the importance of multiple approach for the definition of the reference input motion.

**JSP23/C/U5/W/06-A6**

**1010**

### NEAR-FIELD GROUND MOTIONS

N. AMBRASEYS (Imperial College, London)

The assessment of earthquake hazard of interest to the engineer must be based on the analysis of reliable observational data than on statistics of many records and seismological parameters of questionable quality. Theoretical methods for the prediction of ground motions have become highly developed, whilst knowledge of the observational material is usually lacking. Differences between attenuation laws arise from the size and distribution of the sets of data used in their derivation and from the use of different magnitude scales, which introduce significant bias in the results. In addition, the correction of records and the modelling of attenuation laws and fitting method used to regress the data are sources of systematic errors. Taking some of these differences into consideration we find no significant variation of attenuation laws among different regions for shallow earthquakes, and a remarkable agreement between attenuation laws derived for Europe, western North America and New Zealand. They are all within the standard deviation of the determinations, which are not better than by a factor of 1.7 for accelerations. The importance of the vertical acceleration needs further investigation. However, the observation that the ratio of peak vertical zero-period or spectral value, to that of the horizontal, can be larger than 1.0 does not necessarily imply large vertical accelerations or spectral ordinates, most certainly when these maxima occur simultaneously. Also the assessment of peak and spectral ground displacements, which is of some engineering importance, needs further investigation. Near-field ground motions from medium and large magnitude earthquakes associated with surface faulting or, from sites on low-strength deposits, contain a significant component of permanent displacement, not accounted for in standard base-line correction procedures. An answer to these question is needed in order to rank these effects among other variables, and clarify the need to include or exclude them from building codes.

**JSP23/W/18-A6**

**1050**

### ASSESSMENT OF STRONG EARTHQUAKE GROUND MOTIONS FOR NEAR-FAULT CONDITIONS

Mustafa ERDIK, Eser Durukal (Bogazici University, Kandilli Obs. And Earthq. Res. Inst. 81220 Cengelkoy, Istanbul, Turkey, email: erdik@boun.edu.tr, durukal@boun.edu.tr)

Near-fault ground motions are strongly influenced by the earthquake faulting mechanism. Especially, the motions with periods above 1s may follow certain radiation patterns, predicted by equivalent double-couple source models, and exhibit distinct long period pulses with amplitudes depending on the orientation of the site with respect to the rupture direction. Widely used predictive earthquake engineering tools, such as empirical attenuation relationships and spectral shapes fail in the assessment of such near fault motions. Deterministic theoretical predictions of the ground motion can be achieved by convolution of the Green's Functions and the slip function. Such deterministic predictions cannot be extended into the frequency regions above 1Hz, since, high frequency ground motions are controlled by the heterogeneities in the fault rupture, which cannot be accounted for in a deterministic manner. This requires either the use of stochastic source models or the stochastic treatment of the high frequency components in the ground motions.

Based on these developments a state-of-the art hybrid procedure is developed for the assessment of the time history of the DBE (or SEE) ground motion for important engineering structures near major faults. The essential elements of the procedure can be listed as follows: (1) Assessment of the source parameters of the DBE motion associated with the corresponding return period for specific conditions of site and seismicity; (2) Deterministic assessment of the low frequency (DC-1Hz) ground motion, at the outcrop of a reference soil layer, due to rupture of seismic faults using numerical simulation; (3) Use of a Boore (1983) type stochastic simulation method to complement the deterministic low frequency ground motion with high frequency (1Hz- 50Hz) components; (4) Combination of the two parts of ground motion to yield a site-specific simulation for a frequency range of DC-50 Hz.; and (5) Site response analysis, if required, to include the local wave propagation effects in the soil media above the reference soil layer.

An example that illustrates the application of this procedure is provided.

**JSP23/E/01-A6**

**1110**

### MODIFICATIONS TO SEISMIC HAZARD DUE TO SITE-CITY INTERACTION

Pierre-Yves BARD, Philippe Gueguen (Laboratoire Central des Ponts- et-Chaussées and Observatoire de Grenoble, BP 53 - 38041 Grenoble Cedex - France, email: Pierre-Yves.Bard@lgit.observ.ujf-grenoble.fr); Jean-François Semblat (LCPC, 58 Bd Lefebvre, 75732 Paris Cedex 15 - France); Martin Cardenas and Francisco Chavez- Garcia (Coordinación de Ingeniería Sismológica, Instituto de Ingeniería, UNAM, Ciudad Universitaria, Apdo. Postal 70-472, Coyoacan, 04510 México, D.F)

Soil-structure interaction has long been known to significantly affect the seismic behavior of large buildings on soft soils. A few observations, and several computations as well, recently indicated the possibility for significant feed-back effects from buildings into the soil: the waves radiated back into the soil from the soil-structure interface are trapped in the surface layers when the impedance contrast at depth is large enough, so that the building is acting as a

secondary source of surface waves. This phenomena has been shown to be maximum in case of coincidence between the building and ground natural frequencies: the worst case corresponds to the matching of fundamental frequencies, and induces ground motion modifications of at least 30 % in time-domain amplitudes within distances up to 5 to 10 times the building base dimensions. The question then arises of the possibility of large-scale site-city interaction due to the quasi-random superposition of such phenomena for a large number of buildings in a given city, or in a given quarter, which, in turn, raises two issues: Is the "free-field record" concept relevant in such areas? And will the construction or destruction of some buildings modify locally the hazard? The aim of the presentation is not to answer these questions, but simply to briefly review the reasons why these issues have to be addressed, and to present some preliminary, first order computations exhibiting significant effects not only for "exceptional" configurations such as Mexico City, but also for much more common situations with "ordinary" sediments and "ordinary" buildings.

Saturday 24 July PM

Presiding Chair: D Slejko (Observatorio Geofisico Sperimentale, Trieste, Italy)

JSP23/W/20-A6

1130

### THE CYCLIC BEHAVIOUR OF SOILS AND EFFECTS OF GEOTECHNICAL FACTORS IN MICROZONATION

Atilla ANSAL (Istanbul Technical Uni, Civil Engng., Maslak, Istanbul, Turkey, email:ansal@itu.edu.tr)

The behaviour of soils subjected to cyclic loading is briefly reviewed. The results obtained from cyclic triaxial, simple shear and torsional hollow cylinder tests conducted on undisturbed, normally consolidated clay samples subjected to different shear stress amplitudes and different loading patterns are summarised. Results of the tests conducted under uniform cyclic stresses to evaluate "cyclic yield stress" and "threshold cyclic shear stress" are presented. The effects of cyclic loading on static shear strength and induced settlements due to pore water pressure dissipation are discussed. Cyclic tests performed to evaluate the liquefaction susceptibility of laboratory prepared and undisturbed sands and silty clayey sands are briefly reviewed in the light of the findings reported in the literature.

Geotechnical site conditions is one of the main factors controlling earthquake forces affecting structures. Therefore, in analysing the observed damage in previous earthquakes and for microzonation studies, this factor and its coupled effect with earthquake source characteristics need to be evaluated. The earthquake source characteristics induced by a tectonic source mechanism are on macro level and are not sufficient to explain the variations in structural damage observed within short distances. On the contrary, the geotechnical site conditions that can be very different due to changes in the thickness and properties of soil layers, depth of bedrock and water table, can have more dominant influence on damage distribution. In addition the effect of coupling between site and source characteristics may modify earthquake ground motion characteristics significantly. There are large numbers of instrumental field observations obtained during recent earthquakes reflecting the coupled effects of geotechnical site and earthquake source characteristics. During earthquakes soil layers are subjected to multi-directional cyclic stresses with different amplitudes and frequencies that lead to cyclic deformations and to changes in stress-strain and strength properties of soil layers. Extensive laboratory, model and field studies were conducted concerning response of soils subjected to cyclic stresses. Significant improvements were achieved in the field of insitu tests to obtain more reliable soil properties. Numerous analytical and empirical relationships were developed to model the behaviour of soil deposits subjected to earthquake excitations. From an engineering perspective, it is possible to investigate the properties of geo-technical site conditions in detail and analyse the response of soil layers with sufficient accuracy.

JSP23/E/05-A6

1150

### LOCAL SITE EFFECTS AND DYNAMIC SOIL BEHAVIOUR

Erdal SAFAK (U.S. Geological Survey, Box 25046, MS 966, Denver, CO 80225, USA, email: safak@usgs.gov)

Amplitudes of seismic waves increase significantly as they pass through soft soil layers near the earth's surface. This phenomenon, commonly known as site amplification, is a major factor influencing the amount of damage on structures. It is crucial that site amplification is accounted for when designing structures on soft soil sites. The characteristics of site amplification, at a given site, can be estimated by analytical models, as well as field tests. Analytical models require as inputs the geometry of all soil layers from surface to bedrock, their dynamic properties (e.g., density, wave velocity, damping), and the incident bedrock motions. Field tests involve recording and analyzing the dynamic response of sites to artificial excitations, ambient forces, and actual earthquakes. The most reliable estimates of site amplification are obtained by analyzing the recorded motions of the site during earthquakes.

This paper presents a review of the models and methods that are used to characterise site amplification, and introduces some new ones with better theoretical foundations. The models and methods discussed include spectral and cross-spectral ratios, response spectral ratios, constant amplification factors, parametric models, physical models, time-varying filters, methods for downhole records, single-station methods, and generalised inversion techniques. The paper also examines the validity of one-dimensional models, in comparison to 2D and 3D models, and shows the effects of surface waves and surface-to-bedrock topography on site amplification estimates. The paper concludes that probabilistically cross-spectral ratios give more reliable estimates of site amplification than spectral ratios. Spectral ratios should not be used to determine site amplification from downhole-surface recording pairs because of the feedback in the downhole sensor. Response spectral ratios are appropriate for low frequencies, but overestimate the amplification at high frequencies. One-dimensional site amplification models are not appropriate for sites in deep sedimentary basins that are susceptible to generating surface waves. The surface topography...

JSP23/E/44-A6

1210

### THREE DIMENSIONAL PLATE KINEMATICS IN ROMANIA

Georg Dinter (Department of Geodesy, University of Karlsruhe, D-76128 Karlsruhe, Germany, email: dinter@gik.uni-karlsruhe.de); Guenter SCHMITT (Department of Geodesy, University of Karlsruhe, D-76128 Karlsruhe, Germany, email: schmitt@gik.uni-karlsruhe.de)

Since 1996 the Collaborative Research Center (CRC)461 "Strong Earthquakes: A Challenge for Geosciences and Civil Engineering" is funded by the Deutsche Forschungsgemeinschaft (German Research Foundation) as a German Contribution to the UN initiative "International Decade of Disaster Reduction" (IDNDR). A central project of this CRC is the subproject B1 "Three dimensional Platekinematics in Romania" which is installed to detect borders of the geotectonic plates in Romania, to quantify their three dimensional movement rates and to determine in detail the deformation of each geotectonic unit in the Vrancea Region as a contribution to the research of the tectonic cause of the intermediate depth earthquakes in this region. These aims shall be accomplished by repeated GPS-measurements in a network which has been installed in 1997 and measured until now in 1997 and 1998. This network is consisting of 26 stations, covering an area of 250 x 380 km with the Vrancea area as the centre. The frame is given by six stations of the CEGRN (Central European Geodynamic Regional Network) of the CEI-Initiative CERGOP, for which co-ordinates and velocities in a global tectonic scenario are available. The paper gives information about the tectonic

background, the geodetic network, the GPS-measurements and the achieved accuracy's and first results of deformation analyses.

JSP23/L/06-A6

1400

### EVALUATION OF VULNERABILITY OF CIVIL ENGINEERING STRUCTURES

Mauro DOLCE (Department of Structures, Soil Mechanics, Applied Geology, University of Basilicata, Potenza, Italy)

The impact of earthquakes on man-built systems (buildings, groups of buildings, lifelines, cities, etc.) is usually expressed in terms of losses. Loss assessment is a highly complicated task, involving, besides structural engineering and seismology, many disciplines such as geotechnical, transport, hydraulic and electrical engineering, geology, urban planning, social and economic sciences, etc. However most of the losses results from the consequences of direct damage to civil engineering constructions, particularly buildings. The evaluation of their seismic vulnerability is then a fundamental step in the process of determining the impact of earthquakes on man-built systems. This is usually assessed in terms of seismic risk in a period of time (e.g. one year, hundred years), i.e. in terms of probability or of expectation of losses during that period due to all the possible arriving earthquakes. This representation is very general but presents many drawbacks such as the difficulty of interpreting the results in practical terms and the difficulty of expressing and quantifying losses for territorial systems. In fact they are highly dynamical systems, whose future developments are difficult to forecast, particularly after the occurrence of an earthquake. A long term loss prediction is therefore not much significant, if it is referred to the current situation or even to the current trend.

Recently the interest of researchers and operators has been focused on risk scenarios, where the impact of a given earthquake is investigated and quantified. This approach permits to better understand the behavior of the built environment under study and to take the countermeasures aimed at reducing its impact. Scenarios can be prepared considering different aspects of the earthquake consequences. Different levels of accuracy can be assumed in the preparation of a scenario, starting from the assessment of shaking intensity and characteristics, through damage prediction up to loss assessment. Obviously the accuracy levels in the different steps must be consistent.

The assessment of damage to constructions deserves a special attention. In this respect, two ...

JSP23/L/07-A6

1420

### FROM VULNERABILITY OF OBJECTS TO VULNERABILITY OF SYSTEMS

Carlo GAVARINI (Universita' La Sapienza, Roma, Italy)

First of all the paper outlines the current conceptions relevant to vulnerability of constructions, describing the various approaches and the different research levels, then, in the second part, a more global vision is developed in which the constructions belonging to an aggregate, or a centre, or a city, or a territorial area, are considered as a part of a vulnerable system, with all the complexity that it brings about, in terms of different variables that must be taken in consideration, properties and values that are in danger, disciplinary, cultural and historical aspects that must not be ignored.

Assessment of vulnerability is strictly connected with another basic problem, risk mitigation, that will be briefly considered in the third part, analysing the interrelations between vulnerability and environment aggressions. Also here we must point out how today it is a common exigency, also as regards technical codes, to abandon the sectional vision of objects considered separately and to promote instead the above mentioned "picture in picture" vision applied to systems, better said to complex systems, specially when the areas in question are rich with particular "objects" with a "cultural value", such as historical buildings and monuments.

Lastly, in the fourth part, we return to deal with single objects, giving a short account of problems specific to monuments and in particular to churches subjected to seismic actions; referring to studies regarding the Cathedral of Noto, partially collapsed in 1996 and now in course of reconstruction.

The need for experiments, either real or virtual, is recognized as a key for understanding and classifying the...

JSP23/E/19-A6

1440

### LOSS ESTIMATION: A POWERFUL TOOL FOR RISK ASSESSMENT AND MANAGEMENT

Fouad BENDIMERAD (Risk Management Solutions, Inc., 149 Commonwealth Drive, Menlo Park, CA 94025, USA; email: fouadb@riskinc.com)

Earlier loss estimation studies were limited to investigating particular scenarios and were carried out by highly specialized experts. Today, loss estimation techniques are translated into efficient software applications that are accessible by a large constituency of end-users. These techniques offer a high level of analysis sophistication and enable users to perform various "if-then" scenarios to study the sensitivity of the results, to develop a better understanding of the outcomes and to gain insight on the consequences of the findings and decisions.

Loss estimation techniques have benefited from the advances in information technology. Modularity, encapsulation and a new generation of computer codes such as C++, provide a logical and flexible structure for organizing the analytical procedures involved in loss estimation. These techniques organize the multitude of analytical calculations into modules that are logically inter-related by hierarchical rules. This flexible architecture permits ease in development, testing, validation, maintenance and upgrade. The study region is divided into geographical units (Geo-Units) such as postal codes or census tracts. The data, calculations and results are then associated with the centroid of the Geo-Unit. The aggregated results from the Geo-Units yield the results for the study region. Geographical Information Systems (GIS) and Relational Database Management Systems (RDMS) are used to organize data in data warehouses, to manipulate data during analysis, and to associate results to geographical regions from which they can be queried, aggregated and/or mapped. GIS and RDMS also allow for easy display of input and output (in standard reports and maps) providing a critical functionality for communication of outcomes to end-users. Loss estimation has become a critical tool to the insurance industry and is quickly being adopted by a wide range of users including emergency managers and planners. The key to this expansion is the integration of new information technologies that gave these techniques greater analytical capabilities, flexible architecture, and user-friendliness.



**JSP23/C/U5/E/15-A6 1500**

**GLOBAL SEISMIC HAZARD AND RISK ASSESSMENT**

YONG CHEN, Qi-fu Chen, Ling Chen, Juan Li and Jie Liu (No. 63, Fuxing Avenue, China Seismological Bureau, Beijing 100036, P. R. China)

A global seismic hazard assessment was conducted using the probabilistic approach in conjunction with a modified means of evaluating the seismicity parameters. This method is applicable to both oceanic and continental regions, and for any specific duration of time. It can be used for those regions without detailed geological information or where the relation between existing faults and earthquake occurrence is not clear.

Most seismic risk studies use a probabilistic approach in which predicted damages in various categories of structure and facilities in the region in concern are estimated and added together to obtain a total loss for particular intensity ranges. We have used an alternative means of estimating earthquake losses based on several macroeconomic indices such as the gross domestic product (GDP) and population. A global seismic loss map is then compiled.

The expected losses (in USD) of selected countries and regions for the next 50 years are as follows:

World 949 (USD), Asia 563 (USD), European 184 (USD), N.America 115 (USD), S.America 60 (USD), Oceania 12 (USD), Japan 390 (USD), USA 66 (USD), China 17 (USD)

**JSP23/W/16-A6 1520**

**SEISMIC HAZARD MAPPING FOR ADMINISTRATIVE PURPOSES**

L. Peruzza (C.N.R. Gruppo Nazionale Difesa Terremoti, c/o OGS, Trieste, Italy); A. Rebez and D. SLEJKO (Osservatorio Geofisico Sperimentale, Trieste, Italy, tel: (39)-40-2140248, fax: (39)-40-327307, e-mail: dslejko@ogs.trieste.it)

Local site conditions strongly influence the seismic hazard assessment, even if done using standard probabilistic techniques, with average soil classification. GIS applications, nowadays, enhance these variations, without entering into a detailed microzonation study, that is not possible at wide, regional scale. On the other side, the administrative border of municipalities remains the basic units to face the problems of legislative measurements devoted to risk evaluation and reduction. The aim of this paper is to present maps of different hazard parameter devoted to better represent the free field shakeability in NE Italy. The dominant soil in each municipality has been classified, taking into account the location of buildings and structures: then soil dependent hazard estimates have been performed and mapped, according to the some of the criteria leading the new proposal of seismic classification in Italy.

**JSP23/W/29-A6 1600**

**EARTHQUAKE HAZARD ASSESSMENTS FOR THE GULF OF CORINTH (CENTRAL GREECE) AND KRESNA REGION (SW BULGARIA)**

Vladimír SCHENK, Zdeka Schenková and Pavel Kottbauer (all at Institute of Rock Structure and Mechanics, Academy of Sciences, CZ-182 09 Praha 8, The Czech Republic, email: schenk@irm.cas.cz)

The earthquake hazard calculations were realised for two seismically high-active European zones, for the area round the Gulf of Corinth (Central Greece) and for the Kresna region (SW Bulgaria). To make reliable earthquake hazard calculations all available data were collected. For the Gulf of Corinth data of the National Observatory of Athens compiled by Drakatos, Kalogeris and Papadopoulos and as well the published earthquake catalogues, geological and geophysical materials (Ambraseys & Jackson 1990, Ganas & White 1996, Hatzfeld et al. 1990, Makropoulos 1985, Papazachos 1988, Papazachos & Kiratzi 1993, 1996, Papazachos et al. 1991, 1996, Shebalin et al. 1974) were applied. Simultaneously, for the Kresna region similar available data of the Geophysical Institute, Bulgarian Academy of Sciences, were sent to us by Rangelov and Shanov. All these data allowed seismogenic zones with respect to earthquake occurrence and main tectonic structures to be delineated, dependent events from independent ones to be identified, an earthquake regime per requested observation period and/or a size of the area to be normalised, a maximum possible earthquake to be assessed and an acceptable attenuation law to be applied. Every quantity was statistically tested in order to be possible to introduce the logical tree of the input parameters to the hazard calculations. A reliability of the earthquake hazard calculations in common practice will be discussed. The presented calculations were realised under the EC INCO-Copernicus ASPELEA Project No ERBIC 15CT97 0200.

**JSP23/C/U5/W/09-A6 1620**

**EARTHQUAKE DISASTER MITIGATION AND EMERGENCY RESPONSE SYSTEM (EDMERS) OF SHANGHAI BASED ON GIS**

YANG TING (Geophysics Institute, China Seismological Bureau. Now at Shanghai Seismological Bureau, No.87, Lanxi Rd. Shanghai,China,200062, Email: tyang@263.net) Zhu Yuanqing and Song Jungao (Both at Shanghai Seismological Bureau, No.87, Lanxi Rd. Shanghai, China, 200062)

As the largest city of China, Shanghai is also under the earthquake threat. In order to understand how severe disaster Shanghai will be suffered and what should be done by government when a possible earthquake affects the city, the Earthquake Disaster Mitigation and Emergency Response System (EDMERS) has been developed based on Geographic Information System (GIS). The EDMERS mainly includes two subsystems and several databases. The first subsystem, rapid earthquake damages estimation subsystem, will provide the rapid estimation of all kinds of earthquake damages according to the real earthquake parameters, (the origin time, epicenter location and source depth) which determined by Shanghai Telemetry Seismic Network in minutes while a destructive earthquake occurs. The second subsystem is the emergency response, in which the following emergency responses should be completed in time after a shock: determining the rescue scheme, evacuating victims, coping with dangerous materials, making decisions against fire following earthquake. The databases of EDMERS include building information, lifelines, soil conditions, aerial photographs, historical earthquake catalogues and so on. The following features of EDMERS should be highlighted: first, making use of GIS can enable the system to process the spatial data in a reasonable way, for example, The overlay and buffer functions of GIS can deal with the comprehensive effect of damage of buildings and lifelines. The network analysis of ARC/INFO can be directly used in emergence response such as victim evacuation and pathfinding. Second, emergence response can carry out on the base of real damage conditions by integrating damage estimation subsystem and emergence response subsystem. Third, using remote sensing, namely aerial photograph as an auxiliary tool, make EDMERS visual, vivid and informative.

**JSP23/E/15-A6 1640**

**FIELD SURVEY OF TSUNAMI DISASTER IN PAPUA NEW GUINEA ON 17 JULY 1998**

Yoshiaki KAWATA ( Research Center for Disaster Reduction Systems, DPRI, Kyoto University, Gokasho, Uji, Kyoto 611-0011, Japan, email: kawata@drs.dpri.kyoto-u.ac.jp)

On the evening of Friday 17 July at about 7:30 p.m. a breaking wave from a massive tsunami swept across the sand bar that forms the outer margin of Sissano Lagoon, west Sepik, PNG. Initial reports claimed that the wave was between 7 and 10m and that up to 3,000 persons were killed or missing. This seemed to be an unusually damaging tsunami given the size of the earthquake. Members of the International Tsunami Survey Team decided that a field survey was necessary as soon as possible to try and determine the true value of the maximum run-up and to accurately map the run-up distribution along the coast. The first surveys to the Sissano region confirmed the 7 - 10m wave reports and even found place where the waves were larger - up to 15 m. The severe damage and extreme wave heights were confined to a relatively short (30 km) stretch of coast between Aitape and Sissano Village. The survey was conducted by a multi-national team with representatives from Japan, the United States, Australia, and New Zealand. The team was broken up into two groups, the Japanese and everyone else. By the numerical estimation, it is impossible to get such gigantic tsunamis with the earthquake magnitude of 7.0. We found many marks of liquefaction at the sand bar and many residents reported that they had three earthquakes and middle one was the most severe. Therefore, we concluded that the earthquakes were not slow earthquake. Numerical simulation models of submarine landslide show good agreement with tsunami heights and their longshore distribution.

**JSP23/C/U5/E/23-A6 1700**

**PRECISE TOPOGRAPHIC AND GEOPHYSICAL SURVEYS OFF SISSANO LAGOON, NORTHERN PAPUA NEW GUINEA**

TAKESHI MATSUMOTO(1), David Tappin(2) and R/V KAIREI KR98-13 Cruise Scientific Party 1) Japan Marine Science and Technology Center (JAMSTEC), 2-15, (B)Natsushima-cho, Yokosuka 237-0061, Japan (2) British Geological Survey, Keyworth, Nottingham, UK

The northern coast of Papua New Guinea suffered from a M7.1 earthquake and aftershock events which occurred on July 17, 1998. A large-scale tsunami also occurred just after the earthquakes. KR98-13 Cruise by the Research Vessel KAIREI was carried out in January 1999 in order to locate the possible seismic faults and/or underwater landslides as the source of tsunami. Precise topographic and other geophysical mapping off Sissano Lagoon, in the area of 200km (E-W) and 120km (N-S), was completed after the 9 days' survey.

The study area is characterised by enormous amount of fan sediment supply from Sissano Lagoon, deep-sea canyons on the shelf, arc-shaped slump and offshore strike-slip faults. Straight small-scale submarine canyons and valleys are eroding the shelf slope. The meandering canyon is located on the old shelf to the north of Aitape. Topographic features caused by landslides are recognised at numerous sites of the study area. Most of them are old, and the most recent is located 25km north-east off the Sissano Lagoon. The most prominent of the many tectonic faults located in the study area is E-W trending escarpment, the length of which is about 40 kilometres, recognised 25 kilometres north of Sissano Lagoon.

The result of simplified numerical modelling of tsunami propagation by use of the new bathymetric data shows that the distribution of maximum wave height is in good agreement with the observation. This suggests that the bottom topographic feature is an important factor to amplify the wave and to generate the focused tsunami runup, and that both earthquake faulting and underwater landslide should be taken into account as possible origins of the tsunami.

**JSP23/C/U5/W/19-A6 1720**

**SUPER DENSE REAL-TIME MONITORING OF EARTHQUAKES: SUPREME**

Fumio YAMAZAKI (Institute of Industrial Science, The University of Tokyo, 7-22-1 Roppongi, Minato-ku, Tokyo 106-8558, Japan, email: yamazaki@iis.u-tokyo.ac.jp); Yoshihisa Shimizu, Wataru Nakayama and Ken-ichi Kogaenamaru (all at the Center for Supply Control and Disaster Management, Tokyo Gas Co., Ltd., 1-5-20 Kaigan, Minato-ku, Tokyo 105-8527, Japan, email: yshimizu@tokyo-gas.co.jp)

To cope with earthquake-related secondary disasters, city gas companies in Japan have promoted several countermeasures in the last two decades: increasing seismic resistance of facilities and pipelines, segmentation of gas networks into blocks, earthquake monitoring by seismometers, installation of intelligent gas meters with a seismic sensor etc. As one of such earthquake countermeasures, Tokyo Gas Company introduced an earthquake monitoring and rapid damage assessment system, SIGNAL, with 331 SI-sensors, which measure the peak ground acceleration (PGA) and spectrum intensity (SI) at district regulator stations. The strong motion indices and the results of damage estimation are used for the decision-making whether or not to shut off gas supply.

Recently Tokyo Gas further developed new SI-sensor, having several new functions with the much cheaper price. The new SI-sensor can store acceleration time histories in its IC memory and send monitored strong motion indices to the Supply Control Center through public telecommunication lines. The new sensors will be installed at all the 3,600 district regulator stations with in the next 8 years. The new SI-sensor network is named SUPREME (Super-Dense Real-time Monitoring of Earthquakes), which may be the most dense seismic monitoring network in the world. The data from the network will significantly contribute to the strong ground motion research as well as promote seismic safety of the greater Tokyo Metropolis.

**JSP23/W/00-A6 1740**

**APPLICATION OF POTENTIAL FIELD ANALYSIS ...IN INTRAPLATE SEISMIC RISK ASSESSMENT**

GUO

Abstract not available at the time of going to press



Monday 26 July AM

Presiding Chair: S McLean (NGDC/NOAA, Boulder, Colorado, USA)  
Concurrent Poster Session**NEW PHENOMENA, APPROACHES AND TECHNIQUES****JSP23/C/U5/W/18-B1** Invited **0830****POTENTIAL OF DISRUPTION OF HUMAN ACTIVITIES ON EARTH AND IN SPACE AS A CONSEQUENCE OF THE INTERACTION BETWEEN THE SOLAR CORONA AND EARTH'S MAGNETIC FIELD**

Gordon ROSTOKER (Department of Physics, University of Alberta, Edmonton, Alberta, Canada T6G 2J1, email: rostoker@space.ualberta.ca)

Over the past few decades, mankind has become increasingly dependent on various technologies which have helped greatly to improve the standard of living around the world. Two examples of such technologies that have had an enormous impact on human activities are global communications and the provision of readily available electric energy through the development of large transmission grids. Unfortunately, with the advent of new technologies comes human dependence on them. The use of satellites for communications and position finding purposes serves as a useful example of this dependence. It is now recognised that both geostationary communications satellites and the position-finding GPS satellites are vulnerable to the energetic electron environment in which they orbit. In this paper I shall outline the nature of this vulnerability and what the consequence of the loss of these satellites might be. As well, it is worth noting that large fluctuations in the geomagnetic field at auroral latitudes can induce electric currents in large power transmission grids sometimes causing them to be disabled for significant periods of time. I shall describe the nature of this problem and how space researchers are attempting to develop techniques to predict the potential for power outages. These practical manifestations will be presented in the context of the physical processes through which the solar corona interacts with the earth's magnetic field.

**JSP23/W/00-B1** **0910****REVEALING TEMPORARY MAGNETIC VARIATIONS ASSOCIATED WITH GEODYNAMIC PROCESSES**

EPPELBAURN

Abstract not available at the time of going to press

**JSP23/W/07-B1** **0930****DESTRUCTIVE ATMOSPHERICALLY-GENERATED LONG WAVES: SEPARATION BETWEEN SOURCE AND TOPOGRAPHY**

S. MONSERRAT (1), A.B. Rabinovich (2) and B. Casas (1). (1) Instituto Mediterráneo de Estudios Avanzados, IMEDEA, (CSIC-UIB), Palma de Mallorca, SPAIN, email: dfsmt4@ps.uib.es, (2) Tsunami Center, P.P. Shirshov Institute of Oceanology, Moscow, RUSSIA

Destructive long waves caused by atmospheric disturbances (meteotsunamis) present a significant threat for the Mediterranean coast, in particular, for the Iberian Peninsula and the Balearic Islands. Ciutadella Harbour, Menorca Island, is the place where extreme oscillations, locally known as 'rissaga waves', occur most frequently. The understanding of their origin and generation mechanism is a key scientific and applied problem. A method was first elaborated to suppress the influence of the initial source in order to isolate the general topographic function. The next step was to separate the resonant influence of the outer shelf from the local coastal features (bays or inlets). This second step allows reconstructing the corresponding admittance functions for any bay or inlet, which may be afterward used to predict amplification of meteotsunami but also of tsunami waves in a given location. The data of LAST-97 hydrophysical experiment (June-September, 1997) gave us a good opportunity to test this. A set of bottom pressure recorders were deployed on the shelf of Menorca Island, in two neighboring inlets of this island (Ciutadella and Platja Gran), and in Palma Bay (Mallorca Island); a number of precise microbarographs were working simultaneously. The first step of our analysis allowed reconstructing the open-sea source spectra for several abnormal seiche events recorded in the region of Ciutadella which, after compared with the observed atmospheric spectra, were used to estimate the so-called 'transfer function' between the atmosphere and the sea surface. This function is clearly related to the topography of the source area, but when computed for Ciutadella region, the transfer function was quite similar for different rissaga events suggesting consistency of the basic parameters (phase speed and direction of propagation) of the atmospheric waves generating large seiches. This fact can be used to predict the sea-level spectrum at a given location with the knowledge of the atmospheric pressure spectrum only. The second step of...

**JSP23/L/05-B1** **0950****ASSESSMENT OF GEOMAGNETIC HAZARD TO POWER SYSTEMS**

D. H. BOTELER (Geomagnetic Laboratory, Geological Survey of Canada, Observatory Crescent, Ottawa, Ontario K1A 0Y3, Canada)

During severe geomagnetic disturbances electric currents induced in high voltage power transmission systems can cause transformer saturation resulting in transformer heating, generation of harmonics and increased reactive power demand. These effects can damage transformers, cause misoperation of protective relays and, in the worst case, cause power blackouts. An extensive study has been made to assess the geomagnetic hazard to power systems in Canada. Data from the Canadian Magnetic Observatory Network and conductivity models for different parts of Canada were used to calculate the electric fields produced during different levels of geomagnetic activity. This was combined with statistics on the occurrence of geomagnetic disturbances to determine the electric fields the power systems could expect to experience, on average, once a year and once every ten years. These electric field values were then used as input to power system models which calculated the corresponding levels of geomagnetically induced currents (GIC) in each power system.

**JSP23/W/22-B1** **1010****THE SATELLITE CONCEPTION FOR MONITORING OF IONOSPHERE EXCITATION BY SEISMIC OR TECTONIC PROCESSES.**

Vladimir DOKUKIN, Victor Oraevsky, Yury Ruzhin and Vladimir Alekseev (IZMIRAN, Troitsk-town, Moscow Region, 142092, RUSSIA; E-mail: ruzhin@izmiran.rssi.ru)

The deep tectonic faults are known to be zones of concentration of stresses, canalisation of fluids, aerosols and gases, change of magnetisation and electro- conductivity of rocks,

appearance of high electrical potentials and so on. Also the tectonic faults are associated with the geodynamical structures which form the zones of elevated seismicity (quakes or volcanic eruptions) or zones of dangerous natural hazards. The results of joint processing of the data of low-frequency emission, corpuscular flows as well as temperature and density of plasma permitted us to reveal the previously unknown effect of the generation of low frequency noises in space over the deep faults of the earth crust. The developing now in Russia method of ionosphere tomography also is very perspective for that. The system of the small satellites can be especially important for revealing and research of global and regional net of geological faults in an effort to plan searches of mineral resources and to forecast destructive earthquakes (volcanic eruptions). The first microsatellite COMPASS, weighting about 80 kg, is planned to launch to the circular orbit with height 400 km and inclination 790 for development of the methods of monitoring and forecasting of natural disasters on the base of co-ordinated monitoring at the Earth and from space the pre-earthquake phenomena. COMPASS is composed of several sensors associated to a data processing unit and a large memory in order to record the information all around the Earth independently from telemetry station. The details of the measurements, instruments and general conception of the microsatellite system based on the COMPASS mission are presented in the report.

**JSP23/W/09-B1** **1050****AIR QUALITY AS A GEOPHYSICAL HAZARD**

Tom BEER (CSIRO Atmospheric Research, Aspendale, 3195, Australia, email: Tom.Beer@dar.csiro.au)

Geophysical hazards are usually considered to be earthquakes, volcanic eruptions, landslides, floods, droughts, tsunamis, storm surges, wildfire, tropical cyclones and extreme weather events. Air pollution is not normally considered to be a geophysical hazard. This view has arisen because the causes of air pollution – industrial and motor vehicle emissions – are not geophysical in nature. However, as air pollution regulations succeed in reducing the amount of pollutant emissions, air pollutant episodes become sporadic in nature, and their occurrence depends on a particular combination of meteorological factors. Analyses of air pollution episodes and hospital admissions indicate that there is a significant increase in morbidity and mortality as a result of air pollution episodes. Time-series studies undertaken in Sydney have shown that particulate matter, ozone and nitrogen dioxide are the pollutants that are primarily responsible for adverse health effects. Air quality forecasting systems can play an important role in mitigating the adverse effects of air pollution. The forecasts will affect the behaviour of susceptible individuals, and thus reduce adverse health effects. The outputs from forecasting systems can also be used to provide improved estimates of the total exposure to air pollutants of the inhabitants who are at risk. Such improved estimates can then be used in conjunction with longitudinal studies of health effects to obtain better understanding of the complex interaction between air quality and health. This presentation will illustrate the manner in which air pollution depends on meteorology, review some of the data concerning the resulting health effects, and discuss the future research needed for a better understanding of the interaction between air quality and human health.

**JSP23/W/13-B1** **1110****MULTIFRACTAL ANALYSIS OF TROPICAL ATMOSPHERIC STRUCTURES AND TYPHOON GENERATION.**

I. TCHIGUIRINSKAIA (E.E.&amp;S. Dept., Clemson University, 342 Computer Court, Anderson, SC29625, USA, E-mail: iouliat@clemson.edu); D. Schertzer (L.M.M., Université Pierre et Marie Curie, 4 Place Jussieu F-75252 Paris Cedex 05, France); S. Lovejoy (Physics Dept., McGill University, 3600 University st., Montréal, Qué., H3A 2T8, Canada)

During the last past ten years numerous investigations have been lead on the tropical atmospheric structures: boundary layer coherent structures, tropical storms and typhoons. Emphasis has been often placed on the structural conditions of generation of typhoons. Contrary to other approaches, we investigate this question on a large range of scales and intensities, trying to understand the crucial relationships between extremes events (such as typhoons) and more average ones, how the latter can build up to the appearance of the former. We chose thus a universal multi-fractal approach, since in this case the mean as well as the extreme events are ruled by three fundamental multi-fractal exponents determining the infinite hierarchy of singularities of the field and their corresponding co-dimensions. We analysed data sets obtained during two aircraft expeditions over South China Sea in 1988 and 1989 (Karmazin and Mikhailova, 1991). Measurements were usually done everyday from July to October on 8 or 11 levels from 50 meters up to 5 km heights, every 125 ms along 40 km in the horizontal for each level across the largest clouds bands. In the latter case, some flights were carried at a distance of Ed typhoon center as close as 7 km. Although variations of the estimates of the multi-fractal exponents are present, they do not seem to be significant, since these values remain close to those obtained in mid-latitude boundary layers or wind tunnel experiments (Schmitt et al. 1992). In conclusion, we discuss the rather low critical order of divergence of statistical moments  $q_D=7$  which rules the self organised criticality of extreme wind shears, temperature gradients and generation of related structures, in particular typhoons.

**JSP23/W/32-B1** **1130****LARGE-SCALE EVOLUTIONARY PROCESSES IN HAZARD SYSTEMS OF EARTHQUAKES, A PHENOMENOLOGICAL MODEL BASED UPON SELF-ORGANIZED CRITICALITY [SOC]**

Natalia SMIRNOVA, Vladimir Troyan (both at Institute of Physics, University of St.Petersburg, St.Petersburg 198904, Russia, e-mail: nsmir@snoopy.phys.spbu.ru); Masashi Hayakawa (The University of Electro-Communications, Chofu, Tokyo 182, Japan, e-mail: hayakawa@whistler.ee.ucc.ac.jp); Thomas Peterson (TFPLAB, Cleveland, Ohio 44124-5441, U.S.A., e-mail: TFPLAB@aol.com); Yury Kopytenko (St.Petersburg Filial of IZMIRAN, St. Petersburg 191023, Russia, e-mail: galina@admin.izmi.ras.spbu.ru)

The concept of self-organised criticality (SOC) is now widely used for the interpretation of the behaviour of natural hazard systems. This concept was recently introduced by the present authors as a way to search for earthquake precursory signatures. Here, we continue to consider earthquake region processes on the basis of the SOC concept. We suggest a phenomenological model for large-scale evolutionary processes that occur between violent earthquake episodes. Four principal stages of evolution are proposed and analyzed. They are: random chaos, subcritical, critical, and super-critical. External stimuli such as geomagnetic storms, sharp temporal and spatial variations in atmospheric pressure, and ULF impulses are considered as driving forces for a "cellular automata" process in active seismic regions. We discuss the possibility of using fractal characteristics of signals to study the critical dynamics of a hazard system. The important fingerprints of SOC - temporal and spatial fractal structures are analyzed using seismic and ULF electromagnetic data timed to violent earthquakes near Guam (August 8, 1993,  $M = 8.0$ ) and Kobe (January, 16, 1995,  $M = 7.2$ ). The research was supported by NASDA (Japan) and Russian Foundation for Basic Research (Grants No. 98-05-65554 and 99-05-NNN).

**JSP23/W/10-B1** 1150**ON CONNECTION BETWEEN THE SEISMICITY SPACE-TEMPORAL CHARACTERISTICS AND THE EARTH ROTATION**

Boris W. LEVIN (\*Shirshov Oceanology Institute of RAS and Russian Foundation for Basic Research, 32a Leninsky prosp., Moscow, 117334 Russia; email: levin@rfr.ru) Yeugeny Chirkov (\*\*Union Institute of the Earth Physics of RAS, 10 Bolshaja Gruzinskaja, Moscow, 123810 Russia; email: chirkov@uipe-ras.scgis.ru)

An importance of the Earth's rotation influence to earthquakes occurrence was noted by I.Kant (1756), I.R.Mayer (1893), G.H.Darwin (1908) and was often discussed by geophysicists at present time. Supposing the unpredictability of natural hazards is connected partially with our poor understanding of the planetary processes role, we investigated a geographical distribution of the earthquakes. Using the catalog NEIC, we had created the histograms of the earthquake numbers and its energy as a function of a latitude F from 90 deg. N to 90 deg. S at period of 1900-1993. We had found that the latitude distribution of the event numbers N(F) is similar to the curve describing a dependence R<sup>2</sup>(F) or I(F) where R is a distance from the axis of rotation and I is an inertia momentum of mass unit. Also we discovered the local maximum of the seismicity on so-called "critical latitude" 35 deg. N which was first mentioned by geographer A.Veronne (1912) and was calculated by F.Krasovsky and V.Magnitsky (1941) as a specific parallel for the Earth figure theory. The preliminary analysis of the seismicity-time dependence (more than 100000 events with M>4.0) for different latitude layers showed that the seismicity varies with main period of near 6 years practically at all latitude layers of the Earth.

**JSP23/E/02-B1** 1210**VOLCANIC RISK ASSESMENT AND ZONATION OF THE MAIN ERUPTIVE HAZARDS IN TENERIFE (CANARY ISLANDS)**

Vicente ARAÑA and Alicia Felpeto (Dept. Volcanologia, Museo Nacional de Ciencias Naturales, Jose Gutierrez Abascal 2, 28006 Madrid, Spain); Mar Astiz (Dept. Matematica Aplicada, E.T.S. Arquitectura, U.P.M., Avda. Juan de Herrera, 4, 28040 Madrid, Spain, email: civgv@pinar1.csic.es); Francisca Gomez (Centro di Studio per la Geologia Strutturale e Dinamica dell'Appennino, CNR, Pisa Italy); Alicia Garcia and Ramon Ortiz (Dept.Volcanologia, Museo Nacional de Ciencias Naturales, Jose Gutierrez Abascal 2, 28006 Madrid, Spain, email: mcngg92@pinar1.csic.es and mcnor72@pinar1.csic.es)

Taking into account that the island of Tenerife is a complex case, that one unique volcano and a unique eruptive style cannot be considered, the methodology developed in this paper to define a volcanic hazard-risk zonation in the island consists of: (1) Definition of the different hazards. (2) Numerical gradation of the probability of occurrence of each phenomenon by area. (3) Selection of the areas that show the higher probability of being emission centres. (4) Numerical simulation of the effects of an eruption of the corresponding eruptive style in those areas. The steps (1), (2) and (3) are based on the extensive knowledge of the eruptive activity of Tenerife Island and structural parameters. The results obtained from these three steps and the hazard map are implemented in a GIS and also used for the organisation of the surveillance network in terms of efficiency.

**Monday 26 July PM**

Presiding Chair: B Scott (GNA, CRI, New Zealand)

**JSP23/W/80-B1** 1400**STRESS CHANGES AT THE SOUTH ICELAND SEISMIC ZONE - A MODEL FROM 1706 UP TO THE PRESENT FOR BETTER HAZARD ESTIMATION**

Frank ROTH (Section "Earthquakes & Volcanism", Division "Solid Earth Physics and Disaster Research", GeoForschungsZentrum, Telegrafenberg, D-14473 Potsdam, Fed. Rep. of Germany, email: roth@gfz-potsdam.de)

The South Iceland Seismic Zone is situated between two sections of the mid-Atlantic ridge, i.e. the Reykjanes Ridge SW of Iceland and the Eastern Volcanic Zone on the island. It is a transform zone, though no typical one, as it is not connecting both rifts at right angles. Following this hypothesis, earthquakes should occur on EW-trending left-lateral shear faults, equivalent to conjugate, NS-oriented right-lateral, rupture planes. In fact earthquakes take place on NS-oriented faults, which are indicated by intensity and aftershock distributions, as well as by surface fault traces.

The stress field permanently generated in the fault zone by opening of the adjacent ridges with slightly more than 2 cm per year is computed and superimposed with the stress field changes induced by a series of 11 earthquakes (M >= 6) between 1706 and 1912. For these, different rupture depths are assumed, depending on the distance to the rifts. Finally, the post-seismic stress field of 1912 is extrapolated to the present, to see where highest stresses might have accumulated. In addition, the influence of loads at the Eastern Volcanic Zone on the stress field in the seismic area is studied.

The modelling shows that the stress is released by the series of events in the whole area, even though the ruptures planes are located on parallel NS-striking zones. The pre-seismic stress level for most events is high and pretty stable with the exception of situations when several strong shocks occur over a time span of several days, i.e. display typical main shock-aftershock patterns.

**JSP23/C/U5/W/03-B1** 1420**INITIAL STRUCTURES AND PACKING TRANSFORMATIONS OF LOESS DEPOSITS: IMPLICATIONS FOR THE ANALYSIS OF CATASTROPHIC MASS MOVEMENTS.**

Eleanor PARKER and Tom Dijkstra (Coventry University)

Gradual settlement from aeolian suspension means that loess particles generally form very open initial packing. There is less than 50% solids in a unit volume of soil - unless there is too much water or additional stress which will cause particles to settle in a much denser state. As long as the deposit remains relatively dry, cementation and other bond types will maintain the open structure; the loess is metastable. The potential of metastable loess to collapse is impressive. Rapid transformations from undisturbed packing with dry densities of about 1.3 Mg/m<sup>3</sup> (void ratio e ~ 1), to more closely packed 'deformed' fabrics with dry densities of about 1.65 Mg/m<sup>3</sup> (e = 0.65) after collapse. At failure, significant pore volume reductions (often more than 10%) result in considerable rapid increases in pore pressures (principally related to water pressures, but in loess air pressures are also important). Such pore pressures are necessary ingredients to produce very mobile mass movements, usually in the form of landslides. In situations where pore pressure dissipation is impaired, a lowering of the shearing resistance may last long enough to allow long run-outs and high sliding velocities. The study material is Chinese loess from Gansu province, but there are important parallels with similar collapsible deposits such as the brickearths of South East England.

**JSP23/C/U5/E/04-B1** 1440**EARTHQUAKES PREDICTABILITY: A CASE STUDY**

Valery KOREPANOV, Yevhen Klymovych and Pavlo Maltsev (Lviv Centre of Institute of Space Research, 5-A Naukova str., 290601, Lviv, Ukraine, e-mail: vakor@isr.lviv.ua); Masashi Hayakawa (Dept. of Electronic Engineering, University of Electro-Communications, 1-5-1 Chofugaoka, Chofu, Tokyo 182-8585, Japan, e-mail: hayakawa@whistler.ee.ucc.ac.jp); Katsumi Hattori (International Frontier Program on Earthquake Research, Institute of Physical and Chemical Research (RIKEN), c/o Earthquake Prediction Research Center, Tokai University, 3-20-1, Orido, Shimizu 424, Japan, e-mail: hattori@iord.u-tokai.ac.jp); Victor Tregubenko (Kyiv Branch of Ukrainian Geology Research Institute, 78 Avtozavodska str., 252144 Kyiv, Ukraine, e-mail: direct@kgou.ru.kiev.ua)

It is accepted that large earthquakes (EQ) are accompanied by different electromagnetic phenomena. They are also found to precede the EQ and the most debatable question is whether they can be used as EQ precursors. Two of such positive examples for EQ with M; 4.5 are investigated: near Matsushiro (Japan) 01.07.1998 and near Crimea peninsula (Ukraine) 16.10.1998. In both cases three components of magnetic fluctuations only were studied: for Matsushiro in frequency band from 0.01 to 30 Hz and for Crimea the DC magnetic field was sampled once per 10 seconds. For Matsushiro EQ some preceding events were extracted: short spikes with some features deviating from noisy background and also about 50% overall growth of daily averaged amplitude of ELF emission. For Crimea EQ the variations of mean longitudinal conductivity of the crust were calculated. The resulting curves excellently suit the Scholtz dilatant-diffusional model: for 15 days averaged variations of the conductivity deflection from the mean value before earthquake was about 6% what was fairly beyond mean error ~ 1.2%. Still higher was the deflection for daily averaged variations: more than 25%. The peculiarities of the study and processing methodology are discussed.

**JSP23/C/U5/L/01-B1** 1500**MACRO SCALE MODELLING OF CATASTROPHIC NATURAL HAZARDS**

Adrian STEWART, and Dr Claire McQueen, (EQE International Ltd, 500 Longbarn Boulevard, Warrington, WA2 0XF, UK. Tel: +44 1925 838372, fax +44 121987 654, Email: astewart@eqe.co.uk, cmcqueen@eqe.co.uk.)

Economic losses from Natural disasters over the last few decades have been enormous, as demonstrated by Hurricane Andrew in the US. The impact on the Global economy can reverberate for years after a single event. Assessing the risk to regions and countries is essential in the context of enabling International Organisations, Governments a International Industry and Commerce to plan, mitigate and manage losses.

In terms of risk from damaging earthquake or windstorm events, the risk is a function of the hazard intensity combined with the vulnerability of the properties within any given unit or area. The deterministic results of such studies may also be combined With expected frequencies to obtain probabilistic estimates of risks. In order that the losses expected within an area from an event be estimated accurately, the vulnerability functions and hazard models should be representative of the scale of the area that they are located in. Scale is an important issue. The Hazard Model needs to reflect the reduced risks expected over larger areas. However, the detail needs to remain in order that the spatial resolution of the hazard across an area is accurately represented. The question is whether vulnerability and hazard models can be created for a specific scale, or whether it is possible to calculate losses on a detailed grid and aggregate consistently at any macro scale.

**JSP23/W/39-B1** 1520**SPACE PRECURSORS OF EARTHQUAKE REGISTERED BY SATELLITE AT GEOMAGNETICALLY CONJUGATED AREAS**

Yuri RUZHIN, Vera Larkina and Anna Depueva (IZMIRAN, Troitsk-town, Moscow Region, 142092, RUSSIA; email:ruzhin@izmiran.rssi.ru)

There is some progress in investigations of space plasma precursors of earthquake (EQ) - the magnetic conjugation of VLF pre-seismic emission on satellite orbits was found in both hemispheres. It means that some signature of precursor could be found inside the geomagnetic flux tube (shell) which connected with both conjugated ionosphere regions where the VLF precursors on satellite orbits were registered. Satellites INTERCOSMOS-18 and ALOUETTE data were analyzed from this point of view. Conjugated EQ-precursors are found in very low frequency (VLF) emission and ionosphere F2-layer plasma parameters. It should be pointed out that F2-precursors appears some days before the earthquake, manifest themselves as a plasma anomaly like Appleton anomaly if epicenter of future earthquake is situated near magnetic equator. It is shown that the electric field less than one mV/m have to be generated in the ionosphere. Then we'll be able to observe the above ionosphere phenomena as an equatorial earthquake forerunners. We are able to show that VLF precursors which appears some hours before the earthquake are localized close to magnetic shell corresponding to future earthquake epicenter and have a belt-like structure (longitude aligned on more than some tens thousands kilometers) in bot hemispheres. In the presented work relationship of VLF fields intensity and spectra with energetic electrons flux density are investigated over epicentral zone of the prone earthquake. On the base of our estimations and phenomenological development of the event in the ionosphere (plasmaphere) over the seismic region and over magnetically conjugated region the possibilities of the seismoionospheric anomalies (space precursors of EQ) generation are discussed.

**JSP23/C/U5/W/10-B1** 1600**THE CENTRAL POSITION OF GEOPHYSICS FOR THE EVALUATION OF THE NEAR-FUTURE AND ESPECIALLY THE DISTANT FUTURE**

Nils-Axel MÖRNER, (Paleogeophysics & Geodynamics, S-10691 Stockholm, Sweden, email: morner@pog.su.se)

Geophysics and its paleogeophysical expressions over past periods will always play a central role for all types of predictions and estimations of the future. This applies for the near-future and its evaluation based on our understanding of the natural variability in environmental parameters on a decadal-to-century time scale, and its interaction with induced anthropogenic factors. On the 104-105 year time scale, the selestrial mechanical calculation of the so-called Milankovitch variables form a strong basis in climate prediction. Distant predications and evaluations are, in general, neither simple nor straight-forward. Still, there is a desperate need for safety predictions over 104-106 year time scale when it concerns the long-term stability and safety of high-level nuclear waste repositories. This has added a completely new dimension to geophysics. For a "safe" final bedrock deposition of high-level nuclear waste, we need guarantees for the immense time period of "hundreds of thousands of years". No one can, of course, give meaningful guarantees over such long time periods. The Fennoscandian crystalline bedrock is, by no means, as stable and reliable as sometimes claimed. Only some 10,000 years back in time, the seismic activity was (as a function of the extreme rates of glacial isostatic uplift amounting as much as some 10 cm per year) tremendously high; in amplitude



as well as in frequency. In such an environment – to be repeated at the next future ice age – we can, of course, give no guarantees for a waste disposal in the bedrock; on the contrary, most facts suggest that it would be seriously damaged. In the absence of a true long-term safety, we can only propose that the waste produced: (1) is kept at a minimum, (2) is stored under constant control, and (3) is kept accessible for reparations as well as possible future innovations of how to render the waste harmless.

**JSP23/E/14-B1****1620****LONG-TERM HAZARD FROM RIVER-BED AGGRADATION FOLLOWING VOLCANIC ERUPTIONS**

Thomas C. PIERSON (U.S. Geological Survey, Cascades Volcano Observatory, 5400 MacArthur Blvd., Vancouver, WA 98661, USA, email: tpierson@usgs.gov)

Explosive volcanic eruptions can provide immense volumes of readily erodible volcanoclastic sediment to drainage basins on or near source volcanoes. Post-eruption rainfall, or other types of rapid runoff, mobilizes sediment from hillslopes or from source deposits in upper valleys, episodically moving it downstream during periods of high discharge (probably as long, slow-moving sediment waves). Depending on the volume of sediment added to a fluvial system, this sediment mobilization can result in dramatic and hazardous vertical aggradation of river beds. Data from recent historical eruptions at Mount Pinatubo (Philippines), Mount St. Helens (USA), and other volcanoes demonstrate that river-bed aggradation can occur rapidly (at varying rates as high as 0.4 m/day) in channels up to hundreds of meters wide over extensive downstream reaches in the first year or two following an eruption. Although periods of aggradation may be interrupted by irregular periods of degradation (channel downcutting), river-bed elevations may show net rises of as much as 20 to 30 m within only a matter of months within 50 km of source, and net aggradation of at least 8 m has been documented as far as 280 km from source. Under these conditions, floods and lahars need not have extraordinarily high discharges to be able to reach and inundate previously safe homes, roads, and farmland.

Aggradation may continue for decades before sediment supply from the disturbed areas decreases enough to allow rivers to incise back down to previous bed levels. Tree-ring data from terraces along the Sandy River, 80 km downstream from Mount Hood (USA) indicate that significant re-incision (about 8 m or nearly 50 percent) occurred within about 40 years of the ~200 yBP eruption of Mount Hood, and the river nearly regained its original bed level within about 60 years. Efforts to mitigate river-bed aggradation hazards, such as has been done at Mount St. Helens, should be planned with knowledge of this potentially long-term impact on fluvial systems.

**JSP23/C/U5/W/17-B1****1640****A SEA LEVEL-WAVE JOINT DISTRIBUTION FOR SEVERE STORM SURGE HAZARD ASSESSMENT USING OFFSHORE PLATFORM DATA**

Le KENTANG (Institute of Oceanology, Chinese Academy of Sciences, Qingdao 266071, PRC, email: ktle@ms.qdio.ac.cn)

Generally speaking, the direct economic losses from a severe storm surge disaster consist mainly of that from sea water flooded over land and that from damage caused by high sea. However, the traditional method for storm surge hazard assessment in China is to construct one or two single-parameter distributions by using historical sea level and/or wave data at some coastal stations and/or ocean stations. In this case, apparently, both sea level data and wave data at these stations must be long enough to estimate the return periods needed for mitigation. However, the existing data of sea levels and waves at most of these stations can't meet the needs of the estimation. In this paper we present a method to construct the sea level-wave joint distribution for severe storm surge hazard assessment by using a couple of years data on such a stations. Using a one-year platform data in the Bohai Sea, an example is given to illustrate the capabilities of this methodology.

**JSP23/C/U5/E/08-B1****1700****STATISTICAL METHODS FOR SLUSHFLOW SITUATIONS RECOGNITION, MONITORING AND FORECASTING**

Pavel CHERNOUSS and Olga Tyapkina (Center of Avalanche Safety, "Apatit" JSC, 33a, 50 years of October St., Kirovsk, Murmansk region 184230, Russia, e-mail: P.Chernous@apatit.murmansk.su); Erik Hestnes and Steinar Bakkehoi (both at Norwegian Geotechnical Institute, P.O. Box 3930 Ullevål Hageby, N-0806, Norway, e-mail: eh@ngi.no)

Slushflows - flowing mixtures of water and snow - are a hazardous phenomenon in mountainous regions all over the world. They are most frequent in higher latitudes, i.e. in Norway, Iceland, USA (Alaska), Canada and Russia (northern and eastern parts). Slushflows exert high destructive forces and they are almost unpredictable due to inadequate studies. The work is an attempt to classify meteorological situations at different heights above sea level on "slushflow" and "non-slushflow" with linear discriminant analysis and Bayes' formula. Standard meteorological observations were used as primary parameters to describe the situations. Classification was made on daily base. Data for the mountain regions of Norway and the Khibini Mountains in Russia were taken to derive the classification rules and to carry out a verification of the methods. Different sets of parameters were tried to find out most informative ones. Two parameters have been chosen - daily water income (designed parameter) and snow cover thickness. Classification accuracy, obtained with independent data, was better than 75% for both types of the situations. For more detail slushflow danger monitoring one day moving average values are used. There are two ways to transform the diagnostic methods into forecast ones - by using of forecasted parameters as predictors or by extrapolation of situation probabilities. The methods are an effective tool for slushflow forecaster and realized as software package for the real-time work at the Center of Avalanche Safety of "Apatit" JSC.

**JSP23/W/23-B1****1720****PRESEISMIC ELECTROMAGNETIC SIGNALS GENERATED IN ATMOSPHERE**

Yuri Ruzhin (IZMIRAN, Moscow, 142092, RUSSIA; E-mail: ruzhin@izmiran.rssi.ru); Costas Nomicos (Technological Educational Institute of Athens, GREECE); Filippos Vallianatos (Technological Educational Institute Chania branch, Crete, GREECE)

Electromagnetic (EM) precursors of Earthquakes (EQ's) are modern possibility to monitor pre-earthquake situation and to improve the EQ forecast. Its nature up to now is under the question. The EM signals registered (before the EQ) onboard of satellites is the object of intensively investigations during last decade. Here we overview of EM seismo precursors and present situation with its explanation but the high frequency (HF) precursor (43MHz and 51MHz) is main point of our presentation. It is showed that precursor type HF signals are appeared before the EQ for one-three days and the some new peculiarity is found. This is under horizon epicenter position for main part of events under question. It means that emitted volume must be located at some altitude in atmosphere or ionosphere. The another unusual result is that such pre-seismic signals are responsible for seaquakes (not, as usually, for the

earthquakes!). In result, we made conclusion about existing of some thunderstorm type activity above the sea level before the seismic event. It means that above sea level (up to 3-8 kilometers) the space charge cloud would be generated at one-three days before the active seismicity (under sea floor). Based on above mentioned we can supposed that probably this is new pre-seismic signature which will be used in future EQ forecast. Some additional experimental facts and mechanisms are discussed to explain this HF precursor (EM signals) generation above the epicenter of future seismic activity.

**JSP23/W/87-B1****1740****SIMULATION OF THE DARWIN OBSERVATION OF THE 1835 CHILEAN EARTHQUAKE**

GALIEV

Abstract not available at the time of going to press

**Tuesday 27 July AM**

Presiding Chair: Chen Yong (Seismological Bureau, CHINA)  
Concurrent Poster Session

**DETECTION, MONITORING, EARLY WARNING AND PREDICTION****JSP23/E/18-B2****0930****MONITORING THE CURRENT SUMMIT ERUPTION OF MOUNT ETNA USING INFRARED SATELLITE DATA FROM THE ERS ATSR-2**

Rob WRIGHT, David Rothery, Stephen Blake (Department of Earth Sciences, The Open University, Milton Keynes MK7 6AA, UK, email: r.wright@open.ac.uk); Martin Wooster (Department of Geography, King's College London, Strand, London, WC2R 2LS, UK)

After the unusually quiet period that followed the end of the 1991 to 1993 eruptions, magmatic activity resumed within Etna's summit crater complex in July 1995. All four summit craters have been characterised by strombolian activity while between July 1997 and July 1998 the South East crater was also the site of sustained lava effusion. Intense paroxysmal explosions have also occurred intermittently from the North East crater and La Voragine.

In March 1998, at the request of the Italian Civil Protection Authority, the European Space Agency commissioned the "Empedocles" project. This aim's to assess the role that satellite remote sensing can play in monitoring the volcano, and understanding the nature and future evolution of the current activity. Using data acquired by the ERS-2 along Track Scanning Radiometer (ATSR) we show how the amount of short-wave infrared radiance emitted from the summit crater complex has fluctuated since July 1996. The data reveal patterns that correlate well (on a weekly time scale - ATSR acquires data - every 3 days) with Etna's general level of activity as documented in field reports. Examining the amount of radiation emitted at different wavelengths allows us to distinguish activity associated with high temperature vents from that associated with lava flows. By applying rank order statistics to the ATSR data-set we have inferred changes in the level of activity on Etna that may reflect changes in the eruptive state of the volcano.

**JSP23/C/U5/W/07-B2****0950****THE SPACE VOLCANO OBSERVATORY (SVO) PROJECT**

Pierre BRIOLE (Institut de Physique du Globe, 4 Place Jussieu, F-75005 Paris, email: briole@ipgp.jussieu.fr) and the SVO science team

1500 volcanoes on the earth are potentially active. One third of them have been active during this century and about 70 are presently erupting. At the beginning of the third millennium, 10% of the world population will be living in areas directly threatened by volcanoes. Presently, in spite of the efforts of many countries, only a few volcanoes are monitored by modern observatories. Even in the best equipped of them, real-time data acquisition on the active parts of the edifices during crisis is an extremely difficult and risky task. The only way to provide global, continuous, real-time and all-weather information on volcanoes is to combine observations from space and from the ground. Spaceborne observations (with satellites, helicopters, drones, balloons,...) are mandatory and complement the ground ones that can be implemented on a limited set of volcanoes. A project called SVO (Space Volcano Observatory) has been proposed to the European Space Agency to remotely monitor the deformations and thermal changes of the highest active areas of the volcanoes (lava lakes, lava domes, lava flows, eruptive vents...). These zones are unstable and often deform significantly prior to paroxysmal events (sudden collapses, flank pyroclastic flows, ...). They are also remote and dangerous and cannot be easily equipped with ground equipment. We propose to map at high resolution (1.5m pixel size) the topography and the thermal changes (for pixels above ~ 450°C) of active volcanic areas with a return time of one to three days and an image size of 6 x 6km. Those variations will put constraints on the physical and dynamic processes of the system. Other applications like landslide monitoring, will be possible. The requirement of fast data processing and interpretation imply the set up of several ground-based stations for data collection. The 12-15 major volcanological observatories of the world could host those receiving stations.

**JSP23/E/42-B2****1010****VOLCANIC RISK AND EMERGENCY PLANS OF THE NEAPOLITAN VOLCANOES**

Lucia CIVETTA (Co-ordinator of the technical committee for preparation of the emergency plans Osservatorio Vesuviano, via Manzoni, 249, 80123 Naples, Italy e-mail: civetta@osve.unina.it)

The volcanoes of the Neapolitan area, Vesuvius, Campi Flegrei and Ischia, have generated more than 100 explosive eruptions in the past 10 ka. However, they can lie dormant for many centuries and the great risk posed by volcanic activity in the region was, therefore, not always apparent. Vesuvius has exhibited various types of activity in the past 25 ka. Plinian and subplinian explosive eruptions occurred every few millennia or few centuries, respectively. Strombolian activity, lava effusions and phreatomagmatic eruptions usually follow the plinian and subplinian eruptions until conduit closes. Since the last eruption of 1944, Vesuvius has not shown signs of unrest. Only moderate seismicity and fumarolic emission testify the current state of activity of the volcano. The Vesuvius eruptive history however suggests that the longer is the quiescent period, the more violent is the renewal of the activity. The last eruption of the Campi Flegrei caldera occurred in 1538 AD, at the north-western edge of the La Starza resurgent block. Since that time, after hundreds of years of subsidence, two bradyseismic events occurred in 1969-70 and 1982-84, which totalled a net vertical uplift of 350 cm of the central caldera block, at the harbour of Pozzuoli. The last eruption of Ischia occurred in 1302 AD, at the edge of the resurgent Mt. Epomeo block. Since that time intense fumarolic activity, hot springs and seismicity characterise the island current state. Intense urbanisation and inadequate planning of the Neapolitan territory have significantly contributed to the increment of the volcanic risk since the fifties. In response to the increasing volcanic risk, in 1993 the



## INTER-ASSOCIATION

Minister for Civil Defence appointed a commission to prepare the emergency plan of the Vesuvius area that was completed at the end of 1995. In 1996 the Minister of Civil Defence appointed a new Commission to update the emergency plan of Vesuvius and prepare the scenario of the expected eruption at the Campi Flegrei Caldera and define the guidelines for the Campi Flegrei emergency plan.

**JSP23/E/26-B2**

**1050**

### VOLCANIC HAZARD MAPS OF TENERIFE ISLAND (CANARY ISLANDS)

Alicia FELPETO, Vicente Araña (Dep. Volcanology, Museo Nal. Ciencias Naturales, CSIC, J. Gutiérrez Abascal, 2, 28006 Madrid, Spain, email: mcnaf66@pinar1.csic.es); Mar Astiz (Dep. Matematica Aplicada, E.T.S.A. Universidad Politécnica, Avda. Juan de Herrera 4, 28040 Madrid, Spain); Francisca Gómez (Centro de Estudio per la Geologia Structural e Dinamica dell'Apennino, CNR, via Santa Maria, Pisa, Italy); Alicia García, Ramón Ortiz (Dep. Volcanology, Museo Nal. Ciencias Naturales, CSIC, J. Gutiérrez Abascal 2, 28006 Madrid, Spain)

The first steps for the generation of volcanic hazard maps of Tenerife consists of the definition of the most significant hazards and the selection of the most suitable areas for containing emission centres, taking into account all the data of the eruptive history of the island. Then, for the evaluation of the effects of an eruption, a numerical model for each hazard has been chosen. The application of the different models allows the computation of the probability of each point of the island being affected by each type of eruption, and so, building up the volcanic hazard maps. The methodology proposed, integrated on a GIS framework, allows the automation of the generation of hazard maps for more specific studies of smaller areas of the island or specific risk scenarios. It also represents the starting point for developing risk maps.

**JSP23/C/U5/E/20-B2**

**1110**

### MAPPING AND MONITORING OF VOLCANOES USING SPACE-BORNE SAR

Woolil M. MOON, Lanying Feng and (Geophysics, The University of Manitoba, Winnipeg, Canada R3T 2N2 (email: lfeng@gis.geop.umanitoba.ca, wmoon@cc.umanitoba.ca); DUK-JIN-KIM, K.H. Choi, C.W. Lee and Woolil M. MOON (Earth System Science, Seoul National University (email: wmoon@eos1.snu.ac.kr, djkim@eos1.snu.ac.kr); J. L. Lizca (SERGEOMIN, La Paz, Bolivia ("Jose Luseca" email: abtema@coord.rds.org.bo

In this study, we have investigated several active volcanic areas (Baiktu-san (China-Korea border), Cerro Caquella (Bolivia), and Halla-san (South Korea)) using RADARSAT and JERS-1 SAR data for their geological characteristics and for their application criteria in view of natural hazard monitoring. Baikтусан is located at the junction of northeastern edge of Huabai tectonic block of the Eurasian continent and mid-Cenozoic off-shore Pacific volcanic zone, and have gone through several stages of crustal evolution. According to historical records, Baikтусан had a major eruption in 1002 AD, and several minor eruptions in 16th and 18th century. However, the strategic location of Baikтусан at the political boundary between P. R. China and North Korea, has resulted in a situation with rather poorly surveyed geology maps and inconsistent geological interpretation of recent volcanic activities. The Halla-san volcano has not been active during the historical time, but it is the main feature of the Jeju Island (a volcanic island), which has recently been rapidly developed for increasing human settlement. In the Cerro Caquella region, which is a remote barren Andean range, a detailed DEM could be extracted to investigate morphological changes associated with active volcanic activities, in addition to correlation of the DEM with respect to several other geological and geophysical data collected over the study area. Several sets of JERS-1 SAR and RADARSAT data are acquired for this study with the objectives of investigating the surface geology of Baiktu-san and Halla-san volcanoes and the surrounding area to delineate consistent geological and volcanic characteristics. Both traditional geological remote sensing approach and the space-borne InSAR (SAR interferometry) approach were used (i) for structural geological interpretation of the study area using the pre-processed SAR data, and (ii) for correlation of the interferogram fringe pattern...

**JSP23/C/U5/W/02-B2**

**1130**

### THE MONTSERRAT VOLCANIC ALERT AND WARNING SYSTEM

Lloyd L. LYNCH (Seismic Research Unit, University of the West Indies, St. Augustine, Trinidad W.I., email: sru@wow.net)

From the onset of the Soufriere Hills volcano eruption on July 18, 1995, to the waning stages of the eruption almost three years later most areas of the more developed half of the island of Montserrat faced the threat of devastation. The relatively small size of the island, its complex political and governance structure, and the demographic setting in relationship to the threatening volcano were factors which all combined to make the management of the crisis one of the most challenging of the twentieth century. Compounding matters, was the fact that the eruption followed a style for which there was no well-documented precedent. As in most volcanic crises, an alert and warning system was instituted primarily to facilitate risk and emergency management. The system employed was an adoption of the generic alert and warning system popularised by the UN Volcanic Emergency Handbook. In this article the Montserrat volcano alert and warning system is modelled as network of closely interrelated functional entities comprising of a management subsystem, a detection subsystem and a response subsystem. This provides a comprehensive abstraction of the functions and interaction between the administrative authorities, scientists and the public during the eruption. With aid of this model a detailed analysis of the strengths and shortcomings of the system is performed and presented. Attempt is also made to document the major changes within the subsystems during the crisis. There were several. Among the most remarkable were the many changes in the management personnel such as chief minister, governor and chief scientists. Throughout the crisis key institutions such as the Montserrat Volcano Observatory and the Emergency Operation Center also endured constant evolution. Operational and decision-making policies and procedures within these institutions encountered numerous revisions. Generally, these changes were intended to facilitate the tacit objective of local authorities to maximise life safety while retaining a sustainable level of functionality on the island. In the absence of...

**JSP23/W/24-B2**

**1150**

### A DEVELOPING VOLCANIC CRISIS IN DOMINICA, LESSER ANTILLES

John B. SHEPHERD, Lloyd L. Lynch, Mark Stasiuk, Joan L. Latchman (Seismic Research Unit, UWI, St. Augustine, Trinidad, e-mail: johnshepherd@hotmail.com); Joseph M. Devine (Brown University, Providence, R.I. USA)

The island of Dominica is in the centre of the volcanically active Lesser Antilles island arc. The island is approximately 35 km long by 12 km wide and is composed entirely of Pleistocene to recent volcanoes. Earthquake swarms have been reported from Dominica since it was first settled by Europeans. These originate in all parts of the island but are most common in the southwestern part of the island where there are at least three volcanic vents which have

erupted in the last few thousand years.

The most recent swarm began in September 1998 and is continuing. By January 10 1999 over 1,000 shallow volcanic earthquakes had been recorded by a nine-station digitally recording short period seismograph network. Over 300 earthquakes had been felt in the southwestern part of Dominica causing significant damage. Epicentres were initially located close to Morne Plat Pays volcano but during the swarm have spread to the most of the southwestern region. Focal depth are in the range 1-5 km and are becoming shallower as the swarm progresses. GPS measurements have detected widespread inflation of the epicentral region. An extensive programme of geological mapping is in progress and a response plan has been developed by the civil authorities.

**JSP23/C/U5/W/14-B2**

**1210**

### THE SEISMIC ALERT SYSTEM IN MEXICO CITY AND THE SCHOOL PREVENTION PROGRAM

ESPINOSA ARANDA J M, A Jimenez, G Ibarrola, F Alcantar, A Aguilar, M Inostroza, S Maldonado Director, (Centro de Instrumentacion y Registro Sismico, A.C. Anaxagoras #814, C.P. 03020, Mexico, D.F. E-mail: cires@cires.org.mx Home page: <http://www.cires.org.mx>; ); R Higareda (Director, Direccion de Emergencia Escolar Subsecretaria de Servicios Educativos del Distrito Federal Secretaria de Educacion Publica Callejon de Torresco #12, C.P. 04010, Mexico, D.F. E-mail: rhigareda@yahoo.com)

The Seismic Alert System (SAS) is a public service developed with the sponsorship of the City Government Authorities, with the aim to mitigate seismic disasters. Since August, 1991, after 88 months of continuous operation, the SAS has been capable to detect 714 seismic events in the Guerrero Coast; 12 of them so strong to trigger general alerts in Mexico City, 34 restricted, and one false general alert. The warning ranges strong or restricted correspond to seismic magnitude forecasted great than 6, or great than 5. During the "Copala" M7.3 earthquake, in September 14, 1995 the SAS was activated and issued a general warning signal in Mexico City, 72 seconds prior to the "S" ground motion first arrivals. This earthquake warning reached an estimated population of more than 4 million citizens. The response of children in schools was massive because of the application of an earthquake hazard reduction program. The Copala earthquake helped us to identify the societal response strengths and weaknesses to the earthquake early warning signal. The long-term plan of hazard mitigation of the National Ministry of Public Education, Secretaria de Educacion Publica (SEP), has created awareness to earthquakes in the children that have assisted in these years to various school levels. Even though they did not suffer the disastrous consequences of the 1985 earthquake, they are more aware than the average people that lived through that disastrous event, who still are not trained.

**Tuesday 27 July PM**

Presiding Chair: J M Espinosa-Aranda  
(Centro de instrumentacion y Registro Sismico, Mexico)

**JSP23/W/12-B2**

**1400**

### SEASONAL WARNING FOR CLIMATIC HAZARDS: PROSPECTS AND RESPONSES

T.DOWNING (Environmental Change Unit, 1A Mansfield Road, Oxford, OX1 3TB, Email: tom.downing@ecu.ox.ac.uk)

With climate change, there is increasing concern that climatic hazards will become more frequent and more severe. One of the most promising developments is seasonal climate forecasts. Already forecasts are operational in many parts of the tropics and sub-tropics, and particularly for droughts and floods associated with ENSO events. Prospects for further development of seasonal forecasting for a range of climatic hazards are reviewed, illustrated with case studies in Africa and Europe. A critical evaluation of the utility of seasonal forecasts centres on vulnerability, communication channels, and effective responses. In contrast to short-term prediction, seasonal forecasts raise new issues of preparedness and the use of information.

**JSP23/E/10-B2**

**1420**

### CHANCES FOR A LONG TIME FORECAST OF SEVERE STORM EVENTS IN WESTERN EUROPE WITH RESEPT TO THE NORTH ATLANTIC OSCILLATION

Mattius KLAWA, Uwe Ulbrich and Johannes Wefers (Institut fuer Geophysik und Meteorologie, Kerpener Str. 13, 50923 Koeln, Germany, e-mail: mklawa@meteo.uni-koeln.de, phone: 49 (0)221/470-3689)

The North Atlantic Oscillation is the dominant variability pattern in sea level pressure over the North Atlantic. Spectral analyses of the variations of this pattern show peaks on seasonal, yearly or decadal time scales. Also research proved influence of the NAO on the North Atlantic Stormtracks and on the European climate e.g. rainfall rates, winter temperatures in western Europe. In this presentation extreme storm events in western Europe are evaluated with respect to the NAO. Probabilities for extreme storm events on time scales of 5-10 years dependent on the NAO are estimated. In combination with daily weather regimes (since 1881) the long time series of the NAO pattern (since 1865) is used for a more detailed analyses on European weather events. In a first step damaging storms named by reinsurance companies and meteorological extreme events are compared. Weather regimes associated with these events are used for a description for the atmospheric circulation over Europe and to find out common features of periods around storm events. In a final step the probabilities for storm events are evaluated and interpreted.

**JSP23/E/29-B2**

**1440**

### FRACTURE CRITICALITY: A NEW CRITERIA FOR MONITORING THE ONSET OF EARTHQUAKES AND FRACTURING

Stuart CRAMPIN (Department of Geology & Geophysics, University of Edinburgh, Edinburgh EH9 3JW, UK; email: [scrampin@ed.ac.uk](mailto:scrampin@ed.ac.uk))

Seismic shear-wave splitting, diagnostic of distributions of stress-aligned fluid-saturated grain-boundary cracks and low aspect-ratio pores is seen with very similar characteristics in almost all igneous, metamorphic, and sedimentary rocks with a few well-understood exceptions. There is a minimum shear-wave velocity anisotropy of about 1.5% and a maximum of about 4.5% in intact un-fractured rock below about 1km in the crust. Theory and both field and laboratory observations suggest that this maximum value is close to the level of fracture criticality, associated with the percolation threshold, where rocks are so heavily fractured that shear-strength is lost, through-going fractures propagate, pore-fluids disperse, and earthquakes and fracturing occur. The evolution of such fluid-saturated rock can be modelled with anisotropic poro-elasticity (APE), where the driving mechanism is fluid migration by flow or diffusion along pressure gradient between neighbouring grain-boundary cracks and pores at different orientations to the stress field. APE shows that shear-wave splitting is controlled by the same parameters as control pre-fracturing deformation so that shear-wave splitting can be used to monitor directly the approach of fracture criticality before earthquakes or other failures

by fracturing. The high seismicity of SW Iceland and the extensive SIL seismic network now allow changes in shear-wave splitting before earthquakes to be observed routinely with hindsight. A real-time "stress-forecast" in a narrow magnitude/time window was made with forecasts 17, 15, and 3 days before a M=5 earthquake on 13 November 1998. The key feature is monitoring the increase of stress in the relatively-undisturbed rockmass away from the complications of the earthquake source, and estimating the time at which induced cracking reaches the level of fracture criticality. By monitoring the build-up of stress, such stress-forecasts can give (potentially reliable) estimates of time and magnitude of future earthquakes but cannot give estimates of location. However, forecasts may well stimulate local studies, as was the case in Iceland, where investigations by the Icelandic Meteorological Office correctly identified the rupturing fault.

**JSP23/W/01-B2****1500****THE COASTAL OCEAN MONITORING AND PREDICTION SYSTEM FOR WEST FLORIDA**

MARK E. LUTHER, David Burwell, Meredith Haines, Nan Schmidt, Mark Vincent, Robert Weisberg, and Huijun Yang (University of South Florida Department of Marine Science, 140 Seventh Avenue South, St. Petersburg, FL 33701; Tel: 727/553-1528; Fax: 727/553-1189; E-mail: luther@marine.usf.edu)

Florida is the United States' fourth most populous state, with 80% of the population living in a coastal county. Several recent storms have brought large, unpredicted flooding to Florida's west coast. The coastal sea level response to tropical and extra-tropical storms results from wind forcing over the entire continental shelf. Much of the local response may actually be due to storm winds quite distant from the local area of concern; a case in point being tropical storm Josephine, a modest storm that nevertheless caused extensive flooding in the Tampa Bay area. The University of South Florida is implementing a real-time Coastal Ocean Monitoring and Prediction System (COMPS) for West Florida that will provide additional data needed to give more accurate predictions of ocean storms and coastal flooding by storm surge. This system consists of an array of instrumentation both along the coast and offshore combined with numerical circulation models and builds upon existing in-situ measurements and modelling programs funded by various state and federal agencies. This observing system fulfills all of the requirements of the Coastal Module of the Global Ocean Observing System (CMGOOS). Data and model products are disseminated in real-time to federal, state, and local emergency management officials via the internet (URL <http://comps.marine.usf.edu>).

**JSP23/W/03-B2****1520****EARTHQUAKE PREDICTION AND EARTHQUAKE PREPAREDNESS: CURRENT POSSIBILITIES FOR THE PACIFIC RIM**

Vladimir KOSSOBOKOV, Vladimir Keilis-Borok, (International Institute for Earthquake Prediction Theory and Mathematical Geophysics, Russian Academy of Sciences, 79-2 Warshavskoye Shosse, Moscow 113556, Russia, E-mail: volodya@mitp.ru); John Healy (USGS, Menlo Park, CA 94025, USA, E-mail: jhhealy@aol.com); Donald Turcotte (Department of Geological Sciences Cornell University, Ithaca, NY 14853-1504, USA, E-mail: Turcotte@Geology.Cornell.edu)

The recent results of real-time testing in the Pacific Rim, 1992-1998, have established the high statistical significance of intermediate-term predictions of the largest earthquakes by algorithms M8 and MSc. Among predicted are all earthquakes of magnitude 8 or greater. Predictions are completely reproducible and use precursory activation of seismic static at different space and time ranges to reduce consecutively time and space where disastrous earthquake has to be expected. Although the predictions are of limited accuracy they do create a possibility to prevent part of the damage. This encourages a multi-scale approach to mitigate earthquake disaster. In general, earthquake predictions range from a zero-approximation of seismic zoning through long- and intermediate- to short-term ones. Accordingly, the preparedness measures range from building code, to simulation alarms and reinforcement of high-risk facilities, to the imminent "red alert" (e.g. evacuation of population and introduction of martial law). Different time from decades to seconds is required to undertake different measures; having different cost, they can be realistically maintained during different time periods and in the territories of different size. The key to damage reduction in the area of concern is escalation or de-escalation of preparedness measures depending on the current state of alert. That is the standard practice for mitigation of other major disasters, wars included. The interface between prediction and preparedness is delivered by the recent development of optimal strategies based on a trade-off between total volume of alert and rate of failures-to-predict. We demonstrate case histories of intermediate-term predictions that would have led to preventing a considerable part of losses by low-key safety measures.

**JSP23/E/06-B2****1600****SANARIS PROJECT: A SATELLITE NETWORK FOR NATURAL RISKS MONITORING**

Marta TARRAGA (Dept. Volcanologia, Museo Nacional de Ciencias Naturales, Jose Gutierrez Abascal 2, 28006 Madrid, Spain, email: mcnt184@mncn.csic.es); Alicia Garcia, Ramon Ortiz, Rafael Abella and Javier Peña (Dept. Volcanologia, Museo Nacional de Ciencias Naturales, Jose Gutierrez Abascal 2, 28006 Madrid, Spain, email: mcnp182@mncn.csic.es)

A new satellite communication system specifically designed for low-rate data applications has been developed and prototyped. A validation project is proposed to install a pilot network to be operated during 6 months. One of the target markets related to volcanoes has been selected, so a group of users is integrated in the project. A specific application for this market will be developed regarding data acquisition, processing, storage and dissemination to distant users. The feasibility of using the new satellite system to provide a new Eutelsat service for low-rate data applications will be evaluated from the pilot network performance. According to the Department of Volcanology (M.N.C.N.-C.S.I.C.) experience on the development of systems for volcano monitoring, its role in the project will be: -Co-ordinate the definition of users requirements for the pilot application. Installation of the digital seismic stations. -Maintenance of Teide and/or Timanfaya stations (Canary Islands).

**JSP23/C/U5/E/06-B2****1620****EFFECTIVE EARTHQUAKE MONITORING PROCESS FOR EMERGENCY RESPONSE ON RESCUES (EMPEROR)**

Yutaka NAKAMURA (System and Data Research Co. Ltd., SDR Bldg., 3-25-3 Fujimidai, Kunitachi-shi, Tokyo, 186-0003, JAPAN, E-mail: yutaka@sdr.co.jp)

It has been widely recognised that systematical and continuous monitoring of earthquakes is necessary for the early warning. In this presentation an effective earthquake monitoring process is proposed. DI, Damage Intensity of seismic motion, is defined as an inner product of acceleration vector and velocity vector at each time step dt. The multiplication of DI with mass received seismic motion, indicate the power of the motion act to the object. DI-value, defined as maximum of DI, is generally appeared after S-wave arrival. When P wave arrives, DI increases drastically, and after S wave arrival DI reaches to its maximum value, DI-value,

soon. P wave Index, PI-value, is defined as maximum DI of P wave part. This value is suggested to be used for P wave alarm. DI-value is related with seismic intensity. DI-value has a very important practical advantage, since it can be calculated in real-time soon after the P wave arrives. Additionally, DI-value has a clear physical meaning and it is strongly related with the earthquake damage. This can be concluded as, with the continuous observation of DI, earthquake alarm can be issued efficiently and damage can be estimated precisely. According to combination of S wave and P wave alarms, early and/or reliable alarm is realised. P wave alarms can be issued when PI-value over the pre-set level, and S wave alarm can be issued when ordinary monitored values or DI-value exceed pre-set level. Combining PI, DI values together with K values is promising for the future early warning systems, since it has been clarified with both methods that it is possible to estimate the vulnerabilities of all ground and structures concerned and it is possible to issue the alarm before the real damage occurs.

**JSP23/W/06-B2****1640****HIGH RESOLUTION AEROMAGNETIC SURVEY FOR CONCEALED FAULTS IN THE FUKUI PLAIN, CENTRAL JAPAN**

Shigeo OKUMA, Masahiko Makino and Tadashi Nakatsuka (Geological Survey of Japan, 1-1-3 Higashi, Tsukuba, Ibaraki, 305-8567 Japan, email: okuma@gsj.go.jp)

Geological Survey of Japan (GSJ) has conducted a helicopter-borne high-resolution aeromagnetic survey in the Fukui Plain, Central Japan, to better understand concealed faults associated with the 1948 Fukui Earthquake (June 28, 1948, M=7.3) which brought disastrous damages to this area. The survey was flown along east-west flight lines at an altitude of 150 m above terrain and spaced 300 m apart with a Cesium Vapour magnetometer with a sensitivity of 0.01 nT at a sampling interval of 0.1 second and a differential GPS system. The compiled total intensity map of IGRF residuals shows interesting magnetic features as follows: 1) A broad magnetic high area occupies the western half of the plain with a sharp NNW-SSE trending boundary to the east, which corresponds well to the assumed location of the concealed Fukui Earthquake fault. 2) Three distinctive dipole magnetic anomalies lie in the magnetic high area, two of which lie at the northern edge of the area, implying the existence of intrusions associated with the Awara Hot Spring. 3) Magnetic lows are dominant along the coast line of the Sea of Japan and in its offshore areas, suggesting the existence of reversely magnetised volcanic rocks which lie offshore and maybe outcrop along the coast line.

**JSP23/E/27-B2****1700****LAND SUBSIDENCE OF JAKARTA (INDONESIA) AND ITS GEODETIC-BASED MONITORING SYSTEM**

Hasanuddin Z. ABIDIN, I. Meilano, M. A. Kusuma, J. Kahar (Department of Geodetic Engineering, Institute of Technology Bandung, Jl. Ganesha 10, Bandung, Indonesia, email: hzabidin@indo.net.id and hzabidin@gd.itb.ac.id); Rochman Djaja (National Coordinating Agency for Survey and Mapping, Cibinong, Bogor, Indonesia); Samsul Hadi (Jakarta Provincial Agency of Surveying and Mapping, Jakarta, Indonesia)

Jakarta is the capital city of Indonesia with population of about 12 million peoples, inhabiting the area of about 25-km by 25-km. It has been reported for quite sometimes that several places in Jakarta are subsiding at different rates from place to place. Up to the present times, however, there has been no definitive, detail, and comprehensive information about the characteristics and pattern of land subsidence in Jakarta areas. Usually the land subsidence in several places of Jakarta is estimated using their geological parameters or inferred from the ground water level observations. In order to give a better picture about these land subsidence phenomena in Jakarta, the geodetic-based land subsidence monitoring system has been implemented. The system is based on GPS and levelling measurements.

In this paper the land subsidence study in the city of Jakarta using repeated GPS and levelling surveys will be described and discussed. The land subsidence characteristics of Jakarta and its surrounding area are investigated using the data from three repeated GPS surveys conducted in 1994, 1997, and 1998 and four repeated levelling surveys performed in 1982, 1991, 1993, and 1997. The main goal of this land subsidence study is to understand the characteristics of land subsidence in Jakarta area and their generating forces and factors. Therefore, in this paper, the geological, geophysical, and hydrological aspects of Jakarta area would also be investigated and correlated with the geometrical changes information obtained from geodetic based systems. The paper would be sum up with some closing remarks.

**JSP23/W/38-B2****1720****INTERNATIONAL TECTONIC REAL TIME RADON OBSERVATION AND TRANSMISSION - RELIMINARY RESULTS OF GEODYNAMIC MONITORING**

G.SOBOLEV (United Institute of Physics of the Earth, RAS, Moscow, Russia, email: sobolev@uipe-ras.scgis.ru); S.Balassanian (National Survey for Seismic Protection, Yerevan, Armenia, email: presdint@nssp.yerphi.am); A.Belayev (Vernadsky Institute of geochemistry and analytical chemistry, RAS, Moscow, email: abelayev@chat.ru); S.Bushati (Center of Geophysical and Geochemical Exploration, Tirana, Albania, email: bushati@cgge.tirana.al); E.Lagios (Department of Geophysics and Geothermy, National & Kapodistrian University of Athens, Athens, Greece, email: elagios@atlas.uoa.gr); R.A.Nicholson (British Geological Survey, Keyworth, Nottinghamshire, NG125GG, United Kingdom, email: RAN@wpo.nerc.ac.uk); A.Ponomarev (United Institute of Physics of the Earth, Moscow, email: avp@uipe-ras.scgis.ru); A.Pronin (Geological-technological Scientific Industrial Enterprise "Geotechvims", Naro-Fominsk, Russia); G.Sideris, F.Zervos (GeoMentor, European Economic Interest Grouping, Athens, Greece, email: goemen@otenet.gr).

Seismic activity is a potential threat to populations and commerce throughout the world. Geophysical-geological research institutes and commercial companies in Greece, France and the UK are collaborating with similar organisations from Russia, Armenia and Albania, under the EU-funded Inco-Copernicus (Framework IV) programme, to develop new techniques for the automatic acquisition of gas geochemical data from remote sites using gas-sensing probes and telemetry. The data are being integrated with seismic information acquired in parallel, and used to determine whether or not the technique is a suitable method for monitoring ground disturbance associated with tectonic events. A number of data loggers (transducers/detectors) have already been installed since 1998 at specific locations (base stations) selected by the Project scientists in Caucasus (Southern Russia and Armenia), Greece, Albania and Scotland (UK). The seismic and gas-hydrogeochemical maps as the results of geophysical prospecting were used to select eligible sites for radon monitoring. Each base station includes two data loggers with the latest version of the Barasol MC radon probe incorporating sensors for barometric pressure and temperature combined with local rainfall measurements. These parameters are being transferred to attached cordless modems and are transmitted via INMARSAT global satellite communication system to Greece (Project co-ordinator) where all data are collected for joint processing. Signal processing software has been developed on the base of standard and original approaches. The spectral composition and structure parameters of obtained time series are determined by applying descriptive statistics, causal analysis and methods of the dynamic theory systems. The first stage realisation of Project indicates that telemetry systems are operating satisfactorily and the data are collecting, but that longer-term monitoring is necessary to link seismic measurements to radon exhalations and consider mentioned data acquisition-broadcasting system as real warning system.



**JSP23/C/U3/W/21-B2** **1740**

**DEVELOPMENT OF SEISMIC RAPID REPORTING AND EARLY WARNING SYSTEM IN TAIWAN**

Yih-Min WU, Jen-Kuang Chung, Tzay-Chyn Shin (Central Weather Bureau, 64 Kung Yuan Road, Taipei, Taiwan, email: ludan@sc2.cwb.gov.tw); Yi-Ben Tsai (Institute of Geophysics, National Central University, Chung-li, Taiwan); William H.K. Lee (862 Richardson Court, Palo Alto, CA 94303, USA)

In 1994, two prototype seismic early warning systems have been implemented in Taiwan: (1) a rapid reporting system using a tele-metered network of digital accelerographs spread over the entire island, and (2) an alert system exploring the use of modern technology for the highly seismic area of Hualien. After four-years operation, the rapid reporting system was successfully operated in the seismic monitoring system of the Central Weather Bureau (CWB) for felt earthquake observation (Taiwan Rapid Earthquake Information Release System, TREIRS). It has achieved in the determined of precise earthquake location and magnitude computation about in one minute after the earthquake origin times. On the other hand, the Hualien alert system was phased out in 1998 due to large uncertainty of source parameter determination caused by small station coverage and only using P signal in determining the magnitude. Although it performed a very well reporting time (less than 10s after the earthquake origin time). Recently, the Hualien alert system stations were equipped with the digital accelerograph and combined to the TREIRS system. By adding the Hualien alert system stations to the TREIRS system, we have obtained a good precision for source parameter determination and a well reporting time for Hualien area earthquake monitoring. During the experiment in the past several years, we benefited from these two prototype seismic early warning systems and optimised the TREIRS system. We are encouraged forwards in the development of seismic early warning system based on the successful experience

Friday 23 July AM

**HAZARD AND RISK ASSESSMENT, RISK MITIGATION AND MANAGEMENT**

**JSP23/W/30-A5** **Poster** **0830-01**

**MISLEADING SIGNALS IN HAZARD CATALOGS**

Allen M. HITTELMAN (NOAA's National Geophysical Data Center (NGDC), World Data Center-A (WDC-A for Solid Earth Geophysics, 325 Broadway, Boulder, CO 80303, U. S. A., email: ahittelman@ngdc.noaa.gov); Lowell S. Whiteside and James F. Lander (Co-operative Institute of Research in Environmental Sciences, NOAA, 325 Broadway, Boulder, CO 80303, U. S. A., email: lws@ngdc.noaa.gov)

The primary purpose of natural hazard data catalogs is in the mitigation of future disasters. It is hoped that future natural disasters can be anticipated and populations warned if long term catalogs, which record the regional periodicity of events, are available. While such long-term variations in hazard are possible, we show that many current catalogs of natural hazard data may not be satisfactory to determine whether they actually occur.

Most hazard catalogs cover periods of less than 200 years and are reasonably complete and accurate for only the past 20-50 years. Such catalogs are not sufficient to investigate long term hazard variations. Earthquake, tsunami and volcanic catalogs, acquired and integrated at NGDC, illustrate artificial long-term variations created by cultural and scientific reporting changes, which can introduce unanticipated cyclical variations in the catalogs. These inconsistencies are often related to changes in the way magnitudes are calculated, evolving network equipment, network discontinuities of operation and personnel.

**JSP23/W/35-A5** **Poster** **0830-02**

**DISASTERS CAUSED BY CATASTROPHIC STORMS AND THEIR PREVENTION IN SMALL CATCHMENTS IN THE QIN MOUNTAINS**

Guozhang FENG (College of Water Resources and Architectural Engineering, Northwestern Agricultural University, Yangling, Shaanxi, 712100, China, e-mail: gfeng@public.xa.sn.cn)

Catastrophic storms often cause flash floods and corresponding geophysical hazards in the Qin Mountains in Shaanxi Province, China. The disasters are difficult to be prevented due to their rare occurrence, extremely high severity, non-predictability and too short warning time. The 980709 storm, occurred in a small area in the southeast of the Qin Mountains on 9 July 1998, is the maximum storm event in the records in the region and has an investigated maximum point storm rainfall of approximately 2122 mm during 6 hours and 40 minutes at one of two storm centers, and 1511 mm during 11 hours and 30 minutes at another center. The areas involved inside the isohyets of 1500 mm, 1000 mm, 500 mm and 50 mm's storm rain, are 31.4 km<sup>2</sup>, 45.5 km<sup>2</sup>, 86.8 km<sup>2</sup> and 847.1 km<sup>2</sup>, respectively. The storm formed enormous flash floods, landslides, mud-rock flows and aggradation of the riverbeds. As a combined consequence of the storm related disasters, 82 people and over 2000 thousands livestock were lost, over one hundred families were homeless, and most of the farmlands with growing crops were destroyed in the disaster involved two small catchments, especially in their densely populated valleys. Similar disasters with relatively lower severity frequently occur in the Qin Mountains even during the periods of general storms.

Reconstruction and protection of the areas both under and facing the damages are considerably important. Based on the natural and socio-economic features in the damaged and relevant areas, some integrated reconstruction and protection strategies for mitigation of the disasters and sustainable development of the region as an optimal eco-socio-economic system are proposed. The strategies consist of appropriate flood control standards, optimal land uses, reasonable economic structures, and safe residences and environments, in which some detail measures of engineering and non-engineering are involved. The strategies may be suitable to the similar catchments in the Qin Mountains.

**JSP23/W/08-A5** **Poster** **0830-03**

**VOLCANIC HAZARD ASSESSMENT FOR A PROPOSED HIGH-LEVEL RADIOACTIVE WASTE REPOSITORY AT YUCCA MOUNTAIN, NEVADA, USA**

Charles CONNOR and Brittan Hill (CNWRA, Southwest Research Inst., 6220 Culebra Rd, San Antonio, Tx, 78238, USA, e-mail: cconnor@swri.org); Andrew Woods and Steve Sparks (Centre for Geophysical and Environmental Flows, University of Bristol, Bristol, UK, e-mail: a.w.woods@bristol.ac.uk)

The proposed high-level radioactive waste repository at Yucca Mountain, Nevada, USA, is located within a geologically active basaltic volcanic field. Probabilistic volcanic hazard models for future eruptions through the proposed repository depend heavily on spatial controls on basaltic volcanism, including: Pliocene-Quaternary vent clustering, development of volcanic vent alignments, and localisation of vents along normal faults. When these spatial controls on past volcanism are considered, the probability of volcanic eruptions through the repository is

estimated to be 10<sup>-7</sup> to 10<sup>-8</sup> annually, or 1:1000 during the 10,000 yr performance period for the repository. This estimate is greater than some previous estimates that do not consider structural controls on basaltic volcanism explicitly, primarily because of the location of the proposed repository within a broad density low produced by a half-graben. Modification of spatial hazard models to include this structure, which appears to have controlled past volcanism, provides a mechanism to link patterns in basaltic volcanic activity and crustal extension in a quantitative hazard assessment for the first time. This technique may be widely applicable to assessment of volcanic hazards resulting from small-volume basaltic volcanic fields.

**JSP23/P/05-A5** **Poster** **0830-04**

**A SEISMIC HYDRAULIC BEARING**

Federico BARTOLOZZI (Civil Engineering an Independent Researcher, via dei carracci 4, 21100 varese, Italy, email: ciucizza@iol.it)

The proposed bearing consists of two parts. The fixed part, connected to the building is a steel sliding surface in the shape of a spherical bowl with a safety side spandrel. The movable part, connected to the foundation-soil complex, consists of a movable steel ball (rolling friction) in direct contact with the overhanging spherical bowl; alternatively, the ball may be fixed and coated on the top with Teflon (sliding friction). The lower part of the ball is linked to a movable cylindrical piston housed in the central chamber of a hydraulic device, also having two lateral symmetrical chambers with movable pistons, subjected to the elastic reactions of pre-stressed springs. Two holes connect the lateral chambers with the central one. During an earthquake, the horizontal displacement of the foundation-soil complex slightly affects the rest state of the building and the corresponding seismic energy in the building is negligible. The vertical displacement of the foundation-soil complex does not notably alter the rest state of the building, where there is no danger of resonance occurring due to the damping action of the liquid contained in the hydraulic device. The main advantages of the seismic insulation system, characterised by this type of bearing, are: 1. self-catering of the building after an earthquake; 2. possibility of application to modern and old buildings with any planimetric shape; 3. negligible pendulous effect in the building; 4. economical competitiveness with the existing aseismic systems both with partial and total absorption of seismic energy; 5. negligible psycho-physical effects for the inhabitants.

**JSP23/P/04-A5** **Poster** **0830-05**

**SELF-CENTERING ASEISMIC SYSTEM WITH ELASTIC BEARINGS AND HYDRAULIC DAMPERS**

Federico BARTOLOZZI (Civil Engineer and Independent Researcher, via dei Carracci 4, Varese, Italy, email: ciucizza@iol.it)

The theoretical and experimental analyses emphasise the following characteristics of the proposed system: 1. the self-centring of the building after an earthquake; 2. the undulatory seismic energy in the building is constant and about 1% of the weight, by using bearing with sliding friction (pure Teflon). It is negligible, by using bearings with rolling friction (steel balls). In addition, it is independent on the seismic frequency and the soil displacement; 3. the vertical seismic energy in the building is minor and it increases both with the increase of the ratio between the frequencies (phase opposition) and with its decrease (phase); 4. the building remains almost motionless (negligible displacement) with respect to the horizontal translation of the foundation-soil complex for all values of the direction angle of the motion, of the soil displacement and acceleration; 5. in the interval of emergency vertical seismic frequencies, including the resonance frequency, the automatic starting of the dampers occurs. They progressively decrease the dynamic strain of the springs, which are integral parts of the bearings; 6. because of the sub-undulatory shock, the total load on the bearings increases for upward soil displacements and it decreases in the contrary case, both in phase and in phase opposition conditions; 7. the experimental tests, conducted with reference to the undulatory shock, confirm the theoretical results.

**JSP23/W/00-A5** **Poster** **0830-06**

**A PROPOSAL FOR COASTAL SAFEGUARDS**

MARABINI

Abstract not available at the time of going to press

**JSP23/W/37-A5** **Poster** **0830-07**

**ABOUT THE ENSO IMPACTS IN NORTH-EASTERN ARGENTINE**

Norberto O. GARCIA and Maria del Valle Venencio (Facultad de Ingenieria y Cs. Hidricas - Univ. Nac. del Litoral, CC 495 - (3000), Santa Fe, Argentina. E-mail: nogarcia@fich.unl.edu.ar)

Frequently the North-eastern Argentine Republic is affected by floods on the riversides of the Paraná river, originated in the precipitation on the High Basin, and/or floods caused by the local rainfalls. With the same recurrence characteristic, drought situations take place that also affects the region, going from an extreme to the other in a short time generating emergencies totally different, but equally serious.

The present work makes an analysis of the extreme situations of the Paraná River associating them with the development of the sea surface temperatures on the Pacific Equatorial Ocean (EL NIÑO, LA NIÑA and neutral years). In this sense was found, as it was hoped, that most of the EL NIÑO events were associated with extraordinary floods of the Paraná river; although there were some floods that they were associated with the neutral phase (1959). The phase LA NIÑA (cold events) not always was associated with notable low waters of the river.

The behaviour of the precipitations over the region was non-homogeneous, and not always coincident with what it was hoped from a statistical point of view (Ej. 1983). The situation of EL NIÑO 1997/98 was permanently scanned and climatologically predicted through several models. So much in the river such as in the region the forecasts were completed acceptably. While, the socio-economic impact of the extreme events was very graphically shown in the means of communication.

**JSP23/E/53-A5** **Poster** **0830-08**

**ESTIMATION OF SEISMIC INTENSITY ATTENUATION LAWS FOR BANAT REGION**

AURELIAN PANTEA and Iren-Adelina Moldovan Ivan (National Institute for Earth Physics, P.O. Box MG-2, Bucharest-Magurele, Romania, e-mail: pantea@infp.ifa.ro and iren@infp.ifa.ro)

An attenuation relationship for macroseismic intensities for Banat (Romania) crustal earthquakes has been developed. We have used a data base including macroseismic maps from 21 earthquakes occurred during the period 1900 to present with MGR>4.0. The general form of the attenuation relation used is: log (I)=f1(M)+f2(r,E)+f3(r,M,E)+f4(F)+e (where: I is the



macroseismic intensity,  $M$  is the earthquake magnitude,  $r$  is the hypocentral distance,  $E$  is the tectonic environment,  $f_4(F)$  is a function of fault type and "e" is a random variable representing the uncertainty in  $\log(I)$ . Comparison with other attenuation relationships have been made.

**JSP23/E/48-A5** Poster **0830-09**

#### TROPICAL CYCLONE RISK ASSESSMENT

M.V.RODKIN (Geophysical Center, Russ. Ac. Sci., 117296 Moscow, Molodezhnaya 3, email: rodkin@wdbc.rssi.ru); G.S.Golitsyn (Inst. of Physics of Atmosphere, Russ. Ac. Sci., Moscow); V.F.Pisarenko (Intern. Inst. of Earthquake Prediction Theory and Math. Geophysics, Russ. Ac. Sci., Moscow); M.I.Yaroshevich (NPO Taifun, Rosgidromet, Obninsk, Russia)

A method of statistical estimation of tropical cyclone hazard is suggested. Probabilities of exceeding of certain levels of wind velocity (quantiles of distribution function) at a given area for given time intervals  $T$  are evaluated. The evaluation is based on the following velocity/distance relation:  $V(R)=V_{max}(R/R_{max})^{**2}$ , where  $R_{max}$  is the radius of central part of tropical cyclone where maximum of wind velocity  $V_{max}$  at given moment is observed. Accuracy of this relation is estimated by an error with standard deviation 7 knots. Suggested method is applied to typhoons in the Western Pacific, 1950-1988. The used catalog contains 1013 events. The 50%-quantiles (medians) and 90%- and 95%-quantiles of maximum possible wind velocity for time intervals  $T=1, 2, 5, 10$  and 20 years at 4 areas were evaluated: Tokyo, Hong-Kong, Taiwan Isl., and Vladivostok. Problem of possible temporal change in the typhoons regime is discussed in connection with the solar activity and El-Nino regime. The suggested typhoons risk assessment method can be useful for insurance industry and administration in areas subjected to tropical cyclones.

**JSP23/E/11-A5** Poster **0830-10**

#### LARGE SCALE DESTRUCTIONS OF BUILDINGS, THEIR CONNECTION WITH GROUNDS SPECTRAL PECULIARITIES DURING THE SPITAK EARTHQUAKE OF 12.07.1988 IN LENINAKAN (NOW GIUMRY), ARMENIA

Hrachya ABRAHAMYAN (Institute of Geophysics & Engineering Seismology, NAS RA, Leningradian 5, Gyumri, 377515 Armenia, email: iges@shirak.am)

Severely consequences of Spitak catastrophic earthquake force us to carry out the investigations revealing the causes of much more in quantity destructions. The most interesting aspect of testing the possibility of microvibrations using for prediction the grounds frequency characteristics is the comparison of buildings destructions measure by the grounds frequency elective property giving through the microvibrations. During the earthquake of December 7, 1988 with  $M=7.0$  the full destruction of frame-panel 9-storey buildings (from 138 buildings in Leninakan were undamaged only 6) and frame-stone 5-storey buildings (from 335 buildings were undamaged 87) was observed.

Registrations of buildings natural oscillations before the earthquake and grounds dominant periods by microvibrations after the earthquake showed that statistically the largest amount of destructions were obtained on the parts of town where the grounds natural dominant periods  $T$  were approximately of 0.5-0.6 sec for five-storey frame-stone buildings. On the grounds with  $T=0.2-0.38$  for nine-storey buildings and  $T=0.2-0.3$  for five-storey buildings damages were been of least amounts. Natural periods of nine-storey buildings are of 0.5-0.6 and of five-storey buildings are of 0.25-0.4. The high damages may be explained by strong influence of oscillations due to resonance phenomenon when the ground natural dominant periods tally with the buildings natural periods.

In seismic microzonation of region the possible spectrum of disastrous earthquake must be assessed. By this assessment only the grounds frequency peculiarities may be compared with buildings frequency characteristics. Such a complex approach only enables us to solve correctly the task of connection of possible damages by grounds frequency characteristics. Neglect of this factor will bring to tragic consequences such that were been in Leninakan.

**JSP23/E/32-A5** Poster **0830-11**

#### MINERAL PATHOGENIC DEPOSITS INTO A HUMAN ORGANISM AS A SIGN OF NATURAL HAZARDS

Nadezhda PAL'CHIK (United Institute of Geology, Geophysics and Mineralogy of Siberian Branch of RAS, Koptjug prosp. 3, Novosibirsk 630090, Russia; email: nadezhda@uigm.nsc.ru)

It is known that minerals exist not only into the Earth's crust but also into all human organisms. The pathogenic minerals contained into teeth and bones (as an apatite) are discovered also into pathogenic formations which can be found into different organs and tissues of a human body. We show, using the X-ray diffraction and the infra-red spectroscopy methods, that the apatite is present into urinary calculi, gallstones, dental stones, salivary calculi and also calcified cardiac valves as only phase of a mineral formation. Observations show that the full pathogenic mineralization of all living tissues of an organism occurs in some cases. Such peculiar natural hazard and its geographical distribution require a special attention and further investigation.

**JSP23/W/60-A5** Poster **0830-12**

#### NEGATIVE IMPACT ON HUMAN HEALTH FROM GEOPHYSICAL RISK FACTOR AT THE NORTH

VASSOVA

Abstract not available at the time of going to press

**JSP23/W/61-A5** Poster **0830-13**

#### GEOPHYSICAL RISK FOR HEALTH IN THE CIRCUMPOLAR AURORAL BELT

VINOGRADOV

Abstract not available at the time of going to press

**JSP23/E/30-A5** Poster **0830-14**

#### ASSESSMENT OF LANDSLIDE HAZARDS USING GEOPHYSICAL TOMOGRAPHIES

Simeon KOSTYANEV, Petar Srefanov and Peshka Stoeva (University of Mining & Geology, Sofia-1100, Bulgaria, e-mail: skost@staff.mgu.bg)

Landslides and unstable slopes are among the major natural and man-made hazards affecting mankind and yet their causes, their consequences for human life and property, and possible strategies for mitigating their effect are not very well understood. We will note, that only in Bulgaria

there are over thousand active landslides on populated and health resort areas. The material and social losses have not been calculated yet. But in preliminary data they are enormous. Numerous and dangerous are the landslides and unstable slopes in open-cast coal-mines too.

In this paper we offer methods for combined application of high-resolution electrical tomography and seismic ray tomography for characteristic of landslide hazards and unstable ones. The major aim here is to predict where and when landsliding will occur, establishing their variability in space and time, and appraising their impact on the natural and socio-economical environment.

The above methods are applied for the studying of concrete landslide in Bulgarian Black sea coast and on some unstable slopes in an open-cast coal-mine of Maritza-Iztok area. This combined application of electrical and seismic tomography for assessment of landslide hazard is very useful.

**JSP23/E/45-A5** Poster **0830-15**

#### SEISMICITY AND SEISMIC HAZARD STUDIES IN EGYPT AND SURROUNDING COUNTRIES

Samir RISAD (Geology Department, Assiut University, Egypt), Mahmoud Ghaleb (Geophysics Department, Cairo University, Egypt)

The tectonic setting of the Eastern Mediterranean Region is complicated because of the interacting effect of the principal plates: Africa, Eurasia and Arabia. The highest level of activity occurs at the northern margin of the Arabian plate, where it collides with Turkey and Iran. Strong earthquakes also occur along the western edge of the plate, along the Sea rift and the axis of the Red Sea Gulf of Aden. Egypt has a historical record of earthquake activity extending over the past 4,800 years. The most devastating earthquake in the recent history of Egypt, Dahshour earthquake, occurred some kilometers south of Cairo on the 12th of October 1992 damaged over 1,000 schools and other buildings, and injured over 7,000 people. In addition, other significant earthquakes occurred during this century interrupting the socio-economic development process of Egypt. Vulnerability to earthquakes increases steadily as urbanisation and development occupy more areas that are prone to the effects of significant earthquakes. The uncontrolled growth of cities in such areas are often associated with the construction of seismically unsafe buildings and infrastructures, mostly due to the insufficient knowledge of existing seismic hazard. Moderate and even small earthquakes may turn catastrophic in highly populated areas with poor building construction practice. In addition to the direct socio-economic impact of an earthquake, the long-term effects (the disruption of the economic chain, human resettlement, the reconstruction to modern standards) may last decades and absorb a considerable part of the national budget. In the absence of strong motion records a possible alternate method for seismic risk evaluation is the study of the attenuation of intensity with distance. For this purpose isoseismal maps for 17 historical and instrumental earthquakes that occurred in different parts of Egypt were analysed. Relations for intensity attenuation in different direction for different regions were obtained and have been used to calculate maximum intensity values all over Egypt. In addition, peak ground acceleration maps were produced for exposure time 10, 25, 50, 100 and 250 years, making use of an updated earthquake catalogue for Egypt. More than 20 seismogenic zones in and around Egypt were involved in the calculations. Hazard studies in Egypt have been carried within the framework of the regional IGCP Project 382, entitled "Seismotectonics and Seismic Hazard Assessment in the Mediterranean Basin (SESAME)", and in co-ordination with the activities of RELEMR Project. The results on Egypt were integrated with other available data for the surrounding countries.

**JSP23/E/55-A5** Poster **0830-16**

#### DIRECT AND INDIRECT LOSSES DUE TO EARTHQUAKES

KOFF G.L. (1), Lobatskaya R.M. (2), Frolova N.I. (3), (1) Institute of Lithosphere, Russian Academy of Sciences, Moscow, Russia, (2) Irkutsk University, Irkutsk, Russia, (3) Seismological Center of IGE, Russian Academy of Sciences, Moscow, Russia

The stability of urban area development is strongly depended on the hazardous natural processes. In order to secure the stable development of the territory the expected losses due to future events should be estimated. Direct and indirect economic losses are distinguished. We understood direct economic losses due to natural processes as losses in economy within the current reproductive cycle which are expressed in terms of annual indexes of social economic development. All other losses are referred to indirect ones. They do not influence directly on the achieved results in the economy in the current year. The indirect losses is an estimation of negative consequences resulted from secondary effects. In contradiction to direct losses, indirect ones may arise and manifest within the long time interval. The indirect losses may not have a definite place in space and are usually characterised by cascade effects. Four main groups of factors, which influence upon direct and indirect economic losses due to earthquakes and other natural processes are distinguished; they are the following: origination, susceptibility, cycles and state. Different factors and their influence on losses due to earthquakes are analyzed. For different urban areas it is possible to construct in advance the index system which will allow to estimate the value of mentioned factors. Than it is possible to identify zones according to the weights of different factors which may be used in order to improve prevention, mitigation and response from future events. The system analysis of existing connections of urban areas with other regions will allow to estimate the rate of possible instability of the territory in the case of emergency and to obtain more reliable estimations of acceptable level of economic and ecological risks.

**JSP23/C/U5/W/16-A5** Poster **0830-17**

#### RECENT ANOMALOUS GEODYNAMICS OF PLATFORM FAULTS AS THE NEW ECOLOGICAL RISK FACTOR

CHURIKOV V.A., Kuzmin Yu.O. (both at United Institute of Physics of the Earth, Recent Geodynamic Lab., B. Gruzinskaya Str. 10, Moscow, Russia, email: vt.churik@relcom.ru)

New data on the existence of recent superintensive deformations (SD) of the ground surface are obtained for fault zones in aseismic regions (Russian platform, Pripyatskaya depression (Belorussia), Turanskaya platform (Turkmenistan) and etc.).

These deformations have amplitude approximately 20 - 50 ppm, extension 0.1-1.0 km, velocity of vertical and horizontal displacements up to 5 - 7 cm per year. They have a pulsating character (the duration of the impulses of the activity of 0.5 - 1.5 year). These anomalous deformations call into existence the ecological risk of two types. 1. Direct - by the plums of anomalous fluids during the periods of activating fault zones; 2. Indirect - by the casualties of ecologically dangerous objects (wells on oil field and gas deposits, pipelines, underground depots of gases and toxic wastes, atomic power stations and etc.). The mechanism of SD-processes is suggested based on the parametrical excitation (the induction) of anomalous deformations in fault zones. In this case, the induction is evoked by small disturbances with nature and technogenic origins.

**JSP23/L/08-A5** Poster **0830-18**

**DISASTER MITIGATION PROGRAMMES FOR EARTHQUAKES, CYCLONES, DROUGHTS AND LANDSLIDES**

H.N. SRIVASTAVA (India Meteorological Department, New Delhi-110003, India, email: snb.imd.ernet.in)

Peninsular India earthquake of September 1993 (Latur, Magnitude 6.3) which caused the death of about 10,000 persons and major damage to stone built mud houses led to the development of a World Bank aided project for relief and rehabilitation work besides reconstruction of cheaper but safe dwellings in the area. Under this project, broad band digital seismographs (GSN) were installed in India to improve earthquake risk assessment. Issue of warnings about the land fall of tropical cyclones through INSAT based disaster warning system have helped in saving the lives of people living in coastal areas of peninsular India. Improvement of the rainfall measurements through another World Bank Project for the peninsular India will enable us to study agricultural droughts with greater reliability. Recent landslides and floods in Garhwal and Kumaon regions during May, 1998 in Himalaya which have taken a heavy toll of life and property during August, 1998 have focussed the need for a coordinated approach for landslide zonation integrating seismological, meteorological, remote sensing and other observations.

**JSP23/P/03-A5** Poster **0830-19**

**TOWER OF PISA: STABILITY RESTORATION PROPOSAL TO SAFEGUARD AGAINST SEISMIC RISK**

Federico BARTOLOZZI (Civil Engineer and Independent Researcher, via dei Carracci 4, 21100 Varese, Italy, email: ciuciuza@iol.it)

The proposed technique includes the solution of two problems. The former immediately provides to the removal of the instability due to the rotation in the north-south direction. The second problem consists in preserving the stability against the occurrence of two different phenomena: 1. the restarting of the instability, caused by a possible uneven subsidence of the foundation soil; 2. the instability consequent to an earthquake. Both phenomena could be avoided with the following complex operations: 1. planning and laying of a sub-foundation with geometrical and structural characteristics which ensure the stability of the foundation soil; 2. operation for preserving or decreasing the present inclination and, even, operation for conferring the perfect verticality, as well as, if wanted, the counter-inclination; 3. interruption of the solidarity between the building and the sub-foundation-soil complex, by using multidirectional movable bearings with low sliding or rolling friction, with or without dissipators of sub-undulatory seismic energy and laying laterally or rigid connections with alternative function of elastic linkages. This technique has two important advantages: 1. possibility to remove a future rotation of the Tower, due to an eventual subsidence of the soil; 2. easy maintenance of the sub-foundation structural elements, of the movable bearings and the side connections. The technique permits the removal only of the present instability, disregarding the seismic risk. In this case it is evidently less complicated and expensive. In addition, all operations for preserving or decreasing the present inclination and, even, for conferring the verticality and the counter-inclination are possible.

Saturday 24 July AM

**SEISMIC RISK MAPS AND SCENARIOS: TOOLS FOR PROTECTION AGAINST EARTHQUAKES**

**JSP23/C/U5/E/09-A6** Poster **0830-01**

**THE PREDICTABILITY OF EARTHQUAKE: TWO RECENT CASES IN YUNNAN, CHINA**

Lin RONGHUI (Seismological Bureau of Yunnan Province, Kunming 650041, CHINA); Tel: 86-871-3312339 Fax: 86-871-3315049 E-mail: ydj@public.km.yn.cn

China is one of few countries, which have the stipulation for issuing earthquake prediction and put it in practice. In the past three decades, the Chinese scientists did predict a few events of a certain type and with obvious characteristics. Though on a largely empirical basis such experience is a wealth, as the standpoint of practice should be first and fundamental in the theory of knowledge. The Menglian M7.3 earthquake occurred in the Sino-Burmese border (21°59'N; 99°04'E) at 05:46:41.2 on July 12, 1995. Predictions of the intermediate-term (>1 year), short-term (3 months) and immediate-term (1 day before the mainshock) were made by analyzing in detail the observed seismic and precursory anomalies. The outcome of the prediction effort was only really significant when the immediate-term prediction was made at site just one day ahead of time. The Lijiang M7.0 earthquake occurred in 27°18'N; 100°13'E at 19:14:18.1 on Feb. 3 1996. The observed precursory signals laid bases for making the intermediate- and short-term predictions. Yet, at the time of impending stage, a failure was made to locate the event, due to the superposition of post-precursors caused by Wuding earthquake (M=6.5) which occurred in central Yunnan in later October 1995.

**JSP23/C/U5/E/07-A6** Poster **0830-02**

**CHARACTERISTIC PRECURSORS OF THE 1996 LIJIANG, YUNNAN, EARTHQUAKE (M=7.0)**

Lin RONGHUI (Seismological Bureau of Yunnan Province, Kunming 650041, CHINA); Tel: 86-871-3312339 Fax: 86-871-3315049 E-mail: ydj@public.km.yn.cn

The Lijiang M7.0 earthquake occurred in Yunnan (27°18'N; 100°13'E) at 19:14:18.1 on Feb. 3, 1996. Before the event, precursory anomalies in the regional seismicity pattern were characterized as the absence of moderate-strong and small events around the source area. Since 1925, an average interval between  $M_{\geq 6.0}$  events was 6.4 years in the Lijiang area, northwest Yunnan, with the longest lasting 15 years. The latest Yanyuan M6.7 and Ninglang M6.4 events in the area occurred in 1976, surpassing the longest interval. Along the northern segment of the Zhongdian-Dali seismic belt  $M_{\geq 5.0}$  events were absent from 1983 to 1993, forming a gap of 150 km long. From 1990 to 1995, small events of  $M_{\geq 3.5}$  were also absent in the source area ( $\pm 77$ km). Activity of small events began to increase in the Yhongsheng earthquake window ( $\pm 77$ km) in Dec.1995 and Jan.1996. Around the Eryuan area ( $\pm 122$ km), a foreshock swarm with the maximum magnitude 3.6 occurred on Dec.10, 1995. In addition, in the short and impending stage from Dec.1995 to Jan, 1996, 6 items of abnormal precursors were observed at 7 stations, namely the water level at Jianshui; water temperature at Liuku, Gangyuan, and Lincang; tilt at shipping; water quality (ion of HCO<sub>3</sub><sup>-1</sup>) at Longling; and short leveling and short base line at Yongsheng. Besides, anomalous variations were also obtained from a synthetic analysis of precursory network data in the Lijiang area (which is consisted of 17 deep wells, 20 Radon points, 6 mercury points and 28 hot springs), and from the mobile gravity measurements in the networks of Western Yunnan Test Site before the event. Together with the seismic anomalies, all laid bases for making the intermediate (1-3 years)-, medium-

short (1 year)- and short-term (months) predictions. Yet, at the time of impending stage, a failure was made to locate the event, due to the superposition of post-precursors caused by Wuding earthquake (M=6.5) which took place in later Oct. 1995.

**JSP23/C/U5/E/10-A6** Poster **0830-03**

**RECENT CRUSTAL MOVEMENTS AND SEISMIC ACTIVITY STUDIES IN THE ASWAN REGION, EGYPT**

Abdel Monem S. MOHAMED (National Research Institute of Astronomy and Geophysics, Helwan, Cairo, Egypt, email: moonm98@yahoo.com)

Aswan region is one of the most important regions in Egypt and because it encompasses the vital engineering structure of the High Dam, it has been selected as a pilot project for the present study. Such a choice has been motivated by the fact that both geodetic and seismic data needed for the current investigation have been collected and become available from the Aswan region. So, the main objectives of the current research is to unify the results of the crustal movements and seismic studies which have been made in the Aswan region. This has been done for reaching the best understanding about the geodynamics of the area through investigating the relation between the crustal movements, seismic activity and earthquake occurrence and also for detecting the precursory events associated with earthquake occurrence. For the purpose of monitoring earthquake activity continuously around the Aswan Lake, a radio-telemetry network of 13 seismic stations was established. For monitoring the recent crustal movements several local geodetic networks were established around active faults in the area. Regional geodetic network covering the whole area of the northern part of Aswan Lake was established.

These studies use the seismicity recorded by the Aswan network from December 1981 to December 1997 and analyses different aspects of the data. Geodetic data were collected from local and regional geodetic networks. These studies were initiated to obtain an improved understanding of the seismotectonics in the Aswan region because this information is of importance in assessing the seismic risk.

**JSP23/C/U5/E/19-A6** Poster **0830-04**

**SEISMICITY OF IRANIAN PLATEAU AND ITS BORDERING REGIONS**

Arezou DOROSTIAN (Department of Geophysics, Azad University, North Tehran Branch); M. R. Gheitanchi (Institute of Geophysics, Tehran University, email: mrghchee@chamran.ut.ac.ir)

During the 20th century, from Jan.1, 1900 to Dec.30, 1998, nearly 5100 earthquakes of magnitude 4 and above occurred in the region of 20-40 N and 40-75 E. The area lies along the Alpine-Himalayan belt and surrounded by active seismic faults. This study shows a general aspect of seismicity of different parts of Iranian plateau and bordering regions. Historical and Instrumental data have been collected from several different sources. In order to minimize the uncertainty in magnitude estimation we present a uniform magnitude scale for the calculation of earthquakes. Seismicity maps for periods of time before 1965 and after that in five-year intervals were constructed. Seismic activity in some areas has changed with time. Within major seismic zones, large earthquakes fill gaps in the seismicity pattern. A grid interval of 0.5-degree in Lat. and Lon. covered the whole area. The seismic energy and strain release in each quadrangle were computed for each interval up to 29 years from 1970 to 1999. Maps of tectonic flux and two and three dimensional energy maps were constructed to define the distribution of seismic zones in the area and to give a dynamic measure of their variation. The a and b values for 99 years period are same for some seismotectonic provinces of area and the regions of homogeneous seismicity were constructed. The frequency distribution of earthquakes of different magnitude is discussed. Recurrence curves support a high level of activity for the Zagros zone and they indicate a lower rate of activity for northern Iran faults zone than for other areas in the region. Recurrence curves for central Iran area indicate that the rate of activity in a given region may remain practically constant over periods at least as long as a century, whether or not large earthquakes occur in the region during those periods. Comparisons between seismic hazard, energy maps, faults location and earthquake epicenters distinguish areas which will be damaged or have a heavy casualty.

**JSP23/L/01-A6** Poster **0830-05**

**EXPERIENCES GAINED IN THE RESPONSE TO THE EARTHQUAKE EARLY WARNING SIGNAL IN THE UNIVERSIDAD AUTONOMA METROPOLITANA, CAMPUS IZTAPALAPA IN MEXICO CITY**

Delfino LASCARES, Universidad Autonoma Metropolitana, Iztapalapa Av. Michoacan y Purisima, Col. Vicentina, Delegacion Iztapalapa, C.P. 09340, A.P. 55-535, Mexico D.F. Tels. 724-46-98, FAX 724-46-88, email: held@xanum.uam.mx.

Since June 1997 a radio receiver of the Seismic Alert System of Mexico, City (SAS) was installed in the Universidad Autonoma Metropolitana, Campus Iztapalapa and an integral program for hazard mitigation has been applied in the campus. The population reached by the early warning signal is about 17,000 students and academic personnel, with an average nearby population of 45,000 people. To date 7 early warning signals have been received. During these early warning that occurred in working hours, evacuation has been carried out in an average time of 30 to 60 seconds. Surveys show that, since the SAS warning operation the attitude of the near by population toward earthquake prevention has changed. To date 90 percent of the population respond to the early warning signal. The Seismic Alert System (SAS) was developed by the Centro de Instrumentacion y Registro Sismico (CIRES). The alerts have provided as much as 30 to 60 seconds average in advance warning, before the ground motion sake reach Mexico City.

**JSP23/C/U5/E/05-A6** Poster **0830-06**

**PRECURSORY SEISMIC SIGNALS DURING THE 1998 GUAGUA PICHINCHA CRISIS**

HUGO A., Mario C. Ruiz, Minard L. Hall, Monica Segovia, Alexandra Alvarado, Acinoo Calahorrano, Darwin Villagomez, Diego Viracucha, Patricia Mothes, Andres G. Ruiz, Daniel Andrade; (Instituto Geofisico, Escuela Politecnica Nacional, P.O. Box 17-01-2759, Quito, Ecuador; e-mail: geofisico@accessinter.net)

The Geophysical Institute in Quito, Ecuador, began the instrumental monitoring of Guagua Pichincha volcano in 1981. Until 1988, activity was characterized by a small number of earthquakes and sporadic phreatic explosions, which generated an explosion crater approximately 200 meters in diameter in the bottom of the caldera. In 1988, a swarm of VT earthquakes occurred 9 km southeast of the caldera at a depth of 8-12 km. Moderate phreatic explosions were detected in 1990, 1993, 1995, and 1997 during periods of rain. Between December 1997 and April 1998, three VT earthquake swarms were registered underneath the caldera, and in June 1998, an important swarm of VT earthquakes began 15 km northeast of the caldera. This swarm lasted until October, and at its height more than 100 earthquakes per day with a magnitude between 2.5 and 4.0 were noted. Furthermore, since June 1998, there



have been hybrid earthquakes at depths less than 9 km.

A subduction earthquake with a magnitude of 7.1 occurred on the Ecuadorian coast 220 km from the volcano on 4 August. On 7 August, almost continual explosive activity began at Guagua Pichincha. This activity was characterized in the initial weeks by explosions followed by various days/hours of tremors. Between 7 October and 22 November, the tremors were shorter, with frequencies between 1.8 and 2.0 Hz. Between 22 November and 19 December, the number of explosions diminished with cycles of tremors between 28 and 32 hours. A new cycle of activity began on 19 December with spasmodic tremors and strong explosions followed by short episodes of tremors (<10 minutes) with frequencies of 1.6 Hz. In addition, earthquakes characterized by narrow spectrum (between 2 and 5 Hz) have been registered since 10 September. These earthquakes have originated at shallow depths under the caldera and have accompanied periods of intense phreatic activity. Guagua Pichincha's continuing activity is attributed to various pulses of intrusion of small magmatic bodies, a process, which could ultimately result in a volcanic eruption.

**JSP23/C/U5/E/12-A6** Poster **0830-07**

#### THE HYDROPHYSICAL METHOD OF TSUNAMI ESTIMATION

Yury KOROLYOV and Alexander Poplavsky (Institute of Marine Geology and Geophysics, Sakhalin Scientific Centre, Nauki st., Yuzhno-Sakhalinsk 693002, RUSSIA, email: tsunami@sakmail.sakhalin.ru)

The estimation of tsunami danger is based on seismological data at present. It doesn't take into account inhomogeneity of tsunami source, directivity of tsunami, diffracting effects, which may both amplify and attenuate tsunami waves, and duration of tsunami. Therefore it gives some erroneous forecasts. Information of some level gauges placed on sea may confirm or refute tsunami danger. The hydrophysical method of tsunami estimation using information of some remote level gauges is based on well-known reciprocity principle. This method needs in minimal seismological data (time of beginning and co-ordinates of earthquake), data on sea level in three points and numerical "mareograms" in these points and in point to be warned. These "mareograms" must be obtained by tsunami simulation from some model tsunami sources placed on earthquake epicentre. This method takes into account inhomogeneity of tsunami source, directivity of wave radiation, different diffracting and resonance effects. As a result the time of tsunami attack, form, heights and number of tsunami wave and duration of tsunami alarm are determined. This hydrophysical method will improve the reliability of tsunami warning and allow a creating of networks of local tsunami warning systems. This work was supported by grant 97-05-96625 from Russian Foundation for Basic Researches.

**JSP23/E/56-A6** Poster **0830-08**

#### HISTORICAL DOCUMENTATION OF THE SEISMICITY OF LESVOS ISLAND (E. AEGEAN, GREECE) IN THE SECOND HALF OF THE 19TH CENTURY: COMPARISON WITH THE INSTRUMENTAL PERIOD DATA

Vicki KOUSKOUNA (Department of Geophysics & Geothermy, University of Athens, 157 84 Athens, Greece, email: vkouskou@atlas.uoa.gr); Kostas Taxeidis (Psichari 20, Mytilini 81 100, Greece); Kostas Macropoulos (Department of Geophysics & Geothermy, University of Athens, 157 84 Athens, Greece, email: kmacrop@atlas.uoa.gr)

A total number of 32 earthquakes from Lesbos island for the period 1851-1899 are listed in the existing published catalogues, five of which were destructive and were felt in the Eastern Aegean and Minor Asia. A detailed investigation carried out on the island revealed new, local sources of information (manuscripts, newspapers, etc.) reporting the earthquakes of Lesbos. These sources, together with the existing ones, present a more complete seismic picture of the island, and almost double the total number of its earthquakes, i.e. 34 new single earthquakes (or series of earthquakes) were located, one of which (in 1882) was damaging. The seismicity of the island in the 20th century, as derived from instrumental data, for a time window of 50 years, was compared to the above mentioned period, in an effort to: a) re-evaluate the parameters of the known, major destructive earthquakes by adding the new sources of information, and b) answer to certain questions of tectonic character, i.e. the existence of foreshock/aftershock activity and its characteristics. In this sense, the catalogue of earthquakes of the area is extended backwards up to 1850, and the completeness of its seismicity is tested. This enables the creation of an artificially complete data set, which will therefore contribute to more realistic local seismic hazard assessment and microzonation studies.

**JSP23/E/38-A6** Poster **0830-09**

#### MODULE AND GRADIENT HIGH-SENSITIVITY MEASUREMENTS OF GEOMAGNETIC FIELD VARIATIONS AT THE SEISMIC RESEARCHES

Oleg KUSONSKI (Observatory Arti, Institute of Geophysics, Urals Branch of Russian Academy of Sciences, Geophysics Str., 2a, Arti, Sverdlovsk region, 623350, Russia); Vladimir Sapunov and Olga Dekusar (Ural State Technical University, Quantum Magnetometry Lab, Mira St., 19, Ekaterinburg, 620002, Russia)

The researches are carried out at the observatory Arti (WDC's mnemonic is ARS, coordinates are 56°25.86' N, 58°33.76' E) that is located on the Preduralsky pericratonic trough of the East-European platform. This area is seismically active. Observable here earthquakes have both natural and industrial origin. The last is connected with production of minerals and oil. The magnetic field of this region is characterized by presence of anomaly up to 1200 nT. The module and gradient variations are measured by the proton Overhauser's magnetometer POS-1 with resolution 0.001 nT (sensitivity up to 0.02 nT and 0.01 nT/meter at single measurement). At the same time a registration of super-long-period seismic oscillation (SSO) are made by the ARU IRIS station. A gradiometer allows to control the real measurement sensitivity for absolute value of magnetic fields and to locate geological and technogeneous effects caused by a near zone. The submitted methods and equipment allow to study geoblocks movements creating intensive deformations of mountain breeds, geoblocks response to tectonic factors, SSO excitation mechanism, trigger factors of earthquakes. The data can essentially soften dramatic and economic consequences of earthquakes at the mining enterprises of Ural.

**JSP23/E/45-A6** Poster **0830-10**

#### OBSERVED AND PREDICTED INDUCED SEISMIC IMPACTS IN PREADRIATIC COASTAL AREA OF ALBANIA

Siasi KOCIU (Seismological Institute, Tirana, ALBANIA, email: kociu(sizmo.tirana.al)

Albania, situated on Western Balkans, with a coastal line of 470 km long, represents an attractive area for the future development of tourism. Adriatic seacoast of Albania with many, as one of the most populated areas of the country (where more than 70% of the population is concentrated, with many inhabited centers as those of Durres and Vlora towns in seacoast and Shkodra, Fieri and Tirana (capital), not far away (20-40 km), from the seacoast), represents one of the most

hazardous seismic zones of the country, where many seismic impacts were observed during the past earthquakes and may be developed during expected future earthquakes.

Preadriatic area as a flat area filled mainly by recent very poor Quaternary sediments of thickness down to 100-150 m, with shallow underground water level, represents an area where a lot of soil in stabilities were observed during past earthquakes and can be observed in the future. Based on seismic hazard assessment procedures at local level for two of the biggest coastal cities of Albania ( Durres and Vlora) it is shown that during the expected strong earthquakes induced seismic impacts as liquefaction of sands, new and induced landslides and appearance of fault rupturing on free surface can be observed not only along Adriatic seacoast, but especially within urban areas of these two cities.

**JSP23/E/07-A6** Poster **0830-11**

#### THE RISK OF LARGE VOLCANIC ERUPTIONS AND THE IMPACT OF THIS RISK ON FUTURE OZONE DEPLETION

Howard ROSCOE (British Antarctic Survey/NERC, Madingley Rd, Cambridge CB3 0ET, UK, email: h.roscoe@bas.ac.uk)

Ozone depletion at mid-latitudes due to reactive halogens from man-made halocarbons is enhanced by the increase in stratospheric sulphate aerosol, which follows large volcanic eruptions. Mid-latitude ozone depletion due to halocarbons almost doubled for the two to three years following the eruption of Mt Pinatubo in 1991. Although the Montreal Protocol is expected to reduce amounts of halocarbons in the atmosphere during the next century, the predicted reductions are such that stratospheric ozone will be at risk from such depletion enhancement for the next 50 years. Volcanological mechanisms, models, and measurements in ice cores, suggest that large volcanic eruptions are random and that their global rate is constant over periods of a few centuries. From the rate of large eruptions observed in ice-cores, the probability of one or more eruption, the size of Pinatubo or larger, is 58% in 50 years. This probability is large enough that it should be taken into account in predictions of future ozone loss. Several of the eruptions in the ice-core record were many times larger than Pinatubo, so that a more comprehensive analysis, which also included the probability of eruptions as a function of size, would be beneficial.

**JSP23/E/47-A6** Poster **0830-12**

#### STATISTICS OF EARTHQUAKE HAZARDS

M.V.RODKIN (Geophysical Center, Russ. Ac. Sci., 117296 Moscow, Molodezhnaya 3, email: rodkin@wccb.rssi.ru); V.F.Pisarenko (Intern. Inst. of Earthquake Prediction Theory and Math. Geophysics, Russ. Ac. Sci., Moscow)

Earthquake tolls and economic losses in 1900-1996 years are examined in connection with earthquakes regime and economic conditions in different regions. It was shown that while the number of events with small and moderate number of victims and losses increase with time in a non-linear manner the large losses that constitute the major part of the total number of victims and losses have a linear increase with time. The non-linear increase with time of the total number of victims and losses is caused mainly by the Pareto-law distribution of losses from earthquakes, thus a high non-stationarity of regime of hazards assumed by a few authors is apparent. The limitations inherent to the Pareto-law distribution of losses are discussed and the value of maximum possible seismic hazard is evaluated. The connection of regime of seismic disasters with regional economic situation is discussed also. It was shown that while the losses from earthquakes have a tendency to increase with time, the number of victims and losses we normalised with the national income per capital have a tendency to decrease. A prognosis of number of victims and losses from earthquakes till 2020 year is presented.

**JSP23/E/51-A6** Poster **0830-13**

#### INTERNATIONAL GPS TEST-AREA FOR DEFORMATION FORERUNNERS OF EARTHQUAKE STUDY

Mikhail PRILEPIN (United Institute of Physics of the Earth, B.Gruzinskaya Str., 10, 123810 Moscow, Russia, email: prilepin@uipe-ras.scgis.ru)

One of the reasons why the problem of earthquake prediction is far away from the solution stipulated is the lack of real international co-operation on experimental study and evaluation of significance of different forerunners. Many scientists today share the opinion that deformation forerunners are primary and their study can help in understanding the processes of preparation of earthquakes and prediction of event. The favorable factor nowadays is the availability of very effective GPS technology for the study of deformation forerunners on large territory with high accuracy and with the possibility for automatization of gathering and processing of the data. The next step in instrumentation is combining GPS with SAR interferometry, which is making the first but a very successful step toward the study of geokinematics. In the report discussed, the items dealing with the determination of the epicenter position, magnitude and time of shock using the data accumulated on GPS networks of different levels developed in seismically active areas. The consideration about the selection of place for a test-area, its status, sequence of development of the GPS networks, transition of data, gathering of auxiliary data and activity of the center for processing and analyzing the data are discussed. The consideration about the possibility of united study of different kinds of forerunners: seismic, geoelectromagnetic, variation of ground water level and emanation of noble gases are also presented shortly.

**JSP23/C/U5/P/01-A6** Poster **0830-14**

#### THE THREE STRONG EARTHQUAKES, NORTH CHINA, CHINA AND ITS STRUCTURAL SIGNIFICANCE

Lu PEILING (Centre for Analysis and Prediction, CSB, Beijing (100036), China, Tel: 010-88015557, Fax: 010-68218604)

Abstract The seismic activities before and after strong earthquakes, the source mechanism of mainshocks, and the geological structure of the epicenter area of three strong earthquakes (the 1976(M7.8) Tangshan, the 1989(M6.1)Datong-Yanggao and the 1998 (M6.2)Zhangbei-Shangyi earthquake) have been investigated. The structural significance of the three strong events is also discussed. The results show that 1. In according to the seismic activities before and after mainshocks, three strong events occurred in the north margin of North China faulting block area. The occurrence of three events was resulted from the most recent abrupt slip on a NE-trending Changdong fault zone, a NE-trending Shanxi graben zone and a NWW-trending Zhangjilakou-Bohai fault zone, respectively. 2. In according to the mainshock location, the events was in the intersecting area of the faults, therefore its sequences have the rich aftershock action, the most of strong aftershocks and the energy attenuation slow. 3. The source mechanism solutions of mainshocks are in agreement with the regional stress field with the P axis in the NEE-SWW direction of North China, but there are a difference in the fault motion type, 1976 event shows the northeastern striking high-angle strike-slip faulting



## INTER-ASSOCIATION

mechanism, 1989 event has the strike-slip with the normal faulting motion, and 1998 quake is the thrust fault type. Those might correspond upon the structure of the epicenter area. 4. The epicenters is in or near Cenozoic-aged faulting basins with the Cenozoic -aged basels, the genesis of the strong earthquakes which are derived from basels may be the rising model of the hot material. Due to an action of the local hot stress the earthquakes occurred. 5. The mainshock faults are not at a great active structure, even there is not active fracture in the surface of the epicenter area.

**JSP23/C/U5/P/04-A6** Poster **0830-15**

### SEISMIC HAZARD ASSOCIATED WITH SUBMARINE NEOTECTONIC FAULTS IN GREECE

Joanna PAPOULIA (National Center for Marine Research, Agios Kosmas, Hellinikon, 16604 Athens, GR)

Seismic hazard analyses are associated with large uncertainties when historical data are insufficient to define seismicity rates. These uncertainties may be decreased however in areas where seismicity is shallow, and produced by Quaternary faulting, by incorporating geological data in the analysis of seismic hazard. A tool towards the integration of the so-called prior information of seismicity, obtained from geological data, with historical observations is the Bayesian probability theory. This theory is tested here to estimate the seismic hazard associated with submarine active fault zones in the area of Greece. Prior estimates of seismicity are developed from slip rate measurements obtained from offsets of geological formations. The analysis demonstrates the importance of uncertainty in the Bayesian estimate of seismicity, and subsequently in the estimate of seismic hazard.

**JSP23/C/U4/E/03-A6** Poster **0830-16**

### GUAGUA PICHINCHA: MANAGING THE CRISIS

HUGO A. YEPES; Instituto Geofísico, Escuela Politécnica Nacional, P.O. Box 17-01-2759, Quito, Ecuador; e-mail: geofisico@accessinter.net

Guagua Pichincha is a dacitic volcano located 12 km west of Quito (pop. 1.2 M.), the capital of Ecuador. It has erupted five times in the last 1,030 years (970, 1560, 1575, 1582, and 1660), with a recurrence period of approximately 500 years during Holocene. In July/August 1998, there was a commencement of seismic and explosive activity at levels superceding those seen since the installation of the monitoring network in 1988. The increased activity, which peaked during late September, precipitated the declaration of a yellow alert by the city of Quito on 1 October.

The Geophysical Institute, drawing on its experience and expertise, acted as a catalyst for the city's actions given the city's lack of preparedness and inability to initially grasp the gravity of the situation. The initial step for the government in dealing with the crisis was the designation of the mayor of Quito as the overall response coordinator. The city established an operations/information center; determined populated areas at risk; identified public sectors likely to be affected; and cleared debris from flow areas and potential evacuation routes. Contingency planning included one evacuation drill; periodic meetings of governmental entities; solicitation of heavy equipment and medical supplies from foreign governments and NGOs; the development of ways to minimize impact to the water supply, power grid, and telecommunications; and the planning for ash removal, police deployment, evacuation of aircraft, ingress/egress of the city, and procurement of food and fuel. Educational efforts comprised press conferences, briefings, and press bulletins.

Any crisis has its difficulties. Some problems are unavoidable, some can be mitigated by adequate funding, and others are preventable. Problems encountered by the city have included the inability to control rumors, inability of the government to ameliorate the public's linkage of the alert declaration to local political events, poor management of the initial alert declaration, confusion over alert level definitions, difficulty in maintaining public interest over the long term, the release of overly technical information to the public, delays in developing contingency/evacuation plans, reluctance to disclose all available information on potentially affected areas, the ill-defined role of the operations center, inadequacies in the call-down list, a failure to publicize an alarm system, and insufficient funding. Yet despite these problems, the city has made great progress in recognizing the hazard and addressing the risk.

**JSP23/C/U4/W/01-A6** Poster **0830-17**

### VOLCANIC HAZARD ASSESSMENT AT THE DENSELY INHABITED ISLAND OF ISCHIA

Sandro de VITA, Giovanni Orsi (Osservatorio Vesuviano, 80056 Ercolano -NA- Italy, email: devita@osve.unina.it) Fabio Sansivero (Dip. Geofisica e Vulcanologia. Un. "Federico II", 80138 Napoli, Italy)

Ischia is a volcanic island located in the north-western corner of the Gulf of Naples. Volcanism began more than 150 ka B.P. and the last eruption took place in 1302 A.D. The largest caldera forming eruption generated the Mt. Epomeo Green Tuff and occurred 55 ka B.P. Resurgence of the central part of the caldera began around 28 ka B.P. and caused a net uplift of about 900 m of the Mt. Epomeo block. It occurred through a simple-shear mechanism that determined the conditions for magma to rise to surface only along normal faults within the eastern sector of the resurgent block. Almost all the volcanic vents of the last period of activity (10 ka B.P.-1302 A.D.) are located in the eastern part of the island. During this period 46 eruptions, effusive and explosive, occurred mainly between 2.9 ka B.P. and 1302 A.D. Effusive eruptions produced lava flows and domes; explosive eruptions formed tuff-rings, tuff-cones, and variably dispersed pyroclastic deposits. Eruptions were separated by periods of quiescence that lasted up to few centuries. Slope instability, likely triggered by resurgence dynamics, generated landslides and mud-flows shortly before and after eruptions. The magmatic system is still active, as testified by the intense historical, volcanic and seismic activity, and by widespread thermal springs and fumaroles. The island is inhabited by about 50,000 peoples that greatly increases during summer. Farming, wine industries and a complex network of commercial exchanges with the near city of Naples, contribute to determine a high volcanic risk in this area.

**JSP23/W/72/C/U4/W/03-A6** Poster **0830-18**

### EVIDENCE FOR VOLCANIC INFLUENCES ON MEXICO CITY AEROSOLS

G. B. RAGA (Centro de Ciencias de la Atmósfera, Universidad Nacional Autónoma de México, Ciudad Universitaria, 04510, México DF, México, email: raga@servidor.unam.mx), G. L. Kok (National Center for Atmospheric Research, Boulder, CO 80303, USA, email: kok@ucar.ncar.edu), D. Baumgardner, A. Báez and I. Rosas (all three at: Centro de Ciencias de la Atmósfera, Universidad Nacional Autónoma de México, Ciudad Universitaria, 04510, México DF, México, email: darrel@servidor.unam.mx)

In situ measurements of sulfur dioxide (SO<sub>2</sub>), carbon monoxide (CO) and sulfate mass provide evidence that aerosol composition in Mexico City is affected by emissions from the neighboring volcano, Popocatepetl. The data suggest that there are two distinct pathways by which SO<sub>2</sub> is incorporated into particulates. Periods of high humidity, fog, and rain are accompanied by elevated sulfate mixing ratios, attributed to aqueous chemistry. Similarly, elevated sulfate concentrations in low humidity periods appear to be a result of adsorption onto existing particles. These two mechanisms are important for understanding the processes

associated with particle formation in this highly polluted urban area. Under the influence of volcanic emissions, SO<sub>2</sub> concentration is more than four times the average value and particulate sulfate is a factor of 2 larger.

**JSP23/C/U4/W/05-A6** Poster **0830-19**

### SAN SALVADOR, EL SALVADOR, A HIGH RISK, MULTIPLE HAZARD MEGACITY

D J SOFIELD, J W Vallance, and W I Rose (Geological Engineering and Sciences, Michigan Technological University, Houghton, MI, 49931, email: djsofiel@mtu.edu)

Volcanism and earthquakes are the most dire geological hazards that threaten San Salvador, El Salvador's largest city (population, 1.7 million), with a rapidly growing population, and few plans or resources for hazard mitigation. Financial, transportation, and governmental centers of El Salvador all reside within San Salvador. The city lies on a plain within severe hazard zones of two active volcanoes (San Salvador to the W and Ilopango to the E) and also lies in a zone of major subduction earthquakes.

In the past 60 Ka, a caldera 12 km E of the city now occupied by Lake Ilopango erupted at least four significant pyroclastic deposits, each of which blanketed the valley that San Salvador now occupies. The last of these eruptions devastated all El Salvador in AD 260 and drove pre-Classical Mayan civilization northward into the jungles. A dome eruption in 1880 and small seismic swarms beneath the lake indicate continuing unrest. Neither San Salvador volcano nor its numerous flank vents has erupted catastrophically since European colonization, however numerous explosive eruptions occurred prior to that. San Salvador volcano erupted ash-rich tephra and pyroclastic flows 800 years ago and caused mudslides that would likely kill many thousands today. Because of the frequency of earthquakes, the people of San Salvador are much more aware of seismic risk than volcanic risk. The city has had to rebuild 7 times after earthquakes since 1712. The most recent devastating earthquake in 1986, killed 1500, injured 10,000 and left 100,000 homeless. Thick unconsolidated pyroclastic and tephra deposits amplify the effects of shallow-focus, moderate magnitude earthquakes beneath the city. Timely international involvement could provide the impetus that San Salvador needs to begin effective hazard-assessment, monitoring, and educational programs. A significant part of this work will be to make the population of a volcanic country more aware of its vulnerability to volcanic hazards. The recent occurrence of hurricane Mitch offers an opportunity to advance all hazard work in Central America.

Monday 26 July AM

## NEW PHENOMENA, APPROACHES AND TECHNIQUES

**JSP23/W/28-B1** Poster **0830-01**

### METHODS OF EXTREME SEA LEVEL AND CURRENTS VALUES CALCULATION

Oleg ZILBERSTEIN, Guennady Safronov, Sergei Popov, Mikhail Chumakov (all at State Oceanographic Institute, Kropotkinski per. 6, 119838, Moscow, Russia, email: oleg@soins.msk.ru)

Hydrometeorological support for marine branches of the economy and safety of human activities on offshore regions requires knowledge of the main marine parameters (in particular sea level and current extreme values). As a rule long-term observations in offshore regions are absent. The most dangerous rise and fall of sea level and also extreme currents are result from the combined effect of tides and storm surges. A special automated technology including hydrodynamic and probabilistic modelling was developed. On the basis of historical information and observation series analysis for region of interest, extreme storm cases with corresponding weather maps are selected. Following computation of earth-surface level wind and atmospheric pressure gradients are produced. On the base of this information the hydrodynamic calculation of storms and summary (accounting tides) sea level oscillations and currents are calculated with help of verified 2D and 3D hydrodynamic models. Baroclinic models are actively used last years. With the help of produced probability models, which are based on Gumbel low and Langbein relationship, the results of numerical modelling are processed and long-return period characteristics of sea level and currents at different horizons are determined. Produced complex of models and methods is successfully used within researches and survey for number of designing objects in Barents, Kara, Baltic, Caspian, and Sea of Okhotsk. This approach allows us to produce computer maps of long return period characteristics of sea levels and current

**JSP23/W/33-B1** Poster **0830-02**

### SEARCH FOR THE EARTHQUAKE PRECURSORY SIGNATURES BASED ON FRACTAL ANALYSIS OF THE ULF GEOMAGNETIC DATA

Natalia SMIRNOVA (Institute of Physics, St. Petersburg University, St. Petersburg, 198904, Russia, e-mail: nsmir@snoopy.phys.spbu.ru); Masashi Hayakawa and Tetsuya Ito (The University of Electro-Communications, Chofu, Tokyo 182-8585, Japan, e-mail: hayakawa@whistler.ee.ucc.ac.jp)

An attempt to use fractal methods of time series analysis for searching the earthquake precursory signatures is fulfilled on the basis of ULF geomagnetic data obtained during Guam earthquake (EQ1) on August, 8 1993 (M=8) and Biak earthquake (EQ2) on February, 17 1996 (M=8). The observing places were situated both near the epicenters (Guam, 65 km off EQ1 and Biak, 100 km off EQ2) and far away (Darwin, 1200 km off Biak EQ). The chosen period covered a few months before and after the earthquakes in order to reveal the large-scale dynamics of scaling (fractal) characteristics of the pulsations. It is revealed that in the seismocactive region the ULF spectrum of emissions exhibits a power law behavior which is typical for self-organized critical dynamics. For Guam EQ the slopes of spectra and the fractal dimensions of ULF time series manifested stochastic fluctuations between values 2.5-0.7 with pronounced tendency for slope to decrease and for fractal dimension to increase in the process of the earthquake preparation. Taking into account the certain value of the critical slope we suggest that the gradual increase of the intervals with slopes less than this critical one prior to the earthquake may be considered as an earthquake precursory signature. The peculiarities revealed on the basis of ULF data of Guam EQ is verified on the materials of Biak EQ. The fractal properties of ULF emissions in seismocactive and seismoiquiet regions are compared. The research was supported by Grant 98-05-65554 from Russian Foundation for Basic Research.

**JSP23/C/U5/E/13-B1** Poster **0830-03**

### RESEARCH ON CORRELATION OF ASTRONOMIC FACTORS AND EARTHQUAKES

Hu HUI; Li Yongsheng (Yunnan Observatory, Academia Sinica, Kunming, 650011 China)

The effect of astronomical factors on the major earthquakes in China and the world is discussed in detail in this paper. The results show that the major earthquakes, especially the ones of above magnitude 7.0 are evidently affected by the astronomical factors, such as the Earth rotation, solar activities and lunar orbital motion. Only different seismotectonic belts or zones have different responses to an astronomical factor. The node of the lunar orbit with the earth's orbit

regresses towards the west on the ecliptic, with a period of 18.6 years. The precession of the lunar ascending node causes the inclination between the moon's path and the equator to change continuously from 18.28 to 28.58 degrees. The seismic activities of the main seismic belts in the world are obviously affected by the period of 18.6 years and only their active periods appear alternately, which shows that different locations of the moon correspond to different seismic belts or regions on the Earth. This bears analogy to the fact that the change Earth's climate with a period of a year is caused by the different quantities of arrival of solar radiation due to the inclination of the ecliptic to the equator.

In China, 8 seismic events over M 8.0 occurred since 1820 happened to be during the acceleration of the Earth rotation (DAER). Among the 106 events over M 7.0 occurred in the 20th century, 72% were during the DAER and 71% happened when the inclination changed from the maximum to minimum. Most of the events happened in the descending phases of solar activities.

**JSP23/E/16-B1** Poster **0830-04**

**POINT-LIKE PROCESSES AND CATASTROPHE PREVISION**

Giovanni P. GREGORI (IFA-CNR, via Fosso del Cavaliere 100, 00133 Roma, Italy; e-mail: gregori@atmos.ifa.rm.cnr.it)

A frequent approach when attempting at managing a natural catastrophe is in terms of a numerical model, by which we try at forecasting its occurrence in space and time. Sometimes this results to be difficult or even unrealistic. On a more pragmatic ground we can rather appeal to a formal analysis of the historical time series of every catastrophe of concern. Only approximately, however, such series can be likened to a point-like process, because the "detector-mankind" experienced substantial changes vs. time. Nevertheless, such algorithms can be approximately applied by means of a few suitable assumptions. Four basic viewpoints can be considered: (i) either by assuming that phenomena are periodic; (ii) or by assuming that an event occurs only whenever some energy threshold is attained (calorimetric criterion); (iii) or by assuming that it occurs only whenever the system experiences some abrupt change of its boundary conditions; or (iv), whenever no such algorithm is viable due to scanty observational information, just by applying the box counting method, or some other more or less related and/or equivalent fractal algorithm. The mutual relations, advantages, and drawbacks of either one such approach are briefly discussed, with a few applications. They all lead to an apparently successful long-range forecast of a large flood in northern Italy occurred in 1994, and to the prevision of the next explosive eruption of Vesuvius. But, the success of every such application is closely determined by the quality of the historical database, or by the physical information that is fed into the analysis, rather than by mathematics that per se have only to be concerned with avoiding that some arbitrary non-physical input is added, based only on the human need for simplicity.

**JSP23/W/88-B1** Poster **0830-05**

**SIMULATION OF ANOMALOUS BEHAVIOUR DURING THE NORTHBRIDGE 1994 EARTHQUAKE**

GALIEV

Abstract not available at the time of going to press

**JSP23/E/22-B1** Poster **0830-06**

**PHASE OF MOON, INCLINATION OF MOON'S PATH WITH EQUATOR AND STRONG EARTHQUAKES IN YUNNAN**

Li XIAOMING (Yunnan Observatory, Chinese Academy of Sciences, P.O.Box 110, Kunming; Yunnan Province, 650011, P.R.China)

Yunnan Province lies in the southwestern part of China, adjoining the juncture of the Eurasian plate and Indian plate, with the complicated geological structure, frequent seismic activities and the Mediterranean seismic belt passing through the province itself. It is found from the analyses that the rate of recurrence of earthquakes has close correlation to the position of the Moon at the last quarter and especially near the new Moon and the last quarter of the Moon earthquakes occur frequently. In the 19th and 20th centuries the rates of recurrence of the earthquakes with M 6.2 near the two phases of the Moon are respectively 6.2 times and 4.5 times as frequent as the average rate of recurrence, having a stripe-shaped distribution and the major earthquakes with M 7.0 almost occurred in the maximum and minimum year of the inclination and within two years after or before it in particular. As for the solar and lunar tidal forces, most of the earthquakes occurred in the time interval when the horizontal component of the tidal force made the greatest change. This shows that an earthquake can be excited by the position of the Moon and the tidal forces of the Sun and the Moon.

**JSP23/E/46-B1** Poster **0830-07**

**IMPACT OF THE HYDROLOGIC EXTREMES OVER THE WATER TABLE IN THE "PAMPA HUMEDA" (ARGENTINA) AND ITS RELATIONS WITH THE ENSO**

Maria del Valle VENENCIO and Norberto O. Garcia (Facultad de Ingeniería y Cs. Hídricas - Univ. Nac. del Litoral, CC 495 - (3000) Santa Fe, Argentina. - E-mail: mvv@fich.unl.edu.ar)

This paper aims to create the bases in order to carry out, starting from seasonal and interannual climate prediction, a seasonal and interannual prediction of availability of groundwater resources coming from the unconfined aquifer in the productive areas of the "Pampa Húmeda" in the Argentine Republic.

The regional averages of the depth of the unconfined aquifer get rid suppose affected only for climatic variations. Also, the use of the groundwater resource is considered constant. Keeping in mind that the several water resources states in the region obeys several relationships between the variables precipitation, evaporation and evapotranspiration, it was carried out a serial water balance and correlations between the variability of the precipitation and the depth of the unconfined aquifer.

So, we can say that the precipitation produces decreasing or rising water level. As it was demonstrated the relationship between the ENSO and the precipitation on the Southeastern South America (SSA) by several authors, presently work was aimed to establish relationships between the water table and the ENSO. This correlation also provides useful information about the predictability of the future piezometric levels for sustainability of groundwater resources. Then, the main conclusion of this work is that the water table level is predictable in function of a predictor like El Niño.

**JSP23/E/04-B1** Poster **0830-08**

**LONG REPOSE PERIODS IN THE ERUPTIVE HISTORIES OF RECENT KAMCHATKA VOLCANOES: WHAT VOLCANO CAN BE RECOGNIZED AS EXTINGCT?**

Vera PONOMAREVA, Olga Braitseva, Ivan Melekestsev (Institute of Volcanic Geology and Geochemistry, Piip Ave., 9, Petropavlovsk-Kamchatsky, 683006, Russia, email: ponomareva@geology.ru) Leopold Sulerzhitsky (Geologic Institute, Pyzhevsky per., 7, Moscow, 109017, Russia, email: suler@ginran.msk.ru)

Detailed studies of the eruptive histories of Kamchatka volcanoes, based on geologic mapping, tephrochronology and radiocarbon dating, allowed us to document main repose periods in the lives of most Holocene volcanoes and monogenetic volcanic fields, and to determine their duration. It appeared that dormant periods as long as 500-1000 years were common in the lives of the volcanoes of various morphology, types of activity, and composition of eruptives. The best known example is Bezmianny volcano which was silent for about 1000 years before the 1955-56 large eruption. Longer repose periods up to 2000-3000 years were not rare. The longest repose periods - about 3500 years - were recorded at Kikhpinch and Dikii Greben' volcanoes; after a long dormancy both volcanoes were able to resume their activity. These data suggest that at least in Kamchatka a volcano should be considered potentially active (and thus, potentially hazardous) if it was proved to produce at least one eruption within the last 3-4 thousand years. This approach has allowed us to add some more names to the list of active volcanoes: Taunshits, Khodutka, Dikii Greben', Khangar volcanoes, which have been considered extinct and were not included in any catalogues of active volcanoes, appeared to have large eruptions within the last 3000 years, as well as Tolmachev Plateau and some other volcanic fields.

**JSP23/E/57-B1** Poster **0830-09**

**THE CELLULAR AUTOMATA MODEL SCIARA FOR LAVA FLOW SIMULATION: APPLICATIONS AND RESULTS**

G.M. CRISCI, A. Di Francia, S. Di Gregorio, F. Nicoletta\*, R. Rongo, W. Spataro (Dip. di Scienze della Terra Dip. di Matematica \*Dip. di Chimica ersità della Calabria, I 87036 Arcavacata, Italy)

Cellular Automata (CA) represent a parallel computational method in alternative to differential equations, for modelling very complex phenomena, whose evolution can be considered based exclusively on local interactions. The CA model SCIARA for the simulation of lava flow was developed and subsequently improved several times by our research group. A lava flow is described in SCIARA as a system with discrete time and space; the space is represented by regular cells (square or hexagonal) two-dimensional cells, whose specifications (substates) describe the main physical characteristics of the corresponding portion of space: altitude and, for each lava layer, lava thickness, temperature, lava outflows toward the adjacent cells; furthermore a division in lava layers can be considered in a refinement of the model. The CA evolves changing the state of all cells simultaneously at discrete times. Input for each cell is given by the states in the adjacent cells; the evolution of the phenomenon is mainly given by the computation of the outflow from the cells and the change of the remaining substates. SCIARA was applied in different times to 1986/7 and 1991/2 Mount Etna eruptions. The results were satisfying within limits to forecast the lava flow path, according to the surface covered by lava. The main parameters of the model for Etna lavas were found; then simulations were performed in order to evaluate the risk in some inhabited Etnaean area (the towns of Nicolosi, Pedara and S.Alfio) considering future catastrophic events. We consider the evolution of SCIARA, the main results and a critical discussion for a further improvement of the model, its limits in the application.

**JSP23/W/89-B1** Poster **0830-10**

**UNFAMILIAR HORIZONTAL WAVES IN UPPER LAYERS EXCITED BY ACCELERATION AND OTHER EFFECTS**

GALIEV

Abstract not available at the time of going to press

**JSP23/C/U5/E/18-B1** Poster **0830-11**

**LAVINA - A COMPUTER TOOL FOR AVALANCHE FORECASTER**

Pavel CHERNOUSS and Evgeny Mokrov (Center of Avalanche Safety, "Apati" JSC, 33a, 50 years of October St., Kirovsk, Murmansk region 184230, Russia, e-mail: P.Chernous@apatit.murmansk.su); Alexander Perlikov (Institute of Ecology, Kola Science Centre of the Russian Academy of Sciences, 14a, Fersmana St., Apatity, Murmansk region 184200, Russia)

LAVINA is a software package which assist avalanche forecaster to evaluate avalanche risks. It is an integrated system consist of two main units permitting evaluate probabilities of avalanche occurrence and dynamical parameters of possible avalanches. Probability of avalanche occurrence is evaluated for a whole region or for a separate starting zone. In the first case standard meteorological data and snow drift measurements are used for different types of discriminant analysis and pattern recognition algorithms. Diagnostics is carried on each third hour as current measurements have being made. Probabilistic and categorical conclusions on avalanche releases are the results of data treatment. There is an opportunity to display ten situations closest to current one from archive. Statistical simulation applied to snow thickness, density and shear strength is used for evaluation of snow cover stability in a separate starting zone. The areas of instability of different probabilities are displayed at a computer monitor. The dynamical parameters of a probable avalanche - maximal speed and impact pressure, are calculated at any given point of the avalanche path. LAVINA as a part of computer assisted work place of an avalanche forecaster is in operation at the Center of Avalanche Safety since 1991. The results of its exploitation are discussed and the ways of its improving are considered.

**JSP23/E/52-B1** Poster **0830-12**

**INFLUENCE OF MACROSEISMIC INTENSITY ATTENUATION IN SEISMIC HAZARD EVALUATION FOR FAGARAS (ROMANIA) CRUSTAL SOURCES**

IREN-ADELINA MOLDOVAN (IVAN) and Aurelian Pantea (National Institute for Earth Physics, P.O. Box MG-2, Bucharest-Magurele, Romania, e-mail: pantea@infp.ifa.ro and iren@infp.ifa.ro)

An important step for the correct assessment of seismic hazard is the interpretation of the macroseismic effects distribution from a given seismic zone, as well as the good evaluation of seismic intensity attenuation laws. The attenuation was analysed as a function of distance and azimuth, using nine attenuation laws. The present paper is a study of macroseismic intensity attenuation laws, using 5 crustal earthquakes (MGR>4.0) occurred in Fagaras (Romania) seismic zone, along the following



## INTER-ASSOCIATION

azimuths: E, W, N,S,NE,SW,NW,SE. The evaluation of macroseismic intensity attenuation laws for Fagaras region was imposed by the necessity of seismic hazard assessment in this high seismic potential zone the largest event occurred in this zone: MGR =6.4;  $l_0=IX$ ).

**JSP23/W/90-B1** Poster **0830-13**

### COMPARISON BETWEEN TWO SYSTEMS OF BASE SEISMIC INSULATION

Federico BARTOLOZZI (Civil Engineer and Independent Researcher, via dei Carracci3, 21100 Varese, Italy, email: ciuciuza@iol.it)

One of the proposed systems is with four rigid movable bearings and the other one with four elastic bearings. The two systems share the following characteristics: 1. self-centring of the building after an earthquake; 2. extreme economical competitiveness with all the existing anti-seismic systems, due to the considerable decrease of the seismic energy in the building, which makes possible the use of slenderer carrying structures. The differences between the above systems are: 1. a pendulous effect in the building, during an earthquake, in the system with rigid bearing. It is characterised by a very small vertical rotation of the building, which varies in average from a few seconds to some minutes with soil displacements included between some millimetres and about 150 mm. In addition, this effect is extremely limited and has no repercussions of psycho-physical character for the inhabitants of the building; 2. the verticality and the immobility of the building with respect to the horizontal translation of the foundation-soil complex in the system with elastic bearings. The vertical elastic strain of the springs compensates the variations of rigid deflection relative to the bearings, due to the inclination of their sliding surfaces. The vertical component of the motion, due to the sub-undulatory shock, varies only partially the building behaviour because of two phenomena: minor vertical translation of the building and resonance possibility. In order to prevent the resonance danger, each bearing is equipped with two or four frequency converters automatically started up when the emergency situation, defined by the equality between the vertical component of the earthquake frequency and the building vertical natural frequency, becomes imminent.

**JSP23/C/U5/W/05-B1** Poster **0830-14**

### HIMALAYS CRUST DEFORMATION REGION, RADON EMANATION AND SEISMO WAVE EFFECTS

Vladimir ALEXEEV, Yury Mikhailov (Institute of Terrestrial Magnetism, Ionosphere and Radio Wave Propagation of Russia's Academy of Science, Troitsk, Moscow region, 142092, Russia, e-mail: yumikh@charley.izmiran.rssi.ru)

The Himalays form is available region for study of the deformation processes of continental crust during collision orogeny. Simple shear dominant strains have developed new fabrics parallel to the main thrust zone. Radon fields [1] and aerosols create anomalous electric fields, which may change properties of upper wall of wave-guide earth ionosphere. This process leads to change of penetration of ELF-VLF waves through lower ionosphere and evolution of spectral characteristics of electromagnetic emissions, registered on satellites [2].

- 1 Virk H.S., Singh B. Correlation of radon anomalies with earthquakes in the Kangra Valley. Nucl. Geophys. 1992 V.6. N2. P.293-300.
- 2 Yu.M.Mikhailov, G.A.Mikhailova, O.V.Kapustina. Relation between ELF and VLF emissions on the Intercosmos 24 satellite and concentration of radon in earthquake regions. SSA 15 /GA 118 report of XXII IUGC General Assembly

**JSP23/W/34-B1** Poster **0830-15**

### PHENOMENOLOGICAL MODEL OF THE LARGE-SCALE EVOLUTIONARY PROCESSES IN A HAZARD SYSTEM OF THE EARTHQUAKE BASED ON THE SOC (SELF-ORGANIZED CRITICALITY) CONSIDERATION

Natalia SMIRNOVA, Vladimir Troyan (Institute of Physics, University of St.Petersburg, St.Petersburg 198904, Russia, e-mail: nsmir@snoopy.phys.spbu.ru); Masashi Hayakawa (The University of Electro-Communications, Chofu, Tokyo 182, Japan, e-mail: hayakawa@whistler.ee.ucc.ac.jp); Thomas Peterson (TFPLAB, Cleveland, Ohio 44124-5441, U.S.A., e-mail: TFPLAB@aol.com), and Yury Kopytenko (St.Petersburg Filial of IZMIRAN, St. Petersburg 191023, Russia, e-mail: galina@admin.izmi.ras.spb.ru)

The concept of self-organised criticality (SOC) is now widely used for interpretation of the natural hazard system behaviour. That concept was included as one of the principal point in a complex approach proposed recently by the present authors for searching the earthquake precursory signatures. Here we develop consideration of the processes in the earthquake regions on the basis of SOC concept. We suggest a phenomenological model for large-scale evolutionary processes occurring between two violent earthquakes. Four principal phases of the evolution: random chaos, subcritical, critical and supercritical stages are proposed and analysed consistently. The external stimuli such as geomagnetic storms, sharp temporal and spatial variations of atmospheric pressure, ULF impulses and others are considered as a driving force for "cellular automata" process in a seismoactive region. The important fingerprints of SOC - fractal structures in space and time are analysed using seismicity data and the ULF electromagnetic data timed to violent earthquakes near Guam (August 8, 1993,  $M = 8.0$ ) and Kobe (January, 16, 1995,  $M = 7.2$ ). A possibility to use the fractal characteristics of signals to study critical dynamics of a hazard system is discussed. The research was supported by NASDA (Japan) and Russian Foundation for Basic Research (Grants No. 98-05-65554 and 99-05-NNN).

**JSP23/E/24-B1** Poster **0830-16**

### DYNAMICS OF SELF-DEVELOPING NATURAL PROCESSES AND PROSPECTS OF ITS USE FOR THE FORECAST OF GEOPHYSICAL CATASTROPHES.

Alexander I. MALYSHEV (Institute of Geology and Geochemistry, Urals Branch of RAS, Pochtovy per 7, Ekaterinburg, SU-620151, Russia, email: root@igg.e-burg.su)

Study of patterns of fore-culmination activations present a great interest for the forecast of geophysical catastrophes, such as disastrous earthquakes, strong volcanic eruptions, rock bumps, landslides etc. During the study of Bezymyanni volcano eruptions in 1980-1987 the fact of hyperbolic activation before explosive-effusive eruptions was established. Further studying of the revealed regularities and their comparison with empirical dependencies of the development of various natural processes allowed to conclude that there is a wide class of self-developing natural processes, the dynamics of which is described by non-linear differential equation of the second order. The attempts of using these regularities for the forecast of eruptions were quite successful, however the accuracy of the forecast for the time of eruption did not exceed a semi-quantitative level. At present the methods, allowing confidently to reveal the laws of the development of natural processes, have been developed. As it is shown on the example of a number of Bezymyanni and Shivelutch volcanic eruptions, for the class of eruptions, having stable fore-culmination preparation, this technique allows increasing accuracy

of paroxysm time forecast up to a quantitative level.

The forecast of destructive earthquakes is more complicated. Ivan Tikhonov and me have analyzed the fore-shock-aftershock sequences of destructive earthquakes in southern Kuril arc area. It was established that the development of both of fore-shock, and aftershock sequences corresponds to the equation of the dynamics of self-developing natural processes. However the fore-shock sequences are more poorly expressed. Probably, some updating of seismic observations is required for getting more stable results. The obtained results make it possible to assume that the methods are a perspective for the forecast of these geophysical catastrophes.

Tuesday 27 July AM

## DETECTION, MONITORING, EARLY WARNING AND PREDICTION

**JSP23/W/25-B2** Poster **0830-01**

### EXCESS AND DEFICIENT RAINFALL YEARS OVER INDIA DURING 1871-1996: A BRIEF APPRAISAL

A. A. MUNOT (Indian Institute of Tropical Meteorology Dr. Homi Bhabha Road, Pashan, Pune-411 008, India, e-mail: munot@tropmet.ernet.in)

India, being an agricultural country has its economy closely linked with the performance of the summer monsoon (June-September) which gives 75-90 % of the total annual rainfall. Timely onset and normal distribution of rain in the summer monsoon season generate good amount of food production whereas erratic behavior of monsoon which leads to drought/flood over the country has an adverse effect on the food production and in turn on the economy of the country. Because of this, year to year variation of monsoon rainfall becomes the subject of immense importance. In view of this in this paper an attempt is made to study the inter-annual variability of summer monsoon rainfall for the period 1871-1996. On an average India as a whole receives 852.4 mm of monsoon rainfall with a standard deviation of 84.7 mm and coefficient of variation of 9.9 %. Excess and deficient rainfall years over the country are identified using suitable criterion. There are 22 deficient and 19 excess rainfall years during 1871-1996. The total area of the country under deficient rainfall conditions as well as under excess rainfall conditions have been computed for all the deficient/excess rainfall years. The mean area of the country under deficient rainfall condition in a deficient rainfall year is found to be 42.8% whereas the mean area of the country under excess rainfall condition in a excess rainfall year is found to be 35.7 %. Out of 22 deficient rainfall years, during four years viz. 1877, 1899, 1918 and 1987 more than 60 % area of the country suffered from deficient rain. Similarly out of 19 excess rainfall years during four years viz. 1892, 1917, 1961 and 1988 more than 40 % of the total area of the country was under excess rainfall conditions. Conditional probabilities have been computed for all-India rainfall to be deficient or excess on the basis of June, July and June + July rainfall. It is observed that by the end of July it is possible to anticipate with reasonable degree of accuracy how the performance of the monsoon will be at the end of September, whether it will be normal, deficient or excess. Based on these assessments precautionary measures can be taken in case of monsoon being abnormal.

**JSP23/C/U5/E/11-B2** Poster **0830-02**

### SHORT-TERM EARTHQUAKE PREDICTION: METHODOLOGICAL ADVANTAGES AND WARNING SYSTEM.

Vitali A. MORGOUNOV (Institute of Physics of the Earth, Moscow 123810, B.Grusinskaya 10, Russia, email: vam@uipe-ras.scgis.ru)

What is preferable: to use a chance to win or full ignorance of impending hazard?! Are the cases of real predictions only a blind luck or it is a step to solve the problem? At what extend the uncertainty relation Cognoscibility/Unpredictability of Earthquakes could be improved? Between polar opinions like the dismal prospects for real improvement of the unpredictability (London, November, 7-8, 1996) and unique practical success in China in 1975,1997 there exist a optimum way to solve the most important part of the problem. Progress in the study of short/immediate precursors could be one of the possible path to get over the obstacle due to the following advantages. 1. The final stage of preparation of impending earthquake is characterised by a substantial activation of the process while it's strain rate increase by the orders of magnitude and considerably increase signal-to-noise ratio. That is favourable for identification of critical state of the focal zone through the ground measurements of geophysical fields, in particular by electromagnetic emission, generated by the stress-strain rate of the rock. 2. The avalanche creep process and the worked out instrument make possible to advance the effectivity of the method in relatively short period of time in seismic active areas during the background seismicity ( $M=3-4$ ). 3. The short-term methods suggest the practical utilisation to prevent the casualties and ecological catastrophes. The EM method, experimental results, and Hardware-Software System "Alarm-Seismo" as an acceptable warning instrument are discussed. The System consists of the network of N slave controllers and master station, where in a real time regime the data is processing by PC computer. The distance between the slave stations is defined by the magnitude of expected earthquake, tectonic and geological peculiarities of the region, relief.

**JSP23/W/99-B2** Poster **0830-03**

### MONITORING OF NATURAL HAZARDS USING MULTI-SENSOR DATA

Ramesh P. SINGH, Sudipa Roy and N.C. Mishra (all at Department of Civil Engineering, Indian Institute of Technology, Kanpur - 208016, India, email: ramesh@iitk.ac.in)

The data recorded by the Special Sensor Microwave Imager (SSM/I), IRS-P3 MOS, IRS - LISS and NOAA AVHRR Data over India have been analysed. The brightness temperature deduced from SSM/I data over snow covered region show distinct behaviour which is attributed to the variable snow thickness and snow melting. The routine analysis of SSM/I data will give fairly good idea of snow avalanches and flooding of the river as a result of snow melting. The daily or weekly variations of brightness temperature, liquid water path (LWP) and total precipitable water (TPW) over Arabian sea and Bay of Bengal has given an anomalous characteristics of a tropical cyclone which hit the coast of Bangladesh. The normalised vegetation index (NDVI), vegetation condition index (VCI) and temperature condition index (TCI) deduced from NOAA-AVHRR give information about the vigor of the vegetation which can be used in monitoring of drought conditions. The IRS-P3 MOS data in 14 bands along path 95 of winter and summer seasons have been used in classifying water bodies. The spectral reflectance deduced in 14 bands give information about the water quality> The characteristic peaks in the spectral reflectance data give idea about the type and distribution of contamination in water bodies. The IRS-LISS data has been used for mapping of the lineaments which can be used for the evaluation of seismic hazards of any region. In the present paper the use of multi sensors data will be illustrated and discussed in monitoring various types of natural hazards.



JSP23/W/100-B2 Poster 0830-04

## GEOPHYSICAL HAZARDS: MITIGATION AND WARNING SYSTEMS IN INDIA

K.S. MURTY (E-3 Vishnukamal Apts., 160 Shivajinagar, Nagpur, 440 010 India)

In the last two decades, India was hit by several natural disasters of which the Andhra cyclone of 1977, the Uttarkashi earthquake of 1991, the Latur earthquake of 1993 and the Andhra cyclone of 1996 are typical geophysical phenomena that caused destruction of property and loss of life on a large scale. Relief measures were taken up by government and non-government agencies, while long-term measures like construction of cyclone shelters and new villages to house the affected population were initiated. Cyclone warning systems, flood warning systems, and seismological network in areas that are prone to these geophysical hazards have been set up. Besides, improved infra-structures like road construction have been made part of the development programmes of the concerned areas. These steps have considerably reduced loss of life in some of the more recent natural disasters the country faced.

JSP23/E/12-B2 Poster 0830-05

## AN EMPIRICAL DISPERSION RELATION FOR SEISMIC SIGNALS AND EARTHQUAKE PREDICTIONS

Boris W. LEVIN (Shirshov Oceanology Institute of RAS and Russian Foundation for Basic Research, 32a Leninsky prosp, Moscow, 117334 Russia email: levin@rbr.ru); Elena V. Sassorova (State Oceanographic Institute, 6 Kropotinsky per., Moscow, 119838 Russia; email: sator@geoph.ioras.msk.ru)

We show that faint seismic signals radiated from an earthquake source and acoustic signals foregoing a compression failure of laboratory rock samples can be written by common empirical relationship for waves of period  $T$  and length  $L$ , as follows  $T^2 = dL$ , where  $d$  is dimension coefficient. This leads us to some empirical dispersion relation for seismic signals that is defined by expression  $W^2 = 2^3 \cdot 14^k A k$ , where  $W$  is frequency,  $k$  – wave number,  $A$  – acceleration of stress force. The attempt to find such dispersion relation with theoretical way was made by L.Brevdo (1998) because similar function may, on his opinion, lead to an effective method of some earthquake prediction. We used special developed software package for data processing of 200 earthquake records and had found more than 30 events in which digital records the seismic foregoing signals were discovered. The period-length relation for these signals was well described by presented expression. Although the expression should be studied for using in condition of real seismic region, the presented method can sometimes be used to further improve earthquake disaster mitigation practices.

JSP23/C/U5/W/04-B2 Poster 0830-06

## A VOLCANO MONITORING AND TSUNAMI WARNING SYSTEM FOR GRENADA AND THE SOUTHERN GRENADINE ISLANDS.

Lloyd L. LYNCH, John Shepherd, and Chandradath Ramsingh (Seismic Research Unit, University of the West Indies, St. Augustine, TRINIDAD, email: sru@wow.net).

We propose to develop and establish a volcano monitoring and tsunami warning system for Grenada and the southern Grenadine islands. This region is located close to the Kick 'em Jenny (KeJ) submarine volcano, which has erupted ten times since it was first identified in 1939. Studies that have been done to assess the explosive potential of this volcano and to assess the vulnerability of the East Caribbean Islands to tsunamis, have identified it as a prime tsunami-genic source with Grenada and the southern Grenadines being most vulnerable to its hazards. The studies have also revealed that East Caribbean islands are exposed to tsunamis from other potential sources but to a lesser extent and that the existing regional seismograph and volcano monitoring efforts could be extended and reinforced to mitigate the effects of hazards from KeJ and tsunamis.

The primary aim objective of the volcano monitoring and tsunami warning system is therefore to maximise life safety by providing some level of advanced warning to the vulnerable population. The system is composed two critical components. The first is an integrated network of instruments to detect and rapidly evaluate the nature of increased volcanic activity at the KeJ and events of tsunami generating potential (such as sub-marine landslides or large earthquakes). An array of tide gauges will also be used to track the progress of any sea wave that may be generated. The second component of the system is a set of definitive procedures on how to respond to a tsunami-genic event. All data from the network will be tele-metered to a permanently manned monitoring and warning center to be established near the north coast of Grenada. Warning and alert activities will be co-ordinated through this center. Selected data channels will be relayed to the headquarters of the regional earthquake and volcano-monitoring agency - the Seismic Research Unit (SRU). This agency will widely support the warning center in the areas of equipment installation and maintenance, data processing and interpretation, and staff training. The SRU also plans to assist in educating vulnerable communities about other mitigation techniques that can be used to complement the proposed system.

JSP23/E/49-B2 Poster 0830-07

## TOWARDS UNDERSTANDING LAHAR-TRIGGERING MECHANISMS AT RUAPEHU

Vincent NEALL and Jerome Leconte (Institute of Natural Resources, Massey University, Private Bag 11 222, Palmerston North, New Zealand, email: V.E.Neall@massey.ac.nz); Katy Hodgson (Natural Resources Engineering/Environmental Management and Design Division, Lincoln University, P.O. Box 84, Canterbury, New Zealand, email: Hodgsonk@kea.lincoln.ac.nz)

Over 20 major lahar deposits have been mapped and described from the past 2,000 year B.P. record at Ruapehu. In historical time, a number of different lahar-triggering mechanisms have been observed, so it is pertinent to ascertain how the prehistoric lahar record originated and how this relates to lahar magnitude. We are beginning to recognise specific signatures in the lahar/tephra record that fit models for lahar generation at this volcano. Lahar deposits immediately preceding tephra eruptions are consistent with volcanic activity emptying the crater lake until dry eruptions can occur with resultant ash showers as exemplified by the 1995 eruptions. Lahar deposits immediately following tephra eruptions are consistent with post-eruptive rain-triggering events mobilising tephra accumulations high on the cone. Lahar deposits containing fragile volcanic bombs are clearly indicative of explosion events and eruption-generation of the lahars. Others will be non-eruptive collapse events due to failure of the crater lake wall for a variety of reasons. Currently our programme seeks to: (1) use all sedimentological parameters to characterise the lahar deposits; (2) use petrological matching of lahar clasts to lava flows on the edifice; (3) integrate the complex lahar and tephra record and; (4) provide further precise dating, to elucidate how prehistoric lahars over the last 2,000 years were generated. We thereby hope to understand the environmental conditions one may expect to lead to, or cause any future laharic event.

JSP23/W/27-B2 Poster 0830-08

## ERUPTION FORECASTING AT CERRO NEGRO VOLCANO, NICARAGUA, USING TIME-VOLUME RELATIONSHIPS

Brittain HILL, Charles Connor (CNWRA, Box 28510 San Antonio TX USA 78228, E-mail: bhill@swri.edu)

At the scale of sub-duction-zone tectonics, magma production rates appear constant relative to eruption recurrence rates. Differentiation and mixing processes obscure magma production rates in the mantle, making time-volume relationships complex at differentiated volcanic systems. Cerro Negro (CN) volcano in Nicaragua, however, has erupted relatively homogeneous high-Al basalt 22 times since forming in 1850 A.D. Small petrogenetic variations at CN are produced through minor crystal fractionation-accumulation. Waxing activity from 1850-1900 is followed by a steady-state eruption rate of  $1.8 \times 10^6 \text{ m}^3/\text{yr}$ . Relatively constant petrogenesis of CN basalt suggests eruption rate is controlled by the mantle replenishment rate and thus may follow simple time-volume predictable patterns. Empirically, large-volume eruptions at CN since 1900 are followed by long quiescence, whereas short quiescence follows small-volume eruptions. The timing of CN eruptions  $>5 \times 10^6 \text{ m}^3$  has a linear relationship ( $r^2=0.97$ ) with cumulative volume at the time of each eruption. Eruptions in 1992 and 1995 are successfully forecast within 1 yr of the actual eruption using these relationships. The 1971 eruption occurred 12 yr earlier than expected, also earlier than forecast using a 95% confidence interval (1973-1996). The 1968 eruption occurred 8 yrs

JSP23/E/23-B2 Poster 0830-09

## GEODETIC MONITORING OF FOGO ISLAND (CAPE VERDE ARCHIPELAGO) FOR VOLCANIC HAZARD REDUCTION

Sandra I N HELENO, Joao L Matos and Joao F B D Fonseca (IST, Av Rovisco Pais, 1, 1049-001 LISBOA, Portugal, email: sasilva@alfa.ist.utl.pt); Jos N P Lima and J P Osorio (Centro de Geodesia, Instituto de Investigacao Cientifica e Tropical, Rua da Junqueira, 534, 1300 LISBOA, Portugal, email: cgeod@www.iict.pt); Inocencio J M Barros and Arlindo Rosario (LECV, CP 114, Praia, Republic of Cape Verde, email: lec.mit@mail.cvtelecom.cv); Antonio Berberan (LNEC, Av. Brasil, 101, 1799 LISBOA, Portugal, email: berberan@lnecc.pt); Simon J Day, Benfield Greig Hazard Research Centre, UCL, Gower Street, London WC1E6BT, UK, email: s.day@ucl.ac.uk)

As part of a broader hazard reduction project in Fogo Island, N Atlantic, (Fonseca et al., this issue), a programme of periodic GPS and levelling observations was initiated, with a view to the forecasting of impending eruptions by the detection of associated anomalous crustal deformations. In addition, the data will be used in the characterization of the possible flank instability of the volcanic edifice (Day et al., this issue), which may in itself constitute a significant hazard to the population of the island (33000 inhabitants). This poster describes the observational infrastructure built in the island (23 observation points), emphasising the volcanological criteria behind its design, the care taken in the selection of sites with adequate geology, and the stability requirements of the monuments. Results from the Zero Epoch campaign (September 98) are presented and discussed earlier than forecast, but within a 95% confidence interval (1967-1994). Several intervening small-volume eruptions before the 1968 and 1971 events likely triggered the larger eruptions before source replenishment was complete. The  $8 \times 10^6 \text{ m}^3$  of basalt erupted during 1995 activity at CN indicates the next significant eruption is most likely in 2000+/-1, with a 95% confidence interval to 2006 in the absence of intervening small-volume eruptions.

The work reported here was supported by the U.S. Nuclear Regulatory Commission (Contract NRC-02-97-009). This work is an independent product of the CNWRA and does not necessarily reflect the views or regulatory position of the NRC.

JSP23/E/50-B2 Poster 0830-10

## GLOSEISRISK: A SIMPLIFIED APPROACHING TOOL FOR GLOBAL SEISMIC RISK

QI-FU CHEN and Jie Liu (P. O. Box 166, Center for Analysis and Prediction, CSB, Beijing 100036, P. R. China, email: qcf@cap.ac.cn); Yong Chen (No. 63, Fuxing Avenue, China Seismological Bureau, Beijing 100036, P. R. China, e-mail: yongchen@public.bta.net.cn); Ling Chen (Institute of Geophysics, CSB, Beijing 100081, P. R. China)

A simplified methodology of seismic hazard and risk assessment has been developed by IASPEI working group chaired by Prof. Yong Chen. The new approach includes two analysis methods: One is the seismic hazard analysis method by using earthquake catalogs as basic data and taking area model as potential earthquake sources. A technique is also developed providing the method for integrating individual influences of area sources, near and far, more active or less, into the probability distribution of seismic intensity or peak ground acceleration. Second method addresses exposure bypasses the data collection problems of the traditional method by employing a macroscopic indicator to represent the total exposure directly. The earthquake losses are assessed quickly and approximately by using social wealth represent by Gross Domestic Product and population data.

GloSeisRisk is application software based on Geographic Information System, which is designed to perform analysis and demonstration of seismic hazard and risk with the simplified methodology. The GIS-based GloSeisRisk offers a simplified approach modeling earthquake hazard assessment, loss estimation and earthquake scenario analysis. The GloSeisRisk includes the data analysis and processing programs for seismic catalogue, GDP and population and the seismic risk estimation functions respectively. It can also illustrate the data distribution and seismic risk maps for different print output. The data can be updated readily from available resources in this application tool and easy to update seismic risk analysis.

JSP23/C/U5/E/21-B2 Poster 0830-11

## SCIENCE OR CHANCE? SCORING THE CHINESE ANNUAL EARTHQUAKE PREDICTION FROM 1990 TO 1997

Yaolin SHI (Graduate School, University of Science and Technology of China, Academia Sinica, Beijing 100039, China, email: shiyl@sun.ihep.ac.cn); Jie Liu and Guomin Zhang (Center for Analysis and Prediction, Chinese Seismological Bureau, Beijing 100036, China, email: liujie@cap.ac.cn)

China is the only country in the world that has an official institution dedicated to precursor monitoring and earthquake prediction. About 800 observational stations spread over China, where more than 1700 pre-cursorial elements are monitored on regular basis. Every January, the Chinese (State) Seismological Bureau holds a national consultation meeting on prediction of major earthquake of the year. Deterministic predictions are made in the meeting. Possible risk areas for the year are circled out. These predictions are reported in official documents to the State Council, though kept confidential during the predicted year to avoid unnecessary social panic. In this study, we apply a scheme of success rate score (R-score) to evaluate the disclosed annual predictions in the 90s. A random guess leads to an R-score of 0 and a complete successful prediction has an R-score of +1. The average R-score of the annual prediction in China in the 90s is about 0.10. The probability in achieving equal or better results by random guess for an averaged year is quite high, about 1/3. However, the probability for

## INTER-ASSOCIATION

random prediction to get equal or better scores in 8 successive years is very low, only  $1.5 \times 10^{-4}$ . In conclusion, we believe that earthquake prediction in China is not by chance, even though it is still in a very preliminary stage to fit the definition of science.

**JSP23/E/35-B2** Poster **0830-12**

### CONTRIBUTION OF GEOPHYSICAL INVESTIGATION TO SOLVE AN ENGINEERING PROBLEM, SOUTH EL-KHARGA OASES, EGYPT

Maher A. MESBAH (Department of Geological and Geophysical Engineering; Faculty of Pet. and Min. Eng., Suez, Suez Canal University, e-mail: mmesbah@frcu.eun.eg)

A severe subsidence in the ground has been occurred during the passing of heavy machines which are used in the foundation processes of the base and the sub-base of El-Kharga-Paris railway proposed site. The current geophysical study is directed to determine the causes of this civil engineering problem. Therefore, geoelectric resistivity measurements were done by measuring 25 vertical electrical soundings (VESes) along the proposed line. Also, the previous regional gravity and magnetic surveys were examined in order to obtain the maximum information content from the measured resistivity soundings. In the light of the previous geological, geophysical and geotechnical studies in the area, the measured VESes were manually and automatically processed and interpreted in the light of the drilled boreholes. The analysis and the interpretation of the obtained results should that the maximum monitored depth is 42 m. The resulted geoelectrical models reflects that 3 to 4 geoelectric layers can be determined. A dry surface inhomogeneous layer formed from alluvium deposits covers the investigated site. This surface layer is followed by a soft to hard clay layer. The second geoelectric layer is followed by a hard and compacted clay layer and it was monitored at the most of VESes and didn't at some of them. Therefore, the bedrock layer needed to be a sub-base (or a base) for foundation didn't monitored along the investigated site and special construction requirements are necessary to overcome this conditions of the base.

**JSP23/E/36-B2** Poster **0830-13**

### AUSTRALIA'S IDNDR PROGRAM FOR MITIGATION OF GEOPHYSICAL HAZARDS

Jack RYNN (Member Australian IDNDR Co-ordination Committee, Centre for Earthquake Research in Australia, PO Box 276, Indooroopilly, Queensland 4068, Australia. email: sally.brown@uq.net.au); Alan Hodges (Chair Australian IDNDR Co-ordination Committee, Director General Emergency Management Australia, PO Box 1020 Dickson, ACT 2602, Australia. Email: ahodges@ema.gov.au); Pip Marks, (Manager Australian IDNDR Co-ordination Committee, Emergency Management Australia, PO Box 1020 Dickson, ACT 2602, Australia. Email: pmarks@ema.gov.au)

Following the proclamation by the United Nations of the International Decade for Natural Disaster Reduction (IDNDR) 1990 - 2000, the Australian Committee was established within Emergency Management Australia (EMA) to pursue the ideals and goals of IDNDR pursuant to mitigation measures of natural disasters in Australia. More than 120 projects were successfully undertaken directly relating to the IDNDR targets of risk assessment, mitigation measures (awareness, disaster planning, education, dissemination of information, community involvement) and warning systems, natural hazards. The multi-disciplinary approach involved government agencies (national, state and local), NGO's, academia and the private sector. The Australian projects include tropical cyclone workstation, risk assessments for storm surge and tsunami, earthquake mitigation of cities, flood and landslide awareness, wildfire prediction and warnings, economic guidelines for loss reduction, medical training package, media campaigns, education curricula and community awareness campaigns. Co-operative efforts with 7 Pacific Island countries through the Pacific Region IDNDR (per 1994 Yokohama Statement) completed projects on cyclone, flood, earthquake, tsunami, landslide and volcano. Planning is in progress to continue the IDNDR concept into the 21st century.

**JSP23/E/27-B2** Poster **0830-14**

### VIGIL - A WARNING SYSTEM FOR VOLCANIC ERUPTIONS IN FOGO ISLAND, NORTH ATLANTIC

Joao F B D FONSECA and Sandra I N Heleno (both at Physics Department, IST, Av Rovisco Pais, 1, 1049-001 LISBOA, Portugal, email: fonseca@alfa.ist.utl.pt) Peggy Hellweg and Horst Rademacher (both at Geo Enterprises Orinda, 57 Overhill Road, Orinda, CA 94563-3122, USA, email: HRademacher@compuserve.com) Steve Pauly and Bruce Pauly (both at Digital Technology Associates Inc, USA, 1330A Galaxy Way, Concord, CA94520, USA, email: dta\_pauly@compuserve.com) Nicolas dOreye (ECCGS, Walferdange, G.D.L., email: nicolas.doreye@ecgs.lu) Innocencio J M Barros and Arlindo Rosario (both at LECV, CP 114, Praia, Republic of Cape Verde, email: lec.mit@mail.cvtelecom.cv)

The low-energy strombolian eruption of April 95 in Fogo Island (North Atlantic), following 44 years of quiescence, enhanced the awareness of the risk posed to its 33,000-strong population by the volcanic activity (average interval between eruptions of about 20 years). This created the conditions for the implementation of a volcanological monitoring routine, presently being tested.

This presentation will describe the main components of the monitoring instrumentation, namely, a combined network of broad-band (Guralp CMG-40T) and short-period (Guralp CMG-40T-1) seismic stations, and a network of resistive tiltmeter (AGI702) stations. All the data collected, both in Fogo Island and in the neighbouring Brava Island, are transmitted in real-time to the data acquisition and processing laboratory (located in Praia, Santiago Island) using spread-spectrum transceivers and combiner-repeater modules. Additionally, a network of 23 high-precision geodetic monuments was built in Fogo Island to allow the periodic surveying with GPS receivers and EDM.

**JSP23/C/U5/W/01-B2** Poster **0830-15**

### SPACE - GEODETIC MONITORING OF LANDSLIDE MOVEMENTS USING GPS TECHNIQUES

PRUTIGLIANO, F. Vespe (Centro di Geodesia Spaziale P.O. BOX Aperta, 75100 - Matera ITALY, email: rutigli@asi.it); F. Cafaro, C. Cherubini (Politecnico di Bari - Istituto di Geologia Applicata e Geotecnica, Via Orabona 4, 74100 Bari, Italy)

The use of GPS techniques in monitoring natural hazards like volcanic deformations or landslide motions can be a powerful way to improve disaster mitigation. In this work the experimental setting up of a GPS-based system able to monitor landslide motions is reported. The first step of this work consists in evaluating how much a small simulated landslide movement can be mirrored by GPS data. The landslide simulation has been necessary to calibrate the hardware and the software used in this analysis. The experiment has been done using an array of six receivers placed in a small area around the CGS (Center of Space Geodesy) near Matera, Italy. One receiver has been assumed as reference, working permanently during the whole campaign. The other sites have been occupied for eight hours three times each, in order to obtain an evaluation, of the baseline length between all the receivers and the reference one before and after the displacement of the antenna of a known

quantity (few cm). The main topics under investigation in this step have been:

- The minimum observation time needed to obtain an estimation accuracy level suitable to this application (2-3 cm)
  - The possibility of using one frequency (L1) instead of two frequency (L1/L2) GPS receivers without loss of accuracy in the estimation of the movements
- The second step of the work consists in the planning of a system to constrain solidly the GPS antenna to the ground, necessary to be sure that the possible motions detected with the GPS are representative of the real motion of the landslide.

**JSM24**

**Monday 26 – Tuesday 27 July**

### WATER FLUXES AND WATER AVAILABILITY OVER CONTINENTAL REGIONS (IAMAS, IAHS)

Location: Mechanical Engineering, G34 LR  
Location of Posters: Old Gym

**Monday 26 July AM**

Presiding Chair: Ken Mitchell (NOAA/NWS, Camp Springs, USA)

### SURFACE AND SUB-SURFACE FEATURES

**Introduction 0900**

STEWART, RASCHKE, WILKINSON

**JSM24/E/09-B1**

**0910**

### COMPARISON OF SEASONAL VARIATION OF WATER/HEAT EXCHANGE AT LAND/ATMOSPHERE INTERFACE FOR THREE SITES IN EAST SIBERIA

Tetsuo OHATA, Yuji Kodama (Institute of Low Temperature Science, Hokkaido University, Sapporo, Japan. email: ohata@pop.lowtem.hokudai.ac.jp, kodama@pop.lowtem.hokudai.ac.jp); Takeshi Ohata (Faculty of Agriculture, Iwate University, Morioka, Japan. Email: takeshi@msv.cc.iwate-u.ac.jp)

Within the GAME-Siberia project, three local sites were selected for study of local land surface processes in order to investigate the response characteristics of land surface to the annual atmospheric forcing cycle. These sites are Tiksi facing the Arctic Ocean (vicinity of Yakutsk called Spasskaya Pad where it is Taiga, and Mogot area in the hilly Taiga area. These three sites were selected from the standpoint of surface conditions (Tiksi-tundra, Spasskaya and Mogotarea) and difference in basic climate parameter, precipitation. All have cold winters. Summer temperature is low for Tiksi compared with other two. Precipitation is high for Tiksi and Mogot. Two former sites have already obtained full year data in 1997-1998, and latter one is planned for 1999-2000 but it has past data obtained by State Hydrological Institute in the 1970s to 1980s. These data will be used for preliminary analysis. Result on the comparison of general geographical/topographical/surface/climate conditions, seasonal variations in ground thermal/hydrological conditions, water/energy exchange at the surface and typical processes need to be considered at each sites will be presented. Furthermore, area of further study and needed observation will be discussed.

**JSM24/W/04-B1**

**0930**

### MEASUREMENT OF SENSIBLE AND LATENT HEAT FLUX ON THE TIBETAN PLATEAU

Hirohiko ISHIKAWA, Taiichi Hayashi (both at Disaster Prevention Research Institute, Kyoto University, Gokasho, Uji, 611-0011, Japan, E-mail: ishihawa@srs01.dpri.kyoto-u.ac.jp); Osamu Tsukamoto and Hironori Fudeyasu (both at Faculty of Sciences, Okayama University, 700-0082, Japan, E-mail: tsuka@ccews2.cc.okayama-u.ac.jp); Ichiro Tamagawa (Institute for Hydrospheric-Atmospheric Sciences, Nagoya University, Furo-cho, Chikusa, Nagoya, 464-0814, Japan); Jun Asanuma (Nagaoka University of Technology, Nagaoka, 940-2137, Japan); Yunquiao Qi (School of Agriculture, Kochi University); Shim Miyazaki (Tsukuba University, Tennouai, Tsukuba, 305-0006, Japan); Jieming Wang, Yaoming Ma and Zeyong Hu (at Lanzhou Institute of Plateau Atmospheric Physics, Lanzhou, Gansu, 780000, P. R. China)

As a part of GAME (GEWEX Asian Monsoon Experiment), intensive observation of surface boundary layer of Tibetan Plateau (Amdo,  $32^{\circ} 14.468'N$ ,  $91^{\circ} 37.507'E$ ) was carried out from late May to early September in 1998. The intensive observation includes four components radiation, wind, temperature and humidity profile by a 14 m tower, precipitation and other meteorological parameters. Soil parameters such as ground surface temperature, soil temperature at three depths and soil heat flux at two depths was also monitored continuously. A 3d-sonic anemo-thermometer and an infrared hygrometer were used to measure atmospheric turbulence. The measurement was conducted almost continuously, and more than 4,500 runs of 30 min. 10Hz data were obtained. With these data the land surface-atmosphere interaction is investigated. As compared with other field data, the downward shortwave radiation is the stronger but the downward longwave radiation is the weaker at Amdo. The resultant net radiation is a little greater. The diurnal variation of the surface temperature exceeds 50 degrees in the dry season, which reduced to around 20 degrees after the onset of monsoon. The sensible heat flux was dominant in the dry season, but the latent heat flux becomes comparable with sensible heat flux in the wet season. The surface energy balance is assessed from net radiation, turbulent fluxes and the soil heat flux estimated from soil parameters. The balance is not well established so far. The estimated soil heat flux is smaller than the residual,  $R_n - H - LE$ . In addition to the intensive observation at Amdo, four automatic weather station have been collecting basic meteorological data since August, 1997. The data reveal the south-north contrast of the meteorological condition of the plateau including the winter time.

**JSM24/E/06-B1**

**0950**

### IMPROVEMENT OF MICROWAVE REMOTE SENSING ALGORITHM FOR SNOW AMOUNT ESTIMATION USING GEOLOGICAL INFORMATION

Hiroyuki OHNO (Japan International Research Centre for Agricultural Sciences, 1-2 Ohwasi, Tsukuba, 305-8686, Japan, Email: ohno@jircas.affrc.go.jp); Tetsuo Ohata (Institute of Low Temperature Science, Hokkaido University, 19-8, Kita-ku, Sapporo, 060-0819, Japan, Email: ohata@pop.lowtem.hokudai.ac.jp); Hironori Yabuki (Frontier Research System for Global Change, Institute for Global Change Research, Seavance North 7F, 1-2-1 Shibaura, Minato-ku, 105-6791, Japan, Email: yabuki@frontier.esto.or.jp)

The methods to estimate the amount of deposited snow using microwave remote sensing technique have been studied by many researchers. Many of studies point out that an algorithm, with the form of a polynomial of brightness temperatures, does not have large applicable area. The reason is considered that the microwave emission is affected not only by



the layer of ice particle but also by snow wetness, depth hoar, forest cover and complex mountains terrain. We made linear regression analysis between ground measured snow depth and the difference of microwave brightness temperature (T19v-T37v) observed by SSM/I on DMSP satellite for the data from 1994 to 1998, over more than 500 points ranging eastern part of the Euro-Asian Continent. The result shows that both of the first order (slope) regression coefficient and the standard error of regression has a tendency and to be large in central part of East Siberia. In contrast, only standard error is significant in the area of lower altitude in East Asia, without a clear tendency in slope coefficient. Based upon the result above, we developed a new algorithm being simple and having wider applicable. In the algorithm, the amount of deposited snow is calculated from the linear combination of raster maps of the brightness temperature, slope coefficient and offset coefficient. This procedure has an advantage of representing regional distribution of the error of estimation. We created the maps of the coefficients and the error, by means of multi-valuable regression of geological information of elevation, Id.

**JSM24/E/14-B1****1010****BOREAL FOREST SNOW INTERCEPTION AND SUBLIMATION FLUXES**

POMEROY (1), J. Parviainen (2), N. Hedstrom (1, 2), D.M. Gray (2) (1): National Hydrology Research Centre, Environment Canada, 11 Innovation Blvd., Saskatoon, Sask. S7N 3H5 Canada; (2): Division of Hydrology, University of Saskatchewan, Saskatoon, Sask, S7N 0W0 Canada)

The accumulation, unloading and sublimation of intercepted snow in northern forest canopies is described mathematically and using empirical data. Using fractal mathematics, the physics of interception and sublimation are scaled-up from small-scales, where they are well understood, to forest stand or larger-scale calculations of intercepted snow sublimation. Sublimation rates reached 3 mm per day and could take up to 120 hours after a snowfall. Evaluation of results from the simulation against measured interception and sublimation in a Canadian boreal forest jack pine stand during late winter, found the coupled model provides reasonable approximations of both interception and sublimation losses on half-hourly, daily and event basis. Cumulative errors in estimate of intercepted snow load over 23 days of test were 0.06 mm SWE with a standard deviation of 0.46 mm SWE. Sublimation losses during the evaluation were high, approximately two-thirds of snowfall within this period. Seasonal intercepted snow sublimation as a portion of annual snowfall at the model test site was lower than sublimation during the tests, ranging from 13% for a mixed spruce-aspen, 31% for the mature pine and 40% for a mature spruce stand. The results indicate that sublimation can provide a significant transfer of water vapour from northern forests to the atmosphere and that the transfers can be estimated by application of process-based algorithms can provide a significant transfer of water vapour from northern forests to the atmosphere.

**JSM24/W/02-B1**

Poster

**1030-01****SIMULATION OF PADDY FIELD USING THE SIB2 IN GAME-T**

Wonsik KIM, Taikan Oki, Katsumi Musiaki (Institute of Industrial Science, University of Tokyo, 7-22-1, Roppongi, Minato-ku, Tokyo 106-8558, Japan, Email: wonsik@iis.u-tokyo.ac.jp, taikan@iis.u-tokyo.ac.jp, prof@hydro.iis.u-tokyo.ac.jp)

At present it is being understood that the changes in water and energy cycle in Tropical Asian Monsoon (TAM) influence the water and energy balance of the other climatic systems. However, the changing of energy balance of land surface due to vegetation changes by deforestation in TAM is unknown. As one of the GEWEX Asian Monsoon Experiment-Tropics (GAME-T) projects, experiments to examine the above relationship were launched. One of the experiments was to monitor the energy balance of a paddy field in GAME-T area using a micrometeorological method. Micrometeorological parameters and variables of the paddy field were measured during the period of GAME-T project in Sukhotai, Thailand. Another experiment was performed to simulate the monthly energy balance of this site using the simple biosphere model (SiB2) proposed by Sellers et al.(1996). The leaf area index (LAI) of the vegetation was used as the indicating parameter for the vegetation changes. It was suspected that the changes in the LAI affects predominantly in changing the sensible heat flux and latent heat flux, which are important deciding factors of water and energy cycle.

**JSM24/W/03-B1**

Poster

**1030-02****THE MONITORING OF GROUND HUMIDITY BY METHOD NMR OF THE EARTH'S FIELD**

Anton SABANIN, Vladimir Sapunov, Alexey Denisov (Quantum Magnetometry Laboratory, Physics-Technical Department, Urals State Technical University, Mira 19 St., Ekaterinburg, 620002, Russia. E-mail: ants@dpt.ustu.ru)

NMR measurements are made by manipulating hydrogen protons in fluid molecules. Use of a method NMR gives exact amount of a free fluid, and does not depend on impurity. We have developed and assembled the working model of relaxometer. The relaxometer allows determining saturation of cores by a proton-containing fluid. In updating the equipment the application of the sensor on a surface of ground for monitoring humidity is supposed. Other opportunities of application are considered too.

The method of measurement – Packard-Varian, at which sample is exposed to initial magnetization with the subsequent registration of a signal free precession in the Earth's magnetic field. The times of the longitudinal relaxation time (T1) and the transverse relaxation time (T2) determine character of interaction of a fluid with a sample (ground, sand, etc.), and give the additional information on an opportunity and speed of discharge of water in a ground. Both are directly relate to a porous size. The amplitude of a free precession signal gives the information on amount of a fluid in a sample (Free Fluid index – FFI).

In the paper the accounts original of the noise proof proton sensor of a disk type are submitted. The received signal from such sensor does not depend on orientation of a magnetic field. The registration of a signal occurs in a homogeneous magnetic field of the Earth, that allows to characterize the large volumes of a sample not paying attention on heterogeneity its. In the same time the additional magnetic system is excluded and power consumption is lowered. The mode of accumulation and storage of a signal for case of low-saturated samples is stipulated.

**JSM24/W/07-B1**

Poster

**1030-03****CHARACTERISTICS OF PLANETARY BOUNDARY LAYER STRUCTURE IN CENTRAL TIBET DURING SUMMER SEASON OF 1998**

Nobuhiko ENDO (Frontier Research System for Global Change, c/o National Research Institute for Earth Science and Disaster Prevention, Tsukuba, Ibaraki 305-0006, JAPAN, Email: endo@frontier.bosai.go.jp); Tetsuzo Yasunari (Institute of Geoscience, University of Tsukuba, Tsukuba, Ibaraki 305, JAPAN, Email: yasunari@atm.geo.tsukuba.ac.jp)

Many investigators have previously been evaluated atmospheric heat source and moisture sink over the Tibetan plateau. One of the important processes on the energy and water circulation over the plateau is heat and water transportation mechanism in the planetary boundary layer.

Although several special observations were made in Tibet, regional characteristics of the planetary boundary layer (PBL) are not so clear. The purpose of this paper is to describe the regional characteristics of the PBL structure at Amdo, Central Tibet, during summer of 1998. Using data set is a GAME-TIBET IOP-98 special aerological data which were collected at Amdo (32.25N, 91.63E, 4700ASL) during the GAME-TIBET IOP from June 3 to August 20, 1998. The routine radiosounding observation was made at 00, 06, 12 UTC during IOP. We observed that vertical potential temperature gradient around middle of troposphere was rapidly decreased in June 10. It is coincided with a development of the Tibetan High. Atmospheric moisture content was suddenly increased at June 13. We considered that the monsoon season at Amdo was started around June 13 to June 21 to describe characteristics of the diurnal variation of PBL structure. Observed PBL diurnal variation was very clear. Most obvious character is the atmospheric moisture content was increased and easterly wind was simultaneously prevailed lower most 1000m depth of atmosphere during night. On the other hand, the mixed layer was developed during daytime. Its top reached around 2000m above the ground level. Shallow or deep convective cloud was developed during late afternoon. Those characteristics were almost similar to the CREQ93 radiosonde observation which made at northern side of the Tanggula mountain in 1993. However, the mixed layer depth at Amdo was larger than the case of CREQ93, and the precipitable water content was larger in Amdo. From GMS cloud imagery observation, it is obvious that cloud activity is more vigorous in southern side of the Tanggula mountains. Objective analysis data shows that there is a meridional gradient of water vapour over the plateau.

**JSM24/C/U1/P/03-B1**

Poster

**1030-04****GROUND WATER RECHARGE IN NORTHERN UGANDA**

JAMES MWAMI (Integrated Pastoral Development Project, P.O. Box 964 MBARARA, Uganda, Tel/Fax: 256-485-21395 E-mail: kalisa@swiftuganda.com)

Provision of Potable water supply for Uganda's predominantly (>90%) rural population depends upon the development of ground water. Recent research into ground water resources of Apac District of Northern Uganda indicates that most ground water moves by way of shallow weathered soils (regolith) rather than the underlying bedrock fractures which have traditionally been developed. Indeed, the Lango people have relied upon this shallow source through unprotected spring discharges and land dug "scoop wells". During the last three years a number of agencies (WATSAN-UNICEF, CPAR) have constructed shallow wells with competent yields in the regolith for domestic, hand pump obstruction rates up to 3m<sup>3</sup>/day. However incidents of well failure and waning spring flow have been attributed to presumed fluctuations in the shallow water table and raised concerns over sustainability of ground water development programmes in this region. Nevertheless, studies of ground water recharge in Apac have shown that replenishment is in the order of 0.2m/year and occurs exclusively from intense (>1 Omm/day) rainfall during the monsoons. Monitoring of water levels in the unconfined, regolith aquifer was therefore initiated in June 1994 in order to investigate both the magnitude of water table dynamics in the regolith and the nature of the water table's response to recharge events predicted by developed models of ground water recharge.

**JSM24/W/06-B1****1105****SCALES AND TRENDS OF OBSERVED SOIL MOISTURE VARIATIONS, AND PREDICTED FUTURE VARIATIONS OF SOIL MOISTURE**

Alan ROBOCK (Dept. of Environmental Sciences Rutgers, The State University of New Jersey, 14 College Farm Road, New Brunswick, NJ 08901-8551 USA, email: robock@envsci.rutgers.edu); Konstantin Y. Vinnikov (University of Maryland, USA)

Soil moisture is an important variable in the climate system. Understanding and predicting variations of surface temperature, drought, and flood depend critically on knowledge of soil moisture variations, as do impacts of climate change and seasonal forecasting. An observational data set of actual in situ measurements is crucial for model development and evaluation, and as ground truth for remote sensing. We describe the Global Soil Moisture Data Bank, a web site <http://www.envsci.rutgers.edu/~robock> dedicated to collection, dissemination, and analysis of soil moisture data from around the globe. The Global Soil Moisture Data Bank is a resource for the remote sensing, climate modelling, and climate analysis communities. We currently have soil moisture observations for over 400 stations from a large variety of global climates, including from the former Soviet Union, China, Mongolia, India, and the US. Here we describe the use of several of these data sets to analyse inter-seasonal, inter-annual and inter-decadal variations in soil moisture and determine the important scales of soil moisture variations. In the past, we have used these data to evaluate calculations of soil moisture by land surface models, including PILPS Phase 2(d), the ECMWF ERA-15 reanalysis, the Global Soil Wetness Experiment, to determine the representativeness of our current soil moisture network, to make recommendations about spatial and temporal scales of climate modelling and satellite remote sensing of soil moisture, and as ground truth for passive microwave remote sensing of soil moisture. The scale of temporal variation of soil moisture observed in Illinois, Russia, China, and Mongolia is about 2 months in all cases and the spatial scale in all these regions is about 500 km. We show these analyses and explain how these scales are controlled by atmospheric forcing. This has important implications for climate model evaluation, remote sensing, and design of surface observational networks of soil moisture. Summer desiccation is one of the most serious potential negative consequences of global warming.

**JSM24/E/03-B1****1125****A FIELD STUDY OF ATMOSPHERIC FORCING OF THE SUBSURFACE WATER BUDGET**

Gabriel ROONEY (Met. Research Unit (Field Site), Shortstown, Bedford, MK42 0SY, UK)

Results are presented from a continuing field study of subsurface and atmospheric moisture fluxes at a site near the main drainage stream of a shallow meso-scale (3 km lengthscale) sub-catchment near Bedford, UK. The study, carried out by the UK Meteorological Office Research Unit, began in May 1997 and collects data of precipitation, atmospheric moisture flux and water-table depth, and of subsurface moisture content using a buried vertical array of soil-moisture probes. Wind, radiation, and atmospheric, surface, and subsurface temperatures are also continuously measured.

The soil-moisture evolution is compared with simple force-restore methods for modelling precipitation recharge and drainage and evaporation/transpiration losses. The data show how the soil moisture contents at different depths depend to varying degrees on evaporation as well as precipitation, and how the deep soil moisture over-responds to the precipitation input because of drainage effects, effectively responding to the concentration of precipitation from a wider area. This indicates that one-dimensional modelling of subsurface moisture movement is insufficient in the saturated zone. In addition, it is demonstrated that the timescale for recovery from surface forcing also varies with depth.



**JSM24/E/01-B1 1145****RETRIEVAL OF PLANT-AVAILABLE SOIL MOISTURE THROUGH SATELLITE DATA ASSIMILATION INTO A GLOBAL VEGETATION AND LAND SURFACE MODEL**

Wolfgang KNORR (Max-Planck-Institut fuer Meteorologie, Bundesstrasse 55, D-20146 Hamburg, Germany, email: knorr@dkrz.de); Jan-Peter (Danish Meteorological Institute, Lyngbyvej 100, DK-2100 Copenhagen, Denmark); Bernard Pinty and Michel Verstraete (Space Applications Institute, European Commission Joint Research Center, I-21020 Ispra, Italy); Martin Heimann (Max-Planck-Institut fuer Biogeochemie, Postfach 100164, D-07701 Jena, Germany)

Plants control much of the water balance over continental areas. Therefore, observations of vegetation distribution from satellites can be used as an indicator of the amount of plant-available soil moisture for land surfaces on a global scale. Here, we present a method of inferring land moisture status by a combination of land surface modelling, using observed climate and soils data, and satellite remote sensing. The Biosphere Energy-Transfer and Hydrology model (BETHY) is used to compute photosynthesis, energy and water balance, as well as plant distribution globally. Modelled fields of the fraction of absorbed photosynthetically active radiation (fAPAR) are then compared to satellite data from NOAA-11/AVHRR, and a number of model parameters are adjusted until the agreement reaches an optimum. The results indicate maximum plant available soil moisture of 1000 mm and higher for many parts of the tropics and the arid temperate zones. By a comparison with field measurements, we also demonstrate the importance of consistency between observed greenness and proper surface parameterisation. Modified fields of maximum soil water storage lead to rather large changes in the simulated surface temperature in a general circulation model for a number of regions.

**JSM24/E/11-B1 1205****POSSIBLE ROLE OF SNOW-COVER ON VEGETATION IN ARID AND SEMI-ARID ASIA**

Shao-Fen TIAN (Frontier Research System for Global Change, IGCR, c/o Nat'l Inst. Earth Sci. & Disaster Prevention, Tsukuba, 305-006, Japan, e-mail: tian@frontier.bosai.go.jp); Tetsuzo Yasunari (Institute of Geoscience, University of Tsukuba, Tsukuba, 305-8571, Japan, e-mail: yasanari@atm.geo.tsukuba.ac.jp); Yuuya Adachi (College of Natural Science, University of Tsukuba, Tsukuba, 305-8571, Japan, email: adachi@etesia.geo.tsukuba.ac.jp)

This study examine role of snow-cover on the vegetation activities in arid and semi-arid Asia by comparing the spatial distributions and mean seasonal evolutions of the Normalized Differential Vegetation Index (NDVI), rainfall and snow-cover extent. Particularly, Gobi desert and the surrounding steppe regions are emphasised. Spatial distributions of annually-cumulated NDVI and snow-cover extent reveal that the boundary between Gobi desert and the northern steppe region coincides with the southern limit of regions with seasonal snow-cover. Seasonal evolutions monthly mean NDVI and rainfall shows that green-up in northern Mongolia (with snow-cover) precedes the onset of rainy season. However, the vegetation activity in Gobi desert and Ordos Plateau (without snow-cover) varies almost simultaneously or with a small lag to rainfall. The results suggest that the snow-cover in arid and semi-arid regions may be important for the vegetation activity there. It is implied that decrease in spring snow-cover associated the global warming may bring further northern expanding of the mid-latitude deserts.

**JSM24/E/04-B1 1225****CALCULATION OF RUNOFF IN LPS WITH SUBBASIN GRIDDING METHOD**

Suxia LIU (Department of Hydrology, Institute of Geography, Chinese Academy of Sciences, Beijing 100101, P.R.China, email: liux@sun.igehp.ac.cn)

Almost all of current schemes of land surface Parameterization (LPS) use longitude and latitude to subgrid research areas for regional study. This paper uses sub-basin gridding method to calculate runoff for a region in a typical Yellow River Basin. The regional Climate model is used for the calculation. The results are compared with that by current gridding method which certainly cut off the basin. It is shown that sub-basin gridding method is more reasonable from the point of hydrological view in water fluxes calculation.

**Monday 26 July PM**

Presiding Chair: Burkhardt Rockel (Institute of Atmospheric Physics, Geesthacht, Germany)

**ATMOSPHERIC, BOUNDARY LAYER AND PRECIPITATION FEATURES****JSM24/W/01-B1 1400****WATER BUDGET OF INTENSE CYCLONES IN THE BALTIC REGION**

Burkhardt ROCKEL (Institute of Atmospheric Physics, GKSS Research Centre, Max-Planck-Straße, 21502 Geesthacht, Germany, email: rockel@gkss.de); Ute Karstens (Institute of Atmospheric Physics, GKSS Research Centre, Max-Planck-Straße, 21502 Geesthacht, Germany, email: karstens@gkss.de)

Extra tropical cyclones are one of the major forces driving the hydrological cycle transporting huge masses of moist air and water between different regions of the globe. Within the frame of the Baltic Sea Experiment (BALTEX) the water budget of three intense cyclones was studied. These cyclones occur during the period 28th of August 1995 to 5th of September 1995, which falls into the PIDCAP (BALTEX Pilot Study for Intense Data Collection and Analysis of Precipitation) period where an extended set of observational data was collected. These cyclones were investigated making use of several ground based (e.g. rainfall stations, rain radars, GPS stations) and satellite measurements (e.g. NOAA/AVHRR) as well as analysis data from ECMWF and the German Weather Service. Special emphasis was laid on the 3D-distribution of water components in the cyclones and their temporal development. One of the cyclones staid in the observed area from its formation to its decay, which made it possible to study its whole life cycle. Also the accompanied water transport into the BALTEX region will be shown in this presentation. Furthermore a regional forecast model with a horizontal resolution of less than 20 km was used to simulate these cyclones and compared to the measured and analysed data sets.

**JSM24/W/10-B1 1420****RELATIONSHIP BETWEEN RAINFALL AND GSUT IN TIBETAN PLATEAU IN SUMMER MONSOON SEASON OF GAME/TIBET 1998**

Taiichi HAYASHI (Disaster Prevention Research Institute, Kyoto University, Gokasho, Uji, Kyoto, Japan, email: hayashi@rcde.dpri.kyoto-u.ac.jp)

The Tibetan plateau is the third pole in the world, following the arctic and Antarctic poles, which

affect the Asian monsoon. In the summer monsoon, Rainfall occurred in the afternoon almost everyday after the active development of cumulus in the morning. The wind speed increases suddenly from a few to more than 20-30m/s in only a few ten minutes. At the same time, the wind direction changes and the temperature falls abruptly. Strong solar radiation activates the convection and causes this diurnal variation in spite of the little humidity in the surface of the Tibetan Plateau. The observation of the turbulence in the atmospheric surface layer and clear the existence of the downdraft below the matured cumulus cloud. Enhanced aerological observation, the sensor was launched every 3 hourly, was made from June 7.

**JSM24/E/02-B1 1440****GROUND VALIDATION OF THE TRMM PRECIPITATION RADAR AND MESOSCALE ANALYSES WITH AN X-BAND DOPPLER RADAR SETTLED ON THE TIBETAN PLATEAU**

Shuji SHIMIZU (Earth Observation Research Center, National Space Development Agency of Japan, 1-9-9 Roppongi, Minato-ku, Tokyo 106-0032, JAPAN, email: shimizu@eorc.nasda.go.jp); Ken'ichi Ueno (School of Environmental Science, The University of Shiga Prefecture, 2500 Hassaka-cho Hikone, SHIGA, 522-8533 JAPAN, email: kueno@ses.usp.ac.jp); Hideyuki Fujii (Department of Civil and Environment Engineering, Nagaoka University of Technology, 1603-1 Kamitomioka-cho, Nagaoka, Niigata 940-2137, JAPAN, email: fujii@hydro.nagaokaut.ac.jp); Hiroyuki Yamada (Department of Earth and Planetary Science, Hokkaido University, Nishi-8, Kita-10, Kita-ku, Sapporo, Hokkaido 060-0810, JAPAN, email: yamada@metsun1.sci.hokudai.ac.jp); Ryuichi Shirooka (Department of Rural Development, Hokkaido National Agricultural Experiment Station, 1 Hitsujiogaoka, Toyohira-ku, Sapporo, Hokkaido 062-0045, JAPAN, email: shirooka@cryo.affrc.go.jp); Liping Liu (Lanzhou Institute of Plateau Atmospheric Physics, Chinese Academy of Science, 196 Dong Gang Xi Lu, Lanzhou, PRC, email: wmail2@ns.lzb.ac.cn)

A field observation using an X-band Doppler radar for the ground validation of the TRMM satellite was carried out between May to September 1998 near Naqu, Tibet for the GAME-Tibet project. Midnight rainfall was frequently observed around Naqu area. Stratiform rain lasted for 7 hours from 1600 UTC 1 Aug. 1998. In this case TRMM passed over the radar observation area. The TRMM PR showed that the stratiform echo had small diameter (< 100km) and local rain around Naqu area. PR and ground radar have qualitatively in this case a bright band clearly existed at 0.8km from surface (5.3km above sea level). Time series of vertical profiles of horizontal winds calculated by VAD method shows that beginning time of the northerly wind near the surface coincided with start of rainfall. Then northeasterly wind and convergence dominated around the radar site. The convergence made rain strengthen. It showed that the wind and divergence fields contribute to change of stratiform precipitation.

**JSM24/E/08-B1 1500****REASSESSMENT OF THE MOISTURE SOURCE OVER THE SAHARA DESERT**

ALPERT Pinhas, Yuval Shay-El (Dept. of Geophysics and Planetary Science, Tel Aviv University, 69978, Ramat Aviv, Israel, e-mail: pinhas@cyclone.tau.ac.il)

The components of the moisture balance equation are calculated for the Middle-East North-Africa regions, based on NASA's GEOS-1 DAS multi-year dataset. The annual mean DIV (Q) corresponds well with NCEP analysis by Vitart et al (1996). Over the N. African Sahara desert the moisture flux was shown to converge through the northern and southern boundaries mainly at low levels (~900 hPa) and to diverge through the eastern and western boundaries at higher levels (~700 hPa). Starr and Peixoto(1958) have classified N. Africa as a net moisture source. Area averaging of DIV (Q) over a box with varying dimensions reveals that N. Africa can be classified as a NET SINK if the box is small enough and located over the center of the desert. It is suggested that the earlier finding of a net source might be due to smoothing of the water/land boundaries, or due to atmospheric diffusion processes such as the sea-breeze cycle or clouds intrusion and their dissipation.

**JSM24/W/14-B1 1520****RELATIONSHIP BETWEEN RAINFALL AND DEFORESTATION IN THAILAND**

Shinjirou KANAIE, Taikan Oki, Katumi Musiaki (IIS, University of Tokyo, 7-22-1 Roppongi Minato-ku Tokyo, Japan, email: kanae@iis.u-tokyo.ac.jp)

Observed monthly rainfall data for more than 40 years in Thailand are collected and analyzed, to extract the long-term trend which may reflect the effect of deforestation. Consequently, a remarkable characteristic is found in the analysis of September, which is the peak month on rainfall in Thailand. To investigate the cause of this characteristic, numerical simulations with a regional climate model are carried out. From the analysis of these numerical simulations, it is concluded that the deforestation in Thailand should be the cause of this long-term rainfall change. Also the mechanism how deforestation influence rainfall is discussed.

Presiding Chair: Tetsuo Ohata (Institute of Low Temperature Science, Hokkaido Univ., Japan)

**LARGE SCALE BUDGETS AND FLUXES****JSM24/W/15-B1 1610****WATER AND ENERGY CYCLES IN THE TROPICAL SOUTH EAST ASIA FROM THE INTENSIVE OBSERVATION OF GEWEX ASIAN MONSOON EXPERIMENT IN TROPICS IN 1998**

Taikan OKI, Toshiyuki Nakaegawa, and Katumi Musiaki (Institute of Industrial Science, University of Tokyo 7-22-1 Roppongi, Minato-ku, Tokyo 106-8558, Japan Email: taikan@iis.u-tokyo.ac.jp)

As a part of GEWEX Asian Monsoon Experiment (GAME), GAME-Tropics (GAME-T) is aiming the quantitative monitoring of vapor flux, precipitation, evapotranspiration, radiative flux, and their seasonal, intra-seasonal, and interannual variations in the south-east Asia, and also aiming their applications for water resources management in the region. In order to accomplish these objectives, various field observations and data collections has been planned and implemented. The year 1998 was set to be the Intensive Observation Period (IOP) of GAME and organized field observations and data collections were carried out through the target region. Even though the target area of GAME-T largely covers the warm humid region in the south-east Asia, observational activities were mainly focused in Thailand. Although subsequent or intermittent observations are associated, major IOP activities were done during these two periods; Phase I Monsoon onset: middle of April to middle of June, and Phase II Mature stage of monsoon: middle of August to middle of September. Comprehensive observations includes 4 times daily launch of rawinsonde at 4 sites within Thailand associated with continuous observation by GPS receivers for estimation of precipitable water, digital recording of three weather radars, detailed surface flux observations at three representative land scapes, and ground truth observations for satellite remote sensing such as soil moisture measurement by SAR. From these IOP observations, a hydro-meteorological dataset is being

developed and comparative studies between these two phases are being carried out. Characteristic differences of water and energy cycles between the onset and mature stage of monsoon season was found even in a preliminary summary of the IOP data. Data management, the future linkage with modeling, and the regional reanalysis in high resolution using the IOP data will be discussed as well.

Tuesday 27 July AM

Presiding Chair: Tetsuo Ohata (Institute of Low Temperature Science, Hokkaido Univ., Japan)

JSM24/W/16-B1

1630

### SEASONAL CYCLE AND INTERANNUAL VARIABILITY IN THE AMAZON HYDROLOGIC CYCLE

Dr Ning ZENG (UC Los Angeles, email: zeng@atmos.ucla.edu)

An analysis of the Amazon basin hydrologic cycle has been carried out using the NASA/GEOS-1 atmospheric reanalysis, observed rainfall of Xie and Arkin, and historical Amazon river discharge. Over a seasonal cycle, the precipitation is found to vary by 5 mm day, the runoff by 2 mm day while the evaporation largely remains constant. On interannual time scales, the hydrologic variability both in the atmosphere and at the land-surface is found to be closely related to ENSO. The correlation between the Southern Oscillation Index and Xie-Arkin precipitation is 0.8 for the period 1985-1993 and 0.56 for the period 1979-1996. The precipitation lags behind the Southern Oscillation Index by 3-4 months while the Amazon river discharge lags behind the precipitation by another 3 months. The lagged relationship suggests interesting dynamic mechanisms. The reanalysis moisture convergence and observed discharge are used to diagnose basin average soil water storage. The year to year variation in the annual mean soil water storage is about 200 mm, comparable to the change within a climatological seasonal cycle. In one case, the basin soil water storage increases by 462 mm from September 1987 to March 1989, suggesting the remarkable ability of the tropical rainforest environment to store and take up water.

JSM24/E/05-B1

1650

### RECENT GCIP-SPONSORED ADVANCEMENTS IN COUPLED LAND-SURFACE MODELING AND DATA ASSIMILATION IN THE NCEP MESOSCALE ETA MODEL

Kenneth MITCHELL (National Centres for Environmental Prediction, NOAA/NWS, 5200 Auth Road, Camp Springs, MD 20746-4304, USA, email: Kenneth.Mitchell@noaa.gov); John Schaake (Office of Hydrology, NOAA/NWS, 1325 East-West Highway, Silver Spring, MD 20910-3283, USA, email: John.Schaake@noaa.gov)

With support from the GEWEX Continental-Scale International Project (GCIP), the Environmental Modeling Center (EMC) of NCEP joined with NWS hydrologists in the Office of Hydrology (OH) and satellite land-surface remote sensing experts in NESDIS to develop advancements in the land-surface subsystem (LSS) of the NCEP coupled mesoscale Eta model. Recent advancements include an increase from 2 to 4 soil layers, addition of an explicit vegetation canopy, sub-grid runoff treatments, and satellite-derived a) seasonal cycle of vegetation greenness and b) daily snow cover updates. The Eta LSS is a descendant of the LSS of Oregon State University (Pan and Mahrt, 1987). It carries multiple soil layers for which it predicts a) soil moisture using Richard's equation and soil temperature using the heat equation. In a major NCEP milestone on 03 June 98, the LSS state variables of soil moisture, soil temperature, canopy water, and snow water became fully and continuously cycled state variables in the coupled Eta model's 4-D Data Assimilation System (EDAS). Herein, LSS performance must be good on many time scales (hourly, daily, weekly, monthly, and annual). No nudging of the soil moisture is employed, neither to a soil moisture climatology or otherwise. A vivid example of EDAS soil moisture anomalies in the Texas and Oklahoma drought of summer 1998 will be shown. Additionally, this paper will present Eta LSS performance and validation studies, both from uncoupled intercomparison studies (e.g. PILPS 2a, 2c, 2d) and coupled Eta studies. For example, a new capability to validate LSS skin temperature against hourly 0.50-degree GOES-derived skin temperature will be shown.

JSM24/E/12-B1

1710

### WATER FLUX AND WATER AVAILABILITY OVER CHINA

Xinguo MO (Environment and Ecotechnology Station, Institute of Geography, Chinese Academy of Sciences, Beijing 100101, P.R.China, email: moxg@dls.iog.ac.cn); Suxia Liu (Department of Hydrology, Institute of Geography, Chinese Academy of Sciences, Beijing 100101, P.R.China, email: liux@sun.ihep.ac.cn)

The dataset of soil moisture and meteorological data over 102 agrometeorological stations has been collected over China. A simple regional evapotranspiration model is established which only needs the input from routine meteorological stations and soil moisture. Water flux and water availability is calculated by the model. Compared with the potent-evaporation distribution used currently to guide irrigation and other agriculture management, the results from the model is more accurate and reasonable.

JSM24/L/02-B1

1730

### SPECIAL-SCIENTIFIC THINKING IN HYDROLOGY: A "LABORATORY" FOR UNDERSTANDING OUR PROSPECTS FOR TODAY?

Konstantin A.Sergeyev, Dr. Sci., Prof. (St.-Petersburg State University, History of Philosophy Department, 5 Mendeleyev Line, St.-Petersburg 191002, Russia, email: george@tetrus.dux.ru); Natalia V.PENKOVA, Ph.D (State Hydrological Institute, Water Resources and Water Balance Department, 23 Second Line, St.-Petersburg 199053, Russia, email: george@tetrus.dux.ru); George S.Penkov, Student (St.-Petersburg State University, Social Philosophy Department, 5 Mendeleyev Line, St.-Petersburg 191002, Russia, email: george@tetrus.dux.ru)

Despite the Hydrology data and conclusions almost worldwide are raised now to the level of a state policy, the state of orthodox methodology of the science does not meet modern requirements: theoretical interpretation of Hydrologic problems lags strongly behind an accumulation of an actual material, and new facts frequently conflict with existing theories and hypotheses. Now the fast opening of new problem area - cross-disciplinary researches area in Hydrology (including the person and socio-historical conditions of her activity) is to be observed. Hydrologic researches methodology shifts from "system-ontological" concept to "system-gnosiological" one, which assumes an application of "subject-object" interactive methodology, a personalization of scientific search, a realization of cognitive potential of Hydrologic methods as "reflection, deflection, mental simulation". Thus, not only production of new knowledge, but also intensive "formation and reproduction of the altered subject of cognition" takes place.

At modern level of Hydrology progress all this as "dissolved in vision of a subject intuition" still remains. But an urgent necessity to express the premises, assumptions and consequences of subject cognition in social concepts is emerging. In the study the task on the basis of realizing the "heuristic structure" of the science, and of analysing of various historical and modern forms of human (natural-scientific) thinking experience as "archetypes" that assist us to find "in the

past tactics, way, method, which will help us to be kept in problematic tomorrow" (Ortega Y. Gasset, 1991) is suggested to be investigated.

## LARGE SCALE BUDGETS AND FLUXES

JSM24/W/11-B2

0930

### ANOMALOUS ATMOSPHERIC MOISTURE TRANSPORTS AND VARIATIONS IN THE SOUTHEAST ASIAN MONSOON

Ian SIMMONDS (School of Earth Sciences, The University of Melbourne, Parkville, Victoria, 3052, Australia, email: ihs@met.unimelb.edu.au); Daohua Bi (Antarctic CRC, University of Tasmania, Hobart, Tasmania, 7001, Australia, email: d.bi@utas.edu.au); Pandora Hope (School of Earth Sciences, The University of Melbourne, Parkville, Victoria, 3052, Australia, email: p.hope@met.unimelb.edu.au)

Twice-daily ECMWF/WMO analyses have been used to diagnose the summer moisture transport by the large-scale circulation over China. The horizontal flux of atmospheric water vapour and its divergence has been calculated over two target regions, namely, southeastern China (25-35oN, 110-120oE) and northeastern China (40-50oN, 120-130oE). The time-averaged fluxes show the southeastern Asian and Indian monsoon circulations bringing abundant moisture from the South China Sea and the Bay of Bengal, respectively, to southeastern China while the midlatitude westerlies dominate the moisture transport over northeastern China. The paper addresses the association between the interannual variations of moisture flux and rainfall over China. The comparison (for the period 1980 to 1990) of the fluxes for wet (1980, 1982, 1983) and dry (1981, 1985, 1988) years over the southeast showed there to be, for the former, much stronger moisture transport by the southeastern Asian monsoon through the southern boundary but little change associated with transport by the Indian monsoon. Furthermore, comparison between mean and transient eddy transport budgets in wet and dry years and in the climatological mean shows that the mean component is dominant in the total transport. The moisture convergence associated with the transient eddies assumes its largest values in the eastern part of the country and, for the most part, assumes a sign opposite to that of the moisture flux convergence associated with the time-mean circulation and moisture fields. Our results suggest that the transient eddies do not play a significant role in the initiation and maintenance of the abnormal climate events over our two domains.

JSM24/W/12-B2

0950

### NONLINEAR REACTIONS OF AUSTRALIAN REGION CIRCULATION AND RAINFALL PATTERNS TO NEAR-SURFACE CONTINENTAL WETNESS CHANGES

Ian SIMMONDS, Pandora Hope (School of Earth Sciences, The University of Melbourne, Parkville, Victoria, 3052, Australia, email: ihs@met.unimelb.edu.au)

We have used GCM experiments to examine the interaction of large scale soil moisture anomalies and the atmospheric circulation. The suite of GCM experiments were performed in which the soil was instantaneously saturated and desiccated over the entire Australian continent. These conditions were imposed on the first day of each of the 12 calendar months and anomaly simulations integrated for four months. We discuss the substantial asymmetry in the transient response of the climate system to these Australian wet and dry soil moisture conditions. A significant amount of the asymmetry in the 'wet' and 'dry' cases is seen to be associated with the propagation of surface thermal anomalies into the troposphere. In January the warm anomaly (in the dry case) propagates more rapidly than does the cool anomaly, due to the switch on of convective processes. Hence the troposphere is influenced more rapidly in the dry case and induces at an earlier stage feedbacks associated with anomalous circulation and moisture transports, and cloud cover. By contrast, in the 'dry' July experiment the warming is to a great extent confined to the lower troposphere. This seasonality of the response may be explained in terms of the behaviour of vertical mixing and convection. In general, the vertical stability of the atmosphere is much greater in winter. Hence, any surface warming would be expected to be confined to lower levels. By contrast, in summer conditions are more conducive to deep cumulus and vigorous mixing and thermal anomalies are able to propagate through greater depths of the atmosphere. The presentation will address some of the many nonlinear processes in the land-atmosphere system and the complex roles played by convection, cloud, circulation regimes (including the monsoon), thermal conditions, and horizontal moisture transports.

JSM24/L/01-B2

1010

### THE IMPACT OF CLIMATE CHANGE ON THE WATER RESOURCES OF EASTERN AND SOUTHERN AFRICA

J.R. MEIGH, F.A.K. Farquharson (Institute of Hydrology, Wallingford, Oxfordshire OX10 8BB, UK)

The Institute of Hydrology have taken a novel approach to the problem of assessing the likely impacts of climate change on water resources in Africa and have applied the method to assessing water scarcity. The approach used is believed to offer a realistic and consistent procedure which has been applied across many countries. Water demands, surface flows and groundwater availability were estimated on a gridded basis, and various water availability indices were derived comparing the resource with the projected demand. Surface flows were estimated using a conceptual rainfall-runoff model linking climate to runoff and, in the major river basins, the runoff estimates for individual grid cells were accumulated to give estimates for the total flows at all points of interest. Groundwater availability was derived from hydrogeological maps based on estimates of the potential yield that can be expected from a borehole and the likely maximum borehole density. Estimates of potential groundwater recharge derived from the surface water model were also taken into account. Water demands were based on current and projected population and livestock numbers, and information on irrigation schemes and industrial water use. Results are presented for the application of the model to a region covering the whole of eastern and southern Africa. The main scenario considered includes the combined impact of climate change, population growth and improved living standards to the year 2050. The climate change scenarios applied were those from recent IPCC reports. The results for this scenario show that water scarcity is likely to increase in many countries in the region, with particular problems in the countries around Lake Victoria and in the southernmost parts of the pilot region.



**JSM24/E/07-B2 1055**

**ON THE MACKENZIE BASIN WATER CYCLE DURING TYPICAL AND UNUSUAL WATER YEARS**

Ronald E. STEWART (Atmospheric Environment Service 4905 Dufferin Street Downsview, Ontario Canada M3H 5T4)

The atmospheric, surface, and hydrological components of the Mackenzie Basin's water cycle are described and interpreted in this presentation. Particular attention is paid to the 1994/95 water year that was characterized by slightly below-average precipitation and slightly above-average temperature, but the lowest discharge over the past 40 years.

In general, the water cycle of the Mackenzie Basin is characterized by annual precipitation of approximately 400 mm and about 170 mm of equivalent discharge into the Arctic Ocean. The integrated amount of water vapour over the basin averages about 10 mm and snow covers about 55% of the basin on average. The basin's water cycle appears to become more efficient as its overall temperature decreases in that the fraction of the integrated water vapour that results in discharge is actually higher with lower overall temperature as a result of several feedback processes.

In comparison with long-term averages, the 1994/95 water year resulted in very low discharge. The autumn of 1994 was quite dry, almost no rain fell, and much of the initial snowpack was laid down within one episodic lee cyclogenesis event; the snowpack therefore formed over a dry surface. During the spring melt starting in April 1995, there was a persistent high pressure system covering the basin that was linked with sunny skies, no precipitation, strong winds, and rapid snowmelt. Much of the snowmelt percolated into the dry soil and this is believed to be the major factor (along with enhanced evaporation) leading to the greatly decreased runoff and discharge into the Arctic Ocean, and to some of the lowest lake levels ever experienced over Great Slave Lake. In addition, there was a near normal frequency of summer convection during 1995 but dry surface conditions limited local moisture sources and consequently the amount of rainfall. For this cold climate system, features as surface dryness and atmospheric circulations therefore have immediate as well as long-term impacts on the water cycle.

**JSM24/W/13-B2 1115**

**PLATEAU- AND MESO- SCALE ENERGY AND WATER CYCLE EXPERIMENTS ON THE TIBETAN PLATEAU: GAME-TIBET**

Toshio KOIKE (Nagaoka University of Technology, Nagaoka, 940-2188, Japan, email: tkoiike@nagaokaut.ac.jp); Tetsuzo Yasunari (Institute of Geoscience, University of Tsukuba, Tsukuba, 305-8571, Japan, email: yasanari@atm.geo.tsukuba.ac.jp); Jiemin Wang (Lanzhou Institute of Plateau Atmospheric Physics, Chinese Academy of Sciences, Lanzhou, Gansu 730000, China, email: jimwang@lzu.edu.cn); Thadong Yao (Lanzhou Institute of Glaciology and Geocryology, Chinese Academy of Sciences, Lanzhou, Gansu 730000, China, email: tdyao@public.lz.gs.cn)

To clarify the interactions between the land surface and the atmosphere over the Tibetan Plateau in the context of the Asian monsoon system by taking into account the importance of seasonal variations in key processes, experiments at two different scales, the plateau-scale experiment and the meso-scale experiment, were carried out during the Intensive Observing Period (IOP) from May to September in 1998. For the purposes of improving the quantitative understanding of land-atmosphere interactions over the Tibetan Plateau and developing process models and methods for applying them over large spatial scales, the following measurement systems were deployed and operated continuously during the IOP: the 14 AWSs, PBL tower, two turbulent flux measurement systems, radio-sonde system, 7 barometers, 20 rain gauges, 3-D Doppler radar, snow particle measurement system, microwave radiometer, GPS receiver, 9 soil moisture and temperature measurement systems, and two river water level gauges. To develop and validate satellite-based retrieval methods and to understand characteristics of spatial and seasonal distributions of surface hydrological parameters, soil moisture and temperature, surface roughness and spectral reflectance were measured at 8 areas in the scale of 60m by 60m with 10m interval and in the scale of 1km by 1km scale with 1 km interval once a month during the IOP. For the Isotope studies on the origin of precipitation and its recycling, and formation processes of stable isotopic composition, samples of precipitation, river and lake water and soil water were regularly or temporally taken along the north-south and east-west transects in the plateau-scale and the meso-scale experimental fields.

**JSM24/W/05-B2 1135**

**THE ROLE OF ATMOSPHERE, LAND-SURFACE INTERACTIONS IN HYDROCLIMATOLOGICAL PREDICTABILITY**

Bob OGLESBY (Purdue Univ., W. Lafayette IN 47907, Email: roglesby@purdue.edu); Susan Marshall (Dept. Geog. & Earth Sci., UNC-Charlotte, Charlotte, NC 28233, Email: susanm@uncc.edu); John Roads (Scripps Institution of Oceanography, UCSD-0224, La Jolla, CA 92093, Email: jroads@ucsd.edu) Franklin Robertson (NASA/Marshall Space Flight Center, Global Hydrology and Climate Center, Huntsville, AL 35806, Email: pete.robertson@msfc.nasa.gov)

Wet and dry seasonal composites have been constructed for three separate regions of the Western Hemisphere using long climate model simulations made with the NCAR CCM3 and reanalysis products from NCEP and NASA/DAO. The regions include (1) the high-latitude Mackenzie Basin in northern Canada; (2) the mid-latitude GCIP region of the central US; and (3) the low-latitude LBA region of Brazil. Seasonal anomalies of soil moisture and precipitation are used to construct the composites. Each set of composites is diagnosed to identify the key factors responsible for the wet and dry periods and then the three composites are cross-compared to identify similarities and differences in wet and dry anomalies for these three disparate regions. Our initial emphasis has been on the role of land-surface interactions in accounting for the wet or dry conditions. Predictability experiments using these land surface anomalies are also being developed and will be compared to predictability experiments using sea-surface temperature anomalies. Our ultimate goal is to determine the relative roles of the local land surface forcing and the remote forcing due to SST anomalies.

**JSM24/W/08-B2 1155**

**EVALUATION OF INTERANNUAL VARIATIONS IN RUNOFF FROM LARGE RIVER BASINS**

Andrey B. SHMAKIN (Geophysical Fluid Dynamics Laboratory/NOAA, P. O. Box 308, Princeton, New Jersey 08542, USA, email: abs@efd.gov); P. C. D. Milly (U.S. Geological Survey and Geophysical Fluid Dynamics Laboratory/NOAA, P. O. Box 308, Princeton, New Jersey 08542, USA, email: pcm@efd.gov)

A methodology is proposed and applied for temporal "downscaling" of monthly mean atmospheric data for use as inputs to a land-surface water- and energy-balance model. The general approach, for any model gridpoint, is to modulate 1-year reference input time series of high (e.g., hourly to daily) temporal resolution by multi-year observed monthly means of one or more of the input variables (e.g., precipitation rate). Because the reference inputs are

derived from model-based analyses of atmospheric observations, they express the natural temporal and spatial variability of the inputs, including their space-time correlation structure. The modulation by historical monthly observations allows for temporal and spatial representation of actual historical monthly anomalies. A test of the methodology was conducted using the International Satellite Land Surface Climatology Project (ISLSCP) Initiative I data set (1987-1988) and a simple bucket-type land-surface model for the evaluation of water- and energy-balance components on a global 1-degree grid. Usage of 6-hourly inputs for 1987, modulated by monthly average values of all variables from 1988, gave annual runoff sums, averaged over major river basins, close to those obtained by use of 6-hourly 1988 inputs. The same good correlation was obtained with the years reversed. Furthermore, much of the interannual variability could be reproduced by modulating precipitation and radiation only. In an application of the technique, estimated monthly mean global fields of precipitation and radiation for an eight-year period were used for modulation of the ISLSCP reference time series. The modeled annual basin-mean runoff anomalies were well correlated with observed discharge anomalies for several large river basins.

**JSM24/W/09-B2 1215**

**EVALUATION OF INTERANNUAL VARIABILITY OF RIVER RUNOFF IN EASTERN EUROPE USING ATMOSPHERIC CIRCULATION STATISTICS**

Valeria V. POPOVA (Institute of Geography, Russian Academy of Sciences, Starometny St., 29, Moscow, 109107, Russia, e-mail: climat@ipcom.ru); Andrey B. Shmakin (Geophysical Fluid Dynamics Laboratory, NOAA/Princeton University, e-mail: abs@efd.gov); Natalia L. Shuvaeva (Institute of Geography, Russian Academy of Sciences, Starometny St., 29, Moscow, 109107, Russia, email: climat@ipcom.ru)

The daily air temperature and precipitation data for 1950-85 at 24 stations in Eastern Europe, as well as archive of daily atmospheric circulation types have been used for establishment of statistical relationships between meteorological anomalies and atmospheric circulation patterns. The circulation types archive is based on a classification of large-scale atmospheric processes in the extratropical zone of Northern hemisphere developed by Prof. B.L. Dzerdzeevsky. The relationships were obtained to be various in different regions of the territory according to the direction of main circulation streams, while the strongest negative temperature anomalies (5-7 degrees) extend throughout the whole subcontinent. The absolute values of anomalies averaged for each circulation pattern and for each of four seasons, as well as their statistical confidence and probability of occurrence for all regions were determined. In Eastern Europe, 29 of 41 atmospheric circulation types provide statistically confident deviations of meteorological parameters from the average climatic regime (from 4 to 16 each season in one of 5 large river basins). There were no statistically confident anomalies of precipitation in summer for the studied region. These anomalies were used for evaluation of water/energy exchange by a simple bucket-type land-atmosphere scheme. The meteorological forcing variables for 1987 with 6-hour temporal and 1-degree spatial resolution (ISLSCP Initiative I data set) were transformed according to the occurrence of circulation types during 1950-1985 as compared to 1987. The interannual and decadal variability of river runoff for 5 large basins (Wisla, Neva, Northern Dvina, Pechora and Volga) were reproduced in good agreement with observed data. The approach allows one to obtain interannual variations of river runoff in Eastern Europe (as the main part of runoff there is formed by snow melting, and the absence of relationships between summer precipitation and atmospheric circulation patterns is of less importance).

**CLOSING COMMENTS AND DISCUSSION 1235**

STEWART, RASCHKE, WILKINSON

**JSP25 Monday 26 – Friday 30 July**

**OCEAN/ATMOSPHERE VARIABILITY AND PREDICTABILITY (IAPSO, IAMAS, IAG)**

Location: Arts Building 120 LT  
Location of Posters: Arts Building 101 LR4

**Monday 26 July AM**

Presiding Chair: M. Davey (Meteorological Office, London)  
Concurrent Poster Session

**OCEAN/ATMOSPHERIC VARIABILITY-ENSO EFFECTS, ENSO DECADAL VARIABILITY**

**JSP25/W/24-B1 0850**

**THE EFFECTS OF ENSO ON INDIVIDUAL LARGE-SCALE WEATHER EVENTS**

Joseph J. BARSUGLI, Jeffrey S. Whitaker, Prashant D. Sardeshmukh, Andy Loughe, (all at: NOAA-CIRES Climate Diagnostics Center, University of Colorado, Campus Box 449, Boulder, CO, 80302, USA, email: jjb@cdc.noaa.gov), and Zoltan Toth (NCEP/EMC, 5200 Auth Rd., Camp Springs, MD, 20746, USA, e-mail: zoltan.toth@noaa.gov)

What is the link between ENSO and individual weather events in the extratropics? This question is addressed quantitatively using ensembles of medium-range weather forecasts made with and without tropical sea surface temperature anomalies during the winters of 1997-8 (a record El Nino event) and 1998-9 (a substantial La Nina event).

We find statistically robust sub-seasonal variations in ENSO teleconnections over North America. These sub-seasonal effects can depart dramatically from the seasonally-averaged extratropical pattern classically associated with ENSO. For example, a large tropical influence was detected in the case of the devastating ice storm that hit Canada in January 1998, apparently involving an anomalous atmospheric wavetrain along the Atlantic Coast of North America. Some (though not all) of the variations in the heavy California rains of February 1998 also are associated with sub-seasonal variations in the strength of the ENSO teleconnections. Interesting cases for winter 1998-9 will also be shown.

Some mechanisms, including Rossby wave propagation on time-varying flows, and the effects of transient tropical convective forcing are discussed, as well as the implications for improving medium range forecasts. The inherent limitations of attributing individual weather events to specific causes in a chaotic system is also addressed.



JSP25/W/29-B1

0910

## ENSO WESTERN PACIFIC OSCILLATOR PARADIGM AND THE 1997-98 EL NINO

Chunzai WANG and Robert H. Weisberg (both at Department of Marine Science, University of South Florida, St. Petersburg, FL 33701, USA, email: wang@marine.usf.edu)

A western Pacific oscillator paradigm has been proposed for the El Niño-Southern Oscillation (ENSO). This paradigm emphasizes the importance of western Pacific interannual anomaly patterns for the evolution of ENSO, in addition to eastern Pacific anomaly patterns. During the warm (cold) phase of ENSO, off-equatorial cold (warm) sea surface temperature (SST) and high (low) sea level pressure (SLP) anomalies in the western Pacific produce equatorial easterly (westerly) winds in the western Pacific. These winds force oceanic upwelling (downwelling) responses that evolve eastward tending to decrease (increase) SST in the east, providing a negative feedback for the coupled ocean-atmosphere system to oscillate. The western Pacific oscillator paradigm may work in conjunction with the delayed oscillator paradigm that emphasizes wave reflection at the western boundary as a negative feedback. Observations show that evolution of the 1997-98 El Niño is consistent with the western Pacific oscillator paradigm. From November 1996 to January 1997, the eastern Pacific is characterized by equatorial cold SST and high SLP anomalies, while the western Pacific is marked by off-equatorial warm SST and low SLP anomalies. Corresponding to this distribution are high outgoing longwave radiation (OLR) anomalies in the equatorial central Pacific and low OLR anomalies in the off-equatorial far western Pacific. The off-equatorial low SLP anomalies in the western Pacific are associated with a switch in the equatorial winds over the western Pacific from easterly to westerly. These equatorial westerly anomalies then appear to initiate early SST warmings around the dateline in January/February 1997 and around the far eastern Pacific in March 1997. Subsequently, both the westerly wind and the warm SST anomalies, along with the low OLR anomalies, grow and progress eastward. The eastward propagating warm SST anomalies merge with the slower westward spreading warm SST anomalies from the far eastern Pacific to form large-scale warming in the equatorial eastern and central Pacific. The anomaly patterns in the eastern and central Pacific continue to develop reaching their peak values around December 1997

JSP25/W/30-B1

0930

## A MODELLING STUDY OF THE INFLUENCE OF THE 1997/1998 ENSO ON THE ATLANTIC OCEAN

Stephen JEWSON and Rowan Sutton (both at the Centre for Global Atmospheric Modelling, Department of Meteorology, University of Reading, PO Box 243, Earley Gate, Reading, RG6 6BB, UK, email: steve@met.reading.ac.uk)

The observational record shows us that one of the remote effects of ENSO can be to warm the waters of the northern sub-tropical Atlantic. The recent strong ENSO event was accompanied and followed by large sea surface temperature (SST) anomalies in other parts of the Atlantic as well. This raises the question as to whether these anomalies were also a response to ENSO, and hence whether they might have been predicted in advance. We address this question, and also evaluate the performance of a state of the art coupled model in simulating the whole of the Atlantic response to ENSO.

We have performed ensemble integrations of a global coupled model for the period 1997/1998. Over the tropical Pacific and Indian oceans the model SST is constrained with artificial heat fluxes to follow either the observed evolution for 1997/1998 or climatological SSTs. In the Atlantic, however, the ocean and atmosphere interact freely. In this way we can study the coupled response to a particular ENSO event. The model shows some deficiencies in simulating the observed evolution of Atlantic SST during 1997/1998, while some features are simulated correctly. This leads to insight into both the performance of the model and the role played by ENSO in creating SST anomalies in the Atlantic.

JSP25/W/60-B1

0950

## MECHANISMS FOR THE INDIAN OCEAN WARMING DURING THE 1997-98 EL NINO

Lisan YU (Department of Meteorology, University of Maryland, College Park, MD 20742, USA, email: lyu@atmos.umd.edu); Michele Rienecker (NASA/Goddard Space Flight Center, Greenbelt, MD 20771, USA, email: rienecker@mohawk.gsfc.nasa.gov)

Two major climate events took place in 1997-98: the greatest El Niño of the century in the tropical Pacific Ocean and a record-breaking broad-scale warming in the Indian Ocean. In this study, we examine the primary mechanisms that gave rise to the basin-wide change of the sea surface temperature (SST) in the Indian Ocean during this period and their relationship with the El Niño - Southern Oscillation (ENSO) event in the Pacific. The evolution of some key atmosphere-ocean variables, as revealed in our analyses of multi-source data sets, indicated that the changes of SST in the Indian Ocean were largely attributable to the ENSO impact on the large-scale atmospheric circulation. During June-December 1997, when the El Niño in the Pacific was maturing, the Indian Ocean experienced the reversal of the Walker Circulation and the prolonged equatorward displacement of the southeast trades. The resultant changes of surface wind influenced the SST through the following means. In the equatorial region, the easterly winds associated with the reversed Walker Circulation forced equatorial Kelvin/Rossby waves, which then affected the equatorial ocean heat balance (mainly through upwelling/downwelling) and eventually led to the reversal of the zonal SST gradient in the fall of 1997. The negative SST anomalies in the east and positive anomalies in the west in turn helped maintain and prolong the equatorial easterlies, indicating coupled atmosphere-ocean interactions in operation. Outside of the equatorial waveguide, the broad-scale warming was induced mainly by the changes of latent heat flux associated with the anomalies in wind speed. The most intensive surface warming occurred in the southern Indian Ocean during the summer/fall of 1997 when the southeasterly trade winds weakened significantly, leading to a dramatic reduction of the latent heat release and subsequently a rapid surface warming.

JSP25/W/14-B1

1010

## MJO TRIGGERED 1997/98 ENSO

Tetsuo Nakazawa (Meteorological Research Institute, Tsukuba, Japan 305-0052, Email: nakazawa@mri-jma.go.jp)

The onset phase of the 1997/98 ENSO is described by using several remote-sensing datasets including the ADEOS/NSCAT surface wind data, the NOAA/OLR data, the TOPEX/POSEIDON sea surface height data) as well as the TOGA/TAO buoy data. These data shows that the 1997/98 ENSO is triggered by the Madden-Julian Oscillation with a period of 30-60 days, which is originated in the equatorial Indian Ocean in February 1997 and propagated into the western Pacific in March 1997. Under the warmer condition of the upper ocean in the western Pacific, the strong and persistent westerlies associated with the MJO was favorable to generate the oceanic Kelvin wave in middle of March. This Kelvin wave propagated to the eastern Pacific end of April or early May when the ENSO was initiated.

JSP25/W/26-B1

1050

## DYNAMICS OF TROPICAL DROUGHTS DURING THE 1997-98 EL NINO

J. David NEELIN, Ning Zeng, Chia Chou and Hui Su (University of California at Los Angeles, Dept. of Atmospheric Sciences, UCLA, Los Angeles, CA 90095-1565 USA, e-mail: neelin@ucla.edu)

An intermediate complexity atmospheric model is used to analyse radiative-convective-dynamical interactions in the response to the 1997-98 El Niño sea surface temperature anomalies. The atmospheric model, QTCM1 (quasi-equilibrium tropical circulation model) makes use of properties of the quasi-equilibrium convective closure in the Betts-Miller convective scheme to produce efficient solutions that are accurate in convective regions and reasonable elsewhere. It is coupled to a one-layer land-surface model with interactive soil moisture, and simulates its own tropical climatology. The model is able to reproduce many tropical features in observed anomalies of precipitation, outgoing long-wave radiation, land surface temperature and winds associated with the recent El Niño. The radiative-convective-dynamical balances associated with the subsidence regions around ENSO convective heating regions are examined. We compare the feedbacks over land involved in the Amazon drought with those over the western Pacific/Indonesian ocean region. In both, cloud-radiative interaction affects the dynamics of relative descent in the convection zone. Over parts of the ocean region, ocean dynamical effects are inferred to have played some role. Over land regions adjacent to the SST anomaly, land feedbacks actually simplify the analysis via the surface energy balance condition. The surface temperature response is relatively passive from the dynamical point of view, adjusting to satisfy this condition, and is significantly associated with cloud feedbacks. The convective-radiative-dynamical feedbacks identified in this case likely play a role in most tropical teleconnections involving suppression of convection zones by remote SST anomalies.

JSP25/E/05-B1

1110

## WHAT ROLE DID THE MJO AND ASSOCIATED WESTERLY WIND BURSTS PLAY IN THE DEVELOPMENT OF THE 1997/98 EL NINO

M.K. DAVEY, S. Ineson (both at Hadley Centre for Climate Prediction and Research, UK Met. Office, Bracknell, UK, Email: sineson@meto.gov.uk), J.M. Slingo and R. Bruggé (both at Centre for Global Atmospheric Modelling, Department of Meteorology, University of Reading, Reading, UK.)

The growth of the 1997/98 El Niño was dramatic and significantly faster than normal. It developed in association with strong atmospheric intraseasonal variability, characterised by a series of MJOs with strong Westerly Wind Bursts (WWB) embedded in the active phase of the MJO.

A series of experiments with the UK Met. Office Tropical Pacific OGCM, forced with ECMWF operational analyses for 1996/97, have been made to investigate the impact of the intraseasonal variability in the atmosphere and oceans on the evolution of El Niño. The aim is to test the hypothesis that a series of MJOs and/or WWBs are required to precondition the ocean to El Niño.

JSP25/W/58-B1

1130

## THE BMRC SEASONAL-TO-INTERANNUAL PREDICTION MODEL

Richard Kleeman, Guomin Wang and Neville SMITH (all from the Bureau of Meteorology Research Centre, Melbourne Vic. 3001, AUSTRALIA, email: N.Smith@BOM.GOV.AU)

A global coupled general circulation model has been developed for forecasts of the El Niño-Southern Oscillation. The atmospheric model is an R21L9 version of the BMRC atmospheric climate model. The ocean component is a global general circulation model with resolution focussed in the tropical region and 20 vertical levels. A univariate statistical interpolation method, with 10 day data ingestion windows, is used to assimilate temperature data and initialize the coupled model. Hindcasts have been carried out for the period 1981-1995 for each season (60 in all), for up to 12 months lead-time. This paper will describe these initial experiments and show that the skill comparable to, and in some cases exceeds, that of the present operational intermediate model, and is comparable to that of other published models. The skill of the model is focussed in the central Pacific, which suits seasonal forecasting in the Australian region, but is generally weak in the far eastern Pacific and outside the tropical Pacific. Some of the other attributes and weaknesses of the model will also be discussed. The hindcasts have been extended to the present with a view toward quasi-operational trials.

JSP25/W/66-B1

1150

## A CONCEPTUAL EQUATORIAL OCEAN RECHARGE OSCILLATOR MODEL FOR ENSO

FEI-FEI JIN and Soon-Il An (School of Ocean and Earth Science and Technology, University of Hawaii at Manoa, Honolulu, Hawaii, USA, e-mail: jff@soest.hawaii.edu)

Through the dynamical coupling between ocean and atmosphere, the vertical advection of anomalous subsurface temperature by the mean upwelling and zonal advection of mean sea surface temperature (SST) by anomalous current constitute the so-called the thermocline and zonal advective feedbacks which are essential for El Niño / Southern Oscillation (ENSO) coupled dynamics. In this paper, we demonstrated that these two feedbacks are dynamically linked because of the semi-geostrophic balance the upper ocean zonal current and meridional gradient of the thermocline. Both feedbacks thus play important and similar roles in the growth and phase transition of ENSO. We further proposed a new version of the conceptual recharge oscillator model for ENSO by including these two feedbacks. The new model retains the simplest possible form of a harmonic oscillator, yet presents a more complete description of slow physics for ENSO. Moreover, it also provides the reconciliation between the biased emphases in the ENSO theories on the thermocline and zonal advective feedbacks.

JSP25/W/36-B1

1210

## ASSESSMENT OF THE DIABATIC HEATING DISTRIBUTION AND GLOBAL TELECONNECTION ERRORS IN THE UKMO UNIFIED MODEL DURING ENSO

RICHARD NEALE and Julia Slingo, (CGAM, Department of Meteorology, University of Reading PO BOX 243, Earley Gate, Reading, RG6 6BB)

Interannual variability in tropical sea surface temperatures (SSTs) is able to influence the atmospheric circulation in more remote regions. This is achieved due to a succession of processes, beginning with the generation of convection anomalies through to the impact of global teleconnection patterns. The major source of interannual variability in tropical SSTs is due to ENSO.

AMIP II integrations using the UKMO Unified Model (UM) (version HadAM3) reveal that the global response during ENSO conditions is exaggerated compared to observations. Analyses of these integrations are performed in order to determine the major sources of error in the

## INTER-ASSOCIATION

model. In particular, the ability of the model to reproduce the correct magnitude and spatial distribution of the tropical diabatic heating anomalies in response to ENSO sea surface temperature (SST) distributions will be discussed.

ENSO also influences the more remote tropical climate through known global teleconnection patterns. In the tropics a remote response to ENSO is observed in the tropical Atlantic, primarily through changes in the Walker circulation. During El Niño conditions, increased descent is seen over the tropical Atlantic tending to result in a warming of SSTs. The intensity of this response gives rise to stronger than observed coupling between tropical Pacific and tropical Atlantic SSTs.

The impact of vertical resolution on model skill will also be assessed, with a comparison of 19 level and 58 level versions of the AMIP II UM integrations.

Monday 26 July PM

### OCEAN/ATMOSPHERIC VARIABILITY-ENSO EFFECTS, ENSO DECADEAL VARIABILITY

JSP25/W/22-B1

1400

#### FLUCTUATIONS IN INDIAN OCEAN SST DIPOLE PATTERNS

Robert J. ALLAN (CSIRO Atmospheric Research, Aspendale, Victoria 3195, Australia, email: rob.allan@dar.csiro.au); Ian N. Smith (CSIRO Atmospheric Research, Aspendale, Victoria 3195, Australia, email: ins@dar.csiro.au); Chris J.C. Reason (School of Earth Sciences, University of Melbourne, Parkville, Vic., 3052, Australia, email: cjr@buster.unimelb.edu.au).

Indian Ocean sea surface temperature (SST) dipole patterns are examined in the context of historical, global mean sea level pressure (MSLP) and SST anomalies during the evolution of major El Niño and La Niña events. These SST dipoles occur at various stages during the life cycles of both the more 'canonical' and protracted of El Niño Southern Oscillation (ENSO) phases. When seasonal MSLP and SST fields are filtered on interannual ENSO time scales, the resulting quasi-biennial 2-2.5 year and 'classical' ENSO 2.5-7 year bands often both display SST dipoles, but they may not always be spatially aligned. Superposition of these bands can lead to the annulment of such SST signals. However, if either or both of the above bands is dominant, and carrying SST dipole signals, then an important modulation for rainfall producing systems in various regions of the Indian Ocean basin can emerge. In general, south west-north east oriented dipoles develop during the onset and cessation phases of El Niño or La Niña episodes. During the mature stage of strong ENSO phases a north-south oriented SST dipole structure is usually evident on both bands.

Filtering on lower frequency time scales reveals the presence of additional SST structures, particularly during protracted ENSO phases. This indicates that interannual SST dipoles are modulated further by decadal to interdecadal fluctuations in Indian Ocean SST dipole patterns.

JSP25/W/65-B1

1420

#### DECONSTRUCTING CORRELATIONS: USING PATH ANALYSIS TO DIAGNOSE OCEAN-ATMOSPHERE INTERACTIONS

NEVILLE NICHOLLS, Wasył Drosdowsky, (both at Bureau of Meteorology Research Centre, PO Box 1189K, Melbourne 3001, Australia. E-mail: n.nicholls@bom.gov.au); Tahl Kestin, (CRC for Southern Hemisphere Meteorology, Monash University, Clayton 3168, Australia)

The number of tropical cyclones affecting the Australian region each year is related to the El Niño - Southern Oscillation. The correlation between year-to-year changes in tropical cyclone numbers and year-to-year changes in September-November NINO3.4 sea surface temperature (SST) is -0.62 (n = 48; significant at 1%). Year-to-year changes in tropical cyclone numbers are also correlated with SSTs around northern Australia (r = 0.71) and these SSTs, in turn, are correlated with NINO3.4 SSTs (r = -0.83). Does NINO3.4 SST have an effect on tropical cyclone numbers separate from that arising from acting in concert with local, north Australian SSTs? Path analysis allows us to deconstruct the observed correlations between SSTs and cyclone activity into unique and common effects, ie to separate the unique effect of NINO3.4 SSTs on tropical cyclones from the common effect involving both NINO3.4 and north Australian SSTs. This analysis indicates that the NINO3.4 SST only affects tropical cyclone activity through its common effect with the local, north Australian SSTs. Path analysis, and its more complex relation Structural Equation Modelling, allow us to investigate the underlying correlation structure in situations where there are several inter-related predictor variables all correlated with one or more predictand or response variables. These techniques appear not to have been used in the study of relationships between SSTs and climate variables, despite their obvious utility in such studies. They could, for example, allow the correlation between Indian Ocean SSTs and Indian rainfall to be separated into the contribution arising from the unique effect of Indian Ocean SSTs on rainfall, and the contribution arising from the common relationship of Pacific Ocean and Indian Ocean SSTs with rainfall (through the El Niño - Southern Oscillation). We will illustrate the use of these techniques in separating the effects of Indian and Pacific Ocean SSTs on Indian and Australian rainfall, as well as on tropical cyclone activity, and discuss their relationship to climate model experiments.

JSP25/E/23-B1

1440

#### THE CONNECTION BETWEEN ENSO AND PRECIPITATION IN ISRAEL

Colin PRICE, Pinhas Alpert and Yitzhak Carmona (all at Department of Geophysics and Planetary Sciences, Tel Aviv University, Ramat Aviv, 69978, Israel, email: cprice@flash.tau.ac.il, pinhas@cyclone.tau.ac.il, carmona@cyclone.tau.ac.il); Lewi Stone and Amit Huppert (both at Department of Zoology, Tel Aviv University, Ramat Aviv, 69978, Israel, email: lewi@lanina.tau.ac.il, amit@lanina.tau.ac.il); Balaji Rajagopalan (Lamont-Doherty Earth Observatory, Columbia University, Palisades, NY 10964-8000, USA, email: rbal@rosie.ligo.columbia.edu)

Recent analysis of hydrological data in Israel has revealed some interesting connections between the ENSO phenomenon and weather in Israel. The precipitation season in Israel is during the winter months from October-April, with the maximum precipitation coinciding in phase with the maximum of the ENSO cycle. Hence the anomalous circulation patterns in the atmosphere due to ENSO coincide with the rainy period in Israel.

For this study we used rainfall data from northern Israel, streamflow data from the Jordan river, and lake levels from the Sea of Galilee. The rainfall drains into the watershed of the Jordan river which then flows into the Sea of Galilee. Rainfall data were available from 1922, streamflow from 1967 and lake level data from 1927. We analysed the data on a seasonal basis, and compared the anomalies with both the NINO3 sea surface temperatures and the southern oscillation index, during the same winter months. A highly significant statistical correlation was found between all the hydrological parameters and the ENSO indices. During El Niño years there is generally above average rainfall in the northern parts of Israel, while during La Niña years the opposite is true. By analysing archived data related to global circulation patterns we have noticed that the subtropical jetstream shifts approximately 100-200 km southwards/northwards during El Niño/La Niña years.

It is interesting that the strong connection between ENSO and rainfall in Israel exists only since

the 1970s, with little connection before this period. Whether this is due to a change in the teleconnection patterns since the 1970s is still uncertain. However, it is clear that there has been a change in the frequency and intensity of ENSO events since the 1970s.

JSP25/W/39-B1

1500

#### SEASONAL, DECADEAL, AND ENSO RESPONSES OF THE UPPER LAYERS IN THE NORTHERN GULF OF ALASKA

Thomas C. ROYER (Center for Coastal Physical Oceanography, Department of Oceanography, Old Dominion University, Norfolk, VA 23529 USA, email: royer@ccpo.odu.edu)

Temperature and salinity versus depth to 250 m at the mouth of Resurrection Bay, Alaska (60 N, 149 W) (GAK 1) have been measured since December 1970 with various temporal sampling intervals, ranging from hours to months. The ocean climatology suggests that, seasonally, the temperature and salinity signals propagate downward from the surface to about 100 m. The influences of local upwelling, regional and global atmospheric circulation forcing can be seen in the temperature anomalies along with SOI (Southern Oscillation Index) influences. In contrast with temperature anomalies observed off the California coast, these are coherent with depth. This suggests a barotropic forcing rather than a vertical propagation or baroclinic influence. Amplitudes of the interdecadal temperature fluctuations decrease from more than 6 C at the surface to about 3.6 C at 250 m with those in the lower 150 m being coherent with their greatest variance at low frequencies (15-21 years). Using a threshold level of one standard deviation, positive temperature anomalies at 150 m and deeper since 1974 have corresponded to ENSO events. The 1997-8 ENSO event was accompanied by the largest temperature anomaly yet seen at 250 m (1.43 C) (Feb. 1998), more than 3 SD (1 SD = 0.45 C) above normal. This signal first appeared in Jan. 1998 but by May 1998 had subsided to 0.29 C, below the ENSO threshold. Surface salinity anomalies have significant periods of a 4-5 years whereas the deeper waters (10-100 m) have a decadal periodicity (9-11 years) shifting to 12-15 years for 150-250 m.

JSP25/P/06-B1

1520

#### NUMERICAL SIMULATION RESEARCH ON THE CYCLIC RELATIONSHIP BETWEEN ANOMALOUS EAST-ASIAN WINTER MONSOON AND ENSO

MINGQUAN Mu and Chongyin Li (The Key Laboratory of Numerical Modelling for Atmospheric Sciences and Geophysical Fluid Dynamics (LASG), Institute of Atmospheric Physics (IAP), Chinese Academy of Sciences, P.O.Box 2718, Beijing 10008, China E-mail: mmq@lasg.iap.ac.cn)

This study includes two parts. The first part gives general observational features about mutual relationship between ENSO and anomalous East Asian winter monsoon. On the one hand, stronger (weaker) East Asian winter monsoon can excite happening of El Niño (La Niña) through forced anomalous westerly (easterly) wind and stronger (weaker) convective activity over the tropical Pacific Ocean; on the other hand, the occurrence of El Niño (La Niña) weakens (enhances) East-Asian winter monsoon through the atmospheric teleconnection. Power spectral analyses imply that this cycle mainly locates in the 3-5 years; and quasi-biannual cycle is also clear. The second part mainly focuses on numerical simulations with tropical Pacific ocean model (OGCM) and coupled ocean-atmospheric general circulation model (CGCM). Both of the results reveal that stronger (weaker) winter monsoon is able to lead to El Niño (La Niña) event. The simulation results also indicate that the anomalous oceanic Kelvin waves and atmospheric intraseasonal oscillation, caused separately by anomalous westerly (easterly) and stronger (weaker) convective activity over the tropical Pacific, play an important role in the occurrence of ENSO (El Niño and La Niña). So, both of the observation and simulation have one consistent conclusion: The relationship between anomalous East Asian winter monsoon and ENSO is two-way interaction

Presiding Chair: R.Allan (CSIRO Atmospheric Research, Aspendale, Australia)

JSP25/W/37-B1

1600

#### ENSO VARIABILITY OF THE HYDROLOGICAL CYCLE DERIVED FROM RAINFALL ISOTOPE MEASUREMENTS

Ahmet S Kayaalp and John A T BYE (Faculty of Science and Engineering, Flinders University, GPO Box 2100, Adelaide Australia 5001, email: John.Bye@flinders.edu.au)

Stable isotope measurements in precipitation have been used to obtain the ratio (f) of precipitation to evaporation for 104 stations in the International Atomic Energy Agency archive. The global annual oceanic precipitation fields predicted from published evaporation fields are found to be realistic in comparison with other methods, e.g. from coastal rainfall and MSU satellite data.

The results show that f is well correlated with the wet bulb temperature (Tw) which occurs during rainfall, and in particular that f becomes very large when Tw exceeds about 26°C. This diagnostic has been used to investigate changes in the global hydrological cycle which occur during ENSO.

It is found that the very high MSU derived oceanic rainfall in the central equatorial Pacific Ocean is consistent with the existence of positive Tw anomalies due to positive sea surface temperature anomalies. During the El Niño phase, a corresponding reduction in f occurs in the extra tropical regions. Associated changes in the global hydrological cycle will be discussed.

JSP25/P/07-B1

1620

#### A MODELING ENSO/DECADEAL VARIATIONS IN THE NORTH DURING 1975 TO 1998

Tomonori MATSUURA and Satoshi Iizuka (both at National Research Institute for Earth Science and Disaster Prevention, 3-1 Tennodai Tsukuba, Japan, email: matsuurat@ess.bosai.go.jp)

The El Niño and decadal scale simulation, which is long run from 1975 to 1998, is conducted using an ocean general circulation model (MOM 2). As surface forcings, we used daily fluxes obtained from Louis et al. (1982)'s formulae and NCEP data. We could successfully simulate the El Niño (1976 1979, 1982/83, 1986/87, 1991/92, 1997/98) and the decadal variation, the phase of which changes in 1982, 1989, and 1997. Both the El Niño and decadal signals appear in the North Equatorial Current region (145°E-180°, 10°N-20°N) and the decadal variability of heat content in the subpolar front (145°E-180°, 35°N-45°N) correlated inversely with the North Equatorial Current region. We show that the strong El Niño and La Niñas may play an important role in changing the phase of decadal variability.



JSP25/W/11-B1

1640

## DECADAL MODULATION OF ENSO VARIABILITY IN THE ECHO-G MODEL

Keith RODGERS (Max Planck Institut fuer Meteorologie, Bundesstrasse 55, D-20146 Hamburg, Germany, Email: rodggers@dkrz.de); Mojib Latif (Max Planck Institut fuer Meteorologie, Bundesstrasse 55, D-20146 Hamburg, Germany, Email: latif@dkrz.de); Stefanie Legutke (DKRZ, Bundesstrasse 55, D-20146 Hamburg, Germany, Email: legutke@dkrz.de)

The global coupled ECHO-G (ECHAM4/HOPE) model is examined in order to identify those oceanic processes which modulate the decadal behavior of ENSO. The focus is on inter-gyre exchange of thermocline water between the subtropical Pacific and the upwelling regions of the eastern equatorial Pacific. Three processes which can contribute to changing the thermal structure of the equatorial pycnocline on decadal timescales are considered: Variability in ocean circulation fields, temperature anomalies which subduct in the extratropics and advect equatorward, and changes in diapycnal fluxes within the equatorial pycnocline. Special attention is given to the role of the South Pacific. The growing database of oceanic measurements strongly suggests that the South Pacific plays at least as important a role as the North Pacific in equatorial thermocline ventilation. The ocean model's performance is discussed within the context of hydrographic and tracer measurements.

JSP25/W/87-B1

1700

## TIME SERIES OF SST, SEA-LEVEL PRESSURE, SURFACE WINDS, AND RAINFALL

Todd MITCHELL, (University of Washington, USA, Email: mitchell@atmos.washington.edu)

Time series of SST, sea-level pressure, surface winds, and rainfall are presented to document ENSO variability in the tropics from the 1850s through 1998. The series are derived from area-averages of very large regions and as such emphasize the tropics-scale nature of ENSO-related climate variability. This approach is a complement to the pioneering studies of Quinn and collaborators, which emphasized the historical record of El Nino at the Peru coast. Intercomparison of the series for the different variables will corroborate the identification of the major ENSO episodes and interdecadal variability in the tropics. The resultant series are useful to clarify the relationship between interdecadal variability and the frequency of ENSO episodes.

JSP25/W/41-B1

1720

## WATER VAPOR TRANSPORT OVER THE INDIAN OCEAN AND WESTERN PACIFIC DURING THE WARM AND COLD EVENTS OF EL NINO

Nataly A. VYAZILOVA (Russian Research Institute of Hydrometeorological Information - World Data Center 6, Korolyov St., Obninsk, Kaluga region, 249020, Russia, e-mail: vjaz@meteo.ru)

Using mean monthly and climatic upper-air data of the objective analysis during the period 1982-97, made by the U.S. National Meteorological Center which are presented at the points of the 2.5 step regular grid, the following characteristics of the tropical atmosphere have been calculated for the centers of the 5°5 squares: mean monthly water content in the atmospheric column, water content anomalies for individual months (water content is expressed in percent relative to mean climatic values), mean monthly values of the zone, meridional and resulting water transfer, cross-equatorial water vapour flux. Peculiarities of a space - time distribution of water exchange characteristics are studied in the Tropical Indian ocean and Western Pacific during the summer monsoon in accordance with a type of the monsoon circulation. Four types of the monsoon circulation have been considered as compared to the mean climatic year: Weakened monsoon circulation when an intensive development of El Nino is observed (warm events in 1982, 1987 and 1997);- Weakened monsoon circulation when the El Nino development did not reach its peak (warm event in 1986 );- Developed monsoon circulation (cold events in 1988 and 1996);- Normal monsoon circulation (1989).

JSP25/P/04-B1

1740

## THE ROLE THE INDIAN OCEAN SSTA TAKSE IN THE ENSO TO ASIAN CLIMATE

XIAO Ziniu and Sun Jihua (both at Yunnan Meteorological Observatory, 73 Xichang Road, 650034, Kunming, Yunnan, China); Li Chongyin (LASG, The Institute of Atmosphere Physics, Box 2718, Beijing 100080, China)

During the ENSO event period, the Indian Ocean SST will be anomalous almost simultaneously. But the space structure of the SSTA in the Indian Ocean is not same from time to time. The seesaw structure is a typical pattern of the Indian Ocean SSTA. Based on the IAP-GCM9L model, which is developed in Institute of Atmospheric Physics, the SSTA pattern with warm SST in the western Indian Ocean and cold SST in the eastern India Ocean is simulated during an ENSO period. And its effect to the Asian climate is studied. The results indicated that the Indian Ocean SSTA would mainly influence the climate in Bengal, Indo-China, Indonesia, India and China. During the ENSO period, the SSTA pattern with warm west and cold east SST in India Ocean will enhance the climate anomalous brought by the eastern Pacific Ocean SSTA. Especially, it makes Indo-China more dry and reduce the precipitation over northern China. But it increases the precipitation over the area from southwest China to southeast China obviously. So that, the precipitation will be concentrated in a zonal region around in Changjiang River drainage area and forms zonal drought and flood pattern which is similar to the fact. Therefore, during ENSO period, the Indian Ocean SSTA is important to Asian climate especially to the anomalous precipitation pattern in China.

Tuesday 27 July AM

Presiding Chair: Dr D.B. Stephenson (Meteo-France)  
Concurrent Poster Session

## SEASONAL-DECADAL VARIABILITY

## Enso Related Variability

JSP25/E/27-B2

0930

## IMPACT OF GLOBAL WARMING ON VARIABILITIES OF THE CLIMATE MODES IN A CGCM

Z.-Z. HU, L. Bengtsson, E. Roeckner, M. Christoph, A. Bacher (MPI for Meteorology, Bundesstrasse 55, D-20146 Hamburg, FRG, e-mail: hu@dkrz.de); J. M. Oberhuber (DKRZ, Bundesstrasse 55, D-20146 Hamburg, FRG)

In this study, we investigated the impact of global warming on the linear trend and standard deviation of geopotential height at 500 hPa (H500) in the NH winter, and on the variabilities of the large scale interannual and interdecadal climate modes and the teleconnection patterns with two long term integrations of the ECHAM4/OPYC3 CGCM. One is the control (CTRL) run

with fixed present-day concentrations of greenhouse gases. Another experiment is a simulation of transient greenhouse warming, named GHG run.

In the global warming, the standard deviation of H500 over the tropics is enhanced (reduced) remarkably on the interdecadal (interannual) time scales. Except for the interdecadal mode related to the Southern Oscillation (SO) in the GHG run, the spatial variation patterns are similar for different (interannual+interdecadal, interannual, and interdecadal) time scales both in the GHG and CTRL runs. Spatial distributions of the teleconnection patterns in the GHG run are also similar to those in the CTRL run. But some teleconnection patterns manifest the linear trends and changes of the variances and the frequencies in the global warming scenario. The ENSO cycle has the most significant nonlinear response to the global warming. Besides the linear increasing trend of the SO, the interdecadal modulation to the ENSO cycle is enhanced during the GHG 2040-2099. This is the result of enhancement of the Walker circulation during that period. La Nina event will intensify and El Nino event relatively weaken during the GHG 2070-2090. It is also suggested that the growth of the greenhouse gas concentrations will trigger off the unstable correlation between the SO and the PNA pattern both on the interdecadal and interannual time scales.

JSP25/W/55-B2

0950

## SEA SURFACE TEMPERATURES AND THE MEXICAN MONSOON: MECHANISTIC IMPLICATIONS

DAVID L. MITCHELL (Atmospheric Sciences Center, Desert Research Institute, P.O. Box 60220, Reno, NV 89506, USA; email: mitch@dri.edu); Dorothea Ivanova and Timothy J. Brown (Same address; dorothea@dri.edu, tbwrc@dri.edu)

The North American or Mexican monsoon is responsible for roughly 40% of the annual precipitation in Arizona and New Mexico, USA, and about 60% for northern Mexico. It's regular occurrence in summer also effects precipitation patterns in the mid-western and eastern United States, as well as the North American radiation budget. Recent studies indicate the heat content of the upper layer (e.g. 70 m) in the Gulf of California during spring/summer is primarily due to horizontal advection from the south, allowing sea surface temperatures (SST) to be higher than solar insolation alone would permit. Other studies show the Gulf of California (henceforth the gulf) to be the dominant moisture source for the monsoon. Our study is unique in that it quantitatively relates gulf SSTs to the timing, amount and regional extent of monsoon rainfall. A detailed three season empirical study was conducted based on satellite SST data at 18 km and weekly resolution, along with satellite SSM/I pentad (5 day) precipitation data having a spatial resolution of 0.25 x 0.25 degrees. Four coastal ocean regions (three in the gulf) were evaluated for SSTs, and four land regions northwest of each ocean region (consistent with known moisture transport) were evaluated for rainfall amount. The main results were: (1) Monsoon rainfall did not occur prior to the onset of gulf SSTs exceeding 26 C. (2) The incremental advance of SSTs > 26 C up the mainland coast of Mexico appears necessary for the northward advance of the monsoon. (3) In the southern gulf region, an SST parameter was lag-correlated with rainfall amount in adjacent land regions (r = 0.78) occurring during the 5-15 day period after an SST increase. (4) Relatively heavy rainfall in Arizona and New Mexico depended on two factors: (1) northern gulf SSTs exceeding 29 C, and (2) a neutral or positive along-gulf SST gradient (positive means higher SSTs in the N. gulf). Periods meeting both criteria accounted for 75% of the monsoon rainfall in this region.

JSP25/W/15-B2

1010

## INTERANNUAL VARIABILITY AND PREDICTABILITY IN THE MARITIME CONTINENT

JOHN L MCBRIDE Bureau of Meteorology Research Centre Melbourne Australia and Paulus Winarso, Dodo Gunawan, and Soetanto Meteorological and Geophysical Agency, Jakarta, Indonesia, e-mail: jmb@bom.gov.au

Interannual variability is studied for the maritime continent through analysis of seasonal rainfall data for 102 seasonal forecast districts across Indonesia. These data have been assembled from the records of the Meteorological and geophysical Agency in Indonesia, and form the basis of their seasonal forecasts. Four parameters are available for the 102 districts over the period 1961 to 1998: Onset date for the wet season, onset date for the dry season, total wet season rainfall, total dry season rainfall. From these, two additional derived parameters can be constructed: length of wet season and length of dry season. Linear correlations are calculated for each parameter with the Southern oscillation Index and with amplitudes of various rotated EOFs of global sea surface temperature data. The largest correlations are with the SOI, and these are in the magnitude range of 0.4 to 0.7 across most of the country during the dry months of June to November. Parameters relevant to those months include dry season rainfall and wet season onset, and based on 3-month lag correlations with the SOI, these parameters have a high degree of predictability. Conversely the relationships are quite small in the wet months of December to May; and the predictability is low for parameters whose timing occurs in that half-year, viz: wet season rainfall and dry season onset. These relationships are studied further through calculating correlations with Sea surface temperature patterns as well as cross correlations between the 102 forecast districts. It turns out the parameters related to the SOI are also related to the SST patterns, with smaller but statistically significant correlations with amplitudes of several EOF's. On the other hand parameters occurring during the wet season are not well related to the SST patterns; and they also have close to zero coherence in interannual variations across the domain. The implication is that in this region association with the Southern Oscillation is related to a large scale for spatial coherence in interannual variations. It also suggests that the monsoon or wet season rainfall does not have large scale coherence and is inherently unpredictable.

Presiding Chair: Mitchell D.L

## TROPICAL VARIABILITY

JSP25/W/08-B2

1110

## THE INFLUENCE OF SST PERTURBATIONS ON INTRASEASONAL VARIABILITY OF TROPICAL CONVECTION

Steven WOOLNOUGH and Julia Slingo (Centre for Global Atmospheric Modelling, Department of Meteorology, University of Reading, Earley Gate, PO Box 243, Reading, RG6 6BB, UK, email: s.j.woolnough@rdg.ac.uk); and Brian Hoskins (Department of Meteorology, University of Reading, Earley Gate, PO Box 243, Reading, RG6 6BB, UK)

Results from TOGA-COARE and other studies have shown that convection associated with the intraseasonal oscillation can affect the upper layers of the ocean through changes in the salinity, mixed layer depth and SST. However, the ways in which these changes in SST may feedback on the convection associated with the intraseasonal oscillation are not well understood. A better representation of the intraseasonal oscillation may lead to improvements in seasonal forecasting and the prediction of the onset of El Nino. Results from integrations of an aqua-planet GCM will be presented to demonstrate the sensitivity of intraseasonal variability in convection to SST perturbations. The implications for modelling of the intraseasonal oscillation will be discussed.



JSP25/E/03-B2

1130

## A THREE-DIMENSIONAL SIMULATION OF THE SOUTH CHINA SEA CIRCULATION

QINYU LIU, Haijun Yang (Institute of Physical Oceanography, Ocean University of Qingdao, Qingdao, 266003, P.R.China Email: liuyu@ouqd.edu.cn)

A three-dimensional, sigma-coordinate primitive equation model (Princeton Ocean Model) with a free surface is used to simulate the monthly mean circulation in the South China Sea (SCS). The model has a resolution of  $0.5^\circ$  in the horizontal and 10 sigma layers in the vertical in a region from equator to  $27^\circ\text{N}$  and from  $98^\circ\text{E}$  to  $125^\circ\text{E}$ . There are four openings in the model region, where the inflow and outflow in the Kuroshio, through the Taiwan Strait and Karimata Strait are obtained from the model output of the Parallel Ocean Climate Model (POCM). At the sea surface, the model is forced by monthly averaged climatological wind stress, heat and salinity flux. Several important features are reproduced in the model results. First, for the vertical integrated circulation (VIC), there is a large cyclonic gyre dominated the whole basin in winter, in which a meso-scale cyclonic eddy named Luzon cold eddy (LCE) appears to the northwest of the Luzon island. In spring the large cyclonic gyre becomes weak due to weak wind stress forcing and the LCE moves northwestward. A weak anticyclonic gyre begins to appear in the central SCS ( $10^\circ\text{N}$ - $14^\circ\text{N}$ ) in March. In summer, the VIC is cyclonic in the north half basin and anticyclonic in the south half and the LCE disappears. In fall, the cyclonic gyre expands southward and then occupies the whole basin. Second, the surface current represents the Ekman transport, which direction is nearly perpendicular to that of surface wind. From the sea surface temperature (SST) distribution, there is upwelling between  $11^\circ\text{N}$  to  $13^\circ\text{N}$  off the Vietnam in summertime. Third, in the lower layer, the thermal-wind relation is nearly met between the temperature distribution and the circulation pattern due to relatively weak influence of the surface wind and solar radiation. For example, the LCE is corresponding to a strong upwelling whose center temperature is lower than that of the surroundings by about 2 to 3 degrees. In winter and spring, there is warm water appearing in the central SCS, which corresponds to an anticyclonic gyre there. While in the south of the SCS, there is a cyclonic gyre corresponding to cold water. Finally, the LCE can reach a depth of 200m. Its generation and maintenance should be mainly due to the local wind stress curl. The Kuroshio can not flow directly into the SCS interior but forms an anticyclonic loop in the Luzon Strait, where a small part of Kuroshio water can flow out of the Taiwan Strait along the west coast of the Taiwan island.

JSP25/C/M105/W/01-B2

1150

## ONSET CHARACTERISTICS OF THE 1998 SOUTH CHINA SEA SUMMER MONSOON

Yongguang Wang, JOHNNY C. L. CHAN and Jianjun Xu (Dept. of Physics &amp; Materials Science, City University of Hong Kong; Email: Johnny.Chan@cityu.edu.hk)

The South China Sea Monsoon Experiment (SCSMEX) was conducted in May and June 1998 to study the South China Sea Summer Monsoon (SCSSM). This paper presents the results of a preliminary study of the characteristics of the synoptic-scale conditions related to the SCSSM onset and its maintenance. The onset and break are defined using gridded zonal winds at 850 hPa and observed daily rainfall at Xisha ( $112.33^\circ\text{E}$ ,  $16.83^\circ\text{N}$ ) and Yongshujiao ( $112.88^\circ\text{E}$ ,  $9.53^\circ\text{N}$ ). Four sets of meteorological parameters are examined using the gridded data sets from the Beijing Data Center of SCSMEX: 1) surface and 850-hPa temperatures, 2) mean sea-level pressure (MSLP), 3) surface relative humidity, and 4) surface and upper-level winds. The results show that the summertime meridional temperature gradient and meridional wind circulation as well as high relative humidity are already established before May over the South China Sea (SCS). On the other hand, reversals of the meridional MSLP gradient and the zonal wind circulation occur only at the onset. An active tropical cyclone in the Bay of Bengal is apparently responsible for "leading" the strong southwesterly Somalia jet to the SCS. A vortex over the northern SCS causes a weakening of the subtropical high to change the meridional MSLP gradient over the SCS, and enhances the cross-equator-flow at  $105^\circ\text{E}$ . Westerly flow then sets in at the low levels. The enhanced Southern Asia high at 200 hPa and an upper tropospheric trough over northeastern SCS are related to the establishment of easterly flow at the upper levels.

JSP25/L/01-B2

1210

## INTERANNUAL RAINFALL VARIABILITY

RICHARD WASHINGTON and Martin Todd (School of Geography, University of Oxford; 1 Mansfield Rd, OX1 3TB UK)

The primary mode of interannual rainfall variability over southern Africa and the Southwest Indian Ocean during the austral summer and its relationship with oceanic and atmospheric fields are examined in this paper. Empirical Orthogonal Functions (EOFs) of the Xie-Arkin satellite derived rainfall data are used to determine modes of interannual variability for austral summer months between November and March. In all months it is shown that tropical-temperate troughs linking tropical convection with quasi stationary or propagating transients are the primary mode of rainfall variability. Further analysis of model rainfall from an AGCM (HADAM2A) forced with historical sea surface temperatures from 1904-1994 indicates a similar mode of variability on both interannual and interdecadal time scales.

Sea surface temperatures, moisture fluxes, sea level pressure and other fields are examined to determine the characteristics of oceanic and atmospheric anomalies accompanying extreme years of tropical-temperate trough activity. The NCEP re-analysis data is used in conjunction with the Xie-Arkin (observed) rainfall EOFs and the model data with the model rainfall analysis.

The analysis of both model and observed circulation data focuses on anomalous anticyclonic gyres in near surface atmosphere of the southwest Indian Ocean. Near surface water vapour flux anomalies associated with the anomalous gyres and with extremes in tropical-temperate trough variability are highlighted.

Tuesday 27 July PM

## SEASONAL-DECADAL VARIABILITY

## Asian Monsoon

JSP25/W/89-B2

1400

## MONSOON-ENSO RELATIONSHIP ON INTERANNUAL AND INTERDECADAL TIME SCALES

B N GOSWAMI, Centre for Atmospheric and Oceanic Sciences Indian Institute of Science Bangalore 560012, India e-mail: goswamy@caos.iisc.ernet.in and V. Krishnamurthy Center for Ocean-Land-Atmosphere Studies Institute of Global Environment and Society, Inc. 4041 Powder Mill Road, Suite 302, Calverton, MD 20705, USA e-mail: krishna@cola.iges.org

Empirical evidence is presented to support a hypothesis that the interdecadal variation of the Indian summer monsoon and that of the tropical sea surface temperature (SST) are parts of a

tropical coupled ocean-atmosphere mode. The interdecadal variation of the Indian monsoon rainfall (IMR) is strongly correlated with the interdecadal variations of various indices of El Niño and the Southern Oscillation (ENSO). We also show that the interannual variances of both IMR and ENSO indices vary in phase and follow a common interdecadal variation. However, the correlation between IMR and eastern Pacific SST or between IMR and Southern Oscillation Index (SOI) on the interannual time scale does not follow the interdecadal oscillation. The spatial patterns of SST and sea level pressure (SLP) associated with the interdecadal variation of IMR are nearly identical to those associated with the interdecadal variations of ENSO indices. As has been shown earlier in the case of ENSO, the global patterns associated with the interdecadal and interannual variability of the Indian monsoon are quite similar. The physical link through which ENSO is related to decreased monsoon rainfall on both interannual and interdecadal time scales has been investigated using National Centers for Environmental Prediction/National Center for Atmospheric Research reanalysis products. The decrease in the Indian monsoon rainfall associated with the warm phases of ENSO is due to an anomalous regional Hadley circulation with descending motion over the Indian continent and ascending motion near the equator sustained by the ascending phase of the anomalous Walker circulation in the equatorial Indian Ocean. We show that, to a large extent, both the regional Hadley circulation anomalies and Walker circulation anomalies over the monsoon region associated with the strong (weak) phases of the interdecadal oscillation are similar to those associated with the strong (weak) phases of the interannual variability. However, within a particular phase of the interdecadal oscillation, there are several strong and weak phases of the interannual variation. During a warm eastern Pacific phase of the interdecadal variation, the regional Hadley circulation associated with El Niño reinforces the prevailing anomalous interdecadal Hadley circulation while that associated with La Niña opposes the prevailing interdecadal Hadley circulation. During the warm phase of the interdecadal oscillation, El Niño events are expected to be strongly related to monsoon droughts while La Niña events may not have significant relation. On the other hand, during the cold eastern Pacific phase of the interdecadal SST oscillation, La Niña events are more likely to be strongly related to monsoon floods while El Niño events are unlikely to have a significant relation with the Indian monsoon.

JSP25/E/18-B2

1420

## POST-MONSOON SST ANOMALIES OVER INDIAN AND PACIFIC OCEANS

C. A. BABU and P. V. Joseph (Department of Atmospheric Sciences Cochin University of Science and Technology Cochin - 682 016, INDIA)

We have studied the Sea Surface Temperature (SST) anomalies over the Indian and Pacific Oceans in association with DRY Indian monsoons accompanied or not with El Niño during the period 1961-1985, over the following three seasons September-November (SON), December-February (DJF) and March-May (MAM). The domain studied is between latitudes  $25^\circ\text{S}$  and  $25^\circ\text{N}$  and longitudes  $40^\circ\text{E}$  to  $160^\circ\text{W}$ . In general, a DRY monsoon is followed by a warm SST anomaly over the tropical Indian Ocean and cold SST anomaly over tropical west Pacific ocean. Those DRY monsoons which are co-existing with El Niño are associated with larger SST anomalies.

Examining 3 monthly moving averages, it is found that warm SST anomaly first appear over the western Indian Ocean during JJA and expand in area northward and intensify during the Asian Summer Monsoon (JAS, ASO and SON). During OND this anomaly weakens and spreads to the east and south while a new and stronger SST anomaly appears over the eastern Bay of Bengal and South China Sea, apparently in association with the Asian Winter monsoon. This anomaly intensifies and spreads towards the Australian waters over the following few months. By March to May (MAM) season the entire Indian Ocean about  $10$ - $15$  degrees latitude either side of the equator, has a warm SST anomaly.

JSP25/W/73-B2

1440

## A MODEL OF THE INTRASEASONAL FLUCTUATION OF THE INDIAN MONSOON

MR BRETT SCONCIA and Prof. Brian J. Hoskins, Department of Meteorology, University of Reading, 2 Earley Gate, Whiteknights, PO Box 239, Reading, UK, e-mail: swr96bcs@reading.ac.uk

The dominant mode of intraseasonal variability of the Indian summer monsoon is associated with an alternating position of the tropical convergence zone (TCZ). An "active" period of the monsoon occurs when the TCZ persists over the Indian sub-continent, contrasting with a "break" period that occurs when the TCZ is found in a more southerly position over the equatorial ocean. The heating structures of the atmosphere associated with a typical active and break period are produced from ERA data and are used as forcings to drive a simple numerical model. With the two heatings kept constant, resultant atmospheric flows are consistent with those seen in ERA data. The model is then made time-dependent with a linear combination of the active and break heatings used to drive the model. Characteristics of the low-level flow that are significantly different for the two regimes are used to determine the relative amounts of the two heatings. Results from a 1000-day integration show an apparently chaotic system with some evidence of bi-modality in the probability density function (PDF). Experiments with the time-dependent model to investigate the sensitivity of the PDF distribution to external forcing will be presented.

JSP25/P/03-B2

1500

## IMPACT OF ENSO ON ASIAN MONSOON: NEW PERSPECTIVES

R.H.KRIPALANI and Ashwini Kulkarni (both at Indian Institute of Tropical Meteorology, Pashan, Pune 411008, India, email: rhksup@tropmet.emet.in)

El Niño Southern Oscillation (ENSO) phenomenon is now recognised as the single most important mode of the earth's year-to-year climatic variability. It has been well documented that majority of the ENSO warm (cold) extremes are associated with below (above) normal rainfall over the Asian domain.

Our recent analysis of the 128-year (1871-1998) data reveals that the Indian monsoon rainfall (IMR) exhibits epochal variability. The periods 1880-1895 and 1930-1963 are characterised by above normal rainfall while the periods 1895-1930 and 1963-1990 are characterised by below normal rainfall. Further the impact of El Niño (La Niña) on IMR is more severe during the below (above) normal rainfall epochs. Rainfall data analysis also reveals that the IMR is entering into an above normal epoch with a turning point around 1990 suggesting that the impact of El Niño (La Niña) on IMR may not (may) be severe. This may be a possible reason for India not experiencing a drought during the El Niños after 1990s. In spite of the severe 1997 El Niño the IMR was 102 % of the long-term average. The equatorial Pacific entered into a La Niña phase during the Monsoon of 1998. The IMR for 1998 was 106 % of the normal.

Such phase-locking between the ENSO episodes and epochal variability is also seen over other regions of Asia. Implications of these results on the impact of ENSO during the coming decade will be discussed.

JSP25/E/36-B2

1520

## THE OCEANS' ROLE IN LOW-FREQUENCY VARIABILITY OF THE INDIAN MONSOON

ROXANA C. WAJSOWICZ (Dept. of Meteorology/JCESS, University of Maryland, College Park, MD 20742, U.S.A., e-mail: roxana@atmos.umd.edu); Paul S. Schopf (Institute of Computational Sciences and Informatics, George Mason University, Fairfax, VA 22030, U.S.A., e-mail: schopf@cola.iges.org)

It is proposed that the southern tropical Indian Ocean (STIO) plays an important role in variability of the strength of the Indian summer monsoon. During years of a strong monsoon, its influence is either direct in providing more moisture to precipitate over India, or indirect in draining less heat from the Arabian Sea and so promoting a more energetic atmospheric circulation. Direct influence is supported by analysis of COADS, which shows that the evaporation rate over the STIO is increased as is the cross-equatorial moisture transport by the Findlater jet during boreal summer in strong years. Interestingly, the corresponding SST anomalies in the STIO are positive. In years of below average monsoon rainfall, the opposite is found. Indirect influence occurs because vigorous evaporation over the STIO is sustained during the boreal summer by heat transport from the Arabian Sea and from the western equatorial Pacific Ocean via the Indonesian throughflow. Whereas the heat exchange between the Arabian Sea and STIO has an annual period with a maximum southward transport in boreal summer, that between the western equatorial Pacific and the STIO has a strong semi-annual period with a maximum southwest transport over the upper thermocline during the monsoon transition seasons. Hence, the Indonesian throughflow preconditions the STIO for the ensuing monsoon season. The mutual interactions between these three components, namely the Arabian Sea, STIO and western equatorial Pacific, are illustrated with differently configured GCMs of the seasonal cycle and the last decade.

Presiding Chair: B.N. Goswami (Indian Institute of Science)

## Tropical Atlantic and Connections

JSP25/W/17-B2

1620

## CLIMATIC ANOMALIES DURING THE BOREAL WINTER OF 1997-98: THE ROLE OF ATLANTIC SST

R.T. SUTTON, S.P. Jewson, C. Jones, J. Slingo Centre for Global Atmospheric Modelling, Department of Meteorology, University of Reading, PO Box 243, Earley Gate, Reading RG6 6BB, U.K.

During the boreal winter of 97/98 there were major climate anomalies in many parts of the world. Many of these anomalies were attributed to the El Niño conditions that prevailed at the time, implying a link to SST anomalies in the tropical Pacific. There were, however, significant SST anomalies elsewhere in the world: in the Indian and Atlantic oceans. There is considerable evidence that the Indian Ocean SST anomalies had a major impact on climate. We are investigating the less studied role of the Atlantic Ocean SST anomalies.

We have performed ensemble integrations of an atmospheric General Circulation Model with various SST fields used as lower boundary condition. Our results show that the Atlantic SST anomalies had a significant impact on both the tropical and extratropical atmospheric circulation during DJF 97/98. Our model suggests that this impact included a contribution to a predictable signal over Europe. The response to the Atlantic SST anomalies in the tropics involves intensification of the local Hadley Circulation. Over the North Atlantic an anomalous low is forced. An important question is whether this mid-latitude response is forced by the local Atlantic SST anomalies or is a remote response to the tropical Atlantic SST anomalies. We are presently addressing this question through further experimentation.

JSP24/W/45-B2

1640

## TROPICAL-EXTRATROPICAL CONNECTION IN THE ATLANTIC ATMOSPHERE-OCEAN VARIABILITY

Masahiro WATANABE and Masahide Kimoto (Center for Climate System Research, University of Tokyo, 4-6-1 Komaba, Meguro, Tokyo 153-8904, Japan, email: hiro@ccsr.u-tokyo.ac.jp)

Observations for the recent 40 years show two dominant modes of variability in the tropical Atlantic SST anomalies. One has a monopole structure associated with the El Niño-like signal in the tropical Pacific SST anomalies, while another reveals a north-south dipole straddling the equator. These modes accompany 500-hPa height and SST anomalies in the North Atlantic.

To investigate the physical relationship between the tropical SST variations and the North Atlantic atmosphere-ocean system, a 60-yr long integration was conducted with an AGCM coupled to a 50-m-deep slab ocean except for the tropics where the SST is prescribed to observations (TOGA-ML run). The TOGA-ML run well reproduced the extratropical height and SST anomalies, suggesting an impact of tropical SST anomalies on the North Atlantic air-sea variations. However, linear responses of the dynamical operator of the AGCM to the heating in the tropical Atlantic corresponding to the two modes of SST variability are weak in the North Atlantic and moreover less similar to the observed height anomalies. The height responses resemble the anomalies when associated transient eddy forcing is included. This result implies that the tropical SST variations indirectly influence the North Atlantic atmosphere through changes in the eddy activity. A comparison of the TOGA-ML run with a GCM run coupled to the global slab ocean indicates that the tropical SST variability increases the variance in the extratropical atmosphere, selectively for the North Atlantic Oscillation.

JSP25/L/02-B2

1700

## THE EQUATORIAL ATLANTIC OSCILLATION: A SELF-SUSTAINING CLIMATE OSCILLATION IN THE TROPICAL ATLANTIC

ITSUKI C. HANDOH (School of Environmental Sciences, University of East Anglia, Norwich NR4 7TJ, U.K., e-mail: i.handoh@uea.ac.uk); Grant R. Bigg (School of Environmental Sciences, University of East Anglia, Norwich NR4 7TJ, U.K., e-mail: g.bigg@uea.ac.uk)

The anomalous climate of the Atlantic of 1983-84 has been inferred as being triggered by the 1982/83 El Niño in the Pacific. Other such events have been observed in the tropical Atlantic, typically lagging El Niño events by 4-5 months, although there are not always clear links to such events, as in 1988. Here, using modelling, satellite altimetric and sea surface temperature data, we report an unusual equatorial Atlantic event, starting in autumn 1995 and continuing into the autumn of 1997, which does not seem to be connected to the El Niño ending in early 1995. This Atlantic event contained both a warm and a cold phase, with the latter seemingly being generated, through air-sea coupling, by the former. The propagating signal within each phase is identified in the sea surface height and temperature signatures as both equatorial and off-equatorial Rossby waves in the ocean, with coupling to atmospheric convection. The two-phased climate event appears to have been associated with internal atmospheric and oceanographic variability within the Atlantic basin and hence have been independent of the Pacific climate.

JSP25/W/83-B2

1720

## A LINKAGE FOR DECADEAL CLIMATE VARIATIONS IN THE LABRADOR SEA AND THE TROPICAL ATLANTIC OCEAN

Jiayan YANG (Dept. of Physical Oceanography, Woods Hole Oceanographic Institution, Woods Hole, MA 02543, USA, email: jyang@whoi.edu)

The Labrador Sea Water (LSW) thickness, according to observations, varies significantly on decadal time scales in response to atmospheric forcing and fresh-water flux from the Arctic Ocean. Sea surface temperature (SST) in the tropical Atlantic also exhibits considerably interannual to decadal changes. A distinct mode, as identified in previous studies, is the so-called tropical Atlantic SST dipole -- a cross-equator pattern. Analyses of observations and modeling results indicate that the SST dipole and variations of LSW thickness are linked through the Meridional Overturning Circulation (MOC). Southward transport of LSW along deep western boundary must be compensated by northward flow in the upper ocean. Once the LSW pulse enters the tropics, it affects the cross-equator heat transport and the upper ocean response generates a dipole pattern in the SST field. The correlation between observed LSW thickness and SST is significant with a lag of 5 years. The best correlation occurs in areas off the western boundary where the main cross-equator transport takes place. Results from an ocean model indicate that the time lag between LSW and tropical SST is set by coastal Kelvin waves that propagate from the Labrador Sea to the tropics along the western boundary.

Wednesday 28 July AM

Presiding Chair: M. Alexander (CDC-CIRES)  
Concurrent Poster Session

IA

## SEASONAL-DECADEAL VARIABILITY

## NAO Related Variability

JSP25/E/12-B3

0830

## NORTH ATLANTIC OCEAN VARIABILITY ON DECADEAL TIMESCALES IN THE HADLEY CENTRE COUPLED MODEL

Claire COOPER and Chris Gordon (both at Hadley Centre for Climate Prediction and Research, Meteorological Office, London Road, Bracknell, Berkshire, RG12 2SY, UK. Email: ccooper@meto.gov.uk)

The simulation of decadal variations in the North Atlantic Oscillation (NAO) and related ocean phenomena in a multi-century integration of the latest Hadley Centre coupled model which does not use flux adjustment will be described. Where possible the model simulation is compared with available observations. The ocean component of the model has a 1.25 deg resolution which allows a better representation of the North Atlantic Current (NAC) than in many of the earlier coarser resolution climate models. It has also enabled the relationship between the NAO, high latitude convection and the strength and path of the NAC to be explored in detail. It is shown that the model realistically simulates the NAO in both spatial pattern and time variability and, in addition, the ocean component confirms the observed relationship between convection in the Labrador and Greenland Sea and the phase of the NAO. The model also has propagating decadal timescale sea surface temperature anomalies, similar to those found in the historical observations. The mechanisms of propagation of these anomalies in the coupled model will be discussed.

JSP25/W/53-B3

0850

## FLUCTUATIONS OF THE NAO AND NORTH ATLANTIC STORM TRACK ACTIVITY IN THE ECHAM4/OPYC3 COUPLED AOGCM

M. CHRISTOPH and U. Ulbrich, (Institut für Geophysik und Meteorologie der Universität zu Köln, Kerpener Straße 13, D-50923 Köln, Germany)

In a 300-year control integration of a coupled ocean\_atmosphere GCM (ECHAM4 + OPYC3), a close relation of the North Atlantic Oscillation (NAO) and the eastern part of the Atlantic storm track is confirmed both for the interannual (< 10 years) and the decadal (> 10 years) time scales. Positive anomalies of the NAO are associated with a northward shift and intensification of the storm track, and increased freshwater fluxes into the Iceland and Norwegian Seas. On the other hand, the mean flow anomaly in the atmosphere induces Ekman pumping into the central parts of the subtropical North Atlantic during the positive NAO phase. This contributes to a spin up of the subtropical gyre circulation and thus to northward transports of warm and salty waters within the Gulf stream system. While the existence of such relations on the decadal time scale suggests that the dynamical ocean is important for the NAO and the associated storm track variability, an additional experiment using a 50 m fixed-depth mixed layer ocean proves the contrary. The NAO has very similar space-time behaviour as in the coupled run and amplitudes are only about 10% smaller than using the dynamical ocean. The second EOF of eddy activity over the Atlantic represents the variation of activity in the center of the Atlantic storm track, again both on the interannual and the decadal time scales. This variation exhibits a very weak connection to the NAO or to other coherent SLP variability patterns. Potential factors influencing this region are discussed.

JSP25/E/24-B3

0910

## LONG-TERM CHANGES OF INTERANNUAL SEA LEVEL VARIABILITY IN THE BALTIC SEA AND RELATED CHANGES OF WINTER CLIMATE

Martin EKMAN (Summer Institute for Historical Geophysics Bomarsund Åland Islands)

The world's longest sea level series, that of Stockholm commencing 1774, has earlier been used by the author to study the eustatic rise of sea level. Here, the interannual sea level variability of the Baltic Sea and its relation to climate is studied using the same sea level series, together with equally long temperature and wind series. Long-term changes of the sea level variability are found to be closely related to changes of winter climate. The interannual sea level variability and the interannual winter temperature and winter wind variabilities have all decreased significantly from the end of the 1700s to the beginning of the 1900s; after that they have all increased significantly again. The common origin of these long-term changes turn out to be two consecutive wind processes over the North and Baltic Seas, especially the Baltic entrance: From the end of the 1700s to the beginning of the 1900s there is a rapidly decreasing number of dominating winter winds from northeast, after that there is an increasing number of dominating winter winds from southwest.

**JSP25/E/06-B3 0930**

**IS THE NORTH ATLANTIC OSCILLATION A RANDOM WALK?**

Dr. David B. STEPHENSON (Labo. de Statistiques et Probabilités, Université Paul Sabatier, 118, route de Narbonne, 31062 Toulouse, France. E-mail: stephen@cict.fr); Dr. Valentina Pavan (CINECA, via Magnanelli 6/3, 40033 Casalecchio di Reno, Italy. E-mail: pavan@cineca.it)

A principal component analysis of the Jones gridded land/sea temperature data set reveals that year-to-year differences in global land/sea wintertime surface temperatures are dominated by a) the North Atlantic Oscillation (NAO) and b) the tropical biennial oscillation. The NAO indices exhibit long-memory fluctuations that can be modelled using a simple non-stationary random walk model. The model accounts for both year-to-year reversals and trends in the NAO, and has some slight yet encouraging skill at forecasting the NAO one year ahead. Decadal trends and cycles simulated by this non-stationary stochastic model resemble those in the observed NAO and offer a possible explanation for recent NAO variability.

**JSP25/W/59-B3 0950**

**SEASONAL DEPENDENCE AND TIME EVOLUTION OF THE INTERANNUAL SEESAW BETWEEN THE ALEUTIAN AND ICELANDIC LOWS**

HISASHI NAKAMURA (IGCR, Frontier Research System for Global Change, Tokyo/Dept. Earth, Planetary Physics, Univ. Tokyo, 113-0033, JAPAN; email: hisashi@geoph.s.u-tokyo.ac.jp), Meiji Honda (IGCR, Frontier Research System for Global Change, Tokyo; email: meiji@frontier.esto.or.jp), and Jinro Ukita (IARC, Frontier Research System for Global Change, Tokyo; email: qpee@frontier.esto.or.jp)

It is known that the surface Aleutian and Icelandic lows (AL and IL, respectively) exhibit a seesaw-like oscillation in winter. We examined seasonal dependence of this interannual seesaw by recording the minimum within each of the North Atlantic and North Pacific in the 31-day moving-averaged sea-level pressure (SLP) for each day over 1973-1994 based on the NMC analyses. The correlation coefficient between the 22-year timeseries of thus-defined AL and IL intensities was evaluated for each calendar days. The correlation was found to be strongly negative only in the late winter (February through mid-March). In the rest of the year it is weakly negative or even slightly positive. A similar seesaw is also evident in the SLP field from which ENSO-related anomalies as inferred from a linear regression analysis with SOI were removed.

We defined AI (AL-IL) index as the IL-center pressure subtracted from the AL-center pressure in the 45-day mean SLP for January 31-March 16. In the recognition of the equivalent barotropic structure of the seesaw, we investigated seasonal evolution of the seesaw in the linear lag regression maps between AI index and the mean of the 250-hPa height for each of the fourteen 45-day periods, whose central calendar days are mutually 15 days apart. In the following, we focus on a winter of the weaker AL with the stronger IL. After positive height anomalies gradually develop over the eastern North Pacific in December, a PNA-like wavetrain emanates from the positive anomalies in early January (Dec. 17-Jan. 30) with negative and positive anomalies appear over western Canada and the southeastern US, respectively. Then, another wavetrain emanates from the latter with negative and positive centers to the east of Newfoundland and over northern Europe, respectively. As these wavetrains gradually weaken by early February (Jan. 16-Mar. 1), positive anomalies over the North Pacific fully mature and cover the entire North Pacific, which correspond to the weak AL. At the same time the negative anomalies over the North Atlantic further develop while shifting northward until they mature in the "peak period" (Jan. 31- Mar. 16), when the AL-IL seesaw is the most apparent.

**JSP25/W/52-B3 1010**

**LONG-TERM CHANGES OF THE WINTER SEA LEVEL PRESSURE FIELDS AND RELATED SYNOPTIC ACTIVITY OVER THE NORTH ATLANTIC**

Igor ZVERYAEV (IPRC, SOEST, University of Hawaii, MSB, Room 227, 1000 Pope Rd., Honolulu, HI 96822, USA, email: igorz@soest.hawaii.edu)

Long-term climatic changes of the winter synoptic activity over the North Atlantic are studied in relation to changes of the winter mean sea level pressure (SLP) fields. Analysis of linear trends has revealed a good agreement between long-term (interdecadal) changes of the intensity of synoptic processes and variations of the winter SLP. On the contrary, there was not such agreement found between detrended and low-pass filtered anomalies. There are periods, which are characterized by the enhanced (reduced) synoptic activity attributed to the low (high) index of the North Atlantic Oscillation (NAO). It appears that low-passed anomalies of intramonthly root mean square deviations of SLP are negatively correlated with NAO and East-Atlantic teleconnection patterns over the most of the North Atlantic.

The low-passed winter SLP anomalies demonstrate both propagating and standing patterns. The latter have a period of about 8 years. While meridional dipole-like structures formed by the winter SLP anomalies are shifted to the west (east) of the North Atlantic, related anomalies of synoptic activity tend to be located in the eastern (western) part of the region. When decadal averaged, anomalies in the intensity of synoptic activity are strongly linked to the North Atlantic storm track position. Exception is 1980-1990 decade, characterized by the very high NAO index. During this decade enhanced synoptic activity is observed to the south of the North Atlantic storm track.

Presiding Chair: M. Christoph (Institut für Geophysik und Meteorologie der Universität zu Köln, Germany)

**Predictability**

**JSP25/W/04-B3 1110**

**HYDROCLIMATOLOGICAL PREDICTABILITY OVER THE AMERICAS**

John ROADS (Scripps Institution of Oceanography, UCSD-0224, La Jolla, CA 92093, Email: jroads@ucsd.edu); Susan Marshall (Dept. Geog. & Earth Sci., UNC-Charlotte, Charlotte, NC 28233, Email: susanm@unc.edu); Bob Oglesby (Purdue Univ., W. Lafayette IN 47907, Email: roglesby@purdue.edu); Franklin Robertson (NASA/Marshall Space Flight Center, Global Hydrology and Climate Center, Huntsville, AL 35806, Email: pete.robertson@msfc.nasa.gov)

Hydrologic variations over the Americas associated with interannual sea-surface temperature (SST) anomalies have been identified in long simulations made with the National Center for Atmospheric Centers (NCAR's) community climate model (CCM3) and in the National Centers for Environmental Prediction (NCEP) reanalysis. Corresponding variations in global precipitation climatology project (GPCP) precipitation anomalies provide additional validation of the strength and magnitude of the anomalies. These hydrologic variations are also being compared to the variations associated with local soil moisture anomalies.

The extent to which the response of the CCM3 atmosphere to SST anomalies differs from the response to local soil moisture anomalies serves as the basis for climate predictability

experiments using various combinations of SST and soil moisture anomalies. Preliminary results indicate that in the Mississippi River basin and in the Mackenzie River basin, both soil moisture and SST anomalies have significant influences on monthly to seasonal predictions. By contrast, hydroclimatological variations over the Amazon are governed much more strongly by SST anomalies.

**JSP25/E/33-B3 1130**

**LONG-RANGE PREDICTION OF UK WINDSTORMS**

S. E. GEORGE and M. A. Saunders (both at Department of Space and Climate Physics, Benfield Greig Hazard Research Centre, University College London, UK, Email: seg@mss.ucl.ac.uk)

For the UK and NW Europe, winter storms and floods are the largest cause of economic damage and insurance loss. The skillful prediction of such events several months in advance would allow damage limitation procedures to be implemented. Current dynamical weather forecast models have a limit of predictability measured in weeks rather than months, and are therefore not suitable for such a task. We present a new statistical model for the long range prediction of UK windstorms. Initial results for winter storminess in the South East of England for the period 1958-1996, have shown 70% of the year-to-year variance in storminess can be predicted six months in advance. Physical mechanisms linking the climate predictors we use with UK windspeed several months later will be suggested.

**JSP25/E/08-B3 1150**

**IMPACT OF THE ENSEMBLE SIZE ON MULTIMODEL SEASONAL FORECASTS**

Francisco Javier DOBLAS-REYES and Michel Deque (CNRM, Météo-France, 42, Av. G. Coriolis, 31057 Toulouse Cedex, France)

In the framework of the PROVOST project, the European seasonal prediction experiment, four long-lead ensemble forecast experiments with prescribed SST have been carried out. Each experiment has been run with a different GCM: the ECMWF, CNRM (with two different horizontal resolutions), and UKMO atmospheric models, all integrated from common initial conditions.

The performance of the combination of the different models in a whole ensemble has been compared with the performance of the individual models. The combination increases the ensemble size, providing a good test field for checking the feasibility of probabilistic forecasts in seasonal forecasting. Furthermore, the multimodel forecasts present the advantage of taking into account the role of the model in the forecast divergence. All the models exhibit some skill in the seasonal range in winter. This is also evidenced for the other seasons except for the European region. The hypothesis of a significant gain in skill for multimodel probabilistic forecasts independently of the ensemble size has been tested. Results show that multimodel represents a clear improvement over the tropics.

**Wednesday 28 July PM**

Presiding Chair: Dr D.B. Stephenson (Météo-France)

**SEASONAL-DECADAL VARIABILITY**

**Air-Sea Interaction and the Mixed-Layer**

**JSP25/E/32-B3 1400**

**THE INFLUENCE OF MIDLATITUDE AIR-SEA INTERACTION ON CLIMATE VARIABILITY**

MICHAEL ALEXANDER and James Scott (CDC-CIRES, University of Colorado Boulder, CO 80309, USA e-mail: maa@cdc.noaa.gov)

A coupled atmosphere-ocean model is used to examine the role of air-sea interaction in climate variability. The coupled model consists of the Geophysical Fluid Dynamics Lab (GFDL) atmospheric general circulation model (AGCM) coupled to a grid of independent mixed layer ocean models which is nearly global in extent. The ocean model simulates vertical processes which makes it appropriate for studying aspects of the climate system which operate on interannual time scales in the extratropics. The coupled model has been integrated for 50 years and has been compared to a 50-year control AGCM simulation in which sea surface temperatures (SSTs) corresponding to the long term mean in the coupled run are specified as boundary conditions.

Here we will focus on processes which create SST anomalies and how these anomalies influence the atmospheric circulation. The net surface heat flux is the dominant term in creating SST anomalies over most of the year except in fall when entrainment plays an equal or greater role over parts of the North Pacific and North Atlantic. This allows for the winter-to-winter recurrence of SST anomalies as thermal anomalies created by the net heat flux in late winter, remain below the mixed layer in summer and are then returned to the surface by entrainment in the following winter. Preliminary results indicate that air-sea interaction in the Atlantic influences the storm track and the circulation at 500 mb downstream over Europe.

**JSP25/E/21-B3 1420**

**ERROR PROPAGATION ACROSS THE AIR-OCEAN INTERFACE**

Peter C. CHU, (Naval Postgraduate School, Monterey, CA 93943, USA, Email: chu@nps.navy.mil) Shihua Lu, W. Timothy Liu, and Yuchun Chen

Error propagation across the air-ocean interface is an important factor to determine the ocean/atmosphere predictability. First, we use the Lorenz system (Lorenz, 1963) to show the propagation of boundary error. Second, we use the latest version of the NCAR Community Climate Model (CCM3) to study the propagation of tiny surface temperature error into the model atmosphere. The model was integrated from 1 September 1977 observational data over the globe for 16 months with and without SST disturbances. A time-scale of 20-day is found such that the response increases rapidly within this time-scale and then oscillates at high values. Third, we study the propagation of wind error into ocean model. Finally, some theoretical discussion will also be included.

**JSP25/W/35-B3 1440**

**TESTING THE INFLUENCE OF THE SST ANOMALIES IN THE TROPICAL ATLANTIC UPON THE ATMOSPHERIC CIRCULATION AT 500 HP**

Allaena Mares, C. MARES, Mihaela Mihailescu (National Institute of Meteorology and Hydrology, Bucuresti-Ploiesti 97, Bucharest 71552, Bucharest, Romania Fax : 00-40-1-2303143, E-mail: imares@meteo.inmh.ro)

We have started from the hypothesis that there is a dependence of Markov chain type of the main interaction types between the ocean state and the atmospheric state. The classification



with four states has been used : blocking circulation conditioned by SST negative anomalies, blocking circulation conditioned by SST positive anomalies, zonal circulation conditioned by SST positive anomalies and zonal circulation conditioned by SST negative anomalies.

The probability matrix of the transformations from one state to another, is estimated from monthly mean values of the geopotential at 500 hPa and of the SST in the Atlantic Ocean area, during the period 1965-1987. The geopotential has been considered over the sector: 500W-400E and 350N-650N. The SST data in COADS in the same period have been considered in our processing for the sector: 370S-390N, 740W-100E. The limiting matrix of the Markov chain has become stabilised after 23 steps ( months), indicating a measure of the predictability of the supposed interaction. The statistical significance of the elements of the transition matrix has been established by the Monte Carlo simulation method.

**JSP25/W/94-B3****1500****THE SEASONAL AND INTERANNUAL VARIATION OF THE HEAT BUDGET OF THE MIXED LAYER EVALUATED BY SATELLITE-DERIVED HEAT FLUX AND THE NUMERICAL MODEL VELOCITY FIELD**

Masanori KONDA, Miho Toyoda, Taiyo Kobayashi, Norihisa Imasato (Department of Geophysics, Graduate School of Science, Kyoto University); Kitashirakawa-Oiwake, Sakyō, (Kyoto 606-8502, Japan, E-mail: konda@kugi.kyoto-u.ac.jp) , and Akira Shibata (NASDA/EORC, 14F, Roppongi-1st Bld., 1-9-9 Roppongi, Minato, Tokyo 106-0032, Japan, E-mail: ashibata@eorc.nasda.go.jp )

We evaluate the heat budget in the mixed layer in the global ocean from satellite-derived surface heat flux and the numerical model velocity field, and discussed the seasonal and the interannual variability of it. The surface heat flux data is the sum of the satellite-derived turbulent heat flux and the radiation flux from July 1987 to June 1991, and the seasonal cycle of the surface velocity field is computed by the robust diagnostic model (Kobayashi and Imasato 1998) without the interannual variation. The thermal response of the ocean to the surface heat exchange is very important in the point that the seasonal and the interannual climate changes largely depend on the thermal air-sea interaction. In careful consideration for the validity of using together different types of the data sources as imported from the numerical model computation and the satellite observation, the heat flux at the bottom of the mixed layer is computed as the residual of the surface and the horizontal heat flux and the change of the heat content in the surface layer with a constant depth in the global ocean. The distribution of the heat flux at the bottom of the mixed layer indicates the existence of the significant heat exchange between the surface and the subsurface layer. The seasonal change of the bottom heat flux suggests that the oceanic heat transport by the strong current has relatively greater effect during the season when the sea surface temperature (SST) is increasing, and the surface heat flux when the SST decreasing. Correlation analysis is done to examine how the result of the air-sea heat exchange can be induced to the subsurface ocean, and it is suggested that the change of the thermal condition in the remote area can teleconnectively contribute to the local heat budget through the horizontal heat transport, adding to the local effect of the surface heat flux.

**JSP25/E/17-B3****1520****MIXED-LAYER HEAT BALANCE AND NET SURFACE HEAT FLUX ON A SEASONAL SCALE**

S.A.B. KIM (Satellite Technology Research Center, 373-1, Kusung, Yusong, Taejeon, S. KOREA 305-701, email: sbkim@krsc.kaist.ac.kr. Also at Korean Meteorological Administration)

Heat balance within an ocean mixed layer is important since it describes whether ocean-atmosphere interactions occur locally or remotely. The heat balance mechanism is analysed over the Kuroshio Extension region to identify the significance of the jet, seasonally from October 1992 to September 1995. The horizontal geostrophic heat advection is obtained using current velocities from satellite altimetry. The errors in the monthly and spatial mean values of the zonal and meridional geostrophic heat advection reach respectively 150 % ( $46 \text{ W/m}^2$ ) and 300 % ( $61 \text{ W/m}^2$ ) of the signal. The entrainment heat advection is estimated rigorously on a climatological monthly scale. The heat storage rate is computed using subsurface temperature records. The horizontal Ekman heat advection is derived using ECMWF model wind speeds. The seasonal heat advection by the Kuroshio Extension is <10 % of the heat storage rate in the basin-scale heat balance. The horizontal Ekman heat advection is also insignificant. It is concluded that the heat balance is achieved locally. Monthly net surface heat fluxes are derived from the sum of the heat balance terms. Errors in these fluxes are estimated thoroughly by developing formulae on how errors in the basic fields propagate into the flux. A value of  $30 \text{ W/m}^2$  is obtained for the error in the three-year mean net surface heat flux over the basin. This is smaller in percentage terms than that achieved by the best bulk-formulae method. Horizontal heat advection (Ekman plus geostrophic) contributes  $21 \text{ W/m}^2$  to the error in the three-year mean net surface heat flux.

Presiding Chair: Claire Cooper (Hadley Centre for Climate Prediction and Research, Meteorological Office, Berkshire, UK.)

**JSP25/W/43-B3****1620****INTERNALLY GENERATED MODE WATER VARIABILITY**

Wilco HAZELEGER (KNMI, Oceanogr. Res. Div., PO Box 201, 3730 AE De Bilt, The Netherlands, Email: hazele@knmi.nl) Sybren Drijfhout (KNMI, Oceanogr. Res. Div., PO Box 201, 3730 AE De Bilt, The Netherlands, Email: drjfhout@knmi.nl)

Mode Water formation in the subtropical gyre of the North Atlantic exhibits substantial decadal variability. Here, we present results that indicate a large role of internal oceanic variability in generating this variability. The results are obtained with an isopycnal ocean model, with idealised geometry and forcing. The horizontal resolution is sufficiently high and the friction/diffusion sufficiently low for the flow to become unstable.

Two modes of low frequency variability are found. Both modes consist of westward propagating thickness anomalies. The anomalies have a first baroclinic modal structure. One mode has a time scale of 8 years and a basin wide spatial scale, the other has a time scale of 4.5 years and smaller spatial scale. The modes are damped when the diffusion is increased. In that case, the 8 yr mode can be excited by a spatially coherent stochastic wind stress, but the amplitude is much smaller. The modes are maintained by a release of energy of the mean flow in the thermocline. The instability of the mean flow is determined by the basic stratification, in particular the slope across the midlatitude jet. Finally, it is shown that coupling to the atmosphere and a parameterization of surface mixing are necessary for the low frequency variability to appear in the mixed layer.

**JSP25/E/01-B3****1640****INTER-DECADAL VARIATIONS IN JAPANESE SARDINE AND THE KUROSHIO EXTENSION**

ICHIRO YASUDA (Univ. of Tokyo/ Frontier Research System for Global Change, Hongo 7-3-1, Bunkyo, Tokyo 113-0033, Japan, E-mail: ichiro@geoph.s.u-tokyo.ac.jp); Masayuki Noto (Hokkaido Univ., E-mail: noto@geoph.s.u-tokyo.ac.jp); Tomoki Touzuka (Univ. of Tokyo, E-mail: s72620@vsiron.geoph.s.u-tokyo.ac.jp)

Japanese sardine is known to greatly vary in inter-decadal time scales. In 1988, the catch was over 4 million tons; it declined abruptly since 1989 and was below 1 million tons in 1995. We found the winter-SST in the Kuroshio Extension and its southern recirculation area (KESA: 30-35N, 145-180E) significantly correlates with the mortality coefficient of the Japanese sardine. The warming in the KESA since 1988 possibly causes the collapse of the sardine. The SST variations in the KESA and south of Japan were different from those in the Kuroshio-Oyashio frontal regions in the western/central Pacific (40-45N 145-180E) where a regime-shift around mid-1970s was known: the SSTs in the Kuroshio regions have a longer time scale of over 50 years than in the frontal regions (25 years), and the jump of the Kuroshio SSTs around late-1980s occurred two years earlier in 1988 than in the frontal regions. The shift around mid-1970s in the frontal regions was not observed in the Kuroshio and the KESA where the SST anomalies were already negative in early-1970s. These SST variations well corresponds to sardine catch records. Analyses of heat flux and wind before/after the late-1980s SST jump indicate that the warming since 1988 was caused partly by the decrease in the net heat flux and in the mixed layer depth due to the reduction of wind over the Kuroshio south of Japan and over the Kuroshio Extension regions.

**JSP25/W/72-B3****1700****RECENT VARIATIONS IN THE SURFACE PRESSURE SEMIANNUAL OSCILLATION**

Ian SIMMONDS (School of Earth Sciences, The University of Melbourne, Parkville, Victoria, 3052, Australia, email: ihs@met.unimelb.edu.au); David A. Jones (Bureau of Meteorology Research Centre, 150 Lonsdale Street, Melbourne, Victoria, 3001, Australia, email: d.jones@bom.gov.au)

We present a climatology of the Southern Hemisphere semiannual oscillation of surface pressure and mid tropospheric baroclinicity compiled from 21 years of numerical analyses. In addition, long time series of this feature derived from pressure data from a number of mid and high latitude stations are presented. The results confirm that the oscillation is an important feature of the annual cycle of pressure and meridional temperature gradient. The pressure half-yearly wave attains its greatest amplitudes in the mid latitude ocean basins and on the Antarctic periphery, with a minimum near 55oS. The semiannual oscillation of the temperature gradient is strongest near 60oS, where it explains about 50% of the mean annual variance of monthly data, and the harmonic maxima (strongest gradients) occur during the transition seasons. We document the extent to which the half-yearly wave exhibits variability on interannual to decadal time scales, and consider the extent to which recent changes may be seen as part of such overall variability. In both the mid and high latitudes the temporal variability of the semiannual oscillation of pressure has been found to be statistically related to the variability in the oscillation of the high latitude temperature gradient. Changes in the latter seem to be associated in the greater part with temperature changes at the higher latitudes.

**JSP25/E/19-B3****1720****NATURE OF ATMOSPHERIC VARIABILITY OVER THE NORTH ATLANTIC OCEAN FROM INTERANNUAL TO DECADAL TIME SCALE**

Christophe CASSOU, Laurent Terray, Sophie Valcke (CERFACS, Climate Modelling and Global Change Team, 42, Avenue Gustave Coriolis 31057 Toulouse, FRANCE, EMAIL: cassou@cerfacs.fr)

Predictability is considerably reduced at mid-latitudes especially over the Atlantic Ocean where the variability is mainly controlled by internal atmospheric processes which mask Sea Surface Temperature (SST) influences. In order to quantify and explain the response of the atmosphere to observed SST variability, the ARPEGE-Climat Meteo-France Atmospheric Global Circulation Model is used through 2 types of experiments : a 100-year simulation with a prescribed monthly climatological SST is carried out together with an ensemble of 8 50-year simulations forced by GISSST month to month SST changes from 1948 to 1997 (GOGA simulations hereafter). Predictability is first investigated using ANOVA techniques applied on the ensemble experiment for different seasons. This statistical tool allows to separate in the total variability, the part forced by the SST from the part explained by internal dynamics. The North Atlantic Oscillation (NAO) is then more precisely studied in both experiments. The frequency analysis of the NAO related signal shows a weak 2.5-year peak in the climatological run whereas in GOGA simulations, the same analysis exhibits more energy concentration at longer time scale and a significant 3.7-year peak related to ENSO. This suggests important teleconnections and atmospheric linkages between the Atlantic and the Pacific. The SST impact is then examined using classification techniques in weather regimes; emphasis will be laid on differences between the climatological and the GOGA experiments in terms of spatial weather patterns, their occurrences and transitions. Optimal filter methods finally allow to determine the spatial and time characteristics of the SST pattern which plays a role in setting up the simulated forced atmospheric response. Some preliminary results will also be presented on shorter sensitivity experiments using the detected SST signal superimposed on the climatological background as a new forcing.

**Thursday 29 July AM**

Presiding Chair: S. Minobe (Hokkaido University, Sapporo, Japan)  
Concurrent Poster Session

**GLOBAL VARIABILITY****JSP25/W/61-B4**

Invited

**0930****PATTERNS OF LARGE-SCALE CLIMATIC VARIABILITY IN THE INSTRUMENTAL ERA**

Chris K. FOLLAND (Hadley Centre, Met Office, London Road, Bracknell, Berkshire, RG12 2SY, UK, Email: ckfolland@meto.gov.uk); Rob J. Allan (CSIRO Atmospheric Research, Aspendale, Victoria 3195, Australia, Email: rob.allan@dar.csiro.au); Michael E. Mann (Department of Geosciences Morrill Science Center, University of Massachusetts, Amherst, MA 01003, Email: mann@snow.geo.umass.edu); Scott B. Power (National Climate Centre, Melbourne, Victoria 3001, Australia, Email: s.power@bom.gov.au)

An empirical orthogonal function (EOF) analysis of ocean surface temperature, filtered to highlight periods greater than about 13 years, has been used to identify patterns of low frequency variability. These include a secular pattern of global warming, a 70-80 year interhemispheric pattern associated with interdecadal variations in Sahel rainfall, and a pattern reminiscent of El Niño but with a somewhat different structure that modulates high frequency ENSO influences on Australian climate. More insight can be obtained by carrying out joint EOF

## INTER-ASSOCIATION

analyses of pressure at mean sea level (PMSL) and SST for different spectral bands, and multi-taper singular value decomposition analyses of joint SST and PMSL data. These highlight significant low frequency bands and the secular band, and provide patterns of variability that are mostly consistent between the analyses.

**JSP25/W/49-B4** Invited **0950**

### QUASI-PERIODICITY AND GLOBAL SYMMETRIES IN INTERDECADAL UPPER OCEAN TEMPERATURE VARIABILITY

Warren B. WHITE and Daniel R. (Cayan) Scripps Institution of Oceanography, University of California, San Diego, La Jolla, California, e-mail: wbwhite@ucsd.edu)

Abstract Recent studies find interannual (i.e., 3 to 7 year), decadal (i.e., 9 to 13 year), and interdecadal (i.e., 18 to 23 year) periodicities, and a trend dominating global sea surface temperature (SST) and sea level pressure (SLP) variability over the past hundred years, with the interdecadal signal dominating sub-El Niño-Southern Oscillation (ENSO) frequencies. We isolate interdecadal frequencies in SST and SLP records by band passing with a window admitting 15 to 30 year periods. From 1900 to 1989, the rms of interdecadal-filtered SST and SLP anomalies is largest in the extratropics and eastern boundaries. First-mode empirical orthogonal functions (EOFs) explain about half the interdecadal variance in both variables, with the tropical warm phase peaking near 1900, 1920, 1940, 1960, and 1980. From 1955 to 1994, EOF spatial patterns of interdecadal SST, SLP, and 400m temperature (T400) anomalies reveals global reflection symmetries about the equator and global translation symmetries between ocean basins, with tropical and eastern ocean SSTs warmer (cooler) than normal, covarying with stronger (weaker) extratropical westerly winds, cooler (warmer) SSTs in western-central subtropical and subarctic frontal zones (SAFZs), stronger (weaker) subtropical and subarctic gyre circulations in North Pacific and North Atlantic Oceans, and warmer (cooler) basin and global average SSTs of 0.1°C or so. Evolution of interdecadal variability from the tropical warm phase to the tropical cool phase is propagative, also characterized by reflection and translation symmetries. During the tropical warm phase, cool SST anomalies along western-central SAFZs are advected slowly eastward to the eastern boundaries and subsequently advected poleward and equatorward by the mean gyre circulation, the latter conducting extratropical SST anomalies into the tropics. A delayed action oscillation model is constructed that yields the quasiperiodicity of interdecadal variability in a manner consistent with these global symmetries in both pattern and evolution.

**JSP25/E/02-B4** Invited **1010**

### INTERANNUAL-TO-DECADAL VARIABILITY OF THE TEMPERATURE-SALINITY STRUCTURE OF THE WORLD

SYDNEY LEVITUS (NODC/NOAA, E/OC5, 1315 East West Highway, Room 4362, Silver, Spring MD 20910-3282, Email: slevitus@nodc.noaa.gov)

Analysis of historical upper ocean temperature data suggests the existence of a global mode of upper ocean heat storage. Additional analysis suggests that in the North Atlantic Ocean, both the first (NAO) and second (EAO) modes of sea level pressure are correlated with upper ocean thermal structure demonstrating the existence of coupled modes of oscillation for this ocean. Variability of the temperature-salinity structure of the intermediate and deep waters of various regions of the world ocean will also be described.

Presiding Chair: Chris K. Folland (Hadley Centre, UKMO, Bracknell, UK)

**JSP25/W/71-B4** Invited **1050**

### RELATIONSHIPS AMONG RECENT ATMOSPHERIC CIRCULATION CHANGES, GLOBAL WARMING, AND SATELLITE TEMPERATURES

Jim HURRELL, (NCAR, USA, email: jwhurrell@meto.gov.uk)

There is much debate about our ability to detect a human influence on climate. Part of the problem is that the Earth's climate record includes both natural variability as well as human-induced effects, and the presence of the former makes it difficult to isolate possible anthropogenic signals. This is illustrated by changes in the atmospheric circulation over the past two decades which have contributed strongly to observed global warming patterns. Differences in the vertical structure of the temperature anomalies associated with the circulation changes largely account for discrepancies between temperature trends from surface and satellite-derived lower-atmospheric records. The circulation changes are related to variations in modes of natural variability over the North Atlantic and North Pacific basins. The question of the physical relationship between the variations in these two circulation modes on low frequency time scales, and furthermore their relation to secular changes in ENSO, will be discussed.

**JSP25/W/09-B4** Invited **1110**

### GLOBAL AND REGIONAL TELECONNECTIONS IN ATLANTIC BASIN SST VARIATIONS

YOCHANAN KUSHNIR, Balaji Rajagopalan, Yves Tourre, and Jennifer Miller, (Lamont-Doherty Earth Observatory of Columbia University, Palisades, NY 10964, USA)

To address the extent to which Atlantic climate variability (ACV) is governed by processes internal to the Atlantic Basin, we apply various multivariate analysis methods to a long record of sea surface temperature anomalies. We find evidence for both local and global influences on the leading modes of ACV. Tropical and South Atlantic SST variability appears to be mainly associated with global patterns of SST variability, namely ENSO and an almost-global SST warming trend, between 1930 or so and the present. North Atlantic SST variability appears to be regional with little evidence to other oceanic regions. The characteristic pattern of regional SST variability is its "tri-polar" structure where subtropical and subtropical SST are fluctuating in phase with one another, and out of phase with midlatitude SST. The spectrum of the regional SST fluctuations displays distinct decadal and multi-decadal peaks and a hint of propagating behavior. We compare these results with other recent findings on ACV and discuss their implication.

**JSP25/W/31-B4** Invited **1130**

### DECADAL VARIABILITY IN THE EXTRATROPICAL OCEAN-ATMOSPHERE SYSTEM

Stephen P. MEACHAM, (Atmospheric and Environmental Research Inc., 840 Memorial Dr., Cambridge, MA 02139, USA. Email: smeacham@aer.com)

In the last four decades, a variety of mechanisms have been suggested as potential contributors to decadal variability of the extratropical atmosphere and ocean. It is difficult to unambiguously distinguish individual mechanisms in the complex behavior of a "full" climate model. We describe results from a pair of studies that focus on low frequency variability

associated with redistribution of potential vorticity within the ocean. In the first, a simple baroclinic ocean with an adiabatic interior, forced with a specified double gyre wind stress, is shown to exhibit strong variability on decadal time scales. This variability is associated with the storage and release of potential vorticity in inertial recirculations embedded within the subtropical and subpolar gyres. A necessary condition for this mode of variability is the resolution of mesoscale eddies which are intimately connected with the episodic breakdown of the inertial recirculations. The inter-gyre eddy potential vorticity flux exhibits strong decadal variability. In the second study, a pair of mid-latitude ocean basins is coupled to a quasigeostrophic tropospheric model. The ocean is equipped with an active mixed layer that can store and transport heat. The interior of the ocean is essentially adiabatic. The oceans and atmosphere are coupled primarily through the transfer of potential vorticity: the atmosphere induces Ekman pumping in the ocean while the air-sea heat flux induces atmospheric heating and cooling anomalies which modify the potential vorticity budget of the atmosphere. The active atmosphere exhibits a moderately realistic planetary-scale and synoptic-scale wave regime, with quasistationary subtropical highs over the oceans, and drives subtropical and subpolar gyres in both oceans. Both the atmosphere and ocean exhibit significant low frequency variability. Part of this is the result of potential vorticity accumulation and discharge in the ocean gyres analogous to that seen in the ocean-only model. Another part of the variability can be attributed to coupled "modes" of the ocean-atmosphere-mixed layer system.

**JSP25/E/35-B4** **1150**

### INTERDECADAL OSCILLATIONS WITH A LOW DEGREE OF FREEDOM MODEL OF THE OCEAN-ATMOSPHERE

Alain COLIN DE VERDIERE ( Laboratoire de Physique des Oceans, Universite de Bretagne Occidentale, BP 809, 29285 Brest cedex France, email: acolindv@univ-brest.fr); Thierry Huck ( Geophysical Fluid Dynamics Laboratory, NOAA, Princeton, NJ 08542 USA, email: th@GFDL.GOV)

Oceanic GCMs have been observed to oscillate on time scales in a large number of studies. Under the simplest situation of a temperature dependent equation of state, two conditions are necessary to produce the oscillations for a fixed strength of the overturning: a weak enough damping of SST anomalies (through constant heat flux for instance) and a low enough background eddy diffusivity. We suggest that baroclinic instability in western boundary current outflow regions governs the generation of the oscillations. In the complicated geometry of an oceanic GCM ( as compared to an atmospheric channel), the large scale instability is local, driving planetary waves in the interior that set the period of the oscillations. The situation is not different when the oceanic GCM is coupled to an Atmospheric Energy Balance Model. This is used to construct a two degree of freedom climate model that reproduces a number of features of the coupled Ocean-EBM model such as the Hopf bifurcation to the limit cycle and the damping effect of restoring boundary conditions. It quantifies the relative weight of the various dissipation processes against the instability that feeds on available potential energy. Significant differences appear, however, when the oscillations are in the finite amplitude regime.

**JSP25/W/01-B4** Invited **1210**

### ON THE USE OF WAVELET COHERENCY FOR ANALYZING DECADAL CLIMATE VARIABILITY

TORRENCE, Christopher (National Center for Atmospheric Research/Advanced Study Program, PO Box 3000, Boulder CO 80307-3000 USA, e-mail:torrence@ucar.edu)

The method of wavelet coherency is developed and applied to time series of climate variability. In particular, decadal changes in the El Niño-Southern Oscillation (ENSO) are linked to changes in Indian monsoon rainfall. The wavelet coherency provides a measure of the strength of the ENSO-monsoon connection and how the connection has varied over the last 125 years. Statistical significance tests are used to test the robustness of the results.

**Thursday 29 July PM**

Presiding Chair: Yochanan Kushnir (Columbia University, Palisades, USA)

### VARIABILITY OVER THE ATLANTIC OCEAN

**JSP25/W/47-B4** Invited **1400**

### SIMULATION OF QUASI-DECADAL AND INTERDECADAL VARIABILITY IN THE ATLANTIC OCEAN ASSOCIATED WITH THE NORTH ATLANTIC OSCILLATION

George Halliwell, (MPO/RSMAS, University of Miami, USA)

Over the last several decades, the North Atlantic Oscillation (NAO) index has varied with two distinct time scales, a quasi-decadal oscillation and an interdecadal oscillation with a period of about 50 years. Since high NAO index is associated with anomalously strong Westerlies and Trade Winds, NAO variability is expected to drive Atlantic Ocean climate variability. Properties of this ocean climate variability at both quasi-decadal and interdecadal periods are investigated through analysis of a primitive-equation ocean general circulation model driven by forcing fields derived from the NCEP/NCAR atmospheric reanalysis for 1946-1998. At both time scales, the strong Westerlies and Trade Winds associated with high NAO index generate an SST anomaly pattern characterized by anomalously cold water over the open ocean in both the Westerly and Trade Wind belts and anomalously warm water over the western Sargasso Sea. Model analysis reveals that anomalous SST is driven by local thermodynamical forcing in the two wind belts, and by anomalous heat advection associated with the spin-up of the North Atlantic subtropical gyre in the western Sargasso Sea. The opposite pattern is observed for low NAO index. A two-year time lag is observed in the western Sargasso Sea relative to the basin-wide atmospheric forcing resulting from the baroclinic adjustment of the subtropical gyre. Results suggest that at quasi-decadal periods, the atmosphere is predominantly driving the ocean. An additional time lag between SST anomaly patterns and the NAO index at interdecadal periods suggests that more complicated coupled variability between the atmosphere and ocean occurs at the longer time scales.

**JSP25/W/07-B4** Invited **1420**

### THE FORMATION AND EVOLUTION OF NORTH ATLANTIC HEAT CONTENT ANOMALIES

Graham GLADMAN and Rowan Sutton (Department of Meteorology, University Of Reading, PO BOX 243, Earley Gate, Reading, RG6 6BB, Email: swr97jg@reading.ac.uk)

Observations of the North Atlantic Ocean over the past century reveal decadal timescale fluctuations in heat content and related variables. Many aspects of these fluctuations are intriguing and require explanation. In particular, the mechanisms responsible for the formation and propagation of heat content anomalies are not understood. While such anomalies may be generated by processes internal to the ocean, forcing by the atmosphere is likely to play a key role.

We are investigating the role of atmospheric forcing in the formation and evolution of heat content



anomalies by experimentation with an Atlantic ocean isopycnic GCM. In the first phase we have performed experiments to explore how heat content anomalies develop in response to forcing by idealised windstress anomalies. The interaction between the barotropic response and topography leads to very interesting, and sometimes surprising, behaviour. We will present analyses of both this short timescale response and also the longer timescale baroclinic response. In the second phase of our work we will be investigating the development of specific heat content anomalies observed in the North Atlantic this century.

**JSP25/E/16-B4** Invited **1440**

#### DECADAL VARIATIONS IN TROPICAL ATLANTIC CLIMATE IN OBSERVATIONS AND IN A GLOBAL OCEAN-ATMOSPHERE MODEL

VIKRAM M. MEHTA, (NASA-Univ. of Maryland Joint Center for Earth System Science, Department of Meteorology, Univ. of Maryland, College Park, Maryland 20742, U.S.A.); Tom Delworth, (NOAA/Geophysical Fluid Dynamics Laboratory, P.O. Box 308, Princeton, New Jersey 08542, U.S.A.)

Decadal-multidecadal climate variations are receiving increased attention from the research community in the last one or two decades. It is very important to study decadal-multidecadal climate variability in its own right and also because of its potential to interact with interannual climate variability and anthropogenic climate change. Observed decadal climate variability in the tropical-subtropical Atlantic region and its statistical predictability will be described in this oral presentation. The mechanisms of such climate variability in the GFDL coupled ocean-atmosphere model will also be described.

**JSP25/W/03-B4** **1500**

#### INTERDECADAL MODES OF VARIABILITY IN A SIMPLIFIED COUPLED MODEL

Thierry HUCK and Geoffrey Vallis (GFDL, Princeton University AOS, Forrestal campus, Route 1, Princeton NJ 08542, USA, email: thn@gfdl.gov gkv@gfdl.gov); Alain Colin de Verdiere (Laboratoire de Physique des Océans, Université de Bretagne Occidentale, BP 809, 29285, Brest cedex, France, email: acolindv@univ-brest.fr)

A simplified coupled model is constructed including an ocean general circulation model (MOM3, GFDL) and an atmospheric Energy Balance Model with physical parameterizations for horizontal heat transport and zonal winds. The external forcing comes from constant insolation at the top of the atmosphere (no seasonal cycle). In various idealized and realistic configurations, the model produces interdecadal variability. One mode is clearly related to the thermohaline circulation in the North Atlantic and its sensitivity to parameters and parameterizations is analyzed: it compares very well with the ocean mode under constant surface heat flux. Other modes of variability, involving changes in the subtropical gyres intensity and mid-latitude winds, are investigated. Finally, comparisons are drawn with the observations.

**JSP25/W/20-B4** **1520**

#### DECADAL VARIATIONS OF THE THERMOHALINE CIRCULATION IN MODELS OF THE ATLANTIC OCEAN FORCED BY OBSERVED SURFACE FLUXES

Carsten EDEN, Juergen Willebrand (both at Institut fuer Meereskunde, Duesternbrooker Weg 20, 24105 Kiel, Germany, Email: ceden@ifm.uni-kiel.de, jwillebrand@ifm.uni-kiel.de) and Rene Redler (Alfred Wegener Institut fuer Polar- und Meeresforschung, Bgm.-Smidt Str. 20, 27568 Bremerhaven, Germany, Email: rredler@AWI-Bremerhaven.DE)

The variation of the thermohaline circulation (THC) in the Atlantic Ocean on decadal time scales due to atmospheric surface flux variability is investigated.

A medium-resolution model (4/3 degree horizontal mesh) of the Atlantic Ocean, forced with observed surface fluxes taken from the NCEP-reanalysis dataset, was used to study the induced variations of the THC. Several experiments show that the model THC was sensitive to heat flux anomalies in the Labrador sea, where mixed layer depth variations are correlated with THC-anomalies, which propagate southwards into the subtropical gyre, resembling a first baroclinic mode boundary wave like structure. Atmospheric freshwater flux anomalies seem to be unimportant even under mixed boundary conditions, whereas freshwater flux anomalies originating from sea-ice variability do.

Experiments with an eddy-permitting model (1/3 degree horizontal mesh) of the North Atlantic Ocean were performed to study the impact of the resolution on the variation of the circulation. First results suggest that increased horizontal resolution does not significantly change the oceanic response on the flux variability.

Presiding Chair: Shang-Ping Xie (Hokkaido University, Sapporo, Japan)

**JSP25/E/10-B4** **1620**

#### THE INFLUENCE OF SEA SURFACE TEMPERATURES ON THE NORTH ATLANTIC OSCILLATION AND EUROPEAN CLIMATE IN WINTER

Mark RODWELL, Chris Folland and David Rowell (Hadley Centre, UK Met Office, London Road, Bracknell, RG12 2SY, UK, Email: mjrodwell@meto.gov.uk)

Observational studies have shown that there is a relationship between the North Atlantic Oscillation (NAO) and North Atlantic sea surface temperatures (SSTs). Some of the mechanisms by which the NAO can influence these SSTs are fairly well understood but the opposite link, from SSTs to the NAO, has been unclear. We show for the first time that an atmospheric general circulation model (AGCM), forced with real SSTs and sea-ice extents, can reproduce much of the observed multiannual to multidecadal variations of the NAO over the last half century. The direct effects of greenhouse gases on the atmosphere were not required to achieve this. The SSTs highlighted as important for this NAO simulation are confined to the North Atlantic region and form a tripole pattern, similar to observed correlation patterns between the NAO and SST. We demonstrate that a realistic magnitude of this SST pattern results in local changes to evaporation and atmospheric convective heating that tend to enhance the thermal structure of the NAO. In agreement with observations, there is also a strong modulation of the modelled North Atlantic storm track. NAO-forced Ekman transport appears to provide a positive feedback onto the SST anomaly pattern and this may slow down its rate of damping. Significant multiannual predictability of North Atlantic SSTs has recently been proposed. Our results are therefore encouraging for the prediction of European winter climate features, such as temperature, precipitation and storminess, up to several years ahead.

**JSP25/W/57-B4** Invited **1640**

#### ARCTIC SEA ICE VARIABILITY AND ITS RELATION TO THE NAO

CLARA DESER (National Center for Atmospheric Research, P.O. Box 3000, Boulder, Colorado, USA, e-mail: cdeser@ncar.ucar.edu) John Walsh (University of Illinois, Champaign-Urbana, IL,

USA) Michael Alexander (University of Colorado, Boulder, Colorado, USA) Michael Timlin (University of Colorado, Boulder, Colorado, USA)

Forty years (1958-1997) of gridded monthly sea ice concentration data are used to document variability of Arctic sea ice coverage and its association with atmospheric circulation changes. The dominant pattern of wintertime sea ice variability exhibits out-of-phase fluctuations between the western and eastern North Atlantic, together with a weaker dipole in the North Pacific. This mode is dominated by decadal-scale variations and a longer-term trend of diminishing ice cover east of Greenland and increasing ice cover west of Greenland. The changing sea ice margin, which we suggest is driven by recent trends in the North Atlantic Oscillation (NAO), induces large perturbations (several hundred Watts per square meter) in the surface energy exchange between the atmosphere and ocean. The enhanced upward surface energy flux in the area of ice retreat east of Greenland may have contributed to the observed increase in the number of cyclones over the Greenland Sea during the last 40 years. An ensemble of atmospheric GCM experiments forced by observed trends in sea ice coverage are used to investigate the sensitivity of the circulation to sea ice anomalies.

**JSP25/W/16-B4** Invited **1700**

#### INTER-HEMISPHERE RELATION OF DECADAL CLIMATE VARIATIONS IN ATLANTIC

Youchi TANIMOTO (Institute for Global Change Research, FRSGC, Shibaura 1-2-1, Seavans N Bldg.7F, Minato-ku, Tokyo 105-6791, Japan, email: tanimoto@frontier.esto.or.jp); Shang-Ping, XIE (Graduate School of Environmental Earth Science, Hokkaido University, Sapporo 060-0810, Japan, email: xie@ees.hokudai.ac.jp)

Sea surface temperature (SST) and Sea Level Pressure (SLP) anomaly fields with an equatorial anti-symmetric dipole structure in the tropical Atlantic affects on precipitation in surrounding areas. But zonal mean tropical SST anomalies have decorrelated scatters between 10-20 degree latitudes. The same observation applies to SLP anomalies. Therefore, it seems that there are, at least, two modes in the air-sea coupled field in the tropical Atlantic. The purpose of the present study provides dominant modes, which are physically reasonable, from statistical analyses by taking advantage of the spectral gap between decadal and interannual SST variability in the tropical Atlantic. After we divide the Atlantic basin into two independent parts, north and south of the equator, we compute empirical orthogonal functions (EOFs) for SST and SLP anomalies. Then anomalies are averaged for the boreal winter and filtered through the decadal band (8-16 year). These EOFs of SST (SLP) anomalies explain 44.2% and 43.2% (36.4% and 50.2%) of the band-passed variance on the Northern and Southern Hemispheres, respectively. Two EOFs (spatial patterns) of SST anomalies present meridionally lined up five centers of action. In two EOF of SLP anomalies, we realize subtropical centers of action with opposing polarities in either side of equator. The PCs (time series) of these four EOFs are highly correlated. In the present study, the two subdomains and the two fields are statistically independent and there is no a priori reason for them to be correlated. This indicates that tropical Atlantic SST and SLP anomalies are not always independent in either side of equator, at least on decadal variations, and further that the tropical dipolar oscillation is associated with the inter-hemispheric decadal variability in the Atlantic.

**JSP25/E/14-B4** Invited **1720**

#### RECONSTRUCTIONS OF NORTH ATLANTIC OSCILLATION INDICES

ROSANNE D'ARRIGO, Edward Cook, Heidi Cullen (all at: Lamont-Doherty Earth Observatory, Palisades, NY 10964, TEL 914-365-8617, FAX 914-365-8152, email: druidrd@ldeo.columbia.edu) and Michael Mann (Dept. of Geosciences, Morrill Science Center, University of Massachusetts, Amherst, MA 01003, TEL 413-545-9573, FAX 413-545-1200, email: mann@snow.geo.umass.edu)

The North Atlantic Oscillation (NAO) is one of the dominant features of climate for the North Atlantic and surrounding land areas (Van Loon and Rogers 1978, Rogers and Van Loon 1979, Rogers 1990). Longer records are needed to provide a long-term context for the variability of the recent instrumental record of the NAO (e.g. the persistently high index values of recent decades). Tree-ring width records from North America and Europe have been used to reconstruct the NAO and related time series of North Atlantic climate for the past several hundred years. These include the first reconstruction of the winter (DJF) NAO sea-level pressure (SLP) index (Cook et al. 1998).

We have also produced a reconstruction of a winter (DJFM) NAO sea-surface temperature (SST) index in order to derive a more complete picture of the NAO system. This index is based on SST averaged over five Atlantic regions which are best correlated with NAO SLP, from the Kaplan et al. (1998) analysis. This reconstruction extends from AD 1701 to 1979 and is based on North American and European tree-ring data as well as the long (335 year) Central England instrumental temperature series (CET) (Plaut et al. 1995). The NAO SST reconstruction accounts for 47% of the variance over the calibration period and is well verified using statistical tests typically used to evaluate dendroclimatic reconstructions (Cook and Kairiustis 1990). We have compared the NAO SLP (Cook) and SST (D'Arrigo) reconstructions to several other relevant time series, including an NAO reconstruction (Appenzeller) based on a Greenland ice core record (Appenzeller et al. 1998), and an NAO SST reconstruction based on a network of tree-ring data and other proxies as well as long instrumental temperature records (Mann) Principal components analysis (PCA) scores based on the 4 NAO reconstructions covering 1750-1979 and 3 NAO reconstructions covering the period 1701-1979 (excluding Mann) show verification results that are improved relative to the individual series. The PCA scores of these reconstructions, when compared to global SST, SLP and surface air temperature fields, reflect the characteristic patterns of the NAO.

**JSP25/W/90-B4** **1740**

#### THE PURPOSE OF THIS STUDY IS TO INVESTIGATE THE TEMPORAL STRUCTURE OF TEMPERATURE VARIABILITY

Marina V. SHABALOVA, (Royal Netherlands Meteorological Institute, P.O.Box 201, 3730 AE De Bilt, the Netherlands, email: shabalov@knmi.nl)

The purpose of this study is to investigate the temporal structure of temperature variability on timescales longer than 50 yr, as reflected in a number of long paleo records located in Europe and North America, using a combination of statistical techniques including uni- and multivariate singular spectrum analysis. Two statistically significant modes of temperature variability are identified, one on multidecadal and one on centennial timescales. The first mode is oscillatory, with a timescale ~60-80 yr. Its geographic pattern suggests a connection to the North Atlantic Oscillation. The second mode, confined to high latitudes, describes temperature variations on timescales longer than 100 yr; in the longest records a weak ~120 yr oscillation can be identified with confidence. We show that the temporal pattern of centennial mode is season-dependent in Europe. We also show that paleo records representing the same season and region (e.g. N.Urals versus Fennoscandia) may exhibit a striking difference in their temporal structures on centennial timescales, which is likely to indicate unreliability of centennial timescales in one/both record(s). In a number of seasonally homogeneous records the centennial components of variability are coherent, showing a multiple-phase 'Little Ice Age' and a 'Medieval Warm Period'. We assume that only those centennial signals which are



## INTER-ASSOCIATION

coherent in a number of independent paleo series and are statistically significant against the red noise surrogates at the 95% confidence level represent a genuine mode of temperature variability.

Friday 30 July AM

Presiding Chair: A. Miller (Scripps Inst. of Oceanography, La Jolla, USA)

### VARIABILITY OVER THE PACIFIC OCEAN

**JSP25/W/46-B5** Invited **0830**

#### ON PACIFIC DECADEAL VARIABILITY IN THE CSIRO COUPLED OCEAN-ATMOSPHERE MODEL

Anthony C. HIRST (CRC for Southern Hemisphere Meteorology CSIRO Atmospheric Research PMB 1, Aspendale, Vic., 3196 Australia) Scott B. Power and David Wolland (Bureau of Meteorology GPO Box 1298K, Melbourne, Vic., 3001 Australia Dan Vimont Dept of Atmospheric Sciences University of Washington - JISAO Box 351640, Seattle, WA 98195)

A 1000 year integration of the CSIRO coupled ocean-atmosphere general circulation model is used to study low frequency (decadal to centennial) climate variability. An EOF analysis is applied to selected model fields to show some of the major statistical modes of low frequency variability. The first EOF bears considerable resemblance to observational estimates, it is centered in the Pacific and extends well into the extratropics in both hemispheres. The EOF has a time evolution that appears to be more than just red noise. It modulates both precipitation and temperature globally. In particular, a link to Australian decadal rainfall variability is evident which is of similar character to (though moderately weaker than) that observed. The talk focuses on defining the character of this mode and examining the mechanisms by which it comes about. Comparison is made to both the observed variability and to the patterns of variability found in other coupled general circulation models.

**JSP25/W/91-B5** Invited **0850**

#### DECADEAL TO INTERDECADEAL OCEAN-ATMOSPHERE INTERACTION IN THE PACIFIC BASIN

FEI-FEI JIN, Masahide Kimoto\*, Xiao-Chun Wang School of Ocean and Earth Science and Technology University of Hawaii at Manoa, Honolulu, Hawaii, USA \* Center for Climate System Research University of Tokyo, Tokyo, Japan.

Slow exchanges of mass and heat between the tropical and subtropical ocean gyres, attributed to subtropical oceanic Rossby waves, play a key role in the decadal to interdecadal ocean-atmosphere interactions in the Pacific basin. In this report, with supporting simulations of a global coupled model and analysis of observational data, we developed a simple model to delineate the main physical mechanisms of the decadal to interdecadal oscillations. The subtropical oceanic Rossby waves are found to play a key role in forming a distinct coupled decadal to interdecadal mode and enabling it to modulate the ENSO. Model simulations and observational analysis consistently show that the tropical, and extratropical ocean atmosphere interactions and the teleconnection between the tropics and extratropics in these interactions are responsible for co-variations of the decadal to interdecadal climate fluctuations in the tropical and extratropical Pacific.

**JSP25/W/51-B5** Invited **0910**

#### A DECADEAL SALINITY MODE IN THE TROPICS

Niklas SCHNEIDER (Scripps Institution of Oceanography, University of California, San Diego, Mail Code 0224, 9500 Gilman Drive, La Jolla, CA 92093-0224, USA, email: nschneider@ucsd.edu)

Dynamics of a climate mode in a simulation of a sophisticated coupled ocean-atmosphere model are explored. The mode stems from an interplay in the Pacific of the low-latitude circulation, of advection of thermal and haline anomalies along isopycnal surfaces and of atmospheric wind stress changes due to anomalies in the western equatorial Pacific of the relative importance of temperature and salinity in determining oceanic density. The time scale of the mode is ten years.

In the equatorial region, the arrival in the western Pacific of warm and salty anomalies on isopycnal surfaces slightly increases the across Pacific east-west temperature difference, thus enhances of the trade winds and leads via positive feedbacks to a state of the upper ocean resembling a La Nina. Associated with the strengthening of the wind stress, the North Equatorial current accelerates and, at 10 to 15N in the central Pacific, leads to the generation by anomalous advection across a mean gradient of cool and fresh anomalies on isopycnal surfaces. The anomalies are advected with the mean circulation via the western boundary currents and arrive in the equatorial western Pacific approximately five years later. The arrival there of cool and fresh anomalies decrease the east-west temperature gradient along the equator, reduce the trade winds and flip the system to the opposite phase that resembles El Nino. The associated spin-down of the North Equatorial currents then initiates again warm and salty anomalies at 10 to 15 N whose arrival at the equator five years later close the cycle.

**JSP25/W/88-B5** Invited **0930**

#### AN ISOPYCNAL PRIMITIVE EQUATION OCEAN MODEL

Guillermo AUAD, (Scripps Institution of Oceanography, UCSD, USA, email: guillo@ucsd.edu)

An isopycnal primitive equation ocean model is used to represent the physics of the Pacific Ocean. Observations of winds and surface heat fluxes are used to force the model from 1951 through 1997. The goal of this integration is to detect and understand major decadal and interdecadal changes in both tropics and midlatitudes. Preliminary results show a good agreement with observations of heat content of the upper 400 m of the Pacific Ocean. The central North Pacific and the western equatorial area show maximum variability for oscillations with period between 10-20 y. Additional results and comparisons with observations will be presented at the meeting for sea surface temperature, heat content and thermocline and mixed layer depth.

**JSP25/W/13-B5** Invited **0950**

#### THE IMPACT OF NORTH PACIFIC DECADEAL CLIMATE FLUCTUATIONS ON THE EQUATORIAL PACIFIC

S.VENZKE (MPI fuer Meteorologie, Bundesstr.55, 20146 Hamburg, Germany, email: venzke@dkrz.de); N. Schneider (Scripps Institution of Oceanography, La Jolla, USA, email: niklas@moana.ucsd.edu); M. Latif (MPI fuer Meteorologie, Bundesstr.55, 20146 Hamburg, Germany, email: latif@dkrz.de)

It has been hypothesised that decadal climate variability is caused by the coupling of the central North Pacific to the equatorial thermocline via thermal anomalies that propagate in the oceanic thermocline. While an interpretation of observed upper ocean temperature anomalies appears to provide evidence in support of this hypothesis, consideration of wind stress anomalies using simple steady-state models of the oceanic circulation indicates that tropical variability is mainly driven by low-latitude winds.

To resolve this controversy simulations with the Hamburg Ocean Primitive Equation model (HOPE) driven by different atmospheric forcing conditions have been performed. It is shown that decadal variability within the tropics is largely independent of the arrival of thermal anomalies from midlatitudes.

**JSP25/W/28-B5** Invited **1010**

#### A DYNAMIC COMPARISON OF CLIMATE VARIABILITY IN THE TROPICAL PACIFIC AND ATLANTIC

SHANG-PING XIE, Hideyuki Noguchi (Graduate School of Environmental Earth Science, Hokkaido University, Sapporo 060-0810, Japan, E-mail: xie@ees.hokudai.ac.jp); Taroh Matsuno, Youichi Tanimoto (Frontier Research System for Global Change, Tokyo 105-6791, Japan)

How to characterize the tropical Atlantic sea surface temperature (SST) variability has been highly controversial. New observational evidence is emerging in favor of a dipole-monopole decomposition (Tanimoto and Xie, this volume). Here we examine the physical basis for such an empirical decomposition and address an important question of why such a latitudinally anti-symmetric dipole mode is most pronounced in the Atlantic but apparently not in the Pacific.

For this purpose we develop a coupled ocean-atmosphere model that includes both the feedbacks by ocean dynamics and by surface heat flux. Consistent with observations, an interannual equatorial and a decadal dipole mode emerge from the model and are supported by the Bjerknes and a wind-evaporation-SST feedbacks, respectively. The equatorial and the dipole modes exhibit distinctive growth curves, with the former peaking at the size of the Pacific Ocean while the latter decreasing monotonously with wavenumber. It thus follows that the equatorial mode will dominate the Pacific whereas it will co-exist with a zonally uniform dipole mode, a theoretical outcome that explains observations. Having emphasized the difference between the tropical oceans, we will present evidence for interaction between extratropical North Atlantic and North Pacific, an inter-oceanic link that is particularly pronounced on the quasi-decadal time scale.

Presiding Chair: (A.C. Hirst (CSIRO, Victoria, Australia))

**JSP25/W/05-B5** Invited **1050**

#### OBSERVATIONS AND THEORIES OF PACIFIC OCEAN DECADEAL VARIATIONS

ARTHUR J. MILLER (Scripps Institution of Oceanography, La Jolla, CA 92093-0224. E-mail: ajmiller@ucsd.edu)

Physical fields of the Pacific Ocean are observed to vary over decadal time scales. Different physical mechanisms have been proposed to explain the diverse basin-scale patterns of SST, thermocline depth and horizontal currents, which are linked in various ways. Although observations of upper-ocean temperature and sea-level pressure are limited in temporal and spatial resolution, they can help to put constraints on the various theories. Ocean model hindcasts can also be used to reconstruct the ocean's importance in decadal variations. Various recent theories of Pacific Ocean decadal variability will be summarized and discussed in the context of observations and model hindcasts to attempt to determine which mechanisms are the most plausible.

**JSP25/W/70-B5** **1110**

#### RESONANCE IN BIDECADEAL AND PENTADECADAL CLIMATE OSCILLATIONS OVER THE NORTH PACIFIC: ROLE IN CLIMATIC REGIME SHIFT

SHOSHIRO MINOBE (Division of Earth and Planetary Sciences, Graduate School of Science, Hokkaido University, Sapporo, 060-0810, Japan, Email: minobe@neptune.sci.hokudai.ac.jp)

The roles of interdecadal oscillations in climatic regime shifts, which are observed as rapid strength changes in the Aleutian low in winter and spring seasons in the 1920s, 1940s, and 1970s, have been analyzed. A regime shift results from simultaneous phase reversals between pentadecadal and bidecadal (about 17-years period) variations, which synchronize with one another at a relative period of three. The pentadecadal variation, which is observed in both winter and spring seasons, provides the basic timescale of regime shifts, while the bidecadal variation, which is observed only in winter, characterizes the rapidity of the shifts.

A Monte-Carlo simulation has shown that the simultaneous phase reversals or resonance between the pentadecadal and bidecadal variations reflect a physical linkage between them and do not coincide accidentally. If the synchronization feature continues until the next regime shift, which is likely to occur in the coming decade. The mechanisms of the regime shifts or resonance might be understood by a simple delayed-oscillator model with an external forcing on the bidecadal timescale.

**JSP25/W/48-B5** Invited **1130**

#### THE NORTH PACIFIC DECADEAL CLIMATE VARIABILITY AND OCEANIC FRONTS

HISASHI NAKAMURA (IGCR, Frontier Research System for Global Change, Tokyo/Dept. of Earth, Planetary Physics, Univ. of Tokyo, Tokyo, 113-0033, JAPAN; email: hisashi@geoph.s.u-tokyo.ac.jp); Alexander S. Kazmin (IGCR, Frontier Research System for Global Change, Tokyo; email: kazmin@frontier.esto.or.jp)

Decadal/interdecadal climate events (DICES) observed in the North Pacific over the last several decades are documented. Except in the tropics, the observed wintertime decadal SST variability in the basin is concentrated in the subarctic and subtropical frontal zones (cited to as SAFZ and STFZ, respectively). The decadal SST fluctuations in STFZ, accompanied by the anomalous surface subtropical high, exhibit strong negative simultaneous correlation with the tropical fluctuations, whereas those in SAFZ do not and hence they cannot be attributed to the direct tropical influence via the atmospheric bridge. The decadal SST anomalies in SAFZ are accompanied by the anomalous Aleutian Low and PNA pattern aloft. A wave-activity flux associated with that pattern is strongly divergent over SAFZ, suggesting that the pattern is forced there. It is suggested that the observed DICES in the subpolar gyre and the atmospheric circulation above may be associated with internally-generated variability in the coupled atmosphere-ocean system, although the associated wind anomalies could influence the subtropical gyre. In fact, lag regression analysis indicates a tendency of SST anomaly development in STFZ several years after the maturity of the anomalies in SAFZ, as simulated in coupled GCMs. The decadal SST fluctuations in SAFZ occurred in conjunction with substantial changes in the front. It is evident in high-resolution SST data based on ship measurements that the frontal axis tends to shift equatorward during a cool period and poleward in a warm period. The equatorward shift is associated with the stronger penetration of the Oyashio along the Japanese coast and the cooling in SAFZ and in the northern part of the Kuroshio extension. The decadal shift of SAFZ is confirmed in satellite-derived SST data.

Furthermore, they indicate that the cross-frontal SST contrast tends to be stronger when the front is shifted poleward in a warm period.

**JSP25/W/67-B5** Invited **1150**

#### A 31-YEAR ANALYSIS (1968-1998) OF THE ALASKA SUBPOLAR OCEAN GYRE

Gary LAGERLOEF (Earth and Space Research, 1910 Fairview Ave E, Suite 102, Seattle, WA 98102-3620 USA, email: lagerloef@esr.org)

Surface dynamic topography over the recent three decades is used to assess interdecadal circulation variability of the Alaska Gyre, a cyclonic subpolar gyre in the northeast Pacific Ocean. The data are a composition of conventional upper ocean hydrographic stations for the first 2.5 decades (objectively analyzed), and appended with recent satellite altimetry. The principal mode (positive phase) coincided with elevated dynamic height and SST in the eastern part of the gyre, a weaker circulation, and a slight displacement of the gyre WSW. These features in turn, were coherent with the cold phase of the decadal North Pacific (NP) SST mode and intensified Aleutian Low. The gyre generally exhibited its negative phase for most of the 1970s and 1990s, and positive in the 1980s, with episodic reversals of a few years duration. The dynamics of these decadal variations, including stochastic wind stress curl forcing and heat fluxes, will be discussed along with the relationships of the Alaska gyre variations and other climate indices in the North Pacific sector.

**JSP25/E/01-B5** Invited **1210**

#### INTER-DECADAL VARIATIONS IN JAPANESE SARDINE AND THE KUROSHIO EXTENSION

ICHIRO YASUDA (Univ. of Tokyo/ Frontier Research System for Global Change, Hongo 7-3-1, Bunkyo, Tokyo 113-0033, Japan, E-mail: ichiro@geoph.s.u-tokyo.ac.jp); Masayuki Noto (Hokkaido Univ., E-mail: noto@geoph.s.u-tokyo.ac.jp); Tomoki Touzuka (Univ. of Tokyo, E-mail: s72620@vsiron.geoph.s.u-tokyo.ac.jp)

Japanese sardine is known to greatly vary in inter-decadal time scales. In 1988, the catch was over 4 million tons; it declined abruptly since 1989 and was below 1 million tons in 1995. We found the winter-SST in the Kuroshio Extension and its southern recirculation area (KESA: 30-35N, 145-180E) significantly correlates with the mortality coefficient of the Japanese sardine. The warming in the KESA since 1988 possibly causes the collapse of the sardine. The SST variations in the KESA and south of Japan were different from those in the Kuroshio-Oyashio frontal regions in the western/central Pacific (40-45N 145-180E) where a regime-shift around mid-1970s was known: the SSTs in the Kuroshio regions have a longer time scale of over 50 years than in the frontal regions (25 years), and the jump of the Kuroshio SSTs around late-1980s occurred two years earlier in 1988 than in the frontal regions. The shift around mid-1970s in the frontal regions was not observed in the Kuroshio and the KESA where the SST anomalies were already negative in early-1970s. These SST variations well corresponds to sardine catch records. Analyses of heat flux and wind before/after the late-1980s SST jump indicate that the warming since 1988 was caused partly by the decrease in the net heat flux and in the mixed layer depth due to the reduction of wind over the Kuroshio south of Japan and over the Kuroshio Extension regions.

Friday 30 July PM

Presiding Chair: Lawrence Mysak (McGill University, Montreal, Canada)

#### VARIABILITY OVER THE ARCTIC REGION

**JSP25/W/44-B5** Invited **1400**

#### DECADAL AND LONGER-SCALE VARIABILITY OF THE ARCTIC SEA ICE COVER AND OVERLYING ATMOSPHERIC CIRCULATION

Lawrence A. MYSAK, Dingrong Yi and Silvia A. Venegas (McGill University, Dept. of Atmospheric and Oceanic Sciences, 805 Sherbrook Street West, Montreal, QC H3A 2K6 Canada. E-mail: mysak@zephyr.meteo.mcgill.ca)

The relationship between the Arctic and subarctic sea ice concentration (SIC) anomalies and the overlying atmospheric circulation fluctuations is investigated using the singular value decomposition (SVD) and composite map analysis methods. The data analyzed are monthly SIC and sea level pressure (SLP) anomalies poleward of 45 N which extend over the 38-year period 1954-1991. The association of the SIC anomalies with the decadal-scale "Ice and Salinity Anomalies" (ISAs) observed in the Greenland and Labrador seas during the late 1960s/1970s (by Dickson et al.), the late 1970s/1980s and late 1980s/1990s (by Belkin et al.) is also explored. The SVD1 (first) mode of the coupled variability, which accounts for 54% of the square covariance, is mainly an atmosphere-to-ocean forcing mode characterized by the decadal timescale. The aforementioned ISAs are clearly captured by this mode. We also show that there exists a significant correlation between the decadal SIC variability associated with SVD1 and the North Atlantic Oscillation, whose spectrum also exhibits a quasi-decadal signal. The SVD2 mode accounts for 16% of the square covariance and shows no evidence of a dominant forcing field. This mode exhibits very low frequency variability and reveals that the co-variability of the SIC and SLP fields is mainly concentrated in the northern North Pacific. This is in contrast to SVD1 mode whose variability occurs mainly in the North Atlantic sector.

**JSP25/W/63-B5** Invited **1420**

#### DECADAL VARIABILITY OF THE ARCTIC CLIMATE

ANDREY PROSHUTINSKY (Institute of Marine Science, University of Alaska Fairbanks, P.O. Box 97725-7220, Fairbanks, USA, email: prosh@ims.alaska.edu)

Arctic navigation, oil and gas exploration, and arctic pollutant transport depend on arctic environmental conditions. Existing atlases, manuals, and reference books contain multi-year mean environmental variables and their multi-year mean seasonal variability; however, uncertainties sometimes result from the existing atlases because they do not take into account climate change and climate variability. This presentation is motivated by the recent finding of two regimes (or two climate states) of arctic atmosphere-ice-ocean circulation described by Proshutinsky and Johnson [1997]. Our results show that wind-driven ice and water motion in the Arctic alternates between anti-cyclonic and cyclonic circulation, with each regime persisting for 5-7 years (period is 10-15 years). Based on this work, we demonstrate that seasonal variations in the ice concentration, ice thickness, and ice drift; ocean currents, ocean temperature, and salinity; horizontal and vertical heat fluxes; atmospheric pressure, wind speed, cloudiness, and precipitation; river discharge; and permafrost temperatures are different for cyclonic and anticyclonic arctic climate states. We analyze observational and model data to document decadal variability of the arctic system. The model simulations are validated and aided by oceanic, meteorological, and terrestrial data sets collected over the past 100 years throughout the arctic.

**JSP25/W/82-B5** Invited **1440**

#### HYPERSENSITIVE DECADEAL OSCILLATIONS IN THE COUPLED ATMOSPHERE-ICE-OCEAN SYSTEM OF THE ARCTIC/SUBARCTIC REGIONS

M. IKEDA (Graduate School of Environmental Earth Science, Hokkaido University, Sapporo, Japan, email: mikeda@ees.hokudai.ac.jp); J. Wang (International Arctic Research Center/ Frontier Research System for Global Change, Fairbanks, Alaska); J-P. Zhao (Institute of Oceanology, Chinese Academy of Sciences, Qingdao, China)

Decadal oscillations have become remarkable in the Arctic climate only for last three decades, being superimposed on the global warming trend. The variability is often called the Arctic Oscillation (AO) and characterized by an oscillation between the intensified Polar Vortex connected with the warmer Arctic, having a center of action over Siberia, and the opposite tendency. The air temperature over the Greenland Sea has a reversed phase with that over Siberia. The intense Polar Vortex matches with the lower ice cover in summer and fall over the Canadian Basin, with a two-year lag (ice leads the atmosphere), and the year-round lower ice cover over the Atlantic sector. A conceptual model is developed with a basis on water exchange between the upper layers of the Arctic Ocean, the Greenland-Iceland-Norwegian (GIN) Seas and the Atlantic Ocean. Only the upper-layer volumes (or thicknesses) are considered. Those of the Arctic Ocean and GIN Seas are time-dependent variables, while the Atlantic Ocean is prescribed. An atmosphere-ocean feedback mechanism relates the Arctic Ocean thickness with the flow from Arctic to GIN: i.e., the thinner Arctic upper layer causes warmer Arctic and more intense Polar Vortex, which contributes the flow from Arctic to GIN, or the opposite direction. The other key component is the enhancement of deep water convection caused by the flow from Atlantic to GIN: i.e., the GIN box water is expelled by thermohaline circulation and deep convection, whose rate is increased by the inflow of the more saline Atlantic Water.

The solution is convergent, oscillatory or divergent, depending on efficiencies of the atmosphere-ocean feedback and the deep convection. The higher (lower) efficiency yields divergence (convergence), whereas an oscillation exists only within the limited ranges of these two parameters. The occurrence of the recent AO may be related to the changes in the parameters.

**JSP25/W/27-B5** Invited **1500**

#### DECADAL VARIABILITY OF THE NORTH POLAR VORTEX

Julian X.L. WANG and James K. Angell (NOAA/Air Resources Laboratory, 1315 East-West Highway, Silver Spring, MD 20910, E-mail: julian.wang@noaa.gov)

Using 51 years (1948-1998) of NCEP/NCAR Reanalysis, an assessment on intensity and size of the north polar vortex is made. Three dimensional description of the vortex structure and its decadal variation are shown in geopotential height and surface pressure fields. Preliminary results indicate that the decadal variations of the vortex are closely linked to global tropics, and are associated essentially to the eccentricity of the vortex.

**JSP25/P/05-B5** Invited **1520**

#### MULTIDECADAL VARIABILITY OF NORTHERN HEMISPHERE FUNDAMENTAL CIRCULATION MODES IN A 1.800 YEAR OCEAN-ATMOSPHERE MODEL RUN: IMPLICATIONS FOR CLIMATE CHANGE ASSESSMENT

Hans-F. GRAF and Judith Perlwitz, (Max-Planck-Institute for Meteorology Bundesstr. 55, D-20146 Hamburg, Germany, email: graf@dkrz.de)

The leading mode of coupled stratospheric variability in winter combines the strength of the circumpolar stratospheric vortex with characteristic pressure, temperature and precipitation anomalies in the northern hemispheric troposphere. The loading of this mode has changed significantly from the 1960s to the 1990s towards a stronger polar vortex. Basic features of this mode are also found in climate models. However, there the pattern structure is slightly different and locally explained variance does not reach such large values as in observations. Sensitivity experiments show that the leading variability mode can be exaggerated by external forcing like volcanic aerosol, greenhouse gas concentration and probably ozone changes induced by solar forcing. We studied the similarity between the pattern of observed 40 year circulation trends in the Northern Hemisphere and the corresponding circulation trends in both a 1800-year control run and a IPCC (1996) Scenario A run, carried out with a coupled atmosphere-ocean climate model. We found that even an unforced coupled ocean-atmosphere climate model produces secular variability (in the specific case of a mean period of 76 years), which is strongly pronounced in patterns that resembles the observed trends of the recent 40 years. With greenhouse forcing according to EPCC (1996) Scenario A the leading variability mode becomes exaggerated and remains so. Thus we have to expect an enhanced NAO in the future with mild winters over mid-latitude and northern Eurasia drought in the Mediterranean and a strong, cold and stable stratosphere polar vortex negatively affecting the Arctic stratospheric ozone concentration. The consequences of these results for climate change assessment will be discussed.

Presiding Chair: Fei-Fei Jin (University of Hawaii, Honolulu, USA)

#### CONNECTIONS BETWEEN DIFFERENT TIMESCALES

**JSP25/E/26-B5** Invited **1600**

#### DECADAL TO MULTIDECADAL CLIMATE VARIABILITY IN THE INDIAN OCEAN REGION

Chris J.C. Reason (School of Earth Sciences, University of Melbourne, Parkville, Vic., 3052, Australia, email: cjr@met.unimelb.edu.au); Robert J. ALLAN (CSIRO Atmospheric Research, Aspendale, Vic., 3195, Australia, email: rob.allan@dar.csiro.au)

Decadal to multidecadal climate variability in the Indian Ocean region and potential links with the El Niño Southern Oscillation (ENSO) are examined using observational and modelling approaches. One prominent mode of variability in this region involves a strengthening and weakening of the South Indian Ocean anticyclone and warming and cooling across the southern midlatitudes of the basin. Atmospheric and ocean modelling suggests that local air-sea interaction may play a significant role in the generation of this mode, although evidence also exists of a possible relationship with ENSO.

Band pass filtering of seasonal mean sea level pressure (MSLP) and sea surface temperature (SST) fields for ENSO years on quasidecadal and interdecadal time scales (11-13 year and 15-20 year bands) is used to explore links between ENSO and the lower frequency variability manifested in the Indian Ocean region. This analysis reveals that quasidecadal and interdecadal signals in the climate system provide a modulation of the ENSO phenomenon that may lead to 'protracted' El Niño and La Niña episodes. In the Indian Ocean basin, interactions between these signals can result in periods when SST patterns and rainfall relationships are out-of-phase with 'protracted' ENSO responses across the central-eastern tropical Pacific Ocean.

IA



**JSP25/W/95-B5** Invited **1620**

**WHAT CAUSES INTER-DECADAL CHANGES IN AUSTRALIAN SEASONAL RAINFALL PREDICTABILITY?**

S. POWER (National Climate Centre, email: S.Power@bom.gov.au; GPO Box 1289K, Melbourne, VIC 3001, AUSTRALIA); T. Casey (BMRC), C. Folland and A. Colman (UKMO) and V. Mehta (NASA GSFC).

The success of an ENSO-based statistical rainfall prediction scheme and the influence of ENSO on Australia are shown to vary in association with a coherent, inter-decadal oscillation in surface temperature over the North and South Pacific Oceans. When this Inter-decadal Pacific Oscillation (IPO) raises temperatures in the tropical Pacific Ocean, there is no robust relationship between year-to-year Australian climate variations and ENSO. When the IPO lowers temperature in the same region, on the other hand, year-to-year ENSO variability is closely associated with year-to-year variability in rainfall, surface temperature, river flow and the domestic wheat crop. The contrast in ENSO's influence between the two phases of the IPO is quite remarkable. This highlights exciting new avenues for obtaining improved climate predictions.

**JSP25/E/15-B5** **1640**

**DECADAL-MULTIDECADAL VARIATIONS IN TROPICAL CLIMATE AND ENSO**

VIKRAM M. MEHTA (NASA-Univ. of Maryland Joint Center for Earth System Science Department of Meteorology, Univ. of Maryland College Park, Maryland 20742, U.S.A.)

Decadal-multidecadal climate variations are receiving increased attention from the research community in the last one or two decades. It is very important to study decadal-multidecadal climate variability in its own right and also because of its potential to interact with interannual climate variability and anthropogenic climate change. Observed decadal-multidecadal climate variability in the tropical-subtropical Pacific region, and its influence on long-term modulation of interannual ENSO variability and predictability will be described in this oral presentation. The influence of decadal-multidecadal climate variability in modulating interannual ENSO-global rainfall relationship will also be described.

**JSP25/W/56-B5** **1700**

**INTERDECADAL MODULATION OF INTERANNUAL ATMOSPHERIC AND OCEANIC VARIABILITY OVER THE NORTH PACIFIC**

SHOSHIRO MINOBE (Division of Earth and Planetary Sciences, Graduate School of Science, Hokkaido University, Sapporo 060-0810, Japan, Email: minobe@neptune.sci.hokudai.ac.jp); Nathan Mantua (Joint Institute of Sciences of Atmosphere and Ocean, University of Washington, Seattle, WA 98195-4235, USA, Email: mantua@atmos.washington.edu)

The interdecadal modulation of interannual variability of the atmosphere and ocean is examined over the North Pacific by using Wavelet Transform combined with EOF or SVD analysis. The interannual variability of the wintertime Aleutian Low, identified by either the North Pacific Index or the EOF-1 of North Pacific sea level pressure (SLP), exhibits an interdecadal modulation. Interannual variance in the strength of the Aleutian Low was relatively large from the mid-1920's to mid-1940's and in the mid-1980's, but relatively small in the periods from 1899 to the mid-1920's and from the mid-1940's to the mid-1970's. The periods of high (low) interannual variability roughly coincide with pentadecadal regimes having a time averaged relatively intense (weak) Aleutian Low. The SLP EOF-2, which is related to the North Pacific Oscillation, exhibited a strengthening trend from the beginning of this century to the mid-1960s, and significant weakening after that. Consistent changes are observed in the 500 hPa height and SST fields.

**JSP25/W/19-B5** **1720**

**INTERACTIONS OF DECADAL CLIMATE MODES IN THE NORTH ATLANTIC**

A. GROETZNER and M. Latif (Max-Planck-Institut fuer Meteorologie, Bundestr.55, D-20146 Hamburg, Germany); A. Timmermann (KNMI, Postbus 201, 3730 AE De Bilt, the Netherlands)

Two distinct climate modes of the North Atlantic climate system with decadal timescales have been identified in a millennium integration with the coupled GCM ECHAM3/LSG. Both oscillations rely on a feedback loop between the atmosphere, in particular the North Atlantic Oscillation, and the ocean, which represents the memory of the coupled system. One mode with a period of about 15 years is connected to the wind driven gyre circulation, while the other has a period of about 30-40 years and involves the thermohaline circulation. Since the latter mode has been described already elsewhere, we shall discuss the structure and dynamics of the wind driven mode and its interaction with the thermohaline mode. Since the dynamics of both modes involves large scale SST anomalies in the subtropical North Atlantic and the period of the wind driven mode appears to be roughly half of that of the thermohaline mode, an interaction between the two modes seems to be plausible. By applying various statistical techniques like singular spectrum and wavelet analyses we shall investigate the interactions between the two modes and discuss some implications for climate predictability on decadal timescales.

Monday 26 July AM

**OCEAN/ATMOSPHERIC VARIABILITY AND PREDICTABILITY- ENSO VARIABILITY**

**JSP25/E/30-B1** Poster **0830-01**

**THE INFLUENCE OF THE DECADAL-SCALE VARIABILITY OF SUMMER RAINFALL ON THE IMPACT OF EL NIÑO AND LA NIÑA EVENTS IN SOUTH AFRICA**

A. C. KRUGER, (South African Weather Bureau, Private Bag X097, Pretoria, South Africa)

Regions of correlation between South African late summer rainfall and sea-surface temperature (SST) in the NINO3 region were identified. Regions identified for late summer showed a much better spatial coherence than was the case for early summer. These regions were then compared with eight homogeneous rainfall regions in South Africa. For the period 1955-1991, near-decadal epochs of above- and below-normal late summer rainfall were identified, with Cramer's t-test and cumulative deviations, for five of the eight homogeneous regions, which possessed areas with rainfall correlated with the NINO3 SST time-series. According to these tests, the 1960's and 1980's are characterised by below-normal rainfall, while the 1950's and 1970's are characterised by above-normal rainfall. Turning points between these epochs are around 1959/60, 1970/71, 1980/81 and 1991/92. This corresponds to cycles in summer rainfall in South Africa identified by other authors. To estimate rainfall

anomalies without the effect of El Niño/La Niña, rainfall anomalies due to NINO3 were estimated by a linear regression of rainfall against NINO3 SST's. These were subtracted from the standardised rainfall anomalies to obtain the residual anomalies that give an indication of the rainfall without the effects of El Niño/La Niña. From these time series similar epochs and turning points were evident. El Niño seasons during epochs of below- and above-normal rainfall were compared. The same was done with La Niña seasons. The impact of El Niño and La Niña is influenced in such a way that during an epoch of above-normal rainfall a moderating effect is evident on the severity of El Niño events so that even rainfall above the normal rainfall is experienced on average during such events. The opposite is also true in that an epoch of below-normal rainfall will have a negative effect on the enhancement of rainfall usually associated with a La Niña event. Extreme events of rainfall (droughts and floods), usually occur when an El Niño event occurs during an epoch of below normal rainfall and when a La Niña event occurs during an epoch of above normal rainfall.

**JSP25/E/29-B1** Poster **0830-02**

**ENSO PREDICATION WITH WAVELET METHOD**

Lintao LIU (Institute of Geodesy and Geophysics, Chinese Academy of Sciences, 54 Xudong RD, Wuhan 430077, P. R. China, email: llt@asch.whigg.ac.cn) H. T. Hsu (Institute of Geodesy and Geophysics, Chinese Academy of Sciences, 54 Xudong RD, Wuhan 430077, P. R. China, email: hshu@asch.whigg.ac.cn)

In this contribution, we introduce a new data-analyzing technique: the modified continuous wavelet transform (MCWT). The MCWT technique performs very well in the extraction of instantaneous amplitude and phase of the non-stationary signals. We make time-frequency analyses on the Enso Data (SOI and SST anomaly), resorting to the MCWT technique. The wavelet spectrums of SOI and SST anomaly suggest that the extremes of the Enso circle result from the couplings of the interannual quasi-periodic modes in the Enso circle. The predications of SOI and SST anomaly are made according to their wavelet spectrums, respectively. Our study shows that the wavelet method can play an important role in the prediction of the Enso circle.

**JSP25/C/U2/E/02-B1** Poster **0830-03**

**ON THE SHORT-TERM VARIABILITY OF NORTHERN HEMISPHERE CLIMATE IN CONJUNCTION WITH EL-NINO SOUTHERN OSCILLATION**

Byshev V.I, NEIMAN V.G., Aleynik D.L., Lebedev M.M. (all at P.P.Shirshov Institute of Oceanology, 117851, Nahimovski pr. 36, Moscow, Russia, email: dmitry@clime.ioran.msk.ru)

The main aim of the study was a detection as atmosphere so oceanic in mediate recall for the events of El-Nino Southern Oscillation. It was carried out an analysis of the atmospheric pressure fields at sea level and air temperature and altitude of the H-500 geopotential surface over entire Northern Hemisphere for 20-th century. In results it was acknowledge that certain type variability of processes in ocean and atmosphere appears in obvious temporal correlation with ENSO. Particularly, such variability demonstrates itself by arising of some prominent anomalies in the fields of atmospheric pressure at sea level and air temperature, also by changes of global longitudinal and latitudinal (ocean - continent) thermal gradients as well as variations of lateral temperature shear at sub-polar (Atlantic and sub-arctic Pacific fronts). Taking into account the generally established specific of ocean - atmosphere interrelation during the ENSO it was retraced some regional differences in recall of the climatic system for the event. Thus, in the Pacific and Siberian regions the meteorological fields were found the most sensitive in that respect, while Atlantic and European regions shown relatively much weaker signals. Some interesting additional information can be followed up by face intercomparison of Gulfstream and Kuroshio transport fluctuations with those of quasi-permanent atmospheric highs and lows. Analysis of hydrographic data obtained in 1997-1998 by Russian expeditions in Barents Sea revealed appreciable decrease of its average heat content that conforms eventually with active stage of the last ENSO. Another case of El-Nino related behaviour of atmosphere was traced in phenomenon of Polar anticyclone forcing which controls in turn the hydro-meteorological conditions over whole Arctic area and in the neighbour territories.

**JSP25/C/MI05/W/34-B1** Poster **0830-04**

**CHARACTERISTICS OF THE PLANETARY-SCALE CIRCULATION OVER THE ASIA-PACIFIC REGION DURING A TRANSITION FROM A WARM TO A COLD STATE OF THE ENSO**

Jianjun Xu and JOHNNY C L CHAN (Department of Physics and Materials Science, City University of Hong Kong, Email: APXUJUN@cityu.edu.hk; and Johnny.chan@cityu.edu.hk)

Based on the transition of a significant sea-surface-temperature anomaly (SSTA) over the central equatorial Pacific (the Nino3.4 region) from 0.5°C to -0.5°C after an El Niño episode, three types of transition episodes can be identified: the spring type (SP) in which the SSTA first falls below -0.5°C in April or May after the termination of an El Niño episode; the summer type (SU) in which the SSTA does not reach this threshold until July or later; and no La Niña occurrence type (NON) in which the SSTA never reaches the threshold. A composite of the SSTs in each type suggests that the SP is generally stronger but the SU has two negative peaks during the entire La Niña episode. In the NON type, the positive SSTA gradually damps off. The strength of easterly anomalies over the central equatorial Pacific (CEP) appears to play an active role in the transition from a warm to a cold state of the ENSO cycle. If the easterly anomaly is non-existent or very weak, La Niña will not occur, such as in NON. Convergence over the western equatorial Pacific and divergence over the CEP and eastern equatorial Pacific near the surface appear to be necessary conditions for the development of the easterly anomalies, but their roles are apparently different in the two types of La Niña episodes. The transition from a warm to a cold state of the ENSO cycle is also closely related to anomalies in the Asian-Australian monsoon.

**JSP25/E/34-B1** Poster **0830-05**

**TOWARDS NONLINEAR IDENTIFICATION OF THE ATMOSPHERIC RESPONSE TO ENSO**

A. HANNACHI (Atmospheric Oceanic & Planetary Physics, Clarendon Laboratory, Parks Road, Oxford OX1 3PU, UK, email: han@atm.ox.ac.uk)

The question of estimating the nonlinear atmospheric response to ENSO is addressed here using state-of-the-art General Circulation Models (GCMs) and focussing on the interannual, mainly winter, geopotential height at 500-mb. A set of multidecadal integrations of the Hadley centre GCM model, HADAM1, is used for this purpose. The model is forced by the observed sea surface temperature (SST) and is integrated for 45 years with different initial condition for each run. Simple EOF analysis indicates that the response over the North Pacific is close to being quasi-linear where the internal mode namely Pacific North American (PNA) pattern gets 'synchronized' to the ENSO, while the response over the North Atlantic sector is more likely nonlinear. A probabilistic approach is then introduced to detect this response based on maximizing and



minimizing the respective probability density functions (pdfs) of the ensemble mean and the noise given an estimate of the latter. The method demands that the ensemble mean be split into clusters according to the phase of the southern oscillation (SO) and then the signal pattern in each cluster found. It is then shown in particular that over the North Pacific, in winter, negative phases of the Niño3-SST anomaly (La-Niña) appear to trigger the negative PNA pattern while during positive phases of ENSO (El-Niño) the response bears some similarities to a zonally stretched PNA-like pattern with a weak signature of North Pacific Oscillation, but is not precisely the inverse of the response corresponding to La-Niña (-\$PNA). Over the North Atlantic the two response patterns are different where a dipolar structure with north-south seesaw tilted north-east/south-west is obtained during El-Niño whereas during the opposite phases a tripole response pattern emerged. Finally, investigations of the relationship between the spring atmospheric variability and the ENSO during the spring and the winter, using signal-to-noise ratios and canonical correlations, reveal that the spring atmospheric response is more related to the winter, rather than the spring, east tropical Pacific SST.

**JSP25/E/22-B1** Poster **0830-06**

**PREDICTING THE 1997/98 EL NIÑO USING A COUPLED GCM**

S. INESON and M.K. DAVEY (both at U.K. Meteorological Office, London Road, Bracknell, RG12 2SZ, U.K. Email: sineson@meteo.gov.uk)

The U.K. Met. Office Tropical Pacific/Global Atmosphere CGCM is being used for experimental seasonal predictions. Hindcasts have been made for various periods since the mid-1980's; however, this talk will focus on the recent major El Niño. Six month forecasts have been made at three month intervals with a small ensemble for each start time since December 1997. The forecast system consists of initialisation of the component models followed by the CGCM forecast. The present strategy has been to initialise relative to the coupled model climatology, and to predict anomalies relative to that climatology, with the aim of minimising initial shock on coupling.

In general the onset of the 1997/98 El Niño was forecast well, although the initialisation scheme gave a relative cold bias in the central-east equatorial Pacific SST at this time. Many of the observed regional changes in precipitation in the tropics were captured. Forecasts of the subsequent decline and transition to weak La Niña conditions have not been so successful and have revealed shortcomings in the initialisation technique.

**JSP25/W/06-B1** Poster **0830-07**

**ENSO ACCOMPANYING AND LAGGED VARIATIONS IN THE EXTRATROPIC NORTH PACIFIC SST, METEOROLOGICAL CHARACTERISTICS AND ICE EXTENT**

Vladimir PONOMAREV, Olga Trusenkov, Serge Trousenkov, Dmitry Kaplunenko, and Vladimir Plotnikov (all at Pacific Oceanological Institute, Vladivostok, 690041, Russia, e-mail: archer@linkor.ru, ponomarev%dan86@poi.marine.su)

The ENSO accompanying and lagged variations of the extratropic North Pacific SST and atmospheric circulation patterns, as well as air temperature, precipitation and sea ice extent in the Northwest Pacific margin were studied. The time series of monthly mean SST fields for 32 years were analyzed using Complex EOF method to reveal anomaly development and movement. The linear lagged/unlagged relations between SST anomaly principal components, ice extent, meteorological characteristics and El Niño/Southern Oscillation Indexes were estimated. The extratropic atmospheric circulation patterns were presented by six principal synoptic situations over the North Pacific based on the SLP (Sea Level Pressure) daily field classification developed by Polyakova (1997). These situations are associated mainly with different positions of cyclone tracks and of high/low pressure over the North Pacific and adjacent land areas. Particular classes correspond to known atmospheric circulation patterns over the North Pacific area, namely particularly as Pacific - North American and Subtropical - Zonal. We used time series of frequency of occurrence (days/month) of the mentioned synoptic situations to determine their variations of ENSO-decadal scale related to annual cycle anomalies of the ice extent, air temperature and precipitation over the Northwest Pacific margin. Findings and results imply possible feedbacks between low-frequency variations in Tropic and Extratropic Pacific.

**JSP25/W/76-B1** Poster **0830-08**

**GEARING BETWEEN THE INDO-MONSOON CIRCULATION AND PACIFIC-WALKER CIRCULATION AND THE ENSO**

Wen MENG, (Chinese Academy of Meteorological Sciences, Beijing, 100081, China E-mail: men@lasgsi4.iap.ac.cn); Guoxiong Wu, (State key Laboratory of Numerical Modeling for Atmospheric Geophysical Fluid Dynamics, Institute of Atmospheric Physics, Beijing, 100080, China E-mail: gxwu@lasgsi4.iap.ac.cn)

Most of the existing theories explain the formation of El Niño/Southern Oscillation events in terms of air - sea interaction in the tropical Pacific domain. Prediction of their formation and evolution is still a big scientific challenge. Here we show that air - sea interaction in the equatorial Pacific Ocean and that in the equatorial Indian Ocean are linked to each other due to the close coupling between the monsoonal zonal circulation over the equatorial Indian Ocean and the Walker circulation over the equatorial Pacific Ocean. The coupling of these two circulation cells works in a way much like a pair of gear operating over the equatorial Indian and Pacific: anomalies in the monsoonal zonal flow over the Indian Ocean can affect the air-sea interaction over the central and eastern equatorial Pacific and trigger the occurrence of El Niño/Southern Oscillation events. The finding that El Niño/Southern Oscillation events can be traced back to the origin over the Indian Ocean may enable improved predictions of ENSO formation and evolution.

**JSP25/W/12-B1** Poster **0830-09**

**THE IMPACT OF THE LATEST ENSO EVENTS ON TEMPERATURE AND PRECIPITATION IN ROMANIA**

C. MARES and Ileana Mares ( both at National Institute of Meteorology and Hydrology, Bucuresti-Ploiesti, 97, Bucharest, 71552, Romania, E-mail: cmares@meteo.inmh.ro)

Temperature and precipitation in Romania defined in 31 and 33 stations respectively were filtered by EOF 1, for the interval 1950-1991. In order to quantify the ENSO impact, the SOI values were considered as the measure of this event. Thus, for the interval 1950-1991 simultaneous correlations and of 1 to 12 months delay between the monthly values of the first EOF component of temperature and precipitation in Romania and SOI were taken into account. Usual, biserial and tetrachoric correlations were performed and only the high significant results (1% or more) were considered. For the simultaneous correlations the results showed that the impact of the ENSO event was significant only in July and December for temperature and in August and September for precipitation. For the correlations with up one year delay it resulted that in Romania for the precipitation of April and October the SOI values

of March and August might have been predictors. For temperature, the most significant results were obtained for the months of January, June (with 12 months delay), July (10 months delay) and August (7 months delay). The performed verifications of the last two years in order to assess the impact of the ENSO on the monthly behaviour of temperature and precipitation in Romania, showed that precipitation responded better than temperature to this extreme forcing. Thus, the months extremely rich in precipitation (as compared with normal values), i.e. August 1997 (with monthly anomalies up to 150 mm) and October 1998 (twice exceeded the normal values), could have been forecast taking in account this study. Thus, there are periods when the ENSO influence is significant and can be used in the forecast of monthly temperature and precipitation in Romania.

**JSP25/P/02-B1** Poster **0830-10**

**ENSO OCCURRENCE AND SUB-SURFACE OCEAN TEMPERATURE ANOMALIES IN THE PACIFIC WARM POOL**

Li CHONGYIN, Mu Mingquan, Zhou Guangqing (LASG, Institute of Atmospheric Physics, CAS, P.O. Box 2718, Beijing 100080, China, email: lcy@lasgsi4.iap.ac.cn)

The close relationship of the ENSO occurrence with the sub-surface ocean temperature (SOT) anomalies in the Pacific warm pool region is studied through data analyses and numerical simulation with a CGCM. It is clearly shown that there are continued positive (negative) anomalies of SOT in the warm pool region prior to the El Niño (La Niña), and the outbreak of El Niño (La Niña) is directly associated with the eastward propagation and expanding to the sea surface of positive (negative) SOT anomalies. It is also clear that the eastward propagation of anomalous SOT in the warm pool region is closely related to the zonal wind anomalies over the equatorial centre-western Pacific, which are earlier than the eastward propagation of SOT. A lot of studies have shown that the zonal wind anomalies over the equatorial centre-western Pacific result mainly from anomalous winter monsoon in East Asia. This indicated again that there is close interaction between Asian winter monsoon and the ENSO cycle

Tuesday 27 July AM

**SEASONAL-DECADAL VARIABILITY**

**JSP25/E/25-B2** Poster **0930-01**

**EMPIRICAL SEASONAL FORECAST OF THE NORTH ATLANTIC ATMOSPHERIC ANOMALIES**

Emilia SANCHEZGOMEZ and Maria Jose OrtizBevia (Universidad de Alcalá de Henares, Alcalá, Madrid 28871, Spain, email: emi@pc41.fsc.alcala.es)

In this work an empirical forecast of North Atlantic atmospheric anomalies is carried out using the statistical scheme given by the Singular Value Decomposition (SVD). The goal of SVD is to find linear combinations of two different sets of variables such that these linear combinations explain the maximum possible covariance.

In order to perform our statistical forecast, different meteorological fields are used as predictor and predictand. The predictive potential of these fields is investigated through several experiments: Sea Surface Temperature (SST) anomalies as predictor and 850-mb height air temperature anomalies as predictand and then the predictand field itself.

The air temperature anomalies field is built from the NCAR reanalysis set (Kalnay et al. 1995) and the SST field is built by merging the COADS and the IGOSS datasets. The predictor and predictand spatial domain is restricted to the same geographical region (North Atlantic). These fields both are filtered in time before performing SVD of the covariance matrix at time lag required for the forecast, and subsequently they are spatially filtered taking into account the most representative patterns obtained (20).

The first forecast experiment was carried out for the 90's and the skill (correlation between the predicted and observed field) has significant values in an extended oceanic region, including the subtropics and the central part of midlatitude ocean, while most of the coastal region, east and west, presents negative forecast skill. Other forecast experiments have been performed in order to investigate the spatial and temporal dependence of the correlation skill. The results obtained in these experiments will be discussed, specially those related with the spatial dependence of the skill.

The empirical forecast presented here were intended as the benchmark for the PROVOST project integrations.

**JSP25/E/11-B2** Poster **0930-02**

**SCALE INTERACTIONS IN THE VARIABILITY OF THE TROPICAL ATLANTIC**

Maria Jose OrtizBevia, William CABOSNARVAEZ, Francisco AlvarezGarcia

We analyze the variability of the tropical Atlantic sea surface temperature as simulated in a 250-years time slice of an OPYC-ECHAM coupled model integration, carried out at DKRZ, Hamburg. The statistical methods developed in (OrtizBevia et al., Beyond El Niño: Decadal and interdecadal variability, ed A. Navarra, Springer, 1998) are used to identify the relevant patterns of the interannual variability. Special attention is paid to decadal and ENSO related time scales. Then, we analyse the heat budgets and the dynamics of the mixed layer to seek out the physical mechanisms responsible for the observed patterns. The mechanisms are compared with the ones acting in the case of theseasonal variability. These last are identified by applying the same statistical techniques to the seasonal cycle of the same variables. For a better understanding of the decadal variability of the tropical Atlantic, we study the subsurface circulation of a 50-year period and the relationship between the tropical Atlantic and the tropical RPacific and tropical Indian Oceans, to see their contribution to the Atlantic SST variability. With this communication we make an attempt to contribute to the clarification of the question about the possible modes of variability in the Tropical Atlantic.

**JSP25/E/36-B2** Poster **0930-03**

**TROPICAL-TEMPERATE TROUGHS IN SOUTHERN AFRICA AND THE SOUTH WEST INDIAN OCEAN**

MARTIN TODD (School of Geography, University of Oxford, Mansfield Road, Oxford OX1 3TB, U.K., email: martin.todd@geog.ox.ac.uk); Richard Washington (School of Geography, University of Oxford, Mansfield Road, Oxford OX1 3TB, U.K., email: richard.washington@geog.ox.ac.uk)

Daily rainfall variability over Southern Africa (SA) and the Southwest Indian Ocean (SWIO) during the austral summer months is described objectively using new satellite products. The principle mode of variability in all months is a dipole structure with bands of rainfall orientated north west to south east across the region. These represent the location of cloud bands associated with tropical temperate troughs (TTT). Events characterised by such TTTs occur relatively infrequently with marked inter-annual variability, and contribute disproportionately to total rainfall.

## INTER-ASSOCIATION

On the basis of composites of NCEP reanalysis data the associated atmospheric structure is described. The 2 phases of the rainfall dipole are associated with markedly contrasting circulation patterns. There are also pronounced intra-seasonal variations in the position of the temperate trough and TTT cloud band.

Events in which the TTT cloud band lies primarily over the SWIO, are associated with large scale moisture flux anomalies, confirming TTT events as a major mechanism of poleward transfer of energy and momentum. Moisture is advected from 3 principal sources; (1) the northern or central Indian Ocean (where anomalous fluxes extend eastward to the Maritime Continent), (2) south equatorial Africa and the equatorial Atlantic, (3) from the south within a cyclonic flow around the extratropical trough. Thus, synoptic scale TTT events over SA/SWIO often appear to result from large scale planetary circulation patterns.

TTT development coincides with enhanced tropical convection between 10°-30°E (itself exhibiting periodicity of around 5 days), and often with convergence of eastward and westward propagating convection around 40°E. Harmonic analysis of 200hPa geopotential anomalies show that TTT features are forced by a specific zonally asymmetric wave pattern, with wave 5 dominant or significant in all months except February when quasi-stationary waves 1, 2 and 3 dominate. The relationship of TTT rainfall over SA/SWIO with similar rainfall dipole structures observed in the South Pacific and South Atlantic convergence zones is also analysed. These findings illustrate the importance of tropical and extratropical dynamics in understanding TTT events. Finally, the relationship between patterns of rainfall variability at daily, intra-seasonal and interannual scales, and the implications for predictability are discussed.

**JSP25/L/03-B2** Poster **0930-04**

### STUDIES OF OCEAN-ATMOSPHERE VARIABILITY AND ITS IMPLICATIONS FOR THE CLIMATE SYSTEMS IN WEST AFRICA DURING 1997-98 RAINY SEASONS

OJO O. and Gbuyiro S.(Department Of Geography University Of Lagos, Lagos, Nigeria)

This study applies the use of remote sensing technique to study the variability characteristics of ocean-atmosphere systems during the rainy season of 1997-98 using remote sensing technique. The study begins by examining the climatic background of West Africa with particular reference to the characteristics and significance of the ocean factor of climate in the region. The paper then discusses the elements and factors of climate in the region as they relate to the ocean-atmosphere variability in the region, especially as this relates to the characteristics and consequences of the tropical Atlantic sea-air interactions on the weather and climatic systems in the study region. In this regard, the paper discusses the patterns of migration and pulsation of the Intertropical Convergence Zone (ITC) (commonly known in West Africa as the Inter Tropical Discontinuity (ITD)) with its accompanying maritime Tropical (mT) air and the continental Tropical (cT) air along with their respective south-westerly and north-easterly winds. The paper discusses the macro-, meso- and micro-scale ocean-atmosphere variability as they relate to the Pacific and the Indian oceans and as they affect weather and climatic systems in the study region.

The paper then illustrates the characteristics of the variability in the ocean-atmosphere interactions in the tropical Atlantic Ocean and their impacts on weather and climatic processes during the rainy season of 1997-98 using the satellite photographs. The paper also relates also relates the variability in the air-sea interactions to the general characteristics of the elements and factors of weather and climate in the region, and especially as they affect rainfall and rainfall variability characteristics. The paper finally discusses the significance of this study for predictability of the weather systems and their consequences in the region, emphasise the need for adequate and regular information on satellite data, and advocates for co-operation and co-ordination, more effective monitoring and warning systems, and education and training.

**JSP25/W/02-B2** Poster **0930-05**

### TIME VARIABLE SPECTRA OF SEA LEVEL ANOMALIES COMPUTED BY TOPEX / POSEIDON ALTIMETRY

Wieslaw KOSEK (Space Research Centre, Polish Academy of Sciences, Bartycka 18A, 00-716 Warsaw, Poland, Email: kosek@cbk.waw.pl)

In this paper short period oscillations with periods ranging from 20 to 180 days of sea level anomalies determined from Topex/Poseidon altimetry are presented. The amplitude spectra computed by the Fourier Transform Band Pass Filter (FTBPF) for the whole ocean, equatorial regions, northern and southern hemispheres show that besides the annual oscillation there are oscillations with periods of 182, 120, 90, 60, and 30 days. The mean and variable amplitudes of these oscillations computed by the FTBPF depend on geographic latitude and longitude and are also variable in time. The 182 day oscillation has the biggest amplitude in the Indian and the equatorial Pacific Oceans. The 120-day and 90-day oscillation are very active in the equatorial regions of the Pacific and Indian Oceans as well as at the western parts of each Ocean. The biggest amplitudes of the 60-day oscillation, sometimes of the order of 15 cm, show mostly geographic regions where the M2 tide amplitude is not modelled correctly. In the case of a 30-day oscillation the equidistant spots with amplitudes of the order of 1-2 cm in the Pacific ocean above the equator were detected. These spots can be attributed to the instability waves in the equatorial Pacific. All these oscillations are also very energetic near the east coast of Argentina. In the mentioned geographic regions there are also the biggest changes of amplitudes of these short period oscillations.

**JSP25/P/01-B2** Poster **0930-06**

### ON STRUCTURAL CAUSES OF THE GENESIS OF INTERANNUAL SCALES OUT OF INTRASEASONAL DYNAMICS

Peter CARL (Climate Dynamics Project, c/o Forschungsverbund Berlin, Hausvogteiplatz 5-7, D - 10117 Berlin, Germany, email: pcarl@spclim5.wias-berlin.de)

Of the three types of climate variability found in a conceptual AGCM, a solution is studied in a 200 year run that is dynamically shaped by a torus segment in phase space which imprints a helical winding on the system's trajectories during boreal summer. The geometrical nature of this seasonal cycle bears interannual anomalies that structurally relate to intraseasonal motion systems of the 30-60 days band. The latter are maintained via interhemispheric synchronisation for which two discernible mechanisms are discussed. 2-, 4-, 6-year and longer quasiperiodicities are partially born in three types of re-adjustment in autumn to the annual forcing by the fading summer monsoon. Further structural sources of interannual variability include a generically intraseasonal Southern Oscillation, found as a degenerate monsoon oscillator or as an irregular wander between summer and winter fixpoints in autumn. All these dynamics are reflected in the model's integrals of motion.

To pose the results into perspective, local and global time series of the real world have been studied using methods of time-frequency analysis. The data bear evidence of structured bands, frequency drifts, secular trends and conceptually essential amplitude modulations that altogether point to organised, nonstationary dynamics throughout the century. This leaves the space for variability modes as found, in addition to those not traced back to phase space geometry of a model's atmosphere/land dynamics.

**JSP25/W/40-B2** Poster **0930-07**

### INTERANNUAL AND DECADAL CHANGES IN POLEWARD HEAT TRANSPORT BY THE EAST ASIAN WINTER MONSOON AND PACIFIC STORMTRACK

HISASHI NAKAMURA (IGCR, Frontier Research System for Global Change, Tokyo/Dept. Earth, Planetary Physics, Univ. Tokyo, 113-0033, JAPAN; email: hisashi@geoph.s.u.tokyo.ac.jp), and Takuya Izumi (Dept. Earth, Planetary Physics, Univ. Tokyo)

Interannual variability in the lower-tropospheric poleward sensible heat fluxes over the Northwestern (NW) Pacific associated with migratory baroclinic waves and with standing waves in bimonthly fields is investigated based on the NCEP/NCAR reanalyses for 1979-1995. The former is defined as the covariance (VhTh) of 8-day highpass-filtered temperature and meridional wind, and the latter (VsTs) can be regarded as heat transport by the northwesterly East Asian winter monsoon. Although the climatological-mean VhTh is suppressed in midwinter (Nakamura 1992), its interannual variability is the largest. The first EOF of January-February VhTh, which accounts for nearly 50% of the total interannual variance over the NW Pacific, represents anomalous VhTh along the climatological-mean stormtrack. The linear regression map of VsTs with the first principal component (PC1) timeseries of VhTh shows that the enhanced VsTs tends to be accompanied by the suppressed VhTh along the stormtrack and vice versa. Around 45N anomalous VsTs tends to be largely compensated by anomalous VhTh in the opposite sense, which leaves rather small changes in the total atmospheric sensible heat transport from one winter to another. Associated seasonal-mean circulation anomalies are identified in the linear regression maps with PC1. The enhanced VhTh is associated with anticyclonic SLP (sea-level pressure) anomalies that cover almost entire midlatitude North Pacific and weaker cyclonic anomalies over Siberia; in other words, the weakening of the Aleutian Low and Siberian High. These surface anomalies are accompanied by a PNA-like pattern over the North Pacific in the upper troposphere, and its anticyclonic ÖtaiÖ extends into northern China that is in seewith with cyclonic anomalies over Siberia. This baroclinic structure is consistent with anomalous VsTs over the Far East. Nakamura and Yamagata (1998) pointed out that two of the three dominant modes of the decadal wintertime SST variability over the NW Pacific changed drastically in the second half of the 1980Ös. One is the Ömidlatitude modeÖ characterized by SST anomalies along the subarctic front with the anomalous Aleutian Low and PNA pattern aloft, and the other represents decadal modulation of the East Asian winter monsoon

**JSP25/L/04-B2** Poster **0930-08**

### SOME STUDIES ON THE VARIABILITY OF SURFACE FIELDS OVER THE INDIAN OCEAN DURING ABOVE AND BELOW NORMAL MONSOONS

P.K. Mohanty1 and S.K. Dash2 (1). Marine Science Department, Berhampur University, Berhampur - 76007, Orissa, India (2)Centre for Atmospheric Sciences, Indian Institute of Technology, Delhi, Hauz Khas, New Delhi - 110016, India

Surface fields over the tropics experience oscillations due to solar radiative forcing which contains strong periodicities at annual and semiannual frequencies. Therefore, spectral analysis, an illustrative climate diagnostic tool, and variance, a well known statistical indicator of space-time variability have been employed on sea surface temperature, mean sea level pressure, zonal and meridional wind stress, latent and sensible heat fluxes for four regional domains in the Indian ocean, viz: 1) Arabian Sea, 2) Bay of Bengal, 3) South China Sea and 4) Southern Indian Ocean. Composites of monthly mean, variance, power spectra and cross spectra (Coherence and phase) of the above mentioned surface fields are computed for the below normal (1985, 1986, 1987) and normal/above normal (1988, 1989, 1990) monsoon years. Data for this study consist of the daily uninitialised data (0 UTC) of European Centre for Medium Range Weather Forecasts (ECMWF) for the period 1985 to 1990, FSU observed ship data and NCAR COADS climatology. Time series of surface fields for the composite years of below and above normal monsoons shows the evolution of the surface fields during the course of the annual cycle. However, the contrasts in the monsoons are not well reflected in the composite time series of the surface fields except for latent and sensible heat fluxes. The characteristics of the composite time series are consistent with composite power spectra of the surface fields. Power spectra show that oscillations of the surface fields are explicitly in the annual and semiannual bands in the four regional domains except over the Southern Indian Ocean, where the oscillations are confined to the annual band only and with relatively weak amplitude. Semiannual cycle is predominant in the latent and sensible heat fluxes while the rest of the surface fields exhibit strong annual cycle. The amplitude of annual and semiannual cycles differ from one regional domain to the other and thus there is a distinct role of each regional domain in the monsoon variability. Interestingly, the contrasts in the monsoons are very well reflected in the variance of the surface fields.

Wednesday 28 July AM

### SEASONAL-DECADAL VARIABILITY

**JSP25/W/64-B3** Poster **0830-01**

### VARIABILITY OF THE KUROSHIO VIEWED BY TWO-YEAR-LONG DIRECT CURRENT MEASUREMENTS SOUTH OF JAPAN

Shin-ichiro UMATANI, Motohiko Kashima, Shiro Imawaki (all at Research Institute for Applied Mechanics, Kyushu Univ., Kasuga, 816-8580, Japan, email: umatani@riam.kyushu-u.ac.jp) Hiroshi Uchida (Japan Science and Technology Corporation, Japan), Hiroshi Ichikawa (Kagoshima Univ., Japan), Masao Fukasawa (Tokai Univ., Japan) and ASUKA Group

The Kuroshio, the western boundary current of the North Pacific subtropical gyre, is known as one of major components controlling the earth climate system. A group called ASUKA (Affiliated Surveys of the Kuroshio off Cape Ashizuri) carried out oceanographic observations of the Kuroshio to obtain a long time series of the transport on the basis of direct current measurements. The survey was carried out along a line called ASUKA-line, crossing the Kuroshio from Shikoku coast to 25 °N, during 1993 - 1995. Nine mooring stations were maintained along the line. The shallowest current meter of each station was set nominally at 700 m depth. We also set current meters nominally at depths of 1500 and 3000 m and near the bottom on continental slope. CTD observations were carried out 42 times along the ASUKA-line during the period.

Velocity records from current meters at 700 m nominal depth show remarkable variability which well agrees with north-south movement of the Kuroshio, related to eastward propagation of a small meander of the Kuroshio observed by hydrographic surveys in the upstream region. Temperature of the Kuroshio axis at 650 m depth is estimated to be about 8 °C from temperature and velocity records. The variation of volume transport per unit depth of the Kuroshio, integrated from the coast to the offshore edge of the eastward Kuroshio surface flow, is estimated at depths of 650, 1500 and 3000 m. The shallower two are correlated in some extent with each other but are not correlated with the deepest.

JSP25/W/93-B3 Poster 0830-02

**INTERCOMPARISON OF THE CLIMATIC AND FLUX-DERIVED TEMPERATURE AND SALINITY UPPER LAYER FIELDS IN THE NORTH ATLANTIC**

L.E. AMETISTOVA (1), S.K. Gulev (2), S.A. Dobroliubov (1) (1) Department of Oceanology, Moscow State University, email: diord@ocean.geogr.msu.su (2) (2) P.P. Shirshov Oceanology Institute, Moscow, Russia

The role of air-sea interaction in heat and water budgets in the North Atlantic is examined using temperature and salinity data derived from Levitus Atlas98 and flux fields from NCEP/NCAR Reanalysis data. Four regions in the North Atlantic were taken to represent Gulf Stream (subtropical gyre), Labrador Sea (subpolar gyre), area between the two gyres and the region of Norwegian Current. Mean water temperature TLEV and salinity SLEV of a layer of 250 m were compared to the temperature TCOMP and salinity SCOMP derived from heat and (evaporation-precipitation-river runoff) fluxes on seasonal and interannual scales. TCOMP follows the pattern of TLEV but with greater amplitude. Warmer winters and cooler summers would be observed in all four regions (especially in the Labrador Sea) in case of air-sea interaction as the only term in heat energy budget equation. Heat advection and heat storage changes smooth temperature seasonal cycle. Time-series of salinity and (evaporation-precipitation-river runoff) flux have strong negative correlation in the two gyres. It is most vividly expressed during the Great Salinity Anomaly with smaller values of salinity and predominance of precipitation over evaporation in the subtropical gyre.

JSP25/W/32-B3 Poster 0830-03

**WAVELET ANALYSIS OF LOW FREQUENCY GLOBAL OCEAN VARIABILITY FROM MULTIPLE DATA SOURCES**

O. ANDERSEN (National Survey, Geodetic Division, Copenhagen, Denmark, email: oa@kms.dk) N. L. Bindoff (Antarctic CRC, Hobart, Tasmania, Australia); R. Coleman (University of Tasmania, Hobart, Tasmania, Australia, and at CSIRO Marine Research, Hobart, Tasmania, Australia)

Long period, long-wavelength variations in sea level can be investigated by expanding the sea level variations in low degree spherical harmonic terms. have then been investigated for their using wavelet analysis. The complex Morlet wavelet enables an investigation of characteristics in time of the low degree spherical harmonic terms. The wavelet analysis technique enables a study of the evolution of scales and frequencies with time, and can be used for the identification of the driving forces and their changes with time. The most important physics contributing to the annual and semi annual changes in sea-level change on global space scales, appear to be the wind driven barotropic response and steric sea level changes caused by seasonal solar radiation in the mixed layer.

For the present investigation the low frequency sea level changes have been investigated using the first 6.5 years of TOPEX/POSEIDON altimetry spanning 230 repeats of altimetry. By comparing with long-wavelength height field calculated from NCEP SST and heatflux data, height fields calculated from surface wind data using a simple Sverdrup model, and finally SSH fields of the 1/4 degree WOCE Parallel Ocean Climate Model (Semtner/Chervin) (Stammer, et al., 1996) information on the role of the wind and the heat fluxes on this time and space scales can be gained.

JSP25/W/34-B3 Poster 0830-04

**ANNUAL AND INTER-ANNUAL VARIATIONS IN SEA LEVEL, ATMOSPHERIC PRESSURE AND SEA SURFACE TEMPERATURE FROM SATELLITES**

Per Knudsen and Ole Baltazar Andersen (both at National Survey and Cadastre, Copenhagen NV, Denmark, email: pk@kms.dk, oa@kms.dk)

The sea level is monitored globally from satellites. Five years of atmospheric pressure observations, sea surface temperature data and sea level height for the same period is analysed. Altimetry from the TOPEX/POSEIDON satellite will be used along with low resolution averaged sea surface temperature data from the ATSR 1 and 2 sensor onboard the ERS satellites and AVHRR data from the NOAA satellites.

Global and regional characteristics of annual and interannual variations in sea level, atmospheric pressure and surface temperature during the period from 1992-1997 are investigated. Spatial and temporal correlation between the variations in sea level, atmospheric pressure and sea surface temperature are investigated to decide whether the changes in sea level are related to changes in the heat content of the ocean. Similarly, a bivariate coherency analysis of the sea level together with the atmospheric pressure and sea surface temperature observations is carried out at different spatial scales.

JSP25/W/42-B3 Poster 0830-05

**SEASONAL AND YEAR-TO-YEAR OCEANOGRAPHICS VARIABILITY IN THE NORWEGIAN-GREENLAND REGION**

A. KORABLEV, (Arctic and Antarctic Research Institute, 38, Bering str., St Petersburg, Russia 199397. E-mail: aakor@aari.nw.ru.)

Mean seasonal and year-to-year oceanographic characteristics time series were obtained from historical data base for six regions in the Norwegian-Greenland Seas. Irregularity of the characteristics variability is under the influence of large-scale anomalies and convection activity. The water salinity distribution in the upper layer of the Norwegian and the Greenland Seas is the most typical indicator of the spreading influence of Atlantic and polar water. During GSA'70s passing the mean salinity of upper layer decreasing and not reach the previously value that has a profound influence on the convection activity reduction. Large salinity anomaly were registered early but have not such global consequences. Current system and interannual variability comparison allow to make conclusion that GSA'70s propagation was by to ways: along frontal system and with Norwegian current. Speed of movement and depth level with high anomaly intensity were different. Distributions of temperature, salinity, dissolved oxygen concentration and density seasonal changes for different regions of the Norwegian and Greenland Seas indicate the time of extremums approach at depth levels. Dissolved oxygen concentration and saturation can be used as an index of convection stage. Interannual variability of the oxygen concentration in the different layers of the southern part of the Norwegian Sea is a useful parameter for convection intensity estimation in the Iceland and Greenland Seas.

JSP25/W/25-B3 Poster 0830-06

**INTERANNUAL VARIABILITY OF WATER MASS DISTRIBUTION AND WATER AND HEAT TRANSPORTS ON 37-N OBSERVATION LINE**

Shin-ichi ITO, Osamu Kato and Yugo Shimizu (all at Tohoku National Fisheries Research Institute, Shinhama Shioyama 985-0001, Japan, email: goito@myg.affrc.go.jp); Tomomi Takayama (Shin-Nippon Meteorological & Oceanographical Consultant Co. Ltd., Tamagawa Setagaya, Tokyo, Japan, email: tomomi@notes.metocean.co.jp); Hiroshi Yoshinari and Kensuke Takeuchi (both at Graduate School of Environmental Earth Science, Hokkaido University, Sapporo 060-0810, Japan, email: utatane@ees.hokudai.ac.jp); Ichiro Yasuda (Faculty of Science, Tokyo University, Hongo, Bunkyo 113-0033, Japan, email: ichiro@geoph.s.u-tokyo.ac.jp)

To clarify the interannual variability of water mass distribution and water and heat transports in the Inter-frontal Zone between Oyashio and Kuroshio Fronts in the North Pacific, we analyzed a hydrographic data along the 37-N observation line (extends to 164-E at least) during 1983-1996. Mean structure showed warm water region at 144, 148, 152, 157, 165-E and the variability is relatively high in the warm water region. We applied EOF analysis for historical temperature data and as a result EOF1 (27.2%) showed high amplitude at 144-E and its time variability is consistent with that of 1st crest of the Kuroshio Extension. EOF3 (13.0%) showed whole domain variation and its time variability showed longer period variation with transitions in 1988-1989. After 1989, the zonal inclination of main thermocline lost the steepness. We also estimated the water and heat transports on 37N in 1992-1996 and 1998. Both transports increased rapidly in 1998. The increase of transports again associated with the increase of the zonal inclination of the main thermocline.

JSP25/W/21-B3 Poster 0830-07

**CLIMATIC CHANGES OF SEASONAL CYCLE OF SST IN THE NORTH PACIFIC**

Igor ZVERYAEV (IPRC, SOEST, University of Hawaii, MSB, Room 227, 1000 Pope Rd., Honolulu, HI 96822, USA, email: igorz@soest.hawaii.edu) Konstantin Selemenov (P.P.Shirshov Institute of Oceanology, RAS, Nakhimovskiy Ave. 36, Moscow 117851, RUSSIA, email: selko@gulev.sio.rssi.ru)

Climatic changes in seasonal cycle of sea surface temperature (SST) in the North Pacific during 1951-1995 are studied. These changes are discussed in terms of pentadal anomalies of characteristics of annual and semiannual cycles as well as of anomalies of annual, winter and summer means. Anomalies of annual and seasonal means clearly indicate North Pacific climate shift of mid 70-ties. Quasi-decadal changes are more noticeable before climate shift. Before 1971, anomalies of annual amplitudes tend to result in anomalies of annual means of the same sign, later - in anomalies of opposite sign. It is found out that these changes are due principally to different roles of seasonal anomalies in the formation of the annual cycle of SST. Before 1971, anomalies in annual cycle are defined by summer anomalies. Later, winter anomalies play a leading role in the formation of annual cycle. We note that this switch from the governing role of summer anomalies to that of winter anomalies takes place prior to the North Pacific climate shift.

Comparative analysis of anomalies of annual and semiannual cycles has revealed that enhanced (reduced) annual cycle does not necessarily result in enhanced (reduced) semiannual cycle. I.e. positive anomalies of semiannual cycle can be related both to positive and negative anomalies of annual cycle. The same is true about negative anomalies of the semiannual cycle.

JSP25/E/37-B3 Poster 0830-08

**INTRA-ANNUAL VARIABILITY IN THE DEEP BOTTOM BOUNDARY LAYER OF THE NORTH TROPICAL PACIFIC OCEAN**

Tatiana Demidova (P.P.Shirshov Institute of Oceanology, Moscow, RUSSIA email: evita@redline.ru)

Intra-annual (synoptic and seasonal) current variability and estimates of horizontal mean and fluctuating kinetic energy (MKE and FKE) in the deep-water bottom boundary layer of the Tropical Pacific ocean are considered on the basis of 1 to 2-year time-series from groups of subsurface moorings within two test areas. Data were collected in frameworks of international projects during 1991-1995. The work was fulfilled as a part of the baseline studies aimed to evaluation and prediction of long-term hydrodynamic conditions in the near-bottom layer and in the upper water column in the region of planned deep-water mining.

Quite a stable long-term direction of the near-bottom water flow, controlled, in most cases, by main floor topographic elements, is found. Intraannual-scale spectra were analyzed. Contribution of synoptic as well as meso-scale components in the total fluctuating kinetic energy are estimated. From filtered data, time series of MKE and FKE components are constructed, and time variability of synoptic components of kinetic energy at various levels and in space are analyzed and discussed. Peaks of synoptic-scale fluctuating energy are associated with specific seasonal time periods varying from area to area, and very often they are related to the late fall-winter seasons. There is evidence that high level of synoptic variability in the bottom layer closely associated with synoptic activity on the surface. The comparison of the evaluating current velocity and kinetic energy parameters for different moorings and levels above the bottom contributes in parametrization of synoptic and seasonal processes in high resolution circulation models.

Thursday 29 July AM

DECADAL- CENTENNIAL OCEAN/ATMOSPHERIC VARIABILITY

JSP25/W/68-B4 Poster 0930-01

**DECADAL VARIABILITY IN A COUPLED ATMOSPHERE-OCEAN CIRCULATION MODEL OF MODERATE COMPLEXITY**

Dörthe HANDORF, Klaus Dethloff, and Antje Weisheimer (all at Alfred Wegener Institute for Polar and Marine Research, Telegrafenberg A43, 14473 Potsdam, Germany, e-mail: dhandorf@awi-potsdam.de); Vladimir K. Petoukhov (Obukhov Institute of Atmospheric Physics, Russian Academy of Sciences, Moscow)

In order to improve our knowledge of the influence and extent of internal processes in generating atmospheric variability on time scales of years and decades two 1000 year long integrations of a coupled atmosphere-ocean circulation model of moderate complexity have been performed. This model resolves explicitly the basic features of the large-scale long-term atmospheric and oceanic variables, including the tropo-, strato- and mesosphere, whereas all synoptic-scale processes are parameterized. The main large-scale features of atmospheric circulation have been simulated in agreement with observations. The first run has been performed with the fully coupled model, whereas in the second run the atmosphere is driven by prescribed seasonally varying sea surface temperatures (SST). The combined analyses of both runs reveal strong decadal and interdecadal atmospheric climate variations especially about 9 and 30 years, which show a significant shift from century to century. These modes of variability have been determined by investigations of fields of streamfunctions and



## INTER-ASSOCIATION

temperatures and of the North Atlantic oscillation by means of methods of multivariate statistics and of sophisticated time-frequency analyses (wavelet transformation). The comparison of the coupled with the SST-forced run leads to the conclusion, that the decadal and interdecadal climate variations are forced by nonlinear atmospheric processes and reinforced by oceanic processes.

**JSP25/W/75-B4** Poster **0930-02**

### IS THE ADJOINT METHOD AN APPROPRIATE TOOL TO STUDY CLIMATE VARIABILITY ?

M.JUNGE and T.W.N.Haine, AOPP, University of Oxford, Atmospheric, Oceanic and Planetary Physics, Clarendon Laboratory, Parks Road, Oxford OX1 3PU, UK, e-mail: mmj@atm.ox.ac.uk

A focus of current research in understanding decadal climate variations is the interaction between the atmosphere and the ocean. In order to disentangle these connections we study sensitivities of the upper ocean to the overlying atmosphere on all time scales up to decades. To do so we employ an OGCM (MICOM) in the North Atlantic Domain. Scalar functions such as SST, thermocline depth, upper ocean heat content and gulf stream transport, that comprise the ocean state, are calculated. The adjoint of the OGCM then gives the change in atmospheric conditions due to a change in the scalar function, i.e. the sensitivity of this scalar function to changes in atmospheric forcing.

**JSP25/W/33-B4** Poster **0930-03**

### DECADAL VARIABILITY OF THE ATMOSPHERE IN A COUPLED GLOBAL CIRCULATION MODEL

Antje WEISHEIMER, Klaus Dethloff and Dörthe Handorf (all at Alfred Wegener Institute for Polar and Marine Research, Telegrafenberg A43, 14473 Potsdam, Germany, e-mail: weisheim@awi-pots-dam.de)

Variations of the atmospheric circulation can be caused by external and internal processes. Whereas recently the meaning of external factors had been investigated in detail, the influence and extent of internal processes in generating natural low-frequency atmospheric variability on time scales of years and decades is not very well understood yet.

In this paper we are going to show the results of a 1000-year integration of the coupled general circulation model ECHAM3-T21-LSG without time dependent external forcing except the seasonal cycle in solar insolation. The long-term run was carried out at the MPI for Meteorology in Hamburg. The study is based on monthly mean data of stream functions and temperatures at the surface, in the free troposphere and the lower stratosphere. The structure of the ultra-low-frequency variability with and without seasonal cycle has been investigated by means of EOF and wavelet analysis. The most important EOFs reproduce the spatial structure of the standard deviations, whereas the EOF of higher order reflect the influence of teleconnection patterns on generating atmospheric variability. The power and wavelet spectra of the PC which describe the temporal behaviour of the corresponding spatial patterns have been calculated. They show well pronounced variability on the decadal time scale. Preferred periods exist, especially around 11, 18 and 35 years, changing within the centuries.

**JSP25/W/38-B4** Poster **0930-04**

### LOW-FREQUENCY VARIABILITY IN LOW-ORDER-MODELS OF THE ATMOSPHERE

Antje WEISHEIMER, Klaus Dethloff, Dörthe Handorf and Annette Rinke (all at Alfred Wegener Institute for Polar and Marine Research, Telegrafenberg A43, 14473 Potsdam, Germany, e-mail: weisheim@awi-potsdam.de); Mikhail V. Kurgansky (Obukhov Institute of Atmospheric Physics, Russian Academy of Sciences, Moscow)

Besides the study of external influences on the climate system an improved understanding of atmospheric long-term variations requires also the investigation of internally generated, mostly nonlinear mechanisms of atmospheric dynamics. Because of the limited length of direct measurements of climate variables and temporal as well as spatial inhomogeneities in paleoclimatic data series, long-term integrations of appropriate models with fixed external forcing, however, seem to be one possible way to approach this problem. Analyses of the model's natural low frequency variability on time scales of decades up to centuries might give hints on the behaviour of the real atmosphere. We investigated this problem by running three quasi-geostrophic Low-Order-Models (LOM) of the atmosphere: a one-, a two- and a three-layer LOM with different horizontal resolutions. These models consider nonlinear interactions between the zonal flow, thermally and orographically forced planetary waves and short baroclinic waves. They have been integrated over 1,000 to 10,000 years. The structure of low-frequency variability has been analysed by means of EOF and wavelets. The models reproduce variability on intraseasonal, decadal and even centenary time scales suggesting that the multiscale natural variability is caused by deterministic interactions between the model components and internally driven by short time-scale instabilities and nonlinearities connected with large-scale atmospheric processes.

**JSP25/W/18-B4** Poster **0930-05**

### TEMPERATURE VARIABILITIES IN THE NORTH PACIFIC GENERATED BY MOVEMENTS OF WIND-STRESS ZERO LINE

Yoshio MASUDA and Moto Ikeda (Division of Ocean and Atmospheric Science, Graduated School of Hokkaido University, Sapporo, JAPAN, email: masuda@ees.hokudai.ac.jp)

One and a half layer PE and QG models are used to study decadal temperature variabilities in the north Pacific. In the previous studies southward Ekman transport, air-sea heat flux, and mixed-layer development were suggested to be important for the decadal variabilities. In this study, the effects of curl  $\tau_{\theta=0}$  line movement on the decadal temperature variabilities is investigated. The models are driven by the wind stress which forces the symmetric double-gyre circulation in a rectangular domain. The models retain two mechanisms which can infer temperature variability in the Pacific. One is an interface movement, propagating as a forced Rossby wave, whose zonal wavelength is as long as the longitudinal lengths of the model domains. This wave has some similarity with the observed SST variabilities reversed between the central Pacific and more eastern region. The other mechanism is a cross-gyre transport, which is realized by passive tracers left in the models. When the curl  $\tau_{\theta=0}$  line moves southward, some tracers flowing eastward cross the gyre boundary and penetrate into the subarctic gyre, in particular, near the eastern boundary. This northward movement is consistent with a warm anomaly observed in the Gulf of Alaska. The oscillation of the curl  $\tau_{\theta=0}$  line is the most effective to the temperature variabilities at decadal time scales.

**JSP25/E/31-B4** Poster **0930-06**

### THE THREE-CENTURY CLIMATIC UPHEAVAL OF C. 2000 BC, AND REGIONAL RADIOCARBON DISPARITIES

Douglas J. KEENAN (The Limehouse Cut, London E14 6NQ, U.K.; email: doug.keenan@virgin.net)

Several researchers have previously identified a severe climatic up heaval in tropical North Africa that began just over 4000 years ago and lasted for about three centuries. The upheaval is known to have occurred shortly after a volcanic eruption, and companion work proposes that this eruption was colossal. Here, we suggest how the eruption acted as a trigger for the upheaval: by forcing changes in ocean circulation; although the initial (atmospheric) forcing lasted only a few years, the ocean required three centuries to regain equilibrium. The suggested triggering mechanisms supported by palaeoceanographic, palaeoecological, and archaeo-historical data and by related experiments with a (coupled general-circulation) climate model. We argue that the changes in ocean circulation forced changes in sea-surface temperatures that led to a weakening of the south-west North African monsoon. The upheaval has been proposed to have also encompassed south-western Asia. We argue that it encompassed most of the Northern Hemisphere: we present a variety of palaeoecological and palaeoceanographic evidence and describe the principal underlying climatology. In some areas the upheaval was the most severe since the ice ages. The full scope of the upheaval has previously been missed in part because radiocarbon dates from some areas are centuries too early: palaeoclimatic events in different areas thus appeared asynchronous. (The erroneous radiocarbon dates also misled searches seeking ice-core and tree-ring evidence of the eruption.) The cause of the radiocarbon- dating disparities is identified as a regional deficiency in  $^{14}\text{C}$ , and we locate its source of  $^{14}\text{C}$ -deficient carbon. (An extended version of this abstract will be at <http://freespace.virgin.net/doug.keenan>.)

**JSM26** Monday 26 – Wednesday 28 July

### CHEMISTRY AND TRANSPORT IN THE UPPER TROPOSPHERE AND LOWER STRATOSPHERE (IAMAS, IAVCEI, SPARC)

Location: Mechanical Engineering G31 LT  
Location of Posters: Old Gym

Monday 26 July AM

Presiding Chair: T G Shepherd (Atmospheric Physics Group, Univ. of Toronto, Canada)

**JSM26/E/20-B1** Invited **0830**

### TRANSPORT IN THE LOWER STRATOSPHERE

R. Alan PLUMB (Massachusetts Institute of Technology, Cambridge, MA, USA)

Exchange between troposphere and stratosphere is to a large degree controlled by the large-scale circulation, even though individual transport "events" may occur on smaller scales. Factors controlling the mean meridional circulation will be discussed, especially those that might determine the structure and intensity of lower stratospheric upwelling. Subtle, and poorly understood, aspects of the tropical angular momentum balance may be crucial in determining the relative importance of extratropical wave drag, tropical wave drag, and diabatic heating (in both stratosphere and troposphere). I will also discuss what observations of lower stratospheric tracers, including "age", might tell us about the impact of local (extratropical) stratosphere-troposphere exchange on tracer budgets in the lowermost stratosphere.

**JSM26/W/06-B1** **0900**

### LONG-LIVED FLUORINATED COMPOUNDS AS TRACERS OF THE AGE OF STRATOSPHERIC AIR

WT STURGES, DE Oram, SA Penkett (School of Environmental Sciences, University of East Anglia, Norwich NR4 7TJ, UK, email: w.sturges@uea.ac.uk) PJ Fraser (Division of Atmospheric Research, CSIRO, Private Bag 1, Mordialloc, Victoria 3195, Australia, email: pjf@dar.csiro.au) A Engel (Institute für Meteorologie und Geophysik, J.W.Goethe Universität Frankfurt, D 60325 Frankfurt, Germany, email: a.engel@meteor.uni-frankfurt.de)

Long lived halocarbons have been measured in air collected with a balloon-borne cryogenic sampler at altitudes from the tropopause to 7 hPa (c. 33 km) during flights from the Arctic and Northern mid-latitudes. The compounds measured include C2F6, C3F8, c-C4F8-, CFC-13, CFC-114, CFC-115, SF6 and HFC-23. These compounds have estimated stratospheric lifetimes between several hundred years and ten thousand years, making them potentially ideal tracers of transport to the stratosphere. Shorter-lived HFCs were also measured. Corresponding measurements of the same gases in the Cape Grim, Tasmania air archive allow a direct comparison between stratospheric and tropospheric measurements. C2F6 appears to be an ideal age-of-air tracer in the stratosphere, and agrees well with SF6-derived dates. Air ages at and just above the tropopause appear to be almost contemporaneous with the troposphere. Ages then rapidly increase up to about 20hPa, above which there is little further change in age. Ages at 20hPa are around six to seven years. Atmospheric trends for the other compounds can be reconstructed from the stratospheric profiles to give histories covering more than 10 years (from 1987). The trends are not always consistent with the Cape Grim archive (notably HFC-23 and c-C4F8) suggesting larger stratospheric loss terms than given by current estimates. (This replaces abstract Reference 011528)

**JSM26/W/05-B1** **0920**

### TRANSPORT INTO THE NORTHERN HEMISPHERE LOWERMOST STRATOSPHERE REVEALED BY IN SITU TRACER MEASUREMENTS

Eric A. Ray (1), (2), Fred L. Moore (1), (2), James W. Elkins (1), Geoffrey S. Dutton (1), (2), David W. Fahey (3), Holger Vömel (1), (2), Samuel J. Oltmans (1) and Karen H. Rosenlof (2), (3) (1) NOAA/Climate Monitoring and Diagnostics Laboratory, Boulder, CO (2) Co-operative Institute for Research in Environmental Science (CIRES), Boulder, CO (3) NOAA/Aeronomy Laboratory, Boulder, CO.

The Lightweight Airborne Chromatograph Experiment (LACE) has made in situ measurements of several long-lived trace gases in the upper troposphere and lower to middle stratosphere as part of the Observations of the Middle Stratosphere (OMS) balloon platform. The tracers measured by LACE include several photolytic species (CFC-11, CFC-12 and halon-1211) as well as SF6. LACE measurements of these long-lived tracers as well as nearly simultaneous measurements of water vapor and CO2 are used to investigate transport into the lowermost stratosphere, a region where few in situ measurements exist. The measured photolytic species and water vapor are used in a simple mass balance calculation to estimate the mixture of

tropospheric and overworld ( $\theta > 380$  K) air in the lowermost stratosphere. In the northern mid-latitudes during September 1996 most of the air in the lowermost stratosphere sampled at the flight location (34.5N) was transported quasi-isentropically from the troposphere. Measurements from both a May 1998 mid-latitude flight and a June 1997 high latitude flight (64.5N) revealed the air sampled in the lowermost stratosphere to be dominated by downward advection from the overworld. SF<sub>6</sub> and CO<sub>2</sub> can uniquely reveal time and spatial scales of transport due to these species' large growth rates and subsequent latitudinal surface and free tropospheric gradients. Measurements in the lowermost stratosphere from the September northern mid-latitude flight coupled with surface measurements of these species revealed a transport time scale of no more than 1.5 months from the surface to the lowermost stratosphere. The SF<sub>6</sub> and CO<sub>2</sub> mixing ratios were also consistent with mostly Northern Hemisphere tropospheric air in the lowermost stratosphere. These results point out the usefulness of high-resolution in situ measurements of long-lived tracers to help determine time and spatial scales of transport in the region of the upper troposphere and lowermost stratosphere.

JSM26/W/11-B1

0940

#### TRANSPORT CHARACTERISTICS AND AGE OF AIR IN THE LOWER STRATOSPHERE: SIMULATIONS WITH A 3-D MODEL

W. GROSE, R. Eckman, J. Al Saadi, R. Pierce (NASA LaRC, Hampton, VA, 23681, USA, email: w.l.grose@larc.nasa.gov), D. Fairlie (STC, Hampton, VA 23681, USA) G. Lingenfelter (SAIC, Hampton, VA, 23681, USA)

A multi-year simulation has been conducted with a general circulation model (IMPACT) with coupled radiation, chemistry, and dynamics. IMPACT is a primitive equation, spectral model extending from the surface to approximately 90 km (34 levels). Gas-phase and heterogeneous chemical reactions have been incorporated with 24 species (families) explicitly transported. Discussion will focus on age of air and transport in the lower stratosphere based upon analysis of the model distributions of long-lived species. The age of air spectrum from the model will be compared with that deduced from observations. Diagnosis of the model transport will focus on a modified Lagrangian-mean analysis (developed by Nakamura) of the long-lived species, calculating "equivalent length" distributions for the tracer. Minima in equivalent length occur in polar and subtropical "barrier" regions where the lateral mixing is inhibited. Seasonal evolution of these minima will be presented. Correlation between long-lived species in the model will be compared with similar results from ER-2 airborne data to further evaluate the model transport.

JSM26/W/12-B1

1000

#### A THREE-DIMENSIONAL MODEL SIMULATION OF TRANSPORT OF SEASONALLY VARYING AND LONG-LIVED TRACERS INTO THE LOWER STRATOSPHERE

Lori BRUHWILER (Climate Monitoring and Diagnostics Laboratory, R/E/CG1 325 Broadway, Boulder CO, 80303, USA, email: lbruhwiler@cmdl.noaa.gov); Kevin Hamilton (Geophysical Fluid Dynamics Laboratory, Princeton Forrestal Campus, Rt. 1, Princeton, NJ 08540, USA, email: kph@gfdl.gov)

Due to its seasonal variation, CO<sub>2</sub> is an excellent tracer of transport from the troposphere to the lower tropical stratosphere, and subsequently to the extratropics. Three-dimensional model calculations of CO<sub>2</sub> and other long-lived trace species will be used to quantify the lower stratospheric transport properties of the GFDL SKYHI general circulation model. The responses of the model circulation and transport to parameterisations of momentum forcing due to gravity wave drag and the equatorial stratospheric quasi-biennial oscillation will also be discussed as well as implications for stratospheric photochemical models.

JSM26/E/08-B1

Invited

1040

#### THE EXTRATROPICAL TROPOPAUSE AS A TRANSPORT BARRIER

Peter HAYNES, (Centre for Atmospheric Science, DAMTP, Silver Street, Cambridge, CB3 9EW, United Kingdom, email: phh@damtp.cam.ac.uk)

It has been suggested that there are useful analogies between the extratropical tropopause and the edge of the polar vortex in the stratosphere, in that both are marked by a sharp gradient in potential vorticity and that both appear to act as a partial barrier to transport. These analogies will be discussed in this talk and the implications for our current understanding of the tropopause and stratosphere-troposphere exchange assessed. Two particular aspects will be discussed.

Numerical simulations (performed in collaboration with J. Scinocca) have shown that a quasi-realistic, statistical equilibrium tropopause may form in a simplified numerical model solely through the spatially inhomogeneous stirring of the baroclinic eddies, without any contribution from convection, for example (The mechanism is much the same as that which forms a sharp edge to the polar vortex through the action of Rossby-wave breaking.). At upper levels the stirring is confined in latitude and a sharp edge forms in the potential vorticity field. This is seen as corresponding to the subtropical tropopause. At lower levels there is no latitudinal limit to the stirring. There is a sharp jump in the vertical between the two stirring regimes and this gives rises to a quasi-horizontal tropopause at higher latitudes.

Analysis of the transport properties of isentropic velocity fields from observational datasets, using the 'effective diffusivity' diagnostic (work in collaboration with E. Shuckburgh), has clearly shown the tropopause as a partial barrier to transport on isentropic surfaces and revealed its vertical structure and seasonal evolution. The definition of the tropopause as a transport barrier, e.g. through effective diffusivity, is argued to be the most general and natural definition and is contrasted to more conventional definitions such as by a particular value of potential vorticity.

JSM26/W/30-B1

1110

#### NONLINEAR INTERACTION OF SYNOPTIC-SCALE ROSSBY WAVES AND THE GEOGRAPHIC DISTRIBUTION OF LATERAL TRANSPORT CHANNELS IN THE LOWERMOST STRATOSPHERE

HORINOUCI, T (Department of Atmospheric Science, University of Washington, Seattle, Washington 98195-1640 USA, email: horinout@atmos.washington.edu)

The equatorial westerly duct over the central and eastern Pacific, where the upper tropospheric wind is westerly due to the Walker circulation, is known to allow cross-equatorial propagation of synoptic-scale Rossby waves. By using the middle atmosphere version of the NCAR CCM3 GCM, synoptic scale waves are shown to vigorously propagate to reach the equator through the stratospheric tail of the Pacific westerly duct. Similar propagation is also active though the other westerly duct over the Atlantic. The interaction between these waves and the Walker circulation creates an interesting east-west asymmetry of the potential vorticity (PV) anomalies flanking the westerly flow of the ducts. While persistent wave breaking blurs the PV gradient on west side of an anomaly, the gradient is intensified on the east side. The result is an opening of a PV window which allows air mass exchange between the tropics and the subtropics. This exchange is explained theoretically and demonstrated with a barotropic

model. Trajectory calculations over a boreal winter reveal that the lateral transport between the tropics and the subtropics in the lowermost stratosphere is confined to the vicinity of the westerly ducts especially in the northern hemisphere. On the west-side of the PV anomalies are channels for transport from higher to lower latitudes, while on the east side are those from lower to higher latitudes. These features are consistent with the time-averaged flow, the geographical distribution of wave breaking, and the typical time-dependent flow pattern associated with breaking.

JSM26/W/22-B1

1130

#### STRATOSPHERIC INFLUENCE ON TROPOPAUSE HEIGHT

John THUBURN and George C Craig (Department of Meteorology, University of Reading, Whiteknights, Reading, RG6 6BB, UK, email: swsthubn@met.rdg.ac.uk)

Assuming an approximate balance between absorption of thermal IR radiation upwelling from the troposphere and local emission near the tropopause leads to a minimal quantitative model relating tropopause height to other factors such as tropospheric lapse rate and surface temperature. This minimal model, however, neglects solar heating and dynamical warming or cooling near the tropopause. An extended version of the minimal model including these non-IR warming processes will be presented. It predicts a sensitivity of tropopause height to non-IR warming of a few km per (K/day), with positive warming leading to a lower tropopause. Sensitivities comparable to this are found in GCM experiments in which imposed changes in the ozone distribution or in the driving of the stratospheric residual mean circulation lead to changes in tropopause height.

JSM26/W/32-B1

1150

#### DIAGNOSING STRATOSPHERE-TROPOSPHERE EXCHANGE

Andrew GETTELMAN and Adam H. Sobel, (Department of Atmospheric Sciences, University of Washington, Seattle, WA, USA, email: andrew@atmos.washington.edu)

This study discusses the direct diagnosis of stratosphere-troposphere exchange using different methods. The method introduced by Wei (1987) is applied to the GEOS-1 assimilated data set. A global picture of stratosphere-troposphere exchange for three complete years is presented, from the synoptic scale to the monthly averaged global flux. The same data is also used to derive the net stratosphere-troposphere exchange using monthly averaged mass budgets. We make a detailed comparison with the results of other studies using the same methods and different data sets, as well as comparisons with other methods of estimating stratosphere-troposphere exchange. Sensitivity tests and theoretical considerations indicate that the instantaneous two-way exchange may be significantly exaggerated by the Wei method, due to its being rather sensitive to the noise that is invariably present in observed or assimilated data sets. The method becomes somewhat better conditioned as the results are more heavily averaged, but this also reduces the method's ability to diagnose two-way exchange. Additionally, when the flux across various surfaces is averaged over the globe and the entire year, the result implies unrealistically large imbalances in the annually averaged mass budget of the stratosphere. This could be caused by modest biases in the model used to perform the data assimilation. Since pure model simulations have an internal dynamical consistency that is lacking in observed or assimilated data sets, the analysis appears to explain the fairly large discrepancies between the two way fluxes obtained in studies using models and assimilated data sets. It may also explain the discrepancies between the net fluxes obtained by the Wei method and those obtained by other methods.

JSM26/E/22-B1

1210

#### SEASONAL VARIABILITY OF MIDDLE LATITUDE OZONE IN THE LOWERMOST STRATOSPHERE DERIVED FROM PROBABILITY DISTRIBUTION FUNCTIONS

R B ROOD, M C Cerniglia, A R Douglass, L C Sparling, J E Nielsen (NASA's Goddard Space Flight Center, Greenbelt MD, 20771, email: rrood@dao.gsfc.nasa.gov)

We present a study of the distribution of ozone in the lowermost stratosphere with the goal of understanding the relative contribution to the observations of air of either distinctly tropospheric or stratospheric origin. The air in the lowermost stratosphere is divided into two population groups based on Ertel's potential vorticity at 300 hPa. Conditional probability distribution functions are used to define the statistics of the mix from both observations and model simulations. Two data sources are chosen. First, several years of ozonesonde observations are used to exploit the high vertical resolution. Second, observations made by the Halogen Occultation Experiment [HALOE] on the Upper Atmosphere Research Satellite [UARS] are used to understand the impact on the results of the spatial limitations of the ozonesonde network. Despite the differences in spatial and temporal sampling, the probability distribution functions are similar for the two data sources. Comparisons with the model demonstrate that the model maintains a mix of air in the lowermost stratosphere similar to the observations. The model also simulates a realistic annual cycle. By using the model, possible mechanisms for the maintenance of mix of air in the lowermost stratosphere are revealed.

Monday 26 July PM

Presiding Chair: R B Rood (NASA Goddard Space Flight Center, Greenbelt, USA)

#### TRANSPORT, MIXING AND EXCHANGE

JSM26/E/09-B1

1400

#### LONGITUDINAL VARIATIONS OF THE TROPOPAUSE STRUCTURE IN TROPICS REVEALED BY THE GPS OCCULTATION DATA (GPS/MET)

Toshitaka TSUDA and Masahiro Nishida (Radio Atmospheric Science Center, Kyoto University Uji, Kyoto 611-0011, Japan, email: tsuda@kurasc.kyoto-u.ac.jp, nishida@kurasc.kyoto-u.ac.jp) Christian Rocken and Randolph H. Ware (GPS/MET Project, GPS Science and Technology (GST) Program, UCAR, Boulder, CO 80307-3000, email: rocken@unavco.ucar.edu, ware@unavco.ucar.edu)

Temperature profiles in the upper troposphere and stratosphere have been obtained by means of a radio occultation observation of GPS (Global Positioning System) signals (GPS/MET; GPS Meteorology) during April 1995 and February 1997. The GPS/MET profiles have been found to resolve detailed temperature structure, including sharp inversions and the step-wise increase of the temperature gradient near the tropical tropopause. Taking advantage of the global coverage of the GPS/MET data, we have investigated the longitudinal distribution of the tropopause height and the minimum temperature. The results have strongly suggested that GPS/MET have significant potential to contribute to weather prediction and climate change studies.



**JSM26/W/13-B1** **1420****HIGH-RESOLUTION MEASUREMENTS AND MODELLING OF A SUMMER-TIME TROPOPAUSE FOLD**

Andrew O. LANGFORD (NOAA Aeronomy Laboratory, 325 S. Broadway, R/E/AL6, Boulder, Colorado 80303, email: langford@al.noaa.gov) Stephen J. Reid (National Research Council, Washington, DC and NOAA Aeronomy Laboratory, email: sreid@al.noaa.gov) Jean-François Lamarque (National Center for Atmospheric Research, PO Box 3000, Boulder, Colorado 80307, email: lamar@acd.ucar.edu)

Ground-based lidar measurements of ozone and aerosol backscatter vertical profiles above Fritz Peak Observatory near Boulder, Colorado (39.9° N, 105.3° W) are used in conjunction with radiosonde profiles and satellite water vapor imagery to investigate the structure of a stratospheric intrusion over the western United States on July 11-14, 1997. A high-resolution transect of the equatorward-sloping fold is constructed from 2-minute profiles obtained over nearly 24 hours of continuous lidar operation. These data provide a highly detailed view of the cross-sectional structure of the southward sloping fold and show evidence of small-scale mixing of the intrusion with the surrounding tropospheric air. The observations are compared with potential vorticity analyses obtained from ECMWF data and with model output from the NCAR MM5 mesoscale model.

**JSM26/W/27-B1** **1440****EVIDENCE OF EXCHANGE BETWEEN THE TROPOSPHERE AND STRATOSPHERE IN THE REGION OF THE SUBTROPICAL JET STREAM**

C. Timmis, G. Vaughan (Physics Department, University of Wales, Penglais Hill, Aberystwyth, UK, SY23 3BZ, email: crt@aber.ac.uk, gvx@aber.ac.uk), E. Cuevas (INM, email: ecuevas@inm.es), Z. Xiangdong (Chinese Meteorological Administration, China, email: tangj@public.intercom.com.cn)

The ECMWF T106 31 level model analyses indicates the presence of potential vorticity layering in the latitude band of 30N - 40N. This layering occurs between the isentropic levels of 360K - 380K, which lies above and to the north of the subtropical jet wind maxima (350K). Ozone sondes launched within the subtropical region and in particular from Japan are used to determine whether this feature is a real atmospheric phenomenon. To further verify these results, radiosonde profiles are used to detect this feature as layering in static stability. Results indicate that this layering becomes greatest during the spring when the strength of the subtropical jet stream is strongest and thus suggests that the jet stream may be instrumental in the development of this layering and thus possibly may contribute to irreversible mixing between the stratosphere and troposphere.

During July 1996 Tenerife (28.03N, -16.34E) and Xining (36.43N, 101.45E) launched 21 and 27 ozone sondes respectively. Both of these stations are sub-tropical during the summer months and between the isentropic levels of 340K - 400K the increase of ozone is gradual and no clear ozone tropopause is present. The ozone sondes and the model analyses are used to determine the recent origins of the air in the subtropical upper troposphere and lower stratosphere during the summer months. Trajectory analyses indicates that the Asian summer monsoon is important in the subtropical dynamics during the summer.

**JSM26/W/07-B1** **1500****INTERCOMPARISON OF MOZAIC O3 DATA WITH A CTM: SENSITIVITY TESTS**

Hubert Teysseire, Martyn Chipperfield, Kathy Law & Paul-Henri Plantevin (University of Cambridge, Department of Chemistry, Lensfield Road, Cambridge, CB2 1EW, UK, email: hubert.teysseire@atm.ch.cam.ac.uk, Telephone No: +44-1223 336 524, Fax No: +44-1223 336 362)

An ozone tracer has been included in the TOMCAT chemical transport model and the results compared against in-situ MOZAIC measurements obtained from 5 long-range aircraft. TOMCAT is forced by ECMWF analyses for the year 1996 and uses a simple parametrization for ozone chemistry. An ozone climatology is also prescribed at the top and bottom of the model. The agreement between modelled results and MOZAIC observations is generally good, both in the absolute amount of ozone and the spatial/temporal variability. We have performed several sensitivity experiments to evaluate their effect on the comparison. The effect of the O3 top-boundary condition used in the model, the ozone chemistry parametrization itself and the horizontal resolution have been investigated and the results will be presented.

**JSM26/W/20-B1** **1520****RANDOM-WALK ESTIMATION OF A MEAN VERTICAL DIFFUSIVITY IN THE STRATOSPHERE USING TURBULENT PATCHES STATISTICS**

J. Vanneste(1), J.-R. ALISSE(2) and P. Haynes(3) (1) Dept of Mathematics & Statistics University of Edinburgh Mayfield Road, King's Buildings, Edinburgh EH9 3JZ, UK, (2) Service d'Aeronomie du CNRS BP 3 91371, Verrieres-le-Buisson France, email: alisse@aerov.jussieu.fr (3) DAMTP University of Cambridge Silver Street, CB3 9EW Cambridge UK

Small-scale mixing in the stratosphere is mainly concentrated in isolated patches of three-dimensional turbulence, surrounded by nearly laminar flows. This mixing may lead on average to a diffusive effect in the vertical direction on the large-scale tracer fields. However, the spatially intermittent distribution of the mixing makes the computation of a mean vertical diffusivity somewhat delicate. We present here a theoretical derivation of such a mean vertical diffusivity, following the approach suggested by Dewan (1981) and refined in Vanneste & Haynes (1998). The vertical diffusivity is shown to be related to the variance of the vertical displacements of particles of fluids inside the turbulent patches. Taking into account the observational evidence of imperfect mixing inside the patches, we improve the Dewan's approach by introducing a measure of the mixing efficiency inside each patch. Using high-resolution stratospheric profiles of velocities and temperatures obtained from a balloon-borne experiment, we then estimate this diffusivity, as a function of the hypothetical mean life-time of the patches, which is unknown. For plausible values of the lifetime (between 100 and 100000 s), the mean vertical diffusivity typically lies between 0.01 and 0.02 m<sup>2</sup>/s. These values are of the same order as those recently estimated from aircraft measurements.

**JSM26/E/14-B1** **1540****TRAJECTORY STUDIES OF LOW LATITUDE CROSS TROPOPAUSE TRANSPORT USING MODEL AND ANALYSED WIND FIELDS**

D.R JACKSON (UK Meteorological Office, Bracknell, UK, email: drjackson@meto.gov.uk) J. Methven (Dept. of Meteorology, University of Reading, Reading, UK), V.D Pope (UK Meteorological Office, Bracknell, UK)

Simulations made with a 30-level version of the UK Meteorological Office climate model (HadAM3) show that the model simulation of water vapour near the tropical tropopause is in

reasonable agreement with Halogen Occultation Experiment (HALOE) observations. These results suggest that HadAM3 realistically simulate troposphere to stratosphere transport in the tropics. Accordingly, a detailed examination of such transport is made using an off-line trajectory model driven by model winds. Trajectories were run for ten boreal winter seasons. For each season, a cluster of parcels were initialised in the upper troposphere over the main regions of tropical deep convection (Indonesia, central Pacific, South America and Africa), and forward trajectories over a five day period were calculated. Parcels from all four regions ascend over areas of deep convection, and in addition most are transported rapidly in the horizontal by the Hadley circulation to the subtropics, where they subside. An exception is the central Pacific trajectories, which tend to get transported eastwards by the Walker circulation. Interannual variability is predominantly associated with El Nino and La Nina events, and is greatest in the Pacific. Comparison of HadAM3 trajectories with similar experiments in which the trajectories are driven by ECMWF re-analyses (ERA) shows reasonable agreement, although the ERA experiments show more troposphere to stratosphere transport in deep convective regions.

**JSM26/W/33-B1** **Invited** **1620****PHOTOCHEMICAL AND TRANSPORT STUDIES IN THE HIGH-LATITUDE SUMMER STRATOSPHERE**

D. W. FAHEY, (NOAA Aeronomy Laboratory, 325 Broadway, Boulder CO 80303 USA, email: fahey@al.noaa.gov, Telephone No: 303-497-5277 Fax No: 303-497-5373)

Changes in ozone abundance in the Arctic summer stratosphere were addressed as part of the NASA Photochemistry of Ozone Loss In the Arctic Region in Summer (POLARIS) field campaign in 1997. Significant ozone loss occurs in the Arctic summer stratosphere as a result of continuous solar illumination. A wide variety of stratospheric measurements were made from Alaska with balloon and aircraft platforms between spring and fall of 1997. The measurements included reactive species within the nitrogen, hydrogen, and halogen families; longer-lived species such as N<sub>2</sub>O, ClONO<sub>2</sub>, and O<sub>3</sub>; and aerosol size and number. The data have been used along with photochemical models to address the partitioning within the reactive families and the in situ loss rates of ozone. The use of new laboratory measurements of the reaction rate constants of OH with NO<sub>2</sub> and HNO<sub>3</sub> improve the comparison of modelled and measured NO<sub>2</sub> values. Chemical-transport models were also used to examine the contribution of transport to the observed ozone changes. Results from several of these interpretative studies will be given along with a brief overview of the mission.

**JSM26/W/02-B1** **1650****MODELLING THE BREAKUP OF THE ANTARCTIC OZONE HOLE**

SHUHUA LI, Eugene C. Cordero and David J. Karoly (CRC for Southern Hemisphere Meteorology Monash University, Australia, email: sli@vortex.shm.monash.edu.au)

Understanding the distribution and evolution of stratospheric ozone is important for assessing the springtime break-up of the Antarctic ozone hole. A three-dimensional chemical transport model developed at the Co-operative Research Centre for Southern Hemisphere Meteorology is used to study stratospheric constituent distribution and transport. The model is driven by winds from the GASP (Global Assimilation and Prediction system, Bureau of Meteorology, Australia) global analyses, while chemical processes are parameterised using production and loss rates calculated from a two-dimensional photochemical model. A case study for October 1994 is presented to demonstrate model performance in simulating the vortex structure and ozone evolution in the Southern Hemisphere. Preliminary results indicate good correspondence between modelled ozone fields and observations during the springtime break-up of the polar vortex over Antarctica. Mass flux calculations in the lower stratosphere and upper troposphere will be shown to quantify the exchange rates between the polar vortex and mid-latitudes, as well as the tropical/mid-latitude exchange.

**JSM26/W/36-B1** **1710****MIDDLE ATMOSPHERIC TRANSPORT PROPERTIES OF ASSIMILATED DATASETS**

STEVEN PAWSON (1) and Richard Rood (2) (1)USRA, NASA GSFC, Code 910.3, Greenbelt MD 20771, USA, email: pawson@polska.gsfc.nasa.gov (2)NASA GSFC, Code 910.3, Greenbelt MD 20771, USA

One of the most compelling reasons for performing data assimilation in the middle atmosphere is to obtain global, balanced datasets for studies of trace gas transport and chemistry. This is a major motivation behind the Goddard Earth Observation System-Data Assimilation System (GEOS-DAS). Previous studies have shown that while this and other data assimilation systems can generally obtain good estimates of the extratropical rotational velocity field, the divergent part of the dynamical field is deficient; this impacts the 'residual circulation' and leads to spurious trace gas transport on seasonal and interannual timescales. These problems are impacted by the quality and the method of use of the observational data and by deficiencies in the atmospheric GCM. Whichever the cause at any place and time, the 'solution' is to introduce non-physical forcing terms into the system (the so-called incremental analysis updates); these can directly (thermal) or indirectly (mechanical) affect the residual circulation. This paper will illustrate how the divergent circulation is affected by deficiencies in both observations and models. Theoretical considerations will be illustrated with examples from the GEOS-DAS and from simplified numerical experiments. These are designed to isolate known problems, such as the inability of models to sustain a quasi-biennial oscillation and sparse observational constraints on tropical dynamics, or radiative inconsistencies in the presence of volcanic aerosols.

**JSM26/W/23-B1** **1730****CHAOTIC MIXING IN QUASI-PERIODIC FLOWS OF AN IDEALIZED CIRCUMPOLAR VORTEX OF THE STRATOSPHERE**

Ryo Mizuta and Shigeo YODEN (both at Department of Geophysics, Kyoto University, Kyoto, 606-8502, Japan, email: yoden@kugi.kyoto-u.ac.jp)

A high-resolution two-dimensional spherical model is used to investigate the fundamental process of large-scale horizontal mixing in and out of the circumpolar vortex in the winter stratosphere. Concept and analysis method of the chaotic mixing, which were first introduced to geophysical flow by Pierrehumbert(1991) with a simple kinematical model, are applied to some quasi-periodic and non-periodic solutions obtained in the dynamical model. Ishioka and Yoden(1995) obtained quasi-periodic and non-periodic solutions in an idealised stratospheric model of two-dimensional non-divergent fluid with zonally symmetric zonal-flow forcing and Newtonian-type damping. The forced flow is a barotropically unstable polar-night jet and the obtained solutions mimic the eastward travelling planetary waves in the southern hemisphere upper stratosphere. Some of the typical solutions are analysed in this study. Poincare sections for several particles are used to distinguish the regions of chaotic mixing. Dispersion of lots of particles placed in a limited area in the chaotic region shows the



characteristics of two-dimensionalisation from large scales; fractal dimension (correlation dimension) is estimated to describe the time dependence of the mixing process quantitatively. Stagnation points in the stream function field in the co-moving frame with the dominant wave play an important role in the chaotic mixing. Finite-time Lyapunov stability analysis is also done to obtain quantitative confirmation of the role.

## Tuesday 27 July AM

Presiding Chair: A Tuck, (NOAA, Aeronomy Laboratory, Boulder, USA)

### WATER VAPOR AND CLOUDS

**JSM26/L/01-B2** Invited **0930**

#### WATER VAPOR IN THE UPPER TROPOSPHERE AND LOWER STRATOSPHERE IN THE CONTEXT OF DEEP CONVECTION

Dieter KLEY (Institut für Chemie und Dynamik der Geosphäre, Forschungszentrum Jülich D-52425 Jülich, Germany, email: d.kley@fz-juelich.de)

Water vapor in the upper troposphere and lower stratosphere (UT/LS) is of fundamental importance for atmospheric chemistry and the radiative budget of the atmosphere. The fact that the water substance occurs in all three phases, gas, liquid, solid, together with a strong temperature dependence of its vapor pressure, causes water vapor to be extremely variable in the troposphere and to exhibit a strong negative gradient in the vertical. UT/LS water vapor is difficult to measure with high-precision, accuracy and low uncertainty. The fundamental question, which is not answered to the presence, is whether the control of atmospheric water is by thermodynamic or dynamical principles.

The presentation will review published measurements of water vapor in the tropopause region and in the LS, both from in-situ and satellite instrumentation in the context of data precision and accuracy. Long-term measurements of water vapor in the stratosphere by frost point hygrometers reveal that the concentration in the LS increases at a higher rate than can be explained by methane oxidation alone.

We will also report on H<sub>2</sub>O measurements in the UT from instrumentation on board of commercial aircraft from the ongoing MOZIC project from which four years of water vapor and ozone data are available. The analysis that will concentrate on the tropical UT over the Atlantic ocean and the extra tropical North Atlantic region shows pronounced seasonal variabilities of mixing ratio and relative humidity.

Using simultaneously measured ozone mixing ratios as a quasi-conservative tracer of deep convection we will discuss deep convection in the context of moistening the UT and transport of water vapor to the stratosphere.

**JSM26/E/10-B2** **1000**

#### ON A SOURCE OF ERROR IN THE MEASUREMENT OF UPPER TROPOSPHERIC HUMIDITY BY THE FLUORESCENCE WATER VAPOUR SENSOR ONBOARD THE BRITISH C-130 AIRCRAFT

Iphigenia KERAMITSOGLU, John E. Harries, David J. Colling (Department of Physics, Blackett Laboratory, Imperial College of Science Technology and Medicine, London SW7 2BZ, UK, email: i.keramitsoglou@ic.ac.uk, j.harries@ic.ac.uk, d.colling@ic.ac.uk), Rod A. Barker and John S. Foot (Meteorological Office, Meteorological Research Flight, Building Y46 DRA, Farnborough, Hants GU14 6TD, UK, email: ralbarker@meto.gov.uk, jsfoot@meto.gov.uk)

Water vapour is the most important greenhouse gas in the cloud-free atmosphere. Therefore, the ability to assess and predict any climate change strongly depends on accurate observations of water vapour and its representation in models. However, water vapour's extreme variability on all time and space scales makes accurate measurement a very complicated and difficult task.

The purpose of this study is to analyse and evaluate the performance of the Fluorescence Water Vapour Sensor (FWVS) onboard the British C-130 aircraft. The sensor was built by the Meteorological Research Flight, UK Met. Office, to fulfil the need of fast and accurate in-situ water vapour measurements in the upper troposphere. However, inter-comparisons of coincident flight data with a frost-point hygrometer have shown that the FWVS systematically overestimates humidity by 10-20%, depending on pressure, in comparison to the frost-point instrument. An in depth analysis of the possible sources of error has led to the design of laboratory experiments to better characterise the FWVS instrument. These included the measurement of the source spectrum, and of the effective oxygen absorption cross-section using the sensor itself. Most importantly, though, an original model of the FWVS has been developed, which proved to be a powerful tool in understanding the sensor's behaviour. The laboratory experiments confirmed the emission of wavelengths other than Lyman-alpha by the FWVS source. This result along with the outcome of the sensitivity tests carried out using the new model revealed that a source of error that accounts for up to half of the observed differences is the contaminated lamp spectrum and the underestimation of the oxygen absorption cross-section in the post-flight data processing.

**JSM26/E/02-B2** **1020**

#### WATER VAPOUR TRANSPORT INTO THE LOWER STRATOSPHERE

Antje DETHOF, Alan O'Neill and Julia Slingo (CGAM, Department of Meteorology, University of Reading, RG6 6BB, UK, email: antje@met.rdg.ac.uk)

The climatology of the lowermost stratosphere is not well understood. Tracer distributions in this part of the atmosphere are governed by complicated interactions of dynamical, chemical and radiative processes. In this talk, case studies of isentropic stratosphere-troposphere exchange in the region of the middleworld are presented, and a method is developed, by which isentropic transport of mass and moisture between the tropical troposphere and the extratropical lowermost stratosphere can be quantified.

**JSM26/W/37-B2** Invited **1100**

#### CHLORINE ACTIVATING HETEROGENEOUS REACTIONS

Stephan BORRMAN, (Institute for Stratospheric Chemistry, Germany, email: s.borrmann@fz-juelich.de)

Chlorine activating heterogeneous reactions has been suggested to occur on cirrus clouds as well as in layers of enhanced numbers of small particles, on supercooled cloud droplets and on background aerosol in the tropopause region. The high water content, low temperatures, and slow photochemical recovery times near the tropopause make this region susceptible to heterogeneous processing, just as the extreme cold temperatures over the poles do for dryer air at higher altitudes. Detailed model studies by Solomon et al., 1997, and Hendricks, 1997, revealed that heterogeneous chemistry on the aerosol in the tropopause region could significantly contribute to the ozone depletion in northern mid-latitudes. Input for the model

calculations by Solomon et al., 1997, are climatological SAGE II satellite observations of cirrus cloud optical depths and cloud occurrence frequencies from 1988 and 1989, i.e. years of relative volcanic quiescence. Because of variations in observed cloud occurrence frequency and in photochemical and dynamical time scales, the presence of cirrus clouds likely has its largest effect on ozone near the northern hemispheric mid-latitude tropopause. There the low background ClO mixing ratios could be enhanced by heterogeneous reactions by factors of 30, according to the model results. Due to the lack of extended ClONO<sub>2</sub>, HCl, and ClO observations the processes discussed in this presentation still have to be considered as hypothetical. Measurements of clouds, subvisual cirrus, and recent developments are also discussed in this context.

**JSM26/W/04-B2** **1130**

#### RETHINKING REACTIVE HALOGEN BUDGET IN TROPOSPHERE AND LOWER STRATOSPHERE: IMPLICATIONS FOR MID-LATITUDE OZONE DEPLETION AND DIAGNOSTICS OF CONVECTIVE TRANSPORT

VICTOR L. DVORTSOV (1,2), Marvin A. Geller (3), Susan Solomon (1), Sue M. Schauffler (4), Elliot L. Atlas (4), and Donald R. Blake (5) (1) Co-operative Institute for Research in Environmental Sciences, University of Colorado, Boulder, (2) NOAA, Aeronomy Laboratory, Boulder, Colorado, (3) State University of New York at Stony Brook, Stony Brook, New York, (4) National Center for Atmospheric Research, Boulder, Colorado (5) Department of Chemistry, University of California, Irvine, California

Using bromine species as an example, we use models and observations to show that short-lived halocarbons are able to maintain significant concentration of reactive halogens (e.g., BrO) in the troposphere. Moreover, as evident from both observations and our modeling, at least some of these short-lived source species (e.g., bromoform, CHBr<sub>3</sub>) are present in non-negligible amounts in the upper troposphere. These findings contradict the current beliefs that the short-lived compounds are completely removed in the troposphere, the products being rained out. Therefore, as our modelling further shows, contribution from short-lived halocarbons significantly increases the amount of reactive bromine in the lowermost stratosphere, thus playing an important role in the ozone photochemistry in this region. Depending on the atmospheric humidity and the partitioning of inorganic chlorine, the contribution of bromoform alone increases the model estimates of the ozone trends in the mid-latitude lowermost stratosphere for 20 to 50%. This work has other important implications. As well known, short-lived gases are good tracers of convective transport. For instance, 222 Radon is commonly used for diagnostics of climate model convective parameterizations. However, the utility of 222 Radon for these purposes is limited to the continental convection, as the only source of this gas is ice-free land. On the other hand, the primary source of bromoform and some other short-lived organic halocarbons is ocean, which makes these species useful for diagnostics of the maritime convection. We discuss our implementation of such on-line diagnostics using bromoform in the NCAR Community Climate Model (CCM) version 3.6.

**JSM26/W/31-B2** **1150**

#### FACTORS AFFECTING THE FORMATION OF POLAR STRATOSPHERIC CLOUDS

H.M. STEELE (Dept. of Chemistry, University of Cambridge, CB2 1EW, UK, email: Helen.Steele@atm.ch.cam.ac.uk), K. Hoppel (Naval Research Laboratory, Washington DC 20375, e-mail: hoppel@poomb.nrl.navy.mil), K. Drdla (NASA Ames Research Center, Moffett Field, CA 94035, e-mail: katja@aerosol.arc.nasa.gov), R.M. Bevilacqua (Naval Research Laboratory, Washington DC 20375, e-mail: bevilacqu@map.nrl.navy.mil), R.P. Turco (Dept. of Atmospheric Sciences, UCLA, Los Angeles, CA 90095, e-mail: turco@atmos.ucla.edu).

The formation and development of polar stratospheric clouds are examined in case studies using a comprehensive microphysical model applied along air parcel trajectories. During Antarctic winter specific parcels are sampled over a time span of several days using extinction data from the POAM II satellite instrument. The observed evolution of polar stratospheric cloud spectral opacity is compared to predictions from model simulations. Hence, aerosol growth and decay in response to changing environmental conditions can be observed and interpreted. In some instances good agreement between observations and predictions has been obtained over periods of many days. This analysis suggests that temperature history has a possible role in cloud formation. In order to quantify this role, a statistical study of polar stratospheric cloud formation over three Antarctic winters is carried out using POAM II aerosol observations and back trajectories. Aerosol data are fitted to a theoretical model for cloud growth to retrieve best fit parameters for ambient water vapour concentration and the aerosol sulphate content, and to deduce the rate of dehydration and denitrification throughout the polar winter. An analysis of variance is used to assess the importance of factors such as cooling rate, time spent below the nitric acid trihydrate condensation temperature, and exposure to temperatures below the ice frost point, in the formation of clouds.

**JSM26/W/16-B2** **1210**

#### CONVECTION, CHEMISTRY AND AEROSOLS AT THE TROPICAL TROPOPAUSE: THE APE-THESEO MISSION

ROB MACKENZIE(1), Leopoldo Stefanutti(2), Stefano Balestri(3), Stephan Borrmann(4), Marco Cacciani(5), Ken Carslaw(6, 12), Teo Georgiadis(7), Giorgio Giovannelli(7), Vyacheslav Khattatov(8), Valentin Mitev(9), Piero Mazzinghi(10), Kevin Noone(11), Thomas Peter(12), Wolfgang Renger(13), Vladimir Rudakov(8), Johan Ström(11), Guido Visconti(14), Michael Volk(15), and Vladimir Yushkov(8). (1)Lancaster University, U.K.; (2)IROE-CNR, Italy; (3)APE Management Committee, Italy; (4)Forschungszentrum Jülich, Germany; (5)University of Rome; (6)now at University of Leeds, U.K.; (7)FISBAT-CNR, Italy; (8)Central Aerological Observatory, Russia; (9)Observatoire de Neuchâtel, Switzerland; (10)IEQ, Italy; (11)Stockholm University, Sweden; (12)Max-Planck-Institut für Chemie, Mainz, Germany; (13)DLR-Oberpfaffenhofen, Germany; (14)University of l'Aquila; (15)University of Frankfurt.

APE-THESEO is the Airborne Platform for Earth Observation (APE) contribution to the Third European Stratospheric Experiment on Ozone (THESEO). APE is the facility that manages scientific missions of the Russian high-altitude aircraft, the M-55 Geophysica. The Geophysica is an exciting new platform, well suited to the study of mesoscale processes occurring from the tropopause to 21 km altitude. We describe first results from the deployment of the Geophysica to the tropical tropopause in February-March 1999.

The objectives of APE-THESEO are to measure cloud, aerosol, and trace gas distributions close to, and above, intense tropical convection, in order to understand the processes governing stratospheric dehydration, aerosol formation, and upper tropospheric-lower stratospheric transport. An important additional aspect of APE-THESEO is the collaboration with the Indian Ocean Experiment (INDOEX), which aims to investigate the effect of aerosols on climate in the Indian Ocean.

## CHEMISTRY AND TRANSPORT

JSM26/L/02-B2 Invited 1400

## CHEMISTRY IN THE UPPER TROPOSPHERE AND LOWER STRATOSPHERE

R.A.COX (Department of Chemistry, University of Cambridge, Lensfield Road, Cambridge, CB2 1EW, UK.)

Whilst the gas phase chemistry responsible for the catalytic destruction of ozone in the photochemically controlled regions of the upper stratosphere is now reasonably well known, there remains many interesting problems in the chemistry of the lower stratosphere and upper troposphere.

New observations point to higher fractions of radical species relative to reservoir species in the lower stratosphere, the most extreme examples being in the Polar vortices where essentially all the stratospheric Cl is converted to ClO (or its weakly bound dimer Cl<sub>2</sub>O<sub>2</sub>). The causes of these perturbations are heterogeneous reactions in which stable reservoirs are converted to photolabile radical sources. These processes may also be important in the upper troposphere. Heterogeneous reactions occur on solid ice and NAT particles and on liquid sulphuric acid aerosols at low temperatures. Laboratory studies have provided much new information on the kinetics of these reactions and a picture is now emerging of the key physico-chemical factors affecting reactivity. There have recently been improved laboratory data for the rates and mechanism of several gas phase reactions that are important in the lower stratosphere and upper troposphere.

The presentation will survey recent developments in knowledge of the chemistry of the lower stratosphere and upper troposphere, relevant for ozone loss. Some new kinetics data from our laboratory relating to iodine and bromine chemistry will be used to illustrate the coupled role of gas phase and heterogeneous chemistry in the lower stratosphere.

JSM26/E/05-B2 1430

## DETAILED ATTRIBUTION OF NITROGEN OXIDE SOURCES DETERMINING UPPER TROPOSPHERIC CHEMISTRY IN SONEX

Robert B CHATFIELD (Earth Science/245-5, NASA Ames Research Center, Moffett Field, California 94035 USA, email: chatfield@clio.arc.nasa.gov) Zitian Guo (Research Foundation, San Jose State University, San Jose, California, USA, email: zguo@clio.arc.nasa.gov) Yutaka Kondo (Solar Terrestrial Environment Laboratory, Nagoya University, Honohara, Aichi 442 Japan, email: kondo@stelab.nagoya-u.ac.jp)

We describe the sources of active nitrogen oxides, NO<sub>x</sub>, in the upper troposphere over the North Atlantic for the intensive study period of SONEX, the Subsonic Assessment Program Ozone and Nitrogen Oxide Experiment. Such NO<sub>x</sub> is central in determining the delicate balance determining radiatively important upper tropospheric ozone. Perhaps surprisingly, we find that lightning was frequently a dominant source of NO<sub>x</sub> even in this late fall period, October–November, 1997. Lightning NO<sub>x</sub> in the North Atlantic frequently had sources in from maritime lightning, extending thousands of kilometers off the North American Coast and in the tropical waters of the Gulf and Caribbean. Aircraft and surface sources on NO<sub>x</sub> were also important. Aircraft NO<sub>x</sub> was often more significant for the uppermost troposphere, and surface NO<sub>x</sub> for the middle troposphere. The NO<sub>x</sub>/O<sub>3</sub> ratio associated with stratospheric injections was highly variable.

Our conclusions derive primarily from a tracer model following NO<sub>x</sub> with labeled origin in a model driven by hourly winds and cloud motions. A rich variety of transport processes was revealed. These were derived from MM5 synoptic model reconstructions which was nudged to follow the European Centre analyses. These were compared to the measurements of NO<sub>x</sub> implied by the NO measurements made aboard the NASA DC-8 by the Kondo group as processed by the SONEX data team at Harvard University. Measurements of ozone, hydrocarbons, peroxides, and particles made on the aircraft helped confirm attributions that we made. Aircraft NO<sub>x</sub> accounted for ~30% of upper tropospheric NO<sub>x</sub>. Our ongoing simulations and comparisons will allow us to check this attribution and extend it from the DC-8 flight track to the whole North Atlantic.

JSM26/L/03-B2 1450

## CHANGING STRATOSPHERIC CIRCULATION, THE GREENHOUSE EFFECT AND OZONE LOSS

Hans-F. GRAF and Judith Perlwith, Max-Planck-Institute for Meteorology Bundesstr. 55, D-20146 Hamburg, Germany, email: graf@dkrz.de

Stratospheric climate has changed considerably during the last decades. After elimination of volcanic effects a global mean decreasing lower stratospheric temperature consistent with increased greenhouse effect is detectable. In higher northern latitudes this trend is strongest in spring (March). At this time the reduction in stratospheric ozone is also strongest. However, the trend patterns of stratospheric temperature and geopotential match the ozone trends in March not as well at polar latitudes as in middle latitudes.

Analysis of model runs with prescribed observed ozone changes and with prescribed increased greenhouse gas concentration show that the observed changes cannot be explained by these forcings individually. While reduced stratospheric ozone is responsible for cooling of the stratosphere beginning in April on the northern hemisphere, it does not explain the strengthening of the winter polar vortex. This, according to the results of the greenhouse gas experiment, may be due to initial warming of the troposphere in low latitudes which strengthens the hemispheric geopotential gradient and thus also the polar winter vortex. For realistic forcing the modeled individual effects are weaker than observed. The observed stratospheric changes therefore are suggested to result from a combination of natural and anthropogenic contributions mainly in the troposphere. Initial strengthening and cooling of the polar vortex changes the structure of ultralong planetary waves in the troposphere (including the stabilization of the North Atlantic Oscillation in its positive phase, i.e. with strong Iceland trough and Azores high). This determines the stratospheric ozone concentration mainly in middle latitudes. Inside the intensified vortex cooling sets the precondition for the formation of PSCs and ozone destruction by heterogeneous chemistry in early spring. The reduced ozone leads to negative temperature anomalies that help keeping the vortex stable.

JSM26/W/34-B2 1510

## THE STRATOSPHERE-TROPOSPHERE EXCHANGE SEEN FROM THE SOWER/PACIFIC RESULTS

Fumio Hasebe (Ibaraki University, email: hasebe@mito.ipc.ibaraki.ac.jp), Holger Voemel (University of Colorado/CERES, email: hvommel@cmdl.noaa.gov), MASATO SHIOTANI (Hokkaido University, email: shiotani@ees.hokudai.ac.jp), Noriyuki Nishi (Kyoto University, email: nishi@kugi.kyoto-u.ac.jp), Samuel Oltmans (NOAA/CMDL, email: soltmans@cmdl.noaa.gov), Toshihiro Ogawa (NASDA/EORC, email: t\_ogawa@eorc.nasda.go.jp) Kenneth Gage (NOAA/AL, email: kgage@al.noaa.gov)

Two observational campaigns at San Cristobal, Galapagos (0.90S, 89.62W) as part of the Soundings of Ozone and Water in the Equatorial Region (SOWER)/Pacific mission, have been successfully carried out in March/April and September 1998 and profiles of ozone and water mixing ratio together with those of temperature were obtained. The former (latter) period corresponds to high (low) wave activity in the Northern middle and high latitudes, when extratropical pumping in the stratosphere leads to a higher (lower) and colder (warmer) tropopause in the tropics, though the two periods were highly affected by the end of the very strong El Niño and the condition of the developing cold phase, respectively.

The temperature and ozone profiles show fluctuations typical of those in profiles at other locations in the tropics. These features suggest that wave activity may be responsible for local mass exchange between the troposphere and stratosphere, although that cannot be determined from these data alone. The tropopause is generally colder in March than in September as expected, but its altitude is also likely modified by the waves mentioned above. It is also found that the presence of the upward propagation of the seasonal water vapor signal through the stratosphere, referred to as the tape recorder effect, though profiles are needed at other times of the year for the better definition.

JSM26/W/18-B2 Invited 1550

## UPPER TROPOSPHERIC PHOTOCHEMISTRY: SOME FINDINGS FROM RECENT AIRBORNE STUDIES

H. SINGH (NASA Ames Research Center, MS 245-5, Moffett Field, CA 94035-1000, USA, email: hsingh@mail.arc.nasa.gov); W. Brune, D. Tan and I. Faloona (Penn State Univ., PA), Y. Kondo (Nagoya Univ., Japan), L. Jaegle and D. Jacob (Harvard Univ., MA), D. Davis (Georgia Institute of Technology, GA), B. Heikes (U. Rhode Island, RI), H. Schlager (Wessling, Germany)

Recent airborne missions such as SONEX (SASS Ozone and NO<sub>x</sub> Experiment) and POLINAT (Pollution in North Atlantic Tracks) have provided substantial new data from the upper troposphere/lower stratosphere region of the atmosphere. For SONEX, new state of the art instrumentation has been used to provide measurements of a complete suite of reactive nitrogen (NO<sub>x</sub>, PAN, PPN, HNO<sub>3</sub>, alkyl nitrates, NO<sub>y</sub>, and aerosol nitrate), reactive hydrogen (OH, HO<sub>2</sub>, H<sub>2</sub>O, peroxides, alcohols and carbonyls), and tracer (CO, C<sub>2</sub>Cl<sub>4</sub>, NMHCs) and O<sub>3</sub> measurements. These observational data are complemented by a suite of meteorological products that are useful for interpreting dynamical features of the atmosphere. With these observations and tools, an attempt is made to assess the sources and sinks of a number of key oxygenated species in the troposphere. Factors controlling the rates of ozone production (NO<sub>x</sub>, HO<sub>x</sub> radicals etc.) are examined. Atmospheric observations are compared with photochemical models to assess our knowledge of the photochemistry of the upper troposphere and evaluate the potential impact of anthropogenic perturbations on NO<sub>x</sub> and Ozone. Areas of significant uncertainties are identified. These studies have the potential to greatly enhance our knowledge of the upper tropospheric photochemistry.

PRESENTATION OF POSTERS 1620-1700

JSM26/E/07-B2 Poster 1700-01

## GRAVITY WAVES AND TURBULENCE AROUND THE TROPOPAUSE ABOVE ABERYSTWYTH

E.G. PAVELIN and J.A. Whiteway (Department of Physics, University of Wales, Aberystwyth, Ceredigion, SY23 3BZ, U.K. email: egp98@aber.ac.uk)

The U.K. M.S.T. radar located near Aberystwyth in western Wales has been used to study gravity waves and turbulence in the troposphere and lower stratosphere. Radar velocity measurements have been used to investigate the velocity spectrum of the wind field in regions of varying wave activity and turbulence. Of particular interest are areas of turbulence associated with wave breaking at critical layers, which may be identified with layers of enhanced spectral width. The general objective is to determine whether this turbulence causes significant mixing of constituents (such as ozone and water vapour) near the tropopause; and whether this mixing is significant for exchange between the stratosphere and troposphere.

JSM26/E/19-B2 Poster 1700-02

## THE DYNAMICS OF AIR MASSES SEGREGATED FROM THE SOUTHERN HEMISPHERE POLAR VORTEX IN THE LOWER STRATOSPHERE

Marcelo Behar, Pablo O. CANZIANI (Grupo de Atmosfera Media, Departamento de Ciencias de la Atmosfera, Facultad de Ciencias Exactas y Naturales, Universidad de Buenos Aires, Pabellon II, Ciudad Universitaria, 1428 Capital Federal, ARGENTINA)

The dynamics of the southern polar vortex in the lower stratosphere and of the segregated air masses from the vortex edge are studied, with a special interest on the local impacts to the ozone layer. The air masses the break off the edge of the polar vortex can transport ozone-poor air, with physical and chemical characteristics similar to those found in the inside of the vortex up to latitudes close to 40-35 degrees south. Even if perturbations that these air masses can generate are not significant from the perspective of the total ozone column, it could be possible that the local impacts to the lower stratosphere be significant enough so as to affect the ozone budget there and in consequence modify the energy balance and the characteristics of the tropopause. In this study the break offs from the polar vortex are analysed using a trajectory analysis code together with chemical tracer satellite data. The results are also compared with total ozone measurements. A number of events that took place over the South Atlantic and over Southern South America are discussed, and their evolution is studied.

**JSM26/E/01-B2** Poster **1700-03**

**HIGH SENSITIVITY OF THE POLAR LOWER STRATOSPHERIC PHOTOCHEMICAL SYSTEM TO VARIATIONS OF THE PARAMETERS AND INITIAL CONDITIONS**

A. M. Feigin, I. B. Kononov, M. Y. Kulikov, and A. Y. MUKHINA (Institute of Applied Physics of Russian Academy of Sciences, 46 Ulyanov Str., Nizhny Novgorod, 603600, Russia, e-mail: etanya@appl.sci-nnov.ru)

The qualitative non-linear dynamic properties of the polar lower stratospheric photochemical system (PLS PCS) are investigated on the base of the zero-dimensional photochemical basic dynamical model [Feigin, and Kononov, J. Geophys. Res., 101, 26,023-26,038, 1996 (FK)], which adequately simulates the ozone evolution during the Antarctic ozone hole formation. It is shown that the behaviour of the Antarctic photochemistry is very sensitive to values of concentrations of some chemical species at August, which are considered as initial conditions for our model. The most important result is the high sensitivity of the system to a few parameters: concentration of inorganic chlorine, temperature, surface area of sulphuric aerosol and some others. These results are shown to be a consequence of the nontrivial dynamic properties (NDPs) of PLS PCS [FK; Kononov, Feigin, and Mukhina, J. Geophys. Res., in press], and are of special interest for forecast of the Antarctic photochemistry evolution. At present the question about the possibility of recovering of ozone abundance in polar area due to expected decrease of the chlorine compounds is widely discussed. It is rather understandable that due to NDPs, return of one parameter to the natural level doesn't necessary lead to return of the system to initial state with the other parameters being different. Possible scenarios of the future evolution of ozone hole are investigated for expected future values of other parameters under an assumption that concentration of inorganic chlorine returns to the value of the beginning of 1980s when the Antarctic ozone hole was absent.

**JSM26/E/15-B2** Poster **1700-04**

**CORRELATION OF OZONE AND PV AND OZONE PREDICTION USING MOZAIC MEASUREMENTS**

Olaf MORGENSTERN (Centre for Atmospheric Science, Chemistry Dept., Cambridge University, Cambridge CB2 1EW, UK, email: Olaf.Morgenstern@atm.ch.cam.ac.uk)

Simplified mean ozone analyses are compiled in the equivalent-latitude - potential-temperature space using ozone measurements made within the Measurement of Ozone and Water Vapour by Airbus In-Service Aircraft (MOZAIC) project. The analyses exhibit tropospheric, stratospheric and intermediate tropopause domains. The standard deviations of ozone, relative to the mean, in this parameter space attain maxima south of the subtropical barrier, which is attributed to stratosphere-troposphere exchange. Ozone is inferred from these simplified, two-dimensional representations of ozone for the days following the analyses. It matches measured ozone to a fair degree of accuracy, indicating that in the tropopause region ozone may usefully be described as a function of potential temperature and equivalent latitude, with a seasonal modulation. Differences between inferred and measured ozone appear to be relatively large in regions of low confidence in meteorological analyses.

**JSM26/E/04-B2** Poster **1700-05**

**THE INFLUENCE OF THE STRATOSPHERIC SULFURIC AEROSOL ON THE NONLINEAR DYNAMIC PROPERTIES OF ANTARCTIC PHOTOCHEMICAL SYSTEM AND THEIR TO RELEVANCE IN THE PROCESSES OF THE ANTARCTIC OZONE HOLE FORMATION**

A. M. Feigin, and M. Y. KULIKOV (Institute of Applied Physics of Russian Academy of Sciences, 46 Ulyanov Str., Nizhny Novgorod, 603600, Russia, email: etanya@appl.sci-nnov.ru)

The influence of heterochemical reactions running on the surface of the stratospheric sulphuric aerosol (SSA) on non-linear dynamic properties (NDPs) of the Antarctic photochemical system (PCS) during winter-spring period is investigated. The minimum value of ozone concentration in the region of its season averaged- maximum (heights 17-18 km) is considered as an indicator of this influence. It is shown that the processes change significantly a phase space of the system. In particular, they lead to the appearance of both an additional equilibrium state, and a stable limit cycle. It was obtained that influence of these "aerosol" phase space objects on ozone concentration behaviour depends significantly on a few control parameters, namely, total surface area of SSA particles, prescribed temperature evolution, non-organic chlorine abundance, and power of both denitrification, and dehydration. It is shown that the "aerosol" NDPs may be in close connection with significant increasing of extent of the Antarctic ozone hole extent in the years following powerful volcanic eruptions (e. g., Mount Pinatubo eruption in 1991). An influence of the enhanced SSA level on the NDPs of Antarctic PCS under expected in the future values of other control parameters is analysed. Possible manifestation of these NDPs in the future evolution of Antarctic ozone hole are discussed.

**JSM26/E/18-B2** Poster **1700-06**

**RECONSTRUCTION OF OZONE FIELDS USING PSEUDO-DIABATIC CONTOUR ADVECTION WITH SURGERY**

B. JOSEPH (1), F. Lefevre (2), B. Legras (1) (1) Laboratoire de Meteorologie Dynamique du CNRS, 24 rue Lhomond, 75231 Paris, France (2) CNRS Service d'Aeronomie, Universite Pierre et Marie Curie, BP 102, 4 Place Jussieu, 75252 Paris Cedex 05, France

We explore the feasibility of directly reconstructing fine-scale features in ozone fields in the Northern Hemisphere lower stratosphere from the lower resolution daily output of the three-dimensional REPROBUS (reactive processes ruling the ozone budget in the stratosphere) chemistry transport model (CTM) using pseudo-diabatic contour advection with surgery (PCAS). The PCAS technique, which also assimilates tracer fields as an on-line correction to the advected fields, has been demonstrated in our earlier studies with the potential vorticity (PV) fields to give results, which are superior to the usual contour-advection with surgery (CAS) results, both in the extratropical lower stratosphere as well as in the subtropics. In order to illustrate only the major aspects of the reconstruction of ozone fields, we concentrate our study to the 475 K isentropic surface, typical of the lower stratosphere. When chemistry plays a major role in determining the model ozone fields, we also expect PCAS to play a fundamental role in the reconstruction procedure. We examine high-resolution PCAS reconstructions of both passive and reactive ozone fields from the REPROBUS output and attempt to learn more about the filamentary aspect of transport and its role in the ozone depletion process in the northern lower stratosphere. We will also present a performance evaluation of PCAS reconstructions of PV, passive ozone, and reactive ozone fields on 475 K by comparing with the corresponding observed values from ozone profiles collected during the intensive phase of METRO (MEridional TRansport of Ozone in the lower stratosphere) campaign during 1997-98 and 1998-99 winters.

**JSM26/W/21-B2** Poster **1700-07**

**AGE OF AIR IN THE SLIMCAT CTM: SENSITIVITY TESTS**

Hubert Teyssedre & Martyn Chipperfield (University of Cambridge, Department of Chemistry, Lensfield Road, Cambridge CB2 1EW, UK, email: hubert.teyssedre@atm.ch.cam.ac.uk Telephone No: +44 01223 336524 Fax No: +44 01223 336362)

Deducing the stratospheric age of air [Hall et al., 1999] is a powerful tool to diagnose the quality of the transport representation in an atmospheric model. We have included a tracer with a source (linearly increasing in time) in the tropical lower stratosphere in the SLIMCAT chemical transport model (CTM), which is forced by UKMO/UARS analyses. An initial simulation, at low resolution (7.5 x 7.5 degrees) using 1992 analyses, exhibits an age of air which is too old (by up to 3 years at 30 km) in comparison with values derived from atmospheric SF6 measurements (in contrast to many other reported models). To reduce this discrepancy between our CTM and observations, several sensitivity tests have been performed with SLIMCAT. We will discuss the effect of the model horizontal/vertical resolution, the interannual variability of the analyses used to force the model and the effect of two different radiation schemes (MIDRAD and CCM2) used to calculate the vertical motion, on the modelled age of air. Hall et al., J. Geophys. Res., (in press), 1999.

**JSM26/E/03-B2** Poster **1700-08**

**MULTIPLE EQUILIBRIUM STATES IN THE POLAR LOWER STRATOSPHERIC PHOTOCHEMISTRY**

Igor KONOVALOV, Alexander Feigin, and Anna Mukhina (Institute of Applied Physics of Russian Academy of Sciences, 46 Ulyanov Str., Nizhny Novgorod, 603600, Russia, e-mail: konov@appl.sci-nnov.ru)

Results of our investigations of the polar lower stratospheric photochemical system (PLS PCS) from the point of view of non-linear dynamics are reported. For the investigations the box model of PLS PCS, which includes all the most significant photochemical processes taking place in the polar (both Arctic and Antarctic) lower stratosphere in winter-spring period, and adequately simulates the evolution of the Antarctic ozone hole, has been used. It has been revealed, in particular, that the model can possess simultaneously three equilibrium states (multi-stability) under realistic conditions. Revealing of the origin of this property has allowed to insure that it is not a consequence of any approximation used in the model but is a property inherent in nature of PLS PCS. It is demonstrated that the multi-stability can provide the qualitatively different scenarios of ozone evolution depending on both initial conditions and parameter values. The analysis of the role of the multi-stability in the Antarctic ozone hole phenomenon has shown that the presence of this property may be accounted for the observed steepness of the ozone destruction at 17-18 km of altitude at the mid of 1980s. The possible applications of the knowledge of the non-linear dynamic properties of PLS PCS for the investigations of behaviour of minor constituents in the Arctic region are discussed.

**JSM26/W/29-B2** Poster **1700-09**

**ION-MOLECULE REACTION SCHEMES FOR IN SITU DETERMINATION OF STRATOSPHERIC HNO3 AND HCL CONCENTRATIONS BY CHEMICAL IONIZATION MASS SPECTROMETRY (CIMS)**

A.-M. VAN BAVEL, C. Amelynck, E. Arijis, E. Neefs, D. Nevejans, N. Schoon (Belgian Institute for Space Aeronomy, Ringlaan 3, B-1180 Brussels, Belgium, email: Mieke.VanBavel@bira-iasb.oma.be) V. Catoire, D. Labonnette, G. Poulet, C. Stépien (LPCE-CNRS, 3A, Avenue de la Recherche Scientifique, F-45071 Orléans, France) H.-P. Fink, U. Jenzer, E. Kopp, W. Luthardt (Universität Bern, Sidlerstrasse 5, CH-3012 Bern)

Laboratory measurements (Huey et al. 1995) have shown that CF3O- ions selectively react with several stratospheric minor gases by fluoride transfer. We therefore recently equipped our balloon borne chemical ionization mass spectrometer instrument (MACSIMS) with a new photoelectric ion source producing mainly CF3O- ions. However, flight results obtained with this new ion source revealed that the derivation of trace gas concentrations was complicated by the presence of large amounts of CF3O-H2O (and to a lesser extent CF3O-HF) in the flight spectra. The spectra also indicate that CF3O-H2O and CF3O-HF selectively react with several trace gases (such as HNO3, HCl, ClONO2) by ligand switching, making these ions good CIMS source ion candidates.

In order to adjust the originally proposed fluoride transfer reaction schemes for derivation of HNO3 and HCl concentrations, the gas phase ion-molecule reactions of CF3O-, CF3O-H2O and CF3O-HF with both HCl and HNO3 have been studied at 295 K using our laboratory flowing afterglow apparatus. Rate constants and product ions were determined in the pressure range [0.5-2.4] mbar. Recent HNO3 and HCl mixing ratio height profiles (Gap-Tallard, June 1997) obtained using the adapted reaction scheme are also presented and the usefulness of the applied method is discussed.

**JSM26/W/26-B2** Poster **1700-10**

**MST RADAR AND OZONESONDE OBSERVATIONS OF HIGH-LATITUDE STRATOSPHERE-TROPOSPHERE EXCHANGE**

JOHAN ARVELIUS, Dave Hooper, Hans Nilsson, Sheila Kirkwood and Phil Chilson, (Swedish Institute of Space Physics, Box 812, 981 28 Kiruna, Sweden, email: johan.arvelius@irf.se)

The Esrange MST radar (ESRAD) together with ozonesondes has been used to study the high-latitude tropopause as well as other structures giving rise to strong radar echoes. Such other structures include fronts and the borders of stratospheric air extending deep into the troposphere. Ozonesonde data have been used to compare the radar backscatter data with in-situ measurements. It seems from the measurements made so far that two phenomena of importance for stratosphere troposphere exchange can be studied using the MST radar. One is the characterization of the tropopause, allowing the identification of indefinite tropopause region and troughs, which are likely sites for exchange of stratospheric and tropospheric air. The other phenomenon is the possibility to monitor tongues of stratospheric air extending deep into the troposphere. The radar detects the border between the stratospheric and tropospheric air because of an abrupt change of the radar reflective index, mainly caused by an abrupt change of temperature. Ozonesonde data are required to identify the air-mass as stratospheric, but once identified the air-mass can be monitored by the MST radar.



**JSM26/W/25-B2** Poster **1700-11**

**MODIFIED LAGRANGIAN-MEAN ANALYSIS OF LOW-FREQUENCY VARIATIONS IN THE UPPER TROPOSPHERE OF A SIMPLE GLOBAL CIRCULATION MODEL**

Koji Akahori and Shigeo YODEN (both at Department of Geophysics, Kyoto University, Kyoto, 606-8502, Japan, email: yoden@kugi.kyoto-u.ac.jp)

A modified Lagrangian-mean (MLM) diagnostics of tracer transport in the stratosphere developed by Nakamura(1995) is extended to study the low-frequency variations of the troposphere from a viewpoint of mass conservation. Our method describes the time variation of mass in a volume element enclosed by two nearby surfaces of potential vorticity (PV) and those of potential temperature in terms of non-conservative mass flux through these surfaces. A long time-mean of the MLM mass flux illustrates a direct meridional circulation without eddy flux contributions under the constraints of both dynamics and thermodynamics.

Low-frequency variations of the zonal mean zonal flow and baroclinic eddies in a simple global circulation model, of which dynamics were investigated in the previous paper by the authors (Akahori and Yoden, 1997), are diagnosed by the new method. A characteristic feature is a propagation of the MLM mass anomalies from the tropics to the polar region with a time-scale over 100 days, which sets in rather periodically with a shorter time-scale. The poleward propagation of the mass anomalies is related to that of the zonal-flow anomalies, already found in some observational and numerical studies.

In low latitudes, the mass anomaly is mainly induced by the convergence of the meridional mass flux through PV surfaces, which is related to anticyclonic Rossby-wave breakings in the upper troposphere. In mid-latitudes, on the other hand, it is largely induced by the convergence of the vertical mass flux through isentropic surfaces, which is related to the thermal relaxation. In high latitudes, cyclonic Rossby-wave breakings on the poleward flank of the jet stream become important for the mass anomaly. Rather periodic occurrence of such propagation of the mass anomalies are characterised by a kind of relaxation oscillation which consists of a phase of mechanical mixing by Rossby-wave breakings and a recovery phase due to thermal forcing.

**JSM26/W/35-B2** Poster **1700-12**

**MEASUREMENTS OF THE GROUND-LEVEL SOLAR ULTRAVIOLET RADIATION OVER EAST SIBERIA DURING THE TOTAL OZONE ANOMALY PERIOD**

A.V. Mikhalev, M.A. Chernigovskaya, A.Yu. Shalin, A.B. Beletsky, and E.S. KAZIMIROVSKY (Institute of Solar-Terrestrial Physics, Russian Academy of Sciences, P.O.Box 4026, 664033, Irkutsk, Russia, email: mikhalev@iszf.irk.ru)

Results of spectral measurements of the Solar ground-level UV-radiation (295-345 nm) over East Siberia obtained for the spring time of 1997, are presented. This period was characterised by the greatest total ozone content (TOC) depletion for both the magnitude and the duration in eastern regions of Russia. It is shown that an anomalous ozone decrease in the spring of 1997 was coincided with the high ground-level the Solar UV-radiation as compared with the spring of 1998, when the TOC values were in agreement with long-term average values. However this high level of UV-radiation was smaller than the mean value of the ground-level Solar UV-radiation in the autumn of 1997 for the same Solar elevations when the TOC values were also in agreement with long-term average values.

**JSM26/W/19-B2** Poster **1700-13**

**DETECTING TROPOSPHERE-STRATOSPHERE EXCHANGE USING THE GLOBAL OZONE MONITORING EXPERIMENT (GOME)**

Paul Thomas Quinn, University of Wales, Aberystwyth, Ceredigion, SY23 3BZ, UK (email: ptq94@aber.ac.uk) Richard Siddans(R.Siddans@rl.ac.uk), Brian Kerridge, (email: B.J.Kerridge@rl.ac.uk) both at Rutherford Appleton Laboratory, Chilton, Oxfordshire, OX11 0QX, UK

The observations presented are of a large intrusion of subtropical tropospheric air (3.6(10e15 kg) which was detected in the midlatitude lower stratosphere over Europe in early March 1997. ECMWF trajectory analyses showed that this air was advected isentropically northwards along the 365K surface from near the subtropical tropopause and contained a region with potential vorticity values (2 PVU, consistent with ozone mixing ratios of 80 ppbv observed at Aberystwyth (52.4N, -4E). The feature was seen as a "mini-ozone-hole" in the total ozone fields of both the TOMS and GOME instruments with ozone values <270 Dobson Units. Preliminary ozone profile data from GOME produced by the Rutherford Appleton Laboratory was used to sample the feature at the 12km level, enabling the simultaneous sampling of total column ozone and ozone profile data of a lower stratospheric feature from space. The preliminary data was capable of detecting filaments, which are not seen in T106 ECMWF analyses or the GOME total ozone data, and Reverse Domain Filling trajectories were used to confirm the presence of these features. The data was also able to detect the feature over the Atlantic where no in-situ measurements could be made, and when the feature was not resolved from the background total.

**JSM26/W/14-B2** Poster **1700-14**

**MODEL OF VERTICAL ATMOSPHERE DIFFUSIVITY IN THE UPPER TROPOSPHERE AND LOWER STRATOSPHERE**

A. Belyaev, (Fedorov Institute of Applied Geophysics, Rostokinskaya ul. 9, Moscow, 129128, Russia. E-mail : belyaev@rc.msu.ru)

Height profiles of vertical diffusion coefficients are simulated for upper troposphere - lower stratosphere. Simulations using the original IGW parameterization allowing wave destruction on critical levels are effected in the framework of the one-dimensional atmosphere model with pure zonal wind. In the framework of this parameterization vertical diffusivity values depend on the vertical profile. To demonstrate influence of the wind profile on atmosphere diffusivity two vertical diffusion coefficient profile were calculated. Calculations were done for jet similar and constant wind profiles. The main difference between these diffusivity profiles is the presence of the deep gap in the profile corresponding to jet.

**JSM26/W/08-B2** Poster **1700-15**

**CHLORINE ACTIVATION DURING THE EARLY 1995-1996 ARCTIC WINTER**

STEVEN T. MASSIE, XueXi Tie, and Guy P. Brasseur (National Center for Atmospheric Research, Boulder, CO, email: massie@ucar.edu) Richard M. Bevilacqua and Michael D. Fromm (Naval Research Laboratory, Washington, D. C.) Michelle L. Santee (Jet Propulsion Laboratory, California Institute of Technology, Pasadena, CA)

The coupling of temperature, aerosol area density, and chlorine activation is studied by comparing three-dimensional chemical transport model values with observed temperature, aerosol area density, and ClO values in the Arctic for the time period December 1, 1995 to January 9, 1996. The three-dimensional model uses United Kingdom Meteorological Office (UKMO) winds and temperatures, run on pressure surfaces between 316 and 0.31 hPa, and the model results are examined at 100, 68, 46, 31, and 21 hPa. Polar Ozone and Aerosol Measurement (POAM II) aerosol extinction values are transformed into area density values, and compared to model daily averaged time trends. The model is run in several modes: (i) with gas phase chemistry only, (ii) with gas phase plus sulphate aerosol chemistry, and (iii) the case where gas phase, sulphate aerosol, and polar stratospheric cloud chemistry is active. The study shows that sulphate aerosol is very effective in activating chlorine in the Arctic polar vortex. Furthermore, time trends of five-day averages of model and Upper Atmosphere Research Satellite (UARS) Microwave Limb Sounder (MLS) ClO over extended regions inside and outside the vortex at 21 and 46 hPa agree within the experimental error.

**JSM26/L/04-B2** Poster **1700-16**

**LARGE SCALE TROPOPAUSE FOLDINGS AND EXCHANGES ACROSS THE SUBTROPICAL JET IN THE SOUTHERN HEMISPHERE.**

DANIEL Vincent(1), Barry Jean-Luc(2), Legras Bernard(1), Ancellet Gerard(3). (1) Laboratoire de Meteorologie Dynamique, Ecole Normale Supérieure de Paris, France (2) Laboratoire de Physique de l'atmosphère, Université de la Réunion, France (3) Service d'aéronomie, Université Paris VI, Jussieu, France.

Ozone measurements done at La Reunion and in South Africa with lidars, ozone sounds and Mozaic profiles are showing that the presence of ozone layers is ubiquitous. These ones occur in the mid and upper troposphere on the North side of the Southern hemisphere subtropical jet during winter, in July 1998. Values of 50 to 100 ppbv are often observed at altitudes between 5 and 9 kilometers near 20-25 South. Meridional cross sections of potential vorticity reveal that these layers are related to tropopause folds beneath the jet. Folding appears as quasi permanent and extends over a considerable longitudinal range from mid-Atlantic to Australia. Analysis of divergence, deformation fields and frontogenesis vectors suggest that these structures are due to the stationary forcing of the upper branch of the Hadley circulation during monsoon.

**JSM26/L/05-B2** Poster **1700-17**

**TROPOPAUSE FOLDS AND IRREVERSIBLE MIXING**

YAMAZAKI, Y. H. and W. R. Peltier ( dept. Physics , University of Toronto, 60 St. George Street, Toronto, Ontario, Canada M5S 1A7: email: hiro@atmosp.physics.utoronto.ca)

To assess the significance of small-scale processes associated with the non-linear evolution of synoptic-scale baroclinic waves in the mid-latitudes, we have employed a dry non-hydrostatic anelastic model and executed a series of three-dimensional numerical simulations at very high spatial resolution which explicitly resolve the secondary structures that develop in the troposphere and lower stratosphere. In particular, we evaluate the sensitivity of the degree of tropopause deformation and irreversible mixing to the contrast of stratification between the stratosphere and the troposphere and to the intensity of small-scale turbulent mixing.

The amplitude of the "synoptic-scale deformation" of the tropopause is found to be strongly sensitive to the stratification contrast as one might expect, but the behaviour of the descending "tongue" of the air that constitutes the tropopause folds is found to be relatively insensitive to this influence. In contrast, the strength of the subgrid-scale turbulence that is represented in the model using simple first order closure has little influence on the deformation of tropopause, although it significantly alters the PV generation at the surface front. The degree of irreversible mixing in these non-linear life-cycles has than rigorously evaluated by examining the evolution of the "unavailable" component of the potential energy which reflects only thermodynamic state of the fluid. The intensity of the irreversible mixing was found to be very sensitive to the intensity of turbulent diffusion, as expected.

**Wednesday 28 July AM**

Presiding Chair: M Shiotani (Graduate School of Environmental Earth Science, Hokkaido Univ. Sapporo, Japan)

**CHEMISTRY AND TRANSPORT**

**JSM26/W/09-B3** **0830**

**TRACER TRANSPORT IN THE TROPICAL LOWER STRATOSPHERE IN A CTM SIMULATION**

Yvan J. ORSOLINI (Norwegian Institute for Air Research, Kjeller, Norway; email: orsolini@nilu.no) Martyn Chipperfield (Dept of Chemistry, Cambridge University, UK)

Tracer transport in the lower tropical stratosphere is diagnosed in a high vertical resolution simulation carried out with the isentropic chemical transport model (CTM) SLIMCAT, developed at the U. of Cambridge. The model has 20 levels, extending from the tropical tropopause to near 26 km. The simulation covers February 1996 to February 1998, and uses ECMWF analyses. A suite of 8 idealized tracers is transported, which are injected near the tropical tropopause. In particular, the tracers include two seasonally varying source tracers, an age of air tracer, a tracer with a constant source and two tracers which mimic N2O and CFCs. The later two are initialized with results of a photochemical 2D model, and are decaying with rates calculated from tabulated photodissociation rates as a function of zenith angle and pressure. The model results show a well-pronounced "tape recorder" signal, characterized by slow ascent of seasonally varying anomalies. It takes 10 months for tracer anomalies to rise from 100 mb to near 30 mb. We further examine regions of strong tracer meridional transport. A method for diagnosing regions of enhanced tracer eddy variability has been developed and tested for various seasons.

JSM26/E/13-B3

0850

**RAPID QUASI-ISENTROPIC TRANSPORT IN THE STRATOSPHERIC OVERWORLD DURING WINTER**

C. MARQUARDT, S. Leder and I. Fast, (Freie Universität Berlin, Institut für Meteorologie, Carl-Heinrich-Becker-Weg 6-10, 12165 Berlin, Germany, email: marq@strat01.met.fu-berlin.de)

It is now widely accepted that the transport regime in the "lowermost stratosphere" exhibits rapid meridional quasi-isentropic transport. It is also assumed that transport in this region is more effective than meridional transport in the mid and upper stratosphere: in contrast to the lowermost stratosphere, the tropical and mid-latitude stratosphere are thought to be relatively well separated by a "subtropical transport barrier", which is caused by wintertime planetary wave activity.

By examining two case studies using high-resolution RDF calculations (during northern and southern hemisphere winter, respectively), it is shown that in the presence of sufficiently strong planetary waves quasi-isentropic transport in the stratospheric overworld can be significantly stronger than in the lowermost stratosphere at the same time for a period of several days. Inspection of time series of minimum potential vorticity and meridional transport coefficients indicate that such transport events occur regularly during wintertime on both hemispheres. Some aspects of the low-frequency variability of the transport characteristics are discussed.

JSM26/E/17-B3

0910

**ISENTROPIC STRATOSPHERE-TROPOSPHERE EXCHANGE ACROSS THE SUBTROPICAL BARRIER USING PSEUDO-DIABATIC CONTOUR ADVECTION WITH SURGERY**

B. JOSEPH (1), A. Mariotti (2), B. Legras (1), D. G. Dritschel (3) (1) Laboratoire de Meteorologie Dynamique du CNRS, 24 rue Lhomond, 75231 Paris, France (2) ENEA National Agency - C.R. Casaccia, S.M. di Galeria - ROMA - 00060, Italy (3) School of Mathematical and Computational Sciences, University of St. Andrews, St. Andrews, Fife, Scotland KY16 9AJ, U. K.

We examine the isentropic stratosphere-troposphere exchange (STE) across the subtropical barrier in the Southern Hemisphere during the winter of 1998 (July) by employing pseudo-diabatic contour advection with surgery (PCAS) of potential vorticity (PV) using the ECMWF wind analyses.

PCAS is an extension of the usual contour-advection with surgery (CAS), which also assimilates the non-conservative component of the PV field evolution as an on-line correction to the purely advected PV field. It is demonstrated that PCAS can give superior results than CAS even within 10 days of integration period. One of the results from our study is that during the Southern winter, strong isentropic STE may also occur along uppermost isentropes ( $\approx 370\text{K}$ ) in the middleworld, in addition to that along lowermost isentropes ( $\approx 330\text{K}$ ) in the middleworld already noticed in earlier studies. In agreement with earlier studies, there is little STE along isentropes, which lie between the above two limits. A more stringent test of our results is provided by comparing the CAS and PCAS reconstructions of PV with ozone profiles over La Reunion and South Africa during a strong tropopause folding event, obtained as part of the TRACAS (Transport of Chemical species Across the Subtropical tropopause) field experiment in the Southern hemisphere. Our results suggest that the ozone peaks observed in the middle troposphere are a consequence of isentropic descent of extratropical stratospheric air into the subtropical tropospheric air. Again, PCAS has been found to reconstruct filamentary extrusions of stratospheric air, which are expected from peaks in ozone profiles, more faithfully than the pure CAS.

JSM26/E/11-B3

0930

**UARS MLS OBSERVATIONS OF CROSS-TROPOPAUSE WATER VAPOR TRANSPORT**

John MCCORMACK and Rong Ru (Institute of Atmospheric Physics, University of Arizona, Tucson AZ 85721, USA, email: mcc@atmo.arizona.edu)

UARS MLS measurements of specific humidity at 215hPa provide an opportunity to examine the transport of water vapor between the tropical upper troposphere and the extratropical lower stratosphere. At this level, extratropical stratospheric air is characterized by water vapor mixing ratios of  $\sim 10$  ppmv or less, while mixing ratios in the tropical upper troposphere range from 50 to 300 ppmv. Daily maps of MLS water vapor throughout northern winter and spring show the frequent redistribution of dry stratospheric/moist tropospheric air across 30 degrees N latitude associated with planetary wave activity. Four years of daily MLS upper tropospheric water vapor data (1991-1995) are combined with corresponding analyses of isentropic potential vorticity to create a composite description of this transport. MLS water vapor profile are used to determine the vertical extent of these stratospheric intrusions into the lower latitudes. The influence of equatorward propagating planetary waves on the distribution of water vapor, cloud s, and stability in the upper troposphere over the eastern tropical Pacific region is also examined.

JSM26/W/03-B3

0950

**A ONE-YEAR CLIMATOLOGY OF EXTRA-TROPICAL STRATOSPHERE-TROPOSPHERE EXCHANGE**

Michel BOURQUI and Henry Wernli (Institute for Atmospheric Science, ETHZ, CH-8093 Zuerich, Switzerland)

Stratosphere-troposphere exchange (STE) of mass, moisture and trace gases is a key factor of stratospheric chemistry and dynamics. Direct evaluation of such trans-tropopause exchange in the extra-tropics must take into consideration the (often) sub-synoptic scale and geographically-differentiated nature of the events that accomplish the interchange. In this study, a one-year climatology of the STE flux of air and ozone in the extra-tropics of the Northern Hemisphere is derived by combining (a) the six-hourly ECMWF analysis data (T213L31) for the period May 95 to April 96 and (b) ozone measurements derived in the MOZIC and NOXAR projects. Exchange events are defined using a Lagrangian conception of the air-flow and a dynamical (PV-based) definition of the tropopause. Evaluation of the fluxes entails computing sets of three-dimensional trajectories starting from a regular  $1^\circ \times 1^\circ$  degree grid every six hours throughout the stipulated period and utilising the ozone measurements to obtain the accompanying flux transport. This procedure provides large-scale coverage but with sub-synoptic scale resolution. The results yield illuminating details of the geographical distribution and seasonal variation of the up- and downward trans-tropopause exchange. In addition consideration is given to the sensitivity of the procedure, and a comparison is made with results from other studies.

JSM26/W/10-B3

1010

**ZONALLY SYMMETRIC MODES OF VARIABILITY IN THE ANTARCTIC UPPER TROPOSPHERE AND LOWER STRATOSPHERE AND THEIR INFLUENCE ON TOTAL COLUMN OZONE**

Mark HARVEY (CRC for Southern Hemisphere Meteorology, Monash University, Clayton 3168, Australia, email: mark@vortex.shm.monash.edu.au) Prof. David Karoly (CRC for Southern Hemisphere Meteorology, Monash University, Clayton 3168, Australia, email: djkar@vortex.shm.monash.edu.au) Simon Grainger (CRC for Southern Hemisphere Meteorology, Monash University, Clayton 3168, Australia, email: grainger@vortex.shm.monash.edu.au)

The intent of this study is to use the residual mean circulation as a diagnostic to examine the dominant modes of low-frequency variation of the Southern Hemisphere circulation in 1997. Zonal wind anomalies in the upper troposphere and lower stratosphere and their relationship to eddy fluxes of zonal momentum are also examined.

During the Austral winter and spring when planetary waves are able to penetrate into the stratosphere, these zonal mean zonal wind anomalies amplify with altitude into the lower regions of the polar stratosphere. Total column ozone is employed as a tracer to examine zonally symmetric oscillations between the tropics and higher latitude

JSM26/E/21-B3

1050

**THE INFLUENCE OF THE QBO ON ISENTROPIC MIXING AND TRANSPORT**

EMILY SHUCKBURGH, Peter Haynes, Centre for Atmospheric Science, DAMTP, Silver Street, Cambridge, CB3 9EW, United Kingdom, email: efs20@damtp.cam.ac.uk Alan Iwi, Warwick Norton, Dept. of Atmospheric, Oceanic and Planetary Physics, Clarendon Laboratory, Parks Rd, Oxford OX1 3PU

A 6 year integration with a chemical transport model, using ECMWF winds from 1992-8 has been used to investigate interannual variability in isentropic transport and mixing, in particular the influence of the QBO. The mixing properties of a flow may be characterised by calculating the 'effective diffusivity' (Nakamura: JAS 53 1524-1537 1996) of an advected tracer. The effective diffusivity characterises the geometric structure of a tracer, which is most complex where the mixing is strongest. Effective diffusivity calculated from passive tracer fields advected by observed winds has been used to produce a quantitative characterisation of the transport and mixing structure of the lower and middle stratosphere. This has shown the variation in height and latitude and the seasonal evolution, over the 6 years, of the stratospheric tropical reservoir and of the barrier to transport at the edge of the stratospheric polar vortex.

It is seen that in the tropics, mixing is inhibited when the QBO winds are easterly. When the QBO winds are westerly, the mixing structure suggests that wave disturbances are able to propagate from the extratropics in the winter hemisphere through the westerly winds in the tropics and then break in the weak winds in the tropics or subtropics of the summer hemisphere. The influence of the QBO on the extratropical transport and mixing is also investigated.

Comparison is made between time series of effective diffusivity calculated from ozone fields simulated by the chemical transport model and ozone fields measured by MLS.

JSM26/W/28-B3

1110

**QBO MODULATION OF TROPICAL TRACER TRANSPORT IN THE LOWER STRATOSPHERE**

A. IWI, W. Norton (AOPP, University of Oxford, Clarendon Lab, Parks Road, Oxford OX1 3PU, UK, email: iwi@atm.ox.ac.uk)

A six-year integration of a chemical transport model (CTM) forced by ECMWF analysis is examined as to its simulation of the tropical lower stratosphere. It is found that the quasi-biennial oscillation (QBO) produces marked interannual variability in the distribution of chemical tracers. This has a significant impact on many features including tropical vertical ascent rates, tropical "tape recorder" signal, age of air, and correlation of long-lived tracers. The annual cycle of the subtropical transport barrier will be discussed. Comparison will be made with available observed measurements and with results from other CTMs, which are a part of the EU-funded TOPOZ II project.

JSM26/E/16-B3

1130

**QUANTIFICATION OF FILAMENTS IN THE NORTHERN HEMISPHERE TROPOPAUSE REGION**

O. MORGENSTERN and G. Carver (both at Centre for Atmospheric Science, Chemistry Dept., Cambridge University, Cambridge CB2 1EW, UK, email: Olaf.Morgenstern@atm.ch.cam.ac.uk, Glenn.Carver@atm.ch.cam.ac.uk)

Contour advection simulations are performed of analyzed potential vorticity fields for every day of January and February of the years 1997 and 1998. Filaments are defined as structures of small cross-dimension penetrating in those simulations the finite-thickness tropopause in either direction. Statistics of such structures are derived; episodes of strong hemispheric-mean filamentation are related to the formation of tropospheric cut-off systems evolving in the later stages of Rossby-wave breaking events. Zonal asymmetries occur as these waves favourably break near the end of the North-Atlantic storm track. The results hint at the role of filamentation in accounting for the interannual variability of ozone.

JSM26/W/24-B3

1150

**MONITORING OF STRATOSPHERIC INTRUSIONS USING MST RADAR AND OZONESONDES AT ABERYSTWYTH**

R.M. Worthington, G. Vaughan (Department of Physics, University of Wales, Aberystwyth, SY23 3BZ, U.K. email: rrw@aber.ac.uk, gxv@aber.ac.uk)

This study examines events since 1991 when stratospheric intrusions could be detected and tracked above Aberystwyth ( $52.4\text{N}$ ,  $4.1\text{W}$ ), using extensive data from MST radar, and ozonesondes launched 5 km away. The radar measures height-time structure of wind and wind shear, and the occurrence of increased turbulent mixing shown by Doppler broadening of the radar echoes. The power and anisotropy of the echoes also give information about the static stability. Variability in the evolution of streamers of stratospheric air in the troposphere is studied in terms of their chemical compositions, their changing wind velocity structure, and the intermittency of the turbulent mixing of stratospheric and tropospheric air.

JSM26/W/01-B3

1210

## APPLICATION OF 4D-VAR ASSIMILATION OF STRATOSPHERIC CHEMICAL SPECIES ON THE FIRST CRISTA FLIGHT

Q. ERRERA, D. Fonteyn (Belgish Instituut voor Ruimte Aeronomie, Institut d'Aeronomie Spatial de Belgique, 3 av. circulaire, Brussels, B-1180, Belgium, email: Q.Errera@bira-iasb.oma.be), and M. Rise (Physics Department, University of Wuppertal, Gauss-Str. 20, 42097 Wuppertal, Germany)

For the first time, comparison of model calculations with actual observations is performed by 4D-VAR assimilation. From a general point of view, variational assimilation consists in constraining a model to reproduce the observations and hence find the initial model conditions. In this paper, we present the results of variational assimilation of the stratospheric chemical species performed using CRISTA observations. The CRISTA observations were chosen due to the exceptional spatial data coverage. The 4D-VAR assimilation system and the measurements are briefly described. The chemical composition and its evolution, obtained by these analyses, are discussed as well as the predictive capability of the model. Two main aspects will be considered: from a modelling point of view the 4D-VAR assimilation allows a detailed comparison with observations and thus a validation of the 3D chemical transport model is discussed. The analyses make it possible to perform a predictive model calculation, this gives better a priori information about the composition of the stratosphere. Thus, retrieval algorithms will benefit from this information.

JSA27

Monday 26 July

## HIGH-RESOLUTION GEOPHYSICAL STUDIES OF MINERALIZED ZONES (IAGA, IASPEI)

Location: Muirhead Tower, 112 LR2

Location of Posters: Muirhead Tower, Student Room, (1st Floor)

Monday 26 July AM

Presiding Chairs: Bülent Tezkan (Institut für Geophysik, Univ. Köln, Germany), Bernd Milkereit (Institut für Geophysik, Univ. Köln, Germany)

JSA27/P/05-B1

0900

## A STUDY OF INTEGRATION METHOD OF REMOTE SENSING AND AEROMAGNETICS FOR TECTONIC PROSPECTING OF GOLD ORE DEPOSITS

Zhu ZHENHAI (Institute of Remote Sensing Applications, Chinese Academy of Sciences, Beijing, 100101, P. R. China, email: zhuzh@irsa.irsas.ac.cn); Hao Tianyao (Institute of Geophysics, Chinese Academy of Sciences, Beijing, 100101, P. R. China, email: tyhao@mial.c-geos.ac.cn); Huang Xiaoxia, Wang Hongmei (both at the Institute of Remote Sensing Applications, Chinese Academy of Sciences, Beijing, 100101, P. R. China, email: zhuzh@irsa.irsas.ac.cn)

According to the distribution characteristics of known gold deposits of mid-latitude area of Asia, the obvious regularity of preferentiality of the distribution of a serial of large, rich gold deposits has been discovered. The tectonic prospecting model of gold deposits guided mainly by transverse structures has been established. Because of its diffuse characteristics, the transverse structures are hard to be found by using the conventional geology investigating method. In order to discriminate effectively the transverse structures, we put forward an analytic method of integrating remote sensing and aeromagnetics technology.

The experiment area is mineralization belt of Yin Mountain and Yanliao gold deposits located in northern margin of the northern China Plate. According to the macroscopic interpretation of remote sensing and the new method of "thin shield" for linear tectonics inversion by using aeromagnetic data, the regional distribution of transverse structures has been interpreted. Supporting by the information system of mineral resources, and integrating the analysis of regional strike structure and activity of magnetic rocks and geological background of mineralization, the exploration prospect of large and rich gold ore deposits of Yin Mountain and Yanliao mineralization belt has been put forward.

JSA27/W/02-B1

0920

## GRID-INDEPENDENT ELECTRODE POSITIONING FOR 3D DC AND IP FORWARD MODELING IN MINERAL EXPLORATION

Klaus SPITZER (Joint Geoscientific Research Institute, Stilleweg 2, 30655 Hannover, Germany, email: klaus.spitzer@gga-hannover.de); Michel Chouteau (Ecole Polytechnique, Succ. Centre-Ville, PO Box 6079, Montreal (Qc) H3C 3A7, Canada, email: chouteau@geo.polymtl.ca)

Electric crosshole measurements in mineral exploration require flexible interpretation software because transmitters and receivers are lined up along boreholes that are generally not aligned with the axes of Cartesian coordinate systems. Therefore, we present a 3D DC and IP forward modeling code, which offers grid-independent electrode positioning, i.e. locations of transmitters and receivers may be detached from the grid nodes. This is possible through a singularity removal procedure which splits up the potential in a normal and an anomalous part. The normal part containing the singularity is calculated analytically and is thus independent from the finite difference grid. Consequently, source locations are literally arbitrary. The potential at the receiver positions is calculated via tri-linear interpolation of the anomalous potential. This is superior to interpolating the total potential because the anomalous potential is rather smooth compared with the total potential and shows less steep gradients. Therefore, the accuracy is considerably raised. The new code is applied to a crosshole survey at a gold mine and its advantages (reduction in grid size, decrease in run time) are presented.

JSA27/E/07-B1

0940

## EULER DECONVOLUTION OF GRAVITY TENSOR DATA

Martin F. MUSHAYANDEBVU, Alan B. Reid, J. Derek Fairhead (School of Earth Sciences/GETECH, University of Leeds, Leeds LS2 9JT, UK, email: mushaya@earth.leeds.ac.uk); Changyou Zhang (117-401 Westview St., Coquitlam, B.C., V3K, 3W3, Canada); Mark Odegard (GETECH, 12946 Dairy Ashford, Suite 250, Sugar Land, Texas 77478, USA)

Conventional Euler deconvolution uses 3 orthogonal gradients of any potential quantity as well as the potential quantity itself to determine depths and locations of a source. Gravitational acceleration is a vector with 3 Cartesian components and the gradient is thus a 9 component tensor. Euler deconvolution is developed and modified for the interpretation of gravity tensor gradient data. Using all the measured tensor gradients puts additional constraints on the Euler solutions data forms. The method has also been tested on measured gravity tensor gradient data from the Eugene Island area of the Gulf of Mexico with gridded and profile data forms.

The results from both model and real data show improved performance for the tensor Euler deconvolution.

JSA27/W/01-B1

1000

## GEOLOGICAL DELINEATION OF THE MAIN STRUCTURAL TRENDS AS REVEALED FROM, TOPOGRAPHICAL, AEROMAGNETIC AND AREORADIOSPECTROMETRIC DATA AND THEIR RELATION TO URANIUM REMOBILIZATION IN WADI UM-HAD AREA, CENTRAL EASTERN DESERT, EGYPT

Nasser HASSAN (Geophysics Dept., Fac. of Sc., Ain Shams Univ., Egypt (email: aboashor@asunet.sahams.eun.eg); Magdy A. Gouda, Said I. Rabie, Ahmed A. Ammar (all at Nuclear Materials Authority, P.O.Box 530 Maadi, Cairo, Egypt)

The main objective of the present study is to make use of the different geologic, topographic aeromagnetic and aeroradiospectrometric data in identifying the main directions of the interpreted structural lineaments prevailing in the area of Wadi Um-Had, Central Eastern Desert, Egypt. This objective was quantitatively achieved through the application of combined statistical analysis of trends using the autocovariance function and the successive overlap techniques for all the available data. Such analyses were devoted mainly to try visualize the relationship that might exist between the various interpreted trends and the tectonic pattern. Moreover, they may help reveal the tectonic forces that affected the basement rocks as well as any significant relations reflecting mineralization control. The results attained in this study seem to indicate eight main orientations that take the following particular sequences: N-S, NNW, NW, WNW, E-W, ENE, NE and NNE directions. Three trends (NNW, NW and WNW) out of the recorded eight were found to represent ancient (deep seated) as well as recent (near surface) structures. The E-W trend is interpreted as ancient trend. Besides, the study revealed the insignificant existence of two main trends: N-S and NNE as far as the area under study is considered. It is recommended that the NNW, NW and importance from the point of view of radiospectrometric exploration. The investigated area has been subjected to a maximum principal stress that is nearly oriented in the ENE to NE trend which is perpendicular to the dominant NNW and NW trends. Furthermore, the degree of remobilization of uranium within the different rock units is reflected on the trends of the variations of uranium and thorium with their ratios. It was evident that a strong remobilization of uranium is indicated in the granitic rocks, Nubian sandstones, phosphate formation, gneisses and migmatites as well as the hammamat sediments.

JSA27/P/01-B1

1050

## INTEGRATED GEOLOGICAL AND HIGH-RESOLUTION GEOPHYSICAL STUDIES ON THE COPPER-BEARING PRECAMBRIAN ROCKS AT SOUTH WADI HAMMAD AREA, NORTH EASTERN DESERT OF EGYPT

Aboulhoda M. ELSIRAFY, Mahmoud H. Shalaby (Nuclear Materials Authority of Egypt, P.O Box 530 Elmaadi, Cairo, Egypt)

Field geological studies showed that the copper mineralization at south Wadi Hammad area, located in the northern part of the Egyptian Eastern Desert, is litho-tectonically controlled, and that the composition of the Precambrian metagabbro-diorite rocks, hosting this mineralization is rather complex. These rocks range from diorites, quartz diorites to granodiorites. In case of strong granitization they could approach the granitic composition and are intensely jointed and sheared. This is mainly attributed to their tectonic setting where they lie at the intersection of two regional fault zones. Petrographic investigations, on the other hand, indicated that these rocks are essentially composed of hornblende and plagioclase feldspars with a minor amount of biotite, quartz and orthoclase. The common accessory minerals are zircon, garnet, apatite, beside abundant iron oxides.

Electrical self-potential measurements confirmed the subsurface extensions of the structural zones controlling the copper mineralization down to depth level of 125 m. Further deeper extensions are highly expected. High resolution spectral gamma-ray scanning, carried out within some pre-existing deep exploratory and worked trenches, indicated that uranium enrichment is a phenomenon accompanying the copper mineralizing process. Potassium was also enriched but on a much smaller scale. So, spectral gamma-ray survey is recommended as an efficient geophysical exploration tool for locating further copper-mineralized zones in the same geologic environment. In that regard radioelement ratio measurements will be of higher significance than the absolute abundance.

JSA27/E/09-B1

1110

## 3-D SEISMIC IMAGING OF A DEEP MASSIVE SULPHIDE DEPOSIT

Bernd MILKEREIT (Geosciences, Kiel University, 24118 Kiel, Germany, email: bmilkereit@geophysik.uni-kiel.de); Brian Roberts (Geological Survey of Canada, Ottawa, Booth Street, K1A 0Y3, email: roberts@cg.nrcan.gc.ca)

The Sudbury Basin in Canada was selected for conducting one of the world's first 3-D seismic survey for deep base-metal exploration. Over the past 5 years, an extensive database of geological mapping information, geophysical logs of existing deep drill holes, and core samples for physical rock property studies has been assembled to support the interpretation of seismic data across the Sudbury Structure. In terms of seismic exploration, the contact between the "transparent" SIC Norite and the "reflective" footwall complex represents a clear regional marker horizon, making it possible to map the bottom of the SIC and topography at the impact crater floor (the principle location for Ni-Cu deposits). In addition, the velocity-density field for sulfides (including the pyrrhotite and chalcopyrite assemblages typical for ores in Sudbury) is distinctly different from that for common silicate rocks (such as norite in the hanging wall and gneiss in the footwall), suggesting that massive sulfide bodies should generate prominent seismic reflections. Various stages of the ambitious 3-D seismic exploration study will illustrate: from survey design to helicopter assisted data acquisition and from special processing considerations to final interpretation and groundtruthing of the 3-D seismic data volume. The 3-D seismic experiment confirms that in a geological setting such as the Sudbury North Range, deep massive sulphide bodies cause a characteristic seismic scattering response. This provides an excellent basis for the direct detection of deep massive sulphides in the crystalline crust by seismic methods.

JSA27/E/06-B1

1130

## APPLICATION OF SYNTHETIC APERTURE RADAR (SAR) FOR EXPLORATION OF MINERALIZED ZONES

Wool M. MOON (Earth System Science, Seoul National University, Seoul 151-742, Korea, email: wmoon@eos1.snu.ac.kr or wmoon@cc.umanitoba.ca); W.W. Jiang (Institute of Geophysics, Academia Sinica, Beijing, China); S.G. Choi, S.W. Choi (Earth and Environmental Science, Korea University, Seoul, Korea)

Synthetic Aperture Radar (SAR) is an active sensor which has many advantages over optical sensors for its all-weather capability without solar illumination. For geological applications,



SAR systems can utilize X-, C-, and L-band microwave signals for imaging of the Earth's surface features. Furthermore, multiple polarization capabilities of the SAR antenna have greatly increased the applicability of SAR systems with respect to both surface and volume scattering over geologically anomalous zones such as specific mineralization. Although integrated approach in mineral exploration has become more cost effective and are well accepted, there are many technical and scientific issues to be further investigated and researched. In this study we have reprocessed several sets of previously surveyed exploration data and experimented with fuzzy logic digital fusion of the preprocessed data. The exploration target hypothesis was that there is a W-Mo-F mineralization in the study area. Among the numerous fuzzy logic operators, currently available for data driven integrated exploration strategy, we have used varying combination of fuzzy MIN, fuzzy MAX, and fuzzy SUM operators along with Gamma operator for digital fusion of geochemical, geophysical, and geological information, including the contact metamorphic zone information. In this study, we have also investigated and evaluated the JERS-1 SAR and SIR-C multiple frequency SAR data for differential backscattering effects of microwave with the surface geological material over skarn type ore mineralization. The fuzzy logic derived mineral potential anomaly has almost exactly matched the differential backscattering anomalies on the SIR-C C-band and L-band data overlaid on each other. Although the high degree of correlation is remarkable, the differential backscattering anomaly over the skarn type W-Mo-F ore mineralization in the study area requires further investigation.

JSA27/E/02-B1

1150

#### HIGH RESOLUTION MAGNETIC AND ELECTROMAGNETIC IMAGES OF A CANADIAN MASSIVE SULPHIDE MINING CAMP

Michael THOMAS, Pierre Keating, John Katsube, Neil Rogers, Cees van Staal (all at Geological Survey of Canada, 615 Booth St., Ottawa, Ontario K1A 0E9, Canada, email: mthomas@gsc.nrcan.gc.ca)

A helicopter-borne geophysical survey over the entire Bathurst mining camp in the Canadian Appalachians collected magnetic, electromagnetic and radiometric data at mean terrain clearances of 45 m, 30 m and 60 m, respectively, along flight lines spaced 200 m apart. Resultant high resolution images of measured and derived parameters, particularly those for the magnetic and electromagnetic data sets, provide a unique perspective on the lithological and structural fabric of the bedrock geology, which is largely obscured by a glacial veneer. Calibration of magnetic anomaly and apparent conductivity maps (derived from the 4433 Hz co-planar electromagnetic data) with exposed bedrock indicates various close correlations between magnetic features and mafic volcanics, mafic dykes, gabbroic intrusions and iron formations, and between distinct conductivity features and sedimentary horizons containing black shale and argillite. Geophysical detection of poorly mapped or unmapped iron formations has particular relevance to massive sulphide exploration, given their genetic/spatial association with sulphide deposits. The high resolution maps have been used to enhance geological mapping in the dominantly felsic volcanic, northwest part of the camp. Thin sedimentary and mafic units have been traced geophysically, imparting a tectono-stratigraphic framework to the region. Truncation of units has provided evidence of several thrusts, whose presence must be considered in exploration strategies. Perhaps most importantly for exploration, the new geophysical maps reveal many direct targets for investigation, in the form of roughly circular to elliptical magnetic and conductivity highs. Many correlate with known massive sulphide occurrences, others remain to be examined. One set of co-spatial magnetic and conductivity anomalies that was investigated shortly after completion of the airborne survey resulted in discovery of a small sulphide body.

JSA27/P/04-B1

1210

#### HIGH PRECISION AIRBORNE MAGNETIC AND GAMMA SPECTROMETRIC SURVEY FOR MINERAL EXPLORATION IN THE EASTERN DESERT OF EGYPT

Kadry M. FOUAD (Prof. of Geophysics, Nuclear Materials Authority, P.O. Box 530 Maadi, Cairo, Egypt)

Airborne geophysical exploration activities in Egypt date back to the late fifties. A new king Air Beechcraft C90B aircraft was purchased lately equipped with state-of-the-art magnetic and spectrometric survey systems, as well as navigation and other ancillary equipment. The magnetometer in-flight sensitivity is 0.001 nT, with ten measurements every 1.0 sec. The multichannel airborne gamma-ray spectrometer accepts signals from 50 1 of Na I (Ti) detectors. This system allows the quantitative interpretation of the geochemical parameters indicated by U, Th and K contents in rocks. An airborne differential GPS navigation system receives signals from 12 satellites to provide aircraft positioning in 3-D, accurate to 5 m or better. An IBM compatible data acquisition system accepts and corrects data from the whole system. An advanced software package is utilised for processing the data. The generated contour maps represent the total magnetic field, the total radiometric count, as well as the U, Th and K contents. Powerful techniques are available to help interpret the maps. The power spectrum analysis transfers the magnetic data to the pole, separates the residual and regional fields, delineates the depths to the magnetic interfaces and bodies. The interpreted tectonic framework of the survey area is invaluable in delimiting locations of potential mineralization. Interpretation of the spectrometric data and their ratio maps (U/Th, U/K and Th/K) results in the delineation of the surface distribution of the radioelements. Spots most favorable for U concentration are identified and the direction and degree of its remobilization from the mother rock is indicated. Surface-subsurface configuration of the geological-tectonic setting could be figured out. In addition digital image processing techniques applied to the non-image survey data provided extremely valuable information. Examples of case histories from the Eastern Desert of Egypt are presented.

### Monday 26 July PM

Presiding Chairs: Bülent Tezkan (Institut für Geophysik, Univ. Köln, Germany),  
Bernd Milkereit (Institut für Geophysik, Univ. Köln, Germany),  
Kadry Fouad (Nuclear Materials Authority, Cairo, Egypt)

JSA27/W/03-B1

Poster

1400-01

#### TELEMETRED MULTICHANNEL SYSTEM FOR GEOPHYSICAL CABLE

Florin IONICA (National Institute for Earth Physics, P.O. Box MG-2, Bucharest, Romania presently at University of the West Indies, Earthquake Unit, Mona, Kingston 7, Jamaica W.I., email: fionica@uwimona.edu.jm)

A new telemetred multichannel system for geophysical cable is presented. The investigation of the boreholes is very important to be done using as many measuring channels as possible in order to have fast and effective results. Multiwire cable which are now used in multichannel systems are very problematic due to the connectors, durability and wear. Water tightness must be very high degree because of high pressure which exist in boreholes over 1000 meters. Also noises and disturbances generated by external electromagnetic fields are big problems especially in VSP or HSP measuring where all the signals, also the weakest reflections must be recorded at sufficient resolution. Taking in account these requirements it was designed one modular system which is constructed to function on one coaxial cable where all the channels are located in parallel in frequency domain. This kind of system is called telemetry system and is

used mostly in airplane and space equipment. This telemetry system consist of transducer units (every one with three geophones), circuits to transfer signals to cable, electronic controls and power supply components. These units are connected on a strong main coaxial cable as many as needed. Physically are in series with cable but electrically are in parallel as on a bus line.

JSA27/L/01-B1

Poster

1400-02

#### ORE AUDIOMAGNETOTELLURIC SOUNDINGS (AMTS)

ANTSIFEROV, A.V., Novgorodseva, L.A. Belyavsky V.V., Sukoi L.A.

Abstract not available at time of going to press

JSA27/P/02-B1

Poster

1400-03

#### UTILIZATION OF AERORADIOISPECTROMETRIC SURVEY DATA IN DEFINING RADIOELEMENT ANOMALOUS ZONES IN ELGALALA ELBAHARIYA - ELGALALA ELQIBLIYA, NORTHERN EASTERN DESERT, EGYPT

Ahmed A. AMMAR, Mohamed A. Elsadek (both at Exploration Division, Nuclear Materials Authority, P.O. Box 530 Maadi, Cairo, Egypt); Ahmed M. Sabri (Geophysics Dept., Faculty of Science, Ain Shams Univ., Abbasiya, Cairo, Egypt)

Elgalala Elbahariya - Elgalala Elqibliya area is situated in the Northern Eastern Desert of Egypt. Its surface area, reached about 3000 km<sup>2</sup>. Various rock units are exposed in the study area and are represented by different lithological groups ranging in age from Late Paleozoic to Quaternary. The present work is dedicated to identify the significant aeroradiospectrometric zones of anomalously high "U" and/or "Th" concentrations. Their delineation is based on the techniques of construction of standard deviation (anomaly) contour maps as well as computation of uranium favourability index (U<sub>2</sub>) and the three-elemental effective parameters (F). This study revealed the presence of 76 individual aeroradiospectrometric anomalies which could be assembled into three main groups. These anomalies could be related to either the prevailing faulting system and/or some specific lithologic units and formations. Their aerial eU and eTh values range from 0.50 ppm to 3.60 ppm for eU and between 0.60 ppm to 6.20 ppm for eTh. The eU/eTh, eU/K and eTh/K ratio values differ generally from 0.10, 1.0, and 5.50 to 2.50, 15.0, and 16.0 respectively. The U<sub>2</sub> index and F-parameter oscillate from 0.10 to 1.85 for U<sub>2</sub> and from 0.08 to 0.42 for F. From the economic potential point of view the most promising anomalies are three correlated with El-Galala, Duwi and Mokattam formations as well as Quaternary Sediments and also with the NW- and NE- trending structures.

JSA27/E/04-B1

Poster

1400-04

#### MATHEMATICAL REGIONALIZATION OF THE ORGANIC RESOURCE IN THE EARTH'S CRUST

Tarzadin ULAANBAATAR (Department of Earth Sciences, National University of Mongolia, email: numelect@magincet.mn)

Reliable regionalization of the mineral resource of planet is one of the main bases of successful geophysical exploration. The organic resource in planetary-scale must determine by the reconstruction of the paleotropic and paleosubtropical zones and interglacial epochs when happened agreeable natural conditions for accumulation of the gigantic fauna and flora. In this paper a new mathematical geologic method for regionalization of geographical, climatic zones in accordance with geochronology is shown. The method is based on a 3D model of thermal regime on and near the Earth's surface which includes three simple parameters: number of day from winter solstice, measuring time, geographical latitude. Fortunately, the model parameters have determined geochronologically by studies of paleogeography, paleobotany, paleontology and paleogeocryology. In this paper the paleotemperature regime, insolation regime of geological past time, duration of the daylight, altitude of sun, total insolation in different time interval along interested latitude (zonal), geographical, climatic zones are described. For this reason, based on the mathematical model the organic mineral resources in the earth's crust are shown to be regionalized.

JSA27/L/02-B1

Poster

1400-05

#### RESISTIVITY TOMOGRAPHY WITH INTEGRAL METHOD

QUINGYUN, D Miaoyue, W

Abstract not available at time of going to press

JSA27/E/01-B1

Poster

1400-06

#### PROBLEMS OF HIGH RESOLUTION COMPLEX OF METHODS OF DYNAMIC GEO-ELECTRICITY CREATION FOR INVESTIGATION OF ZONE OF MINERALISATION

Gidroingeo R.TURSUNMETOV (64, Khodjibayev str., Tashkent, Uzbekistan)

Increase of exploration depth in complex geo-structural situation requires more reliable and effective methods of exploration. One of these methods is the method of dynamic geo-electricity which is being now under development. In this method along with rocks' statical properties, connected with linear processes, rocks' dynamic properties, connected with non-linear processes, are studied. Rocks' dynamic properties are bounded mostly with energetically active zones of mineralisation, where electro-chemical and electro-cynetic processes, which, in turn, create intensive natural electric fields. Under electro-magnetic stimulation of these zones results are affected by external phenomena along with phenomena of polarisation that makes difficult their right interpretation. In this connection special investigations were carried out to create high resolution complex of dynamic geo-electric diagnostic methods for zone of mineralisation study, including the following tasks:  
1. study of electro-magnetic properties of rocks dispersion in time and frequency domain and bringing results to the common level, because rocks' electro-magnetic properties differently response to electro-magnetic fields influence, created by different methods of stimulation.  
2. Dynamic electro-magnetic properties of rocks are represented by non-linear parameters of resistance and polarization and by coefficient of heterogeneity of electro-magnetic field. That is why electro-magnetic field distribution under different kinds of stimulation is desirable to use.  
3. While studying electro-magnetic field behavior over zone of mineralisation it is necessary to take into account not only processes, connected with polarization under artificial electric current flow, but also the phenomena taking place before the environment stimulation. This question clarification will permit to study natural electric field with a depth. In order to solve above problems, managed installations are suggested, which allow to create definite current density on the definite depth and obtain information about environment's dynamic properties. Special installations are suggested also to study coefficient of heterogeneity of electro-magnetic field and non-linear parameters of electric resistance.

**JSA27/E/08-B1** Poster **1400-07**

**THE PIEZOELECTRIC MODEL FORMATION NATURAL ELECTRIC FIELD IN THE EARTH**

D.Kh. RASULOEV (Lange Institute of Hydrogeology and Engineering Geology, Tashkent, Uzbekistan, e-mail: root@ariel.tashkent.su)

In the last 50 years the large volume of information stored about natural electric fields in the Earth. Despite of that the question of origin of some of theirs still remained open. The piezoelectric model formation natural electric fields of the Earth is considered in work: formulated the conditions of formation natural piezoelectric fields (NPF) and carried out detailed analysis their fulfillment on the concrete experimental material in natural environment. The principal condition of formation NPF is existence of piezoelectric textures in rocks. By works of previous researchers were ascertained that this condition often to fulfill. Another necessary condition of NPF formation is sufficiently high values of specific electric resistors of reserch rocks: over 1000 Ohm. The additional conditions of NPF formation are existence of the differentiation on rock's tense state and unevenness screening fluence of the cover beds. The piezoelectric model well all peculiarities of manifestation of such natural electric fields as "Changeable in time fields", "Intensive negative anomalies", "Positive anomalies over the pegmatitic veins". The proposed model also explains many unique cases of observations of selfpotential over the sulphide and polymetallic deposits. The piezoelectric model shows how such physical parameters of rocks as temperature, pressure, dampness and selfpotential are correlated.

**JSA27/E/05-B1** Poster **1400-08**

**RADIOWAVE GEINTROSCOPY OF THE ROCKS IN THE INTERWELL AREA (RWGI IWA)**

V. A. ISTRATOV, M. G. Lisov (both at Radionda Ltd. C, 121614, Moscow, Kriilatskie Holmi, G- 614, Box 44, email: radionda@glasnet.ru)

Presented technology for the detailed 3D-mapping non-homogeneous geological strata, having internal peculiarities in electrical properties. The method is based on the relationship of radiowave dissipation in the rock massif strata, depending on electric resistance and dielectric permeability of the rocks situated on the way of radiowave beam. Method is realized by multiple high-frequency raying of the rock massif with dipole source and the following processing of the "radiowave picture" with tomographic, iterative, and other special technique. Applying of the RWGI IWA has resulted in significant reduction of prospecting and exploration drilling amounts, of the time consumption for geological surveys, searches, prospecting and exploration of ores, oil and gas deposits and for means of hydrogeology and engineering geology as well. This method has the most effective application in prospecting and evaluation surveys of deep ore deposits, when high drilling spending are accompanied with the highest business risk. The method can be used with high efficiency in express estimations of the geological researches quality during purchasing of licence for mineral mining. Presently this method can be applied for the interwell distance from 5 meters up to 1.5 kilometers. The biggest for the present time in the world distance is obtained by use relatively low frequency in observation (frequency range: 0.01 - 36 MHz). RWGI IWA method is applied for prospecting and 3D mapping diamond pipes; in oil geology for determination and evaluation transport properties of fracture-porous collectors, mapping oil pools and studying their internal features; in engineering geology during construction and exploitation tunnels (in Moscow Underground), hydropower stations (in permafrost area) and environment high-risk big industrial objects. The method RWGI IWA was applied on different objects in Russia, Spain and South Africa.

**JSA27/E/10-B1** Poster **1400-09**

**DETAILED MAGNETIC INVESTIGATION FOR SEARCHING SHALLOW CHROME OREBODIES**

Arben LULO, Alma Renja (Geophysical and Geochemical Center, L 9, Blloku "Vasil Shanto", Tirana, Albania)

Located in the southern part of Bulqiza Ultrabasic Massif, Albania, the area selected for investigation had rugged topography, deluvial thickness well developed and geological conditions favorable to chrome deposits. The detailed ground magnetic survey was conducted as part of the geological-geophysical study for searching shallow depth chrome orebodies associated with the harzburgite rocks section. Using a proton procession Scintrex magnetometer of 1 nT accuracy the survey net of 40m x 5m was carried out in an area of 4 km<sup>2</sup>. After the data were smoothed, resampled and gridded at a 10m interval the total field magnetic anomaly map was compiled.

In general there is not a good agreement in between the surface geology and the magnetic anomalies in this area. An interpretation of the total field magnetic anomaly map was made transforming it to the magnetization anomaly (susceptibility) map. With a strike filter the results are improved. Zones of the anomalous magnetization (transitory from the negative to the positive magnetic susceptibility intensity) are obtained in this map, interpreted as in agreement with the modeling from the laboratory measurement in chromite samples. It was felt that the shallow orebodies which should influence the surface magnetic data could be more apparently defined in this transformed map. One of the susceptibility anomaly has revealed a shallow chromite deposit about 350m in length in a zone totally covered by overburden.

**JSG28** Monday 26 – Tuesday 27 July

**PROBING THE ATMOSPHERE BY GPS (IAG, IAMAS)**

Location: Haworth Building 203 LT  
Location of Posters: Old Gym

**Monday 26 July AM**

Presiding Chair: Michael Bevis (University of Hawaii, Honolulu, Hawaii, USA)

**Introduction** **0930**

M Bevis (Uni of Hawaii, USA)

**JSG28/E/07-B1** **0950**

**GPS ESTIMATION OF ATMOSPHERIC WATER VAPOUR FROM A MOVING PLATFORM**

Alan DODSON, Wu Chen, Nigel Penna and Helen Baker (IESSG, University of Nottingham, Nottingham, NG7 2RD, UK, Email: alan.dodson@nottingham.ac.uk)

Estimates of atmospheric water vapour are of vital importance to meteorological and climatological modelling, contributing to a wide variety of processes from small scale weather

systems to global climate change. In recent years there has been considerable international interest into the use of ground-based GPS for water vapour estimation and it has been demonstrated that the water vapour can be routinely obtained by GPS with an accuracy of 1 kg per square metre. A reliable method for accurately measuring atmospheric water vapour from a moving platform would be of great benefit to both meteorological and climatological disciplines, and as calibration for satellite-based estimates at coastal locations. It is common knowledge that the sea/air interface is a major contributor to worldwide weather fronts. The measurements of water vapour at strategic locations would provide an important data set for input into climatological models, as well as for meteorological purposes in coastal and near shore regions. In this presentation, a new algorithm is developed to separate the tropospheric delay from the motion of the GPS antenna, especially the height component. The initial test results will also be presented.

**JSG28/W/05-B1** **1010**

**GROUND BASED GPS METEOROLOGY: AN EVALUATION OF DIFFERENT SOFTWARE PACKAGES USING TWO YEARS OF DATA FROM THE SWEDISH NETWORK**

J.M. JOHANSSON, G. Elgered, L.P. Gradinarsky, B.G. Stoew (all at Chalmers, Onsala Space Observatory, SE-439 92 Onsala, Sweden, e-mail: jimj@oso.chalmers.se)

A continuously operating network of ground-based GPS receivers in Sweden has produced data since the summer of 1993. We will here discuss the measurement uncertainty of the derived Integrated Precipitable Water Vapour (IPWV). The quality of the GPS estimates can be assessed through comparisons with independent techniques. We use microwave radiometry and radiosonde observations in order to study the different types of error sources involved.

**JSG28/W/08-B1** **1030**

**A CLOSE RELATIONSHIP BETWEEN TEMPORAL ANOMALIES IN SITE COORDINATE AND ZENITH TROPOSPHERIC DELAY IN GPS ARRAY OVER THE JAPANESE ISLANDS IN SUMMER**

Tetsuya IWABUCHI (The Graduate University for Advanced Studies, Mizusawa, 023-0861, Japan, email: iwabuchi@miz.nao.ac.jp); Isao Naito (National Astronomical Observatory, Mizusawa, 023-0861, Japan, email: naito@miz.nao.ac.jp)

Under a simple assumption of azimuthally homogeneous distribution of water vapor in Global Positioning System (GPS) analysis, a close relationship between horizontal coordinate variation and zenith tropospheric delay (ZTD) is found in the operational analysis of nationwide GPS array of Geographical Survey Institute (GSI) over the Japanese Islands, in particular, during weather conditions that systematic horizontal gradient of water vapor exists in cases of front passages and tropical cyclone. The ZTD gradient of 50 mm per horizontal distance of 100 km is found to cause apparent horizontal coordinate variation of about 10 mm. These relationships become useful information to diagnose if unusually large horizontal coordinate variations retrieved by the GPS analysis reflect net crustal movements or noise due to water vapor distributions.

**JSG28/E/01-B1** **1040**

**COMPARISON AND ACCURACY OF INTEGRATED WATER VAPOR FROM GROUND BASED GPS**

H. Klein Baltink, A.C.A.P. van Lammeren, H. Derks (KNMI, De Bilt) B.A.C. Ambrosius, A.G.A. van der Hoeven, F. Kleijer, H. VAN DER MAREL (Delft University of Technology); A.J.M. Kosters (Survey Department of Rijkswaterstaat, Delft)

Integrated water vapor (IWV) is computed on a routine basis from a ground based GPS network in The Netherlands. The data is stored in a database together with IWV computed from radiosondes and IWV computed from KNMI's regional RACMO model. The standard deviation of the difference of the GPS derived IWV estimates for Kootwijk and radiosonde derived IWV in De Bilt, about 45 km from Kootwijk, is about 1.4 kg/m<sup>2</sup>, with a bias of -0.1 kg/m<sup>2</sup>. Comparison with KNMI's RACMO model showed a good agreement as well. The results of the operational processing are displayed on the internet with a delay of 2 days.

The accuracy of the GPS IWV estimates has been confirmed by four experimental campaigns, where the GPS receiver in Delft was co-located with a microwave radiometer and/or radiosonde launches. Further experiments, using predicted IGS orbit in combination with orbit relaxation, showed that also for less accurate predicted orbit information, which is available in real-time, the same accuracy can be obtained as with rapid orbits. Therefore, near real-time estimation of GPS IWV data for weather forecasting is in principle possible.

**JSG28/E/11-B1** **1120**

**FIRST EXPERIENCE WITH NEAR-REAL TIME WATER VAPOR ESTIMATION IN A GERMAN GROUND-BASED GPS NETWORK**

Christoph Reigber, Galina DICK and Gerd Gendt (GeoForschungsZentrum Potsdam, Telegrafenberg A17, D-14473 Potsdam, Germany, email: dick@gfz-potsdam.de)

Water vapor plays a fundamental role in the transfer of moisture and latent heat in the atmosphere. Its observation remains one of the most complicated subjects and the knowledge of its distribution is yet insufficient. Therefore, continuous and well-distributed measurements of water vapor are of crucial importance for numerical weather predictions and climate research. The GPS technology is likely to become a very effective observing system for this key atmospheric parameter.

The European Union COST Action 716 is aiming at studying the usefulness of GPS-derived integrated water vapor in numerical weather prediction modeling. As a contribution to this study a joint project between GFZ and the German Meteorological Service (DWD) has been initiated in Germany. This project comprises all necessary components - data links and handling, path delay estimation, met data interpolation to GPS location, conversion to water vapor. Ten GPS receivers were installed at DWD synoptic sites in December 1998. The GPS and meteorological data are transmitted in hourly batches to the GFZ and processed with GFZ EPOS software, using predicted GPS orbits estimated at GFZ IGS Analysis Center. First experiences with near-real-time analysis have been obtained and the operational precision determination of water vapor within local GPS networks has been demonstrated. This initial project will be followed by a pilot project in a much denser German DGPS network. The presentation will give insight into all components of the system under development. It will demonstrate the capabilities of the methods used by GFZ for near-real-time processing and will show the strategy to develop from scientific processing to an operational day-to-day service. First results and comparisons will be presented.



JSG28/W/18-B1

1140

## IMPACT OF PRECIPITABLE WATER DERIVED FROM THE GPS NETWORK BY GEOGRAPHICAL SURVEY INSTITUTE OF JAPAN ON NUMERICAL WEATHER PREDICTION

Nobutaka MANNOJI ( Numerical Prediction Division, Japan Meteorological Agency, 1-3-4 Oote-machi, Chiyoda-ku, Tokyo 100-8122, JAPAN, email: nmannoji@npd.kishou.go.jp )

It is important to make accurate prediction of mesoscale phenomena, which often bring torrential rain. In order to achieve the goal with numerical weather prediction (NWP), both the improvement of NWP models and accurate initial condition are needed. Although observation is necessary to make accurate initial condition, operational observation by radiosonde is too coarse in time and space resolution to capture the structure of such phenomena. Precipitable water (PW) retrieved from the zenith total delay of the GPS is revealed to be accurate. Geographical Survey Institute (GSI) of Japan runs a nationwide GPS array composed of 949 observational points as of April 1998 separated typically by 15-30km from one another. Although this array is established to monitoring the crustal deformation, we can derive PW observation over Japan from this dense array with high resolution in time and space. PW retrieved from the GPS array are made use of in initial condition of water vapour in NWP, and the result of NWP with and without GPS PW are compared each other.

JSG28/E/09-B1

1200

## EVALUATION OF WATER VAPOR OBSERVATIONS USING SAR, GPS, AND METEOSAT.

Ramon HANSEN (Delft University of Technology, Thijsseweg 11, 2629 JA, Delft, the Netherlands, Email: hanssen@geo.tudelft.nl); Arnout Feijt (Royal Netherlands Meteorological Institute, P.O.Box 201, 3730 AE, De Bilt, the Netherlands, Email: feijt@knmi.nl); and Roland KLEES (Delft University of Technology, Thijsseweg 11, 2629 JA, Delft, the Netherlands, Email: krees@geo.tudelft.nl).

Water vapor is a key environmental parameter that is not currently measured with sufficient spatial density and accuracy for mesoscale meteorology and forecasting. Spaceborne radiometer observations, such as Meteosat, are available on spatial scales which are currently too coarse for, e.g., quantitative precipitation forecasting or cloud formation studies. Spaceborne geodetic observations such as GPS and radar (SAR) interferometry provide an independent source of meteorological information by analyzing the propagation delay of the electromagnetic signals. Availability of these data on a routine basis will improve numerical forecasting and mesoscale meteorology.

Here we evaluated observations obtained from the Meteosat water vapor channel, GPS stationary zenith delay time series, and SAR interferometry during a cold front passage over the Netherlands in March 1996. Repeat pass SAR interferometry combines two high resolution (20 m) radar images to measure lateral path length differences between the radar and the surface, with an accuracy of a few mm. These delay observations are then transformed to zenith integrated precipitable water (IPW) differences. Meteosat brightness temperature observations are transformed to IPW using a novel algorithm which also applies GPS observations. The GPS IPW measurements are obtained over a stationary site in the center of the cold front area.

An evaluation of the spatial correspondence between Meteosat and ERS SAR observations shows a sudden increase of 6 mm in integrated precipitable water (IPW), corresponding with the location of the cold front. Goodness of fit testing provided modest scaling factors for the dispersion of the difference between the two observations, achieving a standard deviation of 1.2 mm for the IPW observations. Currently, for localized applications of the technique, this is primarily attributed to the Meteosat observations. This spatial water...

JSG28/W/28-B1

1220

## REAL-TIME ESTIMATION OF PRECIPITABLE WATER USING NEW ZEALAND'S CONTINUOUS GPS NETWORK

Mark FALVEY (School of Earth Sciences, Victoria University of Wellington, PO Box 600, Wellington, New Zealand, Email: mfalvey@gamma.gns.cri.nz); John Beavan (Institute of Geological and Nuclear Sciences, PO Box 30368, Lower Hutt, Wellington, New Zealand, Email: J.Beavan@gns.cri.nz)

A network of five GPS receivers is currently in continuous operation in the New Zealand network, with much expansion expected in upcoming years. The primary purpose of the network is to monitor deformation occurring along the Australian-Pacific plate boundary. However the network is also being used to provide estimates of precipitable water (PW). For these to be most useful a real-time capability is required. Because data from all but one of the stations are acquired hourly this will be possible once a successful processing strategy is implemented.

To investigate the potential of real-time PW estimation from our network we have performed simulations of real-time processing. We identify two key factors which degrade the quality of the real-time estimates: (a) inaccuracies in the predicted orbit data used in the processing; and (b) end effects resulting from real-time estimates being made at the end of the data stream. We examine the impact of each of the above. We also discuss techniques we have been using to remove poorly predicted satellite orbits from the estimation procedure. The method analyses the residuals of a first-guess estimation to identify those satellites that are most likely to cause problems. We find this results in a considerable improvement in the quality results.

Monday 26 July PM

Presiding Chair: M. Bevis (Uni of Hawaii)

JSG28/E/22-B1

Poster

1400-01

## ON GPS-DERIVED INTEGRATED WATER VAPOUR DURING FINNISH WINTER

Paavo J. AIRAKSINEN, Jussi Johansson, Hannu Koivula and Martin Vermeer (Finnish Geodetic Institute, P.O.Box 15, FIN-02431 MASALA, Finland; email: pja@fgi.fi, hko@fgi.fi and mv@fgi.fi)

A winter GPS-IWV field campaign was carried out in South-Western Finland in early 1998. The campaign included 6 temporal GPS-receiver sites around Jokioinen meteorological observatory where radiosondes were launched 2-3 times a day. An Ashtech Z12 GPS-receiver was coupled with a meteorological Vaisala PTU200 -transmitter at each site. The data analysis was done using Bernese GPS-software and it shows that GPS-derived-IWV follows quite well the values of radiosonde-derived-IWV.

However during some days there exists systematic differences in the IWV within the mesoscale campaign area. These differences can be explained with horizontal inhomogeneity of IWV during these days. During such days one should put special attention to the selection of the GPS-site against which comparisons of radiosonde-based-IWV are made. The effect of horizontally inhomogeneous atmosphere to IWV comparisons is good to keep in mind also a larger spatial scale (i.e. comparing data from permanent GPS-sites).

The Finnish Permanent GPS-network (FinnRef with 12 sites) and a cooperative station in Xian (China) is now equipped with surface meteorological transmitters. Preliminary calculations of data from these stations in under way. However there are still some challenges to meet before ground based GPS-measurements can be used as an operational year-around source of data

for meteorology in subarctic countries like Finland. During winter snow is temporally gathered on antenna radomes which causes an extra delay that sometimes can be of an order of the IWV or more.

JSG28/W/21-B1

Poster

1400-02

## GPS AND WVR DERIVED TROPOSPHERIC WATER VAPOUR IN THE GERMAN PERMANENT GPS NETWORK AND ITS USE FOR METEOROLOGY

Matthias BECKER, Georg Weber, Peter Franke and Wolfgang Schlueter (all at Bundesamt für Kartographie und Geodäsie, Richard Strauss Allee 11, D-60598 Frankfurt a. Main, Germany, email: becker@ifag.de); Christina Koepken (German Weather Service, Kaiserleistr. 42, D-63067 Offenbach, Germany, email: ckoepken@dwd.4d00.de)

Since middle of 1996 the Federal Agency of Cartography and Geodesy (BKG) computes daily solutions for a set of German and European permanent GPS stations using the Bernese GPS Software. The EUREF-Permanent network is densified by a set of twenty stations within Germany. The BKG processing is used to produce sets of tropospheric zenith path delay parameters in one or two hourly intervals. They are combined and compared with BKG Water Vapour Radiometer data (WVR), observed at the Fundamental Station Wettzell since October 1997. In a joint research project with the German Weather Service the potential use of the vertical integrated water vapour (IWV) content as derived from the tropospheric zenith path delay for the improvement of numerical weather forecast is studied. As a first step, the derived GPS-IWV is compared to IWV derived from weather forecast models. The influence of ancillary numerical model data used in the derivation of GPS IWV is studied. This paper presents re-sults of a test phase selected for a feasibility study and the continuous comparison of the WVR in Wettzell and the GPS estimates.

JSG28/L/01-B1

Poster

1400-03

## GROUND-BASED GPS METEOROLOGY AND CLIMATE RESEARCH

Michael BEVIS, James Foster and Steven Businger (SOEST, University of Hawaii, Honolulu, HI 96822, USA. Email: bevis@soest.hawaii.edu); Yoaz Bar-Sever, Bruce Haines and Jean Dickey (Jet Propulsion Laboratory, Los Angeles, CA 91109, USA); Peng Fang and Yehuda Bock (Scripps Institute of Oceanography, La Jolla, CA 92093, USA)

Ground-based GPS meteorology is now a fairly well established measurement technique. Most researchers engaged in the research and development of 'GPS met' are focusing mainly on its potential use in operational weather analysis and prediction. This is probably the most demanding of all applications identified to date by virtue of its requirement for nearly real-time measurements. Water vapor climatology is a less demanding application since solution latency is not an important consideration.

Nevertheless, using GPS networks for water vapor climatology involves a number of challenging technical problems, some of which are not very prominent in other applications. Our major emphasis to date is on water vapor and delay climatology in oceanic environments. We shall describe the scientific agendas, past experiences, preliminary results and future plans associated with our research programs in the Pacific Ocean and elsewhere.

JSG28/W/15-B1

Poster

1400-04

## MONITORING THE ATMOSPHERE BY GPS AT MATERA SPACE GEODESY CENTRE

Ferraro C. (1), Nardi A. (1), Pacione R. (1), Sciarretta C. (1), Vespe F. (2) (1) Telespazio s.p.a. - Centro di Geodesia Spaziale Italiana - 75100 Matera (2) Agenzia Spaziale Italiana - Centro di Geodesia Spaziale Italiana - 75100 Matera

The Matera Space Geodesy Centre (CGS) has been providing geodetic (positions, baselines) GPS products relevant to the Mediterranean area to the international scientific users, by contributing to the IGS/EUREF project. In addition CGS supports, by its on-line data bank GeoDAF, the needs of the Italian operational and scientific users (e.g. land-surveyors, universities, cadastre,...). Beside the classical geodetic products, are now under testing other GPS by-products relevant to the monitoring of the charged and neutral atmosphere, such as TEC maps and Integrated Precipitable Water Vapour measurements. At present the procedures and the analysis strategy to recover reliably water vapour from tropospheric delays are under testing, mainly to contribute to the MAGIC project, a European joint project aiming to the use of permanent GPS receivers for weather forecast. In this work we want to present extensively a comparison of tropospheric zenith path delays obtained with different SW (GPSY and MicroCosm) and strategies, using data of the Italian GPS Fiducial Network. Moreover the total tropospheric zenith path delay will be divided into dry and wet components using, when available, surface pressure and temperature. As far as the ionosphere is concerned, regional maps (for the Mediterranean latitudes) of Total Electron Content are produced, modelling a single-layered, 450 km high ionosphere by LS estimating the coefficients of the development of TEC as function of latitude and sun-fixed longitude, assuming as observable the 'geometry-free' combination of L1 and L2. Examples of these products are shown and discussed as well as the procedure to obtain them.

JSG28/E/13-B1

Poster

1400-05

## GPS WATER VAPOR OBSERVATIONS OF A LANDFALLING HURRICANE

Seth GUTMAN (NOAA Forecast Systems Laboratory, 325 Broadway R/E/FS3, Boulder, Colorado 80303 USA, Email: gutman@fsl.noaa.gov)

High temporal resolution measurements of total column (integrated) precipitable water vapor during a landfalling Hurricane were successfully carried out this year by NOAA's Forecast Systems Laboratory using ground-based GPS meteorological techniques. GPS-IPW observations were made at NOAA Ground-Based GPS Water Vapor Demonstration Network sites located west and east of the eye of Hurricane Georges as it came ashore along the Gulf Coast of Mississippi on September 28, 1998. Several features of interest, such as the passage of cloud bands and the correlation of IPW maxima with pressure minima, are observed.

JSG28/W/06-B1

Poster

1400-06

## GPS DERIVED WATER VAPOR DISTRIBUTIONS COMPARED WITH SSM AND WVR: THE KILAUEA FIELD EXPERIMENT

Lars Peter KRUSE, Bernd Sierk, Beat Buerki, H.-G.Kahle (all at Geodesy and Geodynamics Laboratory, ETH Zurich, CH, email: kruse@geod.ethz.ch); Mike Lisowsky (US Geological Survey, Hawaiian Volcano Obs., Hawaii, USA); Mike Bevis (University of Hawaii, Hawaii Institute of Geophysics and Planetology, Hawaii, USA); Alan Dodson and Helen Baker (Institute of Engineering Surveying and Space Geodesy, University of Nottingham, UK); Stefan V. Florek (Institute of Spectrochemistry and Applied Spectroscopy Rudower Chaussee 5, 12489 Berlin, Germany)



## INTER-ASSOCIATION

The estimation of total water vapor contents by ground based GPS meteorology is now a well established technique. However, the potential of the method for resolving 4-dimensional distributions of tropospheric water vapor still needs further investigation. In order to validate the capability of GPS, we carried out a field experiment on Hawaii, USA. The ultra dense CGPS network operated at the Mt. Kialuea volcano provides an excellent basis for studies of new processing schemes such as GPS tomography. For comparison of GPS water vapor retrievals we as deployed radiosondes, 3 microwave radiometers and a newly developed Solar Atmospheric Monitoring Spectrometer (SAMOS). The poster presents a comparison of all the complementary techniques, focussing on vertical profiles of water vapor.

**JSG28/W/07-B1** Poster **1400-07**

### AN EXPERIMENTAL CAMPAIGN FOR EVALUATION OF WET DELAY VARIATIONS USING WVRs IN THE KANTO DISTRICT, CENTRAL JAPAN

ICHIKAWA Ryuichi (Kashima Space Research Center, Communications Research Laboratory, 893-1 Hirai, Kashima, Ibaraki 314-0012, Japan, e-mail: richi@rcl.go.jp); Hiroshi Hanado (Communications Research Laboratory, 4-2-1 Nukui-kita, Koganei, Tokyo 184-8795, Japan); Kazumasa Aonashi (Meteorological Research Institute, Japan Meteorological Agency, 1-1 Nagamine, Tsukuba, Ibaraki 305-0052, Japan); Seiichi Shimada (National Research Institute for Earth Science and Disaster Prevention, 3-1 Tennoudai, Tsukuba, Ibaraki 305-0006, Japan); Yuki Hatanaka (Geographical Survey Institute, 1-Kitasato, Tsukuba, Ibaraki 305-0811, JAPAN); Joeta Yamamoto and Tamio Takamura (Center for Environmental Remote Sensing (CEReS), Chiba University, 1-33, Yayoi-cho, Inage-ku, Chiba-shi, Chiba 263-8522 Japan)

Understanding the space-time variability of the atmospheric delay is indispensable for accurate corrections of GPS and VLBI measurements. Recently, several anisotropic mapping functions in which atmospheric gradients are assumed to have a simple linear form have been proposed. On the other hand, meso and local scale phenomena such as passage of cold front, severe storms and land-sea breezes frequently occur in Japan. Thus, we have to evaluate the space-time variability of water vapor quantitatively under these meteorological conditions. For this purpose we carry on an experimental campaign for detecting and characterizing water vapor variations, using water vapor radiometers (WVRs) in the Kanto district of central Japan. WVR observations were started on June 24, 1998 and are still in progress. Our main concerns are (1) What is a dominant scale of disturbances causing significant positioning errors?, (2) Is it enough to use anisotropic mapping functions to remove effects caused by meso and local scale disturbances?, (3) Is it possible and useful to develop a new method for the correction using a Numerical Weather Prediction (NWP) Model? Observed results will be compared with precipitable water fields obtained by the permanent GPS array of the Geographical Survey Institute (GSI) and by the NWP model produced by the Japan Meteorological Agency. Atmospheric gradients estimated using GPS one-way phase residuals will be also compared with these water vapor fields. These analyzed results will be useful to develop an optimum method to handle the anisotropy of the atmosphere.

**JSG28/W/11-B1** Poster **1400-08**

### BEHAVIORS OF GPS RETRIEVED PRECIPITABLE WATER VAPORS OVER THE JAPANESE ISLANDS

Tetsuya IWABUCHI (The Graduate University for Advanced Studies, Mizusawa, 023-0861, Japan, email: iwabuchi@miz.nao.ac.jp); Isao Naito (National Astronomical Observatory, Mizusawa, 023-0861, Japan, email: naito@miz.nao.ac.jp)

Behaviors of precipitable water vapor (PWV) routinely retrieved from the nationwide array of Global Positioning System (GPS) in Geographical Survey Institute (GSI) of Japan for monitoring of crustal deformation are visualized and compared with the Japan area objective analysis data for numerical weather prediction (NWP) in Japan Meteorological Agency (JMA). While a front accompanying with heavy rainfalls moved eastward across the Islands during 9(LST) Sep. 1 - 9(LST) Sep. 3, 1996, the temporal anomalies in GPS PWVs moving along with the front are clearly detected with almost the same space resolution as in the array (50 km) all over the Islands. Comparisons of GPS retrieved PWVs with NWP PWVs show that GPS PWVs have negative biases amounting to 2 - 4 mm not due to the difference in the topographic heights are found all over the islands. The GPS array also retrieve behaviors of the diurnal variation of water vapor induced by thermally excited local circulation in summer over the Islands. Composites ZTD show characteristic tempo-spatial variations of water vapor loosely related to topography of the Islands. In the principal component analysis of composite ZTDs, the first mode with contribution rate is about 75% having sudden increase of ZTD from dawn till dusk and gentle decrease from evening to night is dominant over the Islands especially in mountain area. These are consistent with results of model simulation on thermally excited local water vapor circulation.

**JSG28/W/02-B1** Poster **1400-09**

### REMOTE SENSING WATER VAPOR CONTENT THROUGH GROUND-BASED GPS DATA IN HONG KONG

Y. LIU, H.B.Iz and Y. Chen (Dept. of LSGI, The Hong Kong Polytechnic University, Hong Kong, email: 96980619r@polyu.edu.hk)

Spatial and temporal resolution of water vapor content is useful in improving the accuracy of short-term weather prediction. Dense and continuously tracking regional GPS arrays will play an important role in remote sensing atmospheric water vapor content. Establishment of a dense GPS array in the coming years in Hong Kong is under consideration for multi purpose applications including GPS Meteorology. In this study, we examined the problem of extracting water vapor content information from GPS data. A piecewise linear solution method was used to estimate the Precipitable Water Vapor (PWV) content from GPS observations in Hong Kong. To evaluate the solution accuracy of the water vapor content sensed by GPS, the upper air sounding data (Radiosonde) that are collected locally was used to calculate the precipitable water vapor during the same period. One-month results of PWV from both ground-based GPS sensing technique and Radiosonde method are in agreement within 1-2 mm.

**JSG28/E/18-B1** Poster **1400-10**

### WATER VAPOR DISTRIBUTION IN MIYAKE ISLAND, CENTRAL JAPAN DETECTED BY DENSE GPS MEASUREMENTS

Atsushi MIWA (Division of Earth and Planetary Science, Graduate School of Science, Nagoya University, Furo, Chikusa, Nagoya, 464-8602, JAPAN, email: miwa@eps.nagoya-u.ac.jp); Fumiaki Kimata (Division of Science, G, Nagoya University, email: kimata@seis.nagoya-u.ac.jp)

Miyake Island, one of Izu Islands in Central Japan, is an active volcano and the eruptions have been repeated with intervals of about 20 years. The last eruption is in 1983. So GPS measurements in the island have been occupied continuously at ten stations and repeatedly in the dense network to discuss the crustal movement. Although Miyake Island is a small island

such as 8 x 8 km, the top of the volcanic is 800m above the sea level. As local water vapor does not distribute uniformly over the island, GPS measurement errors show large. In the GPS measurements in 1998, we also made the meteorological observation at the GPS sites, it was raining locally and cap clouds were observed above the top. We would discuss the space-time distribution of water vapor with a B&C (J-) mesoscale analyzing the GPS measurements.

**JSG28/E/26-B1** Poster **1400-11**

### TIME AND SPACE VARIATIONS OF WATER VAPOR DETECTED BY GPS PHASE RESIDUALS

Seiichi SHIMADA (Nat. Res. Inst. for Earth Sc. Disaster Prevention (NIED), 3-1 Ten-nodai, Tsukuba, Ibaraki 305-0006 JAPAN, email: shimada@geo.bosai.go.jp) Kazumasa Aonashi (Meteor. Res. Inst., 1-1 Nagamine, Tsukuba, Ibaraki 305-0052 JAPAN, email: aonashi@mri-jma.go.jp); Thomas A. Herring and Robert W. King (both at Dept. of Earth, Atmospheric and Planetary Sc., Massachusetts Inst. Tech., 77 Massachusetts Av., Cambridge, Massachusetts 02139 USA, email: tah@mtgl.mit.edu)

In usual GPS meteorological analysis, zenith delays of each GPS site are obtained and applied to discuss the water vapor variations. However from the nature of tropospheric phenomena, sometimes local scale inhomogeneity become dominant, and zenith delay, which represents 20 - 30km water vapor around GPS site averaging around 15 - 30 minute, is not suitable to discuss the water vapor time and space variations. Also in the mountainous and humid area like the Japanese Islands, local scale inhomogeneity is very usual. To detect the rapid and local scale water vapor behavior, we propose the GPS phase residual sky mapping obtained after the least-square parameter fitting. Because the traces of the GPS orbits at the short period are very limited, phase residuals in the isolated site may reduce poor water vapor sky distributions. Dense GPS network and/or slow local event like that caused by the tropospheric effect are very useful to apply the phase residual mapping. We also demonstrate the examples of the horizontal mapping of the local scale inhomogeneity of water vapor caused by the local foehn event and the water vapor peak moving associated with the low-elevation clouds both observed in the Japanese GPS network (GEONET).

**JSG28/E/04-B1** Poster **1400-12**

### USE OF GPS FOR SENSING THE PRECIPITABLE WATER VAPOR IN EGYPT: A PROPOSAL

Ashraf MOUSA (National Research Institute of Astronomy and Geophysics, Helwan, Cairo, Egypt, email: ashrafkm@frcu.eun.eg)

Water vapor plays a crucial role in a variety of atmospheric processes that act over a wide range of spatial and temporal scale. It is widely appreciated that improved monitoring of atmospheric water vapor will lead to more accurate forecasts of precipitation and serve numerical weather modeling. However, the traditional tools for water vapor measurements or estimation is not adequate because, water vapor is the most variable of the major constituents of the atmosphere.

Emerging GPS networks invite a new and powerful approach to the remote sensing of the atmospheric water vapor. A GPS-based system for water vapor determination offers the benefits of better resolution of both spatial and temporal variation of the water vapor. This paper reviews the basics behind the use of GPS for water vapor prediction as well as its merits over traditional water vapor measuring tools. Then, the requirements of an operational GPS prediction system in near real time are summarized.

**JSG28/E/10-B1** Poster **1400-13**

### DETECTION OF TROPOSPHERIC DUCTS USING A GROUND-BASED GPS RECEIVER

Kenneth D. ANDERSON (Propagation Division, Space and Naval Warfare Systems Center San Diego D883, 49170 Propagation Path, San Diego CA, 92152-7385, email: kenn@spawar.navy.mil)

Terrestrial propagation of radio waves at frequencies somewhere above 30 MHz is often significantly affected by the composition of the troposphere, especially when both terminals are near a coastline. A famous example of anomalous propagation effects occurred in India during World War II when a 200 MHz radar (with an expected detection range of several hundred miles) detected the coast of Arabia some 2700 km away. Similar effects have been observed along the southern California coast by cell phone users in Los Angeles and San Diego who, instead of connecting with their local cell, are sometimes connected with a remote cell, perhaps 200 km away. Such anomalous effects are usually measured indirectly by sensing atmospheric properties with an instrumented weather balloon, a process that is both time-consuming and expensive. However, recent work with the Global Positioning System (GPS) demonstrates that ground-based measurement of GPS satellite signals can detect these anomalous propagation conditions. Therefore, by capitalizing on the existing technology of GPS, an affordable, all-weather, anomalous effects measurement capability is readily available.

**JSG28/E/16-B1** Poster **1400-14**

### GROUND-BASED GPS WATER VAPOUR ESTIMATION: POTENTIAL FOR METEOROLOGICAL FORECASTING

Helen BAKER, Alan Dodson and Nigel Penna (IESSG, University of Nottingham, University Park, Nottingham, NG7 2RD, UK, Email: helen.baker@nottingham.ac.uk); David Offiler and Mark Higgins (UK Meteorological Office, NWP Satellite Applications, London Road, Bracknell, Berks, RG12 2SZ, UK, Email: doffiler@meto.govt.uk)

In order to assess the impact of ground-based GPS Integrated Water Vapour (IWV) estimates in meteorological forecasting applications, estimates must be available within near real-time and must be of comparable accuracy to existing meteorological measurement techniques. As a prerequisite to assessing the potential benefit of GPS IWV estimates in Numerical Weather Prediction (NWP) models, extensive tests have been performed to examine the effect of various process error models, a-priori constraints and estimation techniques involved within GPS processing procedures, in order to devise a recommended processing strategy. One year of GPS data from a selection of stations, which are co-located with radiosonde launch sites, within the UK permanent GPS network, has been processed to validate these findings. Near real-time estimation issues have subsequently been examined, primarily using a sliding window processing approach to demonstrate the feasibility of producing accurate GPS IWV estimates within the required time frame. Additionally, preliminary work has been performed to assimilate GPS IWV into UK Meteorological Office Numerical Weather Prediction models (post-date), in preparation for impact assessments on the quality of mesoscale weather forecasts.

**JSG28/E/25-B1** Poster **1400-15****ATMOSPHERE PROBING BY GPS FOR SAR INTERFEROMETRY**

Alessandro Bonforte and Giuseppe Puglisi (both at Istituto Internazionale di Vulcanologia - CNR, Piazza Roma, 2, I-95123, Catania, Italy; e-mail: bonforte@iiv.ct.cnr.it, geo@iiv.ct.cnr.it)

GPS measurements were carried out by the Istituto Internazionale di Vulcanologia in Catania (Italy) to evaluate the atmospheric effects on GPS signals. The aim of this work, performed in the framework of an EC project called Monitoring Active Deformation on Volcanoes by Interferometry as an Early Warning System (MADVIEWS), was to give an independent evaluation of the atmospheric artefacts that could affect the SAR interferometric images. The main effort of the IIV team in the project was to estimate the TEC (Total Electron Content) in the ionosphere and the ZPD (Zenith Path Delay) due to the troposphere. To this aim, GPS measurements have been carried out during the ERS-2 passes over Mt. Etna volcano. The knowledge of these parameters can be useful to model the SAR signal propagation respectively in ionosphere and troposphere. Since September 1996 to December 1997 these measurement sessions were carried out monthly, during both ascending and descending passes of the SAR sensor over the investigated area. About the ionosphere, local models were estimated for each ERS pass and TEC variations in the order of 10 TECU were found. Such variations are able to produce a difference in the SAR signal delay up to 20 cm. However, the variation of the TEC in the ionosphere may be considered almost uniform above the area covered by SAR images (about 100 Km X 100 Km). Thus, the result of the measured delay may be a vertical translation of the whole image or eventually a tilt, due to a different gradient in the TEC above the area during the two passes. About the troposphere, the ZPD was estimated for each station at each ERS pass; variation of the ZPD difference between the GPS stations up to 5-6 cm were measured, able to produce up to two fringes on the lower flanks of Etna in the interferograms in the worst conditions, simulating large scale inflations and deflations of the volcanic edifice.

**JSG28/E/20-B1** Poster **1400-16****4D TROPOSPHERIC TOMOGRAPHY USING GPS ESTIMATED SLANT DELAYS**

A. FLORES, G. Ruffini, A. Rius, (Institut d'Estudis Espacials de Catalunya Edif. Nexus 204, C/ Gran Capita 2-4, 08034 Barcelona, Spain)

Retrieval of 4D fields of the tropospheric distribution of water vapor using GPS measurements is an additional and attractive use of the global positioning system. Stochastic GPS tomography has successfully been used in ionospheric studies and a we describe here a similar approach for tropospheric studies. We present here initial results on the tropospheric tomography, comparisons with other sources of data, an error analysis and a study of its resolution capabilities based on simulations. GPS data was tracked at the local permanent network in Kilauea, Hawaii during one day in February 1997. It was then processed using the GPSY-OASIS II software to extract the slant extra delays due to the wet troposphere. The inverse problem is then solved using our in-house software LOTTOS, which has been developed to yield the 4D refractivity field and the solution compared with ECMWF maps. This technique can potentially be used to monitor in a Near Real Time basis the status of the troposphere using a dense local network of receivers.

**JSG28/W/13-B1** Poster **1400-17****AN INTEGRATION OF GPS AND RADISONDE-DERIVED WATER VAPOUR CONTENT USING ARTIFICIAL INTELLIGENT FOR VALIDITY CHECKING**

MANURUNG, Parluhan (Bakosurtanal National Coordination Agency for Survey and Mapping, Jl. Raya Jakarta Bogor Km 46, PO Box 46/CBI, Cibinong 16911 Indonesia, E-mail: parلمان@cbn.net.id Telephone No: +62-21-8764612 Fax No: +62 21 875 2064)

The paper demonstrates a combination of water vapor content (WVC) derived from GPS permanent tracking and radiosonde stations in the Indonesian region. Since the existing radiosonde network consists of 10 stations only, this is still inadequate to represent that of high varying WVC condition of the tropical country, with length and width of about 5000 and 2000 kilometres, respectively. Some efforts to increase the station number are limited due to a radiosonde is disposable resulting in expensive operational cost. Validity checking of GPS-derived WVC were performed using artificial intelligent. The results show that the two types of observations are in close agreement. Since the existing GPS permanent tracking stations in the country are of currently three stations only, the research is limited to provide a model for densification of WVC network. The model should be capable of integrating a number of additional stations as in the future the demand for that of GPS station is growing high, so that an integration of GPS with Radiosonde for determining representative WVC of the region could be achieved.

**JSG28/E/29-B1** Poster **1400-18****SPATIO-TEMPORAL VARIATION OF ATMOSPHERIC DELAY GRADIENT RETRIEVED BY A DENSE GPS ARRAY AND ITS RELATIONSHIP WITH SITE COORDINATE VARIATIONS**

Shin-ichi Miyazaki (Geographical Survey Institute, Tsukuba, 305-0811, Japan, email: miyazaki@gsi-mc.go.jp); Tetsuya Iwabuchi (The Graduate University for Advanced Studies, Mizusawa, 023-0861, Japan, email: iwabuchi@miz.nao.ac.jp); Kosuke Heki (National Astronomical Observatory, Mizusawa, 023-0861, Japan, email: heki@miz.nao.ac.jp) Isao Naito (National Astronomical Observatory, Mizusawa, 023-0861, Japan, email: naito@miz.nao.ac.jp)

We performed a series of GPS analysis with estimating atmospheric delay gradient for the nationwide GPS array of Geographical Survey Institute (GSI) over the Japanese Islands in cases of front passages and tropical cyclone. Clear inverse correlation was found between the wet component of the gradient and the horizontal coordinate variation, and this result agreed with the result of a theoretical study and a simulation study. Furthermore, a large amount of the horizontal coordinate variation found by Iwabuchi and Naito (1999) disappeared when the atmospheric gradient was estimated. Therefore, we can conclude that the estimated gradient reflects the real spatial distribution of water vapor, and estimating the atmospheric gradient significantly improves the repeatability of horizontal coordinate when a systematic horizontal gradient of water vapor exist.

**JSG28/W/16-B1** Poster **1400-19****MEASURING REGIONAL PRECIPITABLE WATER VAPOR VARIATIONS USING THE JAPANESE DENSE GPS NETWORK**

Ryu OHTANI (Univ. Tokyo, Department of Earth and Planetary Physics, 7-3-1 Hongo Bunkyo-ku, Tokyo 113-0033 Japan. E-mail: ryu@epsun01.geoph.s.u-tokyo.ac.); Isao Naito (National Astronomical Observatory)

We investigate the applicability of GPS for sensing water vapor using Japanese nationwide geodetic GPS network (GEONET) established by Geographical Survey Institute (GSI). We made a case study of summer days to see whether the 2 dimensional GPS derived precipitable water vapor (PWV) distribution field could detect the variations of water vapor over a regional scale. We used GPS data collected at about 200 GSI's stations deployed over the central part of Japan with the mean separation of about 25 km. We estimated zenith tropospheric delay every 5 minutes using GIPSY software and converted into PWV using surface pressure and temperature measurements. Then, we made contour maps of PWV every 1 hour plotted with the surface meteorological measurements (wind speed and direction, etc.) obtained by Automated Meteorological Data Acquisition System (AMeDAS) stations deployed by Japan Meteorological Agency all over the Japan islands. We found diurnal variations of PWV field associated with thermally-induced local circulation that drove water vapor from coastal regions to inland mountainous regions, that demonstrate the usefulness of GPS network to study the motions of water vapor with a spatial scale of a few tens of kilometers.

**JSG28/E/02-B1** Poster **1400-20****HIGH TIME RESOLUTION MEASUREMENTS OF PRECIPITABLE WATER VAPOR FROM PROPAGATION DELAY OF GPS SATELLITE SIGNALS**

Takayuki YOSHIHARA, Toshitaka Tsuda (both at Radio Atmospheric Science Center, Kyoto University, Uji, Kyoto, 611-0011, Japan, email: yoshihara@kurasc.kyoto-u.ac.jp) and Kazuro Hirahara (Department of Earth and Planetary Sciences, Graduate School of Science, Nagoya University, Nagoya, 464-8602, Japan, email: hirahara@eps.nagoya-u.ac.jp)

Aiming to apply Global Positioning System (GPS) measurements to an observation of meso-scale phenomena in the atmosphere, we estimated precipitable water vapor (PWV) with a good time resolution from GPS data. To verify such PWVs, we mainly used three meteorological instruments, which were radiosonde, radiometer and ceilometer. We analyzed two GPS campaign data sets, which were observed in Shigaraki, Shiga, Japan in 1995 and in Yamagawa, Kagoshima, Japan in 1996.

From comparison between the GPS and radiosonde results, we found that the GPS result with a high time resolution correctly provides the absolute values of PWV. In the comparison between the GPS and radiometer results (in the zenith direction), general tendency of the GPS results with a time resolution of 6 min. agreed well with the radiometer. Finally, we compared GPS results with the zenith delay caused by water vapor which were contained the lowest cloud layer, whose bottom height and thickness were obtained from a ceilometer measurement. As a result, we obtained good agreement of relative zenith delay perturbations between the results of GPS (estimated every 1 min.) and a ceilometer, especially, in the case of the cloud bottom height was as low as 100 m.

**JSG28/E/14-B1** Poster **1400-21****CALIBRATING SPACEBORNE MICROWAVE RADIOMETERS WITH GPS**

Bruce HAINES, Yoaz Bar-Sever and Shailen Desai (all at Jet Propulsion Laboratory, California Institute of Technology, Pasadena, CA 91109; e-mail: Bruce.J.Haines@jpl.nasa.gov)

Data from terrestrial GPS receivers are being used in growing numbers of applications requiring precise tropospheric sensing. One emerging application is the calibration of water vapor measurements from spaceborne microwave radiometers. An excellent candidate mission for developing this technology is Topex/Poseidon (T/P). A joint U.S./France mission launched in 1992 to measure global ocean circulation and sea level, T/P carries a microwave radiometer to provide measurements of wet path delay with cm-level accuracy. The nadir-looking Topex microwave radiometer (TMR) was included to provide a columnar water vapor delay correction for the altimeter range measurements used in forming the sea-surface height measurements. As such, any spurious drift in the TMR measurements can map significantly into the estimated rate of change in global mean sea level from T/P.

By virtue of their proximity to open-ocean T/P repeat tracks, many stations in the rapidly growing GPS global network are well suited for monitoring the TMR. For these locations, we are constructing time series based on the differences of the instantaneous vertical wet path delay derived independently from the TMR and GPS data at T/P overflight times.

Using data from four GPS stations with the longest and most consistent tracking histories, we concluded that the TMR measurements of wet path delay drifted lower by 1 mm/yr from 1992-97. We discuss the challenges encountered in using these long-term GPS time series as a calibration tool. We also present new TMR drift and scale error estimates from an extended analysis incorporating additional GPS stations. Finally, we discuss plans and prospects for calibrating the radiometer on the T/P follow-on mission (Jason-1), scheduled for launch in May, 2000.

**Tuesday 27 July AM**

Presiding Chair: R Ware (UCAR, Boulder, Colorado, USA)

**JSG28/W/14-B2** **0930****EVALUATIONS OF THE ACCURACY OF PRECIPITABLE WATER VAPOR ESTIMATED FROM GPS OBSERVATIONS WITH RADIOSONDE MEASUREMENTS IN JAPAN**

Ryu OHTANI (Univ. Tokyo, Department of Earth and Planetary Physics, 7-3-1 Hongo Bunkyo-ku, Tokyo 113-0033 Japan. E-mail: ryu@epsun01.geoph.s.u-tokyo.ac.); Isao Naito (National Astronomical Observatory)

We compared precipitable water vapor (PWV) estimated from routine geodetic analyses of Japanese nationwide GPS network (GEONET) with nearby radiosonde observations. It is found that the accuracy of GPS PWVs estimated using GAMIT in 1995 and using Bernese in 1996 are 3.2 mm and 3.6 mm in r.m.s. sense, respectively. However, we found systematic deviation of the biases in both cases; there were significant differences in mean biases between radiosonde launching times (00UT, 12UT) and the PWV differences tend to become large in accordance with the increase of the total PWV. We investigated the causes of the above systematic deviation by analyzing GPS data collected at Tsukuba (IGS station) using different software with different analysis strategy. Comparisons with nearby radiosonde measurements for two years showed the agreement of 2.0 mm in r.m.s. sense though GPS PWV exhibited similar systematic deviation. It was found that incorporating GPS station displacement due to ocean tide loading in the analysis reduced the bias depending on radiosonde launching time. It was also found that adjusting mapping function by incorporating



## INTER-ASSOCIATION

the tropopause height and the surface temperature measurements reduced the systematic deviation that depended on total amount of PWV. These results suggest that the ocean tide loading effect and seasonal variation of the mapping function are important for precise determination of PWV in Japan.

**JSG28/E/05-B2**

**0950**

### MITIGATING THE EFFECTS OF SPACE WEATHER ON THE CANADIAN WAAS

R.B. LANGLEY and P.J. Stewart (Geodetic Research Laboratory, Dept. of Geodesy and Geomatics Engineering, University of New Brunswick, Fredericton, N.B., Canada E3B 5A3. E-mail: lang@unb.ca, pstewart@unb.ca)

GPS receivers typically used in aviation are single-frequency units. They are incapable, therefore, of using the dual-frequency technique of removing the ionospheric propagation delay from their pseudorange measurements. Furthermore, neither the measured pseudorange - carrier-phase divergence nor the predicted corrections provided in the navigation message are sufficiently reliable to provide the required vertical position accuracy for Category I precision approaches. The Wide Area Augmentation System (WAAS), currently being developed under the sponsorship of the U.S. Federal Aviation Administration in concert with Nav Canada, will provide real-time gridded values of vertical ionospheric delay from which user line-of-sight delays can be computed. The vertical delays, together with error-bounding values, will be determined from the measurements by a network of continuously-operating dual-frequency reference receivers and delivered to users via satellite transmission.

Canada's northerly latitude makes mitigation of ionospheric effects a far from trivial task as the ionosphere can be markedly more active in the auroral and polar cap zones and hence more difficult to model. In this paper, we report on an evaluation of the proposed WAAS ionospheric modelling scheme as it would be used in Canadian airspace. Several recommendations concerning reference station location, ionosphere grid spacing, and the effect of ionospheric scintillations will be made.

**JSG28/E/24-B2**

**1010**

### MAPPING AND PREDICTING THE EARTH'S IONOSPHERE BASED ON IGS DATA

Stefan SCHAER and Markus Rothacher and Gerhard Beutler (all at Astronomical Institute, University of Berne, Sidlerstrasse 5, CH-3012 Berne, Switzerland, email: stefan.schaer@aiub.unibe.ch)

CODE, the Center for Orbit Determination in Europe, has been routinely deriving global ionosphere maps (GIMs) from IGS (International GPS Service) data for long time. The current GIMs are represented by a spherical harmonic expansion of degree 12 and order 8 referring to a solar-geomagnetic frame. They describe the total electron content (TEC) with a 2-hour resolution and are made available since June 1998 in the IONEX (IONosphere Map EXchange) format adopted by the IGS.

In mid 1999, the time series of CODE GIMs cover 4.5 years without gaps. The associated time series of global TEC parameters document the evolution of the ionosphere during a period of low solar activity. We discuss series of particular TEC parameters, like the mean and maximum TEC. The series of spherical harmonic coefficients allow to study, for example, autocovariance functions, which may be used in turn to extrapolate signals related to individual coefficients or to predict GIMs. CODE is therefore in a position to generate 1-day as well as 2-day predicted GIMs on a daily basis. Finally, we give time series of differential code biases (DCBs) for GPS - and possibly GLONASS - satellites and for receivers obtained as a by-product of the TEC determination. Other IGS analysis centers also supply TEC/DCB products in the IONEX format. This allows to compare and validate results.

**JSG28/W/12-B2**

**1030**

### STATUS REPORT ON THE OERSTED AND SUNSAT GPS OCCULTATION EXPERIMENTS

E. Robert KURSINSKI and George Hajj (Both at Jet Propulsion Laboratory, California Institute of Technology, Pasadena CA 91109 USA, Email: Rob.Kursinski@jpl.nasa.gov); Per Hoeg (Danish Meteorological Institute, Atmosphere Ionosphere Research Division, Lyngbyvej 100, DK-2100 Copenhagen, DENMARK, E-mail: hoeg@DMI.dk)

With their launch in January 1999, the Oersted and SUNSAT satellites are the first two in a series of orbiting GPS receivers which will acquire occultation data from low Earth orbit over the next several years. Oersted and SUNSAT provide a test bed for evaluating and developing the occultation capability and begin the dramatic increase in sampling density and continuity over that of the prototype GPS/MET experiment. The upcoming group of orbiting receivers will provide sampling comparable to and gradually surpassing that of the present global radiosonde network reaching densities needed to address significant scientific issues in weather, climate and the behavior of the coupled atmosphere-ocean system in general. In this presentation, we will provide a status report on the first 6 months of the occultation experiments on the Oersted and SUNSAT missions including the status of flight instruments and ground network used for clock calibration, and a summary of the data acquired thus far including spatial and temporal sampling and the processing status and availability of archived data. Early validation and analysis results will be presented. Plans for continued data acquisition and the configuration of the instruments will be discussed including data acquisition strategies under the constraint of limited power as necessary.

**JSG28/W/27-B2**

**1110**

### APPLICATIONS OF COSMIC TO METEOROLOGY AND CLIMATE

Richard A. ANTHES, Christian Rocken, and Ying-Hwa Kuo (all at University Corporation for Atmospheric Research, P.O. Box 3000, Boulder CO 80307, USA; email: anthes@ucar.edu)

Based on the success and scientific results of the GPS/MET experiment, Taiwan and the U.S. are working together to develop COSMIC (Constellation Observing System for Meteorology, Ionosphere and Climate), a follow-on project for weather and climate research, climate monitoring, space weather, and geodetic science. COSMIC plans to launch eight LEO satellites in 2002. Each COSMIC satellite will retrieve about 500 daily profiles of key ionospheric and atmospheric properties from the tracked GPS radio-signals as they are occulted behind the Earth limb. The constellation will provide frequent global snapshots of the atmosphere and ionosphere with about 4,000 daily soundings. In meteorology COSMIC will provide high vertical resolution temperature, pressure and water vapor information for a variety of atmospheric process studies and to improve the forecast accuracy of numerical weather prediction (NWP) models. For climate research and monitoring COSMIC will provide an accurate global thermometer that will monitor Earth's atmosphere in all weather with unprecedented long-term stability, resolution, coverage, and accuracy. This paper discusses some of the applications of COSMIC data for meteorology, including NWP, and climate.

**JSG28/W/23-B2**

**1130**

### FIRST RESULTS OF GPS ATMOSPHERE PROFILING FROM THE OERSTED MISSION

P. HOEG (Atmosphere Ionosphere Research Division, Danish Meteorological Institute, Lyngbyvej 100, DK-2100 Copenhagen, Denmark, email: hoeg@DMI.dk), H.-H. Benzon (DMI, email: hhb@DMI.dk), J. Grove-Rasmussen (DMI, email: jgr@DMI.dk), C.O. Jensen (DMI, email: coj@DMI.dk), G.B. Larsen (DMI, email: gbl@DMI.dk), M.D. Mortensen (DMI, email: mdm@DMI.dk), M.B. Sorensen (DMI, email: mbs@DMI.dk), S. Syndergaard (DMI, email: ssy@DMI.dk)

The launch of GPS/MET in 1995 started a range of activities to establish the foundation for GPS atmosphere profiling of the Earth based on observations of GPS signals from a low Earth orbiting satellite. The next satellites able to perform the high-precision atmosphere limb soundings after the GPS/MET proof-of-concept mission are the Danish OERSTED satellite and the South-African SUNSAT satellite (here named the OERSTED mission). The launch of both satellites will take place in January 1999.

The first results from the OERSTED mission of limb soundings will be presented and evaluated in view of the results from the GPS/MET mission. Various effects of the error sources on the final retrieved profiles of refractivity and atmosphere parameters (temperature, pressure and humidity) will be discussed and related to global numerical weather prediction (NWP) model estimates. Additionally will the accuracy of the technique, when applying alternative inversion theories, be addressed.

Preliminary results of the directly integrated limb sounding measurements into NWP models will be laid out along with discussions on the influence of dynamical effects on the retrieved data.

**JSG28/W/10-B2**

**1140**

### GLOBAL IONOSPHERIC MODELS FROM GPS MEASUREMENTS

C. Brunini, A. Meza: (Facultad de Ciencias Astronomicas y Geofisicas, La Plata, Argentina), Kleusberg, D. DETTMERING: (Institute of Navigation, University of Stuttgart, Germany, E-mail: dettmering@nav.uni-stuttgart.de Telephone No: +49 711 121 4137, Fax No: +49 711 121 2755)

GPS signals passing through the earth's atmosphere are affected by refraction in the ionosphere and the lower neutral atmosphere. For many applications these effects are seen as nuisance, but on the other hand refraction effects in GPS measurements contain useful information about the structure of the atmosphere.

In this contribution we focus on the upper part of the atmosphere: the ionosphere. The dispersive nature of this layer gives the opportunity to use two frequency GPS measurements to recover information about the electron density distribution.

Ground-based GPS measurements allow the determination of two dimensional global maps of the Total Electron Content (TEC). To obtain three dimensional models it is necessary to include data collected by one or more space-borne receivers on Low Earth Orbits (LEOs). We present two-dimensional ionospheric maps calculated from data provided by globally distributed IGS stations. In a second part, we discuss the extension of the model into the third dimension and show the possibilities of this approach as well as its limitations. Especially the requirements of the model on the number of LEO satellites and on their orbit parameters are analyzed.

**JSG28/E/12-B2**

**1200**

### VERIFICATION OF GPS/MET TEMPERATURE PROFILES WITH RADIOSONDE AND LIDAR MEASUREMENTS

Masahiro Nishida and Toshitaka TSUDA (Radio Atmospheric Science Center, Kyoto University Uji, Kyoto 611-0011, Japan, Email: nishida@kurasc.kyoto-u.ac.jp, tsuda@kurasc.kyoto-u.ac.jp); Christian Rocken and Randolph H. Ware (GPS/MET Project, GPS Science and Technology (GST) Program, UCAR, Boulder, CO 80307-3000, Email: rocken@unavco.ucar.edu, ware@unavco.ucar.edu); Hideaki Nakane, Nobuo Sugimoto, and Parameswaran S. Namboothiri (National Institute of Environmental Studies (NIES), Tsukuba 305-0053, Japan, Email: nakane@nies.go.jp, sugimoto@nies.go.jp)

This paper is concerned with a comparison of the GPS/MET temperature retrievals with the profiles collected with a balloon-borne radiosonde and a Rayleigh lidar in Indonesia and Japan. We have obtained 33 cases when the GPS/MET profile was determined within several hundred kilometers of two balloon launch sites in Indonesia; Bandung (6.9S, 107.6E) and Pontianak (0.03N, 109.3E). The rms deviation between GPS/MET and radiosonde results was approximately 1 K in the upper troposphere when effects of humidity are small, and about 2 K in the lower stratosphere below about 35 km. We have also compared 18 GPS/MET profiles with Rayleigh lidar measurements in Tsukuba, Japan (36.1N, 140.1E), and found the mean rms difference of 6.0 K and 10.2 K at 30-40 km and 40-60 km altitudes, respectively. These validation studies suggest that the GPS/MET profiles resolve detailed temperature structure, including sharp inversions and the step-wise increase of the temperature gradient near the tropical tropopause.

**JSG28/W/22-B2**

**1220**

### CODE DEVELOPMENT AND ASSESSMENT OF METEOROLOGICAL PARAMETERS DERIVED FROM GPS/MET DATA

Ting-To Yu (Satellite Geoinformatics Research Center, National Cheng Kung University, Tainan, Taiwan, email: yutt@mail.ncku.edu.tw); Ming Yang (Dept. Survey Engineering, National Cheng Kung University, Tainan, Taiwan, email: myang@mail.ncku.edu.tw)

The major mission of ROCSAT III/COSMIC is to retrieve profiles of water vapor, temperature, electron density, and atmospheric refractivity from gathered data globally. Through out the mean of obtaining radio occultation observations from 24 GPS satellites to a constellation of 8 low Earth orbit (LEO) satellites, the variation of electron density within ionosphere, and so is the temporal/spatial change of global meteorological parameters can be estimated. The raw data acquired from GPS/MET satellites handled by certain process can produce the information regarding to the electronic density of ionosphere, and profile of atmospheric refractivity (N). Such processes including the excess delay of GPS signal, bending angle, impact parameter (a) and radius at tangent points. These data thus integrated by the Abel transform to compute the three dimensional distribution of electronic density of ionosphere, and also the global coverage for the profile of atmospheric refractivity (N). From this, one can estimate the meteorological parameters; such is water vapor, pressure, temperature etc. The data processing begin from data set of Level 0, that is the raw science data and satellite attitude and ephemeris. Afterward is the double difference handling to the GPS signal to remove both the clock bias between satellite and receiver, and the selective availability (SA) which deployed by the Department of Defense of United States. With different applied process, the Level 0 to Level 4 data can finally be sorted with developed codes, and the content of Level 4 data mainly is the meteorological parameters, which is the goal of this COSMIC mission. However, the inverting process from atmospheric refractivity to the meteorological parameters is non-linear. It is an interactive and multi-parameters schema, which is difficult to achieve by traditional linear inversion or controlling factors method.



Tuesday 27 July PM

Presiding Chair: D. Ware(UAR, Boulder, Colorado, USA)

**JSG28/E/28-B2** Poster **1400-01****SPATIAL CORRELATION OF IONOSPHERE DURING DISTURBANCES DERIVED FROM GPS MEASUREMENTS**

Lubomir W. BARAN (Institute of Geodesy, Olsztyn University of Agriculture and Technology, 10-957 Olsztyn, Poland, email: baran@moskit.art.olsztyn.pl); Ivan I. Ephishov and Irk I. Shagimuratov (both at West Department of the Institute of Geomagnetism, Ionosphere and Radiowave Propagation of the Russian Academy of Sciences)

The magnetospheric storms create severe ionospheric conditions for precision of geodetic measurements. Storm effect (in value of TEC) depends on latitude and local time. As a result, the spatial correlation of ionosphere at far stations in storm time spoils. We analysed the spatial correlation of ionosphere for storm on 22 November 1997 using the GPS measurements of European IGS stations: Jozefoslaw, Lamkowko, Matera, Mendeleevo, Metsahovi. To exclude the influence of biases the ionospheric Doppler data were used. For quiet day – 21 November 1997 the correlation at distance about 2000 km was 0.9 – 0.8. During storm the correlation decreased. It strongly varied in time. For individual GPS satellite passes the correlation is dropped to become lower than 0.5, at distance 300 km. The analysis of the behaviour of the TEC shows the essential increase of the TID during the storm. It concerns the large as well as medium-scale TID. The correlation of the ionospheric Doppler effect at presence of the TID is lowered down to 0.5, at distances less than 100 km. In the paper we also discuss the behaviour of single-differences between stations during the storm.

**JSG 28/E/23-B2** Poster **1400-02****SOME ASPECTS OF APPLICATION OF IONO- AND TROPOSPHERIC MODELS TO PROCESSING OF PERMANENT GPS OBSERVATIONS.**

Janusz BOGUSZ and Mariusz Figurski (Institute of Geodesy and Geodetic Astronomy, Warsaw University of Technology, 00-661 Warszawa, POLAND, e-mail: jb@gik.pw.edu.pl)

The GPS permanent services in the whole world become more and more important in monitoring of the global geophysical fluids. The accuracy of such measurements is influenced by atmospheric effects, ambiguities of the phase measured, corrections for the rate of satellite clock and the ground reception systems GPS, as well as a number of instrumental errors. With good approximation, these effects may be modelled by using algorithms included in professional software designed to develop high accuracy GPS systems. Of many possible errors to be encountered, we should take into account either the problem of ionospheric refraction or the effect of the tropospheric zenith delay. This paper deals with these two problems occurring in GPS measurements, especially in permanent sites and presents the methods of their solving tested in the Warsaw University of Technology IGS Associate Analysis Centre.

**JSG 28/E/17-B2** Poster **1400-03****GPS-OBSERVED IONOSPHERIC DISTURBANCES AROUND AUSTRALIAN REGION DURING THE 4 MAY 1998 MAGNETIC STORM**

Yue-Jin WANG (IPS Radio and Space Services, Sydney, Australia, email: yuejin@ips.gov.au)

On 4 May 1998, a major magnetic storm was observed at IPS Learmonth Observatory in Western Australia. The storm is explained as being due to the coronal mass ejection associated with an X1 solar flare observed on 2 May 1998. Using data from the Australian Regional GPS Network (ARGN), we have detected some significant ionospheric disturbances during the storm period. In this paper we present the GPS-observed results of ionospheric irregularities by analysing the large gradients of the ionospheric total electron content (TEC) due to the magnetic storm activity. The temporal and spatial variations of TEC are analysed and the potential ionospheric limitations to Wide Area Differential GPS are discussed.

**JSG28/E/27-B2** Poster **1400-04****GPS REMOTE SENSING FOR TEMPERATURE, PRESSURE AND TROPOSPHERIC WATER VAPOR IN THE ATMOSPHERE USING ADDITIONAL WATER VAPOR FREQUENCIES**

Dasheng FENG, Benjamin Herman and David Flittner (Institute of Atmospheric Physics, University of Arizona, Tucson, 85721 U.S.A., email: feng@atmo.arizona.edu); E. Robert Kursinski and Thomas P. Yunck (Jet Propulsion Laboratory, MS 238-600, Pasadena, CA 91109 U.S.A.)

The GPS/MET project has successfully shown that the space-borne radio occultation technique using the GPS L1 and L2 channels can be utilized for remotely sensing pressure and temperature of the Earth's atmosphere from near ground to ~40 km height with unprecedented accuracies. The major observables in GPS/MET are the Doppler-shifted frequencies (phases) of the L1 and L2 signals due in part to the bending of the rays caused by gradients in atmospheric index of refraction. Atmospheric temperature and pressure profiles can then be derived using the bending angles as determined from the measured Doppler shifts. The major disadvantage of this method is the inability to separate water vapor contributions from the dry air contributions to the total atmospheric bending angles with just the L1 and L2 frequencies. Consequently, the retrieved temperatures are considerably different from the real temperatures in the lower part of the troposphere where water vapor is usually plentiful. In addition, water vapor cannot be retrieved from the GPS sounding without additional information and assumptions.

By adding water vapor absorption frequencies around 22 GHz in addition to the standard GPS L1 and L2 frequencies, tropospheric water vapor profile may also be retrieved. Three independent equations are needed for the three variables: temperature, pressure, and water vapor. The first equation comes from the measured atmospheric index of refraction obtained from the GPS L1 and L2 phase measurements; the second equation consists of the measured transmission in the water vapor absorption band; and the third equation is the hydrostatic equation. Solving this closed set of equations, temperature, pressure and tropospheric water vapor can all be retrieved accurately, simultaneously, and independently. Results of our simulation studies, along with a discussion of the results, will be presented.

**JSG28/W/17-B2** Poster **1400-05****ATMOSPHERE WATER VAPOR DETECTION APPLYING GPS LIMB SOUNDING**

J. GROVE-RASMUSSEN (Atmosphere Ionosphere Research Division, Danish Meteorological Institute, Lyngbyvej 100, DK-2100 Copenhagen, Denmark, email: jgr@dmi.dk), P. Hoeg (DMI, email: hoeg@dmi.dk); M.B. Sorensen (DMI, email: mbs@dmi.dk) and S. Syndergaard (DMI, email: sss@dmi.dk)

GPS atmosphere limb soundings on a low Earth orbiter (LEO) have demonstrated the potential of obtaining vertical temperature profiles of the atmosphere. The water vapour profile of the troposphere can be detected by a similar technique. From information on the received phase of the two GPS radio frequencies, precise position and velocity of the involved GPS satellites and LEO, the bending angle of the radio signals, caused by the refraction in the atmosphere, can be determined. Through a relation between the refractivity, temperature, air pressure and water vapour, the dry air temperature can be determined at altitudes above the bulk water vapour content of the troposphere. The water vapour pressure profile is established by comparing the obtained dry temperature profile with an externally determined temperature profile.

The presented initial results from the Danish OERSTED satellite consist of comparisons of derived water vapour profiles with numerical weather prediction analyses and co-located radiosonde observations. Quality testing and error analysis of the retrievals are performed as function of geographical position, enabling tests of moist (tropical) and dry (high latitude) occultation results. The inversion method applied is examined for its ability to measure physical phenomena in the atmosphere and the dependency upon the assumptions throughout the analysis.

Initial results from the OERSTED satellite and the general ability to measure water vapour in the atmosphere by the GPS occultation technique will be presented.

**JSG28/W/10-B2** Poster **1400-06****ANALYSIS OF RADIO OCCULTATION DATA BY MEANS OF THE RADIOHOLOGRAPHIC METHOD**

K. HOCKE, A. Pavelyev, O. Yakovlev, N. Jakowski (DLR-DFD, Kalkhorstweg 53, 17235 Neustrelitz, Germany, e-mail: hocke@nz.dlr.de, IRE RAS, Fryazino, Vvedenskogo sq. 1, 141120 Moscow region, Russia, e-mail: agp117@ire216.msk.su)

The radioholographic method was developed by IRE RAS using radio occultation data of "MIR"-GEO satellites. Recently this method was applied to GPS/MET occultation data by joint efforts of IRE RAS and DLR-DFD. The radio signals received at the LEO satellite are analysed by using a reference beam. From the continuous phase and amplitude measurements at the LEO satellite it is possible to derive high resolution angular spectra as function of time during the occultation event. Subsequently, profiles of bending angle, refractivity and temperature can be retrieved from these angular spectra. This new method is briefly described in the present paper. Angular spectra obtained by various spectral analysis methods are compared, and the corresponding profiles of bending angle and temperature are presented. The potential of the radioholographic method will be discussed in view of enhanced height resolution and detection/removal of multibeam effects.

**JSG28/W/20-B2** Poster **1400-07****COSTELLATION OBSERVING SYSTEM FOR METEOROLOGY, IONOSPHERE, AND CLIMATE---COSMIC: AN OVERVIEW**

Ying-Hwa KUO (UCAR, P.O. Box 3000, Boulder, CO 80307, USA, Email: kuo@ucar.edu); Chris Rocken (UCAR, P.O. Box 3000, Boulder, CO 80307, USA, Email: rocken@ucar.edu); Gerald Liu (NSPO, 8F, 9 Prosperity 1st Road, SBIP, Hsing-Chu, Taiwan, Email: dl13@nsp.gov.tw); Lou Lee (NSPO, 8F, 9 Prosperity 1st Road, SBIP, Hsing-Chu, Taiwan, Email: loulee@nsp.gov.tw)

Constellation Observing System for Meteorology, Ionosphere and Climate---COSMIC is a collaborative science project between the United States and Taiwan. The goal is to launch a constellation of eight small satellites in late 2002. The primary science payload is the latest version of the GPS flight receiver developed by the Jet Propulsion Laboratory. Two secondary payloads are a Tiny Ionospheric Photometer (TIP), developed by the Naval Research Laboratory (NRL) and a Tri-Band Beacon (TBB) transmitter, jointly developed by NRL and Applied Research Laboratory at the University of Texas. COSMIC will produce approximately 4,000 radio occultation sounding every day, in all weather and uniformly distributed around the globe. The TIP and TBB will provide ionospheric measurements that are highly complementary to the GPS occultation soundings. Recent scientific studies have indicated that these soundings and ionospheric measurements will be useful for a variety of weather, climate and ionosphere research and operational applications. COSMIC is a research and operational demonstration program designed to provide atmospheric and ionospheric data in near real time. These data will be provided openly and at the minimum cost of communication and reproduction. In this presentation, we will discuss the preliminary design of the COSMIC system and the program schedule.

**JSG28/W/26-B2** Poster **1400-08****VERTICAL RESOLUTION OF GPS OCCULTATION DATA FROM OERSTED/SUNSAT**

M. D. MORTENSEN, (Atmosphere Ionosphere Research Division, Danish Meteorological Institute, Copenhagen, Denmark, email: mdm@dmi.dk.)

Vertical resolution is an important aspect of all atmospheric remote sensing techniques. In the troposphere there are features with small scale variations - such as the planetary boundary layer and the water vapor concentrations - which requires better vertical resolution than most remote sensing techniques can achieve at the moment. Occultations using the Global Positioning System (GPS) gives vertical profiles of the atmosphere when inverted. These profiles have inherently high vertical resolution but still, the vertical resolution is limited by diffraction effects. Recently developed inversion methods takes diffraction effects into account and thereby improves the resolution. Initial tests indicates that the diffraction methods improves the resolution by a factor of several, down to ~100m. In this talk a brief explanation of the different inversion methods will be given but the main aim is to present high resolution tropo-spheric profiles from real occultation measurements. Hopefully, it will be possible to use Oersted and/or Sunsat data. The results from the different inversion methods will be compared and further-more, comparisons with radiosonde data and ECMWF-data will be presented. Noise and small scale horizontal variations are likely to influence the results. On the other hand the diffraction methods shows great robustness towards noise in the simulations. The focus will be on determining whether the theoretically derived vertical resolution seems likely to be achievable in practise.

**JSG28/E/08-B2** Poster **1400-09****ON THE USE OF GPS MEASUREMENTS ON BOARD OF POSAT - 1 FOR TEC EVALUATION**

Isabel OSORIO and J. Pereira Osorio (both at Faculty of Sciences, University of Porto, Monte da Virgem, 4430 Vila Nova de Gaia, Portugal, email: iposorio@oa.fc.up.pt, posorio@oa.fc.up.pt); J. M. Reborde (INETI / LAER - Aerospace Laboratory, Estrada do Pao do Lumiar, 1699 Lisboa Codex, Portugal, email: jmr@laer.ineti.pt)

On board of the LEO Portuguese micro-satellite PoSAT - 1, codephases and Doppler GPS measurements are available, from a TRIMBLE TANS II receiver. Codephases measurements are ambiguous to the entire number of milliseconds of the signal propagation time, according to the receiver specifications. However, Doppler measurements are good enough to be used

## INTER-ASSOCIATION

on a process of pseudo-ranges smoothing. With this method a new signal of good quality is generated. Sets of fifteen minutes of those measurements, at a cadency of 0.5s, were used, in order to calculate the satellite orbit and the receiver clock error. This can be accomplished with reduced dynamics in a seven states Kalman filter.

Once the Kalman filter convergence is reached, the measurements from the lowest GPS satellite, in the PoSAT - 1 horizon, are used in an inverse process for Total Electron Content (TEC) evaluation, along the signal path, in the upper layers of the ionosphere. So, a contribution is given for the ionosphere knowledge, in directions impossible to be defined from the Earth's surface. The tomography of those zones is, then, possible since TEC values are known in many contiguous directions. In this paper the methods used and the results obtained will be presented.

### JSG28/W/03-B2 Poster 1400-10

#### SAGE III TEMPERATURE MEASUREMENTS

Michael C. PITTS (Science Applications International Corporation, 1 Enterprise Parkway, Hampton, Virginia 23666, USA, email: m.c.pitts@larc.nasa.gov); Larry W. Thomason (Atmospheric Sciences Division, NASA Langley Research Center, Hampton, Virginia 23681, USA, email: l.w.thomason@larc.nasa.gov)

The Stratospheric Aerosol and Gas Experiment (SAGE) III is the fourth generation of solar occultation instruments designed by NASA to measure vertical profiles of aerosols and important trace gases in the atmosphere. As part of NASA's Earth Science Enterprise (ESE), Earth Observing System (EOS) program, SAGE III instruments are currently scheduled to fly onboard the polar-orbiting Meteor-3M satellite in Fall 1999, the International Space Station in 2002, and a future flight of opportunity between 2000 and 2005. Unlike its predecessors, SAGE III has the capability to retrieve profiles of atmospheric temperature and pressure utilizing multi-spectral measurements of the oxygen A-band transmission in the 760-nm spectral region. The profiles will extend from the surface (or cloud top) up to 85 km and their vertical resolution will be approximately one kilometer. Given the inherent insensitivity of solar occultation experiments to long-term instrument degradation and the expected lifetime of the instruments (6+years), the SAGE III suite of instruments should provide a long-term record of self-calibrated, high vertical resolution temperature and pressure measurements. These measurements will be valuable for monitoring temperature trends in the stratosphere and mesosphere and for comparison studies with other temperature data sets. An overview of the SAGE III temperature and pressure retrieval algorithm and results from simulated retrievals using realistic measurement noise will be presented. The expected uncertainties in the retrieved profiles will also be discussed.

### JSG28/W/25-B2 Poster 1400-11

#### SPACEBORNE ATMOSPHERIC PROFILING: RESULTS FROM GPS/MET AND ANALYSIS PLANS FOR COSMIC

Christian ROCKEN, Sergey Sokolovskiy, Bill Schreiner, Doug Hunt, Richard Anthes, Ying-Hwa Kuo, and Randolph Ware (all at University Corporation for Atmospheric Research (UCAR), PO Box 3000, Boulder CO, 80307, USA; email: rocken@ucar.edu)

Data from over 62,000 atmospheric soundings from the GPS/MET experiment have been archived between April 1995 and June 1997. About 11,000 of these soundings have been processed at UCAR to Level 3: atmospheric temperature, pressure and humidity as a function of geometric height. In addition a large number of ionospheric soundings has been analyzed to compute electron density profiles. Based on the GPS/MET experience and results we are now developing the COSMIC Data Analysis and Archive Center (CDAAC). COSMIC will be described in other presentations at this session. CDAAC will process all sounding observations from the eight COSMIC satellites within less than three hours of data collection, for an operational demonstration of the impact of the data on weather forecasting and space weather monitoring and forecasting. Issues that will require special development for the CDAAC analysis system include lower troposphere data analysis, ionospheric correction and profiling, water vapor profiling, multipath in the atmosphere and at the ground fiducial sites, and low Earth satellite orbit prediction. We will summarize the most important results from the GPS/MET mission and outline the planned development and data analysis improvements for the CDAAC.

### JSG28/W/09-B2 Poster 1400-12

#### NEAR REAL-TIME ORBIT DETERMINATION FOR THE COSMIC SATELLITES: METHODOLOGY AND EXPERIMENTAL RESULTS

Ming YANG (Department of Surveying Engineering, National Cheng Kung University, Tainan 701, Taiwan, Email: myang@mail.ncku.edu.tw)

The joint Taiwan-US space program of COSMIC (Constellation of Observing System for Meteorology, Ionosphere and Climate), also known as ROCOSAT-3 in Taiwan, will consist of 8 low-earth orbiting micro-satellites to be launched by the year 2001. The major objective of the project is to conduct atmospheric limb sounding using the GPS/MET radio occultation technique. The GPS/MET soundings will be analyzed within 1 hour of data collection to provide precise, global coverage, and near real-time weather information. Prior to the recovery of atmospheric refractivity in GPS/MET data analysis, precise knowledge of the geometry between the GPS satellites, the COSMIC satellites, and the ground fiducial sites must be resolved first. Therefore, near real-time orbit determination for the COSMIC satellites is needed for the success of the mission. This paper proposes a triple differencing GPS data handling methodology for near real-time orbit estimation. Orbital results obtained from the experimental MicroLab-1 satellite are presented.

### JSG28/W/04-B2 Poster 1400-13

#### ON THE ASSIMILATION OF GPS/MET REFRACTION ANGLE MEASUREMENTS USING THE NCEP'S SSI ANALYSIS SYSTEM

X. ZOU, B. Wang, H. Liu, R. A. Anthes, T. Matsumura and Y.-J. Zhu (Florida State University, Department of Meteorology, 404 Love Building, Tallahassee, FL 32306 4520 USA, E-mail: zou@met.fsu.edu Telephone No: (850) 644-6025 Fax No: (850) 644 9642

In recent work we developed and validated a GPS forward raytracing operator, completed the development of the tangent linear and adjoint of the raytracing operator, and tested the correctness and the characteristics of these operators in several least-square-fit problems. We describe here the implementation of the GPS software and GPS/MET data into the National Centers for Environmental Prediction (NCEP) operational data assimilation system to examine the analysis increment due to the inclusion of GPS/MET refraction angles in the presence of a complete background term.

Additional issues to be addressed are related to the development of a model describing the measurement errors of GPS/MET data, the computational requirements for the forward raytracing and its adjoint operators, and the feasibility of the operational use of GPS data.

### JSG28/E/21-B2 Poster 1400-14

#### AN EVALUATION OF ANISOTROPIC MAPPING FUNCTION BY USING JMA 10KM SPECTRAL MODEL

ICHIKAWA Ryuichi (Kashima Space Research Center, Communications Research Laboratory, 893-1 Hirai, Kashima, Ibaraki 314-0012, Japan, e-mail: richi@crl.go.jp); Michael Bevis and James Foster (Hawaii Institute of Geophysics and Planetology, University of Hawaii, 2525 Correa Road Honolulu, HI, USA 96822); Nobutaka Mannoji (Numerical Prediction Division, Japan Meteorological Agency, 1-3-4 Ohte-machi Chiyoda-ku, Tokyo 100-8122, Japan)

Several anisotropic mapping functions are available for the analysis of GPS and VLBI measurements (MacMillan, 1995; Chen and Herring, 1997). Chen and Herring (1997) have demonstrated good agreement between horizontal gradient parameters estimated using their mapping function and the NCEP (National Center for Environmental Prediction) analysis field that is given on a 2.5degree grid. However, the utility of this anisotropic mapping function has not been evaluated with respect to mesoscale phenomena such as the passing of cold front, heavy rain fall, and severe storms because the NCEP analysis field has insufficient horizontal resolution for this purpose. Accordingly, we evaluate the Chen and Herring mapping function by ray tracing through the 10km spectral model of the Japan Meteorological Agency (JMA). Preliminary results indicate that gradient vectors can be incorrectly estimated in the presence of intense mesoscale disturbances, but that these conditions occur only infrequently.

### JSG28/E/03-B2 Poster 1400-15

#### A STUDY OF SPATIAL WATER VAPOR DISTRIBUTIONS BY USING ONE-WAY RESIDUALS OF GPS PHASE MEASUREMENTS

Takayuki YOSHIHARA, Toshitaka Tsuda (both at Radio Atmospheric Science Center, Kyoto University, Uji, Kyoto, 611-0011, Japan, email: yoshihara@kurasc.kyoto-u.ac.jp); and Kazuro Hirahara (Department of Earth and Planetary Sciences, Graduate School of Science, Nagoya University, Nagoya, 464-8602, Japan, email: hirahara@eps.nagoya-u.ac.jp)

It is very important to investigate characteristics of water vapor distribution in the troposphere, especially in the small scale variations of time and space, for researches on meso-scale phenomena. We aim to find out water vapor distributions by using propagation delays along each signal path from a GPS Satellite to a receiver. We took notice of a potential for pulling out water vapor informations from residuals, which were obtained as by-products of GPS phase data analysis. We analyzed a campaign data set, which was carried out over 12 days in Yamagawa, Kagoshima, Japan on June in 1996. For the analysis of the GPS data, we used GIPSY-OASIS II software. In the observation period, weather condition greatly changed 4 times with the motions of a cold front and a Baiu front, which passed toward north and south above Yamagawa. Time series of "original residuals" (i.e. outputs obtained directly from GPS data analysis) shown rather characteristics of dependences on elevation angles of GPS Satellites than spatial ones of vapors. We calculated "mean residuals" of entire observation period for dependences on elevation angles (for each GPS satellite), and subtracted them from "original residuals". As results, the residuals which calculated by such a method shown differences in spatial distributions as relative values, however, only in several cases of changes of weather condition with the passages of a cold and a Baiu fronts above mentioned.

### JSG28/W/01-B2 Poster 1400-16

#### SUOMINET: A NATIONAL REAL-TIME GPS NETWORK FOR ATMOSPHERIC RESEARCH

Randolph WARE (GST); Dave Fulker (Unidata); Seth Stein (Northwestern U.); David Anderson (U. Colorado); Richard Clark (Millersville U.); Kelvin Droegeheimer (U. Oklahoma); Soroosh Sorooshian (U. Arizona)

The 24 Global Positioning System (GPS) satellites flood the Earth atmosphere with microwave radio signals. Phase delays induced in these signals by the lower and upper atmosphere can be converted into integrated water vapor and total electron content (TEC) along each of the dozen or so ray paths to GPS satellites in view. We have proposed to develop "SuomiNet", a university-based GPS network to provide real time GPS data for atmospheric research and education. Named to honor meteorological satellite pioneer Verner Suomi, the network will make thousands of accurate tropospheric moisture and ionospheric TEC measurements per day during all weather conditions. SuomiNet will demonstrate the concept of a university-based national geophysical instrument providing real time atmospheric data to universities. We describe the proposed network and its potential for research in mesoscale and ionospheric modeling and data assimilation, severe terrestrial and space weather effects, precipitation, cloud dynamics, regional climate, and hydrology. Other potential research applications for SuomiNet data include detection and forecasting of low latitude ionospheric scintillation activity, geomagnetic storm effects at ionospheric mid latitudes, coastal meteorology, atmospheric chemistry, calibration of satellite radiometry, and correction of synthetic aperture radar for crustal deformation applications. The impact of these new data and observation methods on the atmospheric and related sciences may be dramatic, comparable to the impact GPS data have had in a few short years on the solid-Earth sciences.

### JSV29

Monday 26 July

#### MAGMA PHYSICS VERSUS VOLCANO PHYSICS (IAVCEI, IASPEI)

Location: Medical School EF08 LT3

Location of Posters: Arthur Thompson Hall

Monday 26 July PM

Presiding Chairs: D.B. Dingwell (Bayerisches Geoinstitut, Bayreuth, Germany),

B Chouet (Volcano Hazards, USGS, USA)

Concurrent Poster Session

### JSV29/W/07-B1 1400

#### A NUMERICAL INVESTIGATION OF SEISMIC WAVES AND MAGMA DYNAMICS ASSOCIATED WITH A VOLCANIC ERUPTION

Takeshi NISHIMURA (Dept. of Geophysics, Graduate School of Science, Tohoku University, Sendai 980- 8578, Japan, email: nishi@zisin.geophys.tohoku.ac.jp); Bernard Chouet ( U. S. Geological Survey, 345 Middlefield Road, Menlo Park, CA, USA, email: CHOUET@chouet.wr.usgs.gov).

We apply the finite difference method to calculate the magma dynamics and seismic waves associated with a volcanic eruption. Our model consists of a cylindrical reservoir and a narrow cylindrical conduit which are vertically oriented and embedded in a homogeneous half space. A lid caps the vent at the free surface and the magma is overpressurized prior to the eruption.



The eruption is triggered by the instantaneous removal of the lid, at which point the exit pressure becomes equal to the atmospheric pressure. Magma dynamics is expressed by the equations of mass and momentum conservation in a compressible fluid, in which the vesiculation process associated with depressurization is accounted for by a constitutive law between pressure and density (Iida, 1990). Radial velocities and normal stresses are continuous across the conduit and reservoir boundaries. Free slip is allowed at the fluid-solid boundary. Results from our calculations indicate that magma migrates gradually upward in response to the pressure gradient established between the atmosphere and reservoir, which is detected as long-period seismic signals. Superimposed on the long-duration signal associated with mass transport are short-period oscillations of the magma resulting from resonance of the reservoir, which are detected as short period seismic waves. The volume of the reservoir, vent size, and magma properties control the duration of long-period waves and the dominant periods of short-period oscillations.

JSV29/E/05-B1

1420

#### A MODEL OF MAGMA ACCUMULATION AND RELEASE TO DESCRIBE THE RHYTHMS AND STYLES OF VOLCANIC ERUPTIONS

Yoshiaki IIDA (Earthquake Research Institute, University of Tokyo, Yayoi, Bunkyo-ku, Tokyo 113-0032, Japan, email: ida@newsida.eri.u-tokyo.ac.jp)

A simple model of the magmatic process leading to volcanic eruptions is proposed with an elastic magma chamber connected to a shallower cylindrical conduit that opens or closes following inelastic response of the surrounding country rock to the magma pressure. It is further assumed in this model that the magma viscosity depends on the ascending magma flux, reflecting the cooling effect. According to the analysis, suitable coupling of the mechanical and thermal effects allows cyclic flow and episodic effusion of magma for the supply from below at a constant rate. Slow magma accumulation followed by quick release at an eruption is explained by some nonlinear effects included in the model.

Magma migration in a growing fissure from the elastic magma chamber is also modeled. In this case, growth of the magmatic fissure is controlled by the crustal stress as well as the magma pressure. When the initial magma pressure is high enough to suppress the crustal stress, the fissure elongates unlimitedly even to the ground surface while the width finally decreases. When the crustal stress is of sufficiently strong extension, the growth finally stops with the finite length and width of the fissure stabilized in the crustal interior. So the magma migration is either "extrusive" or "intrusive", depending on the crustal stress condition.

JSV29/E/02-B1

1440

#### MAGMA CHAMBERS DYNAMICS OF CRYSTALLISATION AND ERUPTION

C.C. MOURTADA-BONNEFOI (Univ. Blaise Pascal at C.N.R.S., U.M.R. 6524, 5 rue Kessler 63038 Clermont-Ferrand cedex, France; now at University of Bristol, Wills Memorial Building, BS8 1RJ, United Kingdom, email: c.mourtada-bonnefoi@bris.ac.uk); A. Provost (Univ. Blaise Pascal at C.N.R.S., U.M.R. 6524, 5 rue Kessler 63038 Clermont-Ferrand cedex, France, email: provost@opgc.univ-bpclermont.fr); F. Albarede (E.N.S. de Lyon, 46 Allée d'Italie, 69364 Lyon cedex 7, France, email: albarede@geologie.ens-lyon.fr)

On the time scale of their lifetime, most volcanic systems may be modelled as open reservoirs, forced by the input flux of magma and heat loss rate through the wall-rocks, where the magma mixes with input magma, cools, undergoes fractional crystallisation and differentiates.

In a simplified model of a chemically and thermally homogeneous reservoir, the mass, the chemical and the heat balance equations were derived; and their steady state solutions were determined graphically (Mourtada-Bonnefoi et al., 1999). Because of crystallisation kinetics (existence of a maximum crystallisation rate at some undercooling), for some forcing conditions, two stable steady states are possible. The initial conditions determine which of these steady state is realised.

During the lifetime of a volcano, the long term drift of the forcing of the chamber may lead the system to an unstable steady state when the number of stable steady states bifurcates from two to one; it ensues a magmatic catastrophe that implies a brutal increase (or, a decrease) of crystallisation rate, magma differentiation (reverse differentiation), the decrease (increase) of magma undercooling and the decrease (increase) of discharge rate of erupted lava. The model predicts that the magma is maintained at an undercooling of only a few tens of °C in the chamber and that during a magmatic catastrophe, the composition jumps by a few per cent of SiO<sub>2</sub> while the temperature jumps by a few tens of degrees. We suggest that composition gaps in the lava series may be the consequence of magmatic catastrophes. The wide range of lacking compositions, the widths of the gaps, the involvement of fractional crystallisation in lava differentiation and the discontinuity of mineralogy throughout the gap seem compatible with both the qualitative and the quantitative predictions of the model.

JSV29/W/06-B1

1500

#### MAGMA MIXING MODEL IN THE 1991-1995 ERUPTION AT UNZEN VOLCANO

Setsuya NAKADA (Earthquake Res. Inst., Univ. Tokyo, Japan, Email: nakada@eri.u-tokyo.ac.jp), and Chang-Hwa Chen (Inst. Earth Sci., Acad. Sinica, Taipei, Email: china@earth.sinica.edu.tw)

Disequilibrium texture of phenocrysts and the occurrence of enclaves are common in dacite lavas of the latest eruption at Unzen. Glomerophytic aggregation of phenocrysts implies their coexistence either in a crystal mush of the reservoir or in intrusive rocks before eruption. Sr and Nd isotopic ratios of phenocryst species and the groundmass are different from each other. The groundmass is less evolved isotopically than the coexisting hornblende. These facts require that coexisting phenocrysts had spent time as long as 10<sup>5</sup> yr. in a closed system, and that they met a new melt during eruption. A plausible model is either that (1) crystals of old plutonic rocks were incorporated accidentally, or that (2) these phenocrysts had spent a significant time in a stagnate marginal layers of the reservoir. Enclaves are micro-gabbroic in texture with glass in the matrix, isotopically similar to or a little less evolved than the host dacite, having the composition much away from the evolution trend for the Unzen lavas (e.g., in 87Sr/86Sr-FeO\*/MgO plot). The enclaves may represent a sort of cumulate derived from a crystal-mush layer in a cooling magma reservoir, or from a partial-melting zone in the wall rock. Similarly, disequilibrium in texture and chemistry of phenocrysts can be produced either by incorporation of crystals from partial melting zone or by recycling of crystals from a long-lived margin of the reservoir. Thus, disequilibrium can occur as a self-generating process in a cooling magma reservoir rather than as injection of new magma.

JSV29/W/02-B1

1540

#### RECENT MAGMA DISCHARGE RATE AT COLIMA VOLCANO, MEXICO: IMPLICATIONS ON ITS INTERNAL STATE

Juan Manuel ESPÍNDOLA ( Instituto de Geofísica, Universidad Nacional Autónoma de México, Ciudad Universitaria, México 04510 D.F., e-mail: jme@tonatiuh.igeofcu.unam.mx)

The last strong explosive eruption at Colima volcano took place in 1913. That activity produced a crater 350m deep and a jagged rim 400m in diameter. The morphology of the crater varied little during about 18 years. In 1931 the floor of the crater flattened due to a renewed ascent of magma which continued until 1961. At that time the blocky lava accumulating inside the crater reached the northern and lowest part of the rim outpouring and forming a small lava flow. By 1962 the crater had been completely filled and was building up a protruding dome above the level of the former crater rim. We have estimated the volume of material filling the crater in about 44 million cubic meters (mcm), and the volume of the 1961 lava flow in 1.5 mcm. The volume of magma discharged between 1962 and 1984 was estimated through photographs taken in those years from about the same point, some 8 km NE from the crater. From those pictures and topographic maps of the area (scale 1:50,000) we estimated the volume of the dome in 8 mcm. The volcano had other merapien-type eruptions in 1975 and 1982, producing lava flows for which we have estimated a volume of 11 mcm. Thus, we estimate the average annual discharge rate during that period in 0.86 mcm/yr. This estimate and gravity data published previously allow us to formulate a thermal model of the plumbing of Colima volcano, based on a simple conduction model of flow with heat generation due to shearing. We also analyze all the registered seismicity related to the volcano in terms of the model.

JSV29/W/09-B1

1600

#### MAGMA TO SEISMOGRAMS SEISMIC OBSERVATIONS FROM SOUFRIERE HILLS VOLCANO IN MONTSERRAT

Dr Jurgen NEUBERG, (School of Earth Sciences, Leeds, email: locko@earth.leeds.ac.uk)

From Magma to Seismograms Seismic observations from Soufriere Hills volcano in Montserrat reveal a wide variety of low-frequency seismic signals which are considered to play an indicative role in assessing the state of volcanic activity. These events occur usually in swarms, they are associated with tilt, and occasionally merge into tremor, an observation that has shed further light on the generation and composition of harmonic tremor. We use a finite difference method to model several features of low-frequency seismic signatures and compare them with observations. Depth-dependent velocity models for a fluid-filled conduit/dyke are derived by solving the differential equations governing the fluid flow and the resulting pressure fluctuations in the magma. We account for the degassing of the magma and the possible feedback mechanism exerted by the seismic signals. Episodes of tremor which show shifting spectral lines and model those in terms of changes in the gas content of the magma as well as in terms of a time-dependent triggering mechanism of low-frequency resonances. Several models for repetitive triggering mechanisms in a two-phase flow regime are discussed.

JSV29/W/01-B1

1620

#### EXPERIMENTAL STUDIES OF ROCK FAILURE AT NEAR-SOLIDUS TEMPERATURES

P.Sammonds, (Email: p.sammonds@ucl.ac.uk); P.Meredith, (Email: p.meredith@ucl.ac.uk); VROCCHI, (Email: ucfbvro@ucl.ac.uk); (all at University College London, Dept. of Geological Sciences, Rock and Ice Physics Laboratory, Gower St, London WC1E 6BT, UK); C.Kilburn, ( University College London, Benfield Greig Hazard Research Centre, Gower St, London WC1E 6BT, UK Email: c.kilburn@ucl.ac.uk)

Seismicity is a key precursor to volcanic eruptions. As magma approaches the surface, seismicity may be induced by fracturing of country rock and cooled magma (as new conduits form or as existing pathways change shape), and by degassing or dynamic processes within the magma itself. Much of the fracture-induced seismicity is expected to occur in heated rock and solidifying magma at the margins of the feeding dyke or conduit, at nominal temperatures of 500&#61616;-1000&#61616;C. A new rock mechanics cell has been designed to operate at these temperatures and at pressures from atmospheric to 70 MPa (corresponding to depths of 6 Km or less), in order to investigate variations in (1) the compressive and tensile strength of magma, (2) Young's Modulus, and (3) rates of microseismic emission during fracture. The results will provide a coherent database for analysing seismic sequences at volcanoes and for identifying patterns (such as spatial clustering of hypocentres or time increases in seismic rate) that may be diagnostic of an imminent eruption.

JSV29/W/08-B1

1640

#### NUMERICAL SIMULATIONS OF MULTIPHASE NON-EQUILIBRIUM MAGMA ASCENT DYNAMICS WITH COMPOSITIONAL AND PHASE DISTRIBUTION DEPENDENT MAGMA PROPERTIES, STRAIN-INDUCED MAGMA FRAGMENTATION, PUMICE FORMATION, AND CHOKING

Paolo PAPAIE (Istituto Nazionale di Geofisica, via S. Maria 53, I-56126 Pisa, Italy, email: papale@dst.unipi.it)

Steady-state magma ascent along a one-dimensional volcanic conduit is numerically simulated by accounting for the separated flow of homogeneous liquid magma plus crystals, and gas exsolving from the liquid. Relevant properties (density, viscosity, H<sub>2</sub>O or H<sub>2</sub>O+CO<sub>2</sub> saturation) are calculated on the basis of magma composition in terms of 10 major oxides plus two dissolved volatile species, by using most recent and accurate models. Magma viscosity is corrected for the presence of crystals and gas bubbles, and also depends on the stress field with possible pseudoplastic (or shear thinning) and dilatant (or shear thickening) rheology of the magmatic mixture. Magma fragmentation is assumed to occur at either a critical gas volume fraction, or at a critical strain-rate exceeding the inverse of the structural relaxation time of magma and producing strain-induced brittle failure of the liquid continuum. Above fragmentation, the gas phase is transported partly as a continuum, and partly as gas bubbles in liquid+crystal+gas fragments (or droplets) corresponding to pumice; glass shards (or liquid droplets) and free crystals also form at fragmentation. The multiphase magmatic mixture is assumed to choke at the conduit exit, where correspondingly the magmatic pressure can be larger than the atmospheric pressure by several factors. Several simulations have been performed by varying the eruptive conditions in terms of conduit size, mass flow-rate, magma composition, volatile abundance and composition, crystal content and distribution, and assumed amount of pumice formed at fragmentation. The present modeling and the information it supplies can form a basis for a future coupling of magma ascent fluid dynamics with other geophysical disciplines such as volcano seismics and acoustics; such coupling would allow better capability of interpreting signals during eruptions, deriving constraints for the subsurface fluid dynamics, and at the end understanding and predicting volcanic eruptions.



**JSV29/W/04-B1 1700**

**FALL VS FLOW ACTIVITY DURING THE 1991 CLIMACTIC ERUPTION OF MT. PINATUBO (PHILIPPINES)**

Mauro ROSI, Andrea Di Muro and Riccardo Leoni (Universita' degli Studi di Pisa, Pisa I-56126, Italy, E-mail: rosi@dst.unipi.it, dimuro@dst.unipi.it, rleoni@dst.unipi.it); Ma. Lynn o. Paladio-Melosantos and Terecito Bacolcol (Philippine institute of Volcanology and Seismology)

Six years after the 1991 Mt. Pinatubo eruption the deep erosion have superbly exposed pyroclastic deposits enabling us to assess the stratigraphic relationships between climactic fall, flow and surge deposits in the Marella Valley and contiguous ridges on the SW, downwind side of the volcano. In addition maximum clast size measurements of lithics and pumices were carried out on the plinian fall deposit all around the volcano. The maximum height of the convective column obtained using the Carey and Sparks (1986) model is in good agreement with satellite measurements. Field data indicate that the fall bed is normally graded with most of the surge beds intercalated to its upper finer grained portion. The intra-plinian pyroclastic surges propagated up to 10 km from the crater both on valley bottom and contiguous ridges, while post-plinian pyroclastic flows have greater runout and are not associated to ash cloud surges. We believe that during climactic event a progressive shift from an early convective column, to a transitional column feeding both plinian convective plume and radially distributed dilute currents, to a fully collapsing fountain producing only pyroclastic flows without associated plinian fall activity occurred. We believe that the transition from plinian to a large coignimbritic convective column accounts well for the lowering of the plume as measured by the satellites.

**JSV29/E/01-B1 1720**

**PYROCLAST MASS PARTITION OF COLLAPSING AND TRANSITIONAL COLUMNS BY USING NUMERICAL SIMULATIONS**

Andrea di Muro and Mauro Rosi (Universita' degli Studi di Pisa, Pisa I-56126, Italy, Email: dimuro@dst.unipi.it, rosi@dst.unipi.it) Augusto NERI (Consiglio Nazionale delle Ricerche, Pisa I-56126, Italy, Email: neri@dst.unipi.it)

Pyroclast distribution and mass partition between convective and collapsing regions represents a major issue in the understanding of the dynamics of explosive eruptions. The spatial and temporal distribution of pyroclasts during full-collapsing and transitional columns were investigated by using a transient, two-dimensional, and three-phase - one gas phase and two solid phases representative of pyroclasts of different size and density - flow model. Several simulations were carried out by using different water contents of the eruptive mixture and assuming both pressure-balanced and overpressured conditions at the vent region. For full-collapsing columns, simulation results allowed the quantification of the mass of different pyroclasts forming the pyroclastic flow, the co-ignimbrite column, and the thermal plumes rising from the fountain and the deflation zone. The total mass transported in the whole convective system ranges from about 10 up to about 30% of the total mass erupted. With an increase in water content the collapsing character of the column moves towards more transitional behavior. Such a regime is characterized by a greater collapse height, the generation of a more dilute density current, a shorter flow runout, and by a more transient behavior of the column and flow. In these cases, the total mass forming the convective portions can reach values of up to 50% of the erupted pyroclasts with a significant amount of coarse particles. At higher water contents the column becomes Plinian with 100% of the erupted mass feeding the plume.

**JSV29/E/03-B1 1740**

**WHAT IS HAPPENING AT THE DEPTH OF 70 M AT STROMBOLI?**

Sylvie VERGNOLLE (Laboratoire de Dynamique des Systemes Geologiques, Institut de Physique du Globe- 4 place Jussieu - 75252 Paris Cedex 05 FRANCE, email: vergnolle@ipgg.jussieu.fr)

Activity of Stromboli is characterised by a series of explosions, whose origin lies in the breaking of a metric (radius of 0.9 m and length of 15 m), over pressurised bubble (0.031 MPa) at the surface of the magma column. Overpressure at the surface strongly suggests overpressure at depth, when the "slugs" are formed. Here we study the motion of a slug initially over pressurised in a vertical tube of length 70 m and diameter 2 m. The acoustic pressure radiated from the bubble rise at the vent is calculated and compared with acoustic measurements. Because bubbles are formed with an initial overpressure and rise in a tube, they grow mainly by increasing their length (slug flow), overshoot their equilibrium position and the gas compressibility provides the restoring force for their oscillations. The change in the volume of the rising bubble pushes the liquid column up and down, vigorously enough to produce sound waves of low frequency (0.5 Hz). Because the bubbles are relatively long (15 m) compared to their radius (0.9 m), their shape is assumed to be a cylinder whose length oscillates until it stops by viscous dissipation in the magma. Sound is expected at bubble formation around 0.5 Hz and dies quickly after. The strong expansion of the "slug" when it is formed at depth is also able to excite "sloshing waves" at the top of the magma column, whose frequency is between 1 and 3 Hz. The model of acoustic pressure predicts that a peak in acoustic pressure should appear in the frequency range 0-1 Hz (volume mode) simultaneously with a peak in the range 1-3 Hz (sloshing mode), which is what is observed at Stromboli volcano. The amplitude of the precursory signal shows that the "slug" is formed with an overpressure of 14 MPa, an initial length of 0.2 m and at the depth of 70 m. Because "slugs" are formed by the coalescence of a foam layer at the top of the magma chamber, 70 m is its depth.

**Monday 26 July PM**

Presiding Chairs: D.B. Dingwell (Bayerisches Geoinstitut, Bayreuth, Germany); B Chouet (Volcano Hazards, USGS, USA)

**JSV29/W/03-B1 Poster 1400-01**

**SUBSURFACE GEOMETRY OF CALDERA IN RELATION TO DEPTH OF MAGMA CHAMBER, MIOCENE KUMANO CALDERA, SW JAPAN**

Daisuke MIURA (Geology Department, Abiko Research Laboratory, Central Research Institute of Electric Power Industry, 1646 Abiko, Chiba 270-1194, Japan, email: dmiura@criepi.denken.or.jp)

Scaling law of fragmentation and population of fault data with respect to caldera formation produce to evaluate quantitatively subsurface structure of caldera and genetic relationship to the underlying magma chamber. Miocene Kumano caldera, 41 by 23 km in diameter as a whole, southwest Honshu, Japan, is an example to field application based on this idea. Nested piston-cylinder structure is suitable to overall geometry of the caldera.

To select the caldera-related faults, characters of faults, veins, and intrusions in and around the caldera behaved to classify a measured fault data by use of paleo-stress analysis. Comparison of the respective paleo-stress results implies that both tumescence and collapse of country rocks occurred during the caldera formation. Property of the obtained fault set thus

represents the subjective caldera geometry. The exponent of 0.41 on cumulative fault throw distribution produces exponent of 0.6-0.7 on cumulative fragment mass distribution, which reveals a mode of fragmentation of two-dimensional object by vertical stress input. This finding explains well a thin-plaster geometric relation to underlying magma chamber of piston-cylinder caldera, and it suggests that the exponent is useful to chase variation of caldera geometry.

**JSV29/W/05-B1 Poster 1400-02**

**EVALUATION OF SUBSURFACE STRUCTURE AND LONG-TERM STRAIN RATE OF MIOCENE KUMANO CALDERA, JAPAN, BY USE OF FAULT POPULATION DATA**

Daisuke MIURA (Geology Department, Abiko Research Laboratory, Central Research Institute of Electric Power Industry, 1646 Abiko, Chiba 270-1194, Japan, email: dmiura@criepi.denken.or.jp)

Scaling law of fragmentation and population of fault data with respect to caldera formation produce to evaluate quantitatively subsurface structure of caldera. Miocene Kumano caldera, 41 by 23 km in diameter as a whole, southwest Honshu, Japan, is an example to field application based on this idea. Nested piston-cylinder structure is suitable to overall geometry of the caldera.

To select the caldera-related faults, characters of faults, veins, and intrusions in and around the caldera behaved to classify a measured fault data by use of paleo-stress analysis. Comparison of the respective paleo-stress results implies that both tumescence and collapse of country rocks occurred during the caldera formation. Property of the obtained fault set thus represents the subjective caldera geometry. Extrapolation of an exponent of 0.41 on cumulative throw distribution to maximum data and K-Ar ages indicate a long-term strain rate of the caldera development, ca. several cm/year. This value roughly coincides with present short-term rate of caldera and/or of volcano-tectonic depression, as estimated elsewhere.

The exponent of 0.41 produces exponent of 0.6-0.7 on cumulative fragment mass distribution, which reveals a mode of fragmentation of two-dimensional object by vertical stress input. This finding explains well a thin-plaster geometric relation of caldera and underlying magma chamber as proposed to piston-cylinder model, and it suggests that such exponent is an intense variable to chase.

**JSV29/E/04-B1 Poster 1400-03**

**THE INTENSITY AND DEPTH OF THE PRIME HEAT SUPPLY, THE ISOTOPIC CHEMISTRY OF THE OCEAN FLOOR BASALT, BATHYMETRY, AND EQUATION-OF-STATE: A UNIQUE PHENOMENON**

Giovanni P. GREGORI (IFA-CNR, via Fosso del Cavaliere 100, 00133 Roma, Italy; e-mail: gregori@atmos.ifa.rm.cnr.it); and Gino M. Crisci (UNICAL, 87036 Arcavacata di Rende, Cosenza, Italy; e-mail: crisci@fis.unical.it)

The isotopic chemistry of ocean floor basalts is usually interpreted in terms of a mixture of different primitive end-members with reservoirs at different depths ("reservoir rationale"). We show how it can rather be explained in terms of a different melt i ng-depth of every basalt, from a combination of the total prime endogenous heating and of the temporal evolution of its upward propagation. Up to some extent, the equation-of-state relates with each other the prime heat supply, the melting depth, the lav a fluidity, and the bathymetry or topography of the outpoured magma. Therefore, geomagnetic phenomena, the axial bathymetry of mid-ocean ridges and their variation vs. latitude, and the isotopic chemistry of basalts, are correlated with each other. Observations can be interpreted in terms of a chemically spherically isotropic Earth, differentiated vs. geocentric radial distance, and of a spatial variation of the prime endogenous heat supply. Ocean basalts can be distinguished into 5 main categories ("clus t ers"), every one being speculated to correspond to a typical range of prime heat supply ("energy hierarchy"). A wealthier database of isotopic measurements should allow for investigating the temporal evolution of the magmatic history at every site. The g e ographical distribution of the isotopic signature is also proposed. Such mere observational evidences can be interpreted in terms of basically three competing viewpoints: (i) the reservoir rationale; (ii) the trailing continental edge hypothesis; and (ii i ) the energy hierarchy. A tentative model for global volcanism ought to distinguish (i) mid-ocean ridge; (ii) Dupal's; (iii) hot spot and DAVI; and (iv) island arc and Cordilleran volcanoes.

**JSV29/P/01-B1 Poster 1400-04**

**MONITORING OF NATURAL HAZARDS USING MULTI SENSORS DATA**

SINGH, Ramesh (Dept of Civil Engineering, Indian Institute of Technology, Kanpur, 208016, India, Email: ramesh@iitk.ac.in)

Abstract not available at time of going to press

**JSV30 Monday 26 July**

**ARC MAGMATIC ROCKS AS BUILDING BLOCKS FOR THE CONTINENTS (IAVCEI, IASPEI, ILP)**

Location: Medical School, WG11 LT5  
Location of Posters: Arthur Thompson Hall

**Monday 26 July AM**

Presiding Chairs: J.P. Davidson (UCLA, Dept. of Earth and Space Science, Los Angeles, USA); B.M. Wilson (Univ. of Leeds, Dept. of Earth Sciences, Leeds, UK)

**Introduction 0830**

J.P.DAVIDSON

**JSV30/E/07-B1 0840**

**THE ROLE OF HYDRAULIC FRACTURES AND INTERMEDIATE DEPTH EARTHQUAKES IN GENERATING SUBDUCTION ZONE MAGMATISM (SZM)**

J. Huw DAVIES (Dept. of Earth Sci., Univ. of Liverpool, L69 3BX, UK, email: davies@liv.ac.uk)

Hydrous fluxing can unequivocally be shown to be important for generating most present day SZM. Given our present, incomplete, understanding of the connectivity of a hydrous fluid in cold oceanic crust and mantle; it seems that water cannot interconnect and hence percolate out to the hot mantle. So how does the water (released by dehydration of hydrous minerals produced by hydrothermal circulation at the ridge) enter the mantle to generate melting?

Intermediate depth earthquakes are also a puzzle, since the frictional stress preventing slip on a fault plane is greater than the strength of rocks at these depths. One solution is that the pressure of the trapped pore water, which cannot percolate, reduces the effective normal stress (and hence frictional stress). Following the earthquake, the pore water will be temporarily interconnected on the fault plane by the coseismic slip. If this film is sufficiently inter-connected, and exceeds a critical vertical height (>15m-1.5km - range due to uncertainty in fracture properties of rocks at high pressures), then it can span a hydrofracture that will propagate out into the mantle wedge. The volume of water contained will largely control how far they get. The biggest hydrofractures could reach the hottest part of the mantle wedge leading to rapid melting and magma fracturing, while the smallest might stop in the subducted sediments. This process therefore has the potential to explain the wide range of time scales interpreted from short half-life isotopes. A quantitative model for the source region of SZM was developed based on this hypothesis and the recent wet melting experiments of Hirose and Kawamoto. It predicts sensible major element compositions; and a close relationship between water and magma flux.

**JSV30/W/11-B1****0900****HIGH MG# ANDESITES IN THE ALEUTIAN-KAMCHATKA JUNCTION: IMPLICATIONS FOR CONTINENTAL CRUST FORMATION BY SUBDUCTION MAGMATISM**

Gene M. YOGODZINSKI (Dept. of Geology, Dickinson College, Carlisle, PA, U.S.A.); Jonathan M. Lees (Dept. of Geology & Geophysics, Yale University, New Haven, CT, U.S.A.); T. G. Churikova, A. A. Koloskov (both at Inst. of Volcanic Geology and Geochemistry, Petropavlovsk, Kamchatsky, 683006 Russia)

The Aleutian-Kamchatka junction is characterized by unusually high heat flow in the western most Bering Sea, and a shallowing of seismicity northward along the subduction zone from southern Kamchatka (600 km) to the Kamchatka-Bering Fault intersection (100-200 km). If the Pacific plate is torn below the Bering fault, a slab window will be present through which mantle material can flow around the exposed northern edge of the Pacific Plate. In this model slab rollback beneath Kamchatka has induced asthenospheric flow around the northern edge of the subducting plate, and is the cause of the anomalously high magma production from beneath the Kamchatka Central Depression. The northern group volcanoes (Sheveluch, Kharchinsk, Zarechny), which lie in the Aleutian Kamchatka junction immediately above the proposed Pacific Plate edge, are chemically distinct from the adjacent Klyuchevskoi group volcanoes in a way that implies the presence of an anomalously large slab melt contribution to the northern group rocks. Relatively high Mg/Mg+Fe (Mg#) in andesitic rocks of the northern group (55-63% SiO<sub>2</sub>) results in a major element trend that is more strongly calc-alkaline (higher Mg# relative to SiO<sub>2</sub>) than that defined by rocks of the Klyuchevskoi group to the south. The high Mg# andesitic rocks of the northern group also have anomalously low Y and high Sr/Y compared to the Klyuchevskoy rocks, and compared to common arc volcanic rocks world-wide. These features are interpreted to imply the presence of primitive (mantle-derived) andesitic magmas produced by slab melting and melt-peridotite interaction in the mantle wedge beneath the northern group volcanoes (Kay, 1978; J. Volc. & Geoth. Res, v4., p117). The anomalously slab melt contribution is interpreted to result from strong heating of the Pacific Plate by asthenospheric flow around its northern edge. Geochemically, high Mg# andesitic rocks of the Aleutian-Kamchatka junction are broadly like many Archean-age calc-alkaline rocks which were produced at a time when the average age of the subducting lithosphere was relatively young and when melting of the subducting slab may have been more common.

**JSV30/E/06-B1****0920****MID-CRUSTAL ARC LITHOSPHERE AND DEVELOPMENT OF CONTINENTAL CRUST**

PATRICIA FRYER (Hawaii Institute of Geosciences and Planetology, 2525 Correa Rd Honolulu, HI 96822, USA, email: pfryer@soest.hawaii.edu)

A major problem in trying to develop constraints on models for the relationship between evolution of arc and continental crust is understanding the "fundamental paradox" of development of andesitic bulk composition of continental crust despite the basaltic additions that characterize magmatic growth in arcs. Understanding the architecture of the arc crust and aspects of geochemical mass flux into and out of the arc lithosphere in convergent margins are critical to developing models for the evolving composition of continental crust. Recent geophysical studies of the Izu arc have produced a more detailed model for arc velocity structure than ever before. The interpretation that the arc is underlain at mid-crustal levels by a tonalitic layer of considerable thickness is germane to the questions of arc lithosphere composition and evolution. Seismic refraction studies of the Mariana system suggest a similar layer may be present at 18°N, although the data are sparse. The suggested tonalitic layer is too deep beneath the Izu arc to be sampled, but tectonic processes may have exposed a portion of it in the southeastern Mariana forearc. Tonalitic intrusive rocks were dredged from the inner slope of the southeastern Mariana Trench at depths greater than 7000 m. Tectonic erosion has reduced the width of the forearc to approximately 100 km, half that elsewhere (200 km). The region over which these rock types have been recovered is extensive. Nowhere else in an active convergent margin setting are such rocks exposed in close proximity to the active volcanic arc and in an interoceanic setting where influences of continental contamination are minimal. Analyses of these rocks are underway and it will be important to compare the results of these studies with the work that has already been done on the Izu peninsula sequences. A comparison would permit us to test the possibility that mid-crustal arc lithosphere development in these two localities could serve as a model for general interpretation of evolution of arc crust and ultimately of a fundamental process of development of continental crust.

**JSV30/E/05-B1****0940****LONG AND SHORT TERM PETROLOGICAL PROCESSES IN ARC VOLCANOES: IMPLICATIONS FOR CRUSTAL GROWTH FROM MOUNT RUAPEHU, NEW ZEALAND**

John GAMBLE (School of Earth Sciences, Victoria University of Wellington, Wellington, New Zealand, email: John.Gamble@vuw.ac.nz); Richard Price (School of Science & Technology, University of Waikato); Ian Smith (Department of Geology, University of Auckland); Peter Wood (Institute of Geological & Nuclear Sciences); Robert Stewart (Department of Soil Science, Massey University); William McIntosh, Nelia Dunbar (both at Geochronological Laboratory, New Mexico Bureau of Mines)

Mount Ruapehu (2797 m and 110 km<sup>3</sup>) is the largest active andesite – dacite volcano in the Taupo Volcanic Zone. The volcano has been continually active for the past two millennia with small volume (< 0.1 km<sup>3</sup>) eruptions modulated through a vent system beneath a summit crater lake. Since the well documented events of 1945, eruptions of juvenile lava bombs in 1966, 1969, 1971, 1975, 1977, 1995 and 1996, together with reports of activity around 1925, 1895 - 1905 and 1860, have indicated a periodicity of 20 – 30 years for historic times. Because this type of activity was (a) largely phreatomagmatic and (b) minor in volume, little evidence for its existence can be detected on the active edifice, where the dynamic processes of erosion are extreme. However, a complete record of activity is preserved in the tephra sequences on the ring plain and the record can be further constrained by well dated and interbedded rhyolite tephra from the caldera centres to the north. Based upon the tephra records and new

40Ar/39Ar dating studies, we conclude that late Quaternary – Holocene activity on Ruapehu has been pulsatory, with periods of high magma production (~130 ka; 22 ka and 10 ka) bracketed by periods of lower, but more or less continuous activity, which is representative of the situation at present. During periods of high magma production, effusive activity built up thick lava flow sequences, commonly in small time windows. These comprise the bulk of the eroded edifice and eruptive volumes are an order of magnitude larger than the small events. Petrographic and geochemical study of the modern (1945 - 1996) lavas shows that these are generally similar to prehistoric lavas. Conventional geochemical variation diagrams show compositional overlap between modern and prehistoric lavas which satisfy general models of evolution by AFC. Detailed study of the modern and prehistoric samples, based on stratigraphy, reveals complexities requiring the interplay of complex mixing and mingling processes as melts make their way through the crust and into the shallow plumbing system of the volcano.

**JSV30/W/09-B1****1000****THE PETROLOGY OF THE SOUTHERN LONGWOODS COMPLEX, SOUTH ISLAND, NEW ZEALAND: IMPLICATIONS FOR CRUSTAL GROWTH IN SUBDUCTION RELATED MAGMATIC SYSTEMS**

Richard PRICE (School of Science & Technology, University of Waikato, Hamilton, New Zealand, Email: rprice@waikato.ac.nz); Anthony Reay (Department of Geology, University of Otago, Dunedin, New Zealand); Richard Arculus (Department of Geology, Australian National University, Canberra, ACT, Australia)

Intrusive rocks of the Longwood Complex in New Zealand's South Island provide an opportunity to gain insights into the petrological processes operating beneath a subduction related volcanic arc. The complex is of Permian-Triassic age and contains rocks ranging in composition from ultramafic cumulates and gabbros through quartz diorites to granites. All analysed samples show trace element characteristics typical of subduction-related magmas (Cs, Rb, Ba, and K are relatively enriched, Nb is depleted relative to K, U, and La, and Pb is enriched relative to Ce) and quartz diorites are compositionally similar to low to medium K andesites. Gabbroic rocks have some of the features of arc tholeiites [e.g. low K and depleted REE -(La/Yb)<sub>n</sub> = 2.15; (La/Ce)<sub>n</sub> ~ 0.8]. Overall, the geochemical variation in the complex is consistent with a model whereby dioritic rocks were derived by crystal fractionation from mafic precursors represented by the gabbros.

Dykes are abundant within the complex and many are composite with compositions ranging from dolerite through andesite to dacite. Geochemically, the components of composite dykes cannot be related in a simple way to the rocks of the major intrusive units of the complex and they may represent the feeder conduits for andesitic volcanoes that once overlay the intrusive complex. Felsic material in some dykes could be either a residual evolved magma left from earlier recharge events or melt derived by anatexis of the host quartz diorite. Abundant mafic enclaves in quartz dioritic rocks derived by crystal fractionation from magmas represented by the gabbroic rocks of the complex and were incorporated when quartz diorite magmas were intruded into and disrupted evolving basaltic magma chambers. If the quartz diorites are mixed magmas, then the enclaves cannot represent the mafic component of this mixing trajectory.

**JSV30/W/08-B1****1040****PETROLOGY AND PETROGENESIS OF VICO VOLCANO, CENTRAL ITALY**

Giulia PERINI, Jon P. Davidson (both at Department of Earth and Space Sciences, University of California, Los Angeles); Sandro Conticelli (Centro di Geodinamica, Università della Basilicata, Potenza, Italy); Lorella Francalanci (Dipartimento di Scienze della Terra, Università di Firenze, Italy)

Plio-Pleistocene alkaline ultrapotassic magmatism produced several different rock series in Italy. In the same area contemporaneous subalkaline magmas of calcalkaline affinity were also erupted. At Vico volcano and the adjacent area products having distinct petrochemical affinities were erupted in a short period of time. The petrology and petrogenesis of Vico magmas is of importance for unravelling the genetic relationship between the different ultrapotassic rock series, and also between ultrapotassic and subalkaline magmas. Vico volcano has erupted mainly ultrapotassic silica-undersaturated magmas with minor volumes of silica-saturated and -oversaturated magmas. Stratigraphy indicates that the eruptions sampled evolved oversaturated magma at the beginning of Vico's activity and silica-undersaturated magmas toward the end. However, contemporaneous eruptions of primitive silica-saturated and -undersaturated compositions took place during the youngest activity. LILE/HFSE, LREE/HFSE ratios as well as isotope composition (Sr, Nd and Pb isotopes) of the most primitive samples indicate that three non-cogenetic parental magmas having different petrochemical affinities were present in the Vico system. Geochemical and isotope variations indicate that these parental magmas evolved by polybaric fractional crystallization, mixing and crustal assimilation. The oldest silica-oversaturated magmas are the result of mixing between a high potassium calcalkaline magma and an ultrapotassic silica-undersaturated magma. Ultrapotassic primitive silica-saturated magma erupted during the last stage of activity was present in the system earlier than the time of its first eruption.

**JSV30/E/03-B1****1100****FOR A HIGHLY HETEROGENEOUS SUBDUCTION-MODIFIED MANTLEDRAWNKA**

L. BLATTER, Ian S. E. Carmichael (both at Dept. of Geology and Geophysics, University of California, Berkeley, CA. 94720, USA, Email: dblatter@uclink4.berkeley.edu)

Volcanism in the western part of the Mexican Volcanic Belt (MVB) is related to the subduction of the Rivera plate beneath the Jalisco block. Highly potassic absarokites and minettes, along with calc-alkaline basaltic andesites and andesites have erupted within conspicuous grabens at the front of the western MVB. This unusual suite has high oxygen fugacities ranging from NNO +1 to 5, and is thought to be generated by partial fusion of subduction modified mantle wedge material that is extremely oxidized and marbled with veins rich in phlogopite and apatite (Carmichael et al, 1996). Under this hypothesis, the extremely potassic lavas are produced from the phlogopite and apatite-rich material, and the calc-alkaline basaltic andesites and andesites are partial melts of a more typical spinel lherzolite assemblage. Evidently, the ascent and eruption of the entire suite was facilitated by the localized extension of the overriding plate. In central Mexico, MVB-related volcanism overlies the subducted Cocos plate. Like western Mexico, there are prominent extensional fault systems at the front of the MVB in central Mexico, near Valle de Bravo. Although the tectonic setting here is similar to that of the arc-front grabens in western Mexico, highly oxidized minettes and absarokites are not found. Instead, we find Quaternary, fault-associated, high-K andesites and shoshonites, as well as calc-alkaline basaltic andesites, andesites and dacites, all of which have lower Al<sub>2</sub>O<sub>3</sub> concentrations and oxygen fugacities (~NNO -1.0 to NNO +2.7) than their western Mexican equivalents. Small, upper mantle derived, spinel lherzolite xenoliths are hosted in one of these calc-alkaline andesite flows. The xenoliths have oxygen fugacities ranging from NNO +0.7 to 1.6, and many contain abundant hornblende, but no phlogopite or apatite (Blatter and Carmichael, 1998). Based on these observations, we conclude that the mantle beneath the front of the MVB in central Mexico is more refractory and less oxidized than that beneath western Mexico.



**JSV30/W/14-B1 1120**

**HORNBLENDE CRYSTALLISATION AS A BARRIER TO ERUPTION IN HYDROUS BASALTS: AN EXAMPLE FROM THE VOLCANIC FRONT OF WESTERN MEXICO**

J. BARCLAY (1), Ise Carmichael (Dept of Geology and Geophysics, UC Berkeley, USA); (1) Dept de Mineralogie, Université de Geneve, Switzerland.)

The hydrous phase relations of a Quaternary ne-normative trachybasalt from the volcanic front of Western Mexico have been determined experimentally (from 0.1 to 700MPa) in order to elucidate the conditions of ascent and storage of the unusual phenocryst assemblage which includes hornblende as well as apatite, olivine and augite. At fO<sub>2</sub>'s equivalent to NNO+2 hornblende crystallisation occurs at the expense of ol and aug and is found at T < 1040°C and PH<sub>2</sub>O > 130MPa with a positive dP/dT slope of gradient of -1 from 40 to 100MPa. Coexisting liquids evolve from ne-normative basaltic andesite to qtz-normative dacite in the most crystalline experiments, following a shoshonitic 'liquid line of descent'. With the onset of hornblende crystallisation, experimental crystallinities increase dramatically (from ~15-20vol% to >40vol%) with only small degrees of undercooling. This is equivalent to an increase in magma viscosity from ~10Pas to >106Pas, close to the limit of eruptibility of most magmas. Similar increases in sample crystallinity are found in other experimental studies and it is proposed that many hydrous mafic magmas do not erupt in subduction zones as a consequence of this enhanced crystallisation. The subsequent remelting of 'frozen' underplated basalt will produce magmas similar in composition to those of the coexisting experimental liquids. Such magmas are found in subduction zones with low volumes of eruption in regions also usually associated with extensional tectonics.

**JSV30/L/03-B1 Invited 1140**

**THE GUERRERO TERRANE IN WESTERN MEXICO; A MEZOZOIC EXAMPLE OF TRANSITION FROM ARC TO CONTINENTAL CRUST**

Joaquin RUIZ (Dept. of Geosciences, University of Arizona, Tucson, Arizona 85721, USA, email: jruiiz@geo.arizona.edu)

The Guerrero Terrane in western Mexico constitutes about half of Mexico's surface and is a superb example of the transition between accretion of oceanic material, arc magmatism, to formation of continental crust. The basement of the Guerrero terrane, known as the Artega Schist, consists of mid-ocean ridge basalts with pillow structures in places and deformed and metamorphosed sediments with Proterozoic isotopic values. The age of the basement is probably Triassic based on paleontological evidence. Unconformably overlying the Artega Schist is an arc complex with interbedded andesitic flows and pyroclastics and fossiliferous limestone. The accretion of the arc complex to nuclear Mexico was probably in Neocoman times. The whole complex is intruded by Cretaceous calc alkaline and peraluminous granites and then overlain by large Tertiary silicic flows and pyroclastics that are part of the Sierra Madre Occidental volcanic province. Thus the evolution of the region has been from an island arc to a continental arc. This change includes the appropriate change in the chemistry of the igneous rocks from intermediate and mafic to silicic. Although the chemistry of the Guerrero terrane crust is continental-like, the thickness is not always so. In some places the lithosphere is thought to be no more than 12 km. Towards the east, the lithosphere reaches a more reasonable thickness for continental crust. The change in chemistry from island-arc to continental-like crust seems to have been aided by magmatic assimilation of the thick sequence of sediments that were deposited in the ocean floor before accretion by the arc magmatism, and by the loss of deeper parts of the crust after accretion.

**JSV30/W/07-B1 1200**

**MANTLE AND CRUSTAL CONTRIBUTIONS TO PRIMITIVE AND EVOLVED ARC MAGMAS AT THE TATARA-SAN PEDRO COMPLEX (TSPC: 36° S, CHILEAN ANDES): IMPLICATIONS FOR REGIONAL CHEMICAL TRENDS IN THE FRONTAL ARC OF THE SOUTHERN VOLCANIC ZONE (SVZ: 33-41° S)**

Michael DUNGAN (Département de Minéralogie, Université de Genève, 13 rue des Maraichers, 1211 Genève 4, Switzerland, email: dungan@terre.unige.ch)

The long-lived Tatará-San Pedro complex (930 ka - Holocene) is located within the transitional region between thin crust of the southern SVZ (< 40 km; 41-36° S) and thicker, older crust to the north (50-60 km; 33-35° S). For many geochemical parameters the TSPC is intermediate between extremes recorded by centers to the north and south, but previous generalizations concerning systematic along-arc variations among frontal-arc centers as a function of crustal or lithospheric thickness are to some degree confounded by the exceptional diversity of this center (650 analyses). Compositions of primitive, uncontaminated basaltic compositions at the TSPC overlap for most elements with those from the southern SVZ, suggesting less systematic along-arc variability in parent magma composition than previously inferred. However, the major and trace element systematics of evolved mafic magmas (51-53 % SiO<sub>2</sub>) indicate that basalts with 5-6 % MgO are unreliable carriers of source characteristics, as many are either crustally contaminated or mixed with evolved magmas. A range of differentiation trends, some derived dominantly by closed system fractionation of diverse parent magmas and others generated by open system evolution, manifest variable suppression of Y-HREE in evolved magmas relative to enrichments for closed system fractionation. This probably reflects variable incorporation of silicic crustal components with compositions shaped by residual garnet in their source, although other factors may also be involved. Differentiation of variable parent magma compositions by multiple processes, at multiple levels in the crust, and long-term modification of the crustal column beneath the volcano, have contributed to the geochemical diversity of Tatará-San Pedro magmas.

**JSV30/E/13-B1 Invited 1220**

**CONSTRUCTION THROUGH ARC MAGMATISM**

Richard J. ARCULUS (Dept. of Geology, Australian National University, Canberra, ACT 0200, Australia, email: richard.arculus@anu.edu.au)

Genesis of continental crust (CC) is a first-order problem. The granodioritic composition can be produced through: fractional crystallisation of basalt; direct melting of subducted/underplated mafic lithosphere; fractionation of high-Mg andesites generated by wet melting of peridotite. Trace element and isotopic systematics require (at some stage) in CC genesis, low % mantle partial melting; garnet-bearing protolith involvement; fluid/solid elemental fractionation. Temporal changes in CC genesis through Earth history have been important. Post-Proterozoic constraints are: 1. Without recycling of H<sub>2</sub>O, neither melting of subducted slab nor overlying mantle wedge occurs; order of crystalline phase appearance in cooling basalt magmas containing a few % H<sub>2</sub>O is: olivine, pyroxene, plagioclase → delay in plagioclase appearance in the "wet basalt case" enhances concentration of Si, Al, Na, K in residual magmas (key elements characteristic of granites); presence of hydrated minerals (amphibole/biotite) in crystallisation products of wet magmas is also important in generation of granitic magmas during ultra-metamorphism of CC. 2. a key requirement for fractional

crystallisation is for the system to "be left alone" (ie allowed to cool and crystallise) with minimal accompanying magma chamber tapping or replenishment. Neglect is a function of local magma flux, and in arcs, this is ~0.1 of the ridge flux. 3. disposal of ultramafic/mafic crystalline cumulates from basalt fractionation processes is crucial for production of granodioritic crust. Cumulates may be underplated (sub-Moho) as part of the continental lithosphere or dynamically removed. Melts escaping from a supra-subduction zone system are not coupled to crystal cumulates and residual mantle; the latter are advectively dragged by the subducted lithosphere and recycled deep into the mantle.

Monday 26 July PM

Presiding Chairs: J.P. Davidson (UCLA, Dept. of Earth and Space Science, Los Angeles, USA); B.M. Wilson (Univ. of Leeds, Dept. of Earth Sciences, Leeds, UK)

**JSV30/E/08-B1 Poster 1400-01**

**THE PHILIPPINE ISLAND ARC CRUST: THICKNESS, MAGMATIC CONTRIBUTION AND ISSUES**

Eddie L. LISTANCO (National Institute of Geological Sciences, University of the Philippines, Diliman, Quezon City, 1101 Philippines, email: edlist@hotmail.com)

On the basis of the global variations of crustal thickness with Na<sub>2</sub>O<sub>6.0</sub> and CaO<sub>6.0</sub> of island arc volcanic rocks, the thickness of the Philippine arc crust has been estimated to range from 30 to 40 km. Current geochemical database on Philippine volcanoes suggests spatial variations in crustal thickness. The thinnest crust occurs in northern Philippines where xenoliths believed to be of mantle origin are quite common. Incompatible element ratios of volcanic rocks also suggest occasional tapping of non-cogenetic magmas by some volcanic edifices. Variations in the crustal thickness may be partly attributed to age of the crust and to the space-time production rates and emplacement of magmas. Although contributions to volumetric crustal growth can be estimated since the Quaternary, inputs from previous magmatism evident in the underlying volcanogenic sediments and pre-Quaternary volcanics and intrusives remain unresolved.

**JSV30/E/09-B1 Poster 1400-02**

**LATE CRETACEOUS MAGMATISM AND MULTIPLE POST-OROGENIC DENUDATION EVENTS IN THE COASTAL REGION OF SOUTHEAST CHINA**

Cheng-Hong CHEN, Wayne Lin, Chi-Yu Lee (All at: Department of Geology, National Taiwan University, Taipei 106, Taiwan, ROC; e-mail: chenhc@ccms.ntu.edu.tw)

Late Cretaceous I- and A-type granites in the coastal region of SE China were generated in a post-orogenic extensional setting. Voluminous I-type calc-alkaline granites, intruded the late Jurassic/early Cretaceous volcanics at shallow crustal levels during 107-99 Ma., whereas A-type granites emplaced into these preceding plutonic/volcanic suites at 93-90 Ma. Coeval mafic dykes (94-76 Ma) of basic to intermediate composition are also found in this coastal region. They exhibit high-K calc-alkaline trend and lower HFSE abundances similar to I-type granitic suites, but present distinctive Ta and Nb depletions in the spidergram. The geochemical features of A-type granites, such as high silica, alkalis, Ga/Al, Nb, and low Sr, P, Ba contents, are distinguished from those I-type Granites, inferring that A-type magmas in SE China were derived from a separate source other than those of mafic dykes as well as the I-type ones. Lower temperature thermochronological results of these granitic intrusives suggest two distinct episodes of rock mass uplift and denudation during the late Cretaceous. The first episode (~97-84 Ma), deciphered mainly by K-Ar/Ar-Ar biotite and feldspar thermochronology, is possibly controlled by block faulting under the post-orogenic extensional regime, which is accompanied with the development of batholiths subsidence. Syn-extensional mafic dikes emplaced into the faults and joints have been dated coincidentally with this time span. The second episode (84-50 Ma), as indicated by apatite fission-track thermochronology, is possibly a reflection denudation. The amount of rock mass uplift and denudation has been estimated to be about 3 km as indicated by the Al-amphibole geobarometers.

**JSV30/E/10-B1 Poster 1400-03**

**THE MAGMATOLOGY OF BEZYMIANNY VOLCANO: A POSSIBLE MODEL FOR KAMCHATKA ARC VOLCANISM**

G.E. BOGOYAVLENSKAYA (Institute of Volcanology, Petropavlovsk-Kamchatskii, 683006 Russia, email: volcan@svyaz.kamchatka.ru); M.L. Tolstykh and V.B. Naumov (both at Vernadsky Institute, Moscow, 117975 Russia); M.P. Semet (Institut de Physique du Globe, 75252 Paris, email: semet@ipgp.jussieu.fr)

The chemical composition of products emitted throughout the history of Bezymianny volcano is rather typical of those found at a number of Kamchatka active and extinct volcanoes. Lavas are dominantly of andesitic composition and, usually, highly porphyritic. We have investigated the petrogenetic processes responsible for this rather restricted petrographic and chemical variability by a study of a number of samples representative of the evolution of the volcano including a study of the chemistry of glass inclusions in phenocrysts. Plagioclase (on average An<sub>60</sub>) is the most abundant phenocryst in the lavas and is accompanied by modest amounts of both clino- and orthopyroxene. A few modal percent of hornblende and olivine are sometimes present whereas oxides form a constant minor constituent. Glass inclusions were mostly observed in plagioclase crystals and show a range of composition from basic andesitic to rhyolitic. However, the latter composition is the most frequently observed. A conclusion of this is that the andesitic bulk-rock composition results from the presence in about equal proportions of dacitic to rhyolitic liquid and the observed crystals in the magmas feeding the eruptions. The parageneses of the lavas and the volatile contents of the glass inclusions point out to pre-eruptive evolution of the magmas in crustal reservoirs. Because the ultimate source of magmas is from the mantle and of basaltic composition, the above observations require that substantial amounts of material is added to deeper parts of the crust in the form of gabbroic to dioritic complexes as is observed in eroded parts of the peninsula.

**JSV30/W/01-B1 Poster 1400-04**

**40AR/39AR GEOCHRONOLOGY OF THE LAST ERUPTIVE PHASE OF CIOMADUL (CSOMAD) VOLCANO, EAST CARPATHIANS, ROMANIA**

D. KARÁTON (Eötvös University, Department of Physical Geography, 1083 Budapest, Ludovika tér 2, Hungary. Email: dkarat@ludens.elte.hu); L. W. Snee (US Geological Survey, Box 25046, MS913, Federal Center, Denver, CO 80225, USA)

For more than a century it has been well-known that the last volcanic eruptions of the Carpathians occurred at the end of the Pleistocene in the Harghita Mts, at twin-cratered Mt. Ciomadul. In the past years, 14C and K/Ar methods have been employed in attempts to date the youngest units of the volcano. The 14C method has produced controversial dates in the 10- to 40-ka range. K/Ar results have been inadequate because of the very small radiogenic 40Ar



abundances in these samples. Recently we found a new exposure of the products of the last phase of the two craters. These dacitic pumices and lithics are base surge deposits from the eastern crater and the overlying pyroclastic flow and fall deposits mostly from the western crater. At the top of the exposure are the products of the youngest eruption. Biotites from pumices in five distinct units have been separated and will be dated by the  $^{40}\text{Ar}/^{39}\text{Ar}$  method at U.S. Geological Survey laboratory in Denver, CO, USA, using high-sensitivity mass spectrometer with ultra-low blank laser and furnace argon-extraction systems. Argon extraction will be done both by step-heating in the low-blank furnace and by laser-fusion. It is anticipated that our results will clearly define the age of the last eruptive phase of the Carpathians. Here we used data from 1997 and 1998 to assess the influence of the analysis strategy, elevation cut-off angle, and software packages. In all cases IGS orbits and earth orientation products were utilized. The SWEPOS GPS-data are analysed using the GIPSY software package both with traditional network strategies as well as with the precise point positioning method and for different elevation cut-off angles. The tropospheric water vapour content is estimated at each station as a random-walk process with 5 minutes between parameter updates in the Kalman filter. The same data set is also analysed using the Bernese software and the GAMIT software. In this analysis we estimate the water vapour content in a piecewise constant least-squares process.

**JSV30/W/13-B1** Poster 1400-05

#### GENESIS AND GEODYNAMIC IMPLICATIONS OF GARNETS AND GARNET-BEARING MIOCENE CALC-ALKALINE VOLCANIC ROCKS IN THE NORTHERN PANNONIAN BASIN, CENTRAL-EASTERN EUROPE

Szabolcs HARANGI (Department of Petrology & Geochemistry, Eotvos University, H-1088 Budapest, Múzeum krt 4/A, Hungary, e-mail: harangi@iris.geobio.elte.hu); Hilary Downes (Dept of Geological Sciences, Birkbeck College, Malet St., London, WC1E 7HX, UK); Laszlo Kosa, Csaba Szabo (both at Dept of Petrology & Geochemistry, Eotvos University, H-1088 Budapest, Múzeum krt 4/A, Hungary)

Almandine-rich garnets are rare phenocrysts in calc-alkaline volcanic rocks and indicate high-pressure crystallisation and relatively rapid ascent of magma. Thus, occurrences of primary garnet-bearing volcanic rocks appear to indicate a special geodynamic environment. In the Carpathian-Pannonian Region, Miocene to Quaternary calc-alkaline volcanic rocks were formed in a retreating subduction zone. Although a direct relationship has been suggested between volcanism and subduction events in the eastern segment of the Carpathian arc, genesis of the calc-alkaline volcanic rocks of the western segment of the Carpathian arc is more controversial. Volcanism in the western segment of the Carpathian arc started with eruption of garnet-bearing volcanic rocks which in turn are very rare in the eastern part of the arc. Primary garnet phenocrysts occur both in diopside-normative andesites (Type 1 garnets) and corundum-normative dacites and rhyodacites (Type 2 garnets) in the Inner Western Carpathians Volcanic Field, Northern Pannonian Basin. Grossular content of Type 1 garnets is between 8 and 20 mol% and have low  $d_{18}\text{O}$  (6.2-6.5). Type 2 garnets in general show higher grossular content (Gro=8-12 mol%) than majority of garnets from corundum-normative volcanic rocks world-wide and have  $d_{18}\text{O}$ =6.9-7.2. Garnet xenocrysts from these rocks show lower grossular content (Gro=1-8 mol%), typically higher spessartine content (Spes10 mol%) and higher  $d_{18}\text{O}$  (8-10.5) than the primary ones. Sr-Nd isotope ratios of the host rocks indicate that crustal contamination had a major role in the petrogenesis of these rocks. However, the relatively low  $d_{18}\text{O}$  values of the garnets may suggest that they could have been formed from mantle-derived magmas prior the contamination processes. Eruption of garnet-bearing volcanic rocks may indicate a change in the tectonic regime of the area, i.e. transition from compressive to extensional phase

**JSV30/W/02-B1** Poster 1400-06

#### FLUID-CONTROLLED ELEMENTAL TRANSFER FROM SLAB TO CRUST IN THE CENTRAL IZU ARC (NW PACIFIC)

S.M. STRAUB (Geomar Research Center, Wischhofstr.1-3; 24148 Kiel, FRG; e-mail: sstraub@geomar.de); GD Layne (Woods Hole Oceanographic Institution, Woods Hole, MA 02543, USA); A Schmidt, KA Hoernle (Geomar Research Center, Wischhofstr.1-3; 24148 Kiel, FRG)

We investigated fluid-dominated arc front volcanism in the intraoceanic Izu arc (NW Pacific) by approximated arc melts by glasses (matrix shards, melt inclusions) in distal fallout tephra (ODP Site 782A) that ranges from mid-Miocene to Quaternary in age. The glasses show a large range in silica (50-75 wt%  $\text{SiO}_2$ ) that corresponds with a small range in MgO (=6-1 wt%). High-MgO glasses are offset from N-MORBs with similar MgO:  $\text{TiO}_2$  (0.5-1 wt%),  $\text{P}_2\text{O}_5$  (=0.1 wt%),  $\text{Na}_2\text{O}$  (1.5-2 wt%), Be (0.4-0.5 ppm) and F (80-100 ppm) are lower, but  $\text{Al}_2\text{O}_3$  (14-15 wt%) and the incompatible elements B (10-20 ppm), K<sub>2</sub>O (0.2-0.4 wt%), Cl (800-1600 ppm) and H<sub>2</sub>O (up to 4 wt%) are higher. The linear trends of incompatible elements and the only minor Be enrichment from =0.4 to =0.6 ppm with increasing silica suggest that the compositional range of the glasses has been produced by melt mixing. A simple genetic model is that a HFSE-depleted mantle wedge is fluxed by a Be-poor component from the slab, that is differentially enriched in Si, B, K, Li, Cl, F, H (and possibly Na and Al). Unidirectional temporal trends are not apparent in abundances and ratios of incompatible elements. The tephra are nearly homogenous in initial radiogenic isotope ratios ( $^{87}\text{Sr}/^{86}\text{Sr}$  = 0.70339 - 0.70364,  $^{143}\text{Nd}/^{144}\text{Nd}$  = 0.51305 - 0.51311,  $^{206}\text{Pb}/^{204}\text{Pb}$  = 18.36 - 18.46;  $^{207}\text{Pb}/^{204}\text{Pb}$  = 15.50-15.55;  $^{208}\text{Pb}/^{204}\text{Pb}$  = 38.16-38.34). This suggests that fractionation processes are superimposed on the elemental fluxes. The extent of fractionation can vary considerably as indicated by the range in ratios of LLE/Be (e.g. B/Be=20-100) which nearly reaches the global arc range (e.g. B/Be= 5-120). Thus, the glasses provide insights into fluid-controlled fractionation processes that are believed to play an important role in creating the typical elemental signatures of subduction-related magmas.

**JSV30/W/04-B1** Poster 1400-07

#### COMPARATIVE EVOLUTION OF THE CENTRAL IZU AND MARIANA VOLCANIC ARCS DURING THE PAST 15 MILLION YEARS

A. SCHMIDT, S.M. Straub, K.A. Hoernle (Geomar Research Center, Wischhofstr.1-3; 24148 Kiel, FRG; e-mail: aschmidt@geomar.de); A.G. Hochstaedter (Earth Sciences Dept. UC Santa Cruz; CA 95064; USA); C.H. Langmuir (Lamont Doherty Earth Observatory, Palisades, NY 10964, USA); J. Gill (Earth Sciences Dept. UC Santa Cruz; CA 95064; USA)

The intraoceanic Izu and Mariana volcanic arcs (IBM) in the NW Pacific have a similar evolution and many common subduction parameters. However, the chemical signature of arc front volcanic rocks is different, with the Izu arc being less enriched in LILE (e.g. K<sub>2</sub>O: Izu=0.3 wt%; Mariana=0.7 wt%) and radiogenic Pb (e.g.  $^{206}\text{Pb}/^{204}\text{Pb}$ : Izu=18.42; Mariana=18.84) and more depleted in HFSE (e.g. Nb: Izu=0.57 ppm; Mariana=1.07 ppm). Distal tephra layers show that the compositional differences between the Izu and Mariana arcs have persisted for 15 million years. Low K<sub>65</sub> = 0.5 wt% (K<sub>2</sub>O at 65 wt%  $\text{SiO}_2$ ) and a clear separation in low-K and high-K series prevail in the Izu arc in contrast to the Marianas that have a higher K<sub>65</sub> = 1 wt% and display a continuum from low-K to high-K series. It is an open question whether compositions of the various crustal and mantle sources - all else being equal - can account for all differences in isotope and elemental signatures observed. A striking difference between the

Izu and the Mariana arcs are the different angles of the subducting slab (Izu=45°; Mariana=80-90°) beneath the volcanic front and the width of the active volcanic zones (Izu=170 kilometer, Mariana =30 kilometer). Assuming that recycling occurs across a finite p-T-range, the different angles of subduction could result in different horizontal widths across which recycling occurs. If so, the wider volcanic zone in the Izu arc could mirror the larger horizontal vector of the subducting slab. A first order consequence is a better spatial resolution of slab components which are strongly fluid-controlled at the Izu arc front (e.g. high Sr/Nd, high Pb) and but become melt-dominated with increasing depth. In contrast, the steeper angle in the Marianas would result in an "integrated" signal, because fluid- and melt-dominated slab components ascend along a narrower vertical path. Sr-Nd-Pb isotope systematics are consistent with this model but modelling of the elemental budget is needed to further test this hypothesis.

**JSV30/W/10-B1** Poster 1400-08

#### GEOLOGICAL AND PETROGRAPHICAL CHARACTERISTICS OF THE SOFUGAN TECTONIC LINE, IZU-OGASAWARA ARC

Izumi SAKAMOTO, Toshiya Fujiwara (Deep Sea Res. Dept., Japan Marine Science & Technology Center, e-mail: izumis@jamstec.go.jp)

Sofugan Tectonic Line (STL) which is located in the central part of Izu-Ogasawara Arc shows NNE - SSW trending, and cross cutting the whole island arc body. The STL has a 200km-long steep slope (more than 70° and 1000m in height) in this study area. The steep slope observed along the S-E cliff, while the back slope is relatively gentle. Some sea mount with recent volcanic front activity cut the STL in topographically. Lithology of the typical cross section of the STL is divided into the following four units in ascending order: 1) massive volcanic rocks (K-Ar age=3.8 to 2.9 Ma), 2) hyaloclastites, 3) volcanogenic sediment, and 4) mudstone. Alternation with hyaloclastite and mudstone was observed in the upper part of this section. Lithologic changes from pyroclastic fragments to volcanoclastic sediments shows decreasing of volcanic activity. Mudstone includes late Pliocene nanno fossils (CN11B-13b). Altered basalt were sampled from the lower part of unit 1 from the STL, and fresh olivine basalts were collected from middle to upper part of the STL. All of these volcanic rocks are island arc type tholeiite series from the geochemical data (low-K<sub>2</sub>O, low-TiO<sub>2</sub>, and Nb anomaly is observed in MORB normalized spider diagram).

**JSV30/W/12-B1** Poster 1400-09

#### SIMULTANEOUS CRYSTALLIZATION AND MELTING AT BOTH THE ROOF AND FLOOR OF CRUSTAL MAGMA CHAMBERS

Katsuya KANEKO (Central Research Institute of Electric Power Industry, 1646 Abiko, Abiko-city, 270-1194 Chiba, JAPAN, email: katsuya@criepi.denken.or.jp); Takehiro Koyaguchi (Earthquake Research Institute, University of Tokyo, Tokyo 113-0032, JAPAN, email: tak@eri.u-tokyo.ac.jp)

Thermal and compositional evolution of magmas after a basalt emplacement into continental crust has been investigated by means of fluid dynamics experiments using a cold solid mixture with eutectic composition and a hot liquid with higher salinity in the  $\text{NH}_4\text{Cl-H}_2\text{O}$  binary eutectic system. The experiments were designed to simulate the cases where melting occurs at both the roof and floor of crustal magma chambers. The results show that thermal and compositional convection occur simultaneously in the solution; the thermal convection is driven by cooling at the roof and the compositional convection is driven by melting and crystallization at the floor. The roof was rapidly melted by convective heat flux, which resulted in the formation of a separate eutectic melt layer with negligible mixing of the underlying liquid. On the other hand, a mushy cumulate layer formed at the floor. The compositional convection at the floor carried a low heat flux, so that the heat transfer at the floor was basically explained by simple heat conduction. The compositional convection resulted in stabilizing compositional gradient and formation of double-diffusive convecting layers in the solution, which decreased the upward heat flux. These experimental results imply that, when a basalt magma is emplaced in continental crust, floor melting does not always enhance the cooling of the magma, but it may even decrease the total heat loss from the magma to the crusts due to the formation of double-diffusive convecting layers.

**JSV30/E/01-B1** Poster 1400-10

#### TEMPORAL EVOLUTION OF K<sub>2</sub>O CONTENT IN ARC-TYPE VOLCANOES: EXAMPLES FROM NEW ZEALAND AND INDONESIA

Ian E.M. SMITH, Supriyati Andreastuti (Department of Geology, University of Auckland, N.Z., email: ie.smith@auckland.ac.nz); Richard C Price (School of Science and Technology, University of Waikato, N.Z.); Bob Stewart (Department of Soil Science, Massey University, N.Z.)

The correlation of the K<sub>2</sub>O content of magmas erupted from volcanic arcs with depth to the underlying seismic zone (the K-h relationship) has laid the basis for petrogenetic models in which subduction of oceanic lithosphere plays a major role in their petrogenesis. However, detailed studies of individual volcanoes shows that K<sub>2</sub>O contents (and that of geochemically similar elements) show systematic increases with time for equivalent  $\text{SiO}_2$  content. This indicates that interpretation of the K-h relationship in terms of tectonic setting is too simplistic. Ruapehu and Taranaki Volcanos in northern New Zealand occupy frontal and back-arc positions respectively. Merapi Volcano in central Java lies on the arc front. In all three volcanoes the erupted magmas exhibit relatively short time scale (100-1000a) compositional variations which are interpreted as the results of relatively shallow crustal processes probably dominated by fractionation. Longer time scale (1000-10,000a) compositional trends are toward higher K<sub>2</sub>O (and commonly more mafic) compositions and are often correlated with petrographic evidence for recharge of the magmatic system from deeper levels. This trend appears to be independent of tectonic setting and is thought to reflect a process of assimilation of early arc precursors at or near the base of the crust. Our explanation of the observed trends invokes thermal evolution of the arc basement to a stage where reaction between anhydrous mafic cumulates and wall rocks in the amphibole stability field produce progressively more potassic parental magmas as the arc evolves.

**JSV30/E/04-B1** Poster 1400-11

#### CRUSTAL ANATEXIS BENEATH THE TONGA-KERMADEC ARC

Tim J. WORTHINGTON, Ian E.M. Smith (Dept of Geology, University of Auckland, Auckland, New Zealand, e-mail: tj.worthington@auckland.ac.nz / ie.smith@auckland.ac.nz)

Voluminous eruptions of sparsely phryic felsic magma (>10 km<sup>3</sup>) have alternated with eruptions of crystal-rich basaltic-andesitic magma at nine Tonga-Kermadec arc volcanoes since 10 ka. Along-arc variations in felsic and mafic magma composition are dissimilar, and suggest each magma type is derived from a different source. Furthermore, each eruption of felsic magma at Raoul Volcano is geochemically distinct, and these magma batches cannot be related to each other or to a common mafic precursor by simple fractionation processes. The geochemistry of Raoul dacite is modelled by 20-35 % dehydration and 0.6 GPa. Thermal

## INTER-ASSOCIATION

models invoke crustal heating from an ambient 600 °C by underplating and convective cooling of primitive high-Mg magma from 1250 to 1100 °C. Budget calculations based on erupted volumes of dacite and basalt-andesite show that ample heat exists to drive this process (>2.5 times that required). Sub-arc crust is thus transformed to anhydrous granulite + dacitic magma, whereas primitive high-Mg magma evolves to crystal-rich low-Mg magma + cumulates. Crustal anatexis and felsic magmatism are restricted to an adolescent arc window 1-3 m.y. after arc inception if the crust is the sole source of H<sub>2</sub>O. Conversely, anatexis may persist throughout the life of the arc if H<sub>2</sub>O exsolved by primitive magma hydrates the crust. The pulse of felsic magmatism presently sweeping the <3 m.y. Tonga-Kermadec arc, the <2 m.y. Taupo Volcanic Zone, and peaking at 3 Ma in the 5 m.y.-old Mariana arc highlights the role of crustal H<sub>2</sub>O.

**JSV30/W/05-B1** Poster **1400-12**

### ARC MAGMAS PRODUCE CONTINENTAL LITHOSPHERE? (NOT JUST CRUST)

Jon DAVIDSON (Dept. of Earth and Space Sciences, UCLA, Los Angeles, CA 90095, USA, email: davidson@ess.ucla.edu)

Magmatism at convergent plate margins is thought to be the principle mechanism for long-term addition of material to the mantle to the crust. The Andean arc offers an opportunity to test simple models of crust generation. Here, volcanic rocks and their plutonic equivalents are compositionally similar to estimates of "average crust", notwithstanding the chemical differences found in Archean crust. An analysis of magmatic differentiation processes, however, suggests that the similarity is a reflection of large-scale cannibalization – Andean magmatic rocks look like "crust" because they contain a significant component of recycled crust. There is little compelling evidence that the magmas derived from the mantle are different from those encountered at oceanic subduction zones. Here, again accounting for differentiation effects, it is clear that the mass flux from the mantle is fundamentally basaltic. Thus, the composition of material added to the crust instantaneously at subduction zones is very different from the bulk composition of the crust. This observation may suggest that a large fraction of crust formed early in Earth history, by a mechanism different from today's subduction-related magmatogenesis. A more reasonable alternative is that the crust is simply a differentiate of the added material, requiring the existence of an ultramafic complement. The complement may be recycled into the convecting mantle (during arc magmatogenesis or at some later time in an unrelated plate tectonic environment) or may reside in the mantle lithosphere. The issue of crustal growth may therefore seem overly complicated because of our definition of the Moho, which may simply separate feldspar-rich differentiates from ultramafic cumulate.

**JSV30/W/06-B1** Poster **1400-13**

### ORIGINS OF SANIDINE MEGACRYSTS IN ITALIAN ALKALINE ROCKS

Giulia PERINI, Frank J. Tepley III, Jon P. Davidson, (all at Department of Earth and Space Sciences, University of California, Los Angeles, USA); Sandro Conticelli (Centro di Geodinamica, Università della Basilicata, Potenza, Italy)

Sr-isotope compositions were used to determine the origin of sanidine megacrysts found in primitive ultrapotassic and trachytic rocks from the Italian Plio-Pleistocene Volcanic Region. At Cimino volcano, primitive megacryst-bearing rocks are associated with the evolved rocks. The primitive magmas are high-silica lamproite- to transitional-ultrapotassic rocks characterised by high Mg# and high compatible element contents. The evolved rocks are trachytes, which were erupted before the primitive magmas at Cimino. 87Sr/86Sr ratios in the primitive rocks from Cimino volcano vary from 0.713 and 0.716 whereas the more evolved trachytes have ratios between 0.713 and 0.714. Sanidine megacrysts have variable morphologies that range from euhedral in the trachytes to subhedral in the primitive rocks, but in either case they are not fragmented. Core-rim Sr-isotope analyses were performed by the microdrilling technique. 87Sr/86Sr values of sanidine crystals from primitive rocks are between 0.71370 and 0.71398 but cores and rim 87Sr/86Sr ratios are indistinguishable. However, the megacrysts are not in isotopic equilibrium with the host rocks, which are less radiogenic (0.71384-0.71582). Sanidine crystals from a trachyte have similar Sr-isotope compositions to those in the primitive rocks, but the 87Sr/86Sr ratios vary significantly from core (0.71387) to rim (0.71356). Whole-rock Sr-isotope compositions of the trachyte (0.71333) reveal that the sanidine crystals are also not in isotopic equilibrium with their host. We postulate that all of the sanidine megacrysts grew in a relatively low 87Sr/86Sr trachytic magma. Mixing between trachyte and ultrapotassic magmas distributed the megacrysts among all magmas. Sanidine megacrysts hosted in the primitive rocks did not grow in that melt, but were inherited from the trachytic melts, resulting in dissolution of the megacryst rims and the observed subhedral shapes.

**JSV30/E/11-B1** Poster **1400-14**

### VOLCANISM IN THE SAN PEDRO-CEBORUCO GRABEN (NAYARIT, EXICO): COEXISTENCE OF MAGMAS WITH DIFFERENT PETROLOGICAL AFFINITY

C.M. Petrone (1), L. Francalanci (1), S. CONTICELLI (2), L. Ferrari (3) (1: Dipartimento di Scienze della Terra, Università di Firenze; 2: Centro di Geodinamica, Università della Basilicata; 3: Unidad de Ciencias de la Tierra, UNAM, Juriquilla, Mexico)

The San Pedro-Ceboruco graben is a complex asymmetric basin in which calc-alkaline and Na-alkaline magmas coexist in a tectonic setting characterized by active subduction and extension. At least four different volcanic systems, belonging to the Trans-Mexican Volcanic Belt, are set in the San Pedro-Ceboruco graben: 1) alignments of cinder cones and domes arranged parallel to the border of the graben; 2) a volcanic system formed by several domes and a shield volcano, San Pedro-Cerro Grande Volcanic Complex; two polygenetic stratovolcanoes, 3) Tepetitlic and 4) Ceboruco. Calc-alkaline and mildly Na-alkaline rocks coexist in the alignments of cinder cones and domes and in the San Pedro-Cerro Grande Volcanic Complex.

In particular, the shield volcano of the latter has a Na-alkaline composition. Ceboruco and Tepetitlic stratovolcanoes are both calc-alkaline. Mineralogical, chemical and isotopic data have pointed out the existence of at least five different parental magmas whose characteristics encompass the entire compositional range between calc-alkaline and Na-alkaline magmas. They have been interpreted as deriving from a heterogeneous mantle wedge in which MORB-type and OIB-type components coexist.

**JSV30/L/01-B1** Poster **1400-15**

### MAGMATISM IN THE SOUTH SANDWICH ISLANDS AND EAST SCOTIA RIDGE, SOUTH ATLANTIC

P.T. LEAT, J.L. Smellie, R.D. Larter, R.A. Livermore, T.R. Riley, I.L. Millar (British Antarctic Survey, High Cross, Madingley Road, Cambridge CB3 0ET, UK, email: p.leat@bas.ac.uk)

The South Sandwich Islands are a 350 km long, intraoceanic island arc built on the Sandwich plate above west-subducting South American plate. The Sandwich plate is separating from the

Scotia plate at a rate of 6.5-7 cm/yr at the back-arc East Scotia Ridge. This oceanic arc to back-arc system is one of the smallest and tectonically simplest subduction system on Earth. As such, it is an important location for studies of island arc structure and growth, primitive arc composition, and the timing and composition of slab-derived fluxes in the mantle source. It is also an analogue for suprasubduction ophiolites. The islands comprise tholeiitic and rare calc-alkaline basalt to dacite. They are typically ca. 5 km across and represent the subaerial expressions of seven large volcanoes built on the oceanic crust of the Sandwich plate. Marine magnetic anomaly interpretation indicates that the ocean crust beneath the volcanoes was formed at the East Scotia Ridge between anomalies 4 and 5 (ca. 7.5-10 Ma), and that fore-arc erosion of the overriding plate is taking place at the trench. The implication is that earlier volcanic edifices have collapsed into the trench and have been subducted.

Trace element variations indicate that two distinct slab-derived chemical components are present in the arc, a high LREE, high Th/Nb component, probably subducted sediment (end-member: Visokoi Island), and a high Ba,U,Cs/Th, high Sr/Nd component, probably slab-derived fluids (end-member: Vindication Island). Both occur as minor components in back-arc magmas, whose main variations are related to plume mantle (possible migrating westward from Bouvet) entering the back-arc around the edges of the subducting slab and interacting with depleted (MORB-source) mantle.

**JSV30/L/02-B1** Poster **1400-16**

### PHANEROZOIC SUBDUCTION AND THE TTG-MAGMATIC CONSTRUCTION OF ARCHAEOAN CONTINENTAL CRUST

Miles OSMASTON (The White Cottage, Sendmarsh, Ripley, Woking, Surrey, GU23 6JT, UK, email: miles@osmaston.demon.co.uk)

My studies of the evolution of Phanerozoic subduction zones (e.g. IGC1992, IUGG1995), noting their impact upon the geology above them, clearly indicate the presence of two major non-arc processes. (1) Subduction tectonic erosion (STE). In STE the young-plate (<70Ma) downbend mechanism is able to nibble away the hanging wall at the downbend, shallowly and rapidly advancing the downbend position beneath the upper plate by hundreds of kilometers, rendering the margin susceptible to imbrication. STE implies young-plate buoyancy, achievable if a substantial thickness of LVZ material forms an integral part of the plate. This, in turn, provides the heat for (2), post-subduction magmatism (PSM). Here the cessation of subduction gives time for the LVZ heat to soak through the former slab and induce wholesale melting of its subduction interface crustal material, resulting in a several-100km-wide belt of silicic/granitoid magmatism (examples given). The granitoid (TTG) intrusion of Archaean greenstone belts appears consistent with PSM into an extensively STE-undercut margin, as subducted plates would certainly have been young and hot. Key to the much-debated tectonic location and magmatic origin of greenstone belts seems to be my recognition (IGC1992) that Phanerozoic subduction has commonly started in the oceanic domain, reaching continental margins by repeated STE and imbrication. Thus at least the initial forearc is oceanic-crust, having formed a passive margin made by the MOR process before subduction began. In the same way, Archaean greenstone belts may indeed have originated as oceanic crust.

**JSV30/C/JSV22/E/11-B1** Poster **1400-17**

### THE ADAKITE-LIKE AND HIGH-CA BONINITE-LIKE VOLCANIC ROCKS IN CENTRAL AND SOUTHERN TIBET: IMPLICATION FOR TIBETAN TECTONIC RECONSTRUCTION

Chang-Hwa CHEN (Inst. of Earth Science, Academia Sinica., Taiwan, email: china@earth.sinica.edu.tw); Kenneth J. Hsu (Tarim Associates AG, Frohburgstrasse 96, Zurich, Switzerland); Jason Jiun-San Shen (Inst. Earth Sci., Academia Sinica, Taipei, Taiwan); Charles T. Wu (Dept. Geol., Univ. Western Ontario, Canada)

The geochemistry of volcanic rocks in orogenic belts places new constraints on tectonic interpretations of orogenically deformed plate. The adakite-like rocks from Qiangtang Terrane in central Tibet suggested that the magmas were derived from the partial melting of the subducted slab of a young and hot oceanic plate of back-arc basin, not of the Paleotethys ocean plate. The adakite-like rock from Lhasa Terrane in southern Tibet indicated that the magma was derived from the subducted hot ocean crust of a back-arc basin, the Zhabog Back-arc Basin (Hsu et al., 1995, *Inter. Geol. Rev.*, 37, 473-508), not of the Neotethys Ocean plate. Moreover, the High-Ca boninite-like from Amdo along the Banggong-Lujiang suture (BNS) may have been generated from a suboceanic lithosphere by contact melting adjacent to rising MORB source diapirs. Tectonic reconstruction indicates that the Lhasa and Qiangtang Terranes were archipelagos of island-arcs and back-arc basins on the margin of the Gondwana and Cathaysian plates. The Banggong-Lujiang suture (BNS) marks the position of the collision of the two plates.

**JSV30/C/JSV22/E/04-B1** Poster **1400-18**

### PERIODICITY OF MONOGENETIC BASALTIC VOLCANISM AND ITS RELATIONSHIP WITH TECTONIC ACTIVITY AT THE BASIN OF AVACHA RIVER, KAMCHATKA, RUSSIA

Oleg V. DIRKSEN, Ivan V. Melekestsev, Lilia I. Bazanova (Institute of Volcanic Geology and Geochemistry, Piipa blvd. 9, Petropavlovsk-Kamchatsky, 683006, Russia, email: ivgg@svyaz.kamchatka.su)

The research region is situated at 70 km NW of Petropavlovsk-Kamchatsky at a zone of intensive uplifting of the earth surface. We studied 22 Holocene monogenetic centers: 2 maars and 20 scoria cones. Chemically all the eruptive products (except for 1 center) represent basalts (SiO<sub>2</sub> 46.20-53.07 wt %) and usually have high MgO concentration. Maximum MgO concentration is in rocks of Zavaritsky volcano (up to 13 wt %). Using tephrochronological and radiocarbon dating we determined that during the Holocene we can fairly distinguish three outbursts of monogenetic volcanism: I-7700-11000 14C BP (8 centers), II-2500-3000 14C BP (9 centers, 6 of them form volcano Zavaritskogo) and III-600-1600 14C BP (5 centers). The volume of erupted tephra and lava is 0.11 and 0.02 cub km; 0.77 and 0.06 cub km; 0.04 and 0.1 cub km respectively. The studied region is also characterized with a strong tectonic uplifting during the Holocene. This activity is reflected with many river terraces developed over Levaya Avacha river. Our tephrochronological scale allowed us to determine the age of about 30 terraces of different ages. It was clearly identified that in terms of age most of terraces clustered in four time interval: 1) 10000-7700 14C BP, 2) around 4000-3500 14C BP, 3) 2200-1700 14C BP, and about 600 14C BP.

These time intervals correlate well with the periods of volcanic activity. We consider the volcanic outbursts occurred simultaneously with or were preceded by the beginnings of strong tectonic uplifting in studied area. This assumption testifies to close relationship of both volcanic and tectonic processes in this region. In future we plan to continue our investigation to identify the relationship of these phenomena in other parts of Kamchatka.



JSV30/C/JSV22/E/01-B1 Poster 1400-19

## Eocene-Neogene Continental Magmatism in Nechako River Area, Central British Columbia, Canada

Robert G. ANDERSON (Geol. Survey of Canada, 101 – 605 Robson St., Vancouver, B.C., Canada, V6B 5J3)

Eocene and Neogene magmatism in the Nechako River area was widespread, post-accretionary, and well inboard of the Tertiary Canadian Cordilleran continental margin. Several collaborative studies have established the extent, age, structural setting, composition, and isotopic character of the Eocene felsic Ootsa Lake (OLG) and mafic Endako (EG) groups rocks, and Neogene mafic rocks. A fault-bounded, Eocene (53-45 Ma) bimodal, volcano-plutonic complex developed coeval with terminal cooling of a nearby, extensional metamorphic complex and contemporaneous with trans-tensional tectonics. Rhyolitic and dacitic, biotite-quartz-alkali feldspar phytic tuff, pyroclastic rocks, breccia, flows, and siliceous and glassy domes and minor, basal basalt and andesite (OLG) are overlain by amygdaloidal, hypersthene-augite-plagioclase phytic andesite to basaltic andesite flows and hyaloclastite (EG). OLG rocks are silicic, calc-alkaline, very high-K and large ion lithophile-enriched, peraluminous, and have a moderate to marked Eu anomaly. EG mafic flow rocks are mildly alkaline, transitional to calc-alkaline, high-K, and have within-plate and continental affinities. Both units are isotopically primitive (Sri: 0.70401-42; ENd: +1.3 to +3.2). Associated coeval, bimodal and miarolitic leucocratic granite and porphyry plutons are silicic, calc-alkaline, high-K, met- to peraluminous, and are partly of within-plate granite affinity. Neogene (locally Middle Miocene) basaltic and hawaiite flows were erupted from compositionally similar volcanic and diabasic centres which were localized along re-activated? Eocene block faults and characterized by spinel lherzolite and crustal xenoliths. Olivine, pyroxene, plagioclase, and magnetite occur as xenocrysts, megacrysts, and/or phenocrysts. The rocks are typically alkaline (ne-normative), high-K, and encompass within-plate and continental affinities.

JSV30/C/JSV22/E/16-B1 Poster 1400-20

## GEOCHEMISTRY OF MESOZOIC-CENOZOIC IGNEOUS ROCKS IN THE SOUTH SHETLAND ISLANDS, ANTARCTICA

Guang-Fu XING, Qing-Min Jin (both at the Antarctic Research Center, Chinese Academy of Geological Sciences, 534 East Zhongshan Rd., Nanjing, P.R.China, email: nigmr@public1.ptt.js.cn); De-Zi Wang and Wei-Zhou Shen (both at Department of Earth Sciences, Nanjing University, 22 Hankou Rd., Nanjing, P.R.China.)

The South Shetland Islands (SSI) in West Antarctica outcrops extensively Mesozoic-Cenozoic arc volcanic-plutonic rocks (high-alumina basaltic-dacitic). King George Island rocks are 77-14Ma in age but mostly in Tertiary, their (87Sr/86Sr)<sub>i</sub>, =CE=B5Nd(t), 206Pb/204Pb, 207Pb/204Pb and 208Pb/204Pb are 0.70260-0.70387, 2.77-7.28 (mostly >5), 17.776-18.768, 15.506-15.736 and 37.726-38.961, respectively. Rocks from Greenwich and Half Moon islands have (87Sr/86Sr)<sub>i</sub> of 0.70404-0.70475, =CE=B5Nd(t) of 1.14-3.56, 206Pb/204Pb of 17.831-18.487, 207Pb/204Pb of 15.505-15.611, 208Pb/204Pb of 37.829-38.426. Combined with reported Mesozoic igneous rocks from adjoining Livingston, Robert and Nelson islands, arc igneous rocks become younger and younger, i.e., on the whole from late Cretaceous to late Tertiary, and contain more and more radiogenic isotopes along the SSI from SW (Livingston Island) to NE (King George Island). Based on their isotopic compositions, enriched LREE, high LILE/HFSE ratios, negative Ce and Nb anomalies, etc., the authors advance that arc igneous rocks from King George, Greenwich and Half Moon islands derived from upper mantle wedge enriched by metasomatism of CO<sub>2</sub>-rich fluids from subducted carbonate-rich pelagic sediments, and that their evident isotopic variations are ascribed to different degrees of fluid metasomatism rather than crustal contamination.

JSV30/C/JSV22/E/17-B1 Poster 1400-21

## ISOTOPIC GEOCHEMISTRY OF MESOZOIC VOLCANO-INTRUSIVE ROCKS FROM NORTHERN MARGIN OF THE DABIESHAN OROGENE, CHINA

Zhu-Liang YANG, Kui-Yuan Tao, Fang-Gui Xie and Jia-Lin Shen (all at Nanjing Institute of Geology and Mineral Resources, 534 East Zhongshan Rd., Nanjing, P. R. China, email: nigmr@public1.ptt.js.cn); Wei-Zhou Shen (Department of Earth Sciences, Nanjing University, 22 Hankou Rd., Nanjing, P. R. China)

Mesozoic volcanic rocks from northern margin of the Dabieshan orogene can be divided into two episodes, I and II. Episode I (140-126Ma) are mainly andesite and belong to high-K calc-alkaline series. Episode II (126-117Ma) rocks have two different evolution trends, one is the acidic belonging to calc-alkaline series, the other alkaline to shoshonitic series. All of the volcano-intrusive rocks out-cropped in northern margin of the Dabieshan orogene have the following isotopic characteristics: (87Sr/86Sr)<sub>i</sub>>0.708, =EF=81=A5Nd(t)=3D-14.7-21.7, 204Pb=3D1.371-1.439, 206Pb/204Pb=3D15.975-17.363, 207Pb/204Pb=3D15.305-15.537, 208Pb/204Pb=3D36.856-38.816. These indicate that the basement metamorphic rocks play important roles in the petrogeneses of the volcano-intrusive rocks. But two facts must have attention, one is that the direct basement rocks in the area have =EF=81=A5Nd(t) larger than -21.7 (i.e. cannot reach so negative value), the other is that the basement rocks have TDM values (two-stage Nd isotopic depleted mantle model age) less than those of Mesozoic rocks. Recently, we have found the episode I volcanic rocks inside the orogene. All of these show that the Mesozoic rocks were formed in the post-orogeny stage and the basement of the whole orogene and its northern margin is to a great extent akin to the North China Block.

JSV30/C/JSV22/W/01-B1 Poster 1400-22

## ACROSS-ARC MANTLE HETEROGENEITY IN THE SOUTHERN MARIANA

Teruaki ISHII, Hiroshi Sato, Satoru Haraguchi, Shinji Kaneyama (Ocean Res. Inst., Univ. Tokyo, Nakano-Ku, Tokyo 164-8639, Japan; email: ishii@ori.u-tokyo.ac.jp); Hidetsugu Taniguchi (Komazawa Univ. High School, Tokyo, Japan), and Yasuhiko Ohara (Hydrographic Dep. Japan, Tokyo)

Where the ophiolites came from is one of the most interesting problems in the earth science. For these ophiolite problem, we have been investigating on the in situ ophiolite (= proto-ophiolite) in the sea floor, i.e., modern analogue of on-land ophiolites. Trench inner wall of the Southern Mariana shows very steep slope with about 400 km wide having an EWE strike and with about 5000 m high having a southward dip of about 12-15° due to the highly oblique subduction of the Pacific plate beneath the Philippine Sea Plate. The escarpment can be assumed as a huge fault plane. Along the escarpment, several geological cross sections including from crust down to upper mantle successions of the island-arc system with back-arc spreading can be observed, i.e., including the West Mariana Ridge (remnant arc), Mariana Trough (back-arc basin), Mariana Arc (active arc and remnant arc), and Mariana Forearc from west to east. Dredged mantle peridotites can be divided into three groups on the basis of the mineralogical & petrological characteristics and estimated degree of depletion for magmatic components, i.e., Cr-spinel bearing harzburgite (group A), Cr-spinel bearing meta-peridotite (B), and plagioclase bearing spinel lherzolite (C) were collected from diapiric serpentine

seamounts in forearc, back-arc area and forearc area, respectively. Petrological evidences of peridotites and associated effusive rocks suggest that very depleted (=A), moderately depleted (=B) and relatively fertile (=C) peridotites may be refractory residual peridotites after segregation of boninitic magma, arc-tholeiitic magma and back-arc-basin basaltic magma, respectively.

JSV30/C/JSV22/P/02-B1 Poster 1400-23

## GEOCHEMISTRY OF MG-RICH VOLCANIC ROCK SERIES IN ALTAY MT., NORTHWEST CHINA AND ITS GEOLOGIC SIGNIFICANCE

Yu XUEYUAN, Niu Hecai, Xu Jifong, Chen fanrong, Zheng Zuoping (Guangzhou Institute Of Geochemistry, Chinese Academy of Sciences, Guangzhou, 510640, email: yuxueyua@public.guangzhou.gd.cn)

A sequence of rare Mg-rich volcanic rocks has been found in western Altay Mt., Northwest China. It mainly consists of dacite and basalt. They are part of a marine volcanic strata of Middle Devonian epoch. The volcanic rocks are characterized by MgO-rich (2.69-5.24% in the dacites and 9.78-12.19% in the basalts), TiO<sub>2</sub>-poor (0.26-0.31% and 0.55-0.65%), high-SiO<sub>2</sub> (61.93-66.91% and 47.26-53.54%) and strong depletion of HFSE (Zr=29-35ppm and 24-27ppm, Hf=0.39-0.67ppm and 0.27-0.31ppm, Y=10-13ppm and 10-13ppm, P205=0.05-0.07% and 0.10-0.14%). The ratios of <sup>143</sup>Nd/<sup>144</sup>Nd of the Mg-rich rocks are lower (0.512644-0.512712) with  $\epsilon_{\text{Nd}}=+1.1$  - +1.3. Although these geochemical features of the Mg-rich volcanic rocks are similar to boninite, the lack of Mg-rich andesite and associated ophiolite in this area suggests they are more likely to be a Mg-rich volcanic rock series. The high-Mg and strong depletion of HFSE as well as lower ratios of <sup>143</sup>Nd/<sup>144</sup>Nd of the Mg-rich rocks show that they are derived from a depleted source peridotite. Their parent magma might have been formed from the partial melting of residual refractory peridotite of the upper mantle. Two-component mixing modeling (<sup>143</sup>Nd/<sup>144</sup>Nd and 87Sr/86Sr) indicated that the parent magma might have been contaminated by subducted continental crust or oceanic sediment (about 30%). The patterns of incompatible elements for dacites and basalts in this area are similar to those for the primitive plagiogranite of the island arc tholeiitic series and oceanic island arc basalts respectively, suggesting that they may have been formed in the intra-oceanic island arc setting (or fore-arc such as Izu-Bonin arc)...

JSV30/E/03-B1 Poster 1400-24

## WIDESPREAD OIB-TYPE VOLCANISM IN THE MEXICAN VOLCANIC BELT: AN UNUSUAL CONTINENTAL ARC

Surendra P. VERMA (Centro de Investigación en Energía, UNAM, Priv. Xochicalco S/No., Apartado Postal 34, Temixco, Mor. 62580, Mexico, email: spv@mazatl.cie.unam.mx)

Mexican Volcanic Belt (MVB) is a presumably continental arc of Miocene to Recent age, and is probably related to the subduction of Rivera and Cocos plates. It extends approximately 1000 km from the Pacific coast to the coast of Gulf of Mexico in an E-W direction. Although calc-alkaline volcanism dominates, there is also a widespread distribution of Ocean-Island basalt (OIB) type rocks throughout the belt. Furthermore, both types of volcanism seem to be closely related in both space and time. To mention just some of the areas with OIB type volcanism (mainly based on my published and unpublished data) one may state: Tepic-Zacoalco rift in the north-western part of the MVB, Michoacan-Guanajuato and Sierra de Chichinautzin monogenetic volcanic fields in the central MVB, and Los Humeros-Las Derrumbadas and Palma-Sola areas in the eastern MVB.

It seems that the MVB does not share these unusual chemical characteristics with other arcs, including those in the Circum-Pacific area. It is interesting to note that the MVB is probably the only arc in the world that is not parallel to the subduction but makes an angle of about 20° with respect to the Middle-America trench. Although different explanations have been put forth for these unusual characteristics, the most recent one by Márquez et al. (Geology, 1999, in press) is that both plume and subduction-related phenomena coexist in the MVB and therefore it represents a hybrid case with volcanism originating both from the migration of North American plate over a plume and the subduction of Cocos and Rivera plates. The following questions may well be worth addressing. If such a hybrid model is true, what implications does it have for crustal growth? Is there any modern or ancient analog for such an arc?

JSV30/C/U6/E/10-B1 Poster 1400-25

## METASOMATIC MANTLE COLUMN BENEATH BARTOY VOLCANOES

ASHCHEPKOV, I.V. (United Institute of Geology Geophysics and Mineralogy, SD RASC, e-mail: garnet@uiggm.nsc.ru)

Xenoliths from the Quaternary volcanoes SW Trans Baikal represent rare mantle column with the regular changes in metasomatic assemblages from dry sheared Fe-lherzolites to Phl porphyry rhy, Amph-Phl microveined, Dry protogranular, Amph fine equigranular lherzolites. Amount of Cpx megacrystalline (from Ga to Pl bearing) groups (4) coincides. Two first lherzolite groups compile thermally excited branch of geotherm while other are close to SEA. Megacryst further evolve to the Kaers g Kaers-Phl g Kaers- AnClase AnClase-Ti Biotite association. Rarely they reveal direct contacts with lherzolites. Three other evolving magmatic branches: 1) black layered Cpx-Gar-Pl cumulates; 2) large hydrous basalt veins Phl-MegaCpxg Ga-Pl-Kaersg Ga-Ilm-Cpx.; 3) filtration of hydrous melts through lherzolites Ol-Cpx-Kaers g Ol-Amph-Phl-Opx-Cpx-Sp; 4) green low Cr-MegaCpx (+Pargasite)g TwoPx-Ga-Sp hybrid picrite melt fractionation. Temperature groups of cumulate and lherzolite xenoliths represent different level of capturing and interaction of evolving hydrous plume magma with lherzolites. Each of close located volcanoes and portion of lava contain individual set of inclusions increasing in hydrous phases to last stage of mantle activity (1.5-0.8 Ma). (Grant BRFR 93-05-17103) 20

JSV30/C/U6/E/11-B1 Poster 1400-26

## EVOLUTION OF THERMAL CONDITIONS IN MANTLE BENEATH VOLCANIC REGIONS IN BAIKAL RIFT ZONE (OPX THERMOBAROMETRY)

ASHCHEPKOV I.V. (United Institute of Geology Geophysics and Mineralogy, SD RASC, 630090, Novosibirsk, academician V.Koptyug avenue 3, e-mail: garnet@uiggm.nsc.ru)

Thermal conditions beneath volcanic Vitim and Trans Khamar-Daban regions determined on thermal mantle xenoliths for three magmatic stages reveal distinct PT paths and varying mantle layering. Garnet facie part at pre-rifting (1ststage) represented melted and partly solidified mantle diapir with more hot melt percolation zone and plume heat impact zone near 30 kbar. After the lava plateau creation (2nd stage) it consists from steep diapiric and more hot melt percolation branches. Layered mantle column suggests polybaric intrusion of melts with the creation of several local melt filtration zones. The more continuous zones of filtration are pronounced at the 3rd Quaternary stage. Upper cold high gradient lithospheric Spl facie part was thermally excited from basement mainly in last two stages. The depth of melt percolation is close to magma generation level. In Khamar Daban early stage show cold fertile lherzolite



## INTER-ASSOCIATION

with the incompatible element enrichment upward (15-10 kbar) and thermal excitation at about 18 kbar. Later stages are characterized by the deepening of the xenoliths capture and small heating with gradients close to SEA. Pressure estimates are correct for the garnet and fertile spinel lherzolites and less for pyroxenites and depleted peridotites. (Grant RBRF 93-05-17103)

**JSV30/C/U6/E/05-B1** Poster **1400-27**

### GEOCHRONOLOGICAL AND VOLCANOLOGICAL STUDY OF NEOGENE CALC-ALKALINE VOLCANIC ROCKS FROM TRANSCARPATIA, SW UKRAINE

Zoltan PECSKAY (Institute of Nuclear Research of the HAS, H-4001 Debrecen, P.O.Box 51, Hungary, e-mail: balogh@cseles.atomki.hu Ioan Seghedi (Romanian Instit of Geology , Caransebes str. 1., RO-78344 Bucharest 32, Romania. e-mail: seghedi@ns.igr.ro) Hilary Downes (Dept. of Geology, Birkbeck College, Malet St., London, WC1E 7HX, e-mail: hdownes@ucl.ac.uk) Michail Prychodko and Bogdan Mackiv (ZGRE, Geologov 10., UR-295510 Beregov, Ukraine)

The Neogene Carpathian arc is a complex subduction-related magmatic arc, extending from Slovakia into Romania via Hungary and Ukraine. The Transcarpathian region in SW Ukraine comprises the central part of this arc. The volcanic structures of the Transcarpathian region can be divided into three major areas: a. Outer Arc Area; b. Intermediate Area; c. Inner Arc Area. This division reflects the basic tectonic features of the Ukrainian Carpathians, but differs from other parts of the Carpathian arc. Lavas, tuffs and ash deposits of dacitic, rhyodacitic, rhyolitic, andesitic and basaltic-andesitic composition are observed. Lava flows, domes, dykes/sills, volcanic necks, ignimbrites and lahars are characteristic elements of the Middle-Late Miocene volcanic activity. Radiometric dating has yielded K-Ar ages 13.4-9.1 Ma. This time interval (almost 4.3 million years) is identical to that of the neighbouring Carpathian volcanic regions to the west (Tokaj, Hungary) and to the east (Calimani, Romania). Thus there is no evidence in this area for any along-arc migration of volcanism. Volcanic activity started simultaneously in both Outer Arc and Inner Arc volcanic areas (~13.4 Ma). Different peak of volcanic activity was observed, between 12.3-11.6 in the Inner Arc area, interpreted as the major period of generation of the complex of resurgent domes related to a caldera formation and between 11-10.4 Ma in Outer Arc area, representing the main period of volcanoes generation, resulting in a lateral symmetry of the volcanic range. The end of the volcanic activity (9.5-9.1 Ma) is sparse and less voluminous.

**JSS31** Tuesday 27 – Wednesday 28 July

### GEODETTIC CONSTRAINTS ON TECTONIC MODELS (IASPEI, IAG)

Location: Medical School EF08 LT3  
Location of Posters: Arthur Thompson Hall

Tuesday 27 July AM

Presiding Chairs: Dr B.E. Parsons, (University of Oxford, UK)  
Dr R.E. Reilinger, (Massachusetts Institute of Technology, USA)

### GEODETTIC CONSTRAINTS ON TECTONIC MODELS

**JSS31/W/03-B2** **0930**

#### GLOBAL VELOCITIES FROM VLBI

Chopo MA (Space Geodesy Branch, Goddard Space Flight Center, Greenbelt, MD 20771, USA, email: cma@virgo.gsfc.nasa.gov); David Gordon (RITSS, Goddard Space Flight Center, Greenbelt, MD 20771, USA, email: dgg@leo.gsfc.nasa.gov); Daniel MacMillan (NVI, Inc., Goddard Space Flight Center, Greenbelt, MD 20771, USA, email: dsm@aleph.gsfc.nasa.gov)

Precise geodetic VLBI measurements have been made since 1979 at ~130 points on all major tectonic plates, including stable interiors and deformation zones. From the data set of ~2900 observing sessions and ~2.3 million observations, useful three-dimensional velocities can be derived for ~80 sites using an incremental least-squares adjustment of terrestrial, celestial, Earth rotation and site/session-specific parameters. The long history and high precision of the data yield formal errors for horizontal velocity as low as 0.1 mm/yr, but the limitation on the interpretation of individual site velocities is the tie to the terrestrial reference frame. Our studies indicate that the effect of converting precise relative VLBI velocities to individual site velocities is an error floor of ~0.4 mm/yr. Most VLBI horizontal velocities in stable plate interiors agree with the NUVEL-1A model, but there are significant departures in Africa and the Pacific. Vertical precision is worse by a factor of 2-3, and there are significant non-zero values that can be interpreted as post-glacial rebound, regional effects, and local disturbances.

**JSS31/E/08-B2** **0950**

### PRESENT-DAY PATTERN OF CORDILLERAN DEFORMATION IN THE WESTERN UNITED STATES

Richard A. BENNETT, James L. Davis, and James E. Normandeau (Harvard-Smithsonian Center for Astrophysics, 60 Garden Street, Cambridge, Massachusetts 02138, USA, email: rbennett@cfa.harvard.edu); Brian P. Wernicke (California Institute of Technology, 1200 E. California Blvd., Pasadena, California 91125, USA)

We are combining campaign and continuous Global Positioning System (GPS) and very long baseline interferometry (VLBI) observations to infer the pattern of Western United States Cordillera (WUSC) deformation west of longitude 110W, south of latitude 42N, and north of latitude 31N. Preliminary results are consistent with a number of features previously observed through local geodetic studies and very sparse space geodetic studies, including a dominant pattern of right-lateral shear associated with the San Andreas fault, rates of sites along the California coast of 46-48 mm/yr relative to a North America reference frame, and some 11-13 mm/yr of deformation accommodated east of the Sierra Nevada in the Basin and Range province north of latitude 36N. In addition, our results reveal that south of latitude 36N the southernmost San Andreas fault system accommodates effectively all Pacific-North America interplate motion and that the southern Basin and Range is not deforming significantly. At latitude 37N, the eastern California shear zone appears to exhibit simple shear oriented between N20W and N40W relative to North America, with a fairly well defined transition zone from localized shear to diffuse spreading in the Basin and Range. Enigmatically, this transition involves a significant component of contraction normal to the overall shear zone trend, with sites in the Great Basin moving southwestward at up to 5 mm/yr relative to sites within the eastern California shear zone. This apparent shortening may be indicative of "competition" between northwest-southeast plate-boundary shear and eastward buoyancy-driven collapse in the vicinity of latitude 37N. To the north of latitude 37N, in contrast, there appears to be a relatively smooth transition from east-west spreading within the eastern Great Basin to northwest-southeast shear across the westernmost Basin and Range. Our deformation results are available to the community either via the WUSC World-Wide-Web site

(URL: <http://cfa-www.harvard.edu/~rbennett/WUSC>) or via anonymous FTP (<ftp://cfa-ftp.harvard.edu/pub/rbennett/WUSC>). The WUSC web-site is presently being redesigned and we will demonstrate the new features of the redesigned web-site.

**JSS31/E/11-B2** **1010**

### PRESENT-DAY DEFORMATION ACROSS THE BASIN AND RANGE PROVINCE, WESTERN UNITED STATES AND ITS DYNAMICAL IMPLICATIONS

THATCHER, Wayne, (email: [thatcher@usgs.gov](mailto:thatcher@usgs.gov)); Julian, B. R., Svarc, J., E. Quilty, E., Bawden, G (U. S. Geological Survey, MS/977, Menlo Park, CA 94025); Foulger, G. (R. Department of Geological Sciences, University of Durham, Science Laboratories, South Road, Durham DH1 3LE, U. K.)

The distribution of internal deformation across the Basin and Range has been determined from 1992, 1996 and 1998 surveys of an 800-km aperture 63-station GPS network. Internal deformation follows the pattern of Holocene fault distribution and is concentrated in narrow zones near the eastern and western extremities of the province.  $2.8 \pm 0.5$  mm/yr of relative motion occurs across the Wasatch and related faults in central Utah. Little net deformation occurs across the central ~450 km of the network in western Utah and eastern Nevada. Velocities jump abruptly by  $3.7 \pm 0.8$  mm/yr across the central Nevada seismic zone and increase an additional  $6.0 \pm 1.6$  mm/yr towards the Sierra Nevada, indicating partitioning of eastern California shear zone motion between these two zones. Concentration of deformation adjacent to the rigid Sierra Nevada (SN) and Colorado Plateau (CP) blocks indicates plate boundary tractions play a dominant role in driving Basin and Range deformation. There is evidence for local modulation of these forces by extensional stresses generated by internal buoyancy forces due to lateral density gradients and topography near the SN and CP boundaries.

**JSS31/W/10-B2** **1030**

### SOUTHERN CALIFORNIA CRUSTAL DEFORMATION AND ITS TECTONIC IMPLICATIONS

Zheng-Kang SHEN and David D. Jackson (both at Department of Earth & Space Sciences, UCLA, Los Angeles, CA 90095-1567, USA; email: [zshen@ess.ucla.edu](mailto:zshen@ess.ucla.edu))

The Crustal Deformation Working Group of the Southern California Earthquake Center has recently released its Southern California Crustal Deformation Velocity Map 2.0 ([http://www.scecdc.scec.org/group\\_e/release.v2](http://www.scecdc.scec.org/group_e/release.v2)). We analyzed the geodetic data used in the release and derived station velocities before and after the 1992 Landers earthquake. Significant velocity changes were found for sites located within about 60 km of the earthquake epicenter. The average strain rate in the region increased from ~0.10 to ~0.30 micro-radian/yr. We also estimated fault slip rates in southern California using the pre-Landers geodetic velocities and elastic dislocation theory. We used a modified fault model, defined by the California Department of Mine and Geology (USGS Open-file Report 96-706) and derived mainly from geological information, to lay out the fault geometry. We adopted the CDMG fault slip rates and uncertainties as a priori data to constrain the least-squares inversion of geodetic data for fault slip rates. Generally the geodetic and geologic estimates are quite consistent, except for a few places. For example, the geodetic rates are significantly lower than the geologic rates along the Mojave, San Bernardino, and Coachella Valley sections of the San Andreas, but the other way round at the Brawley seismic zone and the Imperial fault. These discrepancies suggest that the current fault slip rate beneath the locking depth along the San Andreas is lower than its long-term average. This may reflect the fact that the San Andreas has experienced no large earthquake since 1857, and the fault has passed the time period of rapid post-seismic deformation and entered one of slow deformation. On the other hand, the Landers and Imperial faults are still being affected by post-seismic deformation caused by the 1992 Landers and the 1940 and 1971 Imperial Valley earthquakes respectively. A second inversion of the geodetic velocities derived from the post-Landers data reveals a substantial reduction of the fault slip rate along the Mojave section of the San Andreas and a significant increase of the fault slip rate along the San Bernardino section of the San Andreas respectively.

**JSS31/W/16-B2** **1110**

### FEM MODELING OF SUBDUCTION DEFORMATION IN THE NANKAI TROUGH

Phil R. CUMMINS, Yoshiyuki Kaneda, and Satoshi Hirano (Frontier Research Program for Subduction Dynamics, Japan Marine Science and Technology Center, 2-15 Natsushima-cho, Yokosuka 237-0061 Japan, email: [cummins@jamstec.go.jp](mailto:cummins@jamstec.go.jp))

The Nankai Trough in southwest Japan is the scene of large, destructive earthquakes which have repeatedly caused substantial loss of life and property in the region. For this reason, measurements of crustal deformation were already being made prior to the last major earthquakes in 1944 and 1946. These measurements continue to the present day, so that the Nankai Trough is said to have the world's most complete record of deformation during the "earthquake cycle". Substantial deformation has been inferred using leveling and tide gauge data, as well as a modern GPS network. However, these observations are typically interpreted using very simple structural models, such as an elastic halfspace or an elastic layer over a viscoelastic halfspace. Such models incorporate none of the structural complexity typical of a subduction zone. We consider whether such complex structure has an important influence on the deformation by performing FEM modeling using a realistic model of subduction zone structure. Our model for the Nankai Trough region is based on a combined OBS/MCS seismic survey performed by JAMSTEC in 1997. Features of this model which may influence the regional deformation include: a plate boundary with very shallow dip, a thin oceanic crust and subducting slab, and a well-developed accretionary prism near the trench. Our results indicate that the influence of complex structure can be important. In particular, the presence of the subducting slab gives rise to a dramatic difference in the coupling of surface deformation to viscoelastic relaxation in the asthenosphere.

**JSS31/W/09-B2** **1130**

### NUMERICAL MODELS OF THE SOUTHERN HIKURANGI TROUGH SUBDUCTION ZONE, NORTH ISLAND, NEW ZEALAND

Steven COHEN (Goddard Space Flight Center, Greenbelt, MD, 20771, USA, email: [scohen@car-noustie.gsfc.nasa.gov](mailto:scohen@car-noustie.gsfc.nasa.gov)); Desmond Darby (Institute of Geological and Nuclear Sciences, Lower Hutt, New Zealand, email: [D.Darby@gns.cri.nz](mailto:D.Darby@gns.cri.nz))

The southern portion of the Hikurangi subduction zone is characterized by oblique convergence with nearly equal components of trench parallel and trench normal motion. Walcott (1978) proposed a slip-partition model in which the motion is accommodated by strike-slip faulting in the North Island Dextral Fault Belt (DFB) and low angle reverse faulting on more trenchward features. We are developing two and three dimensional viscoelastic finite element and elastic dislocation implementations of this model. Constraints come from geological estimates of the fault slip rates, seismicity, and historical and contemporary geodetic data. Of the several strike-slip faults within the DFB the two most important are the Wairarapa fault,

which slipped during an M=8 event in 1855 and the Wellington fault, which has been geologically active and historically quiescent. Shear strain release on the DSZ faults can accommodate most of the right lateral strain accumulating on the locked megathrust provided the slip surface extends to the depth to the locked megathrust. Darby and Beanland (1993) proposed that the slip surface in the 1855 event was listric, with the slip depth extending to at least 20-25 km. If so, the locking depth is greater than that of most strike-slip faults in transform environments. The trench normal strain is accommodated by strain release either along the megathrust or a hypothesized low angle reverse fault lying between the DSZ and the accretionary wedge. The shallowest portions of the plate interface may not be locked or the motion may be accommodated within the accretionary complex.

JSS31/L/01-B2

1150

#### ON THE USE OF SIMPLE ELASTIC DISLOCATION MODELS IN MODELLING STRAIN ACCUMULATION

John BEAVAN and Desmond J Darby (Institute of Geological and Nuclear Sciences, Lower Hutt, New Zealand, email: j.beavan@gns.cri.nz)

We report two examples of the use of dislocation calculations for interpreting GPS-derived horizontal surface deformation resulting from interseismic strain accumulation. In the oblique Hikurangi subduction zone of the southern North Island, New Zealand, we model the state of locking on the subduction interface, and the state of partitioning between thrusting on the interface and strike-slip in the over-riding plate. In the oblique continental convergence zone of the central South Island, we model the ongoing slip rate on a deep extension of the Alpine fault, and the substantial fraction of the plate motion that occurs as distributed deformation well east of the Alpine fault.

We utilise formal inversion techniques using non-linear least-squares methods, and we advance on previous work by propagating the full covariance information from the GPS data analysis through the inversion. We argue that both these features are necessary for optimal application of dislocation methods. The fact that simple dislocation models can usually be found to fit horizontal surface deformation data with high accuracy emphasises one theme of this symposium: that additional information must be included in support of such inversions.

JSS31/E/07-B2

1210

#### NUMERICAL MODELLING OF CRUSTAL DEFORMATION IN THE TIEN SHAN: COMPARISON WITH GPS-MEASUREMENTS

Holger SCHELLE, Christoph Reigber, Detlef Angermann, Jürgen Klotz, and Gero Michel (GeoForschungszentrum Potsdam, Telegrafenberg, D-14473 Potsdam, Germany, email: schell@gfz-potsdam.de)

Numerical simulations were carried out in order to relate crustal deformation processes to the surface motions constrained within different GPS-campaigns between 1992 and 1998. In order to simulate the crustal deformation processes, the 3d - distinct element code 3DEC was used. The main part of the presentation deals with the Ms: 7.3, Aug 19, 1992 Suusamy earthquake and its induced co-seismic surface motions. Aims of the modelling include to check different focal models that explain the earthquake rupture process derived from seismological investigations, and to test different focal parameters. Using information from the measured surface deformations, the model of the earthquake rupture process with the best fit to the GPS-based displacement vectors was selected. The resolving parameters that describe the main shock are: mean stress drop 7 MPa, peak stress drop 11.9 MPa, mean dislocation 1.39 m, and peak dislocation 2.37 m. In addition to the above described models, further numerical simulation has been conducted in order to explain the crustal deformation measured using GPS within the N-Pamirs, Tien Shan and Tarim. The presentation gives an overview of some first and important results.

### Tuesday 27 July PM

Presiding Chairs: Dr B.E. Parsons, (University of Oxford, UK);  
Dr R.E. Reilinger, (Massachusetts Institute of Technology, USA)

JSS31/E/04-B2

1400

#### THE CENTRAL ANDES GPS PROJECT : GEODETIC MEASUREMENTS OF CRUSTAL MOTION AND DEFORMATION IN THE CENTRAL AND SOUTHERN ANDES

Eric Kendrick and Michael BEVIS (HIGP, University of Hawaii, HI 96822, USA, Email: bevis@soest.hawaii.edu); Robert Smalley (CERL, University of Memphis, Memphis, TN 38152, USA); Oscar Cifuentes (Instituto Geográfico Militar, Santiago, Chile); Fernando Galban (Instituto Geográfico Militar, Buenos Aires, Argentina); Thomas Herring (Dept. Earth, Atmospheric & Planetary Sciences, MIT, Cambridge, MA 02139, USA); Rick O'Connell (Dept. Earth & Planetary Science, Harvard University, Cambridge, MA 02138, USA)

We will present velocity fields for the plate boundary zone associated with subduction of the Nazca plate beneath the South American plate. These solutions, which are based on roving and continuous GPS measurements that began in 1993, are presented in a frame that nominally fixes the rigid core of the South American continent. These motions manifest a mixture of interseismic, coseismic and postseismic deformations. Separation of the elastic and anelastic contributions to the deformation field will be a major challenge. The observations allow us to address along-strike segmentation of tectonic style within the Andes, as well as cross-strike partitioning of elastic and anelastic deformation. There are several other major GPS projects working in this region. The GFZ (Potsdam, Germany) network strongly overlaps our own. We have long coordinated the designs of our networks in the sense of minimizing useless spatial redundancy, and we are starting to work on the problem of combining our velocity fields. We also need to combine these results with those obtained further north by project SNAP, which operates in Bolivia and Peru.

JSS31/W/12-B2

1420

#### SPATIAL AND TEMPORAL VARIATION OF GPS-DERIVED DEFORMATION IN THE CENTRAL AND SOUTHERN ANDES

KLOTZ, J., Angermann, D., Michel, G.W., Reigber, (GeoForschungszentrum Potsdam, Telegrafenberg A17, 14473 Potsdam, Germany, e-mail: klotz@gfz-potsdam.de); Cifuentes, O., (Instituto Geográfico Militar de Chile, Santiago, Chile); Barriga, R., (Academia Militar Politécnica, Santiago, Chile Barrientos, S., Univ. de Chile, Santiago, Chile); Perdomo, R., (Univ. Nac. La Plata, Argentina Viramonte, J., Univ. Nac. de Salta, Argentina); Rios, V., (Univ. Nac. Tucuman, Argentina)

In the framework of SAGA (South American Geodynamic Activities) we conducted GPS-measurements at 215 sites covering Chile and parts of Argentina in order to study the surface deformation related to the subduction of the Nazca plate beneath South America. The spatial and temporal distribution of surface deformation related to the 30 July 1995, Mw = 8.0 Antofagasta, Chile, earthquake was studied using 4 datasets of GPS campaigns (70 sites).

Re-observations between Arica and Pto. Montt (18°S to 42°S) indicate strong inter-seismic strain accumulation that slightly varies along strike. Post-seismic displacements of the Antofagasta earthquake area are significantly different from those derived in parts of the net dominated by inter-seismic deformation. We observed a similar post-seismic deformation pattern south of 37°S, in the area of the great Chilean earthquake rupture zone of May 22, 1960.

JSS31/W/14-B2

1440

#### TECTONICS OF INTERIOR ALASKA: A STUDY USING GPS MEASUREMENTS

Hilary J. FLETCHER and Jeffrey T. Freymueller (both at Geophysical Institute, University of Alaska, Fairbanks, AK 99775, email: hilary@giseis.alaska.edu)

To assess the seismic hazard in interior Alaska, it is necessary to understand the tectonics of the area in greater detail. Interior Alaska has produced three earthquakes with magnitudes greater than seven in this century and yet this area has received little study. The Denali fault is an obvious geomorphic feature, extending in a broad arc for more than 2000 km, with up to 400 km of offset over the last 60 million years. Slip rates of 8-12 mm/yr are estimated for the Denali fault based on offset Pleistocene glacial features to the east of Mt. McKinley. Previous geodetic measurements of slip rate along the Denali fault have produced results at odds with this geologic evidence, with two trilateration networks across the Denali fault giving results consistent with a much smaller rate of right lateral shear on the Denali fault than expected based on the Holocene slip rate. Another major tectonic feature in Alaska is the Tintina fault, a large dextral fault system 250km to the north of the Denali fault. The pattern of seismicity in the region between these two fault systems shows NE-SW lineations, which have been interpreted as edges of elongate crustal blocks.

We established a network of GPS sites in interior Alaska between the Denali fault and the Tintina fault in 1995. Velocities at these sites show a low rate of strain accumulation. In 1997 a dense profile of 17 GPS bench marks was installed across the Denali fault. Initial results from surveys of this profile show that some sites in the profile have motion consistent with right lateral shear along the fault. We use an elastic screw dislocation model to invert the estimated site velocities for a slip rate of the Denali fault. We discuss possible tectonic models for interior Alaska in light of our new results

JSS31/E/06-B2

1500

#### GPS GEODETIC CONSTRAINTS ON RIGID CARIBBEAN PLATE MOTION AND PLATE BOUNDARY DEFORMATION

Pamela JANSMA (Dept. of Geology, University of Puerto Rico, Mayaguez, PR 00681 USA, Email: pam@geology.uprm.edu); Roger Bilham, (Dept. of Geological Sciences, University of Colorado, Boulder, CO 80309 USA, Email: bilham@stripe.colorado.edu); Chuck Demets (Dept. of Geology and Geophysics, University of Wisconsin, Madison, WI 53706 USA, Email: chuck@geology.wisc.edu), and Glen Mattioli (Dept. of Geology, University of Puerto Rico, Mayaguez, PR 00681 USA, Email: glen@geology.uprm.edu)

The velocity of the Caribbean plate relative to North America has been estimated at 1-2 cm/yr from traditional sources such as summing seismic moments of earthquakes, deriving velocities from poorly expressed magnetic lineations in the Cayman trough, or calculating closure from global plate circuits. The motion of the Caribbean plate relative to its neighbors remains controversial, however, with proposed intraplate deformation significant enough to produce distinct eastern and western Caribbean plates. Although GPS methods provide instantaneous relative velocities, it has been difficult to obtain measurements from islands outside the zone of active plate boundary deformation defined by diffuse seismicity, and few islands are found in the interior of the plate. We report here measurements obtained in 1994 and 1998 from Aves Island (15.667N, 63.618W) in the eastern interior of the Caribbean plate, which imply motion relative to North America at  $19-20 \pm 2$  mm/yr to the ENE. The similarity within error to GPS-derived velocities at San Andres Island and Cabo Rojo, southern Dominican Republic in the western interior and northern Caribbean, respectively, supports a single, rigid Caribbean plate and allows determination of a stable Caribbean reference frame with which to interpret geodetic results and to quantify deformation in the North and South American plate boundary zones and the Lesser Antilles island arc. Implications for constraints on plate boundary processes will be discussed.

JSS31/L/02-B2

1520

#### TECTONICS OF PAPUA NEW GUINEA FROM GPS OBSERVATIONS

Paul Tregoning, Kurt LAMBECK, Herbert McQueen (all at Research School of Earth Sciences, The Australian National University, Canberra, ACT 0200, Australia, email: Kurt.Lambeck@anu.edu.au); R. Jackson, R. Little (both at Department of Surveying and Land Studies, The Papua New Guinea University of Technology, Lae, Papua New Guinea); Robert Rosa (National Mapping Bureau, PO Box 5665, Boroko, Papua New Guinea); Eli Silver (Earth Sciences Department, University of California, Santa Cruz, CA 95064, USA)

Plate tectonic motions have been estimated in Papua New Guinea from several years of GPS observations on a network of sites spanning most of the country. A tectonic model has been developed comprising three microplates trapped between the colliding Australian and Pacific Plates. This simple model is consistent with the major tectonic features of the region; subduction along the New Britain Trench, spreading on the Woodlark Basin Spreading Centre, convergence along the Ramu-Markham Fault, both strike-slip motion and spreading along different sections of the Bismarck Sea Seismic Lineation. The model predict relative strike-slip motion of ~130 mm/yr between the South Bismarck and Pacific Plates in the southern part of New Ireland. Preliminary GPS results indicate that not all the relative motion occurs on the Weitin Fault; rather, a significant proportion of the convergence is accommodated to the west of the Gazelle Peninsula. A general overview of the tectonics of Papua New Guinea and new results in the East New Britain/New Ireland region will be presented.

JSS31/L/05-B2

1600

#### CRUSTAL MOTION AROUND THE WESTERN SEGMENT OF THE NORTH ANATOLIAN FAULT ZONE : GEODETIC MEASUREMENTS AND GEOPHYSICAL INTERPRETATION

Mehmet Emin AYHAN, Coskun Demir, Ali Kilicoglu, Ilhan Sanli (General Command of Mapping, TR-06100, Ankara, Turkey); S. Mete Nakiboglu (Middle East Technical University, Ankara, Turkey)

Contemporary horizontal crustal motion in the western part of the North Anatolian Fault Zone (NAFZ) is investigated utilizing 25 common points of a triangulation network established in 1940s and a GPS network observed in 1995. The common network, extending about 25 x 103 km<sup>2</sup>, covers the boundary zone of the Anatolian and Eurasian tectonic plates. The GPS network is adjusted on the ITRF94 reference frame using precise orbital information and simultaneous observations to 7 precisely known IGS stations in Europe and Asia within the fiducial network strategy. The repeatabilities of the horizontal coordinates are below about 15



## INTER-ASSOCIATION

mm. The triangulation observations are also adjusted on the same datum by holding the GPS coordinates of two stations as fixed. A comparison of triangulation and GPS coordinates yields the relative displacements in the area ranging from 3.0 m to a few cm with uncertainties of about 25 cm emanating predominately from the triangulation errors. The estimates reveal a westward drift of the Anatolian plate which deviates significantly from a rigid body motion. The relative displacements may be viewed as a combination of rigid body motion and plate boundary deformations which may incorporate co-seismic and/or aseismic components. A cooperative international GPS network covering the same area with 40 different stations observed annually from 1992 to 1998 is re-processed using the precise positioning techniques outlined above. The resulting velocity field reveals the combined effects of rigid body motion and aseismic deformation but no co-seismic deformation as there were no major earthquakes, resulting in fault rupture in the region during this period.

The resulting velocity field is modeled using a least squares Inversion assuming screw dislocations in an elastic half-space. The best estimate of the velocity of Anatolia relative to Eurasia is found to 25 mm/yr. Armutlu Block in the west of the area appears to be moving together with Anatolia, but Almacik Block in the center of the region exhibits a rigid translation of about 15 mm/yr superimposed onto a slow clockwise rotation. The fault segments Ismetpasa- Bolu and Iznik-Sapanca exhibit significant aseismic creep with rates of 7.5 and 14 mm/yr respectively. The Mudurnu Valley and Mekece...

**JSS31/W/11-B2**

**1620**

### SOME ASPECTS OF AEGEAN CONTINENTAL DYNAMICS INFERRED FROM A DECADE OF GPS MEASUREMENTS AND A CENTURY OF TRIANGULATION

PETER CLARKE (Dept. of Geomatics, University of Newcastle, Newcastle NE1 7RU, UK, Email: Peter.Clarke@ncl.ac.uk); Philip England, Barry Parsons (Dept. of Earth Sciences, University of Oxford, UK); Robert Davies (Research School of Earth Sciences, Victoria University, Wellington, NZ); Haris Billiris, Jordan Galanis, Demetris Paradissis, George Veis (Higher Geodesy Laboratory, National Technical University, Athens, Greece); Paul Cross, Paul Cruddace (Dept. of Geomatic Engineering, University College London, UK); Pierre Briole, Helene Lyon-Caen (Institut de Physique du Globe, Paris, France); Hans-Gert Kahle (Institut für Geodäsie und Photogrammetrie, ETH Honggerberg, Zurich, Switzerland); Boudewijn Ambrosius (Faculty of Aerospace Engineering, Delft University of Technology, Netherlands)

We have obtained the velocities at more than 200 sites in Greece using GPS data from over 30 epoch campaigns spanning up to 10 years, under the assumption that short-term inter-seismic velocities are steady and therefore reference frame biases can be estimated. Over 20 of these sites are coincident with or close to pillars in 20- and 100-year-old triangulation networks. By extrapolating a minimal subset of the GPS pillar velocities, we estimate the scale and orientation of the triangulation networks.

We find that the coordinate fit of the triangulation networks fits our model of steady-state velocities well within 95% confidence limits, and observe that the velocity field is generally smooth spatially as well as temporally. From our interpolated velocity field we calculate the strain tensor field and associated derived quantities. We note that the current and recent orientations of faults are consistent with those predicted from the velocity field but oblique to earlier crustal trends. This observation, coupled with the temporal and spatial smoothness of the crustal velocity field, is suggestive of a dynamic model in which brittle-elastic crustal deformation is driven by the ductile lower lithosphere. Further densification and expansion of the GPS network is currently in progress (Cruddace et al., this volume).

**JSS31/W/08-B2**

**1640**

### GPS MEASUREMENT OF CRUSTAL MOTION IN BULGARIA

Valentin KOTZEV (Central Laboratory of Geodesy, Bulgarian Academy of Sciences, ul. 15 noevmvi 1, 1040 Sofia, Bulgaria, email: kotzev@bgcic.acad.bg); Clark Burchfiel and Rob Reilinger (Department of Earth, Atmospheric, and Planetary Sciences, Massachusetts Institute of Technology, 77 Massachusetts Avenue, 54-1010 Cambridge, Massachusetts 02139, USA, email: bcburch@mit.edu)

Active and young deformation in central and southern Bulgaria represents the northernmost extent of the Aegean extensional domain and thus represents an active example of back arc type extension adjacent to a zone of coeval subduction and convergence along the Hellenic subduction boundary. To determine the present day kinematics of the major tectonic elements in Bulgaria, a regional GPS network was established and surveyed in 1996, 1997 and 1998. We present here a solution for the horizontal velocities of 18 sites based on observations performed over the two-year period. We use Kalman filter to estimate a consistent set of coordinates and velocities by combining our loosely constrained solutions with the solutions derived at SOPAC from the analysis of a global tracking network. The reference frame of the computed velocity field is defined through minimizing the departure of the estimated horizontal velocities for 39 core ITRF96 stations from their nominal values. The post-fit of the velocity transformation is 2.6 mm/yr. The relative to Eurasia velocities we estimate are less than 5mm/yr. We obtain one-sigma uncertainties of (0.7 mm/yr for the east components and of (0.4 mm/yr for the north components. Most of the stations indicate N to NE oriented motion at a rate of 3-5 mm/yr. Stations west of the seismically active Struma fault zone show NE motions of 3 mm/yr and those east of the faults show no motions at the 95% confidence level. The two sites located in the west central part indicate NW oriented motion at a rate 3 mm/yr.

**JSS31/E/03-B2**

**1700**

### MODELLING OF VERTICAL MOVEMENTS IN CAUCASUS REGION USING GPS DATA

Mikhail PRILEPIN (United Institute of Physics of the Earth, B.Gruzinskaya Str., 10, 123810 Moscow, Russia, email: prilepin@upei-ras.scgis.ru) Robert E. Reilinger Earth Resources Laboratory, Massachusetts Institute of Technology, 42 Carleton St. Cambridge, Massachusetts 02148

We began GPS-geodynamic measurements in the Caucasus region in 1991 as a part of a cooperative American-Russian-Georgian-Armenian initiative [Reilinger et al., 1997; Prilepin et al., 1997]. Repeat surveys were completed in 1994, 1996 and 1998. The analysis of these observations show that the one-sigma uncertainties for vertical rates for regional sites relative to a reference station on the Skifs platform (100-500 km distance) are about 2-3 mm/year, quite comparable with errors for levelling in mountainous terrains. In spite of short time interval covered (5 yrs), GPS derived vertical motions support some earlier inferences made from repeated leveling surveys, particularly that movements vary substantially between different parts of the Caucasus: the Greater Caucasus experience uplift but the Lesser Caucasus do not reveal any significant vertical movements. Also GPS sites in the Greater Caucasus show larger variations in rates compared to sites in the Lesser Caucasus. The average rates in the Greater Caucasus are about 6-8 mm/year, reaching a maximum of 22 mm/year, while sites in the Lesser Caucasus are characterized by average rates of 3-5 mm/year and a maximum of 8 mm/year. Sites in the eastern and western parts of the GPS network suggest that vertical motions in Caucasus can be described by stepped model, discussed in the report. Four out of five GPS sites in a local network situated in the epicentral area of the 1991, M=7.3, Racha earthquake indicate postseismic (from 3 months after the earthquake to 1996) relative uplift at rates of 2-11 mm/year and only one, most distant from the epicenter,

shows subsidence at a rate of 2 mm/year. New 1998 repeat GPS measurements, which are currently being analyzed, will be presented and should help constrain better the model of vertical motions in the Caucasus region.

**Wednesday 28 July AM**

Presiding Chairs: Dr B.E. Parsons, (University of Oxford, UK);  
Dr R.E. Reilinger, (Massachusetts Institute of Technology, USA)

**JSS31/P/01-B3**

**Poster**

**0830-01**

### A PRELIMINARY RESEARCH ESTABLISHING THE PRESENT-TIME

ZHOU

Abstract not available at time of going to press

**JSS31/W/01-B3**

**Poster**

**0830-02**

### GEODEIC DETECTION OF ACTIVE FAULTS IN SOUTHERN CALIFORNIA

Shimon WDOWINSKI and Yonadav Sudman (both at Department of Geophysics and Planetary Sciences, Tel Aviv University, Ramat Aviv 69978, Israel, email: shimon@geo1.tau.ac.il); Yehuda Bock (Institute for Geophysics and Planetary Physics, Scripps Institution of Oceanography, University of California, San Diego, La Jolla, CA 92093-0225, USA, email: ybock@ucsd.edu)

The steady tectonic motion between the Pacific and North American plates in western North America deforms a broad plate boundary zone, accumulating elastic strain in the lithosphere and creating seismic hazards. Geodetic measurements of the San Andreas fault system have shown a pattern of inhomogeneous strain accumulation, in which strain is localized along active faults where most major (M>6) earthquakes occur. We systematically analyze geodetic determinations of horizontal site velocity fields recently available in southern California to identify and quantify strain localization patterns and active faulting. We find that strain is localized along nine shear belts, which coincide with geologically mapped major strike-slip fault segments and a compressional belt along the northern extent of the Transverse Ranges. Within the highly populated Los Angeles basin, we detect strain localization related to the Newport-Inglewood and Santa Monica faults. We surmise that the steady accumulation of strain pushes the local stress field closer to its yield envelope and hence increases the likelihood of a major earthquake occurring along the geodetically detected active fault segments. Furthermore, the observation that other fault segments, which are known to have significant permanent deformation from geologic and paleoseismic records, are not presently active provides evidence that intraplate strain rates may vary temporally as well as spatially.

**JSS31/W/02-B3**

**Poster**

**0830-03**

### ABOUT THE ISOSTATIC COMPENSATION OF THE EARTH'S CRUST

Nadejda A. CHUJKOVA, Tatiana G. Maximova (Sternberg State Astronomical Institute, Universitetskij pr.13, Moscow, e-mail: chujkova@sai.msu.ru)

The comparative analysis of the harmonic expansions for the heights of the equivalent rock topography for the depth of the Moho discontinuity and for the Earth's gravity field have shown: 1) the Earth's global topography up to expansion of 10 degree is basically isostatically compensated on the Moho surface; 2) the total shift about 20 degrees of the Moho surface relative to the theoretical surface of compensation is observed in direction NE; 3) the surplus geoid flattening is caused by the large surplus flattening of Moho surface relative to theoretical surface of compensation; 4) the estimation of the Moho depth by means of the correlation with the Bouguer anomalies is not confirmed; 5) the correlation of the crust boundaries with the geoid is nonsignificant for expansion up to 10 degree; 6) the correlation of the noncompensated topography with the geoid and the core boundary is partly noticeable

**JSS31/W/04-B3**

**Poster**

**0830-04**

### INVERSION OF STRESS DISTRIBUTION IN JAPAN USING GPS DATA

M. HORI, T. Kameda, and T. Kato, (Earthquake Research Institute, University of Tokyo, Yayoi 1-1-1, Bunkyo, Tokyo 113-0032, JAPAN)

A new inversion method which computes spatial stress distribution from measured displacement distribution is developed. The charm point of this inversion is that it does not have to assume particular constitutive relations. Indeed, the inversion results in solving a well-posed boundary-value problem for unknown stress distribution. Numerical simulation verifies the basic validity of the proposed method, as it succeeds in computing stress distributions of a body with unknown elasto-plastic properties. The method is applied to the GPS data which have been densely measured in Japan. Presented are the current results of the inversion, regarding to the stress distribution and the local constitutive relations of Japan.

**JSS31/W/05-B3**

**Poster**

**0830-05**

### THE KMS99 GLOBAL ALTIMETRIC MARINE GRAVITY FIELD

O. ANDERSEN, P. Knudsen, (both at National Survey and Cadastre, Copenhagen NV, Denmark, email: oa@kms.dk, pk@kms.dk)

The KMS99 altimetric derived global marine gravity field is the latest version of gravity fields derived from ERS-1 and GEOSAT geodetic mission. This presentation describes the new gravity field and the improvements over the older KMS global marine gravity fields as described by Andersen and Knudsen (JGR, 97, ERS special issue). The present resolution of the KMS gravity field is 1/30 degree corresponding to 2 minutes or 4 km at the Equator. In order to improve the capability of the gravity field to map short spatial wavelength in the gravity field, it has been necessary to investigate if data with a higher along track sampling than the present 1Hz data can be used. For the KMS99 gravity field the possibility of using reinterpolated 2 Hz along track observations have been carried out. Some of the other improvements that have been introduced in the new version of the gravity field is the use of repeat track altimetry to improve the spatial resolution at high latitude. Similarly, investigation of a better screening of the raw data have been carried out to improve the gravity field in especially coastal regions.



JSS31/W/06-B3 Poster 0830-06

## INVARIANT GEODYNAMICAL INFORMATION IN GEOMETRIC GEODETIC MEASUREMENTS

Peiliang XU and Torao Tanaka (both at Res. Centre for Earthquake Prediction, Kyoto University at Uji, Uji, Kyoto 611-0011, Japan, email: pxu@rcpe.dpri.kyoto-u.ac.jp); Seiichi Shimada (Natl Res. Inst. for Earth Sc. and Disaster Prevention, Tennodai 3-1, Tsukuba, Ibaraki 305-0006, Japan); Yoichihiro Fujii (Nippo Co. Ltd., 1-8-7, Kodai, Miyamae-ku, Kawasaki 216, Japan)

Repeated geodetic measurements have been used to extract geodynamical quantities such as displacements, velocities of movement and crustal strains. For the geodetic network without tie to an external reference frame, free network adjustment methods have been widely applied to derive geodynamical quantities. Currently, it has been understood that relative displacements can be found uniquely if the geodetic network is geometrically redundant. Strain tensors are then reported to be uniquely determined. We have carried out a theoretical analysis of invariant geodynamical information in geometric geodetic observations and concluded: (1) that relative displacements are not invariant quantities and thus cannot uniquely be determined from free geodetic networks; and (2) all the components of the strain tensors are not invariant and thus cannot individually be determined uniquely from the networks. However, certain combinations of strain components are indeed invariant and can uniquely be determined from geometric geodetic measurements. The theory of invariant information is then applied to analyzing the Tokai first order triangulation/trilateration network spanning over an interval of more than 100 years. The results have shown that the normal strains and the principal strains are significantly affected by the unknown scaling biases and orientation differences; thus any attempt of geophysical interpretation of these quantities must be exercised with great care. If the scaling bias and the orientation difference are small, the shear strain is shown to be practically invariant. The invariant analysis of the Tokai network has also shown that a belt near Shizuoka has been significantly deformed in the past 100 years, which has never been seen in any previous analysis of displacements and/or strains, and may be attributed mainly to the 1923 Kanto Earthquake M7.9, Japan.

JSS31/W/07-B3 Poster 0830-07

## GEODETIC DATUM CONSTRAINTS ON PLATE TECTONIC AND CRUSTAL DEFORMATION MODELS (APKIM9.0)

Hermann DREWES (Deutsches Geodaetisches Forschungsinstitut, Marstallplatz 8, D-80539 Muenchen, Germany, email: drewes@dgfi.badw-muenchen.de)

Various space geodetic techniques (e.g., GPS, SLR, VLBI) contribute to the modelling of Actual Plate Kinematic and crustal deformation Models (APKIM) by providing observed station velocities. A problem in combining these velocities is to homologize the different datum realizations. Each of the technique dependent solutions refers by definition in general to the NNR NUVEL-1A no net rotation plate kinematic model. The realization, however, is quite different by fixing or constraining arbitrarily individual station velocities in each solution. As a consequence we have datum differences resulting in systematic discrepancies between the technique dependent station velocities exceeding by far the observation accuracies.

An actual global no net rotation datum is realized by an integrating procedure of all geodetic observations over the entire surface of the Earth. The Earth's surface is divided into 1\_1 - blocks attributed to either rigid plates or continuous deformation zones, respectively. The plate motion and crustal deformation parameters are estimated by a least squares adjustment or finite element model, respectively. The sum of actual plate motions and crustal deformations is constrained to be zero. The kinematic datums of the individual techniques are simultaneously estimated in the adjustment procedure.

JSS31/W/13-B3 Poster 0830-08

## GEODETIC AND GEOLOGICAL APPROACHES TO DESCRIBE THE GEODYNAMICS OF THE CENTRAL MEDITERRANEAN AREA: A COMBINED INTERPRETATION.

R. Devoti, C. FERRARO, R. Lanotte, V. Luceri, A. Nardi, R. Pacione, P. Rutigliano, C. Sciarretta, F. Vespe (Centro di Geodesia Spaziale -75100 Matera - Italy- Email: vespe@asi.it), E.Gueguen (ITIS/CNR, Centro di Geodesia Spaziale - 75100 Matera - Italy)

Numerous active tectonic zones are present in the Central Mediterranean area. Africa is slowly moving towards Eurasia; southward, the Ionian subduction zone is still active and retreats roughly eastward; during the last 5 My, the Apenninic system has been splitted in two sub-arcs separated by the Tremili line: in the southern segment of the chain the migration of the subduction hinge slowed down, due to the presence of thicker continental crust of the Apulian Platform, whereas in the central and northern part the presence of thin Adriatic lithosphere allowed faster subduction. Nowadays, these movements can be detected not only with a geological approach, based on million years of history impressed in the rocks, but also with geodetic techniques, which give the present movements of the tectonic plates based on few years of data. A dense network of geodetic GPS, SLR and VLBI stations in the Central Mediterranean has been established and long time series of their coordinates and velocities are currently available. This network is a tool to estimate the tectonic velocities and compare them with those derived from geological data in this area, where a high tectonic plates fragmentation is present. We will determine the field of relative velocities in the area and compare the different results in the ITRF96 reference frame. The main stations involved in this work are: Matera (GPS, SLR and VLBI), Medicina (GPS and VLBI), Noto (GPS and VLBI), Cagliari (GPS and SLR), Wettzell (GPS, SLR and VLBI) and Madrid (GPS, SLR and VLBI). Moreover, a particular attention will be given to the interpretation of the vertical movements, which could be the signal of phenomena different from tectonic movements (eg. seasonal effects or subsidence).

JSS31/W/15-B3 Poster 0830-09

## CRUSTAL STRESS IN AUSTRALIA: A MODEL BASED ON GPS VELOCITIES

Y. Zhang (CSIRO Exploration & Mining, PO Box 437, Nedlands, WA 6009, Australia; ph. +61-8-9284-8447; email: zhang@ned.dem.csiro.au); E. Scheibner (CSIRO Exploration & Mining, North Ryde, NSW 2113, Australia; email: erwin.scheibner@dem.csiro.au); P. Morgan (Information Sciences Faculty, Uni. of Canberra, ACT 2601, Australia; email: pjm@mawson.canberra.edu.au); B. E. Hobbs; A. Ord; S. J. D. Cox (all at: CSIRO Exploration & Mining, PO Box 437, Nedlands, WA 6009, Australia; email: b.hobbs@per.dem.csiro.au, a.ord@ned.dem.csiro.au, s.cox@ned.dem.csiro.au)

Regional stress data indicate that the contemporary stress field in SE Australia is dominated by high horizontal compressive stresses in an E-W direction. This is in contrast with the N-S direction of absolute plate motion in Australia over the period Miocene-present, from which one might expect high horizontal stresses oriented N-S. Therefore, the stress pattern of SE Australia cannot be explained simply by considering plate motion-related boundary forces. In this study we aim to model the stress field of the Australian continent using GPS velocities as constraints. The conventional way to model the stress of the Australian plate is to use plate boundary forces as constraints. However, such models do not predict the dominantly E-W oriented stresses in eastern Australia. The E-W compression can be predicted if compressive forces along the

eastern boundary of the plate is introduced, but there is no evidence supporting the existence of such forces. An alternative approach is to use GPS velocities to constrain the model. The idea is that if the true material movements are known, we can use such movements (velocities) as constraints in a mechanical model to simulate the deformation and stress fields. Based on the scope of the existing GPS velocity data which is mostly located on the Australian continent, we have constructed two types of models, including a traditional triangulation model using all the GPS data and a fully mechanical model using the GPS velocity data near the coast. In contrast to the models involving plate boundary forces, the stress results of the present model reproduce the E-W to NEE high compressive regional stress pattern for eastern Australia. The orientation of major horizontal compression seems to vary further inland so that N-S to NE compression dominates. The normalised GPS velocities of Australia show that the eastern seaboard is moving towards the west, that is, there seems to be a contraction between east and west Australia. This probably explains why E-W compression occurs in east Australia. We will continue to refine the data, aiming to build more rigorous models.

JSS31/E/01-B3 Poster 0830-10

## GENETIC ALGORITHM - FINITE ELEMENT INVERSION OF INTRAPLATE STRESS FIELD IN BRAZIL

Yaolin SHI (Graduate School, University of Science and Technology of China, Academia Sinica, Beijing 100039, China, email: shiyl@sun.ihep.ac.cn); Marcelo Assumpcao (Institute of Astronomy and Geophysics University of San Paulo, Brazil, email: marcelo@iag.usp.br)

Genetic Algorithm - Finite Element Method (GA-FEM) provides a way to solve inverse problem of partial differential equations. If stresses or displacements are observed, boundary conditions and material properties can be calculated. Inversion of the effective (or apparent) mechanical property is very important to analyze geodetic observations of faulted blocks.

In this study, we apply GA-FEM to carry out inversion of boundary displacements and nodal forces from observed crustal stress field in Brazil and adjacent areas. Normal, thrust and strike slip types of faulting from earthquake mechanism and geologic observation are also used for additional constraints on the relative magnitude of vertical and horizontal stresses. Our inversion confirms previous studies showing that plate boundary actions are the main controlling factors of regional stress field, and spreading forces at the Andes Mountains and continent-ocean boundaries are important factors. Furthermore, we show that plate bending under vertical load of sedimentation or magma intrusion can affect significantly the local stress field. Our inversion also indicates that, in addition to the well recognized E-W compression in South America, a differential N-S deformation at the northern boundary may exist and play its own role in the regional stress field of northern Brazil. This suggestion is in agreement with recent GPS analysis of relative motion between North and South American plates.

JSS31/E/09-B3 Poster 0830-11

## DETERMINATION BY GPS OF THE DISPLACEMENTS CAUSED BY THE FAIAL SEISM OF 9 JULY 1998

Virgilio B. MENDES (Faculty of Sciences of the Lisbon Classical University, Rua Ernesto de Vasconcelos, Bloco C1, A. 1700 Lisboa, Portugal, email: vmendes@lmc.fc.ul.pt); Jorge Pinto and Helena Ribeiro (both of the Geodetic Department of Portuguese Institute of Cartography and Cadastre, Rua Artilharia 1, 107, 1070 Lisboa, Portugal, email: jtpinto@ipcc.pt and lenarib@ipcc.pt); Joaquim Pagarete (Faculty of Sciences of the Lisbon Classical University, Rua Ernesto de Vasconcelos, Bloco C1, A. 1700 Lisboa, Portugal, email: pagarete@fc.ul.pt)

The authors have already studied the geodynamical behavior of the Central Group from Acores in former presentations, comparing mostly classical geodetic observations from the thirties with GPS observations. Those studies pointed out, especially in Faial case, for a concordance between the displacements deduced from these geodetic observations and the geodynamical model proposed by Madeira y Ribeiro. In July-August 1997, a new GPS campaign was performed by the portuguese geodetic authority (IPCC), covering systematically all the Faial island network. In 9 July of 1998 a strong earthquake took place in Faial, with epicenter some kilometres on the sea between Faial and S. Jorge islands. A month after the seism, IPCC reobserved with GPS, the most affected area of the island, as well as the connection to Pico an S.Jorge Islands. In the present work the authors analyze the results of this post-seismic observations against the former campaigns. This results have a capital importance to help in a correct interpretation of the data recovered by the Geologists and the seismologists during and after the seism. Particularly, this results are an important contribution towards a comprehension about which faults have worked during the main seism and their replicas. The 1998 GPS campaign, which covered almost 60% of the Faial network, allows a rigorous quantification of the displacements inside the island, by comparing it with the 1997 campaign, done a year before the earthquake. Some of these displacements are clearly identifiable by physical evidence in the terrain which could only be caused by the seism. The short interval between the two campaigns, about an year, allows no other cause for the deduced displacements than the seism of 9 July.

JSS31/E/10-B3 Poster 0830-12

## PROGRAM FOR MONITORING CRUSTAL DEFORMATION AND SEISMIC HAZARD ASSESSMENT IN EGYPT USING GEODETIC TECHNIQUES

Ali TEALEB (National Research Institute Of Astronomy And Geophysics, NRIAG, Helwan, Cairo, Egypt, email: salahmm@frcu.eun.eg)

The geodetic methods, terrestrial and space techniques, are considered as one of the most accurate tools for monitoring the vertical and horizontal components of the crustal deformations. Different programs were early initiated since 1983 for recent crustal movement studies in Egypt. The Egyptian programs for monitoring crustal deformations and for seismic hazard assessment include the applications of both the terrestrial and space(GPS) geodetic techniques. The precise terrestrial geodetic techniques(horizontal and vertical methods) as well as the precise gravity measurements were applied since 1983 for monitoring recent crustal movements associated with the earthquake activity in different seismotectonic areas in Egypt. Now-a-days the space geodetic techniques, especially the Global Positioning System (GPS), are widely used for monitoring the relative crustal movements between the continental margins and the Lithospheric plates as well as in regional and study the relative movements between African plates as well as Sinai region. Different applications of the GPS techniques were also carried out to measure regional and local geodetic networks in Egypt. In order to develop and integrate the present programs, the installation of a series of tide gauges and fiducial GPS stations in several locations along the Egyptian shorelines are essential. The collected geodetic data enable the comparison between the sea level changes and the vertical crustal movements. These data may contribute to the seismic hazard assessment in Egypt.

**JSS31/E/12-B3** Poster **0830-13**

**TECTONIC IMPLICATION OF STRAIN RATES DEDUCED FROM REPEATED GPS MEASUREMENTS AROUND GREATER CAIRO, EGYPT**

Ali Tealeb, Salah Mahmoud, Ali Rayan(All at National Research Institute of Astronomy and Geophysics, Helwan, Cairo, Egypt, email: salahmm@frcu.eun.eg) Yoichiro FUJII and Yao Tanaka(both at Nippo, Co.Ltd., 1-8-7, Kodai, Miyama-ku, Kawasaki 2160007, Japan, email: nipposys@bremen.or.jp)

A GPS network consisting of eleven geodetic points near greater Cairo were initially measured during the period from April 27 to May 5, 1996 and measurements were repeated in December, 1996; October, 1997; July, 1998 using Trimble receivers 4000 SSE and SSI. Four dimensional network adjustment has been applied in order to determine strain rates within the network. The results of strain analysis indicate that almost north-south extension is prevailing within the south-eastern part of the GPS network, and the highest rate of maximum shear strain is found to be 0.215  $\mu\text{B/a}$  (J0.202 microstrain/a). The Red Sea is an opening boundary between the Arabian plate and the African plate. The fault system of the Gulf of Elat(Aquaba)-Dead Sea is the transform fault between the Arabian plate and Africa plate. The Gulf of Suez is also a divergent plate boundary between the Sinai peninsula and the African continent. We may assume the Sinai subplate. The tectonic extension of the northern part of the Gulf of Suez is not yet definitely known, while Ben-Menahem, Nur, Vered(1976) assume that north-west extension is across the southern Nile Delta. The geodetic strain deduced from repeated GPS measurements supports an idea of this north-west extension of the western boundary of the Sinai subplate.

**JSS31/E/13-B3** Poster **0830-14**

**THE AMIGO PROJECT: PRESENT-DAY CRUSTAL DEFORMATION OF THE WESTERN SECTION OF THE ALPINE-MEDITERRANEAN PLATE BOUNDARY ZONE**

P. ELOSEGUI(1,2), D. Ben Sari(3), J. M. Davila(4), J. Garate(4), V. Mendes(5), D. Ouazar(3), J. Pagarete(5), R. Relinger(6), A. Rius(2), J. Talaya(7), R. Bennett(1), and J. L. Davis(1)  
 (1) Harvard-Smithsonian Center for Astrophysics, Cambridge, MA, USA; (2) Institut d'Estudis Espacials de Catalunya, Barcelona, Spain; (3) Ecole Mohammadia d'Ingenieurs, Université Mohamed V, Rabat, Morocco; (4) Royal Naval Observatory, San Fernando, Cadiz, Spain; (5) Faculdade de Ciências da Universidade de Lisboa, Portugal; (6) Massachusetts Institute of Technology, Cambridge, MA, USA; (7) Institut Cartogràfic de Catalunya, Barcelona, Spain;

The AMIGO (Atlantic and Mediterranean Interdisciplinary Geophysical Observations) Project is a scientific collaboration among researchers involved in GPS (Global Positioning System) activities along the western section of the Alpine-Mediterranean plate boundary zone. This boundary is made up of a broad transition region between the Eurasia and Africa plates. Its western section extends west-east from the Azores triple junction on the Mid-Atlantic Ridge to Tunisia and Sicily, and is home to a large variety of tectonic processes. Global plate models for this region indicate that the Africa plate is moving northwest relative to Eurasia at a rate of 4-6 mm-yr<sup>-1</sup>. In our presentation, we will describe the objectives of the AMIGO Project, present our most recent GPS measurements of present-day crustal deformation from approximately a year of permanent and campaign data at several sites in this region, and discuss the implications of these, and future measurements for kinematic and dynamic models of this plate boundary zone.

**JSS31/E/14-B3** Poster **0830-15**

**INVESTIGATION OF NAHANNI (CANADA) EARTHQUAKE AREA USING SPACE-BORNE**

Sar Johannes P. RISTAU (Geophysics The University of Manitoba, Winnipeg, Canada R3T 2N2 (email: jrystau@cc.umanitoba.ca) WOOIL M. MOON (Earth System Science, Seoul National University, (email: wmoon@eos1.snu.ac.kr and also with Geophysics, University of Manitoba, Winnipeg, Canada, R3T 2N2 (email: wmoon@cc.umanitoba.ca); Joong-sun Won (Dept. of Earth System Science, Yonsei University, (email: jswon@bubble.yonsei.ac.kr)

The Nahanni River earthquake area in the northeast Cordillera, Northwest Territories, Canada is an intra-plate earthquake area and located in the north-central region of the North American plate and several large earthquakes have recently occurred, including the ones on 5 October 1985 (Ms 6.6), 23 December 1985 (Ms 6.9) and 25 March 1988 (Ms 6.2). The earthquakes occur within a relatively small undeformed plateau, west of the Mackenzie Plain, in the Foreland Fold Belt created along the northeastern Cordillera during the Columbia or Laramide Orogeny. One of the difficulties of studying the geological and tectonic setting of the Nahanni region has been lack of comprehensive geological and geophysical data, perhaps due to remote isolation and logistic difficulties in accessing the study area. In this study an attempt was made to utilize various remote sensing techniques, including the data sets such as CCRS's airborne C- and X-band SAR data and available satellite (Landsat, SPOT, ERS-1, JERS-1, ERS-2, RADARSAT) data for investigation and imaging of the tectonic features. Detailed investigation of the surface structural features of each individual and the final integrated composite images over the epicentral area indicates that there are several new structural features intersecting the major northwest trending Iverson thrust fault and accompanying structures in the vicinity of the earthquake epicentral region. The NW-SE trending structural thrust faults and associated features have been mapped previously but the new N-S trending faults and several NEE-SWW (approximate strike) trending structures (faults) have not been identified before. The single event P-nodal solution plots for the aftershocks M 5.0 and larger (Horner et al., 1989) also confirm the new structures as well as the previously mapped regional features in the Nahanni area. Strikes of the primary and auxiliary fault planes estimated from these large main and aftershocks convincingly outline the structural trends parallel to the Iverson thrust fault. Similarly a newly mapped E-W trending fault intersects the Iverson thrust fault and appears to interact each other. Present results require further detailed ground truthing.

**JSS31/L/03-B3** Poster **0830-16**

**INVESTIGATION OF TECTONIC DEFORMATION ALONG CYPREAN ARC**

Coskun Demir, Ali Turkezzer, General Command of Mapping, Cebeci, 06100 Ankara, Turkey, email: cdemir@hgk.mil.tr

Crustal deformation in the eastern Mediterranean is mainly caused by the northerly motion of the African and Arabian plates relative to Eurasia plate. One of the most important tectonic features in the region is the subduction of the African plate beneath the Eurasia and Anatolian plates along Hellenic and Cyprean arc. Although the tectonic deformation along Hellenic arc is well understood, we have yet no much detailed information about Cyprean arc. In this paper, we have analyzed terrestrial and GPS observations to resolve tectonic deformation along Cyprean arc. The first order network of Turkish Republic of Northern Cyprus of 21 points extending 35 km in N-S direction and 135 km in the E-W direction is situated along the eastern part of the Cyprean arc. A triangulation-trilateration survey was performed in the network in 1987. All the network points, except destroyed one in the northwest, were re-occupied with GPS in 1998. GPS coordinates are determined in the ITRF94 using high precision IGS products

following fiducial network strategy. The triangulation-trilateration network is re-adjusted independently in the various datums defined by holding coordinates of two points fixed in the ITRF94. The adjustment of the terrestrial network results in the precision varying from 2 cm to 4 cm in the investigated area. Then, the comparison of both terrestrial and GPS results spanning 11 years is performed to estimate the horizontal velocity field. Our findings reveals no significant relative motion of the southern part of the network with respect to the northern part.

**JSS31/L/04-B2** Poster **0830-17**

**PLATE MOTIONS AND INTRA-PLATE DEFORMATIONS IN TURKEY FROM 1992-1998 FROM GPS MEASUREMENTS**

MEHMET EMIN AYHAN, Coskun Demir, Muzaffer Kahveci, Ali Kilicoglu, Mustafa Kurt, Onur Lenk, Mustafa Ocak and Ali T (General Command of Mapping (GCM), TR-06100, Ankara, Turkey) Aykut Barka (Istanbul Technical University (ITU), Istanbul, Turkey) Robert Reilinger and Nafi Toksoz (Massachusetts Institute of Technology (MIT), ERL, USA) Hermann Seeger and Y Altiner (Bundesamt f\_r Kartographie und Geodesie (BKG), Frankfurt am Main, Germany).

Turkey is located in the Alpine-Himalayan collision zone, and is characterized by active and complex tectonic deformation. As a result of northward motion of the African and Arabian plates relative to the Eurasian plate, the Anatolian block (bounded by the North Anatolian Fault Zone (NAFZ) on the north, the African plate on the south, the Aegean region on the west, and the East Anatolian Fault Zone (EAFZ) on the east), moves westward. Simultaneously, the Aegean region is being extended in a north-south direction. Hence, Turkey is caught in a complex zone of interaction between various tectonic regimes, including collision, extension, lateral plate extrusion, and other intra-plate and plate boundary deformations. In order to quantify the present-day deformation field, we began GPS measurements for geodynamic studies in Turkey in 1988.

However, satellite orbits and earth rotation parameters accurate enough for determining plate motions have been computed and released to the research community only since 1992. Currently we have 17 GPS campaigns performed from 1992 to 1998. The GPS campaigns included in this study are; 1992, 1994, 1996, 1998 surveys performed throughout Turkey jointly by MIT/GCM/ITU, 1992, 1994, 1996 campaigns conducted as a joint project by the Federal Institute of Technology Zurich(ETHZ)/GCM/ITU in the Marmara Sea region, 1992, 1993, 1995, 1997 surveys along the west end of the NAFZ, and 1992, 1993, 1994, 1997 observations in the Aegean region of western Turkey carried out in collaboration with BKG. We also include in our analysis GPS measurements at tide gauge stations on the Turkish coast and in the European Unified GPS Vertical Network(EUVN) Turkey sub-network performed by GCM in 1995 and 1997 respectively, as well as observations from the 1998 GPS surveys of the Turkish National Fundamental GPS Network. All GPS data were reprocessed by GCM using IGS products and BERNESE V4.0 software following the same processing strategy. The results of all GPS campaigns are combined individually using both BERNESE V4.0/ADDNEQ and GAMIT/GLOBK software to obtain the velocity field in Turkey. We compute site velocities in the ITRF96 reference frame by fixing the velocities of Onsala, Matera, and Wettzell located on the western part of Eurasia, and also estimate velocities relative to Eurasia. The velocity field relative to Eurasia reveals...

**JSM32** Tuesday 27 – Wednesday 28 July

**SMALL-SCALE AND LAYERED PHENOMENA AROUND THE SUMMER MESOPAUSE (IAMAS, IAGA)**

Location: Chemical Engineering, LR112

Tuesday 27 July AM

Presiding Chair: F.-J. Luebken (Physikalisches Institut, Univ. of Bonn, Germany)

**JSM32/W/05-B2** Invited **0930**

**REVIEW OF NLC MEASUREMENTS BY LIDAR**

Jeffrey P. THAYER (SRI International, 333 Ravenswood Avenue, Menlo Park, CA, 94025, USA, Email: thayer@sri.com); Ulf von Zahn and Goertz von Cossart (both at Leibniz-Institute of Atmospheric Physics, D-18225 Kuehlungsborn, Germany, email: vonzahn@iap-kborn.de, vcossart@iap-kborn.de)

Over the past decade high latitude lidar systems have contributed to the study of noctilucent clouds (NLCs) by providing direct measurements of basic cloud properties and their temporal evolution. Since the first definitive lidar detection of a noctilucent cloud by Hansen and von Zahn in 1989, new lidar systems with enhanced capabilities for NLC measurements have been deployed in the arctic. The enhancements made by most of these lidar systems have come in the form of simply increased laser power and increased telescope aperture. These improvements have enabled measurements of NLC characteristics (i.e. height, thickness and backscatter strength) at high temporal and spatial resolution (10's of meters within 10's of seconds) over a range of local times. The Sondrestrom lidar facility in Greenland has, for example, made NLC measurements of this type for the past four summer periods. One facility, the ALOMAR facility in northern Norway, has made the most significant advancements by providing a high power and large aperture lidar system while detecting NLCs at all local times and at three different wavelengths. The multiwavelength measurements allow for the NLC particle size distributions to be derived. The daytime capability permit studies concerned with local time variations in the NLC characteristics. Presently, the ALOMAR facility, followed by the Sondrestrom lidar facility in Greenland, has the most extensive database of NLC detections by lidar systems. Interestingly, these two stations show statistically very different behavior in NLC characteristics. In this presentation, we will review the contributions made by lidar to NLC studies as well as highlight new results and future plans.

**JSM 32/E/04-B2** Invited **1005**

**CURRENT STATUS OF PMC/PMSE OBSERVATIONS**

W. SINGER (Leibniz-Institut fuer Atmosphaerenphysik an der Universitaet Rostock, D-18225 Kuehlungsborn, Germany)

Intensive studies in recent years have shown that the occurrence and morphology of layered structures, such as polar mesosphere summer echoes (PMSE) observed by radars and noctilucent clouds (NLC) observed by optical instruments, are tightly coupled to the thermal and dynamical structure of the mesopause region. PMSE appear in the high latitude summer mesopause region with a large occurrence rate and have been studied at an increasing number of locations. We will briefly address the various radar experiments with special emphasis on new methods. We will review the development of knowledge on PMSE (e.g. connection of PMSE occurrence with seasonal temperature changes and with tidal wind components, correlation between PMSE and NLC).



**JSM32/W/12-B2** Invited **1100**

**ROCKET BORNE MEASUREMENTS OF SMALL SCALE FLUCTUATIONS OF PLASMA, NEUTRAL, AND AEROSOL DENSITIES**

Dr. Tom Arild Blix

The paper will review in situ measurements of plasma, neutral and aerosol densities in the upper mesosphere during Noctilucent Cloud (NLC) and Polar Mesosphere Summer Echoes (PMSE) conditions. Both small-scale (1-10 m) fluctuations and larger scale (100 m - 1 km) variations will be treated. Of special interest is the small-scale variations observed when passing through the PMSE layers. We will discuss possible mechanisms responsible for the observed fluctuations, such as neutral air turbulence and plasma instabilities. We will also discuss the importance of aerosols (1 nm) for the charge balance in the region of NLC and PMSE, and possible size distributions of these particles depending upon the actual temperature and water vapour content at these heights.

**JSM32/W/06-B2** Invited **1135**

**TURBULENCE AND MIXING DUE TO KELVIN-HELMHOLTZ INSTABILITY: IMPLICATIONS FOR LAYERING AND ATMOSPHERIC STRUCTURE**

David C. FRITTS, Joseph A. Werne (Colorado Research Associates, 3380 Mitchell Lane, Boulder, CO 80301, USA)

Numerical simulations of Kelvin-Helmholtz (KH) instabilities have recently described, for the first time, both the transition to turbulence and the dynamics and mixing occurring within the turbulent flow. The morphology of KH billows includes the initial 2D billow roll-up, transition to 3D through the formation of isolated, streamwise-aligned convective rolls, expansion of 3D structures and turbulence throughout the billow cores, homogenization of turbulence horizontally, and restratification of the shear flow as turbulence energy decays. This talk will provide an overview of the dynamics of KH breakdown and turbulence generation, with emphasis on the implications for mixing, formation of layered structures, observations, and inferred dynamics.

**JSM32/W/02-B2** Invited **1210**

**ELECTRIC FIELD STRUCTURE IN THE VICINITY OF NOCTILUCENT CLOUDS AND PMSE**

Alexander M. ZADOROZHNY (Novosibirsk State University, Pirogova 2, Novosibirsk 630090, Russia, email: zadorozh@phys.nsu.ru)

During NLC-91 campaign, disturbances of rocket electric field mill signal of more than 1 V/m were detected at 82.5-84.5 km. The region of the large fields was clearly limited by the noctilucent clouds on the bottom and by the PMSE layer on the top. Both rocket data and laboratory results of a post-flight examination of the field mill probe showed that the perturbations in the field mill signal are caused not only by atmospheric electric fields but also by the impact of solid particles. Simultaneous analysis of the rocket and laboratory data allowed us to estimate sizes of the particles in the PMSE layer to be 13-40 nm and the vertical electric fields at 84 km to be  $-0.9$  V/m. The height correlation of the observed electric field disturbance with the NLC and PMSE positions indicates the importance of the aerosol particles in the generation of the vertical electric fields. A simple gravitational falling of charged aerosol particles could not explain the V/m fields. The main obstacle for the forming of the large fields is a high conductivity of the atmosphere. To explain the V/m fields, we assume the simultaneous existence in the mesosphere both the negative and positive multiply charged aerosol particles. Cho et al. (1992) showed that a presence of charged aerosol in the mesospheric plasma leads to a drastic decrease of effective electron diffusivity when somewhat more than half of the charge is tied up in aerosols. The effective ion diffusivity will be obviously decreased under the same conditions, too. As a result, a large enough charge carried by the particles can reduce effective conductivity of the atmosphere significantly and make it possible of existence of V/m electric fields. The proposed model can explain the existence of the vertical fields observed in the NLC/PMSE vicinity if particles with radius of about 20-25 nm carry 2-4 unit charges.

**Tuesday 27 July PM**

Presiding Chair: T. Blix (Norwegian Def. Res. Establ, Kjeller, Norway)

**JSM32/W/11-B2** Invited **1400**

**THE RELATIONSHIP OF ICE SATURATION AND POLAR MESOSPHERIC CLOUDS**

Gary E. THOMAS (Laboratory for Atmospheric and Space Physics, University of Colorado, CB 392, Boulder, CO 80309, USA, Email: thomas@alcor.colorado.edu)

Polar Mesospheric Clouds (PMC) are thought to be ice crystals which form in the saturated environment of the polar summertime mesopause. The climatology of PMC should therefore be governed by the seasonal cycles of mesospheric temperature and water vapor. This paper examines the latitudinal, seasonal and height dependence of the ice existence region (IER), as determined by satellite measurements of temperature and water vapor, and relates this region to the occurrence statistics of PMC, as observed by UV scattering measurements from the Solar Mesospheric Explorer satellite. In a similar way, the seasonal dependence of a related phenomenon, Polar Mesospheric Summertime Echoes (PMSE) is also related to the IER. PMSE are layers of high radar reflectance observed near the mesopause from fixed ground locations. In general both PMC and PMSE are confined within the IER, but there is a seasonal asymmetry in terms of the beginning and ending dates. There is a curious difference between the beginning of saturation and the onset of PMC and PMSE, and between the end of saturation and the disappearance of PMC/PMSE. Local time dependence of the IER, and its seasonal changes, may be a key factor in the explanation of the asymmetry. Falling-sphere measurements of density (and inferred temperature) at fixed local times, and satellite measurements made at various local times, may be combined to yield information on local time variability of the IER. These empirical relationships will be used in testing the "standard" growth-sedimentation model of PMC.

**JSM32/W/03-B2** **1435**

**PLANETARY WAVE MODULATION OF PMSE AND NLC**

S. KIRKWOOD, A. Réchou, K. Stebel (Swedish Institute of Space Physics, MIR Atmospheric Research Program, Box 812, Kiruna, S-981 28 SWEDEN, e-mail: sheila.kirkwood@irf.se)

PMSE occurrence measured by the ESRAD radar during 3 summer seasons are show significant variation with 4-6 day periodicities. Planetary waves in the same frequency band are extracted from UKMO assimilated analyses (up to 60 km altitude) and compared with the PMSE variations. Good correlation is found for the upper PMSE altitudes, and it is suggested

that the temperature modulation associated with the planetary waves is sufficient to modify the nucleation of aerosols. The possible correlation between noctilucent cloud occurrence and planetary wave activity is also studied, using the observations from the Scottish network and UKMO global meteorological analyses from 1979 - 1999.

**JSM32/E/02-B2** **1500**

**ON THE DIURNAL VARIATION OF POLAR MESOSPHERE SUMMER ECHOES**

J. KLOSTERMEYER (Max-Planck-Institut fuer Aeronomie, 37191 Katlenburg-Lindau, Germany, email: jkloste@gwdg.de)

Observations of polar mesosphere summer echoes yield diurnal variations of the occurrence frequency and the signal-to-noise ratio (SNR) that are characterized by a pronounced maximum and a pronounced minimum near 14 and 20 LT, respectively. A weaker maximum and a weaker minimum may occur between 00 and 10 LT. Several authors suggested a dominant influence of diurnal and semidiurnal tidal wind or temperature variations but excluded any significant effects of the sun's zenith distance and of energetic particle precipitation. A partial regression analysis of published SNR data measured by the ALOMAR-SOUSY radar during July and August 1994 shows on the contrary that SNR is strongly correlated with both the cosine of the sun's zenith distance and the square of the cosmic noise absorption. These results indicate that SNR varies with the square of the electron concentration, in agreement with theoretical predictions. In addition, a negative correlation between SNR and tidal temperature variations is found confirming earlier suggestions and theoretical considerations. After elimination of these effects, the residual time series has an almost white spectrum indicating that other mechanisms had no significant influence on the observed diurnal variation.

**JSM32/W/01-B2** **1600**

**MODELLING OF PARTICLE CHARGING: FINGERPRINTS OF NLC AND PMSE PARTICLES IN THE AMBIENT PLASMA**

M. Rapp, F.-J. LUEBKEN (Physikalisches Institut der Universitaet Bonn, Nussallee 12, D-53115 Bonn, Germany, email: luebken@physik.uni-bonn.de)

Aerosol particles in the polar summer mesosphere which are believed to cause noctilucent clouds (NLC) and polar mesosphere summer echoes (PMSE) lead to a characteristic fingerprint in the height profiles of the ambient electron and positive ion densities mainly as a result of plasma diffusion. Microphysical modelling of aerosol charging shows that specific signatures are expected in the plasma which have indeed been observed in various rocket borne measurements of electron and ion density profiles in the polar summer mesopause region since the late 1960's. We will discuss different scenarios leading to these signatures in terms of the aerosol abundance and composition, as well as the ionization rate and the recombination coefficient. In addition to the frequently observed "bite-out" in the plasma profiles we found that an enhancement of both positive ions and electrons can occur, in agreement with observations. We find a nice agreement of measured and modelled Schmidt numbers in the electron bite-out situation. Special attention will be given to the case of an electron density enhancement which, according to our current understanding, can be caused only by photoemission on the aerosol particles.

**JSM32/W/04-B2** **1625**

**THE ROLE OF METALLIC SPECIES IN THE NUCLEATION OF NOCTILUCENT CLOUDS**

John PLANE (School of Environmental Sciences, University of East Anglia, Norwich NR4 7TJ, UK, email: j.plane@uea.ac.uk)

Two theories have been proposed to provide the source of condensation nuclei for the formation of noctilucent clouds in the high latitude summer mesosphere: ions (either metallic or proton hydrate) and meteoric "smoke". There are difficulties with both theories, such as the presence of sufficient densities of ions below 90 km, and the precise nature and mechanism for the formation of the smoke. This paper will present an alternative theory that combines some elements of the previous two. Meteoric ablation gives rise to the atomic Na layer at 90 km, and we know from a combination of work in our laboratory and atmospheric modelling that the major reservoir for the metal between 80 and 87 km is sodium bicarbonate (NaHCO<sub>3</sub>), with a density in excess of 1e4 cm<sup>-3</sup>. We have recently carried out new high level quantum calculations on this molecule. These show that the molecule is ionised with a substantial dipole moment, and that NaHCO<sub>3</sub> forms very stable complexes with a sequence of H<sub>2</sub>O molecules. Under mesospheric conditions, formation of these clusters will be activated in a narrow temperature range below about 150 K. This feature, together with the estimated number density of NaHCO<sub>3</sub>, makes the molecule (and possibly other metallic compounds with very large dipole moments such as MgCO<sub>3</sub>) attractive candidates as condensation nuclei for NLC.

**JSM32/C/GA2.16/P/1** **1650**

**POLAR MESOSPHERIC CLOUDS SEEN FROM GEOSTATIONARY ORBIT**

M. GADSEN

When the sun is at a declination greater than 9 degrees North or less than 9 degrees South, a geostationary meteorological satellite is in full sunshine at midnight but the Sun is outside the field of view of the radiometer. (The corresponding dates are 13 April-28 August and 19 October-24 February). At this time, forward-scattered sunlight is seen in the atmosphere at high latitudes.

These satellite images allow PMC's to be detected. There are, implicitly, some 20 years of these data available in the geostationary satellite archives, data which refer alternately to the northern and the southern mesospheres. Results of a first-look at this data resource are presented and discussed.

**Wednesday 28 July AM**

Presiding Chair: G. Thomas (Univ. of Colorado, Boulder, USA)

**JSM32/E/03-B3** Invited **0930**

**ON THE INTERHEMISPHERIC DIFFERENCES OF PMSE**

Ben B. BALSLEY (CIRES, Campus Box 216, University of Colorado, Boulder, CO 80309, USA, email: balsley@terra.colorado.edu); Ronald Woodman (Instituto Geofisico del Peru, Apartado 13-0207, Lima 13, Peru, email: ron@geo.igp.gob.pe); Mercedes Huaman (372 Rhodes Hall, Cornell University, Ithaca, NY 14853, email: huaman@ee.cornell.edu)



## INTER-ASSOCIATION

VHF radar observations of PMSE made at Peru's Machu Picchu Radar Facility on King George Island, Antarctica show a marked difference to similar observations made at comparable latitudes in the Northern hemisphere. Basically, PMSE in the Southern hemisphere are between 33-40 dB (i.e. a factor of 2000-10000) weaker than their northern counterparts. This observation is based on some three years of data at Machu Picchu and even more extensive measurements in the Northern hemisphere. The most likely reason for the difference is that summertime high-latitude mesospheric temperatures are somewhat warmer in the southern hemisphere, a possibility that is borne out by a variety of satellite observations and models. The rationale for these warmer temperatures begins with weaker gravity wave activity in the Southern hemisphere that results in reduced mesospheric meridional and vertical winds and a concomitant reduction in near-mesopause cooling. A warmer southern-hemispheric mesosphere is less hospitable to the production of ice particles and the associated phenomena of Polar Mesospheric Clouds (PMC) and PMSE. We will outline a series of recent studies obtained from a variety of observing platforms (satellites, VHF radars, MF radars) that support these ideas.

**JSM32/W/08-B3** Invited **1005**

### SMALL SCALE LAYERS AND TRENDS IN THE MESOSPHERE

F.-J. Luebken (Physikalisches Institut der Universitaet Bonn, Nussallee 12, D-53115 Bonn, Germany)

The occurrence of small scale layered phenomena such as noctilucent clouds (NLC) and polar mesosphere summer echoes (PMSE) in the high latitude summer mesosphere is related to various geophysical parameters, such as temperature, water vapour, and condensation nuclei. The question which one of these parameters is of prime importance is investigated by studying the variations of these phenomena on seasonal and decadal time scales. Recent results from ground based, insitu, and satellite observations suggest that temperature is the prime parameter controlling the morphology of these layers, whereas e.g. water vapour and condensation nuclei are of secondary importance. The experimental evidence for a temperature trend in the mesosphere and its potential impact on the occurrence frequency of NLCs and PMSEs will be critically reviewed in this paper. New experimental results from various techniques will be presented.

**JSM32/W/07-B3** **1100**

### DISTRIBUTIONS OF POLAR MESOSPHERIC CLOUDS OBSERVED BY A MIDDLE ULTRAVIOLET IMAGER

D. MORRISON, J. F. Carbary, G. J. Romick, L. J. Paxton, C.-I. Meng (Johns Hopkins University, Applied Physics Laboratory, 11100 Johns Hopkins Rd., Laurel, MD 20723, USA, email: daniel.morrison@jhuapl.edu)

We report on analysis of images of polar mesospheric clouds (PMC) observed in the middle ultraviolet (235-263 nm). The images were obtained from the UVISI (Ultraviolet and Visible Imaging and Spectrographic Imaging) instrument on the MSX (Midcourse Space Experiment) satellite and cover both the northern and southern polar regions during the arctic summer of 1997 and austral summer of 1997-1998. The imager look-point made multiple trans-polar passes over the Arctic and Antarctic and obtained over 500 images of PMCs at latitudes poleward of 80°. The unprecedented accuracy and stability of the satellite platform (~10 µrad) conferred advantages for investigating both the large-scale (>100 km) and small scale (~1 km) spatial structures of PMCs. The UV imager clearly observed PMCs distinct from the atmospheric backgrounds. Poleward of 70°, the clouds existed in discrete, filamentary structures at altitudes between 80 and 85 km, although most of PMCs appeared at altitudes between 82.5 and 83.0 km. Within these ranges, cloud altitudes were essentially random on a trans-polar scale of ~1000 km. In some instances, the clouds did cluster at common altitudes for distance scales of ~100 km across the polar mesosphere. The PMC altitudes do not appear correlated with latitude or local time on the scale of the observations discussed here. A diffuse signal above the clouds was readily observed in many cases. For some cases comparisons with a co-aligned visible imager will be presented. Analysis of the two dimensional structure of the PMCs in latitude and longitude will be also be presented.

**JSM32/L/01-B3** **1125**

### OBSERVATION OF A NOCTILUCENT CLOUD AT DAVIS, ANTARCTICA IN FEBRUARY 1998

W.J.R. FRENCH (1), G.B. Burns (1), P.A. Greet (1), D.J. Murphy (1), K.J. Quinnell (2) (1: Australian Antarctic Division, Channel Highway, Kingston, Tas. 7050, Australia; 2: Bureau of Meteorology, G.P.O. Box 727G, Hobart Tas 7001, Australia)

This paper reports observation of a Noctilucent Cloud (NLC) from Davis Station, Antarctica (68 35'S; 77 58'E) on 18-FEB-1998, first observed at 1850UT and photographed until it dispersed at 2000UT. These photographs are analysed to determine the cloud's position and extent, and the wavelength, orientation and motion of the wave structures observed. The observation was accompanied by rotational temperature measurements of the OH(6-2) band using a Czerny Turner scanning spectrometer. The OH emission is centered at about 87km altitude, slightly above the typical height of cloud formation. Analysis of these results yields average temperatures considerably lower on the night of the cloud observation than the 7 days prior to and post the event. A dual channel Fabry-Perot spectrometer was also operating, measuring winds and temperatures from OH(6-2) Q1(1) and the Oxygen 558nm emission. Analysis and results of these temperature measurements is also discussed. In addition, data from a 2 MHz MFSa radar, co-located at Davis, is examined for evidence of PMSE's and the meteorological balloon flights surrounding the observation are examined for evidence of stratospheric warming.

**JWS33**

**Tuesday 27 – Wednesday 28 July**

### NEW APPROACHES TO DATA COLLECTION, DATA PROCESSING AND DATA DISSEMINATION (IASPEI, IAGA, IAHS, IAG, IAPSO, SCOSTEP)

Location: Medical School EG12 LT4

Location of Posters: Arthur Thompson Hall

**Tuesday 27 July AM**

Presiding Chair: D C Herzog (US Geological Survey, Denver Federal Center, Denver, USA)

**JWS33/W/29-B2**

**0930**

### THE VIRTUAL WORLD DATA CENTER SYSTEM.

Yu.TYUPKIN (Geophysical Center, Joint Institute of Physics of the Earth, Molodezhnaya 3, Moscow 117296, Russia, email: tyupkin@wdcb.rssi.ru)

The World Data Center system (WDC system) was established in 1957 to serve the International Geophysical Year (IGY) program. Two complex centers were established by USA (WDC A) and USSR (WDC B). These centers realized functions of data acquisition, storage and distribution of most IGY disciplines. In many disciplines there was a special centers known as WDC C1 if in Western Europe and WDC C2 if in Asia or Australia in addition to complex centers. Multiple centers were deemed advisable to guard against catastrophic loss of data, and for the convenience of data providers and users. Because of its success, the WDC system was made permanent and used for post IGY data. Today the WDC system is healthy and available. But new technology of data storage, data access and data processing require new approach to realization of main functions of the WDC system. The conception of Virtual World Data System (VWDCS) is discussed. VWDCS is a distributed automated system on the INTERNET basis. The VWDCS resource is built up by various systematized and reliable information on geosciences that can be reached through Internet and has the main WWW page with the fields filled according to the VWDCS standard. The VWDCS management system must realized functions: 1. The procedure of presentation of a new information resource by the author. 2. The access to Internet informational resources not included in VWDCS. 3. Automatic revision of the informational resources of the VWDCS network. 4. The specific features of work in countries with limited access to Internet. The now existing WDCs should carry out at least three functions in the frame of the VWDC System: - Long-term storage of information. - Provision of means for maintaining control over the quality of information available in VWDCS. - 3. Maintenance and co-ordination of connections with new informational resources on national (WDC A, WDC B, WDC D) and regional (WDC C) levels.

**JWS33/W/10-B2**

**0945**

### WEB EFFECTS: FRONTIERS IN INFORMATION DELIVERY

Allen M. HITTELMAN and Susan J. McLean (NOAA's National Geophysical Data Center, World Data Center for Solid Earth Geophysics, 325 Broadway, Boulder, CO 80303, U. S. A., email: ahittelman@ngdc.noaa.gov)

Without question, one of the most profound impacts on information technology is the advent of the Web. In just a few years, this media has drastically altered our perceptions of information services and created new paradigms for data dissemination. To cope with this unprecedented explosion of change, many of us in the information service business had to re-evaluate organizational goals and objectives. Where once we felt comfortable with our awareness of user needs, now we fell distant due to the impersonal nature of our Web sites (which seem to serve 99% of our scientific clientele's needs).

The National Geophysical Data Center, and its several supported World Data Centers, has pioneered many new innovative methods that enrich data and information delivery on the Web. Examples of these techniques include: the interactive creation of graphical spreadsheets (see <http://swat.ngdc.noaa.gov/cgi-bin/wist/wist.pl>), the satellite browse, display and download features of the Space Physics Interactive Data Resource (SPIDR, see <http://julius.ngdc.noaa.gov:8080/>) and access to gridded relief models (see <http://www.ngdc.noaa.gov/seg/topo/globe.shtml>). Newer techniques are empowering users with the ability to access data and meta-data through GIS-enabled Web servers. We have also explored data mining tools to provide improved understandings of the needs of our Web users -- from where do they come and for what do they search?

**JWS33/W/11-B2**

**1000**

### NEW DIRECTIONS IN NASA EARTH SCIENCE ENTERPRISE DATA MANAGEMENT: PLANS FOR A NEW DATA INFORMATION SYSTEMS AND SERVICES APPROACH (NEW DISS)

Ronald L. S. WEAVER, (National Snow and Ice Data Center, CIRES, Campus Box 449, University of Colorado Boulder, Colorado, 80309)

The NEW DISS effort of the NASA Earth Sciences Enterprise (ESE) has now completed its preliminary report on how to implement data management within the agency in the coming 5-7 year timeframe. The key elements of this plan include more investigator involvement in data management and emphasis on more de-centralized data management services. Design concepts include a modular approach to data system functional elements. The report recognizes the need for distributed, flexible, yet responsive systems and ESE's need to have smaller, more manageable components.

The purpose of this paper is to provide an update on the NEW DISS study team's progress, and to report on the probable course of NASA ESE data management. The author will provide a perspective on these activities based on his involvement as a member of the NEW DISS study Core Team and as an EOSDIS Distributed Active Archive Center (DAAC) Manager.

**JWS33/W/15-B2**

**1015**

### OPEN DISTRIBUTION OF LIVE SEISMIC DATA VIA THE INTERNET

Robert WOODWARD (United States Geological Survey, Albuquerque Seismological Laboratory, Bldg. 10002, Kirtland AFB-E, Albuquerque, NM 87115-5000, USA, e-mail: woodward@asl.cr.usgs.gov)

We have developed a mechanism for the open distribution of digital seismic data, in near-real-time, via the Internet. The seismic data are collected by stations of the Global Seismographic Network at sites on every continent. Data from these seismographic stations are used for a variety of purposes, such as earthquake reporting, tsunami warning, and nuclear monitoring.

The data distribution mechanism, which we call the Live Internet Seismic Server (LISS), is modeled on the concept of a webserver. The LISS accepts a virtually unlimited number of simultaneous client connections via the Internet. Each client simply stays connected to the LISS and receives copies of the digital seismic waveform data which the server is receiving from the seismographic stations. Thus, clients are connecting to the LISS to receive seismic data much like clients connect to a webserver to receive text or images. Latency of data obtained from the LISS is typically less than 30 seconds.

LISS's can be run in a chain, such that one LISS is a client to another LISS. In this way LISS's can be placed at different locations on the Internet to provide redundant paths for accessing the data. At present, auxiliary LISS's are running in Moscow and Beijing and these are forwarding data to the primary LISS at United States Geological Survey's Albuquerque Seismological Laboratory. Data from 30 stations around the world are presently available via the LISS. In addition to distributing these data, the most recent 24 hours of data from each station are plotted in a manner resembling the popular drum style (helicopter) recording mechanism which is widely familiar to the public. These plots are updated every thirty minutes and are accessible via the WWW. These data plots, as well as more information on the LISS, can be obtained via the WWW at the URL: [http://aslwww.cr.usgs.gov/Seismic\\_Data/liss.htm](http://aslwww.cr.usgs.gov/Seismic_Data/liss.htm).

JWS33/W/06-B2

1045

## BASIC PACIFIC TSUNAMI CATALOG AND DATABASE, 47 B.C. - 1998 A.D

V.K.GUSIAKOV (Institute of Computational Mathematics and Mathematical Geophysics, Siberian Division, Russian Academy of Sciences, Novosibirsk 630090, Russia, Email: [gvk@omzg.sssc.ru](mailto:gvk@omzg.sssc.ru))

A compilation of parametric tsunami data for tsunamigenic events occurred in the Pacific from 47 B.C. to 1998 has been made within the joint IUGG Tsunami Commission and ICG/ITSU Project "Basic Pacific Tsunami Catalog and Database". The project is directed to improve the situation with catalogization of historical tsunamis in the Pacific by means of organising them in the form of the database containing all the meaningful historical tsunami data along with additional reference information related to the tsunami problem. Its final goal is the development of the multimedia CDROM "Tsunamis in the Pacific, 47 B.C. - 2000 A.D.". The initial data collection has been made within the relational DBMS dBASE that has been established and being maintained at the Tsunami Laboratory of the Institute of Computational Mathematics and Mathematical Geophysics of SD RAS. A special graphic shell (the GIS-type mapping subsystem) has been developed for easy data manipulation, visualisation and handling. The condensed version of the database (the catalog of the Pacific tsunamigenic events) has been created on the basis of the MS SQL Server 6.5 and available on the following Web site: <http://tsun.sssc.ru/htdbpac/>. This site contains the most comprehensive and constantly updated list of historical tsunamigenic events in the Pacific with their basic source parameters. A set of parameters includes date, time, coordinates of the epicenter, source depth, surface-wave and moment-magnitudes, Abe's tsunami magnitude, tsunami intensity on the SolovievImamura scale, the maximum tsunami run-up height, the number of available run-up observations, cause of the tsunami, validity of the event, coded name of the source region and the main reference to the event. The full version of the database (including the catalog of historical run-up observations with geographical co-ordinates of sites) provided with the Windows-based graphic shell and geographic mapping subsystem is distributed on a CD-ROM. The example of the CD-ROM content can be found at the following URL: [http://omzg.sssc.ru/tsulab/htdb\\_f.html](http://omzg.sssc.ru/tsulab/htdb_f.html).

JWS33/W/13-B2

Invited

1100

## DATA COLLECTION, DATA PROCESSING AND DATA DISSEMINATION IN THE RUSSIAN VIRTUAL GEONETWORK

Pavel PLETCHOV (Geological department, Moscow State University, Moscow, Russia E-mail: [lym@ccas.ru](mailto:lym@ccas.ru)); Eugene Kozlov (Computational Mathematics and Cybernetics department, Moscow State University, Moscow, Russia E-mail: [james@geo.web.ru](mailto:james@geo.web.ru))

RVGN - (Russian Virtual GeoNetwork) is distributed automated system, which ensure systematization, examination and periodic checks of an information on geosciences in a Russian part of Internet. The main server of the RVGN is available by URL: <http://geo.web.ru/>. RVGN is oriented to WWW (HTTP) access to each resource. The RVGN provides automatic checking of the current state of information resources of the net and a system of automatic distribution of information communications. A special robot regularly analyses the content of all informational RVGN resources, and if any changes are revealed made by the authors of the resource, or if a new information resource appears, the robot updates the corresponding information in the central RVGN database. The system automatically formulates communications about the detected changes, from key words draws the distribution list of information to interested users of the net, and transmits communications by the E-mail. RVGN includes a Link Manager program, which support dynamic lists of links. It's like thematic bookmarks or Internet directories, but all RVGN lists of links are constantly updated and automatically checked. Each RVGN expert can support own classification system and edit his classification via ClassEditor. ClassEditor allows create, delete classes and change class attributes. This system support enclosed sections of classification by parent class attribute. If a parent class is HTML file, content of this class will be written to this file. Otherwise, this class is a subsection of a parent class. As a result, dynamic lists of RVGN virtual layer are created daily. RVGN consists of a lot of the connected among themselves programs and user interfaces, which will be discussed in the presentation.

JWS33/E/09-B2

Invited

1115

## AN APPROACH TO ON-LINE INTELLIGENT GEODATA ANALYSIS

V. GITIS, B. Osher, A. Dovgiallo (Institute for Information Transmission Problems, RAS, Moscow, Russia, email: [gitis@ippi.ras.ru](mailto:gitis@ippi.ras.ru)); T. Gergely (Applied Logic Laboratory, Budapest, Hungary, email: [gergely@all.hu](mailto:gergely@all.hu))

An approach to creation of information technology for on-line intelligent geo-information modelling and complex analysis of space-time properties of geological environment is suggested. The technology supports two types of users' queries: (a) Getting knowledge about geological properties of a region; (b) Investigation of properties and solving practical problems of geological and geophysical forecasting. The client part of the system prototype is realised in Java 1.1 and is accessible on address <http://www.iitp.ru/projects/geo> and <http://ta-www.jrc.it/gitis/geoprocessor.html>. Applet supports the following functions of space-time data processing and analysis: (i) Cartographic data representation (map composition, sizes and scale changing, reading a map values, visualisation of crosssections, compiling the maps of similarity with precedents); (ii) Data transformation: (shadow modelling, algebraic and logical raster operations, filtration, learning and testing sample sets formation); (iii) Plausible reasoning of forecast maps: (method of similarity, method of membership function, method of nonparametric regression). The work is partially supported by the project ASPELEA granted by EU Inco-Copernicus Project contract # ERBIC 15CT970200 and by Russian Foundation on Scientific Research, project # 97-07-90326.

JWS33/W/16-B2

1130

## HIGH LEVEL SEARCH TOOLS FOR SPACE PHYSICS DATABASES

Mike HAPGOOD (CLRC Rutherford Appleton Laboratory, Chilton, Didcot, Oxfordshire, OX11 0QX, UK, Email: [M.Hapgood@rl.ac.uk](mailto:M.Hapgood@rl.ac.uk)); Chris Harvey (Centre d'Etude Spatiale des Rayonnements, 9 avenue du Colonel Roche, BP 4346, 31028 Toulouse Cedex 4, FRANCE, Email: [Christopher.Harvey@cesr.fr](mailto:Christopher.Harvey@cesr.fr)); Jim Thieman (National Space Science Data Center, Code 633, NASA/Goddard Space Flight Center, Greenbelt, MD 20771, USA, Email: [thieman@nssdc.gsfc.nasa.gov](mailto:thieman@nssdc.gsfc.nasa.gov))

As the number of space physics data-sets increases internationally it becomes increasingly important to have a method to find and retrieve data of interest wherever they are located on the network. One important method is the use existing web search engines such as AltaVista. This method is suitable for finding data made available by individual scientists and small groups. It requires only that the data are made available via a web page that is well-indexed using search keywords that are intuitive to the user. This method is likely, however, to give a large number of extraneous results as well. Another method, more suited for searching the larger data centres, is the use of a specialised search protocol limited to searching pre-selected sites. This protocol should also support searching for particular types of data recorded at a particular location or during a given time period. A similar protocol is already in use in searches for astrophysics data and includes support for searches over multiple sites. This protocol can be extended to allow simultaneous for overlapping data in selected time intervals or for particular locations. In this paper we discuss and assess the different search methods and describe efforts now underway to implement these ideas in space physics.

JWS33/W/03-B2

1145

## AN INTEGRATED SATELLITE ALTIMETRY, GRAVITY AND GEODESY DATA BASE: ARCHITECTURE, VERIFICATION, DATA PROCESSING, DATA BASE MANAGEMENT SYSTEM

P.P. MEDVEDEV, Yu.S. Tyupkin, S.A. Lebedev (Geophysical Center, Russian Academy of Sciences, Molodezhnaya 3, 117296, Moscow, Russia, email: [pmedv@wdbc.rssi.ru](mailto:pmedv@wdbc.rssi.ru))

The integrated database of satellite altimetry data and supplementary gravity and geodesy information which is necessary for geodesy, geophysics, geology and oceanography applications was created in Geophysical Center of RAS. The satellite altimetry data sets include data measured by the Russian GEOIK geodetic satellites and by GEOSAT, ERS-1, ERS-2 and TOPEX/POSEIDON during the period 1985-1998. Database management system includes problem-oriented modes in addition to the usual DBMS functions. Database consists of three levels: preliminary data, integrated data, results of special processing. The architecture of database, database management system and data processing, future plans and problems are discussed. The work was supported by Russian Basic Research Foundation.

JWS33/W/14-B2

1200

## VIRTUAL DATABASE DEVELOPMENT FOR FLOOD MANAGEMENT IN THE RED RIVER BASIN

Slobodan P. SIMONOVIC (Natural Resources Institute, University of Manitoba, Winnipeg, Canada, R3T 2N2, e-mail: [simon@ce.umanitoba.ca](mailto:simon@ce.umanitoba.ca))

The interim report of the International Red River Basin Task Force (IJC, 1997) provides background on the 1997 flood and describes the development of virtual database as fundamental for success of the study. This paper describes issues involved in the development of a "virtual database" (Data catalog or library) in the form of an internet web site, in sufficient detail to provide the following services: (a) Quickly locate data required for flood reporting and flood fighting in the Red River Basin; and (b) Describe in detail the contents and limitations of the data. Virtual database is searchable by data type, data holder/owner, location, etc. It is proposed that a single link, such as a Web Page, be established that will be the door through which the overall Red River Database is accessed. During the Flood of 1997 numerous Internet "Flood Information" Web pages appeared that provided useful information to data consumers in the basin. However, these sites were not integrated in a way to allow access to all potential sites or sources of information. Based on the International Joint Commission (IJC) public meetings in the Red River Basin and user needs assessment, conducted in July 1998, there is a real need to integrate and make more readily accessible the distributed databases that currently exist and those to be developed in the future. The Red River Basin Virtual Database (RRBVD) has no single data repository thus eliminating the requirement to provide regular updates of data to a data clearinghouse. Some data sets, however, may need to be centralized depending on the preferences of the data set providers. The Red River Basin Virtual Database will be used in three modes: (a) planning and design for flood protection; (b) real time flood emergency; and (c) flood recovery.

JWS33/E/04-B2

1215

## A NEW APPROACH TO GEOPHYSICAL DATA PROCESSING FOR DETECTING EARTHQUAKE PRECURSOR ANOMALY

Yueqing ZHU (Center for Analysis and Prediction, China Seismological Bureau, P. O. Box 166 Beijing, 100036, email: [zhuqy@sun.ihep.ac.cn](mailto:zhuqy@sun.ihep.ac.cn))

Audio-visual and comfortable detection to the earthquake precursor anomalies from geophysical observations is one of the very important aspects for earthquake prediction researches.

The Author and his research group have recently developed a strategy and a related intelligent software system for doing geophysical data processing and also detecting earthquake precursor anomalies from geophysical observations of different disciplines on single station and/or station networks. The results can be also automatically disseminated to a series of expert systems for doing medium-term, short-term and urgent earthquake prediction, which are developed by the author and his other research groups.

The system is consisted of a method-library, synthetic databases, GIS application sub-system, report and table auto-generation sub-system and anomaly feature auto-recognition and recording sub-system. The spatial and temporal variation features of the anomalies detected will be displayed in screen, listed in suitable tables and plotted in maps formed by GIS within suitable text reports in national language or English. It can detect special features of precursors of earthquake generation process and possesses good audio-visual functions.

**JWS33/E/06-B2 1230**

**HIGH-CAPACITY NETWORKING TECHNOLOGY FOR PROCESSING OF THE EARTH'S VIBRATIONAL SOUNDING DATA**

M.S.KHAIRETDINOV, Yu.I.Rodionov, A.P.Grigoryuk, L.G.Dvoretzskaya, G.F.Sedukhina. (Institute of Computational Mathematics and Mathematical Geophysics, Siberian Branch, Russian Academy of Sciences.); M.S.Sevastianov, R.V.Radygin. (Novosibirsk State Technical University, Russia, Novosibirsk.)

The method of deep vibro-seismic sounding of the Earth, because of its high resolution and high accuracy of measurement, has considerable promise for solution of a number of urgent seismological problems. In the first place, these are: problems of monitoring of seismic-prone zones, seismic tomography, precise calibration of traces of seismic wave propagation, etc. Solution of these problems is connected with recording and processing of a large bulk of data, whose capacity can be estimated as  $N=F_d \cdot p \cdot M \cdot L \cdot T$ , where  $F_d$  is the sampling rate of input signal values,  $p$  is word length of sampling values,  $M$  is the number of recording channels,  $L$  is the number of repeating sounding performances,  $T$  is duration of each performance. Selection of the parameters  $L$  and  $T$  determines the noise immunity of vibroseismograms. As applied to solution of the problems in question, for example, to vibromonitoring of seismic-prone zones, an area of 1000 kmx1000 km, the capacity of accumulated information can reach about 100Gb. In order to handle such a large amount of information, the authors have developed a network technology of data processing, which consists of two levels. The lower level of processing is connected to data gathering stations and contains the software for recording and accumulation of initial data with their simultaneous processing, in the first place, calculation vibroseismograms (correlograms) and evaluation of their primary parameters of each of  $M$  channels in the real-time mode in the course of experiment. Because of the latter, the information is  $M \cdot T / T_s$  times compressed, where  $T_s$  is duration of a vibrocorrelogram. In particular, at  $M=500$ ,  $T=3600$ sec,  $T_s=150$ sec, the compression makes about 1000 times, which allows us to essentially decrease the requirements on the channels rate of data transmission to the processing system of the upper level. At the upper level of the system, additional processing ....

**Tuesday 27 July PM**

Presiding Chair: Yu S Tyupkin (Geophysical Center, RAS, Russia)

**JWS33/E/17-B2 1400**

**REAL-TIME INTEGRATION OF SEISMIC DATA USING THE ANTELOPE SYSTEM**

Danny J. HARVEY (Boulder Real Time Technologies, Inc., 2045 Broadway Str., Suite 400, Boulder, CO 80302, USA, email: danny@brtt.com); Frank L. Vernon (Boulder Real Time Technologies, Inc., 2045 Broadway Str., Suite 400, Boulder, CO 80302, USA, email: vernon@palapa.ucsd.edu)

Within the last several years, a new and effective real-time system for transporting and processing seismic data has been developed. This system, known as Antelope, makes it possible to integrate near real-time geophysical data from many diverse and geographically distributed data sources, over the Internet, into a complete real-time processing system. We will show how Antelope has been developed and how it has been used to create global scale "virtual" seismic networks composed of many different individual regional networks and single stations from other more traditional global networks. This has been accomplished with a minimal impact upon the operations of the station owners. In order to integrate real-time geophysical data flows, we make extensive use of both public and private Internet facilities and the standard TCP/IP communications protocols. We will show how Antelope provides important capabilities for geophysical data integration and data sharing that are relevant to all of the earth sciences.

**JWS33/W/25-B2 1415**

**NEW WINDOWS-BASED SOFTWARE FOR GEOMAGNETIC OBSERVATORY DATA PROCESSING**

D.C.HERZOG (USGS Box 25046, MS 966, Denver Federal Centre, Denver, Colorado 80225-0046, USA. Email: herzog@ghmt.cr.usgs.gov)

The U.S. Geological Survey (USGS) has contracted with a commercial vendor to develop a new Windows-based application software program for processing geomagnetic observatory data. This graphical user interface (GUI) program provides a means for loading data from a variety of input formats; displaying it on-screen; deleting values with the aid of "blowup" sections of the plotted values; displaying the calibration baseline values and applying that data directly to the imported data values; and outputting the resulting data in a variety of file types, including the INTERMAGNET CD-ROM and WDC-A formats. The software provides "one-stop" processing capability and greatly improves the efficiency and flexibility with which observatory data can be processed.

**JWS33/W/37-B2 1430**

**ANALOGUE MAGNETOGRAM SERVICE THROUGH INTERNET**

Toshihiko IYEMORI, Masahiko Takeda and Toyohisa Kamei (WDC-C2 for Geomagnetism, Graduate School of Science, Kyoto University, Kyoto 606-8512, Japan, email: iyemori@kugi.kyoto-u.ac.jp, takeda@kugi.kyoto-u.ac.jp, toyo@kugi.kyoto-u.ac.jp); Akinori Saito, Yoshifumi Futaana and Tohru Araki (Geophysical Institute, Graduate School of Science, Kyoto University, Kyoto 606-8502, Japan, E-mail: saitoua@kugi.kyoto-u.ac.jp, futaana@kugi.kyoto-u.ac.jp, araki@kugi.kyoto-u.ac.jp)

In recent years, most of geomagnetic data are provided in digital form through Internet etc.. However, there still exist many observatories, which use analogue magnetometers. At the World Data Centers, there exists a huge archive of analogue magnetograms recorded on microfilms or printed annual reports, which cover for more than 100 years. Although number of the users of these analogue data is decreasing, there still exist considerable amount of data requests. When we investigate the old events before 1980 or some historical events such as the geomagnetic effects of comet Halley's encounter in 1910, we need to look at the analogue magnetograms. To use the analogue data recorded on microfilm, the user have to visit the data center or the staff at the center have to make hard copy of them and send by mail. Users often give-up to use the analogue data because of such procedure which takes time. To improve such situation, we are constructing a system to serve the image files of magnetograms from WWW. We report the method and quality of analogue magnetogram service through Internet and discuss on the problems and future possibility.

**JWS33/W/01-B2 1445**

**THE RUSSIAN MAGNETIC OBSERVATORIES DATA ON CD-ROM**

Alexander ZAITZEV and Vladimir Odintsov (Institute of Terrestrial Magnetism, Ionosphere and Radio Wave Propagation, Troitsk, Moscow Region, 142092, RUSSIA, e-mail: zaitzev@izmiran.rssi.ru)

Despite the general problems of the Russian science, the network of the magnetic observatories of Russia and CIS are still operated. As a rule, all observatories have own hardware and software systems and store an original records on sites which are inaccessible to a wide range of users. We propose to convert the all variational data of magnetic observatories in 1-min binary format and to save it on an optical disk (CD-ROM). In addition of data base production we propose to create the information system for automated data processing. The final CD-ROM we plan to install on Web server to organise a data access via INTERNET . It will allow the broad usage of the magnetic observatories data in the scientific and applied research programs. At the first stage for accommodation on CD-ROM we collect the results of the Moscow observatory data in the form of standard tables of hourly values and 1-min. variational data for period 1991-1998. The variational data was received on experimental digital station CMVS-6. The current observations in the form of variational data are displayed on site: [http://www.izmiran.rssi.ru/magnetism/mos\\_data.htm](http://www.izmiran.rssi.ru/magnetism/mos_data.htm). Beside Moscow data we have a regular 1-min. variational data from expedition site Cape Kamenny (Yamal peninsula), for Jan. 1991 - Sep. 1998, and Cape Schmidt (Chukotka region) observatory for 1995-1997. We call of all our colleagues on Russian magnetic observatories to help us collect the digital data, which might be available for period 1991 and onwards. In the final stage of the project we plan to make enough CD-ROM copies to supply of all scientists interested in Russian magnetic observatories data for period of 1991-1998. The work is supported by Russian Fund of Fundamental Researches Grant 98-07-90278.

**JWS33/E/13-B2 1500**

**PRESENTATION OF THE GEOMAGNETIC DATA BASE OF THE NIEMEKG OBSERVATORY VIA INTERNET AND ITS ACCESS**

Hans-Joachim LINTHE (GFZ Potsdam, Adolf-Schmidt-Observatory, Lindenstr. 7, D-14823 Niemeck, Germany, email: linthe@gfz-potsdam.de)

The Adolf-Schmidt-Observatory Niemeck is in continuous operation since 1890. So the observatory today manages a data series of nearly 110 years. Hourly, monthly and annual mean values are available in a database for the whole period. Additional minute mean values, instantaneous minute values, instantaneous second values and activity indices for longer or shorter periods are also contained in the database. The database is handled by means of the local area network of the observatory, which consists of several PCs, a workstation and software routines. The structure of the data, the data handling and the methods of data access will be presented.

**JWS33/W/30-B2 1515**

**DATA CREATION USING THE SCF SYSTEM**

CARRIE A. GONZALEZ (Instrumentation and Space Research Division, Southwest Research Institute, San Antonio, Texas 78228, e-mail: carrie@pemrac.space.swri.edu)

Many times in the space physics world there arises the need to derive different quantities based upon data parameters that are returned by one or more spacecraft. In some cases, these derived products may be dependent upon values returned from a single instrument; in other cases, the derived products are dependent upon values taken from many instruments. In either case, there is a need to specify data parameters and the algorithms necessary to produce derived data products. To fill this need, a domain specific system has been developed that allows for the definition of the new space data products from an homogeneous, spacecraft/instrument independent primary data format. This system, referred to as the SCF (Science Computation Formulation) software, utilizes a GUI-based definition session in which the user defines the input variables, the temporary variables and the output variables in addition to the actual set of mathematical operations to be performed on the data to produce the derived data products. The input variables are symbolic names given to the data parameters returned by the spacecraft. Temporary variables are symbolic names given to hold constant values (such as pi) or to hold intermediate results during the evaluation of the algorithm (such as the angle between the spacecraft velocity vector and the vector to the sun). Output variables are symbolic names given to the derived data products that are returned by the software. For the algorithm definition, the SCF software recognizes the standard mathematical operations of addition, subtraction, multiplication, and division. These operations are designed to operate on vector-vector, scalar-scalar, or vector-scalar quantities. In the SCF context, a scalar quantity is a single value and a vector quantity is a multi-value entity (an array of values). For the vector-vector operations, the lengths of the vectors must be the same. In addition to the standard mathematical operators, the SCF software supports standard mathematical functions such as square root, sine, cosine, and polynomial expansions to name a few. The SCF software also supports tensor data products. To date, the SCF mathematical library for matrix operations include addition, subtraction, and multiplication. There are functions that return the lower and upper triangular of a given matrix or an identity matrix of a specified order. The trace of a matrix, the transpose of a matrix, the determinant of a matrix and the inverse of a matrix are also supported functions within the SCF mathematical library. The definition of the derived data products is made once and then that information is stored. Realization of the new data ...

**JWS33/P/2-B2 1550**

**EARTHQUAKES AND THEIR SPECTRAL ESTIMATIONS USING EINSTEIN DECONVOLUTION**

Dan LOEWENTHAL, Raymond & Beverly Sackler (Faculty of Exact Sciences Department of Geophysics and Planetary Sciences and Tel Aviv University (Ramat Aviv 69978, Israel. email: danlo@jupiterf.tau.ac.il)

In a recently patented idea, I have conjectured the validity of dual fields theory, which teaches us how seismic or electromagnetic phenomena can be analysed to a much higher precision in comparison to a single field analysis. In its acoustic embodiment these dual fields are the pressure and the particle velocities fields, as registered by hydrophones and geophones, respectively. This can be effectively done in ocean bottom environment. According to this theory both these fields are initiated by the same source. They both solve the same classical wave equation in regions of homogeneous layers but they differ and are nonlinearly coupled through the boundary conditions, where they possess opposite sign reflection coefficients. Since the source is common, it convolves both fields. Thus, its Green's function is estimated by the ratio of these fields defined through its Z transform polynomials. Using transform ratio of these two fields, a rational polynomial presentation of the system is attained, where the source wavelet cancels out. This allows deterministic spectral estimation similar to the maximum entropy or bayesian estimators. But



while the bayesian and maximum entropy estimators are of trial and error statistical approach, our source de-convolution, which is the essence of Einstein-Lorentz velocities additions-subtractions formula, is deterministic in nature.

**JWS33/W/21-B2** 1605

**SEARCH INFORMATION RESOURCE IN THE FIELD OF OCEANOGRAPHY USING INTERNET**

Evgeny D. Vyazilov and Valentine I. Ibragimova (Russian Research Institute of Hydrometeorological Information - World Data Center 6, Korolyov St., Obninsk, Kaluga region, 249020, Russia, e-mail: vjaz@meteo.ru)

An abundance of WEB sites created in INTERNET on oceanography as well as their volume make search and browse of the necessary data very difficult. A lot of servers already are provided with pages containing the list of hat links that are considered useful for the potential users. These addresses are often poorly classified and are not accompanied with information. The most well classified server is IOC WEB site. From viewpoint of search of different organizations' pages, involved in the ocean exploration, this is the best server. Unfortunately, information resources are not presented there. In some research directions the special pages are already created of a general character. Those pages present summaries on information resources in this or that country (e.g. Russian information resources in INTERNET) or separate scientific directions.

That is why there is a strong demand for creation a page for organizing a search of information resources in the field of oceanography. The structure of such a page is as follows: general address (publish house, libraries, magazines, councils, education, hot links, search of work, conferences, funds, plays and other); metadata (platforms, experts, databases, formats, projects, inventories and other); information on organizations (address, functions, projects, in which participate organization); information technology (GIS, software, satellite, ftp).

**JWS 33/E/14-B2** 1620

**ELECTRONIC PUBLISHING ENVIRONMENT IN GEOPHYSICS**

Vitaly NECHITAIENKO (Geophysical Center, Russian Academy of Sciences, 3 Molodezhnaya Str, Moscow 117296, RUSSIA, email: vitaly@wdbc.rssi.ru)

The paper will discuss the state-of-the-art of electronic publishing in geophysics and its recent perspectives with the emphasis on technical issues, especially on creating an integrated environment for collecting and managing both data and results of their analysis.

The discussed EP environment (<http://eos.wdbc.rssi.ru/>) developed at Geophysical Center RAS includes a full set of technologies and tools for preparation of papers from manuscript to print and online versions, including online submissions, peer-review process, updating and revising papers, back- and forward referring, markup language conversion, hyperlinking based on automatic syntax analysis, and interface to data bases and interactive components.

The current EP technologies and tools, and those which will appear in the nearest years, produce strong influence on authors' and publishers', as well as data producers' and data managers', roles and vice versa. In this respect an emphasis will be given to hot and cool technologies and tools, a problem of their harmonization. Main elements of the paper are supported by online presentation.

Presiding Chair: V Gitis (Institute for Information Transmission Problems, RAS, Moscow, Russia)

**JWS33/W/22-B2** Poster 1635-01

**NETDC: A SYSTEM TO NETWORK SEISMOLOGICAL DATA CENTERS**

Tim AHERN and Rob Casey (IRIS Data Management Center, 1408 NE 45th Street, #201, Seattle, WA 98105, USA, Email: tim@iris.washington.edu); Doug Neuhauser and Stephane Zuzlewski (475 McCone Hall, UC Berkeley, Berkeley, CA 94720, USA Email: doug@perry.berkeley.edu); Bernard Dost (ORFEUS Data Center, PO Box 201, 3730 AE De Bilt, the Netherlands, Email: dost@kmi.nl); Genevieve Roullet (Institute de Physique du globe de Paris, Dept. de Sismologie, Programme GEOSCOPE, 4, Place Jussieu, 75252 Paris cedex 05, France, Email: groullet@ipgg.jussieu.fr)

The Federation of Digital Broadband Seismographic Networks (FDSN) has implemented a system that supports data request processing for distributed data centers. The NETDC system allows users to make requests for various types of information to any of the participating data centers, independent of where the data actually reside.

The NETDC system manages the coordination of information requesting and information distribution between the data centers in a manner that is transparent to the seismological data requester. At the present time requests can be made for station inventories, channel response information, and for seismic waveform data. The system is easily extensible to other data types. Currently data centers in Seattle, Washington, Berkeley, California, deBilt, the Netherlands and Paris, France have installed this system. This presentation will summarize how the NETDC system works, what the present status of the system is and hopefully encourage other disciplines to consider a similar method for standardizing methods of coordinating a globally distributed system of data centers.

**JWS33/W/34-B2** Poster 1635-02

**ADVANCES IN CRYOSPHERIC DATA MANGEMENT**

Roger G. BARRY, Ronald L. S. Weaver, Matthew Cross, Gregory Scharfen (National Snow and Ice Data Center, CIRES, Campus Box 449, University of Colorado Boulder, Colorado, 80309)

Over the past 10-15 years the National Snow and Ice Data Center (NSIDC) has played a proactive role in cryospheric data management. Three themes illustrate the advances that have been made. (1) In the areas of new integrative products, three major CD-ROMs were produced. These comprise: the first global assembly of data and information on frozen ground and permafrost; the CAPS CD-ROM which contains digital maps of permafrost, numerous soil temperature and borehole data sets, a 12-language glossary, a cumulative bibliography and an inventory of Russian permafrost maps. A second example is the Polar Pathfinder Sampler CD-ROM that provides combined fields of IR/VIS AVHRR, passive microwave SSM/I and TOVS atmospheric sounder data in a common (Equal Area Scalable Earth Grid) geo-referenced system. A third product is an educational CD (Into the Arctic), designed for schools, using Greenland ice core climate data. (2) NSIDC has provided leadership in data set collection and dissemination through active collaboration with scientific societies and organizations. These include the IPA, the WGMS for glacier inventory data, CONMAP SCAR for the US National Antarctic Data Center for Antarctic metadata, the WMO Commission on Maritime Meteorology for the Global Sea Ice Data Bank and the International Antarctic Buoy Program (IABP). (3) NSIDC's participation in the GCOS TOPC and the IPA Working Group on Data and Information has helped stimulate the organization of a global monitoring network for ground temperature regime (the Circumpolar Active Layer Monitoring Program network),

involving data protocols, site selection etc. at the national level. NSIDC's role in the US NSF ARCSS Data Management and the Antarctic Master Directory contributed to the development of NSF guidelines for investigators to submit data to Data Centers in a timely fashion.

**JWS33/E/05-B2** Poster 1635-03

**DATA COLLECTION AND PROCESSING AT THE ISTITUTO NAZIONALE DI GEOFISICA DATA CENTER**

L. BADIALI, F. Mele, R. Di Giovambattista and A. Basili (Istituto Nazionale di Geofisica, Via di Vigna Murata, 605, I-00143 Roma, Italy. E-mail: BADIALI@ingrm.it)

With the advent of Internet, there was an arise of the request for real time access to seismic data. In an effort to advance the Italian Telemetered Seismic Network (ITSN) we developed a new system for acquiring and processing digital and analog signals that makes extensive use of both standard internet TCP/IP communication protocol and international standard for data exchange. We identify 5 different levels of available information: (1) triggered or continuous seismic signals, (2) automatic picking of seismic phases, (3) automatic determination of earthquake location and magnitude, (4) locations reviewed by a human analyst for prompt alarm and (5) parameters reviewed and analysed by humans after integration with all the available data. Each level of information has its own distribution link.

Data are disseminated in two different ways: (1) the system sends data to a predefined list of targets as soon as they are available or (2) stores them on a server for distribution on request.

**JWS33/W/26-B2** Poster 1635-04

**INCREASED DEMAND FOR RAPID ACCESS TO UK MAGNETIC OBSERVATORY DATA : IMPLICATIONS FOR QUALITY CONTROL PROCEDURES**

Ellen CLARKE and Pamela White (both at Global Seismology and Geomagnetism Group, British Geological Survey, West Mains Road, Edinburgh, EH9 3LA, Scotland. e-mail: e.clarke@bgs.ac.uk)

The scientific and commercial demand for rapid access to UK magnetic observatory data has steadily increased over recent years, prompting the continued development of the data processing procedures and quality control standards. The modern user requirements for accurate as well as timely data has triggered the need for refined automatic quality control procedures. This paper discusses these procedures, highlighting the different user requirements in terms of level of accuracy and speed of dissemination of the data products.

**JWS33/E/10-B2** Poster 1635-05

**DATA PROCESSING IN THE ARCTIC OCEAN DIGITAL BATHYMETRY MODEL**

Elena DANIEL (All-Russia Research Institute for Geology and Mineral Resources of the World Ocean, 1, Angliysky pr., St.-Peterburg, 190121, Russia, email: dani@vniio.nw.ru)

A new computer model of the Arctic Ocean is made under the activity IOC/IASC/IHO project (Macnab & Grikurov, 1997) for building of an international digital bathymetric data base of the Arctic High Seas. The digital model (bathymetry presented as 10 x 10 km grid) is a first relies of the compilation of the various Russian and western bathymetry data. These data include initial observations, digital contours from published bathymetric maps, global data sets. The compilation has started with the collection, digitisation, formatting, editing, and adjustment of bathymetric data. The next step included building a coherent digital data base, gridding and production of computer derived bathymetric maps. The data were processed using common technological procedure for digital compilation of potential fields and other geophysical data. However there are some special items in coherence and gridding of bathymetric data due to higher variability of depth field in comparison with that of magnetic and gravity anomalies. Methods that provide with grid values calculations according to specific features of bottom topography (the existence of linearly extended features, complex mosaic relief, offshore zone, etc.) were used for the constructing of correct digital model. They improved the bathymetry model especially under conditions sparse data distribution in the Arctic Basin. The digital relief model will be distributed on CD-ROM as an ASCII-file containing grid values and as a graphic file that displays bathymetry, and, in addition, as printed maps at a scale of 1:6,000,000.

**JWS33/E/03-B2** Poster 1635-06

**POST-PROCESSING OF SEISMIC EVENTS RECORDED BY THE ISTITUTO NAZIONALE DI GEOFISICA SEISMOGRAPH NETWORK: AN ANALYSIS OF THE ACCURACY OF THE MAIN DISSEMINATED SEISMIC PARAMETERS**

R. DI GIOVAMBATTISTA, F. Mele, A. Marchetti, L. Badiali, S. Baccheschi, P. Battelli, L. Giovani, G. Modica, L. Piccolini, F. Pirro, M. Pirro, R. Tardini and A. Basili (Istituto Nazionale di Geofisica, Via di Vigna Murata, 605, I-00143 Roma, Italy. email: digiovam@martie.ingrm.it)

Some of the most significant advances in seismology have resulted from analysis performed on the seismic parameters reported in the Bulletins and disseminated by the seismological data centers. A large fraction of works on travel time residuals and tomography has relied upon arrival times published by the bulletins. A precise estimate of the onset time of seismic phases is needed to obtain accurate event locations necessary for seismological studies of spatial patterns of earthquake hypocenters. To obtain very precise onset times for all seismic signals, seismological data center mostly rely on the picks provided by their human analysts. However, the increase in the number of analysts and the quality of arrivals reported in bulletins has also been debated. We present the results of an analysis aimed to estimate the quality of phase arrivals. A comparison between the arrival times reported in the Istituto Nazionale di Geofisica (ING) bulletins and those returned in an effort to obtain accurate pickings for a tomographic study is also presented.

**JWS33/W/23 -B2** Poster 1635-07

**GIS TOOLS TO STRUCTURE THE CENTRAL ANDES ON A REGIONAL SCALE**

H.-J. GOETZE and S. Mohr (FU Berlin, Institut fuer Geologie, Geophysik und Geoinformatik, Malteserstr. 74-100, D-12249 Berlin, Germany, email: hajjo@geophysik.fu-berlin.de)

For the last ten years the Central Andes fold belt is focus of scientific investigations conducted within the frame of the "Collaborative Research Center 267 - Deformation Processes in the Andes". Over the years a wealth of data from various disciplines of geosciences has been compiled. To handle this information, and to support an interdisciplinary and international cooperation among involved scientists, the establishment, organization and maintenance of a diversified GIS was necessary, and a data catalogue was set up, which is available on the Web under URL: <http://userpage.fu-berlin.de/~data>.

Application of GIS methods allows structuring of the remote mountainous region of the Central Andes on a regional scale, which is generally marked by a lack of infrastructure and by topographic extremes. Numeric procedures, such as statistical methods, filter techniques or

algorithms of lineament recognition are applied. For example the evaluation and interpretation of geomorphometric data is suited to identify various morpho-structural units of the Andean topography. Investigations of the intensity and direction of inclination and characterization of vertical doming allow to outline the regional strike and identify predominant structural directions. Lineaments, derived from data of topography and gravity grids with objective methods such as algorithms of edge detection or horizontal gradient recognition, which are only in part suitable for correlation with geological data, can also be used for an identification of the structuring of areas under investigation. Investigations of the fractal geometry of contour lines in areal portions warrant a subdivision into morphologically weak and strong structured regions, and reflect the different climatic conditions at the western continental margin of South America.

**JWS33/W/09 -B2** Poster **1635-08**

**EXPORTING IDFS-FORMATTED DATA TO CDF AND NETCDF FORMATS**

Carrie A. GONZALEZ (Instrumentation and Space Research Division, Southwest Research Institute, San Antonio, Texas 78228, e-mail: carrie@pemrac.space.swri.edu)

Southwest Research Institute has developed a data storage format referred to as the Instrument Description File System (IDFS) format. The IDFS format is a data storage format that is designed to be general enough to handle the majority of spacecraft science and engineering data sets. These data sets include raw telemetry, processed data, simulation data and theoretical data. The IDFS paradigm performs a real-time conversion of telemetry data into physical units as the data is accessed. This approach allows for the refinement of calibration factors and processing algorithms without having to reprocess the original data set and avoids the storage of many different unit values. A small core of generic routines services the IDFS format. This covers access of the individual data files through a distributed database, positioning within the data file based on time, access of the data and the real-time conversion of the data to physical units.

Recognising the popularity of the CDF and netCDF file formats, Southwest Research Institute has developed software that extracts and exports data that has been stored in the IDFS format. Currently, IDFS data can be exported to one of three file formats:

- (1) Common Data Format (CDF version 2.6)
- (2) Unidata Network Common Data Form (netCDF version 2.4)
- (3) IDFS - ASCII dump

When the CDF file format is selected, a CDF file is created which contains the requested data parameters and meta data. The meta data is comprised of global-scope attributes that provide information about the data set as an entity. Some of the required global attributes have been selected for potential modification by the user.

**JWS33/W/12-B2** Poster **1635-09**

**DATA PROCESSING AND PRODUCTS AT THE GERMAN SEISMOLOGICAL DATA CENTER**

Gernot HARTMANN (Federal Institute for Geosciences and Natural Resources, Stilleweg 2, 30655 Hannover, Germany, Email: hart@sdac.hannover.bgr.de)

The German Seismological Data Center operates the seismic GERESS array of 25 stations and is responsible for the collection of data from the German Regional Seismic Network (GRSN). This network consists of 13 three-component broadband stations distributed throughout Germany. Real-time data from the GERESS array are recorded continuously at the Data Center. The data from the GRSN stations are automatically retrieved at the end of each day. A seismic alert system provides for rapid epicenter determination of strong events in Germany and adjacent areas. Triggered by a detection algorithm applied to the data of the GERESS array, time segments of the assumed event are retrieved from the GRSN stations for confirmation of the detection and improvement of the epicenter and magnitude determination. The continuously recorded data, as well as the data segments of strong events, are stored on a RAID system until they are archived on CDRs in two jukeboxes with 500 CDs each. This technique provides immediate access to all data, either interactively or by autoDRM via e-mail. This data forms the basis for routine analysis, which includes several newly developed automated procedures:

- (1) event detection, location, and epicenter determination;
- (2) testing of the reliability of the results by several consistency checks;
- (3) screening out explosions from well known quarries and mines.

The interactive analysis of these predefined events ensures the high quality of the determined event parameters, stored in a database management system. The results of automatic and interactive data analysis are published on the homepage of the Data Center. A monthly catalogue of local and regional events is produced by including associated epicenter determinations and phase readings reported from a number of local networks in Germany. A compilation of this catalogue data is published annually as the German Earthquake Data Catalogue. The data processing schemes and their interaction are presented in the poster.

**JWS33/E/08-B2** Poster **1635-10**

**THE SOUTHERN CALIFORNIA EARTHQUAKE CENTER DATA CENTER (SCEC-DC)**

K. HAFNER, R. W. Clayton (Seismological Laboratory, Caltech, California)

The SCEC-DC is the principal archive for seismological waveform and associated parametric data from the Southern California Seismic Network (SCSN). Established in the fall of 1991, the SCEC-DC is now entering a major period of transition. In addition to expanding its archive from a 0.6 Tbyte to a 5 Tbyte WORM mass storage system, the SCEC-DC is developing a new database/archiving system. This system will result in a more interdependent relationship between the SCEC-DC and the real-time data collection/data analysis systems of the SCSN. The system under development has three primary missions: 1) provide rapid access to real-time parametric and waveform earthquake data, 2) consolidate and maintain one oritative database available to the real-time data acquisition systems, the data analysts and the archive facility; and 3) facilitate a seamless exchange of seismological waveform and parametric data with other seismological data centers. In our system, the real-time data collection system populates a local database with parametric earthquake data. This data is "replicated" to a database on the SCEC-DC, where it is accessible within a few minutes of an event. Data analysts interact with and update the database via a java GUI interface, while other users of the data access the database via WWW interfaces on various internet and intranet sites. These interfaces will allow users to search and extract from the earthquake hypocenter and phase catalogs, view and request calibrated waveforms, and view such products as Shakemaps. Once this database comes on-line, it will provide "real-time access" for an average of 26,000 earthquakes/year, in addition to storing the ~400,000 events in the historical Southern California earthquake catalog.

**JWS33/W/10-B2** Poster **1635-11**

**WEB EFFECTS: FRONTIERS IN INFORMATION DELIVERY**

Allen M. HITTELMAN and Susan J. McLean (NOAA's National Geophysical Data Center, World Data Center for Solid Earth Geophysics, 325 Broadway, Boulder, CO 80303, U. S. A., email: ahittelman@ngdc.noaa.gov)

Without question, one of the most profound impacts on information technology is the advent of the Web. In just a few years, this media has drastically altered our perceptions of information services and created new paradigms for data dissemination. To cope with this unprecedented explosion of change, many of us in the information service business had to re-evaluate organisational goals and objectives. Where once we felt comfortable with our awareness of user needs, now we fell distant due to the impersonal nature of our Web sites (which seem to serve 99% of our scientific clientele's needs).

The National Geophysical Data Center, and its several supported World Data Centers, has pioneered many new innovative methods that enrich data and information delivery on the Web. Examples of these techniques include: the interactive creation of graphical spreadsheets (see <http://swat.ngdc.noaa.gov/cgi-bin/wist/wist.pl>), the satellite browse, display and download features of the Space Physics Interactive Data Resource (SPIDR, see <http://julius.ngdc.noaa.gov:8080/>) and access to gridded relief models (see <http://www.ngdc.noaa.gov/seg/topo/globe.shtml>). Newer techniques are empowering users with the ability to access data and metadata through GIS-enabled Web servers. We have also explored data mining tools to provide improved understandings of the needs of our Web users -- from where do they come and for what do they search?

**JWS33/E/06-B2** Poster **1635-12**

**HIGH-CAPACITY NETWORKING TECHNOLOGY FOR PROCESSING OF THE EARTH'S VIBRATIONAL SOUNDING DATA**

M.S.KHAIRETDINOV, Yu.I.Rodionov, A.P.Grigoryuk, L.G.Dvoretzkaya, G.F.Sedukhina. (Institute of Computational Mathematics and Mathematical Geophysics, Siberian Branch, Russian Academy of Sciences.); M.S.Sevastianov, R.V.Radygin. (Novosibirsk State Technical University, Russia, Novosibirsk.)

The method of deep vibroseismic sounding of the Earth, because of its high resolution and high accuracy of measurement, has considerable promise for solution of a number of urgent seismological problems. In the first place, these are: problems of monitoring of seismic-prone zones, seismic tomography, precise calibration of traces of seismic wave propagation, etc. Solution of these problems is connected with recording and processing of a large bulk of data, whose capacity can be estimated as  $N = F_d \cdot p \cdot M \cdot L \cdot T$ , where  $F_d$  is the sampling rate of input signal values,  $p$  is word length of sampling values,  $M$  is the number of recording channels,  $L$  is the number of repeating sounding performances,  $T$  is duration of each performance. Selection of the parameters  $L$  and  $T$  determines the noise immunity of vibroseisograms. As applied to solution of the problems in question, for example, to vibromonitoring of seismic-prone zones, an area of 1000 kmx1000 km, the capacity of accumulated information can reach about 100Gb. In order to handle such a large amount of information, the authors have developed a network technology of data processing, which consists of two levels. The lower level of processing is connected to data gathering stations and contains the software for recording and accumulation of initial data with their simultaneous processing, in the first place, calculation vibroseisograms (correlograms) and evaluation of their primary parameters of each of  $M$  channels in the real-time mode in the course of experiment. Because of the latter, the information is  $M \cdot T / T_s$  times compressed, where  $T_s$  is duration of a vibrocorrelogram. In particular, at  $M=500$ ,  $T=3600$ sec,  $T_s=150$ sec, the compression makes about 1000 times, which allows us to essentially decrease the requirements on the channels rate of data transmission to the processing system of the upper level. At the upper level of the system, additional processing of seismograms is implemented...

**JWS33/E/01-B2** Poster **1635-13**

**THE METHOD OF THE ANALYTICAL AND NUMERICAL DESCRIPTION OF THE GEOMAGNETIC FIELD'S GRADIENTS FOR ITS USING TO SOLVE THE GEOLOGICAL AND NAVIGATION PROBLEMS**

Valentina I. KOLESOVA, Maria A. Effendieva and Sergey V. Hotin (St.-Petersburg filial, Institute of Terrestrial Magnetism, Ionosphere and Radiowave Propagation, Muchnoy per.2, box 188, 191023, St.-Petersburg, Russia, Email: kmp@telecom.lek.ru)

The gradients of the geomagnetic field can be successfully used to investigate the physical processes at the Earth and in the space, to solve scientific and applied problems in the geology and the navigation. Now in general case geomagnetic gradients can be received only by calculation. It was supposed to consider the value of the magnetic field in any point of the space to be the sum of the four components: the main field, the intermediate anomalies field, the regional field and the local field. The gradients of the main field are described the best of all by the Gaussian series. The construction of the fictitious dipole sources approximate the intermediate anomalies. The geometrical parameters of the construction are determined previously at the base of the space spectral analysis. The gradients of regional and local anomalies are calculated using the Poisson's integral. For the essential decreasing of the calculation time and increasing of the result accuracy it was offered to approximate the field by quadratic function at the range of the elementary grid. Then the integral can be calculated analytically in the quadratures using the formula of the highest algebraic accuracy. The method of the magnetic gradients calculation was realised in algorithms and programs, the last were included in the system, which guarantee the functioning of the database. The system gives the opportunity to digitise graphs, maps of graphs, maps of isolines; to include data in the database, to control data, to do the data processing, to create analytical and numerical geomagnetic field models, numeral and graphical charts, to visualise the information.

**JWS33/W/28 -B2** Poster **1635-14**

**FIELD AND OBSERVATORIES MAGNETO-TELLURIC WIDE AREA NETWORK**

Eugene KOPYTENKO, Yury Kopytenko, Andrej Radilov (SPbF IZMIRAN, Muchnoj per.2, Box 188, St.Petersburg, Russia, email: ek@eak.izmi.ras.spb.ru)

SPbF IZMIRAN is continued its developing in the field of high sensitive magnetometric system. On the base of MVC-2DS, multipurpose magnetotelluric station, it was build Wide Area Network for monitoring quick running processes both in magnetic and telluric fields, and in a third (three component) geophysical channel in quasi real time. System consist of Remote Station equipped with high sensitive torsion type magnetometer, 24-bit resolution Analogue to Digital Converter driven by GPS controlled clock, remote PC running under LINUX (UNIX clone OS) and Laboratory's Server. Data are buffered at remote PC. Server collects it and transmits it to the computers, which are included into the list of recipients.



**JWS33/L/1-B2** Poster **1635-14**

**NEW APPROACHES TO DATA COLLECTION, DATA PROCESSING AND DATA DISSEMINATION**

KUDRIASHOV

Abstract not available at time of going to press

**JWS33/E/16-B2** Poster **1635-16**

**ABOUT EARTH'S FREE OSCILLATIONS IN THE FORM OF TILTS AND STRAINS**

Ludmila LATYNINA, Aleksei Ljubushin, Denis Vvedensky (United Institute of Physics of the Earth, RAS, B.Gruzinskay,10, Moscow Russia, 123186 email: lat@uipe-ras.scgis.ru, Fax (095) 2556040

Data of oscillations within the periods of 2 minutes to 2 hours have been obtained at Protvino observatory near Moscow with help of strainmeters and tiltmeters. The recording computer with 16-bit ADC keeps records with resolution equal to 0.1E-09. We consider the Earth free oscillations of last strong Earthquakes and the results of spectral analysis of the observational data during several months. Continuous noticeable oscillations have been observed at the same frequencies (between 3 and 8 mHz) as in works by T.Tanimoto and others and by N.Suda and others (1998). The attempts of long-periodic wave forerunners discovering before strong Earthquakes have been made.

**JWS33/W/17-B2** Poster **1635-17**

**USAGE OF MODERN METHODS OF REFERENCE OCEANOGRAPHIC DATA ORGANISATION**

Igor LEBEDEV, Ludmila Kuznetsova (All-Russian Research Institute of Hydrometeorological Information - World Data Center (RIHMI-WDC), department National Center Oceanographic Data of Russia, 6, Korolyova st., Obninsk, Kaluga region, 249020, Russian Federation; Tel: (7)(08439) 74676; Fax: (7)(095) 2552225; email: lebedev@meteo.ru)

In early 80s Oceanographic Data Centre of Russia pioneered the creation of reference information base on oceanographic data. Since then information base had been used on RV cruises, research projects (programmes), observing platforms, marine institutions and agencies, etc. At the moment reference information data are organised in dbf-tables and are applied under control of DBMS Microsoft FoxPro 2.0. These data are used for obtaining various kinds of reports and references as well as working with observation data.

But there are also a number of drawbacks. These are errors in organising some tables, which are not associated with each other; poor automatization in work with reference data. The need is now obvious for organising reference information into unified database under modern DBMS control that enables one to apply the architecture of client/server computing and the distributed data processing. Besides, a demand arose in publication of some certain reference data on Web. Similar work is already being performed in some data centres abroad.

Some time ago realisation of such a database was started in Oceanographic Data Centre. Oracle8 is used as the DBMS, meeting all the requirements needed. The development of database and its pilot loading has been performed by the present moment. The work is currently underway on refinements of the database structure; working out additional requirements of the final loading of all data as well as development and creation of the client applications.

**JWS33/W/36-B2** Poster **1635-18**

**DISSEMINATING AEROMAGNETIC DATA ON THE WEB**

Susan Mclean (World Data Centre, email: smclean@ngdc.noaa.gov)

The National Geophysical Data Center (NGDC) is undertaking a pilot study to make critical aeromagnetic data sets available via the WWW. The project's goal is to address problems of multiple grid formats, large file size and regionally distributed data. One significant problem when distributing data via the WWW is the potential separation of associated metadata. Proper recognition of the organization or institution that originally collected the data and any value added processes that contributed to the present version of the data set must be retained. A pilot system to access aeromagnetic data via the WWW will be demonstrated by NGDC. The ESRI Spatial Data Engine (SDE) and Oracle database are the heart of the web site. Using these tools, we enable a GIS expert system with dissemination via FTP on-line or CD-R and DVD-R for off-line delivery. In many cases, higher resolution data sets exist. In these circumstances, we provide the proper links and contact information to the original organization. If the large file size presents a data transfer problem, we offer an alternate off-line data distribution method using CD-R or DVD-R.

**JWS33/W/05-B2** Poster **1635-19**

**COMPUTER SYSTEM OF KEEPING, PROCESSING AND ANALYSIS OF GEOMAGNETIC DATA**

Oleg MIKHEEV and Pyotr Djadkov (Institute of Geophysics, av. Acad. Koptuyg, 3, Novosibirsk, 630090, Russia, E-mail: oamih@uiggm.nsc.ru)

Modern development of the geomagnetic instruments is characterized by high accuracy and possibility of digital registration of continuous observations carried out both geomagnetic observatories and stations on different geophysical polygons. Necessity of realisation of modern instrumental possibilities requires a special computer system which allow to operating and suitable performance of the data. Such a system is elaborated now under IDE "Delphi 3" on Windows95 platform. It has several basic aims: 1) maintenance of reliable keeping and initial processing of large data arrays; 2) getting high quality authentic information as result of using special algorithms for elimination of outliers and different artificial and natural geomagnetic noises; 3) opportunities and techniques for detailed special analysis of information. As core for the database access system is using the integrated system - Borland Database Engine. The basic data format is the native dBaseIV-format in which digital primary data are converted by original software. On a contemporary stage the system is interpreted as local database, but afterwards its way can be extended to Intranet/Internet data-access technology. The system is under evaluation on the Baikal geodynamic polygon, where at present time the high-precision observations (up to 0.05 nT) are carried out in a several stations and geomagnetic observatory "Enhalku".

**JWS33/C/ST2/W/02-B2** Poster **1635-20**

**ESTIMATION OF POTENTIAL SEISMIC RISK AREAS BY GIS AND ITS ROLE IN CITY PLANNING - A CASE STUDY**

Naside OZER, Demir Kolcak, Oguz Gundogdu, Yildiz Altinok (all at Department of Geophysical Engineering, Faculty of Engineering, University of Istanbul, Avcilar, 34850, Istanbul, Turkey, Email: naside@istanbul.edu.tr), Recep Cakir and S.Shelton Alexander (both at Department of Geosciences, The Pennsylvania State University, 308 Deike Building, University Park, PA 16802, USA, Email: recep@essc.psu.edu)

A Geographical Information System(GIS) is a data-based Information System that facilitates the integration and joint analysis and interpretation of almost any kinds of spatial data, including maps, aerial photographs, lines and points. It can be used for planning and design, decision making, research and archiving by the central and local governments or by individual groups.

GIS-based investigations are at a very early stage in Turkey and therefore it is necessary to carry out some pilot studies for testing purposes and to gain experience in the use of GIS methodology.

GIS applications explicitly depend on the collection of available spatial data that are relevant to the application. The initial focus for seismic risk applications should be an important places where there exist sufficient data and information from geophysical, geological, and geodetic studies carried out through previous and ongoing national and international projects.

After conversion of the data collected to digital form, GIS utilities(ARC/INFO, ARCVIEW etc.) were used for integration and analysis of data sets to investigate different scenarios relating to hazard and risk for people and infrastructure in populated areas.

Integration of those data and preparing the scenario will offer a knowledge database for contemporary city planning and for central and local governments and private organisations to make informed decisions.

**JWS33/W/20-B2** Poster **1635-21**

**RESTORATION OF SPACE PARTICLE DATA COLLECTIONS**

Nickolay N. PAVLOV, Nickolay N. Kontor and Elmar N. Sosnovets (Skobeltsyn Institute of Nuclear Physics, Moscow State University, Moscow, 119899, Russia, email: nnpavlov@taspd.npi.msu.ru)

Since 1965, Theoretical and Applied Space Physics Division, Institute of Nuclear Physics, Moscow State University carries out monitoring of charged particles in space with use of Russian far spacecraft and satellites. Significant part of the data from old missions is stored only on paper, many data sets have been saved due to special issues published by the WDC-B. The data sets from both paper and old tapes needed to be restored and transferred to the modern computer media. This work has been supported by NASA, grant NAG5-4656. Useful collaboration with NSSDC has also made this project realisable.

Assuming that similar projects are being currently launched by many research groups for the sake of utilisation of the benefits of the new Internet era we would like to share our experience in typical problems, common approaches and software tools used in our work. The main goal is to make the collection living and publicly accessible via Internet. Such issues as data input, data formats, file structure, use of database system, IDL, Java are concerned here. Interactive graphic rectification of raw data sets and creation of the proper documentation are highlighted as the most important for the solving of a key problem of data quality. A simple method of improving the ability of navigation within a multi-spacecraft data collection based on a plain ftp is discussed as well as our approaches to the effective graphic access to the data. Attaching of some simple tools for remote data analysis to the user interface is also considered as a way to make the services more attractive and useful.

**JWS33/W/27-B2** Poster **1635-22**

**DATA COLLECTION, PROCESSING AND DISTRIBUTION FOR THE NASA TIMED MISSION'S GLOBAL ULTRAVIOLET IMAGER (GUVI)**

Larry J. PAXTON (240 228 6871; email: larry.paxton@jhuapl.edu); Michele Weiss (240 228 4806; email: michele.weiss@jhuapl.edu); Rob Barnes (240 228 8134; robin.barnes@jhuapl.edu); Sanae Kubota (240 228 8404; email: sanae.kubota@jhuapl.edu); Rosalyn Pham (240 228 8587; email: rosalypham@jhuapl.edu); Ching-I. Meng (240 228 5409; email: ching.meng@jhuapl.edu) At The Johns Hopkins University Applied Physics Laboratory 11100 Johns Hopkins Rd., Laurel, MD 20723, United States; Andrew Christensen (310 336 7084; email: Andrew.B.Christensen@aero.org) The Aerospace Corporation Space and Environment Technology Center P.O. Box 92957 Los Angeles, CA 90009

The Global Ultraviolet Imager (GUVI) is one of four instruments that on the NASA Thermosphere Ionosphere Mesosphere Energetics and Dynamics (TIMED) spacecraft, the first mission of the NASA Solar Connections program. TIMED, which is scheduled for a May 18, 2000 launch, will be used to study the energetics and dynamics of the mesosphere and lower thermosphere. The focus of the TIMED mission is the processes occurring between altitudes of 60 to 180 kilometers. The other instruments that are a part of the TIMED mission are the Solar EUV Experiment (SEE), the TIMED Doppler Interferometer (TIDI), and SABER (Sounding of the Atmosphere Using Broadband Emission Radiometry). GUVI is a far-ultraviolet (115 to 180 nm) scanning imaging spectrograph that provides horizon-to-horizon images in five selectable wavelength intervals or "colors." These colors (H1 121.6 nm, OI 130.4 nm, OI 135.6 nm, and N2 Lyman-Birge-Hopfield bands 140 to 150 nm and 165 to 180 nm) are chosen in order to produce the GUVI key parameters. These key parameters are produced on a routine basis and will be available via the internet. GUVI supports the TIMED science objectives and will:

- 1) Determine the spatial and temporal variations of constituent number densities and temperature in the thermosphere.
- 2) Determine the relative importance of auroral inputs, Joule heating, and solar EUV for the thermal structure of the lower thermosphere.

Each day GUVI produces 88 MB of raw data which must be processed, vetted, and available for distribution within a day of receipt. This requires the introduction of a rather large amount of software capable of automated processing (about 100,000 lines). In addition there is a graphical user interface, written in Java, that allows users to browse and manipulate the data products locally or over the Internet. GUVI data products and graphical user interface are available at: <http://sd-www.jhuapl.edu/TIMED/GUVI/> and <http://www.aero.org/GUVI/>. These sites document the GUVI project and provide details of the instrument and are the means for accessing the data.

These activities will be demonstrated and discussed.

**JWS33/E/02-B2** Poster **1635-23**

**DESIGN AND OPERATION OF GEOSCIENTIFIC CLEARINGHOUSES AT THE GFZ POTSDAM**

Bernd RITSCHHEL (GFZ Potsdam, Data and Computing Center, 14473 Potsdam, Telegrafenberg A3, email: rit@gfz-potsdam.de)



## INTER-ASSOCIATION

The usage of clearinghouse techniques are a state of the art way to disseminate the digital geoscientific data as well as the information or metadata about the data. A geoscientific clearinghouse consists of a relational database server, a web server and application software for retrieval, presentation and download of data. The client side only needs an internet browser to get access to the clearinghouse features. Metadata are necessary for the operation of clearinghouses. Often the relationships between data and belonging metadata are lost or the metadata itself don't exist. To create from the start a scientific product always as set of a data and a metadata file is an easy way to keep together both digital data and metadata. The product metadata existing as extended DIF documents will be extracted and pumped into a relational database as well as stored as text files together with the data files in a product archive. The extended DIF file contains all attributes are necessary for an aimed and successful geoscientific product retrieval. For the connection of different clearinghouses Z39.50 interfaces and servers are used.

**JWS33/W/04-B2** Poster **1635-24**

### DATABASE OF THE PACIFIC LITHOSPHERE DIGITAL MODELS FROM GEOTRAVERSES

A.G. RODNIKOV, N.A.Sergeeva, M.V.Rodkin, L.P.Zabarinskaya (Geophysical Center, Russian Academy of the Sciences, Molodezhnaya 3, 117296 Moscow, Russia, email: rodnikov@wcb.rssi.ru); (P.A.Stroev Sternberg State Astronomical Institute, Moscow State University, 117296 Moscow, Russia); V.A.Rashidov(Institute of volcanic geology and geochemistry, Petropavlovsk-Kamchatski, Russia)

Within the framework of the Geotraverse Project, a geological/geophysical deep-cross sections of the lithosphere and asthenosphere in the transition zone from Asian continent to the Pacific Ocean has been constructed. A set of bathymetric, magnetic, gravity and geological maps of the area has been made also. The purpose of the research is to study the deep structure of the region having in mind its connection with formation of sedimentary basins, seismic zones, and sea bottom minerageny. Primary geological and geophysical data were collected. The database includes now bathymetric data, gravimetric and magnetic surveys data, heat flow measurements, deep seismic sounding data, catalog of earthquakes, information about magnetic linear anomalies and faults, data on deep structure of the lithosphere and asthenosphere, geological and geophysical data from sea bottom boreholes, and data on sea bottom minerageny. AutoCAD-14 was used for digitizing of graphic images and Surfer32 was used for maps compiling from the primary data. Address of our homepage in Internet is <http://www.wcb.rssi.ru/GCRAS/traverse.html>. The database will include the Okhotsk Sea Geotraverse, the Japan Sea Geotraverse and the Philippine Sea Geotraverse. Now the data on the Philippine Sea Geotraverse and a few maps of the area are presented in Internet only. The Project is sponsored by Russian Foundation for Basic Researches, grant N 98-07-90201.

**JSW33/W/32-B2** Poster **1635-25**

### AN ON-LINE ACCESS SYSTEM FOR THE TRMM DATA

Hualan RUI (Distributed Active Archive Center, NASA/Goddard Space Flight Center, Greenbelt, MD 20770, email: rui@daac.gsfc.nasa.gov)

The Tropical Rainfall Measuring Mission (TRMM), jointly sponsored by the National Aeronautics and Space Administration (NASA) of United States and the National Space Development Agency (NASDA) of Japan, provides visible, infrared, and microwave observations of tropical and subtropical rain system. TRMM satellite was launched on November 27, 1997(EST). Data from TRMM are being archived, processed, and disseminated by Distributed Active Archive Center (DAAC) at the Goddard Space Flight Center (GSFC) of NASA. An online system or user interface is designed for easy, friendly, and quick display and access of the TRMM data. Components, features, and limitations of the system will be demonstrated. The TRMM standard products and variety of the subsets will be shown and their availability will be discussed.

**JWS33/W/08-B2** Poster **1635-26**

### INTERACTIVE POTENTIAL FIELD MODELLING AND INTEGRATION OF CONSTRAINING DATA BY IOGIS

S. SCHMIDT and H.-J. Goetze (FU Berlin, Institut fuer Geologie, Geophysik und Geoinformatik, Maltesersstr. 74-100, D-12249 Berlin, Germany, email: sabine@geophysik.fu-berlin.de); R. Seidemann and A. Siehl (University Bonn, Geologisches Institut, Nussallee 8, D-53115 Bonn); A.B. Cremers, M. Breunig and S. Shumilov (University Bonn, Roemerstr. 164, D-53117 Bonn)

Three-dimensional (3-D) interactive modelling permits an integrated processing and interpretation of geoid, gravity and magnetic fields, yielding an improved geological interpretation. Generally these 3-D models are constructed by triangulated polyhedra with constant density and/or induced and remanent susceptibility. Interactive modifications of model parameters (model coordinates, rock density and susceptibility), access to the numerical modelling process and direct visualization of both, calculated and measured fields of gravity and magnetics, enable the interpreter to design the model as realistic as possible. An approach is described to integrate constraining data into the interactive modelling process by means of visualization and combination of independent data and information together with the density/susceptibility model. This visual combination of 2- and 3-D models (e.g. from seismic reflection or refraction surveys) enables a quantitative comparison and adjustment by the interpreter, and results in a model comprising as much independently derived information as possible. The definition of 'geo-objects', which link geoscientific vocabulary with geometrical elements of the model, provides a comfort environment for interpretations. The modelling method is embedded in an Interoperable Geoinformation System (IOGIS) which uses new object-oriented database management technique. As an example we show results from the southern Northwest German Basin.

**JWS33/W/18-B2** Poster **1635-27**

### DEKORP'S SEISMIC DATA IN THE INTERNET

Christian SEEGRAEF, (Lutz Lesch GeoForschungsZentrum Potsdam, email: seegraef@gfz-potsdam.)

At the GFZ Potsdam a working group was established in 1998 to prepare, archive, and protect seismic data sets, which were originally recorded on common 1/2 inch magnetic tapes, on modern storage media and provide them to the public and scientific community. This is achieved by the establishment of an online-available database. Seismic data in different processing stages (from the field tape to the final line-drawing) will be available for all collected surveys in trace as well as in graphical format together with related information such as coordinate tables, maps, geological interpretations, etc. Final results, such as migrated, depth-converted sections or line-drawings, are kept on a FTP-server for interested users. In addition a possibility should be managed to command data records online and receive them in the form of a CD-ROM. The prime aim is to provide a catalogue-like structure with download-facility using the modern information technologies that are or will be available in the near future.

**JWS33/E/15-B2** Poster **1635-28**

### GIS-BASED ANALYSIS FOR GEOPHYSICAL EXPLORATIONS: IMPROVING POSITIONAL AND ATTRIBUTE DATA MANAGEMENT

SHYLLON E. A., Olaleye J. B and Olunloyo V. O. S (Geoinformatics Laboratory, Faculty of Engineering, University of Lagos, Lagos, Nigeria.)

In a geophysical exploration, the position and attribute of subsurface features are defined using Two-Way-Travel (TWT) time(s) which are interpreted from 3D & 4D reflection seismology or other techniques such as refraction seismology, magnetic, gravity, etc. As a consequence, data management becomes a major task. Then faster means of analyzing and integrating the data sets, and presenting the results are required. A GIS is the means of achieving this for all geospatial data.

The GIS database takes a great variety of explorations geophysical data. In this paper, they are categorized and of many types. The categories distinguish seismic lines and shot points, Magnetic (Geomagnetism and Aeromagnetism), gravity, well log, etc. The data types distinguish such as stratified points samples, interpolated surfaces, etc.

The exploration geophysical data require careful preparation before input into the GIS database. This paper will treat advance data structuring technique of such complex data with position and highly dynamic attributes. It will discuss georeferencing of exploration geophysical data to the Earth system of coordinates; which must be accurate particularly if the results of international and national geophysical observations are to be integrated.

This GIS-based-analysis is a faster means of analyzing these data sets from various sources, and presentation of results to international and national geophysical communities.

**JWS33/W/19-B2** Poster **1635-29**

### A SPACEBASED OCEAN SURFACE EXCHANGE DATA ANALYSIS SYSTEM

Wenqing TANG and W. Timothy Liu (Jet Propulsion Laboratory, Caltech, email: wqt@pacific.jpl.nasa.gov)

Emerging technologies have provided unprecedented opportunities to transform information into knowledge and disseminate them in a much faster, cheaper, and user-friendly mode. We have set up a system to produce and disseminate high level (gridded) ocean surface wind data from the NASA Scatterometer and European Remote Sensing missions. The data system is being expanded to produce real-time gridded ocean surface winds from an improved sensor SeaWinds on the Quikscat Mission. The wind field will be combined with hydrologic parameters from the Tropical Rain Measuring Mission to monitor evolving weather systems and natural hazard in real time. It will form the basis for spacebased Ocean Surface Exchange Data Analysis System (SOSEDAS) which will include the production of ocean surface momentum, heat, and water fluxes needed for interdisciplinary studies of ocean-atmosphere interaction.

Various commercial or non-commercial software tools have been compared and selected in terms of their ability in database management, remote data accessing, graphical interface, data quality, storage needs and transfer speed, etc. Issues regarding system security and user authentication, distributed data archiving and accessing, strategy to compress large-volume geophysical and satellite data/image, and increasing transferring speed are being addressed. A simple and easy way to access information and derive knowledge from spacebased data of multiple missions is being provided. The evolving 'knowledge system' will provide relevant infrastructure to address Earth SystemScience, make inroads in educating an informed populace, and illuminate decision and policy making.

**JWS33/E/12-B2** Poster **1635-30**

### GEOPHYSICAL METADATA SYSTEM OF SLOVENIA

Bojan URAN (Geophysical Survey of Slovenia, Kersnikova 3, 1000 Ljubljana, Slovenia, email: bojan.uran@gov.si); Marjeta Car and Robert Stopar (Institute for Geology, Geotechnics and Geophysics, Dimi eva 14, 1000 Ljubljana, Slovenia, email: mcar@i-ggg.si, rstopar@i-ggg.si)

Geophysical investigations in Slovenia have a long tradition, but until recently we have not got a systematic overview on them. We started to collect data about geophysical investigations in Slovenia from different sources and organised them in a metadata system. The structure of the metadata follows European draft standard for georefered data, so it is easy to combine and correlate our data with geodetic and geologic data as separate layers inside the GIS system. The role of metadata is very important if we want to join data from different sources. It contains basic information of the dataset, its quality and availability. We added also data about geophysical methodology used, aim and scope of the investigations, investor(s), site location, keywords, accessibility of data, short abstract of the results etc. A lot of work and special attention has been paid to critical evaluation of the quality of the observed data and to the harmonised and consistent keyword system. The role of the latter is the possibility of quick and effective searching of data. Additionally, the gravity, geomagnetic, geothermal and geoelectrical resistivity maps have been added. The organisation of information system allows us to use for different purposes. On one hand, it as a metadata system with public access over the Internet. It uses three tier architecture, connecting user with web browser to WWW and database server. On the other hand, it is a full database system, including also raw data, for storage, processing and presentation of data with the GIS tools in an intranet inside the institution.

**JWS33/W/24-B2** Poster **1635-31**

### EVIDENCE FOR MULTIFRACTAL SCALING FROM GEOMAGNETIC DATA

Zoltan VOROS (Geophysical Institute SAS, Komarnanska, 947 01 Hurbanovo, Slovak Republik, email: geomag@geomag.sk); Peter Kovacs and Arpad Juhasz (Eotvos Lorand Geophysical Institute, Budapest, Columbus u. 17-23, Hungary, email: kovacs@elgi.hu)

The question of the higher order statistical analysis of geomagnetic data is propounded. Evidences for multifractal scaling laws describing scale-invariant statistical properties of "geomagnetic turbulence" are presented. The multifractal probability measure constructed from geomagnetic data proved to be singular and distributed on fractal support. The existence of multifractal structure in geomagnetic data is the signature of nonhomogeneous, intermittent energy transfer within the solar wind - magnetosphere - ionosphere system.

**JWS33/W/33-B2** Poster **1635-32**

### POLAR PATHFINDER DATA SAMPLER: NEW DATA FORMATS FOR INTEGRATIVE SCIENCE

Ronald L. S. WEAVER, I. Cheshire, R. Hauser, M. Meshek, M. Marquis, and A. Varani, (National Snow and Ice Data Center [NSIDC], CIRES, Campus Box 449, University of Colorado Boulder, Colorado, 80309); Siri Jodha Singh Khalsa, (Steven Myers and Associates, Space Science and Engineering Division, 9315 Largo Drive West, Largo, MD, 20774)

Impediments to the cross-disciplinary use of remote sensing data are the complexities of data formats, lack of common geographic and temporal referencing systems, and consistent timeseries over the course of a sensor's lifetime. In order to break down some of these barriers specifically found in polar-related remote sensing data, the NOAA-NASA Polar Pathfinder research teams, in conjunction with NSIDC staff embarked on an effort to integrate selected polar remote sensing data. It is a unique effort to provide data sets, which lower the cross-sensor use barriers due to differing geo-referencing, sensor resolution, and temporal schemes.

These data have been packaged on a CD-ROM, which contains selected animations for previewing large-scale atmospheric and surface condition changes. NSIDC has also produced a data access and browse tool based on the commercial off the shelf (COTS) product IDL.

**JWS33/W/35-B2** Poster **1635-33**

**THE BRITISH ATMOSPHERIC DATA CENTRE: DATA FOR UK ATMOSPHERIC SCIENCE**

Simon WILLIAMS and Lesley Gray (British Atmospheric Data Centre, Rutherford Appleton Laboratory, Chilton, Didcot, Oxon, OX11 0QX, UK, email: s.r.williams@rl.ac.uk)

This poster describes data services provided by the British Atmospheric Data Centre (BADC) to the atmospheric science community. We use the example of the support given to atmospheric chemists working on the UK ACSOE (Atmospheric Chemistry Studies in the Oceanic Environment) programme to illustrate the BADC's work. The BADC is the main archive for atmospheric data produced by the UK academic community, but it also holds over 1Tb of 3rd party data sets, such as observational and model data from the Met Office and the European Centre for Medium Range Weather Forecasts (ECMWF). Researchers use our WWW site to find data and then simply copy them over the Internet to their own computers. ACSOE is a research programme of the Natural Environment Research Council, which is working to improve the understanding of the marine atmosphere. Measurements have been made from a remote research station on the west coast of Ireland and from ships and aircraft offshore. The BADC has been actively involved since the outset of the programme and the poster gives an outline of the automatic archive and catalogue system provided by the BADC, which allows the ACSOE researchers to deposit their data and share them efficiently with collaborating groups. It also describes the forecast air parcel trajectories provided to ACSOE through the BADC which researchers found an invaluable aid in planning their measurements. The BADC is funded by the Natural Environment Research Council.

**Wednesday 28 July AM**

Presiding Chair: V Gitis (Institute for Information Transmission Problems, RAS, Moscow, Russia)

**EXTENDED POSTER VIEWING** **0900-1200**

**JWA34** **Tuesday 27 July**

**LONG TERM OCEAN BOTTOM GEOPHYSICAL OBSERVATORIES (IAGA, IASPEI)**

Location: Muirhead Tower G08 LT

**Tuesday 27 July AM**

Presiding Chair: A.W Green (US. Geological Survey, Denver, USA)

**LONG TERM OCEAN BOTTOM GEOPHYSICAL OBSERVATORIES**

**Introduction** **0900**

A.W Green (USGS, USA)

**JWA34/W/07-B2** **0910**

**SHORT CIRCUITING EARTH: A REVIEW OF GLOBAL SCALE GEOELECTRIC FIELD MEASUREMENTS USING SUBMARINE CABLES**

H. SHIMIZU (ERI, University of Tokyo, Tokyo, Japan, email: shimizu@eri.u-tokyo.ac.jp); L. J. Lanzerotti (AT&T Bell Laboratories, Murray Hill, NJ, USA); H. Utada (ERI, Univ. of Tokyo, Tokyo, Japan); and A. Chave (WHOI, Woods Hole, MA, USA)

Over the past decade, more than ten Pacific and three Atlantic submarine telephone cables have been instrumented to monitor the induced geoelectric voltage after their removal from commercial service. These time series are now of significant length, and have been applied to the study of space physics, deep geomagnetic, and oceanographic problems. Both Pacific and Atlantic cables have been used for studies of ionospheric and magnetospheric current systems. In particular, the geoelectric field induced across the Pacific TPC-2 cable (Hawaii to Guam) has been used for studies of the magnetosphere equatorial ring current, and the relationship of the ring current and the induced geoelectric field to interplanetary conditions outside the magnetosphere - the solar wind velocity and the interplanetary magnetic field. An empirical relation has been derived between the induced geoelectric field across this route and the energy input to the magnetosphere from the solar wind. The toroidal geomagnetic field strength and its variation at the CMB have been constrained using both the DC and slowly varying geoelectric potential with an assumed global electrical conductivity structure in the mantle. The constraints are consistent with the results of MHD geodynamo calculations. Regional conductivity structures beneath the Pacific have been estimated using data taken on the HAW-1 and western branches of TPC-1. These inputs are essential to construct a 3D conductivity model of the mantle.

**JWA34/W/01-B2** **0930**

**A JAPANESE CONTRIBUTION TO GLOBAL DEPLOYMENT OF OCEAN BOTTOM GEOPHYSICAL OBSERVATORIES (OHP PROJECT)**

Yoshio FUKAO (Earthquake Research Institute, University of Tokyo, Tokyo 113, Japan, email: fukao@eri.u-tokyo.ac.jp)

The Ocean Hemisphere network Project (OHP) is to establish geophysical observation networks centered on the western Pacific for seismology, geo-electromagnetism, and geodesy. Besides land stations now under construction the OHP network will have the ocean bottom observatories including three ODP borehole seismic stations. We have already established a network of seven retired submarine telephone cables for electrical potential

measurement. Construction of ocean bottom observatories requires various types of system development. (a) Borehole observation system: for the 1999 drilling program we developed a composite sensor string hanging a ultra-sensitive volumetric strainmeter, broadband seismometers, backup seismometers and tiltmeters. (b) Broadband seismometer system: we developed a self-popup system acoustically controlling the tilt of sensors and separation of pressure vessels, with a data logger having a memory capacity of 72 Gbytes. (c) Electromagnetic observatory: we developed a system of eight component geoelectromagnetic sensors with which a long-term observation was conducted at a water depth of 5400m, including an acoustic communication experiment at a data transfer rate of 1200 bps. (d) Crustal movement observation system: our experiment on acoustic distance measurement showed an accuracy of better than 1cm over a 1.35km long baseline on the sea floor, and the experiment on ocean bottom gravity measurement showed a residual fluctuation of 10 microGal after removal of tidal and drift effects. (e) Long-life power supply and acoustic transmission systems: we integrated a sea water battery and a pressure vessel submersible up to 6000m into a system for long-term observations, and completed a system of acoustic data transmission (4800 bps) and satellite communication via a buoy at the surface of relatively shallow ocean.

**JWA34/W/10-B2** **0950**

**GEOSTAR**

Dr Giuseppe Smriglio (Istituto Nazionale di Geofisica, Roma Italy Email: geostar.ing750.ingr.it)

(Geophysical and Oceanographic STation for Abyssal Research) is a project funded by European Commission in the 4th Framework Programme. Aim of the project is the development of the first prototype of a deep sea benthic observatory capable to carry out long-term (up to 1 year) scientific observations at abyssal depths (up to -6000 m). The project is splitted in two phases. The first phase (1995- 1998), was concluded with the demonstration mission in Adriatic Sea at 42m.w.d The second one (1999 - 2001), provides for the completion of the system to be able to operate in near real-time up to -6000 m and for the first long-term deep sea scientific mission scheduled during 2000 for 5-6 months at 3400 m in the Southern Tyrrhenian bathyal plain.. GEOSTAR is characterised by specific solutions enabling the execution of the deep sea mission. Among these solutions: a lightweight and modular frame, active devices for the deployment of specific packages, a dedicated data acquisition and control hardware, autonomous mission control capabilities, multiple possibilities of interfacing with external devices (satellite communication systems, deployment system) for continuous control of system status. The configuration of the Observatory, conceived to be a node of monitoring networks, is made up of two main subsystems: Bottom Station and Active Docker. The Bottom Station includes the acquisition and power systems, the communication system and hosts all the sensors. The Active Docker is a dedicated tool for surface-assisted deployment and recovery. The Bottom Station includes the acquisition and power systems, the communication system and hosts all the sensors, including geophysical, geochemical and oceanographic instruments. The scientific and technological solutions adopted in the first project phase and planned for ongoing second phase are presented and discussed.

**JWA34/W/06-B2** **1010**

**MOISE: A FIRST PROTOTYPE OF A MULTIPARAMETER OCEAN BOTTOM OBSERVATORY**

Amal SEBAI, El'eonore Stutzmann, Wayne Crawford, Jean-Paul Montagner, Genevi'eve Roul, Jean-Francois Karcewski (all at IPGP, Dept.Sismologie, UMR7580, 4 Place Jussieu, 75252 Paris05, France.) Jean-Louis Thiret, Pascal Tarits (both at Universit'e de Bretagne Occidentale, UMR6538, BP809, Brest 29285, France.), Barbara Romanowicz (at UCB Seismological Laboratory, Berkeley CA 94720, U.S.A.), Debra Stakes (MBARI, PO Box 628, Moss Landing, CA95039-0628, U.S.A.).

During the international co-operative pilot experiment MOISE (Monterey Bay Ocean Bottom Seismic Experiment), diverse geophysical data sets were recorded, including seismic signal, temperature, pressure, magnetic field. The experiment successfully conducted from June to September 1997 demonstrates that it is now possible to install of a permanent broadband seismic and geophysical observatory at the bottom of the ocean. The seafloor seismic noise level is comparable to terrestrial station noise for periods smaller than 1 sec. At longer periods, the noise level remains low on the vertical component up to 30 sec, and increases at longer periods. The seismic noise level remains stable during the experiment but varies strongly during the day.

For the three seismic components, the pressure, temperature, current velocity and magnetic field are highly coherent at very low frequencies (below 0.04m Hz), as a consequence of tidal effects. In the frequency range 0.1-0.3m Hz, the seismic signal is more coherent with temperature and pressure than with current velocity or vertical magnetic field. The coherence with temperature breaks down below 0.5mHz.

We also combine pressure signal from an hydrophone installed next to the MOISE observatory with the seismic data to investigate crustal

**JWA34/W/12-B2** **1050**

**A NEW WAY OF REAL-TIME SEISMIC MEASUREMENT: THE GEO-TOC IZU CABLE OBS USING TPC-1, A DECOMMISSIONED SUBMARINE CABLE BETWEEN JAPAN AND GUAM**

Junzo KASAHARA, Toshinori SATO, Hisashi Utada (all at ERI, University of Tokyo, 1-1-1, Yayoi, Bunkyo, Tokyo, Japan, e-mail: kasa2@eri.u-tokyo.ac.jp ; satot@eri.u-tokyo.ac.jp ; utada@eri.u-tokyo.ac.jp); Hajimu Kinoshita (JAMSTEC, 2-15 Natsushima, Yokosuka, Japan, email: jimmy@jamstec.go.jp)

In order to obtain precise images of earthquake generation, tectonics at plate boundaries, and the Earth's deep structures, real-time geophysical measurements in the ocean are required. To achieve the above objectives, we used a decommissioned submarine cable, TPC-1, which runs between Japan and Guam. The cable length is 2,700km. Using TPC-1, an OBS was successfully installed at 2,800m deep on the landward slope of the Izu-Bonin Trench in 1997. The OBS contains three accelerometers, single hydrophone, and a water pressure-temperature sensor. When a Mw6.1 earthquake occurred just below the station at 80 km-deep, accelerometers showed co-seismic and gradual changes after the main shock onset. A pressure sensor showed a 50 cm sea-level change during the earthquake. This suggests a high possibility detecting silent earthquakes or earthquake precursors if they exist. These activities proved that decommissioned submarine cables are great global resources for real-time geophysical measurements on a deep-sea floor. Using such decommissioned submarine cables, cost-effective, real-time measurements will be realized.

**JWA34/W/11-B2** **1110**

**MULTI-DISCIPLINARY GEOPHYSICAL MEASUREMENTS ON THE OCEAN FLOOR USING DECOMMISSIONED SUBMARINE CABLES: VENUS PROJECT**

Junzo Kasahara ( University of Tokyo, Yayoi, Bunkyo, Tokyo, Japan; email: kasa2@eri.u-tokyo.ac.jp); Yuichi shirasaki(k-marine co., Ltd., Nakameguro, Meguro, Tokyo, Japan; email: sirasaki@k-marine.co.jp); Ryoichi iwase, and katsuyuki kawaguchi (both at Jamstec, 2-15

natsushima, yokosuka, Japan, email: iwaser@jamstec.go.jp ; kawak@jamstec.go.jp)

The deployment of an ocean floor geophysical and Multi-disciplinary real-time observatory has been Attempted by reuse of a decommissioned submarine Cable. The venus project reuses the tpc-2, which is one of decommissioned submarine coaxial-cable Systems and runs across the entire philippine sea Plate between guam island and okinawa island. The cable length is 2,500km. The venus system Comprises i) seven sensor units, ii) junction Box, iii)data-telemetry unit, iv)data-coupling Unit, v)main coaxial cables, vi)shore station, And vii) yokosuka data center. There are eight Sensor units including broadband seismometers. The data obtained by the ocean floor observatory Will be transmitted to the yokosuka data center Through the shore cable station. A part of the Bottom equipment was deployed at 2,200 m deep of The landward slope of the ryukyu trench in fall, 1998 and 12 hours tsunami data were obtained. The Tsunami data showed that the system worked well. The whole system is planned to be re-deployed in Summer, 1999.

**JWA34/E/05-B2** Invited **1130**

**THE NEED FOR OCEAN BOTTOM GEOMAGNETIC OBSERVATORIES WITH GOOD BASELINE CONTROL**

GREEN, Arthur W., (U.S. Geological Survey, Golden, CO, USA)

A recent study concluded, that to produce a spherical harmonic model of the Earth's main field with an error range of from 7 to 11 nT would require about 92 high quality observatories evenly spaced around the globe. The spacing would be about 20 degrees. An inventory of existing observatories showed that to achieve the uniform distribution of 92 observatories, some existing sites must be upgraded to INTERMAGNET standards, and that 40 new observatories must be established, of which 8 would be in remote, deep ocean areas. To meet modeling needs, each ocean bottom observatory should have baseline control of less than 5 nT over periods of many years. This would be accomplished by taking weekly measurements by means of independent absolute instruments such as a Declination-Inclination magnetometer and a Proton magnetometer. This process requires accurate knowledge of the local vertical and of the direction of Geographic North. In this paper, we examine the effects of various distributions of observatories and suggest how absolute measurements may be made on the ocean bottom without celestial references.

**JWA34/W/09-B2** **1150**

**THE FRENCH PROGRAM OF SEAFLOOR GEOMAGNETIC OBSERVATORIES**

Pascal TARITS (UBO/IUEM, UMR CNRS ' Domaines Oceaniques' Place Nicolas Copernic, Brest F-29280, France, email: tarits@univ-brest.fr); Mioara Alexandrescu (IPGP, Observatoire Magnetique de Chambon La Foret, Beaune la Rolande F-45340, France , email: mioara@ipgp.jussieu.fr); Dt Insu team (Division Technique de l'INSU)

The accurate determination of the main magnetic field and its secular variation at the global scale remains limited by the number of observatories and their poor distribution over the Earth's surface, particularly over the ocean areas. This biases significantly the determination of the source field geometry even at very long wavelength. We present results illustrating the importance of semi-permanent geomagnetic observatories on islands and seafloor to describe globally the main magnetic field and its secular variation. While the technology to install semi-automatic observatories on islands already exists, seafloor geomagnetic observatories are not yet available for installation. In France, a collaborative action is undertaken to build a semi-permanent seafloor observatory that matches the INTERMAGNET measurement requirements. This observatory comprises a triaxial variometer and an Overhauser magnetometer measuring absolute total field intensity. The main difficulty remains the measurement of the geomagnetic declination, which needs a known geographical reference within a few tens of arc-seconds. We show that the declination may be obtained using a precise mechanical gyro. Preliminary tests to reach this level of precision are presented.

**JWA34/E/02-B2** Invited **1210**

**FULLY AUTOMATIC ABSOLUTE MAGNETOMETER SUITABLE FOR SEA-BOTTOM USE**

JEAN L. RASSON, (Institut Royal Meteorologique, Centre de Physique du Globe, B-5670 Dourbes Belgique)

In this talk, we present our ongoing project to build a fully automatic absolute observatory magnetometer suitable for sea-bottom use. We specifically address the problems of finding true North automatically and of making unattended Diffux measurements. We show that the magnetic cleanliness problems can be solved. Also addressed are the methods of installation and deployment. The dimensions are compatible with cylindrical high-pressure casing.

**JWA34/E/08-B2** **1230**

**DEVELOPMENT OF A SEAFLOOR POSITIONING SYSTEM WITH GPS-ACOUSTIC LINK**

Koichiro OBANA, Hiroshi Katao and Masataka Ando (Disaster Prevention Research Institute, Kyoto University, Gokasho, Uji 611-0011, Japan, email: obana@rcep.dpri.kyoto-u.ac.jp)

The observation of seafloor crustal deformation will contribute significantly to understanding the nature of the tectonic processes at the plate boundaries. We develop a seafloor positioning system for crustal dynamics observation. This system consists of two main components; (1) surface positioning by differential GPS and (2) precise acoustic ranging using the M-sequence between the surface and seafloor references. In this system, the position and attitude (heading, pitch and roll) of the surface GPS-acoustic link unit is determined by the differential GPS observation. The surface unit equips with an acoustic transducer and performs acoustic ranging for the seafloor references. The two-way acoustic travel time between the surface and seafloor is measured. The positions of seafloor references are determined from these observations and assumed sound-speed structure model of the sea water. We performed preliminary seafloor positioning tests. The locations of seafloor reference units are determined as to minimize the two-way travel time residual using the least square method. In these analyses, we used simple 1-D sound-speed structure models. The results show that the positions of the seafloor references are estimated with a ten centimeter-level accuracy. The systematic trend still remains in the residuals. It is important to apply the "real" sound-speed model for more precise positioning.

**LONG TERM OCEAN BOTTOM GEOPHYSICAL OBSERVATORIES**

**JWA34/L/01-B2** Invited **1400**

**AUTOMATICS PRECISION NORTH SEEKER**

GUSINSKY

Abstract not available at time of going to press

**JWA34/E/07-B2** **1420**

**DESIGN FOR AN OCEAN BOTTOM GEOMAGNETIC OBSERVATORY WITH GOOD BASELINE CONTROL**

GREEN, Arthur W., U.S. (Geological Survey, Golden, CO, USA, e-mail: awgreen@gldfs.cr.usgs.gov); Alan Chave, Woods Hole Oceanographic Institution, Woods Hole, MA, USA e-mail: alan@faraday.whoi.edu)

In a previous paper in this session we demonstrated the need for geomagnetic observatories with good baseline control at selected ocean bottom sites. In this paper, we describe an ocean bottom system which will provide the required data to INTERMAGNET standards. The system will be set in place by a Remotely Operated Vehicle (ROV) in depths of 5000 meters or more and will have a lifetime of 4 years or more. After 4 years, the entire system, including the battery package, will be retrieved and replaced by a new system. The data, which consist of one minute filtered values of the three components of the magnetic field plus total field, will be recovered at 6 to 12 month intervals by acoustic interrogation from oceanographic "ships of opportunity". At very remote locations, data recovery will be by messenger buoys which periodically float to the surface and communicate by radio with polar orbiting satellites. We also show how the local vertical and Geographic North may be obtained on the ocean bottom, thus permitting an automated absolute instrument, such as a Declination-Inclination Magnetometer (DIM), to automatically make periodic absolute measurements.

**JWA34/W/04-B2** **1440**

**JAPANESE RESEARCH INITIATIVES IN THE NANKAI TROUGH**

Yoshiyuki KANEDA and the Frontier Research Program for Subduction Dynamics (Japan Marine Science and Technology Center, 2-15 Natsushima-cho, Yokosuka, Japan, email: kaneday@jamstec.go.jp)

More than 80% of the seismic foci of large (M>7) earthquakes around Japan are located in the vicinity of ocean trenches and troughs. It is well known that the Nankai Trough area, offshore southwestern Japan, is one of the most dangerous parts of the world in terms of destructive subduction zone earthquakes. The last earthquakes in the Nankai Trough occurred in 1944 and 1946, and are thought to be successive ruptures in a narrow region along the Nankai Trough. The repeatability of earthquakes in the Nankai Trough region is well established through historical records.

A major effort of the Japanese marine seismological community is the determination of detailed seismic structure in the Nankai Trough region, in order to delineate the seismogenic zone there. Japanese and American scientists will collaborate in a 3-D seismic survey by the US R/V M. Ewing this summer, which will done in combination with refraction and wide-angle surveys using Japanese OBS's. Additional research facilities which are involved in the effort to study the Nankai Trough include: a 150-channel MCS system, more than 100 pop-up OBS's, and a line of cable-connected long-term ocean bottom observatories, which includes three seismographs, two tsunami gauges and other instruments about 120 km to the south of Cape Muroto (Shikoku, Japan). These are utilized in combination with ROV's, manned submersibles, and other conventional research vessels for detailed studies of the Nankai seismogenic zone. the bandaurora and tanspolar arc sometimes occur.

**JWA34/W/08-B2** **1500**

**H2O: THE HAWAII-2 OBSERVATORY**

A.D. CHAVE (Woods Hole Oceanographic Institution, Woods Hole, MA 02543, USA; e-mail: alan@whoi.edu) R. Butler (IRIS, 1200 New York Ave NW, Washington D.C. 20005, USA); F.K. Duennebieber (SOEST, University of Hawaii, Honolulu, HI 96822, USA)

A permanent deep ocean scientific research facility--the Hawaii-2 Observatory or H2O--was installed on a retired submarine telephone cable in September 1998. H2O receives power and communications from a 1960's vintage analog submarine telephone cable. The facility consists of a seafloor junction box located in 5000 m of water near 28°N, 142°W, or about halfway between Hawaii and California. The junction box derives 400 watts of power from the cable and provides bi-directional real time communications through six digital and two analog ports. The H2O junction box is a "smart" design which incorporates full control of instrument and junction box functions from shore. Instruments may be connected to the junction box at wet-mateable connectors using a remotely-operated vehicle. Initial instrumentation at the H2O site includes a broadband three-component seismometer, a short period geophone, a standard hydrophone, and ancillary instruments.

H2O was installed from a large research vessel using the Jason ROV for most installation functions. Initially, the ROV located the cable and cut it at a pre-chosen point for subsequent recovery using the ship's trawl wire. A termination with wet-mateable connector was spliced onto the end of the cable. The termination was then redeployed to the seafloor. The junction box and scientific package were placed nearby and wired up using Jason. Finally, the seismometer was hydraulically buried beneath the sediment-water interface by the ROV.

**JWA34/W/05-B2** **1540**

**RECENT DEVELOPMENTS IN OCEAN BOTTOM SEISMOMETERS AND SEISMIC SENSORS**

Spahr C. WEBB, (Scripps Institution of Oceanography, UCSD, La Jolla, CA 92093. E-mail: scwebb@ucsd.edu)

The ocean floor is a peculiar place to put seismometers or other seismic sensors. The noise climate is different from land, sites are remote and rugged and energy is limited. I describe systems, sensors and strategies optimized for the ocean floor. Recent developments include a broad band pressure sensor, a low power, low noise, low cost, broad band seismic sensor derived from a short period sensor, a long period ocean bottom seismometer based on a LaCoste Romberg gravimeter, and a broad band OBS based on a STS-2. Wave and wind climate determine noise levels at seafloor sites. Some strategies for reducing effective noise levels and for siting instruments are described.



JWA34/E/06-B2

1600

**"CORK" BOREHOLE OBSERVATORIES TO STUDY SUBSEAFLOOR HYDROGEOLOGY**

Keir BECKER (RSMAS, University of Miami, Miami, FL 33149, USA, email: kbecker@rsmas.miami.edu) and Earl Davis (Geological Survey of Canada, PO Box 6000, Sidney, BC, Canada, email: davis@pgc-gsc.nrcan.gc.ca)

CORKs or "Circulation Obviation Retrofit Kits" are hydrogeological observatories that seal ODP boreholes and allow long-term observations to be made with seafloor pressure and temperature sensors and fluid samplers; the instrumentation can be utilized for long-term monitoring of fluid flow processes and direct testing of formation properties using seafloor tidal loading signals or pumps deployed from submersibles. Since 1991, 13 CORKs have been installed in three characteristic seafloor hydrologic settings: the Middle Valley sedimented ridge hydrothermal system on the Juan de Fuca Ridge, accretionary prisms of the Cascadia and Barbados subduction margins, and, ridge-flank hydrothermal systems in young oceanic crust east of the Juan de Fuca Ridge and west of the Mid-Atlantic Ridge. We will review the results, which confirm prior inferences that fluid flow is a key process in all these settings, and clearly demonstrate that the driving forces, permeability structures, and styles of fluid flow vary greatly among settings. We will also discuss plans for future CORKs and opportunities for integration with other seafloor observatory objectives. Major changes are in progress for future Advanced CORKs, to allow for multi-level monitoring in single holes, serviceability by wireline vehicles, and enhanced sensor/sampler capabilities. These changes will allow a greater range of scientific objectives (e.g., in situ studies of gas hydrates and subsurface microbiology) to be addressed with Advanced CORKs that incorporate seal spacing corresponding much more closely to natural permeability structures.

JWA34/W/02-B2

1620

**ABSOLUTE PROTON OVERHAUSER MAGNETOMETERS: DESIGNS AND PROPETIES**

Vladimir SAPUNOV, Dmitry SAVELIEV, Sergey Kiselev, Alex Denisov, Olga Dekusar (Ural State Technical University, Quantum Magnetometry Laboratory, Mira St., 19, Ekaterinburg, 620002, RUSSIA, email: sva@dpt.ustu.ru)

The total geomagnetic field Overhauser's magnetometers are promising for the long term ocean bottom observatories due to low power (1-3 Wt), high sensitivity (0.1 - 0.01 nT), low drift (up to 0.05 nT/year) and precision measurements (absolute accuracy 0.1-1 nT).

In this report, designs and properties of the LETI, GEM Systems, USTU and DTU sensors and magnetometers are considered. The free radicals DNP and ESR properties are a cause for choose of magnetometer mode and/or sensor's design.

The QMLab series of the processor Overhauser sensors POS was developed for observatories and ground application. These magnetometers and gradiometers interfaced only via RS232 port and based on unified proton Larmor counter (0.001 nT resolution at 3 sec sample rate, 0.5 Wt power, size 80x120x15mm). Report presents an actual digital processing of proton signals that afford high sensitivity and broadband operation.

The design of the omnidirectional marine proton Overhauser sensor is submitted. Sensor contains a new stable free radical with very long lifetime up to 10 years. This radical allows to design world's smallest size Overhauser sensors.

JWA34/E/10-B2

1640

**CALIBRATION OF OCEAN BOTTOM MAGNETOMETER**

Valery KOREPANOV and Fedir Dudkin (Lviv Centre of Institute of Space Research, 5-A Naukova str., 290601, Lviv, Ukraine, e-mail: vakor@isr.lviv.ua)

The study of Earth's magnetic field structure around the Globe is one of the most important geophysical problems. Taking into account that 2/3 of the Globe is covered by World Ocean, the installation necessity of long-term autonomous ocean bottom magnetometers is obvious. Practically all technological problems connected with such magnetometers construction, manufacturing, deployment on the bottom and data exchange are sufficiently resolved. The only moment is still waiting appropriate solution - in-situ magnetometer calibration. Here two tasks arise: knowledge of the exact magnetometer axes orientation in order to reduce its data to geomagnetic coordinates and magnetometer calibration: its long-term drift should not surpass 0.005% of the total measured value. The first task seems to be easy to solve with necessary exactness using modern tiltmeters and some mathematics transformations. The attempts to solve the second one trying to automatize the commonly used procedure of absolute measurements are undertaken now but no satisfactory practical results are still obtained. Also the idea to make calibration of the bottom magnetometer using space-born magnetometers of low orbiting satellites was reported. The detailed investigations of the method showed that at present state of its development there is no hope to get necessary calibration precision. Further development of such method is discussed in the report. A floating or towed platform is proposed containing three exact devices: star imager for orientation determination, GPS receiver for platform positioning and reference magnetometer. The possible errors of each device and of the whole system are analyzed, taking into account the main disturbing effects: sea surface and floating platform constant motion and light refraction. The primary estimation is made that practical implementation of the method is possible.

JWA34/E/04-B2

1700

**MAGNETIC FIELDS INDUCED BY STEADY FLOWS AND BY ACOUSTIC WAVES IN THE OCEAN**

Arthur W. GREEN (USGS Denver Federal Center, MS 966 Box25046, USA) Yuri Kopytenko, Polina Serebryanaya, Lidia Nikitina (SPbF IZMIRAN, Muchnoi 2, St.-Petersburg, 191023, Russia, e-mail: gorbunov@neva.spb.ru)

Large vortices are generated along sea and ocean streams and have typical flow velocities of about 0.5 m/s. It was shown that the large-scale structures on a water-area in the presence of Earth's magnetic field induce quasicontant magnetic fields of the order of 10 -100 nT that depend on scale of structures and velocity of flow. It can be used in studies of such physic characteristics of large-scale vortex structures at a water area as, for example, scales and velocities of vortex structures and currents. It was shown that variable magnetic field has the same temporal dependence as the velocity field. This conclusion can be used by consideration an interaction of rarefaction-compression waves on acoustic frequencies with undisturbed ocean surface. The magnitude of induced magnetic field generating by LF acoustic wave was estimated as 0.1pT. Recently investigations of action of acoustic waves on jets or wakes showed a possibility of resonance amplification of turbulent pulsations on acoustic frequencies. This leads to resonance growth of turbulent velocity in a vortex at the forcing frequency. The increase of turbulent velocity by several orders will lead to corresponding amplification of pulsation amplitude of magnetic field under the action of rarefaction-compression wave. The magnetic field can reach to 0.1 81 nT. It can give a useful information about nature processes, accompanying by LF acoustic waves (from earthquakes, aircraft, from active atmospherical formations as typhoons, cyclones).

JWA34/E/03-B2

1720

**INDUCED MAGNETIC FIELDS OVER UNDERWATER VOLCANOES**

Arthur W. GREEN (USGS Denver Federal Center, MS 966 Box 25046, USA) Yuri Kopytenko, Polina Serebryanaya, Lidia NIKITINA (SPbF IZMIRAN, Muchnoi 2, St.-Petersburg, 191023, Russia, e-mail: gorbunov@neva.spb.ru)

It is known that underwater volcanoes activity leads to the appearance of hot-water areas. Hot jet interacting with ambient media creates mesoscale flows over underwater seismic zones. The process of mesoscale flows formation was considered and the basic hydrodynamical parameters of the flow were estimated. In the presence of Earths magnetic field different structures of flow (such as stream or vortex) in conducting sea water induce quasicontant magnetic fields of the order that depends on scale of structures and velocity of flow. Value of magnetic fields induced by mesoscale flow were is about 100 nT. Intensification of tectonic activity near faults and under-water volcanoes is accompanied by rarefaction-compression waves at frequencies in a band 1 - 100 Hz. It is known from laboratory experiments that a strong rarefaction-compression wave interacting with flow leads to resonance amplification of turbulent velocities on forcing frequency. The average amplification of the spectrum is more than 20 dB. Magnetic field has the same temporal dependence as the velocity field. Hence, the increase of turbulent velocity by several orders will lead to corresponding amplification of amplitude of variable magnetic field under the action of rarefaction-compression wave and magnetic fields achieve values of 100 pT. We believe the fluid structures over underwater volcanoes can be used as an indicator of seismic activity of a sea bottom by measuring of anomalous magnetic fields.

JWA34/E/01-B2

1740

**DEEP-WATER ELECTROMAGNETIC UNIT WITH ON-SHORE DATA GATHERING FOR BAYKAL RIFT GEOPHYSICAL STUDY**

Vitaly S. SHNEYER, Igor L. Trofimov and Sergey P. Gaidash (Geelectromagnetic Research Institute of Russian Academy of Sciences, p.o.box 30, Troitsk, Moscow Region, 142092 Russia, email: shneyer@geo.igemi.troitsk.ru, gaidash@helios.izmiran.rssi.ru); Leonid L. Vanyan and Vladimir Kh.Rucol (Shirshov Institute of Oceanology of Russian Academy of Sciences, Nakhimovskiy pr., 36, Moscow, 117851 Russia, email: vanyan@geo.sio.rssi.ru); Vladimir A.Zhukov, Andrey I.Panfilov (Nuclear Research Institute of Russian Academy of Sciences, pr. 60-letiya Octjabrja, 7a, Moscow, 117312 Russia)

We are developing a new method of deep-water measurements with on-shore data gathering of electromagnetic fields for magnetotelluric soundings and seismo-electromagnetic monitoring of geodynamical processes. It is different from traditional method, when full autonomous instruments are used. The advantage of this metod compare with autonomous methods is possibility to get deep-water information in the real time and to control of measuring process. Intracontinental Baykal rift zone is very interesting object for geophysical investigation. Deep-water complex of neutrino telescope NT-200 had been set up 10 years ago on the lake bottom at South-Baykal depression near of deep tectonic fracture . Deep-water unit NT-200 is well connected with data collecting coastal center. In this site will be set up the electromagnetic unit, which consist of three-component electric field instrument and total magnetic field vertical gradient unit. For electromagnetic digital data trasmission the telecommunication lines of NT-200 will be used. The depth of lake at the setting site is 1360 m; the distance from coast is 3600 m. Instruments will be lowered down the lake bottom in winter season through ice hole with NT-200 ancillary equipment use.

JSA35

Monday 26 July

**MIDDLE ATMOSPHERE ELECTRODYNAMICS: INFLUENCES AND PROCESSES (IAGA, IAMAS, SCOSTEP)**

Location: Gisbert Kapp, NG16 LR2

Monday 26 July AM

Presiding Chair: R.Goldberg (NASA/GSFC, Greenbelt, USA)

JSA35/W/08-B1

Invited

0900

**RECENT MULTI-INSTRUMENT OBSERVATIONS OF LAYERING IN THE MLT REGION ABOVE ARECIBO**

KANE, Prof Tim (Penn State, Email: tj7@psu.edu)

During the past year, considerable observational data concerning layering of both neutral and charged constituents above Arecibo, Puerto Rico have been obtained. These include measurements taken by incoherent scatter radar (ISR), VHF coherent scatter radar, lidar, airglow imagers and rocket-borne in-situ payloads. These data shall be presented and probable correlations/causes shall be discussed.

JSA35/E/03-B1

Invited

0930

**ON THE VARIABILITY OF POSITIVE AND NEGATIVE IONS IN THE MIDDLE ATMOSPHERE**

Ernest KOPP (University of Bern, Sidlerstrasse 5, CH-3012 Bern, Switzerland, email: ernest.kopp@phim.unibe.ch)

Primary ions result from ionization of abundant neutral N<sub>2</sub> and O<sub>2</sub> producing N<sub>2</sub><sup>+</sup>, N<sup>+</sup>, O<sub>2</sub><sup>+</sup>, and O<sup>+</sup>. The only but important exception from this is the production of NO<sup>+</sup> by Lyman- $\alpha$  in the mesosphere. Due to a relatively large neutral density below an altitude of 90 km three body reactions become important and the primary ions are transferred to large families of positive and negative ions in a fraction of seconds. This chemistry is controlled by less abundant neutrals such as H<sub>2</sub>O, O<sub>3</sub>, NO, HCl, HNO<sub>3</sub>, H<sub>2</sub>SO<sub>4</sub> in the abundance range of ppm to ppt. Ions are lost by recombination with electrons or ions, and in the stratosphere loss to liquid or solid aerosol surfaces becomes important. Even though the neutral density changes between the mesopause (90 km) and the tropopause (15 km) by a factor of 105 the ion density varies less than two orders of magnitude around 103 cm<sup>-3</sup>. Due to this large decrease of mixing ratios of ions to neutrals, mass spectrometric measurements are much more difficult at lower altitudes.

This review will concentrate on positive and negative ion chemistry in the mesosphere and stratosphere, the natural variability and changes due to the presence of aerosol particles.

## INTER-ASSOCIATION

**JSA35/E/04-B1** Invited **1010**

### CHARGED DUST PARTICLES IN THE EARTH'S MESOSPHERE

Ove HAVNES (Faculty of Science, Department of Physics, University of Tromsø, N-9037 Tromsø, Norway)

The Earth's polar mesosphere is the site of several strange phenomena such as noctilucent clouds and anomalous radar backscattering layers. They occur at heights between 80 and 90 km during the summer season when the mesosphere temperature is low. In situ measurements by rockets have shown that charged dust particles can be present in large numbers and that they can totally dominate the local charge balance. The dust may have positive or negative charges at different occasions. We will discuss the nature of the mesospheric dust, its charges and charging mechanisms, size distribution, number density and influence on other mesospheric phenomena. We have no direct knowledge of the material and structure of the dust particles. Although ice probably is a major constituent other elements with much lower work functions for photoionization must be present in the dust to explain the posit. The dust clouds have similar structure as the radar backscattering layers, which they seem to be closely associated with. The overall cloud thicknesses are of the order of a few km with much internal structure down to thin layers and "holes" of only a few meter thickness. We will discuss the structure of the dust clouds and the effects and forces which influence the structure of them.

We expect to be able to present results from rocket launches during the summer '99, aimed at dust and plasma conditions at different phases of the radar backscattering and noctilucent cloud layers.

**JSA35/W/02-B1** Invited **1050**

### LARGE MIDDLE-ATMOSPHERE ELECTRIC FIELDS AND THEIR RELATIONSHIP TO DUST PARTICLES

Alexander M. ZADOROZHNY (Novosibirsk State University, Pirogova 2, Novosibirsk, 630090, Russia, E-mail: zadorozh@phys.nsu.ru)

During the last two decades, different groups have carried out more than fifty rocket measurements of vertical electric fields in the middle atmosphere with different instruments. In about a half of these measurements a mesospheric maximum of vertical electric field of the order of a few V/m has been observed. In this paper all available rocket measurement data of the vertical electric fields in the middle atmosphere are analysed and a possible mechanism of generation of the fields caused by gravitational sedimentation of charged dust particles is discussed. There are many experimental evidences of the existence of charged dust particles both in the lower mesosphere and in the polar summer mesopause. Simultaneous measurements of the electric field strength, positive ion density and aerosols point out both an ion-aerosol interaction and a connection between the mesospheric electric fields and dust particle content. The observed height correlation of the electric field disturbances with the noctilucent cloud (NLC) position also indicates the importance of the dust particles in the generation of the vertical electric fields under NLC conditions. The simultaneous existence of both negative and positive multiply charged dust particles of different size is assuming for explanation of the V/m vertical electric fields. In this model, more massive charged particles falling with larger velocities initiate a charge separation. Smaller particles carrying charges of other sign are need to reduce the effective conductivity of the atmosphere. The proposed model could explain the existence of the large vertical electric fields observed both in the lower mesosphere and in the NLC vicinity. In both cases, the model predicts the effective conductivity of the atmosphere, which is about two to three orders of magnitude less than the measured ion conductivity.

**JSA35/W/01-B1** **1120**

### EFFECTS OF ELECTRIC FIELDS ON MIDDLE ATMOSPHERE AEROSOLS

S. KIRKWOOD, (Swedish Institute of Space Physics, Box 812, 981 28 Kiruna, Sweden.)

The role of magnetospheric electric fields in producing and modifying sporadic-E layers has become well established in recent years. Such sporadic-E layers are usually observed at heights 95-11 km but have been observed as low as 89 km. In summer, charged aerosol layers (PMSE and NLC) are known to form at only slightly lower altitudes (80-90 km). The expected effects of magnetospheric electric field on PMSE height are significant. Simulations and comparisons with observations (daily variation and specific events) will be presented. It is also of interest to consider whether electric fields can affect stratospheric aerosol layers, such as polar stratospheric clouds at 20- 30 km altitude. Aerosol mobilities at these heights are a thousand times less than at 80-90 km. However, the vertical electric fields are a thousand times stronger. Simulations of expected effects will be presented.

**JSA35/W/05-B1** Invited **1140**

### ELECTRIC FIELDS IN THE POLAR CAP AND CUSP AND THEIR LIKELY EFFECTS ON THE MIDDLE ATMOSPHERE

NILSSON, (Swedish Institute of Space Physics, Box 812, 981 28 Kiruna, Sweden, email: hans.nilsson@irf.se)

The cusp and polar cap ionosphere are the regions in the Earth's upper atmosphere most directly connected to the solar wind / magnetosheath. The source (generator) at the magnetopause is coupled to the load (the ionosphere) through field-aligned currents along a simple magnetic topology. The electric field in the ionosphere will therefore be strongly correlated with source region conditions and thus with interplanetary conditions. However, ionospheric conductance will determine the ionospheric response time and therefore the characteristic time scale of electric field variations observed in the Earth's ionosphere. A short review of the ionospheric electric fields of the cusp and polar cap typically associated with varying solar wind conditions will be presented. For example the signature of a strong well defined flow channel (150 mV/m over 200 km and a very sharp decline of the E field at the borders) will be shown. Finally a brief survey of expected effects in the middle atmosphere will be presented.

**JSA35/E/08-B1** **1210**

### INTERACTION BETWEEN THE GLOBAL ATMOSPHERIC CIRCUIT AND IONOSPHERE-MAGNETOSPHERE PHENOMENA

Evgenia BELOVA, Sheila Kirkwood (MRI Atmospheric Research Programme, Swedish Institute of Space Physics, Box 812, SE-981 28 Kiruna, Sweden, email: belova@irf.se); Tapio Tuomi (Department of Geophysics, Finnish Meteorological Institute, Helsinki, Finland); Hannes Tammet (Department of Environmental Physics, Tartu University, Tartu, Estonia)

Ionosphere-magnetosphere disturbances at high latitudes, such as magnetic substorms, are accompanied by energetic particle precipitation, strong variations of the ionospheric electric

fields and currents. It can result in changed distribution of ionospheric conductivity that can essentially influence the state of the global electric circuit. The aim of this work is to investigate the probable effect of ionosphere-magnetosphere disturbances on atmospheric electricity elements. For this purpose the data of air-earth electric currents were analysed together with the magnetic data. The air-earth electric currents were measured using the similar methods at two points in Northern Scandinavia (Esrange, 68°N, 21°E, Sweden and Sodankylä, 67°N, 27°E, Finland) for time interval from August 1998 to June 1999. The data were sorted to exclude the influence of near-earth winds and others atmospheric factors. Some correlation between the strong magnetic disturbances and variations of the air-earth electric currents was found. Theoretical estimates of magnetic substorm effect on electric current were obtained and compared with observed ones.

**Monday 26 July PM**

Presiding Chair: S.Kirkwood (Swedish Institute of Space Physics, Kiruna, Sweden)

**JSA35/W/06-B1** **1400**

### VARIATIONS OF ATMOSPHERIC ELECTRIC FIELDS IN THE NEAR-POLE REGION RELATED TO THE INTERPLANETARY MAGNETIC FIELD

Alexander Frank-Kamenetsky and Oleg TROSHICHEV (both at Arctic and Antarctic Research Institute, 199397, St.Petersburg, Russia, email: olegtro@aari.nw.ru); Gary Burns (Australian Antarctic Division, Hobart, Tasmania, email: gary\_bur@antdiv.gov.au); Volodya Papitashvili (Space Physics Research Laboratory, University of Michigan, Ann Arbor, MI 48109-2143, USA, email: papita@umich.edu)

The atmospheric vertical electric fields  $E_z$  observed at the Russian Antarctic station Vostok (corrected geomagnetic latitude ( $=-83.3^\circ$ ) in 1979-1980 and 1998 are analyzed. The best days were selected from these intervals satisfying the "good weather" criterion, that is, absence of a strong wind, falling or drifting snow, clouds, and an electric field "pollution" from a station power plant. It is shown that the average diurnal variation of  $E_z$ , derived for these days is close to zero in winter season (May-August) and follows the global geoelectric field "fair-weather" diurnal variation, that is, the so-called Carnegie curve, in summer season (November-February). It is commonly supposed that the Carnegie curve describes the global electric circuit formed by the global thunderstorm activity occurring mostly in the equatorial regions. We found that the vertical electric field measured at Vostok is strongly affected by variations in the interplanetary magnetic field (IMF). The  $E_z$  increases when the IMF By0 and decreases when By<0; however, variations in the IMF Bz component are also important. We conclude that the IMF affects the global electric circuit at high latitudes via the magnetosphere-ionosphere coupling link.

**JSA35/L/01-B1** **1420**

### MESOSPHERIC AEROSOL AND ELECTRODYNAMICS

Les HALE

Although the largest particles that form near the cold summer polar mesopause are clearly visible, there is extensive evidence for "invisible" mesospheric aerosol extending to lower latitudes. Anomalously low mesospheric conductivities were observed as early as 1950 and numerous workers pointed out the need for a fast 2-body process to explain "D-region" data. In the 1966 solar eclipse in Brazil the extremely rapid loss of free electrons during totality confirmed the aerosol hypothesis (a result repeated in 1979 in Kenya and 1980 in Canada). The large ( $\sim 5\%$ ) temperature coefficient of positive conductivity in the cosmic ray region was consistent with ice or ice-coated particles (Chesworth and Hale, GRL 1, 347, 1974), with a Boltzmann partition between water vapor and ice.

The low conductivity of the mesosphere allows the penetration of electromagnetic energy to the base of the ionosphere, usually about 80 km at night. This includes unipolar millisecond "slow tail" wavelets which provide global unipolar fields up to hundreds of millivolts/meter for larger lightning strokes. These are still inadequate to directly explain the several volt/meter vertical mesospheric fields observed by Russian and US groups, which at mid and low latitudes appear to follow the "Carnegie curve" (Zadorozhny). However, they may separate electrons which then attach at lower altitudes to extend the time duration of the fields.

The aerosol particles may be related to "sprites." They can grow at night due to cooling, possibly causing stratified conductivity layers under the influence of gravity waves. They may also provide a source of free electrons (necessary to explain VHF data) due to photo detachment caused by lightning and/or sites for the initiation of breakdown phenomena.

**JSA35/W/07-B1** Invited **1440**

### SPRITE ELECTRODYNAMICS AS SEEN FROM ELECTROMAGNETIC OBSERVATIONS

Steven A. CUMMER (NASA/Goddard Space Flight Center, Greenbelt, MD 20771, USA, Email: steve.cummer@gscf.nasa.gov)

Sprites, the transient high altitude optical flashes which occur in association with some large lightning discharges, are unarguably a spectacular optical phenomenon. High resolution optical observations from the summer of 1998 by a number of research groups have served to confirm this fact. However, much of the current understanding of this phenomenon has not come from optical observations but rather from electrodynamic observations from analysis of the very low frequency (VLF, 3-30 kHz) and extremely low frequency (ELF, 3-3000 Hz) electromagnetic radiation associated with these events. In this talk we will discuss sprite-related electrodynamic observations which have been made in the past five years and have led to discoveries regarding the characteristics of lightning discharges which produce sprites, the discovery of the daytime occurrence of sprites, and the discovery of large electric currents flowing in the sprite itself at mesospheric altitudes. We will discuss the observed magnitudes of these so-called sprite currents and their relationship to the global electric circuit. We will also discuss various theories proposed to explain sprites and the constraints which these electromagnetic obser

**JSA35/E/01-B1** **1510**

### ELECTROSTATIC FIELD ENHANCEMENT DUE TO THE NON-UNIFORM IONISATION CREATED ABOVE A LARGE THUNDERCLOUD

Michael RYCROFT (International Space University, Boul. Gonthier d'Andernach, 6700 Illkirch, France); Mengu Cho (Kyushu Institute of Technology, 1-1 Sensui Tobata-Kitakyushu 804, Japan)

Two-dimensional numerical studies have been conducted to investigate the effects of a positive cloud-to-ground lightning discharge on the upper atmosphere. Electromagnetic waves radiated by a horizontal lightning discharge current interfere with their reflections from the ground and from the ionosphere. This interference leads to a spatially non-uniform distribution of the ionosphere as specified by certain values of the electron density and the electrical conductivity becomes very structured on a scale of a few km, with protrusions pointing downwards (like short lived stalactites). After the positive discharge, a negative

charge remains in the thundercloud and downward electrostatic field is enhanced at the tips of the protrusions, typically by a factor or two. This produces favourable condition for positive streamers to develop downward from these points and to create the cores of columniform sprites

**JSA35/W/04-B1****1550****THE THUNDERSTORM LARGE-SCALE ELECTRIC FIELDS IN THE IONOSPHERE**

V.V. PLOTKIN (Institute of Geophysics SB RAS, Koptyug av., 3, Novosibirsk, 630090, Russia, e-mail: plotkin@uiggm.nsc.ru)

The large-scale electric fields caused by global thunderstorms in the ionosphere are calculated. It is taken into account an assumption for equipotential geomagnetic field lines at ionosphere altitudes. The influence of changes of conductivity high-altitude profiles of an atmosphere in region between the ground and the ionosphere on value of irregularity of ionosphere potential caused by global thunderstorms is investigated. It is shown that electrical fields, penetrating into the ionosphere from below, essentially depend on such important parameters, as integrated conductivity and resistance of an atmosphere. In particular, the average value of potential on the top border depends on resistance of an atmosphere. The irregularity of an ionosphere in a greater degree is determined by integrated conductivity of an atmosphere and with its reduction can become appreciable. In particular, in night conditions, and also in case of conductivity abnormal decrease (for example, during Forbush decrease), the thunderstorm electrical fields in the ionosphere can reach appreciable values.

**JSA35/E/07-B1****1610****TEMPERATURE DEPENDENT REDISTRIBUTION OF GLOBAL LIGHTNING ACTIVITY ON DIFFERENT TIME SCALES AS SHOWN BY SCHUMANN RESONANCES**

Gabriella SATORI (Geodetic and Geophysical Research Institute of the Hungarian Academy of Sciences, Csatskai u. 6-8., H-9400 Sopron, Hungary, email: satori@ggki.hu)

The excitation source of Schumann resonances (SR) is the global lightning activity. As the SR frequencies depend on the source-observer geometry they are responsive for the redistribution of global lightning activity driven by surface temperature variations. This is shown on diurnal, seasonal, annual and El Nino time scales by SR observations at Nagycenk (47.6N, 16.7E, Hungary). The SR frequencies are also indicative to the areal extension of global lightning activity, as well as to the speed of north-south annual migration of thunderstorm regions. It is suggested that the north-south asymmetry of the land/ocean ratio plays an important role in the origin of the spring-autumn asymmetry and the El Nino related redistribution of global lightning activity.

**JSA35/E/05-B1****1630****THE IMPACT OF THE AUGUST 27,1998 GAMMA RAY BURST ON THE SCHUMANN RESONANCE**

Colin PRICE (Department of Geophysics and Planetary Sciences, Tel Aviv University, Ramat Aviv 69978, Israel, email: cprice@flash.tau.ac.il); Vadim Mushak (Box 212 Ulster Heights Road, Woodburne, NY 12788, USA, email: vcm@usa.net)

In 1998 a new Schumann resonance monitoring station in the Negev desert, Israel, started collecting magnetic and electric field data in the extremely low frequency (ELF:1-50 Hz) range. These ELF waves are related primarily to global lightning activity. On 27 August, 1998, at 10:22 UT, and extremely intense gamma ray flare passed through the solar system. The gamma ray burst lasted only 5 minutes and resulted in the ionization of the earth's nightside upper atmosphere to levels found only during the daytime. During this period we were continuously monitoring the ELF waves arriving at our field site in Israel. At the same time a group of researchers at Stanford University were observing this event in the VLF (20 kHz) band. Due to the enormous change in the height of the nighttime ionosphere caused by this event, the Stanford group noticed huge changes in the amplitude of the VLF signals transmitted from Hawaii, and observed in Colorado, during this five minute period. However, our ELF measurements of global lightning signals in Israel showed no influence at all. No change in the ELF time series is seen during the period of the gamma ray burst. In addition, no changes in either amplitude or frequency were observed in the Schumann resonance bands during this period. This is surprising given that the ELF signals from lightning travel around the globe a few times before decaying, and therefore would have to propagate in the earth-ionospheric waveguide that was so strongly influenced by the gamma ray burst. We have performed some theoretical calculations to try explain the different responses in the VLF and ELF frequency bands to this massive gamma ray burst. These results will be presented together with the detailed observations of the Schumann resonances during this short period.

**JSA35/L/01-B1****1650****POLARIZATION STRUCTURE OF THE SCHUMANN FREQUENCY RANGE**

BELYAEV

Abstract not available at time of going to press

**JSA35/L/02-B1****1720****A NEW APPROACH TO THE PROBLEM OF IONOSPHERIC MHD WAVEGUIDE**

BELYAEV

Abstract not available at time of going to press

**JSV36****Wednesday 28 July****UNDERSTANDING VOLCANOES BY GEODESY, SEISMOLOGY, ELECTROMAGNETICS AND GEOCHEMISTRY (IAVCEI, IAGA, IASPEI, IAG, IAMAS, ILP)**

Location: Law Building 303LT

Location of Posters: Old Gym

**Wednesday 28 July AM**Presiding Chair: Jacques Zlotnicki (Laboratoire de Geophysique, France)  
Concurrent Poster Session**JSV36/E/35-B3**

Invited

**0830****A MULTIDISCIPLINARY APPROACH TO UNDERSTANDING VOLCANIC PHENOMENA: THE MOUNT VESUVIUS CASE HISTORY PATELLA**

Domenico PATELLA (Department of Physical Sciences, University Federico II, Naples, Italy, Email: domenico.patella@na.infn.it)

Abstract not available at time of going to press

**JSV36/E/07-B3**

Invited

**0900****THE MERAPI-PROJECT - MULTIPARAMETER MONITORING AND INTERDISCIPLINARY INVESTIGATION OF A HIGH-RISK VOLCANO**

Birger-G. Lühr, Malte Westerhaus and Jochen ZSCHAU (all GFZ-Potsdam, Telegrafenberg Haus E, 14473 Potsdam, Germany, email: zschau@gfz-potsdam.de). Mas Atje Purbawinata (BPPTK, Jl. Cendana 15, Yogyakarta 55166, Indonesia, fax:+62-274-563 630). R. Sukhyar (VSI, Jl. Diponegoro 57, Bandung 40122, Indonesia, fax: +62-22-702761)

Merapi volcano in Central Java belongs to the most active volcanoes in the world. Located at the subduction zone between the Eurasian and the Indo-Australian Plate, the dominant magmatic mechanism is andesitic, i.e. explosive. In 32 of 67 reported historical eruptions, pyroclastic flows took place. Since 1994 pyroclastic flows with a length between 2 km and 8 km occur about once per year. Even small volcanic events are a permanent danger to life and limb within the densely populated area at the flanks of the volcano. IAVCEI has classified Merapi as a high-risk volcano and included it into the list of 15 Decade Volcanoes. In cooperation with the Volcanological Survey of Indonesia and other institutions in Indonesia and Germany, the GeoForschungsZentrum initiated an interdisciplinary monitoring program in 1994, supplementing a number of ongoing national and international activities on this volcano. The MERAPI project (Mechanism Evaluation, Risk Assessment, Prediction Improvement) is supposed to contribute to the development of prediction and warning strategies on different time scales, including intermediate and short term prediction of volcanic events as well as early warning. Special emphasis has been put on continuously monitoring activity indicators such as seismicity, deformation and gas emanation. Directional microphones are expected to facilitate discrimination between shallow volcanic quakes and rock avalanches, which would be of basic importance for an automatically working early warning system. Investigation of the internal structure of the edifice, of magmatism and of the explosive history of the volcano form the basis for a better understanding of the complex processes prior to an eruption.

**JSV36/W/22-B3****0915****AN INTEGRATED APPROACH FOR THE MODELING OF MAGMA PLUMBING SYSTEM AND ERUPTION PREDICTION OF IZU-OSHIMA VOLCANO, JAPAN**

Hidefumi WATANABE (Earthquake Research Institute, University of Tokyo, Yayoi 1-1-1, Bunkyo-ku, Tokyo 113-0032, Japan, email: watanabe@eri.u-tokyo.ac.jp)

An integration of the results of extensive observation before, during and after the 1986 eruption of Izu-Oshima volcano, give us essential information on the physical nature of its magma plumbing system. A gradual rise of seismic activity, inflation of the volcano and anomalous decrease in the geomagnetic total intensity, had continued for more than 10 years until around 1980. After 1981, the volcano showed a small deflation and low seismicity at the caldera area until beginning of the eruption, while we observed anomalous changes in the subsurface resistivity and the magnetic field localised around the summit crater, that indicating a gradual rise of the temperature beneath the crater. By integrating the precursors we propose that the accumulation of magma had continued for more than 10 years until 1980, and then the basalt magma started to rise up through the well-developed conduit. After the 1986 eruption, we clarified the drain-back process of degassed magma in the conduit based on microgravity and magnetic observation around the summit crater. Since 1987 after the eruption, the EDM and GPS measurements have revealed a re-inflation of the volcano. A continuous magma supply and a well-developed conduit connecting the magma reservoir and the summit crater, characterise the magma plumbing system of Izu-Oshima volcano. The convection of volatile-containing and degassed magma might control the ascent and drain-back process in the conduit. The proposed model for the magma plumbing system provides a basis for not only the short-term but also mid-term prediction of the future eruption of Izu-Oshima volcano.

**JSV36/W/02-B3****0930****MODELING VOLCANO-HYDROTHERMAL SYSTEM OF WHITE ISLAND VOLCANO FROM SEISMIC, SELF-POTENTIAL AND AUDIO MAGNETOTELLURIC DATA**

Yuji NISHI, Mituhiko Sugihara, Toshiyuki Toshi, Tuneso Ishido, Yasuo Ogawa (Geological Survey of Japan, Higashi 1-1-3, Tsukuba, Ibaraki 305-8567, Japan, email: uwest@gsgj.go.jp); Bradley J. Scott, Steven Sherburn and Chris Bromley (Institute of Geological &amp; Nuclear Sciences, State Highway 1, Wairakei, Taupo, New Zealand, email: S.Sherburn@gns.cri.nz)

White Island is one of the most active volcanoes in the world and it has vigorous volcano-hydrothermal system that has existed for at least 10,000 years (Giggenbach and Glasby, 1977). Volcano-tectonic earthquakes in this volcano are concentrated in the eastern Main Crater at depths of less than 1 km (Nishi et al., 1996). Space-autocorrelation analysis of seismic tremor suggests an unknown high-velocity layer at very shallow depth beneath the Main Crater floor. Self-potential anomalies suggest subsurface fluid flow patterns (Nishi et al., 1996). Three audio-magnetotelluric soundings in the Main Crater show low resistivity (approx. 10 ohm-m) at a shallow depth (Ogawa et al., 1996). Based on these data, we made a



## INTER-ASSOCIATION

conceptual model of the volcano-hydrothermal system; heat supplied from the deep magmatic system beneath the active vent causes upflow to thermal features along the edge of the subcraters, and downflow overlies at the centre of the eastern sub crater and the north-eastern half of the central subcrater. To integrate the various data, thermohydraulic numerical simulations were also performed.

**JSV36/E/14-B3**

**0945**

### AN APPROACH TO THREE - DIMENSIONAL MAGNETOTELLURIC IMAGING AND MONITORING VOLCANIC ENVIRONMENTS

Vjacheslav SPICHAK (Geophysical Research Centre, Moscow, Russia, e-mail: spichak@dol.ru)

An approach to step-by-step deepening of our knowledge about volcanic interior and long-term forecasting its activity basing on current MT measurements, information available from other methods and sophisticated analysis of past inversion results is suggested. It is based on using methodology of data interpretation, which closely links the monitoring results with knowledge on the internal structure at the moment of the last measurements. Three-dimensional Bayesian inversion and Artificial Neural Network (ANN) - based recognition tools developed recently in (Spichak, 1995; Spichak et al., 1995; Spichak and Popova, 1998) support a new paradigm of MT -data interpretation taking into account the geological information known, noise level in the data, a priori estimates of unknown parameters, new hypotheses formulated in probabilistic terms, data available from other methods and formalized human experience. Imaging volcanic interior and step-by-step updating 3D-conductivity model are carried out via application of the Bayesian inversion procedure after each MT survey. Along this way the ranges of uncertainties of unknown parameters are reduced each time when new MT sounding data or other information are involved into the inversion process. After each cycle of MT data measurement and interpretation a posteriori values and multi-dimensional probability density function of the ensemble of monitored parameters are saved and used then as a priori ones in the next cycle, and so on. Set of these values updated after each new MT survey forms a knowledge base to be used by the ANN - based expert system in order to recognise the tendencies in the parameters' dynamics and to determine the integrated quantitative measure of the risk of future volcanic activity. In order to estimate the effectiveness of the general scheme, simulation of the imaging and monitoring processes using synthetic MT data is carried out.

**JSV36/E/27-B3**

**1040**

### MONITORING THE CHEMICAL COMPOSITION OF VOLCANIC GASES: WHY?

Marino MARTINI (Department of Earth Sciences, University of Florence, Via La Pira 4, 50121, Florence, Italy, email: mmartini@cesit1.unifi.it)

Eruptive activities after short or long periods of quiescence of volcanic systems are always preceded by natural phenomena which can allow some kind of forecast: in extensional areas seismic activities along with ground deformations are mainly recorded as short-term forerunners of effusive events, while in compressional areas important degassing is also expected to occur in advance to any eruptive episode. When considering that, for most of the recent disasters produced by resumed activities at quiescent volcanoes, a clear evidence of forerunning seismicity and deformations is not reported, and that the occurrence of significant phenomena of this kind was not always followed by volcanic activity, the study of fluids released in volcanic areas appears to deserve a special attention, in order to evidenciate chemical anomalies possibly related to the instability of deep-seated magmatic systems. The interaction of uprising hot magmatic fluids with deep or shallow aquifers appears as an important factor in triggering eruptive activities whose characters strongly depend on the mass balance between the energy output from magma bodies and the water availability. Sufficient vapour pressure to initiate explosive eruptions are expected when both components are operating, while effusive phenomena are observed for exceeding heatflows, and substantially hydrothermal activities appear as due to overwhelming water recharges. The results obtained during the last decade through geochemical investigations on volcanic gases from different areas of active or quiescent volcanism, allowed to estimate relative extents of magmatic or geothermal conditions for the systems considered, and not negligible contributions for volcano prediction have been derived; examples are given, and case histories are described.

**JSV36/E/02-B3**

**1100**

### CHEMICAL GAS MONITORING ON MERAPI VOLCANO, INDONESIA

Martin Zimmer (1), Joerg ERZINGER (1) & Yustinus Sulistiyo (2) (1)Geo Forschungs Zentrum Potsdam, Telegrafenberg, D-14473 Potsdam, Germany, email: weihei@gfz-potsdam.de, (2) BPPTK, Jalan Cendana 15, 55166 Yogyakarta, Indonesia

A specially designed device consisting of a gas chromatograph, an alphaszintillometer and a temperature sensor was successfully installed during August and September 1998 at the Merapi summit. The complete unit operates automatically and can be remote controlled by radio link. Concentration levels of H<sub>2</sub>O, CO<sub>2</sub>, SO<sub>2</sub>, N<sub>2</sub>, H<sub>2</sub> and <sup>222</sup>Rn and <sup>220</sup>Rn (thoron) as well as the fumarole temperature were measured every 35 minutes over several weeks. In addition gas and fumarole condensate samples were analysed for C-, He- and H- and O-isotopes at the GeoResearchCenter Potsdam. Results of the on-line gas measurements to date show a significant variation of the volcanic gas composition. Periodically SO<sub>2</sub>, CO<sub>2</sub> and H<sub>2</sub> concentrations increase while H<sub>2</sub>O and N<sub>2</sub> amounts decrease. Simultaneously the <sup>220</sup>Rn concentration increases due to a higher gas velocity. Lower fumarole gas temperatures occur during periods of high water concentrations in the gas. These periodical gas pulses are correlated with higher seismic energies measured in the summit area. The 3He/4He-ratios in Merapi gas samples are between 8-8.8\*10<sup>-6</sup> which are typical for volcanic gases released at convergent plate boundaries. The δ13C-value in CO<sub>2</sub> from Merapi gas is -4.9‰. H- and O-isotope investigations on spring water and fumarole condensate samples indicate that the water present in the fumarole is mainly local rainwater. This cold surface fluid circulates within the volcano edifice and mixes and dilutes with ascending volcanic fluids. A regular stronger degassing of the magma causes an increase in gas flux, gas velocity and gas temperature as well as an increase in the ratio of magmatic gas to meteoric water. This leads to higher CO<sub>2</sub>, SO<sub>2</sub> and H<sub>2</sub> and lower H<sub>2</sub>O and N<sub>2</sub> concentrations in the fumarole gas. The geochemical data series were correlated with geophysical parameters such as seismicity and deformation rates to create a seismo-geochemical model of the Merapi volcano and, thus, to deduce conclusions on the actual amount of ascending magma and herewith very crucial data on dome growth and volcanic activity.

**JSV36/W/04-B3**

**1115**

### HYDROGEOCHEMICAL MONITORING OF THE SEISMIC-VOLCANIC ACTIVITY AT MT. TEIDE, TENERIFE, CANARY ISLANDS, SPAIN

Nemesio PEREZ, José M. L. Salazar, J. M. Navarro (all at Environmental Research Division, ITER, 38594 Granadilla, Tenerife, Canary Islands, Spain; e-mail: nperez@iter.canaria.es), Giovanni Chiodini

(Osservatorio Vesuviano, 80123 Napoli, Italy), and Pedro A. Hernández (Laboratory for Earthquake Chemistry, Univ. Tokyo, Bunkyo-ku, Tokyo 113, Japan)

Mt. Teide (3,716 m of elevation) is a Decade volcano situated at Cañadas caldera, a giant volcanic structure (16 x 9 Km) open to the sea by the north side, in the central part of Tenerife island. Most of the recent volcanic activity at Tenerife takes place along major volcanic rift-zones where had occurred six volcanic eruptions during the last 500 yrs. Most of the fresh water supplies at Tenerife comes from its ground water reserves, and the exploitation of these ground waters by means of thousands of horizontal "gallery" and vertical "well" drillings allow us to reach the volcanic aquifer at many different depth and elevations. These drillings are quite favourable to establish a hydrogeochemical monitoring program for the seismic-volcanic surveillance of Mt. Teide. Monitoring subsurface diffuse degassing of CO<sub>2</sub> from Teide volcano by means of a water mass balance and the total inorganic carbon (TIC) content of the ground waters from the Cañadas caldera's aquifer is one of the most significant part of our hydrogeochemical monitoring program. Our results from 1994 and 1996 surveys showed a steady-state level about 94 t-d<sup>-1</sup> of subsurface diffuse emission of CO<sub>2</sub> from Teide volcano. Controlled and non-controlled discharges of CO<sub>2</sub> into Cañadas' aquifer are estimated about 55 t-d<sup>-1</sup> and 39 t-d<sup>-1</sup>, respectively. Secular variations of physico-chemical components in Tenerife's ground waters are also performed by means of a network of observation sites all over the island. Four monitoring sites are operative since 1997, and the results are quite promising for the seismic-volcano monitoring of Mt. Teide.

**JSV36/P/01-B3**

**1130**

### HYDROTHERMAL FLUIDS ON THE SUBMERGED FLANKS OF VOLCANICALLY ACTIVE ISLANDS IN THE LESSER ANTILLES

Alan Johnson and DAVID CRONAN (both at T. H. Huxley School, Imperial College, London, SW7 2BP, United Kingdom, email: d.cronan@ic.ac.uk)

Submarine hydrothermal activity occurs off St. Lucia, Dominica, Montserrat, St. Kitts, Nevis and Saba in the Lesser Antilles. Minor elements in the hydrothermal fluids show significant enrichments over normal seawater values. Manganese is enriched in almost all the vent fluids sampled and Fe, As, Si and Zn are enriched in many of them. Mg and S are depleted. The composition of the hydrothermal fluids varies off island to island. Observations off Montserrat before and during the early stages of the current eruption showed markedly different degrees of offshore hydrothermal activity, fluid temperature and composition between January 1995 and December 1996. Mn, Fe and As were low in the hydrothermal fluids before the eruption, high at the time of its commencement, and intermediate later. By contrast, terrestrial hydrothermal fluids on Montserrat showed no regular pattern of compositional variation over the same two years. We deduce that the compositional variability of the submarine hydrothermal discharges off Montserrat reflects the variable leaching of magmatic rock by seawater at different stages of the current volcanic cycle. This has important implications in understanding processes under coastal volcanoes and in predicting their eruptions on the basis of monitoring submarine hydrothermal fluid composition. It also implies that inter-island variability in hydrothermal fluid composition will, in part, reflect the stage of its eruptive cycle that each volcanic island is in.

**JSV36/W/05-B3**

**1145**

### MAGMA DEGASSING: IMPACT ON GEOCHEMICAL FIELD PARAMETERS, MODELLING AND IMPLICATIONS FOR VOLCANIC HAZARD

P. Mario Nuccio and Antonio PAONITA (both at Dipartimento di chimica e Fisica della terra ed Applicazioni - CFTA, 90123 Palermo, Italy, e-mail: paonita@cfta.math.unipa.it)

Volatiles are dissolved in magma in concentrations related to genesis, composition and evolution of magma itself. At static pressure, magma degassing normally occurs by diffusion, nevertheless, as a consequence of magma ascent and depressurisation, the principal dissolved volatiles (H<sub>2</sub>O and O<sub>2</sub>) can reach saturation, forming gas bubbles. Composition of partitioned gas phase will depend by equilibrium processes, which will give a different signature with respect to diffusive ones. The progressive improving of knowledge of gas solubility in magmas permits us to quantitatively describe the above processes, following a thermodynamic and numerical approach. Then, given the initial chemical-physical conditions (P, T, X) of a magma, we can theoretically foresee the composition of released gas, on the basis of a degassing model. From an inverse point of view, we can interpret observed geochemical field parameters (i.e. chemical composition of fumarolic gases) and, above all, their time modifications in term of magma degassing process. By using few but regularly sampled volatile species, the degassing model can be parameterised with regard to the input chemical-physical conditions, so to principally know pressure (and depth) of magma and to detect its ascent toward the surface during the time. We can assess the time scale of the process of magma ascent, having the possibility to extrapolate the depth of magmatic body at a fixed time, above all when a consistent time record of the ascent has been acquired. Since volcanic eruption is the final expression of magma ascent, we can use the above modelling to evaluate volcanic hazard and in forecasting of eruptions.

**JSV36/W/18-B3**

**1200**

### DIFFUSE DEGASSING OF POPOCATÉPETL, MEXICO

VARLEY, Nick (Instituto de Geofísica, Ciudad Universitaria, Coyoacan CP 04360 Mexico, email: eruption@iname.com)

The stratovolcano Popocatepetl started its current phase of activity in Dec. 1994. Since then, ash emissions have been occurring and very large quantities of SO<sub>2</sub> and CO<sub>2</sub> have been measured in the summit plume: up to 50,000 tons/day of SO<sub>2</sub>. Pyroclastic deposits from previous eruptions are found beneath nearby Mexico City, and the potential for a catastrophic eruption, affecting a huge number of people, cannot be ignored. It is clear that a vigilant and diverse monitoring program is of the utmost importance. A project was initiated in August 1997 to measure the concentration of various soil gases. Certain other active volcanoes, such as Etna, have been found to have large concentrations of particularly CO<sub>2</sub> in the soil gas. Although generally concentrated along faults, significant levels of magmatic gases can be often found passively diffusing to any point on the edifice. Monitoring soil gases over time has the potential of indicating changes in the dynamics of a volcano, whilst spatial variation can provide important evidence of structural detail. Measurements such as these are particularly important where, as in the case of Popocatepetl, there is an absence of accessible fumaroles. Surprisingly at Popocatepetl the diffuse component of its degassing budget has been found to be low. Over 400 measurements of Rn and CO<sub>2</sub> in soil gas have been performed, using active field methods, with extensive coverage of the volcano. Although levels of up to 14% CO<sub>2</sub> have been measured, 13d values of between -21 and 25‰ suggest a largely biogenic origin. 70%

of the results have concentration of CO<sub>2</sub> less than 2%. Some samples were analysed for He isotopes, with the resulting ratios having values >1 RA, suggesting a radiogenic, rather than magmatic origin. Some large ravines in the edifice are thought to mark the location of faults. Some have shown large displacements, but here too only low concentrations of soil gases have been measured. Interestingly there is no evidence of a geothermal system associated with the volcano. A model for the edifice has been proposed to offer an explanation.

**JSV36/W/26-B3****1215****ANOMALOUS DIFFUSE EMISSION OF CO<sub>2</sub> FROM USU VOLCANO, HOKKAIDO, JAPAN**

Pedro A. HERNÁNDEZ, Toshiya Mori, Kenji Notsu (all at Laboratory for Earthquake Chemistry, University of Tokyo, Bunkyo-ku 113-0033, Japan; e-mail: hernandez@eqchem.s.u-tokyo.ac.jp), Hiromi Okada (Usu Volcano Observatory, Sobetsu-cho, Hokkaido 052-0103, Japan), and Nemesio Pérez (Environmental Research Division, ITER, 38594 Granadilla, Tenerife, Canary Islands, Spain).

Usu volcano is located in the SW of Hokkaido and is one of the most active volcanoes in Japan. Seven major eruptions have been recorded at this volcano since 1663. Fumarole temperatures range from 100°C to 480°C. Large amounts of HF, HCl, SO<sub>2</sub> and H<sub>2</sub> are discharged by high-temperature fumaroles whereas those of low temperatures are CO<sub>2</sub>-rich. To evaluate the diffuse degassing of CO<sub>2</sub> from Usu volcano, a soil CO<sub>2</sub> flux survey of about 210 sampling sites was carried out from August 26 to September 3, 1998. Soil CO<sub>2</sub> flux measurements were performed by using a NDIR spectrophotometer, and the values ranged from 0.7 to 8,210 g-m<sup>-2</sup>-d<sup>-1</sup>. Statistical graphical analysis of the data showed three overlapping populations. The background mean is 37-g-m<sup>-2</sup>-d<sup>-1</sup> and represents 81.5% of the total data. The peak group showed a mean of 2,420-g-m<sup>-2</sup>-d<sup>-1</sup> and represents 9.8% of the total data. The highest levels of diffuse degassing of CO<sub>2</sub> are identified at the summit of Usu and along the Usu-Shinzan fault. Other areas with anomalous CO<sub>2</sub> flux levels are identified along the NW-SE direction, being probably related with the structure of the southern wall of Toya caldera. Spatial distribution of soil CO<sub>2</sub> flux levels shows a good agreement with anomalous soil gas CO<sub>2</sub> concentrations and high soil temperatures (up to 64°C). Carbon isotopic analysis of selected samples range from -32.4‰ to -2.6‰ suggesting a mixed biogenic and magmatic origin for these emanations. An output of 183 t-d<sup>-1</sup> of CO<sub>2</sub> is estimated for the summit of Usu.

**JSV36/E/04-B3****1230****HELIUM ISOTOPES AS TRACERS OF INCIPIENT MAGMATISM FOLLOWING THE 1996/1997 SEISMO-TECTONIC CRISIS ON NISYROS VOLCANO (GREECE)**

Volker J. DIETRICH (Inst. Mineralogy & Petrography ETH Zürich, CH-8092 Zürich, Switzerland, email: wumme@erdw.ethz.ch) Florian M. Schwandner (Inst. Mineralogy & Petrography ETH Zürich, CH-8092 Zürich, Switzerland, email: florimax@erdw.ethz.ch) Rolf Kipfer (EAWAG, CH-8600 Dübendorf, Switzerland, email: kipfer@eawag.ch)

The islands of Nisyros, Santorini, Milos and Methana are considered today the most active areas of the Hellenic Island arc in terms of a potential volcanic reactivation. Although the last volcanic activity on Nisyros dates back at least 25 000 years, the geodynamic activity, expressed by high seismic unrest, fumarolic activity and hydrothermal explosions is continuously present. Violent earthquakes, gas detonations and fire accompanied the most recent hydroclastic eruptions in 1873 and 1888. The latter effects are due to high gas emanations of H<sub>2</sub>S, CO<sub>2</sub>, H<sub>2</sub> and CH<sub>4</sub> from fracture zones, which cut the caldera and extend towards NNW through the vicinity of the village of Mandraki into the island of Yali and even towards Kos. In 1996 and in 1997 high-seismic activity (magnitudes of earthquakes up to 5.5 on the Richter scale) occurred on Nisyros and was accompanied by increased tectonic and fumarolic activity. In this respect, the scheme of events as comparable with the violent activity in 1873 and 1888, required serious examination. Besides the permanent residents of the island of Nisyros, several hundred of tourists enter the hydrothermal field of the Nisyros caldera daily without awareness of the entire risk situation. The high 3He/4He ratios of 5.9 to 7.5 × 10<sup>-6</sup> in the Nisyros fumarolic condensates, sampled in October 1997 after the long period of strong earthquake activity, overlap entirely with the helium isotopic ratios measured in the high temperature fumaroles at Vulcano island (Aeolian island arc) during the magmatic/volcanic crisis in 1988 and 1989. In the case of Nisyros, it may be related to magma degassing, indicating an influx of the gases from a replenished magma reservoir at shallow depth.

**Wednesday 28 July PM**

Presiding Chair: Yasunori Nishida (Department of Earth and Planetary Sciences, Hokkaido University, Japan)  
Concurrent Poster Session

**JSV36/W/07-B3****1400****AN INTEGRATED APPROACH TO THREE-DIMENSIONAL STRATIGRAPHIC RECONSTRUCTIONS OF LONG-LIVED QUATERNARY ARC VOLCANOES: TATARA-SAN PEDRO COMPLEX (TSPC), 36° S, CHILEAN ANDES**

Michael DUNGAN and Brad Singer (Département de Minéralogie, Université de Genève, 13 rue des Maraichers, 1211 Genève 4, Switzerland, email: dungan@terre.unige.ch) Ren Thompson (U.S. Geological Survey MS910, Denver Federal Center, Denver, CO 80225 USA) Laurie Brown, Jim Pickens and Andrew Wulff (Department of Geology and Geography, University of Massachusetts, Amherst, MA 01003)

The TSPC is a large frontal arc center of the Andean Southern Volcanic Zone dissected on all flanks by glacial valleys exposing the eruptive products of seven edifices ranging in age from 930 ka to Holocene (Singer et al, 1997; GSA Bull). Sequences older than 200 ka are remnants of spatially overlapping volcanoes reduced in volume (50-90 %) by glaciation and sector collapse, and preserved remnants generally record short durations relative to intervening lacunae. Digitised photogrammetric projections based on stereo imagery of canyon walls represent stratigraphic relations and the geometries of erosion surfaces in far greater detail and more accurately than conventional mapping would permit. The internal stratigraphy of several sequences has been reconstructed on the basis of geochemical data (650 samples collected in 25 flow-by-flow canyon sections) plus photogrammetric, geochronologic and paleomagnetic constraints. This composite stratigraphy is far more complete than the records present in any single section due to the eccentric distributions of the products of consecutive eruptive events and the effects of erosion. Many stratigraphic successions record temporal trends lacking in evidence for progressive differentiation. The resulting constraints on petrologic models are far different than if apparently co-magmatic lavas were assumed to reflect single-stage differentiation. Most eruptive events reflect arrival of small quantities (<1-2 km<sup>3</sup>) of diverse mafic magma into shallow conduit-reservoir systems where they mixed in varying proportions with variably evolved resident magmas.

**JSV36/C/JSA15/W/34-B3****1415****EVOLUTION OF MONTSERRAT USING 40AR/39AR GEOCHRONOLOGY**

CHLOE L HARFORD and R Stephen J Sparks (Department of Earth Sciences, Bristol University, Bristol BS8 1RJ, UK; email: chloe.harford@bris.ac.uk); Malcolm S Pringle (Scottish Universities Research and Reactor Centre, East Kilbride, UK); Simon R Young (British Geological Survey, Edinburgh, UK)

40Ar/39Ar ages of volcanic rocks representing the major stratigraphic units of Montserrat facilitate a substantial reinterpretation of the evolution of the island. These ages are more precise and significantly different from existing conventional K-Ar ages. We identify three distinct volcanic centres: Silver Hills (c.1.2 to 2.6 Ma); Centre Hills (at least c.950 to 550 ka); Soufriere Hills (at least c.150 ka to present). Volcanism on Montserrat has migrated southwards through time, at a time averaged rate of c. 6 km/m.y. parallel to the trench and c.2 km/m.y. away from the trench, consistent with work elsewhere in the arc.

Six new ages give insights into the life cycle of the youngest centre. The history of the currently active Soufriere Hills Volcano, dominated by andesitic lava dome eruptions, is extended back to 150 ±3 ka (1\_ error), well beyond the oldest radiocarbon age of 31.6 ±0.2 ka. We estimate its time-averaged eruption rate to be c.0.0015 m<sup>3</sup>/s. Ages for three pyroclastic flow deposits and two domes indicate that preservation of domes is incomplete, and large scale collapse may play a significant role in the volcano's history.

An age of 959 ±19 ka from Roche's Bluff, south-east of Perches dome (Soufriere Hills), facilitates the interpretation of this intensely disrupted pyroclastic sequence as part of the uplifted submarine fan of the Centre Hills. We further propose that St George's Hill and Garibaldi Hill to the north-west of the Soufriere Hills are uplifted pyroclastic sequences. An age of 282 ±8 ka from Garibaldi Hill suggests this sequence may represent the early stages of the Soufriere Hills.

Step heating experiments on material from the current eruption give an age indistinguishable from zero (21 ±22 ka) for groundmass separates but an age significantly greater than zero (426 ±95 ka) for separated plagioclase phenocrysts, indicating no extraneous argon in the groundmass but xenocrysts in the plagioclase phenocrysts. Thus, groundmass separates should be used whenever possible for dating crystal-rich andesites.

**JSV36/W/09-B3****1430****SHALLOW SEISMICITY AND CRUSTAL DEFORMATION ASSOCIATED WITH THE 1998 INTRUSION EVENT AT IWATE VOLCANO, NORTH-EASTERN JAPAN**

Satoru TANAKA, Sadato Ueki, Minemori Sato, and Hiroyuki Hamaguchi (all at Graduate School of Science, Tohoku University, Sendai 980-8578, Japan, email: tanaka@aob.geophysics.tohoku.ac.jp)

Since we first observed volcanic tremors in Iwate volcano in September 1995, we have gradually extended seismic stations in and around the volcano and, at the present, we have 20 stations in the area of 15 km x 20 km. We have succeeded to catch a new seismic activity and revealed that the activity is related with intrusion of magmatic fluid beneath the volcano. The activity had started in January 1998 beneath a crater rim adjoining the west of the summit. Magnitudes of the events were less than 0.5, focal depths were 2 - 6 km, and the occurrence rate of the earthquakes was about 10 per month till the middle of March. Suddenly on March 20, the first earthquake swarm had occurred. The source region had extended westward up to 2 km in distance, magnitudes had grown to 0.5 - 1.0, and focal depth had moved to 0-2 km. After this swarm, the rate had increased to about 50 per month till the middle of April. On April 29, the second swarm had occurred. Source region had extended westward more, and earthquakes with magnitude greater than 2 had occurred. After the second swarm, the rate had increased to about 150 per month. Since June, the source region of the seismic activity had gradually extended westward with lapse of time. Then the last geometry of source region is a rectangular shape with 10-km length from east to west and 3km width from north to south in August. Critical comparisons of the above seismicity with crustal deformations observed by borehole strain and tilt meters at 3 stations and GPS (Ueki et al., 1999) clarified upward and westward movements of a pressure source beneath the volcano. Thus we conclude that the both activities are induced from intrusion of fluid like magma. At the final stage of the intrusion event, on September 3, an earthquake M6.1 has occurred at the point close to the western tip of the seismic source region. The mechanism of the earthquake is explained by a thrust type fault presumably affected by the above intrusion.

**JSV36/E/13-B3****1445****APPLICATIONS OF GPS GEODESY ON ACTIVE STRATO-VOLCANOES: CASE STUDIES OF SOUFRIERE HILLS, MONTSERRAT, POPOCATEPETL, MEXICO, AND MISTI, PERU**

Glen MATTIOLI, Lizzette Rodriguez, Alan Smith (all at Department of Geology, University of Puerto Rico, Mayaguez, PR 00681 USA, Email: glen@geology.uprm.edu); Enrique Cabral, Edmundo Norabuena, and Timothy Dixon (all at Department of Marine Geology and Geophysics, RSMAS, University of Miami, Miami, FL 33149 USA, Email: tim@corsica.rsmas.miami.edu)

Ground deformation is important for monitoring volcanoes for hazard assessment and elucidation of sub-surface magmatic processes. GPS geodesy is now used exclusively or in concert with traditional deformation techniques, such as telemetered electronic tiltmeters, precision leveling, and electronic distance measurement, to study volcanic systems at different stages of evolution. While each technique is useful, GPS geodesy has some unique characteristics, which makes it a powerful tool for the study of volcanoes. Continuous GPS (CGPS) systems have special difficulties related to maintenance during intense volcanic activity. We report here results obtained from 1995 to 1999 using mixed-mode and CGPS geodesy from three stratovolcanoes: Soufriere Hills (SH), Montserrat; Popocatepetl (Popo), Mexico; and Misti, Peru. CGPS systems have been deployed at SH and Popo since mid 1996 and Misti since late 1998. In the case of Soufriere Hills, GPS data span the period of phreato-magmatic venting, andesitic lava effusion, dome building and collapse, vulcanian to sub-plinian explosions, and apparent quiescence. CGPS data from Popo span the period of high SO<sub>2</sub> gas emission and venting. While CGPS provides dense temporal sampling, additional mixed-mode and campaign style GPS data are essential to constrain spatially variable deformation fields at the scale of 1 to 10 km. Data spanning distinct eruption events and changes in eruption magnitude or style provide constraints on sub-surface deformation sources. Magma storage depths, volumes, and viscosities may be deduced using elastic and finite-element models.

**JSV36/W/17-B3****1500****REMOTE SENSING AND GPS FOR DIGITAL TERRAIN MODELS EXTRACTION: VALIDATION AND COMPARISON OF OBSERVATIONS FOR VOLCANIC MONTELLING**

Baldi P. - Dip. di Fisica, Università di Bologna, Bonvalot S. - ORSTOM Bondy Briole P. - Institut de Physique du Globe de Paris, Gwinner K. - German Aerospace Center (DLR), Institute of Planetary Exploration, Berlin, Germany M. Coltelli, G. Puglisi - C.N.R. - International Institute of Volcanology (IIV), Catania, Italy MARSELLA M. - DITS, Università di Roma "La Sapienza"



Satellite and airborne remote sensed images provide a powerful tool for Digital Terrain Model (DTM) extraction especially when coupled with the use of Global Positioning System (GPS) techniques for georeferencing and validating results. 3D topographic observations acquired periodically over volcanic areas can be used for deformation monitoring and morphological changes detection. Different studies for monitoring and modelling volcanic processes can be performed depending on the quality and the resolution of the available DTM.

The performance of different methods for DTM extraction are analysed by comparing results over a test area on the Vulcano Island: high resolution DTM obtained by automatic digital processing of airborne stereomages from a photogrammetric camera (Wild RC20) and a High Resolution Stereo Camera (HRSC) are analysed and compared. A SAR interferometric DTM is also derived in support of studies with low accuracy requirements, such as those dedicated to landslides and lava flows monitoring. High accurate height profiles from a GPS kinematic ground survey is used for DTM validation.

**JSV36/W/23-B3 1515**

**DYNAMIC DEFORMATION OF ETNA VOLCANO OBSERVED BY GPS AND SAR INTERFEROMETRY**

P. LUNDGREN, P. Rosen, and F. Webb (Jet Propulsion Laboratory, California Institute of Technology, Pasadena, CA 91109, USA, e-mail: paul@dagobah.jpl.nasa.gov) R. Lanari, M. Tesaro, and E. Ssosti (IRECE, Via Diocleziano, 328, 80124 Napoli, Italy, e-mail: lanari@irece1.irece.na.cnr.it) G. Puglisi, A. Bonforte, and M. Coltellì (Istituto Internazionale di Vulcanologia-CNR, Piazza Roma, 295123 Catania, Italy, e-mail: geo@iiv.ct.cnr.it)

Synthetic aperture radar (SAR) interferometry and GPS have shown that during the quiescent period from 1993-1995 Mt. Etna volcano, Italy inflated. Since the initiation of eruptive activity since late 1995 the deformation has been more contentious. We will explore the detailed deformation during the period from 1995-1996 spanning the late stages of inflation and the beginning of eruptive activity. We use SAR interferometry and GPS data to measure the volcano deformation. We invert the observed deformation for both simple point or tensile crack elastic sources or if warranted for a spheroidal pressure source. In particular, we will examine the evolution of the inflation and the transition to a lesser deflation observed at the end of 1995. We use ERS-1/2 SAR data from both ascending and descending passes to allow for dense temporalsampling of the deformation and to allow us to critically assess atmospheric noise. Preliminary results from interferometry suggest that the inflation rate accelerated prior to resumption of activity in 1995, while GPS data suggest a more steady inflation with some fluctuation following the start of activity. This study will compare and contrast the interferometric SAR and GPS results and will address the strengths and weaknesses of each technique towards volcano deformation studies.

**JSV36/E/01-B3 1610**

**STUDYING THE DEFORMATION CHARACTERISTICS OF GUNTUR VOLCANO (INDONESIA) BY USING GPS, GRAVITY, AND EDM DATA**

Hasanuddin Z. ABIDIN , I. Meilano, M. A. Kusuma , B. Setyadji , J. Kahar (all at Department of Geodetic Engineering, Institute of Technology Bandung, Jl. Ganesha 10, Bandung, Indonesia, email: hzabidin@indo.net.id) Oni K. Suganda, Edi Suhanto, R. Sukhyar (all at Volcanological Survey of Indonesia, Jl. Diponegoro 57, Bandung, Indonesia) Torao Tanaka (Disaster Prevention Research Institute, Kyoto University, Uji, Kyoto, Japan)

Guntur is an andesitic strato volcano and based on the criteria used by the Volcanological Survey of Indonesia it is classified as the type-A volcano, i.e. very active volcano. It is located a few km from town of Garut and about 40-km southeast of Bandung, the capital city of West Java province, Indonesia. Due to its potentially active nature, Guntur volcano is being monitored using several methods, i.e. visual, seismic, deformation (i.e. tiltmeter, EDM, levelling, and GPS survey), and geochemical (i.e. temperature measurements) methods.

In this paper the deformation study of Guntur volcano using repeated GPS surveys, micro gravity surveys, and EDM (Electronic Distance Measurement) methods will be described and discussed. The deformation characteristics of Guntur volcano are investigated using the data from seven repeated GPS surveys, two repeated microgravity surveys, and three EDM surveys that have been conducted in the deformation monitoring network covering Guntur volcano and her surrounding. The main goal of this deformation study is to derive the depth and size of the magma chamber of Guntur volcano from the displacement vectors obtained from the aforementioned surveys, and also to predict the magma supply rate to the volcano and its outgoing volume in case of eruption. This paper will mainly discuss the aspects related to achieving that main goal of deformation study in Guntur. These includes planning and execution of the surveys in the volcano environment, elimination of errors and biases in the data, data processing strategy, deformation modelling, and interpretation of the results. The paper would be sum up with some closing remarks.

**JSV36/E/30-B3 1625**

**MAGMA COMPRESSIBILITY IN SHALLOW CHAMBERS BENEATH CALDERAS**

Hazel RYMER and John B Murray (both at Department of Earth Sciences, The Open University, Walton Hall, Milton Keynes, Bucks, MK7 6AA, UK, email: h.rymer@open.ac.uk); Corinne A Locke and John Cassidy (both at Department of Geology, The University of Auckland, email: c.locke@auckland.ac.nz); Clive Roberts (School of Applied Sciences, University of Wolverhampton, email: in5359@wlv.ac.uk)

The simple and much used Mogi model relates the change in edifice volume (DVe) measured by ground deformation to the change in sub-surface magma chamber volume (DVch). Variations in gravity can also be monitored on active volcanoes and the change in sub-surface magma mass (D Mm) can be quantified. Gravity has been particularly useful in identifying sub-surface mass changes (often interpreted in terms of shallow magma movements within the volcanic edifice) at basaltic and andesitic volcanoes with cones, where the ground deformation is relatively small. At calderas in a state of unrest, the gravity-height gradient is usually close to the free-air-gradient (FAG), but the changes occur over such a large area that Dmm is of the order 1010-1012 kg. At these volcanoes, the source of the ground deformation and gravity changes is likely to be the same, relatively deep magma chamber (2-3 km typically), whereas for stratocones the sources are not necessarily the same (the cone may be fracturing and collapsing while magma is infiltrating a surface feeding conduit). It is remarkable that the range of measured DVe and inferred Dmm observed at calderas in a state of unrest is less than 2 orders of magnitude. A logical conclusion from the similarity in DVe and Dmm might be that the magma and country rock physical properties are similar at each of the sites studied, however subtle variations in the gravity-height gradients (i.e. deviations from the FAG) indicate that there are contrasts in the sub-surface conditions. Since magma movement characteristics are dominated by magma properties rather than by country rock properties, these variations may provide an index of magma fluid dynamic properties, most notably magma compressibility (Km). By assuming a magma density, a relationship between magma and edifice volume change and the ratio between country rock rigidity (me) and Km can be derived.

**JSV36/E/16-B3 1640**

**DISPLACEMENTS, GRAVITY CHANGES AND DEFORMATION FIELD DUE TO DIFFERENT SOURCES OF ANOMALOUS HEAT FLOW IN ELASTIC AND VISCOELASTIC MEDIUM**

Ladislav BRIMICH (Geophysical Institute, Slovak Academy of Sciences, Dubravska 9, 842 28 Bratislava, Slovakia, email: geofbrim@savba.sk)

Theoretical formulae and results of numerical calculation of the deformation field, displacements and gravity changes, due to magmatic bodies approximated by a three dimensional prism embedded in an elastic and viscoelastic halfspace are presented. It is shown that surface displacements cause a pronounced dome in the epicentral region and that surface tensile stresses attain values that compare well with the critical stress required to cause creep or fractures at the surface of the halfspace. Important effect of magmatic bodies is their upward pressure induced by the presence of various hot gases, fluids and by less density of magma in comparison with ambient solid rocks. A concentrated vertical force acting in the elastic halfspace approximates this effect. The results are in good agreement with known patterns of the displacements, the stresses and the faults observed in the regions of near-surface igneous bodies (e.g. laccolithes or diapires).

**JSV36/E/15-B3 1655**

**ON THE INTERPRETATION OF THE MICROGRAVITY AND GPS MEASUREMENTS IN MAYON VOLCANO, PHILIPPINES**

JOSE FERNANDEZ (Institute of Astronomy and Geodesy, Fac. Ciencias Matematicas, Ciudad Universitaria, 28040-Madrid, Spain, email: jft@igmat1.mat.ucm.es) Kristy F. Tiampo (CIRES, University of Colorado, Boulder, CO, USA, email: kristy@fractal.colorado.edu) Gerhard Jentzsch (Institute for Geosciences, FSU Jena, Germany, email: jentzsch@geo.uni-jena.de) John B. Rundle (CIRES, University of Colorado, Boulder, CO, USA, email: rundle@hopfield.colorado.edu).

Mayon volcano is part of the Bicol volcanic chain of the island of Luzon, Philippines. During this century there have been 10 active periods distributed at regular intervals. Because of the dense population living in the vicinity of the volcano, seismological observatories are in operation in addition to measurements of gravity begun in 1992. Two profiles at the slope were established, connected to a regional network around the volcano. The height control is provided by parallel Global Positional System (GPS) measurements. During 5 campaigns within four years the differential GPS gives no significant changes in elevation (around 4 cm), but the gravity increased significantly by up to 1500 nm/s<sup>2</sup> (Jentzsch et al, 1999). Both facts can not be explained with the classical Mogi model (Mogi, 1958). Jentzsch et al. (1999) explain the existing gravity changes without changes in elevation by density changes within a vent system. They do not obtain a perfect fit of data and model results. In this paper we made an interpretation of the geodetic signals observed on Mayon volcano using genetic algorithm inversion technique and considering elastic gravitational Earth models in place of purely elastic ones. The obtained results are described.

**JSV36/E/25-B3 1710**

**THE STROMBOLI VOLCANO AS A NATURAL MULTIDISCIPLINARY LABORATORY A PROPOSAL**

Carlo Bellecci (II Università di Roma, Tor Vergata, Roma, Italy); Gino M. Crisci (UNICAL, Arcavacata di Rende, Cosenza, Italy) Giuseppe de Natale (Osservatorio Vesuviano, Napoli, Italy) Giovanni P. Gregori (IFA-CNR, via Fosso del Cavaliere 100, 00133 Roma, Italy; e-mail: gregori@atmos.ifa.rm.cnr.it) Iginio Marson (Università di Trieste, Italy) Gabriele PAPARO (IDAC-CNR, Roma, Italy), and Domenico Patella (Università Federico II, Napoli, Italy)

Stromboli is a volcanic island slightly North of Sicily, within a tectonic setting characterised by a Benioff zone, that is curved like a Greek theatre opened towards the Tyrrhenian Sea, with very deep earthquakes. It is the unique volcano of entire world that explodes very regularly, every ~15-20 min, since at least ~3,000 years. A permanent Laboratory has recently been established on it, and an extensive interdisciplinary programme is being started. The monitored phenomena are (including their respective time evolution after every volcanic explosion): soil deformation, stress and strain; seismicity, microseismicity and acoustic emissions; gas exhalation and exchanges between soil and atmosphere and/or by submarine fumaroles; shallow and deep geothermic s; geo-e.m. (spontaneous potentials, geomagnetic field, aeromagnetism, Coulomb charge of the ejecta, atmospheric electrical gradient and conductivity, lightning discharges within the plume, eventual coupling between volcanic explosions and ionospheric disturbances); mineralogical, geochemical, and isotopic information; volume and speed of the ejecta; aerosols; atmospheric chemistry and radiative balance; meteorological and environmental impact; boundary layer meteorology either with or without the volcanic injection; etc.

**PANEL DISCUSSION 1720**

Dixon (Univ of Miami, Miami, USA); Hirn (Institut de Physique du Globe Université Paris VI, Paris, France); Martini (Department of Earth Sciences, Univ of Florence, Italy); Mattioli (Univ. Puerto Rico, Dept of Geology, Mayaguez, USA); Shapiro (Institute of Geophysics, Ekaterinburg, Russia); Spichak (Geophysical Research Centre, Moscow, Russia).

Wednesday 28 July AM

**JSV36/W/15-B3 Poster 0900-01**

**SMALL SCALE THERMAL DEMAGNETIZATION AFTER SEISMIC SWARM DETECTED FROM DEENSE OBSERVATION USING ARGOS SYSTEM**

Tsuneomi KAGIYAMA, Maroka Neki and Fumio Masutani (Earthquake Research Institute, University of Tokyo, Tokyo 113-0032, Japan, email: kagiyaama@eri.u-tokyo.ac.jp, neki@eri.u-tokyo.ac.jp, masutani@kirishima.eri.u-tokyo.ac.jp)

Significant information is frequently obtained only at crater zones. Volcano Research Center, ERI developed our own suitable interface for ARGOS system to control the observation and acquisition system to obtain and process the data. Five sets of the ARGOS transmitters were installed just around the crater of Shinmoe-Dake, Kirishima Volcanoes in Japan for total intensity of geomagnetic field and ground temperature. Geomagnetic observation found annual changes up to 1 nT for each site, and clarified an anomalous change up to 2 nT of total intensity from 1993 to 1994 after eliminating the annual changes. The position of this anomalous change is determined within the OShallow Low Resistivity Region<sup>0</sup>, which has already been detected by MT survey and was interpreted as a water saturated layer beneath the crater. After precise seismological and other geophysical observations, it is found that this change followed the outbreak of the earthquake swarm at the top of the ODeep Low Resistivity Region<sup>0</sup>, which is also detected by MT survey, and upward migration of seismic activity. This



evidence suggests that this thermal demagnetization be caused by the increase of the temperature within the ÖSLRRÖ following the supply of magma or magmatic gas associated with the seismic swarm from the top of the ÖDLRRÖ. From the end of 1998, fumarolic temperature was also observed within the crater of Shinmoe-Dake to detect an anomalous change of fumarolic temperature.

**JSV36/E/24-B3** Poster **0900-02**

#### MORPHOLOGICAL INSIGHTS OF SELF-POTENTIAL ANOMALIES

Yasunori NISHIDA (Department of Earth and Planetary Sciences, Hokkaido University, Sapporo, 060-8010 Japan. Email: nishida@ares.hokudai.ac.jp) Jacques Zlotnicki (Laboratoire de physique(a), UMR 6530, 3d av de la recherche scientifique 45071 Orl=E9ans cedex 02, France. Email: jacques.zlotnicki@cnsr-orleans.fr)

During several tens of years Self-Potential (SP) prospectings have been carried out in order to evidence hydrothermal systems associated with geothermal fields. During the last decade a new interest of this technique has appeared. Many teams have tried to extrapolate such studies on volcanoes. Nowadays we have numerous examples of detailed SP mappings on volcanoes; some of them being active. The comparison of the spatial distribution of SP anomalies and their respective amplitudes allow us to synthesise the general features of SP anomalies on volcanoes. - On Mount Pel=E9e (Fr), which is an andestic volcano in a rest period, essentially negative anomalies, up to -1500 mV in amplitude, are observed. They are related to existing calderas and infiltration of meteoric water on the slopes ("topographic effect"). Such anomalies are also observed on Mt Esan (Jp). - On Soufriere=E8re de Guadeloupe (Fr), Komogatake (Jp), Usu (Jp) or Vulcano (It) where an active hydrothermal system produces a strong superficial argillisation, the SP anomalies are smooth and positive. The amplitude generally does not exceed several hundreds mV. - On volcanoes like Piton de la Fournaise (Fr) or Miyake-Jima (Jp) where an hydrothermal system is well-developed in the central part, one can observe the superimposition of sharp and large (< 2 V) positive anomalies. These ones disappear away off the summit where the so-called "topographic effect" is predominant. (Jp: Japan; Fr: France; It: Italy).

**JSV36/E/28-B3** Poster **0900-03**

#### SELF-POTENTIAL MEASUREMENTS ON A CALDERA LAKE

Mitsuhiro SUGIHARA and Tsuneo Ishido (both at Geothermal Research Department, Geological Survey of Japan, 1-1-3, Higashi, Tsukuba, 305-8567, Japan, email: sugihara@gsj.go.jp)

Lake bourne self-potential (SP) measurements can be made by towing electrode pairs behind a boat. The potential gradient distribution are evaluated from the observed potential differences, and integrated into the potential distribution along the track line. Offset between the electrodes must be evaluated accurately because the integration process amplifies it. Outgoing and returning on the same track line is essential to determine the offset value accurately. Continuous kinematic GPS survey makes it possible to evaluate how the track lines coincide with an accuracy of a few centimeters. We succeeded in determining SP distribution with a resolution better than 1 mV on Lake Kutcharo, which is the largest caldera lake in Japan. This experiment shows SP measurements on lake are better in resolution than on land. SP anomalies often observed in volcanic areas. Crater lakes and caldera lakes must be potential fields to apply the lake bourne SP measurements to detect volcanic SP anomalies.

**JSV36/W/25-B3** Poster **0900-04**

#### RESISTIVITY IMAGING AND SELF POTENTIAL MONITORING AT MERAPI

S. FRIEDEL, F. Jacobs (both Institut für Geophysik und Geologie, Universität Leipzig, Talstraße 55, 04103 Leipzig, email: friedel@rz.uni-leipzig.de)

The presentation reports a) results of a near surface resistivity calibration survey in an active solfatara region of Merapi volcano, b) acquisition and processing technology and results of 2.7 km dipole-dipole resistivity survey, and c) results of self potential (SP) mapping and monitoring at the summit.

Near surface resistivity surveys indicate great variability of resistivity in the solfatara region ( $\rho = 2 \dots 2000$  Ohm) depending on fluid saturation and presence of alteration minerals. Resistivity and SP profiles across active solfatara show strong correlation and are consistent with a model of a two-phase convection cell.

A 2.7 km long dipole-dipole profile with was set out radially along the West flank of Merapi between 1300 m and 2000 m above sea level. A special field procedure and data processing schemes are presented. A portable, light-weight DC-transmitter allowed the acquisition of a large number of data despite the rough volcanic terrain. Using 24-bit stand-alone data receiver technology (RefTek) and special data enhancement procedures electrical field amplitudes as low as 100 nV/m could be detected reliably. 2D-Inversion was carried out to a depth of 750 m. The resulting model can be interpreted as a high resistivity top layer of unsaturated pyroclastics ( $\rho = 1 \dots 10$  kOhm,  $t = 200 \dots 350$  m) following an intermediate layer ( $\rho = 100 \dots 500$  Ohm,  $t = 150$  m 200 m) and a low resistivity zone ( $\rho < 100$  Ohm, starting between 350 m and 550 m) of partly saturated and hydrothermally altered pyroclastic and effusive material. SP monitoring at two channels near the solfatara and a remote reference show changes in the order of 10 mV within hours but are only weakly correlated.

**JSV36/W/27-B3** Poster **0900-05**

#### RESISTIVITY STRUCTURE IN THE SOUTHERN KYUSHU AREA, SOUTHWEST JAPAN, REVEALED BY MAGNETOTELLURIC METHODS

Hiroshi MUNEKANE, Tsuneomi Kagiya and Hisashi Utada, Earthquake Research Institute, University of Tokyo, 1-1-1, Yayoi, Bunkyo-ku, Tokyo, 113-0032, Japan (email: munekane@eri.u-tokyo.ac.jp, kagiya@eri.u-tokyo.ac.jp, utada@utada-sun.eri.u-tokyo.ac.jp)

The southern part of Kyushu, southwest Japan, is an area of high volcanic activity in which a number of volcanoes are distributed such as the Kaimon-dake, the Sakura-jima, the Kirishima volcanoes or the Aso. However, distribution of these volcanoes is not spatially uniform, and types of the volcanism have large locality. This apparent heterogeneity of volcanism in this area may be deeply related to that of magma supply system at depths, which may be reflected by the deep crustal structure. The present paper studies the relation between regional volcanism and electrical resistivity structure by Magnetotelluric (MT) method. Prior to the investigation of the resistivity structure, the method to remove galvanic effect developed in Munekane and Utada (1998) is applied to the obtained MT responses. The method has an advantage that it can be theoretically applicable even when a regional structure has three dimensional characteristics, which is a common case in a complex region such as Japan. Although a full 3-D resistivity model should finally be presented, preliminary 1-D modelling show that the resistivity structure in the area have two characteristic features. One is the shallow low resistivity regions (SLRR), which are located at several hundreds of meters depth and have resistivities around 10(Ohm-m) or less. Another feature is the deep low resistivity regions (DLRR), which are located around 10km or deeper and

have resistivities around 10(Ohm-m). The DLRR and SLRR can only be seen in the western part of the volcanic front in this area. The distribution of the SLRR shows good agreement with volcanic regions in Cenozoic era. This implies that the SLRR is possibly related to hydro-thermal activity under this area. The DLRR, on the other hand, not only exists around the Kirishima volcano area but also looks to extend toward north where no volcano exists between the Kirishima and Aso volcanoes. The DLRR may be interpreted as a deep region containing partial melt or free water.

**JSV36/E/08-B3** Poster **0900-06**

#### THE ELECTRICAL STRUCTURE BENEATH WUDALIANCHI VOLCANIC CLUSTER IN HEILONGJIANG PROVINCE OF CHINA

Guozhe ZHAO, Denghai Bai, Yan Zhan, Jijun Wang, Guangwen Jin and Zhao Jiang Institute of Geology, Seismological Bureau of China, Beijing 10029, China email: zhaogz@public.bta.net.cn

Wudalianchi volcanic cluster located in northern part of North-East China, with coordinates of longitude E 126;ã00-126;ã20;ã and latitude of N 48;ã34;ã-48;ã48;ã. It consists of 14 cones. The last eruption of the volcanoes was in the year of 1719 to 1721 and two of cones, Laoheshan cone and Huoshaoshan cone were formed. MT measurement are recently carried out at 71 sites along three EW profiles and four NS profiles in the volcanic cluster and the vicinity in order to study the magma chamber and deep structure and volcanic activity. The periods of the data ranged from 256Hz to about 4096 sec.

The real part of magnetic induction arrows at most of MT sites for periods from several to dozens seconds direct to the cluster center (to high resistivity) showing there is a resistive body in the upper crust. Those for longer periods (around 1000sec) tend to direct to outside of the cluster showing us that there is lower resistivity body in the deeper depth. The 2-D inversion results by RRI method for EW profiles show that there is a high resistivity body like as rivet form from surface to about 20 km depth. The width of the body in EW direction at depth less than 5 km is about 20 km. The width for the lower part of the body is less than 10km. However the tip of the rivet body extends continuously down to several tens kilometers and resistivity decreased with increasing depth. The seismic activity is, recent year, significant in southwestern part of the cluster where low resistivity appeared at depth deeper than 5 km. Most of micro shocks were at shallower depth than 5 km. It is postulated that the high resistivity body with rivet form is a cooling magma chamber. A passage for the magma exited in the deeper depth.

**JSV36/E/23-B3** Poster **0900-07**

#### MAGNETOTELLURIC SOUNDINGS ON MIYAKE-JIMA VOLCANO: A TOOL TO UNDERSTAND THE STRUCTURE AND ITS DYNAMISM

Jacques ZLOTNICKI (Laboratoire de Geophysique(a), UMR 6530, 3d av de la recherche scientifique 45071 Orleans cedex 02, France. Email: jacques.zlotnicki@cnsr-orleans.fr) Yochi Sasai (Earthquake Research Institute(b), Tokyo University, 1-1 yayoi 1-chome, Tokyo, 113 Japan. Email: sasai@eri.u-tokyo.ac.jp) Paul Yvetot(a), Yasunori Nishida (Faculty of Sciences, Sapporo, Japan) & Makoto Uyeshima(b).

Miyake-Jima Island is located on the Izu-Bonin trench extending SSW of Tokyo bay. Miyake-jima is a very active stratobasaltic volcano that can erupt about every twenty years. Large eruptions have occurred in 1940, 1962 and 1983. A new one is expected in the next ten years. To better understand the monitoring of the volcano with electromagnetic methods we have undertaken several campaigns of Magnetotelluric soundings on the island. The objectives were to recognise the existing calderas which form the upper part of the volcano, the main fissural axes along which the last eruptions have taken place, the seawater penetration through the inner part of the island, and the hydrothermal system(s) mainly located in the summit part of the volcano. More than 80 soundings were done in the band 70 kHz-0.1 Hz. We have used an antenna in the band 70 kHz-1 kHz in order to get data when the natural EM field was too weak or in existing. These data give information between a few tens meters and several kilometers deep. The preliminary results are the following: The seawater infiltrates the massif over several hundreds meters depending on existing fissural eruptive axes (SSW, N, NE) and craters bordering the coast. The main fissural axes along which the last eruptions have taken place are well evidenced from the coast to the summit. Some caldera borders are also evidenced; some of them favour the formation of hydrothermal systems in their inner part.

**JSV36/W/12-B3** Poster **0900-08**

#### DIFUSSE DEGASSING OF CO2 AND 222RN IN AND AROUND THE VOLCANIC RIFT-ZONES OF EL HIERRO, CANARY ISLANDS, SPAIN

Ancor TRUJILLO, Yurima Gimeno, Sofia Medina (all at the Faculty of Chemistry, Univ. La Laguna, 38206 La Laguna, Tenerife, Spain), José M. Salazar, José M. Navarro, Nemesio M. Pérez (all at the Environmental Research Division, ITER, 38611 Granadilla, Tenerife, Spain) and Pedro A. Hernández (Lab. for Earthquake Chemistry, Univ. Tokyo, Tokyo 113, Japan)

El Hierro (278 Km<sup>2</sup>) is situated in the southwestern part of the Canary Islands. Subaerial volcanic activity has mainly occurred along three major volcanic rift-zones during the last 1Ma. Gravitational depressions had also occurred at El Hierro, and this type of geological process is responsible for the formation of geomorphological features such as El Golfo Valley. The objective of this study is to evaluate the spatial distribution of soil CO<sub>2</sub> flux and soil gas 222Rn levels for monitoring magma movement and seismicity changes in the island.

A soil gas 222Rn and CO<sub>2</sub> flux survey was performed at 626 sampling sites using a portable radon sensor and a NDIR spectrophotometer, respectively, in 1998. Statistical-graphical analysis of soil gas 222Rn data showed three geochemical populations. The background has a mean of 10.4 pCi/L and represents a 59% of the total data. The peak population showed a mean of 74 pCi/L and represents a 1.8% of the total data. Soil CO<sub>2</sub> flux data showed also three geochemical populations. The background mean is 0.3 g-m<sup>-2</sup>-d<sup>-1</sup> and represents 83% of the total data. The mean of the peak group is 48 g-m<sup>-2</sup>-d<sup>-1</sup> and represents 0.5% of the total data. Anomalous levels of soil CO<sub>2</sub> flux and soil gas 222Rn levels were detected at the intersection of the three major volcanic rift-zones as well as in the central and western part of El Golfo. Other peak values were found along the NE rift-zone, some of them associated to recent fracture/faults. Total diffuse emission of soil CO<sub>2</sub> from El Hierro is about 190 t-d<sup>-1</sup>.

**JSV36/W/20-B3** Poster **0900-09**

#### SOIL CO2 FLUX MONITORING NETWORK FOR THE SEISMIC-VOLCANIC SURVEILLANCE OF TENERIFE, CANARY ISLANDS, SPAIN

Dácil CARBALLO, Carolina Méndez, Francisco Martín (all at Faculty of Chemistry, Univ. La Laguna, 38206 La Laguna, Tenerife, Canary Is., Spain; e-mail: timanfaya@tier.canaria.es), José M. L. Salazar, Nemesio M. Pérez (ITER, 38594 Granadilla, Tenerife, Canary Islands, Spain), and Pedro A. Hernández (Lab. for Earthquake Chemistry, Univ. Tokyo, Bunkyo-ku, Tokyo 113, Japan)

Tenerife is the largest island (2,034 Km<sup>2</sup>) of the Canarian Archipelago. Most of the historical volcanic activity at Tenerife, about 6 eruptions during the last 500 yrs, has occurred along its rift-zones the last eruption being in 1909, Chinyero volcano. Fumarolic degassing (85°C)

occurs just at the summit of Teide volcano (3.716 m of elevation), but diffuse mantle degassing can occur along the rift-zones (Pérez et al., 1996). The role of carbon dioxide as the main pressure-generating component in basaltic magmas, the lack of fumarolic activity, and the geological evidence of significant and recent volcanic activity along the rift-zones support the use of soil CO<sub>2</sub> flux monitoring network as an additional geochemical tool for volcanic surveillance at Tenerife. Soil CO<sub>2</sub> flux measurements are performed since March 1997 by using alkaline traps (NaOH 1N) which are exposed to the soil atmosphere for one week period. This integrated technique for soil CO<sub>2</sub> flux monitoring is being applied at 23 stations which are distributed all over Tenerife. Estimated soil CO<sub>2</sub> flux values are quite similar to those observed by a portable NDIR, especially for low flux levels. Significant spatial variations of soil CO<sub>2</sub> flux levels have been detected. Most of the monitoring stations along the rift-zones showed soil CO<sub>2</sub> flux levels from 1.2 to 27.8 g·m<sup>-2</sup>·d<sup>-1</sup>, and the average level ranged from 8.1 to 11.3 g·m<sup>-2</sup>·d<sup>-1</sup>. In the central part of the island soil CO<sub>2</sub> flux levels were higher, up to 43.1 g·m<sup>-2</sup>·d<sup>-1</sup>, than those observed along the rift-zones. To this date, soil CO<sub>2</sub> flux secular variations are closely related to meteorological fluctuations.

**JSV36/W/16-B3** Poster **0900-10**

**SOIL PH MAPPING TO EVALUATE INTENSIVE MAGMATIC-HYDROTHERMAL DIFFUSE DEGASSING ON ACTIVE VOLCANOES**

Marcos VALIENTE, Belen Meneses, Paqui Rodríguez (all at Faculty of Chemistry, Univ. La Laguna, 38206 La Laguna, Tenerife, Canary Islands, Spain; e-mail: teide@iter.rcanaria.es), José M. L. Salazar, Nemesio Pérez (Environmental Research Division, ITER, 38594 Granadilla, Tenerife, Canary Islands, Spain), and Pedro A. Hernández (Laboratory for Earthquake Chemistry, Univ. Tokyo, Bunkyo-ku, Tokyo 113, Japan)

Soil gas concentration and flux surveys have been applied successfully to understand processes related to magmatic reactivation in active volcanoes, but some problems related to the interpretation of the spatial variations of soil gas content and flux pattern are still significant because of the soil heterogeneity through volcanic edifices. Physico-chemical parameters of the soil environment can affect the distribution pattern of the volatile species and their flux levels because of their effects on the adsorption-desorption, diffusion, and mass transport processes. Therefore, soil pH measurements could be a simple, inexpensive, and "quasi" integrated geochemical tool for detecting areas which are affected by an intensive level of diffuse magmatic-hydrothermal degassing. Soil pH mapping geochemical tool has been performed at Kilauea (Hawaii), Rabaul (Papua New Guinea), Campi Flegrei (Italy), Long Valley (California, USA), Miyake-jima, Usu (Japan), La Palma, El Hierro, and Teide (Canary Islands) volcanoes. Soil pH data of active volcanoes with low levels of magmatic-hydrothermal diffuse degassing showed just one geochemical population: background group. Background soil pH levels showed a range of soil pH average values between 6.5 and 7.5. On the other hand, soil pH data of active volcanoes with high levels of diffuse degassing showed two overlapping geochemical populations: background and an intermediate "threshold" population characterized by soil pH levels (< 4) between background soil pH values (6.5 - 7.5) and typical low pH values (2 - 3) of magmatic-hydrothermal discharges.

**JSV36/W/14-B3** Poster **0900-11**

**GEOCHEMICAL MONITORING OF CUMBRE VIEJA VOLCANO (LA PALMA, CANARY ISLANDS) BY MEANS OF CONTINUOUS MEASUREMENTS OF DISSOLVED GAS 222RN IN GROUND WATER**

Francisco J. HERNÁNDEZ, Jose M. Salazar, Nemesio M. Pérez (all at the Environmental Research Division, ITER, 38594 Granadilla, Tenerife, Spain; email: fhdez@iter.rcanaria.es), George Igarashi, Kenji Notsu, and Pedro A. Hernández (all at the Lab. for Earthquake Chemistry, Univ. of Tokyo, Bunkyo-ku, Tokyo 113, Japan)

La Palma is one of the most active volcanic islands of the Canarian archipelago. Cumbre Vieja volcano is situated in the southern part of La Palma, where had occurred 6 eruptions during the last 500 years. Since fumarolic degassing is not present at Cumbre Vieja volcano, geochemical continuous monitoring of dissolved gases in ground water is a useful tool for volcanic prediction research. With this purpose, continuous monitoring of dissolved gas 222Rn is carried out at Amargavinos well (La Palma) since September 1997. This well is 400 m deep and is located along the NE rift-zone of Cumbre Vieja volcano. The dissolved gas 222Rn monitoring system consist of a 222Rn detection chamber, a 256-channel high-speed analog-to-digital converter (AD) and a personal computer. The 222Rn detection chamber is an electrostatic collector, and the particles emitted mainly by the decays of 214Po and 218Po (daughters of 222Rn) are detected as electrical currents through a PIN photodiode. To this date, dissolved gas 222Rn in ground water at Amargavinos show a steady-state level of 950 pCi/L, and it might be due to the lack of seismic-volcanic activity during this period. The same type of 222Rn monitoring system was used to detect precursory 222Rn signatures related to Kobe (Japan) and Galician (Spain) earthquakes. Other gas components will be soon measured by means of QMS at this observation site to improve our continuous geochemical monitoring of Cumbre Vieja volcano.

**JSV36/W/01-B3** Poster **0900-12**

**SOIL CO<sub>2</sub> AND 222RN DEGASSING AT MIYAKE-JIMA VOLCANO, JAPAN**

Pedro A. HERNANDEZ, Yoichi Shimoike, Toshiya Mori, Kenji Notsu (all at Laboratory for Earthquake Chemistry, Univ. Tokyo, Bunkyo-Ku, Tokyo 113-0033, Japan; e-mail: hernandez@eqchem.s.u-tokyo.ac.jp), José M. L. Salazar, Nemesio M. Pérez (Environmental Research Division, ITER, 38594 Granadilla, Tenerife, Spain), and T. Aotani (Miyake High School, Miyake-jima, Tokyo, Japan).

Miyake-jima is situated about 200 km south of Tokyo and is one of the most active basaltic stratovolcanoes in Japan. During this century, volcanic eruptions have regularly occurred at Miyake-jima, almost every 22 years, and the most recent eruption was on October, 1983. Fumarolic activity (79 to 87°C) is mainly located at the summit cone of Oyama volcano, in the central part of Miyake-jima. A soil gas survey of 150 sampling sites was performed at Miyake-jima from May 23 to June 2, 1998. Soil gas 222Rn and CO<sub>2</sub> flux measurements were performed by using a portable radon sensor and a NDIR spectrophotometer, respectively. Statistical-graphical analysis of soil gas 222Rn measurements showed three overlapping populations. The background mean is 13.1 pCi/L (95% of the total data) and the peak group showed a mean of 43 pCi/L (0.9% of the total data). Soil CO<sub>2</sub> flux measurements showed also three geochemical populations. The background mean is 94 g·m<sup>-2</sup>·d<sup>-1</sup> and represents 59% of the total data. The peak group showed a mean of 9,500 g·m<sup>-2</sup>·d<sup>-1</sup> and represents 2.7% of the total data. Most of the study area showed background levels of diffuse degassing of 222Rn and CO<sub>2</sub>. Anomalous levels of diffuse degassing of 222Rn and CO<sub>2</sub> were identified in the summit crater of Miyake-jima and surrounding areas, showing a good spatial relationship with the radial dike pattern of Miyake-jima. A mixed magmatic and biogenic origin is suggested for the diffuse degassing inside summit crater, while a clear biogenic origin is observed for the CO<sub>2</sub> degassing outside. Diffuse emission of CO<sub>2</sub> from the summit crater is about 327 t·d<sup>-1</sup>.

**JSV36/W/03-B3** Poster **0900-13**

**SECULAR VARIATIONS OF CO<sub>2</sub> DIFFUSE DEGASSING RELATED TO THE 1997 VOLCANIC ACTIVITY AT RABAUL CALDERA, PAPUA NEW GUINEA**

Nemesio PEREZ (Environmental Research Division, ITER, 38594 Granadilla, Tenerife, Canary Islands, Spain; e-mail: nperez@iter.rcanaria.es), David Lokol, Patrice de Saint Ours, and Ben Talai (all at Rabaul Volcano Observatory, P.O. Box 386, Rabaul, East New Britain, Papua New Guinea)

Volcan and Tavurvur volcanoes did erupt simultaneously on September 1994, almost 9 years after the end of the seismic-uplift crisis at Rabaul caldera. An eruptive stage is still taking place at Tavurvur volcano, which had experienced several strombolian eruptions during these recent years. Geophysical conventional techniques are mainly used for monitoring the volcanic activity at Rabaul caldera. In order to establish a multidisciplinary volcano monitoring program research at Rabaul Volcano Observatory, simple geochemical tools were applied for the volcanic surveillance: ash-leachates chemistry and soil CO<sub>2</sub> flux monitoring. A network of 14 observation sites for soil CO<sub>2</sub> flux measurements all over Rabaul caldera was operative from November 1996 to November 1997. During this period two strombolian and lava-producing eruptions occurred on January 1997 and March 14. Other four minor strombolian eruptions did also occur during this period. At each observation site, soil CO<sub>2</sub> flux level was evaluated by means of an integrated technique, which use alkaline solutions (NaOH 1N) exposed to the soil atmosphere for one week period. Estimated soil CO<sub>2</sub> flux values showed significant spatial variations from one observation site to another. The highest levels were detected at the flank of Vulcan and Tavurvur volcanoes, about 70 g·m<sup>-2</sup>·d<sup>-1</sup>, and the lowest levels at Beehives. Anomalous temporal changes of soil CO<sub>2</sub> flux levels had been observed prior to strombolian eruptions during 1997. Even though these levels of soil CO<sub>2</sub> flux could be underestimated, this simple and inexpensive soil CO<sub>2</sub> flux network could be a useful tool for volcano monitoring at Rabaul caldera.

**JSV36/W/08-B3** Poster **0900-14**

**TRACE ELEMENT AND ISOTOPE GEOCHEMISTRY OF HIGH-K CALC-ALKALINE VOLCANIC ROCKS FROM MERAPI VOLCANO, CENTRAL JAVA, INDONESIA**

Ralf GERTISSER and Jörg Keller (Institut für Mineralogie, Petrologie und Geochemie, Universität Freiburg, 79104 Freiburg, Germany, email: gertisse@ruf.uni-freiburg.de, jkeller@ruf.uni-freiburg.de)

Merapi volcano (Central Java, Indonesia) has erupted frequently during Holocene time, producing mainly high-K basaltic andesites with a restricted compositional range from 52-57 wt.% SiO<sub>2</sub>. Mantle-normalised trace element signatures show similar patterns for all Merapi rocks with LILE and Th enrichment relative to LREE and HFSE, as well as negative Nb, Ta and Ti anomalies. REE patterns display LREE enrichment (40-90x chondritic) relative to the HREE (10-15x chondritic). No Eu anomalies are observed. Nd isotope compositions of the studied Merapi samples define a range similar to that given by Whitford et al. (1981) for the Sunda arc in Java. In contrast, Sr isotope ratios of Merapi rocks tend to be more radiogenic than those from adjacent volcanic centers in Java. The elevated values of 87Sr/86Sr for a given 143Nd/144Nd in relation to the "mantle array" point to the presence of a component of altered oceanic crust or sediment in the source region of Merapi magmas. Pb isotope data further illustrate the role of sediments in the genesis of Merapi magmas. Pb isotope ratios of Merapi are distinctly radiogenic and display small-scale variations with linear arrays in 207Pb/204Pb and 208Pb/204Pb vs. 206Pb/204Pb plots, that are steeper than for oceanic basalts. Furthermore our data extend the Pb isotope range for Merapi rocks (McDermott & Hawkesworth, 1991) to more radiogenic Pb isotope ratios, that plot within the field for oceanic sediments adjacent to the West Sunda arc and well outside the Indian Ocean MORB field (Ben Othman et al., 1989). In general, mixing of a suggested MORB-like mantle source with sediments adjacent to the West Sunda arc may account for the observed isotopic variations in Merapi magmas. Trace element and isotope signatures of Merapi are thought to be derived mainly by contamination of the mantle wedge with partial melts of subducted sediments and LILE-enriched slab-derived fluids. The lack of correlation between radiogenic isotope ratios and differentiation indices such as SiO<sub>2</sub> precludes a significant role of crustal contamination by AFC-type processes in the evolution of magma at Merapi.

**JSV36/E/11-B3** Poster **0900-15**

**DYNAMIC MIXING OF THE RECENT POPOCATEPETL (MEXICO) MELTS**

ANA LILLIAN MARTIN (Instituto de Geofísica, UNAM, Ciudad Universitaria, Mexico D.F. 04510, Mexico. Email: analil@tonatiuh.igeofcu.unam.mx) Susanne Straub (Geomar, Wischhofstr 1-3, 24148 Kiel, Germany. Email: sstraub@geomar.de E. Cabral, E. Garcia, G. Cifuentes, G. Sanchez and M. Reyes (all at UNAM)

Geochemical studies of the recent Popocatepetl ejecta (major and trace element data of bulk samples and mineral compositions) correlated with geophysical parameters are consistent with a model of recurrent dynamic mixing between mafic (<57% SiO<sub>2</sub>) and evolved melts (64% SiO<sub>2</sub>). The mafic end member is equilibrated only with olivene (Fo90) and Cr-spinel. Mineral-melt equilibria and clinopyroxene and amphibole barometry suggest that the mafic component rises from over 45km depth and then mixes with the cooler more evolved melt at upper crustal levels. Recurrence of small eruptions spaced mainly over weeks and sometimes days is thought to be related to periodic ascent of mafic melts. Volcanotectonic events generally precede the eruptions by several hours. Small magma pulses are also consistent with magnetic anomalies. Chemical and textural disequilibria (e.g. mineral zoning, quench texture) also suggest a rapid ascent of the mafic melt to crustal levels and mixing with the evolved melt immediately before eruption.

**JSV36/E/22-B3** Poster **0900-16**

**THE GEOCHEMICAL MONITORING SYSTEM (GMS II) PROTOTYPE INSTALLED AT THE "ACQUA DIFESA" WELL (BELPASSO, CATANIA), IN THE ETNA REGION, ADDRESSED TO SEISMIC AND VOLCANIC SURVEILLANCE: FIRST DATA**

Fedora QUATTROCCHI, Luca Pizzino, Francesco Pongetti, Gianni Romeo, Piergiorgio Scarlato, Umberto Sciacca, Giuseppe Urbini. Istituto Nazionale di Geofisica, Via di Vigna Murata 605, 00143, Roma, Italy. E-mail: geochimica@ing750.ingr.it

The drop in the costs/benefits ratio as regard both the hardware (i.e., PC-IBM compatible, electronics box, telecommunication systems, etc.) and sensors devices, as well as the exponential development of different techniques to measure geochemical-hydrologic variables, strongly recommend the continuous monitoring geochemical network strategy, more than discrete monitoring, allowing to obtain scientific results, unthinking since a few time ago. To develop a multidisciplinary approach to seismic/volcanic hazards prediction, using a really multivariable strategy, either in software-hardware as well as in sensors selection, the ING laboratories developed the second prototype of Geochemical Monitoring System (GMS II), that was conceived, designed, assembled and tested in laboratory and in a remote site, specifically addressed to geological-natural hazards surveillance, but it could be easily used for environmental problems too (i.e., bio-geochemical surveillance).



Actually the GMS II prototype is running, recording data every 10 minutes, and the first months of data acquisition have been performed in a test-remote site, "Acqua Difesa" well, located in the Etna region. The results are discussed.

Despite the continuous 222Rn monitoring devices have been assembled still without hardware-station linking and the H2S and He sensor devices are under mounting phase, all the other sensors and the automatic sampler are on line (water temperature, pH, Eh, electrical conductivity, CO2 partial pressure, air temperature, barometric pressure).

**JSV36/E/12-B3** Poster **0900-17**

**A NEW METHOD FOR VOLCANIC GAS FLUX MEASUREMENT: APPLICATION TO KUJU VOLCANO, JAPAN**

Genji SAITO, Kohei Kazahaya, Hiroshi Shinohara, Masaya Yasuhara (Geological Survey of Japan, 1-1-3, Higashi, Tsukuba, Ibaraki, 305-8567, Japan, email: gsaito@gsj.go.jp)

Gas flux from active volcanoes is one of important parameters for evaluation of volcanic activity and magma degassing processes. A new tool for volcanic gas flux measurement was applied at Kuju volcano, Japan. Fumarolic activity existed at Kuju volcano since at least 14th century. A new phreatic eruption began on October 11, 1995 forming new craters, and intense fumarolic activity at these new craters continued till now. Flux measurements of fumarolic gases from the new craters were carried out together with sampling of the fumarolic gases from March 1996 to March 1998. Fluxes of water (steam) from each crater can be calculated based on distribution on the gas velocity (30-70 m/s) in a cross section of each crater outlet (~0.5 m<sup>2</sup>). Flow velocity of the fumarolic gases is obtained by dynamic pressure measured with the Pitot tube and calculated density of the gas at the outlet temperature, according to Bernoulli's theorem. The flux of water from some craters where we could not measure the gas velocity, was estimated by comparing volumetric rate of the plume generation with that from the crater where gas velocity was measured. The plume generation rates were estimated on the base of the plume size and the rising speed observed with a video camera. Total flux of water from the volcano is obtained by summation of these fluxes. Fluxes of magmatic water, meteoric water and other volatile components can be obtained by combination of the total water flux and isotopic and chemical composition of the fumarolic gases. SO<sub>2</sub> flux, estimated by this method, decreased from 140 t/d in March 1996 to 44 t/d in October 1996, that is consistent with the results of COSPEC measurement performed by Kyushu Univ., indicating reliability of the new method. The magmatic gas fluxes have decreased since the eruption, from 23 kt/d in October 1995 to 8 kt/d in October 1996 for magmatic water and from 1600 t/d to 400 t/d for CO<sub>2</sub>, implying decreasing trend of magmatic activity at this volcano.

**JSV36/E/19-B3** Poster **0900-18**

**USING GEOCHEMISTRY TO ASSESS THE POSSIBILITY OF FUTURE LARGE SCALE ERUPTIONS AT MERAPI VOLCANO, CENTRAL JAVA, INDONESIA**

Supriyati Andreausti and Ian SMITH (both at Geology Department, University of Auckland, Private Bag 92019, Auckland, New Zealand, email: s.andreausti@auckland.ac.nz; and ie.smith@auckland.ac.nz) Brent Alloway (Institute of Geological and Nuclear Sciences Ltd, Lower Hutt, New Zealand, email: b.alloway@gns.cri.nz)

Stratigraphic and geochemical studies of historical eruptions (> 3000 BP to 1800 AD) from Merapi Volcano in Central Java have revealed significant changes in the pattern of eruptive behavior through time. This observation allows two levels of volcanic risk to be determined, namely low probability/high risk and high probability/low risk. The average frequency of eruptions during historic times is about once every 80 years; large eruptions occurred every 150 to 500 years and were predominantly sub-plinian to plinian (up to VEI 4) to vulcanian in style. In contrast during recent times (since 1800AD) the return period for large eruptions (up to VEI 3) has been 30 years and for small eruptions 2 years; these events have been mostly dome collapse explosions of vulcanian type.

The frequency and nature of eruptions from Merapi can be correlated with the chemical composition of erupted material on both short (10-100 years) and long (100-1000 years) time scales. Magmatic processes operating at different levels beneath the volcano can explain this. Understanding these processes provides a tool for predicting future activity and associated risk. Merapi is one of the world's most active volcanoes and is situated in a densely populated area. Geochemistry offers the potential for predicting the patterns of future eruptive activity.

**JSV36/E/03-B3** Poster **0900-19**

**HELIUM ISOTOPES TEMPORAL VARIATIONS IN GASES FROM MT ETNA (ITALY)**

F. ITALIANO (Inst. Di Geochemica Dei Fluidi, C.N.R., Via U. La Malfa 153, Palermo, Italy. Email: italiano@igf.pa.cnr.it)

Abstract not available at time of going to press

Wednesday 28 July PM

**JSV36/W/21-B3** Poster **1400-01**

**INVERSION FOR MULTIPLE VOLCANIC SOURCES USING A GENETIC ALGORITHM TECHNIQUE**

K. F. TIAMPO and J. B. Rundle (both at CIRES, University of Colorado, Boulder, CO 80309; Email: kristy@fractal.colorado.edu); Jose M. Fernandez (Instituto de Astronomia y Geodesia (CSIC-UCM), Facultad de Ciencias Matematicas, Ciudad Universitaria, 28040, Madrid, Espana). John Langbein (USGS, Menlo Park, CA, USA).

Significant ground deformation has long been associated with magma injection in volcanic areas. As a result, many such areas are well monitored today, and their activity status is based, at least in part, on the size and pattern of that deformation. We have employed magmatic source models for a prolate ellipsoid, and compared it to spherical sources for an active volcanic area using a genetic algorithm inversion technique (Davis, 1986; Yang and Davis, 1988). A genetic algorithm (GA) is a directed search technique, which combines the principle of survival of the fittest with a prescribed random information exchange. These volcanic source models were compared with deformation data from Long Valley, California. Topographic data from a tri lateration network consisting of both two-colour electronic distance meters (EDMs) and levelling measurements has been in place since 1989 in Long Valley, when the second episode of uplift within a span of 10 years began. Additional features include the capability to invert for both laser altimeter and gravity data in conjunction with the above data types. The GA was used to find and compare the optimal source mechanisms for Long Valley deformation, in conjunction with other potential sources such as faulting.

**JSV36/W/06-B3** Poster **1400-02**

**DEFORMATION MONITORING OF MOUNT MERAPI WITH DINSAR**

C. Gerstenecker, G. LAEUFER (Institute of Physical Geodesy, Darmstadt University of Technology, email: laeuffer@geod.tu-darmstadt.de) B. Wrobel (Institute of Photogrammetry, Darmstadt University of Technology)

Within the Indonesian-German project MERAPI the activities of the volcano Mount Merapi are monitored with different tools. Classical methods of deformation measurements will be combined with spaceborn DINSAR. Differential Interferometric Analysis of Synthetic Aperture Radar data can yield information about areal ground deformation. In a first attempt we are using four SAR-scenes, taken from ERS-1 between April 1996 and October 1996, covering an area of 10,000 km<sup>2</sup>. The interferograms are computed with different software packages as JPL/SIR-C, ENVI/IDL, EASI/ PACE including Antis and JenaSAR. A synthetic interferogram is produced with the help of a Digital Elevation Model (DEM) of the region, which we got by combining SPOT-images, topographic maps, and GPS- measurements. The limits and problems of DINSAR-analysis in tropic regions and steep slopes are discussed and first results of the analysis are given.

**JSV36/W/10-B3** Poster **1400-03**

**INVERSION OF THE GRAVITY FIELD OF MOUNT MERAPI AND MOUNT MERBABU, CENTRAL JAVA, INDONESIA**

C. GERSTENECKER (Darmstadt University of Technology, Darmstadt, FRG, email: gerstenecker@geod.tu-darmstadt.de); S. Kirbani, I. Suyanto (Gadjah Mada University, Yogyakarta, Indonesia)

In winter 1996/97 we have mapped the gravity field of the volcanoes Merapi and Merbabu located in Central Java, Indonesia. Altogether we have measured 380 points covering a range of 50°50 km<sup>2</sup>. Point positioning was done by differential GPS. Gravity values were observed with the LaCoste&Romberg gravimeter LCR-G1029. Bouguer anomalies were corrected for topography using a digital elevation model with 20\*20 m<sup>2</sup> grid size. Surface density was determined using Parasni's method. A 3-parameter linear regression model represents the regional Bouguer anomaly field mostly influenced by the subduction zone South of Java. The residual Bouguer anomalies were merged with gravity data collected by other groups between 1968 and 1994. The inversion is done in two approaches. The first approach is using the program system IGMAS where density subsurface models are fitted interactively to the observed residual Bouguer anomalies. The second method determines the densities of subsurface cubes with the help of L1-norm.

**JSV36/W/13-B3** Poster **1400-04**

**STRUCTURE OF ACTIVE CENTRAL VOLCANOES IN ICELAND DEDUCED FROM GRAVITY MODELLING**

Magnus T. GUDMUNDSSON and Thordis Hognadottir (Science Institute, University of Iceland, Hofsvallagata 54, 107 Reykjavik, Iceland, email: mtg@raunvis.hi.is)

Iceland has an anomalously thick ocean-type crust due to the high magma production rate of the Iceland mantle plume. The volcanic zones in Iceland are divided into volcanic systems consisting of a fissure swarm and one or two central volcanoes. Volcanism is greatest within the central volcanoes, which produce both silicic and basaltic rocks. The gravity field associated with several central volcanoes has now been mapped and the internal structure studied with forward modelling. For the volcanoes studied, the gravity signature can be broadly divided into two categories: the volcanoes that have developed calderas, and those that have not. The calderas are associated with gravity highs (10-40 mGal), caused by massive basic intrusions in the shallow crust. The intrusions are located under the calderas but have a somewhat greater diameter. A relative gravity low is often associated with the center of the caldera while the caldera faults seem to be underlain by dense dyke swarms. Volume of molten magma chambers in the upper crust seems to be only a few percent of the volume of the solid intrusions. The volcanoes that have not developed calderas have a much more subdued gravity signature, suggesting a relatively small volume of basic intrusions. For those volcanic systems that have two central volcanoes, one of the two may be well developed with a large caldera while the other is smaller and without a clear caldera. In some cases, the two are connected by ridge in the gravity field, suggesting a dense dyke swarm. This may imply some of the smaller volcanoes are parasitic, i.e. fed by the larger volcano. The gravity signature of the central volcanoes seems unrelated to exposure of rhyolites on the surface, indicating that the rhyolites are confined to the volcanic edifices and do not make up a significant part of the underlying volume.

**JSV36/W/24-B3** Poster **1400-05**

**DEFORMATION MEASUREMENTS AND DIGITAL ELEVATION MODELS AT MOUNT MERAPI, INDONESIA**

C. Gerstenecker, G. Laeuffer, B. SNITIL (Institute of Physical Geodesy, Darmstadt University of Technology, Germany, email: snitil@geod.tu-darmstadt.de) G. Jentzsch, A. Weise (Institute of Geosciences, Friedrich-Schiller-University Jena, Germany) I.Suyanto (Gadjah Mada University, Yogyakarta, Indonesia)

Mount Merapi, located in Central Java, Indonesia, is one of the most active volcanoes of the world. One of the aims of the Indonesian-German project MERAPI is to determine secular changes of the Earth's gravitational field. Gravity changes in the area of volcanoes may result from vertical movements of the crust, mass displacements inside and outside the Earth and density changes. Together with knowledge of deformation in position and height, the residuals of temporal changes of gravity anomalies will be estimated. For the observation of gravity changes in time a combined gravity and GPS network has been established. The changes in the horizontal and vertical positions of these stations are recorded by using differential GPS measurements. For the estimation of residual gravity changes accurate digital elevation models have to be available. The data of a gravity field mapping campaign, combined with model data based on SPOT images was used to develop a digital elevation model (DEM) of Mount Merapi. Its raster size is 20m\*20m with an altitude accuracy < 50m. Beneath the topographic reduction of gravity anomalies the DEM is used for the correction of seismic and electromagnetic observations as well as for the calculation of synthetic interferograms within the DINSAR-analysis of SAR-images of Merapi.



**JSV36/W/11-B3** Poster **1400-06**

**DEFORMATION AT THE FLANKS OF MERAPI VOLCANO RELATED TO ITS RECENT ACTIVITY**

Dorothee REBSCHER and Hans-Joachim Kuempel (both at Applied Geophysics, University of Bonn, Nussallee 8, 53115 Bonn, Germany, email: rebscher@geo.uni-bonn.de); Malte Westerhaus, Alexander Koerner, Wolfgang Welle, and Jochen Zschau (all at GeoForschungs Zentrum Potsdam, Telegrafenberg A 31, 14473 Potsdam, Germany, email: tilt@gfz-potsdam.de); Arnold Brodscholl and Subandriyo (both at Center for Volcano Research and Technology Development, Jl. Cendana 15, Yogyakarta 55166, Indonesia, email: mvopgm@yogy.wasantara.net.id)

The Indonesian-German deformation experiment, focused on the high-risk volcano Merapi in Central Java, is ingrained in the interdisciplinary research project MERAPI, a contribution to the IDNDR program. Between 1995 and 1997, four multiparameter stations have been installed at the flanks of Merapi, each including one GPS-receiver and an array of three biaxial borehole tiltmeters. In addition, several sensors record local meteorological and hydrological data, permitting the recognition of potentially influencing environmental quantities. In fact, the high resolution of the borehole tiltmeters (0.2 microrad), lets them also be sensitive to small poro-elastic deformations due to rainfall. After correction of the rain-induced tilts, three types of tilt variations of 1 to 8 microrad amplitudes are observed, which appear to be related to volcanic activity: (i) pre-eruptive tilt changes, correlated with an increase of multiphase events preceding the eruptions of Merapi in January 1997 and July 1998; (ii) a co-eruptive tilt anomaly coinciding with the eruption in August 1996; (iii) a local tilt signal, probably a loading effect caused by the mass of debris of pyroclastic flows of the eruption in July 1998. The experimental data conform with numerical modeling results. It is concluded that the recent activity of Merapi is associated with small deformations of the volcano's edifice and, presumably, pressure changes in its interior.

**JSV36/W/19-B3** Poster **1400-07**

**STUDYING KILAUEA VOLCANO'S FAULTS AND RIFTS WITH GPS**

Susan OWEN (Dept. of Earth Sciences, University of Southern California, Los Angeles, CA, 90089-0740, USA, email: owen@seismo.berkeley.edu); Paul Segall (Dept. of Geophysics, Stanford University, Stanford, CA, 94305, USA) Michael Lisowski, and Asta Miklius (both at Hawaiian Volcano Observatory, Hawaii Volcanoes National Park, HI, 96718, USA)

Kilauea Volcano, Hawaii, is the youngest and most recently active subaerial volcano in the Hawaiian Island chain. Kilauea's south flank has generated several large earthquakes in the past twenty-five years (M7.2 1975, M6.1 1989). These earthquakes are generated by seaward displacement along a subhorizontal fault plane approximately 9 km beneath Kilauea's south flank. Since 1983, Kilauea has been erupting almost continuously from Pu'u O'o or Kupaianaha, located near each other along the East Rift Zone. GPS campaigns have been conducted on Kilauea since 1990. In addition, a continuous GPS network was installed starting in 1995. These GPS data have been successfully used to constrain the geometry of the fault and rift zones, understand rift eruptions, and infer the distribution of active fault slip and rift opening.

The horizontal GPS velocities show rapid south flank displacement rates of as much as -8 cm/yr. Subsidence along the rift system occurs at similar rates. The set of sources required to fit these data include rift opening along the upper east and east rift zone, fault slip along a subhorizontal plane near the base of the volcano, and deflation near the summit caldera. In the best-fitting model, the fault plane dips north-northwestward (islandward) and extends offshore. The detailed fault slip modelling results indicate that the highest fault slip rates occur beneath the central south flank. The model includes significant fault slip offshore and in the western south flank, both seismically inactive areas between 1990 and 1996. Fault slip rates are low near the epicenters of the most recent large earthquakes. Model rift dilation extends from the upper east rift zone to Heiheihaihu, ~15 km downrift of Pu'u O'o. The continuous GPS network captured pre-eruptive opening of the east rift zone and contributed data crucial to the interpretation of the January 30, 1997 eruptive event.

**JSV36/E/05-B3** Poster **1400-08**

**DIMENSIONS, TEMPERATURES AND EVOLUTION OF CRUSTAL MAGMA CHAMBERS OF VOLCANOES CALCULATED ON THE BASE OF VOLCANOLOGICAL, GEOPHYSICAL, GEODETICAL, AND PETROLOGICAL DATA**

Sergei A. FEDOTOV, Iona S. Utkin, and Ludmila I. Utkina (Institute of Volcanology, Far East Division, Russian Academy of Sciences, Petropavlovsk-Kamchatsky, 683006 Russia; email: volcan@svyaz.kamchatka.su)

Dimensions, volume, temperature, and evolution of crustal magma chambers of volcanoes are calculated and studied. It is accepted in our model that volcano magma chambers located in the crust are formed mainly by melting, erosion, and removal of their wall rocks. Equations of heat balance of magma flowing through magma feeding system and of its wall rocks are used in calculations. Initial data on magma production rate and chemical composition of erupted products of volcano and their changes in time, on location of magma chambers and the structure of the crust, on geotherm and parameters of magma and wall rocks are taken from results of volcanological, petrological, geophysical, geodetical, and geothermal studies. Calculations were made for representative volcanoes of Kamchatka (Avachinsky, Klyuchevskoy, and others).

The active Avachinsky stratovolcano in Kamchatka is 60000 years old, its products are andesite-basalts and andesites, their volume is 190 km<sup>3</sup>, magma production rate declines in time and equals 2.5\*10<sup>6</sup> t/year during the last 5500 years. The depth of its shallow magma chamber is ~4 km. It was found that magma chamber had reached quasistationary conditions and its maximum radius 2 km and volume 33.4 km<sup>3</sup> during first 15000 years of the volcano activity that magma chamber is decreasing during the last 20000 years and its present radius and volume can be 1 km and 4.2 km<sup>3</sup>.

Such modelling and calculations are useful part of complex studies on features and structure of volcano magma feeding systems, on magma formation and mixing, on evolution of volcanoes and volcanic centers, on potential size of large eruptions and accumulated geothermal resources.

**JSV36/E/17-B3** Poster **1400-09**

**CATALOGUE OF QUATERNARY VOLCANOES IN JAPAN**

Tadahide, UI (Graduate School of Science, Hokkaido University, N10W8, Kita-ku, Sapporo 060-0810, Japan, e-mail: ui@cosmos.sci.hokudai.ac.jp); Shintaro Hayashi (Akita University, e-mail: hayashi@ipc.akita-u.ac.jp); Masaki Takahashi (Ibaraki University, e-mail: takama@mito.ipc.ibaraki.ac.jp); Shigeo Aramaki (Nihon University, e-mail: aramaki@chs.nihon-u.ac.jp); Tatsuro Chiba and Shin Shishikura (Asia Air Survey Co.Ltd, e-mail: sn.shishikura@ajiko.co.jp); Koji Umeda (Nuclear Cycle Development Institute, e-mail: umeda@tono.pnc.go.jp)

We are now compiling a new database on Quaternary volcanoes in Japan. Since the publication of the geologic map of Quaternary volcanoes in Japan (Ono et al., 1981), many research works have been appeared. Number of radiometric age data for volcanic ejecta are drastically increased. This allows us to update the image of Quaternary volcanism in the Japanese Islands. Our database for more than 700 volcanic edifices includes the informations of location of eruption center, area and volume of volcanic ejecta, age of activity, chemistry, representative references and so on. Our database revealed temporal and space variation of Quaternary volcanoes and change of magma production rate during Quaternary period.

**JSV36/E/26-B3** Poster **1400-10**

**GPS CONTROL NETWORK AT FOGO VOLCANO, CAPE VERDE**

J. Nuno LIMA, J. Pereira Osorio, Clara Lazaro (Centro de Geodesia, Instituto de Investigacao Cientifica Tropical, Rua da Junqueira, 534, 1300 Lisboa, Portugal, email: cgeod@iict.pt) Sandra I N Heleno, Joao L Matos and Joao F B D Fonseca (all at IST, Av Rovisco Pais, 1, 1049-001 LISBOA, Portugal, email: sisilva@alfa.ist.utl.pt)

Fogo Island, in Cape Verde Archipelago (North Atlantic), is a roughly conical volcanic edifice with less than 25 Km of base diameter and reaching nearly 3000 m above sea level. Several volcanic eruptions in Fogo have been reported since the discovery of the archipelago in the 15th century. The activity in the 20th century is mainly represented by the two eruptions in 1951 and 1995.

A high precision GPS network for periodic reobservation (campaigns with intervals of about six months) was designed and implemented for supporting the development of models to understand the mechanisms behind seismic or volcanic activity. This network covers all the island and it consists of 23 reinforced concrete pillars with good foundations. The first GPS campaign was performed from September 1 to September 8, 1998, with occupations of all the 23 sites. All the GPS data has been processed with the BERNESE version 4.0 software. In the paper details of the network, the GPS campaign, the data processing and the results obtained so far will be presented.

**JSV36/E/21-B3** Poster **1400-11**

**FRACTAL ROCK FAILURE AND ERUPTION FORECASTS**

S. VINCIGUERRA, C.R.J. Kilburn, V. Rocchi, W.J. McGuire (Benfield Greig Hazard Research Centre, Department of Geological Sciences, University College London, Gower Street, London WC1E 6BT, UK; Email: s.vinciguerra@ucl.ac.uk, c.kilburn@ucl.ac.uk, v.rocchi@ucl.ac.uk, w.mcguire@ucl.ac.uk; Fax: +44-171-3887614.)

The fractal distribution of earthquakes is consistent with a state of 'self-organised criticality' in the earth's crust. Scale invariant hierarchical structure was also observed in volcanic areas where variation of time and spatial fractal properties of seismic patterns have been observed to act at long (order of years), mid (order of months), and short term (order of days). Moreover it has been shown that rates of cracks and the coalescence of minor fractures in major patterns in a rock under stress are ruled too by self-accelerating processes. Thus focusing on the interrelationships between seismicity clustering variation in volcanic areas and cracks patterns evolution under volcano stress conditions are strongly expected to provide relevant information on volcano dynamic processes at different length time scales. Information can be used as a diagnostic tool in volcano hazard evaluation as well as in eruption forecasting.

**JSV36/E/20-B3** Poster **1400-12**

**TIME AND SPACE PROPERTIES OF RECENT SEISMICITY AT CANARY ISLANDS.**

S. Vinciguerra, S.J. DAY and W.J. McGuire (Benfield Greig Hazard Research Centre, Department of Geological Sciences, University College London, Gower Street, London WC1E 6BT, UK, e-mail: s.vinciguerra@ucl.ac.uk, s.day@ucl.ac.uk, w.mcguire@ucl.ac.uk).

A variety of models exist for magmatism in the Canary Islands, some of which imply the development of large - scale regional deformation and seismicity of tectonic origin. However, the many marine seismic surveys around the islands in recent years have revealed the presence of thick sequences of undisturbed sediments around the islands and thus a lack of major regional deformation at least since the middle Tertiary when the oldest volcanic islands in the archipelago appeared. Thus we consider it more likely that seismicity in the Canaries is fundamentally of magmatic origin, although the development of volcano - tectonic or gravitational - loading earthquakes is also possible. Space-time clustering properties of seismic activity at Etna volcano have been shown to be very useful to distinguish variations in the eruptive style as well as volcanic and tectonic processes acting at different time scales. Here variability and origins of recent seismicity (1989 - 1995) of the Canary islands are investigated. 3 periods of activity are recognized: from 1989 to 1991 (the period of the most recent seismic swarm) activity was relatively shallow and strongly clustered, whereas from 1992 to 1994 it was mainly very deep (30 - 60 km depth). More recently, activity has become more widespread and is migrating toward the surface again. We suggest on the basis of these results that a new cycle of magma supply from depth in beginning and that a further seismic crisis or eruption may occur in the next several years.

**JSV36/E/18-B3** Poster **1400-13**

**CRUSTAL DEFORMATION ASSOCIATED WITH THE 1998 SEISMO-VOLCANIC CRISIS OF IWATE VOLCANO, NORTHEASTERN JAPAN, AS OBSERVED BY A DENSE GPS NETWORK**

S.UEKI, S.Miura, T.Sato, K.Tachibana and H.Hamaguchi (all at Graduate School of Science, Tohoku University, Sendai 980-8578, Japan, Email: ueki@aob.geophysics.tohoku.ac.jp)

Iwate volcano is an active volcano located in northeastern Japan and having histories of magmatic eruptions in 1686 and 1732. Unrest of Iwate volcano started in September, 1995 with intermediate-depth tremor. The shallow seismicity in the west of the summit gradually became active in February, 1998, and reached a peak at the end of April. The active seismicity continued till the middle of August. Increase in fumarolic activity was also reported during the same period. Associated with the seismo-volcanic crisis, notable crustal deformation was observed by our dense GPS network. The network consists of 20 stations. At 12 sites, continuous observations have been carried out. We deployed two-frequency receivers at all the stations. The data were collected by using wire telephones, cellular telephones or radio modems for analysis. The radio modems powered by solar panels were newly designed for the stations at the summit area. After smoothing the data for the period from February to August, we obtained significant deformations amounting to about 5 cm in horizontal components and 2 cm in vertical one at the northern and southern foots of the volcano. In general, the pattern of the horizontal displacements is characterised by radial displacements pointing outward from a region of the volcano. The deformation rate raised from less than 0.5 cm/month in February to about 1 cm/month in July. Assuming a simple pressure source, we tried to locate the source for each two months. The result shows that the source was located at about 4 km WSW of the summit and 10 km in depth in February-March, and it moved to a region about 10 km W of the summit and 3 km in depth in June-July. It is noteworthy that the

pressure source projected onto the epicentral distribution is nearly coincided with the western end of the seismic area for each period. The synchronicity of the crustal deformation and seismic activity suggests that the both phenomena were caused by a movement of magmatic liquid from depths beneath the summit to the western shallow part.

**JSV36/E/31-B3** Poster **1400-14**

**GEODETTIC AND SEISMIC CONSTRAINTS ON RECENT ACTIVITY AND SHALLOW MAGMATIC PROPERTIES AT LONG VALLEY CALDERA, CA, USA**

Andrew V. NEWMAN (Department of Geological Sciences, Northwestern University, 1847 Sheridan Rd., Evanston, IL, USA 60208, email: andrew@earth.nwu.edu) Jacqueline E. Dixon & Timothy H. Dixon (both at Rosenstiel School of Marine and Atmospheric Science, University of Miami, 4600 Rickenbacker Cswy., Miami, FL, USA 33149, email: tim@corsica.rsmas.miami.edu, jdixon@rsmas.miami.edu)

The average rate of surface deformation on the resurgent dome of Long Valley Caldera, a volcanic region in east central California, increased by more than an order of magnitude over the six month period July to December 1997, compared to the previous 3 year average. However, the three dimensional location of the immediate (shallow) source of deformation remained essentially constant compared with the earlier period, at a depth of 5-7 km beneath the dome, near the top of the seismically defined magma chamber. Similarly, although the rate of seismic moment release increased dramatically, earthquake locations remained similar to earlier periods. The rate of deformation increased exponentially with a time constant of ~45 days over a period of 5 months, after which it decreased exponentially with about the same time constant. This range of time constants is considerably longer than those characterising typical deformation events at basaltic volcanos, and may be related to the visco-elastic properties of rhyolitic material believed to exist at the top of the density-stratified magma chamber.

**JSV36/P/02-B3** Poster **1400-15**

**TEMPORAL AND THREE-DIMENSIONAL SPATIAL ANALYSES OF THE FREQUENCY-MAGNITUDE DISTRIBUTION NEAR LONG VALLEY CALDERA, CALIFORNIA**

Stephen R. MCNUTT, Stefan Wiemer, and Max Wyss (Geophysical Institute, University of Alaska Fairbanks, P.O. Box 757320, Fairbanks, AK, 99775, USA. email: steve@giseis.alaska.edu, stefan@giseis.alaska.edu, max@giseis.alaska.edu)

The three-dimensional distribution of the b-value of the frequency-magnitude distribution is analysed in the seismically active parts of the crust near Long Valley Caldera, California. The seismicity is sampled in spherical volumes, containing N=150 earthquakes and centred at nodes of a grid separated by 0.3 km. Significant variations in the b-value are detected, with b ranging from b=0.6 to b=2.0. High b-value volumes are located near the resurgent dome, and at depths below 5 km at Mammoth Mountain. b-values are found to be much lower south of the Long Valley Caldera. We interpret this to indicate that an active magma body has advanced from depths below 8 km to depths of 4 to 5 km beneath Mammoth Mountain in 1989, and that anomalous crust, either highly fractured or containing unusually high pore pressure, such as is the case in the vicinity of active magma bodies, exists north of the seismically active area beneath the resurgent dome at all depths. We also investigate the spatial distribution of temporal variations of the frequency-magnitude distribution by introducing differential b-value maps. b-values increased from b=0.8 to b=1.5 underneath Mammoth Mountain at the onset of the 1989 earthquake swarm and remained high thereafter. This suggests that an intrusion permanently altered the average distribution of cracks at 5-10 km depth, or that the pore pressure permanently increased. No significant change in the earthquake size distribution was detected during the 1997 episode of increased activity at Long Valley Caldera. This indicates that a slight stress change caused by the inflation of the magma chamber is causing a significant change in the rate of earthquakes produced, but no change in their size distribution. We propose that high b-values are a necessary (but not sufficient) condition in the vicinity adjacent to a magmatic body, and, therefore, spatial b-value mapping can be used to aid in the identification of active magma bodies.

**JSV36/L/02-B3** Poster **1400-16**

**GEOLOGICAL INVESTIGATION OF VILLA ALOTA-PASTO GRANDE AREA (BOLIVIAN ANDES) USING RADARSAT**

Jose Luis LIZECA (Applied Geology, SERGEOMIN, La Paz, Bolivia Email: abtema@coord.rds.org.bo Woolf M. Moon (Geophysics, The University of Manitoba, Winnipeg, R3T 2N2 Canada ((204)-474-9833 (O); (204)-474-7623 (FAX); Email: wmoon@cc.umanitoba.ca and also with Dept. of Earth System Science, Seoul National University, Seoul 151-742 Korea ((82)-2-880-6526 (O); (82)-2-871-3267(FAX); Email: wmoon@eos1.snu.ac.kr

The Villa Alota - Laguna Past Grande study area in Bolivian Andes is located in the major Cenozoic volcano tectonic province, which appears to represent an effusive andesitic - dacitic volcanism that became active in late Tertiary and that waned in the late Miocene. The average altitude of the study area is between 4,500 m and 5,400 m above sea level and the study area is one of the driest areas on Earth, resulting in extensive evaporite deposits and almost no vegetation cover over the whole study area. A detailed ground truthing, including surface mapping and geochemical sampling, was carried out during the summer of 1998 as a GlobeSAR II campaign. Two RADARSAT image data sets were acquired and processed for this study and interpreted in detail to extract the surface volcanological and geological characteristics over the study area. A number of geochemical samples were also taken mostly from dried evaporite lakes to study chemical and mineralogical composition of the surface material and their dielectric properties. From the pair of RADARSAT data a detailed DEM was also computed to investigate the accuracy and reliability of the morphological characteristics which can be extracted directly from the standard mode RADARSAT data. Preliminary results indicate that (i) for detailed surface feature study, RADARSAT DEM is an effective tool, (ii) for detailed DEM generation, carefully selected ground control points (GCP) are very important, (iii) a large scale volcanological features such as collapsed caldera could easily be mapped using RADARSAT DEM with considerably improved accuracy, and (iv) the changes in dielectric properties over evaporite lakes do neither alter the final DEM nor affect the overall backscattering coefficient values as much as it was expected initially.

**JSV36/C/U6/W/11-B3** Poster **1400-17**

**GEOMAGNETIC STRUCTURES OF THE SUBMARINE CALDERA LOCATED BETWEEN HACHIOJIMA ISLAND AND AOGASHIMA ISLAND, NORTHERN PART OF THE IZU-OGASAWARA ARC**

Mitsuo ISHIDA (School of High-Technology for Human Welfare, University of Tokai, Nishino 317, Numazu, Shizuoka, JAPAN, email: wyvern@wing.ncc.u-tokai.ac.jp); Izumi Sakamoto (Deep Sea Research Dept., Japan Marine Science and Technology Center, Natsushima 2-15, Yokohama, JAPAN, Email: izumis@jamstec.go.jp)

The South-Hachijo Submarine Caldera (SHSC) is located on latitude 32-40.0N, longitude 139-46.0E, about 45 km south from the Hachiojima Island, and situated at southern end of insular shelf of the Hachiojima Island. Positive anomalies are dominant over insular shelf of the Hachiojima Island. The highest positive anomalies are situated in northern part of insular shelf of the Hachiojima Island, where shows higher topographic relief than the around. Central area of the SHSC is covered by weak negative anomalies, which are surrounded by positive anomalies. Positive high anomalies exist in between southern part of central area and southern flank of the SHSC. Positive high anomalies in southern part of central area coincide with the shallowest part of the SHSC. It is considered that positive high anomalies of the SHSC and the northern area of insular shelf of the Hachiojima Island are caused by magnetic bodies near to sea bottom, from the results of analyses of geomagnetic anomalies. It is considered that magnetic body under the SHSC is different from under the insular shelf's, though these magnetic bodies have same magnetization direction as that of present earth's field. SHSC may relate to recent basaltic activity in volcanic front considering the results of geochemical composition of volcanic rocks dredged from the SHSC.

**JSV36/C/U6/W/10-B3** Poster **1400-18**

**GASES OF PLANET EARTH: MANTLE ORIGINS AND ATMOSPHERIC IMPLICATIONS**

Bernard MARTY (Centre de Recherches Pétrographiques et Géochimiques et Ecole Nationale Supérieure de Géologie, BP 20, 54501 Vandoeuvre Cedex France, Email: bmarty@crpg.cnrs-nancy.fr)

Most of volatiles (water, carbon dioxide, nitrogen, halogens, rare gases) present at the Earth's surface were contributed early during accretionary processes. Since then, volcanism is supplying gases in proportions roughly proportional to its activity rate. Part of these volatiles are recycled back into the mantle, so that each species has its own geochemical cycle. Some are cycled between the mantle and the surface with time constants lower than the age of the Earth (e.g., C, S), so that it is possible to derive a mean residence time at the surface. For others (e.g., nitrogen, rare gases), the flux from the mantle to the surface exceeds the return flux, allowing primitive isotope heterogeneities between the surface and the deep Earth to survive. Since the mantle is chemically heterogeneous, it is possible to characterise mantle sources of lavas and corresponding tectonic settings by analysing the isotope composition of some of these elements. Helium provides a sensitive provenance tracer since its isotopic composition in volcanic rocks and gases varies over an order of magnitude between arc-type, and plume-type volcanisms. Rare gases allow also to derive quantitative fluxes of major volatiles (e.g., carbon dioxide), and to model their geochemical history. Volatile isotope geochemistry has recently allowed to demonstrate that major LIP provinces are linked with the development of plumes originating below the convective mantle feeding mid-ocean ridge volcanism. Since the emission of CFB and related felsic volcanism occurs in a limited interval of time, it is likely that such gigantic volcanism has had noticeable climatic impact. The case of the Afar-Ethiopian plume province (CFB and ignimbrite emissions at 30 Ma) will be discussed in this context.

**JSV36/C/U6/W/02-B3** Poster **1400-19**

**THE PRESENT STATE OF THE MAGMATIC SYSTEM OF THE ISCHIA ISLAND (ITALY)**

Monica PIOCHI, Lucia Civetta and Giovanni Orsi (Osservatorio Vesuviano 80056, Ercolano - Napoli, Italy, email: piochi@osve.unina.it)

The island of Ischia, home to about 50,000 people, is an active caldera in the Gulf of Naples. Its volcanism in the past 10 ka was very intense and strictly connected to the resurgence dynamics of the Mt. Epomeo block. The last eruption occurred in 1302 A.D. The eruptions of this period have generated mostly alkali-trachytic and trachytic, and subordinately latitic rocks. Most of the units are composed of homogeneous trachytic and alkali-trachytic rocks that contain crystals in mineralogical and isotopic equilibrium with the groundmass, throughout the sequence. Some units vary in composition from latitic to trachytic and are characterized by complex petrochemical imprint due to mineralogical disequilibrium, chemical inhomogeneity of the glass, and isotopic variability. The main evolutionary magma processes are crystal fractionation and mingling between a highly crystallized alkali-trachytic magma with low Sr-isotope ratio (0.7060-0.7061), and an isotopically distinct (0.7068) latitic-to-trachytic magma. Petrochemical data and modeling of magnetic data suggest that at present the magmatic system includes a deeper, less-evolved magma chamber and shallower, more-evolved bodies. The homogeneous alkali-trachytic and trachytic units were generated by eruptions fed by the shallow magma bodies. The vents for these eruptions were located on the normal faults within the sector of the resurgent block under tensional stress regime. The eruptions that produced units characterized by mineralogical and isotopic disequilibria occurred along parts of regional faults and were generated by mingling of a deep latitic-to-trachytic magma with batches of the shallower alkali-trachytic magma bodies.

**JSV36/C/U6/W/01-B3** Poster **1400-20**

**SURFACE GAS GEOCHEMISTRY OF CO2 AND 222RN AT CUMBRE VIEJA VOLCANO, LA PALMA, CANARY ISLANDS, SPAIN**

Lourdes CÁRDENES, José M. L. Salazar, Nemesio M. Pérez (all at the Environmental Research Division, ITER, 38594 Granadilla, Tenerife, Spain, email: lcardenes@iter.rcanaria.es), José A. Cobas, Gladys Melián (both at Faculty of Chemistry, Univ. La Laguna, 38206 La Laguna, Tenerife, Spain), and Pedro A. Hernández (Laboratory for Earthquake Chemistry, Univ. Tokyo, Bunkyo-Ku, Tokyo 113, Japan)

La Palma is the northwesternmost island of the Canary archipelago and rises 6.5 Km from the surrounding ocean floor. Most of the historical volcanic activity in the Canary Islands has occurred at La Palma where recent volcanic activity is mainly concentrated at Cumbre Vieja volcano, in the southern part of the island. Since fumarolic degassing is not present in and around Cumbre Vieja volcano, spatial distribution analysis of soil gases is an ideal geochemical tool for monitoring magma movement and seismicity changes in this basaltic volcano. Soil gas 222Rn and CO2 flux survey of 470 sampling sites at Cumbre Vieja was performed by using a portable radon sensor and a NDIR spectrophotometer, respectively. Statistical-graphical analysis of soil gas 222Rn measurements showed three overlapping geochemical populations. The background mean is 7.7 pCi/L and represents 21.5% of the total data. The peak population has a mean of 145 pCi/L and represents 7.7% of the total data. Soil CO2 flux measurements showed also three geochemical populations. The background mean is 2.1 g-m-2-d-1 and represents 90% of the total data. The peak population has a mean of 440 g-m-2-d-1 and represents 3% of the total data. Most of the study area and its surroundings showed background and intermediate levels of diffuse degassing of CO2 and 222Rn.



## INTER-ASSOCIATION

Anomalous levels of diffuse degassing of <sup>222</sup>Rn and CO<sub>2</sub> are closely related to the volcanic rift-zones in the southern part of La Palma. Diffuse emission of CO<sub>2</sub> from Cumbre Vieja volcano and its surroundings is about 590 t-d<sup>-1</sup>.

**JSV36/C/U6/W/08-B3** Poster **1400-21**

### CHEMICAL PRECURSORS OF THE 1998 ERUPTION OF COLIMA VOLCANO, MEXICO

Yuri TARAN, Maria Aurora Armenta (Institute of Geophysics, UNAM, Mexico D.F., 04510, Mexico. E-mail: taran@tonatiuh.igeofcu.unam.mx); Juan Carlos Gavilanes, Abel Cortes (Observatorio del Vulcan Colima, University of Colima, Mexico. E-mail: gavil@ucol.mx)

Colima volcano is the most active in Mexico with the last effusive eruption in 1991. Geochemical monitoring of the volcano started in January 1996 with: 1) airborne measurements of the SO<sub>2</sub> flux by COSPEC; 2) collection of fumarolic gases from the summit crater every two months, and 3) monthly collection of water samples from three springs on the S-SW slopes of the volcano. The SO<sub>2</sub> flux from the volcano until September 1998 was at a low level, less than 100 t/d, often below the detection limit of the instrument. A gradual increase in the SO<sub>2</sub> flux has been recorded from 200 t/d in September 1998 to 400+50 t/d two days before the new lava, which occurred on 20 November, 1998. During November 1998, before the eruption started, the SO<sub>2</sub> flux was in a good correlation with seismicity. Chemical compositions of volcanic gases did not show special trends, except of isotopic composition of the volcanic vapor. Starting from the summer of 1997, the volcanic water became gradually enriched in deuterium, which indicates a contribution from deep, less degassed magma. Three main effects in the ground water chemistry can be considered as precursors for the eruption: 1) a gradual increase in Mg/Cl ratio since the summer of 1997; 2) increase in the calculated partial pressure of dissolved CO<sub>2</sub> since the same date, and 3) a two to three-fold "peak" in the boron concentration approximately 4 months before the eruption.

**JSV36/C/U6/E/09-B3** Poster **1400-22**

### ORIGIN CONDITIONS FOR VITIM BASALTS

ASHCHEPKOV I.V. (United Institute of Geology Geophysics and Mineralogy, SD RASC, e-mail: garnet@uiggm.nsc.ru)

Liquidus thermobarometry for Vitim basalts suggest that in initial stage in Bereya block hydrous OIB picrite basalts (mg9270) came from depth of 40-60 kbar heated to 1500°C. Associated Hi-K silicic basalts differentiated in the crust. The main plateau (14-7Ma) (mg9265-60) basanites with the slightly convex down LMREE part originated from peridotites gently U shaped and Cpx deficient as result of melt percolation in 32-25 kbar interval while more differentiated are close to Ga-Sp boundary. Subalkaline ol-basalts interacted with peridotites ascending from garnet to spinel facie with the relic garnet revealing more gentle PT pass. Typical Quaternary OIB Ne-mela-hawaiiites (25-15 kbar) and more differentiated Ne-leico-hawaiiites with hydrous phases demonstrate more cold conditions of differentiation. The later are contaminated in host peridotites as well as Miocene basanites mixed with the DM (MORB) type mantle. Geochemistry of HFSE elements suggest primary OIB type magmas in 1st and last stages to be individual representing heard and tail of the small plume. Megacrystalline pyroxenite assemblages demonstrate intermediate heating conditions between basalts and lherzolites and mixing signatures being originated in pre-eruption small magma chambers or large veins. (Grant RBRF 93-05-17103)

**JSV36/C/U6/W/06-B3** Poster **1400-23**

### TOPOGRAPHICAL AND GEOLOGICAL CHARACTERS OF SUBMARINE CALDERA LOCATED BETWEEN HACHIOJIMA IS. AND AOGASHIMA IS, IZU-OGASAWARA ARC.

Izumi SAKAMOTO, Toshiya FUJIWARA (Deep Sea Res. Dept., Japan Marine Science & Technology Center, email: izumis@jamstec.go.jp), Fumitoshi MURAKAMI (Geological Survey of Japan), and Mitsuo ISHIDA (Univ. TOKAI)

South Hachijyo Submarine Caldera (SHSC) is located between Hachiojima Is. and Aogashima Is., and consisted the recent volcanic front of Izu-Ogasawara Arc. Diameters of SHSC are about 20km (E-W direction) ~13km (N-S direction). Caldera floor is about 5km across with ~500m depth. The somma is consisted with some continuous knolls (height is about 300 m from the caldera floor). A small central cone with 100m in height is observed in the central part of caldera floor.

The acoustic basement in the flank of the SHSC is overlain by thin layer (L-1), and L-1 layer is covered by stratified layer (L-2) unconformably, from single-channel seismic profiles. L-1&2 layers are considered to Hachijyo volcanic ejecta. Stratified layer (L-3) is observed in the caldera, and estimated to volcanic product of SHSC.

Rhyolitic pumices, basalts, and granites were dredged from the SHSC. These volcanic rocks indicate the bimodal volcanism. Trace element pattern from the SHSC rhyolite plotted similar to the granite, rather than the data from volcanic front activity. It is considered that the pumices are caused by remelt of the granite at the time when basaltic activity occurred in the volcanic front recently.

**JSV36/C/U6/E/04-B3** Poster **1400-24**

### LUNDY VOLCANO, BRISTOL CHANNEL, U.K.: FACT OR FICTION?

Clive ROBERTS (School of Applied Sciences, University of Wolverhampton, Wulfruna Street, Wolverhampton WV1 1SB, UK, email: in5359@wlv.ac.uk); Hazel Rymer (Department of Earth Sciences, Open University, Walton Hall, Milton Keynes, MK7 6AA, email: h.rymer@open.ac.uk)

Lundy Island is the southernmost expression of Tertiary volcanism in Great Britain and consists of granite intruded by around 200 dykes. The Lundy Igneous Complex (LIC) as a whole is associated with a large positive gravity anomaly and several small magnetic anomalies. The Lundy Dyke Swarm comprises basalt/dolerite and trachyte to rhyolite intrusions (54.3 to 56.4 Ma) within the host Tertiary granite (58.7 +/- 1.6 Ma) and Devonian sediments. Dykes have a radial disposition superimposed on an ENE-WSW trend.

The LIC is situated close to the intersection of the Variscan Front and Welsh Caledonides massif where the continental thickness is between 25 and 27 km. A large positive gravity anomaly to the north-west of the island (of comparable magnitude to other Tertiary centres in Scotland) does not have a corresponding magnetic signature. Gravity modelling indicates this may reflect dense basement rocks within the Lundy Horst rather than a large near-surface body of basic rocks. Although the heavily fractured nature of the host sediments assisted the passage of magma, the intra-chamber pressure of ponded magma bodies may not have exceeded the overlying lithostatic load to any great extent and so the postulated Lundy Volcano probably did not produce sub-aerial volcanic activity within the outer Bristol Channel.

**JSV36/C/U6/E/08-B3** Poster **1400-25**

### KOMATIITES AND THEIR GEOLOGICAL, GEOCHEMICAL AND GEOPHYSICAL CHARACTERISTICS OF PALEO-YANGTZE PLATE FROM SOUTH CHINA

Yuehua Jiang and Douke Xie N a nging Institute of Geology and Mineral Resources, Nanjing 210016, P. R. China, email: nigmr@public1.ptt.js.cn.

A Paleoproterozoic komatiitic zone (1600-2400Ma) exists in the southeastern margin of Paleo-Yangtze plate from South China, especially along the line of Hunan-Guizhou-Guangxi-Hainan provinces. Komatiitic lavas are 3-50m thick and have spinifex textures. The spinifex of skeletal crystal is 0.3-1.5cm in length and are mainly olivine and pyroxene which have altered into serpentine, hornblende, tremolite or chlorite. Chemical compositions of komatiites are: MgO 11-30%, TiO<sub>2</sub> 0.5-0.9%, (LU/Sm)N<0.7, (La/Sm)N = 2.78-2.88, more than 0.75, 87Sr/86Sr = 0.7039, 143Nd/144Nd=0.5120520. 5 13146, Nd (t)=+2.6+5. 9. MgO content of komatiitic basalts is generally lower (3-9%), but komatiitic basalts also have spinifex textures and are different from those in the other areas of the world. It is considered that komatiites represented palco-volcanic hot-spots of paleo-oceanic plateau which are formed directly by partial melting of rising, deep plume, and were composed of the Lower-Middle Proterozoic growth layers in Paleo-Yangtze plate which are similar to the primitive mantle in isotope. The latest S wave three-dimension velocity plane image displays that there is a columnar low-velocity anomaly area (-0.6%) at depths of 350km and 410km at 110°E and 26-31°N of the middle South China, which verifies that the residual hot paleoplume exists under the lithosphere. The continent crustal structure is closely related to underlying plume structure.

**JSA37**

**Wednesday 28 July**

### EARTH'S GRAVITY AND MAGNETIC FIELDS FROM SPACE (IAGA, IAG, IASPEI, SCOSTEP)

Location: Muirhead Tower, G08 LT

Location of Posters: Muirhead Tower, Student Room (1st floor)

**Wednesday 28 July AM**

Presiding Chair: K. H. Ilk (Inst. f. Theoretische Geodaesie, Univ. Bonn, Germany)

**JSA37/L/02-B3**

**0900**

### AN INTERNATIONAL DECADE OF POTENTIAL FIELD RESEARCH

Eigil FRIIS-CHRISTENSEN (Danish Space Research Institute, Juliane Maries Vej 30, DK-2100 Copenhagen, email: efc@dsri.dk)

During the recent years progress in geopotential field research has been severely limited by the available amount of high precision measurements of the global gravity and geomagnetic field. Since 1980, at the end of the Magsat mission, there have been no further global measurements of the near-Earth magnetic field and there has never been one for the gravity field. This situation will soon change; there are several planned and proposed geopotential field satellites. The scientific community has made an effort to co-ordinate all these endeavours in announcing an "International Decade of Geopotential Field Research" in order to encourage the provision of a set of continuous measurements from space of the Earth's potential fields. Such a continuous and homogeneous series of measurements would have a great impact on the quality of science that can be done and will also provide the foundation for new and improved applications that depend on up-to-date high precision mapping of these fields.

**JSA37/E/01-B3**

**Invited**

**0915**

### DEDICATED GRAVITY FIELD SATELLITE MISSIONS - PRINCIPLES AND AIMS

Reiner RUMMEL (IAPG, Techn.Univ.Muenchen, Arcisstrasse 21, D-80333 Muenchen, Germany, email: rummel@step.iapg.verm.tu-muenchen.de)

All our current global gravity field models are based upon a sophisticated patchwork of satellite orbit perturbations, satellite altimetry, and terrestrial gravity combined with height information. This method has been developed to its very limit. Fundamental further improvement must therefore come from dedicated gravity field satellite missions. The underlying principle for any such mission is the reconstruction of perfect free fall in the Earth's gravitational field of one or more test masses in low orbit. This may be achieved by measuring - with highest possible precision - either (1) the relative motion between the high orbiting GPS satellites and a low orbiter (satellite-to-satellite tracking in the high-low mode (SST hi-lo)), as will be applied for the CHAMP mission, or (2) by combining this concept with the measurement of the relative motion between two low orbiters (satellite-to-satellite tracking in the low-low mode (SST lo-lo)), as for the case of GRACE, or (3) by combining SST hi-lo with satellite gradiometry as proposed for GOCE. Whereas GRACE aims at the recovery of the large and medium spatial scales of the gravity field with ultimate precision so as to reveal its variations in time, GOCE will focus on the determination of the stationary field with maximum spatial resolution. Gradiometry, based on the principle of differential accelerometry, requires the elimination of all possible spurious perturbations on its test masses due to non-gravitational linear accelerations, spacecraft rotation or time-variable self-gravitation. The satellite becomes integral part of the gradiometer. GOCE aims at the resolution of the gravity field up to at least degree and order 200 in terms of spherical harmonics with a cumulative geoid error of below 2cm or gravity anomaly error of below 0.6 mGal.

**JSA37/W/05-B3**

**Invited**

**0945**

### CHAMP AND THE GEOPOTENTIAL FIELDS

Ch. REIGBER, H. Lühr, P. Schwintzer (GeoForschungsZentrum Potsdam, Telegrafenberg A6, 14473 Potsdam, Germany, Email: reigber@gfz-potsdam.de)

CHAMP is the first low-cost satellite mission aiming at the simultaneous precise observation of both the gravity and magnetic field from a low altitude orbit. Thanks to the dedicated orbit design, an unprecedented low altitude in a near polar orbit, its continuous undisturbed observation of the magnetic field vector through scalar and vector magnetometers and its continuous GPS satellite-to-satellite tracking capability together with a direct on-board measurement of the non-gravitational orbit perturbations, a dramatic improvement in the global modelling of the magnetic field and also an order of magnitude improvement for the broad to mesoscale structures of the gravity field can be expected. In addition, due to the designed 5 years mission duration, temporal changes in both fields will be detectable with a higher signal/noise ratio and at increased spatial resolution as it is possible now. Therefore a



number of fast to slowly changing gravity and magnetic signals will become measurable, which are related to processes taking place in the various constituents of the system Earth. The discrimination of various signal sources, the combined use of observed irregularities or variations in time, the inversion and correlation of observed field data will become interesting research issues for atmospheric, ocean and solid Earth sciences. CHAMP fulfils the criteria of a small satellite mission, i.e. short development time through the usage of existing sensors and commercial subsystem components and reduced cost through proto-flight approach, suitable quality standards and streamlined test efforts. The CHAMP development started in January 1997 and the satellite structure, subsystems and payload has been integrated. Launch on a COSMOS rocket is planned for late 1999. The presentation will focus on mission goals, S/C and payload technical characteristics and the expected system performance for the modelling of the gravity and magnetic fields.

**JSA37/E/04-B3****1015****INVESTIGATIONS ON THE POLAR GAP PROBLEM IN ESA'S GRAVITY FIELD AND STEADY-STATE OCEAN CIRCULATION EXPLORER MISSION (GOCE)**

Stephan RUDOLPH, Karl-Heinz Ilk, Juergen Kusche (Institute of Theoretical Geodesy, University of Bonn, Nussallee 17, 53111 Bonn, Germany, email: stephan@theor.geod.uni-bonn.de)

GOCE (Gravity Field and Steady-State Ocean Circulation Explorer Mission) is one of the candidates to become the first ESA's Earth Explorer core mission. It is a high resolution gravity field mission concept based on SGG (satellite gravity gradiometry) combined with GPS-SST (satellite-to-satellite tracking) and will open a completely new range of spatial scales of the earth's gravitational field spectrum down to 100km wavelength. Due to the sun-synchronous orbit the two polar regions with a radius of about 700km cannot be observed. Therefore these regions represent data gaps, resulting in poorly determined frequency bands in the spectral representation of the gravity field. Although these data gaps cover only approximately 2% of the planet's surface, especially the polar regions play an important role in climate change, mass-balance and ocean circulation. From a mathematical point of view, the problem of gravity recovery from observations in satellite altitude is seriously ill-conditioned. The polar gaps additionally aggravate the degree of instability. A theoretical analysis concerning the capabilities of a full tensor gradiometer to "look into" the polar gaps is performed. Special emphasis is laid on the effects of the specific tensor components and of the supplementary high-low SST data. Besides the additional instability effects in the downward continuation process due to the polar gaps are considered. First results using regional recovery strategies are presented.

**JSA37/W/09-B3**

Invited

**1100****THE CONTRIBUTION OF FUTURE DEDICATED SATELLITE GRAVITY MISSIONS TO MEASURING TEMPORAL VARIATIONS OF THE EARTH'S GRAVITATIONAL FIELD**

R.S. NEREM, S.V. Bettadpur, R.J. Eanes, B.D. Tapley (all at the Center for Space Research, The University of Texas at Austin, Austin, TX, 78712, email: nerem@csr.utexas.edu); J. Wahr (Department of Physics, University of Colorado, Boulder, Colorado, 80309-0390, USA, email: wahr@lemond.colorado.edu)

Mass redistributes itself in the coupled Earth system on a variety of temporal and spatial scales reflecting complex interrelated processes in the oceans, atmosphere, groundwater, and glacial/polar ice. The measurement of these variations is thus important for a variety of studies attempting to understand the interactions of the different components of the Earth system, and how they may change with time due to anthropogenic influences. This presentation will discuss the spatial and temporal characteristics of observations of the temporal varying gravity field expected to be made by future dedicated satellite gravity missions (e.g. CHAMP, GRACE, GOCE) early in the next decade. The subject will be introduced by summarizing the relatively limited results available from current space geodetic techniques (e.g. SLR). The spatial and temporal properties of the expected time varying gravity signals arising from different components of the time varying gravity field (ocean mass, atmospheric mass, continental water mass, snow mass, etc.) will be assessed using a variety of geophysical models. These geophysical signals will then be compared to the expected performance of future satellite gravity missions. The limiting error sources influencing these observations will be summarized. Finally, the expected benefits to Earth system science studies will be discussed, based on the magnitude of the signals predicted by the geophysical models, and the expected performance of the satellite measurements. Central to this discussion will be a consideration of how to separate the different sources of mass redistribution given that the satellite observations will reflect contributions from many different components of the Earth system.

**JSA37/E/05-B3****1130****DATA COMBINATION IN ILL-POSED DOWNWARD CONTINUATION PROBLEMS**

Karl Heinz ILK, Juergen Kusche, Stephan Rudolph (Institute of Theoretical Geodesy, University of Bonn, Nussallee 17, D-53115 Bonn, Germany, email ilk@theor.geod.uni-bonn.de)

It is a well-known fact that the computation of gravity field parameters from pure satellite data is improperly posed from a theoretical point of view in so far as the recovery results do not continuously depend on the observations. Despite the fact that the numerical implementation takes the edge out of the problem, at least to a certain amount, it remains a seriously ill-conditioned problem. The standard procedure to overcome this problem is to introduce stochastic prior information, in most cases in form of an appropriate degree variance model. Formally this procedure corresponds to Tikhonov's regularization where the regularization parameter balances the noise and the signal content of the observations. While the combination of data of different origin is comparably well-understood in well-posed problems there are some open questions in combining various data sets in improperly posed problems: What is the information content of the various data, as a set and as individual observations, contributing to the recovered gravity parameters? How does the gravity field parameters change if the observations are changed by minor amounts? Is there a difference of globally and locally defined parameters? What is the effect of data gaps on the spatial and spectral distribution of data? The present investigation tries to tackle a clarification of these questions. Results of simulations of future gravity field mission scenarios are presented to demonstrate the problems. Possibilities to overcome these problems are discussed.

**JSA37/P/01-B3****1145****APPLICATION OF THE TIDAL GRAVITY OBSERVATIONS ON GEODYNAMICS OBTAINED WITH SUPERCONDUCTING GRAVIMETER**

He-Ping SUN, Hou-Tze Hsu, Jian-Qiao Xu, Guo-Qing Tao (Institute of Geodesy and Geophysics, CAS, 54 Xu-dong Road, 430077, Wuhan, China, email: heping@asch.whigg.ac.cn)

The superconducting gravimeter is the most reliable instrument at present on the study of the small change in earth gravity field, since it possess with the wider dynamic linear measuring range and can be used to detect the available signals which are usually below the normal instrumental noise level. The long term (non-) tidal gravity observations for 10 years with

sampling of 20 s observed with superconducting gravimeters at station Wuhan in China are studied comprehensively. The corresponding results at various wave bands are used to study the gravity signals due to (1) the change in the atmospheric pressure; (2) the influence of the oceanic loading; (3) the influence of the dynamics of the Earth's core and (4) the effect of the Earth's rotation.

Using a slipped window function, the abnormal signals as jumps, tares and spikes are detected and eliminated. The missing data due to the power interruptions, earthquakes, refilling liquid helium are filled using a spline interpolation method based on the synthetic tide. Using a symmetric digital low-pass filter with a truncate period of 3 hours, the hourly sampling intervals of the tidal gravity and pressure are obtained after a smoothing processing. The efficiency when using various procedures on improving accuracy of the tidal parameters is discussed. The residual amplitudes and the average standard deviations are determined using the Fast Fourier Transformation method. We used the station air pressure data and the regression method to determine the atmospheric gravity admittances in both temporal and frequency domains. We applied the oceanic loading correction based on the various most recent global ocean tidal models. We used the staking method to determine the resonance parameters of the Nearly Diurnal Free Wobble.

**JSA37/W/04-B3****1200****THE ALPINE SWISS FRENCH AIRBORNE GRAVIMETRY PROJECT**

J. VERDUN (a) (email: verdun@dstu.univ-montp2.fr), R. Bayer (a) (email: roger@dstu.univ-montp2.fr), E. Klingel (b) (email: emile@geod.ethz.ch); M. Cocard (b) (email: cocard@geod.ethz.ch), M. Cerniar (b) (email: mace@geod.ethz.ch), A. Geiger (b) (email: geiger@geod.ethz.ch), M. Halliday (c) (email: MrHalliday@aol.com) [(a) CNRS-ISTEEM, Université de Montpellier II, France; (b) GGL, ETH-Hönggerberg, Zürich, Switzerland; (c) Lacoste&Romberg Gravimeters Inc., Austin, Texas, USA]

This airborne gravity survey was realized in the frame of the "GEOFRANCE 3D Alpes" project in the Western Alps, from the Rhone Valley to the Po-Plain in Italy. Four objectives were followed: accurate airborne measurements of the alpine gravity field, combination of both GPS data and those provided by a classical navigational system (INS), comparison between airborne gravity data and upward prolonged ground data, 3D modelling of the alpine crust using several Bouguer anomaly maps. In February 1998, 18 NS lines were flown, crossed by 16 EW lines, spaced respectively by 10 and 20 km. The survey was performed with a Twin-Hotter aircraft owned by the Swiss Federal Directorate of Cadastral Surveying at barometric altitude of 5100 m above sea level. The aircraft was equipped with 5 GPS receivers (working frequencies: from 1 to 8 Hz) for relative positioning to 7 ground fixed GPS stations and for monitoring both aircraft velocities and accelerations. Gravity field was measured with a L&R airborne gravimeter, type SA, mounted on a laser gyro stabilized platform (working frequencies: 1Hz for the spring tension, 10 Hz for the beam position). Various strategies for computing the kinematic properties of the aircraft (softwares, choice of the reference GPS ground station) are discussed. A preliminary long-wavelength "free-air" anomaly map is presented and compared with some previous published.

**JSA37/E/03-B3****1215****GLOBAL POWER SPECTRAL DENSITIES FOR GRAVITY AND MAGNETIC FIELDS**

Roger HIPKIN, Thomas Kalscheuer (Department of Geology & Geophysics, University of Edinburgh, Kings Buildings, Edinburgh EH9 3JW, UK, email: roger.hipkin@ed.ac.uk)

This paper presents a re-interpretation of the power spectral density of the Earth's gravity field which implies that lithospheric sources dominate the spectrum for spherical harmonic degrees above about 14, the same result as with the geomagnetic spectrum. At lower degrees, both power spectra identify sources largely concentrated at a single depth but, for gravity, they are within the lower mantle, compared with just below the core-mantle boundary for geomagnetism. The low source power from upper mantle asthenosphere results from convection there needing only very small buoyancy forces to overcome viscous drag. Significant sources of the gravity anomaly are thus confined to either the lithosphere (where they are supported by elastic forces), or the lower mantle (where a higher viscosity slows their dissipation).

This result is not due solely to new data: the global gravity models OSU91A and EGM96 have a similar spectrum. Contrary to the conventional picture often described as Kaula's Law, the gravity power spectrum in fact looks very much like the geomagnetic spectrum. Failure to identify this earlier may have been due to a different spherical harmonic normalisation used in geodesy and geomagnetism.

**Wednesday 28 July PM**

Presiding Chair: E. Friis-Christensen  
(Danish Space Research Institute, Copenhagen, Denmark)

**JSA37/E/06-B3**

Invited

**1400****RECENT PROGRESS IN EXPLORING THE NEAR-EARTH MAGNETIC FIELD WITH LOW-ALTITUDE SATELLITES**

Nils OLSEN (Danish Space Research Institute, Juliane Maries Vej 30, DK-2100 Copenhagen, e-mail: nio@dsri.dk)

Data from high-precision geomagnetic satellites in low-altitude orbits are a unique opportunity to investigate the near-Earth magnetic field from space. Almost 20 years after the MAGSAT mission, at least three satellites will provide high-quality data during the next years: Oersted (launched in January 1999), SAC-C/MMP, and CHAMP. They all carry similar high-precision instrumentation for measuring the magnetic field vector with an accuracy better than 2 nT absolute. Each mission, however, has its own advantages given the different altitude, local-time coverage, sampling rate and lifetime of the satellites. Data from single satellite missions are not able to accomplish the accurate determination of the spatial and temporal structure of all sources that contribute to the near-Earth magnetic field. A great challenge is therefore the combined analysis of data from different satellites, and from ground based observatories. This is the only way to take full advantage of the accuracy of the instrumentation, which has improved enormously in comparison to previous missions. The results of such a comprehensive modelling effort will be presented and plans for further improvement of the model will be discussed.

**JSA37/W/08-B3****1430****SEARCHING FOR AN OPTIMAL SATELLITE NETWORK FOR MONITORING FAST CHANGES WITHIN THE EARTH'S MAIN MAGNETIC FIELD**

Benoit LANGLAIS, Pascale Ultré-Guéard, Gauthier Hulot, Yves Cohen, Mioara Manda (Alexandrescu Institut de Physique du Globe de Paris, 4 Place Jussieu, 75252 Paris Cedex 05, France, email: langlais, ultre, gh, cohen, mioara@ipgp.jussieu.fr)

## INTER-ASSOCIATION

In addition to the Danish satellite OERSTED (due to be launched in January 1999), several satellite missions devoted to observing and mapping the Earth's magnetic field are planned to be launched in the near future (e.g., SAC-C, CHAMP). These are one-satellite missions, with both scalar and vectorial magnetometers on board. Combined with observatory data, this data will make it possible to better describe part of the large scale external field and characterise the crustal field, the main field and the secular variation down to time scales of the order of three to six months. Further improvement of our knowledge will only come with the possibility of having missions involving several satellites flying at the same time, such as the proposed SWARM (European) or UNIMAG (Russian and Indian) missions. The purpose of the present study is to assess how much improvement such configurations would bring, especially with respect to our ability to better characterize the evolution of the main field on the shortest time scales. By making use of synthetic data produced by realistic internal and external sources to which a plausible noise is being added, various orbital configurations are being considered. The synthetic data is produced for each satellite and present observatory locations and is then inverted for internal and external sources. It is shown that a very robust configuration would consist in having six vectorial satellites orbiting on polar orbits together with one vectorial satellite orbiting on a near equatorial orbit. It appears for instance that a potential downgrading of the six polar satellites to simple intensity satellites would virtually not affect the quality of main field models which could still be computed on a week by week basis. Adding more satellites would allow to slightly reduce this time step, but this would probably not bring much additional information with respect to the temporal evolution of the main field, the shortest time scales of which are being filtered out by the mantle. By contrast, it will be shown that adding two to three new observatories near the equator would prove very useful.

### JSA37/W/02-B3 1445

#### UNIVERSAL GLOBAL SURVEY OF THE EARTH MAGNETIC FIELD "UNIMAG"

Victor N. Oraevsky, Vadim P. GOLOVKOV (both at IZMIRAN, 142092 Troitsk, Moscow region, Russia, email: golovkov@izmiran.rssi.ru); A.V. Zaitsev (Lavochkin Association, 141400 Leningradskoe sh., 24, Khimki, Moscow region, Russia)

The main goals of UNIMAG mission being the following:

(1).The precise modelling of the main geomagnetic field on epoch of launching and deriving the secular variation model.(2).The Earth's crust magnetic anomaly mapping.(3).The Earth's mantle electrical conductivity mapping.(4).The ionospheric and magnetospheric current systems separation and modelling.for the practical needs the mission will give data for the International Geomagnetic Reference Field modelling as well as for regional geomagnetic field mapping which can be used for:(5). The prospecting and magnetic mapping.(6). The marine and airborne navigation and for other aims of the first necessity. For this aim it is supposed to realise the UNIMAG project by the launching a few small satellites to the orbits separated in altitude and in local time. The first satellite, equipped by the complete set of magnetometers and star imager should be launched to the Sun-synchronised orbit with inclination 96, altitude 500-700 km and local time of the equator crossing - 6 and 18 hour. The second satellite (for anomalous field survey) should be launched as well to the Sun-synchronised orbit with inclination 96, altitude 300-1000 km and local time of equator crossing 6 and 18 hour. Else 3 satellites should be launched on near polar orbits to pass whole range of local time

### JSA37/E/08-B3 Invited 1500

#### SATELLITE MONITORING OF THE MAGNETIC FIELD AND FLUID MOTION AT THE TOP OF THE EARTH'S CORE

A. JACKSON, M. Walker (School of Earth Sciences, Leeds University, Leeds LS2 9JT, UK)

The distribution of magnetic observatories on the Earth's surface is such that accurate monitoring of the conditions at the top of the core necessarily requires spaceborne instrumentation in order to attain full geographical coverage and concomitant accuracy. We are currently entering a new era in spaceborne observation of the geomagnetic field that promises great rewards.

We will describe progress in the analysis of satellite data for core magnetic fields and fluid motions. The overriding limitation on accuracy of the core field is the crustal field, which limits resolution to below spherical harmonic degree 14. We compare the most recent results with models derived from Magsat data in order to analyse the conservation of magnetic flux within the so-called "null-flux patches" on the core surface. Additionally we can address the conservation of radial vorticity within these patches. The construction of magnetic fields conserving such quantities is, we argue, a necessary prerequisite for the self-consistent derivation of fluid motion at the core surface.

### JSA37/W/07-B3 Invited 1600

#### MODELING THE MAGNETIC FIELDS OF IONOSPHERIC AND MAGNETOSPHERIC CURRENTS

Arthur D. RICHMOND (NCAR High Altitude Observatory, P.O. Box 3000, Boulder, CO 80302-3000, USA, email: richmond@ucar.edu)

Electric currents in the ionosphere and magnetosphere produce magnetic perturbation fields on the ground and at low Earth orbit ranging from tens to thousands of nanoteslas. At the ground these are potential fields, but in space there are strong non-potential components, especially those due to geomagnetic-field-aligned currents. This talk describes the simulation modelling of ionospheric and field-aligned currents and their magnetic perturbations. Simplified methods of calculating the perturbations associated with field-aligned currents are presented.

### JSA37/W/03-B3 1630

#### TECHNIQUES FOR IDENTIFYING EXTERNAL FIELD CONTRIBUTIONS IN SATELLITE DATA

H. LUEHR, U. Engels, M. Rother, M. Förster (GeoForschungsZentrum Potsdam, Telegrafenberg, D-14473 Potsdam, Germany)

The upcoming decade will see a whole fleet of geomagnetic field missions. The high resolution of the new and advanced instrumentation can only be fully utilised for main and crustal field modelling, if we succeed in improving the separation between contributions from internal and external field sources.

There is no straightforward mathematical method which could be used for the separation. Our approach is to make intensive use of the special features of external current circuits and include it as a priori information in the calculations. We assume for example that currents at orbital height flow solely along the field lines. All ionospheric currents are confined to a thin layer. If also the electric field is measured, the two currents and the E-field can be combined in a single relation which can be used for consistency checks. Other currents flowing across the field lines occur only further out in the magnetosphere (e.g., ring current, magnetopause, magneto-tail) thus produce large-scale variations.

We have applied our technique to real satellite data. From in situ measurements we estimate

the ionospheric and the field-aligned currents in the vicinity of the satellite orbit. Contributions from the large-scale currents are estimated by employing a magnetospheric current model. Scaling the size of the configuration and the intensity of the currents requires a parameterization of the model. The appropriate parameters have to be deduced from activity indices and/or in situ measurements. First results of our analysis will be presented.

### JSA37/W/06-B3 Invited 1645

#### CRUSTAL MAGNETIC FIELDS

Patrick T. TAYLOR (Geodynamics Branch, Code 921, NASA/GSFC, Greenbelt, MD 20771, USA, email: ptaylor@ltpmail.gsfc.nasa.gov); D. Ravat (Department of Geology, MS 4324, Southern Illinois University at Carbondale, Carbondale, IL 62901, USA, email: tikur@denali.gsfc.nasa.gov); James J. Frawley (Herring Bay Geophysics, Dunkirk, MD 20754, USA, email hbjiff@ltpmail.gsfc.nasa.gov)

Cosmos 49, POGO (OGO-2, 4 and 6) and Magsat have been the only low-earth orbiting satellites to measure the crustal magnetic field on a global scale. These missions revealed the presence of long-wavelength (> 500 km) crustal anomalies predominantly located over continents. Ground based methods were, for the most part, unable to record these very large-scale features; no doubt due to the problems of assembling continental scale maps from numerous smaller surveys acquired over many years. Questions arose as to the source and nature of these long-wavelength anomalies. As a result there was a great stimulant given to the study of the magnetic properties of the lower crust and upper mantle. Some indication as to the nature of these deep sources has been provided by the recent results from the deep crustal drilling programs. In addition, the mechanism of magnetization, induced or remanent, was largely unknown. For computational ease these anomalies were considered to result solely from induced magnetization. However, recent results from MOLA, a magnetometer-bearing mission to Mars, have revealed crustal anomalies with dimensions similar to the largest anomalies on Earth. These Martian features could only have been produced by remanent magnetization, since Mars lacks an inducing field. The origin of long-wavelength crustal anomalies, however, has not been completely determined. Several large crustal magnetic anomalies (e.g., Bangui, Kursk, Kiruna and Central Europe) will be discussed and the role of future satellite magnetometer missions (Orsted, SUNSAT and Champ) in their interpretation evaluated.

### JSA37/E/02-B3 1715

#### MAGSAT ANOMALY CORRELATIONS AMONG THE CONTINENTAL SEGMENTS OF THE EAST GONDWANALAND

O.P. PANDEY, P.K. Agrawal (National Geophysical Research Institute, Uppal Road, Hyderabad 500 007, India, email: postmast@csngri.rec.nic.in)

Long wavelength satellite magnetic (MAGSAT) anomalies have been found very useful in studying geodynamical evolution and regional plate tectonic problems. The present work analyses these and long wavelength gravity signatures together with geotectonic information available over the constituents of East Gondwanaland. We discover that during the pre-breakup period, India together with Madagascar, Sri Lanka and Enderby Land of Antarctica formed a "Super South Indian Shield" till about 130 Ma. The study reveals one to one correspondence between the MAGSAT anomalies across these continents, suggesting that they have common deep seated magnetic properties, which were acquired when all the fragments were joined together. It is observed that the ancient cratonic blocks of Archean-early Proterozoic age, are associated with high order positive MAGSAT anomalies compared to younger counterpart of middle to late Proterozoic age, which are characterised by negative anomalies. Further, the MAGSAT anomaly patterns would also indicate that (i) the Archean Napier complex of Enderby Land (Antarctica) may be continuing underneath the Reyner's complex towards the Lutzow Holm Bay region, and (ii) Madagascar never rifted away from Africa, rather it was a continental fragment of Super Dharwar craton of India till about 88 Ma.

### JSA37/L/01-B3 1730

#### CRUSTAL MAGNETIC ANOMALIES OVER SOUTH EAST ASIA: MAGSAT AND OERSTED

B.P. Singh, Mita RAJARAM (Indian Institute of Geomagnetism, Colaba, Mumbai-400005, INDIA)

The Oersted data will be analysed to prepare a crustal magnetic anomaly map over S.E. Asia to study the lithospheric dynamics and tectonic processes. This map will be compared with the Magsat crustal anomaly map over this region. Although the altitude of the Oersted is higher than Magsat, it is expected that the anomaly maps will have smaller errors and will bring out the broad tectonics of the region.

Presiding Chair: K. H. Ilk (Inst. f. Theoretische Geodaesie, Univ. Bonn, Germany)

### JSA37/W/01-B3 Poster 1745-01

#### THE GEOID HEIGHTS FIELD INTERPRETATION METHODS FOR THE INVESTIGATION OF THE LITHOSPHERE STRUCTURE

A.A. BULYCHEV (Lomonosovs MSU, Geology faculty, Moscow, Leninsky Gory, MSU, Russia, email: bulychev@geophys.geol.msu.ru); A.G. Gainanov (Lomonosovs MSU, Geology faculty, Moscow, Leninsky Gory, MSU, Russia)

The satellite altimetry data acquire particular significance for studying the density inhomogeneities of MOR and adjacent deep-sea basins. Two main approaches to studying the Earth have been developed: the transformation of geoid heights into the gravity field and investigation of deep structure of the Earth using data on geoid height anomalies. The geoid height field, obtained from satellite altimeter data, is the original high-precision information about the Earth-gravity potential. The gravity effect of the water lay must be taken into account in quantitative interpretation the geoid heights field and construction the density models of the tectonosphere. The method of the reduction's computation was worked out. The geoid heights field anomalies in different reductions were computed (Bouger, Glennie and isostatic) for the Angola-Brazil geotranssect (8°-18°) and Bouvet triple junction. The gravity effects of the water lay, bottom topography and deep density inhomogeneities (3-D) were taken into consideration for these reductions. The first 3-D density models of the tectonosphere structure were constructed based on the results the 2-D modeling along the profiles, which crossed the main morphotectonic structures of the investigated areas, and the correlation between bottom age (by the geomagnetic data) and lithosphere deepness. The gravity effects in gravity anomalies and geoid heights were computed from the 3-D density model and then this model was corrected according the residual fields. Residual fields were obtained by subtracting the model's effects from the observed fields. The regional part of the field is very important in the interpretation geoid heights. It was computed by the spherical harmonic of the Earth potential.



JSA37/E/07-B3 Poster 1745-02

## CONCERNING CONFORMITY OF PLANETARY FEATURES OF GRAVITATIONAL AND MAGNETIC FIELDS

D. Kh. RASULOV

The work gives in detail a new piezoelectric model of terrestrial magnetism which permits all the main features of geomagnetic field to be explained from the unified positions. In accordance with the model, piezoelectrical textures may be formed in the Earth's crust which are oriented along a direction close to the geographic parallels. The presence of mechanical strains in Earth's crust rocks caused by an action of terrestrial gravity is to lead to an emergence of a potential difference along the piezoelectric textures. As a result, an electric current runs along these directions forming a weak quasi-stable magnetic field, which direction is to be close to that of the geographic terrestrial axis.

Therefore, in accordance with the model, local gravitational anomalies fixed on the terrestrial surface cause the corresponding local anomalies in the mechanical stressed state of the Earth's crust rocks that must lead to the observed conformity of the planetary features of gravitational and magnetic fields. Mechanical stresses in rocks, naturally, may be caused also by other reasons. These stresses are superimposed to the stress caused by Earth gravitation and may be a reason of various anomalies of the geomagnetic field. Diurnal variations of the geomagnetic field are caused by Sun's and Moon's gravitational attraction to the Earth's crust rocks.

JSP39 Tuesday 27 – Thursday 29 July

## DYNAMICS OF ROTATING AND STRATIFIED FLUIDS (IAPSO, IAMAS, IAGA)

Location: Watson Building, G23 LTA

Location of Posters: Bridge Poynting/Watson

Tuesday 27 July AM

Presiding Chair: D.L. Boyer Arizona State Univ., Tempe, (USA)

JSP39/L/01-B2 Invited 0830

## FLUID DYNAMICS AND SOME KEY APPLICATIONS TO UNDERSTANDING GLOBAL CHEMICAL-CLIMATIC CHANGE

Michael E. McINTYRE (Centre for Atmospheric Science at the Dept. of Applied Mathematics and Theoretical Physics, Cambridge CB3 9EW, UK, email: mem@damtp.cam.ac.uk)

This overview will focus on several very fundamental aspects of our global fluid environment, through some thought-experiments designed to expose key mechanisms controlling global-scale mean circulations in the atmosphere and ocean, and the resulting transports of heat and chemical constituents such as greenhouse gases.

The best understood fluid subsystem is the middle atmosphere - roughly 10-100 km altitude - whose mean stratification is primarily under UV/IR radiative control and whose mean circulation is driven not, as some mythologies have it, by solar heating, but by a persistent mechanical, Coriolis-mediated 'gyroscopic pumping'. The pumping action depends on Rossby and gravity waves propagating or diffracting from below: more precisely, it depends on the interplay of the Coriolis force with the irreversible angular momentum transport that results from wave generation in one place and dissipation in another by breaking and radiative damping.

Viewed as statistical fluctuations about a mean state, the disturbances characteristically have a net effect opposite to what was expected from classical ideas about spatially near-homogeneous 'turbulent' fluctuations. As well as pumping mean circulations, the fluctuations tend to drive the mean state not toward, but away from, a state of solid rotation; and spatial inhomogeneity is an essential, leading-order feature. In the case of Rossby waves, such 'anti-classical' behaviour (seen also in general vortex-interaction scenarios) is almost inevitable consequence of the transport and 'inversion' properties of the Rossby--Ertel potential vorticity. There is an unexpected spinoff for understanding the Sun's interior.

The troposphere and oceans are more complicated, because of the non-global span of stratification surfaces and for other reasons as well. For instance the climate system's 'thermal powerhouse', the tropical troposphere, simplified as a subsystem with a fixed sea-surface temperature, has stable stratification under moist-convective control - temperature profiles clamped to the moist adiabat - and a persistent deep-convective upward mass flux in the intertropical convergence zone consisting of two contributions having somewhat comparable magnitudes, the one controlled by radiative cooling of the tropics and the other by gyroscopic pumping from the extratropics. If both these controls were to be switched off then the deep convection would also switch off. The oceans are more complicated still...

JSP39/W/43-B2 Invited 0900

## THE ROLE OF LABORATORY EXPERIMENTS IN ROTATING STRATIFIED FLOWS

Prof. Paul LINDEN (University of California, San Diego, USA, email: pflinden@ames.ucsd.edu)

This talk will review the role of laboratory experiments in research into the dynamics of rotating stratified flows (RSF) with particular relevance to geophysical fluid dynamics. Experiments have provided a major input into the understanding of RSF, both by revealing new phenomena and by providing data against which theoretical ideas can be tested and developed. The first major impact of experiments came with the annulus studies of the atmospheric circulation in the 1950s, and from that time there has been a (generally) increasing activity in RSF experiments. This talk will outline some of the successes of laboratory experiments in modelling RSF and will describe recent work in which the experiments interface with numerical simulations. The limitations of experiments of geophysical flows will be described and some speculations will be made about possible future developments.

JSP39/W/42-B2 0930

## TURBULENT CONVECTION IN ROTATING AND STRATIFIED FLUIDS

H.J.S. FERNANDO, M.A. Levy (Environmental Fluid Dynamics Program, Arizona State University, Tempe, AZ 85287-9809, USA)

Turbulent convection induced by heating the bottom boundary of a wide, linearly (temperature) stratified, rotating fluid layer is studied using a series of laboratory experiments. It is shown that the growth of the convective mixed-layer is dynamically affected by background rotation (or Coriolis forces) when the parameter  $R = (h^2 W^{**3}/q)^{2/3}$  exceeds a critical value,  $R_1$ , which is approximately 100. Here  $h$  is the depth of the convective layer,  $W$  is the rate of rotation and  $q$  is the buoyancy flux at the bottom boundary. When  $R > R_2$ , where  $R_2$  is approximately

300, the buoyancy gradient in the mixed-layer was profoundly affected by background rotation. Conversely, when  $R < R_1$ , the buoyancy gradient in the convective layer is independent of the rate of rotation and approaches that of convection in non-rotating fluids. When  $R > R_2$ , the entrainment velocity was found to be dependent on the buoyancy frequency of the overlying stratified layer, the rate of rotation and the conventional (Deardorff) convection velocity. A simple theoretical formulation for the rate of entrainment was derived, which was found to be in good agreement with the experimental results. The experimental results also indicate that entrainment in this case is dominated by non-penetrative convection.

JSP39/W/06-B2 0950

## SEPARATION PHENOMENA IN STRATIFIED FLOW ALONG A SLOPING SIDEWALL

Geno PAWLAK, Parker MacCready (School of Oceanography, University of Washington, Box 357940, Seattle, WA 98195, USA, email: gpawlak@ocean.washington.edu)

Experiments examining the separation of a stratified flow along a sloping boundary are presented. Separation phenomena are the source of much of the transfer of vorticity-containing fluid within sidewall boundary layers into the interior inviscid flow, which may contribute to a significant part of the mixing in estuarine and coastal processes. Obstacles along the inclined sidewall induce both cross and along-isopycnal components to the mixing and allow the isolation of the competition between stratification and form induced pressure variations. Experimental results presented, examine obstacles of wavenumber,  $k$ , such that  $N/U \ll k \ll d$ , where  $d$  is the boundary layer thickness. These experiments explore the origin and structure of separation zones for a variety of stratified flow configurations including uniform stratified flow, two-layer and stratified shear flows and tidally modulated stratified flow. Particle imaging velocimetry and flow visualization results are presented along with observations on internal wave generation and drag. Experimental observations are compared to analytical and numerical analyses.

JSP39/L/02-B2 1010

## EDDY-DRIVEN BASIN-SCALE RESPONSE TO LOCALISED FORCING OF A ROTATING STRATIFIED FLUID

J. N. HACKER, S. B. Dalziel (D.A.M.T.P., Cambridge University, Silver Street, Cambridge CB3 9EW, UK; email: j.hacker@damtp.cam.ac.uk), P. F. LINDEN (A.M.E.S., University of California, San Diego, 9500 Gilman Drive, La Jolla, CA 92093-0411, USA)

Mesoscale eddies, produced for example by the instability of density fronts, are a ubiquitous feature of the flow in the oceans. These eddies typically have kinetic energy and vorticity levels exceeding those of the mean motion, and are widely considered to have a profound influence on the flow at larger-scales. Although the nature of this relationship is not well understood at present, the ability of eddies to transport momentum away from regions of eddy production to more quiescent regions may be an important effect influencing the character of the general oceanic circulation. Here we report laboratory experiments in which eddies were produced in a rotating stratified fluid by injecting and withdrawing fluid through sources and sinks situated along some part of the boundary of a laboratory tank. Energetic eddies continually formed and were dissipated at the sources and sinks, but also intermittently escaped from the forcing region, propagating away into the interior of the basin in the form of anticyclone-cyclone pairs. These eddies interacted in the interior of the basin and set up gyre-like circulation patterns. The character and localised nature of the source-sink forcing, together with the geometry of the basin, imposed dynamical constraints on the flow, in particular on the manner in which eddies were produced and the form of eddy interactions, with the results that a coherent basin-scale mean circulation was established.

JSP39/E/19-B2 1050

## LABORATORY EXPERIMENTS ABOUT UPWELLING FRONTS

P. BOURUET-AUBERTOT, P.F. Linden (D.A.M.T.P., Univ. of Cambridge, Silver Street, Cambridge CB9 3EW, U.K.; Dept of Applied Mechanics and Engineering Sciences, Univ. of California San Diego, La Jolla, CA 92093-0411, USA)

We investigate experimentally the instability and later evolution of a front in a two-layer stratification near a coast and over sloping topography. The front is produced through the adjustment of a buoyant fluid that is initially confined within a bottomless cylinder. Typically, a front in quasi-cyclostrophic balance is established after two rotation periods, for appropriate values of the radius of deformation, after which it becomes unstable. We focus here on the influence of the coast and on the effect of conical bottom topography. Quantitative measurements of the velocity and vorticity fields at the surface are made which provide detailed information on the evolution of the front as the instability grows to finite amplitude. The effect of the coast is crucial with respect to the instability of the front and leads to the enhancement of cyclonic eddies consisting of coastal waters. This has significant impact on exchanges across the front. When a conical topography cross-frontal exchanges are weakened as the cyclonic eddies remain confined to the slope region.

JSP39/W/48-B2 1110

## A GRAVITY JET DISCHARGED HORIZONTALLY INTO A ROTATING AND/OR STRATIFIED FLUID

Yoshito IKEHATA (Dept. of Earth System Sci. & Tech., Kyushu University, Japan, email: ikehata@esst.kyushu-u.ac.jp)

A gravity jet discharged horizontally into a rotating and/or stratified fluid is of great interest in oceanography and hydraulics. Two typical examples of such a jet are a high-density current which flows out of the Mediterranean Sea into the Atlantic Ocean and an inflow of muddy river water into an inner bay. Thus a large variety of different scales are associated with the horizontally-discharged gravity jet, which strongly influences coastal and off-shore flow systems. A three-dimensional round jet discharged into a linearly stratified rotating fluid has been investigated experimentally. A 130 x 30 x 30 cm glass water tank was filled with a linearly stratified salt water and placed on a counter-clockwise rotating table with the diameter of 1.0 m. A nozzle with the inside diameter of 3.00 mm was attached horizontally to a smaller side wall of the tank at the height of 18.5 cm. Through this nozzle was discharged horizontally a salt water, which has the same density as the ambient water near the nozzle or a density higher than the ambient water density. The discharged turbulent jet initially moves downward deflecting to the right (when viewed from above the tank) by the action of the Coriolis force. Eventually, the jet reaches a larger side wall and proceeds along it forming a Kelvin-wave like pattern subject to a geostrophic balance and diffusion. In the very long time, steady two-dimensional two to six cellular vortices, were formed in the tank. The jet was marked with a dye and the overall flow patterns were visualized with suspended polystyrene beads. For comparison's sake, the non-rotating case was also investigated. The result shows that similar cellular vortices were formed in the long time, although the horizontal diffusion pattern of the



## INTER-ASSOCIATION

jet was different from that for the rotating case. The behaviour of the horizontally discharged turbulent jet was also analyzed numerically by means of LES. The eddy viscosity was evaluated based on a Smagorinsky type model, which takes into account the turbulence caused by the buoyancy energy of the subgrid scale. The numerical results are generally in accordance with the experimental ones. Such characteristic quantities associated with the jet as the velocity distribution, the vorticity distribution, and the time-series of turbulent spectra are calculated.

**JSP39/W/29-B2** **1130**

### EVOLUTION OF VORTICES GENERATED BY THE COLLAPSE OF A STRATIFIED, TURBULENT WAKE

Alan BRANDT (Johns Hopkins University, Applied Physics Laboratory, Johns Hopkins Road, Laurel MD 20723-6099, USA, email: alan.brandt@jhuapl.edu)

Recent laboratory studies of turbulent wakes of spheres and self-propelled bodies in stratified fluids have shown that late-wake vortices ("pancake eddies") are present over a wide range of Reynolds and Froude numbers and that they persist for very long times. This late-wake, quasi-two dimensional structure results from the stratification induced collapse and transfer of the vertical turbulent energy and the wake-induced shear in the horizontal plane. As the energy supply is non-uniform, due to the turbulent nature of the wake, the resulting vertical vorticity is not uniformly distributed. The late-wake eddies are interconnected and evolve as dipoles with unequal vortex strengths at each pole, and thus do not behave as dipoles that are generated in laminar flow experiments which can be described theoretically. Based on laboratory experiments, a statistical analysis of the late-wake, turbulent dipole evolution has been carried out in order to describe the evolution of the size and motion of the dipoles as a function of Froude number. Implications of these scaling laws for the persistence of eddies in the ocean (that can result from shear induced instabilities and can affect the distribution of the planktonic biomass and anthropogenic pollutants) will also be discussed.

**JSP39/W/08-B2** **1150**

### SPIRAL MONOPOLES AND DIPOLES IN ROTATING STRATIFIED FLUIDS

Sergey VOROPAYEV (Arizona State University, Tempe, AZ 85287-6106, USA and Institute of Oceanology, Russian Academy of Sciences, Moscow, 117851, Russia, email: s.voropayev@asu.edu)

Monopoles and dipoles are most frequent structures observed in the stratified and/or rotating systems. Typical examples are mushroom-like currents in the upper ocean and inter-moocline lenses in the deep ocean. To reproduce these characteristic flows in experiments, a controllable horizontal momentum source (jet emerging from a nozzle into a rotating stratified fluid) was used. The jet either (i) deflects from the direction of injection, forming an anticyclonic spiral monopole (monopole regime), or (ii) propagates along the injection direction, forming a dipolar structure (dipole regime). Which of these flows occurs depends on the system parameters, the Reynolds number  $Re$  and the buoyancy frequency to Coriolis parameter ratio  $N/f$ . A flow regime diagram is developed for a range of these parameters. A theoretical analysis is advanced to explain the conditions under which the monopole or dipole regimes occur, including the transition curve between the two regimes, which is calculated as  $N/f = 2Re^{1/3}$ . The theory is supported by laboratory experiments. In accordance with the flow regime diagram, one may expect that dipolar structures should occur more frequently in the upper ocean, while monopolar structures should occur more frequently in the deep ocean. These conclusions are in agreement with numerous remote observations and direct field measurements.

**JSP39/W/19-B2** **1210**

### INTERACTIONS BETWEEN TOPOGRAPHY AND AN INTERMEDIATE CURRENT: AN EXPERIMENTAL STUDY

Sylvian SADOUX (LEGI-Coriolis, 21 ave des martyrs, Grenoble, 38000, France, email: sadoux@hmg.inpg.fr)

To study the effects of a cape or a canyon upon an intermediate water current, experiments were performed on the 13m diameter tank filled with a linearly stratified fluid. The upstream current was either stable ( $Ro1$ ) or unstable (i.e. anticyclonic lense generating,  $Ro < 0.2$ ) (Sadoux et al., 1999). From horizontal velocity fields recorded in several (up to 29) levels using a Correlation Imaging Velocimetry (CIV) technique it is possible to reconstruct 3D velocity and vorticity fields as functions of time. The cape-current interaction experiments focussed on a simplified model of Cape Saint Vincent at depth 1000m (i.e. a  $70^\circ$  cape). When the upstream current is unstable, they show that there is anticyclonic lense production at the cape; these anticyclonic lenses are at first surrounded by a cyclonic ring. As they propagate, the cyclonic ring tends to weaken but upper and lower (and weaker) cyclones remains attached to the anticyclone. When  $Ro$  increases, (1) there is dipole formation at the cape and (2) the negative to positive vorticity ratio increases too. The formation period, the vorticity and the spin-up time of the lenses generated at the cape agree with in situ observations (Bower et al., 1997). In the canyon-current interaction experiments the mean current level was either above or at the upper bound of the canyon. In both cases, when the upstream current is unstable, the canyon is a possible (but not only) place for anti-cyclonic lense generation. When the upstream current is stable, there is only cyclone generation, starting in the canyon region and growing in diameter with time. These cyclones are then advected downstream by the current. The rate of growth of the cyclones is maximum when the Rossby radius of deformation is larger than the canyon width.

**Tuesday 27 July PM**

Presiding Chair: D. Fearn Univ. of Glasgow, Dept. of Mathematics, (UK)

**JSP39/W/37-B2** **Invited** **1400**

### THE ROLE OF ROTATION & STRATIFICATION IN THE DYNAMICS OF EARTH'S CORE

Paul ROBERTS (Institute of Geophysics and Planetary Physics, UCLA, Los Angeles, CA 90095, USA, email: roberts@math.ucla)

The directional property of the magnetic compass needle is enough to establish how important the rotation of the Earth is for the MHD of its core; of all the forces that act on the core fluid, the Coriolis force alone has a preferred direction. The study of RMHD (rotating MHD) shows how rotation retards most flows, giving them slow time scales that have been identified with those of the geomagnetic secular variation. The time scale of the geostrophic component of flow, and it has been seen in analyses of geomagnetic data.

Most simulations of core RMHD assume that the bulk of the core is weakly but stably stratified because of tiny compositional and thermal superadiabatic gradients that are however large enough to provide the buoyancy necessary to supply kinetic and magnetic energy. It has also been suggested that there is a layer of stably stratified fluid at the top of the core, and

Braginsky has called this "the stratified ocean of the core". This presentation will focus on the present status of the topics adumbrated above.

**JSP39/E/10-B2** **Invited** **1430**

### INFERENCE ON CORE STRUCTURE AND FLOW FROM SURFACE OBSERVATIONS

David CROSSLEY (Saint Louis University, Department of Earth and Atmospheric Sciences, 3507 Laclede Ave., St. Louis, MO 63103, USA, email: crossley@eas.slu.edu)

There can be no direct observations of the Earth's core; all geophysical measurements have to be heavily processed to reveal subtleties that might reflect structure and motions deep within the Earth. The most effective techniques are seismology, gravity, geodesy and geomagnetism. The most likely motions that may be detectable are short period waves (predominantly hydrodynamic) of periods hours to days, rotational phenomena associated with angular momentum changes between the inner core, outer core and mantle with periods of hours to decades, and decadal changes in core flow associated with steady convection of the hydromagnetic fluid. In all successful observational campaigns, three criteria need to be satisfied:

(1) the theoretically possible motions have to be stimulated by a sufficiently energetic source, (2) the signal to noise ratio of the surface phenomena must be adequate and (3) the damping of the motions must be weak (i.e. long) enough to permit the required data to be collected.

This review will begin with the best known data we have at long periods, i.e. the Earth rotation data and the magnetic field variations over several decades to centuries. We will end with the possible observations we may get from seismology and super-conducting gravimeters over the next few years.

**JSP39/W/34-B2** **1500**

### PRECESSION DRIVEN FLOW IN SPHERICAL SHELLS

A. Tilgner, F.H. BUSSE (Institute of Physics, University of Bayreuth, D-95440 Bayreuth, Germany)

Precession has long ago been proposed as a possible driving mechanism for the geodynamo. In the case of exactly spherical boundaries, only viscous forces transmit the motion of the boundaries to the fluid. In the simplest approximation, the flow inside the shell is described as a solid body rotation about an axis that differs from the axis of rotation of the shell. The velocity profile inside processing spherical shells has been investigated numerically for different Ekman numbers, precession rates and gap sizes. The simulations reveal significant deviations from a pure solid body rotation. These deviations determine the shape of internal shear layers and the stability of the flow. The numerical results are compared with analytical expressions in the cases of the full sphere and in the thin shell limit.

**JSP39/E/17-B2** **1520**

### ASYMPTOTIC MODELS FOR RESISTIVE INSTABILITY IN THE EARTH'S OUTER CORE

Steven D. LONDON (Department of Computer and Mathematical Sciences, University of Houston-Downtown, One Main Street, Houston, Texas 77002, USA)

Numerical work indicates that resistive instability may be the dominant mode of instability in the Earth's outer core for realistic core parameter regimes. In this work, we are able to study resistive instability analytically by choosing a parameter regime in which the Elsasser number, while assumed to be large, is an order of magnitude smaller than the magnetic Reynolds number. Applied to an electrically conducting fluid confined to a thin rotating cylindrical shell, these assumptions allow us to analyze the linearized equations of motion using standard analytical techniques. We first discuss the equations which have been linearized about an ambient field which varies only in the direction perpendicular to the axis of rotation. The study is then extended to ambient fields which vary in directions both parallel and perpendicular to the axis of rotation. We will also discuss the extension of this work to spherical geometry.

**JSP39/E/20-B2** **1540**

### HYDRODYNAMIC MODEL OF THE TOPOGRAPHY VARIATIONS ACROSS THE RIDGE CREST

V. CHERNIAVSKI (Paleogeodynamics, Institute of Oceanology of RAS, Moscow, 117851, Russia, email: cherniav@chip.sio.rssi.ru); Suetnova E. (United Institute of the Physics of the Earth of RAS, Moscow, 123810, Russia, email: elena@uipe-ras.scgis.ru)

It is considered the stability of the stationary flow of high viscosity liquid. Well known stationary solution of a jet moving from infinity toward a wall is suggested to be considered as a flow caused by the force acting along the boundary deformable surface. Undisturbed surface is horizontal and horizontal velocity on the surface is the step function. It is studied the developing of infinitesimal disturbances. The disturbed solution is defined by the solutions of two Laplace equations with boundary conditions on the undisturbed surface. It is given a procedure of numerical investigation that is based on the method of conformal mapping the region of the flow to the circle. The problem can be regarded as a model of the topography variations across the ridge crest. It is suggested hydrodynamic model of mantle flow with deformable upper boundary at the mid-ocean ridge crest. It is well known the mantle media can be regarded as a high viscosity liquid (1019-1021puas) at geological intervals of time (1-100 MY). Some observations show that the mantle matter flows from the ridge crest toward borders along the upper boundary. The model is developed under the assumption a hydrodynamic flow causes deformation of the upper boundary depending on time.

**JSP39/W/40-B2** **1620**

### DIFFERENTIAL ROTATION OF LITHOSPHERE AND MANTLE AND ITS BEARING ON PLATE DRIVING FORCES AND THE CAUSES OF INTRAPLATE VOLCANISM

A. MOCHIM (Dept. Earth Sciences, Cheng Kung University, Tainan, Taiwan; email: mochim@mail.ncku.edu.tw); C. Lewis (Dept. Mining & Petroleum Engineering, Cheng Kung University, Tainan, Taiwan)

Uncertainties regarding the relative importance of basal drag and boundary forces in plate tectonic models are a consequence of flawed assumptions imposed by the use of the hotspot reference frame. Velocities of lithospheric plates are influenced not only by lateral boundary forces, but also by basal drag forces resulting from Earth rotation. Drag is exerted on the base of the asthenosphere and motion transmitted upwards to the lithosphere. As the transmission of stress in the mantle is viscosity-dependent, the reduction in viscosity through the asthenosphere results in plates suffering a net westward lag. This differential rotation effect causes continental plates to be more strongly coupled to the deep mantle as they are separated from the mesosphere by only relatively thin regions of asthenosphere. For such plates the calculated drag forces are of the same order of magnitude as boundary forces. The motion of oceanic plates is dominated by conventional plate boundary forces which may either

reinforce or oppose drag from eastward mantle flow. Reinforcement (e.g. Nazca plate) gives rise to Couette flow in the asthenosphere. Opposition (e.g Pacific plate) results in counter-flow. Shear stresses in both regimes are concentrated in the upper asthenosphere and lead to generation of intraplate melts from concentrations of hydrous minerals (wetspots) introduced into the oceanic asthenosphere by lateral asthenospheric flow. Under a counter-flow regime, melt collects in a stationary layer at the crossover point between plate- and mesosphere-induced flow regimes. Release of melt to the surface is governed by lithospheric stress trajectories set up by convergence along plate boundaries, giving an illusion of a series of quasi-fixed melting anomalies, though in reality both these and the lithospheric plates are moving relative to the deep mantle.

**JSP39/E/03-B2****1640****THE NUMERICAL MODELING OF NON-LINEAR TIDE WAVE PROPAGATION IN STRATIFIED OCEAN**

Tatjana TALIPOVA (Laboratory of Hydrophysical and Non-linear Acoustics, Institute of Applied Physics, 46 Uljanov str., Nizhny Novgorod, 603 600 Russia, email: tata@appl.sci-nnov.ru)

The numerical model of the non-linear internal tide evolution in the coastal zone is developed. It is based on the finite-difference scheme of the solution of the generalized Korteweg – de Vries equation. The model includes quadratic and cubic non-linearity, dispersion, the Earth rotation, quadratic bottom friction and horizontal variability of the density stratification. Numerical algorithm is described. Observed data of the density stratification for different shelves in Atlantic and Indian Oceans (North-west Shelf of Australia, Iberian shelf, Malin Edge Shelf, Mediterranean, Baltic and Black Seas) are used to calculate the coefficients of the generalized Korteweg – de Vries equation. Model simulations of the internal sine tide evolution have been done, they show the contribution of the different effects on the non-linear wave evolution for different areas of the World Ocean.

**JSP39/W/36-B2****1700****THE DYNAMICS OF TURBULENCE ACCOMPANYING KELVIN-HELMHOLTZ INSTABILITY**

David C. FRITTS, Joseph A. Werne, Teresa L. Palmer (Colorado Research Associates, 3380 Mitchell Lane Boulder, CO 80301, USA)

Numerical simulations of Kelvin-Helmholtz (KH) instabilities now span sufficient spatial scales to allow a broad inertial range of turbulence accompanying billow breakdown. Turbulence arises in response to secondary and tertiary convective and dynamical instabilities within the KH billows which drive the transition from 2D to 3D flow. These instabilities lead to vortical structures which undergo vigorous subsequent interactions. Vortex interactions lead, in turn, to perturbations of the vortices which contribute to their fragmentation and thus to the cascade to smaller scales of motion. This talk will describe the instability and turbulence dynamics accounting for the transition to and the cascade within the turbulent flow.

**JSP39/W/07-B2****1720****STRATIFIED FLOW AROUND A UNIFORMLY MOVING CYLINDER IN A CONTINUOUSLY STRATIFIED LIQUID**

Yuli D. CHASHECHKIN, Vladimir V. Mitkin (both at the Laboratory of Fluid Mechanics of the Institute for Problems in Mechanics of the RAS, Moscow, prospect Vernadskogo, 101-1, 117526, Russia, email: chakin@ipmnet.ru)

We study experimentally pattern of flow past a horizontal cylinder with diameters 1.5, 2.5, 5 and 7.6 cm. moving with constant velocity from 0.01 to 6 cm/s in a uniformly stratified liquid with buoyancy period from 5.0 to 25.2 s. Visualisation of flow pattern is performed by different schlieren methods (knife, filament natural rainbow), by dyeing and vertical markers. Internal waves are measured by a conductivity probe. On results of more than 800 experiments expanded flow regimes diagram is drawn. Any particular regime of flow is occupied compact domain in the space Froude number-Reynolds number and separated from neighbours ones by sharp boundaries. It is shown that there is no overlapping of regimes in the complete flow regimes cube where axis are Reynolds number-internal Froude number-ratio of external scales. The special class of small scale structures for which thickness of general structure identified elements is determined by effects of viscosity and diffusivity is introduced. Detailed measurements of velocity profiles in a forming and stationary upstream disturbance are carried out. The horizontal size of an area of completely blocked fluid is measured and compared with calculations on different models of upstream wake, the best agreement with the simplest model of singular dipole. Geometry of soaring and imbedded in to the downstream wake vortices and vortex arrays is defined.

**JSP39/L/05-B2****1740****FREE AND LEE WAVES INTERACTION IN NEAR-SURFACE PYCNOCLINE**

Olga SHISHKINA (Institute of Applied Physics, RAS, 16 Uljanovsk st., Nizhni Novgorod, 603600 Russia, email: ols@hydro.appl.sci-nnov.ru)

Experimental results on the lee internal waves' propagation in a fluid with a thermocline-type stratification in the presence of favourable and opposite regular plane internal waves are presented. After stationary background internal wave recording a cylinder of the diameter 0.4m was towed along the tank in both directions with respect to the background waves propagation and resulting internal wave profiles were fixed.

The body's draft T and velocity U were chosen to provide the first and the second internal wave modes generation ( $0.5\pi T/H \leq 1.5$ ,  $0.25\pi U/C_1 \leq 1.5$ , where H is the tank's depth and  $C_1$  is the first mode phase velocity). Background internal waves had first-mode structure at the frequency of  $2/3 N_{max}$  ( $N_{max}$  is the maximum buoyancy frequency). Almost plane lee waves with propagation angles  $60 \text{ deg} \leq \theta \leq 90 \text{ deg}$  provide intensive interaction of two wave systems. The amplitude of internal waves increased almost twice under the influence of favourable background internal waves. This work was supported by the RFBR (grant no.: 99-05-64394)

**JSP39/E/16-B3**

Invited

**0830****CORIOLIS EFFECTS ON OROGRAPHIC AND MESOSCALE FLOWS**

J. C. R. HUNT (Cerfacs and IMFT, Toulouse and Arizona State University); H. Olafsson (Icelandic Met. Services, Reykjavik, Island); P. Bougeault (CNRM, Meteo-France, Toulouse)

Using a theoretical approach based on perturbations to stably stratified flow and on the recently developed understanding of flow over mountains at low Froude number ( $F=U_0/(NH)$ , where N is the buoyancy frequency,  $U_0$  is the wind speed and H is the mountain height), the effects of rotation have been studied. The Rossby number  $Ro=U_0/(fD)$  where f is the Coriolis parameter, and D the diameter of the mountain, is assumed to be a large number. Typically it is found to lie in the range 3-10. The results are compared with the recent numerical simulations. It is found that as the flow impacts on the mountain it turns to the left (with your back to the wind) and wave activity over the top of the mountain is greatest on the left side but the pressure drop is greatest on the right. Over a distance of the order of  $HN/f$ , e.g. 150 km for the Pyrenees, a new wake structure develops that can extend to 1000 km (or a spin down distance). There is a momentum defect within the wake but the wind speed increases either side of the wake. Coriolis forces induce a deflection upward of the isopycnals on the left and downward on the right. This seems to explain some differences in meso-scale weather and climate phenomena between the different sides of mountains and wide valleys and of wakes of mesoscale convection. The large perturbation pressure change predicted by the theory is of the order of  $\rho U^2/F$ , which is consistent with the magnitude of the terms introduced into the recent ECMWF orographic parameterizations. However a fluid-dynamically justified parameterization would allow for asymmetric Rossby number effects on the pressure field and the effective wave flux.

**JSP39/W/21-B3**

Invited

**0900****MEASUREMENT AND MODELING OF THE TRANSPORT OF SNOW, SAND, ICE AND DUST PARTICLES OVER COMPLEX TERRAIN**

Kouichi NISHIMURA (Inst. of Low Temp. Sci., Hokkaido Univ., Sapporo, JAPAN, email: nishi@orange.lowtem.hokudai.ac.jp)

Aeolian particle transports occur in many geophysical contexts, including desert sand, soil erosion and snow drifting, and affect a variety of aspects of human life. For instance, the drift of snow around the structures and transportation systems can cause delays and produces access problems; the mass transport by the blowing snow in the Antarctica can be an important factor in the global climate system. It should be noted the evidence of the aeolian activity has been also found on Mars, Venus and a moon of Saturn. After Bagnold's pioneering work (1941), some progress has been made in the modeling of aeolian particle transport in the last decade, but there are still significant quantitative uncertainties. In this paper, our wind tunnel experiments with spherical particles of different diameters, densities and coefficient of restitution will be also introduced. From the measurements of the ejection velocities of the particles and the mean wind speed profile, the horizontal flux profiles were computed, and compared with our measurements. For the higher wind speeds, we examine the changes in the velocity statistics of the particle as they move randomly under the influence of turbulence in a state of suspension, and examine whether they continue to be ejected from the surface as a result of collision between impacting particles and those in the bed, or whether their movements are more determined by random aerodynamic forces acting on them.

**JSP39/W/46-B3****0930****PHASE RELATIONS BETWEEN MOVING HEATING AND THE RESULTANT TEMPERATURE PERTURBATIONS**

Brian MAPES (NOAA-CIRES Climate Diagnostics Center, Boulder, CO USA 80303-3328, email: bem@cdc.noaa.gov); Matthew Wheeler (National Center for Atmospheric Research, Boulder CO USA, email: mwheeler@cgd.ucar.edu)

In order to interpret observational studies of the thermal structure of waves of tropical convection, we need to understand the thermal structures generated by moving heat sources without any feedback. To this end, we have constructed translating heating processes that resemble observed convective variability, and imposed them in analytical and numerical linear and non-linear atmospheric models. For slowly moving deep heating, a quadrature relation between heating and temperature is established. For more rapidly moving heating, things get more complicated and interesting.

**JSP39/W/27-B3****0950****SUPERCRITICAL CONDITIONS IN THE SUMMER MARINE BOUNDARY LAYER ON THE WEST COAST OF THE UNITED STATES**

Clive DORMAN (Center for Coastal Studies, Scripps Institution of Oceanography, University of California San Diego, La Jolla, CA 92092-0209, USA, email: cdorman@ucsd.edu); David Rogers (Physical Oceanography Research Division, Scripps Institution of Oceanography, University of California San Diego, La Jolla, CA 92092-0209, USA, email: drogers@ucsd.edu); Teddy Holt (Naval Research Laboratory, Marine Meteorology Division, Monterey, CA 93943-5502, USA, email: holt@nrlmry.navy.mil)

Field measurements show that the summer conditions along the US West coast include a strong, subsidence inversion capping a weakly stratified marine boundary layer (MBL). The MBL is lower than the topography lining the coast which forms an eastern wall. Mean surface winds increase to the south along California, reaching a maximum near Pt Conception in Southern California. Mean MBL depths are a broad minimum along California with greater depths north of California and south of Pt Conception, California. Direct aircraft measurements show that the MBL is super-critical along portions of southern Oregon and California that is narrow along Oregon (50 km) and broad off Central California (more than 120 km). In the lee of Capes, the MBL speed accelerates, the depth decreases and the Froude number increases in the nature of an expansion fan with rotation and friction. The tendency for supercritical flow conditions to broaden to the south along California is proposed to be a larger scale expansion fan that is caused by the coast bending to the east as the latitude decreases.

**JSP39/E/08-B3 1010**

**GRAVITY WAVES AND VORTICES IN THE WAKE OF ISOLATED MOUNTAINS**

Dieter ETLING (Institute of Meteorology and Climatology, University Hannover, Herrenhauser Str. 2, 30419 Hannover, Germany, email: etling@muk.uni-hannover.de)

The influence of stable stratification on the wake of obstacles in the laboratory as well as in the atmosphere has been investigated intensively in recent years. Most important, the production of potential vorticity due to non-viscous effects, like gravity wave breaking or flow splitting, has been proposed by several authors. We present some examples where both, gravity waves and Karman vortex streets, can be observed simultaneously in the wake of island mountains. By analysing the meteorological upstream conditions, we will give some insight into the ongoing discussion on PV production in the wake of obstacles in stably stratified flows.

**JSP39/W/14-B3 1050**

**COHERENT VORTICES ALONG THE TROPOPAUSE**

John NIELSEN-GAMMON, John Fulton (Texas A&M University, College Station, TX 77843-3150 USA, email: n-g@tamu.edu)

A climatology of coherent vortices along the tropopause is constructed using the NCEP/NCAR reanalysis data for 1978-1997. Coherent vortices are identified by the presence on multiple isentropic layers of closed contours of the dynamic tropopause (1.5 PVU) which maintain their structure and intensity through several 6-hourly analysis cycles. We find that such vortices are more common in the Southern Hemisphere than the Northern Hemisphere, and occur most often during the winter (SH) and spring (NH). Cyclonic vortices are more frequent than anticyclonic vortices.

Ongoing work will focus on the spatial distribution of coherent vortices with respect to the Earth and to the instantaneous position of the jet stream. We shall also investigate the mechanisms for formation, maintenance, and destruction. Preliminary results indicate that most cyclonic vortices do not dissipate in situ, but instead are ripped apart by an increase in the background horizontal deformation.

**JSP39/W/15-B3 1110**

**DYNAMICS OF ROTATION, CYCLONES AND SCALING GYROSCOPES CASCADE**

I. TCHIGURINSKAYA (E.E.&S. Dept., Clemson University, 342 Computer Court, Anderson, SC29625, USA, E-mail: iouliat@clemson.edu); D. Schertzer (L.M.M., Université Pierre et Marie Curie, 4 Place Jussieu F-75252 Paris Cedex 05, France); S. Lovejoy (Physics Dept., McGill University, 3600 University st., Montréal, Qué., H3A 2T8, Canada)

New experimental data on the structure of the atmospheric boundary layers have indicated that very often despite strong mixing, there are coherent structures. A visual confirmation of the occurrence of such structures in atmospheric boundary layer is given by the ordered "cloud streets" structures observed in photographs of the earth's cloud cover. The stratification of such boundary layers is rather extreme, since the horizontal extension of these structures reach easily hundreds of kilometers, whereas their heights do not exceed 3 kilometers. The expeditions Typhoon 89-91 over South China Sea lead to investigate the stratification, including situations on the periphery and in the eye of tropical cyclones. To understand this phenomena on the theoretical level, we developed the dynamical space-time cascade model for the velocity field, named the Scaling Gyroscopes Cascade. This model was obtained by partial truncations of direct interactions of the Navier-Stokes equations. And it based on the analogy between the Lie structure of the equations of perfect fluid motion inside of rotating ellipsoid and the equations of a rigid body rotation with fixed point (the gyroscope). The effects of viscosity are obtained due to cascade structure of the model. We present high resolution (e.g. scale ratio  $2^{**20}$ ) and long time simulations of this model, leading to universal multifractal behavior which exponents are very close to the empirical estimates for the stratified tropical atmosphere data of Typhoon 89-91 expeditions. It also displays a first order multifractal phase transition with associated self-organized criticality of stratified structures.

**JSP39/W/32-B3 1130**

**THE COUNTER-PROPAGATING ROSSBY WAVE PERSPECTIVE ON INSTABILITY: APPLICATION TO REALISTIC JETS**

John METHVEN (University of Reading, UK); Eyal Heifetz (Tel-Aviv University, Israel) Brian Hoskins (University of Reading, UK); Craig Bishop (Penn-State University, USA)

Bretherton's (1966) view of baroclinic instability as the interaction of two counter-propagating Rossby waves is extended to general zonal flows for which potential vorticity (PV) is conserved. The CRWs are constructed from a growing normal mode and its decaying conjugate so that the material displacements associated with each of the waves (a) have no zonal tilt (b) are orthogonal with respect to each other when density weighted, and (c) are localised in regions of large, opposing PV gradients by the requirement that the CRW displacements are also orthogonal with respect to wave activity. Although each CRW could not continue to exist alone, they can together describe the time development of any zonal flow whose initial conditions can be described by the pair of normal modes.

The structure and interaction of these CRWs is shown for growth on a realistic jet with a tropopause, for a range of zonal wavenumbers,  $m$ . It is found that one CRW is always located on the ground where strong temperature gradients act as large negative PV gradients. The location of the upper CRW's maximum wave activity density varies with  $m$ ; for  $m > 7$  it lies just above the steering level. Both CRW structures are very similar to those from the Charney model. This structure is also seen in inverse Ertel PV,  $(1/P)$ , whilst Ertel PV perturbations,  $P'$ , are large only near the tropopause, even though the tropopause plays virtually no role in the instability. As  $m$  decreases, the depth-scale of the CRWs increases and there is a secondary maximum in upper CRW amplitude at the tropopause. For  $m < 5$  this tropopause perturbation begins to dominate the associated flow and the picture of instability resembles the Eady model. Some examples of finite time baroclinic growth, described by CRWs, are given including development from initial conditions where upper and lower level perturbations are dominant.

**JSP39/W/10-B3 1150**

**EFFECTS OF NEWTONIAN COOLING IN THE SEMIGEOSTROPHIC FRONTGENESIS PROBLEM**

Georgy I. BURDE (Ben-Gurion University, J. Blaustein Institute for Desert Research, Sede Boker Campus 84990, Israel, email: georg@bgumail.bgu.ac.il)

Frontogenesis - the formation of fronts - is a fundamental fluid dynamical problem: it is remarkable that air flow should generate such sharp zones, with horizontal scales in the

atmosphere of only a few tens of kilometers, rather than maintaining a weaker, broader thermal contrast between equator and pole. Because rain and snowfall are concentrated at fronts, the problem is of considerable meteorological importance. The geostrophic momentum model of frontogenesis introduced by Hoskins and Bretherton in 1972 appears to capture basic physical aspects of frontogenesis. Since then semigeostrophic models have remained a mainstay of frontogenesis theory and numerous research papers have emphasized various aspects of the theoretical model. In the present paper, the semigeostrophic, two-dimensional, uniform potential vorticity, Eady-wave model developed by Hoskins and Bretherton has been generalized by embedding the Newtonian (radiative) cooling. The observation, that with this modification the potential vorticity varies in a known manner following fluid particles, has provided the retention of the advantage of analytical representation of the solution inherent in the traditional Eady-wave model. A principal result of this study is that the effects of radiation may critically change the dynamics of semigeostrophic frontogenesis promoted by Eady wave instability even though the radiative damping timescale exceeds significantly the flow time scale. In particular, the formation of a frontal discontinuity from short wave initial disturbances, with the wavenumbers beyond the short wave cutoff of the adiabatic theory, becomes possible.

**JSP39/W/41-B3 1210**

**INSTABILITY OF ZONAL FLOWS IN ROTATING SPHERICAL SHELLS, AN APPLICATION TO JUPITER**

Johannes WICHT (Institut fuer Geophysik, Universitaet Goettingen, Herzberger Landrassse 180, 37075 Goettingen, Germany, email: wicht@willi.uni-geophysik.gwdg.de); Keke Zhang, Chris Jones (both at Mathematics Department, Exeter University, Exeter EX4 4QE, UK, emails: CAJones@maths.exeter.ac.uk and KZhang@maths.exeter.ac.uk)

Measurements from the Galileo probe promote the idea that the zonal winds are deep rooted. Considering Jupiter's high rotation rate and the possible vigor of the convection, it seems indeed likely that the whole outer molecular H/He layer is involved in the flows. Three-dimensional simulations of convection in rotating spherical shells have shown, that these systems are capable of producing strong zonal flows that show as a banded structure on the surface.

Assuming that the primary flows are geostrophic, and that the banded surface structure stretches right through the molecular He/H layer, we examine under which conditions such flows would be stable. As a first step we consider the linear stability of different prescribed banded zonal flows in a rotating spherical shell. Incompressibility is assumed for simplicity, the boundary condition is stress free. We compare solutions for two aspect ratios, for the Earth's outer core and Jupiter's molecular He/H layer, and two Taylor numbers ( $T=10^{**4}$  and  $T=10^{**8}$ ). Convective and shear flow instabilities compete in our system. While the convective instability is of the well-known columnar structure, we find two different shear flow instabilities. At the smaller Taylor number it is similar to the Taylor-Couette instability in rotating annuli, but the flow remains close to geostrophy for the higher Taylor number. Both shear flow instabilities break the azimuthal symmetry.

Since thermal and shear flow instabilities can have different preferred azimuthal wave numbers, we expect an interesting interaction of the two scales in the non-linear regime, which has not been reached so far. We will try to extrapolate our results to Jupiter, in spite of the numerical difficulties in reaching appropriate parameters.

**Wednesday 28 July PM**

Presiding Chair: P.A. Davies., Univ. of Dundee, Dept. of Civil Engineering, Dundee, (UK)

**JSP39/W/13-B3 Poster 1400-01**

**OUTER CORE FLOW DRIVEN BY LATERAL HEAT-FLUX VARIATION AT THE CMB**

Steven John GIBBONS (School of Mathematical Sciences, University of Exeter, Exeter EX4 4QJ, UK, email: sgibbons@maths.ex.ac.uk)

Moving core fluid maintains an isothermal core-mante-boundary (CMB) and so lateral variations in the CMB heat flow result from mantle convection. Such variations will drive thermal wind type flows, even in a layer of stable density stratification at the top of the core. Such flows may contribute to the magnetic secular variation. Large scale equatorially symmetric (ES) heat flux variations at the outer surface of a rapidly rotating spherical shell drive deeply penetrating flows which are strongly suppressed in stratified fluid. Smaller scale ES heat flux variation drives flow less dominated by rotation and so less inhibited by stratification. Equatorially anti-symmetric flux variations drive flows an order of magnitude less energetic than those driven by ES patterns but, due to the nature of the Coriolis force, are less suppressed by stratification. The response of the rotating core fluid to a general CMB heat flow pattern will then depend strongly on the subadiabatic temperature profile.

**JSP39/E/04-B3 Poster 1403-02**

**DYNAMICS OF STRATIFIED, FLUTE STRUCTURED CHARGED PARTICLE JETS AND WAKES IN THE IONOSPHERE UNDER THE GEOMAGNETIC FIELD EFFECT**

Maxim G. PONOMARJOV (Physics Dept., State Academy of Aviation Technology, Promyshlennaya str.1 (Box 22), 152300 Tutaev, Yaroslavl region, Russian Federation, email: png@univ.uniyar.ac.ru)

General methods are proposed for simulations of time-dependent charged particle jets and wakes in the geomagnetic field based on the kinetic approach. The Boltzmann equation solved taking into account the ambient electric and magnetic fields. Using this solution the analytical results are obtained, which describe developing geomagnetic field aligned stratification of charged particle jets in the ionosphere. For geomagnetic field aligned drifting velocity of jets, the formation of flute structures along the edges of the jets is obtained analytically. Using the image method (see [1], [2]) the wakes of different objects in the satellite altitude regime (above 200 km) are simulated. Different kinds of interactions of the ambient particles with object surfaces are considered as absorption, direct and diffuse reflection. The analytical results describe the flute structure of wakes of objects in motion along the geomagnetic field and stratification of wakes in different cases.

References: [1] Ponomarjov M.G., Imaginary emission method for modelling disturbances of all magneto-plasma species: Reflecting and absorbing objects in motion through rarefied plasma at different angles to the ambient magnetic field, Physical Review E, 54, 5591-5598,1996; [2] Ponomarjov M.G., Disturbances of the ambient magneto-plasma due to interactions with the object surfaces. Imaginary emission method. Far-wake of objects moving through a rarefied plasma at different angles to the ambient magnetic field, Planetary and Space Science, 43,1419-1427, 1995.

**JSP39/W/45-B3 Poster 1406-03**

**AN ENSEMBLE OF RANDOM-PHASE INTERNAL GRAVITY WAVES IS CONSIDERED IN THE DYNAMICAL FRAMEWORK OF THE EULER - BOUSSINESQ EQUATIONS**

Vladimir ZEITLIN (Laboratory of Dynamical Meteorology, France, email: zeitlin@lmd.ens.fr)

An ensemble of random-phase internal gravity waves is considered in the dynamical



framework of the Euler - Boussinesq equations. For flows with zero mean potential vorticity a kinetic equation for the mean spectral energy density of the waves is obtained under hypothesis of Gaussian statistics with zero correlation length. Exact stationary scaling solutions of this equation are found for almost vertically propagating waves. The resulting spectra are anisotropic in vertical and horizontal wave numbers. For flows with small but non-zero mean potential vorticity, under the same statistical hypothesis applied to the wave part of the flow, it is shown that the vortex part and the wave part decouple. The vortex part obeys a limiting dynamics equation exhibiting vertical collapse and layering which contaminates the wave-part spectra. Relation of these results to the in situ measurements is discussed.

**JSP39/E/23-B3** Poster **1409-04**

**A FLUID PULSE DISTORTION ON THE SURFACE OF THE OCEAN AS A SOURCE OF WATER MOTION NEAR THE BOTTOM**

Tatiana DEMIDOVA, Nikolai Korchagin (both at Department of Physics, P.P. Shirshov Institute of Oceanology, Moscow 117218, Russia, email: evita@redline.ru)

A model of propagation of a pulse of a surface horizontal water distortion (caused by a non-stationary wind field) from the surface to the bottom in a stratified medium is considered in the frameworks of linear theory of internal waves in a long-wave approximation. In the model, a three-layer fluid is presented as a two-step structure of the density profile with alteration of density discontinuities and homogeneous fluid layers. Rather simple equations for velocities for the first three modes (the barotropic and two baroclinic modes) are derived. The results of calculation show that the presence of sharp discontinuities in density leads to interrelation between the surface and bottom current fields. In this case, the transfer of the surface pulse into deep water is performed by internal wave.

The model of the propagation was tested using experimental moored and cast data as well as time distribution of the surface wind stresses during storms in winter of 1992 at the shelf and slope off the Sakhara coast. Well-developed surface and bottom boundary layers were approximately of the same thickness. High frequency maxima were revealed in energy spectra of the near bottom velocities. Whereas the peak at a period of about 24 min corresponded to the typical buoyancy frequency at the site, the model of the pulse propagation from the surface to the bottom allowed us to explain the peaks at periods 60-70 min. It shows that the model discussed describes one of mechanisms of the increase of current velocities in near-bottom layers.

**JSP39/E/21-B3** Poster **1412-05**

**DYNAMICS OF HYDROTHERMAL TURBULENT JETS IN A STRATIFIED FLUID**

Nikolay KORCHAGIN (P.P. Shirshov Institute of Oceanology, Russian Academy of Sciences, 36, Nakhimovskiyi prospect, 117218, Moscow, Russia, email: niknik@sio.rssi.ru)

A new analytical method to the problem of the closure of the system of integral equations (SIE) describing the dynamics of a buoyant turbulent jet (BTJ) in a stratified fluid is suggested. As a result an analytical expression of the Taylor's "entrainment constant" was obtained from the parameters of the jet flow and a background water stratification. On the other hand, the suggested method of the SIE closure also describing the mechanism of the entrainment of a background fluid into a turbulent area of the same fluid. The numerical model of the SIE solution was made by Runge-Kutta method of the fourth order accuracy. The validity of the numerical model of the BTJ was carried out with using the measurement data of the characteristics of high temperature hydrothermal flows (from "black smokers") and background bottom waters in two ocean regions: the Mid-Atlantic Ridge and the East-Pacific Rising. The model construction of the BTJ was suggested, the use of which in the SIE allowed to obtain the analytical solution of SIE and expression of the maximum height for the rising hydrothermal jet and another characteristics.

**JSP39/E/06-B3** Poster **1415-06**

**OCEANIC UPWELLING AND DOWNWELLING FORCED BY A TROPICAL CYCLONE**

Shin-Ichi SUZUKI (Ocean Research Institutes, University of Tokyo, 1-15-1, Minamidai, Nakano, Tokyo, Japan; E-mail: suzuki@ori.u-tokyo.ac.jp); Hiroshi Niino (email: niino@ori.u-tokyo.ac.jp); Ryuji Kimura (email: kimura@ori.u-tokyo.ac.jp)

While it is generally believed that an oceanic upwelling under a tropical cyclone is caused by the Ekman pumping, previous numerical simulations show that the center of the upwelling is located in the backside of a moving tropical cyclone. Furthermore, our recent numerical simulation with a better vertical resolution and a recent oceanic observation show that even a downwelling exists in the forward side of the cyclone center. The cause and the mechanism of the forward side downwelling and the backside upwelling are investigated by means of a linear theory of a two-dimensional viscous rotating stratified ocean, which is subjected to a prescribed wind stress corresponding to a moving cyclone. The results show that, when the moving speed  $U$  of the cyclone is greater than 10 m/s, the forward side downwelling and backside upwelling take place. The mechanism that causes the vertical motion is further investigated by examining oceanic responses to a moving sinusoidal wind stress with a wavenumber  $k$ . It is found that, when a Rossby number defined by  $Ro = Uk/f$  is less than 1, the vertical motion is mainly caused by the conventional Ekman pumping, where  $f$  is the Coriolis parameter. When the Rossby number is greater than 1, on the other hand, the vertical motion is caused by a horizontal divergence of inertial oscillations forced by the wind stress. The latter mechanism is responsible for the forward side downwelling and backside upwelling.

**JSP39/E/07-B3** Poster **1418-07**

**NON-LINEAR DYNAMICS OF LARGE-AMPLITUDE INTERNAL SOLITARY WAVES**

Tatjana TALIPOVA, Efim Pelinovsky (Laboratory of Hydrophysics and Nonlinear Acoustics, Institute of Applied Physics, 46 Uljanov Str., Nizhny Novgorod, 603600, Russia, email: tata@appl.sci-nnov.ru); Alexey Slunyaev (Advanced School of General and Applied Physics, Nizhny Novgorod State University, 46 Uljanov Str., 603600 Nizhny Novgorod, Russia; email: avs@appl.sci-nnov.ru)

The nonlinear dynamics of large-amplitude long waves in a stratified ocean is studied. Theoretical model is based on the generalised Korteweg - de Vries equation incorporated the effects of the quadratic and cubic nonlinearity. Coefficients of the quadratic and cubic nonlinearity in this equation depend on the density and shear flow stratification and may have either sign. In particular, the coefficient of the cubic nonlinearity is negative for internal waves in the stratified ocean with one-peak distribution of the Vaisal frequency. If the high-order dispersion can be ignored (the corresponding conditions are discussed) the generalised Korteweg - de Vries equation is reduced to the Gardner equation which is integrable nonlinear system. It admits the existence of a large-amplitude "thick" soliton. The processes of the interaction and generation of solitons, including the "thick" solitons are studied. The evolution of the initial impulse disturbance is reported. It is shown that during the evolution process the solitons of the opposite polarity are appeared on the crest of the "thick" soliton.

**JSP39/W/02-B3** Poster **1421-08**

**HYSTERESIS OF WAVE SOLUTIONS IN THE QUASI-GEOSTROPHIC POTENTIAL VORTICITY EQUATIONS WITH A NONLINEAR BASIS STATE**

Gregory M. LEWIS, Wayne Nagata (both of Institute of Applied Mathematics, University of British Columbia, Vancouver, BC, V6T 1Z4, Canada, email: lewis@math.ubc.ca and nagata@math.ubc.ca)

We analyze double-Hopf bifurcations observed in the two layer quasi-geostrophic potential vorticity equations with a non-linear basic state. This bifurcation occurs in the transition from the axisymmetric to the wave regimes when the linear part (of the equations) has two complex conjugate pairs of eigen-values with zero real part. Using center manifold reduction and normal form theory, the behaviour of the full system of partial differential equations near the bifurcation point may be deduced from the two dimensional ordinary differential amplitude equations. Since the non-linear basic state leads to a non-self-adjoint linear part, it is not possible to compute the eigenvalues and eigenfunctions analytically. Therefore, the linear part is discretized and the eigen-values and eigen-functions are approximated from the resulting matrix eigen-value problem. The projection onto the center manifold and reduction to normal form can be done analytically, thus, numerical approximations of the normal form coefficients are obtained upon approximation of the appropriate inner products. The results show that, for the geophysically relevant range of parameters, two periodic solutions (travelling waves with different wave numbers) are simultaneously stable for certain parameter values. This result, which is observed for several wave number pairs, indicates hysteresis of the wave solutions. The quasi-periodicity, which is possible in these types of bifurcations, is not observed. It is straightforward to apply this analytical/numerical method to more complicated models. In particular, preliminary results will be shown of the analysis applied to a model of the differentially heated rotating annulus experiment.

**JSP39/W/33-B3** Poster **1424-09**

**LABORATORY EXPERIMENTS ON ROTATING COMPOSITIONAL CONVECTION AT LOW EKMAN NUMBERS**

Sabine CLASSEN (Institut fuer Geophysik, Herzbergerlandstr. 180, 37075 Goettingen, Germany, email: sac@willi.uni-geophys.gwdg.de); Moritz Heimpel (Department of Earth and Space Sciences, UCLA, 595 Circle Drive East, Los Angeles, CA, USA 90095-1567, email: heimpel@zephyr.ess.ucla.edu)

The onset and structure of compositional convection in a rotating system are investigated experimentally. A vertically oriented cylindrical annulus filled with  $NH_4-H_2O$  solution is cooled from the bottom and can be rotated about its axis at rates ranging up to  $10.5 \text{ rad s}^{-1}$ , corresponding to Ekman numbers down to  $7.5 \times 10^{-6}$ . The Coriolis force has a strong effect on the structure of plumes above the mush-liquid interface. Helical motion of the conduit, which is weakly developed in the non-rotating case, is amplified by Coriolis forces that twist the plume conduits to lie nearly horizontally. This results in secondary plumes (or blobs) that rise from the sub-horizontal primary plume conduits. The rotation has a negligible influence on the solidification process. The main crystallization and convection features we find in the non-rotating system are retained in the presence of rotation. However, rotation seems slightly to speed up the transport of latent heat which controls the growth rate cause the growth rate coefficient increases with the rotation rate.

**JSP39/W/23-B3** Poster **1427-10**

**TURBULENT CONVECTION FROM ISOLATED SOURCES**

Jordi COLOMER (Department of Physics, University of Girona, 17071 Girona, Spain); Boris M. Boubnov, A.M. Obukhov (Institute of Atmospheric Physics, Russian Academy of Sciences, 109017 Moscow, Russia); Harindra J.S. Fernando (Department of Mechanical and Aerospace Engineering, Environmental Fluid Dynamics Program, Arizona State University, Tempe, AZ 85287-9809, USA)

Laboratory experiments were conducted to investigate the evolution of a dense turbulent plume, specified by its buoyancy flux and source diameter  $D$ , issuing into a homogeneous environment. The study was motivated by its applications to geophysical, environmental and engineering flow situations. Special attention was given to study the evolution of plume following its initiation and the flow near the source. At short times, the descent of the plume front can be treated as one-dimensional with negligible lateral (entrainment) mean flow, the plume growth mechanism being the encroachment of underlying non-turbulent fluid. At larger times, the flow achieved a quasi-steady state, in which the plume width first decreases (region I) and then increases (region II). The quasi-steady state velocity and buoyancy measurements in region I showed that they are strongly influenced by the lateral entrainment (and hence  $D$ ), and thus classical free convection scaling is inapplicable to such flows. On the other hand, at large  $z/D$  (in region II), the velocity and buoyancy scalings tend to be independent of  $D$  and follow point source scaling.

**JSP39/W/12-B3** Poster **1430-11**

**LARGE EDDIES BEHIND MANOEUVRING SELF-PROPELLED BODIES IN A STRATIFIED FLUIDS**

Sergey VOROPAYEV (Arizona State University, Tempe, AZ 85287-6106, USA and Institute of Oceanology, Russian Academy of Sciences, Moscow, 117851, Russia, email s.voropayev@asu.edu); Ben McEachern (Arizona State University, Tempe, AZ 85287-6106, USA)

A large number of studies have been reported on wakes in stably stratified fluids either with towed or self-propelled bodies of different shapes. Although these studies have documented many interesting phenomena related with the wake signature, no studies have considered large eddies that may form in the late wakes during the manoeuvring of such bodies. When a self-propelled body makes a manoeuvre (e.g., accelerates or changes its direction of motion), significant horizontal momentum is transported to the surrounding fluid. Our experiments show that in a stratified fluid this may lead to the formation of unusually large eddies, which are much larger and have substantially different characteristics than those produced in the late wake during steady motion. A theory is proposed to explain this effect, and estimates show that when an oceanic submerged vehicle changes its velocity by as little as 10% or its direction of motion by roughly 5 degrees, large structures of characteristic size 1-2 km and with decay times of several days may be expected. Such effect may have potentially important applications and have not been studied previously. This study was supported by NOAA and ONR. For more detail see [1].

1. Voropayev, S.I., McEachern, G.B., Fernando, H.J.S. and Boyer, D.L. 1999. Large vortex structures behind a manoeuvring body in stratified fluids. *Phys. Fluids* (in press).

**JSP39/W/35-B3** Poster **1433-12**

**SELF PROPAGATING QUASI-MONOPOLES IN ROTATING FLUID**

Sergey VOROPAYEV (Arizona State University, Tempe, AZ 85287-6106, USA and Institute of Oceanology, Russian Academy of Sciences, Moscow, 117851, Russia, email: s.voropayev@asu.edu); Ben McEachern (Arizona State University, Tempe, AZ 85287-6106, USA)

Recent results, based on the high-resolution satellite data, demonstrate that a significant dipolar component is present, for example, in most of the Gulf Stream rings. Taking into account the importance of rings and other quasi-monopolar eddies in large scale mixing in the ocean, the need for the developing of models for compact self-propagating vortices becomes obvious. In a recent paper (Stern & Radko, 1998, JPO) an attempt was made in this direction and some basic properties of single self-propagating quasi-monopolar vortex were predicted theoretically and numerically. At present detailed field data are still absent, and the only way to verify the model predictions is to conduct laboratory experiments. The main aim of this communication is (1) to present and discuss the results of laboratory experiments on the formation and dynamics of self-propagating quasi-monopolar vortices, with relatively large angular momentum and small linear momentum, which were generated in a homogeneous rotating fluid of constant depth (f-plane), (2) to make some comparison with the theoretical predictions. The results of our experiment show that such a vortex (1) exists and can be easily generated, (2) is stable and can propagate a significant distance from the origin, (3) survives after a non-elastic collision with a vertical wall and (4) its structure and behavior are very similar to that predicted by Stern and Radko.

**JSP39/W/30-B3** Poster **1436-13**

**BASIC SETS OF STRATIFIED FLOW EQUATIONS INVARIANTS**

Vasily G. BAYDULOV, Yuli D. Chashechkin (both at the Laboratory of Fluid Mechanics of the Institute for Problems in Mechanics of the RAS, Moscow, prospect Vernadskogo, 101-1, 117526, Russia, E-mail: bayd@ipmnet.ru)

We investigated invariant properties of the basic sets of hydro-thermodynamic equations by Lie groups methods. For one component media group classification on stratification type has been performed. Set of equations of double diffusive convection also was classified with respect to type of state equation and thermodynamic properties of all dissipative coefficients. Obtained classifications make possible to compare invariant properties and mutual reducibility of basic 1D, 2D and 3D models of stratified flows. Several types of stratification that are characterised by the widest group of symmetry are distinguished. Invariant properties of governing equations with and without diffusion effects are the same only in case of linear stratification. A wide set of non-trivial groups of self-similarity is constructed when dissipative coefficients (viscosity, diffusivity, thermal conductivity) depend on thermodynamic parameters of the medium. On basis of this groups new exact and self-similar solutions equations of double diffusive convection are constructed. Using the obtained groups to reduce the number of independent variables allows to simplify the search of numerical solutions governing equations. Examples and comparison with laboratory experiments are given.

**JSP39/E/25-B3** Poster **1439-14**

**TURBULENCE MODELING IN COMPRESSIBLE SHEAR LAYERS**

Suresh CHANDRA (Department of Mechanical Engineering, North Carolina A&T State University, Greensboro, NC 27411, USA, Email: chandra@ncat.edu)

For high speed shear layers, variable density extensions of standard incompressible turbulence models have not proven to be adequate in explaining the experimentally observed reduction in growth rate with increase in the convective Mach number. Turbulence modeling for compressible flows has to account for additional correlations involving both thermodynamic quantities and the fluctuating dilatation. In recent years, Sarkar et al. suggested that, in addition to modeling the pressure dilatation, another dilatational correlation (the compressible dissipation) should be considered because of the enhanced dissipation known to be present in compressible turbulence. Specifically, this compressible dissipation correction is proportional to the second and fourth powers of the turbulent Mach number, which is defined in terms of the turbulent kinetic energy and the local speed of sound. Narayan and Sekar have used the compressibility-corrected model - limited to the second power of the turbulent Mach number - with the SPARK code for the computation of high speed reacting layers and have obtained satisfactory agreement with some of the available data.

The simple algebraic compressibility model by Sarkar et al. has been modified to include a fourth order turbulent Mach number term. Comparison of the predictions with results of several analytical models and experimental work has been carried out; both agreement and discrepancies are analyzed. The modified turbulence model presented here has the potential of resolving fluid flows related to Earth's atmosphere as well as internal flows encountered in airbreathing hypersonic vehicles.

**JSP39/W/01-B3** Poster **1442-15**

**FINE STRUCTURE OF A FLOW AROUND STARTING OBSTACLES IN A STRATIFIED FLUID**

Yuli D. CHASHECHKIN, Vasily G. Baydulov, Vladimir V. Mitkin (all at the Laboratory of Fluid Mechanics of the Institute for Problems in Mechanics of the RAS, Moscow, prospect Vernadskogo, 101-1, 117526, Russia, E-mail: chakin@ipmnet.ru)

We study analytically and experimentally onset of a stratified liquid motion around resting and starting plane, channel walls, cylinder and sphere. Analytical solutions are obtained by perturbation theory methods, visualised and compared with laboratory experiments data. Near a body at rest solutions describe diffusion induced transient internal boundary layer which is characterised by different scales of spatial variability of velocity and density or salinity. In limiting cases all solutions are uniformly matched among themselves and with well-known exact solutions. Near a starting body besides the internal boundary layer regular large scale convective motion is formed. Geometry of the flow around starting cylinder and sphere are described by simple trigonometrical functions. Pattern of flow is visualised by different Schlieren methods. Parameters of disturbances are measured by conductivity probes and density markers (vertical wakes past small falling crystal of salt or sugar). Profiles of horizontal component of velocity ahead of the body and perturbations of density gradient are fixed and compared with calculations. Theoretical and experimental results are in good agreement among themselves even beyond of the range of formal applicability of asymptotics.

**JSP39/W/09-B3** Poster **1445-16**

**INTERNAL WAVES AND INTERNAL BOUNDARY CURRENTS PAST A UNIFORMLY MOVING CYLINDER IN A CONTINUOUSLY STRATIFIED LIQUID**

Yuli D. CHASHECHKIN, Vladimir V. Mitkin (both at the Laboratory of Fluid Mechanics of the Institute for Problems in Mechanics of the RAS, Moscow, prospect Vernadskogo, 101-1, 117526, Russia, E-mail: chakin@ipmnet.ru)

We investigate experimentally fine structure of flow around circular horizontal cylinder uniformly moving in a continuously stratified liquid. It was found that the basic elements of motion namely upstream disturbance, internal waves and downstream wake with imbedded or soaring vortices are presented at any large or small values of internal Froude number. General variations of a density containing mean displacement and wavy oscillating components as well as density profiles on the boundary of a density wake are measured by a conductivity probe. In a regime of narrow turbulent wake effect of recurrent and reconnection of downstream adjoined (lee) waves is found. In this regime regular anti-symmetric pattern of lee waves is consequently replaced firstly by irregular waves emitted by vortices inside the turbulent wake and later by system of symmetric waves. Two kinds of thin interfaces inside and outside downstream wake are identified as a new eigen-form of a stratified fluid motion namely as internal boundary currents. These internal soaring boundary currents manifest itself as a surfaces of discontinuity in a wave part of the density gradient field without any features on their leading and trail edges. Sharp interfaces inside a wake are formed due to separation of internal boundary layer on the cylinder surface or directly inside the decaying stratified turbulence.

**JSP39/W/22-B3** Poster **1448-17**

**SIWALL DOUBLE DIFFUSION CONVECTION IN A WEAK GRADIENT**

Yuli D. CHASHECHKIN, Anatoliy V. Kistovich, Vladimir V. Levitskiy (all at the Laboratory of Fluid Mechanics of the Institute for Problems in Mechanics of the RAS, Moscow, prospect Vernadskogo, 101-1, 117526, Russia, E-mail: chakin@ipmnet.ru)

We study theoretically and experimentally onset of a periodic layer structure formation near a heated or cooled sloping wall in a continuously strong or weakly stratified liquid. Analytically it is shown that side-wall heat flux leads to the formation of internal boundary current on a heated surface and of a fast propagating front of injection in a fluid interior. General properties of a double diffusion convection equations are examined by Lee groups method. Dependence of flow geometry parameters above near a point, cylinder or plane heat source on input buoyancy flux and scale of stratification is studied. Parameters of zero frequency internal waves emitted by convection cells in environment fluid are calculated in a linear approximation. Experimentally convection near a sloping wall inclined under the angle 90, 75, 60, 45, 30, 15 degrees to the horizon is studied. Both in a strong (buoyancy period  $T_b < 10$  s) and in a weak ( $T_b > 20$  s) stratified liquid the height of the cell is proportional to the height of potential rise of a heated fluid particle. The fitting coefficient increases with the slope under the heater and weakly depends on it above the heater. The interval of flow formation increases near the critical Rayleigh number. The thickness of interfaces between cells does not depend on the initial density gradient value. In a wide range of flow parameters the number of interfaces is duplicated. Additional interfaces are formed on the upper boundary of inflowing wedge of a cold fluid. Theoretical and experimental results are in a good agreement.

**JSP39/W/44-B3** Poster **1451-18**

**COMPUTATIONS OF AXISYMMETRIC EIGENMODES IN A STABLE STRATIFIED ROTATING SPHERICAL SHELL**

Boris DINTRANS (Observatoire Midi-Pyrenees, France, email: dintrans@obs-mip.fr)

We present computations of axisymmetric eigen-modes in a stable stratified rotating spherical shell using Boussinesq approximation. We first develop a geometric formalism based on the iteration of the underlying characteristics which propagate in the hyperbolic region. Periodic orbits and quasi-periodic orbits have been then found. Computing the corresponding eigen-modes, we prove the link that exists between the characteristic pattern and her associated non-adiabatic structure. Some important spectral consequences have been then deduced both in the adiabatic and non-adiabatic cases.

**JSP39/E/21-B3** Poster **1454-19**

**DYNAMICS OF HYDROTHERMAL TURBULENT JETS IN A STRATIFIED FLUID**

Nikolay KORCHAGIN (P.P. Shirshov Institute of Oceanology, Russian Academy of Sciences, 36, Nakhimovskiy prospect, 117218, Moscow, Russia, email: niknik@sio.rssi.ru)

A new analytical method to the problem of the closure of the system of integral equations (SIE) describing the dynamics of a buoyant turbulent jet (BTJ) in a stratified fluid is suggested. As a result an analytical expression of the Taylor's "entrainment constant" was obtained from the parameters of the jet flow and a background water stratification. On the other hand, the suggested method of the SIE closure also describing the mechanism of the entrainment of a background fluid into a turbulent area of the same fluid. The numerical model of the SIE solution was made by Runge-Kutta method of the fourth order accuracy. The validity of the numerical model of the BTJ was carried out with using the measurement data of the characteristics of high temperature hydrothermal flows (from "black smokers") and background bottom waters in two ocean regions: the Mid-Atlantic Ridge and the East-Pacific Rising. The model construction of the BTJ was suggested, the use of which in the SIE allowed to obtain the analytical solution of SIE and expression of the maximum height for the rising hydrothermal jet and another characteristics.

**JSP39/W/24-B3** Poster **1457-20**

**ABOUT ONE MODELS OF CHAOTIC ADVECTION IN BAROTROPIC BACKGROUND CURRENT**

Vadim Kozlov, Konstantin KOSHEL (both at Pacific Oceanological Institute, FEB RAS, 43 Bultiyskay str., Vladivostok, 690068, Russia, Email: wave@online.vladivostok.ru)

The barotropic model of a chaotic advection in background current is considered [Kozlov V.F., Koshel K.V. A barotropic model of a chaotic advection in background currents [Izv. RAS, FAO, 1998, V.34, in press; Kozlov V.F., Background currents in geophysical hydrodynamics, Izv. RAS, FAO, 1995, V.31, N2, pg. 245-250], representing a sum fixed rotational planetary-topographical and non-stationary irrotational flowing component in a half-disk with a linear contour of bottom and system a radiant - drain in angular points of the boundary. With the help of numerical experiments the process of passive markers passing out from a vortex region in flowing in an outcome of periodic oscillations of the consumption is investigated. The influence

of parameters of oscillation (frequency, amplitude, phase) on a velocity and degree of washing away of markers is investigated. The evaluation of purely chaotic properties of the open system is hampered by standard methods (Lyapunov indexes, Poincare sections) in view of finite life time of trajectories with the most irregular behavior. For a research of zones with a regular and chaotic behavior and evaluation of a degree of intermixing is offered to use distribution of washing away time for markers uniformly distributed on basin. The similar approach is compared to evaluations obtained with the help of Lyapunov indexes and Poincare sections calculated for final time. It is concluded availability of chaotic intermixing in the given system.

**JSP39/E/01-B3** Poster **1500-21**

**SIMILARITY SOLUTIONS FOR TIME-DEPENDENT HORIZONTAL CONVECTION IN A STRATIFIED FLUID SUBJECT TO A DIFFERENTIAL COOLING FROM BELOW**

Atsushi MORI (Department of Astronomy and Earth Science, Tokyo Gakugei University, Koganei-City, Tokyo, 184-8501, Japan, email: mori@buran.u-gakugei.ac.jp); Hiroshi Niino (Division of Marine Meteorology, Ocean Research Institute, University of Tokyo, Minamida, Nakano-Ku, Tokyo, 164-8639, Japan, email: niino@ori.u-tokyo.ac.jp)

Time evolution of a horizontal convection which is caused by cooling a half of the bottom boundary of a viscous stratified Boussinesq fluid is investigated both theoretically and numerically. In the most general situation, the evolution of the convection consists of three distinct stages: During the first stage, the horizontal diffusion of heat is dominant over the horizontal advection. During the second stage, the stratification is still less important. The flow is non-linear and can be regarded as a gravity current in which the vertical scale is determined by the diffusion length scale. Finally, during the third stage, the stratification becomes important and the flow is described by a linear dynamics.

A similarity solution of the time-dependent governing equations which describe the dynamics of each stage has been discovered. The solution for each stage is found to be only a function of the Prandtl number after relevant scalings of the variables are introduced. Numerical experiments with fully non-linear governing equations have confirmed the validity of the similarity solution at each stage. These solutions, for example, are useful for understanding the formation mechanism of an atmospheric heat island circulation in which convections first develop from the two edges of heated area and penetrate into the center to form a steady state convection eventually.

**JSP39/L/04-B3** Poster **1503-22**

**SIMILARITY CRITERIA FOR CONTINUOUSLY STRATIFIED FLOWS OVER OBSTACLES**

Olga SHISHKINA (Institute of Applied Physics, RAS, 16 Uljanovsk st., Nizhni Novgorod, 603600 Russia, email: ols@hydro.appl.sci-nnov.ru)

The comparative analysis of wave-drag coefficient versus 'internal' Froude number for submerged and floating bodies moving uniformly in fluids with different stratification profiles showed similarity of functions  $C_x(F_i)$ . An existence of linear dependence of Froude numbers  $F_i = U/(NR)$  for continuously stratified fluids (a linear stratification and a pycnocline) was observed. Such a phenomenon explanation was based on analysis of wave processes following the drag coefficient increase in the mentioned Froude number range. The similarity of wave induction accompanying the sphere movement in stratified flows with single wave-guide profiles as well as the physical parameters describing those processes of different wave-guide to body heights ratio was observed. A Thorough analysis of known experimental data allowed to choose the phase velocity coincidence of the first IW mode for both the linear stratification and the pycnocline to be the similarity criterion for internal wave processes. This provides an exact choice of the constant buoyancy frequency  $N$  corresponding to the pycnocline conditions.

The induced IW amplitude is proportional to the critical streamline displacement  $(z/R) = F_i$  to interpret the physical meaning of the 'internal' Froude number for continuous stratification  $F_i E^2$  ( $zER$ ) as the relative amplitude of induced IW or as some kind of the performance coefficient for transformation of the flow energy to the energy of the internal waves. This work was supported by the RFBR (grant no. 99-05-64394)

**JSP39/W/26-B3** Poster **1506-23**

**STABILITY OF POLYNOMIAL FLOWS ON A SPHERE**

Yuri SKIBA (Centro de Ciencias de la Atmósfera, Universidad Nacional Autónoma de México, Circuito Exterior, CU, México, D.F., C.P. 04510, México, email: skiba@servidor.unam.mx)

The stability of the Rossby-Haurwitz waves and Legendre-polynomial flows is considered in the framework of an inviscid incompressible fluid on a rotating sphere. A conservation law of arbitrary perturbations of such flows is obtained, and the whole space of the perturbations is divided into four invariant manifolds defined by means of Fjortoft's spectral number of the perturbations. Liapunov instability of non-zonal Rossby-Haurwitz waves of degree  $n > 1$  is shown, and its mechanism is explained. The behavior of the kinetic energy and enstrophy of the perturbations from invariant sets is also considered. In particular, a hyperbolic dependence between the energy and Fjortoft's spectral number of the perturbations is discussed.

In the case that the basic flow has the form of a Legendre polynomial of degree  $n$ , invariant sets of exponentially and algebraically stable infinitesimal perturbations are found. For the other part of infinitesimal perturbations, not belonging to such sets of stable perturbations, it is obtained a necessary condition for the exponential instability, which is more simple than the famous condition by Kuo for the zonal flows.

**JSP39/W/03-B3** Poster **1509-24**

**DOUBLE-COMPONENT CONVECTION DUE TO THE DIFFERENT BOUNDARY CONDITIONS - REVIEW OF COMBINATIONS OF VERTICAL AND HORIZONTAL GRADIENTS**

Naftali TSITVERBLIT (Tel-Aviv University, Tel Aviv, Israel)

The conceptual framework of conventional double-diffusive convection could apply directly to large-scale environmental processes through eddy double-diffusion---instabilities resulting from the unequal perturbed diffusion gradients forming due to the different boundary conditions. The original problem considered by Welander [Tellus 41A, 66 (1989)] is in this context analogous to the conventional diffusive regime, while the inverse type of stratification (Tsitverblit [Phys. Fluids 9(8) 2458 (1997)]) stands for the finger regime. This latter configuration describes the double component Langmuir circulation problem (Leibovich [Ann. Rev. Fluid Mech. 15, 391(1983)]) and, in combination with shear motion (induced, for example, by the horizontal non-uniformity in the temperature distribution), may be relevant to the ocean thermohaline circulation. Decrease of the ratio of the vertical and horizontal diffusion coefficients in this case eventually causes formation of multi-layered structures and may affect the criticality of bifurcations. Like in conventional double-diffusive convection, the instabilities also arise under a combination of the horizontal gradients. This was initially established in application to laterally heated stably stratified systems (Tsitverblit [Phys. Fluids, submitted]). Similar situation is expected when two equal (in terms of their effect on the density) and opposing horizontal gradients attained by the

different boundary conditions at the vertical walls are applied to the fluid being at rest between these boundaries. Trial computations with the equal diffusion coefficients indicated that, when the (joint) horizontal gradient (the  $\text{mbox}\{Rayleigh\}$  number) in this case becomes large enough, the onset of convection indeed takes place, and analysis of this problem with and without vertical stratification due to one of the components is to be reported. Combinations of the above effects arising when the gradients are applied between two inclined planes and their relevance to the ocean are also discussed.

Thursday 29 July AM

Presiding Chair: P.G. Baines., CSIRO, Div. of Atmospheric Research, Aspendale, (Australia)

**JSP39/W/18-B4** **0830**

**THE CURRENT STATE OF OCEANIC FORECASTING (DEEP AND COASTAL OCEANS) AND THE PROSPECTS FOR THE FUTURE**

Prof. Allan R. ROBINSON (Harvard University, Cambridge, MA, USA)

During the last decade remarkable progress has been made in the ability to predict describe, model and forecast the physical synoptic-mesoscale state of the ocean over regional to basin scale domains. This is a result of a new understanding of the underlying dynamical principals and the development of methods significantly and substantially based on data assimilation. (Sub) meso scale phenomena have two important sets of time and space scales - evolutionary and event (scales of intermittency). Multi-scale non-linear interactions are key to determining the underlying dynamics and developing the concomitant predictive capability. Interesting issues relate to validation, verification, predictive capability and limits to predictability. Presently, critically important problems are associated with interdisciplinary dynamics and coupling. The accurate estimation of the physical-acoustical-optical-biological-geochemical ocean is now essential and feasible for modern ocean science.

Such multiscale and multidisciplinary estimation and prediction requires a new level of understanding of the multi-disciplinary hierarchy of complex coupled dynamical processes, with non-linearities and feedbacks which span a multitude of scales in time and space. Fundamental interdisciplinary problems of ocean science, long recognized as of great importance, are now tractable. As the scope of interdisciplinary ocean science expands over the next decade, there will be formidable and challenging research tasks acquired to address the scientific problems through a systems approach.

**JSP39/W/25-B4** **0910**

**FLUCTUATIONS OF SST AND CHL-A CONCENTRATION CAUSED BY BAROCLINIC INERTIA-GRAVITY WAVES**

Roman GLAZMAN (Jet Propulsion Laboratory, Pasadena CA, 91109, USA, email: reg@pacific.jpl.nasa.gov); Peter B. Weichman (Blackhawk Geometrics, Golden, CO 80401, USA, email: pbw@blackhawkgeo.com)

Satellite observations of sea surface temperature and chlorophyll-a concentration permitted detailed statistical analysis of spatial variations of these tracer fields in a broad range of scales. Estimated wave number spectra, on scales from a few to hundreds kilometres - as reported by many authors, display a rather unexpected behaviour: they strongly disagree with predictions of two-dimensional eddy turbulence theory (which requires the SST spectrum to roll off as  $k^{-1}$ ) and they exhibit geographic and seasonal trends which have no simple explanation. Our attention is focused on possible effects of baroclinic inertia-gravity (BIG) wave motions on tracer fields. We present experimental and theoretical results indicating that observed variations are greatly affected by BIG waves, and classical eddy turbulence is not necessarily the main dynamical factor of tracer dispersion. Wave number spectra of BIG wave motions are presented along with observed spectra of SST and Chl-a fields. Typical rates of spectra roll-off, ranging between  $k^{-1.5}$  and  $k^{-3}$ , agree with our theoretical predictions. The fact that BIG wave motions have such a profound effect on fluctuations of ocean tracers has important oceanographic implications.

**JSP39/E/18-B4** **0930**

**PARTICLE DISPERSION IN THE ATLANTIC**

Michel OLLITRAULT (Laboratoire de Physique des Océans, Ifremer, BP 70, 29280 Plouzané, FRANCE, email: mollitra@ifremer.fr); Alain Colin de Verdière, Céline Gabillet (both at Laboratoire de Physique des Océans, Université de Bretagne Occidentale, BP 809, 29280 Brest cedex, FRANCE, email: acolindv@univ-brest.fr)

Absolute and relative dispersion of floats deployed in the Atlantic are estimated at the base of the main thermocline in the North Atlantic subtropical gyre and in the Brazil basin. The initial separations of the floats, a few kilometer to 20 kilometer are small compared to the eddy mesoscale but large compared to dissipation scales so that the results can be usefully compared with the scalings predicted from two dimensional turbulence theory. While the absolute dispersion usually computed from such data dominated by the lowest frequencies, the relative dispersion at scales less than the energy containing scale gives information on the high wave number end of the energy spectrum that is difficult to obtain otherwise. We compare the results of these oceanic field experiments with similar experiments carried out in the atmosphere, in laboratory experiments and in numerical experiments

**JSP39/W/11-B4** **0950**

**GENERATION OF STEP-LIKE STRUCTURE IN STRATIFIED ROTATED BOUNDARY LAYERS**

Iossif LOZOVATSKY (Department of Mechanical and Aerospace Engineering, Arizona State University, Tempe, AZ, 85287-9809, USA; also at P.P. Shirshov Institute of Oceanology, Russian Academy of Sciences, Moscow, 117851, Russia, email: i.lozovatsky@asu.edu); Alexander Ksenofontov (Kabardino-Balkarski State University, Nalchik, Russia, email: ask@ns.kbsu.ru)

Generation of turbulent quasi-homogeneous layers separated by narrow density interfaces in a stratified shear flow with a decreasing buoyancy flux upon increase of stratification has been argued by Phillips (1972). All previous laboratory experiments and theoretical models, which have explored this problem, were limited by non-rotating flows. We added the Coriolis force to this study to verify a rotation impact on the generation, evolution and decay of the layered structure within the pycnocline under the influence of surface stress. It makes our prognostic modeling more geophysical applicable. We employed  $e^{-?}$  and  $e^{-l}$  models of non-stationary, stratified, planetary boundary layer equations ( $e$  is the turbulent kinetic energy,  $?$  is the energy dissipation,  $l$  is a Richardson number dependent turbulent length scale). The numerical simulations clearly showed that the use of  $Re$ -dependent eddy viscosity and diffusivity results in a formation of pycnoclines with a prominent fine structure. It was found that pre-existed background shear is an important external parameter which may influence the development of the step-like structure. Time scale of the fine-structure generation is strongly dependent on inertial oscillations. It was shown that thin homogeneous layers merge each other forming



## INTER-ASSOCIATION

thicker steps owing to shear-induced turbulence at sharp density interfaces. The scales of the layers observed in simulations are close to those observed in the seasonal ocean pycnocline.

### JSP39/W/31-B4 1010

#### THE SHEAR STRESS BETWEEN AIR AND WATER

John A. T. BYE (Faculty of Science and Engineering, Flinders University, GPO Box 2100, Adelaide, South Australia, 5001, Australia, email: John.Bye@flinders.edu.au); Jörg-O. Wolff (Antarctic CRC, University of Tasmania, GPO Box 252-80, Hobart, Tasmania, 7001, Australia, email: j.wolff@utas.edu.au)

Recently a new formulation for the surface shear stress between air and water, which is applicable in the Earth reference frame has been implemented in a quasigeostrophic general circulation model of the Antarctic Circumpolar Current. The results indicate that a momentum balance similar to that observed can be achieved with form stress, without the use of an unrealistically large bottom friction.

This shear stress is quite distinct from that measured in planetary boundary layer studies which use the local reference frame of the surface current. The implications of a shear stress which depends on a reference frame will be discussed. The presentation will be illustrated by experimental data obtained in a novel circular wind wave tank in which a fan drives a rotating air circulation, which generates a complementary water circulation beneath.

### JSP39/W/17-B4 1050

#### A REGIONAL MODEL OF THE SEMI-DIURNAL INTERNAL TIDE ON THE AUSTRALIAN NORTH WEST SHELF

Peter E. HOLLOWAY (School of Geography and Oceanography, University College, University of New South Wales, Australian Defence Force Academy, Canberra ACT 2600, Australia)

The semi-diurnal internal tide on the Australian Northwest Shelf is investigated using a fully three dimensional, non-linear, free surface, hydrostatic, primitive equation numerical model, the Princeton Ocean Model. The model covers a domain 1700 by 700 km using a 4km horizontal grid and 51 vertical sigma levels. Forcing is via specification of the M2 surface elevation along the open boundaries with values taken from the FES-95 global tidal model. The barotropic tidal flow, generated from surface elevation gradients, interacts with the topography and produces an internal tide that is highly variable in space. Depth integrated baroclinic energy fluxes show regions of both onshore and offshore propagation and maximum of approximately 4000 W/m. Model predicted internal tide structures are compared to detailed in-situ observations and show reasonable agreement. The three-dimensional character of the topography is shown to be important in the generation process.

### JSP39/E/12-B4 1110

#### KUROSHIO EDDIES IN THE LUZON STRAIT

Y. HSUEH (Department of Oceanography, Florida State University, Tallahassee, FL 32306-4320, USA, email: hsueh@re.ocean.fsu.edu)

Results from a high-resolution, limited area, primitive-equation model of the circulation of the Asian marginal seas show the Kuroshio bulges into the Luzon Strait and forms a loop current before resuming its northward course. The model run with monthly mean wind forcing indicates that the Southwest monsoon tends to reduce the bulge and the Northeast monsoon tends to promote its growth. In fact, model warm-core eddies often break away from the loop during the winter monsoon season. A reduced-gravity model is constructed to probe the dynamics of the eddy separation in the Luzon Strait. A solution is found in which anticyclonic eddies separate from the loop nearly periodically with a period predicted from an analytic solution. An important aside is the discovery that an anticyclonic eddy is often generated that moves downstream with the Kuroshio. The passage of this eddy produces Kuroshio variabilities detected in recent current measurements.

### JSP39/E/14-B4 1130

#### MEAN FLOW GENERATION BY GEOMETRICALLY FOCUSED GYROSCOPIC WAVES

Leo MAAS (Netherlands Institute for Sea Research, PO Box 59, 1790 AB Texel, Netherlands, email: maas@nioz.nl)

A homogeneous fluid in stationary rotation is stably stratified in angular momentum (increasing radially). When this dynamic equilibrium is periodically perturbed, gyroscopic (or inertial) waves result, that propagate through the fluid along an angle with the vertical determined by the ratio of perturbation frequency to twice the angular frequency. Due to this constraint, in an infinitely long channel, such waves are, upon reflecting from sloping side walls, subject to focusing, much like internal waves are. In a tank of finite azimuthal extent, this result can only be approximately true, as the circular current patterns, associated with the gyroscopic wave, need to accommodate the presence of the plane side walls. As long as the tank is much longer in along-slope than cross-slope direction, attractors might still arise, a suggestion confirmed by a laboratory experiment in which the perturbation is generated by modulating the angular velocity of the tank. Focusing gyroscopic waves lead to mixing of angular momentum at the location where the attractor reflects from the sloping wall. This predicts a mean flow above that location, confirmed by velocity measurements and dye spreading.

### JSP39/W/38-B4 1150

#### HYDROTHERMAL PLUME FROM A WARM LUTOCLINE

Jordi COLOMER, Teresa Serra, Jaume Piera, Elena Roget, Xavier Casamitjana, (Department of Physics, University of Girona, 17071 Girona, Spain)

A hydrothermal plume with vertical and horizontal length scales of 18 and 300m approx., respectively, is generated by a warm lutocline at the mid-depths (29 m) of a karstic lake (lake Banyoles, situated in North-Catalonia, Spain). The rising particle-laden convective plume entrains colder hypolimnetic water and develops upward until it reaches the base of the seasonal thermocline. At the level of neutral buoyancy the plume spreads laterally, mainly to the northeast of the lake, as an hypolimnetic current. Measurements were carried out using a microstructure profiler, a laser in situ scattering and transmissometry probe, and water quality probes.

### JSP39/W/16-B4 1210

#### DIAGNOSTIC MODEL ACCOUNT BAROTROPIC SPEED MODE OF BAROCLINIC OCEAN BY SATELLITE ALTIMETRY DATA

Sergey A. LEBEDEV (Geophysical Center of Russian Academy of Sciences, Molodezhnaya 3, 117296, Moscow, Russia, email: lebedev@wdbc.rssi.ru)

As differentiated satellite altimetry data assimilation the diagnostic analysis of ocean dynamics gives complete hydrodynamic picture on that moment of time or for that temporary interval, when appropriate measurements were made. The given approach permits better to realize as the simulated phenomena, and representation of initial information.

As an initial system of offered model equations are considered equations of ocean dynamics in quasigeostrophic approximation. The boundary condition on surface for vertical mode of speed fields is replaced by «firm cover» condition, and a condition of sliding without friction is at the bottom taken. Integrated stream function, which is necessary for account barotropic speed mode is searched as anomaly from mean season significance. It is reasonably safe to suggest that changes of baroclinic layer thickness are insignificant and density anomaly linearly change by vertical from surface significance to zero on the baroclinic layer bottom border.

The model verification was conducted on independent data: satellite altimetry (ERM mission GEOSAT) and hydrological data (experiment NEWFAEXP-88 the program «Sections») for polygon near island Newfoundland in March 1988. The mean fields of dynamic topography and integrated stream function were determined by known data file LEVITUS.

Thursday 29 July PM

Presiding Chair: C.N.K. Mooers., Univ. of Miami, RSMAS, Miami, FL, (USA)

### JSP39/E/11-B4 Invited 1400

#### MECHANISMS FOR EDDY FORMATION IN DENSE DOWNSLOPE FLOWS IN ROTATING SYSTEMS

Peter G. BAINES (CSIRO Atmospheric Research, PMB No. 1, Aspendale, Australia 3195)

The flow of dense fluid downslope occurs on a large scale in a number of locations in the deep ocean (the Mediterranean outflow, the Denmark Strait overflow, the Bass Strait overflow and at various locations around Antarctica), but there is considerable variety in its observed character for reasons not yet well understood. For steady inviscid flow there is no downslope motion at all, as a "geostrophic" balance obtains between buoyancy and the Coriolis force. Friction is apparently necessary in order to have downslope motion with rotation. Further, eddies have been observed in the Denmark Strait overflow, and in laboratory experiments that aim to provide simple models of these flows (Lane-Serff & Baines 1998, J. Fluid Mech. 63, 229). Bottom Ekman layers are conspicuous in these experiments, and the eddies also have a bearing on the downslope transport.

Three possible mechanisms for eddy production by downslope flows in two-layer systems have been identified by Lane-Serff & Baines. All of these involve stretching of the upper layer fluid column by motion of the lower layer, and consequent spin-up due to potential vorticity conservation. These are: (i) "dragging" of the upper layer fluid by downslope motion of the lower layer before the latter reaches approximate alongslope "geostrophic" balance, in the manner of a "captured" Taylor column; (ii) the collapse (or reduction of thickness) of the lower layer fluid as it approaches this "geostrophic" balance, and (iii) Ekman drainage from the (anticyclonic) lower layer after it reaches this "geostrophic" balance, which also reduces its thickness. The first two only act during geostrophic adjustment, but the last acts continuously. Spall and Price (1998, J. Phys. Oceanog. 28, 1598) have proposed a fourth mechanism (that is similar to (i)) in which the inflow consists of two layers flowing into a third, and the upper inflowing layer is stretched by the motion of lower. They also propose that this process operates in Denmark Strait. A variety of experiments that demonstrate these mechanisms and the situations in which they are dominant will be presented.

### JSP39/W/47-B4 Invited 1430

#### STUDIES OF OCEAN DYNAMICS - FROM SMALL SCALE MIXING TO LARGE SCALE CIRCULATION

Greg IVEY (Department of Environmental Engineering, Centre for Water Research, The University of Western Australia, Nedlands, Western Australia, e-mail: ivey@cwr.uwa.edu.au)

The initiation of a de-stabilizing buoyancy flux across the surface of the ocean produces small-scale convective turbulence and mixing. In the ocean, the small-scale turbulence is only weakly affected by rotation but will erode the underlying stratified fluid. The combination of non-uniform lateral distribution of the surface buoyancy flux and this convectively driven deepening will generate firstly lateral density gradients and then, in turn, a mean circulation. If the scales are large enough, this circulation will be affected by rotation and large-scale baroclinic instabilities dominate the flow field. Recent laboratory studies have provided insight into these flows and have considered cases ranging from open ocean convection, where rotation is of primary importance, through to exchange flows between basins where topographic control is of primary importance. These studies will be reviewed with emphasis on describing how the buoyancy forcing, the ambient stratification, the rotation rate, the depth and the lateral length scales determine both the timescales of evolution of the flow to steady state as well as the final steady state property distributions, circulation and exchange rates.

### JSP39/W/04-B4 1500

#### THE PROPAGATION OF INERTIAL-INTERNAL WAVES OVER SLOPING BOTTOM TOPOGRAPHY: A REVISIT

Christopher N.K. MOOERS (Rosenstiel School of Marine and Atmospheric Science, University of Miami, 4600 Rickenbacker Cswy., Miami, FL33149-1098, USA, email: cmooers@rsmas.miami.edu)

Inertial-internal waves (i.e., waves under the joint influence of the Earth's rotation and density stratification) interact with sloping bottom topography in a fashion that depends upon the ratio of the slope of a frequency-dependent wave parameter (the slope of the wave characteristics or rays) to the slope of the bottom: if the ray slope is greater than the bottom slope, there is forward reflection; if otherwise, there is backward reflection. Of particular interest here is the propagation of inertial-internal waves into a wedge; for relatively high frequencies that are forward-reflected, a given wedge is termed subcritical; conversely, for relatively low frequencies that are backward-reflected, a given wedge is termed supercritical. By analysis of fiducial rays to reduce the frequency-dependent dynamical geometry to characteristic subdomains, a method for constructing solutions is defined for both subcritical and supercritical wedges.

**JSP39/E/02-B4 1520****THE USE OF LABORATORY MEASUREMENTS TO VALIDATE OCEAN NUMERICAL MODELS**

Nicolas PERENNE, David Smith, Don L. Boyer (Environmental Fluid Dynamics Program, Department of Mechanical and Aerospace Engineering, Arizona State University Tempe, AZ 85287-6106, USA, email: perenne@enws606.eas.asu.edu); Dale Haidvogel (Institute of Marine and Coastal Sciences, Rutgers University, P.O. Box 231, New Brunswick, NJ 08903, USA, email: dale@ahab.rutgers.edu)

In order to develop data sets which can be used as benchmarks for current coastal circulation models, laboratory experiments are conducted in a cylindrical tank in which a continuous continental shelf model, interrupted only by a single smooth canyon, is placed along the periphery of the test cell. Prior to experimentation, the tank is filled with a linearly stratified fluid and the tank is then slowly brought up to solid body rotation with Coriolis parameter  $f$ . To initiate the experiments, the turntable rotation rate is then modulated sinusoidally about the background rotation rate  $f/2$ . This effectively drives an oscillatory background current along the coastline. The objectives of the experiments are to (i) observe and better understand the motion field in the vicinity of a submarine canyon and (ii) provide horizontal maps of the velocity, vertical vorticity and horizontal divergence fields, including a determination of the errors associated therewith, that can be compared with current numerical models. The principal governing dynamical parameters are the Rossby, temporal Rossby, Burger and Ekman numbers.

Observations at numerous vertical locations, including those above and below the canyon rim, are presented. Particle tracking techniques are used to delineate the velocity, vorticity and divergence fields. Special attention is given to the mean currents driven by this physical system. Comparisons are made between the laboratory results and two coastal circulation models (i.e., finite difference and finite element). An assessment is made concerning the differences noted between the laboratory and the numerical models.

**JSP39/W/28-B4 1540****MESOSCALE OCEAN EDDY DYNAMICS: HIGH RESOLUTION SHALLOW WATER SIMULATIONS WITH REALISTIC TOPOGRAPHY**

Robert B. SCOTT, Ted Johnson, S. A. Sorenson (Mathematics, UCL, Gower Street, London, WC1E 6BT, UK)

The western boundary current off the southern tip of Africa, the very fast Agulhas current, regularly produces mesoscale eddies. Their westward propagation to the South Atlantic has been captured with TOPEX/Poseidon satellite altimeter data. This provides an excellent opportunity to study the eddy dynamics using simplified models while verifying the accuracy using the real data. We present results produced with a state of the art shallow water code featuring an adaptive grid that provides very high resolution following the eddy. The effects of realistic topography are investigated using the ETOPO5 5 minute resolution data. The possible influences of finer scale topography on eddy spin down is analyzed with artificial topography. Insofar as the most serious limitation of the model is its vertical homogeneity, the comparison between the observations and simulations provides an assessment of the importance of density stratification.

**JSP39/W/39-B4 1620****MIXING EFFICIENCY OF STRONG DENSITY INTERFACES**

J.M. REDONDO, M.A. Sanchez (Dept. Fisica Aplicada, UPC, Barcelona, Spain)

A series of high resolution experiments have been performed in order to examine the structure of a sharp density interface under zero-mean-flow. The evaluation of the mixing efficiency of the grid-stirred turbulence is made comparing the increase of potential energy with the power of the grid. The interface is visualized with a thin laser sheet of 532 nm and rodamine is used to mark the turbulent side of the interface. The structure of the density and velocity fields are imaged using DigImage fluid dynamics software and particle tracking of pilolite suspended near the interface. The reduction of interface thickness with Richardson follows a power law with exponent  $-2/3$ . There is a maximum in mixing efficiency at intermediate  $Ri$  when a high rate of vortex dipoles resonate with the Brunt-Vaisalla frequency at the interface.

**JSP39/E/05-B4 1640****LONG-DISTANCE PROPAGATION AND FEATURES OF TIDAL INTERNAL WAVES IN THE CENTRAL INDIAN OCEAN**

Tatiana Demidova, Eugene MOROZOV (both at Department of Physics, P.P. Shirshov Institute of Oceanology, Moscow 117218, Russia, email: evita@redline.ru)

Propagation of tidal internal waves generated over the slopes of the Mascarene Ridge at a distance over 10 wavelengths in the Central Indian Ocean was studied from a joint analysis of the results of calculations with the use of a non-linear numerical model and experimental cast and mooring data. The barotropic tide over the ridge was assumed to be a 2-D flow in a continuously stratified rotating ocean of changing depth. The modelling was fulfilled for quite large number of steps in time. This allows us to study the evolution of the internal waves at distances over 1500 km from the source. Long-term measurements of temperature and currents at subsurface buoys in direction of the wave propagation were used to get statistically proven experimental parameter of internal waves and to study its time evolution. The results of the modelling and experimental measurements were used to estimate the amplitudes of the waves, the character of their decay and energy flow both near the ridge and at a significant distance from it. Oscillation parameters of the first mode remains unchanged at quite long distances, whereas the higher modes dissipate rapidly already at first periods of oscillation. Approximately 5%-decay per wavelength in the far zone was found. The modelling and measurement results are in a good agreement.

**JSP39/E/24-B4 1700****INTERACTION OF INERTIA-GRAVITY WAVES WITH A POTENTIAL VORTICITY BARRIER**

Gael Huerre, Chantal STAQUET (LEGI, BP 53, 38041 Grenoble cdx 9, France, email: chantal.staquet@hmg.inpg.fr)

The purpose of this work is to investigate the permeability of a dynamical barrier with respect to wave breaking events. This work is motivated by a conjecture proposed by McIntyre (1995) according to which the edge of the polar vortex, which behaves as a dynamical barrier with respect to large scale quasi-two-dimensional turbulence, would be permeable to wave breaking events. McIntyre (1995) suggested that inertia-gravity wave motions, in breaking intermittently near the vortex edge, could give rise to a quasi-horizontal transport across that edge. This conjecture was proposed to account for anomalous behaviours inferred from measurements in the atmosphere, such as low concentration of ozone at mid latitudes. To

investigate this conjecture, we have performed three-dimensional numerical simulations of inertia-gravity waves interacting with the edge of a large scale vortex. Conditions under which breaking may occur have been investigated and the permeability of the vortex edge is studied by following the behaviour of a passive tracer. Preliminary results will be presented at the meeting.

**JSP39/E/13-B4 1720****PARAMETER DEPENDENCE OF LINEAR AND NONLINEAR INSTABILITY OF BAROTROPIC AND BAROCLINIC SHEAR FLOWS**

Kuniko M. YAMAZAKI, Akira Masuda (Dynamics Simulations Research Center, Research Institute for Applied Mechanics, Kyushu University, Kasuga-Koen 6-1, Fukuoka 816-8580, Japan, email: miki@masuda.riam.kyushu-u.ac.jp, masuda@riam.kyushu-u.ac.jp)

We examine the stability of equivalent barotropic and baroclinic shear flows in a periodic domain on an  $f$ -plane and on a beta-plane, as a preliminary to investigating the instability of the Kuroshio Current over the continental slope in the East China Sea. Linear analysis reveals that the instability of the equivalent barotropic shear flow is reduced by stratification, the beta effect, coastal boundaries, and along-flow bottom topography. For the baroclinic flow, however, the influence of stratification is more complex due to the influence of baroclinic instability. The non-linear evolution of such unstable flows is investigated by employing a numerical time-integration technique. An archetypical evolution is found to consist of four stages: primary instability to which linear analysis is applicable, saturated phase characterized by staggered rows of vortices, the onset of a secondary "subharmonic" instability which leads to the development of structures with smaller wavenumbers, and a final stage in which the flow becomes more irregular. It turns out that the long-term non-linear evolution of the flow is drastically altered by the influence of the planetary beta-effect. Furthermore, in the barotropic case, an asymmetry of the profile of the mean shear flow enhances the instability of jets insofar as their development is concerned, although the opposite is the case in the linear regime.

**JSP39/W/20-B4 1740****EDDY-WAVE INTERACTIONS USING A POTENTIAL VORTICITY DIAGNOSTICS**

Maria VALDIVIESO DA COSTA, Alain Colin de Verdiere (both at Laboratoire de Physique des Océans, Université de Bretagne Occidentale, email: mvaldi@deneb-gw.univ-brest.fr)

Process-oriented numerical experiments are carried out to study the dynamics of intermediate density boundary currents and associated lenslike eddies. The model used in the experiments is the pure-isopycnic coordinate primitive equation model of Bleck and Boudra (1986), configured on a semi-open channel with two active layers, and forced by a steady mid-level density flux through one channel wall. Non-linear interactions between neighbouring eddy structures were generally observed within 50 and 100 inertial periods after the geostrophic adjustment phase of the experiments. Most of the clearly visible interactions occurred between large-scale eddies with weak downstream phase velocities, and faster propagating smaller scale waves.

A diagnostic framework based on the model isopycnic potential vorticity (IPV) balance is set out to examine the non-linear interaction processes between these two types of transient features. Specifically, we have calculated four tendency components of the low-frequency IPV field associated with individual large-scale eddies on the framework of the filtered IPV-tendency equation. We then compared each of the tendency components with the (total) observed tendency and the low-frequency IPV field itself. It is found that the sum of the two tendency components induced by each of the internal non-linear interaction processes determines the observed tendency of large-scale eddies. The largest tendency component is the tendency induced by the advection of large-scale eddy structures by the low-frequency component of the total flow, which primarily acts to make large-scale eddies propagate downstream. The tendency component due to self-interaction among high-frequency transients (feedback of high-frequency waves) is nearly out-of-phase with the mean tendency induced by the large-scale advection, retarding, in average, the downstream propagation of large-scale eddies. The tendency component induced by bi-harmonic dissipation of IPV along isopycnal surfaces is in the mean negligible relatively to the other mechanisms.

**JSA40****Wednesday 28 July****SOLID EARTH GEOPHYSICAL DATA FUSION AND ANALYSIS METHODS (IAGA)**

Location: Mairhead Tower Room 112 LR2

Location of Posters: Student Room 1st Floor

**Wednesday 28 July AM**

Presiding Chairs: M. Purucker (Goddard Space Flight Centre, NASA)

L. Ballani (GFZ Potsdam)

**JSA40/W/08-B3 0900****SPECIFICATION OF THE CRUSTAL MAGNETIC FIELD FOR DIRECTIONAL DRILLING**

SUSAN MACMILLAN (British Geological Survey, Murchison House, West Mains Road, Edinburgh EH9 3LA, UK, email: S.Macmillan@bgs.ac.uk) and Paul Williamson (British Geological Survey, Kingsley Dunham Centre, Nicker Hill, Keyworth, Nottingham, NG12 5GG, UK, email: P.Williamson@bgs.ac.uk)

Real-time estimates of the geomagnetic field vector and associated uncertainties, ideally about  $0.1^\circ$  in direction and 50 nT in magnitude, are desired in the drilling of oil and gas wells using magnetic survey tools. To help achieve this level of accuracy a knowledge of the crustal field vector is required and a method to derive this from scalar aeromagnetic data is described. The problem of how to estimate the crustal field contribution and its likely uncertainties at the location of the downhole magnetic survey tool, which is considerably nearer the sources than the aeromagnetic data, is discussed. One possible approach is to use an inversion technique to map the magnetisation distribution, constrained by any available external information such as seismic data. This can then be used to calculate the magnetic anomalies at depths above the sources.



**JSA40/W/12-B3** Invited **0920**

**USE OF EFFECTIVE MEDIUM TECHNIQUES TO INTEGRATE SEISMIC AND ELECTROMAGNETIC DATASETS**

ANTHONY GREER and Martin Sinha University of Cambridge, Department of Earth Sciences, Cambridge, CB3 0EZ, email: greer@esc.cam.ac.uk

The study of rocks containing fluids by seismic or electromagnetic methods can reveal some of the rock's properties - seismic velocity, electrical resistivity - but a single technique can not uniquely determine the pore fractional volume, or the geometrical properties of the pore fraction. Effective medium techniques can be used to jointly interpret the two data types through relationships that map pore fractional volume into variations in resistivity and seismic P-wave velocity, for the case of either aqueous or magmatic fluids filling crustal pore spaces, and for given pore geometries. The models are parameterised using randomly orientated ellipsoidal cracks with variable aspect ratios. Electrical resistivity depends heavily on interconnected pathways of the highly conductive fluid phase, while seismic velocity depends less on interconnected pathways but heavily on pore geometry. Since these two geophysical properties respond differently to variations in pore geometry, it is possible by combining both types of data to overcome the trade off that otherwise exists between pore geometry and pore fractional volume.

We have successfully applied this approach to real, coincident data sets from mid-ocean ridge systems. These are dynamic geological environments where active processes are dominated by the presence of magmatic and hydrothermal fluids. The results provide new constraints on crustal porosity and fluid connectivity.

**JSA40/E/07-B3** **0950**

**TOWARDS AN INTERDISCIPLINARY 3-D MAPPING OF THE LITHOSPHERE AND ASTHENOSPHERE BENEATH ATLANTIC CANADA AND THE ARCTIC. PART-1: APPLICATION OF THE MULTIMODE/MULTISTRUCTURE METHOD OF SEISMOLOGY**

Pierre ROULEAU (Department of Physics, Sir Wilfred Grenfell College, Memorial University of Newfoundland, NF, CANADA, A2H 6P9, email: prouleau@boethuk.swgc.mun.ca), Fred Schwab and Bob Melhman (both at Institute of Geophysics and Planetary Physics, University of California at Los Angeles, Box 95157, Los Angeles, California 90095-1567, USA, email: schwab@cyclop.ess.ucla.edu), Jose Frez and Jose Acosta (both at Centro de Investigacion Cientifica y de Educacion Superior de Ensenada, Av, Espinoza No, 843, Apartado Postal 2732, Ensenada, Baja California, MEXICO, email: jofrez@cicese.mx)

The ultimate goal of our work is to produce a 3-D digital map of the seismic, structural, gravimetric, geochemical, thermal, electromagnetic, and stress field properties beneath the combination of Atlantic Canada and the Arctic down to a nominal depth of 800 km, with a lateral resolution of 10 km. Towards this end, we apply a multi-step, evolving procedure for map improvement, originally elaborated by the IUGG's ICL/ILP Project II-4. The current level includes detailed treatment of geography (topography, bathymetry), geodesy (geoid), surface geology, within the multimode- multi-structure (MM) seismological technique whose aim is to improve an initial model (an "I" data set) by minimising the residuals between complete theoretical seismograms and those recorded experimentally. Using reported data and auxiliary databases (e.g. CRUST 5.1, ETOPO30, EGM96, GLOBE), and specially-constructed software for automating the work, we first built an "I" data set for the Arctic-North Atlantic, and then for the continuation through Atlantic Canada. The current level of formulation of these 3-D maps (electronic databases) is described, as is the allowed variability of the iterative improvement, and the related problems of graphical display of 3-D results. We describe the nuclear, MM technique and its implementation; principally the hardware/software system that we have had to develop for routine 3-D mapping with full control over lateral resolution. We present extensive numerical results of the testing on the Arctic "I" data set; results from the later, preliminary numerical testing on the Atlantic Canada "I" data set are discussed.

**JSA40/E/08-B3** **1005**

**CONSTRAINTS ON CASCADIA SUBDUCTION FROM CONTRASTING MODELS OF CRUSTALAND MANTLE DENSITIES**

Tanya ROMANYUK (IPE, B.Gruzinskaya 10, Moscow, 123 810, Russia, email: t.romanyuk@relcom.ru) Walter Mooney and Richard Blakely (USGS, 345 Middlefield Rd, MS 989, Menlo Park, CA 94025, USA; email: mooney@andreas.wr.usgs.gov; blakely@mojave.wr.usgs.gov)

The style of subduction of the Juan de Fuca plate beneath North America changes markedly along the length of the subduction zone, especially in the angle of subduction, distribution of earthquakes, geologic and seismic structure of the upper plate, and regional horizontal stress. To investigate density characteristics, we conducted detailed modeling experiments of the crust and mantle along two transects across the Cascadia subduction zone, one across Vancouver Island and the Canadian margin, the other across the Oregon margin of the United States. Models of crustal and mantle density were produced with a 2-D linear gravity inversion technique. This technique approximates the crust-mantle cross section by a set of blocks based on published seismic refraction models. Each block is allowed to have a range of densities, constrained where possible by borehole measurements, seismic velocities and petrological arguments. To further constrain the models, we assumed that oceanic crust has the same density-depth ratio at both transects and that the lithosphere is close to isostatic equilibrium in the deep ocean and east of the modern volcanic arc. Our results confirm that the downgoing slab beneath Vancouver Island dips significantly gentler than at Oregon, supporting the idea that the Juan de Fuca plate is segmented from north to south. The Oregon segment has an anomalous block within the mantle situated between the continental crust and the subducting Juan de Fuca plate. This block is located beneath the aseismic Western Cascades and is characterized by a density lower than the mantle density beneath the modern volcanic arc in both segments. This reduced density agrees with observed lower mantle velocities, extensional geodynamic regime, and other characteristics of the Oregon margin.

**JSA40/E/10 -B3** **1025**

**STRENGTHS AND WEAKNESSES OF GLOBAL, LOCAL, AND JOINT-INVERSION APPROACHES IN THE OPTIMISATION OF ELECTRICAL AND EM DATA**

SAURABH K. VERMA (National Geophysical Research Institute, Uppal Road, Hyderabad-500 007, India, email: postmast@csngri.ren.nic.in) Sven-Erik Hjelt, Shashi P. Sharma, and Markku Pirttijarvi (all at Department of Geophysics, University of Oulu, 90750 Oulu, Finland, email: seh@babel.oulu.fi)

Easy accessibility to fast computers has provided an impetus to the application of global inversion methods in the optimisation of geophysical data. Though the appetite of these methods for computer memory and time is enormous, they are guaranteed to converge to a solution. Local inversion methods are computationally efficient but convergence to a solution is not always possible. Joint-inversion (JI) synergistically combines information from two or more data sets to provide a common model acceptable to various data sets. Both local and

global search engines could be utilised to implement a JI scheme. Performance of the above approaches in resolving i) simple and ii) relatively difficult (fine) 1-D structures is compared considering DC and MT sounding data. A comparison of local and global methods is also presented for a 2.5-D 'plate' model considering time-domain EM data. The results reveal that JI based on local search can provide a good resolution of difficult targets most economically. If multi-parametric information is not available to use JI, a local search approach could still be desirable if extraneous information is available to constrain the starting model. Global search may be resorted to only in the absence of multi-parametric data and extraneous information.

**JSA40/E/02-B3** **1045**

**LARGE-SCALE 3-D MODEL FOR THE LITHOSPHERE OF EUROPE INFERRED FROM SEISMIC AND GRAVITY DATA**

Tamara P. YEGOROVA and Vitaly I. Starostenko (both at Institute of Geophysics, National Academy of Sciences, 32 Pr. Palladina, Kiev 252680, Ukraine, e-mail: egorova@igph.kiev.ua)

Presented large-scale 3-D model for the lithosphere of Europe is based on generalised velocity model, compiled by Giese and Pavlenkova and presented by structure maps for "seismic" basement and the Moho, and by a scheme of distribution of average P-wave velocity in the crystalline crust. This model, consisting of three layers (two regional layers - sediments and the crystalline crust and a sea water layer offshore) was converted into its density equivalent with using the conversion functions between velocity and density. Through solving 3-D direct gravity problem an effect from the model has been computed. By removing the calculated effect from the observed gravity field, the residual gravity anomalies of -200 to +200 mGal amplitude, caused by density heterogeneities of the uppermost mantle, have been obtained. Mantle origin of the residual gravity anomalies is confirmed by their correlation with both velocity structure of the upper mantle according to seismotomography and geothermal data. The results of the modelling confirm general division of the lithosphere of the continent on two main blocks - activated Phanerozoic lithosphere of the Western Europe and Precambrian consolidated lithosphere of the East-European Platform.

Against this background there are distinguished two main types of contrast units characterised by negative and positive mantle anomalies. (1) Tapprogonic and rift regime (Western Mediterranean, the Pannonian Basin, North Sea, Rhinegraben) with thin crust, shallow asthenosphere, low-velocity domains in the upper mantle, high-heat flow values and mantle anomalies of -150 to -200 mGal. (2) Orogenic regime (Alps, Pyrenees, Calabria Arc, Dinarides, Caucasus) with thick lithosphere, high velocities in the upper mantle, moderate heat flow values and mantle anomalies -50 to +150 mGal.

**JSA40/W/05-B3** **1120**

**GEOPHYSICAL RECOGNITION OF POSSIBLE OCEANIC PLATEAUS IN THE LOWER CONTINENTAL CRUST**

M Purucker (Geodynamics Branch, Goddard Space Flt Ct, Greenbelt, MD 20771 USA, email: purucker@geomag.gsfc.nasa.gov)

Recent studies of xenoliths and of granulites of the Arunta block suggest the presence of strongly magnetic mafic granulites in the lower crust. These mafic granulites, if present in substantial amounts, will produce significant magnetic anomalies at satellite altitude. What could be the origin of these mafic granulites? One idea is that they may arise from the accretion of oceanic plateaus to continents and the subsequent descent of these oceanic plateaus to lower crustal depths (cf. Condie, J.Geol, 1997,729-736; for counterpoint see Taira and Mann, Fall AGU, 1998). Oceanic plateaus in the present-day ocean exhibit a significant magnetic signature at satellite altitude because they contain a thickened sequence of mafic crust and they are the right size to be seen from satellite altitude. After initial accretion, the oceanic plateau would be largely in the upper crust at greenschist and amphibolite grade. As a general rule, mafic rocks at these metamorphic grades are weakly magnetic, with Fe largely locked up in nonmagnetic minerals such as chlorite and epidote. Granulite grade metamorphism frequently leads to the formation of highly magnetic, low-Ti magnetite. Interrogation of the CRUST 5.1 database for regions in the lower crust with P wave velocities and densities consistent with mafic granulite yields ten areas, five of which host significant satellite magnetic anomalies. Perhaps the lower crust in these regions was derived, at least in part, from oceanic plateaus?

**JSA40/E/03-B3** Invited **1140**

**JOINT GRAVIMETRIC-SEISMIC MODELLING - PITFALLS AND PERSPECTIVES**

Gabriel Strykowski (National Survey and Cadastre, Rentemestervej 8, DK-2400 Copenhagen NV, Denmark, email: gs@kms.min.dk)

The fundamental problem of geophysical modelling is that the information about the subsurface contained in surface data (gravity, seismics and others) is insufficient. It is the limitation in the information content that causes the ambiguity of a solution to the mathematical inverse problem. This explains the apparent paradox. A common sense argument implies the existence of a true and unique (as opposed to ambiguous) distribution of the physical sources of the measured surface signal. In practical modelling, this missing information is provided by 'mathematical assumptions' (such as a limited solution space, a minimization criterion, apriori error statistics, . . . etc), thus, transforming an inherently ill-posed mathematical inverse problem to a well-posed one. The role of joint geophysical modelling is to overcome the above inherent mathematical ill-posedness of monodisciplinary modelling problems by including 'independent information'. However, in practise one faces a problem of coupling different types of information. The obvious question is: Are the sources of different types of surface signals coherent? (For example: Is a seismic reflector always connected to a mass density contrast?) In this contribution we will address such general problems using gravimetric-seismic modelling as a specific example. Furthermore, we will discuss consequence of popular assumptions known in the literature (mass density-seismic velocity relation and apriori fixed mass density contrast across interface separating geological bodies or layers). From this discussion emerges a general frame for joint geophysical modelling. Specifically, for the gravimetric-seismic modelling problem, the hierarchy in which different pieces of information (seismic data, borehole data, and gravimetric data) should be used. All aspects of the general discussion will be illustrated by a field example: modelling of the source (an igneous intrusion within the crust) of Silkeborg Gravity High in Denmark.

**JSA40/W/01-B3** **1205**

**LITOSPHERE AND UPPER MANTLE STRUCTURAL MODELS OF NORTH AMERICA DERIVED FROM INTEGRATED GEOPHYSICAL DATA**

Gildo CALCAGNILE and Vincenzo Del Gaudio (Dipartimento di Geologia e Geofisica and Osservatorio di Geofisica e Fisica Cosmica, Università di Bari, via E. Orabona, 4, Bari, Italy; e-mail: scigeddi@tno.it, delga@geo.uniba.it) Umberto Mascia and Pierpaolo Pierri (Osservatorio di Geofisica e Fisica Cosmica, Università di Bari, via E. Orabona, 4, Bari, Italy; e-mail: mascia@geo.uniba.it, pierri@geo.uniba.it)



Surface dispersion data have been combined with the results of seismic refraction data to derive the regionalisation of lithosphere-asthenosphere system and to investigate the presence of significant heterogeneity in the mantle of North America. The older part of the shield shows lid thickness up to more than 100 km with, if any, weak shear velocity contrast to the underlying layer. The surrounding areas are characterised by a thinner lithosphere in the western and the south-eastern region with a relatively well-developed low-velocity zone (excluding the Colorado Plateau-Sierra Nevada area) where low velocity material may almost rise up to the Moho); in the central stable and eastern regions the contrast may be much milder with higher velocity. Other geophysical features like heat-flow, gravity anomalies and electrical conductivity correlate qualitatively rather well with the characteristics of the lithosphere-asthenosphere system. We attempt a more quantitative approach constraining the obtained seismological models with other geophysical data (mainly gravimetric and thermal data); the results of this integrated approach will be discussed.

JSA40/E/04-B3

1225

#### THE APPLICATIONS OF DYADIC GREEN FUNCTIONS IN 3-DIMENSIONAL MODELLING OF THE EAST AFRICAN RIFT SYSTEM USING BOTH SEISMOLOGY AND MAGNETOTELLURIC METHODS

Ebun Adefunmilayo Oni, Solid Earth and space Physics Research Laboratory, Department of Physics, University of Ibadan, P.O Box 4092, Ibadan, Nigeria. E-mail: ebononi@sesp-ui.ouaiife.edu.ng

The East African Rift System has been under scientific investigation for a long period because of its importance in continental Rifting and modern theory of Plate Tectonics. The 3-Dimensional Mapping of the Lithosphere and Asthenosphere on the African Continent cannot be completed without paying special attention to the 3-Dimensional Modelling of the East African Rift System. In a recent paper, Oni (1995a) developed the use of Dyadic Green Functions for Magnetotelluric in Low Latitudes. The theory can be applied to the 3-Dimensional Modelling of the East African Rift System. In another paper, Oni (1995b) developed the use of Dyadic Green Functions for Seismic Waveguide Theory in 3-Dimensional Seismology. In this paper the Author makes use of the two theories to evolve an integrated Seismology and Magnetotelluric Theory for a 3-Dimensional Modelling of the East African Rift System.

Wednesday 28 July PM

Presiding Chairs: M. Purucker (Goddard Space Flight Centre, NASA)  
L. Ballani (GFZ Potsdam)

JSA40/E/12-B3

Poster

1400-01

#### WAVELET METHOD FOR THE HARMONIC ANALYSIS OF GRAVITY TIDES

H. T. Hsu (Institute of Geodesy and Geophysics, Chinese Academy of Sciences, 54 Xudong RD, Wuhan 430077, P. R. China, email: hshuh@asch.whigg.ac.cn) Lintao LIU (Institute of Geodesy and Geophysics, Chinese Academy of Sciences, 54 Xudong RD, Wuhan 430077, P. R. China, email: llt@asch.whigg.ac.cn)

In this contribution, we propose a new approach to the determination of gravity tidal parameters. Three pairs of compactly supported wavelets are introduced in the approach. They can efficiently extract the aimed tidal signals from the gravity tides. The new approach guarantees a direct and precise analysis of the tidal gravity records of any sampling rate. We apply the new approach to the harmonic analysis to Wuhan superconducting gravimeter records. The results clearly show the resonant effects of the Earth Nearly Diurnal Free Wobble (NDFW).

JSA40/W/15-B3

Poster

1400-02

#### THREE TYPES OF THE EARTH'S MAGNETOACTIVE CRUST

Boris S.Barulin (Geophysical Trust, Novosibirsk, Krasny Prosop.,16, Russia), VLADISLAV N.LUGOVENKO, Aleksandr V.Pchelkin ( both at Institute of Terrestrial Magnetism, Ionosphere and Radio Wave Propagation, Russian Academy of Sciences, Troitsk, Moscow Region, IZMIRAN, 142092, Russia, email: golovkov@izmiran.rssi.ru) Igor V.Lugovenko (Institute of Spectroscopy,Russian Academy of Sciences, Troitsk, Moscow Region, 142092,Russia)

In 1990 (Lugovenko V.N. et al., Proc.Intern. Simp. on Geomagnetism. Shanghai.China. 1990) sufficiently reliable method of estimation of the vertical thickness of the Earth's magnetoactive crust by means of attenuation factor of mean amplitude of magnetic anomaly field by change of survey altitude was suggested.Three types of the Earth's magnetoactive crust (see also Lugovenko V.N. et al.Proc. Intern. Confer. on Marine Electromagnetics.. London, UK, 1997.) were extracted in frame of adopted geophysical model of the Earth's crust at present,using many magnetic anomaly field data for oceans, Russian, USA and Chinese territories:1.Vertical thickness of the typical continental crust of ancient platforms isapproximately 35 km.2.Vertical thickness of the Western-Siberian plate is near 10 km.3.Vertical thickness of the typical oceanic crust of mid-ocean ridges is almost 5 km.

JSA40/W/16-B3

Poster

1400-03

#### FAST CALCULATION OF TEMPERATURE DISTRIBUTION IN OIL BASINS

ZHANG Minghua (Chinese Academy of Geoexploration, 31 College Road, Beijing, 100083, China, Email: zhmh-cag@china2.ygi.edu.cn) Liyan (Xinxing Petroleum Cor., 31 College Road, Beijing, 100083, China)

Temperature is one of the three most important factors for oil maturation, accumulation and transportation. Aimed at small scale, basin belt oil and gas prospecting, geothermal field studies were carried out all over China in the middle 90s, which include direct measurement down drill holes. So far, however, reliable method for calculating temperature distribution and geothermal gradients within a basin has not found, because the boundary conditions for the equation of conductive heat transfer could not be given in high resolution and direct temperature measurement is limited due to drill hole depth. The way we suggest here for fast calculation of thermal field with high resolution consists of two steps. First, determination of Curie depth in high resolution using nonlinear iteration method(Zhang, et al,1997) for aeromagnetic anomaly inversion. Second, solution of the conductive equation by finite-element algorithm with the boundary conditions of Curie depth and temperature, temperature measurement down drill holes, and strata and structure distribution within the basin from both geology and seismic and EM interpretation. We studied Southeast part of Songliao Basin in north China, using the way suggested above in 1997. Geological structure and temperature bore hole data, seismic interpretation and 1:200 000 aeromagnetic data were utilized. Heat production at depth of 10 kilometers under ground  $RH10=1.25mW/cm^3$ . Thermal conductivity of sediments  $K1=1.5W/mK$  and of rocks from basement to Curie depth  $K2=2.6W/mK$ . Surface temperature  $Ts=10j\text{aC}$ . Curie temperature  $Tc=580j\text{aC}$ . The half-space in the earth were divided according to rock types, faults, and strata distribution into homogeneous triangular blocks. Temperature distribution and thermal gradients, heat flux along three long profiles in the basin were calculated. Known reservoirs in the southeast part of Songliao basin are

coincide with the areas where calculated Curie depths are locally shallower in a regional depress, such as Shiwu, Hudian, Qingshan and Nongang. Results of finite-element calculation show that heat flux are from 55-68mW/m2, varying in the same up and down steps as the basement, and that fault angle contributes a lot to the accumulation of heat. A stipend fault...

JSA40/W/17-B3

Poster

1400-04

#### JOINT INVERSION OF LITHOSPHERE STRUCTURE FROM LOVE AND RAYLEIGH WAVE DISPERSIONS

Yang WANG (Lab. for Geothermics, Institute of Geology, Chinese Academy of Sciences, P.O.Box 9825, Beijing 100029, China, email: thalassa@263.net)

Surface wave inversion is the common method to deduce lithosphere structure, but in general Love or Rayleigh wave dispersion data is used separately. We developed the joint inversion methods using both Love and Rayleigh wave dispersion data. Our first method inverts thickness and S-wave velocity of each layer from Love wave dispersion data, then takes the result as constraint to deduce P-wave velocity structure using Rayleigh wave dispersion data. In our second method we apply the overall optimization method, genetic algorithm, to misfit Love and Rayleigh wave dispersion data simultaneously, and obtain thickness, S- and P-wave velocities of each layer. Having S- and P-wave velocities, Poisson ratio is calculated for each layer.

The crustal seismic velocity structure of Tibetan Plateau was studied by our first inversion method, because of lacking Love and Rayleigh wave dispersion data along same path. The densities of sub layers were estimated by the empirical relationships between seismic velocity and rock density. In our results six sub layers are been identified, and the depths of their bottoms are 8, 30, 40, 62, 68, and 75 km separately. The S-wave velocities are 3.13, 3.32, 3.15, 3.92, 3.45, and 3.87 km/s for each layers, and P-wave velocities are 6.00, 6.10, 5.72, 6.35, 6.78, and 6.64 km/s, corresponding Poisson ratios are 0.31, 0.29, 0.28, 0.19, 0.32, and 0.24 separately. Our results were support by waveform modelling (Rodgers & Schwartz, 1998). We estimate the compositions of middle and lower crust of Tibetan plateau using P-wave velocities and Poisson ratios. The lower Poisson ratio of the 4th layer indicates that it maybe a quartz-riched layer, and implies that Indian crust had subducted beneath Tibetan Plateau. The joint inversion using both Love and Rayleigh wave dispersion data can provide the information about Poisson ratio of lithosphere.

JSA40/P/01-B3

Poster

1400-05

#### FLEXURE OF LITHOSPHERE BENEATH EAST CARPATHIAN BELT

Ligia Narciza ATANASIU (Geological Institute of Romania, 1 Caransebes Str., 78344 Bucharest-32, Romania, email: ligia@igr.sfos.ro)

Analysis of deflection and gravity data along a profile crossing the major tectonic units of the East Carpathian Belt.

The late Miocene foredeep basin external to the outer East Carpathian are considered typical molassic foredeep that formed contemporaneously with thrusting in the adjacent mountain belt. A simple mechanical model in which the repose of the lithosphere to loading was approximated by a semi-infinite broken) elastic plate overlying a viscous mantle was used to analyse the deflection of the foredeep assign along a profile perpendicular to the thrust belt.

The deflection of the foreland basement caused by the observed topographic load was calculated for assumed effective plate thickness of 37 Km and several values of flexural rigidities. It can be seen that the maximum predicted depth are only one-half to one-third of the observed Carpathian foredeep, regardless of the flexural rigidities assumed.

We conclude therefore that the load represented by the thrust sheets and foredeep sediments in the profile across the Carpathian is insufficient to cause the observed deflection of the continental basement beneath the foredeep. This result implies the existence of an additional subsurface load that act on the subducted plate. We assume that the presence of the subsurface load is related to the existence of a crust consumption paleozone.

A relative good fit is obtained between the shape predicted by gravity and magnetotelluric data and the results of the computations. Modelling results from the profile give as a thickness of around 47 Km for the sedimentary cover. We obtained for the Moho discontinuity a depth of 38 Km between the Siret Fault and the paleozone subduction zone and 35 Km in the eastern and western part.

JSA40/W/02-B3

Poster

1400-06

#### IMPROVED BP SOFTWARE FOR 3-D GRAVITY INVERSION FOR MULTI-INTERFACES

ZHANG Minghua(Chinese Academy of Geoexploration, 31 College Road, Beijing, 100083, China, Email: zhmh-cag@china2.ygi.edu.cn) Hou Junsheng(China University of Geosciences, 29 College Road, Beijing,100083,China); Liu Kuanhou(The second branch, Chinese Academy of Geoexploration, Longshou Bei Road, Xi'an, 710016, China)

In order to determine depths to multiple strata with high resolution, we improved BP network method software. The measure is to utilize as many as possible geophysical vectors as nodes in the input layer of the network. The ambiguity in inversion is thus reduced. Had passed theoretical tests, the improved BP method software IBPS was applied in Liaohe Oil Field to determine depths to two main density interfaces. Twelve samples scattered over studied area are chosen for training. Each sample consists of Bouguer anomaly and its three directional derivatives, and two depth data to the interfaces. Result showed that inversion was convergent to real depths form lots of drilling and 3-D seismic, and that similarity or paralleling of upper interface to lower one disappeared, and that character of interface does not depend much on the number of samples used to train the network in general. In Huebei Oil Field, reservoirs discovered in recent years are buried mountains of Paleozoic, especially in Ordovician. It is difficult, however, for 2-D Seismic to reveal them because Ordovician is too deep, more than 5000m. IBPS is applied to solve this problem. Two drilling data and depth data at eight reliable points from 2-D seismic interpretation made in 80s are used for training. 1:50000 Bouguer anomaly is used for the network generalization. Three interfaces between upper Tertiary and lower Tertiary, Mesozoic and Paleozoic, and upper Paleozoic and lower Paleozoic, buried mountains and main faults are revealed. A large buried mountain under Dou Zhang is quite clear and some smaller buried mountains can also be recognized. Drilling from gravity interpretation based on IBPS has found a large reservoir at well ZM in Dou Zhang area in November 1998. The effectiveness of IBPS shows that it can be used for 3-D interpretation of gravity anomalies due to multi-interfaces, and that it is better than conventional methods.

JSA40/W/03-B3

Poster

1400-07

#### COUPLED INVERSION OF EARTH ROTATION AND GLOBAL MAGNETIC FIELD IN THE DECADAL TIME SCALE

L.BALLANI, H.Greiner-Mai and D.Stromeyer (all at GeoForschungsZentrum Potsdam, Telegrafenberg, D-14473 Potsdam, Germany, email: bal@gfz-potsdam.de)

## INTER-ASSOCIATION

An overview is given on some inverse problems related to the Earth rotation, the fluid outer core motion and the global magnetic field. Especially, the non-harmonic downward continuation of the surface magnetic field, assuming a non-vanishing electrical mantle conductivity, appears as the solution of an inverse boundary value problem which is connected with the mantle induction equation. It is a suitable tool for calculating the coupling torques numerically. As one example for the joint inversion of the Earth rotation and the magnetic field, the rigid relative rotation of a fluid outer core layer is studied. The amount of an intermediate inertial moment of this layer can be estimated which is responsible for the coupling and the correlation observable in the data.

**JSA40/W/04-B3** Poster **1400-08**

### REGIONAL AND RESIDUAL ISOSTATIC ANOMALIES OF WESTERN TURKEY AND THEIR CORRELATION WITH MAJOR TECTONIC PROVINCES

Mümtaz Hisarlı (Engineering Faculty, University of Istanbul, Avcılar Kampüsü, Istanbul, Turkey, email: mhisarli@istanbul.edu.tr) Naci Orbay (Engineering Faculty, University of Istanbul, Avcılar Kampüsü, Istanbul, Turkey, email: norbay@istanbul.edu.tr)

The aim of this study is to display more clearly gravity anomalies by geologic bodies in the upper parts of the crust of the Western Turkey. The topographic data and gravity data set are taken from National Data Center and Mineral Research and Exploration Institute of Turkey (M.T.A.) which have a resolution 5 by 5 min., respectively. Regional isostatic gravity map is based on an Airy-Heiskanen model of local compensation, which assumes that surface topography is supported by crustal thickening. This model requires a choice of values for three parameters: 1- a depth of compensation for sea level elevations, 2- a density contrast across the bottom of the root, and 3- a density of topographic load. These parameters are determined directly from the topographic elevations, free-air gravity, and Bouguer gravity data set for Western Turkey. The depth of compensation for sea level elevation of 25 km is determined using a spectral method applied to free-air gravity data. The density contrast between the crust and mantle of 0.61 g/cm<sup>3</sup> is determined from crossplots of the Bouguer gravity values versus topographic elevations. The density of topographic load of 2.6 g/cm<sup>3</sup> is determined using fractal technique.

In order to remove the isostatic component from the Bouguer gravity anomalies Airyroot algorithm used. The isostatic residual gravity anomalies are obtained by subtracting the regional isostatic anomaly values from the Bouguer gravity anomaly values of Western Turkey. The obtained residual gravity anomaly map is correlated with the tectonics structure of Western Turkey. As a result, the residual gravity anomalies are correspond to the E-W and NE-SW graben structures of the Western Anatolian.

**JSA40/W/06-B3** Poster **1400-09**

### GEOPHYSICAL INVESTIGATION OF A TERTIARY MAAR NEAR BARUTH (SAXONY, GERMANY)

GABRIEL, G., Pucher, R., Schulz, R., Wiederhold, H., Wonik, T. (Geowissenschaftliche Gemeinschaftsaufgaben, Stilleweg 2, 30657 Hannover, Germany; e-mail: gerald.gabriel@gga-hannover.de)

From regional gravity studies two local minima in the vicinity of Kleinsaubernitz and Baruth (Saxony, Germany) are known. The gravity low of Kleinsaubernitz is caused by 300 m limnic sediments underlying 200 m of miocene series, as could be proofed by drilling in 1970. Therefore, new interpretations proceeded on the assumption that the source of the anomaly Baruth (-7 mGal) is also a tertiary maar, produced by a phreatomagmatic explosion. In 1998 two research boreholes (280 m and 100 m deep) were realized by Geowissenschaftliche Gemeinschaftsaufgaben (Hannover, Germany) in order to enable various geoscientific studies. Extensive preliminary investigations were carried out with the aim to determine the best location for drilling. The different geophysical methods applied comprise gravity, magnetic, geoelectric and seismic surveys. Borehole measurements and VSP complemented these data sets later.

This poster presents a three-dimensional gravity model, that shows a fit of the observed and calculated gravity field better than 0.3 mGal. The geometry of the geological bodies and their densities take into account the results of the different geophysical investigations. Thus, the model can be seen as a synthesis of the actual state of the geoscientific knowledge. The tertiary maar of Baruth is nearly circular symmetric, its lateral extent is about 1200 m, whereas the thickness of the limnic sediments is 200 m.

**JSA40/W/07-B5** Poster **1400-10**

### GEOPHYSICAL CONSTRAINTS ON CONCEALED FAULTS - YORO FAULT AREA, CENTRAL JAPAN

Shigeo OKUMA, Yasuaki Murata, Masahiko Makino and Tadashi Nakatsuka (all at Geological Survey of Japan, 1-1-3 Higashi, Tsukuba, Ibaraki, 305-8567 Japan, email: okuma@gsj.go.jp)

High-resolution gravity and aeromagnetic surveys were conducted to reveal subsurface fault system at the western edge of the Nobi plain, Central Japan. Gravity values were observed at an interval of 20-50 m on the ground along three east-west lines with leveling. The gravity survey was successful to reveal buried faults in the eastern flank of the Yoro Mountains, showing small gravity changes (~ 2 mgal) which were not apparent in regional maps. A 2.5-dimensional model inversion was applied to interpret the gravity anomalies, referring to the result of a seismic reflection survey, which was conducted on the same line as the southernmost gravity profile. The resultant model show a concealed reverse fault, the Yoro fault, lying along the eastern flank of the Yoro Mountains with a vertical uplift of 2,000-3,000 m. The aeromagnetic survey was flown along east-west flight lines at an altitude of 300 m above ground and spaced 300 m apart, employing a kinematic GPS system. A magnetic high lies over the northern edge of the Yoro Mountains, showing a wider distribution of green rocks (altered basaltic volcanic rocks) than was expected. The magnetization intensity map derived from magnetic anomalies clearly shows that a magnetic body lies in the east flank of the northern part of the Yoro Mountains bounded by the assumed Yoro fault to the east. The results of combined analyses of gravity and magnetic anomalies for the area will be presented.

**JSA40/W/09-B3** Poster **1400-11**

### SOME RESULTS FROM THE REPRESENTATION OF THE LIVINGSTON ISLAND MAGNETIC ANOMALIES WITH A SET OF ELEMENTARY SOURCES

Zh. Zhelev (1), T. Petrova (1), V. Stanchev (2), D. Dimov (2) (1) Geophysical Institute, 1113 Sofia, Bulgaria, (2) Sofia University, Sofia, Bulgaria email: Jelelev@geophys.bas.bg / Fax : (3592) - 70 02 26

The Livingston island magnetic anomalies were studied with a set of elementary sources model. After some preliminary polynomial approximations to eliminate some residuals of the regional trend (so that to ease the optimization), the local anomalies together with the rest of the trend are modeled with a set of point sources and a linear trend. The unknown parameters of the suggested model are determined through optimization. The obtained results seems to

be quite in agreement with the intrusive bodies supposed to be in the upper part of the crust at different depths in this region.

**JSA40/W/10-B3** Poster **1400-12**

### SOME NEW RESULTS OF THE REPRESENTATION OF THE ALCALA DEL EBRO (ZARAGOZA) ANOMALY WITH A SET OF ELEMENTARY POINT SOURCES

Zh. Zhelev (1), T. Petrova (1), R. Wiera (2) and F. Montesions (2) (1) Geophysical Institute, 1113 Sofia, Bulgaria, (2) Institute de Astronomia y Geodesia, 28040, Madrid, Spain email: Petrova@geophys.bas.bg / Fax: (3592) - 70 02 26

The Alcala del Ebro (Zaragoza) gravity anomaly was studied with a set of point masses model. After a preliminary polynomial approximation to eliminate the main part of the regional trend (so that to ease the optimization process) the local gravity anomalies together with the rest of the trend are modeled with a set of elementary point sources and a linear trend. The unknown parameters of the suggested model are determined through optimization. The obtained results seems to be quite in agreement with carstic cavities filled with water or sediments supposed to be at depths of 12 to 20m. and the terrain colapses taken place in the last years in this region (Alcala der Ebro villa - Zaragoza, Spain).

**JSA40/W/11-B3** Poster **1400-13**

### SOME RESULTS ON THE REPRESENTATION OF SEVERAL MAGNETIC ANOMALIES OF BULGARIA WITH ELEMENTARY SOURCES

Zh. Zhelev (1), T. Petrova (1) (1) Geophysical Institute, 1113 Sofia, Bulgaria email: Jelelev@geophys.bas.bg / Fax: (3592) - 70 02 26 email: Petrova@geophys.bas.bg / Fax: (3592) - 70 02 26

Several complicated magnetic anomalies from the territory of South Bulgaria are interpreted with a set of elementary sources. The unknown parameters of the model (the depths of the sources and the respective masses) are approximately determined through optimization. A model of the corresponding magnetic field in the obtained results seems to be with a good agreement with the expectations on the base of other independent information.

**JSA40/W/13-B3** Poster **1400-14**

### MODELING AND EXPERIMENTS AT REGIONAL MAGNETIC ANOMALY ON EASTERN EDGE OF THE RUSSIAN PLATFORM

Natalia Fedorova, Sergei Maksimovskikh, Natalia Vinnichuk (Institute of Geophysics, 100 Amundsen str., Ekaterinburg, 620016, Russia. Fax: +7 3432 678872, Email: seva@maglab.mplik.ru

What kind of magnetisation - induced or remanent dominates in rocks in lower part of the crust is the problem under discussion. We examined the problem both by using modelling and experiment in situ at the regional magnetic anomalies located at the eastern part of the Russian platform. The sizes of anomalies are 60-200 km and total field intensities in their epicenters varies from 500 to 1500 nT. According to results of the anomalous magnetic field (AMF) interpretation the centres of magnetic sources disposes at the depths of 15-25 km. We assumed that rocks have only induced magnetisation and modeled changes of the AMF increment for different variations of external geomagnetic field: substorms, SQ and secular variations. In summer periods the total field magnitudes at our latitude are 20-30 nT while change in declination are 0.25 deg. Than according to our model AMF must have increment 0.5-1.5 nT and maximum of the increment must be disposed at the edge of anomaly but not in its epicenter. The induced effect was observed in situ during experiment at Manchag anomaly in summer 1998. Besides the anomalous behaviour of total field secular variation was revealed in the epicenter of the anomaly in 1969-1979. The result of modelling allowed us to explain this phenomenon as the manifestation of induced effect from magnetised rock.

**JSA40/W/14-B3** Poster **1400-15**

### A NEW APPROACH TO 2D INTERPRETATION OF POTENTIAL FIELD ANOMALIES

Nick Kostrov and Valery Kormiltsev (Institute of Geophysics, 100 Amundsen Str., Ekaterinburg, 620016, Russia. Email: root@maglab.mplik.ru, fax: +7 3432 678 880)

We developed a 2D interpretation complex to construct geophysical models of lithosphere utilizing potential fields data. The complex allow us to fit the anomalous magnetic field curves. The models can tell us about a range of magnetic susceptibility of Earth's crust based on potential fields observations. We represent cross-sections of the bodies and inhomogeneities as a set of arbitrary polygons with or without holes because a such delineation is more suitable from the geological point of view. Our method is based on the numerical solution of vector integral equation of Fredholm type 2 by means of triangulation of each source polygon into subareas so small that physical properties within them can be considered as constant. Green's function of a particular triangle is calculated analytically as a difference between inner complex logarithmic potentials of rectangle and outer one of the inscribed triangles adjoining to the particular. Besides, the complex permits to interpret gravity field separately or magnetic and gravity field jointly. There are examples of practical implementation of our method including cases of highly magnetized objects with inhomogeneous distribution of magnetic susceptibility.

**JSA40/E/01-B3** Poster **1400-16**

### THE 3D GEOMETRY OF THE LINGLONG GRANITIC COMPLEX FROM 2D GRAVITY FORWARD MODELLING, SHANDONG PROVINCE, EAST CHINA

HUALIN ZENG( Department of Applied Geophysics, China University of Geosciences (Beijing), 29 Xueyuan Road, Beijing 100083, China. E-mail: hualinzeng@sky.cugb.edu.cn.) Tianfeng Wan(Department of Geology and Mineral Resources, China University of Geosciences (Beijing), 29 Xueyuan Road, Beijing 100083, China. E-mail: wantf@sky.cugb.edu.cn.) Christian Teysier (Department of Geology and Geophysics, University of Minnesota, 108 Pillsburg Hall, 310 Pillsburg Drive S.E., Minneapolis, MN55455, USA. E-mail: teysier@tc.umn.edu.) Changli Yao(Department of Applied Geophysics, China University of Geosciences (Beijing), 29 Xueyuan Road, Beijing 100083, China. E-mail: yaocl@sky.cugb.edu.cn.) Basil Tikoff (Department of Geology and Geophysics, University of Minnesota, 108 Pillsburg Hall, 310 Pillsburg Drive S.E., Minneapolis, MN 55455, USA. E-mail: btikoff@gold.tc.umn.edu.)

The three-dimensional geometry of the Linglong granitic complex, which hosts the largest gold deposit field in China, Shandong Province, East China, is derived from 2D gravity forward modeling, constrained by geological data. A study on the geometry of the granite body at depth is particularly significant in order to better understand emplacement mechanisms and guide gold exploration. The geometry of the granitic complex is analyzed using 2D gravity forward modeling, constrained by the outcrops of the granites along each modeled profile. Anomalies along the profile were modeled using an interactive program derived from 2.5D forward



modeling techniques. The results show that the Linglong granitic complex is a sheet-like body with 3100 km<sup>2</sup> in areal extent, and a maximum thickness of 8 km. It is not a deeply rooted batholith as previously inferred.

**JSA40/E/05-B3** Poster **1400-17**

#### INTEGRATED INTERPRETATION OF THE COMPONENTS OF THE ANOMALOUS OF THE GEOMAGNETIC FIELD IN CUBAN TERRITORY

Rosa ALVAREZ, Jose Luis Cuevas, Lazaro Diaz, Eduardo Perez. (Institute of Geophysics and Astronomy, Science, Technology and Environmental Minister, 212 N. 2906 e/29 y31, La Lisa, Havana, Cuba)

The integration of different interpretation methodologies of the anomalous geomagnetic field in the Cuban territory demonstrated a more effective use of the geomagnetic information in the application of the geology and tectonic studies.

For our purpose were use the vectorial primary information from land surveys in our territory and different kinds of the mathematical and graphical processing as well image processing of the three components and spectral analysis.

Finally, was possible to obtain one and two-dimensional models for the region in dependence of the methods of processing. Also a regional tectonic chart was obtained based on the geomagnetic and gravimetric interpretation

**JSA40/E/06-B3** Poster **1400-18**

#### THE PHYSICAL NATURE OF THERMOELECTRIC EFFECT OF NATURAL MINERALS

RASULOVO D.Kh. Lange Institute of Hydrogeology and Engineering Geology Tashkent, Uzbekistan, e-mail: root@ariel.tashkent.uz

Despite the large volume of laboratory experimental data stored about thermoelectric effect of natural minerals the question of its origin has still remained open. Theoretical models suggested before could not explain the thermoelectric effect peculiarities. Therefore in work proposed the piezoelectric model formation of thermoelectric effect of natural minerals. According to this model, the mechanism of generation piezoelectric polarization take place as follows. Under influence the difference of temperature operating to specimen of mineral in it arise the mechanical tensions. These mechanical tensions stimulate the thrusting pressure of combined water, that contain in minerals. Many natural minerals contain quartz, that is piezoelectric crystal. Under influence of mechanical stress in such crystals form the difference of potentials between opposite faces. Proposed model was made it possible to explain data of experimental observations. From experimental data the author estimated the value of variation mechanical tension of sub-crystalline rocks, when their temperature change on a one degree. This value equals 5000 Pa/degree.

**JSA40/L/01-B3** Poster **1400-19**

#### EDGE ENHANCEMENT ON MAGNETIC DATA IN THE NORTHERN NILE VALLEY, EGYPT

MESBAH Maher A. Dept of Geological and Geophysical Engineering; Faculty of Pet. and Min. Eng., Suez Canal University, e-mail: mmesbah@frcu.eun.eg

Manual methods of the determination of faults from geophysical contour maps are influenced by personal experiences and views. In contrast, automated approaches give unbiased results. Therefore, the edge enhancement technique which is frequently used for mapping lineament on satellite images is adapted for detecting edges (faults) from magnetic data. The technique includes six sequential steps; three of them are typically applied in the digital processing of the remotely sensed images, while new three steps are added. Eight directional components are obtained by applying this technique. The adapted steps include vector to raster transformation, calculation of the directional components and smoothing them, contrast stretching, tracing of edges and frequency analysis of the extracted faults in the eight components. These steps are consequently applied on the reduced to the pole aeromagnetic map of the northern Nile Valley. Results of this application reflect the presence of faults in the eight directional components with various densities, extensions and patterns. Directions of these faults are recognized through eight directions (E-W, N-S, NW-SE, NE-SW, WNW-ESE, NNW, SSE, ENE-WSW, and NNE-SSW). The frequency analysis of these directions showed that the dominant directions of faults are the E-W, N-S, NNE-SSW, NE-SW and ENE-WSW directions, respectively.

**JSA40/L/02-B3** Poster **1400-20**

#### A PROPOSED SEISMIC / GEODETIC SUBSURFACE ANALYSIS BASED ON THE BIHARMONIC EQUIVALENT OF POISSON'S EQUATION

HARDY Rolland L. (International Institutes of Science and Technology, U.S. Post Office Bldg., Suite 202, 305 Avenue B, Bogalusa, LA 70427)

The biharmonic equivalent of Poisson's equation is defined here as follows. The biharmonic operator on potential at a point density is doubled the right hand side of Poisson's equation for the same point density. The mathematical proof of this and other matters are provided in the body of this presentation. This relationship had brought about the replacement of the point mass model with a point density model as the first step of the procedure. The point density model avoids the difficulties associated with point masses. Point masses produce impulse responses at zero distances. Point densities produce null responses at zero distances. Our point density model works extremely well for interpolating scattered geodetic surface data. The unknowns in our system of equations are interpretable as point density anomalies. It is customary to place the point density anomalies at shallow or near zero depths in the vicinity of the surface data. This cannot be done with point masses. We have not been concerned with the possible usefulness of the geodetically estimated point densities for other purposes. They simply provide the basis for smooth interpolation of several geodetic parameters, which fit data values exactly. In any case we are not competing with seismologists who in a sense are measuring densities, instead of estimating them. In fact we believe that geodetic interpolation could be improved with the use of seismic density data. That is why we are proposing a joint venture in seismic/geodetic subsurface analysis.

**JSA40/L/01-B5** Poster **1400-21**

#### PHENOMENOLOGICAL MODEL OF THE LOCAL TIDAL VARIATIONS

A.Zanimonska (Appl. Math. Dep., Kharkiv State Univ., Ukraine) J.Cisak (Institute of Geodesy and Cartography, Warsaw, Poland) Y.ZANIMONSKIY (Institute of Geodesy and Cartography, Warsaw, Poland, tempor.)

In the observatory Borowa Gora near Warsaw for the geodynamic researches the efforts for organization of permanent station with the portable ballistic gravimeter are applied. Due to absence a vibration damping system in this gravimeter, observation were organized during the nights and non-working days. The presence of essential breaks in data series make it

necessary to reduce the spectral leakage of surplus local tidal variations. These variations cannot be calculated by means the ordinary tidal models and are estimated in the data of a relative gravimeter, reaching 0,01mGal. Data processing and modelling were carried out by means it description as an analytical signal with parameters obtained by Hilbert transformation. The basic attention was given to representation and interpretation data in time domain and usage of a short-term spectrum on a subday intervals.

The transitive characteristic with small nonlinearity and delay phenomenologically takes into account the tidal displacements of the TT-zone border. Tidal forces are fully determined and as the signal on the input of a black box make it possible to calculate the local amendments for the any moment of time. The choice of optimal strategy for a tidal gravimeter usage is going to discuss too.

**JSM41**

**Wednesday 28 – Friday 30 July**

#### THE CONTRIBUTION OF SATELLITE OBSERVATIONS TO GLOBAL CLIMATE, OCEAN AND TERRESTRIAL MONITORING

Location: Mechanical Engineering G31 LT

Location of Posters: Old Gym

**Wednesday 28 July AM**

Presiding Chair: G.Ohring (NOAA/NESDIS/Office of Research and Applications, Camp Springs, MD 20746-4304, USA)

#### GLOBAL OBSERVING SYSTEMS

**JSM41/W/26-B3** Invited **0900**

#### TERRESTRIAL CLIMATE-RELATED OBSERVATIONS AND SATELLITE DATA

Josef Cihlar (GCOS/GTOS Terrestrial Observation Panel for Climate c/o Canada Centre for Remote Sensing Ottawa, Ontario, Canada. E-mail: josef@cihlar@ccrs.nrcan.gc.ca)

Concerns about the magnitude and rate of environmental changes at various spatial scales have led to the realization of the need for systematic, sustained observations that would help improve our understanding of these changes as well as facilitate the development and implementation of appropriate response actions. In the climate-terrestrial domain, the climate processes, climate impacts on the ecosystems and feedbacks to climate are of primary interest. To address these issues, the Global Climate Observing System (GCOS) and the Global Terrestrial Observing System (GTOS) have collaborated through a joint Terrestrial Observation Panel for Climate (TOPC). Following an analysis of scientific and modelling issues, TOPC identified a limited number of critical variables that need to be determined at various temporal frequencies and spatial resolutions, globally (GCOS-32). Given the extreme heterogeneity and the logistical as well as financial difficulties of collecting surface measurements, a combination of satellite and surface measurements is the only feasible response to these observation requirements. TOPC proposed a five-tier strategy, with Tier 1 consisting of few sites where many variables are observed using complex instruments (and possibly for a limited period) to Tier 5 consisting of a complete satellite coverage of the global landmass. The intermediate tiers consist of surface observatories focused on ecological, cryospheric, and hydrological processes and related variables. This tier-based framework takes advantage of the existing observation networks, employing their capabilities for climate studies and for an improved use of satellite data. Both surface and satellite observations to date have deficiencies with respect to climate applications because most of these were not intended to be used for this purpose. Aspects such as comprehensiveness of observations, consistency and comparability of methods, calibration, and others therefore need considerable improvements. These improvements, followed up by the establishments of long-term sustained observation programs are a major challenge for the global observing systems. They are being pursued in collaboration with surface regional networks and with the space agencies as part of an Integrated Global Observation Strategy. The numerous present and planned satellite missions will make possible major improvements in global terrestrial observations. The Kyoto Protocol and the importance of terrestrial carbon sinks therein, as well as recent emphasis the need for systematic climate observations by COP-4, have underlined the importance and urgency of these implementation activities.

**JSM41/W/25-B3** Invited **0930**

#### THE ROLE OF SATELLITE DATA IN THE ATMOSPHERIC COMPONENT OF GCOS

M.J. Manton (Bureau of Meteorology Research Centre, Melbourne, Victoria, Australia, Email: m.manton@bom.gov.au)

The Global Climate Observing System (GCOS) is an international program aimed at ensuring that the overall global observing system accounts for the various needs of the world-wide climate community. In addition to supporting regional climate activities, GCOS provides key data for seasonal to inter-annual prediction and for activities under the UN Framework Convention on Climate Change. The atmospheric component of GCOS builds on the existing networks of the World Weather Watch (WWW) and the Global Atmosphere Watch (GAW) of the World Meteorological Organization (WMO). A significant component of the additional benefits of GCOS is the promotion of baseline measurements that allow both for the calibration of regional networks and for the monitoring of global features of the climate system. In situ baseline networks of GCOS are the GCOS Upper Air Network (GUAN) and the GCOS Surface Network (GSN). Satellite data play a vital role in complementing these in situ observations. First satellite observations are used to support the calibration and validation of in situ data, such as GUAN. Secondly they make a vital contribution to data assimilation by providing global coverage of atmospheric variables, and this contribution is especially apparent in reanalysis projects. The third contribution of satellite data is through the generation of specific products, such as cloud analyses and precipitation products. These routine data sets are recognised by GCOS as providing essential global products on the state of the climate system. Satellite data are of fundamental importance to GCOS in the monitoring of the global radiation budget. While satellite data are vital to the overall climate observing system, their value is limited unless rigorous standards of calibration and consistency are established and maintained. Long-term climate monitoring requires much more stringent quality control than that which is normally applied to satellite missions of short-term duration. One of the roles of GCOS is to work with the relevant agencies to ensure that these issues are taken into account in all relevant observation programs.

**JSM41/W/33-B3** Invited **1000**

#### THE OCEAN OBSERVING SYSTEM FOR CLIMATE

Neville SMITH (Bureau of Meteorology Research Centre, Melbourne Vic. 3001, AUSTRALIA,



# INTER-ASSOCIATION

E-mail: N.Smith@BoM.GOV.AU)

The concepts of a Global Ocean Observing System and a Global Climate Observing System (GOOS and GCOS, respectively) were developed nearly ten years ago. Ocean observations for climate lie at the intersection of these two systems. Through the first half of this decade, a conceptual design for the ocean observing system for climate was developed, building upon the technical and scientific advances of Programs like the Tropical Oceans-Global Atmosphere Experiment (TOGA, 1985-94) and the World Ocean Circulation Experiment (WOCE, 1990-). The design described a system that would serve operational seasonal-to-interannual prediction, climate monitoring (e.g., sea level rise) and the development of various other climate products (e.g., global sea surface temperature and surface wind analyses). Subsequently there has been a concerted effort to identify the appropriate methods and mechanisms to implement and maintain the system. The observing system for seasonal-to-interannual prediction was given high priority, as was the development of a global in situ and remote network for monitoring variations in global sea level. A large fraction of the proposed elements now have long-term support. Unlike meteorology, oceanography did not have access to an implementation mechanism dedicated to the cause of ocean and climate observations. Recent decisions have now created such a body, the Joint Technical Commission for Oceanography and Marine Meteorology, to serve GOOS and GCOS plus research needs. Several other strategies are being developed to encourage long-term investment in the ocean observing system. The Global Ocean Data Assimilation Experiment (see Smith, "Toward Operational Oceanography And Climate Prediction", U7 Symposium on Integrated Global Monitoring Networks, this Conference) is being used to develop and promote an integrated approach and to develop and implement the required ocean estimation methods. GODAE is also working hard with the satellite community to ensure the requisite remote sensing systems are available. Argo, an initiative to populate the global oceans with profiling floats, will provide a greatly enhanced capability to sample the subsurface ocean. A set of ocean "observatories", using advanced mooring technology, are being proposed to provide on-going, improved estimates of ocean-atmosphere fluxes and provide extended Eulerian ocean time-series. The recent meeting of the Conference of the Parties to the Framework Convention on Climate Change accepted that increased efforts must be made to address gaps in the Global Observing Networks. Such recommendations have...

**JSM41/L/02-B3** Invited **1050**

## TOWARD A SATELLITE-BASED CLIMATE OBSERVING SYSTEM

Graeme L. Stephens (Colorado State University, Department of Atmospheric Science, Ft. Collins, CO 80523-1371, 970-491-8550 (voice), 970-491-3430 (fax), email: stephens@atmos.colostate.edu, cc: email: linin@atmos.colostate.edu).

Tracking the course of climate change requires a commitment to global-scale observations maintained over periods extending beyond decades and longer. The need to understand the nature of climate change to the point of ultimately assigning cause and effect places stringent and as yet not well understood requirements on these global-scale observations. In a statistical sense it is a difficult enough task to identify (typical) small trends in observed variables above the (typical) observed large climatic variability. This task is made all the more difficult by changing observing practices over the course of time. The problem of observing climate is now at an acute stage given the worldwide demise of conventional meteorological observing networks.

The scientific and programmatic challenge before us is to put in place an observing system or systems that provide observations of key parameters with both sufficient precision and accuracy on time scales that exceed duration of commitment.

The ongoing demise of conventional observing networks places increasing importance on use of satellite measurements not only to fulfil the operational needs of meteorological agencies but also to serve as the basis of a global climate observing system. The regular-in-time and global-in-space nature of these satellite observations makes them particularly attractive for climate research and monitoring purposes. Current operational satellite systems, however, are not optimized for this purpose. In using these operational-based satellite observations, scientists over the past decade have struggled in an attempt to understand and take account of such factors as lack of sensor calibration, sampling problems associated with platform drifts, lack of continuity of observations among a number of other issues.

The definition and design of a climate observing system is a topic of obvious importance in the realm of global climate change. It is also a topic under study by operational satellite agencies which now consider climate either as part of their mandate or are in the process of considering climate requirements in the planning for future observing systems. An example of this consideration has occurred through during the process of the convergence of the US military and civilian meteorological satellite programs under NPOESS.

This talk attempts to discuss critical elements of a climate observing system and will draw on examples and lessons learned from experience in using current satellite data. The distinction between monitoring versus climate process observations will be addressed and some suggestion as to the basic traits of observing systems that address these two distinct aspects of climate will be discussed.

Presiding Chair: P.Schluessel (Meteorologisches Institut, Universitaet Muenchen, Germany)

## ATMOSPHERIC MONITORING

**JSM41/L/05-B3** Invited **1120**

## REANALYSIS OF THE TOVS NOAA/NASA PATHFINDER ARCHIVE: APPLICATION TO CLIMATE RESEARCH

Alain CHEDIN

Improving our understanding of the Earth's climate natural variability as well as detecting potential anthropogenic climate change require, in particular, accurate estimates of many coherently determined surface, atmospheric, thermodynamic, and chemical variables. Among them, some vary quite slowly in time and space while others may vary by several orders of magnitude and in a very complex way, involving many factors. It is now recognized that the value of a global (time and space) description of their characteristics, both in the troposphere and in the stratosphere, is extremely high at this time.

Advances in the ongoing research are based on a multidisciplinary approach, using both modeling and observation. Only by using this approach can such advances be made in the understanding of the earth-ocean-atmosphere system and its sensitivity to anthropogenic changes and allow to make predictions about its short- and medium-term evolution. The basic tool for observing the planet on a global and continuous basis is the satellite, in either a polar or geostationary orbit. In this way, the main components of the Earth system can be observed with instruments which measure the radiances in either high of low spatial or spectral resolutions in a large variety of wavelengths (microwaves, infrared, visible and beyond). A few years ago, NOAA and NASA initiated the Pathfinder programme for the reanalysis of operational meteorological satellite observations.

We present, in this paper, the main characteristics of the TOVS Pathfinder 'Path-B' data set, resulting from the reanalysis of High resolution Infrared Radiation Sounder (HIRS-2) and Microwave Sounding Unit (MSU) observations with the 'Improved Initialization Inversion' (3I)

physico-statistical retrieval algorithm. This method is 'model-independent' (no influence of any forecast of climate model products), and takes great care of eliminating systematic biases that might occur, during one satellite life, or from one satellite to another, between calculated and observed radiances. 3I-derived climate variables are: the temperature and the water vapor vertical structure, the surface temperature and characteristics (emissivity, presence of snow, ice, deserts, etc.), the cloud field description (top, amount, type), and more integrated products like the longwave vertical radiative fluxes. Several auxiliary data sets (RAOBs in-situ measurements, SSM/I, AVHRR or ERBE observations, ISCCP or model analyses, etc.) have been used to carry out extensive validations of 3I-derived variables. If the validation...

**JSM41/E/04-B3** **1150**

## RESULTS FROM THE NOAA AVHRR ATMOSPHERIC PATHFINDER PROJECT

GEORGE OHRING and Herbert Jacobowitz (NOAA/NESDIS Office of Research and Applications 5200 Auth Rd. Suitland, MD 20746-4304)

This paper reports on the data sets of the NOAA AVHRR Atmospheric Pathfinder Program and their applicability to climate studies. As part of the NOAA/NASA Pathfinder Program, NOAA is reprocessing the archived AVHRR observations since 1981 into research quality atmospheric data sets. The raw observations were recalibrated using a vicarious calibration technique for the visible and near-infrared channels and an improved treatment of non-linearity for the infrared channels. State-of-the-art algorithms are used to process the global observations into channel radiances, total cloud amount, the components of the Earth's radiation budget (Outgoing Longwave Radiation and Absorbed Solar Radiation), and aerosol optical thickness (ocean areas only). The radiances and Earth radiation components are determined for clear, cloudy, and all-sky conditions. The output products are generated on an equal area grid with a resolution of approximately 110 km (10 latitude by 10 longitude at the equator), twice daily, and averaged over 5 day (pentad) and monthly periods. Applications of the data sets to radiative forcing, aerosol-cloud interactions, surface temperature/absorbed solar radiation/cloud relationships, and monitoring volcanic aerosols are presented. Problems with the use of the AVHRR for some climate studies are also described.

**JSM41/E/10-B3** **1205**

## INTER-ANNUAL VARIABILITY OF ATMOSPHERIC WATER VAPOR AS SEEN FROM THE TOVS PATHFINDER PATH A DATA SET

AMITA MEHTA and Joel Susskind 910.4, NASA-Goddard Space Flight Center Greenbelt, MD USA 20771

The atmospheric water vapour is a major greenhouse gas and plays a critical role in determining energy and water cycle in the climate system. A new, global, long-term (1985-98) water vapour data set derived from the TIROS Operational Vertical Sounder (TOVS) Path A system will be introduced in the presentation. An assessment of the accuracy of the TOVS Path A water vapour data will be presented. The focus of this oral presentation will be on the inter-annual variability of the water vapour distribution in the atmosphere and how it affects clear-sky outgoing longwave radiation variability. A comparison of water vapour distribution during 1986/97 and 1997/98 ENSO will also be presented.

**JSM41/W/30-B3** **1220**

## DERIVATION OF GLOBAL WATER VAPOUR DISTRIBUTIONS FROM ATSR DATA

Ian BARTON (CSIRO Marine Research, Australia, Email: ian.barton@marine.csiro.au)

A new product to be provided by the ATSR instrument team is a global distribution of averaged infrared brightness temperatures on a spatial scale of 18 km (10 arc-minutes in latitude and longitude). Data for a one-month period are analysed to demonstrate the potential of these data to provide a vertical and horizontal distribution of water vapour amounts over the global oceans. The six ATSR infrared channels (nadir and forward views at three wavelengths) are applied in a similar manner to those on the infrared sounding channels on the operational meteorological satellites. The weighting functions of the ATSR channels are found to give better vertical resolution in the lower troposphere than the typical channels used in the latest operational instruments.

**JSM41/P/01-B3** **1235**

## SEASONAL AND INTERANNUAL VARIABILITY OF BRIGHTNESS TEMPERATURE OVER INDIAN SUBCONTINENT

Ramesh P. SINGH and Nrusingha C. Mshra (both at Department of Civil Engineering, Indian Institute of Technology, Kanpur - 208 016, India, email: ramesh@iitk.ac.in)

The seasonal and yearly variations of brightness temperature measured by SSM/I satellite over land and ocean regions of India during the years 1987 to 1995 show characteristic behaviour. The brightness temperature variations over Indian land region is attributed to the different geological divisions of India. The brightness temperature variations over Arabian ocean and Bay of Bengal show systematic pattern. The brightness temperature changes significantly with latitude which show typical pattern. These systematic and typical pattern is interpreted in relation to seasonal and interannual variability of Monsoon over India and surrounding regions. From the brightness temperature, the snow thickness in the northern part of India, liquid water path (LWP) and total precipitable water (TPW) have been deduced for different seasons and also analysed yearly during 1987 - 1995. The effect of the north-west and south-west monsoon is clearly seen on the seasonal and interannual variations of brightness temperature and meteorological parameters. The role of seasonal and interannual variations of brightness temperature will be discussed in the global change and climatic variations.

Wednesday 28 July PM

**JSM41/W/13-B3** **1400**

## GNSS OCCULTATION SOUNDING FOR CLIMATE MONITORING AND ATMOSPHERIC CHANGE ANALYSIS

Gottfried Kirchengast and Andrea K. STEINER (Institut fuer Meteorologie und Geophysik, Universitaet Graz, Halbaerthgasse 1, A-8010 Graz, Austria, Email: andi.steiner@kfunigraz.ac.at), Luis Kornblueh, Elisa Manzini, and Lennart Bengtsson (Max-Planck-Institut fuer Meteorologie, Bundesstrasse 55, D-20146 Hamburg, Germany)

The Global Navigation Satellite System (GPS) and GLONASS, generically GNSS) based radio occultation technique is an active limb sounding technique exploiting quasi-horizontal transatmospheric sat-to-sat links. Both neutral atmospheric and ionospheric refractive

properties are probed and profiles of associated fundamental atmospheric variables such as temperature, humidity, and electron density can be retrieved with high quality. The method bears great utility for climate studies in providing a unique combination of global coverage, high vertical resolution and accuracy, long-term stability, and all-weather capability. A domain of highest strength of the method is the profiling of the thermal structure in the upper troposphere and stratosphere. As indications exist that the changing thermal structure in this domain is a sensitive indicator of atmospheric change (or climate change) and anthropogenic climatic impacts, respectively, we expect that occultation sounding can furnish unique data to globally monitor this changing structure with unprecedented accuracy.

We undertook to rigorously test the climate monitoring and atmospheric change detection capability of GNSS occultations by an integrated analysis involving: (i) realistic modeling of both the neutral atmosphere (T42L39-GCM up to the mesopause) and ionosphere (empirical, solar-activity dependent 4D model) over the time span 1995 to 2020, (ii) realistic observation system simulations of observables (phases and amplitudes) of a small GNSS receiver constellation (6 satellites) over this time period, (iii) a state-of-the-art occultation data processing chain for temperature profile retrieval in the upper troposphere/stratosphere (core region 8 to 40 km) for establishing a significant set of realistic simulated measurements over the period, (iv) a multivariate statistical analysis of 1996-2020 temporal trends in latitude-height slices of both the "true" states from the atmospheric modeling and the "measured" states from the database of retrieved temperature profiles, and (v) an assessment, by methods of statistical inference, of whether and to what degree the GNSS occultation observing system was able to detect trends in the atmospheric evolution (i.e., atmospheric change) from 1996 to 2020.

This ambitious study is expected to be still in progress at the time of the meeting and the latest status will thus be reported. We will discuss in some detail how we actually implemented steps (i) to (v) noted above, with emphasis on critical scientific and technical areas. Furthermore, we plan to present preliminary results on the climate trend analysis.

**JSM41/E/23-B3****1415****CLOUD-RADIATIVE FORCING TO FORM A COLD AIR-MASS WITH LOW-LEVEL CLOUDS OVER THE SUBARCTIC NORTH PACIFIC DURING SPRING AND SUMMER**

HIROSHI KAWAMURA, Hiroyuki Takeda and Nobuyuki Kikuchi Center for Atmospheric and Oceanic Studies, Tohoku University, Sendai 980, Japan

It is known by the ship observations that the subarctic North Pacific is frequently covered by low-level clouds (LLC) and fogs during spring to summer. It is also confirmed by the historical records of air temperature that the air-mass in the boundary layer over this ocean is rather uniform and colder, by about 5C, than that over lands in the same latitude band. This air mass occasionally blows toward south-west and bring cold summer to Japan, which causes serious agricultural damages and called "Yamase event".

In order to understand formation process of the cold air-mass over the subarctic ocean, the role of LLCs is investigated using the ISCCP (International Cloud Climatogy Project) data set. It is shown that LLC amount over the ocean north of 40N exceeds 70% in summer season, and optical thickness of LLC increases with time and has a peak in July. A core of the optically thick cloud is located in the Bering Sea. To estimate the LLC radiative forcing, radiation at the top of LLC and cloud-free surface is calculated by a radiative transfer code. The ISCCP cloud parameters are used as well as atmospheric parameters of the ECMWF data. The grid and time step of calculation are 280x280km and 1 minute, respectively. The monthly statistics are derived from the estimates obtained for five years of 1988-1992. The short wave radiation is reduced to 50% because of reflection at the cloud top. In contrast, the upward long wave radiation at the cloud top does not differ so much from that at the ocean surface because the altitude of cloud is low and the top temperature is close to SST. The strong contrast in the net radiation over the lands and oceans north of 40N is evident, and this is the main reason for generation of the cold air mass over the subarctic North Pacific during spring to summer.

**JSM41/W/11-B3****1430****A NEW SATELLITE-BASED CLIMATOLOGY OF CLOUDS IN THE NEW ZEALAND REGION**

Howard LARSEN, Warren Gray, and Peter Norris, National Institute for Water and Atmospheric Research, PO Box 14-901, Wellington, New Zealand, email: h.larsen@niwa.cri.nz

A cloud climatology of the New Zealand - South West Pacific region has been derived from AVHRR satellite data using a new cloud classification algorithm. The high-resolution climatology covers a large area of the ocean region around New Zealand, some 3500 km square, from 22°S to 55°S and 150° E to 167° W. It is based on data from May 1997 to the present. Clouds have been classified directly into classes based on their radiative properties and their spatial variability rather than traditional 'cloud type' classes.

Results from the first year of operation show clearly differentiated patterns of cloud coverage at different cloud heights and the effects of the New Zealand landmass. Low, warm clouds, for example, were frequent in a band between 40°S and 50°S but their occurrence is suppressed for several hundred kilometres either side of the New Zealand landmass. Significant seasonal variations in the pattern of cloud cover over the region are also apparent. Current GCM output is not entirely consistent with the measurements represented in the climatology, suggesting refinements are needed in modelling cloud-climate interactions in this region. Some of the discrepancies in modelled low cloud estimates are consistent with ocean-atmosphere interactions.

**JSM41/L/04-B3****1445****CLOUD CLIMATOLOGY FROM NOAA-9 SPLIT WINDOW AND COMPARISON BETWEEN CLOUD TYPE FROM SPLIT WINDOW AND TRMM RAIN OBSERVATIONS**

Toshiro Inoue (Ph.D. Meteorological Research Institute, 1-1, Nagamine, Tsukuba, Ibaraki 305-0052, Japan TEL : +81-298-52-9046(direct) FAX : +81-298-55-2552 e-mail: tinoue@mri-jma.go.jp FAX : +81-298-55-2683)

Using split window data, we can classify optically thin ice cloud and optically thick clouds. We construct the monthly mean cloud cover map for three cloud types (cumulonimbus-, cirrus- and low-level stratocumulus/cumulus- type) over the quasi- global area (50N-50S) in 1987 and 1988 from the split window data on board NOAA-9. The meaning of the cloud type classification by split window is verified using the rainfall information observed from PR (Precipitation Radar) data on board TRMM(Tropical Rainfall Measuring Mission). The TRMM has also VIRS (Visible and Infrared Scanner) and TMI(TRMM Microwave Imager). Using the split window of VIRS, coincident and collocated cloud type information and PR rainfall information are compared. We found optically thicker and colder cloud classified by the split window corresponded well to the PR/TRMM rainfall data.

**JSM41/W/10-B3****1500****VARIABILITY IN SURFACE TEMPERATURE, CLOUDS, AND SEA ICE COVER IN THE POLAR REGIONS INFERRED FROM INFRARED AND PASSIVE MICROWAVE DATA**

JOSEFINO C. COMISO (Laboratory for Hydrospheric Processes, Code 971, NASA/Goddard Space Flight Center, Greenbelt, MD, USA, 20771, email: comiso@joey.gsfc.nasa.gov)

Two decades of satellite infrared and passive microwave data have been analyzed to study seasonal and decadal changes in surface temperature, cloud cover, and sea ice cover in the polar regions. The data analyzed were derived from three key sensors, namely: the Advanced Very High Resolution Radiometer (AVHRR), the Scanning Multichannel Microwave Radiometer (SMMR), and the Special Scanning Microwave Radiometer (SSM/I). To better understand what two decades of data can reveal compared to one or a fraction, we analyzed several decades of in-situ temperature measurements and our results indicate that the trend values tend to stabilize as soon as fifteen to twenty years of data are available. The results of our analysis indicate significant warming in both poles, similar to what has been observed from station data, while the sea ice cover show decreases in extent in the north and no significant change in the south. Large seasonal and interannual variability is however observed, and the presence of the Antarctic Circumpolar Wave in the south, that goes around the continent at a periodicity of eight years, may affect ability to detect changes in the extent of the ice cover. Surface temperatures inferred from infrared data are also biased because of inability to obtain data during cloudy conditions. Cloud statistics from AVHRR data and possible effects on the surface temperature and ice cover will be presented.

**JSM 41/E/28-B3****1515****SIX YEARS OF COMPOSITE INFRA-RED IMAGES SOUTH OF FORTY DEGREES SOUTH AT THREE HOUR INTERVALS**

Charles STEARNS, Bruce Sinkula, Rob Holmes, Matt Lazzara, and J.T. Young (all at Space Science and Engineering Center, University of Wisconsin, 1225 West Dayton Street, Madison, Wisconsin 53711, USA)

At the University of Wisconsin Antarctic Meteorological Research Center (UWAMRC) a composite infrared (IR) image of Antarctica is formed every three hours and saved to an optical disk. The image is of the 11.5 to 12.5 micrometer (surface temperature) band: the image is 1.0 megabyte in size: the resolution is 10km. Regions without data in the 100 minute sampling window white. The initial geostationary satellites used and their longitude are GOES-7, 112 degrees West; GMS, 140 degrees East; Meteosat-3, 0 degrees; Meteosat-4, 75 degrees West,. The initial polar orbiting are NOAA 11 and NOAA 12. The time of the composite images is within 50 minutes of the indicated time on the image. The image extends from the South Pole to approximately 34 degrees South in the corners with New Zealand in the upper left hand corner and to 58 degrees South at the edges closest to the South Pole. A VHS tape of the composite IR images from 31 October 1992 to 30 November 1998 is prepared from the archive at the UWAMRC. The original image resolution is 10 km but the transfer of the images to the tape increases the resolution to about 20 km. Each image is displayed for 0.3 seconds. Images are timed and dated for reference when requesting more detailed data from the UWAMRC.

**JSM41/L/02-B3**

Invited

**1550****A SATELLITE-DERIVED FRESHWATER FLUX CLIMATOLOGY: THE HAMBURG OCEAN ATMOSPHERE PARAMETERS AND FLUXES FROM SATELLITE DATA**

Jörg Schulz , Peter Bauer, Lars Schanz (German Aerospace Center, Linder Höhe, D-51147 Köln, Germany, email: joerg.schulz@dlr.de), Volker Jost (Meteorologisches Institut, Universität Hamburg, Bundesstraße 55, D-20146 Hamburg, Germany, email: jost@dkrz.de), Peter Schlüssel (Meteorologisches Institut, Universität München, Theresienstraße 37, D-80333 München, Germany, email: schluessel@meteo.physik.uni-muenchen.de)

Knowledge of turbulent fluxes between ocean and atmosphere is along with radiative fluxes of great importance to improve our understanding of the large scale climate system. Accurate estimates of these fields can be used as a direct forcing of ocean circulation models or for evaluating the results of coupled climate models that have obviously problems at the air-sea interface. In this talk a climatology of freshwater flux at the sea surface will be presented together with a review of the used retrieval schemes, a comprehensive error assessment, and some examples for the application of such a climatology. The climatology extends over 10.5 years of data and consists of global fields of latent heat flux, freshwater flux, net longwave flux, rainfall, and all associated atmospheric and oceanic parameters. The error assessment is based on validation of the retrieval algorithms and on comparisons to other climatologies constructed from different type of data. As an example comparisons to buoy data gained during the subduction experiment 1991 to 1993 in the eastern subtropical North Atlantic will be shown. This data set is one of the few data sets which are useful to compare not only instantaneous measurements but also long time averages.

Time sampling errors mostly concerning precipitation measurements in the tropics have been assessed by comparisons to radar data gained during TOGA COARE. The sampling error for a grid resolution of 2° by 3° and a sampling time of 3 weeks can be as high as 30% if only one satellite overpass per day was available. If data of two SSM/Is were combined this error can be diminished to less than 4% in the case of 4 overpasses a day.

Improvements of the climatology can be expected if knowledge gained from the Tropical Rainfall Measuring Mission (TRMM) is used to improve SSM/I rainfall algorithms. This shall reflect in both reduction of random error through higher accuracy of TRMM retrievals and reduction of systematic time sampling errors by knowing more about the mean diurnal cycle of precipitation over the ocean.

**JSM41/E/01-B3****1620****GLOBAL MONITORING OF PRECIPITATION ON MONTHLY AND SHORTER TIME SCALES UTILIZING LOW-ORBIT AND GEOSYNCHRONOUS SATELLITE OBSERVATIONS**

ROBERT ADLER, NASA/Goddard Space Flight Center, Code 912, Greenbelt, MD, 20771 ; Scott Curtis, NASA/GSFC, JCE/UMBC, Code 912, Greenbelt, MD, 20771 George Huffman, NASA/GSFC, SSAI, Code 912, Greenbelt, MD, 20771 David Bolvin, NASA/GSFC, SSAI, Code 912, Greenbelt, MD, 20771 Eric Nelkin, NASA/GSFC, SSAI, Code 912, Greenbelt, MD, 20771

A satellite-based system to monitor global precipitation on monthly and shorter time scales is described. The monitoring system is based primarily on the Global Precipitation Climatology Project (GPCP) global, monthly, 2.5fx 2.5f latitude-longitude product which utilizes precipitation estimates from low-orbit microwave sensors (SSM/I) and geosynchronous IR sensors and raingauge information over land. The low-orbit microwave estimates are used to adjust or correct the geosynchronous IR estimates, thereby maximizing the utility of the more physically based microwave estimates and the finer time sampling of the geosynchronous observations. Information from raingauges is blended into the analyses over land. This globally complete, monthly product is available from January 1986 to the present, with an extension



## INTER-ASSOCIATION

back to January 1979 underway using non-SSM/I data.

The monthly GPCP merged data product is augmented in real-time by low-orbit microwave (SSM/I) estimates. Anomalies from climatological means are produced from both the GPCP and microwave fields to monitor the evolution of global precipitation, including the calculation of ENSO precipitation indices for real-time (five-day running means) climate monitoring and comparison with previous ENSO anomalies.

On an even shorter time scale, a new daily,  $1^\circ \times 1^\circ$  latitude-longitude global analysis has been developed starting in January 1997 utilizing low-orbit microwave and geosynchronous IR information using a similar method as is used to produce the monthly GPCP product.

**JSM 41/E/260-B3**

Invited

1635

### SATELLITE REMOTE SENSING OF PRECIPITATION

ERIC BARRETT (School of Geographical Sciences, University of Bristol, Bristol, BS8 1SS, UK, Email: e.c.barrett@bris.ac.uk)

As recently as 30 years ago, knowledge of global precipitation amounts, distributions, and temporal variabilities relied almost entirely on measurements made by rain gauges. Rainfall climatologies even from that era were almost all limited to the continental land masses, excluding Antarctica as well as the North Polar ice cap. More recently, much additional information has been gathered by remote sensing systems, notably by ground-based weather radar, but most of all from meteorological satellites operating passively in the visible, infrared, and microwave regions of the electromagnetic spectrum, and newly (since 1997) actively too, in the microwave region. Thus, although rain gauge networks have generally declined in recent decades, as this paper illustrates our knowledge of global rainfall climatologies today has become much more advanced. This fact is important not only for its own sake, but also on account of the significance of precipitation for global modelling, especially of the atmosphere, hydrosphere, cryosphere and biosphere. This review paper first recalls some of the more significant findings of satellite remote sensing in respect of precipitation since 1969. Next, it identifies some of the greatest problems and challenges facing the satellite precipitation science community today. Finally, it suggests where related resources might be focused most usefully in the near-term future, not least to ensure that appropriate information on global precipitation on time-scales ranging from seasonal-interannual to decadal be secured for a wide range of potential end-users.

**JSM41/W/01-B3**

1705

### A COMBINED INFRARED AND MICROWAVE TECHNIQUE FOR STUDYING THE DIURNAL VARIATION OF RAINFALL OVER AMAZONIA

ANDREW J. NEGRI (1), Emmanouil Anagnostou (2) and Robert F. Adler (1) (1) NASA/GSFC, Laboratory for Atmospheres, Greenbelt, MD 20771, e-mail: negri@erin.gsfc.nasa.gov (2) Dept. of Civil and Environmental Engineering, U. Conn., Storrs, CT 06269

Over 10 years of continuous data from the Special Sensor Microwave Imager (SSM/I) aboard a series of Defense Department satellites has made it possible to construct regional rainfall climatologies at high spatial resolution. Using the Goddard Profiling Algorithm (GPROF), monthly estimates of precipitation were made over the region of northern Brazil, including the Amazon Basin, for 1987 to 1998. GPROF is a physical approach to passive microwave precipitation retrieval, which uses the Goddard Cumulus Ensemble (cloud) model to establish prior probability densities of precipitation structures. Precipitation fields from GPROF were stratified into morning and evening satellite overpasses, and accumulated at monthly intervals at 0.5 degree spatial resolution. Important diurnal effects were noted in the analysis, the most pronounced being a land/sea breeze circulation along the northern coast of Brazil and a mountain/valley circulation along the Andes. There were also indications of morning rainfall maxima along the major rivers, and evening maxima between the rivers. The addition of simultaneous geosynchronous infrared (IR) data leads to the current technique, which takes advantage of the 30 minute sampling and 4 km spatial resolution of the infrared channel and the better physics of the microwave retrieval. The resultant IR method is subsequently used to derive the diurnal variability of rainfall over the Amazon basin, and further, to investigate the relative contribution from its convective and stratiform components.

**JSM41/E/06-B3**

1720

### GLOBAL PRECIPITATION FIELDS FROM ACTIVE MICROWAVE SENSORS

G.D. Quartly, T.H. GUYMER and M.A. Srokosz Southampton Oceanography Centre, Empress Dock, Southampton, Hants, SO17 3SH

For over a decade precipitation information has been available from infrared satellites such as METEOSAT and passive microwave sensors such as SSM/I. Recently developments have been made in the processing of active microwave data from the TOPEX altimeter so that it too can provide information on rain. This talk will summarise the technique and examine the fields produced from 6 years of consistent data from one satellite. The processing yields not only the familiar geographical patterns of rainfall but reasonable estimates of the rain rates involved. The small footprint of the instrument allows studies of the short-scale variations in rainfall, which reveal the organization of rain events typically to have a larger size to the west of ocean basins than to the east. As the altimeter also provides estimates of the wave height and wind speed, we can observe which weather conditions the precipitation is preferentially associated with. We will compare our results with studies using infrared and passive microwave sensors, indicating both the advantages and disadvantages of a TOPEX-derived climatology, and discuss the prospects for further active microwave sensors, such as TRMM (launched in November 1997) and TRMM II.

**JSM41/E/29-B3**

1735

### SSM/I WIND SPEED CLIMATOLOGY OF THE TIME OF MONSOON WIND ONSET IN THE WESTERN ARABIAN SEA

DAVID HALPERN (Jet Propulsion Laboratory, California Institute of Technology, Pasadena, CA 91109-8099, U.S.A., email halpern@pacific.jpl.nasa.gov)

Forecasting the time of onset of monsoon wind in the western Arabian Sea is an important unsolved problem. Prior to measurements of the surface wind field by satellite, there was an absence of suitable surface wind observations over the Arabian Sea. The NASA scatterometer (NSCAT) surface wind vectors revealed that the time of the 1997 onset of 12 m/s south-west monsoon wind speeds in the western Arabian Sea preceded the onset of monsoon rainfall in Goa, India, by 3 - 4 days. Wind speed and direction data were necessary to establish a dynamical mechanism between times of onset of 12 m/s wind speed off Somalia and rainfall in Goa. Except for NSCAT, no satellite scatterometer wind product recorded adequately sampled 2-day  $1^\circ \times 1^\circ$  averaged wind vectors, which are the required space and time scales, to examine the onset of the Somali Jet. However, the greater-than-95% steadiness of summer monsoon winds allows the use of satellite measurements of surface wind speed. The Special

Sensor Microwave Imager (SSM/I) recorded surface wind speed with adequate sampling to produce a 1-day,  $1^\circ \times 1^\circ$  data product during 1988 - 1998. SSM/I data had been uniformly processed throughout the period. Times of onset of SSM/I 12 m/s wind speed off Somalia were 21 May 1988, 24 May 1989, 17 May 1990, 28 May 1991, 8 June 1992, 28 May 1993, 30 May 1994, 7 June 1995, 29 May 1996, 12 June 1997, and 15 May 1998. Uncertainty of the 1992 and 1996 times of onset were increased because of the absence of SSM/I data on 6 and 7 June 1992 and on 30 May 1996. Correlations of the timing of monsoon wind onset with El Niño will be described. The difference between times of onset of 12 m/s wind speed and Goa rainfall will be discussed. At the time of abstract submission, Goa rainfall data have not arrived from the India Meteorological Department.

**JSM41/E/17-B3**

1750

### SIMULTANEOUS REMOTE SENSING OF AEROSOL FEATURES AND SURFACE REFLECTANCE WITH SPACE-BORNE SPECTROMETRY

Daren LU, Mingzhen Duan, (Institute of Atmospheric Physics, Chinese Academy of Sciences, Beijing 100029, CHINA, e-mail: ludr@sun.ihep.ac.cn)

In quantitative remote sensing of atmospheric and earth surface parameters with space-borne optically spectral sensors, atmospheric correction and surface (background) influence deduction are key steps for both surface and atmospheric remote sensing, respectively. In principle, these two steps are with same task, i.e., decoupling or separation of respective contributions to spectral radiance (or normalized reflectance) observed by space-borne sensors. A lot of efforts have been paid to solve this problem. Most of them are using supplementary information obtained by ground-based observation or climatological means for the atmosphere or surfaces. Owing to the limitations of simultaneous surface measurements and temporal and spatial variation of the atmosphere and earth surfaces, above-mentioned efforts are always faced significant error or very limited usefulness. It is commonly recognized that the best or ideal way is simultaneous remote sensing of the atmosphere and surface with space-borne sensors alone (with least assumptions). In general there are three approaches towards simultaneous remote sensing, i.e., multi-angle measurements, multi-spectral measurements, and multi-polarization measurements, and their combinations. In different assumptions, each of them may apply to simultaneous remote sensing. After general discussion, this paper will mainly focus on the approach with multi-spectral observation in Visible-NIR waveband. The present approach includes two steps, the first step is to establish approximate formulae which may explicitly give quantitative contribution of the atmosphere and surface to satellite-borne sensors measurements. The second step is to establish retrieval scheme by using the above mentioned formulae and the spectral dependence of both the atmospheric optical depth and surface reflectance. Details about principle and preliminary results are given in this paper.

Thursday 29 July AM

Presiding Chair: P.Schluessel (Meteorologisches Institut, Universitaet Muenchen, Germany)

## ATMOSPHERIC MODELLING BY MONITORING

**JSM41/W/28-B4**

0930

### POTENTIAL OF METEOSAT SECOND GENERATION TO CLIMATE MONITORING

Yves M. Govaerts, Arlindo Arriaga and Johannes Schmetz (EUMETSAT, Am Kavalleriesand 31, D-64295 Darmstadt, Germany, email govaerts@eumetsat.de, arriaga@eumetsat.de, schmetz@eumetsat.de)

In 2000, EUMETSAT will launch the first Meteosat Second Generation (MSG-1) satellite centred on zero degree longitude. In comparison with the current Meteosat satellites, the MSG system will feature enhanced observation capabilities. Its Spinning Enhanced Visible and Infrared Imager (SEVIRI) provides data in 12 spectral channels instead of 3, distributed throughout the short and long wave parts of the electromagnetic spectrum. The imaging frequency is 15 minutes and the sampling resolution at the sub-satellite point is  $3' \times 3$  km for all channels except the VIS high-resolution band which has a  $1' \times 1$  km nadir resolution. The above enhancements have been driven by the increasingly stringent requirements of the meteorological user community in the areas of nowcasting and numerical weather prediction. The combined improvements in spectral coverage, imaging frequency and ground resolution were needed to better characterise clouds and the vertical structure of the atmosphere, to improve the sampling of dangerous weather patterns, and to derive more accurate atmospheric motion vectors. Calibration of the IR channels is carried out using on-board blackbody operated at two temperatures and vicarious calibration methods. The visible and near infrared channels calibration relies on vicarious method using bright desert targets. Calibration is a critical requirement for climate applications and the expected accuracy will be discussed first. The SEVIRI characteristics, in conjunction with the MSG mission duration (at least 12 years of continuous observations), provide the basis for improved and new products to be used for climate monitoring. The climate observations of SEVIRI are wide spread with enhanced capabilities for observing cloud micro-physical properties, water vapour and land surfaces. In particular, the increased spectral coverage and time-space sampling of MSG imagery are expected to open new avenues for the study of land surface properties, their diurnal variation, and the associated land surface and land-atmosphere interaction processes. Various examples of climate product derived from MSG observations will be given. MSG also carries a radiation budget scanner (GERB), the first instrument of this type in geostationary orbit. Simultaneous observations of spectral radiances from SEVIRI and broadband radiances from GERB will enable novel studies of regional radiation budget parameters.

**JSM41/E/22-B4**

0945

### THE ANTARCTIC METEOROLOGY RESEARCH CENTER: AN INTEGRATED METEOROLOGICAL DATABASE FOR RESEARCH IN THE SOUTHERN HIGH LATITUDES

Matthew Lazzara, George WEIDNER, J.T. Young and Charles Stearns (all at the Space Science and Engineering Center University of Wisconsin, 1225 West Dayton Street, Madison, Wisconsin 53706, USA)

The Antarctic Meteorological Research Center (AMRC) was created in 1992 with funding from the National Science Foundation's United States Antarctic Program (USAP) Office of Polar Programs (OPP) to provide improved access to meteorological data available in Antarctica to the wider scientific community, provide a single source for data from both ground based and satellite derived meteorological data and to provide real-time data to those tasked with providing weather forecasts in support of operations funded by USAP during the Austral Summer field season. Since, meteorological data from Antarctica is only some 40 years old, satellite derived data sets for the Antarctic represent a larger fraction of the recorded data than in other areas. For the Antarctic, the integration of satellite derived data with other data sets provides an important contribution to the study of climate change in the high latitudes and the connections at various time scales between the lower and higher latitudes. Since that time the AMRC has collected, archived and made available to users a significant amount of meteorological data in support of atmospheric research, research in other fields requiring meteorological data, operational forecasting and educational support. A review of the present



set of data collected and archived by the AMRC will be given. These data sets include satellite data from the geostationary and polar-orbiting satellites, synoptic observations, radiosonde observations, automatic weather (AWS) observations and National Meteorological Center's (NMC) Medium Range Forecast Model (MRF) analyses and forecast for use over Antarctica. Recent product additions are a low-mid level infrared wind product and satellite derived winds from the water vapour channel of the GMS-5 satellite in an online archive. Future data from anticipated new satellite platforms will be presented. Examples of the current uses of the AMRC database will be given.

**JSM41/W/08-B4** Poster 1000-01

#### THE STRATOSPHERIC AEROSOL AND GAS EXPERIMENT III

Larry W. Thomason (Atmospheric Sciences Division, NASA Langley Research Center, Hampton, VA 23681 USA, Email: l.w.thomason@larc.nasa.gov), Michael C. PITTS (Science Applications International Corporation, One Enterprise Parkway, Suite 250, Hampton, VA 23666, USA, email: m.c.pitts@larc.nasa.gov)

The Stratospheric Aerosol and Gas Experiment (SAGE) III is the latest in a series of satellite-based instruments to use the polar occultation technique to measure stratospheric and upper tropospheric aerosols and trace gas species. The first instrument will be launched aboard a Russian Meteor 3M platform in Fall 1999. Later flights are scheduled for the International Space Station in 2002 and a Flight-of-Opportunity between 2000 and 2005. SAGE III preserves the robust characteristics of the SAGE series, including self-calibration and high vertical resolution, and adds new capabilities designed to contribute to understanding global climate change. Among these enhancements is a lunar occultation mode in which night time species such as nitrogen trioxide and chlorine dioxide are measured (in addition to ozone and nitrogen dioxide). During solar occultation, measurements of the oxygen A band will be used to infer temperature and pressure profiles from 0 to 85 km. In addition, finer spectral resolution measurements of nitrogen dioxide features near 440 nm and ozone around 600 nm will improve the quality of inferences of those species relative to SAGE II measurements. The spectral coverage of aerosol extinction measurements has been extended to 8 measurements between 385 and 1550 nm compared to SAGE II measurements at 385, 453, 525, and 1020 nm. SAGE III should make significant contributions to understanding the long-term ozone trend and the processes that underlie it. In this presentation, we will discuss the SAGE III instrument design, retrieval algorithm, data products, and plans for validation.

**JSM41/W/31-B4** Poster 1005-02

#### AN EMPIRICAL MODEL FOR GLOBAL ATMOSPHERIC TEMPERATURE ANOMALIES

Olavi KARNER (Tartu Observatory, 61602 Toravere, Estonia, email: olavi@aai.ee)

Global record of temperature fluctuations in the lower troposphere (the lowest 5 miles of the atmosphere) and the lower stratosphere (covering an altitude range of about 9-12 miles) have been monitored by satellite since 1979. The monthly-averaged temperature anomalies for the entire length of record, available online <http://www.ghec.msfc.nasa.gov/temperature/>, have been analysed by means of fitted autoregressive and integrated moving average (ARIMA) models. A nonstationary first order IMA model appears to be appropriate to represent the temporal variability of global temperature anomalies during the period. The model explains about 95 per cent of variance in the stratospheric case. This enables one to use it for short-term predictions of the anomalies. An example will be presented.

**JSM41/E/32-B4** Poster 1010-03

#### RADIOMETRIC CALIBRATION OF THE EARTH'S SCAN IMAGES TRANSMITTED BY GEOSTATIONARY SATELLITE GOMS IN THE VISUAL AND IR SPECTRAL RANGES

S.G.PUGACHEVA, V.V.Shevchenko (both at Sternberg State Astronomical Institute, Moscow University, Universitetskii pr.13, Moscow, 119899, Russia, email: pugach@sai.msu.u)

The technique of calibrating scan images using the Moon's image can be successfully used for the radiometric calibration of the onboard apparatus of the first Russian geostationary artificial meteorological satellite (GOMS) launched on October 31, 1994, in accordance with the program Meteorological Service for the Population. For realization of meteorological observations satellite GOMS has television complex, which gives in actual time scale of the digital images of a cloudy, snow and ice cover and measures of radiation temperature of a surface of an ocean, land and high bound of a clouds. The calibration procedure is based on the comparison of the output data of the onboard apparatus of the geostationary satellite GOMS with a photometric database that includes measured values of brightness and temperature for a large number of lunar-surface areas. To this end, an automated database was created, which contains brightness and temperature values for 1954 areas of the lunar surface, measured by the global scanning of the illuminated lunar disk in the visual (0.445 micron) and infrared (10-12 micron) spectral ranges during a complete lunation. It is known that the emission of the lunar surface in the visual and infrared spectral ranges is stable and constant in space and time and can easily be described analytically. A generalized digital analytical model of the lunar brightness and thermal fields makes it possible to calculate the necessary photometric parameters, surface brightness and temperature for any geometry of the angular parameters of photography and illumination with an accuracy achieved by ground-based photometry. The root-mean-square errors in the determination of the rightness and of the radiation temperature are + 1.5 relative units and + 1.5 K, respectively. The IR channel records thermal fluxes objects with radiation temperatures between 213 and 313 K. The noise level does not exceed 1 K.

**JSM41/W/04-B4** Poster 1015-04

#### HIGH RESOLUTION SYNOPTIC TOTAL OZONE IMAGING FROM A GEOSTATIONARY SATELLITE : A CASE STUDY USING GOES-8 INFRARED RETRIEVALS, GOME OBSERVATIONS AND A NUMERICAL ADVECTION MODEL

Yvan J. ORSOLINI (Norwegian Institute for Air Research; email: orsolini@nilu.no) Fernand Karcher (METEO-FRANCE, Centre National de Recherches Meteorologiques, Toulouse)

The second generation European weather satellite to be launched near the year 2000 is designed to routinely and synoptically monitor total ozone using infrared remote sensing, with a full coverage of the Earth disk. These total ozone observations are likely to convey a wealth of information about dynamical processes in the lower stratosphere. Hence, there is a need for validation and characterization of total ozone structures observed from geostationary satellites before ozone IR remote sensing from such a platform could be routinely used for meteorological applications. A set of high spatial resolution (pixel size near .1 degree) total ozone synoptic images have been produced hourly for the period February 23 to 24 using the GOES-8 IR radiance in 13 channels. The GOES-derived total ozone in the imaging window, covering the eastern US and contiguous maritime areas, is validated against the total ozone measured by GOME. These images show with great detail fine-scale total ozone filaments.

The reality of such features is corroborated by a 5-day numerical simulation of the ozone distribution using analysed ECMWF winds, and an initial 3D ozone field from Microwave Limb Sounder data from the Upper Atmosphere Research Satellite.

Presiding Chair: H.Kawamura (Center for Atmospheric and Oceanic Studies, Tohoku University, Japan)

### OCEAN MONITORING

**JSM41/L/03-B4** Invited 1040

#### GLOBAL SEA SURFACE TEMPERATURE MONITORING FROM SPACE; CURRENT ISSUES OF DEFINITION, ACCURACY AND VALIDATION.

Ian S. Robinson (School of Ocean and Earth Science, University of Southampton, Southampton Oceanography Centre, UK)

Sea surface temperature (SST) is a variable, readily measured from space, which has importance as a driver of air-sea interaction processes, for assimilation into coupled ocean-atmosphere models, and as an indicator of climate change. This talk reviews the differing requirements for accuracy and resolution of global SST data, which are driven by diverse applications of the data. These are compared with the current best achievements of satellite infrared systems in applying corrections for atmospheric effects on the measured radiation. Now that atmospheric correction accuracies using dual-view systems are approaching 0.1 C, it is becoming clear that both the application and the validation of space-derived SST are subject to the thermal structure of the upper ocean. Several reasons are presented to support the proposal that the skin temperature of the upper few microns of the sea surface is the most appropriate measure of SST. This is what is viewed directly by satellite sensors, it is what controls air-sea fluxes, and it is the only definition of SST which is not arbitrarily dependent on the depth of sampling. However, this raises issues of diurnal variability of the skin temperature which need to be handled in a consistent and systematic way in the compilation of SST databases, if SST is to be useful and unambiguous as an indicator of climate change. The potential synergy of geostationary and polar orbiting sensors for generating composite SST fields is considered in this context. Finally the question of validation is addressed, identifying the need for a more comprehensive availability of in situ radiometric measurements of the skin temperature.

**JSM41/W/36-B4** 1110

#### THE USE OF RADIATIVE TRANSFER MODELLING IN IMPROVING SATELLITE SEA SURFACE TEMPERATURE RETRIEVAL

BK MCATEE, M Boterhoven, A Rodger, and MJ Lynch (Remote Sensing and Satellite Research Group, School of Physical Sciences, Curtin University of Technology, GPO Box U1987, Perth WA 6845, Australia, email: pmcateebk@cc.curtin.edu.au) AF Pearce (CSIRO Marine Laboratories, PO Box 20, North Beach WA 6020, Australia, email: alan.pearce@marine.csiro.au)

Satellite-derived sea surface temperature (SST) may be improved by the incorporation of regional atmospheric information into the SST retrieval algorithm. Our discussion of satellite SST retrieval will include computer modelling of radiative transfer as well as the development, performance and sensitivity analysis of SST algorithms.

The algorithms currently under development are designed to improve the accuracy of SST retrieval by accounting for seasonal and latitudinal variation in climatic conditions through the incorporation of the computer simulation of the radiative transfer process into the scheme using an atmospheric transmittance model. Data input to the model may be derived from sources such as radiosonde and TOVS measurement of atmospheric properties.

Progress in algorithm development will be discussed along with the effectiveness of particular algorithms in various scenarios and a description of field measurements of SST and validation of the algorithms.

**JSM41/W/15-B4** 1125

#### SATELLITE OBSERVATIONS OF SEASONAL TO DECADAL VARIABILITY IN THE LARGE-SCALE OCEANIC FRONTAL ZONES

Alexander KAZMIN (Frontier Research System for Global Change/Institute for Global Change Research, SEAVANS N 7F,1-2-1 Shibaura, Minato-ku, Tokyo 105, Japan, email: kazmin@frontier.esto.or.jp)

Sea surface temperature (SST) from weekly global satellite data at 18 km resolution for the period of 1982-97 and estimates of the surface forcing due to wind stress and net heat flux were used to investigate global monthly climatology of the large-scale oceanic frontal zones (OFZ), seasonal and interannual variability of SST gradient in several frontal zones, response of OFZ to decadal climate changes, and the meridional frontogenesis in the North Pacific. A computer animation of the full-resolution monthly climatologies of SST gradient provided detailed dynamic global picture of OFZ seasonal variability. Spectrum analysis of time series of SST gradient revealed a seasonal signal as well as interannual variations that, in the equatorial zone, are related to ENSO events. While 16-year time series is insufficient to detect decadal cycle, it still was useful for documenting the changes in OFZ associated with specific climatic shift of late 1980s from cool to warm conditions in the mid-latitude North Pacific. Both subtropical and subpolar OFZ revealed response to this shift, evident in spatial structure and SST gradient anomalies pattern. Estimates of meridional frontogenesis in the North Pacific due to wind and heat forcing on seasonal and decadal timescales have been compared with observed rates of frontogenesis.

**JSM41/E/20-B4** 1140

#### A REVIEW ON STUDIES OF THE WARM-CORE RING IN THE KUROSHIO-OYASHIO TRANSITION ZONE USING SATELLITE-DERIVED SSTs AND PREDICTION OF ITS SHORT-TERM VARIATIONS

HIROSHI KAWAMURA Center for Atmospheric and Oceanic Studies, Faculty of Science, Tohoku University, Sendai 980, Japan

The Kuroshio and the Oyashio meet in the Pacific ocean east of Japan and a complex oceanic feature associated with warm and cold eddies appears in this region. Therefore, the Kuroshio-Oyashio transition zone is sometime called "the confluence zone" or "the perturbed region". This region is also well known as one of the good commercial fish grounds in the world ocean. Since the large temperature difference between the Kuroshio and Oyashio waters, there appear many temperature fronts. SSTs derived by AVHRR on board the NOAA series satellite have contributed to understand mechanisms of the oceanic variations and to monitor the front locations, which are associated with the promising commercial fish grounds. In the presentation, the oceanographic studies performed in this region using AVHRR-SSTs are reviewed, focusing on the evolution of understanding toward prediction of the short-term variations relating to the warm-core eddies. The contour dynamics was successfully introduced

## INTER-ASSOCIATION

to simulate a drastic variation of two warm-core rings, whose boundaries are visualized by the SST images. Predictability of the contour dynamics is examined for four spring seasons by using daily SST images with high-spatial resolution, and almost of the drastic events are well simulated for about three weeks. This means that combination of SST images and the contour dynamics model can be used to predict the short-term variation of warm-core rings. Social needs and practical methodology of the short-term prediction will be presented.

### JSM41/W/24-B4

1155

#### SPACEBORNE SCATTEROMETERS AND MICROWAVE RADIOMETERS IN THE STUDIES OF OCEAN-ATMOSPHERE INTERACTION

W. Timothy LIU and Wenqing Tang (both at Jet Propulsion Laboratory, Caltech, email: liu@pacific.jpl.nasa.gov)

Spaceborne scatterometers are designed to measure ocean surface wind vectors and, therefore, ocean-atmosphere momentum flux, under both clear and cloudy conditions. The scatterometers on a series of European Remote Sensing Satellites (ERS) have provided surface wind measurements since 1991. The National Aeronautics and Space Administration (NASA) launched scatterometers NSCAT in 1996 and Quikscat in 1999, with continuous improvements in spatial resolution and coverage. The operational Special Sensor Microwave / Imagers (SSM/I) have monitored ocean surface wind speed, integrated water vapor (IWV), and rain since 1987. The Tropical Rain Measuring Mission (TRMM) Microwave Imager (TMI), which was launched in 1997 measures additional frequencies from which all weather sea surface temperature (SST) can be retrieved. Ocean surface evaporation or latent heat flux can be derived from the spacebased measurements of wind speed, IWV, and SST, or it can be retrieved directly from the radiances observed by TMI.

Three examples will be presented to show oceanic responses (as exhibited through spacebased SST and sea level changes) to surface wind and thermal forcing at different temporal and spatial scales - during the transition of a storm, the seasonal changes of monsoons, and an El Nino episode.

### JSM41/E/08-B4

1210

#### SEA SURFACE TEMPERATURE OBSERVATION FROM TRMM MICROWAVE IMAGER

Misako KACHI, Akira Shibata, Hiroshi Murakami and Keiji Imaoka (Earth Observation Research Center (EORC), National Space Development Agency of Japan (NASDA), 1-9-9 Roppongi, Minato-ku, Tokyo 106-0032, JAPAN, email: kachi@eorc.nasda.go.jp)

The Tropical Rainfall Measuring Mission (TRMM) Microwave Imager (TMI) has an added 10 GHz channel compared to the Special Sensor Microwave Imager (SSM/I) which has been operating since 1987. The 10 GHz channel is more sensitive to sea surface temperature (SST) than higher frequency channels. The SST retrieved from TMI is compared to the monthly mean SST produced by Reynolds and Smith (1994), and accuracy of the monthly TMI SST is within 0.5 C, and it satisfies requirement for SST measurement.

In 1998, the El Nino warm episode was diminished from early to mid May, and sudden cooling of SST over the central and eastern equatorial Pacific was clearly observed from TMI. TMI can measure SST under clouds by using microwave signal from the sea surface, while the infrared sensors cannot. Since TRMM carries the visible infrared sensor, we could compare SST coincidentally observed by both microwave and infrared sensors. NASDA will launch ADEOS-II satellite that also carries both microwave sensor, the Advanced Microwave Scanning Radiometer (AMSR) and visible infrared sensor, the Global Imager (GLI) in 2000. In the same year, NASA will also launch the EOS-PM1 satellite, which carries AMSR-E modified from AMSR. We expect that coincidentally observations of SSTs from microwave and infrared sensors will continue after TRMM.

## Thursday 29 July PM

Presiding Chair: H.Kawamura (Center for Atmospheric and Oceanic Studies, Tohoku University, Japan)

### OCEAN MONITORING (CONT)

#### JSM41/E/13-B4

Invited

1400

#### OCEAN COLOR REMOTE SENSING AND JAPANESE OCEAN COLOR SATELLITE ACTIVITIES

JOJI ISHIZAKA (Faculty of Fisheries, Nagasaki Univ., 1-14 Bunkyo, Nagasaki,852-8521 Japan, E-mail: ishizaka@net.nagasaki-u.ac.jp)

Ocean color is the only remote sensing technology to monitor biology in the ocean. The Coastal Zone Color Scanner (CZCS) launched by NASA is the first ocean color sensor specifically designed to detect phytoplankton pigments. The sensor collected data during 1978 to 1986, although the sensor was not continuously operated. The spatial and temporal variability of the CZCS phytoplankton pigments was far larger than the biological oceanographers had been expected. After ten years of blank, Ocean Color and Temperature Sensor (OCTS), developed by National Space Development Agency of Japan (NASDA), was onboard of Advanced Earth Observing Satellite (ADEOS) launched on August 1996. Although the satellite stopped operation on June 1997, OCTS collected 8-months (November to June) of fully global 1-km resolution ocean color data. Global composite data and Intensive Local Area Coverage (LAC) data around Japan of sea surface chlorophyll-a were available through internet with near real time. Those data were verified with sea truth data from the global ocean. The ocean color data time series is now continued by NASA SeaWiFS. Ocean color remote sensing is now facing the new era. Global Imager (GLI) will be onboard of ADEOS-II launched on the fall of 2000 by NASDA. NASA is planning MODIS, and ESA is planning MERIS. Those sensors have larger numbers of channels than previous sensors and should be useful for the monitoring of coastal waters as well as open ocean. Multi-sensor operation should cover global ocean more frequently than by single-sensor operation. Future challenges of the ocean color remote sensing will be discussed.

#### JSM41/E/27-B4

Invited

1430

#### CONTRIBUTIONS OF SATELLITE ALTIMETRY TO GLOBAL OCEAN MONITORING

ROBERT CHENEY (NOAA/NESDIS National Oceanographic Data Center, 1315 East-West Highway, Silver Spring, MD 20910 USA, email: rcheney@nodc.noaa.gov)

An uninterrupted flow of satellite altimeter data has been available since the launch of ERS-1 in 1991 and Topex/Poseidon in 1992. With the Jason-1 and Envisat altimeters due to be launched in 2000, it is likely that we will continue to enjoy this observational wealth for years to come. Satellite altimetry has enabled a variety of phenomena to be monitored in near-real time. Operational applications include tracking of the Loop Current and its eddies in the Gulf of Mexico and assimilation of altimeter sea heights in ocean models used to forecast El Nino. With nearly 7 years of the highly-accurate Topex/Poseidon data already collected, low-

frequency phenomena such as the North Atlantic Oscillation are being studied, and stable values for the rise of global sea level are being obtained. This presentation will review progress in these areas and discuss plans for future altimeter missions.

### JSM41/W/14-B4

1500

#### MONITORING A WESTERN BOUNDARY CURRENT USING SATELLITE AND IN-SITU DATA

Richard COLEMAN, Ken Ridgway, Rick Bailey (CSIRO Marine Research, Hobart, Tasmania, Australia, email: r.coleman@marine.csiro.au), Dave Mickler (University of Colorado, Boulder, Colorado, USA)

We compare the circulation through two sections crossing a western boundary current (East Australian Current, EAC) in the Tasman Sea from in-situ XBT casts and T/P altimeter data. The sections cross the current in the north at 26S (Brisbane-Fiji), where the current intensifies and in the south at 34S, just beyond the main separation point of the EAC mean flow.

Surface steric height relative to 800 db (the depth of the casts) is inferred from the XBTs using a high-resolution T-S climatology with the along section mean (from 20 transects observed between 1992-1999) removed to obtain surface anomalies. We also project the steric height onto a deeper reference level (2000 db) using a regression method derived from historical data. Raw along-track T/P data are first mapped onto the location and date of each XBT cast using optimal interpolation. Both in-situ and satellite data are then 'projected' onto 'standard' sections at a uniform along-track spacing. Over 20 realisations of each data type are available over the common period (Oct 1992 - 1999).

The surface height anomalies from each data type are in good agreement (~3-5 cm rms) down to spatial scales of 300 km. Below this length scale, the in-situ data resolves small changes which are beyond the capability of the interpolated altimeter fields. We also investigate the relative proportions of baroclinic to barotropic variability in the altimeter fields. The deeper reference level is needed to resolve the baroclinic flow associated with the EAC and its eddies within the coastal region. Away from this highly energetic region, the 800 db level is generally sufficient to capture the main baroclinic variability. In the north Tasman Sea we observe a region where the T/P variability is significantly less than that of the in-situ data. This would appear to be related to unresolved barotropic flow. The ability of each data type to resolve both spatial and temporal signals of interest is studied using regression methods, spectral analysis and wavelet techniques. The results provide a basis for designing future monitoring programs which utilise these data techniques in an efficient manner.

Finally, we present results documenting the mean flow and variability of the EAC from the combined dataset. We observe interannual fluctuations in the EAC transport of up to 10 Sverdrups.

### JSM41/W/09-B4

1515

#### VARIATIONS OF GLOBAL MEAN SEA LEVEL OBSERVED DURING THE TOPEX / POSEIDON MISSION

R. S. NEREM, D. P. Chambers, E. W. Leuliette, (all at the Center for Space Research, The University of Texas at Austin, Austin, TX, 78712, email:nerem@csr.utexas.edu) G. T. Mitchum (Dept. of Marine Sciences, University of South Florida, 140 Seventh Ave. South, St. Petersburg, FL, 33701, USA, email: mitchum@seas.marine.usf.edu) B. S. Giese (Dept. of Oceanography, Texas A&M University, College Station, Texas, 77843, USA, email: giese@sweeney.tamu.edu)

The TOPEX/POSEIDON (T/P) satellite altimeter mission has been mapping global sea level every 10 days since its launch in August 1992. One of the objectives of climate change research is to establish the rate at which global mean sea level is increasing, so that it can be compared to similar predictions from global climate models. For this application, interannual variations can be quite troublesome, as they tend to mask the longer-term variations due to climate change. Using the T/P altimeter data, we observed a sharp rise in global mean sea level (~2 cm) during the 1997-1998 ENSO event, followed by a fall in sea level. We find these variations can be reproduced with GFDL's MOM2 ocean model, allowing us to determine the signal is confined to the upper 300 m of the water column. The sea level observations appear to match similar variations observed in satellite measurements of sea surface temperature over the same time period. In addition, they can be represented by the "ENSO modes" of an EOF analysis of the T/P sea level observations. Finally, comparison of the T/P measurements with tide gauge measurements appears to rule out the observed change being caused by an instrumental effect. These ENSO variations have important implications for using altimeter data to detect climate change, the most notable of which is that a time series of several decades in length may be required unless a technique can be found to remove the ENSO variations from the T/P observations. We are experimenting with several statistical/modelling techniques to accomplish this, and will discuss the progress of these efforts. In addition, we will discuss a physical explanation for why ENSO is changing global mean sea level.

### JSM41/W/34-B4

1530

#### ALTIMETRIC SEA SURFACE HEIGHT (SSH), RELATIVE TO THE ELLIPSOID

Dr John Blaha (Institution: Naval Oceanographic Office Email: lahaj@navo.navy.mil)

Altimetric sea surface height (SSH), relative to the ellipsoid, is produced routinely with sub-5 cm accuracy. Global ocean circulation monitoring that would exploit this precision, will require, in addition, determination of the difference of satellite SSH from the geoid. We show comparisons of two methods to remove the effect of the geoid on SSH over the western North Atlantic. The first method fits the time mean of the SSH record on individual satellite groundtracks to a climatological mean of dynamic height. The second method specifies dynamic height by taking in situ observations along selected groundtracks at the times of altimeter overflights. We show the comparisons on 19 TOPEX/POSEIDON groundtracks sampled by aircraft-deployed bathythermographs in the region 25N-40N, 75W-50W. Temperature profiles, from the surface to 800 m, were taken 15-20 km apart (in the along-track sense) within 24 hr of the altimeter measurements. Steric sea level estimates relative to 2000 dbar were computed from these observations. For comparison purposes, differences were computed between the aircraft dynamic heights and the mean-adjusted altimeter heights. This distribution (along tracks crossing the features of the subtropical gyre) shows the competing effects of measurement error in the bathythermograph data and sampling error in the climatological means.

### JSM41/W/06-B4

1545

#### MONITORING ANTARCTIC ICE SHEET WITH SATELLITE RADAR ALTIMETER DATA

V. Nuth (Dept. of Geological Sciences and the Center for Space Research, The University of Texas at Austin, Austin, TX 78712, email: van@csr.utexas.edu), C. R. Wilson (NASA HQ, Geodynamics and Geostintial Fields Code YS, Washington, DC 20546, email: cwilson@hq.nasa.gov) M. K. Cheng (Center for Space Research, email: cheng@csr.utexas.edu) C. K. Shum (Dept. of Civil and Environmental Eng. and Geodetic Science, Ohio State University, email: ckshum@osu.edu)



Since the launch of Seasat, radar altimeter data have contributed enormously to the study of glaciology. Until the launch of ICESAT, spaceborn radar altimeter data remain the only means to monitor ice mass balance on a global scale. However, the rugged ice surface topography has meant that this data set cannot be used readily without significant on-ground reprocessing. We use retracked pairs of altimeter measurements at the satellite cross-over points along with a waveform cross-correlation method to compute the estimate of ice sheet elevation changes over time. We report here results obtained from analysis of ERS-1 data over the Antarctic Ice Sheet. Our elevation time series show that while Antarctica as a whole exhibits a reasonable seasonal signal both in amplitude and phase, selected regions in West Antarctica appear to have undergone large elevation changes which are speculated to be associated with seasonal snowfall and other effects.

**JSM41/W/07-B4** Poster **1620-05**

#### ESTIMATION OF GLOBAL AIR-SEA TRANSFER OF CO<sub>2</sub> USING TOPEX/POSEIDON DUAL-FREQUENCY BACKSCATTER

Nelson FREW, David Glover, Erik Beck, Catherine Goyet, Scott McCue and Richard Healy (Department of Marine Chemistry and Geochemistry, Woods Hole Oceanographic Institution, 360 Woods Hole Rd., Woods Hole, MA 02543 USA, e-mail: nfrew@whoi.edu)

Global and regional estimates of ocean-atmosphere gas fluxes are limited by the uncertainties in current gas transfer velocity parameterizations. These model functions use wind as the sole controlling parameter. However, many other factors, including boundary layer stability, wave age, and surface films strongly affect gas exchange rates.

We outline a new method for estimation of transfer velocity using altimeter backscatter as a more direct measure of sea surface roughness and, therefore, transfer velocity. The algorithm assumes a linear relationship between mean square wave slope and gas transfer velocity for wavenumbers >50 rad/m. Estimates of mean square wave slope from the nadir-looking C- and Ku-band microwave altimeters aboard TOPEX/Poseidon are used to derive monthly global maps of transfer velocity. The monthly maps show a strong correlation with NCEP and FNMOG global winds for the same periods. The transfer velocity fields, combined with in situ observations and ocean colour estimates of biological productivity, are applied in a 3-D ocean GCM to estimate global seasonal and annual CO<sub>2</sub> fluxes. The theoretical background and empirical observations underlying the new algorithm will be presented.

Presiding Chairs: A.Rango (U.S. Department of Agriculture, Beltsville, MD 20705-2350, USA) T.Engman (NASA/GSFC, Greenbelt MD 20771 USA)

#### TERRESTRIAL MONITORING

**JSM41/LL/01-B4** Poster **1625-06**

#### A STUDY OF THE ARCTIC SNOWPACK BY USE OF SYNTHETIC APERTURE RADAR (SAR) IMAGERY

M Johansson and I A BROWN Climate Impacts Research Centre, Björkplan 6A, S-981 42 Kiruna, Sweden email: maria.johansson@natgeo.su.se, iabrown@natgeo.su.se

The extent and properties of the snow cover in polar regions is of great importance to the earth's radiation balance which is influencing the global climate. Therefore snow in the polar regions is an important study object when discussing climate change. A technique using satellite imagery in order to survey and describe the Arctic snowpack would be an important tool in the future, especially as input to global climate models (GCM) and for runoff forecasts made by hydropower companies. The synthetic aperture radar (SAR) is very suitable for operating in polar regions since it is independent of polar nights and cloudy skies. An additional advantage of the SAR-sensor is it's use of microwaves and the microwaves capability to penetrate the surface, i.e. the snowpack and it's substrata, which theoretically gives access to a three dimensional view of the snowpack.

The objective of this work is to investigate the use of SAR-imagery to study snow and snow melt in polar regions. The study focuses on the change in snow distribution and snow composition displayed through backscatter in SAR imagery during one spring season. Field data are collected at two field sites in northern Sweden and Norway at 3-4 occasions at each field site during spring coincident with the acquired satellite imagery. The vertical variation in the snowpack is described by snow depth, dielectric constant, density and temperature measurements at selected profiles distributed over the field sites. The grain size and the stratigraphy of these profiles are ocularly described as well as the surface roughness of the snow cover. Analyses of ERS-1 and Radarsat-1 imagery are compared with the field observations. The field measurements will give a three-dimensional view of the snow cover which will be the background for a discussion highlighting the possibilities to calculate the snow pack status, i.e. liquid water content, density etc. to predict penetration depths, scattering and absorption of the microwaves at the time of satellite overpass. We will also discuss the need of multi-polarisation SAR-data, here HH and VV, within short time spans and the possibilities to follow the change in the snowpack through SAR-backscatter during spring.

**JSM41/W/23-B4** Poster **1630-07**

#### VOLCANIC SO<sub>2</sub> EMISSIONS - A 20-YEAR SATELLITE RECORD

Gregg Bluth (Department of Geological Engineering and Sciences, Michigan Technological University, Houghton, MI 49931, USA, email: gbluth@mtu.edu); Arlin Krueger (Atmospheric Chemistry and Dynamics, NASA/Goddard Space Flight Center, Greenbelt, MD 20771, USA, email: krueger@chapman.gsfc.nasa.gov)

Data from the Total Ozone Mapping Spectrometer (TOMS) instruments have enabled us to develop a near-continuous record of worldwide explosive volcanism since 1978. While the original volcanogenic data product was sulphur dioxide, more recent advances have enabled the detection of ash clouds. In addition to the study of individual eruptions, these data have been used to place constraints on global volcanic SO<sub>2</sub> emissions by explosive-type eruptions, both by infrequent, large eruptions and lower level, but more frequent events.

The current TOMS database includes well over 100 eruptions, including multiple eruptions during a continuous episode of activity. The magnitude of SO<sub>2</sub> clouds range from >10 million tonnes (Mt) to as little as a few kilotonnes (kt). The longevity, and thereby long-term hazards, of the clouds likewise cover a wide range with Pinatubo removal occurring at a rate of 35 days (e-folding time), most mid-sized (200-5000 kt) eruptions from 2 - 10 days, and most small eruptions decaying within 1-2 days. Previous work estimates that explosive volcanic activity emits on the order of 4 Mt SO<sub>2</sub>/yr. However, new work suggests this estimate of annual flux may increase due to more intensive examination of the database focusing on smaller events, such as the prolific Nyamuragira volcano, Zaire. We report on some of the longer term (e.g., multiyear to decadal) trends in global volcanic activity observed through satellite observation, and how these trends may affect hazard planning and mitigation efforts. We also update the progress on a new NASA mission in hazard mitigation, VOLCAM, featuring a TOMS instrument upon a geostationary platform.

**JSM41/E/09-B4** Invited **1635**

#### SATELLITE REMOTE SENSING OF GLOBAL SNOW COVER - A BRIEF HISTORY

R.L. Armstrong, (National Snow and Ice Data Center (NSIDC), Cooperative Institute for Research in Environmental Sciences (CIRES), University of Colorado, Boulder, CO, USA, email: rlax@kryos.colorado.edu)

Snow cover is an important variable for climate and hydrologic processes due to its effect on energy and moisture budgets. In terms of spatial extent, snow cover is the largest single component of the cryosphere with a mean maximum areal extent of 47 million km<sup>2</sup>, about 98% of which is located in the Northern Hemisphere. During the past three decades much important information on Northern Hemisphere snow extent has been provided by the NOAA weekly snow extent charts derived from visible-band satellite imagery (e.g. NOAA-AVHRR, GOES, METEOSAT, GMS). This product represents the longest single time series of any geophysical product obtained from satellite. Beginning in 1997 the spatial and temporal resolution of the original analysis (approx. 190 km and 7 days respectively) was improved to become a daily product with a spatial resolution of 25 km. Limitations associated with visible wavelength data include the inability to acquire information below clouds or during darkness and the fact that data are limited to snow extent only. Because of the ability to penetrate clouds, provide data during darkness and the potential to provide an index of snow depth or water equivalent, passive microwave satellite remote sensing can greatly enhance snow measurements based on visible data alone. It is now possible to monitor the global fluctuation of snow cover over a 20 year period using passive microwave data (Scanning Multichannel Microwave Radiometer (SMMR) 1978-1987 and Special Sensor Microwave/Imager (SSM/I), 1987-present). A comparison of the visible and passive microwave time-series shows the visible data to have higher variability but trends are similar showing a decrease of approximately 0.4 % per year. The passive microwave data indicate less snow-covered area than the visible data throughout the year with the greatest differences in the fall and early winter when the snow cover is shallow. Results from new algorithms designed to reduce this error are presented.

**JSM41/E/07-B4** **1705**

#### TOWARDS AUTOMATED MULTISPECTRAL SNOW MAPPING

PETER ROMANOV, Ivan Csizsar, and Garik Gutman NOAA/NESDIS, Office of Research and Applications, Camp Springs, MD

Current daily and weekly snow products at NOAA are generated by analysts, who use visible imagery from geostationary and polar orbiting satellites. There is no automated satellite-derived product based on the visible and/or infrared data, however. The automated satellite-derived snow product based on SSM/I and/or AMSU microwave observations is used by the analysts only for verification because of the coarse resolution and remaining ambiguities. The present study is based on GOES Imager, NOAA AVHRR and DMSP SSM/I data over North America during the 1998-1999 snow season. The data from all channels on two GOES imagers (East and West) were intercalibrated with NOAA-14 corresponding channels and updated on a bi-monthly basis. The synergy between SSM/I, GOES Imager, and NOAA AVHRR observations has been utilized by taking advantage of the ability to observe ground surface through clouds by SSM/I, frequent views from GOES throughout the day, and the high resolution full coverage of northern latitudes by AVHRR. The SSM/I daily 30-km spatial resolution automated snow maps are produced routinely at NESDIS. They have been used as the primary source for a daily snow map. The shortcomings of the SSM/I-derived maps, such as spatial resolution and snow detection over forests, have been alleviated by a combined use of visible, mid-IR and IR from GOES and AVHRR. Daily composites based on the maximum brightness temperature have been constructed from GOES and AVHRR. All pixels in a daily composite are then classified into snow, snow-free and cloudy. The visible (0.6 5m) reflectances are corrected for angular effects with a semi-empirical kernel driven model. The mid-infrared reflectances were derived from GOES (3.9 5m) and NOAA (3.7 5m) data by subtracting the thermal component from observed radiances. The mid-IR reflectances did not exhibit any significant angular variability. They are then combined with the visible reflectances to form a snow index that is resistant to data contamination by most cloud types. Daily composites of this index are produced over North America from the combined data of the two GOES Imagers and NOAA-14 AVHRR. To produce weekly snow maps, 7-day composites have been formed based on the maximum snow index, reducing cloud contamination even further and filling the data gaps in the daily composites. We conducted validation and comparison of the derived snow maps with reports from ground stations and the current operational snow analysis at NOAA.

**JSM41/W/12-B4** **1720**

#### CRYSYS: COLLABORATIVE APPROACH TO MONITORING AND MODELLING THE CRYOSPHERE IN CANADA

BARRY E. GOODISON, Climate Research Branch, Atmospheric Environment Service, 4905 Dufferin Street, Downsview, Ontario, M3H 5T4 Ross D. Brown, Atmospheric Environment Service, 2121 Trans-Canada Highway, Dorval, Québec, H9P 1J3. Claude R. Duguay, Centre d'études nordiques, Université Laval, Sainte-Foy, Québec, G1K 7P4 Gregory M. Flato, Canadian Centre for Climate Modelling and Analysis, Atmospheric Environment Service, P.O. Box 1700, Victoria, British Columbia, V8W 2Y2 Roy M. Koerner, Glaciology, Terrain Sciences Division, Geological Survey of Canada, 601 Booth St., Ottawa, Ontario K1A 0E8 Ellsworth F. LeDrew, Department of Geography, University of Waterloo, Waterloo, Ontario, N2L 3G1 Anne E. Walker, Climate Research Branch, Atmospheric Environment Service, 4905 Dufferin Street, Downsview, Ontario, M3H 5T4

CRYSYS (Use of the Cryospheric System to Monitor Global Change in Canada) is a Canadian collaborative research effort involving 14 universities, four federal institutions, and one non-profit organization, established originally as an Interdisciplinary Science Investigation (IDS) in NASA's Earth Observing System (EOS) Program. Recognizing the importance of the cryosphere in both the global and regional climate system, CRYSYS has evolved to bring together a wide range of Canadian cryospheric expertise in remote sensing, modelling, field investigations, data integration and data management to provide improved capabilities for monitoring the state of the cryosphere, and a greater understanding of cryospheric processes and variability. The main scientific goals of CRYSYS are: (1) to develop capabilities for monitoring and understanding regional and larger-scale variations in cryospheric variables; (2) to contribute to the development and validation of local, regional and global models of climate/cryospheric processes and dynamics, and to improve understanding of the role of the cryosphere in the climate system; and (3) to assemble, maintain and analyze key historical, operational and research cryospheric data sets to support climate monitoring and model validation. These goals are addressed through the cryospheric components especially important within Canada (sea ice, snow, lake ice, glaciers and ice caps, and permafrost/frozen ground), but recognizing their application in a global context. The team's field expertise and on-going intensive field investigations throughout Canada are key elements in the development and validation of new remote sensing algorithms and techniques (e.g. snow water equivalent, lake ice freeze-up/break-up, sea ice motion, freeze/thaw of frozen ground, growth of glaciers and ice caps), the use of these data for improved model development (e.g. Canadian GCM, CLASS), and the creation of reliable time series for climatological and hydrological analyses.



## INTER-ASSOCIATION

CRYSYS, through its focus on climate/global change in Canada, will continue to contribute to international programs, including EOS, WMO/GCOS through the Canadian cryospheric GCOS activities, and to WMO/WCRP through GEWEX, ACSYS and the new CLIC initiative. This presentation will provide a summary of significant CRYSYS-supported research on monitoring and modelling the cryosphere with remotely sensed and in situ data, will highlight CRYSYS contributions to GCOS objectives, and will provide an assessment of the current state of the cryosphere in Canada.

**JSM41/W/21-B4**

**1735**

### COMPLEMENTARY USE OF SATELLITE AND IN SITU DATA FOR MONITORING SPATIAL AND TEMPORAL CHARACTERISTICS OF SNOW COVER IN CANADA

BARRY GOODISON, Ross Brown and Anne Walker: (Climate Processes and Earth Observation Division, Atmospheric Environment Service, Downsview, Ontario, CANADA, M3H 5T4. E-mail: ross.brown@ec.gc.ca)

Satellite observations are an indispensable component for mapping and monitoring of the cryosphere over large, high latitude land masses, such as Canada, where in-situ data are limited. Satellite sensing of snow cover has been found to be especially important for hydrological and climatological analyses and the assessment of variability and change over a range of spatial and temporal scales including monthly-seasonal and annual-decadal time scales. The CRYSYS project (Use of the Cryospheric System for Monitoring Global Change), a Canadian-led interdisciplinary science project in the NASA/EOS program, supports two important areas of research related to snow that are contributing to an enhanced ability to document spatial and temporal variations in snow cover: (1) the development, validation and refinement of empirical and theoretical algorithms for snow cover properties (extent, water equivalent, wet/dry state) in varying landscapes using passive and active microwave data, and (2) the merging of satellite and in-situ data to extend the satellite record and provide compatible and consistent information for climate variability studies, change detection, and validation of GCM transient climate simulations. This paper will present the results of new research on developing passive microwave SWE algorithms for forested areas, and the development of a satellite-derived SWE time-series (1988/89-1997/98) and climatology for the Prairie region of Canada taking account of the effects of wet snow. The paper will also present results from the merging of in-situ and satellite information that yielded monthly time series of snow cover extent information over North America and Eurasia from 1915. The reconstructed snow cover series show evidence of a significant 20th Century decrease in spring snow cover extent over Eurasia that corresponds with enhanced 20th Century spring warming over this continent. The problem will conclude with recommendations on requirements for monitoring snow cover for the Canadian GCOS program.

**JSM41/E/19-B4**

**1750**

### PASSIVE MICROWAVE REMOTE SENSING OF FROZEN SOILS

T. Zhang, R. ARMSTRONG, and J. Smith, (all at the National Snow and Ice Data Center and Cooperative Institute for Research in Environmental Sciences, University of Colorado, Boulder, CO 80309-0449, USA, email: tzhang@kryos.colorado.edu and rlx@kryos.colorado.edu)

The timing, duration, areal extent, and depth of near-surface soil freezing and thawing are important parameters for regional climatic and hydrologic studies, and changes in these parameters are important climatic indicators and integrators. Conventional point measurements of surface soil freezing and thawing provide information for process studies in local areas. It is impractical to conduct large- or regional-scale investigations of surface soil freezing and thawing by using the point measurement method. In this study, onset, duration and areal extent of near-surface soil freezing and thawing were investigated using passive microwave remote sensing data in North America (30N and 130W to 60N and 50W) during the winter of 1997-1998. The criteria used to detect onset, duration, and areal extent of surface soil freezing include (i) a negative spectral gradient between Tb(37V) and Tb(19V), (ii) a cutoff Tb(37V). The algorithm was partly validated against field measurements in northern Plains of the United States. The primary results obtained indicate that frozen soil extent was generally in good agreement with zero degree Celsius isotherm of air temperature. The boundary of frozen soil extent moved southward as the cold air was invading from north in northern Plains during the early winter. The onset of surface soil freezing ranged from September in northern and mountainous regions to December/January in southern regions. The duration of surface soil freezing varied from a few days in the south to about six months in the north and mountains. Surface soils were generally frozen before snow cover developed. Snow cover extent was also included for comparison. We will discuss the progress and problems concerning the application of passive microwave remote sensing data to study of frozen soils.

## Friday 30 July AM

Presiding Chairs: A.Rango (U.S. Department of Agriculture, Beltsville, MD 20705-2350, USA)  
T.Engman (NASA/GSFC, Greenbelt MD 20771 USA)

## TERRESTRIAL MONITORING

**JSM41/W/19-B5**

Invited

**0900**

### SATELLITE REMOTE SENSING OF SOIL MOISTURE-THE MAXIMUM POTENTIAL OF PAST, CURRENT AND FUTURE SYSTEMS

Thomas J. Jackson, U.S. Department of Agriculture, Agricultural Research Service, Hydrology Lab, 104 Bldg. 007 BARC-West, Beltsville, MD 20705, USA email: jackson@hydrolab.arsusda.gov

The role of surface soil moisture in hydrology and climate has been defined over the past decade. A lack of a physically based soil moisture element and an observational data base for validating such models are recognized as critical sources of uncertainty in simulations and forecasts. Long term spatial soil moisture data have never been available. Although many technologies have been utilized and evaluated, none have been able to provide reliable in-situ measurements in a cost-effective manner. Satellite based microwave remote sensing is an ideal source of surface soil moisture information. Microwave sensors are sensitive to the water content of the soil and satellite sensors can provide updated image (map) products. The geographic domain for soil moisture retrieval is limited by vegetation. Vegetation reduces the sensitivity of the measurement to soil moisture changes. The reduction in sensitivity increases as frequency increases. Satellite agencies have not placed a high priority on providing instruments that are optimized for soil moisture measurement. SSM/I frequencies can only provide information for a few regions with minimal vegetation. There is a better outlook for soil moisture when the AMSR instruments are launched in the year 2000 by the U.S. and Japan. It is possible that by conducting the right kind of calibration activities with these instruments, that the data collected during the nearly ten years of SMMR observations can be more effectively utilized for long term studies. However, the greatest potential for soil moisture remote sensing is at lower frequencies, in particular L band. With current technologies it is possible to implement a spaceborne L band system with a spatial resolution that is compatible with large-scale hydrology and climate. With this system it would be possible to provide soil moisture information for 70% of the Earth's land surfaces.

**JSM41/W/27-B5**

**0930**

### THE SOIL MOISTURE AND OCEAN SALINITY (SMOS) MISSION: AN OVERVIEW

Y.H. Kerr (CESBIO, 18 av E. Belin, 31401 Toulouse cedex, France, email: Yann.Kerr@cesbio.cnes.fr), P. Waldteufel (IPSL, 10-12 av de l'Europe, 78140 Vélizy, France) ; G.S.E. LAGERLOEF (Earth and Space Research, 1910 Fairview Ave E, Suite 102 Seattle WA 98102-3620, USA, email: lagerloef@esr.org) ; J.-P. Wigneron (INRA Bioclimatologie, Agroparc 84914 Avignon Cedex 9, France) J. Font (Dept. of Marine Geology and Physical Oceanography, Institut de Ciències del Mar - CSIC, P. Joan de Borbó s/n, 08039 Barcelona, Spain); J.-M. Martinuzzi (CNES, 18 Avenue Edouard Belin 31401 Toulouse cedex 4, France)

The goal of this paper is to present a space mission aimed at the retrieval of soil moisture and ocean salinity from space. It is now being proposed to the Earth Explorer Opportunity Programme, under the name of SMOS. The sensor is an L-band interferometer based on an innovative concept of bi-dimensional aperture synthesis method. The instrument is a Y shaped structure consisting of 3 co-planar arms consisting of an elongated array of elements operating in H and V polarization and incidence angles ranging from about 0 to 55°. The sensor has new and very significant capabilities especially in terms of multi-angular view configuration. The main goals of this mission are: (i) to provide fields of surface soil moisture and potentially of root zone soil moisture, all over the globe and every 2 to 3 days, (ii) to measure seasonal to interannual variations of sea surface salinity, (iii) to be used over ice and ice caps for research purposes. The ultimate goal is to provide global information on such key parameters (moisture and salinity) for models in the fields of oceanography, meteorology, hydrology and climate. This paper will give an overview of the SMOS Mission objectives and the main mission characteristics together with some of the technical features.

**JSM41/W/02-B5**

**0945**

### DEVELOPMENT OF A SATELLITE SYSTEMS FOR MEASURING SOIL MOISTURE AND SEA SURFACE SALINITY

Edwin T. ENGMAN (Code 974, Hydrological Sciences Branch, Laboratory for Hydrospheric Processes/NASA, Goddard Space Flight Center, Greenbelt, MD 20771, USA, Email: tengman@neptune.gsfc.nasa.gov)

The science need for remotely sensed soil moisture and sea surface salinity has been well established in the hydrologic, oceanographic, climate change and weather forecasting communities. In spite of this well documented science need there are currently no satellite missions flying or funded to make these very important geophysical measurements. There have been a number of experimental programs that have demonstrated the feasibility of using long wave microwave sensors for estimating soil moisture and also a few that have shown the promise for measuring salinity. The principal sensor to accomplish both the soil moisture and salinity measurements is an L-band passive microwave radiometer. Unfortunately, each science driver, soil moisture and salinity, impose quite different technical requirements on the sensor system. Soil moisture is driven by a spatial resolution on the order of 20 to 30 km and achieving this requires a very large antenna. Spatial resolution is not a driver for salinity except for possibly in the littoral zone, however the salinity measurement requires an extremely sensitive radiometer. This paper describes the several alternatives to solve the very large antenna challenge and still meet the radiometer sensitivity requirement for salinity. The paper also discusses the alternatives considered to obtain the necessary ancillary data for characterizing the surface roughness, the surface (land and ocean) temperature and the attenuation affects of vegetation needed to derive the geophysical parameters. Finally, the paper discusses proposed missions and how well they will meet the science requirements.

**JSM41/W/16-B5**

**1000**

### SATELLITE MICROWAVE REMOTE SENSING OF LAND SURFACE HYDROLOGY

Toshio Koike (Nagaoka University of Technology, Nagaoka, 940-2188, Japan, email: tkoike@nagaokaut.ac.jp)

Microwave remote sensing has high potential of measurement of land surface hydrological parameters quantitatively. Their diurnal cycles and heterogeneity also can be measured by non-synchronous satellites and the combination of passive and active sensors, respectively. New algorithms for snow, soil moisture, surface temperature and rain by using passive microwave sensors are developed based on microwave radiative transfer theory. They are applied to the satellite data from the TRMM Microwave Imager (TMI) and the Special Sensor of Microwave Imager (SSM/I) and evaluated by using the ground-based data through the GTS and/or obtained during the GAME-Tibet Intensive Observing Period (IOP) in 1998. The estimated hydrological parameters, snow temperature, surface soil moisture, soil surface temperature and rainfall, show good correspondence to the observed data. An algorithm for soil moisture mapping in permafrost regions is introduced by using two images of L-band Synthetic Aperture Radar (SAR), one in winter and the other in summer. The algorithm is based on a relationship between two surface roughness parameters, r.m.s. height and correlation length, and the scattering model composed by the Integral Equation Method (IEM) and formulation of volume scattering in inhomogeneous medium. This algorithm is applied to the JERS-1 SAR data in the Tibetan Plateau in 1993. The estimated soil moisture shows in good agreement with the observed one obtained during the GAME-Tibet IOP in 1998. Provide fields of surface soil moisture and potentially of root zone soil moisture, all over the globe and every 2 to 3 days, (ii) to provide decadal values of sea surface salinity, (iii) to be used over ice and ice caps for research purposes. The goal is to provide information globally on key parameters (moisture and salinity) for models in the fields of oceanography, meteorology, hydrology to name the main ones. This paper will give an overview of the SMOS Mission objectives and the main mission characteristics together with some of the technical features.

**JSM41/W/22-B5**

**1015**

### ENVIRONMENTAL SIGNALS IN LAND ALTIMETER DATA: POTENTIAL FOR SOIL MOISTURE MEASUREMENT

BERRY, P.A.M., Pinnock, R.A. & Hoogerboord, J.E. Geomatics Unit, De Montfort University, Leicester LE1 9BH, UK, e-mail: pamb@dmu.ac.uk

The development of an expert system for recovery of orthometric heights from land radar altimeter waveforms has now enabled the detection of environmental signals in the altimeter dataset from ERS-1 and ERS-2.

This paper presents initial results from an ongoing research project evaluating the potential for recovery of surface soil moisture from altimeter echoes. With measurements from ERS-1/2 missions now covering almost ten years, and the planned continuation of this datastream with Envisat, radar altimetry presents a unique time series with near global sampling when in ice mode. One focus of the work presented here is on semi-arid areas such as desert margins, where results using the expert system already confirm the presence of quantifiable environmental signals in the individual waveforms

**JSM41/E/24-B5 1030****A STUDY ON SOIL EROSION IN SOUTH CHINA USING REMOTE SENSING AND GIS TECHNIQUE**

ZHANG, Jiahua (Institute of Atmospheric Physics, Chinese Academy of Sciences, Beijing, 100029, P.R.China email: zhangjh@ast590.tea.ac.cn)

Soil erosion seriously impact on global nature resources and ecological environment, in China the total soil erosion area covers 38.26% of total China's area, of which water erosion is 48.77%, and wind erosion accounts 51.22%, the total soil erosion amount annual year is five billion ton, accounting for 10% of the whole world. In the paper hilly land soil erosion condition in Southern China is severe, surface soil has been eroded away, soil fertility drop down, particularly in red earth and granite area, the resistance of erosion is low. Soil erosion and disasters caused by floods, windstorm, landform, slope, soil erodible character and landuse type, among this the human activities including cut down tree and excavate land is main factor. Using study methods of remote sensing and geo-information system can investigate and monitor the degree and of soil erosion, in the meantime dynamic of soil erosion can be analyzed by different period investigate data. The result of investigation based on remote sensing and GIS to Xingqiu country show the soil erosion area and annual soil erosion amount decreased 19.09% and 43.05% respectively from 1958's to 1988's. The gray forecast state that without soil erosion area increasing from 818.04 km<sup>2</sup> in 1988 to 1276.69 km<sup>2</sup> in 1995, in the meantime total soil erosion amount decreased from 607.21A104 t/a in 1988 yr. to 472.12 IA104 t/a in 1995. By comparison to different landuse types, the sediment modulus of woodland is lowest with 177.16-187.75t/km<sup>2</sup> a, on the contrary the bare land is highest with 10626.76-11265.48 t/km<sup>2</sup> a, so high vegetation coverage planting can decrease the soil and water loss. In the end some methods including conservation farming and engineer measures control soil erosion are suggested, by these can control soil erosion, and ecological cycle may take a turn for the better.

**JSM41/E/03-B5 Invited 1105****LAND SURFACE RESPONSE TO HYDROLOGICAL FORCING USING TIME SERIES OF AVHRR AND SMMR 37 GHZ OBSERVATIONS**

Massimo MENENTTI<sup>1</sup>, S. Azzali, G. Roerink, W. Verhoef<sup>2</sup> and S. Leguizamón<sup>3</sup> The Winand Staring Centre (SC-DLO), P.O.B.125, 6700 AC Wageningen, The Netherlands (1) Universite Louis Pasteur-LSIIT, 5 Blvd. S. Brant, 67400, Illkirch, France; e-mail: menenti@sepia.u-strasbg.fr (2)National Aerospace Laboratory (NLR), P.O.B. 153, 8300 AD Emmeloord, The Netherlands (3)Universidad de Mendoza/ CIS, Aristide Villanueva 776,5500 Mendoza, Argentina

In the last few years global satellite data sets have become available to provide observations of changes of land surface conditions over significant periods of time. Although instrument- and orbit-related artefacts still affect the precision of the observations, analyses of time series of satellite observations provide new insights on the response of heterogeneous land surfaces to hydrological forcing. The paper presents highlights of studies on land surface changes in arid (Africa), semi-arid (Mediterranean) and humid (South America) climates. To extract effectively information from such large data sets three algorithms have been developed and applied: Fast Fourier Transform (FFT), Harmonic Analysis of NDVI Time Series (HANTS) and wavelets transform. The analysis (FFT) of 10 years monthly NDVI time series of Africa and South America led to a continental map of vegetation-soil-climate complexes and to document their phenology. The HANTS algorithm was also used to improve the quality of the data sets by removing cloud-contaminated observations still present in the monthly composites. Vegetation type was strongly related to the Budyko aridity index. A detailed change analysis of 10 days 1 km data of the Mediterranean basin led to identify areas most sensitive to drought. Anomalous events in the time series were best detected using the wavelets transform. Notwithstanding the low spatial resolution, the SMMR 37 GHz observations were used to monitor flooding and recession in the Pantanal, a large natural reservoir in Brazil and Paraguay.

**JSM41/E/18-B5 1135****INTERANNUAL CHANGES IN GLOBAL VEGETATION ACTIVITY: COMPARING SATELLITE OBSERVATIONS AND VEGETATION MODELLING**

WOLFGANG KNORR (Max-Planck-Institut fuer Meteorologie, Bundesstrasse 55, D-20146 Hamburg, Germany; Tel.: +49-40-41173-282, Fax: +49-40-41173-298, Email: knorr@dkrz.de) and Garik Gutman (NOAA/NESDIS/ERA12, WWB 712, 5200 Auth Road, Camp Springs, Maryland 20746-4304, U.S.A.)

Remote sensing from satellites offers unique opportunities to monitor the state and evolution of global land vegetation. This is important, because land plants are considered to be of major importance for interannual changes in the global carbon cycle. It is particularly interesting to use remotely sensed imagery to test global models of vegetation activity. In this contribution, we compare interannual changes in vegetation cover inferred from NOAA-AVHRR data over the 1990s with the same changes simulated by the global Biosphere Energy-Transfer and Hydrology model (BETHY). We discuss the implications of differences and agreement between the two fields for the simulated carbon fluxes with BETHY. We find a pronounced impact of the El-Nino/Southern Oscillation phenomenon in both. Comparison with atmospheric CO<sub>2</sub> data also suggests such a link, as it stresses the dominant impact of land vegetation on this time scale. The results suggest that satellite monitoring of vegetation activity could significantly enhance our understanding of the present global carbon cycle.

**JSM41/E/14-B5 1150****THE RESPONSE OF SATELLITE-DERIVED NDVI TO LOCAL CLIMATE VARIATION IN SIBERIA**

Rikie SUZUKI (Frontier Research System for Global Change, c/o NIED, Tsukuba, Ibaraki 305-0006, Japan, email: suzuki@frontier.bosai.go.jp)

The response of the satellite-derived Normalized Difference Vegetation Index (NDVI) to the climate (precipitation and temperature) regionality was investigated in Siberia. The NDVI was obtained from Gallo's monthly Global Vegetation Index (GVI) which is a coarse NDVI data set covering the globe. Since the vegetation in Siberia shows meridional (south-north) transitions corresponding to the climate, two meridional transects were established from arid to taiga (along 75E) and from taiga to tundra (along 110E) vegetation transitions. Using surface station temperature and precipitation data in the CD-ROM "Global Daily Summary", the profiles of NDVI, temperature, and precipitation in the two transects were compared in conjunction with the elevation of each station through 1987 to 1990. As for the temperature, WI(0) which is an annually accumulated monthly mean temperature above 0C was used. In the arid-taiga transect, it was revealed that the NDVI tends to be large at high precipitation stations (the correlation coefficient (r) between the NDVI and precipitation deviations is 0.66). This result shows that the NDVI sensitively fluctuates due to the station-to-station precipitation variation. It was illustrated that the crucial factor in the arid-taiga vegetation transect is precipitation. In taiga-tundra transect, the NDVI tends to be large at high WI(0) stations (r = 0.43 between NDVI and WI(0)), at the same time, a negative correlation between WI(0) and station elevation was

found (r = -0.46). This fact means that the NDVI tends to be larger/smaller corresponding to the higher/lower WI(0) due to several hundreds meters lower/higher elevation of the station. These relationships may be an indication that the temperature factor is critical for the vegetation in taiga-tundra transect.

**JSM41/W/18-B5 1205****MONITORING PHYSICAL AND BIOLOGICAL STATES OF DESERT GRASSLANDS USING REMOTE SENSING**

Jerry C. RITCHIE, Albert Rango, Thomas J. Schumge, and William P. Kustas (all at USDA ARS Hydrology Laboratory, Beltsville, MD 20705, USA, Email: jritchie@hydrolab.arsusda.gov) Frank R. Schiebe (SST Development Group Inc., 824 North Country Club Road, Stillwater, OK 74075, USA, Email: franksch@isc-durant.com)

In 1995 the USDA Agriculture Research Service Hydrology Laboratory began collecting remotely sensed data from ground, aircraft and satellite platforms to provide spatial and temporal data on physical and biological states of desert grasslands in the southwestern United States. These measurements are being used to quantify hydrologic budgets and plant responses to changes in components in the water and energy balance at the Jornada Experimental Range and the Sevilleta Long-Term Ecological Research (LTER) in New Mexico. A range of ground, aircraft, and satellite data have been collected on the physical, vegetative, thermal, and radiometric properties of two ecosystems (grass and shrub) typical of desert grassland in this area. Remote sensing campaigns have been made in dry (May/June) and wet (September/October) periods each year. Data from different platforms will allow the evaluation of landscape properties at a range of scales from meters to kilometers. Radiances measured at ground and aircraft platforms were found to be 3 to 5 % higher for a 30-m<sup>2</sup> area at shrub sites when compared with the grass site. Landscape surface temperatures which were similar in the morning (9 am local time) showed 3 to 5 C higher temperatures at shrub sites when compared with grass sites by 1 pm local time. These differences in albedo and temperature could have significant effects on the energy and water balances of desert grasslands as shrubs continue to expand at the expense of the grass. Landsat and EOS satellite data will be used to extend these data to larger scales. These sites have been selected for EOS validation because of their long history of ground-based studies and ongoing repetitive remote sensing missions.

**JSM41/W/20-B5 1220****COMPARISON OF REMOTE SENSING, MODEL AND FIELD ESTIMATES OF ACTUAL EVAPOTRANSPIRATION**

GEOFF KITE and Peter Droogers, International; Water Management Institute, 35660 Menemen Izmir, Turkey. E-mail: g.kite@cgiar.org

Traditionally, actual evapotranspiration has been computed as a residual in water balance equations, from estimates of potential evapotranspiration or from field measurements by meteorological equipment. Recently, however, researchers have begun using remotely sensed data to estimate regional actual evapotranspiration. A field experiment was carried out in western Turkey over the summer of 1998 to compare the latest methods of estimating areal evapotranspiration using remotely sensed data from NOAA AVHRR and Landsat TM sensors, hydrological models at basin and point scales and field measurements, including scintillometers and net radiometer. This paper introduces the experiment, describes the data set and summarises the different estimation techniques. The results of the different methods are reviewed and compared and recommendations are made as to the suitability of the different methods for different circumstances.

Friday 30 July PM

Presiding Chairs: A.Rango (U.S. Department of Agriculture, Beltsville, MD 20705-2350, USA) T.Engman (NASA/GSFC, Greenbelt MD 20771 USA)

**TERRESTRIAL MONITORING****JSM41/E/30-B5 1400****USING NOAA AVHRR PRODUCTS FOR THE GLOBAL MONITORING OF EL NIÑO IMPACTS**

Garik Gutman, Ivan Csizsar, PETER ROMANOV and Larry Stowe NOAA/NESDIS, Office of Research and Applications, Washington, D.C. 20233, USA

The development of the El Niño Southern Oscillation (ENSO) in 1997-1998, the most intense in this century, has been monitored by space- and ground-based observations. This study discusses the potential of the current products, routinely derived at NOAA from measurements by the Advanced Very High Resolution Radiometer (AVHRR) onboard NOAA polar orbiting satellites, to monitor diverse ENSO impacts over the globe. Generally, ENSO impacts are manifested by droughts, excessive rain, or lack of snow cover, all affecting the agricultural production and often producing natural hazards, such as floods. We analyzed the month-to-month changes in surface-atmosphere conditions in several regions of the world, strongly affected by the 1997-1998 ENSO, using NOAA AVHRR products generated in near-real time, comprising surface and atmospheric variables, such as reflectances, temperatures, vegetation and fire indices, aerosol optical depths over ocean, fractional cloud amount, precipitation, and top-of-the-atmosphere outgoing longwave and absorbed shortwave radiation fluxes. The synergy of many variables allows us to better understand the big picture characterizing the state of the surface-atmosphere system and the relationship between different components of that system. This study demonstrates how the suite of the current NOAA satellite products derived from a single instrument in space can be used to detect ENSO-induced anomalies and to monitor the onset, extent, intensity and duration of ENSO impact on the surface-atmosphere system for diverse regions of the globe. We will discuss also some NOAA AVHRR products that are planned to be included into the suite of products for monitoring ENSO in the near future.

**JSM 41/E/31-B5 1415****MONITORING LAKE LEVEL CHANGES USING TOPEX/POSEIDON AND ERS-1 ALTIMETRIC DATA. COMPARISON WITH REGIONAL HYDROLOGY**

Franck MERCIER and Anny Cazenave (both at Laboratoire d'Etudes en Géophysique et Oceanographie Spatiales, 18 avenue Edouard Belin, 31401 TOULOUSE CEDEX 4, France, email: mercier@boreal-ci.cst.cnes.fr)

Topex/Poseidon and ERS-1 altimeters were primarily designed to measure height of the sea surface. Nevertheless, we can also use satellite altimetry to investigate level changes of continental lakes. We use 6 years of Topex/Poseidon altimetry data to study level changes of African Lakes (lake Malawi, lake Tanganyika, lake Victoria, lake Turkana, lake Tchad and additional smaller lakes). We also analyse the ERS-1 Waveform Altimeter Product raw data set to produce lake level time series. Due to its shorter intertrack spacing, ERS-1 provides a much



## INTER-ASSOCIATION

denser coverage of lakes than Topex/Poseidon. When available, in situ lake level measurements are compared with altimetric time series. In this analysis, we focus on the seasonal and interannual fluctuations of lake levels. Using available regional hydrometeorological data, we further study the water balance over each lake catchment basin. On the annual time-scale, we show a clear correlation between lake level and precipitation fluctuations while on the interannual time-scale, regional as well as global climatic changes are invoked.

### JSM41/W/17-B5 1430

#### MODELING SUSPENDED SEDIMENT TRANSPORT BY INTERNAL TIDES

Li, Jiren (Remote Sensing Technology Application Center, Ministry of Water Resources, 20 West Chegongzhuang Road, Beijing, China 100044, e-mail: ljr@mx.cei.gov.cn)

A sediment transport model was incorporated into an internal tide model to investigate the ability of internal waves to resuspend and advect sediment over continental shelves and slope regions. Internal tides may play a dominant role in controlling the distribution of sediment where the water depth is large enough to attenuate any direct impact upon sediment distributions by wind generated surface waves and currents. A number of numerical experiments were carried out for various idealized slopes and the model was applied to an observed section of the Australian North West Shelf. In all experiments, simulated bottom layer shear stresses were large enough to resuspend sediment. During this talk, the consequences of the non-linearity and asymmetry associated with the internal wave velocity field upon resuspension, deposition, and net sediment fluxes will be discussed.

### JSM41/E/11-B5 1445

#### IMPACT OF CO<sub>2</sub> MULTIPLICATION ON CROP YIELD OF NORTH CHINA PLAIN BASED ON REMOTE SENSING DATA AND PLANT PHOTOSYNTHESIS MODEL

ZHANG Jiahua (Institute of Atmospheric Physics, Chinese Academy of Sciences, Beijing, 100029, P.R.China email: zhangjh@ast590.tea.ac.cn)

In the paper, first considering remote sensing information and crop ecophysiological characteristics, the crop yield estimation model was set up based on NOAA-AVHRR derived variables and plant photosynthesis. Among them, photosynthetic active radiation (PAR), CPAP (Crop Photosynthetic Assimilation Potential, reflects crop photosynthetic time and area), and photosynthetic rate were calculated by remote sensing information and meteorological data. The developed model has been applied to winter wheat yield distributions in North China plain area, shows the model has better precision. Second, taking into account the impact of CO<sub>2</sub> doubling to agro-ecosystem and its influence on winter wheat, the model further developed and the regional crop yield was estimated owe to CO<sub>2</sub> doubled. The further changes of agricultural NPP distributions in North China plain were given using the developed model.

### JSM41/L/01-B5 1500

#### LANDUSE/LAND COVER CHANGE AND ITS IMPLICATIONS FOR DEFORESTATION IN THE HUMID TROPICAL RAINFOREST OF WEST AFRICA: THE EXPERIENCE OF THE LAGOS REGION (NIGERIA)

Simon. O. OJO (Department of Geography, University of Lagos, NIGERIA, e-mail: niomr@linkserve.com.ng)

Using Remote sensing technique, a land use/land cover change study of parts of the tropical rainforest region of West Africa, with emphasis on the Ikorodu area of the Lagos region (Nigeria) is discussed. The main categories of the land uses identified include the built-up areas, agricultural lands, wetlands (vegetated and unvegetated) and the water bodies in addition to barren lands. In addition to these main categories, 5, 2, 3 and 2 sub categories were also identified for the built-up areas, agricultural lands, wetlands and the water bodies respectively. In addition, the barren lands were also identified. Data generated using the 1962 and 1983 photographs were used for the study.

The study showed that between 1962 and 1983, the built-up areas increased by more than 600% from about 82 ha. to about 573 ha. Farmlands also increased by about 13% from about 1419 ha to about 1597 ha while wetlands decreased by about 13% from 2882 ha to about 2514 ha. Water bodies also decreased by about 19% from about 27 ha to about 22 ha. Barren lands also decreased by more than 90% from about 19 ha to about 2 ha. The implications of the results for deforestation in the area in particular, and the tropical rainforest region of West Africa is discussed.

### JSM41/W/05-B5 1515

#### COMPARATIVE ANALYSIS OF GROUND-BASED AND SATELLITE-DERIVED SHORTWAVE SURFACE IRRADIANCE MEASUREMENTS OVER RUSSIA

POKROVSKY O.M., Dalyuk I.V. (both at Main Geophysical Observatory, Karbyshev str.7, St.Petersburg, 194021, Russia, e-mail: pokrov@main.mgo.rssi.ru)

The subject of the study is incoming shortwave surface irradiance, main goal - to increase accuracy of satellite-derived surface radiative budget (SRB) estimates. The study concerns comparison of two types of data: results of retrieval from satellite data performed in the frame of ISCCP/SRB and ground-based measurements for the period 1985-1988 over Russia. In contrast to previous studies the biases between two types of data sets were studied at high temporal resolution - 3-hourly time step. Radiative transfer model exploiting delta-Eddington approximation was used to adopt ground-based data to solar zenith angles corresponding to satellite-derived data. Systematic and random errors for 27 most representative stations from all climatic zones of Russia were analyzed. It was shown that systematic error of monthly mean deviations is 7-10 times lower than standard deviations characterizing variations of instantaneous values of incoming shortwave irradiance. The most attention was paid to the statistical analysis of 2 months having extremal variations, July and March. In July mean deviations of monthly mean values were about 25 wt/m<sup>2</sup>, in March they were about 34 wt/m<sup>2</sup>. The coherence of both types of data is described by mean values of correlation coefficients: 0.74 in July and 0.66 in March. The intra-diurnal deviations of ground and satellite-retrieved data are, too, characterized by systematic and random components. Systematic component changes during the day from 15 to 90 wt/m<sup>2</sup>. Random component has significantly greater amplitude: ±50-150 wt/m<sup>2</sup>. Satellite-derived data values in comparison with ground-based measurements appeared to be overestimated for small values of radiation fluxes (50-200 wt/m<sup>2</sup>) and underestimated for high values of radiation fluxes (700-900 wt/m<sup>2</sup>). Within the interval 400-500 wt/m<sup>2</sup> the biases were minimal.

### JSM41/E/05-B5 1530

#### DEVELOPMENT OF RUSSIA SMALL-SATELLITE SET FOR MONITORING OF GEODYNAMICAL PROCESSES

Vladimir A. ALEKSEEV and Victor N. Oraevsky (Institute of Terrestrial Magnetism, Ionosphere and Radio Wave Propagation, Russian Academy of Sciences (IZMIRAN), Troitsk, Moscow region, 142092 Russia, email: ogm@fly.triniti.troitsk.ru)

To study the Earth and near-Earth space environment and to increase the capabilities of global monitoring, our Institute (IZMIRAN) develops Russia multi-purpose broad small-satellites set together with ground based infrastructure related. In particular, the makes it possible "to see" tectonic faults due to their influence to the ionosphere state by change of an atmospheric electrical field at the degasation of radioactive gases and aerosols in the fault zone. Thus, the whole system of tectonic faults can be fast and effectively mapped, including covert faults. This results in improvement of planning the search of mineral wealths. Changing atmospheric electrical field over faults is a dynamical process. Therefore, with the small-satellites set facilities it is for the first time possible to make monitoring of tectonic activity, using a short sampling interval. This information can help to strike out a new strategy of earthquakes forecasting. Also, (since the small-satellites set considered is a communication satellites system on the basis of high-grade space technologies) the project is aimed at improving the quality of public medicine by promoting the methods of remote consultations, the offered medical aid being able to envelop at once large number of sufferers in the region of a catastrophe.

### JSS42 Thursday 29 – Friday 30 July

#### Tsunami Observations, Modelling and Hazard Reduction (IASPEI, IAPSO, IAVCEI, IUGG Tsunami Commission)

Location: Haworth Building 101LT  
Location of Posters: Old Gym

#### Thursday 29 July AM

Presiding Chairs: V. Gusiakov (Inst. of Computational Mathematics & Mathematical Geophysics, Russia)  
N. Shuto (Iwate Prefectural University, Japan)

#### Tsunami Mitigation and Hazard Reduction

##### Introduction 0930

V. Gusiakov

### JSS42/W/27-B4 0940

#### CONTRIBUTION TO THE IDNDR: TSUNAMI FLOODING MAPS

E.N. Bernard, Tsunami Commission

Since 1989, the IUGG Tsunami Commission has facilitated the dedicated efforts of tsunami scientists to produce over 30 tsunami inundation maps for mitigating the effects of tsunamis in 17 threatened countries. Through a process of planning, proposal acceptance, tsunami data collection, and numerical model development, an internationally accepted methodology for preparing tsunami flooding maps has been created as the tsunami community's contribution to the International Decade of Natural Disaster Reduction. More importantly, scientists in 17 nations were trained to use of this methodology enabling those countries to produce more maps in the future. The value of such maps is that they identify coastal areas that could be flooded by future tsunamis that require some evacuation procedure to remove people from tsunami danger. To accomplish this goal, the tsunami scientific community had to carefully measure the effects of tsunamis and use these data to construct numerical models that could realistically simulate tsunami dynamics. In the past decade 9 destructive tsunamis have killed over 3,200 coastal residents in 7 countries. Each of these tsunamis were surveyed by teams of international tsunami scientists to collect measurements on the extent of flooding along affected coastlines. All surveying scientists generously shared their data with all tsunami scientists quickly and efficiently through internet technology. In addition to new data, a focussed modeling effort was required to convert tsunami flooding data into useful emergency management information. A partnership between the the IUGG Tsunami Commission, the United Nation's Intergovernmental Oceanographic Commission, and Tohoku University in Sendai, Japan was created to support the Tsunami Inundation Modeling Exchange (TIME) project. TIME is a modeling center at Tohoku University, under the leadership of F.Imamura and N. Shuto that trains scientists from other countries to use numerical models to estimate the extent of potential tsunami flooding for any threatened community. So far, these models have been transferred to scientists in seventeen countries, including: Australia, Canada, Chile, Columbia, Costa Rica, Ecuador, Greece, Indonesia, Italy, Japan, Korea, Mexico, New Zealand, Peru, Puerto Rico, Turkey, and the United States who have produced more than 30 inundation maps for tsunami threatened coastal communities. The global emergency management community now has a better tool to mitigate the impact of tsunamis.

### JSS42/E/15-B4 1000

#### TRAFFIC HINDRANCE AFTER TSUNAMI

Nobuo SHUTO (Faculty of Policy Studies, Iwate Prefectural University, Takizawa, Iwate 020-0173, Japan, email: shuto@iwate-pu.ac.jp)

It is important to open coastal traffic after a tsunami, in order to ensure a quick rescue operation within the "Golden 24" hours. Eighty five examples of coastal traffic hindrance were collected, classified and analyzed for 11 tsunamis in Japan. First cause of the traffic hindrance is destruction of structures. (1) Destruction of embankment of roads and railways by overflowing sea water. Destruction might begin with the erosion of slopes of embankment. If an embankment is lower than 0.5 m, and if the thickness of overflowing water is smaller than 1 m, then the embankment is not damaged, with no regard that the road is paved or not paved. (2) Damage due to concentration of water flow. Erosion around a bridge abutment begins at the end of wing walls and develops to the complete destruction of embankment, even though the abutment can withstand. A bridge pier is tilted or turned due to erosion around it. (3) Damage caused by impact of floating materials. Concrete bridges can withstand. Wooden bridges and light steel plate girder bridges are destroyed.



Railways is twisted due to movement of railway bridge. (4) Damage caused by buoyancy. Rails are moved due to buoyancy of wooden sleepers. Second cause is hindrance of function. (1) Standing sea water in low land. (2) Sand and mud deposition on roads and railways. (3) Depositions of logs, ships, houses and debris on roads. (4) Fires on or along roads.

JSS42/E/19-B4

1020

## MITIGATION STRATEGIES BASED ON LOCAL TSUNAMI EFFECTS

JANE PREUSS (Urban Regional Research, 1809 7th Avenue, Suite 1000, Seattle, Washington, 98101 USA, tel.: (206) 624-1669, fax: (206) 626-5324, email: jpreuss@nwlink.com); Razvan Bidoae and Peter E. Raad (Mechanical Engineering Department, Southern Methodist University, Dallas, Texas, 75275-0337 USA, tel.: (214) 768-3043, fax: (214) 768-1473, email: peter@seas.smu.edu

When the local effects imposed on structures are better understood, the knowledge constitutes an important tool that planners and regulators can use when making decisions with respect to land use practices in coastal areas. An initial field inventory defined key vulnerability issues for analysis through numerical simulation. Structures meeting the following three criteria presented the most significant risks: a) potentiality for significant damage, b) high disruption or loss of life, and c) potentiality for interactive damage. In this work, the impact of a water wave with a single, tall structure was numerically simulated and the forces and moments on the structure were calculated. To assess the effects of upstream conditions on the forces experienced by the main structure, four simulations were considered. In the first simulation, the flow path of the wave toward the structure was unobstructed. The results revealed the existence of two large peaks in the force and moment fields. The initial impact (and force peak) occurs at the base of the structure, as expected. The unexpected secondary impact occurs due to the collapse of the water column that ascended along the front face of the structure. In the second simulation, a short, wide obstacle was placed in front of the main structure. The obstacle (dike, shorter building, etc.) causes the initial impact to occur at a higher elevation, giving rise to a significant increase in the moment experienced by the structure. In the third simulation scenario, single and multiple pylons were placed in front of the structure. The results indicated a reduction in the amount of water impacting the structure, but the decreases in impact pressure, force, and moment were not significant. In the fourth simulation, a groove (or trough) was prescribed in front of the structure (the containment dike used around tank farms). This final simulation indicates a significant decrease in the forces and moments exerted on the structure. Land use implications, pertain to structures fronting the water, and also the second and third tiers of buildings, which often differ in building quality (e.g., hotels in front and behind older one or two-story homes). Site planning implications include the layout of structures, relationships of primary to accessory structures such as beach houses, parking lots, and open spaces.

JSS42/E/02-B4

1040

## A FRESH LOOK AT ELEMENTS OF THE TSUNAMI WARNING SYSTEM IN THE PACIFIC

Michael BLACKFORD (International Tsunami Information Center, US National Weather Service, 737 Bishop Street Suite 2200, Honolulu Hawaii 96813-3213, USA, email: michael.blackford@noaa.gov)

In the aftermath following the 1960 Chilean earthquake and tsunami the Tsunami Warning System in the Pacific, was established in 1968 under the auspices of the UNESCO Intergovernmental Oceanographic Commission. An event of similar magnitude has not recurred in the last 30 years, however, thousands of lives have been lost and millions of dollars of damage have been wrought since the System was established. These losses can largely be attributed to insufficient preparation in many areas for tsunami events on a regional or local scale. Although there are several exceptions, the Pacific States have generally moved slowly with regard to the development of adequate tsunami warning subsystems. Are States overwhelmed by subsystem start up costs? Do they believe the centralized System fulfills their needs? This paper looks at recent advances in communications and data acquisition that can bring down dramatically the costs of operating a tsunami warning system. It proposes a fresh look at a System that emphasizes the development of distributed subsystems that can be much more responsive to the needs of those vulnerable to tsunamis.

JSS42/W/24-B4

1120

## U.S. TSUNAMI HAZARD MITIGATION PROGRAM

Bernard, E.N., NOAA/Pacific Marine Environmental Laboratory, email: bernard@pmel.noaa.gov

The National Tsunami Hazard Mitigation Program is a Federal/State partnership (National Oceanic and Atmospheric Administration, Federal Emergency Management Agency, United States Geologic Survey/ Alaska, California, Hawaii, Oregon, and Washington) committed to reducing the vulnerability of U.S. coastal communities to tsunami hazards. Through three interdependent activities of tsunami flooding mapping for coastal communities, tsunami warnings, and education, the program is making progress on a broad range of emergency planning practices to mitigate the effects of tsunamis. A summary of the program's activities for the past 3 years will be given with emphasis on reducing coastal community vulnerability to tsunami hazards. A description of the program can be found at <http://www.pmel.noaa.gov/tsunami-hazard/>.

JSS42/W/25-B4

1140

## EARLY DETECTION AND REAL-TIME REPORTING OF DEEP-OCEAN TSUNAMIS

FI. GONZALEZ, E.N. Bernard, H.B. Milburn and H.O. Mofjeld, (all at NOAA's Pacific Marine Environmental Laboratory, 7600 Sand Point Way, NE, Seattle, WA, 98115)

Current tsunami warnings are based on seismic data and coastal tide gage observations. But neither provides direct measurement of tsunami energy propagating toward coastal communities. As a consequence, an understandably conservative tsunami warning philosophy has produced an unacceptably high false alarm rate -- approximately 75% since 1950. These false alarms are a serious problem because they are expensive, they undermine the credibility of the warning system, and they place citizens at physical risk of accidental injury or death during an evacuation. The speed and accuracy of tsunami warnings can be improved when real-time reports are made of deep ocean tsunami data collected near the source region within a few minutes of generation. Such data will enable a more direct and rapid assessment of the hazard and, when coupled with model forecasting tools, a more accurate prediction of the impact on specific coastal communities. Thus, destructive tsunamis will be identified more reliably and the number of false alarms will be reduced. An added benefit of the real-time data stream is continued offshore tsunami monitoring. Dangerous conditions can persist for several hours after the first wave strikes a community because very large tsunamis can have periods as long as an hour and the largest wave may arrive as late as the third or fourth in a series. So offshore tsunami monitoring will provide important guidance for decision-makers who must judge the risk of deploying rescue and recovery personnel and equipment and, when the area is safe for the return of residents, sound the "all clear." NOAA's Deep-ocean Assessment and Reporting of Tsunamis (DART) Project is an effort of the U.S. National Tsunami Hazard

Mitigation Program to develop this early tsunami detection and real-time reporting capability -- a formidable technological and logistical challenge. DART systems utilize bottom pressure recorders (BPRs) that are capable of detecting and measuring tsunamis with amplitude as small as 1 cm in 6000 m of water. The data are transmitted by acoustic modem to a surface buoy, which then relays the information to a ground station via satellite telecommunications. This design has been tested and refined through several deep ocean deployments of prototype systems. The latest prototype DART system was deployed on September 30, 1998 at Ocean Weather Station PAPA (50 N, 145 W). If this prototype system survives the winter, three additional systems will be deployed in 1999 off Alaska and Oregon as part of a planned six-buoy network in the north Pacific and equatorial region. The network is designed to provide early detection and measurement of tsunamis generated in source regions that threaten U.S. coastal communities: the Alaska Aleutian Subduction Zone, the Cascadia Subduction Zone, and the South American Seismic Zone.

JSS42/W/23-B4

1200

## ELEMENTS OF A TSUNAMI WARNING SYSTEM FOR THE INTRA-AMERICAS SEA

GEORGE A. MAUL, Florida Institute of Technology, 150 West University Boulevard, Melbourne FL 32901 USA, and Douglas M. Martin, NOAA National Ocean Survey, 1305 East-West Highway, Silver Spring MD 20910 USA

At a series of workshops (Barbados, 1995; St. John, 1996; Puerto Rico, 1997; Miami, 1998) the case has been made for significant tsunami hazards in the Intra-Americas Sea (Gulf of Mexico, Caribbean Sea, Bahamas, and Guianas). For example, since the great 1867 US Virgin Islands earthquake and 9 meter-high tsunami, the population density of the region has increased 10-fold, infrastructure development has progressed without a notable natural hazards component, and governments seem to be oblivious to the risk. Accordingly, four essentials comprise the proposed Intra-Americas Sea Tsunami Hazards System: Education, Warning, Management, and Research. The first order of business is to better educate the populace through public information, K-12 student indoctrination, video and other multi-media products, workshops, and popular press articles. The warning component should capitalize on the recently established CPACC (Caribbean Planning for Climate Change) sea-level/weather GOES-reporting network, on existing seismic and meteorological reporting and warning systems, and on active participation with the ICG/ITSU (International Co-ordination Group for the Tsunami Warning System in the Pacific). Management issues include: integration with other natural hazards warning systems; exploration for funds; local warning and evacuation; search and rescue; fire suppression; emergency medical services; damage assessment; inter- and intra-governmental coordination; and, damage and hazard analysis. Research needs are: improved resolution bottom relief data; travel time maps for population centers; earthquake magnitude / depth thresholds; tsunami wave arrival amplitude estimation; potential for Kick'em Jenny and Soufriere (Montserrat) eruption; tsunami and earthquake history improvements; fault locations, activity, and tsunamigenic mechanisms; inundation maps; GPS stations for crustal motion monitoring; and loss estimation studies, amongst others.

JSS42/E/16-B4

1220

## CONTEMPORARY ASSESSMENT OF TSUNAMI RISK AND IMPLICATIONS FOR EARLY WARNINGS FOR AUSTRALIA AND ITS ISLAND TERRITORIES

Jack RYNN (Centre for Earthquake Research in Australia, PO Box 276, Indooroopilly, Queensland 4068 Australia, email: sally.brown@uq.net.au; Jim Davidson (Bureau of Meteorology, GPO Box 413, Brisbane, Queensland 4001, Australia, email: j davidson@bom.gov.au)

The natural hazard of tsunami relative to Australia and its Island Territories is perceived to be of little or no consequence, hence a small risk, when compared to our other more frequent natural disasters. The historical record shows that tsunami damage, although rare, occurred along the eastern seaboard (1877 and 1960 Chile earthquakes), and northwest coast (1983 Krakatoa volcanic eruption and the 1977 and 1994 Indonesian earthquakes). Tsunami mitigation is a need because the island nations of Australia depend on its coastal facilities for sustainable development, with 90% of the population domiciled in this environment. One Australian IDNDR project assessed the tsunami risk to its shorelines and island Territories. A specific methodology invoking a multidisciplinary approach was developed. More than 350 earthquakes and specific submarine volcanoes and landslides were considered as possible tsunamigenic sources. In the period 1788 through 1995 more than 60 registrations on tide-gauge records were identified, together with anecdotal information. The outcomes have been presented as an "information resource" in terms of hazard, vulnerability and risk assessment maps and commentaries, tsunami data base, maps of potential tsunamigenic sources, tsunami travel time charts and relationships between relevant tsunami parameters. This provides practical applications to upgrade the Bureau's warning procedures and emergency services counter disaster planning, including development of a regional tsunami warning system.

Thursday 29 July PM

Presiding Chair: K. Satake (Seismotectonic Section, Geological Survey of Japan)  
S. Tinti (University of Bologna, Italy)

## TSUNAMI GENERATION AND SEISMOTECTONICS

JSS42/W/08-B4

1400

## MODELING FOR TSUNAMI GENERATED BY LANDSLIDING

Fumihiko Imamura; Kazumasa Hashi, Tomohiro Matsumoto, Nobuo Shuto Disaster Control Research Center, School of Eng., Tohoku University, Aoba 06, Sendai 980-8579, Japan, email: imamura@tsunami2.civil.tohoku.ac.jp

The numerical model to simulate tsunami propagation and generation due to a marine as well as land sliding is developed by deriving the governing equation and boundary condition for two layer flows with different density. The governing equation is derived by integration of Euler equation with viscosity, and by using kinetic and dynamic boundary conditions at free surface, interface, and sea bottom. Numerical scheme and procedure is designed the same as the standard model; TUNAMI code for applications. It is found that the front condition of the lower layer as landslide is very important for numerical stability. The form/drag force and interaction of momentum between two layers at the front are introduced to solve the instability. The numerical model is applied to two tsunami cases; the 1741 Oshima-oshima tsunami caused by landsliding on the volcanic island and the 1998 Sissano tsunami in PNG which might be related with a marine landslide. Although a pyroplastic model by Aida could not reproduce the runup heights measured along the peninsula of Oshima, the present model assuming the volume of landslide estimated from the change before and after eruption well simulate the distribution which is energy concentration on Kumaishi in north and Era in south. In the another case for marine landslide, it is demonstrated the interaction between two tsunamis caused by fault motion and landslide, suggesting the energy focus on the Sissano lagoon.

JSS42/W/03-B4

1420

## ENERGY BALANCE IN THE PROBLEM OF LANDSLIDE-INDUCED TSUNAMIS

Stefano Tinti and Cinzia Chiavettieri (both at Dipartimento di Fisica, Settore di Geofisica, Università di Bologna, email: steve@ibogfs.df.unibo.it)

Tsunamis generated by the movement of submerged large masses of sediments accumulated on the sea bottom over long periods of time are not rare and can be even very severe. The body of water and the body of sediments can be physically seen as two interacting systems exchanging energy. The main interest is typically focused on the energy gained by the water and manifesting in form of gravity water waves (the tsunami), but in principle the two systems are fully coupled, with energy flowing in both directions: energy is transmitted by the moving mass to the water giving rise to waves and energy passes from the waves to the mass, which means that the motion of the landslide is influenced by the propagation of the waves. This two-way nonlinear exchange of energy is generally overlooked. Here it is explored and consequences on modeling of tsunamis induced by underwater landslides are discussed.

JSS42/E/06-B4

1440

## LANDSLIDE TSUNAMI 'GENERATION MECHANISM AND ITS DETECTION FOR EARLY TSUNAMI WARNING ISSUE'

S.I.WASAKI (email: cuh@ess.bosai.go.jp) and S.Sakata (both at the National Research Institute for Earth Science and Disaster Prevention, 3-1 Tennodai Tsukuba 305-0006, JAPAN)

The cause of the Papua New Guinea Tsunami was probably landslide triggered by the original earthquake. As this example shows, these kinds of tsunamis generated by non-seismic causes sometimes gave heavy damages. Many reasons can be cited, such as the natural precursor of tsunamis, that is "shaking", were weak or nothing, generation regions were located in near shore regions, almost tsunami warning systems issue the tsunami warnings based on the Magnitude of earthquakes, generation mechanisms are still not fully clear and so on. In this presentation, at first, the simple landslide tsunami generation model will be introduced. Then, using a simplified topography of the ocean off Papua New Guinea coast, differences of wave forms of tsunami generated by a landslide and an earthquake will be discussed. A method to distinguish tsunami generated by an earthquake or a landslide will be shown. Finally, application of newly invented laser tsunami meter will be presented. The main conclusions are as follows; 1. Tsunami generated by a landslide shows strong directivity compared with that generated by an earthquake. 2. For the early tsunami warning issue, detection of tsunami informations at on site is essential. 3. For this aim, the cheaper tsunami warning systems are necessary and the newly invented laser tsunami meter is one of these.

JSS42/E/12-B4

1500

## NUMERICAL SIMULATION OF THE LANDSLIDE-GENERATED TSUNAMI OF NOVEMBER 3, 1994 IN SKAGWAY HARBOR, ALASKA

Evgueni A. Kulikov and Alexander B. RABINOVICH (both at Tsunami Center, Shirshov Institute of Oceanology, 36 Nakhimovskiy Prospekt, Moscow 117851, Russia, e-mail: abr@tsucen.msk.ru); Isaac V. Fine and Brian D. Bornhold (both at International Tsunami Research, Inc. 11321 Chalet Rd., Sidney, BC, V8L 5M1, e-mail: itri@ii.ca); Richard E. Thomson (Institute of Ocean Sciences, 9860 W.Saanich Rd., Sidney, BC, V8L 4B2, Canada, e-mail: thomsonr@dfo-mpo.gc.ca)

We examine the origin and behavior of the catastrophic tsunami that impacted Skagway Harbor, Alaska, on November 3, 1994. Geomorphic and tide gauge data, combined with a rigorous numerical modeling of the event, reveals that the tsunami was generated by an underwater landslide which also resulted in collapse of a cruise-ship dock undergoing construction. The three-dimensional shallow-water numerical model for a viscous landslide with full slide-wave interaction and subaerial slide was used to simulate tsunami waves in Skagway Harbor caused by the failure. The results of the numerical simulation closely agree with the NOAA tide gauge record and eyewitness observations. The landslide has been linked to critical overloading of the slope at a time of extreme low tide and is consistent with similar events in other coastal regions of the world. In general, we conclude that the numerical model of the submarine landslide associated with the dock failure in Skagway Harbor accounts for all aspects of the observed wave field.

JSS42/W/22-B4

1520

## "RED", "GREEN" AND "BLUE" TSUNAMIGENIC EARTHQUAKES: DOES ANY PHYSICAL BASIS FOR THIS CLASSIFICATION EXIST?

V.K. GUSIAKOV (Institute of Computational Mathematics and Mathematical Geophysics, Siberian Division, Russian Academy of Sciences, Novosibirsk 630090, Russia, Email: gvk@omzg.sccc.ru)

In the paper (Chubarov, Gusiakov, 1985), the theoretical dependence of the tsunami intensity  $I$  (on the Soloviev-Imamura scale) on the moment-magnitude  $M_w$  of a submarine earthquake has been obtained ( $I = 3.55M_w - 27.1$ ). This formula can be used for calculation of expected (on the basis of the "piston-like" model of the tsunami generation) tsunami intensity for a submarine earthquake with the known moment-magnitude. In this study, we introduce the formal classification of the Pacific tsunamigenic earthquakes on the basis of their  $dl$  parameter, that is the difference between the actually observed and the expected tsunami intensity ( $dl = I_{obs} - I_{exp}$ ). Based on the  $dl$  value, we divide all tsunamigenic earthquakes with known  $I$  and  $M_w$  into the three groups: "red" ( $dl > 1$ ), "green" ( $-1 < dl < 1$ ), and "blue" ( $dl < -1$ ). From 293 tsunamigenic events that occurred in the Pacific from 1900 to 1998 and which have both  $I$  and  $M_w$  values, 90 events fall within the "red" group, 153 are within the "green" group and 50 events are within the "blue" group. The geographical distribution of these tsunamigenic events shows their clear correlation with the climatic and circumcontinental zonation in the oceanic sedimentation as described in (Lisitzyn, 1996). Namely, two of the five major zones of the oceanic lithogenesis (northern humid zone and equatorial humid zone), that are characterized by the increased rates of the oceanic sedimentation, are clearly indicated by the increased number of the "red" tsunamigenic earthquakes (for instance, 6 of 7 events occurred within the Java trench are "red"). The circumcontinental zonation is clearly expressed by the fact that all the tsunamigenic events occurred in this century in the East China, the Yellow, the Japan, the Okhotsk and the Bering Seas are "red". On the other hand, all major submarine earthquakes that occurred in the remote (from continents) tsunamigenic zones like Guam, Tonga, New Zealand are "green" or "blue". Despite a considerable  $M_w$  value (greater than 7.5), many of these events have generated very minor tsunamis with the run-up heights less than 1 meter. The results of this study show that the earthquake-induced disturbance of the bottom sediments, resulted in submarine slumping, can be the leading factor controlling the tsunami generation mechanism, and these processes should be taken into account in the operational tsunami warning as well as in the coastal tsunamizoneing.

JSS42/W/25-B4

1600

## LIMITATIONS OF FAULT DISLOCATION MODELS FOR TSUNAMI SIMULATIONS ON THE CASCADIA SUBDUCTION ZONE, NORTHWEST COAST, NORTH AMERICA

GEORGE R. PRIEST (Oregon Department of Geology and Mineral Industries, Suite 965, 800 NE Oregon St., #28, Portland, OR 97232, email: george.priest@state.or.us) Edward Myers and António M. Baptista (both at Oregon Graduate Institute of Science and Technology, PO Box 91000, Portland, OR, 97291-91000, email: emyers@ccalmr.ogi.edu; baptista@ccalmr.ogi.edu); Paul Flüch (Swiss Federal Institute of Technology, Zürich, Switzerland); Kelin Wang (Geological Survey of Canada, Pacific Geoscience Centre, P.O. Box 6000, Sidney, B.C. V8L4B2, Canada, email: wang@pgc.emr.ca); Curt D. Peterson (Department of Geology, Portland State University, Portland, OR, 97207-0751, email: curt@ch1.ch.pdx.edu)

Three dimensional fault dislocation models (Okada's (1985) point source solution for an elastic half space) are used here to simulate coseismic ruptures on the Cascadia subduction zone for tsunami simulations. Earthquake recurrence of ~450 years, slip of ~15-20 m, and rupture widths (140 km) extending well onshore fit paleoseismic data. Narrower ruptures (70 km) that occur mostly offshore in Oregon and northern California fit thermal and geodetic data. The wide ruptures produced tsunamis about 30 percent lower than narrow ruptures, all other factors equal. Tsunami height varied directly with total slip. A rupture 1,050 km long with 15-20 m slip produced 6-9 m tsunamis, about twice as high as tsunamis from segmented ruptures 450 km in length with 7-10 m slip. The latter ruptures are most consistent with coupling and aspect (length:width) ratios of world wide analogues to Cascadia. Distribution of paleotsunami deposits appears to favor the 6-9 m tsunamis, but uncertainties in the fault dislocation models preclude assuming that lower slip (450 km) ruptures are not reasonable sources. None of the fault dislocation scenarios accurately depict possible inelastic deformation in the accretionary wedge or deformation from local faults, asperities, and submarine landslides, any of which could strongly modify deformation (and tsunamis) relative to the simulations. Simulation of inelastic deformation in the rheologically weak leading edge of the accretionary wedge was attempted by decreasing slip there. Simulations produced anomalous "spikes" of uplift, because the elastic model treats the area of decreased slip as a strong barrier rather than (as intended) a weak mass. Slip was thus deflected upward at this "barrier," effectively reproducing the same total uplift as full slip, but with a different shape. Tsunami run-up therefore did not decrease as expected.

JSS42/W/18-B4

1620

## THE DESTRUCTIVE SEISMIC ACTIVITY OF 1303 IN THE EASTERN MEDITERRANEAN: A POSSIBLE INTERPRETATION BASED ON REALISTIC SYNTHETIC WAVEFORMS

El-Sayed Attya (Geological Department Mansoura University, Mansoura, Egypt, The Abdus Salam International Center for Theoretical Physics, SAND group, Trieste, Italy and Dipartimento di Scienze della Terra - Università di Trieste, Via Weiss, 4 34127 Trieste, email: elsayed@geosun0.univ.trieste.it) Fabio Romanelli (Gruppo Nazionale per la Difesa dai Terremoti - CNR, Rome, Italy and Dipartimento di Scienze della Terra - Università di Trieste, Via Weiss, 4 34127 Trieste, Italy, email: romanelli@geosun0.univ.trieste.it) Giuliano F. PANZA (Dipartimento di Scienze della Terra - Università di Trieste, Via Weiss, 4 34127 Trieste, Italy and The Abdus Salam International Center for Theoretical Physics, Miramar, Italy, email: panza@geosun0.univ.trieste.it)

The Hellenic Arc is located about 500 km away from the Egyptian border, but earthquakes generated in this area can cause severe effects in Egypt. The observed shaking duration in Lower Egypt due to an event located in the Hellenic Arc is, on average, 3 minutes long. The seismic activity of 8th of August 1303 seems an exception to this pattern in terms of damage and duration of shaking. It was strongly felt in Lower Egypt for about 15 minutes and caused a widespread damage in Crete, Egypt, Rhodes, Jordan, Syria, Palestine, Turkey and Cyprus. The location of the seismic source(s) is ambiguous. Recent seismic activity, synthetic tsunami and ground motion modeling are used to infer the parameters of the possible source(s) from the available historical records. Using as constraint the available macroseismic and tsunami information we propose that two events occurred on the 8th of August of 1303. One earthquake is a shallow event with small to moderate size, located in Egypt, probably to the south of Cairo. This event can be the source of the extensive damage in the Nile Delta, Cairo and Upper Egypt. The other suggested event has a relatively larger size and is situated in the Hellenic Arc at shallow depth. This second event can explain the observed tsunami in the Eastern Mediterranean, the minor to moderate macroseismic effects in a wide area, including sites in, Jordan, Palestine, Syria and Turkey, and the extensive damage in Crete and Alexandria of Egypt.

JSS42/W/10-B4

1640

## NUMERICAL STUDY OF THE SOURCE OF THE JULY 17, 1998 PNG TSUNAMI

Vasily TITOV (NOAA/PMEL, JISAO, 7600 Sand Point Way NE, Seattle WA, 98115; email: titov@pml.noaa.gov) and Frank Gonzalez (NOAA/PMEL, 7600 Sand Point Way NE, Seattle WA, 98115; email: gonzalez@pml.noaa.gov)

The July 17, 1998 Papua New Guinea earthquake produced a tsunami with very high amplitudes, localized in a small area near the earthquake source. The relatively small earthquake magnitude and the concentration of the tsunami impact have prompted questions about the tsunami source mechanism. Possible source scenarios are landslide, bottom deformation, or a combination of the two. A numerical study of the July 17, 1998 Papua New Guinea tsunami is conducted to estimate discrepancies between different source mechanisms. Several source scenarios are simulated using the MOST numerical model, including a landslide source modeled as a viscous sediment flow and a co-seismic bottom deformation. Sources of various sizes at different locations are tested. Computed runup estimates are compared with measurements obtained by the International Tsunami Survey Team. It is found that several computed scenarios produce the runup distributions along the PNG coast which are reasonably close to the observed runup heights. Both pure landslide and bottom deformation are among these possible generation mechanisms, so it is difficult to distinguish between them on the basis of the runup comparison only. Distinctions in the tsunami runup dynamics for different tsunami sources are discussed. In the case of the PNG tsunami, as well as for many other events, runup values alone present too little information to distinguish between different tsunami source mechanisms. Any additional information about tsunamis, such as current velocities, sediments, number of waves and direct measurements in the possible source area, can provide crucial additional information for the tsunami source determination.



JSS42/W/20-B4 1700

## GENERATION OF GRAVITO-ACOUSTICAL WAVES BY BOTTOM DISPLACEMENTS OF FINITE DURATION

M.A. NOSOV, Moscow State University, Faculty of Physics, Russia

The linear potential theory was used for the sake of a comparative study of waves generation by bottom displacements of finite duration in the layer of an ideal incompressible and compressible homogeneous fluid of constant depth in the field of gravity (3-D problem). The analysis of exact analytical solutions to the problem has shown that a substantial difference exists between the behaviour of compressible and incompressible fluids under typical tsunami source conditions. In particular the results of this study indicate that the compressibility of water can not be neglected, if one pretends to give an adequate description of the tsunami generation by bottom displacements of a duration less than 10 H/c, where H is ocean depth in the source region, c is the sound velocity in water. Tsunami source radiates not pure gravitational but a system of gravito-acoustical waves. The further study of the features of these waves could be of interest for tsunami forecasting in terms of tsunami forerunners.

Friday July 23 AM

Presiding Chairs: E.N. Bernard (Pacific marine Environmental Lab, Seattle, USA)  
F. Imamura (Disaster Control Res. Center, Tohoku Univ, Japan)

JSS42/W/14-B5 0830

## STUDY OF TSUNAMI DEPOSITS IN HOKKAIDO, JAPAN: A PROGRESS REPORT

Kenji SATAKE, Futoshi Nanayama, Koichi Shimokawa (all at Earthquake Research Dept., Geological Survey of Japan, Tsukuba, 305-8567 JAPAN, email: satake@gjs.go.jp); K. Shigeno (Meiji consultant co., ltd.)

We are studying tsunami deposits on both the Japan Sea and Pacific coasts of Hokkaido, Japan, to better understand the sedimentology and the history of earthquakes and volcanic eruptions in the region. Our sites include: Taisei town across from Okushiri Island, where we identified tsunami deposits from the 1993 Southwest Hokkaido (Okushiri) earthquake as well as sand deposited by a 1959 typhoon; Ayukawa coast, where we identified tsunami deposits from the 1741 Oshima-oshima eruption; Kiritappu marsh and Bettoga coast, where we found sand layers from at least six tsunamis. The 1993 tsunami deposited four layers at Taisei. We correlate these layers with landward and seaward flows from the two main tsunami waves; the flow directions are shown by imbrication of gravel, current ripples, and the remains of knocked-down plants. On the other hand, the typhoon deposit forms only one layer and its cross bedding records only landward flow. The tsunami's landward-flow layers are mostly marine sand, whereas the seaward flow layers are composed of non-marine sand and a mixture of soil, gravel, and plant remains. The typhoon deposit is composed of mostly marine sand. The 1741 tsunami was associated with the eruption of Oshima-oshima volcano, but the generation mechanism has not been known. We found several cobbles in the tsunami-sand layer in our trench. The Pacific coast of Hokkaido has been affected by tsunamis from subduction-zone earthquakes both nearby and across the Pacific. We found multiple sand layers interbedded with tephra layers: two sand layers above a 1739 tephra, three sand layers between 1694 and the 10th century, and a few more sand layers below the 10th century tephra.

JSS42/W/01-B5 0850

## THE GEOMORPHOLOGY AND SKDIMENTOLOGY OF THE JULY 9TH 1956 AEGEAN SEA TSUNAMI, ASTYPALAEA ISLAND, GREECE

Dale Dominey-Howes (Coventry Centre for Disaster Management, School of the Built Environment, Coventry University, Coventry, CV1 5FB, UK, email: apx124@coventry.ac.uk)

Sediments are described from Livadia and Stavros, Astypalaea Island, Greece and are interpreted to be associated with the Aegean tsunami of 9th July 1956. At Livadia, the marine provenance of the tsunami unit is inferred from two observations. Firstly, the similarity between the clasts comprising the tsunami unit and the contemporary beach sediments from which the sediments are derived, and secondly the inclusion of foraminiferal tests within the sediment matrix. Derivation from the 1956 tsunami, rather than from storm surge is inferred from the uniqueness of the deposits within the sedimentary record, their distinct imbrication and orientation, and <sup>137</sup>Cs and <sup>210</sup>Pb dating of overlying and underlying colluvium. The top of the tsunami sediment layer occurs at +2.00 meters above sea level indicating minimum flood level. At Stavros, the marine provenance of the tsunami sediments is demonstrated by the inclusion of marine mollusca, while the sediments here occur up to an elevation of +10.00 meters above sea level. The minimum flood levels indicated by these deposits are significantly lower than values previously reported. The results presented here represent the first systematic investigation into the geomorphology and sedimentology of modern Aegean tsunami, and, when combined with geomorphological evidence, indicate that previous reports of flooding from the 1956 tsunami were significantly over-estimated. Such over-estimation of flood levels may have important implications for tsunami hazard risk assessment and emergency pre-planning.

JSS42/P/02-B5 0910

## GLOBAL DISTRIBUTIONS OF PEAK FREQUENCY AND THE AMPLITUDE TO THE BIGGEST THREE PACIFIC TSUNAMIS IN THIS CENTURY

Kuniaki Abe (Niigata Junior College, Nippon Dental University, Hamaurachō 1-8, Niigata City, 951-8580, JAPAN, email: abeku@ngt.ndu.ac.jp)

Amplitude spectra were obtained for tide-gage records of the 1952 Kamchatka, 106 Chilean and 1964 Alaska tsunamis in all over the Pacific. Number of used stations are 38 (1952), 42 (1960) and 61 (1964). The spectrum was calculated using Goertzel method for 6 hour's time history including the initial arrival from which tidal level was reduced and plotted for the frequency range from 0 to 2mHz (8.3min in period) at the interval of 0.01 mHz. In the spectrum we noticed a peak frequency and the amplitude. They were discussed in relation to the epicentral distance, which is approximately propagation distance, and azimuth angle of the station to the epicentre.

Average peak frequencies obtained are 0.46 (1952), 0.34 (1960) and 0.36 (1964) in mHz. The difference is mainly attributed to sea-depth at the source because of the proportionality to long wave velocity. The approximate average sea-depths are 2000m, 650m and 150m, respectively. In the amplitude-distance curve amplitude increased or kept a constant value for the distance larger than 1000km. The increase is noticeable for the azimuth direction normal to trench axis. This fact suggests a geometrical contraction of tsunami after passing the critical distance of a quarter of global circumference. The remarkable tendency in the 1952 Kamchatka tsunami is related to station distribution. Azimuth dependences of peak frequency and the amplitude were also observed and support a directivity of wave radiation from the source. Particularly, the largest value in all the peak frequencies for each tsunami is found in the direction approximately normal to the trench axis. If taking into consideration of curving

wave ray, we conclude that tsunami including the highest frequency is radiated to the direction normal to the trench axis.

JSS42/E/05-B5 0930

## DISTRIBUTION FUNCTIONS OF RUNUP HEIGHTS FOR RECENT TSUNAMIS BASED ON OBSERVED DATA

Efim PELINOVSKY (Laboratory of Hydrophysics and Nonlinear Acoustics, Institute of Applied Physics, 46 Ujanov Str., Nizny Novgorod, 603600, Russia, email: enpeli@appl.sci-nnov.ru); Igor Ryabov (Department of Applied Mathematics, Nizhny Novgorod Technical State University, 24 Minin Str., Nizhny Novgorod, 603600, Russia, email: igor@ceed.kis.ru)

Studying the characteristics of the runup heights for several historic tsunamis, Van Dorn, Kajjura and Go have found that the distribution functions of the tsunami heights are described by the log-normal distribution. The aim of this paper is to obtain the distribution functions of the runup heights for recent tsunamis. The observed data of following tsunamis were analysed: Flores (12.12.92); Japan Sea (12.07.93); Java (02.06.94), Shikotan (04.10.94); Mindoro (14.11.94); Sulawesi (01.01.96); Irian Java (17.02.96), Peru (21.02.1996), Papua New Guinea (17.08.98). It is confirmed that the log-normal distribution describes the observed data well, and parameters of this distribution are found. An important problem of the quality of the prognostic characteristics of the tsunami distribution is discussed taking into account different numbers of the observed points.

JSS42/W/21-B5 0950

## IMPACT OF LARGE TSUNAMIS IN THE MESSINA STRAITS, ITALY

Stefano Tinti, Alberto Armigliato and Francesca Fiorini (all at Dipartimento di Fisica, Settore di Geofisica, Università di Bologna, e-mail: steve@ibogfs.df.unibo.it, armigliato@ibogfs.df.unibo.it)

Among the Italian coasts, Messina Straits are one of the most exposed to tsunami attacks. Several historical events are reported for this region, generated both locally and in the surrounding regions, in particular in Thyrrenian Calabria to the north (the 1783 event) and in eastern Sicily to the south (1693). The 28 December 1908 earthquake generated tsunami was the last catastrophic event affecting this region: a large body of documents and reports exists for such event, as well as some tide-gauge records some hundred km away from the source. Nowadays, the Messina Straits coasts are characterised by a large number of urban, industrial and touristic settlements: in addition, towns like Messina and Reggio Calabria represent fundamental nodes for transports. The tsunami hazard assessment for the Messina Straits is then a very relevant problem, which may be faced on the basis of documents available for historical events, of the available geological and seismotectonic information and of numerical modelling and simulations.

JSS42/E/18-B5 1010

## TSUNAMIS IN CENTRAL AMERICA

Mario Fernandez Acre, (Escuela Centroamericana de Geología, Universidad de Costa Rica, San Jose, Costa Rica) Enrique Molina, (Instituto de Sismología, Vulcanología, Hidrología y Meteorología de Guatemala, Guatemala) Jens HAVSKOV and Kuvvet Atakan (both at Institute of Solid Earth Physics, University of Bergen, Allegaten 41, 5007 Bergen, Norway, email: jens@ifij.uib.no)

A catalog of tsunamis has been compiled for Central America containing 49 tsunamis for the time period 1539 to 1996. This is believed to be the most complete catalog made so far. Most of the information (43 events) is reported after 1850. 12 of the tsunamis occurred on the Caribbean side and 37 on the Pacific side. 47 tsunamis were related to local earthquakes while 2 were caused by earthquakes outside the region. On the Caribbean side, there only seem to be a tsunami risk due to local earthquakes in the north and the south while on the Pacific side, the whole coast can experience tsunamis. Here the highest risk is along the coasts from Guatemala to Nicaragua and outside Central Costa Rica. About 500 persons are known to have been killed by tsunamis and the largest known tsunami occurred in Nicaragua in 1992 killing 170 persons. On the Caribbean side, all earthquakes near the coast and larger than Ms have generated a significant tsunami while on the Pacific side only 43% of coastal earthquakes larger than 7 have generated significant tsunamis. These facts will be used as criteria for the new tsunami warning center to be set up in Central America.

JSS42/E/17-B5 1030

## DEVELOPMENT OF LASER TSUNAMIMETER

Shoji SAKATA and Shin'ichi Iwasaki (both at National Research Institute for Earth Science and Disaster Prevention, Ten'nodai 3-1, Tsukuba-shi, Ibaraki-ken, 305-0006, Japan, email: sakata@geo.bosai.go.jp)

Direct observation of tsunami heights in off-shore areas by tsunamimeters installed on the sea bottom is very effective for mitigation of tsunami disasters. We have been developing a new laser tsunamimeter based on the invention by Sakata. The inspiration for this tsunamimeter came from the concept of the borehole laser strainmeter, of which development Sakata has been engaged in. Later Sakata invented an ingenious device for cancellation of effects of temperature change of the sea water around the vessel. By adding this device to the original laser strainmeter the concept of the laser tsunamimeter is completed. This laser tsunamimeter has many advantages over the conventional tsunamimeter of the quartz oscillator type. The change of the diameter of the vessel of the undersea part caused by pressure change due to the tsunami propagation is detected as the change of resonance frequency of the Fabry-Perot interferometer. Due to the simple design of the undersea part, in which neither IC nor mechanically movable part is included, possibility of trouble will be small. Electricity supply to the undersea part is not necessary since it is connected to the land part by only optical fibers. The slender cable needs smaller amount of cost for production and installation. Expected resolution is between 0.1-1cm. Recently we completed the production of the undersea part.

JSS42/W/02-B5 1110

## RECENT TSUNAMIS OF 1990-1998 IN THE PACIFIC: GENERAL OVERVIEW

V.K. GUSIAKOV (Institute of Computational Mathematics and Mathematical Geophysics, Siberian Division, Russian Academy of Sciences, Novosibirsk 630090, Russia, Email: gvk@omzg.ssc.ru); J.F.Lander (National Geophysical Data Center, Boulder, CO 90309, USA, Email: jfl@ngdc.noaa.gov)

A comprehensive list of recent tsunamis occurred in the Pacific during the last nine years has been compiled as part of the joint IUGG Tsunami Commission and ICG/ITSU Project "Basic Pacific Tsunami Catalog and Database, 47 B.C. - 2000 A.D." The list contains 77 tsunamigenic events occurred in the Pacific from 01.01.1990 to 31.12. 1998. From these events, 10 have validity 4 (definite tsunami), 10 - validity 3 (probable tsunami) and 7 events still have validity 2



(questionable tsunami). For all the events, having at least one run-up measurement, the tsunami intensity  $I$  (on the Soloviev - Imamura scale) has been calculated. In terms of this parameter, the smallest but still detectable event was the February 9, 1991 Solomon Islands tsunami ( $I=4.5$ ) with the reported maximum wave height of only 3 cm. The three strongest events within this period were the July 12, 1993 Okushiri tsunami ( $I=3.1$ ) with the highest run-up of 30.6 m, the July 17, 1998 New Guinea tsunami ( $I=3.1$ ) and the September 2, 1992, Nicaragua ( $I=2.8$ ). Several major submarine earthquakes having Ms or Mw value greater than 7.6 generated very minor tsunamis (with the wave height less than 0.5 meter). During this period, 30 regional and 1 Pacificwide warnings were issued by the national and the regional tsunami warning centers. Among them, only 10 warnings can be considered as justified, in other cases the maximum run-up height observed at the coast was less than 1 meter. By different reasons, for 3 damaging tsunami warnings were not issued in time. They are the September 2, 1992, Nicaragua, the December 12, 1992, Flores and the January 1, 1996 Sulawesi tsunamis. Analysis of historical tsunami occurrence in the Pacific in this century shows that the last nine years had the slightly increased level of perceptible ( $I=1$ ) as well as damaging ( $I=2$ ) tsunamis as compared to the long-term average. Their annual rates of occurrence in 1990-98 were 2.2 and 1.1 against 1.7 and 0.75 in 1900-98, respectively.

**JSS42/E/18-B5****1130****A NEW TSUNAMI CATALOGUE FOR EASTERN MEDITERRANEAN SEA**

G. A. PAPAPOPOULOS (Institute of Geodynamics, National Observatory of Athens, 118 10 Athens, Greece, email: g.papad@ege.lasos.gein.noa.gr)

A new catalogue of tsunamis occurring in the area of Eastern Mediterranean Sea from the antiquity to 1998 has been compiled on the basis of original historical documents, previous catalogues, scientific papers as well as geological and archaeological evidence. The format of the catalogue is similar to that arranged by the GITEC group for the new European Tsunami Catalogue. The data incorporated in the new catalogue have been elaborated as for their completeness and reliability described as a function of time and of the particular geographic regions covered.

**JSS42/E/20-B5****1150****OFFSHORE GEOLOGICAL ASPECTS OF THE SISSANO TSUNAMI PAPUA NEW GUINEA**

DAVID R TAPPIN, British Geological Survey, Keyworth, Nottingham, NG12 5GG UK Takeshi Matsumoto, Japan Marine Science and Technology Centre, Natsushima-Cho, Yokosuka, 237-0061, Japan and shipboard scientific party.

A survey to investigate the offshore aspects of the July 1998 Sissano tsunami was carried out in January 1999 by the Research Vessel Kairei. It was coordinated by the Japan Marine Science and Technology Centre and the South Pacific Applied Geoscience Commission and acquired multibeam bathymetry, seabed sonar, sub-bottom profiles and piston cores. Models of the tsunami event have so far been based upon a fault solution. However, other evidence suggests that seabed faulting may be only part of the cause.

The survey results reveal a complex seabed morphology that is attributable to subduction of the Pacific Plate southwards beneath PNG along the New Guinea Trench. A narrow shelf 10 kilometres wide lies offshore of Sissano and passes seaward into an inner trench slope dissected by submarine canyons. Sediment transported from the land mainly bypasses the upper inner trench slope and is transported out into lower slope basins, into the trench and out onto the Pacific Plate. Sediments on the inner trench wall are cohesive clays, whereas in the lower slope basins and the trench they are interbedded fine clays (hemipelagites) and silts (turbidites). The inner trench slope is faulted and bears large arcuate scars interpreted as signs of slope failure. This failure is interpreted as taking place through rotational faulting rather than as debris flows. Nearshore bathymetry off of Sissano suggests a subsided delta front that may provide a focusing mechanism for the Sissano tsunami.

**JSS42/P/01-B5****1210****FLOW STRENGTH ON LAND OF THE 1998 PAPUA NEW GUINEA TSUNAMI**

Hideo MATSUTOMI (Dept. of Civil and Environmental Eng., Akita Univ., Akita, 010-0852, Japan, email: matsuto@ipc.akita-u.ac.jp); Yoshiaki Kawata, Yoshinobu Tsuji, Koji Fujima, Fumihiko Imamura, Masashi Matsuyama, Tomoyuki Takahashi, Norio Maki and Seh-Sub Han (Members of 1st and 2nd International Tsunami Survey Team); Nobuo Shuto (Faculty of Policy Studies, Iwate Prefectural Univ., Iwate, 020-0173, Japan, email: shuto@iwate-pu.ac.jp)

Field survey was conducted two times: during August 3 to 6 and September 30 to October 3, 1998. Main items of the survey were: (1) spatial distribution of both tsunami height and inundation depth in Sissano, Wapapu, Arop 2, Arop 1 and Malol regions, (2) dimension of houses and their floor height, (3) degree of damage to houses and (4) sand erosion depth and sand grain size on the sand spits of Sissano lagoon. Based on these data, (1) current velocities on flat land and on the sand spits, (2) relation between inundation depth and degree of damage to houses, (3) dependency of sand erosion depth on current velocity and so on are discussed. Laboratory experiments were also carried out to confirm the state of flow on the sand spits.

Results indicate that: (1) the largest inundation depth of 10m was found at Arop 2, and the current velocity was estimated greater than 10 m/s, (2) current velocities on flat land had the same tendency as that in past tsunamis, (3) wooden houses which are church were destroyed when the inundation depth exceeded 1 m. This critical depth is very small compared with that in other places and (4) the dependency of sand erosion depth on current velocities on flat land is the same as that in past tsunamis. But, that on the sand spits was different. As a reason, it is considered that undulate jumps would be formed on the lagoon side.

**JSS42/W/15-B5****1230****CLUSTER ANALYSIS OF TSUNAMI MARIGRAMS**

Gerald T. Hebenstreit (SAIC, Ocean Systems Group, 1710 Goodridge Drive, McLean, Virginia, USA, 22102, 703-827-4975, email: gerald.t.hebenstreit@cpm.x.saic.com)

Teletsunamis and some local tsunamis on long coastlines are often marked by surprising differences in the intensity of tsunamis seen in marigrams. One section of a coastline may receive clearly apparent waves, while another section close by may receive much less apparent effects. Cluster analysis is a tool which uses the characteristics of the data to delineate patterns that may not be apparent to visual observation. The analysis makes no assumptions about the data other than that the various pieces can be directly compared. Marigrams from two tsunamis - Chile 1985 and Andeanof Islands 1996 - were examined to identify possible systematic (as opposed to local) patterns in the dispersion of tsunami intensity on coastlines.

Presiding Chairs: F. Gonzalez (Pacific Marine Environmental Lab, Seattle, USA)  
Y. Nishimura (Inst. of Seismology & Volcanology, Hokkaido University, Japan)

**PHYSICAL AND NUMERICAL MODELLING****JSS42/W/06-B5****1400****TSUNAMI RUNUP INTERACTIONS WITH A TEST STRUCTURE**

Harry YEH, Halldor Arnarson, and Catherine Petroff (all at Department of Civil & Environmental Engineering, University of Washington, Seattle, WA 98195-2700, USA, email: haryeh@u.washington.edu); Razvan Bidoae and Peter Raad (both at Department of Mechanical Engineering, Southern Methodist University, Dallas, TX 75275-0337, USA, email: peter@seas.smu.edu)

The hydrodynamics of local tsunami runup interactions with a structure were investigated both experimentally and numerically. A tall, vertical column with a square footprint was used as a model of the structure, and the tsunami runup was assumed to take the form of a uniform turbulent bore. In the laboratory, the impact and transient load forces on the column were measured with a load cell, while detailed temporal and spatial variations of the tsunami runup profiles were obtained with a laser-induced fluorescent technique. Furthermore, water velocities at various locations around the column were measured with a laser Doppler anemometer. The numerical simulations were obtained by the use of the recently developed three-dimensional surface marker and micro cell (3DSMMC) technique, which is a fully three-dimensional finite-volume approach that treats the free-surface dynamics by the use of Lagrangian surface markers defined in more highly resolved surface cells. The transient numerical results are in good agreement with the laboratory results in terms of the net force exerted on the column, the water-surface variations, and the flow velocities around the column. The favorable agreement of the numerical model with the laboratory data demonstrates that the numerical capability can be used with confidence in practical field applications to assess local effects of tsunami runup.

**JSS42/E/21-B5****1420****CHARACTERISTICS OF ON-SHELF TSUNAMIS AND THE ACCURACY OF THE NUMERICAL SIMULATION**

Shun-ichi KOSHIMURA (DCRC, School of engineering, Tohoku University, Aoba 06, Sendai 980-8579, JAPAN, email: kossy@tsunami2.civil.tohoku.ac.jp), Fumihiko Imamura (DCRC, School of engineering, Tohoku University, Aoba 06, Sendai 980-8579, JAPAN, email: imamura@tsunami2.civil.tohoku.ac.jp), Nobuo Shuto (Faculty of Policy Studies, Iwate Prefectural University, Morioka, Japan, email: shuto@poly.iwate-pu.ac.jp)

The waveform and amplitude of obliquely incident tsunamis on a slope such as a continental shelf vary according to the conditions of incidence. However, there are cases that numerical simulation can not predict the characteristics of these on-shelf tsunamis with sufficient accuracy. Especially, if the tsunami is incident almost parallel to the slope, numerical result differ significantly depending on the grid size because of the error associated with the refraction of shallow water waves. So far, there is no criterion for the option of appropriate grid size for the numerical computation except for the specific case such as tsunamis around islands proposed by Fujima et al. (1998).

In the present study, the condition to obtain the accurate result in the numerical simulation of on-shelf tsunamis are discussed by taking the following procedure.

- (1) We derive the analytical solutions of on-shelf tsunamis which is obliquely incident on a constant slope with arbitrary waveform.
- (2) Based on the solutions obtained, the fundamental characteristics of on-shelf tsunamis are discussed for various types of incident waves.
- (3) The numerical solutions of on-shelf tsunamis by the Leap-Frog finite difference method with a variety of grid sizes are compared with the analytical ones obtained by the present study, and the magnitudes of the errors are examined.
- (4) The criterion of the grid size to obtain the sufficiently accurate result in the numerical simulation of on-shelf tsunamis is proposed.

**JSS42/W/26-B5****1440****THE TSUNAMI COMMUNITY MODELING ACTIVITY (TCMA)**

F.I. GONZALEZ, E.N. Bernard and S. Hankin (all at NOAA's Pacific Marine Environmental Laboratory, 7600 Sand Point Way, NE, Seattle, WA, 98115)

Tsunami modeling is a critical community activity that contributes to the overriding goal of saving lives and property. In particular, our community conducts R&D that is focused on model improvement and the development of effective tools for hazard mitigation. A Tsunami Community Modeling Activity (TCMA) is a way to facilitate this R&D process. Community models are well-established as valuable tools in other scientific communities. Good examples are the ocean circulation models maintained at the Institute of Marine and Coastal Sciences at Rutgers University, the Princeton Ocean Model (POM) maintained by Princeton's Program in Atmospheric & Oceanic Sciences, and the Australian Community Ocean Model (ACOM) maintained by the CSIRO Division of Marine Research in Hobart, Tasmania. The value of a community model rests on the following assumption. If easier and more widespread access to models and associated databases is provided, then the R&D to improve model science and develop more effective applications will be accelerated by broadening the user base and providing a mechanism to incorporate and document subsequent innovations and advances. The TCMA will provide a much-needed focal point for the tsunami research community to improve model physics and numerical techniques. Multiple users of the same model and databases will create regular, systematic, and invaluable feedback that will be exploited to improve the models and provide a high degree of quality control on both the model and related databases. A "community memory" will be created and institutionalized, so that important advances are not lost, redundancy and "re-inventing the wheel" is minimized, and the next generation of tsunami modelers will not be obliged to "start from scratch." Finally, and perhaps most importantly from a practical point of view, an optimal environment will be created for the systematic development and improvement of hazard mitigation products. A first step in developing an effective TCMA and enhancing the tsunami modeling R&D environment is the implementation of a distributed facility for the analysis and comparison of tsunami simulations (FACTS) that will allow global, transparent sharing of databases and model results that are resident on servers of participating institutions. FACTS will exploit the World Wide Web and additional existing technologies: Live Access Server software to seamlessly link each server; the FERRET applications package for manipulation, comparison, and analysis capabilities; the NSF/NASA supported Distributed Ocean Data System (DODS) from the University of Rhode Island for networked scientific data communications ...

JSS42/W/07-B5 1500

## OFFSHORE FORECASTING OF ALASKIAN TSUNAMIS IN HAWAII

V.V. TITOV, H.O. Mofjeld, F.I. Gonzalez and J.C. Newman (all at NOAA/PMEL, JISAU/OW, 7600 Sand Point Way NE, Bldg.3, Seattle, WA, 98115, USA, e-mail: titov@pmel.noaa.gov)

This study is an R&D activity conducted in an effort to develop tsunami forecasting tools for the Pacific Disaster Center (PDC). The research includes analytical and numerical sensitivity studies of tsunami wave characteristics offshore of Hawaii, for ranges of earthquake source parameters in the Alaska-Aleutian Subduction Zone (AASZ). The results demonstrate that, for a fixed location and magnitude, there is very weak dependence of the offshore tsunami characteristics on a reasonable range of other AASZ earthquake parameters. This sensitivity study provided guidance for the construction of a database consisting of pre-computed tsunami scenarios. The simulation results are stored as an online database with a WWW interface. A database user can very quickly obtain a model prediction of the tsunami offshore wave heights at chosen locations, for a wide variety of AASZ earthquake scenarios. Direct tsunami observations can be combined with the forecast database to improve the accuracy of the tsunami forecast methodology. Potentially, the best approach to forecasting the impact of a particular tsunami event on a specific coastal site is to perform real-time tsunami model simulations that include real-time data assimilation. As a community, we should work toward this difficult "Holy Grail" of tsunami forecasting. However insufficient real-time earthquake data and a lack of confidence in tsunami generation and inundation modeling, presently render the implementation of such an operational capability imprudent. Fortunately, however, existing numerical models are good enough to provide useful guidance, if exercised with care by an experienced tsunami modeler. Event- and site-specific inundation estimates can be computed far in advance of the earthquake, thoroughly tested and scrutinized for reasonableness and sensitivity to errors, then stored as a database. When an event occurs, the appropriate pre-computed results can be recalled, modified by data assimilation schemes that utilize a user-friendly interface to incorporate real-time tsunami measurements, and then made available to aid hazard assessment and evacuation decision-making.

JSS42/W/09-B5 1520

## TSUNAMI SCOUR MECHANISMS AROUND A CYLINDER

Harry YEH (Department of Civil & Environmental Engineering, University of Washington, Seattle, WA 98195-2700, USA, email: harryeh@u.washington.edu); nji Sato and Norifumi Kato (both at Public Works Research Institute, 1 Asahi, Tsukuba, Japan, email: sato@pwri.go.jp)

It is known that tsunamis cause substantial erosion and scours on shore. The scour mechanisms around on-shore structures are expected to be different from the present understanding of bridge or pier type scour processes in a river or coastal environment. Flows associated with tsunami runup are not steady nor uniform, and the scouring occurs in a short duration, less than half an hour. In order to understand fundamental mechanisms of the scouring, a series of experiments was performed in a 135 m long, 2 m wide, 5 m deep sediment tank; this large facility is necessary because the substantial scale effects are anticipated for the sediment motions. The maximum stroke of the wave paddle is 2.4 m and it was tested and proven to generate, at least, a clean solitary wave of 40 cm high in 3 m deep of water. The circular column is used as a structure model, and is placed upright at three different locations: 1) 4m on-shore from the shoreline, 2) at the shoreline, and 3) 4 m offshore from the shoreline. The cylinder is 50 cm in diameter, made of 1 cm thick Plexiglas. Because of its transparent cylinder wall, the scouring process is conveniently recorded with three miniature CCD video cameras equipped inside of the cylinder, which cover more than 180 degrees of the circumference view. Pore pressure transducers are placed at four locations around the cylinder in the sediment depths of 10 cm, 20 cm and 30 cm. Also placed are the capacitance type wave gages and an electromagnetic flow meter. It was found that the maximum scour occurs during the tsunami drawdown stage and is approximately twice the depth of the final scour configuration. Based on the pore pressure data as well as the video images, sediments around the cylinder appear to become liquefied during the drawdown process.

JSS42/W/17-B5 1600

## NUMERICAL SIMULATION OF 1998 PNG TSUNAMI ON A NEW BATHMETRY BY KAIREI

Masafumi MATSUYAMA, Central Research Institute of Electric Power Industry, 1646 Abiko, Abiko-shi, Chiba-ken, Japan.

The 1998 Papua New Guinea (PNG) tsunami caused devastating damage and casualty along the north coast of PNG, in particular near Sissano lagoon. Surveyed tsunami effects were much greater than the estimated based on the available seismic and bathymetry data. The similar discrepancy is often attributed to the phenomenon so called "the tsunami earthquake." This PNG event does not fit to the characteristics of the tsunami earthquake. The survey also found that only narrow coastal area, approximately 30 km long, around Sissano lagoon was significantly affected by the tsunami; the tsunami effects drastically decrease away from the region. In order to explain the discrepancies, Japan Marine Science and Technology Center (JAMSTEC) and South Pacific Applied Geo-Science Commission (SOPEC) conducted the marine geophysics survey in January, 1999. During the cruise, detailed bathymetry data and sub-bottom profiles are obtained in the offshore area adjacent to Sissano lagoon. With the obtained bathymetry data and the newly discovered fault location, Numerical simulations for the PNG tsunami were performed using the standard seismic model. It was found that significant tsunami-energy focusing toward Sissano lagoon is caused by the bathymetry effects. Furthermore, a possible submarine landslide site was identified, and the initial condition for the landslide generated tsunami is estimated. Even the landslide source area is small (5 km x 7 km), the computed runup heights around Sissano lagoon is significant (approximately one half the measured values). More importantly, the runup height distribution along the shore is qualitatively in good agreement with the simulation. The results demonstrate that the accurate bathymetry and the source location are critical for the predictions for tsunami runup.

JSS42/W/01-B5 1620

## NON-REFLECTIVE OPEN BOUNDARY CONDITION FOR TSUNAMI NUMERICAL SIMULATION

Tomoyuki Takahashi (DRS, DPRI, Kyoto University, Uji, Kyoto 611-0011, Japan, email: tomo@drs.dpri.kyoto-u.ac.jp) Hiroya Ishihara (Fac. of Engineering, Kansai University, Suita, Osaka 564-8680, Japan, email: gj50010@edu.kansai-u.ac.jp) Yoshiaki Kawata (DRS, DPRI, Kyoto University, Uji, Kyoto 611-0011, Japan, email: kawata@drs.dpri.kyoto-u.ac.jp)

In order to carry out numerical simulation stably and with high precision, the setup of suitable boundary condition is indispensable. The boundary condition in tsunami numerical simulation is divided into the land side and the offing side. As for the boundary condition on the land side, there are a vertical wall condition and a runup condition, and a lot of studies about it have been

made so far. Especially, much knowledge about the runup condition has been obtained theoretically and experimentally. On the other hand, as for the boundary condition on the offing side, the method of the long wave approximation, the characteristics method and the method of the virtual non-reflecting plane boundary are used well. However, they have been used without sufficient examination about their accuracy and stability. Although the free penetration of the progressive wave generated inside the computational area needs to be carried out, it turns out that a reflected wave occurs according to open boundary conditions. The reflected wave returns to the computational area and will cause instability and lower accuracy. Especially, the reflected wave occurs mostly by the case when the progressive wave diagonally approach to the boundary and the case where depth is shallow or bottom slope is large in the vicinity of the boundary. To reduce the influence of the reflected wave, the computational area is taken widely. But this makes a problem that the amount of the computation and the computation time become large. Moreover, it is abundant to compute without investigating what reflected wave has occurred at the open boundary. Then, by this research, each non-reflected open boundary condition was compared about the various depth, bottom slope and incident angle, and the applicable condition in tsunami numerical simulation was examined.

JSS42/E/09-B5 1640

## COMPUTATIONAL EXPERIMENTS FOR SIMULATION OF TSUNAMI EFFECTS NEAR SOUTH KURIL ISLANDS

TATYANA IVELSKAYA, Sakhalin Tsunami Warning Center, 78, Zapadnaya str., Yuzhno-Sakhalinsk, 693000, Russia, email: TWC@Sakhalin.ru. Vasily hramushin, Special Research Bureau for Automation of Marine Researches, Far East Branch of Russian Academy of Sciences, 25 Gorky str., Yuzhno-Sakhalinsk, 693013, Russia, email: Khram@Sakhalin.ru;

The tsunamis and storm surges are dangerous sea phenomena, however, these admits the possibilities to organize the actions for the evacuation of peoples, will have earliness from a few minutes or a next hours.

The decision of a problem of numerical simulation with the purpose of operative forecasting of wave processes in a coastal zone for specific tsunami is described in this work.

As initial data for modeling a tsunami parameters of earthquakes, and also the information on displays a tsunami on coast are used the experience of work on realization of similar computational experiments at modeling of real tsunami has shown good results, which give sufficient conformity with records a tsunami.

Presiding Chairs: F. Gonzalez (Pacific Marine Environmental Lab., Seattle, USA)  
Y. Nishimura (Inst. of Seismology & Volcanology, Hokaido University, Japan)

JSS42/W/28-B5 Poster 1700-01

## TSUNAMIS BY VOLCANIC EXPLOSIONS: DEPOSITS AND RUNUP DATA FROM THE 1996 ERUPTION IN KARYMSKOYE LAKE, KAMCHATKA, RUSSIA

Alexander BELOUSOV and Marina Belousova (Institute of Volcanic Geology and Geochemistry, Petropavlovsk-Kamchatsky, Russia, email: Belousov@g23.relcom.ru) Barry Voight (The Pennsylvania State University, USA, email: voight@ems.psu.edu)

The 1996 subaquatic explosive eruption in Karymskoye lake (4 km across, maximal depth 70 m) generated multiple tsunamis. The steep northern shore of the lake adjacent to the crater was violently eroded by the tsunamis, with all plants and soil more than 1.5 m thick stripped off, and poorly consolidated bedrock exposed. Along the rest of the shoreline, more than 1.3 km from the crater, the tsunamis carved new cliffs up to 2 - 3 m high, eroded the upper layer of frozen soil up to 50 cm thick, and inundated adjacent areas as shown by vegetation removal, or destruction of alder bushes. In the band of devastation the tsunamis deposited several discontinuous, finely laminated layers of sand and gravel up to 35 cm thick, with scattered pebbles, fragments of plants and clots of soil. The distinctive band of devastation, and the tsunami deposits, allowed us to measure the runup height of the tsunamis at 24 points around the lake. These data enable determination of a law of attenuation of runup (wave) height for "explosive" tsunami, which is compared with theoretical modelling. For the proximal zone, to radial distances ( $r$ ) up to 1.3 km, the runup height ( $R$ ) shows rapid attenuation (from  $>30\text{m}$  to  $8\text{m}$ ) with distance as  $\log R = -0.56 \log[r] + 5.8$ . For the distal zone,  $r > 1.3\text{ km}$ ,  $R$  decays more slowly (from  $8\text{m}$  to  $3\text{m}$ ) as  $\log R = -1.98 \log[r] + 16.3$ . Rapid decay in proximal zone suggests that in the near field of the explosion the tsunami propagate as a collapsing wave with discontinuous change in height. The break-in-slope of the runup plot at 1.3 km suggests that the tsunami propagate further as a decaying one-dimensional wave in a channel of approximately constant width.

JSS42/W/13-B5 Poster 1700-02

## LOCAL TSUNAMIS GENERATED BY STORM WAVES

GERARD J. FRYER (Hawaii Institute of Geophysics & Planetology, University of Hawaii at Manoa, 2525 Correa Rd, Honolulu, HI 96822, USA, email: gerard@hawaii.edu)

Many orphan tsunamis (events without identifiable sources) have occurred in the two centuries of recorded Hawaiian history. Such "tsunamis" have been commoner in the winter months, when surf can reach 10 m, so they are dismissed in the catalogs as "waves of meteorological origin." Unexplained, however, is occasional inundation far larger than expected even from 10-m surf. Inundation and damage have been so extensive that a true tsunami is the only possible explanation. Without a local earthquake, such an event is assumed to be "a tsunami from a distant but unknown source." The assumption is reasonable: flooding reports are typically from north-facing coastlines, and to the north lie the sparsely-populated Aleutian Islands, where tsumamigenic earthquakes (until the modern era of worldwide instrumentation) might pass unreported. It is now clear, however, that at least three events (in 1860, 1878, and 1903) were not from distant sources. Each of the major Hawaiian Islands has a broad, north-facing bay prone to extreme tsunami runup: Hilo on the Big Island, Kahului on Maui, Waialua on Oahu, and Hanalei on Kauai. A teletsunami producing high runup in one of these bays invariably produces high runup in all. The orphan events, however, affect only Kahului and Waialua Bays, the adjacent coastlines of Maui and Oahu, and the north coast of Molokai. Since the orphans occur only when surf is exceptionally high, it seems probable that by pumping up pore pressures, storm-generated waves drive bottom sediments to failure. The resulting landslide generates a tsunami whose effects are added to the already-large waves. The limited geographic extent of the anomalous flooding clearly identifies the locus of the landslides: the north slope of Molokai.

**JSS42/W/16-B5** Poster **1700-03**

**PALEO-TSUNAMIS NOVEL FINDINGS FROM NORTHWESTERN EUROPE**

Nils-Axel Möner Paleogeophysics & Geodynamics, S-10691 Stockholm, Sweden, email: morner@pog.su.se

Tsunamis are able to cause disastrous damage to coasts and coastal habitation. They are generated by coastal and submarine vertical fault movements or huge submarine slides. It is a well known phenomenon in the Pacific region. The Lisbon 1755 event is classic. In recent years we have also started to appreciate their imprints in our paleorecords. Past events are documented in the Mediterranean region. More surprising are the records from NW Europe. First we learned about the tsunami of the 7200 BP Storegga submarine slide outside Norway and its effect along the coasts of Norway and Scotland. The latest news come from Sweden where we have been able to document a major earthquake (generating liquefaction over 320 km) occurring in the autumn of varve 10,430 BP and a subsequent event occurring in varve 9663 BP (generating seismites over 210 km). Both events generated tsunamis; the first one washed the strait between the Baltic and the North Sea free of ice so that marine water suddenly could invade the Baltic basin (by this creating the Yoldia Sea stage sensu stricto). The second event set up a wave recorded in the sea bed sedimentology and ice marginal shore morphology. A triple sedimentary sequence was recorded indicating sucking motions towards the epicenter, a deformational wave away from the epicenter, and a strong backwash wave depositing high energy accumulations, deforming beds underneath and setting up a turbidite which is recorded in the varve chronology over an area of 210 km (in varve -424 = varve 9663 BP). Other deglacial events are under investigation. An event of more local character has been recorded in a lake system and dated at about 3500 BP. This gives a totally new picture of the long-term seismic hazard and actual occurrence of tsunami events in Sweden and surrounding regions.

**JSS42/E/14-B5** Poster **1700-04**

**IDENTIFICATION OF TSUNAMI DEPOSIT AND ITS APPLICATION FOR EVALUATING HISTORIC TSUNAMI HAZARDS IN HOKKAIDO, NORTHERN JAPAN: A REVIEW**

YUICHI NISHIMURA (Institute of Seismology and Volcanology, Hokkaido University, Sobetsu 59, Utsunomiya, Hokkaido 052-0103, Japan, email: nishi@eos.hokudai.ac.jp) Naomichi Miyaji (Shizuoka Prefectural Agricultural Experiment Station, Godo, Hamaoka-cho, Ogasara-gun, Shizuoka 437-1613, Japan, email: miyaji@ss.sand.agri-exp.pref.shizuoka.jp)

We have studied geological evidence for recent and historic tsunamis which attacked Hokkaido, northern Japan. At various kind of land beside the beach, we made pits to take core samples or excavated trenches, and identified tsunami deposits overlies volcanic ash soil, old dune and peat. These tsunami deposits are found to show some common features: (1) Deposit thickness and mean grain sizes decrease with distance from the sea. (2) The thickness and lithofacies vary according to the original surface undulation. (3) Graded bedding reflecting tsunami runup and backwash is present in thick deposits. It was possible to find coarse tsunami deposits sandwiched by fine dune sands, but hard to specify the original tsunami event except that known volcanic tephra lies closely. On the other hand, the age could be estimated for tsunami deposits in homogeneous peat deposit based on growth rate of the peat. When the upper boundary of a tsunami deposit is traced, we can estimate the minimum height of its corresponding tsunami runup. For the 1640 tsunami caused by an eruption of Hokkaido Komagatake, which killed more than 700 people around Uchiura Bay, we examined documentary descriptions, made numerical computations and traced tsunami deposits. It is useful to combine these independently obtained data to estimate height distribution of a historic tsunami and evaluate its disaster.

**JSS42/E/23-B5** Poster **1700-05**

**1952 NORTH KURIL TSUNAMI: A NEW DATA FROM ARCHIVES**

Victor KAISTRENKO and Valentina Sedaeva (both at Institute of Marine Geology and Geophysics, Far Eastern Division of the Russian Academy of Sciences; Nauki St., Yuzhno-Sakhalinsk, 693002 Russia, email: tsunami@sakhalinmail.sakhalin.ru)

During the long time until 1990th most of data related to the catastrophic 1952 tsunami were secret and last years these data can be investigated. Most essential information is contained in the survey report made by Hydrographic Service of the Russian Navy. Several reports of different commissions were found in Sakhalin archives. Interesting information was received from eye-witness of this event.

Navy's survey team started to work in Severo-Kurilsk next day after the tsunami. Their report contains 10 maps of flooding areas around the settlements on North Kuril Islands and good description of damages due to tsunami and many photos.

The reports in Sakhalin archives give many descriptions of tsunami behavior and contain the lists of damages and lost persons. So, the Okeanskaya settlement was destroyed almost fully by 20-meter tsunami and 460 persons were lost, i.e. about 50 % of population, and 1753 persons were killed by tsunami in this region.

Several descriptions and photos were given by eye-witness. All these data are planned to publish as a book.

**JSS42/E/13-B5** Poster **1700-06**

**RUNUP OF TSUNAMI WAVES ON A VERTICAL WALL AND GENTLE BEACH IN A BASIN OF COMPLEX TOPOGRAPHY**

Efim PELINOVSKY (Laboratory of Hydrophysics and Nonlinear Acoustics, Institute of Applied Physics, 46 Uljanov Str., Nizhny Novgorod, 603600, Russia, email: enpeli@appl.sci-nnov.ru) Elena Troshina (Geophysical Institute, University of Alaska Fairbanks, Fairbanks, AK 99775, USA, email: etroshin@images.alaska.edu) Vladimir Golinko and Natalya Osipenko (both at Department of Applied Mathematics, Nizhny Novgorod Technical University, 24 Minin Str., Nizhny Novgorod, 603600, Russia)

Being able to estimate the flooding area of the coastal zone caused by the tsunami waves is essential for tsunami hazard mitigation. Much progress has been made in applying the one-dimensional nonlinear shallow water theory to the runup height calculation. It was based on the analytical results of the well-known paper by Carrier and Greenspan. This method has been used by many authors to calculate the tsunami wave runup. The exact estimation of the size of the area flooded by tsunami waves requires the solution of two-dimensional shallow-water equations, taking into account the geometry of the coastal line (bays, straits, estuaries, etc.). We study runup of tsunami waves on a vertical wall and gentle beach in a bay of different cross-section using shallow water equations. The characteristics of the nonlinear deformed waves in bays of different cross-section are investigated. The nonlinearity causes the runup height to increase. Several examples of beach topography are considered. The criteria of the wave breaking are discussed.

**JSS42/E/11-B5** Poster **1700-07**

**NUMERICAL SIMULATION OF POTENTIAL SUBMARINE SLOPE FAILURES AND ASSOCIATED TSUNAMIS ALONG THE COAST OF BRITISH COLUMBIA**

Alexander B. RABINOVICH, Evgueni A. Kulikov (both at Tsunami Center, Shirshov Institute of Oceanology, 36 Nakhimovskiy Prospekt, Moscow 117851, Russia, e-mail: abr@tsucen.msk.ru) Richard E. Thomson (Institute of Ocean Sciences, 9860 W.Saanich Rd., Sidney, BC, V8L 4B2, Canada, e-mail: thomsonr@dfo-mpo.gc.ca) Brian D. Bornhold, and Isaac V. Fine (both at International Tsunami Research, Inc. 11321 Chalet Rd., Sidney, BC, V8L 5M1, e-mail: itri@ii.ca)

Studies in coastal areas of British Columbia indicate the high instability of deltaic and nearshore sediments in many areas. Buildings, coastal facilities, pipelines, telecommunication and electrical transmission cable lines are at significant risk of direct damage from subaerial and submarine landslides. Tsunamis generated by these events probably pose an even greater threat in terms of damage and loss of life. We concentrate our attention on two areas of potentially high risk of slope failure: (1) Malaspina Strait, a narrow (5 to 10 km) channel separating Texada Island from the mainland of British Columbia; and (2) the Fraser River delta front in the southern portion of the Strait of Georgia. The main reasons for our interest in these areas are: (1) large volumes of unconsolidated sediments, accumulated there; (2) high risk of instability of these sediments; and (3) location of significant coastal infrastructure, which would be at risk should a failure and tsunami occur. We have developed two types of numerical model to simulate landslide-generated tsunamis: (1) viscous flow, and (2) rigid body. These models bracket the true response of the sea surface to the landslide, with the viscous slide model underestimating the wave response and the rigid body model overestimating the response. Parameters of slide bodies were defined from existing geological and geophysical investigations, and direct video observations. In the case of Malaspina Strait, the failure of the northern lobe of a perched sediment mass on the slope off eastern Texada Island, yielded trough-to-crest waves from 7 to 9 m. Two cases were...

**JSS42/E/25-B5** Poster **1700-08**

**ANALYSIS OF THE ALGERIAN TSUNAMIS ON THE MEDITERRANEAN COAST OF SPAIN**

Alexander B. Rabinovich (IOS, Sidney BC, Canada, Email: RabinovichA@pac.dfo-mpo.gc.ca), Sebastian MONSERRAT (CSIC-UIB, Palma de Mallorca, Spain, Email: dfsmt4@clust.uib.es)

Although tsunamis in the Mediterranean are not so frequent and powerful as in the Pacific, they still present serious threat for the coastal areas. The major risk for the coast of Spain is related to the earthquakes in the northern part of Algeria. The Orleansville Earthquake (1954) with magnitude M = 6.6 and El Asnam Earthquake (1980) with M = 7.3 generated significant tsunamis observed all along the Mediterranean coast of Spain and in the Balearic Islands. These tsunamis were recorded by several tide gauges (Malaga, Ceuta, Alicante, Almeria, Algeciras, etc.). The number of tsunami records in the Mediterranean basin is extremely limited, so examination of these two tsunamis simultaneously measured by the instruments situated in various sites of the Western Mediterranean is of high scientific and applied interest. The method recently proposed by Rabinovich (1997) to separate the influence of source and topography in tsunami spectra was used to analyze the data. The main attention was paid to Alicante records, which were of high quality, especially to the 1980 case when the corresponding tsunami was recorded by two gauges (inside and outside of the harbor). The response characteristics of the harbors were constructed. Several cases of atmospherically generated seiches have been also examined and the results have been compared with results of tsunami analysis.

**JSS42/W/28-B5** Poster **1700-09**

**THE AD1650 MT. COLUMBO (THERA ISLAND) ERUPTION AND TSUNAMI, AEGEAN SEA, GREKCE**

Dale Dominey-Howes (Coventry Centre for Disaster Management, School of the Built Environment, Coventry University, Coventry, CV1 5FB, UK, Kmail:apx124(R)coventry.ac.uk)

This presentation reviews evidence for the eruption and tsunami reported to have occurred in AD1650 in the area of Mt. Columbo, Thera Island, Greece. The tsunami is believed to have been generated as consequence of the eruption of Mt. Columbo 6.5 km NE of Thera Island. Historical documents state that the tsunami flooded up to 2 miles inland and destroyed many engineered structures. Lithostratigraphic evidence from one abandoned trench and two trench excavations close to sea level in the villages of Kamari and Perissa respectively, which lie well within the reported inundation zone of the tsunami. The results presented show that marine- (tsunami) sediments were deposited at these locations. Alternative hypotheses of discontinuous sediment deposition and overestimation of the event magnitude are considered to explain the observations presented here. The data may have important implications for the development of hazard zone maps, risk assessment, vulnerability reduction and for emergency management officials.

**JSS42/E/08-B5** Poster **1700-10**

**MITIGATION OF TSUNAMI RISK FOR THE CITY OF SUVA, FIJI**

Jack RYNN (Centre for Earthquake Research in Australia, PO Box 276, Indooroopilly, Brisbane, Queensland 4068 Australia, email: sally.brown@uq.net.au) Gajendra Prasad (Mineral Resources Department, Government of the Republic of Fiji, Private Mail Bag, Suva, Fiji, email: gajen@mrd.gov.fj); Atu Kaloumaira (Mitigation Advisor, South Pacific Disaster Reduction Management Office, c/o UNDP, Private Mail Bag, Suva, Fiji, email: atu@sopac.com.org)

As part of the UNHDA - South Pacific Programme Office "South Pacific Disaster Reduction Programme", within the auspices of Pacific Region IDNDR and the 1994 Yokohama Statement, the "Suva Earthquake Risk Management Scenario Pilot Project" (SERMP) was facilitated for the Government of the Republic of Fiji. SERMP considered mitigation measures for both earthquake and tsunami impacting upon the City of Suva, with the scenario event based on the real experience of the 1953 Suva earthquake (ML 6.5) and tsunami, which devastated the city, its industrial and harbour facilities. A specific methodology was developed involving a multidisciplinary approach with multi-agency cooperation to address, in both quantitative and qualitative terms, the premise RISK = HAZARD X VULNERABILITY and then integrate the assessments in terms of Fiji's emergency management requirements. The outcomes include hazard, vulnerability and risk zonation maps with commentaries, tsunami parameters and possible damage situations. It was concluded that a significant risk of local tsunami does exist for the City of Suva and its harbour environs. Practical applications of these results, in terms of community vulnerability and reduction of potential losses, and including a simulated tsunami exercise, have been a major element in this project. Fiji is now developing a regional tsunami warning system.



**JSS42/W/05-B5** Poster **1700-11**

**TSUNAMI WAVE SCATTERING IN THE NORTH PACIFIC**

H.O. Mofjeld, V.V. Titov, F.I. González and J.C. Newman NOAA/Pacific Marine Environmental Laboratory Seattle, WA, USA

A theoretical study is being carried out to understand how escarpments, ridges and seamounts affect deep-water tsunami propagation in the Pacific Ocean. The study is also designed to determine the accuracy and resolution of bottom topography that are needed in numerical models to accurately simulate the effects of small-scale ( $\sim 100$  km) topographic features on tsunami propagation. The initial focus of the work is on tsunamis that are generated in the Alaska/Aleutian Subduction Zone (AASZ) and propagate southward to Hawaii. Analytic theory shows that main effects of these features is to scatter energy from the tsunami waves. The amount of scattering depends on the heights of the features relative to the total depth, their spatial extent compared with tsunami wavelengths, and their orientation relative to the direction of wave propagation. 2-D wavelet analyses of the Sandwell/Smith topography (Topo 6.2) are used to identify the spatial scales and locations of scattering features in the North Pacific. Numerical simulations based on the MOST model (with and without small-scale topography) show that deep-water scattering produces only a small amplitude decrease in the first waves of AASZ tsunamis propagating to Hawaii (a few percent in energy). This is compared with the geometric spreading and broad-scale refraction that occurs when the tsunami waves propagate southward from their sources. The primary reason for relatively little deep-water scattering is that the tsunami-scale topographic features between Alaska and Hawaii do not extend vertically over a substantial fraction of the total water depth. However, significant focusing of tsunami waves does occur near Hawaii; this is due to the seamount field north of Kauai, the Emperor Seamount Chain and the Hawaiian Ridge. While deep-water scattering has only a minor influence on the first waves in AASZ tsunamis, it does contribute to the complicated temporal patterns of the waves that occur later in Pacific-wide tsunamis. Scattering processes are much stronger on the upper continental slope and shelf; hence there is a need for accurate topography in these regions. Future work will extend the analysis to shallower water, to other source regions (e.g., Kamchatka, Kuril/Japan and Cascadia) and to other impact regions, especially the U.S. West Coast.

**JSS42/E/03-B5** Poster **1700-12**

**THE TSUNAMI OF 1722.12.27, ALGARVE-PORTUGAL**

M.A. Baptista (Instituto Superior de Engenharia de Lisboa, Lisboa Portugal, email: mariaana@fc.ul.pt, fax + 3511 3953327) C.Lemos (Instituto Hidrográfico - Portugal) J.M.Miranda (Centro de Geofísica da Universidade de Lisboa)

The earthquake of 1722.12.27 generated a tsunami that affect the southern coast of Portugal, mainly in the area of Tavira. The maximum earthquake intensity was X and the magnitude 7.5 (given by Instituto Geográfico Nacional, Madrid Spain). The historical data on this event is rather scarce. However, the earthquake was felt along the whole south Portuguese coast and in Faro and Tavira a rather strong river withdrawal were observed (Mendonça, 1758). The epicentre of the earthquake was located, from isoseismal analysis offshore the south coast of Portugal but the precise location is largely unknown. The aim of this work is the compilation of all geophysical data, and the use of tsunami hydrodynamic modeling to evaluate among a set of fault candidates which is the most probable source of the Tavira earthquake. This work was financially supported by project RIMAR.

**JSS42/E/07-B5** Poster **1700-13**

**TSUNAMI RUN-UP**

C. CORELA and L.A. Mendes Victor (both at ICTE, Instituto de Ciências da Terra e do Espaço, Rua da Escola Politécnica 58, 1200 Lisboa, Portugal, email: ccorela@correo.fc.ul.pt)

The description of the Tsunami run-up is of greatest importance for Tsunami zonation and evaluation of Tsunami Hazard. The difficulties arising here are evident: the complexity of coastal zone morphology and the variety of underlying surfaces changing due to their interaction with the water flows caused by Tsunamis, the possibility of waves breaking and competition of nonlinear and dispersion effects. A numerical method based on the upstream formulation for the advective term is applied to compute the run-up.

**JSS42/E/19-B5** Poster **1700-14**

**THE EXPERIMENTAL ITALIAN TSUNAMI WARNING SYSTEM AT AUGUSTA (EASTERN SICILY)**

Alessandra Maramai, Alessandro Piscini and Giuseppe D Anna (Istituto Nazionale di Geofísica (ING), Via di Vigna Murata 605, Rome - Italy)

In the frame of the GITEC-TWO (Genesis and Impact of Tsunamis on the European Coasts) project, in the Eastern Sicily coasts a "pilot" station of the first Italian Tsunami Warning System (TWS) has been installed. Most of the tsunamis affecting the Italian coasts are generated by local earthquakes with focal region close to the coast, both in land or in the sea. As regards the Eastern Sicily coast, usually the historical tsunamis are characterized by a first withdrawal of the sea, followed within a few minutes by a more or less violent flooding. Taking into account this characteristics, the experimental TWS is conceived for the coastlines affected by tsunamis locally generated, where the waves invest the coast just a few minutes after the earthquake occurrence, so what is needed is an immediate detection of the generated tsunamis. In this context, the Italian TWS is an integrated system designed for the simultaneous acquisition of the seismic signal and the sea level oscillations, for processing both signals, for detecting dangerous conditions and for issuing an alarm message to specific units of the local Civil Protection service. As regards the sea level data, a pressure gauge has been installed in a suitable wharf close to the Augusta harbour. The water level sensor is connected to an automatic station to collect and process the sea level data and many other interesting parameters and to send the data (via radio link) to a TWS "control center". As for the seismic data, the three components (S-13) Augusta seismic station is used and a spectral analysis of the background seismic noise has been done. The TWS control center is equipped with two PC units, connected in LAN network, to collect and process in real time the seismic and the sea level data and to identify anomalous conditions in the two signals, in order to send a useful alarm message. One PC unit is responsible for the seismic signal acquisition and processing, working in a Windows NT environment. The second unit, in UNIX environment, is for both the seismic and the sea level data and it contains specific routines for the detection of sea level anomalous oscillation and for the alarm message transmission code. This unit is also equipped with a specific software for the data management, that is data automatic acquisition, real time data validation, data collection displaying, monitoring of the station activity, etc. The station has been working since July 1998 and at present some preliminary analysis of the registered data sets has been done.

**JSS42/W/11-B5** Poster **1700-15**

**TSUNAMI INUNDATION MODELING FOR SELECTED COMMUNITIES IN KODIAK ISLAND, ALASKA**

Elena N. Suleimani and Roger Hansen (both at Geophysical Institute, University of Alaska Fairbanks, Fairbanks, AK 99775-7320, USA, email: etrosin@images.alaska.edu)

The 28 March 1964 earthquake produced a destructive tsunami in Alaska and on the West Coast of the United States. The event showed avulnerability of Kodiak, a region with a number of relatively high populated communities and significant fishing resources. Over the last ten years there had been substantial growth of Kodiak City and other island communities, a number of engineering projects, and significant changes to the harbor. As part of an ongoing component of the National Tsunami Hazard Mitigation Program and the Alaska Science and Technology Foundation we are providing assistance to threatened communities with potential tsunami inundation assessment. Three of the Kodiak communities were identified as high-priority zones for inundation mapping.

The numerical model is based on the nonlinear shallow-water equations which are solved by a finite-difference method. The historically documented wave runup, mainly from the 1964 Alaska earthquake, is used to calibrate the model. First, the actual ground displacement of the 1964 earthquake is assumed, then, the hypothetical sources are modeled. The results will be presented using a web-based interface. They will allow us to evaluate the potential tsunami hazard for the Kodiak communities and to provide them with the tsunami inundation maps for emergency planning of evacuation routes. Finally, about 10 additional communities are planned for evaluation over the next four years as part of the federal/state mitigation program.

**JSS42/W/12-B5** Poster **1700-16**

**DISPERSIVE TSUNAMI GENERATION BY BOTTOM DISPLACEMENTS WITH COMPLICATED TIME-SPATIAL HISTORY**

M.A. NOSOV, S.V. Mironyuk

The linear potential theory was used to obtain the exact analytical solution of the 3-D problem of gravitational waves generation by bottom displacements of finite duration as double Fourier integrals over components of the wave vector. The integrals were evaluated numerically. In particular it was demonstrated that the bottom displacement should be considered as a process of a finite duration, not as an impulse one. Using some models of bottom displacements of finite duration (piston, membrane-like, traveling, with alternating signs) a certain influence of bottom displacements time-spatial history on amplitude, energy and directivity of tsunami radiation from asymmetric source was revealed. It was also established that as the distance from the source increases, the directivity of energy radiation is preserved, whereas the distribution of wave amplitude characteristics in the azimuthal angle becomes isotropic.

**JSS42/E/04-B5** Poster **1700-17**

**SPECTRAL ANALYZIS OF OCTOBER 5, 1994 SHIKOTAN TSUNAMI RECORDS**

TATYANA IVELSKAYA, Sakhalin Tsunami Warning Center, 78, Zapadnaya St. Youzno-Sakhalinsk, 693000, Russia, George Shevchenko, Institute of Marine Geology and Geophysics, Far East Branch of Russian Academy of Sciences, Nauky str., Yuzhno-Sakhalinsk, 693002, Russia, email: Tsunami@Sakhalin.ru

Spectral characteristics of wave field after strong earthquake that occurred at the October 5, 1994 in the region of Shikotan Island were analyzed. It was shown that main energy of tsunami at the South Kuril stations was concentrated in the relatively high frequency band (with periods about 21 min). Probably, it was induced by the particularities of the seismic processes in the epicentral area of underwater earthquake.

At the same time the energy of tsunami on the coast of Japan was concentrated in the relatively low frequency band (with periods about 28, 36, 48, 60 min). Probably, it was connected not only with particularities of tsunami source, but with the influence of sea bottom topography in this region.

Calculation of spectral-time diagrams shows the complicated structure of wave records that includes five splashes of intensity on the main part of stations. Very likely that these splashes were induced by aftershocks in the epicentral area of underwater earthquake. Spectral-time diagrams detected the early wave groups with wide spectra, and resonance particularities of basins selectively amplify some spectral components.

**JSS42/W/19-B5** Poster **1700-18**

**A FAST AND SIMPLE DIAGNOSTIC METHOD FOR IDENTIFYING TSUNAMIGENIC EARTHQUAKES**

Nikolai. M. SHAPIRO, Shri Krishna Singh, and Javier Pacheco (all at Instituto de Geofísica, Universidad Nacional, Autónoma de México, México D.F., México, e-mail: shapiro@ollin.igeofcu.unam.mx)

An analysis of regional broadband seismograms of moderate and large subduction-zone earthquakes of Mexico shows that the earthquakes which occur near the trench are abnormally depleted in high-frequency radiation. This observation leads to a simple and fast method to assess regional tsunami potential from earthquakes which occur along the Pacific coast of Mexico. A significant advantage of the method is that a single broadband seismograph is sufficient for the purpose. The method is based on the ratio of the total energy to the high-frequency energy (between 1 and 5 Hz), ER, computed from the seismograms. For earthquakes of same seismic moment, ER is an order of magnitude greater for a source area near the trench as compared to that for areas near the coast. The same seismograms are used to compute energy magnitude, Me, which is tied to the moment magnitude, Mw. A regional tsunami may be expected along the coast if  $Me > 6.5$  and ER corresponds to a source near the trench. If, however, ER corresponds to a near-coast source, then Me may have to be greater than about 7.3 for a tsunami of similar size to occur along the coast. The method holds promise for a fast regional tsunami warning in many Pacific basin countries which lack an adequate seismic network.

**JSS42/E/21-B5** Poster **1700-19**

**FUNDAMENTAL STUDY ON TSUNAMIS GENERATED ON A SHELF**

Koji FUJIMA (Department of Civil Engineering, National Defense Academy, Yokosuka 239-8686, Japan, email: fujima@cc.nda.ac.jp)

Based on the linear long wave theory, theoretical solution is obtained for the tsunami propagation >from an arbitrary tsunami source generated on a straight beach with an uniform slope. The solution indicates that the behaviors of tsunami generated on a shelf is governed by the conditions of initial tsunami profile. The edge wave is generated considerably in the

## INTER-ASSOCIATION

case when a tsunami source locates near a coastline. On the contrary, in the case when a tsunami source is generated in a region far from a coastline, the edge wave is not generated and tsunami energy is concentrated in a narrow area. The empirical formulas are derived which evaluate the characteristics of tsunami by those of tsunami source such as the lengths of long-axis and short-axis, the position and direction of tsunami source, and so on. Further, effect of the Coriolis force is also discussed.

**JSS42/E/20-B5** Poster **1700-20**

### THE THREE-DIMENSIONAL TSUNAMI NUMERICAL ANALYSIS WITHOUT ASSUMING THE STEP-TYPE BOTTOM BOUNDARY

Kenji MASAMURA and Koji Fujima (both at Department of Civil Engineering, National Defense Academy, 1-10-20 Hashirimizu, Yokosuka 239-8686, Japan, email: kenji@cc.nda.ac.jp, fujima@cc.nda.ac.jp) Chiaki Goto (Department of Civil Engineering, Tokai University, 1117 Kitakaname, Hiratsuka 259-1292, Japan, email: goto@keyaki.cc.u-tokai.ac.jp)

The conventional numerical analysis of Tsunami based on the shallow water theory cannot reproduce three-dimensional flow. To improve this deficiency, three-dimensional numerical model without using the long wave approximation was developed. This model can compute the propagation of non-linear dispersive waves, because the hydrostatic pressure distribution is not assumed in the model. However, when the complicated geographical features are adopted for the calculation, submarine bottom boundaries are approximated as the stair-shaped step. Therefore, accuracy of calculation tends to become worse at the tip of runup. Thus, in this study, a "permeation rate" is introduced as a new parameter in each surface of the cell. The "permeation rate" is defined by the ratio of the section area of the portion where a water particle can pass through and the area of the surface of the cell. Therefore, the bottom boundary is approximated by a slope crossing the inside of the cell. As the result, runup height can be reproduced with good precision by the present model.

**JSS42/L/01-B5** Poster **1700-21**

### COMBINATION OF BATHYMETRY AND TOPOGRAPHY DATA FOR TSUNAMI MODELING

R.A. KAMPHAUS (NOAA/PMEL, TIME, 2115 SE OSU Drive, Newport, OR 97365, USA; e-mail: kampaush@pmel.noaa.gov), D. Divins (NOAA/NGDC, CIRES, 325 Broadway, Boulder, CO 80303, USA; e-mail: ddivins@ngdc.noaa.gov) and F.L. Gonzalez (NOAA/PMEL, 7600 Sand Point Way NE, Bldg.3, Seattle, WA, 98115, USA, e-mail: gonzalez@pmel.noaa.gov)

Grids that integrate bathymetric and topographic data are needed for effective tsunami inundation modeling. Topographic data in the form of Digital Elevation Models (DEMs) have been available for the majority of the United States for several years from the US Geological Survey (USGS). Bathymetric data, on the other hand, has been more sparse and not available digitally for all areas. As more digital data becomes available through the efforts of data centers such as NOAA's National Geophysical Data Center (NGDC) -- techniques for efficiently incorporating these data into numerical grids are being developed. Using techniques and databases developed at NGDC, the Center for Tsunami Inundation Mapping Efforts (TIME) has created several high quality gridded data sets for tsunami inundation modeling along the coast of California. The grids are assembled by gridding the NOS Hydrographic Database soundings, and supplemental soundings, to the same 3 arc-second (~90 m) resolution and registration as the USGS's 3-arc-second DEMs. In the United States the topographic and bathymetric data are collected in different reference datums; therefore, the data are adjusted to a common datum and a correction for tides is calculated. By adjusting the data to a common vertical datum, and gridding across the shoreline, a smooth transition from ocean bottom to land surface is achieved. The two data sets are then spliced at the NOS medium-resolution vector shoreline. The result is a 3-arc-second elevation grid in which elevations are resolved to 1/10 of a meter. Similar techniques can be used by researchers for different resolution grids and in different areas depending on the availability of data.

**JSM43** Thursday 29 – Friday 30 July

### BOUNDARY-LAYERS OVER COMPLEX TERRAIN AND HETEROGENEOUS SURFACES (IAMAS, IAHS)

Location: Chemical Engineering, 124 LT

Thursday 29 July AM

Presiding Chairs: N.O. Jensen (Risoe Nat. Lab., Roskilde, Denmark), P.A. Taylor (York Univ., Toronto, Canada)

### OBSERVATIONAL STUDIES

**JSM43/W/06-B4** **1030**

### INFLUENCES ON ATMOSPHERIC BOUNDARY LAYER STRUCTURE IN THE NEW ZEALAND SOUTHERN ALPS

Andrew STURMAN (Department of Geography, University of Canterbury, Private Bag 4800, Christchurch, New Zealand, email: a.sturman@geog.canterbury.ac.nz); Hamish McGowan (School of Earth Sciences, Victoria University of Wellington, P.O. Box 600, Wellington, New Zealand, email: Hamish.McGowan@vuw.ac.nz)

The Southern Alps of New Zealand provide an interesting and challenging environment in which to undertake atmospheric boundary layer research, as heterogeneous surface characteristics and mountainous terrain strongly influence the structure of the lower atmosphere. Research has been conducted in the Lake Tekapo region of the South Island since 1991, initially identifying the complexity of the local wind regime in this region with regard to dust dispersion. This complexity results from local and regional variation in surface sensible heat flux, including the effect of Lake Tekapo. In particular, the effects of different scales of motion were noted including the interaction of mountain/valley, land/lake and land/sea breeze systems, as well as with broader scale airflows such as the topographically modified foehn nor'wester. A more comprehensive research programme is under way to understand in greater detail the nature of the wind systems and thermal structures that develop in this region. The current research involves the analysis of data collected using a network of automatic weather stations, surface energy flux measurement systems, pilot balloons, free-flying and tethered sondes, SODAR, and an instrumented light aircraft. Computer simulations using two different mesoscale modelling systems complement the field programme. Some initial results are presented of the interaction of synoptic airflow with locally developed wind systems resulting from slope heating and thermal discontinuities at the surface.

**JSM43/E/01-B4** **1050**

### FLOW OVER THE NEBRASKA SANDHILLS - ANALYSIS OF AIRCRAFT AND TOPOGRAPHIC DATA

Yoseph Mengesha, Peter A. TAYLOR (Dept. of Earth and Atmospheric Sciences, York University, 4700 Keele Street, Toronto, Canada, M3J 1P3, Email: pat@yorku.ca); Donald Lenschow (NCAR, Boulder, Colorado, USA)

In a preliminary investigation of topographic parameters appropriate for drag parametrization we have made a study of the Sand Hills area of Nebraska (USA). Digital topographic data (3 arc seconds, approx 90m) of the Sand Hills terrain were analyzed and parameters (K,L,M) suggested by Baines (1995) to characterize topography were calculated from the topographic data using various horizontal resolutions. Slope-related parameters are highly resolution dependent. Data collected in Aug 1980 by the NCAR Queen Air during low level flights over parts of the region have also been studied. The area overflown has an extensive area of relatively regularly spaced, elongated ridges, of typical peak to trough height of order 75m and crest to crest separation of order 2km. Typical flight levels were about 100m above the terrain but no surface level data were available. We have however computed flight level turbulence statistics and drag coefficients for different sections of the flight and compared these with the mean square slope of the underlying terrain. These preliminary data indicate a potential for a significant increase in aircraft level drag coefficient with topographic slope, but stability effects are also an important factor. Horizontal turbulence values ( $\sigma_u$ ,  $\sigma_v$ ) were about 20-40% higher than one might expect over flat terrain, but vertical components,  $\sigma_w$ , were not significantly affected. The data show a strong variation with static stability and  $u$  and  $v$  spectra have secondary peaks associated with topographic effects.

**JSM43/W/08-B4** **1110**

### THE EFFECTS OF SALT FLATS AND ADJACENT COMPLEX TOPOGRAPHY ON PBL PROPERTIES

Thomas WARNER, Hsiao-Ming Hsu, Chris Davis (National Center for Atmospheric Research Boulder, Colorado, USA); Elford Astling (West Desert Test Center Dugway, Utah, USA)

Salt flats are common in deserts throughout the world and have a profound impact on the PBL thermal, moisture and wind-field properties because of their unique surface characteristics. The desert salt flats often occur near complex terrain, as in the western U.S., and thus the modulation of the PBL properties by the salt flats interacts with that associated with the nearby complex terrain.

In this study, a quadruply nested mesoscale model, with a 1 km grid increment on the finest mesh, is used to simulate the effects of desert salt flats and adjacent mountains on the PBL structure. The use of a complex land-surface model with multi-layer soil physics allows determination of how specific salt-flat characteristics, such as proximity of the water table to the surface, affect the PBL properties. Circulations that result from the thermal contrast between the salt flat and the surrounding desert, referred to as "salt breezes", are as strong as the mountain-valley breezes. Overall, PBL signatures that result from the salt flats are as large as those forced by the adjacent mountains.

**JSM43/E/06-B4** **1130**

### SPATIAL AND TEMPORAL VARIATION OF SOIL MOISTURE AND GROUND TEMPERATURE NEAR THE INTERFACE OF HIGH/LOW STANDS

Xinguo MO (Environment and Eco-technology Station, Institute of Geography, Chinese Academy of Sciences, Beijing 100101, P.R.China, email: moxg@dls.iog.ac.cn); Suxia Liu (Department of Hydrology, Institute of Geography, Chinese Academy of Sciences, Beijing 100101, P.R.China, email: liuxx@sun.ihep.ac.cn)

This paper presents an observational study of the variation of soil moisture and ground temperature with distance of an interface of alfalfa/winter wheat stand. Micro-meteorological elements were observed together. It was found that the influence of the interface on the soil moisture of both high stand (winter wheat) and low stand (alfalfa) is obvious. The difference of soil moisture of high stands and low stands generally increases with the observational sites closing to the interface. The horizontal influence scale is 4~16 meter to the interface. Precipitation and irrigation can fully change this pattern. Ground temperature beneath the surface decreases gradually from relatively hot alfalfa field to cold winter wheat without any influences from the interface. However at the surface, the difference of ground temperature of high and low stands increases with the observational sites closing to the interface, as what we found from the variation of soil moisture. The vertical influence scale is 5 cm. The influence of precipitation and irrigation is less than that of interface. The results of micro-meteorological can help to explain the bigger difference of temperature and soil moisture occurs at the place nearer the interface.

**JSM43/E/09-B4** **1150**

### WIND TUNNEL MEASUREMENTS VS NUMERICAL SIMULATIONS IN COMPLEX TERRAIN

Maria ATHANASSIADOU, Nigel Wood (Met. Office, Bracknell, UK)

Wind tunnel measurements of neutral flow over a series of rough surfaced sinusoidal hills are presented and compared with numerical simulations. The experimental data were taken in the A - Tunnel (4.2m x 0.9m x 0.6m, L x W x H) of the EnFlo Lab at Surrey University as part of a collaborative research project between the UK Met Office and EnFlo. The numerical simulations were performed using BLASIUS, a numerical model designed to simulate turbulent flow over two and three dimensional hills. Issues addressed include the ability of numerical simulations to reliably reproduce turbulent flow over complex terrain, the influence of different boundary conditions employed as well as different turbulence closures. The problem of how to best compare data and results obtained using different methods is also examined.

Thursday 29 July PM

Presiding Chairs: N.O. Jensen (Risoe Nat. Lab., Roskilde, Denmark), P.A. Taylor (York Univ., Toronto, Canada)

### MODELLING STUDIES

**JSM43/W/03-B4** **1400**

### MESOSCALE CIRCULATIONS IN SOUTHERN PORTUGAL: OBSERVATIONS AND NUMERICAL RESULTS

Pedro M. M. SOARES (email: psoares@fc.ul.pt), Carla S. F. Barroso (email: cbarroso@fc.ul.pt), Pedro M. A. Miranda (email: pmiranda@fc.ul.pt), André Barbosa (email: abarbossa@fc.ul.pt) (all at: Centro de Geofísica da Universidade de Lisboa, R. Escola Politécnica 58, 1250 Lisboa, Portugal)

In the last two years, two field experiments were made to better characterise the sea breeze circulation in the South Coast of Portugal, in the perspective of its impact in local meteorology. The campaigns included 2 weeks of measurements during the summer, with a number of surface stations and regular release of radiosondes. The analysis of the observational data also included information from all automatic weather stations in the area. The results showed the expected diurnal cycle of the sea breeze in stations where the near coast is linear, they have also revealed the importance of local orography and coastal irregularity in the shaping of the temporal hodograph of low level wind. Data from inland stations was used to compute the sea breeze penetration in land and the inland velocity. The principal goal of this study was to achieve an experimental confirmation of model predictions for this type of circulations, in the case of complex mesoscale interactions between the sea breeze, coast orography, lake breezes and finally in consequence of coast irregularity. Using the observed atmospheric profiles, a number of numerical simulations were performed, using the NH3D mesoscale model (Miranda and James 1992) coupled with the soil ISBA model (Noilhan and Planton 1989), which are used to perform a detailed analysis of the coastal circulation and to identify the main mechanisms involved in its forcing.

**JSM43/W/13-B4****1420****OBSERVATIONS AND MODELING OF MESOSCALE CIRCULATIONS PRODUCED BY SURFACE HETEROGENEITIES**

Pedro M. A. MIRANDA (Centro de Geofísica and Department of Physics, University of Lisbon, R. Escola Politécnica 58, 1250 Lisboa, Portugal, email: pmiranda@fc.ul.pt); Rui Salgado (Centro de Geofísica, University of Evora); Pedro M. M. Soares and Carla Cardoso (both at Centro de Geofísica, University of Lisbon)

The summer circulation over the Iberian Peninsula is largely dominated by the interaction between a strong sea-breeze effect and up-slope/downslope winds around mesoscale mountains. At the scale of the Peninsula, these effects produce a pulsating thermal low of great regional climatic importance. Locally, these thermal and orographic circulations may be rather distorted by local effects due to surface heterogeneities, in particular in cases where large horizontal gradients of water availability are produced by irrigation patches. Some of these effects are revealed in observations in southern Portugal, which have been organised in the two last years, including a network of continuous surface observations and some radiosonde observations in the summer period. A set of non-linear numerical experiments with a non-hydrostatic mesoscale model, coupled with a soil evolution model, are used to analyse the dynamics of the thermal circulations, including the diurnal evolution of the boundary layer development over land and the horizontal progression of the sea-breeze front.

**JSM43/E/02-B4****1440****MODELLING LONGITUDINAL VORTICES IN BOUNDARY-LAYER AIRFLOW OVER 2D WAVY SURFACES**

Peter A. TAYLOR, Wensong Weng (Dept. of Earth and Atmospheric Sciences, York University, 4700 Keele Street, Toronto, Canada, M3J 1P3, Email: pat@yorku.ca); Stefano Gallino (Department of Physics, University of Genova, Italy)

Gong et al (1996) reported observations of the development of longitudinal vortices in a wind tunnel study of turbulent boundary-layer flow over 2D sinusoidal waves. Large eddy simulations of the same flow showed somewhat similar features but they were less regular or organised. Using a time dependent version of the 3D non-linear mixed spectral finite difference code (NLMSFD) for boundary-layer flow over topography we can simulate the development of similar vortex structures, but their rate of development tends to be rather slower than was observed in the wind tunnel.

Results will be presented showing, amongst other things, a strong dependence of vortex growth rate on the steepness of the waves and on boundary-layer depth. So far these model predictions have not explained a significant disparity between wave crest velocity profile predictions with the 2D NLMSFD model and the profiles measured in the wind tunnel, or differences in the drag on the topography. Potential application of the results to airflow over water waves and to wind wave generation will be discussed.

**JSM43/E/04-B4****1500****SUB-GRID SCALE TOPOGRAPHIC DRAG PARAMETRIZATION FOR LARGE SCALE MODELS - NEUTRAL AND STRATIFIED FLOW**

Peter A. TAYLOR, Wensong Weng, Jingnan Zhou (Dept. of Earth and Atmospheric Sciences, York University, 4700 Keele Street, Toronto, Canada, M3J 1P3, Email: pat@yorku.ca)

At the present time models of neutrally-stratified boundary-layer flow over hills, with Reynolds-averaged flow equations and various turbulence closure schemes, can, in general, do quite well at predicting the "speed-up" of the wind at the summit of isolated low and moderate slope hills, and on the upwind slope. Predictions in the lee of hills with flow separation are more difficult but some progress has been made. It is however proving difficult to obtain reliable results for the form or pressure drag on topography, even in neutrally stratified flows. For stably stratified flow linear inviscid theory appears to provide a reasonable first estimate of the wave drag, at least in terms of comparisons with simplified boundary-layer models. In a boundary-layer context some model results on pressure and wave drag are discussed, and the link between pressure drag on the surface and wave drag aloft illustrated.

**JSM43/W/04-B4****1600****A NUMERICAL STUDY OF TURBULENT BOUNDARY-LAYER FLOW OVER COMPLEX TERRAIN**

Wensong WENG, Peter A. Taylor (Department of Earth and Atmospheric Science, York University, 4700 Keele Street, Toronto, Ontario, Canada M3J 1P3, Email: wweng@yorku.ca)

The Mixed-Spectral Finite Difference (MSFD) and its Non-Linear extension (NLMSFD) models are used to study neutrally-stratified turbulent boundary-layer flow over the real terrain --- Askervein Hill. Three different turbulence closures are used. The model results are compared with the field observations from the Askervein Hill Project of 1982 and 1983 which provided an extensive full-scale data set for studies of wind flow and turbulence over complex terrain. The linear limitation, non-linear effects and impact of different turbulence closures on the model prediction are discussed.

**JSM43/E/12-B4****1620****SURFACE HEAT FLUX AVERAGING IN HETEROGENEOUS TERRAIN**

Niels Otto JENSEN, Charlotte B. Hasager (Risoe National Laboratory, Wind Energy and Atmospheric Physics Dept., 4000 Roskilde, Denmark)

The paper considers the problem of estimating an areal average of the surface heat flux in a terrain consisting of patches in the landscape with different surface temperatures. It is demonstrated analytically as well as with a numerical model that the average stability is not neutral and the heat flux not zero even if the average temperature of the patches equals the air temperature. The numerical modelling focus on non-linear area-averaging of the atmospheric turbulent response between patches in the landscape with variable aerodynamic roughness and surface temperature.

Input to the model are maps of aerodynamic surface roughness and radiative surface temperatures from Landsat TM satellite scenes and meteorological observations of wind speed, wind direction and air temperatures. Aggregation of the heat flux in the landscape is based on a linearized flow equation solved by Fast Fourier Transforms. Stability correction is performed pixelwise. An output of the model is the areal average value of the temperature roughness of the particular terrain. The aggregation model is computationally fast and useful for grid averaging from scales of 30 m to 10-20 km grid cells.

**JSM43/E/10-B4****1640****LARGE-EDDY SIMULATIONS IN COMPLEX TERRAIN**

Nigel Wood, Mike HOBSON (The Meteorological Office, London Road, Bracknell, Berks, RG12 2SZ, UK)

A useful large-eddy simulation of flow over hills is non-trivial. Inevitably it requires a balance between what is desirable in terms of producing the most realistic results possible and what is feasible in terms of computing power. In designing a large-eddy simulation, or a wind tunnel simulation for comparison with one, a key component determining this balance is the ratio of the wavelength of the hill to the roughness length of the surface and much consideration needs to be given to specifying it. Whilst increasing this ratio requires a significant increase in the total number of grid points, decreasing leads to a reduction in resolution within the inner region. It the flow within this region, in particular, in which we are most interested. A consideration of all the factors determining this balance is both an interesting and valuable exercise.

**JSM43/W/11-B4****1700****THE EFFECTS OF LANDSCAPE HETEROGENEITY AND COMPLEX TERRAIN ON THE CONVECTIVE BOUNDARY LAYER**

Roni AVISSAR, S.G. Gopalakrishnan, Somnath Baidya Roy, Tanya Schmidt (Dept. of Environmental Sciences, Rutgers University, 14 College Farm Road, New Brunswick, New Jersey 08901-8551, USA, email: avissar@gaia.rutgers.edu)

The effects on the Convective Boundary Layer (CBL) of surface heterogeneities produced by various topographical features and sensible heat waves with different means, amplitudes, and wavelengths, were investigated with a Large-Eddy Simulation (LES) model. A wavelet analysis was performed on the model outputs to identify the scales of response of the CBL to these various forcing. The major objective of this study was to evaluate at which scale surface heterogeneity starts to significantly affect the heat and momentum fluxes in the CBL. We find that the impact of amplitude and wavelength of the surface heterogeneity is nonlinearly dependent upon the mean heating rate. The circulations (or rolls) resulting from surface heterogeneity are relatively strong when the amplitude and the wavelength of the surface heterogeneity are relatively large, especially at low mean heating rate. In that case the profiles of horizontally-averaged variables are quite strongly modified in the CBL. The potential temperature is not constant with elevation, and the sensible heat flux considerably departs from the linear variation with height obtained in a typical CBL that develop over an homogeneous domain. The mean turbulence kinetic energy (TKE) profile depicts two maxima, one near the ground surface and one near the top of the CBL, corresponding to the strong horizontal flow that develops near the ground surface and the return flow at the top of the CBL. In a dry atmosphere, a relatively weak background wind of 2.5 m/s is strong enough to considerably reduce the impact of ground surface heterogeneity on the CBL. A moderate background wind of 5 m/s virtually eliminates all impacts that could potentially be produced in realistic landscapes. From this study, it can be inferred that as long as the "patchiness" of the landscape has a characteristic length scale smaller than about 5-10 km (even without background wind), the "mosaic of tiles" type of land-surface scheme suggested by Avissar and Pielke (1989) can be applied to represent the land surface in atmospheric models. At larger scales, the impact of landscape heterogeneity may be significant, especially when the atmosphere is humid. Therefore, this study supports previous estimates, which were based on theoretical analyses.

**JSM43/E/07-B4****1720****A TOWN ENERGY BUDGET SCHEME FOR ATMOSPHERIC MODELS SURFACE**

Valery MASSON (CNRM, Météo-France, 42 av Coriolis 31057 Toulouse, FRANCE, email: valery.masson@meteo.fr)

An urban surface model for atmospheric meso-scale models is presented. A generalization of the local canyon geometry is defined instead of the usual bare soil formulation currently used to represent the cities in atmospheric models. This allows to improve the radiative budgets as well as momentum, heat and conduction fluxes. This scheme is aimed to be as general as possible, in order to represent any city in the world, for any time or weather condition (heat island cooling by night, urban wake, water evaporation after rainfall, snow effects). Sensitivity tests and comparison with vegetation schemes outputs on annual forcings (one representative of temperate region, one of continental climate) are discussed. Application in the MESO-NH model to the Paris area for an anticyclonic situation are shown.



Friday 30 July AM

Presiding Chairs: N.O. Jensen (Risoe Nat. Lab., Roskilde, Denmark),  
P.A. Taylor (York Univ., Toronto, Canada)**GENERAL BOUNDARY LAYERS****JSM43/W/10-B5****0900****MEAN WIND AND TURBULENCE CHARACTERISTICS IN THE SURFACE LAYER OVER AN AGRICULTURAL FIELD**

J. S. PILLAI, S. Sivaramkrishnan (Indian Institute of Tropical Meteorology, Pune, India 411008, email: pillai@tropmet.ernet.in)

Evolution of wind and turbulence in the surface layer depends on static stability of the atmosphere and surface cover over different terrains. In this paper we present the wind profile and turbulence measured at two different seasons near the surface of an agriculture field in Anand (22° 35' N, 72°35' E, 45.1 m MSL), India, using a fast response instrument (sonic anemometer at about 9.5 m AGL) and slow response instruments (cup anemometer at 1, 2, 4, 8 m AGL). The power index ( $\alpha$ ) used to describe the wind profile law has been computed between different levels during 1000 to 1600 hrs IST when the atmosphere was unstable/ near neutral at moderate wind speeds. It has been found that  $\alpha$  varies between 0.1 in April to 0.14 in August 1997, agreeing with the rural terrain values. The ratio of vertical turbulence intensity ( $I_w$ ) to longitudinal turbulence intensity ( $I_u$ ) is found to be nearly equal to 0.5 and that of lateral ( $I_v$ ) to longitudinal turbulence intensity ( $I_u$ ) 0.75 - 1.0. The Reynolds stress lies in the range of 0.001 to 0.007 in April and 0.001 to 0.06 in August 1997. The large values of Reynolds stress at 8m AGL, has been observed at Kharagpur (0.005) and at 8m AGL, at Jodhpur(0.02) in India over a gently rolling terrain during the summer monsoon: June- August 1990. High Reynolds stress is also attributed to a change in terrain roughness due to seasonal crops in the upwind sector of the site during April and August 1997.

**JSM43/E/08-B5****0920****ANALYSIS RESULTS OF THE TURBULENCE CHARACTERISTICS AND SPECTRA DURING A COLD FRONT PASSAGE**

Zhang AI-CHEN, Dept. of Geophysics, Peking University, Beijing 100871, China

Based on data from two levels of sonic anemometer/thermometer measurements at the heights of 47 m and 120 m of the IAP (Institute of Atmospheric Physics) meteorological tower, situated at the NW border district of Beijing City, the paper gives some results from calculated and analysed turbulence characteristics during a period where a cold front was passing through. The following interesting results have been shown:

1. The stability parameter Z/L showed slightly negative values over the whole process (including day and night).
2. The values of nondimensional turbulence energy dissipation were smaller than 1.0 during the process.
3. The low frequency portion of the spectrum of U and V wind components, with its energy containing subrange extending to the lower frequencies, covered a wide frequency range compared with the spectrum in calm weather situations.

**JSM43/E/11-B5****0940****THE ANALYSES RESULTS OF THE SEA BREEZE OVER THE COAST REGION OF THE SOUTH CHINA SEA**

Zhang HONG-SHEN, Zhang Ai-chen (Dept. of Geophysics, Beijing University, Beijing 100871, China)

In the winter and Summer 1988, a number of low level radiosondes, wind finding and turbulence instruments was set up in a network in a large area of the Zhu-jiang River Mouth Region, situated along the coast region of The South China Sea. It included one sounding station situated at a small island, seven coast and in-land sounding stations, and two turbulence exploring system. The results showed a set of very typical sea breeze situations, micro fronts and thermal internal boundary layer structures. Results from this exercise will be presented.

**JSM43/W/01-B5****1000****MULTIFRACTAL TURBULENCE OF CHERNOBYL FALL-OUT: HOT SPOTS OF 137CS SOIL CONTAMINATION AND SELF-ORGANIZED CRITICALITY**

I. TCHIGUIRINSKAIA (E.E.&amp;S. Dept., Clemson University, 342 Computer Court, Anderson, SC29625, USA, email: iouliat@clemson.edu); D. Schertzer (L.M.M., Université Pierre et Marie Curie, 4 Place Jussieu F-75252 Paris Cedex 05, France); S. Lovejoy (Physics Dept., McGill University, 3600 University st., Montréal, Qué., H3A 2T8, Canada)

We estimated the average value of the 137Cs soil contamination during years 1986-1991 on 16384 pixels covering a 300 km radius around the Chernobyl area (Ukraine), using a subset of the data base published by the ex-Soviet Hydromet office. The rather complex structures of Chernobyl fall-out at all scales poses nontrivial difficulties for risk assessments since the risks will depend notably on measurements of local doses which have an extreme spatial variability. We consider a new atmospheric dispersion approach based on a multifractal cascade process which leads to an infinite hierarchy of singularities of the multifractal field. We made a special study of the important probability tails associated with the extreme 137Cs soil contamination events ("hot spots"), showing that they are associated with first order multifractal phase transitions and a non classical Self-Organized Criticality. The moment order for the first order phase transition to Self-Organized Criticality is  $q_D=2.2$ . This confirms preliminary empirical studies using the "R.E.M. Chernobyl fall-out data base" covering about 4000 towns over western Europe.

**DISPERSION****JSM43/W/07-B5****1100****MULTISCALE LOCAL FORCING OF THE ARABIAN DESERT DAYTIME BOUNDARY LAYER, AND IMPLICATIONS FOR THE DISPERSION OF SURFACE-RELEASED CONTAMINANTS**

Thomas T. WARNER, Rong-Shyang Sheu (National Center for Atmospheric Research Boulder, Colorado, USA)

Four, six-day simulations were performed, using a mesoscale model run in a data-assimilation mode, of the atmospheric conditions over the Arabian Desert during the time of the 1991 detonation and release of toxic material at the Khamisyah, Iraq weapons depot. These atmospheric simulations are being employed in a forensic analysis of the potential contribution

of the toxic material to the Gulf War illness. The transport and concentration of such surface-released contaminants is strongly related to the planetary boundary layer (PBL) depth and the horizontal wind speed in the PBL. The product of the PBL depth and the mean wind speed within it is referred to as the ventilation, and is used as a metric of the horizontal transport within the PBL. Thus, a corollary study to the larger forensic analysis involves employing the model solutions and available data in an analysis of the multiscale spatial variability of the daytime desert PBL depth and ventilation as they are affected by surface forcing from terrain-elevation variations, coastal circulations and contrasts in surface physical properties. The coarsest computational grid spanned the entire northern Arabian Desert and surrounding areas of the Middle East, and represented the large scale PBL modulation by the orography. The PBL depths were greatest over the high elevations of the western Arabian Peninsula and over the Zagros Mountains in western Iran, and depths were shallowest over water bodies and the lower elevations in the Tigris-Euphrates Valley. Higher resolution grids in the nest (the smallest grid increment being 3.3 km) showed that the PBL depth minimum in the Tigris-Euphrates Valley was likely a consequence of compensating subsidence associated with the thermally forced daytime upward motion over the Zagros Mountains to the east in Iran. Further local modulation of the daytime desert PBL occurred as a result of the inland penetration of the coastal sea-breeze circulation on the west side of the Persian Gulf, where BL depths were suppressed as far as 100 km inland. On the finest scales, significant PBL-depth variability resulted from surface thermal differences associated with contrasts between barren desert and partially vegetated desert. The average 1500 LT ventilation over the Arabian Desert for the six day period varied spatially from less than 4,000 to over 24,000. This represents over a factor-of-six average spatial variation in the ability of the atmosphere to transport contaminants away from a source region.

**JSM43/W/12-B5****1120****SCALING OF BLOWING SNOW FLUXES OVER COMPLEX TERRAIN**

Richard ESSERY (Hadley Centre, Bracknell, UK); John Pomeroy (National Hydrology Research Centre, Saskatoon, Canada), Long Li (Division of Hydrology, University of Saskatchewan, Saskatoon, Canada)

Transport and sublimation rates for wind-blown snow increase rapidly with increasing wind speed and so are highly sensitive to wind speed variations in response to changes in elevation and surface roughness over complex terrain. Sublimation of suspended snow returns moisture to the atmosphere, and redistribution by wind can generate large variations in snow depth which influence the depletion of snow during melt.

A model of windflow over complex terrain and a model of blowing snow over uniform terrain are coupled with a representation of downwind development in a distributed model of blowing snow over complex terrain. Applied to an arctic tundra basin with gentle topography and marked variations in vegetation height, the distributed model is found to give reasonable agreement with measured snow accumulations.

For large-scale modelling applications, scaling relationships are developed between modelled spatial distributions of wind speeds and statistical characteristics of the topography which can be obtained directly from a digital elevation model. These relationships are used to investigate the scaling of blowing snow fluxes over complex terrain.

**JSM43/W/09-B5****1140****THE DISPERSION OF PARTICLES IN HETEROGENEOUS, COMPLEX TERRAIN**

Roni AVISSAR, S.G. Gopalakrishnan (Department of Environmental Sciences, Rutgers University, 14 College Farm Road, New Brunswick, New Jersey 08901-8551, USA, email: avissar@gaia.rutgers.edu)

A systematic analysis of the impacts of heat patches and topographical features on the dispersion of passive materials in a shear-free convective boundary layer (CBL) was performed. A coupled large-eddy simulation (LES) and Lagrangian particle dispersion (LPD) model was used for that purpose. Over a homogeneous, flat terrain the dispersion statistics produced by the model is in excellent agreement with convection tank data and with other model results. Heat flux heterogeneity has a remarkable influence on particle dispersion in the CBL. The horizontal pressure gradients created by these heterogeneities impede vertical mixing. For a near surface release, the particles travel horizontally rather than "lifting-off," increasing the concentration near the ground surface. Particles released at higher elevations reach the surface much slowly than when released above a flat, homogeneous domain. Topography has very little impact on "lift-off," dimensionless crosswind integrated concentration, mean particle height, particle spread and ground level concentration of particles released near the ground surface. This is true even with hills as high as 25% the height of the CBL. However, it has a noticeable effect on the dispersion statistics of particles released from higher elevations. In particular, for a source height located above the height of the CBL, the locus of the maximum concentration in cross-wind integrated plume descends to the surface of a moderate hill noticeably slowly than above a flat, homogeneous domain.

**JSM43/E/03-B5****1200****SOLID AEROSOLS DISPERSION IN URBAN AREA**

K. V. Karelsky, V. V. Papkov, A. S. PETROSYAN (Space Research Institute of the Russian Academy of Sciences, Profsoyuznaya 84/32, Moscow 117810, Russia, email: apetrosoy@iki.rssi.ru)

A new model of solid aerosols dispersion around buildings and street canyons is developed. This is initially based on the description of the multiphase flow problem using the well established non-viscous hydrodynamic equations with full account (in the equation of state) of the changed thermodynamics. The study of multiphase flows is performed using an original idea in which the multiphase flow is simulated by the above-mentioned ideal equations with a finite difference representation which incorporates an internal, i.e. numerical, viscosity. More specifically, the computer calculations are based on the Godunov method which is a first finite difference representation of the non-viscous (Euler) equations of hydrodynamics and has the great advantage of providing the numerical viscosity. This use of the Godunov method has been shown to be practically reliable in important situations when molecular viscosity effects are evidently important. One example is when the boundary layer is heavily loaded with solid particles. It was shown efficiency of developed method for important cases when vertical size of inhomogeneity is in excess of horizontal size and topological diffusion, wake/secondary flow effects and blocking effects exist on complex terrain.

**JSM43/E/05-B5****1220****A NEW MODEL FOR DENSE GAS DISPERSION THROUGH GROUPS OF OBSTACLES**

K. V. Karelsky, V. V. Papkov, A. S. PETROSYAN (Space Research Institute of the Russian Academy of Sciences, Profsoyuznaya 84/32, Moscow 117810, Russia, email: apetrosoy@iki.rssi.ru)

A new model for dense gas dispersion in complex terrain including groups of obstacles is discussed. This model is based on shallow layer equations describing dense gas cloud. It is well known analogy between compressible gas equations and shallow layer equations. This

allows to apply for dense gas description generalised solutions of shallow layer equations which are best adapted for boundary layer including groups of obstacles. A full set of selfsimilar solutions of initial discontinuity decay problem for shallow layer equations will be provided and new computer model based on Godunov method has been shown to be practically useful to predict gas flows in important cases when only two layer model is applicable. One example is when shallow dense gas cloud is located above step inhomogeneity and usual shallow layer equations are non-applicable in the vicinity of terrain discontinuity. Computations for different type of obstacles and terrain will be discussed.

JSS44

Thursday 29 – Friday 30 July

### STRUCTURE OF THE CONTINENTAL LITHOSPHERE FROM INTEGRATED GEOPHYSICAL, GEOLOGICAL AND GEOCHEMICAL STUDIES (IASPEI, IAVCEI, IAGA, IAMAS, ILP)

Location: Medical School, Ext NG26 LT6  
Location of Posters: Arthur Thompson Hall

Thursday 29 July AM

Presiding Chairs: Ron M. Clowes (Univ. of British Columbia, Vancouver, Canada)  
Philip Candela (Univ. of Maryland, USA)  
Concurrent Poster Session

JSS44/E/39-B4

0930

#### THE THERMAL EVOLUTION OF THE SOUTHERN INDIAN SHIELD

R. N. SINGH (CSIR Centre for Mathematical Modelling and Computer Simulation, Bangalore, 560037, India, email: rnsingh@cmmacs.ernet.in); Jibamitra Ganguly (Dept. of Geosciences, University of Arizona, TUCSON, AZ 85721, USA, email: ganguly@geo.arizona.edu)

The southern Indian shield has been a major focus of research among Geoscientists due to its Archean granulite and granite terranes, mantle xenoliths transported by Proterozoic kimberlite eruptions, and intraplate seismicity. Heat flow, magnetic and seismological (tomographic, DSS and teleseismic receiver function) investigations have revealed the deep structure of the shield and the continental roots. The tectonic evolution of the shield has also been a subject of intensive investigation. A comprehensive summary of these studies will be presented in this paper, especially in the context of their importance in understanding the thermal evolution of the Indian shield. We have constructed steady state thermal models of the crust using the available crustal heat flow and heat generation data along with the P-T array of the Proterozoic mantle xenoliths, and accounting for the effect of erosion of the radiogenic layer (Singh, 1984). The latter effect was ignored in our earlier work (Ganguly et al., 1995). These thermal models have been extrapolated to the Archean time taking into consideration the cooling effect in a convecting mantle. A range of transient thermal perturbation models have been calculated to explain the P-T array of the Archean granulites, accounting for the effects of thrusting, CO<sub>2</sub> flux, and irreversible adiabatic decompression of the fluid. As discussed in our earlier work (Ganguly et al., 1995), geophysical data do not support significant magma underplating, whereas thrusting alone could not have produced the thermal perturbation necessary for the formation of granulites. In this work, the magnitude of the required CO<sub>2</sub> flux has been re-evaluated by coupling it to thrusting, and using the revised calculation of steady state initial geotherm. Finally, we discuss the implications of the CO<sub>2</sub> fluxing on the dehydration of crust/lithosphere, its viscosity structure and the stability of continental roots in the light of recent theoretical studies on the mantle convection coupled to moving plates and experimental work on rock rheology.

JSS44/E/09-B4

0950

#### ARCAEAN DHARWAR CRATON, SOUTHERN INDIAN SHIELD: REGIONAL CRUSTAL THERMAL MODEL AND LOCAL DEPARTURES

Sukanta ROY, R.U.M. Rao (National Geophysical Research Institute, PO Bag 724, Uppal Road, Hyderabad 500007, India, email: postmast@csngri.ren.nic.in)

The Archaean Dharwar province in the southern India shield comprises greenstone-granite belts and gneisses which give way to granulites further south. The heat flow regime is found to be low, spanning a range of 25 to 50 milliwatt/sq m. However, the radiogenic heat production of surface rocks is found to vary widely, from 0.2 to 8 microwatt/cu m. Based on considerations of regional geology and crustal sections constrained by deep seismic sounding and gravity data, five 1-D scenarios are envisaged for crustal heat production in the province. These are compatible with the range of the observed surface heat flow and represent the extremes possible in the crustal heat contribution, on a regional scale. A salient outcome is that all result in heat flow at the base of the crust in a very narrow range, 11.5 to 14.5 milliwatt/sq m. This range is about the same as those derived for the Archaean provinces in the Canadian shield and for the Kaapval craton southern Africa. There are locally anomalous areas departing from the regional heat flow - crustal heat production scenarios, where the surface heat flow is well within the regional variation but the surface rocks are incompatibly high in heat production. In such areas, heat flow data constrains the thickness of the high heat producing surficial rocks to thin "veneers" at the top, and further below, the crustal scenario is one among the five envisaged. The regional crustal thermal model also places bounds for crustal temperatures in the province, 280 to 360 deg Celcius at the Moho.

JSS44/E/04-B4

1010

#### MAFIC DYKES AND GEOTECTONIC EVOLUTION OF THE PROTEROZOIC SOUTH INDIAN LITHOSPHERE

T. RADHAKRISHNA, G. Balasubramoniam (both at Centre for Earth Science Studies, Trivandrum, 695 031, India, email: coral@giasmd01.vsnl.net.in)

Proterozoic magmatism manifested as mafic dyke intrusions constitutes an important geological event of the Eon over the Indian shield. The mafic dykes across the South Indian Granulite Terrain (SIGT) and the northern Dharwar Craton (Granite-Greenstone terrain) share many similar geochemical characteristics. These dykes are classified as within plate Fe-rich tholeiites and they possess large ion lithophile and light rare earth element enrichments, depletion of Nb and Ta, high Sr (0.703-0.706) and low Nd values (0 to -6). Their <sup>40</sup>Ar/<sup>39</sup>Ar and K-Ar (limited Rb-Sr and Sm-Nd) isotope age data and the palaeomagnetic data group them into at least four discrete phases between c. 1.6 and 2.1 Ga, while 1.65 Ga episode is the most predominant and widespread. Comparison of palaeomagnetic directions from the dykes of these terrains shows a remarkable correlation for the 1.65 and 1.8 Ga period. Two important geotectonic implications are drawn here for the Proterozoic continental lithospheric configurations. Firstly, the northern Dharwar Craton and the southern SIGT amalgamated at

least by mid- Palaeoproterozoic and thus do not support some of the interpretations extending the Pan-African orogenic belt within the late Proterozoic Gondwana reconstruction across the Indian shield. Secondly, the thermal anomalies associated with these magmatic episodes have initiated the formation of the largest Proterozoic sedimentary (Cuddapah) Basin in Indian shield, but its present large size is mainly related to the widespread 1.65 Ga igneous episode.

JSS44/E/10-B4

1030

#### COMPARISON OF LITHOSPHERIC STRUCTURE BELOW DIAMOND-FERTILE AND DIAMOND-BARREN FIELDS NEAR CUDDAPAH BASIN, INDIA, BASED ON INTEGRATED GEOPHYSICAL, GEOLOGICAL AND GEOCHEMICAL STUDIES

Saurabh K. VERMA (National Geophysical Research Institute, Uppal Road, Hyderabad-500 007, India, email: postmast@csngri.ren.nic.in)

Geophysical, geological, and geochemical characteristics of the lithosphere below two kimberlite fields in the vicinity of Cuddapah Basin, India, are analysed. In the Wajrakurur kimberlite field, located southwest of the basin, 21 pipes have been identified so far and most of them are found to be diamondiferous. On the other hand all the pipes studied so far from a cluster of 31 pipes in the Narayanpet kimberlite field, located north-west of the basin, are non-diamondiferous. While the geophysical data suggests different lithospheric structure below these two fields, the geochemical study provides supportive evidences in terms of pressure, degree of partial melt and oxygen fugacity. All these studies suggest that possibly the lithosphere-asthenosphere structures below the two fields are qualitatively different.

JSS44/W/10-B4

1110

#### SPATIAL AND TEMPORAL RATE VARIATIONS OF ONTINENTAL RIFT MARGIN UPLIFT AND EXHUMATION: THE ASATCH MOUNTAINS, UTAH (USA)

Phillip A. Armstrong, Todd A. EHLERS, David S. Chapman (Dept. of Geology and Geophysics, Univ. of Utah, Salt Lake City, UT 84112, USA, email: paarmstr@mines.utah.edu); Peter J.J. Kamp (Dept. of Earth Sciences, Univ. of Waikato, Hamilton, New Zealand)

The Wasatch Mountains mark the eastern extent of the Basin and Range province and reflect a major continental rift margin uplift. Holocene fault scarps along the range front correspond to apparently long-lived topographic salients and bedrock faults that extend into the range. GPS campaigns across ~N-striking Wasatch Fault segments indicate decadal displacement rates of 3.5 to 5mm/yr for a 55 degree dipping fault. Trenching studies indicate millennium-scale displacement rates of 1-2 mm/yr. (U-Th)/He ages range from 1.6 Ma at the range front to 4.9 Ma ~8 km eastward into the footwall. Helium ages indicate cooling from about 75 degrees C and give apparent exhumation rates of 1-2 mm/yr. at the range front for the last 2 My and 0.3-0.6 mm/yr. for the last 5 My east of the range front. AFT ages from samples that span the E-W extent of the central, pluton-cored section of the range are ~5 Ma adjacent to the range front but increase to ~35 Ma at 35 km eastward. Our preliminary interpretation is that the eastern rocks were rapidly exhumed between ~20 and 35 Ma with little exhumation since whereas the range front rocks were exhumed at 0.5-1.0 mm/yr. for the last ~10-17 My. If range front exhumation and fault displacement rates are assumed to be proxies for one another, then the exhumation and displacement rates have increased by a factor of 3 to 5 between the mid Miocene and present day. Exhumation rates have been relatively low farther east and into the footwall since the middle Miocene, reflecting eastward tilt of the range, which is in agreement with petrographic, fluid inclusion, and structural studies and probably reflects flexural tilt due to tectonic unloading.

JSS44/E/31-B4

1130

#### GEOPHYSICAL CONSEQUENCES OF THE CORDILLERA-CRATON THERMAL TRANSITION IN S. W. CANADA

R.D. Hyndman, Trevor LEWIS (Geological Survey of Canada, Pacific Geoscience Centre, Sidney, B.C. V8L 4B2, Canada)

There is a pronounced increase in heat flow and lithosphere temperatures across the transition from the stable North American Craton to the southeastern Canadian Cordillera. The heat flow increases from 40-60 mWm<sup>-2</sup> in the Craton to 80-100 mWm<sup>-2</sup> in the Cordillera. There are numerous reliable heat flow data in the Cordillera but measurements in the Western Canada Sedimentary Basin overlying the adjacent Craton are in petroleum exploration wells with inherent low accuracy and are affected by hydrological effects. However, the deep thermal boundary is well defined based upon contrasts in several other temperature sensitive geophysical parameters. The boundary is located 100 km west of the mountain front in the region of the Rocky Mountain Trench, and it must occur over a distance of less than 200 km. Temperatures in the deep crust and upper mantle are first computed from the heat flow and radioactive heat generation data. These temperatures are then compared to those estimated from the temperature dependence of uppermost mantle seismic velocity, Pn, and from xenoliths in kimberlites for the Craton, and in Tertiary volcanics for the Cordillera. Pn velocities decrease from about 8.2 km/s in the exposed Craton to 7.8 km/s in the Cordillera. The temperatures just below the Moho are 400-500C for the Craton and 900-1000C beneath the Cordillera based upon all three constraints. Two temperature sensitive changes across the thermal boundary are examined. There is a westward decrease in crustal thickness from 40-50 km for the Craton to 32-34 km for the Cordillera with no significant change in average elevation nor in gravity. Isostatic balance is maintained by thermal expansion and density reduction in the high temperature Cordillera lithosphere. The average temperature to a depth of 150 km is about 400C higher for the Cordillera compared to the Craton. There also is a pronounced westward decrease in lithosphere strength and thus deformation style. In the Craton, the crust and upper mantle are very strong to at least 100km depth. As a result, the foreland belt deep crust and upper mantle have remained undeformed during Late Mesozoic to Early Tertiary tectonics. Shortening occurred primarily in overlying sedimentary thrust sheets, mediated by high pore fluid pressures. In the Cordillera hinterland, the high temperatures result in the rheological lithosphere with significant strength being limited to the upper 10-15 km of the crust. Mesozoic-Cenozoic shortening deformation and subsequent extension included this whole thin lithosphere.

JSS44/L/03-B4

1150

#### ELECTROMAGNETIC IMAGES OF STRUCTURAL AND GEOCHEMICAL EVOLUTION OF OLD CONTINENTAL LITHOSPHERE

J.A. CRAVEN, D.E. Boerner, R.D. Kurtz, (Geological Survey of Canada, Ottawa, Canada, K1A 0E9); I.J. Ferguson (University of Manitoba, Winnipeg, Canada R3T 2N2); R.C. Bailey (University of Toronto, Dept. of Physics, Canada M5S 1A7)

Recent evidence suggests that the geophysical snapshot of the lithosphere is also a viable view into the ancient lithosphere. Deep electromagnetic probing based on the magnetotelluric (MT) method reveals a conductivity structure sensitive to the spatial distribution of minor constituents such as carbon and hydrogen. These elements are important geochemical



## INTER-ASSOCIATION

indicators of lithospheric reworking related to mantle devolatilization and to subduction-related metasomatism. MT surveys across the Archean Hearne and Superior Provinces of Canada contrast the nature of lithospheric reworking during the Proterozoic and Archean. The Archean Hearne Province beneath the Western Canada Sedimentary Basin was substantially weakened during at least three Proterozoic reworking events. One legacy of these events is a strong gradient in the deep electrical conductivity at the margin of the Hearne lithosphere, likely created by modal metasomatism. This view is contrasted by conductivity models of the lithosphere beneath the western Superior Province which is strongly conductive and almost one-dimensional (layered) within the North Caribou subcrustal lithosphere, but spatially juxtaposed against electrically two-dimensional subprovinces to the south. This electrical fabric argues for a stable (primary?) cratonic element in the North Caribou subprovince against which crustal blocks and their lithosphere were coherently accreted during Late Archean. Integration of laboratory and synthetic analyses of the deep conduction mechanisms is the key to unlocking the relationship between the deep electrical geophysics and the on-going evolution of the lithosphere.

**JSS44/L/01-B4**

**1210**

### LITHOPROBE - REVEALING THE EVOLUTION OF A CONTINENT THROUGH MULTIDISCIPLINARY EARTH SCIENCE STUDIES: EXAMPLE FROM THE TRANS-HUDSON OROGEN, CENTRAL CANADA

Ron M. CLOWES (Lithoprobe and Department of Earth & Ocean Sciences, University of British Columbia, 6339 Stores Road, Vancouver, BC, V6T 1Z4, Canada; email: lowes@lithoprobe.ubc.ca) with contributions from many other LITHOPROBE scientists

LITHOPROBE, Canada's national earth science research project, was established in 1984 to develop a comprehensive understanding of the evolution of the northern North American continent. LITHOPROBE's 10 transects (study areas) span the country and 4 b.y. of geological time. A pan-LITHOPROBE synthesis will bring the project to a formal conclusion in 2003. Here we illustrate the multidisciplinary approach and preliminary results of transect synthesis for the Trans-Hudson Orogen Transect. Located in Saskatchewan and Manitoba, the Paleoproterozoic Trans-Hudson Orogen is the best exposed and most complete orogenic belt of a network of such belts formed by collision of older Archean microcontinents. Understanding of its 3D architecture and tectonic history has been changed fundamentally through integration of seismic reflection, seismic refraction, potential field, paleomagnetic, geochemical, geochronological and geological research. An ocean on the scale of the present Pacific Ocean separated Archean blocks that eventually collided. A previously unknown Archean microcontinent, the Sask craton, has been identified in the west central part of the orogen. Crustal thickness over the orogen varies from <40 km to >50 km. Below the central orogen, velocity anomalies in the mantle may represent a preserved mantle suture resulting from the collision of two Archean cratons. The economically important greenstone belt of the Saskatchewan-Manitoba borderland has been revealed to be a collage of oceanic/arc volcanic assemblages that were later intruded and overlain by volcanic, plutonic, and sedimentary rocks. This research has resulted in a new, chronologically well constrained, working model for the tectonic evolution of the orogen between 2.4 and 1.7 Ma, although some inconsistencies remain.

**Thursday 29 July PM**

Presiding Chairs: Sergei Maschenkov (Vini Okeanologiya, St. Petersburg, Russia)  
Ron M. Clowes (Lithoprobe Secretariat, Univ. of British Columbia, Vancouver, Canada)

**JSS44/W/03-B4**

**1400**

### THE 3-D STRUCTURES OF THE TORNGAT AND MAKKOVIK OROGENS AND NAIN PLUTONIC SUITE (LABRADOR) FROM JOINT ANALYSIS OF GEOPHYSICAL AND GEOLOGICAL DATA

Thomas Funck, Keith LOUDEN (both at: Dept. of Oceanography, Dalhousie Univ., Halifax, NS, Canada B3H 4J1, email: tfunck@is.dal.ca); Ian Reid (Danish Lithosphere Centre, Oster Voldgade 10, DK-1350 Copenhagen K, Denmark); Jeremy Hall (Dept. of Earth Sciences, Memorial Univ., St. John's, NF, A1B 3X5 Canada); Dick Wardle (Newfoundland Dept. of Mines and Energy, St. John's, NF, A1B 4F6 Canada)

New geological and geophysical data from the Canadian Lithoprobe's ECSOOT (Eastern Canadian Shield Onshore-Offshore Transect) Program indicate major differences in the deep structures of the Paleoproterozoic Torngat and Makkovik orogens and the Mesoproterozoic anorogenic Nain Plutonic Suite (NPS). These data include recent wide-angle seismic profiles, which allow us to extend interpretation of earlier marine deep MCS profiles onto land where extensive geological studies have been undertaken. For the Torngat Orogen, seismic tomographic inversion images a N-S trending crustal root with a relief of up to 15 km that decreases to the north. The shape of the root in E-W sections across the N-S striking collisional suture changes from asymmetric in the south to symmetric in the north, coincident with changes in the surface geology that indicate N-S variations in late stages of the orogenic development. Preservation of the crustal root and penetration of large-scale shear zones through the entire crust are consistent with an absence of post-orogenic magmatism. In contrast, profiles across the Makkovik orogen, south of the Nain Province, have no crustal root but show signs of significant tectonic modification of the lower crust and upper mantle. An S-shaped reflector separates reworked Archean crust to the north from juvenile Proterozoic crust to the south, but crustal velocities are the same. Finally, the later NPS anorthositic appear to be related to major velocity variations in the mid-to-lower crust.

**JSS44/W/13-B4**

**1420**

### GEOPHYSICAL IMAGES OF THE SVECOFENNIAN OROGEN

Pekka HEIKKINEN, Annakaisa Korja (Institute of Seismology, P.O. Box 26, FIN-00014 University of Helsinki, Finland)

The Svecofennian orogeny took place, when the continental Karelian plate in the east collided with a newly formed Central Finland island arc plate in the west. Later Southern Finland Island Arc Complex amalgamated to this newly formed continent from the south. In the Subjotnian, 200 million years later, an aborted rift was formed within the Southern Finland Island Arc Complex. BABEL lines 1 and 6 image the architecture of the Southern Finland Arc Complex. When the reflection profile data are combined with lithological, new marine gravimetric and seismic wide angle data, the varying reflectivity patterns can be understood in relation to the major processes forming the Svecofennian crust in the region. The unusually thick crust (55-60 km) is cored by unreflective, high density gabbroic intrusions (200km x 50km x 20km), interpreted as a magmatic core of a primitive island arc complex. A highly reflective ramp anticline structure developed against the island arc in the south. The crust was thickened via a sequence of ramp anticlines comprised of the Southern Svecofennian migmatite, schist and volcanic belts. Mantle plume magmatism in the Subjotnian resulted in extensional environment that was expressed by crustal thinning via reflective listric shear zones, that most probably are inverted thrust faults, and via unreflective rapakivi granite magmatism. Shear zones and mafic dyke swarms related to Subjotnian magmatism can be identified from low altitude

aeromagnetic maps and lithological maps. Crustal underplating and intraplating are seen as highly reflective, high velocity lower crust underlain by a 5 km thick, unreflective lower crust, which in turn is cut by a new sharply reflective Moho. BABEL lines 3&4 image reflective NE-dipping suture of the Southern Finland Island arc complex against the Central Finland Arc Complex and the collisional structures of the deformed supracrustal rocks. Ladoga-Bothnian Bay transform fault zone that developed at the Svecofennian Karelian boundary zone is imaged as a 30 km wide, subvertical unreflective band cutting through the crust.

**JSS44/E/02-B4**

**1440**

### INTEGRATED LITHOSPHERIC MODELLING FOR THE STRUCTURE AND OROGENIC EVOLUTION OF THE WESTERN CARPATHIANS AND PANNONIAN BASIN

Miroslav BIELIK (Geophysical Institute, Slovak Academy of Sciences, Dubravska cesta 9, 842 28 Bratislava, Slovak Republic, email: geofmiro@savba.sk); Hermann Zeyen (Department of Earth Sciences, Université de Paris-Sud, Bat. 504, F-91405 Orsay, France, email: zeyen@geol.u-psud.fr); Anco Lankreijer (Institute of Earth Sciences, Vrije Universiteit, 1081 HV Amsterdam, The Netherlands, email: lana@geo.vu.nl)

The contribution focuses on integrated lithospheric modelling for study of the structure and evolution of the continental lithosphere in the Western Carpathian-Pannonian basin region. The integrated 2D modelling algorithm that utilises gravity, local isostasy and thermal analyses is applied to determine lithospheric thermal structure. To improve the knowledge of the continental lithosphere, the rheology of the lithosphere based on extrapolation of failure criteria, lithology and temperature models is also studied. The results show a relatively thin lithosphere underneath the Polish foreland (100-120 km) with indications of a flexural forebulge of about 200 m height. Underneath the Pannonian basin, the lithospheric mantle has to be 5-10 kgm<sup>-3</sup> denser than usual subcrustal mantle which may be explained by enrichment due to a plume. The Carpathians are characterized by a thickened lithosphere which is interpreted as remnants of a subducted slab. Rheological cross-sections show significant variations in rheology of the lithosphere in the Polish foreland, the Western Carpathians and the Pannonian basin with important implications for the tectonic scenarios.

**JSS44/E/18-B4**

**1500**

### ALPINE POLY-STAGE TECTONO- METAMORPHIC EVOLUTION OF THE SOUTH CARPATHIANS AS A PRECURSOR HISTORY OF A YOUNG MOUNTAIN BELT

Viorica IANCU (Geological Institute of Romania, 1 Caransebes Street, Bucharest 32, ROMANIA, RO-78344, Email: viancu@ns.igr.ro); Antoneta Seghedi, Dumitru Ioane (both at Geological Institute of Romania, 1 Caransebes Street, Bucharest 32, Romania, RO-78344, email: geol@igr.sfos.ro)

The structural model of the South Carpathians is based on the idea of a polystage tectono-metamorphic evolution and mountain building. The main tectogenetic events responsible for the compressional and crustal thickening processes are: Mid-Cretaceous ("austrian phase"; 117-118 Ma, by Ar/Ar, Dallmeyer et al., 1996) and Upper Cretaceous ("laramian phase"), the main nape piles including: Danubian, Arjana, Severin, Getic and Supragetic units. The younger history of the belt is dominated by the Miocene tectogenetic events, including thrust of the older nape stacks over Moesian platform, orogen parallel faulting and extension related sedimentation. These structural features of this branch of the Alpine Carpathian mountain belt are strongly supported by structural, petrological and geochronological constraints and are underlined by an integrated analysis of geophysical data: gravity, magnetics, seismics, tellurics. The special features of the alpine history can be underlined by: the successive extensional to compressional tectogenetic events, affecting the same crustal domains, alternating from the Lower Jurassic to Upper Cretaceous, with a period of quiescence in Paleogene, the youngest FT ages being around 30 Ma (Sanders, 1998). The main paroxysmal compressional events alternated with longer periods of extension, magmatism, sedimentation or uplift-erosion; thus, the continent/ocean crust type collision on both sides of the belt, was followed by continent/continent type collision, the alpine mobile belt being attached to the eastern european platforms by the "post-laramian" sedimentary cover during the Neogene. The metamorphic evolution of the alpine cycle has a polystage character in the units of the danubian domain (from chloritoid to prehnite-pumpellyite blastesis in mesozoic covers. In the upper nappes (Getic-Supragetic) the alpine metamorphic imprint is related to high thermal and low-pressure gradients spatially associated with magmatic-arc intrusions (banatitic magmatites) in two pulses: subsequent to late-Albian and intra-Senonian as suggested by U/Pb of 79-75 Ma (Nicolescu, 1998) and K/Ar data (81-68 and 62-45 Ma intervals, cf. Russo-Sandulescu et al., 1994).

**JSS44/L/02-B4**

**1520**

### UPPER MANTLE DOMAINS BENEATH CENTRAL-SOUTHERN ITALY: PETROLOGICAL, GEOCHEMICAL AND GEOPHYSICAL CONSTRAINTS

A. PECCERILLO (Dipartimento di Scienze della Terra, Piazza Universit', 06100 Perugia, Italy, e-mail: peccerang@unipg.it), G. F. Panza (Dipartimento di Scienze della Terra, Universit' di Trieste and the Abdus Salam ICTP, SAND Group, 34124 Trieste, Italy)

The Italian peninsula shows high complexity of the mantle-crust system and of the Plio-Quaternary magmatism. The lithospheric thickness shows remarkable lateral variations from about 110 km to a minimum of about 30 km. Intermediate and deep-focus earthquakes indicate the presence of a lithospheric slab under the Eolian-Calabrian area and at the southern end of Campania. Much less extensive and more shallow seismic activity characterizes the Roman-Tuscan region, where the existence of a relic slab has been hypothesized. The deep seismicity in the southern Tyrrhenian sea is associated with active calcalkaline to shoshonitic volcanism in the Aeolian arc. Alkaline potassic volcanism occurs in central Italy. Finally, potassic lamproitic magmatism coexist with crustal anatectic and various types of hybrid rocks in the Tuscany area. The parallelism between changing magmatism and variations of the structure of the crust-mantle system makes central-southern Italy a key place where petrological and geophysical data can be used to work out an integrated model of the structure and composition of the upper mantle. It is suggested that the upper mantle beneath Tuscany consists of a thick lithospheric lid that has been affected by intensive subduction-related metasomatism. This caused the formation of phlogopite-rich veins that cut through residual spinel-harzburgite and dunite. These veins, possibly partially molten, may be an explanation for the soft mechanical characteristics that are unusual for lithospheric mantle. In the Roman Province, the upper mantle is formed by a thinner lid and by metasomatic fertile peridotite, probably connected with the uprise of an asthenospheric mantle wedge situated above the Apennine subduction zone. Geochemical data indicate that metasomatism, though still related to subduction, had different characteristics and age than in Tuscany. Finally, the upper mantle in the eastern sector of the Aeolian arc and in the Neapolitan area appears to be distinct as in the Roman and Tuscan area and is probably represented by fertile peridotite contaminated by the presently active subduction of the Ionian sea floor. The overall picture of the mantle-crust system in Italy that unfolds from geophysical, petrological and geochemical data is that of a mosaic of various mantle domains that have undergone different evolutionary history in terms of both metasomatism and pre-metasomatic events. The coexistence side by side of these sectors is a key factor that has to be considered by models of the geodynamic evolution of the Central Mediterranean area.



JSS44/E/21-B4

1540

## THE LITHOSPHERIC STRUCTURE OF SOUTHERN ITALY: A CONTRIBUTION FROM GEOCHEMICAL AND GEOPHYSICAL CONSTRAINTS

F. ITALIANO (Istituto di Geochimica dei Fluidi, C.N.R., via U. La Malfa 153, 90146 Palermo, Italy, email: italiano@igf.pa.cnr.it); M. MARTELLI, P.M. Nuccio (both at Dipartimento C.F.T.A., Università di Palermo, via Archirafi 36, 90123 Palermo, Italy, email: marte@neomedia.it); G. Martinelli (Regione Emilia Romagna, Serv. Cartogr. e Geologico, v.le Silvani 4/3,41100 Bologna, Italy, email: g.martinelli@mo.nettuno.it)

Many fluids emissions of the Southern Apennine sedimentary chain are characterised by geochemical features able to furnish new and useful information about the local lithospheric structure. The widespread CO<sub>2</sub>-rich gas emissions of this chain portion are the first geochemical evidence of the geodynamical activity of the area. These emissions display high <sup>3</sup>He fluxes and a <sup>3</sup>He/<sup>4</sup>He ratio as high as 2.84 times the air ratio, clearly testifying an appreciable-to-important contribution of mantle fluids. In particular sites, the presence of intracrustal melt intrusions has been inferred (Italiano et al., 1999). Furthermore, several geophysical data confirm the peculiarity of this crustal portion. Heat-flow displays anomalous values, as high as 215 mW/m<sup>2</sup> (Mongelli et al., 1996); extremely low rock resistivity values beneath 15 km have been evidenced by Lodo et al. (1995), and a deepening of ipocentral depths toward South has been inferred (Doglioni et al., 1996). In relation with these geochemical and geophysical anomalies, we discuss the characteristics of the lithosphere in the investigated zone and its variations in both the apenninic and the antiapenninic directions.

JSS44/E/01-B4

1620

## LITHOSPHERE STRUCTURE OF DEEP BASINS IN NORTHERN EURASIA AND ITS MARGINS

Nina PAVLENKOVA. (Institute for Physics of the Earth, B.Grusinskaja 10, 123810 Moscow, Russia, email: Ninel@Pavlenkova.msk.ru)

Several large and extremely deep basins are outlined in Northern Eurasia and its margins. They are basins formed on cratons and young platforms and in outer and inner seas. Some common features may be determined in their crustal structure and geological carbonate sediments are dominant. Flat bottoms and very steep sides formed by deep faults are typical for the basins. For deep structure the common features are: uplift of the Moho, decreasing of consolidated crust thickness, unusually high velocities (6.5 high seismic velocity intrusions in the lower crust. There is no evidence for large extension. Such basins seem to be formed by a similar process. At the first stage rifting helped to open a channel for transfer of mantle heat and material, starting a ience has been due to the crustal rock modification into more dense phases, to the load of sediments, to effects of thermal blanketing, to a metamorphism of the lower sediments, and to cooling of the formerly intruded hot mantle material.

JSS44/L/04-B4

1640

## INTEGRATED GEOPHYSICAL MODELS OF THE CRUST IN THE NORTH EURASIAN SHELF ON THE BASIS OF NEW COMPUTER DERIVED POTENTIAL FIELD MAPS AND GEOTRANSECTS

MASCHENKOV S.P., Astafurova E.G., Glebovsky V.Yu., Zayonchek A.V., Cherhyh A.A. (All at VNIIOkeangeologia, 1, Angliysky pr., St.-Petersburg, 190121, Russia, e-mail: mascha@vniio.nw.ru)

The deep crustal structure of the North Eurasian shelf was studied on the basis of the integrated interpretation of potential field, seismic refraction and seismic reflection data. To improve the digital magnetic anomaly and gravity data bases in the area a team at VNIIOkeangeologia (St. Petersburg, Russia) has been assembling a bulk of original aeromagnetic profiles and free-air gravity observations. The available seismic cross sections were digitised and compiled. The magnetic and gravity anomaly maps and their derivatives provide with significant information for regional characterisation of major tectonic elements and the deep crustal structure. The basement topography was studied on the basis of comprehensive interpretation of seismic profiles and potential field maps, 2D- and 3-D gravity modelling, and the depth to magnetic source estimations. The position of the Moho evaluated from the gravity modelling along the geotranssects was controlled by deep seismic refraction data where available. The integrated geophysical models allow to distinguish the large-scale structures of the North Eurasian shelf and develop a better understanding of their tectonic history.

JSS44/W/21-B4

1700

## MAPPING LITHOSPHERE-SCALE STRUCTURES IN THE EASTERN SIBERIAN PLATFORM

Yvette H. POUJOM DJOMANI, William L. Griffin, Lev M. Natapov, Suzanne Y. O'Reilly (all at GEMOC ARC National Key Centre, Department of Earth and Planetary Sciences, Macquarie University, NSW 2109, Australia, email: ypoudjom@tilley.es.mq.edu.au); Yuriy Erinchek (VSEGEI, St. Petersburg, Russia 199026, email: erinch@mail.convey.ru)

The Siberian platform consists of several major Archean and Proterozoic basement terranes that have been mapped from regional magnetic data and basement exposures in the Anabar shield. Garnet and chromite concentrates from mantle xenoliths from a chain of Paleozoic to Mesozoic kimberlites across the platform have been used to construct mantle sections showing rock type distribution. These mantle sections reveal that the lithospheric mantle shows significant differences, corresponding to tectonic terranes mapped at the surface, and indicating that the terrane boundaries are trans-lithospheric. Furthermore, the Archean terranes are underlain by the typical depleted Archean lithosphere > 200 km thick, while the Proterozoic terranes are underlain by thinner and less depleted lithosphere. Enhancement of geophysical data shows more strongly negative Bouguer anomalies and a more noisy magnetic anomaly pattern over the Archean terranes than on the Proterozoic terranes. This reflects the difference in the mantle composition beneath the terranes as revealed by mantle-petrology studies. The elevation across the platform is not more than 900 meters. Gravity and topography data have been inverted to estimate the flexural strength, or elastic thickness (Te) of the plate. The results show that although the study area is a geologically stable Precambrian craton, Te is relatively low (< 30km) across most of the area suggesting a weak lithosphere comparable to that of tectonically much younger areas around the world. These results also show a major zone, ~ 150 km wide, of very weak lithosphere (Te < 10 km) running N-S across the western part of the study area which coincides with a zone of thicker lithosphere, lower surface heat flow and thicker lower crust, as well as abnormally high sub-Moho P-wave velocities suggesting an anisotropy in the upper mantle. The kimberlite fields in the Archean part of the platform are localised on the western flank of the zone of weak lithosphere. We suggest that the low Te zone is a mantle shear zone which has been a preferred conduit for magma into the lower crust, and has controlled the emplacement of kimberlites in the study area.

JSS44/E/20-B4

1720

## SECULAR EVOLUTION OF SUBCONTINENTAL LITHOSPHERIC MANTLE

W.L. GRIFFIN, Suzanne Y. O'Reilly (GEMOC, Dept. of Earth and Planetary Sciences, Macquarie University, NSW 2109, Australia, Email: bill.griffin@mq.edu.au); C.G. Ryan (and WLG) CSIRO EM, P.O. Box 136, N. Ryde, NSW 2113, Australia)

Chemical and petrographic observations on mantle-derived xenoliths and xenocrysts define a fundamental distinction between Archean cratonic mantle and Phanerozoic mantle. Archean xenoliths are more depleted on average, and have higher Si/Mg; subcalcic harzburgites are well-represented in Archean xenolith and xenocyst suites, but rare in younger ones. Analysis of >13,000 garnet xenocrysts from volcanic rocks worldwide shows a correlation of garnet composition with the tectonothermal age of the crust penetrated by the volcanic rocks. In xenoliths, the Cr content of garnet correlates well with the Al content of the rock, and Al is closely related to the contents of other major and minor elements. These correlations allow calculation of the mean composition of a mantle section, given the Cr content of garnet xenocrysts from that section. The calculated mean composition of SCLM beneath Archean, Proterozoic and Phanerozoic terranes shows a secular evolution in all measures of depletion, such as Al, Ca, mg#, and Fe/Al; Proterozoic SCLM is intermediate in composition between Archean and Phanerozoic SCLM. Cenozoic SCLM, exemplified by garnet peridotites from young extensional areas (China, Siberia, Australia) is only mildly depleted (~ 10% melt extraction) relative to Primitive Mantle. SCLM beneath some Phanerozoic terranes, especially in Europe, is more depleted and may represent reworked Proterozoic SCLM. Most Archean SCLM probably was derived by high-degree melting at depths ~150 km. Comparison of xenolith suites with ophiolitic and abyssal peridotites suggests that subducted oceanic mantle is not a major component of Phanerozoic SCLM. Most existing Proterozoic and Phanerozoic SCLM probably has been generated in extensional post-orogenic environments. The broad correlation of SCLM composition with crustal age implies quasi-contemporaneous formation of crustal volumes and their underlying SCLM, and crust-mantle coupling over periods of aeons; it also requires an evolution in fundamental processes involved in the formation of continents and their roots.

JSS44/E/32-B4

1740

## THE STRUCTURE OF THE ANABAR SHIELD CRUST

Svet MILANOVSKY, M.K. Kaban (both Institute of Physics of the Earth, Moscow, Russia, email: svet@upei-ras.scgis.ru); A.V.Egorkin (GEONCenter, Moscow, Russia); O.M. Rosen (Institute of Lithosphere, Moscow, Russia)

For the area of Anabar Shield we investigated geology, seismic, gravity and thermal fields. The Earth crust of Anabar presents a relict of most ancient sialic cover of the Earth. From geological point of view the crustal complexes of Anabar Shield are identified and subdivided into passive (terranes) and active (collision zones) tectonic units. Our interest for the study granulitic terranes is caused by the possibility to see the inner structure of the deep eroded crust from the surface geology and in the same time to study it with geophysical technology. Gravity field of the crust within Anabar is characterized by linear maxima which are oriented in NW-SE direction. These maxima coincide with zones of granulites. 3D analysis of gravity field gives the same direction of inclination of high density blocks in the crust that was found from surface geology and seismic model along DSS profile "Shpat". Thermal field of the Anabar Shield is characterized by very low heat flow. The average crustal heat generation was estimated to be 0.36 mW/m<sup>3</sup>. Crustal petrology model was compared with heat generation values, seismic velocity (Vp,Vs) model and 2D density model Moho temperature is about 250-270 gradC on Anabar. We have "frozen" crust with eroded granite-gneiss layer. The present-day crust being a possible model for the consideration of the lower crust consisting of the blocks reflecting collision nature of the Anabar Shield granulites due to intense overthrust movements.

Friday 30 July AM

Presiding Chairs: Prof. Laust B. Pedersen (Dept. of Earth Sciences, Uppsala Univ., Sweden), Sergei Maschenkov (VNIIOkeangeologia, St. Petersburg, Russia)

JSS44/W/02-B5

0930

## IS THICK-SKINNED TECTONICS DUE TO WEAK FAULTS?

M. Cristina Pomposiello (CIRGEO, Ramirez de Velasco 847,1414 Buenos Aires, Argentina, email: cpmposi@mail.retina.ar); John BOOKER, Shenghui Li (both at Geophysics Program, University of Washington, Seattle WA 98195 USA, email: booker@geophysics.washington.edu, shenghui@geophysics.washington.edu); Alicia Favetto, Ana Osella (both at Dpto. De Fisica, Univ. Buenos Aires, Ciudad Universitaria, Pabellon I, 1428 Buenos Aires, Argentina, e-mail: favetto@df.uba.ar, osella@df.uba.ar); Claudia Sainato (Catedra de Fisica, Fac.Agronomia, Univ. Buenos Aires, Av. San Martin 4453, 1417 Buenos Aires, Argentina, email: csainato@ciudad.com.ar)

The Sierras Pampeanas (SP) of Argentina are a region of active thick-skinned deformation between stable cratonic South America and the Andes. The Tucuman Plain (TP) lies at the northern end of the SP between the most easterly active reverse faults of the Andean deformation (which dip west) and the first high ridge (Aconquija) elevated by an eastward dipping reverse fault bounding it to the west. In October 1998, we collected 10 wideband magnetotelluric sites on a 165 km east-west transect of the TP. This transect coincides with industry seismic reflection data reprocessed to image structure to almost 40 km. We observe very low electric resistivity (below 1 Ohm-m) in the lower half of the crust under the western portion of the TP. To the east, the top of this conductor dips eastward roughly orthogonal to the dominant westward dip of the seismically imaged active faults. It continues horizontally eastward in a more subdued form in the mantle under the craton. The active faults bounding the TP and the adjacent Aconquija Ridge are rooted in the very low resistivity zone. Furthermore, the fault that has been traced at high angle to greatest depth (the Guasayan) has a reversely polarized bright reflection below 30 km. Both the low resistivity and reversed seismic reflection polarity lead us to suggest that the thick-skinned faulting beneath the TP is the result of low fault strength due to high fluid pressures. However, the unusually low resistivity under the TP may be due to precipitation of graphite or other very good conductor in the active faults rather than due to the fluid itself.

JSS44/W/08-B5

0850

## ISOSTATIC STATE OF THE CENTRAL ANDES AND RIGIDITY OF ANDEAN LITHOSPHERE

H.-J. GOETZE, M. Koesters (both at FU Berlin, Institut fuer Geologie, Geophysik und Geoinformatik, Malteserstr. 74-100, D-12249 Berlin, Germany, email: hajo@geophysik.fu-berlin.de); A. Kirchner (Shell International Exploration and Production B.V., 2280 AB Rijswijk, Netherlands)

The gravity field of the southern Central Andes and their eastern foreland between 20° to 30°

S was investigated with regard to the isostatic state, the crustal density structure of the orogeny and the rigidity of the Andean Lithosphere. Gravity data-base came from recent field data acquisition in the Central Andes and covers both the area of northern steep subduction zone and the flat slab area in the South. All gravity data analysed in this paper were tied to the IGSN-71 gravity datum and terrain-corrected as well. Bouguer anomaly was evaluated using the sea level datum and a standard density of 2670 kg/m<sup>3</sup> for mass correction. Analysis of Andean topography bases on the 1 km x 1 km mean elevation data grid of the USGS (Bliss and Olson, 1996) and other sources. The gravity effect of the downgoing Nazca Plate was removed from both Bouguer and isostatic residual anomalies (Airy and Vening-Meinesz type) and then correlated with mean topographic heights to identify areas of disturbed isostatic equilibrium. Additionally the balance of topographic surplus and deficit masses of the Andean root was estimated by applying Gauß' theorem to the residual gravity field. As can be expected from the principle of isostasy, isostatic anomalies close to zero dominate, however, clearly shifted to a small positive mean values. Most of the morphological Andean units close to an isostatic equilibrium. Differences were obtained in the Argentine Puna, the south-eastern foreland and along a large NW to SE striking zone crossing the volcanic arc. This structure can be linked to high density crustal remnants of Mesozoic rifting. A novel methodology (Lowry and Smith, 1995) for 2D modelling of lithospheric rigidity which can account for surface and subsurface loads were applied to both topography and gravity field. Rather low values (10 E22 to 10 E23 Nm) were obtained for the area of the inner mountainous basins and 10 E23 to 5x10 E23 Nm were observed for the back arc region which corresponds with an effective elastic thickness of 35 to 45 km.

JSS 44/E/27-B5

0910

## GEODYNAMICS AND STRESSES IN THE ANDEAN SUBDUCTION ZONE AT 21DEG S

Tanya ROMANYUK, Jury Rebetsky (both - Institute Physics of the Earth, B.Gruzinskaya 10, Moscow 123 810, Russia, email: tromanyuk@relcom.ru, reb@uipe-ras.sgis.ru); Hans-Jorgen Goetze (Freie University, Malterstr. 74-100, N, 12249 Berlin, Germany, email: hajo@geophysik.fu-berlin.de)

The most sections of the convergent zones of the Earth are imagined as underthrusting oceanic plates beneath immovable and stable continents. However, we believe that the Andean subduction zone is a region of a global sinking of material from the outer into the deep part of the Earth, with participation by both oceanic, and continental lithosphere. The movement of the material is strongly asymmetrical: the oceanic Nazca plate horizontally moves near trench at ~10cm/y, whereas the cratonic central part of the South America movement is indirectly estimated ~1cm/y. We tested this idea comparing the (1) results of 2D numerical modeling stresses and (2) parameters of present-day stress state. 1) To compile a 2D combining model we summarized information from the seismic refraction profiles, the gravity measurements, a seismic reflection profile of ANCORP group, electro-magnetic profiles and geological data. The densities and rheological properties of rocks, and velocities of the plates movements were used as the input data and boundary conditions for the task. 2) The principal stress axis directions, type of stress ellipsoid and ratio between isotropic pressure and maximum shear stresses were obtained from the earthquake focal mechanisms (CMT - Harvard catalog) with help of an original "cataclastic analysis" method based on the plasticity theory principles. The results of 2D numerical modeling are good agreed with the parameters of present-day tectonic stress state and allows: to allocate zones of tectonic overthrusting compression and extension along subducting slab and maximum intensity areas of stress tensor.

JSS44/W/18-B5

0930

## THE MAGNETIC, PETROMAGNETIC AND EVOLUTION MODELS OF THE CRUST FOR THE EAST EUROPEAN CRATON

M.I. ORLYUK (Institute of Geophysics National Academy of Sciences of the Ukraine, 32 Palladin Ave., 252142 Kiev, Ukraine)

The comprehensive of the interpretation near surface magnetic field, its regional component and MAGSAT anomalies were used for modelling. Petromagnetic data for the upper crust, the depths to the Pre-Riphean basement and to the Mohorovicic discontinuity, chronological and other geodata were used also as a priori information. 3D and 4D magnetic models of the crust have been compiled for the East European Craton (EEC). The EEC consists of the large-scale magnetic provinces with different mean magnetization which are fixed by T-Magsat anomalies. The magnetic provinces are located at the S-S-W and N-N-E margins of the Craton. Within of these provinces the sources of the regional magnetic anomalies of 60-120 km wide, with 1.0-4.0 A/m magnetization intensity of the crust are concentrated. They are presented mainly by femic (basaltoids, basic granulites) and sial-mafic (andesites, diorites) petromagnetic types. The low-magnetic central and S-E part of the EEC are presented by ultramafic-mafic (peridotites, granulites and eclogites) and sial (granitoids and their metamorphic analogues) types. According to 4D magnetic model the high-magnetic body are formed cyclically during the time intervals: 2.90-3.20; 2.25-2.55; 1.60-1.70; 0.90-0.95; 0.35-0.44 Ga. The high-magnetic blocks are related mainly to epochs of extension answering to the tectonic situations as rifts, basic granulite nuclears, subduction zone, while low-magnetic ones are associated with periods of construction of the crust (collisional orogens and compression structures) and may serve as time-markers these stages. In the EEC high-magnetic, deep-seated blocks are indicators of Archean "protorifolds", the Proterozoic and Phanerozoic riftogenetic structures etc.

JSS44/P/03-B5

0950

## GEOPHYSICAL FIELDS AND DEEP STRUCTURE OF THE OKHOTSK SEA

Yuri Neprochnov, Gennady Semenov (both at Institute of Oceanology, Moscow 117585, Russia, email: ypn@geo.sio.rssi.ru); Liu Guangding, Hao TIANYAO (both at Institute of Geophysics, Chinese Academy of Sciences, Beijing, 100101, P.R. China, email: tyhao@mail.c-geos.ac.cn)

A review and integrated interpretation of existing geophysical data from the Okhotsk Sea region is presented. Three types of the earth's crust are revealed in the region: continental (western, northern and eastern marginal areas of the sea), subcontinental (central parts of the sea and the Kuril Island arc), and suboceanic (the Kuril Basin). The crustal thickness changes within the limits of 12-35 km. The central part of the Okhotsk Sea is characterised by rather small isometric anomalies of magnetic field, but positive anomalies of north-eastern direction have found in the Kuril Basin. The free-air gravity anomalies derived from shipboard measurements (25mgal interval) and from satellite altimetry (10mGal interval) were used for the comparative analysis. Mostly positive anomalies prevail in the northern in central parts of the sea, but negative anomalies down to -20 mGal occur in the Kuril Basin. The analysis of heat flow has shown a clear correlation with main tectonic structures: it is rather stable in central part of the sea, high on the rises in its western part and very high on the Kuril Basin. The gravity-seismic modeling was made for several seismic/geological profiles crossing the major tectonic structures of the Okhotsk Sea, and modified 2D and 3D geophysical models were constructed.

JSS44/E/24-B5

1010

## STRUCTURE OF THE LITHOSPHERE IN CONTINENT OF CHINA AND ITS SURROUNDING MARGINAL SEA

Zhu JIESHOU, Yan Zhongqiong, Cao Jamin (Dept. of Geophysics, Chengdu University of Technology, Chengdu 610059, China, email: zhujs@cdut.edu.cn)

The continent of China and its marginal sea were formed by a series of rapid convergence of plates and blocks in the late Paleozoic (about 200-300 Ma). The Indian subcontinent collided with Eurasian continent, causing the crust to be shortened and uplifted in the late Mesozoic to Paleocene epoch, forming the highest plateau of Qinghai-Tibet and Pamir, and orogens of Himalayan and Hindu Kush. Based on the integrated geophysical and geological data, such as Global Geoscience Transects (GGT), the deep seismic refracted and reflected profiles, and the tomographic velocity imaging from seismic body wave and surface wave data, the three-dimensional structure of the lithosphere has been reconstructed for China and its surrounding marginal sea. The studied area ranges from 0o 0N to 60o 0N in latitude and from 60o 0E to 140o 0E in longitude. The Alpine-Himalayan belt throughout the Northern Pakistan (Hindu Kush and Pamir), Qinghai-Tibet plateau including Tarim basin and Tian-Shan mountain chain is characterized by the continent-continent collision zone with a thick crust (50-70 km) and lithosphere (120-250 km). The eastern part influenced by the motion of Pacific plate and has a thin crust (28-40 km) and lithosphere (60-90 km). Several paleonuclei and paleocontinents, such as Tarim, Yangtze, Ordos and Indian shield, show a great thickness of lithosphere (about 130-250 km). The fold belts, such as Altai, Qinlin belt, North-South tectonic belt, southeast continental margin, and the marginal sea (South China Sea, East China Sea, Yellow Sea) have thin lithosphere (about 60-80 km). The central Asia, from Indian subcontinent to Tibet, Xinjiang, Mongolia and Baikal regions is the present largest convergence place in the world.

JSS44/P/04-B5

1050

## CRUST AND UPPER MANTLE STRUCTURE IN THE WEST AND SOUTHWEST MARGIN OF ERDUOS, CHINA, FROM INTEGRATED GEOPHYSICAL, GEOLOGICAL AND GEOCHEMICAL STUDIES

Li QINGHE, Guo Shounian, Lu Dehui (Lanzhou Institute of Seismology, China Seismological Bureau, Lanzhou, Gansu, 730000, P. R. China, email: liqh@lzu.edu.cn)

Erduos Block is a stable platform but with active faults and violent earthquakes around it. The west and southwest margin of Erduos are Qilian, Qinling folding system and located on the Northeast part of the Qinghai-Tibet Plateau. The crust and upper mantle structure in the west and Southwest margin of Erduos, China, were studied. The P- and S- velocity structure, Q-factors were got from Deep Seismic Sounding and seismic tomography. Bouguer anomaly, gravity inversion, density structure were analysed. Magnetic structure, deep faults and Curie isotherm were obtained from aeromagnetic data. The electric resistivity distribution with depth were interpreted from MT profiles. The heat flow and their distribution, thermal conductivity, deep temperature were got from geothermal measurements. The tectonic stress field image is clear from focus mechanism and others. The simultaneous inversion and interpretation for density and velocity, electric resistivity and temperature, electric resistivity and velocity were manipulated. The geophysical model of this field was established. The tectonics, stratum, deep rock fabric, geochemical properties, basin and folding tectonics, fault tectonics, tectonics evolution and so on were studied. Based on the integrated interpretation of deep and shallow faults, geology, geochemistry and geophysics, the crust and upper mantle model was built up. The special geological, geophysical and seismicity features of this field are induced from the motion of Qinghai-Tibet Plateau toward north and north-east, as well as upheaval from the mantle.

JSS44/E/30-B5

1110

## THERMO-TECTONIC MODELING OF P-T-T PATHS OF ULTRA HIGH PRESSURE METAMORPHISM IN THE DABIE MOUNTAIN, CHINA

Yaolin SHI, Taoyuan Fan (both at Graduate School, University of Science and Technology of China, Academia Sinica, Beijing 100039, China, email: shiyl@cc5.gsbustc.ac.cn)

Based on geological observations, we propose a three-stage process of ultra high pressure metamorphism (UHPM) in the Dabie Mountain, and calculate the dynamic and thermal processes by finite element method. In the first stage, the buoyant continental crust was hauled down to more than 100km depth by the subducting oceanic plate, producing a growing prism. In the second stage, continuing subduction of the plate drives a corner flow of low viscosity continental rocks in the prism. In the third stage, the oceanic plate is detached, and continental rocks in the prism is uplifted to lower crust level by buoyancy, and then further uplifted by crustal continental collision tectonics. A Newtonian viscous model is applied to calculate the motion within the prism at different stages. Advective heat transfer then can be included to calculate temperature evolution. P-T-t paths of various blocks can be traced in the modeling and compared with observations at different locations in the Dabie Mountain. It is found that in order to fit the observed P-T-t paths, for normal rate of subduction, frictional/dissipative heating due to rock deformation must be included. A rapid buoyant uplift of UHPM to lower crust level followed by a slow uplift due to collision tectonics are also required. The calculation can further explain the observed spatial distribution of "hot" and "cold" eclogites, and reveal complexities in P-T-t path formation. The complexities indicate that care must be paid in interpretation of observed P-T-t paths.

JSS44/W/06-B5

1130

## THERMAL AND STRENGTH STRUCTURE OF LITHOSPHERE IN QINLING OROGENIC BELT DERIVED FROM SURFACE HEAT FLUX AND GRAVITY OBSERVATIONS

Xiong XIONG, Houtze Hsu (Both at Institute of Geodesy and Geophysics, Chinese Academy of Science, 54 Xudong Road, Wuhan, Hubei 430077, China, email: xxiong@asch.whigg.ac.cn); Rongshan Fu (Department of Earth and Space Science, University of Science and Technology of China, Hefei, Anhui 230026, China, email: frs@ess.ustc.edu.cn)

Since the data of the surface heat flux is very limited, other geophysical observations must be used as constraints to determine the thermal structure of the lithosphere. A algorithm combining the thermal and gravity observations is employed to determine the steady state thermal structure of lithosphere of Qinling orogenic belt. Given the rheological parameters, the strength structure of the lithosphere is also derived. The computation is carried out by using the finite element method. The numerical results show that the thermal regime of Qinling orogenic belt is very inhomogeneous. It is shown that the Qinling orogenic belt can be divided into several blocks with distinct thermal features. The southern Qinling is the hot zone, while the northern Qinling is the cold one. The corresponding features are also shown in the strength structure. The strength of southern Qinling is much greater than that of northern Qinling. The strength structure of southern and northern Qinling indicates that the Yangzi and Huabei blocks might subduct beneath Qinling block. The numerical result fits well with the geological and geophysical observations.



JSS44/W/16-B5 1150

## SEISMIC TOMOGRAPHY IMAGES OF THE QINLING-DABIE OROGENIC BELTS

Ruomei SUN, Futian LIU, Jianhua LIU, Peifen XU (all at Institute of Geophysics, Science Academy of China, 100101 Beijing, CHINA, email: sunrm@sun.ihp.ac.cn)

The Qinling orogen of central China between the Sino-Korea craton and the Yangtze craton began in late Mesozoic. Ultra-High Pressure (UHP) metamorphic rock belt, found in Dabie mountain, is the largest one in the world. We did the P, S wave and Vp/Vs tomographic inversion of North China craton, Qinling-Dabie orogenic belt and Yangtze craton in central China. The results are as follows: 1. The image of the upper crust has a close correlation with surface geology. The North China basin shows obviously low velocity, whereas the orogenic belt expresses high velocity with E-W trend, reflecting old tectonism. However the velocity anomalies at depths 80-110km display a trend in N-S direction, a feature possibly controlled by recent tectonism. 2. The velocity image at depth of 40+ km beneath the Moho shows that the orogenic belt is divided into three sections. West of 108E, the West Qinling displays low velocity anomaly, the crust is thicker than 40km with indications of a mountain root. Between 108°E and 104°E, in the East Qinling, the velocities are high with no indication of mountain root, and the crustal thickness is less than 40km. East of 104°E in the Dabie Mountains, velocities are obviously low, the crustal thickness is not less than 40 km. 3. The image in a profile across the Dabie mountain shows a slab-like high velocity anomaly dipping from south to north, that may be remain of ancient subducted block, which break off around 130-170km. The slab breakoff seems the mechanism of recurvature of UHP metamorphic rock.

JSS44/P/02-B5 1210

## THE QINLING-DABIE COLLISIONAL OROGENIC BELT AND THE EVOLUTION OF LITHOSPHERE IN EASTERN CHINA

Yuan XUECHENG (Chinese Academy of Geosurveying, 31 Xueyuan Road, Beijing, China)

The Qinling-Dabie orogenic belt is the boundary between North China craton and Yangtze craton, and is the largest among the seven UHP belts in the world. Since 1992, the Qinling-Dabie orogenic belt was integrated studying by geology, geophysics, and geochemistry. An integrated geophysical profile, involving seismic reflection, wide-angle seismic reflection, seismic tomography, magneto-telluric sounding, heat flow measurement, gravity, aeromagnetic survey, and petrophysical work was fulfilled across the East Qinling. Another integrated geophysical profile across the Dabie orogeny is undertaken. The geophysical profiling shows that the Qinling orogenic belt is a collisional orogeny, composed by a series of crocodile structures with their mouths towards the north. Seismic tomography in this area discovered that lithosphere in eastern China has been rifted in several places during Mesozoic-Cenozoic period when the Yangtze craton subducted to the North China craton, the hot mantle upwelled to the height near Moho along mantle rifts, overflow in all directions and formed the horizontally layering middle lithosphere, just like the mushroom cloud in a nuclear explosion. UHP metamorphic rocks carried by the upwelling mantle exhumated fast along the "mantle rift" to a height near Moho, and then thrust and outcropped on the surface when the Yangtze craton collided with the North China craton.

Thursday 29 July AM

JSS44/W/19-B4 Poster 0930-01

## DEEP STRUCTURE OF NORTHWESTERN SIERRAS PAMPEANAS (27° S.L. ARGENTINA)

Ernesto CRISTALLINI (Universidad de Buenos Aires, Department of Geological Sciences, Cornell University, Snee Hall, Ithaca NY 14853-1504; e-mail: ernesto@geology.cornell.edu); Alberto Cominquez and Diego Mercerat (CONICET, Departamento de Geofísica Aplicada, Facultad de Ciencias Astronómicas y Geofísicas, Universidad Nacional de La Plata, Paseo del Bosque s/n, La Plata, Argentina; e-mail: coming@fcaglp.edu.ar); Victor Ramos (Laboratorio de Tectónica Andina, Departamento de Ciencias Geológicas, Facultad de Ciencias Exactas y Naturales, Universidad de Buenos Aires, Ciudad Universitaria Pab.II, Cap.Fed., Argentina; e-mail: andes@gl.fcen.uba.ar)

Reprocessing of industrial seismic lines, in eastern and western foothills of Sierra de Aconquija, northwestern Sierras Pampeanas, Argentina, shows the deep structure of the range and the deep geometry of the Andean foreland basin. On the eastern side of Sierra de Aconquija, the structure is characterized by reverse faulting with eastward vergence, with the Guasayán and El Rosario faults exhibiting the most deformation. To the south, the Guasayán fault produces the uplift of the Guasayán basement range over Tertiary deposits, and can be identified in the seismic reflection record down to 40 km depth. On the western side of Sierra de Aconquija, the deep structure of Campo del Arenal is characterized by westward vergent structures controlled by the basement fabric of the Sierra de Aconquija basement. Further to the west, the deformation stile changes to eastward vergence. The cross-cutting relationships between the west and east vergent fault systems, as well as the geometry of the synorogenic deposits permit establishment of the uplift history of Sierra del Aconquija. The uplift started during the Late Miocene, after the Paranense sea transgression, and still continues, as demonstrated by neotectonic activity. Additionally conspicuous sub-horizontal acoustic-reflectors are present at about 18, 25, 30, 40 and 53 km depth, and interpreted as present or pass brittle-ductile transitions.

JSS44/W/05-B4 Poster 0930-02

## MODELING SURFACE WAVE TRAVELLING ACROSS SIERRAS PAMPEANAS, ARGENTINA.

Nora C. SABBIONE, María L. Rosa (both at Depto. de Sismología, Fac. de Cs. Ast. y Geofísicas, Universidad Nacional de La Plata, Paseo del bosque s/n, 1900, La Plata, Pcia de Buenos Aires, Argentina, email: nora@fcaglp.unlp.edu.ar); Ana M. Osella (Dpto. de Física, Fac. Cs. Exactas y Naturales, Universidad de Buenos Aires, Ciudad Universitaria, Pab. I, 1428 Buenos Aires, Argentina, email: osella@df.uba.ar)

Surface-waves group velocity dispersion curves were analyzed from digital data obtained in LPA seismological station (La Plata, Provincia de Buenos Aires), Argentina, using WWSSNLP instruments. The earthquakes chosen since 1995, come from focus such that in their way to the station go through the Sierras Pampeanas province, northwest of Argentina. This mountain block lies over a continental active margin between the Nazca plate and the South American continental plate, constituting a moderate topography system where the foreland deformation structural characteristic coincide with a subductive angle variation from 30° to less than 10°. The applied method is based on the Multiple Filter Technique and on the latter application of an inversion process to the resulting velocities, to obtain finally a lithosphere model of the region being analyzed.

JSS44/E/12-B4 Poster 0930-03

## TECTONIC PATTERN OF SOUTH AMERICA INFERRED FROM TIDAL GRAVITY ANOMALIES

Marta S. M. MANTOVANI (Instituto Astronômico e Geofísico, Universidade de São Paulo, Rua do Matão, 1226 CEP 05505-900 São Paulo, S.P., Brazil, email: marta@iag.usp.br); Vladimir Shukowsky (Instituto Astronômico e Geofísico, Universidade de São Paulo, Rua do Matão, 1226 CEP 05505-900 São Paulo, S.P., Brazil, email: wladimir@iag.usp.br); Sílvia R. C. de Freitas (CPGCG - Centro Politécnico, Universidade Federal do Paraná, PR, Brazil, email: srfreitas@cce.ufrpr.br)

The knowledge of several physical parameters that characterize a tectonic unit is important to evaluate its dynamic evolution and, therefore, its role in the continental evolution. Several methodologies have been used to measure the elastic properties of tectonic units using: seismic waves, the level of coherence between the wavelength pattern of the topography and gravity fields, borehole deformation rate, mineral fabric, etc. In this study, the Earth's dynamic elastic response to gravity tides is applied for measuring the lithosphere effective elastic thickness. This methodology proved to be a good alternative to the conventional coherence method. It was applied over the continent, taking into account the poor gravity coverage in South America and the restricted area of some tectonic units. Results are presented as lateral distribution of the effective elastic thickness in South America.

JSS44/L/05-B4 Poster 0930-04

## INFORMATIONS FROM AEROMAGNETIC AND RADIOMETRIC DATA IN GUYANE FRANCAISE

P. SAILHAC (IPGP, Laboratoire de Géomagnétisme, Institut de Physique du Globe de Paris, 4 Place Jussieu, 75252 PARIS Cedex 05, FRANCE e-mail: sailhac@ipgp.jussieu.fr); A. Galdeano (IPGP), C. Delor BRGM); D. Gibert (Geosciences Rennes); F. Moreau (Geosciences Rennes)

Guyane Française is part of the Guyana Shield (South America), a former part of a main relief of Gondwana. This includes paleoproterozoic rocks, and the nature of the orogen is not yet resolved. A high resolution aeromagnetic survey including radiometric measures has been done during autumn 1996. This provided very precise data reflecting the near underground average properties in U, Th and K on the one hand (radiometry). On the other hand, aeromagnetic data have been analysed via a continuous wavelet transform giving information on the inclination of the magnetization of sources and on their depths. A few additional paleomagnetic data from the ground has completed the survey and helped the analysis of aeromagnetics. These informations have been compared to the Geology and are discussed in term of the ages and positions of structures.

JSS44/W/04-B4 Poster 0930-05

## SEISMICITY AND 3-D VELOCITY STRUCTURE OF THE INTRA-ISLAND-ARC CRUST FROM TRAVEL TIME ANALYSIS OF THE DATA OF THE JOINT SEISMIC OBSERVATION IN THE TOHOKU DISTRICT, THE NORTHEASTERN AREA OF JAPAN

Makoto MATSUBARA, Naoshi Hirata, Shin'ichi Sakai (Earthquake Research Institute, the University of Tokyo, 1-1-1 Yayoi Bunkyo-ku, Tokyo, JAPAN, email: mak@eri.u-tokyo.ac.jp)

To get a new insight of the island-arc crustal dynamics with a relation between seismicity and lateral heterogeneity, we are conducting seismic experiments in the Tohoku area, northeastern Japan, since 1997. One is the Joint Seismic Observation (JSO) since October 1997, and the other is seismic array observation (SAO) of micro-earthquakes in the Kitakami and Senya Faults area in 1998. The SAO was conducted in the area where the JSO is carried out. We need combine the 3-D velocity structures of regional (150 km x 150 km) and local (30 km x 40 km) areas around 39.5 N. We performed the inversion for velocity structure of regional area. We used 412 events comprising 18,475 P- and 8,937 S-wave arrivals. From July 14 to August 20 in 1998, at KK22 (Shiraiawa) in the Kitakami array, we detected 2,359 events, which include natural earthquakes, 13 explosions and earthquake swarm beneath Mt. Iwate. During the same period 3,310 earthquakes were observed by the regional network of the JSO. The number of local events with a S-P time less than 3 s is 577. This seismicity may be related to the fault zone activities, which will be clarified in detail.

JSS44/W/01-B4 Poster 0930-06

## CRUSTAL SECTION ACROSS THE NORTHERN HONSHU ARC, JAPAN, AS REVEALED FROM WIDE-ANGLE SEISMIC DATA

Takaya IWASAKI (Earthquake Research Institute, the Univ. of Tokyo, Tokyo, 113-0032, JAPAN, Email: iwasaki@eri.u-tokyo.ac.jp); W. Kato, T. Takeda, S. Sekine (ERI, the Univ. of Tokyo, Tokyo, JAPAN); T. Moriya (Hokkaido Univ., Sapporo, JAPAN); N. Umino, T. Okada (Tohoku Univ., Sendai, JAPAN); A. Hasemi (Yamagata Univ., Yamagata, JAPAN); K. Miyashita, T. Mizogami (Ibaraki Univ., Mito, JAPAN); T. Matsushima (Kyushu Univ., Shimabara, JAPAN); K. Tashiro (Kyushu Univ., Fukuoka, JAPAN); H. Miyamachi (Kagoshima Univ., Kagoshima, JAPAN)

An extensive wide-angle seismic experiment across the Northern Honshu Island, Japan, in October 1997 provided a new image on the detailed crustal structure of the volcanic arc. Seismic data collected on an E-W profile line of 150-km length indicate remarkable lateral structural changes. The uppermost crust of the eastern (forearc) side of the profile shows a rather simple structure consisting of 0.3-1-km thick surface layer with a velocity of 4.0-5.4 km/s and 5.9-6.1-km/s crystalline basement. These layers were underlain by the 15-20-km thick reflective lower crust. The uppermost crust of western (backarc) side of the profile characterized by thick (3-5 km) sedimentary layers of 2.0-5.4 km/s is severely deformed owing to the process of the back-arc spreading and the following compressional stress regime in this region. The velocity of the basement is relatively low (5.8 km/s) as compared with that in the eastern part. The total crustal thickness in northern Honshu is 35-40 km. The wide-angle reflection from the Moho is very weak which may indicate the existence of structural transition zone from lower crust to mantle. The Pn velocity in the western part of the profile is 7.7-7.8 km/s, approximately 0.2-0.3 km/s lower than that beneath the Sea of Japan.

JSS44/W/07-B4 Poster 0930-07

## DEEP CRUSTAL STRUCTURE OF LARGE-SCALE INTRA-ARC FAILED RIFT, CENTRAL JAPAN

Tetsuya TAKEDA, Takaya Iwasaki, Hiroshi Sato, Shin'ichi Sakai (Earthquake Research Institute, University of Tokyo, 1-1-1 Yayoi, Bunkyo-ku, Tokyo, Japan, 113-0032, email: takeda@eri.u-tokyo.ac.jp, iwasaki@eri.u-tokyo.ac.jp, satow@eri.u-tokyo.ac.jp, coco@eri.u-tokyo.ac.jp)

The Itoigawa-Shizuoka Tectonic Line (ISTL) is a major structural boundary, which divides SW and NE Japan. It was formed as a normal fault under the tensional stress regime associated with the Miocene opening of the Sea of Japan, but has reactivated as a reverse fault owing to



## INTER-ASSOCIATION

subsequent crustal shortening. Reanalysis for three wide-angle reflection data sets provided a new image of the crustal structure around the ISTL. The upper crustal structure was mainly determined from travel time analysis including an inversion method. Deeper part of the crust, on the other hand, was modelled using both travel time and amplitude information. The obtained profiles clearly demonstrate that the northern part of ISTL is characterized by an eastward dipping reverse fault. Tertiary sedimentary rocks with velocity of 3.0-4.0 km/s accumulated along the ISTL at depth of 2-km, suggesting the existence of the Miocene graben. All profiles indicate reflective lower crust, however its depth range shows a clear change across the ISTL. The change was probably caused by the differential tectonic movements of NE and SW Japan blocks and the subsequent different thermal history due to back-arc spreading. Clear Moho is not recognized in all profiles. Highly laminated structure is well developed below 30-40 km depth including the uppermost mantle. It may represent the nature of upper mantle beneath volcanic arc.

**JSS44/W/09-B4** Poster **0930-08**

### INTEGRATED SEISMIC EXPERIMENT IN THE NORTH-EASTERN HONSHU ARC, JAPAN

Naoshi HIRATA, Hiroshi Sato, Takaya Iwasaki (Earthquake Research Institute, The University of Tokyo, Tokyo 113-0032, Japan, e-mail: hirata@eri.u-tokyo.ac.jp, sato@eri.u-tokyo.ac.jp, iwasaki@eri.u-tokyo.ac.jp); Akira Hasegawa, Norihito Umino (Research Center for Prediction of Earthquakes and Volcanic Eruptions, Tohoku University, Sendai 980-8578, Japan, e-mail: hasegawa@aob.geophys.tohoku.ac.jp, umino@aob.geophys.tohoku.ac.jp); Masanao Shinohara (Department of Earth Sciences, Faculty of Science, Chiba University, Chiba 263, Japan, e-mail: mshino@earth.s.chiba-u.ac.jp)

To understand the mechanism of earthquake occurrence in an intra-island-arc crust with its deformation process, we are conducting a large-scale integrated seismic experiment across the North eastern part of Honshu arc at about 40 degree N, Japan, since October 1997, including both passive and active sources, in land and at sea. The target of the experiment is to image the whole crustal section with a special attention to deep structure of active fault systems. The study is also intended to understand the formation process of the island-arc as a part of the continental growth process. We have deployed 50 3-component temporary seismic stations, from which data are transmitted through a satellite communication system. The active experiment includes a 150-km-long refraction profiling on land and 220-km in the Japan Sea. Three 15-km-long reflection surveys were also carried out in the central part of the Tohoku arc. The preliminary results of the seismic profiling indicate that an active fault continues to a detachment fault at a depth of about 15km in the island-arc crust. We found a reflective lower crust in the arc area, which is sometimes detected in a continental crust. The tomography study indicates a correlation with a low velocity area and an active fault area, suggesting a concentration of crustal deformation near the active fault areas.

**JSS44/E/34-B4** Poster **0930-09**

### STRUCTURE OF THE CRUST IN VIETNAM FROM MAGNETIC AND GRAVITY DATA

Cao Dinh TRIEU (Institute of Geophysics, VNCST, Box 411 Buu Dien Bo Ho, Hanoi, Vietnam, email: trieu@igp.ac.vn)

Aeromagnetic and 2d gravity modeling enable the interpretation of the depth to the Moho and crystalline basement. The data used in this study comprise the following: a/ Aeromagnetic anomaly map of the territory of Vietnam at the 1: 500, 000 scale. b/ Bouguer gravity anomaly map of the territory of Vietnam at the 1: 500, 000 scale. c/ Geological map of the territory of Vietnam at the 1:500, 000 scale. The depth of the Moho varies from 30 km to 38 km, the deepest part occurring in Northwest Vietnam. The structure of the basement is fairly similar to that of the dominant geostructural zones. In the Dong Bac zone, the crystalline basement outcrops in positive areas with NW-SE direction. The basement in the Red River depression lies at a depth of about 8-10 km in its central part. In the Tay Bac zone, Fansipan represents the exposed basement. In the Muong Te zone, the depth to the basement varies from 3 up to 5-6 km. In the Truong Son zone, the depth to the basement varies from 1 to 4-5 km and is exposed in the Phu Hoat geoblock. The basement in the Kon Tum zone is exposed over a large area and lies at 1-3 km. The Da Lat zone is characterized by a large negative structure of the basement. In the Cuu Long basin, the depth to the basement varies from 1 to 5 km, and the basement in the Minh Hai-Kien Giang zone lies at a depth of about 3-5 km.

**JSS44/E/41-B4** Poster **0930-10**

### A STUDY ON THE ELECTRICAL CONDUCTIVITY DISTRIBUTION BENEATH AN AREA OF ACTIVE VOLCANISM IN THE NORTHEASTERN PART OF CHINA

Hisashi UTADA, Makoto Uyeshima (both at Earthquake Research Institute, Univ. Tokyo, Tokyo 113-0032, Japan; email: utada@utada-sun.eri.u-tokyo.ac.jp, uyeshima@utada-sun.eri.u-tokyo.ac.jp), Zhao Guozze, Tang Ji (both at Institute of Geology, Seismological Bureau of China, Beijing, China; email: zhaogz@public.bta.net.cn); Ma Mingzhi (Seismological Bureau of Jilin Province, Changchun, China)

Seismic tomography gave us an image of a "stagnant slab" around the depth of 660 discontinuity in various zones of plate subduction in the world (e.g., Fukao et al, 1992). One of the clear examples can be found beneath the North eastern district of China where active Quaternary continental volcanism is widely seen. The cause of this continental volcanism is still controversial, though there have been suggested several models such as hot region (Miyashiro, 1982) or wet region (Iwamori, 1992) in the upper mantle. A study of large-scale deep electrical conductivity structure in this region will give important information for investigating the cause of the volcanism and the lithospheric evolution, as well as their possible relation to the presence of a stagnant slab. For this purpose, a Network-MT experiment was carried out in Jilin Province, NE China, as a collaborative project between China and Japan. This experiment consists of mobile electric field measurements by using telephone lines with typical line length of 30 km and a reference geomagnetic field measurement. This paper presents a preliminary result of this project.

**JSS44/E/05-B4** Poster **0930-11**

### PRE-ALPIAN STRUCTURE OF ZERAVSHAN-HISSAR FOLDED REGION (SOUTH TIEN SHAN) BASED ON THE FREQUENCY ANALYSIS OF PALEOZOIC THRUST PACKETS

Yu. S. RZHEVSKY (Centre for Advanced Professional Education, St.-Petersburg State University; Office 135, 14th line 29, St.-Petersburg, 199178, Russia, email: yurkov@cape.nw.ru)

Southern Tien-Shan as a link of West Ural-Mongolian fold belt emerged after collision of Kirgiz-Kazakh (to North), Karakum-Tajik and Tarim (to South) continents, formerly separated with Turkestan paleo-ocean (a part of the vast Paleo-Tethys Ocean). Relicts of the oceanic crust, mainly sedimentary and igneous rocks that had accumulated on the sea-floor of the Paleo-Tethys, crop out in many places and appear to be largely allochthonous. Complicated tectonic design of accretion wedges is an object of hot discussion. It concerns especially the question

is thrusting of tectonic units in early study of accretion really took place. We used frequency analysis of thrust sheet packets in the Paleozoic of Zeravshan-Hissar region to solve the problem. Results of such an analysis for Zeravshan-Hissar fold belt are done in the paper demonstrated that stratigraphic section had been corrupted by sheet thrusts before folding.

**JSS44/W/14-B4** Poster **0930-12**

### THE POSITION OF NORTH CHINA IN THE GRENVILLE AND CALEDONIAN OROGENIES FROM ND-SR ISOTOPIC STUDIES IN THE QILIAN FOLD BELT

A.D. SMITH, C.-H. Chung, D.-J. Wen, K.-A. Tung, L.-Y. Huang (Department of Earth Sciences, National Cheng Kung University, Tainan, Taiwan; email: mochinn@mail.ncku.edu.tw)

Late Proterozoic plate reconstructions depend heavily on the SWEAT model in which the continental blocks of Asia such as North China and Siberia are placed along the northern margin of North America. Such models require long migration paths for North China to reach the Caledonian position of eastern Gondwana suggested by identical Late Ordovician Rb-Sr isochrons and Middle Proterozoic Sm-Nd TDM model ages for metasediments in the Qilian belt and central Transantarctic Mountains of Antarctica. Rather, the position of North China in the Early Paleozoic suggests it formed part of the megacontinent Laurentia along with North America, the southern tip of South America, and Siberia. Within this continental mass, North China lay in approximately the same position as Mexico today relative to North America with the Qilian-Qinling belts of China continuing into the Famatinian fold belt of South America and the Appalachian fold belt of North America. The Taconic, Famatinian, Qilian and Ross orogenies of the Caledonian stage are thus equivalent. Amphibolite and hornblende-plagioclase gneisses yield common TDM=1.8 to 2.4 Ga Sm-Nd model ages for the basement of the North and Central Qilian terranes with the implication that the latter is a fragment of North China rather than Gondwana. In conjunction with previous geochronological data, a Sm-Nd isochron of 1060±39 Ma with epsilon Nd=-1.2 for granitic gneisses delineates the Central Qilian terrane as a Sibaoan belt and suggests North China may have maintained its inferred position relative to North America since at least the end of the Middle Proterozoic, with the Sibaoan event in North China being equivalent to the Grenville event in North America.

**JSS44/E/40-B4** Poster **0930-13**

### GRAVITY ANOMALIES ACROSS THE NE MARGING OF THE INDIAN PLATE AND THEIR INTERPRETATION IN TERMS OF SURFACE AND SUBSURFACE FEATURES

Carla BRAITENBERG, Maria Zadro (Department of Earth Sciences, University of Trieste, Via Weiss 1, 34100 Trieste, Italy, email: berg@univ.trieste.it, zadro@univ.trieste.it)

The Kohistan-Ladakh Arc (NW-Pakistan) is set between the Northern border of the Indian plate and the Southern border of the Asian plate. The Kohistan sequence has been interpreted as the crust and mantle of an obducted island arc. We study existing, publicly accessible gravity data, extending from the Indian to the Eurasian plates, across the Arc. Apart from the long wavelength field tied to crustal thickening, the gravity anomalies show remarkable variation in the medium to short-wavelength component, which correlates with the major sutures. The features of the gravity values are not explained by the surface geology alone, but indicate the presence of mid crust anomalous masses, which can be interpreted in terms of the collisional process.

**JSS44/E/16-B4** Poster **0930-14**

### INTERPRETATION OF GROUND MAGNETIC DATA OF OIL BEARING CAUVERY BASIN, INDIA

Vinit C. ERRAM, S.P. Anand, Mita Rajaram (Indian Institute of Geomagnetism, Colaba, Mumbai-400 005, India)

The Cauvery basin along the Eastern Continental Margin of India is important from the point of view of oil exploration. Over 200 wells have been drilled, both onshore and offshore, by the Oil and Natural Gas Commission (ONGC) of India. A ground magnetic survey was carried out with readings at every 10km for the magnetic total field 'F' and the vertical field 'Z'. Four major magnetic anomaly trends N-S, E-W, NE-SW and the Cauvery shear trend are evident on the anomaly maps. The major anomalies are constrained within the Eastern Ghat Folding and the anomalies are smooth with very small variation in the region where marine transgression and regression occurred. It is evident from the anomaly maps that the shallow features are superposed on the long wavelength anomalies. The trend in the ground magnetic anomalies corroborates very well with the aeromagnetic maps. Comparison with the marine magnetic data shows that the anomalies continue into the offshore region. The ground and aeromagnetic data are transformed to get second vertical derivative, horizontal gradient of pseudogravity and reduced to pole. These maps distinctly isolate the shallow and deep sources. The ground and aeromagnetic anomalies are compared with gravity, marine magnetic and other available geophysical data and related to the surface geology and subsurface structures. Further, these constraints are used to develop an evolutionary model of the Cauvery basin lying on the rifted continental margin of India.

**JSS44/E/15-B4** Poster **0930-15**

### COMPARATIVE STUDY OF TWO SEDIMENTARY BASINS IN THE EASTERN CONTINENTAL MARGIN OF INDIA

Mita Rajaram, S.P. Anand, Vinit C. ERRAM (Indian Institute of Geomagnetism, Colaba, Mumbai-400005, India)

Krishna Godavari (KG) and Cauvery basins are typical, hydrocarbon bearing sedimentary basins along the Eastern Continental Margin of India (ECMI). The present paper deals with the coarse grid ground magnetic surveys conducted over these basins and the data analysis undertaken to study the tectonic elements of the basins constrained by gravity, magnetotellurics, DSS and borehole data. Available aeromagnetic maps are also analysed. The ground and aeromagnetic total field anomaly maps are transformed to delineate the deep and shallow features. In both the basins the shallow features are showing a NE-SW trend which is in conformity with the Eastern Ghat trend. The KG basin shows distinct NW-SE trends for deeper features which can be related to series of deep seated parallel faults. Along two such prominent faults the Godavari graben is found to extend offshore. On the other hand, the NW-SE trending deep seated fault is dominated by the NE-SW trends in the Cauvery basin. Thus Krishna Godavari basin is formed of two distinct structures while no distinction is seen in the Cauvery basin. The present paper compares these two basins lying on the rifted continental margin of India and relates it to the tectonics and evolution of these basins as the Indian subcontinent separated from Gondwana land in the Mesozoic.

JSS44/E/07-B4 Poster 0930-16

## GEOPHYSICAL STUDY OF THE AHNET BASIN (SW ALGERIA)

A. K. YELLES-CHAOUICHE, R. Ait Ouali, A. Abtout, M.E.M. Derder (Both at C.R.A.A.G., Algerian Research Center of Astronomy, Astrophysics and Geophysics, BP 63 Bouzareua, Algiers, Algeria, e-mail: geoph3@ist.cerist.dz); H. Ghandriche (Head of District 3 of SONATRACH, Algiers)

The Ahnet basin, one of the Algerian Saharan basins, is located at the boundary between the West African Craton and the Hoggar Shield. This particular location indicates that its evolution is influenced by history of the suture between the two main geological domains. During the last twenty years, several geophysical surveys were carried out in this basin due to its importance for the oil companies. Analysis of several seismic lines and others geophysical data (aeromagnetic, gravity...) reveals that: structuration of the basin started at the end of the panafrican orogeny. During the Paleozoic time, the basin was filled by thick sedimentary series. During the Hercynian orogeny the basin was affected by reactivation of the major N-S panafrican accidents with a shortening direction of about N030-040. This stress regime allowed creation of strikeslip faults with an E-W direction and leading to deformation of N-S anticlines. Later, at the Jurassic period and in relation with the opening of the Atlantic ocean, magmatic event affected the basin.

JSS44/P/06-B4 Poster 0930-17

## INTEGRATED USE OF AIRBORNE MAGNETIC, GEOLOGICAL AND SATELLITE IMAGERY DATA IN ELUCIDATING THE STRUCTURAL SETTING OF GABAL AMRIT-GABAL DIF AREA: A SAMPLE AREA FROM THE SOUTH EASTERN DESERT OF EGYPT

Abouelhoda M. ELSIRAFY, Magdy L. Meleik, Ahmed M. Sabri, Alaa Eldin A. Aref (Nuclear Materials Authority of Egypt, P.O Box 530 Elmaadi, Cairo, Egypt)

The study area comprises a wide diversity of igneous, metamorphic and sedimentary rocks ranging in age from Precambrian to the Quaternary. Integration of results obtained from qualitative and quantitative interpretation of the aeromagnetic survey data with the geological and Satellite imagery data, has significantly contributed to the delineation of the regional structural framework of the area under consideration. Analysis of the aerial magnetic data involved the application of some selected 2D-frequency domain filtering operations. 3D-Euler deconvolution was applied to quantify the interpretation of the filtered magnetic anomalies. Furthermore application of standard digital image display and enhancement techniques to these non-imaged magnetic data offered much in terms of structural interpretation of these data. The present study indicated that the study area has been affected by two sets of major deeply rooted faulting structures, trending mainly in the NNW to NW and NNE to NE directions. This faulting pattern is closely related to the development of the Red Sea rifting. The intersection of these two sets of linear tectonic zones has resulted in what is referred to as the block structures, consist mainly of highly magnetic rocks with basic or ultrabasic massifs rocks cut by occasional granitic and pegmatitic bodies. Folding structures are dominant in the eastern part of the area. These have a general NW-SE trending direction, occasionally changed to the NNE-SSW due to faulting and rotation around the stable basic to ultrabasic intrusive rock masses. It was also evident from this study that the gross surface structural fabric of the study area provided a fair expression of the subsurface structures.

JSS44/E/29-B4 Poster 0930-18

## BASEMENT TRENDS AND LITHOSPHERE STRUCTURE IN EGYPT OBTAINED FROM GEOPOTENTIAL DATA

Hassan HOSNEY (Associate Professor, Geophysics Department, Cairo University, Egypt); Samir Riad (Professor of Geophysics, Geology Department, Assuit University, Egypt)

The Bouguer anomaly and RTP aeromagnetic maps of Egypt were utilized to delineate gravity and magnetic trends that are probably due to structures related to basement and deeper horizons within the upper lithosphere. Present trends show that old basement tectonics are controlling the tectonic pattern known to prevail in the whole country. The geophysical lineaments, presumably faults, show a pattern of normal and strike-slip faults that could be explained by either a pure or simple shear stress. In the first case, the acting principal stress is oriented in almost N-S direction, related to the drifting of the African continent and the interaction between the African and European plates. A secondary stress field related to the active Red Sea rift is acting, in addition to the previous one, since the Oligocene time. In the second case, the obtained trends are related to a simple shear stress associated with the transform faulting controlling the spreading of the southern Atlantic.

JSS44/W/15-B4 Poster 0930-19

## CRUSTAL STRUCTURE OF ERATOSTHENES SEAMOUNT (EASTERN MEDITERRANEAN COLLISION ZONE BETWEEN AFRICA AND EURASIA) FROM SEISMIC, PONETICIAL FIELDS AND GEOLOGICAL STUDIES

S.M.Zverev, D.A. ILINSKI (both at Schmidt Institute of the Earth Physics, 123810, Bol.Gruzinskaya 10, Moscow, Russia)

Crustal seismic wide-angle reflection refraction measurements were made across Eratosthenes seamount, during the Soviet research project "Tetis" in 1990. This seamount is located near the southern edge of collision zone between African and European plates. The nature (continental or oceanic) of major Eastern Mediterranean structures such as Eratosthenes seamount is still unclear and under discussion in geological literature. The P-wave velocity cross-section was obtained after evaluation of acquired seismic data. Ray-tracing and full-field acoustic response modeling proves the resulting section. Magnetic and gravity models were built from the basic seismic model. Data from new acquired gravity map of Eastern Mediterranean were used. Crystal rocks with P-wave velocities of 6.0-6.5 km/s uplift under Eratosthenes. Section of the first 10km depth at the Southern part of Eratosthenes has alternation of thin high and thicker low velocity layers. High velocity layers have higher magnetization and density comparing with background structures and could be associated with ancient lava flows. Upper Cretaceous limestone from borehole 967 (DSDP Leg 160) recovered from 2900 meters under the water depth at the north part of Eratosthenes correspond to the same age limestone founded at the south part of the seamount during the dredging (1.3 km water depth). From this evidence we can conclude that northern part of Eratosthenes was lifted down and can explain why the higher velocity and density layers within upper 6 km of the section were not found under the Northern part of the seamount. We suppose that seamount was built in pre-Cretaceous time since limestone covered the Eratosthenes has Senonian age.

JSS44/P/07-B4 Poster 0930-20

## THE CONTACT ZONE BETWEEN PALEOZOIC AND PRECAMBRIAN PLATFORMS IN ROMANIA IN THE LIGHT OF NEW GRAVITY AND MAGNETIC DATA

Ligia Narciza ATANASIU, Dumitru Ioane (both at Geological Institute of Romani, 1 Caransbebes Str., 78344 Bucharest-32, Romania, email: ligia@igr.sfos.ro); Marius Visarion (Romanian Academy, Calea Victoriei, Bucharest, Romania)

One of the major tectonic problems in Europe and in Romania too is the determination of the southwest margin of the East-European platform. A large lithospheric fracture zone, called Tornquist-Teisseyre zone, oriented NW-SE, represents this boundary from North Sea to the Black Sea. It represents the contact zone between East European Platform (Precambrian Platform) and Central European Platform (Paleozoic Platform). In Romania the TTZ is overridden by the Carpathian front. It reappears in Dobrogea, a region between the Danube and Black Sea. The results of this study show that TTZ in Romania is situated between the crustal fault Siret in the eastern part and another crustal fault situated under Central East Carpathian Nappe System or inner nappes, in the Western part. Near Bacau, the TTZ shows an important change in the east and Southeast direction being boarded by the crustal faults: Vaslui-Cetatea Alba Fault, Bistrita Fault and Peceneaga-Camena Fault. The Peceneaga-Camena Fault, which separates the North Dobrogea from the Moesian Platform, is the major fracture of TTZ. The magnetic and gravity anomaly maps shows representative features on the anomalous magnetic and gravity fields in the region of both Paleozoic Platform and Precambrian Platform. The modelling of the gravity and magnetic anomalies which are performed on two regional geological sections offers some information about the geological units, their limits and the total thickness and the positions of the Conrad and Mohorovicic discontinuities.

JSS 44/E/08-B4 Poster 0930-21

## CRUSTAL STRUCTURE IMAGE BASED ON GEOPHYSICAL AND GEOLOGICAL DATA ALONG THE DEEP REFRACTION PROFILE BUCHAREST-BACAU (ROMANIA)

Andrei BALA, Victor Raileanu (both at National Institute for Earth Physics, P.O. Box MG-2, Bucharest, Magurele, Romania, email: bala@infp.ifa.ro)

The most important tectonic feature of Romania, the Carpathian Orogen, is bounded on the north and north - east by the East European Platform and on the east and south by the Moesian Platform; inside the Carpathian Orogen and westward are the Transylvanian Basin and Pannonian Basin separated by the Apuseni Mountains. Three main types of crustal structure have been identified in Romania and they cover the most part of the country: 1. Orogenic belt type: 40 -50 km depth, in Eastern and Southern Carpathians; 2. Platform type: 30 - 40 km depth in Moldavian and Moesian Platform; 3. Depression type: 26 - 30 km depth in Pannonian Depression.

A notable exception from this classification is the crust of the Carpathian Foredeep, especially in front of the Eastern Carpathians Arc Bend (with thickness of 43 - 45 km). This is the place with the most active tectonic and seismogenic forces in Romania. As a result, here are situated the hypocenters of the most numerous and strongest earthquakes in Romania, both at crustal and subcrustal level. A deep refraction profile will be carried out this year in an attempt to clarify the exact position of the most important boundaries of the crustal structure in the area. This profile will cover 200 km from Bacau to Bucharest and will be continued to south- west, until Danube river. The available geophysical and geological data are integrated and represented along path of the refraction profile, to create a state of the art image of the crustal structure as suggested by the present data.

JSS 44/E/23-B4 Poster 0930-22

## REGIONAL LITHOSPHERE STRUCTURE AS INFERRED FROM EARTHQUAKE DISTRIBUTION IN EASTERN ROMANIA

Andrei BALA, Mircea Radulian, Mircea Biter, Zina Malita (all at National Institute for Earth Physics, P.O. Box MG-2, Bucharest - Magurele, 76900 Romania, email: bala@infp.ifa.ro)

The Eastern Carpathian Arc Bend (ECAB) and the Carpathian Foredeep in front of it are the most distinctive tectonic features of Romania. Here is the collision region between at least three tectonic plates: East European plate, Intra-Moesian subplate and Intra-Alpine plate. Some researchers consider the eastern part of the Moesian Platform together with Central Dobruja as representing the Black Sea subplate. Their assumptions are made mainly on the existence of the Intra-moesian Fault which is considered to be still active due to the crustal earthquakes produced on its northern end. This paper focuses the attention on Vrancea zone and the surrounding area, because this is the most active and intense seismogenic area. Here are situated the most numerous, strongest and still unforeseeable earthquakes from Romania. There were represented all the earthquake hypocenters from the period 1982 - 1997 situated in an area which covers Vrancea zone (25° - 28.5° E, 44.5° - 47° N). Because of the great number, they were found to describe well the limits of the tectonic plate (plate fragment?) which is supposed to be subducted in this region until 200km depth. These limits were put in direct relations with the known geology and tectonics of the area. Available fault plane solutions for the crustal earthquakes are analyzed in correlation with the orientation of the principal fault systems in the area. Principal stress vectors are represented as derived from the focal mechanisms of 69 crustal earthquakes. A structural model of this region was derived on the basis of seismological data and linked with fault system in the area as it was established from geological and geophysical researches.

JSS44/W/20-B4 Poster 0930-23

## GEOPHYSICAL MODEL OF THE URALS CRUST ACCORDING TO GEOMAGNETIC DATA

Vsevolod SHAPIRO, Natalia Fedorova, Alexander Chursin (Institute of Geophysics, 100 Amundsen str., Ekaterinburg, 620016, Russia, email: seva@maglab.mplik.ru)

The Urals orogenic belt is one of the greatest structural feature of the Eurasian continent. According to recent point of view Uralian crust was developed during the collision of island arc and micro continental fragments with the structures of East European Craton. The range of geomagnetic investigation of the lithosphere was carried out at the Urals during last two decade. One of the most important part of this research is precise aeromagnetic survey along the network of profiles with the length up to 1200 kms crossing the orogenic belt in latitudinal direction. Besides the airborne survey we used satellite magnetic data and investigated all spectrum of geomagnetic variations from short-period to secular and used new method for interpretation of experimental data. As a consequence of this research we construct the magnetic model of the crust along number of profiles. As a result of study we come to conclusion that the Urals has practically non-magnetic crust in comparison with the magnetisation of the crust of adjacent platforms.



JSS44/E/43-B4 Poster 0930-24

**A "HOT" MODEL OF LOW S VELOCITY ZONE BENEATH THE CENTRAL EUROPE AND AN ORIGIN OF ASTHENOLENSES**

Ya. M. KHAZAN (Institute of Geophysics of Nat. Acad.Sci. Ukr. Palladin pr. 32, Kiev-142, 252680, Ukraine, email: earth@igph.kiev.ua)

Shear wave seismic tomography (Zielhuis and Nolet, 1994) revealed in the transition zone (depth 250±450 km) beneath the central Europe an elongated low S velocity zone (LSVZ) about 500 km wide extending from the Bothnia Gulf to Asia Minor. Just above the LSVZ at subcrustal depths a number of high conductive objects (asthenoleneses) with characteristic dimensions of 50±100 km were found (Burakhovich et al., 1996). In some cases the asthenoleneses correlate with positive heat flow anomalies and topographic uplifts of some hundreds meters amplitude. Thus it seems reasonable to treat them as hot and partially melted bodies. The present paper considers a "hot" model of LSVZ (heating from below) that is an alternative to the "cold" model of Nolet and Zielhuis [1994] and treats the asthenoleneses as resulting from the thermal instability of the uppermost (lying above the melt-solid density crossover) part of partially melted LSVZ.

JSS44/E/19-B4 Poster 0930-25

**3 D TOMOGRAPHY OF THE CRUST IN BELGIUM**

Fabienne COLLIN (Royal Observatory of Belgium, av. Circulaire 3, 1180, Brussels, Belgium, e-mail: F.Collin@oma.be)

A new algorithm for 3D tomography has been build. It's an iterative method inserting Newton method, trust region method and LSQR algorithm. The choice of the parameters is done by an original way in order to limit errors on the travel time evaluation and to optimize the dimensions of the cells. Examples in 2D with synthetic and real data are given. Simulations in 3D are produced and first results are given for the South of Belgium. Comparisons with gravimetrical and geological results are done.

JSS44/E/38-B4 Poster 0930-26

**TOR: DEEP LITHOSPHERE VIA TELESEISMIC TOMOGRAPHY IN NORTHERN EUROPE**

Tor Working Group, reporter Soren GREGERSEN (KMS, Rentemestervej 8, DK-2400 Copenhagen NV, Denmark, email: srg@kms.dk)

We do distinguish very significant deep lithosphere differences in the data of the Tor project, of the largest seismic antenna to this time in Europe. Field work was 1/2 year 1996-1997, data processing 1997-1999. And now preliminary interpretations are available of the project across Germany, Denmark and Sweden. The Tor project has a horizontal resolution of 20-30 km compared to more than 100 km in previous studies. It involves teleseismic tomography as well as studies of receiver functions, S-wave splitting, scattered waves and surface waves. The Tor line goes along a well studied crustal profile of an earlier project, so that the sediments and crustal structure are assumed known, and the inversion efforts are concentrated on the deep lithosphere and asthenosphere differences to depths around 300 km. The investigations can be called two-and-a-half dimensional, being a 900 km profile with 100 km width plus a few seismographs off the profile. The project has established several versions of a 3D crustal/upper mantle model based on existing data, and through ray tracing in the model a picture of the influence on the seismic rays of respectively the known crust and the unknown deep lithosphere/asthenosphere system is established. For several events of the large data base it is shown that the observed travel time anomalies of 1-2 seconds can be divided almost equally between known crustal effects and unknown lower lithosphere/asthenosphere differences. The latter transition is judged to be gradual across Denmark.

JSS44/E/13-B4 Poster 0930-27

**SEISMIC ANISOTROPY AND LARGE-SCALE FABRIC OF THE CONTINENTAL MANTLE LITHOSPHERE**

V. BABUSKA, J. Plomerova (Geophysical Institute, Czech Acad. Sci., 14131 Praha 4, Czech Republic, email: v.babuska@ig.cas.cz)

Seismic anisotropy studies using both surface and body waves provide information on the olivine fabric within the subcrustal lithosphere and asthenosphere. A joint interpretation of P-residual spheres and shear-wave splitting at experimental and permanent seismic stations in the Variscan belt of central Europe and in southern Sweden enable us to model orientations of hexagonal or orthorhombic anisotropic structures within smaller-scale lithospheric blocks and to define first-order sutures separating blocks with different orientations of their fabric. The surface-wave anisotropy beneath the Precambrian shields and platforms world-wide exhibits its maxima at about 100 km depth with  $V_{sv} < V_{sh}$  signature, while beneath Phanerozoic regions it is characterized by  $V_{sh} > V_{sv}$ , with maximum at depths about 70 km. An interpretation of the observed seismic anisotropy by the preferred orientation of olivine crystals results in a model of the mantle lithosphere characterized by anisotropic structures plunging steeply beneath Precambrian shields and platforms, compared with less inclined anisotropies beneath Phanerozoic orogenic belts. The different olivine orientations can result from different processes that lead to the formation of the continental lithosphere in Precambrian, compared with the Phanerozoic, and that probably changed considerably during the Proterozoic.

JSS44/W/11-B4 Poster 0930-28

**INTEGRATED INTERPRETATION OF SEISMIC AND GRAVITY DATA USING A NON-LINEAR DENSITY-VELOCITY RELATIONSHIP**

Elena KOZLOVSKAYA (Department of Geophysics, University of Oulu, POB 3000, FIN-90401 Oulu, Finland, e-mail: elena@babel.oulu.fi); Jukka Yliniemi (Sodankylä Geophysical Observatory, Oulu Unit, POB 3000, FIN-90401 Oulu, Finland, e-mail: jyl@babel.oulu.fi)

The fact that there exists a strong correlation between rock density and seismic waves velocity has been widely used in geophysics for many years for calculating density models from data about velocity of deep structures obtained from seismic investigations. It is a common practice to use for this purpose Birch equation or its modifications. The previous experience of combined interpretation of seismic and gravity data has shown that such equations do not allow to obtain density models that satisfy observed gravity data. To avoid this problem, we have developed a method of integrated interpretation of seismic and gravity data that allows not only to obtain density models of complicated 2-D and 3-D structures, but also to improve the quality of seismic data interpretation.

This method uses a more complicated non-linear relationship connecting density, compressional and shear seismic waves velocity. This equation is obtained as a solution of inverse gravity problem, and it is a very important difference of this technique from the traditional approach. The data on other geophysical and geological measurements are used

as a-priori information necessary to find reliable solution. The equation is then used to calculate density model and its gravity field. The method has been applied to the interpretation of some DSS profile data including LT-7, TTZ profiles in Poland, SVEKA profile in Finland and EUROBRIDGE-95-96 profiles in Lithuania and Belarus. The results allow the conclusion that integrated interpretation of seismic and gravity data with the use of the above technique significantly improves the quality of seismic data interpretation.

JSS44/E/11-B4 Poster 0930-29

**OUTLINE OF PRECAMBRIAN STRUCTURE OF THE FENNOSCANDIAN SHIELD AS REFLECTED BY SOURCES OF POTENTIAL FIELD ANOMALIES**

Juha V. KORHONEN, Tapio Koistinen, Seppo Elo, Heikki Seevuori (all at Geological Survey of Finland, P.O. Box 96, FIN-02151 Espoo, Finland, Email: juha.geofys@gsf.fi); Jussi Kriainen (Finnish Geodetic Institute); Sven Aaro (Geological Survey of Sweden); Larske Haller (National Land Survey of Sweden); Jan Reidar Skilbrei (Geological Survey of Norway); Hans Peter Plag, (Norwegian Mapping Authority); Anatoli Tchepik (Northwest Regional Geological Centre); Anatoli Kulnitch (Petersburg Geophysical Expedition); Lioudmila Jdanova (State Company "Mineral"); Rein Vaher (GeologicalInstitute of Tallinn)

One of the goals of the joint Fennoscandian map project is to find geophysical characteristics, that distinguish exposed Precambrian rocks (Fennoscandian Shield) from the surrounding rocks of the same age, covered by Phanerozoic sediments (East European Platform). The boundary of the shield is not shown in the magnetic, pseudogravimetric or Bouguer anomaly signatures. Instead these anomalies are all low in the central part of the shield and roughly concentric with the Fennoscandian land uplift area. Radially averaged magnetic anomaly field increases from the central part (-120 nT) to +120 nT at a distance of 500 km, steeply decreasing near zero outside. The positive magnetic anomaly ring is associated with Neoproterozoic-Mesoproterozoic igneous rocks, mainly acid in composition. Correlation with petrophysical properties reveals that the anomalies are partly caused by unexposed sources. Study is going on concerning the geological nature of the structure and its possible connections to other lithospheric characteristics of the shield. The shield outside the structure consists of accreted Precambrian terrain of Kola, Svekonorwegian orogeny and Lofoten area. These terrain are characterized by higher magnetization in their central parts, than in the border areas, thus differing in nature of the central geophysical ring structure of the...

JSS44/E/14-B4 Poster 0930-30

**CHARACTERIZATION OF CATACLASTIC FAULT ZONES BY PETROPHYSICAL AND GEOCHEMICAL PROPERTIES APPLYING MULTIVARIATE STATISTICAL METHODS**

Helmuth WINTER (Institut fuer Allgemeine und Angewandte Geophysik der Universitaet Muenchen, Theresienstrasse 41, D-80333 Muenchen, Germany, email: winter@geoelek.geophysik.uni-muenchen.de); Helmut Kuechenhoff (Institut fuer Statistik der Universitaet Muenchen, Akademiestrasse 1, D-80799 Muenchen, Germany, email: helmuth@stat.uni-muenchen.de); Heinrich C. Soffel (Institut fuer Allgemeine und Angewandte Geophysik der Universitaet Muenchen, Theresienstrasse 41, D-80333 Muenchen, Germany, email: soffel@magbakt.geophysik.uni-muenchen.de)

Cataclastic fault zones are important structures in the Earth's crust: they provide paths of migrating fluids, represent seismic reflectors and zones of high electrical conductivity. Analyses of particular samples from scientific drill holes show that composition and physical properties of cataclastic fault zones are different compared to the surrounding not distorted rocks. Direct probing is difficult due to the low strength of the material and, therefore, drill cores from cataclastic fault zones are rare. Data from drill cuttings and borehole measurements are available more easily and in a higher density. They give the basis for our investigation. Multivariate statistical methods are applied to characterize the cataclastic fault zones by petrophysical and geochemical properties. The data sets of the German Continental Deep Drilling Project (KTB) are used which represent a 9-km-deep profile of crystalline rocks, mainly consisting of gneiss and amphibolite, intersected by various cataclastic fault zones in different depth. The calculations lead to a model with characteristic changes in cataclastic fault zones.

JSS44/W/17-B4 Poster 0930-31

**THERMAL EVOLUTION AND EXHUMATION HISTORY OF THE WASATCH NORMAL FAULT, UTAH, USA: RESULTS FROM THERMAL MODELING**

Todd A. EHLERS, Phillip A. Armstrong, David S. Chapman (Dept. of Geology and Geophysics, University of Utah, Salt Lake City, UT, USA 84112; email: tae@mines.utah.edu); Thomas Kohl (Institute for Geophysics, ETH Honggerberg, CH-8093 Zurich)

The thermal regime surrounding an active normal fault is important for the interpretation of thermochronometric data but is complicated by tectonic and topographic processes. The footwall thermal gradient is affected by rates of uplift, erosion, and flexure, whereas the hanging wall gradient is affected by sedimentation and burial. If the exhumation and fault displacement rate are fast enough, an enhanced thermal regime in the footwall is juxtaposed against a depressed regime in the hanging wall, causing lateral heat flow and curved isotherms in the subsurface. Topography causes 3-D variations in isotherms that mimic the topography and are damped in amplitude at several kilometers depth. Exhumation rates calculated from apatite fission track (AFT) and (U-Th)/He analysis are sensitive to the thermal regime surrounding the fault. Our multidimensional thermal models suggest that above a threshold displacement rate isotherms are curved and not horizontal. The depth to the closure temperatures varies with distance from the fault, exhumation duration and rate, and topographic wavelength. Hence, interpretation of fission track data in tectonically active regions necessitates the use of multidimensional thermal models. We interpret spatial variations in exhumation rates from published and new AFT and (U-Th)/He ages using 2-D and 3-D numerical simulations of the Wasatch Mountains. Simulations were run with variable flexural displacement profiles and exhumation rates varying from 0.1 to 5 mm/yr for up to 20 My. Results suggest predicted exhumation rates from multidimensional thermal models differ from commonly used 1-D models by ~40% or more when applied to thermochronologic data.

JSS44/E/42-B4 Poster 0930-32

**DIFFERENCE IN THE THERMOMECHANICAL RESPONSES OF CRATONIC AND MOBILE LITHOSPHERES AND INTEGRATION OF GEODATA SETS**

U. RAVAL, K. Veeraswamy National Geophysical Research Institute, Hyderabad, India

By grouping, the continental lithospheric (CL) region into cratonic and mobile (MBs) domains, large geophysical, geological and geochemical data over the Indian subcontinent could be integrated in a bimodal geodynamical framework consisting of Plate- and Plume-tectonics. The study examines the Meso-Cenozoic tectonothermal development of the Indian CL which exhibits: occurrence of three CFB's over 70 My duration, three breakups (at ~125, 90 & 64 Ma); high plate velocity (up to 16-19 cm/yr during 80-50 Ma), and a continent-continent collision. It is shown that a major thermomechanical difference existing across a -50 mgal



contour could be understood in terms of interaction between cratons/MBs and hotspots. This difference is characterised by high gravity, high heat flow and presence of MBs north of the contour and a relatively low gravity and low heat flow to its south, which does not possess any major mobile zone, because in the southern region major MBs have already participated in the continental break-ups aided by plume activity. The combination of plume & MBs hence appears to be 'fatal' for the continental stability. Concepts of deep rooted (thick), cold, rigid and dry cratonic and relatively thin, warm, weak and wet mobile lithospheres thus allows integration of different data sets and better understanding for the Indian CL.

**JSS44/E/35-B4** Poster **0930-33**

**THERMAL INSTABILITY IN THE UPPER MANTLE: EFFECT OF THE MELT-SOLID DENSITY CROSSOVER**

Ya. M. KHAZAN (Institute of Geophysics of Nat. Acad. Sci. Ukr. Palladin pr., 32, Kiev-142, 252680, Ukraine, email: earth@igph.kiev.ua)

The existence of the melt-solid density crossover (MSDC) at pressure 8-10 GPa (250-300 km) [Rigden et al., 1984; Agee and Walker, 1993] should strongly influence the style of thermal instability in the upper mantle. Below the MSDC the melt is denser than the solid. This implies that partially melted layer heated from below remains stable until the solidus isotherm rises above the MSDC. To estimate scales and increments of the instability of an unstable layer lying in the vicinity of the MSDC the problem is treated as a Rayleigh-Taylor one with additional constraints accounting for a thermal relaxation. It is shown that the instability develops when the unstable layer thickness reaches 10-15 km. Linear stability time (some Myears) and diameter of a body arising from the layer (some tens of km) depend on temperature at the layer bottom and viscosity contrast between undisturbed mantle, unstable layer and intermediate layer. While rising up, the velocity of the body increases about ten times due to both the decompression melting and the increase of the solid - melt density difference away from the MSDC.

**JSS 44/E/36-B4** Poster **0930-34**

**THERMAL HISTORY OF THE EARTH MANTLE AND GLOBAL ASTHENOSPHERE**

Vadim GORDIENKO (Institute of Geophysics of Nat. Acad. Sci. Ukr., Palladin pr., 32, Kiev-142, 252680, Ukraine, email: tectonos@igph.kiev.ua).

Thermal history of the Earth mantle has been analyzed. After the Earth core and crust separation the temperature (25800C at 500km depth and 28600C at 1100 km) exceeded solidus down to 1100km depth and liquidus down to 500km depth. The subsequent evolution included the influence of the radioactive decay, conductive cooling through the Earth surface, advective heat transfer that periodically resumed in activation. By the present a partial melting zone at 800-1000km depth must have remained under the continents and oceans. Its existence is confirmed by geoelectrical data (specific resistance reduced from 5-100Hom<sup>2</sup>m to 0.5-50Hom<sup>2</sup>m) and does not contradict the seismological data (dV/dZ reduced from 3-5\*10<sup>-3</sup>s-1 to 1.5-2\*10<sup>-3</sup>s-1, Vp/Vs reduced from 1.81-1.82 to 1.78-1.79).

**JSS44/E/41-B4** Poster **0930-35**

**REALIZATION OF A TERRESTRIAL REFERENCE FRAME FOR LARGE-SCALE GPS NETWORKS**

Detlef ANGERMANN, Juergen Klotz, Christoph Reigber (GeoForschungsZentrum Potsdam, Telegrafenberg C2, 14473 Potsdam, email: dang@gfz-potsdam.de)

The GFZ Potsdam established GPS networks for geodynamic studies in South America (SAGA), Central Asia (CATS) and South-East Asia (GEODYSSEA), in cooperation with various organizations in the host countries, as well as in Europe and North America. This presentation concentrates on the datum definition of these networks.

The GPS data of the large-scale networks were processed simultaneously with data of the IGS station network using the GFZ software EPOS. The mean station coordinate residuals between our global network solutions and the ITRF96 coordinates are 1 cm horizontally and 1-2 cm vertically. With respect to a regional reference frame the mean station coordinates residuals are in the range of 2-5 mm horizontally and below 1 cm for the height. For the interpretation of our network results we focus on regional tectonics and relative plate motions. To achieve this goal we define the datum of the station velocities in a regional frame. We present results for the datum definition of the SAGA and CATS network.

**JSS44/E/33-B4** Poster **0930-36**

**THE ULTIMATE WIDTHS OF THE 3 OCEANS WHEN CONTINENTAL DRIFT CEASES**

Yi ZHENG (7 Hickling House, Slippers Place, Rotherhithe, London SE16 2ER, UK, email: justicezy@hotmail.com)

Continental drift has been lasting since late Jurassic about 150 Ma ago. However what is the basic cause that makes the continents drift is a quandary in earth science which has been perplexing earth scientists for more than 80 years. Our planet can be taken as a quasi-rigid body rotating around an axis. Its total resultant moment is zero. Thus its angular momentum is conservation. The continental lithospheres as the solid surface layer possessing the maximum distance from the axis play main role in the process of global plate movement because there exists an altitude difference of about 5 km between the average height of continents and the average depth of ocean floors. The rheological asthenosphere is deformable which makes the movement of continental lithospheres over it facilitated. The movement of the continental lithospheres can be divided into longitude drift and latitude drift. The former is that the continental mass tends to move towards equator and is the response of continental mass versus the slowing down of the rotation of the earth. Its results is that the Mediterranean is being squeezed to shrink gradually. The latter is the even distribution of continental mass along latitude and is the response of continental mass versus that the earth's rotation tends to dynamic equilibrium. Its result is that the Pacific Ocean is being squeezed to shrink gradually and with a tendency to break continents. With the aid of oceanic palaeomagnetic data upon which oceanic lithospheric age map can be created, quantitative analyses and calculations indicate that the global continental drift will not continue indefinitely. In about 83 Ma the dynamic equilibrium of the earth's rotation will greatly achieve and the large scale continental drift will turn to cease and the widths of the Pacific, Atlantic and Indian Ocean basins at equator then will be 12,889km, 11,550km and 6,790km respectively.

**JSS44/E/28-B4** Poster **0930-37**

**METAMORPHIC FLUID MOVEMENT IN THE CONVERGENT CONTINENTAL MARGINS AND COLLISIONAL OROGENS**

E. SUETNOVA (United Institute of the Physics of the Earth of RAS, Moscow, 123810, Russia, email: elena@uipe-ras.scgis.ru); Cherniavski V. (Paleogeodynamics, Institute of Oceanology of RAS, Moscow, 117851, Russia, email: cherniav@chip.sio.rssi.ru)

Mathematical model is proposed to describe the process of dehydration and free fluid migration in the lower crust of convergent margins and collision zones. Numerical (using finite-difference scheme) and asymptotic (using parameter expansion) approaches are exploited. Calculations show that fluid can be trapped in the lower crust during the time period of order of a few MY.

**JSS44/E/26-B4** Poster **0930-38**

**LARGE TIME ASYMPTOTIC SOLUTION FOR POROUS MEDIA WITH MOVING BOUNDARY**

E. Suetnova (United Institute of the Physics of the Earth of RAS, Moscow, 123810, Russia, email: elena@uipe-ras.scgis.ru); V. CHERNIAVSKI (Paleogeodynamics, Institute of Oceanology of RAS, Moscow, 117851, Russia, email: cherniav@chip.sio.rssi.ru)

It is investigated the dynamics of evolution of two phase porous layer subject to vertical compaction to simulate large time evolution of low-temperature system where a viscous fluid saturates a viscous matrix under the influence of gravity force. The thickness of the layer is growing with a specific velocity, which is determined by boundary condition (sedimentation rate, for example). It is supposed non-linear dependence of permeability and viscosity on the porosity. It is suggested that impermeable bottom boundary moves downward with constant velocity. Upper boundary is at rest and it is supposed two boundary conditions of constant pressure and definite porosity are posed on it. Numerical modeling shows that the solution of boundary value problem strongly depends on initial conditions at the short and intermediate time level. With the increasing of time, this dependence is decreasing. Analytical modeling has been done to study large time asymptotic solution. Because of investigating evolution when non-dimensional time tends to infinity initial conditions of porosity are not discussed. The width of the region tends to infinity with the same order of rate as time. It is found an exact solution which is valid in a wide region near upper boundary of order of the whole width and can be used in the near bottom region of order unity as a weak solution satisfying integral mass conservation law. The solution is useful to analyze compaction of sedimentary basins and evolution of metamorphic terrains on the geological time scale.

**JSS44/C/JSS07/P/02-B4** Poster **0930-39**

**PHYSICAL EXPERIMENTS OF DYNAMIC PROCESSES ON CONTINENT-CONTINENT COLLISION**

Jiazeng Shan (Institute of Geology, Academia Sinica, P. O. Box 9825, Beijing, China, email: JZ.Shan@ihw.cow.cn)

Physical experiments of continent-continent collision is performed with a new apparatus. The apparatus used in the experimentation consists of large box(100cm long, 70cm high and 12cm wide) with two motors-drive. It is possible that rotational speed of motor-drive changes in 1-2800r/min to simulate drive forces of the mantle convection. Experimental results have indicated that continent-continent collision is one of the principal mechanism leading to lithosphere/crust thickening and mountain building. The models shortened and thickened about 45% and 85% respectively under combined actions by the viscous drag exerted on the base of the lithosphere by lateral motion of the top mantle convection cells from deep mantle and compressive forces from plate movement in the experimental conditions. An evolutionary relationship between napping/mountain building and subducting can be observed from photograph of experimental model.

**JSS44/W/12-B4** Poster **0930-40**

**COUPLED KINEMATIC AND RHEOLOGIC MODEL FOR THE EVOLUTION OF RIFT BASINS**

He LI-JUAN, Xiong Liangping, Wang Jiyang (all at Institute of Geology, Chinese Academy of Sciences, Beijing 100029, China; Email: dsdp@sdbs.cdi.ac.cn)

Coupled kinematic and rheologic model lies between the traditional kinematic model and geodynamic model. It incorporates the advantages of both models, considering simultaneously the effects of heat, stress and rheology on the tectono-thermal evolution of rift basins. On the assumption that the motion of the lithosphere is already known (just like the kinematic model), the model studies the tectono-thermal evolution history of the rheologic lithosphere (just like the geodynamic model). Using this model, we can simulate the multi-phase evolution of the rift basins more flexibly than the geodynamic model by comparison with observed tectonic subsidence values. Much attention must be paid on the consistence of isostatic theory in the coupled kinematic and rheologic forward model and in the backstripping inverse model. Since the flexural isostasy is included in the forward model, tectonic subsidence should be calculated by flexural back stripping too. The effective elastic thickness of the lithosphere, which is affected by the thermal structure of the lithosphere, the sediment loads and the state of stress and strain, may link the forward model with the inverse model. The value of the effective elastic thickness of the lithosphere and its changes with time and space obtained from the forward model, can be used in the inverse flexural back stripping model. We simulated the tectono-thermal evolution history of the Yinggehai basin, South China Sea, which had experienced three phases of extension during the Cenozoic, and satisfied results were obtained should be launched on near polar orbits to pass whole range of local time.

**JSS44/E/45-B4** Poster **0930-41**

**SPATIAL VARIABILITY OF TIDAL GRAVITY ANOMALIES AND ITS CORRELATION WITH THE EFFECTIVE ELASTIC THICKNESS OF THE LITHOSPHERE**

Wladimir SHUKOLSKY (Instituto Astronômico e Geofísico, Universidade de São Paulo, Rua do Matão, 1226 CEP 05505-900 São Paulo, S.P., Brazil, email: wladimir@iag.usp.br) Marta S. M. Mantovani (Instituto Astronômico e Geofísico, Universidade de São Paulo, Rua do Matão, 1226 CEP 05505-900 São Paulo, S.P., Brazil, email: marta@iag.usp.br)

Associations of the Earth tidal gravity response to physical properties of the lithosphere have been attempted at least for the last four decades. Although experimental data suggest this association, rigorous models have not yet been proposed. In this work statistical tests are performed on the available World Gravity Earth Tides data set. Auto-correlation analysis shows that the M2 tidal gravity anomalies are significantly correlated up to a distance of about 500km, with an approximately exponential correlation decay. The analysis of the latitudinal

dependence of the anomalies shows that the anomaly variance, estimated inside of different latitude bands, follows a curve within the latitude interval and defines the noise level for the M2 gravity anomaly data set. The regression analysis between M2 tidal gravity anomaly and the lithosphere Effective Elastic Thickness estimates shows that these quantities are significantly correlated, with a correlation coefficient of -0.82. The wide range of tidal gravity anomaly and effective elastic thickness values, combined with a good global distribution of the data used in the regression analysis, makes the regression equation suitable to be used as a predictor for effective elastic thickness values in areas where M2 tidal gravity anomaly data exist and meet the required quality criteria.

**JSS44/C/U4/W/07-B4** Poster **0930-42**

**SEISMIC REFLECTION RESEARCH ON THE FAULTS IN THE OFFSHORE AREAS TO THE SOUTH OF HAINAN ISLAND CHINA**

Sajjun LIU (Seismological Bureau of Hainan Province, Bailong Road 42, Haikou 570203, China, email: zhengli@pub1.fz.fj.cn); Jinhai Chen (Seismological Bureau of Fujian Province, Hualin Road 203, Fuzhou 350003, China, email: ap35@sdb.csdi.ac.cn)

In the paper, the activities of the large fault in the offshore areas to the South of Hainan Island China were studied in detail by using the data of oil reflection survey. As the boundary fault between the Yingehai and the Southeast Hainan Basin, the No. 1. Fault strike NW is more than 200 km. It is a normal fault dip SW. It stretches to the northwest and connects with the Honghe faults at the north of Vietnam. As an old basement fault, there were movements till the Cenozoic era. Near the point (Long. 1080E, Lat. 190N), it is divided into 2 parts by a pair of faults (NE). And, we find that the fault No.1 is more active in the southeast than the northwest part. Also, there is a gradually strengthening tendency towards SE of Gancheng. The geophysics survey data of the profiles shows that the faults are not any movements in the NW section of Gancheng since the Quaternary period. It shows that in the SE section of Yingehai, however, they had been moving till the early period of the Quaternary Period. And to the south east of the point (1090E, 17.50N) it shows the reduced activities that there were no signs of inheritances in the layer of the Quaternary System. According to the survey data, the fault can be separated into four sections in general. Among them the fault in the Yingehai-Meishan section is more active. In the areas around Gancheng-Lingtou nearby the NE section of the No.1 fault, the earthquake swarm (M=3-4) have occurred since Jan. 1992. The largest one is the earthquake with the Magnitude of 4.5. And the after-earthquakes are lasting till now. The large fault in the offshore areas to the SE Hainan Island was NE-NNE. It turns to the NEE and nearly EW in the waters to the south of Sanya, which is consistent with the gravity and magnetic anomaly belt, the Moho depression and the Arched contact belt. In the NE section, the earthquake (M=6.8) occurred in the 1931. Two earthquakes (M<sub>i</sub> 5.0) took place in the waters around Lingshui in Dec. 1969. The profiles show that from the waters of Yalong Bay of Sanya to the east of the fault, activities are very apparent in the early Quaternary Period still.

**JSS44/L/08-B4** Poster **0930-43**

**WIDE-ANGLE SEISMIC PROFILING: ASEISMIC MODEL OF THE CRUST THROUGH THE BROKEN HILL BLOCK**

J. H. Leven, D. M. FINLAYSON, A. J. Owen, D. W. Johnstone, B.J. Drummond (Australian Geodynamics Cooperative Research Centre, Canberra, Australia, email: jleven@agso.gov.au, dfinlays@agso.gov.au)

The Broken Hill Block, Australia, hosts one of the world's major mineral deposits. It lies just inboard of the Tasman Line, which in this region is coincident with the late Neoproterozoic continental rift margin. In 1997, the Australian Geodynamics Cooperative Research Centre undertook wide-angle seismic profiling across the Broken Hill Block and Tasman Line to investigate the crustal structure beneath and to the east of the Broken Hill Block. Results from this survey indicate:

- Two layer crust: upper layer 5.9 km s<sup>-1</sup> to 6.4 km s<sup>-1</sup> with variable thickness ranging between 20 and 30 km, lower layer 6.8 km s<sup>-1</sup> to 7.2 km s<sup>-1</sup> of relatively constant thickness of around 14 km.
- Moho depth ranges from 35 km on either side of the Broken Hill Block to 43 km beneath it.
- A sub-Moho P-wavespeed of 8.1 km s<sup>-1</sup>.
- Low seismic wavespeeds in the upper crust associated with the region of the Tasman Line.
- Relatively low crustal P-wavespeeds compared with those of eastern Australia, and no evidence of a massive underplated lower crustal layer with P wavespeeds around 7.7 km s<sup>-1</sup>. The structure of the remnant troughs of the Darling Basin which lie to the east of the Broken Hill Block, and the crustal structure as determined from the wide-angle survey suggest that the Broken Hill Block resulted from crustal thickening. The low P-wavespeed upper crustal zone east of the Broken Hill Block is interpreted as a near-surface thrust splay zone, with the leading edge of the thrust sheet defined by the inflection in the Bouguer gravity gradient Southeast of Broken Hill.

**JSS44/L/07-B4** Poster **0930-44**

**SEISMIC IMAGING OF THE LACHLAN TRANSVERSE ZONE, A MAJOR CROSS-CUTTING TECTONIC FEATURE OF EASTERN AUSTRALIA**

Doug FINLAYSON (Australian Geodynamics Cooperative Research Centre (AGCRC), Australian Geological Survey Organisation, Canberra, Australia, email: dfinlays@agso.gov.au); Dick Glen (AGCRC, Geological Survey of New South Wales, St. Leonards, NSW 2065, Australia, email: glen@minerals.nsw.gov.au); Russell Korsch, David Johnstone (AGCRC, Australian Geological Survey Organisation, Canberra, Australia, email: rkorsch@agso.gov.au, djohnsto@agso.gov.au)

The Lachlan Transverse Zone (LTZ) is a newly recognised major yet subtle WNW-trending structure that cuts across the meridional to NNW regional grain of the Neoproterozoic to Mesozoic Tasmanides of South eastern Australia. The LTZ represents the reactivated extension of the southern edge of a WNW trending weak zone that cuts through the Australian continent. The western part of the LTZ separates the Thomson Orogen to the north and Delamerian Orogen to the south. Further east in the Lachlan Orogen, the LTZ has been recently identified as a corridor of repeated faulting and folding since the Early Silurian. The LTZ also controls the localisation of crustal and mantle-derived melts, including Late Ordovician high K (shoshonitic) monzonites and related volcanics that contain major gold and copper deposits in central New South Wales.

In the eastern belt of the Lachlan Orogen, velocity models derived from a 1997 wide-angle seismic profile and reflection profiling across the LTZ have identified significant sub-surface features within the upper and middle crust. These are interpreted to be associated with the Ordovician Macquarie Arc in the north and contrast with features under the Ordovician turbidites and Early Devonian granites to the south. They are inferred to be expressions of the LTZ and related structures in the middle and lower crusts and indicate the lithospheric nature of its character.

**JSA45** **Thursday 29 – Friday 30 July**

**EFFECTS OF SOLAR VARIABILITY, SOLAR WIND AND HIGH ENERGY PARTICLES ON THE MIDDLE ATMOSPHERE (IAGA, IAMAS, SCOSTEP)**

Location: School of Education G33 LT  
Location of Posters: School of Education, Conference Room

**Thursday 29 July AM**

Presiding Chairs: E.S. Kazimirovsky, Institute of Solar-Terrestrial Physics (ISTP), Irkutsk, Russia. B.A. Tinsley, University of Texas, Dallas

**Introduction** **0900**

E.S. Kazimirovsky

**JSA45/E/12-B4** **Invited** **0915**

**EFFECTS OF SOLAR PROTON EVENTS ON THE MIDDLE ATMOSPHERE**

CHARLES H. JACKMAN (Code 916, NASA Goddard Space Flight Center, Greenbelt, Maryland, 20771, U.S.A., email: jackman@assess.gsfc.nasa.gov) Eric L. Fleming (Steven Myers and Associates Corporation, Vienna, Virginia, 22180, U.S.A., email: fleming@kahuna.gsfc.nasa.gov)

Solar proton events (SPEs) can result in increases in both HO<sub>x</sub> (H, OH, HO<sub>2</sub>) and NO<sub>x</sub> (N, NO, NO<sub>2</sub>) constituents in the polar middle atmosphere. Decreases in mesospheric and upper stratospheric ozone caused by HO<sub>x</sub> constituents produced by SPEs have been observed during several events, however, ozone levels generally recover within a few hours after the end of these events because of the short lifetime of the HO<sub>x</sub> species. The NO<sub>x</sub> species feed into the more inclusive odd nitrogen family, NO<sub>y</sub> (N, NO, NO<sub>2</sub>, NO<sub>3</sub>, N<sub>2</sub>O<sub>5</sub>, HNO<sub>3</sub>, HNO<sub>4</sub>, ClONO<sub>2</sub>), over a period of hours to weeks. In low sun and lower altitude conditions, the NO<sub>y</sub> family lasts several months or more in the stratosphere causing prolonged ozone changes over these longer periods. Observations of mesospheric winds during and after SPEs have also indicated some variations as a result of these atmospheric perturbations. An overview of the influence of SPEs on the polar neutral middle atmosphere will be presented in this paper.

**JSA45/E/07-B4** **0945**

**THE LATITUDE EXTENT OF SOLAR PROTON FLUX FROM THE POLAR REGIONS DURING QUIESCENT AND DISTURBED GEOMAGNETIC CONDITIONS**

M.A. SHEA and D.F. Smart (Air Force Research Laboratory, VSBS, 29 Randolph Road, Hanscom AFB, Bedford, MA 01731-3010, U.S.A., email: shea@ph.af.mil)

The extent of most solar proton events is limited to the region of the polar cap above a corrected magnetic latitude of 60 degrees (i.e. quiescent magnetic field L values greater than -4). Approximately 15 percent of the proton events each solar cycle contain protons with energies in excess of 500 MeV which make transient contributions to mid latitude regions. However, during magnetic activity, the polar cap expands equatorward. The combination of a fast interplanetary shock and enhanced geomagnetic activity is the condition for very large solar proton fluence with a distribution of the flux to surprisingly low latitudes. For example, during the October 1989 solar proton event and major geomagnetic disturbance we compute there was a significant flux of protons down to a geographic latitude of ~37 degrees. The cutoff boundaries are surprisingly sharp in the energy range of 30 to several hundred MeV.

**JSA45/E/13-B4** **Invited** **1005**

**SOLAR WIND AND ENERGETIC ELECTRON PRECIPITATION VARIATIONS: EFFECTS ON THE MIDDLE ATMOSPHERE**

LINWOOD B. CALLIS (Atmospheric Sciences Division, NASA Langley Research Center, Hampton, VA 23681-0001, e-mail: lbc@jaguar.larc.nasa.gov)

A solar-atmospheric coupling by electrons (SOLACE) precipitating into the atmosphere which affects global ozone has been reported. This coupling, and the findings required for the confirmation of this coupling, are described. Observations of the solar wind, precipitating electron fluxes, nitric oxide in the thermosphere and mesosphere, and nitrogen dioxide measurements in the lower mesosphere and upper stratosphere confirm the existence of this solar-terrestrial coupling mechanism which is shown to be important to the odd nitrogen budget of the lower thermosphere and the mesosphere. Two-dimensional chemical transport simulations from 1979 through 1987 including a typical trace gas scenario, UV flux variations, and the effects of energetic electron precipitation (EEP) have been carried out to assess the importance of these effects on stratospheric ozone and odd nitrogen. Results indicate that the effects of EEP on ozone extend to the middle latitudes and are comparable to those due to solar UV variations but have significantly different latitudinal distributions of the ozone depletions. Satellite observations of trace species throughout the stratosphere and published three-dimensional tracer simulations, provide evidence for the dispersion to lower latitudes of the odd nitrogen formed by the electrons in the mesosphere and descending into the stratosphere during the late fall, winter, and early spring. The implications of these findings are discussed.

**JSA45/W/05-B4** **Invited** **1055**

**THE INFLUENCE OF AURORAL AND PHOTOELECTRONS ON ODD-NITROGEN, ODD-HYDROGEN AND OZONE IN THE MIDDLE ATMOSPHERE**

Guy P. Brasseur and Rashid Koshravi (both at the National Center for Atmospheric Research, Boulder, Colorado, 80303, USA, email: brasseur@ucar.edu)

SOCRATES, a two-dimensional model of the atmosphere extending from the surface to 120 km altitude has been used to assess the response of the mesosphere and stratosphere to the precipitation of auroral and photoelectrons. This response will be compared to the impact of solar variability on the middle atmosphere, and to the perturbations caused by the release in the atmosphere of anthropogenic chemical compounds.

**JSA45/E/10-B4 1125****MAGNETOSPHERE-THERMOSPHERE COUPLING: COMPARISON OF MEASUREMENTS OF ELECTRON FLUXES IN THE MAGNETOSPHERE AND NITRIC OXIDE IN THE THERMOSPHERE**

D.N. BAKER, C.A. Barth, and S.C. Solomon (Laboratory for Atmospheric and Space Physics, University of Colorado, Campus Box 590, Boulder, Colorado, 80309-0590, USA, e-mail: baker@lynx.colorado.edu); S.M. Bailey (CES, Hampton University, Hampton, VA 23668); S.G. Kanekal (Goddard Space Flight Center, Greenbelt, MD 20771); G.M. Mason (University of Maryland, College Park, MD 20742)

Simultaneous measurements have been made of electrons in several energy ranges (>25keV, >0.4MeV, >1 MeV, 2-6 MeV) with the SAMPEX spacecraft and of nitric oxide density in the lower thermosphere by the SNOE spacecraft for the period March 11, 1998 to December 31, 1998. Comparison of the observations show that during periods of geomagnetic storms, the electron fluxes increase and move to lower L-shells. In response, the nitric oxide density in the auroral region increases and the auroral boundary moves equatorward. These coordinated measurements help to clarify an important solar-terrestrial coupling process.

**JSA45/W/13-B4 1145****THE DEPENDENCE OF JOULE HEATING ON THE SOLAR WIND-MAGNETOSPHERE COUPLING FUNCTION DURING MAGNETIC STORMS**

Ms HUIXIN LIU

By using EISCAT data, Joule heating rates in the auroral ionosphere during different storm events are calculated. The correspondent solar wind-magnetosphere coupling functions,  $\epsilon$ , are derived from IMP8 and WIND satellite data. Through cross-correlation analysis certain relationship is found between the auroral ionospheric Joule heating rate and  $\epsilon$ . And its dependences on solar cycle, season, geomagnetic activities are also presented.

**JSA45/L/03-B4 1205****CHANGES IN ATMOSPHERIC OZONE...**

KASATKINA

Abstract not available at time of going to press

**JSA45/L/04-B4 1225****BEHAVIOUR OF THE DISTRIBUTION...**

SEMENOV

Abstract not available at time of going to press

**Thursday 29 July PM**

Presiding Chairs: C.H. Jackman, NASA Goddard Space Flight Centre, Maryland, USA  
O. Troshichev, Arctic and Antarctic Research Inst. St. Petersburg, Russia

**JSA45/W/03-B4 Invited 1400****THE EFFECTS OF THE VARIABLE SOLAR WIND ON THE GLOBAL ELECTRIC CIRCUIT**

Brian A. TINSLEY, (University of Texas at Dallas, Richardson, TX 75083-0688 USA, e-mail: Tinsley@UTDallas.edu).

The global electric circuit links the troposphere, middle atmosphere, and ionosphere, and the distribution of current density in any one region responds to changes in properties of any of the others. We review models of the global circuit, and of effects on the latitude distribution of ionosphere-earth current density  $J_z$ , due to:

- (1) Changes in the cosmic ray energy spectrum and flux
- (2) Solar proton events
- (3) Changes in polar cap ionospheric potential
- (4) Changes in relativistic electron precipitation (REP) from the magnetosphere. The changes in conductivity in the stratosphere induced by REP and associated Bremsstrahlung X rays can extend down to 35 km. If the stratosphere has been pre-conditioned to a sufficiently low value of conductivity by H<sub>2</sub>SO<sub>4</sub> aerosols and vapor from volcanic injections then the modulation of this conductivity by REP can modulate the vertical column impedance sufficiently to modulate  $J_z$ . Observational data on all four modulations of the latitude distribution of  $J_z$  are sparse and noisy, but consistent with theory. Given that such changes can affect cloud microphysics (as discussed in my paper in JSA16), correlations of atmospheric temperature and dynamics with  $J_z$  and with solar activity can be explained.

**JSA45/W/11-B4 1430****VARIABILITY OF COSMIC RAY FLUXES TO THE EARTH ATMOSPHERE AND CLIMATE CHANGE**

Joan Feynman and Alexander RUZMAIKIN (Jet Propulsion Laboratory, California Institute of Technology, 4800 Oak Grove Dr., Pasadena, CA 91109, USA, email: aruzmaikin@jplsp.jpl.nasa.gov)

High energy cosmic rays may influence the formation of clouds, and thus can have an impact on weather and climate. Cosmic rays in the solar wind are incident on the magnetosphere boundary and are then transmitted through the magnetosphere and atmosphere to reach the upper troposphere. The flux to the troposphere will depend both on the intensity and spectrum of the cosmic rays at the outer boundary of the magnetosphere (magnetopause) and on the configuration of the magnetosphere through which they propagate. Both the incident flux and the magnetospheric transmission have changed systematically during this century due to systematic changes in the solar wind. We show that, early in the century the region of the troposphere open to cosmic ray precipitation was usually confined to a relatively small high-latitude region. As the century progressed there was a systematic increase in the size of this region by over 7 degrees. We suggest that these changes contributed to climate change during the last 100 years.

**JSA45/W/18-B4 1450****INFLUENCE OF FORBUSH DECREASE OF GALACTIC COSMIC RAYS ON ATMOSPHERIC CHARACTERISTICS IN ANTARCTICA**

Larisa Egorova, Valery Vovk and Oleg TROSHICHEV (all at Arctic and Antarctic Research Institute, St.Petersburg, 199397, Russia, email: olegtro@aari.nw.ru)

Relationship between variations of the galactic cosmic rays (GCR) and behavior of atmospheric pressure, temperature and wind speed observed in the region of Antarctic plateau (Vostok station), has been studied for solar cycle 1981-1991. 52 events of Forbush decrease in GCR observed in winter seasons when the solar radiation above Vostok station is absent have been chosen for analysis. It is shown that Forbush decreases affect the temperature profiles at altitudes 0-20 km, the temperature being increased up to maximum (20%) in the near-ground layer (0-3 km). There is a stable correlation between energetic (1-10 GeV) proton flows and variations in tropospheric and near-ground atmospheric pressures, the time delay (0-5 days) being depended on type of solar flare and course of the pressure change before the solar flare. The Ground Level Event in the solar protons led to 2-3 % growth in the atmospheric pressure at altitudes 0-15 km, whereas Forbush decrease produce a 2-8 % reduction in the pressure, the extent of pressure variations at altitudes 10-15 km being much more than that in the near-ground layer. In case of powerful Forbush decreases (20 events) the pressure reduction started simultaneously with decrease in GCR or one day later. In case of less power Forbush decreases the time delay is more, the maximum delay (up to 6 days) being observed when GCR variations occur against the background of the pressure growth. The temperature and pressure differences give rise to changes in a direction of winds observed above Vostok in connection with Forbush decreases. Results of investigation imply that connection between the above mentioned processes is explained by changing of the atmospheric transparency owing to formation of ice particles and small atmospheric components.

**JSA45/E/16-B4 1510****ENERGETIC ELECTRONS AND THEIR EFFECTS ON STRATOSPHERIC AND MESOSPHERIC OZONE IN MAY 1992 AND BEYOND**

W. Dean PESNELL (Nomad Research, Inc., Bowie, MD 20716, USA, email: pesnell@NomadResearch.com) Richard A. Goldberg (NASA Goddard Space Flight Center, Laboratory for Extraterrestrial Physics, Code 690, Greenbelt, MD 20771, USA, email: goldberg@nssdca.gsfc.nasa.gov) David L. Chenette and Edward E. Gaines (both at Research and Development Division, Lockheed Martin, Palo Alto, CA 94304, USA, email: chenette@spasci.com, gaines@spasci.com) Charles H. Jackman (NASA Goddard Space Flight Center, Laboratory for Atmospheres, Code 916, Greenbelt, MD 20771, USA, email: jackman@assess.gsfc.nasa.gov)

The increased fluxes of precipitating energetic electrons ( $E > 1$  MeV) during highly relativistic electron events (HREs) produce ion concentrations in the upper stratosphere and lower mesosphere that exceed the background concentrations. Coupled ion-neutral chemistry models predict that this increased ionization should drive HO<sub>x</sub> reactions and deplete mesospheric ozone by up to 30%. As HREs are more intense and more frequent during solar minimum than maximum, it was also predicted that mesospheric ozone would show long-term effects as a result of these events. To calibrate the effect HREs have on mesospheric ozone, we have studied the May 1992 HRE with several instruments on the UARS. Electron fluxes measured with HEPs give the duration and spatial coverage of the HRE. Ozone data from MLS, CLAES, and HRDI were examined for the chemical signature of the HRE, ozone depletions within the magnetic L-shell limits of  $3 < L < 4$ .

Using the multiple viewing angles of HRDI, we compare mesospheric ozone at similar local solar times before, during, and after the HRE. This removes some of the ambiguity caused by progressive sampling of the diurnal cycle over a yaw cycle of the satellite. Our analysis shows that between altitudes of 55-75 km the ozone mixing ratio is not affected by the particles at the signal-to-noise level of the data. Extrapolating our results to solar timescales requires allowing for the seasonal dependence of water vapor, as well as the occurrence rate, geographic coverage and duration of HREs. Detecting a long-term trend in the ozone driven by precipitating electrons appears to require a substantial increase in the signal-to-noise ratio of the satellite measurements.

**JSA45/W/19-B4 1550****THE SOLAR WIND INFLUENCE ON THE THERMAL REGIME OF THE MIDDLE ATMOSPHERE AT DIFFERENT LATITUDES**

Ludmila MAKAROVA and Alexander Shirochikov (both at Arctic and Antarctic Research Institute, St.-Petersburg, 199397 Russia, e-mail: shirmak@aari.nw.ru)

The reliable evidences are presented which demonstrate that the energetic balance of the middle atmosphere must include energy of the solar wind that under definite conditions can play important role in determination of the middle atmosphere thermal regime. The experimental data used for this study include results of the rocket and balloon measurements performed by the Russian scientists for many years at various polar and midlatitudinal observatories. The measured atmospheric parameters were compared with the concurrent values of the solar wind density ( $n$ ) and its dynamic pressure ( $P_{sw} = m n V^2$ , where  $m$  - proton mass,  $n$  and  $V$  - the solar wind density and velocity, respectively). The solar wind parameters determine value of subsolar distance between the Earth's magnetosphere magnetopause and the Earth. The latter parameter seems to be the universal geophysical index directly proportional to the amount of the solar wind energy transferred into the near - Earth space including the atmosphere. This study reveal a high degree of correlation between the solar wind dynamic pressure and/or the magnetopause position and the following atmospheric processes: a) variability of the thermal regime of the middle atmosphere, b) occurrence of the sudden stratospheric warmings, c) violation of the regular regime of circulation in the middle atmosphere, d) ozone density at definite stratospheric altitudes, e) temperature gradient in the tropopause. These connections are more evident in winter (when UV radiation is weak) and under Eastern QBO orientation. It is noteworthy that the influence of the solar wind on the atmospheric processes has a global scale. A probable physical mechanism responsible for these processes is a version of the global electric circuit with the magnetopause as the external element of this circuit.



JSA45/W/12-B4 1620

Presiding Chair: M.A. Shea, Air Force Research Laboratory, Bedford, USA

## LONG-TERM EFFECTS OF THE VARIABILITY OF SOLAR UV RADIATION ON THE ION CHEMISTRY OF THE MIDDLE ATMOSPHERE

Thomas Ulich<sup>1</sup>, Esa Turunen<sup>1</sup>, Pekka Verronen<sup>2</sup>, Erkki Kyrölä<sup>2</sup> 1Sodankylä Geophysical Observatory, FIN-99600 Sodankylä, Finland; 2Finnish Meteorological Institute, Geophysical Research, P.O.Box 503, FIN-00101, Helsinki, Finland

The solar UV radiation is the main ionising factor in the day-time upper mesosphere during quiet geophysical conditions. The UV radiation varies with the solar activity cycle. This variation is much stronger than the variability of the total solar irradiance or the variability of visible light. We use the detailed 55-ion Sodankylä Ion Chemistry (SIC) model in order to study the effects of changing UV input to the atmosphere. Using available UV data and models as input in the calculation of the ionisation balance, we compare the model results both with long-term data sets from ground based instruments, and with available satellite data.

JSA45/E/02-B4 Invited 1640

## GEOMAGNETIC STORM IMPACT ON ATMOSPHERIC OZONE LAYER

Jan LASTOVICKA (Institute of Atmospheric Physics, Bocni II, 141 31 Prague 4, Czech Republic, email: jla@ufa.cas.cz)

A brief review of effects of strong geomagnetic storms on total ozone content, targeted to effects observed near the latitudinal circle of 50oN, shows that at these latitudes geomagnetic-storm related changes in total ozone can very probably be attributed to storm-related changes in atmospheric circulation. Both ground-based and TOMS data are used. Significant effects of geomagnetic storms on total ozone have been observed only in winter and for strong storms, Ap > 40 or better 60, and only under very specific conditions - high solar activity and the east phase of QBO. This means that it is rather rare effects, as shown by an analysis of data over 1963-1995. The observed effects consist in redistribution of ozone, not in ozone production or loss, which again point out to their dyn origin. They are developed best in the European/North-Eastern Atlantic and East Siberian/Aleutian sectors and invisible in latitudinal average values. In European sector, the effect consists in a significant increase of total ozone with and just after the storm. Overall, the effect at 50oN appears as substantial diminishing of longitudinal variation along this latitudinal circle. The effect of geomagnetic storms is pronounced at 50oN, absent at 40oN (too low latitude), and it does not occur in a systematic manner also along the 60oN latitudinal circle.

No detectable effects of geomagnetic storms on laminae (narrow layers of substantially enhanced ozone concentration) in ozone profiles are found in data from several analyzed ozonesounding stations, even though laminae are generally sensitive to various influences. The effects of geomagnetic storms in circulation in the European/North-Eastern Atlantic area do not support meridional circulation and, therefore, contrary to total ozone no increase in laminae is observed.

JSA45/L/01-B4 Invited 1710

## EFFECTS OF SOLAR CYCLE ULTRAVIOLET VARIATIONS ON OZONE

Lon Hood (Lunar and Planetary Laboratory, University of Arizona, Tucson, Arizona 85721, USA, email: lon@lpl.arizona.edu)

At wavelengths where photo dissociation of molecular oxygen is important in the upper stratosphere, solar spectral irradiance changes from solar minimum to maximum are substantial (~6% at 205 nm). Current two-dimensional chemical/dynamical models predict corresponding changes in ozone of several per cent with maximum amplitude in the middle stratosphere (3--5 mb). However, observations based on satellite measurements since 1979 indicate a solar cycle variation of ozone with maximum amplitude of 4--6% in the upper stratosphere (1--2 mb). The observed solar cycle ozone change approaches zero in the middle stratosphere (4--10 mb) and then increases again in the lower stratosphere. The most probable explanation for the disagreement between observations and models is transport effects on ozone or other species (e.g., methane) that are not included in 2-D models.

In addition to the upper stratospheric ozone variation, a change in total ozone from solar minimum to maximum is observed with global mean amplitude of 1.5--2.0%. According to SBUV-SBUV/2 data, most (about 85%) of this variation occurs in the lower stratosphere (altitudes < 28 km) where 2-D models predict only a small photochemical ozone response. The observed lower stratospheric ozone variation therefore appears to be driven by circulation changes between solar minimum and maximum. These circulation changes are probably associated with the observed quasi-decadal oscillation originally reported by K. Labitzke and H. van Loon. Recent work by S. Chandra and co-workers indicates evidence for changes in tropospheric ozone in the tropics that are out of phase with stratospheric ozone changes on a time scale of a solar cycle. This would imply that the lower stratospheric ozone variation is somewhat larger than previously estimated.

JSA45/E/01-B4 1740

## 11-Y SOLAR MODULATION OF THE INFLUENCE OF THE EQUATORIAL QBO ON TOTAL OZONE AND STRATOSPHERIC CIRCULATION OVER NORTHERN EUROPE

Boris SOUKHAREV (Department of Climatology, St.Petersburg State University, 10 linia, 33, 199178, St.Petersburg, Russia, email: boris@seb.usp.ru)

The monthly mean data of total ozone over Northern Europe and indices of stratospheric circulation at 30 hPa (Cne) over the region for the months from January to March for the period 1957-1996 are used in order to show that the 11-y solar cycle can be a modulator of the remote influence of the equatorial QBO on the interannual variability of ozone and stratospheric dynamics over polar region. Method of the running correlation between the total ozone (and indices Cne) and the equatorial stratospheric zonal wind demonstrates clear modulation of an 11-y solar signal for February and March. The curves of the running correlations show that a sign of correlation between the equatorial stratospheric zonal wind and the studied parameters changes in dependence on solar activity.

Special statistical procedure has been used for the demodulation of an 11-year solar signal from the time-series of ozone and indices Cne. The obtained solar signal which is in phase with the solar cycle, is most clear for February and March. Using the same procedure, an attempt to retrieve the February - March time-series of total ozone and Cne from the data of equatorial zonal wind and 10.7 cm solar radio flux has been made. Correlation coefficients between the retrieved and initial ozone and Cne data for February are about  $r = 0,80$  in the periods of solar extrema. Thus, the present study shows that the most part of the interannual variability of total ozone and stratospheric dynamics over Northern Europe in February - March can be expressed as a product of interaction between the 11-y solar cycle and the equatorial QBO.

JSA45/E/04-B5 Invited 0830

## ARE THERE SOLAR SIGNALS FROM THE MIDDLE ATMOSPHERE IN THE POLAR ICE?

Gisela A. M. DRESCHHOFF (Space Technology Center, University of Kansas, Lawrence, KS 66045, USA) M.A. Shea and D.F. Smart (both at Space Effects Division, Geophysics Directorate/PL, Hanscom AFB, Bedford, MA 01731, USA) K.G. McCracken (Jellora Technologies, Mittagong, NSW, Australia)

Ultra-high resolution measurements of nitrate concentrations in snow and ice from both polar regions revealed the superposition of a number of components such as seasonal variations and longer-term trends. Part of this signal has been interpreted as having been produced in the auroral zone by ionization and modulated by the solar activity cycle. In addition, the fine structure of the nitrate signal reveals the stratospheric ionization effects of large solar proton events such as the solar flare of 1972, which produce distinct pulses of nitrate anomalies that are recognizable over wide areas of the Antarctic and the central Greenland ice sheets. For this reason, local and regional meteorological influences have been effectively eliminated. The presence of such nitrate anomalies retained in the stratigraphy of the continental ice sheets, remains a challenge for model calculations and the parameterization used to represent the chemical and dynamical processes operating at the high magnetic latitudes.

This paper presents a discussion of indirect observations of energetic particle injections into the polar atmosphere, including the frequency of impulsive nitrate events, a quantitative estimate of nitrate production by solar protons, a comparison with the cosmic ray record, and the occurrence of large solar proton events during the time interval 1576-1990.

JSA45/W/10-B5 0900

## SOLAR CYCLE DEPENDENCE OF MIDLATITUDE MESOPAUSE REGION WINDS AND WAVES

Christoph JACOBI and Martin Lange (Institute for Meteorology, University of Leipzig, Germany, email: jacobi@rz.uni-leipzig.de)

Long-term measurements of mesopause region winds performed at Collm, Germany, show a 11-year solar cycle dependence of the of the zonal prevailing wind, so that during solar maximum the spring and summer easterlies in the upper mesosphere are stronger than during solar minimum. The measurements are presented in comparison with model results. The changes of the mean circulation influences the conditions for the excitation of the 2-day wave, so that during solar maximum the quasi 2-day wave is stronger than during solar minimum.

JSA45/L/02-B5 Invited 0920

## AN ADJOINT METHOD OF CALCULATION OF ENERGETIC SOLAR-PARTICLE-EVENT EFFECTS ON THE EARTH'S ATMOSPHERE

K. O'Brien (Northern Arizona University, Flagstaff, AZ 86011 USA), Herbert H. Sauer (CIRES, University of Colorado, Boulder, CO 80303, USA; NOAA Space Environment Center, Boulder, CO 80303, USA)

High energy solar particles, produced in association with solar flares and coronal mass ejections, occasionally bombard the earth's atmosphere, resulting in radiation intensities additional to the already-present cosmic-ray dose rates. Access of these particles to the earth's vicinity during times of geomagnetic disturbance are not adequately described by using static geomagnetic field models. These solar fluxes are also often distributed non-uniformly in space, so that fluxes measured by satellites obtained at great distances from the earth and which sample large volumes of space around the earth cannot be used to predict fluxes locally at the earth's surface. We present here a method which uses the ground-level neutron monitor counting rates as adjoint sources of the flux in the atmosphere immediately above them to obtain solar-particle dose rates as a function of position over the earth's surface. We have applied this approach to the large September 29-30, 1989 event (GLE 42) to obtain the magnitude and distribution of the dose rates from an atypically large event. This approach could easily be adapted to the calculation of other atmospheric quantities of interest, such as ionization and energetic primary and secondary particle fluxes.

JSA45/W/16-B5 0950

## THE ROLE OF PLANETARY WAVE PROPAGATION IN COUPLING THE MIDDLE AND UPPER ATMOSPHERES THROUGH A SOLAR CYCLE

Neil ARNOLD and Terry Robinson (both at the Department of Physics and Astronomy, Leicester, LE1 7RH, UK, email: nfa1@ion.le.ac.uk)

A new three-dimensional model of the middle and upper atmosphere between ~10-350km has been constructed to study the dynamical coupling between the two regions. In addition to more sophisticated radiative transfer calculations in the thermosphere and a better representation of ion drag, a three-dimensional diabatic heating scheme was adopted in the middle atmosphere for the first time. Previously reported results using a simplified upper atmosphere had indicated that there could be significant coupling in the winter hemisphere, especially during warming events, that varied according to solar flux levels. These simulations have been repeated under a range of different initial and boundary conditions using the improved version of the model and the preliminary results compared. Possible implications for the climate of the middle atmosphere will be discussed.

JSA45/E/09-B5 1010

## OZONE RESPONSE AFTER SOLAR PROTON EVENTS IN 1997-1998

Alexei KRIVOLUTSKY, Aleksand Kuminov, Alexandr Repnev (all at Central Aerological Observatory, Pervomayskaya Str.3, Dolgoprudny 141700, Moscow Region, Russia, email: alkriv@mycomp.netclub.ru) Nina Perejaslova and Margarita Nazarova (both Institute of Applied Geophysics, Moscow, Russia)

Solar Proton Events (SPEs) in 1997 and 1998 as a cause of chemical species perturbations in the middle atmosphere has been investigated using numerical photochemical model and energy spectrum of the solar proton fluxes measured by Russian satellite system "Meteor" which has polar orbits with usual inclination about 80-82 degrees. SPE which was in November 1997 was the first event after the solar minimum looked like the manifestation of a new solar cycle growth. Model calculations has been accompanied by UARS data analysis (MLS instrument) at high latitudes of the Southern Hemisphere during November 1997 at 20-80 km range of altitudes. Energy differential spectrum of solar protons was used to calculate a correspondent ionization rates in the middle atmosphere after SPEs. This ionization in accordance to the theory leads to the NO<sub>x</sub> and HO<sub>x</sub> production and disturbs neutral chemical

system of the atmosphere including ozone.

Model calculations has shown short-term negative ozone response in the mesosphere (with increased HOX content) and long-term response in the stratosphere accompanied by increased NOX content.

JSA45/E/11-B5

1030

#### EFFECTS OF TIME VARIABLE SOLAR RADIATION ON THE MIDDLE ATMOSPHERE DYNAMICS

FAHRUTDINOVA A.N., Guryanov V.V., Berdunov N.V., Zaitcev A.V., Fedorov D.V. (Kazan State University, Kazan 42008, Russia, email: Antonina.Fahrutdinova@ksu.ru)

The investigation of effects of time variations of solar radiation in dynamics of middle atmosphere have been conducted by long series of measurements, made by radiometer method within the height interval 80-110 km at Kazan University radiostation (56 N, 49 E) during the period 1986-1995 and by the time series of Katz indexes in Atlantic-European sector at latitude zone 50-70 N for the period 1977-1990. The correlation coefficients of interannual variations of solar radiation and the following dynamics parameters: mean annual values, amplitudes of annual and semiannual oscillations of zonal wind within the height interval 80-110 km, and also mean annual values, amplitudes of annual and semiannual oscillations of Katz indexes at 6 levels within the height interval 0-30 km. It has been found that the level of connection and the sign of correlation are changing depending on the interval of heights of middle atmosphere and the dynamic parameters.

JSA45/E/17-B5

Poster

1110-01

#### THE GLOBAL ATMOSPHERIC-ELECTRICAL CIRCUIT, MESOSPHERIC ELECTRICAL PHENOMENA, AND PARTICLE PRECIPITATION - VOLCANOES LIKE LIGHTNING RODS

C. Bellecci (II Università di Roma, Tor Vergata, Roma, Italy); C. Bianchi, G. de Franceschi, G. di Stefano, G. Romeo, C. Scotto, Q. Taccetti, and B. Zolesi (ING, Roma, Italy); G. M. Crisci (UNICAL, Arcavacata di Rende, Cosenza, Italy); G. P. Gregori (IFA-CNR, via Fosso del Cavaliere 100, 00133 Roma, Italy; e-mail: gregori@atmos.ifa.rm.cnr.it); I. Marson (Università di Trieste, Italy); and G. Paparo (IDAC-CNR, Roma, Italy)

The interpretation appears difficult of several phenomena, such as e.g. the positive charge of the ionosphere, domes of light, noctilucent clouds, elves, sprites, blue rays, lightnings within volcanic plumes, earthquake lights, geo-e.m. earthquake precursors (within either ground, or the ionosphere, or airglow), limb-scanning of the step-like airglow discontinuities and their relation with the South-American anomaly, etc. All such items envisage that some relevant bias forbids a satisfactory assessment of the global atmospheric-electrical circuit. Perhaps, one related key-aspect is concerned with the total Coulomb charge of the precipitating particles over the atmosphere. In fact, until the late '60's they were generally believed to be strictly neutral. Later on, the spectroscopic evidence by polar auroras showed that proton auroras are observed within one large sector of the sky of a given station, while electron auroras are displayed in the remaining part of the sky. Hence, the supposed Coulomb neutrality is achieved only when integrating over a large area. The concern remains about the eventual deviation in time of Coulomb neutrality, and on the time range needed for average neutrality (either seconds, or solar cycle, or else). How could such a feature be observed? Has it ever been discussed? An experiment on the volcanic island of Stromboli is supposed to investigate the electrical relations between volcanic explosions, their Coulomb charge, lightnings, and related ionospheric disturbances. Similar unknown effects could exist over anomalous geothermal areas, etc. High time-resolution ionosondes ought to be collected.

JSA45/E/05-B5

Invited

1110-02

#### HF DOPPLER OBSERVATIONS OF LOWER IONOSPHERE IN SOLAR PROTON EVENTS

Takumi ICHINOSE, Nobuyuki Nakai and Tatehisa Ohta (Department of Electronics, Doshisha University, Kyotanabe, Kyoto 610-0321, Japan, email: tichinos@mail.doshisha.ac.jp) Toru Ogawa (Nagareda, Kamitakano, Kyoto 606-0037, Japan, email: pxi03720@nifty.ne.jp)

Effects of the high-energy solar protons on the lower ionosphere at low magnetic latitude have been observed by the HF Doppler technique. The 5, 8 and 10 MHz standard frequency signals have been received with a horizontal distance of 390 km. The magnetic latitude of the reflection point is about 25 degrees. We analyzed this phenomenon in the last ten years and found its characteristics as follows.

(1) Classes of the solar X-ray flares are between M4 and X1. Because, smaller ones have not enough numbers of emitted particles and larger ones ionize lower E-region to generate fadeouts of the ionospheric propagation. (2) Mean velocity of the particles is larger than ten thousand km/s and it takes only a few hours from the Sun to the Earth. Because, it is necessary to have such high velocity to enter into the lower ionosphere at low-latitude. (3) These events started as a sharp positive pulse of the Doppler shifts that almost coincides with the beginning of the solar proton events observed by the GOES satellites. This pulse was followed by the medium scale TID's. These facts show that the solar protons ionize directly the low-latitude atmosphere, and cause the ionospheric disturbances.

JSA45/E/19-B5

Poster

1110-03

#### VARIATIONS IN THE INTERPLANETARY MAGNETIC FIELD SECTOR STRUCTURE AND QUASI 2-DAY WIND IN THE MIDDLE ATMOSPHERE AT ALTITUDES 80-105 KM

B.L.Kashcheyev, B.V.Kalchenko Kharkov (State Technical University of Radioelectronics)

The paper gives the description of basic results of joint measurements of drift of meteoric trails conducted in course of coordinated programme. The observations were made at different points of Earth during 1968-98. The statistic of measurements is big. In the series of meteor trails observations in the equatorial zone (2 N, 45 E) carried out in 1968-1970 in the meridional direction the 2-days periodicity drift amplitude predominated in 49,6% of cases, the diurnal periodicity amplitude predominated in 36,7% of cases and in semidiurnal periodicity amplitude predominated in 13,7% of cases. In the zonal direction these number were 26,0; 46,5 and 27,5 respectively. The connection of interplanetary magnetic field sector structure variations with quasi 2-day wind in the middle atmosphere at altitudes 80-105 km is discussed. The methods of data processing are discussed as well.

JSA45/W/01-B5

Poster

1110-04

#### THE SIGNAL OF SOLAR/GEOMAGNETIC VARIABILITY IN THE TOTAL OZONE

A.Yu.Belinskaya, Ed. KAZIMIROVSKY, G.K. Matafonov (Institute of Solar-Terrestrial Physics, Russian Academy of Sciences, P.O.Box 4026, 664033, Irkutsk, Russia, email: edkaz@iszf.irk.ru)

The East-Siberian region is the area of special interest for the total ozone content (TOC) variations due to climatic features and record low ozone values during some spring/winter periods. We believe that some part of TOC variability is closely connected with solar variability, solar wind, solar proton events, geomagnetic storms etc. We have tested the possible TOC response on the above mentioned external forcing, first of all for East Siberia and then for some different longitudes along midlatitude circles (database from TOMS, Nimbus-7, USA). We have demonstrated the possible response of TOC depending on solar cycle phases, QBO phases and longitude. We support the hypothesis of redistribution of ozone due to changes in the circulation pattern under external (solar/geomagnetic) forcing.

JSA45/L/05-B5

Poster

1110-05

#### EFFECT OF SOLAR VARIABILITY ON THE ELECTRON DENSITY SMALL SCALED SPECTRA IN THE MIDDLE ATMOSPHERE

Olga G. KHUTOROVA, Guerman M. Teptin (both radioastronomy dep., Physics fac., Kazan State University, 18, Kremlevskaya st., Kazan, Russia, 420008, e-mail: olga@erae.kazan.ru)

The model of electron density small scaled spectra depended on parameters of the middle atmosphere and the lower ionosphere was carried out. The empirical dependence of these parameters on the solar variability is used. The 27-day numerical variance of the electron density spectra are obtained for different heights (80-100 km).

JSA45/E/15-B5

Poster

1110-06

#### UNUSUAL CHANGES OF SOLAR DIURNAL VARIATIONS OF INTENSITY OF COSMIC RAY NEUTRON AND MESON COMPONENTS

Marina Despotashvili, Nugzar NACHKEBIA, Luli Shatashvili (Cosmic Ray Department, Institute of Geophysics, Georgian Academy of Sciences, 1, Aleksidze st., Tbilisi 380093, Georgia, e-mail: nugzar@geophy.acnet.ge; nachkebia@yahoo.com)

The abnormal cases solar diurnal anisotropy of intensity of Cosmic Ray (CR) neutron and meson components for 1976-1986 are considered. There were used, corrected for a barometric effect, hourly data of neutron monitors of stations Kiel and Tokyo, and meson data of surface station of Nagoya. After removal century trend there were calculated Fourier coefficients of the appropriate harmonics for each station. The cases, when value of amplitude solar diurnal anisotropy  $A > 2A_1$  ( $A_1$  is annual value) at least in three cases among the four following days by the data of any considered stations of CR, were studied. 28 cases of abnormal increase of solar diurnal anisotropy of CR intensity are revealed. From the observed events of abnormal increase of solar diurnal anisotropy ~ 40% of cases are unusual - with growing effective rigidity of primary particles amplitude of anisotropy does not decrease, but sometimes it is even increased. Approximately 90% of these cases are connected with sector structure of the interplanetary magnetic field. The appropriate interpretation is given.

JSA45/W/17-B5

Poster

1110-07

#### INFLUENCE OF SOLAR COSMIC RAYS HIGH ENERGY PROTON FLUXES ON THE OZONE DEPLETION DURING ANTARCTIC OZONE HOLE PERIOD

Valery Uljev, Igor Moskvina, Alexander SHIROCHCOV, Ludmila Makarova (all at Arctic and Antarctic Research Institute, Saint-Petersburg, 199397, Russia, e-mail: shirmak@aari.nw.ru)

A two-dimensional chemistry-transport model of polar stratosphere coupled with a model of the calculation of the ionization rate due to the solar cosmic ray (SCR) fluxes is used for study of influence of SCR proton flux of high energy ( $> 200$  MeV) on the ozone content at 15 - 20 km inside antarctic polar cap during August - October period. Two model experiments were performed: model flux was introduced into chemically quiet stratosphere and into chemically disturbed stratosphere simulating antarctic ozone hole. The model flux is that of 4 August 1972 SPE (15 UT) with the flux intensity at the energy  $> 200$  MeV multiplied by 1 - 20 times. In the first experiment no remarkable variation of ozone content was revealed at 15 - 20 km. In the second experiment it was revealed that the model SCR proton flux increases the ozone hole depletion by 5 - 80%. Therefore one can conclude that the impulsive SCR proton flux of high energy and intensity (e.g. during GLE) may decrease ozone content at 15 - 20 km only in chemically disturbed conditions caused in the low stratosphere by polar stratospheric clouds.

JSA45/E/06-B5

Poster

1110-08

#### THE INFLUENCE OF THE 11-Y SOLAR CYCLE ON THE INTERANNUAL VARIABILITY OF TOTAL OZONE OVER NORTHERN EUROPE IN WINTERTIME.

Boris SOUKHAREV (Department of Climatology, St.Petersburg State University, 10 linia, 33, 199178, St.Petersburg, Russia, email: boris@seb.usrpu.ru)

Based on the monthly mean data of total ozone from December till March for the period 1957-1996 for the eight stations of Northern Europe the influence of the 11-y solar cycle on the interannual variability of ozone over the region is investigated. Correlation between the monthly means of total ozone over the studied region and the values of 10,7 cm solar radio flux does not show evident relationship. However, the same analysis conducted on the condition that the data are grouped according to the westerly (W) and easterly (E) phases of the equatorial stratospheric quasi-biennial oscillation (QBO) shows clear positive correlation during the W phase and negative one during the E phase of the QBO. The highest connections are revealed for February ( $r = 0,71$  and  $r = -0,63$  for the W and E QBO phases respectively). It is found that the solar/ozone correlations are much stronger in the periods of solar extrema (peaks and hollows of 11-year solar cycle) than in the periods of transition between solar extremes. Correlation coefficients for February during the periods of solar extrema are  $r = 0,77$  (-0,72) in the W (E) phases while during the transitional periods the coefficients are  $r = -0,58$  (-0,28) in the W (E) phases. The differences E-W between the monthly means of ozone over the region during the E and W QBO phases are about E-W = -30 DU, E-W = 61 DU and E-W = 20 DU during the periods of solar maximum, minimum and transition respectively. Possible physical reasons of the variation of the ozone/QBO relationship on the 11-y solar cycle time scale are discussed.



**JSA45/W/02-B5** Poster **1110-09**

**A SIMPLE EMPIRICAL MODEL FOR GLOBAL DAMAGE UV-B IRRADIANCE**

Vasilyev V.I. (Institute of Experimental Meteorology SPA Typhoon, World Ozone Station 307, 249020 Obninsk, Kaluga Region, Lenin St. 82, Russia, email: iemvasilyev@netscape.net) Tikhonov V.N. (Russian Institute of Agricultural Radiology and Agroecology, 249020 Obninsk, Kaluga Region, Kiev highway 1, Russia, email: tikhon@obninsk.com) Brick N.V. (Biological Department Moscow State Lomonosov University, 119899 Moscow, Russia)

This paper presents first results on the possibility of the short-term forecasting and modelling of the global damage UV-B irradiance (DUV) reaching the ground. The simple mathematical model relating DUV irradiance with solar zenith angle (Za) has been built. The modelled data are based on the experimental measurements performed by Brewer #044 Mark II spectrophotometer at Obninsk (Russia, 55.12 N, 36.6 E) during 1997. Each UV-B global spectrum sampled by Brewer was integrated in the range 290-325 nm by standard DUV routine and compared with the corresponding output of the model which uses the following empirical relation:  $DUV = \exp\{A[\cos(Za)]^{(1/C)+B}\}$  It was found out that most experimental data obtained at the clear sky or direct sun exposures, being plotted in co-ordinates  $\ln(DUV)$  vs.  $[\cos(Za)]^{(1/C)}$ , often form one or two straight lines for each observed day: morning and/or afternoon fits. The best fits were obtained for  $C=2.5 \dots 3$  and statistical analysis indicates that the total amount of ozone has surprisingly little effect on the fitting coefficients A and B. But sum of them, that is  $\ln(DUV)$  for  $Za=0$ , depends on ozone layer thickness with the correlation coefficient being about -0.8. The obtained results may be useful for inter- and extrapolation, filtering and smoothing of experimental data, in procedures for the short-term UV Index forecasting: a few early morning measurements at Za about 80-85 degrees can predict all daily values of DUV with very good accuracy - for the clear sky conditions.

**JSA45/W/04-B5** Poster **1110-10**

**MODELING THE EFFECTS OF SOLAR PROTON EVENTS ON MIDDLE ATMOSPHERE**

Pekka VERRONEN and Erkki Kyrölä (Both at Finnish Meteorological Institute, Geophysical Research, P.O. Box 503, FIN-00101 Helsinki, Finland; email: pekka.verronen@fmi.fi) Esa Turunen and Thomas Ulich (Both at Sodankylä Geophysical Observatory, Tähteläntie 112, FIN-99600 Sodankylä, Finland; email: esa@sgo.fi)

The ionization by solar UV-radiation and energetic particle precipitation causes variation in upper atmosphere constituent concentrations. Ionization and chemical reactions lead to a production of odd nitrogen in the mesosphere, which in turn affects the ozone balance. Under polar night conditions the nitric oxides are long lived and may be carried down into the lower atmosphere, where they can participate in destruction of stratospheric ozone.

Three European satellite missions, Envisat-1, Ørsted, and Odin, will be launched in next two years. Together with the EISCAT incoherent scatter radars and a network of other ground measurements they will provide a so far unique possibility to address this scientific problem in the auroral region.

In order to establish the magnitude of the effects of proton events on middle atmosphere we have added relevant neutral chemistry into the SIC-model and modeled some proton events using a variety of available measurement data.

We will present our project, the latest development of our model, and the preliminary modeling studies.

**JSA45/E/03-B5** Poster **1110-11**

**SOLAR ULTRAVIOLET IRRADIANCE VARIATIONS FROM UARS SOLSTICE**

Thomas N. WOODS, Gary J. Rottman, Giuliana de Toma, Julius London, (all at Laboratory for Atmospheric and Space Physics, University of Colorado, 1234 Innovation Dr., Boulder, CO 80303, USA; e-mail: tom.woods@lasp.colorado.edu), and Dick White (High Altitude Observatory, National Center for Atmospheric Research, PO Box 3000, Boulder, CO 80307, USA)

The SOLAR Stellar Irradiance Comparison Experiment (SOLSTICE) on the Upper Atmosphere Research Satellite (UARS) has been making daily measurements of the solar ultraviolet (UV) irradiance since October 1991. The standard SOLSTICE solar UV irradiance data product covers the 119 to 420 nm range in 1 nm intervals. The solar UV radiation at the shorter wavelengths is deposited in Earth's middle atmosphere; whereas, the solar radiation at the longer UV wavelengths is deposited in the lower atmosphere and much reaches the surface for wavelengths above 320 nm. The solar UV radiation is an important source of energy for the middle atmosphere as well as the driver for the photochemistry in the middle atmosphere. The understanding of the variability of the solar UV irradiance is thus critical to fully understand the variability seen in the middle atmosphere. The variability of the solar UV irradiance is on all time scales with the 27-day solar rotation period and the 22-year solar magnetic cycle being the dominant variability seen in the SOLSTICE data. The longer wavelengths, above 260 nm, show the least amount of variability, 1% or less over the solar cycle. The shorter wavelengths show the most variability, as much as a factor of 2 for some of the solar far UV lines.

**JSS46** Thursday 29 July

**SEISMIC TOMOGRAPHY ON VOLCANOES AND VOLCANIC FIELDS (IASPEI, IAVCEI)**

Location: Medical School, WG11 LT5  
Location of Posters: Arthur Thompson Hall

Thursday 29 July AM

Presiding Chairs: Dr. G.R. Foulger (Univ. of Durham, Dept. Geological Sciences, UK), B.A. Chouet (U.S. Geological Survey, Menlo Park, CA, USA)

Concurrent Poster Session

**JSS46/W/19-B4** **0930**

**THE QUANTIFICATION OF MELT PROPERTIES WITHIN A MAGMA RESERVOIR**

Dr. Mark A.J. TAYLOR (Bullard Laboratories, University of Cambridge, email: taylor@esc.cam.ac.uk)

The quantification of melt properties within a magma reservoir is extremely important in predicting and monitoring of volcanic eruptions. The comparatively low rigidity of magma chambers beneath volcanoes and mid-ocean ridges results in a low-velocity zone. Seismic tomography can provide us information about the wave velocities, and also attenuation and anisotropy of these regions. Here we use effective medium theory to relate this information to, and place subsequent constraints on, the material properties and composition of such

magmatic bodies. Using a combination of the self consistent scheme [Hill, J. Mech. Phys. Solids, 1965, and Budiansky, J. Mech. Phys. Solid, 1965] and differential effective medium theory [Boucher, Rev. Metall., 1976 and McLaughlin, Int. J. Eng. Sci., 1977] in a similar way to Mainprice [Tectonophysics, 1997] we examine the effect of introducing inclusions of melt into a solid matrix on the elastic constants (and hence shear and compressional velocities), attenuation, and anisotropy of the resulting medium. We consider both a homogeneous distribution of spherical inclusions and either aligned or randomly oriented elliptical inclusions. The effect of assuming an isotropic or anisotropic background matrix material is also considered. From this we are able to place some bound on the melt fraction and possible microstructure of magma chambers that is consistent with parameters from seismic inversions. In particular we hope to apply this technique to the data from the 1996 and 1997 land and sea reflection surveys at Mount Vesuvius [Gasparini, EOS, 1998].

**JSS46/W/14-B4** **0950**

**P-WAVES TELESEISMIC VELOCITY TOMOGRAPHY OF THE HOGGAR SWELL (CENTRAL SAHARA, ALGERIA)**

Abdelhakim AYADI (Dept. E.S.S./C.R.A.A.G., BP 63 Bouzaréah 16340 Algiers, Algeria, email: ess1@ist.cerist.dz); Catherine Dorbath (E.O.S.T., 5, Rue René Descartes, F-67084 strasbourg Cédex, France e-mail: cath@mapu.u-strasbg.fr); Alain Lesquer (Centre de Geologie et de Geophysique, Université Montpellier II, e-mail: lesquer@dr13.cnrs.fr); Mourad Bezzegehoud (Deopt. de Fisica, Universidad de Evora, Apartado 94, 7001, Evora, Portugal, email: mourad@uevora.pt)

The Hoggar region is known as one of the important swell in the African continent. Its altitude is ranging from 500m to 2908m at Tahat hill (Atakior). The Hoggar massif and other uplifts (Air, Tibesti, Egheï, Darfur, Cameroon mount) form a system of domal uplifts with semilar scale, morphology and volcanic activity (Lesquer et al., 1988). The knowledge of the structure beneath the Hoggar swell will enable us to understand the origin of the formation of this massif. In order to get an image of the lithosphere in the region we have performed a teleseismic field experiment. This later has been fixed for 3-months, where 33 short-period seismic stations have been installed along a 700-km long NNW-SSE profile crossing the central Hoggar and extend to the In-salah Sahara basin. This P-wave teleseismic tomography, is the only one made on midplate swell in Africa. No similar studies have been found in the literature on the African swells, in order to compare the results especially the nearest one as Air or Tibesti. The high quality of the data recorded during this experiment, enable us to perform a velocity inversion. From various observations compiled with the tomographic results, we can say that the Hoggar swell appears to have an altered lithosphere characterised by a low density, which make the swell in isostatic equilibrium. This low-density body seems to be elongated in the EW direction. The NS structures identified by previous studies seems to have an influence on the distribution of the velocity perturbations. The 4.50° NS megafault and the In Ouzal fault system appeared as a predominant structure in the lithosphere. Northward, the heat flow anomaly in the Sahara basin, could have a mantle origin.

**JSS46/W/03-B4** **1010**

**THREE DIMENSIONAL STRUCTURE OF BANDAI VOLCANO, NORTH-EASTERN JAPAN, DERIVED FROM ARTIFICIAL SOURCE EXPERIMENT**

H. HAMAGUCHI, S. Ueki, S. Tanaka, T. Yamawaki (all at Research Center for Prediction of Earthquakes and Volcanic Eruptions, Graduate School of Science, Tohoku University, email: tanaka@aob.geophys.tohoku.ac.jp); Research Group for Seismic Exploration of Bandai Volcano

Ten universities in Japan and Japan Meteorological Agency jointly performed a seismic exploration with active sources in Bandai volcano to reveal three dimensional structure in October 1997. We installed 292 seismic stations with a short-period seismometer and a portable data logger in and around the volcano over the area of 20 x 15 km<sup>2</sup>. Spaces among stations are about 500 m on the volcano, and about 1 km around the volcano. Eight artificial sources were exploded with dynamite of which charge sizes were 100-250 kg. We have obtained successfully about 2300 travel times of the first motion from the experiment. The travel time data is inverted to obtain three dimensional structure of the volcano. We used the damped least squares for inversion and the pseudo-bending method for the ray trace originally programmed by Zhao et al. (1992). A grid size for inversion is 0.02<sub>r</sub> (nearly 2 km) for horizontal directions and 500 m for a vertical direction. An initial model is two-layered model with laterally varying thickness of the upper layer inferred from the time-term method. The r.m.s. travel time residual is reduced from 0.23 s at the initial model to 0.13 s at the final one. We performed a resolution test with checkerboard-pattern and find that the final model has a good resolution up to 2 km depth from the ground surface. The most characteristic feature of the internal structure of the volcano is extremely high velocity regions (velocity perturbation greater than 20 %) beneath the volcano. This indicates that the basement of the volcano is elevated. The secondary characteristic feature is an extremely low velocity region (velocity perturbation more than 20 %) under the eastern flank of the volcano. The low velocity region is found just under the crater of the volcano and is close to seismic absorption region discovered in a previous fan-shooting experiment by Ueki et al. (1990).

**JSS46/W/06-B4** Invited **1110**

**MONITORING VOLCANOES AND GEOTHERMAL SYSTEMS WITH SEISMIC TOMOGRAPHY.**

B.R. JULIAN (U.S. Geological Survey, 345 Middlefield Rd., Menlo Park, CA 94025, U.S.A., Email: julian@usgs.gov); G.R. Foulger (Dept. Geological Sciences, University of Durham, Durham, DH1 3LE, U.K., Email: g.r.foulger@durham.ac.uk)

Local-earthquake tomography has recently found negative Vp/Vs anomalies at several geothermal systems and volcanoes. At the Hengill-Grensdalur volcanic complex in southwest Iceland, which hosts a mixed-phase hydrothermal system, the shallow parts of the Vp/Vs anomaly underlie areas of surface hot springs, and the deeper parts converge spatially to a small region that is probably a heat source. The Geysers, in northern California, a "dry" steam reservoir, is marked by a strong (~9%) Vp/Vs anomaly that is becoming detectably stronger as steam is extracted for power generation. At Mammoth Mountain, in eastern California, a Vp/Vs anomaly occurs in an area that has experienced massive carbon dioxide emissions since about 1990. All these anomalies can be understood quantitatively using the theory of elasticity of fluid-saturated porous media. The Hengill-Grensdalur anomaly is somewhat too strong to be the effect of variations in only the pore-fluid compressibility, and requires in addition variations in the elasticity of the rock matrix, caused perhaps by hydrothermal alteration. Measurements on core samples from. The Geysers show an unusual increase in the rigidity modulus upon drying (the spaghetti effect), which accounts for much of the observed anomaly. Carbon dioxide is highly compressible even at low temperatures, and carbon dioxide flooding of petroleum reservoirs has been known to change seismic-wave speeds by as much as 10%. Thus a carbon dioxide body might plausibly cause the anomaly at Mammoth Mountain, although knowledge about structure there is currently inadequate to confirm this conjecture.



JSS46/W/04-B4

1130

**MONITORING RESERVOIR DEPLETION AT THE GEYSERS GEOTHERMAL AREA, CALIFORNIA, USING SEISMIC TOMOGRAPHY**

G.R. FOULGER (Dept. Geological Sciences, University of Durham, Durham, DH1 3LE, U.K., email: g.r.foulger@durham.ac.uk); B.R. Julian (U.S. Geological Survey, 345 Middlefield Rd., Menlo Park, CA 94025, U.S.A., email: julian@usgs.gov); R.C. GUNASEKERA (Dept. Geological Sciences, University of Durham, Durham, DH1 3LE, U.K., email: r.c.gunasekera@durham.ac.uk)

Two decades of industrial extraction of steam from The Geysers geothermal reservoir in northern California has caused substantial environmental changes there. These changes include the induction of continuous, small-magnitude earthquakes at a high rate and altering the seismic-wave speeds in the reservoir. The area is continuously monitored by a network of 22 seismic stations operated by the UNOCAL Corporation, whose kind release of the data we gratefully acknowledge. This is an ideal experimental setup for monitoring industrially induced changes in Earth structure using repeated local-earthquake tomography. We conducted tomographic inversions, using the method of Thurber and Eberhart-Phillips, for data from 1991 and 1994. The exploited steam reservoir is associated with a strong (~9%) negative Vp/Vs anomaly, which can be explained as the effect of compressible vapour-phase pore fluid and of drying out of the rock matrix as water flashed to steam during progressive reservoir depletion. Between 1991 and 1994, the magnitude of the Vp/Vs anomaly increased to about 13%, which is consistent with continued pressure reduction and flashing of pore water to steam. These results demonstrate that Vp/Vs tomography is potentially valuable for monitoring geothermal reservoir exploitation and environmental change. This work is continuing with inversions of data from 1993, 1996 and 1998.

JSS46/W/05-B4

Invited

1150

**HIGH-RESOLUTION TOMOGRAPHY OF KILAUEA CALDERA HAWAII**

P.B. DAWSON, B.A. Chouet (U.S. Geological Survey, 345 Middlefield Rd. MS910, Menlo Park, CA 94025, email: dawson@usgs.gov)

A high-resolution velocity model (0.5-km resolution) of the Kilauea caldera region is obtained by tomographic inversion of both first arrival times and S-wave arrival times. Data are from the permanent Hawaiian Volcano Observatory seismic network, a ten-station broadband seismic network, and a temporary array consisting of two concentric rings of stations with diameters of 2 and 4 km centered on the caldera. Between January 8 and February 9, 1996 all three arrays were operating with a total of 300 seismic components being recorded. A total of 4580 first arrivals and 2558 S-wave arrivals from 207 earthquakes were used in the inversion to obtain both the P-wave and Vp/Vs velocity structure of the caldera. Relatively low P-wave velocities are observed within the first km in the center of and along the southern boundary of the caldera, and near the Kilauea Iki Crater. High P-wave velocities are observed in the northeast and southern portions of the caldera and are attributed to ponded, cooled flows. Below this structure a low-velocity volume is imaged beneath the southern caldera and upper-east rift. The velocity contrast between this zone and the surrounding structure is about 10%. This feature persists to a depth of 3 km below sea level. The ratio Vp/Vs beneath the caldera block roughly mimics the P-wave structure and is anomalously high, with values over 2 to depths of 2 km below sea level. The primary difference between the two models is that the Vp/Vs model shows two distinct zones of high Vp/Vs. Below 2 km below sea level Vp/Vs decreases to more normal values near 1.8. The corresponding Poisson ratio is 0.33 in the upper 3 km and 0.25 below 2 km below sea level. The high value of the Poisson ratio in the upper 3 km is consistent with a hot volume which may contain a small fraction of melt. The large-scale features of the velocity structure imaged by high resolution tomography are consistent with results obtained from an earlier larger-scale (2 km resolution) tomographic image of Kilauea Volcano based on HVO network data.

JSS46/W/12-B4

1210

**IMAGING GAS BENEATH AN ACTIVE VOLCANO USING SEISMIC TOMOGRAPHY**

G.R. FOULGER (Dept. Geological Sciences, University of Durham, Durham, DH1 3LE, U.K., Email: g.r.foulger@durham.ac.uk); B.R. Julian, A.M. Pitt and D.P. Hill (All at U.S. Geological Survey, 345 Middlefield Rd., Menlo Park, CA 94025, U.S.A., Email: julian@usgs.gov)

Mammoth Mountain is a volcanic peak on the SW caldera rim of Long Valley, a large, active, silicic volcano in eastern California. It is the site of frequent earthquake swarms, long-period earthquakes and massive surface venting of volcanic carbon dioxide gas, which has killed extensive areas of forest. Local-earthquake tomography using data from 15 temporary stations deployed in 1989 reveals a substantial low-Vp/Vs anomaly in the upper three kilometers whose margins correspond closely to the area of carbon dioxide emission. A network of 14 seismometers was deployed in the area for 3 months in summer 1997, supplementing the 7 permanent stations operated by the U.S. Geological Survey, to gather data to repeat the tomographic inversion and constrain possible changes in the 8-year interim period. These experiments form part of the ongoing Long Valley monitoring project of the U.S. Geological Survey. An excellent set of earthquakes was recorded. Preliminary results of the repeat tomography will be presented.

JSS46/W/01-B4

1230

**P-WAVE ANISOTROPY, STRESS, AND CRACK DISTRIBUTION AT COSO GEOTHERMAL FIELD, CALIFORNIA**

Jonathan M. LEES, Huatao Wu (Dept of Geology and Geophysics, Yale University, New Haven, CT, 06511 email: lees@love.geology.yale.edu)

A new inversion method for P-wave anisotropy [Wu and Lees, GJI, 1999], has been applied to high-precision, microseismic travel-time data collected at Coso geothermal region, California. Direction-dependent P-wave velocity, and thus its perturbation, are represented by a symmetric positive definite matrix A instead of a scalar. The resulting anisotropy distribution is used to estimate variations in crack density, stress distribution and permeability within the producing geothermal field.

A circular dome-like structure is observed at the southwestern part of the geothermal region southwest of Sugarloaf Mountain. Regional deviatoric stress distribution is determined through a linear stress-bulk modulus relation and deviatoric stress is estimated to be 3 -- 6 MPa at geothermal production depths (1 -- 2 km), assuming 20% anisotropy is stress related. The stress field is compressional NNE-SSW and dilational WNW-ESE, coinciding with a previous, independent study using earthquake focal mechanisms. Following a theory on flat, elliptic cracks, residual crack density estimated from P anisotropy is ~0.0078, assuming crack aspect ratios >> 1:60 (i.e. not sufficiently linear) and is ~0.041 when crack aspect ratios are close to 1:60. Residual crack orientation distribution is related to velocity anisotropy. Based on the anisotropic part of crack density distribution function, the anisotropic part of permeability distribution may be calculated by a statistical approach via simple parallel fluid flow along cracks.

JSS46/E/04-B4

1400

**FIRST ARRIVAL TIME TOMOGRAPHY OF MT.VESUVIUS VOLCANO FROM ACTIVE SEISMICS**

Aldo ZOLLO, Andre Herrero, Raffaella De Matteis (Dipartimento di Scienze Fisiche, Universit di Napoli "Federico II); Claudio Chiarabba, Raffaele Di Stefano, Giovanni B.Cimini (ING, Rome); Roberto De Franco, Giancarlo BIELLA, Grazia Caielli, Rosaria TONDI (IRRS, Milan); Jean Virieux, Antony Lomax, Raffaella Montelli (CNRS-UMR GeoAzur, Nice)

Seismic recordings of 17 on land shots from 1994 and 1996 experiments have been used to retrieve the shallow (down to 4-5 km) P wave velocity structure of Mt. Vesuvius. Sources and receivers were deployed along about 30-km long conjugate profiles, crossing the top of the volcano. The recording array was composed by 140 three-component digital, short period seismographs. 250 Kg to 800 Kg of seismic gel was used for each shot. The first arrival time picking vs. distance has been performed using different data pre-processing procedures and representation by reduced travel time curves and NMO correction. The data inversion has been performed using either T(X) and Tau(p) curves and are based on arrival and delay time tomography approaches. In particular, different methods for travel time computations in laterally heterogeneous media are applied based on the exact and approximate ray tracing codes or wavefront tracing techniques like the eikonal method. For the solution of the inverse problem we used both the linearized perturbative approach, which need a well constrained initial model, or a fully non linear global optimization method. A quantitative comparison of the different images of the shallow crustal structure underneath Mt. Vesuvius obtained by applying the various techniques will be shown.

JSS46/E/03-B4

1420

**TOMO VES: AN INTEGRATED SEISMIC PROJECT FOR INVESTIGATING THE STRUCTURE OF MT. VESUVIUS**

Paolo GASPARINI (Dipartimento di Scienze Fisiche, Universita' di Napoli, Italy); Uli Achauer (EOST, Strasbourg, France); Claudio Chiarabba (Ist.Naz.Geofisica, Rome,Italy); Roberto De Franco (Ist.Ric.Rischio Sismico, CNR, Milan, Italy); Giuseppe De Natale (Osservatorio Vesuviano, Naples, Italy); Michel Dietrich (LGIT, Universite' J.Fourier, Grenoble, France); Mario Mango Furnari (Ist. Cibernetica, CNR, Naples, Italy); Dominique Gibert (CNRS-Universite de Rennes, Rennes, France); Eduard Kissling (ETH, Zurich, Switzerland); Roberto Scarpa (Dipartimento di Fisica, Universita' dell'Aquila, Italy); Satish Singh (Dept. Earth Sciences, Bullard Lab. University of Cambridge, UK); Jean Virieux (CNRS, UMR GeoAzur, Nice, France); Aldo Zollo (Dipartimento di Scienze Fisiche, Universita' di Napoli, Italy)

TomoVes project aims at reconstructing the detailed models of Mt. Vesuvius structure using seismic wave velocity and attenuation. It is mainly a controlled source experiment using on-land and offshore energy sources recorded both on land and by OBS. These data are integrated with a selected earthquake set. This project is a reflection/refraction experiment which wants to use the whole information retrievable in the complete incidence angle range (from near vertical to wide angle). Due to the high population density around and on the volcano it has not been possible to design an optimal 3-D acquisition geometry. Therefore to gain 3-D information each shot was recorded both in line and fan receiver configuration. The on-land experiment was integrated by a reflection experiment using about 2000 eight 16-liters aigun shots in the bay of Naples, recorded at few selected sites on-land, mirroring the volcano down to the Moho. Processing and interpretation of these data constitute a EEC supported project involving 12 working teams from France, Italy, Switzerland and UK. The general strategy of data interpretation is to proceed gradually from 1-D to 2-D/3-D models and from shallow to deep. The velocity and attenuation structure of the volcano will be obtained by ad hoc integrated seismic processing tools which are developed and adapted to image the complex volcanic environment in non conventional acquisition geometries. Further products of the project will be the implementation of a seismic, gravity and aeromagnetic data-base for Mt. Vesuvius and a set of methods to be applied for seismic imaging of volcanic complexes.

JSS46/L/01

1440

**SHALLOW VELOCITY MODEL FOR MT. VESUVIUS VOLCANO, ITALY, FROM ARRAY MEASUREMENTS OF SEISMIC NOISE**

R. SCARPA

The use of dense seismic arrays on volcanoes is useful to infer from noise measurements the shallow velocity structure. In the present work results obtained using data from short-period arrays during three experiments carried out in different places on the Vesuvius Volcano are compared. Correlation method was applied on 120-400 seconds time-windows of the noise recorded during all the experiments, allowing to get the shallow velocity structure, up to 500 meters, beneath the investigated sites on volcano. The first two experiments are part of a research project aimed to the high resolution seismic tomography of Mt. Vesuvius using explosive sources. During the first experiment executed in 1994 on the summit crater, the array consisted of two groups of short period geophones, 4.5 Hz natural frequency, formed by 16 and 25 vertical components (plus two horizontal components), distributed along an arc shape. The second experiment was performed in 1996 at about 100 meters a.s.l. on the SE flank of volcano. The 63 channels-array, with circular geometry and an aperture of 200 meters, was equipped with 21 three-component sensors, 4.5 Hz natural frequency. The last experiment was executed in 1998 at about 600 meters a.s.l. on the SW flank of volcano, deploying a seismic array of two three-component and eighteen vertical short period (4.5 Hz extended to 1 Hz) stations, with an aperture of approximately 600 meters, for a seven months operation. The correlation method allowed to define the dispersive characteristics of surface waves composing the noise, from which velocity models of the sub-surface structure were inferred for each investigated site. Results seem to confirm lower seismic velocities beneath the crater compared to those obtained at lower flanks on volcano.

JSS46/W/02-B4

1500

**JOINT INTERPRETATION OF GRAVITY AND SEISMIC TOMOGRAPHY DATA FOR MT. VESUVIUS**

Ulrich ACHAUER (EOST, UMR CNRS-ULP 7516, Strasbourg, France, email: ulrich.achauer@ost.u-strasbg.fr); Giovanna Berrino, Paolo Capuano, Giuseppe De Natale (all at Osservatorio Vesuviano, Naples, Italy); Claudio Chiarabba (ING Rome, Italy); Anne Deschamps (Geosciences AZUR, Nice, France); Paolo Gasparini (Dep. of Geophysics and Volcanology, University of Naples, Italy)

In the framework of the EEC project "Internal structure of Mt. Vesuvius through 3D high resolution seismic tomography (Tomoves)", which focuses on the delineation of the structural

## INTER-ASSOCIATION

setting of Mt. Vesuvius volcano, a joint analysis of gravity and seismic data has been performed. The investigated area covers all the Campanian plain and the Gulf of Naples in order to be able to well-define as well deeper structures. All the available gravity data around Vesuvius and the Campanian area have been quality checked and re-analyzed together with new gravity data collected offshore and along selected profiles in the Vesuvian area. All this data constitute a new gravity database of about 18,000 measurements. The seismic database consists of data collected during the 1994 and 1996 Vesuvius tomography experiments, by teleseismic and regional arrival times. A newly developed joint-inversion program, including 3D-ray tracing and an adaptive grid scheme, is currently being updated in the framework of this project to be used not only for transmission tomography, but for "refraction" type tomography as well. We have opted for a ray-tracer type like in Zhao's inversion program. We perform an analysis on the velocity-density relationship to be used in the joint inversion algorithms, therefore a preliminary modeling of gravity data has been performed. The main goal of this work is to define the morphology of the Moho discontinuity in the Vesuvian area and the shallower main structures or discontinuities like the volcanic sedimentary boundary.

**JSS46/W/11-B4**

**1540**

### EARTHQUAKE DATA BASE FOR SOMMA-VESUVIUS TOMOGRAPHY

Giuseppe DE NATALE (Osservatorio Vesuviano, V.Manconi, 249,80123 Napoli, Italy, email: pino@osve.unina.it); Claudio Chiarabba (ING V.di Vigna Murata,605, Roma, Italy, email: doggydog@netuno.ingr.it); Anne Deschamps (UMR Geo-Azur CNRS/UNSA Rue A. Einstein, 250, F06560, Valbonne, France, email: deschamp@faulle.unice.fr); Edi Kissling (Institute of Geophys., ETH Zurich, CH8093, Switzerland, email: kiss@tomo.ifg.ethz.ch)

In the framework of the TOMOVES Project for Somma -Vesuvius tomography, some field experiments have been performed, aimed to build a data base of local earthquake data. 6 portable digital stations were added to the monitoring networks of OV, five from ETH (Zurich) and 1 broad-band from ING (Roma). The complete network in the period May-August 1996 consisted of 20 stations, located within 15 Km from Vesuvius crater. Several hundreds microearthquakes (ML from 0.2 to 3.2) have been recorded in this period. In addition, during the active experiment some stations from CNRS (Nice) put on active seismic profiles have continuously recorded micro-earthquakes. The coincidence of the active and passive experiment periods with an intense seismic activity allowed to collect a very good earthquake data set. This work presents the data and projects to integrate active and passive data in a high-resolution joint tomography.

**JSS46/W/10-B4**

**1600**

### IMAGING OF THE JEMEZ VOLCANIC FIELD USING KIRCHHOFF MIGRATION OF TELESEISMIC WAVEFIELDS

Claudia Maria APREA, Steven Hildebrand, Michael Fehler, Lee Steck, W. Scott Baldrige, Peter Roberts (all at Earth and Environmental Sciences Division, MS D443, Los Alamos National Laboratory, Los Alamos NM 87545, USA, email: fehler@lanl.gov)

A novel application of a seismic imaging method usually used to search for oil and gas was used to construct an image of the seismic reflectivity of the subsurface of the Jemez Volcanic Field (JVF) in Northern New Mexico, USA. Volcanism began in the JVF about 13 Ma. The region underwent major caldera-forming eruptions at about 1 Ma and a resurgent dome formed. The most recent eruption was about 50-60 Ka. Several geophysical studies have been undertaken to characterize the subsurface of the JVF, the most recent one being a tomographic study using teleseisms as sources. There is clear evidence for the existence of a low velocity zone at mid crustal depths (5-12 km) beneath the region. In an attempt to augment information obtained from the tomography study, we initiated a study of the teleseismic waveforms using a Kirchhoff migration approach. Migration provides an image of the subsurface reflectivity, which is sensitive to strong velocity and density contrasts. We used waveforms recorded on an array of 50 seismometers spread throughout the region. To separate the direct arrival from phases converted at subsurface discontinuities, we used an imaging condition for waves that were first reflected from the Earth's surface. The method provides a remarkably clear image of the subsurface of the JVF. We can clearly see reflections from the base of caldera, the top and bottom of the low velocity zone, and several mid and deep-crustal and/or upper mantle reflectors. Changes in polarity of the reflections provide convincing evidence of the validity of the image and aid in its interpretation.

**JSS46/L/01-B4**

**1620**

### WIDE-ANGLE SEISMIC PROFILING ACROSS THE RABAUOL VOLCANO: A FRAMEWORK FOR TOMOGRAPHIC IMAGING OF CALDERA ARCHITECTURE

Doug FINLAYSON (Australian Geological Survey Organisation, Canberra, Australia email: dfinlays@agso.gov.au); Oli Gudmundsson (Australian National University, Canberra, Australia, email: oli@rsees.anu.edu.au); Wally Johnson (Australian Geological Survey Organisation, Canberra, Australia, email: wjohnson@agso.gov.au); Ima Itikarai (Rabaul Volcanological Observatory, Rabaul, Papua New Guinea, email: rvo@datec.com.pg); Hideki Shimamura and Yuichi Nishimura (Hokkaido University, Sapporo, Japan, email: shima@lobs.sci.hokudai.ac.jp; nishi@eos.hokudai.ac.jp)

The active Rabaul volcanic complex, situated at a triple junction at the eastern end of the island of New Britain, Papua New Guinea, is currently the target of seismic tomography investigations aimed at improving the capabilities of the region's earthquake/volcano monitoring network. Eruptions in 1937 and 1994 resulted in significant fatalities and destruction within and around Rabaul. During 1997, 50 land recorders and 23 OBS were deployed in the region for 6 months. Velocity models derived from wide-angle seismic profiling using marine explosive sources form a framework for the tomographic investigations with earthquake sources (the 1997 Rabaul Earthquake Location and Caldera Structure, RELACS program). A review of earlier 1967-69 seismic data indicates the upper mantle under Rabaul at about 28-30 km depth and a lower crust (14-28 km depth) with a velocity of 7.1-7.2 km/s. Detailed RELACS profiling along two transects indicates that the upper crust is heterogeneous with high P-wave velocities (6.4-6.6 km/s) at shallow depths (3-5 km) on the western side of the currently active volcanic caldera. This may be an element of core basement from early in New Britain's history on the Mid to Late Eocene Caroline plate, or a more recent intrusive body related to faulting/magma conduits for the current volcanic activity.

**JSS46/W/07-B4**

**1640**

### P-VELOCITY TOMOGRAPHY OF SHALLOW STRUCTURE BENEATH RABAUOL CALDERA BASED ON LOCAL EARTHQUAKE AND EXPLOSION DATA

O. GUDMUNDSSON (Australian National University, Canberra, Australia, email: oli@rsees.anu.edu.au); D.M.Finlayson (Australian Geological Survey Organisation, Canberra, Australia, email: dfinlays@agso.gov.au); I. Itikarai (Rabaul Volcano Observatory, Rabaul, Papua New Guinea, email: rvo@datec.com.pg); Y. Nishimura and H. Shimamura (Hokkaido University, Sapporo, Japan, email: nishi@eos.hokudai.ac.jp, shima@lobs.sci.hokudai.ac.jp); R.W. Johnson (Australian Geological Survey Organisation, Canberra, Australia, email: wjohnson@agso.gov.au)

The Rabaul Earthquake Location and Caldera Structure (RELACS) field project was conducted in 1997 to build detailed models of crustal structure around Rabaul caldera, Papua New Guinea, and to improve the precision of focal earthquake location around the volcano. A part of the project is a review of active seismic data from surveys conducted in the 1960s and data collected by the Rabaul Volcano Observatory's monitoring network over the past 25 years. The seismicity of the volcano leading up to the 1994 eruptions defined an oval pattern beneath Blanche Bay, the most recent collapse structure in the caldera, 10 km wide and down to a depth of about 5 km. This pattern is interpreted to represent a ring fault above an underlying magma reservoir. We use arrival times from almost 2500 well located local earthquakes in Rabaul Caldera supplemented by travel times from local explosions conducted in 1967 and 1969 and in 1997 as part of the RELACS project to build an image of P-velocity variations in the top 5 km around Rabaul Caldera. Results show a high level of heterogeneity beneath the caldera which may be related to geothermal activity and intrusive bodies in the roof of an underlying magma reservoir.

**Thursday 29 July AM**

Presiding Chair: Dr. G. R Foulger (Univ of Durham, UK)

**JSS46/W/15-B4**

**Poster**

**0930-01**

### LINEAR JOINT INVERSION OF FIRST ARRIVAL AND REFLECTED TIMES: APPLICATION TO MT. VESUVIUS VOLCANO (ITALY)

Andre HERRERO, Aldo Zollo (both at Dipartimento di Scienze Fisiche, Universita di Napoli, Napoli, Italy, email: herrero@na.infn.it)

The joint inversion of first arrival and reflected times is very useful in presence of a strong interface when the offsets used are large. In this case, the first arrivals are dominated by refracted waves. Thus, the inversion of first arrival times alone doesn't well locate in depth the velocity variations due to the trade off between velocity and depth. The introduction of first reflected times in the inversion process helps to get rid of this problem. The direct problem is solved with Podvin and Lecomte's (1991) method both for first arrivals and first reflected waves. The medium is splitted in two parts by the reflection interface. The velocity is computed in the whole medium with a bicubic spline interpolation from velocities defined at control points. The latter, with the control points vertical position of the interface, are the inversion parameters. The inverse problem is realized by a "pseudo global" search of the misfit function minimum using Downhill Simplex and Montecarlo approaches. To accelerate the inversion processes, an iterative procedure is introduced, increasing little by little the number of inversion parameters. At each iteration, the result of the previous one is taken as a-priori model. The first application is realized with the TomoVes96 data set (Gasparini et al., 1998) on Mt Vesuvius volcano, where the presence of strong limestone interface is expected. The comparison between the inversion results with and without first reflected wave arrival times shows their utility in such a case, even if the cost in computation time is much higher.

**JSS46/E/06-B4**

**Poster**

**0930-02**

### SHALLOW AND DEEP STRUCTURES FROM ACTIVE SEISMIC AND GRAVITY DATA IN THE MT. VESUVIUS AREA (ITALY)

Roberto DE FRANCO, Grazia Caielli, Rosaria Tondi, Giancarlo Biella (Istituto di Ricerca sul Rischio Sismico, CNR, Milano, Italy, email: def@irrs.mi.cnr.it); Riccardo Barzaghi (DIAR, Sezione Rilevamento, Politecnico, Milano, Italy)

An image of shallow and deep structures beneath the Vesuvius and surrounding area is presented. Shallow information were obtained by the results of seismic interpretation of the data acquired during TOMOVES 96 experiment and of the data collected in the active refraction experiment on Vesuvius in 1994. An new integrated sequential inversion seismic-gravity method, has been applied in order to optimize the 2-D initial models down to about 5 km depth in Somma-Vesuvius complex. The deep structures have been obtained by the reinterpretation of old seismic data (1980, 1985, 1994 seismic experiments) and some preliminary new information derived from MAREVES 97 experiment. Using the deep seismic information as constraints a 3-D image of the Moho discontinuity, has been obtained applying a gravity inversion based on the collocation method.

**JSS46/W/08-B4**

**Poster**

**0930-03**

### SEISMIC TOMOGRAPHY OF MT. VESUVIUS VOLCANO WITH BORN'S QUANTITATIVE MIGRATION

E. AUGER (1&2) (email: auger@sungea03.na.infn.it), J. Virieux (2) (email: viri@seisme.unice.fr), A. Zollo (1) (email: aldo@sungea03.na.infn.it) (1) Dip.to di Fisica, Universita' di Napoli Federico II, Naples, Italy); (2)UMR Geosciences-Azur, Nice, France)

We present an improved version of Born's quantitative migration and its application to the data gathered during two seismic active experiments carried out on Mt. Vesuvius. It is based on the analysis of the whole waveform (time+amplitude) of the first reflected waves (PP and PS), done without an initial preprocessing of the data. The existing formalism was extended in such a way as: - to allow for a strongly irregular topography and acquisition system. - to take into account all three components of the ground movement recorded. - to invert for the anelastic attenuation of the propagation media. - to give an estimation of the impedance contrasts associated to the identified reflectors. Theoretical background: The inversion consists in computing a correction to be applied to the initial model in such a way that the L2 norm between perturbed computed and perturbed real seismograms reaches a minimum. The correction from the initial medium is applied as a sum of point-like diffractors over a regular grid. With its linearized form, an analytical gradient and an approximate Hessian can be computed and applied iteratively to the data till the minimum of the residuals is reached. We apply this inversion to the data of two.

**JSS46/E/07-B4**

**Poster**

**0930-04**

### DETERMINATION OF THE MOHO DEPTH IN THE CAMPANIAN VOLCANIC AREA BY P-SV CONVERTED PHASE OF TELESEISMS: PRELIMINARY RESULTS

G. DE NATALE, P. Capuano, C. Troise (Osservatorio Vesuviano, Via Manconi, 249 80123 Napoli, Italy, email: pino@osve.unina.it); B. Rosa, P. Harabaglia (Centro di Geodinamica, Univ. della Basilicata, Potenza, Italy); E. Bertrand, A. Deschamps (CNRS/UNSA, Valbonne (Nice), France, email: deschamp@faulle.unice.it); P. De Gori, C. Chiarabba, G. Cimini (Istituto Nazionale di Geofisica, Via di Vigna Murata, Roma, Italy, email: doggydog@netuno.ingr.it)

In the framework of the TOMOVES project for seismic tomography of the Vesuvius area, we installed, in the summers of 96 and 97, broad-band digital seismic stations in and around the volcanic area of Campania region. The project, called BROADVES, has been exploited in a co-operation among GeoAzur, Nice, I.N.G., Rome and Osservatorio Vesuviano, Naples. It aims to the understanding of the deep and shallow structure of the area at a regional scale, as well as to the characterisation of the local seismicity of the volcanic environments (Vesuvius,



Campi Flegrei and Ischia). We report here the preliminary results of a study of the topography of the Mohorovicic discontinuity under the seismic array. The study is performed by the analysis of P-Sv concerted phases on teleseismic recordings. A receiver function method is used to enhance the useful signal, based on the time domain deconvolution of the vertical traces from the longitudinal ones on the seismograms. For each station the computed receiver functions are summed by a normal-movement stacking technique to image the couple of velocity and Moho depth giving the largest coherence to the P-Sv pulse on seismograms. MOHO depth is then computed, at about 10 different stations, to give the topography of the base of the crust in an area of 4000km<sup>2</sup> which includes the Neapolitan volcanic centers.

**JSS46/W/09-B4** Poster **0930-05**

**SHALLOW VELOCITY MODEL FOR STROMBOLI VOLCANO FROM SURFACE WAVE DISPERSION**

S. PETROSINO, E. Del Pezzo, M. La Rocca, J. Ibanez, R. Maresca (Universit' di Salerno, Salerno, Via S. Allende, Baronissi (SA) 84081, Italy, Tel: 0039 089 953 804, Email: Kilauea@tin.it)

Data recorded during two seismic experiment carried out at Stromboli volcano, Italy, in May 1992 and in September 1997 were used to deduce a shallow velocity model for the north-western and south-western flanks of the volcano. Rayleigh wave group and phase velocity dispersion curves in the 2-8 Hz frequency range were obtained applying Multiple Filter Technique (MFT) and Phase Match Filter (PMF) to the seismic signals produced by the explosion quakes and recorded by a linear seismic array deployed on the north-western flank of the island (Labronzo). These dispersion curves were iteratively inverted to infer the velocity structure to a depth of about 200 m. The velocity model obtained for the north-western flank was compared with the one deduced from an analysis of the volcanic tremor with Aki's correlation technique, showing a good agreement. Multiple Filter Technique and Phase Match Filter were also applied to explosion quakes recorded by a short period seismic antenna installed during the Twin Array Experiment (September, 1997) on the south-western side of the volcano near Ginostra village. Phase velocity dispersion curve was also determined using the Zero-Lag Cross-Correlation technique, to compare it with the one obtained by the MFT and PMF analyses. The velocity model of the south-western flank was then inferred by the inversion of the group and phase velocity dispersion curves. The two investigated areas show a similar shallow velocity structure. Both the models deduced in the present work show an increase of seismic wave velocity with depth, in agreement with the geology of a stratified volcano.

**JSS46/E/01-B4** Poster **0930-06**

**DIFFRACTION AND EMISSION TOMOGRAPHY CRUSYAL STUDY IN THE NORTHERN KANTO, JAPAN**

Irina J. TCHEBOTAREVA, Alexei V.Nikolaev (both at Inst. Earth Physics RAS, B.Gruzinskaya 10, Moscow 117234, Russia, email: chari@synapse.ru); Haruo Sato (Dept.Geoph., Tohoku Un., Aoba-ku, Sendai, 980-8578, Japan, email: sato@zisin.geophys.tohoku.ac.jp)

Method of emission and diffraction tomography was applied for reconstruction of 3D images of passive scatterers and of seismic emission sources within the Earth crust. Temporal array composed from 196 receivers was installed in the volcanic active region of local earthquakes. Both shear and compressional waves have been used for image reconstruction. Obtained images are distinctly similar, that is an indirect sign of reliability of the result. The location of scattering anomalies is in agreement with fontains both scattered and emission component induced by direct P and S waves of earthquakes. Images obtained by 'late coda' show that seismic emission sources differ from the location of the scattering anomalies and relate to the area of the largest ear ear a give rise to this effect. To resolve the problem of relation of the passive scattering and seismic emission in the coda waves it is necessary to study the dependence of the amplitude of the induced component upon the earthquake magnitude.

**JSS46/W/18-B4** Poster **0930-07**

**THREE DIMENSIONAL VELOCITY STRUCTURE CHARACTERIZED BY A LOW VELOCITY ZONE BENEATH THE HIDA MOUNTAINS IN THE CENTRAL HONSHU, JAPAN**

Makoto MATSUBARA, Naoshi Hirata, Shin'ichi Sakai (Earthquake Research Institute, the University of Tokyo, 1-1-1 Yayoi Bunkyo-ku, Tokyo, JAPAN, email: mak@eri.u-tokyo.ac.jp); Ichiro Kawasaki (Toiyama University, 3190 Gofuku Toyama, JAPAN)

Seismic waves suffer strong attenuation when propagating in the crust beneath high mountains. However, details of the region have not yet been clarified which attenuate seismic waves beneath the Hida Mountains located in the central Honshu, Japan. To analyze the region we deployed 44 portable seismographs in a 45-km linear array, three portable seismographs and eight temporary telemetered stations across and around the linear array in the summer of 1996. We obtained 3175 P-wave arrival time data and 2335 S-wave arrival time data from 54 events at 101 stations. We inverted the arrival times to obtain 3-D P- and S-wave velocity models by a damped least squares method (Zhao, 1992). A low velocity zone was found beneath the Hida Mountains at depths of 2 - 4 km and 12 - 20 km. P-wave velocity is 30 % lower and S-wave is 60 % lower than those in the surrounding area. The resolution of inversion was tested by a checker-board method. It is good at depths of 0 - 15 km for both P- and S-wave. A high Vp/Vs ratio (2.7) indicates that a 15 % partially molten rock exists beneath the Hida Mountains, suggesting a magma reservoir in the low velocity area.

**JSS46/E/05-B4** Poster **0930-08**

**CRUSTAL STRUCTURE UNDERNEATH MT. VESUVIUS FROM ONLAND RECORDINGS OF OFFSHORE SHOTS (MAREVES 1997): DATA PRE-PROCESSING AND PRELIMINARY INTERPRETATION**

Jean VIRIEUX (CNRS, UMR GeoAzur, Nice, France); Aldo Zollo, Emmanuel Auger, Maria Rosaria Frattini, Paolo Gasparini (all at Dipartimento di Scienze Fisiche, Universita' di Napoli, Italy); Roberto De Franco, Grazia Caielli (both at Ist.Ric.Rischio Sismico, CNR, Milan, Italy); Giuseppe De Natale, Giovanni Iannaccone, Marcello Martini (all at Osservatorio Vesuviano, Naples, Italy); Roberto Scarpa (Dipartimento di Fisica, Universita' dell'Aquila, Italy)

In February 1997 the oceanographic ship NADIR (IFREMER, Brest, France) performed an offshore seismic campaign in the bay of Naples in the framework of a transit valorisation project. NADIR was equipped with eight 16-liters air guns and operated a dense network of profiles (1690 shots) with one shot per minute (spacing about 150 m) during about 30 hours. The shots were recorded on-land at 16 sites by temporary digital three-component (3C) stations, a 64-channel seismic array and 12 stations of the Osservatorio Vesuviano permanent network. The acquisition layout was designed in order to image the crustal discontinuities down to Moho in the Bay of Napoli, and beneath Mt. Vesuvius and Phlegraean Fields by reflected/converted waves. Most of the recording sites were grouped in three sets at increasing distance from the volcano (maximum offset: 100 km), so to have a continuous space coverage of the crustal reflectors beneath Mt. Vesuvius and the surrounding plain. Each

site was equipped with up to three 3C digital seismographs, in order to improve the signal-to-noise ratio by stacking. The recorded common receiver gathers have been pre-processed, NMO corrected and stacked together in order to enhance the phase identification and the clear detection of main reflection events from crustal discontinuities. In this paper will be shown the pre-processed seismic sections and their preliminary 2-D interpretation.

**JSV47**

**Friday 30 July**

**VOLCANO SEISMOLOGY (IAVCEI, IASPEI)**

Location: Medical School, Ext NG26 LT6

Location of Posters: Arthur Thompson Hall

**Friday 30 July AM**

Presiding Chair: B.A. Chouet (US Geological Survey, Menlo Park, CA, USA), Y. Ida (Univ. of Tokyo, Japan)

**JSV47/E/04-B5**

**0830**

**WAVEFIELD PROPERTIES OF SHALLOW TREMOR AND LONG-PERIOD EVENT AT KILAUEA VOLCANO, HAWAII**

Gilberto SACCOROTTI (Osservatorio Vesuviano, Via Manzoni 249, 80123 Napoli, Italy, E-mail: gilberto@osve.unina.it); Bernard Chouet and Phillip Dawson (U.S. Geological Survey, 345 Middlefield Road, MS 977 94025 Menlo Park, CA, USA, E-mail: chouet@usgs.gov, dawson@usgs.gov)

The wavefields of tremor and a long-period (LP) event associated with the ongoing eruptive activity at Kilauea Volcano, Hawaii, are investigated using a combination of dense small-aperture (300 m) and sparse large-aperture (5 km) arrays deployed in the vicinity of the summit caldera. Measurements of azimuth and slowness for tremor recorded on the small-aperture array indicate a bimodal nature of the observed wavefield. At frequencies below 2 Hz, the wavefield is dominated by body waves impinging the array with steep incidence. These arrivals are attributed to the oceanic microseismic noise. In the 2-6 Hz band, the wavefield is dominated by waves propagating from sources located at shallow depths (<1 km) beneath the eastern edge of the Halemaumau pit crater. The hypocenter of the LP event, determined from frequency-slowness analyses combined with phase picks, appears to be located close to the source of tremor but at a shallower depth (<0.1 km). The wavefields of tremor and LP event are characterized by a complex composition of body and surface waves, whose propagation and polarization properties are strongly affected by topographic and structural features in the summit caldera region. Analyses of the directional properties of the wavefield in the 2-6 Hz band point to the directions of main scattering sources, which are consistent with pronounced velocity contrasts imaged in a high-resolution three-dimensional velocity model of the caldera region. The frequency and Q of the dominant peak observed in the spectra of the LP event may be explained as the dominant oscillation mode of a crack with scale length 20-100 m and aperture of a few centimeters filled with bubbly water. The mechanism driving the shallow tremor appears to be consistent with a sustained excitation originating in the oscillations of a bubble cloud resulting from vesiculation and degassing in the magma.

**JSV47/E/05-B5**

**0845**

**SPATIAL AND TEMPORAL VARIABILITY OF LOW FREQUENCY EARTHQUAKES AND VOLCANIC TREMOR ON MONTSERRAT**

Brian BAPTIE, Richard Luckett (British Geological Survey, Murchison House, Edinburgh, UK); Jurgen Neuberg (School of Earth Sciences, University of Leeds, UK)

Low frequency earthquakes and volcanic tremor at the Soufriere Hills volcano, have been recorded on an array of broadband seismometers. We examine spatial and temporal variability in low frequency earthquakes during the extrusive phase of the eruption, between January and August 1997. Spectral analysis reveals evidence of changes in spectral properties with increasing source energy. The high correlation between spectra of the largest events both within individual swarms and over longer periods of time suggests a highly repeatable source mechanism. In general, we find that spectral properties are not coherent across the array. This leads to the conclusion that the wavefield is dominated by path and site effects characteristic of surface wave propagation. However, we present several episodes of volcanic tremor where the spectra become coherent on all components across the array. The frequency of the spectral peaks is observed to both increase and decrease with time. We observe similar behaviour preceding tremor episodes in the post-extrusive period of the eruption. In this case the tremor is thought to be closely related to ash and steam venting. Such behaviour is clearly a source effect and can be modelled by a sequence of repetitive events whose trigger frequency changes with time.

**JSV47/W/04-B5**

**0900**

**NO RESONATING MAGMA CONDUIT AT KARYMSKY VOLCANO, KAMCHATKA, RUSSIA**

Jonathan M. LEES (Department of Geology and Geophysics, Yale University, New Haven, CT, 06511 email: lees@love.geology.yale.edu); Evgenii Gordeev (Geophysical Services, KOMSP, Russian Academy of Sciences, Petropavlovsk-Kamchatsky, Kamchatka, Russia, email: gord@emsp.iks.ru)

Repeating pulses from an exploding Karymsky volcano contain a rich variety of signals recorded on acoustic and seismic sensors. Several general observations regarding the pulsating train include the following facts: 1) Chugging events always follow an initial explosion, although not all explosions are followed by chugging. 2) There is almost always a lag time between the initial explosion and the commencement of intense chugging. We assume this is a preparation time where the system is building up intensity. 3) The chugging is fairly regular, with a dominant, fundamental frequency that fluctuates from 0.7 to 1.5 s. 4) Individual pulses are very uniform and are near duplicates of the initial explosive pulses. 5) A typical sequence of events has an envelope that grows rapidly in amplitude and later diminishes gradually. The pulsating sequences exhibit behavior that cannot be explained by a resonating conduit. This is clear from the correlation of amplitudes to inter-pulse time intervals. Consistent seismic arrivals appear to be keyed to the size of acoustic recording and not vice-versa, providing evidence for a shallow, oscillatory source near the vent opening. A model consisting of a sequence discrete pulses explains the data and provides a framework for understanding the dynamics of degassing at the vent.



**JSV47/W/27-B5 0915****NATURE OF VOLCANIC EARTHQUAKES AND TREMOR REVEALED BY SEISMIC OBSERVATION VERY CLOSE TO THE SOURCE REGION JUST BELOW THE SUMMIT CRATER OF ASAMA VOLCANO, JAPAN**

Jun OIKAWA, Yoshiaki Ida, Hiroshi Tsuji (Earthquake Research Institute, University of Tokyo, Yayoi 1-1-1, Bunkyo-ku, Tokyo 113-0032, JAPAN, email: oikawa@eri.u-tokyo.ac.jp, ida@newsida.eri.u-tokyo.ac.jp, tsuji@komoro.eri.u-tokyo.ac.jp)

In Asama volcano, additional four seismic stations were recently installed near the summit crater in order to obtain the high quality records in closer distances to the hypocenter regions just below the crater. The waveforms of high frequency earthquakes obtained at the new stations have the sharp first break and the S-phase which has not clearly been recognized before. Low frequency events contain a long coda wave which attenuates monotonically with a dominant frequency of 1 to 3 Hz for 1 minute. Using the new data, the hypocenters of the volcanic earthquakes were determined much more accurately, particularly in depth. High frequency earthquakes and low frequency events are concentrated into a shallow zone above the depths of 1 km underneath the crater. Some high frequency events are also observed below 3 km and there is a seismic gap between the two zones. The seismic gap agrees with the location of the pressure source which is estimated from the ground deformation. It is inferred that the gap zone corresponds to a magma reservoir and that shallower seismic events occur in and around the conduit to the summit crater.

**JSV47/W/31-B5 0930****LOW ATTENUATION RESONANCE OF A SPHERICAL MAGMA CHAMBER: SOURCE MECHANISM OF VOLCANIC TREMOR AT ASAMA VOLCANO, JAPAN**

Eisuke FUJITA (National Research Institute for Earth Science and Disaster Prevention, Tennodai 3-1, Tsukuba, Ibaraki, 300-0006, Japan, email: Fujita@Geo.Bosai.Go.Jp); Yoshiaki Ida (Eri. University Of Tokyo, Yayoi 1-1-1, Bunkyo-ku 113-0032, Japan, email: ida@newsida.eri.u-tokyo.ac.jp)

Volcanic tremor often has oscillating waves with some specific frequencies and attenuation factors of a spherical resonator consisting of volcanic fluid. We have investigated the source mechanism of volcanic tremor, formulating a spherical resonator and found low attenuation modes (lams) in lower modes. Lam takes as low as 0.01 times attenuation factors of higher modes. Some monotonic waveforms of volcanic tremor (lp-events) can be explained by the excitation of lam. Applying the model to the events at asama volcano, japan, both characteristic frequencies and attenuation factors are well fitted and the resonator size, velocity and density contrasts between fluid inside and elastic medium outside are estimated. The resonator about 200m radius contains fluid composed of gas and liquid mixture. Excitation of the resonance is also formulated by expanding the excited wave in the series of the eigen functions and we estimate the excitation function that represents the effect of the applied force on the observed volcanic tremor. It is inferred that the volcanic tremor at asama volcano is triggered by the combination of slow and rapid pulsive forces, suggesting the gas discharge or bubbling in magma and the nearby earthquake, respectively.

**JSV47/W/24-B5 0945****THE COMPLEX FREQUENCIES OF LONG-PERIOD EVENTS AS A PROBE OF FLUID COMPOSITIONS BENEATH VOLCANOES**

Hiroyuki KUMAGI, Bernard A. Chouet (both at U.S. Geological Survey, 345 Middlefield Road, MS 910, Menlo Park, CA 94025, USA, email: kumagai@seis.nagoya-u.ac.jp, chouet@chouet.wr.usgs.gov)

Long-period (LP) events have been widely observed in relation to magmatic and hydrothermal activities in volcanic areas. Their waveforms characterized by their harmonic signature have been interpreted as oscillations of a fluid-filled resonator, and mixtures of liquid and gas in the form of bubbly liquids have been mainly assumed for the fluid.

To investigate the characteristic properties of the resonator system, we analyze waveforms of LP events observed at four different volcanoes in Hawaii, Alaska, Colombia and Japan using a newly developed spectral method. This method allows an estimation of the complex frequencies of decaying sinusoids based on an autoregressive model. The results of our analysis show a wide variety of Q factors ranging between tens and several hundreds.

We compare these complex frequencies with those predicted by the fluid-filled crack model for various mixtures of liquid, gas and ash. While the oscillations of LP events with Q smaller than 50 can be explained by various combinations of liquids and gases, we find that ash-laden gases are required to explain long-lasting oscillations with Q larger than 200. The complex frequencies of LP events yield useful information on the types of fluids, and their temporal and spatial variations can be used as a probe of fluid compositions beneath volcanoes.

**JSV47/W/16-B5 1000****LABORATORY FOAM FLOWS EXHIBITING LP TYPE PRESSURE OSCILLATIONS**

Stephen J LANE (1), Bernard A Chouet (2), Phillip P Dawson (2), Graham A Ryan (1), Jeremy C Phillips (3) (1: Volcanic and Geohazards Research Group, Dept of Environmental Science, Lancaster University Lancaster LA1 4YQ, UK; 2: USGS, 345 Middlefield Road, Menlo Park, California 94025, USA; 3: Centre for Environmental and Geophysical Flows, School of Mathematics, University of Bristol, University Walk, Bristol BS8 1TW, UK)

The two phase gas-liquid flow of fluids in conduits is often considered to lead to the generation of long period and harmonic seismic signals at active volcanoes. These fluids could be magma-steam or water-steam in volcanic systems and could be flowing over a wide range of velocities.

We present pressure oscillation data from the laboratory simulation of magma-steam foam flows using natural gum rosin and a volatile organic solvent. These experiments were carried out over a range of volatile supersaturations generating conditions ranging from gentle unfragmented to violent fragmenting flow. Pressure oscillations were detected over the whole range of flow conditions. Spectral analysis of the oscillations showed that the dominant oscillation frequencies could be attributed to resonant oscillation in both the foam and open gas spaces within the experimental tube. Flows where foam fragmentation occurred showed a broader, higher frequency and more energetic spectrum than unfragmented flows. Some of the experimental pressure data show remarkable qualitative similarity with vertical ground velocity spectra generated by magma flow during the inflation stage of the 1st February 1996 volcanic crisis of Kilauea Volcano, Hawaii. We discuss this in relation to the proposed generation mechanisms within the experiments and Kilauea Volcano.

**JSV47/W/01-B5 1045****LOCATION OF THE SEISMO-VOLCANIC SOURCE AT STROMBOLI VOLCANO USING TWO DISTINCT SEISMIC ANTENNAS**

M. LA ROCCA, E. Del Pezzo, J. Ibanez, J., Almendros, G. Saccorotti, S. Petrosino, G. Alguacil, E. Carmona

In September 1997, two short period, small aperture seismic antennas were installed at Stromboli volcano (Southern Italy), with the main aim of space location of the high frequency source of the explosion quakes. The first antenna, located at Semaforo Labronzo, had an aperture of about 300 m, and consisted of 26 vertical and two 3-D seismometers. The other antenna was deployed near the Ginostra village, located on the western flank of Stromboli, in a flat area named Timpone del Fuoco. It was composed by 15 vertical and three 3-D seismometers. 75 records of explosion quakes triggered both antennas simultaneously, and were used as data set. Slowness spectra, calculated at both arrays for several time windows sliding along the seismograms, track the seismic source in 4 frequency bands centred at 1, 2, 3 and 4 Hz, with the bandwidth of 1 Hz.

Ray parameters and back-azimuths are calculated separately at the two antennas using the Zero Lag Cross-correlation method (ZLCC). Synthetic ray parameters and back-azimuths were then generated for each node of a 3-D grid encompassing the whole volcano and limited by the topography. An approximate ray-tracing in 3-D was used to perform this task, using a velocity model which in the first 200 meters from the surface was derived by a study of velocity dispersion, carried out in the same array sites, and elsewhere was fixed at reasonable values. The search for the grid coordinates which maximise in the least squares sense the probability that the observed data are in fact observed, was performed for both arrays and finally the product of those probability functions gives the final solution. Results show that the epicentral area covers the crater area. Some coherent phases are observed in the late portion of the seismogram, showing the presence of coherent strongly back-scattered arrivals. The present noise is also well correlated in the investigated frequency range, showing similar slowness vectors than those observed for the explosion quakes.

**JSV47/W/18-B5 1100****BROADBAND CHARACTERISTICS OF THE SOURCES OF EXPLOSIONS AT STROMBOLI, ITALY**

Bernard CHOUET, Phillip Dawson (both at U.S. Geological Survey, 345 Middlefield Road, Menlo Park, California 94025, USA, email: chouet@chouet.wr.usgs.gov); Gilberto Saccorotti, Marcello Martini (both at Osservatorio Vesuviano, Via Manzoni 249, 80123 Naples, Italy, email: gilberto@osve.unina.it); Roberto Scarpa (Dipartimento di Fisica, Università degli studi dell'Aquila, 67010 Coppito, L'Aquila, Italy, email: roberto.scarpa@aquila.infn.it); Gaetano De Luca and Giuliano Milana (both at Servizio Sismico Nazionale, Via Curtatone 3, 00185 Rome, Italy, email: gaetano.deluca@aquila.infn.it)

During September-October 1997, 21 three-component broadband (0.02-60 s) seismometers were deployed on the flanks of Stromboli at radial distances of 0.3-2.2 km from the active crater to investigate the source mechanism of Strombolian explosions. Over 1600 minutes of volcanic tremor interspersed with explosions were recorded over a period of 8 days. In the 2-50 s band, the very-long period (VLP) signals associated with explosions are representative of two stationary source mechanisms repeatedly activated in time. VLP particle motions are essentially linear and analyses of semblance and particle motions are consistent with a single point source located 300 m beneath the crater floor and 300 m northwest of the active vents. Similar VLP waveforms are observed at the 21 stations, indicating that the seismograms are source-dominated. The VLP ground displacement response to each explosion is marked by a compression, followed by a dilatation and terminating with another compression, which may be qualitatively interpreted as: (1) pressurization and dilation of the conduit in response to the ascent of a slug of gas; (2) depressurization and collapse of the conduit in response to mass withdrawal (bubble burst) during the eruption; and (3) repressurization and dilation of the conduit associated with the replenishment of the source with fluid. Moment tensor inversions of a subset of VLP data suggest a crack-like geometry for the source centroid. Each eruption corresponds to the evacuation of a volume of gas on the order of 1000 cubic meters.

**JSV47/W/11-B5 1115****DETECTION OF A CRACK-LIKE CONDUIT BENEATH THE ACTIVE CRATER AT ASO VOLCANO FROM DENSE BROADBAND SEISMIC OBSERVATION**

Hitoshi KAWAKATSU, Mare Yamamoto (both at Earthquake Research Institute, University of Tokyo, Yayoi, Bunkyo, Tokyo 113 JAPAN, email: hitosi@eri.u-tokyo.ac.jp); Satoshi Kaneshima (Department of Earth and Planetary Sciences, Faculty of Sciences, Tokyo Institute of Technology); Takehiko Mori, Tomoki Tsutsumi, Yasuaki Sudo (all at Aso Volcanological Laboratory, Kyoto University)

At Aso Volcano in Kyushu, Japan, volcanic signals with unusually long periods (7-15 sec) have been observed in the near-field of the active crater, and their source is known to be located about 1.5km beneath the crater (Sassa, 1935; Kaneshima et al., Science, 1996). In August, 1997, we deployed totally 21 broadband three-component velocity seismometers temporarily around the crater in order to constrain the geometry of the LPT source. Most of these stations were located within 1 km around the Naka-dake 1-st crater and provide a good azimuthal coverage. The observed amplitude variation of LPT reveals that the source of LPT consists of an isotropic component and an inflation (deflation) of an inclined tensile crack almost parallel to the NNW to SSE trending chain of the old craters of Naka-dake. The detected buried crack has a dimension of 1.2km along the strike, which is almost equivalent to that of the old crater chain; its top edge is located about few hundreds meters below the surface, and the crack extends 2-3km downward with a dip of 85 degrees. The fact that the extension of the crack plane meets the active fumarole at the surface suggests that the hydrothermal system beneath the Naka-dake 1st crater causes inflation and deflation of the source region and results in exciting the crack-like conduit to generate LPTs with the period of 15 sec. In November, 1998, we further deployed a dense network of broadband seismometers to observe and constrain the wave propagation along the crack (i.e., crack wave). Analysis of these data will be also presented.

**JSV47/W/22-B5 1130****VERY LONG-PERIOD SEISMIC EVENTS ASSOCIATED WITH THE 1998 ACTIVITY OF IWATE VOLCANO, JAPAN**

Takeshi NISHIMURA, Haruhisa Nakamichi, Satoru Tanaka, Tomokazu Kobayashi, Minemori Sato, Sadato Ueki, Hiroyuki Hamaguchi, Masakazu Ohtake, Haruo Sato, (all at Graduate School of Science, Tohoku University, Sendai 980-8578, Japan, email: nishi@zisin.geophys.tohoku.ac.jp), Eisuke Fujita (NIED, Tukuba 305-0006, Japan)

We have conducted a broad-band seismic observation at Iwate Volcano using six STS-2 seismometers and continuous recording systems (LS8000WD; 24 bit A/D, 50Hz sampling, GPS clock) since April, 1998. We observed a high activity of very long-period seismic events, although there were no significant surface activities of the volcano. The long-period events have a dominant period of about 10s and a duration of 30 s to 60 s, being often accompanied with high-frequency signals (a few Hz) at the beginning and/or the end of the long-period signals. Based on a result that particle orbits at all the stations show elliptical shapes, we estimate the hypocenters to be at a depth of a few kilometer beneath the western region of Iwate Volcano. A detailed semblance analysis further shows that each long-period event moves a few kilometer westward with a speed of a few hundred meters per second. Although pressure sources causing dilatation of the volcano, which are detected by a GPS measurement, migrated upward from an eastern deep part to a western shallow part, the long-

period events observed at the same period do not show any significant temporal changes in their hypocenters. We further determine the source mechanism of long-period events using a moment tensor waveform inversion technique in which a point source is assumed. The results show that a volumetric source in which dilatation and compression occur repeatedly can well explain the observed signals at all stations.

JSV47/W/13-B5

1145

#### NEW INVESTIGATIONS OF NON-DOUBLE-COUPLE EARTHQUAKE MECHANISMS AT LONG VALLEY CALDERA, CALIFORNIA

B.R. JULIAN (U. S. Geological Survey, 345 Middlefield Rd., Menlo Park, CA 94025, USA, email: julian@usgs.gov); G.R. Foulger (Dept. Geological Sciences, University of Durham, Durham, DH1 3LE, UK, email: g.r.foulger@durham.ac.uk)

Some of the earliest evidence of anomalous "non-double-couple" earthquake mechanisms came from Long Valley caldera, in eastern California. Several large (magnitude ~6) earthquakes there in May 1980 produced high-quality seismic data sets that were inconsistent with simple shear faulting, and suggested source processes involving hydraulic fracturing by magmatic fluids. It has so far not proved possible, however, to determine whether the thousands of smaller earthquakes at Long Valley have non-DC mechanisms. In the summer of 1997, a network of 64 three-component digital seismometers, including six with broadband response, was operated in the south moat and around Mammoth Mountain for a three-month period that included the onset of a series of intense earthquake swarms. The stations cover the focal spheres well and provide a wealth of data that greatly improve our ability to resolve earthquake locations and mechanisms. We will present moment-tensor focal mechanisms and high-resolution relative hypocenter locations, which will resolve the question of the mechanisms of small earthquakes at Long Valley.

JSV47/W/09-B5

1200

#### SEISMIC STRAIN AND STRESS PATTERNS AT ETNA VOLCANO, SICILY, BETWEEN 1990 AND 1998

Graziella Barberi, Giancarlo NERI (both at Istituto di Scienze della Terra, University of Messina, Salita Sprone 31, 98166 Messina, Italy, Email: geoforum@imeuniv.unime.it); Ornella Cocina, Eugenio Privitera and Salvatore Spampinato (all at Istituto Internazionale di Vulcanologia, CNR, Piazza Roma 2, 95123 Catania, Italy. Email: cocina@iiv.ct.cnr.it).

The algorithms by Gephart and Forsyth (JGR, 1984) and Wyss et al. (JGR, 1992) for seismic stress and strain tensor computations, respectively, have been applied to shear-type earthquakes occurring beneath the Etna volcano during 1990-1998. Space-time variations of stress and strain parameters have been examined jointly with ground deformation and gravimetric data collected in the same period and reported in the literature or in technical reports by local volcano surveillance institutions. Taking also into account the information available from volcanological observations and structural geology, we propose a volcano activity scheme assuming that hydraulic pumping by magma emplaced in nearly north-south vertical structures produces the east-west orientation of the maximum compressive strain and stress found in the upper 10 Km beneath the crater area. In contrast, regional tectonics deriving from north-south slow convergence between African and European plates appear to play a dominant role in the generation of stress and strain fields at crustal depths deeper than 10 Km in the volcano area. According to our scheme, the progressive magma filling of upper crust in the pre-eruptive phases produces, sequentially, the observed gravity positive changes, cone inflation and unusual seismic strain rate in the upper 10 Km associated to an increased definition of the seismic deformation regime (i.e. very small confidence limits of the orientation). In agreement with this scheme, deflation revealed by ground deformation data during the course of the major 1991-1993 eruption was accompanied by a practically nil level of shallow seismicity.

JSV47/W/07-B5

1215

#### EVIDENCE FOR MAGMA AT INTERMEDIATE CRUSTAL DEPTH BELOW KILAUEA'S EAST RIFT, HAWAII, BASED ON ANOMALOUSLY HIGH B-VALUES IN KILAUEA'S SOUTH FLANK

Max WYSS, Koichiro Nagamine, Stefan Wiemer (Geophysical Institute, University of Alaska, Fairbanks, 99775, email: max@gseis.alaska.edu); Fred Klein (U.S. Geological Survey, Menlo Park, CA, 94025)

The pattern of b-value of the frequency magnitude relation, or mean magnitude, varies little in the Koaiki-Hilea area of Hawaii, and the b-values are normal, with  $b=0.8$  in the top 10 km and somewhat lower values below that depth. We interpret the Koaiki-Hilea area as relatively stable, normal Hawaiian crust. In contrast, the b-value beneath Kilauea's South Flank are anomalously high ( $b=1.3$ ) at depths between 4 and 8 km, with the highest values near the East Rift zone, but extending 5 to 8 km away from the rift. We propose that the anomalously high b-values along and near the East Rift zone are due to the presence of an active magma body beneath the East Rift zone at depths of 4 to 8 km in analogy to other volcanoes where anomalously high b-values correlate with magma chambers. This supports the model of a deep magma body beneath the East Rift zone from Kilauea summit to a distance of at least 40 km down rift. The anomalously high b-values at the center of the South Flank, kilometers away from the rift, may be explained by unusually high pore pressure throughout the South Flank, or alternatively by anomalously strong heterogeneity due to extensive cracking. We hypothesize that the extensive cracking may have been acquired when this part of the South Flank, now several kilometers distant from the rift zone, was generated at the rift zone. Since its generation, this volume may have moved seaward, away from the rift, but earthquakes occurring in this volume still use the preexisting three dimensional crack distribution. Along the decollement plane at 10 km depth the b-values are exceptionally low ( $b=0.5$ ) suggesting a simple one-dimensional crack distribution.

JSV47/E/02-B5

1230

#### A TRIAL FOR DETECTING TEMPORAL VARIATION OF SEISMIC TRANSFER FUNCTION USING ACCURATELY CONTROLLED SINUSOIDS - TOWARDS MONITORING OF GEODYNAMIC STATE

Koshun YAMAOKA, Koji Miyakawa (both at School of Science, Nagoya University, Chikusa, Nagoya 464-8602 Japan. email: yamaoka@seis.nagoya-u.ac.jp); Takahiro Kunitomo, Mineo Kumazawa (both at Tono Geoscience Center, Japan Nuclear Cycle Development Institute, Sonodo, Jorinjii, Tokishi 509-5102, Japan, email: kuni\_tomo@tono.pnc.go.jp), ACROSS development team

We made on-site experiments of a new source-receiver system for seismic sounding, which is named ACROSS (Accurately Controlled Routinely Operated Signal System). The system uses precisely controlled sinusoids, which gives a best way to achieve high signal-to-noise ratio without destroying surrounding ground. One of the final goal of the system is to monitor the temporal variation of geodynamic state such as volcanic activity. The purpose of our experiment is to check the temporal stability of the system and to establish a practical

technique to make a continuous monitoring of seismic structure. In our experimental site the sources which generate 20ton-f with centrifugal force are deployed on the ground surface where granite bedrock is exposed. The emitted elastic wave is received with two borehole seismometers deployed at 800m and 1800m deep near the fracture zones of Nojima fault which generates 1995 Kobe earthquake. We made three one-week runs and a one-month run of experiments. During each run the sources were continuously operated with frequency modulation around 20Hz and 30Hz, which produce plural components of sinusoids of constant frequency interval. The results of these experiments show that the stabilization of source-ground coupling is essential for precise monitoring of the temporal variation of velocity structure. After a correction for the coupling variation we achieved signal stability better than 1% in amplitude and 0.01 radian in phase characteristics, although temporal variation of natural origin is not identified.

Friday 30 July PM

Presiding Chair: B.A. Chouet (U.S. Geological Survey) and Y. Ida (University of Tokyo)

JSV47/E/07-B5

Poster

1400-01

#### PROGRAM FOR LOCATION OF HYPOCENTER COORDINATES OF VOLCANIC EARTHQUAKES USING LOCAL SEISMIC STATIONS NETWORK DATA

V.V. MYACHKIN (Institute of Physics of the Earth, Russian Academy of Sciences, 123810, Bolshaya Gruzinskaya, 10, Moscow, Russia, e-mail: myachkin@uipe-ras.scgis.ru)

The problem of accuracy of hypocentre coordinates determination in case of volcanic earthquakes is more significant than for tectonic earthquakes, because error in hypocentre position about 5 km doesn't allow one to localize the place of the future eruption. Therefore a program for determination of hypocentre parameters of local earthquakes was developed. It can either search for hypocentre coordinates and origin time simultaneously or determine the origin time independently, using 2 modifications of Vadati plot or the so-called robust method which was never used in any other algorithm. Use of external travel times calculated beforehand reduces the time for determination of wave travel times from the source to the station and thus allows the solution function minimum to be searched for at the whole polygon area, without any preliminary suppositions on its character. The program provides a picture of residuals structure near the minimum, i.e. the area of hypocentre existence, showing domains where the residual is 1.5, 2 or 3 times greater than in the minimum point, and we obtained that these domains have rather complicated configuration. Moreover, the solution often has 2 good sharp minima at different depths. The search for the solution function minimum is possible within the given limited depth range, and it allows a solution to be obtained for each minimum individually. The MINIMALM programme is successfully used to determine hypocentre parameters at the region of the Northern volcano group in Kamchatka. Hypocentre coordinates determined by this programme are in good accordance with areas of subsequent volcanic eruptions.

JSV47/E/03-B5

Poster

1400-02

#### SEISMIC OBSERVATIONS AT MT ETNA (ITALY) SUMMIT AREA DURING STROMBOLIAN EXPLOSIONS AND THE BEGINNING OF A LAVA FLOW

Davide EREDITATO (Geological Survey of Japan, 1-1-3, Higashi, Tsukuba, Ibaraki 305, Japan, e-mail: takao@gsj.go.jp); Carmelo Bellia (University of Western Australia, Perth, Australia, e-mail: cbellia@geol.uwa.edu.au); Yuji Nishi (Geological Survey of Japan, 1-1-3, Higashi, Tsukuba, Ibaraki 305, Japan, e-mail: uwest@gsj.go.jp); Matsushima Nobuo (Geological Survey of Japan, 1-1-3, Higashi, Tsukuba, Ibaraki 305, Japan, e-mail: nobuo@gsj.go.jp); Giuseppe Patane (Istituto di Geologia e Geofisica, Universita' di Catania, Corso Italia 55, 95129, Italy); Takao Ohminato (Geological Survey of Japan, 1-1-3 Higashi, Tsukuba, Ibaraki 305, Japan, e-mail: takao@gsj.go.jp)

We conducted seismic observations in close proximity to the summit area of Mt Etna, Italy. During the observations, volcanic activity at the NE, Central, Bocca (Nuova) and SE Craters was characterized by continuous gas emission, frequent small explosions, sporadic explosions and strombolian activity accompanied by a lava flow from SE Crater which started on September 15th.

A seismic network, composed of four Guralp CMG-40 (3-component characteristic frequency  $f_0=0.033$ Hz) and four Mark Products L-22 3 component ( $f_0=2$ Hz) sensors with 16 bit logger LS-8000SH was installed and operated from September 11th to 22th. The seismicity at the summit area of Mt. Etna mainly consists of different types of small earthquakes localized very close to the summit craters and related to their explosive activity. Most earthquakes can be detected only by the seismic stations closest to the summit craters. In addition, we observed some high frequency small earthquakes, with main spectral content above 10 Hz, showing different epicentral location and recorded by all the seismic stations. Seismicity associated with the lava flow from the SE Crater is mainly characterized by the occurrence of many small earthquakes, showing showing similar dominant frequency around 3Hz. A typical increase-decrease pattern of the amplitude of volcanic tremor characterizes the summit activity preceding the summit lava outflow.

JSV47/E/06-B5

Poster

1400-03

#### TEMPORAL EVOLUTION OF VOLCANIC EVENTS SPECTRUM

Javier PEÑA (Dept. Vulcanologia, Museo Nacional de Ciencias Naturales, Jose Gutierrez Abascal 2, 28006 Madrid, Spain, e-mail: mcnp182@mncn.csic.es); Mar Astiz (Dept. Matematica Aplicada, E.T.S. Arquitectura, U.P.M., Avda. Juan de Herrera, 4, 28040 Madrid, Spain, e-mail: civgv@pinar1.csic.es); Alicia Garcia and Ramon Ortiz (Dept. Vulcanologia, Museo Nacional de Ciencias Naturales, Jose Gutierrez Abascal 2, 28006 Madrid, Spain, e-mail: mcng92@pinar1.csic.es and email: mcnor72@pinar1.csic.es)

In this work some results from the analysis of seismic events recorded in the Popocatepetl volcano are presented. The analysis is based on FFT and wavelets methods. The aim is to separate the signals by the temporal evolution of their spectral content. The FFT is only a stationary representation but applying wavelets we can obtain a good time-frequency representation of the signal. The automatic process will allow the seismic classification in real time, while they are recording at the observatory. For volcanic crisis management the fast identification of event type is critical, taking into account that the large volume of recorded information could difficult the work. This method can facilitate this management. The basis of the method and some analysed events are shown.

JSV47/E/08-B5

Poster

1400-04

#### ARRAY ANALYSIS OF SEISMIC NOISE WAVEFIELD AT MT. VESUVIUS VOLCANO, ITALY

G. SACCOROTTI (Dipartimento di Fisica, Università di Salerno, 84081 Baronissi Sa, Italy; e-mail: gilberto@osve.unina.it); R. Maresca (Facoltà di Scienze, Università del Sannio, maresca@physics.unisa.it); E. Del Pezzo (Osservatorio Vesuviano.; delpezzo@osve.unina.it); A. Cirillo (Dipartimento di Fisica, Università di Salerno); S. Petrosino (Osservatorio Vesuviano, e-mail: kilauaea@tin.it)



## INTER-ASSOCIATION

A possible precursor of volcanic eruptions is the insurgence of volcanic tremor, characterised by a sustained signal lasting from several minutes to hours or days, with the distinctive characteristic of absence of clearly recognisable seismic phases. It can be overlapped to cultural ground noise, which in the case of Mt. Vesuvius is extremely high, due to the presence of a huge urban area surrounding the volcano. This is the reason why the discrimination of possible insipient volcanic tremor may become a difficult task. For the above reasons we decided to investigate the spectral characteristics of the noise wave-field at Mt. Vesuvius in the present condition of quiescence. We deployed a seismic array of two three-component and eighteen vertical short period (4.5 Hz extended to 1 Hz) stations, with an aperture of approximately 600 meters, for a 7 months operation, about 1.5 km far away from the summit crater. A detailed spectral analysis of the noise recorded at each station was performed: temporal evolution of the spectra was investigated in short (2 minutes) and long (36 hours) time-windows; possible site effects due to local surface structure were also evaluated using spectral ratios among different stations and array-averaged spectrum. Fourier analysis shows the presence of a persistent peak around 0.5 Hz; the estimated spectral energy of secondary higher frequencies components is strongly time-dependent, showing highest values in the daytime, and so, it is presumably due to human noise sources. The frequency-slowness spectra reveal that only the signals in the frequency band centred at 0.5 Hz is coherent among the array stations, showing a back-azimuth directed toward the South, opposite to the direction of the active crater, and a slowness around 0.7 s/Km. As already observed by different authors in similar conditions (Valle del Tevere, Kilauea), the seismic energy propagating at frequencies lower than 1 Hz is interpreted as associated to marine disturbances. Results show the absence of coherent signals in the frequency band characteristic of the volcanic tremor, as expected in the present state of activity of Mt. Vesuvius.

**JSV47/E/01-B5** Poster **1400-05**

### BOREHOLE STRAINMETERS AND SEISMOMETERS FOR CONTINUOUS MONITORING OF VOLCANOES: RESULTS FROM AN EXPERIMENT ON VESUVIUS VOLCANO, ITALY

Roberto SCARPA, Antonella Amoruso and Alberto Cirella (all at Univ. dell'Aquila, IT), Luca Crescentini (Univ. di Camerino, IT), Gaetano De Luca (Serv. Sism. Naz., IT), Alan Linde and I. Selwyn Sacks (both at Carnegie Institution, Washington D.C., U.S.A.), Mario Castellano, Edoardo Del Pezzo, Mauro Di Vito, Folco Pingue, Marcello Martini, Gilberto Saccorotti and Claudia Troise (all at Osserv. Vesuviano, IT)

This research is focused on the development of borehole very broadband instruments to monitor volcanoes. It has been realized the development and the borehole installation of a strainmeter and a three-component seismometer, to detect very small signals linked to magma chamber pressure variations and magma transport. The borehole strainmeters are the most sensitive instruments developed to detect strain changes (down to  $10^{-12}$ ) with a wide dynamic range (>140 dB) and the borehole three-component seismometers can improve S/N by a factor 10 and will allow a more efficient detection of source parameters from volcanic earthquakes. These instruments have been installed in a hole excavated close to Mt. Vesuvius crater (2.5 km distance from the summit) and the strainmeter has been located in the Campanian ignimbritic layer (wedged grey tuff) at 200 m depth, while two seismometers (Mark L22) have been set up at 70 m depth and at the surface, with a properly designed casing system. This system should constitute the first prototype of a network, consisting of 10 stations, 5 on Vesuvius and 5 on Campi Flegrei, with data transmission of high resolution signals (24 bits) to a real-time data acquisition center and alert system to control a possible reawakening of these potentially destructive volcanoes.

**JSV47/E/09-B5** Poster **1400-06**

### HIGH RESOLUTION SPATIAL AND TEMPORAL MAPPING OF THE FREQUENCY-MAGNITUDE DISTRIBUTION IN VOLCANIC AREAS FOR STRUCTURAL ANALYSIS AND MONITORING - CAPABILITIES AND LIMITATIONS

Stefan WIEMER (Institute of Geophysics, ETH Hoengerberg, CH-8093, Zurich, Switzerland; email: stefan@seismo.ifg.ethz.ch)

High resolution, three dimensional spatial mapping of the frequency-magnitude distribution (FMD) has been performed for 10 seismically active volcanic systems (Mount St. Helens, Long Valley, Mt. Spurr, Mt. Redoubt, Off Ito, Mt. Vesuvius, Mt. Etna, Montserrat, Kilauea, Katmai). Strong and statistically highly significant contrasts in the slope of the FMD (with b-values ranging from 0.6 to 2.0) have been found on the scale of kilometers, defying the commonly held belief that volcanic areas generally exhibit a higher than normal b-value. A more sophisticated analysis reveals that instead pockets of high b-value anomalies ( $b > 1.3$ ) are embedded in normal crust ( $b \sim 0.8$ ). High b-values are particularly concentrated in the vicinity of magmatic bodies, which is to be expected because the physical conditions near a magmatic body (high material heterogeneity, high temperature gradients, low shear stress, and high pore pressures) all favor high b-values. Thus we have proposed that high b-values near magmatic bodies are a necessary, but not sufficient, condition, and, therefore, spatial mapping of the FMD presents a viable tool for structural investigations of volcanic systems. This talk will summarize some of the promise of this relatively new method, but also discuss the limitations and unresolved questions such as: (1) How does the hypocenter accuracy and magnitude determination influence the spatial b-value mapping? (2) Earthquake swarms and families and the resulting bi-modal FMD; (3) How can we resolve the ambiguity in the interpretation of high b-value anomalies? (4) Are temporal variations observed in b actually caused by spatial shifts in activity? (5) Can spatial and temporal mapping be useful for routine monitoring and eruption forecasting?

**JSV47/E/10-B5** Poster **1400-07**

### AN AUTOMATIC OBSERVATORY FOR VOLCANO MONITORING

RAFAEL ABELLA, Alicia Garcia, Ramon Ortiz and Marta Tarraga (all at Departamento de Vulcanologia, Museo Nacional de Ciencias Naturales, CSIC, c/ Jose Gutierrez Abascal 2, 28006 Madrid, Spain, email: mcnam3k@pinar1.csic.es)

The instrumentation in active volcano requires to have equipment handy, adaptable, portable, of low cost and low energy. The tracking of volcanic activity implies open out in a sort time and in a difficult access, the instrumentation have to be able to operate automatically in a crucial conditions. Seismic methods and deformation analysis are the most used for the surveillance and study of volcanoes so we have began with a basic unit constituted by seismic station and extensometer. An acquisition multiparametric system with 8 canals have been developed based on a 16/24 bits analogue digital converter of Analog Devices. The different sensors can be connected, are for example extensometer, clinometer, thermometer, magnetometer. For the first evaluation of this equipment has been installed inside of a volcanic cave in the high part of Villarrica Volcano (Chile), one component seismic station, an extensometer and a thermometer. Also a three component seismic station of sort period have been installed at the base of Villarrica Volcano.

**JSV47/W/15-B5** Poster **1400-08**

### VOLCANO-TECTONIC MICRO-EARTHQUAKE OBSERVED AT A SHORT PERIOD SEISMIC ANTENNA LOCATED AT MT. VESUVIUS (ITALY)

Bianco F., Castellano M., PETROSINO S., Carmona E., La Rocca M., Galluzzo D. and E. Del Pezzo

In November 1997 a short period seismic antenna (array) was installed on the south-western flank of Mt. Vesuvius, about 1.5 Km far from the crater, to record local micro-seismicity. The array was formed by 18 vertical component and 2 three component geophones Mark L15B electronically extended to 1 Hz and cable-connected to the acquisition system (composed by 16 bits A/D converter, anti alias filter and portable PC). The array maximum aperture was about 500 meters, with an average distance between the sensors of 50 meters. The coordinates of the sensors were obtained with differential GPS measurement. The array was in operation for 7 months and during this period it recorded about 300 local micro-earthquakes, more than those triggering the seismic monitoring network. About 40 seismic events were studied with array techniques: the Zero-Lag Cross-Correlation technique was used to calculate backazimuth and apparent velocity for the main direct phases of local micro-earthquakes. Polarisation properties of the first seismic phases were deduced performing a covariance matrix analysis in the time domain and used to constraint the S-wave first onset. Using a simplified 3-D ray-tracing technique we located the seismic source. Source location shows that the earthquakes recorded by the array are quite shallow, with hypocentres not deeper than 4 Km, in agreement with previous studies. The results achieved in this work show that the array techniques are useful to determine the propagation properties of the wave-field associated to micro-earthquakes as well as to discriminate primary seismic phases, becoming an useful complementary tool for the seismic monitoring of the active volcanoes.

**JSV47/W/26-B5** **1400-09**

### A SEISMOLOGICAL STUDY ON REMOTELY TRIGGERED PHREATIC ERUPTION AT AKITA-YAKEYAMA VOLCANO, NORTHEASTERN JAPAN

Hiroyuki HAMAGUCHI, Sadato Ueki, Satoru Tanaka and Haruhisa Nakamichi, (all at Graduate School of Science, Tohoku University, Sendai 980-8578, Japan, email: hama@aob.geophys.tohoku.ac.jp)

We discussed the temporal variations of amplitude and frequency of volcanic tremors and subsequent impulsive long-period signals prior to the simultaneously occurrence of phreatic eruption and debris avalanche at Akita-Yakeyama, northeastern Honshu, Japan on 8:00 May 11, 1997 (JST). Precursory tremors were continuously registered by a short period seismometer ( $T = 1$ sec) at YKY station adjacent to the eruption site (distance; ca 1 km) until a sudden power failure. The small spasmodic harmonic tremors with a frequency of 2.4 Hz began on 17:20, May 10 after 1 min passing of S waves and on 17:41 after 5 min passing the surface waves of the Iran earthquake of M7.2 (epicentral distance; ca 6,000 km). This offers probably first example of remotely triggered volcanic tremors by dynamic strains from a distant large earthquake. After a lapse of about 2 hours, the tremors re-appeared and evolved rapidly from the intermittent appearances with a single peak frequency of 2.1 Hz to the continuous ones with multiple peak frequencies between 0.7 and 2.9 Hz and with an increasing in amplitudes with a time lapse. At the final stage of precursory activity, the apparent seismic (or tremor) quiescence was recognized in the short intervals of 7:54-7:58, May 11 and then impulsive long-period signals were observed at 08:00:05. At this time, phreatic eruptions and the associated wet debris avalanche were eye-witnessed at Sumikawa spa. Long-period waves with a period of 10 sec were interpreted by the single force of 10,000 N excited by the reaction of steam ejection with horizontal column. Time-variable properties of precursory tremors and subsequent steam explosions suggest that a prevailing mechanism is pressure increases within a volume of groundwater at shallow depths.

**JSV47/W/12-B5** Poster **1400-10**

### NON-DOUBLE COUPLE MECHANISMS IN THE SEISMICITY PRECEDING 1991-1993 ETNA VOLCANO ERUPTION

Angela SARAO, Giuliano F. Panza (both at Dipartimento di Scienze della Terra, Universita' di Trieste and The Abdus Salam International Centre for Theoretical Physics, Trieste, Italy, E-mail: angela@geosun0.univ.trieste.it), Eugenio Privitera and Ornella Cocina (both at the Istituto Internazionale di Vulcanologia, CNR, Catania, Italy)

The temporal evolution of the complete moment tensor was investigated for 28 earthquakes occurred at Mt. Etna in the period August 1990- December 1991 just preceding the biggest eruption of the last three centuries. In the seismicity investigated we found the presence of non double couple mechanisms which increase before the outbreak of the Etna eruption. Such mechanisms can be explained as related to magma injection or withdraw process whereas, for some events, the complex interaction between tectonic stress and volcanic activities has to be considered. The aim of this work, is twofold: 1) to contribute to the knowledge of the dynamics of a volcano and 2) to single out systematic features of the seismicity that can be used as alert parameters for volcanic hazard assessment and for monitoring the onset of an eruption mainly in the case of the explosive ones.

**JSV47/W/06-B5** Poster **1400-11**

### DETECTION AND CLASSIFICATION OF SEISMIC SIGNALS OF VOLCANIC ORIGIN AT MT. MERAPI, JAVA, INDONESIA

OHRNBERGER, M., Wassermann, J., and Scherbaum, F. (all at Institute of Geosciences, University of Potsdam, P.O.Box 601553, 14415 Potsdam, E-mail: imao,jowa.fs@geo.uni-potsdam.de)

As being one of the most dangerous active volcanoes due to its location in a densely populated area and its eruptive activity showing doming, dome collapse and pyroclastic flows, Mt. Merapi was chosen as one of the 15 decade volcanoes during the IDNDR. Inside the interdisciplinary joint German-Indonesian research project MERAPI (Mitigation, Evaluation, Risk Assessment, and Prediction Improvement) the seismological investigations are considered as a baseline experiment supplying activity parameters for other experiments.

A continuously operating 12-station, three-component seismic network was installed in July 1997. The station-setup was realized in a combined array-network geometry, each array equipped with one broadband instrument (STS-2) and three short-period seismometers (MARK-L43D) in order to maximize the information about the observed wavefield with a limited number of stations. The enormous amount of data requires new automatic detection and classification algorithms to enable parametrization of the seismic activity with high confidence level.

In this study a feature vector for the detection task is obtained by using the waveform information at the three sub-arrays. In detail we use the maximum beampower and a coherence measure in each subarray per time step for all three components individually. Together with an averaged polarization information this analysis is performed in several frequency bands. After detection, feature vectors are used for training different classes of seismic events performing a cluster analysis in the feature vector space. This analysis is applied to the data recorded during the volcanic eruption cycle in July 1998 and compared to the results given by the Volcanological Survey of Indonesia.



**JSV47/W/03-B5** Poster **1400-12****LONG TERM SEISMICITY AND SOURCE CHANGES DURING DIFFERENT ACTIVITY STAGES OF MT. MERAPI (INDONESIA) USING A TWO SCALE SEISMIC ARRAY**

J. WASSERMANN (Institute of Geosciences, University of Potsdam, P.O.Box 601553, 14415 Potsdam, Germany, email: jowa@geo.uni-potsdam.de), Budi E.N. (Gadjah Mada University, Sekip Utara, Yogyakarta 55281, Indonesia), M. Ohrnberger (same as first author, email: mao@geo.uni-potsdam.de), J. Gossler (GeoForschungsZentrum Potsdam, P.O.Box 600751, 14407 Potsdam, Germany, email: gossler@gfz-potsdam.de)

Research on seismic signals at active volcanoes made two major developments during the last decades. Array techniques are widely used and the deployment of broadband seismometers are supposed to give new insight into source mechanisms of volcano induced seismic signals. Most realizations of these ideas suffer from the short time span of instrument deployments as well as the small aperture of the arrays. To circumvent these drawbacks and to monitor volcanic activity we have deployed a permanent network of both broadband and short-period seismometers at the IDNDR decade volcano Mt. Merapi (Indonesia) in 1997. Located on Central Java (Indonesia) Mt. Merapi is known for his large number of pyroclastic flows according to historic records. This kind of activity is caused mainly by gravitational collapse of subsequent lava domes. The network is arranged in three sub-arrays consisting of four seismometers each. After more than one year of dormancy Mt. Merapi awaked end of June 1998. This enables us to analyze all stages of dome growing, collapse and new inflation of magma using seismic array and network methods. The aim of this talk is to describe the recorded wavefield which finally ends up in source locations for the different kinds of recorded signals. We present a new technique to locate the non-impulsive volcano-induced seismic signals within the 3D structure of the volcano, following the shortest path method and using extensively the coherency of different phases at different array stations. Finally, we also present the result that the different types of signals are linked to different phases of the eruptive cycle.

**JSV47/W/20-B5** Poster **1400-13****PRELIMINARY RESULTS FROM THE 1998-99 DOUBLE SEISMIC ANTENNA EXPERIMENT AT DECEPTION VOLCANO, SOUTH SHETLAND ISLANDS (ANTARCTICA)**

J. ALMENDROS (1), E. Carmona (1), G. Saccorotti (2), J.A. Peña (1) E. Del Pezzo (2,3), J. M. Ibáñez (1,4) and G. Alguacil (1,4). (1) Instituto Andaluz de Geofísica, Universidad de Granada, Campus Universitario de Cartuja s/n, 18071 Granada, Spain. (2) Università degli Studi di Salerno, Dipartimento di Fisica, Via S. Allende, 84081 Baronissi, Salerno, Italy (3) Osservatorio Vesuviano - Via Manzoni 249, 80123 Napoli, Italy (4) Departamento de Física Teórica y del Cosmos. Facultad de Ciencias. Universidad de Granada. 18071 Granada, Spain

During the 1998-1999 austral summer, two dense small-aperture seismic arrays were deployed at Deception volcano, South Shetland Islands, Antarctica. These seismic antennas were deployed on the area in which the last eruption of 1970 took place. Aim of the deployment was a detailed investigation of the wave-field and source properties of the seismic signals associated to the current activity of this part of the volcano. A secondary goal consisted in the observation of the local and regional seismicity associated to the complex dynamics of the Drake-South Shetland subduction zone. Three main types of signals have been identified at both the arrays. The first type consists of short-period pulses probably related to the ice-block fall associated to the ice-melting processes. The second kind consists of short-duration, monochromatic signals with characteristic frequencies spanning the 1-3 Hz frequency interval. Propagation azimuths and slownesses of these signals are consistent with the action of extremely shallow hydrothermal sources located along or in close proximity of the array site fracture system. The last type consists of intermediate-depth tectonic earthquakes, occurring at the Drake-South Shetland subduction zone. Application of the spatial correlation method of Aki (1957, 1965) to background noise recordings from both the arrays has allowed to infer the dispersion properties of Rayleigh waves in the 0.5-8 Hz frequency band. We obtained a good fit between the experimental data and the model, suggesting that the noise wave-field is dominated by surface waves. We found extremely low values of the phase velocities, which indicates a propagation medium characterized by a thick surficial low-velocity layer, which is attributed to the unconsolidated pyroclastic deposits produced during the more recent activity. The three components of ground motion for the background noise are dominated by a broad spectral peak extending below 1 Hz, which remains sustained over time with varying amplitude. Due to the spatial and temporal persistence of this peak, we attribute the energy radiation in that particular band to the oceanic microseismic noise.

**JSV47/W/17-B5** Poster **1400-14****PRELIMINARY ANALYSIS OF HIGH-FREQUENCY EARTHQUAKES AT TIMANFAYA VOLCANO (LANZAROTE ISLAND, SPAIN)**

J.M. IBÁÑEZ (1,2), E. Del Pezzo (3), G. Alguacil (1,2), R. Ortiz (4) and B. Chouet (5). (1) Instituto Andaluz de Geofísica, Universidad de Granada, Campus Universitario de Cartuja s/n, 18071 Granada, Spain. (2) Departamento de Física Teórica y del Cosmos. Facultad de Ciencias. Universidad de Granada. 18071 Granada. Spain (3) Osservatorio Vesuviano - Via Manzoni 249, 80123 Napoli, Italy (4) Departamento de Volcanología. Museo Nacional de Ciencias Naturales. CSIC. C/ J. Gutiérrez Abascal, 2, 28006 Madrid, Spain (5) U. S. Geological Survey, 345 Middlefield Road, MS977, Menlo park, CA 94025. USA

In this work we present the preliminary analysis of thousands of earthquakes recorded in a period of ten years in the volcanic field of Timanfaya (Lanzarote Island, Spain). These earthquakes were recorded in a short-period vertical-component seismometer. The very-local seismicity is characterised by:

- A small magnitude measured using magnitude-duration scales.
- The frequency contain is peaked at frequencies around 10-15 Hz.
- A non-impulsive first onset is observed.
- We could not identify clear S-waves arrivals.
- At some times the seismicity is overlapped on a high frequency tremor with similar spectral characteristics to the aforementioned.
- Although the seismicity seems to appear in isolated events, at some times seismic swarms take place.

The high frequency contain of the seismicity, together with the low magnitude, do not permit to record events far from the source area. The source area is located in a thermal anomaly field with a strong vertical and horizontal temperature gradient. In a few tens of meters of depth the temperature ranges between around 100 degrees of the surface to close to 600°. In order to distinguish the possible different families of earthquakes-sources we compared a select set of events by using cross-correlation techniques in the time domain. Probably the observed small differences are associated with different source positions (depth and distance to the receiver) more than with different focal mechanisms. Therefore, the small differences observed in the time and spectral domain could be associated with path effects.

There are possible mechanisms to explain this seismicity: such as rocks that have been weakened by this gradient of temperature or the possible hydrothermal activity that allows preferential seismic failure. Similar activity has been observed in other volcanoes such as those of Hawaii, White Island (New Zealand) or Vulcano (Italy).

**JSV47/W/05-B5** Poster **1400-15****SEISMIC UNREST AT GUAGUA PICHINCHA VOLCANO, ECUADOR: ANALYSIS OF A POSSIBLE INTRUSIVE PROCESS.**

Jean-Philippe METAXIAN (IRD, Whymper 442 y Coruna, Apartado 17-12-857, Quito, Ecuador, Email: jpmetaxi@uio.satnet.net); Mario Ruiz and Minard Hall (both at Instituto Geofísico, EPN, casilla 1701-2759, Quito, Ecuador, Email: geofisico@accessinter.net).

Guagua Pichincha Volcano (4780m), situated 12 km west of Quito, has been monitored by IGEPN since 1981. Since 1990, the volcanic activity has been characterized by occasional phreatic explosions (< 10/year) occurring in the rainy months. In September 1998, following a 3 month drought, the phreatic activity increased drastically, 24 explosions being registered. On September 28, a phreatic explosion was followed by a swarm of about 50 LP multiplets characterized by an emergent onset, 35 sec durations and a dominant frequency of 1.5 Hz. After 12 hours this series of events was interrupted by a new phreatic explosion which was immediately followed by a swarm of about 900 bimodal events which lasted 17 hours. These events are characterized by an impulsive onset, 30 sec durations and a spectrum composed of two dominant peaks, one at 5-6 Hz corresponding to the first part of the signal and one at 1.5-2 Hz. The spectral analysis shows a slow decrease of the frequency with time. In October, two similar seismic episodes of less intensity were observed. The shallow depth of both LP and bimodal event swarms decreased from September to November. The seismic activity was registered by a network of 10 seismographs equipped with short period and one long period seismometers located around the caldera from 0.8 to 3 km away the dome. These episodes are interpreted to be due to minor magma injection or pressurization in the conduit at shallow depth 2-4 km.

**JSV47/W/19-B5** Poster **1400-16****APPLICATIONS OF AUTOREGRESSIVE AND WAVELET ANALYSIS TO THE DECONVOLUTION OF VOLCANIC LP EVENTS AND HARMONIC TREMOR**

LESAGE, Philippe (LGIT and CRV, Université de Savoie, 73376 Le Bourget-du-Lac, France, email: lesage@univ-savoie.fr) Glangeaud, François and Mars, Jérôme (LIS, INPG, Grenoble, France)

The long-period events (LPE) and harmonic tremor are thought to result from the excitation of a resonator - a fluid-filled cavity - by a disturbance related to the volcanic activity. The recorded signals can be thus considered as the result of the convolution of an excitation function by the impulse response of a resonator and by the propagation function, plus noise. They are characterised by one or a few dominant spectral peaks which generally come from the oscillation modes of the resonator.

We present here some applications of the autoregressive (AR) model and of the wavelet transform to the analysis of this kind of signal. (1) The AR model gives precise estimations of the frequency and attenuation factor of the resonance modes and allows to calculate the equivalent AR filters. (2) The variation with time of the harmonic components amplitudes is obtained by wavelet analysis. (3) Filtering signal by the corresponding inverse MA filters, which use the information given by the equivalent AR filters at step 1, results in the elimination of the main harmonic components and/or of particular spectral component. The residual contains the excitation function and eventually low amplitude phases that were not easily visible in the original record. Several examples are shown where the resulting excitation functions are either of short duration (LPE) or continuous (tremor).

**JSV47/W/02-B5** Poster **1400-17****A STUDY OF TREMOR AND LP EVENTS AT ARENAL VOLCANO, COSTA RICA. FIRST RESULTS OF A SEISMIC EXPERIMENT USING SMALL APERTURE AND RADIAL ARRAYS**

LESAGE, Philippe (LGIT and CRV, Université de Savoie, 73376 Le Bourget-du-Lac, France, email: lesage@univ-savoie.fr) Mora Mauricio (Universidad de Costa Rica, San José, Costa Rica) Dorel Jacques (OPGC and CRV, Clermont-Ferrand, France); Alvarado, Guillermo (ICE, San José, Costa Rica); Métaixian, Jean-Philippe (IRD, Quito, Ecuador)

Arenal volcano has permanent strombolian activity and emits almost continuous lava flows. Its seismic activity includes LP events either associated or not to explosions, but is mainly characterised by several hours of volcanic tremor per day. In the framework of a co-operative project between French and Costarrican institutions, a seismographic experiment has been carried out in 1997 with the aim of studying wave propagation in Arenal structure and improving the knowledge of its seismic sources. Ten small aperture or linear arrays have been set up, occupying 70 sites with seismometers. A 13 stations L-shaped array and 5 tripartite 60 m wide arrays with vertical 1 Hz seismometers were deployed around the volcano in order to test a method of tremor source location. Two semi-circular arrays with 3 components seismometers were set up with the object to obtain information on the seismic structure and wave type by using the spatial correlation method. Seismic signals were also recorded along two radial profiles, respectively of 16 stations, 3 km long to the west and of 9 stations, 1.8 km long to the east, to study the variations with distance of wave amplitude and polarisation. The data set was completed by a continuous recording broadband station, an acoustic sensor and observations from the digital permanent seismic network of OSIVAM-ICE. Among the preliminary results presented here, a striking observation is strong site effects in several stations of both radial profiles. This emphasises that great caution must be used when interpreting spectral, amplitude and polarisation data obtained in isolated stations.

**JSV47/W/25-B5** Poster **1400-18****PRESSURE COOKERS AS VOLCANO ANALOGUES**

Jonathan M. LEES and Edward W. Bolton (both at Department of Geology and Geophysics, Yale University, New Haven, CT, 06511)

We present a quantitative analysis of the oscillations of a household pressure cooker and relate the model to physical parameters in exploding volcanos in Kamchatka, Russia, and Sangay, Ecuador. Degassing of volcanos with viscous plugs produce several levels of periodicity, as does a pressure cooker held in a state of unstable equilibrium. The pressure cooker consists of a sequence of conduits where escaping, high temperature gases are inhibited by a weight that closes, or chokes off, the flow. The balance between the constraining weight and the internal pressure of the main chamber can be shown to produce a variety of oscillatory solutions, some of which exhibit chaotic behavior. We model the pressure cooker behavior by developing a system of coupled differential equations that relate the equation of motion for the constraining weight, pressure in the conduit, temperature and pressure in the boiling chamber, friction and ram effect, and production of gases at the source. Observations at several exploding volcanos show a quasi-periodic explosion cycle that includes, on occasion, a higher frequency (1 Hz) tremor, called chugging. Chugging is a world wide phenomena and has been observed at Kamrysky Volcano, Kamchatka, Sangay Volcano, Ecuador, Langila, Papua-New Guinea, and Semeru, Indonesia. These processes appear to be analogous to physical processes observed in the kitchen pressure cooker.

**JSV47/W/08-B5** Poster **1400-19**

**VARIATIONS IN SOURCE TYPE OF NON-DOUBLE-COUPLE EARTHQUAKES IN VOLCANIC AREAS**

G.R. FOULGER (Dept. Geological Sciences, University of Durham, Durham, DH1 3LE, Email: g.r.foulger@durham.ac.uk) and B.R. Julian (U. S. Geological Survey, 345 Middlefield Rd., Menlo Park, CA 94025, U.S.A., Email: julian@usgs.gov)

Volcanic and volcano-geothermal areas typically generate high levels of small magnitude earthquake activity, sometimes as continuous background activity and sometimes as transient swarms. Industrial exploitation of geothermal resources can also induce earthquakes. Such earthquakes are probably caused by hydraulic or magmatic fracturing or by the rapid transport of fluids. Although the appearance of the seismograms of such earthquakes are generally indistinguishable from those of common "tectonic" earthquakes, they often have non-double-couple focal mechanisms. Whereas such mechanisms were widely disbelieved a decade ago, now several case histories of detailed studies of non-double-couple earthquakes from volcanic and geothermal areas have accumulated. It is clear that there are systematic variations in their source types, as well as common features. Earthquakes from the Hengill-Grensadalur volcano-geothermal area, Iceland, have explosive mechanisms with CLVD components of varying sign and strength. In contrast, industrially-induced earthquakes from The Geysers geothermal area, California, along with other areas, have isotropic components of both signs, which are systematically correlated with the CLVD component. These observed trends have the potential to cast light on the source processes of these exotic types of earthquakes, and thus on fluid motion in magmatic and hydrothermal systems.

**JSV47/W/21-B5** Poster **1400-20**

**A PROBABILISTIC APPROACH FOR THE ESTIMATE OF THE SLOWNESS VECTOR FROM SEISMIC ARRAY DATA**

Dr Gilberto SACCOROTTI (Osservatorio Vesuviano - Centro di Sorveglianza, Via Manzoni 249, Naploio, Italy. Email: giberto@osve.unina.it) and E. Del Pezzo

Array analyses in volcano seismology is the main tool for detecting and quantifying the complex wave-field associated to the volcanic activity, mainly the volcanic tremor and the long period events. The methods based on the analysis of the signal in the frequency domain, or spectral methods (MUSIC algorithm), take the main vantage of both resolving closely-spaced sources and computer speed, but severely fail in the analysis of short duration signals. Conversely, the time domain methods, based on the cross-correlation estimate of signal pairs, can be applied even for short pulses. Both for time and frequency domain techniques, an exhaustive view of the errors associated to the slowness vector estimate does not exist. The estimate of the error is important in the inversion of the slowness vector for source location. In the present work we develop a method based on a probabilistic formalism, which allows for a complete definition of the uncertainties in the estimate of frequency-slowness spectrum based on the measure of the zero-lag cross-correlation. The method is based on the estimation of the theoretical frequency-slowness power spectrum, which can be expressed as the convolution of the true signal with the array response pattern. The application of the Bayes theorem allows for the final estimate of the data probability density function. The method is tested with synthetics using waveforms resembling the most common volcanic earthquakes, and applied to real data as an example.

**JSV47/W/10-B5** Poster **1400-21**

**PROSPECTS OF THE QUANTITATIVE TIME FORECAST OF VOLCANIC ERUPTIONS**

Alexander I. MALYSHEV (Institute of Geology and Geochemistry, Urals Branch of RAS, Pochtovy pr 7, Ekaterinburg, SU-620151, Russia, email: root@igg.e-burg.su)

It is known that many strong eruptions are anticipated by the periods of long-duration and steady increase of volcanic activity. Revealing and study of fore-paroxysmal activations represent large interest for the forecast of strong eruptions. During the study of Bezymjany volcano eruptions in 1980-1987 the fact of hyperbolic activation of deformational-extrusive process before explosive-effusive eruptions was established. Further studying of revealed laws and their comparison with empirical dependences of development of various natural processes have allowed to conclude that there is the wide class of self-developing natural processes, dynamics of which is described by the nonlinear differential equation of the second order. The attempts of using these laws for the forecast of eruptions were quite successful, however the accuracy of time forecast of eruption did not exceed a semiquantitative level. Technique, allowing confidently to reveal laws of development of natural processes, is at the moment developed. For a class of eruptions, with steady fore-culmination prepa-ration, this technique allows to increase accuracy of paroxysm time forecast up to a quantitative level.

**JSV47/W/29-B5** Poster **1400-22**

**DECEPTION ISLAND VOLCANO (ANTARCTICA): SEISMO VOLCANIC SOURCE ANALYSIS**

J.M. IBÁÑEZ (1,2), J. Almendros (1), E. Del Pezzo (3), G. Alguacil (1,2), M. La Rocca (4), A. García (5) and R. Ortiz (5). (1) Instituto Andaluz de Geofísica, Universidad de Granada. Campus de Cartuja s/n. 18071 Granada, Spain. (2) Departamento de Física Teórica y del Cosmos. Facultad de Ciencias, Universidad de Granada. 18071 Granada, Spain. (3) Osservatorio Vesuviano. Via A. Manzoni, 249, 80123 Napoli, Italy. (4) Dipartimento di Fisica. Università di Salerno. Via Salvador Allende. 84081 Baronissi, Salerno, Italy. (5) Departamento de volcanología. Museo Nacional de Ciencias Naturales. CSIC. C/ J. Gutiérrez Abascal, 2, 28006 Madrid, Spain.

During the Antarctic summers of 1994-95, 1995-96 and 1996-97 we monitored the seismic activity of Deception Island volcano (South Shetland Island, Antarctica) by a short-period small-aperture dense seismic array. We recorded thousands of seismic events and analysed hundreds of them in base of their good signal to noise ratio. The main part of the set of seismic events is composed by pure seismo-volcanic signals such, as volcanic tremor and long period events. Other recorded signals presented a shape and spectral contain that permitted us named them as hybrid events. Only some tens of tectonic earthquakes have been recorded and were classified in three groups: volcano-tectonic earthquakes (located inside of the island), regional seismicity and intermediate-focus earthquakes (focal depth between 50 and 120 km). To locate the position of the seismo-volcanic source we used the Zero-Lag Cross-Correlation technique. The back-azimuth between source and array and the apparent slowness of the coherent arrivals were obtained. To determine the epicentral distance of the volcanic signals we have introduced, to the above technique, the approximation of a circular incoming wave front. Using polarisation analysis and energy determination we completed these analyses. From them we can establish the follow observations: All the seismo-volcanic events are composed by two types of seismic waves, P waves and surface waves (mainly Rayleigh waves). No S-waves have been observed in these volcanic events. P-waves are concentrated at high frequencies and surface waves are located at the low-frequency predominant peaks. Volcanic tremor, long period events and hybrid share the same source area and the same array parameters at all frequency bands. It is possible to model the seismic

source, at low frequencies, using the Fluid Driven Crack model, under the assumption of water, as fluid, with gas bubbles (water vapour). From these observations, the interaction of molten water (originated in the extended glacier areas of the island) with hot materials (we have evidences of magma in the vicinity of the source area) could be the most probable source model of the observed volcano-seismicity in Deception Island.

**JSV47/W/30-B5** Poster **1400-23**

**LOCAL SEISMICITY AND ABSENCE OF OBSERVABLE VOLCANIC TREMOR AT TEIDE VOLCANO (CANARY ISLANDS, SPAIN)**

J. ALMENDROS (1), J.M. Ibáñez (1,2), G. Alguacil (1,2), J. Morales (1,2), E. Del Pezzo (3), M. La Rocca (4), R. Ortiz (5), V. Araña (5) and M.J. Blanco (6). (1) Instituto Andaluz de Geofísica. Universidad de Granada. Campus de Cartuja s/n. 18071 Granada, Spain. (2) Departamento de Física Teórica y del Cosmos. Facultad de Ciencias. Universidad de Granada. 18071 Granada, Spain. (3) Osservatorio Vesuviano. Via A. Manzoni, 249, 80123 Napoli, Italy. (4) Dipartimento di Fisica. Università di Salerno. Via Salvador Allende. 84081 Baronissi, Salerno, Italy. (5) Departamento de Vulcanología. Museo Nacional de Ciencias Naturales. CSIC. C/ J. Gutiérrez Abascal, 2, 28006 Madrid, Spain. (6) Delegación Regional del Instituto Geográfico Nacional en Canarias. 38001 Santa Cruz de Tenerife, Spain.

Data analysed in the present work correspond to a 40 days field experiment carried out in Teide volcano (Canary Islands, Spain) with two short-period small-aperture dense seismic antennas in 1994. The objective of this experiment was to detect, analyse and locate the local seismicity. We analysed also the background seismic noise to investigate the possible presence of pure volcanic signals, especially volcanic tremor.

From a set of 76 events, we selected 21 of them in base of their good signal to noise ratio and the possibility to locate their seismic source using the seismic antennas. A visual classification in base of the S-P time and shape has permitted us to establish three groups: local seismicity (S-P time between 3 and 5 seconds), volcano-tectonic earthquakes (S-P time smaller than 3 seconds), and non-natural earthquakes (mainly artificial explosions). These earthquakes have been located by applying the Zero Lag Cross-Correlation technique and the inverse ray-tracing procedure. Those earthquakes that were recorded simultaneously by both seismic antennas were also located by intersecting both back-azimuths.

The analysis of the seismicity has revealed that the amount of seismicity in Teide volcano is moderated. This seismicity could be distributed in three main areas: Inside of the Caldera edifice (below the Teide-Pico Viejo complex), in the border of the Caldera Edifice (possibly related with the 1704-05 eruption) and in the border of the island. At the present, this activity is the only indicator of the volcano dynamic.

The analysis of the back-ground seismic noise has revealed that, at frequencies lower than 2 Hz, the Oceanic Load signal is predominant over other signals, even over local earthquakes with magnitude 2.0. Due to that, although if in the Teide area were present a week volcanic tremor, or other volcanic signals with predominant peaks below 2 Hz, these signals could be very difficult to observe.

**JSV47/P/01-B5** Poster **1400-24**

**SEISMOLOGY DURING VOLCANIC CRISES IN ALASKA, 1989-1998**

Stephen R. McNUTT (Alaska Volcano Observatory, Geophysical Inst, University of Alaska, Fairbanks, USA. Email: steve@giseis.alaska.edu)

Abstract not available at time of going to press

**JSV47/L/01-B5** Poster **1400-25**

**DEFORMATION SIGNALS DERIVED FROM BROADBAND SEISMIC SIGNALS**

NEUBERG

Abstract not available at time of going to press

**JSV47/L/02-B5** Poster **1400-26**

**A NUMERICAL INVESTIGATION OF SEISMIC WAVES AND MAGMA DYNAMICS ASSOCIATED WITH A VOLCANIC ERUPTION**

Takishi NISHIMURA (Dept of Geophysics, Graduate School of Science, Tohoku University, Aoba-ku, Sendai, Japan. Email: nishi@zisin.geophys.tohoku.ac.jp)

Abstract not available at time of going to press

**JSA48** **Friday 30 July**

**CHARACTERIZATION OF THE LITHOSPHERE-ASTHENOSPHERE BOUNDARY (IAGA, IAVCEI, IASPEI, ILP)**

Location: Muirhead Tower, 112 LR2  
Location of Posters: Muirhead Tower, Student Room (1st floor)

**Friday 30 July AM**

**JSA48/E/14-B5** Invited **0830**

**THE AUSTRALIAN UPPER MANTLE - A CONTINENTAL SYNTHESIS**

B.L.N. KENNETT, E. Debayle (Research School of Earth Sciences, Australian National University, Canberra ACT 0200, Australia, email: Brian.Kennett@anu.edu.au); Y. Kaiho (Japan Marine Science and Technology Center, 2-15 Natsushima-cho, Yokosuka 237, Japan)

The combination of body wave and surface wave studies of the Australian continent using the abundant regional seismic sources places strong constraints on the nature of the lithosphere, the underlying asthenosphere and the mantle transition zone. The centre and west of Australia, with Proterozoic to Archaean surface exposure, is characterised by a thick lithosphere characterised by very fast shear wavespeeds extending to at least 200 km. Along the eastern seaboard there is a relatively thin lithosphere with a well developed low velocity zone for shear waves around 150 km deep. In the transitional region the structures are more complex with some high velocity material extending to at least 150 km below Phanerozoic surface rocks. The boundary of the thick lithosphere does not display any simple relation to the "Tasman line" which marks the eastern extent of Precambrian surface rocks. The asthenosphere displays significant seismic attenuation compared with the very low loss in the



cratonic lithosphere. Although the high seismic velocities in central Australia extend to 200 km, the pattern of azimuthal anisotropy derived from Rayleigh waves shows a significant change in pattern with depth a largely east-west pattern of fast wave speeds at 100 km depth is replaced at 150 km by a pattern with a marked trend nearly north-south, in concordance with the current direction of plate motion. This change occurs within the zone of high shear wave speed and so it would appear that deformation must be occurring in the base of the lithosphere.

#### JSA48/E/04-B5 0900

##### POLARIZATION ANISOTROPY IN THE AUSTRALIAN UPPER MANTLE FROM SIMULTANEOUS INVERSION OF RAYLEIGH AND LOVE WAVEFORMS

Y. HIYOSHI, E. Debayle, B.L.N. Kennett (All at Reserach School of Earth Sciences, The Australian National University, Canberra, ACT 0200, Australia. Email: hiyoshi@rse.su.anu.edu.au)

Events from the earthquake belt along the northern continental margin of Australia have been recorded for a decade at several permanent broad-band stations in the continent. The surface wave portion of these seismograms provides a unique opportunity for upper mantle investigation exploiting almost pure continental epicenter-station paths beneath Australia. Simultaneous waveform inversion of Rayleigh and Love seismograms including several overtones allows the determination of the polarization anisotropy of the S waves as well as the SV wave speed and attenuation factor (Q) in the upper mantle beneath each epicenter-station path. This approach has been applied to the vertical and tangential components of seismograms recorded at two permanent stations (NWA0 - IRIS and CAN - GEOSCOPE) in Australia for epicenters are distributed along the northern continental margin. We invert for the anisotropic parameter  $\xi$ , the SV wave speed and the quality factor (Q). Our results suggest that the upper mantle beneath western Australia has (1) a low velocity zone associated with strong attenuation lying between about 200 km and 400 km depth; and (2) polarization anisotropy reaching down to at least 300 km depth.

#### JSA48/E/02-B5 0920

##### MAPPING THE LITHOSPHERE-ASTHENOSPHERE BOUNDARY (LAB) THROUGH CHANGES IN SEISMIC ANISOTROPY

J. PLOMEROVA, V. Babuska, D. Kouba (Geophysical Institute, Czech Acad. Sci., 14131 Praha 4, Czech Republic, email: jpl@ig.cas.cz)

The alignment of olivine crystals is the dominant source of seismic anisotropy in the subcrustal lithosphere and asthenosphere. Different constituents of large-scale anisotropy related to the crust, mantle lithosphere and sub-lithospheric mantle can be traced in depth distributions of the radial and azimuthal anisotropy of surface waves. Thus Earth's boundaries, such as the M-discontinuity or LAB in the upper mantle, as physical boundaries, can be detected by distinct changes of seismic anisotropy. These changes map orientations of a large-scale fabric of different tectonic settings and geological age. The M-discontinuity can be understood as an intra-lithosphere boundary between anisotropic structures of crustal composition and a frozen-in olivine anisotropy in the mantle lithosphere. Similarly, the LAB can represent a change of this frozen-in anisotropy to the present-day anisotropy in the sub-lithospheric mantle related to the upper mantle flow. 3D velocity images of the upper mantle from body wave tomographies map the LAB as a top boundary of the low-velocity zone, considering isotropic wave propagation. Beneath the Precambrian shields and platforms, where a steeply oriented olivine fabric was deduced from surface-wave analyses, the velocity contrast related to the LAB can increase in particular directions. Due to long wave-lengths, the surface waves suffer from laterally integrated effects, but possess a good vertical resolution allowing us to extract gross features of the LAB. Depths of the LAB between 200 and 250 km for the Archean cratons and around 100 km on the average beneath the Phanerozoic regions, are estimated from the radial and azimuthal anisotropy of surface waves.

#### JSA48/P/02-B5 0940

##### DEPTH RESOLUTION OF UPPER MANTLE RESISTIVITY MODELS FROM ELECTRO-MAGNETIC RESPONSES ON CONTINENTS

Ulrich SCHMUCKER (geophysikalisches Institut, Herzberger Landstr. 180, D-37075 Göttingen)

The depth range from 100 to 400 km is the most inaccessible one for electromagnetic induction studies, involving natural source fields between 1 and 6 hours period. At these periods local magnetotelluric MT sounding curves have split at most sites into two distinct branches of maximum and minimum apparent resistivity, at least on continents, while global geomagnetic deep soundings GDS start at 400 km, which is the penetration depth of the fourth harmonic of daily variations. The resulting gap towards unsplit MT results could be closed with regional GDS, notably in jet regions, but this possibility has been rarely used so far. It has been found that MT phases from 6 to 24 hours period reproduce most faithfully global GDS phases of daily variations (for the ra-maximum branch) and thus can be utilized tentatively to close the gap. How does this incomplete knowledge constrain resistivity models for the continental upper mantle, and will it be sufficient for detecting fine structures, which could be associated with Gutenberg's low velocity layer? This question will be addressed, also in conjunction with empirical GDS and MT data. From global GDS alone the upper mantle appears as featureless, moderately resistive region of 70 Wm, which is the expected value for the prevailing temperatures, and no need seems to exist for special effects lowering resistivity in Gutenberg's layer. How accurate would MT phases have to be, from 1 to 6 hours period, for a finer resolution?

#### JSA48/P/01-B5 1000

##### A MAP ON THE CONDUCTIVE ASTHENOSPHERE OF THE PANNONIAN BASIN AND LIMITATION IN ITS CONSTRUCTION

Antal Ádám (Geodetic and Geophysical Research Institute of the Hungarian Academy of Sciences, H-9401 Sopron, POB 5, Hungary, email: adam@ggki.hu)

In the early sixties it has been stated on the basis of deep magnetotelluric soundings that the conductive asthenosphere is upwelling to a depth of 60 km in the central part of the Pannonian Basin (Hungary) in close connection with the high heat flow of the area (~100 mW/m<sup>2</sup>) and it deepens towards the rim of the Basin and reaches in the platforms (e.g. EEP) 100-200 km. Beneath deep extensional basins (e.g. 7 km deep Bækæs graben) the asthenosphere can even reach depth of 40-50 km. It was certainly a plume in the Miocene synrift era having strong ultramafic intrusion in the crust.

It has been tried to construct a map about the depth of the conductive asthenosphere in the Pannonian Basin with correction of the EM distortions (static shift, 3D inhomogeneity  $\mathcal{A}$ E decomposition). The author points to the difficulty of the corrections and compares the map with the results obtained by other geophysical methods (first of all by deep seismics and tomography).

#### JSA48/E/06-B5 Invited 1040

##### PETROLOGIC AND GEOPHYSICAL CHARACTERISTICS OF THE LITHOSPHERE-ASTHENOSPHERE BOUNDARY THROUGH EARTH'S EVOLUTION

Suzanne Y. O'REILLY, William L. Griffin, (GEMOC National Key Centre, Dept of Earth and Planetary Sciences, Macquarie University, NSW, 2109, Australia, Email: sue.oreilly@mq.edu.au, bill.griffin@mq.edu.au; WLG also at CSIRO EM, PO Box 136, N. Ryde, NSW 2113, Australia)

The lithosphere-asthenosphere boundary (LAB) is an interface that reflects the fundamental evolution of the Earth into major geochemical reservoirs driven by global thermal processes. The depth to the LAB varies significantly with the tectonothermal age of lithosphere domains and is a function of the geochemical nature of the lithospheric mantle column and its thermal state which determine its density and rheological response. The Earth's lithospheric mantle is non-convecting and does not mix easily; therefore it carries a geochemical imprint of major melting events and subsequent fluid fluxes (metasomatism). Lithospheric mantle has undergone significant (probably multiple) melting and is depleted in "basaltic" components such as Fe, Al, Ca and Ti. Asthenosphere by contrast, is "fertile" (rich in basaltic components) and geochemically more homogeneous than lithosphere because it is convecting. Mantle xenoliths and their disaggregated minerals (especially garnet and chromite) brought to the surface in basalts and kimberlites, can be used to construct sections of the spatial distribution of rock types with depth in the lithospheric mantle, to estimate empirical palaeogeotherms, and to locate the depth to the LAB. This geochemically determined LAB depth coincides with estimations of depth using geophysical datasets, especially seismic refraction and magnetotelluric. We have established that the mean geochemical composition of the subcontinental lithospheric mantle shows an episodic, secular and apparently irreversible change from Archean to Proterozoic to Phanerozoic. Density and seismic measurements and calculations for these mantle types show increasing density and a decrease in Vp and Vs with decreasing age. Geothermal gradients increase concomitantly and average depths to the LAB decrease from about 220 km to 180 km to 100 km respectively. Density and thermal differences in these distinctive mantle volumes determine the relative buoyancy of the specific lithospheric mantle column relative to asthenosphere. Thus the geochemical composition and thermal state of lithospheric mantle may control the location of the LAB through time and result in the different geophysical signatures.

#### JSA48/E/10-B5 1110

##### HOW THICK IS THE LITHOSPHERE IN THE CENTRAL FENNOSCANDIAN SHIELD? IMPLICATIONS FROM MANTLE XENOLITHS, THERMAL AND RHEOLOGICAL MODELS

Ilmo T. KUKKONEN, Petri Peltonen (both at Geological Survey of Finland, P.O. Box 96, FIN-02151 Espoo, Finland, e-mail: ilmo.kukkonen@gsf.fi)

Thermobarometric studies of kimberlite-hosted mantle xenoliths in eastern Finland, the central Fennoscandian Shield, suggest an exceptionally thick lithosphere in this area, at least 240 km. All recovered xenoliths are lithospheric in character, contain no primary volatile-bearing minerals, and carry no evidence of an asthenosphere. The thermobarometric data were used to calibrate a 2 dimensional thermal lithosphere model, and the xenoliths are in an agreement with a conductive geotherm corresponding to a surface heat flow density value of 36 mW/m<sup>2</sup>. A direct estimate from the thermobarometric data suggests a temperature gradient of 3.7 +/- 0.6 K/km and heat flow density of 11 +/- 4 mW/m<sup>2</sup> in the mantle which is lower than usually considered for the continental mantle. Using the calibrated geotherm, a rheological model of the lithosphere was constructed, and it suggests that the mechanical thickness of the lithosphere is only 130-185 km, depending on the applied values of rheological parameters and creep strength of mantle rocks. The seismic lithosphere thickness is poorly known in this area, but the available data suggest values comparable to the rheological lithosphere thickness. The central part of the shield apparently has a thick root under the rheological lithosphere, and it is transported together with the lithospheric plate as a thermal boundary layer. Our results suggest possible absence or only a very weakly developed partially molten asthenospheric layer under this part of the shield, but do not exclude its existence at depths exceeding 240 km.

#### JSA48/E/08-B5 1130

##### MELT-PERIDOTITE INTERACTION AT THE LITHOSPHERE-PLUME BOUNDARY: IMPLICATION FOR THE MECHANISM OF LITHOSPHERIC THINNING

Yigang XU (Guangzhou Institute of Geochemistry, Chinese Academy of Sciences, 510640 Wushan Guangzhou, P.R. China, email: gdjzh@public.guangzhou.gd.cn); Jean-Louis Bodinier (Geofluides-Bassin-Eau, UMRC5569, CNRS, Université Montpellier 2, F-34095, Montpellier, France); Martin A. Menzies (Geology department, Royal Holloway University of London, Egham, Surrey TW20 0EX, UK)

Poikiloblastic harzburgite xenoliths from Boree, French Massif Central have been interpreted as the deepest spinel facies mantle segments samples by alkalis basalts. However, there exists considerable debate about their petrogenesis. The previous cumulative and isochemical recrystallization models are inadequate when the petrologic characteristics of these poikiloblastic samples are taken into account. On the basis of the newly acquired petrologic, geochemical data and trace element numerical modeling, it is believed that the Boree poikiloblastic peridotites were formed as a results of melt-percolation in a lherzolite precursor during lithospheric erosion by an upwelling plume. If our interpretation is correct, this study provides the evidence for the thermal erosion of the lithosphere accompanied by pervasive porous flow of the asthenospheric melts. This latter process assists the lithospheric erosion by modifying microstructure and modal composition of peridotite and then enhancing permeability of the MBL. Coupled with the thermal effect, this process is able to weaken the lithosphere allowing its mechanical removal by asthenosphere.

#### JSA48/E/07-B5 1150

##### THE THERMAL CHARACTERISTICS OF LAB DEDUCED FROM MAGSAT MODEL

Xiaoping GAO (Lanzhou Institute of Plateau Atmospheric Physics, CAS, 730000 Lanzhou, P.R.China, email: xgao@lzu.edu.cn); Giovanni P. Gregori (Istituto di Fisica dell'Atmosfera, CNR, 00133 Rome, Italy, email: gregori@atmos.ifa.rm.cnr.it)

It is well known that electric currents exist in the Earth. The Earth's magnetic field is produced by the currents. These currents can produce heat because of the resistance of the material of the Earth (called Joule heat). This electric current can be derived from geomagnetic field data



## INTER-ASSOCIATION

or model. Till now, the best geomagnetic field del(MAGSAT) had been gotten by satellite global observation in 1979-1980. By this model, the global distribution of Joule Heat on ALB(Asthenosphere-Lithosphere Boundary) (direct proportion to electric current square) had been calculated. It is found that the distribution of Joule Heat on ALB matches the global geothermal zones very well. And the strongest Joule's Heating is located under Tibet Plateau, the youngest and the highest plateau on the Earth. It seems that the geothermal heat mostly comes from ALB, it is controlled by Joule's Heating process.

**JSA48/P/04-B5**

**1210**

### THE THERMAL CHARACTERISTICS OF THE LITHOSPHERE-ASTHENOSPHERE BOUNDARY

Leonid LEVIN (Centre GEON Regional Geophysical and Geoenvironmental Data, 119034, Chisty per. 4, Moscow, Russia, email: moscow@geon.msk.ru)

A determination of the position of the thermal boundary between the lithosphere and the asthenosphere is based on the data of heat flow used for calculation of depths of the isotherms 600 and 1200°C. This boundary is characterized by inversion of viscosity between the lithosphere and asthenosphere and varies in a wide depth's range from more than 300 km near shields of cratons to less than 5-10 km under rifts of mid-oceanic ridges. At the background of the earth's change, this boundary rises in the zones of the asthenosphere upwelling which are confined to different large tectonic elements of the oceans and continents. In some orogens, there are two boundaries with inversion of viscosity - the upper is above the asthenolenses i.e. intracrustal zones of partial melting and the lower coincides with the top of the asthenosphere proper. The upwelling zones migrated repeatedly in time and space and the recent lithosphere/asthenosphere boundary was formed only at the neotectonic stage.

**JSA48/E/13-B5**

**1230**

### HIGH RESOLUTION IMAGE OF THE LITHOSPHERE-ASTHENOSPHERE BOUNDARY IN CONTINENT OF CHINA AND ITS ADJACENT AREA

Zhu JIESHOU, Cao Jamin, Cao Xiaolin, Zhang Xuemei (Dept. of Geophysics, Chengdu University of Technology, Chengdu 610059, China, email: zhujs@cdut.edu.cn)

Recently, due to the setting and observing of the global observation system of geophysics and geodesy, it became possible to do seismic tomography in detail to view the three-dimensional structure of the deep interior of the Earth. The high resolution seismic surface wave tomographic image for the Lithosphere-Asthenosphere Boundary (LAB) will provide the lateral heterogeneity of the upper mantle, and deep background of craton, mountain ranges, rifts and basins of the continent.

We have collected about more than 4000 long period digital seismic records from 21 stations of GSN and CDSN, which located at China, Japan, Thailand, India, Russia, Indonesia. The high resolution tomographic inversion had been conducted by processing these surface wave data. The three-dimensional velocity image from earthb 60o 0N in latitude and from 60o 0E to 160o 0E in longitude. The lateral variation of LAB mainly reflects the differences of the combinative continental blocks in China and its adjacent area. The thickened lithosphere (140-250 km) located at Tarim, Yangtze, Ordos, Indo-China block and Indian plate. The thinning lithosphere (70o-100 km) mainly appears in rifting zones or graben such as Songliao and North China subsiding zone, and southeastern coastal folding belt, in the orogenic belts such as North-South tectonic belt in central China and Qinling-Dabieshan mountain range, and in the marginal sea (South China Sea, East China Sea, Japan sea, etc). The lower boundary of asthenosphere is clearly shown from 200 to 300 km depth. There obviously exist low velocity asthenosphere which is related with upwelling plume at shallow part of the mantle in west Pacific margin. The hot plumes possibly caused by upwelling heat flow that originated by plate's friction in the subduction zone.

Friday 30 July PM

**JSA48/W/03-B5**

**1400**

### HEAT TRANSPORT IN STAGNANT LID CONVECTION WITH TEMPERATURE AND PRESSURE DEPENDENT NEWTONIAN OR NON-NEWTONIAN RHEOLOGY

Caroline DUMOULIN, M.P. Doin, L. Fleitout (Ecole Normale Supérieure, France, Email: dumoulin@jadeite.ens.fr)

A numerical model of two-dimensional Rayleigh-Benard convection is used to study the relationship between the surface heat flow (or Nusselt number) and the viscosity at the base of the lithosphere. Newtonian or non-Newtonian, temperature and pressure-dependent rheologies are considered. In the high Rayleigh number time-dependent regime, calculations yield:  $Nu$  proportional to  $Ra^{0.33/beff}$ , where  $beff$  is the effective dependence of viscosity with temperature at the base of the upper thermal boundary layer and  $Ra$  is the Rayleigh number calculated with the effective viscosity at the base of the upper thermal boundary layer. The heat flow is the same for Newtonian and non-Newtonian rheologies if the activation energy in the non-Newtonian case is twice the activation energy in the Newtonian case. In this chaotic regime the heat transfer appears to be controlled by secondary instabilities developing in thermal boundary layers. These thermals are advected along the large scale flow. The above relationship is not valid at low heat flow where a stationary regime prevails and for simulations forced into steady state. In these cases, the Nusselt number follows a trend  $Nu$  proportional to  $Ra^{0.2/beff}$  for a Newtonian rheology, as predicted by the boundary layer theory. We argue that the equilibrium lithospheric thickness beneath old oceans or continents is controlled by the development of thermals detaching from the thermal boundary layers. Assuming this, we can estimate the viscosity at the base of the stable oceanic lithosphere. If the contribution of secondary convection to the surface heat flux amounts to 40 to 50 mW.m<sup>-2</sup>, the asthenospheric viscosity is predicted to be between  $2.10^{18}$  and  $3.10^{19}$  Pa.s.

**JSA48/L/01-B5**

**1420**

### MODELS OF SOUTH-WEST PART OF BAIKAL RIFT DEFORMATION BY THE EXPERIMENTAL DATA

Vladimir Timofeev, Dmitry Ardukov (Institute of Geophysics UIGGM SB RAS, Koptug pr. 3, 630090, Novosibirsk, Russia, email: sari@uiggm.nsc.ru); Bernard DUCARME (Observatoire Royal de Belgique, Avenue Circulaire 3, 1180 Bruxelles, Belgium, email: B.Ducarme@oma.be); Arnaudov G.P., Kalish E.N., Stus Y.F. (Institute of Automatic and Electrometry SB RAS, Koptug pr. 1, Novosibirsk, Russia); A.Y. Ribushkin, V.M. Semibalamut (Siberian EMLP GS SB RAS, Lavrientiev pr.13/3, 630090, Novosibirsk, Russia)

Results of 1990-1995 strain measurements in the underground gallery of Talaya station (51.68 N, 103.65 E, Baikal rift) and results of annual measurements of gravity are discussed. Determination of main axis strain were got. Maximum variation were got for shear strain, annual value 3W/10-6, maximum changes was got for strong earthquake M=6.5 period. Deviatoric tectonic stress was near 0.6 MPa. Stability of gravity field by laser gravimeter

GABL-M measurements was near the error level 0.5-1.0 microGal. From this determination level of vertical movement was got near 1mm per year. The Budiasky-Amazigo (fault slip and lithospheric creep) model and Elsasser two-layer (lithosphere-asthenosphere) model were examined by using our experimental results. We got the value of asthenospheric viscosity (1.2W 1020 PaWs) from the calculation with experimental strain results and Elsasser model. The deviatoric tectonic stress for Siberian platform lithospha (18 MPa) was got from the calculation by using the GPS data for Irkutsk station (3cm/ y, 1010N), the value of the asthenospheric viscosity and Elsasser model.

**JSA48/W/02-B5**

**1440**

### TWO STAGE LITHOSPHERE DELAMINATION: A GEODYNAMIC MODEL FOR MESO-CENOZOIC VOLCANISM OF THE NORTH-EASTERN REGION OF NORTH CHINA CRATON AND RELATED DEPTH CHANGE OF LITHOSPHERE-ASTHENOSPHERE BOUNDARY

Yang WANG (Lab. for Geothermics, Institute of Geology, Chinese Academy of Sciences, P.O.Box 9825, Beijing 100029, China, email: thalassa@263.net)

From Triassic to Neogene, five volcanic activities had occurred in the north-eastern region of North China Craton. The first is Triassic small scale basaltic volcanism, which Nd,Sr,Pb isotopes are characterized by the existence of subducted oceanic crust and EM II type mantle source; the second is Jurassic trachyandesitic volcanism, which is dominated by EM I type source; the third is Early Cretaceous rhyolitic volcanism, which is also characterized by EM I source; the fourth and fifth volcanism occurred in Palaeogene and Neogene respectively, which sources represent a mixture of primary mantle(PM) and depleted mantle(DM) components. Related to these volcanism and extension in Cenozoic, the depth of lithosphere-asthenosphere boundary(LAB) ascended from about 150 km in Late Palaeozoic to about 50 km in present. Based on the mineralogical and petrological studies on these volcanic rocks and the mantle fragments in them, and numerical simulation of small scale mantle convection, we proposed a geodynamic model, two stage lithosphere delamination, to explain the origin of volcanism and related geochemical characteristics. The first stage delamination started in Triassic, and the basalt came from the lower part of lithosphere mantle, in where ancient subducted oceanic lithosphere stored. The delamination induced the forced convection of asthenosphere, and Jurassic volcanism was originated by the break off of the upper boundary layer of convection cell. Early Cretaceous volcanism was related to the melting of underplating material which ascended from lower mantle. The LAB under the north-eastern region of North China Craton ascended from ~150 km to ~80 km after the first stage delamination. The second delamination occurred in Cenozoic. It induced the melting of subcontinental lithosphere of North China Craton, which has PM and DM characteristics; and caused the depth of LAB under this region ascending from ~80 km to 50-60 km. Nowadays all of isotope geochemistry, mineralogy and petrology evidences support our idea that, two stage lithosphere delamination induced Meso-Cenozoic volcanism in the north-eastern region of North China Craton, and resulted in the ascending of LAB beneath this region.

**JSA48/E/05-B5**

**1500**

### LITHOSPHERIC STRUCTURE OF DHARWAR CRATON USING MAGNETOTELLURIC STUDIES

S.G. Gokarn, C.K. RAO, Gautam Gupta (Indian Institute of Geomagnetism Colaba, Mumbai, email: kamesh@iig.iigm.res.in)

The Dharwar craton is a part of the South Indian craton, bounded on the north by the Kaladgi and Bhima basins, on the east by the Eastern Ghat mobile belt and on the south by the granulitic terrains of Kerala and Tamilnadu. On the basis of the nature of the metamorphism of the schist belts, Dharwar craton is divided into the eastern and western Dharwar groups, the line of divide coinciding with the Chitradurga fault. The eastern Dharwar rocks show a low pressure metamorphism with younger granitic intrusives, whereas in the western Dharwar region, the intermediate metamorphic grades are observed.

Magnetotelluric studies were conducted over a 350 km long E-W profile with an interstation spacing of 5-10 km. The data shows mostly a one dimensional structure, except some two dimensional effects near Hebsur which is located on the Chitradurga fault. The crustal structure on the east of the Chitradurga fault is "normal as observed in other stable continental regions, with 15-18 km thick crust overlying a mid-crustal conductor. The lower crust and the upper mantle have a resistivity of 1000 ohm-m. A conductive layer is delineated at a depths of about 180 km presumably due to liquid phase, normally associated with the lithosphere-asthenosphere boundary. On the west of Chitradurga fault, the crustal structure is uncharacteristic of the Precambrian cratons. The crustal thickness is higher (22-25 km) and the mid-crustal conductor which is normally observed in the cratonic regions is absent here. The lower crust and upper mantle have a resistivity of 1000 ohm-m. The Chitradurga fault zone is not associated with any appreciable conductivity changes and is thus delineated as a deep vertical divide between the regions with different crustal thicknesses and crustal configurations near Hebsur extending in depth up to the bottom of the upper crust.

**JSA48/E/03-B5**

**1515**

### DEGENERATION OF SUBLITHOSPHERIC MANTLE BENEATH THE CRATONIC AREAS OF THE INDIAN PENINSULAR SHIELD

O.P. PANDEY, P.K. Agrawal (National Geophysical Research Institute, Uppal Road, Hyderabad 500 007, India, email: postmast@csngri.res.nic.in)

Recently, there has been a growing curiosity to understand the deformation of the deep continental roots beneath the Archean- early Proterozoic terrains of the world. These studies suggested the possibility of shearing of sublithospheric mantle caused by plate motion beneath ancient cratonic roots. In the present work, we study the thermal structure beneath the cratonic regions of the Indian shield, which include Aravalli and Singhbhum cratons in the north, Bastar craton in the central, and Dharwar craton and granulite terrain in the southern peninsula. The study reveals a large lithospheric thickness variation from 65 km in the Singhbhum craton to 148 km in the Archean Dharwars. An estimate of 104 km average depth to the top of asthenosphere beneath these cratons conforms well with the findings from other studies and is found to be less than half the 200-400 km thick lithosphere in other stable areas of the earth. Similarly, the average reduced flow of about 35 mW/m<sup>2</sup> and Moho temperature of 555 C (range 400-730 C) in these areas are found much higher than their counterparts in the world. Thus, our study indicates a large scale deformation of the sublithospheric mantle beneath the Indian shield since Meso-Proterozoic times and questions the hitherto believed tectonic stability of the cratons.

JSA48/W/01-B5 1530

## MAGNETOTELLURICS OF UPPER LITOSPHERE ON THE SOUTH RUSSIAN FAR EAST

Alexander VOITENOK (Institute of Tectonics and Geophysics, RUSSIA, Email: u153vaa@rtzi.ru)

During a long period of time in the south of Far East of Russia were carried out magnetotelluric sounding. The works were carried out by the various executors using the equipment with various sensitivity and frequency characteristics. The points of researches are located on a rarefied network of extended profiles. The purpose of the majority soundings was study of conducting formations in the crust and the top mantle. The geoelectric situation in region is dual. On the one hand, in region are absent powerful shallow layers of conducting formations. The sedimentary cover conductivity, as a rule, does not exceed 20 Simens. This factor is favorable for studying depth conducting derivations. On the other hand, the wide circulation of galvanic distortions of impedance dependences is characteristic of high-resistance surface derivations. Everywhere the static shift of dependences have place. So, the data processing method must be oriented on the previous exception of static shifts. Three methods of exception were used. 1) The averaging in square window. This method inevitably lead to the loss of information. It was used in general for old data, with absent phase. 2) Shift of obtained amplitude curves to overlay them low-frequency parts with the normal model's curve. Unfortunately, often is difficult to estimate, how correctly overlay is executed. 3) The simultaneous interpretation of impedance's amplitude and phase for simple 1D layered model with small laves count. Simultaneously with the definition of model parameters, the value of static shift may be defined as one of model parameters. This method, I consider, is more useful and perspective and it is well coordinated with first two methods. After the obtaining of static shift, amplitude curves may be corrected on this shift's value. Then the more exact inverse is carried out for the depth conductivity structure discovering. For studying of distortion effects, which are caused by lateral discontinuities, the finite element's modelling is executed. The following results were obtained: 1) The lower crust's conductive layer is detected almost everywhere, but it is fragmental under ancient geological structures. 2) Thin conductive layer was detected in upper crust of ancient structures on the depth near 10 km. 3) The asthenosphere was not detected under the old structures, but it was detected under the young structures, in particular near to sea coast. So, the main tendency is observed and it show, that the upper lithosphere's conductivity is growing with transition to younger geological structures.

Friday 30 July PM

JSA48/E/01-B5 Poster 1600-01

## LITHOSPHERE-ASTHENOSPHERE BOUNDARY AS A DENSITY DISCONTINUITY

Miroslav BIELIK (Geophysical Institute, Slovak Academy of Sciences, Dúbravská cesta 9, 842 28 Bratislava, Slovak republic, email: geofmiro@savba.sk); Robert Lillie (Dept of Geosciences, Oregon State University, Corvallis, Oregon, 97331-5506, USA, email: lillier@bcc.orst.edu); Jan Sefara (Department of Applied and Environmental Geophysics, Comenius University, Mlynska dolina, 84215 Bratislava, Slovak republic, email: geofyzika@fns.uniba.sk)

Recent extensive gravimetric study involving integrated application of other geophysical and geological constrains in different European collisional and extensional regions indicates that lithosphere-asthenosphere boundary is also observed as a density boundary. Geophysical characterization of the lithosphere-asthenosphere boundary in the Western Carpathians and the Pannonian basin is also presented. Modelling of gravity anomalies by isostatically balancing effects of topography, the crust-mantle boundary and the lithosphere-asthenosphere boundary for the lithosphere-asthenosphere system as a whole suggests a relatively small (about -30 kgm<sup>-3</sup>) density contrast. The results of integrated interpretations in the Eastern Alpine-Carpathian-Pannonian basin-Transylvanian basin region and Scandinavian Caledonides clear show that the lithosphere-asthenosphere boundary is necessary take into consideration for density modelling of long-wavelength gravity anomalies. This boundary is playing important role in analysis and better understanding of the observed gravity anomalies in different tectonic setting.

JSA48/E/15-B5 Poster 1600-02

## JOULE HEAT DISTRIBUTION AND GEOTHERMAL ZONES

Xiaoqing GAO (Lanzhou Institute of Plateau Atmospheric Physics, CAS, 730000 Lanzhou, P.R. China, email: xqgao@lzu.edu.cn); Giovanni P Gregori (Istituto di Fisica dell'Atmosfera, CNR, 00133 Rome, Italy, email: gregori@atmos.ifa.rm.cnr.it)

According to the Geodynamo Theory, electric current exists in the Earth. It can produce heat because of the resistance of the material of the Earth. This electric current can be derived from geomagnetic field data or model. Till now, the best geomagnetic field model (MAGSAT) was gotten by satellite global observation in 1979-1980. By this model, the global distribution of Joule Heat on ALB (Asthenosphere-Lithosphere Boundary) (direct proportion to electric current square) had been gotten. It is surprisingly found that the distribution of Joule Heat on ALB matches the global geothermal zones very well. And the strongest Joule's Heating is located below Tibet Plateau, the youngest and the highest plateau on the Earth. It seems that the geothermal heat mostly comes from ALB, it is controlled by Joule's Heating process.

JSA48/W/07-B5 Poster 1600-03

## SEISMIC IMAGE OF LITHOSPHERE BENEATH THE EASTERN TIBET

G. L. KOSAREV (Institute of Physics of the Earth, B. Gruzinskaya 10, Moscow, 123810, Russia, email: kosarev@synapse.ru), R. Kind, S. V. Sobolev, X. Yuan, W. Hanka (all at GeoForschungsZentrum Potsdam, Telegrafenberg, 14473 Potsdam, Germany), S. Oreshin (Institute of Physics of the Earth, B. Gruzinskaya 10, Moscow, 123810, Russia)

A new method of imaging of the lithosphere structure in a vertical cross-section from a set of receiver functions has been applied to the data of two experiments: 1991-1992 Sino-American Tibet PASSCAL experiment, and 1994 international INDEPTH II experiment. The image along the vertical North-South profile crossing the Tibetan Plateau is analyzed. Moho discontinuity, the inner crustal structure, 410 km, 660 km discontinuities in the mantle transition zone are clearly seen along the whole profile. We were able to resolve the laterally inhomogeneous behavior of low-velocity zones and some discontinuities inside the Earth crust. An inclined discontinuity dipping to the north from the 100 km to 250 km depth is a continuation of earlier discovered inclined structures inside the Earth crust in the Zangbo suture zone. This discontinuity is interpreted as the upper boundary of the subducting Indian lithosphere. Under northern Tibet a less clear south dipping structure is also identified. We are also trying to interpret these observations.

JSA48/W/06-B5 Poster 1600-04

## DEEP SEISMIC STRUCTURE OF THE BAIKAL RIFT: HYPOTHESES AND REALITY

V. V. Mordvinova (Institute of the Earth's Crust, Irkutsk, Russia); L. P. Vinnik, G. L. KOSAREV, S. I. Oreshin, A. V. Treusov (all at Institute of Physics of the Earth, B. Gruzinskaya 10, Moscow, 123810, Russia, email: kosarev@synapse.ru)

We present an analysis of digital seismic records that were obtained in the cooperative Russian-American teleseismic experiment of 1992. It was believed previously that an asthenospheric upwelling, which reaches the bottom of the crust is present underneath the rift zone. Our tomographic analysis indicates, however, that the lithosphere-asthenosphere boundary is indeed uplifted underneath the rift zone, but the depth of the boundary is 100 - 150 km. The value of the scaling coefficient for the lateral variations of the S and P residuals fits the theoretical values for thermal or compositional variations in the absence of melting (around 2.0). The waveforms and amplitudes of the Ps converted phases from the Moho boundary are similar in the rift zone and the neighbouring regions. To summarize, our study reveals a thick subcrustal lithosphere underneath the rift zone and allows first time to reconcile seismic data with the values of heat flow and the estimates of elastic thickness of the lithosphere based on the gravity modelling.

JSA48/E/12-B5 Poster 1600-05

## CHARACTERIZATION OF THE LITHOSPHERE-ASTHENOSPHERE BOUNDARY IN THE PRICASPIAN BASIN, RUSSIA

Uri Shigaev, Leonid ANISSIMOV (Saratov State University, Astrakhanskaya83, Saratov 410026, Russia, email: anisimov.gl.sgu@oda.ssu.runnet.ru)

Examination of electrical conductivity of the crust and mantle in the Pricaspian Basin shows two main layers with high conductivity: the upper layer (10-15 km) with conductivity to 1000 Sm and specific resistivity of 15-20 Omm, and lower layer (70-80 km in the inner part of the basin and 100-110 km in the outer part of the basin) with conductivity to 6000-8000 Sm and specific resistivity of 10 Omm. These layers correspond to low P- and S wave velocity layers. The Basin is characterized by thermal heterogeneity with increased heat flow in the central part. These data prove the point of view that the mantle surface is higher in the central part of the Basin. Mantle uplift is the main reason of the consolidated section thinning and subsiding the Basin during Permian, Triassic and Neogene periods. Basin subsidence formed dilatancy zones along the perimeter of structure and activated he migration processes from the mantle to the sedimentary section. Lithosphere-Asthenosphere boundary is a zone with the fluid generation and rising this surface activates this process. Upper layer with the high conductivity corresponds to upper part of the basement and reflect increasing water content in this interval. Taking into account these data, we presuppose the occurrence of more permeable zones on the contacts: "sedimentary section-crust" and "crust-mantle".

JSA48/E/11-B5 Poster 1600-06

## NETWORK-MT OBSERVATION IN JAPAN AIMING AT DETERMINING REGIONAL SCALE DEEP ELECTRICAL CONDUCTIVITY STRUCTURE

Makoto UYESHIMA (Earthquake Research Institute, Univ. of Tokyo, Tokyo, 113-0032, Japan, email: uyeshima@utada-sun.eri.u-tokyo.ac.jp); Utada, H., Sasai, Y. (ERI, Univ. Tokyo, Japan); Nishida, Y. (Hokkaido Univ., Japan); Mishina, M. (Tohoku Univ., Japan); Nishitani, T. (Akita Univ., Japan); Yamaguchi, S. (Kobe Univ., Japan); Shiozaki, I. (Tottori Univ., Japan); Murakami, H. (Kochi Univ., Japan); Oshiman, N., Sumitomo, N. (DPRI, Kyoto Univ., Japan); Tanaka, Y., Hashimoto, T. (AVL, IGS, Kyoto Univ., Japan); Amita, K. (BGRL, IGS, Kyoto)

In Japan, Network-MT project is now going on, aiming to understand the ongoing tectonics of the Japan island arc by disclosing deep subsurface electrical conductivity structure related to large-scale tectonic features such as the plate subduction. Unlike usual magnetotelluric studies, electric field variations with 10 km scale are measured by employing the commercial telephone line network. Owing to the long electrode spacing, the observed electric field possesses a high S/N ratio and are relatively free Si

JSP49 Friday 30 July

## SMALL-SCALE FLOW, TURBULANCE AND MIXING (IAPSO, IAVCEI, IAMAS)

Location: Watson Building G23 LTA  
Location of Posters: Bridge Poynting/Watson

Friday 30 July AM

Presiding Chair: Peter G. Baines (CSIRO Atmospheric Research, Aspendale, Australia)

JSP49/E/02-B5 Invited 0830

## TIDAL INTERNAL WAVES GENERATION OVER SUBMARINE RIDGES, ENERGY TRANSFER TO HIGH FREQUENCY INTERNAL WAVES AND TURBULENCE

Eugene Morozov (Shirshov Institute of Oceanology, 36, Nakhimovskiy st., 117851, Moscow, Russia, e-mail: internal@redline.ru)

We analyze tidal internal waves generated near the Emperor Ridge in the North Pacific. Internal waves are studied on the basis of data of Russian and US moorings set from both sides of the ridge. A great amount of CTD hydrographic measurements are also available in the region. This allows us to analyze the oceanic turbulence and fine structure which occurs in the ocean due to breaking internal waves. The stations near the ridge show well expressed fine structure with homogeneous steps of tens of meters, the distant stations are more smooth and demonstrate no fine structure. Calculations of spectra from these vertical profiles give different levels of spectral densities. Those near the ridge are significantly above the GM background dropped background spectra. We interpret this as breaking of intensive tidal internal waves, generation of high frequency internal waves, and formation of fine structure. The results of the observations are confirmed by a non-linear numerical model of the generation of tidal internal waves over the ridge. The model describes their propagation and dissipation with generation of short period internal wave trains and turbulence. It is shown that internal tides propagating from submarine ridges strain the vertical structure of hydrographic fields, which can be registered by usual CTD-profiling. Analysis of CTD profiles over great squares in the oceanic basins with account for these properties can indicate areas of intermittent turbulence in the ocean which is caused by breaking internal waves. This analysis

## INTER-ASSOCIATION

of standard oceanographic data is less expensive than special measurements which include deployment of moored buoys in the ocean.

**JSP49/E/03-B5**

**0850**

### REGULAR BURSTS IN THE SEDIMENT-STRATIFIED, OSCILLATING BOTTOM BOUNDARY LAYER: MODEL RESULTS

Boris A. KAGAN and Konstantin B. Utkin (both at Shirshov Institute of Oceanology, Russian Academy of Sciences, St.Petersburg Branch, 30 Pervaya Liniya, 199053 St.Petersburg, Russia, email: kgn@GK3103.spb.edu)

A model based on the 2.5-level turbulence closure scheme and on a parameterization of the processes of sedimentation and entrainment at the top of the bed-load layer is employed to simulate the vertical structure of the sediment-stratified, oscillating bottom boundary layer (BBL). The model predicts regular bursts arising during an oscillation cycle every time when, under certain conditions, entrainment of suspended particles from the bed-load layer is terminated. The regular bursts differ from the random bursts associated with the intermittency of small-scale turbulence in the viscous and buffer sublayers in many respects. In particular, the former are due to the interaction between hydrodynamic and sedimentological processes; more specifically, to the release of the turbulent kinetic energy expended for maintaining particles in suspension. Also, unlike the random bursts, the regular ones do not produce significant contributions to the Reynolds stress, and their timescale is a function of the suspension Froude number, the Reynolds number, the nondimensional critical friction velocity at which sediment particles begin to go into suspension, the relative settling velocity of suspended particles and the Strouhal number. For fixed values of the first four above-mentioned parameters, the regular burst timescale is the smaller the greater is the Strouhal number or, all other factors being the same, the greater is the oscillation frequency. That is apparently why no bursts have been observed in the BBL beneath wind waves, whereas in the tidally induced BBL these have become common.

**JSP49/W/04-B5**

**0910**

### SEAMOUNT TURBULENCE: GENERATION AND DECAY

Iosif Lozovatsky (P.P. Shirshov Institute of Oceanology, Russian Academy of Sciences Moscow, 117851, Russia; also at Department of Mechanical and Aerospace Engineering, Arizona State University, Tempe, AZ, 85287-9809, USA, email: i.lozovatsky@asu.edu)

Turbulent measurements above summits and at the rims of seamounts Erving and Ampere in the Eastern Atlantic revealed an enormous enhancement of turbulent mixing with the mean kinetic energy dissipation rate of  $\approx 6 \times 10^{-8}$  W/kg. The mean eddy and scalar diffusivities are in the range of  $(3.8-5.1) \times 10^{-4}$  m<sup>2</sup>/s with 90% confidence limits of  $(3.1-6.1) \times 10^{-4}$  m<sup>2</sup>/s. This implies that the averaged mixing rate in a 60-mile diameter and 150 m high region surrounding seamount Erving is 30-60 times than that of the far field value. At the place of generation, the diffusivities, averaged over the stratified water column were as high as  $(1-2) \times 10^{-3}$  m<sup>2</sup>/s; a similar result was reported for Fieberling seamount (e.g., Kunze and Tool, 1997). Our observations showed that the turbulent "columns" are possibly detached from the bottom. Their origin appears to be related to the internal-wave shear, rather than to the bottom-roughness induced turbulence. More regular, frictional boundary layers occupy about 30% of the water column above the summit of the Ampere seamount. The dissipation rate within these stratified, non-fully mixed layers was high,  $(1-9) \times 10^{-7}$  W/kg, and corresponding scalar diffusivities ranged  $(5-70) \times 10^{-4}$  m<sup>2</sup>/s. Turbulence upstream of the seamount is almost unaffected by the topography, showing a low background level of  $6 \times 10^{-10}$  W/kg. Downstream of the summit, decreases from  $6 \times 10^{-8}$  to about  $(1-2) \times 10^{-9}$  W/kg, over a distance of 36 miles. This decay can be reasonably approximated by an inverse function of the horizontal distance normalized by the buoyancy mixing scale LB at the site of turbulence generation. The data taken from other regions, e.g. turbulent wakes downstream of the Ampere seamount and small Howland Island, also follow the power law trend  $(x/LB)^{-1}$ , showing the versatility of the results obtained.

**JSP49/W/22-B5**

**0930**

### ABYSSAL TURBULENCE

ROBERT B. SCOTT: Mathematics, UCL, Gower Street, London, WC1E 6BT, UK

Deep ocean turbulent mixing is believed to be important in controlling the large scale meridional overturning rate. Munk suggested in 1966 that deep ocean mixing may be much stronger near boundaries than in the interior, and this has been vindicated by direct measurements of microscale turbulence. While direct measurements reflect local mixing rates, one must use budget studies to indirectly infer the time average volume integrated mixing rates. Wunsch has suggested using the source of mechanical energy as a means of inferring the abyssal mixing rates. Recently it has been demonstrated that the flux of mechanical energy from the winds to the surface geostrophic flow  $F(Kg)$  can be well quantified using TOPEX/Poseidon (TP) data and recent gravity models. Turbulence theory suggests that the geostrophic energy must be dissipated by interactions with the bottom. Thus  $F(Kg)$ , along with tidal forcing, are important in that they provide a power source for driving small scale, abyssal turbulence and mixing. In this work, the time mean field of  $F(Kg)$ , and the factors affecting the reliability of this estimate, are reviewed for the World Ocean. The global mean is comparable to the mean rate of sun and moon tidal forcing. The new results are the presentation of the time variability of  $F(Kg)$  integrated over the World Ocean and various subregions. The time varying component in some cases exceeds the time mean and can result in short periods of atmospheric braking of oceanic surface flow. Factors controlling the variability in  $F(Kg)$  are identified for the TP time period. We also speculate on the longer time scale variability of power sources driving abyssal turbulence and the effects on global circulation and northern climate.

**JSP49/W/10-B5**

**0950**

### DOUBLE DIFFUSIVE MIXING PROCESSES IN THE OYASHIO FRONTAL REGION

Jiro Yoshida, Hideki Nagashima and Moh Nagasaka (all at Department of Ocean Sciences, Tokyo University Fisheries, 4-5-7 Konan, Minato, Tokyo Japan 108-8477, email: jiroy@tokyo-u-fish.ac.jp; nagasima@bimelan.tokyo-u-fish.ac.jp)

Along the north eastern coast of Japan, the Kuroshio (warm and salty water) and the Oyashio (relatively cold and fresh water) directly contact and forms the so-called perturbed area. Warm core rings are sometime detached from the Kuroshio in this area and flows northward. Between this perturbed area and the Oyashio, clear frontal region is formed and is sometimes called as Oyashio Front. At this frontal region, vertical profiles of temperature and salinity often show complex structures such as temperature inversion layers, step structures and so on. These structures sometimes traced over several kilometers in horizontal direction, and were considered to be interleaving processes driven by double diffusive convection. In the present

study, focusing upon these interleaving processes, the time history of layer formation is analyzed by intensive XBT and CTD surveys. The characteristic features of the layer are discussed statistically, and the effective horizontal and vertical diffusivities are estimated by simple advection-diffusion model. These results are compared with the previous ones obtained by Meddy studies, C-SALT, and NATRE, and the role of double diffusive mixing in this area is also significant and might affect the decay processes of Warm core rings

**JSP49/W/08-B5**

**1010**

### INTERNAL WAVES, TURBULENCE AND INTRUSION OF SHELF WATER INTO THE KUROSHIO NEAR THE SHELF BREAK IN THE EAST CHINA SEA

Takeshi MATSUNO, Shotaro Ohsaki and In-Seong Han (Faculty of Fisheries, Nagasaki University, Nagasaki, 852-8521 Japan, email: matsuno@net.nagasaki-u.ac.jp)

Measurements of short time scale fluctuations with moored current meters were carried out near the shelf break in the East China Sea. Short time scale internal waves with periods of 10 to 30 minutes, which is slightly larger than the Brunt-Vaisala period, were frequently detected. Some of internal waves have borelike shape in time series of temperature and current velocity. Propagation speed of the borelike internal waves was 0.5 or 0.6 m/s which was estimated from two moorings with distance of 200 m. Shorter time scale fluctuations often follow the internal waves. This suggests that breaking of internal waves would generate turbulent fluctuations. These turbulent fluctuations could make vertical mixing, however, we did not find distinct occurrence of vertical mixing just after the significant turbulent fluctuations. However, we sometimes found evidences of offshore intrusion of shelf-bottom high turbid water into the Kuroshio. The intrusion tends to be developed when predominant pycnocline is formed just above the shelf break. It is suggested that enhancement of the intrusion should depend on intensification of internal waves associated with turbulent fluctuations, though we did not find a direct evidence yet. Such cross-shelf fluxes related to internal waves and turbulent fluctuations might play an important role on material and energy transports between the shelf water and the Kuroshio.

**JSP49/E/07-B5**

Invited

**1050**

### STRATIFIED FLOW OVER TOPOGRAPHY: THE ROLE OF SMALL SCALE ENTRAINMENT AND MIXING IN FLOW ESTABLISHMENT

David FARMER (Institute of Ocean Sciences, Sidney, B.C., V814B2 Canada, email: farmerd@dfp-mpo.gc.ca) and Laurence Armi (Scripps Institution of Oceanography, La Jolla, California 92093-0230 USA, email: larmi@ucsd.edu)

Stratified flow over topography is examined in the context of its establishment from rest. A key element of numerical and steady state analytical solutions for large amplitude topographic flow is the splitting of streamlines which then enclose a trapped wedge of mixed fluid above the rapidly moving deeper layer. Measurements have been acquired which illustrate the development of this wedge and the role played by small scale instabilities and mixing formed initially by the acceleration of subcritical stratified flow over the obstacle crest. The volume of trapped fluid progressively increases with time, permitting the primary flow to descend beneath it over the lee face of the obstacle. Throughout the evolution of this flow, small scale instability and consequent entrainment would seem to be a prime candidate for producing the weakly stratified wedge, thus allowing establishment of the downslope flow to take place. Velocity structure of instabilities within the entrainment zone is observed and the associated entrainment rate determined. The entrainment is sufficient to produce a slow downstream motion within the upper layer and a density step between the layers that decreases with downstream distance. The resulting internal hydraulic response is explained in terms of a theory which accommodates the spatially variable density difference across the sheared interface. The measurements described here were acquired in a coastal inlet subject to gradually changing tidal currents. It is proposed that the observed mechanism for flow establishment also has application to atmospheric flow over mountains.

**JSP49/L/01-B5**

Invited

**1110**

### STRATIFIED FLOW OVER TOPOGRAPHY: HYDRAULIC FRONTS

Laurence ARMI (Scripps Institution of Oceanography, La Jolla, California 92093-0230 USA, email: larmi@ucsd.edu) and David Farmer (Institute of Ocean Sciences, Sidney, B.C., V814B2 Canada, email: farmerd@dfp-mpo.gc.ca)

When stratified fluid is strongly forced over topography, the resulting flow includes a splitting streamline which then encloses a trapped wedge of mixed fluid above the rapidly moving deeper layer. In response to changes in the forcing, the location of this bifurcation or hydraulic front was observed to move either upstream or downstream. The movement of the hydraulic front is in response to either an increase or decrease of the tidal flow speed or as a result of changes in the density of fluid in the wedge itself. The position of the hydraulic front is explained in terms of a quasisteady theory proposed earlier for two-layer flows and the turbulent structures on the hydraulic front are compared with those observed in recent laboratory experiments on an accelerating baroclinic shear layer. The measurements described here were acquired in a coastal inlet subject to gradually changing tidal currents. It is proposed that the observations also have application to atmospheric flows over mountains.

**JSP49/W/12-B5**

**1130**

### SPATIAL EVOLUTION OF HYDRAULICALLY CONTROLLED FLOWS TO DOWNSLOPE CURRENTS

GENO PAWLAK and Larry Armi (School of Oceanography, University of Washington USA)

The developing region of a steady downslope current in transition from a hydraulically controlled arrested wedge flow is examined through a set of laboratory experiments. The mixing and entrainment mechanisms at the shear interface are explored with the use of imaging techniques. The initial, unstable accelerating region, characterized by rapid development, low shear layer Richardson numbers and high entrainment rates, is quickly limited by the effects of stratification which suppress the vortex pairing mechanism. However, the continuing source of energy from the accelerating flow destabilizes the mixing layer to a shredding type of vortex interaction. The shredding mechanism results in a weakly entraining, well mixed shear layer which evolves towards a steady downslope current for a constant bottom slope. Rates of entrainment of fluid into the turbulent mixing region for each regime are calculated for the various slopes considered.



JSP49/P01-B5 Poster 1210-01

## ENERGY TRANSFER AND MIXING NEAR A DENSITY INTERFACE

A. A. BIDOKHTI and M.Saghafi (both at Institute of Geophysics, Tehran University, P.O. Box 14155-6466: Tehran, Iran. email: bidokhti@chamran.tu.ac.ir)

The problem of mixing and energy transfer across a density interface some distance from the source of turbulent energy, has important applications in geophysical flows. Quite a few experiments have been done, in order to understand and quantify the processes involved (e.g. Turner 1976, Linden 1981 and McGrath et al. 1997).

Results are presented from experiments in which, mechanical grid turbulence is introduced in a homogeneous layer in contact with a stratified layer. Flow visualisation and direct measurements of salinity field (using fast response salinity probes) near the interface, are presented. With a step profile in density, we obtain an entrainment velocity proportional to  $Ri^{-n}$  (where  $Ri$  is the overall Richardson number and  $n \approx 1$ ). Engulfment, eddy impingement are important when the interface is close to the turbulence source. As the distance increases (for  $Ri > 30$ ), internal waves breaking near the interface seems to occur more often (e.g. McGrath et al. 1997). However the case with stratified lower layer (with a linear profile), shows that interfacial internal waves are more pronounced than before. Also some of the energy is transferred to stratified layer and appear as internal waves which seem to have interactions. Internal waves exist in the entire depth of stratified layer. Salinity signals show that the amplitude of the waves decay with depth exponentially. Modulations of the signals indicate the presence of different modes, but the dominant frequency is close to  $N$ , the buoyancy frequency.

JSP49/W/05-B5 Poster 1210-02

## GENERATION AND REFLECTION OF PERIODIC INTERNAL WAVES: EXACT SOLUTIONS AND LABORATORY EXPERIMENTS

Yuli D. Chashechkin, Yuri S. Ilyinikh and Yuri V. Kistovich (all at the Laboratory of Fluid Mechanics of the Institute for Problems in Mechanics of the RAS, Moscow, prospect Vernadskogo, 101-1, 117526, Russia, E-mail: chakin@ipmnet.ru)

We investigate analytically and experimentally 2D and 3D periodic internal waves generation problem in an exponentially stratified viscous fluid. The wave source is plane strip or vertical cylinder tube periodically oscillating along its surface. The linearized governing equations are solved by integral transform method. The exact boundary conditions on the surface of a body as well as the governing equations are satisfied if, in addition to propagating internal wave beams, internal boundary layers on the emitting surfaces are taken into account. On the basis of these two eigen-forms of fluid motion we calculate wave amplitudes and evolution of the wave shape along the beam. The number of maxima in the wave amplitude cross-section depends on the ratio of source width by intrinsic viscous wave scale. The distance from the source where the bi-modal beam is transformed into the uni-modal one is defined. The spatial decay of the wave is different due to the geometry of the problem. Schlieren visualization and probe measurements of a periodic wave pattern confirm the theoretical results for the far wave field. The absolute values of calculated and measured wave amplitudes differ by a factor less than 1.3. Indirect evidences of the internal boundary layers are presented.

JSP49/W/13-B5 Poster 1210-03

## STOKES FLOW INDUCED BY PERIODIC INTERNAL WAVES

Yuli D. Chashechkin and Yuri V. Kistovich (both at the Laboratory of Fluid Mechanics of the Institute for Problems in Mechanics of the RAS, Moscow, prospect Vernadskogo, 101-1, 117526, Russia, E-mail: chakin@ipmnet.ru)

We study problem of propagation non-linear 2D periodic internal waves in exponentially stratified viscous fluid. The solution of complete set of governing equations is expanded in series on harmonics of the main frequency. The average flow is described by the term with zero frequency. As a seed disturbance the infinitesimal solution of linearized equations is taken. In the second order approximation the explicit expression for stream function of the main Stokes flow is received as quadratic differential form of the stream function of seed infinitesimal waves. As an example we calculate Stokes flow induced by a beam of periodic internal waves generated by a point dipole source. Explicit formulae are received in the intrinsic frame where one of the axes is directed along a beam and the other is directed transversely. Total discharge in a beam is absent, that is fluid is moving in one direction in the upper part of a beam and in the opposite direction in the lower part. Patterns of stream lines are calculated for different models of mass source (dipole, quadruple). Stokes flow induced by a single beam tends to zero when kinematic viscosity goes to zero. In a domain of intersection of wave beams from several sources Stokes flow exists even in an ideal fluid. Calculated pattern of stream function describing reflection of an periodic wave beam off a sloping solid plane includes both reflected internal waves and a boundary current on the reflected surface

JSP49/W/06-B5 Poster 1210-04

## ESTIMATES OF DEEP-OCEAN TIDAL DISSIPATION FROM THE TOPEX / POSEIDON GLOBAL TIDE MODELS

JOHN A CHURCH<sup>1,2</sup> Ole B. Anderson<sup>3</sup>, Richard Coleman<sup>1,2,4</sup> and Neil J. White<sup>1,2</sup> 1 Antarctic CRC, Hobart, Tasmania, Australia 2 CSIRO Marine Research, Hobart, Tasmania, Australia 3 National Survey, Geodetic Division, Copenhagen, Denmark 4 University of Tasmania, Hobart, Tasmania, Australia

The TOPEX/POSEIDON models of global sea-surface tidal elevation are used to estimate tidal currents, assuming linear bottom friction. For the M2 tide, the derived currents satisfy the continuity equation to a rms residual of about 0.2 mm s<sup>-1</sup>. However, there is a clear correlation between these residuals and the underlying topographic features. From the surface height fields, the derived current fields and the residuals from the continuity equation, the tidal energy budget can be computed. The energy input by the astronomical potential almost exactly balances the divergence associated with the tidal currents. Residuals from the energy equation, ie the deep water dissipation, are positive almost everywhere and are maximum over major topographic features, such as the mid-ocean ridge in the South Atlantic, around New Zealand and near a number of regions where internal tide generation is known to be strong. The bottom dissipation estimates are combined with hydrographic data to estimate vertical mixing rates in the deep ocean.

JSP49/E/11-B5 Poster 1210-05

## TIDAL ENERGY AVAILABLE FOR DEEP OCEAN MIXING: BOUNDS FROM ALTIMETRY DATA

GARY D. EGBERT (College of Oceanic and Atmospheric Sciences, Oregon State University, 104 Ocean. Admin. Bldg., Corvallis, OR 97331, email: egbert@oce.orst.edu) Richard D. Ray (Goddard Space Flight Center, NASA, Greenbelt, MD, email: rray@geodesy2.gsfc.nasa.gov)

Maintenance of the large-scale thermohaline circulation has long presented a problem to oceanographers. Observed mixing rates in the pelagic ocean are an order of magnitude too small to balance the rate at which dense bottom water is created at high latitudes. Recent observational and theoretical work suggests that much of this mixing may occur in hot spots near areas of rough topography (e.g., mid-ocean ridges and island arcs). Barotropic tidal currents provide a very plausible source of energy to maintain these mixing processes. Topex/Poseidon satellite altimetry data have made precise mapping of open ocean tidal elevations possible for the first time. We can thus obtain empirical, spatially localized, estimates of barotropic tidal dissipation. These provide an upper bound on the amount of tidal energy that is dissipated in the deep ocean, and hence is available for deep mixing. We will present and compare maps of open ocean tidal energy flux divergence, and estimates of tidal energy flux into shallow seas, derived from T/P altimetry data using both formal data assimilation methods and empirical approaches. With the data assimilation methods we can place formal error bars on the fluxes. Our results show that 20-25% of tidal energy dissipation occurs outside of the shallow seas, the traditional sink for tidal energy. This suggests that up to 1 TW of energy may be available from the tides (lunar and solar) for mixing the deep ocean. The dissipation indeed appears to be concentrated over areas of rough topography.

JSP49/W/16-B5 Poster 1210-06

## ENERGY TRANSFER IN THE SMALL-SCALE OCEANIC INTERNAL WAVE SPECTRUM

Ryo FURUE (Center for Climate System Research, University of Tokyo, 4-6-1 Komaba, Meguro-ku, Tokyo 153-8904, Japan, email: furufuru@cscs.u-tokyo.ac.jp)

We examine energy transfers within a high-wavenumber portion of the oceanic internal wave spectrum by direct numerical simulations. The domain is a rectangular box of 100 m x 100 m x 128 m and the flow field is initialized with the Garrett-Munk (GM) spectrum. The GM flow field of larger horizontal scales is represented as a horizontal shear flow of an infinite horizontal scale. We compare cases with and without this shear flow to assess effects of the large scale GM flow field on the energy transfer. We find that wavenumber-local interactions dominate and transfer energy mainly to high horizontal wavenumber regions and that the modeled rate of energy transfer ( $1-4 \times 10^{-10}$  W/kg) is comparable to observed values in the main thermocline. The contribution of the large-scale flow is found to be not very large although the presence of the large-scale flow does enhance vertical transfer by Doppler spreading mechanism. From these results, we propose the following scenario of the energy transfer. There are two paths of energy flux in the spectrum. In one, energy is transferred to vertically small scales at horizontally medium scales, and ultimately to dissipation scales, by scale-separated interactions such as described by the eikonal approximation. In the other, energy is transferred to horizontally small scales, where strong wavenumber-local interactions increasingly dominate and transfer energy to dissipation scales.

JSP49/W/17-B5 Poster 1210-07

## THE IMPACT OF NON-LINEAR WAVES ON THE DISSIPATION OF INTERNAL TIDAL ENERGY AT A SHELF BREAK

Mark E. Inall (University of the Highlands and Islands project, Scottish Association for Marine Science, Dunstaffnage Marine Laboratory, P.O. Box 3, Oban, PA34 4AD, UK, Email: mei@dml.ac.uk), Tom P. Rippeth (School of Ocean Sciences, University of Wales Bangor, Anglesey LL59 5EY, UK), Toby J. Sherwin (UCES, University of Wales Bangor, Anglesey LL59 5EY, UK)

The vertical and temporal structure of the dissipation of turbulent kinetic energy within the internal tide at a location 5 km shoreward of the shelf break on the Malin Shelf has been determined using a combination of the free-fall FLY profiler and Acoustic Doppler Current Profilers (ADCPs). Two distinct internal wave regimes were encountered: Period I in which large amplitude high frequency non-linear internal waves (NIWs) occurred (around neap tides), and Period II in which the internal wave spectral continuum was not dominated by any particular frequency band (around spring tides). Empirical Orthogonal Function (EOF) analysis shows that for the low frequency waves 76% of the variance was described by mode 1, rising to 95% for the high frequency waves. During period I, the dissipation and vertical mixing were dominated by the NIWs, with 70% of the dissipation occurring in the bottom boundary layer. During period II, the depth integrated dissipation was more evenly distributed throughout the tidal cycle, whereas vertical mixing was concentrated in one hour long episode of elevated thermocline dissipation coincident with weakened stratification. During both I and II approximately 30% of the total measured dissipation occurred within the thermocline when averaged over 12.4 hours, the remainder occurred within the BBL. Tidal average values for depth integrated dissipation and vertical eddy diffusivity for regime I (II) were  $1.1 \times 10^{-2}$  Wm<sup>-3</sup> ( $4.0 \times 10^{-2}$  Wm<sup>-3</sup>) and  $5$  cm<sup>2</sup>s<sup>-1</sup> ( $12$  cm<sup>2</sup>s<sup>-1</sup>) respectively.

JSP49/W/19-B5 Poster 1210-08

## OBSERVATIONS AND K-EPS MODEL SIMULATIONS OF TURBULENT MIXING IN STRATIFIED TIDAL FLOW

Josy P. JACOB and Hartmut Peters (both at Rosenstiel School of Marine and Atmospheric Science, University of Miami, USA. email: hpeters@rsmas.miami.edu); Helmut Baumert (Hydromod Scientific Consultants, Wedel, Germany. email: baumert@hydromod.de)

This paper addresses the question how well second-moment turbulence closure models can simulate tidally driven mixing in fast flowing shallow estuaries. We employ a 1-D numerical k-eps model (Burchard and Baumert, 1995; JGR Oceans, 100, 8523), nudging the model velocity and stratification towards the observations. This is necessary because the estuarine momentum and mass balances are not one-dimensional, advective terms being unknown or poorly known. As a result of the nudging, simulated and real turbulence evolve in very similar shear and stratification. The modeled turbulent kinetic energy and dissipation rate are recast into a turbulent length scale and dissipation, both to be compared quantitatively with observations. Extensive observations of the turbulent dissipation rate and of turbulent overturning scales were made in the Hudson River in 1994/95 in conditions of shallow water (15 m depth typical), energetic tides (velocities of 1-2 m/s), mostly strong stratification (2-18 psu top-to-bottom salinity difference) and strong shear. Shear, stratification and turbulent mixing showed pronounced tidal and fortnightly variations.

The k-eps model is able to simulate turbulent dissipation rates and length scales fairly well. Comparing both parameters to their observed counterparts is crucial to determining adjustable model constants.

**JSP49/W/14-B5** Poster **1210-09**

**TURBULENCE PARAMETERIZATION FOR PBL DISPERSION MODELS IN ALL STABILITY CONDITIONS**

Gervásio Annes Degrazia (Universidade Federal de Santa Maria - UFSM, Santa Maria-RS-Brazil, CEP 97.119-900, Email: degrazia@ccne.ufsm.br) CLÁUDIA JACONDINO DE CAMPOS (Universidade Federal de Pelotas-UFPEL, Pelotas-RS-Brazil, CEP 96.010-900, Email: cjcambos@ufpel.tche.br)

Accounting for the current knowledge of the Planetary Boundary Layer (PBL) structure and characteristics, a new set of turbulence parameterizations to be used in atmospheric dispersion models has been derived. The expressions for the vertical profiles of the velocity standard deviation, Lagrangian and Eulerian length scale and time scale and diffusion coefficient are proposed. The classical statistical diffusion theory, the observed spectral properties and measured characteristics of energy containing eddies are used to estimate these parameters. The results of this new method are shown to agree with previously determined parameterizations. In addition, these parameterizations give continuous values for the PBL at all elevations and all stability conditions from unstable, neutral to stable. It is the aim of this work to present the general derivations of these expressions and to show how they compare to previous results. Finally a validation of the present parameterization, obtained by inserting it in a Lagrangian particle model, will be shown. The Copenhagen data set is simulated. This data set is particularly suited for this validation, since most of the Copenhagen tracer experiments were performed in stability conditions that are the result of the relative combination of wind shear and buoyancy forces. As a consequence, a parameterization scheme, able to deal contemporary with neutral and slightly convective condition, is preferred.

**JSP49/E/06-B5** Poster **1210-10**

**COEFFICIENT OF TURBULENT DIFFUSION AT A TROPOSPHERIC ALTITUDES**

George JANDIERI (department of Physics, Georgian Technical University, 77 Kostava str., Tbilisi 380075, Georgia, email: jandieri@access.sanet.ge) Anzor Gvelesiani (Institute of Geophysics of the Georgian Academy of Sciences, 1 Rukhadze str., Tbilisi 380093, Georgia) Zhuzhuna Diasamidze, Vladimir Glonti and Mzia Diasamidze (all three at Department of Physics, Batumi State University, 35 Ninoshvili str., Batumi, Georgia)

New statistical model of the distribution of pollutant mean concentration is presented at lowest atmospheric turbulent layers. Statistical description of turbulent diffusion is payed attention by means of stochastic diffusion equation. Source of pollutant is deterministic function of coordinates and time. Velocity field describes homogeneous and stationary process. General expression of passive impurity concentration distribution is obtained. Coefficient of turbulent diffusion is expressed in terms of coefficient of molecular diffusion and arbitrary correlation tensor of the vector field of velocity fluctuation. Knowledge of the components of the turbulent diffusion coefficient makes it possible to restore the values of spatial-temporal parameters typical of a stochastically inhomogeneous medium. In particular, distribution of pollutant at anomalous meteorological conditions such as calm is of interest. Numerical simulations of normalized concentration distribution against distance are carried out at stationary and nonstationary cases. Globul formation mechanism is observed in nonstationary case for different values of the turbulent flow velocity. They have different linear dimentions and existence time.

**JSP49/E/10-B5** Poster **1210-11**

**THE EFFECT OF DIFFUSION INSTABILITY IN A LOWER TURBULENT ATMOSPHERIC LAYERS**

George JANDIERI (department of Physics, Georgian Technical University, 77 Kostava str., Tbilisi 380075, Georgia, email: jandieri@access.sanet.ge) Anzor Gvelesiani (Institute of Geophysics of the Georgian Academy of Sciences, 1 Rukhadze str., Tbilisi 380093, Georgia) Vladimir Glonti, Guram Varshalomidze and Mzia Diasamidze (all three at Department of Physics, Batumi State University, 35 Ninoshvili str., Batumi, Georgia)

Turbulence favours the mixing of different impurities in random media. Interaction of impurities leads to temporal evolution of medium inhomogeneous structure and it passes to the metastable state. Diffusion instability is investigated by means of solution of stochastic integro-differential equation for the mean concentration of impurities in a randomly inhomogeneous media. Potential energy (PE) of interaction between impurities plays significant role. If PE is positive we can introduce effective diffusion coefficient while it is not justified at any chemical reactions. If PE is negative, critical concentration is exist from which diffusion instability is beginning. Model of PE is supposed using similarity method. Function characterizing PE has potential well at small distances and has wavy character at great distances. New approximation of spatial-temporal distribution of impurity concentration is proposed by solving stochastic diffusion equation using Picard's method. Concentration fluctuations are caused by velocity pulsations. Incompressibility and isotropy of turbulent medium are not use. Knowledge of statistical parameters of fluctuating media and distribution of the mean concentration of impurities allow us to restore characteristic linear dimensions of diffusible particles.

**JSP49W/07-B5** Poster **1210-12**

**DIFFUSING OF A PASSIVE TRACERS IN RANDOM FLOWS. SOME RESULTS OF NUMERICAL SIMULATION.**

KONSTANTIN KOSHEL and Olga Alexandrova (both at Pacific Oceanological Institute, FEB RAS, 43,Bul'tyiskay str., Vladivostok, 690068, Russia, Email: wave@online.vladivostok.ru)

The diffusion of a passive tracers in a two-dimensional random velocity field is considered. On the basis of diffusion equations solution as a functional integral the method of numerical simulation of a problem is offered. By numerical simulation dynamics of formation of cluster structures is studied. The role of molecular diffusion in such situation and degree of effects connected with potential and solenoidal components of velocity fields is estimated. The behavior of a tracers as in diffusion approximation, and for infinite temporary radius of a correlation is investigated.

All calculations are done for one realization of a velocity field. For other realizations the distribution of an impurity essentially varies, however common behaviour defined by parameters of a problem is saved. The results of simulation will be agreed with analytical results obtained by V.I. Klyatskin and A.I. Saichev (JETP. 1997. V. 111. N 4. P. 1297. In Russian). The molecular diffusion renders noticeable influence to distribution of partíñles of an impurity, thereby increasing common square of area occupied by impurity, however influence of this effect to compression of partíñles along trajectory is insignificant. On the other hand an incompressible component in a velocity field poorly influences effect of grouping of partíñles in clusters, but essentially decelerates compression of partíñles along trajectory. Results for case of a velocity field with an infinite radius of correlation on time allow to assume, that the qualitative behaviour of an impurity in this case is saved, however numerical and it is possible also functional performances of process vary. &#137;

**JSP49/W/11-B5** Poster **1210-13**

**DECOMPOSITION OF WIND VELOCITY FLUCTUATIONS INTO WAVE AND TURBULENT SIGNALS USING WAVELET TRANSFORM**

Nisia Krusche (Dept. Geociencias, Fundação Universidade De Rio Grande, C.P. 474, 96201-900 Rio Grande Rs, Brazil) And Osvaldo L. L. Moraes (Dept. Física, Universidade Federal De Santa Maria, 97119-900 Santa Maria, Rs, Brazil)

In the stably stratified atmospheric boundary layer, spectra might be affected by several kinds of Waves. Since the problem of turbulent diffusion is closely related to the spectra of wind velocity Fluctuations, there is a need to separate the contributions of those waves from that of Turbulence. Discrete wavelet transform was applied to temperature and vertical velocity Fluctuations measured in candiota, rs (31o28's, 53o 40'w), sampled with a frequency of 10 Hz. In this data set, waves have been detected through cospectral techniques. As a result, a Wave was identified in both series, which was 90o out of phase, as expected. Therefore, this Method may be used to decompose the series in two signals, one containing the wave and Other corresponding to random turbulence of the flow.

**JSP49/W/23-B5** Poster **1210-14**

**OVERTURNING LENGTH SCALE AS AN INDICATOR OF THE WASTEWATER NEAR FIELD**

Vlado MALACIC (Marine Biological Station, National Institute of Biology, Piran, 6330, Slovenia, email: malacic@nib.si)

During a period of calm weather and stratified water column of a shallow (depth = 21 m) semi-enclosed sea, six surveys of the wastewater near-field of two adjacent submarine diffuser outfalls, with a low sewage outflow rate (usually less than 220 l/s), were conducted with a fine-scale CTD probe. The survey area of 780m\_740m was monitored with the free-falling probe at 30-31 stations. Vertical velocity of the probe was nearly constant, 1 m/s, and the data was retrieved at a frequency of 50 Hz, providing a vertical resolution of 2.5 cm.

When using a fine-scale CTD it has been observed that from the vertical distribution of 'virtual' displacements (Thorpe displacements) of particles with a sampled density, by which each particle would gain a statically stable position, the length scale of overturning events could be estimated, through an appropriate averaging process.

Within the turbulent wastewater field the fluctuations of temperature were of the order of 0.1 oC, and of salinity less than 0.05 psu, generating overturning. The vertical extent of the overturning events could well be determined using the maximum vertical displacement, or the Thorpe length scale. Both scales also indicate the thickness of the neutrally buoyant subsurface wastewater field. Distribution of these length-scales over the diffusers show a clear picture of the wastewater field(s) of a thickness smaller than 1m in windless, stratified conditions, which is otherwise hard to obtain without costly experiments (dye tracers).

**JSP49/E/01-B5** Poster **1210-15**

**PROPAGATION AND DISSIPATION OF TIDAL INTERNAL WAVES IN THE NORTH PACIFIC ON THE BASIS OF THE MEGAPOLYGON DATA, AN EXPERIMENT WITH 170 MOORED BUOYS**

Eugene MOROZOV (Shirshov Institute of Oceanology, 36, Nakhimovskiy st., 117851, Moscow, Russia, e-mail: internal@redline.ru)

Tidal semidiurnal internal waves generated over the Emperor Ridge in the North Pacific are analyzed on the basis of a vast cluster of moorings in the area between 38 - 42 N and 152 - 158 E. The cluster of 170 moored buoys was set for two months in this region with a distance of 24 miles between moorings. The current and temperature meters were set at 120 m and 1200 m levels. This cluster of moorings with current meters forms an antenna to study eddies and tidal internal waves and their variability. The maximum distance between the utmost western and eastern moorings exceeded 450 km. The wave lengths of tidal internal waves vary between 130 and 150 km, while the change of the direction of their propagation is insignificant. Westerly waves are dominating indicating that the Emperor Ridge is the source area. The cluster of buoys was divided into two parts to obtain independent data sets for evaluating wave parameters. The wave lengths and direction of propagation measured at both parts of the study area gave approximately the same results. The results did not change in the analysis of the first and the second months of the time series. The maximum amplitudes of the waves in the eastern part of the study area exceed 40 m, whereas in the western part they were about 15-20 m or less. Decay of the waves is estimated as 5% of the energy over one wave length. Similar results were obtained from the data of US moorings in this area and also from the moorings east of the Emperor Ridge.

**JSP49/W/24-B5** Poster **1210-16**

**A NUMERICAL EXPERIMENT ON THERMOBARIC CONVECTION**

Miyako Naya and Hideki Nagashima (Department of Ocean Sciences, Tokyo University of Fisheries, Konan,Minato, Tokyo Japan 108-8477. E-mail: nagasima@bimelan.tokyo-u-fish.ac.jp)

Predictions of vertical convection and deep water formation in the polar region need to include the nonlinear equation of state. In the present study, a numerical experiment on thermobaric convection is carried out based on the non-linear equation of state in which the thermal expansion coefficient is a function of pressure\_@together with temperature and salinity. A two-dimensional non-hydrostatic model is used with the calculating domain of 8km in horizontal and 4km in vertical directions. The onset of convection is well explained by a linear stability analysis of Rayleigh-Benard problem and the convection develops and reveals thermobaric enhanced turbulence. Next, the double diffusive effect is taken into consideration, because the typical vertical profile in the polar sea shows high activity of double diffusion. In the numerical model, the vertical diffusivities of heat and salt are parameterized by using empirical flux law (Kelly:1990). The result shows that the double diffusive effect reduces the onset of thermobaric convection.

**JSP49/W/20-B5** Poster **1210-17**

**STIMULATION OF LARGE-SCALE ANTICYCLONIC CIRCULATION IN THE OCEAN VIA SALT FINGERS CONVECTION**

Anatoly Pereskokov (Russian Research Institute of Hydrometeorological Information - World Data Centre, 6 Korolyov St., Obninsk 249020, Russia, email: peres@meteo.ru)

A further progress in understanding of the nature of the ocean large-scale circulation relates first of all to the estimate of the processes effectiveness generating the mixing in the ocean pycnocline. Diapycnic transfer due to salt fingers convection appears to be the significant climate-forming factor (Pereskokov, Fedorov, 1985). Evidence of this is the displacement of regions of the increased temperature from equatorial latitudes to the subtropics with the

increase in depth. It is shown that in the core of waters with thermohaline conditions favourable for the development of salt fingers convection which is found in all oceans in the layers between horizons 300 and 600 m, their volumetric shares in the North Pacific, South Pacific, and the Indian ocean are close to 70% and increases to 80% in the South Pacific and almost to 93% - in the North Atlantic. In such a case, an overwhelming majority of the values of density ratio lie within of 1.7-5.0 for the entire World Ocean and within of 1.7-2.5 - for the Atlantic. These limits for the density ratio are typical for conditions in which the effect of salt fingers is most pronounced. Via this vertical heat transfer from upper layers to deep waters salt fingers convection stimulates large-scale anticyclonic circulation contributing to the development of cores of warm (with less density) waters in subtropics. Probably it is not easy to find the numerical support of this hypothesis, but the fact itself that it is already on the level of 200 m that the wind energy can account for only 30% of the observed values of the current speed, is indirect evidence in favour of the assumption made.

**JSP49/W/15-B5** Poster **1210-18**

#### RICHARDSON NUMBER AS AN INDICATOR OF TURBULENT STRATIFICATION AND LARGE EDDY DIFFUSION

Prof. KPR Vittal Murty, (DCM,INPE,Av.dos Astronautos1758,caixa postal 515,Sao jose dos campos-sp-BRAZIL, cep-12201-010, email: murty@met.inpe.br)

Richardson number(Ri), a non-dimensional number which is a ratio of thermal and kinetic forces is an indicator of surface layer turbulence. It is closely associated with turbulence production terms in the equation of turbulent energy balance. In this article the turbulent state of the surface layer is studied as a function of Ri based on Pantanal gradient observation data. Pantanal is located in the western part of central Brazil and is well noted for its flora and fauna. An International Pantanal Experiment (IPE\_1) was conducted in May 1998, which is a part of broad experimental program to study the weather and climate of this region. The gradient observations of wind and temperature obtained in IPE\_1 were used in the present study. The three different forms of Ri namely bulk, gradient and flux form are estimated and compared. The various functions of Ri as envisaged by Pristley, Pasquill, Gurevitch and Rider were estimated and discussed. The variation of horizontal velocity variance with Ri was studied for a clear and cloudy day. This shows an increase of variance with decrease of Ri and the slope which also varies indicate the large eddy diffusion in the area

Friday 30 July PM

Presiding Chair: Peter G. Baines (CSIRO Atmospheric Research, Aspendale, Australia)

**JSP49/E/09-B5** Invited **1400**

#### TURBULENT CONVECTION AND MIXING IN A LABORATORY MODEL OF THE CONVECTIVELY-DRIVEN FLOW IN PARTIALLY-ENCLOSED SEAS

T. MAXWORTHY and Th. Grimm, Department of Aerospace and Mechanical Engineering, University of Southern California, Los Angeles, CA 90089-1191, USA.

Turbulent convection and mixing play a major role in a variety of natural hydrodynamical systems. A special class of such systems are those in which convection drives exchange flows in a channel that is closed at one end and has a lateral contraction and/or a sill at the other, open, end. Typical examples of such "partially-enclosed seas" are the Red and Mediterranean Seas, the Persian Gulf and the fjords that indent many coastlines. The present work focuses on the spatial distribution and scaling of the density difference ( $g'$ ) between the inflowing and outflowing fluid layers at the exit and the characteristics of the turbulent mixing that takes place at the closed end of the sea. Using a long, water-filled channel, fitted with buoyancy sources at its upper surface, experiments were conducted to investigate the influence of the geometry of the strait and the channel as well as the magnitude of the buoyancy flux. Firstly, we have found that the scaling law:

$g' = \text{const. } Bo^{2/3} x/h^{4/3}$   
best describes the distribution of the observed density difference along the channel. Where  $Bo$  is the buoyancy flux,  $x$  the distance from the closed end of the channel and  $h$  its depth at the open end (sill). The numerical value of the constant depends on the hydraulic conditions at the exit and these, in turn, depend on the details of the channel geometry. This scaling law holds for the experimental results and appears to be valid for a number of natural systems as well. Secondly, we discuss, in detail, the flow conditions that are responsible for the turbulence and mixing, at the closed end of the channel, that ultimately account for the observed density distribution.

**JSP49/E/08-B5** **1420**

#### PARTICLE DISPERSION AND MIXING INDUCED BY BREAKING INTERNAL GRAVITY WAVES

P. BOURUET-AUBERTOT, C. Koudella & C. Staquet DAMTP, U. of Cambridge, Silver Street, Cambridge, CB3 9EW, UK Lab. de Physique, E.N.S. de Lyon, 46 allée d'Italie, F69364 Lyon Cedex 07 L.E.G.I., BP 53, F38041 Grenoble Cedex 9

Our study focuses upon diapycnal mixing induced by a breaking gravity wave. The primary wave we consider is of small amplitude (statically stable), a case for which the breaking process mostly involves two-dimensional instabilities. The dynamics of the waves have been previously analyzed by means of two-dimensional direct numerical simulations and three-dimensional calculations will also be reported. Diapycnal mixing is inferred both from particle dispersion and from potential energy budgets, and the two methods are found to lead to the same prediction for the diapycnal diffusivity. This is of particular interest regarding the interpretation of in situ measurements. The diapycnal diffusivity is found to depend on the turbulent Froude number squared, a dependency which we shall relate to the instability process of the primary wave.

**JSP49/E/05-B5** **1440**

#### MIXING IN A STABLY STRATIFIED SHEAR LAYER

Chantal STAQUET (LEGI, BP 53, 38041 Grenoble cdx 9, France, email: Chantal.Staquet@hmg.inpg.fr)

We have investigated the mixing properties of a stably stratified shear layer in two and three dimensions, using a new analysis of mixing proposed by Winters et al. (1995) and Winters and d'Asaro (1996). This analysis provides an exact expression for the diapycnal flux of density; it relies on a stable density profile obtained by sorting adiabatically the fluid parcels so that the heaviest has the lowest altitude. The interest in the new analysis is that mixing rates, such as the mixing efficiency or the diapycnal diffusivity, can be computed instantaneously whatever the flow regime, even if unsteady and strongly nonlinear. We found that the maximum value, as a function of time, of the flux Richardson number depends upon the vertical scale of the instability triggering turbulence, being larger for a larger vertical scale. When the vertical scales of the flow collapse and a weakly nonlinear regime is eventually reached, the predictions of the analysis coincide with those by the Osborn-Cox model. Interestingly, the mixing efficiency relaxes toward an asymptotic value close to 0.25, when the flow is three-

dimensional or two-dimensional with strong stratification. In the latter case, the normalized turbulent diffusivity is found to depend on the inverse of the Richardson number, a parameterization that is identical to that often used in large scale circulation models. It is noteworthy that the same law is found in breaking internal gravity waves.

**JSP49/L/02-B5** **1500**

#### MIXING IN DOWNSLOPE FLOWS INTO STRATIFIED ENVIRONMENTS

Peter G. BAINES, CSIRO Atmospheric Research, PMB No. 1, Aspendale, Australia 3195

The properties of downslope flows may be significantly affected by density variation in the environment. Oceanic examples are downslope flows at high latitudes in the North Atlantic and around Antarctica, driven by surface cooling and brine rejection due to freezing of sea water, and nocturnal flows in the atmosphere driven by radiative surface cooling on slopes.

This paper presents a description of laboratory experiments on downslope flows with stratified environmental fluid, with a dynamical interpretation of the observations, and with measurements of the relevant quantities to enable application of these results to larger scale models. The experiments were carried out in a glass-sided tank 80 cm high and 299 cm long, filled with uniformly salt-stratified water, in which two-dimensional downslope flows of width 23 cm were generated. For each run, a continuous two-dimensional source of dense salty water was introduced at the top of a sloping bottom, for a finite time that depended on the strength of the source and was typically of several minutes duration. Density profiles were measured before the downflow, and some time after it, when all residual motion had ceased. Taking the difference between these two profiles gave quantitative information about the variation of the downflow with downslope distance, the final disposition of the introduced fluid, and the redistribution of the ambient stratification.

A wide range of differing behaviour was observed, depending on the slope angle, the parameter  $M$  (which depends on the mass flux, buoyancy and stratification) and the Reynolds number. The thickness of the density current is generally uniform with downslope distance, but the current exchanges fluid with the environment by the processes of turbulent entrainment into it and more significantly, detrainment from it. The latter is generally the stronger process for small slope angles, where mixing mostly occurs at the upper boundary of the current, but for steeper slope angles (30 degrees and larger) the mixing penetrates deeper, and entrainment is dominant. These processes may be quantified by entrainment and detrainment coefficients for modelling purposes.

**JSP49/W/02-B5** **1520**

#### DEPENDENCE OF MIXING EFFICIENCY ON INITIAL STRATIFICATION IN SHEAR LAYERS

C.P. CAULFIELD (Centre for Environmental and Geophysical Flows and School of Mathematics, University of Bristol, University Walk, Bristol, BS8 1TW, UK, Email: c.p.caulfield@bris.ac.uk) and W.R. PELTIER (Department of Physics, University of Toronto, Toronto, ON M5S 1A7, Canada, Email: peltier@atmos.physics.utoronto.ca)

We investigate the detailed nature of the "mixing transition" through which intense turbulence may develop in stratified free shear layers. We explicitly quantify the time-evolving irreversible mixing which occurs within the flow. We consider in detail the variation in the character of the mixing processes with the initial ambient stratification.

Using the numerical data from a sequence of three-dimensional simulations with varying stratification, we accurately track the nonlinear amplification of streamwise vortex streaks, verifying that they are well-predicted by secondary stability analysis, and that they are due to a convective destabilization of the periphery of a Kelvin-Helmholtz billow. At all times we calculate the minimal potential energy of the system accessible by (notional) adiabatic rearrangement of fluid parcels, and so quantify continuously the irreversible "mixing". Vortex stretching leads eventually to a violent subcritical vortex-vortex collision which drives the dominant mixing process in the flow life cycle. An appropriate definition of the "mixing efficiency" implies that the irreversible small-scale mixing of the density which is triggered by shear layer transition leads inevitably to a density "staircase", with regions of well-mixed fluid separated by narrow regions of relatively strong density gradient.

**JSP49/W/18-B5** **1600**

#### TURBULENT MIXING AND DISSIPATION ACCOMPANYING KELVIN-HELMHOLTZ INSTABILITY

DAVID C. FRITTS and Joseph A. Werne, Colorado Research Associates, 3380 Mitchell Lane, Boulder, CO 80301 USA

The Kelvin-Helmholtz (KH) instability is a major source of turbulence and mixing in stratified and sheared fluids. However, numerical simulations have only recently achieved sufficient resolution to describe the generation and mixing accompanying an extended inertial range of turbulence. Instabilities arise in the outer portions of the KH billows, penetrate into the billow cores thereafter, and lead ultimately to a layer of turbulence that becomes nearly homogeneous horizontally. Turbulence rapidly mixes the fluid initially within the billow cores, leading to a nearly adiabatic layer with large velocity and thermal gradients above and below. Energy and thermal dissipation profiles exhibit considerable spatial and temporal variability and non-Gaussian statistics, particularly at the edges of the mixing zone. As the turbulence layer restratifies, a dynamically stable shear flow is achieved.

**JSP49/W/21-B5** **1620**

#### QUANTITATIVE RESULTS ON TURBULENT PATCHES IN THE STRATOSPHERE

J.-R. ALISSE and C. Sidi Service d'Aéronomie du CNRS BP 3 91371 Verrières-le-Buisson France

The small-scale three-dimensional turbulent activity in the stably stratified atmosphere mainly dwells in isolated patches, with a larger horizontal extent than the vertical one. These structures are usually described as pancakes; they are believed to be completely mixed and hence should display sharp boundary transitions at their edges. Using high-resolution measurements of temperature and velocities profiles, obtained from a balloon-borne instrumentation, we present quantitative results on these patches. From the analysis of Richardson numbers, dissipation rates, Ozmidov, Thorpe and Kolmogorov scales within each layer, a typical pattern emerges, associating low Richardson numbers and significant Thorpe scales. It is noteworthy that the Ozmidov and Thorpe scales are usually quite smaller than the eyeballing thickness of the patches, as observed too in the ocean. Associated with the weak available potential energy dissipation rates, these elements suggest that in almost all the patches the mixing is imperfect. This may be related to the generating processes and life cycle of the patches and has important outcomes for the estimation of a vertical diffusivity on the large-scale tracer fields linked to this small scale turbulent activity.



JSP49/W/01-B5

1640

## DISSIPATION IN SHEAR-FREE TURBULENCE NEAR BOUNDARIES

Miguel A.C.TEIXEIRA and Stephen E. Belcher (both at Department of Meteorology, University of Reading, Earley Gate, PO Box 243, Reading RG6 6BB, UK, email: miguel@met.reading.ac.uk)

Processes such as gas transfer across gas-liquid interfaces are controlled by small-scale turbulence near the interface. Modelling these flows is complex, partly because turbulence dissipation is notoriously difficult to represent in closure models, particularly near boundaries. Hence, we investigate the fundamental dynamics of turbulence near interfaces. Most closure models are developed for solid walls, but recent DNS of shear-free turbulence near boundaries shows significant differences between flows bounded by solid walls and those bounded by free surfaces. Here, we develop a simple model for the rapid distortion of turbulence by such boundaries, which shows how viscous processes lead to the differences between solid walls and free surfaces. The new model produces profiles of Reynolds stresses and turbulence dissipation rates that are in good quantitative agreement with DNS data at short times. As in previous rapid distortion studies, this short time model is able to predict correctly qualitative features of the Reynolds stress and dissipation profiles at longer times. We conclude that the new model captures the essential physics of the problem and that blocking and the dynamics of the viscous boundary layer are the essential factors determining the shape of the turbulent Reynolds stresses and dissipation profiles near the boundary. The differences between model results and DNS data at long times can be attributed both to the neglected nonlinear effects and to turbulence decay due to dissipation. This highlights the importance of correctly representing dissipation in near-wall closure modelling.

JSP49/W/03-B5

1700

## A STUDY OF TURBULENT REGIME AS REVEALED BY VECTORIAL AS WELL AS SCALAR VARIANCE.

PROF.KPR Vittal Murty

This article presents a detailed study of the variances of wind components, temperature and humidity estimated from the data obtained from three dimensional fast response sonic anemometer during May 1998 which is a part of inter-disciplinary Pantanal experiment (IPE-1). Pantanal is the largest wet land in the world. It is located in central-west Brazil. It has ecological and socio-economic significance. There is large seasonal variation in meteorological and hydrological parameters in this region, marked by dry winters and wet summers. The variances of wind components for pure mechanical turbulence are constant and agree fairly with the values reported by Panofsky and Dutton. It should be mentioned that the values of velocity variance lie between the values obtained from earlier expeditions for flat and rolling terrain. This indicates that the terrain features of Pantanal are in between flat and rolling terrains. The vertical variance is scaled with Monin-Obukhov length scale ( $L$ ). It is minimum at neutral condition increasing with stability as well as in-stability. An interesting feature is the relation between horizontal variance and Richardson number. The slope of the curve varies for a clear day and cloudy day thus is a function of synoptic scale disturbance. Both the scalar variances of temperature and humidity showed a similar variation with  $Z/L$  (here  $Z$  is the height of observation and  $L$  Monin-Obukhov length scale). Both the parameters showed a discontinuity at  $Z/L = 0$ .

JSP49/W/09-B5

1720

## SST ANOMALIES, VERTICAL TURBULENT MIXING AND SUBMARINE EARTHQUAKES

M.A. NOSOV, M.V. (Lomonosov Moscow State University Faculty of Physics Moscow State University Russia) B.W Levin., S.N. Skachko

The appearance of large-scale (~500 km) cool SST anomalies were discovered in the epicenter regions of strong underwater earthquakes. In our opinion the mechanism of the SST anomaly origin was certainly connected with an export of cold lower water layers to the ocean surface as a result of intensive turbulent mixing generated by seismic bottom motions. These SST anomalies may lead to some obvious and at the same time important consequences and accompanying phenomena should be studied. Among all the phenomena we single out the following: 1) export of the nutrients toward upper water layers where there is an usual shortage of the substances causing an increase of the productivity (like in an upwelling zone), 2) generation of large amplitude internal waves (much larger than internal tsunami waves) as a result of evolution of the anomaly stratification zone; 3) the appearance of the cool SST anomaly should cause a response of the atmosphere. This study is aimed to reveal the mechanism of the turbulence generation above the moving bottom. The numerical model of the process is based on the equation of the balance of the turbulence energy in stratified fluid and equation of turbulent heat transfer. The results of this study give us grounds to state that submarine earthquakes can produce large scale cool SST anomalies above the pleistoseismic zone by means of intensification of the vertical turbulent exchange.

VS2

Wednesday 28 July

**MAGMA FRAGMENTATION AND EXPLOSIVE ERUPTIVE FLOWS**

Location: Medical School WG11 LT5

Location of Posters: Medical School, Arthur Thompson Hall

Wednesday 28 July AM

Presiding Chairs: G.A. Valentine, (Los Alamos National Laboratory, Los Alamos, USA);  
D.B. Dingwell, (Univeritaet Bayreuth, Germany)

VS2/W/06-B3

0830

**VESICULATION DURING MAGMA ASCENT: GAS PRESSURE, DEHYDRATION AND FRAGMENTATION**

Nadav Lensky, Anatoly Chekhmir, Vladimir Lyakhovsky and Oded NAVON (Institute of Earth Sciences, Hebrew University, Jerusalem, 91904, ISRAEL, email oded@vms.huji.ac.il)

We used experimental and numerical simulations to study the growth of water bubbles in silicic melts under variable pressure. Rhyolitic obsidian was hydrated at 150 MPa (850 C), vesiculated and equilibrated at 110 MPa (700 C) and decompressed gradually, from 110 MPa to 70 MPa. Bubble growth under variable pressure from initial to final radius was documented by comparing photos of individual bubbles before and after decompression. The experiments were simulated using a modification of the model of Lyakhovsky et al. (1995) that accounts for the effects of variable pressure and the dependence of viscosity and diffusivity on both temperature and concentration of water. The excellent agreement of measured and simulated radii confirms the accuracy of the modified code. The model is now combined with conduit flow models in order to examine the evolution of bubbles during magma ascent. The model assumes steady-state flow and a known magma mass discharge through a cylindrical conduit of a given radius. Magma with known initial water content and bubble number density is introduced at the bottom of the conduit and allowed to ascend at a velocity which is determined by the mass flux. The model follows the expansion of bubbles, the ascent velocity and the gas pressure in the bubbles. For a reasonable choice of parameters, the water content of the melt initially follows the equilibrium value and is determined by the ambient pressure. Later, gas pressure increases above ambient, as magma acceleration and increasing melt viscosities prevent equilibrium dehydration of the melt shell around the bubbles. This excess pressure along with increasing viscosity and strain rates may lead to magma fragmentation.

VS2/W/27-B3

0850

**THERMODYNAMIC AND KINETIC CONSIDERATION OF MAGMA FRAGMENTATION AS A RAREFACTION SHOCK WAVE**

ATSUSHI TORAMARU (Department of Earth Sciences, Kanazawa University, Kanazawa, Kakumamachi, Ishikawa 920-1192, Japan, email toratora@kenroku.kanazawa-u.ac.jp)

Fragmentation of magma during explosive volcanic eruptions must be related to the dynamics of vesiculation process such as nucleation, growth, expansion, deformation and coalescence of bubbles. I present the role of magma vesiculation on the magma fragmentation from the view points of the thermodynamics and kinetics. The entropy consideration shows that the fragmentation of magma can possibly propagate as a rarefaction shock wave if the negative curvature part exists on the pressure-specific volume curve (P-V curve). On the P-V curve for a vesiculating magma the negative curvature can exist due to two kinetic effects of vesiculation: nucleation of bubbles and melt viscosity as a function of volatile concentration and time scale of decompression. The former can be called the nucleation wave, the later should be the fragmentation wave. Applying the entropy criterion for the rarefaction shock wave to vesiculating magma and taking into account the viscoelastic rheology of melt, I derive the condition of presence of fragmentation wave as function of decompression rate, silica and water contents. The fragmentation wave as a rarefaction shock wave is caused by the suppressed expansion of bubbles. As an numerical result, the propagation of magma fragmentation can be a rarefaction shock wave if the decompression time scale is approximately less than the relaxation time scale. This stability condition of fragmentation wave as a rarefaction shock wave may correspond to the transition between the explosive eruption to the lava dome growth in eruption styles.

VS2/W/16-B3

0910

**THE INFLUENCE OF FRAGMENTATION CRITERION ON EXPLOSIVE FLOW DYNAMICS IN HIGH-VISCOUS GAS-SATURATED MAGMAS**

Oleg MELNIK (Moscow State University, Institute of Mechanics, 117192, 1-Mitchurinskii prosp, Moscow, Russia, email melnik@inmech.msu.ru); Stephen Sparks (Earth Sciences, Bristol University, Wills Memorial Building, Queen's Road, Bristol, B8S 1RJ, UK, email Steve.Sparks@bristol.ac.uk).

The influence of the fragmentation criterion on the discharge rate of explosive eruption is studied by using unsteady 1D code. Mechanical model takes into account the existence of two different flow regimes - bubbly melt flow and gas-particle dispersion flow. They are separated by a fragmentation region, modelled by means of a discontinuity. To study the influence of fragmentation criterion the problem of initiation of explosive eruption by a lava dome collapse is considered.

Three different fragmentation mechanisms are studied: fixed volume concentration of bubbles before the fragmentation, fixed overpressure in the growing bubble due to the viscous resistance of surrounding melt and strain induced fragmentation. In the case of fixed volume concentration criterion the velocity of the fragmentation wave and discharge rate decrease monotonically and the eruption comes to a steady condition. In case of the two other criteria fragmentation occurs discretely in time. The fragmentation wave stops and magma rise without fragmentation occurs before the conditions become suitable for new fragmentation event. Each fragmentation event causes a pulse in discharge rate. Seismic data and observations for Soufriere Hills volcano explosive eruptions (1995-1998) shows the existence of pulses. The angular platy shapes of pumice ejecta in this eruption also supports a brittle fragmentation mechanism.

VS2/W/18-B3

0930

**THE ASH PROBLEM: HYDRODYNAMIC VERSUS BRITTLE FRAGMENTATION**

Bernd ZIMANOWSKI, Ralf Buettner, and Ines Caffier (all at Physikalisches Vulkanologisches Labor, Universitaet Wuerzburg, Pleichervall 1, D-97070 Wuerzburg, Germany, e-mail: zimano@geologie.uni-wuerzburg.de); Kenneth Wohletz (EES-1, MS D462 Los Alamos National Laboratory, Los Alamos, NM 87545, USA, email: wohletz@lanl.gov)

The deposits of explosive volcanic eruptions are characterized by the abundance of ash-sized pyroclasts. Highly energetic eruptions produce a significantly high proportion of fine ash

particles (diameters < 64 µm). Short time ("explosive") formation of such small particles (in contrary to a grinding process) requires particular fragmentation mechanisms. Currently two different models of fragmentation are generally considered, based upon the relationship between characteristic times for deformation and viscous relaxation; one were viscous relaxation is faster and magma deforms as a liquid, leading to hydrodynamic fragmentation modes; the other were deformation proceeds faster than viscous relaxation, leading to brittle-type fragmentation mechanisms. Combining experimental results and model calculations for the case of basaltic magmas the efficiency of both mechanisms is compared and the requirements for the volcanic apparatus are discussed in respect to a satisfying physical explanation of the particle-size distributions of pyroclastic deposits.

VS2/W/09-B3

0950

**EXPLOSIVE DYNAMICS AND RELATED PHYSICAL FEATURES OF PHREATOMAGMATIC DIATREMES, HOPI BUTTES, ARIZONA, USA**

Jason HOOTEN (Geology Department, Northern Arizona University, Box 4099, Flagstaff, AZ, USA, email: jah23@dana.ucc.nau.edu); Michael Ort (Geology Department, Northern Arizona University, Box 4099, Flagstaff, AZ, USA, email: Michael.Ort@nau.edu)

The Mio-Pliocene Hopi Buttes volcanic field, located in northcentral Arizona, contains approximately 300 individual vents. Within this region, nephelinitic and monchiquite magmas were erupted into water-saturated sediments, resulting in a variety of hydrovolcanic features. Field study of the diatreme portion of these volcanic remnants reveals a consistent change in textural facies within varying levels of the exposed vent structures. At present, the diatremes are exposed 150 to 270 meters below the pre-eruptive surface. Confining pressures calculated for individual diatremes range from 11 to 30 bars, consistent with experimentally derived parameters for optimal explosive effectiveness within fuel-coolant interactions. Approximations of the initial water-melt ratios within individual explosive buds are also consistent with experimental values for mass water-melt ratios necessary for ideal thermodynamic efficiency. The outcrop geometry of many of the diatremes becomes increasingly tabular in shape with greater depth. This change in diatreme morphology is accompanied by a transition in vent facies deposits. Upper diatreme exposures containing massive, pelletal-textured tuffaceous breccias typically grade downward into hypabyssal aphanitic nephelinitic or monchiquite. Inconsistencies between diatreme morphology, facies characteristics, and the current elevation of exposure suggest that the magnitude and/or duration of the eruption controls the boring depth of individual vents.

VS2/E/08-B3

1010

**CONTRASTING FRAGMENTATION AND TRANSPORTATION DYNAMICS IN THE AGNANO MONTE SPINA ERUPTION (4.1 KA) AT PHELGREAN FIELDS (SOUTHERN ITALY)**

Pierfrancesco DELLINO and Luigi La Volpe (both at Dipartimento Geomineralogico, Universita' degli Studi di Bari, Via E. Orabona 4, 70125 -Bari, Italy, email: dellino@lgsxserver.uniba.it) Giovanni Orsi and Roberto Isaia (both at Osservatorio Vesuviano, Via Manzoni, 249, 80132 - Naples, Italy, email: orsi@osve.unina.it)

Pyroclastic deposits of the Agnano - Monte Spina eruption have been studied, in order to define the fragmentation and transportation processes operating in the various phases of activity. The detailed analysis of structural and textural features of deposits has suggested that a complex and variable eruptive style has occurred during the eruption.

To unravel the complexities in the eruption dynamics, grain size and Scanning Electron Microscopy (SEM) data have been elaborated by means of multivariate statistical techniques of the type of Cluster and Factor analyses. Interpretation of results has led to the distinction of end - member deposits due to pure magmatic activity, characterized by coarse pumice fragmentation and emplaced by plinian fallout dynamics, and end - member deposits due to pure hydromagmatic activity, characterized by fine ash fragmentation and emplaced by surge. Between the two end - members, deposits which show the contemporaneous presence of the two fragmentation dynamics have been recognized. Some of the latter are related to energetic and stationary turbulent and dilute surge flows, others to a complex interplay between ash surge flow with contemporaneous ballistic fallout. In this case vesiculated fragments derive from decompression processes occurring as a consequence of the hydromagmatic pulse.

VS2/W/13-B3

1050

**THE PAGOSA PEAK DACITE, SAN JUAN VOLCANIC FIELD, COLORADO: A VOLUMINOUS FOUNTAIN-FED SILICIC PYROCLASTIC DEPOSIT RESULTING FROM BRITTLE MAGMA FRAGMENTATION AT LOW VESICULARITY**

Olivier BACHMANN and Michael Dungan (Département de Minéralogie, Université de Genève, rue des Maraichers, 13, 1211 GENEVE 4, Switzerland, email: bachmann@sc2a.unige.ch) Peter Lipman (U.S. Geological Survey, 345 Middlefield Rd, Menlo Park, CA, USA, email: plipman@mojave.wr.usgs.gov)

The Pagosa Peak dacite, a voluminous (200-300 km<sup>3</sup>) precursor to the enormous 28-Ma Fish Canyon Tuff, was erupted by pyroclastic fountaining and is associated with syn-eruptive block-faulting rather than caldera collapse. Pagosa Peak dacite deposits display a high aspect ratio (~1.50), evidence of rheomorphic flow, coarse granulometry (40-60 % of magmatic "blobs" up to 4 meters in diameter in a fine-grained matrix), and a lack of lithic fragments. Non-welded blobs are less vesicular (20-30 % ves.) than typical silicic pumices (~75 %). These unusual textures are interpreted as a reflection of a low-energy eruptive mechanism due to inefficient fragmentation. Analogous to process observed by Alidibirov and Dingwell (1996; Nature, vol. 380), fragmentation was probably triggered by brittle fracturing of the viscous magma at much lower vesicularities than the common bubble packing limit. Fracture propagation may have been provoked by shear stress, as a consequence of magma ascent in narrow conduits that opened during syn-eruptive block-faulting and subsidence of the magma chamber roof. This inefficient fragmentation mechanism, perhaps associated with partial degassing during relatively slow magma rise, resulted in a low altitude column that fed highly concentrated pyroclastic flows. Rapid emplacement and coarse granulometry maximized heat retention and allowed rheomorphic flow to occur.

VS2/E/02-B3

1110

**THE INFLUENCE OF PYROCLASTIC GRAIN-SIZE DISTRIBUTION ON THE DYNAMICS OF COLLAPSING COLUMNS AND PYROCLASTIC FLOWS**

Augusto NERI (Consiglio Nazionale delle Ricerche, Pisa I-56126, Italy, Email: neri@dst.unipi.it); Giovanni Macedonio (Osservatorio Vesuviano, Napoli I-80123, Italy, Email: macedonio@osve.unina.it) Dimitri Gidaspow (Illinois Institute of Technology, Chicago 60616, USA, Email: gidaspow@charlie.cns.iit.edu) Franco Barberi (Dip. Protezione Civile, Rome I-00185, Italy)

A transient, two-dimensional, thermofluid dynamic flow model was developed to simulate the multiparticle and multicomponent nature of collapsing volcanic columns and pyroclastic flows. The model accounts for full mechanical and thermal non-equilibrium conditions between a multicomponent gas phase and N particulate phases representative of pyroclast distribution.

Pyroclast phases are characterized by specific physical properties such as diameter, density, specific heat, thermal conductivity, and viscosity. The partial differential equations representative of mass, momentum, and energy conservation of each phase were solved numerically on an axisymmetric physical domain. Three simulations were carried out by using different grain-size and gas compositions of the eruptive mixture at the vent. Six particulate phases were considered representative of pyroclasts ranging from a few microns up to a few millimeters in diameter, whereas the gas phase consists of water vapor, carbon dioxide and air. Simulation results show that, with a constant vent diameter, mass flow-rate and water content, fine-grained particle distributions produce thicker and more mobile currents, larger runout distances, and a greater elutriated mass than the coarse-grained distribution.

### VS2/E/13-B3 1130

#### PERIODIC VULCANIAN EXPLOSIONS AT MONTSERRAT (ANTILLES), AUGUST 1997

T. DRUITT (Magmas et Volcans UMR 6524 & CNRS, Clermont-Ferrand, France, and Montserrat Volcano Observatory, druitt@opgc.univ-bpclermont.fr); C. Harford, R. Herd, R., Luckett, B. Voight and others (Montserrat Volcano Observatory)

In August, September, and October 1997, there occurred 75 vulcanian explosions from the South Soufriere Hills lava dome. We present a quantitative analysis of the 11 eruptions that took place between 5 and 12 August, based on measured eruption column heights, video footage, ballistic data, and seismic signals. The August explosions occurred every 10 to 12 hours from a 300 m-diameter crater excavated in the dome. Each lasted several tens of seconds, followed by a waning phase of about an hour. The mass of magma erupted was in each case about 109 kg, with peak discharge rates of 1.5 to 2.5 x 10<sup>7</sup> kgs<sup>-1</sup>. Between 10 and 40 % of this mass collapsed back from 300 to 350 m above the dome to form thin, highly mobile pumice flows, which travelled as far as 5.5 km. The flows had initial speeds of up to 60ms<sup>-1</sup>, then decelerated to about 10 ms<sup>-1</sup>. The convective plumes reached heights of 9 to 14 km and exhibited superbuoyant behaviour, first decelerating, then re-accelerating as they rose. Eruption velocities were between 120 and 170 ms<sup>-1</sup>, and dense blocks 70 cm in diameter were thrown ballistically up to 1.7 km from the dome centre. Each explosion excavated the conduit to a depth of 1 to 1.5 km. The conduit was then re-filled at about 10 m3s<sup>-1</sup> prior to the next explosion. Fragmentation during these eruptions occurred by a brittle spallation mechanism, producing platy pumice clasts. Application of theoretical models suggests fragmentation pressures in the range 3 to 15 MPa and gas contents of 1 to 1.5 wt%. The latter are consistent with bulk-magma water contents estimated from melt inclusion analyses and observed phenocryst contents. This implies that the magma lost little gas during ascent between eruptions and that the explosions were magmatically driven. External water played little role in these eruptions.

### VS2/W/14-B3 1150

#### DYNAMICS OF THE JUNE 25 1997 PYROCLASTIC FLOWS OF SOUFRIERE HILLS VOLCANO, MONTSERRAT

COLE PD, (Dept of Geology, University of Luton, Luton UK, paul.cole@luton.ac.uk), Loughlin S C, (British Geological Survey, Edinburgh, EH9 3LE, UK, s.loughlin@bgs.ac.uk); Luckett R, (Montserrat Volcano Observatory); Sparks RSJ, (Dept of Geology, University of Bristol, Bristol BS8 1RJ, UK); Pyle DM (Dept of Earth Sciences, University of Cambridge CB2 3EQ, UK)

The June 25 1997 pyroclastic flows are some of the largest volume dome collapse events to have occurred during the current eruption. The flows had a total run out of 6.8 km from the dome, and surveys of the deposits indicate that a total of 5 x 10<sup>6</sup> m<sup>3</sup> of dome material was involved. Analysis of video, seismic and eyewitness evidence indicate that there were 3 separate flow pulses that occurred over a 20 minute period. Each flow pulse was more voluminous and energetic than the last. Seismic data allows identification of the onset of each flow pulse. Flow 1 was restricted to the confines of the valley with only minor surge spillage and had a maximum run out of 4.7 km and mean velocity of 15 m/s. Flow pulse 2, which began 2.6 mins after pulse 1, had a run out of 6.8 km and a mean velocity of 16 m/s. Flow pulse 3, which began 8 mins after the onset of pulse 2, had a mean velocity of 22 m/s. These estimates agree well with velocities calculated from super-elevation of flow deposits in medial and distal regions of 20 m/s below Harris at 4 km and 8m/s at 5.8 km. Ash cloud surges detached from flow pulses 2 and 3 along the lower part of Mosquito Ghaut. Surges were particularly extensive with pulse 3, spilled west onto Farrells plain, climbing 60 m up Windy Hill indicating a velocity of between 35 and 37m/s at 2 km. The dilute ash cloud surge transformed into a dense pyroclastic flow moving a further 3.5 km out of the surge effected area down the Dyers River Valley. Calculations using the Chezy flow equation allow partitioning of flow volumes for each flow pulse. The volumes are: 6.5 x 10<sup>5</sup> m<sup>3</sup> (Pulse 1), 1.55 x 10<sup>6</sup> m<sup>3</sup> (Pulse 2), 3.8 x 10<sup>6</sup> m<sup>3</sup> (Pulse 3).

### VS2/W/03-B3 1210

#### CHANGE IN PARTICLE ORIENTATION AND SHAPE IN VOLCANIC BRECCIAS AS A FUNCTION OF TRANSPORT DISTANCE: A PHOTO-STATISTICAL METHOD

D. KARÁTON and T. Telbisz (Eötvös University, Department of Physical Geography, 1083 Budapest, Ludovika tér 2, Hungary) O. Sztanó (Eötvös University, Department of Geology, 1085 Budapest, Múzeum krt. 4/a, Hungary)

Volcanic breccias, such as caldera collapse and lag breccias, block- and ash-flow deposits, and proximal facies of lahars, are investigated by a photo-statistical method. Photos of scaled outcrops from the Carpathians and Japan and some other regions, are scanned, and their fabric is analysed by image-processing and statistical softwares. Numbers of analysed particles, of millimetric to metric size, range from 300 to 1200.

For the orientation of particles, it is found that caldera collapse and lag breccias, with no significant transport, are almost randomly oriented. In contrast, the majority of particles in block- and ash-flow deposits very near (0.5-2 km) to the vent shows a parallel arrangement, corresponding to the inferred flow directions. This orientation is characteristic not only of longitudinal but also of oblique and plan-view sections. In some cases, clast imbrication is also observed.

In deeply eroded, collapsed lava dome products of the Miocene Börzsöny volcano in Hungary, massive or auto-brecciated roots of domes pass upwards into coarse-grained breccias, probably proximal facies of block- and ash-flow deposits. These breccias show random particle orientation relative to more distal counterparts. Particles in these products tend to be more circular and less elongate than the further transported equivalents, perhaps due to the hot, viscous initial fragmentation of the lava dome.

### VS2/E/07-B3 1230

#### ERUPTION OF LAGUNA CALDERA BETWEEN 42,000-47,000 YEARS AGO

Sandra G. CATANE (National Institute of Geological Sciences, University of the Philippines, Diliman, Quezon City, Philippines, email: catane@phivolcs.dost.gov.ph); Ma. Carmencita B. Arpa (Philippine Institute of Volcanology and Seismology, C.P. Garcia Ave., Diliman, Quezon City, Philippines, email: carmen@phivolcs.dost.gov.ph)

Metropolitan Manila sits atop a landmass that was built up from a shallow marine environment mainly by deposition of voluminous pyroclastic materials. At least three episodes of calderagenic eruptions were dated: (1) 5,000 ybp, (2) 27,000-29,000 ybp, and (3) 42,000-47,000 ybp. These eruptions are associated with nearby caldera centers, Taal and Laguna. The earliest eruption (42,000-47,000 ybp) that is related to Laguna caldera had significantly altered the surrounding landscapes by reclaiming part of Manila Bay. The Laguna Lake, which was originally part of Manila Bay, became a separate body of water due to the deposition of voluminous pyroclastic deposits. Pyroclastic flows blanketed wide areas around the caldera and deposits reached as far as 70 km from the source.

The eruption produced a compositionally unique set of deposits – pumiceous units at the base, grading into mixed pumice-scoria deposits at the middle to scoriaceous varieties at the top of the sequence. SiO<sub>2</sub> contents of juvenile clasts range between 54-64%. Texturally, the pyroclastic deposits vary from an unwelded base to strongly welded top reflecting possible changes in composition and volatile content or eruption mechanism. Pyroclastic flows were accompanied by surges but no distinctive plinian fall was recognized. It is likely that pyroclastic flows were fed not by a tall eruption column but rather by a low maintained pyroclastic fountain.

### Wednesday 28 July PM

Presiding Chairs: G.A. Valentine, (Los Alamos National Laboratory, Los Alamos, USA); D.B. Dingwell, (Univeritaet Bayreuth, Germany)

### VS2/W/01-B3 Poster 1400-01

#### MONITORING OF MAGMA FRAGMENTATION BY ELECTRICAL FIELD MEASUREMENTS

Ralf Buettner and Bernd ZIMANOWSKI (both at Physikalisch-Vulkanologisches Labor, Universitaet Wuerzburg, Pleicherwall 1, D-97070 Wuerzburg, Germany, email: zimano@geologie.uni-wuerzburg.de); Helmut Roeder (Institut fuer Geophysik, Universitaet Stuttgart, Richard-Wagner-Straße 44, D-70184 Stuttgart, Germany)

Explosive volcanic eruptions are characterized by intensive magma fragmentation, which dominates the heat transfer from the magma and the conversion to mechanical energy. The fragmentation energy thus represents a proportional part of the total kinetic energy released during explosive volcanism. A method for the quantification of magma fragmentation during the eruption would allow direct measurement of the total kinetic energy release.

If a material gets fragmented on a short time scale its electrostatic equilibrium is disturbed by the formation of new surface. Expansion of the fragmented system results in fluctuations of the electrostatic field. Depending on the electrical properties of the fragmented material and the surrounding media these fluctuations can be detected once a significant amount of new surface area is created. Based on these considerations a method was developed in the lab and successfully tested at Stromboli volcano (Sicily), which allows to distinguish and quantify different eruption styles during real time surveillance operation.

### VS2/W/02-B3 Poster 1400-02

#### FRAGMENTATION BEHAVIOUR OF A LABORATORY ANALOGUE TO EXPLOSIVE MAGMATIC FLOWS

Graham A RYAN<sup>9</sup> (1), Stephen J Lane (2), Jeremy C Phillips (3) (4) (Volcanic and Geohazards Research Group, Department of Environmental Science, Lancaster University Lancaster LA1 4YQ, UK); (3) (Centre for Environmental and Geophysical Flows, School of Mathematics, University of Bristol, University Walk, Bristol BS8 1TW, UK).

The rapid decompression of volumes of gum rosin organic solvent solution to varying degrees of supersaturation results in the generation of a foam flow. The liquid increases in viscosity as the volatile phase degasses in similar fashion to dehydrating magma. Flows of low supersaturation accelerate slowly and no fragmentation is observed. As supersaturation is increased fragmentation occurs and becomes more extensive. The most highly supersaturated flows generate several hundred foam fragments from a few 100 ml of starting solution. We present data on the number, size, velocity and acceleration of fragments from flows with a range of supersaturations. These data show that fragmentation does not take place at a discrete diameter 'fragmentation level'. Fragmentation begins with the development of gas pockets at the tube wall which grow to the of the tube as the foam deforms plastically. The detected increase in foam slug numbers with height in the tube indicates that fragmentation continues along the entire length of the tube. Foam fragments are observed to expand as pressure decreases up the tube, but most of the flow expansion takes place in the gas pockets between the foam slugs. Velocity measurements indicate that the flow is moving at close to sound speed.

### VS2/W/04-B3 Poster 1400-03

#### FORMING OF BEZMYANNI PYROCLASTIC FLOWS, KAMCHATKA

Alexander I. MALYSHEV (Institute of Geology and Geochemistry, Urals Branch of RAS, Pochtovy pr 7, Ekaterinburg, SU-620151, Russia, email root@igg.e-burg.su)

The field observations under forming of Bezmyanniy pyroclastic flows have shown that the movement of pyroclastic flows represents itself a complex self-organizing process. This process has a number of features, which are peculiar both to autoexplosive avalanches, and pyroclastic flows, but at the expense of scale effect more distinctly are traced during the directed paroxysmal eruptions of the volcano. The most essential features are the following.

- 1) Continuous subhorizontal and subvertical differentiation of moving pyroclastic particles on granulometric composition and the speed of movement under the influence of force of weight and energy of extending gases, including the newly formed at the expense of autoexplosivity effect.
- 2) The absence of the precisely expressed border between the heavier bottom part of a flow of heated pyroclastic particles, under which it is usually understood a proper pyroclastic flow, and the lighter top part, usually called the accompanying a pyroclastic flow "ash cloud".
- 3) Specific reaction of a flow of heated pyroclastic particles on the being expressed in the fact that the heavier parts of flow are moving in complete conformity with a relief of a district, and the lighter ones ignore this relief. After pyroclastic flow division into lighter and heavy parts the process of pyroclastic particles differentiation is going on. From the heavier part, of the flow deflected on relief, allocation of lighter and faster pyroclastic particles at once begins, and during the rectilinear movement of the lighter part of the flow in its basement at once it begins to be accumulated more coarse-fragmental material.
- 4) A long interval of time, during which the eruption of a flow heated pyroclastic particles, is going on. Therefore the deposits of final portions of heated pyroclastic particles sharply contrast with primary deposits of a catastrophic pyroclastic flow. These features cause a great variety of pyroclastic deposits.



VS2/W/05-B3 Poster 1400-04

**ANALYSIS OF THE EVOLUTION OF THE ASH CLOUD FROM THE DECEMBER 26, 1997 (BOXING DAY) DOME COLLAPSE OF SOUFRIERE HILLS VOLCANO, MONTSERRAT USING GOES-8 IMAGERY**

Ms. Gari C. MAYBERRY, (Michigan Technological University, Department of Geological Sciences, gcmayber@mtu.edu); Dr. Bill I. Rose, (Michigan Technological University, Department of Geological Sciences); Dr. Gregg Bluth, (Michigan Technological University, Department of Geological Sciences)

There have been many serious incidents of aircraft encountering volcanic clouds in the past. By studying volcanic clouds we can monitor their paths, as well as learn more about their evolution, in an effort to mitigate the hazard they pose to aircraft.

The December 26, 1997 dome collapse of Soufriere Hills volcano, Montserrat resulted in a pyroclastic flow that descended the White River Valley ~4km and traveled across the sea an unknown distance. The slope failure and subsequent dome collapse occurred around 0700Z and lasted approximately 15 minutes and an associated volcanic ash cloud rose to an altitude of 47,000 ft. (14.3 km). The volcanic cloud was observed by the geostationary (GOES-8) satellite every 30 minutes, which resulted in a comprehensive record of its evolution. Seventeen images of the volcanic cloud, between 0715Z and 2345Z, were analyzed. The brightness temperature difference (BTD) between bands 4(10.3-11.3 microns) and 5 (11.5-12.5 microns) of GOES-8 was used to distinguish the ash cloud from meteorological clouds. Ash clouds have a negative BTD while meteorological clouds have a positive BTD (Prata, GRL 16: 1293-1296, 1989). BTD data are used to map the volcanic cloud and retrieve basic data about the area of the cloud, mass of the fine ash particles (<10 microns radius), and the optical depth (Wen and Rose, JGR 99:5421-5431, 1994).

The volcanic cloud moved rapidly 20-28 km/hr to the south east until around 1145Z when it became more transparent and began to dissipate. The largest band 4 optical depth (~3) occurred at 0745Z, shortly after the eruption began, and rapidly decreased to about .3 less than 2 hours after the onset of the eruption. From about 0845Z to 1045Z the ash signal of the volcanic cloud was obscured by "masking", which was caused by a cloud of liquid water droplets with a positive BTD. The cloud with the positive BTD may have overlain or mixed with volcanic cloud, which obscured negative BTD values of the ash cloud. We speculate the water-rich cloud was the result of the interaction of the pyroclastic cloud with the sea, and its subsequent rise and interaction with the volcanic cloud.

VS2/W/07-B3 Poster 1400-05

**BEHAVIOUR OF GASES DURING ERUPTIONS OF BEZMYANNI VOLCANO**

Alexander I. MALYSHEV (Institute of Geology and Geochemistry, Urals Branch of RAS, Pochtovy pr 7, Ekaterinburg, SU-620151, Russia, email root@igg.e-burg.su)

In the report the results of field observations under the behaviour of gases during eruptions of a volcano Bezymyanni are considered. All the variety of character of historical eruptions of Bezymyanni is determined by a mode of expansion of gases. Two groups of eruptions are singled out. The eruptions of the first group correspond to an avalanche degassing of a juvenile material, original wide-ranging break of gases. The character of eruptions of the second group is defined by relatively quiet expansion of gases inside the juvenile material. Four types of degassing processes are fixed: a) degassing of the juvenile material occurs at the expense of migration of gases on long-living zones of the increased cracking in construction of a volcano; b) allocation and quiet expansion of gases inside magma; c) autoexplosive degassing; d) degassing during the provoked explosivity. Dynamics of explosive eruptions of Bezymyanni is determined mainly by autoexplosivity, that is the avalanche degassing of the juvenile material on decompression cracks. High pressure of gases causes the formation of the crack itself, or even of the whole system of the branching cracks extending deep into the aerated and viscous juvenile material. Along the surface of these cracks there is a fragmentation of the juvenile material, and from the surface of cracks deep into the juvenile material it occurs the spreading of a wave of splitting. The gas, extending on cracks, with the seized particles of splitting is taken out on a surface as gas-ash emissions. During intensive receipt on earth surface of the viscous, high-temperature and gas-saturated juvenile material this phenomenon occurs in mass scale and amplifies at the expense of the provoked explosivity. These processes result in an intensive fragmentation of the juvenile material and the formation of pyroclastic flows.

VS2/W/08-B3 Poster 1400-06

**A MODEL OF THE INTERACTION OF A FISSURE ERUPTION WITH A HORIZONTAL TUNNEL**

Andrew WOODS and Steve Sparks, Centre for Environmental and Geophysical Flows, University of Bristol, Bristol, England (e-mail a.w.woods@bris.ac.uk); Chuck Connor and Brittain Hill, Centre for Nuclear Waste Regulatory Analysis, Southwest Research Institute, San Antonio, Texas (e-mail cconnor@swri.edu)

We describe a series of calculations aimed at quantifying the activity which might result when an ascending dike intersects a horizontal tunnel at atmospheric pressure. This allows the magma to decompress rapidly down the tunnel. We examine both water poor basaltic magma, assumed to be incompressible and water-rich basaltic magma (2-3%) as two end member models. The motion of volatile poor magma along the tunnel involves driving pressures up to 10-100 atmospheres and so the magma will advance along the tunnel at speeds up to tens of metres per second. The motion of a volatile rich magma initially produces an expansion wave propagating down the tunnel. We predict that a shock wave develops in the air ahead of the expanding mixture, with a pressure jump across the shock as large as several atmospheres. The fragmented magma-volatile mixture following the shock moves with speeds up to 100-150 m/s. Once the shock wave reaches the end of the tunnel, it is reflected and the pressure in the tunnel gradually builds up. This model of magma behaviour in a horizontal tunnel will be used to constrain the consequences of basaltic volcanic activity, should an eruption occur within the proposed Yucca Mountain, Nevada, high-level radioactive waste repository. This waste storage facility is located within a basaltic volcanic field and is required to isolate radioactive waste in tunnels during its projected 10,000 yr performance period.

VS2/W/10-B3 Poster 1400-07

**CHARACTERIZING THE SHAPES OF PYROCLASTS IN DISTAL FALLOUT MATERIAL TO IMPROVE OUR UNDERSTANDING OF FALLOUT RATES AND TRANSPORT**

C M RILEY, G J S Bluth, W I Rose (All at: Geological Engineering and Sciences, Michigan Technological University, Houghton, MI, 49931, email: cmriley@mtu.edu)

A significant hazard from large-scale volcanic eruptions is ash which can be transported great distances and deposit irregularly and in unusually thick amounts far from the volcanic source. One influence on volcanic ash transport is particle shape which affects the aerodynamic properties responsible for particle separation and fallout, the interaction of particles with the atmosphere, and remote sensing measurements of ash particle concentrations. The main objectives of this study are to characterize the shape and determine terminal settling velocities

for ash particles so that these data can be used to improve transport models and remote sensing algorithms. A total of 1,300 andesitic ash particles were measured from the August 1992 Spurr eruption. The majority of particles are subrounded silicate pumice fragments, with < 10% glass bubble-wall shards. Size distribution data for the sample show the sample is bimodal, which indicates aggregation played a role in fallout. In general, actual mean diameters for each settling velocity group were larger than expected if the particles were assumed spherical. We show that this is due to particle shape influences rather than density effects. The larger than expected diameters for particles in given terminal settling velocity groups suggests that the irregular shape of these particles decreases their settling rate. This is at odds with current transport modeling results which show that particles fall out faster than expected and suggests that another factor such as aggregation may be of greater importance in the fallout of andesitic particles. The Spurr particles are representative of vulcanian to subplinian andesitic eruptions but are unlike more irregular-shaped rhyolitic particles often formed in plinian eruptions.

VS2/W/11-B3 Poster 1400-08

**PRODUCTION OF EXPERIMENTAL PYROCLASTS BY EXPLOSIVE VESICULATION OF A VISCOUS LIQUID**

Jon BLOWER (email Jon.Blower@bris.ac.uk), Heidy Mader (email H.M.Mader@bris.ac.uk); Jeremy Phillips (email J.C.Phillips@bris.ac.uk); (Department of Earth Sciences, Wills Memorial Building, Queens Road, Bristol BS8 1RJ, UK)

In recent years, the study of explosive two-phase flows in the laboratory has revealed much information about the processes operating in a volcanic conduit during an eruption. The experiments discussed here use a solution of gum rosin in acetone (GRA) as an analogue for hydrated magmas. The dependence of the GRA liquid viscosity on its volatile (acetone) content reproduces the dependence of magma (rhyolite) viscosity on its water content. The diffusivities of the corresponding volatile species (water and acetone) are comparable in magnitude. When decompressed from atmospheric pressure to a partial vacuum in a shock-tube, the GRA solution vesiculates into a rapidly-evolving two-phase flow. Under certain experimental conditions the flow may fragment, producing solid foam fragments, which are analogous to volcanic pumice.

Results are presented from a series of experiments in which a range of liquid viscosities and volatile supersaturations are investigated, and a variety of degassing behaviours observed, from gentle boiling to explosive disruption of the liquid. Where solid foam is produced, its vesicularity (volume expansion) is observed to be primarily dependent on the viscosity of the parent GRA liquid, with the volatile supersaturation having a more minor effect. Bubble coalescence and the development of permeability within the foam are also major controls on its expansion. The production and preservation of strained vesicles in the foam is facilitated by high strain rates in the flow and high liquid viscosities. The velocity of the flows (measured from video camera footage) is dependent on both the liquid viscosity and the volatile supersaturation. The fragmentation of the liquid is thought to be ductile, occurring through progressive thinning of bubble walls and bubble coalescence. Bubble growth occurs largely through decompressional expansion, with diffusional mass transfer being less important. Currently in progress is a more detailed comparison of the internal textures of both the experimental pyroclasts and natural pumices. These are related to eruptive processes. The dynamic evolution of the foam is also under close study using high speed cine photography.

VS2/W/12-B3 Poster 1400-09

**SEDIMENTOLOGY OF THE BLAST SURGE DEPOSIT OF DECEMBER 26TH 1997, SOUFRIERE HILLS VOLCANO, MONTSERRAT**

L.J.RITCHIE and P.D.Cole (both at the Centre for Volcanic Studies, Department of Environment, Geography and Geology, Luton University, Park Square, Luton, LU1 3JU); R.S.J.Sparks (Department for Earth Sciences, Bristol University, Bristol, BS8 1RJ)

On 26th December 1997, sector collapse of the Soufriere Hills lava dome resulted in a debris avalanche with subsequent generation of a valley confined pyroclastic flow and associated destructive pyroclastic blast type surge which devastated an area of 9.2km<sup>2</sup>.

The blast surge deposit is characterised by a sandy, fines-rich layer typically overlying a coarser, fines-poor layer, capped by an accretionary lapilli fallout layer. Strong lateral facies variations occur over a wide range of scales with metre scale transitions strongly influenced by topography. The deposit fines and thins rapidly with distance from source. Proximally, extreme lateral facies variations occur with local low angle hummocky breccia sheets being developed. Evidence exists for at least two separate surge/ blast events. Sharp marginal boundaries strongly related to topography delimit a coarse-grained flow deposit on the upper surface which corresponds to the second blast event.

Grainsize analyses show good facies distinction and median diameter v sorting correlations. Evidence indicates that particle size sorting occurred during explosive expansion of the collapsing lava dome such that the resulting surge cloud initially was graded in both size and density. Strong lateral and vertical variations in grainsize indicate further efficient sorting during transport. Experimental modelling of grainsize and density segregation is in progress.

VS2/W/15-B3 Poster 1400-10

**CONSTRAINTS ON SHALLOW BASALTIC SUBVOLCANIC CONDUIT DIMENSIONS**

Brittain HILL, Charles Connor (CNWRA, Box 28510 San Antonio TX USA 78228, bhill@swri.edu), Philip Doubik (State University of New York, Buffalo NY USA 14260)

Shallow (0-2 km) subvolcanic conduit dimensions are important parameters for many eruption process models. Xenoliths from the 1975 Tolbachik (Kamchatka) violent strombolian basaltic eruption constrain changes in conduit dimensions through time. Early phases of the Cone 1 eruption sustained 6-12 km tephra columns, with fall deposits containing 0.001-0.01 vol% crustal xenoliths from Quaternary volcanic (0-1 km deep) and Tertiary sedimentary (1-4 km) rocks. Later eruption stages produced both lavas and 2-5 km high tephra columns, with 0.01-1 vol% xenoliths in falls. The 3x10<sup>5</sup> m<sup>3</sup> (DRE) of xenoliths in Cone 1 juvenile falls represents a cylindrical conduit 15 m in diameter and 1.7 km deep. Simultaneous eruption of tephra and lava suggests an annulus of degassed magma adhered to conduit walls, enhancing entrainment; little entrainment occurred early in an apparent droplet flow regime. The Cone 1 eruption ended with 12 hr of hydromagmatic tephra falls containing 3x10<sup>6</sup> m<sup>3</sup> (70 vol%) xenoliths. The conduit must have widened from 15 to 48 m to produce this xenolith volume.

Subvolcanic conduits in the 4 Ma San Rafael field (USA) are exposed at about 1 km paleodepths. Surveyed conduits (12) range from 2-m diameter buds along dikes with little wall-rock disruption, to 60-m wide cylindrical plugs with variable degrees of wall-rock brecciation and xenolith entrainment. Brecciated conduit margins to 5 m thick appear analogous to annular flow regimes at Cone 1. Several larger conduits, however, have a 0-6 m xenolith-poor annulus with 10-40 m inner core of extensive xenolith breccias and pervasive low-temperature hydrothermal alteration. These conduits appear analogous to late-stage hydromagmatic events at Cone 1. Conduit diameters 40-60 m also occur with relatively low amounts of xenoliths, suggest these eruptions lacked hydromagmatic activity. Models of basaltic cinder cone eruptions should consider subvolcanic conduit diameters on the order of 10-60 m in evaluating mass-flow processes.

**VS2/W/17-B3** Poster **1400-11**

**AN EXPERIMENTAL APPROACH TO QUANTIFYING THE RHEOLOGY OF VESICULATED MELTS**

Ed LLEWELLIN and Heidy Mader (both at Department of Earth Sciences, University of Bristol, Wills Memorial Building, Queens Rd, Bristol BS8 1RJ, UK, e-mail: ed.llewellin@bristol.ac.uk)

Vesiculated flows are ubiquitous in nature. They are known to be non-Newtonian, strongly visco-elastic and subject to breakdown. Whilst some information on the properties of foams and bubble suspensions with very large and very small gas volume fraction is available, the rheological properties of bubble suspensions with gas volume fraction in the geologically important midrange (25-75%) have not been quantified. This represents a serious impediment to the understanding of shallow and surface volcanic processes, especially the multiphase flow of gas and liquids in the upper conduit during explosive and effusive eruptions.

Work is in progress to study the flow properties of foams and bubble suspensions using analogue fluids. Golden syrup foam with intermediate gas volume fraction and bubble size distribution is made using a commercial aerator. The bubble size distribution is determined using a specially-designed cell and image recognition software. Oscillatory viscometry techniques are used to measure the flow properties; a sample of the foam is subjected to a sinusoidally varying shear stress over a range of amplitudes. The strain rate thus induced in the sample also varies sinusoidally but with a phase shift relative to the stress, the magnitude of which depends on the relative importance of the viscous and elastic properties of the foam allowing the two effects to be separated. The amplitudes are chosen to be small enough that the foam is not destroyed by the testing, ensuring that the results are repeatable.

This poster describes oscillatory viscometry, the techniques used for making the foams and measuring bubble size distribution and presents preliminary data relating the viscous and elastic components of deformation to the shear stress applied and the gas volume fraction of the foam. Future work will be carried out using larger net strain and strain rates to explore the parameters which cause the fragmentation of the foams.

**VS2/W/19-B3** Poster **1400-12**

**CONTRASTING ERUPTION MECHANISMS OF COGENETIC, LARGE-VOLUME IGNI MBRITES FROM THE LA PACANA CALDERA, NORTH CHILE**

Jan LINDSAY, Axel Schmitt and Robert Trumbull (GeoForschungsZentrum Potsdam, Division 4.2, Potsdam, Germany, email kiwi@gfz-potsdam.de)

Pre-eruptive H<sub>2</sub>O contents and pumice characteristics of two large-volume ignimbrites (combined minimum volume 1,700 km<sup>3</sup>) from the La Pacana caldera imply different eruption mechanisms. Pumices in the caldera-forming dacitic Atana ignimbrite are dense and crystal rich (35–45% crystals). This ignimbrite occurs as a homogenous single flow unit, and lacks a basal plinian. It overlies the rhyolitic Toconao ignimbrite, which is characterised by distinctive, crystal-poor (<1% crystals) tube pumices, and which has a very thin basal plinian. Stratigraphy and pumice chemistry indicate that these units erupted from a zoned magma chamber. A minimum pressure of 200 MPa is inferred from mineral barometry. The Toconao magma was cooler (735°C) and more volatile rich (6 wt.% H<sub>2</sub>O) than the Atana magma (790°C; 2-3 wt.% H<sub>2</sub>O), and represents the evolved cap of the chamber. Calculated viscosities are distinct for the Toconao and Atana magmas (106 and 108 Pa s respectively).

The contrast in physical characteristics of these two magmas is a function of crystallinity and volatile content. Toconao tube pumices reflect eruption of a relatively viscous, almost aphyric magma, whose high pre-eruptive H<sub>2</sub>O contents facilitated eruption by volatile oversaturation, and sustained a plinian column. In contrast, magmatic water in the Atana was probably too low to build up a critical overpressure in the magma chamber, as the Atana melt was at best only close to H<sub>2</sub>O saturation at inferred pre-eruptive conditions. An external mechanism is therefore needed to trigger eruption of the Atana magma.

**VS2/W/20-B3** Poster **1400-13**

**MAGMA FRAGMENTATION DURING THE PLINIAN PHASE OF THE MINOAN ERUPTION (SANTORINI, GREECE), AS INFERRED BY DEPOSIT FEATURES AND PYROCLAST TEXTURES**

Jacopo TADDEUCCI (Dottorato di Ricerca, Dipartimento di Scienze della Terra, Università "La Sapienza", P.le A. Moro 5, 00185, Roma, Italy. Email: jac.punny@iol.it), Kenneth Wohletz (EES-1 MS D462, Los Alamos National Laboratory, Los Alamos, NM 87545, USA. Email: wohletz@lanl.gov)

Pyroclastic deposits result from a combination of eruptive and transport processes. In study of the Minoan Tephra we describe features of the pumice fall deposit that allow us to distinguish transport from fragmentation effects. A 6-m-thick pumice fall deposit, corresponding to Phase 1 products of the Minoan eruption, as identified by previous workers, shows three interlayered ash flow beds as thick as 10 cm near its top. We collected samples from the base to the top of the section at an interval of 40 cm for the first 5 m, and every 5 cm in the top portion, which includes the flow break. Laboratory studies comprise granulometry with application of the Sequential Fragmentation/Transport theory (SFT), componentry, pumice morphology and crystallinity determination. In addition we use grain-size distributions of artificially broken pumices (of the same deposit) for control and comparison. Concerning the transport process, normal grading of pumices and lithics from the base of the deposit to the ash flow break, and reverse from there to the top, is assumed to record a cycle of column waning before and then waxing after the ash flow break. Transport sorting of pumice and ash at the sample locality is considered to be rather limited because of i) poor sorting coefficient (1-2.7 Phi units) in comparison to other fall deposits, and ii) strong similarity between the size distributions of the artificial shards and of the fall deposit, suggesting that the size distribution of the deposit mainly reflects the fragmentation mechanism and only slightly that of transport. As for the fragmentation mechanism, a development factor, based on SFT parameters of the size distribution, decreases upward from the base of the deposit to the flow break, indicating an increasing efficiency but shorter duration of the fragmentation process. Free crystals are released from the magma through fragmentation process, so the observed increase in the ratio of free crystals content of the deposit vs. crystal content of the pumices confirms a better fragmentation toward the flow break.

**VS2/W/21-B3** Poster **1400-14**

**MULTI-PHASE THERMOFLUID AXISYMMETRIC TRANSIENT DYNAMIC MODELING OF THE AUGUST 1997 VULCANIAN EXPLOSIONS AT SOUFRIERE HILLS VOLCANO, MONTSERRAT: INITIAL CONDUIT CONDITIONS AND PROFILES AND THEIR INFLUENCE ON NEAR-VENT MODEL RESULTS**

A.B. CLARKE (Penn State University, Department of Geosciences, University Park, PA 16802, USA; 814-863-3965; email: aclarke@geosc.psu.edu); A. NERI (CNR-CSGSDA, Department of Earth Sciences, Pisa, Italy); B. Voight (Penn State University); G. Macedonio (Osservatorio Vesuviano, Napoli, ITA); T.H. Druitt (Universite Blaise Pascal, Departement des Sciences de la Terra et URA 10, Clermont-Ferrand, France)

Between August 4 and 12, 1997 at the Soufriere Hills Volcano, Montserrat, 12 discrete, relatively short-duration (tens of seconds) vulcanian eruptions occurred through the andesite dome complex. These eruptions were characterized by an early phase of axisymmetric ballistic throw-out, followed by fountain collapse that sent predominantly pumiceous pyroclastic flows radially from the crater to distances of several km, and by rise of convective plumes to altitudes from 9 to 14 km. We and staff members of the Montserrat Volcano Observatory closely documented the eruptions with photographs, video footage, observation and instrumentation. Previously determined estimates of conduit diameter and magma temperature were used in conjunction with ballistic ranges and angles, pumice vesicularity, and estimated DRE volumes to calculate the length, pressure, and solid/gas volume fraction at the top of the conduit prior to the explosions. Using these well-constrained basic conduit parameters, we have modeled the conduit in several different ways. Models vary from simple to complex, the latter incorporating non-linear gas solubility laws, non-linear viscosity variations, which result in non-linear pressure variations with depth, and losses due to cap rock fracture and fragmentation of magma. Coupling of these conduit models, which provide initial conditions, with a transient multi-phase thermofluid dynamics model allows simulation of the transient, short-pulse eruptions of the Soufriere Hills volcano in 1997. Effects of axisymmetric simplifications are minimized near the event, thus this region is addressed here, although further modeling will explore evolution of phenomena beyond this region. Good qualitative agreement occurs between the observed eruptions and results of some models. Certain models simulate reasonably well important aspects of plume generation, such as behavior and timing, the near-vent cloud shape, and the separation of the cloud into collapsing mixture and convective plume.

**VS2/W/22-B3** Poster **1400-15**

**THE 1983 ERUPTION OF COLO VOLCANO, UNA-UNA ISLAND, INDONESIA**

Raffaello TRIGILA (1) (trigila@axrma.uniroma1.it), Aida M. Conte (2), Carmela Freda (2), Danilo M. Palladin (1), PierGiorgio Scarlato (4), Jacopo Taddeucci (3) (1) Dipartimento di Scienze della Terra, Università "La Sapienza", P.le A. Moro 5, 00185 Roma, Italy; (2) (C.N.R. - C.S.E.S.M.R. c/o Dipartimento di Scienze della Terra, Università "La Sapienza", Roma, Italy); (3) (I.N.G.F. V.d.i Vigna Murata 605, 00143 Roma, Italy); (3) Dottorato di Ricerca, Dipartimento di Scienze della Terra, Università "La Sapienza", Roma Italy)

From July 18 to October 9, 1983, after a repose period of 85 years, an eruption of the Colo Volcano, comprising at least sixty explosive phases, devastated the island of Una-Una, Sulawesi, Indonesia. The eruptive products include a decimeter-thick pumice fall horizon, diffuse ash fall and channelized, massive, lithic-rich pyroclastic flow deposits with associated lahar and alluvial deposits. On the basis of field evidence, grain-size, componentry and SEM data, the eruption dynamics is interpreted in terms of an early climactic, Plinian-type eruptive phase and a number of Vulcanian-type ash explosions characterizing the following activity phases. The eruption, triggered by strong earthquakes with epicenters situated nearby, was initially driven by the volatile pressure increase in a dacitic, crystal rich, water-saturated magma body under closed system conditions. Later on, the magma interaction with external water become a major process responsible for magma fragmentation and repeated, short-lived explosive phases. Crystallization experiments and thermodynamic calculations indicate the magma body crystallizing conditions were approaching 3 km depth; T= 900° C and 3.5 wt% dissolved water content.

**VS2/W/23-B3** Poster **1400-16**

**THE EVOLUTION OF KOKO CRATER TUFF CONE AND KAHALOIA TUFF RING, O'AHU, HAWAII AND THE FACTORS INFLUENCING CONE VERSUS RING GENERATION**

Ian SKILLING (Department of Geology, Rhodes University, Grahamstown, South Africa, email: ips@rock.ru.ac.za)

Kahaloia tuff ring and Koko Crater tuff cone are two immediately adjacent craters which were erupted on the Koko fissure in SE O'ahu about 3000yrs ago. A detailed facies model and stratigraphy is presented. This combined with SEM and petrographic study suggests that Koko was erupted in an open water, relatively sand-free environment but Kahaloia was erupted in a littoral environment with abundant sand. Koko is dominated by "Surtseyan" wet fall deposits and their redeposited equivalents, whilst Kahaloia comprises mostly "Taalian" base surge deposits. Interaction of magma with wet sand rather than water alone may have generated more buoyant eruption plumes and a ring rather than a cone. Alternatively, the fact that surge events at Kahaloia are nearly always preceded by "vent-clearing" blocky fall deposits, suggests that a "closed" vent may have been a factor in the generation of rings rather than cones. The very close proximity (both spatially and temporally) of both craters probably implies that the subsurface hydrology was similar, though hydrological influences on cone versus ring generation cannot be excluded "U-shaped" erosion channels were first described from Koko by Fisher (1977) and attributed to surge erosion. There is little evidence of this at Koko or Kahaloia, were channels and scours appear mostly to have been formed by steep-slope stream drainage, either by cold water and/or hot water condensed from steam during accretionary lapilli-forming events.

**VS2/W/24-B3** Poster **1400-17**

**BASALTIC MAGMA FRAGMENTATION MECHANISMS WITHIN MUDDY TO SANDY WET SEDIMENTS: A TEXTURAL STUDY OF PEPERITES FROM WELGESIEN, SOUTH AFRICA**

Ian SKILLING (Department of Geology, Rhodes University, Grahamstown, South Africa, email: ips@rock.ru.ac.za)

Basaltic peperitic clasts occur within laharic debris flows at Welgesien, South Africa and were examined using SEM and optical microscopy. The basalt was degassed (or was volatile-poor) prior to visco-plastic laminar to convolute mixing with wet muddy to sandy lacustrine sediments, at depths <200m below the palaeosurface. Peperitic textures are almost entirely due to magma interaction with external water in sediment pore space. The peperites preserve an end-member process of magma-water interaction, without the additional factor of accompanying expansion of juvenile volatiles. Basaltic magma laminae or tendrils were fragmented into individual globules or strings of globules by local vesiculation of sediment trapped between areas of magma. Magma fragmentation was essentially a non-explosive process. Peperites are important rocks for the study of magma fragmentation mechanisms as they preserve aspects of the behaviour of the coolant during fragmentation. SEM-scale study is essential to understand the initial stages of magma fragmentation in particular. The importance of such essentially in-situ, fragmentation of magma prior to eruption is not clear, and has important implications for the interpretation of eruption mechanisms from the study of vitriclast morphologies.



**VS2/E/01-B3** Poster **1400-18**
**SEQUENCE AND ERUPTIVE STYLE OF THE 1783 ERUPTION OF ASAMA VOLCANO, CENTRAL JAPAN - A CASE STUDY OF AN EXPLOSIVE ERUPTION OF HETEROGENEOUS, ANDESITIC MAGMA**

MAYA YASUI (Dept. of Earth Sciences, Nihon University, 3-25-40, Sakura-josui, Setagayaku, Tokyo 156-8550, JAPAN, email: yasui@peacock.iis.chs.nihon-u.ac.jp); Takehiro KOYAGUCHI (Earthquake Research Institute, University of Tokyo, 1-1-1, Yayoi, Bunkyo-ku, Tokyo 113-0032, JAPAN, email: tak@eri.u-tokyo.ac.jp)

The 1783 A.D. eruption of Asama Volcano, central Japan is characterized by diverse modes of eruption, abundant eruptive units and a wide variety of petrological heterogeneities. Main events occurred on the last four days in its three-month activity. After 2 August, plinian pumice falls and pyroclastic flows generated alternatively. The climactic phase was initiated with the most intense plinian eruption in the evening of 4 August and followed by generation of pyroclastic flows. A pyroclastic cone built up near the vent associated with the fountaining from the plinian eruption column and it rapidly grew during the climax of the plinian phase. The pyroclastic cone rose out on the steep outer slope of pre-existing volcanic edifice generating clastogenic lava flows. Small-scale pyroclastic flows which originated from partial collapse of the cone occurred as minor events. Bulk rock chemical composition of the 1783 eruptive products range from 60 to 64 wt. % in SiO<sub>2</sub> content. Essential materials of pumice fall deposits is more silicic (typically 63 wt. % SiO<sub>2</sub>) than those of pyroclastic flow deposits (61% SiO<sub>2</sub>), and the lava flow has intermediate composition (62% SiO<sub>2</sub>). The groundmass of the essential materials show compositionally heterogeneous features (e.g. banding or eutaxitic texture) in both hand-specimen scale and microscopic scale. Evidence of magma mixing such as disequilibrium mineral assemblages is common. Phenocrysts in the heterogeneous essential materials are commonly fragmented, which suggests that each essential material experienced repetitive disruption and coalescence during ascent. The complex features of heterogeneity of the 1783 eruptive products can be explained by the following four processes; 1) compositionally zoned magmas were produced before the eruption in a magma chamber, 2) the zoned magma mechanically mingled together within the conduit during magma evacuation, 3) fine-scale heterogeneous texture resulted from repetitive disruption of coalescence of the co-mingled pyroclasts, and 4) these heterogeneous features were further modified by welding and/or secondary flowage after emplacement; partial collapse of densely welded part of the pyroclastic cone resulted in highly homogenized clastogenic lava flow of intermediate composition.

**VS2/E/03-B3** Poster **1400-19**
**FLOW PATTERNS OF OVERPRESSURED VOLCANIC JETS**

Tomaso Esposti Ongaro (Universita' di Pisa and Consiglio Nazionale delle Ricerche, Pisa I-56126, Italy, Email: ongaro@dst.unipi.it) Augusto NERI (Consiglio Nazionale delle Ricerche, Pisa I-56126, Italy, Email: neri@dst.unipi.it)

Volcanic jet dynamics were investigated by using a transient, two-dimensional, and two-phase flow model. The model accounts for mechanical and thermal non-equilibrium between a gas phase and a solid particulate phase representative of pyroclasts. The model equations were solved by a numerical technique able to treat both subsonic and supersonic flows as well as shock waves. Simulation results describe the formation of a vertical jet leaving a vent and expanding by decompression into a volcanic crater. Several simulations were carried out by using different conduit exit conditions and crater geometries. Two types of flow patterns were recognized in good agreement with laboratory experiments. According to the first, decompression and compression waves are repeatedly reflected along the jet axis and boundary. Such a flow pattern appears to be steady and favored by smaller overpressures and crater opening angles. The second flow pattern exhibits a Mach reflection normal to the axis of the jet with the formation of a compressive shock and tangential slip lines. The resulting flow configuration appears to be quite transient and able to produce some instability of the jet. The Mach reflection pattern is obtained with higher overpressures of the jet as well as greater opening angles of the crater.

**VS2/E/05-B3** Poster **1400-20**
**NEAR VENT AND VENT FILLING PYROCLASTIC BRECCIA DEPOSITS OF AN ERODED TUFF RING COMPLEX AT PIGROOT HILL, CENTRAL OTAGO, NEW ZEALAND**

Karoly NEMETH. (Geology Department, University of Otago, PO Box.56., Dunedin, New Zealand, email: karoly.nemeth@stonebow.otago.ac.nz)

The Pigroot Hill is located in Central Otago (Dunedin Volcanic Complex), and is primarily built up by basic volcanoclastic and lava rocks formed between 16-12 Ma. In the lower level of the hill, near vent, subaerial, base surge and fall out beds are exposed, and covered by late Hawaiian spatter deposits with large spindle bombs and small clastogenic lavafalls. The top of the hill is built up by late lava flows and dikes mostly olivine basaltic and andesitic composition. Alongside dikes, remnants of explosion sites are identified. In south, explosion breccias are exposed in 5 well distinguished area with a former collapsed tuff ring rim. Fall out and base surge beds unconformably underlie the coarse grained vent breccia pipes and interpreted as near vent phreatomagmatic deposits of a former tuff ring. The bedded tuff contain large number of features characteristic of base surge origin such as dune bedding, unsorting, undulatory bedding, impact sags, accidental lithics. The bedding clearly indicates sliding and collapse events in near vent position. The juvenile fragments are altered sideromelane glass with highly vesiculated tachylite suggesting phreatomagmatic explosive interaction between subsurface water and uprising magma in shallow level. Large number of angular dense, crystalline fragments represent disrupted clasts from previous volcanic sequences from deep subvolcanic region. Above the bedded lapilli tuff, a coarse grained pyroclastic breccia occur. The breccia consist of large fluidal, vesicular and crystalline, dense olivine basaltic fragments. Cored bombs, irregular shaped, baked mudstone and large limonitic sandstone blocks, small fragments of tuff and deep excavated schist are also common. The well defined distribution of the pyroclastic breccia, the facies relation with the lower bedded lapilli tuff, and the common relation with dikes suggest local explosion pipes where the uprising melt interacted with limited water.

**VS2/E/06-B3** Poster **1400-21**
**COMPLEX COMPOSITIONAL ZONATION IN AN IGNIMBRITE FLOW-UNIT FROM LOS HUMEROS CALDERA, MEXICO**

Gerardo CARRASCO-NUNEZ (Unidad de Investigacion en Ciencias de la Tierra, Instituto de Geologia, Campus Juriquilla, UNAM, Apdo. Postal 1-742, Queretaro, Qro. 76230, Mexico. email: gerardoc@conin.unicit.unam.mx); Michael J. Branney (Department of Geology, University of Leicester, University Road, Leicester LE1, 7RH, United Kingdom, email: MJB26@leicester.ac.uk)

Compositional zoning is a common feature of moderate-to-large volume ignimbrites. Several become more mafic with height, a feature thought to record progressive eruptive withdrawal

from a compositionally stratified agma-chamber, with the eruption progressively tapping deeper, denser parts of the chamber. A single flow unit of the 0.1 Ma Zaragoza ignimbrite (ca. 12 km<sup>3</sup>), in eastern central Mexico, shows unusually complex zonation. Its eruption was accompanied by collapse of Los Potreros caldera, located within the larger Los Humeros caldera (Ferriz and Mahood, 1984). Around 16 km S of Potreros caldera, a basal plinian pumice-fall layer, < 20 cm thick, is overlain by thin surge and flow deposits, totalling < 20 cm-thick, and these are overlain by a single massive ignimbrite flow unit, 15 m thick. The ignimbrite is non-indurated, and generally shows an upward increase in the maximum and mean sizes of pumice lapilli, together with a decrease in sorting.

The colour of the ignimbrite changes gradually upwards, from white at the base through to grey, purple (middle part), pink to yellow at the top. Apart from local oxidation effects, the colour changes correlate in general with changes in the proportion of at least four different types of pumice clast: white and pale-brown rhyodacite pumice (67-68 % SiO<sub>2</sub>), brown-orange and grey dacite pumice (64-66 % SiO<sub>2</sub>), black and dark-grey andesite pumice (58-61 % SiO<sub>2</sub>), and banded (magma-mingled) pumices. The basal part of the deposit comprises entirely rhyodacite pumice. The proportion of dacite, andesite and banded pumice increases with height, toward the middle of the flow-unit, which contain mostly andesite and dacite pumices and without any rhyodacite pumice. Toward the top, rhyodacite pumice appears again, and the proportion of andesite and dacite pumice clasts decreases. The uppermost part is fines-poor, and comprises mostly rhyodacite pumice with rare dacite pumice.

**VS2/E/09-B3** Poster **1400-22**
**THE REASON WHY FRAGMENTATION DEGREE OF FALLOUT ASH VARIED DURING THE 1988-1989 ERUPTIONS OF TOKACHI-DAKE, HOKKAIDO, NORTHERN JAPAN**

Mario YOSHIDA (Graduate School of Science, Hokkaido University, N10W8 Kita-ku, Sapporo 060-0810, JAPAN, Email: mario@cosmos.sci.hokudai.ac.jp); Yuichi Nishimura (Institute of Seismology and Volcanology, Hokkaido University, Sobetsu-onsen 59, Utsunomiya, Hokkaido 052-0103, JAPAN, Email:nishi@eos.hokudai.ac.jp)

Fragmentation degree of fallout ash is defined as weight % of particles finer than 0.125 mm at the site of normalized distance from the vent (i.e., the application of F-value; Walker, 1973). The degree of the fallout ash during the 1988-1989 phreatomagmatic eruptions of Tokachi-dake ranged from 5 % to 98 %. The ash was ejected from the same vent, and main components of the fine ash particles are accessory lithic and mineral fragments in every eruptive phase. Average of roundness (Wadell, 1932) of coarse ash also ranged from 0.3 (subrounded) to 0.6 (well-rounded), and it correlates normally with the fragmentation degree. We assume that the higher degree of fragmentation was due to the longer duration of attrition of the particles when they passed through the conduit. The most likely explanation of the long duration of attrition is stable and mild relieving of the pressure with the progress of clearing and widening of the conduit. Our model is supported by the other observational fact: eruption tremors. The tremors associated with high-fragmented ash eruptions lasted long time (more than several hours) and show spectra in which high-frequency powers are weakened.

**VS2/E/10-B3** Poster **1400-23**
**EXPERIMENTAL POLYDISPERSE SUSPENSION CURRENTS AND IMPLICATIONS FOR PYROCLASTIC FLOW TRANSPORT**

CHOUX C. and Druitt T. (both at Departement des Sciences de la Terre, 5, Rue Kessler, 63000 Clermont Ferrand, France, Email: choux@opgc.univ-bpclermont.fr)

Pyroclastic density currents range from dilute suspensions to highly concentrated granular avalanches. They are highly polydisperse and commonly contain particles of two different densities (pumices and lithics). In order to better understand the segregation processes possible in such currents, we have carried out a series of experiments using aqueous suspension flows with a range of concentrations (1 to 22 vol. %) in a horizontal lock-exchange flume, 5 m. long. The suspensions consist of particles of silicon carbide (3.2 g. cm<sup>-3</sup>; 1mm to 10mm) and dried vegetal matter (1.4 g. cm<sup>-3</sup>; 3mm to 30mm) in equal proportions. Each component population has an approximately log-normal size distribution, and the two populations are in initial hydraulic equivalence. The water-immersed densities of the two components scale to those of lithics and pumices in gas. Some preliminary results are reported in this poster. Particle populations in the deposits from dilute experimental flows are found to be in approximate hydraulic equivalence. With increasing suspension concentration, light particles become increasingly displaced downstream in the deposit due to buoyancy effects in the flow, and the proximal part of the deposit becomes strongly enriched in the dense component. Deposits from concentrated suspensions have two distinct layers, even though the size distribution of the initial suspension is continuous. In one series of experiments (16% concentration), the flows were filmed in order to reconstruct the manner in which the layered deposit aggraded in space and time from the moving flow. The experimental results were compared with vertical and lateral grading observed in some natural ignimbrites.

**VS2/E/11-B3** Poster **1400-24**
**VOLCANIC GLASS STUDY OF VOLCANICLASTIC DEPOSITS OF TIHANY-TYPE AND NORMAL MAAR VOLCANOES OF THE BAKONY-BALATON HIGHLAND VOLCANIC FIELD (BBHV), HUNGARY**

Karoly NEMETH and Ulrike Martin, (Geology Department, University of Otago POBox 56., Dunedin, New Zealand, e-mail: karoly.nemeth@stonebow.otago.ac.nz)

The BBHV, active in late Miocene, is located in the Pannonian Basin and contains two different maar type volcanoes. The water source of phreatomagmatic explosions is from an upper thick, clastic sediment pile and/or from underlying karstwater rich formations. Two different type of maar developed depending on water source. Each has a characteristic volcanic glass type. Where the main water source of phreatomagmatic explosions was restricted to the upper, thick clastic sediment pile, normal maar volcanoes developed. In areas where both the karst water and the relatively thin water rich clastic sediment played important roles to fuel the magma/water interactions, Tihany-type maar volcanoes developed. Microprobe analysis of volcanic glass (94-99 % total) showed composition from basalt, trachy basalt, andesite basalt to andesite or even dacite which data differ from the previous, lava rock based results. The textural analysis showed that there are two types of glass. The common type of glass is non-oriented, microcrystalline, non or slightly vesiculated, slightly elongated, usually fractured. This is formed by strong and sudden cooling of low crystallised magma due to interaction with water. This type of glass are common from normal maar volcanoes. The second glass type is the most common, oriented microcrystalline textured, banded, elongated, slightly vesiculated. It must have been formed when slightly crystallised magma met with water in shallow level. This glass type is common from pyroclastic rocks which are abundant in deep seated (karst water bearing) rock fragments. The paradox of occurrence of deep seated fragments and the "shallow region" (low confining pressure) formed volcanic glass can be solved with operating open, water filled fractures during the explosions, giving free way for karst water to high speed uprising magma to produce phreatomagmatic explosions, and form Tihany-type maar volcanoes.



**VS2/E/14-B3** Poster **1400-25****WET AND DRY SURGE DEPOSITS: FIELD STUDIES AND EXPERIMENTS**

Piero Dellino and Luigi La Volpe (both at Dipartimento Geomineralogico, Università-E0 degli studi di Bari, Via E. Orabona 4, 70125 - Bari, Italy, email: dellino@lgsxserver.uniba.it) Bernd Zimanowski, Ralf Buetner, and Volker Lorenz (all at Physikalisch-Vulkanologisches Labor, Universität Wuerzburg, Pleicherwall 1, D-97070 Wuerzburg, Germany, email: zimano@geologie.uni-wuerzburg.de)

Surge deposits of phreatomagmatic origin, commonly found in volcanic islands, show various structural and textural features and, with respect to the magma/water interaction processes leading to their formation, are subdivided into two types: a) wet surges and b) dry surges. It is assumed, that the amount of external water during explosive fragmentation, transport and deposition controls the characteristics leading to this classification, i.e. wet surge deposits form once the amount of water by far exceeds the volume needed to drive the phreatomagmatic eruption mechanism and dry surge deposits are generated when the amount of external water is more or less restricted to this value. For the case of La Fossa di Vulcano (Sicily) experimental and field studies were combined to investigate the physical frame conditions and the nature of the physical processes that lead to the formation of such deposits. Typical pyroclasts of both types of deposit could be produced in laboratory experiments using remelted volcanic rocks from Vulcano island, that have a composition very close to the magma erupted during the formation of the natural wet and dry surge deposits of La Fossa.

**VS2/E/15-B3** Poster **1400-26****THE ERUPTIVE DEPOSITS OF A SMALL EMERGENT VOLCANO AT THE OTAGO PENINSULA, NEW ZEALAND**

Ulrike MARTIN (Geology Department, Otago University, PO Box 56, Dunedin, New Zealand, email: ulrike.martin@stonebow.otago.ac.nz)

The Sandfly Bay pyroclastic succession at The Otago Peninsula, South Island, New Zealand, comprises partly preserved rim beds of a basaltic tuff cone, belonging to the Miocene Dunedin Volcanic Complex (DVC). The bulk of the DVC is considered to have developed subaerially, but recent studies have delineated several small submarine or Surtseyan volcanoes, one of which is the Sandfly Bay succession. The succession consists of four parts; (1) a vent marked by radiating dikes and peperites, which is approximately 100m in diameter; (2) a thick massive to slightly bedded pillow/hyaloclastite unit; (3) a massive tephra unit; (4) a bedded tephra unit with wave-formed structures at the bottom and well developed unidirectional cross-stratification and sharp bedding planes at the top. Peperites constitute the upper vent-filling, and formed when hot magma intruded wet unconsolidated tephra. Pillow fragments in the massive hyaloclastite unit record initial thermal quenching and fragmentation of erupting basalt. The tephra forming the ring, in both the massive and the bedded unit, comprises juvenile vesiculated sideromelane clasts, sideromelane glass shards, feldspar and large pyroxene crystals up to 1cm. The absence of accidental lithics suggests a shallow explosion level, above the substrate. Beds dip radially outward from the vent at 20-30°. Alternating coarse-grained crystal-rich beds and fine-grained beds form the uppermost unit. The wave-generated structures indicate shoaling of an initially submarine edifice, while the upper part represents the subaerial stage of volcanic activity at Sandfly Bay. The tuff cone is interpreted to have been constructed over a massive hyaloclastite unit that formed below sea level and resulted from a moderately explosive eruption, inferred to have been driven by magma/water interaction in a water-rich environment. The submarine part of the emergent volcano is more massive, coarse-grained and glassy, distinct from the subaerial part.

**VS2/E/17-B3** Poster **1400-27****ON THE FORMATION OF SPINDLE BOMBS IN A SUBMARINE VENT AT BOULDER BEACH, DUNEDIN VOLCANIC COMPLEX, NEW ZEALAND**

Ulrike MARTIN & Karoly Nemeth (Geology Department, Otago University, PO Box 56, Dunedin, New Zealand; email: ulrike.martin@stonebow.otago.ac.nz;

Fusiform "bombs" usually form explosively in subaerial settings such as lava fountain-spatter eruptions, and similar features can develop intrusively when dikes enter unconsolidated wet sediment to form globular peperites. At Boulder Beach unusual kinds of spindle bombs have been formed in a submarine vent. Volcanic rocks of trachytic in composition exposed at Boulder Beach belong to the Dunedin Volcanic Complex (DVC), which makes up the Otago Peninsula near Dunedin, New Zealand. The volcanoclastic deposits record a variety of gravity flows from a subaqueous eruption. The strongly hydrothermally altered vent, which was invaded by dikes, is surrounded by a tephra-ring. The tephra comprises alternating massive coarse-grained and bedded fine-grained layers, formed of pumice, dense crystalline trachytic clasts, glass-shards, feldspar-and quartz crystals and minor sedimentary clasts from underlying strata. Characteristic of the fine-grained beds is cross-stratification, scour-fillings, normal-graded lithic clasts and inverse-graded pumice clasts. Locally present are large lithic clasts up to 20cm, whereas pumice clasts are up to 8 cm. The succession is interpreted to have been formed during shallow marine magmatic/hydromagmatic eruption with deposition from density currents, shed directly from a subaqueous eruption column. The chaotic vent tephra contains fusi-form bombs which were formed while dikes invaded the vent. They formed due to magma/water interaction. The high water/magma ratio led to a mildly explosive fragmentation in the vent slurry. The large bombs retained heat long enough to deform plastically and settled slowly in the fluidized slurry. Fluidisation in the vent sediment is shown as "Schlieren" around the bombs. The spindle-shaped bombs and blocks are vesiculated and vesicles are usually filled with chalcedony. Further away from the feeder-dike there are large bombs with bomb-sags, deposited by backfall during eruption. The original bedding features in the vent have been destroyed due to fluidization along margins of intruding dikes. The basalt-dikes have irregular forms and are strongly chilled.

**VS2/W/25-B3** Poster **1400-28****A SIGNIFICANT HAZARD FROM LARGE-SCALE VOLCANIC ERUPTIONS IS ASH**

C. RILEY (Geological and Engineering Sciences, Michigan Technological University, 1400 Townsend Drive, Houghton, MI, 49931 USA, Email: cmriley@mtu.edu)

A significant hazard from large-scale volcanic eruptions is ash which can be transported great distances and deposit irregularly and in unusually thick amounts far from the volcanic source. One influence on volcanic ash transport is particle shape which affects the aerodynamic properties responsible for particle separation and fallout, the interaction of particles with the atmosphere, and remote sensing measurements of ash particle concentrations. The main objectives of this study are to characterize the shape and determine terminal settling velocities for ash particles so that these data can be used to improve transport models and remote sensing algorithms.

A total of 1,300 andesitic ash particles were measured from the August 1992 Spurr eruption. The majority of particles are subrounded silicate pumice fragments, with < 10% glass bubble-

wall shards. Size distribution data for the sample show the sample is bimodal, which indicates aggregation played a role in fallout. In general, actual mean diameters for each settling velocity group were larger than expected if the particles were assumed spherical. We show that this is due to particle shape influences rather than density effects. The larger than expected diameters for particles in given terminal settling velocity groups suggests that the irregular shape of these particles decreases their settling rate. This is at odds with current transport modeling results which show that particles fall out faster than expected and suggests that another factor such as aggregation may be of greater importance in the fallout of andesitic particles. The Spurr particles are representative of volcanian to subplinian andesitic eruptions but are unlike more irregular-shaped rhyolitic particles often formed in plinian eruptions.

**VS2/W/26-B3** Poster **1400-29****AN APPROACH TO 3D MODEL OF PYROCLASTIC FLOW DYNAMICS AND ITS APPLICATION TO THE AZUFRAL RIVER CHANNEL AT GALERAS VOLCANO, COLOMBIA**

GUSTAVO CORDOBA (Universidad de Nariño, Colombia, email gcordoba@altavista.net); Peter Rutschmann (Laboratory of Hydraulics, Hydrology and Glaciology of the ETHZ, Zurich, email rutschmann@vaw.baug.ethz.ch); Greg Valentine (Los Alamos National Laboratory, USA, email gav@vega.lanl.gov)

Galeras volcano is one of the most active volcanoes in the world, more than 500.000 people are living within its influenced area. The Azufral river channel down directly from the crater zone without topographic barriers and a pyroclastic flow could affect the Consaca town and its surrounding area. The compressible full Navier-Stokes equation is used to describe the 3D motion of a possible pyroclastic flow from a collapsing eruption column from the crater vent in direction to Consaca town descending through the Azufral river basin. The change of the bulk density is taken into account from the variation of the particle volume fraction in the state equation. The resulting set of equations is solved numerically by using the Finite Element Method Toolbox (FEMTOOL) developed at the Laboratory of Hydraulics, Hydrology and Glaciology of the ETHZ, Zurich.

**VS2/W/28-B3** Poster **1400-30****FIVE PARALLEL BRECCIATED FELSIC DIKES, OBSERVED AT CENTRAL KII PENINSULA, SW JAPAN**

Yutaka WADA, (nara University of Education, Japan, email:ywada@nara-edu.ac.jp)

Five parallel brecciated felsic dikes, observed at central Kii Peninsula, SW Japan, show a continuous facies change from magmatic to clastic. Each of dikes is ca. 30-50m wide in maximum, and the maximum length of segments observed is more than 1.5km. Their host rocks are pre-Tertiary sedimentary rocks constituting an accretionary prism (Chichibu belt). The magmatic facies consists of inhomogenous aphyric rhyolite with amoeboid clots (several centimeters in diameter) of porphyritic rhyolite. Perlitic cracks are also developed in the porphyritic clots. The clastic facies is unsorted and consists of juvenile and accidental fragments (maximum diameter is ca. 50cm) and sand-sized matrix with mineral and rock fragments. While the juvenile fragments are mostly of porphyritic rhyolite showing angular with glassy chilled margins or amoeboid in shape, a few aphyric lens- or wisp-shaped rhyolite are also observed. Some accidental fragments are deforming in ductile regime, others are breaking in brittle regime. Based on these observations, it is inferred that after the rhyolitic magmas (porphyritic and aphyric) had intruded into wet and unconsolidated sediment underlying the consolidated accretionary prism, they intruded into the above prism. This emplacement is inferred to be occurred at middle Miocene (13.7-0.7Ma) based on K/Ar dating (K-feldspar). Previously some plant and foraminifera fossils dated Eocene have been reported in the clastic facies, however, suggesting that some part of these dikes were occupied by breccias collapsed down from the above. Furthermore, the dikes seem to be a part of an arc-like distribution as a whole according to the previous works. Thus these dikes may be a possible feeder channel for the pyroclastics and may also suggest a pre-eruptive process within dike fractures feeding magma, although whether it was reached to the earth's surface or not is unclear from the field observations.

**VS2/W/29-B3** Poster **1400-31****STRAIN-INDUCED MAGMA FRAGMENTATION AND NON-EQUILIBRIUM FLOW DYNAMICS IN VOLCANIC CONDUITS**

Paolo PAPALE (Istituto Nazionale di Geofisica, via S. Maria 53, I-56126 Pisa, Italy, email papale@dst.unipi.it)

Magma fragmentation during ascent to the Earth's surface is investigated by numerical simulations of multiphase, non-equilibrium flow of liquid magma, gas exsolving from the liquid, and crystals.

The numerical model uses most recent models to calculate magma properties as a function of magma composition and phase distribution.

The possible occurrence of magma fragmentation as due to overcoming of a critical strain-rate corresponding to rate-limited crossing of the glass transition is investigated, by means of Maxwell relation and published experimental data on fragmentation of thin magma fibers in a rapidly increasing stress field. Such investigation is conducted by means of a parametric study where many different possible eruptive conditions in terms of conduit size, mass flow-rate, magma composition, volatile content and composition, and crystal content and distribution are taken into account. The results show that strain-induced magma fragmentation occurs at a gas volume fraction range identical to the measured range of pumice vesicularity for several eruptions throughout the world, following the development of a narrow region in the conduit where magma viscosity and strain-rate increase more and more rapidly. When plotted against magma viscosity, the gas volume fraction at fragmentation gives a decreasing trend similar to that which has been previously found on the basis of measurements on volcanic products. Furthermore, the model predicts the conditions that do not lead to strain-induced magma fragmentation, that include cases where basaltic magma composition is used, thus allowing to discriminate between explosive and effusive eruption conditions.

**VS2/C/U6/W/12-B3** Poster **1400-32****WE PRESENT THE APPLICATION OF CFD MODELLING OF VOLCANIC JETS ON DIGITAL ELEVATION MODELS (DEM'S)**

Alfredo Mahar Francisco LAGMAY, University of Cambridge, Cambridge, UK, Email: amfal2@esc.cam.ac.uk

We present the application of CFD modelling of volcanic jets on Digital Elevation Models (DEM's) to studies on explosive volcanism. By conducting numerical flow modelling on actual topography (represented by a DEM), we generate output that tell about the dynamics of explosive eruptions. In particular, our results illustrate the remarkable amount contributed by decompression to the radius of the basal gas thrust column. It also shows that the basal region

of the eruption column can be inclined as it exits from asymmetric craters. We present case studies on Mount St. Helens, Mount Pelee, Mayon and Iriga volcanoes to illustrate these effects. The graphic display of the numerical analysis also provides an excellent visualisation tool for generating insights into the nature of volcanic phenomena related to eruption columns such as the formation and emplacement of pyroclastic flows. This type of modelling is useful for hazards assessment and risk mitigation.

**VS2/C/U6/W/13-B3** Poster **1400-33**

**ERUPTIVE PROCESS, EFFECTS AND DEPOSITS OF THE 1996 AND ANCIENT BASALTIC PHREATOMAGMATIC ERUPTIONS IN KARYMSKOYE LAKE, KAMCHATKA, RUSSIA**

Alexander BELOUSOV and Marina Belousova (Institute of Volcanic Geology and Geochemistry, Petropavlovsk-Kamchatsky, Russia, email: A.Belousov@relcom.ru)

On 2-3 January, 1996 an explosive eruption with a discharge rate of basaltic magma of ~106 kg/s occurred in Karymskoye lake through an initial water depth ~50 m. Characteristics of the deposits together with analyses of a videotape of several explosions have allowed us to model the eruptive events. Initial vent-clearing phreatoic explosions ejected blocks of country rocks (up to 3m diameter) to distances up to 1.3 km. Then followed 10 to 20 hours of phreatomagmatic Surtseyan activity (100-200 outbursts of water-gas-pyroclastic mixtures to heights up to 1 km, with initial velocities of 110 m/s). The eruption slugs collapsed back into the lake producing base surges (runout up to 1.3 km; average velocity 12.5 m/s). The eruptive cloud rose to a convective height of 3 km depositing a thin distal fall deposit. The eruption ended with the ejection of scoria crust bombs (specific basaltic bombs with dense core and scoriaceous crust). Pyroclasts of the eruption are mostly poorly to moderately vesicular juvenile basaltic particles shaped by a combination of vesiculation of magma and magma-water interaction. Ninety five percent of the products (0.047 km<sup>3</sup>) formed an underwater tuff ring composed of parallel layers of moderately to poorly sorted lapilli ash and ash lapilli (Md -3.9-0.6f; sorting 1.5-3.2f), each 10-60 cm thick. They were deposited by water-rich base surges that originated from collapses of Surtseyan type slugs. More widespread hazards of the eruption were tsunamis and lahars. At distances less than 1.3 km from the crater, base surges and ballistics were very destructive. Eruptive activity in the lake before 1996 has included two phreatomagmatic eruptions about 4800 14C yrs BP.

**VS2/C/U6/W/14-B3** Poster **1400-34**

**POWERFUL PYROCLASTIC SURGE AT BEZYMIANNY VOLCANO ON MAY 9-10, 1997, KAMCHATKA, RUSSIA**

Marina BELOUSOVA and Alexander Belousov (Institute of Volcanic Geology and Geochemistry, Petropavlovsk-Kamchatsky, Russia, email: A.Belousov@relcom.ru); Barry Voight (The Pennsylvania State University, USA, email: voight@ems.psu.edu)

We have reconstructed the course of the May 9-10, 1997 explosive eruption of Bezymianny volcano from its pyroclastic stratigraphy. The first event of the eruption was an explosive outburst through the top of the dome producing a powerful pyroclastic surge. The surge covered 30km<sup>2</sup> over an elliptical-shaped area, extending as far as 7 km SE from the crater. Its volume is 107m<sup>3</sup>. Temperature of the surge cloud was < 2000C. It deposited a blanket of massive to vaguely laminated gravely sand (Md -1.2...3.7, sorting 1.2...3) of moderately vesiculated andesite. Thickness of the blanket is variable and declines both on ridge crests, and with distance from the source. The maximum observed thickness of the deposit is 30cm, 4km from the dome. The deposit becomes finer grained and better sorted with distance away from the source with maximal diameter of juvenile clasts decreasing from 46cm to 4cm. The surge represented a single short pulse of an inflated, hot, dry gas-pyroclastic mixture, which was likely formed by collapse of the powerful initial explosion fountain. Impact of the surge on several meters of snow filling the crater and the surrounding flank caused extensive lahars which travelled more than 30 km. Following the surge, block-and-ash pyroclastic flows as much as 4.7km long with total volume 0.02km<sup>3</sup> were erupted. They were accompanied by short-lived subplinian eruption column from which widely scattered airfall clasts of pumice, to 10cm diameter, were deposited. The explosive activity destroyed the top of the dome, forming a funnel-shaped crater 200m across, breached to the east. From the crater a short flow of degassed lava was extruded out at the end of the eruption.

**VS2/C/U6/E/01-B3** Poster **1400-35**

**DETAILED HISTORY OF THE ITALIAN EXPLOSIVE VOLCANISM AS DOCUMENTED WITHIN A 110 KA SEDIMENT RECORD OF LAGO GRANDE DI MONTICCHIO (MT. VULTURE, SOUTHERN ITALY)**

Sabine WULF, Jörg F.W. Negendank, Jens Mingram & Bernd Zolitschka (GeoForschungsZentrum Potsdam, PB 3.3 Sedimente und Beckenbildung, Telegrafenberg, D-14473 Potsdam, Germany, email: wulf@gfz-potsdam.de)

Sediment cores from Lago Grande di Monticchio, a maar lake in the Monte Vulture volcanic district (southern Italy), were recovered for interdisciplinary palaeoclimatic and palaeoenvironmental investigations. The partly laminated sediment record spanning the last 110 ka provides 340 tephra layers originating mostly from the Roman Comagmatic Province. Therefore, in addition to radiocarbon and Ar/Ar dates, detailed tephrochronological studies have been initiated in order to confirm the varve- and sedimentation rate chronology of the record. Microscopic studies and geochemical investigations on glass shards using microprobe techniques are in progress to specify the petrology of all tephra layers. At least 33 tephra layers are correlated with Plinian as well as Subplinian eruptions of Somma-Vesuvius (<27 ka). Most of the tephra (>100) originate from explosive eruptions of Ischia (including the "Mt. Epomeo Green Tuff", 56 ka) and the Phlegrean Fields (including the "Campanian Ignimbrite", 33 ka), as well as of the Alban Hills (>20 ka, youngest products) and Sabatini in earlier times ("Tufo di Bracciano", 89 ka). Up to now three tephra layers have been related to explosive eruptions of Etna ("Biancavilla Ignimbrite", 16.5 ka and 18 ka) and Pantelleria ("Ante-Green-Ignimbrite", 74.5 ka). Therefore, studies of the tephrochronological record of Lago Grande di Monticchio will contribute both to a better knowledge of explosive activities of the Campanian volcanoes (e.g. paleowind pattern) and to correlations with isochronous tephra markers of other lacustrine and marine sediments from the Mediterranean (teleconnection).

**VS2/C/U6/E/07-B3** Poster **1400-36**

**WIDESPREAD PUMICE AND ASH (IGNIMBRITE) AT THE NORTHERN CAUCASUS 2.8 MA YEARS AGO**

Nickolai V.Koronovsky (Faculty of Geology, Moscow State Lomonosov University, Moscow 119899, Russia, E-mail: koronovsky@dyname.geol.msu.ru)

Almost instant explosion and following ~2.5 km subsidence of the Upper Chegem caldera (Northern Caucasus) has happened 2.8 years ago that led to northward spreading of rhyolitic ignimbrites at distance about 100 km. Thickness of this sheet was 300 m with area about 1500 square km.

At the periphery this cover (sheet) consists of pumice train. Movement of the masses exploded

was carried out permanently in the aerosole form until the total sheet has been formed. Under compaction volume decreased up to 1/3 of initial value. The rhyolite sheet overlapped late-Miocene quaternary relief. The primary melting magmatic zone was located at depth 20-25 km.

**VS3**

**Wednesday 28 July**

**ENVIRONMENTAL FORCING OF VOLCANIC ERUPTIONS**

Location: Medical School WG11 LT5

Location of Posters: Medical School, Arthur Thompson Hall

**Wednesday 28 July AM**

**VS3/W/26-B3**

Poster

**0900-01**

**RECONSTRUCTING VOLCANIC ERUPTIONS AND GLACIAL EXTENTS USING EVIDENCE OF LAVA-ICE INTERACTION**

David T. LESCINSKY and Jonathan H. Fink (both at Department of Geology, Box 871404, Arizona State University, Tempe, AZ, 85287-1404, United States, e-mail: Lescinsky@asu.edu)

Abundant evidence of lava-ice interaction has been found in the Cascades volcanic arc of the western United States and Canada. Features considered indicative of lava-ice interaction include: thick lava flows with steep marginal walls, abundant glass, and well-developed contraction fractures. These features were produced as lava quenched against steep ice walls caused by erosion and undercutting associated with warm meltwater runoff. Lava-ice interaction features are found on the flanks of volcanoes, and in areas with no current glaciation, indicating that during the lava flow eruptions, glaciers must have been much thicker and more widely distributed.

By identifying features indicative of lava-ice interaction we can reconstruct past eruptions and syn-eruptive glacial extents. Lava quench margins can be used to map out the location and size of the glaciers at the time of eruption. In some locations, preserved quench margins extend all the way to the tops of flows, indicating ice thicknesses greater than several hundred meters. In other locations, quench margins give way to scoriaceous lava consistent with subaerial emplacement. The transition between lava-ice interaction features and apparently subaerial deposits can then be used to map out the upper boundary of the ice. Certain types of lava flow fractures show evidence of abundant water and can be used to indicate where lava flows have traveled subglacially or where meltwater has been trapped. Using these approaches, we have reconstructed the eruptions of the Mazama Ridge flow at Mount Rainier, Washington and a smaller andesite flow near Moraine Lake at South Sister, Oregon. Reconstructions of this sort are important from both volcanic hazards and climatological standpoints. Age-dating of these eruptions allows us to determine the timing and extent of past glaciations. And eruption reconstructions allow us to better assess hazards posed by future lava-ice interaction.

**VS3/E/03-B3**

Poster

**0900-02**

**RECENT STRUCTURAL EVOLUTION OF THE CUMBRE VIEJA VOLCANO, LA PALMA, CANARY ISLANDS AND ITS TIMING RELATIVE TO CLIMATE CHANGE**

S.J. DAY (Benfield Greig Hazard Research Centre, University College London, Gower Street, London WC1E 6BT, U.K.; e-mail s.day@ucl.ac.uk); J.C. Carracedo (Estacion Volcanologica de Canarias, CSIC, 38206 La Laguna, Tenerife, Spain); H. Guillou (Centre des Faibles Radioactivités, CEA-CNRS, 91198 Gif-sur-Yvette, France); P. Gravestock (Dept. of Geography & Geology, Cheltenham & Gloucester College of Higher Education, Cheltenham GL50 4AZ, U.K.).

The Cumbre Vieja volcano is the youngest component of the island of La Palma. It is a very steep - sided oceanic island volcano, of a type which may undergo large - scale lateral collapse with little precursory deformation. Detailed mapping and radiometric dating has revealed structural reconfiguration of the volcanic rift zones and underlying dyke swarms of the volcano, reflecting the onset of incipient flank instability, which can be correlated with climate change events. For most of its history the Cumbre Vieja volcano was characterised by a triple ("Mercedes Star") volcanic rift zone geometry. Radiometric dating indicates that it grew to its present size from about 125 ka onwards, but rapid erosion of exposed hyaloclastites during the syn - glacial low sea level stand produced major coastal cliffs: the resulting stratigraphy of cliff- and platform- forming lavas may be of general use in mapping syn- glacial oceanic island volcanoes. In the post - glacial period the structure of the volcano has evolved rapidly. Since 7 ka the triple - rift geometry has been replaced by a N-S trending rift zone which transects the volcano, and by E-W trending en echelon fissure arrays on the western flank. This structural reconfiguration indicates weakening of the western flank of the volcano, which may be related to an increase in pore fluid pressures resulting from a post - glacial rise in the water table which is also reflected in an increase in the amount of phreatomagmatic explosive activity.

**VS3/E/01-B3**

Poster

**0900-03**

**POSSIBLE RELATIONSHIPS BETWEEN CLIMATE CHANGE, A PAST GIANT LATERAL COLLAPSE AND MODERN FLANK INSTABILITY OF FOGO, CAPE VERDE ISLANDS**

S.J. DAY (Benfield Greig Hazard Research Centre, Department of Geological Sciences, University College London, Gower Street, London WC1E 6BT, U.K., e-mail s.day@ucl.ac.uk); S.I.N. Heleno da Silva & J.F.B.D. Fonseca (both at: Departamento de Fisica, Instituto Superior Tecnico, Av. Rovisco Pais 1, 1049-001 LISBOA, Portugal); P. Harrop & R. Burgess (both at: Department of Geology, University of Manchester, Oxford Road, Manchester M13 9PL, U.K.).

Fogo island is a large and extremely steep oceanic island in the Cape Verde archipelago. It has a large (c. 9 km across) east - facing summit lateral collapse structure, the Monte Amarelo collapse, with a probable volume of at least 150 - 200 km<sup>3</sup>. For most of its history the Monte Amarelo volcano had a small but productive central vent complex, which was removed by the collapse, and radial rift zones fed by laterally - propagating dykes. Shortly before the collapse these were replaced by north - south trending arrays of en echelon, vertically - propagating dykes. Coastal morphology indicates that the relatively recent Monte Amarelo collapse occurred before the end of the last glaciation, and perhaps as far back as the relatively humid early glacial period. The later Cha das Caldeiras volcano which has grown within the collapse scar has undergone a parallel structural reconfiguration during the latter part of the Holocene which suggests that it is evolving towards an unstable condition. The early stages of this structural reconfiguration appear to have occurred during an inferred humid period, most probably the mid - Holocene climatic optimum when adjacent areas of Africa were much wetter than they are at the present day. The likely mechanistic link between climate change and volcano instability is an increase in pore fluid pressurisation effects (Elsworth & Voight 1995; Elsworth & Day, in press) due to elevated water tables in humid periods as discussed elsewhere in this session by Day et al.: radiometric data will provide a test of this hypothesis.



**VS3/E/05-B3** Poster **0900-04**

**EXPLOSIVITY OF SOUTH-ITALIAN VOLCANOES AND CLIMATE CHANGE DURING THE LAST 110,000 YEARS**

Sabine WULF, Jörg F.W. Negendank, Jens Mingram, Bernd Zolitschka (GeoForschungsZentrum Potsdam, PB 3.3 Sedimente und Beckenbildung, Telegrafenberg, D-14473 Potsdam, Germany, email: wulf@gfz-potsdam.de) & Heinz Vos (Forschungszentrum Juelich, Institute for Chemistry and Dynamics of the Geosphere, D-52425 Juelich, Germany, email h.vos@fz-juelich.de)

A 110 ka sediment record, recovered from Lago Grande di Monticchio (Mt. Vulture, southern Italy), provides 340 tephra layers which have been precisely dated by an independent varve and sedimentation rate chronology. Based on tephrochronological studies most tephras originate from Campanian and Roman volcanoes located 100 to 200 km west of Lago Grande di Monticchio. Abundant explosive eruptions are recorded between 110,000 and 75,000 yr, 40,000 and 27,000 yr as well as between 15,000 and 4000 yr ago in the sediment sequence of Monticchio. These intervals are linked to relatively warm periods, e.g. marine oxygen isotope stages 5c, 3 and 1 (the Holocene) reflecting also periods of higher sea levels. We hypothesize that such periods increase the pressure on the roots of the volcanoes, provide larger amounts of ground water reacting with the magma chamber and trigger more explosive eruptions. This is supported by intervals with minor volcanic activity between 75,000 and 40,000 yr and between 27,000 and 15,000 yr ago that can be related to the colder marine oxygen isotope stages 4 and 2 during the last glaciation. However, this may also reflect variations of the Mediterranean wind pattern. Time series analysis of these data is in progress to check whether periodicities like e.g. Milankovich cycles are a detectable feature of the explosive volcanic activity data from Lago Grande di Monticchio.

**VS3/W/27-B3** Poster **0900-05**

**RECORD OF EPISODIC EXPLOSIVE VOLCANISM AND CLIMATE CHANGE OVER THE LAST 6 MA IN THE NORTH ATLANTIC**

Christian LACASSE (GEOMAR, Department of Volcanology and Petrology, Wischhofstrasse 1-3, D-24148 Kiel, Germany, email: clacasse@geomar.de); Hans-Ulrich Schmincke (GEOMAR, Department of Volcanology and Petrology, Wischhofstrasse 1-3, D-24148 Kiel, Germany, email: hschmincke@geomar.de).

A composite record of explosive volcanism in the North Atlantic for the last 6 Ma is presented based on the recovery of tephra layers at five ODP sites: sites 907 (Iceland Plateau), 985 (Norway Basin), 983 and 984 (Iceland Basin) of Leg 162, and site 919 (Irminger Basin) of Leg 152. All the visible tephra layers were systematically sampled in two adjacent drilling holes to study the most complete record of deposition at each site. Age control of about 40 major eruptions was derived from the revised magnetic stratigraphy and full recovery of the sediment. Planktic and benthic oxygen isotope records ( $^{18}O$ , o/o PDB) available for the upper most sequence were used to refine the age model of the eruptions for the 0-1 Ma time interval. Major element analyses of the glass component of the tephra indicate either bimodal compositions (mafic and silicic) with very few intermediate glasses or unimodal compositions. CIPW norms were calculated from the composition of silicic glasses (rhyolitic or trachytic) that are present in more than 95 percents of the tephra layers. Normative plots of silicic glasses in three component system albite-quartz-orthoclase are shown for the six one-million-year time intervals and compared with those obtained from a geochemical database of central volcanoes in Iceland. With the exception of three, likely erupted from volcanic sources along the Jan Mayen ridge, all the tephra layers were derived from large explosive eruptions along the main rift system and the off-rift volcanic zones in Iceland.

Activity along both Icelandic volcanic zones can be traced within each time interval, with the 3-4 Ma period characterized by the highest frequency of eruption, between one and two large events every 100ka. Comparison with a climate proxy record after Shackleton et al. (1984) clearly shows that these more frequent large explosive eruptions occurred during a climatic transition which led to the onset of glaciations in the North Atlantic, but without showing at first sights any direct link such as a possible triggering mechanism (glacier loading/unloading) or feedback mechanism (volcanic winters).

**VS3/P/02-B3** Poster **0900-06**

**DID ASIAN MONSOON DYNAMICS INFLUENCE THE TIMING OF MT. PINATUBO'S ERUPTION?**

Peter CARL (Climate Dynamics Project, c/o Forschungsvorhaben Berlin, Hausvogteiplatz 5-7, D -10117 Berlin, Germany, email: pcarl@spclim5.wias-berlin.de)

The East and South Asian summer monsoon season elapsed dynamically abnormal in 1991. An excessive northern hemisphere atmospheric mass load had been co-operatively built up in 1990 by the tropospheric biennial oscillation and the monsoon's retreat into a pronounced "Indian summer" type autumn. The status of the Southern Oscillation was prepared for El Nino to occur but kept frustrated by this internal asymmetry until autumn 1991. Consistently, both winter and summer monsoons - yet synoptically severe - have been dynamically less excited than normal. Fed by a southwards displaced Western Pacific High, Mei-Yu over East Asia commenced early by a month. Start-up over Kerala of the south-west monsoon dated normal but came along without onset vortex and advanced very fast, to end up in extreme stagnation. Mt. Pinatubo exploded at June 15, just when this monsoon's advance had stopped - as if a valve opened to maintain the angular momentum tendency. The length-of-day record does indeed not show any event-like signal, but global methane data unveil a rare phase coincidence across the annual forcing cycle, resulting in the strong growth rate anomaly that peaks in June 1991. A structural change is also announced in the dynamic interplay between summer and winter monsoon as seen in onset dates from the southern tip of peninsular India. The question arises if internal dynamics of the atmosphere-land system might have triggered this eruption.

**Wednesday 28 July PM**

Presiding Chair: Dr. Chris Kilburn, (Benfield Greig Hazard Research Centre, University College, London)

**VS3/W/28-B3** Invited **1400**

**EXTERNAL MODULATION OF VOLCANIC ACTIVITY**

NEUBERG, Jurgan W (School of Earth Sciences, Leeds, e-mail: locko@earth.leeds.ac.uk)

Time and again seismo-volcanic activity that shows a clear diurnal and semi-diurnal modulation is related to the earth's tidal stress field as an external triggering mechanism. A critical overview is presented here based on several data sets from Stromboli volcano, Italy, Mt Ruapehu, New Zealand, and Merapi, Bromo and Batur, Indonesia, where in some cases also weather data are incorporated. A comparison with theoretical body tides in the spectral domain reveals evidence against any correlation between seismo-volcanic activity and tidal stress. However, other weather parameters such as temperature and barometric pressure

show the same diurnal and semi-diurnal modulation and are, therefore, candidates for possible external modulation. Special emphasis is given to the detection and separation of man-made signals.

**VS3/E/06-B3** **1430**

**SEA-LEVEL CHANGE MODULATION OF EXPLOSIVE VOLCANIC ERUPTIONS**

W. J. McGUIRE, (Benfield Greig Hazard Research Centre, Department of Geological Sciences, University College London, Gower Street, London WC1E 6BT. Email: w.mcguire@ucl.ac.uk)

Volcanic activity has often been linked with dramatic environmental changes in the Quaternary, either by driving climate modification or in response to major changes in the environment. Although the case for large explosive eruptions causing small, brief, falls in global temperatures is convincing, neither the evidence nor the mechanisms for longer episodes of volcano-induced cooling are yet clear. Contrastingly, recent research based on ice-core data suggests that rapid climate change over the past 100,000 years triggered an increase in volcanism. Through examination of the ages of tephra layers in deep-sea sediment cores, a statistical analysis is presented that links the frequency of explosive activity at volcanoes in the Mediterranean to the rate of late Quaternary sea-level change. The non-linear correlation between the two is tentatively explained in terms of the dynamic responses of coastal and island volcanoes to stress-related influences on a range of spatial scales. The correlation supports a mechanism or mechanisms whereby climate-driven growth and decay of large ice sheets can influence the eruptive behaviour of distant volcanic edifices via large, rapid changes in global sea level.

**VS3/E/07-B3** **1450**

**DO GIANT COLLAPSES OF VOLCANOES TEND TO OCCUR IN WARM, WET INTERGLACIAL PERIODS AND IF SO, WHY?**

S.J. DAY and W.J. McGuire (both at: Benfield Greig Hazard Research Centre, Department of Geological Sciences, University College London, Gower Street, London WC1E 6BT, U.K., e-mail s.day@ucl.ac.uk); D. Elsworth (Department of Energy and Geo-Environmental Engineering, The Pennsylvania State University, 110 Hosler Building, University Park PA 16802-5000, U.S.A.); J.C. Carracedo (Estacion Volcanologica de Canarias, CSIC, La Laguna, Tenerife, Spain) & H. Guillou (Centre de Faibles Radioactivités, Laboratoire Mixte CEA - CNRS, 91198 Gif sur Yvette, France).

Giant lateral collapses of oceanic island volcanoes may be triggered by various processes which are influenced by climate. Low sea level stands during glaciations will tend to destabilise volcano flanks by the removal of lateral buttressing forces and intense coastal erosion of hyaloclastite sequences. However, most mid- to low-latitude oceanic islands were arid during glacial periods; the consequent major falls in water tables decreased the pore fluid pressurisation effects which appear to be the dominant mechanism for volcano destabilisation during rift zone eruptions (Elsworth & Voight 1995; Elsworth & Day, in press). Conversely, penetration of salt water into the cores of the volcanoes during dry periods may weaken them by alteration. Most of the destabilising effects of low sea level stands are permanent. In contrast, low-latitude oceanic climates are generally most humid during interglacials and it is in these periods that water tables are highest. Thus, in general, volcano instability will be greatest in the period after the end of glaciations, when the destabilising effects of pore pressure increases are greatest and reinforce the effects of earlier coastal erosion and volcanic core alteration. This prediction is consistent with limited available age data for giant lateral collapses and associated submarine debris avalanches and megaturbidities in the Quaternary. These consistently occur in warm, humid interglacial and interstadial periods, often (but not always) close to their start and not necessarily during periods of rapid sea level change.

**VS3/P/01-B3** **1510**

**ERUPTIONS OF PAVLOF VOLCANO, ALASKA, AND THEIR POSSIBLE MODULATION BY OCEAN LOAD AND TECTONIC STRESSES: RE-EVALUATION OF THE HYPOTHESIS BASED ON NEW DATA FROM 1984-1998**

Stephen R. MCNUTT (Alaska Volcano Observatory, Geophysical Institute, University of Alaska Fairbanks, 903 Koyukuk Drive, P.O. Box 757320, Fairbanks, AK 99775, USA, email: steve@giseis.alaska.edu)

Thirteen of sixteen magmatic eruptions at Pavlof Volcano in nine of the years from 1973 to 1998 have occurred between September 9 and December 29. New statistical tests show that the distribution of eruptions is non-random at a 99.5 percent confidence level. Volumes of erupted material range from 0.3 to 16 x 10<sup>6</sup> m<sup>3</sup> (dense rock equivalent). A significant correlation exists between the eruptions and yearly nontidal variations in sea level and may result from ocean loading. Calculated volume changes beneath the volcano due to ocean loading are from 0.02 to 0.6 times eruption volumes, and it is postulated that the volcano acts as a long-period (several months) volume strain meter, with lava being preferentially erupted when strain beneath the volcano is compressive. Previous observations of a tilt reversal from 1978-1980, and new observations of 1) tectonic activity and eruptions in the spring and summer of 1986, and 2) a M=6.9 earthquake nearby in May 1993, also suggest tectonic modulation of eruptions. The volcano appears to be responsive to small, slow changes in ambient stresses or strains, and these changes may modify or trigger eruptions.

**VS3/E/02-B3** **1550**

**VOLCANICLASTIC SEDIMENTATION IN COASTAL ENVIRONMENTS: THE INTERPLAY BETWEEN VOLCANISM AND QUATERNARY SEA LEVEL CHANGES (LATIUM, CENTRAL ITALY)**

D. DE RITA, M. Fabbri, I. Mazzini, P. Paccara, A. Sposato, A. Trigari, G. Giordano (Dipartimento di Scienze Geologiche, Università Roma Tre, L.go S. Leonardo Murialdo 1, 00146, Roma, Italia)

Quaternary alkali-potassic explosive volcanism developed along the western coast of the Italian peninsula related to back-arc extension of the Tyrrhenian basin. Volcaniclastic sedimentation along the coast of Latium records the interplay of volcanism and Quaternary sea level changes. Most of the large volume pyroclastic flows from Latian volcanoes were erupted during low stands of the sea level; they deposits occur at the base of unconformity bounded stratigraphic units. Detailed stratigraphic correlations between the stratigraphy of volcanic products of Northern Latium and volcaniclastic sedimentation along the coast allowed to identify four first order, regionally extended stratigraphic units (synthems) bounded at the base and top by erosional unconformities that developed during sea level low stands (ice ages) and comprised in age between 0.60 Ma and 0.12 Ma. The area appears to have been relatively stable tectonically, as vertical aggradation is little compared to lateral aggradation. Erosion during low stands of the sea level incised each synthem approximately to the base of the unit, so that successive synthems are laterally juxtaposed rather than vertically.



VS3/W/25-B3

1620

**FIRE AND ICE: IS THERE A CAUSAL RELATIONSHIP BETWEEN GLACIAL MAXIMA AND MINIMA AND THE ERUPTABILITY OF MAGMA AT LARGE CONTINENTAL ARC VOLCANOES?**

Michael DUNGAN, Bradley Singer, and Yann Vinzce. (Département de Minéralogie, Université de Genève, 1211 Genève 4, Switzerland, email dungan@terre.unige.ch); Ren Thompson (U.S. Geological Survey, Denver Federal Center, Denver CO 80225 USA)

Episodic loading by ice during glacial maxima may reduce the eruption probability of mafic magma. Ice accumulation rates on high-standing volcanic edifices greatly exceed the regional average, and erosion during glaciation may remove substantial volumes from the summit and flanks: i.e., the local decrease in compressive stress imposed on conduit systems following ice retreat may be considerable. A petrologic, photogrammetric, paleomagnetic, and geochronological study of the Tatara-San Pedro complex (36° S, Chilean Andes) identified a positive correlation between the ages of basal flows overlying erosional unconformities and the ages of global ice-volume minima inferred from the marine oxygen isotope record (Singer et al., 1997; GSA Bull). New <sup>40</sup>Ar/<sup>39</sup>Ar dates show that some apparent correlations were fortuitous. After elimination of K-Ar dates that give disturbed young ages due to argon loss, the <sup>40</sup>Ar/<sup>39</sup>Ar data still support a correlation between the timing of ice retreat and the ages of basal flows. Present age data from Tatara-San Pedro are too few and insufficiently precise to distinguish definitively between simple preservation of flows emplaced onto erosion surfaces following ice retreat versus suppression of volcanism during glacial maxima followed by high eruption rates after unloading, but they offer hints that large edifices may grow rapidly shortly after ice retreat. Modelling of the intra-edifice stresses imposed by peak ice cover conditions and their consequences for eruptive behavior is an essential step in addressing this question, and field-geochronological investigations of other volcanoes also are needed to test for a general relationship and to assess whether late Quaternary lavas can be dated with sufficient precision to constrain short-term eruption rates.

VS3/W/26-B3

1630

**RECONSTRUCTING VOLCANIC ERUPTIONS AND GLACIAL EXTENTS USING EVIDENCE OF LAVA-ICE INTERACTION**

David T. LESCINSKY and Jonathan H. Fink (both at Department of Geology, Box 871404, Arizona State University, Tempe, AZ, 85287-1404, United States, e-mail: Lescinsky@asu.edu)

Abundant evidence of lava-ice interaction has been found in the Cascades volcanic arc of the western United States and Canada. Features considered indicative of lava-ice interaction include: thick lava flows with steep marginal walls, abundant glass, and well-developed contraction fractures. These features were produced as lava quenched against steep ice walls caused by erosion and undercutting associated with warm meltwater runoff. Lava-ice interaction features are found on the flanks of volcanoes, and in areas with no current glaciation, indicating that during the lava flow eruptions, glaciers must have been much thicker and more widely distributed.

By identifying features indicative of lava-ice interaction we can reconstruct past eruptions and syneruptive glacial extents. Lava quench margins can be used to map out the location and size of the glaciers at the time of eruption. In some locations, preserved quench margins extend all the way to the tops of flows, indicating ice thicknesses greater than several hundred meters. In other locations, quench margins give way to scoriaceous lava consistent with subaerial emplacement. The transition between lava-ice interaction features and apparently subaerial deposits can then be used to map out the upper boundary of the ice. Certain types of lava flow fractures show evidence of abundant water and can be used to indicate where lava flows have traveled subglacially or where meltwater has been trapped. Using these approaches, we have reconstructed the eruptions of the Mazama Ridge flow at Mount Rainier, Washington and a smaller andesite flow near Moraine Lake at South Sister, Oregon.

Reconstructions of this sort are important from both volcanic hazards and climatological standpoints. Age-dating of these eruptions allows us to determine the timing and extent of past glaciations. And eruption reconstructions allow us to better assess hazards posed by future lava-ice interaction.

VS3/E/04-B3

1650

**RELATIONSHIP BETWEEN HISTORICAL ACTIVITY OF FUJI VOLCANO, JAPAN, AND INTERPLATE EARTHQUAKES NEAR THE VOLCANO**

Masato KOYAMA (Faculty of Education, Shizuoka University, 836 Oya, Shizuoka 422-8529, Japan, email: mkoyama@ed.shizuoka.ac.jp)

All available historical documents and paintings, which record abnormal phenomena relating (or possibly relating) to the activity of Fuji Volcano, Japan, were re-examined and classified according to reliability of each document. Reliable descriptions were correlated with eruptive products, and several eruptive events were newly identified. Volcanic activity of Fuji Volcano was in high-level from the 9th to 11th century; in this period at least 7 reliable and 5 possible eruptions occurred. Although only 2 reliable and 1 possible records of eruption exist from the 12th to the early 17th century, this low-level activity is probably due to a lack of enough records. After the middle 17th century, plenty of historical records suggest that the activity is generally low except for the 1707 eruption, which is one of the most voluminous and explosive eruptions in the history of Fuji Volcano. At least thirteen interplate earthquakes (M8 or possible M8 class) have occurred near Fuji Volcano (in east Nankai and Sagami Troughs) since the 9th century. Both the troughs correspond to the convergent boundary between the Philippine Sea plate and the Japan arc. Eleven of the 13 interplate earthquakes occurred coincidentally with volcanic events (eruption, rumbling, or change in geothermal activity) of Fuji Volcano within a interval of +25 years. Most impressive examples are the 1703 rumbling and the 1707 eruption. The former was 35 days behind the 1703 Genroku Kanto earthquake (M7.9-8.2) at Sagami Trough and the latter was 49 days behind the 1707 Hoei Nankai earthquake (M8.4) at Nankai Trough.





**ST3** **Wednesday 28 – Friday 30 July****STRONG GROUND MOTION, EARTHQUAKE HAZARD AND RISK**

Location: Medical School EF08 LT3

Location of Posters: Arthur Thompson Hall

**Wednesday 28 July AM**Presiding Chairs: L.L.Xie (Institute of Engineering Mechanics, China Seismology Bureau, China);  
G.Gibson (Seismology Research Centre, Bundoora, Australia)**ST3/E/33-B3** **Invited** **0830****VERTICAL COMPONENTS OF STRONG GROUND MOTION**

Bruce A. BOLT (Department of Geology and Geophysics, University of California, Berkeley, CA, 94720, USA, email: boltuc@socrates.berkeley.edu)

Differences in wave pattern and coherency between vertical and horizontal components of strong ground motions have been described often in various earthquakes recorded in different parts of the world. Higher frequency content of the vertical ground motions also occurs in alluvial basins compared with the horizontal motions. Reliable estimation of uniform hazard spectra for vertical seismic excitation is dependent on a better understanding of these differences.

Observations from seismic arrays and accelerometers in recent earthquakes provide detail of spectral differences between vertical and horizontal strong seismic motions in alluvial basins. The preferred explanation is that the most energetic of such high-frequency vertical ground accelerations are generated by S-to-P seismic wave conversion within the transition zone between the underlying bedrock and the overlying sedimentary layers. The differences in combined scattering and anelastic attenuation for P and S waves predict the observed spectral differences of the vertical motions between rock and deep alluvium sites. This model also accounts for the frequency content differences between the vertical and horizontal motion ratios at sites in alluvial basins compared with rock sites at similar distance ranges. The high-frequency cut off of the acceleration power spectrum,  $f_{max}$ , is a useful comparison parameter.

**ST3/W/07-B3** **0845****MODELLING THE DIFFERENTIAL MOTION INDUCED BY SEISMIC WAVES AT THE BASE OF BRIDGE PIERS**

Giuliano F. Panza (Dip. di Scienze della Terra, Università di Trieste and The Abdus Salam International Centre for Theoretical Physics, Trieste, Italy, E-mail: panza@geosun0.univ.trieste.it), Fabio Romanelli and Franco Vaccari (both at Dip. di Scienze della Terra, Università di Trieste and GNDT, CNR, Rome, Italy)

The relative motion measured at the base of bridge piers, due to seismic waves generated by nearby and far seismic sources is modelled. Synthetic seismograms are generated by a hybrid technique that combines the advantages of modal summation and finite differences. Relative motion is studied between adjacent piers as well as relative to the extremes of the bridge. The longitudinal, transverse and vertical displacements, velocities and accelerations are considered, in the frequency range up to 6 Hz. It has been found that the relative motion between piers can be of the order of the seismic input amplitude.

**ST3/W/35-B3** **0900****LINEAR AND NONLINEAR BEHAVIORS OF SOFT SOIL LAYERS USING LOTUNG DOWNHOLE ARRAY IN TAIWAN**

HUANG HUEY-CHU, Shieh Chie-Song and Chiu Hung-Chie (Institute of Applied Geophysics National Chung Cheng University Ming-Hsiung, Chia-Yi, 621 Taiwan, R.O.C. TEL: 886-5-2720411 ext.6399 FAX: 886-5-2720807 E-mail: seihuey@eq.ccu.edu.tw)

We analyse the acceleration records of a vertical array to study the linear and nonlinear behaviour of the soft soil layers at LSST site, Lotung, Taiwan. This array includes five triaxial accelerometers deployed at depths of 0m, 6m, 11m, 17m and 47m. During a 6-year operation from 1985 to 1990, 29 earthquakes (4.0-6.5) triggered this array. The maximum PGA value is 257 gals recorded at the surface station. Spectral analyses show that the strong motion causes the peaks of ratio to shift to lower predominant frequencies. The averaged spectral ratio of 15 well recorded weak motion records are selected as a reference, the shift of the maximum predominant frequency can reach 20%. Comparing to the weak motions, the strong motions also decrease the amplification factor. The maximum reduction of the amplification can reach 50%. Besides, the results of waveform simulation show that the linear model based on the Haskell method can well predict the weak motions (PGA < 60 gals) at various depths. However, this linear model does not work for the strong motion data (PGA > 150 gals). Here the non-linear numerical scheme, such as DESRA-2, is required and can significantly improve the simulation results although the PGA value on the surface station is still underestimated. Overall, it is feasible to predict the strong motions for a horizontal layered structure.

**ST3/W/49-B3** **0915****SITE AMPLIFICATIONS ESTIMATES OF THE GEMONA (NE ITALY) ALLUVIAL FAN AND COMPARISON WITH OBSERVATIONS**

Giovanni Costa, Francesco MARRARA and Peter Suhadolc (Dipartimento di Scienze della Terra, University of Trieste, via E. Weiss 1, 34127 Trieste, Italy E-mail: costa@geosun0.univ.trieste.it)

The area of Gemona is characterised by terrigenous sediments, which are covered locally by a thin Quaternary layer, forming a sedimentary basin. The centre of the city of Gemona is located at the margin of this sedimentary basin on an alluvial fan. The city has been completely destroyed during the 1976 Friuli earthquake. Three of the accelerometric stations of the Friuli Strong Motion Network have been installed in the area in order to study the seismic response of the alluvial fan and the sedimentary basin. The seismic response of the April 12, 1997 a  $M=5.6$  event occurred at Bovec (Slovenia) about 40 km from Gemona, has been modelled with a hybrid technique, and the results have been compared with the observations. The hybrid technique combines the analytical method of the modal summation with the numerical method of the finite differences. The seismic response has been analysed in time and frequency domain up to 5 Hz, for the SH and P-SV components. The differences and affinities of the ground-motion as derived from simulation and observation are shown. The comparison of strong motion records with the synthetic signals allow a validation of the prediction and an improvement of the available models, in areas, as Gemona, where few geological and geotechnical data are available. The validated numerical simulations may then be scaled to events with different magnitude, not only to estimate the variability of ground motion in the area, but also to determine the response spectra, the maximum peak ground accelerations, Arias Intensities, and other engineering parameters.

**ST3/W/44-B3** **0930****MEMORY-OPTIMIZED 3D FINITE-ELEMENT MODELING OF SEISMIC GROUND MOTION IN TOPOGRAPHIC STRUCTURES**

Erik Bystricky, Peter MOCZO and Jozef Kristek (all in Geophysical Institute, Slovak Academy of Sciences, Dubravska cesta 9, 84228 Bratislava, Slovak Republic, email: geofpemo@savba.sk)

The existence and importance of an effect of free-surface topography on seismic ground motion is well known. Local topography can cause amplification of ground motion and consequently damage to buildings in the populated areas. Modelling of seismic ground motion in topographic structures is, however, not an easy task if realistic model of medium has to be considered. The finite-element (FE) method allows to include both relatively complex material heterogeneity and free-surface topography. This is because it allows to cover a computational region naturally with irregular mesh of elements of different size and geometry. The problem is that the FE method requires considerable computer memory and time. In order to make the FE modelling more efficient a core memory optimisation is applied to the FE algorithm. The whole computational region can be considered as a set of general surfaces of nodes. In the core memory optimisation only a limited number of surfaces is kept in core memory at one time and the maximum possible number of time updates is performed for these surfaces. The subset of surfaces repeatedly moves throughout the model space until the desired time window is computed. The optimisation significantly reduces core memory requirements and makes the FE method more affordable for seismic ground motion modelling.

**ST3/W/20-B3** **0945****FINITE-DIFFERENCE MODELING OF SITE EFFECTS IN THE GRENOBLE BASIN**

Pierre-Yves BARD (Laboratoire Central des Ponts-et-Chaussées and Observatoire de Grenoble, BP 53 - 38041 Grenoble Cedex - France, email: Pierre-Yves.Bard@lgit.obs.ujf-grenoble.fr), Jozef Kristek, Peter Moczso (both in Geophysical Institute, Slovak Academy of Sciences, Dubravska cesta 9, 842 28 Bratislava, Slovak Republic, email: geofpemo@savba.sk) and Judith Riepl-Thomas (Institut de Protection et de Sureté Nucléaire, 92265 Fontenay-aux-Roses, email: jriep@berlin.far.cea.fr)

The Grenoble area is located at the confluence of three relatively narrow alpine glacier valleys (typically 5 km in width), which are filled with thick quaternary, post-glacial deposits (up to 900 m thick). This geological configuration exhibits a large thickness over width ratio, which is typical of many other alpine valleys. The area is characterised by moderate historic and instrumental seismic activity, with active faults having the potential for at least magnitude 5 to 5.5 events within 10 km of the city. Instrumental recordings obtained at various locations within the city from several local and regional earthquakes consistently exhibit large amplifications over a broad frequency range (a factor exceeding 10 from 0.3 Hz to 5 Hz), as well as very rapid spatial variations and long durations that cannot be explained by 1D modelling. We thus performed a 3D finite-difference modelling using a fourth-order displacement-stress finite-difference scheme with combined memory optimisation developed in Bratislava. The computations are performed for two local, small events that were well recorded inside the town: a magnitude 2.5 located at 10 km to the north-east ("Lancey" event, 21/09/95), and a magnitude 3.5 event located 15 km to the south ("Lafrey" event, 11/01/98). The computations are carried out up to a frequency of 2 Hz, and the source is represented by point sources. A satisfactory quantitative agreement is obtained with observed records, so that we plan to use this FD modelling to anticipate ground motion at other locations inside the valley through an improved understanding of 2D and 3D effects, and for larger events (up to magnitude 5.5) as well.

**ST3/E/31-B3** **1000****CHARACTER OF STRONG GROUND MOTION AND GEOLOGICAL STRUCTURE IN LIJIANG BASIN, CHINA**

Lequn JIANG (Seismological Bureau of Yunnan Province, 650041 Kunming, China, Email: ydj@public.km.yn.cn); Junpei Akamatsu (Disaster Prevention Research Institute, Kyoto University, 611-0011, Uji, Japan, Email: akamatsu@drs.dpri.kyoto-u.ac.jp)

The 1951 Jianchuan earthquake with  $M6.3$  and the 1996 Lijiang earthquake caused serious loss of lives and property in Lijiang basin. Despite lack of instrument recorder of ground motion, the character of strong ground motion was understood through detail investigation of seismic hazard including geographical distribution of human loss in these two earthquakes. Though the epicenter's locations and the strike of seismogenic faults were different, the anomalous intensity distributions caused by two earthquakes were almost the same in Lijiang basin. The serious damages were occurred in Zhonghai village which was about 40 km north-west from the 1951 Jianchuan earthquake's epicenter and also about 40 km south from 1996 Lijiang earthquake's epicenter in these two earthquakes. In order to make sure the local geologic structure which causes anomalous intensity distribution, YSB and Sino-Japanese research team made a lot of research work in Lijiang basin including seismic observation, microtremor survey, deep seismic sounding, reflection survey, gravity survey, boring, underground radar survey and so on. Data analysis shows that there are at least two kinds of geologic structure which cause anomalous distribution of intensity in this area. 1. Bedrock subsides steeply at basin edges by about 400m and the depth to bedrock in the center reaches 1,200m or more. The focussing effect of seismic energy by paraboloid-like bedrock of Lijiang basin is one of the possible causes for the anomalous distribution of intensity. 2. Lijiang area is a geological conjunction zone. Jianchuan-Lijiang fault, Xueshan fault and some other faults divided this area into several tectonic blocks. Effect of the boundaries between crustal blocks is another one of the possible causes for the anomalous distribution of intensity.

**ST3/E/10-B3** **1045****ANALYSES OF STRONG GROUND MOTIONS RECORDED DURING JIASHI EARTHQUAKES**

Li-Li XIE and Mingzhu Guo (Institute of Engineering Mechanics, China Seismological Bureau, 29 Xuefu Road, Harbin, 150080, China, email: llxie@public.hr.hl.cn)

During the four months from the January to the April 1997, there were seven earthquakes of the magnitude greater than  $M_s$  6 occurred in the Jiashi Area of the Xinjiang Uygur Autonomous Region. All the epicenters of the earthquakes were located in a narrow rectangular area of  $18 \times 9$  Km with latitude from  $N39^{\circ}31'$  to  $N39^{\circ}41'$  and longitude  $E76^{\circ}57'$  to  $E77^{\circ}03'$ . During the earthquakes, a small array, consisting of four strong motion accelerographs and about 8.5-170 Km respectively far from the epicentral area, recorded the strong ground motions for all events.

In this paper, the characteristics of the recorded ground motions were analysed. Some interesting results, such as coherency of the ground motions, ratio of vertical to horizontal components, spectral characteristics, etc are presented.



ST3/E/26-B3

1100

## THE LIMITATION OF H/V RATIO IN ESTIMATING THE SITE RESPONSE OF LAYERED MEDIUM

Hung-Chie CHIU, (Institute of Earth Sciences, Academia Sinica, P.O. Box 1-55 Nankang, Taipei, Taiwan, R.O.C., email: chiu@earth.sinica.edu.tw) Ta-liang Teng (Department of Earth Sciences, University of Southern California, Los Angeles, CA 90089-0740, email: lteng@codas.usc.edu) Xiaofei Chen (Department of Geophysics, Peiking University, Beijing, China, email: xfchen@pku.edu.cn)

Spectral ratio between horizontal and vertical components (H/V ratio) has been widely applied to site response estimation recently. However, the physical basis behind this ratio is still unclear. Furthermore, most studies indicated that the H/V ratio only can predict the fundamental resonant frequency but very few researchers claimed that this ratio could estimate the amplification factor. Although many researchers have attempted to verify this method, none of them have fully explored this problem. This paper presents an extensive analysis of the H/V ratio and gives one possible approach to verify the controversial assumptions that made for developing the H/V method. We also give a reasonable explanation to the observations. According to our analyses, the H/V ratio can well estimate the fundamental resonant frequency for a simple layered model with a simple source, and this method may fail in all other cases because of noise, multi-layered-medium or complicate-source effects. Numerical validation based on synthetic seismograms also supports our assessment.

ST3/W/30-B3

1115

## REAL-TIME MAPPING OF POST EARTHQUAKE STRONG-GROUND MOTION

YI-BEN TSAI (Institute of Geophysics, National Central University, Chung-Li, Taiwan, Email: ybtsai@eqm.gcp.ncu.edu.tw), Yih-Min Wu, Jau-Yi Lin (Both at Central Weather Bureau, 64 Kung Yuan Road, Taipei, Taiwan, Email: ludan@ss2.cwb.gov.tw), and Chang-Chi Young (Institute of Geophysics, National Central University, Chung-Li, Taiwan)

We have combined the functions of two advanced accelerograph networks in Taiwan to develop a method for detailed real-time mapping of post-earthquake strong ground motion. The first is a real-time accelerograph network of 60 stations which provides rapid earthquake reports for the public. The station spacings of this network are about 20km x 20km. The second is a stand-alone free-field accelerograph network. The station spacings of this network are about 5km x 5km. Since its first deployment in 1992, the second network has recorded tens of thousands of ground motion accelerograms. We have used these records to establish relative local site response function at each free-field accelerograph station with respect to a nearby real-time network station. By this way, once the real-time network station records strong ground motion from a damaging earthquake, we can immediately calculate the ground motion response spectrum at each station by multiplying the observed response spectrum at the reference station from the earthquake with the relative local site response function. We have tested this method for the Taipei Basin area with excellent results. We are currently expanding the tests to other areas of Taiwan.

ST3/E/25-B3

1130

## A MEASURE OF GROUND MOTION INTENSITY

KOOROSH SHARIF (Institute of Geophysics, Tehran University, email: mraeesi@iman.ut.ac.ir) . R. Gheitanchi (Institute of Geophysics, Tehran University, email: rghchee@chamran.ut.ac.ir)

Quantification of the damage potential of ground motions is desirable for various reasons. Such a quantity facilitates comparison among different types of ground motions. Moreover, rational design limit states may be established by employing a single quantity, which represents the damage potential of the ground motion, expected at a given site. However, this quantity should reflect the influences of basic excitation and system characteristics contributing to the seismic response of structural systems. There are various studies in earthquake engineering literature devoted to the quantification of the damage potential; they describe different physical values in term of different physical units. Arias (1970) introduced a measure of ground motion intensity as the area under the spectrum of total energy absorbed by undamped single degree of freedom (SDOF) system at the end of the ground excitation. But a SDOF system is a discrete system and it does not reflect all characteristics of ground motion. It might be better that we use a continuous system as a vertical elastic rod that is attached to the earth instead of a discrete system that interacts with the excitation. In this paper we introduce the intensity of ground motion as the total energy absorbed by a vertical elastic rod with a length of one meter which is vibrated longitudinally and torsionally by ground motion. The results are in agreement with the observed ground motion intensity.

ST3/E/37-B3

1145

## THE DISTRIBUTION OF GROUND STRAIN AND GROUND FAILURE CAUSED BY A MODERATE EARTHQUAKE IN SOUTHWESTERN TAIWAN

Yeong-Tein Yeh, Han-Yih Peng, Kuo-Liang Wen and Shui-Bei Yu (All at Institute of Earth Sciences, Academia Sinica, Taipei, Taiwan, R.O.C., Email: ytyeh@earth.sinica.edu.tw)

On July 17, 1998, an earthquake with magnitude 6.2 in Richter scale occurred in Rui-Li, Chia-Yi, Taiwan. The epicenter is located at 23°X 30.78°F N and 120°X 37.98°F E and the focal depth is about 6 km. The earthquake caused some ground failure, landslide, and building damage. There are 5 deaths and 17 injuries. It has been the most damaging earthquake occurred in southwestern (SW) Taiwan since 1964. The strong ground motions induced by this earthquake were recorded by 79 out of around 110 observation stations, in SW Taiwan, installed by the Central Weather Bureau, Taiwan in the past years. In this research, we used these strong motion recordings to estimate the distribution of ground strains. First of all, single station estimation method was used to calculate the 9 components of displacement gradient tensors. Then, the co-ordinate strains and/or the principle strains are deduced for each observational site. The observed maximum strain is about 200m in N81°XW at near epicenter distance. In the meantime, the GPS measurements of coseismic ground deformations were also used to estimate the corresponding ground strains for comparison. Finally, the estimated strain distribution will be discussed and compared with the ground damage pattern caused by this earthquake.

ST3/E/39-B3

1200

## ON-LINE WORLD-WIDE STRONG GROUND MOTION DATABASE (SMDB) AND SYNTACTIC WAVEFORM CLASSIFICATION

A.D. GVISHIANI, A.A. Burtsev, M.N. Zhizhin, CGDS, Molodezhnaya Str. 3, GC, Moscow, 117296, Russia; +7-095-1334339; Email: gvi@wdcb.rssi.ru; J. Bonnin, EOPGS, 5 rue Descartes, F-67084 Strasbourg Cedex, France; +33-88416368; Email: bonnin@selene.u-strasbg.fr

The SMDB is a relational seismic waveform data base of accelerograms in the near fields of strong earthquakes, which allows using WWW-browser to retrieve the waveforms together with a set of essential parameters of events, stations and instruments. You may select from more than 23000 records of ground acceleration, velocity and displacement were recorded during well-known strong earthquakes. They describe 786 events recorded by 1235 stations all over the world in the period of time 1933 - 1994. To get data, one may fill in a query form, and retrieve a list of records containing set of essential parameters of related events, sites and instruments. The listed records can be dynamically plotted. One can also find description of recent strong earthquakes on the Web site in half an hour delay. "Syntactic Pattern Recognition Scheme" (SPARS) does classification of the SMDB by wavelet analysis and syntactic pattern recognition. Please consult us to get digital data from SMDB. WWW: <http://www.wdcb.rssi.ru/CGDS/> E-mail: gvi@wdcb.rssi.ru

The problem of seismic resistance and vulnerability of potential building constructions becomes more and more important with time. To do seismic engineering calculations accelerograms recorded in the nearfield of strong earthquakes epicenters occurred in those regions are needed. If they are not available similar records from other regions are used. The principal problem is: what is definition of "similar records" and how to find them? The CGDS/EMSC Strong Motion Data Base (SMDB) and Syntactic Pattern Recognition Scheme tackles this problem.

ST3/E/44-B3

1215

## PRE-INSTRUMENTAL EARTHQUAKES IN A LOW-SEISMICITY REGION: REINTERPRETATION OF THE 16 NOVEMBER 1931 EVENTS IN CENTRAL FINLAND

Paivi MANTYNIEMI (Institute of Seismology, University of Helsinki, Helsinki, Finland, email: paivi@seismo.helsinki.fi)

The largest earthquake known to have occurred in a given region may not have been devastating but is nevertheless of importance when evaluating the seismic hazard. This applies to central Finland, too, where only non-instrumental data are available for the more noted events. This study deals with some of the problems involved in assessing the macro-seismic intensity at the lower degrees where many of the classification factors depend solely on human perception.

The maximum intensities of the main shock in central Finland on 16 November 1931 and its largest aftershock have previously been assessed as 6 and 5 (MCS), respectively. The reconsideration of the data is motivated by some features of the earlier analysis such as a strong emphasis given to local anomalies and a confusion between felt and heard effects.

A total of about 800 reports with noted effects, including questionnaire data, free format descriptions, and interviews, are available for the main shock. For the present study, newspapers were scanned for additional information of the events.

These data are used in assessing the intensity on the European Macro-seismic Scale of 1992 (Gruenthal, 1993). Statistical methods are applied, and the outputs compared with that of the earlier analysis. Special attention is given to assessing the quality of the observations. A brief commentary on the possible effects of a similar earthquake today is included.

## Wednesday 28 July PM

Presiding Chairs: G.F.Panza (Dept. Di Sci. Della Terra, University of Trieste, Italy); H.C.Chiu (Institute of Earth Sciences, Academia Sinica, Taipei, Taiwan)

ST3/W/34-B3

1400

## NEAR-SOURCE INVERSION FOR THE APRIL 12, 1998 BOVEC EARTHQUAKE

Angela Sarao<sup>1</sup> and Peter Suhadolc (both at Dipartimento di Scienze della Terra, Università<sup>1</sup> di Trieste and The Abdus Salam International Centre for Theoretical Physics, Trieste, Italy. E-mail: angela@geosun0.univ.trieste.it)

On April 12, 1998 a 5.6 magnitude earthquake occurred in NW Slovenia near the border with Italy. It was a dextral strike-slip mechanism with small tensile component. The main shock was followed by aftershocks, the strongest one (M=4.6) located few kilometers away from the main shock. To gain insight into the rupture process we have inverted the three-component accelerograms of the main event, recorded by the Friuli accelerometric network, for different sizes and positions of the fault. The results of the inversions allow us to single out the main features of the rupture process which is characterised by two big patches of energy release on the fault. Our results are compared with the geotectonic evidences for the region under study. Solutions obtained inverting velocities and displacements at different frequencies are also discussed.

ST3/W/09-B3

1415

## THE RETRIEVAL OF THE EARTHQUAKE RUPTURING PROCESS BY STRONG MOTION DATA: RESULTS FROM A BLIND TEST

Angela Sarao<sup>1</sup>, Peter Suhadolc (both at Dipartimento di Scienze della Terra, Università<sup>1</sup> di Trieste and The Abdus Salam International Centre for Theoretical Physics, Trieste, Italy. E-mail: angela@geosun0.univ.trieste.it) and Shamita Das (Dept. of Earth Sciences, University of Oxford, England)

A "blind test" has been performed to determine if different methods of analyzing the accelerograms to retrieve details of the earthquake rupturing process lead to similar results. Synthetic accelerograms, to be used as observed data, are computed using the multimodal summation method for an extended source. The moment distribution used to generate the synthetic data was kept secret by one of the authors and only some parameters of the input model such as the seismic moment, focal mechanism and hypocentral location and fault area extension were known. The results obtained by the most suitable procedure for such kind of study, are thoroughly discussed. The inverse problem is solved using the Das-Kostrov method of linear programming with additional physically-based stabilizing constraints. We present the results obtained when 1) each grid is allowed to slip only once; 2) the grids can slip more than once; 3) using only the vertical or the horizontal components; 4) using only seismograms whose amplitudes were comparable to each other. For most of the cases the fit of the waveforms is quite good and the location of the main energy release can be identified on the fault.

**ST3/W/40-B3 1430****SPECTRAL GROUND MOTION ATTENUATION FOR SWITZERLAND AND A FIRST APPLICATION TO SEISMIC HAZARD EVALUATION IN THE VALAIS**

Patrick SMIT (Department of Civil and Environmental Engineering, Imperial College of Science, Technology and Medicine, London SW15 3LR, UK, email: p.smit@ic.ac.uk) Erik Ruttener (Zurich Re, Risk Management, General Guisan-Quai 26, 8022 Zurich, CH, email: erik.ruttener@zurich.com)

The quantitative models used for the anti-seismic design of buildings in Switzerland are based on macro-seismic observations and ground motion acceleration data from adjacent countries. The lack of strong-motion data led in 1983 to the decision to install a national strong-motion network in Switzerland. In 1992 63 digital free-field and dam-related stations were deployed by a governmental working group and subsequently extended to 95 stations. The recordings of this network and the seismograph network, both operated by the Swiss Seismological Service, allow nowadays deriving own attenuation models for peak ground acceleration and spectral ground accelerations. The paper presents the empirical scaling of Fourier amplitude spectra and peak acceleration of earthquake induced ground motion with respect to local-magnitude and hypocentral-distance, valid for rock sites in Switzerland and the adjacent areas. These models are applied to the calculation of seismic hazard curves for the middle and upper Valais (southwestern Switzerland). These areas show the highest seismic activity, historically as well as in this century. The results are in good accordance with estimated macroseismic intensity values for the same return period, as obtained in earlier studies.

**ST3/E/52-B3 1445****STRONG GROUND MOTION ATTENUATION RELATIONSHIPS FOR THE CAUCASUS**

Patrick SMIT (Department of Civil and Environmental Engineering, Imperial College of Science, Technology and Medicine, London SW15 3LR, UK, email: p.smit@ic.ac.uk) Valery ARZOUUMANIAN (National Survey for Seismic Protection of the Republic of Armenia, 375054 Yerevan, Armenia, email: arz@nssp.yerphi.am) Zurab Javakishvili (Institute of Geophysics; Georgian Academy of Sciences, 380093 Tbilisi, Georgia, email: zjavakh@hotmail.com), Sergej Arefiev (Unified Institute Physics of the Earth, Russian Academy of Sciences, 123810 Moscow, Russia, email: arefiev@synapse.ru)

The paper presents the first predictive relation for horizontal and vertical peak ground acceleration and 5% damped maximum absolute acceleration spectrum, appropriate for predicting earthquake ground motion in the Caucasus. The empirical attenuation models were developed based on data from the permanent digital strong motion network installed in 1990 in the epicentral area of the 1988 Spitak (Armenia) earthquake and several temporary networks in the epicentral area of strong earthquakes in the Caucasus and the adjacent area (7.7Ms Manjil, 20.6.1991; 7.0Ms Racha, 29.4.1991; 6.8mb Erzincan, 15.3.1992). The instruments and operation of the permanent and temporary networks were jointly funded by the Swiss Disaster Relief Unit. Today the permanent digital strong-motion network comprises 12 digital free-field stations in the northern part of Armenia and Georgia and are operated by national agencies. This network is complemented by 16 analog strong motion instruments installed all over Armenia and structure-related arrays in the Metsamor nuclear power plant (Armenia) and the Inguri arch dam (Georgia).

The attenuation models, which are considered applicable for estimating free-field ground motions on alluvium from earthquakes in the Caucasus with magnitudes between 3 and 7, were successfully adopted in the calculation of the seismic hazard of Georgia.

**ST3/W/18-B3 1500****REGIONAL WAVE ATTENUATION FROM WEAK MOTION DATA**

P. L. Bragato, A. Govoni and D. SLEJKO (Osservatorio Geofisico Sperimentale, Trieste, Italy, e-mail: dslejko@ogs.trieste.it)

Attenuation relations for the main seismic hazard quantities (peak ground acceleration, spectral acceleration, etc.) are computed from strong motion data and, consequently, are valid in the high to medium magnitude range only. This is reasonable as seismic hazard maps for high seismicity regions are dominated by the contribution of the largest earthquakes. The scarcity of strong motion data limits the definition of specific attenuation relations of geographical and/or tectonic validity. In this work we explore the possibility of using large data sets of digital seismometric data available today for extending and validating attenuation relations in the weak motion regime and getting better spatial resolution at sub-regional scale. Key steps to this goal are reliability of the acquisition process, robustness of inversion procedures, and homogeneity of data set characteristics.

**ST3/E/02-B3 1515****USING DATA FROM SMALL TO MODERATE MAGNITUDE EARTHQUAKES TO CONSTRAIN ATTENUATION FUNCTIONS**

Gary GIBSON (Seismology Research Centre, 2 Park Drive, Bundoora, Victoria 3083, Australia, email: gary@seis.com.au)

Attenuation functions give ground motion as a function of earthquake size and distance. Most have been derived using data from earthquakes in the range from magnitude Mw 5 to Mw 7. This applies for functions giving any measure of ground motion, such as peak ground acceleration, peak ground velocity, intensity, Fourier spectra or response spectra.

Functions have been published for a wide range of tectonic environments, with some functions emphasising smaller events and some larger, and some functions emphasising motion at closer distances and others at greater distances. Superimposed ground motion plots using published functions for earthquakes of magnitude Mw 6 show some scatter. Few on-scale recordings of strong motion data are available from nearby earthquakes in the range from Mw 7 to Mw 9. When computing ground motion recurrence (earthquake hazard), it is necessary to extrapolate out of the magnitude and distance ranges in which the functions were derived. For large events, the various published functions produce much greater scatter in ground motion estimates than for Mw 6. If the same attenuation functions are used to extrapolate to smaller earthquakes, there is a similar very wide scatter in estimated ground motion. In this case data are available, but often have not been used in the derivation of the functions. Although the weaker motion from small earthquakes represents little earthquake hazard, it can constrain the rate of change of ground motion with both magnitude and distance. It can also be used to evaluate methods for dealing with source dimension in attenuation functions. If data from smaller earthquakes are used in the derivation of attenuation functions, then the extrapolation to critical large events should be more reliable. Spectral attenuation functions using data from small nearby events will show their high acceleration, high frequency motion, but with low displacement and low hazard.

**ST3/E/29-B3 1530****THE ATTENUATION RESEARCH OF THE STRONG GROUND DISPLACEMENT IN CHINA**

CHEN PEISHAN Li Baokun Bai Tongxia (Institute of Geophysics, China Seismological Bureau, Beijing, 100081)

We have found from the fracture mechanics rupture model of earthquakes that the peak ground acceleration PGA and velocity PGV and displacement PGD strongly depend on the tectonic ambient shear stress = value =A6=D30. =A6=D30 value is introduced into the predictive equation = of PGD by us, at the same time the dependence of predominant frequency = of PGD fd on magnitude is considered. Based on both improvements, the = predictive equation of PGD(CLB98d) has been derived from theoretical = analysis. It has been tested by observation data that this predictive = equation is suitable for epicentral distance range = =A1=F7=3D10=A1=AA250km and magnitude range Mw=3D4=A1=AA7.2. There are = different =A6=D30 values in different regions all over the world, but = the influence of =A6=D30 value on PGD is not large. =20. Key words: tectonic ambient shear stress field, peak ground = displacement, predictive equation, predominant frequency.=20.

**ST3/E/36-B3 1615****PGA AND RESPONSE SPECTRA ATTENUATION RELATIONS DEDUCED FROM THE GULF OF CORINTH (GREECE) STRONG MOTION DATABANK**

D. DIAGOURTAS and K. Makropoulos (both at Dept. of Geophysics & Geothermy, Univ. of Athens, 157 84 Zografou, Greece, E-mail: ddiagour@cc.uoa.gr)

An extensive databank constructed from high quality strong motion data accumulated during the last 7 years by RASMON (Rion-Anrion Strong Motion) Network, w. Gulf of Corinth (Greece), is used to derive PGA and response spectra local attenuation relationships. The results show remarkable differences between sites located off the north and south coasts of the Gulf which is attributed to corresponding differences in the local geological settings, emphasising thus, the usefulness and necessity of such approach towards a more realistic a-seismic design.

**ST3/W/03-B3 1630****NUMERICAL MODELLING OF THE VRANCEA SOURCE INFLUENCE ON THE LOCAL SEISMIC RESPONSE IN BUCHAREST**

C.L. MOLDOVEANU ([1] National Institute for Earth Physics, Bucharest, Romania; [2] Dipartimento di Scienze della Terra, Universita' di Trieste, Italy; Email: carmen@geosun0.univ.trieste.it) G. F. Panza ([2] Dipartimento di Scienze della Terra, Universita' di Trieste, Italy; [3] The Abdus Salam International Centre for Theoretical Physics, Trieste, Italy; Email: panza@geosun0.univ.trieste.it)

The Vrancea region, characterised by strong intermediate-depth earthquakes, represents the main source to be considered for the seismic risk mapping both at the national (Romania) and the regional level (south-eastern Europe). The mapping of the seismic ground motion in Bucharest, the main city affected by this source, is carried out using a complex hybrid waveform modelling that combines the modal summation and the finite difference schemes, and allows us easy parametric tests. The information necessary for the numerical simulations takes into consideration the source, the averaged regional model and the local structure for Bucharest. The two scenario earthquakes we consider, representative for the seismicity of the region, correspond to the March 4, 1977 (Mw=7.4), and May 30, 1990 (Mw=6.9) Vrancea events. The site effects are analysed in order to define generally valid ground motion parameters, to be used in the seismic hazard estimations. The synthetic signals and the local response are nicely compared with the damage observed in Bucharest for the March 4, 1977 Vrancea event, the strongest earthquake that hit the city in modern time.

We show that using the 2-D hybrid waveform modelling we can make realistic predictions for the possible seismic input which can compensate the lack of strong motion records, available only for a few events that occurred in the last 20-30 years. The synthetic ground motion database can lead to a reliable mapping of the local seismic hazard of Bucharest.

**ST3/W/01-B3 1645****SEISMIC GROUND MOTION SIMULATION FOR THE 1995 KOBE EARTHQUAKE**

Jozef Kristek, Peter MOCZO (both in Geophysical Institute, Slovak Academy of Sciences, Dubravská cesta 9, 84228 Bratislava, Slovak Republic, email: geofpemo@savba.sk), Kojiro Irikura, Tomotaka Iwata and Haruko Sekiguchi (all in Disaster Prevention Research Institute, Kyoto University, Gokasho, Uji, 611, Japan, email: irikura@egmdpri01.dpri.kyoto-u.ac.jp)

The long-period (T>1s) seismic ground motion during the 17 January 1995 Hyogo-ken Nanbu (Kobe), Japan, earthquake is numerically simulated and compared with the recorded ground motions in the Kobe area. Since the main goal is to understand the observed damage belt in Kobe, only a part of the Osaka sedimentary basin is considered in the simulation. A 3D model of the medium is that constructed by Iwata et al. (1998) on the basis of all available geophysical and geologic data. Besides the reference three-layer basin model certain modifications are also considered for comparison. The complex rupture process is modelled using a kinematic fault model of Sekiguchi et al. (1998) obtained by inversion of strong-motion velocity seismograms. The rupture process is simulated by activating point dislocation sources distributed over five fault segments. Both the rupture process and wave propagation are numerically simulated by the 4th-order displacement-stress finite-difference scheme on a staggered grid. Efficiency of the simulation is significantly increased using a discontinuous spatial grid and memory optimisation. A discontinuous grid that combines spatial grids with grid spacings h and 3h reduces the total number of grid points (Kristek et al., 1998). The combined memory optimisation (CDMO, Moczo et al., 1999) reduces core and disk memory requirements. Synthetic ground motion from several simulations are analysed and compared with the recorded ground motion in order to validate the model and discuss main factors forming the ground motion anomaly in the Kobe area.

**ST3/W/50-B3 1700****STRONG MOTION PREDICTION FOR SCENARIO EARTHQUAKES ON ACTIVE FAULTS**

KOJIRO IRIKURA(1) and Katsuhiro Kamae(2) (1) Disaster Prevention Research Institute, Kyoto University, Gokasho, Uji, Kyoto 611-0011, Japan, Phone: 81 774 38 4060, FAX: 81 774 33 5866, Email: irikura@egmdpri01.dpri.kyoto-u.ac.jp; (2) Reactor Research Institute, Kyoto University, Noda, Kumatori-cho, Sennai-gun, Osaka 590-0494, Japan, Phone: 81 724 51 2369, FAX: 81 724 51 2603, Email: kamae@kuca.rrri.kyoto-u.ac.jp

A method of strong motion prediction for future earthquakes is proposed to mitigate earthquake damage in urbanised areas surrounded by seismogenic active faults. The lesson from the 1995 Hyogo-ken Nanbu (Kobe) earthquake shows the importance of evaluating a

synergistic effect of source and local geology effects, which produced killer pulses causing heavy damage in Kobe and adjacent cities. To consider such effects, we propose a hybrid method estimating Green's functions, deterministic and stochastic approaches in low (< 1 Hz) and high (> 1 Hz) frequency range, respectively. Source characterisations of scenario earthquakes shall be made, based on geological investigations of capable earthquake faults and seismological studies of source models. Rupture starting and termination areas of the scenario earthquakes would be evaluated from segmentation and grouping of active faults based on branching features of seismic surface ruptures. The heterogeneous slip distribution in the source area is inferred, based on some statistical analyses of source inversion results using strong ground motion data for recent earthquakes. We examine this method by comparing peak ground velocity and acceleration of estimated ground motion and damage distribution in past damaged earthquakes such as 1948 Fukui and Tottori earthquakes. Then, we apply to simulate strong ground motions for hypothetical large earthquakes in the Osaka metropolitan area.

**ST3/W/37-B3** **1715**

**PHYSICALLY CONSTRAINED SOURCE MODELS FOR BROADBAND GROUND MOTION SYNTHETICS**

ALEXEI TUMARKIN, Institute for Crustal Studies, University of California, Santa Barbara, CA 93106-1100, USA; email: alexei@crustal.ucsb.edu

Reliable ground motion prediction is not possible without a formalised and validated procedure for choosing a detailed description of the rupture time history of the simulated earthquake. While numerous source inversion studies provide valuable information on source complexities, they are limited to low frequencies (below 0.5-1 Hz). An attempt to predict ground motions from a future earthquake by specifying only its seismic moment is doomed to failure. Accordingly the highly successful stochastic approach (Hanks and McGuire, 1981; Boore, 1983) based on the w-squared spectral model (Aki, 1967; Brune, 1970), requires two characteristics - moment and stress parameter. It can be shown, that instead of the formal stress parameter, one can use the apparent stress, that has a clear physical meaning being proportional to the ratio of the total radiated energy and the moment (Randall, 1973; Tumarkin, 1999). The radiated seismic energy was considered as a fundamental quantitative measure of earthquake's size long before the seismic moment or even the magnitude were introduced into practice (Golitzin, 1915; Jeffreys, 1923). The main result of our study is that using two constraints - moment and energy - one can reduce the model uncertainty of predictions by narrowing the range of possible combinations of slip, rise time, rupture time and hypocenter location for any extended source model. Our studies of the temporal evolution of the apparent stress revealed an interesting feature observed both for earthquakes and dynamic rupture models. The initial stage of a rupture process is characterised by a sharp increase of the apparent stress to values exceeding the final number by a factor of 3-4, then it quickly stabilises around its final value. This characteristic behaviour can be used to further constrain the source models.

**ST3/W/46-B3** **1730**

**HYBRID-EMPIRICAL MODEL FOR ESTIMATING STRONG GROUND MOTION IN REGIONS OF FEW STRONG-MOTION RECORDINGS**

KENNETH W. CAMPBELL (EQE International, 6555 S. Olympus Dr., Evergreen, CO 80439, USA, email: KCampbell@eqe.com)

The hybrid-empirical model is an alternative to the purely theoretical models commonly used to estimate strong ground motion in regions of few recordings. Theoretical models have become the de facto engineering standard for estimating ground motions in such regions. However, theoretical models lack the empirical basis that is inherent in purely empirical models. The model is considered a "hybrid" because it uses modified empirical estimates from a host region other than that for which the predictions are made. These empirical estimates are modified using simple theoretical techniques to account for differences in the source, propagation, and site characteristics between the host and target regions. An inherent strength of the hybrid-empirical model is its reliance on ground-motion models that are well constrained by actual strong-motion recordings. As a result, observations rather than theoretical assumptions control the magnitude- and distance-scaling characteristics of the model. The aspect of the model is particularly important for ground-motion estimates in the near-source region of large-magnitude earthquakes, which are strongly affected by the complex characteristics of the rupture process. Additional strengths of the model are its explicit incorporation of uncertainty and its reliance on relative rather than absolute theoretical ground-motion predictions. In its current form, the hybrid-empirical model is applied to a selected target region as follows. First, several candidate empirical attenuation relationships for generic rock are selected from a host region (e.g., California). Second, seismological and crustal parameters are selected for both the host and target regions to use in the theoretical estimation of ground motion in these regions. Third, a theoretical stochastic simulation model is used to develop ratios of peak and spectral strong-motion parameters between the target and host regions. Fourth, the ratios are used to adjust the empirical ground-motion estimates from the host region. Finally, the adjusted empirical estimates are weighted and used to develop scenario response spectra and/or regional attenuation relationships for the target region.

**ST3/P/03-B3** **1730**

**STRONG-MOTION SIMULATION FROM ACCELEROGRAMS OF ALBORZ-AZARBAYEJAN NORTH AND NORTHWEST OF IRAN**

HAFIZI, Mohammed Kazem, University of Tehran, Iran

Abstract not available at time of going to press

**Thursday 29 July AM**

Presiding Chairs: B.William (USGS, Menlo Park, CA 94025, USA);

V.Mihailov (Institute of Earthquake Engineering and Engineering Seismology, University of St. Cyril and Methodius, Skopje, Republic of Macedonia)  
Concurrent Poster Session

**ST3/E/46-B4** **0930**

**STUDIES ON TECTONICS, SEISMICITY AND OCCURRENCES OF MAJOR EARTHQUAKES IN NORTH-EAST INIDA**

D.Shanker (Department of Earthquake Engineering, University of Roorkee Roorkee-247667, India. E-Mail: quake@rurkiu.ernet.in)

Last two decades have witnessed considerable development in the field of seismological investigations. A number of approaches have been given for seismic hazard evaluation and earthquake prediction. The north-east India region (18° to 32° N and 84° to 100° east). The

stress pattern in the basin is directed towards northeast. The seismicity and stress distribution pattern of Burmese arc are due to downward bending of the zone around 24° N caused by southeast flow of Tibetan plateau. The region also exhibits

**ST3/W/04-B4** **0945**

**PALEOSEISMIC INVESTIGATIONS ALONG THE ROER VALLEY GRABEN**

Bernard Dost, Laslo Evers (both at KNMI, P.O.Box 201, 3730 AE De Bilt, the Netherlands), br Ad Lokhorst (NITG-TNO, Postbus 157, 2000 AD Haarlem, the Netherlands) Meindert W. van den Berg (NITG-TNO, Postbus 511, 8000 AM Zwolle, the Netherlands)

The seismic risk of the Netherlands and immediate surroundings is calculated on the basis of historical seismicity. The region is regarded a low seismicity area, although in 1992 the Roermond earthquake (M<sub>L</sub>= 5.8) showed the impact of an occasional larger event. The historical period is rather short and large events occurring at a longer return rate will be missed in the analysis. In order to estimate the significance of possible prehistoric events a palaeoseismic investigation is being carried out along the Peel boundary fault, bordering the seismic active Roer valley graben to the North. During 1998 site selection was made for the construction of a trench. Important criteria in the site selection are the detection of a surface expression of the scarp and the possibility of dating at a high time resolution. The availability of different sources of data (aerial photographs, seismic reflection lines, geomorphological data) provided a starting point. In particular a 117 years long time series of levelling data provided rates of vertical movements in the area. Accurate dating is envisaged by selection of the trench in river terraces, which are very well dated. Zooming in on possible trench locations further requires the acquisition of shallow reflection seismics, electrical tomography and ground penetrating radar. It is planned to finalise site selection early 1999 and to start trenching in April/May 1999. In the presentation an overview will be given of the status of the project and future plans. The project is part of the EC funded PALEOSIS program.

**ST3/E/07-B4** **1000**

**REAPPRAISAL OF A XVI CENTURY EARTHQUAKE COMBINING HISTORICAL, GEOLOGICAL AND INSTRUMENTAL INFORMATION**

Gianluca Valensise (Istituto Nazionale di Geofisica, Roma, Italy); MARCO MUCCIARELLI (Universit' della Basilicata, Potenza, Italy, email: mucciarelli@unibas.it) Maria Rosaria Gallipoli (I.M.A.A.A.-C.N.R., Tito Scalco, Italy); Riccardo Caputo (Universit' della Basilicata, Potenza, Italy)

The earthquake occurred during 1561 in Southern Italy heavily struck a Zone known as Vallo di Diano. This is the only destructive earthquake whose epicenter is attributed to that valley. Two problems arise about this epicentral location: 1) the distribution of reported effect is highly asymmetrical, possibly reflecting population distribution at that time, 2) some geologist maintain that there is no evidence for ongoing active tectonics in the Vallo di Diano area. Further doubts are cast by the fact that there is a very well known active zone few km away: the Val d'Agri, whose 1857 event is described in the monumental work of Robert Mallet, and for which no data is available about the 1561 event. The basic question behind our work is the following: Is it possible that both expert judgement and computer techniques have up to now placed the 1561 epicentre in the wrong place, driven by asymmetrical distribution of observations and by site effects enhancing damage in the alluvial valley? To try to answer this question, we performed site amplification measurements to have a sort of "station correction" for each locality involved, so to be able to understand if the intensity assigned on the basis of historical information is somehow biased by the presence of local effects. Then we studied some plausible scenarios of rupture propagation on finite faults to derive the best fit possible between observed intensity and theoretical models compatible with geological information.

**ST3/P/02-B4** **1015**

**IZOSEISMAL MAP AND TECTONICAL POSITION OF THE KOMAROM EARTHQUAKE OF 1763.**

Rudolf Gutdeutsch (Institute of Meteorology and Geophysics, University Wien, Nordbergstr. 17, A-1090 Wien) Goyo Szeidovitz and PÉTER VARGA (Geodetic and Geophysical Research Institute of HAS, 9401 Sopron, P.O.Box 5. Hungary, email: varga@ggki.hu)

One of the largest earthquakes of the last five centuries in Carpathian basin occurred in Komárom on 28. June 1763. The earthquake was felt over a very large area. This earthquake is significant not only because of its seismotectonic implication, but also for the earthquake hazard assessment of Gabčíkovo/Nagyymaros Barrage System. On the damages caused by this earthquake quite correct pictures and texts are at authors disposal from Győr and Komárom what allows an accurate determination of the seismic intensities in these cities. On the areal distribution of the shocks informations were collected from the notice of losses recorded by the expert groups commissioned by Queen Maria Theresia. These committees consisted of bricklayer, carpenter, and mayor's counsellor. The reconstruction cost of every church, the manor houses and public houses was listed in detail and the sum of rebuilding of farm houses was given. (In this relation ethnographic informations on the architecture of village buildings was also considered). Based on the above data the isoseismal map of the earthquake of 1763 was completed with significant reliability. The detailed study of the tertier basin morphology and different geophysical data (magnetotelluric and seismic profiles, gravimetric and magnetic maps) allows to interpret the tectonic position of this seismic event and to estimate its focal depth. Based on the reinterpretation of the earthquake of 1763 the statistics of the regional seismicity was also carried out.

**ST3/W/42-B4** **1030**

**PROBABILISTIC SEISMIC HAZARD MAPPING IN NORTHERN EGYPT**

MOHAMMAD G. AL-IBIARY (Geology Dept., Faculty of Science, Helwan University, Cairo 11795, Egypt, e-mail: ibiary@frcu.eun.eg) Ramses Albert (National Research Institute of Astronomy and Geophysics, Helwan, Cairo, Egypt); Ahmed Abuel-Atta (Geophysics Dept, Faculty of Science, Ain-Shams University, Cairo, Egypt) and Ahmed Deif (National Research Institute of Astronomy and Geophysics, Helwan, Cairo, Egypt)

The expected ground motion at different return periods in Northern Egypt is mapped employing the probabilistic approach. The seismic sources were defined and their boundaries were delineated utilising the seismicity of the Eastern Mediterranean region, slip rates, maximum observed intensity, maximum expected earthquake magnitude, maximum expected acceleration and their fault plane solutions correlating the earthquake epicenters with the geological and geophysical data.

For the sake of for seismic risk evaluation, eight intensity-dependent attenuation models were produced in the present study for eight different directions around the epicenter (the north, north-east, east, south-east, south, south-west, west, and north-west). They were converted from intensity into acceleration models using a simple intensity-acceleration relationship. A regional acceleration-dependent model was also derived.



Using an appropriate seismic hazard model, the maximum expected acceleration with a probability of 90% not being occurred during the next 50, 100, and 500 years in Northern Egypt are calculated and contoured. The authors aim to contribute new hazard maps that can be used in the Building Codes, regional land-use planning, emergency preparedness and in the reinsurance analyses. The contributed maps also serve in designating several regions in Northern Egypt for subsequent seismological, geological and geophysical research.

ST3/W/21-B4

1115

## NEW METHODOLOGY AND THE SEISMIC HAZARD MAPS OF NORTHERN EURASIA

Valentin I. ULOMOV (Schmidt United Institute of Physics of the Earth, Russian Academy of Sciences, Bol'shaya Gruzinskaya, 10, Moscow, 123810 Russia, email: ulomov@uipe-ras.scgis.ru

Comprehensive studies on the General Seismic Zoning (GSZ-97) of Northern Eurasia, including the territories of the Russia and other CIS republics and adjacent seismic regions, have been accomplished. The basic differences between the new methods and the previously used ones are as follows: the harmonized and standardized Lineament-Domain-Focal (LDF) model of earthquake source zones (ESZ) based on the fractal lattice regularization of the seismogeodynamic processes was developed; for the entire territory of Northern Eurasia the uniform ESZ model was created; seismic source size and orientation (rather than point sources previously considered) were used at all GSZ stages, from the identification of ESZ to the evaluation of strong ground motions; various non-standard data on regional seismicity (fractal structure; nonlinear earthquake recurrence; nonlinear seismic effect attenuation etc.) and earthquake sources (size, orientation, predominantly distance between sources with different magnitude etc.) were applied. The new method of creation of the ESZ model and their application to the seismic hazard assessment is named EAST -97 (Earthquake Adequate Source Technology). The GSZ-97 complete set consists of three maps: (1) GSZ-97-A, (2) GSZ-97-B and (3) GSZ-97-C, which 90%-s', 95%-s' and 99%-s' probability of not excess of MSK-64 intensity in 50 years. The GSZ-97-A map of Northern Eurasia was submitted in peak accelerations (PGA) and will enter by some component of the GSHAP Map (look <http://seismo.ethz.ch/hazard/gshap/>). For territory of Russia the GSZ-97 (A,B,C) maps were officially included in National Building Code. All materials are submitted in the electronic form with use of Geographical Information System (GIS ESRI).

ST3/E/43-B4

1130

## ON THE METHOD OF SEISMIC REGIONALIZATION OF THE FENNOSCANDIAN SHIELD

BELA ASSINOVSKAYA (Geodynamical Laboratory, CAO RAS, Bolshoi pr.50G, V.O., 199034, Saint-Petersburg, Russia, email: bela@ba2248.spb.edu)

The seismic regionalisation methods are probably the least developed and formalised among the all seismic hazard assessment stages. Due to this fact certain regions especially with weak seismic activity areas such as the Fennoscandian Shield seem groundlessly large and generalised. Whereas the maximum earthquake magnitude ( $M_{max}$ ) is low as for the Fennoscandian Shield the simple cell square for assessment of  $M_{max}$  should not exceed the area 10x10 km. Development of  $M_{max}$  determination method described by us earlier is suggested. The method is based on the geological information and the most possible full data on the rock mechanical properties of the crust simple cell. This work uses relationships between accumulated energy and calculated strike slip rock strength at the depth of earthquake sources taking into account pressure and temperature. In the Fennoscandian Shield conditions Early Proterozoic granite batholite intrusions formed in compression environment have the most seismotectonic potential that becomes less as geometry intrusion changing. Gneissic rocks with the same quartz contents as in granite, have lesser strike slip strength. The method was used to estimate  $M_{max}$  in the region of seismic profile Kostamuksha -Pechenga on the north-east of the Fennoscandian Shield.

ST3/E/18-B4

1145

## A PROBABILISTIC SEISMIC HAZARD MAP OF INDIA AND ADJOINING REGIONS: AN EXERCISE TOWARDS GSHAP

S C BHATIA and H K Gupta (Both at National Geophysical Research Institute, Uppal Road, Hyderabad-500007, India, E-mail: postmast@csngri.res.nic.in)

This paper presents the results of the seismic hazard assessment exercise carried out in the framework of GSHAP (Global Seismic Hazard Assessment Program) over the Indian region, in the back drop of a review of the seismic hazard / zoning maps of India. The GSHAP exercise for India region started with computations over the GSHAP Test Area #8, bounded by latitudes 20N - 40N and longitudes 85E-105E. In continuation of the test area exercise, the region bounded by latitudes 0N-40N and longitudes 65E-100E was considered for the preparation of a seismic hazard map of India and adjoining regions. Based on the seismotectonic information, 86 potential seismic source zones were delineated. A catalog of main shocks was prepared by merging several local catalogs with the NOAA catalog, and removing duplicates, aftershocks and earthquakes without any magnitude. Using the probabilistic hazard assessment approach of McGuire, adopted by GSHAP, the Peak Ground Accelerations (PGA) were computed for exceedence level for 10% probability in 50 years, as per the hazard definition adopted by GSHAP, at locations defined by a grid of 0.5 X 0.5 degrees. Since no reliable estimates of attenuation values are available for the Indian region, the global attenuation relation of Joyner and Boore was used. The PGA values over the grid were contoured to obtain a seismic hazard map. The hazard map depicts prominent highs of the order of 0.35g in the seismically active zones like the Burmese arc, North-eastern India, eastern Himalaya, etc. The other seismically active zones indicate PGA values of the order of 0.25 g. The major concerns that have emerged are that the Indian region poses a lot of problems for data homogenisation and the seismic hazard maps are strongly influenced by the size and shape of seismic source zones.

ST3/P/05-B4

1200

## SEISMIC ZONING MAPS OF THE REGION OF ALGIERS (ALGERIA)

Youcef BOUHADAD, Laouami, Nacer. and Djamel El-Foul. (National center of applied Research in Earthquakes Engineering (CGS), 1, Rue Kadour Rahim, H.Dey Alger-Algérie).

For the large city of Algiers earthquake hazard constitutes a serious and permanent threat for human lives as well as for properties. In the past, it was strongly hit by destructive earthquakes such as the 1716 event whose intensity reached X (Mercalli scale) and which claimed about twenty thousand human lives. In this paper it is proposed to predict seismic hazard in terms of values of maximum accelerations in some characteristic sites within the studied region. A seismic zoning was done by calculating hazard at different sites in the grid of 10 km X 10 Km using the probabilistic approach. In this study, the steps described below were performed:

1) Identification of all seismic sources capable of generating earthquakes in the future. The Algiers region lying in a compressive inter-plate region, earthquakes are mainly produced by

active faults which are sometimes blind and associated to asymmetric folds. New techniques such as the digital elevation models to identify such faults are used.

2) Source parameters such as b-value,  $N(mO)$ , Slip rate, maximum magnitude, and dip are assessed for each seismic source.

3) Concerning the ground motion attenuation a locally strong motion data was collected during the  $M_s=6.1$  Chenoua earthquake of October 29, 1989 and the  $M_s=5.6$  Ain Benian-Algiers earthquake of September 4, 1996 using the local accelerometer Network as a part of the National Network previously deployed in the North of Algeria. Based on this data, a local attenuation relationship is developed. We used also the Worldwide developed attenuation relationships such as Ambraseys (1995) and Sadigh & al. (1989).

Results are presented as relationships between amplitudes of Peak Ground Accelerations (PGA) and annual frequencies of exceedence of those amplitudes as well as maps of the mean values of PGA for different return periods.

Key words: Earthquakes- Algiers-Hazard- strong motion- maps- seismic zoning- active fault- seismotectonics- probabilistics.

ST3/W/36-B4

1215

## NEW TRENDS IN SEISMIC HAZARD EVALUATION IN GREECE

Stylianios KOUTRAKIS (Geophysical Laboratory, School of Geology, Aristotle University of Thessaloniki, Thessaloniki 540 06, Greece, email: stelios@lemnos.geo.auth.gr); Vassilios N. Margaris and Panagiotis K. Koliopoulos (both at Institute of Engineering Seismology and Earthquake Engineering, P.O. Box 53, 55102 Finikas, Thessaloniki, Greece, email: margaris@itsak.gr); George F. Karakaisis (Geophysical Laboratory, School of Geology, Aristotle University of Thessaloniki, Thessaloniki 540 06, Greece, email: karakais@geo.auth.gr)

Based on a growing number of observations indicating that some strong motion parameters, such as the peak ground acceleration and the peak ground velocity and ground displacement, exhibit rather weak correlation with the observed damage distribution, many researchers have suggested that the study of the strong ground motion duration, as well as of its energy content, may enhance the ability of choosing the proper design earthquake. Moreover, in some cases of the earthquake-resistant design the seismic hazard assessment is required to be represented in the form of acceleration time histories, in which the duration and energy characteristics play a significant role.

In the present study, a considerable number of strong ground motion components concerning recent, moderate to strong, earthquakes which occurred in Greece are used. For most of them the significant (or Husid) duration and several values of bracketed duration, corresponding to levels between 0% and 10%, have been taken from the existing literature, while for earthquakes which occurred in Greece since 1994, these duration-related parameters are calculated and attenuation relationships are derived. On the basis of these data, the seismic hazard for the area of Greece for various return periods is calculated, in terms of the expected strong motion duration. The results are subsequently compared with existing seismic hazard maps based on other strong motion parameters (e.g. pga, etc).

ST3/E/53-B4

1230

## SEISMIC HAZARD ANALYSIS AND SENSITIVITY ANALYSIS FOR THE KRESNA REGION (SW BULGARIA)

TORILD VAN ECK (Seismological Division, KNMI, PO Box 201, 3730 AE De Bilt, Netherlands. E-mail: vaneck@knmi.nl); Savka Dineva (Geophysical Institute, BAS, Ac.G Bonchev st. bl.3, 1113 Sofia, Bulgaria. E-mail: dgm-sid@geophys.bas.bg); Renata Rotondi (Consiglio Nazionale della Ricerche, Via Ampere 56, 20131 Milan, Italy. E-mail: reni@iami.mi.cnr.it) and Valeri Gitis (Inst. Information & Transmission Problems, RAS, B. Karetny 19, Moscow, Russia. E-mail: gitis@iitp.ru)

The region around Kresna (SW-Bulgaria) is tectonically complicated. The NNW-SSE oriented Struma lineament, a fault zone of older tectonic origin, is overlain by younger, SW-NE oriented, seismic active faults. A re-analysis of the observed seismicity since 1985 provided new locations, a new crustal velocity model and stress tensors. Further, the available earthquake catalogue for the region has been re-analysed in order to obtain a seismicity model. This seismicity model together with all available seismotectonic and geophysical data have been analysed to evaluate possible non-linear relationships between seismic activity, b-value or fractal dimension, RTL criterion and available geoscientific data.

This new information has been interpreted into a seismotectonic model of the region for a Probabilistic Seismic Hazard Analysis (PSHA). Presently, few ground acceleration measurements are available. Therefore using different peak ground acceleration relations and different PSHA approaches with a variety of models we made a sensitivity analysis. This enables us to access the major source of uncertainty, besides the ground motion attenuation.

Thursday 29 July PM

Presiding Chairs: V.Schenk (Inst. Of Rock Structure and Mechanics, Acad. Sc., Czech Republic), V.Mihailov (Institute of Earthquake Engineering and Engineering Seismology, University of St. Cyril and Methodius, Skopje, Republic of Macedonia)  
Concurrent Poster Session

ST3/W/53-B4

1400

## SOME RESULTS OF SEISMIC HAZARD ANALYSIS OF BELGIUM

VLADIMIR MIHAILOV(1), Dragi Dojcinovski(1), Thierry Camelbeek(2) and Roland Verbeiren(2)  
1)Institute of Earthquake Engineering and Engineering Seismology at the University St. Cyril and Methodius; P.O.Box. 101, 91000 Skopje, Republic of Macedonia 2)Royal Observatory of Belgium, Av. Circulaire 3,B-1180 Brussels, Belgium

In recent years, the seismic hazard analysis has been recognised as an important part of earthquake engineering. Most of parameters and aspects associated with the seismic hazard analysis, however, have been studied for a long time, but an increasing interest in this field has been observed in the past fifteen years. As a result of this interest currently, there is a considerable work done in the area of probabilistic estimations of seismic load parameters. Since the best practical presentation of seismic loading for a given region or site is in term of seismic hazard maps (e.g. isoseismal and iso-acceleration maps), a lot of maps for different geographical regions were developed. The usefulness of such maps is to a considerable extent a function of the type and amount of information they contain. The seismicity in Belgium is an example of an intraplate zone with low seismic activity and sporadic large events. The region can be subdivided in seven seismogenic zones with different tectonic characteristics. Based on existing seismological and tectonic data, a model of the seismicity of Belgium and the neighbouring countries was elaborated. Using on all these data and the assumptions related to the nature of occurrence of earthquakes, analysis of the seismic hazard has been carried out for the territory of Belgium and several maps and diagrams have been obtained. The purpose of this paper is to outline briefly the factors believed to be important in preparation of the seismic zoning maps (seismic hazard maps), to present the concept of mapping technique, together with some seismic hazard maps of Belgium.

## SEISMIC HAZARD ANALYSIS OF THE CITY OF SOFIA

Slavey SLAVOV (Department of Meteorology&Geophysics, University of Sofia, 5 James Bourchier Blvd, Sofia-1126, Bulgaria, email: slav@phys.uni-sofia.bg); Franco VACCARI and Giuliano Francesco PANZA (both at Department of Earth Sciences, University of Trieste, 4 Weiss street, Trieste-34127, Italy, email: panza@geosun0.univ.trieste.it)

The importance of Sofia, as an administrative and economical center of Bulgaria defines the significance of the seismological investigations in the city. During the past century, Sofia has suffered damages caused by shallow depth earthquakes. The strongest earthquake in the region occurred on 18.09.1858. The hypocenter has been under the town itself and the intensity is evaluated to be destructive - IX MSK. The last strong event M=5 has occurred in 1928 and following the recurrence relationship for the Sofia valley, we have to expect next strong event within next 5 years. The lack of strong recent earthquakes makes crucial the using of realistic modelling techniques for defining the seismic input for Sofia. The necessary input data have been critically discussed. The influence of the both distant and local sources has been estimated. A hybrid technique, based on modal summation and finite differences is used to simulate the strong ground motion in the city of Sofia. The results of the numerical modelling are presented as acceleration time series, PGA maps, PGV/PGA plots and spectral amplifications for different cross sections. Detailed modelling of the ground motions for realistic heterogeneous media up to 10 Hz can be immediately used in the design of new seismic-resistant constructions and in the reinforcement of existing buildings, without having to wait for a strong earthquake to occur.

## LOCAL RECURRENCE TIME, A NEW CONCEPT IN EARTHQUAKE HAZARD ASSESSMENT

M. WYSS, S. Wiemer Geophysical Institute, University of Alaska, Fairbanks, AK, 99775-7320, email: max@giseis.alaska.edu, 907 474 5529 D. Schorlemmer, Technische Universitaet, Berlin.

We define TL(M) as the recurrence time calculated from the local b- and a-values of the frequency magnitude distribution (earthquakes within 5 to 10 km from each point of interest). The value of TL(M) varies by several orders of magnitude over distances of 10 km because b- and a-values vary strongly. We argue that the hazard due to earth-quake (of any magnitude) more than about 10 km distant from the site of interest is negligible compared to the hazard posed by the largest earthquake that can occur be-low a site, without rupturing the surface. The TL(M) estimates the probability of this earthquake happening. Earthquake recurrence times and hazard maps are routinely computed using a single overall b-value and a smoothed a-value distribution. We propose that a more accurate description of the hazard can be obtained by computing TL(M). Spatially separating low and high b-value zones may be key to improving hazard mapping, because only the highly stressed (hence low b-value) volumes contain information about recurrence time. Adding events from neighboring low stress areas of faults (high b-value volumes) only biases the recurrence time estimate towards unrealistically long intervals. Further we propose that anomalously low TL(M)-values map asperities, based on the correlation of TL(M) minima along the Parkfield and the Mor-gan Hill segments of the San Andreas fault system with known asperities. Testing this hypothesis along the San Jacinto-Elsinore faults we found that out of six historic main shocks (1899-1968), five ruptured substantial parts of four asperities mapped by our method, based on the modern earthquake catalog (M<sup>1.2</sup>, 1981.0-1998.7). We estimate the probability for this correlation to occur at random as 7 10<sup>-4</sup>. The Anza gap is mapped as an asperity by our method. The b-values range from 0.5 to 1.8 over distances of 10 km. Volumes with approximately constant b-values have radii of r=8\*6 km. The observation of five minima of TL(M) along the SJ, compared to only two along the E fault zone agrees with the geologically estimated slip rates along the two fault systems (about a factor of two higher on the SJ than on the E fault).

## IMPROVING AFTERSHOCK HAZARD ASSESSMENT BY INCORPORATING THE SPATIAL VARIABILITY OF AFTERSHOCK ACTIVITY

Stefan WIEMER (Institute of Geophysics, ETH Hoenggerberg, CH-8093, Zurich, Switzerland; email: stefan@seismo.ifg.ethz.ch)

We propose that real-time probabilistic aftershock hazard assessment can be significantly improved by incorporating spatial information about the characteristics of the aftershock decay rate, the local activity, and the earthquake size distribution. There is solid evidence from several aftershock sequences that the characteristics of aftershocks, and hence the probabilities of moderate magnitude aftershocks, vary strongly as a function of space. In recent studies, it has been demonstrated that both the b- and p-values vary significantly and systematically by up to a factor of three along the strike of aftershock zones. The observed variations are likely related to both the slip history as well as the tectonic setting. High b-values are often in the vicinity of high slip areas. For the Landers case, the slowest aftershock decay rate (lowest p-value) coincides with the Kickapoo shear zone and may be related to high pore pressure in this region. In addition, the seismicity rates (as measured by 'a' in log N = a-bM) vary spatially, possibly proportional to the static stress change caused by the main shock. Because the generally used estimation of the aftershock hazard assessment, introduced by Reasenberg and Jones, relies on all three of these parameters (a, b and p), we find that the probability of a large and potentially damaging aftershock varies substantially and significantly with location. The results for the Landers and Northridge aftershock sequences confirm that the aftershock probability indeed varies with location by several orders of magnitude.

## PROBABILISTIC MODELS FOR EARTHQUAKE HAZARD ASSESSMENT IN THE INDIAN AND SURROUNDING REGIONS

Avadh RAM:Harsh Singh (Both at Dept. of Geophysics, Banaras Hindu University, Varanasi-221005, India; tel: +91 542 317074; email: aram@banaras.ernet.in)

A seismicity map of the Indian subcontinent has been prepared using the earthquakes obtained from the National Earthquake Information Centre and International Seismological Centre for the period 1963-1994. The seismicity in the main Himalayan seismic belt is due to the collision between the Indian plate and the Eurasian plate. The earthquakes in this region are generally correlated with the known regional thrusts like the Main Boundary Thrust and the Main Central Thrust. Six different zones have been identified on the basis of clustering of events (5-M<7) from the seismicity map starting from the Sulaiman & Kirthar ranges in the north-west, Hindukush and Pamir, Central Himalayas, north-east Himalaya and part of Andaman. The probability of different magnitude threshold has been evaluated using the Gutenberg - Richter formula logN=a-bM for magnitude distribution. The constants a and b have been computed for each region and found to vary within different limits. The Lognormal, Weibull, Gamma and Exponential portability models have been used to find the distribution of events from each region. The method of moments and the method of maximum likelihood

estimates have been used to compute and verify model parameters for different sets of data. It has been found that the Lognormal and Weibull models are more plausible as compared to the other two models. The probability of occurrence of an earthquake rises between 0.9 and 1.0 at the time period of 100 months for the region A, C and E. The regions BS and BD have the time period of 90 and 50 months respectively for the high probability values. The region D and F indicate the time period of more than 100 months. The peak ground acceleration associated with the observed data has also been computed. This diagram illustrates the higher peak ground acceleration in the area of shallow focus earthquakes and lower accelerations in the regions of deep focus earthquakes.

## INTENSITY OBSERVATIONS AND SOURCE PARAMETERS OF CALIFORNIA EARTHQUAKES

W. H. BAKUN (U S Geological Survey, 345 Middlefield Rd MS977, Menlo Park, CA 94025, USA. E-mail: bakun@andreas.wr.usgs.gov)

Seismologists use intensity values to assign source parameters to historical earthquakes, using empirical relations calibrated with the instrumental source parameters of recent shocks. While a good estimate of the magnitude of an historical earthquake is our primary goal, we also want to know, among other things, the location of the earthquake and the causative fault or tectonic structure. Independent estimates of the magnitude and location of historical shocks often do not differ significantly, but the subjective techniques usually used (e.g., contouring the intensity data and estimating an isoseismal area) rarely provide the objective estimates of the parameter uncertainty that are useful in seismic hazard assessment.

Analysis of Modified Mercalli intensity (MMI) observations for recent California earthquakes provides a strategy for bounding the moment magnitude M and the epicentral region of historical California earthquakes for different levels of confidence and number of MMI (W. H. Bakun and C. M. Wentworth, Earthquake location and magnitude from seismic intensity data, Bull. Seismol. Soc. Am., v. 87, pp. 1502-1521, 1997). Estimates of M from intensities are in good agreement with the instrumental magnitudes for M > 5.5 northern California shocks since 1900. The intensity center is the geographic point that best satisfies the MMI data in a least-squares sense; the intensity center corresponds more to the moment centroid of the earthquake source than to the epicenter. The geographic locations of confidence level contours bounding the epicentral region are controlled by the number of MMI available, by the degree to which MMI observations are available at near distances for all azimuth sectors from the epicenter, and by the internal consistency of the MMI observations. Even for recent California earthquakes with hundreds of reliable MMI observations, the confidence level contours bounding the epicentral region usually contain more than one active fault, so that the causative fault of historical California shocks cannot be determined with high confidence from MMI observations alone.

## RENEWAL RECURRENCE MODELS FOR LARGE EARTHQUAKES IN JAPAN

Kunihiko Shimazaki (Earthquake Research Institute, University of Tokyo, 1-1-1 Yayoi, Bunkyo-ku, Tokyo 113-0032, Japan, email: nikosh@eri.u-tokyo.ac.jp) Kazushige Kawase (Science and Technology Agency, Now at Geographical Survey Institute, Japan, email: kawase@gsi-mc.go.jp); Kenji Satake (Geological Survey of Japan, email: satake@gsj.go.jp); Yasuhiro Suzuki (Aichi Prefect. Univ., Japan, email: y-suzuki@ist.aichi-pu.ac.jp); Yoshihiko Ogata (Inst. Statistical Mathematics, Japan, email: ogata@sunyo.ism.ac.jp); Masajiro Imoto (Inst. Disaster Prevention and Earth Sci., Japan, email: imoto@bosai.go.jp) and Takashi Kumamoto (Tokyo Metropolitan Univ., Japan, email: kuma@geog.metro-u.ac.jp)

Four renewal models, i.e. log normal, gamma, Weibull, and double exponential distributions together with exponential distribution (i.e. Poisson process) are examined on how well these models apply to actual data of inter-event intervals of large earthquakes in Japan. In contrast to Nishenko and Buland's study in 1987, we treat a small number of sequences with relatively many events, i.e. six sequences and total of forty inter-event intervals; eighteen and twenty-two repeat times for two interplate and four intraplate sequences, respectively. The maximum likelihood estimates of the parameters for the above statistical models are obtained for each sequence, and Akaike's Information Criterion (AIC) is calculated for each model. In all cases the Poisson process shows the worst fit to the data, significantly poorer than other models. Among the rest of the models, none is significantly better than the others. We tentatively choose log normal and assume a common standard deviation for the intraplate sequences. We found that AIC for the common standard deviation is smaller than AIC for the case with different standard deviations estimated for each sequence. It shows that the common standard deviation explains the data set better than different standard deviations for each sequence so far as the four examples of Japanese intraplate earthquake sequence are concerned. For the time being, we plan to apply this common standard deviation of 0.23 to other intraplate sequences with small number of inter-event intervals.

## DETERMINISTIC HAZARD COMPUTATION FOR ROMANIAN CRUSTAL AND SUBCRUSTAL EARTHQUAKES

M. Radulian ([1] National Institute for Earth Physics, P. O. Box MG-2, Bucharest, Romania, Email: mircea@infp.ifa.ro) C. L. MOLDOVEANU ([1] National Institute for Earth Physics, Bucharest, Romania; [2] Dipartimento di Scienze della Terra, Universita' di Trieste, Italy; Email: carmen@geosun0.univ.trieste.it) F. Vaccari ([2] Dipartimento di Scienze della Terra, Universita' di Trieste, Italy; [3] GNDT - CNR, Rome, Italy; Email: vaccari@geosun0.univ.trieste.it) N. Mandrescu ([1] National Institute for Earth Physics, P. O. Box MG-2, Bucharest, Romania, Email: mandrescu@infp.ifa.ro) G. F. Panza ([2] Dipartimento di Scienze della Terra, Universita' di Trieste, Italy; [4] The Abdus Salam International Centre for Theoretical Physics, SAND Group, Trieste, Italy; Email: panza@geosun0.univ.trieste.it)

The evaluation of the seismic hazard for the Romanian territory is carried out separately for crustal (h < 60 km) and subcrustal (h > 60 km) earthquakes. Synthetic P-SV and SH seismograms are generated by the modal summation technique (Panza, 1985; Florsch et al., 1991) on a regular grid covering the whole territory of the country. The structural input modelling consists of 14 polygons with 1-D average structure, and the source modelling consists of 13 seismogenic zones with specific seismicity and focal mechanism. The frequency range spans the interval 0.005 - 1 Hz and a scaled point double-couple models the source process. The results are expressed in terms of maximum displacement, maximum velocity and design ground acceleration. Vrancea subcrustal earthquakes control the resulted seismic hazard. The previous hazard maps underestimate the hazard level in the southeastern part of the country due to the crustal earthquakes in the Shabla area.

The deterministic method addresses some issues largely neglected in probabilistic hazard analysis, e.g. how crustal properties affect attenuation. The parametric study shows that the hazard level is very sensitive to the maximum magnitude, average depth and focal mechanism variation. Possible scenarios can be easily constructed for different source and structural parameters.



ST3/W/19-B4

1630

**A MUTUALLY CONSISTENT SEISMIC-HAZARD SOURCE MODEL FOR SOUTHERN CALIFORNIA**

Edward H FIELD, James F. Dolan (both at Dept. of Earth Sciences, University of Southern California, Los Angeles, CA 90089-0740, USA, Email: field@usc.edu), and David D. Jackson (Dept. of Earth and Space Sciences, University of California, Los Angeles, 405 Hilgard Ave., Los Angeles, CA 90024-1567, USA)

The first attempt to integrate geological, geodetic, and observed seismicity data into a probabilistic-hazard source model predicted a rate of magnitude 6 to 7 earthquakes significantly greater than that observed historically (WGCEP, 1995). One explanation was that the discrepancy, or apparent earthquake deficit, is an artefact of the upper magnitude limit built into the model. This was controversial, however, because removing the discrepancy required earthquakes larger than are seen in the geological record, and larger than implied from empirical relationships between fault dimension and magnitude. Although several papers have addressed this issue, an alternative, integrated source model without an apparent deficit has not yet appeared. We present a simple geologically based approach for constructing such a model which agrees well with the historical record and does not invoke any unsubstantiated phenomena. The following factors are found to be influential: the b-value and minimum magnitude applied to Gutenberg-Richter seismicity; the percentage of moment released in characteristic earthquakes; a round-off error in the moment-magnitude definition; bias due to historical catalog incompleteness; careful adherence to the conservation of seismic moment rate; uncertainty in magnitudes estimates obtained from empirical regressions; allowing multi-segment ruptures (cascades); and the time dependence of recurrence rates. The previous apparent deficit is shown to have resulted from a combination of these factors. None alone caused the problem, nor solves it. The model presented here is relatively robust with respect to these factors.

ST3/W/02-B4

1645

**DETERMINISTIC SEISMIC HAZARD IN THE CIRCUM-MEDITERRANEAN DOMAIN**

Giuliano F. PANZA (Dip. di Scienze della Terra, Università di Trieste and The Abdus Salam International Centre for Theoretical Physics, Trieste, Italy. E-mail: panza@geosun0.univ.trieste.it), and Franco Vaccari (Dip. di Scienze della Terra, Università di Trieste and CNR-GNDT, Rome, Italy)

The deterministic procedure for seismic hazard assessment developed at the Department of Earth Sciences of the University of Trieste in the framework of the CNR-GNDT activities has been applied to several countries in the Mediterranean and Circumpannonian regions as the result of comprehensive international cooperations. The main effort has been to harmonize Eastern and Western Europe in terms of seismic safety compliance. Characteristic parameters of seismogenic zones and regional structural models have been assembled and synthetic seismograms have been computed for a dense grid of sites covering the investigated area. Special attention has been paid to the intermediate depth events occurring in Vrancea (Romania). Results are shown in terms of maximum displacement, velocities and Design Ground Acceleration.

ST3/W/29-B4

1700

**THE DETERMINATION OF EARTHQUAKE MAGNITUDE FROM HISTORICAL DATA IN THE EUROPEAN PARAMETRIC CATALOGUES: A REVIEW**

Alessandro Rebez (Osservatorio Geofisico Sperimentale, Trieste, Italy, Email: rebez@ogs.trieste.it), Massimiliano STUCCHI (Istituto di Ricerca sul Rischio Sismico, CNR, Milano, Italy, Email: stucchi@irrs.mi.cnr.it), Ruben Tatevossian (Institute of Physics of the Earth, Moscow, Russia, Email: tatev@synapse.ru).

Magnitude determination from historical data is one of the most controversial issues in the compilation of parametric earthquake catalogues. In Europe, where more than 30 parametric catalogues cover a rather limited area, several, different procedures are in use, giving rise to large in-homogeneity in the data available to the users. In the frame of the EC project "A Basic European Earthquake Catalogue..." a survey was performed with the aim of investigating which procedures are used, in theory and in practice. The results show either largely inhomogeneous procedures, or even gaps from theory to practice, probably due to the introduction of "hidden" assumptions or personal judgement. Gaps are easily detectable for earthquakes located in areas covered by more catalogues (e.g. frontier areas, where the same events can be given varied sizes), while they are not for earthquakes located in distant areas. As a result of the survey and the work carried out in the project, some conclusions can be drawn. First, that intensity data points allow the use of formalised, repeatable procedures which limit, to a certain extent, the subjectivity of most procedures, including the drawing of isoseismal maps. Second, that such procedures may require case-by-case calibration, due to unavoidable inhomogeneous data distribution. Third, that such procedures can be applied to a limited number of strong events and that, therefore, lot of efforts are required for moderate to minor earthquakes.

ST3/E/21-B4

1715

**METHODOLOGICAL CONSIDERATIONS OF PROBABILISTIC SEISMIC HAZARD MAPPING**

R.M.W. MUSSON (British Geological Survey, West Mains Road, Edinburgh, EH9 3LA, UK, Email: R.Musson@bgs.ac.uk)

The study of seismic hazard is perhaps the most practically oriented aspect of earthquake seismology. As such, it should not be treated in an idealised or academic manner, but with regard to the needs of the consumers of the final product. This has important consequences when it comes to the topic of probabilistic seismic hazard maps. Who are these for? Historically, early studies of probabilistic seismic hazard tended to be done for engineers for specific design requirements. Consequently, there has been a tendency to treat seismic hazard maps as a sort of pan-national study for engineers, who can identify the design requirements for any site by picking them from the map. A dissenting point of view argues that seismic hazard maps are by their very nature too generalised to be used in this way; that such maps provide a first indication of relative hazard and should not be a substitute for site studies. There are, therefore, a number of interesting and important methodological questions to be asked: what are the practical differences in undertaking a seismic hazard map from calculating hazard for a site? Should probabilistic seismic hazard maps have the same degree of conservatism as site studies? How can seismologists meet the needs of different audiences? An engineer may think in terms of ground acceleration, but this parameter probably means little to people in other professions who still need access to seismic hazard data, but in a form they can understand. These are questions that need to be addressed directly; one should not leave them to be answered by default.

ST3/E/27-B4

1730

**SEISMIC MOMENT RATE IN THE SEISMIC HAZARD ASSESSMENT IN NORTH VIETNAM AND SURROUNDING AREA**

PHAN -TRONG Trinh (1), Thierry Winter (2) 1. Institute of Geological Science, NCNST, Vien Dia Chat, Nghiado, Cau giay, Hanoi, Vietnam, Fax : 84 4 8362886, E-mail: ptrinh@refer.edu.vn. 2.Bureau Geologique et Mine, Paris, France

The estimation of seismic risk in Vietnam is carried out in following successive stages: A seismic hazard assessment carried out through both the connections, at various scales, of the structural geology with seismicity. The estimate of the seismogenic capability of the active faults identified through satellite image, topographic and geological map, field survey and earthquake catalogue. A seismic risk assessment of the regional seismic hazard on the site corresponding to the occurrence of design earthquake magnitude such as: maximum credible earthquake (MCE), maximum design earthquake (MDE) consisting of an earthquake having 10% risk of occurrence during the service-life of dam (100 years), the operating basis earthquake (OBE) consisting of an earthquake having a 50% risk of occurrence during the service life of dam and peak ground acceleration (PGA) corresponding to MCE, MDE and OBE., Maximum credible Earthquake is estimated from combination of various methods: fault segment, fault surface, seismic moment and fault slip rate. We test to combine seismic data and geological data by using seismic moment rate to estimate maximum credible earthquake. Some examples in the estimation of seismic risk for hydropower dam design are presented. Many arguments of remote sensing, geomorphology, geology, geodesy, state of stress attest the intensive actual tectonic activity in Vietnam. However, the poorness of the seismological network prevents accurate localisation of moderate seismicity. For this region, using pure probabilistic model or historical approaches to select a seismic risk in structure design will be quite random. The combination of the deterministic and probabilistic analysis was performed in several stages. The application of the seismic risk assessment for many hydropower sites in Vietnam such as: Song Ca, Hoa Binh and Son La stations is presented in detail. MDE is 6.3 - 6.5 for Song Ca fault, 6.9 - 7.0 for Nam Chou fault. OBE is 5.6 - 6.1 for Song Ca fault, 6.3 - 6.5 for Nam Chou fault. Various attenuation laws based on world wide data recorded in near field (Campbell) and by Xiang based on Yunnan data (next to Vietnam) are used to calculate Peak Ground Acceleration. The above-mentioned MDE magnitude should induce at the dam site a PGA of about 0.35 - 0.39 g. The OBE magnitude should induce at the dam site a PGA of about 0.24 - 0.31 g.

ST3/E/45-B4

1745

**PECULIARITIES OF SEISMIC REACTION ON MOLDOVA REPUBLIC'S TERRITORY**

Vasile Alkaz, Anatol ROMAN and Eugene Isichko (all at Institute of Geophysics and Geology, Moldavian Academy of Sciences, Academy str. 3, Kishinev, MD-2028, Moldova, email: drumea@geo.moldova.su)

Systematic instrumental engineering observations were started in Moldova in the 1970-s. Three subsequent strong intermediate-depth Carpathian earthquakes: 4.03.1077 (M=7.2), 30.08.1986 (M=7.0), 30.05.1990 (M=6.9) provided rich instrumental and macro-seismic data. Joint analysis of that material has revealed some peculiarities in the manifestation of different local geologic-engineering factors during the above mentioned earthquakes. The difference in the estimated intensity values at various sites reach 2 points and more (MSK-64 scale). The recordings are the wide frequency band processes: considerably predominating are the oscillations with periods 0.1 - 0.7 s. Comparisons of the observed response spectra with design spectra are made. Real impacts exceed 1.5 - 1.8 times those given in the normative document in the high frequency range (0.1 - 0.3 s). In the 0.3 - 0.6 interval normative curve overlaps the real impact on the ground. In the range of long periods (over 0.7 s) the real seismic loads again exceed the rated ones. A proposal has been made to improve the national seismic design code taking into consideration the results obtained from the experimental data. It has been shown that for specific regional conditions such factors as thickness of soft soil, shear waves velocity, high impedance contrast between the clay-sandy layers and limestone basement play a decisive role in forming the amplitude level and spectral composition on motions occurring on surface. It has also been established that the influence of water-logging, lithology is less than traditionally adopted. The unusually high level of damage to modern structures has been observed, resulting from resonance phenomena pertinent to soil-structure system.

Friday 30 July AM

Presiding Chairs: G.F.Panza (Dept. Di Sci. Della Terra, University of Trieste, Italy), C.Yong (China Seismology Bureau, Beijing, China)

ST3/W/25-B5

0830

**INTERNATIONAL DECADE FOR NATURAL DISASTER REDUCTION (IDNDR)**

Robert M. HAMILTON (Chair, IDNDR Scientific and Technical Committee, National Research Council, Washington, DC, USA, Email: bhamilton@nas.edu)

The IDNDR was adopted for the 1990s to focus world attention on opportunities to reduce the impacts of natural hazards, including earthquakes, windstorms, tsunamis, floods, landslides, volcanic eruptions, wildfires, grasshopper and locust infestations, and drought and desertification. Substantial losses in many industrialized and developing countries prompted this initiative. Its importance is underscored by migration of populations into hazard-prone areas and their concentration in megacities, which are particularly vulnerable owing to their complex infrastructures. In looking beyond the Decade, the IDNDR Scientific and Technical Committee identified five major challenges: 1) Integrated risk management - Natural disaster mitigation can be effective only if it is an integral, high-priority part of the overall planning and development process. 2) Mega-disasters - Megacities are poorly prepared to face the disruption that a natural disaster brings and face losses on an unprecedented scale. 3) Ecosystem vulnerability - Natural hazards can substantially impact landscape and habitat and can combine with human-induced hazards into a greatly enhanced threat. 4) Disaster management capabilities of developing countries - Expertise must be increased in many developing countries to promote adoption of sound disaster prevention practices. 5) Co-ordination and implementation - The growing impact of natural disasters demonstrates the need to further advance mitigation through well co-ordinated activities. This will require a UN oversight unit to co-ordinate activities in the program areas of: advancing the frontiers of hazard mitigation science and technology; implementing programs of education, training and technology transfer; monitoring hazards phenomena, and providing early warning where possible; and promoting and implementing mitigation as an integral part of economic development.



ST3/E/40-B5

0845

## SEISMIC RISK ASSESSMENT IN REPUBLIC OF MOLDOVA

Vasile ALKAZ, Anatol Drumea and Eugene Isichko (all at Institute of Geophysics and Geology, Moldavian Academy of Sciences, Academy str. 3, Kishinev, MD-2028, Moldova, email: drumea@geo.moldova.eu)

The contribution presents the first attempt to evaluate the seismic risk distribution in Republic of Moldova. This territory systematically suffers heavy damage and losses as a consequence of the intermediate depth earthquakes sources located in Vrancea zone, Romania. So, the disaster effect of the last strong earthquake (August, 30, 1986, M=7.0) was represented by 2 deaths, 561 injured persons, 1169 completely destroyed buildings, 800 millions US \$ direct loss. In the framework of investigation the seismic risk has been determined as a convolution of earthquake hazard and seismic vulnerability. Earthquake hazard has been evaluated on the basis of the map of maximum seismic intensity observed. The seismic vulnerability was determined as a convolution of physical environment vulnerability, quality of structures (number of suffered earthquakes), population features and relative value of loss. The vulnerability of physical environment was estimated on the basis of the map, which was produced taking into account the areas affected by landsliding, liquefaction, different densification capacity and degree of slope abruptness. The spatial distribution and density of the population were considered the main important factors, determining the population features in the investigated territory. As a measure of relative value of loss the index of economical activity each of districts was assumed. On the basis of these data the map of relative seismic risk has been performed. According to it, the seismic risk reaches levels of concern - first of all in Kishinev city and regions, were secondary effects of earthquakes are more likely.

ST3/W/43-B5

0900

## RE-EVALUATION OF THE LARGEST EARTHQUAKES IN THE NORTHERN UPPER RHINEGRABEN (GERMANY) SINCE THE YEAR 858

Diethelm KAISER (Institut für Geowissenschaften, Friedrich-Schiller-Universität Jena, Burgweg 11, 07749 Jena, Germany, email: kaiser@geo.uni-jena.de) Christa Hammerl, Rolf Gutdeutsch (both at Institut für Meteorologie und Geophysik, Universität Wien, Nordbergstraße 14, 1090 Wien, Austria, email: rudolf.gutdeutsch@univie.ac.at)

The northern part of the Upper Rhinegraben is part of the European Cenozoic rift system and displays moderate seismic activity. Six entries of this region in the earthquake catalogue of Germany have been verified by the investigation of historical records: (1) Mainz 1. January 858, I0=VII-VIII, N=3; (2) Mainz 14. February 1445, I0=VIII, N=1; (3) Mainz-Münchweiler 18. May 1733, I0=VII, N=33; (4) Groß-Gerau 1. November 1869 4:07, I0=VII, N=172; (5) Lorsch 10. February 1871 I0=VII, N=128; (6) Lorsch 16. February 1871 I0=VII, N=0; (N=number of towns with reported effects). Entry (1) is so poorly documented that it was not possible to determine the epicenter and the maximum intensity. Entry (2) indicates ground subsidence but not an earthquake. Entry (3) is associated with an earthquake with epicentral co-ordinates 7.95°E, 49.68°N, I0=VII without a specified focal depth. Earthquake (4) was downgraded to I0=VI-VII using the criteria of the European Macroseismic Scale. The epicentral intensity and co-ordinates of earthquake (5) have been confirmed; the focal depth was estimated to 7 km. Entry (6) is the result of a dating error and was deleted.

In addition we verified and developed empirical relations between I0, local magnitude ML, felt area, and focal depth. The equation relating ML with the felt area as developed by Musson (1996) for earthquakes in the U.K. appeared as the most reliable as compared to others (e.g. Kárník 1969). For earthquake (5) we determined ML=4.9. The re-evaluation of the largest earthquakes in the northern Upper Rhinegraben has a significant influence on seismic hazard estimates.

ST3/W/13-B5

0915

## INPUT EARTHQUAKE HAZARD VALUES OF THE THIVA-OROPOS REGION(CENTRAL GREECE) FOR SEISMIC RISK ESTIMATES

Vladimír SCHENK, Zdeňka Schenková and Pavel Kottbauer (all at Institute of Rock Structure and Mechanics, Academy of Sciences, CZ-182 09 Praha 8, The Czech Republic, email: schenk@irm.cas.cz)

Recent seismic risk estimates need reliable earthquake hazard inputs that have to involve damage effects caused both by tectonic structures of area and by seismogeological site conditions. The Thiva-Oropos zone belongs to seismically high-active zones of central Greece that neighbours on its south-west margin with the area of the Gulf of Corinth and is elongated to north-east direction. That elongation could be joined with an existence of geological structures that further, in the north-east part of Greece, can possibly coincide with structures close to the North Anatolian fault. For the hazard calculations all available published data as well as unpublished seismic data monitored by the local seismic array of the National Observatory of Athens (Drakatos, Kalogeras and Papadopoulos) were applied. At the beginning the standard earthquake hazard assessment for the Thiva-Oropos seismoactive zone will be presented. This approach uses an earthquake data base to which statistical methods are applied in order to determine the "regional" hazard values for the whole area. Then seismogeological site conditions at the studied area will be introduced into the earthquake hazard process. The site conditions, characterised mostly by differences in seismic wave velocities and bulk densities, will show how big variety in the hazard outputs can appear. An attempt to introduce any corrections caused by the presence of active tectonic elements will be demonstrated. Finally, the earthquake hazard outputs will be discussed from the viewpoint of their direct application to the seismic risk estimates. The presented calculations were realised under the EC INCO-Copernicus ASPELEA Project No ERBIC 15CT97 0200.

ST3/E/05-B5

0930

## AN EXPERIMENT OF SEISMIC RISK ASSESSMENT FOR SOFIA CITY

Larionov V.I.\*, Rangelov B.\*\*, FROLOVA N.I.\*\*\*, Ugarov A.N.\*\*\*\* Agency on Monitoring and Forecast of Emergency Situations, Ministry of Emergency Situations of Russian Federation \*\*Geophysical Institute, Bulgarian Academy of Sciences\*\*\*Seismological Center of IGE, Russian Academy of Sciences\*\*\*\*Extreme Situations Research Center

The territory of Bulgaria is characterized by high level of seismic hazard. According to the map of possible seismic sources the earthquakes with intensity 9 (MSK scale) may occur in its capital. The population of the city is 1 350 000. In order to plan preventive measures and reduce possible social and economic losses due to future events the seismic risk assessment was carried out for the Sofia City territory. The special geographic information system (GIS) developed in the Russian Agency on Monitoring and Forecast of Emergency Situations was implemented. The different input data on seismic hazard level with taking into account secondary processes and different scenario a were used for losses computations (number of fatalities, number of people injured, distribution of different buildings type according to damage states). The existing building stock is not homogenous. The information about different types

buildings' distribution was taken from the city territory map (scale 1:10 000). The influence of vulnerability functions for different buildings types on the expected social and economic losses was studied. The parameters of fragility laws were computed for typical buildings and structures in the area under consideration. The maps of damage states distribution caused by scenario earthquakes are compiled for the whole city and its districts. Individual seismic risk computations were carried out with GIS application and the corresponding maps are presented. The output modelled information can be used by decision makers, insurance companies and others. The GIS applied in this study, as well as the input data collected during many years may be integrated into the city information system in order to increase the efficiency of response measures in the case of emergency situations.

ST3/E/17-B5

0945

## THE ERZINDZAN EARTHQUAKE AT 1939 - A CASE OF A MULTIDISASTER EVENT

Boyko RANGUELOV (Geophysical Institute, Sofia 1113, Bulgaria, email: bkr@geophys.bas.bg) Arnd Bornaerts (Bordesholmer Str.14a, Hamburg 22143, Germany)

A bad thing never came alone. The famous Erzindzan earthquake (M=8.0) on 30 December 1939 generated many effects - surface ruptures, landslides, macroseismic intensities up to 11 degree, tsunami in the Black see, as well as big destructions and many human deaths (more 30-40 000). There are very clear descriptions from this time (mainly by the newspapers) about the anomalous behaviour of the meteorological weather in the epicentral area - extremely low temperatures, very large snowfalls, freeze winds, big storms. All these events make very difficult all rescue operations. During the following days, very large rains to the south and south east generated very big flooding and mudflows to the southern, eastern and south-eastern parts of Turkey. These negative meteorological events add more than several thousands deaths and many injured accompanied by destruction of the buildings and expected summer harvest. Our hypothesis follows the general possible explanations of the observed negative events: bad, very sensitive meteorological conditions, (the lowest air pressure as a probable influence for the earthquake generation), the strong earthquake itself, generation of tsunami in the Black sea, very probable influence of the mixed sea water to the weather conditions, storms observed on the coast followed by cold air invasion, followed by the snowfalls and freezing weather. Than to the south, generation of the big rainfalls, followed by the floodings and mudflows. The interconnection between all these events brings many tragedies, bad economical consequences and human deaths. To check this hypothesis is very difficult and the problems are under discussion. But the observed events, provide the opportunity to discuss and to try to obtain more reliable information about these very destructive events.

ST3/E/41-B5

1000

## SEISMIC RISK ASSESSMENT FOR CATALONIA (SPAIN)

Chavez, J., Fleta, J., GOULA.X., Roca, A., Secanell, R. & Susagna, T. (Institut Cartogràfic de Catalunya, Parc de Montjuïc, E08038 Barcelona. Email: xgoula@icc.es)

Following Spanish regulations for Civil Defence, the Civil Defence Agency of the Catalan government has promoted an evaluation of the seismic risk in Catalonia. A new parametric catalogue of seismicity, in terms of macroseismic intensities and a new seismotectonic zonation of the area under study (32000 km2) and surrounding regions (in total about 220 000 km2 surface) are the basis of a hazard analysis. Deterministic and probabilistic approaches with different models of earthquake occurrence have been used; a quasi-stationary behaviour is deduced. Uncertainties of the results are estimated by Montecarlo technique. For return periods of 500 years standard deviations less than half degree of intensity are obtained. A map of seismic zones combining deterministic and probabilistic approaches is proposed for average soil conditions. The final map is modified, for urban areas, considering site effects estimated from geological maps. An estimation of vulnerability of dwelling buildings is carried out together with the assessment of seismic risk for people and of earthquake losses in all municipalities of Catalonia on the basis of the map of seismic zones. The methodology developed is summarised in four steps: 1) Classification of the existing buildings in vulnerability classes according to EMS-92, 2) estimation of damage in buildings, 3) assessment of the human casualties, and 4) evaluation of economical losses.

ST3/E/49-B5

1045

## ABOUT THE PROGNOSIS OF SEISMIC INFLUENCES FOR THE CAPITAL OF KYRGYSTAN

Aleksandra Frolova, Institute of Seismology NAS of the Kyrgyz Republic (SI NAS KR), Bishkek, E-mail: kis@imfiko.bishkek.su Svetlana Uranova, Kyrgyz Scientific and Design Construction Institute of the ministry of Architecture and Construction of the Kyrgyz Republic (KyrghyzNIIPC), Bishkek, E-mail: uran@imfiko.bishkek

The capital of Kyrgyzstan Bishkek is located in the seismic hazardous Chu Depression. The map of maximum accelerations was calculated in isolines for Chu Depression. The most part of this territory may be exposed to shaking more than 600 cm/sec<sup>2</sup> (0.6g). Amplitudes of accelerations are in accordance with new facts of strong movements. The possible response spectrum and values of resonance periods and maximum accelerations were calculated for Bishkek from different source zones. The possible amplitude of shaking is 0.6g for Bishkek for average soils. This acceleration corresponds to the intensity 9 according to the MSC-scale.

ST3/E/48-B5

1100

## RISK ANALYSIS IN KOLA; SEISMIC LOADS AND WEATHER FACTORS IN SIMULATIONS OF AVALANCHE HAZARDS IN THE KHBINY MASSIF

Pavel Chernous and Evgeny Mokrov (Centre of Avalanche Safety, 33a, 50-years of October St., Kirovsk, 184230 Russia; email: P.Chernous@apatit.murmansk.su); Yura Fedorenko and Sergey Morozov (INEP, KSC RAS, Fersman str. 14, Apatity, 184200 Russia, email: morozov@inep.ksc.ru); Eystein S. HUSEBYE (IFJ, UoBergen, Allegaten 41,N-5007, Norway, email: eystein.husebye@ifj.uib.no)

The Khibiny Massif, Kola is well known for many avalanches in winter some of which have caused losses of human life in the past. In order to mitigate this hazard the Avalanche Safety Service (Apatity JSC) monitors weather conditions, estimates snow transport and measures snow depths over slopes close to open pit mines. These data are used for predicting avalanche risk and issue warnings for miners. Occasionally explosives are used for preventive triggering of avalanches which also may cause avalanches elsewhere. However, outside mining areas safety measures are less rigid so tourists and weekend skiers are at risk. Hence, we are undertaking as a first step in risk mitigation to model mathematically avalanches (snow drifts) per se and their potential for being released. The snow slab is modeled as an elastic non-moment shell which parameterization is obtained via field measurements. Critical parameters are snow thickness, shear and tensile properties and friction coefficient. Avalanche initiation is tied to exceedance of a critical stress threshold. For hazard extrapolation to non-mining areas meteo data from the Rassvumchor plateau (1100m height)

were used to evaluate prevailing wind conditions via the Navier-Stokes eqs. Trigger levels were tied to ground accelerations of mining and other explosions as measured at the new NANSEN 3-comp. station within the massif. On this basis we have calculated snow thicknesses in Khibiny and in addition also singled out areas likely to be hazardous. During spring 99 we expect to get observational data on real snow thicknesses and areas where avalanches have taken place thus ensuring direct comparisons to the theoretical predictions made.

ST3/P/4-B5

1115

## INTENSITY ESTIMATION USING THE GRAPHIC FORM OF THE EMS-98 SCALE

Peter LABÁK (Geophysical Institute, Slovak Academy of Sciences, Dúbravská cesta 9, 842 28 Bratislava, Slovak Republic); Christa Hammerl (Institute of Meteorology and Geophysics, University of Vienna, UZA II, Althanstrasse 14, A-1090 Vienna, Austria); Jirí Pospíšil (Geophysical Institute, Academy of Sciences of the Czech Republic, Bocni II, 141 31 Prague, Czech Republic)

A new graphic form of the EMS-98 scale is presented. The effects on humans, and objects and nature are displayed in the form of tables. The tables include the size of the effects for all intensities. The definition of damage to buildings is displayed in the form of vulnerability class vs. damage grade table for each intensity degree. The tables enable us to identify how the observed effects obtained either from questionnaires and damage data for recent earthquakes or from damage data for historical earthquakes correspond to the defined effects for an intensity degree.

We used the graphic form of the EMS-98 scale for the intensity estimation for two recent and two historical earthquakes - the April 12, 1998 Slovenia, the 1997 Umbria-Marche, the January 15, 1858 Zilina (Slovakia), and February 4, 1794 Leoben (Austria) earthquakes. We used the Slovak and Czech questionnaire data for the Slovenian earthquake, the damage data collected by ESC WG Macroseismology (Stucchi, ed., 1998) for the Umbria-Marche earthquakes and the damage data from the studies by Hammerl & Labák (1999) and Hammerl (1996) for the historical earthquakes. The use of the proposed graphic form of the EMS-98 scale allowed us to identify inconsistencies of the Slovak and Czech questionnaires (originally proposed for the MSK-64 scale) with the new EMS-98 scale. The problems of the intensity estimation for both recent and historical earthquakes under study are also discussed.

ST3/E/14-B5

1130

## SEISMIC HAZARD AND MICROZONATION IN CENTRAL AMERICA

LINDHOLM C. D.1, H. Bungum1 and F. Nadim2 1) NORSAR, Box 51, 2007 Kjeller, Norway 2) Norwegian Geotechnical Institute, Box 3939 Ullevål Hageby, Oslo, Norway

Central America has experienced repeated earthquake disasters in this century, and with the current economical growth the vulnerability will increase unless the main urban centers firmly commit themselves to precautions. The first steps in reducing vulnerability is proper mapping of hazards and risks and the engagement of competent scientists on the national level within these fields. As part of a regional project, seismic microzonation for main urban centers in Panama, Costa Rica and Nicaragua have now been undertaken, and seismic hazard evaluations are being made for Honduras, El Salvador and Guatemala. The microzonation studies implies computation of seismic hazard based on a probabilistic approach, integrated with modelling of ground motion contributions from local, active faults. The hazard results, which are also based on locally developed ground motion relations, were presented both in terms of peak ground acceleration maps and in terms of pseudo-velocity spectra. Geological investigations were undertaken to map the potentials of local faults, applying analysis of air photos and satellite data as well as morphologic evaluation with trenching and fault dating. The geologic investigations were particularly extensive in Panama and Nicaragua and involved extensive regional co-operation. Local soil amplification has been focused on through analytical as well as empirical methods. Data from local strong motion networks that have been used in spectral ratio analysis have been compared with results from analytical analyses (such as through the computer code SHAKE). Finally also Spectral Analysis of Surface Waves (SASW) experiments have been carried out. The societal needs have been attended to in these studies through active participation of city councils and national emergency commissions as users of the microzonation products, and through reporting on city growth perspectives.

ST3/E/47-B5

1145

## DETERMINISTIC VS. PROBABILISTIC EARTHQUAKE HAZARDS AND RISKS

ROBIN K. MCGUIRE (Risk Engineering, Inc., 4155 Darley Ave, Suite A, Boulder, Colorado, 80403, USA, email: mcguire@riskeng.com)

Deterministic vs. probabilistic approaches to assessing earthquake hazards and risks have differences, advantages, and disadvantages that often preclude the use of one over the other. Factors that influence the choice include the decision to be made (i.e. the purpose of the hazard or risk assessment), the seismic environment (whether the location is in a high, moderate, or low seismic risk region), and the scope of the assessment (a single-site risk, a multi-site risk, or risk to a region). Decisions coming from earthquake assessments include selection of design or retrofit criteria and levels, financial planning for earthquake losses, and planning for emergency response and long-term recovery. The more quantitative the decision to be made, the more appropriate is probabilistic hazard and risk assessment. For high seismic regions (e.g. California or Japan) where the largest earthquakes occur every 100-300 years), a deterministic scenario for the largest event will allow details to be examined such as ground motion effects caused by rupture propagation. In low seismic regions, extreme deterministic scenarios will have probabilities of occurrence that are too low to be useful for most decision purposes. Specific site analyses generally require a probabilistic approach. Multiple-site analyses (e.g. for a portfolio of exposed or insured properties, or a lifeline) often require a probabilistic analysis because of multiple variables and complexities of the system, and a deterministic check can be misleading. Regional assessments often benefit most from deterministic models.

ST3/E/23-B5

1200

## COMPARISON OF SOME MACROSEISMIC EPICENTRE LOCATION METHODS

R.M.W. MUSSON (British Geological Survey, West Mains Road, Edinburgh, EH9 3LA, UK, Email: R.Musson@bgs.ac.uk)

The provision of spatial co-ordinates for historical earthquakes, derived from macroseismic data, can follow one of two objectives. The first is to try to determine, from macroseismic evidence, what point would have been cited as the epicentre in the sense that this term is used in modern instrumental catalogues. The second is to determine some conventional point representing the focus from which the strongest shaking appears to radiate. The term barycentre has been suggested for such a point. It can be argued that the latter approach is

more appropriate for seismic hazard studies, in which the aim is to characterise the field of strong shaking of future earthquakes. On the other hand, such an approach, if it is to be pursued consistently, requires one to jettison all instrumental earthquake catalogues, which may not be practical. This paper compares some simple approaches to making automatic epicentre determinations from macroseismic data and examines their accuracy with respect to instrumentally determined epicentres.

ST3/E/28-B5

1215

## A COMPARATIVE STUDY OF SEISMIC RISK ASSESSMENT

Zhi-xian YANG (Institute of Crustal Dynamics, CSB, P.O.Box 2855 Beijing 100085, China, email: zhixian@public.bta.net.cn) Pei-zhen Zhang (Institute of Geology, CSB, P.O.Box 634, Beijing 100029, China, email: peizhen@public3.bta.net.cn)

Calculated seismic hazards by different programs are slightly different. Results from programs SEISRISK6 (Bernice Bender and David Perkins), FRISK-88M (R. McGuire) and SEISRISK-CH (used for seismic zoning mapping in China) using same attenuation relation and same seismicity parameters are compared in this study. The features of the differences for high seismicity as well as low seismicity region are described. The authors propose that resolution of the calculations is the major factor that affects this difference. Spatial distribution of seismicity is not uniform. In seismic hazard assessment, in order to emphasize the non-uniformity of seismicity appropriate weighting procedures should be used. A procedure of weighting on seismicity parameters before calculating seismic hazard is adopted by Chinese seismologists in the past decade. Recently an alternative procedure of weighting on calculated seismic hazard based on the delineation of seismic sources is adopted by US seismologists. In the later procedure seismic sources include not only the area with high seismicity but also the area with low seismicity historically but potentially prone to major earthquakes known as background zone. We applied these two weighting procedures to the same area and compared the results obtained. We also compare the results from the combined source models with and without background zone. The comparisons indicate that the procedure of weighting on the seismicity parameters is appropriate for emphasis of high seismic hazard in a special seismic zone, while the procedure of weighting on calculated seismic hazard is appropriate for evaluation of seismic hazards in the area with low seismicity.

ST3/P/06-B5

1230

## REINTERPRETATION OF THE JANUARY 15, 1858 ZILINA (SLOVAKIA) EARTHQUAKE

Christa HAMMERL (Institute of Meteorology and Geophysics, University of Vienna, UZA II, Althanstrasse 14, A-1090 Vienna, Austria); Peter Labák (Geophysical Institute, Slovak Academy of Sciences, Dúbravská cesta 9, 842 28 Bratislava, Slovak Republic)

The January 15, 1858 Zilina earthquake is the first earthquake on the territory of Slovakia for which a systematic collection and analysis of the data was performed by earthquake contemporary researchers. The most recent isoseismal map by Brouek (published in Atlas of Isoseismal Maps for Central and Eastern Europe, Procházková & Kárník, 1978) includes 196 intensity data points. Comparing five detailed earthquake contemporary studies (original documents by Jetteles, 1858; Jetteles, 1858; Kornhuber, 1858; Schmidt, 1858- Hunfalvy 1859) we found their supplementary character. In this special case the procedure of comparing different contemporary studies was very fruitful. We identified more than 600 localities (including negative reports). Names of localities are given in Slovak, German and Hungarian languages. We studied their "history" to avoid duplications. Further it should be stressed that Jetteles used some kind of questionnaires and distributed them in the affected area. The questionnaires were focused on the time, the direction, the number and the duration of the shock(s), the air temperature, the barometer reading, about noise, air- and light phenomena, movement of waters, impression to man and animals, mechanical effects and other consequences. The answers served as a good basis for damage estimation. We used the EMS-98 scale for the estimation of the site intensities (the method of intensity estimation is presented in the contribution by Labák et al. at this conference). Comparison with Kárník's and Brouek's intensity estimations and estimation of the focal parameters is also shown.

Friday 30 July PM

Presiding Chair: V.Schenk (Inst. Of Rock Structure and Mechanics, Acad. Sc., Czech Republic)

ST3/E/01-B5

1400

## GEOINFORMATION SYSTEM FOR OPERATIVE COMPUTATION OF SOCIAL LOSSES DUE TO EARTHQUAKES

Larionov V.I. (1), Aptikaev F.F. (2), FROLOVA N.I. (3), Ugarov A.N. (4)

(1) Agency on Monitoring and Forecast of Emergency Situations, Ministry of Emergency Situations of Russian Federation (2) Joint Institute of Physics of the Earth, Russian Academy of Sciences (3) Seismological Center of IGE, Russian Academy of Sciences (4) Extreme Situations Research Center

The extreme estimations of macroseismic effects gained from past strong earthquakes was used in special Geographic Information System (GIS) in order to compute social losses. In the present study 1025 earthquakes with  $M=3$  and above, characterized by anomalous high macroseismic effect from ancient time up to 1998 are analyzed. The relationship between the number of fatalities and people injured and different magnitudes are proposed for the estimation of possible social losses from earthquakes. These relationships are valid for two groups of countries, where the most part of buildings was constructed with or without taking into account earthquake resistant measures. As well as the most probable (median) number of casualties and the ratio of number of fatalities and people injured are estimated as a function of seismic intensity for these two groups of countries. For each group of countries the estimations error was characterized by quantile equal to 0.3 lg (factor 2). These relationships are very conservative for both groups of countries within last tens years. The GIS contains cartographic base data about the states boundaries and global geographical grid. The obtained statistical relationships are used as the GIS mathematical models. The co-ordinates of earthquake epicenters and their magnitudes are used as input data for losses computations. The output results are presented as tables. The comparison of losses estimations obtained with the help of the GIS and another GIS, which uses simulation models, gives good agreement. For the Northern Caucasian region the divergence does not exceed 15%. The proposed GIS may be easily integrated into INTERNET and used by wide range of end-users in earthquake-prone areas for taking a decision about immediate response in the case of emergency.

ST3/E/42-B5

1415

## VULNERABILITY ANALYSIS BASED ON MACROECONOMIC DATA

YONG CHEN, Qi-fu Chen and Ling Chen (No. 63, Fuxing Avenue, China Seismological Bureau, Beijing 100036, P. R. China)

When we employ readily available macroeconomic data -GDP- as the basis for the vulnerability analysis, the vulnerability is defined as the ratio of physical economic loss to the GDP within a given area resulting from the occurrence of earthquakes, which we called as macroscopic vulnerability.

The vulnerability in inventory method varies with the type of buildings. For those buildings with very poor quality, such as the adobe in Costa Rica or the old civil houses in mainland of China, the vulnerabilities of them are almost the same, which represent the vulnerability in the worst cases. On the other hand, for those buildings with high quality and with seismic design, such as the reinforced masonry in Middle East or the reinforced concrete building in China, the vulnerabilities are also the same, which represent the vulnerability in the best cases due to employing the state-of-the-art design and construction techniques. The same results obtained by different authors are not strange because they represent the two extreme situations under the contemporary conditions: the best one and the worst one.

The plots of macroscopic vulnerabilities vs. seismic intensity just fall in the variation ranges limited by two extreme plots from inventory study. It is easy to understand because the total loss is the sum of different building and facilities loss, therefore, the macroscopic vulnerability should be greater than that of the worst situation in inventory study, and less than the one from the best situation. The use of macroscopic vulnerability in earthquake loss estimate is easy, simple and feasible. Present study provides a possible link between the building vulnerability of inventory method and macroscopic vulnerability.

ST3/W/12-B5

1430

## REALISTIC MODELING OF SEISMIC INPUT FOR MEGACITIES AND LARGE URBAN AREAS: THE IUGS-UNESCO IGCP PROJECT 414

Giuliano F. PANZA (Dipartimento di Scienze della Terra – Università di Trieste, Via Weiss, 4 34127 Trieste, Italy and The Abdus Salam International Center for Theoretical Physics, Miramare, Italy, email: panza@geosun0.univ.trieste.it); Fabio Vaccari and Fabio Romanelli (both at Gruppo Nazionale per la Difesa dai Terremoti - CNR, Rome, Italy and Dipartimento di Scienze della Terra –Università di Trieste, Via Weiss, 4 34127 Trieste, Italy, email: vaccari@geosun0.univ.trieste.it, romanel@geosun0.univ.trieste.it)

The project addresses the problem of pre-disaster orientation: hazard prediction, risk assessment, and hazard mapping, in connection with seismic activity and man-induced vibrations. The definition of realistic seismic input can be obtained from the computation of a wide set of time histories and spectral information, corresponding to possible seismotectonic scenarios for different source and structural models. The availability of realistic numerical simulations enables us to estimate the amplification effects in complex structures exploiting the available geotechnical, lithological, geophysical parameters, topography of the medium, tectonic, historical, palaeo-seismological data, and seismotectonic models. The realistic modelling of the ground motion is a very important base of knowledge that can be very fruitfully used by civil engineers in the design of new seismo-resistant constructions and in the reinforcement of the existing built environment, and, therefore, supplies a particularly powerful tool for the prevention aspects of Civil Defense. At present, the project is active in Antananarivo, Bangalore, Beijing, Bucharest, Budapest, Cairo, Catania, Damascus, Delhi, Kathmandu, Ljubljana, Mexicali, Mexico City, Naples, Rome, Santiago de Chile, Santiago de Cuba, Silistra, Sofia, hessaloniki, Tijuana and Zagreb.

ST3/W/38-B5

1445

## MAXIMUM POSSIBLE EARTHQUAKES AS THE UPPER THRESHOLD OF SEISMIC POTENTIAL ESTIMATES OF EARTHQUAKE ACTIVE ZONES

Vladimír SCHENK, Zdeňka Schenková and Pavel Kottbauer (all at Institute of Rock Structure and Mechanics, Academy of Sciences, CZ-182 09 Praha 8, The Czech Republic, email: schenk@irms.cas.cz)

The seismic potential is commonly understood as the upper threshold of an ability of seismogenic zone to originate the maximum earthquake. To test some approaches of statistical evaluations of the seismic potential two earthquake zones, the Gulf of Corinth area (Central Greece) and Kresna region (SW Bulgaria), that belong to seismically high-active European areas, were used. There are several published earthquake catalogues (Makropoulos 1985, Papazachos 1988, Shebalin et al. 1974) and unpublished data on earthquake occurrences monitored by local arrays of the National Observatory of Athens and the Geophysical Institute, Bulgarian Academy of Sciences. Array data were compiled by Drakatos, Kalogeras, Papadopoulos and Rangelov and were obtained from both organisations within the joint activity in the EC INCO-Copernicus Project ASPELEA. The presentation attempts to extend standard procedures for some additional seismogenic zone quantities as a seismoactive layer thickness, a characteristic earthquake estimate, a linkage of active part of zone to known tectonic data, etc. Obtained seismic potential evaluations will be discussed from the viewpoint of a reliability of an applied methodology. The presented research was realised under the EC INCO-Copernicus ASPELEA Project No ERBIC 15CT97 0200.

ST3/W/15-B5

1500

## MAGNITUDE FROM DOCUMENTARY DATA: CURRENT TOPICS AND OPEN PROBLEMS

DARIO ALBARELLO (Dept. of Earth Sciences, University of Siena, Via Laterana 8, 53100 Siena, email: dario@ibogfs.df.unibo.it)

By following standard statistical approaches, several empirical relationships have been so far proposed in the literature for the macroseismic estimate of magnitude. However, the heterogeneous character of the variables involved in this kind of analysis, and in particular the ordinal and discrete character of Intensity, prevents from the safe use of the usual statistical methods. As an example, it can be shown that, when linear empirical relationships are considered, the uneven sampling of data combined with the peculiar frequency distribution of magnitude values result in biased parameterizations. Suitable distribution-free statistical approaches can be adopted to overcome such kind of problems. These new procedures could help to evaluate the actual constraining power of the explicative variables so far proposed and to allow a more reliable treatment of the involved uncertainties. Furthermore, these methodologies could be useful to better understand the dependence of magnitude-intensity relationships on local seismotectonic features. In fact, despite the critical role of regionalization in the assessment of magnitude-intensity relationships, the development of suitable statistical procedures remains an open problem. To this purpose, a new procedure is discussed and tentatively applied in the Mediterranean region.

ST3/E/22-B5

1515

## IN SITU MEASUREMENT OF SITE EFFECTS AND BUILDING DYNAMIC BEHAVIOUR RELATED TO DAMAGE OBSERVED DURING THREE RECENT EARTHQUAKES

MARCO MUCCIARELLI (Universit` della Basilicata, Potenza, Italy); Maria Rosaria Gallipoli (I.M.A.A.-C.N.R., Tito Scalco, Italy); Giancarlo Monachesi (O.G.S.M., Macerata, Italy)

After three events (Marche-Umbria, 1997; Slovenia, 1998; Southern Italy, 1998) a series of in-situ measurements were undertaken. In the aftermath of mainshocks, HVSR were measured using aftershocks, microtremors and man-made excitations. The measurements were performed both on free-field and inside damaged buildings. It was possible to see how the enhancement of damage can be attributed to a double resonance effect observed when a building fundamental mode approaches soil resonance frequency, and how displacements provide a better relationship with damage rather than accelerations, especially using IDI. Some more interesting effect were observed, namely: 1) the increase of site effect close to fault gauge zones not activated by the event; 2) the coupling of frequency of adjacent building with different characteristics (RC and stone masonry); different damage in buildings that appear to be exactly similar but that show different fundamental frequency.

Thursday 29 July AM

Presiding Chairs: L.L.Xie (Institute of Engineering Mechanics, China Seismology Bureau, China), G.Gibson (Seismology Research Centre, Bundoora, Australia)

ST3/W/14-B4

Poster

0930-01

## SEISMIC GROUND MOTION MODELLING FOR THE LJUBLJANA BASIN

Andrej GOSAR and Mladen Zivcic (both at Min. of the Environ. and Physical Planning, Geophysical Survey of Slovenia, Pot na Golovec 25, SI-1000 Ljubljana, Slovenia, email: andrej.gosar@gov.si); Peter Suhadolc and Francesco Marrara (both at Dep. of Earth Sciences, University of Trieste, Via Weiss 1, 34127 Trieste, Italy, email: suhadolc@geosun0.univ.trieste.it)

Ljubljana, the capital of Slovenia, is situated in a Plio-Quaternary tectonic basin characterised by almost flat surface and rough bedrock topography. The basin is filled up with lacustrine sediments and carbonate gravel, up to 200 m thick. Site effects can have, therefore, strong influence on seismic ground motion. The strongest earthquake in the history of the city occurred in 1895 (M=6.1, I=VIII-X MCS). The lack of stronger recent seismic activity and observational data increases the importance of numerical modelling for hazard assessment. The data from a revised earthquake catalogue and newly determined fault plane solutions were combined with available geological data to determine the parameters of possible seismic sources. These are related mainly to dextral strike-slip faults running south-west of Ljubljana at a distance from 30 to 120 km. The largest historical earthquake in this area was in 1511 with an assessed magnitude of 6.8. A 3D structural model of the Ljubljana basin was built from the results of numerous geophysical investigations and borehole data. From this we extracted a profile towards the active area of Mt. Sneznik, lying 50 km SW of Ljubljana, for which strong motion records of an MLV=4.7 event were recorded both on sediments and on bedrock. The hybrid technique which combines the modal summation and finite-difference methods was used to calculate three-component synthetic seismograms in 2D media. A great influence of bedrock topography on the shape, duration and amplitude of the signal was observed. Comparison with available records shows a good match of the shape and amplitude of the principal phases, but an underestimation of the signal duration.

ST3/W/11-B4

Poster

0930-02

## LARGE FLUCTUATION OF WAVE AMPLITUDE PRODUCED BY SMALL FLUCTUATION OF VELOCITY STRUCTURE - FOR CASE OF SPHERICAL WAVE

Mitsuyuki HOSHIBA (Meteorological Research Institute, Tsukuba, 305-0052, Japan, e-mail: mhoshiba@mri-jma.go.jp) Takashi Furumura (Hokkaido University of Education, Iwamizawa, 068-0835, Japan, e-mail: furumura@atson.iwa.hokkyodai.ac.jp)

Seismic velocity structure of the real Earth is described by a combination of deterministic large-scale structure and small-scale fluctuation. When waves propagate in media having the small-scale fluctuation, the fluctuation makes the rays bent and introduces focussing and defocussing, and then produces the fluctuation of wave amplitude. To estimate how large fluctuation of the wave amplitude is made due to the velocity fluctuation, the average and the variance of wave amplitudes are evaluated as a function of propagation distance from numerical simulations of scalar wave propagation in 3D random media having Gaussian or exponential autocorrelation functions. Phase screen method and pseudospectral method are used considering Ricker wavelet as source time function. Comparing the cases of point sources with those of plane wave source, the decay rate of maximum amplitude with distance is small for point source because the effect of stochastic dispersion is weak for point source. For small propagation distance the variance for point source is smaller than that for plane wave, and for large distance that for point source is larger than that for plane wave. The variance of maximum amplitude is larger than the square of its average (i.e., large fluctuation of wave amplitude) even for several % of velocity fluctuation. These results suggest how small error and how fine resolution are necessary for velocity structure model for the discussion of wave amplitude.

ST3/W/26-B4

Poster

0930-03

## MODELLING THE AMPLIFICATION OF S-WAVES AT ZUIDLAARDERVEEN

Theo DE CROOK (Royal Netherlands Meteorological Institute, Seismology Division, P.O. Box 201, 3730 AE De Bilt, The Netherlands, email: crookde@knmi.nl)

The aim of this study is to investigate the influence of shallow soil deposits on the amplification of S-waves in the borehole station Zuidlaarderveen (ZLV) and its vicinity. This amplification is important in terms of seismic hazard. The amplification in the borehole station ZLV is observed mainly in the upper 25 meters. The soil deposits are modelled with a one-dimensional model. The records of local earthquakes recorded in the borehole station are used as input motions for the model and to validate the model. Site investigations are carried out in the upper 50 meters to determine accurate soil parameters. The amplification function, calculated with the SHAKE program, approximately matches the measured amplification in the upper 25-meter for frequencies below 15 Hz.

In the vicinity of the station ZLV the soil deposits vary strongly over a few hundred meters and consist of mainly sands with clay and peat layers. In this area representative soil profiles are selected. For these profiles the amplification factors of the m



ST3/W/22-B4 Poster 0930-04

## THE EFFECTS OF SOURCE PARAMETERS ON STRONG GROUND MOTIONS

Midori KAWAHARA and Masatake Ichikawa (both at Tokyo Electric Power Services Co. Ltd., 3-3-3 Higashi-Ueno, Taito-ku, Tokyo, 110-0015 Japan, email: kawahara@aed.tepsc.co.jp); Tomoyoshi Takeda and Hiroyuki Ishikawa (both at Tokyo Electric Power Company, 4-1, Egasaki-Cho, Tsurumi-ku, Yokohama, 230-8510 Japan)

It is an important problem to decide rupture processes in predicting strong ground motions due to future earthquakes. The detailed rupture processes of past earthquakes have been derived by the inversion analysis using waveforms or envelopes of the strong ground motions. Statistically analysing of these rupture processes, slip models for future earthquakes have also been derived. Though the characteristics of asperity sizes have been clarified, it is still difficult to identify locations of starting points of rupture and distributions of asperity. Therefore, it is necessary to know to what extent the simplified source models are applicable, in other words, to investigate which source parameters greatly influence strong ground motions. In this study, using the rupture processes derived from the inversion analysis as the true model, we estimated how the characteristics of strong ground motions are changed by simplifying each source parameter. Using a discrete wave number method for waveform synthesis, we analysed long period seismograms (< 2Hz), which are determined directly by the rupture processes. We assumed two simplified models, one with a constant slip magnitude, and the other with a constant slip direction. We found that in both cases the ratios of maximums of the displacements for the simplified models to those for the true one range from 0.3 to 2.0. Correlation between the waveforms for each simple model and the true one is high, especially in the case of the constant slip magnitude. We will also investigate the effects due to locations of starting points of rupture and distributions of asperity.

ST3/W/06-B4 Poster 0930-05

## PILOT SYSTEM FOR AUTOMATIC DETERMINATION OF EARTHQUAKE SOURCE PARAMETERS USING BROADBAND STRONG-MOTION WAVEFORM DATA

Keiko KUGE (Department of Geophysics, Kyoto University, Kyoto 606-8502 Japan; email: keiko@kugi.kyoto-u.ac.jp) Tomotaka Iwata and Kojiro Irikura (both at DPRI, Kyoto University, Uji 611-0011 Japan)

Strong ground motions in a near-fault region are controlled by earthquake source parameters including geometry and dimension of the fault plane, rupture direction, and locations and sizes of asperities. To estimate the distribution of strong ground motions in a short time, we should rapidly determine the source parameters in an automated method. In order to test ability of the automatic determination, especially with broadband strong-motion waveform data, we have been running a pilot system automated for earthquakes in south-western Japan, using data from K-NET. Finding a new data set in the data center, the system starts to determine the moment tensor solution by modelling the three components of waveform that include P and S waves. Since 1996 the system has determined more than twenty moment tensor solutions of earthquakes with magnitudes from 3.4 to 5.5, distributing the results through the e-mails and home pages. For large earthquakes, we are expanding the system to automatically determine the fault planes and ruptured areas by using aligned-point-source modelling. The ability of the modelling was tested and approved for recent inland earthquakes with magnitudes of 6 to 7, which include the 16 January 1995 Kobe (Mw6.9), 26 March 1997 Kagoshima (Mw6.1), and 25 June 1997 Yamaguchi (Mw5.9) earthquakes, and numerical experiments. With a source of real-time waveform data, the automated system will enable rapid determination of source parameters, leading to quick estimation of ground motions for the obtained source parameters.

ST3/W/16-B4 Poster 0930-06

## RUPTURE DIRECTIVITY EFFECTS ON SOURCE SPECTRA IN NEAR-SOURCE AREA

Hiroe MIYAKE, Tomotaka Iwata, and Kojiro Irikura (Disaster Prevention Research Institute, Kyoto University, Uji, Kyoto, 611-0011, Japan, email: miyake@egmdpri01.dpri.kyoto-u.ac.jp)

Rupture directivity effects on far-field seismic waves have been widely discussed in its azimuthal variation. It is also important to clarify directivity effects in near-source area for studying rupture processes and strong ground motions. We propose a method of determining the rupture area and direction from the directivity effects obtained from seismic spectra. We examined five crustal earthquakes (Mjma5.7-7.2) using K-NET records at more than 20 stations located less than 50km from the epicenter. Source processes of these events were estimated by the waveform inversion in the low frequency range (<1Hz). Based on the inversions results, we classified the observed spectra into those at forward, side-ward, and backward stations. To remove site and propagation effects in observed spectra, we took spectral ratios of main shock to aftershock (Mjma4.0-4.7). We used a frequency range below the aftershock corner frequencies. When the rupture propagated horizontally along strike unilaterally, forward, side-ward, and backward directivity effects were clearly found in the spectral ratios. Source displacement spectra of the main shock at forward stations had higher corner frequencies and steeper high-frequency decays compared with those at side-ward stations. Results at backward stations were contrary to those at forward. When the rupture propagated predominantly up-dip direction, forward directivity effects were observed only in the epicentral area. In case of the bilateral rupture event, forward directivity effects were observed near the rupture end. To examine the directivity effects on the spectra, we made numerical tests in which finite extended fault planes were expressed as a sum of sub-faults. Seismic waves from the sub-faults were calculated using the Boore's stochastic simulations. From the numerical tests, we confirmed that the spatial variations of source spectra are expressed as a function of rupture area and direction.

ST3/W/24-B4 Poster 0930-07

## 3-D FDM SIMULATION OF THE 1995 HYOGO-KEN NANBU EARTHQUAKE WITH DISCONTINUOUS GRIDS

Shin Aoi (National Research Institute for Earth Science and Disaster Prevention, 3-1 Tenoudai, Tsukuba-city, Ibaraki 305 Japan, email: aoi@geo.bosai.go.jp); Haruko Sekiguchi (Disaster Prevention Research Institute, Kyoto University, Gokasho, Uji, Kyoto 611-0011, Japan, email: haru@egmdpri01.dpri.kyoto-u.ac.jp); Tomotaka Iwata (Disaster Prevention Research Institute, Kyoto University, Gokasho, Uji, Kyoto 611-0011, Japan; email: iwata@egmdpri01.dpri.kyoto-u.ac.jp); Hiroyuki Fujiwara (National Research Institute for Earth Science and Disaster Prevention, 3-1 Tenoudai, Tsukuba-city, Ibaraki 305 Japan, email: fujiwara@ess.bosai.go.jp)

We use 3-D fourth-order finite-difference method (FDM) using discontinuous grids in order to simulate ground motions in source area during the 1995 Hyogo-ken Nanbu Earthquake. Discontinuous FDM grids adapted to the velocity structure is highly effective when they are used for synthesizing waveforms of large-scale basins (Aoi and Fujiwara, 1998, submitted to BSSA). Most 3-D simulations of Hyogo-ken Nanbu Earthquake employed coarse grids with the spacing of more than 100 m for finite-difference calculations, and hence the models with the S-wave velocity of approximately 600 m/s at the superficial layer, resulting in underestimated

amplitude. We use the discontinuous grids, that consist of small grids (50 m spacing) up to the depth of 2.5 km where there exist sedimentary layers and coarse grids (150 m spacing) from that depth up to 25 km that is the lower bound of the fault plane. It is suggested by geophysical explorations that the S-wave velocity of the superficial layer is about 400 m/s. The use of the discontinuous grids enables us to treat a model with such S-wave velocity, with frequency of up to more than 1 Hz. Compared to the case with the S-wave velocity at the superficial layer of 600 m/s, the velocity amplitude of the synthetics at the observation point on the sedimentary layer becomes several dozens percent larger.

ST3/W/08-B4 Poster 0930-08

## EFFECTS OF SURFACE GEOLOGY ON EARTHQUAKE GROUND MOTION IN THE CITY OF BARCELONA, SPAIN

Maria-Jose JIMENEZ, Mariano Garcia-Fernandez (Institute of Earth Sciences "Jaume Almera"/C.S.I.C., Lluís Sole i Sabaris, s/n, E-08028 Barcelona, Spain, email: mjimenez@ija.csic.es, mgarcia@ija.csic.es); Gaetano Zonno (Istituto di Ricerca sul Rischio Sismico/C.N.R., Via Bassini, 15, I-20133 Milano, Italy, email: zonno@irrs.mi.cnr.it)

This paper presents the results on earthquake hazard scenarios for Barcelona urban area as evaluated through a component of the computer prototype developed within the European project SERGISAI. Maps of soil response for the city of Barcelona have been for the first time obtained through a GIS environment, which integrates the different analysis procedures within a single application. The approach followed in order to obtain the hazard scenarios involves: collection of all data relevant to local geology and soil conditions, implementation of geotechnical models into the GIS, estimation of the level of seismic action, generation of strong-motion time histories and implementation of 1D analytical method for soil response calculations. The resulting predictive hazard maps of predominant periods and amplification ratios delineate potential variations on ground shaking and constitute a first approximation towards an integrated approach to Barcelona urban area microzonation. A comparison with empirical values from ambient noise measurements shows that most of the observed differences can be explained in terms of the physical parameters of subsurface layers. The interpretation of observed differences through a detailed analysis of empirical and analytical results is twofold. First to determine site dependence suitability and reliability of both methodologies, and second to both extract information on at-present inaccessible parameters needed for the characterisation of physical properties of soil and delimit areas where further in-depth survey research is needed for a proper seismic hazard assessment.

ST3/E/32-B4 Poster 0930-09

## SITE EFFECT EVALUATION USING COMBINATION OF SOURCE SACLING MODELS AND GROUND MOTION RECORDS

Vladimir SOKOLOV (National Center for Research on Earthquake Engineering, 200, Sec.3, Hsinhai Rd., Taipei, Taiwan, E-mail: vova@email.ncree.gov.tw)

A set of acceleration records obtained during recent Caucasian earthquakes (the Spitak, Armenia 1988, M=6.8; the Ratchi, Georgia 1991, M=7.1) was used to evaluate the site response. The soil/bedrock spectral ratios (SBSR) (mean values and deviations) were determined within frequency interval 0.6-10 Hz as ratios between spectra of the records and spectra that have been simulated for rock outcrop using w-squared Brune's model. The frequency dependence of amplification clearly exhibits the influence of soil deposits of various thickness, as well as the affect of surface topography. The generalises regional SBSR functions for so-called "reference shallow-soil site" were calculated using accelerograms recorded on various stations. The amplification functions were used for prediction of ground motion parameters expected during future earthquakes.

ST3/E/20-B4 Poster 0930-10

## SOURCE SPECTRA SCALING AND ATTENUATION MODELS FOR DIFFERENT SEISMOGENIC REGIONS

Vladimir SOKOLOV (National Center for Research on Earthquake Engineering, 200, Sec.3, Hsinhai Rd., Taipei, Taiwan, E-mail: vova@email.ncree.gov.tw)

Fourier-amplitude spectrum is one of the most important parameters describing earthquake ground motion, and it is widely used for estimating seismic hazard and strong ground motion prediction. At the present there is no doubt that Fourier spectra source scaling and attenuation models may differ in various seismogenic regions. In this study, relationships between Fourier-acceleration spectra, earthquake magnitude and distance were analysed for different active regions using ground motion recordings of small to moderate (M < 6.5) shallow earthquakes. Two characteristic models are used to describe amplitude spectra as a function of earthquake energy and distance: so-called "w-squared" Brune's source spectra model, and empirical model based on statistical analyses of recorded accelerograms. Stochastic simulation of ground motions (peak ground acceleration and response spectra) using obtained models of source spectra and attenuation shows good agreement with observed data.

ST3/E/06-B4 Poster 0930-11

## RESPONSE SPECTRA OF STRONG EARTHQUAKES OF KYRGYZSTAN

Aleksandra FROLOVA (Institute of Seismology, National Academy of Sciences, Asanbai 52/1, Bishkek 720060, Kyrgyzstan, email: kis@imfiko.bishkek.su)

Response spectra for the time history were calculated at strong earthquakes records in terms of displacements, velocities and accelerations. Three parameters were used for analysis of spectra diversity: maximum level, resonance period and logarithmic width of spectrum on three levels from maximum. Characteristics of distribution these values were estimated. Average normalised response spectra were received, which are characteristic for strong earthquakes of Kyrgyzstan.

ST3/E/38-B4 Poster 0930-12

## LOW VELOCITY LOVE WAVE IN HIGH DENSITY STRONG MOTION SEISMOGRAPH NETWORK DATA: RE-EXAMINATION OF UPPERMOST CRUST MODEL IN SOUTHERN METROPOLITAN AREA OF JAPAN

Yasushi ISHIIHARA and Masanori Saito (both at Faculty of Science, Yokohama City University, Seto 22-2, Kanazawa-ku, Yokohama, 236-0027, JAPAN, email: ishiihara@yokohama-cu.ac.jp) Masayuki Kikuchi (Earthquake Research Institute, University of Tokyo)

Highly condense seismic array network is a powerful tool to research the details of uppermost crust structure and subsurface characteristics of seismic ground motion. We had constructed the strong motion seismograph network in Yokohama city, southern metropolitan area of

Japan, which consists of 150 observatories in about 400 kilometer square area. This region has sediment layer of 3-4km thick which is estimated by artificial seismic refraction survey and surface wave velocity by other sparse network. The thick sediment layer excites slightly long (5-10 sec) period surface waves. This network observed the Love wave excited by relatively nearby and shallow middle-scale earthquake with strike-slip fault mechanism. As the phase-time mapping and band-passed seismograms aligned by epicentral distance, phase velocity and propagation direction of Love wave is estimated with high accuracy. The group velocity is not resolved well because of local magnification and severe long coda duration. This analysis brings the dispersion curve in 5 - 20 sec period range. The phase velocity at 10 sec period is about 2.0 km/s, which is less than one of previous studies. The phase velocity curve does not indicate strong dispersive character in this range. The theoretical study expects that sediment layer is lower velocity and/or thicker than standard structure model, however the sufficient interpretation is not reached. The phase-time mapping shows the heterogeneous seismic propagation affected by westward high velocity mountain region.

**ST3/E/30-B4** Poster **0930-13**

**MODELING SUBSURFACE STRUCTURE IN A SEDIMENTARY BASIN USING SEISMIC RECORDS OF VERTICAL ARRAY AND VARIOUS GEOPHYSICAL DATA**

Hitoshi MORIKAWA (Graduate School of Civil Engineering, Kyoto University, Yoshida-Hon'machi, Sakyo-ku, Kyoto 606-8501, Japan, E-mail: morika@quake.kuciv.kyoto-u.ac.jp), Junpei Akamatsu (Disaster Prevention Research Institute, Kyoto University, Gokasho, Uji, Kyoto 611-0011, Japan, E-mail: akamatsu@dri.kyoto-u.ac.jp), Akito Uchida (Nara National Cultural Properties Research Institute, Nijo, Nara 630-8002, Japan).

We discuss a method to estimate accurately subsurface structure in a deep sedimentary basin with use of seismic observation with vertical array, and to assess reliability of resultant structure model on the basis of cross-check of theoretical horizontal-to-vertical spectral ratios (H/V) for S-waves and phase velocities of Rayleigh waves (CR). Study area is Heijo-Kyo, the northernmost part of Nara basin, Japan. The depth to bedrock is known to be about 600m from a nearby deep-borehole. In addition, we could utilize the other geophysical data such as microseism array data obtained by previous works, which provide information of CR. 3-component seismic observations have been carry out at GL 0m, -20m, -42m, and -100m in a borehole, and 70 local and regional events with magnitude of 3.2 to 7.7 were recorded in 1997 and 1998. We analyzed (1) difference in onset time between S-to-P converted wave and S-wave, (2) surface-to-underground spectral ratios (S/UG), and (3)H/V at each depth. It is noteworthy that, spectral ratios of S/UG peak at depth-dependent frequencies of nearly odd multiples (up to third higher mode), and that H/V from earthquake motions and that from microseisms resemble each other. From the analysis, a model of S-wave velocity structure is proposed. To verify the model, we used both of CR and peak period of H/V for S-waves (Tp) calculated from models. Comparison was made with models obtained from the other data such as CR of microseisms and small-scale refraction survey. Although parameters of each model contain the coefficients of variance of 5 to 10%, theoretical CR and Tp for the models coincide respectively in a range of one standard deviation. This enable us, therefore, to use the least squared method to develop a more reliable model satisfying all the available data.

**ST3/E/35-B4** Poster **0930-14**

**COMPARISON OF VARIOUS METHODS TO ESTIMATE THE GROUND STRUCTURE**

Hitoshi MORIKAWA (Graduate School of Civil Engineering, Kyoto University, Yoshida-Hon'machi, Sakyo-ku, Kyoto 606-8501, Japan, E-mail: morika@quake.kuciv.kyoto-u.ac.jp), Junpei Akamatsu (Disaster Prevention Research Institute, Kyoto University, Gokasho, Uji, Kyoto 611-0011, Japan, E-mail: akamatsu@dri.kyoto-u.ac.jp), Akito Uchida (Nara National Cultural Properties Research Institute, Nijyo, Nara 630-8002, Japan).

Various methods have been presented to estimate S-wave velocity structure of sediment which will be a basic information for prevention of earthquake disaster. We discuss a method to estimate accurately ground structure in this study, comparing the structure obtained from vertical array observation records of earthquakes with that from other method. For this purpose, using the velocity type seismometers, we carried out the observation in a borehole at Heijo-Kyo where is located at north of Nara basin, Japan. The seismometers consist of three components and are set at GL 0m, -20m, -42m, and -100m. In this site, the government plans to construct a large wooden structure, which has long predominant period, to restore the ancient capital of Japan. As a priori information, some data obtained from microseisms observations and deep borehole are available to estimation of ground structure. According to these data, the depth to the bedrock, whose velocity of shear waves is 3.2km/s, is about 600m and we can model this structure in two sedimentary layers. The observation systems have recorded about 70 events in these two years. Using these records, (1) running time of S-P converted waves, (2) spectral ratio between different depth, and (3) horizontal/vertical spectral ratio (H/V) at each depth are calculated and a model of S-wave velocity structure is developed for this site. To verify the development, we compare the obtained model with various models estimated from other data, that is, deep borehole data, dispersion curves from array observation of microseisms, H/V of microseisms around this site, Bouguer anomalies, small-scale refraction surveys. While the S-wave velocity structures estimated from these various data contain the coefficient of variance, whose value is 5 to 10%, they share the same value in range of mean plus/minus standard deviation. Using the least squared method, therefore, we can develop a more accurate model of ground structure which satisfies the various data.

**ST3/E/03-B4** Poster **0930-15**

**AZIMUTH VARIATIONS OF THE AVERAGE ATTENUATION COEFFICIENTS**

Lenka S. TIMIOVSKA (Institute of Earthquake Engineering and Engineering of Seismology, Salvador Ajlende 73, Skopje, Macedonia)

Within the frames of a project for computation of seismic risk in Macedonia, there arose the need of investigating the variation of seismic intensity attenuation. Defined from the isoseismals of some earthquakes were the coefficients of average attenuation, and their azimuth variations. Due to the wide range of attenuation coefficients, the application of complex attenuation laws becomes a necessity in determination of the anisotropy of energy expansion. The obtained relationship shows a fairly good agreement with isoseismals of many large events on the whole investigation region and may therefore be useful in providing realistic estimates of spatial attenuation and hence of design earthquakes for a given site. It can also be sometimes useful in estimating the epicentral intensity for an earthquake whose maximum intensity is not reliably known. In general speaking, the results point to the fact that the use of average attenuation values or approximation of the first order is not sufficient enough for corresponding definition of attenuation, but approximations of a higher order are necessary. Investigation to a greater depth could enable prediction of the possibility of obtaining attenuation laws depending on magnitudes on one hand, while on the other, the possibility to work with revised data.

**ST3/W/28-B4** Poster **0930-16**

**NUMERICAL SIMULATION OF NONLINEAR SITE-RESPONSE EFFECTS**

Olga PAVLENKO (Institute of Physics of the Earth, B.Gruzinskaya 10, Moscow 123810, Russia, e-mail: olga@synapse.ru)

To study nonlinear site-response effects, numerical simulation is performed of propagation of Gaussian white-noise seismic signals of various intensities in horizontally layered sedimentary soils. The behaviour of soils under loading is described by nonlinear hysteretic Iwan model, linear elastic model, or linear visco-elastic model. For these models, nonlinear system identification techniques were applied: the spectra and bispectra of output signals are computed, which characterise in frequency domain the linear and nonlinear (due to quadratic nonlinearity) parts of the medium response to a seismic action. It was shown that, for the nonlinear model, increasing the intensity of the input signal gives rise to the signal distortion in the process of its propagation, the shape of the power spectral density curve transforms, and, for intense input signals (corresponding to acceleration of higher than 0.4g), takes the form  $E \sim f^{-k}$ ; bispectral amplitudes of the output signals increase in the high-frequency and low-frequency domains due to generation of combinative frequency harmonics. This is in accordance with theoretically predicted shape of spectrum and bispectrum in the case of interaction of a large number of seismic waves, in the approximation of chaotic phases. The inverse problem is solved of estimating coefficients of the power series describing the nonlinear hysteretic curve of soil behaviour by spectral and bispectral amplitudes. Power spectral density of the seismic noise also decreases with frequency as  $E \sim f^{-k}$ , this can indicate the presence of a nonlinear component of the medium response to a seismic action in the seismic noise. Estimates of this component for areas with various geological structure are made by bispectra of seismic noise.

**ST3/W/17-B4** Poster **0930-17**

**ANOMALOUS (-1G) PEAK ACCELERATIONS RECORDED AT STATION KRUGLYI, KAMCHATKA.**

PETUKHIN A.G.(1), Dontsov O.V.(1), Egorov O.N.(2), Melekkestev I.V.(2) and Sinityn V.I.(1) (1) Kamchatka Experimental and Methodical Seismological Department; (2) Institute of Volcanic Geology and Geochemistry; 9 Piip Blvd., Petropavlovsk-Kamchatsky, 683006, RUSSIA, email: gusev@emsd.iks.ru

In 1993yr, during strong earthquakes on June 8 (Mw=7.5) and November 13 (Mw=7.0) near South Kamchatka, at ground strong-motion station Kruglyi accelerograms were recorded with unusually large peak accelerations:  $A_{max} = 991$  gal and 897 gal. Hypocentral distances were  $R=104$  and 60 km, respectively. The both records have high frequency content: amplitude Fourier spectra have broad peaks at 5-10 Hz with maximum amplitudes about 30 times greater than it could be expected on rock in Kamchatka from earthquakes with the same values of Mw and R. To find out the reasons of these anomalies, we investigated the geological environment at the station Kruglyi and estimated the station spectral corrections by two methods: (1) the ratio of Fourier amplitudes of micro-seismic noise at the investigated point and at the base rock point; (2) the ratio of the accelerogram spectrum at station Kruglyi and the average spectrum for Kamchatka on rock for the same magnitude and distance. The both spectral corrections are fitted well, i.e., the source of the spectral anomaly is located near the station, at a distance much shorter than the distance between the investigated and the base points. The most probable candidate for such anomaly is the pocket of hydro-thermally altered rocks (sand + clay, 70 m. width, the distance from the accelerometer to the nearest boundary is 30-40 meters, while the accelerometer itself is located on rock). Dried hydrothermal system looks like a soft inclusion in rock with vertical parallel walls and produces a resonator/waveguide; this can lead to the observed phenomenon.

**ST3/W/23-B4** Poster **0930-18**

**SPATIAL VARIATIONS OF SITE RESPONSE AND RESONANCE SITE EFFECTS IN SOILS**

Rufet URDUKHANOV and Olga Pavlenko (both at Institute of Physics of the Earth, B.Gruzinskaya 10, Moscow 123810, Russia)

The medium response to a seismic action is often substantially determined by resonant oscillations of various inhomogeneities in the earth's crust, i.e., separate layers, wave guides, or inclusions, excited by propagating seismic waves. An experiment is carried out at a test-site of the Institute of Physics of the Earth with a vibrator seismic source, aimed at a detailed study of the medium transfer functions within a small area. A 3-component receiver was placed in the center of a circle of the 100 m- radius, and the vibrator moved along the circle and radiated signals at frequencies of 10 Hz, 14 Hz, 16 Hz, 18 Hz, and 20 Hz at points having azimuths of 0°, 30°, 60°, 90°, 120°, 150°, 180°, 210°, 240°, 270°, 300°, and 330°. The upper part of the medium are sand and clay layers up to depths of 1000-1200 m. The results of the experiment show: 1) substantial difference in the transfer functions of the medium for different azimuths; 2) noticeable amplification of seismic amplitudes at some frequencies and some frequency bands; 3) amplification of oscillations at a frequency of 17 Hz for all azimuths and resonant oscillations at 17 Hz for one direction, the Q-value is rather high and testifies to contrast boundaries and contrast impedance properties of the resonant structure. According to the scheme of the experiment, we can conclude that the resonant structure is located near the surface, and its dimensions are about some meters. The numerical simulation is performed of propagating of seismic signals in the medium with the geological structure and physical properties depending on depth, as it was determined for the test-site, and the same medium with slight variations in its parameters, assuming deep and subsurface wave guides; estimates of characteristics of the resonant structure are made based on the whole set of available seismic recordings.

**ST3/E/50-B4** Poster **0930-19**

**CALCULATION OF LONG-PERIOD GROUND MOTION RESPONSE SPECTRUM BY USING BROAD-BAND DIGITAL RECORD**

YU, Yanxiang, WANG, Suyun and HU, Yuxian (Institute of Geophysics, China Seismological Bureau, Beijing 100081, China, email: yanxiang@cdsindm.csb.gov)

There is an increasing need to study the characteristic of long-period ground motion with the construction of many large scale structures whose natural period are around 10 sec. Although the digital strong motion accelerographs are used for many years and a number of such high-quality records are obtained, recent studies show that it is still difficult to obtain reliable response spectrum due to the low signal-to-noise ratio when the period exceeds 10 sec. The broadband digital seismographs used by seismologist have many excellent characteristics such as broadband, high-resolution and low-noise, which are also needed in study of earthquake engineering. The seismograms recorded by these seismographs might be used in studying long-period ground motion in certain conditions. In this paper we have a detailed study to these records in the aspects of instrument response, resuming of ground motion, correction, spectrum analysis of signal and noise to demonstrate their feasibility in studying



long-period ground motion. Over 70 broad-band (BB or VBB) or low-gain accelerograph (LG) records of the Chinese Digital Seismograph Network (CDSN) and VBB records of GEOSCOPE in Wushi seismic station are used to calculate the horizontal response spectra in the period range up to 20 sec.

The BB system has a very flat amplitude response in the period range up to about 20 sec. The VBB or LG system of CDSN and VBB system of GEOSCOPE have flat amplitude response in the period up to several hundred sec. So these seismographs can record the long-period ground motion which we concern. The ground motion displacement, velocity or acceleration can be expediently resumed by applying the transfer function of the system to the record. Tests in this study show that, as to one earthquake, the ground motions resumed from records of different seismographs are very similar. The baseline correction and high-pass filtering are required before calculating the response spectrum. The baseline drift is removed and a high-pass filter which the cut-off period is 40 sec is applied. No other correction process is used in order to further reserve long-period ground motion information. In order to analyze the signal-to-noise level, noise is extracted from the first 62.5 sec of the pre-event recording while the signal is from the thereafter 125 sec recording. Their Fourier amplitude...

**ST3/W/52-B4** Poster **0930-20**

#### NEW INSTRUMENTATION OF THE UKRAINIAN NATIONAL NETWORK FOR SEISMIC OBSERVATIONS

Yu. LOKSHYN, N. Petrov, V. Baranov (all at State Scientific Industrial Association "Metrology", 42 Mironositskaya st., 310002 Kharkov, Ukraine, fax: +380 572 43 61 93)

The possible earthquakes are very strong hazard for population safety and could cause the essential economic disasters and environment catastrophes. The problem of the earthquakes prediction and anti-seismic protection has the most importance in Ukraine, where the large industrial units, in particular, the nuclear power stations, are situated in the seismic active regions near large cities. In this sense, Ukraine needs a modern and broad network of the permanent seismic observations. At present, one of the main directions to improve the national seismic observations network is its re-supplying with new seismic control instruments, in particular, with accelerometers and seismic sensors for low and infra-low frequency. Such re-supplying also foresees to perfect the metrological traceability in the vibration acceleration measurement area. The Complex State Program to develop the national system of the seismic observations and to raise the population safety in the seismic hazardous regions has been worked out in Ukraine. In frame of that program the State Scientific Industrial Association (SSIA) "Metrology" develops, manufactures and tests the various types of tri-axis accelerometers and seismic sensors based on that accelerometers intended for operation at the nuclear power stations in the anti-seismic protection systems. To verify those accelerometers and seismic sensors SSIA "Metrology" also develops the Special Standard consisting of Pendulum and Rotating Calibrators. The Pendulum Calibrator has been already manufactured and tested. To make use new accelerometers, seismic sensors and instruments for their verification allows to upgrade the national seismic observations network, to improve its reliability and trustworthy of observations and to mitigate risk of the nuclear power stations maintenance.

**Thursday 29 July PM**

Presiding Chairs: C.McQueen (EQE International Ltd, Warrington, UK),

V.Ginsari (Institute of Geophysics and Geology, Moldavian Academy of Sciences, Moldova)

**ST3/W/33-B4** Poster **1400-01**

#### STUDY OF THE SITE EFFECT IN ROME AS INFERRED FROM MACROSEISMIC SURVEYS

Andrea Tertulliani ( Istituto Nazionale di Geofisica, Via di Vigna Murata, 605 Roma, Italy, email: tertul@ing750.ingrm.it.); Francesca Fuciniello, Stefano Donati and Francesca Cifelli (Dept. of Geology, University of Roma Tre, Largo S. L. Murialdo, 00146 Roma, Italy, email: sdonati@uniroma3.it)

An original methodology has been prepared for high density macroseismic surveys in urban areas by Istituto Nazionale di Geofisica, Department of Geology of University Roma Tre and many high schools of Rome. Such a method was applied to Rome during the seismic sequence started in Central Italy in September 1997, studying two earthquakes largely felt in the city: the October 14, 1997 earthquake ( $M_w=5.7$ ) and the March 26, 1998 earthquake ( $M_w=5.3$ ). The two events were different in depth and epicentral distance from Rome. The systematic collection of macroseismic data allowed us to plot 669 and 928 observation points respectively for the two events, all in the roman urban area. The high density of information revealed in a great detail the variation of intensity in the urban frame, showing a very good correlation with local geology. The analysis of the intensity variation has shown, as expected, an amplification of the seismic effects on Holocene deposits, in particular on the alluvial deposits of Tevere valley, and on the alluvial deposits of the minor tributaries. This last evidence is new, as those areas have been never studied before from a seismological point of view. Recent alluvial sites have in general shown, for both earthquakes, major effects in comparison with sites on pre-holocene formations (bedrock); the increasing in term of MCS scale has been one degree or more. The whole research provides a good confirmation of the important role of the very local geological variations in the seismic response of the city. Our experimental evidences are in good agreement with numerical simulations and modelling of seismic response, that are available only for the historical centre of Rome. These results can provide a significant contribution to the seismic risk evaluation of Roman area, assessing the correct hazard to the recent alluvial deposits.

**ST3/W/32-B4** Poster **1400-02**

#### EFFECTS OF 12 APRIL 1998 KRN, SLOVENIA, EARTHQUAKE ( $M_w=5.8$ ) ON NATURAL SURROUNDINGS AND THEIR INTENSITY-RELATED DISTRIBUTION

Andrej GOSAR and Polona Zupancic (both at Min. of the Environ. and Physical Planning, Geophysical Survey of Slovenia, Pot na Golovec 25, SI-1000 Ljubljana, Slovenia, email: andrej.gosar@gov.si)

On Easter day, 1998 at 10:55 UTC the strongest earthquake reported in this century in Slovenia ( $M_w=5.8$ ) occurred near the border with Italy. The epicenter was in uninhabited area of Krn mountains (Julian Alps) in a complex built area at the junction of External Dinarides and Southern Alps. Preliminary depth of the hypocenter is about 15 km and the focal mechanism shows almost pure dextral strike-slip (NW-SE). The earthquake caused extensive damage in several villages and in the city of Bovec located 10 km from the epicenter. The maximum intensity VII-VIII EMS-98 was assessed. The earthquake caused several massive rock-falls, few landslides and affected the flow of some springs in epicentral area. Due to the fact that this mountain area was unpopulated during the earthquake (very bad weather and high snow), it was useful to grade the damage to natural surroundings and to study intensity-related distribution. An analysis of these effects was therefore made to assess the reliability of the data and their relation to other macroseismic data. The area of greatest rock-falls as well as the area of aftershocks is elongated in direction of the structures. Attention was needed because rock-falls are not rare events in Julian Alps (two larger occurred in last 10 years), that are built mainly of highly fractured carbonates. The maximum assessed intensity from the damage to

buildings corresponds to the lower intensity limit, according to EMS-98, at which the observed effects on nature occur. For the landslide of the Bohinj lake bank (15 km away), there is no evidence of the liquefaction, characteristic for higher intensities. Waves on standing water were observed in wider area as well as substantial changes to the level of ground water. Only small damage for few isolated stone buildings in epicentral mountain area was also reported. None of these effects are sufficient to quantify the higher EMS-98 intensity.

**ST3/E/19-B4** Poster **1400-03**

#### MACROSEISMIC EFFECTS OF 12 APRIL 1998 KRN, SLOVENIA, EARTHQUAKE: AN OVERVIEW

Ina CECIC, Matjaz Godec, Polona Zupancic and David Dolenc (all at Ministry of the Envir. and Physical Planning, Geophysical Survey of Slovenia, Ljubljana, Slovenia, email: ina.cecic@gov.si)

On Easter 1998 at 10:55 UTC (12:55 local time) the strongest earthquake reported in this century in Slovenia ( $M_w=5.8$ ) occurred near the border with Italy. The epicentre was in uninhabited area of Krn mountains (Julian Alps). The earthquake caused extensive damage in several villages and in the city of Bovec (approx. 10 km NW from the epicentre). The maximum intensity was estimated to be VII-VIII EMS-98. One person in Bovec died of a heart attack. The earthquake was also felt in nine European countries, where the data were collected and evaluated by the institutions in charge. After the main shock the questionnaire forms were distributed by mail to all observers in the Slovene database (more than 4300). Several field trips were made in order to collect the macroseismic data in the wider epicentral area. The collaboration with other governmental teams that were collecting and evaluating the damage was established and their data were made available for our use. More than 1000 houses were examined by civil engineers and the damage was described in detail. Older fieldstone and simple stone objects with wooden floors and bad quality mortar suffered the damage most often. Many of them were already damaged in the 1976 Friuli earthquake, but the retrofitting and the reinforcement of the buildings were done poorly or not at all. Some recently built buildings were damaged as well, in many cases due to the unfavorable soil conditions. The data on damage and the data from questionnaires were combined into a database which enables us to obtain good quality EMS-98 intensity estimates as well as to study single effect distributions. The earthquake caused many effects on nature (huge rockfalls, landslides, etc.) that were also documented.

**ST3/E/34-B4** Poster **1400-04**

#### SEISMIC RISK IN CENTRAL AMERICA - A SIMPLIFIED APPROACH

YONG CHEN (China Seismological Bureau, 100036 Beijing, China, email: yongchen@public.bta.net.cn) Federico Giendel (Universidad Nacional, Apdo. 86-3000, Heredia, Costa Rica, email: fgu@geofys.uu.se) Ota Kulhánek (University of Uppsala, Villavägen 16, 752-36, Uppsala, Sweden, email: Ota.Kulhanek@seismo.uu.se)

Seismic hazard in Central America (in 50 years, 10% probability of exceedence), is assessed on a 5' x 5' grid by making use of available earthquake catalogs and attenuation formulae. In the simplified seismic risk approach used, the time consuming and costly vulnerability analysis is replaced by macro-economic indicators, such as the Gross Domestic Product and population distribution, which are easy to compile. Calculated losses correlate well with the distribution of seismic hazard and social wealth. In Central America, the largest losses of US \$ 2.5 billion are expected in Guatemala (50-year interval, 10% probability of exceedence). For Costa Rica and El Salvador the respective figures are US\$ 1.6 and 1.5 billions. In Honduras, Nicaragua and Panama the expected losses are significantly below US\$ 1 billion.

**ST3/E/15-B4** Poster **1400-05**

#### 1995 NEFTEGORSK EARTHQUAKE STATISTICS OF OIL PIPE LINE SYSTEMS

KOFF G.L. (1), Frolova N.I. (2), Zverev L.A. (3) (1)Institute of Lithosphere, Russian Academy of Sciences Moscow, Russia (2) Seismological Center of IGE, Russian Academy of Sciences, Moscow, Russia (3)VNIPI "Morneftegas", Okha, Russia

The Neftegorsk earthquake ( $M=7.1$ ) occurred on May 28, 1995. It resulted in large social and economic losses. The number of fatalities reached 1958 people, about one thousand inhabitants were severely injured. Damage rate of almost all existing buildings was discovered to be 4 (heavy damage) and 5 (total collapse). The earthquake caused more 30 breaks of the oil pipe line system in the Northern Sakhalin. Three major oil pipelines Tungur-Sabo, Sabo-Blockpost 3, Okha-Komsomolsk-na-Amure were inspected. The diameter of the damaged pipelines varies from 325 mm up to 426 mm. The main damage to pipe lines occurred due to ground layers displacement and failure. Cracks from 20 to 100 cm wide and offsets up to 30 cm have been measured throughout the observed pipe line routes. The typical damage to pipe lines is cracks in joints, total failure of joints. The detailed description of the inspected pipe line breaks is given. The most severe damage to pipe lines was found at distances from 10-12 km up to 16-20 km from Neftegorsk. Little damage was observed at distance of 35 km. Most of oil pipe line damage during the earthquake were observed in the areas characterized by unfavourable ground conditions and local dislocations, as well as in the vicinity of moving blocks of Verkhne-Pitulsky and Gyrgylaninsky active regional faults. The engineering geological conditions and physical mechanical soil properties were studied in the areas of pipeline breaks. The engineering recommendations for the oil pipeline restoration and future construction are given.

**ST3/P/16-B4** Poster **1400-06**

#### A METHOD OF EARTHQUAKE RISK ASSESSMENT

LUO WEI (Seismological Bureau of Beijing, CSB No.28 Suzhou Street, Haidian District, Beijing, 100080, China, email: weiluo@public.bta.net.cn)

The violent earthquake activity on a global scale is mainly concentrated in the relatively narrow zones of the plate boundaries. However, there are also violent neotectonic movement and earthquake activity within the plates and continents. The most typical region where intraplate earthquakes happen is a large triangle situated in the continental China and its environs. This is a specific phenomenon from the action of the strong plate boundary force by the collision between the Indian and Eurasian plates at the Himalayan Arc. On the basis of the theoretical and experimental results, the epicentral distribution, the surfaces rupture belts and focal mechanism solutions, the seismicity framework is suggested. The framework is formed by the two groups of neotectonic slip lines approximate to logarithmic spirals; that is, the zones where the maximum shear stress and shear strain are concentrated. The netlike structure makes a spatial framework dominating over the neotectonic movement and earthquake activity, and provides a new method for studying and predicting strong earthquake risk areas. The spatial distribution of the large earthquakes ( $M \geq 7$ ) in the continental China is changed from along the neotectonic slip lines to an area within a plan rectangular co-ordinate. We found out that the earthquakes obviously concentrated on two narrow and interesting zones similar to the X type rupture. It is useful for us to reduce the areas where we attempt to explore the large



earthquake occurrence. According to the dynamic developing process of the moderate events ( $M \geq 5$ ) along the neotectonic slip lines in every year since 1900, it is found out that the events increased before a large earthquake with magnitude greater than or equal to 7 occurrence. The moderate events mainly occurred at the special locations on or near the slip lines related to the future large earthquake epicenters. In fact, most of the large earthquakes of the recent years do occur as above descriptions.

**ST3/W/41-B4** Poster **1400-07**

**INVESTIGATING CONSISTENCY BETWEEN ESTIMATES OF SEISMIC HAZARD: A COMPARATIVE EVALUATION OF THREE METHODOLOGIES**

CLAIRE McQUEEN EQE International Ltd, The Genesis Centre, Science Park South, Birchwood, Warrington, UK, WA3 7BH

Raised awareness of the threat posed by natural hazards such as earthquakes has led to an increase in the number of studies attempting to quantify these risks. Several methods are available for this purpose which prompts the question: "What degree of consistency, if any, may be expected between results produced by each method?" This study uses Cornell type, Historical Parametric, and Extreme Value methods to assess the seismic hazard across the South Eastern Caribbean, a region for which a detailed and complete catalogue exists. Hazard levels are displayed as contour maps showing Peak Ground Acceleration (PGA) with a 10% probability of exceedence in any 50 year time period. For each method, a number of sensitivity tests are performed, yielding results that are then used to produce a suite of maps illustrating the dependency of results on various input variables. Comparisons are also made for modelling scale and attenuation relationships, and inter-methodological consistency is examined.

The results suggest that of all the input variables, the attenuation relationship chosen to model ground motion has the greatest effect on the results. As far as consistency between methods is concerned, providing that a historically complete catalogue is available, the methods produce contour maps with a similar spatial distribution of hazard. However, absolute ground motions are highly dependent upon the attenuation model applied.

Given the importance of hazard continuity, it is recommended that caution be exercised when using composite hazard maps taken from sources that favour different methodologies. For risk assessment purposes, since results from individual studies are often not directly comparable, super-zone hazard maps covering areas that are not delimited by political or national boundaries should be created; thus necessitating further discussion of standardisation of data collection and hazard assessment methodology.

**ST3/W/39-B4** Poster **1400-08**

**SIGNIFICANCE OF FAULT-RELATED BEDROCK-STRUCTURE IN MICROZONING OF A DEEP SEDIMENTARY BASIN: STUDY ON THE 1996 LIJIANG EARTHQUAKE, YUNNAN, CHINA (IDNDR JOINT-RESEARCH)**

J.AKAMATSU(Disas. Prev. Res. Inst., Kyoto Univ., Uji, Kyoto 611-0011, Japan, e-mail: akamatsu@drs.dpri.kyoto-u.ac.jp), K.Nishimura(Dep. Informatics, Okayama Univ. of Science), H.Morikawa(Graduate School of Civil Eng., Kyoto Univ.), K.Onoue(DPRI, Kyoto Univ.), N.Seto, M.Nakamura(both at Earthq. Res. Inst., Univ. of Tokyo), M.Komazawa(Geological Survey of Japan), L.Jiang(Seismological Bureau of Yunnan Prov.), K.Li(Seismological Bureau of Lijiang Pref.), Q.Lao and Y.Wang(both at Inst. of Structural Theory, Tongji Univ.)

The Lijiang Earthquake of February 3, 1996 ( $M7.0$ ) brought serious damage to Lijiang basin. Its seismogenic fault is considered to be Xueshan fault lying along the western edge of the basin. There is another large fault, called Lijiang-Jianchuan fault, which crosses the basin in the southern part. What is important to note is that anomalous distribution of damage to wooden houses and RC buildings was observed in the basin. This involves an issue of microzoning. Thus we studied the subsurface structure of the basin, mainly the configuration of bedrock related to the faults, on the basis of array observations of microseisms, large and small scale seismic refraction surveys and gravity survey. The results show that, the depth to bedrock reaches 1,200m or more in the central part, and bedrock subsides steeply by more than 700m along Xueshan fault at the western edge, whereas subsidence of bedrock across Lijiang-Jianchuan fault is not significant. We suggest from these results that the irregular configuration of bedrock related to the faults has played an important role in amplification of ground motions, and consequently the anomalous distribution of damage. In conclusion it is pointed that configuration of bedrock should be taken into account for microzoning study, for which combined analysis of microseisms and Bouguer gravity anomalies is very useful.

**ST3/E/51-B4** Poster **1400-09**

**DETERMINATION OF THE EPICENTERS, MAGNITUDES AND DEPTHS OF PHILIPPINE HISTORICAL EARTHQUAKES**

MA. LEONILA P. BAUTISTA1,2, Bartolome C. Bautista1,2 and Kazuo Oike1(1Dept of Earth and Planetary Sciences, Graduate School of Science, Kyoto University, Sakyo, Kyoto, Japan, 606-8502; 2Philippine Institute of Volcanology and Seismology, C. P. Garcia Avenue, UP Diliman campus, Diliman, Quezon City 1100, Philippines)

A large volume of Philippine historical earthquake descriptions from 1589 to 1897 is reviewed, evaluated and interpreted in order to estimate their magnitudes, epicenters and depths. Historical earthquake data are obtained, as much as possible, from primary sources in libraries and archives in the Philippines and Spain since the period under study is also the time when Spain started its more than 300-year colonial rule of the Philippines. More than 3000 events consisting of about 6679 intensity reports are catalogued, interpreted and their intensities determined by considering the possible effects of local site conditions, type of construction and the number and locations of existing towns to assess completeness of reporting. Epicenters of 487 historical events are determined based on the resulting generalized isoseismal maps augmented by information on recent seismicity and location of known tectonic structures. Their historical magnitudes are estimated by using previously determined magnitude-felt area equations for recent events. These equations were derived using intensity data of eighty-eight recent, shallow Philippine earthquakes. Meanwhile, depths were calculated using the depth estimation software of Musson (1998) that uses intensity at epicenter ( $I_0$ ) and felt areas at different intensity levels. Results show that about half of the evaluated events have less than 50-km depths while the rest are deeper than 50 km.

The epicenters are found to mostly lie along known tectonic structures. As compared with recent seismicity, however, the eastern Philippine region and Mindanao island showed low seismicity as compared to recent data. The quality of epicenter and magnitude determination was also assessed based on the number of intensity reports. Most earthquakes earlier than 1850 had only 9 or less reports. Good quality reports start to be collected from 1850 probably correlative to an increase in the number of reporting towns. Comparing with the number of recent earthquakes, the results show that there are still a large number of events especially during the pre-1850 period that remains "missing" or unevaluated due to meager historical accounts.

**ST3/W/48-B4** Poster **1400-10**

**SENSITIVITY ASPECTS OF SEISMIC HAZARD ASSESSMENT – CASE STUDY FOR THE GERA-RONNEBURG REGION (GERMANY)**

Dieter KRACKE, Roswitha Heinrich, Diethelm Kaiser Institut für Geowissenschaften, Friedrich-Schiller-Universität Jena, Burgweg 11, D-07749 Jena, Germany, email: kracke@geo.uni-jena.de

The region Gera-Ronneburg is part of the large Kyffhäuser-Jachymov-fault zone and displays moderate seismicity. But its seismic hazard is significantly higher than that of the surrounding area. The earthquake catalogue of Germany contains for this region, besides the well investigated Central German Earthquake (March 1872,  $I_0=VII-VIII$ ), entries of up to  $I_0=VIII$  (14th century). Epicentral intensity and coordinates of these earthquakes are considered as uncertain. In seismic hazard analysis historical events which are uncertain are often neglected. But, especially in regions of moderate seismicity, the time window considered should be extended as far as possible. Apart from the necessity to study the historical sources of the strongest 14th century earthquakes we investigate the influence of these events on the seismic hazard, taking into account all uncertainties of their size and location. Macroseismic observations, especially from the Central German Earthquake (1872), show strong lateral variations of local intensities in the epicentral area. These variations correlate with local geology. To verify the influence of site effects we recorded and analysed local events and noise at selected sites. The influence of the local site effects on the seismic hazard is included in the sensitivity analysis.

**ST3/E/54-B4** Poster **1400-11**

**EARTHQUAKE PREDICTION: PROBLEMS AND RESULTS**

Oleg KHAVROSHKIN, Vladislav Tsyplakov and Natalia Vidmont (United Institute of Physics of the Earth, Russian Academy of Sciences, B.Gruzinskaya 10, 123810 Moscow D242 Russia, Email: khavole@upei-ras.scgis.ru)

The history of the problem mentioned in the head is full of dramatic collisions. Methods of many branches of modern science are applied for its solving. Thus, we shall invent general aspects of this problem without detail: 1. The monitoring of the energetic state of investigated region. 2. Physical models. 3. The paradigm of the prediction and courses of its deadlock. 4. Nets of seismic stations. 5. What to do: abandonment of the old paradigm, the prediction in the open non-linear system, etc.

The analysis based on the scheme proposed leads to sad prognosis on complete decision of the problem in nearest 10-20 years. The only way is to abandon on the existing paradigm and development of the scheme of operative prediction of individual using (OPIU). We propose the scheme of OPIU that can be realized just now. It is based on the analysis of the emission seismic response of geophysical media in the region learned by the user, to local variations of strained state. We suppose, that the great part of seismological information is contained in the emission seismic noise. Thus, this noise must be recorded in dangerous areas permanently.

**ST3/E/04-B4** Poster **1400-12**

**NEW PROBABILISTIC HAZARD ASSESSMENT FOR SWITZERLAND**

Francesca BAY, Swiss Seismological Service, Institute of Geophysics, ETH-Hoenggerberg HPP, CH-8093 Zuerich, email: bay@seismo.ifg.ethz.ch Souad Sellami, Donat Faeh & Domenico Giardini, Swiss Seismological Service, Institute of Geophysics, ETH-Hoenggerberg HPP, CH-8093 Zuerich Juan José Egozcue, Dep. Matemática Aplicada III, U. Politècnica de Catalunya, Gran Capitán s/n, E-08034 Barcelona, Spain

Switzerland is a country of moderate seismicity but high economical risk. Probabilistic seismic hazard studies have been conducted for Switzerland in the past in terms of macroseismic intensities, mostly due to the lack of strong motion data. Engineering needs and the international norms require the assessment of the seismic hazard in terms of physical parameters. The classical probabilistic hazard methods do poorly take into account the uncertainties of the input parameters (as location, magnitude, intensities and attenuation). A method to evaluate uncertainties using Bayesian statistics, was developed and applied to estimate the return period for different intensities at different sites (Egozcue and Ruettener, Natural Hazards 14: 91-112,1997). The new earthquake catalogue is a compilation of the macroseismic earthquake catalogue which covers the time period from 1021 to 1997 for intensities 4 to 9 and instrumental data since 1942 for magnitudes ranging from 3.5 to 5.2. Empirical relationships for Switzerland are used to convert magnitudes from Intensities. Seismotectonic investigations and paleoseismological observations are under studies. Recently acquired attenuation relations (Smit 1996, Ph.D ETH Zuerich) are based on the data of the short period network of the SED which is operated since 1974 and the strong motion network which has been installed in 1992. The attenuation relations are in terms of peak ground- and spectral acceleration with respect to magnitude (ML) and hypocentral distance. The Bayesian method was further developed to deal with the incomplete part of the catalogue and applied at chosen sites in order to compare the hazard. This poster presents new results of seismic hazard assessment in terms of peak ground- and spectral acceleration and sensitivity analyses of the input parameters.

**ST3/E/08-B4** Poster **1400-13**

**THE PROBABILITY ESTIMATION OF STRONG VRANCEAN EARTHQUAKES ON THE BASIS OF MAXIMUM ENTROPY PRINCIPLE**

Victoria GINSARI (Institute of Geophysics and Geology Moldavian Academy of Sciences, Academy str. 3, Kishinev, MD-2028, Moldova, email: postmaster@geo.moldova.us)

Some results of seismic hazard assessment, conditioned by vrancean intermediate earthquakes, are presented in this paper. It was used maximum entropy principle (MEP), known by application in many engineering fields. Later, some researchers adopted MER for using in seismic hazard analysis, especially, for the estimation of the strong earthquakes recurrence. MEP indicates an alternative way for the recurrence and probability estimations not rejecting, but supplementing the results, obtained by use of least-squares fit, maximum likelihood method or some other method.

Taking into account the scatter in  $M$  max value for Vrancea zone according to the different authors investigations (7.5-8.0), and specificity of method MEP, we have been set apriory by three values of  $M$  max: 8.25, 8.0, 7.75. In this case, the recurrence interval of a magnitude 7.5 earthquake, the most realistic estimation of the observed value of the strongest vrancean earthquake during the millennium, is found to be 104, 115 or 159 years, respectively. For three apriory taken  $M$  max: 8.0, 7.75, 7.5, the magnitude of an earthquake with a 10% probability of exceedence in 50 years is determined to be 7.84, 7.66, 7.45. It should be noted that computed values of earthquake recurrence with  $M=7.0$  are invariant to  $M$  max and are equal to 37 years. The comparison of both recurrence estimations and probability density functions, obtained on the basis of MER and other methods (by using the same data set) shows that recurrence intervals for the earthquakes with  $M=7.25$ , computed by MEP, are higher, than that one computed by other method. The difference is increased considerable with increasing of magnitude. Thus, if the results, based on the MEP, were not taking into account, the seismic hazard would have been overestimated.

**ST3/E/09-B4** Poster **1400-14****SEISMIC HAZARD ASSESSMENT IN PORTUGAL, A COMPLEX INTRAPLATE SETTING**

Susana P VILANOVA, Joao F B D Fonseca, Alexandra Paula and Carlos A S Oliveira (all at IST, Av. Rovisco Pais, 1, 1049-001 LISBOA, Portugal, email: vilanovs@fisica.ist.utl.pt)

This poster describes an effort towards the assessment of seismic hazard in Portugal, emphasising the problems inherent to most intraplate settings, such as the lack of instrumental data and the uncertainties about the attenuation laws. In Portugal these difficulties are increased by the complexity of the tectonic environment: continental margin under compression on the W, zone of continental convergence on the SE, and a dense network of Late Hercynian faults cutting the basement throughout the region. Strong motion data from intraplate earthquakes in continental regions, both stable and active (excluding the very specific environments), were analysed and used to "calibrate" the existent (but limited) macroseismic database for Portugal. Different assumptions for the attenuation curves for several source zones lead to different scenarios used as input for the Seismic Hazard Analysis. We compare the results obtained in this study with previous hazard estimates.

**ST3/E/13-B4** Poster **1400-15****SEISMIC ZONATION FOR NORWAY**

LINDHOLM C. D.1, H. Bungum1, A. Dahle1, F. Nadim2, J. Holme2 and G. Woo3 1) NORSAR, Box 51, 2007 Kjeller, Norway 2) Norwegian Geotechnical Institute, Box 3939 Ullevel Hageby, Oslo, Norway 3) EQE International Ltd., 18 Mansell St., London E18AA, England

Eurocode 8 "Design provisions for resistance structures", comprising earthquake resistant design, is expected soon to be implemented in many European countries. Norway has prepared for adaption to these codes through a National Application Document, which also includes results from a national seismic zonation study. This means that earthquake resistant design can be incorporated without extensive site studies on seismic loading unless strict safety criteria are calling for a site-specific analysis. The basic seismic zonation study was done for Norwegian onshore and offshore regions with a unique international co-operation from the British side. Through this co-operation the seismic hazard results across the national boundaries were prepared in a joint effort. The results were utilizing recent ground motion attenuation models and a newly developed earthquake source zone definition, based on a quality controlled earthquake catalogue where all magnitudes were converted to moment magnitude. The results were presented in terms of peak ground acceleration (PGA) maps for four annual probabilities together with normalized pseudo velocity spectra with corresponding time histories. The smoothed maps were based on computations in a 50 km x 50 km grid, and one normalized spectrum was found representative for all Norwegian regions. Furthermore relations for computation of vertical spectra and duration were presented allowing for flexible application of the results. Soil amplification of earthquake loads were defined for three main onshore categories (rock, moraine and clay, silt and sand) for which response spectra were developed and for typical offshore soil conditions.

**ST3/E/12-B4** Poster **1400-16****SEISMIC HAZARD ASSESSMENT INCORPORATING SITE EFFECT: PROBABILISTIC MICROZONATION**

Vladimir SOKOLOV (National Center for Research on Earthquake Engineering, 200, Sec.3, Hsinhai Rd., Taipei, Taiwan, E-mail: vova@email.ncee.gov.tw); Yuri Chernov (SK IGC, 185 Dzerzhinsky pr., Stavropol, Russia 355105)

The problem of accounting for local soil effect on earthquake ground motion is especially urgent when assessing of seismic hazard - recent needs of earthquake engineering require for including effects of surface geology into hazard maps. When evaluating of seismic hazard, it is necessary to account dangerous earthquakes of various magnitudes that may occur at different distances and, therefore, to consider soil response on different excitation levels. Recently developed by authors method of seismic hazard calculations allows us to create hazard maps involving influence of local soil conditions using soil/bedrock spectral ratios. Probabilistic microzoning maps may be constructed showing Macroseismic Intensity, Peak Ground Acceleration, Response and Design Spectra, as well as ground motion time series (accelerograms) for various return periods (probability of exceedence), that allow to optimize engineering decisions. The results of the approach utilization are presented.

**ST3/E/11-B4** Poster **1400-17****COMPARISON OF RECENT STRONG EARTHQUAKES EFFECT AND SEISMIC HAZARD MAPS: AN OPPORTUNITY TO EVALUATE HAZARD ASSESSMENT TECHNIQUE**

Vladimir SOKOLOV (National Center for Research on Earthquake Engineering, 200, Sec. 3, Hsinhai Rd., Taipei, Taiwan, E-mail: vova@email.ncee.gov.tw); Yuri Chernov (SK IGC, 185 Dzerzhinsky pr., Stavropol, Russia 355105)

Results of seismic hazard analysis are used as a basis for engineering decisions, and design ground motion parameters, so-called "basic seismicity", (MMI (MSK) intensity, PGA values and response spectra) are dictated in Building Codes. Recent strong earthquakes, occurred throughout the world, showed that the assessment of seismic hazard in some respective regions must be revised. New assessment of "basic seismicity" in terms of MMI (MSK) intensity, PGA values and response spectra were carried out for some regions of the former USSR (the Caucasus, Central Asia, Sakhalin island) using technique of probabilistic seismic hazard assessment developed by the authors. When employing the method, we used the data on the seismicity that were available before recent strong earthquakes. Therefore, this study may be considered as a test of the approach. The results demonstrate that our assessment of "basic seismicity" (MSK intensity, PGA values and response spectra) for 1000-years return period (0.05 probability of exceedence in 50 years) confirm the observed data, and they may be used as a reliable basis for Building Code provisions.

**ST3/E/55-B4** Poster **1400-18****SUBSURFACE STRUCTURE BELOW OHMI BASIN, SOUTHWEST JAPAN, AS DEDUCED FROM GEOPHYSICAL EXPLORATION AND ITS POSSIBLE EFFECTS ON EARTHQUAKE HAZARD AND RISK**

Keiichi Nishimura(Faculty of Informatics, Okayama University of Science, Okayama 700-0005, Japan, email: nisimura@big.ous.ac.jp), Masao Komazawa (Geological Survey of Japan, Tsukuba 305-8567, Japan, email: koma@gsj.go.jp), Tomoki Tsutsui(Aso Volcanological Laboratory, Kyoto University, Kumamoto 869-1404, Japan, email: tom@aso.vgs.kyoto-u.ac.jp) and Masao Takabayashi (Seta Senior High School, Ohtsu 520-2132, Japan, email: setahspc@mx.biwa.or.jp)

Ohmi basin, situated to the east of Lake Biwa, southwest Japan, is a sedimentary basin filled with late Pliocene-to-Pleistocene lacustrine deposits and surrounded by mountains both on the east and on the south. In the basin, anomalously high seismic intensities have been recorded from large historic earthquakes, including fairly distant Nankai-trough events that occurred south off Honshu Island. This involves a issue of microzoning. Thus we studied the subsurface structure below the basin using data of seismic refraction exploration, long-period microtremors and Bouguer gravity anomaly; in addition, well information from two deep drillings, performed inside the Lake and in the eastern part of the basin, was used to constrain structural models to be obtained. The result of analysis shows fairly complicated configuration of bedrock below the basin: the thickness of lacustrine deposits is greatest near along the eastern edge of the basin, possibly implying fault-related subsidence of bedrock; toward the west, after being thinnest in the central part of basin, the deposits are thickened again near the coast of the Lake where they are overlain by reclamation land. It is highly probable that such complicated surface geology has significant effects on seismic ground motion, thereby bringing anomalous distribution of earthquake damages in the basin.

**ST3/E/16-B4** Poster **1400-19****UNCERTAINTY STUDIES IN SEISMIC HAZARD ASSESSMENTS APPLIED TO SELECTED SITES IN CENTRAL EUROPE**

Gottfried GRUENTHAL, Rutger Wahlstrom (both at GeoForschungsZentrum Potsdam, Telegrafenberg, 14473 Potsdam, Germany, email: ggroe@gfz-potsdam.de)

An essential element in the current practice of seismic hazard assessments consists in the consideration on uncertainties in the procedure. The presented seismic hazard study is based on a logic tree approach applied to selected sites in seismically most active parts of central Europe. The influence of various input parameters and their combinations is analyzed with respect to resulting mean, median and fractiles of the hazard curves. Emphasis is given to constraints on attenuation relations of peak and spectral accelerations as well as intensities, focal depth distributions, magnitude frequency relations, lower and upper bound magnitudes (the latter being also depth dependent) and the source regionalizations.

**ST3/E/56-B4** Poster **1400-20****THE GSHAP WORLD MAP OF SEISMIC HAZARD**

D. GIARDINI (ETH, 8093 Zurich, Switzerland, email: giardini@seismo.ifg.ethz.ch) G. Grunthal (GFZ, Potsdam, Germany), H. Gupta (NGRI, Hyderabad, India), D. Mayer-Rosa and S. Sellami (ETH, Zurich, Switzerland), K. Shedlock (USGS, Boulder, USA), P. Zhang (SSB, Beijing, China), T. Annaka (Tokyo Electric Power Services, Japan), M. G.-Ashtiany (IIEES, Tehran, Iran), K. Atakan (Bergen University, Norway), S. Balassanian (NSSP, Yerevan, Armenia), P. Basham (CTBTO, Vienna, Austria), C. Dimate (Ingeominas, Bogota, Colombia), M. Erdik (Kandilli Obs., Istanbul, Turkey), M. Garcia (CSIC, Barcelona, Spain), Giesecke (CERESIS, Lima, Peru), K. McCue (AGSO, Canberra, Australia), R. McGuire (Risk Engineering, Boulder, USA), R. Musson (BGS, Edinburgh, UK), S. Riad (Assiut University, Cairo, Egypt), D. Slejko (OGS, Trieste, Italy), V. Ulomov (JIPE, Moscow, Russia), the Working Groups of the GSHAP regions: Central-North America, Central-Northern Europe, Eastern Asia, Northern Eurasia, Ibero-Maghreb, Adria, the working Groups of the projects: PILOTO, CAUCAS, RELEMR, SESAME, PAIGH-IDRC, EU-QSEZ-CIRPAN.

The Global Seismic Hazard Assessment Program (GSHAP) was launched in 1992 by ILP and ICSU and endorsed as a demonstration program by the UN/IDNDR. The GSHAP promoted a regionally co-ordinated, homogeneous approach to seismic hazard evaluation. Regional activities were concluded in 1992-98; the results have now been compiled in a uniform set of databases and in a world map of seismic hazard expressed in PGA. Support for the GSHAP implementation was provided by ING, Roma, by national and regional institutions, by IASPEI, UNESCO, ICSU, ILP, IDNDR, EU, NATO, INTAS and IGCP. All GSHAP materials (regional report, maps, datasets) can be retrieved on the GSHAP web site at <http://seismo.ethz.ch/GSHAP/>. The GSHAP world map of seismic hazard will be presented for the first time at the IUGG assembly and will be available for distribution at the assembly.

**ST3/P/08-B4** Poster **1400-21****MEASUREMENTS OF HORIZONTAL CRUSTAL DEFORMATIONS AT THE BAIKAL GEODYNAMIC POLYGON**

VI. KUPKO, V.Strelets (all at Kharkov State Research Institute of Metrology, Ukraine, fax +380 572 43 61 93)

Results of horizontal crustal deformations in the Baikal Lake region will be reported. A high-precision range-finder developed and produced at the Kharkov State Research Inst. Of Metrology is used to detect three-year crustal movements. The used range-finder is based on a double frequency optical laser interferometer and is able to measure a distance from 1m to 5 km with an uncertainty of the order 0.05mm. Yearly variations of +11.7 mm/1.5 km; +12.3 mm/3 km; +6.2 mm/700 m ; -0.3 mm/700 m are detected in various directions. Possible geophysical interpretations will be given.

**ST3/P/09-B4** Poster **1400-22****HIGH PRECISION LASER COMPLEX TO MONITOR LINEAR-ANGULAR MOVEMENTS IN GEOPHYSICS**

VI.KUPKO, S.Kovshov, I.Lukin, V.Sobol, G.Pushkariov(all at Kharkov State Research Institute of Metrology, Ukraine, fax +380 572 43 61 93)

The Kharkov State Research Institute of Metrology has developed a new high precision laser complex for linear-angular measurements in a range 1m to 5 km with an uncertainty of 0.05 mm (linear) and in a range ±180 degrees (horizontal) with an uncertainty of 2" (angular). The complex combines the following main components: a high precision laser range-finder which is heading the state hierarchy scheme; an angular measuring system based on photo-electric transformers; a complex system for measurements various parameters of atmosphere (temperature, pressure, humidity); a special algorithm to take a current air refraction index into account. The developed complex can operate under influence of non-stationary disturbances. Some technical details of the complex and first obtained field measurement results will be given in this presentation.

**ST3/P/10-B4** Poster **1400-23****VERIFICATION COMPLEX FOR GEODETIC LENGTH MEASURING EQUIPMENT**

VI. KUPKO, N.Kravchenko (all at Kharkov State Research Institute of Metrology, Ukraine, fax +380 572 43 61 93)

High precision length measurements in a range from meters to kilometers are of great



importance in geodesy since it is necessary to detect earth crustal deformations as well as to establish reference networks and monitor conditions of great industrial constructions. To verify all the used instrumentation, special laser interferometric comparators are usually created. In this presentation we report on a unique verification complex consisting of length base of 168 m created in Armenia. This base is located in an underground tunnel (depth is 70 m, diameter is 4 m). A complex consists of various retroreflectors, microscopes, half-transparent mirrors, centering devices, railways etc. Performed interferometric measurements show an achieved accuracy of the length of the base of the order of  $\pm 0.03$  mm (standard error). The first obtained results on observations of crustal deformations using the length base will be reported.

**ST3/E/57-B4** Poster **1400-24**

#### MACRO SCALE MODELLING OF CATASTROPHIC NATURAL HAZARDS

ADRIAN STEWART, and Dr Claire McQueen, (both at EQE International Ltd, 500 Longbarn Boulevard, Warrington, WA2 0XF, UK. Tel:- +44 1925 838372, fax =44 121987 654, Email: astewart@eqe.co.uk, cmcqueen@eqe.co.uk.

Economic losses from Natural disasters over the last few decades have been enormous, as demonstrated by Hurricane Andrew in the US. The impact on the global economy can reverberate for years after a single event. Assessing the risk to regions and countries is essential in the context of enabling International Organisations, Governments and International Industry and Commerce to plan, mitigate and manage losses. In terms of risk from damaging earthquake or windstorm events, the risk is a function of the hazard intensity combined with the vulnerability of the properties within any given unit or area. The deterministic results of such studies may also be combined with expected frequencies to obtain probabilistic estimates of risks. In order that the losses expected within an area from an event be estimated accurately, the vulnerability functions and hazard models should be representative of the scale of the area that they are located in. Scale is an important issue. The Hazard Model needs to reflect the reduced risks expected over larger areas. However, the detail needs to remain in order that the spatial resolution of the hazard across an area is accurately represented. The question is whether vulnerability and hazard models can be created for a specific scale, or whether it is possible to calculate losses on a detailed grid and aggregate consistently at any macro scale.

**ST3/L/01-B4** Poster **1400-25**

#### THE S. BALKAN DBANK OF SHALLOW AND INTERMEDIATE DEPTH EARTHQUAKE MACROSEISMIC DATA

B. C. Papazachos, A. A. Savaidis (both at Geophysical Laboratory, University of Thessaloniki, GR-54006 Greece); Ch. A. PAPAIOANNOU, C. B. Papazachos (both at ITSAK, P. O. Box 53 Foinikas, GR-55102 Thessaloniki, Greece, email: chpapai@itsak.gr)

In the present paper information is given on the data bank of macroseismic observation and the basic source parameters of earthquakes in the southern Balkan area starting from the 6th century BC. This data bank includes about 37500 macroseismic observation of 577 strong ( $M \geq 6.0$ ) shallow earthquakes for the time interval 550 BC-1996 AD, of 300 shallow earthquakes of the present century with magnitude  $4.1 \leq M < 5.9$  and 60 intermediate depth (60km  $< h < 150$ km) earthquakes of the present century with magnitude  $5.5 \leq M < 7.9$ . The input data for this data bank were either site-specific intensities or grouped data derived from published macroseismic maps. All the intensity values were converted to the MM scale. For all cases the geographical coordinates are given. The intensities are homogeneous, that is, the different degree of vulnerability of structures through the time periods spanned by the data was also considered. The data were elaborated using published scaling empirical relations, based on present century data, holding between macroseismic intensities versus distance and instrumental magnitude, in order to determine the macroseismic magnitude. Furthermore based on the macroseismic pattern and the scaling relations, the epicenter and the magnitude of the historical earthquakes were determined. For cases of shallow earthquakes where an adequate number ( $N > 10$ ) of observations was available, synthetic isoseismals were compiled considering anisotropic radiation of the seismic energy at the source.

In the dBank for every populated site in the southern Balkan area there are intensities caused by at least 20 earthquakes. The macroseismic observations for every site and the magnitude and epicentral distance in the data bank were used both for the determination of site specific attenuation relations, which are important for any hazard assessment, as well as a hazard map depicting the distribution of the observed intensities  $I > VIII$  for every site. Moreover, a map depicting the maximum observed intensities for the study area was compiled.

**ST4** Monday 26 – Wednesday 28 July

#### EARTH STRUCTURE AND GEODYNAMICS

Location: Medical School EG12 LT4 and Ext NG26 LT6\*

Location of Posters: Arthur Thompson Hall

*Note:	Monday 26 July	Room No. EG12 LT4
	Tuesday 27 July	Room No. Ext NG26 LT6
	Wednesday 28 July	Room No. Ext NG26 LT6

**Monday 26 July AM**

Presiding Chair: I.T.Kukkonen (Geological Survey of Finland, Espoo, Finland)  
Concurrent Poster Session

#### THERMAL STUDIES

**ST4/W/13-B1** **0840**

#### EVALUATION OF THERMALLY RELEVANT PROCESSES FOR TEMPERATURE PROGNOSIS IN ALPINE TUNNELS

Thomas KOHL, Andreas Busslinger, Ladislaus Rybach Institute of Geophysics ETH Hönggerberg, CH-8093 Zurich, Switzerland

The present day temperature field results from the complex interplay of several factors and processes. The analyses of the subsurface temperature fields have been performed customarily by treating individually and separately involved mechanisms such as steady-state topography effects, transient palaeoclimatic effects, lateral and vertical heterogeneities,  $P/T$  dependency of thermal parameters, forced and free convection, radioactive heat production, erosion / sedimentation. Such treatment neglects the potentially important interplay of these effects and processes. In this paper a combined 3-D analysis is presented for a well studied situation along a major Alpine Swiss engineering project: the new Gotthard base tunnel

project which will cross the mountains at a level of maximum 550 m a.s.l. and below an overburden of up to 2500 m. The design of the tunnel ventilation and climate system during construction and operation requires a sophisticated temperature prognosis which has to account for all possible thermal transport mechanisms.

The basic concept for our numerical (FE) study is the evaluation of the topographical influence on transient temperature signals in mountain areas. In the important depth range, primary thermally relevant effects result from morphological situations and fluid advection. Also important for the alteration of the local temperature fields are the climatic history since the last Ice Age and the combination of uplift and erosion. The results highlight the necessity for topographical correction of temperature data in the areas not affected by fluid movement which yield maximum temperatures above 40°C. In the highly permeable fault zones, however, the fluid advection may wash out any transient effect.

**ST4/W/65-B1** **0900**

#### NUMERICAL MODELS OF THE CONDUCTIVE THERMAL REGIME IN LONG VALLEY, CALIFORNIA

S. HURTER and D. Pribnow (all at: Joint Geoscientific Research GGA, Hannover, Germany)

Within the International Continental Drilling Program (ICDP) and Long Valley Coring Project (LVCP), numerical models are applied to explain the lower than expected temperatures down to depths of 3 km and to understand the deeper thermal regime of this active caldera. Conductive and convective heat transport at various rates and timescales are expected. Full advantage is taken from the fact that numerical models allow the effects of several processes to be evaluated separately or jointly. The first step was to set up a background steady state thermal field neglecting fluid flow. The model is based upon knowledge of the regional setting surrounding the caldera so that future and more complete models can distinguish local anomalies due to the caldera itself from the regional thermal field. Long Valley caldera is situated within the transition from Sierra Nevada to Basin and Range, two contrasting physiographic provinces. Sierra Nevada has thicker stable crust, lower heat flow at the surface, while Basin and Range is characterised by volcanism, higher seismicity, normal faulting, higher upper mantle temperatures and higher heat flow. An E-W section was discretized into a 2-D model. The heat conduction equation was solved by a finite difference scheme (SHEMAT) at 500 x 220 gridpoints. The surface temperature was fixed at 8 °C. The side boundaries were insulating. Radioactive heat production in the crust followed an exponential decrease with depth. Model temperatures are lower than those measured in the Long Valley Exploration Well. In a second step, the existence of a long-lived magma chamber at a depth of 7km underneath the eastern half of the caldera was examined by imposing a temperature of 800 °C at each magma chamber node. The resulting model temperatures at 2km depth are 200 °C higher than those measured. Transient models of the cooling of this magma chamber suggest that its thermal signal should still be detected in the present-day, more than 750 000 years since the great Bishop Tuff eruption. However, the conductive background model in the absence of magma at depth matches the measured temperatures much better.

**ST4/E/14-B1** **0920**

#### GEOTHERMAL CHARACTERISTICS OF THE RIES IMPACT STRUCTURE (GERMANY)

Yuri POPOV (Moscow State Geological Prospecting Academy, Miklukho- Maklai str., 39-1-191, Moscow 117485, Russia, email: Yurpopov@mgga-sec.msk.ru) Jean Pohl and Heinrich Soffel (Institute of Geophysics, Muenchen Ludwig-Maximilians-University, Theresien str. 41, D-80333 Muenchen, Germany, email: pohl@alice.geophysik.uni-muenchen.de, soffel@magbakt.geophysik.uni-muenchen.de) Raissa Romushkevich (Moscow State Geological Prospecting Academy)

Rock thermal conductivity measurements were carried out on 530 dry and water-saturated cores from the 1206m deep Noerdlingen borehole drilled in 1973 in the Ries impact structure (Bavaria, Germany). It was found that different structural-lithological complexes and different rock types are characterized by essentially different values of both thermal conductivity and thermal inhomogeneity factors. The thermal conductivity data from dry rocks and the porosity, calculated using theoretical models and experimental data, correlate well with other logs, especially with sonic, electric and neutron gamma logs. Thermal anisotropy of gneisses is found to be negligible although significant anisotropy for these rocks is usually observed. Average heat flow density values vary from 117 mW/m<sup>2</sup> in the depth interval of 70-250m to 68mW/m<sup>2</sup> in the depth interval of 250-500 m, to 72mW/m<sup>2</sup> in the depth interval of 500-870m and are predicted to be 77 mW/m<sup>2</sup> in the depth interval of 870-1200m, i.e. 33-45% higher for these depths than in previously published data. Significant differences in temporal variations of the temperature gradient determined from the temperature logs measured at different times after termination of drilling (from 1 day up to 10 months) indicate significant variations in strata permeability and fluid activity.

**ST4/W/84-B1** **0940**

#### TECTONIC LEAKAGE OF FAULT BOUNDED AQUIFERS SUBJECT TO NON-ISOTHERMAL RECHARGE: A POSSIBLE MECHANISM GENERATING THERMAL PRECURSORS TO SEISMIC EVENTS

Valiya M. HAMZA (Observatório Nacional – CNPq, Rio de Janeiro, Brazil)

The thermal consequences of flow transients generated by deformation induced leakage at fault zones intersecting confined aquifers have been examined using a simple analytical model. The recharge of the aquifer is assumed to take place by vertical infiltration through the confining layers. The energy equation relevant in this case can be derived by evaluating enthalpy fluxes associated with lateral and vertical components of fluid flows as well as that due to volume changes in the permeable layer, generated by deformation induced alterations in the hydraulic head. Results of numerical simulations indicate that thermal transients arise during the stress build-up period as a consequence of mixing of the infiltrating fluids with those in the aquifer. Steady state conditions are attained within relatively short periods of time due to rapid energy exchange. On the other hand, when deformation ceases infiltration is drastically reduced and consequently return to equilibrium thermal conditions is quite rapid. Thus, under favorable conditions, relatively small changes in deformation pattern can easily lead to abrupt and substantial changes in the thermal regime. Model results also indicate that the characteristics of thermal precursors depend on a number of factors such as duration of stress build-up, direction of recharge flux, permeability contrast between the confining layer and the aquifer as well as local geothermal gradient.

Examination of available observational records of temperature variations in bore holes in tectonically active areas indicates that occurrence of transient thermal anomalies with characteristics similar to those predicted by the 'deformation induced leakage' model is not uncommon. Examples are presented illustrating model fits to thermal transients, identified as precursors to seismic events, in Firjusa (Turkmenistan) and Izu peninsula (Japan). The results indicate the possibility of obtaining complementary information on processes controlling fluid flow during pre-seismic periods. It appears that the occurrence of thermal anomalies associated with small scale tectonic deformation may be quite widespread, but its detection would require long term monitoring using high precision temperature sensors.



**ST4/W/46-B1 1000****THERMAL EVOLUTION, TECTONIC SUBSIDENCE ANALYSES AND DEEP GEOPHYSICAL CHARACTER OF BOHAI BAY BASIN, EAST CHINA**

HU Shengbiao and Wang Jiyang (both at Institute of Geology, Chinese Academy of Sciences, Beijing 100029, China, Email: sbhu@mail.igcas.ac.cn)

Heat flow measurements and thermal history reconstruction, using vitrinite reflectance and apatite fission track data, indicate that Bohai Bay Basin is characterized by lower present-day heat flow varying between 50 and 65mW/m<sup>2</sup> with a background heat flow value of 63.6mW/m<sup>2</sup>, and that the basin experienced a much higher heat flow (70-90mW/m<sup>2</sup>) period prior to 25Ma. Tectonic subsidence analysis shows that the subsidence of Bohai Basin can be divided into two phases: earlier (25-50Ma) initial (rift) and later (Since 25Ma) thermal subsidence. The earlier rift phase is composed of two sub-rift episodes with quick subsidence, and the later thermal subsidence was superimposed with rapid subsidence since 12Ma, which can be related to crustal isostasy induced by mantle decoupling as revealed by seismic tomography. The lower present-day heat flow and the higher palaeo-heat flow corresponding to initial subsidence stage as well as the typical rift subsidence style in Bohai Basin support its feature of intraplate, pull-apart rift basin, and provided with some insight to the tectonic-thermal evolution of the basin.

**ST4/W/38-B1 1100****HEAT FLOW IN AND AROUND THE MARGINAL SEAS OF THE NORTHWEST PACIFIC**

Lili JIANG (Institute of Geophysics, Chinese Academy of Sciences, 11 Datun Road, Chaoyang District, Beijing 100101)

In this paper, the marginal seas of the northwest Pacific include the Bering Sea, Okhotsk Sea, Japan Sea, East China Sea, South China Sea and Philippine Sea. The adjacent areas comprise the continent around these marginal seas, the islands and the trenches outside of these seas. Since the first heat flow measurements in the area were taken in 1957 around the Japanese islands and the first marine heat flow measurements were carried in Bering Sea in 1961, more than 4,000 heat flow values have been obtained. The numerical value of the mean heat flow in the area is somewhere between those of the continent and ocean. The results of the heat flow measurements between the east of Eurasia plate and the west of Pacific Ocean Plate imply that the thermal state of the lithosphere in this area is also the thermal transition zone between continent and ocean plate. The thermal anomalies of these marginal seas and their adjacent areas have four characteristics: First, there is no clear borderline among continent, marginal seas and islands in the heat flow anomaly bodies. Second, the low heat flow anomaly boundary gives the outline of the trench system in the northwest Pacific Ocean. Third, in general, the high heat flow anomaly bodies trend towards NE direction, the exceptions being Komandorskaya Basin, the Izo-Ogasawara(Bonin) arc and Marina Trough, they extend towards NW direction. Finally, the area of high heat flow corresponds to strong tectonic activity and the most important is that the local geology structure controls the shapes of local heat flow anomaly bodies.

**ST4/W/22-B1 1120****HEAT FLOW PATTERN AND THERMAL STRUCTURE OF LITHOSPHERE IN CONTINENTAL AREA OF CHINA**

WANG Ji-Yang (Institute of Geology, Chinese Academy of Sciences, Beijing 100029, China, E-mail: JYWLPX@public3.bta.net.cn)

To date, altogether 730 heat flow values were obtained in continental area of China. The mean heat flow value turns out to be 65.2±1.6 mW/m<sup>2</sup>, which is in good accordance with the global continental mean of 65±1.6 mW/m<sup>2</sup> (Pollack et al., 1993). Heat flow pattern in continental area of China is characterized by "high in the East & South" and "low in the North & West". The lowest heat flow appears in the NW part of China. For example, the average heat flow in Tarim Basin exhibits to be 50mW/m<sup>2</sup> and in Jungar Basin, 45mW/m<sup>2</sup>. The highest heat flow has been observed in southern Tibet where the mean value may reach up to 80-100mW/m<sup>2</sup> and more. There's a good relationship between heat flow and the geological age of the terrain. But there's no good correlation between heat flow and the last tectono-thermal events of the terrain. Generally, relatively high heat flow is observed in old terrain affected by the latter tectonic activity and/or tectono-thermal events. Thermal structure of the lithosphere in continental area of China exhibits that there exists so called "hot crust & cold mantle" thermal structure for the western part of China whereas "cold crust & hot mantle" is inherent for the eastern part of China. The above-mentioned heat flow pattern and thermal structure of lithosphere are resulted from the Pacific plate subduction from the East and continent-continent collision between India and Eurasia plates since Meso-Cenozoic era.

**ST4/E/13-B1 1140****UNCERTAINTIES OF LITHOSPHERIC THERMAL MODELS: THE BOUNDARY BETWEEN FACT AND FICTION**

Ilmo T. KUKKONEN and Jarkko Jokinen (both at Geological Survey of Finland, P.O. Box 96, FIN-02151 Espoo, Finland, e-mail: ilmo.kukkonen@gsf.fi) Ulf Seipold (GeoForschungsZentrum Potsdam, Post Box 600751, 14407 Potsdam, Germany, e-mail: seip@gfz-potsdam.de)

Any geothermal model used for calculating the lithospheric thermal regime is sensitive to uncertainties in the model parameters, namely, thermal conductivity, its temperature and pressure dependence, heat production rate and applied boundary conditions (surface heat flow, mantle heat flow or mantle temperature). We have investigated the uncertainties of lithospheric conductive models using a random simulation technique with a 4-layer model representative of 155 km thick shield-type lithosphere (50 km thick 3-layer crust). Model parameters were varied according to predetermined probability functions and standard deviations were calculated for lithospheric temperature and heat flow density after 1500 independent simulations. For instance, assuming relative uncertainties of 20-30 % for the individual parameters, the highest variations in Moho temperatures (+/- 40-50 K) are due to conductivity and heat production, whereas the temperature and pressure dependencies of conductivity have much smaller effects (< 20 K). When all parameters vary simultaneously, it does not seem possible to estimate the Moho temperature with an uncertainty smaller than +/- 100-130 K, and in the mantle the value increases approximately linearly to about +/- 220-270 K at the base of the lithosphere. Improving results from these values requires deep temperature and heat flow estimates independent of the model as well as of heat flow measurements in shallow boreholes, which often are disturbed by palaeoclimatic or hydrogeological factors.

**ST4/E/16-B1 1200****THERMAL STRUCTURE OF THE LITHOSPHERE SURROUNDING WESTERN MARGIN OF INDIA AND LATE CRETACEOUS GEODYNAMICS**

O.P. PANDEY and P.K. Agrawal (National Geophysical Research Institute, Uppal Road, Hyderabad 500 007, India email: postmast@csngri.res.nic.in)

Passive continental margin of western India is an elongated, anomalous, degenerated, seismically active and rifted part of the Indian peninsula. In the present paper, we analyse the available geothermic data to study the sublithospheric thermal structure. The anomalous nature of the lithosphere beneath this region is well reflected in the heat flow and geothermal gradient distribution, the latter varying widely from 15°C/km to 78°C/km with an average of over 30°C/km. The gradients are particularly high in the north Cambay graben, Konkan belt, northern and eastern part of the Bombay offshore and off the Cochin coast. The average gradients in the first three regions herein referred to as West Coast Thermal Anomaly Zone, are of the order of 50 to 60°C/km. Curie depth analysis using MAGSAT data also indicates a high gradient of about 31°C/km within the upper crustal column. As expected, heat flow is quite high in the West Coast Thermal Anomaly Zone averaging over 80mW/m<sup>2</sup>. In the major part of this region, gravity anomalies usually have positive bias in an overall low gravity environment, indicating shallowing of Moho 18 to 30km. The asthenosphere beneath this margin is situated between 30 and 70km. The unusual thermal behaviour of this region could be ascribed to catastrophic and geodynamic events which took place during the last 130 Ma.

**ST4/E/26-B1 1220****VARIATIONAL MODELLING OF RADIOGENIC HEAT DISTRIBUTION IN THE CONTINENTAL CRUST**

R. N. SINGH (CSIR Centre for Mathematical Modelling and Computer Simulation, Wind Tunnel Road, BANGALORE 560 037, India, email: rnsingh@cmmacs.ernet.in) Ajay Manglik (National Geophysical Research Institute, Uppal Road, HYDERABAD 500 007, India, email: postmast@csngri.res.nic.in (Attn: AMANGLIK))

The linear surface heat flow-heat generation relationship has been used to quantify the nature of shallow vs. deep source for the surface heat flow.

The radiogenic heat sources are concentrated in the shallow regions in the continental crust and this contributes significantly to the surface heat flow and temperature distribution in the crust. Amongst various models of radiogenic heat sources, the exponential model has been shown as an optimal model using a variational approach to one dimensional steady heat conduction equation by Singh & Negi(1980 a,b). This approach has been extended to include advective heat transport by Bodri & Cermak (1993) who again obtained an exponential model plus a constant term for the radiogenic heat distribution. In the present work, the above studies have been generalised for a stratified model of the crust undergoing both heat conduction and advection transports using a variational approach. The results give a model of the radiogenic heat distribution which is more complex than a simple exponential function. Numerical results show that the concentration of radiogenic sources at various depths would vary with strength of fluid advection for a given set of values of surface heat flow, surface radiogenic heat concentration and reduced heat flow.

Monday 26 July PM

Presiding Chair: W.Mooney (US Geological Survey)

**CRUSTAL STRUCTURE AND DYNAMICS****ST4/W/34-B1 1400****HETEROGENEOUS CRUSTAL STRUCTURE IN FOREARC SLOPE OF THE JAPAN TRENCH USING OCEAN BOTTOM SEISMOMETERS**

Gou Fujie and Junzo KASAHARA (both at Earthquake Research Institute, University of Tokyo, 1-1-1 Yayoi, Bunkyo, Tokyo, Japan, Email: fujie@eri.u-tokyo.ac.jp) Shinobu Ito (Geological Survey of Japan, 1-1-3 Higashi, Tsukuba, Ibaraki, Japan, Email: ito@gsj.go.jp) Ryota Hino (Research Center for Prediction of Earthquakes and Volcanic Eruptions, Tohoku University, Sendai, Japan, Email: hino@aob.geophys.tohoku.ac.jp) Masanao Shinohara (Faculty of Science, Chiba University, Chiba, Japan, Email: mshino@earth.s.chiba-u.ac.jp) Kiyoshi Suyehiro (Ocean Research Institute, University of Tokyo, 1-15-1 Minamidai, Nakano, Tokyo, Japan, Email: suyehiro@ori.u-tokyo.ac.jp)

A seismic reflection-refraction experiment with Ocean Bottom Seismometers(OBS's) was conducted in 1996 in the Japan Trench in order to clarify the crustal structure in the subduction area. The experiment was conducted along two lines, one was parallel to the trench axis, which is called Line2, and another was perpendicular to the axis, which is called Line1.

To determine the velocity structure beneath the both lines, we applied the tau-p, reflection analysis of multi channel hydrophone streamer data and the iterative non-linear traveltimes inversion method, which uses traveltimes of reflections as well as of first arrivals.

Along Line 2, the depth of the plate boundary is not uniform and we found velocity anomaly around there. The seismic activity since 1985 in this area also has not been uniform. According to the observed data along the Line 1, the dipping angle of subducting Pacific Plate becomes steeper toward west of around 143.5E. We observed the oceanic Pn phases at 142.9E station from the trench side shots at distance further than 70km.

**ST4/E/35-B1 1420****WHY ARE THE PALAU AND YAP TRENCHES SO DEEP AND BARE ?**

Kazuo KOBAYASHI (Japan Marine Science and Technology Center, 2-15 Natsushima, Yokosuka 237-0061 Japan, email: kobayashik@jamstec.go.jp)

Rates of plate convergence at the Palau and Yap Trenches in the western Pacific are very small. Neither deep-focus earthquakes nor active volcanoes are observed in the arcs adjacent to the trenches. Nevertheless, both trenches are deeper than 8,000 m. In the north-central Yap Trench a deep as great as 8946 m was recently found by R. V. Yokosuka. In spite of large amounts of slope failure deposits collapsed from the steep trench inner (landward) walls identified by visual observation from a manned submersible Shinkai 6500, most of the axial zones of these trenches are kept bare with V-shaped bathymetric cross-section. The Palau and Yap Islands composed of old volcanic and metamorphic rocks fringed with coral-reef limestones are situated in abnormally close proximity of the trench axis and being uplifted, although no evidence of collision is found. I would like to draw your attention to high rates of northwestward horizontal motion of both trenches relative to underlying asthenosphere amounting to about 9 cm/yr. It seems likely that resistance of subducted slab moving on the asthenosphere generates uplifting force in front of the moving slab just like a plow working in the farmyard in addition to enhanced tectonic erosion along the subducting slab.

**ST4/W/12-B1** 1440**CRUSTAL STRUCTURE OF ICELAND FROM RECEIVER FUNCTIONS**

V. SCHLINDWEIN, G. R. Foulger, Z. J. Du, (Department of Geological Sciences, University of Durham, Science Laboratories, South Road, Durham DH1 3LE, UK)

Despite a wealth of geophysical data available for Iceland, the nature of the crust there is poorly understood. The long-standing debate, whether the Icelandic crust is thin and hot or thick and cold, focusses on a key problem: What and where is the "Moho" underneath Iceland? Some seismic refraction profiles show reflections at 20-35 km depth which are interpreted as the "Moho", but on other profiles a similar reflector is absent. We take a new approach to the problem using teleseismic receiver functions. The HOTSPOT network, a temporary seismic network consisting of 30 broadband seismometers distributed over all Iceland, provided excellent data for this purpose. Receiver functions are sensitive to velocity contrasts beneath the seismometer site, such as the Moho or intracrustal reflectors. However, they do not contain information about absolute seismic velocities. We overcome this problem by incorporating independent geophysical data into the study. Our first results indicate considerable lateral variability of crustal structure. The waveforms of the receiver functions show strong azimuthal dependence. Scattered energy characterizes the receiver functions close to active volcanoes, for example at Askja. In general, seismic velocities increase rapidly in the upper crust. Below about 10 km depth, vertical velocity gradients are small. A velocity inversion occurs in some areas. A strong P-S converted phase stemming from a potential first order discontinuity at depths of 20-35 km is generally not observed.

**ST4/W/61-B1** 1500**VARIATION IN THE CRUSTAL STRUCTURE BENEATH NORTH-WESTERN ICELAND**

DU, Z.J. and Foulger, G.R.

Five broadband seismic stations were operated in northwest Iceland from 1996 - 1998, as part of the Iceland HOTSPOT project of Durham University. Structures beneath these stations were determined by the modelling and the joint inversion of teleseismic P-wave receiver functions and regional surface wave phase velocity data. More than 40 teleseismic events and a few regional events containing high-quality surface wave trains were used. Although the middle period passband of the seismograms contains micro oceanic noise, which prevents us from interpreting some structural details, the inversion reveals major crustal features.  $P_{-}(s)$  conversions, appearing about at  $3s$  after the P wave, are observable on nearly all traces of the radial receiver functions. These conversions characterize a reflector at depths greater than about  $23s$  (1t km). The other common major crustal features are high velocity gradients in the upper crust, and high but nearly constant velocity in the middle crust. The data also clearly indicate azimuthal structural variation. However this could not be verified using tangential arrivals because of high noise contamination.

**ST4/E/05-B1** 1520**CRUSTAL THICKNESSES IN SE BRAZILIAN SHIELD BY RECEIVER FUNCTION ANALYSIS: IMPLICATIONS FOR ISOSTATIC COMPENSATION**

M. ASSUMPCAO (IAG-USP, Sao Paulo, Brazil, 05508-900, Email: marcelo@iag.usp.br); D. James (Carnegie Institution of Washington) and Arthur Snoke (Virginia Tech, USA).

The Brazilian Lithosphere Seismic Project (a joint project by University of Sao Paulo and Carnegie Institution, 1992-1998) operated 20 temporary broad-band stations (STS-2 with RefTeks) in the SE Brazilian shield. The area, about 1000 km long and 300 km wide, covers different geological provinces: an Archean block in the Sao Francisco craton, the adjacent Brasiliano (700-500 Ma) fold belts, and the Parana basin of Paleozoic origin. Crustal thicknesses were estimated for 16 sites using receiver functions. The P-to-S Moho converted phase was clearly identified at most sites. Crustal thicknesses were estimated using an average crustal P-wave velocity of 6.45 km/s.  $V_p/V_s$  ratios of 1.70 were used for the stations in the craton and adjacent fold belt (based on small, local earthquakes), and 1.73 for the other stations. Crustal thicknesses ranged from 35 to 48 km.

Despite a clear correlation between topography and Bouguer gravity anomalies in the area, Moho depths show the opposite pattern from the expected: areas of low topography and less negative Bouguer anomalies, (Parana basin) have thicker crust (40 to 48 km) compared with the high elevation areas of the craton and fold belt (37 to 43 km). Two hypotheses are proposed to explain the data: 1) lower density (contrast of -0.03 to -0.04 g/cm<sup>3</sup>) in the lithospheric mantle under the Archean block is responsible for maintaining the high elevations in the plateau area: low density and high P-wave velocity are compatible with a depleted (low FeO) composition for the Archean lithosphere; 2) alternatively, if the density contrasts between Archean and Proterozoic lithospheres is smaller than the values above, then the crust beneath the Parana basin must be more dense than that of the craton: higher crustal density and high Poisson's ratio would be consistent with underplating in the lower crust beneath the Parana basin.

**ST4/W/54-B1** 1620**SHEAR WAVE VELOCITY STRUCTURE BENEATH EAST AND SOUTHERN AFRICA FROM SURFACE WAVE DISPERSION**

Vunganai MIDZI, Jens Havskov and Kuvvet Atakan (all at Institute of Solid Earth Physics, University of Bergen, Allegt. 41, N-5007 Bergen, Norway, email: vunganai@ifj.uib.no, V. Midzi also at Department of Meteorological Services, Goetz Observatory, P.O.Box AC65, Ascot, Bulawayo, Zimbabwe); D.D. Singh (National Geophysical Research Institute, Hyderabad - 500 007, India, email: postmaster@csngri.ren.nic.in)

The fundamental mode Love and Rayleigh waves generated by eight earthquakes, which occurred in central Africa and recorded at BOSA, TSUM, LBTB and SLR seismic stations in southeast Africa, are used to estimate the shear wave velocity structure beneath the region. The observed group velocity of Love and Rayleigh waves are computed using the Multiple Filter Technique (MFT) at the period of 5 to 50 seconds. The inversion of observed dispersion data shows a 33km thick crust with a low velocity layer of 2.5km thickness and shear wave velocity of 3.13 km/sec centred at a depth of 13.2km from the surface. Another low velocity zone (LVZ) of 15km thickness is estimated in the upper mantle beneath a depth of 132.2km from the surface. A shear wave velocity of 3.44km/sec to 3.84km/sec is estimated in the lower part of the crust whilst the upper crustal layers have a shear wave velocity of 3.07km/sec to 3.64 km/sec. The brittle-ductile transition zone may be interpreted as starting at a depth of 15.7km from the surface (the LVZ in the upper crust) which matches with the focal depth of most earthquakes occurring in the region.

**ST4/W/49-B1** 1640**CRUSTAL DYNAMICS AND ADVECTIVE HEAT TRANSPORT IN CONTINENTAL RIFT ZONES INDICATED BY THERMAL AND HELIUM TRACERS**

Christoph CLAUSER, Joint Geoscientific Research Institute, D-30631 Hannover, Germany, Email: c.clouser@gga-hannover.de; Erika Griesshaber (Geological Institute, University of Tübingen, Sigwartstr. 10, D-72076 Tübingen, Germany, Email: erika.griesshaber@uni-tuebingen.de); Horst J. Neugebauer (Geodynamics, University of Bonn, Nussallee 8, D-563115 Bonn, Germany, Email: neugbr@geo.uni-bonn.de)

Continental rift zones are characterized by increased permeability due to crustal extension and brittle block faulting of their basement. Numerical simulations of groundwater and heat flow in a two-dimensional type-model of the upper crust show that the dominant mode of heat transport changes from conduction to advection within the permeability range  $5E-18$  m<sup>2</sup> -  $3E-17$  m<sup>2</sup>, typical values for basement and metamorphic rocks. Depending on the host-rock permeability, faults and fracture zones either serve as preferred conduits for pervasive infiltration or for free convection within these structures. Three characteristic patterns evolve in the temperature and flow fields, depending on the relation of forced to free convection. Inspection of a real continental rift zone, the Rhine graben, shows that these patterns cannot be distinguished only on the basis of thermal data. The ratio  $3He/4He$  of the stable helium isotopes provides an additional, independent tracer for transport. Mantle helium varies from 75-50 % in the Eifel volcanic region and 15-25 % at the Miocene Kaiserstuhl volcano in the south to less than 3 % close to the thermal anomalies in the north. Finally, a combination of numerical simulations and a joint interpretation of thermal, helium isotope, and hydro-chemical data shows: (1) The thermal anomalies of the Rhine graben are caused by an E-W groundwater flow system and not directly linked to a mantle intrusion; (2) The  $3He/4He$  anomaly in the Eifel volcanic region and around the Kaiserstuhl volcano is not accompanied by a thermal anomaly. The present-day helium signature evidently trails behind the volcanic thermal signal and is not accompanied by thermally efficient mass flow rates.

**ST4/W/67-B1** 1700**GEODYNAMIC INVESTIGATIONS OF THE HARZ MOUNTAINS/GERMANY: FINITE ELEMENT STUDIES AND INTERPRETATIONS**

Dr Thomas JAHR (Institute for Geosciences)

The Harz Mountains belong to these geological complexes, which were reinvestigated intensively as one common structure due to the political changes at the beginning of the nineties. The FE modelings are conceived by large scale and subsection modelings: A regional large scale model is developed describing the evolution process of the European Variscides. The results yield to the boundary conditions of the rhenohercynian submodel. The local modeling simulate the geodynamic evolution of the Harz Mountains of the Carboniferous up to Quaternary with characteristics of the geological main epochs. The most important boundary conditions derived from rhenohercynian modelings. The numerical simulation indicates on one side the significant influence of the horizontal stress component: In the case of realistic parameters of the Earths crust this stress field cause a vertical uplift of the Harz Mountains which corresponds to geological aspects and the appearance of the orogenic complex nowadays. On the other side the most important role of the intrusion tectonics, which produced main vertical impulses, is pointed out specially for the evolution of the Harz Mountains. The results show that the introduced method come up to an instrument for the geophysical quantification of geological processes. Keywords Geodynamics, FE-modeling, orogenic processes, tectonics, gravity field.

**ST4/W/63-B1** 1720**SEISMIC STRAIN RATES OF THE NORTHERN EURASIAN FOLD BELTS**

Sergei YUNGA (Institute of physics of the Earth, Moscow, 123810, B.Gruzinskaya, 10, Email: syunga@uipe-ras.scgis.ru)

A comparative study of focal mechanisms, seismic and structural data from the Northern Eurasian Fold Belts is presented. The method of representation of the focal mechanisms statistics by a cloud of points in a classification diagrams is developed. On the basis of extensive statistics specific features of the regional seismotectonic deformation field are analysed in great detail for the Alpine fold belt, represented here by the Pamir-Tien Shan and Caucasus-Kopet-Dag orogens, where reverse and strike-slip faults are concentrated. The seismotectonic deformation of the Altai-Sayan seismic belt, where strike-slip faulting is widespread, and the Baikal Rift zone, where normal faulting prevails were characterised sufficiently. Farther to the east, in the Olekma-Stanovoi zones of Yakutia, seismotectonic deformation in mainly marked by individual focal mechanisms or by their groups. It is shown that the distribution of seismicity and seismic strain trajectories in the Alpine-Himalayan fold belt are interpreted mainly as the response of a stable Eurasian block to the on-going south-north India - North Eurasia convergence, as well as controlled by the influence of the shape and rheological properties of major structural units. Thus, deformation of the not dominant orientations and types caused by superposition of structural, rheological and others factors acting probably under neotectonic and recent conditions develops in some particular zones at the flanks of reactivated pre-existing structures. This work was partly supported by the RFBR, grant N 98-05-65159.

**ST4/W/52-B1** 1740**MULTIFRACTAL HETEROGENEITY IN THE UPPER CRYSTALLINE CRUST**

David MARSAN, Chris Bean (both at Geology Dept., University College Dublin, Belfield, Dublin 4, Ireland)

Analyses of the p-sonic velocity and of the gamma log of the Main KTB Borehole indicate the heterogeneous scaling of both logs, which are shown to exhibit multifractal properties. Contrary to their homogeneous, monofractal counterparts, multifractals are characterised by a scaling variability in the local fractal dimensionality, and therefore are more heterogeneous. Consequently, the velocity gradients, a proxy for the seismic reflectivity, follow non-Gaussian distributions, leading to more pronounced scattering of seismic wavelets propagating in such media. While such multifractal properties for the sonic velocity can be linked to a multifractal clustering of fractures as observed for other boreholes, the lithological distribution also appears to be multifractal but with a different scaling, as shown by the gamma log. It can be expected that such properties for the sonic log are related to many different contributions.

Tuesday 27 July AM

Presiding Chair: B.L.N.Kennett (Research School of Earth Sciences, Australian National University, Canberra, Australia)

**MANTLE STRUCTURE AND DYNAMICS****ST4/W/06-B2** Poster **0930-01****TOWARD FULLY SELF-CONSISTENT MODELING OF AVERAGE CONTINENTAL GEOTHERMS**

Louis MORESI (Australian Geodynamics CRC, CSIRO Exploration & Mining, PO Box 437, Nedlands, 6008, Western Australia; Adrian Lenardic, Department of Geology and Geophysics, University of California, Berkeley, CA 94720, USA)

The forward modeling of average continental geotherms appears to be a relatively simple task. Given the stability and large lateral extent of the continental crust, one solves a one dimensional conduction equation (in a layered medium) for suitable values of thermal conductivity, internal heat generation and mantle heat flux.

One problem with such a model, however, is that the mantle heat flux is not an independent parameter. Heat from the mantle escapes through convective transport to a surface boundary layer where conduction then dominates. The balance between the convective transport and conduction is a sensitive function of the coupled mechanical and thermal properties of the boundary layer. Furthermore, this balance is inherently not one-dimensional: continual horizontal transport of cooling material along the boundary layer is required to sustain the vertical heat conduction.

In the oceanic case, the lithosphere thermal and mechanical structure is readily modeled (at least when less than ~80Myr old) by a cooling half-space conduction profile attached to a material point in accordance with simple boundary layer theory. However, the presence of buoyant continental crust, and depleted sub-continental mantle lithosphere, prevents convection from determining the thickness of the upper boundary layer. Therefore, the thermal structure of the crust, sub-continental mantle lithosphere, and convecting mantle must be solved as a coupled system in which the convection pattern and associated heat transport is not known in advance. A further complexity is that the continents are finite in extent - the partitioning of mantle heat flow between continents and oceans is another unknown which must be modeled. We present a number of convection simulations in which we incorporate realistic models of the oceanic lithosphere with continental blocks of varying size and shape and with different relative thermal conductivities and heat generation rates. We solve for the velocity and temperature everywhere in the crust and mantle during several mantle overturns. We track geotherms for a number of points within the continental blocks to determine the long-time average profiles, the variance, and the extreme values of the profiles in response to the underlying convection.

As one example we compare geotherms obtained from continental margins with those from the continental interior, and examine the influence of steps in the thickness of the depleted mantle root. Computed geotherms are compared to approximations obtained using 1D conduction modeling to demonstrate the conditions under which the 1D assumption may fail. We also compare the computed geotherms for the continental margin with analytic solutions in 2D for flow under a changing boundary condition.

**ST4/W/43-B2** Poster **0930-02****THE RELATIONSHIP BETWEEN THE RATE OF SUBSIDENCE OF THE OCEANIC LITHOSPHERE AND THE HEIGHT OF THE RIDGE: A CONSEQUENCE OF VARIATIONS IN THE COOLING RATE?**

C. DUMOULIN, M.P. Doin and L. Fleitout (Laboratoire de Geologie de l'ENS, 24 rue Lhomond, 75231 Paris cedex 05, France, email: dumoulin@jadeite.ens.fr)

Previous studies on the dependence of seafloor depth on crustal age have shown a linear relationship between subsidence rate and axial depths. The physical models used to interpret this dependence involve lithospheric cooling by conduction with variations of upper mantle's temperature. The lithosphere associated with high ridges and hot mantle subsides more. However, some processes, such as crustal thickness variations, deep mantle temperature variations, sea-mounts, crustal faults etc, can perturb the topography and induce a 'random noise' superimposed on the cooling signal.

We show theoretically that such a 'noise' could be responsible of a linear relationship between subsidence rate and axial depth with a slope equal to the average of the age's square root. In order to quantify the influence of this 'noise' and understand what can be linked to the cooling of the lithosphere in the ridge-height versus subsidence-rate relationship, we study the bathymetry versus age in the South-East Indian and the South Atlantic oceans. Profiles along flow lines and profiles along an arbitrary direction diagonal to the flow lines are compared.

**ST4/W/35-B2** Poster **0930-03****IMAGING THE UPPER MANTLE P-WAVE VELOCITY STRUCTURE OF THE APENNINES (ITALY) BY NONLINEAR INVERSION OF TELESEISMIC TRAVEL TIME RESIDUALS**

Giovanni Battista CIMINI (Istituto Nazionale di Geofisica, Via di Vigna Murata 605, 00143 Rome, Italy, email: cimini@nettuno.ingrm.it)

Over 4,000 handpicked arrival times from high-quality teleseismic waveforms digitally recorded by the stations of the National Seismic Network during the past ten years are used to invert for the aspherical velocity structure of the upper mantle beneath the Apenninic chain. The data used in the tomographic reconstruction are the travel time residuals of P, pP, sP, PcP, PKP<sub>df</sub> and PKP<sub>bc</sub> phases computed with respect to the improved global 1-D velocity model ak135. The imaging algorithm applied employs a three-dimensional minimum travel time ray tracing within a standard nonlinear inversion scheme that repeatedly solve the linearized problem and recalculate the ray trajectories after each iteration. The data kernel matrix computed for a weighted damped least square solution of the problem is inverted by using the singular value decomposition (SVD) method to better test the resolution capabilities of the dataset and the reliability of the inversion result. The resulting lateral heterogeneities delineate a very complex pattern, with the anomalies of the P-wave velocity amplitude reaching 10%. A pronounced high velocity anomaly is imaged beneath the internal part of the northern Apenninic arc from the uppermost mantle down to a depth of about 400 km. Below Central and Southern Apennines a low velocity zone is recognized between 0 and 100 km depth. It overlies a complex shape high-velocity region located beneath the belt between 100 and 300 km depth. Velocity contrasts between this feature and the contiguous mantle are less strong than those characterizing the high velocity zone under the Northern Apennines, suggesting a less dense, probably continental, subducted lithosphere.

**ST4/W/11-B2** Poster **0930-04****REFLECTION OF MANTLE AND LITHOSPHERIC HETEROGENETIES IN SEISMIC FIELD OF KAMCHATKA REGION**

Sergey A. Boldyrev, Victor V. MYACHKIN, Maria S. Solovieva (all - Institute of Physics of the Earth, Russian Academy of Sciences, Bolshaya Gruzinskaya, 10, Moscow 123810, Russia, e-mail: sabold@iuepe-ras.segis.ru)

Properties and structural organisation of shallow seismicity ( $H < 50$ km) in North-West sector of Pacific Ocean in joint region of Kuril-Kamchatka and Aleutian Islands arc are analysed with the use of data of detailed seismological observations during 1962 - 1997. The maps of seismicity parameters distribution, of kinematic and dissipative peculiarities of elastic waves propagation including their azimuthal characteristics were made. At least two hierarchic systems of lineaments were distinguished. The main one repeats configuration of the main morphological structures of the region and is represented by interchange of three belts, the distance between extremums varies from 60 - 80km at the south to 40 - 60km at the north. Anomalies intensity decreases towards the ocean. The sub-meridional zones of low viscosity of material (low velocity and high attenuation of elastic waves, predominance of comparatively weak earthquakes etc.) were distinguished with the use of a complex of parameters. Positive relief structures continuing headlands of East Kamchatka, and magnetic anomalies, which are traced on the land and beyond the trench as well, correspond to these zones. Areas where the azimuthal dependence of velocity and attenuation of elastic waves are most obvious coincide with the selected system of lineaments as a whole. Maximum velocity values and increased attenuation of elastic waves are typical for the tracks along Kamchatka (except the region of Kronotsky peninsula), and as a whole they coincide with the extension of the planes of motion in the local earthquakes foci. It allows one to connect the origin of azimuthal dependence of the parameters under study with the tectonic deformations. The monotonous character of the parameters under study alteration through the area and coincidence of the anomalous zones according to different data suggest their connection with lateral variations of the composing substance properties caused by geotectonic development of the region.

**ST4/L/04-B2** Poster **0930-05****TRAVEL TIME TOMOGRAPHY FOR UPPER LITHOSPHERE VELOCITY STRUCTURE OF THE RUSSIAN FAR EAST**

Alexander VOITENOK (Institute of Tectonics and Geophysics Far Eastern, Branch of RAS, Khabarovsk, Voroshilova street, 9-63, Russia, 680051 email: u153vaa@rtzi.ru)

During 1975-1990 years on a continental part of Far East of Russia the network of regional seismic stations operated. The data, obtained by them, about seismic waves arrival times are used for specification of upper lithosphere velocity structure. I used an iterative two-stage algorithm for definition of 3D velocity model. At the first stage, proceeding from a previously determined velocity model, the specified situations of earthquakes and origin times are determined. Initially is used the standard velocity model. At the second stage the task of definition of abnormal velocities is solved. Usual methods of linear inversion were used. This sequence repeats up to achievement of a required error. Travel paths are calculated by numerical solution of the eikonal equation for an inhomogeneous medium. For full completion of solution the common error of the computing scheme is estimated. With this objective the initial data about a situations of hypocenters and origin times are distorted by casual noise according to an error of their definition. The difference of definitions on the source and deformed data characterizes stability of a method. The definition of a model is executed for both P and S- waves, though data about travel times of S-waves is significant less. Therefore for S- waves the simplified scheme is used.

**ST4/E/66-B2** Poster **0930-06****SHEAR-WAVE SPLITTING IN THE UPPER MANTLE BENEATH THE AEGEAN AREA**

K. MAKROPOULOS, P. Papadimitriou, G. Kaviris, I. Kasarass (all at Department of Geophysics, University of Athens, 157 84 Athens, Greece, email: kmakrop@cc.uoa.gr); D. Hatzfeld (LGIT, UJF, Grenoble, France, email: Denis.Hatzfeld@obs.ujf-grenoble.fr); H. Lyon-Caen (Institut de Physique du Globe de Paris, France, email: lyoncaen@jadeite.ens.fr); A. Kiratzi (Geophysical Laboratory, University of Thessaloniki, Greece, email: kiratzi@geo.auth.gr); L. Vinnik (Institute of Physics of the Earth, Moscow, Russia, email: vinnik@synapse.ru)

The Aegean Sea is a region characterized by subduction and back-arc spreading. In this study, data on the deformations and flow in the upper mantle of the region are presented. These data are obtained from a temporary broadband seismological network installed over the Aegean. The network was in operation for six months (February-July 1997). In spite of the relatively short time span and the high noise level at some stations, we were able to detect teleseismic SKS and SKKS phases coming from different azimuths and with a high signal to noise ratio. The inversion of the recorded particle motions for shear-wave splitting indicates that the dominant direction of polarization of the fast shear wave is close to North-South. This anisotropy indicates an approximately North-South extension in the upper mantle, slightly different from the geodetic data on the deformations in the region. The obtained anisotropy directions are possibly related with the internal deformation of the Aegean. At some stations a complicated pattern of shear-wave splitting was observed, which suggests that anisotropy in the subcrustal lithosphere and asthenosphere could be different.

**ST4/E/46-B2** Poster **0930-07****A SEISMIC ANISOTROPY OF THE LITHOSPHERE AROUND THE TRANS-EUROPEAN SUTURE ZONE (TESZ) BASED ON SHEAR-WAVE SPLITTING DATA OF THE TOR EXPERIMENT**

J. PLOMEROVA, D. Kouba, L. Vecsey and V. Babuska (Geophysical Institute, Czech Acad. Sci., 14131 Praha 4, Czech Republic, email: jpl@ig.cas.cz) TOR Working Group

The Trans-European Suture Zone (TESZ) is the most prominent tectono-geological boundary within Europe separating mobile Phanerozoic terranes in the western part from the Precambrian East-European Platform in the eastern part. Distinct changes of seismic anisotropy of the mantle lithosphere are related to this intra-continental suture. The effect is observable in various wavelengths as well as seismic wave types. In the long-period range, the radial anisotropy of surface waves differs distinctly in the lithosphere on both sides of the TESZ. In the short-period range of body waves, the P residual spheres detected changes in the lithospheric anisotropy related the various blocks around the TESZ as well. A passive teleseismic field experiment -TOR- traversing the northern part of the TESZ in Germany, Denmark and Sweden was conducted during 1996-1997. The array recorded data for teleseismic tomography of the upper mantle with a high lateral resolution, about few tens of km, including data for seismic anisotropy studies. Our analysis of shear-wave data recorded at broad-band stations during the field measurements aims at retrieving a 3D orientation of anisotropy around the TESZ and mapping lateral changes of the 3D orientation of anisotropic structures along the TOR antenna. An interpretation of the observed seismic anisotropy by the



preferred orientation of olivine crystals results in a model of the mantle lithosphere characterized by plunging anisotropic structures. It is evident that different orientations of large-scale olivine fabrics on both sides of this major suture zone extend through the whole lithosphere.

**ST4/W/27-B2** Poster **0930-08**

**REGIONAL SURFACE - WAVE GROUP VELOCITY INVERSION BY SPHERICAL HARMONIC METHOD**

Liangbao ZHU and Qing Xu (Department of Geophysics, Peking University, Beijing 100871,China)

If one complex surface-wave velocity function defined on a regional sphere area is imitated directly by spherical harmonic functions, maybe very high order spherical harmonic coefficients are needed. By conformal mapping in which the surface-wave velocities keep unchanged, a regional area on a sphere surface can be extended to a much larger spherical segment area. Then we extend the spherical segment area to the whole sphere by analytic continuation, and the continuation of the velocity is arbitrary. Imitating the velocities by spherical harmonic expansion on the sphere after transformation can greatly reduce the number of spherical harmonic coefficients needed. The inversion of surface-wave velocities turns into the linear inversion of spherical harmonic coefficients. The resolution kernel and the root square deviation of inversion can be obtained by analyzing the spherical harmonic coefficients. The algorithm has advantages in the sense that: the computing speed is fast, the contours are smooth, and the tectonic boundaries are clear. Theoretically, this method is not only applicable to the surface-wave group velocity inversion, but also to a wide variety of analyses of regional fields.

**ST4/W/28-B2** Poster **0930-09**

**CAN THE LOVE-RAYLEIGH DISCREPANCY BE CAUSED BY ISOTROPIC LATERAL HETEROGENEITIES?**

Valerie MAUPIN (Dept of Geophysics, Univ. of Oslo, PO Box 1022 Blindern, 0315 Oslo, Norway; email: valerie.maupin@geofysikk.uio.no)

At global as well as at regional scale, the lithosphere appears faster to Love waves than to Rayleigh waves. This Love-Rayleigh discrepancy can be modelled by introducing transverse isotropy in the upper mantle. In the oceanic lithosphere, transverse isotropy is usually associated with azimuthal anisotropy and can be explained by the orientation of olivine crystals, at least partly. The situation is more complex in the continental lithosphere, where azimuthal anisotropy is not necessarily associated with transverse isotropy. Although a more complex structure of the olivine orientation or horizontal layers of partially molten material could explain this situation, the Love-Rayleigh discrepancy could also partly originate from the presence of isotropic lateral heterogeneities, as noted by Levshin and Ratnikova (1984). Using recent mode-coupling methods for modelling surface wave propagation in 3-D structures, we explore if any kind of isotropic laterally heterogeneous model of the mantle could produce the systematic Love-Rayleigh discrepancy observed in continental regions.

**ST4/P/01-B2** Poster **0930-10**

**REFINED SEISMIC STRUCTURE OF THE INDIAN LITHOSPHERE-ASTHENOSPHERE**

Avadh RAM, Pati Patel (Both at Department of Geophysics, Banares Hindu University, Varanasi-221005, India; Tel: +91 542 317123; Fax: +91 542 317074; email: aram@banares.ernet.in)

The Indian subcontinent is of particular interest to geoscientific community of the world because of the manner it has moved northward and collided with the Eurasian plate. Himalayan mountains to the north and mid-oceanic ridges to the south and earthquake belt surrounding the Indian plate all show that the lithosphere-asthenosphere structure in this region must have some significant lateral and vertical variations. Several scientists have tried to find one dimensional velocity models in the past using the seismic wave data. It has been confirmed by the study of the Gauribidanur seismic array data from the Indian subcontinent (Ram & Mereu, 1997) that the region has two prominent anomalous zones lying around "400km" and "650km" depths with varying thicknesses. Seismic structures associated with these anomalous zones have also been clearly identified using the other methods.

We have also obtained the variation of P-wave seismic velocity in x-y plane for various depths. These velocity models for continental and oceanic regions have been refined using other imaging techniques for travel-time and slowness data and the uncertainties are demarcated with the help of envelopes. The dynamic interaction and modelling processes are discussed. Anelasticity and scattering effects have also been considered in refinements of the models. Further, an attempt has also been made to map the structure three dimensionally on the basis of the methodology and computer programs developed by ILP Task Group II-4, where initially; an "I" data set has been prepared. Various linear features have been identified using multimode/multistructure procedures. Finally, a refined seismic structure of the part of Indian lithosphere-asthenosphere has been delineated.

**ST4/W/56-B2** Poster **0930-11**

**MAPPING THE LITHOSPHERE-ASTHENOSPHERE SYSTEM IN THE CENTRAL MEDITERRANEAN SEA FROM SN WAVE ATTENUATION**

Giuliana MELE (Istituto Nazionale di Geofisica)

The lithosphere-asthenosphere system is mapped over the central Mediterranean area using regional shear wave propagation characteristics. The shear Sn phase in a good indicator of the presence of asthenosphere at shallow depth, i.e., of discontinuities in the lithospheric mantle. A large number of raypaths crossing the study area from different azimuths provided useful information and constraints on the extent of low-strength attenuative zones in the uppermost mantle. A previous study of Sn attenuation in Italy showed that the asthenosphere replaces the lithosphere at shallow depth beneath the northern part of the Apennine chain, and a lithospheric delamination has been hypothesized. A Sn high attenuation zone is also found beneath the southern Tyrrhenian Sea. In this case the uprising of asthenosphere is expected, and it is consistent with other geological and geophysical evidences of a back-arc process. The lateral extent and the continuity at depth of the south Tyrrhenian subduction zone has been also mapped using deep S phases. In the present study the continuity of the mantle lid is investigated over the area of the Ionian Sea, south of Italy, and across the Sicily Channel, between Africa and Sicily.

**ST4/L/05-B2** Poster **0930-12**

**A PRIMARY STUDY ON LITHOSPHERE STRUCTURE IN EASTERN REGION OF QINGHAI-TIBET PLATEAU**

LIU Hongbing, Kong xiangu and Yan yongli(all at Institute of Geophysics, Chinese Academy of Sciences, Beijing, 100101, P. R. China, Email: bliu@mail.c-geos.ac.cn)

In Oct of 1998, A geophysical survey including Magnetotelluric sounding(MT), gravity and geomagnetism was carried out by Institute of Geophysics, Chinese Academy of Sciences in eastern region of Qinghai-Tibet plateau. It is known from tectonic mapping that study area was divided into four blocks by three large sutures, but we have very little information on deep-seated structure which have close relationship with evolution of Tibet plateau, the purpose of research is to find some evidences of deep matters The geophysical study region is located in range of 97-98oE and 35-26oN, the profile with the length of 900km runs through Bayanhar, Qingtang and Gandise block in NS direction, 349 gravity and geomagnetic data were acquired simultaneously, and 31 MT sites are be placed along the profile with about 18km-interval to detect electrical conductive feature, MT recording period (256Hz to 4096s) is long enough to reach the bottom of lithosphere. By data processing, the crustal thickness from gravity data is about u and Cayu region is only 90km deep, the distribution of the high conductive layers in crust were complicate, most of those is about 25km deep, but near the Banggongco-Nujing and Jingshajing sutures the depth of the layers are only about 20km. Besides, all of geophysical data show that their amplitude of the variation in southern region are stronger than those in northern region. A further integrated study is being conducted, the primary result show that in the southern region of profile the tectonic act!

**ST4/W/47-B2** Poster **0930-13**

**RAYLEIGH WAVE GROUP VELOCITY MAPS OF EAST ASIA**

Liangbao ZHU and Qing Xu (Department of Geophysics, Peking University, Beijing 100871,China)

Rayleigh waves are used in a tomographic inversion to obtain group velocity maps from 10s to 120s periods of East Asia (70°E-145°E, 10°N-55°N). Due to the dense path coverage and the good azimuthal distribution of paths, we obtain some new results. The Tarim Basin is obviously recognizable in the maps of 10s-15s periods, appearing as a low velocity structure, but it can't be seen in the maps of 16s-33s periods, and then appears as an area of high velocity in the maps of 36s-85s. This indicates that there is a deep root under the Tarim Basin. With clear demarcation lines to the Indian plate on the south and to the Tarim Basin and Qaidam Basin on the north, Tibetan plateau is the most prominent low velocity block in the maps of 44s-110s, and the velocity in its central and western portion is lower than that in the east. The South-North seismic belt appears to be one with high group velocity gradient, which divides the China continent into eastern part and western part; the velocities in the east are noticeably higher than that in the west. The central South China Sea, the Japan Sea, and Philippine Sea appear as oceanic crust. The image of Philippine Sea is completely consistent with the topography and the seismic zone. Around the Philippine Sea and the Japan Sea, there is a low velocity belt of about 400km wide, and it may be a zone with magmatic activities. In the vicinity of Chiang Mai, Thailand we can see a low velocity zone with scale of 1000km, which may be created as the mass of Tibetan plateau migrates south-east.

**ST4/W/48-B2** Poster **0930-14**

**UPPER MANTLE SEISMIC STRUCTURE BENEATH THE PHILIPPINE SEA REGION INFERRED FROM SURFACE WAVE PHASE VELOCITIES**

Yasuyuki NAKAMURA and Takuo Shibutani (both at Disaster Prevention Research Institute, Kyoto University, Gokasho, Uji, Kyoto, 611-0011 Japan, Email: saru@rcep.dpri.kyoto-u.ac.jp, shibutan@rcep.dpri.kyoto-u.ac.jp)

The distribution of anisotropic seismic structure in the upper mantle beneath the Philippine Sea region was obtained using surface wave dispersion data both of Rayleigh and Love waves.

About 800 Rayleigh and Love wave phase velocity curves were calculated with the non-linear waveform inversion (Trampert and Woodhouse, 1995) in the periods of 30-100s. The calculated phase velocity curves were inverted for Rayleigh and Love wave phase velocity maps by 2-D tomographic inversion for each period. The block parameterization where the block size was 2.5 degree-times-2.5 degree was adopted in the tomographic inversion.

The Rayleigh and Love wave phase velocities were converted to eigenperiods of the fundamental spheroidal and toroidal modes respectively. The eigenperiods were inverted for the upper mantle seismic structure with transversely isotropic features in each block down to the 220km depth.

In the depth range 80-100km, resultant shear wave velocity structure distributions well correlate with the tectonic evolution history suggested in the Philippine Sea. The older western part of the Philippine Sea has high velocity, and the younger eastern part indicates low velocity. The averaged shear wave velocities for the Philippine Sea is about 4.3km/s in the depths of 50-220km, which is slower than the PREM model. This slow upper mantle is also seen in other back arc basins, for example Lau basin.

**ST4/W/19-B2** Poster **0930-15**

**MODELLING OF TELESEISMIC WAVES IN DIPPING ANISOTROPIC STRUCTURES**

Andrew W. Frederiksen and Michael G. BOSTOCK (both at Department of Earth and Ocean Sciences, U.B.C., Vancouver, B.C., V6T 1Z4, CANADA, Email: andy@geop.ubc.ca, bostock@geop.ubc.ca)

The existence of seismic discontinuities within the continental upper mantle has long been recognized, with more recent studies often indicating an association with strong elastic anisotropy. Structural relations with surface geology have, in a number of instances, established a correspondence of such features with ancient subducted lithosphere, thereby underlining their importance in understanding the assembly and stabilization of continental lithosphere. The near vertical sampling of teleseismic P, S, and SKS waves provide a convenient means of characterizing mantle discontinuities but computationally efficient methods of calculating synthetic seismograms are required for structures that exhibit lateral variability. We consider mantle lithospheric models consisting of planar, homogeneous anisotropic layers with arbitrary dip. Reflectivity techniques cannot be used to model dipping layers, while fully 3-D ray tracing in anisotropic media is computationally involved owing to its reliance on shooting or bending methods. The travel time equation of Diebold (1987) for dipping layered media is adopted as the basis for a high-frequency asymptotic method that does not require ray tracing. Travel times of plane waves in anisotropic media are calculated from simple analytic formulae involving the depths of layers beneath a station and associated vertical phase slownesses. Amplitudes are computed using the reflection and transmission matrices for planar interfaces separating anisotropic layers. Preliminary results from simple models indicate that upper-mantle seismic responses depend in a complex fashion on both layer dip and anisotropy, particularly in the case of converted phases. Rotation of energy onto the transverse component from Ps conversions is induced by both dip and

anisotropy, the dip having greater influence on travel time. The S response is further complicated by a marked dependence on the polarization of the incident wave, while the behavior of Sp conversions is strongly influenced by dip. Applications of this method to both P and S data from the Yellowknife broadband seismic array will be presented.

**ST4/E/19-B2** Poster **0930-16**

#### ON CORRELATION AND DE-CORRELATION OF MANTLE TRANSITION ZONE DISCONTINUITIES

D.S.RAMESH (National Geophysical Research Institute, Uppal Road, Hyderabad-500 007, India, email: postmast@csngri.res.nic.in)

Recent advances in secondary phase identification and recognition of precursor arrivals to major seismic phases (e.g. SS, PP) enable to image the fine structure of the mantle transition zone. As is typical in studies dealing with weak signals, the attendant methods of data processing and analyses besides data quality contribute to variations in the final results. Also, signal enhancement strategies like stacking for a small region with fewer seismograms accompanied by lower signal to noise ratio (SNR) can yield dubious results. Recent studies do indeed present conflicting results both in global scale and for smaller regions as well. The ongoing debate on whether the 410-km and 660-km discontinuities in the mantle transition zone are globally anti-correlated or de-correlated perhaps owes its origin to factors mentioned above. It is also interesting to recognise possible positive correlation of these discontinuities, albeit, locally in regions of active tectonics (e.g. northwest Pacific Ocean). The northwest Pacific Ocean is taken up as a case study with about 1700 broadband seismograms applying simple yet refreshingly innovative strategies to study the nature of the mantle transition zone discontinuities and their disposition. A novelty in the present study involves replacement of the stacking procedure by display of 'time-movement' corrected seismograms facilitating identification of precursors in individual seismograms. In addition, the seismograms are sorted by bouncepoint longitude. Possible latitudinal variations are also studied, by both viewing the seismogram section in latitude corridors and latitude-wise sorted sections. Also, the bouncepoints are projected on to appropriate direction profiles (eg. NorthWest) to better document signatures of subduction zone. Such a presentation of seismograms hopefully registered narrow zone signatures of smaller wavelength related to subduction. Due to the opposing signs of Clapeyron slopes, the 410-km and 660-km boundaries are expected to be negatively correlated. However, recent studies based on high-pressure experiments, thermodynamic calculations and numerical simulations suggest that the Clapeyron slope of the spinel-perovskite phase transition at a depth of 660-km changes from negative ( $dP/dT < 0$ ) to positive ( $dP/dT > 0$ ) in the triple point temperature region 1700\_x\_C-2000\_x\_C for a pyrolyte composition mantle. This change in Clapeyron slope to positive ( $dP/dT > 0$ ) would thus enable the 660-km discontinuity to be positively correlated with the overlying 410-km discontinuity which is indeed reflected in our seismological observations for the study region.

**ST4/E/67-B2** Poster **0930-17**

#### WHOLE EARTH STRUCTURE ESTIMATED FROM SEISMIC TRAVEL TIME DATA

L. R. JOHNSON and D. W. Vasco (both at Center for Computational Seismology and Seismological Laboratory, University of California, Berkeley, CA 94720, USA)

Seismic travel time data for a suite of P and S body wave phases are used to infer the three-dimensional velocity structure for the entire earth. Ray tracing in a three-dimensional model is used to relocate the seismic events. The model is described in terms of volumetric cells and a general inverse problem is formulated to determine the P velocity, S velocity, and anisotropy within the cells. The topography on major internal velocity discontinuities is also included in the inversion. The model parameters are estimated using an iterative Lanczos algorithm to obtain a partial singular value decomposition. With such a decomposition, it is possible to also obtain estimates of model resolution and uncertainty. The results are similar to those obtained with other inversions of body wave data, with the uneven sampling of the earth due to the non-uniform distribution of sources and receivers playing a dominant role in the resolution. The crust and uppermost mantle of the model are well resolved under continents, particularly in the northern hemisphere, and the velocity anomalies correlate strongly with surface tectonics. The magnitude of the velocity heterogeneity decreases with depth in the mantle before it increases again in regin D\*, although the resolution is limited in this region at the bottom of the mantle. There is evidence of lateral variation of the P velocity in the outer core which appears to be resolved. There is also evidence for anisotropy in the P velocity within the inner core, but this feature trades off strongly with velocity heterogeneity.

**ST4/L/09-B2** Poster **0930-18**

#### A WHOLE MANTLE P WAVE ATTENUATION STRUCTURE OBTAINED FROM THE ISC AMPLITUDE DATA

Hiroaki NEGISHI (Disaster Prevention Research Institute, Kyoto University, Gokasho, Uji, Kyoto 611-0011, JAPAN, email: negi@rcp.dpri.kyoto-u.ac.jp)

The 3-d structure of P-wave attenuation was obtained in the whole mantle by applying the tomographic method to the amplitude data of the Bulletin of the International Seismological Centre (ISC). The 115,418 amplitude data of the 2,721 events occurring from 1984 to 1995, observed at 718 stations, were analyzed after the focal mechanism correction. AK135 velocity model (Kennett et al., GJI, 1995) was used for the ray tracing and the geometrical spreading correction. The simultaneous inversion technique was adopted for determining source amplitude, site amplification factor and 1-D  $Q_p^{-1}$  structure down to 2,720 km depth, and 3-D  $Q_p^{-1}$  perturbation distribution from the 1-D model was obtained. The attenuation at the upper mantle is relatively stronger than that at the lower mantle. Such pattern is also seen in the various earth models that obtained by the Earth's free-oscillation analyses. The lateral variations in long wavelength show a similar pattern to the previous P-wave velocity studies. Two major high attenuation zones appear to be located at the middle and lower mantle beneath the Central Pacific and northern Africa, while low attenuation body is spreading at the upper and middle mantle beneath the Eurasia continental shield. This is the first result that delineates the whole mantle attenuation heterogeneity of the short-period body waves. This new information will become important for investigations of geothermal and geodynamical features of the Earth.

**ST4/E/17-B2** Poster **0930-19**

#### GLOBAL SEISMIC BOUNDARIES AND WEAK ZONES IN THE CRUST AND UPPER MANTLE

Nina PAVLENKOVA (Institute for Physics of the Earth, B.Grusinskaja 10, 123810 Moscow, Russia, email: Ninel@Pavlenkova.msk.ru)

Long range seismic profiling revealed a fine stratification of the crust and upper mantle: high velocity layers alternate with lower velocity ones and strong reflection boundaries often separate the layers. A change of velocity pattern where the block structure is transformed into

a subhorizontal layering and a local isostatic equilibrium are typical at the boundaries. These structural features and other geophysical data suggest that the boundaries separates brittle and weak layers. Several such boundaries layers have a global significance and suggest rheological stratification of the lithosphere. In the continental crust weak zones are determined at depth of 10-20 km and at the Moho level. A rheologically weak layer underlain by the reflection boundary N is distinguished at a depth of 80-100 km. It is located inside the thermal lithosphere beneath old platforms (East-European, Siberian, North-American) and at the bottom of the lithosphere beneath active tectonic areas (West Europe) and in oceans (Angoa-Brazil Geotraverse). The nature of these boundary layers may be explained by changes of mechanical properties of the matter. The velocity inversions which are often characterized by higher electrical conductivity may be a result of fluids or melt concentration at the critical depths. The high velocity boundaries suggest the anisotropic layers formed by the mantle matter flows. Together with deep faults the weak layers form a channel system for the mantle fluids and matter transportation. During tectonic activation the lithosphere weak layers are transformed by partial melting in asthenolites which are important for the plume tectonics. The crustal weak zones and the plastic flows at the Moho level help the crustal blocks to move at local plate tectonics. (The study is a part of RBRF project 99-05-64799)

**ST4/E/03-B2** Poster **0930-20**

#### BROAD-BAND SEISMIC PROFILE TO IMAGE THE CRUST AND MANTLE STRUCTURE BENEATH THE INDIAN CRATON AND THE HIMALAYAS

K.S.Prakasam and S.S.RAI (both at National Geophysical Research Institute, Uppal Road, Hyderabad-500 007,India, email: postmast@csngri.res.nic.in)

Seismic structure of the Indian crust and mantle is being investigated using array of broad-band seismic stations. The array of 30 broadband seismic station will operate over 3000 km from the Archean terrains in the south (8 degree North) to the Himalayas (30 degree North). Proposed profile would operate in three phases. Beginning January 1999 first phase of the array is operating over the Dharwar craton (Archean granite gneiss and metamorphic terranes), Proterozoic Cuddapah basin and Deccan Volcanic Province. While the investigation concentrate on the Indian region, it will help answer several global questions like how thick is lithosphere in different geological terranes/ages; structure and composition of the crust; nature of dissimilarity between Archean, Proterozoic and Phanerozoic provinces; crust and lithospheric structure beneath the Ganga basin and the Himalayas. We present initial result from broad-band array focussing the nature of crust and upper mantle in Dharwar Craton.

**ST4/E/69-B2** Poster **0930-21**

#### MANTLE Q AT PERIOD 12.4 HOURS: NEW ESTIMATES FROM SATELLITE TRACKING AND ALTIMETRY

R D RAY (NASA Goddard Space Flight Center, Code 926, Greenbelt MD, USA; email: richard.ray@gsfc.nasa.gov)

The most convincing estimates of mantle Q at periods of many hours have historically come from extrapolating seismic and free-oscillation estimates via some assumed frequency dependence, sometimes contrained by estimates from the Chandler Wobble. At the semi-diurnal tidal period, direct estimates of Q have been difficult to obtain because of the dominating signals of the ocean tides, which account for more than 95% of the tidal energy dissipation. But knowledge of the ocean tides has been rapidly improving, primarily owing to satellite altimetry, and in 1996 we reported (NATURE, 381, 595-7) an estimate of solid-earth tidal energy dissipation and mantle Q based on combining satellite altimeter measurements with tracking observations of tidally induced satellite orbit perturbations. Tidal estimates from both reveal a small systematic difference in the quadrature component of the degree-2, order-2 spherical harmonic coefficients, which we attribute to a small lag in the earth's body tide. The formalism accounts for this lag in both the altimeter and tracking solutions and also accounts for a very small contribution from the lunar atmospheric tide. Since this original report, both altimeter and tracking estimates have improved. Recent solutions for the body-tide lag at the M2 period are 0.20 +/- 0.09 degrees, implying an energy dissipation of 100 +/- 50 gigawatts and a solid-earth Q of 300. Further new solutions will be discussed, as will the prospects for significantly reducing error bars and for obtaining estimates from other tides in the diurnal band.

**ST4/E/37-B2** Poster **0930-22**

#### GLOBAL ANOMALIES IN TIDAL GRAVITY AND LOWER MANTLE STRUCTURE

A.KOPEV (Astronomical Institute of Moscow University, Universitetski prosp. 13, Moscow, 119899, Russia; fax: +7-095-9328841; e-mail: kopev@sai.msu.ru)

Direct modelling of the tidal delta-factors and phase lag anomalies caused by upper and lower mantle heterogeneities has been carried out for M2, O1 and Mf tidal waves using the approach of S.Molodenski (1980) and SH8/U4L8 seismic model. Resulting lateral anomalies of delta-factors are less than 0.1 % and correlate with CMB-topography and should not be observable at the current accuracy level in tidal gravimetry. Nevertheless, highest quality tidal gravity data selected from ICET Data Bank reveal global anomalies that correlate modelled with modelled anomalies although the former ones are one order larger in magnitude (up to 1 %). This discrepancy may reflect inapplicability of mantle elastic parameters deduced from seismic data to tidal frequencies (i.e. mantle' elastic parameters for tidal frequencies are higher than for seismic ones) and/or suspected lateral anomalies in lower mantle viscosity.

**ST4/E/72-B2** Poster **0930-23**

#### BIRTH AND DEATH OF A GEOPHYSICAL ANOMALY

U. RAVAL and K. Veeraswamy National Geophysical Research Institute, Hyderabad, India

Most lithospheric geophysical anomalies originate due to (1) Plate (horizontal) and/or (2) Plume (vertical) tectonics. Since these thermomechanical causes are finite in space and time, their geo-physical effects would tend to decay when the sources become weak or inoperative. For example, an asthenospheric upwelling would result in both short- and long-living lithospheric anomalies. Thus, (a) swells/ uplifts, doming, subsidence, long wavelength gravity low and low seismic velocity layers (LVLS) etc. form short period features and (b) high density, seismic velocity (HVLS), electrical conductivity (HCL), magnetic susceptibility etc., frozen in the crust, are long living until a major rejuvenation/ orogeny. Thus, while the cratons have long-living fetures, the mobile belt features have relatively shorter life. The heat and mass transfer during magmatic underplating may result in a gravity high after sufficient cooling and also in high seismic velocity and magnetic susceptibility. From such heating and cooling follows a cycle from low (when hot) to high (when cold) anomalies. The Meso-Cenozoic dynamics of the Indiancontinental lithosphere giving rise to birth and death of certain geophysical anomalies over the subcontinent is discussed.



**ST4/E/24-B2** Poster **0930-24**

**THE EFFORTS APPLIED ON ALL OF PLATE'S AROUND AND ITS BASE BY GLOBAL MANTLE FLOW**

Xunying SUN (Department of Geology, Peking University, Beijing, 100871, P.R.China, email: dszxy@pubms.pku.edu.cn); Guoping Liang, Yuezhi Sun, Jinzhao Liu and Huai Zhang (Mathematical Institute, Chinese Science Academy, Beijing, 100081, P.R.China, email: ling@public.east.cn.net)

Every Plate or massif is one part of the earth surface. Its tectonic movement as a result of thermal motion of global mantle is driven by the efforts applied not only on all of its around but also on its base by global. So, if the tectonic effect will be studied, the efforts acting on the plates must be studied clearly. The following questions should be answered: How do act the efforts on the plate or massif? How do distribute the efforts?

We use 3-D finite element method for Newtonian medium to calculate the global mantle and crust creep flow. The LDDA (Lagrangian Discontinuity Deformation Analysis) technique is used to treat the contact problems of plate boundaries such as subduction zones and collision belts. The LDDM (Lagrangian Domain Decomposition Method) and parallel algorithm are employed to calculate with parallel computer. The CMM (Combinatorial Mesh Method) is employed to handle the multiscale problem, for example, the problem of different meshes between global and local plate or massif.

First of all, on the basis of fitting the velocities of divergent and convergent boundaries of the plates, the velocity field is obtained as well as the temperature and the pressure fields. Then, the stresses acting on preceding boundaries and bases are calculated. Finally, obtained the efforts applied on the plates or massifs by global.

**ST4/E/71-B2** Poster **0930-25**

**TECTONIC AND SOLAR CYCLES, MOVEMENT OF CONTINENTS, CLIMATE**

D.SADYKOV, I.Levchenko, E.Bukreeva, A.Baimoldaeva (all at Abay University, Almaty, MD Koktem-1, 28-12, 480090 Almaty, Republic of Kazakhstan, email: 89284974@public.asdc.kz)

Tectonic and the solar cycles depend on galactic year (220 Ma). At an equatorial part of the Earth the compression is possible for 55-110, 165-330, 385-440, 495-550, 605-660, 715-770, 825-880Ma, and the stretching is possible at high breadths of the Earth at the same intervals of time. The compression at its polar part is possible for 0-55, 110-165, 220-275, 330-385, 440-495, 550-605, 660-715, 770-825Ma. The change of character of deformational processes happens at the time of transition of solar system through the special points of a galaxy in 55Ma, where the solar system crosses area where the galactic weight is at its flat part. These processes result in the change of temperature of ocean and change of climate of the Earth. The increase of a level of ocean and flooding of continents happen basically in 40-60Ma, and reduction of ocean level in 44-60Ma. These intervals of change of a climate will be coordinated to the interval 55Ma. The occurrence of the glacier periods on the Earth depends on places of a place of continents at the given interval of time. All continents were in the area of South Pole at 600Ma and then were drifting to North, under the theory of tectonic plates. In these situations the exact fixing of the glacier periods is complicated. Therefore changes of a climate for 0-600Ma are better correlated with change of a level of ocean for 600Ma and forms 0.00003cm p.a. This parameter characterizes the tendency of reduction of the world ocean level and will be coordinated to amount of weight of water leaving the Earth annually. The given data are a background for an estimation of change of a climate for shorter periods: tens - hundreds years. Thus the role of solar cycles varied within 10Ma-6 years grows.

**ST4/E/39-B2** Poster **0930-26**

**ENDOGENOUS HEAT SUPPLY FROM THE CMB AND/OR FROM THE ALB VOLCANISM AND HEAT FLOW**

Giovanni P. GREGORI (IFA-CNR, via Fosso del Cavaliere 100, 00133 Roma, Italy; e-mail: gregori@atmos.ifa.rm.cnr.it)

According to a tide-driven dynamo model (Gregori, PEPI, 77, 39, 1993), three main sources of endogenous Joule's heating ought to be recognised corresponding to the ICB, CMB, and ALB, respectively. Their total energy is sufficient for justifying even the entire internal energy budget of the Earth. Upward propagation of endogenous energy occurs (1) from the ICB by convection within the fluid outer core, and (2) from the CMB or the ALB by Hamilton's principle at a speed of the order of magnitude of  $\sim 10 \text{ cm year}^{-1}$  ("electric soldering iron mechanism", *ibid.*). Allowance ought to be given, however, also for frictional heating from the ALB, consequent to transformation of plate kinetic energy, a process that seems to be typical of island arcs, or that follows e.g. a superswell upheaval originated by the "electric soldering iron". It is possible to estimate the percent vs. time of endogenous energy from different sources, released during the last  $\sim 70 \text{ Ma}$ , by means of an analysis of the Hawaii - Emperor Seamount chain, also considering geomagnetic reversals. Such an entire scheme appears to be significantly supported by several and as yet otherwise unexplained observational features.

**ST4/P/02-B2** Poster **0930-27**

**SOME CONSIDERATIONS ABOUT THE OLD EARTH DILATATION IDEA: SHOULD IT BE RE-EVALUATED?**

Giancarlo SCALERA (Istituto Nazionale di Geofisica, via di Vigna Murata 605, 00143 - Roma, Italy)

The idea of Earth dilatation, more than a century old, has been tested performing computer assisted cartography and paleogeography. After the recognition of a new class of conformities in the Pacific hemisphere, which is strong clues favouring the possibility of a considerable dilatation of the planet, a more complete series of paleogeographical reconstructions has been performed starting from Palaeozoic and using as boundary conditions paleomagnetic data, geochronological data, paleontological data and the same conformities.

The good self-consistency of the set of reconstructions has deserved the tentative elaboration of a tectonic model of evolution of the trench-arc-backarc zones in agreement with a dilatational planet. Some new argument linking the global expanding tectonics to the Earth rotation are presented.

**ST4/W/58-B2** Poster **0930-28**

**ON SOME ASPECTS OF THE INTERNATIONAL PROJECT "CREATION OF A SOFTWARE FOR THE STUDY OF THE EARTH STRUCTURE EVOLUTION IN THE INTERESTS OF THE EARTH SCIENCES"**

E.Ya.SMIRNOV (Interdisciplinary Centre for Advanced Professional Education, St.Petersburg State University, 14th Line 29, St.Petersburg, Russia)

The project is based on an original concept of the Earth structure evolution. According to this concept, the core of the modern Earth is solid and practically wholly consists of a magnetized iron at a temperature close to absolute zero. Between the cold solid core and the hot fluid mantle there is a sort of a thermonuclear reactor processing the substance of the core surface into the mantle substance, thus monotonously increasing the Earth volume. The Earth crust consists of at least two solid layers split into deformed tectonic plates and monotonously rotating relatively to each other, their interaction basically determining the mechanisms of tectonic processes. The proposed concept of the Earth structure evolution, unlike the previous concepts of this kind, does not contradict the presently available information on the processes going on in the Earth. Besides, even without full implementation of the proposed project, it allows to obtain more adequate idea on the Earth core properties on the basis of the presently available seismic measurements and develop more effective methods of the forecast of earthquakes with epicenters located either within the Earth crust or near the boundary between the core and the mantle. There are certain ideas of development of the necessary techniques. They are based on the character of tectonic plates interaction and on the "drift" of seismic waves in the area of the Earth thermonuclear reactor containing powerful flows of particles with their velocities substantially exceeding those of seismic waves. The description of the project is available in Internet at the address <http://www.ecosafe.nw.ru/geya/project.htm>

**ST4/L/06-B2** Poster **0930-29**

**THE SNAKE RIVER EXPERIMENT REVISITED. EVIDENCE FOR THE PRESENCE OF FARALLON PLATE FRAGMENT IN THE TRANSITION ZONE**

Eric BEUCLER, Sebastien Chevrot and Jean-Paul Montagner, Institut de Physique du Globe de Paris, Laboratoire de Sismologie globale, 4, place Jussieu 75005 PARIS FRANCE

The analysis of the 93 PASSCAL-OREGON SRP experiment data [Dueker & Sheehan, 1997] has been reconsidered. New techniques have been applied in the processing of PdS waves, converted from P to S from seismic discontinuities at depth  $d$  in the receiver region. The data set cannot be explained by a one dimension velocity model. Consequently we performed a migration using the linear array distribution, lined up with two great seismic regions (South America on one side, Kuril islands and Aleutians on the other side). The 410-km discontinuity presents a noisy aspect, which prevents from observing the discontinuity topography variations. The 660-km discontinuity is clearly more visible, but it seems to vanish or become largely deflected in a large part of the profile. This anomalous behaviour and the noisy aspect of the transition zone could be associated with the presence of a Farallon plate fragment, already described by van der Lee & Nolet (1997).

**ST4/c/GA1.01/E/17-B2** Poster **0930-30**

**ON THE PLATE TECTONIC DYNAMICS AND GIANT METEORITE IMPACT**

Wan TIANFENG (Department of Geology and Mineral Resources, China University of Geosciences, Beijing 100083, CHINA, email: wantf@sky.cugb.edu.cn) Yin Yanhong (Institute of Marine Geology, MLR, Qingdao 266071, CHINA)

Depending on the data of rock deformation, the change of stress concentration, the periodicity of plate migration, and the periodicity of giant meteorite impact coincides with that the palaeomagnetic inversion, biotic extinction, change of sea level, the solar system's crossing of the galactic plane (about 33 Ma) or cosmic year (about 280 Ma), we proposed a working hypothesis - the microtektite impact induced the plate motion, the essential of that are as follows: (1) The giant meteorite impact has a periodicity of about 33 Ma, coincident with the time for the solar system to cross the galactic plane, where more intense interstellar material would cause meteorite impacts and induce the motion of plates. (2) The angle and orientation of meteorite impact on the Earth surface will influence the direction of plate motion. (3) The giant meteorite will produce a great crater and induce the partial material debility in the upper lithosphere. (4) Because of the thin oceanic lithosphere (50-60 km), the impact of giant meteorite is most likely to destroy the lithosphere, sea floor spreading and change the orientation of migration of oceanic plates.

Presiding Chair: T.Owens (Dept. of Geological Sciences, University of Carolina, Columbia, USA)

**MANTLE STRUCTURE AND DYNAMICS 1**

**ST4/W/21-B2** **1120**

**THE NATURE OF THE CONTINENTAL LITHOSPHERE: INTERPRETATION OF LATERAL VELOCITY ANOMALIES BENEATH NORTH AMERICA**

J. Michael BROWN (Geophysics Program, University of Washington, Seattle, WA 98195, USA, Email: brown@geophys.washington.edu)

New data for the elasticity of upper mantle constituents (single crystal olivines, pyroxenes, and garnets) have been obtained as a function of composition under mantle pressures and elevated temperatures. These experimental constraints for essential derivatives (and cross derivatives) with respect to pressure, temperature, and composition, in conjunction with phase equilibria and elemental partitioning calculations, aid in understanding the seismic structure of the upper mantle. Observed lateral variations in velocity are rationalized through a combination of intrinsic temperature effects and changes in mineral modes and elemental partitioning (caused both by temperature and composition variation). Most of the approximately 9% lateral velocity difference between "cratonic" and "tectonic" North America is so accounted for. The complex velocity structure beneath western North America appears to reflect extremes in compositional and temperature heterogeneity. Although anelastic behavior and melting are expected to further reduce velocities in high temperature regions, pervasive partial melt within the upper mantle is not required. Additional observations of rock fabric will be needed to better link single crystal elasticity to seismic determinations of mantle anisotropy.

**ST4/W/40-B2** **1140**

**MANTLE STRATIGRAPHY AND EVOLUTION OF THE SLAVE PROVINCE**

Michael BOSTOCK (Department of Earth and Ocean Sciences, University of British Columbia, Vancouver, V6T 1Z4 Canada, email: bostock@geop.ubc.ca)

A data set of 1033 three-component, P wave seismograms from five broadband stations at the Yellowknife Array is assembled to investigate mantle structure below the southern Slave province in Canada's Northwest Territories. Following wave field decomposition, seismograms are source-normalized through simultaneous deconvolution to estimate the near-receiver impulse response as a function of epicentral distance and back azimuth. Images of impulse response reveal a well-developed mantle stratigraphy, anisotropic in part, extending from the Mohorovicic discontinuity to the transition zone. A layer of depth-localized anisotropy (+/-5%), termed H, is situated between  $\sim 70$  and 80 km depth with an average shear velocity



comparable to that of the ambient mantle and a sharp upper boundary less than 100 m in transition width. The absence of free surface crustal reverberations on the transverse component affords a window into the upper mantle between 100 and 200 km depth. A sequence of at least two layers between 120-150 km depth, collectively termed X, is most clearly evident to the north and is underlain by a second structure L which dips from 170 km in the west to 230 km into the center of the Slave province. The deepest interface above the transition zone W marks a shear velocity inversion near 350 km depth whose signature is restricted to the SV component signalling a dominantly isotropic response. Consideration of these observations in light of data acquired in a recent Lithoprobe seismic reflection traverse and in petrological studies of kimberlite xenoliths prompts speculation into the role of subduction in craton stabilization. It is suggested that the proto-Slave craton was assembled through processes of shallow subduction resulting in a near-horizontal mantle stratigraphy (i.e., H, X) both compositional and rheological in nature. Interpretation of L as the continuation of dipping reflectors on the seismic reflection profile argues for a final phase of craton assembly involving oblique underplating of subducted lithosphere in the Proterozoic. Subsequent modification of the lithosphere, as manifest by Phanerozoic kimberlite volcanism, may be related to W if an interpretation as the top of a layer containing a dense silicate melt fraction is invoked.

**ST4/W/06-B2****1200****TOWARD FULLY SELF-CONSISTENT MODELING OF AVERAGE CONTINENTAL GEOTHERMS**

Louis MORESI (Australian Geodynamics CRC, CSIRO Exploration & Mining, PO Box 437, Nedlands, 6008, Western Australia); Adrian Lenardic (Department of Geology and Geophysics, University of California, Berkeley, CA 94720, USA)

The forward modeling of average continental geotherms appears to be a relatively simple task. Given the stability and large lateral extent of the continental crust, one solves a one dimensional conduction equation (in a layered medium) for suitable values of thermal conductivity, internal heat generation and mantle heat flux.

One problem with such a model, however, is that the mantle heat flux is not an independent parameter. Heat from the mantle escapes through convective transport to a surface boundary layer where conduction then dominates. The balance between the convective transport and conduction is a sensitive function of the coupled mechanical and thermal properties of the boundary layer. Furthermore, this balance is inherently not one-dimensional: continual horizontal transport of cooling material along the boundary layer is required to sustain the vertical heat conduction.

In the oceanic case, the lithosphere thermal and mechanical structure is readily modeled (at least when less than ~80Myr old) by a cooling half-space conduction profile attached to a material point in accordance with simple boundary layer theory.

However, the presence of buoyant continental crust, and depleted sub-continental mantle lithosphere, prevents convection from determining the thickness of the upper boundary layer. Therefore, the thermal structure of the crust, sub-continental mantle lithosphere, and convecting mantle must be solved as a coupled system in which the convection pattern and associated heat transport is not known in advance. A further complexity is that the continents are finite in extent - the partitioning of mantle heat flow between continents and oceans is another unknown which must be modeled.

We present a number of convection simulations in which we incorporate realistic models of the oceanic lithosphere with continental blocks of varying size and shape and with different relative thermal conductivities and heat generation rates. We solve for the velocity and temperature everywhere in the crust and mantle during several mantle overturns. We track geotherms for a number of points within the continental blocks to determine the long-time average profiles, the variance, and the extreme values of the profiles in response to the underlying convection.

As one example we compare geotherms obtained from continental margins with those from the continental interior, and examine the influence of steps in the thickness of the depleted mantle root. Computed geotherms are compared to approximations obtained using 1D conduction modeling to demonstrate the conditions under which the 1D assumption may fail. We also compare the computed geotherms for the continental margin with analytic solutions in 2D for flow under a changing boundary condition.

**ST4/W/50-B2****1220****CONNECTION BETWEEN STRUCTURE, DYNAMICS AND INSTABILITY OF THE LITHOSPHERE**

Andrei Gabrielov (Departments of Mathematics and Geophysics, Purdue University, W. Lafayette, IN 47907-1395, USA, email: agabriel@math.purdue.edu); Vladimir KEILIS-BOROK (International Institute of Earthquake Prediction Theory and Mathematical Geophysics, Russian Academy of Sciences, Warshavskoye shosse 79 kor.2, Moscow 113556, Russia, email: vkborok@mitp.ru); David Jackson (Department of Earth and Space Sciences, UCLA, Los Angeles, CA 90095-1567, USA, email: jackson@ucla.edu)

Structure of the lithosphere imposes strong limitations on its stationary dynamics. Inconsistency between structure and dynamics leads to instability, expressed in accumulation of stress, deformation, fracturing, and the change of geometry of the system. Two integral measures of such instability are introduced: geometric incompatibility G, depicting instability concentrated near the faults' junctions, and kinematic (Saint Venant's) incompatibility depicting inconsistency between absolute movements of the blocks and relative movement on the faults. The estimates of G and K link together the structure and dynamics of the lithosphere, the driving forces included. An analog of Stokes formula is found, allowing to estimate instability of the structure from observations on its boundary.

**Tuesday 27 July PM**

Presiding Chair: M.Bostock (Dept. of Earth and Ocean Sciences, University of British Columbia, Canada)

**MANTLE STRUCTURE AND DYNAMICS 2****ST4/W/30-B2****1400****IMAGING OF THE LITHOSPHERE AND MANTLE TRANSITION ZONE BENEATH THE TANZANIAN CRATON AND SURROUNDING MOBILE BELTS, EAST AFRICA: IMPLICATIONS FOR CRATONIC STABILITY AND THE ORIGIN OF EAST AFRICAN UPLIFT AND TECTONISM**

T.J. OWENS (Department of Geological Sciences, University of South Carolina, Columbia, SC 29208 USA, Email: owens@sc.edu); A.A. Nyblade and C.A. Langston (Department of Geosciences, Penn State University, College Park, PA); H.Gurrola (Department of Geosciences, Texas Tech University, Lubbock, TX); J. Ritsema (Seismological Laboratory, California Technical University, Pasadena, CA)

Results of a 20-station broadband seismic array experiment deployed in and around the Archean Tanzania Craton in 1994-95 shed new light on issues of both the stability of cratonic lithosphere and the origin of the East African uplift and tectonism. We utilized crustal and upper mantle receiver function analysis, teleseismic travel-time tomography, and regional earthquake waveform modeling to generate three-dimensional images of the upper 700 km of the earth in this region. Due to the natural distribution of teleseismic earthquakes relative to Tanzania, our resolution is best in the eastern half of the craton, the eastern rift, and the continental margin of Africa. Our derived images help constrain the existence of a seismically fast cratonic keel extending to at least 200km depth beneath the Tanzanian Craton. Beneath this fast zone, anomalously low velocities extend down into the mantle transition zone. On the margins of the craton, low seismic velocities extend from the transition zone up to shallow depths beneath rifted mobile belts. These observations suggest a deep-seated origin for the uplift, rifting and volcanism of East Africa that can be explained most easily by a mantle plume. A process in which this plume rises beneath the cratonic keel and is deflected around the sides of the keel is consistent with our observations. It is also consistent with the uplift of the broad East African Plateau, and focussing of rifting and volcanism in the surrounding mobile belts and suggests that the Archean craton is relatively resistance to thermal erosion during this plume event.

**ST4/W/55-B2****1420****SMALL-SCALE CONVECTION WITHIN UPPER MANTLE BENEATH TIBETAN PLATEAU AND ITS CONTRIBUTION TO THE UPLIFT OF THE PLATEAU**

Xiong XIONG, Houtze Hsu (Both at Institute of Geodesy and Geophysics, Chinese Academy of Science, 54 Xudong Road, Wuhan, Hubei 430077, China, email: xxiong@asch.whigg.ac.cn); Rongshan Fu (Department of Earth and Space Science, University of Science and Technology of China, Hefei 230026, China, email: frs@ess.ustc.edu.cn)

Although many mechanisms have been proposed to clarify the uplift of the Tibetan Plateau, the mechanism of mantle dynamics is paid little attention. The evolution of the upper mantle flow under the Tibetan Plateau in the past 200 million years and its contribution to the uplift of the plateau has been investigated by the numerical experiment in the paper. In the experiment the effects of several geological factors, such as a subductive oceanic lithosphere, the Tarim Basin and the moving Indian Plate, are considered. The results show that there is an upper mantle convective system beneath the Tibetan Plateau. The upwelling locates in the central northern part of the plateau, while the downwelling locates in the south and northmost parts. The uplift amount of the Tibetan Plateau includes two parts, mechanical component, which is caused by the boundary stress induced by the small-scale convection within the upper mantle, and the thermal one, which is caused by the heating of the mantle upwelling. At the time scale corresponding to the present, the mechanical component is about 100m, while the thermal one is about 550m. The numerical results suggest that the thermal action is an important factor for the uplift of Tibetan Plateau which can not be ignored.

**ST4/W/18-B2****1440****THE STRUCTURE OF THE MANTLE BELOW THE EURO-MEDITERRANEAN REGION**

Piromallo C., MORELLI A., Olivieri M. (Istituto Nazionale di Geofisica, 00143 Rome, Italy; email: piromallo@ing750.ingrm.it)

Knowledge of the structure of the upper mantle and transition zone in a region of plate collision, such as the Mediterranean, is a key to understanding the tectonics and dynamics of active and past processes. We have analyzed P-wave delay times from regional and teleseismic earthquakes in our new tomographic study of the Alpine-Mediterranean area. Well defined high velocity structures mark subducted slabs (Alboran, Apenninic-Calabrian arc, Dinaro-Hellenic arc, Carpathian arc) and stable cold lithosphere (Eastern Mediterranean, Adriatic, Western Mediterranean), whereas low velocity regions are connected to high heat flux (Aegean, Tyrrhenian, Pannonian basin, Central Massif, Central Italy volcanic provinces). Seismic fast and slow velocities are usually explained as due to thermal anomalies. In order to calibrate our tomographic results, we also model variations of the depth of mineralogical phase transitions at 410 and 660km - also affected by temperature - by time-domain inversion of teleseismic P waveforms for transfer functions. We find evidence for small-scale topography of the discontinuities, translating into maximum lateral thermal anomalies of the order of 400K. Recent deployment of seismographs in areas with previously insufficient illumination significantly improved ray coverage for tomography, but the availability of broadband data outside continental Europe is still limited to few stations.

**ST4/E/68-B2****1500****PRELIMINARY RESULTS ON THE STRUCTURE OF THE UPPER MANTLE OF THE AEGEAN AREA, FROM TELESEISMIC SURFACE WAVES MEASUREMENTS**

K. MAKROPOULOS, I. Kassaras, P. Papadimitriou (all at Department of Geophysics, University of Athens, 157 84 Athens, Greece, email: kmakrop@cc.uoa.gr); D. Hatzfeld, H. Pedersen (LGIT/UFJ, Grenoble, France, email: Denis.Hatzfeld@obs.ujf-grenoble.fr); H. Lyon-Caen (Institut de Physique du Globe de Paris, France, email: lyoncaen@jadete.ens.fr); Kiratzi (Geophysical Laboratory, University of Thessaloniki, Greece, email: kiratzi@geo.auth.gr)

In 1997, for a period of six months, we deployed a temporary broadband array of 30 digital seismological stations over the Aegean area. About 110 teleseismic events with magnitude greater than 5.5 were recorded, comprising a unique database for the northeastern Mediterranean region. Seismograms of 12 long-period instruments of the network, are analyzed to determine the dispersion of Rayleigh and Love waves, by the two station method. Phase velocities from fundamental and higher-mode data are obtained over the period range 10-100s, along selected paths. Furthermore, the calculated phase velocities are inverted with the linear approach, providing constraints on the upper mantle shear velocity structure, along the propagation paths. In this study, we will present the first preliminary results on the structure of the lower lithosphere and the upper mantle beneath the Aegean, focusing on the possible effect-relation of the defined structure to the observed complex geodynamics of the area.

**ST4/E/65-B2****1520****UPPER MANTLE SEISMIC VELOCITY STRUCTURE BENEATH SE BRAZIL**

M. SCHIMMEL, M. Assumpcao (both at Dept of Geophysics, University of Sao Paulo, Rua do Matao 1226, 05508-900 Sao Paulo - SP, Brazil); and J. VanDecar (Carnegie Institution of Washington, 5241 Broad Branch Road, NW, Washington DC 20015, USA)

We present preliminary results from teleseismic travel-time inversions for P- and S-wave data mainly recorded at portable broad band stations in SE Brazil. The stations have been employed at more than 25 sites within an area of about 500km x 1000 km during the years 1992 - 1998. Most stations are from a joint project (BLSP92) of the Carnegie Institution of Washington and the University of Sao Paulo (USP) and from a continuation of this project by

the USP (BLSP95). The P and S data base consists of relative travel times (P, PKP and S, ScS, SKS, SKKS-waves) which we obtained from the wave forms by a multi-channel cross-correlation technique (VanDecar and Crosson, 1990) using a new coherence functional (Schimmel, in prep.). The inversion follows the approach described by (VanDecar, James, and Assumpcao; 1995). Our results confirm the main features revealed by VanDecar et al. (1995): a shallow high-velocity region beneath the Sao Francisco craton, deep high velocities to the southwest, and a low-velocity cylindrical structure in the upper mantle to a depth of at least 500 - 600km. The cylindrical structure has been interpreted as the fossil conduit through which the initial Tristan da Cunha plume head traveled to generate the Parana flood basalts. This structure continues to lie beneath the Parana basin indicating that the upper mantle has been in coupled motion with the overlying plate since the opening of the South Atlantic Ocean. The increased aperture of the seismic network, amount of station sites, and data permit a more detailed separation of geological structures such as the Sao Francisco craton and an extension of the study to larger depth. The greater resolution at depth is important for determining the base of the inferred conduit and therefore for characterizing the coupling between upper and lower mantle beneath SE Brazil.

**ST4/E/55-B2****1620****SEISMIC BODY WAVE ATTENUATION IN THE UPPER MANTLE**

H.X. CHENG, B.L.N. Kennett (Both at Research School of Earth Sciences, Australian National University, ACT 0200, Australia, email:chx@rse.ses.anu.edu.au)

The main challenge in measuring and developing models for attenuation structure in the Earth is the separation of anelastic effects from both propagation and source effects. The slope of logarithm of the spectral ratio between P and S wave arrivals on the same record can be used to determine the  $t^*$  (differential attenuation) between P and S because the frequency dependent factors common to the two wave types are canceled through the spectral ratio. The use of the logarithmic slope also minimises the influence of absolute amplitude variations. Tests on noise treatment show that the noise spectrum can be represented by a mean base line. The noise can then be removed from signal based on the assumption that noises are same in both signal and noise spectral windows. Tests using synthetic seismograms show that the  $t^*$  can be recovered quite well but also that the influence of surface reflected phases within the P and S wave spectral windows can be important.

The systematic application of the spectral ratio approach to the estimation of the  $t^*$  between P and S to the broadband data from Australian stations provides a measurements along nearly 2000 refracted raypaths mostly sampling the northern part of the continent. The measurements also clearly delineate major variations in attenuation between the cratonic structures in the centre and west and the eastern part of Australia.

With our knowledge of the variations in velocity structure, the  $t^*$  along the different paths can begin to be interpreted in terms of attenuation structure in 3-D. In central and western Australia strong attenuation of S waves is required in the asthenosphere beneath a lithosphere with comparatively low attenuation. In the east the zone of high attenuation is shallower.

**ST4/W/44-B2****1640****RESOLVING UPPER-MANTLE ATTENUATION STRUCTURE BY ANALYZING HIGH-FREQUENCY P AND PP SPECTRA**

Linda M. WARREN and Peter M. Shearer (Scripps Institution of Oceanography, University of California, San Diego, La Jolla, CA, 92037-0225; email: lwarren@ucsd.edu)

We study the P-wave attenuation structure in the upper mantle by computing the spectra for more than 22,000 P and 4000 PP waves using selected seismograms from the global seismic networks between 1988 and 1997. Each spectrum is the product of source, propagation, and receiver response functions. Since there are multiple receivers for each source and multiple sources for each receiver, we can approximate the source and receiver responses by stacking the appropriate P spectra. The resulting source-specific response functions include both the source spectra and the effect of near-source attenuation in the upper mantle; the receiver stacks include the instrument and site responses and near-receiver Q structure. Next, we correct the PP spectra using the source and receiver stacks found from the P waves. For each PP path, the remaining spectrum, which represents the propagation response, is used to estimate  $t^*$  at frequencies between 0.55 and 1.95 Hz. Since we have accounted for the source- and receiver-side effects and attenuation in the lower mantle is small, most of the residual  $t^*$  is accumulated in the upper mantle at the PP bounce point. Maps of our  $t^*$  measurements plotted at their surface bounce points show remarkably coherent patterns. Eurasia is less attenuating while the northeast Pacific is more attenuating than the global average. The patterns of more and less attenuating regions that we see are similar to those in the S-wave attenuation model QR19 [Romanowicz, 1995]. Our  $t^*$  measurements for oceanic bounce points demonstrate a good correlation between the age of the ocean floor and the amount of attenuation.

**ST4/W/14-B2****1700****ANISOTROPY, MANTLE FLOW AND SCATTERED SURFACE WAVES IN THE KAMCHATKA REGION**

Jeffrey PARK, Vadim Levin, Valerie Peyton, Jonathan Lees, Mark Brandon (all at Dept of Geology and Geophysics, Yale University, POB 208109, New Haven CT 06520 USA; email: park@hess.geology.yale.edu); Evgenii Gordeev, Victor Chebrov (OMSP, Petropavlovsk-Kamchatsky, Kamchatka, Russia) and Alexei Ozerov (Institute of Volcanology, Petropavlovsk-Kamchatsky, Kamchatka, Russia)

Active subduction of the Pacific plate beneath the Kamchatka peninsula appears to terminate at its intersection with the Aleutian Island chain, where a transform plate boundary forms a "corner" with the subduction zone. The near-absence of seismicity north of the Aleutian junction suggests that the subducting Pacific plate terminates at this point, dangling a slab edge into the ambient upper mantle flow. By analogy with the Lau Basin in the Tonga region, slab rollback at the Aleutian corner would lead to east-west extension in the upper mantle beneath central Kamchatka, slab-parallel flow on the seaward side of the trench, and possibly transport of fore-arc asthenosphere eastward to the back-arc side. In an alternative scenario a contiguous slab that is currently aseismic might extend north of the Aleutian junction, forming a barrier for the east-west asthenospheric flow. Mantle flow leads to peridotite deformation, preferred alignment of mantle minerals, and elastic anisotropy. Sharp lateral gradients of anisotropy would be developed in likely models for mantle flow in the Kamchatka region. These would induce quasi-Love waves (Love-to-Rayleigh surface-wave scattering) at periods longer than 50 seconds. Preliminary analyses of data from the GSN station PET in Kamchatka and ADK at Adak Is. in the Aleutians show strong quasi-Love waves, presumably associated with mantle flow near the local plate boundaries. In August 1998 a joint team of US and Russian investigators installed a network of 15 broadband portable seismometers on the Kamchatka peninsula. Initial data records from selected stations in the portable network display long-period quasi-Love waves, similar to those seen at PET. We will report on attempts to combine data from the Kamchatka network and Aleutian-Island stations to infer mantle flow in this region.

**ST4/W/25-B2****1720****ANISOTROPIC TOMOGRAPHY OF THE ATLANTIC OCEAN**

Graca SILVEIRA (Centro de Geofisica da Universidade de Lisboa,Rua da Escola Politecnica, 58, P-1250 LISBOA) , Eleonore Stutzmann, Jean-Paul Montagner (both at Departement de Sismologie, Institut de Physique du Globe, 4 place Jussieu, 75252 PARIS-CEDEX 05, France.) and Luis Mendes Victor (Centro de Geofisica da Universidade de Lisboa)

The depth extent of the Mid Atlantic Ridge and the role of hotspots in the Atlantic opening are still a matter of debate. In order to constrain the structure and the geodynamic processes below the Atlantic Ocean, we provide the first anisotropic phase velocity and S-wave velocity maps of this area, obtained at a regional scale. We have determined Rayleigh wave phase velocities along 1311 direct epicentre-to-station paths. After shallow layer corrections, the phase velocities are inverted, without a priori constraints, to obtain anisotropic phase velocity lateral variations in the period range 50 - 250s. In a second step, the inversion versus depth enables to retrieve S-wave velocity structures. The ridge axis corresponds to a low velocity anomaly visible down to 150km in the North Atlantic and down to 200km in the South Atlantic. A good correlation between hotspot locations and low velocity anomalies is obtained down to the deepest depth inverted. Furthermore, a low velocity anomaly elongated along a North-South direction is visible at every depth and seems to be correlated with hotspot positions. On average, the North Atlantic is associated with higher velocities than the South Atlantic. The maps of phase velocity anisotropy under the Atlantic Ocean are interpreted in the Mid-Atlantic area where we have the best resolution. Close to the ridge, the fast axis of Rayleigh wave phase velocity is found perpendicular to the ridge axis. A comparison of anisotropy directions and plate motion shows that seismic anisotropy integrates also deeper phenomena such as mantle convection.

**ST4/W/51-B2****1740****DEPTH DISTRIBUTION OF ANISOTROPY USING CONVERTED WAVES**

Takashi IIDAKA and Fenglin Niu (both at Earthquake Research Institute, the University of Tokyo, 1-1-1 Yayoi, Bunkyo-ku, Tokyo 113, Japan, Email: iidaka@eri.u-tokyo.ac.jp, niu@eri.u-tokyo.ac.jp)

Depth distribution of the anisotropy inside the earth has been an important problem to be solved. The shear-wave splitting analysis using converted waves makes it possible to estimate the anisotropy at each layer; i.e. crust, upper mantle, lower mantle, and D" layers, if the clear converted waves caused by each boundary are observed. We researched shear-wave splitting in the east China region to know the depth distribution of the anisotropy by comparing the waveform splitting by the use of SKS, P-SmS(P-S converted at the free surface and reflected Moho discontinuity) and P660s(P-S converted waves at the '660km' discontinuity) waves. However, 660s and P-SmS waves were only observed at HIA and three stations (ENH, MDJ and SSE), respectively. We can not restrict which parts of the anisotropic region should be attributed. The analysis of P-SmS wave indicates crustal anisotropy is estimated to be less than 0.05 sec at the most eastern China region.

The time-lag values of the shear-wave splitting caused by the lower mantle and upper mantle including crustal anisotropy are about 0.4 sec and 0.2 sec beneath the HIA station, respectively. The shear-wave splitting analysis of the converted waves makes it possible to reveal the depth distribution of anisotropy.

**Wednesday 28 July AM**

Presiding Chair: J.H.Davies (Dept. of Earth Sciences, University of Liverpool, UK)  
Concurrent Poster Session

**MANTLE STRUCTURE AND DYNAMICS 3****ST4/W/20-B3****0840****A SMALL DENSITY JUMP ACROSS THE 660KM DISCONTINUITY INFERRED FROM PP AND SS PRECURSOR AMPLITUDES**

Peter M. SHEARER and Megan P. Flanagan (University of California, San Diego, La Jolla, California 92093-0225, USA, e-mail: pshearer@ucsd.edu)

Globally averaged depths to the 410- and 660-km discontinuities are now constrained rather precisely from studies of seismic reflections off these boundaries. However, the amplitudes of the velocity and density jumps at the interfaces are known much more poorly, and results from different studies show scatter of a factor of two or more. The density jumps, critical parameters for modeling of mantle dynamics, are particularly hard to measure and are often based on velocity versus density scaling relationships rather than direct observational constraints. Seismic reflections at near-vertical incidence are sensitive to the impedance changes at the interfaces and cannot separately resolve the velocity and density jumps. However, at shallower ray angles the reflection coefficients respond differently to the velocity and density changes. Thus, in principle, by studying the behavior of reflection coefficients as a function of ray angle, the velocity and density jumps can be separately resolved. We adopt this approach to modeling the range dependence in the amplitude of long-period SS and PP precursors resulting from underside reflections off the 410 and 660km discontinuities. We stack over 20,000 long-period seismograms to obtain measures of the range dependence in PdP and SdS amplitudes. We estimate error bounds on our observed amplitudes using a bootstrap resampling approach. Using synthetic seismogram modeling, we then compute confidence ellipses within the three-parameter model space of changes in P velocity, S velocity and density across each interface. Our results show that the PREM model is within the 95% confidence ellipse for the 410km discontinuity but well outside the allowed jumps across the 660km discontinuity. In particular, the density jump across the 660km discontinuity is constrained to lie between 4 and 6%, substantially below the PREM value of 9.3%. Many convection models have assumed the PREM density jump at 660km in computing the barrier to mantle flow caused by a negative 660km Clapeyron slope. Our results suggest that these studies may be overestimating the influence of the 660km discontinuity on mantle flow.

**ST4/E/02-B3****0900****MANTLE DISCONTINUITIES BENEATH NORTHEAST OF CHINA AND ITS GEODYNAMIC IMPLICATION**

Shaonian ZANG and Yuanze Zhou(both at Department of Geophysics, Peking University, Beijing 100871, China, email: szzang@ibmstone.pku.edu.cn, zyz@www.geophy.pku.edu.cn )

In this study we investigate the mantle discontinuities beneath the northeast part of China where the Japan sea subducting slab reached and try to find some clues for interaction between subducting slab and discontinuities. The converted waves of P-SV were used to study the discontinuities. The seismological records from eight stations were used. The three directions of record UD, NS and EW were transformed to P, SV and SH coordinate system.



The polarization filter was applied to the three components P, SV and SH in time domain, then the P-SV phases were picked out from the time window of 15 -110seconds after P arrival by comparison the P and SV components. The methods of cross-correlation and waveform analysis were also applied to select the converted wave phases. According to the converted phases, the converted points were obtained basing on the PREM velocity model and concentrated nearly on the depths of 150km, 220km, 400km, 520km, 660km, 900km and 1100km respectively. There are obvious velocity contrasts. It was also noted that some converted points are distributed between 220km and 400km as well as 660km and 900km. The reason for that was analysed. The big attention has been paid to the 660km discontinuity. The depth of the discontinuity from the east part of the region to west part along the subducting direction is slightly changed. It may imply that the subducting slab does not penetrate through the 660km discontinuity, but is bended and extended horizontally from east to west.

**ST4/E/49-B3****0920****MAPPING LOWER MANTLE TOPOGRAPHY USING A HIGH RESOLUTION MIGRATION TECHNIQUE**

Aoife O'MONGAIN (British Geological Survey, Murchison House, West Mains Road, Edinburgh EH9 3LA, UK, email: aom@mail.nmh.ac.uk) Jurgen Neuberg (School of Earth Sciences, University of Leeds, Leeds LS2 9JT, UK, email: j.neuberg@earth.leeds.ac.uk)

P-waves recorded on the Northern California Seismic Network provide the high resolution required to investigate the heterogeneity in the lower mantle which is associated with the intermittent detection of a D'' discontinuity. The overlapping Fresnel zones of the bounce points in the lower mantle facilitates the development of models which are significantly more consistent than previous models created using data from single stations or sparse arrays. An advanced processing scheme which involved the use of the vespagram, FK and matched filter methods, was developed to enhance anomalous lower mantle P phases and retrieve all possible parameters which could be used to determine their origin and character. Analysis of the effect of reflector topography on the lower mantle phases led to the development of a migration scheme. Differential travel times, slowness and azimuth values obtained from the array processing techniques were used in the migration scheme, which does not constrain the positioning of the scatterers to one depth, but accounts for reflector topography or for the occurrence of lower mantle scattering bodies. Realistic structures could be inferred from the migration results; D'' structures larger than the effective Fresnel zone size were observed. Mountainous D'' topography with a height of 300km above a base level of 3616km is suggested for the bounce point region south of the Aleutian Island Arc. The central Pacific region shows evidence for a D'' discontinuity with considerable topography (150km topography above a base level of 3766km) and also the presence of a low velocity layer at the base of the mantle. In contrast, distinctive scattering bodies, which are all greater than effective Fresnel zone size, are observed in the bounce point region off the coast of Central America. For the first time the size of the scattering bodies responsible for the observed transverse isotropy beneath Central America is constrained.

**ST4/E/10-B3****0940****A COMPLETE P WAVEFORM MIGRATION IN THE LOWERMOST MANTLE BENEATH NORTHERN SIBERIA**

Marion FREYBOURGER (email: marion@quake.mit.edu), Sebastien Chevrot (both at EAPS, MIT, Cambridge, MA02139, USA), Frank Krueger (Institut fuer Geowissenschaften, Potsdam, 14415, Germany) and Ulrich Achauer (EOST, UMR 7516 CNRS-ULP, Strasbourg, 67084, France)

More than 15 years of PcP and ScS precursor studies failed to give enough constraints for an appropriate explanation of the origin of the highly variable discontinuity on top of D'' (2 to 3% velocity contrast, 150 to 400 km above the core-mantle boundary). Whether there indeed exists a discontinuity with topography or rapidly varying velocity contrast, or scatterers non uniformly distributed within D'' is still debated. Classical 1D or 2D forward modelling appear unsatisfactory. The larger amount of high quality broadband data now available has thus recently stimulated the development of migration techniques in order to take into account potential non great circle paths resulting from 3D effects and to extract the information from larger datasets. A new migration scheme is here introduced to address the issue of the origin of PcP precursors. This is to our knowledge the first complete waveform migration scheme for the investigation of the lowermost mantle. The method is tested on synthetics and then applied to a dense dataset of Kuril events recorded in Western Europe which samples D'' beneath Northern Siberia. The migration reveals the existence of a finite size scatterer with highly anisotropic scattering diagram, some 2600-2650km beneath the Tajmyr peninsula (around 70 deg N, 80 deg E).

**ST4/E/15-B3****1000****LOW SOUTHERN HEMISPHERE CORE-MANTLE BOUNDARY P WAVESPEEDS DERIVED BY PKP A-POINT LOCATION AND DIFFRACTED PKP(AB) SLOWNESS**

George HELFFRICH (Earth Sciences, U. of Bristol, Bristol UK), Paul Silver (DTM/Carnegie Institution of Washington, Washington DC USA)

Records from a portable array of broadband seismometers deployed in South America contain near-antipodal P wave arrivals through the core (PKP). The 50-100 km instrument spacing permits the waveforms and distance decay of PKP frequency content of PKP to be analyzed in detail to establish the A-point position in the PKP travel time curve, which at 184 degrees, is farther than specified in contemporary radial earth models (PREM, IASP91, SP6, AK135). The A-point position and array analysis of slowness anomalies of the major arc branch of PKP(AB) reveal ~5% slower CMB wavespeeds under the south Atlantic and Indian Ocean, locations not previously recognized as anomalous. Wave speeds 5% slower than ambient must exist at both the source- and receiver-side of the CMB. While the southern Atlantic site lies below the Tristan hotspot, there is no similar feature above the CMB interaction point at the source side.

**ST4/W/01-B3****1100****DYNAMIC CONSTRAINTS ON THE STRUCTURE AT THE BASE OF THE MANTLE**

Igor Sidorin, Michael GURNIS, and Donald V. Helmsberger (all at Seismological Laboratory, Caltech, Pasadena, CA 91125 USA, email: gurnis@caltech.edu)

The lowermost mantle, D'', contains substantial variations in seismic velocity both radially and laterally on ~10 km to >1,000 km scales. Seismic phases related to D'' are widely used to study the structure at the base of the mantle. We use dynamic forward modeling (thermo-chemical models of mantle convection with imposed plate tectonics) to predict the seismic structure in the deep mantle. By computing synthetic waveforms and comparing them with data, we select dynamic models consistent with seismological observations. Thermal anomalies from slabs

alone do not give rise to a sufficiently strong triplication. The geographical patterns of the triplication caused by a basal phase change agree with seismic observations better than those caused by a chemical layer. By comparing the predicted trends in amplitude and travel time distributions with regional data, we obtain constraints on the (P,T) conditions and the value of Clapeyron slope of such a phase change that yield best agreement with seismological data. We geographically predict the elevation of the discontinuity above the core-mantle boundary using thermal anomalies inferred from tomographic inversions. The discontinuity is imposed on the large-scale structure predicted by tomographic models with an appropriate compensation for the added velocity increase. Synthetic waveforms are computed for many 2-D sections of this composite seismic structure. We find that the strength of D'' (Scd) is strongest beneath seismically fast regions (like the Caribbean) and weakest in slow regions, such as the mid Pacific, consistent with observed waveforms.

**ST4/W/08-B3****1120****A MODEL OF WHOLE-MANTLE HETEROGENEITY DERIVED FROM WAVEFORM DATA**

Charles MEGNIN, Barbara Romanowicz & Ludovic Breger (Berkeley Seismological Laboratory, U.C. Berkeley, 94720)

We present a new mantle model of VSH heterogeneity calculated from the inversion of handpicked waveforms of Love waves, body waves and first and second order higher mode arrivals. Our model is developed laterally up to spherical harmonic degree 18 and radially on 16 cubic spline knots spaced according to the depth sampling. The waveform modeling is done with the mode coupling formalism 'NACT' of Li & Romanowicz (1995) that is appropriate for the modeling of both surface and body wave energy. We invert iteratively for mantle heterogeneity and for CMTs until a stable solution is obtained. The set of a priori is determined by performing an inversion for the set of damping parameters that optimizes the retrieval of the 3D convection model GEMLAB1 of Bunge et al (1998). This model incorporates the effects of phase transitions at 410 km & 670 km, partial bottom heating, viscosity contrast between upper and lower mantle and the history of plate motions since the mid-Mesozoic.

Cross-sections across subduction zones such as Tonga-Kermadec, Farallon, Peru-Chile show continuous fast structure penetrating the lower mantle, although the depth of penetration fluctuates from one region to the next. In contrast, fast anomaly appears to accumulate at the 670 km discontinuity under the Kurile, Japan trench and Izu-Bonin arc, with no penetration in the lower mantle, in agreement with the results of Fukao et al (1992). Continuity across the whole mantle of the slow anomaly below the African continent is observed, suggesting a deep origin to the African superswell.

To test the model in the lowermost mantle, we selected S-SKS differential traveltimes for narrow azimuthal corridors between the Fiji Islands region and North American stations and compared them with synthetic ones. The trends observed in the data are compatible with those predicted by the model.

Finally, we separate the model into its positive and negative parts. In the lower mantle, the spectral image of the "slow" model shows wavelengths that increase progressively with radius, from a degree two peak near the CMB to a degree six maximum at 700km. In contrast, the "fast" part exhibits little variation with depth with spectral peaks at degrees two and three throughout the lower mantle. This image suggests that upwellings become increasingly diffuse as they ascend, while the downwellings remain comparatively coherent.

**ST4/E/22-B3****1140****EVIDENCE FOR RADIAL ANISOTROPY IN THE EARTH'S MANTLE**

Lapo BOSCHI and Adam M. Dziewonski (both at Department of Earth and Planetary Sciences, Harvard University, 20 Oxford street, Cambridge MA 02138, U.S.A.) Email: boschi@seismology.harvard.edu

In the last twenty years or so, numerous authors have used the techniques of global tomography to obtain three-dimensional images of the laterally heterogeneous structure of the Earth. During this time, the number of available seismic measurements was increased enormously, and the inversion methods were constantly refined. Today, velocity models obtained with different datasets and very different approaches often show an encouraging consistency between each other. Nevertheless, recent results suggest that seismic tomography might be capable of constraining geophysical observables that were not accounted for by earlier studies; Ekstrom and Dziewonski (1998), for example, were able to find a robust regional anomaly in elastic anisotropy, located in the Pacific upper mantle. Vasco and Johnson (1998) suggested that the travel-time measurements associated with phases traveling through the Earth's core are best explained by allowing the outer core to be laterally heterogeneous. In general, such results seem to indicate that the many seismic data that are now available probably contain some valuable information that we might as yet have neglected. Our research focuses on the possibility of radial anisotropy throughout the mantle. We perform joint inversions for lateral anomalies in horizontal and radial P-velocity (the "A" and "C" parameters) in the Earth's mantle, and in the topography of the CMB, using P, PKP, and PcP travel-time data and a block-parameterization of high nominal resolution. We interpret our results in the framework of the above mentioned recent studies; in particular, radial anisotropy of the mantle can be an alternative way, without requiring outer-core lateral heterogeneities, to fit the travel-time data associated with core-phases. Furthermore, an anisotropic map of the mantle can provide new constraints on our geophysical interpretation of tomographic images.

**ST4/E/23-B3****1200****SEISMIC TOMOGRAPHY, 3D SPHERICAL MANTLE CONVECTION, AND GEODYNAMICS: THE MUTUAL BENEFITS**

J. Huw DAVIES (Dept. of Earth Sci., Univ. of Liverpool, L69 3BX, UK, email: davies@liv.ac.uk); H.-P. Bunge (Dept. of Geological Sciences, Princeton Univ., Princeton, NJ, USA)

The best way to demonstrate understanding of the dynamics of the mantle is by developing successful mantle circulation models that explain a wide body of data. Spatially, the most testing data come from seismic tomography. We have started on the road of directly testing realistic 3D high Rayleigh number (node spacing down to 25km) spherical mantle circulation models which incorporate recent subduction history. The lateral temperature variations are converted to seismic velocity perturbations then, using exactly the same 2.5D ray-set as used in our tomography we predict the travel-time residuals. These are then inverted using exactly the same joint structure location inversion algorithm i.e. the model data go through exactly the same 'filter' as the actual data. These results can be compared directly with the P body-wave data inversions implemented using a 3D a-priori model constructed with geodynamical constraints. The circulation models predict well the downwellings but as expected do not match the locations of the hot upwelling plumes found crossing from the lower to upper mantle in the tomography. The mantle circulation and a-priori seismic models provide excellent realistic synthetic models with which to investigate the practice of global seismic tomography. For example one can quantify: the trade-off between relocation and structure, the optimum damping parameters, the best model parameterization, and the degree of aliasing. For example we find that the histogram of the synthetic travel time residuals is never Gaussian, rarely unimodal, and not centred around zero. This for example brings into question



procedures (e.g. L2 norm, source relocation) that theoretically assume such a distribution. The non-zero mean questions using 'true' global reference earth models constrained by free oscillations as initial models for body-wave inversions.

ST4/L/01

1420

#### SUBDUCTION PROCESSES AND FLUID/ROCK INTERACTIONS IN THE CENTRAL ANDES IMAGINED BY GEOPHYSICAL OBSERVATIONS

Günther Asch, Christian. Haberland, Frank Schilling, Xiaohui Yuan, Henry Brasse, PETER GIESE, Stefan Lueth, Peter Wigger

The lithosphere of the Central Andes (21° and 24°S) has been investigated by the interdisciplinary research program "Deformation processes in the Andes" carried out by geoscientists of the Freie Universität Berlin, Technische Universität Berlin, the GeoForschungsZentrum Potsdam and the Universität Potsdam in co-operation with institutions in Southern America. Here geophysical studies are presented which monitor fluid/rock interactions in the downgoing slab and the overlying slab. The pattern of intermediate depth seismicity as double seismic zone portrays the shape of the isotherms in the temperature range 500°-700°C. Tomographic sections of the parameters  $v_p/v_s$  and  $Q$  display regions of hydration and melting in the upper plate. Extreme low velocity regions indicate the distribution of partly molten rocks in the uppermost crust. Sections derived from receiver functions reveal the transition from basalt to eclogite in the downgoing slab. There are well expressed changes in the petrophysical structure of the lithosphere in the upper plate in N-S direction, which may be correlated the recent volcanic activities in the magmatic arc.

Wednesday 28 July PM

Presiding Chair: G.Helffrich (Dept. of Earth Sciences, University of Bristol, UK)

#### SLABS AND PLUMES

ST4/E/01-B3

1400

#### SEISMIC STRUCTURE OF SUBDUCTION ZONES: IMPLICATIONS FOR ARC MAGMATISM, SEISMOTECTONICS AND GEODYNAMICS

Dapeng ZHAO (Department of Earth Sciences, Ehime University, Matsuyama 790-8577, JAPAN; E-mail: zhao@sci.ehime-u.ac.jp)

High-resolution 3-D seismic structure of several subduction regions including Japan, Alaska, and Tonga is determined down to 700 km depth by using high-quality data recorded by regional seismic networks. Major findings are summarized as follows. (1) The subducting Pacific slab is imaged as a high-velocity zone with a thickness of 50-90 km and a P-wave velocity 4-6 percent faster than the normal mantle. (2) The subducting Philippine Sea slab in west Japan is also detected. It has a thickness of 30-35 km and a P-wave velocity 3-5 percent faster. (3) In the crust and mantle wedge, low seismic velocities are visible beneath active volcanoes. The mantle wedge low-velocity zones are related to the arc magmatism caused by the convective circulation process in the mantle wedge and dehydration reactions in the subducting slab. (4) The hypocenter of the 1995 Kobe earthquake (M 7.2) in west Japan was located in a distinctive zone characterized by low seismic velocity and high Poisson's ratio. This anomaly may represent a fluid-filled, fractured rock matrix that contributed to the initiation of the Kobe earthquake. Evidence shows that the fluids mainly due to the dehydration of the subducting Philippine Sea slab. (5) Large crustal earthquakes (M 5.7-8.0) from 1885 to 1998 in Japan occurred in or around crustal low-velocity zones which may represent weak sections of the seismogenic crust and be caused by active volcanoes and/or magma chambers in volcanic areas and by fluids in fault zones in non-volcanic areas. The weak sections of the crust are subject to the tectonic stress and prone to large earthquakes. These results indicate that large earthquakes do not strike anywhere, but only anomalous areas which may be detected with geophysical methods.

ST4/E/48-B3

1420

#### LABORATORY EXPERIMENTS ON SUBDUCTION AND BACKARC EXTENSION

Francesca FUNICIELLO (Dip. Scienze Geologiche, Univ. Roma Tre, Largo S. L. Murialdo 1, 00146, Roma Italy, Institute of Geophysics, ETH, 8093 Zurich Switzerland e-mail: ffunicie@geo.uniroma3.it), Claudio FACCENNA (Dip. Scienze Geologiche, Univ. Roma Tre, Largo S. L. Murialdo 1, 00146, Roma Italy, e-mail: faccenna@uniroma3.it), Domenico GIARDINI (Institute of Geophysics, ETH, 8093 Zurich Switzerland)

We have performed 2D and 3D laboratory experiments to investigate the way the oceanic lithosphere sink into the mantle. Models have been performed with silicone putty, simulating the viscous behaviour of an oceanic lithosphere subjected to long term deformation and glucose syrup, simulating the mantle. We tested the influence of two parameters on the style of mantle convection: (1) lateral boundary conditions, i.e. box width, (2) deep discontinuity in the mantle resembling the 670km transition. We expressed the results in terms of: rate of trench retreat, rate of subduction, dip of subduction and state of strain of the upper plate. Our results show how the slab trajectory into the mantle is influenced by the presence/absence of deep discontinuity.

ST4/W/36-B3

1440

#### THERMAL MODELING IN TORN, SUBDUCTED PLATE EDGES

Jonathan M. LEES (Department of Geology and Geophysics, Yale University, New Haven, CT, 06511 email: lees@love.geology.yale.edu); Anne Davaille (Universite Paris 7, Institut Physique du Globe, Paris, France email: davaille@ipgp.jussieu.fr)

In this paper we investigate the implications for a tear in the Pacific plate at the northern limit of the Kamchatka volcanic arc. The Kamchatka-Bering juncture is characterized by unusual volcanic products and distribution of heat flow below the Komandorsky basin, and shallowing of seismicity along the subduction zone from Southern Kamchatka (600 km) to relatively shallow seismicity near the Kamchatka-Bering Fault intersection (100-200 km). If the Pacific plate is torn below the Bering fault, a slab window will be present through which mantle material can flow around the exposed Pacific plate edge, below the northern extent of active volcanism in Kamchatka. The exposed edge and subsequent mantle flow have a significant effect on internal structure of the subducting slab, as seen, to first order, by the shallowing seismicity. To investigate this model, we use a combination of laboratory experiments, numerical and theoretical modeling.

A subducting slab with three sides exposed to the mantle will heat up faster than a semi-infinite slab. Analytical solutions for the thermal evolution of a torn slab with high Peclet number (fast subduction) show that conduction alone cannot explain the shallowing seismicity. On the other hand, numerical solutions of the thermal evolution of a slab thinned toward the edge simulates the seismological data: minimum temperature isotherms inside the slab shift inward, producing

a lack of deep seismicity near the edge. Older plates are thinned and fragilized on their edge by small-scale convection. Preliminary laboratory experiments show that in this case, applying a mantle flow around the fragilized edge is sufficient to produce, in a few Myr, the necessary amount of thinning.

ST4/W/15-B3

1500

#### HUNTING BIG SLAB IN KAMCHATKA

Jeffrey PARK, Vadim Levin, Valerie Peyton, Jonathan Lees, Mark Brandon (all at Dept of Geology and Geophysics, Yale University, POB 208109, New Haven CT 06520 USA; email: park@hess.geology.yale.edu); Evgenii Gordeev, Victor Chebrov (OMSP, Petropavlovsk-Kamchatsky, Kamchatka, Russia) and Alexei Ozerov (Institute of Volcanology, Petropavlovsk-Kamchatsky, Kamchatka, Russia).

The Pacific-North America plate boundary takes a sharp turn where the Aleutian Islands meet the Kamchatka Peninsula, changing from strike-slip to convergent motion. Active subduction of the Pacific plate beneath the Eurasian landmass appears to terminate here, though past plate convergence farther north can be inferred from the continuity of accreted terranes across the Aleutian intersection. The history of subduction in this region should be reflected in the geometry of high-velocity slab material in the upper mantle. Hypotheses include (1) a dangling slab edge that ablates down-dip as it warms in the upper mantle; (2) a "tablecloth bulge" if a contiguous slab drapes over the boundary corner; and (3) a contiguous slab that parallels the full coastline of Kamchatka. Option (3) would imply that subduction of the Bering Sea plate fragment is still proceeding north of the Aleutians, but has been quiescent in historical times. We investigate the Kamchatka slab with broadband receiver functions. From P-coda this method reconstructs P-to-S converted phases from velocity interfaces beneath a seismic station. Preliminary analysis of data from the GSN station PET at Petropavlovsk-Kamchatsky shows a strong P-to-S converted phase from the upper surface of the slab, including a splendid lowpassed conversion from the large P-diffracted arrival from the 9 June 1994 deep-Bolivia event. In August 1998 a joint team of US and Russian investigators installed a network of 15 broadband portable seismometers on the Kamchatka peninsula, both north and south of the Aleutian junction. Initial data records from stations in the portable network have quality sufficient to detect similar conversions from elsewhere on the slab's upper surface. We will report on attempts to map the existence, location and strength of P-to-S converted phases, to distinguish between models for mantle flow in this region.

ST4/E/04-B3

1550

#### ANTI-CORRELATION OF THE 410 AND 660KM DISCONTINUITIES AND SUBDUCTION ZONE STRUCTURE

Jonathan COLLIER and George Helffrich (Department of Earth Sciences, University of Bristol, Wills Memorial Building, Queens Road, Bristol, BS8 1RJ, UK, email: jonathan@gly.bris.ac.uk)

Seismic mantle discontinuities at global average depths of 410 and 660km are believed to arise from pressure induced phase changes. Thermodynamically refined Clapeyron slopes suggest elevation of the 410km discontinuity and depression of the 660 in cool regions of the mantle. We test this hypothesis by investigating the response of these discontinuities to cold downwelling material in subduction zones. A slant stacking technique with regional seismic network data is used to enhance weak arrivals in the time window between P and sP for teleseismic events in the northwest Pacific and South America. In stacked data arrivals resulting from interactions with the 410 and 660km discontinuity are enhanced above the background noise level. Use of networks in the western US and the UK coupled with the location of the largest number of source earthquakes provides the best data coverage in the Izu-Bonin region. Here we clearly image elevation of the 410km discontinuity of up to 60km in the core of the subducting slab and a broad depression of the 660km discontinuity by up to 40km consistent with expected Clapeyron slopes. The observations of the 410km discontinuity are incompatible with the presence of a significant metastable wedge. In the Kurile Islands region elevation of the 410 in the slab is also seen whereas under the Japan Sea a more regional elevation is observed. Beneath Chile little deflection of the 410 is seen indicating either absence of subducting slab in the aseismic region or the weak cooling effect of a relatively young slab on the mantle.

ST4/E/32-B3

1610

#### 410KM DISCONTINUITY UPLIFT IN SLAB INCOMPATIBLE WITH METASTABLE WEDGE

Jonathan Collier, George HELFFRICH (Earth Sciences, Univ. Bristol, Bristol BS8 1RJ, UK)

Deep earthquakes occur at temperatures and pressures where the brittle failure associated with shallow earthquakes cannot occur. The transformational faulting hypothesis for deep earthquakes holds that when olivine is in a metastable state due to the kinetically hindered transition to a denser phase, and is nonhydrostatically deformed, planar faulting is possible when the olivine transforms. The hypothesis requires a metastable wedge of untransformed olivine in the slab. We test this hypothesis by seeking the position of the 410 km discontinuity inside a slab where deep earthquakes occur. Using short-period regional network data from Europe and North America, we located the 410 in the Izu-Bonin deep seismic zone using underside pP- and sP-like reflections from the discontinuity. The discontinuity topography that we observe is consistent with the maximum elevation expected from numerical modelling and Clapeyron slope estimates, up to 60 km relative to the 410 depth outside the slab. We see uplift on both the oceanward and the trenchward sides of the seismicity, ruling out the uplift as being an artifact of the velocity contrast at the formerly oceanic crust side of the slab/mantle interface. Thus a crucial element of the transformational faulting model for deep earthquakes is missing in one deep seismic zone. Whatever the mechanism of deep earthquakes, it must operate when the olivine transformation progresses under essentially equilibrium conditions.

ST4/W/03-B3

1630

#### A TELESEISMIC TOMOGRAPHIC IMAGE OF THE ICELAND MANTLE PLUME

G.R. FOULGER, M.J. Pritchard (Both at Dept. Geological Sciences, University of Durham, Durham, DH1 3LE, Email: g.r.foulger@durham.ac.uk); B. R. Julian (U. S. Geological Survey, 345 Middlefield Rd., Menlo Park, CA 94025, U.S.A., Email: julian@usgs.gov), G. Nolet, W.J. Morgan, R. M. Allen (All at Dept. Geosciences, Princeton University, Princeton, NJ, U.S.A., Email: guust@weasel.princeton.edu), B.H. Bergsson, P. Erlendsson, S. Jakobsdottir, S. Ragnarsson and R. Stefansson (All at Vedurstofa Islands, Reykjavik, Iceland, Email: ragnar@veduris).

A major passive seismic experiment is currently underway to map the structure of the crust and upper mantle over the whole of the Iceland hotspot. Thirty-four broadband seismic stations, distributed over the whole of Iceland, were operated for the two-year period 1996 - 1998. An extremely rich dataset that includes teleseismic, regional and local earthquakes was collected. The data have been used to obtain a teleseismic tomography image of the Iceland plume from the surface down to about 600km. For this study we also used data from 8 stations

of the permanent Icelandic network, and thus a total of 42 seismic stations contributed data. About 120 earthquakes were used with a good azimuthal distribution around Iceland. The data included about 4500 P-wave arrival times, including the phases P, pP, PP, PpP and PkIKP, and about 2000 S-wave arrival times, including the phases S, sS, SS and SKS. We performed many inversions, varying the initial starting model, damping and the inversion program used. Our final results will be presented for the first time in this talk.

ST4/W/10-B3

1650

#### PLUME-RIDGE-INTERACTION: THE INFLUENCE OF STRONGLY TEMPERATURE DEPENDENT VISCOSITY

Michael ALBERS and Ulrich Christensen (both at Institute of Geophysics, University of Goettingen, Herzberger Landstr. 180, 37075 Goettingen, Germany, email: mab@geo.physik.uni-goettingen.de)

Many hotspots of the Earth are located on or nearby mid-ocean ridges. Geophysical as well as geochemical observations indicate that abnormal plume material may interact over long distances with ridges. These observations are often explained by flow of plume material from the hotspot along the ridge axis. However, in previous numerical models no significant channeling of plume material has been found. We investigate the interaction of mantle plumes with mid-ocean ridges in 3-D numerical convection models. Using a multigrid technique with local grid refinements, we are able to incorporate a much stronger temperature-dependence of viscosity than was possible in previous models. This allows lateral viscosity variations of more than 6 orders of magnitude, which is realistic in a ridge situation. Results for ridge-centered plumes are presented. The maximum extent of plume material along the ridge is systematically determined in dependence on various model parameters, like the heat flux of the plume, the spreading rate of the ridge and the viscosity contrast between plume and ambient mantle. It turns out that a plume viscosity in the order of  $10E-17$  Pas and a slow spreading rate are necessary for significant flow of plume material along the ridge axis.

ST4/E/64-B3

1710

#### DYNAMICAL EFFECTS OF MELTING IN THE HAWAIIAN PLUME

Neil Ribe (Dept. of Geology and Geophysics, Yale University) Laszlo Cserepes (Eotvos University, Budapest) Ulrich CHRISTENSEN (University of Goettingen)

We use a 3D variable viscosity convection model to study the effect of the reduced density (depletion buoyancy) of the residuum after melt extraction and the loading of the surface by melt deposition on the geoid and topographic anomalies produced by the Hawaiian plume. In addition, we study the spatial distribution of melting in the plume and compare with the temporal evolution of individual Hawaiian volcanoes. We use the melting parameterization of McKenzie & Bickle (1988) and assume rapid extraction to the surface. From a set of model calculations, we derive scaling laws for melt production rate and topographic uplift depending on the plume's thermal flux and excess temperature and the lithospheric thickness. The observed topography is well matched by models with about 250 K excess temperature and 4000 kg/sec buoyancy flux. The effects of surface loading reduce the apparent geoid-topography ratio obtained by applying standard spatial filtering procedures to the "observed" range of 4-6 m/km. All the melt is drawn from the hottest part of the plume, implying no direct melting of asthenosphere or lithosphere. 99% of the melt is erupted in a region within 200 km of the plume center with a distribution that is skewed downstream. We also find a secondary melting region about 400 km downstream from the plume that is separated from the main region. This provides an explanation for the late-stage "rejuvenated" volcanism of the Hawaiian islands.

Monday 20 July AM

Presiding Chair: J.Kasahara (ERI, University of Tokyo)

### CRUSTAL STRUCTURE AND DYNAMICS

ST4/W/57-B1

Poster

0830-01

#### A COMPARISON OF THE GEOPHYSICAL SIGNATURES BETWEEN GREECE AND ITALY AS DERIVED BY GEODETIC DATA

M.G. Doufexopoulou & V.N. PAGOUNIS (Dept. Rural and Surveying Eng. NTU Athens, Heroon Politichniou 9, Zografos - Athens, Greece, email: vassilios.pagounis@survey.ntua.gr)

The difference between GPS geometric height and leveled or trigonometric heights gives point undulations of the geoid that have an estimated accuracy of  $\pm 0.10$  cm. By subtracting from these local signals, the model values at the same points computed with the EGM96 and OSU91a coefficients at various truncation degrees and lag intervals various residual point field undulations are produced. These signals are rich in geophysical information without biased assumptions on the analytic structure of the local gravity field, or the used density values. Several statistical procedures enable to eliminate the global model gravity field contribution and to trace tectonic signatures in geographical sense. On the other hand the numerical computation of raw variance and variability spectra provides a simple method to draw conclusions on the relative difference in the depth of the main sources above each tectonic block. We present results of this methodology using GPS and leveled data from Greece and Italy.

ST4/L/01-B1

Poster

0830-02

#### 3D REFLECTION IMAGING OF THE PUGET LOWLANDS, CASCADIA, USA

L.A. PRESTON (Geophysics Program, Box 351650, University of Washington, Seattle, WA, 98195-1650; email: preston@geophys.washington.edu), K.C. Creager, R.S. Crosson (Geophysics Program, Box 351650, University of Washington, Seattle, WA, 98195-1650), T.L. Pratt, C. Weaver (U.S. Geological Survey, PO Box 351650, University of Washington, Seattle, WA, 98195), M.A. Fisher, T. Parsons, T.M. Brocher (U.S. Geological Survey, 345 Middlefield Rd., Menlo Park, CA 94025)

The 1998 Seismic Hazards in Puget Sound (SHIPS) experiment used closely spaced airgun sources and uniformly distributed seismometers to gain a better understanding of the crustal structure of the densely populated Puget Sound region, Washington. The Seattle Basin is an area of low-velocity sediments up to 10km thick underlying the metropolitan area and Puget Sound. Evidence for large earthquakes on the Cascadia subduction zone and on regional fault systems underscores the need to know the 3D structure of the Seattle Basin to assess the hazards due to reverberation and seismic focusing. 3D tomography and borehole sonic logs have shown that the compressional-wave velocities within the Seattle Basin are as low as 2-3 km/s. 2D reflection profiles, collected along the waterways of Puget Sound, have provided a high resolution image of the shape of this basin along a north-south section. During the SHIPS experiment, 6500 airgun shots within Lake Washington, Puget Sound, and Hood Canal were recorded at an array of 150 onshore seismometers spaced about 10km apart in the Puget

Lowlands. We are using a 3D seismic reflection software package to produce a high resolution image of discontinuities within the Puget Lowlands crust. These low-fold 3D reflection images will improve and extend the lateral and vertical resolution of the Seattle Basin and other crustal features previously studied using 3D seismic tomography and 2D seismic reflection.

ST4/W/37-B1

Poster

0830-03

#### INTERPRETATION OF LINE TEST-02 AROUND GANOS VAULT FROM THE SEA OF MARMARA

AKKARGAN Sahin (The University of Istanbul, Faculty of Engineering, Turkey, email: sahin@istanbul.edu.tr)

The control of Geophysicist on seismic data has increased due to developments of digital seismic recording and analyzing technology. Thus, seismic data processing techniques have been applying more efficiently with saving time to analyse data. In this study I present a seismic section (line TEST-02) which constitutes part of the data acquired by R/V MTA Sismik-1 on the Sea of Marmara under TUBITAK's National Marine Geological and Geophysical Program. Line TEST-02 is a stacked and migrated seismic section recruited from 302 shots. My preliminary interpretations of line TEST-02 reveal a polarity reversal between CDP's 1150 and 1500 most probably caused by an antithetic fault surrounded by some other minor faults indicating a potential hydrocarbon (gas) trap. This interpretation, however, must be justified by additional seismic line shoots in the vicinity of the region under construction.

ST4/L/03-B1

Poster

0830-04

#### STRUCTURAL MODEL OF THE ERZURUM BASIN (EASTERN TURKEY) BASED ON THE GEOPHYSICAL PROFILES

M.Salih BAYRAKTUTAN (Earthquake Res. Centre, Atatürk Univ,Erzurum Turkey, Fax +90 442 2187140, email: msalih @ rocketmail.com ) Azer Kadırovcı (E R C , Ataturk University, Erzurum, Turkey) Ali Aliyev (Geological Survey, Huseyn Cahid Prospekt, Bakü, Azerbaijan)

The Erzurum Basin (EB) is located in the centralsegment of almost E-W striking active Erzurum Faults,between Erzincan and Igdır Basins, in East Anatolian Convergence Zone. EB is bounded along both northern and southern margins, by sinistral strike slip faults with large reverse components and thrusts. Geophysical data obtained from four gravity-magnetic and one seismic profile have been analyzed for structural features. Basin floor topography has rough relief with two major trough shaped depressions extending in NE-SW and NNW-SSE. One positive structural feature separates the north western segment (Daphan Plain) from the main depression (Karasu Plain). This threshold at about 800m depth and the thicknesses of clastic deposits (Late Pliocene-Quaternary) on both sides reaches about 1.2 and 1.6 km, respectively. The secondary depression to the NW of Ilıca with 4x16 km dimensions reflect the deepest part of the Pliocene lacustrine area in which fan delta deposits emerged from continental high at NW. Basin floor deepens southwards (and east). Basement folds in volcanic units with ENE-WSW extending axis are cut by two sets of active faults striking at NNE-SSW and NNW-SSE. Gravity map displayed +10 ( to +30) mGal positive and -14 ( to -16 ) mGal anomaly differences. All magnetic profiles showed sharp changes along N and S margins which are well coincided with gravity anomalies. Consequently, geophysical data revealed three main stages of structural deformation in the history of basin inversion.

ST4/E/53-B1

Poster

0830-05

#### DYNAMIC RESTORATION OF CROSS-SECTIONS WITH DIAPYRIC STRUCTURES

Alik ISMAIL-ZADEH (International Institute of Earthquake Prediction Theory and Mathematical Geophysics, Russian Academy of Sciences, Varshavskoye shosse 79, kor. 2, Moscow 113556, Russia, email: aismail@mitp.ru) Christopher Talbot (Institute of Earth Sciences, Uppsala University, Villavagen 16, SE-752 36 Uppsala, Sweden) Yuri Volozh (Institute of Geology, Russian Academy of Sciences, Pyzhevsky per. 7, Moscow 109017, Russia)

The backstripping method widely used in basin analysis sometimes fails in studying salt-bearing basins, because salt greatly affects the deformation of salt overburden. We present a numerical approach for dynamic restoration of cross-sections to their earlier depositional stages in regions of salt tectonics where deformation is confined to salt and its overburden. The technique combines the Galerkin-spline finite-element method with interface tracking and a backstripping method. We formulate a model concept where a viscous material filling a model rectangular box is divided into layers by advected boundaries (horizons), across which physical parameters (density and viscosity) change discontinuously. The model approximates a stratified geological cross-section. The evolution of salt-affected structures is restored by using backstripping and decompaction of sediments. We demonstrate the applicability of the suggested technique by reconstructions of upbuilt and downbuilt diapirs. The technique is applied to restore a depth converted cross-section through the south-eastern margin of the Pricaspian salt basin. The section is characterised by mature downbuilt salt diapirs and a remnant salt sheet, which are shown to emerge from an originally continuous salt sheet modified by differential sedimentary loading. The numerical approach is well suited for restoration of cross-sections with ductile overburdens.

ST4/E/31-B1

Poster

0830-06

#### MOSAIC AND CRUSTAL STRUCTURE OF THE DEFORMED BLOCKS IN THE CENTRAL INDIAN OCEAN BASIN FROM SEISMIC AND GRAVITY INVESTIGATIONS

D. Gopala RAO, K.S. Krishna (National Institute of Oceanography, Dona Paula, Goa-403004, India, email: gopalrao@csnio.ren.nic.in, krishna@csnio.ren.nic.in); Yu.P. Neprochnov, B.N. Grinko (P.P. Shirshov Institute of Oceanology, 36 Nakhimovskiy prospect, Moscow-117851, Russia, email: ypn@geo.sio.rssi.ru, gas@sio.rssi.ru)

Seismic reflection and refraction, free-air gravity (shipborne and satellite derived) and bathymetric data of the Central Indian Ocean Basin are analysed to map the mosaic of all the deformed crustal blocks and to determine crustal structure beneath some of the blocks. The deformed blocks in the form of anticlinal basement rises, zones of high angle faults, low amplitude broad basement rises associated with high angle faults and reactivated pre-existing structures are trending in NE-SW direction. The deformation zone comprises of 22 such blocks originated at different ages. Besides, linear chain of circular gravity anomalies that are identified near parallel to 82 degrees 30 minutes E longitude might be due to volcanic constructs. The seismic sequence stratigraphic studies have revealed 2 to 3 km thick sediments consisting of five seismic sequences H1 to H5 separated by Oligocene (?), upper Miocene, lower Pliocene and upper Pleistocene unconformities and underlain by mid-Cretaceous oceanic basement. Model studies of the Ocean Bottom Seismic refraction and free-air gravity (satellite derived) data across the three deformed blocks and in between troughs in the north (along 81.5 degrees E longitude) have revealed structure of the crust and deformation occurs within the crust only. The NE-SW deformed crustal blocks can be accounted due to the NW-SE compression, anti-clockwise rotational forces and different mechanical strength of the

rocks in the area. Serpentinites, low velocity layer possibly occur at sub-crustal depths and appear to facilitate the deformation of the crust from time to time.

**ST4/W/80-B1** Poster **0830-07**

**SEDIMENTARY DYNAMICS OF KASHI DEPRESSION IN TARIM BASIN**

LI Tie-Jun and Luo Xiao-rong (Inst. Of Geology, Chinese Academy of Sciences, Beijing, China, 100029)

Kashi Depression is a secondary depression of Tarim Basin in north-western China. On its south and north sides, there are Kunlun Shan and Tian Shan orogenic belts. Influenced by the India-Asia collision, the western Kunlun Shan and the southern Tian Shan were reactivated during Neogene and Quaternary. And these two orogenic belts have overthrust to Kashi depression during this period. Controlled by the thrust activities and Airy isostatic adjustments, the crust thickness of Kashi depression has been significantly increased, and the present crust thickness ranges between 52 and 54 km. Accompanied with the emplacement of the foreland thrust-fold belts, the lithosphere in the area was deflected greatly and foreland basins were formed before the western Kunlun Shan and the southern Tian Shan. But it is because the interval between the two orogenic belts was not long enough and the foreland basins couldn't be distinguished effectively. Different from the typical foreland basins, Kashi depression was a composite symmetric foreland basin which was controlled by the two orogenic belts on its southern and northern sides, and the subsidence amount was the sum of the subsidence amounts before the two mountains. According to the studies of seismic data, gravity and magnetotellurics, the Cenozoic sedimentary thickness in Kashi depression are more than 12,000 m and the maximum of Quaternary conglomerate thickness is more than 8,000m, which corresponds to the most intense tectonic activity stage.

**ST4/P/10-B1** Poster **0830-08**

**HIGH RESOLUTION TOMOGRAPHIC IMAGING IN SOUTH CHINA SEA**

ZHU Jieshou, Yan Zhongqun, Cao Jamin, Cao Xiaolin, and Zhang Xuemi (Dept. of Geophysics) Chengdu University of Technology, Chengdu 610059, China, email: zhujs@cdit.edu)

The most of west Pacific marginal basins showed that they were spreading in 32-15 Ma and ended the opening turned to compressible closure after 17-15 Ma. Recently, due to the setting and observing of the global observation system of geophysics and geodesy, it became possible to do seismic tomography in detail to view the three-dimensional structure of the deep interior of the Earth. The high resolution seismic surface wave tomographic imaging for the South China sea and other surrounding marginal basins, such as Sulu sea, Celebes basin and Andaman sea, west Philippine basin. We have collected about more than 500 long period digital seismic records from 7 stations of GSN and CDSN, which located at China, Thailand, Indonesia. The high resolution tomographic inversion had been conducted by processing these surface wave data. The three-dimensional velocity image from earth's surface to 6 00 km depth, ranges from - 10°S to 3 0°N in latitude and from 94°E to 136°E in longitude. The image mainly reflects the lithosphere/asthenosphere system of the spreading marginal basins. South China sea had a thinning lithosphere (60-70km) and thickened asthenosphere. The very low  $v_{\text{at}}$  also appears in the asthenosphere beneath the basin, which is related with upwelling plume in the upper mantle in west Pacific marginal sea. In contrast the continents and islands go around the South China sea, such as south China block, Indochina block, Sumatra, Java, Philippine, show the high velocity in the lithosphere.

**ST4/W/45-B1** Poster **0830-09**

**ANOMALIES OF ELECTRICAL CONDUCTIVITY AND ELASTIC PROPERTIES OF THE CRUST IN THE SAYAN-BAIKAL PROVINCE THEIR RELATIONS AND NATURE**

POPOV A.M.(Institute of the Earth's Crust, Siberian Branch of the Russian Academy of Sciences. E-mail:popov@earth.crust.irk.ru)

There exists a hypothesis that layers of enhanced electrical conductivity in the crust physical and spatially coincide with waveguides. However, detailed analysis of spatial relationship between the two anomalies on the example of the Sayan-Baikal province showed inconsistency of this hypothesis. The crustal conductor observed within the province is evident both beneath the craton and in its tectonically active surroundings between 11 and 55 km below the surface, shallowing up toward the active areas. It is 15-20 km thick and has a conductivity ranging from 100 to 2000 S. The waveguide is absent within the stable Siberian craton but occurs beneath activated areas at depths between 11 and 22 km. It is 5 km thick and laterally discontinuous showing tectonic layering of the medium and a velocity deficit of - 0.2-0.3 km/s. Therefore, the two anomalous layers are spatially discordant. It is suggested that the behaviour of elastic and conductive properties of the medium depends on its rheology, fluids playing an active part. Electrical conductivity increases in the brittle-ductile medium favourable for origination of interconnected fluid-filled microcracks whereas seismic velocities there either remain the same (Berge et al., 1995) or likewise increase (Nur, 1974; Petkevich, 1965). Seismic velocities decrease producing a waveguide in the brittle medium (uppermost crust) where cracks are isolated and not, at least fully, filled with fluids. Such a relationship between elastic and conductive properties implies that fractured medium is favourable for origination of the anomalies in point.

**ST4/E/60-B1** Poster **0830-10**

**KAMCHATKA: DEEP STRUCTURE OF THE AVACHA -KORYAKSKY GROUP OF ACTIVE VOLCANOES BY THE GEOPHYSICAL DATA**

MOROZOV Yu.F. (Gontovaya L.I., Institute of Volcanic Geology and Geochemistry, FED RAS. Petropavlovsk-Kamchatsky, 683006, Russia (4150058293); e-mail: ivgv@svyaz.Kamchatka.su)

Two 3D models for lithosphere of the area of Avacha-Koryaksky group of volcanoes were developed based on the data of seismology, gravimetry and magnetotelluric sounding; a model of elastic and density properties and a geoelectrical one. It is shown that active volcanoes are confined to the boundary of the lithosphere blocks with various values of P-wave velocity, density and electric conductivity. The first block involves crustal layer of increased electric conductivity at the depth of 25-40km. This layer rises to the depth of (10km in the area of volcanoes. The second block is characterised by the velocity inversion in the middle crust and by the absence of the crustal layer of increased electric conductivity. By seismic data obtained from the explosive source and from the earthquakes beneath active volcanoes two zones are distinguished: zone of increased velocity in the middle crust at a depth of 10-25km and zone of anomalous absorption of the seismic waves under the cone of Avachinsky volcano. A wave guide is fixed in the basement of Avachinsky graben; here zone of anomalously increased values of electric conductivity is also present. Based on the analysis of distribution of the physical parameters in the studied volume of lithosphere, areas of magmatic chambers are revealed: crustal at the depth of 10-20km and peripheral at the

depth of 0-2km. The latter is probably connected with the zone of geophysical anomalies in the basement of Avachinsky graben either. Considering peculiarities of distribution of the physical parameters in the studied volume of lithosphere a possible mechanism of magma feeding for the volcanoes is suggested. Recent dynamic processes and formation of magmatic chambers are mainly determined by the geothermal solutions penetrating to the upper part of the crust from the depth of 25-40km.

**ST4/P/6-B1** Poster **0830-11**

**AVERAGE CRUSTAL STRUCTURE OF THE WESTERN BRANCH OF THE EAST AFRICAN RIFT AND RELOCATION OF EARTHQUAKES BETWEEN 1° N AND 12° S**

Richard W. FERDINAND (Department of Earth Sciences, Seismology, Uppsala University, Villavägen 16, S-752 36, Uppsala Sweden, email: rf@geofys.uu.se Thierry Camelbeeck (Royal Observatory of Belgium, Avenue Circulaire, 3, 1180 Brussels, Belgium, email: Thierry.Camelbeeck@mailserv.oma.be)

Arrival time data from 56 regional events recorded by 21 stations of the East and Southern African network and a local network in south-western Tanzania were used in estimation of average crustal model for the region bounding the western branch of East African rift system, between 1° N and 12°S. The model is characterised by 38 km crust thickness, with an average velocity of 6.32 km/sec and 3.61 km/sec for P and S waves respectively. Upper mantle velocities for Pn and Sn phases are 8.11 km/sec and 4.67 km/sec respectively. These velocities are not different from those obtained for the African shield. Relocated regional earthquakes using our model show low epicenter errors of less than 10 km. Good agreement between locations of these events and those corresponding and reported by ISC bulletines, demonstrate the importance of these networks to locate regional earthquakes and hence improvement in event location capability in eastern Africa.

**ST5/E/18-B1** Poster **0830-12**

**INVESTIGATING THE LIGURIAN SEA (WESTERN MEDITERRANEAN SEA) BY MEANS OF LOCAL EARTHQUAKE TOMOGRAPHY**

EVA E, Spallarossa D. (Dipteris, Universita' di Genova, Viale Benedetto XV,5, 16132 Genova, Italy, email: elena@dister.unige.it) Solorino S. (Institute of Geophysics, ETH-Hoenggerberg, Zuerich, CH-8093, Switzerland, email: stefano@tomo.ig.erdw.ethz.ch) EVA C. (Dipteris, Universita' di Genova, Viale Benedetto XV,5, 16132 Genova, Italy, email: elena@dister.unige.it)

In the last decade the knowledge and quality of seismological data for the Ligurian Sea greatly improved due to several seismic surveys conducted both off and on shore and especially due to the installation and running of a permanent seismic network equipped with 1C and 3C stations. The revision of the seismic catalogue, completed by waveforms and phase picking provided by the surrounding networks, and a quite restrictive selection on the data yielded a high quality dataset that has been used to improve the knowledge of the role of the Ligurian Sea in the Mediterranean region. Computation of a reference velocity model and tomographic inversion of local earthquakes data lead to a detailed frame of the distribution of velocity structure. As a consequence, reliable three dimensional locations constrained the map of seismicity for the area. Computation of focal mechanisms using 3D velocity models outlined the distribution of forces acting on this puzzling area. Basically, it turns out that seismicity affects the foot of the continental slope in correspondence with some crustal faults while another seismicity band seems to delimit the northern side of the Corsica block. Tomographic images outline a very shallow Moho in the center of the Ligurian Seadeepening down to 25 km beneath the coastal regions.

**ST5/E/27-B1** Poster **0830-13**

**VELOCITY HETEROGENEITIES OF EARTH CRUST AND SEISMICITY (TIEN-SHAN)**

Tamara SABITOVA and Albina Adamova ( both at Institute of Seismology, National Academy of Science, Asanbai 52/1, Bishkek 720060, Kyrgyz Republic, email: kis@imfiko.bishkek.su) Oksana Lesik (Experiment-Methodical Expedition of IVTRAN RAS, 720049, Bishkek 720049, Kyrgyz Republic, email: olesik@gdir.ru)

Complex analysis of deep structure data has been carried out for the kyrgyz part of Tien-Shan. based on results of tomography imaging ( P- and S- wave velocity variations maps for each of the crustal and uppermost mantle layers, velocity sections) and subsequent zoning of region under investigation on type of velocity sections. Epicenters map considering the earthquake intensity shows the seismic activity over period from 0001 till 1998. It is shown that there are some differences in velocity variations which are characteristic for crust structure of strong (M>6.5) and moderate (M=5-6) earthquakes focal zones. Strong earthquakes originate, as a rule, in layered crust, for which were revealed following features: high gradient zones with low velocity layer at different depth levels, and mainly in lower crust (35-50km) and subvertical weakened channels. Focal zones of moderate events also confined to contacts of different velocity blocks in upper crust (0-20km). These contacts sometime are zones of known faults, dividing different geological blocks. In that reducing of velocity and existence of subvertical weakened channels can not be observed. Background seismicity (M<5) apparently connected with less marked velocity heterogeneities. Mentioned patterns allow to account for difference in observed source location for strong and moderate events: few strong earthquakes look as if they contour the region under study reflecting by it the presence of low velocity zone over most part of Northern and several areas of Southern Tien-Shan; high seismic activity zone (and epicenters density) being located in Southern Tien-Shan, indicates strongly marked mosaic structure of upper crust of this region.

**ST4/E/29-B1** Poster **0830-14**

**3-D VELOCITY TOMOGRAPHY OF THE CRUST AND THE UPPER MANTLE IN THE CENTRAL KOREAN PENINSULA AND ITS VICINITY**

So Gu KIM (The Seismological Institute, Hanyang University, Ahnsan, Kyonggi-do, 427-791, South Korea; Tel: +82-345-400-5532; Fax: +82-345-400-5830, email sogukim@mail.hanyang.ac.kr) Qinghe Li(Lanzhou Seismological Institute, SSB, Lanzhou, 73000, China)

Pg, Sg, PmP, SmS, Pn, and Sn arrival times of 32 events with 404 seismic rays are inverted for location and crustal structure. 5 (1° along the latitude)\* 6 (0.5° along the longitude)\* 8 block (4 km each layer) model was inverted. 3-D seismic crustal velocity tomography including eight sections from the surface to the Moho, thirteen profiles (but only eight presented here) along latitude and longitude, the Moho depth distribution was determined. (1) the average velocity and thickness of sediment are 5.15 km/sec and 3-4 km, and the velocity of the basement is 6.12 km/sec. (2) the velocities fluctuate strongly in the upper crust and those of the lower crust under Conrad appear horizontal. (3) the average depth and velocity of the Moho are 29.8 km and 7.97 km/sec. (4) the Chugaryong Rift Zone can be located from the cross section profiles. (5) we note that there are big anisotropy bodies near Hongsung and north of Seoul in the upper crust, implying that they may be related to the Chugaryong Rift Zone and deep fault systems, respectively.



From 3-D velocity tomography in the upper mantle, we found that the Benioff-Wadati subduction zones are dipping about 30 degree up to 700km in the east side of the Korean Peninsula, and there are low velocity anomalies in the upper mantle, especially near Mt. Paektu indicating that they may be related to the low velocity bodies of partial melting. 660km- and 410km discontinuities are also found to be in the inner continental side and in the outer continental side of the the East Sea(Japan Sea), respectively.

**ST4/E/12-B1** Poster **0830-15**

#### SEISMIC TOMOGRAPHY IMAGES OF THE QINLING-DABIE OROGENIC BELT

SUN Ruomei, LIU Futian, LIU Jianhua, Xu Peifen (all in the Institute of Geophysics, Science Academy of China, 100101 Beijing, CHINA, email: sunrm@sun.igep.ac.cn)

The Qinling orogen of central China between the Sino-Korea craton and the Yangtze craton began in late Mesozoic. Ultra-High Pressure (UHP) metamorphic rock belt, found in Dabie mountain, is the largest one in the world. We did the P, S wave and Vp/Vs tomographic inversion of North China craton, Qinling-Dabie orogenic belt and Yangtze craton in central China. The results are as follows: 1. The image of the upper crust has a close correlation with surface geology. The North China basin shows obviously low velocity, whereas the orogenic belt expresses high velocity with E-W trend, reflecting old tectonism. However the velocity anomalies at depths 80-110km display a trend in N-S direction, a feature possibly controlled by recent tectonism. 2. The velocity image at depth of 40+ km beneath the Moho shows that the orogenic belt is divided into three sections. West of 108E, the West Qinling displays low velocity anomaly, the crust is thicker than 40km with indications of a mountain root. Between 1080E and 1040E, in the East Qinling, the velocities are high with no indication of mountain root, and the crustal thickness is less than 40km. East of 1040E in the Dabie Mountains, velocities are obviously low, the crustal thickness is not less than 40km. 3.The image in a profile across the Dabie mountain shows a slab-like high velocity anomaly dipping from south to north, that may be remain of ancient subducted block, which break off around 130-170km. The slab breakoff seems the mechanism of recurvature of UHP metamorphic rock.

**ST4/E/30-B1** Poster **0830-16**

#### A MODEL OF LITHOSPHERIC STRENGTH WITH A MINIMUM FOR SEISMOGENIC ZONE

Mitsuhiro SHIMADA (Research Center for Earthquake Prediction, Disaster Prevention Research Institute, Kyoto University, Uji, Kyoto 611-0011, Japan, email: shimada@rcep.dpri.kyoto-u.ac.jp)

The brittle-ductile hypothesis for seismogenic zones in the intraplate crust (e.g., Meissner & Strehlau, 1982; Sibson, 1984; Ito, 1990, 1993) is principally based on the strength envelope of the lithosphere (Goetze & Evans, 1979; Brace & Kohlstedt, 1980) inferred from laboratory experiments on frictional strength and steady-state creep strength. The hypothesis is also based on the similarity between the strength envelope and the frequency-depth distribution of earthquakes, which implies that the possibility of earthquake occurrence is higher at the depth where the strength of the crust is higher, or that the stronger part of the crust has the ability to generate more earthquakes.

Here, we show a modified model of lithospheric strength inferred from our laboratory experiments indicating that strength values of a granite are unusually low between 200\_Bo\_(Band 280\_Bo\_(BC with a minimum at around 250\_Bo\_(B in the high-pressure type fracture regime (Shimada et al, 1983; Shimada & Cho, 1990; Shimada, 1992) that occurs when the compressive strength equals the frictional strength. The lithospheric strength inferred from these experimental results and our previous assumption that the high-pressure type fracture occurs in the crust considering the size effect of rock strength, suggests a low-strength zone between 8 and 12 km depth. This suggestion could provide an alternative explanation for the brittle-ductile hypothesis: earthquakes could occur or nucleate more easily where the strength is low. A similar suggestion has been proposed by a model for the frictional strength profile with a minimum, assuming high (near lithostatic) pore fluid pressure (Streit, 1997). Our model could be applicable to the moderate pore pressure or even dry condition.

**ST4/W/59-B1** Poster **0830-17**

#### USE OF CODA OF LOCAL EARTHQUAKES AND SEISMIC NOISE FOR STUDY OF THE EARTH'S STRUCTURE AND MONITORING OF GEODINAMIC PROCESSES

Irina J.TCHEBOTAREVA(Inst. Earth Physics RAS,B.Gruzinskaya 10,Moscow 117234, Russia, email: chari@synapse.ru) Haruo Sato(Dept.Geoph.,Tohoku Un., Aoba-ku, Sendai, 980-8578, Japan, email: sato@zisin.geophys.tohoku.ac.jp)

Conventional methods of study of the structure of the Earth's crust and mantle consider only passive reradiation of seismic energy by structural heterogeneities. They do not consider the seismic component connected with emission from the active volumes of the energy-saturated medium. Our study of coda of local earthquakes and seismic noise shows that both noise and coda contain the emission component from the deep active sources. Method of emission tomography was applied for analysis of the data obtained by "The 1993 Joint Seismic Observation Group in and around the Nikko area"; the dense seismic array composed from 3-component stations was set in the volcanic area in northern Kanto, Japan. Analysis of seismic noise before P wave of earthquakes reveals active volumes emitting a weak seismic signal, the largest of them are connected with the mid-crust magma body and area of large earthquakes. The study of records after the direct S waves shows that coda waves are composed from both a scattered component and emission one induced by the direct waves from earthquake, moreover the scattered component decreases with time and the induced component increases. The volumes of induced emission received from the 'late coda' differ from the scattering structure received from the 'early coda' and are the same as the active volumes detected from seismic noise. The emission radiation from the active volumes is a response to the change in the stress field and can be used for seismic monitoring of geodynamic processes. By means of choice of a suitable frequency band and array aperture we can make study in different scales, from the crustal to the global one.

**ST4/W/26-B1** Poster **0830-18**

#### BASIN FORMING PROCESS AND FAULT DISTRIBUTION AT THE TERMINATION OF THE RIGHT-LATERAL LEFT-STEPPING FAULTS: A CASE STUDY OF OSAKA BAY BASIN, KINKI DISTRICT IN JAPAN

Shigekazu KUSUMOTO (Department of Geophysics, Graduate School of Science, Kyoto University, Kitashirakawa oiwake-cho, Sakyo-ku, Kyoto 606- 8502, Japan. E-mail: kusu@kugi.kyoto-u.ac.jp), Yoichi Fukuda, Keiji Takemura and Shuzo Takemoto (Department of Geophysics, Graduate School of Science, Kyoto University, Kitashirakawa oiwake- cho, Sakyo-ku, Kyoto 606-8502, Japan.)

Osaka Bay basin, Kinki district in Japan, is a sedimentary basin that is filled with Quaternary sediments. This basin is sandwiched between the Median Tectonic Line (MTL) and Arima-Takatsuki Tectonic Line (ATL). These tectonic lines are right-lateral strike-slip faults with reverse component and form a left-stepping en echelon arrangement. Although the right-

lateral left- stepping en echelon faults generally develop an upheaval structure at the termination, the Osaka Bay does not fit in the case. In addition, the MTL and ATL have more than one fault at their end with reverse and lateral motion components.

In order to understand the formation of a sedimentary basin at the termination of the right-lateral left-stepping faults, we numerically simulated the behavior and distribution of secondary faults caused by the strike-slip motion. The results of simulations show that 1) the depression structure can be formed only when the secondary fault is reverse and its displacement is larger than 20 % of the lateral motion, 2) faults at the end of the MTL and ATL are developed by the secondary ruptures due to strike-slip motion and 3) distribution of the secondary faults indicates the change of the past maximum compressive stress in Kinki district. We thus conclude that Osaka Bay basin was formed by the evolution of the secondary reverse faults due to the same strike-slip motions.

**ST4/E/57-B1** Poster **0830-19**

#### NUMERICAL MODELING OF A COLLISION STAGE OF CONTINENTAL CRUST FORMATION IN KOLA SUPERDEEP REGION (THE BALTIC SHIELD)

PARPHENUK Olga (Institute of Physics of the Earth RAS, 10 B. Gruzinskaya, Moscow, 123 810, Russia, email: olg@upei-ras.scgis.ru)

Thermal-mechanical model of continental collision including brittle overthrusting in the upper crust and lower crustal viscous flow is developed and applied to the modeling of the Northern Pechenga formation in the vicinity of the Kola Superdeep borehole along the Luchlompolsky thrust fault (the Baltic Shield). The uniqueness of the Baltic Shield data is defined by the Kola Superdeep drilling results, which give an excellent opportunity to evaluate all the results including seismic interpretation. Finite-element 2- D modeling was used to examine the conditions under which ductile flow of the rheologically layered lower crust and upper mantle can produce the structure with crustal roots and surface uplift as a result of shortening, loading and erosion. The numerical calculations of shortening and overthrusting along the Luchlompolsky thrust fault for the rate of 1 cm/yr during 60 Myrs and erosion rate 0.1 cm/yr demonstrated the possibility of the structural formation with thickened upper crust and progressively increasing level of erosion, which reflects the exhumation of the rocks from different depths to the surface. The shape of the crustal root for the initial deep angle of fault assumed for the structure has the wavelength of topography which can lead to its relaxation by viscous flow.

**ST4/W/02-B1** Poster **0830-20**

#### RELATIVE DISPLACEMENT ACROSS THE FRACTURE ZONE

Keisuke TANIGUCHI (Kyoto University of Education, Fushimi-ku, Kyoto, 612-8255, JAPAN, Email: taniguti@wsml.kyokyo-u.ac.jp)

Geodetic survey and continuous observation of crustal deformation across faults or fracture zones have led to many evidences that crust was consisted of loosely coupled blocks mostly bounded by faults or fracture zones. In order to study the relative movement of two crustal blocks bounded by the fracture zone in the tunnel of Hokuriku observatory of Kyoto University in Japan, three dimensional relative displacement meters were designed and has been set up across that fracture zone since 1986. They have measured tidal and seismic relative displacements between two fixed points in three orthogonal directions. Results are as follows, 1) Tidal strain across the fracture zone was about four times as large as the theoretical, whereas the observed near the fracture zone was only half of the theoretical. Strain seismograms across the fracture zone are from 5 to 15 times as large as at the neighborhood and larger than the calculated strain seismograms with STS type seismographs set up in the same tunnel. 2) The vector of each tidal and seismic relative displacement across the fracture zone is almost fixed at any term. This may be caused by the existence of plane-like fracture zone. 3) Amplification factor is related to propagation azimuth of each earthquake. And dip angle of propagation is smaller, the amplification factor is larger. These results indicate that the change of fracture zone width, in other words, compress- extension motion at the fracture zone causes the amplification of seismic waves. 4) It was confirmed that block bounded by that fracture zone spreads in horizontal. And calculation with FFT indicates that fracture zone extends to several km in dip direction. 5) Seismic waves which frequency are larger than 1Hz only cause the amplification.

**ST4/E/58-B1** Poster **0830-21**

#### THERMAL REGIME AND DYNAMICS OF COLLISION ZONE: RESULTS OF MODELING

Vladimir S.ZAKHAROV (Moscow State University, Geological Dept., Dynamic Geology Chair, Vorobiovy Gory, Moscow, 119899, Russia. Email: zakharov@dynamo.geol.msu.ru)

This paper will report on a quantitative model of mechanical and thermal processes under collisions in rheologically stratified lithosphere (upper elastic crust, lower plastic crust, elastic mantle lithosphere). In the area of collision delamination and subduction of the mantle lithosphere of undermoving plate takes place resulted in the development of plastic deformation in the lower crust. Results of modeling indicate significant (up to 65 km in 20 m.y.) increase of the crust thickness in the collisions area. Though formation of orogen occurs in the condition of general compression, in the central part of orogen on late stages of collisions and in postcollision phase an area of extension arise, connected with gravitational spreading of the formed raising. The dissipative heat generation originates in the process of the lower crust material viscous flow . It brings about heating both the crust and undercrust mantles as well. Simulation of heat regime shows that the area of significant temperature rise on the base of crust (50 - 200oC in 20 m.y.) has a thickness of about 10 km and hundreds of kilometers in other dimensions. Substantially heated (up to 100 oC) an upper part of the mantle lithosphere (near 10 km thick). Temperature of the crust base under wide range of parameters reaches the wet granite liquidus point. The partial melting of the lower crust material has been made possible. Thus, premise conditions for origin of the postcollision granitoid magmatism are formed. This mechanism of dissipative heat generation can also explain the existence of deep metamorphism.

**ST4/W/24-B1** Poster **0830-22**

#### PHASE TRANSITIONS IN THE GROWTH OF CONTINENTAL CRUST

Carlo GIUNCHI (Istituto Nazionale di Geofisica, Via di Vigna Murata 605, 00143 Roma, Italy, Email: giunchi@gea.df.unibo.it); Yanick Ricard (ENS Lyon, 46 Allée d'Italie, 69364 Lyon Cedex 07, France)

We investigate the thermal and petrological behaviour of the continental crust and its growth due to events of continental collision. The evolution of the thermal profile and of an univariant phase transition in the lower crust, during the thickening and the following relaxation and erosion, is computed by a numerical model. In case of fast collision events, the rise of the topography is isostatically favoured, but it is counteracted by a fast transition to the dense

phase. Depending on the density contrast, this may cause even a topographic collapse. The thermal relaxation following the collision is able to trigger the re-transformation of the dense phase, but this time the topographic rise may be affected by erosion rate. We study the interplay between these factors trying to model and to put constraints on the evolution of the topography of mountain belts.

**ST4/W/31-B1** Poster **0830-23**

**DYNAMIC PROCESSES OF THE STRESS CHANGES IN CENTRAL KYUSHU, JAPAN**

Shigekazu KUSUMOTO (Department of Geophysics, Graduate School of Science, Kyoto University, Kitashirakawa oiwake-cho, Sakyo-ku, Kyoto 606-8502, Japan. E-mail: kusu@kugi.kyoto-u.ac.jp), Yoichi Fukuda, Shuzo Takemoto and Keiji Takemura (Department of Geophysics, Graduate School of Science, Kyoto University, Kitashirakawa oiwake-cho, Sakyo-ku, Kyoto 606-8502, Japan.)

The eastern part of central Kyushu is a key area for understanding the tectonic history of Southwest Japan because the region is located at an intersection of tectonic lines and is near an inflection point of the subducting Philippine Sea plate margin. This region is also characterized by gravity lows which are caused by the tectonic and volcanic depression structures. All tectonic depression structures and gravity lows in this region can be restored by considering the following two mechanical processes; 1) the formation of the half-graben under the N-S extension before 1.5 Ma, 2) the formation of the pull-apart basins under the W-E compression after 1.5 Ma.

In order to explain the source of the regional stress field and of its variation, the effects of the convergence direction of the subducting Philippine Sea plate, interplate coupling between the Eurasian and Philippine Sea plates and upwelling flow were evaluated by means of the finite element analyses. The results show; 1) the extension in central Kyushu before 1.5 Ma is not the passive extension but the active extension caused by the upwelling flow, 2) the upwelling flow gives the maximum shear stress of 5 - 6 MPa on the base of the lithosphere and 3) the W-E compression field required in central Kyushu after 1.5 Ma can be explained by the change of the convergence direction of the Philippine Sea plate and the decrease of the maximum shear stress on the base of the lithosphere.

**ST4/E/08-B1** Poster **0830-24**

**THE CONJECTURAL GEODYNAMIC MODEL OF MODERN DEVELOPMENT OF THE CENTRAL ASIAN REGION**

Leonid Bogomolov, Vitaly BRAGIN and Yuri Trapeznikov (all at International Research Center - Geodynamic Proving Ground in Bishkek, 720049, Bishkek, Kyrgyz Republic. E-mail: bragin@laurel.gdirc.ru)

For the Central Asian region, including Gindukush, the distribution of 9-13 class earthquakes was reviewed for 25 years. A choice of energy diapason for earthquakes to be investigated is determined, from the bottom, by their statistic importance for the whole region and from the top, by the sufficiency of quantity of earthquakes for the comparative analysis of their number from year to year on  $10^6 \pm 10^8$  cells. Spatial time analysis of these seismic events showed, that normalized frequency of origin of earthquakes has a natural spatial distribution in the region remaining from year to year. This is determined, that frequency changing of these classes earthquakes origin occurs in synchronism within the territory under consideration. The calculations made and compared with pattern of earthquakes distribution under observation demonstrate, that it impossible to explain the given picture by transmission of horizontal stresses in resilient plastic substance. The detailed distribution of earthquake origin frequency and earthquake synchronous on time changing within the region can be explained by presence of substance flow in quasi-plastic layer at depths of middle crust - upper mantle and by exposure of this flow to the above-laying levels of crust. The supposition of substance flow presence in quasi-plastic level with roof laying at a depth of 20 and more kilometers is bore out by quantities and directions of the earth's surface movement on the Tien Shan territory ascertained with the aid of GPS measuring and by data about the presence of indivisible conducting horizon received by means of magnetotellurics. The main component of flow has a radial character and a center situated in the Gindukush area and direction outgoing from it.

**ST4/W/81-B1** Poster **0830-25**

**WEIGHTED STATISTICAL ANALYSIS OF THE OBSERVED GLOBAL STRESS ORIENTATIONS**

WEI, Dongping (Graduate School at Beijing, University of Science and Technology of China, P.O.BOX 3908, Beijing, 100039, P.R. China, email: dongping@earth.gsbsustc.ac.cn) SENO, Tetsuzo (Earthquake Research Institute, University of Tokyo, Yayoi 1-1-1, Bunkyo-ku, Tokyo 113-0032, Japan, email: seno@eri.u-tokyo.ac.jp)

Over 7000 global stress indicators have been compiled in a digital database in the World Stress Map Project (WSMP). Five qualities from highest quality A to lowest E were defined in WSMP database in ranking the data. Previous study (Coblentz and Richardson, 1995) has presented a statistical analysis of the WSMP stress indicators with the aim of quantifying trends in both the SHmax orientations and stress regimes. The analyses was carried out with 5x5 degree bins which provide a resolution of several hundred kilometres by using 4537 high-quality WSMP indicators with the rating A to C.

In the present study, we mainly deal with the SHmax orientation with the weighted statistical analysis. The WSMP datum with an error of SHmax orientation within 10-15 degree is quality A, within 15-20 degree is B, with 25 degree is C, bigger than 25 degree is quality D, and that with no useful SHmax orientation information is quality E. So here we exclude E type data, and assign different weight coefficients to A-D data on the basis of their qualities of SHmax orientations, i.e. 1/12.5 (12.5 is the mean of 10 and 15), 1/17.5, 1/25 and 1/75 to each A,B,C and D quality indicators, respectively. For simplicity, we convert all these weight coefficients to integers, so here the weight coefficients of 6,4,3 and 1 are assigned to A,B,C, and D quality data, respectively.

We apply a Rayleigh test, a standard statistical method in the analysis of directional data, to check whether the distribution of SHmax orientation in the defined bin is random. An important aspect of this study is the choice of different weight coefficients drawn from quantitative inspection of the WSMP database. We also compare our result with previous study which assigned the same weighted coefficient 1 to quality data A to C. The mean SHmax orientations within the bins are slightly different between the weighted coefficient and equal weight coefficient cases. The average deviation of the average SHmax orientations for all the global plates between these two cases is about 4.8 degrees. However, some continental regions and convergent boundary regions, for example, Baikal rift, Iran plateau, and Aegean Sea regions etc., have relatively large difference up to about 12 degrees for the above two cases. Our analyses also indicate that more bins are rejected as sampling a random distribution at each confidence level. This is because the weighted coefficients strengthen the importance of the stress indicator with a higher orientation accuracy, thus decrease a possibility of random distribution.

**ST4/E/20-B1** Poster **0830-26**

**REFLECTION AND TRANSMISSION OF LOVE WAVE IN PRESENCE OF SUDDEN CHANGE IN CRUSTAL THICKNESS**

A.ROY and R.K.Bhattacharyya (Department of Applied Mathematics, Calcutta University, 92, A.P.C.Road, Calcutta 700009, India. e-mail: aroy@cucc.ernet.in)

In order to investigate the transmission of Love wave through laterally varying structure, we consider the mode conversion of Love wave in presence a sudden change in the layer thickness. The integral equation that arises in the problem is solved by means of Wiener Hopf technique combined with mode matching method. In the limiting case of change when the layer thickness is small, some numerical computation both for transmission and reflection coefficient are given. As a special case we also derive the results for laterally varying structure and also discuss the reflection and transmission of Love wave across a vertical discontinuity between two welded media.

**ST4/E/34-B1** Poster **0830-27**

**DETERMINATION OF GREEN'S TENSOR FOR A GRANULAR ELASTIC MEDIUM AND APPLICATION TO WAVE PROPAGATION IN A RANDOM MEDIUM**

Gayatri Chattopadhyay (Department of Mathematics, Surendranath College, Calcutta 700009, India) and R.K.Bhattacharyya (DST Project, Department of Applied Mathematics, Calcutta University, 92, A.P.C.Road, Calcutta 700009, India. e-mail: aroy@cucc.ernet.in)

Green's tensor for a granular elastic medium is computed and used to study the wave propagation in a random granular elastic medium by employing J.B.Keller's perturbation technique. Four different types of body waves are shown to propagate through the medium. The propagation is affected by random inhomogeneities of the medium. The effects have been calculated in terms of correlation functions. Particular forms of correlation functions are assumed to show that the waves attenuate as they propagate. Numerical results are obtained.

**ST4/E/40-B1** Poster **0830-28**

**ON WAVE PROPAGATION IN A RANDOM CONDUCTING MAGNETO-VISCOELASTIC MEDIUM**

Gayatri Chattopadhyay (Department of Mathematics, Surendranath College, Calcutta 700009, India); Rabindra Kumar BHATTACHARYYA (DST Project, Department of Applied Mathematics, Calcutta University, Science College, Calcutta 700009, India.)

The problem of wave propagation in arandom conducting magneto-viscoelastic medium is investigated by employing perturbation technique. The appropriate Green's matrix has been evaluated and used to obtain the wave velocity equation. It has been shown that the propagation of body waves depends upon the random inhomogeneities of the medium. The expressions measuring deviations resulting from random fluctuations of the material properties have been derived in terms correlation functions between parameters of the medium. The body waves attenuate due to randomness as they propagate through the medium. A numerical solution is being attempted on the assumption of particular forms of correlation functions.

**ST4/W/33-B1** Poster **0830-29**

**TWO DIMENSIONAL INTERPRETATION OF DIRECT CURRENT RESISTIVITY TRVERSING DATA FOR STUDYING SHEAR ZONE, EASTERN INDIA**

K.K.ROY (Department of Geology and Geophysics, Indian Institute of Technology, Kharagpur - 721 302, West Bengal, India, Email: kkroy@gg.iitkgp.ernet.in) L.K.Das and K.K. Mukherjee (both at Geological Survey of India, Ratnakar Building, 4, Chowringhee Lane, Calcutta - 700 016) P.S. Routh (Department of Geophysics and Astronomy, University of British Columbia, Vancouver, Canada) M.K. Sen and R. Chunduru (both at Institute of Geophysics and Department of Geological Sciences, The University of Texas at Austin, 8701 Mopae Express way, Texas 78759-8397, USA)

Direct current resistivity traversing was done across the Singhbhum shear zone near Ghatshila - Mosabani, Eastern India using the collinear dipole dipole configuration with dipole length of 500m and dipole separation varied from 500m to 6kms. Two-dimensional forward modeling was done using finite difference method and the inversion was done using Very Fast Simulated Annealing and Ridge Regression. The same data were inverted by three different institutions with different software and common features of these three interpretations are accepted with certain degree of confidence. It is observed that important geological signatures along this traverse are reflected in all the models but the geometrical shapes of the high and low resistive zone came different in different interpretations. Singhbhum shear zone is 1.5km thick and dip increases with depth. The shear zone is vertical at a depth of 1km from the surface. The north Singhbhum fold belt composed of Garnet, Kyanite, Silliminate, Staraulite schist is highly resistive and running parallel to Singhbhum shear zone for about 150km. Since the level of nonuniqueness in 2-D inversion is much higher than in 1-D inversion, the same data should preferably be inverted using different software based one different techniques.

**ST4/W/32-B1** Poster **0830-30**

**TWO DIMENSIONAL DIRECT CURRENT INVERSE PROBLEM USING GENETIC ALGORITHM AND SIMULATED ANNEALING**

K.K. ROY and N.S.R. Murthy (both at Department of Geology and Geophysics, Indian Institute of Technology, Kharagpur - 721 302, India, Email: kkroy@gg.iitkgp.ernet.in) B.K. Kumar (MBT, Pune, India) D. Sarkar (School of Geology and Geophysics, University of Oklahoma Norman, USA)

Two dimensional direct current resistivity forward problem was solved developing the source codes in finite difference and finite element modeling. Global optimization methods were used for 2-D inversion. Source codes for Genetic Algorithm (GA) and Very Fast Simulated Annealing (VFSA) are developed by the authors and the programs are tested for simpler structures. Resistivity traversing data collected across the Singhbhum shear zone near Rajkharwan Singhbhum Archaon Craton, Eastern India were inverted using both GA and VFSA. The results show that the shear zone is highly conducting and is about 2km thick. Just north of the shear zone highly resistive Proterozoic north Singhbhum fold belt is the prominent feature in the model. 2D resistivity modeling for cultural studies with dipole length of 500m and total electrode separation of 6 to 7km is possible. There are some common features in both GA and VFSA interpretations. Global optimization tools appear to be powerful in 2D inversion. About 50% of the model features may reflect the subsurface.

ST4/W/53-B1 Poster 0830-31

## THE EXCITEMENT OF WAVES IN THE EARTH ATMOSPHERE CAUSED BY A WIND FIELD

A.Pataraya, Z.khvedelidze, A.Chitaladze (Tbilisi State University, Chavchavadze Ave 3, Nanking, Taipei, Tbilisi 380028, Georgia. Email: sciteco@access.sanet.ge)

The experiment of the gravitational and acoustic waves in the Earth atmosphere is investigated in work. The atmosphere is assumed to be an ideally isothermally stratified and the waves excite by the inhomogeneous wind.

The amplitude reaches its maximal value on certain moment. The maximal amplitude of the gravitational wave is larger than that of the acoustic waves. These results can explain the perturbation of the ionosphere before and after the earthquake.

ST4/L/40-B1 Poster 0830-32

## DISCUSSION OF METHOD FOR JOINT INVERSION OF SEISMIC SURFACE WAVES AND GRAVITY DATA FOR THREE-DIMENSIONAL DENSITY STRUCTURE

Chongbing LIU and Jinsheng Ning(both at Department of Geodesy,Wuhan Technical University of Surveying and Mapping,Wuhan,430079,P.R.China, e-mail: cblu@dns.wtusm.edu.cn), Yushen Zhang (at Institute of Geophysics, Academia Sinica, Beijing,100101,P.R.China)

Seismic surface waves have been a very useful tool to study the Earth's upper mantle. But as a geophysical inverse problem, inversion of seismic surface waves can only reach a non-unique solution. In order to reduce the nonuniqueness, one important approach is to increase the data set, namely, include data of other disciplines into the inversion. In this paper, a method for joint inversion of seismic surface waves and gravity data, is proposed and formulated to investigate three-dimensional density structure of the upper mantle. The results of simulation experiment indicate that (1) the inclusion of gravity data can reduce the number of relatively small singular values of the kernel coefficient matrix, (2) the trade-off curve of joint inversion is located left-down to that of inversion using seismic data only, and both the variance and resolution of the solution estimation of joint inversion are improved, and (3) the resulting three-dimensional density structure of joint inversion approach to the theoretical density model closer than do that of inversion using seismic data only, especially within the depth range of 0-300km. Using this method, a three-dimensional density structure of upper mantle in North China is constructed, and the result is of interesting tectonic implication.

Monday 26 July PM

Presiding Chair: V.Cermak (Geophysical Institute, Czech Acad. Sci., Praha, Czech Republic)

## THERMAL STUDIES

ST4/W/41-B1 Poster 1400-01

## HEAT FLOW AND THERMAL HISTORY OF YINGGEHAI BASIN, SOUTH CHINA SEA

XIONG Liang-Ping, He Li-juan and Wang Ji-yang (Institute of Geology, Chinese Academy of Sciences, Beijing 100029, China, E-mail: JYWLPX@public3.bta.net.cn)

Yinggehai Basin is a shearing-extensional basin in South China sea. Based on temperature measurements in 56 wells and thermal conductivity determinations on 68 rock samples, mean heat flow value has been calculated and it turns out to be 84.1 mW/m<sup>2</sup>. This is the highest value so far observed in oil-gas bearing basins in China. The high heat flow is the results of three-phase extension of the basin since Cenozoic era. The first-phase extension occurred during 50-45 Ma followed by thermal subsidence till 28 Ma. The second-phase extension happened during 28-22 Ma and the third-phase extension, 5.2-1.9 Ma. After every extension, the basal heat flow at the bottom of the basin has been raised, starting from 60 mW/m<sup>2</sup> and reaching the highest value of 72 mW/m<sup>2</sup> at 1.9 Ma. If the radiogenic heat from the thick sediments is added, the surface heat flow may reach up to about 80 mW/m<sup>2</sup> which is consistent with the observations. Another words, the Yinggehai basin is becoming hotter and hotter after every extension and the highest value is observed nowadays.

ST4/E/38-B1 Poster 1400-02

## TEMPERATURE REGIME IN THE SURFACE RUPTURE ZONE OF THE 1993 LATUR EARTHQUAKE, INDIA : RESULTS FROM DRILLING

Sukanta ROY and R U M Rao (National Geophysical Research Institute, PO Bag 724, Uppal Road, Hyderabad 500 007, India, email: postmast@cnsri.res.nic.in)

Faults associated with shallow focus earthquakes are often associated with a complex configuration of fractures in the near surface zone. Drilling in such zones may connect two previously unconnected fractures causing vertical movement of water (and heat) inside the borehole. Precise temperature measurements made in boreholes clearly reveal zones of entry and/or exit of water causing characteristic perturbations in the temperature field over the affected depth sections. The 1993 Mw 6.1 Latur earthquake had a centroid depth of 2.6 km and was associated with a surface rupture zone (SRZ) near Kilarī. Detailed seismological, soil-gas helium and drilling investigations in the area confirmed the existence of a thrust fault dipping SSW at 50 degrees. Two boreholes, KLR-1 and KLR-3, on the hanging wall, penetrated the entire 338 m flood basalt cover and KLR-1 was deepened into the Archaean granite-gneiss basement up to 617 m. KLR-2 was drilled up to 270 m on the footwall. Heavy loss of drilling fluids, poor core recovery and slickensides characterised the depths where the fault was met with in the holes. The temperature profiles for all the holes revealed a "constant temperature zone (CTZ)" up to a depth of ~262 m after which they tend to return to normal formation temperatures. This is attributable to entry of water in the holes at shallow depths and its exit through a major fracture zone around 262 m. The basaltic section below 300 m and the granite-gneiss basement section yielded undisturbed temperature profiles and identical heat flow values. Three other holes located outside the SR in the Kilarī area yielded undisturbed temperature profiles pointing to the uniqueness of the perturbations in the SRZ.

ST4/E/52-B1 Poster 1400-03

## HYDROGEOLOGY OF THE UPPER CRUST NEAR KOLA HOLE - GEOTHERMAL ASPECTS

MILANOVSKY Svet (Institute of Physics of the Earth, Moscow, email: svet@uipe-ras.scgis.ru, Moscow), L. V. Borevsky (HYDEC Research Company, Moscow), V. I. Morgachev and V.N.Orlov (both Pechenganickel Kombinat, Nickel)

The paper presents data about hydro-geothermal field in crystalline rocks of the upper crust. These data were obtained during long term field observation in prospecting holes drilled on the territory of copper-nickel ore deposit which belongs to Pechenga Structure of Baltic Shield. Our interest to this study was stimulated by results of Kola superdeep drilling project. In the area of Kola hole we have the unique opportunity to investigate in details relationship between space peculiarities of thermal field, hydrogeology, fracturing of crystalline rocks and stress-field. In many prospecting holes situated near Kola hole we analyzed thermal field, hydrogeodynamics and geochemistry of groundwater. The zone of exogenous fissuring about 800m (up to 2000m) depth was established by hydrogeological study on Pechenga and Kola Peninsula as well. The observed thermal field seems to be closely connected with permeability (cracked-tie) of metamorphic rocks belonging to this zone. For the upper, fractured crust we observe: increasing with depth thermal gradient and heat flow, neg- correlation between filtration coefficient and geothermal gradient, space inhomogeneity of geothermal and filtration parameters, reflecting anisotropy of transport properties of fracture system. The permeability of this zone depends on tectonic and lithological factors. The result of the study of space peculiarities of permeability in the upper crust gives us an opportunity to take out realistic parameters for numerical model of heat- mass transfer.

ST4/E/21-B1 Poster 1400-04

## JOULE HEAT DISTRIBUTION AND GEOTHERMAL ZONES

Xiaoqing GAO(Lanzhou Institute of Plateau Atmospheric Physics,CAS, 730000 Lanzhou, P.R.China, email: xqgao@lzu.edu.cn); Giovanni P Gregori(Istituto di Fisica dell'Atmosfera, CNR, 00133 Rome, Italy, email: gregori@atmos.ifa.rm.cnr.it)

According to the Geodynamo Theory, electric current exists in the Earth. It can produce heat because of the resistance of the material of the Earth. This electric current can be derived from geomagnetic field data or model. Till now, the best geomagnetic field model(MAGSAT) was gotten by satellite global observation in 1979-1980. By this model, the global distribution of Joule Heat on ALB(Asthenosphere-Lithosphere Boundary) (direct proportion to electric current square) had been gotten. It is surprisingly found that the distribution of Joule Heat on ALB matches the global geothermal zones very well. And the strongest Joule's Heating is located below Tibet Plateau, the youngest and the highest plateau on the Earth. It seems that the geothermal heat mostly comes from ALB, it is controlled by Joule's Heating process.

ST4/E/61-B1 Poster 1400-05

## GEOTHERMAL GRADIENT VARIATIONS IN SOUTHERN IRAN AND ITS EFFECTS ON HYDROCARBON MATURATION

JAMSHID HASSANZADEH (Institute of Geophysics, Tehran University, P.O. Box 14155-6466, Tehran, Iran, email: jhassan@chamran.ut.ac.ir); Minoo Kosarian (Institute of Geophysics, Tehran University, P.O. Box, 14155-6466, Tehran, Iran, email: minoo@iman.ut.ac.ir)

A preliminary geothermal gradient map of Iran is constructed using all bottom hole temperatures previously measured in drill holes for oil, gas, and coal explorations. Data from few geothermal fields in N and NW Iran are also included in this map. With the exception of Zagros simply folded belt and the Persian Gulf, the geothermal data are generally sparse for the rest of the country. The range and pattern of gradient variations in Iran is far more complicated than inferred from the global heat flow map. Geothermal gradient contours in the Zagros generally run parallel to the folding axes and values increase to the south (from ~ 10 C/km in the northern folded Zagros to ~ 40 C/km in the southeastern part of the Persian Gulf). Moho depth decrease in the same direction. The Qatar-Kazeroun lineament divides the Zagros-Persian Gulf area into two zones with different thermal gradients. To the east of this divide, average gradient is remarkably higher than in the western Zagros. The regional thermal anomaly in the east is due to the Infracambrian Hormoz salt series intruding the overlying strata. Salt, in general, is a very effective heat conductor; however, the Hormoz salt has also a great potential of radioactive heat generation due to its abundant uranium-rich rock fragments. The abnormal heat flow explains the dominance of gaseous hydrocarbons in the eastern Zagros-Persian Gulf region. This is an example of shallow source for surface heat flow on the edge of a cold continental shield.

ST4/E/25-B1 Poster 1400-06

## HEAT FLOW IN THE ALGARVE BASIN, SOUTH PORTUGAL

M. Rosa DUQUE (Departamento de Física, Universidade de Evora, Rua Romão Ramalho 59, 7000 Evora, Portugal, email: mrad@uevora.pt)

The Algarve Basin is a Mesozoic-Cenozoic sedimentary basin located in the South of Portugal, with an East-West axis extending mainly in the offshore areas. This basin evolved in a constrictive compressive stress field during the Quaternary but its positive and negative vertical movements are mainly flexural, possibly associated with deep located lithospheric mechanisms. Two heat flow values were obtained in boreholes Ruivo 1 and Algarve 1. This values were obtained using BHT values and thermal conductivity data from thermal conductivity tables. In this work, the heat flow in this basin is analysed using data from five boreholes drilled for oil prospecting. Temperature data were obtained from BHT measurements. Gamma-ray logs were used to obtain heat production from radioactive elements in the region. Samples from one borehole were used to obtain thermal conductivity data in laboratory. Information about porosity was obtained from sonic and formation density logs. An estimation of the heat flow and temperature values at the bottom of the basin was found from heat flow values obtained in the holes and heat generated in the basin.

ST4/W/39-B1 Poster 1400-07

## THE NUMERICAL SIMULATION OF COUPLED FLUID FLOW, TEMPERATURE AND PRESSURE IN YINGGEHAI BASIN

XU Hehua, Zhang Jian, Xiong Liangping (Institute of Geology, Chinese Academy of Sciences, Beijing)

The numerical simulation is a useful method in quantitative analysis of sedimentary basin. During basin evolution, all kind of observed variables interplay and influence each other. It is very important to couple temperature, pressure and flow in basin modeling. In this paper, the nonlinear numerical modeling method to couple temperature, pressure and flow is introduced. Yinghai Basin in South China Sea is rich in oil and gas with high temperature and high over-pressure, so temperature, pressure and flow is of nonlinear relation. We apply this numerical model to simulate fluid migration in Yinghai basin. Finite element method is adopted in solving control equation. Results of calculation indicated that this numerical modeling is applicable in Yinghai basin. In Dong-Fang 1-1 structure, there exists large-scale movement of hot liquid with high temperature and high over-pressure. The movement of hot liquid is either horizontal or vertical. The fluid passage of hot liquid is at depth of 1250m to 1500m along fractures caused by mud diapir. We simulated the effect of seepage to thermal evolution and the results indicated that the flux of liquid is an important factor to the temperature distribution.



ST4/W/07-B1 Poster 1400-08

## THERMAL HISTORY OF TARIM BASIN DERIVED FROM FISSION TRACK ANALYSIS

WANG shejiao(Research Institute of Petroleum Exploration and Development Xue Yuan Road 20 Beijing 100083,P. R. China, email: sbhu@mail.igcas.ac.cn)

Thermal history and timing of hydrocarbon generation of the Tarim Basin are evaluated by fission track analyses. The results show that the temperature-gradient during late Paleozoic is very high which is caused by igneous activities in the basin. Cooling from elevated palaeotemperature was caused by late Permian and late Triassic uplift and erosion of 0.8jA0.2km and 1.0jA0.2km respectively. The increase of temperature during Cenozoic was due to the rapid depression corresponding to foreland basin. The timing of hydrocarbon generation can be determined. The main source rocks of Cambrian and Ordovician passed into the oil generation window during the middle Paleozoic and into the zone of gas production during the middle Mesozoic. At present, most of these source rocks are still in the zone of gas production but part of them are in the zone of dry gas production. As another important source rocks, Triassic and Jurassic have not been heated enough to be mature at present time, only in the Kuche depression, north part of the Tarim Basin, the source rocks passed into oil window. by fission track analyses. The results show that the temperature-gradient during late Paleozoic is very high which is caused by igneous activities in the basin. Cooling from elevated palaeotemperature was caused by late Permian and late Triassic uplift and erosion of 0.8jA0.2km and 1.0jA0.2km respectively. The increase of temperature during Cenozoic was due to the rapid depression corresponding to foreland basin. The timing of hydrocarbon generation can be determined. The main source rocks of Cambrian and Ordovician passed into the oil generation window during the middle Paleozoic and into the zone of gas production during the middle Mesozoic. At present, most of these source rocks are still in the zone of gas production but part of them are in the zone of dry gas production. As another important source rocks, Triassic and Jurassic have not been heated enough to be mature at present time, only in the Kuche depression, north part of the Tarim Basin, the source rocks passed into oil window.

ST4/E/43-B1 Poster 1400-09

## LITHOSPHERIC THERMAL STRUCTURE AND EVOLUTION OF THE TRANSYLVANIAN DEPRESSION - INSIGHTS FROM NEW GEOTHERMAL MEASUREMENTS AND MODELING RESULTS

Crisan DEMETRESCU (Institute of Geodynamics, 19-21 J.L.Calderon Str.,R-70201, Bucharest, Romania) Soren Bom Nielsen (Department of Earth Sciences, Geophysical Laboratory, The University of Aarhus, Finlandsgade 8, DK-8200 Aarhus N, Denmark) Mirel Ene, Delia Zemira Serban, Gabriela Polonic, Maria Andreescu (all at The Institute of Geodynamics, 19-21 J.L.Calderon Str., R-70201, Bucharest, Romania) Aurel Pop (ROMGAZ-SA Medias, Romania) Niels Balling (Department of Earth Sciences, The University of Aarhus)

The surface heat flow density pattern of the Transylvanian Depression (TD) represents a marked high amplitude short wavelength low in a region of generally elevated heat flow. Detailed temperature-depth profiles obtained by continuous temperature logging in 24 thermally stabilized wells to a maximum depth of 1400 m, combined with a finite element modeling of topographic and fluid flow effects support the conclusion that the observed thermal gradient in the TD truly represents the rate of heat loss of the subsurface. Modeling results show that the transient effects of sedimentation and erosion mean an overall 5-7 mW/m2 reduction in heat flow compared to the steady state value and that a low mantle heat flow and a low crustal heat production rate in the TD are necessary to explain the heat flow anomaly. The shape of the Neogene depression is roughly circular with radius 60 km with sediment thickness increasing toward the centre where it reaches more than 4000 m. A system of roughly circular faults borders the basin. The TD has a length scale in all directions which is similar to the thickness of the lithosphere and calls for three-dimensional modeling. As a first approach we invoke a rheological lithosphere model of alternate radial compression and extension to model the Neogene subsidence. The compressional phases are related to the Old Styrian (20-17 Ma), Young Styrian (16-15 Ma) and Moldavian (13-11.5 Ma) tectogeneses active in the Carpathians, while weak extensional phases account for the uplift of the basin in Pannonian (5.5-0 Ma).

ST4/W/23-B1 Poster 1400-10

## DEEP-SEATED GEOTHERMAL RESOURCES SURVEY PROJECT IN THE KAKKONDA GEOTHERMAL FIELD, JAPAN

Takao OHMINATO, Yasukuni Okubo, and Kouhei Akaku (New Energy and Industrial Technology Development Organization, Sunshine-60, 3-1-1 Higashi-Ikebukuro, Toshima-ku, Tokyo, Japan, email: ominatoko@nedo.go.jp, okuboysk@nedo.go.jp, akakukhi@nedo.go.jp)Nobuo Doi (Japan Metals and Chemicals Co. Ltd., 72 Sasamori, Ukai-aza, Takizawa, Iwate-gun, Iwate, Japan, email: doi@geothermal.co.jp)

The New Energy and Industrial Technology Development Organization (NEDO) has been conducting a research project named "Deep-Seated Geothermal Resources Survey" since 1992 in order to establish a desired direction for development of deep geothermal resources which exist beneath the already-developed shallow reservoirs. Deep wells WD-1a (3729m) and WD-1b (2963m, side tracked from WD-1a) were drilled in the Kakkonda geothermal field, north-eastern Japan, for this project. WD-1a penetrated Quaternary granite body named Kakkonda Granite for about 870m and reached the temperature over 500C. WD-1b encountered highly permeable fracture zone, which WD-1a missed.

Various types of survey methods, including well geological survey, well loggings, electro-magnetic survey, and micro-earthquake monitoring have been conducted and new results have been obtained; (1) Highly permeable fracture system is not observed in the region hotter than 400C, suggesting that this temperature corresponds to the limit of the productive geothermal reservoir, (2) Beneath the swarms of micro-earthquake hypocenters, deep drillholes, including Wd-1b, often encounter lost circulation which indicates the existence of productive zone,(3) Hypocenter distribution of micro-earthquakes has a lower limit which corresponds to the temperature range of 320-350C. At the well WD-1b, production tests were also conducted and geochemical samples have been obtained, as well. More detailed analyses are now going on and the series of results of this project will be used to make guidelines for the development of deep-seated geothermal resources all over Japan.

ST4/E/45-B1 Poster 1400-11

## GEOTHERMAL GRADIENTS AND ESTIMATES OF THERMAL STRUCTURE OF THE JAPANESE ISLANDS

Yasukuni OKUBO, Akiko Tanaka and Yusaku Yano (Geological Survey of Japan, 1-1-3 Higashi Tsukuba Japan 305, email: okubo@gsj.go.jp)

Geothermal gradients have been estimated from temperature logging data of 1809 drillholes and heat flow data of 108 sites in the Japanese Islands. Most of the geothermal gradients in

volcanic areas are greater than 100 K/km. Non-volcanic areas, on the other hand, represent values less than 30 K/km. A spatial mesh data set of geothermal gradient is created by the two-dimensional interpolation of spline fit from the measured geothermal gradients. Although the measured data include errors, the high density data coverage allows one to delineate the regional geothermal structures of the Japanese Islands. Then the depths of 350 deg. and 580 deg. isotherms are mapped based on the following assumptions: (1) 10 deg. at the ground level; (2) a one-dimensional and steady state model; (3) constant thermal conductivities of 2.5 W/m K for the upper crust and 2.0 W/m K for the lower crust; (4) constant heat productions of 1.5 mW/m3 for the upper crust and 0.15 mW/m3 for the lower crust. Comparison with the thermal structure indicates that the Curie point depths deduced from magnetic analysis represent the 580 deg. isotherm. The map of 350 deg. isotherm, which could correspond to the cutoff depth of seismic activity, marks shallow depths in the volcanic areas and varied depths in the surrounding areas.

ST4/W/64-B1 Poster 1400-12

## HEAT- AND FLUID-FLOW AT THE SOULTZ HOT-DRY-ROCK SYSTEM IN THE RHINE GRABEN

D PRIBNOW and C Clauser (both at: Joint Geoscientific Research Institute GGA, Stilleweg 2, 30655 Hannover, Germany, Email: dan.pribnow@gga-hannover.de)

Hot-Dry-Rock (HDR) is a concept for using Earth's heat as an energy resource. An artificial underground heat exchanger at a depth of 3.0 to 3.5 km has been created in the granitic basement of the Rhine Graben, close to the town of Soultz in France, by hydraulically connecting two deep boreholes over a horizontal distance of 500 m with the hydrofracture-technique. During a 4-month circulation test, over 240,000 m3 of water have been injected and produced at flow rates of 20 to 25 l/s and with outflow temperatures above 140 degC. The net output of thermal power exceeded 10 MW. The experiments indicate that the circulation system in the underground is hydraulically open. Numerical models of coupled heat- and fluid-flow help to understand the observations. At the regional scale, previous models suggested deep fluid circulation from East to West through a sandstone aquifer across the Rhine Graben causing a heat flow anomaly at Soultz. This is in contradiction to recent geochemical analyses of pore fluids. Models of the regional flow-system that agree with the pore-fluid chemistry include deep flow through the granitic basement. These models show that in the area of the HDR heat exchanger fluids generally move upwards. The results of the regional simulations are incorporated as boundary conditions in a local 3-D model of the underground heat exchanger at Soultz. This model is based on flow of two kinds: (1) Darcy-flow in the artificially fractured (stimulated) areas of the granite and (2) channelled flow on natural faults. The stimulated volume is a heat exchanger in the classical HDR concept: it is the hydraulic connection between injection and production hole and it provides the surface for heat absorption of the fluid flowing through the fractured rock. Additionally, the hydraulic fracturing of the granite created a connection with the regional fault system of the graben. Although not part of the HDR concept, this extension of the involved hydraulic system improves the long-term heat extraction process because the regional fault system acts as a buffer for temperature and pressure. The numerical models are used to predict the performance of a pilot plant that is planned to utilize an underground heat exchanger at 200 degC.

ST4/E/54-B1 Poster 1400-13

## INFLUENCE OF WATER AND DRILLING FLUID ON THE STRUCTURE AND PERMEABILITY PROPERTIES OF METAMORPHIC ROCKS AT THE DEPTH 7-12 KM IN KOLA WELL

Abdrakhimov M.Z. (RIC "GERS", Tver), MILANOVSKY Svet (Institute of Physics of the Earth RAS, Moscow, email: svet@uipe-ras.scgis.ru) and M.Z.Traskin (Moscow State University )

A number of data obtained at the Kola Superdeep well give the evidence of rock volume discompaction in-situ below 7-8 km: low seismic velocities, high porosity, increasing drilling rate and hole cavity, core disking, etc... The series of experiments connected with thermo-barotest of rocks for in-situ conditions at various depths of Kola well has confirmed the assumption that on depth 10-12 km, rocks in environment of water or drilling liquid, can tend to discompaction of rocks. We observed pronounced fluid-induced embrittlement effects on amphibolite and gneiss specimens strength was reduced to about a half of the initial value. It enabled us to estimate surface energy decrease and adsorption on the basis of Griffith brittle fracture criterion and Gibbs adsorption isotherm. Microstructure researches of core have shown, that that its specific features in particular the frequent occurrence of intergranular microcracks increasing with depth from 9 to 12 km are consistent with the hypothesis about the Rehbindler effect or stress corrosion as the mechanism of spontaneous penetration of drilling fluid along grain boundaries under Gibbs-Smith condition. Our study have demonstrated that the surface activity of water as the principal constituent part of the drilling fluid, combined with elevated temperatures and differential stresses, contributes to the development of intergranular micr cracks under conditions for the lower part of superdeep well.

ST4/E/18-B1 Poster 1400-14

## LONG-TERM TEMPERATURE MEASUREMENTS IN THE VOROTILOVO DEEP GEOLABORATORY

Yuri POPOV (Moscow State Geological Prospecting Academy, Miklukho- Maklai str., 39-1-191, Moscow 117485, Russia, email: Ypopov@mgga-sec.msk.ru) Lev Pevzner ("NEDRA", State Scientific and Industrial Enterprise on Superdeep Drilling, Svoboda str. 8/38, Yaroslavl 150000, Russia, email: root@nedra.yar.ru)

Data on spatial and temporal variations of temperature and temperature gradient in the Vorotilovo deep borehole (5374m in depth, without a casing tube, drilled in 1989-1992 in the Puchezh- Katunk impact structure, Russia) were inferred from 28 temperature logs obtained in 1992-1998. At present the thermal regime of the strata can be considered to be close to equilibrium. The maximum temperature value is about 98 C. Different rate of thermal equilibrium restoration for various depth intervals of the strata was observed. Regular temporal variations in temperature gradient within the depth interval of 3700-4800m are negligible inspite of a monotonous increase in temperature (by 4-6%). Significant systematic changes in temperature gradient value are being observed within the depth interval of 0-1700 m although there are short depth intervals with insignificant temporal variations in temperature gradient. Basically a degree of temporal changes of temperature gradient decreases with depth and corresponds to a decrease in rock porosity values. Dependence of vertical variations in temperature gradient on borehole diameter changes and some technological factors are found out.

ST4/W/68-B1 Poster 1400-15

## USING HELIUM ISOTOPE RATIO TO ESTIMATE CRUST AND MANTLE COMPONENTS OF SURFACE HEAT FLOW

Yang WANG (Lab. for Geothermics, Institute of Geology, Chinese Academy of Sciences, P.O.Box 9825, Beijing 100029, China, email: thalassa@263.net)

The ratio between crust and mantle heat flow component ( $Q_c/Q_m$ ) can be estimated by helium isotope ratio ( $He3/He4$ ).  $He4$  is the product from decay of uranium and thorium; and  $He3$  comes from mantle by degassing. Because U and Th (and K) mainly concentrate in crust, so  $He4$  is approximately proportional to the heat flux of crust.  $He3$  is associated with mantle heat flux. However, the specific relations between heat flux and  $He3$  or  $He4$  flux may be considerably modified by transport processes. But the  $He3/He4$  ratio can be used to constrain the  $Q_c/Q_m$  ratio. Using the  $He3/He4$  ratio and  $Q_c/Q_m$  data in basins of North China and Eastern China, and that of MORB, which  $He3/He4$  ratio is 8 RA (atmospheric  $He3/He4$  value) and  $Q_c/Q_m$  approximately equals zero, we obtain the relation between  $He3/He4$  and  $Q_c/Q_m$ :  $Q_c/Q_m = 0.87 - 0.39 \cdot \ln(He3/He4)$  (1) in which the unit of  $He3/He4$  is RA. Furthermore, the crust and mantle heat flow components can be taken from surface heat flow and  $Q_c/Q_m$  value. We had used formula (1) to estimate the crust heat flow ( $Q_c$ ) and the mantle heat flow ( $Q_m$ ) for some terrains in China. The  $Q_c$  and  $Q_m$  are  $\sim 70$  and  $\sim 30$  mW/m<sup>2</sup> in South Tibet; and in Tarim Basin they are  $\sim 30$  and  $\sim 14$  mW/m<sup>2</sup> respectively; and in Sichuan Basin,  $Q_c$  equals  $\sim 39$  mW/m<sup>2</sup>,  $Q_m$  is  $\sim 16$  mW/m<sup>2</sup>; but they are  $\sim 31$  and  $\sim 39$  mW/m<sup>2</sup> respectively in Songliao Basin, NE China. Our results were confirmed by previous geothermal studies. Helium isotope ratio ( $He3/He4$ ) may be a useful parameter for separating crust and mantle components from surface heat flux.

ST4/W/29-B1 Poster 1400-16

## SEPARATING SHALLOW AND DEEP COMPONENTS OF SURFACE HEAT FLOW BY WAVELET TRANSFORM

Yang WANG (Lab. for Geothermics, Institute of Geology, Chinese Academy of Sciences, P.O.Box 9825, Beijing 100029, China, email: thalassa@263.net)

The surface heat flow are superposition of some components which correspond to different sources within the Earth. The large scale feature of surface heat flow field corresponds to deep source (i.e. mantle) because lithosphere is a low-pass filter for conductive heat; and the small scale feature of the field is related to shallow processes due to the heterogeneity of thermal properties in crust. It is necessary to decompose the heat flow field into different scales in order to separate shallow and deep heat flux components. Wavelet analysis is a powerful tool for field decomposition, because of the local feature of wavelet functions; and it was tested by numerical experiment. Based on Mallat's pyramidal algorithm, we developed the code for 1-D multiscale analysis which are then applied to decompose the heat flow profile along East European Geotraverse 5 (EEG5) and the profile along 115 degree E in China. The decomposition produces a series of heat flux component profile related to different scales. Among these results, the high order details of the wavelet transform (e.g. D6) correspond to the heat flux of 60 km depth; the low order details (e.g. D3) is related to crustal heat flux; and the base function of wavelet transform (e.g. A6) reflects the trend of heat flux change along the profile. The decomposition result of EEG5 profile shows that, the main component of heat flow in Pannonian Basin comes from mantle, and mantle heat flow decreases toward east and west; the relative high surface heat flow in Saxothuringicum and Eastern Carpathians are due to high crustal heat flux which corresponds to the thick crust or high heat production in crust. The decomposition on 115 degree E in China demonstrates that, the mantle heat flow beneath Northern China is higher than that beneath Southern China; but the crustal heat flow of Southern China is much higher than Northern China. Previous studies on EEG5 and China confirmed our results (Shen et al., 1990, Wang J. et al., 1996).

ST4/E/27-B1 Poster 1400-17

## HEAT FLOW, SEISMICITY AND CRUSTAL STRUCTURE IN SOUTH PORTUGAL

M. ROSA DUQUE, José F. Borges and Maria João Costa (Physics Department, University of Evora, Rua Romão Ramalho 59, 7000 Evora, Portugal, email: mrad@uevora.pt)

The Variscan Fold Belt SW suture zone in Iberia involves several different units. From South to North we find: the South Portuguese Zone (SPZ), the Pulo de Lobo Formation (PLF), the Beja-Acebuches Ophiolitic Complex (BAOC), the Beja Igneous Complex (BIC) and the Ossa Morena zone (OMZ).

Aeromagnetic data suggest the existence of continental crust under the OMZ and SPZ forming a thin plate over a décollement zone. The SPZ corresponds to an accretionary prism that evolved to a typical foreland thrust belt with décollement of Carboniferous to Upper Devonian sediments above a Pre-Upper Devonian Paleozoic sedimentary sequence resting on a Precambrian basement. A Variscan suture that evolved to a continent-continent collision exists between the OMZ and SPZ. Flake tectonics in the Lower Devonian produced obduction to the North followed by a subduction in the same sense. Several heat flow data obtained in boreholes drilled for mineral prospecting were used in this work. Seismicity and hypocenter location in the area were studied and compared with heat flow density values. Temperature values at the surface, estimated from boreholes, were compared with surface temperature values obtained from other sources of data. Crustal structure in the region was obtained from seismic and MT data. Geotherms for the region were calculated and a preliminary rheological model for the SPZ was obtained.

ST4/E/06-B1 Poster 1400-18

## CONTACT METAMORPHISM OF SEDIMENTARY STRATA BY A BASALTIC SILL: COMPUTER SIMULATIONS AND GEOLOGICAL EVIDENCE

J. Safanda (Geophysical Institute, CZ-14131 Praha, Boci II/1401, Czech Republic, email: jsa@ig.cas.cz); V. Suchy and K. Melka (Geological Institute, CZ-16500 Praha, Rozvojova 135, email: suchy@gli.cas.cz); I. Sykora (Inst. of Rock Structure and Mechanics, CZ-18209, email: sykora@alpha.irm.cas.cz); P. Dobes (Czech Geological Survey, CZ-11821 Praha, Klarov 3/131, P.O.B. 85); M. Stejskal (Chemical Univ., Dept. of Oil Technology and Petrochemistry, CZ-16628 Praha)

Thermal influence of a 4 m-thick basaltic sill on adjacent organic matter-rich shale has been studied in detail at Kosov Quarry, the Barrandian basin (Silurian and Devonian), Czech Republic. Computer simulation of the thermal effect was based on the finite-difference transient solution of the heat conduction equation in 3-D axially symmetric geothermal model of the sill and its surroundings taking into account the heat of the magma crystallization. A different extent of the fluid convection, the initial magma temperature and the depth of the intrusion were considered. The results predict the thermal effect of hundreds of degrees C limited to the close surroundings (of a few metres) of the sill. The common feature of all the versions was a short duration of the heat pulse - a few years at most, during which the contact metamorphism of sediments had to occur. A range of independent geological thermometers (organic matter reflectance, illite and chlorite "crystallinity", analysis of fluid inclusions and isoprenoid distribution) have been employed to compare these predicted values with actual

geological evidence. All the thermal indicators generally show an appreciable increase of paleotemperatures toward the contact of the sill with enclosing sediments. A thermometer based on graptolite reflectance confirms relatively short-lived heating at maximum temperatures of about 500 C that were attained in a narrow (about 1 m thick) zone adjacent to the intrusion. Aqueous and hydrocarbon fluid inclusions in secondary calcite and quartz cements evidence substantially lower temperatures (from 60 to 150 C) that dominated within the igneous body upon cooling.

ST4/E/42-B1 Poster 1400-19

## HEAT FLOW ANOMALIES AND GEODYNAMIC IN THE NORTH-WESTERN PART OF THE BLACK SEA

Roman Kutas, Vladimir KOBOLEV and Vladimir Tsvyaschenko (Institute of Geophysics Acad. of Sciences, av. Palladin 32, 252142 Kyiv, Ukraine)

More than 500 heat flow measurements were performed in the Central part of the Black Sea. Low values (20-40 mW/m<sup>2</sup>) are now predominant. However last years geothermal anomaly has been revealed in the north-western part of the Black Sea (south-westwards from the Crimean peninsula). Within the anomaly heat flows are 70-90 mW/m<sup>2</sup> being increased up to 130-150 mW/m<sup>2</sup> on the local areas. Geothermal anomaly is situated on the continental slope in the zone of the deep Odessa-Sinop fault. In this area a mass of igneous rocks (from basic to pacific) was found on the continental slope. Their age varies from 135 to 26 Ma. In Pliocene-Quaternary the north-eastern part of the Black Sea adjacent to Crimea subsided. Along the Odessa-Sinop fault shear movements was evolved. Mutual movements of plates are expressed in the modern intensive seismic activity along Crimean peninsula. Interpretation of the geothermal data shows that the heat flow anomaly is due to the young tectonic and magmatic processes. Significant differentiation of thermal field and intensive local anomalies which are situated along the fault at the foot of the slope are created by hydrothermal processes. In this zone many water and gas expulsion have been revealed.

ST4/E/51-B1 Poster 1400-20

## THERMAL LITHOSPHERIC STRUCTURE AND GEOTHERMAL MODELING ALONG AND ACROSS THE GULF OF SUEZ

Sherif EL-HADY (email: Srozza@frcu.eun.eg); Imam Marzouk and Mohamed Dessoky (all at National Research Institute of Astronomy and Geophysics, Helwan, Cairo, Egypt)

One- and two-dimensional geothermal modeling were performed along and across the Gulf of Suez basin to study the thermal regime of the basin and its relation to the lithospheric structure. The FINITEG computer Program (Lee et al., 1980) was used for managing one- and two-dimensional geothermal modeling along the studied areas. Many modifications were made by the present authors in the FINITEG program to agree with the recent techniques used for temperature modeling. Most of these modifications were concentrated on the way of calculation of thermo-physical parameters (heat production, thermal conductivity and thermal diffusivity), which used for solving the geothermal modeling problem in the studied areas. It is found from the results of one-dimensional thermal lithospheric structure that, the average lithosphere thickness of Northern Egypt is ranged from 107 Km to 122 km. The last lithosphere thickness value is considered to represent the initial lithosphere thickness at the beginning of the Gulf of Suez rifting. Two-dimensional thermal lithosphere structure for the Gulf of Suez is performed through two profiles. The two profiles are chosen to pass through the new estimated heat flow areas in the Gulf of Suez. The first profile (A) is about 100 km in length and passes through Shadwan seismically active area and Esh El-Mellaha area towards the Eastern Desert. The second profile (B) is about 110 km in length and passes through the Gulf of Suez Basin, started from Shadwan area and end to Ramadan oil field. In each profile, the thermal lithospheric structure is calculated by a time step of one million year from the beginning of rifting (24 My) till the present situation. The thermal lithosphere structure of each time step is considered to represent the initial thermal lithospheric structure of the next time step. It is found from the results of the two dimensional geothermal modeling in the Gulf of Suez that, the lithosphere/asthenosphere boundary is very shallow (32-33 km) just below Shadwan seismically active area, while it reached to about 50 km just below Ramadan Field. It is found also that, the shallow hot swelled lithosphere/asthenosphere boundary could be only the sufficient factor which governs the observed geothermal anomaly along the Gulf of Suez.

ST4/E/41-B1 Poster 1400-21

## GEOTHERMAL EVOLUTION OF A MIOCENE SUBDUCTION AREA: THE EASTERN CARPATHIANS

Serban VELICIU (Geological Institute of Romania, Caransebes, 1; 78344 Bucharest, Romania, e-mail veliciu@igr.sfos.ro)

The geological structure of the Carpathians is now viewed as a collection of effects of the plate tectonics; on the other hand it is possible to construct various geothermal models that provide some insight into the tectonic history. These models must be reconciled with the knowledge of the structure of the lithosphere, petrophysical properties of rocks and the thermal regime of the Earth as inferred from the observations at its surface. The Eastern Carpathians area is relatively young and it is characterised by less than 25 m.y. since the last thermo-tectonic event; consequently, a dynamic model should be adopted. In order to explain the high heat flow (73-126 mW/m<sup>2</sup>) observed at the inner part of the Eastern Carpathians, a 2-D model which takes into account the radiogenic heat generation and the descent of a lithospheric plate has been elaborated. Calculated geotherms by finite element method indicate the presence of a high temperature anomaly (exceeding 1000 deg.C) localised in the upper mantle. The geothermal data suggest that both the high heat flow and the building up of the Pliocene-Quaternary volcanic chain are consequences of the lithospheric Miocene subduction in the Carpathians area.

ST4/E/62-B1 Poster 1400-22

## THE RELATIONSHIP BETWEEN GEOTHERMAL VORTEX AND EARTHQUAKE

Maocang Tang and Xiaoqing GAO (both in Lanzhou Institute of Plateau Atmospheric Physics, CAS, Lanzhou 730000, P.R.China, email: xqgao@lzu.edu.cn)

Earthquake always accompanied by thermal process. The change of soil temperature at different depths shows the underground thermal process. The data of soil temperature observed in more than 180 meteorological observatories in China for the period of 1980-1993 have been analyzed. And the concept of Geothermal Vortex was proposed and defined. The result shows that there are close relationship between geothermal vortex and earthquake. Earthquake always happened at the edge, with high gradient, of geothermal vortex. The stronger the geothermal vortex, the stronger the earthquake. It is possible to predict dangerous areas of earthquake by following the movement of geothermal vortices. Based on the statistical facts, a thermal-dynamic process linking geothermal vortex and earthquake has been proposed.



**ST4/E/36-B1** Poster **1400-23**

**TIDE GRAVITY NEAR MT. ELBRUS - NO EVIDENCE FOR HEAT FLOW INFLUENCE**

A.KOPEAEV, V.Yushkin (both at Astronomical Institute of Moscow University, Universitetski prosp. 13, Moscow, 119899, Russia; fax: +7-095-9328841; e-mail: kopaev@sai.msu.ru)

We chose tectonically active region of Central Caucasus to check independently the famous hypothesis of prof. Melchior concerning the correlation between the tide gravity anomalies and heat flow, as well-known tests (i.e. Baker et al, 1989) covered the area of Central Europe where loading tides may affect the 'purity of experiment' generally. Tide gravity observations have been carried out at the Bakstan station located 15 km apart from the highest top of Europe, sleeping volcano Mt. Elbrus, using quartz tide gravimeter DELTA-1 (modernized from Sodin-209 with addition of CCD, special tilting device for absolute in-situ calibration, etc) after its attestation at the ORB, Brussels. Elaborate processing of available gravity data (7 months altogether) gives delta-factors for M2 and O1 that agree with model values 'Wahr-Dehant' plus Schwiderski) within the error bars of 0.3 % resp. 0.5 %. So, there are no serious discrepancies (larger than 0.3 %) between the tide gravity observations and models in 'geophysically hot' areas even at the distance of 3300 km from the nearest ocean.

**Wednesday 28 July AM**

Presiding Chair: L.Moresi (Australian Geodynamics CRC, CSIRO Exploration & Mining, Western Australia)

**SLABS AND PLUMES**

**ST4/W/60-B3** Poster **0830-01**

**RHEOLOGY AND DEFORMATION OF THE TYRRHENIAN PLATE**

Carlo GIUNCHI (Istituto Nazionale di Geofisica, Via di Vigna Murata 605, 00143 Roma, Italy, Email: carlo@gea.dfn.unibo.it). Spina Cianetti e Paolo Gasperini (Dipartimento di Fisica, Settore Geofisica, Universita' di Bologna, Viale B. Pichat 8, 40127 Bologna, Italy)

The deformation of the Tyrrhenian plate is investigated by a thin plate model with realistic rheology for the crust/lithosphere system. The Tyrrhenian and peri-Tyrrhenian basins are trapped between the convergence of the two major African and Eurasian plates, resulting in the subduction of the African lithosphere underneath the Calabrian arc and the formation of the Alpine and Apenninic belts. We try to include in the model forces acting at the plate boundaries that better represent the observed deformation. The work focus on the interplay between the push of the African plate, the roll-back of the Tyrrhenian plate and other potential sources of intraplate deformation. It is found that the rheological heterogeneities in the Tyrrhenian plate are needed to describe the partitioning of the deformation in the Apenninic and Calabrian arc, and in the plate itself.

**ST4/W/04-B3** Poster **0830-02**

**TIME-DEPENDENT DYNAMICS OF THE TONGA-KERMADEC SUBDUCTION ZONE**

Lijie Han, Michael GURNIS, and Hendrik van Heijst (all at Seismological Laboratory, Caltech, Pasadena, CA 91125, USA, email: gurnis@caltech.edu.); Carmen Gaina and R. Dietmar Mueller (Department of Geology and Geophysics, University of Sydney, Sydney, NSW 2006, Australia, e-mail: dietmar@es.su.oz.au)

We formulate regional, time-dependent dynamic models of the Tonga-Kermadec subduction system from 40 Ma to the present. The goal of our approach is to explore the sensitivity of outcomes to both uncertainties in plate tectonic reconstructions and lateral and radial variations in mantle properties. The regional models have a spherical geometry, but the flow is solved only within the area of interest. The full convection problem within a viscously dominated fluid is solved with the coupled momentum and energy equations. The rheology is linear, but highly pressure and temperature dependent. Plate kinematics are imposed as velocity boundary conditions with weak plate margins at the inferred evolving position of trenches. The plate tectonic model is characterized by the initiation of subduction at about 40 Ma at the Norfolk ridge and with subsequent opening of the Norfolk, South Fiji, and Lau basins. Moreover, the New Hebrides trench sweeps southwest from the Late Miocene to the present. The dynamics of the slab are influenced by the rapid motion of the trench both along strike and oceanward. The shape of the slab in the dynamic models are compared with relocated hypocenters within the upper mantle. In global seismic tomographic inversions, the Tonga-Kermadec system is characterized by strong fast anomalies within the transition zone and top of the lower mantle but does not appear to extend below ~1000 to ~1200 km depth. This is consistent with the Eocene initiation of subduction. The conclusion is quantified by comparing the outcomes of dynamic models with seismic tomography.

**ST4/W/09-B3** Poster **0830-03**

**THE PARAMETERIZED MIXED MANTLE CONVECTION MODELS OF CONTINENT AND OCEAN**

ZHANG Jian, (Institute of Geology, Chinese Academy of Sciences, Beijing, 100029, China); Shi Yaolin (Graduate School, University of Science and Technology of China, Academia Sinica, Beijing 100039, China. E-mail: shiyl@sun.ihep.ac.cn)

Recent studies reveal that mantle convection could be mixed, that is, convection penetrates the 670km boundary and involves whole mantle in some places, while convection is layered in some other places. Therefore, we carry out the parameterized mixed mantle convection model to modeling the penetrative mantle convecting beneath Oceanic and Continental lithosphere. In model, we introduce a time-dependent penetration parameter  $F$ , which denotes the ratio of mantle material involved in whole mantle convection over the entire mantle. Completely whole mantle convection is achieved if  $F$  approaches 1, and convection is completely layered if  $F$  approaches 0. When layered convection dominates, the temperature difference between upper mantle and lower mantle, until the thermal driving force can overcome the phase barrier to slab penetration. With the parameter  $F$ , thermal evolution of mantle convection state can be calculated, temperatures and heat losses can also calculate respectively. It is found that there is a nonsynchronous of the overturn between oceanic and continental mantle. This nonsynchronous can cause the tectonic activity and geothermal anomaly in the marginal zone between Oceanic and Continental lithosphere. Such results offer a physical interpretation of the observed geothermal anomaly in South China Sea. For example, Yinghai basin which lies in the marginal zone of Pacific and Euroasian plate has elevated temperature and pressure background that could be created by the nonsynchronous of the overturn between oceanic and continental mantle.

**ST4/W/62-B3** Poster **0830-04**

**APPLICATION OF CONTINUUM PLASTICITY MODELING TO 2D SIMULATIONS OF PLATE TECTONICS**

Louis MORESI and Hans Muhlhaus (Australian Geodynamics CRC, CSIRO Exploration & Mining, PO Box 437, Nedlands, 6008, Western Australia)

We use a Lagrangian Particle Finite Element code to study the problem of convection in a fluid with material properties which are a strong function of composition and strain history. The method is applied to the study of the manner in which the Earth's lithosphere is mobilized and subducted. The lithosphere is treated as the cool thermal boundary layer of a convecting fluid with strongly temperature dependent viscosity. In such a system, the lithosphere will be entirely stagnant unless the boundary layer yields under relatively high stresses. This yielding, mimicking pervasive brittle failure of the lithosphere, has been demonstrated to produce convection with plate-like surface motions and a boundary layer structure similar to the cooling oceanic lithosphere. In the Earth, plate boundaries are strongly localized along narrow zones dominated by major fault systems and can easily be picked out in maps of global seismicity. Several studies have shown that it is important to consider the history dependence of the yielding of the lithosphere in order to reproduce well-defined, narrow plate boundaries in convection models (i.e. to consider the fact that plate boundaries which have accumulated significant slip appear to be weaker than newly yielding lithosphere). Such modeling requires that the strain history of a particular parcel of material must be tracked for at least the period of time it remains part of the brittle lithosphere. At the same time, the large-scale convecting system must be modeled for a number of overturns. Together these requirements make the problem difficult to solve - requiring the tracking of a highly deforming lagrangian reference frame while also retaining computational efficiency so that an enormous number of timesteps can be completed. Lagrangian Particle methods give us a simple way to track history variables in a highly deforming fluid while retaining the computational efficiency of a multigrid fluid-dynamics finite element code. Our model uses a strain-softening yield criterion for each material parcel in the convecting system to study the influence of history dependent rheology on the form taken by the structures which allow the thermal boundary layer to founder. The introduction of this history dependence immediately induces a strong localization of deformation in converging regions into narrow shear bands. The development of these shear bands tends to stabilize the convection ...

**ST4/L/02-B3** Poster **0830-05**

**DIFFERENTIAL CORE-MANTLE ROTATION AS A SOURCE OF ADDITIONAL HEATING AND ORIGINATING OF DEEP PLUMES**

Natasha Petrova, Alexander Gusev (Department of Astronomy and GRG, Kazan University, Kremlevskaja Str., 18, Kazan, 420008, Russia, E-mail: petrova@astro.ksu.ras.ru)

Modern tectonophysics of plumes determines the region of plume origin in ultra-low velocity zone of the core-mantle boundary (D' zone) being a power heat source. On evidence derived from seismotomography the earth core has a very rough surface that has ledges and depressions with the amplitude up to 5-6-km. The thickness of intermediate layer is varied from 100 to 300-km according to different data. Dissipative effects, arising from the different core-mantle rotation, are of particular interest as the source of additional heating of the Earth interior. The friction power extracted from differential core-mantle rotational kinetic energy of the Earth depends on the flattening of the core, size and viscosity of D' layer. It may be transformed into heat and then create instability of the D' thermal layer, leading to the generation of upwelling vortical plume. According to the theory of differential rotation for two-layer Earth (rigid mantle and liquid core) (Getino, Fernandez, 1995; M.Greff, H.Legros, 1998; Petrova, Gusev, 1997), which predict two eigen-modes: Chandler Wobble and Free-Core Nutation, we estimated frictional dissipative power that is approximately equal to 10% from the total Earth' heat flow.

**ST4/W/17-B3** Poster **0830-06**

**EXPERIMENTAL INVESTIGATION OF WAVE PROPAGATION IN THERMAL PLUMES**

Nils LAUDENBACH / Ulrich R. Christensen, (Institute of Geophysics Goettingen)

In laboratory experiments thermal plumes are created by injecting hot corn syrup into a column of cold syrup. The viscosity contrast is up to a factor of 1000. The experimental apparatus is able to generate laboratory plumes with well defined volume fluxes. Solitary waves, that propagate upwards in the plume conduit, are generated by enhancing the injection rate for a few seconds. For the measurement of the thermal structure of the plume we have implemented a method based on the deflection of a laser beam passing through the plume. Continuous scanning provides a new radial temperature profile each second, which allows detailed studies of the thermal structure of solitary waves. Because of thermal diffusion, the conduit widens with height, while its central temperature decreases. The solitary waves start with the same temperature as the unperturbed conduit, however, we find that the temperature in the waves decreases less rapidly with rising height. This can be explained by the faster upward propagation and the trapping of fluid within the soliton. If solitary waves exist in mantle plumes, this would imply that they arrive at the bottom of the lithosphere with a larger excess temperature than what the plumes normally exhibit, which could explain strong variations of melt generation with time.

**ST4/L/10-B3** Poster **0830-07**

**VORTEX VOLGA-KAMA'S PLUME UNDER RUSSIAN CRATON**

Alexander GUSEV, Natasha Petrova, Dpt. of Astronomy and GRG, Kazan University, Kremlevskaja Str., 18, Kazan, 420008, Russia, E-mail: gusev@astro.ksu.ras.ru

Tectonophysics of plumes is based on the modern jet-theory of viscose matter including and adapting convective structure of ascending and descending flows of mantle matter. The plume source is located at ULVZ, which is characterised by large contrast in density, viscosity, material flow rates, chemistry and thermodynamical parameters. The vortex plume penetrating lower and upper mantle is considered as plausible pattern. Such vortex plume is more stable under influence of different motions in the mantle, under cross-section of various phase transition zones: spinel to oxides, perovskite (670km), olivine to spinel (410km). The vortex plume increases an additional pressure on the crust, causing notable elevation of Moho boundary (4-5 km) and sedimentary cover (2-3 km), such as the South-Tatar Crest in the Volga-Kama's region. The top of vortex plume pins to the Earth's crust, melting the matter and creating local intensive heat flow (74 mW) at the surface. It discretely moves under the plate, conserving mushroom-like pluto-bodies (30-50km) in crust and causing the gravitational anomalies. By this means, under motion of the plates the plume's top remain its track ("hot-spot" track) at the plate surface in the form of volcanic islands archipelago in ocean region or in the form of pluto-like bodies, dome-shaped uplifts and arch lineaments chains in the thick continental plates such as Euro-Asian one. Investigating the "hot -spot" tracks we can conclude about



velocity and direction of plate motion like Russian craton ( $5.2 \pm 3.3$  mm/year, south-western line) in the hot-spot reference frame. This value is confirmed by the method of zero kinetic plate moment (Euler's theorem for the sphere) and by analytical extension of velocity of neighboring plates.

**ST4/E/48-B3**

Poster

**0830-08****LABORATORY EXPERIMENTS ON SUBDUCTION AND BACKARC EXTENSION**

Francesca FUNICIELLO (Dip. Scienze Geologiche, Univ. Roma Tre, Largo S. L. Murialdo 1, 00146, Roma Italy, Institute of Geophysics, ETH, 8093 Zurich Switzerland e-mail: ffunicie@geo.uniroma3.it), Claudio Faccenna, (Dip. Scienze Geologiche, Univ. Roma Tre, Largo S. L. Murialdo 1, 00146, Roma Italy, e-mail: faccenna@uniroma3.it), Domenico Giardini (Institute of Geophysics, ETH, 8093 Zurich Switzerland)

We have performed 2D and 3D laboratory experiments to investigate the way the oceanic lithosphere sink into the mantle. Models have been performed with silicone putty, simulating the viscous behaviour of an oceanic lithosphere subjected to long term deformation and glucose syrup, simulating the mantle. We tested the influence of two parameters on the style of mantle convection: (1) lateral boundary conditions, i.e. box width, (2) deep discontinuity in the mantle resembling the 670km transition. We expressed the results in terms of: rate of trench retreat, rate of subduction, dip of subduction and state of strain of the upper plate. Our results show how the slab trajectory into the mantle is influenced by the presence/absence of deep discontinuity.

**ST5****Wednesday 28 – Friday 30 July****SEISMOLOGICAL OBSERVATION AND INTERPRETATION (LINKED TO U7,U8, JWA34 AND JSA40)**

Location: Medical School EG12 LT4

Location of Posters: Arthur Thompson Hall

**Wednesday 28 July AM**

Presiding Chair: Torild Van Eck (KNMI, the Netherlands)

Concurrent Poster Session

**SEISMOLOGICAL OBSERVATION AND INTERPRETATION: NETWORKS****ST5/E/34-B3****0830****A NEW BROAD-BAND SEISMIC NETWORK WITH SATELLITE TRANSMISSION IN CATALONIA (SPAIN)**

Figueras, S.; Fleta, J.; GOULA, X.; Olivera, C.; Olmedillas, J.C.; Roca, A. and Susagna, T. Institut Cartogràfic de Catalunya, Parc de Montjuïc, E-08038 Barcelona. email: xarxasimica@icc.es; http://www.icc.es

Technological advances in the field of telecommunications make possible now to use continuous satellite data transmission for geophysical applications at a very affordable economical cost compared to other transmission systems. The use of low consumption VSAT platforms gives more freedom to choose stations sites, in particular in mountainous areas as the Pyrenees. The capacity and flexibility of available systems make possible the installation of multisensor field stations that can send data to different reception and acquisition centres simultaneously. The project of the Institut Cartogràfic de Catalunya includes the installation of 20 broadband, high dynamic range seismic stations in our territory (aprox. 32000 km<sup>2</sup>) with continuous transmission to the recording centre at Barcelona. Some of these stations will also contain dual frequency continuous transmission GPS receivers. The recording centre and 3 first field stations will be installed on April 1999 and it is expected that an operative network of 10 stations with fast automatic location and early warning systems will be ready on January 2000. High importance will be given to the automatic data distribution which should include: 1) data interchange among centres responsible for data acquisition and dissemination of information; 2) early warning with information to various agencies, in particular to responsible for civil defence and 3) good quality data dissemination to the scientific community.

**ST5/W/17-B3****0850****A NEW MEXICAN NATIONAL SEISMOGRAPHIC NETWORK**

D.A. Novelo-Casanova, S.K. Singh, and J. Pacheco (all at Instituto de Geofísica, Universidad Nacional Autónoma de México, Ciudad Universitaria, México, email: david@ollin.igeofcu.unam.mx)

The new Mexican National Seismographic Network (MNSN) will have great impact in regional advanced seismic research and in local seismic mitigation programs. At present, 18 broadband observatories in south-central Mexico are operating. Each remote station has a STS-2 seismometer, a FBA-23 accelerometer, a Quanterra processor Q680/LT-G and a GPS clock. In addition to the broadband network, MNSN operates other seismic networks located at strategic sites (Mexican Valley, Guerrero, Popocatepetl). All this instrumentation, together with the national short-period network, provides the means for: (1) detailed studies of the Mexican seismicity; (2) rapid response to earthquake disaster prevention measures; and (3) earthquake engineering research.

**ST5/W/21-B3****0910****THE ALERT SYSTEM OF THE SIL NETWORK AND EARLY WARNINGS OF EARTHQUAKES AND VOLCANIC ERUPTIONS**

Steinnun S. JAKOBSDÓTTIR and Ragnar Stefánsson ( both at Department of Geophysics, The Icelandic Meteorological Office, Bústa\_avegi 9, IS-150 Reykjavík, Iceland, email: ssj@vedur.is, ragnar@vedur.is)

The SIL system is an advanced seismic network in Iceland, automatically locating earthquakes, estimating moment magnitudes and "local" magnitudes and calculating fault plain solutions. It has facilities to monitor on routine basis active faults with a relative accuracy of tens of meters, to monitor on routine basis the orientation of individual fault plains and comparing direction of fault planes to direction of the active fault. An automatic alert system is

in continuous development in the SIL system. The alert system is two-fold, a central alert based on the automatic bulletin and a station alert that reports directly on ground motion at the site stations. For the central alert Iceland is divided into alert regions. The size of each region and its preset thresholds for expected number and magnitude of events, depend on the seismicity in the area and the station spacing. The station alert reports on big amplitudes and on increase in the background noise. Alerts given by the automatic system are evaluated by seismologists, which then decide if warnings should be forwarded to The Civil Defence and local authorities. To do that they use the facilities of the SIL system to carry out what might be called a real-time research to find out what is really happening. The aim is to include all new understanding, as gained from earthquake prediction research, directly into the system to improve it. The alert system was started in september 1992. Since then there have been two eruptions in Iceland, both within the glacier Vatnajökull, and two periods of earthquake swarms, with earthquakes reaching magnitude 5. Both eruptions were predicted and warnings issued to The Civil Defence and aviation authorities before the eruption. The alert system issued automatic warnings both few days and few hours before the big events. An overview over automatic alerts and warnings issued by seismologist before these events will be given in the talk.

**ST5/W/52-B3****0930****UPDATING THE ISC BULLETIN**

Raymond J WILLEMANN and Dmitry Storchak (International Seismological Centre, Pipers Lane, Thatcham, Berkshire RG19 4NS, UK, email: ray@isc.ac.uk)

Internationally funded to publish the definitive global seismicity bulletin, the ISC has avoided changes that might alter the fundamental content of the Bulletin. This conservative approach has been mandated by the need for hypocentres, magnitudes and other earthquake parameters that are as uniform as possible. It is now possible, however, to compute new locations and magnitudes for the ISC's entire Bulletin back to 1964 and to provide data more flexibly, for example giving users residuals with respect to their own choice of location or earth model. Thus, the ISC could now change models or procedures occasionally as required to best serve seismologists, and compute new parameters of past events according to the updated practices. Over more than 30 years of operation, possibilities for many types of changes have arisen. Seismologists might be well-served by adding new features to the Bulletin as soon as they are ready, but most would probably prefer a single change of all procedures for computing earthquake location and size. Changes that the ISC may consider over the next few years include

- Using updated travel times, based on a modern homogenous earth model such as IASP91 or PREM, a 3-dimensional or anisotropic model, or regional models.
- Computing locations from more phases (S or PKP) and more readings (vector slowness).
- Using station travel time and amplitude corrections, either static or source-dependent.
- Implementing alternative location algorithms, e.g., epicentres from only differences of arrival time, depths from waveform fits, or relative locations using JHD.
- Computing magnitude on alternative scales, such as ML or MW.

**ST5/E/21-B3****0950****REAL-TIME SEISMIC INFORMATION SYSTEM BY FREESIA PROJECT**

Mizuho ISHIDA (National Research Institute for Earth Science and Disaster Prevention, 3-1 Tennodai, Tsukuba-shi, Ibaraki-ken 305-0006, Japan, email: ishida@geo.bosai.go.jp)

FREESIA (Fundamental Research on Earthquakes and Earth Interior's Anomalies) project started in 1994. The major objectives of the project are; to develop a broad-band network for real-time earthquake monitoring and subsequent data analysis; to co-install strong motion seismographs to record large earthquakes; to open, in quasi-real time basis, the information about source mechanism and ground motion for earthquakes with magnitudes down to around 3.0 in and around Japan. The Freesia network now consists of twenty stations covering whole Japan. Each station is equipped with three-component broad band seismometers and strong motion sensors, with 24-bit digital data recording at a sampling rate of 80 Hz. Data from eleven stations are transmitted to NIED (National Research Institute for Earth Science and Disaster Prevention) through continuous telemetry, continuously stored in the data mass storage and are available through internet. Data from the remaining data from nine stations by a dial-up telephone link. We develop a software of automated moment tensor determination by using on-line broadband seismic waveforms from the FREESIA networks. The location and origin time which are broadcasted by Japan Meteorological Agency by e-mail are used. The moment tensor solution determined by using long period waveforms (from 20 to 50 seconds) of 3 stations are automatically displayed on the World Wide Web within five minutes after the e-mail information was received. The FREESIA program is cooperative project between NIED and several universities and is supported by NIED.

**ST5/E/39-B3****1125****CLOSE-RANGE SEISMIC MONITORING OF THE MINING AREA NEAR APATITY, KOLA**

Yura V. Fedorenko (IFJ/UoBergen and Inst. North Ecology Problems, Kola Science Centre, RAS, Fersman Str. 14, Apatity, 184200 Murmansk Reg., Russia; Email: yura.fedorenko@ifjf.uib.no) Lena Beketova (Geological Inst., Kola Science Centre, RAS, Fersman Str. 14, Apatity, 184200 Murmansk Reg., Russia) Eystein S. HUSEBYE (IFJ, UoBergen, Allegaten 41,N-5007, Norway, email: eystein.husebye@ifjf.uib.no)

A truly nuisance in monitoring CTBT compliance is small areas of high mining activities like that near Apatity, Kola. The numerous chemical explosions here are occasionally recorded at teleseismic distances but very frequently at local and regional ranges. Since every signal recorded would necessitate some processing and possibly analyst inspections these explosions constitute a significant extra workload to seismic monitoring tasks on any data center level. Our approach to resolve this problem was to install on an experimental basis a 3-component seismic station NANSEN (NKK;33.84N,67.60E) in the Apatity mining district. The self-constructed data logger is flexible with respect to sampling rates, detector design, data storage and transfer to a local center. Timing is via GPS-clock and the station operation is remotely controlled and calibrated. In the initial stages of NKK-operations the emphasis is aimed at automatically to identify explosion signals and the associated mine locations. Here we are using the algorithms for explosion site recognition presented elsewhere (Husebye & Fedorenko, IUGG99 Abstract). There are many mines in the Apatity area but today only 5 are in operation. The explosion signals from these mines were always correctly 'recognized' as such. We are also expanding this aspect of NKK-operation that is to recognize other mines on Kola on the basis of signals recorded. The hardware cost of the NANSEN station was less than US \$ 2000. which we rate a modest investment for significantly reducing analysis at data centers at local/regional distances from Apatity. This aspect of 'explosion' monitoring is easily transportable to other areas with numerous mining and/or quarry explosions. There is also an environmental aspect of the NANSEN station operation namely to monitor seismic loading on the free surface which may trigger snow avalanches (Chernous et al.; IUGG99 Abstract).

ST5/W/19-B3

1145

**CALIXTO'99: STATUS QUO OF AN ONGOING HIGH RESOLUTION TOMOGRAPHICAL EXPERIMENT IN ROMANIA.**

FRANK P. LORENZ, M. Martin, F. Wenzel, (Geophysical Institute, University of Karlsruhe, Germany, email: Frank.Lorenz@phys.uni-karlsruhe.de) and the CALIXTO Group (National Institute for Earth Physics, Bucharest, Romania; Faculty of Geology and Geophysics, University Bucharest, Romania; Institute of Geophysics, ETH Hoenggerberg, Zuerich, Switzerland; Ecole et Observatoire des Sciences de la Terre, Strasbourg, France; Istituto Ricerca Rischio Sismico, Milano, Italy; Department of Geological Sciences, Northwestern University, Evanston, ILL, USA; GeoForschungsZentrum Potsdam, Germany).

A status report of the Carpathian Arc Lithosphere X-Tomography (CALIXTO) seismic experiment is given. An international group is operating a large scale high resolution passive seismic experiment between 1999 and end of May 2000. Over 150 mobile acquisition systems, with a large number of broadband sensors is deployed in an area between 24E-28E and 44N-47N investigating the Vrancea Zone, an extraordinary earthquake area with very high seismic activity in intermediate-depth range. We show the results of extended synthetic numerical calculations for optimizing the station distribution and give a proof for distinct Moho-topography within the epicentral area. Our studies include teleseismic and local earthquake data. We give better constraints for seismic hazard assessment for this former subduction zone, by revealing the dimensions of a high-velocity body, which embeds all intermediate-depth seismicity. The P-wave velocity perturbation is about 3%, and we reach an accuracy of about 10km x 10km blocksize with satisfying resolution down to a depth of about 400km.

ST5/E/19-B3

1205

**SOURCES OF SEISMIC NOISE AT AUSTRALIAN STATIONS**

Mark Leonard (Australian Geological Survey Organisation, PO Box 378, Canberra City, ACT 2601, Australia, email: mleonard@agso.gov.au)

The source of microseismic noise has long been accepted as standing waves in the ocean which are generated by the interaction of two sets of oceans waves travelling in approximately opposite directions. Various authors have suggested the phenomena is due to fast moving storms at sea over-riding themselves, others have suggested it is due to ocean waves interacting with their own reflection of off a coastline.

Data from a regional array of three component broadband seismometers and the Skipky deployment of three component broadband seismometers across Australia has provided a unique set of data for studying the seismological properties of the Australian region. In this study the deployments are used to study the nature and sources of microseismic noise in Australia. Results will be presented showing the correlation of noise peaks with storms in the surrounding oceans and periods of high seas impacting on the Australian coast.

ST5/W/61-B3

1225

**OCEANIC WAVEHEIGHT MODELS AND MICROSEISMS**

David A. McCormack (Geological Survey of Canada, 1 Observatory Crescent, Ottawa, Ontario K1S 2H1, Canada email: mccormack@seismo.nrcan.gc.ca)

Waveheight maps covering the world's oceans have recently become available to the scientific community. Such maps permit direct comparison between observed microseismic wavefields and microseisms predicted by source generation models. This presentation examines the correlation between observed microseisms and the microseismic signals predicted from measured waveheights. In addition to waveheight maps, simple physical models permit forecasting of waveheights up to seven days in advance. The reliability of such waveheight forecasts for prediction of microseismic noise amplitudes is examined.

Wednesday 28 July PM

Presiding Chair: Prof. Y.T. Chen, Director, Institute of Geophysics, Beijing, China  
Concurrent Poster Session

**SEISMOLOGICAL OBSERVATION AND INTERPRETATION: TECHNIQUES**

ST5/E/02-B3

1400

**SYNTACTIC PATTERN RECOGNITION FOR WARNING SYSTEMS AND SUPPORTING DATA BASES**

M.N. ZHIZHIN, A.D. Gvishiani, A.A. Burtsev CGDS, Molodezhnaya Str. 3, GC, Moscow, 117296, Russia; +7-095-1334339; Email: jjn@wdbc.rssi.ru J. Bonnin, D. Rouland, EOPGS, 5 rue Descartes, F-67084 Strasbourg Cedex, France; +33-88416368; Email: bonnin@selene.u-strasbg.fr

Syntactic Pattern Recognition Scheme (SPARS) has been applied to classify seismograms from different seismic source zones (Fiji, Tonga and Vanuatu) in New Caledonia region. Several GEOSCOPE stations based in that region provided with the initial data set. The supporting relational database contains a large number of broad-band waveforms of local and regional seismic events. The result of SPARS application to the database analysis is a set of algorithms and software tools for pattern recognition and classification of seismic records in quasi real time.

ST5/W/03-B3

1420

**AUTOMATIC S-PHASE PICKING IN BROAD-BAND SEISMOGRAMS USING THE DISCRETE WAVELET TRANSFORM**

Reinoud SLEEMAN, Torild van Eck (Royal Netherlands Meteorological Institute, P.O. Box 201, 3730 AE, De Bilt, Netherlands, email: sleeman@kmi.nl) Patrick J. Oonincx (Centre for Mathematics and Computer Science, P.O. Box 94079, 1090 GB, Amsterdam, Netherlands)

We present an algorithm for the automatic picking of seismic S-phases at a single three component broad-band station, in which the discrete wavelet transform (DWT) and classical polarization techniques are combined.

A common strategy to detect and pick seismic phases in seismic recordings is the construction of characteristic functions. These functions describe specific properties of the seismic signal. For the detection of S-phases the following functions are used from polarization analysis: (1) ratio of energy in the Q, T-plane and total energy, (2) deflection angle and (3) degree of polarization.

This strategy can be improved by applying DWT prior to the polarization analysis. DWT decomposes the three components of the seismogram at different scales. In this way, different seismic phases are separated at different scales. At each scale the signal is de-noised using

the wavelet coefficients prior to the P-phase. Then, the polarization technique is applied at those scales where the S-phase dominates. Results of this algorithm on a large data-set are compared with results based on classical polarization analysis, and show an improvement in performance.

ST5/W/05-B3

1440

**IMPROVING PRECISION OF FREQUENCY-TIME ANALYSIS OF SURFACE WAVES**

Helle PEDERSEN (1)Laboratoire de Geophysique Interne et Tectonophysique, BP 53x, F-38041 Grenoble Cedex, email: Helle.Pedersen@obs.ujf-grenoble.fr Jerome Mars, Pierre-Olivier Amblard (2)Laboratoire des Images et des Signaux, ENSIEG, BP 46, 38402 Saint Martin d'Heres, FRANCE Anne-Lise Bard (1 and 2)

Group velocity dispersion curves of seismic surface waves are either directly inverted to obtain earth models, or used to apply frequency-time ('phase-match') filtering prior to further data processing. Unfortunately, the multiple filter analysis commonly used for the estimation of group velocities is not very precise due to the trade-off of precision between the time and frequency domains. To avoid this problem and to improve the measurement of the group velocities, we suggest to develop from the multiple filter analysis, a treatment based on the temporal and spectral reallocation of the energy map. This process, called reassignment multiple filter analysis, is included in the process of the multiple filter analysis, and reassigns the energy attributed to the centre of a time and frequency window to the gravitational energy centre calculated for the same window. This reallocation that concentrates the energy for the width of the band-pass filters applied, allows us a significant gain in terms of resolution and therefore significantly reduces the uncertainty of the group velocity measurement. We test the method on synthetic seismograms for plane layered models, with and without noise, and we apply the method to improve frequency-time filtering on a data set from the TOR experiment from northern Europe. The method is stable, and makes it possible to significantly improve the signal to noise ratio of fundamental mode Rayleigh waves prior to phase velocity measurements.

ST5/W/12-B3

1500

**AUTOMATIC ASSOCIATION AT THE ISC**

Noureddine BEGHOU, Raymond J Willemann and Dmitry A Storchak, (all at International Seismological Centre, Pipers Lane, Thatcham, Berkshire RG19 4NS, UK, email: nour@isc.ac.uk)

Each year, the ISC receives two million readings from more than 2000 stations and nearly 200,000 preliminary event locations from dozens of agencies. The number of data in the Bulletin has increased many-fold since the ISC began operations, and programs now in use produce at least one misassociation in most events. The common causes for misassociations include readings from unreported events, gross errors in preliminary hypocentres, large lateral velocity variations, and readings with initial phases excluded from the Jeffreys-Bullen tables. Sometimes a reading simply fits the expected arrival time from a small distant earthquake better than the expected time from an approximately located nearby hypocentre.

We plan to change the association process used at the ISC. We want to reduce the number of misassociations, use more data reported to the ISC, be flexible, rank alternative associations, and not associate a reading when no fit is good. We will define misassociations as departures from associations made by ISC seismologists preparing past Bulletins. Additional data to consider include reported associations and phase identifications, reporting patterns (e.g., some stations report readings only from local earthquakes), and measurements such as S-P time, slowness and azimuth. Flexibility will allow us to improve the performance of the association algorithm, for example by changing the weight given to each type of data, perhaps on a station-by-station basis. When a seismologist finds a misassociation, ranked alternatives could be used to suggest other possibilities.

ST5/W/43-B3

1520

**A TEST FOR DISTINGUISHING CONVERTED PHASES FROM UPPER MANTLE DISCONTINUITIES USING COMPONENT COMPOSITION, NON-LINEAR STACKING AND POLARISATION ANALYSIS FOR DATA FROM AN ARRAY OF PORTABLE BROAD BAND INSTRUMENTS**

Huilan Zhou\* and B.L.N. Kennett (Research School of Earth Sciences, Australian National University, GPO Box, Canberra ACT 2601, Australia); \* permanent address: Department of Earth Science, Graduate School at Beijing, University of Science and Technology of China, P.R.China

In this work, we have tried to combine the stacking procedures with other signal enhancement tools with the aim of isolating weak converted arrivals from the upper mantle transitions. As a test, only 6 events and their broadband seismic records at Kimba Array in the Northwestern Australia were used. We introduce the resultant vector U formed by the composition of the R and Z components in R-Z plane, and have then applied the phase weighted stack (PWS) method to these U traces of each event, with comparison to analysis using the R and Z components. The synthetic examination and real data treatment show that the converted phases at U from P to SV or from SV to P at the discontinuities in the upper mantle, such as near 410km and 660km, could be much clearer than at R and Z. From the data analyses, we have had a clear impression that the composite component U is more effective to search the weak phases after non-linear stacking, although this effectiveness is different from data to data, as well as other methods.

The polarization analysis method used to be applied to distinguish the converted phases at single seismic trace. However, this method was combined with linear and non-linear stacking in our work, and a comparison was made between them. The results show that it could become more effective after combined with other procedures. Pre- and post-stack polarization analysis were also tested, and were found which can also help with the identification of weak arrivals. More tests are worth to do.

ST5/W/13-B3

1640

**UTILIZATION OF WAVEFORM CORRELATION IN REAL-TIME SEISMOLOGICAL NETWORK OPERATION**

REYNIR BODVARSSON, Dep. of Earth Sciences, Uppsala University Sigurdur Th. Rognvaldsson, Icelandic Meteorological Office Ragnar Slunga, Dep. of Earth Sciences, Uppsala University Einar Kjartansson, National Energy Authority, Iceland

It is well established that accurate measurements of the arrival time difference between similar earthquakes can be used to constrain the relative locations of the earthquakes. The arrival time differences are measured through cross-correlation of the similar seismograms. This method is used routinely in the South Iceland Lowland (SIL) seismic network to accurately map active subsurface faults. Based on the positive results of the correlation techniques used in the relative location algorithm a new approach is being taken regarding the automatic operation of the SIL network. Experience shows that a substantial fraction of the events occurring within a given area belongs to a few clusters or families of earthquakes,

characterized by highly similar waveforms. The cross correlation of seismograms at individual stations can be used to identify such clusters. We are currently working on a method for using cross correlation of neighboring events to automatically determine the onsets of P and S waves with accuracy comparable to or better than achieved in the interactive analysis. The aim is to reduce the need for manual inspection of seismograms from local and regional earthquakes and to improve the quality of the readings in the icro earthquake database. The objective is to create a Geographically Indexed Database (GID) where different classes of earthquakes will be stored. When creating the GID, each event within a given cell is correlated with all other earthquakes in the cell. The results of the correlation are used to group the earthquakes into classes. A few events of each class are stored in the GID. As new earthquakes are recorded by the network, the system automatically looks for similar waveforms in the GID and if found takes the onset picks from there. For events not found in the GID the onsets are estimated through interactive analysis.

ST5/W/18-B3

1700

#### NEAR-REAL-TIME AND AUTOMATED ESTIMATION OF SOURCE PROCESS USING TELESEISMIC P-WAVE

Yoshiko YAMANAKA and Masayuki Kikuchi (both at Earthquake Research Institute, University of Tokyo, Tokyo 113-0032, Japan, e-mail: sanchu@eri.u-tokyo.ac.jp)

Recently we can get CMT solutions within several hours after earthquakes via E-mail or WWW. Some of these solutions are determined automatically using the long-period surface and body wave data of the global broadband seismograph network. From the viewpoint of disaster mitigation, we need more detailed and earlier information.

For this we have developed automated analysis system to obtain the information such as the direction and duration of rupture propagation. Our analysis is based on Kikuchi and Kanamori (1991) to use teleseismic broadband body waves filtered 0.5-250sec. We assume a triangular source time function, whose pulse width,  $t$ , is calculated from QED magnitude with the help of an empirical relation between  $M$  and  $t$ .

As compared with the long-period surface wave analysis, uncertainty of arrival time with even a few seconds results in timing error causes a serious change in the solution. It is also important to check the quality of used waveform data automatically. We attempt to resolve these difficulties to obtain more reliable information about the direction of rupture propagation. Currently we aim to determine the above source parameters automatically within half an hour for large events occurred in Japan.

ST5/E/24-B3

1720

#### WAVEFORM INVERSION VIA ENSEMBLE INFERENCE

Malcolm Sambridge (Research School of Earth Sciences, Australian National University, Canberra ACT 0200, Australia; email: malcolm@rse.anu.edu.au)

Over the past decade the availability of digital broad band seismic data has led to extensive use of body and surface waveforms to constrain earth structure. Inversion methods have been developed and applied to a wide range of problems, from the 1m - 1km distance scales of reflection and refraction studies, to regional and global studies using surface and body waveforms. In most cases the objective is to find a single earth model, which provides the best fit to the observations, and from this make inferences on earth structure.

In this work an alternative approach is examined where inferences are based on an ensemble of seismic earth models, with a range of data fits. The inverse problem then falls into two parts (1) generate an ensemble of earth models which preferentially sample regions of model space with high data fit. (2) draw quantitative inferences on the earth from this ensemble. A new Monte Carlo algorithm is presented which can be used for both stages of the problem. The algorithm will be illustrated with an application to the inversion of crustal receiver functions. With the new approach all earth models contribute to the information measures retrieved from the data. In some cases models which fit the observations poorly may tell us just as much as those that fit it well.

ST5/W/38-B3

1740

#### FINITE DIFFERENCE MODELING OF PATH EFFECTS IN WESTERN CHINA

L. E. JONES and C. R. Bradley, Geoanalysis, MS-F665 Los Alamos National Laboratory, Los Alamos, NM 87545, USA

Robust velocity models are imperative for full- waveform modeling of structure and for determination of source mechanism and depth. While a carefully determined one-dimensional model may be adequate on a local to regional scale and at longer periods, complexity introduced by lateral heterogeneity may require two or three- dimensional modeling. Surface waves are often the only phases recorded for small magnitude events at regional distances, since they are, in general, much larger in amplitude than body waves. Thus, for moderately-sized ( $M_b$  4.5-5.5) earthquakes in the Lop Nor region (China) we obtain near-regional to regional distance group velocity measurements and use these to construct a family of simple one- dimensional velocity structures for crustal, lithospheric and uppermost mantle structure in Western China and Tibet, for stations AAK, MAK, LSA and LZH. The initial models are determined either via forward modeling of group velocities, or by inversion of combined group and phase velocity measurements. We then test the validity of the one-dimensional models by full waveform (forward) modeling and comparison to data. Results obtained from dispersion measurements are thus incorporated into existing models for full- waveform [Finite Difference] modeling, and used as initial models for iterative forward modeling. We then compare results from these simple one- dimensional models with two-dimensional composite models incorporating basin structure and moho topography into the original one-dimensional velocity structures.

Thursday 29 July AM

Presiding Chair: Dr. Seiji Tsuboi, (Department of Geoscience National Defense Academy, Yokosuka, Japan)  
Concurrent Poster Session

#### SEISMOLOGICAL OBSERVATION AND INTERPRETATION: THEORY

ST5/W/24-B4

0930

#### ENVELOPE BROADENING OF OUTGOING WAVES IN RANDOM MEDIA: A COMPARISON BETWEEN THE MARKOV APPROXIMATION AND THE FINITE DIFFERENCE SIMULATION IN 2D

Haruo SATO (Dept. of Geophysics, Graduate School of Science, Tohoku University, Aoba-ku, Sendai-shi, 980-8578, Japan, email: sato@zisin.geophys.tohoku.ac.jp) Mike Fehler (Los Alamos National Laboratory, Los Alamos, New Mexico, USA, email: fehler@mukthinath.lanl.gov)

The envelope broadening of seismic waves after traveling a long distance is one of the most prominent pieces of evidence for the existence of random heterogeneity in the earth medium. It can be interpreted to be a result of multiple forward scattering of waves. By using the Markov approximation for the parabolic wave equation, Sato [1989] directly simulated the envelope and quantitatively explained the observed envelope broadening. However, his model was applicable only for plane-wave propagation. Here, we introduce a method for the direct simulation of envelopes of outgoing waves radiated from a point source in a random media in 3D according to Shishov [1974], and extend it to 2D. The resultant envelope is broadened and the maximum amplitude decreases with the reciprocal of travel distance times the amount attributed to simple geometrical spreading. For the evaluation of this simulation, we compare the envelope derived with waveforms that are numerically simulated by the finite difference method in 2D. There is a good coincidence between them around the maximum peak. But the coda level of the finite difference method is a little larger than that of the Markov approximation since the large angle scattering is accurately modeled only in the finite difference method. We may use the envelope broadening as a quantitative measure of randomness from forward scattering, where we note the coda excitation is a measure of back-scattering strength.

ST5/W/25-B4

0950

#### THE 'GAP' BETWEEN SEISMIC RAY THEORY AND 'FULL' WAVEFIELD EXTRAPOLATION

C. J. THOMSON, Geological Sciences, Queen's University, Kingston, ON K7L 3N6, Canada. 613-533 6178, email: thomson@geol.queensu.ca

A new derivation is given of the factorization of the anisotropic, elastic body-wave equation into two operators which are 1st-order wrt to a preferred direction of propagation. The solution to one of these gives the waves propagating in the forward direction. A 3 by 3 matrix notation is used which emphasizes the role of the Christoffel equation (or what might be called its "projection" onto the preferred direction) familiar from ray theory. To see this it helps first to obtain an exact factorization of the wave equation for homogeneous elastic media. When inhomogeneities exist it is necessary to use a Fourier representation for differential operators wrt the transverse coordinates, but still the Christoffel equation is the key. The so-called "square root operator" required in the factorization becomes more correctly the "root of an operator quadratic equation" intimately connected to the Christoffel equation. The factorization does not assume narrow-angle propagation or involve an a priori reference phase. It includes the P and two S waves and forward coupling between them. It remains valid at slowness-surface singularities (e.g. conical points, a.k.a. acoustic axes --- a most stringent test) and for folded wavefronts.

The one-way equation can be solved "analytically" by using "Path Integrals". These in turn may be reduced by stationary-phase arguments to standard ray theory, Maslov theory and Kirchhoff representations. In this sense the "gap" between ray theory and the numerical solution of the full wave equation is bridged or filled out.

Alternatively, the one-way pseudodifferential wave equation can be solved by numerical "forward-stepping" algorithms and here again a number of choices are available. Some of these are intimately related to (in fact, effectively reduce to) the "phase screen" approach of Wu and others.

ST5/W/47-B4

1010

#### SYNTHETIC SEISMOGRAMS IN COMPLEX CRUSTAL WAVEGUIDES WITH SURFACE TOPOGRAPHY USING HALF-SPACE SCREEN PROPAGATORS

Ru-Shan WU and Xiao-Bi Xie (both at Institute of Tectonics, Univ. of California, Santa Cruz, CA 95064, USA, email: wrs@es.ucsc.edu, xie@es.ucsc.edu)

The half-space GSP (generalized screen propagator) is a variation of GSP with free surface taken into the formulation. The method is based on the one-way wave equation theory and has a fast dual-domain implementation. The GSP method is several orders of magnitude faster than finite-difference methods with a similar accuracy for certain problems. It has been used for the simulation of wave propagation for high-frequency waves (1 - 20 Hz) to a regional distance (greater than 1000 km). In this study, we extend the GSP method by incorporating a coordinate transform into the method for the surface topography problems. Comparison with other methods, such as the boundary element method, through numerical simulations showed that the extended method worked well for mild topographies. Accuracy improvement for rough topography has been also discussed. Numerical simulations have been conducted for various crustal waveguide structures, including both deterministic structures and small-scale random heterogeneities and random rough surfaces. Influence of random heterogeneities and rough surfaces on Lg amplitude attenuation and Lg coda formation are shown to be significant.

ST5/E/29-B4

1030

#### FREQUENCY DEPENDENT SEISMIC Q IN FRAGMENTED CRUST: SCALING ABSORPTION BY SQUEEZE-FLOW FROM MICRO TO MACRO SCALE

Pierre ROULEAU (Department of Physics, Sir Wilfred Grenfell College, Memorial University of Newfoundland, NF, CANADA, A2H 6P9, email: prouleau@beothuk.swgc.mun.ca)

Preferentially localised squeeze-flow of interstitial viscous fluid in rock samples produces significant frequency-dependent absorption of elastic energy in the kHz range. When transposed to the pore space of natural rough-walled fractures, this microscopic absorption mechanism can produce significant, frequency-dependent absorption in the crustal seismic band (i. e. 0.08 to 20 Hz). In the modelling which yields this result, the dimensions of absorption loci are constrained by the critical slip distance of seismic faulting and by crustal permeability estimates from reservoir induced seismicity observations. A characteristic absorption locus is idealised by a narrow gap of cylindrical shape surrounded by a deformable permeable ring, which leads to analytical solutions of the squeeze-flow governing equation in terms of a complex stiffness. The real and imaginary parts of this micromechanical stiffness form the basis for defining a macroscopic quality factor, appropriate for a fractured medium modelled as a tight packing of randomly ordered spheres whose surfaces are rough (fractal) and lubricated. For given thermodynamic conditions, upward scaling of the microscopic absorption requires estimating: 1) the macroscopic stiffnesses of rough fractures (normal and tangential); 2) the microscopic (ring) and macroscopic (crustal) porosity and permeability; and 3) packing parameters (coordination number and fragment dimensions), all of which can be inferred from field-based geological and geophysical observations. Macroscopic Q results for a generic crustal model composed of fractured layers show that in-situ absorption by squeeze-flow can be significant, with peak values remaining well within the crustal seismic band down to midcrustal depths.

ST5/W/08-B4

1145

#### WAVE SCATTERING ON FLUCTUATIONS OF ELASTIC CONSTANTS AND DENSITIES

Evgeni M. CHESNOKOV, Yuri A. Kukhareenko (both at the Institute of Physics of the Earth, Russian Academy of Sciences, email: e.chesnokov@ucl.ac.uk, echesn@uipe-ras.scgis.ru), John Quenn (Conoco



Inc., Seismic Imaging Technology Center, 1000 S.Pine, P.O.Box 1267, 4487 RW, Ponca City, OK - 74602-1267, USA) and Peter Yu. Kukharenko (at the Institute of Physics of the Earth, Russian Academy of Sciences, email: e.chesnokov@ucl.ac.uk, echesn@uipe-ras.scgis.ru)

The fluctuating wavefields generated by scattering of elastic waves from randomly distributed inhomogeneities arising from fluctuations of elastic constants and densities is investigated. The average dynamic Green function and scattering cross section are calculated using a Feynman diagram technique. A relation between the scattering cross section and the spatial correlation functions of densities and elastic constants is obtained. The scattering cross section is calculated without any assumptions on the size of the inhomogeneities relative to the wavelength. The cases of random and correlated spatial locations of inclusions are considered. The dependence of scattering cross section on inclusion shape, correlation radius, and wavelength are investigated. Limited cases are studied analytically, while general cases are studied numerically.

**ST5/E/01-B4****1205****LONG WAVE IN AN ARBITRARY IRREGULAR MULTI-LAYERED MEDIUM (2)**

Xiaofei CHEN (Department of Geophysics, Peking University, Beijing 100871, P.R.China, email: xfchen@pku.edu.cn)

The classic theory of seismic surface waves was established upon the laterally homogeneous earth model. However, the laterally homogeneous model is only an approximate and idealized medium model. In many actual problems, the lateral heterogeneity of media cannot be ignored, thus new theories for surface waves in laterally heterogeneous medium is needed. So far, the most of theories for seismic surface waves in laterally heterogeneous medium is established upon the hypothesis of "localization", i.e. the classic surface theory can be applied to each local "quasi 1-D" (quasi-stratified medium) structure by ignoring the interactions among different normal modes. Obviously, this hypothesis is appropriate for weak lateral variation and it is questionable for strong lateral heterogeneity. However, there is little study to devote systematically discussing the appropriateness of such hypothesis. As presented in part 1 of this series study we have derived an analytic theory of Love in an irregular multi-layered medium by using the global generalized reflection/transmission matrix method without making "localization" hypothesis. As the part 2 of this series study, we shall use this accurate theory of Love in an arbitrarily irregular multi-layered medium to investigate the appropriateness of "localization" in laterally heterogeneous medium. According to our preliminary study, we find that "localization" hypothesis is generally applicable at lower frequency case or weaker lateral variation of the medium, and it is inappropriate for higher frequency case or stronger lateral variation.

**ST5/W/11-B4****1225****CAUSAL CONSTRAINT ON THE SCATTERING ATTENUATION IN ACOUSTIC RANDOM MEDIA**

Jun KAWAHARA (Department of Environmental Sciences, Ibaraki University, Mito 310-8512, Japan, email: joker@mito.ipc.ibaraki.ac.jp)

The observed nature of seismic attenuation is successfully explained by a well-known theory of scattering attenuation established by Wu (1982) and Sato (1982). The theory deals with the scattering in randomly inhomogeneous media based on the Born approximation, neglecting multiple scattering as well as diffraction. The key is to eliminate the contribution of forward scattering within a cutoff scattering angle (CSA) (or equivalently, to correct the travel-time fluctuations caused by long-scale velocity fluctuations) when evaluating the scattering attenuation. This is essential to avoid the overestimation of attenuation at high frequencies. However, the value of the CSA is not objectively determined in the theory. Although several researchers evaluated the CSA by numerical and laboratory experiments, their results disagreed with each other's. Hence the choice of the CSA remained unsolved until recently. In this study, we investigate the constraint by causality on the choice of the CSA in cases of acoustic random media. The densities are assumed to be constant for simplicity. Based on the Kramers-Kronig relation, we derive simple relations among the phase velocities in the high- and low-frequency limits and the CSA, in both three- and two-dimensional cases. After some consideration on the phase velocities, we further show that the CSA is uniquely determined as 60 (about 65) degrees in three- (two-) dimensional cases. It is surprising that these values are independent of the types of inhomogeneity.

**Thursday 29 July PM**

Presiding Chair: Dr. Gary Gibson, RMIT University, Victoria, Australia  
Concurrent Poster Session

**SEISMOLOGICAL OBSERVATION AND INTERPRETATION EARTHQUAKES****ST5/W/15-B4****1400****SEISMIC PARAMETERS OF STRONG EARTHQUAKES IN BULGARIA AND SPAIN FROM HISTORICAL SEISMOGRAMS**

S.Dineva, D.Mihaylov (both at Geophysical Institute, BAS, Acad. G. Bonchev Str. bl.3, 1113 Sofia, Bulgaria. Email: dgm-sid@geophys.bas.bg) J.BATLLO (Escuela Universitaria de Ciencias Empresariales Dr. Manyà, E-43500 Tortosa, Spain. Email: jbo@tinet.fut.es), T. van Eck (Seismological Division, KNMI, PO Box 201, 3730 AE De Bilt, Netherlands. Email: vaneck@knmi.nl).

All available instrumental data about earthquakes within the territory of Bulgaria and Spain with magnitude larger than 6 from 1904 to 1928 have been collected and analysed. This data include - arrival times and amplitudes from station- and international- bulletins and historical seismograms from the whole world.

New hypocenter locations and magnitude estimations are obtained on the basis of collected arrival times and amplitudes from the bulletins and seismogram readings. The seismograms are digitised and are corrected for the curvature and for the instrument response. The estimated ground motion records are used to obtain spectra of P and S waves and determination of the seismic moment and Mw.

The obtained results are useful for seismic hazard estimations and seismotectonic interpretations in both countries.

**ST5/E/11-B4****1420****THE SPACIAL EVOLUTION OF SEISMIC SERIES IN THE BETIC RANGE**

Daniel Stich, Gerardo Alguacil (Instituto Andaluz de Geofísica, Universidad de Granada, Spain, email: daniel@iag.ugr.es)

One characteristic of the seismic activity in the Betic Range (Andalucía, Spain) is the spatial

and temporal clustering of the vast majority of events. Subject of this research is especially an area on the coast around the towns of Adra and Berja. In Dec. 23, 1993 an earthquake of magnitude 5.0 occurred there and, eleven days later, there was a second earthquake of the same magnitude with epicentre some 20 km apart. Both main shocks were followed by high seismic activity in the area, apparently as two series, spatially separated and close to the main shock locations. Increased activity continued, including further maxima in 1995 and 1996. Altogether, our local network has recorded more than 700 events in the area.

The clustering of events results in the occurrence of similar earthquakes. Similarity is quantified as the maximum cross-correlation value of wave-arrivals of two events. Using this criterion, we detect groups of similar events among our data. For events of sufficient similarity, the interpolated time shift of the cross-correlation maximum, just as well as the slope of the cross-spectrum phase, indicate the time difference of the arrivals. From the relative delay times at various stations, high-precision relative hypocenter locations of the similar events are calculated. Several authors have described these techniques during the recent years. By applying to our data, we want to obtain information on the location, shape and behaviour of the active fault zones, using the spatial distribution of the relocated events as well as the clustering properties and the temporal development of the seismicity. The extensions and potential connections of the seismic zones touch seismic hazard estimation, the area has been affected by destructive historical earthquakes, the last one (Magnitude 6.4) in 1910.

**ST 5/E/04-B4****1440****NOVEMBER 6TH 1990, FORK (DARAB-IRAN) EARTHQUAKE**

M. RAEESSI (Geophysics Institute, Univ. Of Tehran, Tehran, Iran. email: mraeesi@iman.ut.ac.ir) M. R. Gheitanchi and Z. Zariifi (Raeesi) (Both at the above address, email: mrghchee@chamran.ut.ac.ir and zariifi@iman.ut.ac.ir) and A. Zamani (Dept. of Geology, Shiraz Univ., Shiraz, Iran.)

Southeastern part of Zagros continent-continent collision zone is the most active part of this seismogenic belt. On Nov. 6th 1990 at 18:45:53 GMT a destructive earthquake (Ms 6.9) shook Fork region in this part of Zagros. Twenty-two victims, 100 injuries, 300 buildings with total destruction and 2000 structures with partial damage resulted from this event. A reverse surface rupture about 15.1km in length, 273 degrees in azimuth and dipping toward north, two collapse structures and several landslides accompanied the quake. The greater collapse structure is 60m in diameter and 80m in depth. What discriminates this event from thousands recorded-earthquakes in Zagros seismic belt, is the occurrence of surface rupture. There have been only three earthquakes with reported surface rupture inside and along the limits of Zagros belt before the happening of Fork event. The one inside the belt (July 2nd 1972, 12:56:06, mb 5.4) has a normal fault, while the other two quakes (23 Jan. 1909, 02:48:18, M 7.4 and 16 Aug. 1958, 19:13:43, M 6.6) at northern contact of the belt with neighboring zone have thrust faults with strike-slip components. Then it can be said that the Fork earthquake has the first reported reverse surface rupture inside Zagros belt. Zagros is a sequence of folded marginal sediments with thickness about 12-15km and rarely 18km. About 6 to 7km of these, are competent sediments which are surrounded by incompetent layers. Lower incompetent layer is highly plastic and has a thickness about 1000m and plays a very important role in tectonics of Zagros, especially in separating sedimentary cover from bedrock which prevents from reaching of bedrock breaks to earth surface. Causes of reaching the rupture of Fork quake to surface and seismological aspects of the event with especial concern to aftershock distribution and waveform modeling are discussed.

**ST5/E/16-B4****1500****DETERMINATION OF SOURCE PARAMETERS OF 1940'S DESTRUCTIVE EARTHQUAKES IN JAPAN USING SMOKED PAPER SEISMOGRAMS**

Masayuki KIKUCHI (Earthquake Research Institute, University of Tokyo, Tokyo 113-0032 Japan, email: kikuchi@eri.u-tokyo.ac.jp), Misao Nakamura (NGP, Tokyo 143-0027 Japan, email: misao@ba2.so-net.or.jp) Makoto Yamada (Waseda University, Tokyo 162-0044 Japan, email: yamadamk@mn.waseda.ac.jp)

In 1940's there occurred several destructive earthquakes in western Japan. Seismograms in this period were usually recorded on smoked paper. Owing to the recent development of photocopy and image processing techniques, we can reconstruct feasible waveform data by tracing, digitizing, and correcting the arc effect due to inclined lever. In the waveform inversion we consider the uncertainty of instrumental constants (pendulum period, magnification and damping constant), timing, and chart speed. Thus we allow a certain deviation of these constants from the face values given in literatures, and determine the source parameters in the least-squares manner.

So far examined are the Fukui earthquake (M 7.1) of June 28, 1948, and the Tonankai earthquake (M 7.9) of December 7, 1944. We used low gain strong motion data at several observatories of Japan Meteorological Agency, with epicentral distance shorter than about 150 km. In both earthquakes a few subevents were identified including a small introductory rupture with a source duration of several seconds. Another destructive earthquake: the Mikawa earthquake (M 6.8) of January 13, 1945 is also being examined.

**ST 5/E/37-B4****1520****AN INVERSION TECHNIQUE FOR THE TEMPO-SPATIAL DISTRIBUTION OF SLIP ON THE FAULT PLANE AND ITS APPLICATION TO THREE RECENT LARGE EARTHQUAKES IN QINGHAI-XIZANG (TIBETAN) PLATEAU OF CHINA**

Li-sheng XU and Yun-tai Chen (both at Institute of Geophysics, China Seismological Bureau, Beijing 100081, People's Republic of China; email: chenyt@public.bta.net.cn)

A time domain inversion technique is developed to invert the azimuth dependent source time function (STF) for the tempo-spatial distribution of slip on the fault plane. In this technique we begin by using the moment tensor inversion technique to invert for the focal mechanism of the earthquake. Then we use the de-convolution technique to retrieve the azimuth dependent STF. Finally we translate the azimuth dependence of the STFs of the earthquake into the tempo-spatial pattern of the slip distribution on the fault plane. To stabilize the inversion an inequality constraint that no reverse slip occur, is imposed. Using the data from the China Digital Seismograph Network (CDSN), this technique is applied to study the source processes of recent large earthquakes occurred in the Qinghai-Xizang (Tibetan) plateau of China. Among these earthquakes are the April 26, 1990 Gonghe Ms=6.9, the February 3, 1996 Ms=7.0 and the November 8, 1997 Mani MS=7.9 earthquakes. It is demonstrated that the inversion technique is efficient in retrieving the tempo-spatial complexities of earthquake rupture process, even in the case that the available data only come from a few stations.

**ST5/W/31-B4****1640****FULL MOMENT TENSOR RETRIEVAL FROM WAVEFORM INVERSION: AN APPLICATION TO THE BOVEC EVENT (SLOVENIA) AND ITS SWARM**

Stefano KRAVANJA, Giovanni Costa (Dipartimento di Scienze della Terra, Università degli Studi di Trieste, via E. Weiss 4, 34142 Trieste, Italy) Giuliano Francesco Panza, Peter Suhadolc (Dipartimento

di Scienze della Terra, Università degli Studi di Trieste, via E. Weiss 4, 34142 Trieste, Italy and International Centre for Theoretical Physics, SAND Group, Miramare, 34100 Trieste, Italy)

The destructive event occurred in Slovenia on April 12, 1998 and the swarm associated to the main event has been studied by applying the waveform inversion algorithm developed by Sileny et al (1992). The algorithm is a two-step procedure; the first step is the waveform inversion for moment tensor rate functions retrieval; the second step is the factorization of the moment tensor rate functions to obtain a moment tensor and a source time function for total, deviatoric and volumetric components. Using only the waveforms recorded by the Friuli accelerometric network, operated by the Department of Earth Sciences of the University of Trieste, for the main shock we get a source mechanism in agreement with the CMT solution retrieved by Harvard and a smooth source time function. The processed aftershocks have their fault plane solutions characterized by a nodal plane oriented NW-SE, in agreement with the fault plane of the main shock.

References: Sileny J., Panza G.F., Campus P., 1992. Waveform inversion for point source moment tensor retrieval with variable hypocentral depth and structural model. *Geophys. J. Int.*, 109, 259-274.

ST5/E/22-B4

1700

#### VARIATIONS IN WORLD SEISMICITY: REAL OR IMAGINARY?

A. Douglas (1), J. B. YOUNG (2), M. A. Chinnery (3), email: alan@blacknest.gov.uk (1 and 2) AWE Blacknest, Brimpton, Reading, RG7 4RS, UK (3) NGDC, NOAA, Boulder, USA. (Retired)

Studies of earthquakes with magnitudes over mb 5.0 reported by the International Seismological Centre (ISC) show an apparent variation in world seismicity occurring over the 33 year period 1964 - 1996. Part of this variation appears to be roughly periodic. Initial thoughts suggested links to the solar cycle and sun-spots or to meteorological effects such as El Nino. However, studies using maximum-likelihood methods to recompute magnitudes show that the network of stations used has a far greater effect than any geophysical agents. The ISC has no fixed station network for computing magnitudes and contributing stations can change month by month. For example, it can be shown that an increase in the number of contributing stations actually decreases the number of earthquakes over mb 5.0. By using maximum likelihood methods to re-compute magnitudes with a fixed network of stations which report to the ISC it is shown there is little variation with time in world seismicity.

ST5/P/04-B4

1720

#### SOME ASPECTS OF SEISMOLOGICAL STUDIES OF JABALPUR EARTHQUAKE 1997 THROUGH GSN BROAD BAND DATA

H.N. SRIVASTAVA (India Meteorological Department, New Delhi-110003, India, e-mail: snb@imd.ernet.in)

Jabalpur earthquake of magnitude 6.1 on 22 May, 1997, caused the loss of about 45 human lives and major damage to property in the city and neighbouring regions.

The focal depth of the main earthquake was reported as about 30 km. through a depth phase from GSN data by India Meteorological Department and other agencies. However, Sg phases identified on seismograms suggest that the focal depth of the earthquake could be shallower than 30 km as the crustal structure close to Jabalpur based on deep seismic sounding explosion data showed the thickness of granitic layer as 20 km. only.

Based on synthetic seismograms using Broad band GSN long period data, the best crustal velocity giving least errors was seen to fit with a Pn velocity of 7.9 km/sec. This is in contrast with the local crustal velocity model based on deep seismic sounding explosion data wherein Pn velocity was found to be 8.1 km/sec. The results suggest the need for developing improved methodology for utilisation of broad band seismological data.

ST5/E/38-B4

1740

#### ON THE GLOBAL COMPONENT IN THE SEISMIC ACTIVITY AND ITS CONNECTION WITH OBSERVED PECULIARITIES ON THE EARTH'S SPIN

Alexey Fridman (Institute of Astronomy, Russian Academy of Sciences, 10917, Moscow, Pjatsnikskaja ulitsa, 48, Email: flexa@glas.apc.org), Nikolay Gorkavyy (The Crimea Astrophysical Observatory: email: gorkav@catpeak.crimea.ua) Yuri. TRAPEZNIKOV (International Research Center - Geodynamic Proving Ground in Bishkek, email: tua@laurel.gdirc.ru)

Analysis of the data from the catalog of the National Earthquake Information Center (1964-1988) U.S. Geological Survey shows the possibility to identify three components in the seismic activity of the Earth: (1) the global, or T component, which is a general feature for all the hemispheres and large regions of the Earth's globe; (2) the mirror symmetrical, or M component for the submeridional and sublatitudinal seismogenerating structures which is characterized by reducing activity in the first at the time when seismicity in the second is intensified (and vice versa). This is particular clearly showed within the Pacific Ocean region; and (3) the linear, or R component, characterized by a durable drop or, conversely, growth of seismic activity. Using also the Morrison's year-mean data on the variations in the Earth's spin, we prove the connection of the global component of the seismic process with observed peculiarities in the Earth's spin. We calculated the coefficients of correlation of the Earth's angular speed  $W(t)$  and the modulus of its time derivative  $|dW(t)/dt|$  with the earthquake number  $N(t)$ . These correlations depend qualitatively on the value of magnitude. The correlation coefficient between  $N(t)$  and  $W(t)$  is great for earthquakes with  $M > 4.0$ , but its value systematically decreases with increasing magnitude. The correlation between  $N(t)$  and  $W(t)$  entirely absent for Earth quakes with  $M > 5.5$ . An opposite dependence is demonstrated by the correlation between  $N(t)$  and  $|dW(t)/dt|$ . There is no correlation for earthquakes of  $M > 4.0$ , but the correlation coefficient systematically increases with magnitude and reaches a significant value at  $M > 5.5$ . Also the analysis of changing these correlation coefficients depending on the depth distribution of hypocenters of earthquakes was carried out. Spreading and subduction zones were studied specially. Furthermore, a high value of the coefficient of correlation between  $N(t)$  and  $|dW(t)/dt|$  was found on averaging the two graphs over several years and shifting the graph  $N(t)$  to the past time. The latter fact may be indicative of change in the Earth's angular velocity as one of the causes of increasing seismic activity or the both things are connected with some third cause.

## SEISMOLOGICAL OBSERVATION AND INTERPRETATION: APPLICATIONS

ST5/E/35-B5

0830

#### ANISOTROPY STUDY IN THE GULF OF CORINTH (GREECE) USING MICROEARTHQUAKES RECORDED BY THE CORNET NETWORK

P. Papadimitriou, G. Kaviris and K. Makropoulos (all at Department of Geophysics, University of Athens, 157 84 Athens, Greece, email: ppapadim@cc.uoa.gr)

The analysis of local earthquakes recorded by the Cornet network and located in the Gulf of Corinth (Greece) has revealed the existence of shear-wave splitting. The visual inspection technique is used to estimate the polarization direction of the fast shear wave and the time delay between the two split shear waves. The selected earthquakes are located close to one of the Cornet stations. Most of these earthquakes are recorded by only one station and their azimuth and angle of incidence are estimated using the covariance matrix decomposition method combined with the P-wave polarization direction. Polarigrams plotted for the horizontal components present a clear linear and almost constant polarization for each station, independent of the azimuth of the earthquake, except for one station where different Sfast polarization directions are observed. The mean direction of the fast shear wave polarization at Paradeisi station is N146°, at Sofiko station N104° and at Villia station N142°. At Desfina station two different main Sfast polarization directions were observed, one N143° and the other N55°. The calculated time delays between the two split shear waves are higher for the stations located in the eastern part of the Gulf. Comparing the mean Sfast polarization direction with the direction of local faulting, we observe that they are approximately parallel at Sofiko station, while at Villia station they are almost perpendicular. In general, the obtained mean Sfast polarization directions at the CORNET stations are perpendicular to the direction of the extension of the Gulf which is NNE-SSW and consistent with the extensive dilatancy anisotropy model.

ST5/E/32-B5

0850

#### STUDY ON MANTLE DISCONTINUITIES USING THE P-SV CONVERTED PHASES

Shaonian ZANG and Yuanze Zhou (both at Department of Geophysics, Peking University, Beijing 100871, China, email: sxzang@ibmstone.pku.edu.cn, zyz@www.geophy.pku.edu.cn) Y. L. Chen (Department of geological sciences, University of South California, U.S.A.)

The discontinuities were studied using P-SV converted phases. The earthquake, which were recorded at CN2, YNB, BNX, NZN, MIH, MDJ and HIA stations, with epicenter distances from 40 to 90 km were selected to study the discontinuities. The records are different in the eight stations. The records are digital and broadband recording in MDJ and HIA, optical analog recording (by SK instrument) and mechanical analog recording (by DK-1 instrument) in CN2 and YNB, mechanical analog recording (by DK-1) in BNX, YLN, NZN and MIH. The analog records were digitized and selected. Both the analog and digital data in MDJ station were used for comparison of the two kinds of data. Both optical and mechanical analog data in CN2 and YNB stations were also used. The method for picking out the P-SV converted phases was studied. The filter of rectilinearity, direction analysis and phase comparison were applied to determine the P-SV converted phases. The discontinuities near the depth of 520 km and 660 km were found by the different kinds of records. There are two things needed to mention from the results. Firstly, it was found that the analog records, even the mechanical analog records can be used to study the discontinuities.

Secondly, the discontinuities are not as simple as single interface, they may have certain structure and there may be some anomalous bodies in different depth between the discontinuities.

ST5/W/39-B5

0910

#### AN EXAMINATION OF LINEAR AND NON-LINEAR EARTHQUAKE LOCATIONS USING SYNTHETIC TRAVEL TIMES FROM A 3D MODEL

Anthony LOMAX and Jean Virieux (both at Géosciences-Azur, Universitèy of Nice - Sophia Antipolis, 250 Rue Albert Einstein, 06560 Valbonne, France, email: lomax@faillie.unice.fr) Philippe Volant and Catherine Berge-Thierry (both at IPSN, BP6 92265 Fontenay-aux-Roses, France)

We generate synthetic P and S travel-times in a 3D velocity model for known sources at various depths on a vertical plane passing through a station network with the geometry of the IPSN-Durance micro-seismic network in southern France. With these times we "locate" the sources using non-linear grid and Metropolis-Gibbs searches (valid in 3D models) to obtain a probability density function and equivalent Gaussian uncertainty statistics, and we use the linear method Hypoellipse (Lahr, 1989; valid for layered models) to obtain hypocentres and associated Gaussian uncertainties. We also obtain estimates of the known focal mechanisms using synthetic P wave first motions. To validate the non-linear algorithms and to study a near ideal, but unrealizable location scenario, we examine the locations and uncertainties obtained from the 3D synthetic times using the correct 3D velocity model.

To investigate a more realistic location scenario, we use the 3D travel times with added station static shifts, and locate with a 1D layered model. We compare the locations, uncertainties, and focal mechanisms obtained with the linear and non-linear location methods. We find that with both methods the locations can be strongly biased with respect to the "true" locations of the known sources. For events inside of the network, the linear and non-linear locations and uncertainties are similar, but they can differ significantly (particularly in depth) outside of the network. These differences reflect the limitations of linear inversion in the presence of irregular, highly non-gaussian location uncertainties.

ST5/W/46-B5

0930

#### REASONS FOR PIDC MISLOCATIONS: A VIEW FROM THE ISC

DMITRY A STORCHAK (International Seismological Centre, Pipers lane, Thatcham, Berkshire, RG19 4NS, UK, email: dmitry@isc.ac.uk)

The prototype IDC (Arlington, USA) provides a rapid first determination of seismic events to aid in the swift identification of suspected non-natural events and publishes the Revised Event Bulletin (REB). The REB is also of great value to non-explosion seismology, including its contribution to the ISC Bulletin. Although the pIDC network was incomplete, discrepancies between ISC and REB locations provide insight into the utility of data from the higher density of stations reporting to the ISC.

Nearly two years of the ISC Bulletin are now available for comparison with the REB. Differences greater than 1 degree are rare. They occur most often when an REB epicentre is supported by only a few stations in a limited azimuth range. Another common cause of large

discrepancies is identification of depth phases as primary waves in the REB, resulting in phantom events quickly following some deep earthquakes. Both of these problems could be excluded based on a careful selection from the REB alone. Another cause of discrepancies is REB locations computed from phases that additional data available to the ISC show to come from two different origins. Mislocations of this type might be especially difficult to spot based on even the most careful review of REB data alone.

**ST5/W/48-B5****0950****HYOSAT - AN SEISMIC EVENT LOCATION PROGRAM**

Johannes Schweitzer (NORSAR, P.O.Box 51, N-2007 Kjeller, Norway)

Since summer 1996 a program package to locate seismic sources was developed that attempts to use as much of the available information as possible to invert the parameters of the hypocenter. The following input parameters are used: travel times, travel-time differences between different phases observed at the same station, backazimuth, and ray parameter. The weighting of all input parameters follows the observed standard deviations and the inversion is done with a generalized matrix inversion code. All partial derivatives are internally recalculated for each iteration. A starting solution with 'a priori' uncertainties can be given or calculated as the intersection of all backazimuth observations. If S observations are available, a source time is estimated using the Wadati formula. Observations of all seismic phases as defined in the IASP91 software can be used for the inversion. Implemented global Earth models are Jeffreys-Bullen, PREM, IASP91, SP6 and AK135. In addition, self defined horizontally layered local or regional models, or the crustal structure of Mooney et al. (1998), can be used to localize seismic events. The observed travel times are corrected for the ellipticity of the Earth, and corrections for the elevation of the seismic stations are calculated using the local P and S velocities below the stations. The global crustal model can also be used to correct reflections at the Earth's surface (e.g. pP, sP, PP, SS, P'P') at their reflection points.

The program package can be copied via anonymous ftp from ftp.norsar.no under /pub/outgoing/johannes/hyosat.

**ST5/W/60-B5****1125****2-D SEISMIC RAY TRACING AND ARRIVAL TIME INVERSION USING A SPECTRAL DECOMPOSED PROPAGATION MEDIUM**

R. DE MATTEIS (Universita' del Sannio, Via Caio Pontio Telesino, 82100 Benevento, Italy; e-mail: raffa@sungea03.na.infn.it), A. Zollo (Dipartimento di Scienze Fisiche, Universita' di Napoli "Federico II", Mostra d'Oltremare pad. 16, 80125 Napoli, Italy; e-mail: aldo@sungea03.na.infn.it) L. D'Auria (Dipartimento di Scienze Fisiche, Universita' di Napoli "Federico II", Mostra d'Oltremare pad. 16, 80125 Napoli, Italy; e-mail: luca@sungea03.na.infn.it), J. Virieux (Geoscience Azur, CNRS-UNR, Universite' de Nice-Sophia Antipolis, Valbonne, France; e-mail: viri@seisme.unice.fr)

We propose a new method for exact 2-D ray-tracing and body arrival time computation based on series expansion representation of medium velocities. The velocity field is represented by the sum of a polynomial and wavenumber spectral Fourier decomposed functions which accounts for the long wavelength velocity variations and short wavelength anomalies. In this case the ray vector equation is resolved locally by setting the initial conditions for ray position and parameter. We provide the iterative analytic expression for computing ray coordinates in a heterogeneous elastic 2-D medium. Synthetic examples show the effect of medium spectral features on the arrival times and ray paths and they allow us to suggest a criterion to estimate the higher wavenumber corners for a given acquisition geometry and arrival time uncertainty. This spectral approach turns to be very efficient for applications to seismic tomography problems where the medium spectral content and the minimum resolved wavelength are generally unknown. In fact, a medium description through a Fourier series enables one to estimate by arrival time data inversion both the medium properties and the minimum resolvable wavelength. We further developed a method for a non linear inversion of Tau-p curves based on travel time computation in a 2-D spectral decomposed propagation medium. This method is based on a global optimization technique (SIMPLEX and Montecarlo methods) which explore the whole parameter space i.e. the coefficients of the polynomial and spectral Fourier functions. Preliminary applications to synthetic and real data from an active seismic experiment will be presented.

**ST5/W/04-B5****1145****ADAPTIVE AUTOMATIC PHASE REPICKING FOR HIGH-PRECISION HYPOCENTER RELOCATION IN LARGE SEISMIC DATA SETS**

Charlotte ROWE and Richard Aster (both at Dept. of Earth and Environmental Science, New Mexico Tech, Socorro, New Mexico, U.S.A., email: char@dutchman.nmt.edu), Michael Fehler and W. Scott Phillips (both at Los Alamos National Laboratory, Los Alamos, New Mexico, U.S.A., email: fehler@muktinath.lanl.gov)

We report on the development of an efficient algorithm to adjust inconsistent phase picks and produce high-precision hypocenter estimates for large data sets with preliminary phase picks. The technique first estimates a large number of lag constraints for appropriate seismogram pairs by invoking a combination of adaptive coherency-driven prefiltering for coarse alignment and robust coherency-weighted evaluation of the minimum L-1 norm cross-spectral phase slope. Additional correlation processing which may significantly improve repicking and relocation of events in some data sets includes correlation of signal envelopes and adaptive band-rejection of coherent energy in pre-pick time windows. Pre-pick-based filtering is expected to be especially important for data sets exhibiting coherent background noise such as oceanic microseisms or harmonic volcanic tremor, and in improving the consistent picking of S-waves, which may be superimposed on significant coherent energy from the P-wave coda. Events are assigned to similarity classes based on a weighted function of median waveform and/or envelope crosscorrelation maxima. Within each similarity class, pick adjustments from interevent lag constraints are independently estimated using a memory-conservative conjugate gradient approach which minimizes the L-1 norm misfit. We demonstrate the technique using a collection of induced microearthquakes from the Soultz, France hot dry rock geothermal reservoir. This data set is especially well suited for a demonstration of the technique because of its finely detailed seismogenic features corresponding to intersecting joint structures, and because of a large previously-existing data set of manually-estimated consistent picks against which to gauge the success of the algorithm.

**ST5/E/33-B5****1205****MOMENT TENSOR INVERSION OF REGIONAL WAVEFORMS : STUDY OF THE SIGNIFICANCE OF THE ISOTROPIC COMPONENT**

Valerie TEYSSONEYRE and Bruno Feignier (both at Laboratoire de Detection et de Geophysique, CEA, BP12, 91680 Bruyeres le Chatel, France, email: teyssone@ldg.bruyeres.cea.fr)

The aim of our study consists of discriminating between isotropic and deviatoric sources, particularly to study the significance of the isotropic component in the results from moment tensor inversion using data recorded at regional distances. At such distances, high frequencies are still observed in the waveforms, therefore requiring the use of complex propagation models to compute the Green's functions. In a first step, we have tested our inversion program on a synthetic case. This was done by generating "real" seismograms with the reflectivity method in a flat layered medium and the same model was used to calculate the corresponding Green's functions. We successfully retrieved the correct moment tensor and were able to reconstruct the original signals. This set-up was also used to estimate the influence of the azimuthal station coverage and the number of stations used in the inversion on the resulting moment tensor. Results showing the significance of the obtained isotropic component will be presented. In a second step, we apply our method to an event which occurred near the town of Halle in Germany and was due to a mine collapse. Thus, the nature, location, and geometry of this source is known. Therefore, we were able to test the influence of inadequate Green's functions and measure their impact on the moment tensor obtained, particularly concerning the isotropic component.

**ST5/W/55-B5****1225****OBSERVATIONS OF T-WAVES IN SEISMIC STATIONS IN SOUTHERN SPAIN FROM EARTHQUAKES OF THE NORTH COAST OF MOROCCO**

J.M. IBÁÑEZ (1,2), E. Carmona (1) and G. Alguacil (1,2). (1) Instituto Andaluz de Geofísica, Universidad de Granada, Campus Universitario de Cartuja s/n, 18071 Granada, Spain.; (2) Departamento de Física Teórica y del Cosmos, Facultad de Ciencias, Universidad de Granada. 18071 Granada, Spain.

In the present work we show observations of the arrival in short-period vertical seismic stations, placed in southern Spain, of converted T-waves from earthquakes located in the North coast of Morocco. The observation of this type of waves is common for big earthquakes and oceanic paths in which the presence of a SOFAR channel is well known. The novelty of this study is the appearance of this type of wave for earthquakes with moderate and low magnitude ( $m < 4.0$ ) in a short sea path (less than 180 km) and with the presence of strong sea streams (this area is close to the Strait of Gibraltar).

The main characteristics of the converted T-waves are:

- They are observed only in the stations placed close to the coast. For stations located more than 40 km from the coast line there are no observations of them.
- They are observed for earthquakes located in a few areas of the coast of North of Morocco. Not all the seismogenic sources of this region show these arrivals.
- The spectral content of these converted T-waves is different to the coda spectral form on which they are overlapped. The spectral shape is richer in high frequencies and very similar to the P or S waves packet.
- By assuming that the T-waves have been originated in the same area as the earthquakes, their average propagation speed is around 1024 m/s, the same as the sound speed in water. We have calculated the attenuation factor of these converted T-waves by comparing the spectral level of the signal among stations located near the coast line and inland. The Q-value is very low and different to the coda-Q of the area, and similar to the expected surface Q-value. This observation, among others, permits us to infer that these converted T-waves are basically Rayleigh waves. Measuring the time delay among these seismic stations we could establish the possible area in which the T-waves are converted to Rayleigh waves. This zone is located around 1 km inside the sea in the Spanish coast.

**Friday 30 July PM**

Presiding Chair: Prof. J.J. Park, Department of Geology and Geophysics, New Haven, U.S.A  
Concurrent Poster Session

**SEISMOLOGICAL OBSERVATION AND INTERPRETATION: LOW FREQUENCY****ST5/W/42-B5****1400****AUTOREGRESSIVE ESTIMATION OF SPLITTING MATRICES AND THE ROTATION OF THE INNER CORE.**

G. Laské, G. Masters, and F. Gilbert (IGPP, Scripps Inst. of Oceanography, U.C. San Diego SIO-0225, La Jolla, CA 92093; ph. 619-534-2470; e-mail: fgilbert@ucsd.edu)

Recent large earthquakes, recorded by the rapidly growing global seismic networks, have produced a vast amount of high quality data. This new dataset allows us to re-evaluate the techniques used to determine the coupling and splitting characteristics of modes, and hence the three dimensional structure of the earth. Current techniques tend to be computationally intensive and require detailed models of earthquake sources (which may be unavailable for the large and often complicated events used in free-oscillation research). Here, we introduce a new technique that allows us to solve for the most general form of the splitting matrix without knowledge of the earthquake sources. This technique is based on the autoregressive property of combinations of seismograms for each event allowing the splitting matrix to be estimated in a non-iterative, one-step process. We apply this technique to anomalously split modes which are sensitive to the inner core and get extremely reliable estimates of their splitting matrices. These splitting matrices can be used to compute theoretical splitting matrices for past earthquakes assuming different relative rotation rates for the inner core. We find that very small relative rotation rates (less than 0.3 degrees per year) are consistent with our data which is in agreement with new analyses of body-wave data.

**ST5/E/12-B5****1420****THE EMERGENCE OF NEW NORMAL MODE CONSTRAINTS ON LONG-WAVELENGTH 3-D DENSITY STRUCTURE**

Joseph Resovsky and Michael Ritzwoller (Department of Physics, University of Colorado, Boulder, Campus Box 390, Boulder, CO, 80301, email: resovsky@abdu.colorado.edu)

The acquisition of new normal mode constraints on mantle structure from the 3-6 mHz frequency band should prove to be one of the key components to the development of reliable models of long-wavelength density structure. We have developed an approximate method of modeling the along-branch coupling of the fundamental modes that are the dominant signal in this frequency domain. Modeling of these surface-wave fundamentals enables precise measurements of important lower mantle sensitive modes that are otherwise obscured by the fundamentals, as well as the acquisition of new constraints on upper mantle structures, including anelastic heterogeneity. We show the results of tests which confirm the accuracy of our approximation, and present examples of the new structure coefficients that have been estimated through the application of this technique to a much larger database of long-duration seismograms than that employed in any previous normal mode inversions.



ST5/E/13-B5 1440

## ON SUPER CONDUCTING GRAVIMETER OBSERVATIONS IN SEISMIC SPECTRAL BAND AT THE METSAHOVI STATION, FINLAND

Heikki VIRTANEN (Finnish Geodetic Institute, Geodeetinrinne 2, PL 15, FIN-02431 Masala, Finland)

The summary of four years observations from lowest spheroidal normal mode 0S2 with the GWR T020 superconducting gravimeter, participating Global Geodynamics Project at the Metsahovi station, Finland, are given. Big earthquakes cause excitation of free oscillation of the Earth; modes decaying during few days, except the mode 0S0, which is observable in weeks after some major events at nanogal level. The main attention, however, is paid to find evidences for excitations of normal modes without quaking at the level near to noise limit. The causes of excitation could be slow or silent earthquakes, or the atmospheric-solid earth interaction. Some examples of the excitation are given in seismically silent periods. In addition, the seismic background noise at the site, in the region of microseismicity up to 300 mHz is reviewed.

ST5/W/58-B5 1500

## OBSERVATIONS OF ULF SEISMIC ACTIVITY AND INTERNAL WAVES IN THE SHELF ZONE OF SEA

Vadim V. NAVROTSKY, Vadim V. Novotryasov, Grigoriy I. Dolguikh (Pacific Oceanological Institute, 43 Baltiyskaya Str., Vladivostok, 690041, Russia, email: navr@online.vladivostok.ru)

The laser interferometer (LI) of the Pacific Oceanological Institute with measuring base of 52.5 m has linear frequency response in the 0-300 Hz range and can detect relative displacements of the Earth crust with the accuracy of 1 picometer. It is important to identify different mechanisms of ultra-low frequency vibrations of the Earth crust. The spectral analysis of LI and water temperature records was made in the range from tidal till short internal wave frequencies. The amplitudes of the registered seismic deformations were 7.0 microns for the 24-hour tide and 8.7 microns for the half-day tide. Comparisons of the registered deformations with theoretical calculations for lithosphere were made. Basing on model calculations and observational results we can maintain that internal waves in the shelf zone of sea can be the cause of rather stable maximum in the spectra of near-shore lithosphere deformations. We suppose that basing on these results a new method of remote sensing of important hydrophysical processes in the shelf zone of sea can be developed.

ST5/E/08-B5 1520

## DIRECT CALCULATION OF EIGENFUNCTIONS AND EIGENFREQUENCIES OF FREE OSCILLATIONS OF THE ROTATING ELLIPTIC EARTH

Vladimir GORBUNOV (Vavilov State Optical Institute, Birzhevaya 12, St.-Petersburg, 199034, Russia, E-mail: gorbunov@neva.spb.ru) Polina Serebryanaya (SPbF IZMIRAN, Muchnoi 2, St.-Petersburg, 191023, Russia, Email: gorbunov@neva.spb.ru)

The earth's rotation and ellipticity of figure cause the splitting of seismic normal modes that is commonly evaluated by perturbation theory. We present here the results of numerical computations of normal modes of rotating, elliptical and oceanless earth model obtained by another way. Our numerical procedure is direct integration of linearized equations of motion by using expansions in vector spherical harmonics to reduce the problem to infinite set of coupled ordinary differential equations over radius. This approach has been already used by M. Smith in the study of the Slichter triplet of inner core translational oscillations, by J. Wahrtrid response. The motivation for the present work is the idea that it is more simple way then perturbation theory to obtain the eigenfunctions of a multiplet because a good accuracy is reached with a truncated system by taking a few neighboring terms in the expansion of the displacement field. The scheme we use to convert vector equations with boundary conditions to scalar equations is considerably modified. Among other things it does not require the ellipticity to be small. In this report we examine the multiplets of lower spheroidal mode of degree 2 and its overtones by taking only three terms: spheroidal displacement of degree 2 and toroidal displacements of degree 1 and 3. In particular, we have found that the center member of the fundamental multiplet is shifted in period by 2.27 s to corresponding degenerate eigenfrequency (perturbation theory gives 0.88 s). This method is convenient for investigation of near-resonance multiplet coupling that has strong effect on eigenfunctions. The study of such quasi-degenerate multiplets (when two eigenfrequencies are close together) offers a possibility in evaluation of asymmetry in the Earth's model of the odd degree.

## Wednesday 28 July AM

Presiding Chair: Prof. J.P. Montagner, Institut de Physique du Globe, Paris, France

## SEISMOLOGICAL OBSERVATION AND INTERPRETATION: NETWORKS

ST5/W/56-B3 Poster 0900-01

## USE OF A PORTABLE DENSE SEISMIC ANTENNA TO STUDY VERY LOCAL MICROEARTHQUAKES: APPLICATION TO SEVERAL VOLCANIC AREAS

G. ALGUACIL (1,2), R. Ortiz (3), E. Del Pezzo (4), J.M. Ibáñez (1), J. Almendros (1), J. Morales (1,2), G. Saccorotti (5,4), E. Carmona (1), S. Petrosino (4), M. Abril (1), M. La Rocca (5), F. Bianco (4) and M. Castellano (4); (1) Instituto Andaluz de Geofísica, Universidad de Granada, Campus Universitario de Cartuja s/n, 18071 Granada, Spain; (2) Departamento de Física Teórica y del Cosmos, Facultad de Ciencias, Universidad de Granada, 18071 Granada, Spain; (3) Departamento de Volcanología, Museo Nacional de Ciencias Naturales, CSIC, C/ J. Gutiérrez Abascal, 2, 28006 Madrid, Spain; (4) Osservatorio Vesuviano - Via Manzoni 249, 80123 Napoli, Italy; (5) Università degli Studi di Salerno, Dipartimento di Fisica, Via S.Allende, 84081 Baronissi, Salerno, Italy

The present work shows: the design of a digital portable dense short-period seismic antenna, thought out to study very local microearthquakes; some techniques developed to determine the position of the seismic source; and its application to several volcanic areas.

The seismic antenna is composed of several eight channels modules. Each module has 8 seismometers with preamplifiers close to them that permits to send the signal via cable to the data logger, a data acquisition system and a GPS time receiver. The seismometers used in the experiments were Mark L15 and L25, with natural frequency in 4.5 Hz and electronically extended to 1 Hz, or Mark L4C, with natural frequency in 1 Hz, that sometimes was extended to 0.1 Hz. The data acquisition system is composed of an eight channel anti-alias Butterworth multipole filter at 48 Hz, a multiplexer that samples the channels every 5 ms and a 16 bits A/D converter. The internal clock is synchronised by GPS time every second and the sampling rate used was 200 sps. The control of the whole system and the storage of the data are done by a portable PC. The triggering algorithm is based on the STA/LTA ratio and with the possibility of a continuous registration.

Two techniques were used to locate the position of the seismic sources: in the time domain we

used the named Zero Lag Cross Correlation, and in the frequency domain the called MUSIC algorithm. Parallel to that we improved the ZLCC method introducing the approximation of a circular wave-front incoming to the seismic antenna. Also, a probabilistic approach for the estimate of the slowness vector from these data was used.

Since 1994 these instruments and techniques have been deployed and applied to several volcanic areas: Teide volcano (Spain), Deception island (Antarctica), Stromboli and Vesuvius (Italy) and Llaima (Chile). In some of them (Deception, Vesuvius or Llaima) only one dense antenna was deployed. In others (Teide, Stromboli and also Deception) two dense seismic antennas were deployed in order to obtain a joint location of the seismic source. These and other applications of the seismic antennas are presented in the sessions ST5, JSS46 and JSV47.

ST5/L/02-B3 Poster 0900-02

## THE SWISS EARTHQUAKE MONITORING SYSTEM (CH-NET)

M. BAER, D. Giardini, U. Kradolfer, E. Spuehler and P. Zweifel, Swiss Seismological Service, ETH, CH-8053 Zurich, Switzerland (email: sed@seismo.ethz.ch)

The Swiss Seismological Service (SED) is responsible for earthquake monitoring in Switzerland and is upgrading the existing seismic networks and individual instruments to establish a modern, integrated monitoring system to serve the earthquake surveillance needs of Switzerland. The new Swiss Earthquake Monitoring System (CH-NET) will replace in the year 2000 the former analog national seismic network and upgrade the existing strong-motion instrumentation. The upgrade will be completed in the 1997-1999 period and is supported by ETHZ. The new CH-NET includes four modules: 1. the Swiss Digital Seismographic Network: 29 broad-band digital stations (Streckeisen STS-2 sensors, Nanometrics HRD 24-bit digitizers) with homogeneous coverage of the Swiss territory and continuous digital data transmission through a protected federal computer network; six BB stations and the central acquisition system are now in operation; 1. the Swiss digital Strong-Motion Network: five arrays (34 stations) monitoring large dams and 63 free-field stations, with concentrations in areas of expected higher strong motions (Basel, Wallis, E. Rhine Valley), equipped with wide-band sensor, DCF-radio clock, and phone connection for automatic data retrieval; 2. the Data Management Center unifies the acquisition, storage and distribution of waveforms from the seismographic and strong-motion networks and fulfills the SED duties of earthquake monitoring; 3. the portable seismographic and strong-motion networks.

ST5/W/36-B3 Poster 0900-03

## INVESTIGATION OF THE PHYSICAL ORIGIN OF THE LONG-PERIOD VERTICAL SEISMIC NOISE

Yuri Starovoit, IIEP RAN, Warshavskoye sh. 79, k1, Moscow, Russia. email: yuri.starovoit@ctbo.org.

Combination facilities of colocated broad band seismometer STS-1 in OBN (Russia) and microbarometer is an effective tool for observation of coupling effects in the boundary between atmosphere and the Earth surface. Even vertical instrument, whose protection against influence of pressure changes much better than horizontal one, sometimes in good agreement with ambient pressure variations in the range 0.8mHz<f<40mHz. The mechanism of this residual correlation was a subject for investigations. Despite uncertainty in absolute values of thermal sensitivity of seismometer's spring and time constants of temperature penetration through the chain of cases, the spectrum of apparent displacement caused by temperature variations was estimated. As a result, an observational spectrum of vertical seismic noise reduced to the pressure variations could be explained as a combination of two effects, which dominate in different passband. First effect, in the range 0.8mHz<f<1.5mHz, could be a result of direct influence on the pendulum by temperature changes in the vault, caused by pressure variations. For computations it was used the values of thermoelastic constant of the leaf spring in the range  $3 \cdot 10^{-6} - 3 \cdot 10^{-7}$  1/K. Ground movements induced by pressure variations dominate in the frequency range f>3mHz. For computations of the transfer function between pressure changes and ground movements it was considered a model of changeable load applied to the elastic halfspace. The spatial correlation of the pressure field was chosen as a variable. Playing with a parameter a good agreement with experimental curve was obtained for reasonable values of spatial correlation of the pressure variations.

ST5/E/15-B3 Poster 0900-04

## SUPERPLUME PROJECT: SOUTH PACIFIC BROAD BAND SEISMIC NETWORK (SPANET)

Mizuho ISHIDA (National Research Institute for Earth Science and Disaster Prevention, 3-1 Tennodai, Tsukuba-shi, Ibaraki-ken 305-0006, Japan, email: ishida@geo.bosai.go.jp)

The "Super Plume" project is to examine the recent working hypothesis of "super plume tectonics" in the light of newly obtained from a broad range of earth sciences; seismology, geology, high-pressure experiments, geodesy, and numerical simulation of mantle convection. The seismological part of this project includes construction of three seismic networks: JISNET (Japan-Indonesia Seismic Network: temporal array of broadband seismic stations in Indonesia), GARNET (Global Alliance of Regional NETWORKs: integrated digital data base from local networks) and SPANET ( explanation follows) under the generic name of PANSY (Pacific Networks for Seismology). The main objective of SPANET (South Pacific Broadband Seismic Network ) is to resolve the mantle structures beneath the South Pacific where a large scale slow anomaly in global tomographic image has been considered to represent a superplume ascending from the core-mantle boundary. For this purpose we will deploy, by the end of 2000, sixteen broad-band seismographic stations in and around the relevant region, including ten stations in collaboration with IRIS Incorporated Research Institutions for Seismology). We have already established six CMG-3T stations by cooperation with Australia, Fiji, Tonga, Niue and Cook Islands. All the data from the above three networks are archived at DMC (Data Management Center) of NIED (National Research Institute for Earth Science and Disaster Prevention) in cooperative with IRIS and the collaborated countries. The program is financially supported by STA (Science and Technology Agency), which is started in 1996 and is scheduled to be completed in 2000 (First period:1996-\$BIA\_(B1998, Second period:1999-\$BIA\_(B2000).

ST5/W/01-B3 Poster 0900-05

## DATA PROCESSING AND DISSEMINATION IN THE CANADIAN NATIONAL SEISMOGRAPH NETWORK

Jim Lyons, Philip Munro, John Adams, and David MCCORMACK (Geological Survey of Canada, 7 Observatory Crescent, Ottawa, Ontario, K1A 0Y3, CANADA, email: jlyons@seismo.nrcan.gc.ca)

The Canadian National Seismograph Network (CNSN) comprises about 100 automatic, unattended digital seismographs installed across Canada. Continuous data from each site are formatted into 6-second packets and transmitted to dual (for redundancy) network centres located in Ottawa, Ontario and Sidney, BC. Data telemetry employs a variety of dedicated full- and half-duplex links over domestic VSAT satellite, terrestrial telephone, and UHF radio. At the

National Seismology Data Centre (NSDC) in Ottawa, almost a gigabyte of continuous, compressed data from 150 seismic components and a 4-element infrasound array are acquired, quality controlled, processed, and archived on a daily basis. For significant local and regional events, automatic event detection, event location, and e-mail alerts are accomplished within minutes. Automatic processing of Yellowknife Array (YKA) data allows global events to be detected, locations refined, and e-mail alerts issued to national and international subscribers within three minutes of p-wave arrival. The National Earthquake Database (NEDB) provides the national repository/index for all phase measurements, and derived parameters. The National Waveform Archive (NWA) holds all digital waveform data. The NSDC acts as Canada's National Data Centre for the CTBT International Monitoring System, forwarding continuous data in near real-time from YKA and 3 other primary seismic stations, a hydroacoustic station, the Infrasound Array, and eventually 4 radionuclide stations, to both the Vienna International Data Centre (IDC) and the prototype IDC in Arlington, VA. The IDC regularly requests additional data from 6 secondary seismic stations via AutoDRM. Continuous data from 10 broad band sites designated "Federation" (FDSN) stations are supplied to the IRIS DMC within weeks of real time for archive. Event-related digital waveforms since 1975 are available from regional networks in Eastern and Western Canada, as are continuous CNSN data since 1992. AutoDRM provides convenient access to on-line waveform data plus selected bulletins, etc. from the NEDB. Once the NWA has been transcribed to a new automated library system (hopefully next year), our entire digital waveform data holdings will be available online. Our Web server, active since April 1995, provides ready dissemination of data to both the scientific community and the general public.

**ST5/W/14-B3** Poster **0900-06**

#### HOT SPOT OBSERVATORY ON ICELAND - A PROPOSAL ON MULTINATIONAL EFFORT

REYNIR BODVARSSON Dep. of Earth Sciences, Uppsala University Ragnar Stefansson Icelandic Meteorological Office Freysteinn Sigmundsson Nordic Volcanological Institute, Iceland Axel Bjornsson Nordic Volcanological Institute, Iceland

The Iceland Hot Spot is a large scale feature on Earth, a plume located beneath the Mid-Atlantic Ridge showing effects over an area of several hundreds thousands square kilometers (gravity). The role of the plume in the deformation processes acting on the crust is poorly understood. There are indications that the plume up-flow and rifting of the adjacent parts of the Mid-Atlantic ridge have observable influence on the crustal stress in the continents of northern Europe and America. Flow of basaltic fluids into the crust and stresses exerted by the plume cause large variations in the seismicity rate as well as the rate of volcanic activity in Iceland. The intensified monitoring in Iceland related to seismic risk mitigation has indicated that strain waves related to intrusive episodes can be monitored over large distances (several hundreds of kilometers). The aim of this poster is to put forward an idea of a multinational effort regarding design and construction of a multidisciplinary multistation geophysical observatory for monitoring various geophysical signals from the plume. Continuous geodetic measurements using GPS, gravity, volume strain-meters in bore-holes, long period MT measurements, radioactive gases and microearthquakes are among the observations suggested. The challenge is not only of scientific nature, but also technical as an unmanned observatory with good communication facilities is to be constructed in a mountain area at a latitude of 65 deg N. In this poster we also demonstrate the existing monitoring facilities.

**ST5/W/33-B3** Poster **0900-07**

#### GEOSCOPE 2000

Genevieve ROULT, Jean-Paul MONTAGNER, Jean-Francois KARCZEWSKI and Eleonore STUTZMANN (Departement de Sismologie, Institut de Physique du Globe, 4 place Jussieu, 75252 PARIS-Cedex 05, France)

The GEOSCOPE program corresponds to 28 stations (25 permanent stations and three contributing stations) well distributed. All of them are in the VBB configuration (144db, 24bits), except two of them which have to be transformed. Four channels are recorded, VH and LH channels continuously with respectively a sampling rate of 0.1sps and 1sps, MH which is triggered with a sampling rate of 5sps, and BH which is triggered in 14 stations and continuously recorded in 14 stations. The scientific and technical staffs of GEOSCOPE are defining a new digitizer (144db, 24bits, BH continuously recorded at 20sps for a STS1 sensor, and triggered at 80sps for a STS2 sensor). All stations of the GEOSCOPE program will be equipped in the next future, not only with seismometers, but also with magnetometers, a set of microbarometers, a set of microthermometers, inclinometers, GPS... in order to transform each station in a multi-parameter observatory. GEOSCOPE 2000 is coordinating with OFM program (Ocean Bottom Observatory) in order to fill the instrumental geographical desert of the oceanic regions, and to install new multi-parameters observatories.

In the future ten GEOSCOPE stations will be teletransmitted by commercial satellite in real time, in cooperation with the french agency CEALD/G.

**ST5/W/35-B3** Poster **0900-08**

#### ORFEUS: STATUS AND RECENT DEVELOPMENTS

TORILD VAN ECK, Bernard Dost, Reinoud Sleeman and Laslo Evers ORFEUS, c/o Seismological Division, Royal Netherlands Meteorological Institute, PO Box 201, 3730 AE De Bilt, The Netherlands. <http://orfeus.knmi.nl>, E-mail: [vaneck@knmi.nl](mailto:vaneck@knmi.nl).

ORFEUS is rapidly developing. Crucial is the exponential growth of the number of installed and operating broad-band seismograph stations in the European-Mediterranean area, rapid developments in data exchange and internet facilities and extended interests from research institutes. This last factor is obvious in the increased activities within ORFEUS four working groups (Station siting, Technical assistance, Mobile equipment and Seismological Software). The Orfeus Data Center (ODC), the core activity of the organisation, is taking advantage of the improved data exchange and internet facilities, with 1) its Near Real Time (NRT) data base and EuroSpyder and 2) extended use of AutoDRM and NetDC. In 1998 the ODC has produced 15 CD-ROM's (10 GB data from 1992 and 1993) and continued providing on-line Spyder(R) and SEED data. The challenge in 1999 will be to continue providing an increasing amount of data from an increasing diversity of sources in a user friendly way. Within the Orfeus working groups activities continue with, among others, the EuroMed stationbook, technical overviews, developing lecture notes, equipment and project overviews, the ORFEUS Seismological Software Library. Further, two workshops: 'Installing, operating and data processing of mobile seismograph station deployments' and 'Java in seismology' are planned for the autumn 1999. Information on new developments and on-going activities will be reported in the ORFEUS Electronic Newsletter.

**ST5/W/45-B3** Poster **0900-09**

#### ACCESSING DATA FROM THE ISC

Anna SURGUY and Raymond J Willemann (International Seismological Centre, Pipers Lane, Thatcham, Berkshire RG19 4NS, UK, email: [anna@isc.ac.uk](mailto:anna@isc.ac.uk))

The ISC has distributed its data in print, as the Bulletin and Catalogue, since its inception. We have provided data in digital format on custom-written tapes and other media since early in the Centre's history and we continue to provide outcomes from specialised searches of our data. During this period, the Centre established a policy of distribution at a price just sufficient to cover the cost of reproduction. Starting in 1995, we released a series of CDs that now provide our complete data set in computer-readable form, at lower cost than custom products. Since 1997, we have made all of our analysed data freely available on the Internet from our web site. In the future we plan to continue improving the accessibility of our data and the ease of integrating it with other data. New query tools on our web site will provide greater flexibility in selecting data. We have implemented mechanisms to generate focused links to other Internet nodes and insert them in our on-line Bulletin. The objective is not to merely tell users of other data sources, but to link them directly to a moment tensor, waveform collection or velocity model needed for further analysis of the event they have found in the Bulletin. We are working with other seismic data centres to help define more widely useful standards for data exchange and CORBA-compliant object classes. We are evaluating the possibility of distributing functions written in Fortran, C and other languages to allow users to more easily access our data from within their own programs.

**ST5/W/54-B3** Poster **0900-10**

#### NETWORK BROADBAND SEISMOGRAM DATABASE BASED ON JAVA

Seiji TSUBOI (Department of Geoscience, National Defense Academy, Yokosuka 238-8686, Japan, email: [tsuboi@cc.nda.ac.jp](mailto:tsuboi@cc.nda.ac.jp)) Shingo Watada and Yoshio Fukao (both at earthquake Research Institute, University of Tokyo, Tokyo 113, Japan, email: [watada@eri.u-tokyo.ac.jp](mailto:watada@eri.u-tokyo.ac.jp))

We have developed Network Data Center software by using Java-RMI so that users can retrieve, in a standardized format, the data from different data centers in different format, through a common web site without connecting each data center. Java-RMI (Remote Method Invocation) realizes a CORBA-like Object Oriented environment. We have defined several classes based on Java-RMI to retrieve both continuous and event seismograms from remote data centers. We put RMI dispatcher and RMI server at each data center which provides broadband seismograms. The requests received at local RMI dispatcher are delivered to corresponding RMI server at remote data center. When the requested data is found, then the data are sent back to local dispatcher. Users can download the data through the browser such as Netscape. Currently, prototype system is actually running at Ocean Hemisphere Network Data Center at Earthquake Research Institute of University of Tokyo. This Network Data Center software will be quite useful if there are several data centers that provide seismograms from different network in different format, such as in the case of PACIFIC21 which is a generic name of the integrated broadband seismogram database in Japan.

**ST5/W/63/B3** Poster **0900-11**

#### SEISMIC NOISE LEVEL IN THE GEOSCOPE STATIONS

El'eonore STUTZMANN, Genevieve Roullet (both at D'epartement de Sismologie, Institut de Physique du Globe, 4 place Jussieu, 75252 PARIS- CEDEX 05, France.) and Luciana Astiz (at IGPP-SIO, 9500 Gilman Dr, La Jolla, CA 92093-0225, USA)

The seismic noise level of GEOSCOPE stations has been studied for the year 1995 to quantify the station quality. On the horizontal components, the seismic noise varies in most stations as a function of local time for periods greater than 20 seconds. It is higher during the day than during the night. Only stations located in cold areas with little daily temperature variations and stations installed on a long tunnel do not display these daily noise variations. There is no seasonal variation of short period seismic noise (periods less than 7 sec). On some continental stations, we observe variations of the amplitude of the 7 sec microseismic peak during the year. On all 3 components, the peak amplitude is higher and shifted toward longer periods in fall and winter than in spring and summer. This phenomenon can be explained by an increase of the number and the amplitude of oceanic storms in autumn and winter. For some stations, long period seismic noise (periods greater than 30 seconds) also varies as a function of the season but no systematic characteristic has been observed.

The seismic noise level is lowest at continental stations. Island stations have a similar low noise level at long period but a high noise level for periods shorter than 10 seconds, in particular at the period range of the microseismic peak. Finally, some coastal stations have a low noise level similar to the level at continental stations.

The systematic installation of thermometers and microbarometers at future GEOSCOPE stations will allow the quantification of the environmental influence on seismic noise. These data will be used to reduce the noise level of seismic data.

**ST5/W/L/03-B3** Poster **0900-12**

#### RESULTS FROM THE HAWAIIAN SWELL EXPERIMENT

G. Laske, J. Phipps Morgan and J. Orcutt (IGPP, Scripps Inst. of Oceanography, U.C. San Diego SIO-0225, La Jolla, CA 92093; ph. 619-534-8774; e-mail: [glaske@ucsd.edu](mailto:glaske@ucsd.edu))

The SWELL experiment (Seismic Wave Exploration in the Lower Lithosphere) is designed to map the 3-dimensional seismic structure of the lithosphere and upper asthenosphere beneath the Hawaiian Swell, using intermediate-period Rayleigh waves. The experiment is a multiple-deployment experiment where we use 8 ocean bottom differential pressure gauges in a hexagonal array, with station spacing of about 200km. In successive redeployments, this array will be placed in a leap-frog manner around the Hawaiian Island Chain. Our low-cost seafloor dataloggers (L-CHEAPOs) enable us to conduct sea-going experiments on a reasonable financial level. This experiment provides a genuine alternative to land-based seismic studies where the resolution power is either too low (global studies) or the station coverage is insufficient (regional studies) to map the fine-scale structure of the entire swell.

We recently recovered the instruments of the 12-month pilot deployment which was co-located with the pilot OSN borehole experiment to the southwest of the Hawaiian Islands. We have analyzed waveforms for more than 65 events and are able to obtain stable estimates of Rayleigh wave dispersion at periods between 15 and 70s. In this period range, the recorded waveforms are remarkably consistent with the recordings of the global broad-band station KIP on Oahu. The good azimuthal data coverage allows us to obtain an unbiased estimate of the average structure beneath the array which corresponds to that of lithosphere between 50 and 100-Myr of age. We therefore conclude that the generation of the Hawaiian Swell is inconsistent with thermal rejuvenation in its pure form. While there is little lateral heterogeneity across the array, we find evidence for significantly lower phase velocities under stations which are closest to the islands. The low velocities, which are in concordance with the results of other recent land-based studies, imply a rather narrow channel of hot plume asthenosphere which



has been dragged along the Hawaiian Island Chain. The good data coverage also allows us to study the azimuthal dependence of phase velocity, hence lets us constrain flow patterns in the mantle.

The results of the pilot experiment, together with those of the re-deployments will allow us to explore to which extent each of the proposed mechanisms are involved in the generation of the Hawaiian Swell: (1) thermal rejuvenation, (2) compositional underplating, (3) dragging of hot plume asthenosphere.

**ST5/W/L/04-B3** Poster **0900-13**

#### MODERN, DIGITAL MULTI-FUNCTIONAL REAL-TIME SEISMOGRAPHIC NETWORK FOR SOUTHERN CALIFORNIA, US: TRINET

Jones, L. M., D. Given, D. Wald (USGS, 525 S. Wilson Ave., Pasadena, CA 91106), and Hauksson, E., R. Clayton, K. Hafner, T. Heaton, K. Hutton, H. Kanamori, P. Maechling, J. Goltz (Seismo. Lab. 252-21, Calif. Insti. Tech., Pasadena, CA 91125);

The United States Geological Survey, the California Institute of Technology, and the California Department of Conservation are deploying a new generation of seismographic network in southern California. The purpose of this network, called TriNet, is to record and analyze earthquake ground motions in southern California, and distribute that information quickly, to improve our understanding of earthquakes and their effects, to contribute to improving building codes and structural design, and to facilitate emergency response in cooperation with other agencies. TriNet has two elements with the California Department of Conservation element concentrating on engineering applications and the Caltech/USGS element (SCSN/ TriNet) concentrating on seismological and emergency response aspects.

To fulfill its part of the mission, SCSN/TriNet must have capabilities beyond what has previously been designed into any seismographic network. Rapid acquisition and processing of digital data streams exceeding 2 Mbytes/second, realtime ground motion estimations and hardened data distribution channels are some of the new requirements. We have prepared system specifications for SCSN/ TriNet to ensure achievement of five goals: First, operate a hardened seismographic network, that is sufficiently dense to document the true distribution of ground motions at kilometer resolution and robust enough to operate successfully in even the largest possible earthquakes. Second, cooperate with other agencies working to mitigate the earthquake hazard in southern California in the recording, analysis and distribution of information. Third, create an easily accessible database of earth-quake information in southern California for seismological and engineering research. Fourth, distribute information about an earthquake rapidly after occurrence to save lives and property, by facilitating decision making and mitigating actions such as search and rescue, fire prevention, and deployment of engineers and inspectors for building inspection. Fifth, develop a pilot early warning system that would allow us to know that an earthquake has begun before damaging shaking arrives at more distant sites and conduct social science research on the use of such data to be ready to implement once funds for future SCSN/TriNet enhancements, including sufficient stations, are obtained.

**ST5/L/01-B3** Poster **0900-14**

#### DYNAMICAL CHARACTERISTICS OF SEISMIC NOISE LEVEL OF STATIONS OF KAZAKHSTANI SEISMOLOGICAL NETWORK

ZLATA I. SINYOVA, Natalia N. Mikhailova, Igor I. Komarov (email: igr@kaskelen.almaty.kz)

Data of eight seismic stations, located in the northern, eastern and south-eastern parts of Kazakhstan were used in the present study of seismic noise level. These are the following stations, belonging to the National Nuclear Center of Kazakhstan Republic: Kurchatov, Borovoye, Vostochnoye, Zerenda, Chkalov, Aktymbinsk, Makanchi; and Talgar. Starting from 1994, all of these stations are equipped with STS-2 and CMG-3 seismometers. The spectral and dynamical characteristics of seismic noise were studied for all three components (vertical and two horizontal), covering frequency diapason from 20 Hz to 0,001 Hz. All seismometers are installed on bedrock foundation. The spectral density of seismic noise was computed in acceleration domain. For each component the following parameters were computed: median, variance, and histogram of distribution of seismic noise level for a number of frequencies (5 Hz, 1 Hz, 0,1 Hz). The shapes of curves of median values of spectral density on all stations are rather similar. However, there exist a clear difference between curves of spectral density for short-period seismic noise (for frequencies high than 0,2 Hz). At frequency 10 Hz a variation of noise level between quietest and noisiest stations reaches 20 dB; at frequency 1 Hz - accordingly, 7 dB; and there is no statistically significant difference between noise level of different stations at frequencies lower than 0,2 Hz. The low level of seismic noise, as well as a small daily variations of seismic noise, allows to consider the Kazakhstani network as a very effective for monitoring of nuclear explosions and earthquakes, especially for regions of Central and Southern Asia.

Wednesday 28 July PM

Presiding Chair: Prof. Y.T. Chen, Director, Institute of Geophysics, Beijing, China

#### SEISMOLOGICAL OBSERVATION AND INTERPRETATION: TECHNIQUES

**ST5/W/65-B3** Poster **1400-01**

#### A PROBABILISTIC APPROACH FOR THE ESTIMATE OF THE SLOWNESS VECTOR FROM SEISMIC ARRAY DATA

G. SACCOROTTI, Università di Salerno, Via Salvador Allende 84081 Baronissi (SA), e-mail: gilberto@osve.unina.it; E. Del Pezzo, Università di Salerno, Via Salvador Allende 84081 Baronissi (SA), Osservatorio Vesuviano, Via Manzoni 249, 80123 Napoli; e-mail: delpezzo@osve.unina.it.

Array analyses in volcano seismology is the main tool for detecting and quantifying the complex wave-field associated to the volcanic activity, mainly the volcanic tremor and the long period events. The methods based on the analysis of the signal in the frequency domain, or spectral methods (MUSIC algorithm), take the main vantage of both resolving closely-spaced sources and computer speed, but severely fail in the analysis of short duration signals. Conversely, the time domain methods, based on the cross-correlation estimate of signal pairs, can be applied even for short pulses. Both for time and frequency domain techniques, an exhaustive view of the errors associated to the slowness vector estimate does not exist. The estimate of the error is important in the inversion of the slowness vector for source location. In the present work we develop a method based on a probabilistic formalism, which allows for a complete definition of the uncertainties in the estimate of frequency-slowness spectrum based on the measure of the zero-lag cross-correlation. The method is based on the estimation of the theoretical frequency-slowness power spectrum, which can be expressed as the convolution of the true signal with the array response pattern. The application of the Bayes theorem allows for the final estimate of the data probability density function. The method is tested with synthetics using waveforms resembling the most common volcanic earthquakes, and applied to real data as an example.

**ST5/W/29-B3** Poster **1400-02**

#### WHY THE ISC CONTINUES TO SEARCH FOR "UNREPORTED" EVENTS

Since 1974 the International Seismological Centre has searched its unassociated phase readings to find events not reported by other agencies. About 100 to 200 such events are found each month, and while the number of events published by the ISC has risen dramatically over the decades, the number of "new" events has remained steady. Many are genuine new events located in remote areas, such as oceanic ridges, where instrumental coverage by national agencies is poor, or situated near national boundaries, where no single country can obtain a solution with its own stations alone.

One example of a new event was the first earthquake to be confirmed as occurring in continental Antarctica, in 1982. Many new events are already known to local agencies, but their origins are not reported to ISC because they are too small, or are known to be of non-seismic origin, such as mining explosions. In early years the distribution of new events was widespread, but recent improved global location capability of agencies such as the Prototype International Data Center has greatly reduced their number in remote areas. A few are still found, however, in Hindu Kush, Myanmar, and around the Pacific Rim. Many more events are now being found in areas with good local coverage, such as Alaska, Mexico, Andean South America and New Zealand, where for various reasons not all locally determined origins are reported to ISC. Also, the new events seldom have teleseismic amplitude and period readings for ISC to determine a magnitude, and locally determined values of ML are rarely available. Reviewing these events takes a considerable proportion of ISC's analysis effort, and ISC plans to review the procedure to ensure that genuine new events, particularly in remote areas, continue to be discovered without devoting undue effort to rediscovering events already known. We report on regional variation in the proportion of new events not in local catalogues, particularly those requiring data from two or more networks.

**ST5/W/06-B3** Poster **1400-03**

#### HIGH FREQUENCY WAVEFORM INVERSION OF CROSSWELL DATA

Henk Keers, Lane Johnson, Don Vasco (Dept of Geology and Geophysics, Lawrence Berkeley National Lab, UC Berkeley, Berkeley CA 94720, email: henk@ccs.lbl.gov)

Seismic waveforms are inverted using an asymptotic method. The asymptotic method provides an efficient way of computing partial derivatives of the data with respect to the model. The partial derivatives enable the formulation of a waveform inversion algorithm, which is applied to a laboratory crosswell experiment. The goal of the laboratory experiment was the detection of a non-aqueous phase liquid (NAPL) in water saturated sand. The sand was imaged before and after injection of the NAPL. Using the waveform inversion method, low velocity anomalies were imaged that correlate well with post-experiment determination of NAPL concentrations. The low velocity anomaly defocuses the seismic energy. However the observed amplitude reduction due to the low velocity anomaly is not enough to explain the observed low amplitudes. We suggest that other mechanisms (such as multiple scattering, scattering on pore scale), not included in the waveform modeling, play an important role in decreasing the amplitude.

**ST5/E/28-B3** Poster **1400-04**

#### COMPARISON OF MANUAL AND AUTOMATIC ONSET TIME PICKS

Mark Leonard (Australian Geological Survey Organisation, PO Box 378, Canberra City, ACT 2601, Australia, email: mleonard@agso.gov.au)

A data set consisting of analyst onset picks from 60 teleseismic waveforms recorded at an array was used to test the accuracy of automatically generated arrival times from two onset picking algorithms. The 60 picks are picks which an analyst considered could be picked to within 0.2 seconds. They have small to moderate SNRs. Four comparisons were made: the single trace with the beam for the four analysts; the four analysts with each other; the analysts with the ES method (Earl, P. and Shearer, P. (1994) and an AR method similar to Kvaerna, T. (1995).

On average an event manually read on a beam was picked 0.125 seconds earlier than the single trace, with a standard deviation (std) of 0.18 seconds. For the single trace the analysts picks differed on average by 0.1 seconds with a std of 0.15 seconds (0.05 and 0.11 for the beam). The ES method produced similar times to the analysts for large events but performed poorly for small amplitude events. The AR onset time picker typically picked 0.1 seconds after the analyst with a std of 0.2 seconds (0.8 and 0.15 for the beam). There were three events which the AR picker picked more than 0.2 seconds before an analyst but there was no single event where the AR picker differed significantly. Generally the AR picker picks at the same time or slightly later than an analyst.

These findings suggest that for modest sized iP phases the AR onset time picker can pick events with a similar accuracy as an experienced seismic analyst.

**ST5/E/30-B3** Poster **1400-05**

#### WAVELET TRANSFORM BASED S PHASE PICKER

Bojan Uran (Geophysical Survey of Slovenia, Kersnikova 3, 1000 Ljubljana, Slovenia, email: bojan.uran@gov.si)

Single-station three-component seismogram processing in the nearly real time is important for automatic location of earthquakes, distributed data processing and early warning systems. There exist many successful algorithms for P phase arrival picking, but picking of S phase is more difficult. Wavelet transform is used for interscale analysis of polarisation data of the three-component seismograms. Tests have been done with standard wavelet basis functions for a typical set of local and regional seismograms. Newer techniques, like wavelet packets, Malvar wavelets, lifting scheme and matching pursuit were also used to best match the S wave recording and obtain the best estimate for the S phase arrival.

**ST5/W/L/05-B3** Poster **1400-06**

#### DETERMINATION OF UPPER MANTLE S-WAVE STRUCTURE BENEATH CENTRAL EUROPE USING WAVEFORM TOMOGRAPHY

T. Meier, P.G. Malischewsky, U. Walzer, (Institute for Geosciences, Friedrich Schiller University Jena, Burgweg 11, D-07749 Jena, Germany, email: meier@geo.uni-jena.de)

A regional upper mantle S-wave velocity model for Central Europe is obtained by inversion of longperiod waveforms. Synthetic waveforms for the vertical component are matched to measured waveforms in a frequency range between 6 mHz and 40 mHz. The synthetics are calculated by summation of Rayleigh modes. While the fundamental mode gives resolution in depths between the Moho and about 300 km higher modes allow to map heterogeneity between about 300 km and 660 km depth. The model is interpreted tectonically. For selected paths one-dimensional models for the vertical component obtained by summation of Rayleigh



modes are compared to one-dimensional models based on the inversion of the transverse component and summation of Love modes.

**ST5/L/03-B4** Poster **0930-09**

#### ANNUAL CHANGING RATE OF THE CRUSTAL STRAIN-ENERGY DENSITY AND ACTIVITY OF STRONG EARTHQUAKES IN CHINESE MAINLAND

ZHANG Dongning and XU Zhonghui

The annual changing rates of the crustal strain-energy density in Chinese mainland are calculated by using the finite element method, and the calculation is constrained with the tectonic stress field and the GPS results of the crust motion. The numerical model is constructed with 3-D elasto-viscous body, and some large-scale active faults are involved. Gravity and buoyancy forces in Tibetan Plateau are considered. Some boundary loading is applied as convergence of Eurasia plate with Pacific plate and Indian plate.

The calculation results are compared with the distribution map of strong earthquakes in China. The transitional zones of the positive and negative strain-energy changing rate areas are just corresponding to Longmenshan fault, Yanshan-Yinshan E-W tectonic zone, Tianshan tectonic zone, Xianshuihe-Xiaojiang fault, Honghe fault and faults around Erdos block, which are all the strong earthquake zones in history. The average recurrence interval of the strong earthquakes is evaluated with the calculation results of the changing rates of the crustal strain-energy density. The average recurrence interval in western China should be 250 years or so, and it may be longer in eastern China.

**ST5/L/04-B4** Poster **0930-10**

#### CRUSTAL STRUCTURE IN NORTH MARGIN OF TIANSHAN MOUNTAINS, CHINA

Chun-Yong

The fine crustal structure in the area of 1906 Manas ( $M=7.7$ ) earthquake, the north margin of Tianshan mountains, is obtained from a deep seismic reflection profile, which stretches across the northern Tianshan piedmont and has a nearly north-south trend. The CDP stack section is characterized by a thin-skinned piggyback structure of crust. The profile is divided into two parts and bounded by the Manas reverse fault. The south part of the profile is transition zone of the Tianshan block and the Junggar block. There are anticlines (Qingshuihe anticline and Manas anticline) and detachments in upper crust. A detachment at depth of 8(10)km relates the Manas anticline to the Qingshuihe reverse fault. The north part of the profile belongs in the Junggar block. There exists a 12(14)km thick sedimentary cover in the depression. The Moho discontinuity beneath the basin is located at the depth of about 45km and deepens southwards.

The hypocenter of 1906 Manas earthquake is inferred at the junction of the Qingshuihe reverse fault and the detachment, and the epicenter is about 40km far from the Manas reverse fault, where the surface rupture of the Manas earthquake was discovered. It is implicated that the seismotectonics of the earthquake is a fault system constituted by the Qingshuihe reverse fault, detachment and shallow ramp.

**ST5/L/01-B4** Poster **0930-11**

#### NUMERICAL STUDY OF ENVELOPE BROADENING IN RANDOM MEDIA

M.FEHLER and Lian-Jie Huang

Observed long duration of S-waves from earthquakes at depths between 100 and 200 km beneath Japan can be explained as being caused by multiple forward scattering between the source and receiver. For the study of multiple forward scattering effects, we calculated wavefields using two numerical methods: (1) the local Rytov Fourier method, which models forward scattering effects more reliably than the split-step Fourier method and is computationally fast and (2) finite difference solution of the acoustic wave equation, which gives complete wavefields. In addition, we compare envelopes calculated using the Markov approximation, which allows the direct calculation of seismogram envelopes in statistically characterized random media. We calculate the time trace of the RMS envelope averaged over 65 simulations at a distance of 200 km from a point source, where the source waveform is a 2 Hz Ricker wavelet. We used a 2D random media characterized by a correlation distance of 5 km, a RMS fractional fluctuation of 5%, and an average velocity of 4 km/s. The delay between the first arrival and the time that the envelope reaches its peak amplitude is slightly greater and the amplitude of the later portion of envelope is slightly larger for the finite difference solutions than the local Rytov solutions. The envelope calculated using the local Rytov approximation is nearly identical to that calculated analytically using the Markov approximation. Our results show that the local Rytov simulation and the Markov approximation provide reliable information about envelope shapes for forward scattered wavefields but that the influence of wide-angle scattering and backscattering have some influence on envelope shapes and should be considered when analyzing data using random media models.

Thursday 29 July AM

Presiding Chair: Dr. Seiji Tsuboi, Department of Geoscience National Defense Academy, Yokosuka, Japan

#### SEISMOLOGICAL OBSERVATION AND INTERPRETATION: THEORY

**ST5/W/34-B4** **0930-01**

#### SIMULATION OF COMPLETE WAVE FIELD PROPAGATION IN VOLCANIC STRUCTURES

Guido Russo, Aldo Zollo (both at Dipartimento di Scienze Fisiche, Universita' di Napoli "Federico II", Mostra d'Oltremare, Pad. 16, 80125 Naples, Italy, Email: russog@na.infn.it, aldo@sungeo3.na.infn.it), Mario Mango Furnari and Alberto Imparato (both at Istituto di Cibernetica, C.N.R., via Toiano 6, 70082 Arco Felice (Naples), Italy, Email: mf@cib.na.cnr.it, a.imparato@cib.na.cnr.it)

We have implemented a finite difference (FD) code as part of the interpretation tools developed in the framework of TomoVes project that is aimed at reconstructing the crustal structures underneath Mt. Vesuvius (Italy) by active and passive seismics. The FD code is based on stress-velocity approach implemented by an explicit method on a staggered grid with fourth order spatial operators. It can handle 2D elastic heterogeneous models. To simulate the effect of topography (an essential feature in almost every volcanic area) we adopted a technique consisting in gradually reducing the stress components to zero. The code undergoes a constant upgrading of its performances by hardware and software improvements. Also, we are developing the code to include anelastic attenuation. We extensively used the FD code to simulate the complete wavefield propagation in heterogeneous volcanic models obtained by tomographic inversion of first arrival times. Synthetic and observed seismic sections recorded along the main profiles of TomoVes96 experiment are compared in order

to validate arrival times models and verify their consistency with the observed waveform amplitudes.

**ST5/W/14-B4** Poster **0930-02**

#### MODELLING SEISMIC WAVE PROPAGATION IN 2-D CYLINDRICAL WHOLE EARTH MODEL BY PSEUDOSPECTRAL METHOD

Yanbin WANG, Hiroshi Takenaka (both at Department of Earth and Planetary Sciences, Faculty of Science, Kyushu University, Hakozaki 6-10-1, Higashi-ku, Fukuoka 812-8581, Japan, Email: wang@geo.kyushu-u.ac.jp, takenaka@geo.kyushu-u.ac.jp) and Takashi Furumura (Faculty of Education, Hokkaido University of Education, Midorigaoka 2-34-1, Iwamizawa 068-0835, Japan, Email: furumura@atson.iwa.hokkyodai.ac.jp)

We present a method for solving the elastodynamic equations in 2-D cylindrical coordinates using the pseudospectral method (PSM). The model and the wavefield are defined in the angular and radial directions, and the derivatives of wavefield are approximated by using the fast Fourier transform in both of the directions.

To solve the 2-D cylindrical elastodynamic equations for whole earth, singularity arises at the center ( $r=0$ ) of the earth. To avoid this singularity, we develop a scheme that uses extension of field variables in the radial direction. Wavefield at the center and the wave propagation through the center can be calculated by this scheme. The time interval used in the calculation is chosen according to the smallest grid spacing in the grid. In cylindrical coordinate system, the smallest grid spacing is located around the center in the angular direction that is much smaller than the grid spacing in radial direction. Generally, the smallest angular grid spacing around center is so small that the calculation is too time consuming to be carried out. We adopt a multidomain scheme (Takenaka & Wang, 1999) to increase the smallest angular spacing and increase the time interval that is large enough to make the calculation for the whole earth model to be implemented on a general computation resource.

We apply the algorithm to the PREM model in a 2-D slice of the whole earth firstly, and then apply it in the forward modelling of wave propagation in more complex models considering subduction, mantle convection.

**ST5/W/16-B4** Poster **0930-03**

#### LASTIC MODELLING BY A MULTIDOMAIN APPROACH OF THE FOURIER PSEUDOSPECTRAL METHOD USING DISCONTINUOUS GRIDS

Hiroshi TAKENAKA and Yanbin Wang (both at Dept. Earth & Planetary Sciences, Kyushu Univ., Hakozaki 6-10-1, Fukuoka 812-8581, Japan, email: takenaka@geo.kyushu-u.ac.jp)

The pseudospectral method is a high-accuracy numerical modelling technique that requires less computer memory and computation time than the traditional techniques such as the finite-difference method. These advantages of the pseudospectral method have enabled us to practically apply this method to modelling seismic wavefields in realistic models that have complex structures such as a sedimentary basin. However, if the sedimentary layers are included in the model, high velocity contrasts arise because of the very low S-wave velocities of the sediments as compared with the bedrock. The grid spacing then has to be very small, which leads to a spatial oversampling in regions with higher velocities. As a result, we also have to use very small time interval for time marching so that the computation requires much CPU time. A breakthrough of this problem is use of a multidomain approach that can employ different grid spacing in different regions, i.e. "discontinuous grids". In this study we propose a scheme of the Fourier pseudospectral method for discontinuous grids, which uses an interpolation by the FFT. This scheme can reduce the computation time as compared with the conventional one. In the presentation we also show the accuracy and efficiency of our approach.

**ST5/W/40-B4** Poster **0930-04**

#### NUMERICAL CALCULATIONS OF SEISMIC WAVES BASED ON SOME NONLINEAR VISCOELASTIC MODEL

Dmitry N. Mikhailov, Institute of Physics of the Earth, Russian Academy of Sciences. B. Gruzinskaya 10, Moscow, 123810, Russia, email: dmikch@uipe-ras.scgis.ru.

Effects of nonlinear propagation of seismic waves in the Earth crust are actively studied recently. The estimates of nonlinear parameters of real rocks show that these media have coefficient of nonlinearity, which exceeds coefficient of nonlinearity of homogeneous solid on 2 - 3 order. Such high value of nonlinearity can be related with a mesostructural heterogeneity of geological media, that is with presence in such media of pores, cracks, grains, blocks, etc. The experimental study of features of seismic waves in the Earth crust have shown, that this process generates oscillations of higher or combinative harmonic, distorting a basic seismic wave. The nonlinear attenuation, formation of solitons and other nonlinear effects were observed in experiments.

The generalized viscoelastic rheology model, including an interior linear scale of a media and nonlinear parameter, was suggested for theoretical study of seismic wave propagation. This model consist of equations of mass and impulse balances and rheology equation (relation between strain and stress). The rheology equation was built on base of combination of some mass and viscoelastic rheological elements. Some type of nonlinear relationships between strain and stress were used.

It was shown that in a long wavelength approximation and at a small period of a spreading wave compare with a relaxation time, the resulting equations are reduced asymptotically to the Burgers equation. The numerical calculations of seismic wave propagation were performed on the base of this model. The results were compared with the data of physical experiments. The dependencies of attenuation and velocity of seismic waves on frequencies were found.

These results may be useful for study and construction of real models of seismoactive zones and for development of new types of prediction of earthquakes based on usage of nonlinear effects (for example, variation of higher harmonic intensity).

**ST5/W/28-B4** Poster **0930-05**

#### SYNTHETIC SEISMOGRAMS OF BODY WAVES IN MULTILAYERED ANISOTROPIC MEDIA

EVGENI M. CHESNOKOV, Alexander A. Vikhorev, and Sergey S. Abaseev (all at the Institute of Physics of the Earth, Russian Academy of Sciences, ul. Bol'shaya Gruzinskaya 10, Moscow, 123810 Russia, email: echesn@uipe-ras.scgis.ru, e.chesnokov@ucl.ac.uk)

For seismology, of importance is to develop the methods for efficient solving the general wave equation, which describe the dynamics of inhomogeneities in arbitrary anisotropic medium. In this work, we present a technique for calculating the Green function of the general wave equation, which is based on summing the normal modes of natural oscillations of the medium. The technique allows one (1) to avoid the pole integrals unacceptable in numerical modelling and (2) to modify the problem of calculating the Green function for inhomogeneous anisotropic medium, successively introducing of inhomogeneities varying from horizontal layers to finite

three-dimensional inclusions. The time needed for numerical calculus also decreases, since the solution is found for relatively great observation times:  $t \gg w(\min)$ , where  $w(\min)$  is the lower bound for signal frequency recorded. The Green function of the layered anisotropic medium with finite three-dimensional inclusions of arbitrary shape is represented as definite integral over two-dimensional sphere, whose integrand is regular function. Attention is paid to the difference between the Green function and theoretical seismogram, obtained as a result of filtering the Green function by the model filter being an analog of receiving apparatus.

**ST5/W/02-B4** Poster **0930-06**

#### INFLUENCE OF SHAPE AND SIZE OF MICROINHOMOGENEITIES ON EFFECTIVE STATIC ELASTIC CONSTANTS

EVGENI M. CHESNOKOV, Yuri A. Kukhareno (both at Institute of Physics of the Earth, Russian Academy of Sciences, B.Gruzinskaya,10, Moscow 123810), John Queen (at Conoco Inc., Seismic Imaging Technology Center, 1000 S.Pine,P.O.Box 1267, 4487 RW, Ponca City, OK -74602-1267, USA), and Peter Yu. Kukhareno (at Institute of Physics of the Earth, Russian Academy of Sciences, B.Gruzinskaya,10, Moscow 123810)

Investigations of the influence of inhomogeneities on the tensor of effective elastic constants usually assume elliptically shaped inclusions. The usefulness of this assumption is quite broad because a wide range of shapes, from needles to spheres, can be represented. At the same time this approximation is rather narrow, because elliptical inclusions imply a uniform or homogeneous strain field throughout the inclusion. This does not correspond to the real situation found in inhomogeneous rocks.

In this paper inclusions of an arbitrary shape are considered. A method for the description of the shape of inhomogeneities is developed. This allows us to calculate analytically the influence of shape on elastic constants of media containing spheres of various radii, hemispheres and spherical segments. Combining these segments allows us to model media with "flower" shaped inclusions. In this case "flowers" can have different petals. Mathematically this means that in integration over wave vector, we can take into account Fourier components which are determined by the shape of the inclusions.

A numerical procedure for the calculation of the effective elastic tensor elements including the influence of various shapes of inclusions is developed. This procedure also accounts for structural correlations in locations and size of inclusions.

**ST5/W/27-B4** Poster **0930-07**

#### MATHEMATICAL MODELING THE PHYSICAL PROPERTIES OF ARTIFICIAL AND NATURAL ROCK SAMPLES

Alexander A. Vikhorev, EVGENI M. CHESNOKOV, and Irina O. Bayuk (all at Institute of Physics of the Earth Russian Academy of Sciences, ul. Bol'shaya Gruzinskaya 10, Moscow, 123810 Russia, email: echesn@uipe-ras.scgis.ru)

Effective physical characteristics of porous-cracked anisotropic media were calculated. In order to find the effective elastic tensor, the generalized singular approximation was applied. The effective tensor was used to compute the angular dependencies of longitudinal and shear wave velocities. The dependencies were compared with experimental data obtained for artificial samples of porous-cracked media. A good agreement between theoretical and experimental values of the body waves were established. For the effective medium in question, the theoretical seismograms of longitudinal and shear waves were calculated, which were compared with the oscillograms observed in experimental study (Rathore et al., 1995).

**ST5/L/02-B4** Poster **0930-08**

#### EARTHQUAKES AND THEIR SPECTRAL ESTIMATIONS USING EINSTEIN DECONVOLUTION

Dan LOEWENTHAL, Raymond & Beverly Sackler (Faculty of Exact Sciences Department of Geophysics and Planetary Sciences and Tel Aviv University (Ramat Aviv 69978, Israel. email: danlo@jupitier.tau.ac.il)

In a recently patented idea, I have conjectured the validity of dual fields theory, which teaches us how seismic or electromagnetic phenomena can be analysed to a much higher precision in comparison to a single field analysis.

In its acoustic embodiment these dual fields are the pressure and the particle velocities fields, as registered by hydrophones and geophones, respectively. This can be effectively done in ocean bottom environment. According to this theory both these fields are initiated by the same source. They both solve the same classical wave equation in regions of homogeneous layers but they differ and are nonlinearly coupled through the boundary conditions, where they possess opposite sign reflection coefficients. Since the source is common, it convolves both fields. Thus, its Green's function is estimated by the ratio of these fields defined through its Z transform polynomials. Using transform ratio of these two fields, a rational polynomial presentation of the system is attained, where the source wavelet cancels out. This allows deterministic spectral estimation similar to the maximum entropy or Bayesian estimators. But while the Bayesian and maximum entropy estimators are of trial and error statistical approach, our source de-convolution, which is the essence of Einstein-Lorentz velocities additions-subtractions formula, is deterministic in nature.

**Thursday 29 July PM**

Presiding Chair: Dr. Gary Gibson, RMIT University, Victoria, Australia

#### SEISMOLOGICAL OBSERVATION AND INTERPRETATION: EARTHQUAKES

**ST5/E/03-B4** Poster **1400-01**

#### AFTERSHOCKS SEQUENCE OF THE 1997 ZIRKUH (GHAEN-BIRJAND) EARTHQUAKE IN EAST-CENTRAL IRAN

M.R. GHEITANCHI (Geophysics Institute, University of Tehran, Tehran, Iran. email: mrghchee@chamran.ut.ac.ir) M. Raeesi (Geophysics Institute, University of Tehran, Tehran, Iran. Email: mraeesi@iman.ut.ac.ir)

On 10th May 1997, a shallow destructive earthquake occurred in east-central Iran (07:57:29.7 GMT, 33.825N, 59.809E, depth 10km, mb 6.4, Ms 7.3, Mw 7.1; USGS). The mainshock happened along the southern extension of an earlier quake in 1979 and caused extensive damage and 1563 human lost. The field study reported 113km NW-SE trending new discontinuous surface faulting produced by the mainshock. The predominant faulting was right-lateral strike-slip. The recorded waveforms are complicated. Furthermore, the reported long duration of shaking also indicated that the faulting during the mainshock was complex. In order to study the aftershock activity, a temporary seismic network was deployed within the meizoseismal area shortly after the occurrence of the mainshock. The seismic activity was monitored for two months. The network included seven portable digital PDAS and three analog Sprengnethers MEQ-800 systems. The aftershocks were determined by using the HYPO71PC

software and good locations were selected on the basis of RMS smaller than 0.3s. The distribution of epicenters suggests that aftershock activity appeared to be close to the macroseismic epicenter having focal depths in the range of 1-20 km. This indicates that the faulting is mainly taking place in the upper crust. Aftershocks extend over an approximately 120km long zone with a general NW-ES elongation. The seismicity appears to be more scattered than along a fault zone. Three barriers were determined by aftershock distribution which two of them coincide with gaps between surface rupture segments. As the number of the seismic stations is very limited, focal mechanism solutions for a single event cannot be drawn. An attempt has been made to determine composite focal mechanisms for various aftershock clusters.

**ST 5/E/05-B4** Poster **1400-02**

#### SOURCE CHARACTERISTICS OF THE 1998 GOLBAF, SOUTH-EAST IRAN, EARTHQUAKE

M.R. GHEITANCHI (Geophysics Institute, University of Tehran, Tehran, Iran. email: mrghchee@chamran.ut.ac.ir)

Golbaf in Kerman province, south-east Iran, is one of the seismically active regions in the country. On 14 March 1998 at 19h 40m 27.1 GMT, a strong earthquake occurred in Golbaf. The earthquake killed 5 people, injured 50, destroyed 2000 homes and left 10,000 homeless in the Golbaf area. The USGS located the mainshock as 30.15N-57.57E with magnitude mb=5.9, Ms=6.9, and Mw 6.6. Harvard University reported a Centroid Moment Tensor analysis for the mainshock. It shows two nodal planes striking 153 (dipping 65 SW) and 61 (dipping 86 SE). A similar solution was given by USGS. The mainshock was associated with a fresh surface faulting and preliminary focal depth determination indicated a shallow focal depth.

Shortly after the occurrence of the mainshock, the University of Tehran deployed a temporary seismic network in the affected area to observe the aftershock sequence and carried on field investigation. In this study, using the results of field observation and aftershocks study the teleseismic body waveforms of this earthquake are inverted to their sources to investigate the source characteristics. The result of this study suggests that the mainshock was a single event having a strike-slip mechanism. Rupture during the Golbaf earthquake initiated in the epicentral area and propagated bilaterally to southeast and northwest. Assuming a NW-SE direction for the fault strike, as revealed from the field investigation, the mainshock has a right-lateral strike-slip mechanism, which is predominant in this region. The seismic moment is calculated to be  $M_0 = 7.12 \cdot 10^{25}$  dyne-cm. Approximating the rupture area by  $L \cdot (L/3)$  and the fault length  $L = 30$  km, the average stress drop will be about 35 bar and the estimated static displacement is about 80 cm.

**ST5/W/22-B4** Poster **1400-03**

#### ON THE STUDY OF STRESS STATE OF EARTH CRUST AT TATARSTAN OIL REGION

Kamil MIRZOEVI ("TATaria-Oil", Tatarian prospecting, Chernyushevsky 6/2, 420503, Kazan, Russia Email: seismo@kazan.su), Albert Lukk , Sergei Yunga (both at Institute of physics of the Earth, Moscow, 123810, B.Gruzinskaya, 10, Email: syunga@uipe-ras.scgis.ru)

One of the first attempt to estimate some features of stress state of Russian plate is presented. This new evidences of stress-strain state are obtained for a territory of Tatarstan. Stress state study presented here is available through small earthquakes data acquisition and processing. They are based on our instrumental seismological observations of numerous weak local earthquakes and their fault plane solutions. Local seismic network consist from more than 10 stations. Determination of composite earthquake focal mechanism is performed on the base of P-wave first arrivals in the framework of standard approach. Preliminary results of the SE-NW compression stresses are obtained. Proceeding from these representations, it is possible to believe, that the recent tectogenesis process should be displayed in more preferable development strike-slip faults on systems of submeridional and sublatitudinal orientations, as well as thrust and overthrust faults on planes of south-east and north-west incidence. These results are correspond to really observable dominant orientation of tectonical joints and microfractures.

Corresponding indication on prevailing development on a territory of Tatarstan and Bashkortostan regional bend of microfractures of north-east direction is reported by Stepanov et al, 1994, 1995. There are the basis to believe, that between fracture tectonics and recent evidences of tectonical and seismic activity there is reasonably close interrelation. It can assists in the establishment of geological correlation models with regard to migration of hydrocarbons.

**ST5/E/17-B4** Poster **1400-04**

#### RUPTURE CHARACTERISTICS OF THE 25 MARCH 1998 ANTARCTIC EARTHQUAKE

Masayuki KIKUCHI and Yoshiko Yamanaka (both at Earthquake Research Institute, University of Tokyo, Tokyo 113-0032 Japan, email: kikuchi@eri.u-tokyo.ac.jp) Keiko Kuge (Department of Geophysics, Kyoto University, Kyoto 606-8502 Japan) Tatsuhiro Hara (International Institute of Seismology and Earthquake Engineering, Building Research Institute, Tsukuba 305-0802 Japan)

A very curious earthquake occurred in an ocean area of the Antarctic plate. We investigate the rupture characteristics of this earthquake using the teleseismic body waves and long-period surface waves recorded by IRIS network. The results of body-wave inversion show two clusters of subevents.

The first cluster consists of a few subevents propagating 60 km to the west during the initial 60 s. The other subevent cluster, which is located at about 120 km west of the epicenter, ruptures during 70-90 s after the initial break. The focal mechanism has a nearly pure strike-slip with NW-SE tension, and almost unchanged during the main process. The westward rupture is also observed in the radiation of long-period surface waves, for which we obtain a total rupture length of about 150 km by assuming two-subevent rupture. The moment tensor solution determined from the surface waves is characterized by strike-slip faulting with NW-SE tension with a large non-double-couple component (NDCC). The NDCC is so significant that it cannot be attributed to long-wavelength lateral heterogeneity of the Earth interior. A temporal and spatial separation of the subevent clusters alone cannot also explain this NDCC, which seems to require other origin than the earthquake source.

**ST5/W/32-B4** Poster **1400-05**

#### STATISTICS OF SEISMICITY AND SOURCE PROCESSES OF EARTHQUAKE SWARM AROUND KAMIKOUCHI, JAPAN, IN 1998

Hiroshi Aoyama, Satoshi IDE, Minoru Takeo and Naoshi Hirata (all at Earthquake Research Institute, Univ. of Tokyo, 1-1-1 Yayoi Bunkyo, Tokyo, 113-0032 Japan, E-mail: aoyama@eri.u-tokyo.ac.jp, ide@eri.u-tokyo.ac.jp)

On August 7, 1998, an earthquake swarm activity began from Kamikochi, Nagano pref., Japan. To make detailed analysis Earthquake Observation Center (EOC), Earthquake Research Institute (ERI), University of Tokyo, installed two broadband seismometers in the

swarm region. These data are used for hypocenter determination and various analyses together with routine seismic networks. During first 4 months of the activity, about 7500 hypocenters are manually determined. We first made statistical studies of the seismicity. Because it has been reported that b-value of Gutenberg-Richter law exceeds 1 in some volcanic active regions, we investigated frequency-size relation of the seismicity and determined b-value. The b-value of overall activity is almost 1 and that for each cluster decreases to 0.5-0.8. This study alone cannot probe the relation to the volcano. We also studied the source rupture process for 17 earthquakes of ERI magnitude 4 or larger, using empirical Green's function method. The rupture of the largest event (Mw 5.2), which mainly propagated to the west and was the largest moment release, occurred 2 s after rupture initiation. More than a half of 17 events show such pre-process before the main moment release. This must be a regional feature of earthquake source process and might be related to some inhomogeneity of crustal structure.

**ST5/W/66-B4** Poster **1400-06**

**SPATIAL AND TEMPORAL ANALYSIS, BY USING BAYESIAN AND CLUSTERING TECHNIQUES, OF A SEISMIC SERIES IN GRANADA BASIN (SPAIN)**

E. CARMONA (1), G. Saccorotti (2), A.M. Posadas (1, 3), J.M. Ibáñez (1, 4), E. Del Pezzo (5), G. Alguacil (1,3) and J. Morales (1, 3). Instituto Andaluz de Geofísica. Universidad de Granada. Campus de Cartuja s/n. 18071 Granada. Spain.; Departamento de Física. Università di Salerno. Via Salvador Allende. 84081 Baronissi, Salerno, Italy. Departamento de Física Aplicada. Universidad de Almería. 04071 Almería, Spain. Departamento de Física Teórica y del Cosmos. Facultad de Ciencias. Universidad de Granada. 18071 Granada, Spain. Osservatorio Vesuviano. Via A. Manzoni, 249. 80123 Napoli, Italy.

A seismic swarm located in the centre of Granada Basin (Spain) occurred between December 1988 and February 1989 is analysed in the present work. From more than 400 events we selected 132 earthquakes and micro-earthquakes recorded in at least four digital stations and with magnitudes ranging between 1.5 and 4.1. The first analysis procedure was to relocate the whole subset picking the first P-wave onset and its uncertainty interval. This analysis was done by standard location procedure as HIPO77. Second, the Bayesian analysis (a probabilistical approach) was applied, from the preliminary location, to the above data in order to obtain regions with maximum likelihood of hypocentral location at every event. The overlapping of these volumes provides the most probable distribution of the source volume. Third, the principle component analysis was applied to the hypocentral distribution obtained in the step one. This analysis has provided the main fault plane that was active during the swarm and other secondary planes.

We compared the focal mechanisms obtained by the inversion of the polarity of the first motion of the P-wave with the planes observed in the above analysis and with the source volume focused with the Bayesian analysis.

Finally we are comparing, by using cross correlation techniques, the different events located inside the source volume in order to distinguish families of events. This analysis is the previous step in case of a Master event location procedure.

**ST4/E/11-B4** Poster **1400-07**

**HIGHER DEGREE MOMENT TENSOR INVERSION OF 1997 TIBETAN EARTHQUAKE (MS=7.4) USING FAR-FIELD BROAD-BAND RECORDING**

Liu Rui Feng (Institute of Geophysics, China Seismological Bureau, Beijing 100081, CHINA, email: liurf@cndsndmc.css.gov)

We used a method presented by T. Dahm and F. Krueger to estimate parameters of the extended earthquake source using higher degree moment tensors at 27 centroid locations. A Taylor series expansion of Green's function around a single centroid is not accurate enough when working with seismic wave periods and wavelengths in the range of rupture duration and spatial extent of the fault, respectively. Introducing a grid of 27 centroid locations on the fault and using higher degree moment tensors we are able to adequately model body and surface waves with periods and wavelengths smaller than rupture duration and fault dimensions, under simplifying assumption an iterative inversion scheme is coded to estimate parameters of planar, Haskell-type faults. We have inverted the higher degree moment tensor of November 8, 1997 Tibetan earthquake using far-field broad-band recording of GSN, the best fit uni-directional rupture model indicated that rupture duration  $T=19.0$  sec, fault length  $L=47$  km, fault width  $W=28$  km, scalar moment  $M_0=2.1E20$  Nm, strike=77 dip=88 rake=0. The result show that uni-directional moments, rupture direction, fault and auxiliary plane and kinematic source dimension and time can be constrained with teleseismic body or surface wave.

**ST5/L/06-B4** Poster **1400-08**

**INFLUENCE OF WEAK SEISMIC IMPACTS ON THE SEISMIC REGIME.**

Nikolay T. TARASOV (OGGGGN Russian Academy of Sciences, Leninskiy ave. 32a, Moscow, 117993, Russia, email: geodep@ipsun.ras.ru) Nadezhda V. Tarasova (United Institute of the Physics of the Earth, Russian Academy of Sciences, B.Gruzinskaya, 10, 123810 Moscow, Russia, email: tarasov@uipe-ras.scgis.ru)

The influence of the Semipalatinsk underground nuclear explosions on the seismic regime of the Garm region located at 1400 km from the test site has been studied. It was found that the occurrence of large events ( $K>10$ ) and microearthquakes ( $K<5$ ) after tests became higher than before them. The occurrence of earthquakes of  $5<K<10$  remains the same. High level activity of small earthquakes was observed from 1 to 30 days. Large earthquakes occurred in 5-7 days cycles. It was found that cycling of seismicity after explosions was connected with periodic discrete changes of activity maximum time delays in different geological structures. Explosions cause release of tectonic deformation process. The energy releases in the series of relatively weak earthquakes instead of one catastrophic event. These results were confirmed in the worldwide seismicity investigation from 1900 to 1997 years.

**Friday 30 July AM**

Presiding Chair: Prof. D. Giardini, Institute of Geophysics, Zurich, Switzerland

**SEISMOLOGICAL OBSERVATION AND INTERPRETATION: APPLICATIONS**

**ST5/W/30-B5** Poster **0930-01**

**OBSERVATIONS OF LOCAL CODA USING A THREE-DIMENSIONAL SEISMIC ARRAY NEAR THE ATOTSUGAWA FAULT, CENTRAL JAPAN**

Masahiro KOSUGA and Tomomi Saito (both at Faculty of Science and Technology, Hiroaki University, Hiroaki 036-8561, Japan, email: mkos@cc.hiroaki-u.ac.jp) Noriko Tsumura (Faculty of

Science, Chiba University, Chiba 263-0022, Japan) Kazushige Obara (National Research Institute for Earth Science and Disaster Prevention, Tsukuba, 305-0006, Japan)

We have examined the characteristics of local coda using data from a small-aperture three-dimensional seismic array deployed near the Atotsugawa fault, the one of the most active strike-slip faults in Japan. The array consists of two subarrays; an L-shaped subarray with 36 seismometers and a spiral subarray with 40 sensors. The use of three-dimensional array with a vertical extent of 230 m gives a unique opportunity to directly estimate the vertical slowness.

We applied a semblance analysis to measure the time variation of coherence, back-azimuth, incident angle, and slowness of waves that pass the array. From close inspection of back-azimuth, we found that the incident azimuth of S-wave is systematically rotated clockwise from the theoretical one for both the earthquakes located to the NE and to the SW of the array. This observation is qualitatively explained by either local velocity heterogeneity or crustal anisotropy. We also found that some coherent phases arrive about 8 s after the P wave, making a flattening or even transient increasing of RMS amplitude. These phases have nearly the same slowness as the P-wave and show a steep incident to the array. Considering the lapse time from the P-wave, these phases are probably the scattered and/or reflected P-waves from the lower crust. The long duration (3-4 s) of coherent arrival suggests that the scattering and/or reflection is occurring in a thick zone rather than a thin sheet.

**ST5/E/23-B5** Poster **0930-02**

**ON THE NATURE OF UNUSUAL SEISMIC PHASE, BEING OBSERVED IN SHORT-PERIOD S-CODA IN THE NORTH TIEN SHAN REGION**

Yuri KOPNICHEV (Complex Seismological Expedition, Joint Institute of Physics of the Earth, Kamo str. 8a, Talgar, Almaty region, 483310, Kazakhstan, email: adm@cse.academ.alma-ata.su)

At the border between the mountainous areas of the North Tien Shan and the Chu and Ili basins an unusual seismic phase sharply stands out against a background of short-period coda on seismograms of local earthquakes and quarry blasts. This phase, which we denoted as SL, is observed most clearly at small epicentral distances (up to 30 km). It presents a compact tandem of almost monochromatic oscillations with periods of 1.5-1.8 sec and duration of ~6-10 sec. The lapse time, corresponding to a maximum amplitude in SL phase (tm), varied from 102 to 131 sec. In a relatively 'quiet' tectonic situation, at the border between the Kendykta range and the Chu basin, the particle motion in SL wave is in a horizontal plane. Apparent velocities of this phase are very low (they reach of ~70-80 m/sec). Very strong variations of tm values are observed in the Zailii deep fault zone: to the south from the fault, in the Zailii Alatau range area they are considerably higher, than to the north from it, in the Almaty depression area. This correlates with data on a big difference of shear wave attenuation in the lithosphere on both sides of the fault. On the basis of an analysis of experimental data it can be concluded, that SL group is formed by shear waves, being reflected from a thin layer with a large impedance contrast, which is located in the upper mantle at a depth of about 220-240 km. Possible reasons of an existence of this layer are discussed.

**ST5/W/23-B5** Poster **0930-03**

**THE MORPHOLOGY OF THE SUBDUCTING SLAB BENEATH NORTHERN TAIWAN**

KUO-FONG MA and Pei-Ru Jian (both at Institute of Geophysics, National Central University, Chuang-Li, 320-54, Taiwan, ROC, email: fong@sal.gep.ncu.edu.tw) Ban-Yan Kuo (Institute of Earth Sciences, Academia Sinica, Taiwan, ROC)

The converted phases from upper plate boundary of the subducting slab denoted as SP phases recorded by the CWBSN (Central Weather Bureau Seismographic Network) for events in northern Taiwan (24.0°N latitude ± 26.0°N, 121°E longitude ± 122°E, 60km depth ± 300km, and  $M_L \geq 4.0$ ) provide us an advantageous opportunity to construct the morphology of descending slab. We apply the polarization filter and theoretical travel time analysis to the 3-component records to identify the conceivable SP converted waves. The initial velocity model with subducting slab used as theoretical travel time calculation was based on the recent tomographic results. The model is constructed by considering that the velocity contrasts among the discontinuities are fixed, while the upper boundary of the slab is allowed to change. We separate the events into several groups according to their paths to stations. Considering the travel time residual of ts-tsp between the observed and the constructed models for different groups, we make out the upper boundary of the subducting Philippine plate beneath northern Taiwan for various profiles. The results show that the subducting slab has a dip angle of about 45 to 50 degree and reaches to the depth of about 100 km beneath northern Taiwan. The subduction also tends deeper to the east, while shallower to the west.

**ST5/W/50-B5** Poster **0930-04**

**SHEAR WAVE SPLITTING AND ANISOTROPY OF THE EARTH'S CRUST: OBSERVATIONS AND MATHEMATICAL MODELLING**

Maria A. KRASNOVA, Alexander A. Vikhorev, Irina O. Bayuk and Evgeni M. Chesnokov (all at Institute of Physics of the Earth, Russian Academy of Sciences, B.Gruzinskaya 10, Moscow, 123810, Russia, email: mkrasnova@uipe-ras.scgis.ru)

An experimental study of the structure of the Earth's crust based on the records of shear waves from low energy earthquakes was carried out for two regions: the south-western seismic zone of Iceland and the Germab seismoactive zone in the Ashkhabad test site. The goal of the study was to distinguish anisotropy of elastic properties and to estimate the depth to the anisotropic layer, its thickness, seismic velocities and composition. The results of the study of 241 three-component seismic records from 50 crustal earthquakes permit to assign a 20% anisotropy of elastic parameters in the central part of the south-western seismic zone of Iceland to 1.75 km layer at the depth of 3 km. The study of 418 seismograms from 81 earthquakes, recorded by seven three-component seismic stations, revealed a 5 km thick upper crustal layer in the Germab seismoactive zone with 14% of elastic anisotropy. Mineralogical models of the crustal composition in the regions of study were used to calculate effective elastic moduli and crustal density by the method of generalized singular approximation. Spatial distribution of seismic velocities and synthetic seismograms were calculated for the estimated elastic moduli and densities and for the set of hypocenters, corresponding to the observed one. The comparison of the calculated and observed seismic velocity distribution, as well as of real and synthetic seismograms permitted to specify the structure and the composition of anisotropic layers.

**ST5/L/01-B5** Poster **0930-05**

**WESTERN US MANTLE STRAIN PROVINCES INFERRED FROM SHEAR WAVE SPLITTING**

D. SCHUTT, University of Oregon, US (email: schutt@newberry.uoregon.edu)

Three tectonic provinces lie near the Yellowstone Hotspot: the Yellowstone Swell, deformed by the passage of the hotspot; the extensional Basin and Range; and the Precambrian craton.



Of these three provinces, only the Yellowstone Swell produces shear wave splitting measurements that are easily explained. In this region, the fast polarization direction of the SKS phase is nearly constant, and is most reasonably explained by the simple shear of the Yellowstone Hotspot asthenosphere as the North America plate moves southwesterly with respect to the more stable interior of the Earth. In contrast, newly analyzed data from three arrays outside the Yellowstone Swell (in conjunction with previous studies) show complex anisotropy, and imply that the Swell is a distinct anisotropic province within the western United States. We find measured fast axis orientation changes with back azimuth at individual stations, and also changes from station to station for a given event. That no obvious strong anisotropic fabric has developed beneath North America, particularly in the Basin and Range where the asthenosphere should be well-developed, suggests that the upper mantle is not deforming in a simple, homogeneous manner.

**ST5/W/62-B5** Poster **0930-06**

#### OPTIMIZING MODEL PARAMETERIZATION IN 2D SEISMIC TRAVELTIME TOMOGRAPHY

Zoltán WÉBER (Seismological Observatory of the Hungarian Academy of Sciences, H-1112 Budapest, Mérédek u. 18., Hungary, email: weber@seismology.hu)

In seismic traveltime tomography a set of linear equations is to be solved for the unknown slowness perturbations. The matrix of this set of equations (the raypath matrix) is usually ill-conditioned because the model space contains more details than can be resolved using the available data. The condition of the raypath matrix can be characterized by its singular value spectrum: the larger the area under the normalized singular value curve and the greater the rank of the matrix, the better the condition of the inversion problem and the more independent pieces of information may be gained from the data. The structure of the raypath matrix depends on the source-receiver configuration and the model parameterization. Since the source-receiver geometry is often fixed (e.g. in earthquake tomography), conditioning can only be influenced through the model parameterization, i.e. the structure of the model space.

In this paper we illustrate a method for finding an optimal, irregular triangular cell parameterization that best suits the raypath geometry. We present a practical measure of conditioning that is to be minimized. Since this measure depends on the model parameterization in a highly nonlinear manner, a simulated annealing algorithm is used to find the optimal parameterization. We show that the condition of the raypath matrix corresponding to the parameterization determined by optimization is much better than that corresponding to a regular rectangular parameterization with the same dimension. The method is demonstrated through some cross-borehole tomographic examples with given acquisition geometries.

**ST5/W/53-B5** Poster **0930-07**

#### EMISSION TOMOGRAPHY - FRUITFUL APPROACH FOR SEISMIC STUDY IN THE 21ST CENTURY

Irina J.TCHEBOTAREVA (Inst. Earth Physics RAS, B.Gruzinskaya 10, Moscow 117234, Russia, email: chari@synapse.ru)

Seismic observation by means of a dense seismic array composed from 3-component stations allows us to develop new advanced methods of study of the fine structure of the Earth and seismic emission. One of such methods is emission tomography which permits to locate sources of weak continuous seismic signals, to estimate amplitude and spectrum of underground radiation from the active sources and scatterers. Different parts of seismic records supply different kind of geophysical information. Using records of the direct P and S waves of a seismic event, we receive images of the source of the event. Analysis of the coda part of seismic records gives the 3-D image of a scattering structure and a distribution of active volumes of seismic radiation induced by direct waves. Analysis of a seismic noise detects the active volumes of seismic emission being a kind of trigger effect in the energy-saturated Earth. Emission tomography is a device for seismic monitoring in the volcanic and tectonic active areas, mines and oil and gas deposits: a set of images in the consequent time windows shows the evolution of seismic sources distribution. The possibilities of emission tomography are illustrated by the results of computer modeling and study of the data of seismic observation over volcanic front in the northern Kanto, Japan. Detected scattering and emission anomalies relate to the real geological objects. Active volumes revealed from noise analysis are the same that the volumes of induced emission in the 'late' coda. Now the emission tomography studies are unique because of a small number of suitable observations but in the nearest future, with a developing of seismic designs, this powerful method can become a routine one. By means of choice of a suitable frequency band and array aperture we can carry out study in different scales, from the crustal to the global one.

**ST5/E/10-B5** Poster **0930-08**

#### RELOCATION OF LARGE HISTORICAL EARTHQUAKES GLOBALLY USING MODERN TECHNIQUES

A VILLASENOR, T M Boyd (Colorado School of Mines, Golden, CO 80401 USA, ph. 1-303-273-8590; e-mail: antonio@gldage.cr.usgs.gov) E R Engdahl, K M Shedlock (U.S. Geological Survey, Denver, CO 80225 USA)

Although earthquakes have been instrumentally recorded for nearly 100 years, source parameters (epicenter location, depth and magnitude) for events that occurred before the full implementation of the World-Wide Standardized Seismograph Network (WWSSN) during the early 1960's are poorly constrained. In most cases, this is simply because modern data analysis techniques have yet to be applied to the available observations, which, for the most part, are preserved as written records, not in a computer-ready, digital data format.

We have undertaken the uniform relocation of all earthquakes reported prior to 1964 in the International Seismological Summary (ISS), the Bureau Central International de Seismologie (BCIS) Bulletin and other available bulletins. Arrival times tabulated in these bulletins are converted to computer-readable form using optical character recognition (OCR) software. After examining the observations for obvious translation errors and establishing the locations and codes of the recording stations, the arrival times are converted to a standard format (ISC 96-byte). Each earthquake is then relocated using the ak135 earth model, and P, S PKP, and re-identified depth phases (pP, sP and pWP).

In this presentation, we show and discuss results from relocations of earthquakes of magnitude equal to or greater than 6.5 during this period. This systematic re-determination of historical earthquake locations permits the better definition of seismic zones globally, which can be readily applied to a range of seismicity, seismotectonic and seismic hazard investigations.

**ST5/E/07-B5** Poster **0930-09**

#### RELOCATION OF FRENCH NUCLEAR EXPLOSIONS IN THE TUAMOTU ARCHIPELAGO

Eric BERGMAN (Global Seismological Services, 601 16th St., #C390, Golden, Colorado 80401, USA, ph/fax: 1-303-278-4089, email: bergman@seismo.com) E. R. Engdahl (Department of Physics, University of Colorado, Campus Box 390, Boulder, Colorado 80309-0390 USA, ph: 1-303-735-4853,

fax: 1-303-492-7935, email: engdahl@lemond.colorado.edu)

Between 1968 and 1996 the French government conducted nuclear tests at Mururoa and Fangataufa, atolls of the Tuamotu Archipelago in the south central Pacific. Although the true locations and origin times of these tests have never been released, the limited extent of the atolls allows strong constraints to be placed on the true locations. The ISC Bulletin and USGS datasets contain arrival time data for 91 explosions, which comprise a particularly attractive dataset for methods of multiple event relocation. We applied the Hypocentroidal Decomposition (HCD) method to examine the effects of network coverage and the use of different phase sets on the estimation of epicenters and origin times. Relocations are performed using several phase sets: P only, and P plus PKP phases, with distance-dependent phase weighting based on observed variances. One useful criterion of success is the ability to separate Mururoa events from the nearby Fangataufa events. The statistical rigor of the HCD method allows such a distinction to be made in most cases. Confidence ellipses are calculated separately for the relative locations of the events with respect to the cluster's centroid and for the centroid itself. The relative locations form a pattern which may be shifted to provide an optimal match with the shape of the atolls. Comparing this shift with the location of the centroid provides insight into the applicability of the travel time model (ak135). The improved locations and origin times should have application as a known source for studies of deep earth structure.

**ST5/W/26-B5** Poster **0930-10**

#### EARTHQUAKE LOCATION ON IRREGULAR GRIDS

Todd Nicholson, MALCOLM SAMBRIDGE, OLI GUDMUNDSSON (Research School of Earth Sciences, Australian National University, Canberra ACT 0200, Australia; email: malcolm@rsees.anu.edu.au.)

Over the past five years the advent of high performance computing has led to increased interest in grid search methods for earthquake location. This approach has several advantages over matrix methods in that it overcomes numerical stability problems associated with matrix inversion, avoids the calculation of derivatives and allows flexibility in choice of data fit measure. Previously grid search methods have been restricted to simple, or nested, regular grids (i.e. based on rectangular cells) in three or four dimensions, which are searched for a best fit solution. Even with modern computers this often involves a search over an enormous number of possible solutions and may not be practical for routine use. Here we propose a simple procedure for locating hypocenters on a completely unstructured mesh. The advantage is that the mesh may be generated automatically from a set of nodes with any chosen distribution, allowing finer discretization in regions where events are more likely, e.g. defined by previous seismicity, local geology or other factors. We illustrate the approach by building an irregular mesh from global seismicity using Delaunay tetrahedra, and locating earthquakes by a process of pattern matching with previous events. The novelty is that no seismic earth model is required.

**ST5/W/69-B5** Poster **0930-11**

#### ACCURATE HYPOCENTER DETERMINATION USING STATION CORRECTIONS: IN THE CASE OF SOUTH-WEST OFF HOKKAIDO IN JAPAN

Masaki Nakamura (Seismology & Volcanology Research Department, Meteorological Research Institute, 1-1 Nagamine, Tsukuba, Ibaraki, 305-0052, Japan, email: mnakamur@mri-jma.go.jp)

One of the approaches of accurate hypocenter determination is the station correction method. This method is usually applied to earthquake activity in relatively small area, such as swarm. HURUKAWA and OHMI (1993) proposed a new method where station corrections vary as a function of hypocenter coordinates. They applied it to the earthquake observation network covering about 200 km \* 200 km, and showed its effectiveness. But their method encounters difficulties when earthquakes are poorly surrounded by stations, as is often the case of earthquakes in the sea. We still expect good results if we can combine their method with some accurate hypocenters for reference. This is shown in this study. After 1993 Hokkaido Nansei-Oki Earthquake which occurred south-west off Hokkaido in 1993, HINO et al. (1994) installed 18 pop-up type oceanbottom seismometers covering the focal region at intervals of 5 - 30 km, and determined focal parameters of aftershocks. Then station corrections as a function of hypocenter coordinates are obtained based on them, and focal parameters of earthquakes occurred in the region are re-determined. Main results are the following: 1. Hypocenters determined by Japan Meteorological Agency (JMA) and those re-determined by the conventional method of station corrections based on them, are mostly distributed shallower than 40 km, while hypocenters re-determined in this study are mostly distributed shallower than 20 km. 2. Aftershock segments, especially the segment north-west of Okushiri island, are smaller than those of JMA hypocenters etc. 3. If data of Okushiri station near the analyzed region are excluded, hypocenter distribution becomes remarkably thicker. It will be possible to determine accurate hypocenters all over Japan by this above method, if accurate reference hypocenters are available which are determined by pop-up type oceanbottom seismometers, depth phase, and so on. I thank to the members of HINO et al. (1994) for providing hypocenters.

**ST5/E/26-B5** Poster **0930-12**

#### THE CALIBRATING CURVES FOR MACROSEISMIC MAGNITUDE DETERMINATION IN THE AREA OF CAUCASUS, TURKMENISTAN, TURKEY

Ye.A. Khrometskaya (United Institute of the Earth Russian Academy of Sciences, Moscow, 123810 Russia; 0952541564; e-mail: kondor@uipe-ras.scgis.ru)

The macroseismic magnitude (MMC) is determined as an average macroseismic intensity MCK-68 reduced to the hypocentral distance 30 km by calibrating curve. The MMC values are correlated with MLH, MPVA and logE (Rautian, 1982). The curves were obtained for Caucasus, Turkmenistan, Turkey. The scale can be used for determination of magnitudes of historical earthquakes from macroseismic data. The calibrating curves were used for redetermination of macroseismic magnitudes of several strong earthquakes in this area.

**ST5/E/06-B5** Poster **0930-13**

#### LOCAL MAGNITUDE SCALE CALIBRATION FOR VRANCEA (ROMANIA) INTERMEDIATE-DEPTH EARTHQUAKES

Olivia Bazacliu (National Institute for Earth Physics, P.O. Box MG-2, 76900 Bucharest, Romania, email: olivia@infp.ifa.ro) Mircea RADULIAN (National Institute for Earth Physics, P.O. Box MG-2, 76900 Bucharest, Romania, email: mircea@infp.ifa.ro)

The present paper is focused on two main problems: (1) the determination of a reference curve for magnitude computation in case of Vrancea intermediate-depth earthquakes, and (2) the correlation between the new proposed local scale magnitudes and other source- or propagation-related parameters (seismic moment, stress drop, peak ground motion values etc.). To this purpose an extended waveform data set provided by the Romanian local seismic

networks of S13 instruments (short-period velocities, vertical components) and K2 instruments (accelerations, three components) is investigated. More than 100 events with magnitude between 2.5 and 7.1, located in the depth range from 60 to 180 km, are considered. Peak displacements and velocities and spectral values (P- and S- body waves) are used to obtain the reference curve (amplitude versus hypocentral distance). Influences of site amplification factor, focal mechanism and focal depth are estimated. The calibration of the computed magnitude with the seismic moment and a rapid earthquake quantification procedure are analyzed.

**ST5/E/36-B5** Poster **0930-14**

**SEISMOLOGICAL NETWORK IN REPUBLIC OF MACEDONIA: HOMOGENEOUS MAGNITUDE SYSTEM**

Dragana Cernih (Seismological Observatory, P.O.Box 422, 91000, Skopje, Republic of Macedonia, email: dcernih@seismobsko.pmf.ukim.edu.mk) Lazo PEKEVSKI (Seismological Observatory, Faculty of Natural Sciences and Mathematics, Sts Cyril and Methodius University, Skopje, Republic of Macedonia, email: lpekevski@seismobsko.pmf.ukim.edu.mk)

A Homogeneous Magnitude System (HMS) has been determined for the territory of the Republic of Macedonia, for the four telemetred seismological stations: Skopje (SKO), Valandovo (VAY), Ohrid (OHR) and Bitola (BIT). Earthquake network magnitudes (NM) can be estimated for weak regional earthquakes using amplitude observations from these stations. Method of basic station for determining station corrections and a combined method, based mainly on the graphical method and on the method of moving averages, for determining improved magnitude calibrating function were used. The station corrections for VAY, BIT and OHR, relative to SKO, and the improved calibrating function for Sg waves observed for the range of epicentral distances 55-205 km, were obtained through four successive iterations using 450 HMS station amplitude observations. The calibrating function for Lgh and Sg waves determined by Karnik (1968) was used as the initial calibrating function.

**Friday 30 July PM**

Presiding Chair: Prof. J.J. Park, Department of Geology and Geophysics, New Haven, USA

**SEISMOLOGICAL OBSERVATION AND INTERPRETATION: LOW FREQUENCY**

**ST5/W/57-B5** Poster **1400-01**

**WHY DOES THE EARTH OSCILLATE CONTINUOUSLY?**

Genevieve Roult and Nicolas Denis (both at Institut de Physique du Globe de Paris, 75252 Paris-Cedex 05, France; groutt@ipgg.jussieu)

It is well established that the fundamental modes of the Earth are excited even on seismically quiet days and the Earth is oscillating continuously, because of still unexplained dynamic processes. The GEOSCOPE network, which started in 1982, provides us with long time high quality seismic data to better observe this phenomenon. We can now detect the resonance frequencies of the Earth even in absence of earthquakes. Analysis of the WUS station (the GEOSCOPE station with the lowest noise level), and the TAM station (with simultaneous recording of a microbarograph) helps us to make a preliminary interpretation of these background oscillations. While the exact causes are not clear, they may be of internal origin (for example tectonic motions) or external origin (for example atmospheric turbulence). These oscillations may be an interesting example of atmosphere-solid earth interaction, but we must first eliminate possible sources including small earthquakes usually ignored in the data processing, undetected earthquakes, slow and silent earthquakes.

**SW1**

**Friday 30 July**

**NEW SYSTEMATIC APPROACHES IN SEISMIC HAZARD AND EARTHQUAKE PREDICTION RESEARCH**

Location: Medical School WG11 LT5  
Location of Posters: Arthur Thompson Hall

**Friday 30 July AM**

Presiding Chair: V.G. Gitis, IITP RAN, Moscow, Russia  
D.A. Rhoades, Institute of Geological and Nuclear Sciences, New Zealand  
Concurrent Poster Session

**SW1/E/09-B5** **0830**

**THE THERMAL CHARACTERISTICS OF LAB DEDUCED FROM MAGSAT MODEL**

Xiaogang GAO (Lanzhou Institute of Plateau Atmospheric Physics, CAS, 730000 Lanzhou, P.R.China, email: xgao@lzu.edu.cn) Giovanni P Gregori (Istituto di Fisica dell'Atmosfera, CNR, 00133 Rome, Italy, email: gregori@atmos.ifa.rm.cnr.it)

It is well known that electric currents exist in the Earth. The Earth's magnetic field is produced the currents. These currents can produce heat because of the resistance of the material of the Earth (called Joule heat). This electric current can be derived from geomagnetic field data or model. Till now, the best geomagnetic field model (MAGSAT) had been gotten by satellite global observation in 1979-1980. By this model, the global distribution of Joule Heat on ALB (Asthenosphere-Lithosphere Boundary) (direct proportion to electric current square) had been calculated. It is found that the distribution of Joule Heat on ALB matches the global geothermal zones very well. And the strongest Joule's Heating is located below Tibet Plateau, the youngest and the highest plateau on the Earth. It seems that the geothermal heat mostly comes from ALB, it is controlled by Joule's Heating process.

**SW1/E/04-B5** **0845**

**THE RELATIONSHIP BETWEEN GEOTHERMAL VORTEX AND EARTHQUAKE**

Maocang Tang and Xiaogang GAO (both in Lanzhou Institute of Plateau Atmospheric Physics, CAS, Lanzhou 730000, P.R.China, email: xgao@lzu.edu.cn)

Earthquake always accompanies by thermal process. The change of soil temperature at different depths shows the underground thermal process. The data of soil temperature observed in more than 180 meteorological observatories in China for the period of 1980-1993 have been

analyzed. And the concept of Geothermal Vortex was proposed and defined. The result shows that there are close relationship between geothermal vortex and earthquake. Earthquake always happened at the edge, with high gradient, of geothermal vortex. The stronger the geothermal vortex, the stronger.

The earthquake. It is possible to predict dangerous areas of earthquake by following the movement of geothermal vortices. Based on the statistical facts, a thermal-dynamic process linking geothermal vortex and earthquake has been proposed.

**SW1/W/05-B5** **0900**

**PROBABILISTIC ASSESSMENT OF EARTHQUAKE HAZARD IN THE INDIAN SUBCONTINENT**

IMTIYAZ A. PARVEZ (Department of Geology, Kumaun University, Nainital, INDIA. Presently at the Department of Earth Sciences, University of Trieste, ITALY, email: parvez@geosun0.univ.trieste.it)

Avadh Ram (Department of Geophysics, Banaras Hindu University, Varanasi - 221005, INDIA)

The Indian subcontinent is one of the most seismic prone areas of the world. Himalayan mountains in the north, mid-oceanic ridges in the south and earthquake belts surrounding the Indian plate all show that the subcontinent has undergone through extensive geological and tectonic processes in the past. The probability of the occurrence of earthquakes with magnitude  $6 < M_b < 7$  during a specified interval of time have been estimated on the basis of four probabilistic models namely Lognormal, Weibull, Gamma and Exponential distribution for the Indian subcontinent. The seismicity map has been prepared using the earthquake catalogue from the period 1963-1994 and six different zones have been identified on the basis of clustering of events. The model parameters have been estimated by the method of Maximum Likelihood Estimates (MLE) and Method of Moments (MOM). A computer program package has been developed for all the four models which represents the distributions of time intervals fairly well. The logarithmic of likelihood (lnL) are estimated for testing the models and different models have been found to be plausible. The probability of different magnitude threshold has been evaluated using Gutenberg-Richter formula  $\text{Log}N = a - bM$  for magnitude distribution. The constants a and b have been computed for each region and found to be varying between 5.46-8.53 and 0.87-1.34 respectively.

**SW1/P/01-B5** **0915**

**MODELLING EARTHQUAKE SWARMS NEAR VALSAD (GUJRAT), INDIA USING CHAOTIC DYNAMICS**

H.N. SRIVASTAVA and S.N. Bhattacharya (both at India Meteorological Department, New Delhi-110003, India, e-mail: snb@imd.ernet.in) D.T. Rao and Sanjay Srivastava (both at Gujarat Engineering Research Institute, Vadodara-50007, India)

Valsad district in South Gujarat near the western coast of the Peninsular India experienced earthquake swarms since early February, 1986. A total number of 21,830 earthquakes were recorded during March 1986 to June 1988. The daily frequency of earthquakes for this period was utilised to examine deterministic chaos through evaluation of dimension of strange attractor and Lyapunov exponent. The low dimension of 2.1 for the strange attractor and positive value of the largest Lyapunov exponent suggested chaotic dynamics in Valsad earthquake swarms. In the neighbouring Koyana region, strange attractor dimension of 3.41 suggested it to be a new measure of seismotectonics. These results have been compared with the modelling parameters needed near the continent-continent collision type of Indian-Eurasian plate boundary. It is found that based on dynamical concepts, more reliable techniques for earthquake hazard assessment can be developed as compared to that using Gutenberg frequency magnitude relationship attempted so far.

**SW1/W/06-B5** **0930**

**"PARAMETRIC-HISTORIC" PROCEDURE FOR SEISMIC HAZARD ASSESSMENT AND ITS APPLICATION FOR EARTHQUAKE HAZARD MAPPING IN SUB-SAHARAN AFRICA**

Andrzej KIJKO (Council for Geoscience, Geological Survey of South Africa, Private Bag X112, Pretoria 0001, South Africa, Email: kijko@geoscience.org.za); Gerhard Graham, (Council for Geoscience, Geological Survey of South Africa, Private Bag X112, Pretoria 0001, South Africa, Email: gerhardg@geoscience.org.za)

A new methodology for probabilistic seismic hazard analysis (PSHA), is described. The approach combines the best features of the "deductive" (Cornell, 1968) and "historical" (Veneziano et al., 1984) procedures. The maximum regional magnitude  $m_{max}$  is of paramount importance in this approach and the authors present some of the statistical techniques that can be used for evaluation of this important parameter. The approach permits the utilisation of incomplete earthquake catalogues. It is assumed that typical catalogues contain two types of information: historical macroseismic events that occurred over a period of a few hundred years, and recent instrumental data. The historical part of the catalogue contains only the strongest events, whereas the complete part can be divided into several subcatalogues, each assumed complete above a specified threshold of magnitude. The approach also takes into account uncertainty in the determination of earthquake magnitude. The technique has been developed specifically for the estimation of seismic hazard at individual sites, without the subjective judgement involved in the definition of seismic-source zones, when specific active faults have not been mapped and identified, and where the causes of seismicity are not well understood. As an example of the application of the new technique, the results of a typical hazard analysis for a hypothetical engineering structure, frequency dependent hazard maps for South Africa and Sub-Saharan Africa are presented.

**SW1/W/01-B5** **0945**

**SOME STATISTICAL CHARACTERISTICS OBTAINED FROM A LARGE NUMBER OF EARTHQUAKES IN CHINA BY SINGLE-LINK CLUSTER METHOD**

Yanlu MaHuilan Zhou (Graduate School at Beijing, University of Science and Technology of China, 100039 Beijing, China)

We have used SLC method, introduced by C. Frohlich etc, to analyze the spatial and temporal properties of 43,260 earthquakes ( $M_s \geq 3.0$ ) occurred in China and its neighbors between 1970 and March 1998.

After computing the space-time SLC frame of these earthquakes, we have got three results: (1) The earthquake clusters obtained from cutting all the links exceeding a special cut-off length D show an obvious fractal characteristic. The number of clusters and the number of earthquakes within the cluster exhibit explicitly a scaling invariance. This characteristic is maintained when D is varied between 30 and 100 km. (2) We considered two distribution functions about the link length in the frame:  $w_1(r) = N(\langle r \rangle / N_0)$ ,  $w_2(r) = L(\langle r \rangle / L_0)$ . The function  $w_1(r)$  is the statistical empiric distribution function of link length that is treated as a random variable.  $N_0$  is the total number of links,  $N(\langle r \rangle)$  is the number of links which lengths are shorter than r.

The function  $w_2(r)$  is closely related to the fragmentation distribution.  $L_0$  is the total length of links.  $L(<r)$  is the sum of link lengths which are shorter than  $r$ . We find that Weibull function  $w(r)=1-\exp[-(kr)^d]$  fits  $w_2(r)$  very well. We can also match  $w_1(r)$  with a Weibull function, but the fitting result can not pass the Kolmogorov non-parametric test. So we can not say that the links obey Weibull distribution. And we can not conclude that they do not obey Weibull distribution, because the non-random sample of links can also explain the result. When we delete the pre- and after shocks, we can get a new catalog and a new frame which distribution of link length can pass the statistic test. (3) We considered that slips of a frame in a time interval. We can use the variation of parameters-  $d$  and  $k$  in  $w(r)$  to describe the variation of distribution of earthquakes in space and time. We found the  $d$  value declined so much in 1976, which may be concerned with the high level of seismicity in that period. However, the variation of year by year can only show some gross information in such a large region.

**SW1/W/02-B5****1000****THE PECULIARITIES OF THE SEISMICITY LATITUDE DISTRIBUTION AND THE EARTH ROTATION**

Boris W. LEVIN (\*Shirshov Oceanology Institute of RAS and Russian Foundation for Basic Research, 32a Leninsky prosp., Moscow, 117334 Russia; levin@rbr.ru) Yeugeny Chirkov (\*\*Union Institute of the Earth Physics of RAS, 10 Bolshaja Gruzinskaja, Moscow, 123810 Russia; email: chirkov@uipe-ras.scgis.ru)

The analysis of the latitude distribution of the earthquakes number and its energy on the base of NEIC catalogues (1900-1993) is presented. The peculiarities of the latitude distribution of the seismicity connected with the Earth's rotation has been found. We had made the histograms of the earthquake numbers and its energy as a function of a latitude  $F$  from 90 deg. N to 90 deg. S at period of 1900-1993. We had found that the latitude distribution of the event numbers  $N(F)$  is similar to the curve describing a dependence  $R^2(F)$  or  $I(F)$  where  $R$  is a distance from the axis of rotation and  $I$  is an inertia momentum of mass unit of the Earth crust. It was also discovered the local maximum of the earthquake number in the region of so-called "critical parallel"  $\approx 35$  deg. N which was introduced by A. Verone (1912) and theoretically grounded by F.Krasovsky and V. Magnitsky (1941). The comparison of the seismicity latitude distribution in West hemisphere and in the East one showed that most of local maximums of the seismicity for first hemisphere is coincident with the corresponding local minimums of seismicity in other hemisphere as rule, and on the contrary. Revealed peculiarities confirm the axis symmetry of the seismicity distribution that may be considered as sign of connection between seismicity and the Earth rotation.

**SW1/E/03-B5****1015****A NEW SYNTHETIC EXPERT SYSTEM FOR QUICK SEISMIC HAZARD ASSESSMENT AND LOSS ESTIMATION**

Yueqing Zhu, Ping Hao (Center for Analysis and Prediction, China Seismological Bureau, P.O.Box 166 Beijing, 100036, email: zhuyq@sun.ihep.ac.cn)

Earthquakes usually make very serious catastrophes to humanity. It is necessary very much to have a quick assessment and estimation on the hazard and risk caused or will be made by the strong earthquake for all the countermeasures for preparedness prior to earthquakes and also search, rescue and relief operations post quakes, not only for the decision-makers, commanders, but also for the public, which had been shown by many historical lessons obviously. But what to do and how to do it is an important problem.

The Author and his research group have completed a new approach of the methodology and also software system development on a synthetic expert system for quick seismic hazard assessment and loss estimation. This system is consisted of several modules on data management, evidence acquisition, knowledge processing, reasoning, decision-making and output, contents different functions on geological, engineering hydrological, site soil dynamics, seismological, construction, population and economical conditions recognition and seismic wave attenuation and people activity laws application and some additional functions. It is an intelligent system combined several different disciplines, an advanced software system integrated functions of different software environments (such as VP, GIS et al.), also a practical earthquake hazard assessment and loss estimation system.

**SW1/W/09-B5****1100****STUDY ON SOME SEISMOLOGICAL PREDICTION INDEXES AND SYNTHETIC PREDICTION METHODS FOR 5 SEISMIC ZONES OF SICHUAN PROVINCE, CHINA**

Weibin Han and Guixi Yi et al.(Seismological Bureau of Sichuan Province, Chengdu, 610041,P. R. China, email: Hanwb@mail.sc.cninfo.net)

In this paper, 6 seismological prediction indexes: variation rates of capacity dimension and information dimension, algorithmic complexity, seismicity quiescence index,  $b$  value, mean square deviation from  $Ig N=a-bM$  and total area of faults, and 4 synthetic prediction methods: combined probability, pattern recognition, fuzzy clustering and neural net method have been carefully studied for 5 major seismic zones of Sichuan and its neighbour region, China. Using more than 20 years' data since the beginning of 1970' for the 5 seismic zones, the change curves of the 6 seismological prediction indexes with time have been calculated, taking 1 a as the time window and 0.5 a as step length. After selected and determined the criterions of recognizing precursor and prediction regulations, the prediction ability of the 6 seismological indexes have been tested by using prediction mark  $R$ . Then 4 synthetic prediction methods based on the 6 seismological indexes have been researched, and their prediction ability have been tested and compared by using prediction mark  $R$ , too.

The results show: (1) For most of the seismic zones, indexes and synthetic prediction methods, the prediction marks  $R$  are higher than the critical mark value  $R_0$  for assessing random prediction at the confidence level of 97.5%. (2) Generally, the prediction ability can be raised by using any one of 4 synthetic prediction methods. (3) When the prediction ability of the 4 synthetic prediction methods are compared, it seems that the  $R$  value of the combined probability method and pattern recognition method are higher.

**SW1/W/03-B5****1115****VARIATION OF ATMOSPHERIC INGREDIENT CONCENTRATION BEFORE EARTHQUAKES**

Tokiyoshi MATSUDA, Hiroshi Matsumoto and Motoji Ikeya (Department of Earth and Space Science, Graduate school of Science, Osaka University, 1-1 Machikaneyama, Toyonaka, Osaka 560-0043, Japan, Email: toki@ess.sci.osaka-u.ac.jp)

We proposed an electromagnetic model of fault to explain seismic electromagnetic signals (SEMS) in which electric charges are induced around the epicenter before earthquakes by the piezo-electricity of quartz [1]. Nitrogen oxide (NO) is produced by natural electric discharge phenomena of atmospheric lightning [2]. Earthquake lightning before the Kobe Earthquake

(Hyogo Pref. Jan. 17, 1995,  $M=7.2$ ) due to dark atmospheric discharge is reported, which might produce NO [3]. We analyzed the variation and distribution of NO concentration at atmosphere monitoring stations affiliated to local Environmental Protection Agencies (EPA), near epicenters of large earthquakes. In case of the Kobe Earthquake, the concentration of NO was 199 ppb, about 7 times as large as average level for a few hours, 8 days before the earthquake. There was an increase in radon concentration in deep well water on the same day [4]. Count of SEMS at LF (163 kHz) also increased [5]. Thunderstorm was more than 150 - km away from the epicenter. Since it is hard to consider that the NO is generated by thunder (atmospheric lightning). The EPA data related with other major earthquakes ( $M > 6.0$ ) also indicate the increase concentration of NO. About earthquake in Kagoshima (Kagoshima Pref. 1997 Mar. 26,  $M=6.2$ ), the NO concentration increased to 30 ppb, about 3.5 times more than average level for one hour, 8 days before the earthquake. The results of the analysis suggest the relation between NO concentration and large earthquakes.

**SW1/W/07-B5****1130****FROM INTERMEDIATE-TERM CN PREDICTIONS TO MICROZONING: HOW TO USE AVAILABLE INFORMATION TO INCREASE EARTHQUAKE PREPAREDNESS**

ANTONELLA PERESAN (Department of Earth Sciences, University of Trieste, via Weiss 4, 34127 Trieste, Italy, Email: anto@geosun0.univ.trieste.it) Giuliano F. Panza (Department of Earth Sciences, University of Trieste, via Weiss 4, 34127 Trieste, Italy and The Abdus Salam International Centre for Theoretical Physics, SAND Group, Trieste, Italy)

The possibility to combine CN intermediate-term earthquake predictions, pattern recognition of earthquake-prone areas and deterministic hazard maps, in order to associate CN Times of Increased Probability (TIPs) to a set of appropriate scenarios of damage, is examined. The algorithm CN indicates the probable occurrence, inside a given space-time window, of events with magnitude greater than a fixed threshold  $M_0$ , on the basis of a quantitative analysis of the seismic flow. Hence, when a TIP is given, it is feasible to select from the available databases, produced for seismic hazard estimations and based on historical and instrumental data, the subset of expected sources included within the monitored region. This source data-set can be used as seismic input for the realistic modelling of ground motion, thus identifying, inside the confined region alerted by CN, the zones where is possible an optimisation of the mitigation measures. The advantage of this procedure mainly consists in the time information provided by predictions, indicating the urgency of intermediate-term actions oriented to damage reduction within relatively limited areas.

In a further step, pattern recognition methods can be applied to identify, independently from seismicity information, sites where events with magnitude larger than 6.5 may occur, based on the assumption that such earthquake-prone areas are associated to unstable tectonic structures formed by faults or lineament intersections. This procedure and CN algorithm can be viewed as independent experts, therefore when CN indicates a TIP, it is also possible to identify a set of scenarios of damage for the strongest events, associated to the earthquake-prone areas included in the region. This procedure will provide useful information to increase preparedness of safety measures and to indicate a priority for detailed seismic risk studies to be performed on a smaller scale, such as the microzoning of the built environment.

**SW1/E/10-B5****1145****SOFTWARE PACKAGE FOR DETECTION OF LOCAL EARTHQUAKE PREPARATION SIGNS (LOW-FREQUENCY FOREGOING SEISMIC SIGNALS).**

Elena V. Satorova ( State Oceanographic Institute, 6 Kropotinsky per., Moscow, 119838 Russia; email: sator@geoph.ioras.msk.ru)

It is discussed the properties of low-frequency seismic signals foregoing main shock and the methods developed for its detection. The foregoing low-frequency seismic (FLFS) signals were already described as a sign of the earthquake preparation (B.W. Levin, E.V.Satorova, 1994, 1996; P.F.Ihmle, T.H.Jordan, 1994; L.Brevdo, 1998). These signals have: a period from 3 to 200 s, forecast time before P-wave arrival in area from 20s to 1.5 hours, small amplitude. Richter magnitude for such events were above 5.5. It should be noted that the real data have the signal to noise ratios well below than unit ( sometimes less than 0.001), that the FLFS signals may appear as a packet of pulses several times in pre-history period. In this case it is more efficient to use simultaneously wellknown canonical methods as well as unorthodox data processing methods for extraction, description and quantitative estimations of the measured signals. It is discussed software package developed for picking up FLFS signals, for detection of the faint modification of the observed data, for analysis of the signal structure, for extraction of the repetitive groups of the alike signals. This package is based on the using unorthodox data processing methods such as extremal statistics, pattern recognition, linguistic description and linguistic recognition, the neural networks, fuzzy set methods. It may be used for data processing any one of multi-channel geophysical data and for simultaneously processing of different data type.

**SW1/W/04-B5****1200****SPACE-TIME ANALYSIS OF MULTIDISCIPLINARY GEOPHYSICAL OBSERVATIONS ASSOCIATED WITH EARTHQUAKE ACTIVITIES IN NORTHERN PART OF NORTH CHINA ( $6 < M < 6.5$ ) IN 1989-1998**

Jiadong QIAN, Cao Aiming, Meng Guojie (all at Center for Analysis and Prediction, China Seismological Bureau, P.O.Box 166, 63 Fuxing Ave., Beijing, 100036, China, email: jqdian@sdb.csi.ac.cn) A.V. Ponomarev, G.A. Sobolev (both at United Institute of Physics of the Earth, Russian Academy of Sciences, Moscow, Russia, email: avp@uipe-ras.scgis.ru) V.G.Gitis (Institute for Information Transmission Problems, Russian Academy of Sciences, Moscow, Russia, email: gitis@ipipi.ras.ru)

Northern part of North China is one of special regions in the researches of earthquake prediction in China, where a densest monitoring network of geophysical observations for searching precursors, in the whole China, has been working for over the past 30 years since 1966 till now, and the seismicities in the same period of time could be characterised by 3 stages: the strong one in 1966-1976, the quiet one in 1977-1988 and the medium-strong one since 1989.

A space-time analysis of multidisciplinary geophysical observations associated with the third stage in which three medium-strong earthquakes ( $6 < M < 6.5$ ) has occurred, is described in this paper on the basis of Geotime computer environment through a joint project of Sino-Russia co-operation. In comparison with the analysis for the case study of 1976 Tangshan earthquake in the previous time of the co-operation, the analysis shown in this paper was done on the following approaches: (1) The stability of the analysis in Geotime environment had been checked as some stations involved in it was replaced by the others. (2) Some modifications for the program had been made in order to continue the analysis whenever some interruption of observations might take place so that the modified program could be applied not only for the retrospective predictions in the case studies, but also for the test of earthquake predictions in the real time. (3) The separations in the time series had been made into two parts with high and low frequency component respectively.

Final results from the space-time analysis are given in this paper to show that there seems to



be a pretty good relation between the dynamic pattern and the earthquake occurrence of Zhangbei-Shanyi earthquake ( $M=6.2$ , Jan. 10, 1998, Hebei Province), 200 km northwest of the capital.

SW1/E/06-B5

1215

#### ANALYSIS OF SPACE-TIME PARAMETERS OF SEISMIC PROCESS FOR CORINTHOS GULF AND THIVA-OROPOS REGIONS IN GEOTIME INSTRUMENTAL ENVIRONMENT

V.GITIS, (Institute for Information Transmission Problems, RAS, Moscow, Russia email: gitis@iitp.ru)  
B.V.Osher (Institute Physics of the Earth, RAS, Moscow, Russia, email: osher@iitp.ru),  
G.Papadopoulos (Institute of Geodynamics, National Observatory of Athens,  
email: g.papad@egelados.gein.noa.gr)

The main idea of GeoTime technology is based on the alternative method of data representation and analysis. The time variations of geophysical parameters synchronously measured at different points of the region and the data of the earthquake catalogue are transformed into 3D rasters with two spatial and one temporal co-ordinate. It is assumed that after elimination of seasonal rhythms in the absence of earthquake preparation the 3D-raster fields are inhomogeneous in space, but quasistationary in time. The appearance of a precursor, which occupies a certain related subset of elements of the raster, violates the stationarity of the process. Statistical hypotheses testing techniques are used to determine the non-stationarity and to estimate its level of significance. Space-time analysis of seismic data for Corinthos Gulf and Thiva-Oropos regions was made in GeoTime environment. 3D-rasters of representativity of earthquake catalogues, seismic activity, b-value, fractal dimension and RTL criterion are discussed. This work is supported within INCO-COPERNICUS Project ASPELEA, contract number ERBIC-ISCT-97-0200

Friday 30 July AM

Presiding Chair: J. Qian, Centre for Analysis and Prediction, China Seismological Bureau, Beijing, China

SW1/E/02-B5

Poster

1030-01

#### SPATIAL-ENERGY INDICES OF ACOUSTIC EMISSION AND SEISMIC PROCESSES

E. YURKOV (Institute for Information Transmission Problems, RAS, Moscow, Russia, email: jork@iitp.ru)

Acoustic emission arising with destruction of rock samples under pressure is analogue of seismic process. Such known indices as b-value, frequency of seismic events and others are widely used for analysis of seismic and acoustic processes. Here the new indices describing spatial-energy variability of acoustic and seismic sequences are offered. The inertial index is based on use of inertia tensor in application to an acoustic (seismic) sequence. The inertia tensor is calculated how it is accepted in the mechanics, provided that mass proportional to energy is attributed to each acoustic event. The index of spatial variability is a special case of the inertial index, provided that energies of all acoustic events are equal. This index has statistical meaning, as it is connected to hypothesis test about distinction between two random sets. These and other indices were calculated during processing the acoustic emission data received in experiments on destruction of rock samples. The results of the analysis have shown that the offered indices are especially sensitive to spatial-energy variability of acoustic process. The work is partially supported by Russian Foundation on Scientific Research, project # 97-07-90326.

SW1/E/07-B5

Poster

1030-02

#### VARIATIONS OF THE LOW FREQUENCY MICROTREMORS PARAMETERS AS EARTHQUAKES INDICATOR.

Yury Tarasenko and ELENA MUSIENKO ( both at Institute of Seismology, Asanbai 52/1, 720060 Bishkek, Kyrgyzstan, email: kis@imfiko.bishkek.su)

The space-time the strong earthquake ( $M>5.0$ ) distribution in the Tien-Shan region and variations of azimuth and amplitude of the low frequency wave filtered from microtremors records on periods 60 sec and 120 sec have been analysed to improve understanding of physical processes closely connected with earthquakes phenomenon. We used digital records of microtremors velocity (nm/sec) selected daily in the same quietest time for periods 1992 (100 days), whole 1995 and 1997 and 1998 (152 days). During this time 6 earthquakes with  $M>5.0$  occurred in the radius 400 km. Software SAC was applied to estimate mathematically maximum amplitude of the low frequency wave on one of horizontal components at certain azimuth. Observation for the time periods mentioned above have shown that stability of the wave amplitude and azimuth are closely connected with strong earthquakes ( $M>5.0$ ) occurrence. Sharp variations of the wave azimuth (from 10 to 90 degrees) and either amplitude amplification or decrease tens times as much were beginning at all points of observation for 35-45 days before each strong event. Then the low frequency wave parameters were being stable during 5-15 days before events and later. These facts put on an idea that reconstruction of the crustle stress field is completed for 5-15 days before strong events. As for small earthquakes ( $M<5.0$ ) similar wave parameters variations took place only at a few points situated in the radius 100 km from source.

SW1/E/08-B5

Poster

1030-03

#### PHYSICAL BASIS OF A FORECASTING METHOD FOR EARTHQUAKES AND VOLCANOS' ACTIVITY ACCORDING OBSERVATIONS OF VARIATIONS OF NEUTRON FLUX NEAR THE EARTH'S CRUST

Beliaeva E.A., Kuzhevskij B.M., Nechaev O.Yu., Skobeltsyn Institute of Nuclear Physics, Moscow State University, Vorobjovy Gory, 119899, Moscow, Russia, e-mail: bmksrdlan.npi.msu.su

Made during many years (from 1990) observations of variations of thermal and slow neutrons' fluxes in seismo-active (Pamir) and seismo-quiet (Moscow) regions of the Earth allow to prove following: 1. Earth's crust makes a substantial contribution into full flux of such neutrons near the crust. 2. There are observed variations of neutron flux with in amplitude and different duration, part of which correlate with tidal wave in the Earth's crust, which is induced by interaction of the Earth and the Moon. These two claims result in followin one: deformations of the Earth's crust cause variations of thermal and slow neutrons' flux near the Earth's crust, especially displayed in the seismo-active reagions. Methods for forecasting of earthquakes and volcanos' activity are developed on this basis.

P11

Wednesday 28 – Friday 30 July

**CLOSED, SEMI-ENCLOSED AND MARGINAL SEAS PHYSICAL, CHEMICAL AND BIOLOGICAL PROPERTIES (JOINT IAPSO/IABO)**Location: Poynting Physics, S02 LT  
Location of Posters: Bridge Physics/Watson

Wednesday 28 July AM

Presiding Chair: Prof. P. Malanotte-Rizzoli

**GENERAL PRESENTATIONS**

P11/E/10-B3

0830

**SIMULATION OF PHYTOPLANKTON ANNUAL CYCLE IN LAKE BAIKAL, ECOLOGY CONTROLLING BY HYDRODYNAMIC AND OPTICS**

Sergei V.SEMOVSKI (Limnological Institute SB RAS, P.O.Box 4199, Irkutsk, 664033 Russia, email: Semovsky@lin.irk.ru)

Lake Baikal is the deepest and the most voluminous freshwater basin in the World. Great depth and narrow shelf produce the peculiar horizontal and vertical exchange of water masses. Many processes in the lake can be considered as analogy of those typical for the deep ocean and marginal seas. From other hand, highly endemic lake Baikal ecosystem is under studies for long time, many features are known there much better than those in oceans and seas.

The model is presented for Baikal epipelagial ecosystem annual variability focusing on dynamics of main taxonomical phytoplankton groups. Bio-optical block of underwater optical field simulation includes impact of all optically active components of ecosystem.

Main features that should be described using the model are the follows: winter-spring under-ice diatoms bloom (the most abundant is *Aulacoseira baicalensis*) that is controlled by under-ice convection and optical properties of ice; spring deep mixing and blocking of phytoplankton development; summer picophytoplankton bloom (with prevailing green-blue *Synechocystis limnetica* Popovsk.); autumn diatoms (*Cyclotella minuta*) bloom, autumn deep mixing and *Aulacoseira* spores transport from bottom zone into surface layer. The main objectives of the model development is to investigate factors influencing known interannual variability in spring diatoms bloom, full diatoms extinction during cold paleoclimates, autumnal diatoms prevailing during 16-19 century, etc.

P11/W/20-B3

0850

**ROCK LOBSTER JASUS EDWARDSII LAVAL RETENTION BY THE WAIRARAPA EDDY OFF NEW ZEALAND**

STEPHEN M.CHISWELL (National Institute of Water and Atmospheric Research, NIWA, PO Box 14-901, Kilbirnie, Wellington, New Zealand, email: s.chiswell@niwa.cri.nz)

In February 1988, *Jasus edwardsii* larval catches off the east coast of New Zealand were binomial in size and stage of development. Mid-stage larvae (presumed to be from the 1997 cohort) appear to be contained within a large permanent eddy found offshore known as the Wairarapa Eddy. Late-stage larvae (1996 cohort) have a statistically distinguishable different distribution from the mid-stage larvae, being found closer inshore of the eddy. Pueruli (also 1996 cohort) were found well inshore of the eddy. Surface currents derived from TOPEX/Poseidon altimeter measurements of sea level are used to model passive tracer distributions designed to simulate larval concentrations. The numerical simulations show that the different distributions of the three groups cannot be explained on the basis of their different time histories to advection alone. Mid-stage concentrations appear to be well described by passive drift alone, but the simulations suggest some mechanism inducing shoreward transport is needed for both pueruli and late-stage phyllosomas. Observed pueruli concentrations are best matched by adding a shorewards-directed speed of 8-10 cm/s for between 1 to 3 weeks before the date of the cruise. Late-stage phyllosoma concentrations are best matched by adding speeds of 4-6 cm/s. Sustained shorewards swimming speeds of 8-10 cm/s are well within the estimates of swimming speed that have been reported elsewhere for pueruli. To our knowledge, directed horizontal swimming has not been reported for phyllosomas, yet in the final stage, the pleopods are as well developed, as they are in the pueruli. These final stage larvae could well use forward pleopod propulsion to allow them to swim.

P11/E/07-B3

0910

**CIRCULATION AND DEEP WATER VENTILATION PROCESSES IN THE CASPIAN SEA SIMULATION USING 3-D PEM AND THERMODYNAMIC ICE MODEL**

Rashit A. IBRAYEV and Artem S. Sarkisyan (Institute of Numerical Mathematics, Russian Academy of Sciences, Gubkin str.8, 117951, Moscow, Russia, email: ibrayev@inn.ras.ru) Emin Ozsoy and Halil I. Sur (Institute of Marine Sciences, Middle East Technical University, P.K.28 Erdemli-Icel, 33731, Turkey, email: ozsoy@inn.metu.edu.tr) Corinna Schrum (Institute of Oceanography, University of Hamburg, Tropicowitz str.7, Hamburg, D- 22529, Germany, email: schrum@dkrz.de)

A 3-D PE GCM coupled with an ice sub-model is used for the study of seasonal and interannual variability of the Caspian sea circulation. ECMWF derived fluxes, and river inflows are used to force the model. Wind-driven shelf currents and basin-scale interconnected recirculation gyres define the horizontal pattern of circulation. Our results support the earlier hypothesis that the Volga river inflow plays a significant role in driving the southward longshore currents along the western coast. Predominant southward and westward winds create downwelling along the western shelf and upwelling along the eastern shelf, supported by consistent satellite observations. Gravitational sinking of dense water on the northern shelf slope occurs as a result of local freezing and vertical mixing of cold water originally formed on the northern and eastern shelves. Changes of sea level and production of dense water under ice sheet occur in response to interannual changes in the water balance based on river inflow and evaporation fluxes. As a result, ventilation of the deep water is decreased when the sea level rises. Our model results are in agreement with the analyses of historical and recent data, indicating decreasing oxygen in the deep waters of the Middle Caspian Basin during the epochs of rising sea level.

P11/E/04-B3

0930

**OBSERVATIONS OF SEDIMENT RESUSPENSION AND TRANSPORT IN THE COASTAL AND BOTTOM BOUNDARY LAYERS OF LARGE LAKES WITH ACOUSTIC DOPPLER CURRENT PROFILERS**

JAMES H. SAYLOR and Gerald S. Miller (Both at: National Oceanic and Atmospheric Administration,

Great Lakes Environmental Research Laboratory, 2205 Commonwealth Blvd., Ann Arbor, MI 48105; e-mail: saylor@glerl.noaa.gov)

Data from Acoustic Doppler Current Profilers (ADCP) deployed in the nearshore region of southeastern Lake Michigan provide evidence of sediment resuspension and the cross-shelf transport of these materials during episodes of winter wind storms. Significant increases (+20 dB) in echo intensity and current velocity correlate well with satellite imagery of a sediment-laden plume transporting material in a cyclonic flow around the basin perimeter. A decrease in echo intensity to near background levels following the resuspension event suggests that the larger particles settle out, leaving the very fine material that remains visible in satellite imagery for many days. In Lake Champlain, a long, narrow and deep lake that forms the boundary between the states of New York and Vermont, bottom sediment resuspension caused by surges and gravity currents in the density-stratified lake water has also been documented in acoustic profiler records. Although no concurrent measurements of Total Suspended Material have been achieved in either lake, the ADCP results show that resuspension events can be detected using these instruments. With calibration of sediment concentration and echo intensity at each site, it appears that quantitative values of sediment fluxes can be determined.

P11/W/16-B3

0950

**ABSOLUTE FLUXES UTILISING DIRECT VELOCITIES, ACROSS 8.5N IN THE ARABIAN SEA IN JUNE 1995**

L. M. BEAL, (Lamont-Doherty Earth Observatory, Palisades, NY 10964, USA email: lbeal@ideo.columbia.edu); A. Field, R. L. Molinari and W. D. Wilson

Meridional volume fluxes into the Arabian Sea have been estimated using a combination of the geostrophic approximation and direct velocity measurements. The data were collected during the southwest monsoon of June 1995, as NOAA repeat line I1R, nominally along 8.5N. Direct velocity measurements show that winds drive strong southward fluxes of (about 19 Sv) over the upper 50 m, which appear to be partially compensated by a northward flow of subsurface waters between 50 and 290 m depth in the interior, and by the intense northward flow of the Somali Current at the western boundary. The cumulative transport in this surface layer was found to be 8 +/- 2 Sv from on-station shipboard and lowered ADCP velocity profiles. Below 290 m, velocities and shears are generally an order of magnitude smaller than in the surface intensified flows. Here, where we expect the flow to be dominated by rotation, geostrophic velocity has been referenced to the detided, cross stream component of LADCP velocity. The resultant structure of the section transport per-unit-depth from geostrophy and from LADCP is quite different. Geostrophic fluxes suggest a deep overturning, with northward transport below 2400 m of 22 Sv, while LADCP suggests 0.4 Sv. Since the Arabian Sea is closed to the north of the I1R section, the former transport would require an unrealistic scale of upwelling throughout the basin, and hence, evidently the LADCP-referencing scheme would appear to be flawed, certainly for this low baroclinic mode circulation. For comparison, taking geostrophy referenced to 2000 dbar across the section, the overturning is 13.3 Sv; still rather large. The horizontal transport structure, on the other hand, shows that geostrophic and LADCP fluxes are well matched; largely an artifact of the referencing method used. The depth-integrated transport structure is dominated by bands of alternating northward and southward fluxes, with particularly strong circulations to the east of the Carlsberg and Chagos-Laccadives Ridges. The accumulated transport along the section (below 290 m) is about 22 Sv. The next step for this analysis is to establish the representativeness of the one-time section and, subsequently, to enforce a mass balance on the circulation.

P11/E/06-B3

1010

**THE RESPONSE OF SEMI-ENCLOSED SEAS TO SYNOPTIC ATMOSPHERIC FORCING**

Christopher N.K. MOOERS, HeeSook Kang, and Lianmei Gao (OPEL/RSMAS, University of Miami, 4600 Rickenbacker Cswy., Miami, FL 33149-1098, USA, email: cmooers@rsmas.miami.edu, hkang@rsmas.miami.edu, lgao@rsmas.miami.edu)

Semi-enclosed seas are under the influence of atmospheric forcing (wind stress, surface pressure, heating/cooling, and evaporation/precipitation) on a variety of space and time scales from mesoscale to synoptic scale to intra-seasonal, seasonal/annual, inter-annual, and so forth. Here, the primary interest is in the oceanic response to synoptic scale forcing. Because of the joint effects of Earth's rotation, ocean density stratification, and continental margin topography, the response of semi-enclosed seas to synoptic forcing can be rich, ranging from transient coastal upwelling or downwelling, to coastally trapped waves, storm surges, transient jets and fronts, transient surface and bottom mixed layers, convection/ventilation, and so forth.

Numerical simulations (using POM) of the response of the Japan (East) Sea to wintertime extratropical cyclone/cold front outbreaks, and the Intra-Americas Sea to summertime tropical cyclones, are used as examples. The synoptic atmospheric forcing (with mesoscale resolution) utilized is provided by relatively new sources; e.g., a spaceborne scatterometer (NSCAT) and a mesoscale atmospheric model (MM5). By comparing with the response to more conventional, lower-resolution atmospheric forcing fields, the sensitivity of semi-enclosed seas is illustrated. Conversely, the space-time-amplitude resolution and accuracy requirements of atmospheric forcing for quality simulations of semi-enclosed seas circulation are beginning to be better defined by these response studies.

Looking ahead, the new sources of synoptic atmospheric forcing information (with mesoscale resolution) offer the potential for driving simulation and predictive models of circulation in semi-enclosed seas with higher accuracy on a routine (operational) basis.

Presiding Chair: Prof. P. Malanotte-Rizzoli

JAPAN SEA

P11/E/13-B3

1050

**THE SOUTH CHINA SEA RESPONSE TO TROPICAL CYCLONE ERNIE 1996**

Peter C. CHU (Naval Postgraduate Research, Monterey, CA 93943, USA Email: chu@nps.navy.mil); and Joseph Veneziano

We study the response of the South China Sea (SCS) to a tropical cyclone using the Princeton Ocean Model (POM) with 20 km horizontal resolution and 23 sigma levels conforming to a realistic bottom topography. A high-resolution surface wind field was established to represent Tropical over the SCS. Its translational velocity is determined using the best track storm course and speed from post-storm analysis by the United States Navy Joint Typhoon Warning Center at Guam (JTWC), and its relative velocity to a storm center is determined using a recently developed tropical cyclone wind profile model (TCWPM). To obtain the wind field both inside and outside a tropical storm, a background (climatological) wind field is blended. The calculated wind field is verified using the JTWC analyzed wind profile data. The integration of the POM model was divided into pre-experimental and experimental stages. During the pre-experimental stage the model was integrated for 34 months and three days from an initial at rest state with three-dimensional climatological January temperature and salinity fields, forced by the climatological monthly mean wind stress. The final state from the pre-experimental run

was taken as the SCS condition for 4 November 1996, the initial condition for the experimental stage. During the experimental stage, the POM model was forced by TCWPM modeled wind field, simulating Tropical Cyclone Ernie, for eighteen days. Our results show that the POM adequately simulated ocean responses to tropical cyclone forcing. Near-surface ocean responses simulated by the POM included strong asymmetrical divergent currents with near-inertial oscillations, significant sea surface temperature cooling, biased to the right of the storm track, and sea surface depressions in the wake of the storm. Subsurface responses included intense upwelling and cooling at the base of the mixed layer to the right of the storm track. Several unique features used by coastal interactions with storm forcing, were also simulated by the model. Along the coast of Luzon a sub-surface alongshore jet was formed, a warm anomaly off the northern tip of Luzon was significantly enhanced by surface layer convergence and storm surges simulated along the coasts of nd Vietnam.

**P11/E/14-B3 1110**

**A COASTAL AIR-OCEAN COUPLED SYSTEM (CAOCS) FOR THE SOUTH CHINA SEA MULTI-EDDY STRUCTURE**

Peter C. CHU, (Naval Postgraduate Research, Monterey, CA93943, USA Email: chu@nps.navy.mil) Shihua Lu, and Yuchun Chen

A coastal atmosphere-ocean coupled system (CAOCS) is developed to study the South China Sea (SCS) mesoscale eddy formation in May 1995. The oceanic component consists of the Princeton Ocean Model (POM) with 20 km horizontal resolution and 23 sigma levels conforming to a realistic bottom topography. The atmospheric component consists of a recent version of the regional climate model (RegCM2) with 40 km horizontal resolution and 16 vertical levels. The model domain (98.84-121.16 degree E, 3.06 degree S-25.07 degree N) covers the whole SCS and surrounding land and islands. The lateral boundary conditions for the atmospheric component come from European Center for Medium-Range Weather Forecasts (ECMWF) analyses of observations, and for the oceanic component come from observational oceanic inflow/outflow at the open boundaries. The surface fluxes of water, heat (excluding solar radiation), and momentum are applied synchronously with opposite signs in the atmosphere and ocean. Flux adjustments are not used. The CAOCS model simulation agrees well with an extensive airborne expendable bathythermograph (AXBT) survey of the South China Sea (SCS) conducted in May 1995, and shows the capability of simulating the SCS multi-eddy structure in May 1995: a central SCS warm-core anticyclonic eddy surrounded by several cool-core and warm-core eddies.

**P11/E/15-B3 1130**

**AN AIRBORNE EXPENDABLE BATHY THERMOGRAPH SURVEY OF THE SOUTH CHINA SEA, MAY 1995**

Peter C. CHU (Naval Postgraduate Research, Monterey, CA93943, USA Email: chu@nps.navy.mil), C.W. Fan, C.J. Lozano, J.L. Kirling

An extensive airborne expendable bathythermograph survey of the South China Sea (SCS) conducted in May 1995 and historical data are used to analyze and infer the upper layer (300 m) synoptic structure and general circulation. The primary thermal feature observed was a central SCS warm pool surrounded by several cool pools. The size of the warm pool decreased with depth from approximately 200,000 square kilometers at 50 m depth to about 70,000 square kilometers at 300 m depth. The maximum temperature of the warm pool was 30 degree C, appearing near the surface. At the depth of 50 m, the temperature of the central SCS warm pool was 29 degree C, and the temperature of the five surrounding cool pools ranged from 26 degree C to 22 degree C. A three-dimensional estimate of the absolute velocity field was obtained from the observed temperature field and a climatological salinity field using the P-vector inverse method. Striking circulation features were the existence of dual anticyclonic eddies in the central SCS warm pool and the existence of cyclonic eddies associated with the cool pools. In the upper layer the tangential velocity of the dual central SCS anticyclonic warm-core eddies is around 30-40 cm/s and that of the five cyclonic cool-core eddies varies from 10 cm/s to 40 cm/s. The tangential velocity of all the eddies decreased with depth. At 300 m depth, it became less than 5 cm/s for all the eddies.

**P11/E/22-B3 1150**

**WARMING AND LONG-TERM VARIATION IN THE EAST/JAPAN SEA; A GLOBAL IMPLICATION**

Kuh KIM and Kyung-Ryul Kim (both at Research Institute of Oceanography, Seoul National University, Seoul 151-742, Korea, email: kuhkim@ocean.snu.ac.kr); Young Oh Kwon (School of Oceanography, University of Washington, Seattle WA 98195 USA, email: yokwon@ocean.washington.edu)

Potential temperature in the East Sea has risen about 0.03 deg C at 3000 m and 0.25 deg C at 500 m since 1940s. Salinity has undergone a differential change with depth at the same time; an increase above 1200 m, but a decrease below it since 1965. During the same period the concentration of the dissolved oxygen has changed in three layers; a decrease in the upper 500 m, an increase at 500-1400 m and another decrease below 1400 m. The warming and reduction in the dissolved oxygen in deep and bottom waters indicate that the rapid ventilation which kept the East Sea rich in oxygen as high as 6.0 ml/L in the past may have stopped or have been reduced significantly. Meanwhile increase of both salinity and dissolved oxygen at intermediate depths is possible only through introduction of a new water mass at this depth. A simple one-dimensional model suggests that continuation of this process would deplete the bottom water in 30 years. The East Sea seems to act as a miniature ocean for monitoring and prediction of the change in the thermohaline circulation in oceans associated with the global warming.

Wednesday 28 July PM

Presiding Chair: Prof. P. Malanotte-Rizzoli

**JAPAN SEA**

**P11/W/25-B3 1400**

**A NOTE ON THE TAIWAN WARM CURRENT**

Le KENTANG (Institute of Oceanology, CAS, Qingdao 266071, PRC, email: ktle@ms.qdio.ac.cn)

The Taiwan Warm Current is one of the major currents in the East China Sea. It is traditionally believed that the Taiwan Warm Current (TWC) is to the east of the East China Sea Coastal Current and flows roughly along the coast of the Zhejiang and Fujian Provinces from the southwest to the north. However, with the increase of the field data it is found that the origin of the TWC Water varies seasonally. In other words, it can originate from the Taiwan Strait or from the intrusion of Kuroshio northeast of Taiwan or from the both. On the other hand, some

contour maps of the isopycnal surface given by Su and Pan in 1987 suggested that the TWC actually had two branches, one inshore and one offshore. However, the plane distributions of the monthly-mean temperature and salinity in <<Marine Atlas of Bohai Sea, Yellow Sea and East China Sea>> (1992) have shown that the hydrological structure in the region north of Taiwan has remarkable annual variations due to monsoon, coastal currents off the continent, intrusion of Kuroshio. Also, the seasonal surface current maps in it have displayed that the surface currents in the same region have different seasonal patterns and the so-called inshore and offshore of the TWC may have different origins. It would be better to suggest that the inshore one still remain its traditional nomenclature, the TWC, and the offshore one can be named as the East China Sea Warm Current.

**P11/E/03-B3 1420**

**CURRENTS AND EDDIES IN THE ABYSSAL WATER OF THE JAPAN SEA**

Masaki Takematsu, Alexander G. Ostrovskii (both at Research Institute for Applied Mechanics, Kyushu University, Kasuga 816-8580, Japan, email: takematu@hikari.riam.kyushu-u.ac.jp)

Moored current measurements were made for the first time at seven sites in the Japan Basin, the northern half of the Japan Sea, in an attempt to directly explore the velocity field in the highly homogeneous abyssal water of the semi-enclosed marginal sea. Duration of the current measurements was 1 to 3 years depending on specific site.

The current meter data thus collected revealed that the abyssal water of the Japan Basin is very energetic with vertically coherent currents and eddies of the order of 10cm/s. Surprisingly, the currents and eddies exhibit marked seasonal variability even in the deepest layers. The observed new current features are discussed in comparison with remotely sensed data (sea surface temperature and drifter tracks) and results of numerical simulation with Princeton Ocean Model. New findings about the Liman Current along the Primorye coast are also described.

Presiding Chair: Prof. P. Malanotte-Rizzoli

**NORTHERN SEAS**

**P11/W/18-B3 1440**

**VALIDATING MULTIYEAR OCEAN-MODEL RUNS FOR MARGINAL SEAS**

Frank Janssen and Corinna Schrum (both at Institut of Oceanography, University of Hamburg, Tloplowitzstr.7, D-22529 Hamburg, Germany, email: janssen@ifm.uni-hamburg.de)

Many ocean scientist believe that the time has come to leave the global scale in climate modelling. Much hope lies in the enhancement of our knowledge of interannual and decadal variability of the ocean from regional coupled model experiments. Semi-enclosed and marginal seas are highly preferable areas for these kind of studies, not only because of the sensitivity of their physical and biological systems to small climate changes, but also their great importance for men. But a detailed analysis of model results only makes sense if it can be guaranteed that the model system is able to give the wanted answers with the needed accuracy: Systematic model validation is therefore of utmost importance! First steps of a systematic validation procedure for a shelf sea model, integrated up to the decadal time scale, will be presented. Model results are taken from a 15 year model run with the HAMSOM (Hamburg Shelf Ocean Model) forced by ECMWF re-analysis data. The model area is the North Sea/Baltic Sea system, which is one of the areas with the highest coverage of observed data worldwide. This area can be seen as a kind of test case. If we fail to come to a consistent validation with the amount of available observations here, there is little hope that this will be possible elsewhere.

**P11/W/09-B3 1500**

**TRANSPORT AND STRUCTURE OF THE ATLANTIC INFLOW TO THE NORTHERN SEAS BASED ON LONG TERM CURRENT MEASUREMENTS**

Kjell Arild ORVIK, Øystein Skagseth and Martin Mork (Geophysical Institute, University of Bergen, Allegaten 70, N-5007 Bergen, Norway)

This study deals with the inflow of warm and saline North Atlantic water to the Northern Seas, this important factor for climate, ecology and biological production in Northern Europe. The investigations are carried out in the Svinøy Section just to the north of the Faroe-Shetland Channel cutting through the core of the Atlantic inflow to the Norwegian Sea. This is because recent investigations show that different branches of the Atlantic inflow through the Scotland-Greenland gaps merge through confluence in a two-branch flow crossing the Svinøy Section, making this site very suitable for monitoring the Atlantic inflow. Based on long term current measurements from 3-5 mooring lines from April 1995 to October 1998 in combination with shipboard ADCP, SeaSoar-CTD and CTD transects, transport estimates and spatial current structures will be presented. For the first time the two-branched Norwegian Atlantic Current has been revealed with a striking inner and outer branch. The inner branch shows properties as a 30-50 km wide, nearly barotropic flow trapped over the steepest slope between depths of 200 m and 900 m, while the outer branch makes its appearance about 200 km further offshore just above the 2000 m isobath as a 30-50 km wide jet with baroclinic properties extending down to 400 m depth. In between the observations show strong spatial variabilities in an eddy and recirculation pattern. The Atlantic inflow shows variabilities over a broad frequency band with periods from days to weeks. Seasonal and interannual variabilities are also prominent. Presumably, high inflow events are forced by wind impact which is also revealed in the high correlation with the North Atlantic Oscillation (NAO) index, mirroring the strength of the westerly wind-field in the North Atlantic. Thus, the most dominant seasonal signal is found in the seasonality of the winds.

**P11/W/29-B3 1520**

**USE OF AN OPTICAL SATELLITE SENSOR SUCH AS SEAWIFS...**

Dr Bernard WALTER (NorthWest Research Associates, USA)

Use of an optical satellite sensor such as SeaWiFS is limited in its ability to adequately monitor spatial and temporal changes in biological productivity in an area frequently covered by clouds such as over the Southeast Bering Sea shelf. In order to extend this monitoring capability we study the relationship between patterns seen in Synthetic Aperture Radar (SAR) imagery, which is not affected by cloud cover, and those seen in ocean color measurements from SeaWiFS imagery over this area during a period in June, 1998. We attempt to identify characteristic patterns or features in SAR imagery associated with areas of high (low) biological activity. The link between biological activity and SAR is through the fact that planktonic material produce fatty acids and alkanes that produce films on the ocean surface. These natural films cause damping of capillary and short gravity waves sensed by SAR thus producing dark slick signatures in SAR imagery. We focus on the period: June 19-22, 1998



where we have coincident SAR and SeaWiFS imagery. Winds were generally light (3-5 m/s) during the period. The SeaWiFS images show a large region over the SE Bering Sea shelf with low chlorophyll concentration (1 mg/m<sup>3</sup>) associated with a coccolithophore bloom. There was a large increase in chlorophyll concentration near 57.5-58.5 deg N, 168 deg W with values 10 mg/m<sup>3</sup> southward toward St. Paul Island. The SAR images during this period consistently show striking differences in radar backscatter patterns between the areas indicated as having high chlorophyll concentration and low chlorophyll concentration in the SeaWiFS images. In general in the areas of high chlorophyll, the SAR images show considerable eddy activity delineated by dark bands presumably caused by the natural surfactants from the biological activity. There is a definite transition in backscatter pattern in the region of high horizontal chlorophyll gradient, from the eddy activity to a rather featureless backscatter pattern. We will explore the use of texture analysis as a way of quantifying the differences in backscatter patterns between the high and low chlorophyll regions and investigate the effects of wind forcing on these results. These preliminary results point to the possibility that SAR imagery may be able to delineate regions of high and low biological activity.

**P11/E/26-B3****1600****ON WATER AND SALT EXCHANGE IN A FRICTIONALLY DOMINATED STRAIT - CONNECTING THE BALTIC WITH THE NORTH SEA**

BERTIL HAKANSSON (Swedish Meteorological and Hydrological Institute, S-60176 Norrköping, Sweden, email: bertil.hakansson@smhi.se)

A hydraulic model is applied to one of the straits in the transition area between the Baltic and the North Sea. It is calibrated and validated with independent datasets of ship-borne ADCP transect measurements and an array of moored current meters. The model is able to explain 0.91 and 0.79 of the variance, respectively. It is forced with sea level data, which representativity is studied in some detail. The 1993 volume and salt exchange are investigated. It is found that the annual salt import is of the same magnitude as during a Major Baltic Inflow event. A twenty-year time series of calculated water exchange is used to estimate the average export of water. This estimate is used in a Baltic Sea water budget to evaluate the mean water exchange in Öresund and the Great Belt strait. It is found that the mean water outflow is distributed as 1.9:1 between the two straits, indicating that Öresund has a more efficient barotropic water exchange than the Great Belt. It is also demonstrated that the water exchange anomalies, on a decadal time-scale, closely follow the Baltic drainage area runoff anomalies.

**P11/E/09-B3****1620****SOME ASPECTS OF THE STUDY OF THE BALTIC SEA**

Natalia STASHCHUK, Vasily Vlasenko (both Marine Hydrophysical Institute, Kapitanskaya Str. 2, Sevastopol, 335000, Ukraine, email: vlasta@ukrcom.sebastopol.ua); Vadim Paka and Nikolay Golenko (both Atlantic Branch of P.P. Shirshov Oceanology Institute, Mira Street 1, Kaliningrad, 236000, Russia, email: paka@ioran.kern.ru)

Two interesting phenomena revealed in the Baltic Sea during 29 Cruise of R/V "Professor Shtokman" are investigated. The first one is the local widening of a pycnocline with vertical scope of about 30 m and horizontal scale of 12-20 km near a shelf break of the Gotland Deep. Two possible mechanisms of the formation were investigated by means of mathematical modeling. At first the in-situ data were explained as an "internal surf", generated by seiches in the region of a steep slope. A comparison of the in-situ data with the results of mathematical modeling rejected the hypothesis. The more realistic one is that baroclinic seiches oscillations can form local zones of a shear instability. This leads to a widening of a pycnocline in these zones due to a mixing.

Analysis of the in-situ measurements conducted in Stolpe Channel after the salty water inflow has shown the narrowing and uprising of isohalines to a sea surface on the northern periphery of the channel and their widening and deepening in the southern part of it. It was supposed that the system of near bottom currents generated during inflow was the reason of marked structure. By use of mathematical modeling it was obtained that the North Sea waters moving eastward along the channel form a bottom boundary layer.

The Ekman drift excited due to the Coriolis force generates the water transport across the channel in the bottom boundary layer. It can lead to the formation of an asymmetrical structure of hydrophysical fields across the channel.

**P11/W/13-B3****1640****BOTTOM BOUNDARY LAYER DYNAMICS IN THE BALTIC SEA TYPICAL SUBREGIONS**

Jüri ELKEN and Urmas Raudsepp (Estonian Marine Institute, Paldiski St. 1, 10137 Tallinn, Estonia, email: elken@phys.sea.ee, raudsepp@phys.sea.ee); Tarmo Kouts (Estonian National Maritime Board, Hydrographic Service, Lasnamäe St. 48, 11413 Tallinn, email: kouts@gwb.ee)

Observational data are presented for slopes and interior of deep basins (Gotland Deep), shallow straits (Irbe Strait) and medium-deep semi-enclosed basins (Gulf of Riga). The strongest signal in near-bottom currents comes from wind-forced barotropic motions of the basins. In the flat-bottom areas, the current speed may exceed 15-20 cm/s (Ruhnu Deep in the Gulf of Riga, full depth 53 m). Barotropic motions are more amplified on the slopes and connecting straits. In the Irbe Strait, resonance with the Baltic Sea seiches drives 24-h period current oscillations which amplitude may exceed 60 cm/s at stronger winds. Apart from the fluctuating part, steady density-driven current components are evident in the channels and on the slopes. The 3D-circulation model (a free surface version of the Bryan-Cox model) is used to further investigate the bottom boundary layer dynamics. The modelled current response to the major forcing factors is in agreement with the observed current dynamics. A sediment dynamics model and a Lagrangian particle transport model are superimposed on the circulation model. The calculations are used to estimate the sediment resuspension/deposition and redistribution. The results are compared with the observed fluff layer dynamics and sediment distributions.

**P11/W/02-B3****1700****GAS BUBBLE CONCENTRATIONS IN THE BALTIC SEA AND THEIR ROLE IN GAS EXCHANGE**

Jaromir Jakacki (1), Zygmunt Klusek (1) and (2) (1: Institute of Oceanology, PAS, ul. Powstańców Warszawy 55, 81-712 Sopot, Poland; 2: Pedagogical University, ul. Arciszewskiego 22, S\_upsk, Poland)

Gas bubble concentrations in the surficial water layer in the Baltic sea were measured using the multi-frequency acoustical system. The concentration estimations were performed using non-linear response of bubble in an acoustical field of high intensity. Dependence of bubble concentrations on wind speed and on the depth have been established. Gas fluxes carried into sea water by the bubble population were estimated.

**MEDITERRANEAN SEA****P11/W/06-B4****0930****RADIATIVE EQUATIONS AND CLIMATIC BEHAVIOUR OF THE MEDITERRANEAN BASIN.**

Maria Elisabetta SCHIANO and Mireno Borghini (both at Istituto per lo studio dell'Oceanografia Fisica-CNR, Forte S. Teresa, 19036, La Spezia, Italy, email: schiano@estof.santateresa.enea.it; Costante Luttazzi (Istituto di Fisica dell'Atmosfera-CNR, Rome, Italy)

An analysis is performed on the systematic discrepancies observed over the Mediterranean Sea between direct measured radiative fluxes and predictions obtained by the most widely used bulk formulae. The investigation has been carried out using direct measurements of solar radiation, atmospheric radiation, sea surface temperature and meteorological parameters collected over the Mediterranean Sea in the last ten years. The climatic features of the basin are charged for the failure of the equations. Particularly, it is shown that formulae developed for the mid-latitude oceans cannot be applied over the Mediterranean Sea owing to the interactions between the warm sea surface and the lower atmosphere. These strongly affect the surface parameters producing some conditions very different from typical mid-latitude situation. Moreover, the analysis reveals that, due to the strong variability, a single equation is unable to reproduce the fluxes at the surface of the Mediterranean Sea all year round. The twofold climatic behaviour of the Mediterranean region, where are present both tropical and mid-latitude aspects, requires distinct equations, probably involving different surface variables.

**P11/W/23-B4****0950****MODELLING THE MEDITERRANEAN UNDER DERIVED FLUX FORCING**

Paul Myers and Keith HAINES (both at Department of Meteorology, University of Edinburgh, JCMB, Kings Buildings, Edinburgh, EH9 3JZ, U.K., email: paulm@met.ed.ac.uk; kh@met.ed.ac.uk)

A long term integration of a Mediterranean model is performed with surface forcing of derived heat and freshwater fluxes. The model remains stable under these fluxes over a 100 year integration, reproducing the major water masses of the Mediterranean quite accurately. With the flux surface boundary condition, internal variability at interannual and interdecadal periods is enhanced. Levantine Intermediate Water (LIW) production of \$1.3\$ Sv occurs and a detailed examination of LIW budgets in the model is given. Interannual variability in the production of LIW is shown to be related to changes of the main path of the Mid-Mediterranean Jet and the advection of Modified Atlantic Water to the west or east of Cyprus. Furthermore, the flux boundary conditions permit the discovery of multiple equilibria in the basin's thermohaline circulation, with a second state involving a circulation collapse, with only intermediate water formation. This state is similar to that hypothesized for sapropel formation in the Holocene. Both states are characterized by similar hydraulic conditions at the Strait of Gibraltar, with significantly submaximal volume transport and large freshwater transport. A further intermediate state exists with near maximal transport and small freshwater transport.

**P11/E/25-B4****1010****NUTRIENT TRANSPORT MECHANISMS AND THE DYNAMICS OF THE PLANKTON PRODUCTION IN THE NORTHEASTERN MEDITERRANEAN**

Aysen YILMAZ, Ilkay SALIHOGLU, Suleyman TUGRUL, Dilek EDIGER, Yesim COBAN YILDIZ and Mehmet YAYLA (Middle East Technical University Institute of Marine Sciences, P.O.Box 28, 33731, Erdemli-Icel / TURKEY)

The eastern Mediterranean is one of the well known region of low productivity in the world due to limited nutrient supply to its surface layer from external and internal sources. The seasonality and the magnitude of primary productivity are principally determined by the extent and duration of winter mixing which provides nutrient input from intermediate layers to the euphotic zone. Chlorophyll-a concentrations measured in the last 10 years ranged from 0.01-0.5 µg/L in summer to 0.1-1 µg/L during the late winter-early spring bloom period. A well-developed deep chlorophyll maximum (DCM) near the base of the euphotic zone is a characteristic feature of the Northeastern Mediterranean throughout almost the whole year while this peak was broadened and observed at shallower depths during bloom periods. Nevertheless this prominent feature disappeared under severe winter conditions, as experienced in the winters of 1992, 1993 and 1995. The chlorophyll-a concentrations up to 3 µg/L were observed and the thickness of the euphotic zone decreased from 60-80m to 50-55m in the Rhodes cyclonic eddy and its peripheries. Such exceptional events in terms of phytoplankton activity attributed to the instant changes in the nutrient transport mechanisms since chimney type of structures were observed and the euphotic zone was fully enriched by the nutrients due to extreme hydrodynamical events experienced in these years.

The deep water of the Northeastern Mediterranean is relatively rich in dissolved inorganic nutrients (NO<sub>3</sub>=4-6 µM and PO<sub>4</sub>=0.15-0.22 µM) but it posses a relatively high N:P ratio (=26-28) compared to the deep oceanic values (=14-17). Therefore, nutrient inputs from the deep layer to the surface waters by advective and convective mixing in winter occur with the indicated high ratios. This process most probably leads to phosphorus-limited algal growth in the euphotic zone of the eastern Mediterranean. The bioassay experiments proceeded in the last two years supported this phenomenon and when the excess amount nutrients were provided to the phytoplankton populations, phosphorus seems to stimulate the growth. Moreover, the limited nutrient supply from the deep waters with relatively high N/P molar ratios of dissolved nutrients is expected to affect the chemical composition of biogenic particles synthesized in the euphotic zone and it has been shown that N/P molar ratio in POM is generally higher than the Redfield ratio.

**P11/E/11-B4****1050****THE POEM-BC PROGRAMME (PHYSICAL OCEANOGRAPHY OF THE EASTERN MEDITERRANEAN BIOLOGY AND CHEMISTRY): A REVIEW OF ITS DISCOVERIES**

Paola MALANOTTE-RIZZOLI (Bldg. 54-1416, Department of Earth, Atmospheric, and Planetary Sciences, Massachusetts Institute of Technology, 77 Massachusetts Ave., Cambridge, MA 02139, USA, Email: rizzoli@ocean.mit.edu)

Physical Oceanography of the Eastern Mediterranean (POEM), an international collaborative program sponsored by the United Nations Educational Scientific and Cultural Organization and the Intergovernmental Oceanographic Commission, has studied the Eastern Mediterranean since 1985. After a preparation phase, POEM studied circulation and physical processes from 1985 to 1990, resulting in three unexpected findings.

Researchers discovered a closed thermohaline cell in the deep-bottom layers of water that originates in the Southern Adriatic and spreads into the Eastern Levantine, the Eastern Mediterranean "conveyor belt" [Roether and Schlitzer, 1991]. Also found were multiple scales of interacting motions that define the general circulation at the basin, sub-basin, and

mesoscale [Malanotte-Rizzoli and Robinson, 1988; POEM Group, 1992]. And two convective regions with related water mass formation were found. The first is a deep convection cell in the Southern Adriatic, where the Eastern Mediterranean Deep Water (EMDW) was formed between 1985 and 1987.

Second, a convective region exists, rather more extensive than previously recognized, surrounding the Levantine Rhodes gyre where intermediate convection leads to the formation of Levantine Intermediate Water (LIW). Deep convection has also been observed in the Rhodes gyre leading to the formation of Levantine Deep Water (LDW) [Ozsoy et al., 1993]. The results of POEM Phase I are summarized in a group paper [POEM Group, 1992] and in a special issue of Deep Sea Research devoted to POEM results [Robinson and Malanotte-Rizzoli, 1993]. In 1990, POEM evolved into POEM-BC, an interdisciplinary project with a biology and chemistry component. Field work began with a basin-wide interdisciplinary survey carried out in October 1991 by five research vessels from Greece, Israel, Turkey, and Italy, which contributed two research vessels. A second interdisciplinary survey was carried out in March 1992 in the Ionian and Cretan Seas by two of the research vessels. The data set collected is helping to quantify the distributions of major inorganic nutrients and biological properties in the context of the physical processes of the basin. A major observational effort was finally carried out in winter 1995 with the execution of the LIW formation experiment. The three objectives of the experiment were to define the process of LIW formation through the successive phases of preconditioning, convection and formation, and spreading and dispersion; to study the internal (deep) and external...

**P11/W/24-B4****1130****CHANGES IN THE SALT INVENTORY OF THE EASTERN MEDITERRANEAN AND THEIR RELATION TO RECENT SHIFTS IN WATER MASS FORMATION AREAS**

Birgit KLEIN (Uni of Bremen, Institute of Environ Physics P.O.Box 330440 D28334 Germany Email: Ulf.Klein@uni-bremen.de); and Wolfgang Roether

Large scale hydrographic and tracer surveys performed in the framework of POEM and POEM-BC/MATER have provided snapshots of the dramatic change in the thermohaline circulation of the Eastern Mediterranean that has taken place between the late 1980ties and the mid 1990ties. During this period the Aegean was established as a source of deep waters, discharge of which had pronounced effects on water mass properties and on circulation within the deep water regime. The most prominent effect of the new deep water source is the strong increase in salinity over much of the deep waters. An open question to date has been to identify the source of this salinity increase. Three scenarios are possible: internal redistribution of salt in the basin, changes in the fresh water fluxes through the surface or changes in the salt transport through the Strait of Sicily and the Bosphorus.

In order to investigate this question salt inventories of the Eastern Mediterranean have been computed for the period before 1988 and for 1995. The comparison of these inventories indicates an apparent increase in salt content of  $5.7 \cdot 10^{11}$  kg. It assumes a constant volume and changes in water volume through variations in the fresh water flux have therefore to be removed from the estimate. Internal redistribution of salt is also noted and links salinity changes between intermediate and deep water masses on sub-basin scale. An increase of the net E-P flux of 20 cm/ly averaging over 8 consecutive years would be required to explain the apparent salt content increase. Available estimates of evaporation and precipitation confirm increases in the net evaporation rate for the period concerned but of a much lower magnitude, accounting only for about 40% of the apparent salt content increase. We find that the required import of salt into the Eastern Mediterranean to close the budget is related to changes in water mass characteristics in the Strait of Sicily. Hydrographic data from the Strait of Sicily indicate a strong increase in salinity of the inflowing water from the Western Mediterranean. The effect of the flow through the Bosphorus is assumed to be small.

**P11/E/19-B4****1150****UPDATING EASTERN MEDITERRANEAN TRANSIENT**

BENIAMINO BRUNO MANCA, Osservatorio Geofisico Sperimentale, Trieste, 34016 Italy, email: bmanca@ogs.trieste.it Giuseppe Civitarese, Istituto Talassografico di Trieste - CNR, Trieste, Italy, email: civitarese@TS.CNR.IT Maurizio Ribera d'Alcala', Stazione Zoologica "A. Dohrn", Napoli, 80121 Italy, email: maurizio@alpha.szn.it

The recent change in the thermohaline circulation of the Eastern Mediterranean has been characterized by a large outflow of Cretan water at Deep and Intermediate layers. Especially the second one has, apparently, replaced the LIW as the main Intermediate Water Mass in the Eastern Ionian Sea. In addition, a significant modification in the nutrient distributions with an uplift of the main nutrient by several hundred meters has been observed. A basin-wide cruise, carried on December 1998-January 1999, in the Ionian Sea allows to determine the present characteristic and distribution of water masses as well as the chemical and biological fields. The aim of the cruise is to reveal regions where the local dynamics could enhance the vertical flux of nutrients and eventually affect the pool of the photic zone. Cruises conducted in previous years after the first observations on the "new state" of the Eastern Mediterranean reveal that the new properties in water masses have rapidly affected the marginal seas and the Western Mediterranean, which in turn suggests that a new steady state will be probably reached relatively soon. We discuss data collected during the cruise in connection with a possible reconstruction of the damping process occurring in the Adriatic and Ionian Seas.

**Thursday 29 July PM**

Presiding Chair: Dr. Mario Astraldi

**MEDITERRANEAN SEA****P11/W/28-B4****1400****A WINTER INTERMEDIATE WATER EDDY EAST OF THE ALBORAN SEA**

D. A. SMEED and J. T. Allen (Southampton Oceanography Centre, Empress Dock, Southampton. SO14 3ZH, email: das@soc.soton.ac.uk) J. Tintoré (Universitat de les Illes Balears, Palma de Mallorca)

During the second cruise of the OMEGA project the towed CTD SeaSoar was deployed to survey the upper 350m of the water column in the eastern Alboran Sea and extreme western Algerian basin. Fluorescence, optical back scatter and light were measured along with conductivity and temperature with an effective along track resolution of 4km. The combined data sets have enabled a detailed description of the different upper ocean water types and the fronts that separate them. The Almeria Oran front forms at the eastern boundary of the Alboran Sea gyre system, in the upper 150- 200 m of the water column, and separates waters of predominantly Atlantic origin from those formed in the Western Mediterranean Sea. Below these surface waters, but above the Levantine Intermediate Water, Winter Intermediate Water, believed to be formed to the north of the Balearic Sea, is often observed. However, to our knowledge, this is the first time a discreet eddy of Winter Intermediate Water, a "WEDDY", has been found in the extreme western Algerian basin. Repeated surveys of the region allowed us to observe the evolution of the eddy over a period of 40 days.

**P11/E/16-B4****1420****MESOSCALE VARIABILITY IN THE EASTERN ALBORAN SEA IN DECEMBER 1997 JANUARY 1998**

Yves GRATTON (INRS-Océanologie, Rimouski, Qc, Canada, G5L 3A1. Email: yves\_gratton@uqar.quebec.ca); Louis Prieur (LPCM, 06230 Villefranche-sur-mer, France. Email: lprieur@ccrv.obs-uvfr.fr); Caroline Lafleur (INRS-Océanologie, Rimouski, Qc, Canada, G5L 3A1. Email: caroline\_lafleur@uqar.quebec.ca)

This paper describes the slow evolution of the mesoscale coherent structures observed in the Eastern Alboran Sea aboard the MV Atalante between November 30, 1997, and January 16, 1998. This scientific cruise was the second segment of the french Almofront (ALMeria-Oran front) program. The observed initial configuration is characterized by the Atlantic Jet meandering around an anticyclonic eddy. In this configuration the density front lies exactly on the imaginary line between Almería (Spain) and Oran (Algeria). Three weeks later, the meander structure is more pronounced and the front has moved eastward. A mushroom-shaped structure can be observed in the satellite IR image of December 23. Another three weeks later, the eddy has moved eastward and the coherent structures observed on the thermal images are much more difficult to interpret, but the jet and the density front can still be observed in the density-velocity field. We also show that, contrary to what was observed in April-May 1991 (Almofront I), the structures observed in the satellite thermal images correspond to the deeper, geostrophic structures.

**P11/E/05-B4****1440****ANALYSIS OF FLOW AND TRANSPORT MEASUREMENTS IN THE STRAIT OF GIBRALTAR**

Burkard BASCHKE and Uwe Send (both at Institut fuer Meereskunde, Meeresphysik, Duesternbrooker Weg 20, D-24105 Kiel, Germany, Email: bbaschke@ifm.uni-kiel.de)

To resolve the net inflow into the Mediterranean Sea, as well as the temporal changes of the exchange flow, transport estimates at the Strait of Gibraltar have to have an accuracy of at least 0.1 Sv. This is still a challenge in physical oceanography and requires measurements with a high temporal and spatial resolution. These were carried out during the EU-Projet CANIGO (Canary Island Azores Gibraltar Experiment) between October 1995 und June 1998. Extensive measurements with vessel-mounted ADCP, CTD, IADCP and XBT during the research cruises 'Poseidon 217' and 'Poseidon 234' were focused on the eastern entrance of the Strait of Gibraltar and were complemented by moorings in this region.

This data set was used to develop an inverse model to describe the currents and the vertical movement of the interface at the eastern entrance of the Strait of Gibraltar as a function of 2-D space and time. With this model the mean current speed and the volume transports in both layers were integrated across the section, where the correlation between tidal currents and the movement of the interface was included in the transport estimates.

In addition, acoustic transmission across the strait, which was tested during the CANIGO-Project, were compared with the model transports and the longperiodic components of the currents were determined after removing the tidal currents from the observations. Seasonably varying hydraulic effects are visible in the data and were accounted for in the analysis.

**P11/W/19-B4****1500****OBSERVATIONS OF BIOPHYSICAL INTERACTION AT THE ALMERIA-ORAN FRONT**

S. FIELDING, J. T. Allen, N. Crisp, D. A. Smeed and H. S. Roe (Southampton Oceanography Centre, Empress Dock, Southampton, email: sof@soc.soton.ac.uk); P. Velez (Universitat de les Illes Balears, Palma de Mallorca, Spain)

The Almeria-Oran front forms at the eastern boundary of the Alboran Sea gyre system. During RRS Discovery cruise 224 (part of the observational phase of EU MAST 3 project OMEGA) five repeat, high resolution, multidisciplinary surveys were made of the Almeria-Oran front. Hydrographic data were obtained with the towed undulating vehicle, SeaSoar. Concurrent with this, in-situ and remotely sensed biological data were collected using sensors fitted to SeaSoar, an optical plankton counter (OPC) and a fluorometer, as well as a hull mounted RDI ADCP and towed Simrad EK500 multifrequency sonar. Phytoplankton and zooplankton samples were collected to compliment and calibrate the in situ and remotely sensed data. Analysis of temperature and salinity on density surfaces, derived from the detailed hydrographic data, traced the high salinity, high temperature signature of Mediterranean surface waters entrained into the frontal jet and drawn down and across the front with a subduction velocity estimated to be 30-40 m/day. From the rapid repetition of the surveys we infer the advection of vorticity and predict regions of vertical motion. Solving the quasi-geostrophic omega equation, we have calculated vertical velocities (~15-20 m/day) and have compared the diagnostic picture of mesoscale vertical motion with that inferred from isopycnal maps of salinity and potential vorticity. Fluorescence data show that phytoplankton is also subducted at the front. Similar advection of zooplankton is also seen using acoustic backscatter data from both the ADCP and EK500 data. A high level of acoustic backscatter mirrors the downward subduction of the phytoplankton, persisting at times when diel migratory behaviour takes other zooplankton upwards towards the surface. Biological distributions in the vicinity of the front therefore result from interactions between physical processes and animal behaviour. OPC data and acoustic backscatter data (used in combination with net data and appropriate scattering models) can distinguish different biological communities in different water masses.

**P11/W/07-B4****1520****ATMOSPHERE-OCEAN FLUXES, CLIMATIC VARIABILITY AND EXCHANGES BETWEEN THE EASTERN MEDITERRANEAN AND THE BLACK SEA**

Emin OZSOY (Institute of Marine Sciences, Middle East Technical University, P.K. 28 Erdemli - Icel 33731 Turkey, Email: ozsoy@ims.metu.edu.tr), Leonid I. Ivanov and Vladimir Belokopytov (Marine Hydrophysical Institute, Kapitanskaya St., 2a, Sevastopol, 335000, Ukraine, Email: leonid@alpha.mhi.iuf.net)

The Eastern Mediterranean Basin and the Black Sea constitute two largely isolated water bodies of the world ocean, surrounded by land and constrained by exchanges through straits. Both regions appear highly sensitive to anthropogenic or climatic change, as a result of their isolation, enclosed geometry, being subject to large gradients in properties, transport from land, and their relatively small inertia in comparison to the ocean. Comparable effects of anthropogenic and natural variability in the ocean-atmosphere-land system makes diagnosis of environmental issues difficult. The marine environmental changes are most readily felt near the coast, adjacent to the continental shelf and abyssal regions.

Typical circulations, coherent features, convective mixing and upwelling events in the two interconnected Seas, their short and long-term variability, as well as synchronisms, differences and similarities in terms of intrinsic scales and forcing functions, are displayed, based on intensive oceanographic and satellite observations in the last decades. Local forcing and remote atmospheric connections to systems such as the North Atlantic Oscillation are exemplified. Decadal and longer term climatic atmospheric variability, with intensified effects

on air-sea fluxes in the region, their coincidence with convective events are studied, based on the analyses of atmospheric, oceanographic and satellite data. Coincidence of recent changes with the massive formation of Eastern Mediterranean deep waters during the Great Aegean Anomaly, and with pycnocline mixing in the Black Sea are investigated.

Atmospheric fluxes of momentum and heat obtained from ECMWF re-analysis data sets of 1979-1993, simultaneous satellite based and in-situ air and sea-surface temperatures, as well as marine heat storage and mixing characteristics based on time series of oceanographic measurements in the two seas are used to analyse their variability and interrelations. The results indicate a great degree of synchronism on interannual and decadal scales, and suggests strong atmospheric events and climatic variables linked to water mass formation.

The Turkish Straits, connecting the Two Seas through the Bosphorus and Dardanelles Straits and the Sea of Marmara serves as a transition between them and reflects the changes taking place in the adjacent seas. However, the variability of both the forcing and the response affecting this relatively small, dynamic system is much greater. Various types of forcing and mass budgets, including river discharges into the Black Sea, atmospheric pressure and wind stress in the adjacent seas, and internal dynamics of the Straits determine the response. In addition, the mixing taking place along the Straits and the exit regions have strong consequences for the circulation and mixing in the adjacent Seas. These aspects are studied, based on available measurements and information.

P11/E/17-B4

1600

#### PHYSICAL-BIOLOGICAL INTERACTION DURING DEEP WINTER MIXING IN AN EASTERN MEDITERRANEAN WARM CORE EDDY

Stephen BRENNER, Nurit Kress (both at National Institute of Oceanography, Israel Oceanographic and Limnological Research, Haifa 31080 Israel, Email: sbrenner@mail.biu.ac.il), Tamar Zohary (Kinneret Limnological Laboratory, Israel Oceanographic and Limnological Research, Tiberias 14102, Israel) and Michael D. Krom (Department of Earth Sciences, Leeds University, Leeds LS2 9JT, UK)

The Shikmona gyre, a recurrent warm core eddy located to the south of Cyprus, has been observed during nearly every cruise conducted in this region since 1982. Detailed CTD data collected during the period 1987-1992 showed that the water in the core of the eddy is renewed every 2-3 years. Winter sampling of the eddy on two different occasions (Feb 1989 and Mar 1992) showed that a phytoplankton bloom occurs in late winter during the deep mixing phase. The bloom was not delayed until the establishment of springtime stratification as has been observed in other warm core eddies. In Mar 1992 viable phytoplankton and bacteria were found uniformly distributed throughout most of the deep mixed layer, from the surface to 500 m which is well below the euphotic zone. As a first step in studying the physical and biological processes involved, an NPZD model coupled to a Mellor-Yamada turbulence model was used to simulate the bloom dynamics.

P11/W/22-B4

1620

#### BOTTOM WATER OUTFLOW IN THE STRAIT OF OTRANTO – SEASONAL AND YEAR-TO-YEAR VARIABILITY

Miroslav GACIC, Dino Viezzoli and Vanessa Cardin (Osservatorio Geofisico Sperimentale, P.O.Box 2011, 34016 Opicina (Ts) Italy, email: mgacic@ogs.trieste.it, dviezzoli@ogs.trieste.it and vcardin@ogs.trieste.it)

A bottom water outflow from the Adriatic Sea has been monitored with three bottom mounted ADCP's since March 1997. The most energetic low-frequency sub-inertial variability of the Adriatic outflowing current component occurs at time scales of the order of a week. Superimposed on these variations are seasonal and year-to-year fluctuations. Spatial distribution of the bottom flow suggests that the vein of the outflowing bottom water has horizontal dimensions of about 15 km while in the vertical the vein is about 100 m thick. Sub-inertial variations at weekly time scales manifest in occasional current reversals. Seasonal variations are of the order of 1 cm/sec while the interannual variability is slightly stronger. Seasonal variations show a maximum in the outflow in May and a minimum in November which can be explained in terms of the filling up/emptying the South Adriatic Pit dense water reservoir. Year-to-year variations in the bottom water outflow have been shown to be correlated with the surface buoyancy losses and consequently with the intensity of the vertical convection and the deep water formation. Calculations of the average bottom water fluxes separately for the pre-conditioning and for the post-convection periods have confirmed importance of both the year-to-year and seasonal signal. The estimates of the Adriatic Bottom Water fluxes are in the range from 0.13 Sv. in a post-convection of the winter 1997/98, to 0.08 Sv. occurring in a pre-conditioning period of the same winter. The obtained values are about 50% smaller than those obtained previously (winter 1994/95). It is not clear whether these differences are due to the uncertainties in estimating the water fluxes or make part of the long-term variability (the winter 1994/95 surface buoyancy losses were stronger than in both 1996/97 and 1997/98).

P11/W/12-B4

1640

#### INTERANNUAL VARIABILITY OF THE PHYSICAL AND BIOCHEMICAL PROPERTIES OF THE WATER MASSES IN THE STRAIT OF SICILY

Mario ASTRALDI, Gian Pietro Gasparini, Anna Vetrano, Stefano Vignudelli (all at CNR-IOF, La Spezia, IT, email: astraldi@estof.santateresa.enea.it) Fabio Conversano, Maurizio Ribera d'Alcala' (both at Stazione Zoologica, Napoli, IT)

The Strait of Sicily is a key-region for the control of the waters flowing between the Eastern and Western Mediterranean. While the surface layer is entirely occupied by Modified Atlantic Water, repeated hydrographic measurements have allowed to identify two different water types coming from the Eastern Mediterranean: the classical Levantine Intermediate Water and a colder water type flowing next to the bottom and identified as uplifted Eastern Mediterranean Deep Water (EMDW). Both of them enter the Tyrrhenian Basin, where the EMDW progressively sinks at about 1600-1800m of depth and mixes with the resident Tyrrhenian Deep Water. The long term monitoring of the hydrographic properties of these water masses permitted to evidence significant trends in temperature, salinity and in other biochemical properties, which seem to be in agreement with the recent modifications observed in the Eastern Basin. These changes, influencing the characteristics of the outflow from the Eastern Basin, induce significant variations of the physical and biochemical properties in the sub-surface layers of the western Mediterranean Basin.

P11/E/21-B4

1700

#### THE MEDITERRANEAN OLIGOTROPHY AND THE GIBRALTAR CONSTRAINT

MAURIZIO RIBERA D'ALCALA' (Stazione Zoologica "A. Dohrn", Napoli, 80121 Italy, email: maurizio@alpha.szn.it); Giuseppe Civitarese (Istituto Talassografico di Trieste - CNR, Trieste, Italy, email: civitarese@TS.CNR.IT); Fabio Conversano (Stazione Zoologica "A. Dohrn", Napoli, 80121 Italy, email: fabio@alpha.szn.it); Alessandro Crise (Osservatorio Geofisico Sperimentale, Trieste, Italy, email: Crise@oce715b.ogs.trieste.it)

Present Mediterranean Sea is widely considered an oligotrophic basin, both in terms of production and upper layer nutrient stock. This statement has been questioned a few times stressing the role of short duration intense episodes in proximity of fronts, sub-basin gyres etc. observed in situ and from satellites on the overall budget. Nevertheless a reliable estimate of average annual production for the basin does not exceed 80-100 g C m<sup>-2</sup> for the Western Med and 30-50 g C m<sup>-2</sup> for the Eastern Basin. This is not very far from the average values of the neighboring Atlantic Ocean at same latitudes but, probably because of the extremely low values in the Eastern Mediterranean, this feature called for an explanation linked to some specificity of the Sea. The main characteristic of the extant Mediterranean is the inverse estuarine circulation that also causes a net loss of nutrients at Gibraltar. The evidence of this negative balance generated the paradigm of the Mediterranean being oligotrophic because it exports nutrients to the Atlantic.

We question this recurrent explanation of Mediterranean oligotrophy showing that the internal dynamics of the basin and the fluxes at the boundaries basically determine the functioning of the system and that the "Gibraltar constraint" is only of minor relevance in determining its low level of production.

P11/E/20-B4

1720

#### HINDCAST AND FORECAST OF THE IMPACT OF MEDITERRANEAN TRANSIENT ON THE ECOSYSTEM

Alessandro CRISE (Osservatorio Geofisico Sperimentale, CP 2011 Opicina, Borgo Grotta Gigante 42/C, Sgonico, Trieste, 34016 Italy, email: scrise@ogs.trieste.it); Giuseppe Civitarese (Istituto Talassografico di Trieste - CNR, Trieste, Italy, email: civitarese@TS.CNR.IT); Beniamino Bruno Manca (Osservatorio Geofisico Sperimentale, Trieste, 34016 Italy, email: bmanca@ogs.trieste.it); Maurizio Ribera d'Alcala' (Stazione Zoologica "A. Dohrn", Napoli, 80121 Italy, email: maurizio@alpha.szn.it)

After the observation of the transition in the thermohaline circulation in the Eastern Mediterranean the hypothesis of a quantitative and qualitative change in basin biological production, because of the nutrient redistribution, has puzzled the Mediterranean scientific community. Several cruises have been conducted since then, mostly on sub-regions of the Ionian and Levantine seas, whereas the hypothesized redistribution, would have impact on the whole basin, albeit with different effects. To verify the consistency of the above hypothesis an implementation of MOM-NPZD, a coupled eco-hydrodynamical three-dimensional model will be used to study ongoing processes as diagnostic tool for hindcasting and forecasting changes on short time scales. Data deriving from a January 1999 Cruise will be blended with model estimates for the same period in order to obtain new initial conditions for further integration, so to improve present knowledge on the ongoing change. A comparison with available low resolution SeaWiFS data will also be carried out. For the first time in this area, the results of this study would track changes in ecosystem structure due to climatic transients while they are occurring.

P11/W/15-B4

1740

#### MODELLING OF THE MEDITERRANEAN SYSTEM CHANGES UNDER CLIMATE VARIATIONS AND HUMAN IMPACT

Vladimir MADERICH (Institute of Mathematical Machine and System Problems NASU, Pr. Glushkova, 42, Kiev, 252187, Ukraine, Email: vlad@maderich.pp.kiev.ua)

The one-and-a-half dimension multilayer Lagrangian model LATOX was supplemented by models of straits to simulate changes in the system of the Mediterranean seas, forced by the climate variations and anthropogenic factors. A comparison is given of the Black Sea, Eastern and Western Mediterranean response on (a) the fallout of radionuclide dating back 60th, (b) the increase of the freshwater consumption and (c) post-glacial climate changes. The results of simulation show that the interaction through straits plays key role in variability of thermohaline fields and matter transport in the Mediterranean sub-basins on the scale of decades. Among other things, an exchange through straits and freshwater balance result in the difference in the temporal evolution of total amount of 137Cs in the Black Sea, Western and Eastern Mediterranean. It was shown a sensitivity of the Mediterranean to the changes in the freshwater balance. It should be pointed out that recent river diversions are as yet distinctly smaller than the natural variability of the freshwater balance in the Mediterranean and Black seas. The calculations showed that the process of transition of the Black Sea from closed water body with low salinity 7000 years ago to the recent state was not accompanied by the deep convection events. These latter with appearance of hydrogen sulphide in the surface layer can take place under the conditions of steep growth of the water consumption in the sea drainage basin superimposed on the climate change effects.

Friday 30 July AM

Presiding Chair: Dr. Mario Astraldi

MEDITERRANEAN SEA

P11/L/01-B5

0830

#### INTERMEDIATE AND DEEP WATER MASS DISTRIBUTION IN THE EASTERN CHANNEL OF SICILY AND WESTERN IONIAN SEA AS OBSERVED DURING SYMPLEX EXPERIMENT

Salvatore Marullo and Bruno Buongiorno Nardelli (Centro Ricerche Casaccia - ENEA, Via Anguillarese 301, 00060 S. Maria di Galeria (Roma), Italy, email: salva@gorgona.casaccia.enea.it); Rosalia Santoleri (Istituto di Fisica dell'Atmosfera, CNR, Via del Fosso del Cavaliere, 100 Roma, Italy, email lia@oceanofia.rm.cnr.it); Paola Malanotte Rizzoli (Department of Earth, Atmospheric, and Planetary Sciences - MIT - 77 Massachusetts Avenue, Cambridge, MA 02139, USA, email: rizzoli@ocean.mit.edu)

In the framework of the SYMPLEX (SYnoptic Mesoscale PLankton EXperiment) experiment, the eastern area of the Sicily Channel and neighbouring western Ionian Sea were surveyed from 1996 to 1998. About 600 CTD casts have been collected during three surveys and the data have been analysed in order to study the intermediate water exchanges between the eastern Mediterranean Sea and the Sicily Channel. It has been found that Levantine Intermediate Water (LIW) enters the Sicily Channel from a southern passage between Medina bank and the Tunisian shelf, at depth of 200-300 m, being characterised by a salinity of 38.76\*0.1 and a temperature of 13.9\*0.2 °C. A second possible pathway for the LIW is the eastern sill, between Malta island and Medina bank. In that sill, LIW was flowing eastward during 1996 and 1997 surveys, while a westward inflow has been observed in 1998. In correspondence to the inversion of the flow at the eastern sill, a clear increase of the salinity (from 38.70 to 38.74) and temperature (from 13.35 to 13.45 °C) at 2500-3000 m has been observed in the CTD stations of the neighbouring western Ionian Sea, associated to the spreading of the Cretan Deep Water (CDW) in the Ionian Sea.



P11/L/02-B5

0850

**POTENTIAL VORTICITY AND VERTICAL MOTION AT A MEANDERING UPPER OCEAN FRONT**

Bruno Buongiorno Nardelli (Centro Ricerche Casaccia – ENEA, Via Anguillarese 301, 00060 S. Maria di Galeria (Roma) – Italy – email: bruno@gorgona.casaccia.enea.it); Sefania Sarnocchia (Istituto Sperimentale Talassografico di Trieste, Viale Romolo Gessi 2, 34100 Trieste – Italy, email: sparnocchia@ts.cnr.it); Rosalia Santoleri and Fabrizio D'Ortenzio (Istituto di Fisica dell'Atmosfera – CNR, Via del Fosso del Cavaliere 100, Roma, Italy, email: lia@oceanofa.rm.cnr.it)

The 8-km horizontal resolution data collected by R/V Urania during SYMPLEX 1998 survey (SYNOptic Mesoscale PLancton EXperiment) have been analysed to describe the structure and dynamics of the upper 250 m in a small region along a frontal structure east of Capo Passero (western Ionian Sea).

The geostrophic field is inferred by adjusting the velocities derived from an Acoustic Doppler Current Profiler (ADCP) to the density field measured by a CTD (Conductivity Temperature Depth), with the constraint of no horizontal divergence and of thermal wind balance. Data were optimally interpolated over a regular 3-dimensional grid and used to compute the vertical component of the ageostrophic circulation by solution of the omega equation. The relative importance of stratification, relative vorticity and twisting terms in the Rossby-Ertel potential vorticity is then examined along selected isopycnals, together with the associated vertical motions and vortex stretching.

P11/L/03-B5

0910

**THE THERMOHALINE CIRCULATION OF THE MEDITERRANEAN SEA FROM LAGRANGIAN NUMERICAL STUDIES**

Volfango Rupolo, Vincenzo Artale (C.R. Casaccia ENEA, 00060 S. Maria di Galeria, Roma, Italy, email: volfango@canaletto.casaccia.enea.it); Bruno Blanke, Sabrina Speich (Laboratoire de Physique des Océans, Cnrs-Ifremer-Ubo, Brest, France, Sabrina.Speich@univ-brest.fr); Daniele Iudicone, Rosalia Santoleri (Istituto di Fisica dell'Atmosfera – CNR, Via del Fosso del Cavaliere 100, Roma, Italy, email: daniele@oceanofa.rm.cnr.it)

Integration of Lagrangian particles in velocity output from a numerical circulation model were used to study the thermohaline circulation of the Mediterranean Sea. This study is developed in the context of TRACMASS, a EEC-MAST III project. Particle trajectories were computed off line using an appropriate scheme that fully respects the non divergence of the 3D flow. Lagrangian analysis allows to evaluate accurately mass transfer between various sections of the basin and make easier visualisation of water mass pathways. Velocity output from different model experiments were used in order to study sensitivity to the surface forcing time variability. The dependence of the results from the time sampling of the eulerian velocity field is studied.

P11/L/04-B5

0930

**A SENSITIVITY STUDY OF THE CIRCULATION OF THE ALBORAN SEA AND THE GULF OF CADIZ: THE RESPONSE TO A REALISTIC TOPOGRAPHY**

Gianmaria SANNINO (CASPUR – Università "La Sapienza" – Via Aldo Moro, 15, Roma, Italy, email: sannino@caspur.it); Vincenzo Artale (Centro Ricerche Casaccia – ENEA, Via Anguillarese 301, 00060 S. Maria di Galeria, Roma, Italy, email: vincenzo@casaccia.enea.it); Roberto Conversano (Istituto di Fisica, Università "La Sapienza" Via Aldo Moro, 15, Roma, Italy, email: sannino@gorgona.casaccia.enea.it)

The three-dimensional sigma-coordinate Princeton Ocean Model is used to investigate the influence of the topography on the surface and deep circulation of the Alboran Sea and the Gulf of Cadiz. The topography constraint is analysed by comparing an experiment with a flat bottom with an experiment with an experiment with a real bathymetry. In the present study horizontal model domain covers the area from 13W to 0 longitude and from 33N to 38N in latitude, the grid resolution is variable: the horizontal ranging from about 2km within the Strait to 10km in the western and 9 km in the eastern end. The realistic topography is obtained by merging the very high resolution LODYC data (about 1km) with the standard ETOPO5 data. In all the numerical experiments the ocean starts from rest; the Gibraltar Strait is "closed by dam" that separate two reservoirs filled with water of different densities and is opened at the initial time. In order to remove spurious oscillations found in the frontal zone during the spinup phase the Smolarkiewicz upstream-corrected advective scheme was implemented and used in the model instead of the standard centred advection scheme.

P11/E/28-B5

0950

**THE STUDY ON THE ANNUAL OSCILLATION IN ALTIMETRY DATA**

DEL ROSARIO Alonso, J.J Catalan Perez-Urquioloa (1)(Dept of Applied Physics, Poligono del Rio San Pedro, Cadiz, Spain, Email: rosario@galeon.uca.es); M. Catalan-Morollon (Real Observatorio de Armada, C/Cecilio Pujazon s/n 11100, San Fernando, Cadiz); M. Bruno Mejias (1) M Ruiz Canavate(1) A. Villares-Duran(1)

One of the common characteristics of the inspection of altimetric data records is the presence of a annual oscillation. When a classical spectral analysis is carried out the frequency of the annual oscillation is close to 1 cycle/year (Sa tidal wave). However a more advanced frequency analysis gives that such an oscillation is not always centred at such a frequency. Sometimes is shifted right or left.

With this a very important questions is opened. When the annual oscillation is eliminated some energy persists around such a frequency, so the source of such extra energy must be identified. In order to carry out this study we have selected a large area, from the Cape Juby (North Africa) to England on a meridian. Data record have been four years at the crossover points of the Topex Poseidon mission in the selected area.

The scientific contribution of this work can be summarised as follows. We present a method for isolating the annual the annual oscillation from altimetric data records taken as a basis the tide generation potential RATGP95 as an application of the Empirical Orthogonal Function Decomposition. We have also made an analysis of the evolution of the amplitude and phasa lag of the annual wave is latitude. The same procedure is applied on the residual data where energy is still at the annual frequency giving the evolution of the amplitude with h elatitude.

P11/L/05-B5

1010

**INTERANNUAL CHANGES OF THE NUTRIENT EXCHANGE BETWEEN THE CRETAN SEA AND THE EASTERN MEDITERRANEAN**

Ekatzerini SOUVERMEZOGLOU, Evangelia Krasakopoulou (both at National Centre for Marine Research, Institute of Oceanography, Hellinikon 16604, Athens, Greece, email: katerina@fl.ncmr.gr, ekras@fl.ncmr.gr)

The systematic study of the nutrient regime in the Eastern Mediterranean since 1985 permitted to identify the chemical signature of the recent drastic changes in the deep thermohaline circulation.

Within the period of 1986-1987 Adriatic Sea is still the main contributor to the Eastern Mediterranean Deep Water (EMDW). The sporadic contribution of the Aegean Sea in this period is manifested by the intermittent outflow of the Cretan Deep Water (CDW) in form of "high oxygen -low nutrient" patches detected in the vicinity of Cretan Arc regions.

In the years following 1987 both density and transport rates of CDW are increased resulting to the addition of very dense and well oxygenated waters in the deep and bottom sections of the Eastern Mediterranean displacing upwards the waters of Adriatic origin. The oxygen increase and the nitrate decrease in the deep and bottom layers of the Eastern Mediterranean is in the order 0.3 ml/l and 1mM respectively.

Important modifications on the nutrient and oxygen distribution in the intermediate layers of the Eastern Mediterranean derived by the changes in the deep circulation through the straits. The lifting of the deep waters enriched in nutrients the intermediate layers of the basin. The concentration of nutrients in the intermediate layer of the Cretan Sea are found sometimes double than those observed during the previous years, due to the intrusion of this "nutrient rich -oxygen poor" layer compensating the deep water outflow.

Presiding Chair: Prof. T. Oguz

**THE BLACK SEA**

P11/E/29-B5

1050

**MODELLING TOP-DOWN CONTROL IN THE BLACK SEA PELAGIC FOOD WEB BY GELATINOUS CARNIVORES**

Temel OGUZ (Middle East Technical University, Institute of Marine Sciences, Erdemli, Icel, Turkey, e-mail: oguz@ims.metu.edu.tr); Hugh W. Ducklow (Virginia Institute of Marine Sciences, The College of William and Mary, Gloucester Point, VA, USA, e-mail: duck@vims.edu); Paola Malanotte-Rizzoli (Massachusetts Institute of Technology, Department of Earth, Atmospheric and Planetary Sciences, Cambridge, MA, USA, e-mail: rizzoli@mit.edu)

The changes taking place in the overall annual plankton structure of the Black Sea ecosystem in response to increasing grazing pressure by gelatinous carnivores are studied by a series of simulations using a one dimensional, vertically resolved, coupled physical-biochemical model. The pelagic food web is represented by two groups of phytoplankton (diatoms and dinoflagellates), bacterioplankton, microzooplankton, omnivorous mesozooplankton, carnivorous mesozooplankton (dominated by medusae), the ctenophore Mnemiopsis leidyi and the giant omnivorous dinoflagellate Noctiluca scintillans. Dissolved and particulate organic nitrogen as well as nitrate, nitrite and ammonium constitute its other components.

This study demonstrates the combined role of bottom-up forcing by anthropogenic nutrient enrichment and top-down control by gelatinous predators on the Black Sea plankton system. The model is first shown to reproduce reasonably well the observed planktonic food web structure at a particular location of the Black Sea for which a year-long data set with 2-to-4 week intervals is available from 1978. This simulation represents the typical eutrophic ecosystem conditions of the late 1970's and early 1980's. Additional simulations are performed for the eutrophication-free (unperturbed) ecosystem conditions of the late 1960's, and to explore the role of Mnemiopsis leidyi introduced into the already perturbed ecosystem of the late 1980's. These simulations are also validated by extended observations from specific years. The results indicate that much weaker and almost uniform plankton distributions characterize the unperturbed ecosystem of the 1960's for most of the year. The increased anthropogenic nutrient load together with population explosions in the opportunistic species during the 1970's lead to practically uninterrupted phytoplankton blooms. Mass development of the ctenophore Mnemiopsis leidyi causes even more pronounced and longer-lasting phytoplankton blooms due to stronger "top-down" control introduced into the ecosystem.

P11/E/27-B5

1130

**THE RECENT CHANGES IN THE NUTRIENT COMPOSITION OF THE BLACK SEA AND OBSERVATIONS ON THE PHYTOPLANKTON PRODUCTION**

Aysen YILMAZ, Mehmet YAYLA, Yesim COBAN YILDIZ, Suleyman TUGRUL and Ilkay SALIHOGLU (Middle East Technical University, Institute of Marine Sciences, P.O.Box 28, 33731, Erdemli-Icel/TURKEY, phone: 090-3245213434, Fax: 090-3245212327, e-mail: yilmaz@ims.metu.edu.tr)

Recent changes have been documented in the riverine discharge in the northwestern shelf of the Black Sea in both diminished flow and in nutrient concentrations (decrease in Si and increase in NO<sub>3</sub>) and these changes have caused increases in both amplitude and frequency of phytoplankton blooms with major shifts in taxonomic groups. Between the 1960-1980 the proportion of non-diatoms has increased eight-fold and during 1980s average phytoplankton biomass in the NW shelf increased eight-fold. These changes are evident in the deep region of the sea as rates of primary production and chlorophyll-a concentrations have both doubled between the mid 1970s and early 1990s. In 1970s and 1980s, primary production in the Black Sea displayed two phytoplankton maxima throughout the year; the major one occurred in early spring while a secondary peak appeared in autumn. Recently (1990s), additional summer blooms have frequently been observed in both the coastal and open waters. Water transparency has significantly changed in the Black Sea in the recent years. Secchi disk depth had decreased from 20-21m to 15-16m between 1920-1980. The values in excess of 15m were no longer observed after 1990 and the mean values were only 6-10 m in the 1990-1993 period and then it started to increase again after 1993. The main reason for the drastic decrease in the water transparency was the enhanced bloom of Peridinium and Coccolitophores during 1986-1992 period. The interannual variations observed in the chlorophyll-a concentrations after 1990s were more significant and pronounced than the ones observed in 1970s and 1980s. It was observed that the general trend was the increasing of different index of pelagic productivity during the last 40-50 years (1950s, 1960-1990s).

Coastal waters of the Black Sea are principally fed by the riverine input whereas the cyclonically dominated open ecosystem is mainly controlled by the influx of nutrients from the oxygenated lower layers by vertical diffusion and wind induced mixing processes that is much effective in winter. However, the input from the anoxic layer is limited due to the presence of a permanent halocline in the Black Sea. Halocline coincides with the suboxic zone where intense denitrification and redox-dependent processes also limit nitrogen and phosphorus input to the productive layer. In comparison, the role of atmospheric sources of nutrients appears to be marginal.

**INTRODUCTION TO POSTERS 1150****P11/P/01-B5 Poster 1150-01****STUDY OF LAYERED STRUCTURES IN SEMI-ENCLOSED SEAS (PERSIAN GULF)**

A.A.BIDOKHTI and M.Sagliafi (both at Institute of Geophysics, Tehran University, P.O.Box 14155-6466: Tehran, Iran. email: bidokhti@chamran.tu.ac.ir).

Excessive evaporation in semi-enclosed shallow seas as the Persian Gulf, specially in summer, can lead to a buoyancy driven exchange between these waters and the open sea. Such exchange leads to a strongly stratified sea (mainly two layer, warm fresher water, over cold salty water). In the middle of the Gulf, fine layered structure is observed in CTD records. Such layered structure with good regularity can be due to, two mechanisms; one regular internal waves which can break and produce fine structures. The other mechanism, which is the more probable one is the double diffusive convection, which can occur near the middle of the Gulf where colder fresher water from the north meets warm salty water from the south. Near such a frontal region, the double diffusive regime can lead to layered structures. Typical thickness of the layers is about 3–5 m. This is in agreement with calculations based on typical horizontal temperature gradient and vertical salinity gradient. Typical CTD of such layered water will be shown, including their spatial spectrum. These regular structures, will be discussed in terms of the two proposed mechanisms. Meanwhile, some results of laboratory simulation of the double diffusion, with horizontal temperature gradient of salt stratified fluid will also be presented.

**P11/P/02-B5 Poster 1150-02****OIL POLLUTION IN MUSCAT COAST, GULF OF OMAN**

EL Samra M.I., TAREK OTHMAN and AL Kharousy, L. G. (National Institute of Oceanography and Fisheries, Suez-Egypt, P.O.182)

The oceanic region including the Arabian Gulf, Strait of Hormuz and Gulf of Oman is one of the most important waterways in the world. One of the most important ports in the region is Mina Al-Fahal. It is located at The coast of Muscat. All of petroleum activities such as loading/unloading and refining operations in Sultanate of Oman are concentrated there. In addition, there are four operating companies concerned with the production, storage, refining, marketing and transport of Oman export blend crude and refined products, and also importing refined petroleum products.

Water and sediment samples were collected from the marine area of Muscat City, during winter and summer, 1995. Concentrations of total hydrocarbons were measured using spectrofluorometer, while the identification of different fractions was investigated in detail using GC/MS technique. The types of PAHs whither, substituted or unsubstituted were discussed relevant to the source of pollution. Long chain alkylated hydrocarbons and alkyl-substituted aromatic hydrocarbons were identified in Muscat coast. Levels up to 499.77 ppb of phthalate were measured in sediments of the port of Mina Al-Fahal.

**P11/P/03-B5 Poster 1150-03****DISSOLVED PETROLEUM COMPONENTS ALONG SUEZ SUEZ CANAL**

TAREK OT and EL Samra M.I. (National Institute of Oceanography and Fisheries, Suez-Egypt P.O.182)

The Suez Canal area is subject to oil pollution from ship's oil and refuse, atmospheric fallout (result from oil refineries) and domestic usage (sewage and agricultural wastes). The total annual oil tanker traffic in the Suez Canal routes amounts to 2472 vessels or a quantity of oil estimate is ~98 million tons during 1997.

Water and sediments samples were collected from the Suez Canal during, 1997. Examination of these samples using spectrofluorometric technique to assess the contents of petroleum hydrocarbons reveals that the area is moderately polluted. Levels of polycyclic aromatic hydrocarbons (PAHs) were measured in water of the Suez Canal. Advanced technique GC/MS was used for the analysis. The presence of fluorene is reported at low concentration ranges from 0.14 - 0.21 µg/L in the Suez Canal as a result from heavy traffic ships in addition to atmospheric fallout of automobile exhausts in cities and towns distributed along the Canal. Phthalate was found in the middle of the Canal reflecting the degradation of high parent molecular weight fractions. Concentrations and molecular structures were formulated and discussed in detail.

**P11/P/04-B5 Poster 1150-04****A COMPARISON OF FLUORENCE AND GC FOR DETERMINATION OF AROMATIC HYDROCARBONS**

OTHMAN Tarek, (National Institute of Oceanography and Fisheries, Suez, PO182, Egypt)

Abstract not available at time of going to press

**P11/P/05-B5 Poster 1150-05****THE HYDROGRAPHY OF THE GULF OF AQ ABA**

Ibrahim A. A. Maiyya, Ahmed Ramadan HASSAN (both at NIOF, Suez P.O. Box 182, EGYPT, Tel (062) 360015, Fax 002(062) 360016, Leila Saado Balloemel, and Lobna Mohammed Salah (both at Physics Department, Faculty of Science, Cairo University).

The Gulf of Aqaba (29–29.5°N and 34–35°E, 70–km long, 14–26 km wide and up to 1829 m deep) is the NE segment of the Red Sea. A narrow sill at the Straits of Tiran separates it from the Red Sea. The major factors influencing the hydrographic regime are the physiographic elements and its climatic setting within an arid area. The water masses in the Gulf are almost one in winter due to the vertical convection. In spring the surface layer tend to separate due to the surface heating and the exchange with waters of Red Sea origin. In summer and autumn distinct three water masses appeared. A surface one, which is a mixture of Aqaba and Red Sea waters. A subsurface one of Red Sea origin enter the Gulf at the Straits zone and as a new Gulf water mass created at the northern zone and turn back southerly, partially emerge to the Red Sea as a subsurface current and partially as result of many factors turn back to the bottom of the Gulf. A deep water mass, which in some cases can be divided, into deep and near bottom water masses. The water masses can be differing in magnitude and space depending to some extended on the interannual variability, which play an important role in the hydrography of the Gulf of Aqaba. The central zone participates the northern zone as a source of the Gulf deep water, at which the Red Sea water start to slope downward. The wind system, which may change suddenly in magnitude and/or direction, has great influence on the hydrographic regime of the Gulf of Aqaba.

**P11/W/03-B5 Poster 1150-06****COASTAL BENTHIC COMMUNITY OF THE PECHORA SEA**

Nikita V. Kucheruk, Pavel V. RYBINKOV, Filipp V. Sapozhnikov (all from Oceanology Institute RAS, Nakhymovsky 36, 117518 Moscow, Russia, email: fisher@ecosys.sio.rssi.ru)

Investigations of the Eastern shallow water part of the Pechora sea were carried out in 1998 August-October. About 200 samples of macrobenthos, 90 samples of meiobenthos and 130 samples of microphytobenthos were taken in 50 station at 5-25 m depths. The peculiarity of the region was the minimal macrobenthos diversity and biomass at shallowest (5-10 m) stations. Maximal macrobenthos biomass and species richness was found for >20 m depth at constantly negative temperature values. Maximal biomass of meiobenthos at the area studied barely exceeded 0.5 g/m<sup>2</sup>. At that, contribution of pseudomeiobenthos reached in average 40-50%. In all samples treated numerical dominants were nematods, but their mass share amounted only 20% . Approximately the same contributions to total biomass made Harpacticoida and Ostracoda. In general meiobenthos fauna of the Pechora sea coastal part was quite poor both from qualitative and quantitative point of view. Microphytobenthos of bottom sediments upper layers was mainly represented by diatoms. Their biomass amounted 180-720 g/m<sup>2</sup>. There were totally 173 species identified. All the diatoms may be divided in two groups: species, settled down from water column (Melosira and Thalassiosira) and initially benthic forms (Raphoneis, Navicula and Nitzschia). The pattern observed, may derive from cooling of sea water in the end of October.

**P11/W/11-B5 Poster 1150-07****OCEAN CLIMATE OF THE BALTIC SEA AND KATTEGAT-ANALYSIS OF HISTORICAL DATA OF SALINITY AND SEA LEVEL.**

Peter WINSOR (Earth Science Center, Box 460, Gvteborg, Sweden, Email: pewi@oce.gu.se)

As a part of the Swedish regional climate modelling programme SWECLIM the ocean climate of the Baltic Sea and the Kattegat is examined by means of analyzing historical data series. Defining today's climate state and its natural variability is necessary in order to be able to model future climate change. The data consists of long time series (about 100 years) of salinity, temperature, sea level, and river runoff. These series are analyzed statistically regarding the variability on different time scales. The integrated estimates include the vertically integrated freshwater height  $F (F=1/Sref*\sum[Sref-S(z)]dz$ , where Sref is a reference ocean salinity), the sea level, the barotropic water exchange between the Kattegat and the Baltic Sea, and the ice extent of the Baltic Sea. Prominent findings include:

Most of the variability of the freshwater height of the Baltic Sea is on time scales of months or longer, whereas nearly all variability in the Kattegat is on months or less. Furthermore, about half of the Baltic Sea freshwater variability can be explained in terms of the interannual variability of the runoff to the Baltic Sea. The rest of the variability is related to variations of the intermediate or deep water inflows from the Kattegat.

For periods longer than one month Samuelsson and Stigebrant 1996 have shown that the Baltic Sea acts as an open fjord with increasing amplitudes from the mouth and inwards. Most of the sea level variance on time scales longer than two months is due to external forcing, i.e., the sea level in the Kattegat and the freshwater supply to the Baltic Sea.

**P11/W/14-B5 Poster 1150-08****SEASONAL VARIABILITY OF THE LA PEROUSE STRAIT WATER STRUCTURE AND WATER MASSES**

Pishchalnik V.M., ARKHIPKIN V.S. (1)SakhNIRO Yuzhno-Sakhalinsk 693016 Russia email: pvm@tinro.sakhalin.ru; 2)Department of Oceanology Moscow State University Vorobiyevy Gory Moscow 119899 Russia email: arkip@ocean.geogr.msu.su)

In this report the quantitative estimate of a seasonal variability of volumes and heat content of the La Perouse Strait water masses is given. For this purpose the data on temperature and salinity on 48 standard oceanographic stations for period with 1948 on 1994 were used. In total about 10000 observations. The analysis of obtained outcomes allows to make the following conclusions. In without ice period in the La Perouse Strait three water masses are selected: Surface Water (SW), Okhotsk Water (OW) and Japan Surface Water (JW). The singularities of spatial distribution of water masses in research region cause presence of two types of a water structure: subarctic and subtropical. In the spring, summer and autumn a majority of strait volume (70-80 %) takes waters of the subarctic structure. The subarctic water structure consists of two water masses - SW and OW. The subtropical structure of waters is submitted by warm the Soya Current and places in a narrow coastal zone (10-15 miles) near the Hokkaido Island. On mean stations the parameters of water vertical stability in both structures are calculated. Values of common vertical stability of water in the subarctic structure much more, than in subtropical. In the spring and summer in both structures the contribution of temperature in common vertical stability much greater, than the contribution of salinity. In the autumn this ratio a converse. The significant seasonal variability of the SW and JW characteristics is detected. OW within all year has the stable characteristics. In the summer the main reserve of heat is concentrated in Surface (48 %) and Japan Surface (42 %) Waters. Because of seasonal oscillations of volumes of water of a subtropical structure is appreciated seasonal variability of the consumption of the Soya Current, which can reach 0.4-0.5 Sv.

**P11/W/21-B5 Poster 1150-09****FORMATION AND CIRCULATION OF THE INTERMEDIATE WATER IN THE NORTHWESTERN JAPAN SEA AND THEIR DECADEAL CHANGES ACCOMPANIED BY CLIMATE CHANGE**

Tatsuro WATANABE (Japan Sea National Fisheries Research Institute, Niigata, Japan, email: tatsuro@jsnf.affrc.go.jp); Akifumi Nakata (Hokkaido Fisheries Experimental Station, Yoichi, Japan)

By using winter CTDO data, isopycnal analyses were done to clarify the formation and circulation of the intermediate water in the northwestern Japan Sea. On the surface of 26.8 sigma-theta, since the Tsushima Warm Current (TWC) outcrops around 42.5N, extremely high salinity water of TWC can be cooled directly there. On the surface of the density from 27.2 to 27.34 sigma-theta, high salinity and high dissolved-oxygen water can be seen in the northwestern Japan Sea, off the Hokkaido Island. Since there are not any origins of high salinity except TWC, it is suggested that TWC is the origins of the intermediate water of the Japan Sea. By using historical data of the temperature and the salinity distributions in the northwestern Japan Sea, it can be shown good agreements with the variability of the formation of the intermediate water and the intensity of surface cooling and the supply of high salinity water by TWC.

**P11/W/26-B5** Poster **1150-10**

**MUSSEL (MYTILUS EDULIS) FILTERING OF THE BALTIC-SEA OUTFLOW THROUGH THE ÖRESUND - AN EXAMPLE OF A LARGE-SCALE ECOSYSTEM RESTORATION**

Johan RODHE (Göteborg University, Department of Oceanography, Box 460, S-405 30 Göteborg, Sweden, email: joro@oce.gu.se) Joel Haamer (National Board of Fisheries, Institute of Coastal Research, Nya varvet, byggnad 31, S-42 671 Västra Frölunda, Sweden)

Investigations were undertaken, aiming at a quantification of the filtering capacity by the mussels at the sill in Öresund, one of the straits connecting the Baltic Sea with the Kattegat. The investigations included observations of hydrography and currents together with the content of nutrients in the water, chlorophyll-a and phytoplankton. Following the water over the vast mussel banks at the sill, we found that about 75% of the phytoplankton biomass was removed from the water. The clearance rate, defined as the volume of water cleared from organic matter per unit time and unit ash-free dry-weight of soft tissues of the mussels (AFWD), was estimated at 7 l h<sup>-1</sup> g<sup>-1</sup>. Judging from the total amount of mussels, we found that the mussels at the sill have the capacity to clear the outflow from the Baltic Sea, through Öresund, almost completely. We also found that the plankton biomass recovered after the passage of the sill.

**P11/W/27-B5** Poster **1150-11**

**COASTAL BENTHIC COMMUNITY OF THE PECHORA SEA**

KUCHERUK N.V (Oceanology Institute Ras Nakhymovsfy 36, Moscow, Russia, Email: Kucheruk@ecosys.sio.rssi.ru)

Abstract not available at time of going to press

**P11/W/30-B5** **1150-12**

**CONSIDERATION IS GIVEN TO THE PROBLEM OF DEFINING A MIXING ZONE NEAR AN OUTFALL**

SHERWIN T (Uni of Wales, Bangor, Wales, UK Email: tjs@uces.bangor.ac.uk)

Consideration is given to the problem of defining a mixing zone near an outfall, particularly when the zone is to be used to examine eutrophication problems. It is demonstrated that long term, and often non-tidal, coastal residual currents play an important part in flushing nutrients away from a long sea outfall, and can render the definition of a mixing zone in terms of the tidal excursion irrelevant when a pollutant has a long decay time. Consequently far field effects, such as the interaction of neighbouring outfalls, may be more important than is implied by the mixing zone concept. These ideas run counter to the guidelines published by the Comprehensive Studies Task Team for the application of the European Union Urban Waste Water Treatment Directive in UK waters, which emphasises the use of a tidal mixing zone for eutrophication problems.

**Friday 30 July PM**

Presiding Chair: Prof. T. Oguz

**THE BLACK SEA**

**P11/W/17-B5** **1400**

**HYDRO-OPTICAL INVESTIGATIONS IN THE EASTERN MEDITERRANEAN AND WESTERN BLACK SEA FROM RV HORIZONT, 1998**

Viktor I. Man'kovsky, Alexey V.MISHONOV, Mark V. Solov'ev (Marine Hydrophysical Institute, National Academy of Science of Ukraine, 2 Kapitanskaya St., Sevastopol, 335000, Crimea, Ukraine, email: mishonov@alpha.mhi.iuf.net)

Scientists from MHI NASU performed a cruise on R.V. Horizont from 5 May to 4 June 1998. The beam attenuation coefficient (BAC), Secchi disk depth and watercolours, by the Forele-Ulle scale, were measured in the eastern Mediterranean and the western Black Sea. The main research areas were the Levantine Sea (Crete-Rhodes area), the Aegean Sea (Dardanelles Straits region), and the Black Sea (continental slope area westward of the Crimean peninsula). The BAC was measured at seven wavelengths in samples taken from Nansen bottles from different depths on stations and surface samples were taken from a bucket en passage. BAC fields at 0, 40, and 80 meters depth, Secchi disk depth field, and watercolour field were obtained from these areas. Results from the BAC spatial field, obtained from the Rhodes-gyre area, showed upwelling deep water. This was demonstrated at all depths (0, 40 and 80m). The spectral distribution of the BAC showed different shaped spectra for upwelling waters compared to down-welling waters. The optical assessment of the Levantine Sea waters shows it to be oligotrophic waters. This confirms previous research in 1981-1983. In the Dardanelles Straits area the frontal zone, where waters from the Marmara Sea mix with Aegean Sea waters, was recognised from the BAC field as well as from Secchi disk data. This frontal zone was 15 - 18 nautical miles wide. The SeaWiFS images for this period shows this feature in the chlorophyll-a concentration field. The spectral distribution of the BAC in this area shows increased light attenuation in the violet range of the spectra and a shift of minimal values to the yellow area. This is evidence of high concentration of "yellow matter" in this area. In the Black Sea the optical properties were measured twice on one transect along 34°E at the beginning and at the end of the cruise. A further polygon survey was carried out westward of the Crimea. A quasi-stationary anti-cyclone gyre was observed from the data, which is well known for this area and relates to the interaction between the main Black Sea current and the continental slope. The spatial distribution of the optical properties in this area correlates well with the hydrographic data, which were obtained simultaneously. The spectral distribution of the BAC in this region indicates a significant increase in the violet-green spectral range with minimal values in yellow area. The concentration of "yellow matter" in this area is high and these waters can be classified as meso/euphotrophic. Results obtained from this cruise allowed assessments to be made of the optical conditions and comparisons between the different, but connected, parts of the Mediterranean basin. These data are very important for the continuation of the long-time series data, which have been collected by the MHI NASU for the Mediterranean and Black Seas.

**P11/E/23-B5** **1420**

**WINTER MIXING EVENTS IN THE BLACK SEA**

Leonid I. IVANOV, Vladimir Belokopytov (Marine Hydrophysical Institute, Kapitanskaya St., Sevastopol, 335000, UKRAINE; e-mail: leonid@alpha.mhi.iuf.net); Emin Ozsoy (Institute of Marine Sciences, Middle East Technical University, P.K. 28 Erdemli - Icel 33731 Turkey; e-mail: ozsoy@ims.metu.edu.tr)

A scientific assessment of the role of winter mixing and water mass formation in the Black Sea is essential for a better understanding of the impacts on the transports of pollutants and

organic matter, and on the evolution of the suboxic layer and the chemocline, as well as on the entrainment of nutrients from the pycnocline into the euphotic zone. We present results on the history of winter mixing events over the period from 1923 to present to discuss the depth dependence of the magnitude and phase of long-term temperature fluctuations in the pycnocline, and to provide estimates of the heat flux through the pycnocline for characteristically mild, moderate and severe winter atmospheric conditions. Temporal and spatial variability is analysed as a function of depth, salinity and density. The effects of winter mixing events are well preserved in the T,S structure, while the individual convection events have limited effect in modifying main pycnocline on a seasonal time scale. The magnitude of temperature fluctuations decreases exponentially with increasing depth. Major cooling periods, with a net decrease of temperature in the entire pycnocline above 16.5 sigma-t, occurred in the late 20's - early 30's, early 50's, middle 80's and early 90's. An analysis of surface fluxes and heat content of the pycnocline on a regional basis allows to infer that, typically, the pycnocline is exposed to cooling for a short periods in confined areas.

**P11/E/01-B5** **1440**

**NITROGEN IN THE BLACK SEA: FLUXES, CYCLING AND BUDGET**

Sergey KONOVALOV, Leonid Ivanov and Anatoly Samodurov (all at Marine Hydrophysical Institute, Kapitanskaya 2a, Sevastopol 335000, Crimea, Ukraine, email: sergey@alpha.mhi.iuf.net, leonid@alpha.mhi.iuf.net)

Drastic eutrophication has been primarily recognized as the reason of adverse changes in the Black Sea ecosystem over the last three decades. This is true for many other semi-enclosed and marginal seas all over the world. Nitrogen is considered as the leading nutrient among the others to be responsible for various aspects and results of eutrophication. While the source of nitrogen in the Black Sea is well known, the budget, cycling and loss of this nutrient are poorly investigated. To fill this gap 1.5-D model of vertical exchange in the Black Sea pycnocline has been applied to assess nitrogen fluxes and losses, as well as to reconstruct its budget, in the oxic/anoxic transition zone of the Black Sea. Field data on distribution of nitrogen and other basic properties (oxygen, sulfide, temperature and salinity) have been analyzed in order to verify the results of modeling and to estimate changes in the overall budget of nitrogen in the Black Sea. The results demonstrate notable increase in the overall inventory of nitrogen (mainly in form of ammonia). They also reveal that the main part of the load of inorganic nitrogen is stored in water column. Vertical exchange in the pycnocline plays important role in governing cycling and losses of nitrogen in the Black Sea. The flux of ammonia from the anoxic zone is enough to compensate the down ward flux of nitrate supporting hypothesis of effective denitrification in the layer of pycnocline. The amount of nitrogen that is annually replenished in the oxic/anoxic layer from external sources is close to 30% of the river-born load into the basin. Unlike ammonia, residence time of nitrate in the layer of the main pycnocline is fairly short and it lies on scale of a year.

**P11/E/08-B5** **1500**

**SULPHIDE BUDGET IN THE BLACK SEA**

Leonid I. IVANOV, Sergey Kononov and Anatoly Samodurov (Marine Hydrophysical Institute, Kapitanskaya St., 2a, Sevastopol, 335000, UKRAINE; e-mail: leonid@alpha.mhi.iuf.net)

The Black Sea, an example of an estuary basin, being globally the largest body of anoxic waters, presently, is facing rapid environmental degradation. An assessment of its present state and prediction of its future, among other issues, implies better understanding of the processes maintaining vertical structure of the anoxic layer. The specific objective of this study was to estimate the sulphide production rates and fluxes. The 1.5-dimensional model of vertical exchange in the Black Sea has been applied to calculate vertical fluxes of sulphide and a distributive lateral flux of dissolved oxygen into the suboxic and anoxic layers. The latter is maintained by the Bosphorus effluent. Calculations were based on stratification and sulphide vertical distribution averaged over the period from 1985 to 1995. The results, however, are not sensitive to the period of averaging. This is especially true for the upper layer of the anoxic zone where vertical gradients of sulphide are proved to be practically unchanged in recent decades.

The magnitude of the sulphide total flux (advective and diffusive) for the entire basin reaches its maximum, 13E10 M/yr, at about 300 meters. From that point it decreases upward to about 6E10 M/yr at the top boundary of the anoxic layer and downward to less than 4E10 M/yr at 1000 meters. A remarkable feature of the flux vertical distribution is absence of a general resemblance with the profile for the flux of ammonia, which should be expected, unless their losses are controlled by different mechanisms. Oxidation of sulphide takes place within the sulphidic layer, but not only at the top boundary as for ammonia. The sulphide production rate, calculated with the consideration of oxidising capacity of Bosphorus inflow, shows general decrease with increasing depth.

**P11/E/18-B5** **1520**

**THE STUDY OF MESOSCALE MOTIONS IN THE SHELF ZONE OF THE BLACK SEA**

Vasily VLASENKO, Natalia Stashchuk, Vitaliy Ivanov (Marine Hydrophysical Institute, Kapitanskaya Str. 2, Sevastopol, 335000, Ukraine, e-mail: vlasta@ukrcm.sebastopol.ua)

The response of the Black Sea shelf zone to a short period (up to one day) wind action is investigated. The analysis is carried out on the basis of in-situ and remote sensing data and with the help of mathematical modeling. It was found that the vertical stationary circulation cell was formed in the shelf interior due to the wind action. It characterized by virtue of water ascent near the coast and descent in the region of the shelf break. Near inertial horizontal oscillations in the open part of the sea and vertical oscillations over the slope are generated. The inertial oscillations may lead to meandering of the Black Sea rim current and its interaction with the shelf edge. That, in turn, gives rise the considerable vertical displacements of a pycnocline above the shelf edge, which, in the long run, generate progressive internal waves. The shoreward-oriented long internal wave, due to the nonlinearity of the wave process, disintegrates into a packet of intensive shortperiod internal waves, many times measured in the shelf zone of the Crimea.

The nearcoastal upwelling and mesoscale motions have also an essential influence on the dynamics of the upper boundary of the Black Sea hydrogen sulphide zone. The upward fluxes of cold bottom water are accompanied by the displacement of the upper boundary of the hydrogen sulphide zone and its penetration into the layer enriched by oxygen. As a result, an extensive co-existence zone is formed over the shelf-break area in place of upwelled water. As was obtained theoretically an confirmed experimentally, the area with small oxygen concentration remains over the shelf break after the end of the chemical reaction between two dissolved gases. This extended area with low oxygen concentration may be considered as a "trace" of the upwelling event.



P11/W/08-B5

1600

## THE RESPONSE OF THE BLACK SEA ECOSYSTEM TO SOME PHYSICAL PROCESSES

J. Staneva, E. Stanev (both at the University of Sofia, 5, J. Bourchier Street, Sofia 1126, Bulgaria, e-mail: joana@phys.uni-sofia.bg); Ch. Lancelot (Universite Libre de Bruxelles, CP221, B-1050, Belgium, e-mail: lancelot@ulb.ac.be)

This study presents the state of the art of the 3D coupled physical-biological model of the Black Sea ecosystem resulting from the online coupling of the Modular Ocean Model modified for its application in the Black Sea with the mechanistic ecological model BIOGEN. Both models were developed, tested and analyzed separately before their online coupling. The Modular Ocean Model was implemented in the Black Sea with two horizontal resolutions: 5, or 15 min. New parametrizations were added in order to take into account the specific physical processes prevailing in this almost enclosed ocean basin. The diapycnal mixing was calibrated against independent measurements of chemical tracers. Data on Chernobyl tracer penetration were used for Model validation. This comparison shows that the model simulates correctly the pathways and the rates of penetration of signals originating at sea surface and presents a reliable tool for water mass and ecological modeling. BIOGEN is a mechanistic ecological model of high trophic complexity (34 biogeochemical state variables) that was established in order to assess the response of the north-western Black Sea ecosystem to human-induced changes and predict its future evolution. The model was first implemented by coupling it with physical models of increasing spatio-temporal complexity and running it with different human-induced forcings in order to analyse its ability to reproduce correctly historical ecological events recorded since the 1960. Preliminary results of the performance of coupled 3-D physical-biological models are analysed. The impact of some physical processes on the Black Sea ecosystem as well as the role of the physical processes in driving interannual variability in ocean primary production is studied. The simulated phytoplankton patterns are compared with the CZCS and SeaWiFS satellite data.

P11/W/01-B5

1620

## DEEP-SEA ZERNOV'S PHYLOPHORA MEADOW IN THE BLACK SEA: THE COMBINED RESULT OF HYDRODYNAMICS AND ECO-MORPHOLOGICAL PLASTICITY OF PHYLOPHORA NERVOSA (D.C.) GREV. (RHODOPHYTA, GIGARTINALES)

Olga V. MAXIMOVA, Nikita V. Kucheruk, (both from Oceanology Institute RAS, Nakhimovskiy 36, 117851 Moscow, Russia, email: kucheruk@ecosys.sio.rssi.ru)

Zernov's Phyllophora Meadow is a unique deep-sea (up to 60 m) ecosystem of unattached form of red alga *Phyllophora nervosa*. It had been discovered in 1908 and since that time was intensively explored and used for agar-containing biomass prey. Its area up to the 60-th was about 10 km<sup>2</sup> but now it is decreasing each year due to anthropogenic eutrophication of Black Sea. Our investigation is based on the last information about the current system of the North-western Black Sea and original experimental data on *Phyllophora*'s morphological transformations. The Meadow has a near-shore origin in the thickets of attached *Phyllophora nervosa* form. From our point of view, the currents and circulations ensure the stability of Meadow's spatial location, and *Phyllophora*'s eco-physiological peculiarities give the opportunity for its existence in the form of self-dependent semi-closed population.

P11/E/12-B5

1640

## "CLOSED, SEMIENCLOSED AND MARGINAL SEAS: PHYSICAL, CHEMICAL AND BIOLOGICAL PROPERTIES". LIGHT ABSORPTION BY PHYTOPLANKTON, DETRITUS AND DISSOLVED ORGANIC SUBSTANCES DURING DIATOM AND COCCOLITHOPHORE BLOOMS IN THE BLACK SEA: IMPACT ON ALGORITHMS FOR REMOTE SENSING

Churilova T.I., Berseneva G.P., Georgieva L.V. (Institute of Biology of the Southern Seas of National Academy of Science of Ukraine Crimea, Ukraine, Sevastopol, 335011, P.O.Box 13, e-mail: churil@ukrom.sebastopol.ua); Stanichny S.V. (Marine Hydrophysical Institute of National Academy of Science of Ukraine, 2 Kapitanskaya st., 335000, Sevastopol, Crimea, Ukraine, e-mail: odmi@alpha.mhi.iuf.net)

The satellite-based remote sensing of the water leaving radiance allow to assessing the surface chlorophyll concentration. Standard algorithms for estimating chlorophyll a concentrations perform quite well for regions of the ocean where scattering and absorbing components of seawater covary with these pigments. The development of realistic models, require algorithms with reflect variability in biological and optical characteristics. The work presented here is an analysis of data collected during the monitoring of bio-optical properties (chlorophyll a and pheophytin a concentrations, light absorption spectra by particles, phytoplankton, detritus and dissolved organic substances, species composition of phytoplankton, cells and biomass concentration) of surface water which was conducted in the central western part of Black sea in February-December 1998. The blooming of big diatom (*Rhizosolenia alata*) was observed in March and blooming of coccolithophore (*Emiliania huxleyi*) – in June. The high concentration of pigment (1.9 mg.m<sup>-3</sup>) were corresponding to big diatom bloom. During the diatom bloom the chl-a specific absorption coefficient ( $\text{aph}^*$ ) was decreased due to high degree of packaging of pigment in cells. The values of  $\text{aph}^*$  in blue maximum (678nm) were 0.015-0.016 m<sup>2</sup>.mg<sup>-1</sup>, the ratio between red and blue maximum of absorption spectra (R) - 1.8. The contribution of detritus to total light absorption by particles ( $\text{ad}(440)/\text{ap}(440)$ ) is decreased to 19 %. During coccolithophore bloom chlorophyll a concentrations were 0.15-0.21 mg.m<sup>-3</sup>, the values of  $\text{aph}^*(678)$ - 0.019-0.023 m<sup>2</sup>.mg<sup>-1</sup>, the ratio R 2.5-2.6. The contribution of detritus to total light absorption reached to 58 %. It is apparent that light absorption by dissolved organic matter (as) for both blooming was practically not variable.

P11/W/05-B5

1700

## VARIATIONS OF THE BLACK SEA ECOSYSTEM MEASURED FROM REMOTE SENSING

NEZLIN N.P. (Shirshov Inst of Oceanology, Russian Academy of Science, 36 Nakhimovskiy Ave, Moscow, Russia, Email: nezlin@ecosys.sio.rssi.ru)

Abstract not available at time of going to press

P11/W/10-B5

1715

## VERTICAL MIXING ON THE BLACK SEA SHELF

Iossif Lozovatsky (P.P. Shirshov Institute of Oceanology, Russian Academy of Sciences Moscow, 117851, Russia; also at Department of Mechanical and Aerospace Engineering, Arizona State University, Tempe, AZ, 85287-9809, USA, Email: i.lozovatsky@asu.edu); Sergei Shapovalov (P.P. Shirshov Institute of Oceanology, Russian Academy of Sciences Moscow, 117851, Russia, email: smshap@glas.apc.org)

Study of turbulence in the regions essentially free of tidal forcing may have some resemblance to laboratory experiments that have been carried out under idealized conditions (with only a few energy input mechanisms), making comparison of laboratory and field data possible. The measurements of the kinetic energy and scalar dissipation in the shallow shelf waters of Black Sea were accompanied by meteorological and hydrological background observations. The power spectra of turbulent fluctuations and corresponding correlations between buoyancy length scales are discussed. The dependence between normalized Thorpe scale and patch Reynolds and Richardson numbers found in our measurements give more insight on a scaling problem for stratified microstructure patches. The regions with active and fossil turbulence were identified at different depths using the relationship between the mixing activity parameter and the buoyancy Reynolds number. Statistics of the mixing coefficients for certain turbulent regions, calculated from the probability distribution functions of eddy and scalar diffusivities and by using the bootstrap method are presented. The domain-averaged turbulent diffusivities vary from 4 cm<sup>2</sup>/s in the boundary layers to 0.2 cm<sup>2</sup>/s in quasi-homogeneous patches inside the thermocline. An appropriate averaging of microstructure variables taken separately for each specific turbulent regions leads to substantial improvement of the correlation between eddy and scalar vertical diffusivities. Influence of inertial oscillations on small-scale shelf dynamics is discussed.

P11/L/06-B5

1730

## PECULIARITY OF VERTICAL CHLOROPHYLL DISTRIBUTION IN THE BLACK AND MEDITERRANEAN SEA

Oleg A. YUNEVI, Zosim Z. Finenkol, Vladimir I. Vedernikov2, Aysen Yilmaz3 (Institute of Biology of Southern Seas, National Academy of Sciences of Ukraine, Sevastopol/UKRAINE; 2 P.P. Shirshov Institute of Oceanology, Russian Academy of Sciences, Moscow/RUSSIA; 3 Middle East Technical University, Institute of Marine Sciences, Erdemli-Icel/TURKEY)

From oceanographic studies carried out in the last two decades it is clear that the mechanisms controlling the biochemical cycle are not uniform throughout the World Ocean. Phytoplankton, the major component responsible for the primary production in the sea, has a principal influence on biochemical cycling from local to global scales. A major objective in oceanography today is estimating the mean and the variance of all parameters describing process of photosynthesis in the sea on a global basis. The greatest variability of the primary production characteristics is observed in basins (to which the Black and Mediterranean Seas can be concerned) with vastly expressed seasonal changeability.

The aim of this investigation is the research of common features in vertical chlorophyll (CHL) distribution in various seasons and in different parts of two interconnected basins with use of mathematical representation of vertical CHL profiles.

In the present study the data obtained in Ukrainian, Russian and Turkish cruises during the last twenty years on the vertical CHL and CHL fluorescence in situ (FLU) distribution in both seas were analysed and parameterised. The CHL profiles with as few as six data points were admitted for parameter estimation. These were found to be adequate to characterize the profile, provided that the data points were well distributed around the peak. For the calculation of CHL and FLU profiles parameters and statistical estimation we used a package of the applied computer programs SigmaPlot for Windows and ANOVA.

The analysis of the Black Sea data has shown, that the forms of vertical CHL and FLU distribution have some types: 1) quasi-homogeneous; 2) with one well advanced and symmetric maximum; 3) with an asymmetrical maximum in the upper half of photosynthetic zone 4) with two maxima (or more than two), which are comparable or differ on amplitude; 5) distribution, when CHL and FLU gradually decreases with depth beginning from a surface.

The first of the listed types is characteristic of a winter period in the Black Sea, when there is the vertical mixing or active upward transporting nutrients from the bottom layers into euphotic layer. The profiles of the second and fourth types are more often observed in summer-autumn period, when the temperature stratification of water mass is a barrier to penetration of additional nutrients from the bottom layers into the well-lit surface layer. The vertical distribution of the third type is characteristic of spring....

P11/L/07-B5

1745

## INFLUENCE OF WATER MASS DYNAMIC ACTIVITY ON NUTRITIONAL CONDITION OF CALANUS EUXINUS IN THE SOUTHERN BLACK SEA

Tatyana V. YUNEVAI, Oleg A. Yunev, Ferit Bingel2, Ahmet E. Kideys2, Georgy E. Shulman1 (Institute of Biology of Southern Seas, National Academy of Sciences of Ukraine, Sevastopol/UKRAINE; 2 Middle East Technical University, Institute of Marine Sciences, Erdemli-Icel/TURKEY)

*Calanus euxinus* is the main trophic link between phytoplankton and many fish species in open part of the Black Sea. *Calanus* food supply, and consequently their fecundity and abundance are characterized by significant spatial variability (Vinogradov et al., 1992). It is possible to assume, that the reason of such variability are the non-uniform hydrophysical conditions of plankton environment.

For confirmation of this hypothesis we investigated dependence between lipid content in the body of *Calanus* as result of food supply (nutritional condition) (Sargent and Henderson, 1986) and dynamic activity of water mass in the places of copepods stay. The samples were collected in the southern part of the Black Sea at two cruises RV "Bilim" (Institute of Marine Sciences, Erdemli, Turkey) during period of steady density stratification (September-October 1996 and July 1997). The bottom border of aerobic layer was used as pattern of dynamic activity; this value is determined as the depth location of density  $\sigma_t = 16.2$ . In the Black Sea location of  $\sigma_t = 16.2$  at the depth of 100-120 m was indicative of cyclonic gyre and descend to 160-200 in depth - of anticyclonic eddy (Murray et al., 1993). Physical patterns (T, S<sub>00</sub>,  $\sigma_t$ ) were measured at the stations using Sea Bird Electronics Model 9 CTD System. *Calanus euxinus* were captured by Nansen plankton net (112 mm mesh size, 0.7 m diameter). Females of the size range 3.3-3.5 mm were used for analyses.

It was shown significant spatial variability of the lipids content in the body of *Calanus* (30 -120 mg per individual). There is close negative correlation ( $r = 0.79-0.90$ ;  $n = 26$ ;  $P < 0.01$ ) between the level of reserve lipids (wax esters and triacylglycerols) and total lipids too (composed in average on 72 % of first ones and on 10 % of second ones) and the depth location of  $\sigma_t = 16.2$  in the places of copepods stay. The structure lipid (phospholipid) contents had not significant correlation ( $r = 0.3$ ). It is important to note, that quantitative expressions for the relationships in 1996 and 1997 were similar to each other, despite of temporal and spatial differences in sampling stations.

P13

Monday 26 – Tuesday 27 July

**DYNAMICS OF SEA ICE AND OCEAN IN POLAR SEAS (IAPSO)**

Location: Arts Building 125 LR1

Location of Posters: Arts Building 126 LR2

Monday 26 July AM

Presiding Chairs: P. Wadhams (Scott Polar Res. Institute, Univ. of Cambridge, UK);  
A.J. Willmott (Dept. of Mathematics, Keele Univ., UK)

P13/E/01-B1

Invited

0830

**LATERAL OCEAN TRANSPORT PROCESSES IN THE ARCTIC BASIN**

Robin D. MUENCH (Earth &amp; Space Research, 1910 Fairview East., Suite 102, Seattle, WA 98102-3620, USA, email: rmuench@esr.org)

The relative importance of mechanisms that laterally transport water, heat and dissolved materials differs in the Arctic from that at lower latitudes because of the low energy levels and small baroclinicities that typify high latitude oceans. The primary mechanism for advective transport in the Arctic Ocean, below the upper mixed layer which is frictionally coupled to a wind-driven ice cover, is by way of strongly barotropic boundary currents that overlie the steep continental slopes around the peripheries of the basins. These currents provide the Arctic Ocean with a cyclonic overall circulation and bifurcate into branches that overlie the steep flanks of the several mid-ocean ridge systems to comprise an interlocking family of closed or partially closed gyres. There are regions, such as surrounding the Chukchi Rise and along the Alpha-Mendeleyev and Arctic Mid-Ocean ridges, where significant gaps exist in our understanding of the circulation. The central basins remote from steep bottom slopes and the associated currents are low in energy. Small-scale structures observed across the Makarov, Amundsen and Nansen basins suggest that molecular processes such as double diffusion play a significant if uncertain role in lateral transport there. Our understanding of these structures remains at the level of hypothesis development. Isolated observations of both warm and cold-core eddies in the central basins suggests that these, too, are important to central basin property transports. The role of fronts remains uncertain, as does the importance of dynamic interaction between the peripheral currents and complex bathymetric features. The balance of transport mechanisms results in relative isolation of the central basin waters when compared to the peripheral or ridge-oriented systems. More quantitative understanding of this balance awaits improved field and theoretically-based analyses of the dominant mechanisms.

P13/E/12-B1

0910

**A TWO-DIMENSIONAL TIME-DEPENDENT MODEL OF A WIND-DRIVEN COASTAL POLYNYA: APPLICATION TO THE ST. LAWRENCE ISLAND POLYNYA**

M. A. MORALES MAQUEDA, A. J. Willmott (both at Department of Mathematics, Keele University, Keele, Staffordshire ST5 5BG, UK, email: m.a.morales.maqueda@maths.keele.ac.uk)

We present a two-dimensional model of the temporal evolution of a wind-driven coastal polynya. Given the time-varying surface winds and heat fluxes, the model calculates the growth rate, distribution and motion of frazil ice within the polynya, and the mass fluxes of frazil ice and consolidated new ice at the polynya edge. The difference between these two mass fluxes determines the velocity of advance/retreat of the polynya edge. Analytical solutions of the model are found for the case when the coastline is a straight line segment of length  $D$  (an idealised representation of an island). Two time-scales and two spatial scales are shown to be important in characterising the polynya: the consolidated new ice and frazil ice time-scales,  $t_c$  and  $t_f$ , respectively, and the offshore and alongshore adjustment length-scales,  $R_o$  and  $R_a$ , respectively. The time-scale  $t_c$  is the time required for the polynya to grow ice of thickness equal to the collection thickness of frazil at the polynya edge. The time-scale  $t_f$  is the time it takes frazil to cross the equilibrium width of the polynya, which is, in turn, determined by the length-scale  $R_o$ . In combination,  $t_c$  and  $t_f$  control the time-scale for the polynya to respond to variations in the atmospheric forcing. The length-scale  $R_a$  measures the sensitivity of the polynya edge to alongshore variations in the coastline geometry. It is shown that if  $R_a$  is comparable to  $D$  then the offshore dimension of the polynya and the time-scale for the polynya to reach equilibrium can be very different from those obtained from a one-dimensional formulation. The model is applied to the study of seasonal and short-term variability of the St. Lawrence Island Polynya.

P13/E/04-B1

0930

**THE PAST ANALOGIES OF RECENT CHANGES OF THE ARCTIC BASIN T,S CHARACTERISTICS.**

PISAREV S.V. ( P.P. Shirshov Institute of Oceanology, RAS, 36 Nachimovskiy ave., 117218, Moscow, Russia, email: sergey@pisarev.msk.ru)

Large and widespread warming of the Atlantic layer, salting of the upper layer of the Eurasian Basin, substantially retreating of the cold halocline from the Eurasian Basin were selected among others recent remarkable changes of the Arctic Ocean to try to reveal the similar phenomena in the past.

All available unclassified observed T,S data of the Arctic Basin, including WODB98, MOODS, and data from old Russian collections, were used to describe the incomplete picture of the past variability. To characterise the recent changes, the results of well known measurements of "Rossiya"-90, "Oden"-91, "Henry Larsen and Polar Star"-93, "Polarstern"-93,96, "SCICEXs"-93,95,96, "TAPEX-94", "Louis S. St.-Laurent"- 94 were collected. The published results of these expeditions and, partly, observed data were used. The data of "Lance"-93,94,95, "Logachev"-94, "Yasnogorsk"- 95, and "Ak.Fedorov"-98, that not widely discussed before, were also added to represent modern changes. The winter and summer T,S fields of EWG (1997,98) were applied as climatology to compare scarce observed stations with each other. The analogies in the past were found, in one or another degree, for all recent changes.

P13/E/17-B1

0950

**TRANSFORMATION OF ATLANTIC WATERS IN THE BARENTS SEA AND THEIR FLOW TO THE EURASIAN BASIN THROUGH ST. ANNA TROUGH**

Ursula SCHAUER (Alfred-Wegener-Institut fuer Polar- und Meeresforschung, D-27515 Bremerhaven, Germany, email: uschauer@awi-bremerhaven.de), Bert Rudels (Finnish Institute of Marine Research, FIN-00931 Helsinki Finland) Harald Loeng (Institute of Marine Research, N-5024 Bergen-Nordnes, Norway), Robin Muench (Earth &amp; Space Research, Seattle, WA 98102-3699 USA) Jim Swift (UCSD Scripps Institution of Oceanography, La Jolla, CA92093-0214, USA)

The ventilation of the Arctic Ocean basins is largely associated with the input of water from the Barents and Kara Seas. Using hydrographic observations, made in the Barents Sea and along

the shelf edge of the Kara Sea between 1991 and 1996, and time series of current, temperature and salinity from moorings in the eastern Barents Sea, we discuss the flow and the modification of the water masses between the western Barents Sea and the St. Anna Trough. The inflow of warm, saline Atlantic-derived water from the Norwegian Sea and the low salinity Norwegian Coastal Current feed a permanent eastward flow. An additional input of fresh water is melted ice which is advected from the central Arctic Ocean and the Kara Sea. These three water masses are modified through cooling and the freezing/melting cycle. Two distinct modes are formed, which leave the Barents Sea eastward and descend down the St. Anna Trough. The lighter mode is winter water of low salinity, thus confined to the upper layers, which leaves the Barents Sea seasonally at temperatures close to freezing point. The largest and most dense contribution consists in more saline but only moderately cold bottom water which is formed in the polynya west of Novaya Zemlya through highly brine-enriched water. Subsequent lateral mixing with warmer Atlantic water feeds a bottom-intensified flow throughout the year. At present conditions, both modes form a low salinity input of about 2 Sv to intermediate depths of the Arctic Ocean.

P13/W/26-B1

1010

**INTERANNUAL VARIABILITY OF SUMMER SEA-ICE THICKNESS IN THE LAPTEV SEA AND THE TRANSPOLAR DRIFT**

Hajo EICKEN (Geophysical Institute, University of Alaska, Fairbanks, AK 99775-7320, USA, Email: hajo.eicken@gi.alaska.edu); Christian Haas (Alfred Wegener Institute, D-27515 Bremerhaven, Germany)

The dominant sea-ice circulation pattern in the Eurasian sector of the Arctic Ocean is the Transpolar Drift (TPD), exporting ice from the Siberian shelves across the central Arctic Ocean into the Greenland and Barents Seas. Large-scale sea-ice models indicate that the highest net ice production rates in the interior Arctic (on the order of 2-3 m/yr) are found in the Laptev Sea in the upper reaches of the TPD. The present study focusses on the interannual variability of sea-ice thickness in the source area of the TPD and how contrasting atmospheric circulation regimes impact ice thickening in the Laptev Sea and adjacent sectors of the Arctic. Ice-thickness data sets were collected during icebreaker expeditions in the summers of 1991, 1993, 1995 and 1996 through electromagnetic induction measurements and drilling. Level-ice thickness varied considerably in the Laptev Sea, with modal thicknesses at the end of the melt season ranging between 1.2 and 1.9 m. Higher mean and modal thicknesses in 1993 and 1996 are associated with recirculation of second-year ice over the Laptev Shelf and severely reduced summer melt, both strongly influenced by the dominant spring and summer atmospheric circulation patterns with low pressure dominating over the central Arctic. Low ice thicknesses in August of 1995, a year of a record minimum summer ice extent, are mostly the result of excessive surface melt, associated with advection of warm air from the Siberian continent. A Lagrangian thickness-evolution study and an analysis of the thickness and composition of level ice downstream in the TPD indicates that (level-)ice thickness anomalies tend to decay as they are advected across the Arctic Basin due to both dynamic and thermodynamic processes.

P13/W/22-B1

1050

**ADVANCED MODELING OF RECENT VARIABILITIES IN THE ARCTIC OCEAN**

Wieslaw MASLOWSKI, Albert Semtner (both at Department of Oceanography, Naval Postgraduate School, Monterey, CA 93943, USA, email: maslowsk@ucar.edu), Bob Newton, Peter Schlosser, Douglas Martinson (all at Lamont-Doherty Earth Observatory, Palisades, NY 10964, USA, email: bnewton@ldeo.columbia.edu)

Recent observations of the Arctic Ice Pack and the upper ocean circulation and water mass structure indicate dramatic changes taking place in this region, as compared to known climatologies. Submarine observations, sea ice buoy data, and various hydrographic sections made in the 1990s show large scale and large magnitude anomalies in distribution and in characteristics of sea ice, fresh water, and Atlantic Water in the Arctic Ocean. Those changes seem to be strongly associated with variability of the atmospheric circulation in the northern high latitudes. Changes in the atmospheric circulation manifested by prolonged summer cyclonic activity in the central Arctic and weakening of the high pressure system over Greenland have been known to occur in that region since the late 1980s.

In order to understand the Arctic Ocean system response to such variable atmospheric forcing, a high resolution, basin-scale, coupled ice-ocean model of the Arctic is used. This model is forced with ECMWF re-analyzed atmospheric forcing for 1979-93 to simulate sea ice and ocean conditions before and during the 1990s. Results from the 15-year simulation show changes in large scale ice and ocean circulation, including the distribution of arctic river runoff and Pacific Water. Comparison of model results for the 1980s and 1990s shows basin-scale changes in the distribution of sea ice and water masses in the upper ocean. Circulation of fresh water on the arctic shelves (as modeled by multiple river tracers), communication with deep basins and its export through Fram Strait and through the Canadian Archipelago vary significantly throughout the time of simulation. Relationships of sea ice and oceanic fluxes to the large scale atmospheric systems as represented by Arctic Oscillation (AO) and North Atlantic Oscillation (NAO) are investigated.

P13/W/25-B1

1110

**SIMULATION OF THE INTERANNUAL VARIABILITY OF THE WIND DRIVEN ARCTIC SEA ICE COVER DURING 1958-98**

Gilles ARFEUILLE, (National Institute for Earth Physics, PO Box M.G 2 Bucharest, Romania Email: ardel@infp.ifa.ro) Lawrence A. Mysak, Louis-Bruno Tremblay

A thermodynamic-dynamic sea ice model based on a granular material rheology developed by Tremblay and Mysak is used to study the interannual variability of the Arctic sea ice cover during the 41-year period 1958-98.

Monthly wind stress forcing derived from the National Centers for Environmental Prediction (NCEP) Reanalysis data is used to produce the year-to-year variations in the sea ice circulation and thickness. We focus on analyzing the variability of the sea ice volume in the Arctic Basin and the subsequent changes in sea ice export into the Greenland Sea via Fram Strait. The relative contributions of the Fram Strait sea ice thickness and velocity anomalies to the sea ice export anomalies are first investigated, and the former is shown to be particularly important during several large export events.

The sea ice export anomalies for these events are next related to prior sea ice volume anomalies in the Arctic Basin. The origin and evolution of the sea ice volume anomalies are then related to the sea ice circulation and atmospheric forcing patterns in the Arctic. Large sea ice export anomalies are generally preceded by large volume anomalies formed along the East Siberian coast due to anomalous winds which occur when the Arctic High is centered closer than usual to this coastal area. When the center of this High relocates over the Beaufort Sea and the Icelandic Low extends far into the Arctic Basin, the above ice volume anomalies are transported to the Fram Strait region via the Transpolar Drift Stream. Finally, the link between the sea ice export and the North Atlantic Oscillation (NAO) index is briefly discussed. The overall results from this study show that the Arctic Basin and its ice volume anomalies must be considered in order to fully understand the export through Fram Strait.



P13/W/24-B1

1130

## PARAMETRIZATION OF ICE CATEGORIES IN A COUPLED ICE-OCEAN MODEL

Hitoshi Shinkai, Motoyoshi IKEDA (Graduate School of Environmental Earth Science, Hokkaido University, Sapporo, Japan, email: shinkai@ees.hokudai.ac.jp); Tatsuro Watanabe (Japan Sea National Fisheries Research Institute, Fisheries Agency, Niigata, Japan)

Parametrization of ice categories in a sea ice model for the simulation of a seasonal ice cover is investigated. In various sea ice models, only two idealized thickness levels (two category model) are used: i.e., thick and thin, which is taken to have zero thickness and treated as open water. Hence, new ice freezing over open water is forced to merge immediately with the thick ice. However, in the situation of low ice concentration at lower latitudes, such as the Okhotsk Sea, the two category ice model may overestimate air-sea heat flux through thin ice (open water). We propose three ice categories: thick ice, open water and thin ice which is produced over open water and stays to be thin until it is deformed mechanically. The thin ice among the thick ice has much weaker effects on ice pressure, and a higher ice concentration is preserved than the two category model. The thin ice in the three category model prevents air-sea heat flux resulting in less ice formation. The consequences during a decay period is faster melting, because smaller ice volume overcomes the albedo effects of the thin ice (vs. open water). The parametrization of thin ice is found to be important for simulation of the seasonal ice cover in the Sea of Okhotsk, and a step-by-step toward a multicategory ice model.

P13/W/01-B1

1150

## CONVECTION IN THE STRATIFIED OCEAN WITH BACKGROUND GEOSTROPHIC CURRENT

Yutaka YOSHIKAWA, Kazunori Akimoto, and Toshiyuki Awaji (Department of Geophysics, Graduate School of Science, Kyoto University, Kyoto, 606-8502, Japan. email: yosikawa@kugi.kyoto-u.ac.jp)

Numerical experiments are performed using a 3D nonhydrostatic model to understand convective and water formation processes in the stratified ocean with background geostrophic current. The model ocean is a rectangular one (50km x 50km x 1km) on an f-plane. Background current is initially given, geostrophically balancing with upward- domed density structure. With the beginning of uniform surface cooling, convective plumes of about 1-km scale develop and vertically homogenize the water column in the upper layer. At the same time, they accelerate the growth of baroclinic instability; unstable waves of 5-km wavelength develop at the periphery of the dome more rapidly than unstable waves due to pure baroclinic instability. Another effect of convection is to induce significant vertical motion in the preferred place provided by baroclinic unstable waves, upward motion on the ridge and downward on the trough. These up- and downward motions extend to greater depths along isopycnal surfaces, compared with those due solely to either convective or baroclinic instability. As a result, the upper layer water is effectively subducted to form patches with anticyclonic eddy at around the base of pycnocline. This is a possible formation process of eddies containing newly ventilated water as observed south of the Labrador Sea

P13/W/27-B1

1210

## POLYNYA SIMULATIONS: A COMPARISON OF A FLUX MODEL AND A HIGH RESOLUTION DYNAMIC-THERMODYNAMIC SEA ICE MODEL

H. BJORNSSON, L.A. Mysak (Department of Atmospheric and Oceanic Sciences, McGill University, Montreal, Canada), Andrew J. Willmott and Miquel M. Morales (Department of Mathematics, Keele University, Keele, Staffordshire, UK)

The current theoretical understanding of wind-driven polynyas is based on flux models, which are generalizations of the steady state models of Lebedev and Pease. In these flux models, a polynya will evolve according to the balance of the nearshore ice formation and the offshore wind-driven ice transport. In these models, two types of ice are considered: the newly formed frazil ice, and the consolidated frazil ice pack. The boundary between the two ice types is the polynya edge. The influence of internal ice stresses is not considered, and thus the flux models are limited in that they employ no ice rheology.

Ice rheology is employed in traditional dynamic-thermodynamic sea ice models. However they do not consider different ice types (i.e. frazil and consolidated ice), which means that even though they correctly model the same thermodynamic processes as the flux models do, a clear polynya edge is not guaranteed. We apply a recently developed sea ice model to simulate a polynya edge in a semi-enclosed channel for several different wind directions, and compared the results with those obtained with a flux model.

We show that in the cases where the ice flow is not affected by internal ice stresses (eg, along-channel winds), the results from the two types of model compare extremely well, although the definition of the polynya edge in the ice rheology model becomes arbitrary. For the cases where there is an onshore wind component, the ice rheology model gives a clear polynya region and an ice pack region with a polynya edge separating the two. In this case, however, there were greater differences in the results for the two types of models, unless special care was taken to ensure that the effects of rheology were implicitly accounted for in the flux model. We performed sensitivity experiments to see if the flux model results depended on the spatial non-uniformity of ice production within the polynya and the along-channel motion of the ice pack. We found only a slight sensitivity to these variables. The flux model proved to be more sensitive to the spatial variability in the cross-channel velocity component of the ice pack. This is the variable in the ice model that is most affected by rheology. Using the same cross-channel velocity component in both models gave results that compared quite favorably.

Monday 26 July PM

Presiding Chairs: P. Wadhams (Scott Polar Res. Institute, Univ. of Cambridge, UK); A.J. Willmott (Dept. of Mathematics, Keele Univ., UK)

## DYNAMICS OF OCEAN IN POLAR SEAS

P13/E/10-B1

1400

## ON THE SENSITIVITY OF SOUTHERN OCEAN SEA-ICE TO THE SURFACE FRESH WATER FLUX: A MODEL STUDY

S. J. MARSLAND (Max-Planck-Institut fuer Meteorologie, Hamburg, Germany, Email: simon.marsland@utas.edu.au) J.-O. Wolff (ICBM, University of Oldenburg, Oldenburg, Germany, Email: wolff@icbm.de)

An investigation of the ocean/sea-ice interaction in the Southern Ocean has been carried out using the Hamburg Ocean Primitive Equation Model (HOPE). Coupled to this is a thermodynamic model of sea-ice growth and melt, and a dynamic model of the sea-ice momentum balance employing a viscous-plastic rheology. Two versions of the model have been formulated: a high resolution re-entrant channel model along the East Antarctic coastline; and a medium resolution model of the entire southern hemisphere. Both models are found to be very sensitive to the magnitude of the surface fresh water flux (SFWF). The high resolution model has been tested for a range of values of a space and time constant precipitation minus

evaporation (P-E). The time mean sea-ice extent is found to be linearly correlated to the magnitude of the P-E, and for the case of zero P-E there is a complete breakdown of the seasonal cycle of sea-ice advance and retreat, characterised by large scale oceanic convection and above freezing sea surface temperature. In the medium resolution version the occurrence of a large scale convective polynya in the Weddell Sea is found to depend critically on the magnitude of SFWF. There the polynya forms for two of the three P-E climatologies considered when no glacial meltwater is added to the SFWF, but does not form for any of the P-E climatologies when a contribution (10 cm/annum) due to glacial melt water is added to the region south of 60 degrees South. It is concluded that the Weddell Sea is the most marginally stable region of the Southern Ocean, and given this, that a negative anomaly in the P-E to that region in the early 1970's would be sufficient cause to explain the observed Weddell Polynya.

P13/E/07-B1

1420

## STRUCTURE AND CHARACTERISTICS OF DICOTHERMAL LAYER IN THE ANTARCTIC OCEAN

BENNY N. PETER (Department of Physical Oceanography, Cochin University of Science & Technology, Fine Arts Ave, Cochin, India 682016, email: benny@md2.vsnl.net.in)

Dicothermal layer, a peculiar temperature structure of cold water, sandwiched between the warm waters above and below is observed in the surface layers of high latitude oceans, and is conspicuous only during summer. From the vertical section of temperature along various longitudes in the Antarctic Ocean the dicothermal layer has been identified. This layer occupies between 50 and 150m depth and extends upto about 52 degree south from the Antarctic Coast. Characteristics such as salinity, temperature, thermocline anomaly, oxyt and sound velocity in the dicothermal layer have been analysed. The dicothermal layer is associated with relatively high gradient of temperature, salinity, density and oxyt. The sound velocity decreases with depth in the dicothermal layer and attains a minimum at the core of the layer and then increases downwards. Thus, the sound wave is less attenuated along this channel. The dicothermal layer shows much spatial variation in the Antarctic Ocean. The occurrence and extent of this layer mainly depends on mixing processes.

P13/E/11-B1

1440

## A SIMPLE ICE-OCEAN COUPLED MODEL IN THE ANTARCTIC MELTING SEASON

Kay I. OHSHIMA (Institute of Low Temperature Science, Hokkaido University, Kita-19, Nishi-8, Kita-ku, Sapporo 060-0819, Japan, email: ohshima@soya.lowtem.hokudai.ac.jp)

In the Antarctic Ocean, sea ice melts mostly on the bottom and lateral faces by the heat input (mainly solar radiation) through the open water area. We propose a simple ice-upper ocean coupled model in which sea ice melts only by the ocean heat supplied from the air. The model shows that the relation between ice concentration and upper ocean temperature (CT-relation) converges to a certain asymptotic curve with time, which explains the relation observed in the Antarctic summer by Ohshima et al. (1998). The model also shows that the ratio of the heat used for the melting to the heat input into the open water from the air is determined by the ice concentration at that time. When the model is applied to the summer condition in the Antarctic Ocean, it roughly reproduces meridional retreat of sea ice, suggesting that the melting of sea ice is determined by the local balance to the first approximation. When the model is extended to two-dimensional in the meridional direction with the inclusion of the wind-drift effects, reproduction of the sea ice retreat has further progressed. This two-dimensional model can describe the following ice albedo feedback effect; once the ice concentration is decreased by the divergent wind field, the heat input to the upper ocean is enhanced, leading to further decrease of ice concentration. This mechanism can partly explain the year to year variation of the sea ice retreat in the Antarctic Ocean. Best-fit value of heat transfer coefficient, the key parameter in this model, becomes almost the same value both from CT-relation and meridional retreat of sea ice, and the value is also consistent with the result of McPhee (1992).

P13/E/14-B1

1500

## THE DYNAMICS OF THE ANTARCTIC CIRCUMPOLAR CURRENT

A. GREZIO (School of Ocean and Earth Sciences, University of Southampton, Southampton Oceanography Centre, Southampton S0 14 3ZH, U.K., E-mail: a.grezio@soc.soton.ac.uk); N. C. Wells (Department of Oceanography, University of Southampton, Southampton Oceanography Centre, Southampton S0 14 3ZH, U.K., E-mail: n.c.wells@soc.soton.ac.uk)

The Antarctic Circumpolar Current (ACC) is the only current which flows around the globe without interruptions and connects all oceans to the South Polar regions. The ACC current is driven eastward by a strong wind field, and eddies together with topographic obstacles are crucial in the ACC dynamics. Eddies transfer heat from the lower latitudes to the higher latitudes. They also transfer momentum downward from the surface to the lower layers in the ACC. It is already known that the ACC undergoes interannual changes of the volume transport. Studies on the ACC transport are important for understanding of how rapidly these transfers take place. The dynamics of the ACC is investigated by two partial eddy-resolving models (Fine Resolution Antarctic Model -FRAM- and Ocean Circulation and Climate Advanced Model -OCCAM-). Those models are used in order to understand the role that eddies play in the main balance of the mean circulation in the dynamics of the ACC. Results from the vorticity budget in the OCCAM will be presented and compared with previous studies in the FRAM. Significant differences arise in the two models because of the wind forcing, the rigid-lid condition (in FRAM) and the free-surface condition (in OCCAM). Seasonal and interannual transport variability are going to be evaluated in OCCAM at the Drake Passage in order to analyse the mechanisms that control temporal variability in the Antarctic Circumpolar Current.

P13/E/05-B1

1520

## OPEN OCEAN CONVECTION AND POLYNYA FORMATION IN A LARGE-SCALE ICE/OCEAN MODEL

H. GooSe, T. FICHEFET (both at Institut d'Astronomie et de Geophysique G. Lemaitre, Universite catholique de Louvain, Chemin du Cyclotron, 2, 1348 Louvain-la-Neuve, Belgium, email: hgs@astr.ucl.ac.be)

The formation of an offshore polynya located in the Southern Ocean near the Greenwich meridian is analysed in a large-scale ice-ocean model. This area, which receives at depth an inflow of relatively warm water from the Antarctic Circumpolar Current (ACC), is preconditioned for convection in the model by a wind-driven upwelling and by the convection that has occurred the preceding year. In autumn and early winter, the brine release during ice formation, which is enhanced due to ice divergence, is sufficient to remove the fresh layer caused by summer ice melting and to induce a deepening of the mixed layer. This incorporates warm water in the surface layer which, in a first step, slows down ice formation followed by ice melting in a second step. Then, the freshwater forcing associated with ice melting tends to stabilise the



water column, but the destabilising effect of the oceanic cooling has a large magnitude, even though ice transport convergence prevails now. As a result, convection continues until the total disappearance of the ice at the end of September. Convection stops only when the atmosphere warms up in November. This mechanism of polynya formation seems fairly realistic and the polynya is located in a region where such features have been frequently observed. Nevertheless, the polynya is too wide and persistent in the model, probably because of a too low density at depth and because of the coarse resolution of the model. A passive tracer released in the polynya area shows that the polynya area contributes significantly to the renewal of deep water in the Weddell gyre and that it is major component of the Antarctic Bottom Water (AABW) inflow to the Atlantic.

**P13/W/16-B1****1600****NUMERICAL MODELING OF THE CIRCULATION AND SEA ICE IN THE REGION OF PRYDZ BAY, ANTARCTICA**

Le KENTANG, Shi Jiuxin (Institute of Oceanology, Chinese Academy of Sciences, Qingdao 266071, PRC, email: ktle@ms.qdio.ac.cn)

A coupled sea ice-mixed layer-isopycnal general circulation model formulated on isopycnal coordinates is used to simulate annual variations of the circulation and sea ice in the region of Prydz Bay, Antarctica. Both dynamic and thermodynamic processes are included in this model. The initial condition and forcing fields were calculated from the monthly-mean observed data. To obtain a resolution sufficient enough for the study region, the grid space was to be designed as a varying one.

The simulated circulation pattern and sea ice cover agree reasonably well with the observations. Some new phenomena were found. The computed circulation show that there is a clockwise gyre with annual and inter-annual variation in Prydz Bay. The water exchange between both inside and outside the bay is weak, which mainly occurs in the mouth of the bay, where vertical mixing probably exists. The eastward Antarctic Circumpolar Current in the northern deep region is not really zonal due to topography. The ACC is changeable with seasons. The amplitude of the current is widest in spring. The divergence zone exists between the westward and eastward currents. Many eddies appear in this region. The sea ice cover in this region has a obvious asymmetry annual cycle (the freezing period is longer than the thawing period, which is well consistent with the observation one).

**P13/W/08-B1****1620****ON THE COMMUNICATION BETWEEN THE WEDDELL AND SCOTIA SEAS**

M.P. SCHODLOK, H.H. Hellmer (Alfred-Wegener Institute for Polar and Marine Research, D-27568 Bremerhaven, FR. Germany, e-mail: mschodlok@awi-bremerhaven.de)

The Scotia Sea is filled with newly ventilated Weddell Sea Deep Water (WSDW) which in turn is a vital part for the ventilation of the World Ocean abyss. Depending on the formation process and/or its location along the Weddell Sea periphery, deep and bottom water masses follow different routes to fill the Scotia Sea. Observations along the South Scotia Ridge, i.e. including the Weddell-Scotia confluence region, are limited in space and time possibly leaving escape-routes undiscovered. As a part of the BRIOS (Bremerhaven Regional Ice-Ocean Simulations) project a stand alone ocean model (SPEM) is focused on the Weddell-Scotia confluence region with a resolution of ~20 km. The model is initialized with hydrographic data from Southern Ocean Atlas. The surface forcing data are averaged monthly means from a stand alone sea ice-mixed layer model, based on 6-hourly ECMWF (1985-1993) re-analysis data. Lagrangian floats deployed at different locations served as a tool to examine various pathways for deep and bottom water renewal within the Scotia Sea. Modelled characteristics of the WSDW throughflow into the Scotia Sea through Orkney Passage (~40W) are shown and compared to observations.

**P13/W/05-B1****1640****EAST ANTARCTIC SEA-ICE DRIFT: OBSERVATIONS AND MODELLING**

Petra HEIL (Antarctic CRC, Hobart, Tasmania, Australia, email: petra.heil@utas.edu.au); Xingren Wu, Ian Allison (Antarctic CRC and Australian Antarctic Division, Hobart, Tasmania, Australia, email: x.wu@utas.edu.au, ian.allison@utas.edu.au)

Many of the characteristics of polar sea ice that are important to global climate processes are influenced by the ice drift and deformation. This work presents an overview of the buoy-derived sea-ice drift off East Antarctica (20 - 160E) and compares these data with modelled ice drift fields. Possible improvements in the simulation of sea-ice dynamics over this region are suggested.

The buoy-derived velocity field confirms the broad-scale feature of East Antarctic sea-ice drift. This consists of a westward drift in the coastal current, an eastward current north of the Antarctic Divergence, and a broad region of northward ice transport in Prydz Bay. Sea-ice velocities in the coastal current (0.22 m/s) are generally higher than elsewhere (0.17 m/s), and the flow in the coastal current appears to be steered by the shelf break. In the region between 20 and 152.5E the average meridional component of the coastal current is southward, but small. This average is strongly influenced by a southward component in the flow west of Cape Anne (45E). In contrast, persistent northward ice outlets from the coastal current are found in the region east of Prydz Bay. Although these northward transport rates are smaller than in Prydz Bay itself, they contribute considerably to the divergent character of the region. The drift pattern appears to be largely robust with time, with some variance in the meridional flow. There is some evidence of a seasonal cycle in the sea ice drift speed. The length of the buoy-data record (1985 - 1998) is not sufficient to derive long-term changes, however interannual variability has been identified in the region east of Prydz Bay.

A coupled atmosphere-sea ice model is used to simulate the sea ice over this region. A simple scheme for sea-ice dynamics is currently applied in the model with only the compressive stresses effective in the sea ice. Ice of low concentration moves in free drift from atmospheric wind forcing. At high ice concentration the resistance of sea ice is considered. Preliminary results suggest that the model can simulate the broad structure for the sea-ice drift over this region. However, comparison with the buoy-derived sea-ice field suggests that there is a general tendency for northward transport in the model; also the magnitude of the sea-ice speed appears to be underestimated. Improvement of the ice rheology should remedy the simulations. Some experiments with modified sea-ice dynamics are underway. We will present results from these simulations.

**P13/W/10-B1****1700****OBSERVED WATER MASS PROPERTIES AND OUTFLOW ACROSS THE WEDDELL-SCOTIA CONFLUENCE: A SPANISH CONTRIBUTION TO THE DOVETAIL PROJECT**

Ileana BLADE, Marc A. Garcia (both at Laboratori d'Enginyeria Marítima, Universitat Politècnica de Catalunya, c/ Jordi Girona 1-3, Edifici D-1, 08034 Barcelona, Spain, email: garcial@etsecpb.upc.es)

As part of the international DOVETAIL project, a series of CTD stations were obtained in the Weddell-Scotia Confluence (WSC) region in January-February 1998, in an attempt to

characterize the source waters for the WSC and quantify the Weddell Sea outflow into the Scotia Sea through the Confluence. Due to adverse ice conditions, the two projected meridional transects across the Confluence, to the west and east of the South Orkney Islands, could not extend poleward of 61S. Nevertheless, it is clear that the waters in the WSC are characterized by weakened CDW temperature and salinity maxima compared to those found in the adjacent Scotia Sea waters to the north and at a station farther southwest in the NW Weddell Sea -- though nowhere was the water colder than 0°C, in contrast to previous summer observations in that area. On the basis of this one Weddell Sea station available, it appears that the WSC waters, at densities of 27.8 kg/m<sup>3</sup>, cannot result from an isopycnal mixture between waters to the north and south, which supports earlier results calling for a shelf water contribution to the mixture. As for the Weddell Sea outflow into the Scotia Sea, geostrophic transports computed across a zonal section along the WSC and the ridge separating Powell Basin from the Scotia Sea reveal inflow into the Scotia Sea of both Warm Deep Water (1.7 Sv) and Weddell Sea Deep Water (1 Sv). Neutral density surfaces show sinking of Weddell Warm Deep Water from depths of 1000-1500 m on the southern side of the ridge to depths below 2500 m in the northern Scotia Sea (58S). On the other hand, the meridional flow across the gap to the east of the South Orkneys between Bruce Bank and Laurie Island is directed poleward. These results confirm that waters from the NW Weddell Sea, presumably mixed with (colder, fresher) waters from the eastern shelf off the Antarctic Peninsula, contribute to the deep ventilation of the Scotia basin.

**P13/W/03-B1****1720****THE INFLUENCE OF MAUD RISE ON OCEAN CIRCULATION AND SEA ICE DISTRIBUTION IN THE WEDDELL SEA**

Ralph TIMMERMANN and Aike Beckmann (both at Alfred-Wegener-Institute for Polar and Marine Research, D-27568 Bremerhaven, Germany, email: rtimmern@awi-bremerhaven.de)

Water mass circulation and sea ice distribution in the Southern Ocean are generally assumed to be strongly affected by the bottom topography in the eastern Weddell Sea. Maud Rise is the most prominent bathymetric feature in this area. As a part of the BRIOS (Bremerhaven Regional Ice-Ocean Simulations) project a coupled ice-ocean model for the the Weddell Sea has been developed. A sigma-coordinate primitive equation ocean model (SPEM) is coupled to a dynamic-thermodynamic sea ice-model with viscous-plastic rheology (based on Hibler/Lemke). Model runs are initialized with data from the Hydrographic Atlas of the Southern Ocean and forced with wind, cloudiness and temperature fields of the 6h-reanalyses of the European Centre for Medium Range Weather Forecasts (ECMWF). In the reference integration, the simulated circulation in the Weddell Sector of the Southern Ocean features a double cell structure of the Weddell Gyre. Its vertical structure is revealed by trajectories of (numerical) floats which are deployed at different depth levels along the Greenwich meridian. Sensitivity studies using a modified bottom topography in the eastern Weddell Sea indicate that the double cell structure of the Weddell Gyre is strongly controlled by the presence of Maud Rise while the effect on the sea ice distribution seems to be less pronounced.

**P13/L/02-B1****1740****VARIOUS NATURE OF INTERNAL WAVES GENERATION BY AN ICEBERG IN SHELF ZONE**

Lyudmila Pisarevskaya (Arctic and Antarctic Research Institute, 38 Bering st., 199397, St.-Petersburg, Russia) Olga SHISHKINA (Institute of Applied Physics, Russian Academy of Sciences, 46 Ul'janov st., Nizhny Novgorod, 603600, Russia, email: ols@hydro.appl.sci-nnov.ru) Valeriya Vasilieva (State Marine Technical University, 3 Lotsmanskaya st., 190008, St.-Petersburg, Russia)

One of the typical features of the Arctic zone of the ocean is a sharp pycnocline presence in summer time. Such a natural condition provides internal waves induction in the near-surface water layers. Previous theoretical and experimental investigations proved that under some conditions drifting icebergs may act as sources of short-period internal waves.

In the present work both theoretical and experimental study of both stationary and nonstationary internal waves generation by an iceberg drifting under water flow and wind influence was fulfilled. Some experimental data on plane regular internal waves interaction with the wave system induced by the drifting iceberg will be presented. Conditions of nonlinearity influence on internal waves formation were analysed. Experimental results on lee internal waves propagation in a fluid with the pycnocline - type stratification in the presence of regular plane internal waves are presented. Internal waves generation by the agrounded iceberg in the shelf zone taking into account its melting followed by intensive air bubbles injection (up to 10% of melting water volume) was considered as well. It occurs due to the pycnocline upwelling following bubbles emerge. Natural observations of the 6-meters pycnocline shift near the agrounded iceberg are presented.

**Tuesday 27 July AM**

Presiding Chairs: P. Wadhams (Univ. of Cambridge, Scott Polar Res. Institute, UK), A.J. Willmott (Keele Univ., Dept. of Mathematics, UK)

**DYNAMICS OF SEA AND OCEAN IN POLAR SEAS****P13/W/19-B2****0930****SIMULATIONS OF ANTARCTIC SEA ICE IN GLOBAL CLIMATE MODELS**

Siobhan P. O'FARRELL (CSIRO Atmospheric Research Aspendale, 3195, Australia, email: Siobhan.O'Farrell@dar.csiro.au)

The CSIRO coupled ocean-ice-atmosphere climate model includes a full dynamic thermodynamic ice model with cavitating fluid rheology. A number of simulations have been undertaken with the model for different greenhouse forcings and for different formulations of ocean eddy mixing (the latter alters the density structure in the Southern Ocean). This talk will examine the response of the ice in the Southern Ocean to the greenhouse signal. A number of simulations will be presented: a) where the seasonal cycle has been improved over the original simulation and b) simulations where different values for the ocean-ice heat flux have been employed.

One of the shortcomings of the CSIRO coupled model is the coarse resolution (3.2 degrees in latitude by 5.6 degrees in longitude). While this enables more climate simulations to be undertaken, the ice is poorly resolved around the Antarctic continent which leads to problems with the seasonal cycle of ice retreat in some locations and poor representation of the thicker ice of the Weddell sea. These shortcomings do have significant implications for the freshwater coupling between the ice and ocean components of the coupled model. Currently the Antarctic bottom water generated in the coupled model is driven more by salinity flux adjustment terms than by levels of brine release onto the continental shelf in areas of high ice production.

The experience gained in running the atmosphere- ice component of the coupled model at higher resolution has been used in the upgraded CSIRO climate model which is at finer resolution (1.875 degrees in latitude and longitude). Results from this new atmosphere-ice model will be shown. The improved rates of ice freezing around Antarctica will reduce the dependence on flux adjustment terms in the coupling process. It is noted that two of the recent generation coupled models which have been run without flux adjustment terms (NCAR CSM,

HADCM3) still encounter some of their greatest problems in the Antarctic region where the models have difficulty getting the ice to drive realistic amounts of bottom water. There has been some discussion recently over the likelihood of the rates of formation of Antarctic bottom water decreasing under a warmer climate. To be able to predict such changes with any confidence, it is crucial that the model has realistic ice production rates which may balance any increases in freshwater from precipitation and glacial melt.

P13/E/09-B2

0950

## SEA-ICE WITH FREE-DRIFT DYNAMICS IN THE HADLEY CENTRE GCM

Doug CRESSWELL and Jonathan Gregory (Hadley Centre for Climate Prediction and Research, The UK Met. Office, London Road, Bracknell, Berkshire, RG12 2SY, UK, email: dcresswell@meto.gov.uk, jmgregory@meto.gov.uk)

Results are presented from the current Hadley Centre coupled model, HadCM3, which has completed a 1000 year simulation of pre-industrial climate. The model comprises a 2.5 x 3.75 degree latitude longitude atmospheric GCM coupled to a 1.25x1.25 degree ocean model and a sea-ice model based on Semtner zero layer thermodynamics in which the ice drifts with the ocean current. The coupled model runs stably without flux adjustment. The drift in global-average surface air temperature is only 0.1K in the first 1000 years. The sea-ice climatology of the model will be described, and compared with observations. The model ice has a realistic seasonal cycle, slightly over-estimating the extent of the ice in winter. There is good agreement with satellite data on the geographical distribution of the ice.

A revised version of the model has been run with free-drift sea-ice dynamics, in which the ice has an independent velocity calculated to give a balance of forces, including the effect of windstress. The rheology of the ice is represented in both schemes by a restriction on the convergence of thick ice. The free-drift scheme generally increases ice velocity and causes an increase of ice volume in winter. An improvement was seen in the simulation of the areas of ice production off the Siberian and Antarctic coasts. Results of these experiments will be presented.

P13/E/06-B2

1010

## ICE CLASSES BASED MODELLING OF ICE THICKNESS REDISTRIBUTION

Jari HAAPALA (Department of Geophysics, P.O. Box 4, FIN-00014 University of Helsinki, Finland, Email: Jari.J.Haapala@helsinki.fi)

Pack ice is a mixture of several ice types and open water. Each ice type has its own characteristic thickness, temperature, roughness etc., and has a specific effect on the ice dynamics, and heat and momentum exchange between the atmosphere and the ocean. Present ice models resolve an amount of the open water, the mean ice thickness and distinguish ridged ice from level ice. That approach has been extended and a new ice thickness redistribution model has been formulated where the pack ice is decomposed to open water, two different type of undeformed ice, and rafted, rubble and ridged ice. The ice thickness distribution model has been included to a coupled ice-ocean model and numerical experiments have been made for the simulation of the Baltic Sea ice season. The benefits of the extended ice classification are a separation of the thermally and mechanically produced ice and a better description of the minimum ice strength. Also different thermodynamic growth/melting rates of the ice types can be introduced to the model, hence giving more detailed seasonal evolution of the pack ice. In addition, the six level ice thickness distribution model gives more information about the surface properties (surface temperature, albedo, roughness) of pack ice.

P13/W/02-B2

1050

## OPEN-OCEAN DEEP CONVECTION DUE TO THERMOBARICITY

Kazunori AKITOMO (Department of Geophysics, Kyoto University, Kyoto 606-8502, JAPAN, Email: akimoto@kugi.kyoto-u.ac.jp)

Properties of open-ocean deep convection due to thermobaricity at high latitudes have been investigated. Scaling argument shows that two types of open-ocean deep convection are possible. The first type appears in a homogeneous ocean, or in a deepening mixed layer. The increased apparent buoyancy flux due to thermobaricity makes the scales of convective properties larger than those without thermobaricity. The ratio of thermobaric to nonthermobaric scales is determined only by the ratio of the nonthermobaric convective size to the characteristic depth for thermobaricity to be effective. In a nonrotating frame, then, thermobaricity becomes effective when the ocean depth is comparable with the characteristic depth, as previous studies showed. In a rotating frame, thermobaricity is most effective with slow rotation and low temperatures. In the actual situation, thus, thermobaricity is not so effective even in polar oceans because the earth rotation confines the convective size to a smaller level. The second type of deep convection is driven by pure thermobaric instability in a two-layer ocean where a cold, fresh mixed layer overlies a warm, saline deep layer, as often observed in polar oceans. It causes an abrupt overturning of the water column. Scales of convective properties are dependent on the difference of water temperature between the two layers, the initial size of plume and the Coriolis parameter (or time), but not on the surface cooling rate directly. With actual parameters, convective properties and the associated buoyancy flux are much larger than those of the first type. Observed vertical profiles of water temperature and salinity suggest that the first type of deep convection could occur in the Greenland Basin while the second type in the Weddell Sea. Numerical experiments with a three-dimensional nonhydrostatic model confirms the above results based on the scaling argument except that the convective size is determined by the product of characteristic scales of velocity and time whether the ocean is shallow or deep, rotating or nonrotating.

P13/W/12-B2

1110

## REGIONAL FOCUS OF A GLOBAL TIDAL MODEL: THE POLAR REGIONS

F. LEFEVRE (email: Fabien.Lefevre@cnes.fr), F. Lyard (email: Florent.Lyard@cnes.fr), C. Le Provost (email: Christian.Le-Provost@cnes.fr) (all at LEGOS/GRGS, UMR5566 CNES-CNRS-UPS, 14 Avenue E. Belin, 31400 Toulouse, France)

The CEFMO hydrodynamic model and the associated data assimilation code is the only one global model to include the ice-shelf covered seas like the Weddell Sea, the Ross Sea, or the Amery ice shelf basin. A new version of our hydrodynamic finite element tide model combined with a revised data assimilation procedure is now available, referred as the FES98 solutions. These global solutions, including the polar regions which are not included in the altimetric empirical models, show now an overall accuracy comparable with the one of the latter. The modelling of the tides in the polar regions is made more difficult due to the lack of accurate data, especially on the ocean bottom topography. The situation is even more complicated below the permanent ice shelves. Nevertheless, a significant effort was made to prescribe the correct water column height and grounding line in these regions. Its finite element

discretization allows a realistic modelling in the coastal areas (with horizontal resolution ranging from 10 to 1 kilometer). The model output are the tidal elevation and currents. The tides can interact with many processes, such as, among others, the ice melting below the ice shelves (through a background turbulence) or transport, grounding line variations, the water mixing etc... Actually, the regions with intense tidal dissipation are known to show strong water mixing. In addition, the tides can be responsible of a mean transport, which is somehow connected to the tidal energy flux. A collection of model zooms on regions of interest are presented, with a particular focus on ice covered seas, shelf edges and energetically active regions.

P13/P/01-B2

1130

## ICE AND SALT TRANSPORTS IN THE WEDDELL SEA

Sabine HARMS, Eberhard Fahrback, Volker H. Strass (all at Alfred Wegener Institute for Polar and Marine Research, Postfach 12 01 61, 27515 Bremerhaven, Germany, email: sharms@awi-bremerhaven.de).

Time series of ice thickness in the Weddell Sea are evaluated together with hydrographic observations and ice drift for estimation of the freshwater fluxes into and out of the Weddell Sea. Ice draft is measured with moored Upward Looking Sonars (ULS) since 1989 along two transects across the Weddell Sea. One transect, extending from the tip of the Antarctic Peninsula to Kapp Norvegia, covers the flow into and out of the southern Weddell Sea. The other transect, extending from the Antarctic continent northward along the Greenwich Meridian, covers the exchange of water masses between the eastern and the western Weddell Sea. On average wind and current force a westward ice transport in the east into the Weddell Sea and a northward ice transport in the west out of the Weddell Sea. Near the coast, in the southern Weddell Sea and along the tip of the Antarctic Peninsula, offshore winds push ice away from the coast and new ice is continuously formed in these regions, indicated by low ice draft modes (< 0.3 m) and high surface salinities (> 34.25). When offshore winds weaken or reverse to onshore ice is deformed. In the presence of opposing currents and the coast the ice thickness increases. On its way along the southern part of the Weddell Gyre the ice grows continuously. The mean ice draft increases from 1.6m in the eastern inflow at the Greenwich Meridian to 2.2m in near Kapp Norvegia and 2.7m in the western outflow. The mean ice export out of the Weddell Sea is  $(57 \pm 21) \times 10^3 \text{ m}^3 \text{ s}^{-1}$ , corresponding to a net freshwater export due to drifting sea ice of  $(0.06 \pm 0.02) \text{ Sv}$ . This freshwater export exceeds the average amount of freshwater gained by precipitation (Bromwich and Cullather, 1997) by a factor of three. The net amount of salt gained by sea ice formation is  $(15 \pm 7) \times 10^5 \text{ kg s}^{-1}$ .

P13/L/01-B2

1150

## A LINK BETWEEN SEA ICE EXPORT FROM THE ARCTIC AND THE NAO

Bruno TREMBLAY (Lamont-Doherty Earth Observatory of Columbia University, USA)

In the past decade, an increasing trend in the North Atlantic Oscillation (NAO) index has been observed. A high NAO index will influence the strength of the westerlies in the mid-latitude of the North Atlantic and could also result in different atmospheric circulation pattern in the Arctic. Since regional and large scale anomalous wind patterns in this region can produce fluctuations in ice export from the Arctic through Fram Strait, a link between the state of the NAO and the export of ice out of the Arctic is possible. A dynamic-thermodynamic sea-ice model is used to study the interannual variability of the sea ice export from the Arctic through Fram Strait during the 1958-98 period. The model is forced with monthly varying wind stresses and air temperatures from the NCEP reanalysis data. The simulation results show a significant correlation between the ice export and the NAO index time series. When the NAO index is positive, the Icelandic Low is extending further north into the eastern Arctic and the Arctic High is located closer to the Beaufort Sea. During those periods, the Transpolar Drift Stream (TDS) is well developed, leading to a large ice export from the Arctic. During a negative phase of the NAO, the Arctic High moves closer to the Siberian coast and the TDS tends to feed into the Beaufort Gyre leading to a smaller ice export. During these periods, the atmospheric circulation is such that more ice is found in the East Siberian Sea (at the source of the TDS); these ice thickness anomalies are advected out of the Arctic during subsequent periods of high exports, tending to reinforced the ice export anomalies.

Tuesday 27 July PM

Presiding Chairs: P. Wadhams (Scott Polar Res. Institute, Univ. of Cambridge, UK), A.J. Willmott (Dept. of Mathematics, Keele Univ., UK)

P13/E/02-B2

Invited

1400

## SATELLITE OBSERVED SEASONAL AND INTERANNUAL VARIABILITY OF THE ODDEN FROM 1973 THROUGH 1997 AND ENVIRONMENTAL EFFECTS

Josefino C. COMISO (Laboratory for Hydropheric Processes, Code 971, NASA/GSFC, Greenbelt, MD, USA, 20771, email: comiso@joey.gsfc.nasa.gov), Peter Wadhams (Scotts Polar Research Institute, University of Cambridge, Cambridge, England, email: pw11@cam.ac.uk), and Lef Toudal Pedersen, Technical University of Denmark, Dept. of Electromagnetic Systems, Bygning 348, DK-2800 Lyngby, Danmark, email: ltp@emi.dtu.dk)

The Odden is a regular ice feature phenomenon in the Greenland Sea that is believed to have a profound influence on the convection and circulation characteristics of the ocean in the region. Although it had been observed and reported by early explorers, it was not until the satellite era that its size, shape, and characteristics became apparent. It usually occurs early in the winter and forms as an ice tongue, a bulge, or an island depending on atmospheric and oceanographic forcing. The most frequently observed development of the Odden is as an area of locally-grown frazil and pancake ice along the cold polar Jan Mayen Current which diverts eastward from the East Greenland Current. Such composition has been confirmed during field programs carried out in this region. However, on some occasions, the ice cover in the Odden has been observed late in the season to be made up of multiyear or old ice advected from the Arctic Ocean through the Fram Strait and the Greenland Sea. Our study makes use of satellite passive microwave historical data to investigate the seasonal and interannual variability of the size, extent, and type of the Odden since 1973. High resolution satellite SAR and AVHRR data was used to improve our interpretation of the passive microwave data, the resolution of which is relatively poor. Our analysis reveals large interannual variability in time of occurrence, persistence, and type. Also, the Odden appeared every year except in 1984, 1994, and 1995. We observed that the size and extent varies with wind and surface temperature but the correlation of the distribution of the ice cover with the bathymetry is weak although the feature is usually along the Jan Mayen fracture zone. Analysis of the influence of environmental effects that sometimes cause transitions from a bulge feature to an ice tongue, and from an ice tongue to an island will be presented. Also, the potential impact of rapid ice growth to convection and of the presence of multiyear and old ice in late spring to the carbon cycle in the region will be discussed.



**P13/E/16-B2** 1440**SATELLITE-DERIVED DYNAMICS OF SOUTHERN OCEAN SEA ICE**

Mark R. DRINKWATER and Xiang Liu (Jet Propulsion Laboratory MS: 300-323, 4800 Oak Grove Drive, Pasadena, CA 91109, USA, email: mrd@pacific.jpl.nasa.gov)

Antarctic ERS-2, RADARSAT Synthetic Aperture Radar and ERS-1/2 Scatterometer images were analyzed with SMMI radiometer image time-series data to investigate seasonal variability in satellite-tracked sea-ice dynamics in the Southern Ocean during 1992. Supporting field data were acquired during 'in-situ' experiments including the winter 1992 Ice Station Weddell and Winter Weddell Gyre studies. A variety of surface measurements were made during these experiments including Argos-buoy deployment and GPS drift measurements. These are used in conjunction with International Program for Antarctic Buoys drift trajectories for ice-motion tracking validation. Comparisons between gridded SSMI ice-motion vectors and ECMWF/NCEP analyses indicate that large-scale drift is forced predominantly by the long-term mean, large-scale synoptic pressure field. Only sub-daily SAR sea-ice tracking can capture high-frequency fluctuations, driven by polar lows or tidal forcing. In these cases, sea-ice drift can respond rapidly to changes in forcing on semi-diurnal time scales depending on the location with respect to the coastline. Seasonality of ice drift, particularly in the Weddell and Ross Seas, is linked to ice extent and compactness, and internal ice stresses transmitted through the pack ice from the coast. Three-monthly seasonal climatologies are presented of austral winter of ice drift in the Southern Ocean. The large Weddell and Ross Sea gyres are clearly resolved along with key seasonal and spatial attributes of their cyclonic circulation. Regional time series of ice dynamics parameters are used to illustrate correlations with meteorological forcing. Persistent divergence such as that occurring in the Ronne-Filchner polynya system results in large fractions of new ice. Similarly, convergence zones produce large fractions of deformed ice and characterize the dynamics of regions where perennial ice is observed. High shear strains also help delineate the axis of the Antarctic divergence in many places in the ice cover. In these regions, the separation between the coastal 'east wind drift' and ACC-dominated drift regimes is characterised by zonally extended regions of intense shear.

**P13/E/15-B2** 1500**SEA ICE THICKNESS DERIVED FROM ERS-1 AND 2 ALTIMETER OBSERVATIONS**

Neil PEACOCK, Seymour Laxon (University College London 17-19 Gordon Street, London, WC1H 0AH, UK)

A new technique to directly measure sea ice freeboard from ERS-1 and 2 spaceborne altimetry has recently been developed. This offers the potential to provide up to 250,000 estimates of ice thickness per month over a large fraction of the Arctic Ocean. There is a critical need to calibrate and validate these thickness estimates prior to their widespread application to climate-related problems.

In this paper, we present the results of comparisons of these measurements, obtained between 1993 and 1998, with in situ Upward-Looking Sonar (ULS) measurements from moored buoys in Fram Strait, and ULS measurements made from US Navy submarines. The statistical properties of the thickness data sets acquired using these methods will also be investigated, and estimates of the corresponding errors in our thickness measurements will be derived.

Potential applications of this unique data set will then be discussed, which include the monitoring of ice thickness in the Arctic Ocean and Fram Strait, and the ability to estimate ice flux from the Arctic Ocean into the Greenland Sea. Future spaceborne altimeter missions, such as ENVISAT, will allow observations of this important climatological parameter well into the next century.

**P13/W/14-B2** 1520**POLAR SEA ICE MOTIONS CHARACTERIZED FROM 20 YEARS OF PASSIVE MICROWAVE SATELLITE IMAGERY**

W.J. EMERY, C. Fowler, J.A. Maslanik (CCAR Box 431, University of Colorado, Boulder, CO 80309, USA)

An approximately 20 year time series of daily passive microwave maps of polar sea ice have been constructed using the Special Sensor Microwave/ Imager (SSM/I) for the years 1987-1997, and the Scanning Multichannel Microwave Radiometer (SMMR) for the years 1979-1987. While the sensor channels and the specific ice concentration algorithms are different for these two sensors the basic imaging of the ice surface as used for the computation of sea ice motion, is quite similar between the two instruments. Arctic sea ice motions are analyzed in conjunction with ice trajectories from the Arctic ice buoy program while the Antarctic ice motions are based on the passive microwave imagery alone. Means are calculated for the entire time period, for both decades and then for individual years to characterize the interannual variability of the ice motion fields. Standard deviations for these same periods reveal where the ice movements are most variable. Empirical orthogonal functions (EOFs) are computed from the ice motion maps to indicate the basic patterns of ice motion. These patterns are found to correlate well with structures of the atmospheric pressure and hence geostrophic wind patterns. The EOFs for the Arctic and the Antarctic are quite different reflecting the very different forcing functions operating in the Antarctic.

**P13/E/13-B2** Poster 1600-01**THE ESTIMATIONS OF SEA ICE EXCHANGE BETWEEN THE ARCTIC SHELF SEAS AND THE ARCTIC BASIN**

Alexander MAKSHITAS and Sergey Shoutilin (both at Arctic and Antarctic Research Institute, 38 Bering Street, St.Petersburg, 199397, Russia, email: maksh@aari.nw.ru)

Sea ice exchange between the Barents, Kara and Laptev seas and the Arctic Basin was investigated using a large-scale dynamic-thermodynamic model (for period 1958 - 1997 years) and semi-empirical method, based on empirical relation between atmospheric surface pressure gradient and drift velocity (for period 1936 - 1996 years). Estimates of sea ice exchange of the Laptev sea, calculated using empirical relation between ice flux and air pressure difference at polar stations Kotelnny and Cape Cheluskin, showed strong seasonal and interannual variability with an absolute minimum of sea ice export to the Arctic Basin in 1957 year and did not reveal significant trends for the entire period. In opposite estimates for the Kara sea, obtained with the same method and atmospheric surface pressure data from meteorological stations Cape Arcticheskiy and Ostrov Rudolf, showed strong positive trend of ice export to the Arctic Basin, especially during last three decades, when sea ice export from the Kara sea almost reached values from the Laptev sea. The dynamic-thermodynamic model, validated with empirical method for sea ice area exchange allowed to estimate sea ice mass exchange and to make some numerical experiments on sensitivity of the Arctic Basin sea ice cover to the hypothetical Arctic climate changes. This experiments showed strong dependence of sea ice mass exchange to increasing of atmospheric surface layer temperature and incoming longwave radiation.

**P13/E/08-B2** Poster 1600-02**INTERANNUAL AND DECADEAL VARIABILITY OF THE GIN/BARENTS SEAS SYSTEM**

S. PIACSEK, A.Warn-Varnas, R.Allard (Ocean Science Division, Naval Research Laboratory, Stennis Space Center, MS, 39529, USA; email: piacsek@nrlssc.navy.mil); A.Mehra, D.Dietrich (CAST, Mississippi State University, Stennis Space Center, MS, 39529)

The variability of the Greenland-Iceland-Norwegian (GIN)/ Barents Seas system has been investigated via analysis of hydrographic data and numerical models. Data has been extracted mainly from the NODC's WOA94 database and from 9 successive cruises by the SACLANT Research Center in the 1986-1993 period. A watermass census was performed for regions where the data density warranted it.

Model results were generated with two models, one spherical including the North Atlantic and one polar stereographic including the whole Arctic Basin. Forcing was derived from the NCEP reanalysis files (2.5 deg) and the US Navy's NOGAPS GCM output (1 deg).

The model results revealed an increased inflow of Atlantic water (AW) into the Arctic Basin during the 90's, with the dominant circulation patterns and transport magnitudes shifting from the West Spitsbergen Current to the Barents Sea branch flowing north along the Novaya Zemlya coast. A recirculation of AW southward along the east coast of Svalbard, very prominent in the '80s, almost disappeared except for 1994. The outflow of deep water (DW) from the Arctic through the Fram Strait consisted of two branches, one fed by waters coming from the Eurasian Basin and one from the Canadian Basin. The hydrographic data analysis revealed a gradual decrease of AW until 1989, and then a gradual increase in the 90's.

The DW exhibited an opposite behavior, peaking in 1989 and then decreasing. Furthermore, the DW constitution changed from Norwegian Sea Deep Water (NSDW) to a class warmer than -5 deg C.

**P13/E/03-B2** Poster 1600-03**SPATIAL AND TEMPORAL VARIABILITY OF WATER MASSES IN FRANZ-VICTORIA TROUGH**

Ivanov V.V., Korabev A.A. (Arctic and Antarctic Research Institute, 38 Bering st., 199397, St.Peterburg, Russia, email: vivan@aari.nw.ru); PISAREV S.V. (P.P.Shirshov Institute of Oceanology, RAS, 36 Nachimovsky ave., 117218, Moscow, Russia, email: sergey@pisarev.msk.ru)

The WODB-98, MOODS, local Russian and Norwegian databases, recent measurements of RV "Polarstern" in 1993 and RV "Lance" in 1993,94,95 were used to describe the spatial and temporal variability of water masses in Franz-Victoria Trough (between the Victoria Isl. and Franz Joseph Land). The data obtained during the multidisciplinary research cruise carried out in October 1998 from the board of Russian RV "Ak. Fedorov" were used also. About 750 stations were collected for 1923-1998. The water masses of the Franz-Victoria Trough were classified based mainly on the T,S characteristics. It was noted, that the main features of spatial distribution of the water masses of the region were determined by bottom relief. The conclusion concerning general circulation within the Trough was made. The interannual variability of atlantic water temperature, heat content, and spreading was also determined.

**P13/W/06-B2** Poster 1600-04**DEVELOPMENT OF AN IMPROVED DYNAMIC-THERMODYNAMIC SEA ICE THICKNESS DISTRIBUTION MODEL FOR CLIMATE APPLICATIONS**

Todd ARBETTER (McGill University, Montreal, Quebec, CANADA); Judy Curry, Julie Schramm (University of Colorado,Boulder, Colorado, USA)

One of the major challenges in climate modeling is development and implementation into general circulation models of a sea ice model that accurately predicts sea ice mass balance, ice extent, interfacial fluxes, and the associated feedbacks with the atmosphere and ocean. Initially, general circulation models contained simple parameterizations of sea ice thermodynamic and dynamic processes. The development of sophisticated stand-alone ice dynamic models facilitated improvement in the treatment of ice dynamics in GCMs. However, while there has been substantial progress in the development of single-column thermodynamic sea ice models, little work has been done to unify sophisticated thermodynamics and dynamics into a single model.

Towards this end, a new sea ice model is described which incorporates the sophisticated thermodynamics of a single-column sea ice model developed at the University of Colorado into an existing basin-scale dynamic-thermodynamic model. Using a viscous-plastic dynamic model and an ice strength parameterization which accounts for a distribution of sea ice thicknesses, the model resolves a domain covering the Arctic Ocean and much of its surrounding seas. Beneath the ice at each grid cell is an interactive ocean mixed layer. A preliminary comparison of baseline characteristics of the model with observations indicates that the new model performs reasonably well in terms of its reproduction of ice surface albedo, ice surface temperature, and ice thickness distribution.

**P13/W/09-B2** Poster 1600-05**CHANGES IN THE NORTH SLOPE CLIMATE AND THE SEA ICE CONCENTRATION IN THE ADJACENT BEAUFORT SEA**

Gerd WENDLER and Blake Moore (both at Geophysical Institute, University of Alaska, Fairbanks. 903 Koyukuk Dr., Fairbanks, AK, 99775-7320 USA, email: gerd@gi.alaska.edu)

Significant climate change has been observed in recent decades in the Western Arctic. Two climate variables in particular show this quite clearly; temperature and sea ice concentration. Western Arctic temperatures have increased; the observed temperature rise, however, varies significantly from one season to another (it is most pronounced in the winter and spring) and over multi-year time scales. This makes it difficult to explain the trend as a direct consequence of increasing greenhouse gases in the atmosphere. At the same time, the sea ice concentration has decreased in the southern Beaufort Sea. Temperature variations were found to correlate with changes in cloudiness associated with specific synoptic patterns. Increased cloudiness was correlated with a warming of the temperature in winter, but with a cooling in summer, indicating that the temperature regime in winter is strongly influenced by the long wave radiation. We were able to analyze systematically the area in the southern Beaufort Sea using a portion of the international Sea Ice Grid (SIGRID) produced by National Ice Center. Weekly sea ice concentration consisting of 0.25 degree latitude by 0.50 degree longitude grids derived from satellites for the period 1972-1994. We limited our preliminary study to the coastal Beaufort Sea south of 72° North, and between 142° and 152° West. There are two main processes which influence the sea ice conditions, namely thermodynamics and dynamics. The thermodynamics determines the formation and decay of the sea ice and is directly related to the surface energy budget, while the dynamics determines the transport of sea ice, which is strongly related to atmospheric dynamics. Other factors such as ocean currents also play a major role.

The annual average ice concentrations shows a decreasing ice concentration. Forcing the best linear fit through the data points, a decrease in the yearly average sea ice concentration from over 88% to 81% can be observed for the 24 year time period. A temperature increase of about



1°C was also observed during this time. If the annual temperature values are plotted against the annual values of the sea ice concentration, a good statistical variance ( $r^2 = 0.48$ ) was found. For shorter time periods, especially during times when the ice concentration can vary considerably (e.g. fall), the relationships become even better. This presentation will concentrate on the underlying causes of these changes which are not well understood. The primary forcing mechanisms that underlie these changes will be discussed. The observed trend of decreasing sea ice concentration is continuing. This fall (1998) the lowest ice concentration since the start of the record has been observed.

**P13/W/18-B2** Poster **1600-06**

#### THE ROLE OF TRANSIENT EDDIES IN ACC DYNAMICS IN CROZET PLATEAU REGION OF THE SOUTHERN OCEAN

Vladimir IVCHENKO (Jet Propulsion Laboratory/NASA, M/S 300-323, 4800 Oak Grove Drive, Pasadena, CA 91109, USA, Email: voi@sundog.jpl.nasa.gov)

A vigorous eddy field is observed in TOPEX altimeter data around the Crozet Plateau, especially around the northern flank and downstream of the Plateau. The important question that is addressed in this study is how transient eddies affect the mean flow? This problem has been studied using the output of two fine resolution numerical models: the Fine Resolution Antarctic Model (FRAM) and the Parallel Ocean Program (POP). The level of eddy kinetic energy (EKE) throughout the region is much greater in POP than FRAM, due to better horizontal resolution.

Although maximum values in FRAM are just as high as in POP, these values are restricted around the northern flank and downstream of the Plateau. The most important source of the EKE is the eddy buoyancy term. In both models instability analysis showed that baroclinic instability is likely to be the main mechanism responsible for generating EKE. Transient eddies are found to be responsible in shaping the flow structure and transferring momentum in both the horizontal and vertical directions. The eddy flux of the potential vorticity has been split into rotating and divergent parts by solving a Poisson-type equation, using iteration schemes with appropriate boundary conditions. The rotational part is found to be quite large in the western and north-western part of the Crozet storm track.

**P13/W/17-B2** Poster **1600-07**

#### BEAUFORT AND CHUKCHI SEA SEASONAL VARIABILITY

Tatiana Proshutinsky and Andrey PROSHUTINSKY (Institute of Marine Science, University of Alaska Fairbanks, Fairbanks, AK 99775-7220, USA email: prosh@ims.alaska.edu) James Maslanik (Colorado Center for Astrodynamic Research, University of Colorado, Boulder, CO 80309 USA, e-mail: jimmm@northwind.colorado.edu)

Arctic navigation, oil and gas exploration, and arctic pollutant transport depend on arctic environmental conditions. Existing atlases, manuals, and reference books contain multi-year mean environmental variables and their multi-year mean seasonal variability; however, uncertainties sometimes result from the existing atlases because they do not take into account climate change and climate variability. Our work is motivated by the recent finding of two regimes (or two climate states) of arctic atmosphere-ice-ocean circulation described by Proshutinsky and Johnson [1997]. Seasonal variations in the ice concentration, ice thickness, and ice drift, ocean currents, ocean temperature, and salinity, atmospheric pressure, wind speed, cloudiness, and precipitation, river discharge, and permafrost temperature are different for cyclonic and anticyclonic arctic climate states. In this poster we present the atmospheric, ice, oceanic, and terrestrial signals showing seasonal variability of environmental parameters during cyclonic and anticyclonic climate states in the Beaufort and Chukchi seas using observational data and results of numerical modeling.

**P13/W/20-B2** Poster **1600-08**

#### THE COUPLED ATMOSPHERIC BOUNDARY LAYER- SEA ICE - UPPER LAYER - DEEP OCEAN MODEL FOR INVESTIGATION OF SEASONAL, INTERANNUAL AND INTERDECADE VARIABILITY OF WATER CIRCULATION AND TERMOHALINE STRUCTURE IN THE ARCTIC AND ATLANTIC OCEANS

G.A. SEMYONOV (Arctic and Antarctic Research Institute, 38 Bering St., St-Petersburg, 199397, Russia)

For simulation and investigation of climate large-scale circulation evaluation in the Atlantic Ocean (AO) and the Arctic basin (AB) the three-dimensional efficient hydro-thermodynamical model, based on the primitive equations with used of a hydrostatics and Boussinesque approximation with free surface, was built. The calculating area includes the regions from the equator to the Bering strait. To improve the finite-difference approximation in the Denmark, Fram and Faeroe-Shetland straits the spherical coordinate system with pole placed in point 75 N & 40 W (in Greenland) was designed. The ocean model has a variable resolution from 28 km (Greenland Sea) to 312 km (near equator). The model uses a total of 47 levels in the vertical. The method of solving equations this model is based on the split method. The atmospheric boundary layer is parametrized with the help of integrated model. The model of n ice cover is based on the primitive equations of dynamics both thermodynamics of ice and snow. The upper mixed - layer of ocean is parametrized by using the K - theory, that allows to calculate coefficients of vertical turbulent exchange of momentum, heat and salt by solving the equation of balance of kinetic turbulent energy. Application of the effective non-explicit numerical schemes allows to execute calculation using time steps equal 24 hour for period of 100 years and more. The model reproduces three-dimensional circulation of waters, evolution of a sea surface elevation, termohalin of structure, annual course of variability of an ice cover, distribution of a firm suspension and various pollutions both on a surface of the sea and in thickly waters at the task of temperature of air and height of geopotential of 850 mb of a surface above the AB and AO.

**P13/W/04-B2** Poster **1600-09**

#### NEW OBSERVATIONS FROM BOTTOM PRESSURE RECORDERS IN THE WEDDELL SEA

M.J. SMITHSON (CCMS-Proudman Oceanographic Laboratory, Birkenhead, Merseyside, L43 7RA, U.K., e-mail: msm@ccms.ac.uk)

Recent studies of the southern Weddell Sea using a hydrodynamic numerical tide model have shown that it is not possible to model simultaneously the tides of the open ocean and the tidal motion of the ice shelves (Ronne and Filchner). Specifically, in order to reproduce the ice shelf movement near the grounding line unrealistic model parameters in the region of permanent ice cover, in particular the bottom friction coefficient, must be used. The effect of this is to destroy any agreement between model and observations in the open ocean, especially near to the permanent ice front. Existing observational data indicate the presence of an amphidrome in the principal semidiurnal tides close to the Ronne Ice Shelf but its position is uncertain. Its existence is also borne out by the model results and its position is very sensitive to model parameters. A number of bottom pressure recorders were deployed in the region at the beginning of 1998, from H.M.S. Endurance. These are due to be recovered in January/February 1999. The data

from them should provide valuable information to help fix the location of the amphidrome and hence reduce significantly the uncertainties in the model parameters.

**P13/W/15-B2** Poster **1600-10**

#### A STRONG FRONT OVER THE NORTHERN ARCTIC MID-OCEAN RIDGE

Robin D. MUENCH, John T. Gunn (Earth & Space Research, 1910 Fairview East, Suite 102, Seattle, WA 98102-3620, USA, email: rmuench@esr.org); Tim Boyd (College of Oceanic and Atmospheric Sciences, Oregon State University, Corvallis, OR, 97330, USA, email: tboyd@oce.orst.edu)

Oceanographic temperature (T), salinity (S) and dissolved oxygen concentration (O2) were measured continuously along a closely spaced array of transects that were made across and roughly normal to the northern portion of the Arctic Mid-Ocean Ridge system from the U.S. Navy submarine Hawkbill. Additional T and S data were collected as vertical profiles at selected sites using expendable probes. The transects were run at a sensor depth of 212m, and the vertical profiles extended from about 20m down to 1000m depths, providing detailed documentation of the Atlantic Water layer. A strong T and S front was seen to coincide approximately with the axis of the Ridge. Maximum Atlantic Water T increased from about 1.1°C to nearly 2.3°C across the front from north to south, and S increased by about 0.06 psu. The frontal distributions of T and S showed complex wavelike undulations and discrete features. Some were consistent with the presence of mesoscale eddies, while others appeared to be associated with the bottom topography. An eastward flowing current filament about 20 km wide coincided over part of the system with the southern slope of the central rift valley. Current speeds in this filament were estimated based on offsets in the cruise track to exceed 25 cm/s. Neither the high T nor the eastward current is consistent with the concept of a cyclonic gyre occupying the Nansen Basin. The eastward current, whose presence is consistent with topographic control by the steep axial rift valley, may be an extension of a continuous northward flow through Fram Strait. The high T suggests, also, a more direct route from Fram Strait than would be consistent with flow within a large cyclonic gyre.

**P13/W/13-B2** Poster **1600-11**

#### MODELLING OF THE SEASONAL DYNAMICS OF THE WATER MASSES, ICE AND RADIONUCLIDE TRANSPORT IN THE KARA SEA

Liudmila Koziy, Vladimir Maderich, Nugzar MARGVELASHVILI, Mark Zheleznyak (all at Institute of Mathematical Machine and System Problems NASU, Glushkova pr. 42, Kiev 252187, Ukraine.)

The numerical THREETOX code was used to simulate 3-D hydrodynamic fields, ice transport, suspended sediment transport and the dispersion of the radionuclide in the Kara Sea and adjacent areas of the Barents Sea and Arctic Ocean. The code includes the hydrodynamics sub-model, ice sub-model, suspended sediment transport and radionuclide transport sub-models. The hydrodynamics is simulated using the, time-dependent, free surface, primitive equation model. The modified Hilber type dynamic-thermodynamic model describes the momentum balance, nonlinear ice rheology, mass balance and the ice strength. The ice thickness distribution is a two-level representation (compactness and ice thickness). An important role of seasonally varying ice cover in the seasonal dynamics of the Kara Sea was shown. At summer, the western and northern flows of the Ob and Enisey plume are transformed in the slope current that flows to the Severnaya Zemlya. Another current flows along the north coast of the Novaya Zemlya. The residual tidal currents are important in narrows (e.g. Karskie Vorota Strait and Ob and Enisey estuary mouths). The water exchange through the Karskie vorota is bi-directional. At winter the ice sheet covers almost all area of the Kara Sea. The strong current flows from the Karskie Vorota and merges with Ob-Enisey flow in the northern part of the sea. The numerical results agree quite well with the observations. These peculiarities of the Kara Sea circulation strongly affected on the radionuclide transport. Weak and seasonally varied currents near Novaya Zemlya coast result in the long residence time for radionuclides dumped in the Novaya Zemlya fjords and the Novaya Zemlya trough.

**P13/W/21-B2** Poster **1600-12**

#### ON PHYSICAL NATURE OF LARGE-SCALE ANTICYCLONIC GYRE IN THE NORWEGIAN SEA WATER DEPTH

Anatoly PERESKOKOV (Russian Research Institute of Hydrometeorological Information - World Data Center, 6 Korolyov St, Obninsk 249020, Russia, email: peres@meteo.ru)

Anticyclonic vorticity in the thick layer of deep water over Lofoten lows in the Norwegian Sea is a paradox, especially in view of the cyclonic winds of the Icelandic hollow, and the fact that neither the density field nor the available measurements suggest an anticyclonic circulation of the surface waters. No doubt, the topography largely determines the characteristic features of the stationary circulation of the Norwegian Sea waters. However, the circumstantial evidence suggests that an important role may be attributed to a redistribution of the Atlantic waters heat from upper layers to the lower ones through salt finger convection. Our calculations show close agreement between the area with the highest likelihood for salt fingers, given through the density ratio, and the region of the relative temperature maximum at every horizontal surface of 800-1500 m water thickness. The centre of the temperature maximum is quasi-stationary in this deep layer near 69.5 N, 3.5 E. A quite natural response to the generation of this quasi-stationary horizontal inhomogeneity of physical and topographical origin (with less density) is the initiation of an anticyclonic circulation. Since variations in the gyre intensity can not but influence the transfer of the Atlantic waters heat to the higher latitudes, the monitoring of the parameters of dynamic and thermal regime at some certain depths could possibly be the positive contribution to the ice prediction.

**P13/W/23-B2** Poster **1600-13**

#### THERMAL INSTABILITY OF WATER SATURATED SEA ICE SHEET BOUNDED BY MELT POND

Pjotr BOGORODSKY (Arctic & Antarctic Research Institute, 38 Bering str., 199397 St.Petersburg, Russia, email: vivanv@aari.nw.ru)

Fresh melting water accumulates during summer period in the melt ponds at the ice surface and percolate it forming so-called "underice melt ponds". Heating from above by radiation flux can induce convection resulting intensifying processes of air-sea energy and mass exchange. However, the permeability of intermediate ice sheet provides interaction of fresh liquid layers by the way that all they form unit combine system. At the present work the analysis of its convective stability is performed. The external boundaries of the system are considered as free or hard surfaces with constant heat fluxes. The critical values of Rayleigh numbers depending of determining parameters (coefficients of heat diffusivity of ice and fresh water, thickness and permeability of ice) are found out from the analysis of linearized spectrum problem. At deduction of equations for eigenvalues the method of series expansion is used. The study is restricted by the longwave instability of monotonic perturbations. The simplicity of such an approach allows to easy transform to extreme cases cases of approximation of

dimensionless ice thickness to zero (unit). In these cases the expression obtained for critical Rayleigh number transforms to the known value for single liquid (porous) layer with heat insulated boundaries. When summerizing results it may be concluded that 1) the dynamical boundary conditions on the system outer surfaces do not principally affect the instability character; 2) the ice sheet permeability changes at its fixed thickness do not influence on the value of critical Rayleigh numbers; 3) the increasing ice sheet thickness lead to significant stabilization on the longwave mode of instability.

**P13/L/01** Poster **1600-14**

#### MODELING SEA-ICE AND WINTER PROCESSES IN THE LABRADOR SEA

C.L.TANG

Sea-ice and winter processes in the Labrador Sea are studied with an hierarchy of numerical models: (a) 1-D mixed-layer model; (b) 3-D coupled ice-mixed layer-ocean model; (c) 3-D coupled ice-Princeton Ocean Model. The re-analysis data of ECMWF and NCEP are used for the calculations of heat and water fluxes. The archived oceanographic data at BIO are objectively analyzed to produce the initial ocean state. The models successfully simulate the seasonal change of sea-ice coverage. Ice grows in the inner shelf and melts in the outer shelf regions. Heat loss of the ocean reaches a maximum at the end of January. The highest heat loss, 250 to 400 W/m<sup>2</sup>, occurs in the northern Labrador Sea between 56N and 63N in ice-free waters near the ice edge. Sea ice significantly reduces the heat loss with a typical values of 50 W/m<sup>2</sup>. In the open sea, surface cooling causes the mixed layer to deepen continuously through winter. The mixed layer reaches a maximum depth of 150m to 450m in late March. Across the southern shelf, observations indicate that the mixed-layer depth decreases from 80m in mid-shelf where the water is completely covered by ice to 25m at the ice edge. The temperature under the pack ice is near the freezing temperature and increases to 0 deg at the ice edge. The variation of the mixed-layer properties across the shelf is simulated by the D mixed-layer model. The relative contributions from wind mixing, buoyancy production and short-wave radiation to the mixed-layer properties vary with space and time, and are closely related to sea ice.

**P15** **Wednesday 28 – Thursday 29 July**

#### OPTICAL OCEANOGRAPHY AND UV RADIATION (CO SPONSORED BY IOP AND EOS)

Location: Arts Building, 125 LR1

**Wednesday 28 July AM**

Presiding Chair: Jim Aiken (Plymouth Marine Laboratory, Prospect Place, Plymouth)

#### OPTICAL AND BIO-OPTICAL MEASUREMENTS

**Introduction** **0900**

Jim Aiken, Ray Smith and Andre Morel

**P15/E/02-B3** **Invited** **0915**

#### NEW BIO-OPTICAL MEASUREMENTS FROM AUTONOMOUS PLATFORMS

T. DICKEY (University of California at Santa Barbara, 6487 Calle Real, Suite A, Goleta, CA 93117, (805) 893-7354; email: tommy@icess.ucsb.edu)

During the past few years, our group and collaborators have made bio-optical and physical observations using autonomous platforms including moorings and autonomous underwater vehicles (AUVs). The variety of optical (and chemical) measurements is expanding rapidly. Our work has focused on the development of new systems capitalizing on emerging multi-spectral sensors, novel platforms, and specialized telemetry technologies. In this review, examples of these new interdisciplinary sampling systems, data acquired with the systems, and interpretation of these data will be discussed. Sites for the studies include the North Atlantic near Bermuda (Bermuda Testbed Mooring) and coastal waters off the east coast of the United States. Phenomena including eddies, fronts, internal waves, sediment resuspension, and ocean response to hurricanes have been captured during these studies. The relations among physical, biological, and optical properties and processes are being explored and modeled using these data sets.

**P15/W/01-B3** **1000**

#### MEASUREMENTS AND MODELS OF THE BACKWARD SCATTERING COEFFICIENT

Robert A. MAFFIONE (Hydro-Optics, Biology, and Instrumentation Laboratories, 55 Penny Lane, Watsonville, CA 95076, email: maffione@hobilabs.com)

The backward-scattering coefficient,  $bb$ , has historically been one of the most undersampled ocean-optical properties. Yet it is a key optical parameter for ocean-color remote sensing and underwater visibility. Due to the difficulty in measuring  $bb$ , most investigators have resorted to modeling it based on other optical parameters which can be measured and on chlorophyll concentration. Now, with the availability of new instrumentation, namely the HydroScat backscattering sensors,  $bb$  can be easily and accurately measured at selected wavelengths across the visible spectrum. How  $bb$  is measured with the HydroScat will be presented, along with results from a number of cruises in coastal waters around the east and west coasts of the United States. Results include not only spectral measurements of  $bb$ , but also concomitant measurements of the spectral absorption and beam attenuation coefficients, remote-sensing reflectance, chlorophyll concentration, and particle size distributions. These results were used to both test published models involving  $bb$ , and to derive new models based on more complete data set than has historically been available.

**P15/W/03-B3** **1025**

#### BIO-OPTICAL INVESTIGATION OF THE AMAZON OUTFLOW REGION IN DIFFERENT SEASONS

Evgeny Afonin, Alexey MISHONOV, (Marine Hydrophysical Institute, 2 Kapitanskaya St., 335000, Sevastopol, Ukraine, e-mail: mishonov@alpha.mhi.iuf.net); Oleg Yunev (Institute of Biology of the Southern Seas, 2 Nakhimov Ave., 335011, Sevastopol, Ukraine, e-mail: yunev@ibss.iuf.net); Bob Williams (Plymouth Marine Laboratory, Prospect Place, The Hoe, Plymouth, PL1 3DH, United Kingdom, e-mail: bw@ccms.ac.uk).

A large data set of bio-optical parameters: upwelling radiation spectra, Secchi disk depth, colour of the seawater and concentration of phytoplankton pigments was obtained in the western tropical Atlantic during three expeditions of the RV Akademik Vernadsky (36th, 37th & 41st cruises). Research was carried out during different seasons (spring, summer & autumn) and against a background of different hydrographic situations. The region where the Amazon water mixes with oceanic water produces a wide variety of conditions in optical, biological and hydrographic properties. Remotely sensed seawater colour data for this region, obtained from CZCS and SeaWiFS sensors, were analysed to build up pictures of seasonal patterns. These patterns were correlated against ship collected spectrophotometer data and parameters measured in-situ in the three seasons. Measurements were taken of water transparency, chlorophyll concentration, number & biomass of the phytoplankton cells. These data were obtained from surface samples simultaneously together with hydrographic data. Changes in water colour in frontal zones were investigated and described.

**P15/L/26-B3** **1110**

#### PARTICULATE ABSORPTION VARIABILITY IN THE ARABIAN SEA DURING BRITISH AND US JGOFS CRUISES

C.C. TREES (Center for Hydro-Optics & Remote Sensing, San Diego State University, 6505 Alvarado Rd., Suite 206, San Diego, CA 92120, email: ctrees@chors.sdsu.edu); J. Aiken (Plymouth Marine Laboratory, Prospect Place, Plymouth, United Kingdom); R. Bidigare (Department of Oceanography, University of Hawaii, Honolulu, HI 96822); J. Marra (Lamont-Doherty Earth Observatory, Columbia University, Palisades, NY 10964)

Bio-optical properties were measured in the Arabian Sea and the Gulf of Oman during two British and five US JGOFS cruises (August 1994 to December 1995). Remote sensing algorithms have been developed relating water-leaving radiance ratios to diffuse attenuation coefficients, HPLC measured pigments and particulate absorption coefficients. Pigment specific total particulate and phytoplankton absorptions, when normalized to HPLC measured chlorophyll *a*, showed no spatial or temporal trends, indicating that the 'pigment packaging effect' is minimal. The variability in the pigment specific absorption coefficient is so large that for primary productivity modelling efforts, the use of a constant coefficient is probably not appropriate for this region.

**P15/L/22-B3** **1135**

#### ACTIVE IMAGING THROUGH TURBID WATER USING POLARIZED LIGHT

J G WALKER, P C Y Chang, E Jakeman K I Hopcraft, B Ablitt, (University of Nottingham, University Park, Nottingham, NG7 2RD, UK) D L Jordan and G D Lewis (Defence Research Agency, Malvern, Worcestershire WR14 3PS, UK)

Results are presented of a Monte Carlo study of the influence of using polarising optics in underwater imaging. The study considers a number of single-ended illumination and imaging geometries. The study is concerned with active illumination systems and considers both linear and circular polarisation illuminations. The simulation tracks the propagation of the light through the multiply scattering medium and rigorously calculates the Stokes vectors describing the polarisation state of each ray as it propagates. Results are presented for three types of scattering particles; spherical Rayleigh particles, non-spherical Rayleigh particles and spherical Mie particles. The object is treated as a planar diffuse reflector with various polarisation properties; namely, a target which preserves the incident polarisation state and a target which randomises the polarisation state of the light it scatters. The results clearly indicate that the effectiveness of polarisation discrimination in active-illumination imaging systems in overcoming the effects of light scattering are critically dependent on the polarisation properties of the surface to be imaged as well as those of the scattering medium.

Presiding Chair: Andre Morel

#### RADIATIVE TRANSFER AND BIO-OPTICAL MODELLING

**P15/L/28-B3** **Invited** **1200**

#### APPARENT OPTICAL PROPERTIES AND LAMBERT-BEER'S LAW, A NEW THEORETICAL APPROACH

Robert MAFFIONE (Hydro-Optics, Biology, and Instrumentation Laboratories, 55 Penny Lane, Watsonville, CA 95076, email: maffione@hobilabs.com)

In the development of simplified radiative transfer or bio-optical models, a common approach is to apply the so-called Lambert-Beer's law to diffuse attenuation coefficients, usually referred to as apparent optical properties (AOP's). The diffuse attenuation coefficients are therefore treated as a linear sum of the individual attenuation coefficients of the various constituents of sea water. It is straightforward to show that this is theoretically incorrect, although this approach is thought to be a fairly good approximation. However, there is also a problem with the interpretation of the constituent attenuation coefficients that seems to have been overlooked. By a proper redefinition of the constituent attenuation coefficients, given here, a more useful interpretation arises and, moreover, the Lambert-Beer's law is shown to apply in a completely consistent mathematical fashion. Other useful mathematical results from this redefinition are described.

**Wednesday 28 July PM**

Presiding Chair: Andre Morel

#### RADIATIVE TRANSFER AND BIO-OPTICAL MODELLING

**P15/W/02-B3** **1400**

#### USING ANALYTICAL OPTIC CHANGES PREDICTIONS OF PLANKTON DEMOGRAPHY

Liu Cheng-Cheng (Huxley School, Imperial College, London SW7 2BP email: c.c.liu@ic.ac.uk); John Woods (Huxley School, Imperial College, London SW7 2BP email: j.woods@ic.ac.uk)

We report the first successful use of the Radiative Transfer Equation (RTE) to compute the irradiance profile interactively in a plankton ecosystem model. We have done so by incorporating a modified version of the analytical Hydrolight code (Mobley 1994) into the WB plankton ecosystem model (Woods and Barkmann 1994), which previously followed normal practice in using an empirical code (Morel 1988) to compute the vertical distribution of solar irradiance. When integrated by the Lagrangian Ensemble method (Woods and Barkmann 1994) the model simulates the demographics of explicit populations of diatoms and copepods treated as individuals. We have compared the annual cycle of those demographics in simulations based on the two optical methods: analytical and empirical. The former simulates BOFS (Lowry and Cramer 1994) data much better than the latter. However, the empirical code

provides a good first order simulation of the annual cycle in plankton demography. Compared with the empirical method, the analytical method predicts that the peak of the spring bloom in phytoplankton occurs 10 days later, and that copepod reproduction is 15% lower. Analytical optics provides a better prediction of satellite observations of the spring bloom.

**P15/W/06-B3****1420**

#### MODELLING THE SPECTRAL ALBEDO OF THE SEA JUST ABOVE THE WATER SURFACE FOR DIFFERENT TROPHIC TYPES OF CASE I WATERS

Slawomir B. WOZNIAK (Institute of Oceanology, Polish Academy of Sciences (PAS), ul.Powstancow Warszawy 55, Sopot, PL 81-712, Poland, email: woznjr@iopan.gda.pl)

A theoretical spectral model for calculating albedo of the sea just above the surface is developed. Model takes into account a part of irradiance reflected from the sea surface, as well as a part of irradiance scattered backward in the water body. As a 'surface part' of the model the previously developed model of downwelling and upwelling irradiance reflectance from and transmittance through a wind-ruffled sea surface was used. As an 'underwater part' of the model the theoretical formulae for distribution of radiance just below the sea surface (quasi single scattering model) and semi-empirical spectral model of absorption and backscattering were used. Based on the mathematical apparatus of the model the numerical calculations for different meteorological and hydrodynamic conditions and different trophic types of water were performed. Selected parts of calculations containing complex spherical integration were approximated with the polynomial functions. That procedure enabled to develop the simplified polynomial method for estimating the values of the albedo of the sea.

**P15/E/03-B3****1440**

#### DETERMINATION OF INHERENT OPTICAL PROPERTIES FROM SEAWIFS IMAGES

Gerald MOORE (CCMS, Plymouth Marine Laboratory, Prospect Place, Plymouth PL1 3DH, UK, email: G.Moore@CCMS.AC.UK); Jim Aiken (Plymouth Marine Laboratory, Prospect Place, Plymouth PL1 3DH, UK, email: J.Aiken@CCMS.AC.UK)

Models that invert inherent optical properties (IOPs) from satellite observations of reflectance provide an important intermediate stage in deriving remote sensed products that can be tuned for regional optical properties. The spectral reflectance derived from satellite observations is dependant on the absorption (a) and backscatter (bb) of the water itself, the a and bb of the biogeochemical constituents of the water column, the solar illumination and viewing geometry. Results from the Atlantic Meridional Transect (AMT) cruises and other published studies indicate that a and bb are highly constrained by the biogeochemistry. These biogeochemical constraints on the IOPs have been used to develop a model that can be solved by an iterative procedure to determine the IOPs of both Case I and Case II waters, from measurements of above and below surface radiance reflectance, and irradiance reflectance. The effects of the viewing geometry are resolved by using discrete optical models for each viewing geometry. The procedure thus accounts for the BDRF effects on reflectance and enables the determination of the true normalised water reflectance and the diffuse attenuation coefficient. Results are shown for SeaWiFS imagery concurrent with the AMT-6 and AMT-6B cruises. Results from the model are validated against in-situ absorption, bio-optical measures and HPLC pigment analysis.

**P15/L/19-B3****1500**

#### BIO-OPTICAL MODELLING IN THE GULF OF AQABA (EILAT)

L. SOKOLETSKY, Z. Dubinsky, N. Stambler, D. Iluz and M. Shoshany (Bar-Ilan University, 52900 Ramat-Gan, Israel tel.: 972-3-5340856, 972-3-5358283; e-mail: sokolel@mail.biu.ac.il)

According to recently carried out Monte-Carlo simulations of H. R. Gordon and co-workers, four factors influence the upwelling radiance beneath the sea surface (Lu): the downwelling irradiance (Ed), the attenuation coefficient of Ed(Kd), the backscattering coefficient (bb) and the solar zenith angle beneath the sea surface (tetaw). We examine these factors on the basis of statistical processing of measured marine and atmospheric optical characteristics and of chlorophyll a (Chl a) and pheophytin concentrations, during the period 1990-1998 in the Gulf of Aqaba (Eilat) at different layers. We show that Lu is: (1) proportional to Ed; (2) decreases slowly with increase in Kd; (3) does not have a significant connection with bb and tetaw. Simple relationships between Kd, Ed and Lu at the wavelength of 443 nm were obtained. Analogous, highly significant relationships between Chl a and these optical characteristics were also established. Our regional results, validated by us from ground-truth data for the northern Red Sea, will be compared with the global multichannel relationships used today by satellite sensors, such as SeaWiFS. Our aim will be to develop an optimal algorithm in term of precision and simplicity to suit the seasonally variable meso-oligotrophic waters under investigation.

**DISCUSSION****1520**

Presiding Chair: Ray Smith (Institute for Computational Earth System Science (ICESS) University of California, USA)

#### REMOTE SENSING, CALIBRATION, VALIDATION, INTERPRETATION AND METHODOLOGY

**P15/L/29-B3**

Invited

**1550**

#### CAN REMOTELY SENSED MEASUREMENTS PROVIDE ALL THE VARIABLES REQUIRED FOR OCEANIC CARBON CYCLE MODELS?

Jim AIKEN (Plymouth Marine Laboratory, Prospect Place, Plymouth PL1 3DH, UK, email: J.Aiken@CCMS.AC.UK)

Biological production drives all the processes in the ocean which relate to natural resources, fisheries and the sustainability of ecosystems and the air-sea exchange of biogenic gases, which are implicated in or responsive to the role of the oceans in the natural and anthropogenically forced green house effect and global climate change. A holistic approach, coupling large-area satellite remotely sensed observations of the marine environment, with oceanographic measurements of process rates and parameter values for models is a widely accepted approach for biological oceanography. Models can be used with remote sensing data, to extrapolate the in situ measurements horizontally to ocean basin scales and vertically to sub-surface layers, not measured by most remote sensors in space. Ultimately models will be used to predict the effects of pelagic primary production on the global biosphere and the responses of oceanic ecosystems to climate change.

Recent innovations of new measurements of phytoplankton photosynthetic parameter values (by Fast Repetition Rate Fluorometry, FRRF), new ocean colour sensors (SeaWiFS) and novel analytical bio-optical models have advanced the prospects for improved accuracy of basin

scale productivity and carbon-cycle models. The models will be discussed, the availability of remotely sensed data assessed and the extrapolation to sub-surface layers considered.

**P15/W/05-B3****1630**

#### SATELLITE SENSING AND IN-SITU VALIDATION OF OCEANIC WATERS OF WESTERN AUSTRALIA

Peter RCS FEARNES, James E Davies, Mervyn J LYNCH (Remote Sensing and Satellite Research Group, School of Physical Sciences, Curtin University of Technology, GPO Box U1987, Perth WA 6845, Australia); Wilma J Vincent (School of Environmental Biology, Curtin University of Technology, GPO Box U1987, Perth WA 6845, Australia); Alan F Pearce (CSIRO Marine Laboratories, PO Box 20 North Beach WA 6020, Australia)

Curtin University researchers, in association with scientists from the CSIRO Marine Research and Fisheries Western Australia, have been conducting in situ validation of remotely sensed ocean colour products off Perth, Western Australia. On a monthly basis over a 27-month period, numerous biological and physical measurements have been made along a 40 km transect west of Hillarys Marina (20 km north of Perth). The 1997 launch of the ocean colour sensor SeaWiFS (Sea-viewing Wide Field-of-view Sensor) provided remotely sensed ocean products coincident with in situ measurements along the Hillarys transect between November 1997 and December 1998. This paper presents a review of the in situ validation measurements of chlorophyll concentration, phytoplankton species counts, sea surface temperature (SST), temperature profiles, salinity profiles, and comparisons with satellite derived chlorophyll and SST measurements.

**P15/W/07-B3****1650**

#### HANDLING, PROCESSING AND FIRST INTERPRETATION OF SEAWIFS DATA IN THE GEOSONAR PROJECT

T. KNUDSEN, N. F. Carlsen, O. B. Andersen, and P. Knudsen (all at National Survey and Cadastre, Copenhagen NV, Denmark, email: thk@kms.dk); A. A. Nielsen, K. B. Hilger (both at IMM, Technical University of Denmark, Lyngby, Denmark)

The interdisciplinary project GEOSONAR (funded by the Danish Earth observation programme) analyses multi-disciplinary contributions to sea level and its variations on different time scales. This includes geodetic, oceanographic and meteorological effects on sea level, focussed in the North Atlantic and particularly the North Sea. In addition to traditional geodetic remote sensing techniques, such as altimetry, this project also involves the use of multi-channel scanning radiometers data, in the visible and infrared wavelengths. Data have been obtained from the Sea-viewing Wide Field-of-view Sensor (SeaWiFS), as well as from the NOAA advanced very high resolution radiometer (AVHRR), and the ERS along track scanning radiometer (ATSR). The results of a new handling and enhanced cloud removal scheme for SeaWiFS data is presented and the results are compared with data processed using the existing cloud removal scheme. This new cloud removal technique is based on maximum auto-correlation factors analysis (MAF). Extracting geodetic and oceanographic signal from these merged multi-channel data sources is non-trivial, however, the MAF analysis tool has also proven to be valuable in the processing and initial interpretation of the data.

**P15/W/08-B3****1710**

#### SEASONAL BLENDED IN-SITU AND REMOTELY-SENSED OCEAN CHLOROPHYLL CLIMATOLOGIES

M.E. CONKRIGHT (NOAA/NODC, Ocean Climate Laboratory E/OC5, 1315 East-West Highway, Silver Spring, MD, 20910, USA, Email: mconkright@nodc.noaa.gov; W.W. Gregg (NASA/GSFC, Laboratory for Hydrospheric processes, Greenbelt, MD, USA, Email: gregg@cabin.gsfc.nasa.gov)

We have developed global seasonal climatologies of ocean chlorophyll, through the blending of in situ data (NOAA/NODC archives) and remotely-sensed data (NASA/GSFC archives) using the Conditional Relaxation Analysis Method. Blending of in situ chlorophyll and satellite remotely-sensed provides us with an enhanced data set by maximizing the strengths of each observational platform. Satellite chlorophyll data provide large horizontal coverage and improved temporal resolution but poor accuracy whereas in-situ data provide high quality (accuracy) but poor spatial and temporal coverage.

We focus on historical data from the Coastal Zone Color Scanner (CZCS) era (1978-1986), since sufficient in situ data are available for this time period. Differences between the blended and CZCS seasonal chlorophyll climatologies are observed primarily in coastal regions for all seasons. The blended climatologies are higher in these areas than the satellite data. These differences may have several sources, including time mismatches, sampling bias, and interannual variability. As data become available from satellites (e.g., from the Ocean Color and Temperature Scanner and Sea-Viewing Wide Field-of-View Sensor), and corresponding in-situ data are obtained, these methods will be expanded to produce a long-term blended data set encompassing the years 1978-1986 (years when CZCS was operational) and 1997-2002 (the period for which ocean color mission data are expected to be available).

**P15/L/24-B3****1730**

#### DERIVING BATHYMETRY FROM HYPERSPECTRAL DATA

W. D. PHILPOT (email: wdp2@cornell.edu, Cornell University, 220 Hollister Hall, Ithaca, NY 14853); and D.D. Kohler (email: ddk6@cornell.edu, Cornell University, 220 Hollister Hall, Ithaca, NY 14853)

Deriving bathymetric maps from passive remotely sensed imagery is an appealing prospect, but one that is prone to large errors and uncertainties. The advent of hyperspectral imagery raises the possibility of deriving more accurate bathymetric maps. Greater accuracy may be possible using standard analysis procedures but optimizing solutions using the greater number of spectral bands. It is more likely that new analysis procedures based on the spectral content of the data will yield greater accuracy in depth estimates as well as providing some information as to water quality and bottom reflectance. A new procedure that does take this extra information into account has been developed. The technique which is based on the use of spectral derivatives, significantly improves the accuracy of the depth estimates in test data. The technique is being adapted for use with hyperspectral image data.

**DISCUSSION****1750**



**REMOTE SENSING, CALIBRATION, VALIDATION,  
INTERPRETATION AND METHODOLOGY (Continued)****P15/E/01-B4****0900****ATMOSPHERIC CORRECTION OF SEAWIFS IMAGERY OVER HIGHLY TURBID CASE II WATERS**

Samantha LAVENDER (CCMS, Plymouth Marine Laboratory, Prospect Place, Plymouth PL1 3DH, UK, email: S.Lavender@CCMS.AC.UK); Gerald Moore (CCMS, Plymouth Marine Laboratory, Prospect Place, Plymouth PL1 3DH, UK, email: G.Moore@CCMS.AC.UK)

The successful exploitation of remotely sensed observations of water colour requires the development of atmospheric correction methods in coastal waters, and the determination of the concentration of suspended particulate matter (SPM) concentrations in gravimetric units for use in mass flux studies and hydrodynamic models. The remote sensing of turbid waters (Case II) using SeaWiFS requires new approaches for the atmospheric correction of the data. Unlike open ocean waters (Case I) there is significant water leaving radiance at infrared wavelengths, so conventional 'dark pixel' atmospheric correction procedures are invalid. A coupled hydrological atmosphere model is described that solves the water leaving radiance and atmospheric path radiance in the near infra-red (NIR) over Case II turbid waters. The theoretical basis of this model is described, together with its implementation in the current CCMS/PML processing architecture called the SeaWiFS Automated data processing system (SeaAPS). SeaAPS and the resulting products are being validated using both in-situ measurements of water-leaving radiance and suspended particulate matter, in collaboration with European research projects. This research is an important step in deriving biogeochemical parameters for turbid Case II waters.

**P15/L/21-B4****0925****ESTIMATION OF AEROSOL PROPERTIES FROM OCTS AND POLDER DATA FOR OCEAN COLOR REMOTE SENSING**

Yasushi MITOMI (1), Riko HIGUTCH (1), Hajime FUKUSHIMA (2), and Tamio TAKAMURA (3).

(1) Remote Sensing Technology Center of Japan, Roppongi First Bldg. 8F, 1-9-9, Roppongi, Minato-ku, Tokyo 106-0032, Japan, Email: mitomi@restec.or.jp, hriko@restec.or.jp  
(2) School of High-Technology for Human Welfare, Tokai University, 317 Nishino, Numazu 410-0395, Japan, Email: hajime@fks.h.fc.u-tokai.ac.jp  
(3) Center for Environmental Remote Sensing, Chiba University, 1-33 Yayoi-cho, Inage-ku, Chiba 263-8522, Japan

The atmospheric correction in ocean color remote sensing seeks to retrieve the water leaving radiances from the total radiances observed at satellite altitude. Its accuracy depends on the estimation error of the radiance scattered and absorbed by aerosol which is highly variable in both space and time. ADEOS/OCTS has three observation bands (670, 765, and 865nm) in the near-infrared region to measure aerosol properties (eg., aerosol type and optical thickness) and the radiances at 670 and 865nm are used to generate NASDA's OCTS ocean color products. POLDER onboard ADEOS together with OCTS has the aerosol observation bands similar to the OCTS and also has multi-angle polarization data, but its spatial resolution (7km \* 6km) is inferior to the OCTS (700m at nadir). In this research, the aerosol informations derived by OCTS and POLDER were compared. Furthermore, an estimation method of the aerosol properties by the composite data from the two different sensors was discussed in order to improve an accuracy of the atmospheric correction. These results are reported in this presentation.

Presiding Chair: John Cullen (Center for Environmental Observation Technology and Research, Department of Oceanography, Nova Scotia Canada,)

**PRIMARY PRODUCTION AND BIOGEOCHEMICAL FLUXES****P15/L/30-B4**

Invited

**0950****PRIMARY PRODUCTION FROM NEW SATELLITE OCEAN COLOUR SENSORS**

André Morel and David Antoine

Based on a spectral light-photosynthesis model, previously operated in conjunction with the CZCS imagery, the primary production at global (and basin) scales has been derived from SeaWiFS data, namely from the monthly composites of the chlorophyll distribution, and over a period of one year. Climatological fields of temperature and mixed layer depth have been utilised for the derivation. The actual cloudiness fields, contemporaneous of the SeaWiFS data capture are not yet available, so that the climatological cloudiness fields (ISCCP data base, for the 1983-1990 period, previously used with the CZCS data) were again used to estimate the incident irradiation at the ocean surface, which is an input for the model.

Therefore the difference between the primary production estimates based on the data delivered by the two sensors (CZCS and SeaWiFS) can only originate from differences in the chlorophyll fields and in their temporal evolutions. The excellent consistency between the chlorophyll determinations made by the two sensors leads to an excellent agreement between the derived annual primary production at global and basin scales, despite slightly differing temporal evolution (in Pacific, in particular). Chlorophyll data from the OCTS instrument are also transformed in the same way into primary production maps, for a 8 months period, prior to the launch of the SeaWiFS instrument. A more realistic and accurate comparison between these results will be possible as soon as the actual cloudiness distribution for the involved periods are available. Sensitivity analyses effected with the model allow to predict that replacing an « academic » cloud field by an actual one will not entail large differences in terms of production.

**P15/W/04-B4****1055****STATISTICAL RELATIONSHIPS BETWEEN LIGHT CONDITIONS IN THE SEA AND PHOTO-PHYSIOLOGICAL CHARACTERISTICS OF MARINE ALGAE.**

Bogdan WOZNIAK (1,2), Jerzy Dera (1), Dariusz Ficek (2), Roman Majchrowski (2), Slawomir Kaczmarek (1), Mirosława Ostrowska (1), Olga J. Koblentz-Mishke (3).1) Institute of Oceanology, Polish Academy of Sciences (PAS), ul. Powstancow Warszawy 55, Sopot, Poland, PL 81-712, e-mail: wozniak@iopan.gda.pl 2) Institute of Physics, Pedagogical University in Slupsk, ul Arciszewskiego 22, Slupsk, Poland, PL 76-200 3) Shirshov Institute of Oceanology, Russian Academy of Sciences (RAS), ul. Krasikova 23, Moscow, Russia 117218.

Due to photo- and chromatic - acclimation processes of phytoplankton cells the light conditions in the sea affect the particular photosynthetic and photoprotecting pigments contents in marine phytoplankton cells. It is manifested in diversity of spectral absorption properties of phytoplankton and has also indirect influence on quantum yield of photosynthesis. The aim of this work is to find relationships between spectral composition and absolute level of the PAR irradiance in the sea and photophysiological characteristic of algae. This aim was achieved with statistical analysis of appropriate data sets from a few hundred stations from the world oceans. As a result the model which allows to estimate as follow: the phytoplankton pigments composition, the light absorption coefficient for all pigments and its components from photosynthetic and photoprotecting pigments for the given light conditions in the sea, was worked out. This model also allows to determine variability of quantum yield of photosynthesis due to changes in proportions between photosynthetic and photoprotecting phytoplankton pigments.

**P15/W/09-B4****1115****MODELLED AND MEASURED PRIMARY PRODUCTION DISTRIBUTION IN THE BALTIC**

Slawomir Kaczmarek (1), Mirosława Ostrowska (1), Olga J. Koblentz-Mishke (2), Bogdan Wozniak (1). 1) Institute of Oceanology, Polish Academy of Sciences (PAS), ul. Powstancow Warszawy 55, Sopot, Poland, PL 81-712, e-mail: kaczmar@iopan.gda.pl. 2) Shirshov Institute of Oceanology, Russian Academy of Sciences (RAS), ul. Krasikova 23, Moscow, Russia 117218.

The results of primary production modelling for the Baltic Sea, which is typical case 2 waters basin, are presented. Earlier established, the bio-optical relationships for oceanic case 1 water were a base of a primary production model. Using the empirical data gathered from the Baltic Sea the model's parameters were adopted to obtain a model appropriate for the Baltic. This model was used to estimate primary production in the Southern Baltic region, divided into 20 sub-regions. The mean monthly primary production have been calculated for each month of the year. As the model input data, the long-term (over 20 years) monthly means of hydro-meteorological parameters and surface chlorophyll a concentration have been used. The model results were compared with the map of yearly primary production obtained after analyses of long-term "in situ" measured data. Both data sets relate to the same period. Such comparison allows discuss the advantages and limitations of the primary production bio-optical modelling especially in the context of remote sensing data assimilation.

**P15/E/04-B4****1135****DETERMINATION OF PHYTOPLANKTON PHOTOSYNTHETIC CHARACTERISTICS AND PRODUCTION FROM REMOTE SENSED REFLECTANCE.**

Gerald MOORE (CCMS, Plymouth Marine Laboratory, Prospect Place, Plymouth PL1 3DH, UK, email: G.Moore@CCMS.AC.UK); Jim Aiken (Plymouth Marine Laboratory, Prospect Place, Plymouth PL1 3DH, UK, email: J.Aiken@CCMS.AC.UK)

Currently available remote sensed algorithms supply information in terms of biomass normalised to chlorophyll concentration. In addition, these algorithms implicitly fix the spectral shape of the absorption characteristics of phytoplankton, by using simple band ratios, and assume that optically active dissolved organic material (DOM) is a fixed proportion of phytoplankton absorption. The use of an algorithm that inverts remote sensed reflectance to the IOPs of spectral absorption (a) and backscatter (bb) enables the determination of the major pigment classes chlorophyll, photosynthetic carotenoids, photoprotectant carotenoids, and co-varying ODOM concentration.

The results from the optical model have been used to differentiate the rate of phytoplankton photosynthetic pigment absorption from non-photosynthetic absorption, and thus derive production estimates based on fixed quantum yield.

The absorption model measurements are compared with data from the Atlantic Meridional Transect (AMT) cruise using in-situ absorption and simulated absorption derived HPLC pigment concentrations. The production estimates are compared with 14C measurements taken on the AMT-6 cruise. Production maps of the AMT cruise region are computed from data from the SeaWiFS sensor.

**DISCUSSION****1155****P15/L/01-B4**

Invited

**1205****PRIMARY PRODUCTIVITY OF THE WESTERN ANTARCTIC PENINSULA REGION AND THE SOUTHERN OCEAN**

Raymond SMITH & Heidi Dierssen (Institute for Computational Earth System Science (ICESS); University of California, Santa Barbara, CA, 93106, USA, email: ray@icess.ucsb.edu, dierssen@icess.ucsb.edu); Karen Baker & Maria Vernet (Scripps Institution of Oceanography (SIO/MRD); University of California, San Diego, La Jolla, CA 92093-0218, USA, email: kbaker@ucsd.edu, mvernet@ucsd.edu)

Phytoplankton production in the Southern Ocean is poorly known compared to temperate ecosystems. The relative inaccessibility, paucity of data, large area, extreme environmental conditions, and the potential role of the Southern Ocean carbon cycle in response to rising atmospheric CO<sub>2</sub> are compelling reasons for optimizing models for the estimation of phytoplankton production remotely. Further, there is now strong evidence that the bio-optical properties of these Antarctic waters are significantly different than temperate waters. Consequently, both the retrieval of chlorophyll concentrations and the subsequent estimation of phytoplankton production from satellite sensed reflectance measurements require regional specific algorithms for optimum accuracy. Based upon data from the Palmer Long Term Ecological Research (PAL/LTER) program we have optimized retrieval algorithms and utilized a depth-integrated primary productivity model to estimate biomass and productivity in Antarctic waters. Productivity results are compared with previous published estimates and sensitivity studies evaluated. The space-time distribution and the seasonal and interannual variability are discussed within the context of contribution to the overall Southern Ocean marine ecology.

**UV RADIATION MEASUREMENTS AND ECOLOGICAL CONSEQUENCES****P15/L/18-B4****1400****ESTIMATING UV ATTENUATION AND PHOTOCHEMICAL REACTION RATES FROM REMOTE SENSING OF OCEAN COLOR**

John J. CULLEN, Richard F. Davis, Barbara Nieke (all at Center for Environmental Observation Technology and Research, Department of Oceanography, Dalhousie University, Halifax, Nova Scotia B3H 4J1, Canada, Email: John.Cullen@Dal.ca, Richard.Davis@Dal.ca, bnieke@raptor.ocean.dal.ca,

Sophia Johannessen and William L. Miller (both at Department of Oceanography, Dalhousie University, Email: schjohan@is2.dal.ca, William.Miller@Dal.ca).

Previously, we outlined a method for using measurements of upwelling radiance in the visible to quantify UV-dependent processes in aquatic systems: 1) attenuation coefficients for UV and visible irradiance are estimated from spectra of upwelling radiance at the surface, based on empirical relationships between ratios of upwelling radiance and near-surface diffuse attenuation coefficients; 2) total absorption is related to attenuation by accounting for geometry of the radiance field; 3) total absorption is partitioned among colored dissolved organic matter (CDOM; essential to photochemistry), water, and particulate matter using published coefficients for water, estimates of chlorophyll from blue:green reflectance ratios, and assumed chlorophyll-specific particulate absorption spectra; 4) solar irradiance at the surface is calculated from a model, tuned with observations from a filter-based radiometer; and 5) laboratory-derived action spectra, modeled irradiance, and estimated CDOM vs total absorption are used to quantify rates of photochemical transformation. In principle, this approach can yield synoptic estimates of photochemistry from airborne sensors. Here, we parameterize the model with recently obtained data from several marine environments, along with an action spectrum for photochemical production of carbon monoxide from CDOM, to estimate the photochemical production of CO using aircraft remote sensing of ocean color. The precision of key empirical relationships (e.g., between diffuse attenuation coefficients in the UV and ratios of upwelling radiance in the visible) is assessed, and the uncertainty of estimates is partially described.

#### P15/E/05-B4 1445

##### PENETRATION OF UVB IRRADIANCE INTO THE NORDIC SEAS AND ADJACENT COASTAL WATERS

Eyvind AAS (Department of Geophysics, University of Oslo, N-0315 Oslo, Norway, Email: eyvind.aas@geofysikk.uio.no); Niels K. Høejerlev (Niels Bohr Institute of Astronomy, Physics and Geophysics, University of Copenhagen, DK-2100 Copenhagen O, Denmark, Email: nk@fy.ku.dk)

Data for downward UVB irradiance at about 200 stations in the Nordic Seas and the adjacent coastal waters have been analysed. The depth where the irradiance is reduced to 10% of its surface value,  $Z(10\%)$ , ranges from 0.1 to 16 m. For comparison very clear ocean water (Gulf of Mexico) has a  $Z(10\%)$  value around 35 m. In the German Bight the mean value of  $Z(10\%)$  is 0.8 m, in the Kattegat 0.9 m, and in the Skagerrak 2.5 m. In the Norwegian Coastal Current the observed mean value is 4.6 m, while the mean values of  $Z(10\%)$  in Svalbard waters have been observed to be either 5 or 10 m, depending on season. The Norwegian Atlantic Current has the mean value 15 m during non-bloom conditions, but phytoplankton blooms seem to be able to reduce  $Z(10\%)$  by a factor of up to 3. Yellow substance, suspended organic and inorganic matter all contribute to the variation of  $Z(10\%)$  in highly different proportions depending on both location and season. Solar elevations have a minor effect on  $Z(10\%)$  according to the measurements performed in the region considered. Finally, penetration of UVB irradiance in waters dominated by yellow substance is not straightforward to model based on spectral irradiance measurements in the visible part of the spectrum. This is due to the fact that the spectral absorbance of yellow substance is much more complex than previously and traditionally anticipated.

#### P15/L/16-B4 1505

##### SEASONAL VARIABILITY IN THE RELATIVE PENETRATION OF UVR AND PAR IN TEMPERATE COASTAL WATERS

KUWAHARA, V. S. I., H. Ogawa2, T. Toda1, T. Kikuchi3, S. Taguchi1; (Faculty of Engineering, Soka University1; Faculty of Ocean Research, Tokyo University2; Faculty of Education and Human Sciences, Yokohama National University3)

Seasonal UVR penetration variability was surveyed for three consecutive years in the temperate coastal waters of Sagami Bay, Japan. Integrated mixed layer samples of sea-water were concurrently collected for chlorophyll a analysis. Dissolved organic carbon (DOC), particulate organic carbon (POC), and the absorption coefficient of the dissolved (acDM) and particulate material (acPM) were also measured during one year. The 1% attenuation depth of 305, 320, 340 and 380nm calculated from the diffuse attenuation coefficient (Kd) averaged 11.4Å)6.34, 14.06Å)8.30, 18.68±10.90, and 29.81Å)15.79m, respectively for the three years with minimum penetration occurring near summer solstice. Breaks in the slopes of Kd (multiple Kd patterns) were also observed during particular summer months for 340nm, 380nm, and PAR. The relative penetration of UVR into the euphotic zone (1% penetration depth of PAR) averaged 19Å)9% for 305nm, 24Å)11% for 320nm, 32Å)14% for 340nm, and 49Å)20% for 380nm accordingly. Seasonal variability in UVR transparency was attributable to changes in concentrations of DOC, Chl a, and POC. This was further supported by results from the acDM and acPM analysis. The percent contribution of acDM and acPM varied with season.

#### DISCUSSION 1525

#### P15/L/17-B4 1550

##### FLUX OF CARBONYL SULFIDE FROM THE OCEANS USING SEAWIFS CHLOROPHYLL CONCENTRATION ESTIMATES.

J. KETTLE, T. S. Rhee, M. V. Hobe, and M. O. Andreae (Biogeochemistry Department, Max Planck Institute for Chemistry, P. O. Box 3060, D-55020 Mainz, Germany, email: ajkettle@mpch-mainz.mpg.de)

Carbonyl sulfide (COS) is a long lived atmospheric molecule which is oxidized in the stratosphere to sulfate particles which may alter the radiation budget of the earth's surface. One of the more important sources of COS is the upper ocean where it is produced photochemically as the result of the interaction of solar ultraviolet light with colored dissolved organic matter. The principal sinks of the molecule from the oceanic mixed layer are hydrolysis and surface outgassing to the atmosphere. The interaction between the production and loss terms controls the flux of the molecule to the atmosphere. The recent meridional transect of the James Clark Ross from England to the Falkland Islands in September-October, 1998 provided an opportunity to investigate the flux of COS to the atmosphere. During the cruise, atmospheric and sea surface concentrations of COS were measured, in addition to the ultraviolet absorbance and fluorescence of seawater, chlorophyll concentration, insolation, wind speed, and other meteorological parameters. Earlier measurements have suggested a relationship between the ultraviolet absorbance of seawater and the chlorophyll concentration. Using this relationship, it is proposed that the SEAWIFS data can be used to estimate the global CDOM absorbance. The global photochemical production of COS can then be

estimated using climatological information for insolation. Using climatological temperature fields to constrain the physical hydrolysis process and climatological mixed layer depths to constrain the amount of dilution of the tracer, it is possible to develop a simple model of global COS near surface concentration and outgassing to the atmosphere. The results of the ship expedition are used to verify the predictions of this simple model.

#### P15/L/05-B4 1610

##### RESPONSE OF BACTERIOPLANKTON TO DIFFERENT INTENSITIES OF ULTRAVIOLET-B RADIATION: A MESOCOSM STUDY

Khaled CHATILA, Serge Demers, Behzad Mostajir, Jean-Pierre Chanut (all at Groupe de Recherche en Environnement Côtier, Institut des Sciences de la Mer de Rimouski (ISMER), Université du Québec à Rimouski, 310 Allée des Ursulines, Rimouski (Québec), Canada, G5L 3A1, email: khaled\_chatila@uqar.quebec.ca) Patrick Monfort (Laboratoire d'Hydrobiologie Marine et Continentale, Unité Mixte de Recherche "Écosystèmes lagunaires", Université Montpellier II - CNRS (UMR 5556) Case 093, F-34095 Montpellier Cedex 05, France, email: pmonfort@crit.univ-montp2.fr)

The recent decreasing trends of stratospheric ozone concentration and the subsequent increases of ultraviolet-B radiation (UVBR) reaching the Earth's surface have raised concern about the possible impact of this radiation on aquatic ecosystems. In July 1996, the effects of excluded, natural and artificially enhanced UVBR on the summer planktonic community (<240mm) of the lower St. Lawrence Estuary (Québec, Canada) were studied during a week-long mesocosm experiment. Experimental water was continuously mixed by a pumping system. The present work was a part of this experiment and addressed the response of bacteria to the tested light regimes. Our data suggest that UVBR may have both inhibiting (by directly acting on cellular processes) and stimulating effects on bacterioplankton (by increasing the release of labile substrates from UVBR stressed phytoplankton or by decreasing cells removal by UVBR sensitive bacterivores). On an ecosystem level, overall bacterial response to UVBR will be the net result of these competing processes.

#### P15/L/27-B4 1630

##### GLOBAL MAPPING OF UNDERWATER UV FLUXES AND DNA-WEIGHTED EXPOSURES USING TOMS AND SEAWIFS DATA PRODUCTS

Alexander VASILKOV, Nickolay Krotkov (both at Raytheon ITSS Co., 4400 Forbes Blvd., Lanham, 20706 USA), Jay Herman (NASA/Goddard Space Flight Center, Greenbelt, 20771 USA)

The global stratospheric ozone layer depletion results in an increase in biologically harmful ultraviolet (UV) radiation reaching the surface and penetrating to ecologically significant depths in the natural waters. Such an increase could be estimated on a global scale by combining satellite estimates of the UV irradiance at the ocean surface from the Total Ozone Mapping Spectrometer (TOMS) satellite instrument with the satellite ocean color measurements in the visible spectral region from the SeaWiFS instrument. In this paper we propose a model of seawater optical properties in the UV spectral region based on the Case 1 water model in the visible range. The inputs of the model are standard products of ocean color sensors: chlorophyll concentration and the diffuse attenuation coefficient at 490 nm. Penetration of solar UV radiation at different depths into open ocean waters is calculated using the quasi-single scattering approximation of the radiative transfer (RT) in the water. The separation of the ocean and atmospheric RT problems in the UV spectral region is discussed. The accuracy of the RT approximation in the water is tested using accurate Monte Carlo modeling. The sensitivity study of the underwater UV irradiance to atmospheric and oceanic optical properties is performed based on the model proposed. The simulations have shown that the main environmental parameters controlling the levels of the most harmful UVB (280-320nm) radiation underwater for clear sky conditions are: solar zenith angle, water optical properties and total ozone. Weekly maps of underwater UV irradiance and DNA weighted exposure are calculated using monthly mean SeaWiFS chlorophyll a and diffuse attenuation coefficient products and the TOMS-derived surface UV irradiance weekly maps. The final products include global maps of depths, at which UVB flux and DNA weighted dose rate are equal to 10% of their surface values.

#### CONCLUDING DISCUSSIONS 1650

#### P16 Friday 30 July

##### RECENT IMPROVEMENTS TO DEEP-SEA RESEARCH THROUGH USE OF SUBMERSIBLES, ACOUSTIC TOMOGRAPHY AND IN-SITU LONG TERM OBSERVATIONS (IAPSO)

Location: Arts Building, 125 LR1

#### Friday 30 July AM

Presiding Chairs: A. Flosadottir (Univ. of Washington, Seattle, USA), R. Iwase (Deep-Sea Res., JAMSTEC, Yokosuka, Japan)

#### P16/W/05-B5 0830

##### LONG-TERM MONITORING OF OCEANIC SEISMICITY USING UNDERWATER ACOUSTIC TECHNIQUES

Christopher G. FOX, Robert P. Dziak (both at NOAA, Pacific Marine Environmental Laboratory, 2115 S.E. OSU Drive, Newport, OR 97365 USA email: fox@pmel.noaa.gov)

Monitoring oceanic seismicity using underwater acoustic techniques offers several advantages over land-based seismic networks, including a lower detection threshold, improved location accuracy, and the ability to monitor large areas of the ocean with relatively few sensors. The availability of the U.S. Navy's SOUND SURVEILLANCE System (SOSUS) to the scientific community has allowed long-term monitoring of seismicity in the North Pacific Ocean to be accomplished at relatively low cost. Detailed maps of overall seismicity are now available for structural interpretation of plate tectonic activity. Episodes of volcanic seismicity associated with seafloor spreading, generally with magnitudes less than 3.0, have been successfully detected by SOSUS three times and verified in the field. Patterns of intraplate deformation have also been discovered, including both isolated intraplate earthquakes and patterns of intraplate activity relating to large-scale stresses on the plate. Based on the success of its SOSUS efforts, NOAA developed and deployed an array of autonomous hydrophones in the equatorial Pacific in May, 1996. Seismicity from the equatorial region of the Pacific shows a similar pattern to that in the northeast Pacific, with most activity confined to subduction zones and transform fault zones, with some indications of intraplate seismicity and volcanic seismicity along the ridge crest. The inferred volcanic episodes along the fast-spreading-rate



East Pacific Rise (EPR) are of short duration relative to confirmed activity along the medium-spreading-rate Juan deFuca/ Gorda Ridges (hours-days versus days-weeks). These shorter volcanic episodes may simply represent the nature of the activity or perhaps reflect lower seismic magnitudes due to a thin brittle layer. In February 1999, a second array of hydrophones was deployed in the North Atlantic between 10N and 40N in a two-year experiment to monitor the Mid-Atlantic Ridge (D. Smith, WHOI; M Tolstoy, LDEO; C. Fox, NOAA, Pls). Analogy to the Pacific examples would predict fewer, longer duration volcanic episodes and larger magnitude fault plane earthquakes. Additional monitoring efforts, based on either routine ship access or the establishment of permanent ocean stations, will depend on partnerships with the international research community and other U.S. agencies, but could eventually lead to a global acoustic monitoring system.

P16/L/01-B5

0910

#### FOUR-YEARS' CHANGE OF THE TAG HYDROTHERMAL MOUND OBSERVED BY SUBMERSIBLESHINKAI 6500

Kantaro FUJIOKA (Deep Sea Research Department, Japan Marine Science & Technology Center, Yokosuka, 237-0061 JAPAN, email: fujiokek@jamstec.go.jp), Hitoshi Chiba (Institute for study of the Earth's Interior, Okayama University, 827 Yamada, Misasa, Tottori, 682-0193 JAPAN, email: hchiba@misasa.okayama-u.ac.jp), Harue Masuda (Department of Geophysics, Osaka City University, 3-3-138 Sugimoto, Sumiyoshi-ku, Osaka, 558-8585 JAPAN, email: harue@sci.osaka-cu.ac.jp), MEGATRIN scientific party

The TAG hydrothermal mound is one of the largest hydrothermal mounds known in the world. Since the first finding of the mound its whole edifice, stratigraphy and structure, chemistry and long-term change were made clear by the previous studies. Here we present new data sets on the location of active vents, type of smokers, and chemistry of the hydrothermal fluids. The TAG hydrothermal mound is migrating with NNE-SSW trending fault movement since 1994 to form the two new black smoker mounds east of the Central Blacksmoker Complex previously existed. The chemical compositions of the vent fluids did not change at all even 17 ODP drill holes were dug up on and around the TAG mound. We detected big change of the Eh, pH, CDT and gamma ray intensity along the vents and faults on the mound. We also found the existence of the plume structure by the measurements during the descent and ascent the submersible. The TAG hydrothermal mound is now migration together with fault system suggesting that the pass way of the hydrothermal fluid changes without any reaction with the mound forming materials since 1994.

P16/E/03-B5

0930

#### DEEP-SEA SUBMERSIBLE MAGNETICS ACROSS A MID-OCEAN RIDGE

J. DYMENT, M. Ravilly (both at CNRS, IUEM, Univ. Bretagne Occidentale, Plouzané, France; email: jerome@univ-brest.fr); C. Honsho (Ocean Research Institute, Univ. Tokyo, Japan); M. Perrin (CNRS, ISTEEM, Univ. Montpellier II, Montpellier, France); H. Horen (Ecole Normale Supérieure, Paris, France); P. Gente (CNRS, IUEM, Univ. Bretagne Occidentale, Plouzané, France)

A unique set of magnetic data has been acquired on the Mid-Atlantic Ridge spreading segment at about 21°40'N during the Tamar cruise of R/V Nadir and deep sea submersible Nautilie. The data include surface scalar magnetic field collected by the ship, sea-bottom vector magnetic field continuously measured along the dive track by a three component magnetometer attached to Nautilie, and measurements of rock magnetic properties and absolute paleointensities on samples collected by the submersible. Fifteen dives make three almost-continuous traverses of the spreading center, and four additional dives at the axis allow examination of magnetic variations along the axis. The surface magnetic anomaly and the long-wavelength part of the sea-bottom magnetic anomaly were inverted to equivalent magnetization. Because they were measured close to the seafloor, the observed sea bottom anomalies contains short-wavelength variations produced by the topography and the up-and-down motion of the submersible. We estimate the magnetisation of the seafloor along the dive tracks by comparing the amplitude of these short-wavelengths with synthetics calculated for different uniform magnetisation of the seafloor. About 130 direct measurements of the natural remanent magnetisation and magnetic susceptibility have been made on the samples. In addition, successful determinations of the geomagnetic field paleointensity by the Thellier method have been obtained for 34 samples of the two traverses located in the segment center. These data offer a unique opportunity to study the structure and magnetic properties of the oceanic crust and the source of marine magnetic anomalies.

P16/E/13-B5

0950

#### LONG TERM DEEP SEAFLOOR MONITORING AT COLD SEEPAGE SITE OFF HATSUSHIMA ISLAND IN SAGAMI BAY

Ryoichi IWASE, Hiroyasu Momma, Kyohiko Mitsuzawa and Katsuyoshi Kawaguchi (Deep Sea Research Department, Japan Marine Science and Technology Center, 2-15 Natsushima-cho, Yokosuka, 237-0061, Japan, email: iwaser@jamstec.go.jp)

Real time deep seafloor monitoring has been carried out for more than 5 years by the cable-connected observatory which was deployed at the cold seep community site at a depth of 1174m off Hatsushima Island in Sagami Bay, central Japan in 1993. It is equipped with video cameras, subbottom temperature probes, a current meter, a CTD, a seismometer and a hydrophone. Through 5 year monitoring, seasonal variations of subbottom temperatures which increased in spring and had a peak in April or May were observed, although the seasonal variations of water temperature were not so obvious. The increase of the amount of suspended particles which are considered to be produced by the spring bloom in the shallow water were also observed in spring by the video camera. The sedimentation of these particles seems to affect the subbottom temperatures. The daily variations of subbottom temperatures which correlated with the variation of hydraulic pressure i.e. ocean tide were also observed. These are considered to have some relation with the behaviour of cold seepage. When the earthquake swarms occurred at about 7 km southwest of the observatory in March, 1997 and in April and May, 1998, mudflows were observed by the observatory. Considering from video images, bottom current profiles and the results of deep-tow survey around the observatory after the earthquake in 1997, mudflows seem to be caused by the landslides of the unstable surface sediment on the slope in the west of the observatory. The subbottom temperatures increased more than 1 degree C in only several days just after the occurrence of mudflows. These seem to be caused mainly by rapid sedimentation associated with mudflows.

P16/E/10-B5

1010

#### COMPREHENSIVE DEEP SEAFLOOR MONITORING SYSTEM OFF CAPE MURATO, WESTERN JAPAN

Hiroyasu MOMMA (Ocean Engineering Department, JAMSTEC, 2-15 Natsushimacho Yokosuka 237-0061, Japan, e-mail: mommah@jamstec.go.jp)

Great submarine earthquakes at a scale of magnitude 8 (M8) occurred successively in 1944 and 1946 in the Nankai Trough off Cape Muroto and Kii Peninsula, the western region of Japan. Since similar great earthquakes have repeated at intervals between 100 and 150 years, there has been no seafloor seismic network in this area. As a step to increase the seafloor network, a comprehensive deep seafloor monitoring system was developed by the JAMSTEC to monitor the seismic activity and deep-sea environment in the Nankai Trough off Cape Muroto. The system consists of observatories with a cable and without cable. The cabled observatory comprises of two accelerometer type seismometers, two Tsunami pressure gauges, a multi-sensor cable-end station with video camera, CTD, current meter, etc., 125 km long optical submarine cable, and a land station at Muroto. All the data are sent and stored in real time to the land station, and they are also transmitted to JAMSTEC and Meteorological Agency of Japan. It was deployed at water depths between 1,290 meters and 3,572 meters in March 1997. The observatory without cable comprises of a multi-sensor mother station and four satellite stations. The mother station is equipped with a velocity type seismometer, a Tsunami pressure gauge, a digital camera with flash, a CTD, an electro-magnetic current meter, two heat flow temperature probes, a hydrophone and 16 pop-up buoys. The data in mother station could be monitored monthly through satellites by releasing pop-up buoys. After one year long observation, all the data in 8 GB hard disc is retrieved by recovering the station. Each satellite station comprises of a long-term velocity type digital ocean bottom seismometer (OBS) which could be recorded three -component seismic data continuously for two months. The data in 2 GB Exabyte tape could be retrieved by recovering the station. The observatory without cable finished preliminary observation in 1998 for four months at a depth around 1,400 meters. In total, five systems, similar to that off Cape Muroto, will be deployed around Japan.

P16/E/04-B5

1050

#### MONITORING THE MID-ATLANTIC RIDGE: THE MOMAR PROJECT

Pascal TARITS and the Momar Working Group (IUEM/UBO, UMR CNRS 'Domaines Océaniques', Place Nicolas Copernic, F-2980, Plouzané, France, email: tarits@univ-brest.fr)

Over the coming years, the European and international community of multidisciplinary ridge researchers is seeking to initiate a comprehensive long-term program to monitor the Mid Atlantic Ridge (MAR) near the Azores (MOMAR). This program is designed to conduct in-depth inquiries into the issues of:

How does this mid-oceanic ridge environment change with time (in terms of seismicity, volcanism, hydrothermal venting and the distribution and characteristics of biological populations)? How do these changes affect heat and chemical transfer to the overlying ocean, ecosystem development, faunal succession and biological productivity? What are the components and space/time extent of the subseafloor biosphere? What are the dominant controls on volcanism, hydrothermalism and faulting at this ridge axis, and how are these processes connected?

This program is being initiated by InterRidge, an international program for the coordination of ridge studies that has a strong European component (7 out of the 9 member countries are European). It is planned to be the most ambitious and comprehensive effort to date for the multidisciplinary monitoring of a mid-ocean ridge system. It will follow up on previous experiments carried out by American researchers in the Pacific (mainly on the Juan de Fuca ridge) and by Japanese researchers on the East Pacific Rise. The program will extend the scope of these experiments beyond the monitoring of individual volcanoes or vent sites, to integrated monitoring of all axial processes in the studied region.

The MOMAR project will include the deployment in the Azores region of a variety of monitoring tools, some of which have been successfully deployed in the past, while some will need to be specifically designed. Efforts will be made to involve engineering specialists from industry backgrounds in the development of these tools, and to publicise their potential for monitoring other active underwater environments. The use of submarine cables and moored buoys to transmit data and provide the energy necessary to work these tools are also envisioned as part of the project and will require co-ordinated technological efforts on the part of the participating countries.

P16/W/03-B5

1110

#### NEPTUNE: A FIBER OPTIC TELESCOPE TO INNER SPACE

A.D. CHAVE (Woods Hole Oceanographic Institution, Woods Hole, MA 02543, USA; e-mail: alan@whoi.edu), J.R. Delaney (University of Washington, Seattle, WA 98195, USA)

Investigation of the Earth as a dynamic system will require new intellectual approaches in the ocean sciences. We submit that it will also require a co-ordinated investment in a new mode of conducting oceanographic investigations through the establishment of long-term (i.e., "permanent") observatories on the seafloor. To effectively model the complex interactions involved in ocean systems, a submarine presence must be used which returns four-dimensional (three spatial dimensions plus time) data sets from multiple arrays of physical, chemical, and biological sensors deployed specifically to characterise the covariant nonlinear behaviour of the major planetary systems. North East Pacific Time-integrated Undersea Networked Experiments (NEPTUNE) is a concept for a series of interactive seafloor observatories to investigate highly active plate tectonic and oceanographic systems off the Washington-Oregon coast. This can be accomplished by establishing a series of strategically-located, state-of-the-art seafloor observatories capable of 1) real-time transmission of data and images from many hundreds of instruments, 2) routine robotic responses controlled from shore, and 3) distribution of power to the system. The single-most important technology required to achieve this capability is a fibre-optic cable system, designed to link a series of seafloor communication nodes to shore, enabling and controlling the data flow and power transmission required for comprehensive long-term observations and routine remote interventions. In fact, with such a facility, individual seafloor instruments or arrays can become virtual Internet sites from which data retrieval, instrument control, or robotic intervention may be accomplished remotely by designated shore-side users.

P16/W/04-B5

1130

#### GLOBAL MULTIDISCIPLINARY OBSERVATIONS FROM SEAFLOOR OCEAN OBSERVATORIES

Dr. John A. ORCUTT IGPP (0225) (Scripps Institution of Oceanography, La Jolla, CA 92093, USA, email: jorcutt@igpp.ucsd.edu), Dr. Adam Schultz (Institute of Theoretical Geophysics, Department of Earth Sciences, Downing Street, Cambridge, CB2 3EQ, UK)

Oceanography, in contrast to many other Earth Sciences, has advanced almost solely through expeditions which examine phenomena in a limited area over a very limited time. Technology can now support, and scientific problems demand, continuous observations on a broad range of scales in understanding the dynamics involved in global processes in addition to the traditional approach of exploration. For example, the observation of change can only be accomplished by such continuous observations, whether a change in a climate system or the eruption of sections of a mid-ocean ridge. It is essential that oceanographers pursue the development, deployment, and operation of an integrated, permanent ocean observing system for seismology, oceanography, geomagnetism, geodesy, climate and other critical



observations. Such observations will lead directly to fundamental discoveries about the physical, chemical, and biological processes that, on all time scales, determine the structure, evolution, and climate of our planet. We envision a coherent network of observatories in the oceans with data broadly available to scientists, students, commercial interests, and other individuals and organisations. While the emphasis is on long-term observations at fixed, globally-distributed locations, it is essential that shorter-term, smaller-scale studies be promoted to minimise aliasing of important phenomena. The network will include 20-30 observatories distributed globally to provide measurements of geophysical phenomena. Most of these sites are in isolated regions and near-real-time delivery of data and the supply of power require specially-designed, long-life buoys which will be serviced annually (SeaStation) or less frequently (SeaBase). The buoys designed for global observations must be used to support shorter term (2 - 4 years) regional observations with plug-in access for individual experiments. These will be complemented by autonomous stations to ensure that the variety of spatial scales which characterise all geophysical fields can be sampled. 5 - 10 additional observatories will be required for this more temporary component of the global network.

**P16/L/02-B5****1150**

#### A BENTHOPELAGIC CONTACT ZONE IN THE OCEAN PATTERNS OF THE PLANKTON DISTRIBUTION IN THE NEAR-BOTTOM LAYER

Alexander L. VERESHCHAKA (Institute of Oceanology, Moscow, Russian Academy of Sciences. E-mail: alv@ecosys.sio.rssi.ru)

During 12 biological dives in the North Atlantic (hydrothermal fields Rainbow, Broken Spur, Logachev, Norwegian Sea, off Newfoundland, depths range from 1700 m to 3800 m), methods of the planktonic visual observations have been developed. This has become possible due to the huge energetic store (1.5-2 times more than in any other submersible) which characterises "Mir" submersibles and allows illumination of the water column during many hours of observations. Emphasis has been made on the detailed observations of the plankton distribution and biology within few hundreds of meter above bottom. All planktonic animals were shown to be divided into 2 principal groups: pelagic (not related to the bottom) and benthopelagic (associated with the sea-floor, this group may be subdivided further). Each group is characterised by certain patterns of distribution, behaviour, and feeding. Near the bottom there is an area called benthopelagic contact zone, where benthopelagic animals dominate and biological processes related to the bottom define the structure and function of the near bottom communities. This zone seems to be ubiquitous in the deep ocean, and was found at all studied depths both above hydrothermal fields and background areas. The thickness of this zone depends upon various biotic and abiotic parameters (examples given), the structure of this zone may be very complex (exemplified by the Broken Spur contact zone). The concept of a benthopelagic contact zone allows more perfect understanding of the biological structure of the ocean.

**Friday 30 July PM**

Presiding Chairs: C. Fox (Pacific Marine Environmental Lab., Newport, USA); I. Nakano (Affiliation Ocean Obs.-Res. Div., JAMSTEC, Yokosuka, Japan)

**P16/E/07-B5****1400**

#### UNDERWATER CABLE OBSERVATIONS OF OCEAN VARIABILITY IN THE NORTH PACIFIC

Agusta FLOSADOTTIR (Joint Institute for Studies of the Atmosphere and Ocean, JISAO/PMEL, Box 357941, University of Washington, Seattle, WA98115, U.S.A., email: agusta@pmel.noaa.gov)

Ocean current variability is a major contributor to the large-scale voltage differences observed between points on the sea floor. An example of successful interpretation of a voltage time series in terms of ocean transport variability has been given by J.C. Larsen's ongoing time series of cross-stream voltages in the Straits of Florida on time scales from days and now approaching the inter-decadal. Until recently, the Florida Current work was the only long underwater cable voltage time series in existence. Over the last few years, however, a network of basin-scale voltage measurements has been established in the North Pacific by the groups of L.J. Lanzertotti at Lucent Technologies' Bell Laboratories and A.D. Chave at WHOI in collaboration with the group of H. Utada at Tokyo University. The two longest time series are Hawaii-California, since 1990, and Guam-Japan, since 1992. While these data have been used in applications ranging from the Earth's geophysical structure to space weather, a large part of the frequency range has been shown to be dominated by signals of oceanic origin. Oceanographic analysis, however, has so far been based on what is by now less than half of the time series. An overview will be given of the cable voltage observations in the North Pacific, and their place among other large-scale ocean observations. The full Hawaii-California time series will be presented and discussed in terms of ocean variability.

**P16/E/11-B5****1440**

#### CENTRAL EQUATORIAL PACIFIC TOMOGRAPHY EXPERIMENT: PLANS AND PRELIMINARY RESULT

Iwao NAKANO, Toshiaki Nakamura, Hidetoshi Fujimori (Japan Marine Science and Technology Center, 2-15 Natsumishima-cho, Yokosuka, Japan Email: nakanoi@jamstec.go.jp) and Bruce Howe (Applied Physics Laboratory, University of Washington, Seattle, USA, email: howe@apl.washington.edu)

JAMSTEC and APL made and started a joint program to set the acoustic tomography system to measure a shallow overturning which is thought to be related to interdecadal climate variability (Gu and Philander, Science 1997) as well as to measure the heat storage variation due to El Nino for two years (1998-2000). The acoustic tomography system was successfully deployed by the JAMSTEC tomography team in the Central Equatorial Pacific Region (0.5N to 13.6N, 177.7E to 172.1E) in early January, 1999. This system has a capability to transfer measured data for the experiment sites to the Land Station in real-time in addition to store it in the internal HDD. These transferred data is to be analyzed to reconstruct temperature and current fields in the region using the tomographic inversion. Topics at the early stage of the experiment will be presented and mentioned to the relation of El Nino.

**P16/E/06-B5****1500**

#### SIMULTANEOUS TRANSMISSION OF FIVE TRANSCIEVERS BY THE USE OF MULTIPLE M-SEQUENCES IN THE CENTRAL EQUATORIAL PACIFIC TOMOGRAPHY EXPERIMENTS

Toshiaki NAKAMURA, Tomoyuki Kanaizumi, Hidetoshi Fujimori, Iwao Nakano, (Japan Marine Science and Technology Center, Japan); Kurt Metzger (Michigan University, USA); and Bruce Howe (Applied Physics Laboratories, University of Washington, USA)

A tomography array which consists of five 200 Hz transceivers were deployed in the Central Equatorial Pacific in December 1998 and are under measurements for two years. The objective of this experiment which is an international collaborative work between JAMSTEC

and APL-UW is to Monitor the variability of water temperature and current in relation to the El Nino. In our previous experiments, each transceiver transmitted in order every 30 minutes, and the total turn-around time was 2.5 hours. In this experiment, we intend to shorten a measurement time by a simultaneous transmission of five transceivers, which improves an accuracy of measurement for water current velocity due to reduce the effects of internal waves. In this case, however, each transceiver receives an overlapped signal of other transceivers. Multiple M-sequence signals are needed to discriminate mutual signals among transceivers. Five sets of M-sequences were chosen carefully and a simulation for discrimination of the overlapped signals were conducted under the condition of the practical geometry of the five transceivers. As the result, it is expected that the signal of each transceiver can be received with the S/N ratio of over 20 dB.

**P16/E/01-B5****1520**

#### THE APPLICATION OF HIGH DATA RATE TRANSMISSION ON OCEANOGRAPHIC RESEARCH

XU Tianzeng (Department of Oceanography, Xiamen University, Xiamen, 361005, China, email: xmxu@jingxian.xmu.edu.cn)

Over the last decade, more attentions have been paid to underwater acoustic data transmission techniques. The partial reason is the increasing requirements of developing underwater vehicle, such as manned research submersibles, ROV and AUV. But the mission of high data rate transmission through underwater acoustical channel have to face a variety of serious and difficult problems arising from the channel: multipath spread, noise, fluctuation and so forth. With experiments, we have studied on some statistical characteristics of signal, multipath and noise as the theoretical foundation of signal processing in underwater acoustic channels for many years. Theoretical analyses and experimental results show that the techniques based on MFSK, together with corresponding anti-multipath, anti-fluctuation and anti-noise is an effective signal processing method suitable for high data rate transmission in the channels. Combined with the respective characters of acoustic data telemetry, digital speech communication and video image transmission, the corresponding experimental prototypes have been developed. These prototypes were tested in Xiamen harbor and got good results, for example, the video image can be transmitted omni-directionally to about 10km at the data rate of 8kbits/s by occupying 5 kHz frequency bandwidth, the speech communication can be transmitted to the same distance at 6kbits/s by occupying 4kHz bandwidth. We also developed the deep-sea transducer. For the acoustical conditions in the deep-sea are much better than in the shallow-sea, the prototypes would be used to transmit the relative signals in the deep-sea research.

**P16/E/02-B5****1600**

#### ARCTIC CLIMATE OBSERVATIONS USING UNDERWATER SOUND (ACOUS)

Peter N. MIKHALEVSKY (Science Applications International Corporation, Ocean Sciences Division, 1710 Goodridge Dr., McLean, VA 22101, USA)

Since the early 1990's it appears that inflow of warmer Atlantic Water into the Arctic Ocean increased resulting in temperature increases in the Atlantic Layer that are continuing until today. Point measurements from icebreakers in 1991 and 1993 showed temperature increases of several tenths of a degree C over historical climatologies. In 1994 acoustic transmissions were made from a site north of the Svalbard Archipelago across the entire Arctic Ocean to receiver arrays located in the Lincoln Sea and the Beaufort Sea. The travel time measurements revealed an average .4 C increase in the Atlantic Layer. This was the first basin scale measurement of this large scale warming. Since 1994 there have been annual trans-Arctic submarine cruises and one trans-Arctic icebreaker cruise that have also observed these changes. The 1999 submarine SCICEX cruise in the Arctic is likely to be the last such cruise to be undertaken for some time. A network of sources and receive arrays (the latter cabled to shore) would be able to provide year-round real-time measurements. Acoustic energy traverses the Arctic basin in approximately 30 mins. providing an integrated measurement of the Arctic Ocean temperature. Observations can be made on many acoustic paths over the Arctic on time scales unachievable by submarine, icebreaker or ice camps. Coupled atmosphere-ice-ocean modelling and analysis of recent data appear to support a decadal scale oscillation in the atmospheric and ocean circulation in the Arctic that may explain the recent warming and portend a return to cooler temperatures. The need for year-round real-time data from the Arctic is evident. A program called Arctic Climate Observations using Underwater Sound (ACOUS, from the Greek word "akous" meaning "listen!") is underway to establish an acoustic monitoring network in the Arctic. The first source and receive array were installed in Oct. 1998. Funding constraints limited the array to be autonomous, but a cabled array is being planned for installation in the spring of 2000. In addition to using the travel time measurements to obtain ocean temperature, research is underway to use the acoustic attenuation changes to measure changes in average sea ice roughness and thickness, and the use of multiple frequencies to measure the depth of the thermocline and thus the thickness of the upper mixed layer in the Arctic Ocean.

**P16/W/01-B5****1620**

#### COHERENCE OF BOTTOM AND SUB-SURFACE PRESSURES AND SEA LEVELS AROUND ANTARCTICA

PL. WOODWORTH, C.W. Hughes, M. Smithson and J.M. Vassie (Proudman Oceanographic Laboratory, Bidston Observatory, Birkenhead, Merseyside L43 7RA, UK, email: plw@pol.ac.uk) T. Whitworth (Department of Oceanography, Texas A&M University, College Station, TX 77843, USA, email: twhitworth@tamu.edu) and other US Collaborators R.M.V. Summerson (National Resource Information Centre, Canberra ACT 2600, Australia, email: rupert.summerson@brs.gov.au)

Since the late 1980s, the Proudman Oceanographic Laboratory (POL) and Texas A&M University have deployed bottom pressure recorders (BPRs) either side of, and in the middle of, the Antarctic Circumpolar Current (ACC) 'choke points' at the Drake Passage and south of South Africa and Australia. The object has been to provide information for the World Ocean Circulation Experiment (WOCE) on ACC transports for comparison to those obtained from coastal tide gauges, satellite altimetry and numerical models. This presentation shows some of the findings from the BP deployments, tide gauges and models. One significant feature observed is that large-scale coherence at the several mbar (cm) level does appear to exist between BPR sites and gauges many 1000s of kilometres apart from low frequencies (e.g. annual) to timescales of order 10 days. The data analysis is continuing, but so far the signals appear to be larger than those suggested by numerical models such as FRAM and OCCAM. Ongoing BP deployments will continue to be required beyond the WOCE observational phase, in order to acquire an extended time series of ACC transport, aided by the constant improvement in technology (e.g. via the use of air-launched 'expendable' BPRs). In addition, the availability and suitability of data from the Antarctic coastal sites (e.g. Faraday, Syowa, Mawson, Dumont d'Urville and several other sites) suggest that they might be appropriate data sources of ACC variability, although perhaps containing a greater degree of near-coastal local 'noise'. The continued development of the GLOSS tide gauge network in this part of the world is essential.

**DEPARTURES FROM THE INVERSE BAROMETER MODEL OBSERVED IN TIDE GAUGE AND ALTIMETER DATA AND IN A GLOBAL BAROTROPIC NUMERICAL MODEL**

Lucy MATHERS, Philip Woodworth (both at Proudman Oceanographic Laboratory, Bidston Observatory, Birkenhead L43 7RA, UK, email: lucy@pol.ac.uk)

The 'local inverse barometer' (LIB) model provides a simple description of the response of sea level to forcing from air pressure changes. It is widely used in oceanography as a correction to sea level data prior to ocean circulation studies. At high frequencies (periods typically less than 2 days), at very low frequencies (periods typically seasonal and longer), and in certain areas at particular timescales (e.g. in tropical areas at periods of around 5 days), the LIB model is known not to work well. In most other parts of the temporal spectrum, it is assumed to work reasonably well. In this presentation, results will be given of a worldwide search for departures from the simple LIB model using tide gauge data from about 100 sites in the global network and from the TOPEX/POSEIDON altimeter satellite. In addition, results will be presented from a coarse-grid global barotropic model (a development of the coastal tide-surge model of Flather) forced by ECMWF air pressure and wind fields. Apparent dynamical features evident in all three data sets will be discussed.

**MC02 Monday 26 – Tuesday 27 July****DETECTION AND ATTRIBUTION OF CLIMATE CHANGE (ICCL)**

Location: Mechanical Engineering, G28 LRE

Location of Posters: Old Gym

**Monday 26 July AM**

Presiding Chair: David Chapman (Dept. of Geology and Geophysics, Univ. of Utah, USA)

**MC02/W/12-B1 Invited 0900****CLIMATE CHANGE REVEALED BY SUBSURFACE TEMPERATURES: A GLOBAL PERSPECTIVE**

Henry N. POLLACK, Shaopeng Huang (Department of Geological Sciences, University of Michigan, Ann Arbor, MI 48109-1063; email: hpollack@umich.edu; shaopeng@umich.edu); Po Yu Shen (Dept. of Earth Sciences, University of Western Ontario, London, Ontario N6A 5B7, Canada, email: pys@julian.uwo.ca)

Temperature changes at the Earth's surface propagate slowly downward into the rocks beneath the surface and modify the ambient thermal regime. Thus present-day subsurface temperatures provide evidence of temperature changes that have occurred at the surface in the past, a valuable complement to instrumentally-acquired temperature data and various temperature proxies in understanding the Earth's recent surface temperature history. With support from the international heat flow community, a global database of borehole temperatures has been assembled for the special purpose of climate reconstruction. In this paper we present a global perspective of climate change over the last five centuries based on analyses of temperature measurements in more than 600 boreholes from North America, Europe, Africa, Australia, Asia, and South America. The ensemble of individual reconstructions shows that in the 20th century the average surface temperature of the Earth has increased by about 0.5 K, and that the 20th century has been the warmest century of the past five. Almost 80% of the sites experienced a net warming over the past five centuries. The mean of the cumulative temperature change over the past five centuries is a warming of about 1.0 K. Many multi-proxy reconstructions also show the 20th century to be the warmest century in their respective reconstruction time intervals. The geothermal analysis, based on direct temperature data and a methodology totally different from the multi-proxy investigations, thus provides independent confirmation of the unusual character of 20th century climate.

**MC02/W/14-B1 0930****INTEGRATIVE RECONSTRUCTION OF A GLOBAL GROUND SURFACE TEMPERATURE HISTORY FROM BOREHOLE TEMPERATURES AND OTHER PROXIES**

Shaopeng HUANG, Henry N. Pollack (Dept. of Geological Sciences, University of Michigan, Ann Arbor, MI 48109-1063, email: shaopeng@umich.edu; hpollack@umich.edu)

Paleoclimatic proxies such as tree-ring density, pollen characteristics, and ice core isotope ratios all yield projections of past climate changes. Each proxy has its own strengths and limitations in reconstructing climate history. Borehole temperatures offer yet another perspective that can be integrated with traditional proxies to yield a composite reconstruction. Because of the selective filtering of thermal diffusion, borehole temperatures record only longer term trends of climate variation at increasing depths. A ground surface temperature history derived from a conventional inversion approach is typically characterized by robust determination of a long term mean temperature, but with increasingly poorer resolution of variations towards the remote past. In this study we integrate higher resolution proxy information into the inversion of borehole temperatures for the reconstruction of a global average ground surface temperature (GST) history. This approach comprises two steps. Subsurface temperatures from more than 600 boreholes from North America, Europe, Africa, Australia, Asia, and South America were respectively preprocessed with a standardized Bayesian inversion scheme with an a priori null hypothesis. The derived transient subsurface temperature components of the individual boreholes were assembled into a single average transient temperature profile. This global average borehole temperature profile was then inverted for a GST history reconstruction. To incorporate information made available by other disciplines, we employed proxy reconstructions as the a priori hypotheses in the second phase inversion. The second step inversion embeds the high resolution proxy reconstructions into the longer term trends determined from subsurface temperatures. The proxy reconstructions complement the borehole data with high frequency information and bridge the gaps due to sparse or missing data. Results show a general increase of about 1K in the GST over the last five centuries, with an increasingly strong warming trend in the 20th century.

**MC02/E/10-B1 0950****BOREHOLE TEMPERATURES, CLIMATE CHANGE AND LAND DEVELOPMENT: EVIDENCE FROM CUBA**

V. CERMAK, J. Safanda (Geoph. Inst., Czech Acad.Sci., 141-31 Praha, Czech Rep., email: cermak@ig.cas.cz); L Bodri (Geoph. Dept., Hung. Acad. Sci., 1083 Budapest, Hungary, email: bodri@gis.elte.hu)

Inversion of borehole temperatures to reconstruct ground surface temperature (GST) history is a good method to obtain both the long-term average GST and variations in the past GST at a site. To interpret the results in terms of climate change, the knowledge of the relation between the GST and the surface air temperature (SAT) is essential. Several researchers demonstrated that inverted GST history might comprise an apparent component reflecting temporal variations in land (vegetation) cover. Anomalous curvature observed in the uppermost 200-250 m of the measured T(z)-profiles in more than 30 boreholes in Cuba indicated a pronounced change in the past GST conditions. The calculated magnitude of the apparent recent warming revealed values as high as 5-8 K, which cannot be attributed to the natural climate variability. It was demonstrated that land cultivation may have contributed to the effective increase of the GST due to deforestation and consequent land exposure to solar radiation. The resulting GST change may thus by far surpassed the proper climate effect. To estimate the "vegetation correction" which is closely related to GST-SAT coupling, the measured T(z) data were first "corrected" by forward application of the long-term meteorological record of the mean annual air-temperatures in the Caribbean area.

**MC02/E/07-B1 1010****ANALYSIS OF BOREHOLE TEMPERATURE RECORDS FOR GROUND TEMPERATURE HISTORY: FIRST RESULTS FROM INDIA**

Roy SUKANTA, R. U. M. Rao (National Geophysical Research Institute, PO Bag 724, Uppal Road, Hyderabad 500 007, India, email: postmast@csnrg.ren.nic.in)

Surface air temperature (SAT) changes can cause concomitant changes in ground temperature which diffuse downward by conduction causing a systematic perturbation to the subsurface temperature field generally in the top 100-150 m. Therefore the present day borehole temperature records hold a Ground Temperature History (GTH). A set of sixteen carefully selected borehole temperature records, covering different parts of India and a depth range of 150 to 700 m, have been analysed for GTH. A simple linear increase in surface temperature, D, that started t years ago, was found to provide excellent fits to the ground warming related anomalies in all the temperature profiles. The D values range 1 to 2.5 Celcius degrees and t values, generally 50 to 150 years, and in a few cases 200 to 250 years. The trends are consistent with the long term trends of SAT increases from the Indian meteorological records. No spatial variation pattern could, however, be gleaned because of the limited data set. A more detailed coverage, with good number of properly sited boreholes would yield an improved picture. These results, the first from low latitudes (12-28 deg N) are in consonance with the trends in GTH delineated in higher latitudes, North America and Europe. Signals of cooling immediately preceding the recent warming found in Eastern Canada are however not observable in the present records.

Presiding Chair: Henry Pollack (Dept. of Geological Sciences, University of Michigan, USA)

**MC02/E/08-B1 Invited 1100****QUANTIFICATION OF NATURAL CLIMATE VARIABILITY IN CENTRAL GREENLAND AND EAST ANTARCTICA USING BOREHOLE PALEOTHERMOMETRY**

Gary D. CLOW (U.S. Geological Survey, Climate History Program, Denver Federal Center, Box 25046, MS980, Denver, CO 80225, USA; email: clow@usgs.gov); Edwin D. Waddington (Univ. of Washington, Geophysics Program, Box 351650, Seattle, WA 98195, USA; email: edw@geophys.washington.edu)

The most accurate way to determine the magnitude of past temperature changes in polar regions is through "borehole paleothermometry" in the ice sheets. We have used this technique to quantify the magnitude of natural climate variability during the Holocene at two locations: 1) GISP2 - central Greenland, 2) Taylor Dome - East Antarctica. At GISP2, there was a general decline in temperatures during the Holocene that parallels the drop in summer insolation at this latitude. The decline was weak from 10 ka to the mid-Holocene Optimum (MHO) at 4 ka. Temperatures then dropped 2 K from the MHO into the Little Ice Age (LIA). This cooling was briefly interrupted by a 0.5 K warming during the Medieval Warm Period (MWP) at 1 ka. Temperatures in central Greenland are currently 1.3 K colder than during the MHO and 0.4 K colder than during the MWP. At Taylor Dome, there too was a general decline in temperatures following the MHO. However, rather than experiencing the MWP at 1 ka, temperatures reached their coldest value of the last 4 kyr. During the "LIA", the Taylor Dome region experienced a dramatic 2 K warming. Thus, temperature changes on the multi-hundred year timescale during the MWP and LIA were anti-correlated in Greenland and the Taylor Dome sector of Antarctica.

This may be related to changes in the oceanic "conveyor" system. Within the context of Holocene natural climate variability, current temperatures in Greenland are not unusual while those at Taylor Dome are unusually warm.

**MC02/E/19-B1 1130****BOREHOLE TEMPERATURES, METEOROLOGICAL DATA AND CLIMATE CHANGE**

David S. CHAPMAN, Scott N. Putnam (Dept. of Geology and Geophysics, Univ. of Utah, Salt Lake City, UT 84112, USA, email: dchapman@mines.utah.edu); Robert N. Harris (RSMAS, Univ. of Miami, Miami FL 33143, USA)

The seminal analysis of borehole temperatures on the north coast of Alaska (Lachenbruch and Marshall, Science, 234, 1986) had two significant impacts. The study alerted us to 2-5 oC of surface warming in this century at high latitudes. An the detailed description of using temperature-depth profiles in boreholes to study global warming prompted many geothermal laboratories into serious study of the geothermics of climate change. At Utah we concentrated our efforts on understanding the geothermal signal of climate change in low latitudes where the global warming signal is predicted to be small, on combining ground and air temperature records at the regional scale, and, at the local scale on establishing a geothermal climate-change observatory. Our work allows the following conclusions and observations: 1. Six borehole sites in northwest Utah in homogeneous granite yield warming trends about 0.3 oC at the century time scale. Variability in the borehole results is comparable to variability in local surface air temperatures (SAT) warming trends. 2. Eight borehole sites in southeast Utah, in the layered sedimentary rocks of the Colorado Plateau, yield warming of 0.6 oC over the past 200 years, less than warming computed from 100-year SAT records. 3. Synthetic temperature-depth profiles computed in remarkable detail the temperature profiles at nearby borehole sites. 4. Weather station temperature records can be combined with borehole temperature logs to estimate mean surface air temperatures prior to the instrumental SATs. This 19th century baseline temperature in Utah is 0.6+-0.1 oC below the 1951-1970 mean temperature for the region. 5. Our Emigrant Pass Observatory has been operated for 4 years and has produced a wealth of meteorological data acquired simultaneously with subsurface temperature data. Ground and air temperature track each other but with important time-varying offsets.

**MC02/E/11-B1 1150****INVERSION OF BOREHOLE THERMAL DATA: NINETEENTH CENTURY WARMING IN CENTRAL CANADA CAUSED BY LAND DEVELOPMENT**

Trevor LEWIS (Sidney Geophysical Consultants Ltd. and Geological Survey of Canada, Sidney, B.C. V8L 4B2, Canada)

Borehole temperatures within the conductive regime of the solid earth to depths of hundreds of metres often reflect a constant heat flow from below on which are superimposed temperature anomalies propagating downward from the surface of the earth. Such data can be inverted to obtain past temperatures at the top of the conductive zone, called here the ground surface temperature (GST). This boundary may be cms or metres below the actual ground-air interface. Analyses of such data show that 1-3 K increases of the past GST occur at the times of local deforestation at many, differing sites. The amount of heat formerly required for transpiration is approximately the amount required for this warming, and reduction in the evaporated water mainly increases summer temperatures. The water no longer transpired increases the runoff. In colder climates where there is seasonally frozen ground but no permafrost, the latent heat of ground moisture in the top several cms of the overburden buffers the underlying bedrock from freezing temperatures, causing average GSTs to be warmer than the average air temperatures. The GST is limited to following only changes in the air temperature above freezing and never goes below freezing. However, the effects of deforestation are undiminished in these climates. The widely observed regional warming of the GST in southern and central Ontario correlates with the period of deforestation and is attributed to the creation of farmlands in the nineteenth century. Warming is to be expected wherever the ground cover is decreased, or has been decreased in the past.



MC02/E/22-B1

1210

## COMPARISON OF SOIL TEMPERATURE DATA DERIVED FROM BOREHOLE OBSERVATIONS WITH METEOROLOGICAL RECORDS

Serban VELICIU (Geological Institute of Romania, Caransebes 1; 78344 Bucharest, Romania, email: veliciu@igr.sfos.ro)

Comparison of surface temperature change estimated from borehole temperature profiles and observed surface air temperature and precipitation time series for periods in which the three signals overlap can strengthen the confidence in geothermal method for climatic reconstruction. To illustrate this will draw an example from the north Danube Plain, Romania, geographically located near the north 45 lat., where the meteorological records of temperature change against temperature-depth measurements have previously been interpreted in terms of temporal variations of ground surface temperature for the last two centuries. In order to quantify correlations of meteorological and geothermal data, the earth's response to surface air temperature as recorded in the nearby weather stations, has been modelled using the finite element method. For the weather stations from the Danube Plain the meteorological records indicate an average rise of temperature over the time interval 1850-1995, showing the century-long trend of +0.22 to +0.84 deg. C, determined by the least-square regression. This is also exhibited by the reconstructed ground surface temperature history deduced from temperature measurements in the wells. The inverse method used for the geothermal data set for Romania was based on the simple theory of 1-D heat conduction using the least square computing technique. The employed parametrisation scheme constrains the ground surface temperature history to a few changes. The ground surface temperature fluctuations for the considered time period do not generally exceed +2 or +3 deg. C and the quality of the measured temperature logs permitted to resolve not more than 2-3 climatic events.

The results from the measurements in the studied boreholes could be suspicious not because they indicate warming, but because the amplitude of warming that they indicate, as compared with the meteorological records. The suspicion concerns the question whether the perturbations observed in the boreholes are only climatic. However, direct comparison of the borehole temperature profiles and surface air temperature records is not possible for two main reasons: first, ground temperature is generally warmer than air temperature by 1-5 deg. C, second, changes in the earth's surface temperature are filtered and attenuated in the earth's surface by the process of heat conduction.

Monday 26 July PM

Presiding Chair: Phil Jones (Climatic Research Unit, Univ. of East Anglia, UK)

MC02/E/17-B1

Invited

1400

## UPDATE ON THE USE OF TEMPERATURE RESPONSE TO SEQUENCES OF VOLCANIC ERUPTIONS TO DETERMINE CLIMATE SENSITIVITY

Richard S. LINDZEN (54-1720, MIT, Cambridge, MA 02139, USA); Constantine Giannitsis

A detailed consideration of the greenhouse effect permits a convenient determination of the ratio of surface flux changes relative to top-of-atmosphere changes associated with changes in atmospheric carbon dioxide. This has, in turn, permitted us to properly calibrate the recent attempt by Lindzen and Giannitsis to determine climate sensitivity on the basis of the observed temperature response to a sequence of volcanic eruptions. We have, furthermore developed a simple statistical analysis to ascertain the significance of the distinction between various sensitivities determined by this method.

MC02/W/05-B1

1430

## IS THERE A SOLAR SIGNAL IN RECENT VARIATIONS IN GLOBAL CLOUDINESS AND CLOUD RADIATIVE FORCING?

Jon Egill KRISTJÁNSSON, Jørn Kristiansen (University of Oslo, Norway)

We have explored the possibility of a link between solar activity (via cosmic rays), cloudiness and climate, recently proposed as a factor in explaining global warming. Multi-year datasets of cloud cover from ISCCP- and DMSP-based satellite estimates have been investigated, as well as ERBE estimates of cloud radiative "forcing".

Comparing cosmic ray flux and global cloud cover from ISCCP we find a good correlation between 1986 and 1990, but between 1990 and 1993 the correlation is lower. A similar result is found when data over land as well as over the tropical regions are excluded. Those areas would be expected to be the least sensitive to an extra-terrestrial source of CCN, if this were to exist. The correlation between cosmic ray flux and DMSP cloud cover for the period 1987-1998 is even lower than when ISCCP data are used, but it should be noted that those data only cover water clouds. Furthermore, there does not appear to be any simple relationship between the cloud coverage and the radiative impact of clouds. This is probably due to year-to-year variations in cloud height and in the spatial distribution of clouds.

Our findings seem to undermine the alleged relationship between solar activity and climate through the proposed effect on cloud cover. The implication seems to be that other factors, e.g., El Niño or natural variability, play a larger role in determining year-to-year variations in cloudiness and cloud radiative forcing than any potential cosmic ray forcing.

MC02/E/23-B1

1450

## EMPIRICAL ESTIMATES OF CLOUD EFFECTS ON THE NEAR-SURFACE AIR TEMPERATURE: COMPARISON WITH GCMs

Pavel Ya. GROISMAN (ICAR Project Scientist, National Climatic Data Center, Ashville, North Carolina, USA); Bomin Sun, Raymond S. Bradley, Frank Keimig (Dept. of Geosciences, University of Massachusetts, Amherst, MA, USA)

Using synoptic data for the past several decades over the Northern Hemisphere and tropics we estimate a normalised overall cloud effect on temperature, NOCET, as a sensitivity of near-surface air temperature, T, to the presence of cloud cover, CL, (NOCET = dT/dCL) and parameterise this derivative as a function of atmospheric humidity and snow cover. In humid tropics the effects of humidity and snow cover on NOCET vanish and asymptotic values of NOCET become spatially and seasonally unvarying an equal approximately -0.75 K/(tenth of cloud cover) for daytime and -0.2 K/(tenth of cloud cover) at night. Clouds are an internal component of the climatic system and "forcing" is not a proper term in describing their effects on the system. But this terminology is commonly used, and, using the terminology, we produced empirical estimates of cloud cover "forcing" of the present climate system.

We believe that it is important for GCMs (used in climate sensitivity studies, e.g., for contemporary and future climate change analyses), to properly reproduce the interaction (internal relationships) in the contemporary climatic system among cloud, snow cover, and near-surface humidity and temperature. Geographical patterns and time series of NOCET will be discussed and compared to similar estimates derived from several GCM simulations. The results indicate that a proper estimation of the sensitivity of surface air temperature to cloud cover is still a challenge to most of the GCMs tested. This impedes the accuracy of climate change assessments based on these models

MC02/W/07-B1

1510

## PROXY AND MODEL-BASED ANALYSIS OF PATTERNS OF TEMPERATURE ASSOCIATED WITH SOLAR IRRADIANCE OVER THE LAST SEVERAL CENTURIES

Anne M. WAPLE, Michael E. Mann, Raymond S. Bradley (Department of Geosciences, University of Massachusetts, Amherst, MA, 0100359; email: awaple@geo.umass.edu, mann@snow.geo.umass.edu, rbradley@geo.umass.edu)

The multi-proxy temperature reconstruction of Mann et al. (1998) and irradiance reconstruction of Lean et al. (1995) as well as climate model data have been used to assess the degree to which characteristic spatial temperature patterns exist as a result of changes in solar irradiance over the last several centuries. The last 300-400 years contains the Maunder minimum as well as the Dalton Minimum and a period of relatively higher irradiance for comparison with the surface temperature. A band of tropical warmth in runs of a solar-forced coupled model (Cubasch et al. 1997) is corroborated by a positive correlation between irradiance and tropical Atlantic SSTs in the proxy reconstruction. However, much higher significant positive correlation exists in SE Asia and the western Pacific. This is despite high interannual variability in the region which matches well with reconstructed El Niño events identified by Quinn and Neal (1987). The high correlation in this area with irradiance forcing is in accordance with arguments suggesting a positive feedback mechanism in the western Pacific (Clement et al.1996) and this feedback is a phenomenon not adequately represented in the GCMs. In contrast, higher latitude Pacific temperatures show no coherence at all.

A land-sea contrast is an important feature in the correlation of irradiance and the proxy reconstruction. While Cubasch et al. (1997) also determine that a land-sea contrast is one of the major 'fingerprints' of a solar as well as the greenhouse gas signal, they find a 10-year lag provides the optimum response over most regions, however a 25-30-year lag is more appropriate over the ocean. We find that a 30-year lag provides the best correlation in many areas of the globe; a notable exception being the northern North Atlantic which has higher correlation at a 15-year lag. These patterns are also examined in the coarser solar-forced GISS atmospheric GCM of Rind and Lean (1998) which does not display the land-sea contrast evident in the coupled model. The correlation is more consistently positive over the globe and there is also a band of high correlation between irradiance and temperature in the tropics.

Presiding Chair: Phil Jones (Climatic Research Unit, University of East Anglia, Norwich, UK)

MC02/W/10-B1

Poster

1600-01

## A MULTICENTURY CORAL GROWTH RECORD FROM FRENCH POLYNESIA: INTERANNUAL AND DECADEAL SEA SURFACE TEMPERATURE AND SOLAR ACTIVITY VARIABILITY IN THE SOUTH CENTRAL PACIFIC

Frederic BESSAT (University of Sorbonne, 191 Rue St-Jacques 75 000 Paris, France, email: Frederic.Bessat@paris4.sorbonne.fr)

Since 25 years, annual density banding patterns in massive coral skeletons have promised to be the key to a wealth of proxy climate information for ocean areas in the tropics. Living corals promise information covering the past several centuries with annual or better resolution. This paper present coral research designed to develop a multi-proxy approach to coral-based paleoclimatology. A new understanding and measurements (by computerized tomography) of coral growth has led to a refined 190 years record of calcification in massive coral from Moorea Island (17°30' S, 149°50' W, French Polynesia). Time series analysis (MTM analysis) of the coral density banding records reveals a concentration of variance at El Niño-Southern Oscillation (3-6 years) frequency bands. In addition, interdecadal spectral peaks are notable; 9.5 - 11.5 and 21.9 years peaks are found. These and others (stable isotope record) results indicate that the French Polynesia coral record is a valuable source of information on south central Pacific climate history.

MC02/E/13-B1

Poster

1600-02

## THE NATURAL CLIMATE CHANGE DUE TO THE ACTIVITY OF GEOSPHERE

Xiaoqing GAO, Maocang Tang(both in Lanzhou Institute of Plateau Atmospheric Physics, Chinese Academy of Sciences, Lanzhou 730000, P.R.China, email: xgao@lzu.edu.cn)

Over the past few decades, the most important advance in the earth sciences has been the development of the concept of a system: of a climate system and of an earth system. These concepts mark milestones toward the achievement of an adequate methodology for our discipline. It has now come to be realized that climate change can be deeply influenced by the lithosphere as well as hydrosphere, the biosphere, and human activity, by ways of interaction(mass and energy fluctuations) at the boundaries of these spheres. But, the causal connections of interactions among these spheres remain poorly understood.

In this paper, the focus is on the influence of geothermal heat flux anomaly on climate change. The soil temperature at different depths (0.00m, 0.05m, 0.10m, 0.20m, 0.40m, 0.80m, 1.6m, and 3.2m) has been observed in more than 180 observatories in China, now. It is found that the heat flux anomaly is of a stable persistence, and has a good relationship with short term precipitation anomaly. It is meaningful for climate prediction.

MC02/E/03-B1

Poster

1600-03

## TRENDS IN 500 HPA WINDS OVER ESTONIA

Sirje KEEVALLIK (Tartu Observatory, 61602 Toravere, Estonia)

It is widely recognised that changes have taken place in frequencies of different circulation patterns in Europe during recent decades. The aim of the present paper is to find out if respective changes can be noticed also in the 500 hpa wind components above Estonia. For this purpose, data on wind direction and velocity have been drawn from vertical soundings at Tallinn aerological station. Situations in January and July have been analysed during a 30-year period of 1961- 1990. It can be said that in

MC02/W/08-B1

Poster

1600-04

## AIR-GROUND TEMPERATURE TRACKING IN NORTH DAKOTA

William SCHMIDT (Univ. of North Dakota, Dept. of Geology and Geological Engineering, PO Box 8358, Grand Forks, ND 58202-8358, USA, email: wischmid@badlands.nodak.edu)

Understanding the long-term tracking of air and ground surface temperatures is necessary for any borehole paleoclimate study, particularly in regions of snow cover and ground freezing. The duration of the surface air temperature record is insufficient to determine if observed global warming is due to anthropogenic effects or natural climatic fluctuations. The geothermal record enables better spatial and longer temporal resolution of climate change. Several borehole

climate change studies have demonstrated warming in North America in the past five centuries. However, most published results have been based on the assumption of consistent and uniform tracking of air and ground temperatures. This assumption may be valid in some cases, but it is likely that parameters in the soil that affect energy transfer undergo seasonal or decade scale variations. Secular variations in these parameters produce regional discrepancies in climate change magnitudes as determined by borehole records and recorded surface air temperatures. We examined a data set recorded between October 1980 and April 1990 at Fargo, North Dakota. Standard climatic variables, as well as 21 subsurface values ranging in depth from 1 cm to 1170 cm, were recorded. The heat flow at the site is completely conductive, with no non-climatic effects present. A 2-D numerical conduction model produced temperatures within  $\pm 0.2$  K of observed temperatures below 1 m depth. The two main factors causing winter divergence of air and subsurface temperatures are insulation due to snow cover and latent energy due to soil moisture freezing. Latent energy holds the ground temperatures at freezing until all the water present has frozen. The extent of this warming effect is dependent on volumetric moisture content at the onset of ground freezing. Volumetric heat production in the model simulates latent energy due to ground freezing and thawing. Modelled annual heat production values during ground freezing show a correlation ( $r^2 = .61$ ) with total precipitation 3 months prior to ground freezing. Decade-scale warming in the upper few centimeters of the ground surface is due to an increase in the number of days with snow cover. January the frequency of the westerlies has increased and the frequency of the easterlies decreased. A general increase in the wind velocity can be noticed. In July main changes are associated with meridional winds: the frequency of the northerlies has increased and that of the southerlies decreased. Wind velocity has increased for the easterlies and southerlies and decreased for the westerlies. These tendencies have been analysed from the point of view of the European circulation patterns (Grosswetterlagen) - a synoptic-climatological classification of surface and upper-air pressure patterns elaborated in 1944 by F. Baur, P. Hess, and H. Nagel.

**MC02/E/06-B1** Poster **1600-05**

#### PECULIARITIES OF CLIMATIC IMPACT OF THE ORBITAL FORCING IN VARIOUS GEOLOGICAL PERIODS

V. A. BOL'SHAKOV (Geographical Dept., Moscow State University, 119899, Moscow, Russia)

It is known that periodicities of orbital elements variations (OEV) were nearly constant during the Mesozoic and Cenozoic. However, climatic influence of the orbital forcing varied from one geological period to another. OEV determined the rhythm of glaciations and deglaciations in the Quaternary. Periodicity in lake-level cycles connected with OEV was discovered in Late Triassic sediments. It should be noted that relative importance of the various orbital parameters in controlling climate has varied through geologic time. Precessional cycle (nearly 23 Kyr.) was detected primarily in warm periods of the Earth's geological history such as Miocene and Late Triassic. Climatic influence of the eccentricity cycle (about 100 Kyr.) was predominant in the Upper Pleistocene according to oxygen isotope data. The obliquity cycle (nearly 41 Kyr.) was the most important in the Lower Pleistocene. These data allow us to conclude that climatic impact of the orbital forcing depends not only upon orbital elements variations peculiarities but also upon terrestrial factors and possibly some other cosmic factors.

**MC02/W/04-B1** Poster **1600-06**

#### DIABATIC AND ADIABATIC CONTRIBUTIONS TO THE DYNAMICALLY INDUCED CLIMATE OSCILLATIONS

Roman BELKRYAEV (Arctic and Antarctic Research Institute, 38 Bering str., 199397, St.-Petersburg, Russia, email: bekryaev@aari.nw.ru)

Global air surface temperature is one of the most important indices of climate variations. The typical point of view connects variations of the global mean air surface temperature with the fluctuations of the heat fluxes only. Diabatic heating or cooling (connected, for example, with changes in planetary albedo, cloudiness or heat fluxes from the ocean) are the most important causes of such variability. However, more than half of the extra-tropical mean air surface temperature variability is dynamically contributed and can be associated with the COWL (Cold Ocean Warm Land) structures (Wallace et al., 1995), NAO indices (Hurrell, 1996) or Arctic Oscillations (Wallace, 1998). Particularly, warm winters in the Northern Hemisphere are associated with the warm air anomaly over the continents and cold air anomaly over the ocean (and vice versa). Typical explanation is the following: the heat capacity of the underlying surface has a major influence in amplifying surface temperature changes over land while moderating them over the ocean. Strong variability of the large-scale atmospheric circulation and some other circumstances allow the hypothesis that an additional mechanism of global air surface temperature fluctuation exists. We suggest that short-term variations of the global surface air temperature may be partly a result of adiabatic vertical mixing. For the purpose of research a run of a global atmospheric model, T10-L14 (Main Geophysical Observatory, St.-Petersburg, Russia) in the regime of perpetual January for 200 years' was carried out. An additional set of numerical 14-year runs with the T30-L14 MGO model, using annual cycle of incoming solar radiation and the sea surface temperature, has also been performed. Using Wallace et al's (1995) method of analysis and the results of the long-term MGO model integration, we have revealed the structures of the temperature field at the AT-1000 level, and outgoing long-wave radiation fields at the top boundary of the atmosphere. Using monthly data, we have demonstrated the so-called COWL structures (Wallace 1995, 1996) in the temperature field; these are well correlated with the global mean air surface temperature ( $r=0.8$  for daily and  $r=0.7$  for monthly averaged data). We have found very strong negative correlation ( $r=-0.9$ ) between the indices of the COWL pattern and eddy available potential energy in the low troposphere. These results allow us to suggest that at least part of the short-term air surface temperature variations can be...

**MC02/E/20-B1** Poster **1600-07**

#### EXTREME TEMPERATURES OVER ARGENTINA. ENSO AS A CLIMATIC VARIABILITY FACTOR

Matilde RUSTICUCCI, Walter Vargas (Detp. De Cs. De la Atmosfera, Universidad de Buenos Aires, 1428 Buenos Aires, Argentina, email: mati@at1.fcen.uba.ar)

The relevance of ENSO phases on temperature extreme situations in Argentina is presented here. Warm and cold spells of Maximum and Minimum daily temperatures are analysed from 40-year station data series in 24 stations covering all climatic zones, using the third quartile of each distribution of persistence and intensity to compare extreme situations. Each month was classified as extremely warm, cold or normal or El Niño, La Niña or Neutral. Cold spells are more persistent in northern Argentina with an autumn maximum. The maximum values persist from autumn to summer, only in the northeast. In general, maximum intensity values occurred in winter in the northern regions, and during the summer in central-southern Argentina, the exception being cases of extreme cold winters having extremely cold waves, in the south. Over the Andes Mountains, intensity values present a minimum. The third Quartile persistence values are between 3-5 days in a normal year, reaching 11 days in a cold year and between

2 and 4 in a warm one. This appears to be the key parameter to classify a month as warm or cold. Data from Northern Argentina present a more significant ENSO signal. In the south there is no significant difference between phases. In central Argentina, cold winter spells are more significant during La Niña. In spring, these waves are more persistent and intense than a normal year, and in some regions even than a cold one. In Winter both parameters are similar to those of a cold year, except in the south, where a cold summer is not explained by any of the ENSO phases. The relationship Niño-warm/Niño-cold is clearest in Northern Argentina, with the strongest Niña signal present in the spring. In general, the effects of El Niño or closer to give a normal month than a Neutral does. The third quartile values are lower when the data are classified according to ENSO phases than in warm / cold / normal cases, so the effect of ENSO phase differences on temperature regime is lower than the extreme climatic differences. Warm waves are more persistent but equally intense than cold ones. The ENSO effect is also highest over the northern regions, presenting largest values in winter, in opposite phase with the south, a characteristic also exhibited by cold waves. El Niño events bring more intense and persistent warm waves in the north, and more regionally homogeneous than La Niña ones. An extremely warm summer has more intense and persistent warm waves than any ENSO phase, while El Niño could better explain a warm winter in the north.

**MC02/E/05-B1** Poster **1600-08**

#### MILANKOVITCH THEORY: NEW CONCEPT

V.A. BOL'SHAKOV (Geographical Dept., Moscow State University, 119899, Moscow, Russia); P.V. Bol'shakov (NBZ Community, Olimpiyskiy pr., 30, 129272, Moscow, Russia)

The recent version of the astronomical theory of paleoclimate (ATP) - Milankovitch theory (MT) - meet some problems which retard further development of this theory and its practical applications. The main of them are the followings. 1. Discrepancy between the quantity and dates of glaciations according to Milankovitch diagram and OI data. 2. Period about 100 kyr. is of prevailing significance in OI records during the past million years. However, precisely this period correlated with variations of eccentricity is absent in the Milankovitch theory. 3. Glacial (even) OI stages coincides with the intervals of low eccentricity values. MT can not explain this fact too.

The analysis of MT, deep-sea oxygen isotope records, solar activity variations and its correlation with climate change allows us to propose the new concept of MT. "Insolation-climatic" (IC) diagram was constructed according to this new concept. IC diagram has a good visual correlation with OI data for the last million years. So this new view on MT provides more full and direct confirmation of climate orbital forcing because our concept implies the climatic influence of all three orbital elements (including eccentricity) and it gives the opportunity of direct correlation of IC and OI graphs. Our new concept contains simple and real solving of the 100-kyr cycle problem.

**MC02/E/24-B1** Poster **1600-09**

#### SEASON'S PENDULATION AND CLIMATIC JUMPS

Ionel HAIDU (University "Babes-Bolyai", 1 Kogalniceanu Str., 3400 Cluj-Napoca, Romania, email: haidu@bioge.ubbcluj.ro)

This paper examines the hypothesis of season's pendulation at an interannual time scale and its statistical links with the climatic jumps. The work is done on observed time series of precipitation totals and mean surface air temperature, and on some derived time series. Several stations in Europe, representative positionally, were taken into account having more than 100 years of observations. The maximum and minimum season has been defined upon quantitative criteria. As consequence, both, the extreme seasons has no constant position within the year. Thus, the series of moments of occurring of maximum / minimum season within every year has been defined. Also, the time series of amplitudes between the extreme seasons has been considered. Abrupt changes and jumps in the annual and seasonal variations of precipitation total and mean surface air temperature were investigated using the Iwashima method. The jumps and the changes of the mean show a relative synchronism and have a regional character. Significant jumps or changes of the mean are to be noticed in the periods: 1800-1830, 1840-1860, 1870-1900, 1910-1930, around 1950 and 1980. From a statistical point of view, there are links between the season's pendulation, local trend and the climatic jumps. Some of the maximum season's pendulation seem to time correlated with some major volcanic eruptions.

**MC02/E/21-B1** Poster **1600-10**

#### GEOHERMAL EVIDENCE OF RECENT WARMING IN THE URALS

Dmitry DEMEZHKO (Institute of Geophysics, Ural Branch of Russian Academy of Science, 100 Amundsen Str., 620016 Ekaterinburg, Russia, email: ddem@igeoph.mplik.ru)

Ground temperature changes, associated with climate changes, disturb the stationary underground temperature field. Thus borehole temperature measurements performed at present contain information about ground surface temperature (GST) changes in the past. 66 temperature-depth profiles recorded in the Urals (50-61° E Long) were investigated with the aim to reconstruct GST history. The mean GST history curve shows a cold period with temperature minimum in the 17-18 centuries followed by a fast warming in the 19th century (at the rate of 0.8-1.5K/100 years) and a moderate warming in the first 70 years of the 20th century (at the rate of 0.4K/100 years). The latest GST rising rate is lower than that for surface air temperature in the same period (0.8K/100 years) derived from meteorological data. Also some non-uniform spatial distribution of recent GST rising rate was noticed. It varies from about 0.5-0.9K/100 years in the southern one, and it appears no rising in the northern part. It is assumed that GST changes in the Urals are determined by a combined influence of surface air temperature changes and snow cover height oscillation. Statistical relationship between mean annual soil-air temperature difference and snow cover height has been established. Decrease in snow height about 10 cm may cause GST decrease about 0.6-0.7 K at stable air temperature.

**MC02/E/12-B1** Poster **1600-11**

#### LONGWAVE RADIATION IN THE SWISS ALPS

CH. MARTY(1), R. Philipona(1), C. Frohlich(1), A. Ohmura(2) ((1)Physikalisch-Meteorologisches Observatorium Davos, World Radiation Center, PMOD/WRC, CH-7260 Davos, Switzerland; (2)Institute of Geography, ETH, CH-8057 Zurich, Switzerland)

Monitoring of longwave downward radiation is one possibility to determine the effect of increasing greenhouse gases. A total of eleven stations between 400 and 3600m a.s.l. in the Swiss Alps are measuring short- and longwave radiation. The 4 years of data show the dependence on elevation, which is mainly due to water vapor content. Together with the shortwave measurement, information about the cloud forcing and its change with altitude is extracted.

**MC02/E/01-B1** Poster **1600-12**

**ANOMALY METHOD FOR SELECTION OF THE GLOBAL, REGIONAL AND LOCAL CLIMATE**

Tarzadin ULAANBAATAR (Department of Earth Sciences, National University of Mongolia, email: numelect@maginnet.mn)

The detailed and realistic maps of climate zones of the Earth must be prepared by mathematical selection of the global, regional and local climate. Present geographical, climate maps are shown the integrated impact of the geospheres, geographical objects and Sun on the weather. But climate is a whole hierarchy of complexity of global, regional and local climate regime. A best way of the theoretical description of successful prediction, realization, mitigation, rehabilitation strategies of climate change is to select it in global, regional and local scale. In aspect of this goal, I endeavoured to create a mathematically adopted unswerving climate model, which is necessary to play key role for theoretical standard climate regime and to be fundamental background for selection of the climate change in regional and local scale. In this paper, based on a new climate model, so-called anomaly method of their selection is presented.

**MC02/E/15-B1** Poster **1600-13**

**PALEOCLIMATIC SIGNALS FROM TRANSYLVANIAN TEMPERATURE LOGS**

Delia Zemira SERBAN (Institute of Geodynamics, 19-21 J.L. Calderon Str., R-70201, Bucharest, Romania, email: delias@geodin.ro); Soren Bom Nielsen (Department of Earth Sciences, Geophysical Laboratory, The University of Aarhus, Finlandsvej 8, DK-8200 Aarhus N, Denmark, email: geofsb@au.dk); Crisan Demetrescu (Institute of Geodynamics, 19-21 J.L. Calderon Str., R-70201, Bucharest, Romania, email: crisan@geodin.ro)

Continuous temperature logs to depths of 1400 m in the Transylvanian Basin, Romania, in many cases show temperature gradient variations with depth which cannot be explained by depth variations in thermal conductivity, topography and groundwater flow. The only possible responsible agent seems to be the past surface temperature variations. The temperature logs have been interpreted by least squares inverse modelling with the surface temperature history and background heat flow as unknown parameters. The temperature data are too shallow to contain information about the temperature rise at the end of the last glaciation. However, several temperature profiles are consistent with a postglacial warming. Measurement technique, inversion methods and modelling results are discussed.

**MC02/L/01-B1** Poster **1600-14**

**ASYMMETRIC CLIMATIC CHANGE OVER COASTAL CALIFORNIA: CAUSES AND CONSEQUENCES**

Michael A. White, Ramakrishna R. Nemani, Daniel R. Cayan, Gregory V. Jones, Steven W. Running and Joseph C. Coughlan

Climatic change in coastal California has been dominated by asymmetric air temperature changes associated with dewpoint temperature increases. Regional mean California air temperature increases were tightly coupled to near-coastal Pacific sea surface temperatures, which in turn were highly correlated with Pacific specific humidity and California dewpoint temperature. Higher dewpoint led to advection of high humidity air masses over coastal California. Biological consequences of such symmetric climate change can be significant. In Napa/Sonoma valleys, the center of premium California wine production, climatic change has dramatically improved the viticultural environment. Changes include: 65-day increase in frost-free growing season; 71% reduction in frost occurrence; 3.14°C decrease in growing season diurnal temperature range; 14% increase in growing season growing degree days; an estimated 23-day advance in flowering date; and a 7% decline in growing season vapor pressure deficit. Over 1951-1997, there has also been significant improvements in both wine quality and grape yield. Finally, since annual temperature patterns are generally forecast by winter sea circulation patterns, there appears to be some potential in forecasting wine quality from winter conditions.

**Tuesday 27 July AM**

Presiding Chair: David Karoly (Monash University, Clayton, Australia)

**MC02/E/09-B2** Invited **0900**

**A QUANTITATIVE ASSESSMENT OF THE ASSOCIATION BETWEEN WINTERTIME NORTHERN HEMISPHERE CIRCULATION INDICES AND TEMPERATURE**

Anthony J. BROCCOLI, Thomas L. Delworth (both at NOAA/Geophysical Fluid Dynamics Laboratory, Princeton, NJ 08542, USA, email: ajb@gfdl.gov)

The North Atlantic Oscillation (NAO) and Arctic Oscillation (AO) are related measures of the regional and hemispheric strength of the Northern Hemisphere midlatitude westerlies. A number of studies, focusing on the winter season, have reported an association between Northern Hemisphere temperatures (both local and spatially averaged) and the NAO and AO indices. Accurately assessing the amount of recent warming associated with such changes in circulation is an important aspect of the detection and attribution of climate change. Using both observations and model output, we investigate the hypothesis that the coexistence of long-term trends in the NAO/AO indices and temperature during recent decades has led to an overestimation of the strength of the association between circulation and hemispheric mean temperature.

**MC02/W/03-B2** **0930**

**MODEL SIMULATION OF THE ARCTIC OSCILLATION TREND: IMPLICATIONS FOR ATTRIBUTION OF OBSERVED GLOBAL WARMING**

Drew SHINDELL, Ron L. Miller, Gavin Schmidt (NASA Goddard Institute for Space Studies and Center for Climate Systems Research/Dept. of Applied Physics, Columbia University, New York, NY USA); Lionel Pandolfo (Dept. of Earth and Ocean Science, University of British Columbia, Vancouver, BC Canada)

The Arctic Oscillation (AO), a hemispheric-scale version of the North Atlantic Oscillation (NAO), is a prominent feature of climate variability. Changes in sea-level pressure (SLP) are highly correlated with wintertime variations in Northern Hemisphere surface air temperature, and the more than 10 K warming over Eurasia during recent decades is associated with a decrease in

Arctic SLP and an increase in mid-latitude SLP. We present climate model results demonstrating that the observed trend, including its magnitude, can be induced by increasing greenhouse gases. This suggests that although the warming appears through a naturally occurring mode of variability, it is likely attributable to anthropogenic activities. The AO mode extends from the surface to the stratosphere. Our results indicate that stratospheric changes may have a significant effect on surface climate, and that dynamical forcing of climate change by greenhouse gases may be quite important, in addition to the direct radiative forcing. Because the AO is associated with a distinctive, large regional signature of warming, proper simulation of anthropogenic impacts on this mode is important for the detection of climate change.

**MC02/W/16-B2**

**0950**

**AN ENSEMBLE OF CLIMATE CHANGE SIMULATIONS WITH GFDL'S COUPLED CLIMATE MODEL**

Tapio SCHNEIDER (Atmospheric and Oceanic Sciences Program, Princeton University, Princeton, NJ 08544-0710 Email: tapio@splash.Princeton.edu)

Climate change detection has come to be viewed as the problem of detecting a climate change "signal" that is contaminated by the "noise" of natural variability. The signal is usually taken as the simulated difference between a reference climate and a changed climate, and the natural variability noise is assumed to be linearly superimposed on the signal and unaffected by climate change. Detection of climate change in the observed record is taken to mean that the projection of the observations onto the simulated signal is, in a statistically significant manner, greater than the projection of the simulated natural variability onto the signal.

In this paper, a view of climate change detection is proposed that does not rest upon a linear decomposition of the data into a signal and noise and does not require the assumption of an unchanging natural variability. Instead of framing climate change detection as a signal transmission problem and defining a signal as the difference between two climatic states, we seek those climatic features that, on the average, best separate several groups of climatic states, groups defined, for example, as probable decadal climates in a climate change scenario. Detecting a climate change in the observed record at a certain time then amounts to verifying the following: first, in the simulations the separating climatic features discriminate reliably between the climate at that time and a reference climate; second, the simulation of the separating climatic features is consistent with observations.

**MC02/P/01-B2**

**1010**

**CLIMATE CHANGE ASSESSMENT OVER INDIA USING METEOROLOGICAL, TIDE GAUGE OBSERVATIONS AND REGIONAL MODELS**

H. N. SRIVASTAVA (India Meteorological Department New Delhi-110003, India, email: snb@imd.ernet.in)

Surface and upper air meteorological observations have been used for 475 surface and 31 upper air observatories data for 1901 to 1986 and 1951 to 1980 respectively to understand the decadal and 30 years trend over India for maximum and minimum temperatures, rainfall, frequencies of cyclonic storms and western disturbances and sea level changes using tide gauge observations.

It is found that the regional variation in surface air temperature is well marked over the country showing a rising trend south of 23°N and a fall north of this latitude. For the country as a whole, the temperatures have shown slight rise similar to global observations. Rainfall variations are within the statistical limits except over hilly regions where they show a decrease. The frequency of cyclonic storms and western disturbances does not show a marked change on the decadal scale. The tide gauge observations do not indicate a significant trend over the coastal region of the country. Although regional climate models need considerable modification, some agreement with the surface air temperature variations over India has been found and discussed. The agreement with rainfall predictions is poor suggesting finer scale grid models.

Presiding Chair: Mike MacCracken (Co-convenor)

**MC02/W/01-B2**

Invited

**1100**

**A MULTI-VARIABLE APPROACH TO CLIMATE-CHANGE DETECTION**

B. D. Santer, K. E. TAYLOR (Program for Climate Model Diagnosis and Intercomparison, Lawrence Livermore National Laboratory, Livermore, CA 94550, U.S.A., email: ktaylor@pcmdi.llnl.gov), E. Roeckner, T. M.L. Wigley, T. P. Barnett, C. Doutriaux, K. Hasselmann, G. C. Hegerl, J. J. Hnilo, P. D. Jones, and U. Mikolajewicz

To date, virtually all studies attempting to identify human effects on global climate have compared modeled and observed temperature fields. Here, we consider whether these effects can be more readily identified by considering the joint behavior of several different climate variables rather than the behavior of a single variable. Our multi-variable representation of the climate system (in both models and data) comprises roughly 25-30 indices. The indices are very large-scale spatial averages, incorporating information on the atmospheric general circulation, temperature and moisture. Index time series are computed in comparable ways from models and observations, using both high-pass and low-pass filtered data. The model-based multi-variable signal and noise estimates are taken from perturbation experiments and a control integration performed recently with the ECHAM4/OPYC coupled model developed in Hamburg. The experiments involve time-varying changes in well-mixed greenhouse gases, tropospheric ozone and sulfate aerosol direct and indirect effects. We first attempt to identify the model-predicted multi-variable fingerprints in the observations. We then compute EOFs of the normalized modeled and observed index time series and apply an "optimal detection" strategy to enhance signal-to-noise ratios. Preliminary results indicate that this approach is useful in climate-change detection and attribution studies and also offers a useful internal consistency check on the "between-variable" covariance relationships in models and data.

**MC02/W/02-B2**

**1130**

**CLIMATE CHANGE DETECTION AND ATTRIBUTION USING SIMPLE GLOBAL INDICES**

David KAROLY, Karl Braganza, Tony Hirst, Scott Power (Meteorology CRC, Monash University, Clayton, VIC 3168, Australia, E-mail: dj@vortex.shm.monash.edu.au)

Initial studies of global climate change have sought to identify significant changes in global mean surface temperature and to attribute such changes to human influences. However, cause-and-effect are difficult to identify unequivocally in such a simple globally-averaged measure. More recent studies have focussed on fingerprint methods, which make use of the spatial patterns of temperature change to try to attribute the observed changes to one or more climate forcing factors. However, fingerprint methods also make use of more complex multi-variate statistics and the results may be harder to interpret or to communicate than those using global mean temperature.



In this study, we seek to follow the detection and attribution methodologies used in fingerprint detection studies but apply them using a small number of indices of global climate change. These indices have been selected based on earlier studies of climate change detection and on some of the key features identified in the climate change fingerprints that have been used commonly. They include the global mean temperature, the global mean temperature contrast between land and ocean, the mean meridional temperature gradient between high and low latitudes, and the mean magnitude of the seasonal temperature cycle and of the diurnal temperature cycle on land.

First, the observed trends in these global indices are compared with estimates of natural variability from control coupled climate model simulations to detect significant changes. Next, they are compared with forced climate model simulations to try to attribute the observed changes to one or more causes. The combination of these simple global indices has more power to attribute climate change than does the use of global mean temperature alone. While this approach may not be as statistically powerful as the fingerprint method, it is easier to explain.

MC02/E/18-B2

1150

#### DETECTION AND ATTRIBUTION OF ANTHROPOGENIC GLOBAL WARMING USING OBSERVED TRENDS IN NORTHERN HEMISPHERE SNOW COVER AND SEA ICE AREAS

Alan ROBOCK (Dept. of Environmental Sciences, Rutgers - The State University of New Jersey, 14 College Farm Rd., New Brunswick, NJ 08901-8551, USA, email: robock@envsci.rutgers.edu); Konstantin Y. Vinnikov (Univ. of Maryland, USA); Ronald J. Stouffer (NOAA Geophysical Fluid Dynamics Lab., Princeton Univ., USA); David Robinson (Rutgers Univ., USA); John Walsh (Univ. of Illinois, USA)

We compare existing observed data on variations in Northern Hemisphere sea ice and snow cover areas with those from equilibrium and transient climate model runs. We plan to present results from the GFDL and Hadley Centre GCMs. Northern Hemisphere sea ice area has been decreasing during the last five decades. The observed trend and inter-annual variability of sea ice area are in a good agreement with the GFDL transient (aerosol +1%/yr CO<sub>2</sub>) scenario of global warming, and the observed trend exceeds the limits of its natural variability, as determined by a long GCM control run. Northern Hemisphere snow cover area has also been decreasing during the past three decades. The observed trend and inter-annual variability of snow cover area are larger than those in the GFDL transient scenario of global warming, but can be explained as an effect of model resolution, in which the model cannot reproduce small scale summer snow variations. The observed snow cover trend is also very significant. Thus, we claim that the observed decreases in Northern Hemisphere snow and sea ice are fingerprints of the anthropogenic effect on climate. Seasonal distributions of the observed trends in Northern Hemisphere sea ice and snow cover areas are different from the model predicted scenario of global warming, and we will examine possible reasons for this. We will examine the predications of snow and ice by other GFDL simulations and by the Hadley Centre GCMs to determine how dependent these results are on the particular climate model we used.

MC02/W/11-B2

1210

#### INFLUENCE OF CIRCULATION AND SHORT WAVE RADIATION ON REGIONAL AIR TEMPERATURE VARIABILITY IN CENTRAL EUROPE

Ingeborg Auer, Reinhard BÖHM (Central Institute for Meteorology and Geodynamics, Hohe Warte 38, A-1190 Vienna, Austria, email: reinhard.boehm@zamg.ac.at)

A new instrumental climatic data set is used to investigate two natural factors to explain central European temperature variability and its regional deviations from global mean variability. The data set has been elaborated during the past two years (project ALOCLIM: Austrian long-term climate). It covers Austria and parts of the surrounding countries. It has been homogenised carefully using both meta data information for documented breaks in the series and three different relative homogeneity tests for quantitatively non documented breaks. It covers more than 200 years thus reaching far to the pre-industrial period. With four high level sites in altitudes up to 3100m asl. (700hPa) and 10 to 50 low level sites it introduces also the third (vertical) component into climate time series analyses. As it consists of time series of 15 to 20 single climate elements, it is a multiple data set usable for real climatic analyses considering not only single elements but also their possible interactions, dependencies and forcings. In this contribution the data set is used to analyse two factors that explain to a high degree the regional temperature variability in the east alpine region. Circulation is the real background forcing factor – directly by heat advection and indirectly by its influence on cloudiness and radiation in the mountainous region of investigation. Circulation is studied by NAO (explaining up to 60% of temperature variance) and by local air pressure series which show a stupendously high correlation with temperature. The indirect circulation forcing via radiation is studied by the co-analysis of temperature and sunshine series. Also for those two climate elements there is a high correlation both for high frequent and low frequent variability. The conclusion is that regional temperature variability in central Europe is strongly governed by

Tuesday 27 July PM

Presiding Chair: Mike MacCracken

MC02/E/02-B2

1400

#### ANTHROPOGENIC AND NATURAL CAUSES OF TWENTIETH CENTURY TEMPERATURE CHANGE

Peter A. STOTT, Gareth S. Jones, Simon F. B. Tett Hadley Centre for Climate Prediction and Research, U.K. Met. Office, London Road, Bracknell, Berkshire RG12 2SY, UK.

A new coupled ocean atmosphere general circulation model that does not include flux correction has been used for the first time to attribute twentieth century climate change to anthropogenic and natural causes. We have made two ensembles of climate runs, initialised from different starting conditions, one of which includes natural forcings due to volcanic dust and changes in total solar irradiance and the other of which includes changes due to well mixed greenhouse gases, sulphate aerosols (both direct and indirect effects) and tropospheric ozone. Our modelling represents a significant advance on previous work by including the atmospheric sulphur cycle and representing well mixed greenhouse gases explicitly. We compare spatial and temporal patterns of near-surface temperature change from the model and observations using an "optimal fingerprinting" methodology. First we determine whether any linear combination of the response to natural forcings and internal variability can account for the warming observed this century. Next we include anthropogenic effects and attribute the observed change to natural and anthropogenic factors.

MC02/W/13-B2

1430

#### DISTINGUISHING BETWEEN NATURAL AND ANTHROPOGENIC INFLUENCE ON ATMOSPHERIC VERTICAL TEMPERATURE STRUCTURE

D.C. HILL (Rutherford Appleton Laboratory, Chilton, Didcot, Oxfordshire, OX11 0QX); M.R. Allen (Rutherford Appleton Laboratory, Chilton, Didcot, Oxfordshire OX11 0QX); S.F.B. Tett (Hadley Centre, UK Met. Office, London Rd., Bracknell, RG12 2SY)

Current approaches to the detection and attribution of an anthropogenic influence on climate involve quantifying the level of agreement between one or more model-predicted forced-response patterns and observed changes in the recent climate record. Studies (e.g. Allen and Tett 1999) have shown that, for a decadal mean diagnostic of zonally averaged vertical temperature, a zero response to greenhouse gases can be excluded, while a zero response to the combined influence of anthropogenic sulphate aerosols and stratospheric ozone depletion cannot. It is thought that more information may be found in a seasonally resolved approach since the impacts of sulphate and ozone are seasonally modulated. Hence, a study on vertical temperature patterns for 3 monthly averaged data is carried out, including patterns consisting of concatenated winter and summer data. The results which exclude a zero response to greenhouse gases have not explicitly taken into account solar and volcanic activity. Output from runs of the Hadley Centre's HadCM2 model for various forcings (including greenhouse gases, greenhouse gases and sulphate aerosols, changing solar activity and volcanic aerosols) is used in an optimal fingerprinting study to evaluate the evidence for these natural and anthropogenic forcings in radiosonde observations of atmospheric temperature structure.

MC02/E/14-B2

1450

#### DETECTION AND ATTRIBUTION OF 20TH CENTURY CLIMATE CHANGE USING A SEASONALLY OPTIMISED DETECTION METHOD

Gareth S. JONES, Peter Stott, Simon Tett (Hadley Centre for Climate Prediction and Research, Meteorological Office, London Road, Bracknell, RG12 2SY, UK, email: gsjones@meto.gov.uk)

We present the results of an 'optimal detection' analysis on the near surface temperature record and simulations of a climate model (HadCM2). The analysis is over latitude, longitude, time and additionally seasons. Optimising over seasons increases the signal to noise ratio of detection of climate signals above that of an annual analysis. The influence of greenhouse gases and anthropogenic sulphate aerosols is detectable in the latter part of the twentieth century and the influence of greenhouse gases and solar irradiance changes is detectable in the early part of this century.

MC02/E/04-B2

1510

#### LOCAL VERSUS GLOBAL CLIMATE CHANGE DETECTION PROBLEMS IN ISRAEL

Alpert PINHAS (Dept. of Geophysics and Planetary Science, Tel Aviv University 69978 Ramat Aviv, Israel, e-mail: pinhas@cyclone.tau.ac.il); Tehilla Ben-Gai, Arie Bitan, Alexander Manes (Dept. of Geography, Tel Aviv University, 69978 Ramat Aviv, Israel.)

Significant changes in land usage have taken place since the National Water Carrier operation in the early 1960's. Such changes are reflected in the spatial distribution of the surface albedo pattern, obviously resulting in changes in the surface radiation balance and, subsequently, modifying the surface heat fluxes and the stability conditions of the Planetary Boundary Layer (PBL). This process of changes in momentum, moisture, and heat fluxes, known as the ANTI-DESERTIFICATION process, should also affect climatic parameters of the boundary layer: rainfall patterns, temperature patterns, moisture, air pressure and wind, followed by changes in instability that could affect synoptic systems and rainfall amounts. Estimations of the temporal changes in the albedo values for the last sixty years show large differences (of up to 0.2) in the surface reflection. A gamma distribution function that was fitted to the annual and monthly rainfall at 60 station for two normal periods, reveal appreciable changes, especially in the Southern part of the country, with more than 60 percent increase in the shape parameter. The monthly distribution revealed considerable changes in October, November and March. Daily maximum and minimum temperatures in Israel revealed a significant decreasing trend of both the daily maximum and minimum temperature, during the cool season (November to March), and an increasing trend during the warm season (April to October), resulting in increasing seasonal temperature range. Teleconnections with changing patterns of temperature and pressure anomalies observed in Israel showed Relatively high correlation of -0.8 and +0.9 between the North Atlantic Oscillation(NAO) Index anomalies and the cool season temperature and surface pressure anomalies in Israel, respectively. Radiosonde records from the Bet-Dagan aerological station of the Israel Meteorological Service reveals a clearly defined increasing trend in the moisture content, mainly during summer. The stability of the surface layer, characterized by the Bulk Richardson Number, shows a decreasing trend since early 1960s. Though it seems that the changes in climatic parameters, point to a possible link to land use changes, connections with global trends should also be considered. The relatively high correlation between temperature anomalies and the North Atlantic Oscillation supports this connection. No link was found to the Southern Oscillation. We will discuss the more general detection and attribution problems as discovered by the Israel complex case.

Presiding Chair: Phil Jones (Climatic Research Unit, University of East Anglia, Norwich, UK)

MC02/W/09-B2

Invited

1600

#### BAYESIAN PARAMETER ESTIMATION AND HYPOTHESIS TESTING OF CLIMATE CHANGE

Haroon S. KHESHSI, Benjamin S. White (both at Exxon Research and Engineering Company, Route 22 East, Annandale, NJ 08801, USA, email: hskhesh@erej.com)

Comparisons between climate data and climate model results are generally used to i) improve estimates of future climate, i.e. estimate parameters, and to ii) attribute the causes of changes in observed climate, i.e. test hypotheses. We use related Bayesian statistical frameworks to treat these two tasks on a common basis. For hypothesis testing we apply the Neyman-Pearson Lemma to construct the most powerful test for a variety of climate models and attribution questions, and compute the relationship between false-negative and false-positive errors for this optimal test. Both statistical frameworks depend on the characterization -- including uncertainty -- of climate records, climate variability, and the expected climate signal. We apply these frameworks to aggregated model/data comparison -- global and hemispheric temperatures.

MC02/W/06-B2

1630

### THE ASSOCIATION BETWEEN THE INTENSITY OF MELBOURNE'S URBAN HEAT ISLAND AND THE REGIONAL SURFACE PRESSURE DISTRIBUTION

C. Jon Morris, Ian SIMMONDS (both at School of Earth Sciences, The University of Melbourne, Parkville, Victoria, 3052, Australia, email: ihs@met.unimelb.edu.au)

In using urban weather records to detect global climate change one must be careful to allow for the effects of urban heat islands (UHIs) (and how these may change with time). In this study we quantify the UHI in Melbourne as the difference between the 0600 temperature within the CBD and the mean of three non-urban airport sites (all located between 16.6 and 20.5 km from the CBD, and at different points of the compass). The analysis has been performed for the period 1973-91.

The daily data are binned into 1°C 'boxes', with all those exhibiting UHI of (-1°C and > 3°C considered in two separate bins. (About 75% of the UHI values fell between 0 and 2°C, while 3.6% of days exhibited a UHI in excess of 3°C.) The composite anomalous synoptic patterns (from the NCEP reanalysis data) associated with each of these UHI bins will be shown and interpreted. Not surprisingly, the strongest heat islands in Melbourne are associated anticyclonic conditions. However, one of the interesting results to come out of this work is the composite anomalous anticyclone is not centered directly over Melbourne but is located at some distance, lying to the east and south east of Tasmania.

MC02/W/15-B2

1650

### TRENDS OF CLIMATE EXTREMES IN CHINA DURING THE LAST DECADES

Chi YANG, Zhongwei Yan (both at Institute of Atmospheric Physics, Chinese Academy of Sciences, Beijing 100029, China, email: yangchi@ihw.com.cn)

Based on the daily weather observations of 61 stations during the 1951-1997, we analyzed the trends of the climate extremes in precipitation, maximum and minimum temperatures and wind speed over China. The least square fit method and Mann-Kendall's trend test were applied to define the linear changing rates and their significance. Some nationwide significant trends were found. At most of the stations, the number of days without precipitation increased during the last decades by a few days to weeks, whereas the number of days with the least precipitation (recorded as 0 mm) decreases. There is little trend in the strength of the extreme precipitation events. The minimum temperature significantly increased by more than 1 °C in northern China and about 0.5 °C in southern China, whereas the maximum temperature decreased but not very significantly. The extreme wind speed decreased about 1 m/s throughout China. A Singular Value Decomposition analysis was performed in order to find the principal correlation modes among the changes in the different variables.

MC02/P/03-B2

1710

### GLOBAL CLIMATE CHANGE AND ITS EMPIRICAL DIAGNOSTICS

V.N. Adamenko (Marine Academy, 16 Kosaya Liniya, St.Petersburg, Russia); K. Ya. KONDRATYEV (Russian Academy of Sciences, Research Centre for Ecological Safety, 18 Korpusnaya St., 197110 St. Petersburg, Russia, email: nansen@online.ru)

A hypothesis that global climate warming observed during the last century had been due to anthropogenically induced carbon dioxide concentration growth provoked controversial response. In this context, general considerations have been discussed which support the viewpoint that the 'greenhouse' global warming hypothesis is doubtful. One of the strongest arguments in favour of the above hypothesis is a conclusion drawn from numerical climate modelling data that there must be an enhancement of the 'greenhouse signal' with latitude. Some results of surface air temperature (SAT) observations in the Arctic during the last 20-30 years have been discussed which demonstrate a reduction in SAT in a number of Arctic regions. Some dendro-climatic data for the last 20-30 years relevant to tree growth near the northern forest boundary have also been considered. Analysis of these data reveals that not only the conclusion about polar enhancement of climate warming is wrong but the warming itself could hardly be realistic. So it may be concluded that no non-controversial information exists that can support the hypothesis of global 'greenhouse' warming.

MC02/P/02-B2

1730

### GROWING SEASONAL SYNCHRONY BETWEEN GLOBAL TRACE GAS LOADS AND WORLDWIDE GAS PRODUCTION?

Peter CARL (Climate Dynamics Project, c/o Forschungsverbund Berlin Hausvogteiplatz 5-7, D -10117 Berlin, Germany, email: pcarl@spclim5.wias-berlin.de)

Time-frequency analyses are presented for both the global NOAA records of atmospheric CO<sub>2</sub> and CH<sub>4</sub> and the OGJ figures of worldwide oil and gas production. The strong CH<sub>4</sub> growth rate anomaly of the early 90th is situated just at the common (1990-94) stagnation phase in both production records. Though decline of eastern economies and Mt. Pinatubo's eruption may be blamed, a longer-term climatic contribution is suggested from monsoon time series of the century that point to a change, at the lower-frequency ENSO timescale, in the dynamic interplay of the monsoons of both hemispheres.

Except a moderate seasonal cycle, sub- to inter-annual variability dies largely out in oil production after recovery from stagnation. In contrast, gas production maintains rich variability that is dominated by far, however, by a strong and increasing seasonal cycle. The latter shows growing yet complex coincidence with the same cycle in atmospheric methane - which itself loses much of its sub-annual variability during the 80th to become more harmonic. In parallel, the growth rate of global atmospheric methane has continuously decreased. CO<sub>2</sub> shows a similar structural evolution except for semiannual variability which increases in amplitude together with the seasonal CO<sub>2</sub> cycle. If the northern hemisphere heating period becomes more directly involved in the seasonal radiative forcing, this would not necessarily saturate together with the CH<sub>4</sub> growth rate.

MC03

Thursday 29 July

### SUDDEN CLIMATE CHANGE (ICCL)

Location of Symposium: Mechanical Engineering G29 LT

Thursday 29 July AM

MC03/E/02-B4

0930

### SUDDEN CLIMATE SHIFTS IN THE GLACIAL NORTH AND SOUTH ATLANTIC OCEANS

GERARD BOND (Lamont-Doherty Earth Observatory, Rt. 9W, Palisades, NY, 10964, email: gcb@lamont.ldeo.columbia.edu)

Millennial time-scale climate variability in the North and South Atlantic, revealed by radiocarbon dated surface and deep ocean proxies, exhibits complex phasing that may arise from major shifts in the ocean's thermohaline circulation. In the northwestern limb of the present-day Gulf Stream, ocean surface temperatures are strongly antiphased with respect to those to the north in the subpolar gyre. The most striking antiphased patterns occur during the North Atlantic's Heinrich events. Carbon isotopic compositions of benthic foraminifera suggest that the antiphased patterns developed at times of significant reductions in the formation of North Atlantic Deep Water. Antiphased surface temperatures in the two regions also appear in the late Holocene, and may have been associated changes in deep water formation then as well. In the South Atlantic, a series of millennial-scale ice rafting events appears to be correlated, within error of radiocarbon dating, to ice rafting events in the North Atlantic. The most robust evidence is in recurring increases in percent of volcanic glass carried on ice drifting from the Scotia Arc. The North Atlantic ice rafting events are tied to Greenland's Dansgaard-Oeschger cycles, and hence, the ice core record appears to be imprinted in the Southern Ocean. During correlatives of Heinrich events, however, the South Atlantic ocean surface warmed, thereby implying the same strong antiphasing with respect to temperature in the subpolar North Atlantic as found in the northern Gulf Stream. The antiphased patterns in the North and South Atlantic Oceans are consistent with temperature anomalies produced in coupled ocean-atmosphere GCMs by a shut down of North Atlantic Deep Water formation. In the North Atlantic the antiphased shifts result from changes in the separation point of the Gulf Stream. In the South Atlantic, they arise from changes in cross-equatorial heat transport. If antiphased climate patterns are a common product of perturbations to global thermohaline circulation, their identification in paleoclimate records provides further constraint on the role of ocean circulation in climate change.

MC03/W/05-B4

0950

### THE GLOBAL SYNCHRONY OF GLACIAL-INTERGLACIAL EVENTS

A. Clement, Université de Paris 6, LODYC, etage 4, CASE 100, 4 place Jussieu, 75005 Paris, France. CEDEX 05. E-mail: aclocl@ipsl.jussieu.fr

The global synchrony of glacial-interglacial events is one of the major problems in understanding the link between Milankovich forcing and the climate of the late Pleistocene. In this study, we isolate a part of the climate system, the tropical Pacific, and test its sensitivity to changes in solar forcing associated with changes in the Earth's orbital parameters. We use a simplified coupled ocean-atmosphere model which is run for 150,000 years, and forced with Milankovich changes in the solar insolation. This system responds primarily to the precessional cycle in solar forcing, and is capable of generating an annual mean response to the changes in the seasonal distribution of solar radiation even while the annual mean insolation is roughly constant. The mechanism responsible for the annual mean response is the interaction between an altered seasonal cycle and the El Niño–Southern Oscillation. Changes in the ENSO behavior result in a mean tropical climate change which can be relatively abrupt. The hypothesis is advanced that such a change in the tropical climate can generate a globally synchronous climate response to Milankovich forcing.

MC03/E/09-B4

1010

### ABRUPT CLIMATE CHANGES DURING THE LAST 6 600 YEARS IN SOUTH AFRICA

PETER TYSON (Climatology Research Group, University of the Witwatersrand, Johannesburg, South Africa, email: ptdt@org.bpb.wits.ac.za) Wibjorn Karlén and Karin Holmgren (Department of Physical Geography, Stockholm University email: karlen@natgeo.su.se and karin@natgeo.su.se)

Five high-resolution time series are available for subtropical latitudes in the southern hemisphere that permit the determination of sudden climate shifts and changing patterns of variability during the last six millennia. Recently, a quasi-decadal resolution, 6 600-year proxy climate record has been determined from a stalagmite taken from a cave in the Makapansgat Valley in northern South Africa.

The series is characterised by periods of relative stability, periods of rapid change and times when rapid changes between extreme conditions were dominant. Rapidly changing patterns of variability with time are shown to be a feature of the entire record. The most extreme and prolonged episode in the entire record is shown to have occurred in the five centuries of cooling that constituted the Little Ice Age from 1300 to 1800. The depression of annual maximum temperature below the present-day 1961-1990 mean at the time of maximum cooling at 1700 was 1-2 °C. Following maximum cooling at 1700, conditions ameliorated rapidly to revert to above-normal within fifty years. Other extreme shifts in the record are shown to have occurred within a decade or two. Changes in variability with time will be illustrated by determining the decadal variability in moving two-century time periods traversing the entire 6 600-year series.

Comparison of the stable isotope record for the Makapansgat valley with a similar high-resolution stalagmite isotope data for the Cango Cave in southern South Africa and an even higher-resolution record derived from corals on the south-western coast of Madagascar reveals that the Little Ice Age was a pronounced regional event over a large area of southern Africa. The spatial extent of the abrupt changes and sudden climate ...

MC03/W/03-B4

1030

### IDENTIFICATION OF CLIMATE SUDDEN CHANGE EVENTS IN QUATERNARY SEDIMENTARY RECORD BY WAVELET TRANSFORM

Yang WANG (Lab. for Geothermics, Institute of Geology, Chinese Academy of Sciences, P.O.Box 9825, Beijing 100029, China, email: thalassa@263.net)

The previous studies on climate change in Quaternary are mostly based on classical Fourier analysis method which only provides the frequency information about climate change periods. Wavelet analysis is a powerful tool for signal processing, owing to the local feature of wavelet functions. It means the function has non-zero values in a finite range, beyond the range values

approximate fast to zero; and this range is called the window of wavelet. Making convolution of signal and wavelet function, the singularity points of signal sequence can be identified; and we can find singularity points in different time (period) scales by changing the width of wavelet's window. When we take climate record as time dependent signal sequence, sudden change points in record are singularity points. Mexican Sombbrero Wavelet (MSW) is the second derivative of Gaussian Function, the convolution of signal and MSW corresponds to smoothing signal by Gaussian Function and then making two derivations. This means that sudden change points are inflection points (a kind of singularity) of convolution function. The climate change signals from a Quaternary loess sequence in Xifeng, NW China, had been processed by wavelet transform. It was found that six sudden change events occurred in 1.32, 1.11, 0.58, 0.41, and 0.16 Ma BP, and demonstrates a quasi period in scaling of  $-0.4 \sim -0.7$  Ma. Thirteen sudden change events were identified on  $\sim 0.1$  Ma scale, and more sudden change events were found in shorter period scales. This result reveals the hierarchical structure of Quaternary climate signals and corresponds to the fractal nature of climate system.

### MC03/W/04-B4 1110

#### ON RAPID AND PROTRACTED CHANGE IN THE SOUTHERN OCEAN CIRCULATION UNDER MODERATE GLOBAL WARMING

ANTHONY C. HIRST CRC for Southern Hemisphere Meteorology CSIRO Atmospheric Research PMB 1, Aspendale, Vic., 3196 Australia William F. Budd, Dave Bi and Xingren Wu Antarctic CRC University of Tasmania GPO Box 252-80, Hobart, Tas. 7001 Australia

Recent work using the the CSIRO coupled ocean-atmosphere model suggests that certain aspects of the Southern Ocean circulation may be very sensitive to global warming. We present results from three integrations of this model where the equivalent CO2 concentration is increased according to the IS92a radiative forcing scenario from 1880 AD to (1) 2000 AD, (2) 2033 AD and (3) 2083 AD, and then held steady for several centuries at, respectively, (1) 1.5 times, (2) 2 times and (3) 3 times the 1880 level. The oceanic changes occurring at high Southern latitude in the doubled and tripled equivalent CO2 integrations are quite profound, and include an major increase in strength of the near-surface halocline and the cessation of convection and bottom water formation. In both cases, this collapsed thermohaline state continues for several centuries of stable elevated equivalent CO2 to the end of the integrations. Further, the integration featuring a mere increase in equivalent CO2 by 50 percent (approximately present day levels) produces a substantial thermohaline slow-down which lasts at least several centuries. Importantly, these changes occurring in the 1.5 times and doubled equivalent CO2 integrations develop progressively during the 21st century despite stable levels of equivalent CO2.

The sensitivity of the Southern Ocean circulation to global warming is potentially important for several reasons. Firstly, convection and thermohaline overturning are important in bringing warm, salty subsurface water into the upper mixed layer, and so a slowing of this exchange may reduce the rate of regional surface warming. Secondly, changes in the surface/deep ocean exchange rate may affect the ability of the ocean to sequester anthropogenic CO2. Thirdly, these same exchange rate changes may affect...

### MC03/E/03-B4 1130

#### SUDDEN CLIMATIC CHANGE WITHIN A MILLENNIAL COUPLED MODEL SIMULATION

B.G.HUNT (CSIRO Atmospheric Research, Australia, email: bgh@dar.csiro.au)

The CSIRO Mark 2 coupled global climatic model has been used to generate 1000 years of simulated climate for present conditions (i.e. constant CO2). The model has 9 vertical levels in the atmosphere and 12 in the ocean and a horizontal resolution of R21. A comprehensive land surface scheme and a dynamical sea-ice formulation are included in the model. Examination of the model output provides many examples of sudden climatic change. These changes can be simple examples of year-to-year variability, or periods of sustained (10 years or longer) climatic anomalies of opposite sign to those preceding a change. Rainfall, surface temperature and surface wind stress provide particularly good case studies for sudden climatic changes. Normally the duration of sustained changes was between 10 and 15 years, depending on the climatic variable concerned. Preferred geographical regions were easily identified. Oceanic temperature anomalies appear to play a major role in sustaining other climatic anomalies, with oceanic temperature anomalies being identifiable down to several hundred metres depth. All the sudden climatic changes in the simulation can be attributed to natural climatic variability within the model system, and as such provide possible estimates of the duration, geographical regions, frequency of occurrence and amplitude of changes which might be observable.

### MC 03/E/01-B4 1150

#### THE IMPACT LARGE LAKES ON CLIMATE

Potemkin V. (Limnological Institute, Irkutsk, 664033 Russia, email: klimat@lin.irk.ru)

Ice-age periods and interglacials - main and the most essential changes of global climate in modern quaternary period (about 2 million years). The intensive development of paleoclimatology, the integration of extensive information from different sources, including the data from annual layers of ice cores and sediments on the bottom of lakes and seas, have allowed to receive a detailed picture of a condition of all climatic system in ice period. According to the data obtained during research in modern lakes it is known that large, long not frozen in the winter reservoirs of middle latitudes can cause fall out of additional "lakes" snowfalls on their leeward coast. In this connection there is a supposition that the existing huge lake Mansi in Late Pleistocene (20-25 thousand years ago) on the territory of West-Siberian Lowland could be the reason of the occurrence of powerful mountainous ice-sheets in Siberia. The preliminary quantitative valuations of this effect are under discussion in this paper.

### MC03/W/02-B4 1210

#### OCEAN CIRCULATION AND SUDDEN CLIMATIC CHANGES

Nils-Axel Mörner, Paleogeophysics & Geodynamics, S-10691 Stockholm, Sweden, email: morner@pog.su.se

There is a strong linkage between Earth's rate of rotation - total as well as differential - and the changes in ocean surface circulation. The ocean circulation changes are, in their turn, strongly linked to the paleoclimatic evolution of the bordering land masses. This is due to the high heat-storing capacity of the oceans, the ocean/atmosphere heat flux, and the ocean/land interaction via heat transport by the winds. Consequently, we see a causal connection between Earth's rotation, oceanic circulation, ocean/atmosphere heating, atmospheric (wind) heat transport and continental paleoclimatic changes. We propose that the paleoclimatic changes on the decadal-to-millennial time scale are primarily driven by this mechanism. Observational data of changes in ocean water masses and paleoclimate are presented for the 20 Ka situation, for the "sudden"

high-amplitude changes 13-10 Ka ago, for the decadal-to-century changes during the Holocene, for the last centuries' instrumental data and for the ENSO-events. This implies that the oceanic system (the ocean surface circulation system) has a much more important role than previously appreciated for the understanding of short-term changes in climate as well as in sea level. It provides a logical mechanism for the interpretation of "sudden changes in climate" as well as for globally differentiated (even opposite) responsesignals. The cold periods (or "Little Ice Ages") recorded in NW Europe in 1440-1460, 1687-1703 and 1808-1821 in approximate association with the Spörer, Maunder and Dalton sunspot minima seem all to represent oceanographic circulation changes due to rotational increases.

### MC04 Monday 26 – Tuesday 27 July

#### QUANTITATIVE PRECIPITATION FORECASTING (ICCP) (IAMAS)

Location: Mechanical Engineering, G33 LT

### Monday 26 July AM

Presiding Chair: H. Sundqvist (Stockholm Univ., Dept. of Meteorology, Sweden)

#### UNDERSTANDING HEAVY PRECIPITATION SYSTEMS AND IMPACTS

##### Introduction 0900

R. CARBONE

### MC04/W/15-B1 0915

#### THE TYPICAL CONCEPTUAL MODEL OF MOIST CONVECTIVE OVERTURNING

George BRYAN (Pennsylvania State University, USA, Email: bryan@essc.psu.edu)

The typical conceptual model of moist convective overturning depicts an ensemble of individual cumulus clouds emanating from a well-mixed convective boundary layer. This model fits with the accepted notion and theoretically supported view that atmospheric overturning will be dominated by fast-growing non-hydrostatic modes, i.e., thunderstorms. However, the atmosphere sometimes overturns in a manner that resembles mesoscale slabs (or sheets) of ascending air overrunning slabs of descending air. The ascending slabs, which are typically several hundred km in length and width, are usually forced upward by a front or convective outflow layer. As a slab ascends, a substantial portion, sometimes several hundred mb deep, reaches saturation. Since the ambient environmental lapse rate is steeper than moist adiabatic, the MESOSCALE lifting and subsequent saturation of the slab results in a moist absolutely unstable layer (MAUL). If the magnitude of MESOSCALE vertical motion exceeds the magnitude of the vertical motions that result from buoyancy forcing, the atmosphere can maintain (through a process of continual creation) the MAUL. Moreover, with continued mesoscale ascent, a solid swath along the front or outflow boundary reaches saturation and the convective overturning takes the form of a highly turbulent slab instead of discrete convective cells with intervening subsaturated areas.

Evidence of slab convective overturning of MAULs was compiled using Doppler radar data and the U.S.A. sounding network. Several examples documenting this mode of overturning are presented. The results from a non-hydrostatic cloud-scale-resolution numerical simulation of an event which featured a MAUL are also presented. It is argued that adjusting our conceptual models to view mesoscale moist convective overturning as vertically expanding slabs of saturated buoyantly turbulent flow would help explain several features often observed in mesoscale convective systems. Further, it forces us to address a fundamental problem with convective parameterization in mesoscale models, i.e., that buoyant parcels sometimes follow slantwise paths and affect more than a single gridelement at a time.

### MC04/W/17-B1 0940

#### MESOSCALE CONVECTIVE SYSTEMS IN THE TAIWAN MEI-YU SEASON

JOU, Ben Jong-Dao (Department of Atmospheric Sciences, National Taiwan University, Taipei, Taiwan, 106, email: jou@hp715.as.ntu.edu.tw)

Individual thunderstorms developed into organised thunderstorm lines (squall lines) or complex convective storms are commonly observed. The spatial scale of these convective systems is about hundred kilometers and the time scale spans from a few hours to about a day. Significant precipitation and rapid changes of wind and temperature are frequently observed at the surface stations during the passage of these storms. We call these storm systems: Mesoscale Convective Systems (MCSs). From many observational and numerical studies in the past 40 years, it is known by the meteorological community that the favourable environmental conditions for development of these storms are availability of convective available potential energy (CAPE) and pronounced vertical wind shear.

Mei-Yu period in Taiwan, i.e., May and June, is a season with transition. In this season, the cold air mass from Siberia is weakening and the warm air mass from Tropics is strengthening. The boundary of these two air masses forms a stationary front in the subtropical area, extending from south of Japan to Taiwan and southern China. Accompanying with the stationary front, a wide cloud band with embedded organized convective systems are commonly observed from satellite images. Strong interaction between Taiwan topography and the frontal system induced many interesting local weather phenomena along the coast and over the island. This paper, by using radar images, to show the precipitation patterns and evolution of the mesoscale convective systems occurred in the Taiwan area and its vicinity during the Mei-Yu season.

Four different kinds of mesoscale convective systems, i.e., mountain convection, prefrontal squall lines, frontal rainbands, and tropical convection, total 16 cases observed by the conventional and Doppler radars around the island will be discussed. Cases observed during TAMEX\_Taiwan Area Mesoscale Experiment, i.e., data from NCAR CP4 and NOAA TOGA radars, are also included. More details will be given during the meeting.

### MC04/E/10-B1 1035

#### WARM SEASON PRECIPITATION EPISODES IN CENTRAL NORTH AMERICA

R. E. CARBONE, J. Tuttle, L. J. Miller, S. Trier (NCAR, Boulder, CO, USA)

Our purpose is to improve the understanding and prediction of heavy precipitation episodes that result from clusters of mesoscale convective systems (MCSs). In the US, WSR-88D Level II radar data, GOES Rapid Scan satellite data, and NWS Family of Services data have been acquired over 1000 to 2500 km domains for periods of 18 to 72 h. The radar and satellite data are conditioned and gridded in a manner that preserves their native spatial and temporal



resolution (1 to 4 km; 5 to 15 min), while permitting their use for integrated analyses, retrievals, and as a basis for initializing and verifying simulations with the MM5 model. Eight precipitation episodes were selected from the 1998 warm season for diagnostic analyses and simulations. The initial analyses focus on retrieval of wind fields and condensate fields over the regional domain. Wind fields and some 1st order derivatives thereof are retrieved through harmonic Doppler techniques and auto-correlation tracking techniques using both radar and multi-spectral GOES data in addition to UHF profiler and other NWS analyses. The three dimensional condensate fields are retrieved from a combination of radar reflectivity factor and GOES cloud cover information, where emphasis is placed on (1) precipitation-sized condensate to establish diabatic effects resulting from phase change of water, and (2) the radiative effects of optically-dense, non-precipitating cloud cover. Our preliminary analyses of the 1998 episodes explore several factors including the influences of topography; the role of travelling free-tropospheric disturbances, such as fronts and mesoscale convective vortices; and the larger scale role of various planetary boundary layer convergence lines, which are well established as a major factor in convection initiation at smaller scales.

#### MC04/L/01-B1 1100

##### LONG-LIVED MESOSCALE CYCLONIC VORTICES AND THEIR ASSOCIATION WITH SUBSEQUENT DEEP CONVECTION WITHIN HEAVY PRECIPITATION EPISODES

S. B. TRIER, C. A. Davis, W. C. Skamarock, and J. D. Tuttle, National Center for Atmospheric Research, P. O. Box 3000, Boulder, Colorado USA 80307-3000

Midlevel cyclonic vortices (MCVs) generated by mesoscale convective systems (MCSs) can persist after the dissipation of deep convection, and in some cases, may focus subsequent convective development within long-lived discontinuous heavy precipitation episodes. Thus, MCV behavior may be an important aspect of the warm-season quantitative precipitation forecast problem in many midlatitude locations.

Observations taken from the modernized United States Weather Service data network have been used to assess the frequency and general characteristics of MCVs induced by MCSs. Results from the 1998 convective season over the central United States suggest that long-lived MCVs, which persist after the dissipation of the initiating MCS, are more common than previously documented. The ambient vertical shear in the path of these long-lived MCVs tends to be weaker than the shear in the path of dissipating MCSs from which no detectable MCVs were spawned. New convection was observed on the downshear flank of the MCVs (i.e. in the direction of the ambient 0.5 to 2.5 km vertical shear vector) given appropriate preexisting thermodynamic conditions (i.e., weak convective inhibition).

Supporting numerical simulations with a primitive equation model indicate that lifting that results from the interaction of the MCV with the ambient shear produces vertical parcel displacements sufficient to saturate portions of the lower troposphere on the downshear flank of the MCV in model environments representative of those found in the observations. In addition to confirming the importance of weak ambient shear for MCV longevity, the simulations have also illustrated the importance of internal vortex parameters such as the initial size and strength of the vortex and also its location relative to the ambient shear layer for both MCV longevity and their ability to generate subsequent convection. Additional numerical experiments that examine the interaction between convection induced by the MCV and the subsequent evolution of the MCV itself will be presented. Understanding the life cycles of MCVs is expected to improve prediction of a large class of long-lived heavy precipitation episodes.

#### MC04/E/09-B1 1130

##### SHORT-TERM FORECASTING OF SEVERE STORMS WITH A NUMERICAL MODEL AND ITS ADJOINT

Andrew CROOK, Juanzhen Sun and Tom Warner (National Center for Atmospheric Research, P.O. Box 3000, Boulder, Colorado, USA, 80307-3000, email: crook@ucar.edu)

Over the past decade we have been developing methods to initialize a numerical cloud model with Doppler radar observations for the purpose of short-term storm forecasting. The system uses the adjoint method to assimilate observations from either single or multiple Doppler radars. The goal is to produce initial conditions for the full dynamical, thermodynamical and microphysical fields that optimally fit a numerical cloud model to all available radar observations.

We have applied the adjoint method to observations of a flash flood producing storm in the Front Range of the Rocky Mountains. The storm of interest moved slowly over the Buffalo Creek, Colorado watershed producing over 75 mm of rain in less than one hour. A number of 1-2 hour forecasts of this storm have been performed starting at different times in the storm evolution. In general, the numerical forecasts outperform other methods based on persistence, extrapolation and rule-based techniques. Some of the outstanding issues and problems in short-term numerical prediction of thunderstorms will be discussed at the Conference along with future planned research.

#### MC04/L/03-B1 1205

##### PRECIPITATION AND FISH KILLS: ARE THEY RELATED?

L. J. PIETRAFESA; L. Xie (Dept. of MEAS, N.C. State University, Box 8208, Raleigh, NC 27695-8208, USA); N. E. Huang (Laboratory for Hydrospheric Processes/Oceans and Ice Branch, NASA Goddard Space Flight Center, Greenbelt, MD 20771, USA)

Quantifying precipitation presents an important challenge, particularly as it relates to societal impacts. One such area of concern is the combination of precipitation and ensuing drainage of fresh, buoyant and often nutrient-rich water into coastal regions. Fishermen and coastal residents have long been witness to the occurrences of fish kills in river and estuary waters. Causes are often ascribed to natural environmental events which result in anoxic conditions. In recent years, fish kill occurrences have received massive public attention and political scrutiny because of the perceived increased exposure of people who are dependent upon the use and health of coastal and estuarine waters for their livelihood, eg. Fishing, agriculture and ecotourism. As an outcome of the public debate that has ensued, state and federally subsidised studies in support of determining causes, effects and solutions have been established. Albeit, to date few of these studies has focused on the time history of fish kill occurrences and their potential correlation with environmental factors. A pre-conditioning of the water environment which places the fish community at risk is a possibility. This paper looks at the documented history of fish kills, reported over eleven years in two adjacent North Carolina river estuaries in relation to several environmental factors: including precipitation, river discharge, atmospheric temperature and winds. A new empirical mode decomposition technique is used to analyse the non-linear, non-stationary time series used in the analyses. Results indicate that quantitative precipitation forecasting at river basin scales is key to coastal management strategies.

### SIMULATIONS OF EXTREME EVENTS, EDUCATION AND TRAINING

#### MC04/W/11-B2 1400

##### QUANTITATIVE PRECIPITATION FORECASTING OF EXTREME PRECIPITATION EVENTS

Deborah J. ABBS (CSIRO Atmospheric Research, Private Bag No. 1, Aspendale, Vic. 3195, Australia, Email: debbie.abbs@dar.csiro.au)

The CSU Regional Atmospheric Modelling System (RAMS) has been used to model extreme precipitation events that have occurred along the steep, coastal escarpment of the Sydney-Illawarra region of south-eastern Australia. Results have been obtained at a horizontal resolution of 7 km. Two types of synoptic-scale systems have been modelled, (i) an east-coast low and (ii) an upper-level cut-off low. Both cases were associated with 24-hr rainfall in excess of 300 mm. East coast lows have been identified as the major cause of flood-producing rains on the east coast of Australia, and are characterised by heavy rainfall and strong winds. In contrast, upper-level cut-off lows are usually associated with intense thunderstorms. For each system, simulations both with and without parameterised convection on the finest mesh have been performed. We have found that the use of an appropriate convective parameterisation scheme at these resolutions has the effect of triggering convection at both the correct location and time and produces good quantitative precipitation forecasts. In this presentation we will (a) show that a convective parameterisation scheme may need to be used at grid resolutions of the order of 10 km and (b) investigate the coupling between the convective scheme and boundary layer processes that occurs in these case studies.

#### MC04/W/08-B1 1425

##### NUMERICAL SIMULATION OF THE 28 JULY 1997 FORT COLLINS, COLORADO, FLASH FLOOD

C. Travis ASHBY (Department of Atmospheric Science, Colorado State University, Fort Collins, Colorado 80523, USA, Email: ashby@chubasco.atmos.colostate.edu); Dr. William R. Cotton (Department of Atmospheric Science, Colorado State University, Fort Collins, Colorado 80523, USA, Email: cotton@isis.atmos.colostate.edu)

The Regional Atmospheric Modelling System (RAMS) is being used to simulate the 28 July 1997 Fort Collins, Colorado, flash flood. Nested model grids are used, allowing explicit simulation of synoptic, meso and convective scale motions. The processes responsible for initiating and maintaining the quasi-stationary, flood-producing convection are investigated. The mechanisms for modulating the precipitation intensity during the event are also examined. This includes the observed acceleration of easterly winds preceding the time of heaviest precipitation. The convective bands which were observed to originate over central and north-central Colorado and propagate north-eastward over the Front Range at the time of flooding are also present in this simulation. The influence of these convective bands in intensifying the pre-existing convection over the northern foothills of the Front Range is also studied. Several experiments are being conducted to determine the sensitivity of the simulation to the initial conditions and model physics. The varying parameters in these sensitivity tests include soil moisture, topography resolution, initial cloud amount and distribution, initial wind and moisture perturbations, hydrometeor size distribution and complexity of moist thermodynamics (liquid phase only vs. mixed phase microphysics). These simulations indicate that initial cloud cover characteristics can influence storm outflow properties and storm propagation characteristics through the model surface temperature and low-level moisture fields.

#### MC04/W/06-B1 1450

##### NUMERICAL SIMULATION OF THE 16-19 OCTOBER 1994 SOUTH-EAST TEXAS HEAVY RAIN EVENT

Thomas PETROSKI, John nielsen-gammon (Texas A&M University, College Station, TX, 77843-3150, USA; email: n-g@tamu.edu)

During the period from 16 October through 19 October 1994, a mesoscale convective system developed within a weakly forced large-scale environment resulting in very heavy rainfall with subsequent widespread flash flooding that affected much of south-east Texas. Liberty, Texas, about 55 km north-east of Houston recorded 77.5 cm of rain and an area greater than the state of South Carolina received in excess of 25.4 cm of rain.

Simulations using the PSU-NCAR Mesoscale Model are conducted to explore the degree to which a high resolution model can reproduce this heavy rain event. In order to include synoptic and mesoscale features into the analysis which are important for correctly simulating a heavy rainfall event, initial conditions are generated using four dimensional data assimilation techniques. Model simulations utilise the Grell cumulus parameterisation scheme, the Reisner mixed-phase explicit scheme, and high resolution grids (i.e. 36 and 12 km). Preliminary model results show precipitation totals and distributions are very sensitive to the choice of grid resolution. The convective scheme initiates and maintains convection over much of the Gulf of Mexico even though none was occurring in the real case. Since we are interested in determining the critical mesoscale elements important for simulating a heavy rain event, future simulations will test higher grid resolutions (e.g. 4 km) over south-east Texas using only an explicit parameterisation scheme.

#### MC04/W/10-B1 1515

##### SIMULATIONS OF EXTREME PRECIPITATION EVENTS IN THE SOUTHERN UNITED STATES: SENSITIVITY TO GRID RESOLUTION

John NIELSEN-GAMMON, John Strack (Texas A&M University, College Station, TX, 77843-3150, USA; e-mail: n-g@tamu.edu)

We test the performance of the Penn State/NCAR Mesoscale Model, Version 5.2 in simulating five extreme precipitation events that occurred in the south-eastern United States during the past five years. All five events produced point totals of close to 1 m of rainfall in a short period of time, and were generally not of the same nature as the more widely studied continental mesoscale convective systems. The sensitivity of the model to grid resolution is tested by performing a large number of simulations at a wide range of resolutions using both explicit and parameterised convection. Based on preliminary results, we expect to find extreme sensitivity to explicit versus parameterised convection and fairly high sensitivity to grid resolution. We shall also explore the extent to which increases in grid resolution cause the model simulations to converge toward a particular solution.

MC04/W/16-B1

1620

**IMPACT OF CHOICE OF CONVECTIVE PARAMETERIZATION ON MODEL QPF-HORIZONTAL RESOLUTION DEPENDENCE**

William A. GALLUS Jr. (Iowa State University, USA, E-mail: wgalus@iastate.edu)

A workstation version of the Eta model is used to simulate three excessive rainfall events in the Central United States. The episodes reflect a wide range of meteorological situations: (i) a warm core cyclone in June 1996 generated a meso-beta scale region of excessive rainfall from echo training in its warm sector while producing excessive overrunning rainfall to the north of the warm front, (ii) a fairly typical mesoscale convective complex in July 1996 produced excessive rainfall and (iii) tornadic thunderstorms in May 1997 resulted in small-scale excessive rains. Model peak QPF sensitivity to horizontal resolution is investigated using grid spacing of 78, 39, 22 and 12 km. In addition, both the operational Betts-Miller-Janjic (BMJ) and Kain-Fritsch (KF) convective parameterizations are used. The three cases exhibit strikingly different QPF behavior as resolution is refined, and differences are shown to be related to the design of the convective parameterizations. The aggressive BMJ scheme tends to reduce the resolution dependence of QPF by preventing a significant grid-resolved component of precipitation under moist conditions with modest instability. In some cases, peak precipitation may actually decrease as resolution improves. Under the same conditions, the KF scheme promotes the grid-resolved component, resulting in large sensitivity of QPF to resolution. In the July MCS case for instance, peak QPF increased by nearly 1800% as resolution improved from 78 km to 12 km. In cases with extreme instability (such as the May 1997 case), a stronger resolution dependence occurs with the BMJ scheme; the KF scheme triggers too quickly in the strongly forced environment, with a different simulated evolution of events. The variability of results suggests that an understanding of convective parameterizations would benefit forecasters, and implies that an ensemble approach to the prediction of excessive rainfall may be of more benefit than the use of just one especially high resolution model simulation.

MC04/W/07-B1

1700

**EXCESSIVE SHORT-DURATION RAINFALL FROM WARM SEASON CONVECTION**

Matthew KELSCH (UCAR/COMET, USA, e-mail: kelsch@comet.ucar.edu)

Short-duration, localized excessive rainfall is among the most difficult to forecast due to the rapid storm evolution and complex storm-scale interactions involved. The storm complexes responsible for such events are often focused by terrain, pre-existing mesoscale boundaries, and meteorological boundaries generated by the storm system itself. When the precipitation occurs over hydrologically sensitive areas, such as steep terrain or small urbanized basins, severe flash flooding can result. Accurate Quantitative Precipitation Forecasts (QPF) for such events requires detailed understanding of the mesoscale processes that result in enhanced precipitation efficiency and prolonged duration over a localized area. The Cooperative Program for Operational Meteorology, Education and Training (COMET) at the University Corporation for Atmospheric Research (UCAR) in Boulder, Colorado, USA, has developed a thorough set of multimedia material for training in the hydrometeorological sciences. These materials exist in electronic form on compact discs, in Web-based material, and in an online case study library. In addition, a Hydrometeorology course as offered at the classroom facility. Participants receive presentations from experts on various topics in hydrology and meteorology. Laboratory exercises use a variety of flood events, including several warm-season events involving intense, localized precipitation. The material is designed to demonstrate the utility of mesoscale observing and modeling methodologies as well as the importance of the human forecaster in flash flood situations.

Tuesday 27 July AM

Presiding Chair: A.J. Illingworth (Univ. of Reading, Dept. of Meteorology, UK)

**RAINFALL ESTIMATION TECHNIQUES AND GLOBAL MODEL PERFORMANCE**

MC04/W/12-B2

0925

**REAL TIME SATELLITE RAINFALL ESTIMATION OF HEAVY PRECIPITATION IN THE TROPICS AND SUBTROPICS - EXPERIENCE WITH AN EXPERIMENTAL/OPERATIONAL TECHNIQUE**

Gilberto A. VICENTE, Rod A. Scofield (NOAA/NESDIS, Office of Research and Applications, E/NP2 4700 Silver Hill Road, Washington, DC, 20233-9910, USA, email: gvicente@nesdis.noaa.gov)

An automatic precipitation estimation technique (called the Auto-Estimator) has been developed for GOES-8/9/10 data, Vicente et al., 1998. This algorithm has been used experimentally in NESDIS for estimating rainfall from convective systems during flash flood situations for 3 years. Recently it was used by the US National Weather Service during 6 weeks in August/September on the test/operational environment. Characteristics of the Auto-Estimator include a rain rate curve based on the 10.7 micron temperature, and adjustments for cloud growth, cloud gradients, and moisture. Currently, the Auto-Estimator uses half hour data to compute 4 by 4 Km resolution real time 1-hour estimates and 3-hour totals every half hour, 6-hour totals every hour and 24-hour totals once a day. The 1-hour estimates and 24-hour totals have been archived since September/96 for sub-synoptic and mesoscale analyses. The Auto-Estimator takes into account orograph and wind information and adopts cloud top satellite parallax corrections for better location and estimation of the heavy precipitation cores on the cloud system. The objective of the presentation is to show results of the NOAA/NESDIS experience in dealing with flash flood watch and warning situations using an automated rainfall estimation technique in combination with other information sources [ground observations (radar and gauges) and models (wind speed and direction, precipitable water, relative humidity)]. We will discuss the advantages and disadvantages of the automated technique in comparison with the more established manual Interactive Flash Flood Analyzer technique (IFFA, Scofield 1987) in operational use by NOAA/NESDIS US National Weather Service for the last 15 years. Attention also will be given to the use of an extension of the US version of the Auto-Estimator to South America and the possibilities for the use and implementation of the same technique for every tropical and subtropical region in the globe.

MC04/E/02-B2

0950

**RADAR VALIDATION OF CONVECTIVE AND DYNAMIC PRECIPITATION FORECASTS**

Anthony J. ILLINGWORTH (Department of Meteorology, University of Reading, Reading RG6 6BB, UK, email: a.j.illingworth@reading.ac.uk)

Radar is one of the most attractive means of validating quantitative precipitation forecasts because its spatial coverage is superior to that of a point rain gauge. The shortcomings of radar estimates of rainfall are well known: two of the major ones are the vertical profile of reflectivity and absolute calibration of the return power in terms of reflectivity, Z. In this paper

we will indicate how corrections for vertical profile can be made by using two profiles, one for bright band and one for non-bright band cases, by using a threshold value of Z of 30dBZ at a height 1.5km above the freezing level to indicate when a bright band is absent. The two classes of profile should also provide a separation into convective and dynamic rainfall and provide validation of the contributions made by the two precipitation schemes in mesoscale forecasting models. Accurate calibration of the Z return to within 0.5Db can be provided by exploiting the redundancy of two of the polarisation parameters when observed in rain: the differential reflectivity and differential phase shift. This automatic calibration of the reflectivity values every time there is moderate or heavy rain could turn out to be one of the most powerful uses of the polarisation technique.

MC04/W/13-B2

1050

**QUANTITATIVE PRECIPITATION FORECASTS BASED ON OPERATIONAL NWP MODEL PRECIPITATION FIELDS**

John L. McBRIDE, E. Ebert, and K. Puri (Bureau of Meteorology Research Centre, Melbourne, Australia)

Results are presented of recent developments in operational QPF in the Bureau of Meteorology. Real-time gridded 24-hour precipitation forecasts from seven operational NWP models are verified over two large subregions of the Australian continent: the Northern tropical monsoon regime, and the south-east subtropical regime. All forecasts have been mapped to a one-degree latitude / longitude grid and have been verified against an operational daily rainfall analysis, mapped to the same grid. Verification statistics include bias score, probability of detection, false alarm ratio, root mean square error, correlation and mean absolute error. Our main measure of skill, however, is the Hanssen and Kuipers score, and its two components: accuracy for events and accuracy for non-events. The aim is to establish the current skill level in both regions as a basis for comparison with later models and longer lead-time forecasts. Results are calculated as a function of rain threshold; and a compact presentation of results is obtained through the use of phase-space diagrams, with HK score, accuracy for non-events as the three co-ordinates.

The same seven operational models are used to develop a combined model forecast, based on a weighted average of the seven models. Methods of combining include simple averaging and weighted averages based on inverse error variances. Other methods of combining forecasts are explored based on multiple linear regression and stepwise regression. We also experiment with correcting the individual models before averaging based on errors in either rain volume or rain area. Lastly, the weights are calculated for a three month period, then recalculated at monthly intervals as a form of adaptive filter.

Other aspects of our development will be briefly described, including a graphical user interface for operational forecasters to obtain maps and line plots of analysed rain, QPF and verification statistics for all models. Also we will describe some results on the concept of verifying contiguous rain areas (or CRAs) rather than single point measures.

MC04/W/14-B2

1115

**THE DIURNAL CYCLE OF PRECIPITATION IN THE ECMWF GLOBAL FORECAST MODEL: DESCRIPTION AND SENSITIVITY**

D. GREGORY (ECMWF, Shinfield Park, Reading RG2 9AX United Kingdom E-mail: dgregory@ecmwf.int)

In common with many NWP and climate models, the ECMWF global forecast model has tendency to predict the onset of diurnally driven convection too early. This leads to an over prediction of precipitation before local noon over continental regions during the summer season. The early onset of convection is due to the response of the convection scheme to the rapid transition of the dry boundary layer from stable conditions during the night to an unstable profile soon after sunrise. Failure of the convection scheme to respond to longwave cooling of the mid-troposphere during the night exacerbates the problem, allows instability to build towards sunrise assisting the rapid development of intense convection.

Revision of the triggering algorithm used to diagnose the presence of convection and its impact upon the diurnal cycle of convection will be discussed. The formulation of lateral entrainment above cloud base also has an impact upon the onset of precipitating convection. A new formulation in which entrainment is linked to the buoyancy of a parcel inhibits the development of convection to a greater extent than the fixed values of the current scheme.

MC04/E/03-B2

1140

**THE STUDY OF THE PRECIPITATION FORECASTS IN THE SL-AV GLOBAL NWP MODEL**

Mikhail TOLSTYKH, Igor Esau (both at Institute of Numerical Mathematics, Russian Academy of Sciences, 8 Gubkina str., 117951 GSP-1 Moscow, Russia, e-mail: tolstykh@inn.ras.ru)

This work studies the quality of medium-range precipitation forecasts in the recently developed global semi-Lagrangian model SL-AV with the resolution 1.5 degrees and 28 vertical levels. The basic version of this model uses the parameterizations of subgrid-scale processes from the French operational model ARPEGE/IFS, where the convection is parameterized by a mass-flux scheme. The experimental version includes the modified Betts-Miller scheme and the modified Smith scheme for stratiform precipitations. The latter allows to take into account the variability of precipitation related with the Ns-type cloudiness. The results for the series of five-day forecasts with the basic and experimental versions of the model and their comparison with the observations are described.

MC 04/E/08-B2

1205

**A NEW IDEA TO IMPROVE CHINA SUMMER PRECIPITATION FORECASTING**

DONG Wenjie, Wei Zhigang (both at Lanzhou Institute of Plateau Atmospheric Physics, Chinese Academy of Sciences, Lanzhou, Gansu, 730000, P.R.China, email: dwj@ns.lzb.ac.cn)

At present, the dynamic model method and the statistical climatic method are used at flood-season precipitation forecasting. The difficulty of the dynamic method is that it is too far a way to fit an operational prediction's requirement and the limit of the statistical method is that it has no power facing the case that the multi-factors are simultaneously abnormal. By the examples to predict the precipitation of summer in 1998 in China, a new idea of the dynamical-statistical forecasting combination is found out: In the case that two or more factors are simultaneously abnormal, use the dynamical model to separate and diagnose the dependent contribution of each abnormal factor and the combining contribution of multiple abnormal factors. The EOF analysis is applied to the numerical experiment to predict summer precipitation anomalies. The main forecasting result accords with the real distribution of summer precipitation anomalies in 1998 in China.



Tuesday 27 July PM

Presiding Chair: A. Crook (NCAR, Boulder, USA)

**DATA ASSIMILATION, VERIFICATION AND NON-DYNAMICAL FORECAST SYSTEMS****MC04/E/01-B2****1400****EFFECTS OF MIXED-PHASE PROCESSES ON SHORT-RANGE RUC QPF**

John M. BROWN, Georg Grell, Stan Benjamin, and Tanya Smirnova (NOAA/Forecast Systems Lab; 325 Broadway, Boulder, Colorado 80303 USA, Email: jmbrown@fsl.noaa.gov)

The Rapid Update Cycle (RUC) running at NCEP in the U.S. includes in its forecast model a detailed mixed-phase bulk microphysics scheme adopted from the NCAR/Penn State MM5 model. This scheme includes explicit forecasts of mixing ratios of 5 different hydrometeor species. Previous experiments showed that the inclusion of this scheme into the RUC improved QPF over that previously produced by a simple supersaturation removal. In this study, we investigate the overall effect of ice processes as well as the role of specific water-to-ice conversion processes on the 3-D structure of model-predicted precipitating systems and on the resulting QPF.

**MC04/E/07-B2****1425****EFFECTS OF GOES CLOUD-TOP ASSIMILATION INTO RUC MIXED-PHASE CLOUDS ON SHORT-RANGE QPF**

Stan BENJAMIN, Dongsoo Kim, Tanya Smirnova, and J. M. Brown (NOAA/Forecast Systems Laboratory, Boulder, CO 80303 USA, email: benjamin@fsl.noaa.gov)

Initial conditions of water vapor and hydrometeors are clearly critical to an accurate very short-range precipitation forecast. The Rapid Update Cycle (RUC) is a high-frequency (1-h) short-range assimilation/forecast system running at NCEP in the United States. The RUC includes a mixed-phase bulk microphysics scheme in its forecast model. At present, the RUC initializes hydrometeors by simply using the 3-D distribution of hydrometeor mixing ratios from the previous 1-h RUC forecast. Recognizing that these forecasts have significant errors resulting in large part from errors in initial conditions, FSL has begun experiments combining cloud-top pressure data from GOES with the model 1-h forecast for modified initial conditions of cloud water and ice. In this paper, we will present a study on the effects on 3-6h precipitation forecasts of this GOES cloud-top assimilation.

**MC04/E/06-B2****1450****VERIFICATION OF SHORT RANGE RUC PRECIPITATION FORECASTS USING THE NCEP EXPERIMENTAL STAGE-4 HOURLY PRECIPITATION ANALYSES**

Barry SCHWARTZ, Stan Benjamin (NOAA/Forecast Systems Laboratory; 325 Broadway, Boulder, CO 80303 USA, Email: schwartz@fsl.noaa.gov, benjamin@fsl.noaa.gov)

The Rapid Update Cycle (RUC) is a model that was developed at NOAA's Forecast Systems Laboratory and has been implemented operationally at the National Centers for Environmental Prediction (NCEP). The RUC has a unique role within the U.S. National Weather Service in that it is the only operational system that provides updated national scale Numerical Weather Prediction (NWP) analyses and forecasts more often than once every 6 hours. QPF forecasts from the RUC are produced hourly out to 3-h in advance, and 3-hourly out to 12-h in advance of the initial cycle run time. At NCEP an experimental real-time hourly, multi-sensor U.S. National Precipitation Analysis (NPA) was developed in the mid 1990s. Over the lower 48 states, this analysis merges approximately 2500 hourly raingauge observations obtained in real-time with hourly digital precipitation radar estimates. The NPA and the RUC give us a unique opportunity to examine frequently updated short-range QPF characteristics of an operational NWP model. Standard QPF Skill scores for 1- and 3-h accumulated RUC precipitation forecasts will be presented for part of the winter and the spring of 1999. A brief discussion of the ongoing development of the RUC and NPA systems will be included.

**MC04/W/05-B2****1515****QUANTITATIVE EVALUATION OF CUMULUS PARAMETERIZATION SCHEMES IN AN OPERATIONAL MESOSCALE MODEL**

Chi-Sann LIU (Naval Research Laboratory, Monterey, CA, USA)

Three cumulus parameterization schemes: relaxed Arakawa-Schubert, Kain-Fritsch, and Kuo are evaluated within the US Navy operational model of Coupled Ocean/Atmosphere Mesoscale Prediction System (COAMPS). The operational model has been run with the three cumulus parameterization schemes for 20 days in winter 98/99 over the US with two-level nested grids of 81km and 27km resolution. Equitable threat scores and biases are computed and compared among the three schemes to serve as objective measures of the quantitative precipitation forecast skills. In addition, two heavy rainfall cases, one in subtropical and the other in mid-latitude areas, are selected to examine in details the forecast skills of the three cumulus parameterizations in severe weather situations. In the case studies, 9km third-mesh grids are also included in the evaluation. The preliminary results indicate that the Kuo scheme over-predicts while the Kain-Fritsch scheme under-predicts precipitation in COAMPS.

**MC04/W/09-B2****1600****THIRTY THREE YEARS OF QUANTITATIVE PRECIPITATION FORECASTING DURING THE SUMMER CONVECTIVE SEASON IN THE UNITED STATES**

David W. REYNOLDS (Hydrometeorological Prediction Center, 5200 Auth Road Room 410, Camp Springs, MD 20746, USA, Email: david.reynolds@noaa.gov); Bruce Terry (Hydrometeorological Prediction Center, 5200 Auth Road Room 410, Camp Springs, MD 20746, USA, Email: bruce.terry@noaa.gov)

The HPC (Hydrometeorological Prediction Center), a service center within the National Weather Service's National Center for Environmental Prediction, has been producing quantitative precipitation forecasts for over thirty years. These are 24-hour forecasts out through 24 and 48 hours. The forecast includes a graphical depiction of isohyets using .25, .5, 1.2, 3 ... inch amounts. In addition, the HPC has been computing 6 hour QPF's since 1981 for the 6 to 12 and 12 to 18 hour period. During the past three years we have expanded the 6-hour forecast to include the 0 to 6 as well as the 18 to 24 and 24 to 30 hour forecasts. The HPC has been keeping verification scores of all forecasts since its inception, both for the 24-hour and 6-hour forecasts. Not only are these forecasts verified against observations, but are also compared to the QPF as produced by the operational NWP (numerical weather prediction) models run at NCEP. This paper will concentrate on the verification statistics for the

convective season, May through August, for both the manual as well as the model forecast. As many of the more significant rainfall events during the US convective season are produced by mesoscale convective systems, by concentrating on the verification scores for the one and two inch isohyets, one can try to isolate how well the rainfall from these systems can be forecast. Year to year trends in scores will be related to either improvements in NWP or improvements in the knowledge base of the forecaster. Of special concern is the difference in skill between the 24 hour and six hour forecast amounts. As flash floods are more sensitive to rain-rate and thus the short term QPF, it will be important that the six-hour forecasts show sufficient skill as it is these values that are input to hydrologic forecast models. These results should provide the audience with the "state of the science" in QPF forecasting for convective systems, at least in the US.

**MC04/E/04-B2****1625****ASSIMILATING SATELLITE AND RADAR OBSERVATIONS INTO THE ETA MODEL TO IMPROVE CLOUD AND PRECIPITATION FORECASTS**

Qingyun ZHAO, Geoffrey J. DiMego, David F. Parrish, Ying Lin, Michael Baldwin, Eric Rogers, Kenneth A. Campana (Environmental Modeling Center, National Centers for Environmental Prediction, Washington, D.C. 20233, USA, Email: wd20cl@next4.wvrb.noaa.gov)

To further improve the model's cloud and quantitative precipitation forecasts and to study the method of optimally using various type of data in the data assimilation, an algorithm has been developed to combine the satellite data with radar observations in the Eta Data Assimilation System (EDAS). The Real-time, three-dimensional Neph-analyses (RTNEPH) from the US Air Force Global Weather Center are used in the data assimilation procedures to indicate the cloud locations both in the horizontal and in the vertical directions. Hourly precipitation analyses derived from NEXRAD observations over the United States are also employed to retrieve the total cloud water content. Several cases have been chosen to study the effects of the data assimilation on model precipitation forecasts. This algorithm was also continuously tested for about a month during a winter time. Results from all tests showed significant improvement in precipitation forecast during the 48-hour free forecast period. Efforts are also being made to expand this algorithm to use more observed data resources available at NCEP, such as GOES cloud images and radar reflectivity data from NEXRAD network. As progress is being made, more interesting results from this study will come out and be represented at the conference.

**MC04/L/02-B2****1650****THE MARITIME CONTINENT RAINFALL FORECASTING BY USING NEURAL ARTIFICIAL NETWORK METHOD**

Joko WIRATMO (Dept. of Geophysics & Meteorology, Institute of Technology, Bandung Jl. Ganesha 10 Bandung 40132 West Java, Indonesia, email: wiratmo@geoph.itb.ac.id)

Rainfall is the main weather element with an important role in tropically maritime continent region. The rainfall cycle is controlled by many predictable and unpredictable factors. Therefore, it is not easy to forecast rainfall quantity in any specific area. At the same time, the need for an accurate quantity of rainfall is acutely felt. Learning rainfall pattern is needed to build a forecasting model. One method to recognise the rainfall pattern is neural artificial network method that is better than the statistical extrapolation techniques. The aim of this paper is to apply neural artificial network to forecast rainfall quantitatively.

**MC04/E/05-B2****1715****NOWCASTS OF CONVECTIVE PRECIPITATION USING AN OBJECT-ORIENTED LIFE CYCLE MODEL OF A CONVECTIVE CELL**

Andrew COOPER, Clive Pierce (Forecasting Products, UK Met. Office, London Road, Bracknell, Berkshire, RG12 2SZ, UK, email: amcooper@meto.gov.uk)

Extensive operational trials of an object-oriented convective precipitation model (or object-oriented model) have recently been completed by the UK Meteorological Office, in collaboration with the Environment Agency (responsible for flood warning in England and Wales). This Object-Oriented Model (OOM) incorporates a conceptual model of the life cycle of a shower cloud, such as might be observed in mid-latitudes. Five developmental or cell stages are recognised. These encompass the developing, mature and dissipating phases in the life of a typical convective cloud. Cell stages are distinguished on the basis of vertical instantaneous rain rate profiles, derived from multiple beam C-band radar data. The vigour or development potential of a cell may vary, accounting for variations in cell duration, the quantity of precipitation produced, and whether or not the cell can trigger daughter cell development in its mature phase. Operational trials of the OOM have demonstrated its capability for generating reliable, very shortrange (0-3 hours ahead), high resolution (10 minute time step, 2 km resolution) precipitation forecasts during periods of airmass convection. In June 1999, the model will be implemented operationally within an automated nowcasting system known as GANDOLF (Generating Advanced Nowcasts for Deployment in Operational Land-based flood Forecasts). This system is designed to run the model when conditions suit. During periods of airmass convection, the OOM will run on a 15 minute cycle, and generate 10 minute instantaneous rain rate and 15 minute accumulation forecasts with lead times out to T+180 minutes. These forecasts may be relayed directly to Flood Warning Centres where they can be used by the Environment Agency in river flow modelling and flood prediction. In this presentation we will review the design of the OOM and consider strengths and weaknesses revealed by the operational trials. Case study material will also be presented to demonstrate the model's behaviour.

**MC05****Thursday 29 July****LAND-FALLING TROPICAL CYCLONES (ICCP)**

Location: Mechanical Engineering G33 LT

**Thursday 29 July AM**

Presiding Chair: Dr Kendal McGuffie

**Introduction****0900**

Dr. Kendal McGuffie

**MC05/E/01-B4****0910**



**UPWARD TREND IN GLOBAL INTENSE AND SUPER-INTENSE TROPICAL CYCLONE NUMBERS 1969-1997**

F. P. Roberts and M. A. SAUNDERS (both at Benfield Greig Hazard Research Centre, Department of Space and Climate Physics, University College London, Holmbury St Mary, Dorking, Surrey RH5 6NT, UK, email: mas@mssl.ucl.ac.uk)

We report the results of a study of the trends in global intense (maximum sustained winds of 33ms<sup>-1</sup>) and super-intense (maximum sustained winds of 50ms<sup>-1</sup>) tropical cyclone numbers for 1969-1997. We also examine trends in global intense landfalling events and 'high-impact' landfalling events. We define the latter by a population density threshold of 180 people/km<sup>2</sup>. We find that the annual (and seasonal) number of intense and super-intense events have increased by 32% and 59% respectively for 1969-1997. These upward trends are significant to 99%. Over the same period, the annual number of super-intense landfalling events has increased by 57% (significant to 91%), and the annual number of high-impact landfalling events has increased by 53% (significant to 84%). Similar trends occur for 1979-1997.

We discuss possible causes for these upward increases. While artificial biases produced by inhomogeneous retrieval methods may be a contributory factor, they are unlikely to have an influence on the similar upward trends found in the global number of landfalling and 'high impact' tropical cyclones.

**MC05/E/04-B4 0930****LANDFALLING TROPICAL CYCLONES IN THE ATLANTIC BASIN**

Jenni L. EVANS and Robert Hart (Department of Meteorology, The Pennsylvania State University University Park PA 16802 USA)

Rainfall induced damages associated with landfalling tropical cyclones are a major source of devastation in the United States. Recent climatologies of tropical cyclone rainfall impacts on the northeast United States and Canada reveal that tropical cyclones are the cause of major rainfall events every 2-3 years over most of this region. Locations, such as Boston and Cape Cod, which are particularly susceptible, with individual events every 5-6 years in which twice the normal monthly rainfall is measured as the result of a single tropical cyclone passage. At the time that these tropical cyclones are delivering such copious rainfalls, they are often undergoing complex structural changes that are poorly understood. These may result in the system simply decaying or it may evolve toward a new, extratropical-like system. Environmental indicators that discriminate between the lifecycle of the tropical cyclone through to a hybrid or truly extratropical cyclone will be presented and a theoretical underpinning for this evolution will be elucidated here.

**MC05/E/07-B4 0950****SECONDARY PRESSURE MINIMUM OBSERVED IN TYPHOON MIREILLE (T9119) INTERACTING WITH THE POLAR FRONT**

Toshihisa ITANO (Department of Geoscience, National Defense Academy, Yokosuka 239-8686, JAPAN, email: itano@cc.nda.ac.jp)

**MC05/E/02-B4 1010****LONG-RANGE FORECASTING OF U.S. LANDFALLING HURRICANES**

M. A. SAUNDERS and C. J. Merchant (both at Benfield Greig Hazard Research Centre, Department of Space and Climate Physics, University College London, Holmbury St Mary, Dorking, Surrey RH5 6NT, UK, email: mas@mssl.ucl.ac.uk)

**MC05/W/03-B4 1030****A NEW METHOD FOR PREDICTING LAND-FALLING TROPICAL CYCLONES**

Remata S. REDDY and Lail S. Hossain (Dept. of Physics, Atmospheric Sciences, and General Science, Jackson State University, Jackson, MS 39217, USA, e-mail: rsreddy@ccaix.jsums.edu) Richard L. Miller (NASA Earth System Science Office, Stennis Space Center, MS 39529, USA, e-mail: miller@Wpogate.ssc.nasa.gov)

Under the NASA/JOVE Program a study has been undertaken to investigate the ocean-atmosphere interactions over the Gulf of Mexico and their relation in the formation and development of tropical cyclones/hurricanes. Hurricane Predictive Index (HPI), a new method, has been developed for predicting the formation and development of land-falling tropical cyclones/hurricanes over Gulf of Mexico. This index characterizes the ocean-atmosphere interactions over the Marine Boundary Layer (MBL) in terms of heat, momentum, and moisture fluxes, scale height, pressure tendency, kinetic energy and instability. A positive index indicates no sign of formation of cyclones/hurricanes. A negative index indicates a significant formation and development of hurricanes. The index has been tested for the hurricane Opal which formed on October 4, 1995 over the Gulf of Mexico and made a land-falling on the same day. A strong negative index was noticed 2-3 days prior to the formation (Reddy et al., 1998). In the present study, the index has been further tested for hurricane Roxanne which formed and developed on October 10, 1995 over the Gulf of Mexico. Satellite images of Advanced Very High Resolution Radiometer (AVHRR) Sea Surface Temperature (SST) and NOAA's buoy data from the National Data Buoy Center at Stennis are used in this study. The study has indicated a strong negative index (-0.5 to -3.0) 2-3 days prior to the formation of hurricane Roxanne. The results were in good agreement with those of hurricane Opal. This method is useful to disaster relief agencies for reducing property damage and loss of life during these events.

**MC05/E/05-B4 1110****PLANS FOR THE USWRP HURRICANE LANDFALL PROGRAM**

Russell L. ELSBERRY (Department of Meteorology, Naval Postgraduate School, Monterey, California, 93943, USA, E-mail: elsberry@met.nps.navy.mil)

The United States Weather Research Program (USWRP) has adopted Hurricane Landfall as one of its three main foci. Whereas the USWRP has been in a planning and developmental stage, a major increase in funding is expected for a five-year program beginning 1 October 1999. The Hurricane Landfall program has five thrusts: (i) Improved prediction of the tracks of landfalling hurricanes; (ii) Understanding and prediction of the outer and inner wind structure; (iii) Observing and understanding the modification of the hurricane structure as the hurricane crosses the coast; (iv) Quantitative precipitation estimation and prediction during and following landfall; and (v) Understanding the socio-economic impacts of landfall. The goals and strategies in each of these thrusts will be presented.

**MC05/W/02-B4 1130****EVALUATION OF CHANGES IN TROPICAL CYCLONE WARNINGS SINCE 1964**

Kendal MCGUFFIE and Joanne Hall, Department of Applied Physics, University of Technology, Sydney, PO Box 123, Broadway, NSW 2007

Tropical cyclones cause considerable destruction, disruption of human activity and loss of life as they impact the coast. Over the last thirty years, forecast accuracy for tropical cyclone tracks has improved considerably. This improvement has come as a result of enhanced satellite observing systems and analysis techniques and as a result of greatly enhanced numerical weather prediction capabilities. There has, however, been little in the way of evaluation of the changes in tropical cyclone warnings issued as a result of these considerably improved forecasts. In this paper, the results of a preliminary study of forty tropical cyclones impacting the Coral Sea coast of Queensland, Australia are presented and the changes in cyclone warnings issued are evaluated. Interpretation of results from this preliminary study is not straightforward. The study was confined to the evaluation of the duration of the warning period and the linear length (measured as a straight line) of coastline warned. Preliminary results indicate slight decreases in the level of warning (time of warning and length of coastline warned) associated with cyclones in this region, although the factors influencing warnings are not restricted to meteorological factors and more work is needed to evaluate these changes.

**MC05/W/01-B4 1150****NUMERICAL SIMULATIONS OF LAND-FALLING TROPICAL CYCLONES WITH A HIGH-RESOLUTION MOVABLE MESH COUPLED TROPICAL CYCLONE-OCEAN PREDICTION SYSTEM**

Isaac GINIS and Clark Rowley (both at Graduate School of Oceanography, University of Rhode Island, Narragansett, Rhode Island, USA email: i.ginis@gso.uri.edu, c.rowley@gso.uri.edu)

A new coupled tropical cyclone-ocean model has been developed to study air-sea interaction under tropical cyclones. The tropical cyclone model is the GFDL/NOAA hurricane forecast model that is now in operational use by the US National Weather Service and by the US Navy. The ocean model is a new movable nested-mesh ocean model developed for air-sea interaction studies. Using a movable nested-mesh system for both the tropical cyclone and ocean models allows matching high horizontal resolutions to be maintained for the atmosphere and ocean in the vicinity of the storm. Both idealised and real-case simulations have been configured to test the performance of the coupled model and to examine the influence of the ocean coupling on the storm structure and intensity during landfall. The model is presently applied for tropical cyclone simulations in the eastern and western Pacific.

**MC05/E/03-B4 1210****HOW WELL DO NUMERICAL WEATHER PREDICTION MODELS ESTIMATE ATMOSPHERIC WATER VAPOR DURING A LAND-FALLING TROPICAL CYCLONE?**

Seth GUTMAN, Nicole Radziwill, Stan Benjamin, and Tracy Smith (all at NOAA Forecast Systems Laboratory, 325 Broadway R/E/FS3, Boulder, Colorado 80303 USA, Email: gutman@fsl.noaa.gov)

A brief introduction to ground-based GPS meteorology, emphasizing the ability to make accurate integrated precipitable water vapor measurements under all weather conditions, is presented. Independent GPS water vapor observations of a land-falling tropical cyclone (Hurricane Georges) are compared with estimates of total column water vapor produced by the NOAA Forecast Systems Laboratory MAPS/RUC-2 numerical weather prediction model. The potential impact of these observations on NWP forecast accuracy of land-falling tropical cyclones is discussed.

**MC05/E/06-B4 1230****STORM TIDE RISK IN TWO COMMUNITIES IN QUEENSLAND, AUSTRALIA**

Ken GRANGER (Australian Geological Survey Organisation, GPO Box 762, Brisbane, Queensland, 4001, Australia, Email: kgranger.agso@bom.gov.au)

Three major storm tide events, causing loss of life and substantial damage, have been experienced along the Queensland (Australia) coast over the past 100 years. The most lethal event, on 5 March 1899, was a storm tide, reported to have reached 14.5m above sea level, which killed at least 307 people from the pearling fleet sheltering in Bathurst Bay in the far north of the state, together with possibly 100 aboriginal people on shore. On 21 January 1918 a severe tropical cyclone struck the town of Mackay on the central coast, killing 30 people, of whom at least 13 were drowned in the storm tide that reached about 5.3m above sea level. Seven weeks later, on 10 March 1918, an even stronger cyclone struck the Innisfail area, 500km to the north of Mackay, killing perhaps 100 people with as many as 60 being drowned in the storm tide that reached at least 5.6m above sea level.

Whilst the Queensland coast has been crossed by at least 80 tropical cyclones since 1918, there has, fortunately, been no repetition of these earlier tragic storm tide impacts, though there have been several near misses. Over the same 80 year period, the population of coastal settlements has grown enormously to the point where today, almost three million Queenslanders (or 86% of the total) live within 50km of the coast. As many as a quarter of these are potentially exposed to the direct impact of storm tide.

The magnitude of this risk has only recently become apparent to the current generation of disaster managers and the local governments at risk, largely as the result of research conducted under the Tropical Cyclone Coastal Impacts Program (TCCIP) - a multi-agency and multi-disciplinary research program coordinated by the Australian Bureau of Meteorology. TCCIP researchers have adopted a comprehensive risk-based approach which takes account of both the hazardous phenomena associated with tropical cyclones (wind, rain and storm surge) and the elements at risk within the community (the people, buildings and infrastructure) and their vulnerability to hazard impact. Two Queensland cities, Cairns (a major tourist destination, service and sugar growing centre with a population 125 000) and Mackay (a rural service centre and transport node with a population of 55 000), have been studied in detail, with a particular focus on their exposure to the impact of storm tide.

This paper reports on the outcomes of this storm tide risk research and describes the quantitative risk analysis and risk assessment techniques employed. Particular emphasis is given to the data collected and the geographic information systems and spatial modelling tools developed to produce information of use to local officials to develop risk reduction strategies and disaster management options.

One of the potentially life-saving outcomes of this work is the capacity to forecast inundation levels for all buildings and roads in each community well before a threatening cyclone crosses the coast. This information will greatly enhance the process of evacuation and the allocation of shelter should a storm tide, of the magnitude of those experienced historically in Queensland, were to occur today.

## PLANETARY ATMOSPHERES AND THEIR EVOLUTION (ICPAE)

Location: Chemical Engineering, G35 LT  
Location of Posters: Old Gym

Tuesday 27 July AM

Presiding Chair: F.W. Taylor (Oxford University, Clarendon Lab., UK)  
Concurrent Poster Session

## TITAN'S ATMOSPHERE FROM ISO OBSERVATIONS

COUSTENIS Athena (Paris Observatory, France, Email: coustenis@obspm.fr)

Observations of Titan in the thermal infrared (2.36-45.2 micron) were performed by ISO, in Jan. and Dec. 1997, with resolving powers between 1500 and 3000 in the Grating mode and up to 30000 in the Fabry-Perot mode. Two pure rotational water lines were observed for the first time using the ISO/SWS/Grating (R=2000) at 39.4 and 43.9 micron, with fluxes of about 2 Jy over a continuum of 60 Jy [1], with S/N of about 8. The flux observed can be reproduced with a constant abundance of about 0.4 ppb, or with a recent photochemical profile [2] multiplied by a factor of 0.4. This yields a water vapor mole fraction of about 10 ppb at the 400 km altitude level). The inferred water influx at Titan at 700 km of altitude is compatible with the CO<sub>2</sub> observed abundance and similar to that found at Saturn [3]. This suggests that infalling material from Saturn rings may not be the dominant source of Saturn's water. The analysis of the 233-1500 cm<sup>-1</sup> spectrum of ISO/SWS has provided the thermal and compositional structure of Titan on a disk-average [4]. We have also tested available vertical profiles and inferred upper limits for a few likely candidates in Titan's stratosphere (such as benzene and allene) [4]. References: [1] COUSTENIS, A., et al., 1998. *Astron. Astrophys.* 336, L85. [2] LARA, L. M., et al., 1996. *J. Geophys. Res.-Planets*, 101, 23261-23283. [3] FEUCHTGRUBER, H., et al., 1997. *Nature*, 389, 159-162. [4] COUSTENIS, A., et al., 1999. Submitted for publication.

## MARS WATER ABUNDANCE BASED ON ISOTOPIC ANALYSIS

Suchita GHOSH (Department of Physics, Rajendra College, J. P. University, Chapra, Bihar 84 1301, India)

Isotopic composition of Martian water is extremely important for understanding the evolution of the planet's atmosphere. Water on Mars is present primarily as vapor in the atmosphere, adsorbed gas in the regolith, residual polar ice caps and subsurface ices. We have constructed a simple analytical model to estimate the amount of water based on the fractionation in deuterium to hydrogen (D/H) given loss of hydrogen to space and irreversible loss to the surface. Reported measurements of D/H from SNC meteorites and spectroscopic observations using Earth-based telescopes are employed to characterize the D/H evolution process. The D/H ratio in some of the SNC meteorites is found to be nearly equal to the present day value in the Mars atmosphere. This enrichment in D/H ratio is thought to reflect an interaction process involving water operating between atmosphere, regolith and rocks in SNC meteorites. Such exchange may have operated in aqueous or hydrothermal environment. The effects of replenishment of water from outgassing have also been examined. Our results show that atmospheric enrichment in D/H has occurred primarily through thermal escape of hydrogen to space. Although there is uncertainty in the interpretation of these results, they suggest a substantial loss of water to surface if Mars exchangeable global inventory of water has undergone transition from an initial large abundance to a meagre quantity at present.

## MIXING HEIGHT OF THE MARTIAN BOUNDARY LAYER

Ari-Matti Harri (FMI, Vuorikatu 15A, 00101 Helsinki), Arakel PETROSYAN (IKI, Profsoyuznaya 84/32, Moscow 117810, Russia, email: apetro@iki.rssi.ru)

The key features of the Martian boundary layer allow us to assume that its role on the global-scale and meso-scale atmospheric flows in Mars are different from the one at the Earth. At first Mars has a complicated nonhomogeneous terrain making the formation of a shear driven turbulent boundary-layer easy during the night, and further, it makes boundary-layer nonhomogeneous in convective conditions. At second, all diagnostic evaluations of the Martian boundary layer height predict it not to be small in comparison of the tropospheric height. All above mentioned makes the mixing height a key parameter in the Mars atmosphere studies. In suggested presentation we discuss different prognostic models for Mars mixing height determination and predict its diurnal evolution for Viking landing sites. In our mixing height model for Mars we assume that in the morning the mixing layer is nearly neutrally stratified. Hence the height of the shear driven turbulent boundary layer in the morning is used as the initial condition to solve prediction equations for the mixing height. The main model assumption in Mars mixing modelling is that development of an unstable boundary layer is governed by same kind of similarity relations that are also applicable at the surface layer with new dimensionless characteristics connected with mixing height.

## DOPPLER IMAGING OF PLANETARY ATMOSPHERES

N. MURPHY, S. Gillam, E.J. Smith (Jet Propulsion Laboratory, 4800 Oak Grove Dr., Pasadena, CA 91109, USA), W. Rodgers (The Eddy Company, Apple Valley, CA 92308, USA), A. Cacciani (University of Rome 'La Sapienza', P.le A. Moro 2, 00185-Roma, Italy), W. Wild, R. Rosner (University of Chicago, Dept. of Astronomy and Astrophysics, Chicago, USA)

Typically, planetary atmospheric motions are deduced by tracing the motions of visible cloud features or by measurements from in-situ instruments. While both these techniques have provided considerable insight into the atmospheric dynamics of our planetary neighbours, they suffer from obvious disadvantages: Only visible features can be tracked and in-situ measurements are difficult to accomplish and provide limited spatial information.

We have explored an additional technique, Doppler imaging, which takes advantage of the small Doppler shifts imposed on reflected solar absorption lines by planetary atmospheric motions. These small Doppler shifts are measured using a magneto optical filter (MOF) (Cacciani and Fofi, *Solar Phys.* 59, 179-189, 1978) mounted on the Table Mountain 1.2m telescope. They provide a snapshot of the line-of-sight atmospheric motions and can also be used to build a synoptic map of large-scale atmospheric circulation.

We will discuss the application of this technique to the atmospheres of Jupiter, Saturn and Mars and explore its strengths and weaknesses. Using the data we have collected so far we will estimate the increased spatial and velocity resolution available via Doppler imaging with larger telescopes.

## EFFECTS OF MAGNETIC FIELD ON THE DAYSIDE AND NIGHTSIDE IONOSPHERE OF MARS: SOLAR WIND - MARS INTERACTION

S.A. HAIDER (Physical Research Laboratory, Ahmedabad 380 009, India, email: haider@prl.ernet.in), S.P. Seth (Bhavan's R. A. College of Science, Ahmedabad 380 001, India) Anil Bhardwaj (Space Physics Laboratory, Vikram Sarabhai Space Centre, Trivandrum 650 022, India)

The magnetometer onboard Mars Global surveyor spacecraft has observed magnetic field above 100 km from the surface. This suggests that solar wind interaction with Mars is similar to that at Venus and active comets, that is, primarily an ionospheric-atmospheric interaction. To understand the solar wind - Mars interaction and its dynamical effect on the dayside and nightside ionosphere of Mars, a theoretical model is developed to study the magnetized and unmagnetized ionosphere of Mars. In the model the continuity and momentum equations are solved self consistently. Using this model the two dimensional profiles of ion and electron densities are obtained. It is found that the density decreases gradually with solar zenith angle up to 80 degree and then it drops rapidly near terminator. In the nightside region the electron densities below 150 km where O<sub>2</sub><sup>+</sup> is the major ion drop dramatically because of the lack of a photoionization source.

OXYGEN AND OZONE PRODUCTION IN CO<sub>2</sub>-RICH PLANETARY ATMOSPHERES

Ilias VARDAVAS, Georgia Vlastou (Department of Physics, University of Crete and Foundation for Research and Technology - Hellas Heraklion, Crete, Greece)

We use a 1-D radiative-convective photochemical model for an Earth-like planet with an atmosphere consisting of nitrogen and carbon dioxide at different atmospheric pressures. The planet's atmosphere is irradiated by different levels of ultraviolet radiation. The model computes the vertical temperature and chemical composition from the planet's surface to the lower thermosphere. We show that both at low and at high CO<sub>2</sub> pressures the production of oxygen and ozone is not significant. At pressures between 0.1 and 10 bar significant oxygen and ozone layers are formed. In addition it is found that ultraviolet flux enhancement towards Lyman-alpha reduces oxygen production. The results have important ramifications for biological evolution in CO<sub>2</sub>-rich planetary atmospheres.

## SEARCH FOR STRONGEST ALBEDO AND THERMAL INERTIA VARIATION INDUCED CIRCULATIONS IN THE MARTIAN ATMOSPHERE

Tero SILLI (Finnish Meteorological Institute, Geophysical Research, P.O.BOX 503, FIN-00101 Helsinki, Finland, Email: Tero.Siili@Fmi.Fi)

Modelling [1] has shown the plausibility of mesoscale circulations – albeit relatively weak – driven by variations in surface albedo (a) and/or soil thermal inertia (I). These circulations can be overwhelmed by stronger mesoscale circulations (e.g., slope winds) and large-scale flows (e.g., baroclinic disturbances). The anticorrelation of the a and I variations also tends to cause the two forcings to cancel out. For conditions conducive for observation of these circulations, as pronounced a and I variations, as high solar insolation and a season of as quiescent large-scale flows as possible are desirable. In this work a search for suitable combinations of surface areas (in the Martian equatorial and subtropical regions) and seasons has been conducted. Subsequently simulations corresponding to those regions and seasons have been made with the Department of Meteorology / University of Helsinki 2-D Mars Mesoscale Circulation Model (MMCM). Results of the simulations are presented as well as their relevance to, e.g., the site selection of the planned European NeLander mission are discussed. [1] Siili, T., 1996. *J. Geophys. Res.* 101, 14957- 14968.

## WAVE DISTURBANCES FROM THE COMET SL-9 IMPACTS IN JUPITER'S ATMOSPHERE

G. SCHUBERT (Dep't Earth & Space Sciences, UCLA, Los Angeles, CA, 90095-1567 USA, email: schubert@ucla.edu); R.L. Walterscheid, D. G. Brinkman (Space Sciences Laboratory, The Aerospace Corporation, Los Angeles, CA 90009, USA)

Wave disturbances due to the Shoemaker-Levy 9 (SL-9) cometary impacts into Jupiter's atmosphere have been simulated with a fully compressible (non-hydrostatic), time-dependent, non-linear, axisymmetric, f-plane, finite difference computational scheme. Energy is released in a cylindrical region with a radius of 250 to 1000 km as suggested by models of the re-entry of impact ejecta following the initial explosion. The model produces outward moving gravity waves at stratospheric altitudes with speeds and relative amplitudes in agreement with observations. The waves emerge from a cylindrical region of alternating inflow and outflow that extends high into the atmosphere in the main region of energy release. The disturbances originate as horizontally propagating waves at the periphery of this region thereby providing an explanation for the observed large initial radius (~450-700 km) of the main ring. The model results suggest that the waves are made visible by the inflow of particulate impact debris into outward moving rings of wave horizontal convergence. The results of this study remove the necessity to invoke a stable, water-rich, wave-trapping layer in Jupiter's atmosphere in order to understand the Comet SL-9 observations of dark wave-like rings expanding radially away from the impact sites.

Tuesday 27 July PM

Presiding Chair: S.K. Atreya (Univ. Michigan, Dept. of Atmospheres, Oceanic & Space Sciences, USA)

## SCIENTIFIC INTERPRETATION OF RECENT OBSERVATIONS OF THE GIANT PLANET ATMOSPHERES: EXCITEMENT AND CAUTION

Sushil ATREYA (Dept. of Atmospheric, Oceanic and Space Sciences, University of Michigan, Ann Arbor, Michigan 48109-2143, USA, email: atreya@umich.edu), Toby Owen (Institute for Astronomy, University of Hawaii, Honolulu, Hawaii, 96822, USA)

Without a doubt, recent observations from the Infrared Space Observatory and the Galileo Probe have contributed immensely to our understanding of the composition, structure and origin of the giant planet atmospheres. At the same time, they have revealed that the interpretation of these new data, exciting as they are, requires caution. We illustrate this point with several examples, particularly those derived from the ISO observations with relevance to hydrocarbon photochemistry on the giant planets, and from the Galileo Probe as related to the composition and structure of the clouds and the origin of Jupiter's atmosphere. These



illustrations are meant to alert the planetary community of the pitfalls that can be avoided with timely work on the relevant laboratory measurements and theoretical models, especially as we embark on an ambitious set of observations of Saturn and Titan from Cassini orbiter and the Huygens probe beginning in 2004.

**MC09/L/02-B2** Invited **1430**

#### THE ATMOSPHERE OF EUROPA AND ITS EVOLUTION IN THE ENVIRONMENT OF THE JOVIAN MAGNETOSPHERE

Darrell F. STROBEL (Johns Hopkins University, Baltimore, MD, 21218, USA)

This talk will first review the observational evidence for an oxygen atmosphere on Europa based on Hubble Space Telescope observations in 1994 and 1996 (Hall et al., Nature, 373, 677, 1995; Astrophys. J., 499, 475, 1998) and for an ionosphere on Europa detected by the Galileo spacecraft radio occultation measurements. Then I will summarise the salient conclusions from the recent model of Saur et al. (J. Geophys. Res., 103, 19,947, 1998) which provides a theoretical framework to interpret the observational data.

Suprathermal torus ions with a contribution from thermal ions sputter O<sub>2</sub> from the water ice surface and thermal torus ions remove the O<sub>2</sub> atmosphere by sputtering. For an oxygen column density of  $5 \times 10^{14} \text{ cm}^{-2}$  the calculated intensities of the oxygen lines 130.4 nm and 135.6 nm produced by electron impact dissociation are in excellent agreement with the observations by the Hubble Space Telescope. Mass balance is also consistent with this column density with a net atmospheric mass loss of  $50 \text{ kg s}^{-1}$ . Accordingly the atmosphere has a residence time of ~2 day in the presence of ion sputtering. The exobase is approximately 70 km above the surface. The dominant heat source in the atmosphere is Joule heating with magnitude of  $3 \times 10^{10} \text{ W}$ .

**MC09/W/11-B2** **1500**

#### BAND MODEL PARAMETERS OF LABORATORY MEASURED METHANE BANDS AND THEIR IMPACT ON THE INTERPRETATION OF NIMS SPECTRA

Kamaljit SIHRA (University of Reading, Department of Meteorology, 2 Earley Gate, Whiteknights, PO Box 239, Reading RG6 2AU, UK, email: sws98ks@met.rdg.ac.uk); John Remedios (University of Oxford, Atmospheric, Oceanic & Planetary Physics, Parks Road, Oxford OX1 3PU); Kimberly Strong (University of Toronto, Department of Physics, 60 St. George Street, Toronto, Ontario, M5S 1A7, Canada). Simon Calcutt and Frederic Taylor (University of Oxford)

The Jovian atmosphere, in the spectral region sounded by the Near-Infrared Mapping Spectrometer (NIMS) on the Galileo spacecraft, is dominated by methane and ammonia absorption bands. In support of the NIMS/GALILEO project, laboratory measurements of methane transmittances have been obtained in the 1800-9500 cm<sup>-1</sup> region, at an original resolution of 0.2 cm<sup>-1</sup>, for gas pressures from 0.2670 to 4965 mb and temperatures from 100 to 340 K. For the analysis of NIMS spectra, methane transmittances were degraded to 10 cm<sup>-1</sup> and fitted using random band models, with the Goody-Voigt band model with a continuum limit term providing the best fit. The fitting errors are discussed and the uncertainty in the parameterised variables are assessed. Selected self-broadened spectra of this study were also fitted with hydrogen-broadened spectra of Strong (1992) to determine the ratio of self-to-hydrogen broadening for methane. This is important for application of these band model results to Jovian conditions. An average value of  $1.40 \pm 0.07$  was determined for this ratio. The band model parameters were also used in a simple radiative transfer atmospheric model to assess the impact of these spectra on the interpretation of NIMS spectral data. The implication of these results are also discussed.

**MC09/W/10-B2** **1515**

#### JOVIAN ATMOSPHERIC STUDIES WITH THE GALILEO NEAR INFRARED MAPPING SPECTROMETER: AN UPDATE

F.W. TAYLOR (1), R.W. CARLSON (2), K.H. BAINES (2), P. IRWIN (1), A. WEIR (1), P. CAMPBELL-SMITH (1), S. CALCUTT (1), T. ENCRENAZ (3), P. DROSSART (3), M. ROOS-SEROTE (3), E. LELLOUCH (3), and G. ORTON (2). (1) Atmospheric, Oceanic & Planetary Physics, Oxford University, United Kingdom (2) Jet Propulsion Laboratory, Pasadena, USA (3) Département Spatial (CNRS URA 264), Observatoire de Paris, Section de Meudon, email: Francef.taylor@physics.oxford.ac.uk

In its first two years of operation since arrival at Jupiter in December 1995, the Near Infrared Mapping Spectrometer on the Galileo orbiter spacecraft obtained extensive coverage of the planet, including detailed coverage of the NEB 'hot spot' region and the Great Red Spot. The status of the analysis of this data will be presented, including recent results on the abundances and variability of several minor constituents (H<sub>2</sub>O, CH<sub>4</sub>, NH<sub>3</sub>, GeH<sub>4</sub>, CH<sub>3</sub>D, and PH<sub>3</sub>) and the cloud structure and morphology.

**MC09/L/03-B2** **1530**

#### IMPACT OF THE BEHAVIOUR OF THE EARTH'S INTERIOR UPON THE EVOLUTION OF THE EARTH'S ATMOSPHERE AND THE RISE OF OXYGEN

Miles OSMASTON (The White Cottage, Sendmarsh, Ripley, Woking, Surrey GU23 6JT, UK. E-mail: miles@osmaston.demon.co.uk)

At IUGG95 I outlined a new history of the Earth's internal evolution. That history can now be elaborated and its impact upon evolution of the atmosphere outlined. The story begins in the later stages of planetary accretion, with magmatic Fe<sub>2</sub>O<sub>3</sub> being reduced by the nebular atmosphere to Fe and 'subducted' to form the core. Some of the huge amount of water thus produced (several 100 Vocean) gave the early Earth a wet mantle with a low viscosity well able to convect away the great heat. Throughout the Archaean, a low-pH ocean (topped by a shallow oxygenated water layer beneath a dense CO<sub>2</sub>-N atmosphere) accumulated Fe<sup>++</sup> in solution. At 2.8Ga the ocean floor began to deepen, marking declining MOR height and mantle heat, and foreshadowing the 2.45-2.2 Ga 'hiatus' in mantle overturn seen as a gap in orogenic granitoid dates. Deepening ocean basins exposed the cratons to massive weathering. This lowered CO<sub>2</sub> and resulted in the Earth's first glaciation at 2.65Ga, followed at 2.35Ga by the Huronian glaciation during the 4km+ lowering of sea-level by the hiatus proper. During the hiatus the supply of reducing gases from MORs was shut off and oxygenic life was at last enabled to begin to win its battle against the Earth's reducing power. This resulted in deposition of uniquely vast amounts of banded ironstone formation during the 2.45-2.2Ga interval. Carbonates with a major positive excursion in  $\delta^{13}\text{C}$  at 2.2Ga mark the florescence of oxygenic life presented with non-acid shallow seas over planated cratons as renewed MOR activity raised sea-level. Thus both the lowering of CO<sub>2</sub> in the Earth's atmosphere and the rise of oxygen stem from changes in the Earth's internal behaviour, not from biological innovation.

**MC09/E/01-B2** **1545**

#### A NEW MODEL FOR THE INFRARED RADIATION OF THE MARTIAN ATMOSPHERE

Alexander KUTEPOV and Oleg Gusev (both at the Institute for Astronomy and Astrophysics, University of Munich, Scheinerstr. 1, 81679 Munich, Germany, email: aak@usm.uni-muenchen.de)

We present a new line-by-line model of the formation of the infrared radiation in the ro-vibrational bands of CO<sub>2</sub> and CO molecules in the Martian atmosphere. The model accounts for both vibrational and rotational non-LTE, line-overlapping effects, extinction due to dust particles, effects of the ground albedo, and absorption and transformation of the near-infrared solar radiation. The number of vibrational levels and bands treated is substantially extended when compared to previous models. The collisional kinetic inputs are also updated. The model utilises the accelerated lambda-iteration technique for the solution of the system of kinetic equations and the Feautrier radiative transfer algorithm. Vibrational temperatures, radiative cooling/heating, and the limb radiances in a few spectral regions are compared with those for less sophisticated models.

**MC09/W/06-B2** Invited **1630**

#### THE VERTICAL STRUCTURE OF MAJOR METEOROLOGICAL FEATURES ON JUPITER: THE GREAT RED SPOT AND WHITE OVALS BC AND DE

Kevin H. BAINES and Robert W. Carlson (CSIRO Atmospheric Research, PMB No. 1, Aspendale, 3195, Australia. E-mail: peter.baines@dar.csiro.au)

Multi-spectral imagery of Jupiter's Great Red Spot (GRS) and two White Ovals acquired by the Galileo/NIMS are used to constrain the spatial variability of the vertical aerosol structure and the distribution of ammonia in and around these most-prominent anti-cyclonic features. All three features exhibit a high-altitude core spanning about 3/4 of their visual size when viewed with moderate absorption wavelengths, indicating a bulk elliptical, "wedding cake" shape in their overall three-dimensional cloud structure. A distinctive spiral pattern within the GRS core is seen in moderate methane and hydrogen absorption bandpasses. This pattern - which has been modelled to show a 2 km variation in cloudtop pressure within the GRS - is inconsistent with a different spiral-shaped pattern observed in ammonia-sensitive wavelengths, thus indicating spatial variability not only in the column abundance of ammonia within the GRS, but in its mixing ratio as well.

White Ovals BC and DE were observed in February 1997, just a year before their unusual merger into a single feature. At the time of these observations, the centers of the two anticyclones were ~16 degrees apart, separated by a complex cyclonic feature which exhibited unusual spatial variability in its appearance in images acquired at ammonia-sensitive wavelengths. In particular, the northern half of this feature has the largest ammonia column abundance seen within the environs around the white ovals, indicating unusual variability in either cloud structure/altitude and/or ammonia humidity within the cyclone.

**MC09/E/09-B2** **1700**

#### ABRUPT CLIMATE CHANGES DURING THE LAST 6 600 YEARS IN SOUTH AFRICA

Peter TYSON (Climatology Research Group, University of the Witwatersrand, Johannesburg, South Africa, e-mail: ptd@crg.bpb.wits.ac.za); Wibjorn Karl and Karin Holmgren (Department of Physical Geography, Stockholm University, Stockholm, e-mails: karlen@natgeo.su.se and karin@natgeo.su.se)

Few high-resolution time series are available for subtropical latitudes in the southern hemisphere that permit the determination of sudden climate shifts and changing patterns of variability during the last six millennia. Recently, a quasi-decadal resolution, 6 600-year proxy climate record has been determined from a stalagmite taken from a cave in the Makapansgat Valley in northern South Africa. The series is characterised by periods of relative stability, periods of rapid change and times when rapid changes between extreme conditions were dominant. Rapidly changing patterns of variability with time are shown to be a feature of the entire record. The most extreme and prolonged episode in the entire record is shown to have occurred in the five centuries of cooling that constituted the Little Ice Age from 1300 to 1800. The depression of annual maximum temperature below the present-day 1961-1990 mean at the time of maximum cooling at 1700 was  $1-2 = 0.0\text{C}$ . Following maximum cooling at 1700, conditions ameliorated rapidly to revert to above-normal within fifty years. Other extreme shifts in the record are shown to have occurred within a decade or two. Changes in variability with time will be illustrated by determining the decadal variability in moving two-century time periods traversing the entire 6 600-year series.

Comparison of the stable isotope record for the Makapansgat valley with a similar high-resolution stalagmite isotope data for the Cango Cave in southern South Africa and an even higher-resolution record derived from corals on the south-western coast of Madagascar reveals that the Little Ice Age was a pronounced regional event over a large area of southern Africa. The spatial extent of the abrupt changes and sudden climate shifts at the different widely separated sites during the Little Ice Age will be assessed. Likewise, regional differences in temporal variability will be considered.

Finally, the nature of the regional atmospheric circulation changes forcing the abrupt shifts in climate over the last few millennia, particularly during the Little Ice Age event, will be considered. It will be shown how a combination of changes occurring in both mid-latitude baroclinic and tropical barotropic circulation features, together with sea surface temperature changes within and beyond the region, modulate the regional climate on annual to millennial time scales. A framework for the validation of regional climate models will be proposed.

**MC09/E/02-B2** **1715**

#### MODELING OF GRAVITY WAVE HEATING IN JUPITER'S THERMOSPHERE

Michael P. HICKEY (Department of Physics and Astronomy, 308 Kinard Laboratory, Clemson University, Clemson, SC 29634-1911, USA); Richard L. Walterscheid (Space and Environment Technology Center, The Aerospace Corporation, Los Angeles, CA 90009, USA); Gerald Schubert (Department of Earth and Space Sciences, University of California at Los Angeles, Los Angeles, CA 90095-1567, USA)

Measurements of Jupiter's upper atmosphere by the atmosphere structure instrument on the Galileo Probe revealed wave-like variations in the derived temperature profile that have been attributed to internal gravity waves. The possibility that these waves could be providing the energy required to maintain the relatively high (~900 K) thermospheric temperatures has been previously explored using WKB models describing gravity wave propagation. However, the observations have shown that the waves have large vertical wavelengths (~100 km), for which WKB analyses are not always expected to provide realistic results. In this paper we discuss the application of a full-wave model to characterise two waves observed in Jupiter's thermosphere having large vertical wavelengths. The horizontal wavelengths used are derived from published analyses. The model includes inhomogeneities due to the effects of eddy and molecular diffusion of heat and momentum, Rayleigh friction, Newtonian cooling, and the Coriolis force. The mean state required for the computations is provided by the Galileo Probe observations. The wave period required for the computations is calculated iteratively using



Newton's method constrained by prescribing a value of vertical wavelength at a reference altitude. Second-order wave energy terms are derived and used in the heat-flow equation to solve for the steady-state thermospheric temperatures. The whole process is repeated until convergence is achieved. We discuss the ability of the waves to maintain the high thermospheric temperatures.

**MC09/E/06-B2****1730****ON THE STREAM VELOCITIES IN THE JOVIAN ATMOSPHERE**

V.V.SHEVCHENKO, V.I.Chikmachev, S.I.Ivanov (Sternberg State Astronomical Institute, Moscow University, Universitetskii pr. 13, Moscow 119899, Russia, e-mail: shev@sai.msu.u)

It was studied the process of the dynamic development of postimpact formations in the Jovian atmosphere using results of photographic observations of Jupiter in the period of the impacts of the nucleus fragments of comet Shoemaker-Levy 9. The images were obtained by the AZT-22 telescope at the Maidanak Observatory. The structure of newly formed features was revealed, and the dynamics of their development during approximately 12 revolution periods of the planet was followed. The spatial structure of the largest details comprises a central column (plume) and a peripheral cloud of scattered ejection products. Within the accuracy of measurements carried out, the extent of the central ejecta plume remains roughly constant. The average top height of the plume over the level of the visible cloud layer is about 2500 km. The peripheral ejecta cloud is virtually at the level of the cloud layer. The tops of the central ejecta plumes have no proper motion in the latitudinal direction with respect to the rotating coordinate system III. Consequently, the images of these features can serve as reference points to study the dynamics of peripheral ejecta clouds. The measurements of the extent of largest new features in longitude, made in the photographs, showed that the peripheral clouds expand predominantly from west to east with respect to longitudinal position of the central ejecta plumes. Since, according to our estimation, the peripheral clouds are localised just on the level of the surface cloud layer of Jovian atmosphere, the dynamics of the new-born features will develop under the influence of local atmospheric streams. The velocities of the streams are from zero to 40 m/s in the different latitudes. The results are compared with Galileo's data concerning the clouds dynamics in the Jovian atmosphere.

**ICPAE MEETING****1745****Tuesday 27 July AM**

Presiding Chair: F.W. Taylor (Oxford Univ., Clarendon Lab., UK)

**MC09/W/07B2**

Poster

**0930-01****ATMOSPHERIC SCIENCE EXPERIMENT AT MARS - NETLANDER MISSION IN 2005**

A.-M. HARRI 1, A. Angrilli, S. Calcutt, D. Crisp, J.-P. Pommereau, F. Forget, V. Formisano, M. Fulchignoni, R.M. Haberle, S. Larsen, V. Linkin, T. Mäkinen, A. Petrosyan, J. Polkko, H. Savijärvi, T. Siili and J.E. Tillman. (1 Finnish Meteorological Institute, Geophysical Research, P.O.Box 503, FIN-00101 Helsinki, e-mail: Ari-Matti.Harri@fmi.fi)

ATMIS (Atmospheric and Meteorological Instrumentation System) is a versatile suite of atmospheric instrumentation to be accommodated onboard the Netlander Mission slated for launch in 2005. Four Netlanders are planned to form a geophysical measurement network on the surface of Mars. The atmospheric sciences are among the scientific disciplines benefiting most of the network concept. The goal of the ATMIS instrument is to provide new data on the atmospheric vertical structure, regional and global circulation phenomena, the Martian Planetary Boundary Layer (PBL) and atmosphere-surface interactions, dust storm triggering mechanisms, as well as the climatological cycles of H<sub>2</sub>O, dust and CO<sub>2</sub>. To achieve these goals the in situ observations made by the ATMIS sensors will be supported by extensive modelling efforts.

The ATMIS comprises sensors for the vertical profile of atmospheric pressure, temperature and density, as well as for surface pressure, temperature, wind, optical thickness and humidity. The ATMIS benefits from the heritage of instruments already built for missions as Mars-96, Huygens, Pathfinder, as well as the Mars Polar Lander. The characteristics of the atmospheric conditions and phenomena anticipated to occur at tentative NetLander landing regions, as well as the design and the predicted performance of the ATMIS are discussed.

**MC09/E/03-B2**

Poster

**0930-02****REEXAMINATION OF THOMPSON'S MECHANISM ON THE SPHERE**

Masahiro TAKAGI and Yoshihisa Matsuda (Department of Earth and Planetary Physics, University of Tokyo, 7-3-1 Hongo, Bunkyo-ku, Tokyo 113-0033, Japan, email: takagi@geoph.s.u-tokyo.ac.jp)

Thompson (1970) proposed a generation mechanism of a mean shear flow by the tilting instability of convection on a two-dimensional plane in order to explain the super-rotation of Venus atmosphere. In our study, Thompson's mechanism is reexamined both on the nonrotating and rotating spheres. First, two-dimensional Thompson's mechanism is reexamined. It is shown that a mean shear flow is generated not by a purely dynamical process neglecting temperature field but by a positive feedback among the mean shear flow, tilting convective motion and tilting temperature distribution. Second, a three-dimensional model is constructed in order to numerically obtain steady solutions which represent three-dimensional convection between the day and night sides on the sphere. The stability of the steady solutions is examined by linear analysis. For the case of no planetary rotation, the convection pattern is axisymmetric about a line between the subsolar and antisolar points. This convection pattern on the vertical section on the equator is very similar to that obtained in Thompson (1970). However, it is shown that this convection solution is stable. When the planetary rotation is considered, in some parameter ranges, the convection pattern is modified and restricted to the equatorial region by the Coriolis force. In this case, since the meridional flow becomes weak, it may be possible that the instability due to Thompson's mechanism takes place. However, it is found that the convection solution remains stable. These results suggest that Thompson's mechanism proposed for two-dimensional convection is not applicable to three-dimensional convection on the sphere.

**MC09/E/05-B2**

Poster

**0930-03****A MECHANISM OF THE SUPER-ROTATION ON THE VENUS ATMOSPHERE: MERIDIONAL CIRCULATION AND BAROTROPIC INSTABILITY**

Shinichi IGA and Yoshihisa Matsuda (Department of Earth and Planetary Physics, University of Tokyo, 7-3-1 Hongo, Bunkyo-ku, Tokyo 113-0033, Japan, email: iga@atmos5.geoph.s.u-tokyo.ac.jp)

The Venus atmosphere at the cloud top level rotates 60 times faster than the solid part. In this study, this super-rotation is investigated in the light of the upward transport of angular momentum by meridional circulation.

First, the generation of the super-rotation by this mechanism is examined by a 2-dimensional meridional model with very large horizontal viscosity. The super-rotation with mid-latitude jet is produced for some range of parameter values. The parameter-dependency of magnitude of super-rotation is examined in detail.

Second, the origin of the assumed "very large horizontal viscosity" is investigated in the light of barotropic instability. In our "barotropic" model, meridional and vertical advections of mean zonal flow by the meridional circulation are considered. The barotropic instability occurs intermittently and produces horizontal mixing of angular momentum. Two more interesting results are also obtained. One is oscillation of magnitude of the super-rotation and the other is a dipole structure in the polar regions. The former may be related to the observed variation of zonal wind distribution. The latter seems consistent with the infrared observations, except in size.

**MC09/W/01-B2**

Poster

**0930-04****SEARCH FOR STRONGEST ALBEDO AND THERMAL INERTIA VARIATION INDUCED CIRCULATIONS IN THE MARTIAN ATMOSPHERE**

Tero Siili (Finnish Meteorological Institute, Geophysical Research, P.O.Box 503, FIN-00101 Helsinki, Finland, Email: Tero.Siili@Fmi.Fi)

Modelling [1] has shown the plausibility of mesoscale circulations – albeit relatively weak – driven by variations in surface albedo (a) and/or soil thermal inertia (I). These circulations can be overwhelmed by stronger mesoscale circulations (e.g., slope winds) and large-scale flows (e.g., baroclinic disturbances). The anticorrelation of the a and I variations also tends to cause the two forcings to cancel out. For conditions conducive for observation of these circulations, as pronounced a and I variations, as high solar insolation and a season of as quiescent large-scale flows as possible are desirable. In this work a search for suitable combinations of surface areas (in the Martian equatorial and subtropical regions) and seasons has been conducted. Subsequently simulations corresponding to those regions and seasons have been made with the Department of Meteorology / University of Helsinki 2-D Mars Mesoscale Circulation Model (MMCM). Results of the simulations are presented as well as their relevance to, e.g., the site selection of the planned European NetLander mission are discussed.

[1]Siili, T., 1996. J. Geophys. Res. 101, 14957- 14968.

**MC10****Monday 26 July****SUBTROPICAL ANTICYCLONE DYNAMICS (ICDM)**

Location: Chemical Engineering G35 LT

**Monday 26 July AM**

Presiding Chair: Guo-Xiong Wu, (Chinese Academy of Sciences, Beijing, China)

**MC10/P/03-B1**

Invited

**0900****A REVIEW OF SUBTROPICAL ANTICYCLONES AS PART OF THE CLIMATE SYSTEM**

B.J. HOSKINS (Department of Meteorology, Reading University, Berkshire, UK)

In each hemisphere the winter subtropical anticyclone belt may be described to first order as the lower tropospheric part of the region of the descending branch of the Hadley Cell. However, there are significant zonal asymmetries. In the summertime these asymmetries are dominant. The summer subtropical anticyclones are intimately connected with continental monsoon behaviour. The ITCZs occur on their equatorial flanks and radiatively important stratus on their eastern sides. They act as important drivers for oceanic motions and surface temperatures.

**MC 10/E/01-B1****0950****THE ROLE OF MONSOONS IN THE EXISTENCE AND STRENGTH OF SUMMER SUBTROPICAL ANTICYCLONES**

Mark RODWELL (Hadley Centre, UK Met Office, London Road, Bracknell, RG12 2SY, UK, E-mail: mjrodwell@meto.gov.uk); Brian Hoskins (Department of Meteorology, University of Reading, PO Box 243, Earley Gate, Reading, RG6 6BB, UK, E-mail: B.J.Hoskins@reading.ac.uk)

The subtropical anticyclones (STAs), which occupy about 30% of the earth's surface, are usually related to radiative cooling and the descending arm of the zonal mean Hadley Cell. This explanation works well for the winter anticyclone belt. However, the summer STAs are generally stronger and more longitudinally localized to the oceanic regions than in winter. We have used a global atmospheric primitive equation model to investigate the summer and winter subtropical circulations. For the winter, we find that the interaction between the zonal mean flow and orography is sufficient to reproduce the observed STAs. For the summer season, we have focused on the North and South Pacific and North Atlantic anticyclones. We suggest that the basic cause of each summer STA is the latent heating over the continental monsoon region to the east. As this monsoonal heating moves poleward to near 25 degrees latitude, it can induce descent and equatorward motion over the eastern subtropical oceans. Orography acts to localize this motion. The descending air warms adiabatically leading to an enhancement of radiative cooling and an amplification of the descent. The suppression of convection is viewed in a similar way. The equatorward motion forms part of the eastern branch of the STA, which is thought to drive oceanic upwelling, leading to cold sea surface temperatures and reinforcement of the suppression of convection. Our results also suggest that the west African monsoon plays little part in forcing the North Atlantic STA through this mechanism. Instead, the forcing comes from the Asian summer monsoon which, although more remote, extends much further north. The extent of the Andes is such that they also have an appreciable impact on the summer South Pacific STA through interaction with the zonal mean flow.

**MC10/W/04-B1****0955****SIMULATION OF THE NORTH PACIFIC SUMMER SUBTROPICAL HIGH AND ITS SENSITIVITY**

Riyu Lu and Brian J. HOSKINS (Department of Meteorology, University of Reading, PO Box 243, Earley Gate, Reading, RG6 6BB, UK)

In summer, the intensity and position of the subtropical high over the North Pacific are closely associated with the intensity and seasonal progress of the East Asian summer monsoon. Rodwell and Hoskins (Hoskins, 1996) have proposed that the North American summer monsoon is important for setting the scene for this North Pacific subtropical anticyclone. To explore these issues further, we have used the UK Meteorological Office Unified Model, and

examined simulations with and without seasonal cycles. In the simulation without seasonal cycles (perpetual runs), the solar radiation is fixed on 1 July. The simulation with seasonal cycles captures very well both the temporal and spatial characteristics of the subtropical anticyclones, while in the perpetual runs the subtropical anticyclone over the North Pacific is simulated too far poleward. This is consistent with the proposal that the heating over the continents is important for this anticyclone. Analysis of both the seasonal cycle simulations and ECMWF re-analysis data shows that the subtropical high over the North Pacific shifts poleward in summer, whereas, the subtropical high over the North Atlantic remains at a relatively stable position. To examine the hypothesized sensitivity of the North Pacific subtropical anticyclone to the conditions on its eastward flank, simulations in which the cold sea surface temperatures near the western coast of North America are removed and in which the North American monsoon is suppressed are being performed. The results will be presented and conclusion made.

**MC10/E/02-B1****1040****SEASONAL EVOLUTION OF THE SUBTROPICAL HIGH DURING ASIAN MONSOON**

Hailan WANG (Department of Atmospheric Sciences, University of Illinois at Urbana-Champaign, Urbana, IL 61801, U.S.A., e-mail: h-wang1@atmos.uiuc.edu); Mingfang Ting (Department of Atmospheric Sciences, University of Illinois at Urbana-Champaign, Urbana, IL 61801, U.S.A., e-mail: ting@atmos.uiuc.edu)

The seasonal evolution of the subtropical Pacific high in northern summer has been found to be one of the important indicators for the East Asian monsoon onset and evolution. In this study, the dynamical mechanisms for the evolution of this high are investigated by using the GFDL general circulation model (GCM) data and the NCEP/NCAR Reanalysis. The data are divided into overlapping 30-day averages for the period April through September with a time interval of 10 days. A nonlinear stationary wave model is employed to investigate the forcing mechanisms for the seasonal evolutions of the location and intensity of the subtropical high. There is a systematic northward movement of the subtropical high from April to July in the GCM data and the NCEP/NCAR Reanalysis, and the movement is mainly related to the enhancement of heating in the tropics. A similarly significant southward movement is found from August to September. We are currently investigating the regional tropical heating centers that are most influential to the position of the subtropical high using Green's function analysis on different climatological basic states. The effect of the El Niño heating on the location and strength of the subtropical high is also under investigation. The relatively long record of the NCEP/NCAR Reanalysis data set can help reveal the interannual variability of the subtropical high. The results may be useful for understanding the variability of China monsoon rainfall as well as the monsoon evolution. Some interesting differences between the GCM and the NCEP/NCAR reanalysis will be discussed. A third dataset, the ECMWF reanalysis will also be used to shed light on the credibility of the reanalysis as a prototype for observations.

**MC10/E/04-B1****1105****A CLIMATOLOGY STUDY OF THE SOUTH ATLANTIC SUBTROPICAL ANTICYCLONE AND YOUR POSSIBLE INFLUENCE IN WEATHER SYSTEMS**

Ester Regina Kazuko Ito and Tércio AMBRIZZI (both at Departamento de Ciências Atmosféricas, Instituto Astronômico e Geofísico, Universidade de São Paulo, Rua do Matão, 1226 - CEP 05508-900, São Paulo, SP, Brazil, Emails: esterito@model.iag.usp.br, ambrizzi@model.iag.usp.br)

An automated procedure for finding and tracking high pressure centres has been applied for mean sea level pressure data set daily for 15 years period (1981-1996) from the NCEP (National Centers for Environmental Prediction) Reanalysis to investigate the behaviour of the South Atlantic Subtropical High (SASH). The area of interest extends from 0 - 60°S latitude and 20°E - 70°W longitude. We defined the climatology of the latitudinal and longitudinal variations of the high centre and analysed its function as "blocking anticyclone" and its influence in the general characteristics of the atmospheric circulation. This study was first done for winter months (June, July and August), period in which the SASH is most intensified. Once defined the climatology, a case study of the anomalous winter of 1995 was studied. During this winter the SASH was anomalously intense and worked as a strong atmospheric blocking acting on the dynamic-synoptic characteristics of the South America.

**MC10/W/02-B1****1130****SENSIBLE HEAT DRIVING AIR PUMP OVER THE TIBETAN PLATEAU AND THE SOUTH ASIAN SUBTROPICAL HIGH**

Weiping LI and Guoxiong Wu (State Key Lab of Atmospheric Sciences and Geophysical Fluid Dynamics (LASG), Institute of Atmospheric Physics, Academia Sinica, P.O. Box 2718, Beijing 100080, China, Email: lwp@lasgsg4.iap.ac.cn)

Based upon numerical simulations by using the IAP/LASG GOALS climate model, it is shown that the downward motion in winter and upward motion in summer of the air column over the Tibetan Plateau act as an air pump. This air pump is mainly driven by the surface sensible heat flux over the plateau and is therefore named as "Sensible Heat driving Air pump"(SHAP). The pumping of the SHAP on the air at high levels pushes the atmosphere to move outward, hence forms a divergence center in summer. This, together with the strong negative vorticity forcing produced from the strong surface sensible heating over the Plateau, generates a strong South Asian Subtropical High. Through its pumping and suction on the air, the SHAP strongly regulates the activities of the atmospheric semi-permanent activity centers in mid- and high latitudes, and the monsoon systems in tropics. It is mainly the SHAP that causes the northward jump of the South Asian Subtropical High. It is also shown that in middle summer, the suction of the SHAP on the warm and moist air at low levels maintains the precipitation of the plateau area, and modulates the climate over East and South Asia; whereas the pumping of the SHAP in the upper atmosphere can affect global climate through energy dispersion along Rossby wave trains.

**MC10/W/07-B1****1155****CLOUD RADIATIVE FORCING OF THE SUBTROPICAL CIRCULATION: LINEAR CALCULATIONS**

John W. BERGMAN (University of Colorado, USA, E-mail: jwb@cdc.noaa.gov)

The role of clouds for low-latitude atmospheric circulations is examined in a linearized calculation forced by diabatic heating rates. The circulation calculated from total diabatic heating, obtained from reanalysis data, determines which aspects of the calculated circulation are realistic and which are not. The role of clouds is quantified by the circulation forced by cloud radiative forcing that has been calculated in a radiative transfer model from cloud properties observed in ISCCP. In general, cloud radiative forcing contributes about 20% to the

magnitude of low-latitude maritime circulations and it typically reinforces the circulation that is driven by convective latent heating. However, cloud radiative forcing has a much stronger influence in the subtropics, where it accounts for more than half of the strength of the anticyclonic flow over the eastern Pacific. Cloud radiative forcing tends to have a stronger influence in the lower troposphere than at upper levels and influences local circulations more than remote ones. In particular, cloud radiative forcing from local stratus decks is the dominant source of diabatic heating influencing subtropical circulations over the eastern oceans. Cloud radiative forcing in the subtropical stratus decks is also found to be important for seasonal variations of meridional winds over the cold tongue in the east Pacific, indicating that atmospheric cloud radiative forcing in stratus clouds is important for ocean-atmospheric coupling there.

**Monday 26 July PM**

Presiding Chair: Brian J. Hoskins, The University of Reading, UK

**MC10/W/01-B1**

Invited

**1400****BASIC DYNAMICS AND SIMULATION OF SUBTROPICAL ANTICYCLONE**

Guoxiong WU (email: gxwu@lasgsg4.iap.ac.cn), Yimin Liu (email: lym@lasgsg4.iap.ac.cn) (State Key Lab of Atmospheric Sciences and Geophysical Fluid Dynamics (LASG) Institute of Atmospheric Physics, Academia Sinica, Beijing P.O. 2718, 100080 China)

Based on the equation of Ertel potential vorticity, a complete form of equation of vertical vorticity tendency is developed for the study of subtropical anticyclone dynamics. In addition to those terms appearing in the corresponding classical equation, this new equation includes a term representing "internal forcing" which is associated with the thermal structure of the atmosphere and the terms representing "external forcing" associated with frictional dissipation and diabatic heating. Scaling analysis shows that the vertically non-uniform diabatic heating prevails over the horizontally non-uniform diabatic heating in the breakdown into asymmetric centers of the zonal symmetric subtropical anticyclone. A theory of thermal adaptation linking atmospheric circulation to external forcing and a new concept of "overshooting" are then proposed for the study. According to these, ascending and cold anticyclonic flow must exist in the atmospheric layers above the low-level heating even though there is no diabatic heating within these layers. It was concluded that along the subtropical belt where the Burger number is approximately unity, strong surface sensible heating can excite anticyclone to its west in the lower layer and to its east in the upper layer; whereas deep convective condensation heating can generate anticyclone to its east in the lower layer and to its west in the upper layer. This is examined by using the NCEP/NCAR reanalysis data and verified by a series of numerical experiments by using the IAP/LASG GOALS climate model.

**MC10/W/03-B1**

Invited

**1430****IMPACTS OF SURFACE SENSIBLE HEATING ON THE FORMATION OF SUBTROPICAL ANTICYCLONE IN BOREAL SUMMER**

Yimin LIU (email: lym@lasgsg4.iap.ac.cn.); Guoxiong Wu, Ping Liu (State Key Lab of Atmospheric Sciences and Geophysical Fluid Dynamics (LASG), Institute of Atmospheric Physics, Academia Sinica, Beijing P.O. 2718, 100080 China)

The mechanism linking the formation of subtropical anticyclone in boreal summer to zonally asymmetric surface sensible heating (SH) is investigated via data diagnosis and numerical experiment. The complete form of the tendency equation for vertical vorticity development, the NCEP/NCAR reanalysis data, and the IAP/LASG GOALS climate model are employed for the study. Based on the NCEP/NCAR data, it is shown that, in boreal summer in the Northern American region and at 500hPa, vorticity advection and beta-term in the vorticity equation are the main terms in balancing external vorticity forcing due to surface SH. Then a series of numerical experiments have been carried out. The results from idealized SH heating show that advection makes the subtropical anticyclone appear to the east of the surface sensible heating region. Whereas near the surface, beta-effect makes the subtropical anticyclone appear to its west. However, sensible heating over one single region along the subtropics only generates weak subtropical anticyclone. Only the heating over two continental regions can generate subtropical anticyclones over two oceans with intensity of reasonable extent. Further numerical simulation has proved that, continental sensible heating is essential for the formation of subtropical anticyclones over the two oceans in the lower troposphere. It also contributes to the formation of the following systems at 500hPa: the North American High, North Africa High, and the Iran High. Finally, the results from diagnosing the interannual variability by using the NCEP/NCAR reanalysis data support and verify above results.

**MC10/W/08-B1****1455****SUBTROPICAL ANTICYCLONES FORCED BY ATMOSPHERIC DIABATIC HEATING**

Ping CHEN (NOAA-CIRES Climate Diagnostics Center, USA Email: pc@cdc.noaa.gov)

A general formula is derived for thermally-forced atmospheric responses in a linear quasi-geostrophic beta-plane model. The analytic solutions forced by a realistic monsoonal heating resemble the observed summertime circulation in the subtropics: there is a trough (ridge) in the lower (upper) levels in the heating region; and there is a low-level anticyclone about one-to-two quarter wavelength downstream of the heating maximum. The strength of the anticyclone is proportional to the intensity of the heating and inversely proportional to the magnitude of the zonal westerly. The location of the low-level anticyclone moves eastward as the zonal westerly decreases. All these features agree with the annual cycle of the observed subtropical anticyclones. It is therefore proposed that the observed subtropical anticyclones are part of an atmospheric circulation forced by zonally asymmetric atmospheric diabatic heating rather than forced by the descending branch of the Hadley Cell.

**MC10/E/03-B1****1500****ON THE ANOMALY OF THE SUBTROPICAL ANTICYCLONE OVER THE WESTERN PACIFIC IN 1998**

Ping LIU (e-mail: liup@lasgsg4.iap.ac.cn.); Yimin Liu (State Key Lab of Atmospheric Sciences and Geophysical Fluid Dynamics (LASG), Institute of Atmospheric Physics, Academia Sinica, Beijing P.O. 2718, 100080 China)

In the summer of 1998, China suffered from extremely severe flood along the Yangtze River. The anomalously southward shifting of the subtropical anticyclone over the western Pacific, or SAWP in short, is pertinent to the flooding. The wind anomaly at 850hPa also shows a strong anticyclonic pattern persisting to the western Pacific Ocean. Meanwhile, the easterly near the equator is abnormally strong. The flooding and the aforementioned anomaly of the SAWP have been successfully simulated by using the IAP/GOALS climate model. A series of

numerical experiments on the mechanism are carried out mainly taking the sea surface temperature anomaly (SSTA) in the equatorial Pacific and Indian Ocean into consideration. Results show that there is strong equatorial easterly wind anomaly at 850hPa with the forcing of actual SSTA pattern. Such wind anomaly is due to the strong negative SSTA around Niño 3 area and positive one in the Indian Ocean. The results also show it is the strong anomaly of latent heat release in south-east Asia that leads to the southward shifting of the SAWP.

**MC10/P/02-B1****1610****ROLES OF SUBTROPICAL RIDGE IN TROPICAL PACIFIC SST – EAST ASIAN MONSOON INTERACTIONS**

C.-P. Chang (email: cpchang@nps.navy.mil); Yongsheng Zhang; Tim LI (Dept. of Meteorology, Naval Postgraduate School, Monterey, CA. E-mail: li@nrlmyr.navy.mil)

The interannual relationship between East Asian summer monsoon and tropical Pacific sea-surface temperatures (SST) is studied using rainfall data in the Yangtze River Valley and the NCEP reanalysis for 1951-1996. The date sets are also partitioned between 1951-77 and 1978-96 to study the interdecadal variations of this relationship.

A wet May-June summer monsoon is preceded by a warm equatorial eastern Pacific (EEP) in the previous winter and followed by a cold EEP in the following fall. In a wet year, the western Pacific subtropical ridge is stronger form the previous winter to the following fall, resulting in an 850 hPa anomalous anticyclone near the southeast coast of China. The anticyclone (1) blocks the pre-Meiyu/Meiyu fronts thereby extending the period of the stationary rainfall, (2) enhances the pressure gradient to its northwest resulting in a more intense front, and (3) warms the South China Sea surface through increased downwelling. A positive feedback may lead to an intensification of the anomalous anticyclone. This relationship is observed in both the interannual time scale within each interdecadal period and in the interdecadal scale. The SST anomalies (SSTA) change sign in northern spring and resemble a tropospheric biennial oscillation pattern during 1951-77. In 1978-96 the sign change occurs in fall and the SSTA pattern is of a longer time scale. This interdecadal variation appears to result from a change of the basic state. Apparently through ocean wave anticyclone starts to propagate slowly eastward in May and June towards EEP, carrying with it a cooling effect on the SST. In 1951-77 this effect is insignificant as the EEP SSTA already change from warm to cold in northern spring. In 1978-96 the EEP has a warmer mean SST. A stronger positive feedback with the Walker circulation during a warm phase tends to keep the SSTA warm until northern fall, when the eastward propagating easterly wind anomaly reaches the EEP and reserves the SSTA.

**MC10/E/07-B1****1635****LOW-LATITUDE BEHAVIOUR OF ROSSBY WAVEPACKETS IN ZONALLY-VARYING BASIC FLOWS**

Takeshi ENOMOTO, Yoshihisa Matsuda (both at Dept. of Earth and Planetary Physics, University of Tokyo, Tokyo 113-0033, Japan, e-mail: eno@geoph.s.u-tokyo.ac.jp)

With a non-divergent barotropic model on a sphere, a numerical study has been conducted to clarify the behaviour of Rossby wavepackets in zonally varying flows. Zonally varying basic flows with concentrated and less-concentrated westerly jets are considered to show two different mechanisms for low-latitude reflection of Rossby waves. Associated with the zonal variations of the basic state, a subtropical high exists. The subtropical high is more prominent for the basic flow with a weaker meridional shear. The position of subtropical forcing with a divergent vorticity source is varied along the latitude circle in our experiments. Wavepackets forced at the jet entrance exhibit a low-latitude reflection in the both basic states. In the basic flow with a concentrated jet, a wavepacket tends to propagate along the jet. Closer inspections, however, reveal a slight meridional propagation and an associated reflection near the shear maximum, where the stationary Rossby wavenumber squared is negative. It is considered that a reflection occurs due to a basic-state 'reflector' associated with turning latitudes. No such 'reflector' exists in the basic flow with a less-concentrated jet. A reflection in this basic flow, by contrast, occurs due to the advection of vorticity anomalies in the subtropical high. The tilt of phase lines of anomalies are changed from NE-ADSW to NW-ADSE by the clockwise flow associated with the subtropical high. Such reflections are found both in linear and nonlinear experiments. This result suggests that the nonlinear terms are less important in the critical layer of a zonally varying flow. Our results imply that the applicability of the SWW solution to upper tropospheric phenomena is questionable.

The intensity of the subtropical high in our experiments is found to be varied by the stagnated vorticity anomalies superimposed on the subtropical high. The superposition of incident and reflecting anomalies probably acts to maintain the amplitude and position of the stagnated anomalies.

**MC10/W/06-B1****1700****EFFECT OF SSTAS OVER EQUATORIAL PACIFIC ON SUBTROPICAL HIGH OVER WESTERN PACIFIC**

LONG Zhenxia (Institute of Atmospheric Physics, CAS, email: lzx@lasgsg4.iap.ac.cn); Li Chongyin (Institute of Atmospheric Physics, CAS, email: lcy@lasgsg4.iap.ac.cn)

LASG 9-level spectral model and IAP 2-level model have been employed to study the effect of SSTAs in equatorial Pacific on the summer subtropical high over western Pacific. Positive or negative SSTAs with different duration (Similar to the SSTA distribution during the years next to El Niño or La Niña) over equatorial eastern Pacific are prescribed. Anomalous subtropical high is defined as the difference between anomalous experiment and control experiment. The results suggest that the anomalous subtropical high shows insensitive to the details of SSTAs in equatorial Pacific. The insensitivity is independent of model. Further analyses suggest that the atmospheric internal dynamic process may be responsible for the insensitivity of anomalous subtropical high to the details of SSTA in equatorial Pacific. For example, the weakened intraseasonal oscillation may be responsible for the insensitivity during the warm event. This result will change the traditional theory with which the summer subtropical high over western Pacific can be predicted based on the SSTAs over equatorial Pacific.

**MC10/P/01-B1****1720****LOCAL HADLEY CELL, LOCAL WALKER CELL AND SUBTROPICAL CELL**

Ming XU (Department of Atmospheric Science, Lanzhou University, Lanzhou, China, New address: Graduate Department, Beijing Meteorological College, Beijing, 100081, China)

The relationship of subtropical cell and local Hadley cell and local Walker cell is still an unsettled problem. In this paper, the indexes of local Hadley cell, local Walker cell and subtropical cell are defined. By using these indexes, the relationship of subtropical cell and local Hadley cell, subtropical cell and local Walker cell are diagnosed. The results show, local Hadley cell and local Walker cell play distinct roles in different subtropical cells. In Southern

Hemisphere, subtropical cells are mainly affected by local Hadley cell. However, in Northern Hemisphere, subtropical cells are affected by both local Hadley cells and Walker cells. Subtropical cell in Southern Hemisphere seems like trade wind system, while in Northern Hemisphere it seems like monsoon system. The mechanism that local Hadley cell and local Walker cell influence subtropical cell is also discussed.

**MC11****Wednesday 28 – Thursday 29 July****ON THE USE OF COUPLED MODELS FOR PALEOCLIMATE STUDIES (ICCL) (IAMAS)**

Location: Law Building, 116 LR3

**Wednesday July 28 AM****LONG-TERM CLIMATIC SIMULATIONS****Introduction****0830**

N. de NOBLET (LSCE, Saclay, France)

**MC11/E/18-B3****Invited****0850****INFLUENCE OF CO<sub>2</sub> THRESHOLDS IN THE RESPONSE OF THE LLN CLIMATE MODEL TO THE ASTRONOMICAL FORCING**

André BERGER, Marie-France Loutre (Université catholique de Louvain, Institut d'Astronomie et de Géophysique G. Lemaître, 2 Chemin du Cyclotron, B-1348 Louvain-la-Neuve, Belgium, e-mail: berger@astr.ucl.ac.be)

The LLN 2-D northern hemisphere climate model has been used to reconstruct the long-term climatic variations over the Quaternary Ice Age. Sensitivity analyses to the astronomically-driven insolation changes and to the CO<sub>2</sub> atmospheric concentration have been performed. In particular, an atmospheric CO<sub>2</sub> concentration decreasing linearly from 320 ppmv at 3 Myr BP (Late Pliocene) to 200 ppmv at the Last Glacial Maximum was used to force the model in addition to the insolation. Under such condition, the model simulates the intensification of glaciation around 2.75 Myr BP, the late Pliocene-early Pleistocene 41-kyr cycle, the emergence of the 100-kyr cycle around 900 kyr BP, and the glacial-interglacial cycles of the last 600 kyr. Using a reconstructed CO<sub>2</sub> concentration over the last 600 kyr from a regression based upon SPECMAP, it has been shown that stage 11 and stage 1 request a high CO<sub>2</sub> to reach the interglacial level. The insolation profile at both stages and modelling results tend to show that stage 11 might be a better analogue for our future climate than the Eem. Sensitivity analyses have also demonstrated that CO<sub>2</sub> thresholds do control the response of the LLN climate model to the orbital forcing. Between 4 and 3 Myr BP CO<sub>2</sub> must exceed 450 ppmv to prevent ice sheets to develop, in particular at about 3.8 Myr BP. The mid-Pleistocene transition between the 41 kyr and 100 kyr periodicities is associated to CO<sub>2</sub> values lower than 240 ppmv. Over the last 200 kyr, CO<sub>2</sub> threshold values depend upon the global climate itself. The global warming expected over the next centuries require to study deeply periods during which temperature and CO<sub>2</sub> higher than to-day, e.g. the late Pliocene.

**MC11/W/03-B3****0930****AN ATMOSPHERE-MIXED LAYER OCEAN MODEL'S RESPONSE TO ORBITAL VARIATIONS OVER THE PAST 120,000 YEARS**

Charles JACKSON (Program in Atmospheric and Oceanic Sciences, Princeton University, Princeton, New Jersey 08542, email: csj@gfdl.gov); Anthony Broccoli (Geophysical Fluid Dynamics Laboratory/NOAA, Princeton University, Princeton, New Jersey 08542, email: ajb@gfdl.gov)

The atmosphere's response to variations in Earth's orbital configuration over the past 120,000 years is considered using a 9 layer R15 atmospheric general circulation model coupled to a static mixed-layer ocean and dynamic/thermodynamic sea ice model. The large computational cost of simulating the equilibrium response to orbital variations over this long time period is reduced by accelerating orbital variations by a factor of 30 which can be justified by the relatively short response time of the atmosphere-mixed layer ocean system. Of interest are the internal processes by which the model adjusts to temporally and spatially varying insolation. The response for any given location should include factors that are local as well as remote, immediate as well as long term. The advantage of the present model experiment over equilibrium simulations with fixed orbital parameters is that it can produce the time evolving response to the complete spectrum of orbital variations. In so doing, the nature of model processes can be illustrated by the way they filter or translate a given variation in radiative forcing to model climate. Model results will also be compared to various paleoclimate records. Similarities obtained from these comparisons can be helpful in diagnosing the degree to which the observed record can be understood in terms of the physics of an atmosphere-mixed layer ocean model given one of the known variations in palaeoclimate forcings.

**MC11/P/02-B3****0950****SIMULATIONS WITH THE WATER ISOTOPE SUB-MODEL OF THE GISS AND THE ECHAM ATMOSPHERIC GENERAL CIRCULATION MODELS: RESULTS FROM 7 TIME SLICE CALCULATIONS FROM THE RECENT HOLOCENE TO THE LAST GLACIAL MAXIMUM**

G.HOFFMANN1, R.Koster2, G.Delaygue1, M.Werner3, Jjouze11 (1. Lab. Des Sciences du Climat et de l'Environnement, CEA/CNRS, Gif sur Yvette, France, 2. NASA, GSFC, Greenbelt, Maryland, USA, 3. MPI f.Meteorologie, Hamburg, Germany)

Since long time the isotopic composition of water (18O,D) is used to quantitatively estimate past temperatures. In mid and high latitudes a strong relationship has been found between the isotopic composition of modern precipitation and the corresponding mean temperature. The basic assumption for using the water isotopes in paleo climatology now is the equivalence between this spatial isotope-temperature gradient and the temporal gradient at a fix location. The spatial relation serves then as a modern analogue for the temporal gradient subsequently applied on temporal series of reconstructed isotopic composition of precipitation. For the application of this modern analogue method to be valid several preconditions must hold, e.g. an approximately constant contribution of vapour from different source regions or a constant seasonality of precipitation under even completely different climate conditions such as the last glacial maximum (LGM). Recently new results came up that imply that this assumption, i.e. the equivalence of the spatial and the temporal gradient, is not valid at least for Greenland ice cores. Different and independent methods using borehole temperatures or trace gases enclosed in the ice showed that the temporal isotope-temperature gradient most probably is overestimated by about 50% (modern spatial gradient over Greenland. 0.69‰/°C, estimates



based on borehole temperatures: 0.33-0.36‰/°C).

GCMs coupled with a water isotope sub-model are in principal perfectly suited to address this problem. They take into account for example atmospheric circulation changes, varying source conditions or changes in the seasonality of precipitation for calculating the isotopic composition of precipitation under different climate conditions. The model experiments done until now showed only a slight diminution of the temporal gradient (Control-LGM) over Greenland compared to the calculated spatial gradient. In all other regions the analogue method was justified by GCM simulations. For testing the robustness of these results we performed a set of time slice calculations with two of the above mentioned GCMs, the GISS model (in its high resolution version of 4°\*5° degrees) and the ECHAM4 model (T30 resolution). These time slice calculations were done in time steps of 3kyrs through the entire Holocene to the last glacial maximum, 21kyr BP. The computed gradual changes of the temporal versus the spatial isotope-temperature gradients are discussed in terms of the continuously increasing glacial conditions at high latitude regions of both the northern and the southern hemisphere.

**MC11/E/17-B3**

**1010**

**THE ROLE OF SEA-LEVEL AND VEGETATION IN THE ASTRONOMICAL THEORY OF PALAEOCLIMATES**

BERGER, André, Dutrieux A., Loutre M.F. (Université catholique de Louvain, Institut d'Astronomie et de Géophysique G. Lemaître, 2 Chemin du Cyclotron, B-1348 Louvain-la-Neuve, Belgium, email: berger@astr.ucl.ac.be)

Sensitivity experiments have been made over the last glacial-interglacial climatic cycle using the Louvain-la-Neuve 2-dimension Northern and Southern hemispheres climate model. The continental ice volume was simulated for the last 122 kyr in response to changes of both the insolation and CO2 atmospheric concentration. The sensitivity of such a response to sea level changes and to the taiga-tundra - snow albedo feedback indicates that the 100-kyr cycle cannot be sustained if these processes are not taken into account.

**INCEPTION OF GLACIAL TIMES AND DEGLACIATION**

**MC11/W/06-B3**

**1100**

**THE ROLE OF THE THERMOHALINE CIRCULATION IN THE INITIATION OF GLACIATION**

Zhaomin WANG, Lawrence A. Mysak (Department Of Atmospheric and Oceanic Sciences McGill University 805 Sherbrooke West Montreal Quebec H3A 2K6 Canada email: Zhaomin@whale.meteo.mcgill.ca)

We present a new coupled atmosphere-ocean-sea ice-land surface model for long-term climate change studies which incorporates the seasonal cycle. The three major ocean basins, the Antarctic Circumpolar Current region and the major continents are resolved.

The model components are coupled together using flux adjustments (for heat and fresh water) in order to first simulate the present day climate. The major features of this simulation are consistent with observations and the general results of GCMs. In a global warming (cooling) experiment, the thermohaline circulation (THC) in the North Atlantic Ocean is weakened (intensified) mainly due to the increased (reduced) moisture transport to the northern high latitudes and warming (cooling) in the high latitudes of the North Atlantic.

Lastly, the coupled model is employed to investigate the initiation of glaciation by slowly reducing the solar radiation and increasing the planetary emissivity, only in the northern high latitudes. When land ice is growing, the THC in the North Atlantic Ocean is intensified, resulting in a warm subpolar North Atlantic Ocean, which is in agreement with the observations of Ruddiman and McIntyre. The intensified THC maintains large land-ocean thermal contrast at high latitudes and hence enhances land ice accumulation, which is consistent with the rapid ice sheet growth during the first 10 ka of the last glacial period that was observed by Johnson and Andrews. We conclude that a cold climate is not responsible for a weak or collapsed THC in the North Atlantic Ocean; rather we suggest that increased fresh water or massive iceberg discharge from land is responsible for such a state.

**MC11/W/08-B3**

**1120**

**ATMOSPHERE-CRYOSPHERE INTERACTION FROM EEMEAN TO HOLOCENE CLIMATE SIMULATIONS WITH A COUPLED AGCM-ICE SHEET MODEL**

G. VETTORETTI, W. R. Peltier (both at Dept. of Physics, University of Toronto, Toronto, Ontario, M5S 1A7, Canada); N. A. McFarlane (Canadian Climate Centre for Modelling and Analysis, University of Victoria, Victoria, British Columbia, V8W 2Y2, Canada)

Atmospheric-Cryospheric interaction in the earth system is fundamental to the long-term dynamical evolution of global climate. A series of simulations of climate state at key epochs within the last glacial cycle have been performed using the CCCma atmospheric general circulation model (AGCM). The focus in this paper will be upon investigations of the Last Glacial Maximum (LGM) at 21 000 years before present (21 Kyrs BP) and post Eemean Glacial Inception (117 to 112 Kyrs BP). The AGCM has also been asynchronously coupled to a much simpler Energy Balance-Ice Sheet Model (ISM/EBM) to connect the AGCM hydrological cycle and atmospheric energy balance with the dynamics of the ISM/EBM.

We will demonstrate that the resolution of the T32 AGCM cannot adequately capture the detailed mass-balance along the ablation zones of the Laurentide ice complex at LGM. Also, changes in the LGM northern hemisphere stationary wave patterns over Eastern Canada reveal an increased cold southerly geostrophic air flow being driven directly to the southern lobes of the Laurentide ice sheet which extended into the New England region of the United States at LGM. An AGCM sensitivity study of post Eemean Glacial Inception was conducted with modified orbital parameters, orography and model surface hydrology. To adequately resolve the initial evolution of the glacial cycle over many thousands of years, we have coupled the AGCM to the ISM/EBM in order to simulate the evolution of continental scale glacial advance during the last interglacial. We will demonstrate that this combination provides an opportunity to determine ice sheet mass balance over periods which the AGCM alone could not simulate given current computational restraints.

**MC11/W/05-B3**

**1140**

**THE CLIMATE-ICE SHEET INTERACTIONS IN A SIMPLE CLIMATE MODEL**

Lawrence A. MYSK, Zhaomin Wang (Department Of Atmospheric and Oceanic Sciences, McGill University, 805 Sherbrooke West, Montreal, Quebec, H3A 2K6, Canada, E-mail: Mysak@zephyr.meteo.mcgill.ca; Zhaomin@whale.meteo.mcgill.ca)

A zonally averaged ice sheet model used by Gallee et al. has been coupled to a simple climate model, which incorporates an energy-moisture balance atmospheric model, a zonally averaged ocean model of Wright and Stocker, a zero-layer thermodynamic sea ice model and a simple land surface model. The ice sheets are initiated by reducing the solar insolation and

planetary emissivity in the northern high latitudes.

The ice sheets grow rapidly during the first 10 ka due to the strong thermohaline circulation (THC) in the North Atlantic and very small lateral discharge of ice mass. However, during this stage, the climate in the northern high latitudes is only cooled down slightly and ice sheets cannot advance southward easily. On the other hand, if the planetary emissivity is reduced globally, which can mimic the drop of the concentration of carbon dioxide and water vapor after the initiation of glaciation, the ice sheets may extend southward significantly. Also, the weakening of the THC due to the large ice mass discharge leads to the southward advance of sea ice and a significant cooling of the climate.

Since there exist two flow regimes (steady flow and rapid ice mass discharge) of ice sheets, the ice mass discharge to the ocean is suddenly increased once the ice flow reaches a critical value. This causes the drop of ice volume and weakens the THC. The weak THC leads to the advance of sea ice, which cools down the climate further and slows down the growth of ice sheets. When the large ice mass discharge stops, the THC is restored and the sea ice cover retreats. Then the ice sheets grow relatively rapidly and the critical situation is reached again, which causes another large ice mass discharge.

**MC11/L/03-B3**

**1200**

**TWO-WAY AGCM-ISM COUPLING**

Christophe GENTHON and Catherine Ritz (both at Laboratoire de Glaciologie et Géophysique de l'Environnement, CNRS, BP96, F-38402 Saint Martin d'Hères Cedex, France, E-mail: genthon@glaciog.ujf-grenoble.fr)

Coupling an Atmospheric General Circulation Model (AGCM) and an Ice Sheet Model (ISM) poses sharp constraints on the AGCM computing efficiency. Because the climate of ice sheets is very sensitive to resolution, low resolution is not an acceptable option.

We use a stretchable-grid AGCM to reach reasonable resolution (about 300km) where major ice sheets develop during an ice age at affordable computing cost. Asynchronous coupling is nevertheless inescapable. Because the topography of the ice sheets can significantly evolve between two coupling steps [O(1000 years)], interpolation in time of the atmospheric forcing must be done. Simulations of the atmosphere of an ice age with different ice sheet topographies have been performed, from which simple parameterizations of temperature and mass balance at the surface of ice sheets will be developed. After testing the equilibrium of the ice age ice sheets by fully (two-way) coupling the atmospheric and ice models, a full deglaciation will be covered. Results available at the time of the symposium will be presented.

**MC11/E/12-B3**

**1220**

**THE NORTHERN HEMISPHERE ICE COVER SIMULATED WITH A COUPLED CLIMATE-SYSTEM MODEL**

Reinhard CALOV, Andrey Ganopolski, Martin Claussen (all at Potsdam Institute for Climate Impact Research, PO Box 60 12 03, D-14412 Potsdam, Germany, Email: calov@pik-potsdam.de)

We study the temporal evolution of the northern Hemisphere's ice sheets through the last glacial cycle with special emphasis on the inception of glaciation and deglaciation using the climate-system model CLIMBER-2 (CLIMate and BiosPHERE model) coupled to the polythermal ice-sheet model SICOPOLIS (Simulation Code for POLYthermal Ice Sheets). CLIMBER-2 is a coarse resolution climate-system of intermediate complexity. It describes the atmosphere, sea ice, ocean, and the biosphere. The polythermal ice sheet model SICOPOLIS simulates the time-dependent extent of thickness, velocity, temperature, water-content and age for grounded ice sheets. The bedrock responds to the load of the ice through the buoyancy forces of the asthenosphere. SICOPOLIS provides CLIMBER-2 with the temporal change of orography and areas of land and ice sheets. Inversely, the climate characteristics (air temperature and humidity, long-wave and short-wave radiation, precipitation) on the coarse grid of CLIMBER-2 are used to calculate the energy and mass balance on the fine grid of SICOPOLIS accounting for the orography on the fine grid. The only external forcing for CLIMBER-2 are the Milankovitch insolation and the atmospheric CO2-concentration.

The validation of the new coupled model CLIMBER-2/SICOPOLIS shows, in particular, that the modeled present-day surface mass balance and precipitation of Greenland are in good agreement with observations, and that the modeled northern Hemisphere's ice cover at LGM corresponds to the geological findings. Here, we study the role of different factors for the inception of glaciation (at 115 kyr BP) and deglaciation (after 21 kyr BP) of the northern Hemisphere. These factors are in particular the oceanic transport, the sea ice, the vegetation, the atmospheric dust and the flow properties of ice. Furthermore, we compare the importance of these factors for glaciation and deglaciation.

Wednesday July 28 PM

**INCEPTION OF GLACIAL TIMES AND DEGLACIATION.**

**PANEL DISCUSSION**

**1400**

**HOW CAN TRANSIENT SIMULATIONS IMPROVE OUR UNDERSTANDING OF THE GLACIAL WORLD?**

Paul VALDES (UGAMP, UK)

**CLIMATE OF THE LAST GLACIAL MAXIMUM (21,000 YEARS AGO)**

**MC11/L/01-B3**

Invited

**1440**

**MODELLING THE LAST GLACIAL MAXIMUM CLIMATE: STATUS AND UNCERTAINTIES**

Sophie PINOT, Sandy P. Harrison, Gilles Ramstein

Simulations of the last glacial maximum (LGM) have been performed within the Palaeoclimate Modelling Intercomparison Project (PMIP) using atmospheric general circulation models (AGCMs) with both prescribed (CLIMAP) sea-surface temperatures (SSTs) and with SSTs computed using a mixed-layer slab ocean. The simulations use the same boundary conditions for CO2, insolation, and ice sheet extent and height, in order to determine which responses are model-dependent. Evaluations of these simulations have been made using offline vegetation (BIOME 3.5), in order to facilitate comparison with global data sets of pollen-based reconstructions of vegetation patterns. Although all of the models simulate generally colder and drier conditions at the LGM, the global comparisons show that they underestimate the degree of cooling and drying shown by the data. A more quantitative evaluation of the simulated climates can be made using new reconstructions of the temperature lowering at the LGM across the tropics. The simulations with prescribed CLIMAP SSTs underestimate the observed tropical cooling. However, three models with computed SSTs (CCM1, CCC2 and UKMO) simulate a mean annual cooling consistent with the terrestrial reconstructions. Two of the models produce a rather uniform cooling across the tropics; only the UKMO model simulates the spatial patterning in the cooling shown by pollen-data from lowland tropical areas and alkenone-based estimates of SSTs. A sensitivity experiment in which the simulated

SSTs field from the UKMO experiment was used to drive an AGCM (LMD5) shows that it is possible to reconcile marine and terrestrial estimates of the tropical cooling at the LGM. The implausibility of uniform tropical cooling is confirmed by sensitivity experiments with an AGCM asynchronously-coupled to an ocean general circulation model which show that the eastern tropical Pacific must be at least 2°C colder than the western tropical Pacific in order to explain the observed 3-dimensional structure of the tropical ocean.

**MC11/E/05-B3****1440****CLIMATE-VEGETATION FEEDBACKS DURING THE LAST GLACIAL MAXIMUM**

SAMUEL LEVIS (National Center for Atmospheric Research, PO Box 3000, Boulder CO 80307-3000, USA, Email: slevis@ucar.edu) Jonathan A. Foley (Climate, People and Environment Program, University of Wisconsin, Madison WI 53706, USA) David Pollard (Earth System Science Center, Pennsylvania State University, University Park PA 16802, USA)

We operate the fully coupled GENESIS-IBIS climate-vegetation model with last glacial maximum boundary conditions (~21000 years before present). We find that grasslands and tundra largely replace temperate and boreal forests primarily due to colder and drier simulated conditions. Also, mainly due to reduced plant productivity under lowered CO<sub>2</sub> concentrations, tropical and subtropical forests retreat and C4 grasses advance. These shifting vegetation patterns produce significant climatic feedbacks when isolated from the radiative effects of lowered CO<sub>2</sub> on this epoch's climate. In particular, a positive feedback process which depends on the difference in albedo between tundra and forest regions results in additional middle and high latitude cooling. On the other hand, sparser vegetation cover in the tropics and subtropics results in significant decreases in the evapotranspiration, leading to warmer and drier conditions in these regions when compared to the simulation results without vegetation feedbacks. These results, and particularly the changes in vegetation cover simulated for the tropics and subtropics, are supported by some observational reconstructions but refuted by others. Progress must be made in the reconstruction of palaeobotanical maps for the tropics, in order to evaluate model results such as these.

**MC11/E/02-B3****1540****CONTINENTAL BIOSPHERE CARBON STORAGE AT 21KYR**

Dr. Caroline ROELANDT (Max Planck Institute for Biogeochemistry, Tatzendpromenade 1a, D-07745 Jena, Germany, e-mail: caroline.roelandt@bgc-jena.mpg.de)

An integrated land-surface biosphere model: ALBIOC (ALbedo - BIOSphere - Carbon), which simulates the potential distribution of vegetation, terrestrial carbon storage and land-surface properties, as a function of climate, has been applied to estimate changes in the continental biosphere carbon storage at 21kyr (the Last Glacial Maximum). These experiments were made using 17 atmospheric general circulation model simulation done within the Palaeoclimate Modelling Intercomparison Project (PMIP). The simulated vegetation patterns are compared with vegetation reconstructions based on pollen- and macro-fossil data from the BIOME6000 project. The simulated carbon storage values compare well with previous estimate of LGM carbon storage.

**MC11/E/04-B3****1620****COMPARISON OF VEGETATION DISTRIBUTIONS AND TERRESTRIAL CARBON BUDGETS RECONSTRUCTED FOR THE LAST GLACIAL MAXIMUM WITH FOUR DIFFERENT BIOSPHERE MODELS**

Louis FRANCOIS (1), Dominique Otto (1), Jed Kaplan (2), Pierre Friedlingstein (3), Caroline Roelandt (2), Gilles Ramstein (3), Nathalie de Noblet (3), Pierre Warnant (1), Colin Prentice (2) (1 Laboratoire de Physique Atmosphérique et Planétaire, Université de Liège, Liège, Belgium, e-mail: francois@astro.ulg.ac.be) (2 Max-Planck Institut für Biogeochemie, Jena, Germany) (3 Laboratoire des Sciences du Climat et de l'Environnement, Unité mixte de Recherche CEA-CNRS, Gif-sur-Yvette, France)

Model reconstructions of vegetation distribution and carbon sequestration in the land biosphere at several key periods in the past have been attempted in recent years by many research groups. These reconstructions are based upon the use of biosphere models forced with climatic outputs from general circulation models. This methodology applied to the Last Glacial Maximum (LGM) provides results which vary significantly from one reconstruction to the other. The question can thus be raised whether this variability in the results are mainly due to the use of different biosphere models or to the different climate reconstructions adopted in these studies. In order to answer this question, an intercomparison of biosphere models forced with a common set of climate reconstructions is necessary. Such a work has been initiated in the frame of the "Paleo-Carbon Cycle Modelling Intercomparison Project (PCCMIP)", a sub-project of the "Paleoclimate Modelling Intercomparison Project (PMIP)". Here, we present some preliminary results obtained with four biosphere models participating in this project: BIOME3, CARAIB, ALBIOC and SLAVE. These models differ widely from each other. The first two use a mechanistic description of photosynthesis and stomatal regulation and predict the biome distribution from a physiologically-based approach in which the net primary productivities of different plant functional types are compared. ALBIOC also incorporates a mechanistic model of photosynthesis and provides a detailed formulation of land surface processes. SLAVE simulates biome distribution in a more simple way, but has the advantage of including a nitrogen cycle. These biosphere models are forced with a common subset of the LGM climatic reconstructions available within PMIP. The predicted vegetation distributions, carbon fluxes (e.g. the net primary productivity) and stocks are compared. Some results regarding the 13C biospheric changes between the LGM and pre-industrial times are also presented.

**MC11/E/13-B3****1640****GLOBAL SIMULATIONS OF THE EFFECTS OF LOW ATMOSPHERIC CO<sub>2</sub> ON VEGETATION PROCESSES WHICH AFFECT ATMOSPHERIC ENERGY TRANSFER AND CARBON CYCLING**

SA COWLING (Climate Impacts Group, Lund University, S223 62 Lund, Sweden. (tel) +46 (0)46 222 3132, (email) Sharon.Cowling@planteco.lu.se)

Atmospheric CO<sub>2</sub> during the last ice-age was between 35 and 50% lower than today, and was probably an important modifier of glacial vegetation. Global modelling experiments using a biogeography-biochemical vegetation model (BIOME3) and palaeoclimate reconstructions from an atmospheric general circulation model (NCAR-CCM1) will be used in a two-by-two factorial design to test the independent and interactive effects of climate and CO<sub>2</sub> on leaf area index (LAI), net primary production (NPP) and vegetation distributions at the Last Glacial Maximum (LGM). Regional differences in the sensitivity of vegetation to low atmospheric CO<sub>2</sub> is expected, with sub-tropical vegetation predicted to show the greatest response. Low CO<sub>2</sub>

increases stomatal conductance, which in turn can lower plant water-use efficiency (WUE, ratio of photosynthesis to transpiration) and augment plant water stress. The contribution of LGM climate and LGM CO<sub>2</sub> in altering plant-water relations will be quantified by comparing combinations of simulations, and implications for feedbacks on atmospheric energy transfer and carbon cycling will be addressed.

**MC11/E/16-B3****1700****DUST SOURCES AND DEPOSITION DURING THE LAST GLACIAL MAXIMUM AND CURRENT CLIMATE: A COMPARISON OF MODEL RESULTS WITH PALEODATA FROM ICE CORES AND MARINE SEDIMENTS**

Natalie MAHOWALD (Department of Meteorology, Stockholm University, S-106 91 Stockholm, Sweden. Now at Donald Bren School of Environmental Science and Management, University of California, Santa Barbara, CA 93106, USA.); Karen E. Kohfeld (Dynamic Palaeoclimatology, Lund University); Margareta Hansson (Department of Meteorology, Stockholm University); Yves Balkanski (Laboratoire des Sciences du Climat et de l'Environnement); Sandy P. Harrison (Dynamic Palaeoclimatology, Lund University); Colin Prentice (Max Planck Institute for Biogeochemistry); Michael Schulz (Institute for Inorganic and Applied Chemistry, University of Hamburg); Henning Rodhe (Department of Meteorology, Stockholm University)

Mineral dust aerosols in the atmosphere have the potential to affect the global climate by influencing the radiative balance of the atmosphere and the supply of micronutrients to the ocean. Ice and marine sediment cores indicate that dust deposition from the atmosphere was on average 2-20 times enhanced (depending on location) during glacial periods. Differences in atmospheric dust loadings between the last glacial maximum (LGM) and Holocene might therefore have contributed to climate change on glacial-interglacial time scales. As a first step to addressing this possibility, we have used a terrestrial biosphere model (BIOME3), a simple dust source model, and an atmospheric transport model (TM3) in an attempt to simulate the dust cycle in the atmosphere for current and last glacial maximum climates, as simulated by an atmospheric general circulation model (ECHAM3). We obtain a 2.5-fold higher dust loading in the entire atmosphere and a 20-fold higher loading in high latitudes, relative to present. Based on a compilation of atmosphere-to-surface dust flux estimates for LGM and present in marine sediment and ice cores, we show that the simulated flux ratios are broadly in agreement with observations both in the high latitudes and elsewhere; differences between the modelled and observed deposition nevertheless suggest that further improvements in the simple dust model could be made. Changes in atmospheric transport alone do not produce such a large increase in dustiness at the LGM in this model, although enhanced transport can account for some specific geographic features of the marine dust record. The simulated increase in high-latitude dustiness depends on the expansion of unvegetated (potential dust source) areas, especially in the high latitudes and in central Asia, caused by a combination of increased aridity and low atmospheric [CO<sub>2</sub>]. The existence of these dust source areas at the LGM is supported by pollen data and loess distribution in the northern continents, and by geochemical sourcing of LGM dust in polar ice cores. These results point to a role for vegetation feedbacks, including climate effects and physiological effects of low [CO<sub>2</sub>], in modulating the atmospheric distribution of dust.

**MC11/L/02-B3****1720****SENSITIVITY TO THE SSTs FORCING IN PALEOCLIMATE SIMULATIONS**

Isabelle MARSAT, Paul J Valdes (Department of Meteorology, University of Reading, Whiteknights, PO Box 243, Reading, RG6 6BB UK, e-mail: marsiat@met.rdg.ac.uk)

The role of prescribing Sea Surface Temperature in paleoclimate atmospheric simulations has been investigated by comparing GCMs experiments using different SSTs data sets as well as coupled atmosphere/oceanic mixed layer models. We found that the SST forcing is as important as the ice sheet orographic forcing. Changes in the SSTs and sea ice margin generate different patterns of zonal asymmetries in the atmospheric circulation that are responsible of reorganisation of heat and moisture transport, leading to important variations of northern hemisphere regional climates. Sensitivity experiments have been carried over to isolate the individual role of North Pacific and North Atlantic SSTs.

**MC11/W/04-B3****1740****PRESENT DAY AND LAST GLACIAL MAXIMUM OCEAN THERMOHALINE CIRCULATION IN A ZONALLY AVERAGED COUPLED OCEAN-SEA ICE-ATMOSPHERE MODEL**

H. BJORNSSON, and L.A. Mysak, Department of Atmospheric and Oceanic Sciences, McGill University, Montreal Canada, H3A 2K6

Using a simple three-basin zonally averaged ocean model coupled to an energy moisture balance atmospheric model and a thermodynamic sea ice model we investigate the stability of the thermohaline circulation during the last glaciation.

First we determine whether the model can be used to simulate the "present day" climate conditions, and following that we spin the model up for the conditions resembling those of the last glacial maximum (LGM). In the first case, the model has an ocean "conveyor belt" (thermohaline) circulation in which the overturning in the North Atlantic is slightly more than 15 Sv.

Two methods are used to spin up the model to the LGM climate. First, a cool state is obtained by running the coupled model with a reduced model greenhouse effect and increased albedo, but without making any explicit changes to the hydrological cycle. In the second method, the model is directly set up for LGM conditions, in a manner similar to the method used to simulate the present day climate. In both cases the computed LGM sea surface temperatures are reasonable, but only in the second case a realistic ocean thermohaline circulation obtained.

The LGM conveyor belt circulation is stable and no self-sustained millennial-scale oscillations are present. The absence of these oscillations in this model and their presence in other models are discussed, and it is suggested how ocean modelling results combined with paleoceanographic data might be used to determine whether the glacial conveyor indeed exhibited such oscillations.

Thursday July 29 AM

**CLIMATE OF THE LAST GLACIAL MAXIMUM (21,000 YEARS AGO)****MC11/E/06-B4****0900****A PERIODICALLY-SYNCHRONOUSLY COUPLED ATMOSPHERE-OCEAN GENERAL CIRCULATION MODEL (ECHAM-LSG) FOR SIMULATION OF PALEOCLIMATES**

LORENZ, S. J. and Paul, A. (University of Bremen, Postfach 330440 D-28334 Bremen, Germany, e-mail slor@palmmod.uni-bremen.de)

For modelling past climates, boundary conditions at the atmosphere-ocean interface are not generally available on a global scale. Coupled atmosphere-ocean general circulation models (GCM) have the potential to make these boundary conditions superfluous. Synchronously



coupled GCMs have been developed for studying anthropogenic greenhouse warming with a typical simulation time of 200 years. Due to the long response time of the deep ocean this is too short for simulating an equilibrium state of the atmosphere-ocean system. In order to reduce the computing time the method of periodically-synchronous coupling is applied to the coupled ECHAM-LSG GCM. In this method, short periods of synchronous coupling alternate with long ocean-only periods. Our application on paleoclimatic time scales enables an integration over some thousand model years within a reasonable computing time. We present stationary states of the ocean-only model and the coupled atmosphere-ocean GCM forced by modern and paleoclimatic boundary conditions. The ocean model simulation of the last glacial maximum at about 20,000 years B.P. exhibits a weaker and shallower Atlantic conveyor belt circulation. The next step is a simulation of the glacial climate with the coupled model. Resultant global data sets at the atmosphere-ocean interface can be used for an independent comparison to the CLIMAP data set.

MC11/E/14-B4

0920

#### ARE DEEP DECOUPLING OSCILLATIONS OF ATLANTIC THERMOHALINE CIRCULATION THE CAUSE OF DANSGAARD-OESCHGER CYCLES: MODEL RESULTS VS. PALEOCEANOGRAPHIC DATA

Michael SCHULZ(1), Shirley van Kreveld(1), Michael Samthein(1) and Simon Jung(2), (1)Institute for Geosciences, University of Kiel, Olshausenstr. 40, D-24118 Kiel (2)Institute of Earth Sciences, Free University, De Boelelaan, 1085, NL-1081 HV Amsterdam

Based on model experiments it has been postulated that thermohaline circulation of the Atlantic Ocean may exhibit self-sustained oscillations on centennial to millennial time scales (Winton, 1993; 1997). These deep decoupling oscillations are not a feature of the coupled ocean-atmosphere system, but are solely due to internal ocean dynamics. Depending on model parameters, the periodicity of these oscillations ranges from approximately 700-4000 years, and thus includes the periodicity of the Dansgaard-Oeschger (D-O) oscillations (1450 years). To test whether this model is capable of explaining the D-O oscillations, we compare model predictions with paleoceanographic data from the North Atlantic. We use a simple box model of the Atlantic Ocean to simulate the deep decoupling oscillations. This model predicts temperature variations of the subsurface water in the North Atlantic by about 3-5°C over the course of an oscillation. In contrast, benthic oxygen isotope as well as Mg/Ca data from the North Atlantic indicate only an average temperature change of approximately 2 °C during a D-O cycle. Furthermore, the model predicts steady warming of subsurface water masses in the North Atlantic during the cold phase of a D-O cycle. This is at variance with our data, which clearly depict a warming of the subsurface water during the warm phase of a D-O cycle. Hence, we regard it as unlikely that deep decoupling oscillations are a suitable mechanism to explain the observed D-O oscillations. We will discuss alternative modeling approaches, which predict temperature variations during D-O cycles, which are consistent with the paleoceanographic record.

PANEL DISCUSSION

0940

#### HOW IMPORTANT IS THE INITIALIZATION OF FRESHWATER INPUTS TO THE CORRECT SIMULATION OF THE COUPLED OCEAN/ATMOSPHERE SYSTEM AT THE LGM?

Bette OTTO-BLIESNER, NCAR.

CLIMATE OF THE MID-HOLOCENE (6,000 YEARS AGO)

MC11/E/15-B4

Invited

1045

#### MODEL UNCERTAINTIES IN SIMULATING MID-HOLOCENE CLIMATES

Paul J VALDES and Buwen Dong (Department of Meteorology, University of Reading, Whiteknights, PO Box 243, Reading, RG6 6BB UK, email: P.J.Valdes@reading.ac.uk)

The mid-Holocene climate of North Africa has received much recent attention. GCM simulations have suggested that changes in ocean circulation and land surfaces have played a major role in climate change in this region. We will present results from a number of simulations using the UGAMP GCM with different land surface conditions, sea surface temperatures and different model parameterisation schemes. The results show that all contribute towards increased monsoon strength during the mid-Holocene although the changes remain smaller than implied by palaeodata. The results will also be used to help interpret the PMIP simulations.

MC11/E/07-B4

1125

#### MID-HOLOCENE GREENING OF THE SAHARA, WITH THE HELP OF FEEDBACKS FROM THE TERRESTRIAL BIOSPHERE

Nathalie DE NOBLET, Pascale Braconnot, Sylvie Joussaume and Olivier Marti (Laboratoire des Sciences du Climat et de l'Environnement, Unite mixte de Recherche CEA-CNRS, Bat. 709 / Orme des Merisiers, 91191 Gif-sur-Yvette, FRANCE, email: noblet@lscce.saclay.cea.fr)

One characteristic of the Mid-Holocene climate (6000 years ago) is the enhanced seasonal cycle of insolation in the northern hemisphere. As a result, African and Asian monsoons are strongly increased and accompanied, in northern Africa, by the so-called 'greening' of the Sahara. Pollen data are indeed showing that moisture-demanding vegetation types were present in now arid regions. Simulations of the mid-Holocene climate carried out within the Paleoclimate Modelling Intercomparison project (PMIP) demonstrated that Atmosphere General Circulation Models (AGCMs), using fixed present-day SSTs and land-surface characteristics, are unable to explain the intensity of the observed signal in northern Africa in response to the sole prescribed change in orbital forcing. Feedbacks from the ocean and the biosphere, to name only the most important ones, may therefore be required to reconcile models and data. We will present results from simulations of increasing complexity to test the role of feedbacks from the terrestrial biosphere in the Mid-Holocene climate simulated by the LMD1 AGCM. In the first and simplest one, desert in the Sahara is replaced by a prescribed combination of xerophytic woods/scrub and warm grassland, in agreement with vegetation reconstructed using pollen data. The second simulation uses an interactive biosphere, i.e. the BIOME1 model is asynchronously coupled to our AGCM while SSTs are still fixed to present-day conditions. In the third and more complex simulation, the AGCM is also being coupled, synchronously, to a three-dimensional oceanic model.

MC11/E/19-B4

Invited

1145

#### STABILITY ANALYSIS OF THE CLIMATE-VEGETATION SYSTEM WITH THE CLIMBER-2 MODEL

Victor BROVKIN, Martin Claussen, Andrey Ganopolski, Claudia Kubatzki, and Vladimir Petoukhov. (Potsdam Institute for Climate Impact Research, PO Box 601203, D-14412, Potsdam, Germany,

Email: victor@pik-potsdam.de)

The interaction among different compartments of the climate system can lead to multiple steady states which evolve during the history of the Earth system. While the existence of multiple steady states in zero- and one-dimensional climate models is rather certain, the multistability phenomenon is interesting to analyse with geographically explicit models of the climate system. We concentrate our efforts on the interaction between climate and vegetation and analyse the system dynamics with assistance of a climate system model of intermediate complexity CLIMBER-2. It includes a 2.5-dimensional dynamical-statistical atmosphere model; a multi-basin, zonally averaged ocean model including a sea ice model; a surface parameterization scheme based on BATS; and a terrestrial vegetation model, VECODE, based on the continuous bioclimatic classification. Vegetation is described as a composition of plant functional types (trees and grasses), and the equilibrium vegetation cover depends only on climate. VECODE estimates changes in vegetation structure and the terrestrial carbon cycle in response to climate change, and the model has been validated globally for present-day climate. Oceanic carbon cycle is represented by models of inorganic carbon uptake and marine biota.

We perform a series of transient runs of the coupled climate-vegetation model from the early Holocene to present day under the external forcing of the Milankovich insolation. The two main candidates for multistability regions are: near-ocean subtropical deserts like the Sahara where precipitation-vegetation feedback is quite significant, and high latitude land regions where interaction between forest cover and air temperature is amplified by sea ice-albedo feedback. While conceptual models point to the possibility of multistable equilibria in both geographical regions, the experiment results in a unique stable equilibrium. However, we see a rather abrupt change from a vegetation covered Sahara in the mid-Holocene to the present-day desert Sahara. At the high latitude region, we obtain a slow retreat of the treeline from the northwards extended position in the mid-Holocene to the present-day boundary. The biogeochemical feedback through the carbon cycle plays a stabilising role in the system dynamics.

MC11/W/01-B4

1205

#### A GREEN PLANET VERSUS A DESERT WORLD: ESTIMATING THE MAXIMUM EFFECT OF VEGETATION ON THE ATMOSPHERE

Klaus FRAEDRICH, Axel Kleidon, and Frank Lunkeit (Meteorologische Institut, Universitaet Hamburg, Bundesstr. 55, D-20146 Hamburg, Germany, email: fraedrich@dkrz.de)

The effect of vegetation extremes on the general circulation is estimated by two atmospheric GCM simulations using global desert and forest boundary conditions over land. The difference between the climates of a 'green planet' and a 'desert world' is dominated by the changes of the hydrological cycle, which is intensified substantially. Enhanced evapotranspiration over land reduces the near surface temperatures; enhanced precipitation leads to a warmer mid- and upper troposphere extending from the subtropics (induced by ITCZ, Monsoon and Hadley cell dynamics) to the mid-latitudes (over the cyclogenesis area of NH storm tracks). These regional changes of the surface water and energy balances, and of the atmospheric circulation have potential impact on the ocean and the atmospheric greenhouse: The ocean is reduced to the prescribed annual cycle of the sea surface temperatures, which are associated with the present day climate. Therefore, both 'green planet' and 'desert world' are expected to generate a net heat exchange between ocean and atmosphere which does not balance in the climatological global average. This global imbalance amounts to a loss of  $0.6 \cdot 10^{14}$  W for the oceans in a desert world and a gain of  $1.2 \cdot 10^{14}$  W on the 'green planet'. The atmosphere and its implied CO<sub>2</sub>-induced greenhouse warming may be substantially influenced by a 'green planet'. The near surface cooling (associated with a more stable troposphere) reduces the greenhouse effect.

MC11/E/01-B4

1225

#### THE ROLE OF VEGETATION IN CLIMATE INTERACTION AND INTERANNUAL VARIABILITY IN SHAPING THE AFRICAN SAVANNAH

NING ZENG and David Neelin, Dept. of Atmospheric Sciences and Inst. of Geophysics and Planetary Physics Univ. of California, Los Angeles

Using a coupled atmosphere-land-vegetation model of intermediate complexity, we explore how vegetation-climate interaction and internal climate variability might influence the vegetation distribution in Africa. When the model is forced by observed climatological sea surface temperature (SST), multi-equilibrium states are found in the climatologically sensitive zones, namely, the Sahel and southern Africa. Depending on the initial condition, these regions can settle on either a forest-like or a desert-like vegetation cover. When forced by interannually varying SST that corresponds to observed wet and dry years in the Sahel, these stable equilibria are driven toward an intermediate grass-like vegetation due to the nonlinearity in the coupled system. In comparison with the traditional view of vegetation as a mere response to environmental conditions, our results suggest a new mechanism involving vegetation playing an active role in shaping the subtropical savanna ecosystem and modifying the regional climate.

CLIMATE OF THE MID-HOLOCENE (6,000 YEARS AGO).

MC11/E/11-B4

1400

#### PAIN - THE PALAEO-ARCTIC INITIATIVE

Jed O. KAPLAN 1, and Nancy Bigelow 2 (1Max Planck Institute for Biogeochemistry, Jena, Germany) (2Alaska Quaternary Center, University of Alaska Fairbanks, Fairbanks, AK, USA)

Many recent studies have shown the high sensitivity of arctic ecosystems to climate change, especially with respect to short-term melting of permafrost soils and the consequent release of CO<sub>2</sub> and CH<sub>4</sub> to the atmosphere. Over longer time scales changing climate in the high-latitudes has had significant impact on the distribution and productivity of vegetation with important feedbacks to the ocean-atmosphere system. The Palaeo-Arctic Initiative (PAIN) is an informal, multidisciplinary project to quantify both vegetation changes through the past and simulate those changes using coupled biosphere and circulation models. This approach of parallel data synthesis and model development allowed us to validate and improve both reconstruction methods and the model results in an efficient way. The activity has three main components, 1. Assembling floristic and physiological information regarding the present distribution of vegetation in the Arctic, 2. Determining the extent and timing of vegetation changes in the Arctic since the Last Glacial Maximum (LGM) mainly through use of the pollen record, and 3. Modelling vegetation changes through time with a biosphere model driven by GCM output. We made pollen-based reconstructions of Arctic vegetation during three important time slices: at the LGM, 6000 yr. BP, and in the present day using the widely applied biomisation technique. The modern biomisation was calibrated to a new map of potential natural vegetation for the Arctic. The vegetation map was also used in the development of a new version of the biosphere model driven by present-day mean climatology. Results indicate that reconstructing regional vegetation history from the pollen record is difficult. Several indicator genera are not well represented in the Arctic pollen record. We applied a novel approach to the biomisation method to extract important distinctions in vegetation type. The model successfully simulated the range of different Arctic vegetation types observed today.



However, under different climate regimes, changes in Arctic vegetation were not possible to simulate with the simple, time-slice coupling performed here. Substantial feedbacks between the vegetation and the atmosphere-ocean system may be responsible for the model's inability to match the pollen-based reconstruction.

## PANEL DISCUSSION 1420

### THE LAND-SURFACE IS MORE THAN VEGETATION.

Sandy HARRISON, MPI Jena.

Thursday July 29 PM

## MC11/E/10-B4 1500

### THE CLIMATE OF 6000 YEARS BP IN NEAR-EQUILIBRIUM SIMULATIONS WITH A COUPLED AOGCM

Uwe MIKOLAJEWICZ and Reinhard VOSS (Max-Planck Institut fuer Meteorologie, Bundesstr 55, D-20146 Hamburg, Germany email: mikolajewicz@dkrz.de, reinhard.voss@dkrz.de)

One focus point for application of complex models in palaeoclimate studies is the time slice 6000 years before present. Most of these studies have been performed using uncoupled atmosphere general circulation models (AGCMs) forced with insolation and CO<sub>2</sub> concentration of the mid-Holocene and prescribing present-day sea surface temperatures (SSTs) and sea-ice distributions. First results from coupled atmosphere-ocean general circulation models (AOGCMs) with identical CO<sub>2</sub> and insolation forcing, however, show a marked effect of resulting SST changes on the atmospheric circulation. We have performed a set of coupled AOGCM simulations to investigate the impact of insolation and CO<sub>2</sub> changes including a control run with present-day forcing. In one simulation, both, insolation and CO<sub>2</sub> forcing were applied. In a second run the mid-Holocene CO<sub>2</sub> forcing and modern insolation were prescribed. The 000 years length each to permit the ocean circulation to adjust to the changes in forcing. In order to derive an estimate of the error induced by the use of present-day SST fields, corresponding uncoupled AGCM experiments have been performed. In the coupled runs the insolation and CO<sub>2</sub> changes lead to an decrease of the global mean near surface temperature of 0.3 K after 1000 years. Regarding only the CO<sub>2</sub> changes the cooling is 0.5 K. Where as the cooling dominates in most regions, the high northern latitudes show a warming in connection with a reduced ice coverage and intensified thermohaline circulation of the Atlantic. Cooler tropical SSTs lead to a weaker monsoon response compared to the uncoupled simulations.

## MC11/E/09-B4 1520

### THE AFRICAN MONSOON AND THE GREEN SAHARA 6000 YEARS AGO: INFLUENCE OF OCEAN-ATMOSPHERE FEEDBACKS IN A COUPLED MODEL

Olivier MARTI, Pascale Braconnot, Nathalie de Noblet, Sylvie Joussaume Laboratoire des Sciences du Climat et de l'Environnement, CEA Saclay, DSM/LSCE, F91191 Gif sur Yvette Cidex, France. Email: olivier.marti@cea.fr.

6000 years ago, the insolation at the top of the atmosphere was characterised by an enhanced seasonal contrast in the Northern hemisphere. African and Asian monsoons were stronger than today, and pollen and lakes data show that in Africa the vegetation was covering the Sahara, suggesting a northward extension of the summer monsoon. Simulations of the Paleoclimate Modelling Intercomparison Project (PMIP) with atmosphere general circulation models qualitatively reproduce this humidification of the Sahara, but underestimate the magnitude of the change. Part of the mismatch could therefore be attributed to the neglected feedbacks from ocean and vegetation. To study the impact ocean on climate of this period, we have used of the IPSL coupled ocean-atmosphere model. It significantly improves the simulation of the African monsoon, which reacts to an increased land-sea temperature contrast. For the 6000 years ago simulation, only the orbital parameters have been changed and set to those of this period, compared to a coupled control simulation. As observed in ocean sediment cores, the simulated sea surface temperature (SST) changes between 6 kyears and present are small. However, the changes of SST seasonality in the Atlantic has a large impact on monsoon seasonality and amplitude, and of the northward migration of the intertropical convergence zone over Africa. The relative role of changes in atmospheric heat fluxes and in oceanic heat transport on the SST show that ocean dynamic plays a major role, through the change of Ekman layer heat transport within the tropics and subtropics. We discuss the relationship between the change of atmospheric circulation (trade winds) and oceanic one.

## MC11/E/08-B4 1540

### MODES OF ATMOSPHERIC CIRCULATION AND THEIR CONNECTIONS TO NORTHERN HEMISPHERE TEMPERATURE AND PRECIPITATION DURING THE MID-HOLOCENE

Bette L. OTTO-BLIESNER (National Center for Atmospheric Research Address: P.O. Box 3000 Boulder, CO 80307 USA Association: E-mail: otobli@ncar.ucar.edu Phone: 303-497-1723 Fax: 303-497-1348)

Analyses of instrumental data quantify the roles of two circulation modes, the North Atlantic Oscillation (NAO) and the Southern Oscillation (SO), in explaining regional temperature and precipitation anomaly patterns over North America, Europe, and the North Atlantic. Their roles in explaining interannual to decadal variability during the mid-Holocene is investigated using the fully coupled atmosphere-land-ocean-sea ice model developed at the National Center for Atmospheric Research. The results show prominent Northern Hemisphere teleconnections for the North Atlantic Oscillation but reduced teleconnections for the Southern Oscillation.

## MC11/W/07-B4 1630

### A COUPLED MODEL EXPERIMENT OF THE MID-HOLOCENE OPTIMUM

WEBER, N., KNMI (P.O. Box 201, 3730 AE De Bilt, The Netherlands. E-mail: weber@knmi.nl)

A coupled atmosphere-ocean model of intermediate complexity (ECBilt; Opsteegh et al., 1998) is applied to the simulation of the mid-Holocene Optimum at 6000 BP. At this time, which was identified by PMIP as a key period for evaluating model performance, the seasonality of insolation was enhanced compared to present-day values. The computational efficiency of ECBilt makes it feasible to perform simulations in coupled mode over time periods of the order of thousands of years. In ECBilt the enhanced summer insolation gives rise to warmer summer temperatures over the NH continents and an enhanced hydrological cycle, consistent with PMIP results for atmosphere-only models. The response in ocean temperature and salinity is small. However, the ocean overturning circulation shows a marked response with a decreased intensity in the Atlantic ocean and an increased overturning in the Pacific domain. The mechanism for this Atlantic-Pacific connection is described. The ocean response evolves

during the integration, due to the long adjustment times of the deep ocean. The associated sensitivity of the atmospheric response to the length of the integration (as well as the averaging period) is discussed. As the Holocene insolation is characterised by enhanced seasonality over large time periods the present results might have implications for transient model experiments.

## MC11/W/02-B4 1650

### THE PRESENT-DAY AND HOLOCENE CLIMATES SIMULATED WITH MOBIDIC

Philippe TULKENS (email: ptulkens@astr.ucl.ac.be); Marie-France Loutre (email: loutre@astr.ucl.ac.be); Michel Crucifix (email: crucifix@astr.ucl.ac.be); Thierry Fichefet (email: fichefet@astr.ucl.ac.be); Andre Berger (email: berger@astr.ucl.ac.be)

MoBidiC is a zonally averaged climate model in which a quasi-geostrophic atmosphere model is coupled to a three-basin (latitude-depth) ocean-sea-ice model. The main continental ice sheets are also represented. The atmospheric component of MoBidiC contains an interactive representation of the hydrological cycle based on meridional transport of moisture and zonal redistribution of precipitation. The sea-ice model enables to represent explicitly the climatic effect of ice formation and ablation and their consequences on the ocean circulation. The inter-connected ocean basins allow this model to simulate the main thermohaline circulation processes. MoBidiC is designed for long-term climate simulations and has a low computational cost.

We present temperature, precipitation and ocean circulation patterns simulated for the present-day climate. Despite shortcomings in the representation of atmospheric dynamics and in the distribution of ocean salinity, the values obtained are realistic. Then we discuss a first palaeoclimatic application of the model: the climate of the Holocene is simulated forcing the model with the variations of CO<sub>2</sub> and insolation over that period.

## PANEL DISCUSSION 1710

### CAN WE ASSESS THE VARIABILITY OF THE COUPLED ATMOSPHERE/OCEAN SYSTEM DURING THE MID-HOLOCENE?

S. LORENZ, University Of Bremen.

## MI04/MI10 Monday 26 – Thursday 29 July

### CLOUDS - THEIR DYNAMICS, PHYSICS AND PARAMETERIZATION

Location: Chemical Engineering 124 LT

Location of Posters: Old Gym

Monday 26 July AM

Presiding Chair: D Gregory (ECMWF, Reading, Berkshire)  
Concurrent Poster Session

## MULTI-SCALE CLOUD SYSTEMS AND TROPICAL CIRCULATION

Introduction 0830

MONCRIEFF (National Centre for Atmos Research, USA)

## MI04/L/04-B1 0840

### A STATISTICAL EQUILIBRIUM THEORY FOR CUMULUS CONVECTION

GEORGE C. CRAIG (University of Reading, UK)

Cumulus parameterization is based on the assumption that, in a convecting atmosphere, the ensemble of cumulus clouds is in some sort of equilibrium with the large-scale forcings that destabilize the atmosphere. The various closure hypotheses in parameterization schemes predict mean properties of the ensemble, but in the absence of a complete statistical theory, it is impossible to determine when these mean properties will be achieved in the atmosphere. In this talk, cumulus convection will be considered from the point of view of equilibrium and non-equilibrium statistical mechanics. A theory will be presented for an ideal convective ensemble ("ideal" implying that the clouds do not interact). The theory will reduce to a standard closure hypothesis (boundary-layer quasi-equilibrium) for the mean properties of the ensemble, but will also make predictions for the distribution of convection in space and time. Fundamental results from statistical mechanics, including the fluctuation-dissipation theorem and the Curie symmetry principle, will be used to identify limits on the parameterizability of cumulus convection and to propose new observational tests.

## MI04/W/32-B1 0900

### IDEALIZED SIMULATIONS OF RADIATIVE-CONVECTIVE EQUILIBRIUM

Adrian TOMPKINS (Max Planck Institute for Meteorology, email: Tompkins@dkrz.de Tompkins@dkrz.de)

Cloud resolving models have been used previously to examine bulk statistics of deep convection in long-term simulations of radiative-convective equilibrium. Here we focus on highly resolved deep convection, with statistics based on individual cloud units, tracing cloud volumes, cross-sectional areas, and transport properties in a pseudo-Lagrangian fashion. The sensitivity of such properties to 'external' factors such as large-scale temperature and humidity profiles and boundary layer properties will be examined, using a domain large enough to continuously contain an ensemble of deep convective clouds, and with a horizontal resolution of 400m to attempt to resolve some of their internal structure.

## MI04/W/13-B1 0915

### RADIATION AND SURFACE ENERGY BUDGETS SIMULATED BY NCAR CLOUD-RESOLVING MODEL AND COMMUNITY CLIMATE MODEL

Xiaoqing WU (Email: xiaoqing@ucar.edu) and Mitchell W. Moncrieff (National Centre for Atmos Research, Mesoscale and Microscale Met., Boulder, USA, Email: moncreif@ncar.ucar.edu)

The representation of cloud systems and the simulation of sea surface temperature (SST) are two major uncertainties in coupled ocean-atmosphere general circulation models (GCMs). Clouds affect the ocean-atmosphere system through their influence on the earth radiation budget and the surface energy budget, momentum flux and precipitation. In order to improve

the representation of physical processes in the coupled GCMs, a comparison of cloud properties, radiative properties and surface energy budget is conducted using the NCAR cloud-resolving model (CRM) and community climate model (CCM3). CRM that combines evolving large-scale observations with cloud-scale models has shown great potential for producing realizations of tropical cloud systems and dynamically consistent cloud-scale datasets. The model-produced data can be quantitatively evaluated against various independent data sources, such as satellite radiative fluxes, albedo, cloud radiative forcing, surface heat fluxes, radar rainfall data, among others. The results show that the successful representation of cloud systems is of great importance for models to realistically simulate the radiative fluxes and surface energy budget. It suggests that the ocean-atmosphere coupling may be down to mesoscale and cloud-scale processes. The dynamically consistent cloud properties and surface forcing provide valuable long-term datasets for improving the parameterization of cloud radiative properties and understanding the role of clouds in the coupled ocean-atmosphere system.

MI10/W/25-B1

0930

#### CIRRUS CLOUD PROPERTIES DERIVED FROM AN EXTENSIVE RECORD OF SURFACE-BASED SENSOR DATA

Gerald G. MACE, (Uni of Utah Email: mace@atmos.met.utah.edu); E.E Clothiaux and T.P Ackerman, (Penn State University)

In the efforts toward improved characterization of cloud-related processes in global models two general trains of thought have emerged.

One approach is to use global data sets to characterise the influence of clouds on the energy budget and then to parameterise the infra-red physical processes in the models.

The canonical example of this is the use of Earth Radiation Budget Experiment (ERBE) data to validate the top of atmosphere energy budget of most general circulation models. Another equally viable approach that is now emerging is to use highly detailed extended time observations of a single vertical column to characterise the statistics of the physical processes that occur within that column and then to compare the statistics of the observations to those predicted by a global model. We have been active in this latter approach largely through the analysis of Atmospheric Radiation Measurement Program data. We are in the process of developing new and implementing already published cloud retrievals schemes on the operational cloud radar data streams available from the various ARM sites. At the conference we will present the latest results of this effort. Specifically, we will explore the statistical distributions that are now emerging from this undertaking regarding cirrus and boundary layer clouds and our ongoing to compare these distributions to predictions by the ECMWF model.

MI04/L/13-B1

0945

#### CIRRUS DETRAINMENT-TEMPERATURE FEEDBACK

DAVID NEELIN and Chia Chou (Dept. of Atmospheric Sciences, UCLA, Los Angeles, California, USA)

To unravel the role of cirriform clouds in climate change, it is important to distinguish among the relationships of different high cloud types to large-scale atmospheric dynamics. While cirrostratus and cirrocumulus (CsCc) have a clear relation to deep convective sources, the ensemble behavior of cirrus is more subtle. An empirical relation is found between cirrus fraction and deep cloud top temperature that points to detrainment temperature as a dominant factor governing tropical and subtropical cirrus. This cirrus-detrainment-temperature (CDT) relation provides a target for modelers, and suggests an additional cloud-climate feedback. As surface temperatures warm, detrainment temperatures cool as deep cloud top height increases. The CDT relation implies that cirrus fraction increases. Because cirrus are optically thinner than CsCc, the competition between longwave feedbacks and cloud albedo feedbacks leads to a hypothesized positive climate feedback by cirrus fraction.

MI10/W/15-B1

1000

#### LONG TERM CLOUD AND RADIATION MEASUREMENTS IN THE TROPICAL WESTERN PACIFIC

Charles N. LONG, James Mather, and Tomas P. Ackerman (Pennsylvania State University Department of Meteorology University Park, PA, USA 16802)

The tropical western Pacific region is characterized by high sea surface temperatures and frequent deep convection. It also plays an important role in the global atmospheric circulation, acting as a driver for mass and energy export into higher latitudes. The US Department of Energy Atmospheric Radiation Measurement (ARM) Program has recently installed two Atmospheric Radiation and Cloud monitoring Stations (ARCS) in the area. The first ARCS was installed in September-November of 1996 on the island of Manus, Papua New Guinea. The second ARCS has more recently become operational as of November, 1998, on the island of Nauru. This paper describes the instrumentation included with each ARCS deployment, focusing on the capabilities of these instruments in the quantification of cloud properties and the study of cloud effects on the surface energy budget. Each ARCS includes standard surface meteorological instrumentation (pressure, temperature, RH, winds, etc.) as well as radiometers to measure the complete surface radiative energy budget. Additional instrumentation, including balloon borne radiosondes, measures properties of the atmospheric state. Instruments, especially at Nauru, particularly suited to measure cloud properties include a lidar, a millimeter cloud radar, a whole sky radiance and cloud instrument, a microwave radiometer, a narrow field of view 10 micron radiometer, and an Infrared Fourier Transform Interferometer. With these instruments, we can observe vertical (lidar and cloud radar) and horizontal (sky imager) distributions of clouds over the site. With the microwave radiometer and the infrared instruments we can determine column water vapor and liquid water amounts, and cloud optical properties. The ARCS combination of active and passive sensors gives a comprehensive view of the cloud field over each site, and measurements of the effect at the surface. The ARM program intends to operate these two, and other, ARCS sites for at least a 10 year period. We will present examples of retrieved cloud properties and the attendant effect of clouds on the surface radiative energy budget from the first six months of data collected at the Nauru site, and a comparison with over two years of data collected at the Manus site.

MI04/W/34-B1

1045

#### RADAR STATISTICS IN TROPICAL PACIFIC CLOUD FIELDS

Brian MAPES (NOAA-CIRES Climate Diagnostics Center, Boulder, CO USA 80303-3328, email: bem@cdc.noaa.gov)

Shipborne Doppler radar data from several month-long cruises in the equatorial Pacific have been analyzed by binning the observations in a coarse cylindrical grid. This analysis reduces the data volume tremendously, allowing nimble exploration. The cylindrical coordinate system respects the perverse nature of radar data, and facilitates quantitative use of single Doppler

data. Reflectivity, wind, and horizontal wind divergence statistics from unprecedentedly large samples of Pacific precipitating cloud fields are presented. Systematic differences between radar-derived and sonde-derived winds indicate the vertical flux of horizontal momentum.

MI10/W/12-B1

1100

#### A MULTISCALE NUMERICAL SIMULATION OF A HIGH LATITUDE CLOUD SYSTEM

M.K.YAU (Department of Atmospheric and Oceanic Sciences, McGill University, Montreal, Quebec, Canada H3A 2K6, email: yau@rainband.meteo.mcgill.ca)

In this study, the cloud system associated with the 30 September 1994 Arctic low which passed over the southern Beaufort Sea area of northern Canada is simulated using the Canadian Mesoscale Community Model (MC2) in a one-way nested mode. The model utilizes simultaneously a cumulus parameterization scheme and an explicit microphysics scheme to simulate the evolution of the larger-scale flows over the coarser-mesh domain (20km grid size). Over the fine-mesh domains at a grid size of 5km and 2 km respectively, the storm is resolved with the explicit scheme containing prognostic equations for cloud water, ice, rainwater, snow and graupel. The model is initialized with the Canadian Meteorological Center (CMC) analysis and is integrated for 36 h which covers the development stage and the mature stage of the storm.

As verified against various observations and the best analysis, the model captures reasonably well many of the fine-scale structures of the cloud system associated with the storm, including the cloud head, the banded cloud features, and the warm frontal clouds. In particular, the model reproduces the observed dry slot at the front edge of the storm. The effects of the frontal circulation, sublimation, horizontal shear and conditional symmetric instability in the evolution of the cloud system are also investigated.

MI04/E/12-B1

1115

#### NONLINEAR KELVIN WAVES AND INTRASEASONAL OSCILLATIONS IN THE EQUATORIAL

HAN-RU CHO (Department Of Physics University Of Toronto Toronto Ontario Canada m5s 1a7 FAX: 416-978-8905 e-mail: cho@physics.utoronto.ca)

Equatorial Kelvin wave-CISK has been proposed as the possible mechanism to explain equatorial intraseasonal oscillations. This paper will discuss certain nonlinear aspects of Kelvin wave-CISK propagation. This study is motivated by the fact that if one adopts the so called "CISK parameterization", then, as pointed out by a number of authors, CISK is an essentially nonlinear process which is nonlinear even in the small amplitude approximation.

Since Kelvin wave is a non-dispersive wave, its solution can be obtained from the method of characteristics. In applying the methods we find that CISK process doesn't exist in Kelvin waves. In other words, Kelvin waves with cumulus heating is always stable. This is the central conclusion of this paper. Furthermore we found another problem with the so called "CISK parameterization". In the trailing edge of the cloud region, we show that discontinuity will develop. Because of the so called "CISK parameterization" we show the discontinuity begin to appear at the initial time. Furthermore, we will show that the discontinuity in the cloud heating parameter introduced in the so called "CISK parameterization" is incompatible with the "jump condition". A jump condition is what we must have when a discontinuous solution is applied to a conservation law.

In the leading edge of the cloud region the solution of the wave will involve the so called "rarefaction wave". A method used to drive a rarefaction wave will also be discussed.

MI04/E/19-B1

1130

#### ORGANISED DEEP CONVECTION AND ITS RELATION TO SST AND HUMIDITY

C. A. BABU and P. V. Joseph (Department of Atmospheric Sciences, Cochin University of Science and Technology, Cochin - 682 016, INDIA)

We have examined the relationship of SST and humidity at 850 hPa level with organised deep convection over tropical Indian Ocean and Western Pacific Ocean. SST is obtained from COADS data set and humidity field is from NCEP data set while HRC data set as derived by Garcia (1985) is used to represent deep convection. SST and HRC data sets are monthly mean values during the period 1971 to 1986 and humidity field is from 1979 to 1986, averaged over 4 deg. latitude X 4 deg. longitude squares. The response of convection to SST is of two types: one the TROUGH type and the other the SUBSIDENCE Type. In the Equatorial Convective Cloudiness Maximum (ECCM) area convection is large (HRC 4-6 days/month) and occurs with SST in the range 28 to 30 C. To the north and south of the ECCM, convection is feeble (HRC less than 2 days/month) due to the subsidence zones associated with the descending limb of tropical Hadley circulation and in these areas convection increases with SST in the range 26 C to 29 C.

Decrease in convection above 29 C is also noticed as found by Walliser (1993). Another component examined is the response of convection to SST over the ECCM cloud band during January and February (Austral summer) over the Australian Seas, Indian Ocean and in the equatorial central Pacific. Trough type pattern occurs over the Australian Seas and other two areas show Subsidence type pattern with high HRC values. This can be interpreted due to sinking motion associated with the Walker circulation with rising motion over the Australian Seas. The response of convection to SST in El Nino case is also discussed. Humidity - convection results indicate that humidity at 850 hPa has influence in organised deep convection.

MI04/L/12-B1

1145

#### STATISTICAL ANALYSIS OF THE MAXIMUM VERTICAL WIND VELOCITY IN THE WESTERN PACIFIC

Philippe NAVEAU and Mitch Moncrieff (National Centre for Atmos Research, Mesoscale and Microscale Met., Boulder, USA, Email: moncreif@ncar.ucar.edu)

To model the atmospheric characteristics of mesoscale clouds system in the Western Pacific, a variety of simulated numerical models has been generated and studied in the past. One important output from these models is the time series of the maximum vertical wind velocity on the domain. Our data constitutes of two different sets of observations. The first set is generated by a two-dimensional, two-nested Cloud Resolving Model (CRM) with a large outer domain (4500 \* 30 km) initialized by an idealization of December 1992 westerly wind burst in the Tropical Oceans Global Atmosphere Coupled Ocean-Atmosphere Research Experiment region (TOGA COARE). The second set of observations is generated by a different two-dimensional CRM initialized by a thermodynamic sounding typical of those observed during TOGA COARE but with different idealized wind profile (for more details see Wu and Moncrieff (1995) and Liu and Moncrieff (1997)).

A key aspect in this study is the relationship between the maximum vertical wind velocity and two distinct regimes, highly organized squall-line-like convection and less organized non-squall cloud clusters. Applying the statistical theory of extreme values, we first analyze the

statistical distribution of the maximum vertical wind velocity as a mixture of two Generalized Extreme Distributions. Since the maximum vertical wind velocity time series is not stationary, we develop then a stochastic model that takes into account the non-stationary temporal dependence and the regime type dependence. Our stochastic model can be describe like a random game with two players, and can reproduce the different regimes, squall-lines, non-squall lines cluster and scattered. We show that the behaviour of the maximum vertical wind velocity can be simulated by using few parameters. These parameters are set according to the behaviour of the cloud system that you want to reproduce.

#### MI04/W/10-B1 1200

##### A COMPREHENSIVE TREATMENT OF CLOUDS AND CONVECTION FOR USE IN A REGIONAL CLIMATE MODEL

Colin G. JONES, Ulrika Willen, Markku Rummukainen & Anders Ullerstig (Rosby Centre, SMHI, Norrköping SE601 76 Sweden)

The SWELIM program has as a goal to model climate change in the NORDIC region, over the next 50-100 years. To achieve this the High Resolution Limited Area Model (HIRLAM) is being developed into a Regional Climate Model (RCA), incorporating an atmospheric component, 3D model of the Baltic Sea and a sophisticated treatment of the surface and subsurface hydrology. For climate change experiments the RCA is commonly run at a resolution between 20-80km. Crucial to these climate integrations is an accurate treatment of the water cycle. In particular, precipitation and cloud cover/content and its radiative interaction. The HIRLAM model contains a detailed parameterisation of cloud microphysics and formation, due to Sundqvist (1988,1993). The treatment of convection is less detailed, being a Kuo type scheme. In an attempt to improve the representation of convection in the RCA, the Kain-Fritsch convection parameterisation has been implemented. This scheme was designed specifically for mesoscale applications. Amongst other features, it contains a CAPE based closure, a trigger function controlling the onset of convection in an unstable atmosphere and both moist updrafts and downdrafts. Cloud water is a prognostic quantity in the RCA, water detrained from the convective updrafts and downdrafts is passed to the cloud microphysics parameterisation for cloud formation and may also interact directly with the resolved dynamics. This talk will outline the impact of the Kain-Fritsch scheme on simulations with the RCA on both synoptic forecast timescales through to multi annual climate timescales. Key parameters analysed include precipitation, cloud cover/content and its radiative interaction and the overall water budget of the atmosphere.

#### MI04/L/19-B1 1215

##### THE FEATURES OF CLOUD-RADIATION OVER TIBETAN PLATEAU

WANG

Abstract not available at time of going to press

**Monday 26 July PM**

Presiding Chair: R Abbey (Office of Naval Research)

#### PARAMETERIZATION AND LARGE-SCALE MODELLING

#### MI04/W/24-B1 1400

##### A PARAMETERIZATION OF CLOUD AND PRECIPITATION OVERLAP FOR USE IN GENERAL CIRCULATION MODELS

Christian JAKOB (1) and Stephen A. Klein (2); (1) European Centre for Medium-Range Weather Forecasts (2) Geophysical Fluid Dynamics Laboratory/NOAA

Global Circulation Models (GCMs) have generally treated only the radiative impacts of vertically varying cloud fraction by use of a cloud overlap assumption. In a recent study Jakob and Klein (1999) have attempted to evaluate the importance of the "cloud macrophysics", i.e., the treatment of cloud cover and its vertical overlap, for the parameterization of microphysical processes. They used a simple microphysical scheme as it is implemented in the current ECMWF model to show that a more detailed treatment of cloud fraction and its overlap can lead to large differences in the parameterized precipitation and evaporation rates. The method they employed was to subdivide each model grid box in a number of smaller boxes and solve the cloud microphysics parameterization for each of the sub boxes individually after applying a cloud overlap assumption. This method increased the runtime of the ECMWF model by about 20 %. Given the large uncertainties in both the microphysical parameterization themselves and in the description of the cloud overlap it seems inadequate to apply their "sub-grid precipitation scheme" directly in a GCM. However, it can also be argued that the use of a complex microphysical parameterization, which undoubtedly also increases model cost enormously, is not useful before addressing the cloud and precipitation overlap issues. This paper describes a simple parameterization that tries to address the problems raised in JK99 without significantly increasing the model cost. The basic idea of the parameterization is to divide the precipitation flux in each grid box into a cloudy and a clear-sky part. That division together with a description of the area coverage of each of the flux components and their overlap captures the main features of the sub-grid precipitation formulation of Jakob and Klein (1999) at a much reduced cost. Results from both climate simulations and forecasts will be presented to demonstrate the impact the new treatment has on the ECMWF model simulations.

#### MI04/E/09-B1 1420

##### ASSESSING CLOUD OVERLAP ASSUMPTIONS USING LARGE EDDY MODEL RESULTS

Jon PETCH, John Edwards and Mike Gray (UK Met Office, London Rd, Bracknell, Berks, RG12 2SZ. e-mail: jpetch@meto.gov.uk)

A Large Eddy Model (LEM), using a horizontal grid length of 2 km and a domain size of 256 km, has been run for 6 days of the TOGA-COARE Intensive Observational Period (IOP). 2-D and 3-D simulations have been carried out to give detailed temperature, moisture, cloud and radiation fields. A radiation scheme from a climate model has then been run on the domain average fields and compared to the heating rates calculated within the LEM. Sensitivities to the cloud overlap assumption used in the climate model radiation scheme are presented. Further sensitivities to the treatment of precipitation sized hydrometeors in the radiation schemes are also shown.

#### MI04/E/15-B1 1435

##### IMPROVEMENT OF CUMULUS-SCALE PARAMETERIZATION IN A TROPICAL CYCLONE MODEL

Tomoe NASUNO and Masanori Yamasaki (Department of Earth and Planetary Physics, Faculty of Science, University of Tokyo, Hongo 7-3-1, Bunkyo-ku, Tokyo, 113-0033, Japan, email: nasuno@atmos0.geoph.s.u-tokyo.ac.jp, yamas@atmos0.geoph.s.u-tokyo.ac.jp)

It is important to treat cumulus convection properly in tropical cyclone models. Especially, the significance of expressing mesoscale organized convection(MC), which is known as a basic component in TC rainband (Yamasaki,1983), has been emphasized(Yamasaki,1986). In the present study a new non-hydrostatic 10km grid model including cumulus-scale parameterization is constructed, based upon Yamasaki(1986). At present axi-symmetric model is used for understanding and results are evaluated in comparison with cloud resolving case (1km grid).In order to express MC cloud water and rainwater are predicted following Yamasaki(1986). Cumulus-scale heating is included by Kuo's(1965) method, different from Yamasaki(1986). Water vapor consumed as cumulus-scale condensation is converted to cumulus-scale cloud water, and cumulus-scale cloud water and rainwater are also treated as predictable variables. By including cumulus-scale effects convection grows to high levels and maintains with intense rainfall, and decays within several hours as cold pool develops. Tropical cyclone scale circulaion gradually develops through continuous formation of MC. The life cycle of MC and development of the tropical cyclone qualitatively express the main characteristics of the cloud-resolving case and consistent with observational facts.

#### MI04/W/20-B1 1450

##### A PARAMETERIZATION OF CONVECTIVE CLOUDS FOR LARGE-SCALE MODELS

RONI AVISSAR, Yongqiang Liu and Chris Weaver (Department of Environmental Sciences, Rutgers University, 14 College Farm Road, New Brunswick, New Jersey 08901-8551, USA, email: avissar@gaia.rutgers.edu)

To develop a parameterization of shallow convective clouds and precipitation induced by land-surface processes in large-scale atmospheric models, a set of simulations was performed with a high-resolution 3D atmospheric model. Results indicate that landscape discontinuities could significantly affect the timing of onset of clouds, and the intensity and distribution of precipitation. In most cases, landscape discontinuities enhance precipitation. Current parameterizations of clouds and precipitation in atmospheric models do not account for such effects. Similarity theory was used to develop such a parameterization. For this purpose, Buckingham Pi Theory, a systematic method for performing dimensional analysis, was used to derive a set of dimensionless groups, which describes the large-scale atmospheric background conditions, the spatial variability of surface sensible heat flux, and the characteristic structure of the landscape. These dimensionless groups were used to calculate the coefficients of a Chebyshev polynomial, which represents the self similar vertical profiles of dimensionless mesoscale heat fluxes obtained for a broad range of large-scale atmospheric conditions and different landscapes. The numerous 3D numerical experiments performed to evaluate this similarity relationship suggest that the parameterization provides reasonable results.

#### MI04/W/01-B1 1505

##### TOWARDS PARAMETERIZING CONVECTIVE MOMENTUM TRANSPORTS BY ORGANISED CONVECTION

D. GREGORY and M.Miller (ECMWF, Shinfield Park, Reading RG2 9AX, United Kingdom Email: dgregory@ecmwf.int)

In recent years several schemes for representing convective momentum transports have been incorporated into GCMs, differing in their treatment of the across-cloud pressure gradient which plays an important role in determining the vertical variation of updraught horizontal momentum. At ECMWF, the convection scheme represents the pressure gradient through enhanced horizontal mixing (Miller, personal communication), while the scheme in use at the UK Met. Office uses a parameterization with dependency upon verticals heat and cloud mass flux (Gregory et al, 1997).

Further analysis suggests that a combination of the two approaches may provide a more accurate parameterization of the pressure gradient. The various approaches are contrasted in the ECMWF convection scheme for cases of shallow and both unorganised and organised deep convection using results from CRM simulations. Comments will also be made regarding the ability of the combined approach to represent "up-gradient" transports associated with organised convection through use of the "lateral mixing" component of the pressure gradient formulation.

#### MI04/L/11-B1 1520

##### DYNAMICAL MODELS OF MOMENTUM TRANSPORT BY ORGANIZED CONVECTION

Mitchell W. MONCRIEFF (National Center for Atmospheric Research, Boulder, CO 80307-3000, USA email: moncrieff@ucar.edu)

Convective momentum transport (CMT) is categorized in terms of two regimes; namely, i) down-gradient flux and ii) up-gradient flux as paradigms for organized transport in constant shear and in jet-like mean flow, respectively. Archetypal models are derived, as the term implies, as the simplest possible representation of momentum flux, simple enough to be applied in mass-flux-based parameterization.

These dynamical models represent the total momentum flux rather than the eddy flux associated with the standard Reynolds-averaging principle on which standard convective parameterization is based. This concept and the modeled momentum fluxes are evaluated against transports derived from fine-scale simulations of organized convection. The entraining plume used in convective parameterization is argued to be an inappropriate model of CMT by organized flows. This points to shortcomings in its (universal) application in convective parameterization. Finally, it is suggested how existing parameterization methods for CMT should be modified, at least to test the impact of organized fluxes in global models if not as a fundamental concept.

#### MI04/W/33-B1 1535

##### PARAMETERIZATION OF THE INTERACTION BETWEEN CUMULUS CONVECTION AND THE SUBCLOUD LAYER

A. Pier SIEBESMA (European Centre for Medium-Range Weather Forecasts, Shinfield Park, Reading, RG29AX, England. email: siebesma@ecmwf.int.) and Roel Neggers (Royal Netherlands Meteorological Institute, P.O. Box 201, De Bilt AE3730, the Netherlands. Email: neggers@knmi.nl.)



It is well known that the roots of cumulus convection reside in strong convective plumes that originate from the surface layer. Yet, in large-scale weather and climate models it is still common practice to parameterize the dry boundary layer and the cloud layer separately. This results in unwanted overlaps between the schemes and double counting of the transport mechanisms. It also has the additional disadvantage that it requires extra boundary conditions for the convective fluxes at cloud base, which is usually referred to as the closure problem. To overcome these problems a mass flux parameterization is proposed and analysed for strong thermals in the convective boundary layer. Lower boundary conditions can be formulated using the surface layer similarity theory. By subsequently solving updraft equations for vertical velocity, temperature and moisture, this parameterization estimates the non-local convective transport of heat and moisture by strong thermals in the sub-cloud cloud layer that transform into cumulus updrafts in the cumulus cloud layer above the level of condensation (LCL). This way the closure problem is simply shifted to the surface layer and the interaction of cumulus convection with the sub-cloud layer is established in a natural way. The parameterization scheme is tested and developed using Large Eddy Simulation (LES) results and its impact is evaluated using the ECMWF model.

MI10/W/21-B1

1620

#### INTERACTIONS BETWEEN CLOUD MICROPHYSICS AND CUMULUS CONVECTION IN THE CSU GENERAL CIRCULATION MODEL

Laura D. Fowler and David A. Randall (Department of Atmospheric Science Colorado State University Fort Collins, CO 80523, e-mail: laura@slirkrock.atmos.colostate.edu)

In the Colorado State University General Circulation Model (CSU GCM), cumulus detrainment of cloud water and cloud ice is the only coupling between convective and large-scale condensation processes. This one-way interaction from the convective to the large-scale environment parameterizes, in a highly simplified manner, the growth of horizontally spreading anvils at the tops of narrow cumulus updrafts. The reverse interaction from the large-scale to the convective environment through which large-scale cloud water and cloud ice can modify microphysical processes occurring in individual convective updrafts is presently missing. In the EAU cup parameterization of convection, large-scale water vapor, cloud water, and cloud ice are let to enter the sides of the convective updraft, and be lifted to the top of the cloud. As the different water species are being lifted, cloud microphysical processes are taking place, removing excess supersaturation in the form of cloud water and cloud ice, and converting excess cloud water and cloud ice in the form of precipitation of rain and snow. The partitioning between cloud water and cloud ice, and that between rain and snow are based on temperature, as in the EAUliq parameterization of large-scale cloud microphysical processes. As in the CONTROL parameterization of convection, cumulus precipitation of rain is assumed to instantaneously fall to the surface. In contrast, the treatment of the cumulus precipitation of snow varies, from assuming that snow completely detrains at the top of cumulus towers, to assuming that snow falls through the updraft and melts, or to assuming that snow falls outside of the updraft and may evaporate. Differences between climate simulations obtained with the EAUcup and CONTROL parameterizations of convection are discussed. Emphasis is given on the impact of the treatment of the precipitation of snow formed by convection on the simulated climate. The importance of parameterizing a two-way interaction between convective and large-scale condensation processes is emphasised.

MI04/W/17-B1

1635

#### ATMOSPHERIC GENERAL CIRCULATION MODELS: CAN SEASONAL AND LATITUDINAL CHANGES OF CLOUD-RADIATIVE FORCING BE USED TO VALIDATE CLOUD- CLIMATE FEEDBACK?

Robert D. CESS (Marine Sciences Research Center, State University of New York, Stony Brook, NY 11794-5000, email: cess@atmsci.msrc.sunysb.edu)

Seasonal and latitudinal changes in cloud-radiative forcing at the top of the atmosphere have been evaluated from 18 atmospheric general circulation models. These same models have been used to evaluate cloud-climate feedback for one type of climate-changes simulation. These two separate studies thus provide a means of addressing the question as to whether seasonal and latitudinal changes of cloud-radiative forcing can be used to validate cloud-climate feedback.

MI04/E/08-B1

1650

#### STUDY OF CLOUD PARAMETERIZATIONS AND THEIR INTERACTION WITH CONVECTION IN AN OPERATIONAL NWP MODEL

Qingyun ZHAO, Thomas L. Black, and Song-You Hong (Environmental Modeling Center, National Centers for Environmental Prediction, Washington, D. C. 20233, Email: wd20cl@next4.www.noaa.gov)

A package of cloud and precipitation parameterization schemes has been incorporated into the National Centers for Environmental Prediction (NCEP) Eta Model for testing. This package combines the operational Eta Model cloud parameterization scheme (Zhao and Carr, 1997, Zhao et al., 1997) with the precipitation physics package developed by Hong et al. (1998). The schemes in this package are designed with different levels of sophistication in microphysics for different model configurations and/or for different reanalysis and operational purposes. Currently, there are three cloud and precipitation schemes in this package. The CLD2 scheme contains only one prognostic variable, cloud water/ice mixing ratio, and is basically for uses in large-scale NWP models and GCMs. This scheme has been in operational use in the Eta Model at NCEP since 1995 and is being incorporated and tested in the NCEP MRF Model. The CLD3 scheme contains two species of hydrometeors, namely, cloud water/ice and rain/snow, and is designed to improve the cloud and precipitation forecasts in the mesoscale Eta Model where model resolution is high and the horizontal advection of precipitation (rain and snow) is important due to the small model grid size. The CLD5 is the most sophisticated scheme in this package and has four prognostic variables: cloud liquid water, cloud ice, rain and snow. This scheme is developed for the future uses for the Eta Model with very high model resolution. The CLD3 and CLD5 schemes have been tested with the NCEP Regional Spectral Model (Hong et al., 1998). The whole package is coded with a plug-in ability for easy uses with other models and it is easy to switch from one cloud scheme to another without changing the model codes. The objectives of this research are to study the effects of cloud parameterization with different schemes on the model's cloud and precipitation forecasts and to learn how cloud parameterization interacts with convection. For this purpose, tests with all these cloud parameterization schemes have been carried out with the same model configuration. Preliminary results show that a simple scheme sometimes performs better than complicated ones in a large-scale model. Experiments have also been performed with and without cloud microphysics in the model's convective parameterization. Studies of these experiments are underway and results will be represented at the Symposium.

MI04/E/27-B1

1705

#### IMPACTS OF CONVECTION PARAMETERS ON CLIMATE SIMULATIONS USING THE ARIES GCM

Julio T. BACMEISTER (University Space Research Association, 7501 Forbes Blvd #206, Seabrook, MD 20706-2253 USA e-mail: bacmj@janus.gsfc.nasa.gov); Max J. Suarez (Code 913, NASA Goddard Space Flight Center, Greenbelt, MD 20771 USA)

Results from multi-year simulations at 2.5x2 degree resolution using the ARIES GCM are shown. ARIES includes a relaxed Arakawa-Schubert scheme (RAS) to represent the effects of atmospheric convection. We examine the climatological impact of several physical processes represented in RAS, including the efficiency of precipitation conversion and re-evaporation, and the existence of "triggers" for convection. Large impacts are found when rain-re- evaporation is included. Persistent errors in the model's global precipitation, such as the existence of a "double ITCZ" are reduced or eliminated. Interactions between RAS and a new prognostic liquid water scheme for ARIES will also be discussed.

MI04/L/08-B1

1720

#### SENSITIVITY OF CLIMATE SIMULATION TO THE RADIATIVE...

LI

Abstract not available at time of going to press

PANEL DISCUSSION

1735

Tuesday 27 July AM

Presiding Chair: J Joseph (Tel-Aviv University, Tel-Aviv, Israel)

RADIATIVE TRANSFER AND CLOUD FIELD MORPHOLOGY

MI10/E/03-B2

0930

#### CLOUD SPATIAL STRUCTURE AND 3D RADIATIVE TRANSFER

ROBERT F. CAHALAN (NASA/Goddard Space Flight Center, Greenbelt, MD 20771 USA)

Cloud radiative properties are sensitive to drop size and other parameters of cloud micro-structure, but also to cloud shape, spacing, and other parameters of cloud macro-structure, including internal fractal structure. New information on cloud structure is being derived from a variety of cloud radars, and ongoing field programs such as DoE/ARM are improving the measurement and modelling of physical and radiative properties of clouds. A parallel effort is underway to improve cloud remote sensing, especially from the new suite of EOS-AM1 instruments which will provide higher spectral, spatial resolution, and/or angular resolution. Key parameters for improving pixel-scale retrievals are cloud thickness and photon mean-free-path, which together determine the scale of "radiative smoothing" of cloud fluxes and radiances. This scale has been observed as a change in the spatial spectrum of Landsat cloud radiances, and was also recently found with the Goddard micropulse lidar, by searching for returns from directions nonparallel to the incident beam. "Offbeam" Lidar returns are now being used to estimate the cloud "radiative Green's function", G, which depends on cloud thickness and may be used to retrieve that important quantity. G is also being applied to improving simple IPA estimates of cloud radiative properties. This and other measurements of 3D transfer in clouds, coupled with Monte Carlo and other 3D transfer methods, are beginning to provide a better understanding of the dependence of radiation on cloud inhomogeneity, and to suggest new retrieval and parameterization algorithms which take account of cloud inhomogeneity. An international "Intercorparison of 3D Radiation Codes" or I3RC, program is beginning to coordinate and evaluate the variety of 3D radiative transfer methods now available, and to make them more widely available. Information is on the Web at: <http://climate.gsfc.nasa.gov/I3RC>. Input consists of selected cloud fields derived from data sources such as radar, microwave and satellite, and from models involved in the GEWEX Cloud Systems Studies. Output is selected radiative quantities that characterize the large-scale properties of the fields of radiative fluxes and heating. Several example cloud fields will be used to illustrate.

MI04/E/26-B2

0950

#### THE RETRIEVAL OF CIRRUS CLOUD MICROPHYSICAL AND BULK PROPERTIES USING RADIANCE DATA FROM THE MULTI-SPECTRAL AND DUAL-VIEWING ALONG TRACK SCANNING RADIOMETER

Sarah K. WATTS (Department of Atmospheric, Oceanic and Planetary Physics, Oxford University, Parks Road, Oxford OX1 3PU, UK, Email: swatts@atm.ox.ac.uk); Anthony J. Baran (Satellite Soundings, UK Meteorological Office, Email: abaran@meto.gov.uk); Philip D. Watts (Rutherford Appleton Laboratory Email: p.d.watts@rl.ac.uk); Mark J. Webb (Hadley Centre, UK Meteorological Office, Email: mjwebb@meto.gov.uk Ping Yang, Department of Atmospheric Sciences, University of California, Email: yang@atmos.ucla.edu)

The Along Track Scanning Radiometer (ATSR-2) instrument on the ERS-2 platform has multi-spectral and dual look capabilities providing the means for retrieving cirrus cloud parameters such as optical depth, crystal effective size and estimates of crystal habit and ice water path. In the retrieval scheme, cloud is modelled as a single, homogeneous layer, specified by the single scattering albedo, the optical depth and the scattering phase function. Assuming a particular crystal shape (or habit), it is usual to assume the geometric optics approximation in calculating crystal optical properties and single scattering phase function. The limitations of the geometric optics method are well known. However, in this paper we present retrievals based on the Finite Difference Time Domain (FDTD) method. The FDTD method is exact and has been used to calculate all crystal optical properties and single scattering phase functions for hexagonal plates, hexagonal columns, bullet rosettes and complex aggregates at the wavelengths of 0.55, 0.87, 1.6 and 3.7 microns. Selected tropical and mid-latitude cirrus cases are presented. For these cases we use the dual-view geometry of ATSR-2 at 0.87 microns to estimate the dominant crystal habit, thereby testing the FDTD predictions of the scattering phase functions representing the various crystal habits. The 0.55, 1.6 and 3.7 micron ATSR-2 channels are used to retrieve the bulk optical depth and crystal effective diameter (De), and these two independent retrievals allow the estimation of ice water path (IWP). Preliminary comparisons of retrieved De and IWP will be made with the UK Meteorological Office HadAM4 model predictions of ice water path for selected case studies in the tropical Pacific.

MI10/W/06-B2

1005

**A STATISTICALLY BASED PARAMETERIZATION OF SHORTWAVE CLOUD RADIATIVE FLUXES OF INHOMOGENEOUS MIXED PHASE CLOUDS**

Andreas MACKE, Ronald Scheirer, and Lueder v. Bremen (Institute for Oceanography, University of Kiel, Duesternbrookerweg 20, D-24105Kiel, Germany, email: amacke@ifm.uni-kiel.de)

Shortwave (SW) cloud radiative fluxes and radiance fields for inhomogeneous mixed-phase clouds have been calculated by means of a Monte Carlo radiative transfer model. Single scattering properties of water droplets, ice, snow and graupel particles, as well as raindrops are considered as realistically as possible. Furthermore, scattering and absorption at the spatially inhomogeneous distributions of dry air and water vapour is taken into account. Cloud geometries and cloud microphysical properties have been obtained from a large number of mesoscale cloud model results and various cloud radar measurements. The calculated SW albedo, transmission, and absorption differ considerably from those obtained by a homogeneous plane-parallel cloud idealisation. These qualitatively well known deviations have been quantified with respect to bulk cloud physical properties such as cloud height, cloud liquid water, cloud ice, and cloud top temperature. First results of a principal component analysis correlating the radiative fluxes with the most relevant bulk properties will be discussed. These statistically based parameterisation of solar broadband cloud radiative properties provides a promising tool to improve cloud radiation schemes in atmospheric circulation models.

MI10/W/05-B2

1020

**USING MEASUREMENT-BASED THREE-DIMENSIONAL CLOUD DEPICTIONS IN NUMERICAL WEATHER PREDICTION**

Donald C. NORQUIST, (AFRL/VSBE, c/o AFWA/DNX, 106 Peacekeeper Dr, Offutt AFB, NE 68113-4039 USA; Telephone: 402-232-8282, Fax: 402-294-2892, E-mail: Donald.Norquist@afwa.af.mil)

Mesoscale and global-scale numerical weather prediction (NWP) models are now predicting near-future distributions of clouds in three-dimensions. In most cases, the prognostic cloud variable is cloud water content in both ice and liquid states. Unfortunately, initialization of such predictions have lagged behind the mechanics of the predictions themselves. Modellers find themselves having to use less than adequate means to initialize the cloud water content, usually either with a zero state or a previous forecast. This is because direct cloud water measurements, unlike other NWP prognostic variables, are not available. What are widely available are the "observed" cloud quantities like fractional cloud coverage and cloud top temperature. Satellite imagery processing algorithms have been developed to estimate additional quantities, such as cloud top altitude, cloud emissivity, cloud optical depth, and cloud type. What is needed is a way to convert these observed or derived cloud properties based on satellite imagery into cloud water content that can be used to initialize NWP models. In this project, we have placed aircraft-borne in situ cloud particle measurements, ground-based cloud radar measurements, and satellite observed and derived cloud properties in three-dimensional grids. The in situ and radar measurements were used to derive cloud water content which were placed in grid cells on grids synoptic with satellite imagery from a geostationary satellite. The imagery-based cloud properties were also placed in the grids in their respective locations. From these grids, co-located and synoptic grid values of cloud water content and observed/derived satellite-based cloud properties were matched to derive empirical relationships for the former as a function of the latter. These relationships were tested on subsequent days of field experiment data to evaluate their effectiveness in estimating cloud water content from the satellite-based cloud properties. We plan to use the relationships as a module in a cloud water analysis procedure to convert satellite imagery data to cloud water estimates that, in correcting a mesoscale NWP model prediction of cloud water, can result in realistic initial cloud water conditions for a subsequent model prediction. Three-dimensional cloud data grids and empirical cloud water - cloud property relationships will be shown at the conference.

MI10/W/01-B2

1035

**FRACTAL ANALYSIS OF AN UPPER TROPICAL TROPOSPHERIC CIRRUS SHIELD AND OF AN ARCTIC POLAR STRATOSPHERIC CLOUD**

Adrian TUCK (NOAA Aeronomy Laboratory, 325 Broadway, Boulder CO 80303-3328, USA, email: tuck@al.noaa.gov); Susan Hovde (CIRES/NOAA Aeronomy Laboratory, 325 Broadway, Boulder CO 80303-3328, USA, email: hovde@al.noaa.gov)

The ER-2 high altitude research aircraft made over 200 flights in the lower stratosphere between 90N and 72S, with some penetrations into the upper tropical troposphere between 1987 and 1997. Here, we describe a fractal analysis using the Hurst exponent measure H to examine the cirrus shield associated with tropical cyclone Jason over the Gulf of Carpentaria 19870208. We show that all variables measured (CN, water vapor, total water, ice saturation mixing ratio, temperature, pressure, horizontal wind speed and direction, vertical wind speed, ozone and NOy) are fractal, with cases of random (H=0.5), persistent (H>0.5) and anti-persistent (H<0.5) self-affine behaviour. It is shown that total water shows a value of H indicating that it was subject to a process which was variable on small scales and which did not operate on the other measured variables; gravitational settlement is suggested as a viable candidate. In the case of a polar stratospheric cloud over Scandinavia on 19890124, the relative dispersion measure is used in conjunction with H to examine the behaviour of the above variables plus the particle number densities in the 0.50-0.55 and 0.55-0.60 micron size bins. We argue that at the edge of the cloud the measures show variabilities in certain of the observables which correlate with the particle number densities in the former range but not the latter, yielding insight into how the processes are related. In neither tropical or polar case would it have been possible to deduce the relationships among variables without using the measures.

MI04/W/14-B2

1120

**CLOUD MODULATION OF ZENITH SKY OXYGEN PHOTON PATHLENGTHS OVER BOULDER COLORADO: MEASUREMENTS VS. MODEL**

Robert PORTMANN, Susan Solomon, Ryan Sanders and John Daniel (NOAA Aeronomy Lab, 325 Broadway, Boulder, CO, USA, email: portmann@al.noaa.gov); Ellsworth Dutton (NOAA Climate Monitoring and Diagnostics Lab, 325 Broadway, Boulder, CO, USA)

Cloud sky average photon path lengths were measured using the 628nm gamma band of oxygen on many days over Boulder, Colorado using a zenith looking spectrograph. These photon pathlengths show very large variations as the cloud field overhead evolves. They are compared with detailed line-by-line model calculations based on the HITRAN database and the DISORT radiative transfer code. Clouds are modeled as temporally varying in optical depth but uniform vertically and horizontally, with cloud top and bottom heights estimated from radar and ceilometer data. Reasonable agreement between the measured and modeled pathlengths is obtained when the cloud optical depth is retrieved from broadband flux measurements taken

at a nearby location (approximately 2 km distant). Thus, the relationship between the cloud scattering induced reflection (which dominates changes in the broadband flux at the ground) and enhanced photon pathlengths is usually (surprisingly) well modeled by current plane parallel radiative transfer codes, at least when cloud cover is relatively uniform. The implication of these results to the "anomalous absorption" problem are discussed.

MI04/W/28-B2

1135

**SURFACE RADIATION BUDGET AND CLOUD COVER DIURNAL PATTERN MODEL**

Oleg POKROVSKY (Main Geophysical Observatory, Karbyshev str.7, St.Petersburg, 194021, Russia, e-mail: pokrov@main.mgo.rssi.ru)

Surface radiation budget (SRB) variables are not synoptically observed or input daily as a boundary condition into global models. SRB data sets could be used to identify systematic errors and to improve land surface and boundary layer parametrization for global models. This study is prompted by the need to investigate the climatology of surface variables diurnal cycles. The solar terms are the dominant terms during daytime and in summer. It is difficult to calculate the SRB to sufficient accuracy in global forecast and climate models. Many of models underestimate the absorption or reflection of solar radiation in atmosphere, either by clouds or aerosol, that are poorly modeled with the results that they overestimate the incoming solar radiation at surface. Proposed method bases on "fuzzy" logic approach, aiming the maximization of intercluster distances under the minimum of each cluster scattering measures. A basis for our researches were hourly observational data for several sites of North-West region of Russia for 1984-93. Diurnal cycle of total solar downward radiation in summer is the most significant due to amplitudes. The obtained results on average diurnal cycle in clusters support the simple interpretation. The upper curve corresponds to conditions of clear sky, and lower one to overcast cloud cover. Intermediate curves correspond to conditions of a fractional cloud cover, which can vary during a day. Results of empirical classification of a day time cycle of cloud cover, presented in climatological works, are closely linked with our conclusions. The complete set of classes changes from 3 in the winter up to 6 in the summer. To substantiate the interpretation of classification results parallel calculations of day time distribution of downward SW radiation for the latitude 60° and height of the Sun, adequate to the middle of an appropriate month of the year, were performed. The calculations were carried out on the base of the Delta-Eddington approximation technique for one-layer cloud model, with optical thickness equal to 30, the single scattering albedo was equal to 0.99 and asymmetry factor of the phase function  $g=0.85$ . Bi-diurnal SRB patterns also are considered. Main result of this research is not only study of non-stationary diurnal and multi-diurnal oscillations (modes), but also the definition of elementary neural network for modeling diurnal cycles and multi-diurnal patterns of SRB.

MI10/W/10-B2

1150

**TEMPORAL VARIABILITY OF CUMULUS CLOUD FIELD SPATIAL DISTRIBUTIONS OVER TEXAS**

U. S. NAIR and R. M. Welch (Department of Atmospheric Sciences, University of Alabama in Huntsville, Global Hydrology and Climate Center, 977 Explorer Avenue, Huntsville, AL 35899 USA, E-mail: nair@atmos.uah.edu)

The spatial arrangement of clouds within cumulus cloud fields has been an area of considerable controversy. The majority of studies in this area have been conducted using SKYLAB, LANDSAT and AVHRR satellite imagery. GOES satellite imagery shows significant temporal variation in the spatial arrangement within cumulus cloud fields. For a four month period of time, cumulus cloud fields over Texas are identified using an automated cumulus cloud detection scheme. Then for individual cloud fields, the morphological features and spatial arrangements within cumulus cloud fields are examined as a function of time and atmospheric properties. The spatial arrangements within cloud fields are analyzed using the nearest neighbor distance cumulative distribution function. The interaction between clouds within the cloud field are examined using the radial cloud number density function. The general pattern observed is that cloud fields tend to be clustered during the early stages of growth. As the cloud fields mature, their spatial distributions tend towards randomness, but with some tendencies towards regularity. During later stages of cloud field development the spatial distributions tend towards randomness and some clustering. The Colorado State University Regional Atmospheric Modeling System (CSU RAMS) is used to model the cloud fields for a few selected days. The modeled cloud fields are compared against the satellite observed cloud fields.

MI10/W/03-B2

1205

**AUTOMATIC DETERMINATION OF DAYTIME AND NIGHTTIME CLOUD FRACTION**

Dave SOWLE (Mission Research Corporation, P. O. Drawer 719, Santa Barbara, CA 93102, email: sowle@mrcsb.com); Tim Tooman (Sandia Corporation, Livermore CA, email: tooman@ca.sandia.gov); Sean Moore (Mission Research Corporation, P. O. Drawer 719, Santa Barbara, CA 93102, email: moore@mrcsb.com)

The Atmospheric Radiation Measurements Program of the U. S. Department of Energy developed a Whole Sky Imager. This instrument measures absolute atmospheric radiance with approximately 0.3-degree resolution between zenith and 2-degrees below the horizon. Copies of the instrument are deployed over a wide geographical area. An objective of the instrument is to provide automated cloud fraction measurements at ten-minute intervals, or more frequently, over the complete diurnal cycle continuously for periods up to decades. Our daytime algorithm compares measured radiance in blue, red, and near infrared bands to those calculated for a pristine clear sky. Comparing measured to calculated band radiance allows classification of each pixel as clear, aerosol burdened, or cloudy. Thus resolution is approximately 0.3-degrees. Results were calibrated against known sky conditions. Our night-time algorithm has resolution of tens of degrees, rather than tenths of degrees. It compares, for a specific set of bright stars, the difference between stellar and nearby sky radiance to that measured on a night known to be clear. The portion of sky represented by a particular star is then classified as clear, thin clouds, or thick clouds.

MI10/W/08-B2

1220

**VALIDATION OF CUMULUS CLOUD PARAMETERIZATIONS FOR LONGWAVE RADIATION CALCULATIONS**

Robert G. ELLINGSON, Dejiang Han and Zhaohui Cheng (Department of Meteorology, University of Maryland, College Park, MD 20742, email: bobe@atmos.umd.edu)

Measurements at the Atmospheric Radiation Measurement (ARM) program site in Oklahoma, USA have been used to estimate many characteristics of small cumulus clouds, including the effective cloud cover, actual cloud cover, and aspect ratio. Different parameterizations of the longwave radiative effective cloud fraction have been tested by comparing observations with calculations from several different parameterizations using observed cloud variables as input.



The results show agreement to within about 10% between observed and estimated effective cloud fraction for absolute cloud fractions less than about 50%. Such errors result in longwave flux uncertainties of a few Watts per sq. m. Reductions of the errors below this level require refinements in the specification of the cloud spatial and size distributions.

**Tuesday 27 July PM**

Presiding Chair: R.Cahalan (NASA Goddard, Greenbelt, USA)

## RADIATIVE TRANSFER AND CLOUD FIELD MORPHOLOGY

MI10/E/06-B2

1400

### PARAMETRISEMENT OF FLUX RADIATIVE TRANSFER THROUGH LOW CONVECTIVE CLOUD LAYERS.

Ofer Yaron and Joachim H. JOSEPH (Dept of Geophysics and Planetary Sciences, TAU, Tel- Aviv 69978, Israel, e- mail: yoya@jupiter1.tau.ac.il)

We present in this study a parameterisation of cloud optical depth in terms of the multifractal parameter C1. This parameterisation makes it possible to include the 2D characteristics of a Stratocumulus layer cloud into a 1D plane- parallel radiative transfer model. Our study was based on a 2D Monte Carlo simulation of the flux radiative transfer that used a 1D bounded cascade model to represent a fractal, inhomogeneous cloud layer. The simulations were carried out for a range of the C1 parameter determined from analysis of digital cloud field images and a range of typical optical depths. The resulting albedos as a function of average optical depth, C1 and solar zenith angle were linked with those obtained from a delta-Eddington approximation for a plane- parallel layer. This linkage made it possible to define- for use in the plane parallel case- effective optical depths that depend on C1, for any given average optical depth of the cloud layer.

MI10/W/23-B2

1420

### ABSORPTION OF SOLAR RADIATION BY THE CLOUDY ATMOSPHERE: FURTHER INTERPRETATIONS OF COLLOCATED AIRCRAFT MEASUREMENTS ROBERT

D. CESS and Minghua Zhang (both at Marine Sciences Research Center, State University of New York, Stony Brook, NY 11794-5000, email: cessa@atmsci.msrc.sunysb.edu); Francisco P. J. Valero, Shelly K. Pope, Anthony Bucholtz and Brett Bush (all at Atmospheric Research Laboratory, University of California, San Diego, Scripps Institution of Oceanography, 0221, La Jolla, California 92093-0221, email: fvalero@ucsd.edu); Charles S. Zender (National Center for Atmospheric Research, P. O. Box 3000, Boulder, CO 80307, email: zender@ncar.ucar.edu); John Vitko, Jr. (Sandia National Laboratory, Org. 8102, P. O. Box 969, 7011 E. Avenue, Livermore, CA 94551-0969, email: john\_vitko@sandia.gov)

We have extended the interpretations made in two prior studies of the aircraft shortwave radiation measurements that were obtained as part of the Atmospheric Radiation Measurements (ARM) Enhanced Shortwave Experiments (ARESE). These extended interpretations use the 500 nm (10 nm bandwidth) measurements to minimize sampling errors in the broadband measurements. It is indicated that the clouds present during this experiment absorb more shortwave radiation than predicted by clear skies and thus by theoretical models, that at least some (less than 20%) of this enhanced cloud absorption occurs at wavelengths less than 680 nm, and that the observed cloud absorption does not appear to be an artifact of sampling errors nor of instrument calibration errors.

MI10/W/16-B2

1435

### A STUDY OF CLOUD GEOMETRY EFFECTS ON ATMOSPHERIC SOLAR ABSORPTION

Qiang FU, M.C. Cribb, (both at the Department of Oceanography, Dalhousie University, Halifax, Nova Scotia B3H 4J1, Canada. Email: qfu@atm.dal.ca), and H.W. Barker (Atmospheric Environment Service, Downsview, ON, Canada)

A 3D broadband solar radiative transfer scheme is formulated by integrating a Monte Carlo photon transport algorithm with the Fu-Liou radiation model. It is applied to fields of tropical mesoscale convective clouds and subtropical marine boundary layer clouds; they were generated by a cloud resolving model. The effects of cloud geometry on the radiative energy budget are examined by comparing the full resolution Monte Carlo results with those from the independent column approximation (ICA) which applies the plane-parallel radiation model to each column. We also investigate the effects of cloud geometry on the absorption of solar radiation by black carbon aerosol and a water vapor continuum.

MI04/W/35-B2

1450

### THE ABSORPTION OF SOLAR RADIATION BY THE ATMOSPHERE AS DETERMINED USING CONSISTENT SATELLITE, AIRCRAFT AND SURFACE DATA DURING THE ARM ENHANCED SHORT-WAVE EXPERIMENT (ARESE)

Francisco P. J. VALERO, Shelly K. Pope, Anthony Bucholtz Atmospheric Research Laboratory, Center for Atmospheric Sciences, Scripps Institution of Oceanography, University of California, San Diego, 9500 Gilman Dr, La Jolla, Ca 92093-0242 Patrick Minnis, NASA Langley Research Center, David R. Doelling, AS&M, Inc., Hampton, Virginia

Radiometric data sets acquired during the ARESE experiment using simultaneous measurements from five different, independent platforms (GOES 8 geostationary satellite, ER-2, Egrett and Twin Otter aircraft and surface) are analyzed for consistency. It is found that a very robust data set can be built on the basis of the observations from these multiple platforms. The aircraft data are further analyzed to determine atmospheric absorption of solar radiation applying the flux divergence method, and the GOES 8 and surface data are combined to determine the relationship between top of the atmosphere albedo and surface transmittance. The results of the aircraft data analysis and the GOES 8 versus surface analysis are in excellent agreement. It is found that there is strong evidence for excess absorption by the atmosphere in the presence of clouds, compared to model estimates, and that such excess absorption increases with cloud amount. These results are in agreement with recent findings that are the subject of some controversy, but here an exceptionally robust data set that brings together totally independent observations (satellite, surface and aircraft) is used.

MI10/E/07-B3

1505

### SPATIAL-TEMPORARY VARIATIONS OF TOTAL CLOUDINESS OVER THE GEORGIAN TERRITORY

Avtandil Amirashvili, VAZHA AMIRANASHVILI, Tengiz Gzirishvili (all at the Institute of Geophysics of Georgian Academy of Sciences, 1, M. Aleksidze Str., Tbilisi 380093, Georgia, email: vazha@excite.com); Kukuri Tavartkiladze (Institute of Geography of Georgian Academy of Sciences, 12, M. Aleksidze Str., Tbilisi 380093, Georgia)

The results of investigations of total cloudiness (G) and its variations from 1936 to 1991 over the Georgian territory are presented. With this purpose data of 46 meteorological stations on mean monthly values of G were analysed.

Mean annual, cold and warm season, January and July distribution maps of total cloudiness values on the Georgian territory in the mentioned time period are presented. Mean monthly trends of G are studied from 1936 to 1991 and peculiarities of total cloudiness variations for various regions of Georgia are revealed. Maps of variations of G in the mentioned months and seasons are composed.

In Georgia in the cold season and on the average per year small negative trends of G are observed: decrease in 1991 in comparison to 1936 by 5% and 0.9% in Western Georgia and by 5% and 1.8% in Eastern Georgia correspondingly. In the warm season small positive trends are characteristic for the whole Georgian territory: increase by 2.8% in 1991 in Western Georgia and by 1.9% in Eastern Georgia.

For a number of stations and certain months variations of total cloudiness in the mentioned period are quite considerable and range from +67% (station Dmanisi, August) to -31% (station Jvari Pass, February).

MI10/E/14-B2

1520

### UNBOUNDED CASCADE MODELS OF CLOUD FIELDS AND THE ANOMALOUS RADIATIVE ABSORPTION

D. SCHERTZNER, M. Larchevêque (LMM, CNRS UMR 7607, Case 162, Université P.&M. Curie, Paris, France, 4 Pl. Jussieu, 75252 Paris Cedex 05, France); S. Lovejoy (Physics dept, McGill University, 3600 University St., Montréal, Québec, H3A 2T8, Canada); C. Naud (Space and Atmospheric Physics, Blackett Laboratory, Imperial College London SW7 2BZ)

We first clarify the reasons to consider unbounded cascade models of cloud fields, rather than bounded cascade models. Second, we show that this distinction is extremely important for radiative transfer studies, in particular to explore the question of the atmospheric anomalous absorption. The difference between the two types of models is related to the fundamental distinction between the fields (e.g., velocity, temperature, liquid water content) and the corresponding turbulent fluxes (e.g., energy flux, scalar variance flux). In the case of the bounded cascade models, one tries to use a rather standard model of flux, i.e., a multiplicative cascade process, for the concentration field itself. As it does not yield smooth enough statistics, one is compelled to introduce an ad-hoc bounding operation step-by-step. Not only is the physics soon lost, since fluxes are no more defined, but so is the logical coherence of cascades: the bounding breaks down the scaling of the cascade process! There is no need to proceed this way: the difference of scaling and smoothness between fields and fluxes is easily taken into account by a fractional integration, as done in multifractal Fractionally Integrated Flux (FIF) models. Furthermore, keeping the direct contact with physics of turbulence is indispensable to understand and quantify the anomalous absorption in an apparently nearly perfect scattering case. Indeed, the case of perfect scattering corresponds to the rather naive 'external' solution of a singular perturbation problem. On the contrary, the 'internal' solution estimates the effect of the thin but primarily important 'boundary layers' where occur most of the increase of the 'effective' absorption which is quite larger than the 'bare' absorption coefficient. We present the internal solutions of the FIF models.

MI10/E/01-B2

1535

### CLOUD TOP HEIGHTS AND WINDS FROM STEREO METHODS USING ATSR DATA

R M DUNDAS, J P Muller and C Vogt (Geomatic Engineering, University College London, Gower Street, London WC1E 6BT, UK, Email: rdundas@ge.ucl.ac.uk)

Clouds considerably influence the radiation interaction between the surface and space. Satellite images offer the possibility of obtaining cloud top heights over a large area using techniques such as Stereo. Stereoscopic methods require two images of the same geographical area from two different view angles. The resulting parallax between the two images of an observed feature is then proportional to its height. These techniques will be applied to data from the dual view Along Track Scanning Radiometer, (ATSR) and evaluation will include a comparison with brightness temperature derived cloud top heights, a comparison of cloud free heights against a ground terrain model and ground based 94GHz radar measurements. Winds will also be derived.

MI10/W/17-B2

1620

### CLOUD-FIELD VARIABILITY DURING CLARA: ACTIVE INSTRUMENT SIGNALS

DAVID P. DONOVAN, A.C.A.P. Van Lammeren, A. Feijt (Royal Netherlands Meteorological Institute (KNMI), Postbus 201, 3730 AE, De Bilt, The Netherlands, Email: donovan@knmi.nl)

The degree of cloud variability has obvious implications with regards to cloud remote sensing. By combining measurements made with different instruments in principle it is possible to extract much more information than is the case by using each instrument in isolation. However, in the real world, different instruments may have different footprints and sampling rates as well there may be some spatial and/or temporal separation between the measurements made by the different sensors. Hence, it is necessary to know to what extent two spatially and/or temporally separated soundings may be meaningfully compared. Further complicate matters, the degree of signal variability in space and time depends not only on the physical variability of the cloud field itself but also on what exactly a given instrument is measuring.

During the CLARA (Clouds And Radiation) campaigns carried out in 1996 in the Netherlands a large number of co-located lidar and radar cloud soundings were carried out. In addition, two nearly identical lidar systems were operated within 4 km of each other so the CLARA data can be used to explore cloud variability by comparing the spatially separated data as well using standard spectral analysis techniques on the single instrument lidar and radar data.

In this presentation, an overview of the temporal and spatial cloud signal variability encountered during CLARA is presented. In addition, the difference in the behavior between the lidar and radar signals will be explored with the aid of a simple analytic model linking the lidar and radar signals to fluctuations in the physical state of the clouds themselves.

MI10/W/20-B2

1635

### INVESTIGATION OF THE TWO-DIMENSIONAL SECOND ORDER STRUCTURE FUNCTION OF SATELLITE-RETRIEVED OPTICAL DEPTH AND EFFECTIVE RADIUS

Gregory M. LEWIS (Institute of Applied Mathematics, University of British Columbia, Vancouver, BC, V6T 1Z4, Canada, Email: lewis@math.ubc.ca); Philip H. Austin (Atmospheric Science Programme, University of British Columbia, #217 Geography, Vancouver, BC, V6T 1Z2, Canada, Email: phil@geog.ubc.ca).

We investigate the scaling behaviour of satellite-retrieved optical depth and cloud top effective radius in marine stratocumulus clouds found over the eastern Pacific Ocean and the Southern Ocean near Tasmania. Using the algorithm of Nakajima and Nakajima, the optical depth and



effective radius are inferred from radiance measurements made by the AVHRR (Advanced Very High Resolution Radiometer) on board four NOAA polar orbiting satellites. The second order structure functions of twenty-five scenes are examined. Many of the isotropic structure functions indicate a possible scale break at a spatial scale of approximately 10km. However, when the two dimensional structure functions are calculated, it is found that many of the scenes are characterized by their anisotropy, indicating that in some cases the isotropic structure function may not be the appropriate scaling function. The structure function averaged over all scenes still exhibits anisotropy and the scale break is still seen (although it seems clearer that it is a transition between two different scaling regimes). The possibility that the scale break is a result of the anisotropy will be discussed. We will also contrast the scaling and anisotropy of the raw data versus the transformed data. We find that although the isotropic structure functions are similar there is a marked change in the anisotropy. This is expected since the anisotropy due to external variables, in particular the dependence of reflectivity on solar zenith angle, has been corrected for in the transformed data. We will also investigate the sensitivity of the scaling with domain size.

**MI10/W/13-B2****1650****A GCM PARAMETERIZATION OF BIMODAL SIZE SPECTRA FOR ICE CLOUDS**

D.L.Mitchell, (Desert Research Institute, Atmospheric Sciences Centre, P.O.Box 60220, Reno, Nevada, 89506 USA. E-mail: mitch@dri.edu)

As the global radiation budget is sensitive to the effective radius assumed for water clouds, so also it is sensitive to the effective diameter ( $D_e$ ) assumed for ice clouds. While many GCMs assume an effective radius for ice clouds around 30  $\mu\text{m}$ ,  $D_e$  is known to vary due to changes in size distribution with temperature by over an order of magnitude.

Based on existing field measurements of size spectra from 10 frontal cloud studies, ARM, FIRE and SUCCESS cirrus case studies, 7 tropical cirrus clouds and 8 other mid-latitude cirrus flights, a scheme was formulated by which the small and large particle modes of the observed bimodal size distribution could be estimated as a function of temperature and ice water mixing ratio (or IWC), as provided by a GCM.

The size distribution slope of both modes was related to temperature, where size spectra were averaged over horizontal transects exceeding 5 km, which eliminated much variability. To calculate the bimodal spectra, the total IWC needed to be partitioned between both modes. The IWC for each mode was calculated from measured spectra, and the resultant partitioning was well described solely in terms of the slope (or mean length) of the large particle mode. Hence, by only knowing temperature and the total IWC, the complete bimodal size spectrum can be estimated, which agreed reasonably well with measured leg-averaged spectra having the same temperature and IWC.

**MI10/E/10-B2****1705****THE MULTIFRACTAL CONTINUUM IN RAIN AND CLOUDS FROM 0.2MM TO 5000KM**

S. LOVEJOY, N. Desaulniers-Soucy, J. D. Stanway, (all at Physics dept, McGill University, 3600 University St., Montréal, Québec, H3A 2T8, Canada) D. Schertzer (LMM, case 162, Université P. et M. Curie, 4 pl. Jussieu, Paris F-75252 Cedex 05, France)

Using stereophotography of rain drops and large numbers of satellite and ground based cloud images, we empirically examine two key assumptions of classical meteorology and rain/cloud physics. We first investigate the standard homogeneity assumptions used for modelling drop growth, aggregation or the interpretation of radar reflectivities from rain or snow. This standard "continuum" hypothesis for the hydrometeors implies that particle size distributions can be well defined independently of the measurement volume/scale. On the contrary, over the accessible range (0.2mm to 2m) we find multiscaling statistics with an inner scale very close to the mean inter particle distance; the continuum is multifractal. The second key assumption we investigate is that at scales of roughly 10km (the vertical pressure scale) there is a "meso-scale gap" in the (horizontal) spectrum separating the small scales (assumed to be isotropic homogeneous 3-D turbulence) and the large scales (assumed to be the corresponding 2-D turbulence). On the contrary, by analyzing nearly a thousand visible and infra red cloud images from geostationary (GMS), polar orbiting (NOAA 12, 14, SPOT) satellites as well as ground based imagers (roughly 100 times more data than that used on any comparable study) over the range 5000km to 50cm we found (as predicted by the unified scaling model), a) that the scaling is well respected over the entire range (there is no "meso-scale gap"), b) We obtain the first direct evidence for multiplicative cascades and direct estimates of the outer scale (planetary scale), c) the radiance fields are indeed very close to what is expected for universal multifractals. In the latter, the infinite hierarchy of exponents (e.g. dimensions/codimensions) is described by only three universal exponents which we estimate.

**MI04/L/21-B2****1720****RADIATIVE TRANSFER THROUGH FAIR-WEATHER CUMULI**

Paquita ZUIDEMA (Program in Atmospheric and Oceanic Sciences, University of Colorado-Boulder, Boulder, CO USA 80309-0311, email: zuidema@monsoon.colorado.edu) and Frank Evans

The two-dimensional radiative transfer behavior of ten fair-weather cumulus clouds observed by cloud radar in the equatorial Pacific is examined. A recently-introduced radiative transfer approximation, the tilted independent pixel (TIP; Varnai and Davies, 1998) is evaluated. TIPA is similar to the independent pixel approximation except that TIPA evaluates the optical depth columns as seen tilted towards the Sun rather than vertically-projected optical depth columns. Major results are:

- TIPA captures the two-dimensional domain-averaged albedo quite well at all Sun angles, performing much better than IPA.
- Most of TIPA's successful performance can be attributed to its use of the apparent cloud fraction as seen by the Sun.
- 2D-TIPA albedo differences under low Sun vary with optical depth and with cloud shape details related to the cloud aspect ratio. This differs from what is seen in Varnai and Davies (1998).
- Knowledge of the mean cloud optical depth and aspect ratio, when utilized within TIPA, is often enough information with which to successfully capture the true domain-averaged albedo. The results are thought to apply to many tropical fair-weather cumuli although more work needs to be done to establish the representativeness of the cloud radar-derived cloud sample. This study extends Varnai and Davies' (1998) work by examining more realistic clouds with a different range of optical depths and aspect ratios than is present within the cloud fields utilized by Varnai and Davies' (1998).

**MI10/W/18-B2****1735****ESTIMATION OF FRACTIONAL SKY COVER FROM BROADBAND SW RADIOMETER MEASUREMENTS**

Charles N. LONG and Thomas P. Ackerman., (Penn State University Dept. of Meteorology, John J. DeLuise, NOAA ARL Surface Radiation Research Branch. E-mail: long@essc.psu.edu)

One of the greatest uncertainties in global climate change research is the changes, if any, in cloud amount and the resultant effect on global radiative energy balance. Only satellites afford the global coverage needed to study cloud amount on a global scale. However, as with other satellite-derived variables, the accuracy of satellite cloud fraction retrievals must be verified with surface measurements. Previous comparisons have in large part depended on surface observer reports, which include temporal and spatial mis-matches and observer subjectivity that add uncertainty to the comparison.

Our previous work has provided a means to infer the effect of clouds on the downwelling SW irradiance at the surface. We have now additionally developed a technique to infer fractional sky cover from the same surface broadband global and diffuse SW measurements. While the absolute accuracy of these sky cover retrievals depends on the particular division of clear sky - cloudy sky boundary, comparisons with NOAA/ARL/Surface Radiation Research Branch (SRRB) Hemispheric Sky Imager data suggest the retrieved sky cover values are accurate to better than an RMS Standard Deviation of 0.1. The retrieval method does not appear to be system or location dependent. Comparisons of three independent surface radiation measurement systems collocated at the Atmospheric Radiation Measurement (ARM) Program site near Lamont, OK yield RMS standard deviations better than 0.04 for retrieved sky cover. Thus, this method affords a consistent, non-subjective estimation of fractional sky cover at high temporal resolution for use in verifying satellite derived cloud fractions, and provides both SW cloud effect and sky cover for climate change studies.

We present details of the method, as well as comparisons with sky cover measurements and collocated retrievals to illustrate accuracy and precision. Examples of retrieved SW cloud effect and sky cover will be included, along with analysis and comparison of multi-year time series using ARM Southern Great Plains and Tropical Western Pacific, and SRRB SURFRAD data.

**MI04/C/MC07/W/21****1750****EFFECT OF CIRRUS CLOUDS ON LONGWAVE OUTGOING RADIATION IN THE FAR INFRARED**

C.NAUD, J. E. Russell and J. E. Harries (both Space and Atmospheric Physics group, Imperial College, London SW7 2BZ, email: j.e.russell@ic.ac.uk, j.harries@ic.ac.uk)

We have performed simulations of the impact of cirrus clouds on radiances at the top of the atmosphere, and on atmospheric heating rates in the far infrared region from 100 to 1000  $\text{cm}^{-1}$ . Using a high resolution data base for the atmospheric gases optical properties, and a multiple scattering radiative transfer scheme, we look at the effect of changes in parameters such as the shape and size of ice crystals, and the height and ice water content of the clouds. We show that cirrus clouds have a strong effect on the reduction of the outgoing radiation in the far infrared, this part of the total infrared spectrum contributing to nearly 20% of the overall reduction. Calculation of the atmospheric heating rates shows that ice clouds cool the atmosphere at their top and heat the atmosphere below compared to clear sky conditions. This effect is enhanced for higher heights of clouds, and, by comparing different shapes of ice crystals, we show that spheroids (distorted spheres) have a bigger effect than spheres for a same cloud ice water content. The main consequence is that cirrus clouds warm the troposphere and cool the stratosphere in the far infrared, whereas they warm the local atmosphere in the window region.

We used these calculations to study the effect of changes in the global cirrus cloud amount on the local atmospheric heating rates and the relation to changes in upper troposphere and lower stratosphere temperatures, for a variety of shapes and size distributions of ice crystals. Using NCEP data for changes in temperature trends and ISCCP data for cirrus trends, we consider whether these changes are compatible with each other given our calculations of the radiative effect of any change in clouds.

**Wednesday 28 July AM**

Presiding Chair: K Browning (Univ. of Reading, Reading)

**PRECIPITATING CONVECTIVE CLOUD SYSTEMS****MI04/W/26-B3****0830****AN OVERVIEW OF PROFILER OBSERVATIONS OF TROPICAL PRECIPITATING CLOUD SYSTEMS**

Kenneth S GAGE ( NOAA Aeronomy Laboratory, Boulder, CO 80303; email: kgage@al.noaa.gov); Warner L. Ecklund and Christopher R. Williams (University of Colorado/CIRES, Boulder, CO 80309; 303-497-5322; e-mail: wecklund@al.noaa.gov; chris@al.noaa.gov)

During the past decade Doppler radar profilers that operate at 915 MHz were developed at the NOAA Aeronomy Laboratory and are now in widespread use primarily for wind measurement in the lower troposphere. The profilers are also very sensitive to hydrometeors and can be very useful tools for precipitation studies. During the TOGA COARE field campaign, these profilers were utilized for wind and precipitation measurements at four island sites and on two research ships. Following TOGA COARE the Aeronomy Laboratory developed an S-band (2835 MHz) profiler that is about 20 dB more sensitive to hydrometeors than the 915 MHz profiler.

This paper presents an overview of observations and analyses of the structure and evolution of precipitating cloud systems over the western Pacific region obtained during COARE and subsequent field campaigns including the Maritime Continent Thunderstorm Experiment (MCTEX) that took place near Darwin Australia in November - December 1995 and the Combined Sensor Program (CSP) that took place in the vicinity of Manus Island, Papua New Guinea in March 1996. The latter two campaigns utilized collocated 915 MHz and S-band profilers which have been intercompared to unambiguously separate backscattering from hydrometeors and atmospheric turbulence.

Profilers observations yield time height cross-sections of equivalent reflectivity, Doppler velocity and spectral width that illustrate the evolution of precipitating clouds systems. In the presence of precipitating clouds back-scattering from hydrometeors is dominant and the Doppler velocity provides a measure of the fall velocity of hydrometeors. The vertical structure of these parameters has been used to classify the precipitating cloud systems into several different categories. These observations document the prevalence of deep anvil cloud systems over the Pacific warm pool region. These optically thick clouds are present up to 25% of the time. While precipitation occurs at the surface less than about 10% of the time.

**MI04/W/09-B3****0850****RAINFALL AND RADIATIVE HEATING RATE ESTIMATES FOR TOGA COARE**

RICHARD H. JOHNSON and Paul E. Ciesielski (Department of Atmospheric Science, Colorado State University, Fort Collins, CO 80523, USA, email: rhj@vortex.atmos.colostate.edu)

Atmospheric heat and moisture budgets are used to determine rainfall and radiative heating rates over the western Pacific warm pool during TOGA COARE. Using the COARE bulk flux algorithm to estimate surface evaporation over the Intensive Flux Array (IFA), the IFA moisture budget-derived average rainfall for the 120-day Intensive Observing Period (IOP) is 8.2 mm/day. However, for a smaller area within the IFA comprising the rain-mapping domain of the

TOGA and MIT radars, the atmospheric budget for the 101-day radar deployment yields a much smaller value, 5.2 mm/day. This estimate agrees well with the independent radar rainrate estimate of 5.4 mm/day. Further analysis indicates that the TOGA and MIT radars were located within a relatively dry region of the IFA and their deployments were during relatively dry periods of the IOP.

Computation of the vertically integrated net radiative heating rate as a residual from the heat and moisture budgets yields an IFA-IOP average of  $-0.31$  C/day. This net cooling rate is smaller than many previous estimates for the Tropics, but is within the range of independent COARE estimates based on radiation models and observations. This small value may arise from decreased longwave emission to space due to abundant cirrus over the warm pool and may also reflect some short-wave absorption by cirrus.

**MI04/L/02-B3**

**0905**

**A COMPARISON OF COARE RADAR OBSERVATIONS WITH AN NCAR 2-D CLOUD RESOLVING MODEL**

Scott J. CARPENTER, (Colorado State Uni, Fort Collins co80523, USA, Email: Rhj@vortex.atmos.colostate.edu); Steven A. Rutledge, Xiaoqing Wu, and Mitchell W. Moncrieff

A two-dimensional cloud resolving modeling study was performed at NCAR for a 39-day period (5 December 1992 through 12 January 1993) during the Tropical Ocean Global Atmosphere (TOGA) Coupled Ocean-Atmosphere Response Experiment (COARE). The study was motivated by the need to study the complex coupling of processes over climatically key areas as well as the need to quantify the collective effects of cloud systems which will help to improve future parameterizations for general circulation models (GCMs). The work presented here was performed to test the consistency of the model output with the observed radar data from the MIT and TOGA Radars which were stationed on the R/V John V. Vickers and PRC ship Xiangyonghang No. 5, respectively. The model's convective response to the overall forcing was analyzed by comparing model simulations and radar observations of rainfall rate distribution, diurnal rainfall rate signals, and reflectivity characteristics. The forcing data originated from numerous other platforms in operation during COARE (radiosondes, buoys, etc.) and was added to the model at six hour intervals. The model output condensate mixing ratios were used to derive reflectivity values using reflectivity to liquid water content relationships (Z-M relationships), so that a direct comparison with radar reflectivities could be performed. The model derived rainfall rate data was compared to the rainfall rate files prepared from the combined TOGA and MIT radars using cumulative and percent frequency distributions. Initial results indicated that the model and radar results were in agreement for rainfall rates near 10 mm/hr. About 0.5% of the radar and model grid points had rainfall rates greater than 10 mm/hr. The model overestimated the areal coverage of smaller rainfall rates (between 10 mm/hr and 0.1 mm/hr) by between 0.5% and 1.5%, and underestimated areal coverage for rainfall rates greater than 10 mm/hr. The latter fact is probably due to the model's inability to resolve the short lived, narrow, very intense convective cells which produced very heavy precipitation.

The TOGA-COARE radar data set has also shown that there exists a trimodal distribution of convective echoes, with peaks at heights typical of cumulus, cumulus congestus, and cumulonimbus. Analysis of whether or not this cloud-resolving model (CRM) can simulate the trimodal distribution of convective echoes is ongoing.

**MI10/E/08-B3**

**0920**

**THE COMPARISON OF MICROWAVE BRIGHTNESS TEMPERATURES SIMULATED BY A 3-D CLOUD-RESOLVING MODEL WITH OBSERVATIONS**

Philip R.A. BROWN and David C. Jones (Meteorological Office, London Road, Bracknell, RG12 2SZ, UK, email: prabrown@meto.gov.uk, dcjones@meto.gov.uk)

Recent intercomparisons of both 2- and 3-d cloud-resolving models (CRMs) on cases of tropical convection observed during the TOGA-COARE experiment have shown that they can produce widely-differing vertical profiles of hydrometeors, particularly in the widespread ice anvil region. It is in this part of the cloud system that most of the radiative heating is generated, hence the models indicate differing feedbacks between convection, cloud and radiation. It is of great importance to the use of such CRMs for cloud parametrization development to determine whether their simulated hydrometeor profiles are realistic.

Microwave brightness temperatures measured by aircraft and/or spaceborne instruments have been used to retrieve the total ice and liquid water paths, using both statistical and physically-based retrieval methods. The latter do, however, usually rely on some a priori knowledge or assumption of the relative vertical distribution of ice hydrometeor species. In the present study, we use the Eddington approximation for plane-parallel radiative transfer to calculate the upwelling microwave brightness temperatures over clouds simulated by a 3-d cloud-resolving model, which has a 1.25 km grid spacing in the horizontal. The simulated brightness temperatures are then averaged over the instantaneous field of the view of the simulated observing instrument. The primary aim is to examine the sensitivity of modelled brightness temperatures to changes in the vertical hydrometeor profiles caused by changes to the model's microphysics parametrization scheme. We then examine whether the available aircraft and spaceborne microwave observations of the case are able to distinguish between the model simulations and give guidance as to which is generating the most realistic ice and water cloud distributions. We also consider the uncertainties introduced by the representation of the strongly structured hydrometeor fields by a plane-parallel radiative transfer model.

**MI04/E/28-B3**

**0935**

**UNDERSTANDING HECTOR: THE DYNAMICS OF ISLAND THUNDERSTORMS**

Andrew CROOK (National Center for Atmospheric Research P.O. Box 3000, Boulder, CO, USA, 80307-3000, email: crook@ucar.edu)

Hector is the name given to a thunderstorm complex that develops over the Tiwi Islands just north of mainland Australia during the wet season. The regular occurrence of the storms over isolated, basically flat, terrain make the islands an excellent testing ground for observational and modeling studies. The thunderstorm complex is particularly suitable for studies which include convection initiation, microphysical development, electrification, radiation, and convectively-generated gravity waves.

In this study we will examine the convective response to changes in the large-scale thermal forcing provided by the islands. A model of the large-scale forcing is first developed by solving the linear equations for flow past an isolated heat source. The model predicts that the maximum convergence occurs along a narrow band in the downwind half of the heat source. The dependence of the convergence strength on a number of features such as flow speed and direction is then examined.

The predictions of the linear model are then tested in a nonlinear, cloud-resolving, model. The nonlinear model simulates a number of features such as sea-breezes, gust fronts and moist convection that are not captured by the linear model. Nevertheless, the dependence of convective strength on the large-scale flow predicted by the linear model is borne out by the nonlinear simulations. However, one major difference is that the storms generally do not form along a band in the downwind half of the island but rather at a point where that band intersects

a cold pool formed by the moist convection. We end with a discussion on the controversial question of whether or not the sea breezes from opposite coastlines collide.

**MI04/L/16-B3**

**0950**

**MECHANISMS RESPONSIBLE FOR THE DEVELOPMENT AND MAINTENANCE OF LONG-LIVED SQUALL LINES**

TAKEMI

The mechanisms responsible for the development and maintenance of long-lived squall lines in dry environments are investigated through two-dimensional numerical experiments by using a nonhydrostatic cloud model. The squall-line environments are characterized by a low convective available potential energy (CAPE), low moisture content, and a high level of free convection (LFC), which are based on observations of a squall line over an arid region in China. Although these environments seem to be unfavorable for the development of convective systems, a long-lived squall line is simulated in the environment of a well-mixed moisture profile within a deep, mixed boundary layer. During the mature stage of this simulated squall line, the air parcels originating in the upper part of the mixed layer ahead of a surface cold-air pool are lifted to the upper troposphere. On the other hand, the air parcels originating in the lower part of the mixed layer are forced to go rearward, never reaching the upper levels. The low pressure just above the surface cold pool plays an important role in determining these parcel trajectories. The sensitivity experiments in which the mixed-layer height and vertical profile of moisture within the mixed layer are varied illuminate the mechanisms for the development and maintenance of the simulated squall lines in the dry environments. First, the presence of a deep mixed layer is indispensable for the squall-line development. Second, a moisture profile that is nearly constant with height is favorable for the long-lived squall lines, although the CAPE value for the surface air parcel is small (250 J/kg). In this moisture condition, air parcels in the upper part of the mixed layer have moderate CAPE values of 50-150 J/kg, and the differences between the source levels of these parcels and their LFCs are very small. These parcels are easily lifted to their LFCs without experiencing substantial inhibition of convection, thus releasing their CAPE. The vertical distribution of CAPE values in the mixed layer is very important for the squall-line maintenance in dry environments. Another sensitivity experiment in which the mid-to-upper level vertical shear of horizontal winds is varied shows that upper-level shear plays an important role in characterizing the structure and longevity of squall lines. The upper level shear is necessary for the development of vigorous squall lines.

**MI04/W/23-B3**

**1035**

**A NONHYDROSTATIC NUMERICAL MODELING STUDY OF MESOSCALE CONVECTIVE SYSTEMS ALONG THE BAIU FRONT OVER KYUSHU, JAPAN ON 17 JULY 1988**

Zhe-Min TAN (1) Kozo Nakamura (2) Tokao Takeda (Frontier Research System for Global Change, Institute for Global Change Research), (2) Ocean Research Institute Tokyo University) & (Institute of Hydrospheric-Atmospheric Sciences Nogoya University)

Numerical simulations and the analysis of observational data are employed to understand the structure and development of meso-scale convective systems along the Baiu front over Kyushu, Japan on 16 July 1988. The National Center for Atmospheric Research (NCAR) / The Pennsylvania State University (PSU) Mesoscale Model Version 5 (MM5) was used to simulate 24h on a 30-km domain with 10-km and 3.33-km nests. The model includes microphysics with cloud, rains, snow/graupeil; ice processes on all domains' resolved scales. The Grell cumulus parameterization scheme is adopted only on the 10-km and coarser domains.

In the relatively coarse horizontal resolution (e.g. 10-km), the numerical simulation has captured the major features of observed convective systems development very well. The sensitivity experiments are done to isolate the effects of topography, latent heat release and sea surface temperature. The results showed that the latent heat release plays the key role for the development of convective system along the Baiu front. Using of the cloud-resolving 3.33-km resolution model investigated the organization and maintenance of rainband in this event. The results showed that structure and evolution of rainband are closely related to the large-scale forcing and different choices of subgrid-scale convective parameterization for a coarse domain.

**MI04/W/03-B3**

**1050**

**THE MODEL SIMULATION OF AN ISOLATED CUMULONIMBUS CLOUD WHICH MOVES ALONG A VALLEY**

Mladjen CURIC, Dejan Janc and Vladan Vuckovic (Institute of Meteorology, University of Belgrade, Yugoslavia)

In the summer season the isolated severe hail clouds are often formed on the western portion of the Western Morava valley named Zlatibor plateau which mean height is approximately 1 km (Western Serbia). They move roughly from WNW to ESE direction. The environmental wind of the mean troposphere is nearly parallel with valley direction, while the low-level air motion is in the opposite direction to the cloud motion. The basic purpose of this study is to simulate the development of such hail cloud which occurred in the Western Morava valley by help of the ARPS three-dimensional mesoscale model with improved hail microphysics and local orography. The model simulation shows that a cloud came down from a plateau to the valley. A strong downdraft of the cold air occurs since the land slopes down to a valley. The warm air motion toward the mountainside is amplified due to the forced lifting of a warm air above the cold air and the local low pressure. Further, the strong updraft in the front side of the cloud occurs and after that the hail appears on the ground. The cold air spreads out in a valley direction. The model simulation clearly shows the gust front formation in front of the main cloud, whose height oscillates with time. This is fairly illustrated by the patterns of the reflectivity factor in x-y plane whose maxima values are concentrated in the valley area. As a consequence of such cloud processes, the hail produced on the ground has the hailstreaks form separated about 10 km.

**MI04/W/06-B3**

**1105**

**THE DEPENDENCE ON GRID RESOLUTION OF NUMERICALLY SIMULATED CONVECTIVE CLOUD SYSTEMS USING ICE MICROPHYSICS**

Scott A. BRAUN, Wei-Kuo Tao, Stephen E. Lang, and Bradley S. Ferrier (NASA/GSFC, Code 912, Greenbelt, MD 20771, USA)

As model resolution increases from scales  $>10$  km to scales on the order of a few kilometers, the representation of cloud processes shifts from cumulus parameterizations to grid-resolvable bulk microphysics. It is not uncommon these days to see mesoscale models run with fine grids of about 4-10 km for storms such as fronts, squall lines, and hurricanes. Bulk cloud microphysical parameterizations that include detailed ice microphysics (e.g., common 3-ice class schemes) were designed for models using high-resolution ( $<1$  km) grids. An important question that remains to be addressed is to what extent models with grid sizes  $>1$  km can represent cloud structures obtained with higher resolution grids using common ice



microphysical parameterizations? In this study, we compare simulations from 2-D models of convective cloud systems using 1-, 2-, and 4-km grids and show how the cloud and circulation structures change as resolution is decreased. Implications for mesoscale modeling will be discussed.

**MI04/E/13-B3****1120****DYNAMICS OF THUNDERSTORMS EMBEDDED WITHIN THE SHEAR FLOW**

R.B.ZARIPOV. (Department of Meteorology and Climate, Geographic Faculty, Moscow State University, Vorobjovi Gori, 119899 Moscow, RUSSIA, email: pressman@rhmc.mecom.ru)

The impact of horizontally homogeneous large-scale flow on the dynamics of thunderstorm is studied numerically with the use of three-dimensional Cb cloud based on the anelastic equations. The cloud and precipitation microphysics in the liquid and ice phases is parameterized. The interaction of several thunderstorms is achieved by posing the periodic boundary conditions at the side walls. The series of numerical experiments with different wind hodographs: plane-parallel and veering flows have been performed. The influence of different velocity profiles on the internal cloud dynamics is studied in terms of kinetic energy, vorticity, helicity and the other flow characteristics. The analysis of production (and sink) of vorticity and helicity is presented. The results of this study agree qualitatively with those obtained in the previous works for the cases of isolated thunderstorms. The mayor difference is that in the case of interacting clouds the effects of basic flow helicity are less pronounced than in the case of isolated storm, particularly in terms of storm longevity.

**MI04/W/22-B3****1135****WHAT CAN WE LEARN ABOUT CLOUD PROCESSES FROM A SIMPLE MODEL?**

Olaf STILLER (Uni of Reading, Dept of Meteorology, Earley Gate, RG6 6BB, UK, Email: o.stiller@reading.ac.uk); and George C. Craig

The parameterisation of cloud processes is a delicate task due to the lack of understanding of the basic dynamics comprising mixing processes and momentum transport. Experimental data are limited and not always conclusive and also numerical investigations are difficult due to the systems complexity and often obscured by the large number of parameters involved in a realistic representation of moist processes. Using the large eddy model of the British Meteorological office to investigate the dynamics of single clouds (updrafts) we have extracted a largely idealised version of the model which possesses basic features of the full model but has fewer parameters and thus permits a more systematic analysis facilitating conclusions concerning cause and effect of the observed phenomena. The idealised model has a drastically simplified microphysics which still includes condensation and re-evaporation of cloud water but the parameterisation of rain is reduced to the fact that the content of cloud water has an upper limit above which the water is irreversibly taken out of the system. The saturation value of water vapour is taken to depend only on height and to decrease linearly with height. As a consequence a sounding with a constant dry lapse rate also possesses a constant moist lapse rate. To investigate mixing processes we are considering situations where the height reached by the updraft is entirely determined by mixing processes. This means we consider a sounding which is neutral with respect to moist convection. In particular we find that a dryer atmosphere enhances mixing and decreases the height reached by the updraft. This can be explained by the increased release of negative buoyancy from re-evaporation processes which enhances the vortices responsible for the mixing. Similarities and differences of the model dynamics and those from simulations with the full large eddy model are discussed.

**MI04/C/MI06/W/10-B3****1150****RELATIONSHIPS BETWEEN THE MICROSTRUCTURE OF CONVECTIVE CLOUDS AND THEIR RAINFALL PRODUCTION**

Daniel ROSENFELD (Atmospheric Sciences, The Hebrew University, Jerusalem, Israel, email: daniel@vms.huji.ac.il); William L. Woodley, Woodley (Weather Consultants, Littleton, Colorado Bernard A. Silverman, Meteorological Consultant, Englewood, CO, USA)

Radar tracking and aircraft measurements of nearly 400 convective clouds during 5 years over northwestern Thailand provided for each cloud the following information: (1) the extent of warm rain processes, indexed into three categories; (2) the integrated rainfall in time and space; (3) maximum echo top height. Analysis of the rain production as a function of precipitation echo top height and warm rain index revealed that: 1. Clouds with tops smaller than 10 km precipitate more than 10 times as much rainfall with active coalescence as compared to clouds with little coalescence. 2. Clouds with tops taller than 10 km (i.e., deep Cb) precipitate 3.5 times as much as clouds with little coalescence. All the results are statistically highly significant. Some of the ramifications of these findings are: Mainly anthropogenic aerosols, such as biomass burning smoke and air pollution cause the lack of coalescence, in the study area as elsewhere, as has been shown by Rosenfeld and Lensky (BAMS, 11/1988). That means a very large impact detrimental impact of these aerosols on rainfall. That has major climatic, economical and sociological implications, which must be brought to the front of the attention of the climate change community.

**MI04/W/02-B3****1205****A LAGRANGIAN MODEL FOR THE BAROCLINIC GENESIS OF MESOSCALE VORTICES**

Robert Davies JONES (National Severe Storms Lab., NOAA, Norman, OK 73069 USA, email: bobdj@nssl.noaa.gov)

Baroclinically generated mesoscale vortices play vital roles in the genesis of near-ground mesocyclones, jets of strong surface winds and tornadoes in supercell and bow-echo storms. An analytical Lagrangian model is based on the decomposition in inviscid isentropic flows of vorticity into barotropic and baroclinic components. The model is tested by showing that it correctly predicts the formation of baroclinic lee vortices in stratified flow over hills. It is then used to show that air on the left (right) side of a cool downdraft in an unstably stratified environment acquires cyclonic (anticyclonic) baroclinic vorticity during descent. The cyclonic spin is greatly amplified if the air on the left side passes out of the downdraft along the ground into an updraft. This scenario explains many observed features of severe storms, and leads to the conclusion is that the rain curtains associated with hook-shaped appendages to radar echoes are the insigators (not just passive indicators) of tornadoes.

**MI04/P/01-B3****1220****LIDAR SOUNDING OF LOW AND MIDDLE LEVEL CLOUD PROPERTIES OVER A TROPICAL STATION**

P.C.S. DEVARA, P.E. Raj, R.S. Mahes Kumar, K.K. Dani and Y. Jaya Rao (Indian Institute of Tropical Meteorology, Pune 411 008, India, email: devara@tropmet.emet.in)

Clouds in the lower part of the atmosphere play vital role in pollution transfer and boundary layer and radiative processes. Unlike the clear air, cloud medium generates strong lidar return signals which can be used for the purpose of cloud parameterisation involving ceiling and base heights, and the location of discontinuities (layer clouds). The fine-scale variations in scattered signal strength in the sub-cloud air, layer and polarisation characteristics provide more insight into the structure and composition of clouds. These measurements at multiple laser probing wavelengths offer more reliable means to study cloud evolution and microphysics. Shallow clouds generally allow penetration of low power laser beams and hence both cloud base and top height measurements are possible. In the case of high dense clouds, the corresponding parameters can be determined in the lower part of the cloud without regard for the influence of multiple scattering effects.

The bistatic, continuous wave, Argon-ion lidar system at the Indian Institute of Tropical Meteorology (IITM), Pune (18°32'N, 73°51'E), India has been used to study the base heights (above ground level) of clouds over the station during 1986-1993. Subsequently, this lidar was equipped with an optical polariser to enlarge the scope of cloud studies. In this paper, cloud base and top heights, multi-layer cloud structures, interface between cloud condensation nuclei in the sub-cloud- layer and in the vicinity of cloud base and depolarisation characteristics studied from the data archived during 1997-1998 together with the cloud lidar database built with the observations collected during the past 12-year period from October 1986 through September 1998 are presented.

**Wednesday 28 July PM**

Presiding Chair: D Randall (Colorado State University, Colorado, USA)

**PBL, SHALLOW CONVECTION AND NONPRECIPITATING LAYER CLOUDS****MI04/L/06-B3****1400****GENERATION OF MESOSCALE FLUCTUATIONS IN CONVECTIVE ATMOSPHERIC BOUNDARY LAYERS**

Peter G. DUYNKERKE and Harm J.J. Jonker (Princetonplein 5,3584 CC Utrecht, The Netherlands Tel: 31 30 2532909, Fax: 31 30 2543163 Email: P.G.Duynkerke@phys.uu.nl)

The goal of this study is to obtain a better understanding of the generation of mesoscale fluctuations in different types of convective (buoyancy driven) atmospheric boundary layers. To this end we will use Large Eddy Simulations (LES) with a domain size large enough to accommodate mesoscale fluctuations, but with a resolution fine enough to resolve the three-dimensional turbulence structure. Moreover we will use observations of GATE and ASTEX to illustrate our findings.

The research on the generation of mesoscale fluctuations has until now mainly focused on investigating the effect of diabatic heat sources, associated with clouds, such as radiative cooling at cloud top and latent heat release. Recently (Jonker et al, 1999; <http://www.phys.uu.nl/~hjonker>) we have shown that in a clear convective boundary layer (without diabatic heat sources) passive scalars can possess significant mesoscale fluctuations, while at the same time the dynamics (velocity and temperature fields) do not show fluctuations on the mesoscale.

First we will investigate why passive scalars in the dry convective boundary layer (CBL) become dominated by mesoscale fluctuations, while the dynamics does not. Since the dry CBL can be regarded as the most elementary but still relevant boundary layer, we will endeavour to fundamentally understand the mechanism of mesoscale generation in this case. Next, we will step by step increase the complexity of the boundary layers, by including radiative cooling, and latent heat effects and studying their separate effect on mesoscale generation. Finally, we will consider the cloudy boundary layer, where all these processes simultaneously play a role.

The methodology will consist of spectrally decomposing the variances of the turbulence variables in the LES model into a microscale and mesoscale contribution, and determining the budget terms (sources and sinks) of the separate evolution equations in the numerical model.

**MI04/E/12-B3****1420****IMPROVED STRATOCUMULUS SIMULATION IN A CLIMATE MODEL**

Andrew C BUSHELL (Hadley Centre, London Road, Bracknell, Berks., RG12 2SY, UK.)

Cloud simulations in Atmospheric General Circulation Models (AGCMs) result from a combination of the chosen physical parameterization for cloud with the dynamical structure of the local environments in which the cloud parameterization activates. In particular, stratocumulus is highly sensitive to the state of the atmospheric boundary layer, and the main regions of persistent stratocumulus, off the coasts of Namibia, Peru and California, are generally recognized by AGCM modellers as problem areas.

Current developments to the Meteorological Office Unified Model (UM) include the introduction of a new dynamical core, which has been tested in a research AGCM with a state-of-the-art package of physical parameterizations, including a new boundary layer scheme. This offers a rare opportunity to examine the behaviour of the main stratocumulus regions in an alternative dynamical realization for which the model physics is kept as far as possible constant. It will be shown that this leads to a much improved representation of stratocumulus.

**MI10/W/07-B3****1435****ON THE ESTIMATION OF ENTRAINMENT IN SHALLOW AND DEEP CONVECTION II.**

GREGORY (ECMWF, Shinfield Park, Reading RG2 9AX, United Kingdom Email: dgregory@ecmwf.int); H.J.Jonker and A.P.Siebesma (KNMI, De Bilt, AE 3730, The Netherlands Email: jonker@knmi.nl and siebesma@knmi.nl)

A key parameter in the mass flux approach to convective parameterization is the lateral entrainment rate, which determines the rate of mixing of an ascending parcel with environmental air. Although mass flux schemes are now in wide use this parameter remains poorly defined, although recent LES and CRM studies have provide insight into both its magnitude and vertical variation in several cases of deep and shallow convection. Considering the vertical velocity equation of an up draught a formulation for entrainment is suggested, emphasising the effect of entrainment upon the vertical kinetic energy budget of an ascending parcel rather than on the mixing of thermodynamics quantities. The success of the approach depends upon estimating the vertical velocity within the cloud up draught. An approximate form of the vertical velocity equation for use in simple cloud models is suggested, including a parameterization of the vertical pressure gradient in terms of shear and net inflow and outflow. Comparison is made to the vertical kinetic energy budget derived from LES and CRM simulations.

The formulation gives reasonable estimates of entrainment rates for both shallow and deep convection compared to LES and CRM simulations. The entrainment rate is sensitive to the environmental profile and may allow convective parameterization schemes to be more sensitive to situations (such as a dry middle troposphere) where deep convection is inhibited.



MI04/W/31-B3

1450

## A NEW PARAMETERIZATION OF THE PBL

Bjorn STEVENS (Max Planck-Institut für Meteorologie & University of California, Los Angeles, Email: stevens@dkrz.de)

We present a new parameterization of the planetary boundary layer. Although still general, the parameterization has been developed to better address the physics of subtropical stratocumulus clouds. Thus it contains an explicit representation of boundary layer depth and entrainment, and is formulated to perform adequately on coarse (order 250 - 500m) vertical grids.

The main conceptual distinction of this model is its explicit specification of a bulk entrainment rate, following the work of the European Center (Beljaars and colleagues) and the GEWEX cloud systems studies (GCSS) working group one, and the use of profile reconstruction. Profile reconstruction allows for air in an intermediate layer (diagnosed to contain the top of the PBL) to be partitioned into PBL air and free-tropospheric air, on the basis of the properties of adjacent layers. In the limit of smooth profiles above the inversion, and strong forcing, the method allows one to diagnostically track the depth of the boundary layer as it moves through a coarse grid, and thus maintain very high accuracy at very coarse resolution. Key additional features that provide resolution independence are the formal coupling of the PBL model to the large-scale advection and radiative forcing in a way that is consistent with the profile reconstruction. That is we show that spurious grid-scale-dependent effects are only eliminated if radiative and advective tendencies are applied in a manner consistent with the dynamic and numerical assumptions of the PBL model.

Single column results will be shown comparing the performance of the model with both large-eddy simulation, and measurements of stratocumulus taken during the DYCOMS experiment. Preliminary results, with the model implemented in the ECHAM GCM will also be presented.

MI04/E/18-B3

1505

## A NON-LOCAL PARAMETRIZATION OF BOUNDARY LAYER MIXING WITH EXPLICIT ENTRAINMENT AND ITS IMPACT ON CLOUD SIMULATIONS IN THE UKMO UNIFIED MODEL

A.PLOCK, A.R.Brown, M.Bush, A.L.M.Grant, G.M.Martin, R.N.B.Smith, (UK Meteorological Office, London Road, Bracknell, RG12 2SZ, UK; email: aplock@meto.gov.uk)

Accurate representation of boundary layer clouds is essential in all forecast models, from short term mesoscale forecasts to global climate simulations. A realistic representation of boundary layer mixing is crucial to the simulation of such clouds. In the Unified Model's current boundary layer scheme, the local Richardson number profile determines the calculated mixing coefficients within the boundary layer. Studies have shown that turbulent fluxes between the boundary layer and the free atmosphere cannot be represented accurately by such a scheme. A new boundary layer mixing scheme, which includes non-local turbulent mixing, an explicit parameterisation of cloud-top entrainment, and diagnosis and treatment of decoupled boundary layers, has been tested in different configurations of the Unified Model. One of the main benefits is in allowing a specific diagnosis and treatment of different cloudy boundary layer types, extending the basic stable/unstable separation to recognising well-mixed, decoupled and cumulus-capped boundary layers. Results from the mesoscale model show better discrimination between layer cloud and convective cloud in the boundary layer in unstable conditions. In the climate model (where this scheme is introduced along with increased vertical resolution below 600 hPa), the tendency for the boundary layer to be excessively shallow in the sub-tropical stratocumulus regions is reduced, although cloud amounts remain underestimated. The treatment of decoupling allows the transition between stratocumulus and trade cumulus to be represented realistically.

MI04/L/10-B3

1520

## ATMOSPHERIC BOUNDARY LAYER DEPTH EVALUATION USING A GCM AND AVHRR CLOUD DATA

A.MATHIEU (Centre d'Etude des Environnements Terrestre et Planétaire (CETP), 10-12 av. de l'Europe 78140 Velizy, France, Email: nne.mathieu@cetp.ipsl.fr); G.Seze (Laboratoire de Meteorologie Dynamique LMD, Paris); A.Weill (CETP); H.Giordanni (Meteo-France CNRM/GMGC, Toulouse); H.Dupuis (Departement de Geologie et d'Océanographie, Bordeaux)

We propose a method to compare Marine Atmospheric Boundary Layer height as determined from a GCM and corresponding information as retrieved from AVHRR satellite cloud analysis over oceanic mid-latitudes. We use the Holtslag et al. (J. of Climate, 92) algorithm and the French Met GCM : RPEGE.

First, a cloud classification of AVHRR images is used to discriminate low level Strato-Cumuli, from which are derived cloud top temperature fields. Secondly, from the GCM output, we determine the MABL altitude. The temperature correspondence between the two fields is worked out to evaluate the ability of the GCM to give realistic characteristics of the MABL. The method is applied to the SEMAPHORE experiment, held in sept-Nov 1993 over the Azores basin (North. MidAtlantic) using ARPEGE re-analysed with the SEMAPHORE observations. The advantage to use a combined information of GCM with relatively good surface information but poor determination of the cloud layer and remote sensing with relatively accurate data is demonstrated.

MI04/W/18-B3

1600

## HEAT AND MOISTURE BUDGETS IN STRATOCUMULUS AND TRADE CUMULUS REGIMES: SYNOPTIC AND DIURNAL VARIABILITY

Paul E. CIESIELSKI, Wayne H. Schubert, and Richard H. Johnson, (Department of Atmospheric Science, Colorado State University, Fort Collins, Colorado 80523, USA, email: paulc@tornado.atmos.colostate.edu)

Rawinsonde data collected from the Atlantic Stratocumulus Transition Experiment (ASTEX) are used to investigate the mean and temporal characteristics of large-scale heat and moisture budgets for a two-week period in June 1992. During this period a large apparent heat sink and apparent moisture source are observed near inversion base (around 1500 m) which resulted from evaporation of cloud droplets which detrained near this level. Analyses from other budget studies such as BOMEX (Barbados Oceanographic and Meteorological Experiment) show that similar convective signatures (i.e., low-level apparent moistening and cooling) occur in a wide variety of regimes when trade-wind type inversions are present. The vertical eddy flux of moist static energy over the ASTEX domain (centered at 33N with an average sea-surface temperature of 19.4 C) is about half that observed in the undisturbed trade-wind regime of BOMEX (centered at 15N with an average sea-surface temperature of 28.1 C). The apparent heat source, apparent moisture sink and convective flux of moist static energy over ASTEX are strongly modulated on a synoptic time scale by the passage of fronts and by fluctuations in the subsidence rate associated with changes in the strength and position of the subtropical high.

The influence of mid-latitude distinguishes this region from trade-wind and tropical regimes. We will also examine the diurnal variability of large-scale motion fields over ASTEX and compare these results to other regions in order to deepen our understanding of why regional phase and amplitude differences exist in the diurnal cycle.

MI10/W/11-B3

1615

## IMPROVEMENTS IN THE REPRESENTATION OF STRATOCUMULUS IN THE ECMWF MODEL

Joao TEIXEIRA, Anton Beljaars, Christian Jakob and Pier Siebesma (ECMWF, Shinfield Park, Reading, RG2 9AX, UK, email: teixeira@ecmwf.int)

It has been recognized for many years that clouds play a fundamental role in the climate system. Stratocumulus, in particular, have a strong influence on the global climate due to its impact on the Earth's radiation budget. This implies that the ability to represent stratocumulus in global models in a realistic way is a crucial scientific issue in climate modelling. Comparisons of the ECMWF Re-Analysis stratocumulus with observations have shown that the model largely underestimates the observed stratocumulus clouds. This problem can have serious negative consequences in the ocean surface fluxes produced by the model. Other diagnostic studies based on the NWP model or the single-column version of the ECMWF model also point on the same direction. An improved boundary layer vertical resolution configuration has been tested at ECMWF. The first studies were performed using the single-column model, and they have shown that the stratocumulus clouds and the transition to cumulus clouds is better captured with the increased resolution. In long integrations, the new configuration improves the cloud cover, liquid water path, surface shortwave radiation and the net surface flux over the stratocumulus areas. A major impact of the improved resolution is also seen in the thermodynamic structure of the boundary layer profiles: the new resolution has sharper inversions and the inversion heights are closer to the observations. One of the missing processes in the ECMWF model is the vertical turbulent mixing of cloud variables, that is only partially done by cloud top entrainment. A parameterization for the turbulent mixing of cloud variables is shown to have a positive impact on the simulation of stratocumulus. Improvements in the representation of stratocumulus due to the introduction of a revised parameterization for the evaporation of precipitation are also discussed.

MI04/W/12-B3

1630

## SIMULATION OF THE CLOUD-TOPPED BOUNDARY LAYER WITH A SINGLE-COLUMN MODEL

Jean-Christophe GOLAZ (Department of Atmospheric Science, Colorado State University, Fort Collins, CO 80523, USA, email: golaz@tofu.atmos.colostate.edu); William R. Cotton (Department of Atmospheric Science, Colorado State University, Fort Collins, CO 80523, USA, email: cotton@isis.atmos.colostate.edu)

Accurate representation of boundary layer clouds in large-scale models remains a formidable task. Single-column models, which can be viewed as isolated columns from a large-scale model, offer the ability to develop parameterizations without the complexity of the full model. A single-column model for simulating the cloudy boundary layer is presented. The model offers different turbulence parameterizations including several low order closure schemes as well as a plume decomposition. A microphysical scheme is also included, making it possible to simulate liquid and mixed-phase precipitation processes and their influence on the cloudy boundary layer.

The model has been applied to different marine boundary layer regimes such as stratocumulus, cumulus and cumulus under stratus. Sensitivity to sea surface temperature and drizzle is explored. It is, for instance, shown that for a stratocumulus-topped boundary layer, evaporation of drizzle can produce a two-layer structure by stabilizing the subcloud layer with respect to the cloud layer. This stabilization does not necessarily lead to a decoupling of the boundary layer.

MI04/E/21-B3

1645

## CLOUD, AEROSOL AND BOUNDARY LAYER EVOLUTION MEASURED DURING THE ACE-2 LAGRANGIAN EXPERIMENTS

D.W.JOHNSON, S.Osborne and R.Wood (Meteorological Office, Meteorological Research Flight, Building Y46, DERA, Farnborough, Hants GU14 6TD, UK.)

On three occasions during June and July 1997 as part of the Aerosol Characterisation Experiment (ACE-2), "smart" balloons and PFC tracers were released into the boundary layer off the Portuguese coast. On each occasion the balloons were tracked for up to two days using instrumented aircraft as they were advected south westwards in the trade winds towards the Canary Islands. Results will be presented of the analysis of the measurements made on the UK Meteorological Research Flight C-130 aircraft which describe how the cloud conditions, aerosol characteristics and boundary layer thermodynamics and dynamics evolve with time.

The three Lagrangian experiments showed a great deal of diversity in the cloud and aerosol characteristics encountered and in particular how the aerosol evolved within the boundary layer. The boundary layer was always relatively deep and highly structured in the vertical with a well mixed surface layer decoupled from the cloud layer. In the first Lagrangian the air mass had originated from the centre of the Atlantic and was unpolluted. In the other two Lagrangians anthropogenic sources over western Europe had considerably polluted the air parcel. The influence of the boundary layer structure on the cloud, and the feedback between the cloud microphysics and the aerosol characteristics will be detailed.

MI04/E/05-B3

1700

## DEVELOPMENT OF A PARTIALLY CLOUDY BOUNDARY LAYER

J.D. PRICE (Met. Research Unit, Cardington, Beds, MK42 0SY, UK)

A case study of a partially cloudy boundary layer consisting of cumulus and stratocumulus is presented, and the main dynamical processes responsible for its evolution are identified. Measurements were made with the UK Meteorological Office tethered balloon facility which was located in Hampshire, Southern England, during the Doppler Radar Observation Project, September 1998.

Results show fair weather cumulus formed during the morning and quickly overdeveloped into patches of stratocumulus. A characteristic of this day was a relatively weak capping inversion, which allowed a significant amount of encroachment/entrainment to occur. Between 1100 and 1400GMT this was calculated at 102kgm<sup>-2</sup>. The ratio of entrainment to encroachment was found to be 0.5. Data show, together with a simple model, that entrainment of warm air into the upper part of the boundary layer significantly increased the stability there and caused a reduction in the cloud area.

**MI10/W/19-B3** 1715**TEST OF THE VOLUME-OF-FLUID METHOD ON MARINE BOUNDARY LAYER CLOUDS**

C.-Y. J. KAO, Y. H. Hang, J. M. Reisner, and W. S. Smith (Earth and Environment Sciences Division, Los Alamos National Laboratory, Los Alamos, NM 87545, USA. E-mail: kao@lanl.gov)

The impact of using grid-averaged thermodynamic properties (i.e., neglecting their sub-grid variability due to partial cloudiness) to represent forcings for condensation or evaporation has long been recognized. In particular, numerical difficulties in terms of spurious oscillations and/or diffusion in the vicinity of a cloud-environment interface have been encountered in most of the conventional finite-difference Eulerian advection schemes. This problem is equivalent to the inability of models to accurately track the cloud boundary within a grid cell, which eventually leads to spurious production or destruction of cloud water at leading or trailing edges of clouds. In this paper, we employ a specialized technique called "Volume of Fluid" (VOF) method to better parameterize the subgrid-scale advection process that accounts for the transport of material interfaces. VOF also determines where the partial cloudiness actually sits within a grid box. Consequently, relevant microphysical parameterizations in mixed cells can be consistently applied in "cloudy" and "clear" regions. We have incorporated the VOF technique in a two-dimensional hydrodynamic model to simulate the diurnal cycle of the marine stratocumulus-capped boundary layer. The fidelity of VOF to advection-condensation processes under a diurnal radiative forcing is assessed by comparing the model simulation with data taken during the ISCCP FIRE observational period as well as with results from simulations without VOF. Our study shows that the VOF method indeed suppresses the spurious cloud boundary instability and supports a multi-day cloud evolution as observed. For the case without VOF, the spurious instability near the cloud top causes the dissipation of the entire cloud layer within a half of a diurnal cycle.

**MI04/E/29-B3** 1730**ON TOP-HAT REPRESENTATION OF TURBULENCE STATISTICS IN CLOUD-TOPPED MARINE BOUNDARY LAYER: A LARGE-EDDY SIMULATION**

Shouping WANG (Universities Space Research Ass, 977 Explorer Blvd, Huntsville AL 35806, USA Email: wangsx@vmcs.msfc.nasa.gov)

Large-eddy simulation is used to study top-hat parameterizations of second- and third-order scalar statistics in cumulus and stratocumulus cloud-topped boundary layers (CTBLs). Although the top-hat parameterizations based on commonly used conditional sampling methods is a useful approach to modeling the vertical fluxes in the simulated CTBLs, it fails to realistically represent the scalar variances. The reason is because the common sampling methods are based at least in part on the sign of vertical velocity, but not the sign of scalars, and because scalars and velocity are not perfectly correlated such methods cannot guarantee uniqueness of the sign of the scalar fluctuations in each individually defined plume. The cancellation between the positive and negative fluctuations induced by the physical processes such as cloud-top entrainment, radiative cooling, small-scale mixing between the different plumes considerably reduces the top-hat contribution to the variances, but has significantly less effect on the fluxes. For the vertical velocity-scalar related third-order moments, the top-hat model gives reasonable estimates for the cumulus CTBL; but not for the stratocumulus CTBL. These differences between the two CTBLs are explained by structural differences (tied to circulation differences in the two CTBLs) in their respective joint probability density functions of vertical velocity and various scalars.

**MI10/E/05-B3** 1745**MORPHOLOGY OF LOW CONVECTIVE CLOUD FIELDS**

Joachim H. JOSEPH and Ofer Heyman (Dept. of Geophysics and Planetary Sciences, Tel-Aviv University, Tel-Aviv 69978, Israel, email: yoya@jupiter1.tau.ac.il)

Morphological and fractal analysis of digital, spectral images, acquired from air-planes during the SCAR-B mission at different times of day, has been carried out for the purpose of supplying detailed data on the structure of low-level convective cloud fields. Morphological and fractal characteristics of clouds as well as holes in clouds have been derived and are compared. The morphological characteristics have been applied to develop two new parameters- the "Stratiformity" and the Maximal Area/Median Area ratio. These can be used for an automatic discrimination between low-level convective cloud types.

**Thursday 29 July AM**

Presiding Chair: G Isaac (AES, Toronto, Canada)

**MICROPHYSICAL PROCESSES AND UPPER-TROPOSPHERE CLOUDS****MI04/E/25-B4** 0930**ESTIMATION OF THE PARTICLE SIZE DISTRIBUTION IN TROPICAL CIRRUS CLOUDS - HOW IMPORTANT ARE SMALL PARTICLES?**

C. Martin R. PLATT (Department of Atmospheric Science, Colorado State University, Fort Collins, CO, 80523); R. T. Austin (Department of Atmospheric Science, Colorado State University, Fort Collins, CO, 80523); S. A. Young, CSIRO, Atmospheric Research, P. Bag 1, Aspendale, VIC, 3195, Australia); D. L. Mitchell (Atmospheric Sciences Center, Desert Research Institute, P.O. Box 60220 Reno, NV 89506); Stephen M. Sekelsky (Dept. of Electrical &amp; Computer Engineering, University of Massachusetts, Amherst, MA 01003)

Recent ground-based remote sensing observations have shown that small particles are prevalent, and sometimes dominant, in cold tropical cirrus near the tropopause. These clouds are found to have significant infrared optical depths, but, because of their small particle size, even higher visible solar optical depths. Combined lidar, radar and infrared radiometric observations provide the opportunity to deduce an effective particle radius. Particle sizes in the small-particle range are inferred from lidar-IR radiometer observations, whereas the larger particle range is inferred from combined lidar and millimeter radar data. A set of such data obtained in the Maritime Continent Thunderstorm Experiment (MCTEX) on the Tiwi Islands, Northern Australia in November-December, 1995, included cirrus clouds with temperatures covering the range from -80C to -20C. In some of the higher cloud decks, the millimeter radar could not detect any returns. The lidar-radiometer technique then indicated small particles in the 1 micron to 20 micron range. In the warmer cloud decks, the millimeter radar easily detected most of the cloud (except near cloud top) and the lidar-radar method was able to give effective radii. The methods require an assumption of a particle size distribution. Three models are employed here to assess the sensitivity of the method to such assumptions. The importance of the very high cold clouds of small particles to the radiation budget is discussed.

**MI10/W/04-B4** 0950**ON THE MAINTENANCE OF HIGH TROPICAL CIRRUS**

M.T. BOEHM (Dept. of Meteorology, Pennsylvania State University, 503, Walker Building, University Park, PA 16802, USA., email: boehm@essc.psu.edu)

Observations reveal that cirrus clouds are ubiquitous in the tropics and therefore significantly impact the radiation budget in this region. Numerical studies are conducted using a two-dimensional cloud resolving model with explicit microphysics to study the processes that lead to the maintenance of tropical cirrus. In particular, radiative destabilization is investigated as a possible maintenance mechanism. It is found that, despite significant differences in the cloud dynamics among the simulations performed, the model is unable to maintain a cloud against the processes of sedimentation and evaporation under the assumed environmental conditions, leading to the conclusion that radiative destabilization is not able to maintain tropical cirrus. It is hypothesized that maintenance requires a source of large-scale upward motion.

**MI04/E/23-B4** 1005**NUMERICAL SIMULATIONS OF DROP SPECTRA EVOLUTION IN TROPICAL CONVECTIVE CLOUDS OVER LAND AND SEA**

Lester ALFONSO, Daniel Martínez (Instituto de Meteorología, A.P. 17032, La Habana 17, Cuba, email: finubes@met.inf.cu); Alberto A. García (Centro de Investigación y Estudios Avanzados del I.P.N., A.P. 14740, México D.F.); Carlos A. Pérez (Martínez (Instituto de Meteorología, A.P. 17032, La Habana 17, Cuba, email: finubes@met.inf.cu)

A one dimensional cloud model with detailed microphysics was used to simulate the evolution of drop spectra in tropical convective clouds. The model considers the processes of activation, condensation, coalescence, break-up, deposition and advection. Two types of cloud base activated droplet spectra were used, corresponding to clouds developing over land and sea. These droplet spectra were measured in young cloud bases over the central part of Camaguey, Cuba and over the Caribbean Sea, near the Camaguey coast, respectively. As initial environmental conditions, a sounding of the Camaguey rawinsond stations was used. Sub-cloud layer sounding data were modified for the simulations over sea. Comparisons were made between modeled and experimental raindrop spectra.

**MI04/W/21-B4** 1020**DO ICE NUCLEATION RATES DEPEND ON CRYSTAL SHAPE?**

D.I. MITCHELL (Desert Research Institute, Atmospheric Sciences Centre, P.O. Box 60220, Reno, Nevada, 89506, USA, email: mitch@dri.edu)

A snow growth model based on an analytical solution to the ice particle number density equation to date has been tested against 9 case studies with consistent favorable agreement between observed and predicted mean particle size and number concentration, N. The model physics for diffusional growth predicts N to be very sensitive to crystal habit. This can be understood if nucleation rates depend largely on the level of supersaturation, Si. In the absence of water droplets, Si depends on the surface area of the size distribution. Cloud regions characterized by crystals with low surface area-to-volume ratios tend to develop higher Si than regions characterized by higher ratios, and the higher Si is, the higher is N. This reasoning was tested in a parcel model, which predicted N in the isometric crystal regime (-7 to -11 C) to be 2 to 7 times greater than N in the dendritic regime. While this assumes no droplets, other detailed microphysical modeling indicates cloud droplets are generally rapidly depleted through riming within snowbands, leaving Si governed by the ice phase. In another test, size spectra predicted by the snow growth model were compared with those from a frontal cloud where enhanced N was attributed to the rime-splintering mechanism. The snow growth model, which implicitly includes the above physics but no rime splintering mechanism, successfully reproduced the observed height evolution of size spectra and N.

**MI04/E/04-B4** 1035**VALIDATION AND IMPROVEMENT OF STRATIFORM CLOUD FRACTION PARAMETERISATION IN GCMS USING AIRCRAFT DATA**

Robert WOOD, Paul R. Field, Doug Johnson, Stephen Cusack, Mark Webb, Gill Martin, Roy Kershaw and Damian Wilson (United Kingdom Meteorological Office, London Road, Bracknell, UK, email: robwood@meto.gov.uk)

Cloud fraction is an important parameter in global circulation models (GCMs) as it can affect both the surface radiation balance and the production of precipitation. The majority of cloud schemes currently used in GCMs diagnose cloud fraction as a function of grid-box mean relative humidity. Results are presented of an attempt to validate several diagnostic cloud fraction schemes with aircraft data collected using the Meteorological Research Flight C-130 aircraft in both warm and cold stratiform cloud. It is shown that one of the most commonly used schemes results in a substantial underprediction of cloud fraction. A scheme based upon a fit to the aircraft data is tested in the UK Meteorological Office Unified Model and results in a significant improvement in the prediction of cloud fraction especially in the stratocumulus sheets over the oceans to the west of continents. The scheme also results in an improvement to the TOA short-wave radiation in these regions and, through feedback, produces boundary layers with more realistic inversion heights and specific humidities.

**MI04/E/11-B4** 1120**ICE PARTICLE NUCLEATION IN AN A DIABATIC PARCEL MODEL**

Richard COTTON, Doug Johnson (The Met. Office, Meteorological Research Flight, Y46, DERA Farnborough, Hants, GU14 0LX, UK, email: rcotton@meto.gov.uk)

Ice particle production by the processes of homogeneous freezing and heterogeneous nucleation in orographic cirrus clouds is studied using a simple adiabatic ascending air parcel model. Case studies being used in the GEWEX Cloud System Study (GCSS) WG2 have been used to initialise this model and results will be shown here. Homogeneous freezing rates in the model are based on Jeffery's (1997) formulation, which matches with observed rates, modified according to the solution effect. Different parameterisations of the heterogeneous nucleation processes have been incorporated into the model and sensitivity studies have been carried out. The model initial conditions are:

100 cm<sup>-3</sup> CCN H<sub>2</sub>SO<sub>4</sub> particles, lognormally distributed 0.02 - 1.0µm radius, a range of updraught velocities 0.04, 0.2, 1.0 ms<sup>-1</sup>, warm case model run starting at -40 C (height 8.3km, pressure 340mb), and cold case model run starting at -60 C (height 13.4km, pressure 170mb).



MI04/E/27-B4 1135

## ICE CLOUD DIABATIC PROCESSES AND MESOSCALE STRUCTURE IN FRONTAL ZONES

R.M.FORBES (Joint Centre for Mesoscale Meteorology (UK Met Office), University of Reading, Reading, RG6 6BB, UK. email: rnforges@meto.gov.uk)

Ice cloud can have a significant dynamical effect through the sublimation of precipitation that may be important in determining mesoscale structure in frontal zones. Observations from FASTEX, a major observational campaign over the North Atlantic, are used to investigate this relationship. The FASTEX dataset includes airborne Doppler radar data, in situ observations from aircrafts, and series of dropsondes which are objectively analysed on isentropic surfaces to form vertical cross sections along the aircraft track. Information regarding heat and moisture budget will be derived from the observational data, and implications for the representation of diabatic processes in a numerical model will be discussed.

MI04/E/22-B4 1150

## A CIRRUS CLOUD MODEL WITH EXPLICIT MICROPHYSICS

Ken-ichi MARUYAMA, Naomi Kuba (Institute of Global Change Research, @frontier.esto.or.jp, N.Kuba: kuba@frontier.esto.or.jp); Ryosuke Nakamura (Information Processing Center, Kobe University, Japan, email ryosuke@komadori.planet.sci.kobe-u.ac.jp); Yasushi Fujiyoshi (Institute of Low Temperature Science, Hokkaido University, Japan, email: fujiyo@stellar.lowtem.hokudai.ac.jp, Frontier Research System of Global Change); Takao Takeda (Institute for Hydrospheric-Atmospheric Sciences, Nagoya University, Japan, email: takeda@ihas.nagoya-u.ac.jp, Frontier Research System for Global Change)

It is well known that cirrus clouds play an important role in the radiative heat balance of the earth. Since their radiative properties critically depend on microphysical properties, we are developing a new cirrus model that explicitly calculates such microphysical processes as nucleation of cloud condensation nuclei, nucleation of ice nuclei, condensational growth/evaporation of droplets, growth/sublimation of ice crystals due to accretion, freezing of droplets and stochastic collection between ice crystals and droplets. To simulate the stochastic collection process rigorously, the Monte Carlo algorithm (Gillespie, 1975) is used for calculation of collection and coalescence of ice crystals. Although this calculation technique takes much more CPU-time than other conventional schemes (e.g., Berry and Reinhardt, 1974, Bott, 1998), this model can produce realistic development of ice crystals within cirrus clouds. In addition our model can describe the growth processes of individual ice particles and simulate the shapes of aggregates by applying a cluster formation model.

MI10/E/09-B4 1205

## A COMPARISON BETWEEN ISCCP CLOUD OPTICAL DEPTHS AND VALUES ESTIMATED FROM IN-SITU AIRCRAFT DATA FOR CIRRUS CLOUDS OBSERVED DURING FIRE-II

Samantha SMITH (Columbia University, 2880 Broadway, New York, NY 10025, USA, email: ssmith@giis.nasa.gov); Anthony D. DelGenio (NASA Goddard Institute for Space Studies, 2880 Broadway, New York, NY 10025, USA)

The results of a comparison between ISCCP retrieved optical depths and FIRE-II in-situ aircraft measurements are presented. Conditions must be examined closely to omit cases with underlying cloud and to choose a satellite scene representative of the aircraft flight region. Comparison is very good for well-sampled homogeneous cirrus layers when cloud fraction is accounted for, with locally averaged ISCCP optical depth values within 4 to 9% of the in-situ derived values. Locally averaged ISCCP optical depths differ from in-situ values by up to 70% for inhomogeneous cloud fields (optical depth standard deviation greater than 4), although individual pixel values may give better agreement if that part of the cirrus happens to be similar to that sampled by the aircraft. Conditions that change in time cause even more problems. Although individual histograms of in-situ ice water contents are not necessarily the same shape as the ISCCP optical depth histogram, their overall behavior with cloud fraction is the same. At low cloud fractions the histograms peak at the highest measurable value. At larger cloud fractions the distributions are wider, tending towards a Gaussian shape. The standard deviations of the ISCCP optical depths are proportional to the average values, as for in-situ ice data.

MI04/E/16-B4 1220

## THE EFFECTS OF EMBEDDED CONVECTION ON THE PARAMETERISATION OF LAYER CLOUD

T.W. CHOULARTON, K.N. Bower and J. Cardwell (Department of Physics, UMIST, P.O.Box 88, Manchester M60 1QD, UK, email: t.w.choularton@umist.ac.uk)

A model of the microphysical development of a nimbostratus cloud with embedded convective cells has been developed. The cloud model contains a full description of mixed phase cloud microphysics including droplet growth, ice nucleation, ice crystal growth by vapour diffusion, riming and aggregation. The model is used to predict the precipitation rate from the cloud as a function of time and the ice and liquid water contents as a function of position and time in the cloud. The results are compared with a similar model but using the parameterised cloud microphysics developed at the UK Meteorological office by Wilson and Kershaw. The results of both these model runs are then compared with a single column cloud model which does not resolve the embedded convection but in which the total water flux into the cloud is the same as the models. The paper will comment on the results of this intercomparison and the implications for treating such clouds in Global Climate Models. The work is supported by the UK Meteorological Office.

Thursday 29 July PM

Presiding Chair: Tom Choularton (UMIST, Physics Dept Manchester)

## MICROPHYSICAL PROCESSES AND UPPER-TROPOSPHERE CLOUDS

MI04/W/07-B4 1400

## CLOUD MICROPHYSICAL PARAMETERIZATION: VARIABILITY IN THE DERIVED RELATIONSHIPS

G.A. ISAAC and I. Gultepe (Cloud Physics Research Division, Atmospheric Environment Service, Toronto, Ontario, M3H 5T4, Canada, e-mail: george.isaac@ec.gc.ca and ismail.gultepe@ec.gc.ca)

This study shows uncertainties in cloud parameterizations using observations collected during

Canadian field projects conducted in the 1980s to 1990s. Microphysical and dynamical measurements were collected by instruments mounted on National Research Council aircraft. Observations represent various cloud types including both maritime and continental stratus, at mid and high latitudes. Models use relationships which have parameters such as liquid water content (LWC), ice water content (IWC), total particle concentration (aerosol, ice, and droplets), temperature, vertical air velocity, and particle size. In parameterized equations, the following concepts have been used: 1) continental clouds have higher concentrations than maritime clouds, 2) droplet number concentration increases with particle concentration and decreasing droplet size, 3) LWC and IWC decreases with altitude, 4) ice crystal number concentration increases with decreasing temperature, and 5) increasing vertical air velocity results in large number concentrations. Most of the earlier relationships were based on observations collected during the 1950s-70s. In earlier studies, scale effects for averaging were not considered, and breaks in the clouds were ignored. The results from this study will be used to show the variability and profiles of cloud microphysical parameters, and the importance of vertical air velocity on number concentration. Also, comparisons with ice crystal number concentration-temperature relationships will be summarized, and their importance to model results will be discussed.

MI04/W/15-B4 1420

## IMPROVED IN SITU OBSERVATIONS OF CLOUD PARTICLE CHARACTERISTICS AND IMPLICATIONS ON CLOUD MICROPHYSICS AND RADIATION

R. Paul LAWSON (SPEC Incorporated, 5401 Western Ave., Suite B, Boulder, CO 80301, USA, email: plawson@specinc.com)

A new airborne device, the cloud particle imager (CPI), records high-resolution (2.3 um) digital images of cloud particles "on the fly" as they pass through the instrument sample volume. The CPI now makes it possible to study the detailed structure of ice crystals and discriminate them from water drops in clouds. The CPI is a sophisticated instrument that has been carefully designed to provide extensive information on cloud particle characteristics. In addition to high-resolution images, the CPI sizes the particles in real-time, records particle detection sensitivity, arrival time, transit time, dead time, total particle count and several other critical parameters. Analysis of data recently collected by the CPI in Arctic stratus, mid-latitude cirrus, and organized convection in Texas and Florida, suggests the presence of very high (5,000 - 10,000 per liter) concentrations of small ice particles in some of these clouds. In the outflow of convective clouds, regions of exceptionally high ice particle concentration are located in juxtaposition with regions with substantially lower concentrations. The visual characteristics of the ice particles in the two adjacent regions are noticeably different. The particles found in high concentrations generally show evidence of riming and contain pockets with high concentrations of small particles. Regions with lower particle concentrations are usually more faceted, showing less evidence of riming and fewer small particles. When the high concentrations of small particles are detected, they are typically found to be inhomogeneously distributed in small clusters. If the clusters of small particles are real, (i.e., not artifacts of the sampling process) they would have previously gone undetected by conventional digital imaging probes and undercounted by scattering probes. In this paper we compare data from the CPI with measurements from the conventional imaging and scattering probes. The likelihood that clusters of small particles exist, their possible origins, the impact on cloud microphysics and radiation are considered.

MI04/W/08-B4 1435

## LABORATORY STUDIES OF AEROSOLS AND ICE FORMATION IN CIRRUS

Paul J. DEMOTT (Department of Atmospheric Science, Colorado State University, Fort Collins, CO, USA 80523-1371, Email: pdemott@lamar.colostate.edu)

The role of aerosols in catalyzing ice formation in clouds, an indirect pathway to altering cloud properties that potentially affect climate, is poorly understood. This area of study is receiving renewed interest world-wide and nowhere is this more evident than in laboratory studies of cirrus ice formation. Cirrus ice formation is often envisioned as a straightforward process involving the freezing of haze particles composed of binary solutions of water and sulfuric acid or ammonium sulfate. Some observations do exist to support the view that cirrus ice formation is primarily by homogeneous freezing nucleation and on this basis a number of numerical studies have investigated the expected relationships between aerosol properties, thermodynamics and ice formation. Nevertheless, the fundamental hydration and freezing behaviours of liquid aerosol particles have not been well documented and there are a host of potential complexities involved under cirrus conditions. First, there are many ways that the cloud nuclei may arrive at cirrus levels or be modified along the way, so there are many potential compositions to be investigated. It is certain that secondary phase transition behaviours of aerosol particles also impact cirrus formation and there may be additional kinetic limitations to a problem that is often viewed thermodynamically. Finally, there are several alternate pathways to ice formation in cirrus, including all the hypothesized heterogeneous ice nucleation mechanisms. This presentation will highlight recent advances in understanding that have been obtained through laboratory studies of ice formation on aerosol particles under cirrus conditions. These new research results provide guidance for theoretical developments, focused field study, and parameterization of ice formation processes for numerical cloud models. This contribution updates a recent textbook contribution in this rapidly evolving research area.

MI04/E/01-B4 1450

## EVOLUTION OF BIMODAL ICE SPECTRA

Paul R. FIELD, Doug Johnson (United Kingdom Meteorological Office, London Road, Bracknell, UK, email: prfield@meto.gov.uk)

Frontal clouds were sampled with the UKMO C-130 research aircraft. The aircraft advected with the wind and descended from cloud top to cloud base with an average descent rate close to the average fall speed of the observed ice crystals. The ice crystal size spectra from 5 descents exhibited very similar evolutions: a mode formed at small crystal diameters and high concentrations migrated to larger diameters and lower concentrations with increased depth from cloud top. Quantitative relations for the observed evolution of bimodal ice size spectra and conclusions about the relative importance of aggregation and diffusional growth processes will be presented.

MI04/W/29-B4 1505

## IS THE DETAILED PATTERN OF SNOW ACCUMULATION OVER ANTARCTICA PREDICTED BY GLOBAL MODELS?

Tom LACHLAN-COPE, Russell Ladkin and Steven Leonard (British Antarctic Survey, High Cross, Madingley Road, Cambridge CB3 0ET. email: t.lachlan-cope@bas.ac.uk)



During the 1998/99 summer a series of 10m firn cores were taken in a traverse inland from the coast in the Bryan Coast area of Antarctica. The annual accumulation was determined from these cores using the Electrical Conductivity Method (ECM) in the field using a new portable ECM instrument developed for this project. The results give a detailed picture of how the accumulation varies with height during 1997 and 1998. The results are compared with the annual precipitation, over the same period, given by the UK Met Office operational forecast model, the ECMWF operational model and a Lagrangian version of the UK Met. Office single column model.

A detailed comparison of the accumulation will show any gross errors in the parameterisation of clouds and precipitation processes in numerical models. Some thought is given to possible differences between the precipitation predicted and the accumulation measured, in particular the effect of blowing snow will be considered.

**DISCUSSION**

1520

Monday 26 July AM

**MI10/E/11-B1**

Poster

0900-01

**THE DYNAMICS OF HAIL PROCESSES IN THE KAKHETI REGION OF GEORGIA IN 1967-1998**

Vazha AMIRANASHVILI, Avtandil Amiranashvili, (Institute of Geophysics of Georgian Academy of Sciences, 1, M. Aleksidze Str., Tbilisi 380093, Georgia, email: vazha@excite.com); Muraz Bakhsoliani (Main Department of Hydrometeorology and Environmental Monitoring of Georgia.); Nodar Begalishvili (Institute of Hydrometeorology of Georgian Academy of Sciences); Kukuri Tavartkiladze (Institute of Geography of Georgian Academy of Sciences)

An analysis of the hail processes from 1967 to 1998 in the Kakheti Region of Georgia is carried out, where until 1989 hail suppression activities were conducted.

Within the period of activities of the hail suppression service (1967-1989) positive trends of the following characteristics of hail processes were detected: the number of hail-dangerous clouds exposed to the modification, the part of protected territory inflected by hail per 100%, the expected number of hail cases, the actual number of hail cases.

Within the same period a negative trend of hail suppression efficiency was detected, which on the average amounted to 80%. The part of protected territory inflected by hail per 100% in 1967-1989 amounted on the average to 0.44%. After the cancellation of the hail suppression activities in 1990-1998 this value rose up to 2.9% versus 2% before the launching of the activities.

Thus, within the last decade in Kakheti an intensification of hail processes has taken place. It is supposed that one of the reasons of this represents the regional climate change and increase of the anthropogenic air pollution. In the nearest future it is planned to renew the hail suppression activities and the above factors should be taken into account for a more precise development of the hail clouds modification methodology.

**MI04/W/11-B1**

Poster

0900-02

**CHARACTERIZATION OF CIRRUS CLOUD PROCESSES USING A CLOUD RESOLVING MODEL WITH AN ADVANCED RADIATIVE TRANSFER SCHEME**

Angela BENEDETTI and Graeme L. Stephens (Department of Atmospheric Sciences, Colorado State University, Fort Collins, CO 80523, Email: angela@moa.atmos.colostate.edu, stephens@langley.atmos.colostate.edu)

The understanding of ice cloud properties and their sensitivity to different atmospheric conditions is very important for the proper parameterization of such clouds in forecasting models, from mesoscale to the global scale. A two-dimensional cloud resolving model, including dynamical and microphysical processes, is coupled with an advanced radiative transfer model to simulate cirrus clouds. The latter is computationally extremely efficient, deriving its speed by an approximate, robust perturbation technique developed at CSU. The fields provided by the cirrus model are ice water content, crystal number concentration, radiative fluxes, heating rates and vertical velocities. Analysis of these fields will provide insight into the variables that play important roles in the evolution of cirrus clouds. The results of these simulations will also be compared against benchmarks to determine the accuracy and integrity of the cirrus model.

**MI04/W/25-B1**

Poster

0900-03

**IMPROVED NUMERICAL MODELING OF THE LIFECYCLE OF A THUNDERSTORM CELL BASED ON OGURA - TAKAHASHI'S MODEL**

Sohaila Javanmard (Department of Agricultural Meteorology, Faculty of Agriculture, Kyushu University, Hakozaki, Fukuoka 812-8581, Japan, email: jbjp8scp@mbox.nc.kyushu-u.ac.jp); JAVAD BODAGHJAMALI (Department of Physics, Faculty of Science, Kyushu University, Hakozaki, Fukuoka 812-8581, Japan, email: jbjp8scp@mbox.nc.kyushu-u.ac.jp); Golamali Kamali (IR of Iran Meteorological Organization, Meradj Ave., email: Tehran@13185-361, Islamic Republic of Iran)

Ogura-Takahashi's numerical modeling of the life cycle of a thunderstorm has been improved in microphysical processes, specially in autoconversion of cloud droplets to form raindrops, as well as in glaciation of raindrops to form hail and fall velocities of raindrops and hail. The results of the improved modeling are shown that the rainfall intensity became much heavier with using the Kessler's bulk parameterization. Besides, the second peak of rainfall intensity disappeared with using the Bigg's freezing probability of supercooling water, and also the rainfall intensity became much heavier and sharper with using the Lin et al's bulk parameterization for fall velocities of the rain and hail in comparing to the Ogura-Takahashi's original model. The rainfall profile has much similarities to the observations. The modified Ogura-Takahashi's model can be useful not only for the construction of mesoscale cloud model including clouds and precipitation, but also for the study of the seeding effect on rain evolution.

**MI10/W/22-B1**

Poster

0900-04

**ONE-DIMENSIONAL NUMERICAL CLOUD NODER STUDY ABOUT THE EFFECTS OF ICE MULTIPLICATION AND ICE NUCLEI CONCENTRATION ON PRECIPITATION**

Javad BODAGHJAMALI (Department of Physics, Faculty of Science, Kyushu University, Hakozaki, Fukuoka 812-8581, Japan, email: jbjp8scp@mbox.nc.kyushu-u.ac.jp); Sohaila Javanmard (Department of Agricultural Meteorology, Faculty of Agriculture, Kyushu University, Hakozaki, Fukuoka 812-8581, Japan, email: jbjp8scp@mbox.nc.kyushu-u.ac.jp); Golamali Kamali (IR of Iran Meteorological Organization, Meradj Ave., email: Tehran@13185-361, Islamic Republic of Iran)

The effects of ice multiplication and variation of natural ice nuclei concentration on rain evolution and precipitation have been studied by using a time-dependent, one-dimensional numerical cloud model. The dynamics and thermodynamics of the model is according to Ogura-Takahashi's cloud model. Six forms of water substance (water vapor, cloud water, cloud

ice, rain, snow, and hail) have been simulated. The model utilizes the "bulk water" microphysical parameterization technique according to Lin et al's bulk parameterization. When ice multiplication was used, model produced more intense rainfall peak and precipitation efficiency reached to 24%. Besides, when ice nuclei concentration was increased about 1000 times of standard value, rainfall intensity peak appeared 8 minutes earlier and precipitation efficiency reached to 13%.

**MI10/W/14-B1**

Poster

0900-05

**NUMERICAL MODELING OF LOW LEVEL HORIZONTAL PENETRATION OF LIQUID CARBON DIOXIDE SEEDING IN SUPERCOOLED CLOUD IN NORTHERN KYUSHU OF JAPAN**

JAVAD BODAGHJAMALI (Faculty of Science, Kyushu University, Hakozaki, Fukuoka 812-8581, Japan, e-mail: jbjp8scp@mbox.nc.kyushu-u.ac.jp) Norihiko Fukuta (Department of Meteorology, University of Utah, Salt Lake City, Utah, USA, e-mail: nfukuta@sohaila.javanmard, Yoshinori Suzuki, Kouji Nishiyama and Kenji Wakimizu (all at Faculty of Agriculture, Kyushu University, Hakozaki, Fukuoka 812-8581, Japan) Golamali Kamali (IR of Iran Meteorological Organization, Meradj Ave., Tehran 13185-361, Islamic Republic of Iran)

In order to achieve effective modification of supercooled clouds, Fukuta (1996) formulated a new seeding method which avoids the problems associated with dry ice and silver iodide seedings and maximizes the seeding reactions involved. The method causes RETHIT (Roll-up Expansion of Twin Horizontal Ice-crystal Thermal) process followed by FILAS (Falling-growth Induced Lateral Air Spreading) process, with a low level horizontal penetration seeding of liquid carbon dioxide (LC). The two-dimensional and time-dependent numerical modeling of the LC seeding method has been carried out for standard atmosphere, where the cloud base temperature and the thickness of cloud were 0 C and 3 km, respectively, in one of our previous work. In this paper, the above mentioned model has been performed to test the feasibility of precipitation enhancement by LC seeding in Northern Kyushu of Japan (Fukuoka). The sounding data of the Fukuoka on 4 November 1998 is used to test the seeding effect. The cloud base and cloud top temperatures are -12 C and -22 C, respectively, and the thickness of cloud is about 2 km. The modeling results of microphysics and dynamics interactions of LC seeding effect shows that the seeded ice crystal thermal has arrived the cloud top in 11 minutes and the amount of precipitation at the ground is obtained about 1.0 mm which is about the maximum releasable precipitation of the supercooled cloud with liquid water content of 0.5 gram per cubic meter and 2000 m thick.

**MI04/E/14-B1**

Poster

0900-06

**MODELLING THE FORMATION AND GROWTH OF ICE SNOWFLAKES IN DEEP LAYER CLOUD**

J. CARDWELL, T.W. Chouarton (Physics Department, UMIST, P.O. Box 88, Manchester, M60 1QD, UK) and P.R. Field (Meteorological Research Flight, DERA, Farnborough, Hants)

The UK Meteorological Office C-130 aircraft made measurements in a deep layer cloud of the evolution of the ice crystal and snowflake spectrum from cloud top down to cloud base. A detailed microphysical model has been used to investigate the contribution of the range of physical processes to the evolution of the ice crystals. Comparison of the model and observations shows that: a. The initial ice crystal spectrum grows and descends from cloud top. This can be explained by the known mechanisms of primary nucleation and growth by vapour diffusion. b. Aggregation is required to explain the ice crystal spectrum lower down in the cloud. The results suggest that aggregation is more important at low temperatures than previously thought. c. A mechanism of secondary ice particle production is required to explain the large number of small ice particles observed at all levels below cloud top. This is consistent with laboratory studies of the fragmentation of ice crystals during evaporation.

**MI04/E/03-B1**

Poster

0900-07

**DETECTION OF VERTICAL FINE STRUCTURES IN THE FREE ATMOSPHERE**

Takashi CHUDA, Ryuji Kimura, Hiroshi Niino (Ocean Research Institute, University of Tokyo, 1-15-1 Minamida, Nakano-ku Tokyo, 164-8639, Japan, email: chuda@ori.u-tokyo.ac.jp)

Using raw insonde data with vertical resolution of about 10 m, we have detected vertical fine-structures of temperature and specific humidity between 1 and 8 km MSL. An average vertical scale of these structures is about 300 m. Mean amplitudes of temperature and specific humidity are 0.4 K and 0.4 g/kg, respectively, which are significantly larger than the accuracy of the sensors, where the fine-structures of temperature and specific humidity are defined as deviations from running means.

In most fine-structures, perturbations of temperature and specific humidity have a significant negative correlation: For 167 vertical soundings obtained in Kyushu island in the southern part of Japan during the summer of 1996, more than 90 percents of those had negative correlation. To assess the generality of these features found for the soundings in Kyushu, additional studies were made for rawinsonde soundings in different seasons and in different districts of Japan. Most of the soundings exhibited similar features of the fine-structures of temperature and specific humidity. Thus, it is considered that these are common features that exist in the troposphere. Such fine-structures of specific humidity seem to be consistent with occasional observations of cap clouds with multiple layered structure over an isolated mountain.

**MI04/W/04-B1**

Poster

0900-08

**RADIATION-INDUCED DYNAMICS IN ARCTIC STRATUS CLOUDS**

Dietmar FREESE and Joerg Hartmann (Alfred Wegener Institute, 27515 Bremerhaven, Germany, email: dfrees@awi-bremerhaven.de)

To study the interaction between radiation, cloud microphysics and dynamic processes, the experiment REFLEX III (Radiation and Eddy Flux Experiment) was conducted in summer 1995 in the European Arctic north of Svalbard. It was shown that radiative cooling at the top of a stratus cloud deck can lead to a dynamic formation of cell structures within the entire stratus layer.

Airborne measurements were taken of the three wind components, of the temperature and humidity, of the solar and of the terrestrial irradiance and of the particle spectra on flights through the stratus cloud cover over sea ice. Results from measurement on 27 July 1995 are presented, when a stratus cloud was at first shielded by a higher altocumulus cloud. The lower cloud then drifted into a region without higher clouds leading to the onset of radiation cooling at the top. Complex cell structures formed in the stratus layer due to radiative cooling and are visualised by a tomography method.

MI04/E/20-B1 Poster 0900-09

**THE EFFECT OF INHOMOGENEOUS SUPERSATURATION HISTORY ON THE DROPLET SPECTRA IN STRATOCUMULUS CLOUDS**

Sarah L. IRONS (Department of Physics, UMIST, Manchester, UK, email: sarah@sneezy.phy.umist.ac.uk); Peter R. Jonas (Department of Physics, UMIST, Manchester, UK, e-mail: peter.jonas@umist.ac.uk)

This work is concerned with the impact of a turbulent updraught on the nucleation processes and droplet spectral evolution within stratocumulus cloud. It has previously been shown that turbulent variations in the updraught result in fluctuations of supersaturation. Fluctuations in the updraught velocity cause local values of the supersaturation which may be much larger than those occurring in a cloud experiencing a constant vertical velocity equal to the mean of the fluctuating updraught. This leads to increased droplet nucleation as well as enhanced growth rates for pre-existing droplets in the regions of higher than average updraught. The effect is investigated using an explicit microphysical model which has been developed to simulate a marine stratocumulus cloud deck. It is shown that while the fluctuations give rise to local variations in droplet concentration, effects on the development of the mean droplet spectrum are however limited due to the short vertical scale over which the velocity fluctuations are correlated.

MI04/W/05-B1 Poster 0900-10

**FREEZING OF CLOUD DROPS ON THE GRAUPEL SURFACE - THEORETICAL STUDY**

Tzveta KASSABOVA (Department of Meteorology and Geophysics, Sofia University, P.O.Box 44, Sofia 1164, BULGARIA, email: rumypm@phys.uni-sofia.bg) and Martin Kassabov (Department of Mathematics, Yale University, 276 Prospect Str., #211, New Haven, CT 06511, USA)

A new approach to the freezing process of water droplets on the graupel surface is proposed. The model takes into account the influence of the freezing of droplets on the temperature inside the graupel. The surface temperature of the graupel is a parameter in the Macklin & Payne (1967) equation. Its change during the freezing process brings an additional heat flow in the original equation. The impact of droplets size, cloud temperature and liquid water content on freezing time of cloud droplets and on graupel surface temperature will be discussed. References: Macklin W. C. and G. S. Payne, 1967, Quart. J. Roy. Meteor. Soc., 93, 195 \_

MI10/W/02-B1 Poster 0900-11

**A LONG-TERM ANALYSIS OF THE GLOBAL CLOUD MICROPHYSICS DERIVED FROM AVHRR DATA**

Kazuaki KAWAMOTO and Teruyuki Nakajima (Center for Climate System Research, University of Tokyo, Meguro-ku, Tokyo, 153-8904, Japan, e-mail: kawamoto@ccsr.u-tokyo.ac.jp)

An algorithm is developed for determining the cloud optical thickness and effective particle radius (the cloud microphysics) simultaneously on a global scale using AVHRR (Advanced Very High Resolution Radiometer) multi-spectral radiance data. In the algorithm, the treatment of thermal radiation in Nakajima and Nakajima (1995) is improved by reformulating the thermal emission in the atmospheric layers. At the same time, the look-up table for thermal emission is parameterized in terms of the effective water vapor path in order to include the effect of various vertical water vapor profiles. This algorithm has been applied to four-month (Jan., Apr., Jul. and Oct.) data to generate the annual-mean global distributions of the cloud optical thickness and effective particle radius for every 0.5 (deg.) x 0.5 (deg.) box in a -60 (deg.) to 60 (deg.) latitudinal region. Various features of the cloud optical thickness and effective particle radius such as the ocean-land contrast and the altitude dependence are obtained. Moreover, a long-term analysis of the cloud microphysics from 1985 to 1994 has been performed. We have obtained a result that the effective particle radius decreased gradually both over ocean and land during this period. As one of the major reasons, we like to suggest an increase of anthropogenic aerosols originating from industrial production and biomass burning.

MI104/E/02-B1 Poster 0900-12

**CONCERNING TO IDENTIFICATION OF THUNDER CLOUDS**

T. G. Salukvadze, N. V. KHELAIJA, E. I. Khelaia Nodia (Institute of Geophysics, Academy of Sciences of Georgia Georgia, Tbilisi 380093 Aleksidze str. 1)

The investigation of radar observations on several hundred convective clouds to overwhelm thunder phenomena, with the aim to express the modeling possibilities on atmospheric electricity processes have been carried out. From date archives of many years radar observations on hail and thunder clouds, that had been carried out on Alazany Valley in East Georgia, were selected such clouds, the evolution of the parameters of which was tracked by their natural development. According this the following 8 radar and aerological parameters have been used: Hm km – the radioecho height maximum above sea level; tHm (c – the temperature in the free atmosphere over the Hm level; h-/h+ - the ratio radio-echo thickness of the part of cloud that is above zero isothermal (h-) level on that isothermal height, that is above place level (h+); Hzm km – the radar reflectivity locations height maximum above sea level; tHzm (c - the temperature of the free atmosphere on the Hzm level; (h km – the increased reflectivity thickness zones that are placed above zero isotherm's level; t(h (c - the temperature in the free atmosphere on the level of the upper bound; lgzm - the logarithm of maximum radar reflectivity. The distribution curves for the values of were found where rain and thunderstorm clouds separate unambiguously. The informativeness of all parameters according to Makhalanobis distance was estimated.

MI04/E/17-B1 Poster 0900-13

**TROPOSPHERIC STATIC STABILITY AND CONVECTIVE RAINFALL IN CAMAGÜEY, CUBA.**

Daniel MARTINEZ, Lester Alfonso, and Ieng Jo (Instituto de Meteorología, A.P. 17032, La Habana 17, Cuba, Email: finubus@met.inf.cu)

Convective available potential energy (CAPE), stability indices, moisture and wind shear related magnitudes were calculated from 413 afternoon soundings of the Camagüey rawinsond station, located in the Central-Eastern part of Cuba. These and other magnitudes, derived from a simple stationary cloudy parcel model with lateral entrainment were related with 24 hour mean and maximum rainfall for a dense rain gauge network centered in the rawinsond station. Regression and discriminant analysis techniques were applied. Positive correlation was found between rainfall and moisture related parameters. If inter-seasonal variations are considered, slightly positive correlations are obtained between rainfall and static stability parameters, which becomes negative if only rainy season soundings are included. The results are discussed on the base of cloud physics arguments based on data and numerical modeling results.

MI04/E/07-B1 Poster 0900-14

**SHALLOW CONVECTION IMPACT UPON MEDIUM-RANGE NUMERICAL WEATHER FORECASTS**

Georgui V. MOSTOVOI and Elena D. Astakhova (Hydrometeorological Centre of Russia, Bol'shoi Predtechensky per., 9-13, Moscow, 123242, Russia, email: most@rhmc.mecom.ru)

The description of a new parameterization scheme of shallow convection (SC) and results of numerical experiments, carried out with the help of an operational version of Russian Hydrometeorological Centre spectral model (T40L31 sigma model) are presented. Experiments were carried out for estimating the impact of a new SC scheme on the model performance for 6-day forecasts. The scheme takes into account the terminal size and deformation of a small cumulus cloud during its life cycle. Therefore in comparison with other schemes based on a parcel method it is more adequate for reproducing thermodynamic structure of small clouds. Influence of the new parameterization scheme of SC upon large-scale thermodynamic fields is assessed. Sample estimations of the model skill for some meteorological elements are considered. They allow to note existence of clear tendency toward small improvement of 850 hPa geopotential height and air temperature forecasting quality for 6-day period at the expense of SC parameterization. Noticeable positive response of forecast skill is observed in the tropics. The quality of surface pressure forecasts remains about the same everywhere. Influence of SC parameterization upon spatial distribution of precipitations in midlatitudes is discussed for few individual forecasts.

MI10/E/04-B1 Poster 0900-15

**PARAMETERIZATION SCHEME OF SHALLOW CONVECTIVE CLOUDS BASED ON TWO-DIMENSIONAL NUMERICAL MODELLING**

Georgui V. MOSTOVOI (Hydrometeorological Centre of Russia, Bol'shoi Predtechensky per., 9-13, Moscow, 123242, Russia, email: most@rhmc.mecom.ru)

The parcel concept based on one-dimensional, steady-state cloud models is widely used in atmospheric convection (AC) parameterization schemes. These models are generally restricted to the prescribed cloud geometry and neglect some important features relating to the spatial structure of the AC. The current research is carried out to refine a parcel method taking into account the terminal size and deformation of a small cumulus cloud during its life cycle. Numerical experiments with nonhydrostatic two-dimensional shallow AC model with fine spatial resolution of 30m aimed for simulation of a cumulus cloud evolution represent a necessary framework for the parcel method improvement. Model thermodynamical variables are: the liquid water potential temperature and the total moisture content (TMC) mixing ratio. AC is initiated by the overheated dome-like area in the form of a semicircle placed at the bottom boundary on a central axis of the model domain. The initial thermodynamic profiles, chosen for numerical experiments, reflected various conditions of large-scale stratification for small cumulus development in the tropics and midlatitudes. A quasi-conservative property of the TMC mixing ratio is taken into account to track displacements of atmospheric layers in the course of AC and to consider the composition of the cloudy air from the viewpoint of air parcel history. Peculiarities of cumuli life cycle revealed in numerical experiments form a basis for the proposed parameterization scheme of small cumulus clouds in large-scale atmospheric models. A comparison with other parameterization methods is done. The scheme provides more adequate estimation for a cloud top height and thermodynamic parameters.

MI10/W/09-B1 Poster 0900-16

**CHARACTERISTICS OF THE VERTICAL AND HORIZONTAL DISTRIBUTION OF CLOUDS FROM LITE OBSERVATIONS**

Kathleen A. POWELL (NASA Langley Research Center, MS 475, Hampton, VA 23681 USA, email: k.a.powell@larc.nasa.gov) David M. Winker (NASA Langley Research Center, MS 475, Hampton, VA 23681 USA, email: d.m.winker@larc.nasa.gov)

Clouds play a major role in determining the Earth radiation budget. The feedback between clouds and the climate system are not well understood, however. This is due in part to the limitations of passive satellite sensors for observing thin and multi-layer clouds and for measuring characteristics such as cloud height and the 3-D spatial organization of cloud. The Lidar In-space Technology Experiment (LITE) was flown on Space Shuttle mission STS-64 in September 1994. High vertical resolution, high sensitivity, the ability to observe multi-layer clouds, and near-global coverage provide a unique dataset for the study of cloud distribution. As an example of the information available from LITE, preliminary results on cloud brokenness and on the characteristics of the overlap of multilayer clouds are presented. These results have implications for the design of satellite sensors for observing clouds and can be used to test the validity of cloud parameterizations in global climate models.

MI04/E/24-B1 Poster 0900-17

**A SIMPLE MODEL OF CIRRUS HORIZONTAL INHOMOGENEITY AND CLOUD FRACTION**

Samantha SMITH (Columbia University, 2880 Broadway, New York, NY 10025, USA, email: ssmith@giss.nasa.gov); Anthony D. DelGenio, (NASA Goddard Institute for Space Studies, 2880 Broadway, New York, NY 10025, USA)

A simple model of horizontal inhomogeneity and cloud fraction in cirrus clouds has been formulated on the basis that all internal horizontal inhomogeneity in the ice mixing ratio is due to variations in the cloud depth, which are assumed to be Gaussian. The use of such a model was justified by the observed relationship between the normalized variability of the ice water mixing ratio (and extinction) and the normalized variability of cloud depth. Using radar cloud depth data as input, the model reproduced well the in-cloud ice water mixing ratio histograms obtained from horizontal runs during the FIRE-II cirrus campaign. For totally overcast cases the histograms were almost Gaussian, but changed as cloud fraction decreased to exponential distributions which peaked at the lowest nonzero ice value for cloud fractions below 90%. Cloud fractions predicted by the model were always within 28% of the observed value. The predicted average ice water mixing ratios were within 34% of the observed values. This model could be used in a GCM to produce the ice mixing ratio probability distribution function and to estimate cloud fraction. It only requires basic meteorological parameters, the depth of the saturated layer and the standard deviation of cloud depth as input.

MI04/L/15-B1 Poster 0900-18

**USING LEM TO INVESTIGATE THE DYNAMICS OF SINGLE CLOUDS**

STILLER (Address not available at time of going to press)

The parameterisation of cloud processes is a delicate task due to the lack of understanding of the basic dynamics comprising mixing processes and momentum transport. Experimental data

are limited and not always conclusive and also numerical investigations are difficult due to the systems complexity and often obscured by the large number of parameters involved in a realistic representation of moist processes. Using the large eddy model of the British Meteorological office to investigate the dynamics of single clouds (updrafts) we have extracted a largely idealised version of the model which possesses basic features of the full model but has fewer parameters and thus permits a more systematic analysis facilitating conclusions concerning cause and effect of the observed phenomena. The idealised model has a drastically simplified microphysics which still includes condensation and reevaporation of cloud water but the parametrisation of rain is reduced to the fact that the content of cloud water has an upper limit above which the water is irreversibly taken out of the system. The saturation value of water vapour is taken to depend only on height and to decrease linearly with height. As a consequence a sounding with a constant dry lapse rate also possesses a constant moist lapse rate. To investigate mixing processes we are considering situations where the height reached by the updraft is entirely determined by mixing processes. This means we consider a sounding which is neutral with respect to moist convection. In particular we find that a dryer atmosphere enhances mixing and decreases the height reached by the updraft. This can be explained by the increased release of negative buoyancy from reevaporation processes which enhances the vortices responsible for the mixing. Similarities and differences of the model dynamics and those from simulations with the full large eddy model are discussed.

**MI04/L/18-B1** Poster **0900-19**

**PHYSICAL ASPECTS OF THE PRECIPITATION PROCESS IN MONSOON CLOUDS**

TINMAKER

Abstract not available at time of going to press

**MI04/W/27-B1** Poster **0900-20**

**ON SIMULATING INTRASEASONAL OSCILLATIONS IN A GCM**

G.K.WALKER, Y.C.Sud, K.-M. Lau (Laboratory for Atmospheres, NASA Goddard Space Flight Center, Greenbelt, MD 20771, USA), and D.A.Randall (Colorado State University, Fort Collins, CO, USA)

One of the least understood phenomenon of tropical motions is the interaction among physical and dynamical processes that cause intra-seasonal oscillations commonly known as Madden-Julian Oscillations, or MJOs. Only a few general circulations models (GCMs) were able to simulate decent MJOs in the Atmospheric Model Inter-comparison Project (AMIP I). A few GCMs that had decent MJOs in one version lost them in another so-called improved version; consequently considerable diagnostic and model development research is necessary to understand the processes that affect MJOs. Such research not only would help to understand MJOs, but also would enable modelers to improve tropical moist processes in GCMs. The GLA GCM in AMIP I, which is a version of the GEOS GCM with an improved physical package, had fairly decent MJOs. In this research, we show how several changes in moist convection, rain- evaporation, and downdraft parameterizations would influence simulation of MJOs. The investigations are in the form of sensitivity studies in which the influence of inclusion or removal of the above noted physical processes on MJOs is examined. Our preliminary results show that elimination of a physical process leads to slow degradation of MJOs. In this way, simulation of MJOs is ultimately related to realistic simulation of vertical heating profiles and depth of moist convection. The details of the episodic structure and intensity of convection is also identified.

**MI04/L/20-B1** Poster **0900-21**

**A ONE DIMENSIONAL LAGRANGIAN SIMULATION OF STRATOCUMULOUS EVOLUTION IN SEA-BREEZE CIRCULATIONS IN CALIFORNIA COAST**

WANG

Abstract not available at time of going to press

**MI06** **Monday 26 – Tuesday 27 July**

**REMOTE SENSING OF THE ATMOSPHERE FOR WEATHERFORECASTING AND CLIMATE APPLICATIONS (ICDM, ICCL, IRC)**

Location: Mechanical Engineering G29 LT

**Monday 26 July AM**

Presiding Chair: R.G. Ellingson (University of Maryland, Maryland,USA)

**TECHNIQUES AND SURFACE PROPERTIES**

**Introduction** **0900**

D.R. Hudak

**MI06/W/15-B1** **0910**

**LAND USE AND TERRAIN IMPACTS ON CLOUD FIELD DEVELOPMENT ON THE CARIBBEAN SLOPE OF COSTA RICA AND NICARAGUA**

R. M. WELCH, R. O. Lawton and U.S. Nair

It has long been hypothesized that landscape changes alter regional climates, but direct evidence has been lacking. Analysis of satellite imagery acquired during the Central American dry season reveals that the trade wind cumulus cloud fields over the Caribbean slope of northern Costa Rica and adjacent southern Nicaragua are influenced by several classes of terrain features and by human land use practices. In Costa Rica, deforestation of the southern margins of the Llanura de Tortuguero, the Llanura de San Carlos and the Llanura de los Guatusos began in the 1950s but expanded rapidly on the northern margins in the 1970s and has continued until the present. Social conditions in southeastern Nicaragua have limited agricultural expansion in that time frame, so that area remains forested, as do tracts protected within the Costa Rican Parque Nacional de Tortuguero and the Regugio de Fauna Silvestre de Barro Colorado. Twenty years of Landsat imagery shows that deforestation and establishment of a mixed agricultural landscape in Costa Rica is associated with significantly decreased cumulus development. Indeed, many images show complete

suppression of cloud development over deforested areas, while nearby forested regions are covered by trade wind cumulus.

**MI06/W/09-B1** **0930**

**NAST-I: AN AIRBORNE DEMONSTRATION OF FORTHCOMING SATELLITE CAPABILITIES FOR HIGH SPECTRAL RESOLUTION INFRARED REMOTE SENSING OF WEATHER AND CLIMATE VARIABLES**

William L. SMITH (NASA Langley Research Center, Mail Stop 401, Bldg 1250, 21 Langley Blvd. Hampton, VA 23681 USA, email: bill.l.smith@larc.nasa.gov Tel: 757-864-5380, Fax No: 757-864-8197)

The NPOESS Airborne Sounder Testbed-Interferometer (NAST-I) is a new high spectral resolution (0.25cm-1) and high spatial resolution (2.6 km at nadir and 3.6 X 5.2 km at 45 degrees) scanning (46 km swath) Fourier Transform Spectrometer flying on NASA high altitude (~20 km) ER-2 aircraft. The NAST-I has been flown during several field measurement campaigns to provide experimental observations needed to finalize the specifications and to test proposed designs for future satellite instruments, particularly the Cross-track Infrared Sounder (CrIS) set to fly on the National Polar-orbiting Operational Environmental Satellite System (NPOESS). The data are also being used to test and validate forward radiative transfer models and retrieval algorithms designed for the upcoming launch of the EOS-PM platform Advanced Infrared Sounder (AIRS) and the METOP Infrared Atmospheric Sounding Interferometer (IASI). The NAST-I instrument provides new and exciting observations of the mesoscale structure of the atmosphere and the Earth's surface. The fine scale thermodynamic characteristics of tropical cyclones (Hurricane Bonnie and Hurricane Georges, Atlantic Basin 1998 Hurricane Season) and extra-tropical storm systems have been observed to date. The detailed horizontal structure of ocean, and land, surface temperature and spectral emissivity features can be observed with high accuracy afforded by a high spectral resolution and precision of the radiance measurements. The spatial resolution and scan geometry of this instrument enables observation of the fine spatial structure of cloud radiation and implied cloud microphysical properties. The NAST-I instrument provides atmospheric sounding measurements with an unprecedented vertical and horizontal resolution. Surface and atmospheric remote sensing results obtained during several airborne measurement campaigns have already provided a glimpse of the advanced global remote sensing capabilities which will soon be realized from meteorological satellites.

**MI06/L/04-B1** **0950**

**AN INSTRUMENT FOR GRADIENT FIELD MAPPING IN WEATHER SYSTEMS**

Dr. William E. SHARP, ITT Aerospace Communications, Fort Wayne, IN 46801, 219-451-6147, email: wesharp@itt.com. Dr Mark Abrams, ITT Aerospace Communications, Fort Wayne, IN 46801, 219-451-6822, email: mcabrams@itt.com

Storm formation occurs in the boundary regions between airmasses with very different temperatures, pressures, water content, and aerosol loading. Severe storm tracking and forecasting utilizes the discontinuities in observed fields and gradient fields to diagnose and forecast the formation, evolution, and motion of severe storms. Heat islands, super-regional pollution, and rain shower formation are each the result of temporal and spatial gradients present in the atmosphere. Diagnosing and forecasting such event requires an ability to map atmospheric gradients and discontinuities in real-time on micro to meso-scales in the atmosphere. A new measurement concept, the Geostationary Severe Storm Imager (GSSI), is described which demonstrate a class of autonomous event identification, monitoring and tracking sensor. The GSSI combines high spatial resolution (0.5-1 km) imaging with high spectral resolution (0.25 cm-1 across the mid infrared 3-10 microns) in time intervals of a few seconds. This electronically programmable infrared camera combines a large-format focal plane array with a Fourier transform spectrometer and builds on currently fielded airborne demonstration systems and an instrument concept in development for the Next Generation Space Telescope (NGST). The GSSI concept is revolutionary in several aspects: 2-10 fold increase in spatial resolution, 2 fold increase in spectral resolution, 30 fold increase in temporal resolution; in combination the measurement concept would require a 100-600 fold increase in telemetry bandwidth without a new approach to imaging. GSSI breaks this paradigm with a new approach to hyperspectral imaging. Four innovations enable this measurement concept: GSSI will: (a) directly observe the gradient fields, (b) Nyquist sample the image, (c) have Multi-channel detection of gradient regions, and (d) have an autonomous targeting and tracking system that identifies, subsets, and follows regions with significant discontinuities (i.e., regions where severe storms, toxic pollution, heat islands, or rain/thunderstorms will form). An analysis of the excellent spectral data and images from an airborne experiment demonstrates the utility of the GSSI concept.

**MI06/W/29-B1** **1010**

**MEASURING ATMOSPHERIC WATER VAPOR, TEMPERATURE AND GEOPOTENTIAL USING SATELLITE OCCULTATION OBSERVATIONS NEAR 22 GHZ**

E. Robert KURSINSKI, Thomas Yunck (Both at Jet Propulsion Laboratory, California Institute of Technology, Pasadena CA 91109, Email: Rob.Kursinski@jpl.nasa.gov), Benjamin Herman, Dashing Feng (Both at Institute of Atmospheric Physics, University of Arizona, Tucson, AZ 85712)

Atmospheric water plays fundamental roles in energy transfer, atmospheric circulation and defining the continental biosphere via precipitation. Accurate predictions of weather and changes in climate require detailed knowledge of the distribution of atmospheric water in clear and cloudy conditions, at sufficient spatial and temporal scales over the entire range of climatic conditions. Observations must capture aspects of the distributions from which to infer the mechanisms and predict how they will change in a changing climate. In particular, both specific and relative humidity are needed to infer the processes involving water phase changes and moisture advection.

Spacecraft radio occultations near 22 GHz can address many of these objectives as well as improve knowledge of temperature and geopotential on a global scale. The concept is to make occultation measurements near the 22 GHz water line of both propagation delay and absorption to derive the wet and dry density structure of the atmosphere in a limb viewing geometry. Recovery of dry density versus height yields hydrostatic pressure versus altitude or equivalently the geopotential of pressure surfaces. Estimated specific humidity accuracy is ~1 to 2% in the lower and middle troposphere and 3 to 5 ppm in the upper troposphere. Relative humidity can be estimated at the few percent level through much of the troposphere. Profiles of cloud liquid water will be derived as well. Temperatures with sub-kelvin accuracy and geopotential heights accurate to ~10 m or better should extend from near the surface to ~60 km altitude.

The presentation will discuss the measurement and retrieval concept, estimated accuracy and plans for development of this system.



Presiding Chair: R.A. Brown (University of Washington, Seattle, USA)

**ATMOSPHERIC PROFILING****MI06/E/13-B1****1100****FIELDS OF NO<sub>2</sub> AND O<sub>3</sub> TOTAL CONTENT: MEASUREMENTS, VALIDATION, NUMERICAL SIMULATION**

Yuriy M. TIMOFEEV, Dmitriy, V. Ionov, Vladimir, V. Ionov (St.Petersburg State University, Ulyanovskaya 1, St.Petersburg-Petrodvorets, 198904 Russia, e-mail: tim@troll.phys.spbu.ru). Nikolay F. Elansky, Aleksandr S. Elokhov, Alexandr M. Gruzdev, Oleg V. Postlyakov (Institute of Atmospheric Physics RAS, Pyshevsky per. 3, Moscow, 109017 Russia, e-mail: Nikolai@selansky.home.bio.msu.ru). Igor L. Karol, Vladimir Zubov, Arkadiy M. Shalamyansky (Main Geophysical Observatory, Karbysheva 7, St.Petersburg, 194018 Russia, e-mail: ozon@peterlink.ru). Eugene Rozanov, M. Schlesinger (University of Illinois, S.Gregory Ave 105, Urbana, IL 61801 USA, e-mail: rozanov@atmos.uiuc.edu). John P. Burrows (University of Bremen, Bibliothekstr. 1, Bremen,330440 Germany, e-mail: burrows@gome3.physik.uni-bremen).

Information on global fields of the O<sub>3</sub> and NO<sub>2</sub> content is retrieved from the GOME satellite measurements of reflected and scattered solar radiation in UV and visible spectral ranges. Data of ground-based Russian network are used for estimating the quality of the satellite measurements. Russian network of ground-based measurements of atmospheric gaseous constituents by optical methods is characterized. Accuracy of measuring the O<sub>3</sub> and NO<sub>2</sub> column amount and the methods of device calibration and interpretation of measurement data are clarified. Comparison of the GOME O<sub>3</sub> and NO<sub>2</sub> data with network measurements over the 1996-1998 period is carried out for North-West and Central Russia. Systematical deviations between the GOME satellite and M-124 ozonometer ground-based measurements are revealed. Comparisons of the M-124 and the TOMS data testified to a high accuracy of ground-based measurements. Essential deviations are also observed between the NO<sub>2</sub> total column amount retrieved from the GOME and ground-based measurements. Possible sources of the mismatches revealed has been analyzed. Some examples of comparing the O<sub>3</sub> and NO<sub>2</sub> satellite and ground-based measurements with the results of numerical modeling the total content by the global three-dimensional model are given.

**MI06/E/03-B1****1120****THE MOISTURE CONTENT OF MID-LATITUDE WEATHER SYSTEMS IN THE NEW ZEALAND REGION FROM GPS PRECIPITABLE WATER AND GMS-5 SATELLITE IMAGERY**

James MCGREGOR (School of Earth Sciences, Victoria University of Wellington, PO Box 600, Wellington, New Zealand, Email: mcgregor@vuw.ac.nz); Mark Falvey (School of Earth Sciences, Victoria University of Wellington, PO Box 600, Wellington, New Zealand, Email: mfallvey@gamma.gns.cri.nz)

Video animations of infrared and upper tropospheric water vapour channel data from the Geostationary Meteorological satellite, GMS-5 satellite reveal the passage of a number of interesting mid-latitude weather systems in the vicinity of New Zealand during February - March 1997. The water content of the atmosphere during these events is examined in detail using GMS-5 satellite data, GPS Total Precipitable Water data and rainfall data from the New Zealand Climate database (CLIDB). Comparisons are also made to six hourly data derived from European Centre for Medium Range weather Forecasting (ECMWF) global analysis fields. In this study we pay particular attention to mesoscale variations in the moisture observed in the GMS water vapour channel and its relationship to short term temporal variations in the GPS PW time series at four stations around the NZ region. By combining the upper tropospheric information of the GMS data with the total column information provided by GPS-PW, we also obtain a greater insight into the vertical distribution of moisture content of the various weather systems.

**MI06/E/05-B1****1140****RETRIEVAL OF HUMIDITY PROFILES FROM GMS-5 DATA USING BAYESIAN DISCRIMINATION AND REGRESSION**

Niels BORMANN, Crispin J. Marks, James A. Renwick (NIWA/VUW Centre of Excellence, PO Box 14 901, Kilbirnie, Wellington, New Zealand/Aotearoa, email: n.bormann@niwa.cri.nz)

We describe and characterise a statistical method to estimate humidity profiles based on data from the Geostationary Meteorological Satellite (GMS-5). The method incorporates data from all four GMS channels (0.6 $\mu$ m, 6.7 $\mu$ m, 11.5 $\mu$ m, 12.5 $\mu$ m), and it is developed for the New Zealand region, i.e. for an oceanic midlatitude environment with very few conventional observations. Results from the validation of the retrievals are discussed and compared to results from other algorithms based on similar satellite data (e.g. Garand 1993).

The retrieval method uses various predictors derived from atmospheric background fields and scenes of the satellite data, and it is based on clustering and cluster-specific regression models for standard pressure levels, similar to Garand 1993. Clustering allows the separation of different physical regimes similar to cloud-classification, and we use multivariate Bayesian discrimination to distinguish between the clusters (e.g. Uddstrom and Gray 1996). The algorithm is developed by collocating 33 months worth of radiosonde profiles with satellite data. The algorithm shows significant skill in estimating humidity profiles. The retrievals are better for upper levels (700hPa and above) due to contributions of the 6.7 $\mu$ m channel, though poorer at lower levels as these are often obscured by clouds in the satellite data. The Bayesian approach allows the identification of poorer retrievals and can be used to significantly improve the algorithm performance. We highlight the benefits and limitations of the scheme with a view to assimilating the retrievals into a regional numerical model.

**MI06/W/22-B1****1200****THERMODYNAMIC PROFILING OF THE LOWER 10-20 METRES OF THE ATMOSPHERIC MARINE BOUNDARY LAYER USING HIGH SPECTRAL RESOLUTION INFRARED INTERFEROMETRY**

BJ Osborne, MJ LYNCH (Remote Sensing and Satellite Research Group, School of Physical Sciences, Curtin University of Technology, GPO Box U1987, Perth WA 6845, Australia, email: posbornebj@cc.curtin.edu.au); RO Knuteson (Space Science and Engineering Center, University of Wisconsin-Madison, 1225 W. Dayton Street, Madison, WI 53706, USA)

This paper will describe the information content of high spectral resolution infrared radiance observations in the 15 micron region, for the purpose of retrieving near-surface marine boundary layer air temperature and temperature profiles. Using atmospheric transmittance models and radiometric data from the Marine Atmospheric Emitted Radiance Interferometer (MAERI), the potential for down-looking sounding of temperature from ship deck altitude is assessed. Factors impacting such retrievals, such as spectral selection, the sea surface emissivity, reflected downwelling radiation and instrument specifications will also be

discussed. It is anticipated that such profiles may be useful estimators of ocean heat flux. Preliminary investigations comparing MAERI-derived air temperature with an in-situ sensor and the response of temperature profiles to ocean heat flux will be discussed.

**MI06/W/07-B1****1220****ATMOSPHERIC BOUNDARY LAYER DEPTH EVALUATION USING A GCM AND AVHRR CLOUD DATA**

A.MATHIEU (Centre d'Etude des Environnements Terrestre et Planetaire (CETP), 10-12 av. De l'Europe 78140 Velizy, Email: anne.mathieu@cetp.ipsl.fr); G.Seze (Laboratoire de Meteorologie Dynamique (LMD, Paris); A.Weill (CETP, Velizy); H.Giordani (Meteo-France CNRM/GMGEC, Toulouse); H.Dupuis (Departement de Geologie et d'Océanographie, Bordeaux)

We propose a method to compare Marine Atmospheric Boundary Layer (MABL) height as determined from a GCM and corresponding information as retrieved from AVHRR satellite cloud analysis over oceanic mid-latitudes. We use the Holtzlag et al. (J. of Climate, 92) algorithm and the French Met GCM : ARPEGE. First, a cloud classification of AVHRR images is used to discriminate low level Strato-Cumuli, from which are derived cloud top temperature fields. Secondly, from the GCM output we determine the MABL altitude. The temperature correspondence between the two fields is worked out to evaluate the ability of the GCM to give realistic characteristics of the MABL. The method is applied to the SEMAPHORE experiment, held in sept-nov 1993 over the Azores basin (North. MidAtlantic) using ARPEGE re-analysed with the SEMAPHORE observations. The advantage to use a combined information of GCM with relatively good surface information but poor determination of the cloud layer and remote sensing with relatively accurate data is demonstrated.

**Monday 26 July PM****MI06/W/08-B1****Poster****1400-01****GROUND - BASED OBSERVATIONS OF O<sub>3</sub>, CO<sub>2</sub>, NO<sub>2</sub>, H<sub>2</sub>O AND VISIBLE SPECTRAL IRRADIANCE OVER EURASIA CENTRAL PART**

Vladimir N. Aref'ev, Nikita Ye. Kamenogradsky, Felix V. Kashin, Vladimir K. Semyonov, Valery P. Sinyakov, Konstantin K. VISHERATIN (all at Institute of Experimental Meteorology, SPA "Typhoon", Obninsk, Kaluga region, 82 Lenina Avenue, Russia, email: typhoon.meteo.ru)

Since 1979, regular carbon dioxide, water vapor, total ozone, nitrogen dioxide and visible spectral irradiance measurements have been made over central part of Eurasia (42.6 N, 76.7 E, 1650 m above sea level). The instrumentation and measurements procedures are outlined, and results from 1979-1998 are discussed. The daily as well as monthly averages have been examined to find the trends and other statistical characteristics. The trend values are 6.1% (carbon dioxide), 11% (water vapor), -4.0% (total ozone), 4.3% (nitrogen dioxide) and 4.7% (visible spectral irradiance) per decade. The spectral analysis of the observations has been used to obtain the periodical oscillations and the comparisons are made with variations of the solar activity and quasi-biennial oscillation (QBO).

**MI06/E/11-B1****Poster****1400-02****NOAA GROUND-BASED GPS WATER VAPOR DEMONSTRATION NETWORK**

Seth GUTMAN, Kirk Holub, and Nicole Radziwill, (all at NOAA Forecast Systems Laboratory, 325 Broadway R/E/FS3, Boulder, Colorado 80303 USA, Email: gutman@fsl.noaa.gov)

An overview and status report on the Forecast Systems Laboratory's efforts to develop a GPS water vapor demonstration network for NOAA is presented. This project was initiated to evaluate the engineering and scientific bases of ground-based GPS meteorology, as well as the utility of ground-based GPS observations for improved weather forecasting and climate monitoring. An increased number of observations are needed to assess the impact of these data on short-term weather forecast accuracy in a timely manner. As a consequence, FSL plans to expand the demonstration network to about 200 sites in the next 3-5 years. Some examples of data acquired by the network are presented.

**MI06/W/11-B1****Poster****1400-03****CHANNEL SELECTION FOR HIGH-RESOLUTION REMOTE SOUNDING INSTRUMENTS**

V.L.BENNETT, A.Dudhia, C.D.Rodgers (Atmospheric, Oceanic and Planetary Physics, Oxford University, Oxford OX1 3PU, UK, e-mail: vbennett@atm.ox.ac.uk, dudhia@atm.ox.ac.uk, rogers@atm.ox.ac.uk)

**MI06/W/18-B1****Poster****1400-04****HIGH RESOLUTION SOLAR SPECTROMETER FOR RETRIEVAL OF TROPOSPHERIC WATER VAPOR: FIRST RESULTS AND COMPARISONS**

Bernd SIERK (Institute of Geodesy and Photogrammetry, Swiss Federal Institute of Technology (ETH), ETH-Hoenggerberg 8093 Zurich email: bernd@geod.ethz.ch); Stefan V. Florek and Helmut Becker-Ross (Institute of Spectrochemistry and Applied Spectroscopy Rudower Chaussee 5, 12489 Berlin, Germany); Beat Bürki, Lars Kruse and Hans-Gert Kahle (Institute of Geodesy and Photogrammetry, Swiss Federal Institute of Technology (ETH), ETH-Hoenggerberg 8093 Zurich)

Based on previous studies of Differential Optical Absorption Spectroscopy (DOAS) using solar radiation, we developed a field spectrometer which is specially designed to measure water vapor in the troposphere. The Solar Atmospheric Monitoring Spectrometer (SAMOS) is capable of monitoring single absorption lines of H<sub>2</sub>O in the visible and near infrared spectral region (600-900 nm). The high resolution of the instrument allows accurate retrievals of columnar precipitable water. In addition we investigate the possibility to derive information on vertical humidity profiles. The distribution of molecules along the line of sight towards the Sun determines the shape as well as the total absorption of each individual line. Simulation studies show that profile information can be retrieved from the spectra, provided spectral line parameters are known and simple models of pressure and temperature profiles are assumed. In addition to the instrumental design we will present results from a field campaign carried out on Hawaii. The water vapor retrievals from SAMOS-data will be compared with those from radiosondes, microwave radiometers and Global Positioning System (GPS) receivers.

**MI06/C/MI01/W/24-B1** Poster **1400-05**

**CHARACTERISTICS OF THE VERTICAL AND HORIZONTAL DISTRIBUTION OF CLOUDS FROM LITE OBSERVATIONS**

Kathleen A. POWELL (NASA Langley Research Center, MS 475, Hampton, VA 23681 USA, email: k.a.powell@larc.nasa.gov) David M. Winker (NASA Langley Research Center, MS 475, Hampton, VA 23681 USA, email: d.m.winker@larc.nasa.gov)

Clouds play a major role in determining the Earth radiation budget. The feedbacks between clouds and the climate system are not well understood, however. This is due in part to the limitations of passive satellite sensors for observing thin and multilayer clouds and for measuring characteristics such as cloud height and the 3-D spatial organization of cloud. The Lidar In-space Technology Experiment (LITE) was flown on Space Shuttle mission STS-64 in September 1994. High vertical resolution, high sensitivity, the ability to observe multilayer clouds, and near-global coverage provide a unique dataset for the study of cloud distribution. As an example of the information available from LITE, preliminary results on cloud brokenness and on the characteristics of the overlap of multilayer clouds are presented. These results have implications for the design of satellite sensors for observing clouds and can be used to test the validity of cloud parameterizations in global climate models.

**MI06/W/05-B1** Poster **1400-06**

**CLOUD COVER OBSERVED SIMULTANEOUSLY FROM POLDER AND METEOSAT**

Genevieve SEZE(1), Claudine Vanbauce(2), Jean-Claude Buriez(2), Frederic Parol(2), Pierre Couvert(3); (1)Laboratoire de Meteorologie Dynamique du CNRS; (2)Laboratoire d'Optique Atmosphérique Université des Sciences de Lille; (3)Laboratoire de Modelisation du Climat

The POLDER instrument that was aboard the Japanese ADEOS platform between August 1996 and June 1997, is designed to the global observation of the polarization and directionality of the sunlight reflected by the earthatmosphere system. The cloud detection from POLDER takes advantage of the original capabilities of the instrument (spectral polarization and directionality). This cloud scheme uses 5 threshold tests based on pressure, reflectance, polarized reflectance, spectral variability. The results of the POLDER cloud detection scheme are compared to those of the LMD dynamical clustering method applied to visible and infrared METEOSAT data and local spatial variability of these two parameters. Special focus is given to the detection capabilities of the two kind of measurements for cloud situations such as small cumulus, thin cirrus. It is shown also the interest of combining the two kind of measurements to improve the identification and separation of cloud types such as low clouds, middle clouds, multi-layer clouds, thick cirrus, high convective clouds, is shown. Results of this comparison will give some insight on the behavior of the International Satellite Cloud Climatology (ISCCP) built mainly from visible and infrared measurements.

**MI06/W/20-B1** Poster **1400-07**

**THE NATURE OF ARCTIC CLOUD SYSTEMS**

D. HUDAK, B. Currie, R. Stewart, and V. Kezys ( Atmospheric Environment Service, 14780 Jane Street, King City, Ontario L7B 1A3 Canada. E-mail: David.Hudak@ec.gc.ca Telephone No: 905-833-3896,x242 Fax No: 905-833-0398)

The Mackenzie GEWEX Study (MAGS) represents the Canadian contribution to the international GEWEX effort. It involves a coordinated series of process, remote sensing, and modelling studies within the Mackenzie River Basin, a high latitude, cold region climate system. The McMaster University IPIX radar, a portable X-band, polarized, Doppler radar with high sensitivity, was deployed in the middle of the basin at Fort Simpson, NT, as part of the remote sensing studies on MAGS. The role of the IPIX radar was to take the necessary observations that will contribute to i) the quantification of the atmospheric component of the hydrological cycle; ii) the development of new observing techniques that combine surface and satellite based sensors; and iii) the improvement in regional climate models. To that end, a series of observational campaigns each lasting about three weeks took place during the fall, winter and spring of 1998/99.

Preliminary analyses included extended time height representations of radar intensity and vertical Doppler velocity for cloud systems that originated in both the Pacific and the Arctic Oceans from each of the three seasons. The descriptions of these cloud systems included the degree of layering, the cloud top height, and an assessment of their horizontal homogeneity and predominant precipitation formation mechanism. This information was combined with AVHRR data from the NOAA polar orbiting satellites to characterize the typical cloud systems. These findings were compared with objective analysis fields from the Canadian Meteorological Centre Global Environmental Multiscale model. An assessment of the ability of the model to replicate the essential features of these systems was then made.

An improved understanding of these cloud systems and the role they play in the global climate system is expected to be derived from this study.

**MI06/W/13-B1** Poster **1400-08**

**ANALYSIS OF ERRORS IN RETRIEVALS OF CLOUD OPTICAL THICKNESS AND DROPLET SIZE IN 3-D CLOUD FIELDS**

K-S KUO and R. M. Welch, Department of Atmospheric Science, University of Alabama in Huntsville

Cloud optical thickness and droplet size are retrieved from satellite imagery by assuming that plane-parallel approaches are valid. However, broken cloud fields produce reflected radiances which are significantly different from those produced by the plane-parallel assumption. The 3-D Picard Iterative method is used to simulate the radiances produced by broken cloud fields. Then cloud optical thickness' and droplet sizes are retrieved from these radiance values using the standard plane-parallel retrieval scheme. Resulting cloud optical thickness' are underestimated from the true values, while droplet sizes are overestimated. Results will be shown for a number of cloud field simulations in terms of cloud size, cloud cover and cloud aspect ratios. Even with these cloud property retrieval errors the important question is to what extent the resultant radiative fluxes from the cloud field are altered. To answer this question, radiative fluxes derived from the retrieved values are compared with those fluxes derived from the actual cloud properties. It is found that significant errors (in W/m<sup>2</sup>) occur in broken cloud fields.

**MI06/E/07-B1** Poster **1400-09**

**THE IMPACT OF ADVANCED TOVS DATA ON NUMERICAL WEATHER PREDICTION**

Caroline POULSEN, Andrew Collard, Paul Dibben, Steve English, Peter Rayer, Richard Renshaw, Andrew Smith, (all at UK Met. Office, London road Bracknell, RG12 2SZ)

Radiance observations measured by infrared and microwave radiometers on polar-orbiting satellites are used by assimilation schemes of numerical weather prediction models to provide a more accurate three-dimensional analysis of temperature and humidity in data sparse regions. In May 1998 the Advanced TOVS instrument was launched on NOAA-15 as a replacement for the TOVS system which had operated on a succession of NOAA satellites since 1978. The Advanced Microwave Sounding Unit is the main difference between Advanced TOVS and TOVS. It has twelve temperature sounding channels, three humidity sounding channels and five window channels which can also provide information on lower tropospheric water vapour. The main purpose of the Advanced Microwave Sounding Unit is to provide temperature and humidity information in cloudy areas. The observed brightness temperatures have been compared with brightness temperatures calculated using the numerical weather prediction model background (a short range forecast). This has shown we can model these channels very accurately, typically achieving standard deviations of the difference between observed and modelled brightness temperatures of 0.2-0.5K for mid tropospheric channels. The radiances have been assimilated into a 3DVAR assimilation scheme in the form of retrievals generated using a 1DVAR method. The direct assimilation of the radiances themselves has also been tested. The differences between observed and modelled brightness temperatures and the results of the assimilation experiments will be presented.

**MI06/W/27-B1** Poster **1400-11**

**NEURAL NETWORK BASED SATELLITE SCATTEROMETER FORWARD AND INVERSE MODELS**

Dan CORNFORD and Ian T Nabney (Neural Computing Research Group, Aston University, Aston Triangle, Birmingham B4 7ET, UK, Email: d.cornford@aston.ac.uk)

Satellite scatterometer forward sensor models, relating wind vectors over the ocean to the backscatter measurements, such as CMOD4, are generally based on highly parameterised statistical models. Even the physically based models, such as VIERS-1, are significantly calibrated from observational data. We propose an alternative, dual approach to the retrieval of scatterometer winds. We describe the development of a hybrid forward model, which combines the physical knowledge incorporated in CMOD4 with the flexibility of neural networks. A Bayesian framework is adopted to train the networks accounting for the 'input noise' on the Numerical Weather Prediction (NWP) model wind vectors and this significantly improves the model. However, inversion of forward models is generally computationally expensive. We show how neural network based methods can be used to create local, direct inverse models. We compare the results of local wind vector retrieval from our forward and direct inverse models with those from CMOD4. We then indicate an appropriate framework for the use of the local models for wind field retrieval and contrast the results of wind field retrieval with local wind vector retrieval.

**MI06/W/30-B1** Poster **1400-11**

**SATELLITE SCATTEROMETER MODEL FUNCTIONS**

P.A. BROWN, University of Washington, Seattle, Washington, 98105, USA, email rabrown@atmos.washington.edu

The model functions (correlations of geophysical parameters to backscatter coefficients) are examined. The wind, stress and surface pressure model functions are examined. The pressure model function is described, compared to ECMWF analyses, and used to infer basic information on the planetary boundary layer state.

**MI06/E/09-B1** Poster **1400-13**

**THE SURFACE AND ATMOSPHERIC RADIATION BUDGET: VERTICAL PROFILES OF FLUXES RETRIEVED BY CERES FOR JANUARY 1998**

Fred G. ROSE (A.S.&M., Suite 300, 1 Enterprise Parkway, Hampton VA 23666, Email: f.g.rose@larc.nasa.gov), Thomas P. Charlock (NASA Langley Research Center, Mail Stop 420, Hampton, Virginia 23681, USA, Email: t.p.charlock@larc.nasa.gov), and Jean-Jacques Morcrette (ECMWF, Shinfield Park, Reading, Berkshire, England, Email: pam@ecmwf.int)

The surface and atmospheric radiation budget (SARB) has been retrieved by applying a variational analysis which incorporates broadband CERES data at the top of the atmosphere (TOA), temperature and humidity profiles from ECMWF, cloud optical properties from the VIRS imager, and the Fu-Liou radiative transfer code. The analysis constrains (adjusts) surface temperature, humidity profile, aerosol optical depth, cloud top altitude, cloud fractional area, cloud optical depth, surface albedo, and the TOA broadband fluxes. The initial cloud properties were retrieved with Minnis' technique, which uses numerous VIRS pixels within the larger CERES footprints. Our broadband radiative transfer calculations are iterated at each footprint. The analysis to date covers January 1998 for 35N-35S SW and LW fluxes were retrieved and archived at the surface, 500 hPa, 200 hPa, 70 hPa, and TOA. The ensemble mean adjustments produced mean reductions of 0.192 K in skin temperature, 0.006 cm in precipitable water, 0.002 in surface albedo, 0.006 in aerosol optical depth, 0.821 in cloud optical depth, 1.527 K for cloud top temperature, and 0.01 in cloud fraction. The first results were biased. We are revising our algorithm to reduce the biases. One revision incorporates the CERES broadband LW and 8-12 micron window channels, making separate adjustments for upper and lower tropospheric humidity. Results with the revised algorithm will be shown at IUGG.

**MI06/W/06-B1** Poster **1400-14**

**VALIDATED SURFACE RADIATION INFERRED FROM METEOROLOGICAL SATELLITE DATA**

Franz H. BERGER (Dresden University of Technology, Institute of Hydrology and Meteorology, Piennstr. 9, D-01173 Tharandt, Germany, email: berger@forst.tu-dresden.de)

For episodes (with periods up to two months) within a few experiments in Europe, like BALTIX, RESMEDES, LITFASS and MAP, meteorological satellite data could be analysed. The analysis of NOAA-AVHRR and Meteosat data included a detailed cloud classification, the determination of cloud optical properties, and the computation of surface radiation. Concerning the surface radiation all radiation components could be inferred. The analysis of surface radiation as well as of cloud optical properties is based on an inverse remote sensing

technique, where intensive calculations of atmospheric radiative transfer could be carried out in advance. These calculations consider all relevant atmospheric (temperature and humidity profiles, aerosol content in the PBL) and geometrical (solar zenith angle, satellite viewing angle) conditions.

After the computation of surface radiation from remotely sensed data, different validation with ground based observations could be done. And this validation show a general slight underestimation of the inferred satellite radiation with respect to the ground based measurements. More detailed results (correlation, variances) will be given. Thus, diurnal variations of surface radiation for the experiment periods will be presented, which show the influence of individual clouds on the surface fluxes. A comparison with modelled surface radiation, carried out with the regional model REMO, will close this contribution.

**MI06/L/02-B1** Poster **1400-15**

**A STUDY OF RELATIONSHIP BETWEEN SATELLITE DERIVED CLOUD PROPERTIES AND PRECIPITATION.**

Muloshi, Department of Meteorology, P.O.Box 30200, Lusaka 10101, ZAMBIA, Telefax: (+260-1) 251889, E-mail: zmd@zamnet.zm

The satellite sub-system constitutes a part of the WWW Global Observing System. Information is received from near-polar orbiting and geostationary satellites. Current observations from these satellites provide information about the most important meteorological elements, such as cloud and wind fields, location of precipitation areas and their intensity and components of radiation balance just to mention a few. The information received from these satellites by interpreting images have been important to meteorologists and have proved to be of immense value to operational weather forecasting, agro-meteorological research and many other environment monitoring applications. At Zambia Meteorological Department, one of the application of the satellite information is in rainfall estimation by correlating Cold Cloud Duration (CCD) information at a given threshold temperature on daily or 10 days basis with observed rainfall measured using standard rain gauge. This is more useful in areas which are not accessible or the density of the standard rain gauge is very low. This paper presents a statistical analysis of the relationship between CCD values in hours and measured rainfall (mm) at 10 meteorological stations in Zambia. The data studied is for the three decades of November to April for a period of four years (1992 - 1996). The correlation method employed in this study revealed a significant positive value of  $r = 0.99$  for all the stations. The result seems to suggest that a strong relationship exists between the CCD images and rainfall. Least square regression shows that the increase in the amount of CCD values at a given temperature threshold corresponds to an increase in rainfall.

**MI06/W/03-B1** Poster **1400-16**

**PRINCIPAL COMPONENT ANALYSIS FOR RAINDROPS AND ITS APPLICATION TO THE REMOTE SENSING OF RAIN**

JONATHAN MEAGHER (MS 300-227, Jet Propulsion Lab, 4800 Oak Grove Drive, Pasadena, CA 91109-8099, USA, email: meagher@radar-sci.jpl.nasa.gov) Ziad Haddad (MS 300-227, Jet Propulsion Lab, 4800 Oak Grove Drive, Pasadena, CA 91109-8099, USA, email: zsh@titan.jpl.nasa.gov)

In the problem of inverting remote-sensing measurements of rain, current representations of the raindrop size distribution (DSD) suffer crucially from the expedient but unjustified and empirically ill-fitting assumption that the distribution has a known closed-form shape. Indeed, statistical tests for goodness of fit have repeatedly failed to support the assumption that the sampled drops are consistent with a Gamma or lognormal distribution. The Gamma and lognormal fits are especially bad when large drops occur, and in cases where the DSD exhibits peaks at two or more drop diameters. This produces biases in subsequent estimates of the rain. Yet fitting the DSD with a closed form expression does conveniently reduce the entire description of the rain to the knowledge of two or three parameters. One approach to obtain such a description without bias would be to discretize the range of drop diameters and use as DSD variables the numbers of drops in each discrete size bin. The drawback is that this requires a few dozen parameters to characterize a DSD. Grouping adjacent size bins into single variables is counter-productive since it drastically increases the resulting error. Using a "principal-component" analysis, we identify those four linear combinations of the equivalent-liquid-water in the drop size bin which embody the essential description of the DSD. Moreover, being eigenvectors of the covariance matrix, these four parameters are mutually uncorrelated. This characterization of DSDs using four parameters appears quite robust. The results obtained using a ground distrometer did not differ significantly from those obtained using airborne probes, in spite of the vastly different measurement uncertainties, implying that this description can be used for rain aloft and near the surface. Moreover, the horizontal autocorrelation shows that three of the four variables can be assumed constant on small spatial scales.

**MI06/E/16-B1** Poster **1400-17**

**THE EVOLUTION OF AVHRR-DERIVED TEMPERATURES OVER BOREAL LAKES FROM BREAKUP TO FREEZE-UP**

Normand Bussières (Climate Processes and Earth Observation Division, Climate Research Branch, Environment Canada, 4905 Dufferin St., Downsview, Ontario, Canada, M3H 5T4, Normand. email: Bussières@ec.gc.ca) Ian McPherson (Flight Research Laboratory, Institute for Aerospace Research, National Research Council Canada, Room 223, Building U-61, Ottawa, Ontario, Canada, K1A 0R6, email: Ian.Mcpherson@nrc.ca)

Thermal IR observations were extracted from NOAA AVHRR satellite data over the period from April 1st, 1994 to August 31st, 1994. These were collected in order to set up the lake temperature boundary conditions for a land surface model. The IR temperatures were calibrated and atmospherically adjusted for the intervening atmosphere. For each of these days, polar stereographic scenes of temperatures were generated for a 1000 km by 1000 km rectangular region extending from about 110°W, 60°N over the Northern part of the Canadian Province of Alberta to about 97°W, 50°N in Southern Manitoba. The average daytime variance of the daily AVHRR-based water surface temperature estimations under cloud-free conditions is 2 °C. Independent aircraft data confirms the validity of the AVHRR-based temperature estimates. There are 134 water bodies of area larger than 100 km<sup>2</sup>. The temperature cycle over these water bodies can give an accurate estimation of break-up date, which can serve to complete other types of data sources like passive microwave observations of the larger lakes.

**MI06/W/02-B1** Poster **1400-18**

**STUDY OF VERTICAL VELOCITIES WITH THE MU RADAR MULTIBEAM/INTERFEROMETRY OBSERVATIONS**

N.KAWANO, M. Yamamoto and S. Fukao (Radio Atmospheric Science Center, Kyoto University, Uji, Kyoto 611-0011, Japan, Email: kawano@kurasc.kyoto-u.ac.jp)

Atmospheric radar observations are useful for the wide height range and continuous observations. The Doppler technique is utilized as a standard technique. However, there are reports of possible errors of vertical velocities determined as Doppler velocities in a vertical beam if turbulent layers are tilted. It is also reported that such error in the vertical velocity could be corrected by measuring the tilt angle of turbulent layers with the interferometry technique. Based on some more data from the multibeam/interferometry observations with the MU radar, behavior of the vertical velocity fields and its relationship to such anisotropic scattering layers will be discussed.

Presiding Chairs: D. Rosenfeld (Hebrews University of Jerusalem); P. Bauer (German, Kolin, Germany)

**RAIN**

**MI06/W/10-B1** **1500**

**ESTIMATIONS FROM SYNERGY OF ACTIVE AND PASSIVE MICROWAVE SENSORS ONBOARD TRMM**

Peter Bauer German Aerospace Center, Linder Höhe, 51147 Köln, Germany phone: (+49) 2203 601 2995, fax: (+49) 2203 68309, email: peter.bauer@dlr.de

New rainfall retrieval was developed aiming at optimization of accuracy and computer efficiency considerations to be applied to the Tropical Rainfall Measuring Mission (TRMM) Microwave Imager (TMI) and the Precipitation Radar (PR) over oceans. The technique involves single sensor retrievals and their combination to provide the retrieval accuracy introduced by the PR on the narrow swath (220 km) and its transfer to the TMI-retrievals on the broad swath (760 km). For the PR-estimates the TRMM standard product 2A25, i.e., rainrate profiles, were used. The TMI-component is based on extensive, three-dimensional radiative transfer simulations through various cloud systems obtained from dynamical cloud models which form the database for the inversion procedure. The retrieval comprises (1) the deconvolution of the TMI 10.7 GHz channel to provide better surface resolution and signal dynamic range; (2) the inclusion of local estimates of surface conditions (SST, near-surface wind speed) and zenith angle; (3) the derivation of additional parameters such as effective sensing altitude where retrieval accuracy is maximized; (4) the non-linear calibration of TMI-by PR-estimates on a unified resolution across the narrow swath; (5) the calibration of TMI-estimates on the wide swath; (6) application to case studies as well as large data amounts allowing climatological analyses. The outline of the algorithm and its major features as well as some aspects of database generation will be presented. Various inversion principles such as multiple linear regressions, a neuronal network, and database search routines are intercompared. The algorithm performance is demonstrated by examples from TRMM data covering various meteorological situations and geographical regions. Major error sources seem to be introduced by the database rather than the retrieval procedure. Particle size distributions, ice microphysics, and inhomogeneous particles are candidates which require attention when better algorithm performance is sought.

**MI06/E/14-B1** **1520**

**A COMBINED SATELLITE INFRARED AND PASSIVE MICROWAVE TECHNIQUE FOR ESTIMATION OF SMALL SCALE RAINFALL OVER THE GLOBAL TROPICS AND SUBTROPICS**

MARTIN TODD (School of Geography, University of Oxford, Mansfield Road, Oxford, OX1 3TB, U.K, email: martin.todd@geog.ox.ac.uk) Dominic Kniveton (Department of Geography, University of Leicester, University Road, Leicester, UK, email: drk5@le.ac.uk)

The accurate estimation of rainfall at small spatial and temporal scales (0.5 degree or less/daily and below) presents problems for satellite based methods. Passive (PMW) and active microwave (rain radar) algorithms are able to provide accurate estimation of instantaneous rainrates, but the poor temporal sampling of low earth orbiting satellites makes them most suitable for estimation over longer periods of perhaps a month. In contrast, infrared (IR) satellite algorithms benefit from the high temporal sampling of geostationary satellites, but IR radiances from cloud tops have only a weak, indirect relationship with surface rainfall. Accordingly, many simple IR algorithms rely on the effects of scale averaging to improve accuracy. Whilst global satellite (and merged) precipitation products at monthly/2.5 degree resolution are now routinely available, there is an absence of rainfall information at smaller scales, over extended periods for the globe as a whole. There are numerous applications in climatology where accurate information of this kind would be invaluable. Only since 1996 have daily/1 degree satellite IR products using the Goes Precipitation Index been archived. Here we introduce a technique which combines the information content of both satellite IR and PMW data. Rainfall estimates are produced at the high temporal frequency of the IR data using rainfall information from the PMW data. The technique first uses coincident instantaneous PMW and IR observations over a 1 month period to calculate at each 0.5 degree grid cell (a) an optimum IR temperature threshold to identify rainfall and (b) the conditional rainrate. These variables are then applied to each hourly IR slot over the entire month period. Unlike existing IR algorithms therefore the IR threshold and rainrate parameters are spatially and temporally variable. The results of a validation exercise are presented.

**MI06/E/01-B1** **1610**

**CORRECTION OF RADAR SURFACE RAINFALL ESTIMATES FOR THE EFFECTS OF THE VERTICAL PROFILE OF REFLECTIVITY USING TYPICAL SHAPE FUNCTIONS**

Warren Gray and Michael Uddstrom (National Institute of Water and Atmosphere, PO Box 14 - 901, Wellington New Zealand, Email: w.gray@niwa.cri.nz)

As the distance from the radar increases, so does the height at which radar samples rainfall. Variations in the relationship between these observations aloft and the rain rate at the ground need to be accounted for if good estimates of surface rain rate are to be formulated. A hypothesis was formed that a few typical shapes can describe the variations in the vertical profile of reflectivity and that these shapes are useful in estimating the surface rain rate. An archive of radar volume scan information was formed from data interpolated on to 10 constant height levels at 250m intervals. The heights were chosen so that the melting layer always lay at height level 6. Five typical shape functions (TSF) classes were found in the vertical profile of reflectivity archive. Bayesian equations were formulated that related the observations aloft to the shape class. Linear equations were found which relate the observations aloft to surface reflectivity for each TSF class. The results showed that 62% of the dependent sample was



correctly classified into its TSF class. This approach increased the variation of the surface reflectivity explained by observations aloft from 59.5% to 77.4%. An assessment of the skill of the surface rainfall estimate was also produced.

**MI06/E/04-B1****1630****NEW METHODS FOR RETRIEVAL OF RAINFALL RATE WITH SSM/I DATA**

Daren LU, Haibing Sun, Jianchun Bian, Hongbin Chen, Jinli Liu, Mingzhen Duan, (Institute of Atmospheric Physics, Chinese Academy of Sciences, Beijing 100029, CHINA, e-mail: ludr@sun.ihep.ac.cn)

Space-borne microwave (MW) remote sensing of rainfall distribution with multi-channel radiometers has been proved as a powerful tool in past decade, in particular with DMSP's SSM/I and recently TRMM data. Similar instruments but with different channel combinations, such as ADEOS-II/AMSR are being developed. Although there have been several schemes used for research and operational application, improvement of retrieval accuracy is still an important subject. As part of a NASDA project for ADEOS-II/AMSR retrieval algorithm development and Chinese National High-tech R&D program for space Technology, we proposed two kinds of retrieval algorithms for rainfall rate over ocean and land with SSM/I data. The first kind of algorithm is based on probability pairing method, in which three different retrieval rain indices composed with different combination of SSM/I's channels are used as pairing indices with surface rainfall rate data provided by NASDA, Japan. Three different empirical rainfall rate- rain index relationship are produced. The second kind of algorithm is based on the method of self Organization feature Mapping (SOM), a kind of artificial neural network (ANN). SSM/I data and co-located surface rainfall data are put into SOM and clustering procedure is self-trained. After training, 154 clustering centers are formed and for each cluster a regressive relationship between retrieved rainfall rate and SSM/I data is established. In this paper, these two kinds of algorithm are briefly reviewed with their developments and validation. Comparison of these retrieved methods and with other published methods are discussed.

**MI06/E/17-B1****1650****TRMM PRECIPITATION RADAR (PR) GROUND VALIDATION USING GROUND BASED DATA FROM JAPAN**

Riko OKI, Kinji Furukawa and Misako Kachi (Earth Observation Research Center (EORC), National Space Development Agency of Japan (NASDA), 1-9-9 Roppongi Minato-ku, Tokyo 106-0032, Japan, email: riko@eorc.nasda.go.jp)

The Precipitation Radar (PR) on the Tropical Rainfall Measuring Mission (TRMM) satellite is the first space-borne precipitation radar that can observe the three-dimensional structure of rainfall over the tropics. Ground validation of the PR using ground based data from Japan and its results are presented in this paper.

In the Ishigaki-Miyako Campaign Experiment for TRMM (IMCET), several simultaneous observations were conducted by the PR and Japan Meteorological Agency (JMA)'s ground-based radars. Horizontal and vertical patterns of radar reflectivities obtained by those different radars agreed well. In addition to the radar reflectivity, estimated rain rates are compared with rain rates estimated from ground-based radar and rain gauges. Rain rates estimated by the standard algorithm (2A25) appear to be reasonable in spatial patterns, compared with rain rates obtained from JMA's Radar-AMeDAS and AMeDAS rain gauges. To compare AMeDAS rain gauges and 2A25 rain rates, both data were averaged in 0.5 degree by 0.5 degree boxes respectively. A seasonal dependency of rain intensity estimated by 2A25 is found. That is, in winter PR rain rates are higher than rain gauges, however the 2A25 algorithm seems to estimate rain rate lower than rain gauges especially in summer. In winter, there is a possibility that estimated rain rates were affected by bright bands. Also a comparison of rain amount in climatological sense will be reported.

**MI06/W/04-B1****1710****A MICROPHYSICALLY BASED IR NIGHTTIME METHOD TO DELINEATE RAINFALL IN CLOUDS WITH TOPS WARMER THAN 245K**

ITAMAR M. LENSKEY, Atmospheric Science, The Hebrew University, Jerusalem, Israel. email: itamarl@cc.huji.ac.il ; Daniel Rosenfeld, Atmospheric Science, The Hebrew University, Jerusalem, Israel. email: daniel@vms.huji.ac.il

The Tropical Rainfall Measuring Mission (TRMM) data have been used for developing and validating a microphysically based method to delineate precipitating clouds with tops that are warmer than the temperature at which much ice and thus precipitation always develops in optically thick clouds. That temperature threshold is 245K. Optically thick clouds with colder tops have been identified as precipitating by the currently available VIS/IR methods. The existence or lack of precipitation processes near the top of the clouds is inferred from the 3.7 micron emissivity of their tops. Clouds with small particles have low emissivity. Such clouds also typically are devoid of precipitation forming processes. An algorithm, based on the 3.7, 10.8 and 12.0 micron channels of the TRMM VIRS (Visible IR Scanner) is using that principle to delineate the precipitating clouds.

That algorithm was developed as part of the package for the Global Imager (GLI) onboard the ADEOS-2 satellite, for NASDA. Therefore, the algorithm is named hereafter the "GLI" algorithm. Results of the GLI rain algorithm were validated against the actual measurements of precipitation by the TRMM precipitation radar (PR). The performance was compared to that of the TRMM microwave imager (TMI) rainfall delineation.

The GLI algorithm detected significant amount of precipitation that the TMI missed, especially over land in the mid-latitude, but not exclusively. The GLI algorithm correctly detected non-precipitating microphysically continental clouds over sea, which the TMI falsely identified as precipitating. This was found often over the Mediterranean Sea. The added microphysical information from visible/IR sensors, in both day and nighttime, is potentially valuable for cloud radiative and precipitation parameterization, and for improvement of rainfall measurements from space.

**Tuesday 27 July AM**

Presiding Chair: D.R. Hudak, Environment Canada, Ontario, Canada  
R.J. Hogan, University of Reading, UK

**CLOUDS****MI06/W/23-B2****0930****COMPARISON OF ECMWF MODEL CLOUD COVER WITH RADAR DERIVED VALUES**

Robin Hogan (Department of Meteorology, University of Reading, UK; email: R.J.Hogan@reading.ac.uk), Christian Jakob (ECMWF, Reading, UK), Anthony Illingworth (Department of Meteorology, University of Reading, UK)

Clouds represent one of the major uncertainties in climate modelling. The limited resolution available to global climate models means that clouds cannot be resolved explicitly and it is necessary for some estimate of the sub-gridscale fluctuation of cloudiness to be included in radiative transfer calculations. However there is little physical basis behind the diagnosis of cloud cover from prognostic model variables, and errors in model radiative fluxes are often blamed on poor model cloud cover. It is therefore vital for climate simulations that this parameter can be calculated accurately. Previous attempts to validate the cloud cover in the ECMWF model have used AVHRR data to estimate the total cloud cover for a model gridbox through the whole depth of the atmosphere, but there is clearly a need for vertically-resolved observations of cloud cover to be used to perform the validation at each model level. In this study, ECMWF cloud cover is compared with that derived by three active instruments located at Chilbolton, England, for a month-long period. Throughout most of the depth of the atmosphere one of two cloud radars (operating at 35 and 94 GHz) is used, but in the lowest 500 metres where ground clutter and leakage from the transmit pulse can be a problem, we use data from a lidar ceilometer.

**MI06/W/28-B2****0950****PROFILING CLOUD LIQUID WATER BY COMBINATION OF A CLOUD RADAR AND A PASSIVE MICROWAVE RADIOMETER**

Ulrich LOEHNERT (Meteorologisches Institut der Universitaet Bonn, Auf dem Huegel 20, 53121 Bonn, Germany, Email: uloe@uni-bonn.de) Andreas Macke (Institut fuer Maritime Meteorologie Kiel, Duesternbrooker Weg 20, 24105 Kiel, Germany, Email: amacke@ifm.uni-kiel.de)

To derive cloud liquid water profiles (LWC) a combination of a cloud radar and a passive microwave radiometer is proposed. A cloud radar can measure radar reflectivities (Z) with an accuracy of -30 dBZ in 10 km distance, but conventional algorithms for LWC based on Z alone show errors of up to an order of one magnitude. Collocated measurements of integrated cloud liquid water (ILW) (10 - 20 % relative accuracy) with a dual-channel microwave radiometer can, together with a cloud radar, provide a constrained estimate of the LWC profile. Previous studies of the Z-LWC relation have used either fixed or statistically varied drop size distributions. In this work a 1.5-dimensional dynamic cloud model is used to investigate the dynamical dependencies of the Z-LWC relationship. The spectral model, which calculates drop size spectra prognostically, allows a detailed study of the statistics of the Z-LWC relationship concerning height and time, which can prove valuable in algorithm development. Difficulties arise in mixed-phase clouds and precipitation, where scattering and attenuation become difficult to handle. First collocated measurements of the 95 GHz polarimetric cloud radar MIRACLE (GKSS, Geesthacht, Germany) and corresponding values of ILW of the dual-wavelength (20/30 GHz) RESCOM radiometer (Institute for Marine Sciences Kiel, Germany), which are currently being recorded, will be shown.

**MI06/W/14-B2****1010****LIDAR/RADAR REMOTE SENSING OF CLOUD PARTICLE EFFECTIVE RADIUS DURING CLARA**

DAVID P. DONOVAN, A.C.A.P. Van Lammeren, H.R. Bloemink, A. Feijt (Royal Netherlands Meteorological Institute (KNMI), Postbus 201, 3730 AE, De Bilt, The Netherlands)

During 1996 three intensive cloud measurement campaigns were carried out in the Netherlands. The CLARA (CLouds And RAdiation) program was headed by the Royal Netherlands Meteorological Institute (KNMI) and involved participation from several other Dutch institutions and universities. During CLARA, cloud measurements were obtained using a ground-based 3 GHz radar system, several lidar systems, microwave and IR radiometers as well as an aircraft mounted FSSP particle size probe. The goal of the CLARA program was mainly to investigate the radiative effects of the clouds using the data obtained from the various diverse instruments.

It is well known that the scattering properties per unit mass for cloud particles can be well represented in terms of their effective radius. Since lidars and radars operate at very different frequencies they are capable of providing complementary information which may be used to infer the effective radius of the sampled cloud particle size distribution. In this presentation, a new procedure for determining effective radii profiles using a combination of microwave radar and near-infrared lidar measurements is outlined. Several examples of the application of this procedure to cloud measurements made during the CLARA campaigns are presented and compared to the results of in-situ FSSP-100 airborne particle probes.

**MI06/W/16-B2****1030****REMOTE SENSING AND AIRCRAFT OBSERVATIONS OF PHASE AND SIZE OF PARTICLES DURING FIRE-ACE**

I.GULTEPE, and G. A. Isaac (both at Atmospheric Environment Service, Cloud Physics Res. Div., Downsview, Ontario, M3H 5T4, Canada, e-mail: ismail.gultepe@ec.gc.ca and george.isaac@ec.gc.ca); R. Hoff, and K. Strawbridge (both at Atmospheric Environment Service, Air Quality Proc. Res. Div., Downsview, Ontario, M3H 5T4, Canada, e-mail: ray.hoff@ec.gc.ca and kevin.strawbridge@ec.gc.ca); D. L. Mitchell (Desert Research Institute, Reno, NV 89506, USA, e-mail: mitch@dri.edu); A.Macke (Institut fuer Meereskunde, Abt. Maritime Meteorologie, Duesternbrooker, Weg 20, 24105, Kiel, Germany, e-mail: amacke@ifm.uni-kiel.de)

In this study, observations collected during the First International Satellite Cloud Climatology Project (ISCCP) Regional Experiment - Arctic Cloud Experiment (FIRE-ACE) which took place over the Arctic Ocean during April 1998 were utilized. Measurements from aircraft microphysical probes, an Arizona radiometer, a LANDSAT simulator, a simultaneous upward/downward lidar with depolarization capability, and LANDSAT were used to understand phase separation, and particle size estimation in the Arctic clouds. Five individual cases, representing different microphysical characteristics, were analyzed. Each case had either mixed phase or one phase. Cases of liquid phase were mostly observed when aircraft were over the leads or polynya. Aircraft microphysical data obtained by the hot-wire probes, Rosemount icing detector, the Particle Measuring Systems (PMS) forward scattering spectrometer probe (FSSP) and 2 dimensional cloud (2D-C) probes indicated water and ice regions. Using information from different channels e.g. near infrared (1.6 and 2.21) and visible channel (0.83) in the various remote sensing platforms, particle size and phase of the particles were obtained. Near-infrared channels have lower reflectance compared to those of visible channels. Arizona radiometer, LANDSAT simulator, and lidar observations showed the open water surfaces that were likely the source of warm and moist air. Results showed that in-situ cloud microphysical information obtained using various platforms were comparable with those of the remote sensing platforms. Theoretical calculations using a Monte-Carlo radiative transfer model will also be made for further validation of the observations, and summary of the results related to climate change studies will be given.

Remote Sensing of the Atmosphere for Weather Forecasting and Climate Applications, IAMAS Inter-Commission Symposia, IUGG99 General Assembly in Birmingham, UK, 18-30 July 1999

MI06/W/26-B2

1110

## AEROSOL AND CLOUD PROCESS STUDIES USING AIRBORNE LIDAR OBSERVATIONS OF STRATOSPHERIC CLOUDS - NEW TECHNIQUES AND FUTURE APPLICATIONS

KENNETH S. CARSLAW (Environment Centre, University of Leeds, Leeds LS2 9JT, UK, E-mail: carslaw@lec.leeds.ac.uk), Th. Peter, A. Tsias, T. Trautmann, B.P. Luo (Max Planck Institute for Chemistry, Mainz, Germany) M. Wirth, W. Renger (Deutsche Forschungsanstalt für Luft- und Raumfahrt, Oberpfaffenhofen, Germany)

Lidar observations can yield detailed optical information, such as backscatter ratio and depolarisation properties, of atmospheric aerosols and clouds. However, it is often difficult to convert such measurements into microphysical information, such as particle sizes, which are needed to validate atmospheric models.

We describe a technique for probing polar stratospheric clouds with dual wavelength airborne depolarisation lidar, combined with optical and microphysical model simulations, which can yield detailed information on the evolution of individual cloud elements. The technique has so far been restricted to stratospheric aerosols and clouds, but could also be applied to thin cirrus. The technique is based on quasi-Lagrangian observations of small scale clouds (i.e. with the aircraft heading parallel with the wind at the level of the cloud). Microphysical properties of the clouds, such as particle sizes, aerosol growth and ice nucleation conditions, are then derived by combining an optical simulation of the lidar signal with a microphysical model in an iterative procedure.

We have so far applied this new technique to interpret measurements made with the DLR OLEX lidar on board Transall and Falcon aircraft during two Arctic ozone and aerosol campaigns. Our interpretation of lidar data has yielded unprecedented information on polar stratospheric cloud properties. Important results include a determination of ice particle number densities in mother-of-pearl clouds and the first determination of the supercooled required to form such clouds.

MI06/W/25-B2

1130

## MULTIWAVELENGTH LIDAR OBSERVATIONS OF THIN CLOUDS AND AEROSOLS

SATYANARAYANA. M., Ramakrishna Rao, D. Mohankumar., S.V., Presennakumar. B., Sreelatha. P. and Veerabuthiran. S. (Atmospheric Lidars Branch, Space Physics Laboratory, Vikram Sarabhai Space Centre, Trivandrum - 695 022, India, email: spl\_vssc@vssc.org)

This paper describes a pulsed monostatic high resolution Multiwavelength Lidar (MWL) system designed and developed for use in detailed scientific studies on clouds, atmospheric aerosols, ozone and temperature variations (upto 70 km) at a tropical station Trivandrum (Geog. Lat. - 8.6°N, Geog. Long. - 77°E) India. Nd:YAG laser is the main transmitting source operating at wavelengths 1064 nm, 532 nm, 355 nm and 266 nm with a pulse energy of about 600 mJ at 532 nm. The backscattered signals are received using a 500 m Cassegrain telescope. To obtain usable data upto 70-80 km, both the analog and photon counting modes of data acquisition have been incorporated in the system. Further, the PC based Data Acquisition System (DAS) has a two step digitization scheme with 8 bit resolution and a maximum sampling rate of 100 MSPS in the analog mode. The MWL system can also be used in the polarization lidar mode by using suitable polarizers in the receiving system. Scientific observations on the simultaneous measurement on aerosols and thin clouds made for about 15 days spread over 3 months using the above system will be described. A new lidar inversion technique developed for obtaining extinction coefficient of both aerosols and clouds will be presented. Preliminary results on the characteristics of clouds and aerosols at this tropical coastal station are presented.

MI06/E/10-B2

1150

## USE OF DIFFERENT PHASE FUNCTIONS TO RETRIEVE THE POLDER DIRECTIONAL OPTICAL THICKNESS

M. DOUTRIAUX-BOUCHER, J.-C. Buriez, L. C.-Labonnote, G. Brogniez (Laboratoire d'Optique Atmosphérique, Université des Sciences et Technologies de Lille, Villeneuve d'Ascq, France, e-mail: mdoutri@loa.univ-lille1.fr) A. J. Baran (UK Meteorological Office, Bracknell, Berkshire, England)

POLDER uses an original concept to observe clouds and their properties. Angular reflectance measurements obtained from the POLDER instrument are used to retrieve, for each scene, the cloud visible optical thickness. POLDER also has a capability to distinguish between liquid and ice clouds from polarisation measurements. The algorithm presently used to retrieve cloud properties can be improved. Especially, in the present version of the algorithm, cloud optical thickness is calculated assuming the cloud is composed of 10 micrometer droplets, without distinction between liquid and ice clouds. However, it is well known that the droplet size distribution may vary and that the single scattering properties of ice crystals differ substantially from those of liquid droplets. We test here the scattering phase functions of several cloud particle models, such as 5 micrometer cloud droplets, ice polycrystals, hexagonal monocrystals as well as a synthesised phase function fitted from aircraft observations, in order to retrieve ice cloud properties using the POLDER algorithm. We show that the directional cloud optical thickness measured by POLDER is very dependent on the cloud particle models chosen for the inversion.

MI06/W/31-B2

1210

## HIGH RESOLUTION INFRARED SPECTRA OF ICE CLOUDS

R. J. Bantges, J. E. Russell, J. D. Haigh and C. Naud (All at Space & Atmospheric Physics, Blackett Laboratory, Imperial College, London SW7 2BZ, UK, email: r.bantges@ic.ac.uk)

High spectral resolution top of atmosphere brightness temperatures have been simulated in the infrared (600-2500cm<sup>-1</sup>) for an absorbing, emitting, multiple-scattering cirrus cloud placed in a realistic atmosphere. Single scattering properties of the ice crystals were calculated using Mie theory for spheres, ray-tracing optics for hexagonal columns and T-matrix method for spheroids. The sensitivity to a variety of assumptions concerning the cirrus cloud properties, (ice crystal sizes, shapes and size distributions) has been studied. Comparisons between simulations and data obtained from the High resolution Interferometer Sounder have been made. A statistical method has been applied to the simulated spectra to highlight wavelength combinations which may be used to exploit the retrieval of cirrus cloud properties from data anticipated from the next generation of spaceborne high resolution spectrometers, such as the Infrared Atmospheric Sounding Interferometer, due for launch on METOP-I in 2003.

MI06/W/19-B2

1230

## OBSERVED EFFECTS OF CLOUD DROPLET CONCENTRATION ON ALBEDO FOR LOW-LEVEL CLOUDS USING SATELLITE DATA

Qingyuan Han(1), William B. Rossow(2), Joyce Chou(1) and R. M. Welch(1) (1)Department of Atmospheric Science, University of Alabama in Huntsville (2)NASA Goddard Institute for Space Studies, New York, NY

This study presents retrieved effects of enhanced cloud droplet concentration on cloud albedo for low-level clouds on a near-global scale using ISCCP data. A new parameter, column cloud susceptibility, is introduced so that no assumptions of constant liquid water content and cloud geometrical thickness are required in the retrieval. This greatly reduces the uncertainties caused by these approximations. The results show that the cloud albedo sensitivity to the percentage change of cloud droplet concentration is more than two times larger than predicted by model calculations based on the assumption of constant liquid water path. Regions close to and within most continents are already saturated, so that cloud albedo is insensitive to cloud droplet changes. The derived relationships such as column susceptibility and column droplet concentration, column susceptibility and cloud albedo, and the distribution of column susceptibility can be used as a basis for model studies and guidance for selection of future field campaigns.

Tuesday 27 July PM

POSTER VIEWING

1400-1500

Presiding Chair: W.L. Smith (NASA Langley Research Centre, USA)

RADIATION

MI06/W/12-B2

1500

## A STUDY OF THE DIURNAL CYCLE OF OLR WITH IMPLICATIONS TO ERBE AND CERES ANALYSES

ROBERT G. ELLINGSON, and Mamadou Ba (Department of Meteorology, University of Maryland, College Park, MD 20742, email: bobe@atmos.umd.edu)

A multi-spectral outgoing longwave radiation (OLR) estimation technique is being applied to GOES sounder data to study the diurnal cycle of OLR. Currently, all satellite-based OLR estimation techniques require the use of models of the diurnal cycle in order to estimate time-averaged OLR from any scene. In this study we use July 1998 hourly GOES sounder radiance observations with the Ellingson et al. (1994) multi-spectral OLR estimation technique to determine the instantaneous, daily- and monthly- averaged OLR from 100 square km scenes over North America and the adjacent Gulf of Mexico. The instantaneous data are compared with collocated data from the TRMM/CERES and NOAA-14 HIRS to establish the instantaneous accuracy of the multi-spectral estimation techniques for homogeneous scenes. The time-averaged data are used to estimate the accuracy of the ERBE/CERES and HIRS diurnal cycle models as applied to daily- and monthly- averaged products at different spatial resolutions. The presentation will concentrate on the effects of the uncertainties in the diurnal models on monthly-average OLR products at different spatial resolutions.

MI06/E/02-B2

1520

## OUTGOING LONGWAVE RADIATION AND CLOUD RADIATIVE FORCING OF THE TIBETAN PLATEAU

WENYING SU, Jietai Mao, Fei Ji, Dept of Geophysics, Peking University, LSSR, Beijing, 100871

In this paper two years' GMS5 satellite data are analyzed to study the monthly mean outgoing longwave radiation (OLR) and the cloud radiative forcing (CRF) of the Tibetan Plateau. A method was developed to compute the OLR by using radiative transfer model DISORT together with the radiosonde profile of the Tibetan Plateau. Since the location of the Tibetan Plateau is nearly out of the effective observational range of the GMS5 satellite, the regression results of GMS5's split-window channels and the water-vapor channel are corrected by using simultaneous retrieved results from TOVS. The correlation coefficient between them is 0.8426. During winter season the OLR distribution exhibits low value over the Tibetan Plateau but high value for areas off the Tibetan Plateau and during summer season the OLR of the southern part is smaller than that of the northern part. The temporal resolution of GMS5 data which is one hour and can help us to study the diurnal variations of OLR. The diurnal variations of OLR are affected by diurnal cycles of cloud amount and surface temperature. The relief of the Tibetan Plateau is very high and the radiative heating is intense after sunrise, so the OLR is much influenced by the surface and reaches maximum soon after sunrise. But for the emergence time of minimum OLR it is varied. The monthly mean clear-sky components of OLR and albedo are obtained from the ISCCP cloud detection algorithm. The CRF over the Tibetan Plateau is negative most of the time which means the CRF is dominated by cooling effects and the distribution pattern is mainly determined by the shortwave CRF component. While the CRF to the southern and the northern of the Tibetan Plateau is different, it shows obvious annual variations which demonstrates heating effects in summer-autumn season and cooling effects in winter-spring season.

Presiding Chair: D.C. Jones (UK Met Office, Bracknell)

DATA ASSIMILATION

MI06/W/32-B2

1610

## NEURAL NETWORKS AS A GENERIC TOOL FOR RETRIEVAL ALGORITHM DEVELOPMENT AND DIRECT ASSIMILATION

Vladimir KRASNOPOLSKY (EMC/NCEP/NOAA, 5200 Auth Rd., Camp Springs, MD 20746, USA, Email: kvladimir@ncep.noaa.gov)

Retrievals (geophysical parameters derived from the remote sensing satellite measurements) are used by operational meteorology, for assimilation into atmospheric and oceanic models, etc. Two different ways of producing retrievals from satellite remote sensing data are discussed. Variational retrievals (direct assimilation) use data assimilation systems of atmospheric or oceanic models to produce fields of retrieved geophysical parameters. Forward models (FM) which convert geophysical parameters into satellite measurements are required for variational retrievals.

Traditional retrievals use retrieval algorithms, which approximate the transfer functions (TF) of various satellite instruments, to convert satellite data into geophysical parameters. TFs can be estimated theoretically or/and empirically from observed or simulated data. Direct assimilation requires simple and fast FMs, whereas existing FMs are often too complex and slow. Because

both FM and TF can be considered as continuous mappings, and neural networks (NNs) are well suited to approximate continuous mappings, they can provide accurate mathematical models for a broad class of FMs and TFs. NN FMs are simple and fast, they are well suited for using in direct assimilation. NNs can also be used for accelerating existing FMs. A NN tutorial and approach to solving the forward and retrieval problems in satellite remote sensing are presented. NN are also well suited for multi-parameter retrievals, which advantages vs. single-parameter retrievals are discussed.

Recently developed NN SSM/I retrieval algorithm, which retrieves wind speed, W, columnar water vapor, V, columnar liquid water, L, and SST, using only satellite data, and NN SSM/I FM, which generates SSM/I brightness temperatures given W, V, L, and SST, are used for illustration. New NN TF and FM are compared with physically based and other empirical TFs and FMs.

#### MI06/E/08-B2 1630

##### A ONE DIMENSIONAL VARIATIONAL SCHEME FOR THE SIMULTANEOUS RETRIEVAL OF TEMPERATURE AND HUMIDITY INFORMATION FROM GPS RADIO OCCULTATION REFRACTIVITY PROFILES.

S.B.HEALY, Numerical Weather Prediction, Meteorological Office, Bracknell, Berkshire, United Kingdom, RG12 2SZ.

A one dimensional variational (1dvar) scheme for the simultaneous retrieval of temperature and humidity information from GPS radio occultation (RO) refractivity profiles will be outlined. The method combines information contained in the measurements with a priori (or background) data in statistically optimal way, in order to find the most probable atmospheric state. It will be demonstrated, using both simulated and real measurement data, that the "water vapour ambiguity" inherent in more conventional RO inversion techniques is resolved with this approach. Comparisons with alternative "sub-optimal" water vapour retrieval methods will be presented. Furthermore, it will be shown that the measurements can also provide significant surface pressure information.

#### MI06/E/12-B2 1650

##### ASSIMILATION OF SATELLITE DATA AND OBJECTIVE ANALYSIS

Willy S Goma, Zambia Meteorological Department, P.o Box 310095, Lusaka 15301, Zambia. Fax: (260)-1-251889 E-mail: zmd@zamnet.zm

Although Zambia lies entirely within the tropics, its weather is influenced to a large extent by the migratory synoptic systems of the southern mid-latitude (Mumba et al., 1984). During the wet season the main weather system responsible for rainfall occurrence in Zambia as a whole is the Inter-tropical Convergence Zone. In this regard Forecasting had continued in the past to be a problem in Zambia especially when it came to forecasting climatic anomalies e.g drought, floods and weather associated with synoptic features such as Angolan Low and easterly waves. Since most of the practical forecasting was mostly subjective, little progress had occurred. This was due to lack of upper air data from Zambia. As such we were relying on upper air data from our neighbouring countries. Secondly, it was due to lack of computing facilities. However, since then automation has been introduced in the department. The main weather systems considered in this discussion are the Inter-tropical Convergence Zone (ITCZ) and frontal systems in the Atlantic and the Indian Oceans. The satellite images and the corresponding surface charts have been examined for similarities in position of the above mentioned weather systems. The objective of this paper is to examine satellite images and try to incorporate the inherent details into charts that have been objectively analysed and these charts may be either (a) the ECMF forecast data or (b) the real time surface chart. In the case of ECMF products it is important to find out if a link exists between the forecast position of the synoptic systems and that of the satellite image together with the actual real time surface charts depicted at a given time.

#### MI06/W/01-B2 1710

##### ASSIMILATING SATELLITE MEASUREMENTS OF CLOUD COVER IN THE REGIONAL ATMOSPHERIC MODEL SYSTEM (RAMS)

ISMAIL YUCEL, W. James Shuttleworth, and James Toth (all at Department of Hydrology and Water Resources, University of Arizona, Tucson, 85721, AZ, USA, Email: yucel@hwr.arizona.edu)

The goal of this study is to provide an improved, high-resolution regional diagnosis of three of the important controls on the land surface energy and water balance, namely the downward shortwave and downward longwave surface radiation fluxes, and precipitation. Cloud cover is a key parameter linking and controlling these three terms. An automatic procedure was developed to derive high resolution (4km X 4km) fields of fractional cloud cover from visible band, (GOES series) geostationary satellite data using a novel tracking procedure to determine the clear-sky composite image. In our initial data assimilation studies, the surface shortwave radiation fluxes calculated by RAMS were simply replaced by the equivalent estimated values obtained by applying this high-resolution satellite-derived cloud cover in the University of Maryland (UMD) GEWEX/SRB Model. However, the cloud cover simulated in RAMS remained unchanged and this led to inconsistencies in areas modeled by RAMS as being cloud-free. Specifically, the modeled downward longwave fluxes retain their relatively low, clear-sky values rather than assuming higher values appropriate to cloud covered areas. In semi-arid areas such as Southern Arizona--the area used in this study--the difference in longwave radiation between cloud-free and cloud-covered areas can exceed 100 watts per square meter. A further important inconsistency is that RAMS can generate precipitation where the sky is clear. It was recognized that the UMD GEWEX/SRB Model and RAMS both use essentially identical descriptions of atmospheric radiative transfer. To diagnose shortwave radiation, both models use a multidimensional lookup table which is precalculated for fixed intervals of cloud optical depth, solar zenith angle, spectral band, total ozone and water vapor absorption, and both models assume the same relationship between optical depth and vertically integrated cloud water/ice. Recognizing these similarities, our research then focused on exploring the feasibility of directly assimilating cloud cover into RAMS by converting the measured fractional cloud cover (via cloud optical depth) into vertically integrated cloud water/ice. The potential advantages of this approach are that, not only is the surface solar radiation field better estimated, but RAMS may also be better able to diagnose the true spatial pattern of longwave radiation and precipitation. However, the procedure is complicated by the need realistically to distribute the cloud water/ice within the vertical profile for each modeled grid square. This paper describes our progress towards directly assimilating satellite-derived cloud cover into RAMS and validating the model-calculated surface fields against field data.

#### MI06/E/15-B2 1730

##### EXPERIMENTS ON THE ASSIMILATION OF TROPICAL CONVECTIVE RAINFALL ESTIMATES IN THE UKMO GLOBAL FORECAST MODEL

MARK RINGER (U.K. Met. Office, Bracknell RG12 2SZ, U.K.)

Results are presented from a set of experiments which aim to test the impact of assimilating satellite-derived estimates of tropical convective rainfall in the U.K. Met. Office's global numerical weather prediction model. The rainfall estimates are derived from infrared brightness temperatures using three different methods. The data are assimilated using a latent heat nudging method currently used in the UKMO's operational mesoscale model. Latent heating profiles are calculated by considering the condensational heating within the model physics step. Increments to the potential temperature are then derived within the assimilation scheme, based on a scaling of the profiles by the ratio of the observed and model first-guess rainfall rates. The aim is to cause the model to adjust so that the diagnosed rainfall rate agrees more closely with the observations. The practical considerations involved in applying this technique (e.g. the optimal spatial resolution of the observations) are briefly discussed. The impacts of assimilating the rainfall data on the model analyses and forecasts are then examined. Independent validation data sets from SSM/I, CERES and TRMM are used for this purpose. Particular attention is focussed on the location of rainfall events, the sensitivity of the technique to the choice of the rainfall estimation method and the effects on model spin-up time. A brief comparison with other assimilation experiments currently being undertaken at the UKMO is presented.

MI11

Friday 30 July

#### NON-LINEAR DYNAMICS AND CLIMATE PREDICTION

Location: Mechanical Engineering G29 LT

Friday 30 July AM

Presiding Chair: S. Lovejoy, (McGill University, Montreal, Quebec)

#### ATMOSPHERIC AND OCEANIC STUDIES

#### MI11/W/01-B5 Invited 0830

##### SIGNATURE OF CLIMATE CHANGE IN ATMOSPHERIC CIRCULATION-REGIME FREQUENCIES

T.N.PALMER (ECMWF, Reading, UK), S.Corti and F. Molteni (CINECA, Bologna, Italy)  
E-mail: tim.palmer@ecmwf.int

Based on analyses of mid-tropospheric geopotential data, evidence is presented that trends in northern hemisphere climate over recent decades can be explained by changes in the frequency of preferred nonlinear naturally-occurring circulation regimes. These results support a nonlinear paradigm that the climatic response to anthropogenic forcing may project principally on the dominant patterns of natural climatic variability, even though such natural variability may be manifest predominantly on timescales much shorter than that of the imposed forcing.

#### MI11/E/08-B5 0900

##### CLIMATIC INTRA-DECADAL QUASI-CYCLES AND THEIR NONLINEAR EVOLUTION

Igor I. MOKHOV (A.M.Obukhov Institute of Atmospheric Physics RAS, 3 Pyzhevsky, Moscow 109017, Russia, email: mokhov@omega.ifaran.ru)

Global climate system is considered as a dynamics system with potential attractors of the cyclic behaviour in the interannual evolution. The diagnostics of intra-decadal quasi-cyclic features in the temporal series of different thermodynamical and dynamical climatic characteristics is performed. Analysis of phase portraits and their changes during the last century displays the nonlinear effects of a general increase of amplitudes with an increase of periods, in particular for quasi-biennial (QBO) and quasi 5-year period (QFO) oscillations of global surface air temperature (GSAT), El-Nino/ Southern Oscillation (ENSO) characteristics and zonal wind in the equatorial stratosphere. The applicability of adiabatic invariants for climate dynamics system is estimated using models of an oscillator with slowly evolving period and a system of two coupled oscillators (TCO). In particular, the dependence of the QBO amplitude on its period for zonal wind in the lower equatorial stratosphere is quite well approximated by the power function with the power index close to 1/2 as it follows from adiabatic invariant theory. The TCO model is used for interpretation of relative variations of QBO and QFO peaks in spectra of the NH surface air temperature during last decades. In some cases there are significant differences between amplitude-period relation following from observations and from quasi-adiabatic model results. The general tendency of the QFO period decrease of GSAT under global warming during last century is exhibited. This effect is related to El-Nino-like phenomena. The displayed nonlinear dynamics and tendencies of its change can effect the resonance properties of the system (particularly in the case of the QBO realization as a parametric resonance phenomenon) and its variability.

#### MI11/W/07-B5 0915

##### SENSITIVITY ANALYSIS OF THE CLIMATE OF A CHAOTIC SYSTEM

J.A. HANSEN (1,2) and M.R. Allen (1,3) (1) Rutherford Appleton Laboratory, Space Science Department, Chilton/Didcot, OXON, OX11 0QX, UK, (2) Mathematical Institute, University of Oxford, Oxford, OX1 3LB, UK, (3) Department of Physics, Clarendon Laboratory, Parks Road, Oxford, OX1 3PU, UK.

The dominant source of uncertainty in climate prediction is likely to be model error, in contrast to the exponential growth of uncertainty in initial conditions which dominates short-range forecasting. A formal treatment of uncertainty in model structure remains virtually impossible, but parametric uncertainty can, at least in principle, be addressed through ensemble predictions varying model parameters. The challenge is to determine which parameters must be varied to span the range of possible forecasts with a limited ensemble. Model linearisation techniques have proved useful in the analysis of initial-condition uncertainty, but the utility of the conventional approach in the analysis of parametric uncertainty is limited by the exponential growth of perturbations in state space. For long enough trajectories, linear uncertainty growth in both fast and slow manifold processes can become too large to be useful. Extendible methodologies to address the issues of linearisation optimisation time and multiple time-scales are demonstrated.



MI11/E/01-B5 0930

## CORRELATIONS BETWEEN THE STRUCTURES OF ERRORS AND LYAPUNOV AND SINGULAR VECTORS IN BAROTROPIC DYNAMICS

Mozheng WEI and Jorgen S. Frederiksen CRC for Southern Hemisphere Meteorology CSIRO Atmospheric Research, PMB 1, Aspendale Victoria 3195, Australia email: mozheng.wei@dar.csiro.au

Singular vectors (SVs) and Lyapunov vectors (LVs) are compared with structures of evolved randomly generated errors during the cases of block development in the S.H. in 1989. A tangent linear model with time-dependent basic states taken from observations is employed to describe the error growth. The statistics of 100 evolved errors are studied for six day period and compared with the growth and structures of fast growing LVs and SVs in enstrophy, kinetic energy and streamfunction norms. The amplification factors of most random errors are slightly less than those of LV 1 for the same time-interval; while the amplification factors of all the random errors are much smaller than those of SVs 1 in all three norms, as expected.

The probability distributions, the mean and standard deviations of pattern correlations between each of the 100 evolved error fields and the five fastest growing LVs and SVs have been calculated. The mean of the largest pattern correlation, taken over the five fastest growing LVs (or SVs), increases with increasing time interval. The mean pattern correlation between 100 evolved random errors and LV 1 is smaller than those of evolved SVs 1. In about 3-4 days, the structures of evolved SVs start to show the similarity to the evolved random errors and take up large scale dipole structures. The random errors and evolved SVs 1 converge to LV 1 after about 20 days.

MI11/P/02-B5 0945

## STRANGE ATTRACTOR IN CLIMATIC PARAMETERS OVER INDIA AND THEIR COMPOUNDING

H.N. SRIVASTAVA (India Meteorological Department New Delhi-110003, India, e-mail: snb@imd.ernet.in)

Strange attractor characteristics have been determined for the climatic parameters like maximum and minimum temperature and atmospheric pressure for Indian stations representing different climatic regimes. It was found that the strange attractors lie between 5 and 6 over the Indian region. Similar computation for monsoon rainfall have shown larger variations between 4 and 7 for different meteorological sub-divisions of India and the country as a whole. It was found that the predictability of these parameters lies in the medium range namely 8 to 10 days. On the other hand, icecore results by other workers have reported climatic changes on much longer time scale.

A question arises whether the rainfall over the country, as a whole, for which long range forecast is issued using 16 parameters could be modelled when predictability of individual meteorological parameters lies in the medium range. Using the concept of 'compound chaos', it has been found that the technique based on strange attractor could have limitation for climatic predictions since compounding two parameters gives a predictability of less than 8 days.

MI11/E/12-B5 1000

## STOCHASTIC DYNAMICS OF EL NINO-SOUTHERN OSCILLATION

Bin WANG (Department of Meteorology, University of Hawaii, 2525 Correa Road, Honolulu, HI 96822, USA, email: bwang@soest.hawaii.edu) Albert Barcion (Department of Meteorology and GFDDI, the Florida State University, email: barcion@joanna.gfdl.fsu.edu) and Zheng Fang (Department of Meteorology, University of Hawaii, email: zfang@soest.hawaii.edu)

A stochastically forced nonlinear dynamic model for El Nino-Southern Oscillation (ENSO) is advanced to explore the nature of the highly irregular ENSO cycle. The model physics includes nonlinear dynamics of the coupled ocean-atmosphere system, high-frequency stochastic forcing, and the annual forcing of a prescribed climatological basic state.

The model irregular ENSO-like oscillation arises from three different origins: stochastic resonance, coupled nonlinear instability, and stochastic transition. When the basic state is stable, the stochastic forcing excites irregular oscillations by stochastic resonance. When the system is unstable and the coupled dynamics sustains a nonlinear oscillation (stable limit cycle), the stochastic forcing perturbs the deterministic trajectory of the limit cycle in the phase-space, generating irregularities and modifying the oscillation period. When the system possesses multi-equilibrium states, the stochastic forcing may render the system oscillatory by randomly switching the system between a warm and a cold stable steady state.

The stochastic response depends not only on the nonlinear dynamic regimes of the ENSO system but also on the temporal structure (spectrum) and strength of the stochastic forcing. White and red noises are shown to be much more effective than band-limited white noises in stochastic resonance. The intraseasonal noise can alter the dominant period of intrinsic nonlinear oscillation, favoring biennial oscillation, especially when the intraseasonal forcing is modulated by monsoon (annual cycle). A sufficiently strong white noise forcing can destroy the nonlinear or resonant oscillation, leading to a Markovian process.

The model results suggest that ENSO may arise from multi-mechanisms. The different mechanisms may be at work in various phases of the ENSO evolution, depending on the basic state and the nonlinear dynamics of the system. The monsoon may affect ENSO through modulation of intraseasonal stochastic forcing, enhancing the biennial component of ENSO.

MI11/W/06-B5 1100

## A NEW DYNAMICAL SYSTEMS THEORY OF INCOMPRESSIBLE FLOWS AND APPLICATIONS TO GENERAL OCEAN CIRCULATIONS

Shouhong WANG (Department of Mathematics, Indiana University, Bloomington, IN 47405, USA, E-mail: showang@indiana.edu)

I shall present in this talk a new dynamical systems theory of two-dimensional incompressible flows from the Lagrangian point of view, as well as its applications to large scale ocean circulations. The theory is developed recently jointly with T. Ma. On the theoretical side, I shall address a) the global structural classification of divergence-free vector fields, b) structural and block stability of divergence-free vector fields, c) structural bifurcation of the solutions of the 2D Navier-Stokes equations, and d) structural stability of solutions of the Navier-Stokes equations. The results and methods involved will be presented with simple schematic pictures. Then I shall apply the theoretical results and methods to the structure analysis of a wind-driven, double gyre, QG ocean model, as well as a two and half layer shallow water model. Several features related to climate low frequency variabilities shall be discussed. The work on double gyre circulations is joint with M. Ghil, K. Ide, E. Simonnet, J. Shen, T. Tachim Medjo and R. Temam.

MI11/L/01-B5 1130

## REMARKS ON THE BOUNDARY LAYER ON THE WEST COAST OF A WIND DRIVEN OCEAN

TREMAM

Abstract not available at time of going to press

MI11/E/07-B5 1200

## VERIFYING NONLINEAR CLIMATE CONCEPTIONS FROM TIME SERIES: METHODOLOGICAL BRICKS

PETER CARL (Climate Dynamics Project, c/o Forschungsverbund Berlin, Hausvogteiplatz 5--7, D - 10117 Berlin, Germany, email: pcarl@spclim5.wias-berlin.de)

Given that low-dimensional behaviour of higher-dimensional systems should realize itself via synchronized motions, the search for rational frequency relationships in observational data may become a key issue in the goal of puzzling out what contribution to the explanation (and prediction) of real world phenomena can be gained from nonlinear systems conceptions of climate dynamics. Evolutionary spectra are mapped to this end on the Farey tree of rational numbers thus facilitating the study of complex, nonstationary modal structures with a view on frequency 'aggregations' and their (changing) coupling strength and structures, both internal and with respect to cyclic external forcing. The method is applied to different time-frequency representations, including windowed Fourier and Maximum Entropy spectra, the continuous wavelet transform and projection-based 'pursuits' using either empirical orthogonal functions in the time domain or highly redundant dictionaries of Gabor 'time-frequency atoms' and other functions. These "Projection" and "Matching" Pursuits are shown to be best suited for the present purpose using a number of real world time series including monsoon, trace gas, SO<sub>2</sub>, NAO and Earth rotation data. The sensitive point of adequate representation of atmospheric variability in the models used for prediction is approached in a preliminary, demonstrative study using a conceptual, coarse-resolution, tropospheric GCM.

MI11/E/09-B5 1215

## NON-MARKOVIAN DYNAMICS OF WEATHER REGIMES IN A T21L3 QUASI-GEOSTROPHIC MODEL

S. VANNITSEM, Royal Meteorological Institute of Belgium, Avenue Circulaire, 3, 1180 Brussels, Belgium.

The dynamics between successive weather regimes generated by a Quasi-Geostrophic model are investigated. A new clustering procedure of the anomaly weather fields based on the local Kolmogorov entropy is first performed, leading to three distinct clusters. It is shown that two of these correspond to large and small expansion rates, suggesting that these regimes display different predictability properties. The dynamics of the symbolic sequence as provided by the three clusters is subsequently investigated and shown to be non-Markovian. A simple model of this behaviour is developed and the implications for long term prediction are discussed.

MI11/W/03-B5 1230

## STEADY RESPONSE OF BAROTROPIC ATMOSPHERE TO THE SMALL PERTURBATIONS OF EXTERNAL FORCING. THEORY AND NUMERICAL EXPERIMENTS

A. GRITSOUN and V. Dymnikov (both at Institute of Numerical Mathematics RAS, Gubkina 8, 117951, GSP-1, Moscow, Russia, e-mail: andrusha@inn.ras.ru)

In this study we consider the barotropic model of the low-frequency atmospheric variability. Using Monte-Carlo method, we construct the operator that describes the model response to small constant external perturbations. It is shown that this operator can be considered as linear with high accuracy. Moreover, it turns out, that maximum response of the system is close to its dominant low-frequency EOF. Next we investigate the possibility to describe the response of barotropic model by means of the linear dynamical-stochastic model. To this end we construct the linear dynamical-stochastic model with low frequency variability is identical to that of original system. The linear operator of this model can be calculated using original model data and right hand side represents some random process. The singular vectors of the linear system matrix turn to be close to that of the original system response matrix. In addition we demonstrate that autocovariance matrix of right hand side of linear model can be selected as  $cI$ , where  $I$  is unity matrix and  $c$  is some number. The consequence of this fact is that the maximum responses of linear and original systems are close to the leading low-frequency EOF of the model circulation. In sum one can conclude that the use of the linear approach to predict the sensitivity of the barotropic atmosphere model leads to the satisfactory results.

Friday 30 July PM

Presiding Chair: S. Lovejoy, (McGill University, Montreal, Quebec)

INTERMITTENCY, DETERMINISTIC CHAOS, STOCHASTICITY

MI11/E/02-B5 1400

## MULTIFRACTAL PROCESSES AND STOCHASTIC CHAOS IN THE WEATHER AND CLIMATE

S. LOVEJOY, (Physics dept, McGill University, 3600 University St., Montréal, Québec, H3A 2T8, Canada); D. Schertzer (LMM, case 162, Université P. et M. Curie, 4 pl. Jussieu, Paris F-75252 Cedex 05, France)

Real world systems - especially weather and climate systems - have many chaotic features. These include apparently continuous change interrupted by sudden (often catastrophic) transitions, spatial structures spanning wide ranges of scale (mountains, clouds, "eddies"). Furthermore, the systematic study of nonlinear systems with few degrees of freedom - "deterministic chaos" - has led to a profound change in the way we think about such nonlinear systems. We now expect their behaviour to be "chaotic". However, in spite of this important philosophical impact, deterministic chaos has actually led to surprisingly few direct applications. We argue that the reason is that most interesting nonlinear systems involve large numbers of degrees of freedom; "stochastic chaos". When such systems obey the (non-classical) symmetry of scale invariance, then the outcome will be multifractal fields. Since these multifractal processes possess stable and attractive generators, "universal" features emerge with the attendant theoretical and analytical simplifications. We illustrate these ideas using a range of atmospheric examples, and show how they can be used to produce realistic space-time stochastic models. Finally, we compare and contrast the prediction limits for deterministic and stochastic forecasts.

**MI11/E/04-B5** **1430****NONLINEAR DYNAMICS, MULTIFRACTAL INTERMITTENCY AND THE RENORMALIZATION OF THE GENERATING EQUATIONS**

D. SCHERTZER, M. Larchevêque (LMM, CNRS UMR 7607, Case 162, Université P.&amp;M. Curie, Paris, France, 4 Pl. Jussieu, 75252 Paris Cedex 05, France) S. Lovejoy (Physics dept, McGill University, 3600 University St., Montréal, Québec, H3A 2T8, Canada)

Nonlinear dynamics of the climate system are strongly intermittent: the activity or efficiency of nonlinear couplings is highly inhomogeneous in time and space. Developments of multifractal notions and models have recently led to a deeper understanding of the phenomenology of intermittency. Indeed, wild probability distributions and corresponding coherent structures are a direct outcome of the multifractal processes, whereas they remain beyond the scope of the classical analytical/renormalization theories. Therefore, we are faced with a paradoxical situation: a deeper and deeper understanding of intermittency, but a looser contact with the structure of the generating equations. Contrary to a pessimistic recent viewpoint, we show that there is a way of bridging up this gap. We clarify that the failure of renormalization techniques is due to (rather implicit) quasi-gaussian assumptions concerning not only the fields, but also their adjoint fields that define the (non linear) infinitesimal response of the former to perturbations. With the help of multifractal Fractionally Integrated Flux (FIF) models, we define a renormalized forcing which is strongly non gaussian, and therefore, with the help of the corresponding renormalization of the propagator, obtain intermittent models built directly on the structures of the generating equations.

**MI11/W/08-B5** **1500****INTERMITTENCY IN A MODEL OF NON-LINEAR PLANETARY WAVE INTERACTION**

Roman BEKRYAEV (Arctic and Antarctic Research Institute, 38 Bering st., 199397, St.-Petersburg, Russia, e-mail: bekryaev@aari.nw.ru)

We consider the connection of bifurcations and statistical properties of the quasisoloidal horizontally baroclinic model of the nonlinear interaction between planetary atmospheric waves in a zonal channel. Research of a low-order model has shown that in the conditions of inhomogeneous underlying surface the stationary state chaos-intermittency can be observed. Slow laminar stage of intermittency is connected with the blocking of zonal thermal west-east flow. We have shown that distribution of laminar interval length is bimodal. This property is typical to the first kind of intermittency connected with saddle-nodule bifurcation. A mechanism leading the intermittent fluctuations has been investigated analytically. It has been shown that in our case the intermittency is determined by intersection of Hopf bifurcation line with saddle-nodule boundary of Whitney set. The laminar phase of the intermittency is connected with gathering of the trajectories to "fantom" of the stationary stable point. The numerical experiments have shown that exponential scattering of trajectories can be observed only in the periods of chaotic dynamics. The error of prediction does not grow during the laminar stage of intermittency.

The work presented here was supported in part by the Russian Fund of Basic Research under Grant number: 96 05 - 64960.

**MI11/W/04-B5** **1515****CONTRASTING "LOCAL" AND GLOBAL LYAPUNOV EXPONENTS**

Christine ZIEHLANN (University of Potsdam, Institute of Physics, Am Neuen Palais 19, PF 601553, D-14415 Potsdam, Germany. E-mail: chriss@agnld.uni-potsdam.de) and LEONARD A. SMITH (University of Oxford, Mathematical Institute, 26 St. Giles, Oxford OX1 3LB, UK. email: lenny@maths.ox.ac.uk)

In the thirty years since their introduction, both global Lyapunov exponents (LE) (Oseledec 1968), and their local counterparts (Lorenz 1965), have been widely employed to quantify the predictability. Distinct entities (with different properties) have been dubbed "local Lyapunov exponents", creating some confusion; two of these, finite time LE and finite sample LE are defined in Ziehlmann et al. 1999. Relations between the finite time, the finite sample and the global Lyapunov exponents are noted. For predictions over finite periods of time, the finite time and the finite sample LE may provide completely different estimates of predictability for the same initial state. As long as the uncertainties remain small enough to be approximated by the tangent dynamics, the finite time LE appear more relevant; details may depend on the assimilation scheme employed. Contrasting the distributions of finite time LE and finite sample LE, provides a new tool for estimating the uncertainty remaining in a global LE computation. Results are presented for two chaotic maps, the Henon system and the Ikeda system; it is proven that true "return of skill" exists in some chaotic systems. All Lyapunov exponents represent "effective" rates, and thus they are all fundamentally limited in terms of quantifying predictability inasmuch as, by definition, they require the selection of a timescale a priori. The advantages of an alternative approach, computing uncertainty growth timescales directly, are discussed.

References: E.N. Lorenz (1965): A study of the predictability of a 28-variable atmospheric model, *Tellus*, 17, 321-333. V.I. Oseledec (1968): A multiplicative ergodic theorem. Lyapunov characteristic numbers for dynamical systems. *Transactions of the Moscow Mathematical Society*, 19, 197-231. C. Ziehlmann, L.A. Smith and J. Kurths (1999): The Bootstrap and Lyapunov Exponents in Deterministic Chaos, *Physica D* (in press).

**MI11/W/02-B5** **1530****INERTIAL MANIFOLD OF THE ATMOSPHERIC EQUATIONS**

LI Jianping (State Key Laboratory of Numerical modelling for Atmospheric Sciences and Geophysical Fluid Dynamics (LASG), Institute of Atmospheric Physical, Chinese Academy of Sciences, Beijing 100080, China Chou Jifan Department of atmospheric sciences, Lanzhou University, Lanzhou 730000, China)

Abstract For a class of non-linear evolution equations, we study their global attractors and discuss the existence of their inertial manifolds using the truncated method. Then, on the basis of the properties of operators of the atmospheric equations, it is proved that the operator equation of the atmospheric motion with dissipation and external forcing belongs to this class of non-linear evolution equations. Therefore, it is got that there exists an inertial manifold of the atmospheric equations if the spectral gap condition for the dissipation operator is satisfied. These results furnish a basis for studying further dynamical properties of global attractor of the atmospheric equations and for designing better numerical scheme. Key words: Inertial manifold, Non-linear evolution equation, Global attractor, Operator Equation, Operator.

**MI11/W/05-B5** **1545****ELIMINATING COMPUTATIONAL UNCERTAINTY AND ITS METEOROLOGICAL USES**

Qing ZHONG (Institute of Atmospheric Physics, Chinese Academy of Sciences, Beijing 100029 CHINA. E-mail: zhongq@sgj50s.iap.ac.cn)

A computational intermittent turbulence like Uncertainty in a non-linear Lorenz's system is revealed in this work. The origin of this Uncertainty is analysed, and its unfavourable meteorological sequence in relation with predictability of numerical models for short range and long term integration is also discussed. Moreover, a successful approach to eliminating this kind of Uncertainty is discovered, formulated as well as tested. In addition, some applications of this approach is also discussed as a new way to reduce failures in actual numerical weather forecast and reduce Uncertainty in actual numerical climate forecast and simulation.

**MI11/E/05-B5** **1630****LIMITATION OF CLIMATE PREDICTION**

Prof. Peter C. CHU

The limitation of climate prediction is due to uncertain initial and boundary conditions. Much of the predictability studies (e.g., Lorenz, 1974) have been done on the sensitivity of model behaviour to tiny disturbances in the initial field. We may ask: What is the sensitivity of model behaviour to tiny disturbances boundary conditions, such as in the sea surface temperature (SST) anomaly. First, we use the Lorenz system (Lorenz, 1963) to show the existence of two kinds of predictability, in terms of initial error (first kind) and of the boundary error (second kind). Second, we use the latest version of the NCAR Community Climate Model (CCM3) to study the model response to tiny surface temperature disturbances. The model was integrated from 1 September 1977 observational data over the globe for 16 months with and without SST disturbances. A time-scale of 20-day is found such that the response increases rapidly within this time-scale and then oscillates at high values. Finally, some theoretical discussion will also be included.

**MI11/E/10-B5** **1645****NON-LINEAR STABILITY AND INSTABILITY IN ATMOSPHERIC DYNAMICS: THEORY AND APPLICATION**

Mu MU, Wu Yonghui, Wang Jiafeng (all at LASG, Institute of Atmospheric Physics, Chinese Academy of Sciences, Beijing 100029, China, e-mail: mumu@sun.ihep.ac.cn) Liu Yongming (Department of Mathematics, East China Normal University, Shanghai, 200062, China)

This paper is concerned with the non-linear stability and instability in atmospheric dynamics and its applications.

First, Arnold's non-linear stability theorems of barotropic motions obtained by energy - Casimir method are applied to diagnose the maintenance or breakdown of the zonal flows in the middle and high latitudes. The primary results show that the analyses correspond well to the evolution of the real atmospheric motions.

Second, the basic states, which are guaranteed to be nonlinearly stable or unstable by the non-linear stability criteria, are utilised to study the validity and limitation of tangent linear model (TLM) and the singular vectors (SVs). In the barotropic context, numerical results show that the validity period of the TLM and SVs depend essentially on the non-linear stability and instability of the motion. The energy of the fastest growing disturbance obtained by SV method, could less than significantly the energy of certain kind of disturbance gained by using non-linear model in case that the basic state is nonlinearly unstable.

Finally, the non-linear stability criterion of continuously stratified quasigeostrophic generalised Eady's model is established, which demonstrates the short-wave cut-off phenomenon and the impact of the Beta parameter.

**MI11/E/06-B5** **1715****THE RELATIONSHIP BETWEEN PRECIPITATION IN SOUTHERN BRAZIL AND SEA SURFACE TEMPERATURE IN SOUTHERN HEMISPHERE**

Valentina M. KHAN (Russian State Center of Hydrometeorology, Moscow, Russia, e-mail: odpp@glasnet.ru)

The relationship between rainfall anomalies in Southern Brazil and SST in Southern Hemisphere, with temporal lags varying from 0 to 12 months, is investigated using linear correlation analysis. The precipitation data represent monthly historical record from 13 meteorological stations objectively grouped in 5 classes. The data covered the period between 1911 and 1995. The historical SST data used in the work are the monthly averages that were compiled from different sources. Significant correlations were detected between precipitation in the study region and anomalies of SST in the belt of Antarctic Circumpolar Current. This teleconnection may be associated with ENSO-correlated perturbations in SST that translate around the Antarctic Circumpolar Current (the so-called "Antarctic Circumpolar Wave"). Significant relationship was also observed between regional precipitation in southern part of Brazil and SST anomalies in South Pacific Convergence zone, South Indian Convergence zone and the El Niño zone in the eastern equatorial Pacific. The possible mechanisms that control the connections between the anomalies of regional rainfall and SST in the detected specific areas of Southern Hemisphere are discussed.

**MI11/W/09-B5** **1730****ADAPTIVE ALGORITHM FOR LONG-TERM PROGNOSIS OF OBSERVED CHAOTIC DYNAMICS**

Mr Dmitry N. MUKHIN (Institute of applied physics RAS)

The work is aimed to develop a new approach to long-term prognosis of the nonautonomous non-linear dynamic system behaviour. The essence of this approach, which is discussed in another IUGG99 report of the authors, is derivation of a special "prognostic" model from the observed chaotic time series. This article is devoted to significant enhancing the capabilities of the approach through special adaptive procedure elaborated. The procedure is "self-educated" and concludes an optimisation of prognostic model parameters via comparison of predicted system behaviour with a newly measured data. A specific arisen problem, which was overcome, is lack of information extracted from the new data. This lack results from system bifurcation from more complicated behaviour to simpler one. The algorithm is applied to time series obtained due to numerical experiment with dynamical models of atmospheric photochemical systems as well as a few classical models (e.g. Rossler model), in which trends of control parameters were entered. As a result, entire bifurcation sequences of these systems were predicted and both the bifurcation values of parameters, and a ranges of changes of the dynamic variables magnitudes were reproduced. Note that all mentioned predictions are quantitatively very close to corresponding characteristics of the modelled systems.

MI11/E/03-B5

1745

## PROGNOSTIC MODELS OF NON-LINEAR DYNAMIC SYSTEMS

Alexander M. FEIGIN, Eugene M. Loskutov, Yaroslav I. Molkov and Dmitry N. Mukhin (all at Institute of Applied Physics, Russian Academy of Sciences, 46 Ulyanov St., Nizhny Novgorod, 603600, Russia, email: feigin@appl.sci-nnov.ru)

A new approach to long-term prediction of bifurcations of nonautonomous non-linear dynamic system behaviour is suggested. The approach is based on the derivation of a special dynamic model through an analysis of observed chaotic oscillations of the system. This model not only reproduces a current system behaviour, but carries also information about dependencies of intrinsic characteristics of the system on parameters, which underwent slow trends during the observation period. The last point transforms the model into prognostic one, which is suitable for prediction of bifurcations of the system behaviour resulting from expected in the future variations of the parameters. The prognostic model is aimed to finding bifurcation values of the parameters as well as evaluating changes of magnitudes of the dynamic variables caused by the system bifurcations. The suggested approach has been elaborated and confirmed both by a few "classical" model dynamic systems (e.g. Rossler and Lorenz models), and a recently elaborated model of the mesospheric photochemical system forced by diurnal modulation of photolysis rates. All systems considered exhibit, depending on the parameter values, various types of non-linear dynamic behaviour (including chaotic oscillations) as well as different kinds of bifurcations. This gives possibility to analyse a broad spectrum of the representative situations which can be observed, and reveal both the advantages of the approach, and problems arisen, as well as propose ways for these problems overcoming. The derivation of the prognostic model from really observed time series is discussed.

MI12

Thursday 29 – Friday 30 July

## SOURCES OF VARIABILITY IN THE MIDDLE ATMOSPHERE (ICMA, SCOSTEP, SPARC)

Location: Mechanical Engineering, G28 LRE

Thursday 29 July AM

Presiding Chair: A. O'Neill (University of Reading, UK)

Introduction

0930

A.O'Neill

MI12/W/09-B4

Invited

0945

## PLANETARY SCALE ASPECTS OF MIDDLE ATMOSPHERE VARIABILITY

William J. RANDEL (NCAR, PO Box 3000, Boulder, Colorado, 80307-3000, USA, e-mail: randel@ucar.edu)

Long records of satellite observations and meteorological analyses provide global perspective to seasonal and interannual variability of the stratosphere. Planetary waves provide a strong coupling mechanism between the troposphere and stratosphere in winter; their effects extend to the near-global scale, with influence from the tropical tropopause to the polar vortex. The contrasts between Northern and Southern Hemisphere polar vortex structure further demonstrates the influence of planetary waves. Interannual variability of the stratosphere is dominated by the quasi-biennial oscillation (QBO) in the tropics and low latitudes; variability of the polar vortices are more closely related to forcing from the troposphere. Observed low-frequency changes (trends) in the stratosphere will be discussed, with focus on the recent springtime polar cooling observed in both hemispheres.

MI12/W/07-B4

1030

## IS THERE A LONG-TERM TREND OF PLANETARY WAVES IN THE NORTHERN WINTER STRATOSPHERE?

Kirstin KRUEGER(1), Steven Pawson(2), Ulrike Langematz(1). (1 Institut fuer Meteorologie, FU Berlin, 12165, Berlin, Germany email: krueger@strat01.met.fu-berlin.de) (2 Universities Space Research Association, NASA GSFC, Greenbelt, MD 20771, USA)

A possible long-term change of the polar vortex spin up, duration and break-down in the northern winter stratosphere is studied over the period 1964-1998. The long-term DJF-climatology of the polar vortex reveals a zonally-asymmetric structure, which can be interpreted in terms of planetary waves. To analyse such changes of the polar vortex structure, a trend analysis of planetary waves (amplitudes, phases and corresponding fluxes) and the mean zonal mean wind during pre-, mid-, and late winter is calculated from the Free University Berlin (FUB) observational data. Possible dynamical feedbacks of observed stratospheric ozone decrease on planetary wave dynamics are discussed by comparing the results of the trend analysis with those from two multiyear simulations with the Berlin Climate-Middle-Atmosphere-model. In the model runs, either a climatological ozone field of the 1980s or an ozone field with observed ozone trends was used.

MI12/W/05-B4

1115

## THE EFFECT OF INERTIAL INSTABILITY ON THE EVOLUTION OF A MODELLED STRATOSPHERIC WARMING

EUAIN F. DRYSDALE (Rutherford Appleton Laboratory, Chilton, Didcot, OX11 0QX, UK, email: e.drysdale@rl.ac.uk), Lesley J. Gray (Rutherford Appleton Laboratory, Chilton, Didcot, OX11 0QX, UK, E-mail: L.J.Gray@rl.ac.uk) and Suzanne M. Rosier (Department of Meteorology, University of Reading, Earley Gate, Whiteknights, P.O. Box 243, Reading, RG6 6BB. E-mail: S.M.Rosier@reading.ac.uk)

The effect of inertial instability on the evolution of a northern hemisphere stratospheric sudden warming is investigated in a modelling study. In the tropical upper stratosphere and lower mesosphere, the model (and indeed the atmosphere) are often in an inertially unstable state. This inertial instability results in the formation of flat 'pancake rolls' consisting of stacked layers of meridional wind with alternating directions. These rolls will act to stabilise the flow and it is hypothesised that they inhibit the advection of low latitude air into the extra-tropics and through this mechanism will prevent or delay stratospheric warmings. A vertical diffusion parameterisation is added to the model, and changes in the evolution of the modelled winter are seen. The main action of the applied vertical diffusion is to limit the formation of the small

vertical scale rolls formed as a result of inertial instability. The effect of these rolls on a stratospheric warming is investigated by applying the vertical diffusion in a variety of model runs and observing the changes in both the evolution of this warming directly and the transport in the model. It is seen that restricting the model adjustment to inertial instability has the effect of advancing and strengthening the warming observed.

MI12/W/12-B4

1135

## CAN THERE BE INTRASEASONAL AND INTERANNUAL VARIATIONS IN THE MIDDLE ATMOSPHERE IF THOSE VARIATIONS ARE NOT PRESENT AT THE LOWER BOUNDARY?

Mingyue Chen (Climate Prediction Center/National Centers for Environmental Prediction, Camp Springs, MD 20746); Carlos R. MECHOSO and J.D. Farrara (both at Department of Atmospheric Sciences, University of California, Los Angeles, CA 90095-1565, e-mail: mechoso@atmos.ucla.edu)

The answer to the question posed in the title of this talk is sought in the framework of a quasi-geostrophic, beta-plane, channel model of the middle atmosphere in the presence of conditions at the lower boundary that are either steady or whose zonal component is time-varying but without interannual variations. The model uses different spectral truncations in the horizontal and finite-differencing in the vertical. The circulation is driven by zonally-independent differential radiative heating, which is either time-independent or time-varying without interannual variations.

It is shown that intraseasonal variations can be obtained with steady conditions at the model's lower boundary and time-independent winter-type radiative forcing. In this case, the model's steady solutions are found and their dependence on truncation is analysed in detail when either one or both of the two longest zonal and meridional modes are retained. The number and stability properties of those solutions can depend strongly on model truncation. Model integrations in time illustrate that the variations appear as flow transitions between steady solutions.

It is also shown that significant interannual variability can be obtained for particular values of the model parameters in the case when both the zonal component of the conditions prescribed at the model's lower boundary and the radiative heating include a seasonal cycle. These variations resemble those observed during final warmings in the southern hemisphere.

MI12/W/13-B4

1155

## INTERNAL VARIABILITY OF THE WINTER STRATOSPHERE THROUGH THE TROPOSPHERE-STRATOSPHERE DYNAMICAL LINK IN A SIMPLE GLOBAL CIRCULATION MODEL

Masakazu Taguchi, Takashi Yamaga and Shigeo YODEN (Department of Geophysics, Kyoto University, Kyoto, 606-8502, Japan, e-mail: yoden@kugi.kyoto-u.ac.jp)

We perform numerical experiments with an idealized troposphere-stratosphere global circulation model to investigate internal variability of the winter stratosphere which arises from the vertical dynamical link. While the model is simplified in some ways (dry atmosphere, no physical process except for Rayleigh friction at the surface, and perpetual external conditions), it explicitly describes dynamical processes related to the vertical link: excitation of planetary waves by the surface topography and their interaction with baroclinic eddies in the troposphere as well as their upward propagation and interaction with the mean zonal flow in the stratosphere. Amplitude of a sinusoidal surface topography is chosen as an experimental parameter to examine the relative importance of the forced planetary waves: 1000-day integrations are done for each of about 50 runs with different amplitude. The obtained winter stratospheric circulations can be classified into 5 regimes dependent on the topography amplitude: (1) nearly radiative-equilibrium state, (2) weak undulation of a strong polar vortex, (3) quasi-periodic occurrence of minor sudden warmings, (4) intermittent occurrence of major warmings, and (5) weak and warm polar vortex at all times. Time variations of the stratospheric circulation in some parameter ranges resemble those of the real atmosphere, and interhemispheric differences in the winter stratosphere can be understood as the regime difference. The southern hemisphere winter corresponds to the second or the third regime, while the northern hemisphere winter does to the fourth regime. Dynamical diagnosis is also done for some typical runs to clarify the excitation process of planetary waves and their interaction with the mean zonal flow and baroclinic waves in the troposphere and the lower stratosphere

MI12/W/15-B4

1215

## THE WAVE-1 STRATOSPHERIC WARMING AND INTERNAL VARIABILITY

Andrew GREGORY, Alan O'Neill and John Thuburn (CGAM, Department of Meteorology, University of Reading, PO Box 243, Earley Gate, Reading, RG6 6BB)

Standard textbook theory links the stratospheric sudden warming to the development of planetary waves in the troposphere. This theory can be difficult to apply to many observed warmings notably warmings dominated by zonal-wavenumber 1 (a 'wave-1 warming'). Such warmings are associated with the strengthening of a quasi-stationary anticyclone (the Aleutian high). Usually this happens as the quasi-stationary anticyclone merges with a second travelling anticyclone in the upper stratosphere. A series of seasonal integrations with a new stratosphere-mesosphere model has been performed with the idealisation of constant tropospheric wave forcing. It is found that with constant wave forcing of 300m, an amplitude comparable to that observed, the model stratosphere generates a series of travelling anticyclones which merge with a quasi-stationary anticyclone in a manner that can be closely compared to observations. It is argued that, although the resulting model warming is weaker than is often observed, the model shows that a wave-1 warming can be generated as a result of the stratosphere's internal variability and need not be linked with tropospheric wave development. Consequences for the success of simulations of observed wave-1 warmings with stratosphere-mesosphere models are also discussed.

Thursday 29 July PM

Presiding Chair: S. Yodon (Kyoto University, Japan)

MI12/W/03-B4

1400

## EXCITATION MECHANISM OF QUASI STATIONARY ROSSBY WAVES IN THE SOUTHERN HEMISPHERE

Yasunobu MIYOSHI (Department of Earth and Planetary Sciences, Kyushu University, Hakozaki, Fukuoka, Japan, e-mail: miyoshi@rossby.geo.kyushu-u.ac.jp)

Quasi stationary Rossby waves with zonal wavenumber 1 (QS-wave 1) have large amplitude in winter-spring of the middle atmosphere. However, excitation mechanism of QS-wave 1 in the southern hemisphere has not been well understood. In this paper, excitation mechanism of QS-wave 1 in the southern hemisphere is studied. Effects of the zonal asymmetry of SST distributions in low and middle latitudes on excitation of QS-wave 1 are investigated by a series of GCM experiments. The GCM used in this study is T21L37 model, which is developed



at Kyushu University. Results indicate that the zonal asymmetry of the SST in low latitudes is essential for excitation of QS-wave 1. The interannual variation of QS-wave1 in the stratosphere and its relation to the interannual variation of SST(ENSO) will be discussed.

**MI12/W/01-B4** **1420**

**STRATOSPHERIC VARIABILITY AND REPRODUCIBILITY IN SEASONAL ENSEMBLE INTEGRATIONS WITH A TROPOSPHERE - STRATOSPHERE GCM**

W.A. LAHOZ and A. O'Neill (CGAM, University of Reading, Department of Meteorology, Reading, RG6 6BB, UK. E-mail: wal@met.reading.ac.uk)

The Centre for Global Atmospheric Modelling (CGAM) has participated in the EU-funded PROVOST project to assess the capabilities of GCMs for seasonal forecasting. CGAM has used a troposphere-stratosphere version of the Unified Model developed at the UK Meteorological Office. It has 58 levels in the vertical and a horizontal resolution of 2.5deg latitude by 3.75deg longitude. It has the same tropospheric configuration and representation of physical processes as the current climate version of the Hadley Centre's version of the Unified Model (with so-called HADAM3 physics). A nine-member ensemble of four-month integrations has been run for the 18 northern winters from 1979 to 1997, each one started during the last nine days of November. Experiments were run in hind-cast mode with sea-surface temperatures prescribed with observational data. The simulated variability in the extratropical stratosphere during each winter, and the variability between winters will be discussed and analysed by comparison with ERA-15 data. The reproducibility of the seasonal cycle and of the intraseasonal variability among ensemble members will be assessed to determine the impact of ocean-surface boundary conditions on stratospheric variability.

**MI12/W/04-B4** **1440**

**INTERANNUAL VARIABILITY IN A MECHANISTIC MIDDLE ATMOSPHERE MODEL**

Euain F. DRYSDALE (537 Rutherford Appleton Laboratory, Chilton, Didcot, OX11 0QX, UK. E-mail: e.drysdale@rl.ac.uk); Lesley J. Gray (Rutherford Appleton Laboratory, Chilton, Didcot, OX11 0QX, UK. E-mail: L.J.Gray@rl.ac.uk)

A series of long model runs are performed using the UKMO Stratosphere-Mesosphere Model and the interannual variability in the northern polar vortex is compared. This model used is a mechanistic model, with a vertical domain spanning 100 to 0.01 hPa. The troposphere is represented by supplying the model with a lower boundary condition of the geopotential height of the 100 hPa pressure surface. In these experiments, the model is run with a bottom boundary that is taken from a single years data and repeated in a loop to form a continuous data set. This eliminates any tropospheric interannual variability from the simulation while still providing the model with a realistic annual cycle in the bottom boundary. Two experiments are performed where different years data are used to supply the lower boundary and long runs are performed. The interannual variability observed in each of these two experiments is found to be quite different. One run produces a large amount of interannual variability (January temperature variations, for example, are comparable to those observed in the real atmosphere) whereas the other experiment produces very much less interannual variability. Initial inspection of the height fields yields no obvious reason why the model produces very different amounts of interannual variability, and a more detailed examination of the bottom boundaries is performed.

**MI12/E/06-B4** **1500**

**ON THE PRESENCE OF A WAVE-GUIDE FOR PLANETARY WAVES IN THE STRATOSPHERE DUE TO THE RADIATIVE AND PHOTOCHEMICAL PROCESSES**

Igor KONOVALOV (Institute of Applied Physics of Russian Academy of Sciences, 46 Ulyanov Str., Nizhny Novgorod, 603600, Russia. E-mail: konov@appl.sci-nnov.ru)

Qualitative effects appearing due to coupling of radiative and photochemical processes (RPP), and planetary-scale motions in the stratosphere are analysed using a quasi-geostrophic mechanistic model. The analysis has been fulfilled both for the stationary atmosphere case which roughly corresponds to the situation at April-May and September-October periods and for the summertime atmosphere case. The results for the former have been published earlier [Konovvalov I. B., Izv. Atm. Ocean. Phys., v. 33, 475-482, 1997] and this report is mainly focused on the latter. It is shown that RPP can significantly perturb a vertical profile of an index of refraction so that to provide its wave-guide-like structure and cause the existence of a distinctive mode of planetary waves whose energy is mostly concentrated at heights of 30-40 km. It is discussed that this mode with zonal wavenumber 1 and meridional wavenumber 6 or 7 may be accounted for the observed distinctive wave phenomenon in the summertime stratosphere [Muench H., J. Atmos. Sci., v.25, 1108-1115, 1968]. Both the vertical structure and period of our mode are close to those of the observed wave. However, the model provides rather short damping time (approximately 1.5 periods), what is an obstacle for the complete identification of the observed and simulated waves. It is shown, though, that the value of the damping time is very sensitive to the parameters of the model (it is not so for the period and vertical structure) and thus the more accurate modelling approach is necessary to obtain the reliable value of the damping time.

**MI12/E/03-B4** **1520**

**ON THE SENSITIVITY OF SUDDEN WARMINGS TO EQUATORIAL WINDS AND TEMPERATURES**

lesley GRAY and Euain Drysdale (Rutherford Appleton Laboratory, Chilton, Didcot, Oxon., OX11 0QE, U.K. Tel: +44 1235 446745, Fax: +44 1235 445848, e-mail: lesley.gray@rl.ac.uk)

A 30 year simulation of a stratosphere mesosphere model is described in which the modelled winds are relaxed towards observations in the lower equatorial stratosphere so that a realistic quasi biennial oscillation (QBO) is reproduced. The influence of these lower stratospheric winds on the synoptic evolution of the Northern Hemisphere winter and timing of the stratospheric sudden warming is examined. Although there is some correlation between the QBO and the general evolution of the winter circulation in the expected sense i.e. warm, disturbed winters in the easterly QBO phase years and cold, undisturbed winters in the westerly QBO phase years, this is by no means universal. In fact, there are several examples that exhibit a strong anti-correlation, suggesting additional source(s) of variability that are more important in these years. These winters are examined in detail. In particular, we investigate whether there is in any sense a 'memory' of the previous winter carried over into the following year. The model experiments show that the synoptic evolution of the winter circulation and the nature of the stratospheric warmings exhibit significant sensitivity to the temperature distribution at the equatorial tropopause.

**MI12/E/01-B4** **1610**

**ON THE POSSIBLE CAUSES OF THE INTERANNUAL VARIABILITY OF THE PLANETARY WAVE ACTIVITY IN THE WINTER POLAR STRATOSPHERE**

Boris SOUKHAREV, Olga Kozlova, Svetlana Renyova, Irina Gorodetskaya and Ekaterina Kutuzova (all at Department of Climatology, St.Petersburg State University, 10 linia, 33, 199178, St.Petersburg, Russia, e-mail: boris@seb.usr.pu.ru)

The varying activity of the planetary waves is responsible for the interannual variability of the polar stratosphere. As the planetary height-waves 1 and 2 explains most of the total spatial variance of the winter polar stratosphere, the interannual variability of the two waves at the four stratospheric levels (100, 50, 30 and 10 hPa) for the period 1957-1996 in months from November to March is studied. Amplitudes of height-waves 1 and 2 at 60 degree North are used as parameters of the wave activity because the two waves reach their peaks between 60 and 70 degrees North. Correlation coefficients between the amplitudes of height-wave 1 and equatorial stratospheric zonal winds are negative in November and December at all considered levels. But in January - March the signal of the equatorial QBO in the planetary waves amplitudes is very weak. It is evident that most of the interannual variability of the waves amplitudes in January - March depends on other factors. If the data are grouped according to the extremes (peaks and hollows) of 11-year solar cycle then strong opposite correlations between the amplitudes of height-wave 1 in February and March and equatorial zonal winds (positive correlations at solar minima and negative ones at solar maxima) are revealed. In the periods of transition between solar extremes the connections are not so evident. The differences E-W between the February mean amplitudes of height-wave 1 at 30 hPa during the easterly (E) and westerly (W) QBO phases are about E-W = 199 gpdm and E-W = -176 gpdm for the periods of solar maximum and minimum respectively. Thus, the solar/QBO interaction can be considered as important cause of the interannual variability of planetary wave activity.

**MI12/W/02-B4** **1630**

**PROPAGATION OF THE ARCTIC OSCILLATION FROM THE STRATOSPHERE TO THE TROPOSPHERE**

MARK P. BALDWIN and Timothy J. Dunkerton (Northwest Research Associates, Bellevue, Washington, 98009-3027 USA. E-mail: mark@nwra.com)

Geopotential anomalies ranging from the earth's surface to the middle stratosphere in the northern hemisphere are dominated by a mode of variability known as the Arctic Oscillation (AO). The AO is represented herein by the leading mode (the first empirical orthogonal function) of variability of wintertime geopotential between 1000 and 10 hPa. In the middle stratosphere the signature of the AO is a nearly zonally symmetric pattern representing a strong or weak polar vortex. At 1000 hPa the AO is similar to the North Atlantic Oscillation, but with more zonal symmetry, especially at high latitudes. In zonal-mean zonal wind the AO is seen as a north-south dipole centered on 40-45°N; in zonal-mean temperature it is seen as a deep warm or cold polar anomaly from the upper troposphere to ~10 hPa. By examining separately time series of AO signatures at tropospheric and stratospheric levels, it is shown that AO anomalies typically appear first in the stratosphere and propagate downward. The midwinter correlation between the 90-day low-pass filtered 10-hPa anomaly and the 1000-hPa anomaly exceeds 0.65 when the surface anomaly time series is lagged by about three weeks. The tropospheric signature of the anomaly is characterized by substantial changes to the storm tracks and strength of the mid-tropospheric flow, especially over the North Atlantic and Europe. The implications of large stratospheric anomalies as precursors to changes in tropospheric weather patterns are discussed.

**MI12/W/10-B4** **1650**

**INTERANNUAL VARIABILITY OF THE GENERAL CIRCULATION DUE TO OZONE HOLE CHANGES: A GENERAL CIRCULATION MODEL EXPERIMENT**

T. Hirooka, S. WATANABE, T. Nishiyoshi and S. Miyahara (all at Department of Earth and Planetary Sciences, Kyushu University, 6-10-1, Hakozaki, Fukuoka 812-8581, Japan, email: hirook@geo.kyushu-u.ac.jp)

A general circulation model developed at Kyushu University has been used to examine effects of interannual variation of Arctic and Antarctic ozone holes on the general circulation of the middle atmosphere. In the model, ozone photochemistry is calculated by a parameterized Chapman cycle and is interactively coupled with radiation and dynamics. In order to simulate the ozone hole, the polar ozone destruction is expressed by a parameterized loss term added in a continuity equation for the ozone mixing ratio, which is initiated under suitable switch-on conditions. We have performed the experiment over successive five years with the interannual variation of ozone holes which is produced by internal nonlinear atmospheric dynamics as well as by slightly changing the threshold values of the switch-on conditions and in good agreement with observations. The general circulation exhibits interannual variability owing to feedback processes of the ozone holes. The degree and spatial structure of the variability are discussed with relation to those of the ozone holes, compared with corresponding observations.

**MI12/W/08-B4** **1710**

**STRATOSPHERIC OZONE VARIABILITY RESULTING FROM UNCERTAINTIES IN THE NOX PRODUCTION FROM LIGHTNING**

Sergei P. SMYSHLYAEV (Russian State Hydrometeorological Institute, 98 Maloostinskiy, St.Petersburg 195196, Russia, e-mail: smyshl@meteo.shmi.spb.ru)

A two-dimensional chemistry transport model with input parameters from a global circulation model is used to evaluate stratospheric ozone sensitivity to the strength of NOx lightning production. NOx production from lightning is one of the most important sources of reactive nitrogen in the atmosphere. Recent studies of NOx produced from lightning have concluded that the magnitude of this source is likely to be between 2 and 25 Tg N/year and cannot be better quantified at this time. Major variability in the effect of lightning on the background levels of atmospheric nitrogen oxides may lead to variability of ozone in the lower stratosphere and to uncertainties in the calculated effects of man-made impacts on the atmospheric ozone layer. To examine the role of NOx lightning production uncertainties in the atmospheric ozone variability, we have done a number of numerical experiments with the SUNY-SPB two-dimensional model. The amount of nitrogen oxides produced by lightning discharges was varied from 2 to 25 TgN/year. Results of model calculations show that ozone distribution in the lower atmosphere is very sensitive to the strength of NOx production from lightning. Assessment of man-made impacts on the ozone layer, such as chlorofluorocarbons and halons emissions and aircraft ejections are especially sensitive to the nitrogen lightning production.

Friday 30 July AM

Presiding Chair: M. Baldwin, (Northwest Research Associates, Bellevue, USA)

MI12/W/06-B5

Invited

0900

## GRAVITY WAVE VARIABILITY IN THE MIDDLE ATMOSPHERE

Robert A. VINCENT (Department of Physics and Mathematical Physics, University of Adelaide, Adelaide 5005, Australia, e-mail: rvincent@physics.adelaide.edu.au)

The seasonal and geographical variability of gravity wave activity in the middle atmosphere has been studied by a variety of techniques, including rockets, radiosondes, radar, lidar and satellites. The aims of these studies include the statistical description of the wave field and determining sources. Recent observations will be reviewed and some of the factors that influence their interpretation, such as the filtering effects of the background winds and observational selection, discussed.

MI12/W/11-B5

0945

## LONG-TERM TRENDS IN LOWER STRATOSPHERIC CIRCULATION AND THEIR INFLUENCE ON COLUMN OZONE TRENDS AT NORTHERN MID-LATITUDES

Lon HOOD, S. Rossi, and M. Beulen (Lunar and Planetary Laboratory, University of Arizona, Tucson, Arizona 85721, USA, e-mail: lon@lpl.arizona.edu)

It is well established that a major cause of global column ozone trends is heterogeneous chemical losses on lower stratospheric aerosols in the presence of increasing concentrations of anthropogenic chlorine and bromine. However, at northern mid-latitudes, several studies have obtained empirical evidence that a significant fraction (as much as 40 per cent) of the zonally averaged column ozone trend in winter and early spring is attributable to differences in ozone transport associated with long-term changes in lower stratospheric circulation. At certain longitudes, e.g., over western Europe, the contribution to ozone trends from this source is well over 50 per cent. We investigate here the origin of changes in lower stratospheric circulation in winter that have been responsible for this effective contribution to mid-latitude ozone trends. The primary signature of the circulation trend consists of a modification of the zonal wind field in the upper troposphere and lower stratosphere such that the winter vortex is strengthened near 60 N and weakened near 30 N. This results in a less cyclonic mid-latitude meridional wind shear that favors the occurrence of more anticyclonic breaking events. The acceleration of the vortex near 60 N is associated with polar cooling and has been predicted by some GCM's that include greenhouse gas forcing. However, a portion of the polar cooling is also attributable to chemical ozone depletion.

MI12/W/14-B5

1005

## A CHANGE IN THE ABUNDANCE OF SUB-TROPICAL INCURSIONS INTO THE MID-LATITUDE LOWER STRATOSPHERE

Stephen J. REID (National Research Council, Washington D.C./NOAA Aeronomy Laboratory); Adrian F. Tuck and George N. Kiladis (NOAA Aeronomy Laboratory, Boulder, Colorado 80303, USA)

Incursions of tropical and subtropical air into the middle latitude lower stratosphere have been modelled by a number of researchers. The presence of a lower-stratospheric minimum in ozone, identified by an ozone content of  $\sim 200$  ppbv, reduces the total column by 10-15% over several million square kilometres. According to the 30-year record of ozone data archived by the World Ozone Data Center in Canada, the number of minima entering the northern mid-latitude lower stratosphere has increased in recent years. The lowest ozone concentrations within the ozone minima are generally found in the isentropic range 370-380K, coincident with the altitude of the subtropical tropopause break. Clusters of back trajectories from each minimum detected at mid-latitude ozonesonde stations demonstrate that air containing an ozone minimum is subtropical in origin. An increase in the number of such events has implications for the mid-latitude ozone trend. In-situ measurements obtained by NASA's ER-2 aircraft in the subtropics and mid-latitudes show the presence of ozone minima. The suite of onboard instruments also reveals corresponding maxima in N<sub>2</sub>O, CH<sub>4</sub> and CO, coupled with low H<sub>2</sub>O. The concentrations of N<sub>2</sub>O and H<sub>2</sub>O in particular suggest a strong tropical tropospheric component in these air masses. The global distribution of ozone minima, and minima/maxima in several other tracers, are provided by HALOE and SAGE II data. Evidence for dynamical changes which may be responsible for the increased numbers of mid-latitude ozone minima is provided by a statistical treatment of the NCEP re-analyses data set.

MI12/W/17-B5

1055

## MEASURES OF SMALL SCALE VARIABILITY AND FRACTALITY IN TIME SERIES OF STRATOSPHERIC AIRCRAFT AND BALLOON DATA

Adrian TUCK (NOAA Aeronomy Laboratory, 325 Broadway, Boulder CO 80303-3328, USA, e-mail: tuck@al.noaa.gov); Susan Hovde (CIRES/NOAA Aeronomy Laboratory, 325 Broadway, Boulder CO 80303-3328, USA, e-mail: hovde@al.noaa.gov); Michael Proffitt (CIRES/NOAA Aeronomy Laboratory, 325 Broadway, Boulder CO 80303-3328, USA, e-mail: proffitt@al.noaa.gov)

Four measures of variability are applied to time series of meteorological and chemical quantities observed from the ER-2, WB57F and balloons. Modulation factor and relative dispersion give results that show maximum values in regions of sharp gradients, that is to say edges of filaments and laminae. The calipers measure, used in a way preserving phase information, shows minimum values at the centre of filament edges and maxima elsewhere; the fraction of 1 Hz time intervals having zero variability above instrument noise reveals a maximum scale of 3.2 km (16 s) for unmixed filament edges. The measure also reveals that over scales larger than about 60 km ozone has near maximum possible variability, and that about 65% of all 1 Hz bins are still inhomogeneous at 600 m. The Hurst exponent H is used to examine fractality, with the result that all quantities observed with adequate S/N ratio are indeed self-affine fractals; ozone and horizontal wind speed are random (H=0.5), wind direction has a small tendency to persistence (H>0.5), temperature is persistent (H>0.5) and vertical wind speed is antipersistent (H<0.5). It is argued that the measures together provide a sharper instrument than traditional power spectral analysis. The implications for stratospheric mixing and its affect upon calculations of chemical loss rates are discussed. Balloon data are examined up to 40 km, where the slow motion relative to the air and low pressure extend the examination for homogeneity as a function of scale.

MI12/E/02-B5

1115

## TIME SERIES OF REACTIVE BROMINE, CHLORINE, AND NITROGEN SPECIES TOGETHER WITH OZONE OBSERVED AT ARRIVAL HEIGHTS (77.8S), ANTARCTICA

Karin KREHER, Gregory E. Bodeker, Stephen W. Wood, Brian J. Connor, and Paul V. Johnston (National Institute of Water and Atmospheric Research, Private Bag 50061, Omakau, 9182, New

Zealand, email: k.kreher@niwa.cri.nz, g.bodeker@niwa.cri.nz, s.wood@niwa.cri.nz, b.connor@niwa.cri.nz, p.johnston@niwa.cri.nz) Philip M. Solomon (Dept. of Physics and Astronomy, State University of New York at Stony Brook Stony Brook, NY, email: psolomon@sbastk.ess.sunysb.edu)

Since 1993 ground-based measurements of OCIO and NO<sub>2</sub> have been made at Arrival Heights with a new diode array spectrometer. In 1995 measurements of BrO and ozone were added using the same instrument. Spectra in the UV/visible wavelength region are taken throughout the day and during the twilight period (solar zenith angle < 96) using zenith sky absorption spectroscopy.

Total column measurements of OCIO, BrO and NO<sub>2</sub> are presented to show diurnal, seasonal and interannual changes. These observations are discussed in the context of supplementary data sets such as total columns of ClO, HCl, HNO<sub>3</sub> and NMC temperatures. Due to dynamically induced displacements of the vortex, observations at Arrival Heights are made in three regions: inside the polar vortex, in the vortex boundary region and outside the vortex. For a quantitative analysis, Ertel's potential vorticity and wind fields from the NCEP/NCAR reanalysis data set and the UKMO data set are used to define these three dynamically distinct regions and to investigate differences in stratospheric chemistry in these regions based on the observations discussed above.

MI12/E/05-B5

1135

## MID-LATITUDE PLANETARY WAVE INFLUENCE ON THE SEVERITY OF ANTARCTIC OZONE DEPLETION

G.E. BODEKER, J.G. Keys and B.J. Connor (National Institute of Water and Atmospheric Research, Lauder, Private Bag 50061, Omakau, Central Otago, 9182, New Zealand)

Previous studies [Bodeker and Scourfield, 1995; Shindell et al., 1997] have shown that mid-latitude planetary waves play an important role in modulating the inter-annual variability in Antarctic ozone depletion. Planetary waves affect vortex temperatures above 25 to 30 km through heat transport, affect vortex area and isolation by eroding material from its edge, and affect sunlight conditions inside the vortex by elongating it and displacing its center from the pole. The purpose of this paper is to use global ozone and meteorological measurements to demonstrate more quantitatively these wave-vortex interactions and to better understand how they determine the severity of Antarctic ozone depletion.

Daily global total column ozone data from 1978 to 1997 were obtained from four different Total Ozone Mapping Spectrometer (TOMS) experiments and the Global Ozone Monitoring Experiment (GOME). These data were regridded by equivalent latitude calculated on the 450 K surface [Nash, 1996] and zonal means were calculated. Equivalent latitude mapping provides a vortex centered co-ordinate system which preserves steep meridional gradients across the vortex boundary when calculating zonal means. Likewise, daily 450 K NCEP/NCAR reanalysis temperatures for the same time period were regridded by equivalent latitude and zonal means were calculated. A measure of the strength of the polar vortex was derived by multiplying the first derivative of 450 K potential vorticity with the mean wind field along PV isolines as in Nash [1996]. The meridional maximum in this quantity defines the vortex edge and allows calculation of the vortex area. Mid-latitude planetary wave amplitudes for the first 6 wave modes are diagnosed by Fourier analyses of daily 20 hPa geopotential heights. Daily Antarctic depleted ozone mass values [Bodeker and Scourfield, 1995] are used to quantify the severity of Antarctic ozone depletion. The chain of events linking mid-latitude planetary wave variability to variability in the severity of Antarctic ozone depletion is investigated through lagged cross-correlation and linear least squares regression analyses of time series derived from the data sets discussed above. By examining the time lags revealed by these cross-correlations we plan to test the modelling based observation [Shindell et al., 1997] that midwinter wave activity may be the best predictor of the severity of the ozone hole the following spring.

MI12/E/04-B5

1155

## INTERANNUAL VARIABILITY OF THE SOUTHERN WINTER POLAR VORTEX RELATED TO THE EQUATORIAL QBO

Yoko NAITO and Isamu Hirota (both at Department of Geophysics, Kyoto University, Kyoto 606-8502, Japan E-mail: naito@kugi.kyoto-u.ac.jp)

The correlation between the polar vortex in the northern winter and the equatorial quasi-biennial oscillation (QBO) has been studied long time since Holton and Tan (1980).

On the other hand, the evolution of the stratospheric circulation in the southern winter is different from that in the northern winter. Any major warming is not observed, and the polar-night jet shifts poleward and downward in late winter to early spring. The year-to-year variation of the timing of this shift-down makes the large interannual variability in connection with the planetary wave activity.

In order to investigate the variability, we made statistical analysis by using the NCEP/NCAR reanalysis data over 40 years (1958-1997). Unlike the northern winter, the polar-night jet in the southern winter has the largest correlation with the QBO in spring. It is found that, in November, the jet is stronger (weaker) in the westerly (easterly) category of the QBO. Further discussion is made in term of the planetary wave propagation and its interaction with the mean flow.

MI12/W/16-B5

1215

## EFFECT OF THE QUASI-BIENNIAL OSCILLATION (QBO) ON TRACER TRANSPORT - INTEGRATION WITH KASIMA (KARLSRUHE SIMULATION MODEL OF THE MIDDLE ATMOSPHERE)

Irmgard LANGBEIN and Wolfgang Kouker (Institut fuer Meteorologie und Klimaforschung Forschungszentrum Karlsruhe, Postfach 3640, D-76021 Karlsruhe, Germany)

The quasi-biennial oscillation (QBO) of the zonal wind in the equatorial tropical stratosphere significantly influences the transport of long-lived tracers and their distribution in the stratosphere. To see what role the QBO plays in the transport of tracers, a perturbation has been applied to the model wind field of the Karlsruhe Simulation Model of the Middle Atmosphere (KASIMA, a 3-dimensional primitive equation model), to simulate the effect of the QBO.

From the ECMWF dataset of the period from 1979 to 1994 the mean zonal wind was calculated and the time-height cross section showed a QBO in the equatorial region. From a harmonical analysis of this oscillation we determined the amplitudes and phases as a function of height and latitude. By applying a band pass filter, high and low frequent oscillations are suppressed. A zonal wind with an idealised QBO is reconstructed from this amplitudes and phases.

A zonal mean zonal force is applied to the model in the tropics in form of a Rayleigh friction type relaxation term with the idealized QBO-wind as equilibrium wind and a relocation time of 3 days. With this model version the QBO-induced mean meridional circulation, the correlated temperature signal and the influence on the transport of passive tracers are studied in detail and results are discussed.



**MI12/C/MW08/W/08-B5** **1235****THE LARGE-SCALE ZONALLY ASYMMETRIC OZONE DISTRIBUTION**

Dieter H.W. PETERS (Institute für Atmosphärenphysik an der University of Kuhlungsborn, Meckleburg-Vorpommern, D-18225, Germany, E-mail: peters@iap-kborn.de)

The large-scale zonally asymmetric ozone distribution is mainly determined by advective transport of quasi-stationary waves in winter of northern and southern hemisphere. It is well known, that a decadal change of the quasi-stationary wave structure in the 80ies caused a change of the large-scale ozone distribution, especially in January over Europe, here we found a total ozone decrease of the same order as the zonal mean trend. In this paper we want to examine the role of quasi-stationary wave structure changes for changes of the zonally asymmetric ozone field in the 60ies and 70ies on the basis of re-analyses data. A linear transport model is used to perform transport calculations as a function of given geopotential and zonal mean ozone. A comparison and discussion of the model results for the North Atlantic European region with results received for the 80ies are presented.

**MW02****Wednesday 28 July****ON THE USE OF GLOBAL DATASETS TO VALIDATE AND IMPROVE ATMOSPHERIC PROCESSES IN CLIMATE MODELS**

Location: Chemical Engineering G35 LT

**Wednesday 28 July AM**

Presiding Chair: G. Tselioudis (NASA/GISS New York, USA)

**Introduction** **0830**

G. Tselioudis

**MW02/E/08-B3** **0840****HOW DOES THE GLOBAL-SCALE ATMOSPHERIC CIRCULATION PRODUCE CLOUDS?**

William B. ROSSOW (NASA Goddard Institute for Space Studies, 2880 Broadway, New York, NY 10025, USA, e-mail: wrossow@giss.nasa.gov)

Although clouds are produced by "micro-scale" processes, these processes operate as a response to global-scale atmospheric motions to produce the complex geographic distribution of clouds on Earth. One way to attack this larger-scale problem is to combine global-scale satellite observations of cloud property variations with global-scale determinations of the atmospheric circulation. Such a global data analyses can be used to describe the mean characteristics of clouds and their variations, to identify systematic relations among observed cloud properties and atmospheric motions, or to estimate, directly, the derivative relations of the processes at work using statistical life-cycle-composites of cloud system evolution. Another approach is to find what characteristics of the global atmospheric circulation are revealed in observed global-scale cloud variations. All of these results can be used to verify the cloud representations in global climate models. For the first time last type of analysis is possible with the advent of global, satellite-based cloud (ISCCP), precipitation (microwave-based), and water vapor (merged infrared and microwave) datasets, together with global wind datasets (ECMWF and NCEP re-analyses), all of which resolve features at least down to the upper end of the mesoscale and cover more than a decade. We report on some preliminary attempts to identify quantitative relationships between atmospheric motions and cloud properties that are relevant to cloud processes. Three examples are given: (1) cloud variations at the smallest scales and what they reveal about the nature of small-scale turbulence in the atmospheric boundary layer, (2) cloud variations at "moderate" weather-scales and what they reveal about meteorological storm systems, and (3) cloud variations at the largest scales and what they indicate about interannual variations of climate.

**MW02/W/04-B3** **0910****THE CHARACTERISTICS OF CLOUD FIELDS AND ENERGY DISTRIBUTION ASSOCIATED WITH SYNOPTIC-SCALE CIRCULATION SYSTEM IN A GENERAL CIRCULATION MODEL**

Cheng-Ta CHEN (Dept. of Earth Sciences, National Taiwan Normal University, Taipei, Taiwan, R. O. C., e-mail: chen@cloud.geos.ntnu.edu.tw) Erich Roeckner (Max Planck Institute for Meteorology, Hamburg, F. R. Germany)

Cloud fields and concurrent atmospheric dynamical structures associated with extratropical cyclone in a general circulation model are constructed using the ensemble mean of the cloud systems traced. The composite pictures of these simulated features are in good agreement with both the recent observational study using satellite cloud climatology and operational analyses and the classical conceptual model for the organization of cloud properties near cold and warm frontal zones. The vertical structure and wave characteristics of various dynamical and hydrological fields linked to the mid-latitude circulation system in the model are resemble to those observed feature characteristics of a baroclinic wave. The new approach to investigate the general properties of cloud system embedded in the focused midlatitude baroclinic activities enables the depiction of the interactions between cloud and circulation in the model. The impact of extratropical frontal system on the ambient atmosphere and its energy and water budget can be easily deduced from the dynamically consistent model data and their direct links to the physical processes in the model. The method provides an unique way to reveal the cloud systems in different climate regimes. Constrained by the empirical and theoretical findings, the composite pattern from the simulation can help in guiding the development of physical parameterization in the model.

**MW02/W/05-B3** **0930****MIDLATITUDE CLOUD VARIATIONS WITH DYNAMIC REGIME IN OBSERVATIONS AND GENERAL CIRCULATION MODELS**

Christian Jakob 1, George Tselioudis 2, and Ulrike Lohmann 3, 1. ECMWF Shinfield Park Reading, RG2 9AX, UK, Tel: (0118) 949-9735, FAX: (0118) 986-9450, e-mail: cjakob@ecmwf.int 2. NASA Goddard Institute for Space Studies, New York, N.Y., U.S.A.; 3. Dalhousie University, Halifax, Nova Scotia, Canada

General Circulation Model simulations of the current climate show large deficiencies in their radiative balance calculations in the midlatitude regions. Many GCMs allow excessive amounts of sunlight to reach the midlatitude surface, casting doubt on the atmospheric models'

climate sensitivity and their ability to drive the ocean circulation when coupled to ocean models. One primary contributor to the midlatitude radiative balance is clouds formed by baroclinic storms. This study will examine the relationship between the structure and strength of the synoptic scale atmospheric patterns and the cloud fields. The 12-hourly NCEP sea level pressure data are used to define three dynamic regimes based on local sea-level pressure anomaly in the midlatitude regions, and the ISCCP dataset is used to accumulate the cloud type distributions in the three regimes. The same analysis method is subsequently applied to current-climate simulations of the GISS, ECHAM, and ECMWF GCMs, in order to try and identify the cloud structure deficiencies that may be responsible for the radiative imbalances in the models' midlatitudes. The ECMWF model will be used to investigate the role model resolution (horizontal and vertical), running mode (short-range forecasts vs. climate simulation), and the cloud parameterization play in the model's ability to represent midlatitude clouds in the different regimes.

**MW02/W/10-B3** **0950****SENSITIVITY STUDIES WITH A NUDGED VERSION OF ECHAM4 FOR THE PURPOSE OF CLOUD VALIDATION**

Hans-Stefan BAUER and Lennart Bengtsson

Clouds are an important regulator of the Earth's radiation budget and present a major link between radiation and the hydrological cycle.

To improve the representation of clouds in our general circulation model ECHAM4 we first validated the model for specific synoptic situations. This was accomplished by using the so-called nudging technique, which enables the validation against observational data. In our simulations vorticity, divergence, temperature and surface pressure are nudged with ECMWF reanalysis fields.

We performed simulations with the resolutions T42 and T106 and diagnosed some systematic differences between the model and ISCCP DX satellite data.

From this basis we performed sensitivity studies with the lower resolution T42 of the nudged model in which we investigate the effects of small changes in the various parameterization schemes. They show the influences of different physical processes on the representation of clouds in distinct synoptic systems.

**MW02/E/03-B3** **1010****THE NORTHERN HEMISPHERE WINTERTIME STORM TRACKS IN HADAM3 AND THE ERA (ECMWF RE-ANALYSIS) DATASET**

L. SHAFFREY AND P. Berrisford (CGAM, Department of Meteorology, University of Reading, Reading, RG6 6BB, U.K., email: L.C.Shaffrey@reading.ac.uk) K. Hodges (ESSC, University of Reading, Reading, U. K., email: Kevin.Hodges@mail.nerc-essc.ac.uk)

The Northern Hemisphere wintertime atmospheric flow is characterised by two regions of synoptic-scale high-frequency eddies which are located over the North Atlantic and North Pacific Oceans, i.e. the Atlantic and Pacific storm tracks.

There are number of ways that the shape, location and strength of the storm tracks can be determined from observations or AGCMs (Atmospheric Global Circulation Models). One method is to use time-filtered variance and co-variance measures such as the high-pass eddy kinetic energy and the high-pass poleward temperature flux. Another method focuses on individual weather systems and involves using a feature tracking algorithm to determine the magnitudes, paths, propagation speeds and growth rates of extra-tropical cyclones as they move through the storm track. Both methods, though conceptually very different, provide complimentary information about the synoptic-scale variability of the mid-latitudes in both models and observations.

In this study the different measures of synoptic-scale variability are calculated from a ten member wintertime ensemble of the United Kingdom Meteorological Office's Atmospheric Climate Model, HadAM3, and are compared with the same measures from the ERA dataset. The prominent differences between the observed and modelled storm tracks are the slow propagation speeds of extra-tropical cyclones in HadAM3 as they move through the Atlantic storm track, and the shape of the Atlantic storm track which is more zonal in the model than in observations. Both these differences can be related to the structures of the time-mean jet streams and steering level flows in HadAM3 and the ERA dataset.

**MW02/E/05-B3** **1100****SENSITIVITY OF THE TROPICAL CLOUD RADIATIVE FORCING TO SEA SURFACE TEMPERATURE: TOWARD AN ASSESEMENT OF CLIMATE MODELS?**

Sandrine BONY, Herve Le Treut (LMD/CNRS, Paris, France); Jean-Jacques Morcrette (ECMWF, Reading, UK); Catherine Senior, Mark Webb (Hadley Center, Bracknell, UK)

We investigate the sensitivity to sea surface temperature changes of the cloud amount, cloud optical properties and cloud radiative forcing derived from satellite observations and from climate model simulations. The following specific questions are addressed: how does the sensitivity vary among climate models, among coupled and uncoupled simulations, and between short-term climate variability and global warming experiments? Implications with regards to the validation of cloud feedbacks produced by climate models will be discussed.

**MW02/W/02-B3** **1120****THE USE OF SATELLITE BRIGHTNESS TEMPERATURE DATA FOR EVALUATING THE DIURNAL CYCLE IN TROPICAL CONVECTION AS SIMULATED BY THE UK METEOROLOGICAL OFFICE UNIFIED MODEL**

Guiying Yang and Julia SLINGO (both at Centre for Global Atmospheric Modelling, Department of Meteorology, University of Reading, Earley Gate, Reading, RG6 6BB, UK. Email: J.M.Slingo@reading.ac.uk)

A global archive of window brightness temperature with high spatial (0.5 degree longitude/latitude) and temporal (3 hourly) resolution has recently been constructed for the period 1983-1996 by the EU Project, 'Cloud archive User Service (CLAUS)'. This contiguous dataset has enabled a range of studies of the temporal and spatial characteristics of tropical convection. The high temporal sampling of the CLAUS dataset has been used to perform a detailed study of the diurnal cycle in tropical convection and clear sky land surface temperatures. The phase and amplitude of the diurnal cycle for different regimes (e.g. deep oceanic convection) have been computed. The results have confirmed the early morning maximum in convection over the tropical oceans, whereas continental convection tends to peak in the late afternoon and early evening. This analysis has been used to evaluate the simulation of the tropical diurnal cycle by the latest version of the atmospheric component of the Hadley Centre climate model (HadAM3). The results have shown that the model has various systematic errors in its simulation which can be related to aspects of the physical parameterizations.



MW02/E/04-B3

1140

**HOW WELL CAN CCM3 SIMULATE THE RESPONSE OF UPPER TROPOSPHERE AND LOWER STRATOSPHERE WATER VAPOR AND CIRRUS CLOUDS TO A PERTURBATION IN TROPICAL CONVECTION?**

RONG FU, Mingxiang Chen and John McCormack (Department of Atmospheric Sciences, The University of Arizona, 1118 E. 4th. St., Rm. 576, P.O. Box 210081, Tucson, AZ 85721-0081, USA; 602-621-6955; e-mail: fu@atmo.arizona.edu)

Evaluating the responses of upper troposphere and lower stratosphere water vapor and cirrus clouds to a perturbation in tropical convection in climate models enables us to assess the adequacy of these models in simulating the physical and dynamic processes that determine water vapor and cloud feedbacks. We have used UARS MLS, SAGE II, ISCCP and TOVS data sets to examine both horizontal and vertical structures of water vapor and cirrus clouds in responding to changes in tropical convection. The results suggest that CCM3 appears to adequately capture the sensitivity of water vapor between 500 mb and 200 mb to perturbations in the tropical Pacific in the subtropical clear sky region, although the magnitude of water vapor anomalies disagrees with observation due to errors in convection. The sensitivity of water vapor above 200mb appears to be opposite in sign in large subtropical areas, as suggested by both UARS MLS and SAGE II data. Whether CCM3 can simulate this vertical dependence of water vapor sensitivity on convection and the underlying processes will be discussed. The responses of water vapor and cirrus clouds to changes in continental atmospheric deep convection, as in the Amazon basin, will also be evaluated.

MW02/W/03-B3

1200

**CONSISTENCY BETWEEN TROPICAL DIVERGENT CIRCULATIONS FROM REANALYSIS DATA SETS AND SATELLITE-DERIVED PRECIPITATION, RADIATION, AND SURFACE FLUXES**

IFranklin R. ROBERTSON, 2John Roads,3H.-I. Lu, 3Eugene W. McCaul, 1NASA / Marshall Space Flight Center, Global Hydrology and Climate Center, Huntsville, AL 35806, 2Scripps Institution of Oceanography, UCSD, 0224 , La Jolla, CA 92093-0224 , 3Universities Space Research Association, Global Hydrology and Climate Center, Huntsville, AL 35806

Large-scale divergent circulations are part of the atmospheric dynamic response to diabatic heating from condensation, radiative processes, and surface heat fluxes. Vertical motion and the associated divergent wind is thus intimately tied to the hydrologic cycle and the global heat balance. Vertical motions are recovered diagnostically from reanalyses and, as such, are subject to shortcomings in model physics, numerics, and data availability. We use several GEWEX EOS data sets derived from satellite data to assess interannual divergent flow anomalies in the NCEP, GSFC, and GSFC DAO analyses. Among the data sets are monthly, 2.5 degree gridded precipitation (MSU and SSM/I-based), TOA radiative fluxes from ERBS, surface radiative fluxes from the SRB project, and surface latent and sensible flux estimates from SSM/I. These data sets can be considered as independent of the reanalysis fields. We focus largely on the period 1987-1989 encompassing a strong El Niño / La Niña couplet. Consequently we emphasize interannual changes as well as climatological aspects of the reanalyses. In the processes of this study we use simple integral constraints enforced through the satellite-derived data sets to derive corrections to the divergent circulation produced from the reanalyses. We examine the implications of these corrections in describing how perturbations to the tropical heat balance evolve during a warm / cool couplet. In particular the perturbations to the planetary scale water vapor transport, and the resulting changes in TOA and surface radiative fluxes are considered.

MW02/L/01-B3

1220

**MOISTURE TRANSPORT OVER THE AUSTRALIAN CONTINENTAL IN THE 1997/1998 ENSO EVENT: COMPARISON OF MODEL RESULTS WITH NCAR/NCEP REANALYSIS**

HUQIANG ZHANG (Environment Division, Australian Nuclear Science and Technology Organisation, PMB 1, Menai, NSW 2234, Australia); Carsten Frederiksen (Bureau of Meteorology Research Centre, GPO BOX 1289K, VIC 3001, Australia); Ann Henderson-Sellers (Environment Division, Australian Nuclear Science and Technology Organisation, PMB 1, Menai, NSW 2234, Australia).

Every El Niño event has its own unique development. In addition, the regional and global impacts of the associated large tropical SST anomalies may vary between different events. For example, the 1997/1998 El Niño event did not produce as severe a drought over the Australian continent as was expected. Both statistical and numerical models showed limited skill in forecasting Australian rainfall anomalies. Improving our understanding of how large tropical SST anomalies affect Australian rainfall requires more diagnostic and modelling studies of the related physical and dynamical processes. In the current study, we focus our attention on the water vapour budget and horizontal moisture transport over the Australian continent. A climatology of regional moisture transport is established using the 40-year (1958-1997) NCAR/NCEP reanalysis data. From the analysis we note that there are some biases between the observed Australian rainfall climatology and that derived from the reanalysis data. We discuss how the biases affect our analysis and validation. Using monthly averaged reanalysis data, several past El Niño events covered by the reanalysis period are synthesized to give a general picture of how moisture transport changes during the El Niño events. We then study the changes of moisture transport and water vapour budget during the 1997/1998 El Niño event in more detail. Results from a set of AGCM experiments conducted in the 1997/1998 period by using persistent SST anomalies are compared with the results from the reanalysis data. The aim is to try to understand how the simulated changes of horizontal moisture transports affect the model rainfall forecasts and which factors contribute to those differences seen between the model and reanalysis results. The importance of soil moisture initialization and parameterization is also discussed.

Wednesday 28 July PM

Presiding Chair: H. LeTreut (LMD, University P. et M. Curie, Paris, France)

MW02/W/09-B3

1400

**GLOBAL SATELLITE CLOUD OBSERVATION DATA SETS**

G. Garrett CAMPBELL (CIRA/CSU, Ft. Collins, CO 80523)

Two distinct satellite based cloud climatologies are available for comparison to model simulation: ISCCP and the Pathfinder Atmospheric Cloud products. ISCCP assigns 100% cloudiness to pixels which are colder or brighter than a background radiance. Patmos constructs a similar background, but then assigns a cloud fraction using a radiation budget approach to account for partly cloudy pixels. These two data sets will be compared for the period 1983 to 1993. Generally Patmos measures less cloudiness than ISCCP. These measurements should bracket model simulations of the Earth's climate. An NCAR Community Climate Model simulation of the variation of cloudiness for this period will also

be compared. This run used the monthly sea surface temperature observations to force the model, so the month to month cloud variations can be compared, not just the seasonal cycle. In most cases this model shows more cloudiness than either ISCCP or Patmos.

Better matches between the observations and the simulations occur when the seasonal cycle is removed: anomaly series. The most obvious feature is the El Niño events over the last 2 decades. In addition the model and observations match in the Atlantic area. The model and the real atmosphere are forced by the sea surface temperature in tropical areas. Some results can be viewed at <http://acamar.cira.colostate.edu/>.

MW02/W/08-B3

1420

**GLOBAL PRECIPITATION DATASETS OF GPCP: RESOLUTION, QUALITY-CONTROL AND ERROR ASSESSMENT**

Bruno RUDOLF, Deutscher Wetterdienst, Offenbach/Germany

The objective is to provide the climate research community with gridded datasets of global precipitation derived from observational data. The continents are covered by more or less dense raingauge networks supplying in-situ observations, which are the most reliable data base, while satellite-based estimates are subject to larger biases and stochastic errors and need to be adjusted to conventionally measured data. The reference-status of in-situ data requires very careful handling and quality-control of the data, compensation of systematic errors and assessment of remaining stochastic errors. The Global Precipitation Climatology Centre (GPCC) disseminates gridded datasets of precipitation derived from 6,000 to 7,000 near-realtime data for the landsurface on a monthly routine basis. The gridded results are available on internet for the period beginning with January 1986 and are complemented regularly month by month under the name 'GPCC Monitoring Product' with a lag of two months after observation. Analyses including additional data from 40,000 stations supplied by the individual countries are in preparation.

MW02/E/07-B3

1440

**ON THE TEMPORAL SAMPLING ERRORS IN GLOBAL DATASETS**

ISAMU YAGAI, Takahiro Kayahara, and Kimpei Ichiyagagi National Research Institute for Earth Science and Disaster Prevention, Tsukuba Ibaraki 305, Japan

Recent development of orbital satellite such as TRMM (Tropical Rainfall Measuring Mission) makes very high spatial resolution observation of physical quantity but the sampling time is poor compared to the ordinary routine observation. Therefore, when they make monthly mean distributions of rainfall or other variables from TRMM observations, they have to experience sampling time error problems. Although the sampling problems in the observations are not new ones, we obtained interesting results by using the sophisticated climate model and REANALYSES data by ECMWF. The model used here has twenty-one layers in the vertical with the top level at 10 hPa, and a horizontal resolution of T42. The time integration starts at 31 December 1980; the initial condition of the model atmosphere adopted from the value in the long time integration. We used two kinds of data sampling interval. One is 6 hours which can analyze diurnal variations and the other 30 hours for climate analyses. When we compare the monthly mean values for each different sampling time case, relatively large temperature difference about 2.5 K appeared at high latitudes in the troposphere in the northern hemisphere. There are also large values about 4.5 K seen at high latitudes in the stratosphere due to stratospheric sudden warmings. For specific humidity the situation is quite different; large differences appeared near the boundary between land and sea at 925hPa. At 100hPa level large difference are seen near the equator since the moisture at this level is brought up by the cumulus convection and the convections have strong diurnal variations. Sampling time errors are seen in particular area in the globe, which are different in each physical quantities and associated phenomena.

MW02/W/07-B3

1500

**PARAMETERIZING UNRESOLVED SCALE INTERACTIONS**

E. KAAS, A. Gulberg, W. May, Danish Meteorological Institute, Denmark and M. Deque, Meteo-France, France.

A parameterisation of non-linear dynamical interactions with unresolved scales - usually referred to as horizontal diffusion - is needed in most atmospheric models to ensure realistic fluxes of energy and enstrophy near and at the truncation limit. In this paper a minimisation of tendency errors in low to medium resolution versions of the ARPEGE/IFS and the ECHAM4 general circulation models is sought in order to obtain spectral empirical interaction functions (EIFs) to be used in the formulation of horizontal diffusion. The tendency errors are calculated relative to reanalysis data and high resolution adiabatic versions of the models themselves. Different EIFs are obtained for vorticity, divergence and temperature. The most striking feature is that the vorticity and partly the temperature EIF has non-negligible negative values for low wave numbers in large parts of the troposphere. This implies that these waves are enhanced in amplitude due to non-linear scale interactions with unresolved scales. At low resolution the generation/dissipation of kinetic energy due to the interactions is not well parameterised by neither the standard horizontal diffusion nor when using the EIFs in this parameterisation. When the EIFs are used in the formulation of horizontal diffusion it is seen that the spectrum of kinetic energy is closer to observations than in the original model versions. Furthermore, the large scale systematic model errors are reduced in a medium resolution simulation, while less clear improvement is seen in a simulation at low resolution.

MW02/E/09-B3

1520

**OBSERVATIONAL AND MODELED ESTIMATES OF TEMPERATURE CHANGE IN THE FREE ATMOSPHERE**

JUSTIN J. HNILO, Benjamin D. Santer and James Boyle (all at Program for Climate Model Diagnosis and Intercomparison, Lawrence Livermore National Lab, Livermore, CA, USA, Email: hnilo@pcmdi.llnl.gov)

Observed Microwave Sounding Unit (MSU) brightness temperatures have been the focus of much spirited debate within the atmospheric science community given their lack of any significant lower tropospheric warming trend. This work uses observed and model data to compare different methods of producing simulated MSU temperatures. Data used herein are the ECMWF and NCEP reanalyses, the Comprehensive Aerological Reference Dataset (CARDS), the Hadley Centre radiosonde datasets (versions 1.1 and 1.2) and where possible, preliminary results from participant AMIP II models. Two methods of deriving a simulated MSU temperature will be employed. The first is a view angle resolving radiative transfer model which incorporates both skin and profiles of temperature as well as profiles of moisture and variations of surface emissivity. The second method is a simpler global weighting function applied directly to the profile of temperature. Global and hemispheric simulated values for these two methods are highly correlated and yield similar decadal trends and variability. At smaller scales,

however, the two methods exhibit much larger differences, particularly in the troposphere. These regional differences are largely attributable to differences in the vertical coherence of temperature profiles and in the spatial variability of moisture changes. On regional scales, therefore, the use of two different methods to simulate a satellite signal from the same data can yield two different answers.

**MW02/W/06-B3****1600****HEAT TRANSPORT IN THE ATMOSPHERE AND OCEAN**

Paul BERRISFORD and Alan O'Neill (CGAM Department of Meteorology University of Reading Reading RG6 6BB U.K.).

Over long timescales the Earth absorbs more solar radiation in tropical regions than it does at higher latitudes. Similarly, more longwave radiation is emitted to space in the tropics than at high latitudes. However, the net effect of these two processes is that energy is absorbed at low latitudes and emitted to space at high latitudes.

Assuming that over long timescales the heat storage in the Earth's atmosphere and oceans does not change then the atmosphere and ocean must transport heat from the tropical regions to high latitudes. Heat transport in the atmosphere and ocean is investigated using the European Centre for Medium-Range Weather Forecasts (ECMWF) Re-Analysis (ERA) dataset covering the period January 1979 through to December 1993. The heat transports of the atmosphere, ocean and the combined system are computed separately for the fifteen year climatology and the individual annual means. These results can be compared with previous estimates of the heat transports. Given that the heat transports in the atmosphere and ocean add up to that required for the combined system, an intercomparison of the heat transports in the three systems allows an estimation of the internal consistency of the ERA data to be made. This gives an indication of how reliable the results are.

Heat transports are also calculated from the AMIP-II dataset and these results are compared with the results from the ERA.

**MW02/W/01-B3****1620****RELATIONSHIP OF OPTICAL DEPTH WITH EFFECTIVE RADIUS IN ECHAM AND OBSERVATIONS**

Ulrike LOHMANN (Dept. of Physics, Dalhousie University, Halifax, NS, B3H 3J5, Canada, email: Ulrike.Lohmann@Dal.Ca)

ISCCP data were analyzed in terms of the relationship of cloud albedo and liquid water path with droplet size. It was found that only for optically thick clouds (with an optical depth > 15) and for clouds over land the cloud albedo increase with decreasing droplet size, which is the underlying assumption for the indirect aerosol effect. For optically thinner clouds (with an optical depth < 15) the time available for droplet growth leads to an increase in liquid water path and cloud albedo with increasing droplet size. For all warm clouds the liquid water path increases with increasing effective radius as to be expected in the droplet growth state where CDNC is almost constant. The ECHAM model was analyzed and the opposite behavior for optically thin and thick clouds over the oceans is captured. However, the land-sea contrast for optically thin clouds is not simulated. Here we want to investigate why optically thin and thick clouds behave so different with changing effective radius.

**MW02/E/02-B3****1640****VALIDATION OF TOA RADIATION AND CLOUD SIMULATIONS BY DIFFERENT LMD GCM VERSIONS IN MIDDLE AND EQUATORIAL LATITUDES**

Igor I. MOKHOV (A.M.Obukhov Institute of Atmospheric Physics RAS, 3 Pyzhevsky, Moscow 109017, Russia, e-mail: mokhov@omega.ifaran.ru) Marie Doutriaux-Boucher (Laboratoire d'Optique Atmosphérique, Université de Lille-1, e-mail: mdoutri@loa.univ-lille1.fr) Alexey V. Eliseev (A.M.Obukhov Institute of Atmospheric Physics RAS) Herve Le Treut (Laboratoire de Meteorologie Dynamique, Université PetM Curie, e-mail: Herve.Letreut@lmd.jussieu.fr)

The ERBE data are used for validation of radiation fluxes at the top of the atmosphere (TOA) in the three LMD GCM versions with a quite different parameterizations of physical processes. The objective of this analysis is to show that a restricted number of key longitudinal profiles offers a good insight into the behaviour of different model versions. Detailed analysis is done for selected sections in middle and equatorial latitudes with a remarkable cloudiness due to intensive cyclonic or convective activity. The satellite ISCCP data together with ground-based data for clouds of different types have been used for the combined analysis of the causes of systematic model errors. Significant problem exhibit simulations of cloud radiative forcing (CRF) over oceans in the middle NH latitudes, especially in winter. It is related with simulation of clouds and CRF over storm tracks. Overestimation by models of the longwave CRF with not too strong negative shortwave CRF lead to the significant overestimation of the net CRF. It can result in the too strong positive cloud-related feedback with the increase of model sensitivity (at least at the regional scale) to different influences, particularly to the anthropogenic one. One of the important conclusions can be done for equatorial regions, in particular for Pacific regions with the realization of ENSO effects.

**MW02/E/01-B3****1700****SURFACE CLEAR-SKY LONGWAVE IRRADIANCES IN CLIMATE MODELS**

J.R.GARRATT (CSIRO Atmospheric Research, Aspendale, Vic.3195, Australia)

The clear-sky longwave irradiance at the surface (Clis) is an important property of climate and climate change and one of the principal drivers of the planet's greenhouse effect. We use mean monthly, grid-point results from three climate model simulations (NCAR, UKMO and CSIRO) and from the NCEP-NCAR re-analysis (based on the NCEP climate model) to investigate the seasonal and regional behaviour of Clis. In addition, we utilise global datasets of observed column water vapour (W) and screen-air or surface temperature (T) to validate indirectly the model simulations using the algorithm of Dilley and O'Brien (1998 - Quart. J. Roy. Meteorol. Soc., 124A, 1391-1401) for predicting Clis (to ~ 5W per square metre). Over the oceans, annually-averaged Clis in the model simulations is a strong function of T, but less so over land. The main reason relates to the close link between W and sea-surface temperature. For monthly Clis (January and July) over the oceans, the dependence upon T forms two distinct branches according to hemisphere, with greatest January - July differences occurring in middle to high northern latitudes in both Atlantic and Pacific Oceans. This is closely linked to the analogous branching of the seasonal column water vapour variation with surface temperature, related to effects of large-scale dynamics on water vapour transport (Webb et al., 1993 - Clim. Dynamics, 9, 117-129). Regional January and July algorithm-determined fluxes (typical values of 250 to 350 W per square metre), using both observed and model-generated fields of W and T, are mostly within \* 5 to 15 W per square metre of model fluxes. The analysis provides further support for the Dilley-O'Brien algorithm in determining mean monthly values of Clis from W and T, particularly when more detailed radiative models are either unavailable or their use impractical.

**MW02/E/06-B3****1720****A GLOBAL COMPARISON OF GPCP PRECIPITATION OBSERVATIONS WITH MODEL-GENERATED ESTIMATES**

SCOTT CURTIS (JCET/UMBC NASA/GSFC, Code 912, Greenbelt, MD, 20771); Robert Adler (NASA/GSFC, Code 912, Greenbelt, MD, 20771); George Huffman (NASA/GSFC, Code 912, Greenbelt, MD, 20771).

The Global Precipitation Climatology Project (GPCP) community dataset blends satellite observations (SSM/I, IR, TOVS) and rain gauge data into a globally complete monthly product, available from January 1986 to present. This dataset is useful for monitoring climate variability on the synoptic scale. A primary objective is to validate model precipitation output with GPCP observations. Global satellite-derived precipitation estimates on smaller time and space scales will also be used for these purposes, including pentad averages of the SSM/I-based Goddard Profiling Algorithm (GPROF) and the new one degree daily (1DD) microwave-adjusted, IR-based estimates. In a recent study, Janowiak et al. (1998) quantified differences between GPCP observations and the NCEP reanalysis. In light of the fact that NCEP does not assimilate precipitation observations in their reanalysis product, substantial differences were found in the globally averaged precipitation rates, seasonal cycle, and interannual variability. NCEP is somewhat higher (3.0 mm day<sup>-1</sup>) than GPCP (2.8 mm day<sup>-1</sup>) in the global average which is mainly due to tropical rainfall. Our investigations into the 1997-98 ENSO revealed that NCEP tended to produce more positive than negative precipitation anomalies. For example, NCEP showed wet conditions over the Indian sub-continent, while GPCP observations did not. Also, NCEP did not have the extremes in rainfall observed in the tropical Pacific.

The precipitation estimates of other models will also be compared to satellite derived observations on a range of time and space scales. Finally, a component of this study will compare GPCP with model-produced circulation fields (divergence, vertical motion, precipitable water) to help us better represent and understand the global hydrologic cycle and elucidate improvements to the model's representation of atmospheric processes.

Janowiak, J. E., A. Gruber, C. R. Kondragunta, R. E. Livezey, G. J. Huffman, 1998: A comparison of the NCEP-NCAR reanalysis precipitation and the GPCP rain gauge-satellite combined dataset with observational error considerations. J. Climate, 11, 2960-2979.

**MW03****Thursday 29 July****DEVELOPMENT OF HIGH RESOLUTION CLIMATE MODELS (ICCL)**

Location: Chemical Engineering G35 LT

**Thursday 29 July AM**

Presiding Chairs: C R Mechoso (Univ. of California, Los Angeles); J L McGregor (CSIRO Atmospheric Research, Victoria, Australia)

**Introduction****0930**

M. Sugi (Meteorological Research Institute)

**MW03/E/06-B4****0935****THE IMPACT OF INCREASING HORIZONTAL RESOLUTION ON THE HADLEY CENTRE MODEL HADAM3**

Rachel STRATTON (Hadley Centre for Climate Prediction and Research, Met Office, London Road, Bracknell, RG12 2SY, UK. Email: rastratton@meto.gov.uk)

HadAM3, the latest version of the atmospheric part of the Hadley Centre climate model, has been used for a series of AMIP II integrations to investigate the sensitivity of the model to horizontal resolution. The investigation has been done using a higher vertical resolution (roughly 50hPa in and around the troposphere) than previously used for most climate resolution studies. Three integrations have been performed, all with the same 30 vertical levels, as follows:

Name resolution	lat x long	timestep	physics	dynamics of run at midlatitudes	length resolution in km
SRES	2.5 x 3.75	15 min	15 min	17 years	300
MRES	1.25 x 1.875	15 min	15 min	17 years	150
HRES	0.888 x 1.25	10 min	5 min	10 years	100

where SRES is the horizontal resolution usually used for climate simulations. The HRES simulation is comparable in resolution to recent operational forecast models. For example it is comparable with that used for the ECMWF reanalysis project (ERA).

A comparison of the first 10 year means show that on increasing resolution the westerly jets move polewards in both hemispheres. The mean sea level pressure decreases over the poles and increases between 30 and 60 N/S. At mid-latitudes the troposphere warms, specific humidity decreases, the standard deviations of vertical velocity increases, eddy kinetic energy and eddy fluxes of heat momentum and moisture increase. On the whole the changes due to increased resolution improve agreement with ERA (ECMWF reanalyses for 1979-88). The most significant changes occur in going from SRES to MRES and are mainly due to a better resolution of synoptic scale disturbances.

**MW03/E/02-B4****0950****THE IMPACT OF HORIZONTAL RESOLUTION ON THREE ATMOSPHERIC GCMS**

DOBLAS-REYES, Francisco Javier and Michel Deque (CNRM, Météo-France, 42, Av. G. Coriolis, 31057 Toulouse Cedex, France)

In the HIRETYCS project, a European research project funded by the Environment and Climate programme of the European Commission, the analysis of two AMIP I-type experiments has been undertaken. The experiments use a standard (T42 or equivalent) and a high (T106 or equivalent) horizontal resolutions. Three models have been run under these conditions to simulate the climate of 1979-88, namely the CNRM model, the Hadley Centre model, and the MPI model. The impact of the resolution increase is not systematically positive. The mean climate is in the best cases slightly improved and sometimes degraded. The most remarkable improvements are obtained on the climate variability, since this feature of the GCM is rarely tuned by a choice of empirical parameters which favours the version used in the tuning process, i.e. the standard resolution. Another interesting feature is the fact that the models are very different, and has thus very different systematic errors. But, in many instances, the impact of the resolution increase on this systematic error (which can be either positive or negative) is similar between the three models.



MW03/E/10-B4

1005

**A STUDY ON THE INFLUENCE OF GLOBAL WARMING ON TYPHOON CLIMATOLOGY USING A HIGH RESOLUTION AGCM**

MASATO SUGI, Jun Yoshimura and Akira Noda (Meteorological Research Institute, 1-1 Nagamine, Tsukuba, Ibaraki 305-0052, Japan, email: msugi@mri-jma.go.jp, jyoshimu@mri-jma.go.jp, noda@mri-jma.go.jp)

Influence of global warming on tropical cyclone climatology is studied using two ten-year integrations of the Japan Meteorological Agency (JMA) global model at T106 horizontal resolution. First integration (CNTL run), forced with observed sea surface temperature (SST) for the period 1979-1988, could simulate current tropical cyclone climatology reasonably well. The second integration (2xCO<sub>2</sub> run) has been conducted with the SST increase corresponding to global warming and with doubled atmospheric CO<sub>2</sub> concentration. The SST increase is estimated from the results of transient CO<sub>2</sub> experiment with a low resolution coupled model, MRI-CGCM. Comparison of the two integrations has revealed significant reduction in the number of tropical cyclones due to global warming. The reduction in the tropical cyclone frequency seems to be associated with the weakening of the tropical circulation due to the increased atmospheric stability by global warming. Several additional experiments have been conducted to see the sensitivity of the results to convection scheme and pattern of SST increase. The results of these experiments further confirmed the reduction in tropical cyclone frequencies due to global warming. However, it is strongly suggested that we need much higher

MW03/L/01-B4

1020

**RESEARCH AND DEVELOPMENT FOR MEDIUM AND EXTENDED-RANGE FORECASTS: METHODS, RESULTS, AND PROSPECTS**

A. HOLLINGSWORTH, M. Capaldo, A. Simmons (ECMWF, Shinfield Park Reading RG2 9AX, UK)

ECMWF's prime long-term goal is to deliver operational medium-range-weather forecasts of increasingly high quality, over the range from three to ten days and beyond. A complementary long-term goal is to establish and deliver a reliable operational seasonal forecasting capability. Overall success will depend crucially on new and improved satellite observations, on improvements in the data-assimilation system, and on improvements in the forecast models. Ensemble prediction will play a major role in attaining both goals.

Medium-range and seasonal-to-interannual weather forecasting have attained new levels of achievement and continue to offer exciting prospects for further development. A new generation of operational and research satellites is coming on stream; four-dimensional variational assimilation is established as a powerful and effective method to use all observations; numerical methods continue to provide improved accuracy and substantial economies; parametrization schemes are improving steadily through new approaches which jointly exploit field experiments, large-eddy simulations and operational data assimilation; ensemble prediction systems are providing a new dimension in probabilistic forecasting; the development of simplified Kalman filters, based on singular vectors, will benefit both the assimilation systems and the ensemble prediction systems; coupled atmosphere-chemistry models offer new ways to improve the initialisation of forecast models; coupled atmosphere-ocean models have delivered successful ensemble forecasts of the 1997-98 El Niño event; and computer vendors are confident they can meet the requirements for computational power in an affordable manner. These developments will undoubtedly lead to further gains in medium-range and seasonal-to-interannual forecast skill.

The new satellite data essential to achieve these goals over the next decade will be provided as a result of investments of 3B or more by Europe (EUM= ETSAT and ESA), 3B or more by Japan and 10B or more by the USA. By the end of 1999, in readiness to exploit the new satellite data, ECMWF will have implemented an advanced operational Earth-system model and data assimilation system. ECMWF's Earth-system model will comprise the following coupled modules:

- Atmosphere an atmospheric general circulation model
- Ocean circulation: an ocean general circulation model ocean ice processes
- Ocean surface waves ocean surface wave dynamics model
- Land land biosphere module land surface, soil, hydrological and snow model
- Ozone parametrized stratospheric ozone chemistry

Some modules of the model are already quite sophisticated, but others are at an early stage of development.

ECMWF's advanced four-dimensional

MW03/W/08-B4

1035

**ASPECTS OF ATMOSPHERIC CIRCULATION SIMULATED IN A GLOBAL CLIMATE MODEL WITH 30 KM HORIZONTAL GRID SPACING**

KEVIN HAMILTON and Richard Hemler (Geophysical Fluid Dynamics Lab/NOAA, P.O. Box 308, Princeton, New Jersey 08542, USA, Email: kph@princeton.edu); Frederic Vitart (European Centre for Medium Range Weather Forecasts, Reading, UK)

A version of the GFDL SKYHI global general circulation model with 30 km horizontal grid spacing and 40 vertical levels has been integrated for more than 8 months. This talk will examine aspects of the simulation including the large-scale wind and temperature structure in both the troposphere and the middle atmosphere. Also discussed will be the statistics of intense rainfall events including simulated tropical cyclones.

MW03/W/07-B4

1115

**SIMULATION OF THE MESOSCALE SPECTRAL REGIME IN HIGH-RESOLUTION VERSIONS OF A GLOBAL CLIMATE MODEL**

JOHN KOSHYK (Department of Physics, University of Toronto, Toronto, Ontario, Canada, Email: koshyk@mam.physics.utoronto.ca); Kevin Hamilton (Geophysical Fluid Dynamics Lab/NOAA, P.O. Box 308, Princeton, New Jersey, USA)

This paper will discuss the mesoscale variability found in the upper troposphere and lower stratosphere in simulations of the atmospheric circulation made with very high spatial resolution versions of the GFDL SKYHI GCM. Included will be one integration with horizontal grid-spacing of 30 km, and another with horizontal spacing of 100 km, but vertical level-spacing less than 400 m in the lower stratosphere. The horizontal spectra of winds in the simulations display two separate regimes: one at large scales (>1000 km) with steep power law behaviour and a shallower regime in the mesoscale. This is in general accord with the usual observational picture of tropospheric/lower stratospheric meteorology. In fact, the model-simulated kinetic energy spectrum near the tropopause compares quantitatively with the observations in the GASP archive of data taken during thousands of commercial aircraft flights. Detailed analysis of the spectral kinetic energy budget will be presented.

MW03/E/09-B4

1130

**A LOOSE COUPLING OF GENERAL CIRCULATION MODEL WITH CHEMICAL TRANSPORT MODEL AND ITS APPLICATION TO OZONE DATA ASSIMILATION**

Toshiki IWASAKI (Geophysical Institute, Graduate School of Science, Tohoku University, Aoba-ku, Sendai, 980-8578, JAPAN, Email: iwasaki@wind.geophys.tohoku.ac.jp); Hisashi. Kato, Atsuya Kinoshita and Toru Sasaki (Japan Meteorological Agency, Otemachi 1-3-4, Chiyodaku, 100-8122, JAPAN, email: tsasaki@naps.kishou.go.jp)

We are developing a high resolution General Circulation Model (GCM) coupled with a chemical transport model (CTM) to study interactions between the atmospheric circulations and the global distributions of minor constituents. CTMs have too many prognostic variables and vertical levels to increase horizontal resolutions under limited computational resources. GCMs, on the other hand, are expected to run high resolution simulations in the horizontal. To save computational resources, the time step length should be different between two models. Thus, we are concerned about a loose coupling technique of GCM and CTM which adopts different space and/or time resolutions between two models.

What is important for the loose coupling is to estimate vertical velocity used for advection of minor constituents in the CTM. Distributions of minor constituents of minor constituents, such as ozone, are very sensitive to vertical velocity because of large vertical gradients of its mixing ratio. When GCM-produced vertical velocities are used to advect minor constituents, the CTM may be subject to time truncation errors related to high frequency gravity modes. In the actual simulation, the predicted constituent distributions tend to have spurious spreading and bias. In order to get rid of time truncation errors, we estimate vertical velocities from the thermodynamic equation with diabatic terms.

A preliminary test is conducted focusing on data assimilation of ozone in comparison with satellite-derived total ozone amount. The T63 or T213 version of JMS's global NWP model is coupled with a CTM in 2.5 or 5 degree longitude-latitude co-ordinates. Prognostic variables are exchanged between GCMs and CTMs every 3 or 6 hours. The time step for CTM is set at 30 minutes, which is longer than that for GCM to save computational resources. Diabatically diagnosed vertical velocities allow us to successfully reproduce observed distributions of total ozone amounts. Further experiments are underway on impacts of vertical and horizontal resolutions of the CTM.

MW03/E/05-B4

1145

**TOWARD THE REALIZATION OF CLOUD CLUSTER-RESOLVING GLOBAL ATMOSPHERE MODELS**

Taroh MATSUNO (Institute of Global Change Research, Frontier System for Global Change, Seavans-N Bldg 7thF, Shibaura 1-2-1, Minatoku 105-6791, Japan, e-mail: taguchik@jamstec.go.jp)

Considering the recent development of computer technology it will become possible to use numerical J models of the global atmosphere having the horizontal grid-size of about 10km in the near future (probably within 3 years). For such high resolution models parameterization of convective clouds as usually used in current atmosphere models becomes inadequate because convection in the vast area of tropics takes place as meso-scale convective systems (cloud clusters) whose horizontal dimension is larger than 10km. Thus we are forced to jump to construct models to resolve cloud clusters. Judging from the observed structure of cloud clusters, the required horizontal grid-size may be around 5km at the greatest which could be attained not so far in the future. Development of such high resolution atmosphere models can be done basically by extending currently existing meso-scale cloud models to cover much larger areas, but we need to know much more about dynamics of meso-scale processes of J atmosphere such as generation of internal gravity waves, down-cascade of enstrophy, turbulent energy dissipation due to shear instability and so on. In current models, they are parameterized as double laplacian diffusion process or vertical eddy viscosity and their representation and the values of coefficients are determined more or less ambiguously and the physical reality of these processes have not been, discussed so far. Some elementary considerations on these problems will be made.

MW03/E/07-B4

1200

**PROBLEMS IN NUMERICAL MODELING USING VERY HIGH RESOLUTION**

Yoshio KURIHARA (Frontier Research System for Global Change, Sumitomo-Hamamatsucho Bldg. 4F, 1-18-16 Hamamatsucho, Minato-ku, Tokyo, 105-0013, Japan. email: ykuri@frontier.esto.or.jp)

A climate model with very high horizontal resolution of the order of 10km is expected to be capable of realistically describing climatic features peculiar to each of different regions or localities, as well as of simulating the structure and behavior of the mesoscale systems more accurately than models with coarse resolution. Construction of such models requires, on the one hand, rigorous evaluation of numerical schemes, which treat dynamical core of the model. These schemes are formulated once the grid configuration or the spectrum domain is determined. On the other hand, a guideline has to be developed for dealing with model physics in a very high-resolution model and performance of the numerical schemes representing it has to be tested. Among a number of problems concerning treatment of model physics, the most intriguing one is, perhaps, how to incorporate effects of convection and condensation processes into the model. One may consider usage of a cloud-resolving model despite a fact that the horizontal resolution of the order of 10 km may be too coarse and can cause bias of the model climate. Another approach is to rely on a scheme of parameterization. The basic environmental parameters controlling free convection are the atmospheric stability and the moisture content. If the size of cloud, i.e., a fundamental cloud property, is specified, one can derive a formula which defines the critical relative humidity for free convection with that cloud size to occur in the atmosphere of given static stability. A scheme of parameterization developed along this line has been used in the GFDL (Geophysical Fluid Dynamics Laboratory, NOAA) hurricane model. In the present paper, a method will be proposed to utilize the same formula in the estimate of cloud amount. The cloud amount is an important quantity, which substantially influences radiation budget. Also, in the evaluation of the radiation budget in high-resolution models, effects of detailed topography may have to be taken into consideration.

MW03/W/10-B4

1215

**ON THE COMPUTATIONAL REQUIREMENTS OF HIGH-RESOLUTION CLIMATE MODELS**

Carlos R. MECHOSO and Leroy A. Drummond (Department of Atmospheric Sciences, University of California, Los Angeles, CA 90024 USA, email: mechoso@atmos.ucla.edu)

Climate models are among the archetypical computer-demanding applications, a characteristic that is exacerbated by increases in resolution. This presentation discusses design and machine requirements of high-resolution climate models, viewed as a set of modules (e.g., atmospheric and oceanic codes) with different spatial/temporal resolutions and periodic/sporadic data exchanges. First, there is the problem of load-balancing of individual codes. Methods are presented and



their impact on performance is discussed. Second, there is the load-balancing of different codes sharing computational resources. Since the scalability of a code decreases with increasing number of processors, it can be more efficient to simultaneously run several modules in sub-sets of processors than sequentially run individual modules in all available processors. Third, there is the problem of efficient data transfers between different modules running in parallel. A novel system for parallel data exchanges (Distributed Data Broker) is presented. Finally, there are aspects involving data mining and real-time visualization of very large model output.

These issues are discussed in the framework of the UCLA Earth System Model, which combines atmospheric and oceanic dynamics and chemistry codes. The models are both global and regional and have multiple resolutions. The potential for performances at the TFLOP level is examined.

**MW03/W/03-B4****1230****A PLATFORM FOR THE STUDY OF GLOBAL CLIMATE MODEL STUDY WITH HIGH RESOLUTION**

Takahiro INOUE, Yukio Tanaka, Yonejiro Yamagishi and Hisashi Nakamura (Research Organization for Information Science and Technology, 1-18-16, Hamamatsu-cho, Minato-ku, Tokyo 105-0013, Japan, email: don@tokyo.rist.or.jp)

A high-resolution, coupled atmosphere-ocean climate model, called 'NJR', has been developed. NJR is parallel software and designed as a platform for high-resolution climate model study. NJR consists of AGCM, OGCM and atmosphere-ocean coupler. As a total system, pre/post-processes of data are also well equipped. The AGCM has two alternative dynamics part as an option, one uses spectral method and the other uses finite difference method. They use common physics packages. The OGCM also has two alternative co-ordinate systems, one use sigma-co-ordinate and the other uses z-co-ordinate in vertical. Each component or sub-process is modularised and users can add or modify any sub-process model. NJR uses domain decomposition as the parallel algorithm and the MPI as the message passing library. Therefore, it runs on almost all parallel machines, such as SX-4, SR2201, or even on workstation clusters. NJR will be mainly optimised and used on the 'Earth Simulator', which is a very large-scale distributed and shared memory vector parallel machine currently under development. Through NJR with these high performance machines, such as the Earth Simulator, users will be provided a useful tool for high-resolution climate model studies. Although, there are still some questions such as: What would happen on 10km mesh climate model? Would it be valid on such a high-resolution model that physics sub-process models currently used? What would be needed to handle massive data from such a large-scale simulation? etc. Until 1998, basic part of NJR was completed and released as version 1.00 to users. Some validation studies of each component, in AGCM, OGCM, and coupled model, are proceeded in order to evaluate its performance in climatological and parallel aspects. In the presentation, we will show description of NJR and some results of our experiments.

**Thursday 29 July PM**

Presiding Chairs: H Kida (University of Kyoto, Japan)

T Matsuno (Frontier Research System for Global Change, Tokyo, Japan)

**MW03/W/06-B4****1400****THE CSIRO CONFORMAL-CUBIC GCM**

John L. Mcgregor and Martin R. Dix (CSIRO Atmospheric Research, Melbourne, Australia)

A new global primitive equations model has been developed at CSIRO. It has the unique feature that it is based on the conformal-cubic grid (Rancic et al., QJRM, 1996). The model utilises 2-time-level semi-Lagrangian advection (McGregor, 1996). A recent significant improvement is a modification to carry the velocities on a quasi-staggered grid which has superior dispersion properties for geostrophic adjustment, when compared to the A, B and C grids. This improvement is evident for standard test cases of the shallow water equations as well as for the 3D dynamic core test, compared to the previous C-grid scheme. The model employs a semi-implicit treatment for gravity waves; a simple tri-colour successive over-relaxation scheme has been developed to solve the associated Helmholtz equations. Major attractions of the model are its quasi-uniform resolution, and absence of the Gibbs' phenomena which occur for spectral models. The model is computationally efficient and its architecture should be suitable for massively parallel computers. The talk will describe selected aspects of the model formulation and implementation. A complete set of physical parameterizations has been incorporated. The parameterizations are essentially the same as those used by the CSIRO spectral GCM and by the regional climate model DARAM. The computational efficiency of the model will be discussed, and results presented for present-day AMIP-style climate runs. Results will also be presented for a version where the Schmidt (1977) stretching transformation has been applied to the grid. McGregor, J. L., 1996: Semi-Lagrangian advection on conformal-cubic grids. *Mon. Wea. Rev.*, 124, 1311-1322. Rancic, M., R. J. Purser and F. Mesinger, 1996: A global shallow-water model using an expanded spherical cube: Gnomonic versus conformal co-ordinates. *Quart. J. Roy. Meteor. Soc.*, 122, 959-982. Schmidt, F., 1977: Variable fine mesh in spectral global model. *Beitr. Phys. Atmos.*, 50, 211-217.

**MW03/W/04-B4****1415****THE CUBED SPHERE: A NEW METHOD FOR THE HIGH RESOLUTION SIMULATION OF GLOBAL ATMOSPHERIC DYNAMICS**

R. Iacono, P.M. Ruti and G. Pisacane (ENEA, Rome)

The Cubed Sphere (CS) [1] is a new gridding technique that has been successfully applied to the solution of the shallow water equations in spherical geometry. In fact, a detailed study of the performance of the method for the suite of test cases proposed by Williamson et al. has shown that CS can achieve accuracies comparable to those obtained by the spectral transform method, with substantial savings in computing time. Here we discuss the problems associated with the extension of CS to three-dimensional geometry and present the first results of a Navier-Stokes primitive equations solver based on this method. The performances of CS are compared to those of traditional methods in the test cases proposed by Held and Suarez for studying the behaviour of the dynamical core of GCMs in climatic integration.

**MW03/W/12-B4****1430****AN EFFICIENT PREDICTION MODEL FOR ALL SCALES**

Ferdinand BAER (Dept. of Meteorology, University of Maryland, College Park, MD 20742, USA, email: baer@atmos.umd.edu); Mark Taylor (LANL, X-HM Mail Stop D413, Los Alamos, NM 87545, USA, email: mt@lanl.gov)

A Spectral Element Atmospheric Model (SEAM) has been developed for prediction on all time

scales and a variety of space scales over a spherical Earth. The computational domain is broken into rectangular regions called elements using spectral element discretization, and within each element all variables are approximated by polynomial expansions; herein those functions are Legendre polynomials. The vertical discretization selected is finite differencing and uses sigma co-ordinates following the NCAR/CCM3. The advantages of this model are numerous, but most dramatically it allows for arbitrary resolution in each element to provide regional predictions at any or all locations. The model is ideally suited to computation on parallel processors because it minimises communication requirements. It has been tested with the shallow water test suite and we will present results demonstrating its skill when compared with other models. The model's success in fully three-dimensional predictions using the Held-Suarez test conditions will also be demonstrated, indicating its feasibility as a GCM dynamical core. Additional applications with the model to be discussed include the incorporation of a state-of-the-art physics package, and three-dimensional small-scale (high-resolution) turbulence studies.

**MW03/W/01-B4****1445****ON THE MODELLING OF THE SURFACE ENERGY EXCHANGE PROCESSES BY COMBINED "FUZZY SETS AND NEURAL NETWORKS" APPROACH**

Oleg POKROVSKY (Main Geophysical Observatory, Karbyshev str.7, St.Petersburg, 194021, Russia, e-mail: pokrov@main.mgo.rssi.ru)

Climate numerical models depend on many surface energy variables. Principal variables are land/water and air temperatures and moisture, solar downward irradiance, albedo, reflected and emitted radiances, heat fluxes into ground and atmosphere, latent and eddy heat fluxes. Its values are mainly determined by individual optical, physical and chemical properties of a given homogeneous land/water pattern. The pattern scale, depending heavily on landscape peculiarities, could vary from several meters to several kilometers (or even to tens or hundreds km in desert areas). However, there are two weak sides of these data implementation in ecological model. First side is that all mentioned variables with the exception of air temperature and moisture are not synoptically observed and become available for users with one month delay at least. Second one is due to substantial departures between observed and modeled diurnal values of these variables. These differences are so grade that often exceed 100% level. New approach to surface variable diurnal cycle modelling was proposed in order to overcome this problem. The joint statistical distribution of principal meteorological variables is investigated. Ten-year length time series of one-hour temporal resolution for several meteorological sites of Russian North-West Region are used. The data set of simultaneous observations (for all variables and stations) allows to reveal main features of joint diurnal distributions by means of known "min-max" fuzzy set approach. Known and novel interrelationships between various meteorological and linked soil variables are reviewed. The revealed relationships between solar downward radiative fluxes and soil temperature diurnal patterns allow to simulate all principal elements of surface energy exchange: longwave outgoing radiative fluxes in the atmosphere, soil heat fluxes, available, turbulent and latent heat fluxes. It was found out that the most complicated links take place for fuzzy sets, corresponding to fractional cloudiness diurnal patterns. Proposed approach could be used as a part of downscaling procedure.

**MW03/E/08-B4****1500****ROLE OF THE SHADE IN EXISTENCE OF THE MICROCLIMATE ZONES**

Tarzadin ULAANBAATAR (Department of Earth Sciences, National University of Mongolia, email: numelect@magicnet.mn)

The shade influences powerfully and constantly on the microclimate zones and their extents in regional and local scale. But it does not calculated and drawn on any climate model and charts. Its precise calculation is one of the key factors for more realistic and detailed simulation of the climate zones, result of which will provide an opportunity for detailed comparisons of model results with recent weather and climate observations, as well for development of high resolution climate model, and more reliable predictions of global climate and climate change. The success of detailed simulation, precision and comparison of the coupled model depends on 1) how well are the high resolution airborne, space and geodesy images on which the shade is drawn by computer due to the model calculation, 2) how punctual does described the mathematical base of model.

In this paper methodology of a 3D mathematical model for representation of the shadow impact on the climate and geographical zones and method for computer drawing of shadow on the high resolution geographical and climate maps are described brand-newly. Resolution of this model is limited only by map resolution.

**MW03/W/09-B4****1515****A REGIONAL MODELING APPROACH FOR STUDYING CLIMATE AND ENVIRONMENT OVER EAST ASIA**

WEI-CHYUNG WANG and Wei Gong (Atmospheric Sciences Research Center, State University of New York at Albany)

In recent years, efforts to study regional climate change and the associated environmental impact have significantly increased, partly due to concerns over regional responses caused by the enhanced greenhouse effect, increased sulfates, and changes of atmospheric ozone. The climate over East Asia is the result of multi-scale interactions, including large-scale circulation (e.g., subtropical high and upper level jet) and regional-scale factors (e.g., topography, surface characteristics, and thermal and dynamic heating). Regional climate models, which incorporate in detail these regional factors with prescribed large-scale circulation as the boundary condition, is a useful tool for evaluating these scale interactions, and for studying the physical, chemical, and dynamical processes and their interactions. The continued development of the SUNYA regional model to study climate and environment over East Asia is presented. The initial focus is on the model's capability to simulate key climate characteristics, such as the summer monsoon. As a test case, we run the model with different objective analysis data (ECMWF-TOGA analysis, ECWMF-reanalysis and NCEP/NCAR-reanalysis) as the initial and lateral boundary conditions to simulate the 1991 severe flood over the Yangtze-Huai River Valley. The model is capable of reproducing the five-day mean features of monsoon circulation, anomalous rainfall in the Yangtze-Huai River Valley and the large- and regional-scale circulation statistics. The model is also used to simulate the interannual variability of the rainfall movement during the 1990s. Plans for using the regional model for climate change and environmental studies will be discussed. Further, the regional modeling approach will be addressed within the context of high-resolution global climate models.

MW03/W/05-B4

1530

## DEVELOPMENT OF A REGIONAL CLIMATE MODEL FOR EAST ASIA BASED ON CSU-RAMS

Seita EMORI, Toru Nozawa (Atmospheric Environment Division, National Institute for Environmental Studies, 16-2 Onogawa, Tsukuba, Ibaraki, 305-0053 Japan, email: emori@nies.go.jp, nozawa@nies.go.jp); Atsui Numaguti (Center for Climate System Research, University of Tokyo, 4-6-1 Komaba, Meguro, Tokyo, 153-8904 Japan, email: numaguti@ccsr.u-tokyo.ac.jp); and Itsushi Uno (Research Institute for Applied Mechanics, Kyushu University, 6-1 Kasuga-Park, Kasuga, Fukuoka, 816-8580 Japan, email: iuno@riam.kyushu-u.ac.jp)

In order to evaluate the regional scale climate change over East Asia, a regional climate model is developed. The model is based on the Regional Atmospheric Modeling System developed at Colorado State University, which adopts compressible non-hydrostatic basic equations and a cloud microphysics parameterization. Several processes including radiation, cumulus convection and land surface are modified to make a long-term integration. A year-long integration targeting the regional climate of 1994 is conducted to evaluate the performance of the model. Twice-daily ECMWF analysis data are used for initial and boundary conditions. The horizontal grid resolution is set to 40km. The model simulated the spatial pattern of precipitation in wintertime over East Asia and the annual temporal variations of precipitation over various regions of Japan fairly well. It is suggested that the simulation of Baiu, the persistent precipitation band over Japan islands mainly in June, is strongly sensitive to cumulus parameterization. An Arakawa-Schubert type cumulus scheme tends to fail the simulation of Baiu, while the simulation is improved when the scheme is modified to consider the suppression of cumulus convection under a dry environment. The results of one-way nesting with a GCM, which adopts the same physical parameterizations as the regional climate model does, will be also presented.

MW03/E/04-B4

1610

## NUMERICAL SIMULATIONS OF JAPANESE CLIMATE USING A HIGH-RESOLUTION NESTED REGIONAL SPECTRAL MODEL

Hideji KIDA (Department of Geophysics, Kyoto University, Kyoto 606-8502, Japan, Email: kida@kugi.kyoto-u.ac.jp) and Hidetaka Sasaki (Meteorological Institute, Tsukuba, Ibaraki 305-0052, Japan, Email: hsasaki@mri-jma.go.jp)

The necessity of higher resolution climate models increases in order to simulate the more realistic local climates and environments including the small-scale orography and patched distribution of vegetation systems. A way to such a high-resolution model is obtained by applying a limited-area model to climate simulations of the interested regions. This approach is not always completely in a mathematical view, but fully usable in a practical view to get quick results to so long-term integrations necessary for climate change simulations such as more than in the 1-10 thousand years scale, or very high-resolution climate simulations such as less than in 1-10 thousand meters.

The authors (1991) proposed a new method to nest a high-resolution model in a lower-resolution model such as GCMs. Here is presented some results from some experiments for winter climate simulations over the Japanese area to test its performance to local climates. The climatological contrast features of snow and temperature distributions both in Japan sea side and Pacific Ocean side of Japan islands are well simulated using 10-100 km resolution models. Furthermore, precipitation in the rainy season is fairly realistic over Japan as well. This suggests that the high-resolution nested model is usable for simulations of local climates provided that the large-scale simulation is well done.

MW03/E/03-B4

1625

## A 2 X CO2 REGIONAL CLIMATE PREDICTION EXPERIMENT OVER JAPAN IN WINTER WITH AN MRI REGIONAL CLIMATE MODEL

Yasuo SATO, Hidetaka Sasaki, Kazuyo Adachi, Akira Noda & Seiji Yukimoto (Meteorological Research Institute, 1-1 Nagamine, Tsukuba, Ibaraki 305-0052, Japan, email: ysato@mri-jma.go.jp)

A high resolution regional climate model is integrated using output of a transient CO2 experiment with the Meteorological Research Institute coupled atmosphere-ocean global climate model (MRI/CGCM) as initial and lateral boundary conditions. We use two-step nesting due to a coarser grid size of the CGCM, whose grid size in an atmospheric component is 5 degrees in longitude and 4 degrees in latitude and that of an oceanic component is two-times finer than that of the atmospheric component. Then, an East Asian model with horizontal grid size of 120km is nested in the CGCM. Further, a Japanese islands model with horizontal grid size of 40km is nested in the East Asian model. We have conducted several experiments under a January condition for two runs: one (referred to as CTRL hereafter) is a control experiment under the present-day CO2 concentration (1 x CO2) and the other (referred to as TRAN hereafter) a regional climate experiment under the doubled CO2 condition. Both experiments firstly do 10 runs each of which is 40 day prediction in each of 10 years predicted by either a constant CO2 concentration or a gradual increase (at a compound annual rate of 1%) in CO2 concentration experiment of CGCM for 71st through 80th year. Then the above 10 runs with the last 30-day results for both CTRL and TRAN are averaged as the predicted regional climate for January. Both runs can simulate detailed features over the land. Differences (warming signal) of the surface air temperature between two cases are about 2.5 degrees on the western part of Japan and about 3 degrees on the northern part of Japan, which are larger than biases (1 x CO2 - observed climate) over the land. As to precipitation, both cases show much precipitation belt along the north-western part of the main island facing the Japan Sea than the other side facing the Pacific. This feature in CTRL simulates well the present climate and much better than the simulation in a CGCM control experiment. Differences of TRAN from CTRL ...

MW03/P/01-B4

1640

## NUMERICAL SIMULATIONS ON IMPACTS OF THREE GORGES RESERVOIR ON SUMMER MONSOON RAINFALL OVER EAST ASIA

Zongci ZHAO and Yong Luo (National Climate Centre, Baishiqiaolu, No.46, Beijing, 100081, P.R.China, email: zhaoc@sun.ihep.ac.cn)

Three Gorges reservoir along the Yangtze River Valley of China is going to be reconstructed. The numerical simulations of Three Gorges reservoir have been conducted by using a regional climate model (RegCM2/EA) which was based on the NCAR RegCM2. The model has a domain of about 100-150E and 10-45N with a horizontal resolution of 60kmX60km and a vertical resolution of 23 layers.

A sensitive experiment was designed a water body at around the Three Gorges region with 45 grid points and 50m or 100m of water depth to replace the vegetation of the present time. To compare the simulations of Three Gorges' reservoir run with the control run, it is found that the

summer rainfall over some regions where are near the Three Gorges reservoir such as Southwest China, Yangtze-Huaihe River Valley and Hetao might be increased clearly. Impacts of the Three Gorges reservoir on other variables have also been investigated in this research. The numerical experiments with the different areas and depths of this reservoir were also conducted.

MW03/E/01-B4

1655

## ORIGIN AND MAINTENANCE OF THE TEXAS-OKLAHOMA DROUGHT OF 1998

Song-you Hong (1) and EUGENIA KALNAY (1), (2) (1) National Centers for Environmental Prediction(2) School of Meteorology, University of Oklahoma

The drought of the summer of 1998 was extremely strong and persistent. The Oklahoma mesonet showed that the soil moisture reached levels comparable or lower to those of the 1930's Dust Bowl (Ken Crawford, pers. comm., 1998). By May, a mid-summer circulation had been established, with high temperatures and low precipitation typical of July and August, and it persisted until early October throughout most of Oklahoma and Texas, except in some areas of southern Texas, where it rained in August and September (Figs. 1a-d from NCDC). Since 1997/1998 also underwent a very strong El Niño that produced many major changes in the global circulation, it is natural to assume that the Texas-Oklahoma (TXOK) drought could be "blamed on El Niño". However, the El Niño/Southern Oscillation (ENSO) episode faded in the beginning of the summer (Fig. 2, SOI), and the drought persisted until the fall, so that it is necessary to establish the processes that maintained it beyond the anomalous ENSO circulation.

In this study we make use of the NCEP/NCAR Reanalysis initial and boundary conditions to drive the NCEP Regional Spectral model (RSM). Comparisons of the soil moisture in the reanalysis indicate that the Reanalysis shows an anomalously low soil moisture level over most of central US on 14 April 1998, compared with 1993, a year with high precipitation. The RSM reproduces very well the precipitation for MJJ (Fig. 3) even though the only information it receives is through the boundary conditions (BC). Using 1993 initial soil moisture for 14 April 1998 does not increase the pp over TXOK (Fig. 4). This agrees well with the notion that El Niño anomalous circulation has forced the drought, since its influence is felt through the BC.

We will explore whether during July and August, after the end of the ENSO episode, low soil moisture and high albedo contributed to the maintenance of the drought through a local positive feedback (Atlas et al, 1990), or if it was still driven and maintained by the large scale circulation. The results will be presented at the conference.

MW03/W/02-B4

1710

## APPLICATION OF THE CANADIAN REGIONAL CLIMATE MODEL OVER SWITZERLAND: ON THE SENSITIVITY OF MODEL'S RESOLUTION ON THE SIMULATED WIND AT THE SURFACE.

STEPHANE GOYETTE and Martin Beniston (Institute of Geography, University of Fribourg, Switzerland)

Switzerland is characterised by highly complex orography which has a determining influence on climate winds. In many instances, wind extremes impact more heavily upon the natural environment and human infrastructure than changes in mean wind conditions. We are interested in evaluating the manner in which the Canadian regional climate model (CRCM) is capable of reproducing extreme climatic events in the Swiss Alps using the multiple self-nesting technique. This is a very useful feature of the model when aiming to run at very F. More specifically, we are here looking on the sensitivity of the surface winds to model horizontal and vertical resolution, and on the way it impacts on simulated wind extremes. High spatial resolution in the horizontal is required for the orography and other surface characteristics to be resolved accurately. In the vertical, high resolution in the lower layers permits a better representation of the boundary layer and a better representation of the surface winds. This paper thus describe the results of the CRCM, applied to the European Alpine area using different resolutions to simulate extreme wind events during the February 1900 VIVIAN windstorm.

MW03/W/11-B4

1725

## HIGH RESOLUTION SIMULATIONS OF EXTREME METEOROLOGICAL EVENTS OVER BELGIUM

BRASSEUR O. (Institut d'Astronomie et de Géophysique G. Lemaître, Université catholique de Louvain, Chemin du Cyclotron 2, B-1348 Louvain-la-Neuve, Belgium); Tricot C. (Climatology Department, Royal Meteorological Institute of Belgium, Avenue Circulaire 3, B-1180 Bruxelles, Belgium)

There are two ways of considering the improvement of an atmospheric model: refining the resolution, and improving the physics. Both these aspects are important and cannot be separately investigated because of the interactions between dynamics and physics. As the horizontal resolution is refined, some problems occur: phenomena considered at larger scales as subgrid processes can partly become explicitly represented by model. Such difficulties therefore imply a reconsideration of the physical parameterisations. An interesting test for current regional models is the simulation of extreme events that allow assessing of their limits. Moreover, these events are an important concern in the framework of operational weather forecast as well as climate change at the regional scale.

The MAR - Modèle Atmosphérique Régional - mesoscale model (developed at the University of Louvain-la-Neuve, Belgium) has been tested on several short-range (a few days) and medium-range (a few months) extreme situations characterised by extreme temperatures, storms originating from explosive cyclogenesis, and thunderstorms. The MAR includes sophisticated parameterisations of microphysics, turbulence, deep convection, and soil-vegetation-atmosphere interactions. The horizontal resolution generally ranges between 10 and 50 km. The simulation domain is centred on Belgium, and covers Western Europe or a sub-region of Europe depending on the resolution.

Simulated results have shown a very good accuracy for all these considered events. In particular, the MAR has underlined the relevant role of mesoscale circulations (gravity winds, breezes) in the prediction of extreme temperatures over Belgium. The deepening rate and the frontal structure of intense cyclones during the period from January to March 1990 are particularly well represented. Precipitation associated with fronts and represented by the convective parameterisation is in correct agreement with observations. We note also that the horizontal resolution of 20 or 25 km is probably the best compromise to represent all considered extreme events: the 50-km resolution is generally not accurate enough, while the 10-km resolution causes scale separation problem for the representation of deep convection.





**HS1 Thursday 29 – Friday 30 July****HYDROLOGICAL EXTREMES: UNDERSTANDING, PREDICTING, MITIGATING (ICWRS, ICSW; COLLABORATING ASSOCIATION: IAMAS)**

Location: Barber Institute, Concert Hall

Location of Posters: Guild of Students, Room 46&amp;47

**Thursday 29 July AM**

Presiding Chair: Lars Gottschalk (University of Oslo, Norway)

**UNDERSTANDING – CIRCULATION PATTERNS****Introduction 0900**

Lars Gottschalk(University of Oslo, Norway)

**HS1/W/22-B4 0905****LARGE-SCALE ATMOSPHERIC AND SEA SURFACE PROCESSES LEADING TO EXCESSIVE RAINFALL IN TUSCANY, ITALY**

Francesco MENEGUZZO, Alfonso Crisci (Applied Meteorology Foundation (FMA), Via Einstein 35, I-50013 Campi Bisenzio, Firenze, Italy); Bernardo GOZZINI, Daniele Grifoni (Laboratory for Meteorology, Climatology and Environmental Modelling (LaMMA); Via Einstein 35, I-50013 Campi Bisenzio, Firenze, Italy); Stefano Pagliara (Dipartimento di Ingegneria Edile, Idraulica e del Territorio, University of Pisa, Via Gabba 22, I-56126 Pisa, Italy)

Monthly extreme rainfalls at several gauges and several durations (1, 3 and 5 days) in Tuscany, Italy, are compared with simultaneous and previous patterns of large-scale circulation, synthesized by the North Atlantic Oscillation (NAO) index, and patterns of sea surface temperature (SSTa) in central-western Mediterranean. Several statistical methods are employed, from simple contingency tables to frequency histogram. Scenarios of global change in terms of changes in Mediterranean SSTa anomalies are considered and the quantitative consequences in terms of extreme rainfalls are derived.

**HS1/W/49-B4 0925****IMPACTS OF CLIMATE CHANGE ON MID-EUROPEAN RIVER BASIN HYDROLOGY**

A. BÁRDOSSY, H. Giese, G. Hartmann (Institut für Wasserbau, Universität Stuttgart, Pfaffenwaldring 61, D-70550 Stuttgart, Germany); H. P. Nachtnebel, W. Diernhofer, K. Hebenstreit (IWHW, Universität für Bodenkultur, Nußdorfer Lände 11, A-1190 Wien, Austria)

The impact of climate change on the hydrologic regimes of medium-scale rivers in Europe is investigated in this work. The main aim is to predict hydrological changes at a medium time scale (referring to several decades) for medium-scale river catchments in Europe. A downscaling approach is used to apply GCM data for this: large-scale pressure distribution patterns were classified as a base for conditional statistics of rainfall and temperature data. These were utilized for the calibration of statistical models of local rainfall and temperature. Using appropriate interpolation methods, these data were then used as input for runoff models of medium-scale river catchments in Europe. This method was finally applied to GCM outputs representing a doubled CO<sub>2</sub>-scenario. Using the calibration for the historical data delivers a prediction about the impact of climate changes on the local weather parameters and changes in hydrological regimes. Application of the methodology and results are illustrated on the Neckar catchment (Germany) and the Enns catchment (Austria). In both catchments changes in temperature and runoff for the 2\_CO<sub>2</sub>-scenario simulations are observed. However, due to the shortness of simulated time-series no detailed conclusions with respect to extreme events are possible.

**HS1/W/29-B4 0945****INVESTIGATING THE INFLUENCE OF ATMOSPHERIC CIRCULATION PATTERNS ON REGIONAL STREAMFLOW DROUGHT IN SOUTHERN GERMANY**

Kerstin STAHL and Siegfried Demuth (Institute of Hydrology, University of Freiburg, Fahrenbergplatz, D-79098 Freiburg, Germany, email: kstahl@uni-freiburg.de)

This study investigated the influence of synoptic meteorology on streamflow drought in a region with highly variable hydrological characteristics. First, groups of catchments with similar drought characteristics were identified by cluster analysis. A regional drought index (RDI) derived from aggregating the streamflow drought series of a cluster provided the basis for the link to the occurrence of atmospheric circulation patterns (CPs). Frequency cross-tabulation revealed important information about the regionally different influence of CPs on drought events. Based on the results of the cross-tabulation, the CPs were classified and reduced to eight groups. Finally, the possibility of simulating the regional drought index by CP-group occurrence was tested using a logistic regression model. The results show that high pressure over central Europe and the British Isles as well as anticyclonic CPs with easterly air flow were strongly associated with summer streamflow drought in all regions.

**HS1/W/48-B4 1005****ATMOSPHERIC PROCESSES LEADING TO DROUGHTY PERIODS IN ROMANIA**

Mary-Jeanne ADLER, Aristita Busuioc, Monica Ghioca (National Institute of Meteorology and Hydrology, Sos. Bucuresti-Ploiesti 97, 71552 Bucharest, Romania); Sabina Stefan (University of Bucharest, Faculty of Physics, Dept. of Atmospheric Physics, PO Box MG-11, Bucharest, Romania)

The study of climate variability is important for a better understanding of the hydrological and atmospheric processes that lead to droughty periods in Romania. The variability of the seasonal and annual precipitation at Romanian rain gauge stations are examined for characteristics of droughty periods in the atmospheric processes. The discharge series were statistical analyzed to complete the image of the water resources behavior in Romania. The changes identified in the time series of data by means of statistical methods, using Canonical Correlation Analysis, were shown to be correlated with the large atmospheric circulation.

**HS1/W/36-B4 Poster 1025-01****EFFECTS OF QUASI-STATIONARY WAVE ANOMALIES ON THE REGIONAL HYDROLOGIC CYCLE IN THE CONTINENTAL UNITED STATES**

Zaitao PAN, Moti Segal, Raymond W. Arritt, Tsing-Chang Chen and Shu-Ping Weng (Department of Agronomy, Iowa State University, Ames, Iowa 50011, USA, email: rwarritt@iastate.edu)

The interaction of large-scale quasi-stationary waves with regional forcing in the drought of 1988 and flood of 1993 in the north central United States was examined using a mesoscale numerical model. When the observed large-scale quasi-stationary wave anomalies in the dynamic and thermo-dynamic fields were filtered through adjustment of the observationally-based lateral boundary conditions, predicted rainfall and meteorological fields over the drought and flood regions tended toward those for normal years. This method for quantifying, isolating and filtering the relevant large-scale anomalies allows us to infer specific scale interaction mechanisms that produce regional hydrologic consequences of large-scale circulation patterns.

Presiding Chair: Dan Rosbjerg (Technical University of Denmark, Lyngby, Denmark)

**UNDERSTANDING–NONSTATIONARY****HS1/W/06-B4 1100****CLUSTER-BASED HYDROLOGICAL ANALYSIS AND PREDICTION OF LONG-TERM CLIMATE CHANGE AND DROUGHT DISCHARGE**

Toshiharu KOJIRI (Water Resources Research Center, DPRI, Kyoto University, Gokasho, Uji, Kyoto 611-0011, Japan, email: tkojiri@wrcn2.dpri.kyoto-u.ac.jp)

Partly due to climate change, natural disasters such as flood inundation or drought have recently caused heavy damage in many places in the world. Estimation and prediction of the present climate situation will provide significant information to reduce these damages. In this paper, pattern classification methodologies are introduced to analyse global warming effects and spatial relationships of considered meteorological events from a global viewpoint. Furthermore, the advanced AI technology of neural networks is applied to predict regional and local precipitation magnitudes and features.

**HS1/W/21-B4 1120****CLIMATIC VARIABILITY AND ITS IMPACT ON RAINFALL EXTREMES AND URBAN RUNOFF DESIGN IN TUSCANY**

Alfonso CRISCI, Bernardo Gozzini (Laboratory for Meteorology, Climatology and Environmental Modelling (LaMMA), Via Einstein 35, I-50013 Campi Bisenzio, Firenze, Italy); Daniele Grifoni, Francesco Meneguzzo, Gaetano Zipoli (Applied Meteorology Foundation (FMA), Via Einstein 35, I-50013 Campi Bisenzio, Firenze, Italy); Stefano Pagliara (Dipartimento di Ingegneria Edile, Idraulica e del Territorio, University of Pisa, Via Gabba 22, I-56100 Pisa, Italy)

The distinct role of errors in the extremal statistics used to infer design storms of any duration and any return period and trend in the extremal time series are analysed to derive uncertainties affecting the estimates of the design storms. Several extremal time series collected at gauges in Tuscany, Italy, are considered. The Generalized Extreme Value (GEV) distribution is employed to compute the design storms, and the uncertainties in the estimates are derived through the maximum likelihood method. Design storms are then computed for several consecutive 30-year moving time windows (step of one year) to evaluate intrinsic (climatological) uncertainties in the series. The climatological uncertainties in the evaluations are connected to trends and oscillations affecting general circulation features, tentatively expressed by the North Atlantic Oscillation (NAO) index. The hydrological consequences of climate variability are shown to have a major impact on the design of hydraulic works in an urban drainage network.

**HS1/W/07-B4 1140****FORECASTING THE OCCURRENCE OF LOW PRECIPITATION THREE TO TWELVE MONTHS AHEAD**

Ian CORDERY (School of Civil & Environmental Engineering, The University of New South Wales, Sydney, New South Wales 2052, Australia, email: ianc@civil.civeng.unsw.edu.au); Mark MCCall (Bureau of Meteorology, 300 Elizabeth Street, Sydney, New South Wales 2000, Australia); M. Jafar Nazemosadat (Agricultural Faculty, Shiraz University, Shiraz, Iran)

To be accepted and acted upon, forecasts of drought need to be seen to be reliable. A simple partitioning model is presented here in which occurrence of one variable (say geopotential height) within a specified range of values points to the existence of a strong relationship between another variable (say Southern Oscillation Index) in the same season and precipitation one to four seasons later. Partition relations are demonstrated to explain more than 65% of the variance in the precipitation in the next season for areas of up to 500 000 km<sup>2</sup> in Australia, and 50% of the variance in the precipitation four seasons (one year) ahead for similar sized areas.

**HS1/W/14-B4 1200****STUDIES ON HYDROLOGICAL EXTREMES—ENSO SIGNAL**

A. A. L. N. SARMA, B. Padma Kumari & S. Srinivas (Department of Meteorology & Oceanography, Andhra University, Visakhapatnam 530 003, Andhra Pradesh, India)

The Krishna River basin is one of the major river systems of south India. Its hydrological regime is studied using a season climate concept based on a water balance model. Proneness to humid and drought events along with frequency distributions of climate types for selected stations of the river basin are reported. The statistical correlation of the river discharge with the Southern Oscillation Index (SOI) and Sea Surface Temperature (SST) of the Niño3 region of the equatorial Pacific Ocean is also analysed.

**UNDERSTANDING-NONSTATIONARY****HS1/W/39-B4 1400****DEPENDENCE OF THE FREQUENCY AND MAGNITUDE OF EXTREME FLOODS IN COSTA RICA ON THE SOUTHERN OSCILLATION INDEX**

Irina KRASOVSKAIA (Department of Earth Sciences, University of Uppsala, Villavägen 16, S-75236 Uppsala, Sweden, email: irina.gottschalk@hoganas.mail.telia.com); Lars Gottschalk (Department of Geophysics, University of Oslo, Box 1022, N-0315 Oslo, Norway); Alexis Rodríguez and Sadí Laporte (Department of Basic Studies, Instituto Costarricense de Electricidad, Apartado 10032, 1000 San José, Costa Rica)

For the Caribbean and Central America, the positive values of the Southern Oscillation Index (SOI) are generally associated with drought and the negative ones with excess rainfall. For hydropower, as well as for many environmental problems, the existence of non-stationarity in the extreme events is of prime importance. The effect of the Southern Oscillation, described by SOI, on the frequency and magnitude of extreme floods in Costa Rica is investigated by applying a partial duration approach to the total of 91 mean daily runoff series. Statistical analyses of these data indicated that, in the majority of the cases, an assumption of randomness, widely used in operational extreme value analyses, is violated. The analysis of the extensive data sample indicates dependence between the frequency of extreme flood events and the SOI anomalies, while no clear connection can be noted for the magnitude of the extreme floods.

**HS1/W/44-B4 1420****TRENDS AND VARIABILITY IN SWEDISH FLOODS**

Göran LINDSTRÖM (Swedish Meteorological and Hydrological Institute, S-60176 Norrköping, Sweden, email: goran.lindstrom@smhi.se)

Trend analysis was carried out for time series of annual and seasonal extremes at 65 unregulated discharge stations in Sweden. The stations are clearly not independent, as shown by the occurrence of large floods in many basins at the same time. Neither the results from statistical trend tests nor visual inspection of the data suggest any change in flood frequency. Furthermore, the end period, 1995, was not chosen arbitrarily, since the reason for initiating this study was the many observed floods in recent years.

**HS1/W/64-B4 1440****RECENT CHANGE AND PREDICTION OF GLACIER DAMMED LAKE OUTBURST FLOODS FROM KUNMALIK RIVER IN SOUTHERN TIEN SHAN, CHINA**

LIU JINGSHI & Yoshihiro Fukushima (Institute for Atmospheric & Hydrospheric Sciences, Nagoya University, Nagoya 464-01, Japan, email: liu@hydro.nagaokaut.ac.jp)

Glacier Lake Outburst Flood (GLOF) from a glacier dammed lake in the Central Tien Shan has occurred during almost 100 years. Recent records of the GLOF events in the 1990's has indicated that the lake volume and peak discharge are becoming larger and larger corresponding to a warming and wetting of the inner Asian continent. Two extraordinary events of GLOF in summer 1994 and winter 1996 are investigated and described. There is evidence of a change in the magnitude and frequency of floods and in the extension of the glacier and the lake systems. A possible change of the GLOF for next 50 years is predicted by reviewing the history of GLOF events combined with water and heat indices of the current climate. The maximum peak discharge and the flood volume will be enlarged by 50% and 20% respectively, and the date of GLOF occurrence will be shifted to early summer and/or winter. The spring flow will be enlarged due to base flow originating from meltwater.

**HS1/W/65-B4 1500****A STUDY OF EXTREME FLOODS IN CHINA FOR THE PAST 100 YEARS**

Guowei LIU & Jingping Wang (Nanjing Institute of Hydrology and Water Resources, 1 Xikang Road, Nanjing 210024, China)

The peak flow and volume characteristics of the extreme floods of China are discussed, together with their seasonal and geographic distribution. Their secular variation is reviewed and a comparison made between extreme floods of the 20th century and the past 500 years, and with the world extreme flood records. Some characteristics of heavy and large area storms—the causes of extreme floods—are discussed. The conclusions contribute to a better understanding of characteristics of extreme floods of China.

**HS1/W/74-B4 1600****EFFECT OF NOISE IN NONLINEAR HYDROLOGICAL TIME SERIES ANALYSIS AND PREDICTION**

A. W. JAYAWARDENA & A. B. Gurung (Department of Civil Engineering, The University of Hong Kong, Hong Kong, China, email: hrecjaw@hkucc.hku.hk)

Hydrological time series are considered as the outcome of deterministic systems, which may become "chaotic" at times. Identification of such systems requires the data to be noise free. In this study three non-linear noise reduction techniques have been applied to two sets of hydrological data: daily river flow and sea surface temperature anomaly index (S-index). The correlation dimensions have been computed and predictions made before and after noise reduction. The results show that convergence in the correlation dimension as well as increase in the prediction accuracy can be achieved in the noise-reduced data.

**HS1/W/19-B4 Poster 1620-01****JOKULHLAUP CHARACTERISTICS OF LAKE MERTZBAKHER IN THE TIANSHAN MTS AND ITS RELATION TO CLIMATE CHANGE**

S. LIU (Department of Hydrology, Institute of Geography, Chinese Academy of Sciences, Beijing 100101, PR China)

Abstract not available at time of going to press

**HS1/W/42-B4 Poster 1625-02****VARIABILITY IN SPECTRAL CHARACTERISTICS OF HYDROLOGIC DATA**

Khaled H. HAMED (Irrigation and Hydraulics Department, Faculty of Engineering, Cairo University, Giza, Egypt); A. R. RAO (School of Civil Engineering, Purdue University, West Lafayette, Indiana 47907, USA, email: rao@ecn.purdue.edu)

Conventionally, hydrologic time series have been studied in both the time and frequency domains. However, neither the time domain nor the frequency domain is adequate for revealing the underlying structure of such time series. Hydrologic time series can be shown to consist of a stochastic component with a continuous spectrum in addition to a number of added components with discrete spectra. These added components are often interpreted as the effect of a number of natural phenomena such as the sunspot activity, El-Niño Southern Oscillations (ENSO), Quasi-Biennial Oscillations (QBO) and others. However, these components are usually not well defined in hydrologic time series. This study investigates the variability in both the frequency and amplitude of the cyclic components in hydrologic time series. For this purpose, the Multi-Taper spectral analysis method (MTM) (Thomson, 1982) coupled with evolutionary spectral analysis (Priestley, 1965) are used to analyse a number of rainfall, flow, and temperature time series from the Midwest region of the United States. The results from evolutionary spectral analysis indicate variability in both the frequency and magnitude of the cyclic components in the studied time series. Furthermore, a statistical test of stationarity indicates that the continuous part of the spectrum varies significantly with time, indicating nonstationarity of the stochastic processes producing these hydrologic time series.

Presiding Chair: E Servat (IRD, Montpellier, France)

**PREDICTION – DROUGHT****HS1/W/04-B4 1640****GLOBAL MODELLING OF RUNOFF AND IRRIGATION REQUIREMENTS IN TYPICAL DRY YEARS**

Petra DÖLL, Frank Kaspar, Stefan Siebert and Joseph Alcamo (Center for Environmental Systems Research, University of Kassel, D-34109 Kassel, Germany, email: doell@usf.uni-kassel.de)

In order to assess the impact of global change on water scarcity, it is appropriate to look at the situation not only under average climatic conditions but also in dry years. With our global model of water availability and water use in drainage basins (WaterGAP) we calculated runoff and irrigation water use under average climatic conditions and in basin-specific typical dry years. On 33% of the global land area, runoff in the meteorological 1-in-10 dry year differs from runoff in the hydrological 1-in-10 dry year by more than 10%. Besides, years with high irrigation requirements do not necessarily coincide with either type of typical dry year. Therefore, it is necessary to analyse the water situation during three types of basin-specific 1-in-10 dry years that are defined based on (a) precipitation, (b) runoff and (c) irrigation requirements.

**HS1/W/17-B4 1700****REGIONAL PARTIAL DURATION SERIES MODELLING OF HYDROLOGICAL DROUGHTS IN ZIMBABWEAN RIVERS USING A TWO-COMPONENT EXPONENTIAL DISTRIBUTION**

Thomas R. KJELDSEN, Allan Lundorf and Dan Rosbjerg (Department of Hydrodynamics and Water Resources, Technical University of Denmark, Building 115, DK-2800 Lyngby, Denmark, email: trk@email.isva.dtu.dk)

A regional analysis of hydrological droughts is conducted using the partial duration series model with the two-component exponential (TCE) distribution as exceedance distribution. The index-flood method is applied in order to obtain more efficient estimates of the T-year events. Only one of the three parameters of the TCE distribution contributes significantly to the uncertainty of the T-year events and, therefore, only this parameter is regionalized. In total 25 gauging stations covering most of Zimbabwe were used to identify sufficiently homogeneous regions for use with the index-flood method. Separation of the stations according to mean annual precipitation indicated the existence of three or possibly more homogeneous regions, though the limited number of available stations did not allow for any rigorous conclusions.

**HS1/W/45-B4 1720****MODÉLISATION DE L'OCCURRENCE DES ÉTIAGES À PARTIR DES DÉBITS MOYENS JOURNALIERS À L'AIDE DES PROCESSUS PONCTUELS**

Assia CHEBCHOUB (Département de Mathématiques et Informatique, INSAT, BP 676, 1080 Tunis, Tunisie, email: assia.chebchoub@insat.rnu.tn); Zoubeida Bargaoui (Département de Génie Civil, ENIT, BP 37, 1002 Tunis, Tunisie); Irene Abi-Zeid (DRE-Valcartier, 2459 Pie-XI Boulevard North, Val-Bélair, Québec, Canada G3J 1X5); Bernard Bobée (INRS-Eau 2800, Rue Einstein, CP 7500, Sainte-Foy, Québec, Canada G1V 4C7)

La définition des événements de type étiages ou surplus à partir des débits moyens journaliers se fait généralement sur la base d'un débit seuil. Pour les étiages, ce débit représente par exemple le débit atteint ou dépassé 75% ou 90% des jours de l'année. L'application d'un tel critère est apparu inadéquate dans le cas d'un bassin versant tunisien de superficie 448 km<sup>2</sup>. Afin de prendre en compte le caractère fortement intermittent des écoulements, il est proposé de baser la sélection des événements sur un seuil plus élevé correspondant au débit caractéristique de crue (DCC), débit moyen journalier atteint ou dépassé 10 jours par an. L'examen du nombre et de la répartition des événements sur l'année a cependant montré la nécessité d'introduire un deuxième seuil permettant de réduire le nombre d'événements isolés (surplus et étiages). Il s'agit du DC1, débit moyen journalier atteint ou dépassé 30 jours par an. Ainsi, deux seuils de débit au lieu d'un seul sont proposés pour la définition des événements. En outre, un paramètre supplémentaire représentant une durée minimum d'étiage a été introduit. La modélisation de l'occurrence des étiages ainsi définis fait appel aux processus ponctuels alternés surplus/étiage. L'estimation des paramètres des fonctions d'intensités se fait par la méthode du maximum de vraisemblance. Ces estimateurs permettent de prédéterminer l'occurrence des étiages et la loi des durées d'étiages.

**HS1/W/02-B4** Poster **1740-01**

**ON THE NECESSITY TO USE THREE-DIMENSIONAL GROUNDWATER MODELS FOR DESCRIBING IMPACT OF DROUGHT CONDITIONS ON STREAMFLOW REGIMES**

Alain DASSARGUES, Jean-Christophe Marechal, Guy Carabin (Laboratoires de Géologie de l'Ingénieur, d'Hydrogéologie et de Prospection Géophysique (LGIH), University of Liège, Bat. B19, B-4000 Liège, Belgium, email: adassarg@lgih.ulg.ac.be); Olivier Sels (Hydrogéologie, Institut voor Aardwetenschappen, Katholieke Universiteit Leuven, Redingenstraat 16, B-3000 Leuven, Belgium)

Integrated hydrological models are used to assess the impact of global climatic changes on the water cycle. Very often, they are supposed to represent with physical consistency the exchanged water flows between the different parts of the hydrological cycle. In drought conditions, it is particularly important to study with accuracy the baseflow groundwater component for a good assessment of the streamflow. However, in most of the integrated models, the contribution of groundwater in the total streamflow is calculated by use of an empirical or lumped coefficient (i.e. recession coefficient). Due to the lack of recharge during the long drought periods, a general piezometric drop is induced. In heterogeneous and especially in fissured aquifers, the baseflow is changed due essentially to desaturation of the upper zone. By this way, the geometry of the groundwater basin and the local values of hydraulic permeability and effective porosity are influencing the groundwater contribution. Consequently, three-dimensional groundwater models are strongly recommended in order to be able to describe locally different hydrodynamic characteristics in the aquifer. These models should be able to describe explicitly the river-aquifer exchanges with physical consistency, including space and time variations of the baseflow component.

**HS1/W/12-B4** Poster **1745-02**

**DEEP FREEZING OF CRYOLITHOZONE RIVERS**

Svetlana ARZHAKOVA (Department of Land Hydrology, Russian State Hydrometeorological University, 98 Malookhtinsky Avenue, St Petersburg 195196, Russia, email: lobanova@rgmi.spb.su)

The discharge of ground water and the regime of the cryolithozone have been studied to characterize freezing of the rivers in Yakutia. Methods for computations of freezing characteristics based on their dependence upon the length of a river as the principle parameter have been worked out. Average relative estimation errors do not exceed 20 percent, which is acceptable in hydrological practice.

**HS1/W/51-B4** Poster **1750-03**

**INCIDENCES ÉVENTUELLES SUR LA RELATION PLUIE-DÉBIT D'UN CONTEXTE RÉGIONAL DE DIMINUTION DES RESSOURCES EN EAU EN AFRIQUE DE L'OUEST ET CENTRALE NON SAHÉLIENNE**

M. OUÉDRAOGO, E. Servat, J. E. Paturel, B. Kouamé, M. Travaglio (06 BP 1203 Cidex 1, Abidjan 06, Côte d'Ivoire, email: eric.servat@mpl.ird.fr); H. Lubès-Niel (BP 5045, F-34032 Montpellier Cedex, France, email: helene.lubes-niel@mpl.ird.fr); J. M. Masson (Laboratoire Géofluides-Bassins-Eau, URA-CNRS 1767, Université Montpellier II, Place Eugène Bataillon, F-34095 Montpellier Cedex 5, France)

L'Afrique de l'Ouest et Centrale connaît, depuis 1970 environ, des conditions exceptionnelles, en intensité et en durée, de déficits pluviométrique et hydrométrique. Les pays de la zone non sahélienne (appelée zone "humide") ressentent également ces aléas climatiques et présentent des diminutions sensibles de la pluviométrie annuelle (20–25%) et des écoulements (modules en baisse de plus de 35–40% en général). Il apparaît, alors, légitime de s'interroger sur les liens éventuels entre un tel phénomène et la relation pluie-débit elle-même. Pour mener cette étude, on a eu recours à la modélisation de la relation pluie-débit. Le principe a consisté, essentiellement, à ajuster les mêmes modèles sur les deux périodes "humide" et "sèche", puis à tester si les paramètres obtenus sur les deux périodes variaient significativement.

**Friday 30 July AM**

Presiding Chair: J. C. Olivery (IRD, Montpellier, France)

**FORECASTING OF FLOODS**

**HS1/W/08-B5** Poster **0830-01**

**HYDROLOGICAL MAXIMA IN PLAIN RIVERS OF RUSSIA**

Elena ASABINA (Russian Research Institute of Water Resources Management, Mira Street 23, Ekaterinburg 620049, Russia)

Vast territory is characterized with great differences in both climatic factors and local conditions influencing upon origin and development of hydrological maxima. Particularity of hydrological regime is in different causes of maximum origin. The flood peaks may be formed both from snowmelt in spring (snow maxima) and from rain storms in summer and autumn (rain maxima). Usually the snow maxima exceed the rain maxima in plain rivers of Russia. Snow falls and covers territory during 2–6 months. Its melting takes several days or weeks and embraces whole watershed almost simultaneously. The conditions lead to flood with high and long period peak. Usually the maximum stays during some hours or days. Whole flood wave retains from 2 weeks to 2 months and takes place every year in all streams and rivers. The height and total duration of the flood waves change only from year to year depending on water storage in snow. The water storage in snow is the main estimating variable effecting upon all quantitative relations of hydrometeorological processes in snow and soil. In some years, it is possible for rain maxima to exceed snow ones. Rain floods have another time frames. Usually rain storms continue from several minutes to 2–4 h, but with high intensity. These floods have not high peaks and their peak duration continues from several minutes to one hour usually. Whole rain floods takes several days and weeks sometime. Location of them in a basin ties to places of rain storm event and does not embrace whole watershed. Rain floods may be unobserved during a year and may appear several times. Its height and duration change from year to year and from event to event in a year. The main estimating variable of rain floods is day maximum of precipitation and rainfall intensity. Probability of excess of rain maxima over snow maxima of low frequency (1 event per 100 years) is subject of special interest.

**HS1/W/13-B5** Poster **0830-02**

**THE ROLE OF SPATIAL RAINFALL DISTRIBUTION IN FLOOD FORMATION: USING A DISTRIBUTED HYDROLOGICAL MODEL**

Huaxia YAO and Michio Hashino (Department of Civil Engineering, The University of Tokushima, 2-1 Minami-Josanjima, Tokushima 770-8506, Tokushima, Japan, email: yao@ce.tokushima-u.ac.jp)

Hydrological events of flood, their magnitude and occurrence time, are determined by rainfall distribution in a basin and the basin's topography-soil-landuse conditions. The role of rainfall distribution could be interpreted and simulated by a distributed model taking consideration of spatial difference of these controlling factors. In this research a grid-cell-type distributed model is firstly constructed and calibrated for the upper and middle area of Fuji River in central Japan. Daily temperature at every grid-cell is derived from data of in-situ weather stations and GIS, using relationships of temperature and geographical variables such as altitude and latitude. Hourly rainfall at each grid is allocated from in-situ data or from radar rainfall data. Then evapotranspiration, soil water adjusting, and various outflows from soil and aquifer in each grid are estimated with the grid sub-model, and outflows at all grids are routed through a river network onto the outlet, using a river routing sub-model. And the parameters are spatially calibrated with discharge and GIS data. In order to check the validation of model, several rainfall events are selected and the estimated discharge hydrographs are compared with the observed ones. The model shows good reproduction of hydrograph at two gauges along the river. Then supposed rainfall scenarios are applied to explain the effects of distribution on flood formation. Three types of distribution: concentrated on the upper, on the lower parts and uniform on whole area, are considered. But they have same rainfall volume and same timely pattern. Model's outputs shows that these types of rainfall produce rather different flood responses. The rainfall concentrated on upper parts produces the most delayed and flattest flood shape, the rainfall concentrated on the lower parts produces the quickest and sharpest flood, and the uniform rainfall produces a mediating flood between the two cases. Furthermore, a rainfall moving in the basin is also considered. Two directions of movement are supposed. The partly-area-covering rainfall

**HS1/W/26-B5** Poster **0830-03**

**PREDICTION OF VARIABILITY IN THE AMUDARYA RIVER FLOW ON THE BASIS OF HELIOGEOGRAPHICAL OBSERVATIONS**

E. SHERMATOV, B. S. Nutaav (Central Asian Research Institute for Irrigation (SANIIRI), Karasu 4/11, Tashkent 700187, Uzbekistan)

There is no doubt that an interrelation exists between Amudarya River water supply and meteorological data (Tcinzerling, 1924) and identification of this relationship could clarify the possibility of river regime prediction. At present, the problem of climate or over long-term hydrometeorological prediction is not decided. We believe the above tasks can be solved using the accumulated database of many years observations. The current situation can be characterized as a conversion period from climatology (descriptive) to physical climatology. In order to understand climate change and development of hydrological events it is necessary to face the problem Sun–Earth. Heliogeographical data can help in climatology in the theoretical identification of the climate cinematic components and elaborate theoretical basis of climate predictions. In accordance with current ideas, the effect of the sun on climate is about 60%, and of the moon 15%. The influence of the sun is already known – plot to ground water table fluctuation. In Uzbekistan eleven years regime cycle have been observed with one maximum and one minimum. Maximum concurs with minimum of Sun phase and minimum of the contrary. Generalized consideration of Sun activity fluctuations, temperatures of air, precipitation's and Amudarya River flow for a period of more than 100 years are demonstrated close interrelation. Hydrological events have been enforced by fluctuations (or autooscillation) through Sun activity-climate relation. Annual water content of Amudarya River can be calculated as by  $Q = Ae^{BT}$ , where Q is water discharge, T is temperature (Kelvin) of North Hemisphere (latitudes 85–85), and A and B are statistical parameters. The correlation coefficient from 0.88 to 0.98 between temperature and Amudarya River flow, near Kerkey, for the period 1910–1952 before anthropogenic impact to river.

**HS1/W/28-B5** Poster **0830-04**

**SHORT LEAD-TIME RIVER FLOW FORECASTING ON THE YANGHE RESERVOIR BASIN**

Suxia LIU (Department of Hydrology, Institute of Geography, Chinese Academy of Sciences, Beijing 100101, PR China)

With mighty advance of computers and automatic techniques being made and the need for reservoir operation and flood control, allowances have been made for considering river flow forecasting in which lead time is very short. Using a data set of precipitation, evaporation and discharge with 15-min time intervals collected in Yanghe Reservoir basin of north China, where the concentration distance is short and the velocity of flow is high, some experiences are obtained by applying four UCG models. All the chosen 16 floods are considered as continuous time series data. For the Simple Linear model, the relationship between the memory length and the model efficiency is shown monotonous. The favorable memory length is 130 quaters. For simple linear-API model, there seems two optimal points when the memory length is equal to 70 and 140 quaters. Comparing with the shape of the unit hydrography, memory length being 140 quaters is more reasonable. The memory length for both UCGSMAR2 and UCGXIN2 is 75 quaters. The models were both designed for daily data, 75 is the upper limit of the memory length given. The unit hydrography shape of the four models are favourable agreeable with each other. It is promising to apply UCG models to short lead time river flow forecasting from flood event data. By comparing the discharge observed and estimated by the four UCG model, the model efficiency of UGXIN2 model is a little higher than other three models. Based on fluid dynamics of porous media, an water transfer equation is build. By comparing analysis, it is found that when the unsaturated soil is considered as one layer and the river reach is not divided into subreaches, the simulation result of UCGXIN2 is in agreement with that of the equation solution. We have reason to conclude that UCGXIN2 model is a better model to forecast short lead-time river flow.

**HS1/W/38-B5** Poster **0830-05**

**USE OF WEATHER RADAR DATA FOR A FLOOD WARNING SYSTEM**

H. BERGMANN & R. Schatzl (Institute of Hydraulics and Hydrology, Technical University, Graz, Austria)

Since 1979, the Institute of Hydraulics and Hydrology of the Technical University in Graz operates an experimental area on hydrological aspects in the Pöllau basin near Hartberg in the eastern Styria, in which step by step a measuring net with high density of gauges for scientific purposes was equipped. The area includes seven raingauges, four gauging stations as well as a meteorological station in a catchment area of 58.3 km<sup>2</sup>. Extensive analysis is made as preliminary work for the development of a rainfall-runoff model based on weather radar data in the course of a flood warning system for flood endangered zones in western



Styria, in which the Institute for Hydraulics and Hydrology will also be engaged, whereas hydrological data from the Pöllau basin serve as basis, which are available in very detailed form because of the high density of the measuring net and the high discrimination of the measuring instruments. This concerns the precipitation, which is recorded on data loggers in time-variable form as well as the discharge. A comparative analysis of the weather radar data and the terrestrial precipitation measurement is the substance of the paper. Aim of the analysis is to make declarations about the origin of floods, whereas special attention is directed to the comparison of raingauge data with weather radar data. Radar data are intensity data (mm h<sup>-1</sup>), which are recorded in intervals of 10 min and for grids of 2 × 2 km but which are in the form, which is at present available, affected with great unreliability's. To get a basis as well-founded as possible for the flood warning system it must be tried to put these unreliability's to a minimum. For this purpose, the radar data have to be compared with the precipitation data measured at the raingauges and furthermore they have to be calibrated, whereas the following proceeding is chosen: with the aid of a method, which was developed at the Institute for Hydraulics and Hydrology, it is possible to convert the precipitation data measured at the rain gauges into field precipitation data, which are orientated to the grid of the weather radar. Now it is possible to make correlations...

**HS1/W/53-B5** Poster **0830-06**

**HALF-SELF ADAPTIVE UPDATING KALMAN FILTER MODEL OF CHANNEL FLOW ROUTING**

LI ZHIJIA (Department of Water Resources and Hydrology, Hohai University, Nanjing 210024, China, email: lizhijia@public.1.ptt.js.cn)

The half-self adaptive updating Kalman filter model of channel flow routing has been developed for real time application to flood forecasts. The model is based on the Kalman filter theory and Muskingum method. In the model, the measurement error covariance matrix can be estimated in real time through on the innovation sequence. A reasonable and simple model is used in the inflow errors. Examples are given of how the method works for the reaches of rivers. The results show the model are reasonable.

**HS1/W/62-B5** Poster **0830-07**

**APPLICATION OF A PHYSICALLY-BASED DISTRIBUTED MODEL FOR RUNOFF ESTIMATION**

U. C. KOTHYARI (Department of Civil Engineering, University of Roorkee, Roorkee, India)

The occurrence of hydrological extremes in a stream such as the floods or the droughts is greatly dependent upon the process of runoff generation in its catchment. The physically-based distributed modelling for stream runoff enables one to improve the understanding on the processes involved and to help solve the urgent environmental problems associated with man's impact on hydrological cycle e.g. soil erosion and water quality (Kothyari et al., 1997). In recent times a lot of work has been done on physically-based models for runoff generation and these are found to be reliable in estimation of runoff in a catchment. These models include TOP model (Beven, 1996), SHE model (Abbott et al., 1986), ARNO model (Todini, 1989) etc. Nevertheless, most of the existing physically-based models need for their use elaborate data on hydro-climatic, topographic, soil and land-use characteristics of the catchment and also the number of input parameters for most of these models is very large (Kothyari & Jain, 1997). Therefore, in the present study a simpler approach is adopted for runoff modelling which is mainly based on the concepts of Field (1982) and Field & Williams (1987). Rain falling into a catchment surface storage is considered to supply the flow to the main channel and also the ground water storage which then also feeds the main channel is routed by a kinematic wave model. Conventionally, in the kinematic wave model for flow in a channel, a unique relation is assumed between the storage and discharge (Singh, 1996). However, in practice such a relation is not unique and is found to form a loop. To account for this feature the following form of flux law (storage–discharge relation) is considered:

$Ar = aQ1/m b(\partial Q/\partial x)$  where Q is channel discharge Ar is stream cross-sectional area, x is distance, m is channel conveyance exponent and a and b are coefficients. The main feature of present study is the use of above generalized flux law along with the conventional kinematic wave equations. The above generalized flow law is derived by combining the power and the gradient type flux laws and the same is also termed as the Burger's flux law. The model for runoff generation derived as above is applied to the daily rainfall-runoff data of river Narmada in India and is found to satisfactorily simulate the runoff values for the catchments studied.

**HS1/W/72-B5** Poster **0830-08**

**INTEGRATED UNDERSTANDING AND MITIGATION OF FLOODS AND DROUGHTS IN NORTHERN INDIA**

R. B. SINGH (Department of Geography, University of Delhi, Delhi 110007, India)

India is endowed with not only vast and varied geosystems and glaciers but also huge network of river basins. The changing ecohydrology of the catchment areas of the major rivers is also affected by the potential background of the snow cover melting and, consequently, increasing the water potentiality of these rivers. Geographical monitoring considers glaciers as a prime natural capital for development, utilization and conservation of water resources for human sustenance and sustainable mountain development. On the other hand, as increasing uncertainty with the water in streams and rivers, rainfall and snowfall, the natural disasters like floods and droughts are becoming frequent events. Conditions vary widely from region to region. Whereas, some are drought-affected, others are frequently flooded. Hydrological systems as a linking element between land and water are very sensitive to unsustainable and unadopted anthropogenic activities in the highlands as well as in the lowlands. The occurrence of hydrological extreme events are becoming a common feature in Northern India. It is very difficult to say that the hazards are mainly produced by natural fragility of the region or the biotic degradation and land use practices more significant for the flood disaster processes. Flood region covers eight major river valleys spread over 40 million hectares of area in the entire country. This affects 260 million population of India. In recent years with increasing uncertainty in rainfall, drought occurred regularly in north India. Drought conditions are aggravated due to land degradation, loss of top soil and vegetative cover, unregulated surface run off and poor recharge of ground water aquifers with limited landholdings and crop production dependent on erratic rainfall. The drought region covers 14 states and affects a population of 86 million. Drought mitigation is closely linked with groundwater management. An integrated understanding and mitigation strategy is needed to reduce the impact of both flood and drought disasters. A balanced and regular distribution of water harvesting ponds will store excess monsoon rainfall which may be used during the drought period. Flood control measures...

**HS1/W/75-B5** Poster **0830-09**

**MODELISATION DE LA PROPOGATION DES ECOULEMENTS A SURFACE LIBRE PAR REGLES FLOUES**

M. S. LALIAM and L. Duckstein (LATE Hydram, Departement de Genie Rural, EPFL, Suisse)

Le but du présent article est d'exposer d'une manière simplifiée, la faisabilité de modéliser les équations de St Venant grâce à logique floue. Les sources d'erreurs en modélisation hydrologique comprennent des facteurs hydrométrique, topographique et de représentativité comme lorsqu'une équation n'épouse pas fidèlement le phénomène réel. L'un des points forts de la logique floue est qu'elle offre la possibilité de manipuler à souhait des informations de nature incertaine, subjective ou imprécise telle que des informations linguistiques out des données entachées d'erreurs. Ici, l'application de la logique floue se fait grâce à des règles floues. Un modèle flou contient un ensemble de règles floues, chacune de ces règles est composée d'ensembles flous explicatifs et d'ensembles flous réponses. Dans le présent article, ce nouveau concept de modélisation sera décrit en exposant les points suivants: (a) établissement du modèle—les règles floues s'ont obtenues après la génération des ensembles flous explicatifs selon l'avis du concepteur hydroauien et des ensembles flous réponses obtenues grace a l'application des équations classiques et reconnues des phénomènes considérés; et (b) la modélisation s'effectue par une pondération, mathématique, des règles floues. Cette manipulation s'opère par pondération puis combinaison des règles puis fuzzification et defuzzification successives.

Presiding Chair: J.C.Olivery (IRD, Montpellier, France)

**PREDICTION-FLOODS**

**HS1/W/03-B5** **0920**

**ON THE DISTRIBUTION FUNCTION OF EXTREME FLOOD DISCHARGE**

Mikhail V. BOLGOV (Water Problems Institute, Russian Academy of Science, Gubkin Street 3, 117971 Moscow, Russia, email: bolgov@iwapr.msk.su); Vladilen F. Pisarenko (International Institute of Earthquake Theory and Prediction, Russian Academy of Science, Moscow, Russia); Marina I. Fortus (Institute of Atmospheric Physics, Russian Academy of Science, Moscow, Russia)

The examination of sample histograms of river runoff data for the Pacific coast of Russia revealed that it is reasonable to consider the hypothesis that the distribution density of annual maximum of runoff values must include a component with the so-called "fat tail". To describe the tails of maximum runoff histograms, we recommend using the distribution in the form of a mixture of two densities: the normal distribution for the main region and the Pareto distribution providing the slow decrease of the density in the tail region. To estimate the parameters of the mixture, the numerical method of solution of the maximum likelihood equations is proposed.

**HS1/W/09-B5** **0940**

**PRACTICAL APPLICATION OF HISTORICAL FLOOD INFORMATION TO FLOOD ESTIMATION**

David ARCHER (Jeremy Benn Associates, The North Barn, Broughton Hall, Skipton, North Yorkshire BD23 3AE, UK, email: david.archer@jeremybenn.co.uk)

Recent UK legislation requires assessment of 100-year return period flood levels for flood plain planning control. Typical gauged data lengths give an unreliable estimate and the merits of regionalization and the use of historic data are discussed. Typically, existing methods of incorporating historic data require the assessment of event discharges when often all that can be assessed from available sources is the number of events in a specified period over a threshold. Whilst this may be considered statistically as a binomial censored sample, a graphical procedure based on the exceedence of the largest gauged discharge is demonstrated for two contrasting cases of the Rivers Wansbeck and Leam in England using data covering a period of over 200 years. These demonstrate both the limitations and the usefulness of incorporating historical flood data.

**HS1/W/23-B5** **1000**

**ANALYSE DES PLUIES EXTRÊMES ANNUELLES SUR LA RÉGION DE MINAS GERAIS (BRÉSIL): MODELE DE RÉGIONALISATION TCEV**

Bruno Rabelo VERSIANI (Departamento de Engenharia Hidráulica e Recursos Hídricos, Escola de Engenharia da Universidade Federal de Minas Gerais, Av. do Contorno, 842, 30110-060, Belo Horizonte, Brésil, email: versiani@ehr.ufmg.br); Eber José de Andrade Pinto (CPRM, Serviço Geológico do Brasil, Av. Brasil, 1731, 30140-002, Belo Horizonte, Brésil); Philippe Bois (Laboratoire d'Etude des Transferts en Hydrologie et Environnement (LTHE), Domaine Universitaire, BP 53, F-38041 Grenoble Cedex, France)

Cet article présente la méthode de régionalisation des pluies maximales basée sur la fonction de distribution TCEV (Two Component Extreme Value), proposée par Rossi et al. (1984) et son application à des séries de pluies journalières maximales annuelles dans la région de Minas Gerais (Brésil). Ce modèle statistique est composé du produit de deux exponentielles, chacune représentant un processus de Poisson: le premier correspond aux pluies maximales générées plus fréquemment et l'autre aux pluies maximales plus rares, les horsains ("outliers"). Les aspects théoriques du modèle et de la méthode de régionalisation sont brièvement présentés. La région d'étude est un bassin de 50 000 km<sup>2</sup> situé dans une zone représentative du climat tropical de la région sudest du Brésil. La procédure utilisée permet de faire une analyse des horsains et d'identifier deux régions homogènes.

Presiding Chair: I.Cordery (School of Civil & Environmental Engineering, The University of New South Wales, Sydney, Australia)

**HS1/W/32-B5** **1100**

**REASSESSMENT OF FLOOD RISK FOR SCOTTISH RIVERS USING SYNTHETIC RUNOFF DATA**

Michael E. STEEL, Andrew R. Black, Alan Werritty (Department of Geography, University of Dundee, Dundee DD1 4HN, UK, email: m.steel@dundee.ac.uk); Ian G. Littlewood (Institute of Hydrology, Wallingford, Oxfordshire OX10 8BB, UK)

Increased hydroclimatic variability in recent years and the resultant flooding raise questions concerning flood risk estimation from short flow records in Scotland. Long peak flow series have been simulated using historical rainfall to reassess flood risk estimates for 11 selected rivers. Changes of >10% in the estimated value of the 100-year flood are reported for three rivers, as a result of the synthetic record extension achieved. Future changes in flood risk, as a result of possible changes in atmospheric circulation, are discussed briefly.

**HS1/W/34-B5** 1120**PREDICTING SHORT DURATION DESIGN STORMS IN SOUTH AFRICA USING INADEQUATE DATA**

Jeffrey SMITHERS, Roland Schulze (Department of Agricultural Engineering, University of Natal, Pietermaritzburg, South Africa, email: smithers@agua.ccwr.ac.za); Geoffrey Pegram (Department of Civil Engineering, University of Natal, Durban, South Africa)

Relatively few recording raingauges with long, reliable records are available in South Africa for the estimation of short duration ( $E_{24}$  h) design rainfalls. Hence approaches to estimating short duration design rainfalls have been developed which are based on daily rainfall data measured by standard, non-recording raingauges at fixed 24 h periods ending at 08:00. These approaches include the use of regional frequency analyses, scaling the moments of the extreme events and stochastic modelling of the rainfall process. This paper presents results from estimating short duration design rainfalls at selected sites in South Africa, using synthetic rainfall series generated by a stochastic model with parameters derived from daily rainfall data.

**HS1/W/59-B5** 1140**SPATIAL-TEMPORAL STOCHASTIC RAINFALL MODELLING FOR HYDROLOGICAL DESIGN**

Paul J. NORTHROP, Richard E. Chandler, Valerie S. Isham (Department of Statistical Science, University College London, Gower Street, London WC1E 6BT, UK); Christian Onof, Howard S. Wheater (Department of Civil and Environmental Engineering, Imperial College, Imperial College Road, London SW7 2BU, UK, email: c.onof@ic.ac.uk)

The concept of the design storm has its limitations because of its inability to take into account antecedent conditions and the consequent difference between the return periods of the storm and the flood it generates. Stochastic rainfall point models have been developed to model rainfall raingauge data at a single site and, through continuous simulation, provide a new design tool. In the case of many hydrological catchments however, the spatial variability of rainfall becomes crucial to the runoff generation. We present a model in which rain cell origins arrive according to a clustered point process in space and time. The model is fitted using a generalized method of moments. Results are presented for the simulation of individual storms over the Brue catchment in southwest England. These show that the spatial and temporal correlation structures are well reproduced. The model also provides a good fit to the observed marginal intensity and cumulative depth distributions.

**HS1/W/67-B5** 1200**FOCUSED GROWTH ESTIMATION AND THE FLOOD ESTIMATION HANDBOOK**

Duncan W. REED, (Institute of Hydrology, Wallingford, Oxfordshire OX10 8BB, UK, email: d.reed@mail.nwl.ac.uk)

Abstract not available at time of going to press

**Friday 30 July PM**

Presiding Chair: B R Versiani (Univ. Federal de Minas Gerais, Brazil)

**HS1/W/68-B5** 1400**ESTIMATING FLOODS IN PERMEABLE DRAINAGE BASINS**

Duncan S. FAULKNER and Alice J. Robson (Institute of Hydrology, Wallingford, Oxfordshire OX10 8BB, UK, email: dsf@mail.nwl.ac.uk)

Basins with permeable soils and geology pose problems for flood frequency analysis. Several approaches to statistical flood estimation are reviewed which can account for the infrequency of flooding on rivers draining permeable basins. One method which makes efficient use of annual maximum flow data is based on conditional probability. This technique can be applied to single sites or to regional flood estimation, by allowing for the presence of years with no substantial flood. The approach is suited for use in cases where L-moments are used for flood frequency estimation. Examples illustrate that this can avoid underestimation of design floods. The method forms part of the new UK Flood Estimation Handbook procedures.

**HS1/W/24-B5** 1420**FACTORS AFFECTING THE RELATIONSHIP BETWEEN THE FREQUENCY OF A FLOOD AND ITS CAUSATIVE RAINFALL**

Paul WEBSTER (School of Civil Engineering, The University of Birmingham, Edgbaston, Birmingham B15 2TT, UK, email: p.webster@bham.ac.uk)

The paper describes the use of a rainfall-runoff model for investigation of the relationship between the frequency of a flood and that of its causative rainfall. Previous investigation had shown that the annual maximum floods of a given return period were generally caused by storms of lesser return period than implied by the UK Flood Studies Report (FSR) design procedures. Further investigations were carried out to examine the effect of scale, soil type and climate change upon this relationship. It was found that the form of the relationship was applicable across a wide range of scales, and soil types. However, the relationship was characterized by considerable scatter for permeable catchments due to the influence of alternative modes of flood generation. The design event approach to flood estimation is not considered to be appropriate in such catchments. The relationship was little altered under elementary climate change scenarios.

**HS1/W/27-B5** Poster 1500-01**INVESTIGATION ON THE PROBABILITY OF FLOOD EVENTS IN SMALL UNGAUGED AUSTRIAN CATCHMENT AREAS USING BASIN CHARACTERISTICS**

Evelyn KRALL (Institute of Hydraulics and Hydrology, Technical University Graz, Mandellstrasse 9, A-8010 Graz, Austria, email: evi@hydro.tu-graz.ac.at)

For many projects concerning flood control it is necessary to base the flood design on parameters such as the flood peak discharge or the flood hydrograph of a certain probability of occurrence. Here an attempt is made to show the interaction between basin characteristics and those parameters, which are decisive for determining a design flood hydrograph. The knowledge of easily available basin characteristics makes it possible to estimate a design flood event of a certain probability for small ungauged catchment areas. The approach is exemplified on data from the River Raab in eastern Styria.

**HS1/W/37-B5** Poster 1505-02**REGIONAL ESTIMATION OF DESIGN SUMMER FLOOD DISCHARGES IN SMALL CATCHMENTS OF NORTHERN SLOVAKIA**

Silvia KOHNOVÁ and Ján Szolgay (Department of Land and Water Resources Management, Faculty of Civil Engineering, Slovak Technical University, Radlinského 11, 813 68 Bratislava, Slovakia, email: kohnova@us.svf.stuba.sk)

Design floods in ungauged small and mid-sized basins in Slovakia are usually computed from simple regional flood formulae. In this paper other regional approaches have been tested in the flysh region in northern Slovakia. Sub-regions were constructed using hydrologic reasoning based on basin properties and K-means clustering of 17 physiographic basin characteristics and annual summer flood statistics from 43 basins. Regional formulae for the computation of the mean annual summer flood and its standard deviation were derived. Comparison of flood quantiles computed from data and from the formulae showed similar results for all tested methods. The practical applicability of the derived formulae is limited and possible reasons for this are discussed.

**HS1/W/54-B5** Poster 1510-03**DESIGN DISCHARGE OF THE LARGE RIVERS IN THE NETHERLANDS - TOWARDS A NEW METHODOLOGY**

Bart PARMET (Institute of Inland Water Management and Waste Water Treatment (RIZA), PO Box 9072, NL-6800 ED Arnhem, The Netherlands); T. Adri Buishand, Theo Brandsma (Royal Netherlands Meteorological Institute (KNMI), PO Box 201, NL-3730 AE De Bilt, The Netherlands); Rainer Mülders (Federal Institute of Hydrology (BfG), PO Box 309, D-56003 Koblenz, Germany)

The design discharge of the large rivers in the Netherlands has been derived from statistical analyses of time series of peak discharges. Because the available time series are relatively short compared to the required mean recurrence period of 1250 years, and may also be non-homogeneous, the estimated design discharge is subject to large uncertainties. In order to reduce these uncertainties, a new methodology is being developed, consisting of a stochastic multivariate weather generator and a hydrological/hydraulic model. Preliminary results are presented for the Rhine basin.

**HS1/W/61-B5** Poster 1515-04**SEASONALITY OF FLOOD PROCESSES IN AUSTRIA**

R. MERZ, U. Ploock-Ellena, G. Blöschl & D. Gutknecht (Institut für Hydraulik, Gewässerkunde und Wasserwirtschaft, Technische Universität Wien, Karlsplatz 13/223, A-1040 Vienna, Austria)

Work towards an approach to flood regionalization is presented in which the seasonality of runoff and precipitation is used to infer the main flood producing processes which can in turn be used for delineating homogeneous regions. The rationale behind this study is that we believe that similarities in the seasonality of these hydrological variables are often a consequence of similarities in the underlying hydrological and meteorological processes. The analysis of the data shows, for example, that in all high Alpine catchments the mean date of occurrence of floods is in summer and the variability in the flood dates is low. Clearly, this similarity is due to glacier and snowmelt being the main flood producing processes. More detailed process interpretations are presented which are corroborated by examining the seasonality of mean monthly streamflow (i.e. runoff regime), the seasonality of mean monthly precipitation and the seasonality of annual maximum daily precipitation.

Presiding Chair: Duncan Reed (Institute of Hydrology, Wallingford, UK)

**MITIGATION****HS1/W/77-B5** Invited 1600**FLOOD MITIGATION EFFORTS IN THE RED RIVER BASIN: PRACTICAL CONSIDERATIONS**

S P SIMONOVIC

Abstract not available at time of going to press

**HS1/W/50-B5** 1640**INFLUENCES COMBINÉES DE LA SÉCHERESSE ET DE LA PRESSION ANTHROPIQUE SUR UN SYSTÈME D'EAU AMÉNAGÉ EN AFRIQUE DE L'OUEST. CAS DU BASSIN DU BANDAMA (CÔTE D'IVOIRE)**

AKA Akpa, Eric Servat, Jean Emmanuel Paturel (BP 1203 Cidex 1, Abidjan 06, Côte d'Ivoire); Alain Dezetter (01 BP 182, Ouagadougou 01, Burkina Faso); Helene Lubès-Niel, Jean Marie Fritsch (BP 5045, F-34032 Montpellier Cedex, France); Jean Marie Masson (Laboratoire Géofluides-Bassin-Eau, UMR-CNRS 5569, Université Montpellier II, Place Eugène Bataillon, F-34095 Montpellier Cedex 5, France)

La sécheresse que connaît le Sahel se fait également ressentir dans les régions dites humides de l'Afrique de l'Ouest où la gestion des ressources naturelles est un élément important de la stratégie de développement. L'étude entreprise a pour objet d'étudier les conséquences de la sécheresse et de la pression anthropique sur l'utilisation des ressources en eaux dans le bassin du Bandama en Côte d'Ivoire. L'examen des séries de modules de quatre stations montre une diminution de près de 50% des apports annuels en phase avec les perturbations observées au Sahel. Fort de ce constat, le fonctionnement de deux schémas du système d'eau du Bandama a été simulé sur deux ans sous différents scénarios climatiques en termes de pénurie et de défaillance. Les résultats permettent de caractériser tant l'importance du phénomène de sécheresse sur la détérioration des performances du système que celle d'une pression anthropique sans cesse croissante dans un pays africain en voie de développement.

**HS1/W/20-B5** 1700**EVALUATION OF SEASONAL FORECASTING METHODS FOR WATER RESOURCE MANAGEMENT IN THE BRAZILIAN NORTHEAST**

Carlos Oliveira GALVÃO (Department of Civil Engineering, Federal University of Paraíba, Caixa Postal 505, Campina Grande, Paraíba 58100-970, Brazil, email: galvao@if.ufrgs.br); Robin T. Clarke (Institute of Hydraulic Research, Federal University of Rio Grande do Sul, Caixa Postal 15029, Porto Alegre, Rio Grande do Sul 91501-970, Brazil); Trevor D. Davies and Phil D. Jones (Climatic Research Unit, University of East Anglia, Norwich NR4 7TJ, UK)

Rain in the semiarid and drought-prone Northeast of Brazil is highly variable in space and time. Recently available forecasts of seasonal rainfall are at the regional or at the general circulation

model (GCM) grid-square scales, and their usefulness for water management will depend on how far they can be disaggregated to give forecasts at the drainage-basin scale. In this paper seasonal rainfall forecasts produced by two methods—a statistical-empirical and a GCM—are used to derive forecasts of flow volumes, using downscaling and resampling procedures. Performance measures show significant information loss where forecasts of seasonal rainfall are converted to runoff sequences intended for use in water resource management, although some gain is verified in a simulation of the operation of a reservoir using the forecasts.

**HS1/W/31-B5** Poster **1720-01**

**OCCURRENCE, SEVERITY AND MAGNITUDE OF HYDROLOGICAL DROUGHT IN ZAMBIA: IMPACTS AND IMPLICATIONS**

Henry M. SICHINGABULA (Department of Geography, University of Zambia, PO Box 32379, Lusaka, Zambia, email: hsichingabula@natsci.unza.zm); Happy Sikazwe (Department of Water Affairs, P. O. Box 50280, Lusaka, Zambia)

Persistent occurrence of drought under increasing water supply demands for municipalities and agriculture and under increased threat of global warming, requires increased understanding of drought characteristics and sustainable use of water resources. Using the theory of runs, several hydrological drought parameters of frequency of occurrence, run length, magnitude and run intensity, were investigated for the Kafue and Zambezi rivers. Objectives were to (a) determine magnitude-frequency characteristics of hydrological droughts; (b) determine some drought run parameters and frequency of their occurrence and (c) propose a new approach for increasing Zambia's utilization of its water resources without jeopardizing international relations with neighbouring countries. Better understanding of droughts and assessment of Zambia's present and future water requirements will enable planners and decision makers to bring increased economic benefits to citizens. Zambia's drought and water scarcity problems are outlined and linked to some proposed regional water projects designed to divert water from the Zambezi River system. One possible solution to problems of drought and dwindling water levels on Kafue River is proposed.

**HS1/W/76-B5** Poster **1725-02**

**FLOODING IN MONSOON RIVERS: COMPLEX HYDROMETEOROLOGICAL RISK ANALYSIS**

Boris GARTSMAN (Pacific Institute of Geography FEB RAS, Radio Street 7, Vladivostok 69041, Russia); Mark Karasyov (Far-Eastern Hydrometeorological Research Institute, Fontannaya Street 24, Vladivostok 690600, Russia)

Hydrometeorological risk is understood as the probability of the occurrence of hazardous events and is estimated from long series of observations. Here a complete analysis of risk related to flooding in monsoon rivers has been carried out. The analysis includes a study of destructive factors; a spatial analysis of flooding with the help of scenarios produced by a multi-site stochastic model; a regional risk classification of sections of river valleys, and a construction of risk maps in different scales for using in water and land-use management.

**HS1/W/73-B5** Poster **1730-03**

**PERFORMANCE EVALUATION OF A STORAGE RESERVOIR: A CASE STUDY**

Ivan MUZIK (Department of Civil Engineering, University of Calgary, Calgary, Alberta, Canada T2N 1N4)

The Dixon dam reservoir, located on the Red Deer River in central Alberta, Canada, was constructed in 1983. The drainage area of the reservoir is 5600 km<sup>2</sup> and its purpose is mainly to augment the downstream flows for municipal and agricultural use. At the time of design of the reservoir, there were 61 years of historic mean monthly flows available some 60 river kilometers downstream of the dam site. Using regionalization techniques, 61 years of mean monthly flows were estimated at the dam site. The reservoir storage capacities required to meet certain water demands, and their associated probabilities of failure, were determined using: (a) the recorded historic sequence of streamflow, (b) a generated flow sequence of 9900 years by a stochastic model [ARMA (1,1)] and (c) synthetic mass curves of reservoir inflows obtained by statistical analysis of the historic flows. The three methods are briefly outlined and results of the design analysis presented. The paper objective is to take a first look at the reservoir performance using a thirteen year post-construction sequence of observed reservoir outflows and water levels. It is found that during this post-construction period the observed storages confirm design values obtained by the three methods of analysis.

**HS2** Monday 26 – Tuesday 27 July

**INTERACTIONS BETWEEN THE CRYOSPHERE, CLIMATE AND GREENHOUSE GASES (ICSI WITH INVOLVEMENT OF ICT, ICWQ, IAMAS)**

Location: Barber Institute Concert Hall

Monday 26 July AM

Presiding Chair: H G Jones (INRS-Eau, QUEBEC)

**INTERACTIONS BETWEEN CLIMATE, SNOW AND PERMAFROST**

**HS2/W/01-B1** **0900**

**SIMULATION OF THE NORTHERN HEMISPHERE SNOW COVER**

Pierre ETCHEVERS, Hervé DOUVILLE, Eric MARTIN. (CNRM, Météo-France, avenue G.Coriolis, 31057 Toulouse Cedex, France.)

Within the framework of the GSW (Global Soil Wetness) Project, a comprehensive data set of meteorological and surface parameters is provided, enabling the simulation of the northern hemisphere snow cover for the years 1987 and 1988. Two snow models are tested: ISBA (the operational land surface scheme of Météo-France) and Crocus, a multi-layer snow model used for avalanche risk forecasting. The results are compared with two observed data sets: the USAF snow depth climatology and the NESDIS weekly satellite measurement of snow cover. The comparison shows a reasonable agreement between simulations and observations on the global scale. The main discrepancy is the early apparition of snow in autumn and snowmelt in spring. Differences between models are mainly noticeable in mountainous and high latitude areas. They can be interpreted in the light of physical phenomena taken into account in Crocus and simplified in ISBA, such as the snow type dependence of albedo or liquid water retention in the snow pack.

**HS2/W/02-B1** **0920**

**THE INFLUENCE OF EURASIAN SNOW COVER ON NORTHERN HEMISPHERE CLIMATE VARIABILITY**

Judah COHEN and Dara Entekhabi (Massachusetts Institute of Technology, Cambridge, Massachusetts, U.S.A.)

Numerical and observational evidence will be presented demonstrating dynamic interactions and feedback between the extent of multi-seasonal snow cover and the characteristics of wintertime circulation anomalies over mid-high latitudes. The cooling effect of Eurasian snow cover results in a strengthened and more expansive Siberian high with more frequent, topographically constrained intrusions of Arctic air west and north. Early-season snow cover variability results in altered general circulation patterns consistent with the dominant mode of winter variability observed in the Northern Hemisphere. The implications of the surface-atmosphere coupling for seasonal predictability will also be discussed.

**HS2/W/03-B1** **0940**

**TRENDS IN TURBULENT HEAT FLUXES OVER NORTHERN EURASIA**

Pavel Ya. GROISMAN (National Climatic Data Center, 151 Patton Avenue, Asheville, North Carolina, 28801, USA), Eugene L. Genikhovich (Main Geophysical Observatory, Koroleva St. 7, St. Petersburg, 194021, Russia), Raymond S. Bradley AND Sun Bomin (Department of Geosciences, University of Massachusetts, Amherst, 01003, USA)

Recently we developed a method to obtain direct estimates of surface turbulent heat fluxes (latent heat fluxes are estimated only for saturated surfaces, wet and/or snow-covered) using routine meteorological observations. This was possible for the former USSR territory and some other countries, where the standard practice of hourly observations includes measurements of temperature at the atmosphere - land surface boundary and state of the ground. The method has been tested on several observational data sets and is now applied to Northern Eurasia. We use the 3- / 6-hourly station data for the past several decades to assess the trends of sensible heat fluxes and latent heat fluxes from well saturated surfaces, including snow cover, for the period 1960 to 1990. Large-scale changes in these fluxes, near-surface temperature inversions and wind speed have been revealed over all of Northern Eurasia during the cold season.

**HS2/W/04-B1** **1000**

**INTERANNUAL VARIABILITY OF THE ANOMALIES STRUCTURE OF SNOW COVER OVER THE FORMER SOVIET UNION IN CONNECTION WITH CLIMATE CHANGES**

A.N. Krenke, L.M. Kitaev, and T.N. Vegener (Russian Academy of Sciences)

Abstract not available at time of going to press

**HS2/W/05-B1** **1020**

**A MULTICHANNEL THRESHOLD TECHNIQUE FOR NOAA-AVHRR DATA TO MONITOR THE EXTENT OF SNOW COVER IN THE SWISS ALPS**

Stefan Voigt, Michael Koch, Michael F. Baumgartner (Department of Geography, University of Bern, Hallerstrasse 12, 3012 Bern, Switzerland)

A multi-channel threshold technique is presented that allows monitoring of snow cover in mountainous terrain such as the Swiss Alps using NOAA-AVHRR data. The data preparation and calibration steps necessary to apply the method on time series are described. While some of the classification thresholds are stable with time others vary over the season. The classification skill proves to be better than that of supervised and unsupervised classification approaches. Comparison with ground measurements displays accordance between 60 % and 90 %. The method shows to be reliable and easy to apply and is therefore well suited for operational snow cover monitoring.

**HS2/W/06-B1** **1120**

**SNOWFALL RESPONSES OVER THE U.S.A. TO PHASE AND AMPLITUDE VARIATIONS IN THE TROPOSPHERIC WAVETRAIN**

Martyn P. Clark and Mark C. Serreze (Cryospheric and Polar Processes Division, Co-operative Institute for Research in Environmental Sciences, Campus Box 449, University of Colorado, Boulder Colorado 80309-0449, USA.)

Variability in snowfall over the United States is examined with respect to changes in the phase and amplitude of the tropospheric wavetrain. Results are based on composites constructed for both high and low amplitude cases when the ridge axis of the wave train was located in each of six 10o longitude bands between 160oW and 100oW. The most striking signals occur over the central U.S. when the wavetrain is of high amplitude and just west of its mean position. Positive precipitation anomalies and negative temperature anomalies combine to provide positive snowfall signals. Over the western U.S.A., the strongest positive snowfall signals are found when the wave train is of low amplitude, and the ridge lies west of its preferred position. Temperature and precipitation anomalies again play reinforcing roles. Widespread decreases in snowfall occur when the wavetrain is amplified and lies on or east of its preferred location, reflecting high temperatures and low precipitation totals. Significant regional snowfall increases in some composites occur in the absence of positive precipitation anomalies, best expressed in the transient snow regions (e.g., the eastern U.S.) where precipitation phase is the limiting factor on snowfall.

**HS2/W/07-B1** **1120**

**INTERANNUAL VARIATIONS IN SNOW MELT ONSET AND LINKS TO 500 HPA ATMOSPHERIC ANOMALIES OVER THE ARCTIC**

Sheldon DROBOT (Department of Geosciences, University of Nebraska, Lincoln, Nebraska, USA, 68588), Mark ANDERSON (Department of Geosciences, University of Nebraska, Lincoln, Nebraska, USA, 68588)

Interannual variations in the melt onset of snow provide a mechanism to observe climatic fluctuations. Timing of initial ablation is associated with certain poorly defined overlying atmospheric conditions. This paper investigates the spatial and temporal patterns in melt onset dates and associated 500 hPa height anomalies over the Arctic region from 1982 – 1992. Melt onset dates are derived from Scanning Multichannel Microwave Radiometer (SMMR) and Special Sensor Microwave Imager (SSM/I) data, while 500 hPa height anomalies are



computed from the National Centers for Environmental Protection (NCEP) reanalysis models. Results indicate significant interannual variations in the spatial pattern and timing of melt onset. With the assistance of principal component analysis (PCA) links between the melt onset dates and the 500 hPa height anomaly field are highlighted.

**HS2/W/08-B1****1140****CLIMATE CHANGE AND SIERRA NEVADA SNOWPACK**

Tammy JOHNSON (Department of Geography, University of California, Santa Barbara, 3611 Ellison Hall, Santa Barbara, California 93106-4060, USA); Jeff Dozier (Donald Bren School of Environmental Science and Management, University of California, Santa Barbara, 4670 Physical Sciences North, Santa Barbara, California 93106-5131, USA); Joel Michaelsen (Department of Geography, University of California, Santa Barbara, 3611 Ellison Hall, Santa Barbara, California 93106-4060, USA)

Most of California's water resources accumulate within the snowpack on mountains until it melts, which is usually in the spring. This study uses a statistical model which links snow water equivalent (SWE) measurements over a 60-year time-series to clarify the spatial characteristics of snow accumulation trends in the Sierra Nevada. To determine the effects of a monthly and irregular sampling schedule we analyzed daily snow sensor data spanning 28 years. Results are presented for monthly and seasonal maximum changes by range-wide elevation bins and by river basin groupings. We found a strong linear elevational component to monthly SWE accumulation trends. Below 2400 meters, less snow is accumulating and it is melting earlier. Higher elevations exhibit greater variability, with most stations accumulating more snow and melting earlier. This could be the result of warmer air masses having higher moisture contents.

**HS2/W/09-B1****1200****MAPPING THE SENSITIVITY OF CANADIAN PERMAFROST TO CLIMATE WARMING**

Sharon L. SMITH and Margo M. Burgess (Geological Survey of Canada, 601 Booth St. Ottawa, Canada, K1A 0E8)

A major concern in climate change impact studies in polar regions is the effect of warming on permafrost. Under climate warming scenarios, permafrost may ultimately disappear from about half of the present Canadian permafrost region. The Geological Survey of Canada, as part of a set of national syntheses of geological responses to climate change, is preparing maps to characterise the response of permafrost to climate warming. Digital data layers of factors that influence permafrost response have been combined to produce maps classifying permafrost within the zone where it may ultimately disappear according to i) the relative rate of response of its thermal regime to warming, and ii) the relative magnitude of the impact of permafrost thaw. A final map then combines these two components into one sensitivity index.

**Monday 26 July PM**

Presiding Chair: Angela Gurnell (Birmingham)

**MONITORING AND MODELLING SNOWCOVER****HS2/W/10-B1****1400****PRE-OPERATIONAL SNOWMELT FORECASTING BASED ON AN INTEGRATION OF GROUND MEASUREMENTS, METEOROLOGICAL FORECASTS AND SATELLITE DATA**

Hannes Kleindienst, Markus Pfister, Michael F. Baumgartner (Department of Geography, University of Bern, Hallerstrasse 12, 3012 Bern, Switzerland)

A method for short term snowmelt runoff forecast based on a degree-day snowmelt model is discussed. Snow maps derived from NOAA-AVHRR satellite images, meteorological forecast data from a limited area model and data from several snow gauges are used to define daily input for the model. A test run for the main ablation period 1996 showed average errors of 12.6% and 16.6% for a one and two days forecast respectively. A modified forecast system based on the experiences presented here will be applied in real time for the ablation period 1999.

**HS2/W/11-B1****1420****MODELLING SNOW-ATMOSPHERE INTERACTIONS IN COLD CONTINENTAL ENVIRONMENT**

J. W. Pomeroy (National Hydrology Research Centre, 11 Innovation Blvd., Saskatoon S7N 3H5 Canada), R. L. H. Essery, D. M. Gray, K. R. Shook, B. Toth (Division of Hydrology, University of Saskatchewan, Saskatoon S7N 0W0 Canada), P. Marsh (National Hydrology Research Centre, 11 Innovation Blvd., Saskatoon S7N 3H5 Canada)

Land surface process schemes are very sensitive to snow cover and snow processes. However many of these schemes are deficient in their representation of snow processes, as they are manifested in cold continental interior climates. The next generation of GCMs, meso-scale models and coupled hydrological models will require improved representations of snow surface processes. To this end, new algorithms have been developed and verified by field measurements to improve snow process representations for prairie and arctic environments. Based on the algorithm results, recommendations for advances in snow modelling are made regarding: redistribution of snow cover by blowing snow, sublimation loss during blowing snow, turbulent transfer during snowmelt and ground heat flux during percolation of snowmelt water through the snowpack and infiltration into frozen soil.

**HS2/W/32-B2****1440****SPATIAL VARIATIONS IN ENERGY BALANCE OF PATCHY ARCTIC SNOW COVERS**

P Marsh, N Neuman, J. Pomeroy and R. Essery (NHRI, Saskatoon)

Abstract not available at time of going to press

**HS2/W/12-B1****1540****SHAPE CHARACTERISTICS OF FRESHLY FALLEN SNOWFLAKES AND THEIR SHORT-TERM CHANGES**

S.R. FASSNACHT, E.D. Soulis & N. Kouwen (Department of Civil Engineering, University of Waterloo, Waterloo, Ontario N2L 3G1, Canada)

The shape of newly formed snowflakes is an important qualitative parameter as input to the development of a snowpack, and for potential atmospheric scavenging, while changes in the shape of freshly fallen crystals influence the metamorphosis and transport of snow and contaminants. This paper uses known spatial properties to simulate the variety of crystal structures that can occur in the range of -4 to -6°C. Probability distribution functions (pdfs) are derived for the surface area to mass ratio, ranging from 0.10 to 0.20 m<sup>2</sup>.g<sup>-1</sup>. Observations of freshly fallen flakes are compared to predicted pdfs. The modification in the snow crystal shape, immediately after accumulation, is estimated from laboratory experiments that measured sublimation rates directly from the pack. For fresh flakes, there is a rapid decrease in the effective surface area up to 50% over only 2-3 days.

**HS2/W/13-B1****1600****IMPACT OF CLIMATE VARIABILITY ON SNOW COVER REDISTRIBUTION AND SNOWMELT RUNOFF REGIMES IN MOUNTAINOUS REGION**

Wang Jian and Li Wenjun (Lanzhou Institute of Glaciology and Geocryology, Chinese Academy of Sciences, 730000 Lanzhou Gansu, P. R. China)

As a matter of fact, the annual average air temperature increases 1.4° C in test basin from 1956 to 1996. The results of analysis show that snow cover distribution and runoff regimes in western China has been obviously effected by globe warming and rising air temperature since 1960. Commonly, in the middle latitude mountainous region, the snow cover area reduces in the winter because of the accumulation period to be shortened while in the summer the snow cover extent increases for the adding of snowfall days. Snowmelt runoff will be increment in yearly round with higher melting rate, earlier melting starting data and longer melting interval. For vital reason is the permanent snowfield and glaciers would play two sensitive roles in melting period for flow supply by rising temperature. Based on the scenarios of 4° C rising in air temperature, the simulating discharges would be discussed in hydrological year of 1986.

**HS2/W/14-B1****1620****EFFECT OF CLIMATIC FACTORS ON STREAMFLOW IN THE INTERIOR MOUNTAINOUS CATCHMENT, NORTHWESTERN CHINA**

Ding Yongjian, Ye Baisheng and Liu Shiyong (Lanzhou Institute of Glaciology and Geocryology)

Abstract not available at time of going to press

**Tuesday 27 July AM**

Presiding Chair: John Pomeroy (NHRI, Saskatoon)

**ICE MASS VARIABILITY****HS2/W/15-B2****0900****INTERANNUAL VARIABILITY OF GLACIERS AND SNOW COVER**

A.N. Krenke, T.E. Khromova and L.P. Chernova (Russian Academy of Sciences)

Abstract not available at time of going to press

**HS2/W/16-B2****0920****REGIONAL CHARACTERISTICS OF GLACIER MASS BALANCE VARIATIONS IN HIGH ASIA**

Liu Shiyin, Wang Ninglian, Ding Yongjian (Lanzhou Institute of Glaciology and Geocryology, Chinese Academy of Sciences, Lanzhou 730000, PR. China), Xie Zichu (Department of Resources and Environment, Hunan Normal university, Changsha 410081, PR. China)

The High Asia, broad in area with numerous huge mountainous ranges, is one of regions with existing glaciers mostly concentrated. However glacier mass balance measurements can not be extended on much more glaciers covering most of the mountains because of the high altitudes and complex topography. Analyzing the temporal and spatial variations of mass balance sequences from presently observed High Asia glaciers is therefore of help to evaluate the regional regularities of balance variations and their response to the global warming. 17 sequences of mass balance obtained in various sources for glaciers in different mountains of Altay, Tianshan, Pamir-Alai Mountains and the Himalayas are selected for present analysis by means of frequency filtering, spectral analysis, principal component analysis (PCA) as well as Mann-Kendall non parameter rank statistic. Results indicate that mass balance series have a similar variation pattern when glaciers are within the vicinity of a short distance while regional inhomogeneity in balance variations appears when the spatial distance extends to a large range. This conclusion gives a fundamental base for establishing a plausible regional network of glacier mass balance monitoring. Furthermore, most of the balance sequences show a quasi-2 years periodical fluctuations corresponding to that of the climatic parameters in the region. It is also found that there exists an abrupt change in the variations of mass balance of almost all glaciers. Based on the PCA method balance sequence from the area-weighted average of all observed mass balance can roughly represent the variations of different glaciers in the region.

**HS2/W/17-B2****0940****IDENTIFYING LINKS BETWEEN LARGE-SCALE ATMOSPHERIC CIRCULATION AND LOCAL GLACIER ABLATION CLIMATES IN THE FRENCH PYRÉNÉES**

David M. Hannah, Angela M. Gurnell & Glenn R. Mcgregor (School of Geography, University of Birmingham, Edgbaston, Birmingham. B15 2TT. UK.)

This paper adopts a synoptic climatological approach to elucidate associations between large-scale atmospheric circulation and local summer ablation climates for a small cirque glacier (Taillon Glacier, French Pyrénées), located at the climatically-sensitive southern limit of contemporary European glaciation. The air-mass categories identified possess differential influences on snow and ice melt dependent upon their thermodynamic properties. The observed climate-glacier links are employed to predict the impact of a shift in air-mass type frequency on Pyrénéan snowpacks and glaciers. Typically, cyclonic patterns are associated with low ablation whereas high melt is associated with anticyclonic systems. An extension of the North African-Mediterranean subtropical ridge with an associated polar shift in the westerlies, as proposed under global warming, would favour an increase in the prevalence of high-energy air-masses, thus enhancing Pyrénéan ablation climates. Further work is required to extend this air-mass identification scheme over a number of years and to

**HS2/W/18-B2 1000****ENERGY BALANCE MEASUREMENTS ON A CANADIAN HIGH ARCTIC GLACIER AND THEIR IMPLICATIONS FOR MASS BALANCE MODELING**

Anthony ARENDT and Martin Sharp (Department of Earth and Atmospheric Sciences, University of Alberta, Edmonton, Alberta, T6G 2E3, Canada)

Meteorological measurements from 3 weather stations on John Evans Glacier were used to show that (a) lapse rates in air temperature were highly variable (values ranged between -0.02 and -0.63°C per 100 m), and generally lower than assumed in degree-day mass balance models; and (b) degree-day factors, calculated from energy balance measurements at the 3 stations, tended to increase throughout the melt season. Degree-day factors correlated well with measured surface albedo ( $r^2$  as high as 0.50), and relationships were consistent between years. A simple albedo algorithm implemented within a degree-day model for John Evans Glacier resulted in average melt predictions that were up to 0.13 m WE closer to observed values than those produced by simulations which relied upon constant degree-day factors used in previous studies.

**HS2/W/19-B2 1020****VARIATIONS OF GLACIER MASS BALANCE AND THEIR CLIMATIC IMPLICATION OVER THE NORTHERN HEMISPHERE IN PAST FORTY YEARS**

Ding YONGJIAN, Liu Shiyin, YE Baisheng And Zhou Wenjuan (Lanzhou Institute of Glaciology and Geocryology, Chinese Academy of Sciences, Lanzhou 730000, P. R. CHINA)

Based on mass-balance data continuously measured at 40 glaciers from the last thirty to forty-years, some characteristics of mass balance variations of main glacial areas of the Northern Hemisphere have been analysed. The connection and difference of mass balance records and variations of mass balance and ELA have been discussed. Finally, relation between mass balance and climate in the hemispherical range is also analysed. Sensitivity of mass balance to climatic warming is approximately -800 mm/yr/°C according to recorded data.

**HS2/W/20-B2 1040****ON THE CHARACTERISTICS OF GLACIER FLUCTUATIONS DURING THE LAST 30 YEARS IN THE URUMQI RIVER BASIN AND THE ESTIMATION OF TEMPERATURE RISE IN THE HIGH MOUNTAIN AREA**

Liu Shiyin, Wang Ninglian, Ding Yongjian (Lanzhou Institute of Glaciology and Geocryology, Chinese Academy of Sciences, Lanzhou 730000, PR. China ), Xie Zichu (Department of Resource and Environment, Hunan Normal University, Changsha 410081, PR. China)

Based on field observations and repeated photo-grammetry, representative glacier and all the other glaciers in the Urumqi River basin have experienced definite shrinkage since the end of 1950s and the beginning of 1960s. It's found that the decreases in length, area and ice volume of glaciers show a close relationship with glacier dimensions, that is, the larger the glaciers, the bigger their retreats and vice versa. Analysis indicates that statistical relations can be established for the absolute and relative changes in length, area and volume of glaciers against with glacier lengths, which can be adapted to glaciers in other mountainous regions, if we conduct some supplementary measurements of glacier fluctuations. With this concept, an evaluation can be made for glacier fluctuations in a regional scale. Further calculation demonstrates that glacier shrinkage in the last 30 years corresponded to a warming of about 0.35?0.27? in the high mountain region of the Urumqi River.

**HS2/W/21-B2 1120****HYDROLOGICAL RESPONSE OF MELT-WATER FROM GLACIER COVERED MOUNTAIN WATERSHEDS TO CLIMATE CHANGE IN THE NORTHWEST CHINA**

Liu Jingshi Yoshihiro Fukushima Tetsuya Hiyama (Institute for Hydrospheric & Atmospheric Science, Nagoya University, Nagoya 464-01, Japan)

Most rivers in the Northwest China are recharged by snow and ice melt-water from the glacier covered area in the mountains. An obvious change in the regional climate with 0.5?h warming in annual air temperature and 10% - 20% increasing in the precipitation has occurred in the inner land Xinjiang of China since the late 1970s, relevant variation in the stream flow from grouped two typical glaciers covered watersheds in the North and the South Tien Shan Mts., the Pamirs, the Mts. Karakoram and the West Kunlun were analyzed based on hydro-meteorological records for 40 years. Results indicated that the stream meltwater didn't produce a response of increase to climatic fluctuation in the 1980s, the stream-flow in most rivers appeared a little decrease, and increase only in one basin with delayed about 5-6 years, summer discharge also performed the delaying and a little increase in the same period due to a little increase in summer precipitation and under a stable summer temperature. The most sensitive response with biggest variability of 15%-20% among the melt-water components to the climate fluctuation was from seasonal flow in May and the annual maximum flood in the smaller watershed with low glacier coverage. It is favourable to glacier development due to more snow accumulation and lower air temperature in summer in the high mountains under the current climate.

**HS2/W/22-B2 1140****MASS BALANCE STUDY ON COLLINS ICE CAP, KING GEORGE ISLAND, ANTARCTICA: SPATIAL AND TEMPORAL VARIATION**

Han Jiankang Xie Zichu (Hunan Normal University, Changsha, 410006, P.R. China), Wen Jiahong Kang Jiancheng (Polar Research Institute of China, Shanghai, 200129, P.R. China), Zhu Guocai Jin Xiaoping Gao Xinsheng (Lanzhou Institute of Glaciology and Geocryology, Chinese Academy of Sciences, Lanzhou 730000, P.R. China)

The mass balance study carried out during Oct.1991 to Nov.1992 on Collins Ice Cap, King George Island, Antarctica suggested that the equilibrium line for 1991-1992 was at the elevation of 140m a.s.l., but the mean equilibrium line altitude for multiple years is at 160m a.s.l.. The net mass balance shows an increasing trend with altitudes, having a maximum up to 2480kg-m<sup>-2</sup>-a<sup>-1</sup> in water equivalent on the summit. Using a relation between mean summer temperature and the total ablation, the variation of annual net mass balance during the period of 1971-1992 at the Low Dome was worked out. It showed that the mass balance of the ice cap was negative mostly in the years 1971/1972-1983/1984, while kept positive mainly from 1984/1985 to 1991/1992. The cumulative net balance during the 21 years was near zero.

**HS2/W/23-B2 1200****SENSITIVITY OF AN ANNUAL MEAN ENERGY-MOISTURE BALANCE MODEL WITH A PLASTIC ICE SHEET**

M M Maqueda, G. Kainyck, and A.J. Willmot (Keele University, UK)

Abstract not available at time of going to press

**HS2/W/24-B2 1220****A STUDY OF CLIMATE AND ENVIRONMENT DURING LAST MAXIMUM GLACIAL PERIOD IN WESTERN CHINA**

Ye BAISHENG Ding Yongjian Shi Yafeng Zheng Benxing (Lanzhou Institute of Glaciology and Geocryology, Chinese Academy of Sciences, Lanzhou 730000, China)

Since last maximum glacial period, mountain glacier in western China has been affected by global climatic warming and neotectonic uplift. To study climatic characteristics in last maximum glacial period, seven sites, source area of Urumqi River in Tianshan Mountains, east slope in A'Nyemaqen Mountains, Dongkemadi in Tanggula Mountains, Chongce in West Kunlun Mountains, Rongbu in Qomolangma Mount, Hailuoguo in Gongga Mount and Yulungxueshan in Hengduan Mountains, were selected for comparing, where include almost all main mountains in western China. Based on sizes of glaciers in these sites during last maximum glacial period, the conditions of air temperature and precipitation are recovered using the method of glacier dynamics. The results show that precipitation in last maximum glacial period only is only 20-30% in comparison with that of present in central and eastern Qinghai-Xizang (Tibet) Plateau and Tianshan area. In the south part of the Plateau, Gongga and Yulungxueshan areas, precipitation is identical to or slightly over that of the present, but in the western side of the Plateau it is 60-70% of the today's. If effect of neotectonic uplift on climate is not considered, air temperature in summer in that time is 4.6-6.0° C lower than that of present in the eastern part and the southern part of Tibet Plateau and Tianshan area, and 2-3.5° C lower in the western side and the central part of the Plateau. Estimated air temperature in summer is relatively low in comparison with the results from other methods, because effect of neotectonic movement has been from the last glacial period to now. Differences of the temperature rising in varied regions of the Plateau reflect discrepancy of neotectonic lift. If air temperature in summer in last maximum glacial period is 6.0° C lower than today's, the amount of neotectonic lift can be roughly estimated by difference between supposed and estimated air temperatures. The central and the western parts of the Plateau have risen to a maximum of 400-600m since last maximum glacial period, and of which West Kunlun and Qomolangma areas raised about 650m. Relatively small rising of 100-200m occurred in the eastern and southern parts of Plateau and Tianshan area.

**HS2/W/25-B2 1240****HIGH RESOLUTION CLIMATIC RECORD FROM THE TIBETAN ICE CORES**

Yao Tandong (Lanzhou Institute of Glaciology and Geocryology, CAS, Lanzhou, China)

Based on ice core studies, climatic history since the Last Interglacial on the Tibetan Plateau has been reconstructed. Climate reconstructed from ice cores since the Little Ice Age indicated three cold sub-stages and three warm sub-stages. However, the date, duration and magnitude of each corresponding cold and warm sub-stage in the two records are different. The climatic changes in the past 2000 years were also carefully studied. In both precipitation and temperature records, there are gradual increasing trends from the past to present with many fluctuations. However, the magnitude and phase of each corresponding fluctuation is different in the two records. The most important progress in Tibetan ice core study is the climatic reconstruction since the Last Interglacial from the Guliya ice core. There are several features in this long record. Firstly, the major climatic events from deep-sea core were well recorded in the Guliya ice core. Secondly, the transition from warm to cold period was abrupt. Third, the temperature fluctuation indicated by the Guliya record is closely related to insolation. It is, therefore, speculated that insolation might be a major driving force of the major climatic events recorded in the guliya ice core.

**Tuesday 27 July PM**

Presiding Chair: Jake Peters (USGS)

**CHEMICAL PROCESSES IN THE CRYOSPHERE****HS2/W/26-B2 1400****THE TRANSMISSION OF SOIL GASES THROUGH SEASONAL SNOW COVER: AN EXPERIMENT TO DETERMINE THE DIFFUSIVITY OF N<sub>2</sub>O IN SNOW IN SITU**

H.G. JONES (INRS-Eau, Ste-Foy, Quebec, Canada.), E. van Bochove and N. Bertrand (Agriculture and Agri-Food Canada, Ste-Foy, Quebec, Canada)

This study reports on an experiment to better estimate gas diffusion coefficients for N<sub>2</sub>O emitted from agricultural soils using a gas diffusion system composed of a mass flow controller, a diffusion enclosure and a diffusion chamber installed in situ. From the observed values of D<sub>s</sub> and the known value of the diffusion co-efficient of N<sub>2</sub>O in air, the Aresistance factor @, Rs, of snow to gaseous diffusion was calculated. Rs is a parameter that integrates the different transport rates of the gas due to structural differences in the snow. A Rs value of 1 shows the snow to be an unimpeded diffusion matrix; a Rs of less than 1 shows that diffusion is restricted. The results demonstrated that Rs values (0.60 -1.0) varied with time and could be related to the degree of heterogeneity of the snow cover as the winter season progressed.

**HS2/W/27-B2 1420****A STUDY ON SPATIAL AND TEMPORAL DISTRIBUTION OF 18O ON PRECIPITATION IN THE TIBET PLATEAU**

Zhang Xinping, Yao Tandong and Tian Lide (Hunan Normal University)

Abstract not available at time of going to press

**HS2/W/28-B2 1440****RESPONSE OF MAGNITUDE OF 18O IN SHALLOW ICE CORE OF DASUOPU GLACIER IN TIBET PLATEAU TO LARGE SCALE SEA-AIR INTERACTION**

Zhang Xinping, Yao Tandong and Xie Zichu (Hunan Normal University)

Abstract not available at time of going to press

**HS2/W/29-B2 1540****BICARBONATE AND BICARBONATE-DERIVED CARBON FLUXES FROM 3 POLYTHERMAL GLACIER BASINS IN SVALBARD, NORWEGIAN HIGH ARCTIC**

A J Hodson (University of Sheffield) and M. Tranter (Bristol Glaciology Centre, School of Geographical Sciences, University of Bristol, University Road, Bristol. BS8 1SS. U.K.)

Abstract not available at time of going to press

**HS2/W/30-B2 1600****COMPARATIVE FLUXES OF HCO<sub>3</sub><sup>-</sup> AND SI FROM GLACIATED AND NON-GLACIATED TERRAIN DURING THE LAST DEGLACIATION**

I. W. Jones, G. Munhoven & M. Tranter (Bristol Glaciology Centre, School of Geographical Sciences, University of Bristol, University Road, Bristol. BS8 1SS. U.K.)

There is current interest in the riverine fluxes of HCO<sub>3</sub><sup>-</sup> and Si at the last glacial maximum (LGM), since modelling suggests that these were higher than today (Gibbs and Kump, 1994; Froelich et al., 1992). If this is the case, removal of atmospheric CO<sub>2</sub> by silicate weathering is also likely to have been greater at the LGM (Munhoven and Francois, 1996), so contributing to the lower atmospheric CO<sub>2</sub> recorded by ice cores (Barnola et al., 1987). To date, the magnitude of glacial chemical erosion on HCO<sub>3</sub><sup>-</sup> and Si fluxes at the LGM is poorly quantified, and the locus of the inferred doubled terrestrial Si flux is unknown. This paper aims to provide first estimates of the relative fluxes of HCO<sub>3</sub><sup>-</sup> and Si fluxes from ice-free and glaciated terrain for five time steps between the LGM (21ka), by extending the modelling approach of Gibbs and Kump (1994) and incorporating new data on glacial solute fluxes (Tranter et al., submitted).

**HS2/W/31-B2 1620****CARBON DIOXIDE CONSUMPTION AND BICARBONATE PRODUCTION RATES BY CONTINENTAL WEATHERING AT THE LGM AND AT PRESENT-DAY—AN UPDATE**

Guy Munhoven (Bristol Glaciology Centre, School of Geographical Sciences, University of Bristol, Bristol BS8 1SS, UK)

There is currently major debate on the variations of CO<sub>2</sub> consumption and HCO<sub>3</sub><sup>-</sup> production rates by continental weathering processes on glacial-interglacial time scales. In this study, we use two models of continental weathering to calculate the bicarbonate production rates from the distributions of drainage intensity and rock type exposure (lithology). A range of estimates for the distribution of runoff at the Last Glacial Maximum (LGM) is obtained by combining four different climatologies from General Circulation Models with two different runoff data sets for the present-day. Although there is some variability in the results derived from the different runoff estimates, both weathering models consistently indicate that the global production of HCO<sub>3</sub><sup>-</sup> was about 30–40% higher at the LGM than at present-day. This increase is significantly larger than previous estimates of 20% based upon a similar approach. CO<sub>2</sub> consumption was about 25–35% higher. The increase of the HCO<sub>3</sub><sup>-</sup> production on the exposed continental margin counterbalances the reduction due to presence of ice sheets by a factor of about 3–4; for CO<sub>2</sub> consumption, this factor is about 2.3–3.7. Areas exposed both at the LGM and at the present-day present only small variations, comparable to the range of uncertainty estimated for the global net change. Both models furthermore predict a higher consumption rate of CO<sub>2</sub> at the LGM. For silicate weathering, results are contradictory, but indicate that variations were at least 2.5 times lower than those calculated by Munhoven and Francois (1996). Finally, sensitivity tests regarding the lithology of the exposed shelf were performed. These tests illustrate the wide range of variability that possibly affects our estimates of CO<sub>2</sub> consumption rates by weathering in this environment at the LGM. They also emphasise the different sensitivities of both weathering models.

**HW2 Monday 26 – Tuesday 27 July****HYDRO-ECOLOGY: RIVERINE ECOLOGICAL RESPONSE TO CHANGES IN HYDROLOGICAL REGIME, SEDIMENT TRANSPORT, AND NUTRIENT LOADING (ICSW, ICWQ, ICCE, ICASVR)**

Location: Guild of Students, Council Chamber

Location of Posters: Guild of Students, Room 46&47

Monday 26 July AM

Concurrent Poster Session

**GENERAL INTRODUCTION 0900****Introduction 0910**

Chairman

**HW2/W/01-B1 0920****RIVER HABITATS, RIVER FLOWS AND RIVER MANAGEMENT**

David HARPER (Dept of Zoology, Uni of Leicester, Leicester, UK, Email: dmh@le.ac.uk); Joanna Kemp and Benoît Demars

Habitats and habitat structure of river channels, play important roles in UK monitoring and management. Water quality, fisheries quality and wildlife quality assessments are all habitat-based. Biotic indices for water quality assessment which were initially derived from single-habitat sampling ('stony riffles') are now calculated from field collections made from all habitats in proportion to their abundance and one index, the 'Lincoln Index' takes 'habitat-poor' sites in account in its derivation. Assessment of fisheries used 'HABSCORE' - a means of evaluating the habitat features of importance to successful fish growth and recruitment in a reach. More recently, PHABSIM habitat modelling for individual species based upon MS methodology has been evaluated in several rivers. Assessment of conservation status, initially based on 'River Corridor Surveys' in the 1970s and 1980s, is now based on 'River Habitat Surveys' - both identifying habitat features and highlighting rare or unusual ones.

These uses of the concept of habitat are all based upon habitat structure. Additional uses, based upon the habitat-scale processes, are needed for future management applications and three under development are discussed. Firstly, biological species traits related to the 'habitat template' concept already provide better perspectives than existing systems for a bio-monitoring

tool, such as relative independence of bio-geographical area and better sensitivity to a wide range of specific human impacts. Secondly, the idea of habitats as the basic unit for a river's metabolic processes provides a very clear link between habitat structure and water quality. Thirdly, the extent to which habitat structure changes in a predictable fashion with both discharge regime, extends the scale (beyond that of species) at which we can set ecological flow targets, as well as integrating the combined effects of channel morphology and flow regime.

**HW2/W/02-B1 0940****VERTICAL INTEGRATION OF SPATIAL AND HYDRAULIC DATA FOR IMPROVED HABITAT MODELLING IN GIS**

Thomas B. HARDY (Institute for Natural Systems Engineering, Utah State Univ, Logan, USA, Email: hardy@aron.cce.usu.edu), Craig Addley

This paper highlights the application of several technologies for the spatial delineation and characterisation of river ecosystems for evaluating habitat quantity and quality. Spatial characterisation based on remotely sensed data using multi-spectral digital imagery and image classification is demonstrated to delineate aquatic habitat types and riparian vegetation community distributions. Derivation of high resolution digital terrain models for use in 1-, 2-, or 3-dimensional hydraulic modelling from the integrated application of low elevation aerial photogrammetry with precision real-time GPS hydro-acoustic mapping of channel topographies, substrates, and 3-dimensional velocity fields are demonstrated. The spatial characterisation of the river using remotely sensed data and hydraulic modelling results based on the digital terrain models are vertically integrated in a GIS to derive habitat based prediction in terms of quantity and quality. Vertical integration of these data in a GIS is also utilised to predict expected fish positions based on bio-energetics of feeding locations, which incorporate food availability and temperature. The use of a GIS for validation of modelling results is demonstrated for hydraulic model predictions and fish distributions relative to habitat quality and fish position choice based bio-energetic modelling predictions.

**DISCUSSION 1000****HW2/W/03-B1 1100****BROAD SCALE RIVER DRAINAGE DENSITY AND IN-STREAM ECOSYSTEM CHARACTERISTICS: SOME PRACTICAL ISSUES FOR HYDRAULIC WORK IMPACT ASSESSMENT**

Pascal BREIL (Division Hydrologie-Hydraulique, Cemagref, Lyon, France, Email: pascal.breil@cemagref.fr)

As written by a number of authors, the variability of flow conditions seems to be a major factor that influence running water ecosystem strategies. At a local scale, high flow variability is often linked to headwater system where observed fish species are known to have a wide range of capability to adapt to this high aquatic habitat temporal variability. At a broad scale of description, not limited to the upstream part of a basin, a high river drainage system density can be related to a high flow variability. This is a physical consequence of time efficiency to transfer flow variations in any part of the river network. Does it mean that such river basin characteristics could sustain specific and more flexible running water ecosystem strategies than in the case of more linear extended river networks? This question is of interest for hydraulic works impact in a all.

Hydraulic works have variable effects on flow regimes and by consequence variable impacts on freshwater ecosystems. A rough relationship exists between hydraulic work size and impacted length of river. However depending on the river network density we can make the hypothesis that physical effects can be rapidly diluted downstream hydraulic works. Same hypothesis concerns biological response which is determined both by an adaptation of the freshwater ecosystem to the overall unaffected flow regime and by refuges capacity that offers a high drainage density by the way of connected sub-streams. Validation of a such hypothesis is based, firstly, on a regional scale studies to verify existence of some range of regional flow characteristics, in accordance with major broad scale physical basin characteristics. Secondly, we try to verify biological hypothesis using a number of local scale studies based on fish surveys. Depending on regional community patterns distribution and case study located just downstream hydraulic works, we could verify if it exist a mitigation length of stream, depending on the river drainage density.

Practical applications of such regional coherence for eco-hydrological flow regimes concerns broad scale freshwater management objectives for society. As an example, in some areas, addition of hydraulic works could have a limited impact on the long term running fresh water ecosystem dynamics. As biological indicators are used as water health indicators, it means a reduced physical impact on the overall surface water resource in a region.

**HW2/W/04-B1 1120****THE HYDRO-ECOLOGICAL FUNCTION OF LARGE WOODY DEBRIS IN BRITISH HEADWATER RIVERS**

Conor LINSTEAD (Institute of Hydrology, Crowmarsh Gifford, Wallingford, Oxfordshire, UK, Email: clin@ioh.ac.uk)

The role of large woody debris (LWD) in the ecological functioning of streams has been the subject of much research in the US. The ecological importance of LWD in terms of habitat formation and maintenance, sediment storage and regulation and the retention of organic matter within the fluvial ecosystem has been clearly demonstrated by these studies. There have, however, been few published studies of LWD in the UK. Those studies that have been carried out in the UK demonstrate that, although the LWD in UK streams provides similar functions to that in the US, the morphology and dynamics are very different.

LWD is routinely removed from streams in the UK, principally due to the flood risk posed by excessive accumulations. However, the ecological benefits of LWD has been brought to the attention of some river managers and, recently, attempts have been made to incorporate LWD addition in stream restoration schemes. There is, therefore, clearly a need to understand both the processes surrounding LWD and the wider context of LWD in UK streams in order to provide scientifically based management recommendations for in-stream LWD.

In order to investigate the reach scale hydraulic effect of LWD accumulations, detailed studies were carried out in the New Forest and Forest of Dean (UK). The impacts of LWD on flow depth, velocity, channel roughness and the diversity of hydraulic conditions over a range of discharges and for a range of LWD accumulation morphologies were examined.

The Environment Agency's River Habitat Survey (RHS) database provides a unique opportunity to assess large scale patterns in LWD abundance in the UK and place the results of the reach scale hydraulic analysis of LWD into a larger spatial context. Analysis of the LWD data within the RHS database has supported and extended the results of previous studies into the catchment scale distribution of LWD, which found that abundance is strongly influenced by channel width and riparian landuse. The extent of the influence of channel clearance on the spatial distribution of LWD can also be estimated by comparing the data from the RHS database with detailed surveys of LWD density and distribution carried out in semi-natural catchments in the UK.



**HW2/W/05-B1 1140****AN ASSESSMENT OF PHYSICAL HABITAT MODELLING IN A LOWLAND UK RIVER**

ELLIOTT, C.R.N.(CIRIA, 6 Storey's Gate, Westminster, London, UK, Email: craig.elliott@ciria.org.uk); Ibbotson, A., Gowing, I.M., Acreman, M.C., & Dunbar, M.J.

The application of the Physical Habitat Simulation (PHABSIM) system (a component part of the Instream Flow Incremental Methodology) forms a useful tool for the assessment of water resource issues in the UK and elsewhere. The operational application of the model in the UK has increased over the last 10 years and hydro-ecological modelling techniques such as the IFIM/PHABSIM are, and have been, the focus of a large amount of research and development work. Due to the multi-disciplinary nature of the IFIM/PHABSIM and other habitat models, there are still issues within the modelling procedure where further study is required.

This paper reports on some of the findings of a NERC funded study which has assessed the application of the IFIM/PHABSIM to Mill Stream, a side channel of the River Frome, Dorset. The study examines the links between habitat availability (predicted using PHABSIM) and fish populations (e.g. Dace (*Leuciscus leuciscus*)). It also assesses the effects of macrophyte growth on habitat prediction and examines other issues which may cause uncertainty interpreting model outputs.

**DISCUSSION 1200**

Monday 26 July PM

**Introduction 1400****HW2/W/06-B1 1410****GEOMORPHOLOGY: THE LINK BETWEEN THE HYDROLOGY AND ECOLOGY OF RIVER SYSTEMS**

G.E. PETTS (Dept of Environmental Research and Mangement School of Geography, Uni of Birmingham, Edgbaston, UK, Email: g.e.petts@bham.ac.uk); and A.M. Gurnell

The ecology of river channels, exposed riverine sediments and vegetated riparian zones is heavily influenced by their geomorphology (i.e. their form and sedimentary structure) as well as by their hydrology. This paper presents a series of in-channel and riparian studies undertaken at spatial scales ranging from individual river bends to complete river corridors. It illustrates the complexities of hydrology-geomorphology-ecology interactions and the ways in which hydrological and geomorphological change impact upon plant and animal communities in British rivers.

**HW2/W/07-B1 1430****GEOMORPHOLOGICAL AND VEGETATION COMMUNITY RESPONSES TO THE FLOW REGIME OF A SEMI ARID RIVER**

M.W. ROUNTREE, G.L. Heritage(Dept of Geography, Peel Building, Uni of Salford, Manchester, UK, Email: g.l.heritage@geography.salford.ac.uk); and K.H. Rogers

Unlike many temperate river systems, semi arid river systems display highly variable flow regimes, with floods that can be two orders of magnitude greater than average daily flows. These infrequent flooding events have been shown to cause extensive stripping of vegetation and sedimentary features from the river channel. The prolonged 'recovery periods' following flooding events are influenced by the positive feedback mechanisms which exist between channel hydraulics, vegetation establishment and the geomorphological development of sedimentary bars. The nature and scale of these inter-relationships was investigated in the Olifants River, Kruger National Park, South Africa. Like most other rivers in the Kruger National Park, the Olifants River has extensive areas of considerable bedrock influence, creating a wide variety of channel types including anastomosing, pool-rapid, braided and single thread reaches. Five sets of aerial photographs (1944, 1965, 1974, 1986 and 1996) spanning a 50 year period were available to document the changes in vegetation and geomorphology which have occurred in response to progressive sedimentation and decreased flow. The 1996 aerial photographs recorded the effects of a high magnitude flood that resulted in catastrophic stripping of vegetation and sediment, exposing the underlying bedrock. This aerial photo set was used to infer the initial condition of the river prior to the decreased flow conditions and associated enhanced sedimentation observed in the other aerial photographs. At the broadest scale bedrock influenced channel types were observed to switch to more alluvial influenced channel types with increased sedimentation. This was reflected in an associated change in vegetation communities. Changes recorded for a particular channel type revealed distinct patterns of vegetation and geomorphological development and their interactions were found to be more complex in anastomosing reaches of the river, where the bedrock influence on the river is greatest, than in the more geomorphologically homogenous single thread reaches. In the single thread channel types vegetation distribution appears to be primarily a function of the geomorphic unit upon which it grows. Elevation above and distance...

**HW2/W/08-B1 1450****HYDRO-ECOLOGICAL VARIABILITY WITHIN A GROUNDWATER-DOMINATED STREAM**

Paul WOOD(Geographical and Environmental Sciences, Uni of Huddersfield, Queensgate, Huddersfield, UK, Email: p.j.wood@hud.ac.uk)

Excessive groundwater abstraction and drought has resulted in severe low-flows in many stream and rivers in the UK in the last decade. The response of in-stream ecology has been relatively hard to quantify in many cases due to the absence of long-term baseline data. Some of the most severe problems have been experienced in chalk streams where up to 80% of the discharge may be derived from groundwater sources. In some extreme cases previously perennial streams have become dry along some of their length. A long-term study of Little Stour River (Kent) commenced in 1992 following three winters of low rainfall. Drought and excessive groundwater abstraction resulted in severe low flow conditions and the desiccation of two sections of the stream. The recovery of the system was monitored until 1995 when a second drought commenced, leading to the de-watering of one section of the stream again. Fine sediment composition and low flow velocities resulted in deterioration of instream habitats, elimination of macrophytes and degradation of salmonid spawning habitats in the absence of flushing flows. The response of the macro-invertebrate community in the stream has been examined in detail throughout the period. Clear changes in the structure and composition of the macro-invertebrate community can be detected in response to hydrological variability. The relative abundance of macro-invertebrates was markedly lower during periods of hydrological stress. However, few taxa were eliminated and some were more common during drought periods. The paper highlights the threat posed by flow depletion to groundwater-dominated systems, and examines the need and value of long-term hydro-ecological studies.

**DISCUSSION 1510****HW2/W/09-B1 1600****SECONDARY PRODUCTION AND HABITAT FREQUENCIES IN EAFS DEFINITION IN AN ITALIAN ALPINE RIVER**

Andrea BUFFAGNI (Water Research Institute-CNR, Via della Mornera, 25, 20047 Brugherio MI, Italy, Email: buffagni@server-mi.irsra.rm.cnr.it)

The identification or developing of simple, economically acceptable and ecologically sound methods are now required for Italy as new national rules regulating water abstractions are being set. In Italy, the definition of Ecologically Acceptable Flows has a short history, as laws and local rules on this topic started to be stated since a few years only. This led to a delay in application of existing methodologies and promotion of new methods suitable for the Italian geographical and socio-economical situation. Many commonly used hydrological methods to set standard flows can hardly be employed in Italian rivers for the lack of hydrological data and existing biological based methodologies to define optimum or minimum flows can find only local applications mainly because of uncertainties on ecological assumptions and target species selection. This paper presents the results of a study aimed at identifying optimum and minimum flow conditions for the benthic community in an Italian alpine river (R. Pioverna, Valsassina, LC). The field data collection was performed to link benthos secondary production and flows by means of the functional habitat concept. Production of benthic taxa is different among different in-stream habitats - four functional habitats were identified in the Pioverna river - and habitat frequencies vary with flow. Based on single habitat production and on habitat frequencies as a function of flow, the expected benthic production of the river can be estimated. The relationship between instream flow and total production is then established. The identification of inflection points on the curve, together with the selection of natural-like or desired habitat frequencies, is used to suggest optimum or minimum discharges to be set for the river. In its last step, the method is close to the approach adopted within PHABSIM, as it assumes that river secondary production (or biomass) can be related to flow and that notable discharge values, of ecological value, can be identified. To overcome the need of hydraulic simulation, flow is related to habitat occurrence and not directly to biota preferences for water depth and velocity. To use more information, attention is here given to the invertebrate community, on which fish species feed, and the most comprehensive representation of success for populations and assemblages ...

**HW2/W/10-B1 1620****ECO-ENVIRONMENT QUALITY ASSESSMENT: A CASE STUDY ON NING XIA, WEST-NORTHERN ARID AND SEMI-ARID REGION IN CHINA**

Jun Xia (College of Water Resources and Hydropower, Wuhan University of Hydraulic and Electric Engineering, 430073, China Email: jxia@wuhee.deu.cn); Zhonggen WANG

As a developing country, China is facing increasing problems in managing its water resources. The new ethic of "sustainable development" not only reinforces but also extends the main principles of water resources management. In China, the emphasis has been and is currently on "elementary environmental care", i.e. oriented primarily to meeting basic water supply needs, for domestic use and wastewater disposal. The environmental management aspects of water engineering continue to be of major significance to the profession. One of the more important aspects of sustainable water management should be the inculcation of concern for ecosystem preservation and protection. Within China, this is especially important in the semi-arid and arid regions where the ecosystem significantly relies on water availability, which has been greatly reduced in the last several decades. The competition for limited freshwater resources between the economy and the ecosystem in these regions is extremely great. Rapid development of these regions has posed an increasingly greater pressure on water systems. The sharp competition for limited freshwater resources, coupled with irrational water utilization practices, induced a host of ecological problems. Desertification, soil salinization, vegetation degradation, the shrinking and disappearance of rivers and lakes are now commonly occurring in these regions. Ecological degradation has become a major threat to the sustainable development of related oases where social and economic activities of the local inhabitants are concentrated.

This paper focuses on ecological quality assessment that considered need to be integrated into the traditional development and economy oriented water resource management research areas of study. The studies on the index system applied to regional Eco-environmental quality assessment, Eco-environmental quality standards, Eco-environmental quality assessment methodology and applications on the West-Northern arid and semi-arid region in China were done. This systems involve... six folds, i.e., (1) the Forest Quality (e.g., arbors, bush, cover degree, underground water level, salinity content etc.); (2) Meadow Quality...

**HW2/W/11-B1 1640****MODIFICATION OF NIGER DELTA PHYSICAL ECOLOGY: THE ROLE OF DAMS AND RESERVOIRS**

Kingdon ABAM (Niger Delta Environmental Survey, NAL Tower, 8th Floor, 20 Marina, Lagos Island, POBox 56299, Falomo-Ikoyi, Lagos, Nigeria, Email: mosesb33@hotmail.com)

The Niger delta has a fragile ecology with a complex river network in which fresh and saline water and their underground extensions maintain a dynamic equilibrium. Large scale upstream impoundment in dams and reservoirs have drastically reduced flow and sediment delivery to the coast resulting in adjustments to ecological boundaries, coastline geometry, lowered flood water levels and upstream migration of tidal influences. Although the effects of dams and reservoirs are cumulative, the large capacity dams cause the most spontaneous impacts.

**DISCUSSION 1700**

Tuesday 27 July AM

**Introduction 0900**

Chairman

**HW2/W/12-B2 0910****STREAMFLOW REGIME CHANGE AND ECOLOGICAL RESPONSE IN THE LAKE CHAD BASIN IN NIGERIA**

Lekan OYEBANDE (Faculty of Environmental Science, Uni of Lagos, Nigeria, Email: lekan@info.web.abs.net)

Lake Chad basin in Nigeria consists of five river systems, including the Komadugu-Yobe. The

Yobe River system, which empties into Lake Chad is the focus of the present study. It comprises three main rivers, the Hadejia, Jama and the Misau with their tributaries. All the rivers derive their headwaters from wetter highland to the east and south of Lake Chad and most of them have high sediment carrying capacity. As they descend from the crystalline basement complex onto the ancient lacustrine basin of Lake Chad however, their gradient reduces abruptly, and they deposit their load of silt and fine sand to produce aggraded valley in which the channel becomes poorly defined and characterised by numerous small oxbow lakes.

Two major factors account for the streamflow regime change in the study area: the prolonged Sahelian drought since the mid-sixties and the management practices adopted by the operators of the water projects in the basin. For instance, two consecutive years of low runoff driven by drought were followed in 1974 by the closure of the oversized Tiga dam on the main tributary of the River Hadejia. Both events reduced the level of flood flows reaching the bifurcation of the river and River Burum Gana downstream. The reduction promoted rapid decline of R. Hadejia due to weed growth and silting. Test releases in 1996 from Tiga and Challawa Dams show that virtually no water from the Hadejia River system leaves the Hadejia-Nguru wetlands due to weed blockages (Typha reed beds), and siltation of the river bed in the zone of the wetlands.

During the pre-dam period, (1974), there was a very high concentration of the river flow during June-October, accounting for 98-99% of the annual flow. The post-dam period witnessed a reduction to 78-79% concentration. Correspondingly, the extent of wetlands fed by floods progressively decreased from 2,350 km<sup>2</sup> in 1969 to 700 in 1987, 893 km<sup>2</sup> in 1991, 387 km<sup>2</sup> in 1993, but was 1728 km<sup>2</sup> and 967 km<sup>2</sup> in 1994 and 1995 respectively. The effect of such decreased flooding on the ecology of traditional agricultural production and fisheries as well as groundwater recharge has been severe. Elsewhere however, the cultural landscape has been transformed in an otherwise semi arid environment by blossoms of agricultural crops made possible by water released from dam reservoirs. Also as the Lake Chad recedes, lake bed farming replaces water coverage with crop cover.

**HW2/W/14-B2****0930****UPSTREAM INFLUENCE ON THE WETLANDS OF THE BAHR EL JEBEL**

John SUTCLIFFE (Heathbarton, Manor Road, Goring-on-Thames, Oxfordshire, UK Tel: +44 1491 872268);& Yvonne Parks

Hydrological processes evidently control the ecology of riverine wetlands. Thus upstream influences, like land use change or reservoir control, on the nature of inundation of a downstream flood plain will change the local environment. However, prediction of the consequence of a hydrological change should depend on understanding of the chain of control. An example of a direct link between hydrological regime and wetland vegetation is given by the Bahr el Jebel floodplain in the southern Sudan.

Until the present the hydrological regime of the Bahr el Jebel has been natural, but there are sufficient differences between different locations and also time periods to deduce the means of control of vegetation by flooding. Analysis of flooding and vegetation distribution in two sample areas showed that the link was based on duration, maximum depth and range of inundation. These jointly determined the vegetation distribution by elevation and thus over the floodplain. Between two surveys of the same area, in 1951 and 1982, the hydrological regime altered following the rise of Lake Victoria; this led to doubled river flows and greatly increased flooding from the Bahr el Jebel. Monitoring of changes in flooding regime and vegetation showed that the controls deduced were reasonable.

Because of the effect of evaporation within the wetlands, the outflow is about half the inflow. Various measures, like upstream storage operation and diversion of the natural river through the Jonglei Canal, have been proposed. Understanding of the mode of control makes it possible to make reasonable predictions of such operation on the vegetation, which is vital to the local economy. It also suggests ways in which the operation might be amended to minimise the adverse local effects.

**HW2/W/15-B2****0950****THE FLOODPLAIN MODEL MOVER FOR PREDICTING ECOLOGICAL IMPACTS CAUSED BY ALTERATIONS IN MEAN RIVER STAGES**

Dr. E. FUCHS (German Federal Institute of Hydrology, Kaiserin-Augusta-Anlagen 15-17, D-56068, Kobenz, Germany, Email: fuchs@bafg.de)

One aspect of changes in the hydrological regime of rivers is the long term lowering of mean river stages. This effect can be observed in some German rivers used as national waterways. Such changes of river water stages may have natural or anthropogenic causes. Well known are progressing river bed erosion or interference with water levels due to construction works. Logically the ecology of the floodplain will be affected by this shift in hydrological conditions. The riparian vegetation and fauna will react by changes in their communities.

Against this background and because of the growing importance of ecological aspects in river engineering the Waterways and Shipping Administration of the Federal Republic of Germany (WSV) decided to have the ecological impacts of long term river stage variations to be examined and to be evaluated. The German Federal Institute of Hydrology (BfG) was assigned to develop a respective methodology. In the meantime this project is installed as a basic research and development project within the framework of the main tasks of the BfG. The development of the methodology is carried out with a 15 km<sup>2</sup> study area on the Lower Rhine. The results of comprehensive field studies covering abiotic and biotic parameters serve as the data basis for the model development.

In the first step the model focuses the riparian vegetation, because for the time being ecological impacts due to changes of mean water stages are defined as changes in vegetation units. Considerations on the conceptual idea of the model led to the fundamental thesis of the model: with view to ecosystem relations in floodplains and to the dependency of these relations on model scale the water regime is the most crucial site factor for determining riparian plant communities.

For the development of the ecological model the main regional dependent processes for the existence of riparian vegetation have to be enlightened and to be parameterised. This job was done by multivariate statistical analyses of the abiotic and biotic field data and moreover by intensive literature enquiries. The Model for Vegetation Response in floodplains MOVER is based on a combination of modelling the abiotic floodplain...

**DISCUSSION****1010****HW2/W/16-B2****1100****ECOLOGICAL FLOW SETTING USING MACRO-INVERTEBRATES**

Chris EXTENCE (Environmental Agency, Kingfisher House, Orton Goldhay, Peterborough, UK, Tel: 44 1733 371811)

A method linking qualitative and semi-quantitative change in benthic macro-invertebrate communities, to prevailing flow regimes in lotic systems, is proposed. The Lotic-invertebrate Index for Flow Evaluation (LIFE) technique is based on data derived from established survey methods, which incorporate sampling strategies considered highly appropriate for assessing

the impact of variable flows on benthic riverine populations.

Results from a number of contrasting rivers in England are presented and discussed, and LIFE scores are linked with flow regimes after determining specific relationships with an extended range of hydrological variables. This process identifies those features of flow which are of critical importance in influencing community structure at individual river sites. These distinct responses provide the opportunity to set highly relevant ecological flow objectives, and the Waithe Beck, a Lincolnshire chalk stream, is used as an example to show how this might be accomplished. Employing the LIFE methodology provides ample scope for analysing and elucidating hydroecological relationships in some detail, and a number of additional ancillary applications are outlined and discussed.

Key areas of further work are identified, including the need to provide rational and realistic procedures for setting ecological flow targets, and investigation of habitat quality and life score relationships, in both natural and degraded river reaches.

**HW2/W/17-B2****1120****MODELLING ABIOTIC AND BIOTIC LINKS IN THE RIVERS OF THE KRUGER NATIONAL PARK, MPUMALANGA, SOUTH AFRICA: A KNOWLEDGE-BASED APPROACH**

G.P.W. JEWITT, D.C. Weeks, G. Heritage, A.H.M. Görgens (all at Dept of Agricultural Engineering, Uni of Natal, P BAG X01, Scottsville, 3209, Republic of South Africa, Email: jewitt@aquac.cvr.ac.za)

The Kruger National Park (KNP) is South Africa's premiere national park and a major attraction to local and foreign tourists. The park is dependent upon several rivers for its water supply, all of which rise outside of the Park's borders. These catchments are increasingly affected by agricultural, forestry and industrial development. A need to develop water supplies for a burgeoning human population has exacerbated the effects of this development on water quality and quantity in the KNP rivers and is placing its aquatic ecosystems under threat.

The Kruger National Park Rivers Research Programme (KNPRRP) is an interdisciplinary and co-operative endeavour aimed at contributing to the development of decision support tools for the conservation of the natural environment of rivers. These tools include models to predict responses of the aquatic biota to natural and anthropogenic influences. The development of such models is described in this paper and some important conceptual and scientific problems are discussed and analysed, including:

1. Abiotic-biotic linkages and difficulties for hydrologists and engineers (abiotic disciplines) in developing predictive tools in collaboration with ecological scientists (largely biotic disciplines) whose disciplinary fields have not traditionally focused on simulation.

2. Resolution of scale issues, emanating from linking information that is measured, developed and utilised by different biotic and abiotic disciplines acting at different spatial and temporal scales within a catchment.

3. inter-disciplinary research complexities.

Results from the construction and theoretical operation of qualitative rule-based models (RBMs) suggest that these may provide an effective means of integrating abiotic and biotic components of a catchment in a modelling system, and that this approach may assist in resolving the interdisciplinary and scale issues associated with such projects. Such RBMs are demonstrated through practical application of a spatial decision support system which includes an integrated suite of hydrology, geomorphology and fish models, developed to assess the impact of upstream development scenarios.

The development of knowledge-based...

**HW2/W/18-B2****1140****A TECHNIQUE FOR PREDICTION OF HYDRO-ECOLOGICAL EFFECTS FOR THE ECOLOGICAL ASSESSMENT OF WATER PROJECTS**

Elke FREISTÜHLER, Antje Giers, Hermann Josef Bauer, Gert A. Schultz (all at Institute of Hydrology, Water Resources Management and Environmental Techniques, Ruhr Uni OF Bochum, Germany, Email: elke.frestuehler@ruhr-uni-bochum.de)

In a current research project a computer-based hydro-ecological information and evaluation system is developed as a planning instrument in water resources management. The first step of the assessment method is a spatially detailed evaluation of the present ecological state of the area under consideration. Secondly, the expected degree of ecological damage caused by the planned construction is estimated and evaluated. Finally, the ordinal values resulting from the first two evaluation steps are aggregated to an ecological risk value for the affected area. A fictitiously planned dam construction in a small river valley in the mountainous region of the "Hochsauerland" in western Germany serves as a case study.

Here a major task is to determine the degree of damage to the in-stream ecosystem. First of all this requires a detailed ecological effect analysis which allows to answer the following questions:

Which abiotic changes (emissions) are to be expected from the project?

Which organisms (receptors) could be affected by these emissions?

By combining each single emission with its specific receptors, so-called "pairs of effect" are formed (e.g. hyporheic interstitial filled with fine material – benthic invertebrates). This effect analysis is based on information gained from literature and studies of comparable projects. Next, we apply the results to the situation in the planning area by a specific effect prediction. To this end the intensity and the spatial extent of each single emission have to be assessed. Accordingly, the specific biotic response of the receptor (single effect) must be forecast. Subsequently, the degree of damage can be determined by aggregating these single effects. This procedure considers explicitly the cause-effect relationship between abiotic and biotic changes caused by the project.

There are, however, two basic problems when evaluating hydro-ecological effects in practice: In many cases the ecological knowledge is still too vague and incomplete for an exact forecast of biotic responses, a detailed modelling of abiotic processes might often be similarly complicated. Therefore...

**DISCUSSION****1200****Tuesday 27 July PM****EXPLANATION OF WORKING GROUP SESSIONS****1345****WORKING GROUP SESSION 1****1400****WORKING GROUP SESSION 2****1530****PRESENTATION OF WORKING GROUP REPORTS****1630****DISCUSSION****1700**

**HW2/W/19-B1** Poster **0900-01****FIELD OBSERVATIONS ON WOODY DEBRIS IN A WATERSHED DISTURBED BY A POWERFUL TYPHON, SOUTHWEST JAPAN**

Y MIYABUCHI, A Shimizu, Y Ogawa and T Shimizu

A powerful typhoon in September 1991 severely damaged the northern part of Kyushu, Southwestern Japan, and produced large amounts of blown-down trees on hillslopes. Subsequent storm-triggered shallow slope failures deposited timber along streambeds. Distribution of woody debris and sediment and their characteristics were examined in a mountain stream three and half years after the typhoon. Log jams of various sizes occurred in the channel; the largest log jam as 100 m long, had a volume of 3,100 cubic meters, and was located along the middle reach of the research section. Principal component analysis of channel morphology and volume of woody debris and sediment suggests that sediment deposition is controlled by tractive force decrease owing to broad channel width and gentle gradient. The analysis demonstrates that there is no conspicuous relationship between volume of woody debris and geomorphic factors such as gradient and sinuosity. Field observations reveal that most log jams occur behind large boulders in the research section. Our results indicate that woody debris accumulation is influenced more by topographic barriers such as large boulders than by channel morphology. We believe that the supply of boulders from sideslopes greatly influences the storage of woody debris in the investigated stream.

**HW2/W/20-B1** Poster **0900-02****DEPOSITION OF CARBON, SULPHUR AND PHOSPHORUS IN THE FLOODPLAIN SEDIMENTS OF THE YAMUNA RIVER BASIN INDIA IN THE RECENT PAST**

D.P.SAXENA

Floodplains are in large measures produced by physical process of river deposition. Floodplain have a history of recording the environmental changes of recent past. It can be an important accumulation zones of pollutants that are dispersed by fluvial activity.

In the present study the floodplains of river Yamuna has been studied, which is the largest tributary of the river Ganga, guided by the Himalayas watershed. It originates from the Yamunotri Glacier, near Bunderpunch in the Mussorie range of the lower Himalayas at an elevation of about 6320 m above the mean sea level (MSL).

The sediments core were collected from the floodplains of Yamuna river basin at five sampling stations : Saharanpur (next to Himalayas), Delhi , Jagmanpur, Hamirpur and Allahabad (river confluence with Ganga). The biogeochemical indicators Carbon, Sulphur, and Phosphorus were analysed in the core sediments .

Phosphorus concentrations ranges from 272 ug/g to 940ug/g, these values are comparable to the range of average content phosphorus in the sediments of Indian rivers, 11000 ug/g (Subramanian, 1989) Delhi core sediments has highest value ( 321 - 940 ug/g) in the present study.

Carbon and Sulphur values are higher in younger strata (upper ) than older strata of floodplains .Land use is currently extremely rapid and its consequences are more evident in the tropical regions and is part because of the disproportionate share of human population growth that is taking place in the tropics land clearing and conversion causes substantial loss of Sulphur and Phosphorus from cleared site in most region climate change and increased nutrient deposition from the atmosphere, soils plants productivity and biogeochemical cycles The same pattern observed in the Yamuna river basin, Carbon, Phosphorus and Sulphur values are higher in Yamuna strata than the older strata as it reflect high use of fertilisers and detergents by human population. It signifies the change in nutrition of Yamuna river basin in recent past as a result of anthropogenic activities.

**HW2/W/21-B1** Poster **0900-03****SOURCES, DISTRIBUTION AND FATE OF ARSENIC ALONG THE TOLIMAN RIVER, ZIMAPAN, MEXICO**

M A ARMIENTA

The Tolimán river is located in the Zimapán basin, approximately 200 km north of México City. Arsenic pollution has been detected in the groundwaters of the Zimapán valley by previous studies. Sediments taken in 54 points along 35.8 km of the Tolimán river-bed were analyzed in order to quantify their total arsenic contents, and to identify the possible arsenic pollution sources. Besides, some samples were analyzed by a sequential extraction procedure to determine arsenic speciation. The fractions of arsenic bound to carbonates, to Fe and Mn oxides and oxyhydroxides, to organic matter and amorphous sulfides, and residual, were determined. Arsenic was quantified by electrothermal atomic absorption spectrometry. The granulometry of the sediment samples was also obtained by standard procedures. Total arsenic concentrations ranged from 96 to 6575 mg/kg. The greatest arsenic contents were found in front of the tailing dumps settled on the river shore south of Zimapán town, and in the mineralized zones of E1 Carrizal and La Luz. The residual and the Fe and Mn Oxides and oxyhydroxides fractions were found to contain most of the arsenic. In addition to its mobility from arsenic sources, parameters like grain size and pH determined the high and low contents of arsenic in the sediments. Samples with middle grain-size of fine sand had greater contents of total arsenic, whereas samples with middle grain-size of coarse silt had a lower content. Lower total arsenic concentrations were found in the samples with high pH(>8), whereas samples with a pH between 7 and 7.5 had higher As concentration. Two main sources of arsenic were identified in the Tolimán river. The first one is a natural source due to the presence of the As-bearing minerals, and the second one is due to human activities related to mining operations. The speciation of arsenic showed that it will remain table in the sediments under oxidant and near-neutral pH condition. Changes of the pH to extreme values and more reducing conditions will allow As mobilization, increase its bio-availability as well as its environmental risk.

**HW2/W/22-B1** Poster **0900-04****MULTIVARIATE ANALYSIS OF SLOVENIAN RIVER WATER CHEMICAL COMPOSITION**

J UHAN M ZUPAN

Slovenia is a country with very different types of landscape, which is a consequence of heterogeneous climatic conditions (alpine, sub-mediterranean and continental) with 1570 mm annual average quantity of precipitation (from 800 to over 3000 mm) on the contact of three tectonic units (Alps, Dinarides and Panonic basin). The same facts cause very different hydrological conditions, from steep mountain streams to slow flowing rivers in flat land areas. Trough very dense stream net (1.32 km/km<sup>2</sup>) flows in average 590 m<sup>3</sup>/s of water from Slovenia territory to the Black See (catchment area 16.370 km<sup>2</sup>) and the rest to the Adriatic See (catchment area 3.860 km<sup>2</sup>).

The variability in chemical composition of water and the quantity of suspended solids and

sediment is very high as well. Analysis of variance permitted to estimate the temporal and spatial variability of hydrochemical data. The variability in chemical composition of river water is influenced as by human impact as by climatic, hydrological and geological conditions in individual river basins. The selection of most important factors that caused variability in chemical composition of river water were estimated by multivariate statistical analysis (cluster analysis and principal component analysis). As groundwater we have chosen all available data from national water quality and quantity monitoring database for the 15-year period (1983-1997). To the national water quality monitoring program are included all rivers with mean annual flow higher than 4 m<sup>3</sup>/s (102 sampling points on 54 rivers). The result of three factors model was reduction of the data matrix and quantification of pollution, pedological and geochemical factor, as well as detection the distribution pattern of the most important factors in national scale.

**HW2/W/23-B1** Poster **0900-05****CHANGES OF NITROGEN FLOWS FROM A RIVER BASIN IN A 100 YEARS PERSPECTIVE**

L ANDERSSON

Sings of eutrophication in the Baltic sea were found already in the first half of this century, and questions have been raised about the causes of long term change in river loads of nitrogen. The aim of this project is to analyse how changes in land use, but also of the wetness of the landscape during the latest 100 years have affected flow of nitrogen to the Baltic. Our hypothesis, which seems to be verified, is that a change in retention capacity, both in soil, watercourses and lakes, due to changed hydrology is a dominant factor for changes in nitrogen flow.

The nitrogen transport from the Svartå river basin (1 905 km<sup>2</sup>) was modelled with HBV-N, a conceptual hydrological model with nitrogen routines. The model considers soil leaching from fallow, ley and cereals, forest and non-classified land. In addition atmospheric deposition at water surfaces, discharge from water treatment plants and industries are considered. The model calculates, on a daily basis, retention for 26 subcatchments, and net transport from all sources to the outlet of the basin. The model is dynamic and considers that retention depends on loads, transit times and climate.

Much of the used statistics is based on data collected for the included parishes. GIS was used to determine the distribution in the sub-catchments and to determine other spatial parameters, such as distribution of soil-types and land-use.

As input to the HBV-N model, nitrogen concentrations in water leached from arable land, fallow and ley, on different soil types were calculated with the deterministic SOIL-N model for each decade from 1875-1995. Although there has been discussions about nitrogen saturation in the forests, still the N-exports from forests play a minor role, and they were therefore set to unchanged during the studied time period.

The HBV-N model was set up for each of the decades, using the calculated soil leaching from the SOIL-N model. Water was then transitioned... through groundwater, streams and lakes, until it reached the outlet of the catchment. The effect of an increasing amount of underdrained land was simulated, in addition to changes in lake percentages, and wetlands. To make it possible to compare the land-use and hydrology of the different time-steps...

**HW2/W/24-B1** Poster **0900-06****TRANSPORT OF RADIUM ISOTOPE (RA-226) BY THE VISTULA RIVER DUE TO COAL MINE ACTIVITY IN THE SILESIA REGION.**

J. Pociask-KARTECZKA, J. Jasinska, J.W. Mieltski, J. Krupa

One of a major source of radiation in the Silesia Region results from hard coal mining activity. The Silesia has been recognized as a natural radiohydroanomaly since the 70. this century. Coal, deep circulation waters and deposits contain significant quantities of Ra-226 (0-121 Bq/kg, 0.7-100 kBq/m<sup>3</sup>, 110-133200 Bq/kg respectively). Radium is an extremely important member of the uranium decay series. The isotope Ra-226 is a particularly significant nuclide because of its relatively high radiotoxicity. The Silesian mines Ra-226 input to the environment reached about 306 MBq/d. in 1993, ie. two times less than in the beginning of the 1980s. Present and former discharge of radium with mine waters caused enhanced natural radioactivity not only in the Salsia Region; also in the vicinity of it.

In our previous piloting work we have studied radium activity in Vistula river sediments. The aim of the presentation has been to find out the proportion between the radium content in soluble and not soluble form in river waters according to transport process. The second goal has been just to find the range of radium activity in waters (clay and colloids may carry a predominantly role in radium isotopes transport; so sorption process can have predominant role in Ra-226 transport for a long distance).

Samples were collected the Vistula River at 7 different locations. In the same time another water samples were collected one from each of the 6 tributaries of the Vistula River: the Chech\_o, Przemsa, Bieruń, Gostynia, Pszczyńka and Dunajec. Each sample were of two litre volume, and were put into plastic vessel. Immediately after sample arriving to the laboratory they were acceded. Then they were filtrate on paper filter and then second time filtrate on a membrane filter (with pore diameter equal to 0.7 mm). Dried membrane filters were measured on gamma-rays spectrometer for Ra-226 and Ra-228 (Ac-228). The residues from paper filters were ashen in 600 C. Those ashes and a half of a litre of filtrate water from each sample were taken separately for radiochemical analyses. The Pb and Ba carriers were added along with radiochemical tracer (Ba-133, 55 Bq/sample). Ashes were wet mineralised using concentrate acid solutions (HF, HNO<sub>3</sub>, HCl) and then transferred to diluted HNO<sub>3</sub> solution. Separation of radium for both kind of samples were done by co-precipitation with PbCrO<sub>4</sub>. Centrifuged residues were then dissolved with hot 0.1 M DTPA solution, and then second co-precipitation with ca 100 micrograms of barium sulphate were performed to obtain thin, alpha spectrometric source. Each source were measured on gamma-spectrometer for the determination of chemical yield (recovery of Ba-133 activity) and for the determination of Ra-228 content via Ac-228 measurement. Then samples were measured on alpha-spectrometer.

**HW3** Thursday 29 – Friday 30 July**HYDROLOGY OF ICE-COVERED RIVERS (ICSI, ICCE)**

Location: Guild of Students, Council Chamber

Location of Posters: Guild of Students, Rooms 46 &amp; 47

**Thursday 29 July AM**

Presiding Chairs: Phil Marsh (National Water Res. Inst. Canada)  
and R D Moore (Simon Fraser Univ., Canada)  
Concurrent Poster Session

**Introduction** **0900**

Michael G FERRICK (USA CRREL) and Terry D Prowse



Presiding Chair: Phil Marsh (National Water Res. Inst. Canada)

**TRENDS AND VARIABILITY IN ICE-COVERED RIVERS AND LAKES****HW3/W/01-B4 0915****EFFECTS OF CLIMATE ON MID-WINTER ICE JAMS**

BELTAOS. S

Abstract not available at time of going to press

**HW3/W/02-B4 0940****RIVER ICE TRENDS OF COASTAL RIVERS IN ATLANTIC CANADA**

Bill BRIMLEY and Bridget Thomas (Atmospheric Environment Branch, Environment Canada, 16th Floor, 45 Alderney Dr., Dartmouth, NS, Canada, B2Y 2N6)

The presence of ice in streams and rivers is detected by observation and by the backwater effect that occurs due to the changing hydraulic characteristics of the streamflow. Ice data are recorded as part of the hydrometric record collected by Environment Canada. Preliminary analyses of data from long term hydrometric stations in the Reference Basin Hydrologic Network reveals a significant trend in the presence of ice in the river and the duration of the ice season in certain streams in Atlantic Canada. Data from hydrometric stations in Nova Scotia and Newfoundland show that the number of days with ice in the river has significantly increased since 1955 (when the ice data became part of the hydrometric record). Initial comparisons of ice data with winter season air temperatures showed that there was a cause and effect relationship between the temperature and ice. Links to the cold North Atlantic Current and the winter period of the North Atlantic Oscillation appear to support the winter cooling of this area. The downturn in the northern cod fishery has been linked to these colder waters however the potential impacts on the Atlantic Coast aqua-culture industry and the fresh water habitat are not fully understood.

**HW3/W/03-B4 1005****LONG-TERM CHANGES AND ANNUAL VARIABILITY IN ICE COVER ACROSS THE NORTHERN HEMISPHERE OVER THE PAST 170 YEARS**

D.M. ROBERTSON, US Geological Survey, WRD, USA (email: dzrobert@usgs.gov); J.J. Magnuson, Center For Limnology (University of Wisconsin-Madison, USA); and R.H. Wynne, Dept. of Forestry (Virginia Polytechnic Institute and State University, Blacksburg, VA, USA.)

Freeze and break-up dates from lakes and rivers across the Northern Hemisphere were assembled as part of a meeting of an ad hoc group of international scientists (Lake Ice Analysis Group, LIAG). Twenty-six of the sites had ice records over 100 years in length. These sites were used to quantify the long-term changes and interannual variability in ice cover and examine the causes of these changes and variability. Consistent long-term changes (later freeze dates and earlier break-up dates in recent years) were found throughout the Northern Hemisphere, indicative of late fall, winter, and spring warming. Most of the changes in these records occurred rather abruptly around the 1880's and 1970's rather than as long-term monotonic changes. The records were also examined to determine if consistent annual anomalies occurred during El Niño events. Freeze dates were consistently later during years of the mature phase of strong El Niños than in other years throughout the 1900's, indicative of warmer early winter air temperatures. Similarly, since 1940, years during the mature phase of strong El Niños were characterised by early break-up dates throughout North America, indicative of warmer spring temperatures; however, break-up dates in Europe and Asia were later than other years, indicative of cooler temperatures. From 1900 to 1940, this pattern in unusual break-up dates is reversed for North America and Asia; that is, break-up tended to be early in Asia and late in North America.

Presiding Chair: R D Moore (Simon Fraser Univ., Canada)

**Ecological Aspects of Ice-Covered Rivers****HW3/W/04-B4 1050****DISSOLVED OXYGEN DECLINES IN ICE-COVERED RIVERS: CAUSES AND ENVIRONMENTAL CONSEQUENCES**

CHAMBERS P.A., and A. Pietroniro

Abstract not available at time of going to press

**HW3/W/05-B4 1115****INCORPORATING ICE AND EFFECTS OF ICE INTO THE NORWEGIAN HABITAT ASSESSMENT STRATEGIES AND THE HABITAT PROGRAM SYSTEM**

Knut ALFREDSSEN and Einar Tesaker (SINTEF Civil &amp; Environmental Engineering, Water Resources)

Habitat assessment through application of computer based simulation tools has been applied to several Norwegian rivers over the past decade. Over the last few years, the HABITAT program system has been upgraded to incorporate both more advanced hydraulic simulation tools and new strategies for habitat assessment. Current research involves the use of metrics to better classify spatial habitat arrangements, and research into habitat assessment through energetic modeling. Cold water conditions are incorporated into the habitat assessment process through cold water preferences for the target species, but direct and indirect impacts on available habitat by river ice are currently on the research and development stage. Ice poses several challenges to the traditional habitat modeling process, both regarding the biological responses in an ice covered environment and the hydraulic modeling of rivers influenced by ice. Typical problems may be 1) the study of under ice fish behaviour, both to create fish preference curves and to validate model predictions, 2) the effects of anchor ice on habitat selection and fish migration, 3) under ice hydraulics and 4) the dynamics of ice formation and breakup on the micro scale. Since habitat selection is a micro scale process, changes in habitat structure through ice induced erosion may also be an important topic. This paper outlines our ideas on how the effects of river ice could be incorporated into the habitat simulation system.

**HW3/W/06-B4 1140****THE ROLE OF RIVER ICE COVERS IN THE HYDROLOGY AND ECOLOGY OF THE MACKENZIE DELTA**

MARSH P. and L. Lesack

Abstract not available at time of going to press

**HW3/W/07-B4 1205****BIOLOGICAL AND PHYSIOLOGICAL RESPONSE OF TROUT TO WINTER HABITATS IN WYOMING, USA**

Thomas C. ANNEAR (Wyoming Game and Fish Department, Cheyenne, WY) and Wayne Hubert (Co-operative Fishery and Wildlife Research Unit, University of Wyoming, Laramie, WY)

Fisheries managers of have long known that survival of trout during the winter is a major factor affecting population densities in many stream ecosystems in the Rocky Mountains. In Wyoming, trout population reductions in excess of 90% have been documented in some reservoir tailwaters. Though biologists have surmised that these reductions were the result of either mortality or emigration from some river sections, the specific mechanism was not defined and the factors leading to the trout loss were unknown. Between 1991 and 1998 the Wyoming Game and Fish Department funded four different studies in addition to conducting other work with department staff to better understand the extent of over winter losses, identify some of the mechanisms leading to those conditions and develop management strategies to help avoid those impacts. Winter studies were conducted on tailwater fisheries in the Green, North Platte, Bighorn and Shoshone Rivers to document trout population dynamics, assess physical habitat availability, evaluate trout movement and habitat selection, and understand the relationships between food availability and bioenergetic relationships. Preliminary results indicate that winter trout losses are extreme in some years, that trout movement and habitat selection is directly affected by super-cooled flows and that mortality is probably not directly due to reduced body condition (starvation). The combination of physiological impairment with frequently altered habitat availability probably leads to indirect mortality from predators and other factors.

Thursday 29 July PM

Presiding Chair: Daqing Yang (Inst. For Global Change Res., Tokyo, Japan)

**RIVER ICE, LOW FLOW AND HYDRAULIC STRUCTURES****DISCUSSION 1400****RESEARCH DIRECTIONS IN CLIMATE CHANGE AND ECOLOGICAL ASPECTS OF ICE-COVERED RIVERS AND LAKES****RIVER AND LAKE ICE COVERS****HW3/W/08-B4 1430****SEDIMENT CONTENT IN THE ICE COVER OF THE TANANA RIVER**

CHACHO E.

Abstract not available at time of going to press

**HW3/W/09-B4 1455****STABLE ENVIRONMENTAL ISOTOPES IN LAKE AND RIVER ICE CORES**

M.G. FERRICK, D.J. Calkins, N.M. Perron (U.S.A. Cold Regions Research and Engineering Laboratory, Hanover, NH) and C. Kendall (U.S. Geological Survey, Menlo Park, CA)

This study was initiated to assess the possibilities of using the stable isotopes of water from ice cores to capture the temporal isotopic signature of river water during the winter and as tracers of ice coming from different tributaries in a river system. A review of the literature revealed that ice growing at rates commonly measured in rivers and lakes experiences nonequilibrium fractionation of stable isotopes. Laboratory experiments conducted at small scales and sea ice data both show a strong correlation between ice growth velocity and the fractionation factor. Also, stirring of the water in laboratory experiments gave dramatically different results for similar ice growth rates, indicating the presence of a boundary layer in the water. Our objectives were to determine the isotopic composition and corresponding crystalline structure of river and lake ice cores, and to use these data to test the analytical diffusion model of Burton et al. (1953) that simulates the fractionation process. The field sites used for sampling were Post Pond, a small, deep lake with minimal inflow during winter, and Wilder Reservoir, an impoundment of the Connecticut River with minimal storage and significant through flow. Ice cores were collected weekly along with water and snow samples from each site. Ice thickness, snow depth and water velocity were routinely measured at the sites, and daily meteorological observations were made throughout the sampling period. The ice growth patterns at the sites were different, with later formation and lower growth rates at the river site, a result of heat conveyed to the ice by the flow. Flow velocities of up to 0.3 m/s just under the ice also caused greater mixing in the river compared to the pond. Application of the fractionation model revealed comparable boundary layer thickness at the two sites, an unexpected result. Apparently, most of the ice growth at the river site occurs during the night while the flow is minimal. We conducted large-scale laboratory experiments to verify this hypothesis and to more effectively test the diffusion model.

**HW3/W/10-B4 1520****RECONSTRUCTING TEMPORAL ISOTOPIC VARIATIONS IN WINTER STREAM FLOW FROM RIVER-ICE ARCHIVES**

J.J. GIBSON (Wetlands Research Centre, University of Waterloo, Waterloo, ON, N2L 3G1 Canada; email: jggibson@fes.uwaterloo.ca) and T.D. Prowse (National Water Research Institute, 11 Innovation Blvd., Saskatoon SK, S7N 3H5 Canada)

Isotope stratigraphy of river-ice covers can be applied to reconstruct time-series of the stable isotopic composition of winter stream flow, although careful attention to ice type, morphology and location of sampling is required to obtain useful results. Ice surveys conducted in the Liard River Basin, north-western Canada during 1997 and 1998, suggest that the isotopic composition of winter stream flow is relatively invariant along the main river stem. Systematic isotopic shifts in winter stream flow are evident in ice-core records obtained from numerous tributaries. This effect is discussed and potential mechanisms are reviewed. Early analysis suggests that systematic isotopic shifts are tracing the winter base flow recession, and are

indicative of temporal shifts in the fraction of flow derived from groundwater vs. surface water sources. In combination with direct water sampling conducted during open-water periods, ice-core records are used to assemble near-continuous multi-year records of isotopic variations in stream flow in remote, low-accessibility areas.

Presiding Chair: Daqing Yang (Inst. For Global Change Res., Tokyo, Japan)

### RIVER ICE AND HYDRAULIC STRUCTURES

**HW3/W/11-B4** **1610**

#### PECULIARITIES OF THE DEVELOPMENT OF FILTRATION PROCESS IN THE RIGHT - BANK CONTIGUITY OF VILUI DAM

Svet MILANOVSKY (Institute of Physics of the Earth, Moscow, email: svet@uipe-ras.scgis.ru , Moscow); Toloshinov A.V. (Vilui Dam Cascade), Velikin S.A., Snegirev A.M., Kuchmin O.A. (Vilui Permafrost Research Station of Permafrost Institute RAS, Chernishevski)

The dam of Vilui hydro-engineering unit is the first one among big hydro-technical constructions raised in permafrost zone. Many parameters of this dam are unique therefore it's exploitation needs continual attention. Until the end of 70th - beginning of 80th the state of right-bank contiguity as well of the whole dam was considered acceptable. To obtain more electric power after proper preparation of the construction the water level was lifted above project level. Quick thawing of frozen ground in the basement of right-bank contiguity and appearance of filtration flow transferring heat has begun in 1995. We present results of complex experimental control observation of the development of filtration process. On the base of detailed surface and boreholes geophysical observations the numerical model of the part of right-bank contiguity was done. The model shows the behavior of filtration flow and thawing zone as a function of air and water temperature, water level in the headwater, lithology, thermal and other properties of the section. Forecasting possibilities of the model are shown as well as possibilities of model's improvement.

**HW3/W/12-B4** **1635**

#### GEOPHYSICAL MONITORING OF HYDROTECHNICAL OBJECTS IN PERMAFROST ZONE

Svet MILANOVSKY (Institute of Physics of the Earth, Moscow, email: svet@uipe-ras.scgis.ru , Moscow); Velikin S.A., Snegirev A.M., Kuchmin O.A. (Vilui Permafrost Research Station of Permafrost Institute RAS, Chernishevski); Kalitin V.T., Sergievsky V.V.(both "Diamonds of Russia" Company, Mirni)

Hydroengineering unit is constructed in the middle reaches of Vilui River between the estuary of its tributary Malaya Botubiya and the dam of the operating Vilui Hydropower Station - I and 2. This area is characterized by a complex geocryological situation. The edges of the valley at the gage site carry traces of their processing by landsliding. Nowadays the landslide activity is blocked by permafrost. The shore border massif of the reservoir are composed of terrigenous-carbonate rocks. The salinity (mostly of sulfate composition) of frozen grounds is up to 2%. The foot of the reservoir borders is occupied by grounds at the temperatures below zero but saturated with saline waters (cryopegs). The content of salts (mostly sodium chloride) in these waters is 40 g/l or more. After the reservoir filling, the increased water pressure may induce penetration of brines into the frozen mass through their weakened sites, melting of natural ground ice and initiate, respectively, the degradation of frozen grounds and activity of landslide processes. Due to a difficult and hardly predictable geocryological situation in this area, the geophysical methods were included into the system of local monitoring. We demonstrate several examples showing the possibilities of geophysical methods for monitoring of different types of instability in the system: frozen rocks-river (like landsliding, changing position of the boundaries of thawed and frozen grounds, development of filtration flows, etc.). Besides, it was taken into account that during a future exploitation of the reservoir the systematic geophysical observations would be highly useful for the inspection of the state of the shoreline at the upper water level which is also characterized as endangered because of the presence of ancient landslide systems in its structure.

**HW3/W/13-B4** **1700**

#### PECULIARITIES OF ICE EVENTS IN THE RIVERS OF THE ARCTIC ZONE OF RUSSIA

VUGLINSKY V.S

Abstract not available at time of going to press

**HW3/W/14-B4** **1725**

#### RIVER ICE CHARACTERISTIC AND THE ASSOCIATED LOW-FLOWS OF SIBERIAN RIVERS

Daqing YANG (Inst. for Global Change Research, SEAVANS Building North, 7th floor, 1-2-1 Shibaura, Minato-ku, Tokyo 105-6791, Japan, email: dyang@frontier.esto.or.jp); Tetsuo Ohata (The Institute of Low Temperature Science, Hokkaido University, Kita-19, Nishi-8, Kita-ku Sapporo 060-0819, Japan, email: ohata@pop.lowtem.hokudai.ac.jp)

River ice is one of the important components of hydrological processes in cold regions. To accurately quantify hydrological cycle in cold regions, it is necessary to observe and study river ice. In Siberian regions, river ice thickness, date of river freeze-up, stream water temperature, and discharge have been measured since late 1940's for many large rivers (i.e. Lena, Yenisey and Obi rivers) and the observation records were archived by Russian Hydrological Services. These data are now available for the period of 1950 to 1988 to the GEWEX/GAME-Siberia project. These valuable data sets were analyzed in this study, with special emphases on: (1) temporal variation and spatial distribution of the river ice (thickness) and associated low-flows; (2) effect of river ice on low-flows for various basin scales; and, (3) relation of river freeze-up to air temperature and river discharge in different basins. The results indicate the significant influence of regional climate variation on river ice conditions (i.e. ice thickness and the timing of the river freeze-up) and also on the winter low-flows. Possible future changes of the river ice conditions and winter low-flows under a warmer climate scenario were predicted based on the identified dependence of river ice/low-flow on climate conditions. The results of this study will be useful for understanding the impact of climate variation on cold-region hydrological processes and for improving land-surface hydrological modeling particularly for large river basins in the high latitudes.

### HYDROLOGY OF ICE-COVERED RIVERS AND LAKES

**HW3/W/15-B5** **0835**

#### FREEZE-UP STORAGE: THE "MISSING LINK" IN SPRING SNOWMELT

PROWSE T.D.

Abstract not available at time of going to press

**HW3/W/16-B5** **0900**

#### ASPECTS OF RIVER ICE HYDROLOGY IN JAPAN

Ken-ichi HIRAYAMA (Iwate University, Morioka, Japan); Makoto Yamazaki (Hokkaido Electric Power Co., Inc., Ebetsu, Japan) and Hung Tao Shen (Clarkson University, Potsdam, NY, U.S.A.)

Rivers in Hokkaido and northern Honshu generally originated from mountains and discharge to the sea over relative short distances. The slopes are usually very steep, in the order of 1/100 to 1/300, especially in the upstream reaches. These rivers usually have very low discharges in the winter. In the steep upstream reaches, the ice covers are typically discontinuous and form step pools along the river. Considerable daily oscillations in water temperature and frazil ice production are observed in open water reaches due to the small discharges in these rivers. Daily oscillations in river discharge are also observed due to the formation and release of hanging dams and anchor ice. These processes will first be discussed in the paper. In addition, hydrological aspects of ice jam formation will also be discussed. Although geometric and hydraulic characteristics of Hokkaido rivers are ideal for ice jam formation, ice jam does not occur very often. This is due to the fact that Hokkaido winters do not have mid-winter thaw as often-observed in North America or other areas. River basins are covered by heavy snow accumulation that usually remains until the end of the winter and melt out slowly as the ice covers are also deteriorating due to the rising water temperature. Ice jam events occurred during the winter of 1995 will be used to demonstrate the hydrological process that caused the ice jam formation in Hokkaido rivers.

**HW3/W/17-B5** **0925**

#### WINTER STREAM FLOW VARIABILITY, YUKON TERRITORY, CANADA

MOORE R.D., A.S. HAMILTON, AND J. SCIBEK

Abstract not available at time of going of press

**HW3/W/18-B5** **0950**

#### ASPECTS OF WEATHERING AND SOLUTE ACQUISITION PROCESSES CONTROLLING CHEMISTRY OF SUB ALPINE PROGLACIAL STREAMS OF GARHWAL HIMALAYA, INDIA

SINGH, A.K. AND S.I. HASNAIN

Abstract not available at time of going to press

**HW3/W/19-B5** **1015**

#### EFFECTS OF DOUBLE FREEZE-FRACTIONATION UPON NACL EXCLUSION FROM RIVER AND LAKE ICE

CRAGIN, J.H., M.G. Ferrick, and M. Yushak

Abstract not available at time of going to press

**DISCUSSION** **1100**

#### PHYSICAL AND CHEMICAL HYDROLOGY OF ICE-COVERED RIVERS AND LAKES - RESEARCH DIRECTIONS

**WORKING GROUP** **1130**

#### FORMATION OF A WORKING GROUP TO REPRESENT THE RIVER AND LAKE ICE COMMUNITY WITHIN IAHS AND OTHER INTERNATIONAL SCIENTIFIC SOCIETY

**HW3/W/20-B4** **Poster** **0900-01**

#### RIVERS OF THE ARCTIC BASIN, THEIR SEASON THERMOHALINE FLUX AT TIDELWATER AFFECTING THE HABITATS, ECOLOGY AND DISTRIBUTION OF FISHES

Richard Gordon MILLER (University of Arizona and Foresta Institute for ocean and Mountain Studies)

Boreal and Arctic north-flowing rivers of Eurasia and America have earliest spring thaws in their southern highlands, carrying fresher waters and ice downstream onto still frozen river channels. Ice dams build up at tidewater impounding the seasons runoff in broad lakes and ponds that last into summer when they are released by the break-up of the bay ice. This becomes a deluge of fresh water into the brackish and saline strata in the estuary and shore waters. The extremes of thermohaline flux thus imposed on the habitats of native fishes and other biota cause ecologic stress, not yet well studied. Fish populations, their feeding, nesting, reproduction and the dispersal of larvae and young are largely conjectural. Some inferences are gathered from nursery waters in the Antarctic. This project maps the known and conjectural distribution of four species of Arctic Sculpin (family Cottidae, Order Scorpaeniformes). It poses hypotheses on the origin, physiological and behavioral adaptations resulting from life in these troubled waters. The physical dynamics of these watersheds is a study that must be urged.

**HW4 Tuesday 27 – Wednesday 28 July**

**REGIONALISATION OF PARAMETERS OF HYDROGEOLOGICAL AND ATMOSPHERIC LANDSURFACE MODELS (IAHS/WMO WORKING GROUP FOR GEWEX, ICRSDT, IAMAS)**

Location: Physics West 809 LT

Location of Posters: Guild of Students, Rooms 46&47

**Tuesday 27 July AM**

Presiding Chair: J.Wallace  
Concurrent Poster Session

**REGIONAL PARAMETER ESTIMATION ISSUES**

**Introduction 0900**

Alan HALL

**HW4/E/12-B2 0930**

**OPPORTUNITIES FOR IMPROVED ESTIMATION OF PARAMETERS OF HYDROLOGICAL MODELS**

J. Schaake, Q Duan and V.Koren

Abstract not available at time of going to press

**HW4/W/02-B2 1000**

**OBJECTIVE DISTRIBUTED-PARAMETER ESTIMATION METHODS AND TOOLS IN THE USGS MODULAR MODELING SYSTEM (MMS)**

GEORGE LEAVESLEY, Roland Viger, and Lauren Hay (all at U.S. Geological Survey, MS 412, Denver Federal Center, Denver, CO, 80225, USA, email: george@usgs.gov)

Objective parameter-estimation methods and tools are being developed and evaluated using the U.S. Geological Survey (USGS) Modular Modeling System (MMS). MMS is an integrated system of computer software developed to provide a framework for the development, integration, application, and analysis of hydrologic and ecosystem models. A geographic information system (GIS) interface permits application of a variety of GIS tools to delineate, characterize, and parameterize topographical, hydrological, and biological basin features for use in a variety of lumped- and distributed-parameter modeling approaches. Current methods are being developed using the USGS Precipitation-Runoff Modeling System (PRMS). Digital databases used for parameter estimation include USGS 3-arc second digital elevation models, State Soils Geographic (STATSGO) 1-km gridded soils data, and Forest Service 1-km gridded vegetation type and density data. Basin parameters estimated include slope, aspect, elevation, soil type, available water-holding capacity of the soil, vegetation type, vegetation cover density, solar radiation transmission coefficient, and interception-storage capacity. Precipitation- and temperature-distribution parameters are also estimated. Parameter-estimation methodologies, and evaluation of estimated parameters and their regionalization, are presented for selected basins within the MOPEX data sets and other USGS data sets for a variety of climatic and physiographic regions in the United States. While initial evaluation efforts are focused on PRMS applications, the tools are generic and applicable to a wide variety of models and geographic regions.

**HW4/E/04-B2 1100**

**ASSESSING THE REGIONALISATION POTENTIAL OF HYDROLOGICAL MODELS**

Matthew LEES, Thorsten Wagener, Howard Wheaton (Department of Civil and Environmental Engineering, Imperial College of Science, Technology and Medicine, London, SW7 2BU, e-mail: m.lees@ic.ac.uk) Keith Beven (Institute of Environmental and Biological Sciences, Lancaster University, LA1 4YQ)

To date, only extremely simple event based models have been successfully regionalised. Developments in parsimonious continuous modelling, allied with progress in calibration techniques, promises a new generation of regionalised models for use in applications as diverse as global water cycling studies, water resources assessment and flood design. However, since models are commonly regionalised through a regression relationship between their parameters and catchment characteristics, parameter uncertainty is a crucial factor in model regionalisation. To improve the potential success of a multiple catchment exercise, it is proposed that a prior assessment of regionalisation potential should be made through an examination of the model's identifiability. Synthetic data sets, generated from parsimonious hybrid conceptual-metric rainfall-runoff models, incorporating realistic model structure errors, input and output data errors, will be used to investigate different methods of parameter estimation and associated parameter and output uncertainty. A number of commonly used calibration methods including: SCE-UA; system identification; and GLUE will be applied prior to an investigation of the relationship between model complexity and errors, and model parameter and output response uncertainty. Also the role of objective functions will be investigated with three major aims: (1) assess the suitability of different objective functions for identification of individual parameters; (2) investigate the use of multi-objective optimisation to both constrain behavioral parameter space, and estimate uncertainty; and, (3) investigate the use of different objective functions due to the purpose of the modelling effort.

**HW4/E/11-B2 1130**

**ASSESSMENT OF PARAMETER UNCERTAINTY IN HYDROLOGICAL MODELS**

Charles Perrin and Claude Michel

Abstract not available at time of going to press

**HW4/W/01-B2 1200**

**EFFECT OF AREAL VERSUS POINT INFORMATION IN THE PARAMETER IDENTIFICATION OF LAND-SURFACE SCHEMES USING MULTI-CRITERIA METHODS**

Luis BASTIDAS (Department of Hydrology and Water Resources, University of Arizona, Tucson, AZ 85721, USA, email: lucho@hwr.arizona.edu) Hoshin Gupta, Soroosh Sorooshian, and W. James Shuttleworth (Department of Hydrology and Water Resources, University of Arizona, Tucson, AZ 85721, USA, email: hoshin@hwr.arizona.edu)

*This page may be copied freely*

Multi-criteria methods provide a useful framework for the calibration and regionalization of land surface parameterizations. This presentation describes and presents preliminary results of an on-going research project in which data collected at the ARM-CART site in Oklahoma/Kansas is being used to study how the information from different point locations, but with similar regional conditions, affects the parameter identification and the sensitivity of a land-surface model, the Biosphere-Atmosphere Transfer Scheme (BATS). Issues of areal averaging and/or aggregation are also addressed. Multi-criteria methods are used for carrying out the optimization procedures involved in both parameter identification and sensitivity analysis.

**Tuesday 27 July PM**

Presiding Chair: J. Schaake

**CASE STUDIES**

**HW4/E/08-B2 1400**

**PARAMETERIZATION OF A CONCEPTUAL CONTINUOUS RAINFALL RUNOFF MODEL BY MEANS OF CATCHMENT CHARACTERISTICS**

Hubert HOLZMANN and Hans Peter Nachtnebel (both at Department of Water Management, Hydrology and Hydraulic Engineering, University of Natural Sciences BOKU, Muthgasse 18, A-1190 Vienna, Austria, email: holz@edv2.boku.ac.at)

At the IWHW a conceptual continuous rainfall runoff model was developed. Input and output data deal with daily time series. The model consists of a snowmelt module and a runoff formation module. The first is based on a simple day degree method, but uses detailed altitudinal discretization by means of a digital elevation model. Temperature profiles refer to observations or empirical gradients. Furthermore the areal precipitation is required. The runoff formation module uses the concept of linear storages. The upper storage with two outlets represents the (near)surface flow and the interflow, the lower storage the base flow component. First estimates of the storage coefficients are made by analysis of the specific discharges at the catchment outlets. The depth of the interflow outlet can be interpreted as the mean plant available water content (field capacity minus wilting point) multiplied with the root depth of the vegetation. The surplus of the upper outlet characterizes the retention capacity of the near surface layer which can be a function of soil permeability, texture and vegetation type. The model works in a broad range of areas (from about 10 km<sup>2</sup> to 10000 km<sup>2</sup>). The experiences refer to catchments of the Austrian Danube. Test results of some MOPEX catchments with a priori estimates of model parameters will be presented.

**HW4/W/05-B2 1420**

**SOIL HYDRAULIC PROPERTIES FROM RIVER FLOW**

E.M.BLYTH

Data on soil hydraulic properties are sparse and often unreliable: based on small samples from a medium that is highly heterogeneous. On the other hand, data on large scale hydrological phenomena, such as river flow, are available world-wide. The seasonal pattern of river flow gives an indication of the porosity of the soil in the catchment: in porous soils, rainfall is transferred rapidly to the groundwater store. The river flow is therefore dominated by baseflow and is relatively uniform through the year. The opposite is true for non-porous soils. Using a simple layered soil model with a groundwater store, a method has been developed to calibrate soil parameters of an evaporation model for use in GCMs using monthly river flow.

**HW4/E/19-B2 1440**

**DEVELOPMENT OF REGIONAL SOIL HYDRAULIC PROPERTIES**

Walter RAWLS and Curt Reynolds

Abstract not available at time of going to press

**HW4/E/06-B2 1500**

**A MULTIPLE PATCH SVAT MODEL CONDITIONED ON ESTIMATES OF LATENT HEAT FLUXES AS INFERRED FROM REMOTELY SENSED DATA**

STEWART W. FRANKS (Department of Civil, Surveying and Environmental Engineering, University of Newcastle, Callaghan, New South Wales, 2308, Australia. email: ceswf@civeng.newcastle.edu.au); KEITH J. BEVEN (Institute of Environmental and Natural Sciences, Lancaster University, U.K.)

It has been shown that the calibration of SVAT models is inherently uncertain, even when data is available over a relatively limited homogeneous area. The representation of sub-grid scale variability of fluxes is not easily achieved due to the lack of information available about appropriate parameter distributions and their covariance. However, remote sensing of thermal surface responses offers the possibility of obtaining distributed estimates of surface fluxes. In this paper, multiple LANDSAT-TM images are used to derive uncertain estimates of the land surface - atmosphere sensible and latent fluxes over a period of time. Employing a novel 'function'-based framework, the parameter space representing all feasible 1-D parameterisations of a SVAT model are examined with respect to these image estimates. Areal weightings for a number of functional types of flux behaviour are then derived through which the temporal evolution of surface fluxes can be estimated.

**HW4/E/16-B2 1520**

**MULTISCALE HYDROLOGICAL PARAMETER ESTIMATION AND MODELLING – THE SEIG EXPERIMENT**

Prof W-A Flugel, K Bongartz, M Klenke, C Michl and H Staudenrausch

Abstract not available at time of going to press

**HW4/E/17-B2 1610**

**PREDICTIVE VALUE OF LAND-SURFACE-CHARACTERISTIC DATA SETS IN THE CALCULATION OF WATER AND ENERGY FLUXES OF LARGE RIVER BASINS**

P.C.D Milly and A.B.Shmakin

Abstract not available at time of going to press



**HW4/E/01-B2 1630****REGIONALIZATION OF PARAMETERS FOR THE MODELLING OF AREAL EVAPOTRANSPIRATION**

LUCAS MENZEL (Potsdam-Institute for Climate Impact Research, P.O. Box 601203, 14412 Potsdam, Germany, email: menzel@pik-potsdam.de)

In order to determine areal distribution patterns of evapotranspiration across the entire area of Switzerland a model to deliver evapotranspiration over complex terrain was developed. Intensive field studies at various sites of an alpine valley (Dischma, eastern Swiss Alps) and a prealpine location (Rietholzbach experimental basin) served to study relationships between atmospheric conditions, soil moisture and transpiration/interception evaporation over various land cover types.

Different submodels were used, e.g. to describe transpiration (Penman-Monteith equation with variation of canopy resistances), or evaporation of water from bare or vegetated surfaces. A series of model parameters were determined through field measurements and related experience. These parameters mainly include a proper description of plant physiological conditions and land surface characteristics like vegetation cover, canopy height, LAI development, albedo, interception storage capacity etc.

To regionalize the evapotranspiration model with all its components simplifications and estimations of the model parameters had to be carried out. In order to apply the whole model for longer time periods further submodels, e.g. to describe snow accumulation, snow melt and snow albedo, had to be elaborated. In addition, interpolation of the meteorological input data over the complex terrain was a difficult task. It was solved through a combination of inverse distance weighting techniques and altitude regressions. Slope inclination, slope exposition and terrain shadowing were calculated using a digital terrain model.

**HW4/E/05-B2 1645****THE EXPERIENCE OF APPLICATION OF DIFFERENT TECHNIQUES FOR REGIONALIZATION OF HEAT AND WATER EXCHANGE AT THE LAND SURFACE**

Yeugeniy GUSEV and Olga Nasonova (both at the Institute of Water Problems, Russian Academy of Sciences, Gubkina St. 3, 117971 Moscow, Russia, email: sowa@ipcom.ru)

Results of application of three approaches to regionalization of heat and water exchange at the land surface are presented. The first approach is to apply the existing point land surface schemes provided with so-called effective values for surface parameters instead of their point values. The second approach is explicit accounting for spatial heterogeneity when heterogeneous area is divided into a number of independent relatively homogeneous patches, or mosaic tiles, with different deterministic values of land surface parameters and with the same area-averaged atmospheric forcings. The components of heat and water budget are calculated separately for each mosaic tile and then averaged over the whole area. The third approach is statistical. In so doing, heterogeneous area is presented as statistical ensemble of patches for which the appropriate factors are treated to be random variables with known statistical parameters. In this case the problem consists in analytical or numerical solution of equations describing the dynamics of statistical moments of output variables or their distribution functions rather than the dynamics of outputs themselves. Application of the above mentioned approaches for regionalization of hydrological processes at different spatial scales is illustrated using the data for several catchments within the Arkansas-Red River basin (USA) as well as for the Kursk and Kiev regions (Russia). A set of various meso-scale models describing the processes of heat and water exchange at heterogeneous surfaces during both the warm and cold periods of a year is developed.

The magnitudes of spatial variability of the main influencing factors (precipitation, leaf area index, field capacity, and hydraulic conductivity at saturation) and statistical parameters of their distribution functions for the Kursk and Kiev regions are found.

**HW4/E/20-B2 1700****THE EXPERIENCE OF APPLICATION OF DIFFERENT TECHNIQUES FOR REGIONALIZATION OF HEAT AND WATER EXCHANGE AT THE LAND SURFACE**

Yeugeniy GUSEV and Olga Nasonova

Abstract not available at time of going to press

**HW4/E/11-B2 1715****GIS - BASED INTERPOLATION AND REGIONALIZATION OF MONTHLY LUMPED MODEL PARAMETERS**

IONEL HAIDU (University "Babes-Bolyai", 1 Kogalniceanu Str., 3400 Cluj-Napoca, Romania, email: haidu@bioge.ubbcluj.ro) Calin Haidu (Hydropower Company "Somes", 2-4 Napoca Str., 3400 Cluj-Napoca, Romania, email: giss@codex.ro)

The main purpose of the paper is to check the ability of some GIS procedures in order to interpolate and regionalise hydrological model parameters. First step is to estimate model parameters at basin scale which is important to runoff response. A parsimonious model, having a little number of parameter and physical meaning is preferable because, in the next step, they will be regionalized. Therefore, a monthly rainfall - runoff model on basin scale (VUB model - Type 1) was applied to the available 40 basins of Arkansas - Red river basin. It results three filter parameters which stand for the evapotranspiration equations, slow flow equations and for the fast flow equations. In the second step we passed from the lumped representation of the space to the distributed representation. Starting from the 3 x 40 lumped parameters, now, the purpose is to derive significant parameter values for each grid point. The GIS procedures offered by SPANS packages were used: TIN, Krigging, Density, Potential Mapping. The resulted layers (thematical maps) reveal some links with the basin characteristics. In the regionalization step we try to design hydrological homogeneous units (regions) using the classification facilities of the GIS. Some of the working steps are user depend and as consequences, the results have to be confronted with the reality of the terrain.

**HW4/E/W/03-B2 1730****PARAMETERISATION OF DISTRIBUTED RUNOFF MODELS BY USE OF OBJECTIVE FUNCTIONS AND MULTIPLE STATE VARIABLES**

Ing. T. RIJNTJES, Prof.dr.ir. C. van den Akker 1 and Prof.dr.ir. P. van der Veer 2 (1 Delft University of Technology, section Hydrology and Ecology, TUDelft Faculty of Civil Engineering, Stevinweg 1, 2628 CN Delft; (2) Delft University of Technology, Faculty of Civil Engineering, Stevinweg 1, 2628 CN Delft; section Civil Engineering Informatics)

The rainfall response of a catchment is expressed by a runoff hydrograph at the catchment outlet where the hydrograph is interpreted as an integrated response function of the various

(dominant) runoff processes. In runoff modelling it is common practice that only this hydrograph is used for model calibration. In distributed runoff models the calibration becomes unreliable by the large number of model parameters (e.g. Grayson et al., 1992a, b). Nowadays it is generally accepted that the model performance of distributed runoff models is doubtful by the over-parameterisation of these models. Models produce equally satisfactory model output (i.e. the catchment hydrograph) by use of different sets of parameter (values). Some ten years ago, groundwater modellers also were confronted with the phenomena of over-parameterisation in distributed groundwater models. In order to improve the reliability of distributed runoff models, the use of automated calibration procedures such as proposed by Carrera and Neuman [1986] is advocated in this article.

A catchment will be regarded as a set of interacting sub-systems where for each sub-system one or two model parameters and state variables must be defined. For model calibration, a maximum of four to five parameters must be selected for optimisation while the values of the other parameters must be fixed to a certain value. For the calibration of a model, automated calibration procedures must be employed where multiple state variables must be used for calibration. The use of automated calibration procedures in the field of physically based runoff modelling is advocated since a) multiple parameters can be optimised simultaneously with consideration of multiple state variables and b) parameter estimation is achieved for the model domain as a whole.

Variables to be used for calibration are the channel flow hydrograph, the ground-water table and the soil moisture content. By usage of an objective function in which the 'observation to measurement' discrepancies of state variables and parameters are minimised, it is believed that the model calibration procedure and so the model performance will improve.

For the modelling of catchment response in a distributed manner, the event based computer code 'Flowsim' has been developed within the Delft University of Technology. In this code a number of flow equations are used: overland flow and channel flow are described by 2-D and 1-D Strickler-Manning equations respectively; unsaturated sub-surface flow is described by Richards flow equation while groundwater flow is described by the Darcy flow equation. For model calibration the Gauss-Marquart-Levenburg algorithm will be applied. Model calibration and parameter estimation is achieved by usage of the Parameter ESTimation (PEST) programme (Watermark Computing, 1994).

Wednesday 28 July AM

Presiding Chair: J. Wallace

**WORKSHOP DISCUSSION****DISCUSSION 0900****ADDITIONAL INSIGHTS FROM POSTER PRESENTATIONS**

A. Becker

**DISCUSSION 1100****PROMISING APPROACHES TO PARAMETER ESTIMATION**

J. Schaake

Wednesday 28 July PM

Presiding Chair: A. Becker

**WORKSHOP DISCUSSION****DISCUSSION 1400****DATA REQUIREMENTS AND STRATEGIES**

J. Wallace

**DISCUSSION 1645****FUTURE MOPEX ACTIVITIES**

A. Hall

Tuesday 27 July AM

Presiding Chair: A. Becker

**HW4/E/23-B2 Poster 0900-01****REGIONALIZATION OF HYDROLOGICAL CHARACTERISTICS OF WATER BALANCE MATHEMATICAL MODEL IN THE REGION OF RAY ISLAND IN SLOVAKIA**

SUTOR Julius and STEKAUEROVA Vlasta

Abstract not available at time of going to press

**HW4/E/24-B2 Poster 0900-02****FLOOD CYCLE MODEL FOR SMALL RIVER BASIN WITHIN MONSOON ZONE: DIRECT AND INDICATIVE EVALUATION OF PARAMETERS**

Boris GARTMAN

Abstract not available at time of going to press

**HW4/E/25-B2 Poster 0900-03****THE SOUTHERN GREAT PLAINS 1997 HYDROLOGY EXPERIMENT DATA BASES**

Thomas JACKSON

Abstract not available at time of going to press

**HW4/E/26-B2 Poster 0900-04****A METHODOLOGY FOR MODEL VERIFICATION**

Richard VOGEL

Abstract not available at time of going to press

**HW4/E/27-B2** Poster **0900-05**

**REGIONALIZATION OF HYDROLOGICAL PARAMETERS OF THEQDF MODEL**

Pierre JAVELLE

Abstract not available at time of going to press

**HW4/E/07-B2** Poster **0900-06**

**THE CALCULATION OF EVAPORATION OVER LUOHE BASIN BY A SVAT MODEL AND USE OF IT TO CALCULATE THE RIVER FLOW**

XINGUO MO (Environment and ecotechnology Station, Institute of Geography, Chinese Academy of Sciences, Beijing 100101, P.R.China, email: moxg@dls.ig.ac.cn); Suxia Liu (Department of Hydrology, Institute of Geography, Chinese Academy of Sciences, Beijing 100101, P.R.China, email: liusx@sun.ihp.ac.cn) Zhonghui Lin (the same as Xinguo Mo); Weimin Zhao (Hydrological Bureau, the Huanghe(Yellow River) Water resources Commission, Zhengzhou 450004, P.R.China, e-mail: wiminz@usant.net)

Evaporation is usually calculated by experiential method in hydrological watershed model. When calculating annual river flow, evaporation is even more important. A Soil-Vegetation-Atmosphere water and energy Transfer model is established to calculate evaporation over Luohe basin, a typical catchment of Yellow river. Xinanjiang model with the improvement in evaporation by this SVAT model is used to calculate river flow for the basin. The results is useful for the solution to "yellow river without water now", one of the key water problems of China in 21 century.

**HW4/W/04-B2** Poster **0900-07**

**SENSITIVITY ANALYSIS ON SWAT MODEL TO ASSESS EFFECTIVE EVAPOTRANSPIRATION: THE VIRGINIOLIO BASIN CASE STUDY**

Giovanni Mariotto, Marco Mancini, NICOLA MONTALDO e Renzo Rosso (all at DIIAR, Politecnico di Milano, Milano, 20133 Milano, Italy, email: montaldo@idra1.iar.polimi.it) Peter A. Troch (Laboratory of Hydrology and Water Management, University of Gent, Coupure Links 653, Gent B-9000, Belgium)

A soil vegetation transfer scheme model has been applied to an experimental basin (Virginiolo, Italy) of about 5 sqkm to quantify the effect of canopy and soil parameters on the effective evapotranspiration, so that the large number of parameter used by these kinds of models can be reduced. It is well known how difficult is the data acquisition needed for a complete model parameterization. A sensitivity analysis is carried on in this respect. comparing estimated and observed evapotranspiration data for a field campaign during the summer 1997.

**HW4/E/03-B2** Poster **0900-08**

**COULD BE REGIONALIZED THE STOCHASTICAL MODEL PARAMETERS ?**

Ionel HAIDU (University "Babes-Bolyai", 1 Kogalniceanu Str., 3400 Cluj-Napoca, Romania, email: haidu@bioge.ubbcluj.ro)

The regionalization procedures of any hydrological model parameter require an existing spatial relationship between the data point. But, the parameter values of a stochastic model being the result of a mathematical optimization procedure are considered to be independent of any physiographical basin characteristic. Also, because the possible climatic change and the stochasticity of the runoff process, the parameter values would be time dependent. The apparent conclusion is that no any reason to make regionalization of such parameters. However, one purpose of the paper is to check if exist physically and statistically significant relationships between some monthly stochastic models and physiographical basin characteristics. For a such analysis just the very small basins (area under 150 - 200 sq.km.) from a continuous area are suitable, because the higher degree of intern homogeneity of basins characteristics. The monthly flow of 60 very small basins and their physiographical characteristics (like geology, slope, mean altitude, mean specific runoff etc.) from Northern Romania represent the data for this study. In order to have a limited number of parameter, two parsimonious stochastic models were derived: the Simplified Thomas - Fiering model (STF) which has 2 parameters (except for the monthly means) and an Extreme Parsimonious model (EP) which has only 1 parameter (except for the monthly indices of seasonality). The both models have been passed the specific tests on residuals and on simulation. Regional maps of these parameters were obtained using GIS procedure. The regional maps of stochastic parameters are used to test the procedures in order to compute runoff for ungaged catchments, but not all the cases are fulfilled. The conclusions is that the regionalization of stochastic parameters is model specific and limited to the considered area.

**HW4/E/29-B2** Poster **0900-09**

**MODEL OF GLACIERS RUNOFF FOR CENTRAL AASIA REGION**

V.G.KONOVALOV

Abstract not available at time of going to press

**HW4/E/30-B2** Poster **0900-10**

**UTILISATION OF ENTROPY FOR STRUCTURING OF GRID-BASED HYDROLOGICAL MODELS**

J. Geyer and A.H.Schmann

Abstract not available at time of going to press

**HW4/E/09-B2** Poster **0900-11**

**NUMERICAL EXPERIMENT OF CO<sub>2</sub> LATENT/SENSIBLE HEAT EXCHANGE BETWEEN ATMOSPHERE AND DIFFERENT PLANT CANOPIES**

Katsunori TANAKA (Frontier Research System for Global Change, Tokyo, Japan, email: ktanaka@frontier.est.or.jp) Masakazu Suzuki (Graduate School of Agricultural and Life Sciences, University of Tokyo, email: suzuki@fra.u-tokyo.ac.jp) and Nipon Tangtham (Faculty of Forestry, Kasetsart University email: ffrompt@ku.ac.th)

To clarify the mechanism of CO<sub>2</sub>, latent heat and sensible heat exchange between a plant community and the atmosphere, a multilayer model of these exchange has been developed.

This model includes a feedback function and takes account of the canopy intercept of rainfall. It can calculate not only a profile of these fluxes within and above a canopy, but also the profile of meteorological elements within and above the canopy, such as solar radiation, long wave radiation, air/leaf temperature, specific humidity, wind velocity, and CO<sub>2</sub> concentration. These profiles are calculated by using the information on the canopy structure, leaf characteristics, and the meteorological elements observed over the plant community. In order to validate the reproducibility of these fluxes over a tropical monsoon forest by this model, we observed CO<sub>2</sub>, latent heat and sensible heat flux over a canopy in Kog-Ma experimental basin in Thailand, which is one of target areas in GAME-Tropics, on several days in rainy season. As a result of the application of this model, we found that it could successfully reproduce CO<sub>2</sub>, latent heat and sensible heat flux over a canopy. Moreover, numerical experiments on CO<sub>2</sub>, latent heat and sensible heat flux were carried out using this model to investigate the influence of the characteristics of the canopy structure. I could consider about exchange of CO<sub>2</sub>, latent heat and sensible heat within and above a plant community, from the point of view of the canopy structure.

**HW4/E/31-B2** Poster **0900-12**

**VARIABILITY OF PARAMETERS OF THE SACRAMENTO MODEL IN THE CZECH PART OF THE ELBE RIVER BASIN**

Josef Buchtele and Jioi Zezilak

Abstract not available at time of going to press

**HW4/E/32-B2** Poster **0900-13**

**LARGE SCALE HYDROLOGIC PARAMETRIZATION FOR INTEGRATED MODELLING IN NORTHEAST BRAZIL**

Axel BRONSTERT, Martin Krol, J. Krywkow, Anne Jaeger

Abstract not available at time of going to press

**HW4/E/02-B2** Poster **0900-14**

**MODELLING SEDIMENT AND SOLUTE YIELDS OF THE RIVER WYE CATCHMENT, UK**

DAVID J. MITCHELL (School of Applied Sciences, University of Wolverhampton, Wolverhampton West Midlands WV1 1SB UK, email: d.mitchell@wlv.ac.uk)

The sediment and solute yields of the River Wye Catchment (4010 sq.km) and nine sub-catchments were modelled using hydrometric and basin parameters. Although large data sets exist for the Wye Catchment, the following problems arise in the application of data to statistical models:-

- 1.The historical format of data is usually perpetuated.
  - 2.Data if often in the form of point values rather than areal values.
  - 3.Temporal lag effects occur due to increasing catchment area.
  - 4.Spatial patterns of basin characteristics are often complex.
- In order to model sediment and solute yields traditional data sets were modified to overcome the above problems, using a mixture of standard manipulative procedures and the introduction of surrogate parameters. Using national archives and large scale maps, 36 hydrometric variable, 3 seasonal factors and 29 catchment characteristics (geological, pedological, land use and morphometric) were derived on an extensive scale.

**HW4/E/33-B2** Poster **0900-15**

**PARAMETERIZATION OF LATERAL HYDROLOGICAL PROCESSES BASED ON GEOMORPHOLOGIC UNITS**

Andrea Gunter and Axel Bronstert

Abstract not available at time of going to press





**GA1.03 Monday 26 – Wednesday 28 July****PALEOMAGNETIC FIELD BEHAVIOUR**

Location: Barber Institute LT

**Monday 26 July AM**Presiding Chairs: P Rochette (Cerege, Aix en Provence, France),  
P Camps (Univ. Montpellier, France)**PALEOMAGNETIC FIELD BEHAVIOUR 1****GA1.03/W/29-B1 0900****PALEOMAGNETIC EXCURSION AT 1.4 MA IN ASO VOLCANO, KYUSHU ISLAND, JAPAN**

H. SHIBUYA, S. Honjo, K. Hirata and T. Yamasaki (Dep't Earth Sci., Kumamoto Univ., Kumamoto 860- 8555, Japan.)

A paleomagnetic excursion was found in Aso Volcano, Kyushu Island, Japan. Aso-2 pyroclastic flow was found to have a paleomagnetic direction of very steep inclination. The pyroclastic flow is one of the four major widely spread pyroclastic flows of Aso Volcano. Those have been very well studied because they are, as well as their tuffs are, used as good keybeds not only in Kyushu Island but all over the Japanese Islands. The age of the Aso-2 pyroclastic flow had been determined to be 0.141±0.005Ma. To investigate that the anomalous direction was not by a rotation of a small block or by a local magnetic anomaly, we took the samples from multiple sites of the Aso-2 pyroclastic flow. As it spreads in an area of about 50km in diameter, it is easy to avoid a local disturbance of the paleomagnetic direction. The average direction of five sites distributed in the area was  $Dm=6.6$ ,  $Im=78.9$ ,  $a95=5.4$  and  $k=198.2$ , and the corresponding VGP was at 54.2N and 135.1E. If the criterion of an excursion is set at 60 in VGP latitude, it is called an excursion, though the difference of the direction from the geocentric axial dipole field is only about 25. The good concentration of the magnetic directions of widely distributed sites indicates that the direction anomaly is not due to a crustal source. The  $k$  value was not much different from that of paleomagnetic directions of Aso-4 pyroclastic flow, which had typical normal direction ( $N=15$ ,  $Dm=-3.8$ ,  $Im=42.4$ ,  $a95=2.6$  and  $k=198.2$ ). It may indicate that the paleointensity at the Aso-2 excursion was not significantly weak to be affected by the local magnetic anomaly. It was also confirmed by the preliminary paleointensity. Seven Thellier experiments of the strongly welded part gave 0.023mT to 0.048mT. They were as strong as or only slightly weaker than the present geomagnetic field.

**GA1.03/W/13-B1 0920****FIELD BEHAVIOUR DURING A REVERSAL EVENT IN A LAVA SEQUENCE FROM WAI'ANA'E VOLCANO, O'AHU, HAWAII**

STEVE OPENSHAW, John Shaw (Geomagnetism Laboratory, Department of Earth Sciences, Oliver Lodge Laboratories, Peach Street, Liverpool, L69 7ZE, UK. Email: steveo@liv.ac.uk); Emilio Herrero-Bervera (Hawaii Institute of Geophysics and Planetology, University of Hawaii, 2525 Correa Rd., Honolulu, HI 96822, USA Email: hererro@soest.hawaii.edu).

A suite of samples taken from lava flows on the Hawaiian Island of O'ahu are currently being investigated to illustrate field behaviour during a short period geomagnetic event. K-Ar dating has provided a date of 3.29 Ma at the base of the flow units. This corresponds to the onset of the Gauss Normal Epoch and includes the period of the Lower Mammoth polarity transition (3.06 - 2.94 Ma). Not only are we interested in the directional behaviour of the field during the transition but we are also attempting to produce a continuous palaeointensity record spanning the transition. Demagnetisation and palaeointensity studies are being performed on oriented 5mm diameter 1mm thick disk samples using an 8.2 GHz microwave demag / magnetisation SQUID system which avoids chemical alteration at temperature because the sample matrix is not directly heated. In addition to directional and palaeointensity determinations we present rock magnetic results obtained using a Variable Field Translation Balance (VFTB) which characterise the magnetic mineralogy throughout the flow.

**GA1.03/L/01-B1 0940****PALEOMAGNETIC STUDY OF THE SOCIETY ISLANDS: ITS IMPLICATION FOR THE PAST 5MA PALEOSECULAR VARIATION**

Hideo Tsunakawa, Koichiro SHIMURA, and Tetsu Kogiso (Department of Earth &amp; Planetary Sciences, Tokyo Institute of Technology, Ookayama, Meguro, Tokyo 152-8551, Japan, email: kshimura@geo.titech.ac.jp, htsuna@geo.titech.ac.jp, kogiso@geo.titech.ac.jp); Hans G. Barscuz (GfE, Université de Montpellier II, 34095 Montpellier, France, email: barscuz@dstu.univ-montp2.fr)

Reliable paleomagnetic data have recently accumulated but those from the southern hemisphere have not yet been enough. We have performed the paleomagnetic study of the Society Islands except for Tahiti, that is, Maupiti, Borabora, Tahaa, Raiatea, Huahine, and Moorea. The K-Ar ages of 1.5-4.8Ma were reported for the studied islands while Tahiti has younger ages (e.g. White and Duncan, 1996). Duncan (1975) reported the first systematic study of the paleosecular variation (PSV) in the Society Islands. Roperch and Duncan (1990) and Chauvin et al. (1990) carried out the detailed measurement of directions and paleointensities for the lava sequences in Huahine and Tahiti, respectively. The objective of this study is to obtain a number of reliable paleomagnetic direction and intensity data from the islands. We report the preliminary result of PSV from these six islands.

More than 5 cores were collected from 134 units of lavas and dikes by a portable gasoline engine drill and sun or magnetic compasses. Three specimens from each unit were subjected to stepwise thermal demagnetization. Most of the specimens show primary components while some units cannot. As a result, 68 normal, 39 reversed, and 10 intermediate directions were measured when a threshold VGP latitude of 45 deg is applied. The angular standard deviation (ASD) is calculated from these normal and reversed VGPs to be 14.8 deg. This value is similar to that of Tahiti (13.9 deg; Chauvin et al., 1990) and the global trend calculated from IGRF 1965 (McFadden et al., 1988) but larger than the Hawaiian PSV (11.2 deg; McWilliams et al., 1982).

**GA1.03/W/01-B1 1000****PALEOMAGNETISM OF VOLCANIC ROCKS FROM KERGUELEN ARCHIPELAGO (24-30 MA): IMPLICATIONS FOR THE PALEOSECULAR VARIATION IN SOUTHERN INDIAN OCEAN**

P. CAMPS (ISTEEM, University of Montpellier 2 case 060, France, email: camps@dstu.univ-montp2.fr); B. Henry (IPGP, 75252 Paris, France, email: henry@ipgp.jussieu.fr) and M. Prévot (ISTEEM, email: prevot@dstu.univ-montp2.fr).

We report a survey carried out on the flood basalts from Kerguelen Archipelago (indian ocean)

for purposes of extending records of paleomagnetic directional fluctuations from a site in the southern hemisphere. We have sampled a hundred lava flows (667 oriented cores) from 5 stratigraphic sections from diverse regions of the archipelago. The 40Ar/39Ar estimated age of the sampled lava ranges from 24 to 30 Ma (Nicolaysen et al. 1999). The paleomagnetic treatment (stepwise thermal or alternating field demagnetization) is still in progress. Our preliminary results, obtained from 4 sections on the basis of NRM measurement for each core plus one pilot sample demagnetized per flow, revealed the presence of normally and reversely magnetized lavas but no transitional directions between the two polarities. For the 4 sections, we obtained a N-R-N, R-N-R, R-N and N-R stratigraphic sequences, respectively. Lavas seem not suitable for paleointensity determinations because we observe in most cases a contamination of the natural remanent magnetization by large viscous component. These results will be discussed by means of a paleomagnetic secular variation model describing the temporal changes in the geomagnetic field.

**GA1.03/W/23-B1 1040****PALEOMAGNETISM AND K-AR AGES OF LAVAS FROM SUDURDALUR, EASTERN ICELAND**

Saneyuki UDAGAWA (Earthquake Research Institute, University of Tokyo), Hajime Kitagawa (Patent Agency, MITI), Takehiro Koyaguchi (University of Tokyo), and Masaru Kono (Okayama University)

Two sequences of successive lava flows were sampled in Sudurdalur, Eastern Iceland. They are composed of 46 and 54 lava flows, respectively. These sampling sites are located in the valley adjacent to Nordurdalur studied by Liverpool group in 1970s. Paleomagnetic directions of all lava flows were determined after AF demagnetization to 50 mT. In most cases, secondary components could be removed by about 20 mT demagnetization.

K-Ar ages were obtained from about 30 lavas and they range between 3.0 and 6.0 Ma. The ages are generally consistent with the stratigraphy and shows that two sections overlap partially. Combining our data with Watkins and Walker (1977) and McDougall et al. (1976), we obtain a composite of reversal history in this area, which may be reconciled with the geomagnetic polarity timescale of Gauss to Epoch 5, derived from marine magnetic anomalies.

**GA1.03/P/01-B1 1100****LOW-LATITUDE VIRTUAL GEOMAGNETIC POLES IN NEOGENE ICELANDIC LAVA SEQUENCES**

Leo KRISTJANSSON (Geophysics Division, Science Institute, University of Iceland, Hagi, Hofsvallagata 53, 107 Reykjavik, Iceland, email: leo@raunvis.hi.is)

Two paleomagnetic studies on altogether about 1400 lava flows from the subaerial Neogene basalt lava sequences of Iceland were published in 1977. In these collections, about 10% of the reliably determined remanence directions corresponded to virtual pole (VGP) positions below 40° latitude. This was a larger proportion than found in most other volcanic locations. To explain it, Harrison (1980) suggested that some 10% of the observed virtual geomagnetic poles from Iceland might be distributed at random over the globe. Such "random poles" can be envisaged as dating from periods when the geomagnetic field is weak and dominated by variable non-dipole terms. Remanence directions and intensities in additional collections of lava flows were analysed by Kristjansson & McDougall (1982); in these studies the within-flow directional uncertainties were generally smaller than in the work published in 1977. Not much change from the original results of Harrison (1980) was however observed in the overall distribution of poles. In collections completed after 1982, improved sampling and demagnetisation procedures are yielding further reductions in within-flow scatter (Kristjansson 1995, and work in progress). Poles below 40° latitude continue to amount to at least 10% of the total, and altogether 20% lie below 50° latitude. The poles have a fairly uniform distribution in longitude, and there is no significant difference between normal and reverse poles. The average strength of the virtual dipole falls by a factor of 3-4 between the geographic poles and Equator. Normalising of remanence intensity data by the use of anhysteretic remanence may improve the resolution of this type of analysis. There is some evidence for long-term variations in the amount of between-flow scatter of poles from Icelandic lava flows emplaced in the last 15 M.y.

**GA1.03/E/07-B1 1120****MORE EVIDENCES FOR LARGE TERTIARY NON DIPOLE FIELD**

Pierre ROCHETTE, Didier Vandamme and Y. Touchard (CEREGE, BP80 13545 Aix en Provence Cdx 4, France; email: rochette@cerege.fr)

A new well-documented pole for Africa at 30 Ma has been obtained in the Ethiopian traps (77N 208E, N=53 A95=3.7). This pole is far sided by 6 degree with respect to the synthetic pole from Besse and Courtillot but agree with other synchronous poles from African volcanic rocks, together with the pole derived by Schneider et al. (1990) from inclination data of ODP sites. We resampled two South Indian Ocean ODP sections at 30 Ma and found consistent inclinations with the Ethiopian data. The convergence of evidences from volcanic rocks and oceanic sediments widely distributed within the African plate clearly impose a large (>10% quadrupole and octupole) NDF at 30 Ma. This NDF is averaged out in the synthetic data because of longitude distribution of the sites in the global database but is visible when averaging on longitude sectors. It also accounts for the widespread paleolatitude problem encountered in the Eurasian data.

Another interesting feature of the Ethiopian traps data is that directions show clearly non-Fisherian distribution while VGPs do. Other equatorial data like from the Galapagos Islands (0-5 Ma) exhibit the reverse behavior (Fisherian directions, not VGPs). Does such a behavior relates to non-dipole field?

**GA1.03/W/04-B1 1140****ANOMALOUSLY LOW ANGULAR DISPERSION DURING THE EARLY CRETACEOUS**

Jonathan M.G. GLEN (Berkeley Geochronology Center, 2455 Ridge Rd., Berkeley, CA 94709 USA; Earth Sciences Department, University of California, Santa Cruz, CA, 95064, USA; and Laboratoire de Paleomagnetisme, Institut de Physique du Globe 4 Place Jussieu, 75252 Paris Cedex 05, France); Paul R. Renne (Berkeley Geochronology Center, 2455 Ridge Rd., Berkeley, CA 94709 USA); Robert S. Coe (Earth Sciences Department, University of California, Santa Cruz, CA, 95064, USA), and Simon C. Milner (Geological Survey of Namibia, PO Box 2168 Windhoek, Republic of Namibia)

we have sampled rocks from the parana-etendeka igneous province, one of the largest flood volcanic provinces in the world that formed 132 my ago, roughly coincident with the rifting of south america and africa in the south atlantic. paleomagnetic measurements yielded generally well defined characteristic components. mean paleomagnetic directions from normally and reversely magnetized units are indistinguishable at the 99% confidence level, confirming that primary directions of magnetization have been adequately isolated. geochemical and magnetostratigraphic correlations of sections reveal that the data span several polarity chrons

-- long enough to average out secular variation. however, the data surprisingly yield an anomalously low estimate of the angular standard deviation (asd), falling significantly below the expected value based on a compilation of data spanning 110 to 195 ma. most likely this indicates that the early cretaceous was a time of unusually low asd, as has been suggested for the immediately following cretaceous superchron because of its low reversal rate. if this observation holds up with additional data, it furnishes a critical test for models of the geodynamo.

**Monday 26 July PM**

Presiding Chairs: J Carlut ( Inst. Du Physique du Globe, France) and U Draeger (Univ. California Santa Cruz, California)

**PALEOMAGNETIC FIELD BEHAVIOUR 2**

**GA1.03/W/08-B1 1400**

**CRM EXPERIMENTS AND PALEOINTENSITY MEASUREMENTS ON VOLCANIC ROCKS WITH INITIALLY LOW CURIE TEMPERATURE**

Ulrike DRAEGER (University of California Santa Cruz, Institute of Tectonics, Santa Cruz, CA 95064, USA, email: draeger@earthsci.ucsc.edu); Michel Prévot and Thierry Poidras (Laboratoire de Géophysique et Tectonique, Université de Montpellier 2, 34095 Montpellier Cédex 05, France, email: prevot@dstu.univ-montp2.fr)

There is some evidence that the primary remanence of basaltic rocks which are oxidized at high temperatures can be a thermochemical magnetization (TCRM) rather than a TRM. This can cause errors in determination of the paleointensity of the Earth's magnetic field. In order to simulate two different kinds of oxidation processes we produced a CRM at a constant temperature of oxidation and a TCRM at a very slowly decreasing temperature. The original samples were carrying titanomagnetite with Curie temperatures far below the oxidation temperatures of the experiment. Subsequent Thellier experiments on the oxidized samples yielded different values for the intensity of the 'paleofield' (here: field which was applied during acquisition of CRM), depending on the oxidation experiment. While the apparent paleointensity estimated from a pure CRM is lower than the actual magnetizing field and is dependent on the oxidation temperature, the TCRM provides an almost correct apparent paleointensity. Performed rock magnetic experiments let us assume that we produce a CRM by crystal growth of a Ti-poor mineral like magnetite in the original titanomagnetite. Long-term heating experiments, paleointensity experiments and rockmagnetic studies are presented.

**GA1.03/W/19-B1 1420**

**SHORT TERM VARIATIONS IN GEOMAGNETIC FIELD STRENGTH FROM MICROWAVE ANALYSIS OF PERUVIAN, CHINESE AND EGYPTIAN CERAMICS**

JOHN SHAW and Shanlin Yang (Geomagnetism Laboratory, University of Liverpool, UK); Derek Walton (Department of Physics, McMaster university, Canada.); Hatem Odah (NRIAG, Cairo, Egypt.)

Microwave heating of the magnetic system within ceramic samples has allowed the determination of the ancient geomagnetic field strength without causing laboratory alteration. Application of the microwave palaeointensity method to ceramics from North West China, Peru and Northern Egypt has revealed smoothly varying changes in the strength of the geomagnetic field with time. The major source of change appears to be the movement of non-dipole anomalies. Further application of the new microwave archaeointensity method will allow us to construct a global map of dipole and non-dipole field strength changes over archaeological time.

**GA1.03/W/24-B1 1440**

**ROCK-MAGNETIC CHARACTERISTICS AND PALAEOINTENSITY RESULTS: A STUDY ON HISTORICAL LAVES FROM MT. ETNA**

Manuel CALVO (Dep. de Física, Universidad de Burgos, Spain. Email: mcalvo@ubu.es); Mireille Perrin and Michel Prévot (Lab. de Géophysique et Tectonique, UMR CNRS 5573, Univ. Montpellier II, France. Email: perrin@dstu.univ-montp2.fr and prevot@dstu.univ-montp2.fr)

In palaeointensity studies, a high percentage of samples do not yield reliable results and dispersion is often high. The aim of the present study is to obtain information about the effect on palaeointensity determinations of the presence of MD-grains and mineralogical, chemical and/or physical changes during heating in Thellier-type palaeointensity experiments. For this purpose, a refined palaeointensity experiment was devised, which could allow determination of CRM created during the experiment and recognition and quantification of the effect of MD-grains on palaeointensity. In addition, rock-magnetic experiments aimed to obtain information about carriers of remanence, their stability and the presence of MD-grains were carried out. Different carriers of remanence and different behaviour during heating are reflected in the obtained k-T curves, although no direct correlation is observed between them and value and quality of palaeointensity determinations. The mean palaeointensity obtained in this study is in accordance with the expected one, although scatter of single values around the mean is considerable. If samples are analysed individually, four cases can be distinguished: apparently correct palaeointensity determinations are accompanied either by correct and incorrect "quality indicators", and the same holds for incorrect palaeointensity determinations.

**GA1.03/W/07-B1 1500**

**MAGNETIC INVESTIGATION, PAYING PARTICULAR ATTENTION TO THE INTENSITY, OF A RECENT HAWAIIAN LAVA FLOW**

Mimii J. HILL and John Shaw (The Geomagnetism Laboratory, The University of Liverpool, L69 7ZE, UK) and Emilio Herrero-Bervera (Hawaii Institute of Geophysics and Planetology, University of Hawaii, HI 96822, USA.)

Detailed investigation of historic lava flows where the field behaviour is well known permits a clearer understanding of the recording process that occurs in lava to be obtained. It has been shown (Rolph, 1997 and Böhnell et al, 1997) that there can be considerable variation in the magnetic properties within a single lava flow. Two vertical sections, approximately 16 m apart, of the 1960 lava flow in Puna were sampled. One section is 75 cm thick and the other 1 m thick. 2.5 cm diameter cores were taken at a vertical spacing of 5 cm.

We present rock magnetic, directional and palaeointensity results. Microwave demagnetisation / remagnetisation has been used for the intensity and directional analysis. The microwave method allows the magnetic minerals to be directly heated without heating the bulk sample (Walton et al, 1993) thus minimising the problems associated with alteration during experimentation. It is required for palaeointensity determinations that the NRM is a TRM and not a CRM. Many of the samples showed two distinct intensity components, a low microwave power / blocking temperature component and a high power / blocking temperature component with the low power intensity being considerably higher than expected. It is

suggested that the higher intensity value could be due to a natural CRM. Using the high power component where two components were present, the evaluated intensity does show some variation though the flow but the average for the whole flow is within the limits of the expected value.

**GA1.03/L/04-B1 1520**

**PALEOINTENSITY STUDIES OF A LAVA SUCCESSION FROM JILIN PROVINCE, NORTHEASTERN CHINA: AN EVIDENCE FOR THE BLAKE EVENT**

Rixiang ZHU and Yongxi Pan (Institute of Geophysics, Chinese Academy of Sciences, Beijing 100101, email: rxzhu@mail.c-geos.ac.cn)

Geomagnetic reversals and short geomagnetic events are well-documented modes of behavior of the Earth's magnetic field. One such convincingly demonstrated geomagnetic event is so-called Blake event, which was first reported by Smith & Foster (1969). This geomagnetic event has subsequently been reported in different lithologic and places and therefore appears to be a global event. Here we present a new study of absolute intensities for the period 210-88 kyr obtained from a sequence lava flows from the Tianchi lava flows (42.05°N, 128.0°E), Jilin Province, Northeastern China. The lava flows are formed entirely of alkali basalt located in the center of Changbaishan Mts lying to Sino-North Korean boundary. 5 lava flows can be recognized from the presence of stratigraphic discontinuities. The age of the lower flow named lava1 is 210 kyr, which is overlain by other series lavas labeled as 2-5. 123±7 and 123±10 have been dated for the lava3 and lava4 respectively, and 88 kyr for the lava5. Total 275 oriented core samples were collected within these 5 lava flows. Rock magnetic analyses and reflected light microscopy indicate that the magnetic mineralogy of the lava flows is dominated by magnetite containing a significant fraction of single-domain grains. Stable characteristic remanence (ChRM) can be thermally isolated above 150-200°C. Two intermediate directions held by the lavas with a age of ~123 kyr correspond to the Blake event, their virtual geomagnetic poles (VGPs) are located at the Eastern Asia and Australia. Over 121 samples are used to paleointensity determinations carried out with Thellier method in an argon atmosphere. Of these, only 34 samples yield reliable results, with within-flow scatter lower than 15%. The results indicate that marked intensity low is coinciding with intermediate directions.

**GA1.03/W/27-B1 1600**

**ABSOLUTE PALEOINTENSITY OF 0-1 MA OLD LAVA FLOWS FROM LA GUADELOUPE ISLAND: COMPARISON WITH SEDIMENTARY AND VOLCANIC DATASETS**

J. CARLUT (email: carlut@ipgp.jussieu.fr, Lab. de Paleomagnetisme, IPGP, 4 Place Jussieu, 75252 Paris Cedex 05, FRANCE) and X. QUIDELLEUR (email: quidel@geol.u-psud.fr, Lab. de géochronologie UPS- IPGP, Bat.504, Univ. Paris Sud, 91405 Orsay, FRANCE)

Ten absolute paleointensity determinations covering the Brunhes chron have been obtained on andesitic lava flows from La Guadeloupe Island, French West Indies. The Thellier and Thellier method performed on 124 specimens under either ambient or argon atmosphere allows reliable determinations from high temperature steps. The average virtual axial dipole moment (VADM) for normal polarity flows from the Brunhes chron is compatible with the present day field. A paleointensity decrease of a factor of ten is observed for flows emitted during the Matuyama-Brunhes transition, as already observed in other records of this reversal. Each flow from this study is associated with a K/Ar age (Blanc, 1983; Carlut et al., 1999) obtained using the Cassinot technique (Gillot and Cornette, 1986). This allows us to compare the present dataset with other records from the Brunhes interval. The ten VADM values obtained show a relatively good agreement with the global variations of the axial dipole strength, as displayed by the deep sea composite record (SINT800) of relative paleointensity, when rapid fluctuations of about 15% amplitude due to the non-dipole components are taken into account. We present a new global dataset including all recent studies with good age determinations. Within the most documented interval, a well defined 20 kyr long oscillation observed in the volcanic VADM can be attributed to the long term evolution of the axial dipole part of the field. Because a large area of the Globe around the Caribbean Islands was previously devoid of data, the present dataset fills a gap towards construction of a global paleointensity database for the Brunhes chron.

**GA1.03/L/03-B1 1620**

**A PALEOMAGNETIC STUDY OF JURASSIC INTRUSIVES...**

THOMAS

Abstract not available at time of going to press

**GA1.03/L/02-B1 1640**

**FILLING GAPS IN THE PHANEROZOIC PALEOINTENSITY...**

THOMAS

Abstract not available at time of going to press

**Tuesday 27 July AM**

Presiding Chairs: E Schnepf (Inst. Fur Geophysik, Gottingen, Germany) and B Clement (Univ. Florida Int, Florida, USA)

**PALEOMAGNETIC FIELD BEHAVIOR 3**

**GA1.03/E/06-B2 0900**

**REPEATED PATTERNS OF GEOMAGNETIC FIELD BEHAVIOUR ON THOUSAND YEAR TIME-SCALES IN THE LOWER CRETACEOUS**

IORIO, M. (Geomare Sud, Via Vespucci 9, Napoli 80142, Italy Email: iorio@gms01.na.cnr.it); TARLING, D.H. (Geological Sciences, University, Plymouth PL4 8AA, UK Email: d.tarling@plymouth.ac.uk) and D'Argenio, B. (Scienze della Terra, Università Federico II di Napoli, Napoli 80138, Italy Email: ciclisiti@gms01.na.cnr.it)

Some twelve patterns in the directional behaviour of the palaeomagnetic signal have been recognised in shallow-water carbonate bore-core accumulated during some 3.2 Ma some 127 Ma ago. These patterns are each of several ka duration and follow consistent sequences during constant polarities and transitional polarities. The directional patterns do not appear to be related to changes in intensity or susceptibility. These sequential patterns appear to be attributable to the behaviour of the geomagnetic dipole as the individual measurements average out secular variations on time-scales of up to 2-5 ka.



GA1.03/E/08-B2

0920

## THE GERMAN ARCHAEOMAGNETIC SECULAR VARIATION CURVE

Elisabeth SCHNEPP (Institut für Geophysik, Herzberger Landstr. 180, 37075 Göttingen, Germany, email: Grubenhagen@t-online.de); Rudolf Pucher (Geowissenschaftliche Gemeinschaftsaufgaben, Postfach 510153, 30631 Hannover, Germany, email: R.Pucher@bgr.de)

The archaeomagnetic secular variation (SV) curve for Germany is based on recent palaeomagnetic measurements carried out on 36 archaeological sites in Germany and on a collection of further 103 published or unpublished archaeodirections also from the neighbouring countries. All sites are located in an area ranging from 3 to 15°E in geographical longitude and 47 to 57°N in latitude. The German sites have been investigated by using standard palaeomagnetic and rock magnetic methods. Samples come mainly from various kilns which were preserved from the epoch between the early middle age and the 18th century, mainly dated with the radiocarbon or thermoluminescence method. Although, geographical and age distribution of the data set is still uneven, for the time interval 900 to 1800 AD six to 26 data points per 50 year interval can be used to calculate an average SV curve. This curve clearly deviates from the neighbored French or British archaeomagnetic SV master curves. The German curve shows a delay in time of up to 75 years and around 1300 AD the inclination was about 5° higher than in France and Britain. It seems that the SV pattern changed considerably from mediaeval to modern times in Europe. This feature will be clarified with palaeomagnetic measurements on further six mediaeval kilns under investigation situated in the eastern part of Germany. Furthermore the archaeomagnetic SV curves were compared with historical magnetic data. The correlation is for the overlapping time interval of about 200 years is not satisfying, presumably because geographic areas taken for the archaeomagnetic SV curves are too large.

GA1.03/W/06-B2

0940

## RELIABILITY OF RELATIVE PALAEOINTENSITY OF SEDIMENTS WITH STRONG CLIMATICALLY AFFECTED MAGNETISATION CHANGES

Maja HAAG (Institut für Geophysik, ETH-Hönggerberg, CH-8093 Zürich, Switzerland  
Email: maja@mag.ig.erdw.ethz.ch)

A late Pleistocene deep-sea core taken in the Central Atlantic along the coast of Mauritania (W-Africa) shows large variations of magnetic properties, such as natural and anhysteretic remanent magnetisation (NRM, ARM), low field susceptibility (k) as well as their ratios NRM/k and ARM/k. These rock magnetic parameters coincide with rapid changes of the stable oxygen isotope ratio which indicate climate changes, i.e. correspond to glacial stage or substage boundaries. Warm periods mainly correspond to high magnetisation intensity and cold periods to low intensity. Such intensity variations are due to changes in chemistry and concentration of ferromagnetic minerals and thus normally hinder the determination of reliable measurements of relative palaeointensity of the Earth's magnetic field. Previous investigations established the boundary conditions for the maximum variation of the ferromagnetic minerals and related magnetic properties necessary for reliable relative palaeointensity measurements. The mineralogical variations of the present study are much above these limits. However, the NRM/ARM ratio which is mostly used for relative palaeointensity determinations varies differently with depth than the other parameters and therefore reflects to a lesser degree such mineral changes. The most prominent lows of the NRM/ARM ratio are observed at ca. 17 kyr, 35-40 kyr, 60-65 kyr, 90-120 kyr, 128-132 kyr, 150-155 kyr and 180-195 kyr. The minimal relative palaeointensity is at 185 kyr. The most distinguished highs are visible at ca. 45-52 kyr, 125 kyr, 135-145 kyr and at 220 kyr. The maximal relative palaeointensities are at 52

GA1.03/W/03-B2

1000

## RELATIVE PALAEOINTENSITY OF THE GEOMAGNETIC FIELD DURING BRUNHES CHRON RECORDED IN NORTH PACIFIC DEEP-SEA SEDIMENT CORES: ORBITAL FORCING?

Toshitsugu YAMAZAKI (Geological Survey of Japan, Tsukuba 305-8567, Japan,  
e-mail: yamazaki@gsj.go.jp)

Relative palaeointensity records of the geomagnetic field during the Brunhes Chron were obtained from two sediment cores in the North Pacific near the Hess Rise. The cores, taken below the carbonate compensation depth (CCD), showed an oxidized environment, and accompany little paleoclimatically induced lithological changes. Utilization of such sediments has the advantage of avoiding paleoclimatic contamination to relative palaeointensity through rock-magnetic changes, although relatively slow sedimentation limits resolution. Homogeneity of magnetic mineralogy and magnetic grain size, which is prerequisite for sedimentary palaeointensity, was thoroughly examined using various techniques including low-temperature magnetometry, room-temperature hysteresis parameters, and S ratio. The IRM was used as a normalizer of the natural remanent magnetization (NRM). The appropriateness of the normalization was checked by the absence of correlation between the normalized intensity (NRM/IRM) and the normalizer (IRM). The relative palaeointensity records obtained are in general similar to the dataset from the east and central equatorial Pacific [1, 2]. The average geomagnetic field intensity during the Brunhes Chron is not lower than the present as suggested previously [3]. Spectral analysis of the relative palaeointensity showed significant power at the orbital eccentricity (100 kyr) frequency. The eccentricity frequency is not dominant in bulk magnetic properties. This suggests orbital forcing of geomagnetic field intensity.

GA1.03/W/05-B2

1040

## LATE MATUYAMA GEOMAGNETIC FIELD BEHAVIOR AS RECORDED AT HIGH SEDIMENTATION RATE SITE IN THE NORTHWEST ATLANTIC

BRAD CLEMENT and Zhong Yang (Dept of Geology, Florida International University, Miami, FL, email: clementb@fiu.edu); Gary Acton (Ocean Drilling Program, Texas A&M University, College Station, TX); Steve Lund (Dept. of Geology, University of Southern California, Los Angeles, California); Trevor Williams (Borehole Research, Department of Geology, University of Leicester, Leicester United Kingdom)

Recent results of  $^{40}\text{Ar}/^{39}\text{Ar}$  dating of basalts suggest a more complicated polarity reversal pattern during the late Matuyama than previously accepted. Dating of lavas on Maui and on Tahiti has produced dates of normal polarity flows that have been interpreted as being significantly different from ages consistent with the Brunhes, Jaramillo or Cobb Mountain polarity intervals. If correct, these results indicate the presence of additional excursions or short normal polarity subchrons during the late Matuyama. The fact that the proposed short polarity intervals have not been widely recognized in stratigraphic records of field behavior means that they must be very short intervals if they are truly present.

Ocean Drilling Program Leg 172 recovered very high sedimentation rate upper Matuyama sequences at Sites 1060, 1061, located on the Blake Outer Ridge, and Site 1063, located on the Bermuda Rise. Sedimentation rates in these sequences range up to 25-30 m/m.y. providing very high resolution of the geomagnetic field during this time. The paleomagnetism of these intervals was measured by collecting U channel samples from the cores and

measuring the U-channels at 1 cm intervals on pass-through cryogenic magnetometer. The results exhibit a very high degree of coherence between the different sites even though they are separated by more than 1000 km. The high resolution nature of these records makes it possible to place upper limits on the duration of the proposed new short polarity intervals that are not observed, assuming that these intervals are in fact, global features of the earth's magnetic field.

GA1.03/E/09-B2

1100

## RELATIVE GEOMAGNETIC FIELD INTENSITY ACROSS THE JARAMILLO SUBCHRON IN SEDIMENTS FROM THE CALIFORNIA MARGIN (ODP LEG 167)

Roman LEONHARDT ( Department of Geophysics, University of Munich, Theresienstr. 41, 80333 München, Germany, email: leon@rockmag.geophysik.uni-muenchen.de ); Franz HEIDER (GFZ Potsdam, Telegrafenberg Haus C, 14473 Potsdam, Germany, email: fheider@gfz-potsdam.de ); Akira Hayashida (Science and Engineering Research Institute, Doshisha University, Kyoto 610-0321, Japan, email: ahay@doshisha.ac.jp)

A sedimentary relative paleointensity record of the Jaramillo subchron was obtained at Site 1010 during the Ocean Drilling Program Leg 167 on the California margin. The demagnetization of the natural remanent magnetization of discrete samples revealed a vertical drilling overprint. Reversal tests on the characteristic remanent magnetization of the discrete samples showed that the drilling overprint had been removed successfully by alternating field demagnetization at 20-mT. Rock magnetic criteria for determining relative paleointensities are fulfilled. Normalization with various magnetic parameters yielded similar results and contributions from viscous remanent magnetization could not be detected. Several intensity features are detectable in the record of Site 1010, displaying a maximum in intensity shortly above the lower Jaramillo transition, a prominent local minimum in the middle of the subchron and a gradual decrease toward the upper Jaramillo reversal. A comparison of the record from the California margin with several other records of relative paleointensity across the Jaramillo subchron with different sedimentation rates and sediment composition shows reasonable agreement between the paleointensity patterns but also differences in amplitudes. The amplitude differences suggest an influence of post depositional magnetization processes which were not removed during normalization.

GA1.03/W/31-B2

1120

## MAGNETOSTRATIGRAPHY AND RELATIVE PALAEOINTENSITY OF PELAGIC SEDIMENTS AT ODP LEG 167 SITE 1010 OFF BAJA CALIFORNIA

Akira HAYASHIDA (Doshisha University, Kyo-Tanabe, Kyoto 610-0321, Japan; e-mail: ahay@doshisha.ac.jp); Kenneth L. Verosub (University of California, Davis); Franz Heider and Roman Leonhardt (Ludwig-Maximilians- Universität, Muenchen)

Sediments recovered from the most seaward site of the Baja Transect of the California Margin (ODP Leg 167) yielded a high fidelity magnetostratigraphic record spanning the last 6 m.y. Using a long-core cryogenic magnetometer, we made NRM measurements of 59 u-channel samples, which cover the interval from 0 to 78.5 mcd (meters composite depth) of the spliced section of Holes 1010C and 1010E. Stepwise AF demagnetization between 20 and 60 mT showed that the remanence is essentially composed of a single stable component, which was not affected by a coring-induced magnetization. The investigated section can be divided into at least 25 polarity intervals, which are assigned to the chrons from C3A.n2 to the Brunhes (C1n). The sedimentation rate was nearly constant at about 13 m/m.y., except for a reduction to 9 m/m.y. between 4 and 5 Ma. ARM and IRM measurements of the u-channels revealed that the sediments below 23 mcd exhibit sharp drops in magnetic concentration at several horizons, but the upper part has relatively uniform magnetic concentration, containing magnetite of pseudo-single domain size. The upper interval yielded consistent relative intensity records when normalized with ARM, IRM and shipboard susceptibility data. Several peaks in the relative intensity variations correspond to the drops in the S-ratio or to anomalous peaks in the IRM and magnetic susceptibility profiles, suggesting that the normalized intensity record is partly influenced by episodic changes in the flux of magnetic grains. The normalized intensity for the intervals younger than 1.2 Ma shows similarities with published paleointensity records from the equatorial Pacific, including results from ODP Leg 138. In particular, intensity minima at 0.05, 0.11, 0.18 and 0.29 Ma and those associated with the onset and termination of the Jaramillo Subchron are well correlated.

GA1.03/W/28-B2

1140

## DETAILED RECORD OF PALEOMAGNETIC FIELD CHANGE FROM SEARLES LAKE, CALIFORNIA (2) THE GAUSS/MATUYAMA POLARITY REVERSAL

Jonathan M.G. GLEN (Earth Sciences Department, University of California, Santa Cruz, CA 5064, and Berkeley Geochronology Center, 2455 Ridge Rd., Berkeley, CA 94709, email: jglen@bgc.org), Robert R.S. Coe (Earth Sciences Department, University of California, Santa Cruz, CA 95064, email: rcoe@earthsci.ucsc.edu), and Joseph C. Liddicoat (Environmental Sciences, Barnard College, NY 10027, email: jliddicoat@barnard.columbia.edu)

This new study of the Gauss/Matuyama transition from Searles Lake, CA conjoined with other records from the western US, provides interesting insights into the structure of the reversing magnetic field. The present study employs improved measurement and data reduction techniques, multiple parallel strings of samples, and a finer sampling interval than was used in the original study by Liddicoat (1982). Particularly crucial to this investigation was the use of overprint directions to reconstruct declinations, required because the core was rotary drilled. The results of this technique were corroborated by employing an independent method that uses anisotropy of magnetic susceptibility to resolve a sediment fabric: the fabric facilitated the alignment of core segments. The new record reveals that the main swing of the transition occurs over a significantly shorter time span than was found in the original study. In addition, it brings out several small scale variations that were absent in the old record, some of which take the form of relatively rapid jumps in direction that punctuate more steadily varying changes. This alternating steady and rapid field change is similar to behaviour observed in volcanic records, which argues that such behaviour is not merely an artefact of episodic volcanism. The Searles Lake record is strongly non-zonal, and is defined in the northern hemisphere by a swath of virtual geomagnetic poles (VGPs) stretching from northern Eurasia to west Africa and to the northwest Pacific. Glen et al. (1994) showed that a collection (spanning >15 my) of western North American transition and excursion records displays this same pattern, indicating that the VGP swath is a persistent feature of the transitional field. In addition, the compilation reveals that the swath extends into the southern hemisphere, outlining a region marked by an absence of poles that is centred on the Indian Ocean. The fact that this pattern is offset from a similar one seen in global compilations suggests that the persistent fields have a significant nondipolar component. Six additional records are now available, making the w.NA dataset perhaps the finest regional set of high resolution records consisting of both igneous and sedimentary records. The new records, which provide an important test of the existence of the VGP pattern, strongly support the findings that reveal the presence of persistent, long-term (>15 my) nondipolar transitional fields.



**PALEOMAGNETIC FIELD BEHAVIOR 4**

**GA1.03/W/11-B2 1400**

**A DETAILED RECORD OF THE BRUNHES-MATUYAMA TRANSITION FROM A MARINE CLAY OF A 1700-M CORE OF OSAKA BAY, SOUTHWESTERN JAPAN**

Dipak Kumar BISWAS (Graduate School of Science and Technology, Kobe University, Kobe 657-8501, Japan, E-mail: dipak@kobe-u.ac.jp); Masayuki Hyodo (Research Center for Inland Seas, Kobe University, Kobe 657-8501, Japan, E-mail: mhyodo@kobe-u.ac.jp)

A detailed record of the Brunhes-Matuyama transition in a marine clay of a 1700-m core from Osaka Bay, south-western Japan revealed 5 conspicuous reversal episodes: three predating and two post-dating. Using a reasonable constant accumulation rate of 1.4 mm/yr, the mid-ages (duration) of the predating episodes are estimated to be about 3100(420), 800(143), 340(130) yr before the reversal and the mid-ages(duration) of the two post-dating reversal episodes are estimated to be about 370(90) and 1200(220) yr after the reversal. Decrease in field intensity during the transition process was apparently started about 4.6 kyr before the reversal. Highest intensity decay by about 15-20 % of the original value was observed about 2.1 kyr before the reversal. Reversal occurred during a period when intensity was gradually recovering and at the reversal boundary, intensity was about 17 % of its original value. By about 1.2 kyr after the reversal, intensity returned to its original value. The duration of decay and recovery of field strength is about 5.8 kyr

**GA1.03/W/10-B2 1420**

**A LATE HOLOCENE GEOMAGNETIC SECULAR VARIATION RECORD FROM ERHAI LAKE, SOUTHWEST CHINA**

Masayuki HYODO (Research Center for Inland Seas, Kobe University, Kobe 657-8501, Japan, Email: mhyodo@kobe-u.ac.jp); Arata Yoshihara (University of Tokyo); Kenji Kashiwaya (Kanazawa University); Takashi Okimura (Kobe University); Toshiyuki Masuzawa (Nagoya University); Ryotaro Nomura, Shingo Tanaka (Kobe University); Tang Bang Xing, Liu Su Qing, and Liu Shi Jian (Chinese Academy of Sciences, Chengdu, China)

A secular variation record of the geomagnetic field direction for the last 6.5 kyr has been obtained from the magnetization of sediment cores in Erhai Lake, Southwest China. In order to make a comparison with this record, secular variation in east central China was investigated by combining magnetic field data from historical records of observations and archeomagnetic measurements since about 350BC. The secular variation in Erhai Lake shows features consistent with the combined record, except for the oldest three observed declination swings in Sian from 720-900AD. Many features of declination and inclination in China also occur in Japan. From 500 to 1000AD, declination was westerly ranging from about -20 to -5 in Erhai Lake, east central China, and Japan. The three declination data observed in Sian from 720-900AD, which are easterly-ranging from +5 to +15, are probably erroneous.

**GA1.03/W/25-B2 1440**

**A 4-32 KYR BP PSV RECORD FROM LAKE BIWA, JAPAN: IMPRINTS OF AN EXCURSION AT 23000 YR BP**

MOHAMMAD ALI (Geoscience Laboratory, Geological Survey of Pakistan, Shahzad Town, National Park Road, Islamabad, Pakistan., email: ali@gsl.sdnk.undp.org); Y. Kuniko, H. Kitagawa, K. Takemura, A. Hayashida and M. Torii (email: torii@big.ous.ac.jp)

A paleomagnetic record of the geomagnetic field secular variation for the period of 4 to 32 ky bp. has been obtained from a single core sediment recovered from Lake Biwa, central Japan. A total of 615 discrete samples from the core show strong and stable remanence, which is carried by magnetite. Time constraint is provided by the nine radiocarbon age determinations of leaves & total organic carbon (TOC) and five known tephra from the core. Comparison of the top ~5000 years record with the respective period of the Holocene master PSV record shows good agreement of morphology. However the amplitudes are subdued in the present record owing relatively low sedimentation rate of about 40 cm per ky. Our inclination record agrees well in morphology and time frame with the paleomagnetic secular variation (PSV) record from marine sediments off Shikoku Island. Thus for having high resolution and record for both declinations and inclinations the present record could be used for reconstructing chronology of sedimentary records in southwest Japan. We have found anomaly in the direction around 23 ky bp. that has close resemblance with fine details of PSV and virtual geomagnetic poles (VGPs) looping with that of the Mono Lake excursion. Furthermore, correlation with other reported similar excursions around mid-latitude in the northern hemisphere indicate a possible westward drift of non-dipole field at the rate of 2.18 degrees per century.

**GA1.03/W/17-B2 1500**

**HOLOCENE PALEOMAGNETIC SECULAR VARIATION: A MASTER CURVE FOR JAPAN**

MOHAMMAD ALI (Geoscience Laboratory, Geological Survey of Pakistan, Shahzad Town, National Park Road, Islamabad, Pakistan., email: ali@gsl.sdnk.undp.org); H. Oda, H. Kitagawa, A. Hayashida, K. Takemura and M. Torii, (email: torii@big.ous.ac.jp)

Master paleomagnetic secular variation (PSV) curves for different regions are required to date local sedimentary sequences and to use them as source data in geomagnetic modelling. There have been many attempts to develop such curves for Holocene around the world including Japan. The PSV over Japan remains a matter of discussion because of the large discrepancies found in the proposed curves. Recently a development of a composite PSV record from a site in Lake Biwa, central Japan provided a master curve for the Holocene. The composite PSV record based on a total of 1430 samples from three cores, which shows strong and stable remanence carried by pseudo-single-domain magnetite. Paleomagnetic records from the individual cores show little scattering of directions, and excellent correlation among them. The age model is based on two wide-spread tephra layers and nine radiocarbon dates. Our result shows that the declinations and inclinations are strikingly similar to the archeomagnetic data from southwest Japan for last 2000 years. Furthermore, on the basis of this record we are able to resolve the apparent discrepancies observed in so far proposed PSV curves from the region. We can therefore, reliably use the master curve for age estimation of other sedimentary sequences. The record also shows positive correlation with those from the Britain and the western America, suggesting dominance of dipole nature of geomagnetic field for the last 10,000 years.

**GA1.03/W/12-B2 1520**

**PALEOMAGNETIC AND PALEOENVIRONMENTAL HOLOCENE-PLEISTOCENE RECORDS FROM ESCONDIDO LAKE (41° S 71°30'O), PATAGONIA-ARGENTINA**

Claudia S. G. GOGORZA (IFAS-UNCPBA, Pinto 399, 7000 Tandil, Argentina; email: cgogorza@ifas.exa.unicen.edu.ar); Ana M. Sinito (CONICET-IFAS-UNCPBA, Pinto 399, 7000 Tandil, Argentina; email: asinito@ifas.exa.unicen.edu.ar); Juan F. Vilas and María E. Rodríguez (CONICET-Lab. D. Valencio-UBA C. Universitaria, P.2, 1428 Bs. As., Argentina; email: vilas@glg.fcen.uba.ar); Héctor Nuñez and Juan M. Lirio (IAA, Cerrito 1248, Bs. As., Argentina; e-mail: nunez@siscor.bibnal.edu.ar)

This work describes the preliminary results of an investigation on sediments from Escondido Lake in south western Argentina. Four cores up to 12 m long were taken with a push-corer. About 1300 subsamples for paleomagnetic studies were obtained. The intensity and directions of the natural remanent magnetisation were measured using a 2G magnetometer. Isothermal remanent magnetisation curves were obtained using a pulse magnetiser. The directions of the stable remanent magnetisation were compared with previous results obtained from shorter cores from the same lake, extracted by a Mackereth corer. This comparison allowed evaluating the reliability of the results obtained with the push-corer. The sedimentary sequence shows different lithologies related to different environments; they are varves, with isolated clusters, grey clays with thin tephra layers, light brown clays with thicker tephra layers and dark brown clayey mud with abundant organic material. These lithologies have unlike magnetic behaviour.

**GA1.03/E/04-B2 1600**

**DETAILED RECORDS OF RELATIVE PALEOINTENSITY VARIATIONS ACROSS THE LASCHAMP AND MONO LAKE GEOMAGNETIC EVENTS - IMPLICATIONS FOR A STRONGLY DYNAMIC GEOMAGNETIC FIELD**

Norbert R. NOWACZYK (GeoForschungsZentrum Potsdam, Haus C, Telegrafenberg, D-14473 Potsdam, Germany, email: nowa@gfz-potsdam.de)

The Laschamp geomagnetic event is one of the most prominent features in magnetostratigraphic records from northern high latitudes. It could be verified in a region from 69°N, 20°W to 82°N, 110°E. The generally high NRM intensity and a homogenous magneto-mineralogy of the mainly lithogenic sediments of the Norwegian-Greenland Sea and the Arctic Ocean, in combination with minimum or even absent bioturbation, and very low contents of organic matter, that could cause dissolution of magnetite, are ideal conditions for recording high-frequency geomagnetic directional as well as intensity variations. An increasing number of AMS-14C ages and oxygen isotope stratigraphic records now provide a sufficient time frame especially for the younger sediments in order to analyse the documented geomagnetic variations with respect to time. Together with the Mono Lake excursion and other directional fluctuations older than 50 ka the obtained records revealed a strongly dynamic character of the earth's magnetic field with pronounced lows in intensity linked with directional variations, i.e. excursions and polarity events. Only longer events, such as the Laschamp event, are characterized by an increase of relative paleointensity during the reversed state of the geomagnetic field vector.

**GA1.03/E/03-B2 1620**

**A LATE HOLOCENE RECORD OF GEOMAGNETIC SECULAR VARIATIONS FROM LAGO DI MEZZANO, CENTRAL ITALY**

Ute BRANDT, Norbert R. Nowaczyk and Jörg F.W. Negendank (GeoForschungsZentrum Potsdam, Telegrafenberg, D-14474 Potsdam, Germany, email: brandt@gfz-potsdam.de) Antje Ramrath (Dept. of Geography, University of Western Australia, Nedlands, WA6907, Australia)

A high resolution record of geomagnetic secular variation back to 8000 years has been obtained from four, 1.1 m to 26.7 m long, sediment cores from Lago di Mezzano. Dating of the sediments is based on varve counting, interpolated sedimentation rates and AMS-14C-dating on bulk sediment. Intra lake correlation was carried out using the data of continuous high resolution susceptibility measurements. Magnetite in the pseudo-single range was identified as the main carrier of the remanence. AF-demagnetization of the NRM intensity revealed a high stability of the magnetization directions after removing a viscous overprint at 15 mT. The ChRM directions were determined by vector analysis of the demagnetization results. Correlating the records for the single cores with the archaeomagnetic secular variation records from Eastern Europe and France and the records for historical lavas in Sicily, the lock-in time for the sediments investigated could be estimated to be about 300 years. This corresponds with a lock-in depth of 70 cm. The stacked inclination record from Lago di Mezzano generally agrees with those from other sites in Europe, especially with the British mastercurve, the records from the Eifel maars, Germany and from Lake Aslikul, Russia.

**GA1.03/E/05-B2 1640**

**A LACUSTRINE RECORD OF RELATIVE PALAEOINTENSITY FROM LAGO DI MEZZANO, CENTRAL ITALY**

Ute BRANDT, Norbert R. Nowaczyk and Jörg F.W. Negendank (GeoForschungsZentrum Potsdam, Telegrafenberg, D-14474 Potsdam, Germany, email: brandt@gfz-potsdam.de)

Two 27 and 17 m long sediment cores from Lago di Mezzano (central Italy) were subjected to detailed palaeo- and rockmagnetic investigations in order to obtain a high resolution record of relative palaeointensity for the last 31 ka. The investigations comprise magnetic susceptibility (kLF), ARM and IRM acquisition, hysteresis loops and backfield as well as thermomagnetic measurements. Magnetite in the pseudosingle to multidomain range was identified as the main carrier of the remanence. The relative palaeointensities were estimated normalizing the NRM intensities after demagnetization at 20 mT by kLF, the ARM intensities at the same demagnetization level and the SIRM, yielding not only slightly differences between the curves obtained by different methods, but also between the results of both cores. Those differences could clearly be attributed to changes in the relative grain size of the magnetite as reflected by the ratio kARM/SIRM due to sedimentation and dissolution processes. A new method was developed to eliminate the influence of the grain size of the remanence carrier in order to stack the records of relative palaeointensity obtained for both cores. The reconstructed palaeointensity record for Lago di Mezzano generally agrees with those from other sites around the globe.

Wednesday 28 July AM

Presiding Chairs: M Kono (Inst. Study Earth Int, Okayama Univ., Japan) and V Pavlov (United Institute of the Physics of the Earth, Moscow, Russia)

**PALEOMAGNETIC FIELD BEHAVIOR 5**

**GA1.03/W/22-B3**

**0900**

**A RIGOROUS STATISTICAL APPROACH TO PALEOMAGNETIC FIELD MODELLING**

A.KHOKHLOV (International Institute of Earthquake Prediction Theory and Mathematical Geophysics 79, b2, Varshavskoe shosse 113556 Moscow, Russia, email: khokhlov@mitp.ru); G. Hulot, J. Carlot, V. Courtillot (Institut de Physique du Globe de Paris, 4, Place Jussieu, 75252, Paris, France, email: gh@ipgp.jussieu.fr)

Modern studies of the paleomagnetic field behaviour in the recent past (0-5 M.y), all rely on statistical analysis of mainly directional data randomly distributed in both time and space. Such studies are not as straightforward as one would wish. The data is quite sparse and ill distributed. In addition, directional parameters are non-linear and correlated functions of the local field. Up to now these difficulties have usually been ignored or taken into account by relying on some simplification (linearization, neglecting of internal correlation, etc). Such approximations can be justified only if the field behaves in a simple way but not if the field contains some amount of complexity. Whether this is the case, is a matter of current debate and it would therefore be desirable to propose a rigorous statistical approach to the problem. The purpose of the present paper is precisely to present such an approach based on standard tools in Information Theory. It is designed to test any statistical model of the paleomagnetic field against any given dataset of directional data, when the field model is being defined in terms of the statistical behaviour of its Gauss coefficients (along the lines pioneered by Constable and Parker in 1988). This approach can equally be used to test the models on a site by site basis, or on regional and global scales. Examples of tests will be provided.

**GA1.03/W/02-B3**

**0920**

**CORRELATION FUNCTIONS BETWEEN HOLOCENE PALEOMAGNETIC SECULAR VARIATIONS TO SYNTHETIC SECULAR VARIATION CAUSED BY A DRIFTING RADIAL DIPOLE**

Chizu ITOTA (Department of Management Information, Osaka College, Mihara, Osaka 587-8555, Japan, email: citota@osaka-c.ac.jp)

Correlation functions between Holocene paleomagnetic secular variation records from Japan, Britain and North America and synthetic secular variations caused by a single drifting radial dipole of various drifting rates were calculated. The radial dipole of fixed intensity located at the core surface was drifted westward along the equator. The synthetic data were obtained by the geocentric axial dipole and the radial dipole drifting from +90o to -90o to the longitude of the observing site. Drifting rates were set to 0.36 - 0.09o/yr. In the results, good correlations are observed between the paleomagnetic records and the synthetic data of some rates for the three sites. In Japan, a synthetic variation, which a radial dipole was pointing upward and its drifting rate was 0.2o/yr, showed a good correlation to the paleomagnetic record at 3250yrBP. In Britain, the variation, which a radial dipole was pointing downward and the rate was 0.3o/yr, was correlated well at 2250yrBP. Furthermore, in North America, the synthetic variation caused by an upward-pointing radial dipole with drifting rates both at 0.15o/yr and 0.3o/yr were correlated at 8500 and 6100, and 1850yrBPs, respectively. These results may indicate that a maximum or minimum focus of non-dipole field passes through the sites' meridian at the time when the maximum correlations were obtained. Unfortunately, peaks of these correlation functions among sites considered them as introduced by the same radial dipole were not observed.

**GA1.03/W/16-B3**

**0940**

**PLUNGE AND AZIMUTH - AN ALTERNATIVE WAY TO REPRESENT THE DIRECTION OF THE MAGNETIC FIELD**

Masaru KONO (Institute for the Study of the Earth's Interior, Okayama University, Misasa, Tottori-ken 682-0193)

Paleomagnetic directions are almost always described by inclination and declination. With the addition of the intensity, they form the spherical co-ordinates, which can easily be converted to any other co-ordinates, such as cartesian elements. As representations by any co-ordinate system is equivalent, inclination-declination representation is satisfactory to represent the direction of the field as any other co-ordinates. This does not apply when we have statistically distributed data, which is usual in paleomagnetism. As is well known, the mean of inclinations are always biased, while declination loses much significance when we are dealing with high-latitude data. Kono (PEPI, 1997) proposed the use of two alternative angles plunge and azimuth. While inclination and declination are defined with the coordinate axis in the vertical direction, plunge and azimuth have the co-ordinate axis in horizontally east west. As the field is quite unlikely to be near this co-ordinate axis, plunge and azimuth co-ordinates are not plagued by the singularity associated with the axis. The use of these two angles is particularly useful in paleosecular variation studies.

**GA1.03/W/21-B3**

**1000**

**STATISTICAL ANALYSIS OF CENOZOIC VGP AND MODELS OF GEOMAGNETIC FIELD DURING POLARITY INVERTIONS**

Mabel MENA (CONICET- Fac. de Cs. Exactas y Naturales- UBA- Ciudad Universitaria - Pab.2, 1428 Ciudad de Buenos Aires, Argentina, email: mena@tango.glfen.uba.ar); Ana M. SINITO (CONICET- IFAS - UNCPBA - Pinto 399, 7000 Tandil, Argentina, email: asinito@ifas.exa.unicen.edu.ar)

To study the behaviour of the geomagnetic field during polarity transitions, an statistical analysis of cenozoic VGP positions was carried out. Data from the Blake event and all transitions from the last 5MA, registered in the Global Paleomagnetic Database (McElhinny & Lock, 1996) were analysed. Those VGP were obtained from volcanic and sedimentary rocks as well as deep marine sediments from sites spanning the 360° of longitude. To perform this analysis the VGPs were classified in 12 latitude stripes of 15° each. A test for uniform distribution of longitudes was rejected in most cases for the stripes between latitudes of +60° and -60°. An analysis of the shape of longitude distribution using eigen values shows that the stripes ranging between latitudes of +30° have the best defined bipolar distribution with maximal around 300° and 120° meridians. A simple morphological model of geomagnetic field, consisting of two centred oblique dipole with magnetic poles at about 60oN, 120oE and 60oN, 300oE, respectively, which change their intensities sinusoidally and have an additional small precession around the mean position is postulated. This model suggests the existence of two equally stable states when both dipoles have the same polarity, and unstable states when dipoles have opposite polarities. The main implications of this model are that VGPs recording excursions describe similar paths and that the patches suggested by Hoffman agree with the pole positions of both dipoles.

**GA1.03/W/26-B3**

**1040**

**DIPOLE NATURE OF PALEOMAGNETIC FIELD OBSERVED IN THE SHAPE OF ANGULAR DISPERSION**

Hidefumi TANAKA (Faculty of Education, Kochi University, Kochi 780-8520, Japan, email: hidefumi@cc.kochi-u.ac.jp)

Paleomagnetic secular variation (PSV) from lavas shows latitude dependent variation of angular standard deviation (ASD); the higher the latitude, the smaller in field directions and the larger in VGP positions. On the other hand, distribution is distorted when field is transferred to pole or vice versa, as mathematical formulation was given by Cox (1970). Only a few authors, however, payed attention to the shape of distribution of paleomagnetic field.

This study applies a Bingham statistics to paleomagnetic dataset from lavas for the last 5 my, and studies the shape of distribution in field and VGP. When data of distinct site is examined, dataset from Hawaii clearly shows an oval shaped distribution of field directions, elongated along a plane of the meridian, while distribution of VGP is almost circular. This indicates that most of PSV at Hawaii was caused from a dipole wobble. This tendency is also observed in the combined data along a latitudinal band of lower latitude. Although this elongated shape in field distribution is not clear for most of distinct site data, anisotropy analysis of the distribution depict this feature at almost all sites.

**GA1.03/W/34-B3**

**1100**

**CORRELATION BETWEEN VARIATION OF GEOMAGNETIC FIELD PALAEOINTENSITY AND THE EARTH'S ROTATION RATE IN THE PHANEROZOIC**

V. P. APARIN (Inst. of Physics SB RAS, Krasnoyarsk, Russia, 660036, email: dir@iph.krasnoyarsk.su); V. T. Sarychev (Tomsk State University, 634050, Russia); M. V. Kiselev, N.Y. Romanova, V. V. Vilisov (All of Krasnoyarsk State University, 660071, Russia)

Phanerozoic time series of geomagnetic field palaeointensity (Ha) and angular rate of the Earth's rotation (W) were approximated by cubic splines and are underwent to spectral analyses by new modification of maximum entropy method. Cycle about 250 Myr is revealed in Ha(t) and W(t) variations. Cycle about 700 Myr is shown in the Earth's rotation. Negative correlation between Ha(t) and acceleration of the Earth's rotation suppose the existence of whole regulation mechanism of these two processes. Probably main contribution belongs here to mantle convection, which by means of plate kinematics change the Earth's rotation and geomagnetic field generation.

**GA1.03/E/01-B3**

**1120**

**AN APPROACH TO REGIONALLY MODELLING THE GEOMAGNETIC FIELD FOR EUROPE FROM DIRECTIONAL ARCHAEOMAGNETIC DATA**

J. Miquel TORTA, Lluís Gaya-Pique (Observatori de l'Ebre, CSIC, 43520 Roquetes, Tarragona, Spain, email: ebre.jmorta@readysoft.es); Juan I. Nunez, Maria L. Osete (Departamento de Física de la Tierra, Astronomía y Astrofísica, Universidad Complutense de Madrid, email: juanig@eucmos.sim.ucm.es); Angelo De Santis (Istituto Nazionale di Geofisica, email: desantisag@ing750.ingrm.it)

The recent compilations of declination and inclination data obtained from baked archaeological materials offer an unprecedented opportunity for advances in the analysis of the spatial-temporal behavior of the ancient magnetic field. However, the temporal and, especially, the spatial distributions of these data are far from being uniform and they only allow for very low degree spherical harmonic models to be determined. In Europe, the density of these records is greater than anywhere else in the world, so that smaller scale features can be represented by means of an appropriate regional modelling scheme. The results from the few previously determined low-degree global models are used to provide the necessary boundary conditions to fill-in an adequate spherical cap region, and a time-varying spherical cap harmonic analysis has been attempted, first for the centuries bracketing the Roman Epoch, and afterwards from that epoch to recent. Geographical and age distribution of the data set is still very uneven but our results suggest that, at least for Europe, some of the nondipole archaeomagnetic field can be discriminated.

**GA1.03/E/02-B3**

**1140**

**ON APPLICATION OF WAVELET ANALYSIS TO GEOMAGNETIC POLARITY TIME SERIES**

Maxim RESHETNYAK, Vladimir PAVLOV (United Institute of the Physics of the Earth, Moscow, Russia, 123810, email: pavlov@uipe-ras.scgis.ru and rm@uipe.srcc.msu.su)

Usually, the analysis of the geomagnetic time scale reduces to investigation of the reversals frequency (e.g., Mazaud et al., 1983), or to distribution of the lengths of magnetozones of constant polarity proposed by Gallet & Hulot (1997). Nevertheless, the signal of polarity itself contains much more information, which can be useful for understanding of the geodynamo process nature. The difficulty of direct application of the Fourier or MEM analysis is concerned with the fact that the signal of polarity P is a step function: P(t)=+/- 1, and the traditional approaches leads to existence of artificial noise in the spectra. On contrary, the wavelet approach looks to be a good candidate for this purpose. We present the wavelet analysis of the geomagnetic polarity signal over the last 165Ma. Using the additional information about paleointensity of the magnetic field (Perrin & Shcherbakov, 1997), we distinguish the four different regimes of geomagnetic field generation. The scenario of the geodynamo system evolution in terms of aw-model (Pechersky et al., 1998) is discussed.

Wednesday 28 July PM

Presiding Chairs: P P Kruijer (Fort Hoofddijk, Utrecht University, Utrecht) and C G Langeris (Fort Hoofddijk, Utrecht University, Utrecht)

**PALEOMAGNETIC FIELD BEHAVIOR 6**

**GA1.03/W/30-B3**

**1400**

**ARCHAEOINTENSITY DATA CORRECTION FROM GREEK CERAMICS**

V.SPATHARAS1 and N.Jordanova2 1-(Dept.Of Geophysics, Aristotle University of Thessaloniki) 2-(Geophysical Institute, Bas, Bulgaria)

It is known that in an isotropic medium the direction of a remanent magnetization vector coincides with the direction of the ancient magnetic field. But in the case of a significant anisotropy, it is necessary to involve a correction factor in order to obtain the true direction of the ancient field. The causes of magnetic anisotropy of rocks have been summarized by Hrouda (1982) and are related, among others, to shape, lattice or magnetic domain alignment. It has been shown (Aitken et al., 1981) that ancient ceramics exhibit significant magnetic anisotropy due to the way in which they have been manufactured and explained by the "easy



plane" of magnetization. The detection of this anisotropy and the calculation of an "anisotropy factor" are of crucial importance during Thellier experiments aiming to the determination of the ancient geomagnetic field. Pottery as well as bricks anisotropy affect the direction and the intensity of the NRM. After Thellier's experiment for the definition of archaeointensity into 12 samples for which we obtained good results, we made an attempt to study the effect of the texture's anisotropy as well as to calculate the coefficient for the correction of the archaeointensity. The calculation of the anisotropy parameters as well as that of the magnetic susceptibility is done by the device of the K-bridge according in the methodology suggested by Jelinek (1977). Stephenson et al (1986) show that IRM and TRM anisotropy ellipsoids are of identical shape. We used this result to apply the method for correcting archaeointensity, proposed by Veitch et al. (1984). The rates of the parameter  $P'$  are high, those rates become bigger after Thellier's experiment (during the whole experiment, we studied the change of the magnetic susceptibility). For the studied collection the correction factor (f) varies from 0.90 to 1.05 for bricks and from 0.93 to 1.27 for pottery. The internal agreement among the archaeointensity results improves after applying the correction for anisotropy.

**GA1.03/W/20-B3 1420**

**PALAEOMAGNETIC RECORDS WITHIN ISOTOPE STAGE 9 TRAVERTINES FROM BAD CANNSTATT, GERMANY.**

STEVE OPENSHAW, John Shaw, David Heslop (Geomagnetism Laboratory, Department of Earth Sciences, Oliver Lodge Laboratories, Peach Street, Liverpool, L69 7ZE. UK, email: steveo@liv.ac.uk); and Ulrich Hambach (Universitat zu Koln, Zulpicher Str 49a, D-50674 Koln, Germany, email: Uli.Hambach@uni-koeln.de).

Travertine is a calcium carbonate deposit produced when CaCO<sub>3</sub> saturated groundwaters reach the open environment and precipitate hard crystalline carbonate through CO<sub>2</sub> degassing. In temperate regions travertine deposition is thought to coincide with the warmer and wetter phases of glacial / interglacial cycles and in addition lamination within travertine deposits may represent seasonal climatic variation. We have begun a study of several travertine deposits in Germany including massive sheet deposits and a 30-40cm thick annually laminated deposit in a Roman water pipe representing around 200 years of continuous precipitation. We aim to develop magnetic characterisation parameters for both the magnetic recording processes and to enable palaeo-environmental reconstruction. We present here preliminary palaeomagnetic results from a 26m thick deposit of travertine found in a quarry on a river terrace of the River Neckar at Bad Cannstatt, Stuttgart. TIMS uranium-series dating suggests deposition over the period of MIS stage 9 (300 kyr). The lower travertine is broken by three thin (~1m) loess layers which represent shorter periods of cooling and termination of travertine deposition. Alternating Field (AF) demagnetisation yields stable, single component remanence vectors which are easily measurable on a LN<sub>2</sub> SQUID magnetometer despite being magnetically very weak (6-30 x10<sup>-8</sup> Am<sup>2</sup> kg<sup>-1</sup>).

**GA1.03/W/14-B3 1440**

**A GEOMAGNETIC EXCURSION OBSERVED IN A TRAVERTINE-COMPLEX FROM STUTTGART - UNTERTUERKHEIM (GERMANY)**

Jan REINDERS and Ulrich Hambach (Department of Geology, University of Cologne, Zulpicher Str. 49 a, 50674 Cologne, Germany, email: jan.reinders@newmail.net)

The Biedermann-travertine is situated on a river Neckar terrace. U-series dating of the complex suggests that it grew from 109 to 101 ka bp with a rate of 0.91 mm/year (Frank et al. subm. Quat. Res.). Oriented samples were taken from a 7.5 thick section, and three 1.0 m thick parallel sections (2.5 cm average spacing). Rock magnetic investigations indicate that the mineral magnetic assemblage consists of varying relative amounts of maghemite and hematite. Alternating field demagnetization reveals a stable, characteristic remanent magnetization (ChRM) after 27mT. The high fidelity of the paleomagnetic signal is corroborated by the good correlation of the ChRM amongst parallel sections, laterally (contemporary) differing paleo-environmental conditions. The Biedermann-paleofield record (BM-PFR) suggests that a reversed stationary flux patch north of the observation site predominates from 105.0 - 102.0 ka bp. It culminates in an excursion of the geomagnetic field between 103.0 and 102.6 ka bp. A geomagnetic field model derived from the BM-PFR and literature data favours a regionally restricted efficiency of the reversed flux and puts forward transitional field models inhibiting a temporary predominance of non-dipole components.

**GA1.03/W/09-B3 1520**

**PALEOMAGNETIC REVERSALS IN AN ARCHEAN BANDED IRON FORMATION AND POSSIBILITIES OF THEIR ORIGIN**

Tadahiro HATAKEYAMA, Ikuro Sumita and Yozo Hamano (Univ.of Tokyo, Japan)

For an Archean banded iron formation (BIF) outcropped in the Cleaverville region (ca. 3.3Ga) of the Pilbara craton, north Western Australia, we have made paleomagnetic and rockmagnetic measurements and have obtained following results: (1) the main ferromagnetic mineral and remanence carrying mineral is hematite, (2) most of the specimens have single components of the natural remanence and (3) many paleomagnetic reversals were discovered. The smallest scale of the one magnetic polarity is less than the size of specimen; about 1cm, which is larger than the thickness of the visible bands ("mesobands") which is generally several millimeters. However, the paleomagnetic results from two columns 2m apart from each other show that the distribution of the magnetic polarities from these columns do not coincide but seem shifted. From these results two or more possibilities of the origin of the characteristic remanent magnetization can be considered; one is depositional origin; DRM, PDRM or CRM in the process of the deposition-diagenesis in the Archean era, the other is due to weathering (lateritization) where secondary CRM was acquired after the upheaval and long after the deposition. From the measurements of paleomagnetism and rockmagnetism, we discuss how we can constrain the origin of the remanent magnetization.

**GA1.03/W/15-B3 1540**

**PALEOSECLAR VARIATION DURING THE KIAMAN REVERSED SUPERCHRON**

PP. KRUIVER, C.G. Langereis, M. J. Dekkers (Paleomagnetic Laboratory Fort Hoofddijk, Utrecht University, Budapestlaan 17, 3584 CD Utrecht, The Netherlands, e-mail: kruiver@geo.uu.nl)

The Permian red beds of Dôme de Barrot (Southern France) were deposited during the Kiaman Reversed Superchron near the paleo-equator. The natural remanent magnetisation (NRM) of these sediments resides in hematite. It is very resistant against both alternating field and thermal demagnetisation. Thin section studies suggest that the hematite is of primary origin. The patterns and amplitudes observed in declination and inclination resemble those of present-day secular variation. The high magnitude of paleosecular variation (PSV) during a Superchron contrasts with current dynamo theories which suggest that the magnitude of PSV is argued to be less in the stationary mode of the geomagnetic field.

To verify secular variation during a Superchron, an accurate time control is required. This is hampered by the absence of fossils and the single polarity. However, the cyclic sedimentation pattern of red and purple layers provides control on duration, if we assume that these cycles are caused by climate (Milankovitch) forcing. We argue the probability of Milankovitch cycles in the ed beds on the basis of (spectral analyses of) sedimentological, magnetic and other data.

**GA1.03/W/18-B3 1600**

**SHORT GEOMAGNETIC EVENT RECORDED IN CHINESE LOESS-SOIL SEQUENCES**

Guo BIN (Institute of Geophysics, Chinese Academy of Sciences, Beijing 100101, China, email: guobin@mail.c-geos.ac.cn.); Lin Mian (Institute of mechanics, Chinese Academy of Sciences, Beijing 100080, China)

The nature of geomagnetic field behavior during polarity transitions is one of the most highly debated issues in modern geophysics. The detailed study of geomagnetic reversals and excursions has provided some insights on fluid motion in the Earth's core. Since the short geomagnetic event within the Jaramillo normal subchron had been discovered in the Wanganu Basin, New Zealand, the similar phenomena had also been uncovered in the Weinan and Jiuzhoutai, China. Its global nature and even their existence, however, are still debated. Recently, the detailed rock magnetic and paleomagnetic investigations had been carried out in Chinese loess-paleosol sequences at Jinbian (37.4°N, 108.8°E), China. It has been shown that both loess and paleosol in the northern margin of the Chinese loess plateau can capture geomagnetic variation during the polarity transition, also that a reversal bounding the onset of a reversed-polarity zone within the Jaramillo normal subchron was recorded. Rock magnetic and paleomagnetic studies demonstrate that this short-term feature is geomagnetic signals, rather than artefacts. The relative paleointensity records determined also confirm that the weakest geomagnetic field intensity correspond to the short-term feature. Therefore, we conclude that this short-term feature is an independent geomagnetic event. The statistical analysis reveal that the VGP paths of the short geomagnetic event are predominantly situated in the longitudinal sector over the America continent and its antipodal longitudes, while the VGP paths of upper Jaramillo recorded in the same loess-paleosol sequence exhibits a tight cluster located at western Australia. It suggests that the transitional field is very complex, VGP paths for

**GA1.07 Tuesday 27 July**

**SEPARATION OF INTERNAL AND EXTERNAL FIELD VARIATIONS**

Location: Muirhead Tower 112 LR2  
Location of Posters: Student Room (1st floor)

**Tuesday 27 July AM**

Presiding Chairs: N.Olsen (Danish Space Research Institute, Copenhagen), B.Arora (Indian Institute of Geomagnetism, Colaba, Mumbai)  
Concurrent Poster Session

**SEPARATION OF INTERNAL AND EXTERNAL FIELD VARIATIONS**

**GA1.07/W/03-B2 0900**

**A PROBLEM IN USING SPHERICAL CAP HARMONIC ANALYSIS TO SEPARATE INTERNAL AND EXTERNAL FIELDS**

Frank LOWES (Physics Department, University of Newcastle, Newcastle Upon Tyne NE1 7RU, UK, e-mail: f.j.lowes@ncl.ac.uk)

Spherical Cap Harmonic Analysis (SCHA) is useful when analysing data available only over a limited area on the Earth's surface, but it does have limitations when used for separation of the observed surface field into its parts of internal and external origin. Such separation involves (in effect if not explicitly) comparing the results of separate analyses of the horizontal and vertical parts of the field vector. In this context, analysing the horizontal component is essentially the same as making a least squares' fit to the scalar potential, while analysing the vertical component involves a least squares' fit to the radial derivative of the potential. However, even if all the field were of, say, purely internal origin, SCHA will give different solutions for the potential for these two situations, so a separation analysis would wrongly indicate the presence of a significant contribution of external origin. So in a real situation significant errors could be expected. A simulation was done using a model of the surface Sq over a 50 degree polar cap. Although the total (internal + external) field was fitted to 0.1%, the separated internal/external fields had errors ranging from 10 to 40%. It is therefore doubtful if the results of such an analysis are very useful. This problem is not unique to SCHA, but will occur in any method which uses observations over only a small part of the surface.

**GA1.07/W/05-B2 0920**

**DIFFERENTIAL VECTOR MAGNETOMETRY (DVM) - A NEW METHOD FOR REMOTE DETERMINATION OF MAGNETIC PROPERTIES OF ANOMALY SOURCES AND IMPROVED DRILL TARGETTING**

David A. CLARK (CSIRO Exploration and Mining, PO Box 136, North Ryde NSW 1670, Australia, email: d.clark@syd.dem.csiro.au); Phillip W. Schmidt, David A. Coward and Mark P. Huddleston (all at CSIRO Exploration and Mining, PO Box 136, North Ryde, NSW 1670, Australia)

The local perturbation of the geomagnetic variations arising from a subsurface magnetic body can be determined by simultaneous monitoring of geomagnetic variations at two sites: one within the static magnetic anomaly associated with the body and another at a remote base station. Monitoring of all three field components at the on-anomaly and base stations allows the components of the second order gradient tensor of the anomalous pseudogravitational potential to be determined. This tensor depends only on the source geometry and the measurement location and is independent of the nature (remanent or induced), magnitude or direction of the source magnetisation. Without making any assumptions about source geometry or location, the Koenigsberger ratio (Q), the direction of remanence and the direction of total magnetisation can be obtained from the components of this tensor. This information can constrain magnetic modelling prior to drilling and remove a major source of ambiguity in magnetic interpretation. The direction to the centre of a compact source can be determined directly from diagonalisation of the tensor. Values of Q constrain the magnetic mineralogy of the source and the remanence direction can discriminate sources of different ages or geological histories. Thus the method can also alleviate the geological ambiguity that afflicts magnetic interpretation. Field trials of differential vector magnetometry (DVM) at several sites, including the Tallawang magnetite deposit, New South Wales, have demonstrated the validity of the proposed in situ method. However, a number of technical difficulties must be resolved before this method can be used routinely.



GA1.07/W/01-B2

0940

## SEPARATION OF THE MAGNETIC FIELD INTO EXTERNAL AND INTERNAL PARTS AT THE SURFACE OF PROLATE SPHEROID

ZVEREVA Tatjana I (Institute of Terrestrial Magnetism, Ionosphere and Radio Wave Propagation, Troitsk, Moscow Region, 142092, Russia, email: golovkov@izmiran.rssi.ru)

We solve the problem of separation of a magnetic field, measured at the surface of a body having the special form of a prolate spheroid, into two parts, one of which is external with respect to this body while the other is its own magnetic field. This problem is considered in the orthogonal co-ordinate system of a prolate spheroid where this body is one of co-ordinate surfaces. By presenting of the solution of the Laplace equation in this co-ordinate system in the form of an infinite series of expansion in terms of spheroidal functions, separation of the field into the external and internal parts is carried out formally, but mathematically correctly, without dwelling on its origin. The results may be used in magnetic cartography and magnetic navigation.

GA1.07/E/02-B2

1000

## PRINCIPAL COMPONENTS ANALYSIS OF THE (INTERMITTENT) GLOBAL GEOMAGNETIC OBSERVATORY ARRAY

Gary D. EGBERT (College of Oceanic and Atmospheric Sciences, Oregon State University, 104 Ocean Admin. Bldg, Corvallis, OR 97331, e-mail: egbert@oce.orst.edu)

Magnetometer arrays are inevitably sparse and/or of limited spatial extent. As a result, direct application of formulae from classical potential theory to separate the observed fields into internal and external components is generally problematic. We discuss a statistical approach to this problem based on generalised (multivariate) transfer function methods. In essence, the idea is to take advantage of the very different properties of internal and external sources. Internal sources are inhomogeneous, and are largely determined by conductivity variations of fixed geometry inside the earth. Geometries of external sources are generally more transient, and, in a time averaged sense, often exhibit some degree of statistical homogeneity. (E.g., the statistical properties of external parts of daily variations should be approximately independent of absolute longitude.) Without making any specific assumptions about internal and external sources, a principal components (or EOF) analysis can generally be used to project the observed data (internal+external) onto a small set "array modes". This initial step greatly facilitates separation, by reducing noise and allowing us to more reasonably impose a priori constraints on the external portion of the projected data. These constraints can be hard (assuming a simple form for external sources) or soft (assuming a semi-homogeneous statistical model for sources). We consider application of these ideas to the global array of geomagnetic observatories. To allow for the many data gaps in the observatory record we have developed specialised EOF methods. These allow us to provide a characterisation of statistically averaged global source geometries which makes use of a large part of the historical observatory data base. Application to geomagnetic induction studies of deep mantle conductivity will be considered.

GA1.07/E/01-B2

1020

## ELECTROMAGNETIC RESPONSE AND SOURCE FIELD CHARACTERISATION FROM MERIDIONAL CHAIN OF GEOMAGNETIC OBSERVATORIES

B.R. ARORA (Indian Institute of Geomagnetism, Colaba, Mumbai 400 005, India, e-mail: bra@iig.iigm.res.in)

With a purpose to estimate electromagnetic (EM) response of the Earth at long periods, the space-time characteristics of natural EM sources are established by subjecting the geomagnetic field variations for a dense chain of geomagnetic observatories along the Indian-Russian sector to Singular Spectrum Analysis and Principal Component Analysis. The alignment of geomagnetic observatories along a single meridian, extending from equator to the pole, is used to test the assumption of zonal morphology for each principal component describing the spatial structure of the fields at a given period. Besides facilitating separation of long period geomagnetic field into external and internal parts, the approach helps to isolate sources not compatible with zonal approximation. The possible contamination of the EM response function from sources other than zonal terms, is evidenced by the marked differences in the single-station response function using both the Z.Y and Z.H. The contamination resulting from the near-surface conductivity structures also hamper the reliable estimation of the EM response functions. The results show that effects of localised sources and continuation from lateral conductivity contrast, if not guarded for, lead to totally spurious model of electrical conductivity structure. The significance of establishing the source characteristics in deriving EM response free from the source field structure and lateral conductivity continuation is discussed.

GA1.07/W/04-B2

1100

## USES OF SATELLITE DATA FOR SEPARATION OF INTERNAL AND EXTERNAL SOURCES IN GEOMAGNETIC FIELD MODELLING

Benoit LANGLAIS, Pascale Ultré-Guérand and Mioara Manda Alexandrescu (Institut de Physique du Globe de Paris 4 Place Jussieu 75252 Paris Cedex 05 France email: langlais, ultre, mioara@ipgp.jussieu.fr)

Satellite measurements are an important source of data for improving our knowledge of the Earth's magnetic field. Oersted has been launched in January 1999 and several others are planned in the next few years (e.g. SAC-C, CHAMP). There have been no reliable vector measurements by satellite since MAGSAT, which operated for six months in 1979/1980 with a tri-axial magnetometer. In this study we compute geomagnetic field models by using MAGSAT data together with hourly means values of observatories for the same epoch. In this kind of study, the crucial point is the separation of external sources, i.e. ionospheric and the magnetospheric fields from internal ones. Indeed, satellite measurements are made above ionospheric currents, which can then be described as internal sources. Furthermore, internal and external fields are not fixed by the same parameters: the internal part is fixed by geographic location, while the external part is fixed by both dipole and sun location. So we have to take into account the periodic variations of the external fields (from diurnal to yearly variations). A geomagnetic potential is used in the spherical harmonic expansion in order to separate the ionospheric contribution from the internal (core and crust) and the external (magnetosphere) sources. We discuss of quiet-time data selection, using geomagnetic activity indices, and especially those computed by sectors of longitude. Moreover, we show that the magnetospheric contribution and the corresponding induced effects can be estimated by using a linear relationship between the first degree Gauss coefficients of the external and internal field, and the Dst indices.

GA1.07/P/01-B2

1120

## SOURCE CONSIDERATIONS FOR ELECTROMAGNETIC RESPONSE ESTIMATES WITH GEOMAGNETIC SURFACE DATA

Ulrich SCHMUCKER (Geophysikalisches Institut, Herzberger Landstr. 180, D-37075 Göttingen)

While in magnetotellurics source effects are of second order and thus are usually ignored, knowledge about the inducing source geometry may be essential for response estimates from geomagnetic observations alone. Three alternative methods exist for deriving such responses: (i) The source geometry is given a single-term description, in spherical or Fourier spatial harmonics, and responses are derived from local Z:H or Z:D ratios.

(ii) A single or multiple-term description is used in conjunction with a separation of external and internal parts, yielding from their relationship global response estimates.

(iii) Ideally, source and response informations should be derived in a single computational process which on a regional scale can be achieved with the gradient method, based on relations between local Z and spatial derivatives of H and D. As a rule, in this third approach no attention is given to the implications of the inserted spatial derivatives with respect to meaningful source geometries.

Each of the three approaches has its own problems. In local responses the observed H:D relation may be in conflict with the single-term description, in global responses information about radially symmetric Earth models may be mixed with that of large-scale deviations from such symmetry and the same applies on a regional scale to results obtained with the gradient method. - An attempt is made to interconnect the approaches. Since separations into external parts are without any restrictive assumptions (except that the source is tangential-electric and quasi-stationary) and since the derivation of external parts is a fairly stable process, the external source geometry of various well defined types of variations are combined with first order layered Earth models to derive H:D relations and spatial gradients of H and D, which are consistent with such sources and of sufficient general validity to be utilised, when no global data are available for a separation analysis.

GA1.07/E/03-B2

1140

## A ZONALLY DOMINANT STOCHASTIC PROCESS ON THE SPHERE FOR STATISTICAL MODELING OF LONG-PERIOD EXTERNAL SOURCE FIELDS

Gary D. EGBERT (College of Oceanic and Atmospheric Sciences, Oregon State University, 104 Ocean Admin. Bldg, Corvallis, OR 97331, e-mail: egbert@oce.orst.edu)

Long period ( $T > 1$  day) external magnetic source fields are dominantly (but not exactly) zonal, and fluctuate over time. I consider here stochastic processes on the sphere suitable for modelling the spatial behaviour of these fields. By constructing the process as a superposition of purely zonal random processes with randomly varying axes of symmetry, an inhomogeneous (but not-overly parameterised) random process on the sphere can be generated which has many properties in common with the external source variations observed on the real earth. The random process (which is motivated by the observation that there is no single, well-defined axis of symmetry for external source processes), is zonally dominant, but not exactly zonal; the most extreme departures from zonal dominance occur at high latitudes, around the mean symmetry axis. I will discuss procedures for fitting free model parameters, and the adequacy of the model in describing the spatial statistics of hourly mean observatory data. Application of the model as prior information to improve separation of internal and external field components will be discussed.

GA1.07/W/06-B2

1200

## SQ STUDIES ON A GLOBAL SCALE - INDUCTION IN A 3D EARTH

GRAMMATIKA, Nafsika (UBO-IVEM, UMR Domaines Oceaniques, Place Nicolas Copernic, Plouzane Email: naphsica@sdt.univ-brest.fr)

The first global analysis of the solar magnetic tide was that of Schuster(1889) based on a spherical harmonic analysis of magnetic daily variations. This method assumes that the daily variation is dependent on local time alone, its relation to the universal time UT being identified to the dependence on longitude. With the aim of describing the Sq field globally as closely as possible, we discuss two different methods for the determination of the spherical harmonic coefficients. Observatory data acquired during the period of the Magsat mission is used. In one method, the spherical harmonic coefficients are estimated by a singular value decomposition method. In the second method, the spherical harmonic coefficients are estimated using a MCMC (Monte Carlo Markov Chain) method. In the latter, the result is described in terms of a posteriori probability density function of the coefficients which is the invariant probability of the Markov chain. It is estimated by means of the average of the transition probabilities of the Markov Chain. The internal field induced by the estimated Sq variation is calculated, at Magsat local times and for a selected range of Magsat altitudes, using a heterogeneous earth model, dominated by the electrical conductivity contrast between the oceans and the continents. The calculated total field is compared to Magsat observations.

GA1.07/W/07-B2

1220

## SPHERICAL CAP HARMONICS ANALYSIS OF GEOMAGNETIC VARIATIONS OVER HIGH LATITUDES

Irina A. Burdelnaya, Vladimir GOLOVKOV and Tatjana I. Zvereva (all at Institute of Terrestrial Magnetism, Ionosphere and Radio Wave Propagation, Troitsk, Moscow Region, 142092, Russia, e-mail: golovkov@izmiran.rssi.ru); Vladimir O Papatashvili\*, O Rasmussen, and P Stauning (all at Danish Meteorological Institute, Lyngbyvej 100, DK-2100, Copenhagen, Denmark, e-mail: vp@dmu.dk; \* also at SPRL, University of Michigan)

The complexity of ionospheric current systems and insufficient network of polar magnetic observatories makes difficult to model magnetic variations at high latitudes. Combining observatory data with the low-altitude satellite surveys, researchers are able, at least, to obtain realistic distributions of high latitude magnetic variations and then apply various techniques for their modelling. The proposed algorithm for that kind of modelling is a two-step approach. First, the 1-min data from magnetic observatories are utilised in the framework of the Natural Orthogonal Component (NOC) algebra. Then the obtained models of magnetic variations for each observatory are subjected to the Spherical Cap Harmonics Analysis (SCHA) together with existed magnetic satellite data. Presented examples of analysis of the polar cap observatory data and MAGSAT magnetic survey show high resolution of the proposed technique in describing high latitude magnetic variations produced by different current systems. Application of the technique to the analysis of Orsted magnetic satellite data are also discussed.

**GA1.07/W/02-B2** Poster **0900-01**

**DECOMPOSITION OF MAGNETIC ANOMALIES ALONG SOUTH CHINA SEA GEOSCIENCE TRANSECT BY WAVELET TRANSFORM**

Yang WANG (Lab. for Geothermics, Institute of Geology, Chinese Academy of Sciences, P.O.Box 9825, Beijing 100029, China, email: thalassa@263.net)

The regional magnetic anomalies provide information about magnetic properties of the crust. However, magnetic fields are superposition of some components which correspond to different scales, patterns, and buried depths of sources within the crust. It is necessary to decompose magnetic field into their components in order to identify magnetic features of crust on different scales. Numerical tests have shown that the wavelet transform is a powerful tool for decomposition of regional potential field. According to the principle of multi-scale analysis, a signal function can be decomposed as the sum of wavelet detail function (D1) and base function (A1); then we can decompose the base function A1 into second order detail function (D2) and second order base function (A2), and so on. Finally we can obtain the details of signal function in different scales. Using the technique of multi-scale analysis, we decompose the magnetic anomalies along South China Sea Geoscience Transect, which extends from Guangzhou to Palawan, into multi-scale components. The original data comes from the 500 km long oceanic crust segment of the Transect. The decomposition produces a series of magnetic anomalies profile related to different scales. Among them, the low order details of the wavelet transform (e.g. D1, D2 etc.) correspond to magnetic feature of small space scale, and the high order details (e.g. D5, D6 etc.) is related to the feature of large scale. We find that there is a ~100 km wavelength structure of the third order wavelet details, which correspond to shallow magnetic layer (oceanic layer 2A). The high order base function of wavelet transform (e.g. A6) reflects the regional trend of anomalies, which change from negative in north to positive in south. These negative anomalies in the north part is caused by deep magnetic source which is the relics of continental crust, and those positive anomalies in the middle and south part is originated by deep mafic magma chambers which were products of sea floor expanding. Furthermore, the relative high positive anomalies in south are possibly superposed by sea mounts located in there.

**GA1.07/W/08-B2** Poster **0900-02**

**INTERNAL PART OF THE GEOMAGNETIC SQ FIELD**

Masahiko TAKEDA (Data Analysis Center for Geomagnetism and Space Magnetism, Graduate school of Science, Kyoto University Kyoto 606-8501, Japan, e-mail: takeda@kugi.kyoto-u.ac.jp)

Internal part of the geomagnetic Sq field has long been used to study the conductivity of the upper mantle. In the present study, spherical harmonics analysis was applied to the geomagnetic Sq field for the several years. The monthly averaged values of the internal and external parts are used to the estimation of the conductivity distribution and its stability of the result. Effect of the currents induced in the ocean will be also discussed.

**GA1.15** **Thursday 29 July**

**MAGNETOSTRATIGRAPHY AND TIME SCALES FROM EXCURSIONS TO SUPERCHRONS**

Location: Muirhead Tower 112 LR2  
Location of Posters: Student Room (1st Floor)

**Thursday 29 July PM**

Presiding Chair: Lauri Brown (Dept. of Geosciences, Massachusetts, USA)  
Concurrent Poster Session

**GA1.15/W/09-B4** **1400**

**AN ASTRONOMICAL POLARITY TIME SCALE FOR THE MIDDLE MIOCENE BASED ON A CONTINENTAL SUCCESSION (CALATAYUD BASIN, N.E. SPAIN)**

H. Abdul Aziz, F.J. Hilgen, W. Krijgsman, E. Sanz, J.P. Calvo, M. Hoyos (Faculty of Earth Sciences, Utrecht University, Utrecht, The Netherlands, Email: krijgsma@geo.uu.nl)

In the vicinity of Orera village (Calatayud Basin, NE Spain), an extraordinary cyclic succession of distal alluvial fan-floodplain, lacustrine and palustrine sediments of middle Miocene age is developed. The sections comprise grey, occasionally red, clays and dolomitic marls alternating with white palustrine carbonates. In the succession, sedimentary cycles can be recognised at four different scales varying from basic small-scale cycles up to large-scale cycle patterns. Cyclostratigraphy and magnetostratigraphy of several subsections were used to construct the composite record. The magnetostratigraphy was correlated to the Geomagnetic Polarity Time Scale (GPTS) of Cande & Kent (CK95), providing an age of 10.7 to 12.8 Ma for the entire succession.

Colour measurements of the sedimentary cycles proved an excellent tool for an objective recognition of these different scales of sedimentary cycles. Spectral analysis of the colour data set resulted in several peaks with frequencies similar to the periodicity of earth's orbital parameters. The average periodicity of the basic small-scale cycles arrives at about 23 kyr implying that these cycles are related to the earth's orbital cycle of precession. The large-scale cycles, characterised by the intervals of well developed small-scale cycles with distinct carbonate beds alternated with more clay-rich with less well defined small-scale cycles, are related to the 100 and 400 kyr eccentricity cycles. The sedimentary cycles were correlated to the eccentricity, precession and summer insolation curves of Laskar 93, thereby assuming that the carbonates represent higher lake levels and thus correspond to precession minima and eccentricity maxima. This correlation provides astronomical ages for the individual sedimentary cycles and for the polarity reversals whereby the latter results in an extension of the Astronomical Polarity Time Scale (APTS) into the middle Miocene.

**GA1.15/W/01-B4** **1415**

**THE TIMING OF REVERSALS IN VARIOUS MIOCENE RED BEDS**

P.P. KRUIVER, W. Krijgsman, C.G. Langereis, M. J. Dekkers (Paleomagnetic Laboratory Fort Hoofddijk, Utrecht University, Budapestlaan 17, 3584 CD Utrecht, The Netherlands, e-mail: kruiver@geo.uu.nl)

In Spain extensive Miocene continental sections are present, of which an important part consists of red beds. The sedimentation patterns in these sections appear to be cyclic and are driven by Milankovitch forcing. Therefore, these sections are extremely suitable for

comparison of Milankovitch cyclicity between the continental and the marine realm. Moreover, these sections provide excellent means for the extension of the Astronomical Polarity Time Scale (APTS). We have studied two continental sections from different sedimentary environments, with emphasis on the timing of the acquisition of the natural remanent magnetisation (NRM). The Librilla section (southern Spain) consists of an alternation of red (fan delta) and grey (lacustrine) sediments. The La Gloria section (central Spain) consists of red (flood plain) deposits with a regular alternation of clay and caliche rich beds. The interpretation of the magnetic signal is not always straightforward. In a large interval of Librilla the grey lithology has a reversed polarity whereas the red lithology displays normal polarity. We interpret the reversed polarity as a complete overprint related to the Messinian salinity crisis. The overprinting occurred long after deposition of the sediment. In the red bed section of La Gloria one polarity reversal (C5n to C4Ar) is investigated in detail. The polarity transition is recorded by different magnetic minerals at different depths. The NRM displays three components. At least one of these components is interpreted as a diagenetic overprint. The overprinting was effective on a much shorter time scale than in Librilla. In the light of magnetostratigraphy the error in dating is small for La Gloria. However, the error in timing of the reversals in Librilla would be severe and would seriously distort the calibration of the APTS.

**GA1.15/E/03-B4** **1430**

**STRATIGRAPHY AND PALAEOMAGNETISM OF A 2.8 KM LAVA SUCCESSION IN CENTRAL N ICELAND**

Bjorn S. Hardarson and Malcolm S. PRINGLE (both at Scottish Universities Research and Reactor Centre, Scottish Enterprise Technology Park, East Kilbride, G75 0QF, UK, e-mail: bjorn@glg.ed.ac.uk, m.pringle@surr.gla.ac.uk); Leo Kristjansson (Geophysics Division, Science Institute, University of Iceland, Hagi, Hofsvallagata 53, 107 Reykjavik, Iceland, e-mail: leo@raunvis.hi.is); Agust Gudmundsson (AGVST Geological Services, Armuli 4, 108 Reykjavik, Iceland); Haukur Johannesson (Icelandic Institute of Natural History, Hlemmur, 101 Reykjavik, Iceland, e-mail: haukur@nattf.is)

We have carried out detailed geological and magnetic mapping of a lava pile in Eyjafjardardalur and OExnadalur in central N Iceland. The succession consists of 7 overlapping profiles comprising tholeiitic lava flows (olivine basalt through to rhyolite in composition) and interbedded sediments representing a continuous 2800 m (235 lava flows) geological record. The sediments generally indicate warm climate which became colder at the top of the succession. Preliminary radiometric data, using 40Ar-39Ar incremental heating analyses on whole-rock cores show that the lavas were erupted from about 8.9 to less than 4.8 m.y. ago which corresponds to an accumulation rate of about 700m/m.y. This is a significantly slower rate than the 4000m/m.y. observed in the upper part of a 5 km lava succession located immediately below the one reported here (Saemundsson et al., J.Geophys. Res., 85, 3628-3646, 1980). Combined geomagnetic polarity measurements and radiometric data imply that the geological record in the study area embraces the polarity time scale between C4An and C3n,3n (Sidufjall) and our data indicate that at least 16 Normal Polarity Chrons, Subchrons (and possibly excursions) may have occurred during this period. This exceeds the number of reversals generally accepted. We hope to solve some of these discrepancies by detailed 40Ar-39Ar analysis of transitional lavas in the succession.

**GA1.15/W/08-B4** **1445**

**MESSINIAN ASTROCHRONOLOGY: THE SOLUTION TO AN OLD PROBLEM**

W. KRIJGSMA, F.J. Hilgen, I. Raffi, F.J. Sierro, D.S. Wilson (Faculty of Earth Sciences, Utrecht University, Utrecht, The Netherlands, Email: krijgsma@geo.uu.nl)

Recently, we established an astronomical polarity time scale (APTS) for the Late Miocene (6.7-9.7) based on cyclically bedded sequences in the Mediterranean. The astronomical ages of the Messinian polarity reversals are much older (up to 166 kyr) than expected from CK95. Because the previous APTS covered the last 5.3 m.y., we still have a "Messinian gap" from 5.3 to 6.7 Ma. This gap is caused by the notoriously complex history of the Mediterranean during the so-called "Messinian salinity crisis" and the deposition of less-favourable sediments (diatomites and evaporites) during this time interval.

However, most of these Messinian sediments display a very clear sedimentary cyclicity what makes them especially suitable for cyclostratigraphic calibration to the astronomical curves. Field observations indicate that the cyclicity in the Messinian diatomites and evaporites are related to precession/insolation with an average periodicity of 21 kyr. We will present the results of our detailed integrated stratigraphic studies on various sections located throughout the Mediterranean. This will close the "Messinian gap" and, for the first time, provide an accurate and reliable time frame for the Mediterranean Messinian in which several important palaeoceanographic and tectonic events are now accurately dated.

**GA1.15/W/04-B4** **1500**

**APPLICATION OF HIGH-RESOLUTION DATING OF DIFFERENT LACUSTRINE ENVIRONMENTS**

Nicole VAN VUGT, Cor Langereis, Joris Steenbrink (Faculty of Earth Sciences, Utrecht University, Budapestlaan 4, 3584 CD Utrecht, the Netherlands, e-mail: vanvugt@geo.uu.nl)

Study of the timing of cyclic environmental changes or bed-to-bed comparison of different sedimentary settings over hundreds of kilometers has become possible using high-resolution dating based on combination of magneto- and cyclostratigraphy. We compare three coal-bearing lacustrine basin fills: the Lower Pliocene (Gilbert) lignite/carbonate system of Ptolemais (N. Greece); the time-equivalent lignite/detrital system of Lupoia (Romania); and the Pleistocene (Brunhes) lignite/detrital system of Megalopolis (S. Greece). All these sequences have been dated using biostratigraphy, magnetostratigraphy, cyclostratigraphy and, in two cases, 40Ar/39Ar dating. The Megalopolis sequence is dominated by eccentricity, as are the marine Brunhes archives from both the Atlantic and the Pacific, where the ice ages were registered during eccentricity minima. The Pliocene lithological cycles of Ptolemais are forced by precession, but unlike the Mediterranean reference section of the same age (Rossello composite), influence of eccentricity is virtually absent. In the parallel Lupoia section, however, eccentricity controls the occurrence of cyclic coal seams, with precession only playing a minor role. Strikingly, the Lupoia and Megalopolis deposits were formed in similar environments. Certain lacustrine sedimentary environments are apparently more influenced by eccentricity, while others are more susceptible to precessional forcing. Similar as for different marine basins, e.g. the precession dominance in the Mediterranean at times when obliquity is the main driving force behind the Atlantic and Pacific cycles.

GA1.15/E/04-B4

1515

## THE LOCATION OF THE KAEANA POLARITY CHRON

E. HERRERO-BERVERA (Hawaii Institute of Geophysics, University of Hawaii, Honolulu HI 96822, USA, e-mail: herrero@soest.hawaii.edu); D.H. Tarling (Geological Sciences, University, Plymouth PL4 8AA, UK, E-mail: d.tarling@plymouth.ac.uk)

There is some confusion about where the Kaeana Reversed Polarity chron was originally identified on Oahu, Hawaii. Re-examination of the available records suggest that one of the key radiometrically dated sites may well have been in a different part of the Waianaea Series. However, the original quarry site cited in the original naming of the chron is now under-water and the surrounding rocks are of normal polarity, overlain by rocks of reversed polarity. On the basis of re-evaluation of the earlier sparse studies, a detailed sampling campaign of several sequences in the Waianaea Formation suggests that the transition from normal to reversed polarity was rapid, relative to the eruption rate, usually comprising of less than two lavas. The results from these sequences are only now providing sufficient data for magnetostratigraphic zonation of this Formation.

Presiding Chair: Malcolm Pringle (Scottish Universities Research and Reactor Centre, UK)

GA1.15/P/01-B4

1630

## AR40-AR39 DATING OF TRANSITIONAL LAVAS AT TWO POLARITY BOUNDARIES IN THE SKARDSHEIDI AND AKRAFJALL MOUNTAINS, SW-ICELAND

Leo KRISTJANSSON (Geophysics Division, Science Institute, University of Iceland, Hagi, Hofsvallagata 53, 107 Reykjavik, Iceland, email: leo@raunvis.hi.is); Malcolm S. Pringle and Björn S. Hardarson (both at Scottish Universities Research and Reactor Centre, Scottish Enterprise Technology Park, East Kilbride, G75 0QF, U.K., email: m.pringle@surre.gla.ac.uk and bjorn@glg.ed.ac.uk); Agust Gudmundsson (AGVST Geological Services, Armuli 4, 108 Reykjavik, Iceland)

We have obtained radiometric dates on lava flows at two polarity zone boundaries in the lava pile of SW- Iceland, by using 40Ar-39Ar incremental heating analysis. One location is in the NE part of Mt. Skardsheidi where previous paleomagnetic laboratory measurements showed that ten transitional flows (units SH 9-18 in Kristjansson and Sigurgeirsson, J. Geomag. Geol. 1993) occur at a R-N boundary. Duplicate age determinations on a sample from flow SH 12 yield a weighted mean of 3.613 +/- 0.058 M.y., and flow SH 19 similarly yields a mean age of 3.612 +/- 0.039 M.y. We have now sampled over 100 lavas in two profiles on the S side of Skardsheidi for paleomagnetic measurements; in these the number of transitional flows at the same R-N boundary is one and three respectively. Some other reversals and excursions are also recorded in Skardsheidi.

Our other location is in Mt. Akrafjall which lies about 20 km south-west of Skardsheidi and is at a similar stratigraphic level. In the profile FA (Kristjansson et al., J. Geophys. 1980) in Akrafjall intermediate directions are not found at a R-N polarity zone boundary which is correlated with the one in profile SH mentioned above, but four flows FA 45-48 with a cluster of low-latitude virtual poles are found at the overlying N-R zone boundary. The weighted mean age of the units FA 46 and 47 which were measured in duplicate, is 3.285 +/- 0.018 M.y. Our results agree well with other recent estimates of the ages of the Gilbert-Gauss and Lower Mammoth transitions.

GA1.15/E/06-B4

1645

## 40AR/39AR AGES AND PALAEOMAGNETIC DATA FROM CERRO FRAILE, ARGENTINA: FURTHER CONSTRAINTS ON TIMING OF REVERSALS DURING THE MATUYAMA CHRON

Bradley Singer (Department of Geology and Geophysics, University of Wisconsin, Madison, WI 53706, USA, e-mail: bsinger@geology.wisc.edu); Laurie BROWN (Department of Geosciences, University of Massachusetts, email: lbrown@geo.umass.edu); Hervi Guillou (Centre des Faibles Radioactivités, CEA/CNRS); Jorge Rabassa (Universidad Nacional del Comahue); Lyn Gualtieri (Department of Geosciences, University of Massachusetts)

Cerro Fraile (50.5 S, 72.7W), located 40 km east of the crest of the Andean Cordillera in southwestern Patagonia, is a splendid exposure of meseta-capping Plio-Pleistocene basaltic lava flows interbedded with glacial tills. Classic K-Ar and paleomagnetic work by Fleck et al. (1972) provided the first age constraints on multiple early Pleistocene glaciations in the Southern Hemisphere. In addition, the confirmation of several polarity subchrons between 2.2 and 1.0 Ma contributed to early refinements of the GPTS. Revisions of the GPTS over the past several years reflecting problems with K-Ar dated samples prompted us to reassess the Cerro Fraile section using modern geochronologic and paleomagnetic methods. Oriented cores and geochronologic samples were collected in 1996 and 1998 from 10 lava flows interbedded among 7 glacial tills.

Detailed 40Ar/39Ar incremental-heating experiments on 9 of the 10 lavas found to comprise the 200 m thick section along the northwestern escarpment of Cerro Fraile, plus one unspiked K-Ar age from the ninth flow in the sequence, gave the following isochron ages\* in ascending stratigraphic order: 2.16 +/- 0.06 Ma; 2.24 +/- 0.09 Ma; 2.07 +/- 0.04 Ma; 1.89 +/- 0.03 Ma; 1.95 +/- 0.01 Ma; 1.89 +/- 0.03 Ma; 1.83 +/- 0.03 Ma; 1.76 +/- 0.04 Ma; 1.43 +/- 0.02 Ma; 1.08 +/- 0.01 Ma. New paleomagnetic results on the same flows indicate strong, stable, uni-vectorial magnetizations for flows with normal or reversed polarities. Three flows have weaker magnetizations with greater directional variability during demagnetization and characteristic directions classified as transitional. Magneto-stratigraphy, corresponding to the above age determinations, is: R-T-N-R-R-T-N-R-T-N. All reversed flows correspond to the Matuyama chron, while the normally magnetized lavas record the Reunion event, the Olduvai event, and the Jaramillo subchron. The new age determinations lead us to suggest that the lower two transitional flows actually record the reversal process marking the onset of the Reunion and Olduvai events, whereas the uppermost transitional flow, K-Ar dated at 1.43 +/- 0.02 Ma, may correspond to one of several short events suggested in the mid Matuyama between the well-established Gilsa and Cobb Mountain events. The 1.08 +/- 0.01 Ma age for the uppermost normally magnetized lava coincides with the astronomically determined age of 1.07 Ma for the onset of the Jaramillo Normal Subchron, and together with recent results from a Tahitian lava sequence indicates, that the Jaramillo Normal Subchron lasted about 80 k.y. between 1.07 Ma and 0.99 Ma.

\*All 40Ar/39Ar ages are relative to the Taylor Creek Rhyolite sanidine standard @ 27.92 Ma

GA1.15/W/02-B4

1700

## SHORT GEOMAGNETIC EVENTS IN THE EARLY BRUNHES AND MIDDLE MATUYAMA CHRON IN THE 1700-M BORING CORE FROM OSAKA BAY, SOUTHWEST JAPAN

Masayuki HYODO (Research Center for Inland Seas, Kobe University, Kobe 657-8501, Japan, E-mail: mhyodo@kobe-u.ac.jp); Dipak Kumar Biswas (Graduate school of Science and Technology, Kobe University, Kobe 657-8501, Japan, E-mail: dipak@kobe-u.ac.jp)

Paleomagnetic measurements of Plio-Pleistocene sediments were made in a 1700-m core

from the Osaka Basin. Two short geomagnetic events of reverse polarity including excursions were found in a marine clay Ma5, over a section of 3.7 m thick around the lower boundary and over a thin section of 80 cm in the topmost part. The lower event was reproduced in another core at a site 14 km separated. The marine layer Ma5 deposited during a period of eustatic high sea level corresponding to the marine isotope stage 17. Assuming a constant accumulation rate of 0.50 mm/yr between the Brunhes/Matuyama boundary and the AT tuff dated as 24.5 ka, the short events are dated to be about 0.69 Ma. This estimate is consistent with the age of the marine isotope stage 17.3. The Delta event is correlated to them. A short geomagnetic normal polarity event was found in a zone from 910.9-921.7m and in between the Cobb Mountain and Olduvai subchrons. This event began with an excursions field of steep inclination, and became dominated by normal polarity fields in the latter half. The age range is estimated to be 1.60-1.62 Ma with a duration of about 18 kyr, assuming a constant accumulation rate of 0.61 mm/yr between the mid-point of the Cobb Mountain subchron and the Upper Olduvai boundary. A duration of about 8 kyr is estimated for a zone with only positive inclinations. This event is correlated to the Gilsa event, the Stage 54 event, and the event preceded the Sangiran Excursion.

GA 1.15/E/01-B4

1715

## GEOMAGNETIC EVENTS AND RELATIVE PALEOINTENSITY VARIATIONS WITHIN THE BRUNHES CHRON AS INFERRED FROM MARINE NORTHERN HIGH LATITUDE SEDIMENTS

Norbert R. NOWACZYK (GeoForschungsZentrum Potsdam, Haus C, Telegrafenberg, D-14473 Potsdam, Germany, e-mail: nowa@gfz-potsdam.de)

Numerous magnetostratigraphic results especially from northern high latitudes revealed the existence of a whole series of short reversals of the earth's magnetic field during the last 3000 ka of the Brunhes Chron (the last 780 ka). These short events with estimated durations from 1 to about 5 ka can be traced from the Iceland Sea across about 30 coring sites into the Arctic Ocean, covering a distance of more than 3000 km. At least the longer events have also been found at other locations over the globe. All geomagnetic events are linked with pronounced lows in the relative paleointensity variation record, as estimated by different techniques. Especially the polarity transitions are characterised by relative intensities of sometimes less than 5% of the preceding intensity maximum. The polarity transition is completed mostly within less than 1 ka whereas the intensity decay (and increase) takes about 10 ka. The overall pattern of relative paleointensity together with directional variations within the Brunhes Chron indicate a strongly dynamic character of the geodynamo as the source of the Earth's magnetic field.

GA1.15/W/05-B4

1730

## GEOMAGNETIC EXCURSION DURING THE LAST INTERGLACIAL / GLACIAL RECORDED IN LACUSTRINE SEDIMENTS FROM SALAWUSU, INNER MONGOLIA, CHINA

Su PU. (Department of Geosciences, Taiyuan University of Technology, Taiyuan, Shanxi 030024, China, e-mail: supu@hotmail.com); Reidar Løvlie. (Institute of Solid Earth Physics, University of Bergen, Norway, e-mail: reidar.lovlie@ifj.uib.no); Fan Xingzhao. (Department of Geosciences, Taiyuan University of Technology, Taiyuan, Shanxi 030024, China, e-mail: supu@public.ty.sx.cn).

The Salawusu section is located in Inner Mongolia (North China) and consists of a suite of aeolian-fluvial-lacustrine sediments with a total thickness of 70m. The lower 50m is composed of layers of fluvial-lacustrine sediments deposited between 124.9±15.8 and 70±1.2ka B.P. (TL, ERS) corresponding to the last interglacial period. The overlying 20m consist of aeolian derived sand with ages ranging from 70.9±1.2 to 9.7±0.1ka B.P. (C14, TL, ERS) corresponding to the last glacial period. Paleomagnetic and rock magnetic investigation on some 390 samples collected along this section is reported. Susceptibility and NRM intensity reflect clear relationships to lithology; the sand at the top carry lower values compared to the fine-grained silt-clay intervals. Magnetic fabric, based on AMS measurements, reveals typically depositional features; oblate susceptibility ellipsoids associated with sub-horizontal kMAX axes. Remanent coercivity analysis indicates a uniform composition of magnetic minerals within the lower 50m that is dominated by magnetite with a small contribution of hematite. Alternating field demagnetisation reveals single component magnetisation defining a northerly distribution around the present geomagnetic fields with inclinations around 45°. Two or three short intervals at the bottom carry anomalous magnetisation with negative inclinations, possibly representing the Blake geomagnetic excursions (117ka).

GA1.15/W/10-B4

1745

## ETRUSIA EXCURSION IN HOLOCENE DEPOSITS OF THE WESTERN SIBERIA

Z.N. GNIBIDENKO, L.A. Orlova (United Institute of Geology, Geophysics and Mineralogy, SB RAS, Novosibirsk, Russia)

Complex palaeomagnetic, palinological and chronological investigations of Holocene deposits of high flood-lands of the Aley river in the south of the Western Siberia have been accomplished by us. From the investigated section (6 m in thickness), which is represented by loesslike loams, sandy loams and buried soils two dates 14C - 3185 year (SOAN-3146) and 3080 years (SOAN-3146) were obtained by humus, which make it possible to ascribe the deposits of high flood-lands to the subboreal period (SB-2, SB-3) of the Late Holocene. In the obtained palaeomagnetic recording of the rocks of this section, characterised by normal polarity (Brunhes chron), the horizon of rocks (0.4 m in thickness) with reverse magnetisation has been revealed. The composition of ferromagnetic minerals, behaviour of magnetic susceptibility and natural remanent magnetisation permit to judge about the geophysical nature of reverse magnetisation of this interval of rocks and to ascribe it to the excursions of the geomagnetic field. Obtained for this interval dates by 14C - 3185 years and 3080 years make it possible to identify this excursion with the Etrussia excursion. As palinological data showed, in the south of the Western Siberia this excursion coincides with the phase of rise in temperature at the end of subboreal period.

Thursday 29 July PM

Presiding Chair: Cor Langereis (Utrecht University, the Netherlands)

GA1.15/E/05-B4

Poster

1530-01

## MAGNETOSTRATIGRAPHY AND MILANKOVITCH CYCLICITY IN SHALLOW WATER CARBONATES DURING THE LOWER CRETACEOUS

B. D'Argenio (Scienze della Terra, Università Federico II di Napoli, Napoli 80138, Italy E-mail: ciclisiti@gms01.na.cnr.it); Iorio, M. (Geomare Sud, Via Vespucci 9, Napoli 80142, Italy Email iorio@gms01.na.cnr.it); D.H. TARLING, (Geological Sciences, University, Plymouth PL4 8AA, UK E-mail: d.tarling@plymouth.ac.uk)

Cyclites in the sedimentological and textural features in a Lower Cretaceous 88 m carbonate



bore-core from southern Italy correspond with the predicted Milankovitch cyclicities for that time. Identical spectral peaks are observed in the palaeomagnetic properties - intensity, inclination and declination - although there are no linear correlations between the geological and palaeomagnetic parameters. The spectral similarities enable the thickness to be related to directly to the astronomical time-scale; an average thickness of 1 cm equating with an average time interval of 360 years. As a range of spectral peaks in uncorrelated parameters are involved, it is also possible to estimate the standard deviation on this time equivalent as some  $\pm 16$  years. When smoothed, this directional polarity record can be compared with the sea-floor magnetic anomaly intensity record of the same time. Such comparison also shows some Milankovitch cyclicities are also present in the anomaly records. This enables the linkage of astronomical and magnetostratigraphic dating techniques for extremely high precision dating under suitable circumstances.

**GA1.15/E/02-B4** Poster **1530-02**

**MAGNETOSTRATIGRAPHY ACROSS THE J/K BOUNDARY STRATA AT PUERTO ESCANO (S. SPAIN): CORRELATION WITH HIGH-RESOLUTION DATA AT BRODNO AND BOSSO VALLEY**

Václav Hou\_a, Miroslav KRS, Otakar Man, Petr Pruner, Daniela Venhodoová (Institute of Geology, Academy of Sciences, Rozvojová 135, 165 02 Prague 6 - Lysolaje, Czech Republic, e-mail: housa@gli.cas.cz); José M. Tavera and Federico Oloriz (Departamento de Estratigrafía y Paleontología, Instituto Andaluz de Geología Mediterránea, Universidad de Granada, 18071 Granada, Spain, e-mail: jtavera@goliat.ugr.es; foloriz@goliat.ugr.es)

This study presents first results of magnetostratigraphic investigations across Jurassic/Cretaceous (J/K) boundary limestones in Puerto Escano, Province of Córdoba, S. Spain. This locality was chosen because of the concomitant presence of calcionellids and ammonites. The aim is to prepare the background for the correlation of Late Tithonian and Early Berriasian biostratigraphic zonation with the geomagnetic events (manifested in detailed magnetostratigraphy), between the Tethyan realm and other regions on the Earth, particularly the Boreal and Pacific realms. Laboratory tests using the MAVACS apparatus showed extremely suitable physical properties of the studied limestones allowing a precise derivation of A-, B- and C-components of remanence. The C-component is clearly of pre-folding origin and indicates normally and reversely polarized magnetozones. Two reverse subzones were detected in the Puerto Escano section within the magnetozones M20n and M1 K-boundary in the Tethyan realm are already available, two of them (Brodno and Bosso Valley) being high-resolution profiles. Due to palaeontological significance of the Puerto Escano section, it will be subjected to next detailed magnetostratigraphic investigation.

**GA1.15/W/11-B4** Poster **1530-03**

**DIRECT INTERCALIBRATION OF ASTRONOMICAL AND RADIOISOTOPIC TIME IN THE MEDITERRANEAN NEOGENE**

Klaudia KUIPER and Jan Wijbrans (both at Department of Isotope Geochemistry, Vrije Universiteit, De Boelelaan 1085, 1081 HV Amsterdam, The Netherlands, e-mail: kuik@geo.vu.nl, wjij@geo.vu.nl); Frits Hilgen, Wout Krijgsman and Joris Steenbrink (all at the Faculty of Earth Sciences, Utrecht University, Budapestlaan 4, 3584 CD Utrecht, The Netherlands, email: fhilgen@geo.uu.nl, krijgsma@geo.uu.nl, jsteen@geo.uu.nl)

Cyclically bedded sediments in the Mediterranean Neogene form a continuous record of dominantly precession controlled climatic oscillations during the Pliocene and Miocene. This signal can be identified in both marine and continental (lacustrine) records. Astronomical tuning of these sediments allows the calculation of discrete ages for individual beds of the sedimentary cycles. Thus astronomical ages can be assigned to volcanic ash beds intercalated in these successions. Sedimentary basins containing suitable tephra intercalated in astronomically dated cyclically bedded successions occur in southern Spain, Morocco, Italy, Greece and Turkey. Biotite and sanidine separates from the tephra layers in these successions have been dated by the  $^{40}\text{Ar}/^{39}\text{Ar}$  laserprobe technique (both multiple single fusion and incremental heating techniques are used) and the  $^{40}\text{Ar}/^{39}\text{Ar}$  ages are compared with astronomical ages for the same volcanic ash beds.

Research carried out on the Ptolemais section in northern Greece and the Phaneromeni section on northeastern Crete indicate that 1) the cyclically bedded successions are of Pliocene age and follow the 21.7 kyr precession cycle, and 2) a discrepancy in absolute age of ca 200 kyr exists between the astronomical derived ages and the isotopic ages, where the  $^{40}\text{Ar}/^{39}\text{Ar}$  ages are significantly younger. Only part of the problem might be explained by the use of erroneously young ages for the neutron fluence monitors, and/or incorrect values for the decay constants of  $^{40}\text{K}$ .

**GA1.15/W/06-B4** Poster **1530-04**

**MAGNETOSTRATIGRAPHY OF MIDDLE-LOWER JURASSIC SECTIONS FROM BETIC CORDILLERA (SOUTHERN SPAIN): BAJOCIAN-BATHONIAN AND TOARCIAN-AALENIAN BOUNDARIES**

OSETE, C., Osete, M.L. (Departamento de Geofísica de la Facultad de Ciencias Físicas de la Universidad Complutense de Madrid, Spain, e-mail: crisol@eucmos.sim.ucm.es) Sandoval, J. (Departamento de Estratigrafía y Paleontología, Universidad de Granada, Spain, e-mail: sandoval@goliat.ugr.es)

A detailed palaeomagnetic study was carried out in two sections (Sierra Lúgar and Cerro Méndez) in the Betic Cordillera (Southern Spain). Both sections contain a well-preserved and complete record of ammonite assemblages. The boundaries Bajocian-Bathonian and Toarcian-Aalenian in Sierra Lúgar and Cerro Méndez respectively, are represented by a uniform succession of marls, nodular marly-limestones and nodular limestones ("ammonitic rosso" facies) with abundant Bositra filaments and Conoglobigerina. The initial NRM in the samples are between 2.7 10<sup>-3</sup> and 4 10<sup>-4</sup> A/m. In all the samples three magnetisation components could be identified by thermal cleaning. A low unblocking temperature component, close to the present field, was generally isolated between 80°C and 200°C. The second component has been observed in all samples as well and it is responsible for the major part of the non-viscous fraction of the NRM. It's maximum unblocking temperature 450°C and is always of normal polarity. The third component presents low intensity. It's maximum unblocking temperature ranges are between 550-600°C. This component exhibits both reversed and normal polarities and it is interpreted as the primary magnetisation.

**GA1.15/W/07-B4** Poster **1530-05**

**MAGNETOSTRATIGRAPHY OF THREE LOWER TOARCIAN SECTIONS FROM THE IBERIAN RANGES (CENTRAL SPAIN)**

Paola Romana GIALANELLA (Dept. of Earth Science, Univ of Naples "FedericoII", Italy.), Maria Luisa Osete (Dept. Geofísica, F. CC Físicas, Complutense University, Madrid 28040, Spain, E-mail: mlosete@eucmax.sim.ucm.es); Juan José Villalafin (Escuela Politécnica Superior, Burgos University, Spain); Friedrich Heller (Institut für Geophysik, ETH, Zurich, Switzerland); Antonio Goy (Dept. Estratigrafía y Paleontología, Complutense University, Madrid 28040, Spain)

Three well dated sections (Arino1, Arino2 and Sierra Palomera) covering the lower Toarcian (from Tenuicostatum to Variabilis subzones) have been palaeomagnetically investigated. The sections are located in the central part of the Iberian Ranges (Central Spain). The lower Toarcian are represented in the three investigated sections by an exceptionally thick and uniform succession of marls and marly limestones. The successions contain a well-preserved and complete record of ammonite assemblages. About 180 oriented samples were collected. Specimens are characterised by a multicomponent NRM. After initial removal of a viscous component, an intermediate component was isolated between 250°C and 450°C. This component has always normal polarity and it is interpreted on basis of previous palaeomagnetic studies in this region as a Cretaceous remagnetisation. The characteristic component is isolated after 450°C and presents a maximum unblocking temperature up to 575°C and carries both normal and reversed polarities. The magnetostratigraphic columns obtained in the three sections can be easily correlated.

**GA1.15/W/03-B4** Poster **1530-06**

**PALAEOMAGNETIC RESULTS OF THE MIDDLE-LATE TRIASSIC IN THE WESTERN IBERIAN RANGES**

Vicente Carlos RUIZ-MARTÍNEZ and Maria Luisa Osete (both at the Dpto. de Geofísica, Facultad de CC. Físicas, Universidad Complutense de Madrid, 28040 Madrid, Spain, e-mail: vcarlos@eucmax.sim.ucm.es & mlosete@eucmax.sim.ucm.es); Daniel Rey (Facultad de CC. del Mar, Universidad de Vigo, Apdo. 874, 36200 Vigo, Spain, email: ); Juan Jose Villalafin (Dpto. Física Aplicada, E.U. Politécnica, Universidad de Burgos, 09006 Burgos, Spain, e-mail: villa@ubu.es); Paola Gialanella (Dip. Scienze della Terra, Università degli Studi di Napoli "Federico II", Lgo S. Marcellino 10, I-80138, Napoli, Italy); Alfonso Sopena (Instituto de Geología Económica, Consejo Superior de Investigaciones Científicas, Universidad Complutense de Madrid, 28040 Madrid, Spain, e-mail: sopena@eucmax.sim.ucm.es)

Middle-Late Triassic strata of the Cuevas de Ayllón section and Late Triassic correlated strata of the Licerias section (westernmost margin of the Iberian Ranges, Spain) present predominantly reverse polarity characteristic magnetisations of high coercivity and distributed unblocking temperatures up to 700°C. Samples of these formations (interbedded mudstones and sandstones dipping gently to the north) also contain normal polarity secondary remagnetisations, interpreted as result of the overlapping of the present field and an older overprint probably related with the extensional phases of the Iberian Basin in the Cretaceous. Primary remanence is better preserved in the finer-grained beds, with a lower overlapping degree with the high temperature overprint. The palaeomagnetic poles obtained in this study contribute to fit more accurately the apparent polar wander path of Stable Iberia for the Middle-Late Triassic time span.

**GA1.15/C/U6/W/05-B4** Poster **1530-07**

**MAGNETOSTRATIGRAPHY OF THE NUUANU AND WAILAU GIANT HAWAIIAN SUBMARINE LANDSLIDES**

Gary McMURTRY and Emilio Herrero-Bervera (both at SOEST University of Hawaii, 1000 Pope Road, Honolulu, Hawaii, 96822, USA, email: garym@soest.hawaii.edu) Toshiya Kanamatsu (JAMSTEC, 2-15 Natsushima-Cho, Yokosuka 237, JAPAN, email: toshiyak@jamstec.go.jp)

A joint Japan-USA investigation on the origin of giant Hawaiian submarine landslides was launched in 1998 with the JAMSTEC R/V Kairei and ROV Kaiko. Four 7 meters long piston cores were recovered from the vicinity of the Nuuanu and Wailau giant submarine landslide, which dispersed onto the seafloor some 10s to 100s of km NE of Oahu and N of Molokai Islands, respectively. Three of the four 7 m long piston cores collected NE of Oahu contain distinct buried turbidites composed primarily of volcanic ash with some included forams, whereas the fourth core, located on a large detached slide block near Molokai displays a complex stratigraphy that contains numerous turbidites from that island. The three cores so far investigated contain reversals and excursions of the geomagnetic field, as revealed by marked changes in the inclination, declination and intensity profiles taken at 5-cm intervals. Preliminary ages (not yet constrained by radioisotope and/or paleontological dating) assigned to the polarity events yield sedimentation rates of 1-52 mm/k.y. for Kairei cores KR98-01,02 and 03. The changes in sedimentation from relatively fast rates to the Matuyama-Brunhes reversal to slower rates afterward are similar to a nearby core site (KK-78O30, 19 N, 160 W) but are generally lower in magnitude, perhaps reflecting increasing winnowing near the islands. A single distinct turbidite buried within the carbonate ooze atop Tuscaloosa Seamount (PC-01), a very large detached slide block of the Nuuanu landslide, and that within a pelagic red clay ~50 km in front of the seamount (PC-03) both date to approximately 1 Ma BP. The PC-03 turbidite ash suggest a mixed Koolau (Oahu) basalt composition (M. Garcia, pers. comm., 1998), whereas the turbidite atop Tuscaloosa likely deposited from the Wailau giant submarine landslide. If so, the maximum age of the Nuuanu landslide is presently best constrained by a lack of turbidite deposits in core PC-02, ~100km in front of the slide, to >1.8 Ma BP, with the minimum age or last phase of the Nuuanu landslide deposition at approx. 1 Ma BP, followed closely in time by the Wailau event. It may be significant that this latter date was a time of eustatic sealevel rise. The Wailau and Nuuanu landslides apparently occurred near the apex of shield building for East Molokai volcano (from 1.75 to 0.75 Ma BP--Naughton et al., 1980; J. Moore, pers. comm., 1998) and perhaps also for Koolau volcano (from 2.6 to 1.8 Ma BP-- Doell and Dalrymple, 1973). Longer cores will likely reveal earlier landslide events in this area.

**GA2.02** Thursday 29 – Friday 30 July

**ELECTRODYNAMIC PROCESSES IN THE GENERATION OF IONOSPHERIC IRREGULARITIES (OBSERVATIONS, THEORY, SIMULATIONS)**

Location: Gisbert Kapp E203 LT1  
Location of Posters: Gisbert Kapp Coffee Room

**Thursday 29 July AM**

Presiding Chair: A.M. Hamza (Univ of Brunswick, Canada)  
Concurrent Poster Session

**ELECTRODYNAMIC PROCESSES – MID-LATITUDE IRREGULARITIES**

**GA2.02/W/09-B4** **0900**

**COORDINATED OBSERVATION OF THE FIELD-ALIGNED IRREGULARITIES IN MID-LATITUDE F-REGION IONOSPHERE WITH THE MU RADAR AND GPS**

S. FUKAO, M. Yamamoto, M. Nishimura and Y. Otsuka (Radio Atmospheric Science Center, Kyoto University, Uji 611-0011, Japan, Email: fukao@kurasc.kyoto-u.ac.jp) A. Saito (Department of Geophysics, Kyoto University, Kyoto 606-8502, Japan, Email: saitoua@kugi.kyoto-u.ac.jp) S. Miyazaki (Geographical Survey Institute, Tsukuba 305-0811, Japan, Email: miyazaki@gsi-mc.jp) K. Shiokawa, M. Ejiri and T. Ogawa (Solar-Terrestrial Environment Laboratory, Nagoya University, Toyokawa 442-8507, Japan, Email: shiokawa@stelab.nagoya-u.ac.jp) M. Kubota, M. Ishii and F. Isoda (Communication Research Laboratory, Koganei 184-8795, Japan, Email: mkubota@crl.go.jp) K. Nakajima and T. Sakanou (Graduate School of Science, Tohoku University, Aoba-ku, Sendai 980-8578, Japan, Email: ken@pat.geophys.tohoku.ac.jp)

The mid-latitude F-region field-aligned irregularities (FAls) observed with the MU radar show marked upwelling structures with large Doppler velocities up to 200 m/s. A coordinated observation, F-region Radio and Optical measurement of Nighttime TIDs (FRONT), was conducted with the MU radar, the GEONET GPS receiver array, and several optical instruments during May 16-24, 1998. While the MU radar detected intense F-region FAls, horizontal distributions of the total electron content were measured by 900 GPS receivers. Also, five all-sky CCD imagers observed emission of the air-glow in a wide ionospheric area over Japan and a Fabry-Perot interferometer observed thermospheric neutral wind velocities at two sites. Based on these variety of data, generation mechanisms of FAls will be discussed.

**GA2.02/W/10-B4****0920****FIRST 50 MHZ CONTINUOUS WAVE INTERFEROMETRY MEASUREMENTS OF LOCALIZED BACKSCATTER REGIONS IN THE MIDLATITUDE E-REGION IONOSPHERE**

Christos HALDOUPIS and Anastasios Kamburelis (Physics Department, University of Crete, Iraklion, Crete, 710 03 Greece, Email: haldoupis@talos.cc.ucl.gr) Kristian Schlegel (Max-Planck-Institut fuer Aeronomie, Katlenburg-Lindau, Germany, Email: schlegel@linmpi.mpg.de); Mirela Voiculescu (Physics Department, University of Galati, Galati, Romania, Email: mvoic@phys.ugal.ro)

The radar interferometer technique, which has been applied in the past years to studies of short wavelength plasma turbulence in the earth's ionosphere, can provide, in addition to the Doppler spectrum, estimates of mean size, mean angular position, and velocity transverse to the viewing direction. Here we describe the conversion of SESCAT (Sporadic E Scatter experiment, a bistatic 50 MHz continuous wave (CW) Doppler radar located in the island of Crete, Greece) to an interferometer that is capable to investigate short term dynamics of localized scattering regions in the midlatitude E region ionosphere with mean transverse sizes as small as a couple of kilometers. The first results show that SESCAT, which provides high quality spectra and excellent temporal resolution, has its measurement capabilities enhanced significantly when operated as interferometer. In this paper we will present and discuss results of azimuthal SESCAT interferometry for typical midlatitude echoes, that is, type II echoes characterized by small mean Doppler velocities. In addition we will present examples of uncommon echoes characterized by large line-of-sight velocities due to elevated electric fields. In the latter case, the cross-phase changes with time indicate rapid zonal movements of backscatter regions, presumably due to neutral winds, having at times velocities as high as at least 150 m/s, that is, well above typical neutral wind velocities at midlatitude. Finally, an effort is made to interpret the interferometry findings within the framework of our present theoretical understanding.

**GA2.02/L/06-B4****0940****A PHYSICAL MODEL FOR 3.2-M AND 6.1-M BACKSCATTER FROM MIDLATITUDE E REGION**

Ludmila M. Kagan (Radiophysical Research Institute, B.Pecherskaya st.25, Nizhny Novgorod 603600, Russia, e-mail: kagmil@nirfi.sci.nov.ru) Tadahiko Ogawa (Solar-Terrestrial Environment Laboratory, Nagoya University, Toyokawa, Aichi 3-13, Japan, e-mail: ogawa@stet1.nagoya-u.ac.jp) Mamoru Yamamoto and Shoichiro Fukao (both at Radio Atmospheric Science Center, Kyoto University, Uji, Kyoto 611-0011, Japan, e-mail: fukao@kurasc.kyoto-u.ac.jp, yamamoto@kurasc.kyoto-u.ac.jp)

We propose that backscatter from 3.2-m and 6.1-m field-aligned irregularities observed by MU and FAR radars over Japan within a 90-150 km altitude range is caused by a presence of the same source, neutral motions, which due to different values of ionospheric parameters result in different dominating processes (and so different backscatter echo types) at different altitudes. Such an approach allows to explain the QP-echoes by the gradient drift processes [1] and the continuous, thick continuous and high-altitude echo types by the thermal processes [2].

**GA2.02/L/01-B4****1000****ROCKET/RADAR SPORADIC-E EXPERIMENT CONDUCTED DURING THE EL COQUI II CAMPAIGN**

R.F. Pfaff, M. Acuña, S. Bounds, H. Freudenreich (NASA Goddard Space Flight Center, Greenbelt, MD), J. Clemmons (Aerospace Corporation, El Segundo, CA), G. Earle, R. Heelis (Univ. of Texas at Dallas, Richardson, TX), E. Kudeki, S. Franke (Univ. of Illinois, Urbana-Champaign, IL), M. Larsen (Clemson University, Clemson, SC), S. Gonazales, C. Tepley (Arecibo Observatory, Puerto Rico), C. Hanuise (LSEET, Toulon, France), A. Bourdillon (Univ. of Rennes, Rennes, France), W. Swartz (Cornell University, Ithaca, NY)

In order to investigate the complex electrodynamics and neutral-plasma coupling inherent to sporadic-E layers in the earth's mid-latitude ionosphere, a series of rocket/radar experiments were planned as part of the NASA El Coqui II Campaign from Tortuguero Launch Range, Puerto Rico, in March-April, 1998. The rocket experiments consisted of two pairs of "mother-daughter" payloads with limited apogees so that the payloads "hovered" in the sporadic-E region (95-125 km). Each payload pair included vector DC and AC electric field detectors, a highly accurate flux-gate DC magnetometer, an ion mass spectrometer, an ionization gauge, and spaced-electric field receivers to measure the wavelength and phase velocity of the unstable plasma waves. Separate rockets were included to simultaneously carry aloft TMA trails to measure the neutral wind and its velocity shear, believed responsible for the sporadic-E layer formation. In addition to the rocket experiments, incoherent scatter radar measurements of plasma density and drift velocity were gathered almost every night during the 3 week campaign. Continuous VHF backscatter radar operations were carried out from a site near Salinas, Puerto Rico, where 3-m backscatter echoes were observed associated with sporadic-E and other types of low altitude ionospheric layers. Other radars that operated during the campaign included an HF backscatter system near Ponce, Puerto Rico, and a second VHF backscatter radar set up near Aguadilla, Puerto Rico. On 24 March 1998, one of the instrumented rockets was launched, attaining an apogee of 129 km. The payloads successfully pierced an intense sporadic-E layer observed by both the Arecibo radar and the in-situ density and ion mass spectrometer probes. In-situ DC electric fields revealed very low (-1.2 mV/m) ambient fields with small amplitude structures of the same order. No high frequency (short scale) waves were observed, consistent with the VHF backscatter observations at the time of the launch. An overview of the observations will be presented

**GA2.02/E/13-B4****1100****INTENSE 630NM AIRGLOW OBSERVED IN JAPAN DURING A STORM-TIME SUBSTORM ON AUGUST 26, 1998**

Kazuo SHIOKAWA and Tadahiko Ogawa (Solar-Terrestrial Environment Laboratory, Nagoya University, 3-13, Honohara, Toyokawa, Aichi 442-8507, Japan, Email: shiokawa@stelab.nagoya-u.ac.jp) Akinori Saito (Department of Geophysics, Kyoto University, Sakyo-ku, Kyoto 606-8502, Japan, Email: saitoua@kugi.kyoto-u.ac.jp) Shinichi Miyazaki (Geographical Survey Institute, Kitagou, Tsukuba 305-0811, Japan, Email: miyazaki@gsi-mc.jp) Kiyoshi Igarashi (Communication Research Laboratory, 4-2-1, Nukuijita, Koganei 184-8795, Japan, Email: igarashi@crl.go.jp) Frederick J. Rich (USAF Research Laboratory, 29 Randolph Road, Hanscom Air Force Base, MA 01731, USA, Email: rich@plh.af.mil) Kiyohumi Yumoto (Department of Earth and Planetary Sciences, Kyushu University, 6-10-1, Hakozaki, Higashi-ku, Fukuoka 812-8581, Japan, Email: yumoto@geo.kyushu-u.ac.jp)

We show an enhancement of OI 630nm airglow emission observed at Shigaraki (34.8N, 136.1E) for 15:10-16:10UT (00:10-0110LT) on August 26, 1998 using data from a north-south meridian scanning photometer and an all-sky cooled-CCD camera. The maximum zenith emission rate reached up to 250 R. The enhancement was mainly seen in the southern sky of Shigaraki. Ground magnetometer data indicate that a substorm occurred coincide with the airglow enhancement during the initial phase of a magnetic storm. Total electron content (TEC) data obtained by more than 900 GPS receiver network in Japan show similar enhancement in the southern part of Japan associated with the substorm. Intense subauroral ion drift (SAID - westward ion flow) was observed at 15:19UT in the evening sector (20MLT, 55-60MLAT) by the DMSF-F12 satellite at an altitude of 800 km, suggesting a penetration of magnetospheric electric field to subauroral latitudes. The F-region virtual height obtained at four stations of the Communication Research Laboratory in Japan show upward (at higher latitudes) and downward (at lower latitudes) motions of the ionosphere associated with the substorm. Based on these data, we discuss possible mechanisms that caused observed airglow and TEC enhancements during the storm-time substorm.

**GA2.02/W/06-B4****1120****EVIDENCE FOR PLANETARY WAVE EFFECTS ON MIDLATITUDE BACKSCATTER AND SPORADIC E LAYER OCCURRENCE**

Mirela VOICULESCU (Department of Physics, Faculty of Sciences, University "Dunarea de Jos" of Galati, Str. Domneasca nr. 111, Galati 6200, Romania, Email: mvoic@phys.ugal.ro); Christos Haldoupis (Physics Department, University of Crete, Iraklion, 710 03, Crete, Greece, Email: haldoupis@talos.cc.ucl.gr); Kristian Schlegel (Max-Planck Institute fur Aeronomie, D-37191, Katlenburg-Lindau, Germany, Email: schlegel@linmpi.mpg.de)

A large database of midlatitude E region coherent backscatter, obtained with a 50 MHz Doppler system, is used in this paper to investigate the long-term variability in echo occurrence. The backscatter is found to be dominated by pronounced quasi-periodic variations with periods in the range from 2 to 9 days that persist for time intervals from about 10 to more than 20 days and have no relation to geomagnetic activity. The most commonly observed periods appear in two preferential bands, that is 2-3 day and 4-6 day band. Using concurrent ionosonde data we find the variations in backscatter to be exactly in phase with similar periodicities in the occurrence of relatively strong sporadic E layers. The present findings support the possibility that planetary waves are responsible for the observed long-term periodicities which also indicates a close relation between planetary waves and the well-known, but not well understood, seasonal sporadic E layer dependence. We suggest that the planetary wave option constitutes a new component into the research of midlatitude sporadic E layer formation and occurrence that needs to be considered and closely investigated.

**GA2.02/W/26-B4****1140****SIMULATION OF THE IONOSPHERIC AND THERMOSPHERIC IRREGULARITIES DURING MAGNETIC DISTURBANCES**

N.A.KILIFARSKA, Geophysical Institute, Bulgarian Academy of Sciences, Sofia 1113, BULGARIA

A theoretical ionospheric model (TIM), combined with a special procedure for updating the input parameters of the model, is applied to model the spatial/temporal irregularities in mid-latitude ionosphere during the storm-time period 9-11 October 1988. The moment distributions of thermospheric dynamic and composition (particularly, the ratio O/N<sub>2</sub>), determined from real measurements of foF<sub>2</sub> and hmF<sub>2</sub> in a meridional chain of VI stations are also presented. It was found that the main contribution to the ionospheric plasma depletion are the changes in O/N<sub>2</sub> ratio, reaching 50-70% deflection from its median values, while electron density is decreased more than 70%. The variations of the vertical plasma drift (W), induced by electric fields and thermospheric winds, are much smaller. The maximum deflections of W from its median state are ±30%, detected in 04:00 and 16:00 UT respectively. The accuracy of TIM model in foF<sub>2</sub> simulation is presented by spatial relative errors e(lat, long) between measured and calculated values. The most typical values of e are ±10% during the most hours of the disturbed period. The real measurements of foF<sub>2</sub> in all available mid-latitude stations in the Northern hemisphere have been used as criteria for the models accuracy.

**Thursday 29 July PM**

Presiding Chair: C. Haldoupis (Univ of New Crete, Greece)

**ELECTRODYNAMIC PROCESSES - HIGH LATITUDE IRREGULARITIES****GA2.02/W/31-B4****1400****COMPARISONS BETWEEN RADAR SIGNATURES OF THE FARLEY-BUNEMAN AND THE ELECTRON PEDERSEN CONDUCTIVITY INSTABILITIES**

Ranvir Singh Dhillon, University of Leicester, UK, email: rsd6@ion.le.ac.uk

Recent theoretical and experimental work directed towards the D-region and lower E-region, at altitudes of around 80-95km, has indicated the existence of a new type of plasma instability. This instability, the Electron Pedersen Conductivity Instability (EPCI), excites waves that propagate preferentially along a direction parallel to the bisector between the electric field and ExB directions. The differences between radar backscatter signatures for the EPCI and the more widely known E-region Farley-Buneman Instability (FBI) are discussed and characterised. The data were collected using CUTLASS, a bistatic component of the HF SuperDARN array with sites in Iceland and Finland, and STARE, a bistatic coherent scatter radar with sites in Finland and Norway. A summary of previous experimental studies, providing possible confirmation of the EPCI, is also presented.

**GA2.02/E/06-B4 1420**

**BACKSCATTER FROM THE AURORAL E-REGION AT ASPECT ANGLES CLOSE TO 90 DEGREES**

R.RUESTER and K.Schlegel Max-Planck-Institut fuer Aeronomie, 37191 Katlenburg-Lindau, Germany

Backscatter from E-region irregularities at aspect angles close to 90 degrees (i.e. almost parallel to the direction of the magnetic field) was observed at 53 MHz using the ALOMAR SOUSY Radar at Andoya/Norway. Strong electric fields and increased E-region electron temperatures simultaneously measured with the incoherent scatter facility EISCAT, indicate that the Farley-Buneman plasma instability was excited. In addition strong particle precipitation as inferred from EISCAT electron densities shows that the gradient drift instability may have been active, too. Auroral backscatter at such large aspect angles was not expected and has not been observed before. The characteristics of the backscatter are in many aspects completely different from usual auroral radar observations: the velocities are only of the order of 10 m/s, the half-width of the spectra is about 5 m/s and the echoes occur at altitudes well below 100 km. It is concluded, therefore, that the observed strong radar echoes are not directly caused by the above mentioned instabilities and that other mechanisms have to be considered to explain these observations.

**GA2.02/L/8-B4 1440**

**CAN FIELD ALIGNED CURRENTS GENERATE RADAR BACKSCATTER AT VERY LARGE ASPECT ANGLES?**

T R Robinson (Department of Physics, University of Leicester, Leicester LE1 7RH, UK, email: txr@ion.le.ac.uk); K Schlegel (Max-Planck-Institut fuer Aeronomie, Katlenburg-Lindau, Germany)

Recent ALOMAR SOUSY radar observations indicate that radar backscatter at 50MHz can arise in the lower E-region of the auroral ionosphere when the radar beam is pointing in a direction close to that of the geomagnetic field. If this scatter is due to 3 m plasma density irregularities then these would have to be propagating in a direction almost parallel to the geomagnetic field. There is strong evidence to suggest that field aligned currents are usually present during these large aspect angle backscatter events. This paper explores the theoretical possibility of a causal connection between the large field aligned currents and the backscatter. In particular the role of electron inertia is examined, together with thermal effects which accompany frictional heating by rapidly moving field parallel electron streams. The effects of ionisation of neutrals by fast electron impact on the stability of small scale plasma irregularities is also considered. Attention is also given to particle beam effects as well as bulk electron motion.

**GA2.02/W/01-B4 1500**

**OBSERVATIONS OF E REGION DENSITY CAVITIES**

HANS NILSSON (Swedish Institute of Space Physics, Box 812, 981 28 Kiruna, Sweden, email: hans.nilsson@irf.se)

Incoherent scatter radar observations of deep E region density cavities are reported. The observed cavities occur at the altitude of peak Pedersen conductivity and are thus likely related to downward field-aligned currents (electrons going out of the ionosphere). The cavities have electron density decreases of 30 - 50 % as compared to the background (solar EUV produced) plasma and were observed during midday in the cusp region. It appears that the seeding of the cavity may be from conductivity structures caused by cusp (proton) precipitation, causing the initial field-aligned current.

**GA2.02/W/33-B4 1520**

**A REVIEW OF THE PERKINS INSTABILITY**

Abdelhaq M. Hamza, University of New Brunswick, Canada, email: ahamza@unb.ca

A thorough review of the Perkins instability is presented in this paper. We introduce two new elements to the earlier model presented by (vit Perkins) [1973], namely the neutral wind velocity and gradients in the background field line-integrated density and Pedersen conductivity respectively. We derive the eigenfrequency and growth rate for the new instability, and recover the limiting cases discussed by (vit Perkins) [1973], and (vit Miller) [1997].

**GA2.02/W/19-B4 1600**

**FLOW ANGLE DISTRIBUTION OF THE ION AND ELECTRON TEMPERATURES ACROSS THE STATIONARY CONE OF THE PRIMARY MODIFIED FARLEY-BUNEMAN WAVES**

E E TIMOFEEV (Polar Geophysical Institute of the Russian Academy, Murmansk, Russia); M K Vallinkoski, J Kangas, P Pollari (Department of Physics, University of Oulu, Finland); T Virdi, P J Williams (Department of Physics, University of Aberystwyth, Wales, U.K.); E Nielsen (Max-Planck-Institute fuer Aeronomie, Katlenburg-Lindau, Germany)

As it has been shown in the accompanying our IAGA paper devoted to the experimental study of the thermal effects in the excitation of the Farley-Buneman (FB) waves, the primary cone of the modified FB waves with about 45 degree half-width exists permanently within the Finnish STARE radar echo layer (108\_6 km altitudes) for small (near-threshold radar echo) level of the DC ionospheric electric fields. The present paper deals with analysis of the flow angle properties of the electron (Te) and ion (Ti) temperatures as averaged within the echo layer and over 30 degree flow angle bins. It is found that: 1) both temperatures are minimal in the center of the cone while their local maxima are at the edges of the cone; the temperatures decrease beyond the cone limits; 2) both temperatures are essentially flow angle asymmetric. Ti (Te) has its absolute maximum at -45 (+45) degree flow angle bin. As a result, such a puzzling phenomenon as cooling of electrons relatively to ions stationary exists near the negative flow angle edge of the cone. The difference of temperatures (Ti-Te) is of about 50 K degrees; 3) standard deviation of the Ti (Te) sharply (2-5 times) increases near the negative (positive) flow angle edge of the cone, respectively.

**GA2.02/W/32-B4 1620**

**INTEGRAL CONDUCTIVITY OF THE TURBULENT IONOSPHERE**

Leonid ALPEROVICH (Department of Geophysics and Planetary Sciences, Tel Aviv University, 69978 Israel. Email: leonid@jupiter1.tau.ac.il )

The influence of local and random inclusions on the ionospheric conductivity has been analyzed. The calculations have demonstrated strong influence of small perturbations of the electron concentrations on the effective Pedersen conductivity in the D- and E-layers even during weak ionospheric turbulization. This is connected with the anisotropy in a strong magnetic field where the electron Pedersen conductivity which is small usually in the homogeneous ionosphere increases drastically due to an engagement with the electron Hall conductivity because of the polarization fields of ionospheric irregularities. It is found a general expression for the effective conductivity valid for both high- and low-latitude ionosphere. One can be hold for example that the effective integral conductivity of the equatorial electrojet region is almost nonsensitive to sporadic electron irregularities. Conversely, the integral conductivity of the middle latitude ionosphere and the ionosphere of the outlying regions of the polar electrojet and the polar cap can be changed drastically even during small perturbations of the electron density.

**GA2.02/E/12-B4 1640**

**STATISTICAL RELATIONSHIP AMONG ECHO POWER, DOPPLER VELOCITY AND SPECTRAL WIDTH OF HF RADAR ECHOES FROM THE HIGH-LATITUDE F REGION**

Masaaki Fukumoto, Nozomu Nishitani and Tadahiko OGAWA (Solar-Terrestrial Environment Laboratory, Nagoya University, 3-13 Honohara, Toyokawa, Aichi 442-8507, Japan, email: ogawa@stelab.nagoya-u.ac.jp) Natsuo Sato, H. Yamagishi and A. S. Yukimatu (National Institute of Polar Research, 1-9-10 Kaga, Itabashi, Tokyo 173-8515, Japan)

Three parameters (echo power, Doppler velocity and spectral width) derived from ionospheric HF and VHF radar echoes have been very useful to study the characteristics of equatorial and high-latitude E region irregularities, their generation mechanisms and nonlinear plasma state. The generation mechanisms of F region irregularities at high-latitude seem to be more complicated than those at the equator and mid-latitude because, in addition to electric fields, particle precipitation (field-aligned current) from the magnetosphere may play a part in producing the high-latitude F region irregularities. In this paper, we present some statistical relationships among the three parameters in the auroral and polar cap F regions obtained from the Syowa Station HF radar in Antarctica. Although data points are largely scattered, there exists an indication of positive correlation between the Doppler velocity and echo power and also between the Doppler velocity and spectral width (and therefore, between the echo power and spectral width). Based on these results, we discuss possible generation mechanism(s) of the F region irregularities responsible for the HF radar backscatter.

**GA2.02/W/04-B4 1700**

**COHERENT HF RADAR BACKSCATTER CHARACTERISTICS ASSOCIATED WITH AURORAL FORMS IDENTIFIED BY INCOHERENT RADAR TECHNIQUES: CUTLASS AND EISCAT**

S E MILAN, J A Davies, M Lester (All at Department of Physics and Astronomy, Leicester University, Leicester LE1 7RH, UK. Email: Steve.Milan@ion.le.ac.uk)

CUTLASS Finland HF coherent radar backscatter from decametre-wavelength field-aligned F region irregularities is compared with common-volume plasma parameters and the electric field deduced by the EISCAT UHF incoherent radar system, for a 12 hour period from the 18 and 19 June 1996. During this interval we find an excellent agreement between irregularity Doppler velocity and bulk ion drift resolved along the CUTLASS beam. Furthermore, backscatter is found to exist only in regions of non-zero electric field, as the ExB instability growth rate is dependent on E. Also, no backscatter is observed in regions where the E region Pedersen conductivity is greatly enhanced, as the perturbation electric field associated with the F region irregularities is shorted-out and the instability growth is quenched. The presence of auroral arcs within the scatter volume increases both the intensity and spectral width of backscatter returns. We show how this allows the location of precipitation features within the field-

**GA2.02/W/22-B4 1720**

**ORIENTATION OF SMALL-SCALE ELECTRON DENSITY FLUCTUATIONS AND THE DIRECTION OF PLASMA FLOW IN THE IONOSPHERIC F LAYER**

T Nygren (Department of Physical Sciences, University of Oulu, FIN-90570 Oulu, Finland, email: tuomo.nygren@oulu.fi), E.D. Tereshchenko, B.Z. Khudukon and M.O. Kozlova (Polar Geophysical Institute, 183010, Murmansk, Russia)

A new method of determining the anisotropy parameters of ionospheric field-aligned electron density fluctuations is presented. The method makes use of amplitude scintillation of a signal from a satellite to a ground-based receiver. In simple terms, the method is based on the fact that sheeetlike irregularities cause maximal scintillation when the ray from the radio source to the receiver lies in the plane of the irregularity sheets. Hence, due to a straightforward geometric effect, a maximum scintillation level should be met in some specific ray direction during the satellite passage. Using the known geomagnetic field and a reasonable assumption of the height range of the irregularities, the variation of the scintillation level around this direction allows the determination of both the field-aligned and field-perpendicular anisotropy as well as the orientation of the field-perpendicular anisotropy of the spatial spectrum of the density fluctuations. Results are shown from an experimental campaign where satellite scintillation was observed at three sites at high latitudes and, simultaneously, the F region plasma flow was measured by the near-by EISCAT incoherent scatter radar. The orientation of the anisotropy determined from the scintillation observations is compared with the direction of F region plasma flow. The results indicate that, in cases where the observed irregularities lie close to the theastatic radar volume and the experimental errors of the radar velocity measurement are not great, a good agreement between the two directions is obtained.

**GA2.02/E/02-B4 1740**

**DYNAMICS OF THE POLAR CAP IONOSPHERE: A STUDY OF POLAR PATCHES ABOVE CASEY, ANTARCTICA.**

A.M. Breed(1), T.M. Maddern(1), P.L. Dyson(2), R.J. MORRIS(1) (1) Australian Antarctic Division, Channel Highway, Kingston, Tas. 7050, Australia. (2) School of Physics, La Trobe University, Bundoora, Vic. 3083, Australia.

A Lowell Digital Ionosonde (DPS-4) has operated at the Australian Antarctic polar cap station Casey (-80.6o CGM latitude), since early 1993, primarily to study the dynamics of the southern



polar cap ionosphere. To gain a better understanding of the ionospheric motions involved, animated data displays have been developed using ionospheric drift and ionogram data combined together with other geophysical data sets to help identify dynamical features. These displays generally show ionospheric sky maps (echo locations), drift velocities and Doppler ionograms (vertical profiles), produced with a resolution of up to a frame every 2 minutes. Ionospheric changes can then be viewed frame by frame using commercial animation software. This provides a simple means of viewing large amounts of data and identifying, for example, drifting polar patches, or the response of ionospheric drift to changes in the IMF. Since the ionosonde takes measurements throughout the bottomside ionosphere, different height regions (eg. E and F) can be examined independently or compared directly. Doppler and directional information featured in the animations provide a powerful technique for studying the evolution of ionospheric phenomena, such as polar patches. This paper will demonstrate the applications of the 'ionomovie' animations, and then present results of a study of polar patches.

Friday 30 July AM

Presiding Chair: S. Fukao (Kyoto University, Japan)

## ELECTRODYNAMIC PROCESSES – LOW-LATITUDE IRREGULARITIES

GA2.02/W/05-B5

0900

### ZONAL WIND VARIATIONS FROM HF/VHF RADAR OBSERVATIONS OF THE EQUATORIAL ELECTROJET REGION

C.V. DEVASIA, Sudha Ravindran, K.S. Viswanathan and K.S.V. Subbarao (Space Physics Laboratory, Vikram Sarabhai Space Centre, Trivandrum - 695022, India, email: spl\_vssc@vssc.org)

The electric fields generated by local east-west wind structures in the electrojet region are very important as they are involved in many other ionospheric processes in addition to the generation of currents which modulate the normal electrojet current. Depending on the height structure of the wind, the wind generated polarization field can have a much greater fine structure in height compared to the smooth altitude structure of the normal vertical polarization electric field due to the height-invariant global east-west electric field present in the electrojet region. The height structure of the wind generated electric field can have a large variability on different time scales due to the large variability of the causative wind structure. These characteristics of the wind generated polarization field are manifested in the height structure of the type II plasma phase velocities as observed by the HF and VHF backscatter radars at Trivandrum (Dip 0.5 deg. N) as the radar measured phase velocities are proportional to the polarization field in the electrojet region. The inverse problem of deducing the zonal wind velocities at the electrojet altitudes from the radar measurements thus provide a simple method for studying the wind variations in the electrojet region. The characteristics of zonal winds deduced from the radar measurements are discussed in detail in terms of their spatial and temporal variations.

GA2.02/W/08-B5

0920

### FIRST RESULTS OF EQUATORIAL ELECTROJET OBSERVATIONS USING INPE'S 50 MHZ COHERENT BACK-SCATTER RADAR

M. A. Abdu, J. H. A. Sobral, Clezio M. Dinardini, I. S. Batista, P. Muralikrishna, E. R. de Paula (Instituto Nacional de Pesquisas Espaciais- INPE, 12201-970 Sao Jose dos Campos, Brazil.)

A VHF coherent back-scatter radar developed at INPE is now partially operational at the magnetic equatorial site, Sao Luis (2.33° S, 44.2° W dip angle: -5°) in Brazil. The radar operating at 50 MHz is projected for a nominal transmitting peak pulse power of 120 kW although only a partial capability of ~40kW was used in its first measurements of the electrojet irregularity dynamics carried out in a one-week campaign conducted in August 1998. The radar employs a coaxial-colinear type antenna system arranged in a phased array of 16 parabolic antennas (each having 48 half wave dipoles) arranged in 8 pairs each fed by one of the 8 units of its modular transmitter system. Backscattered echos are received by the same antenna through the use of T/R switches. Doppler velocity spectra of the 3-m irregularities of the electrojet were recorded at 2.6 km height resolution between 90 and 120 kms. The measurements to be reported here were made in a time sharing mode between the antenna beam oriented vertically and at 30° tilted eastward. The few days of observation covered a disturbance interval associated with the major magnetic storm of 26 August 1998. The velocity spectrum and intensity distribution of electrojet irregularities showed large fluctuations in response to prompt penetration of magnetospheric electric field to equatorial latitudes as indicated by the simultaneous fluctuations observed in the auroral activity indices and in local magnetogram. Instances of total inhibition of the plasma instability process was also observed possibly caused by disturbance dynamo electric field associated with the storm. Results of a detailed analysis of the data set will be presented in this paper.

GA2.02/E/09-B5

0940

### IONOSPHERIC E REGION IRREGULARITIES DURING COUNTER ELECTROJET

R.G.RASTOGI, Department of Physics, Gujarat University, and Physical Research Laboratory, Ahmedabad 380 009, India e-mail: parvs@prl.ernet.in V.V.Somayajulu, Space Physics Laboratory, Vikram Sarabhai Space Centre, Thiruvananthapuram 695 022, India

The paper describes the ionospheric observations at Thumba during intense midday equatorial counter electrojet events, which occur on a series of days of December solstitial months. It is shown that Es-q type of plasma irregularities or blanketing type of sporadic E layer are often generated during westward electric field. On certain events the occurrence of these irregularities are preceded by the down drifting of intermediate E2 layer from 150 km to below 100 km level. Possible suggestions for such events are made.

GA2.02/W/28-B5

1000

### VHF RADAR OBSERVATIONS OF E REGION IRREGULARITIES OFF THE MAGNETIC EQUATOR OVER GADANKI

K.S. VISWANATHAN (Space Physics Laboratory, Vikram Sarabhai Space Centre, Trivandrum 695 022, India, email: spl\_vssc@vssc.org) A.K. Patra (Department of Physics, K.O. College, Gumla 835 207, India) K.S. Raina and P.B.Rao (both at National MST Radar Facility, P.O. Box 123, Tirupati 517 502, India, email: nmrf@isro.ernet.in)

The MST radar, located at Gadanki (13.5 deg.N, 79.2 deg.E; dip 12.5 deg.N), has been operated in ionospheric coherent backscatter mode for mapping the structure and dynamics of E region field aligned irregularities on several days during summer and equinoctial months since 1994. The observations are presented in the form of Doppler power spectra, height-time-intensity (HTI) maps and height-time variations of Doppler velocity and velocity spectral width.

The spectra are found to be quasi-Gaussian, showing variations in both height and time that are more intense during nighttime compared to daytime. During daytime, the E region is found to be unstable in two distinct height ranges, nominally 85-95 km and 100-115 km and they merge during nighttime. The signals are found to drop out, in general, for 3 to 4 hr. around noontime at Gadanki, in contrast to that observed over the equator. The signal intensity often undergoes quasi-periodic variations with periods of few tens of min which seem to be a manifestation of medium-scale gravity waves. The Doppler velocities in the higher height range are mostly upward during daytime and downward during nighttime with values generally not exceeding 40 m/s and are clearly of electrodynamic origin. In the lower height range, however, the drift velocities are downward during daytime and upward during nighttime with values less than about 30 m/s and seem to be due mainly to the meridional component of the neutral wind. The velocity spectral width, representing turbulence, often exceeds 100 m/s and is thus greater to the mean Doppler velocity.

GA2.02/E/14-B5

1040

### STUDY OF ELECTROJET ASSOCIATED IONOSPHERIC IRREGULARITIES THROUGH VHF SCINTILLATION

B.M.PATHAN,D.R.K.Rao and S.Banola(all at Indian Institute of Geomagnetism Colaba, Mumbai 400 005 India, email: bmpathan@iig.iigm.res.in)

Daytime scintillations observed at the equatorial region are attributed to the instabilities in the electrojet currents flowing in the E-region of the equatorial ionosphere. These scintillations are rather weak and hence have a narrow latitudinal coverage. The occurrence of Esq associated weak scintillations is maximum (~ 90%) near the dip equator while on few occasions strong scintillations associated with blanketing type of Es are seen near the edge of the electrojet. Strong scintillations (S4-0.8) with moderate fade rate (~ 13 fades per min) on 250 MHz signal were recorded at Pondicherry (4.4 deg. dip lat.) on 05 May 1998 (Ap=42) during 16-17 hr IST. Ionosonde operated at a nearby station Kodaikanal indicated the presence of multi layer blanketing Es at about 100 km altitude. The high frequency asymptotes of power spectra have yielded two dimensional irregularity power spectrum index of about 3 over wave lengths of 100-700 m which are close to the theoretical prediction of 8/3 for type I and type II irregularities. The transverse drift speed of the irregularity as determined from the Fresnel frequency is about 70 m/s. The results are discussed in terms of variation in electrojet characteristics.

GA2.02/E/08-B5

1100

### SHAPE AND SPATIAL DISTRIBUTION OF F-REGION ELECTRON DENSITY IRREGULARITIES AS OBSERVED BY THREE DIFFERENT PLASMA PROBES DURING THE GUARA CAMPAIGN

P. MURALIKRISHNA, M.A. Abdu, M.G.S. Aquino (all at Instituto Nacional de Pesquisas Espaciais - INPE/MCT, C.P. 515, 12201-970, Sco Josi dos Campos - SP, Brazil, email: murali@dae.inpe.br), J LaBelle (Department of Physics and Astronomy, Dartmouth College, Hanover, NH 03755, USA, email: jlabelle@einstein.dartmouth.edu)

Nighttime F-region electron density height profile and the amplitude of the electron density fluctuations were measured simultaneously by three different plasma density probes during the Guara campaign, conducted from Alcantara in Brazil in the year 1994. During this campaign a Black Brant X sounding rocket was launched on 14-th October 1994 at 1955hrs (LT) to investigate into the phenomenon of high-altitude equatorial spread-F events. The rocket, as expected passed through an active topside spread-F event, monitored simultaneously by several ground-based instruments. A High Frequency Capacitance (HFC) probe, a conventional Langmuir Probe (LP) and a Plasma Frequency Probe (PFP) were used to measure the electron density and the spatial fluctuations in it. While the PFP and HFC measurements (except for an estimated plasma sheath factor for the HFC probe) provide the absolute electron density, the LP gives the relative variation in the electron density. The spatial resolutions that can be obtained from the three probes are also different. While the HFC probe has the lowest spatial resolution and thus can be used to study the shape of large scale irregularities, the PFP has the highest spatial resolution and thus can be used to study the shape of small scale irregularities. The LP has an intermediate spatial resolution. Thus, the three probes provided data, which could be used not only to obtain reliable electron density data, but also to study the shape and spatial distribution of the electron density irregularities over a wide range of scale sizes. The shape of the irregularities is seen to change not only with the range of their scale size but also from one height region to another. These spatial characteristics of the irregularities are presented and discussed here in the light of the plasma instability mechanisms responsible for their generation.

GA2.02/E/05-B5

1120

### FIRST SIMULTANEOUS MEASUREMENT OF ELECTRON DENSITY AND ELECTRIC FIELD FLUCTUATIONS FROM THE INDIAN ZONE

H.S.S. SINHA, Shikha Raizada and R.N. Misra, Physical Research Laboratory, Navrangpura, Ahmedabad -380 009, INDIA

Simultaneous measurements of electron density and electric field were made from SHAR (13°N, 80°E) using a Langmuir probe and two pairs of double probes respectively onboard a RH-560 rocket. This constituted the first simultaneous in-situ measurement of electric field and electron density from the Indian zone. The aim of the experiment was to study the nature of irregularities during a fully developed phase of ESF. It was observed that the electric field and electron density fluctuations were co-located in the altitude regions between 165-175 km, 210-260 km, and 295-330 km.

The electron density profile exhibited new type of irregularities in 165-175 km altitude region. Structures with vertical scale sizes with wavelengths of about 40 km, were seen in this region. Presence of fluctuations with such scale sizes suggests that gravity waves might be playing a dominant role in producing irregularities in this region. Smaller scale perturbations with scale sizes less than 6 km superimposed on large perturbations were prominent in this altitude region. Power spectral analysis of the irregularities showed the presence of perturbations with scale sizes from 15 m to 1 km in 165 - 175 km region. These irregularities display very steep spectral indices which were not seen in earlier experiments and cannot be explained by Generalized Rayleigh Taylor Instability (GRTI), Gradient Drift Instability (GDI) or image striation theory. We conjecture that these perturbations might be due to the cascade of larger scale structures as in the case of neutral turbulence in the lower atmosphere.

**GA2.02/W/27-B5 1140**

**INTRINSIC LOCALIZED MODES AND ONSET OF THE EQUATORIAL SPREAD F**

BAMANDAS BASU (Air Force Research Laboratory, Hanscom Air Force Base, MA, 01731, USA, Email: basub@plh.af.mil); Bruno Coppi (Department of Physics, Massachusetts Institute of Technology, Cambridge, MA, 02139, USA, Email: coppi@pc.mit.edu)

A theoretical model for the onset of the Equatorial Spread F (ESF) is introduced considering all the effects of the electric fields that are present together with those of the neutral wind velocity, of gravity, and of the density gradient. These impose well-defined topological constraints on the modes that can be excited. The horizontal (east-west) ion velocity is shown to be one of the key factors for the intrinsic vertical localization of modes that are driven unstable by the effective vertical gravity (including the E-field contribution). The width of the layer of localization is related to the vertical gradient of the ion horizontal velocity, of the neutral wind velocity, and of the ion-neutral collision frequency. The "horizontal gravity" resulting from the difference between the horizontal ion and neutral velocities is shown not to be a driving factor for the instability, when the eastward electric field is included in the analysis, but to have an important influence on the mode topology (vertical profile). An explicit analytical solution is found for the relevant dispersion equation that includes the contribution of a vertical ion velocity. The mode vertical profile under realistic conditions is found. It is suggested that the onset of the ESF is determined by the necessary conditions for the intrinsic localization of the modes, and that this fact may explain why the onset is not observed to correlate only with the formation of steep density gradients. The mode ballooning structure, along the magnetic field, including the effect of the plasma finite resistivity is also described.

Friday 30 July PM

Presiding Chair: M. Abdu (Instituto Nacional de Pesquisas Espaciais, Brazil)

**ELECTRODYNAMIC PROCESSES – LOW-LATITUDE IRREGULARITIES – PART 2**

**GA2.02/E/01-B5 1400**

**INTERACTION OF TWO LONG WAVELENGTH MODES IN THE NONLINEAR EVOLUTION OF EQUATORIAL SPREAD-F**

R. SEKAR and E. A. Kherani (Physical Research Laboratory, Navrangpura, Ahmedabad, India, email: rsekar@prl.ernet.in); P. B. Rao and A. K. Patra (National MST Radar Facility, Gadanki, India).

Plasma irregularities during nighttime in the equatorial F-region (ESF) manifest themselves in many different forms on VHF radars, ranging from spectacular rising plumes and multipulses to modest bottomside spread-F events. The plumes which extend from bottomside to the topside of the ionosphere were identified earlier as the manifestation of large scale plasma bubbles generated by the action of generalized Rayleigh-Taylor instability. For seeding the above instability, gravity waves in the neutral atmosphere is thought to be a potential source. As the spectra associated with the gravity waves are diverse, it becomes important to investigate the development of ESF with different modes simultaneously. As a first step, an investigation is made with two long wavelength modes as initial perturbation in the nonlinear simulation model of ESF. It is demonstrated that the longer wavelength mode developed into a bottomside structure, while the second mode developed into multiple plumes. Further, the interaction between the modes has been shown to modify the electric field structures. The results obtained from this investigation explain some of the unique patterns of plumes and their Doppler velocities observed by the Indian MST Radar in ionospheric mode.

**GA2.02/W/34-B5 1420**

**ROCSAT-1 OBSERVATIONS OF LOW LATITUDE: IONOSPHERIC IRREGULARITIES**

Y. C. Yeh, J. M. Wu, S. Y. Su, and H. C. Yeh (all at Institute of Space Science, National Central University, Chung-Li, 320, Taiwan, email: ycye@ccsrd.csr.ncu.edu.tw); R. A. Heelis (University of Texas at Dallas, email: heelis@utdallas.edu)

The ion density observation from Ion Trap(IT) of IPEI payload onboard the ROCSAT-1 at 600 km altitude is capable of sampling at 1024 Hz to obtain the high spatial resolution of density variations in the ionospheric bubble event. The fast variations in densities developed on the steep walls of convection bubble will be presented. The general morphology of the bubbles will also be presented.

**GA2.02/W/18-B5 1440**

**ROCSAT-1 OBSERVATIONS OF LOW LATITUDE IONOSPHERIC IRREGULARITIES - PLASMA FLOW OBSERVATIONS**

J.M.Wu, Y.C. Yeh, S.Y. Su, H.C. Yeh (Institute of Space Science, National Central University, Chung-Li 320, Taiwan, ROC. email: jmwwu@ccsrd.csr.ncu.edu.tw) R.A. Heelis (University of Texas at Dallas, email: heelis@utdallas.edu)

The ion drift meter (IDM) of the IPEI payload on board ROCSAT-1 is designed to take in-situ measurement of ion drift velocity over a large dynamic range with high accuracy. The IPEI ion drift data observed at the high sampling rate (32 Hz in Normal mode, and 1024 Hz in Fast Mode) will provide ion flow structures in the ionosphere at middle and low latitudes at 600 km altitude. In this report, horizontal and vertical ion drift data from the ROCSAT1 will be used to determine the average zonal and vertical plasma flow characteristics during a disturbed ionospheric condition when mid-latitude irregularities and/or low-latitude spread-F have occurred. Detail comparison of the flow patterns for these two difference ionospheric phenomena will be presented. of AMS particularly for sediments.

**GA2.02/W/24-B5 1500**

**CONTRIBUTION OF MULTI-LATITUDINAL MEASUREMENTS OF TEC ON THE UNDERSTANDING OF THE DEVELOPMENT OF LOW-LATITUDE SCINTILLATIONS**

C.E. Valladares, R. Sheehan (Institute for Scientific Research, Boston College, Chestnut Hill, MA 02167; 781-863-5928; email: cesar@dl5000.bc.edu) A. Mazzella (Northwest Research Associates, Bellevue, WA) J. W. Meriwether (Department of Physics and Astronomy, Clemson University, Clemson, SC 29634; 864-656-0915; email: john.meriwether@ces.clemson.edu)

Measurements of the total electron content (TEC) using four stations (Bogota, Ancon, Arequipa, and Santiago) located near the west coast of South America were used to obtain long-term statistics of the preferred conditions of the low-latitude ionospheric plasma during the occurrence of scintillations at the magnetic equator. The scintillation activity is quantified using the S4 index gathered both in the UHF- and L-bands at two stations (Ancon and Antofagasta). The first site is placed near the magnetic equator and the second station is

situated close to the equatorial anomaly. The multiple site measurements allow us to infer the altitude extension of the layers containing irregularities and the distribution of TEC along the magnetic field lines. We have also used measurements of the zonal and meridional winds at the Arequipa station, first to understand the latitudinal distribution of TEC and secondly to observe the dominant conditions of the electrodynamics driving zonal winds during the onset of irregularities. We present here measurements of the degree of symmetry/asymmetry that can exist between the southern and northward anomalies during times of the development of the equatorial irregularities and values of the neutral wind during these times.

**GA2.02/P/01-B5 1520**

**ON THE 01 630.0 NM, 557.7 NM AND 777.4 NM NIGHTGLOW MEASUREMENTS OF EQUATORIAL PLASMA DEPLETIONS DURING SPREAD-F-EVENTS**

G.K. Mukherjee, L. Carlo and S.H. Mahajan, Indian Institute of Geomagnetism Colaba, Mumbai 400 005, India e-mail: gkm@iig.res.in

During the period January-April 1998, a good series of measurements of the 01 630.0 nm, 557.7 nm and 777.4 nm nightglow emissions of equatorial plasma depletion have been obtained during spread-F condition of the ionosphere using an All-Sky Camera at Kolhapur (16.8 deg N, 74.2 deg E; dip lat. 10.6 deg N). The All-Sky Camera offers broad and instantaneous coverage of the movement of large scale size irregularities (depletions or bubbles) over a region of horizontal diameter of 1800 km at about 300 km. The location of the station is important as a single image at a given instant maps the irregularities over a large area starting from the geomagnetic equator to the anomaly region. The images also show altitude-latitude extent of the plasma depleted fluxtubes and it is observed that most of the bubbles rise to an altitude of 1000 km over the magnetic equator, only few of them could exceed the height of 1500 km which corresponds to the northern edge of the image. The characteristics of bubbles at this longitude zone have been brought out. The maximum number of depletions occur during the equinoctial months, March. Simultaneously the data from other complementary experiments such as VHF scintillation, ionosonde and photometers are presented to study the characteristics of small and large scale size irregularities. Using the field aligned movement of the bubbles, the bubble rise velocities at the equator have been estimated and compared with other experimental results.

**GA2.02/E/11-B5 1600**

**FURTHER RESULTS REFERRING TO THE NEUTRAL DENSITY DEPLETIONS ATTRIBUTED TO PLASMA BUBBLES**

Pal BENCZE (Geodetic and Geophysical Research Institute, Hungarian Academy of Sciences, H-9401 Sopron, P.O.B. 5, Hungary, email: bencze@ggki.hu) Ivan Almar and Erzsebet Illes-Almar (both at Konkoly Observatory, H-1525 Budapest, P.O.B. 67, Hungary, email: almar@ogyalla.konkoly.hu) Csilla Nemeth (H-1112 Budapest, Koerberki u. 37, Hungary)

Our former investigations have indicated that short period depletions of the total neutral density - found in the data of the high temporal resolution accelerometer measurements of the San Marco V satellite - might be attributed to plasma bubbles in the vicinity of the equator. As it is known, plasma bubbles are generated by the Rayleigh-Taylor instability, the growth rate of which depends on the vertical gradient of the electron density. This gradient is greatest by night and in the winter months. Furthermore, the occurrence of plasma bubbles depends on geomagnetic activity as indicated by the occurrence frequency of spread F. Therefore the temporal variation of the occurrence frequency of the total neutral density depletions was investigated to confirm the assumption that these depletions in the vicinity of the equator are due to plasma bubbles.

**GA2.02/W/07-B5 1620**

**THERMOSPHERIC MERIDIONAL WINDS AND ITS RELATION TO SPREAD-F**

N. JYOTI and C.V. Devasia (Space Physics Laboratory, Vikram Sarabhai Space Centre, Trivandrum-695 022, India, email: spl\_vssc@vssc.org)

One of the important characteristics of the night time equatorial F-region is the occurrence of F-region plasma density irregularities known as equatorial spread-F(ESF). Experimental evidences have shown that a rapid vertical plasma drift due to enhanced zonal electric fields of F-region dynamo action which becomes prominent over the E-region dynamo action in the post sunset period leads to an elevated F-region ,thus providing the prerequisite for the onset of ESF. The above physical condition is conducive for a fast growth of Rayleigh-Taylor (R-T) plasma instability processes which account for ESF generation .Still there remains some observational aspects of ESF which are not clearly explained. Using the ionograms recorded during March-April, 1998, under I-STEP campaign, we attempt to ascertain the ambient ionosphere-thermosphere conditions especially the role of meridional winds in the occurrence of ESF at Trivandrum, an electrojet station and SHAR, a non-electrojet station both over India. A large wind velocity significantly reduces the instability ,even if a large upward ExB drift velocity is applied and the wind effect is more prominent when the reversal time of the ExB drift is late. We also attempt to assess whether the favourable or unfavourable conditions found are related to geomagnetic activity or merely extreme forms of the day to day variability.

**GA2.02/W/23-B5 1640**

**MODELLING SECTIONS OF THE EQUATORIAL F-REGION DURING SUNRISE AND SOLAR ECLIPSE**

O.P.KOLOMITSEV (1), I.B.Egorov (1), B.M.Reddy (2), V.A.Surotkin (1) (1) IZMIRAN, Troitsk 142092 Moscow Region, Russia (2) National Physical Laboratory, New Delhi 110012, India

The description of numerical-analytical method of construction of vertical structure ionospheric plasma is caused. The method permits to reproduce two-dimensional the sections of F-region - isolines of plasma frequency in coordinates height-time (height-distance) under various solar-geophysical conditions: the initial conditions, solar activity, season, photochemistry, geomagnetic disturbance, diffusion, and vertical drift of the ionospheric plasma. The method was used for construction of the ionospheric sections to sunrise and eclipse periods. For example, the results of accounts to equator present, where in the ionospheric F-layer near sunrise or at eclipse for certain conditions a hole of lower electron density can arise, which is situated between the F-layers surviving after the night and the new morning F-layer. It is shown that near to total phase of eclipse below of maximum Ne the decrease Ne is observed. This spot of perturbation of eclipse Ne with increase of height is run and displaces aside of midday. On vertical it covers the region of heights 150-270 km, till time of ~30 min with maxima shifted to midday concerning to total phase eclipse on 10-15 min. Solar eclipse renders also the influence and on rate run of night F-layer, and layer actually disappears by 07.40 LT, i.e. the hole lifetime increases, and without eclipse it already disappears by 07.05 LT. The total lifetime of the hole (the sunrise and solar eclipse effects) is equal ~120 min.

**GA2.02/E/10-B5** **1700**

**MEASUREMENT OF EXPLOSION-INDUCED GEOMAGNETIC DISTURBANCES\***

D. LYNN SHAEFFER, Donald R. Rock, J. Patrick Lewis, and Stephen I. Warshaw (all at Lawrence Livermore National Laboratory, P.O. Box 808, L-183, Livermore, California, U.S.A. 94550, email: shaeffer1@llnl.gov)

The Black Thunder Coal Mine (BTCM) near Gillette, Wyoming was used as a test bed to determine the feasibility of detecting explosion-induced geomagnetic disturbances with ground-based induction magnetometers. Two magnetic observatories were fielded at distances of 50 km and 64 km geomagnetically north from BTCM. Each observatory consisted of three mutually orthogonal magnetometers, Global Positioning System (GPS) timing, battery and solar power, a data acquisition and storage system, and a three-axis seismometer. Explosions with yields of 1 to 3 kT of TNT equivalent occur approximately every three weeks at BTCM. Explosion-induced acoustic waves propagate upward and interact collisionally with the ionosphere to produce ionospheric electron density perturbations that act as sources for geomagnetic disturbances. These disturbances propagate through an ionospheric Alfvén waveguide that we postulate to be leaky. Consequently, wave energy may be observed on the ground. We observed Q-bursts that appear to be excited in the earth-ionosphere cavity by Alfvén solitons that may have been generated by the explosion-induced acoustic waves reaching the ionospheric E and F regions and that subsequently propagate down through the ionosphere to the atmosphere. In addition, we observed late time (> 800 s) ultra low frequency (ULF) geomagnetic perturbations that appear to originate in the upper F region (~ 300 km) and appear to be caused by the explosion-induced acoustic wave. We suggest that explosion-induced Q-bursts may be discriminated from naturally occurring Q-bursts by association of the former with the late time explosion-induced ULF perturbations. Experimental results, analyses, and conclusions will be presented. (... This work was performed under the auspices of the U.S. Department of Energy by Lawrence Livermore National Laboratory under contract No. W-7405-Eng-48.)

**Thursday 29 July AM**

Presiding Chair: R.F. Pfaff (NASA, USA)

**GA2.02/W/17-B4** **Poster** **0930-01**

**SPATIAL DISTRIBUTION OF E-REGION DECAMETRE WAVELENGTH IRREGULARITIES OBSERVED BY THE HIGH FREQUENCY VALENSOLE RADAR**

Glenn Hussey (Institute of Space and Atmospheric Studies, University of Saskatchewan, Saskatoon, Canada); Christos HALDOUPIS (Physics Department, University of Crete, Iraklion, Crete, 710 03 Greece, Email: haldoupis@talos.cc.uoh.gr) ; Alain Bourdillon (Laboratoire Radiocommunications, URA CNRS 834, Université de Rennes 1, Rennes, France); Jean Delloue (Laboratoire de Physique de l'Exosphère, Université Pierre et Marie Curie, Paris, France); Dieter Andre (Institute of Space and Atmospheric Studies, University of Saskatchewan, Saskatoon, Canada)

We use data from a high frequency (HF) Doppler radar experiment at midlatitudes to perform a statistical analysis of the spatial occurrence of \$E\$ region decametre backscatter. The radar, which is located near Valensole in Southern France made multifrequency measurements of high resolution spectra simultaneously at four frequencies, namely, 9.23, 11.03, 12.71 and 16.09 MHz, which correspond to backscatter from field-aligned, E region irregularities with wavelengths of 16.3, 13.6, 11.8 and 9.3 m, respectively. Based on the premise that E region scattering is fully magnetic aspect sensitive, the spatial occurrence statistics show that the aspect sensitive region moves towards the radar (southward) with respect to line-of-sight propagation calculations with the lower frequency echoes being closer towards the radar than the higher frequency ones, in agreement with refraction theory predictions. Ray-tracing calculations inside nighttime midlatitude electron density profiles augmented with dense sporadic Es layers was used to calculate the expected echoing region and, indeed, good agreement with the observed region was found. Another finding is the angular distribution of backscatter inside the wide azimuthal sector covered by the radar scan. The spatial distribution of echo occurrence has its maximum at small azimuths at and about the geomagnetic north, suggesting that statistically the meridional direction is strongly preferred for backscatter. Under the postulation that these are secondary decametre waves, we conclude that the observed angular anisotropy in spatial occurrence is at odds with the concept of strong isotropic plasma turbulence (i.e., see Sudan, JGR, 88, 4853, 1983), but in general agreement with the two step instability theory of secondary wave generation proposed earlier (i.e., see Sudan et al., JGR, 78, 240, 1973).

**GA2.02/W/03-B4** **Poster** **0930-02**

**LARGE POLARIZATION ELECTRIC FIELDS ASSOCIATED WITH MIDLATITUDE SPORADIC E**

Sergei Shalimov (Institute of Physics of the Earth, Moscow, Russia, Email: shalimov@upei-ras.scgis.ru)Christos HALDOUPIS (Physics Department, University of Crete, Iraklion, Crete, 710 03 Greece, Email: haldoupis@talos.cc.uoh.gr)Kristian Schlegel (Max-Planck-Institut fuer Aeronomie, Katlenburg-Lindau, Germany, Email: schlegel@linmpi.mpg.de)

Recent 50 MHz E region coherent backscatter observations and in situ rocket measurements established the existence of enhanced electric fields in the midlatitude ionosphere that can become at times sufficiently large to excite the Farley-Buneman instability. To understand the origin of these fields, we present a simple quantitative model that relates to a local polarization process acting inside spatially confined, nighttime sporadic E layers of dense ionization. By including the effects of field-aligned currents in the current continuity equation we estimate the necessary conditions on the relative horizontal E layer extent and the ratio of integrated Pedersen conductivities above and inside the layer for the generation of both zonal and meridional polarization fields. We show that the polarization process can account for the elevated electric fields of several millivolts per meter, which are implied often from backscatter Doppler measurements during unstable E region conditions at midlatitude. The polarization process can become much more effective for dense and strongly elongated Es layers under the action of an enhanced ambient electric field. In this case, large polarization fields that may be capable of exciting Farley-Buneman plasma waves can be sustained. The stringent requirements for strongly elongated sporadic E layers with sharp boundaries, low ionospheric Pedersen conductivities above the layer in relation to those inside, and relatively large ambient electric fields would explain why type 1 echoes are so rare in midlatitude E region backscatter.

**GA2.02/W/29-B4** **Poster** **0930-03**

**THE GENERATION OF IONOSPHERIC IRREGULARITIES DUE TO INSTABILITY OF ACOUSTIC-GRAVITY WAVES IN THE ELECTRIC FIELD**

Valery SOROKIN and Vitaly Chmyrev (both at: Institute of Terrestrial Magnetism, Ionosphere and Radio Wave Propagation, Russian Academy of Sciences, IZMIRAN, Troitsk, Moscow Region, Russia, 142092, email: sova@izmiran.rssi.ru)

The generation mechanism of small – scale ionospheric irregularities is presented. The critical factor of the mechanism is excitation of super threshold DC electric field in the lower ionosphere initiating the AGW instability and the formation of periodic structure of Pedersen conductivity, field – aligned electric currents and the related plasma density inhomogeneities in the upper ionosphere. The electric field energy transforms to the energy of acoustic oscillations without a change in the medium thermal balance. The instability increment is proportional to the square of external electric field. In the presence of external DC electric field the conductivity variations in E-layer lead to an appearance of polarization electric fields propagating into the upper ionosphere and generating the plasma density variations at these altitudes. Estimates of the space-time and amplitude characteristics of the excited ionospheric disturbances and their comparison with the satellite data show that the developed mechanism can be applied to explanation of some properties of auroral ionosphere irregularities, as well as to generation model of earthquake related small-scale plasma inhomogeneities in the upper ionosphere.

**GA2.02/W/30-B4** **Poster** **0930-04**

**DIFFERENCES AND CHARACTERISTICS IN THE FORMATION OF DIFFERENT TYPES OF THE IONOSPHERIC E-REGION SPORADIC LAYERS FROM INOSPHERIC SOUNDING DATA OBTAINED IN THE EAST-SIBERIAN REGION**

V.F.Petrukhin, E.A.Ponomarev and N.A.Sutyryn (Institut of Solar-Terrestrial Physics, Irkutsk, Russia, email: nasut@iszf.irk.ru)

Presented are results derived from analyzing the data on the ionospheric Es-layer behavior over East Siberia for the time interval 1975-1996. The analysis was carried out by using a filter separating the data into daytime and nighttime intervals (from the solar zenith angle), as well as without it. It is shown that the formation conditions of type "1" and "f" Es differ from those for type "c" Es. The highest formation probabilities of type "1" and "f" Es coincide with the passage time of the morning and evening terminators, and the formation probabilities are higher in the case of the evening terminator when compared with the morning terminator. The formation conditions of type "1" and "f" Es are largely associated with the annual variation of the solar zenith angle. Also, the formation probabilities and heights of type "f" and "1" Es are differ from each other. The formation conditions of type "c" Es are different. The height-time variation of its formation probabilities is similar to that of the semi-diurnal temperature component in the ionospheric E region obtained in terms of the MSIS model.

**GA2.02/L/02-B4** **Poster** **0930-05**

**NONEQUILIBRUM PROCESSES AND ORGANIZED STRUCTURES IN NEAR COSMIC SPACE**

Vjacheslav M. Somsikov (Institute of Ionosphere, Kameskoe Plato, 480068 Alma-Ata, Republic of Kazakhstan, email: nes@kaznet.kz) Gennadiy V. KHREBTOV and Ibragim E. Suleimenov (both at Institute of Ionosphere, Kameskoe Plato, 480068 Alma-Ata, Republic of Kazakstan, email: gn@ionos.alma-ata.su)

Transition processes in Near Cosmic Space during magnetic storms and in sunrise-sunset hours of day has been investigation by the methods of nonequilibrium dynamics. By joint processing of experimental records of variations of a magnetic field, cosmic rays and ionosphere of parameters the occurrence of dynamic chaos final Hausdorff dimension in variations of a magnetic field and ionosphere of concentration in transitive periods is established. It was found that at transitive hours in ionosphere parameters the additional oscillatory mode has appeared. The comparative analysis of results of processing of records of cosmic rays and magnetic fields, has allowed to assume that the variations, registered on ground, of a magnetic field and variations of cosmic rays in a minute range of frequencies arise on ionosphere heights. Therefore our results testify to presence of the determined chaos in Near Cosmic Space in transitive periods of days.

**GA2.02/L/03-B4** **Poster** **0930-06**

**TURBULENT FLUCTUATIONS OF ELECTRON DENSITY GRADIENT IN THE LOWER IONOSPHERE**

Olga G. KHUTOROVA, Dmitry V. Paponov (both radioastronomy dep., Physics fac., Kazan State University, 18, Kremlevskaya st., Kazan, Russia, 420008, e-mail: olga@erae.kazan.ru)

The numerical model of spectrum of turbulent fluctuations of gradient of electron concentration at various heights from 80 to 110 km is carried out versus of the irregularities horizontal size. The model takes into account the seasonal and geophysical changes in ionosphere. The analytical kind of the spectrum is found with using of the theory of dimensions. The spectrum has a maximum near the internal scale of turbulence. Spectrum model is based on empirical ionospheric models.

**GA2.02/L/04-B4** **Poster** **0930-07**

**FORMATION OF FAST IONOSPHERIC PLASMA FLUCTUATIONS CAUSED BY METEOR IONIZATION.**

Nicolay S. Andrianov, Guerman M. TEPTIN (both radioastronomy dep., Physics fac., Kazan State University, 18, Kremlevskaya st., Kazan, Russia, 420008, e-mail: teptin@erae.kazan.ru)

Meteor ionization makes significant contribution to dynamics of plasma irregularities at heights 80-100 km. Several thousands of meteor particles penetrate during one hour with space velocities, leaving after themselves plasma trails with electron densities 10 fi 10 per meter, several kilometers by length and with diameter by the order of the one meter. Our theoretical investigations and simulation have shown that these irregularities are explained by the influence of turbulent winds and it is well confirmed by experiment. Parameters of turbulent motions and parameters of meteor trails are accounted in the model when dissipative processes are operative (attachment, ambipolar and turbulent diffusion). Estimates were fulfilled by Monte-Carlo method.



**GA2.02/L/07-B4** Poster **0930-08**

**NEUTRAL WIND DRIVEN GRADIENT DRIFT INSTABILITY IN THE MIDLATITUDE E REGION**

Ludmila Kagan (Radiophysical Research Institute, B.Pecherskaya 25, Nizhny Novgorod 603600, Russia, e-mail: kagmil@nirfi.sci-nnov.ru) Michael Kelley (School of Electric Engineering, Cornell University, Ithaca, NY 14853, USA, e-mail: mikel@ee.cornell.edu)

We propose a new explanation for medium- to small-scale irregularities in the mid-latitude E region. We show that the very wind field that forms thin layers of ionization can also create plasma instabilities. To date, the application of gradient drift instability theory has been restricted to free energy sources involving the ambient electric field. We show that a vertical shear in the zonal wind not only leads to layer formation, but also to unstable regions on both sides of the layer. The mechanism thus does not suffer from the problem inherent in electric field-driven processes, namely, that the mapping of electric fields along magnetic field lines leads to stabilizing conditions on one side of the layer, even if the other side is unstable. Evidence is given that anomalous diffusion due to such waves affects the evolution of the layers.

**GA2.02/W/14-B4** Poster **0930-09**

**SPECTRAL AND FLOW ANGLE CHARACTERISTICS OF BACKSCATTER FROM DECAMETRE IRREGULARITIES IN THE AURORAL ELECTROJETS**

S E MILAN, M Lester (Both at Department of Physics and Astronomy, Leicester University, Leicester LE1 7RH, UK. Email: Steve.Milan@ion.le.ac.uk)

Measurements are presented of backscatter spectra from 15 m ionospheric irregularities in the auroral electrojets by the CUTLASS Iceland coherent HF radar. The scanning nature of the radar allows the flow angle dependence of the spectral characteristics to be determined and interferometric techniques allow the altitude of the scatter volume (E-, upper E-, or F-region) to be estimated. Several populations of backscatter spectra are observed, each with distinct velocity-spectral width and velocity-flow angle behaviours. At E-region altitudes, two populations appear to correspond to the type I (two-stream instability) and type II (gradient drift instability) spectra observed with VHF radars. However, two E- or upper E-region spectral populations with velocities up to 1000 m/s, above the typical ion-acoustic speed, are also observed. Furthermore, a population with Doppler shifts of the opposite sense to the main body.

**GA2.02/E/04-B4** Poster **0930-10**

**STATISTICAL ANALYSES OF ELECTRON DENSITY DISTRIBUTION AT HIGH LATITUDE**

Yasuyuki Sato, Hiroaki MISAWA, Akira Morioka (all at Upper Atmosphere and Space Research Laboratory, Tohoku University, Sendai, 980-8578, Japan, email: misawa@stpp2.geophys.tohoku.ac.jp) Hiroshi Oya (Department of Astronomy and Geophysics, Tohoku University, Sendai, 980-8578, Japan, email: oya@stpp1.geophys.tohoku.ac.jp) Toshifumi Mukai (Institute of Space and Astronautical Science, Sagami-hara, 229-8510, Japan, email: mukai@fujitubo.gtl.isas.ac.jp)

Statistical profiles of electron density distribution have been derived for the high latitude regions by using the data measured with Plasma Wave and Sounder experiment (PWS) on board the EXOS-D (AKEBONO) satellite. We have analyzed the data of 1989 to 1994 for the altitude range of 300 km to 10,000 km and the invariant latitude range of 50 to 90 degrees. An electron density was derived by detecting upper hybrid resonance frequency and/or cut-off frequency of whistler mode waves. The data of electron density were classified according to local-time, season and geomagnetic activity, then, statistical profiles have been determined as averaged values for the bins of every 50 km height and every 1 degree in invariant latitude. The major results of this study are as follows. 1) There is little difference between the density profiles of summer and winter for the invariant latitude below 60 degrees, while, the densities in winter are smaller than that in summer for the latitude over 60 degrees and the altitude below 6,000 km. This result suggests a possibility of the close relation of back-ground electron densities with the seasonal variations of occurrence of auroral electron accelerations and AKR events. 2) There is a density enhancement region particularly in day-side at the altitude of thousands km and the invariant latitude around 80 degrees. The region corresponds to that of downward electron flux with hundreds eV observed with the LEP instrument on board AKEBONO. 3) A set of fitting functions of electron density profiles is empirically

**GA2.02/W/25-B4** Poster **0930-11**

**FLOW ANGLE PROPERTIES OF THE 1-M IONOSPHERIC PLASMA WAVE TURBULENCE**

E E TIMOFEEV (Polar Geophysical Institute of the Russian Academy, Murmansk, Russia); M K Vallinkoski, J Kangas, P Pollari (Department of Physics, University of Oulu, Finland); T Virdi, P J Williams (Department of Physics, University of Aberystwyth, Wales, U.K.); E Nielsen (Max-Planck-Institute fuer Aeronomie, Katlenburg-Lindau, Germany)

The coordinated STARE-EISCAT data stored for the multi-event ERRRIS campaign are used to study the flow angle properties of threshold ionospheric parameters controlling the STARE radar echo appearance. The selected data with  $0\text{db} < \text{SNR} < 1\text{db}$  contain 64 and 128 cases observed by the Finnish (F-radar) and Norwegian (N-radar) STARE radar, respectively. The echo is supposed to come from different echo-layers corresponding to the zero aspect angles: from 100.6 km and 108.6 km altitudes over Tromso for the N-radar and F- radar, respectively. Electron and current densities are averaged over the echo-layer altitudes and over 30-degree flow angle bins. It is found that: 1) for the F-radar the threshold E-field strength is drift-aligned, and therefore anisotropic. Besides, there is a systematic decrease of the strength when going from positive to negative flow angles. For the N-radar the threshold E-fields are practically independent of flow angle, and therefore isotropic; 2) the average threshold E-fields are systematically lower but the threshold electron densities are higher in the westjet than within the eastjet for either radar. The difference of the fields is about 25% (50%) but of the densities is factor of 2.25 (1.5) for the N- and the F- radar, respectively; 3) the threshold electron density level is higher in the F-radar than in the N-radar echo layer by a factor of 3 (4) within the westjet (eastjet), respectively.

The nonlinearity of the dynamo layer plasma waves responsible for the F-radar echo is concluded even for small near-threshold E-fields. It is conjectured that the plasma wave turbulence level is enhanced (damped) due to the gradient-drift mechanism within the eastjet (westjet), respectively.

**GA2.02/W/15-B4** Poster **0930-12**

**THE THERMAL EFFECTS IN THE EXCITATION OF THE FARLEY-BUNEMAN WAVES**

E E TIMOFEEV (Polar Geophysical Institute of the Russian Academy, Murmansk, Russia); M K Vallinkoski, J Kangas, P Pollari (Department of Physics, University of Oulu, Finland); T Virdi, P J Williams (Department of Physics, University of Aberystwyth, Wales, U.K.); E Nielsen (Max-Planck-Institute fuer Aeronomie, Katlenburg-Lindau, Germany)

Properties of the threshold E-fields of a radar echo appearance are analyzed from statistics of the coordinated STARE-EISCAT measurements stored during the multi-event ERRRIS campaign. The selected data pool with  $0\text{db} < \text{SNR} < 1\text{db}$  contains 64 cases observed by the Finnish STARE radar (F-radar). The radar echo is supposed to come from the zero-aspect angle layer (echo-layer): 108.6 km altitudes over Tromso. Electron (Te) and ion (Ti) temperatures are analyzed as being averaged over the echo-layer width and over 30-deg flow angle bins. Properties of the threshold ratio of the electron drift to-ion-acoustic velocities (Vd/Cs) dependence on the Te/Ti ratio are analyzed for the following set of the half-widths of the flow angle cone: 15, 30, 45 and  $> 45$  degrees. It is found that: 1) In about 90% of all threshold cases the Vd/Cs is less than 1; 2) the properties are essentially different within and beyond .45 degree flow angle cone that is interpreted as a primary cone of the modified FB-waves. Within the cone Vd/Cs achieves its maximum for Te/Ti of about 0.8 and has a tendency to decrease both for Te/Ti $>$ 1 and for Te/Ti $<$ 1. Beyond the cone Vd/Cs is minimum for Te/Ti of about 0.8 and has a tendency to increase both for Te/Ti $>$ 1 and for Te/Ti $<$ 1; 3) within (beyond) the cone the properties of the histograms of the threshold radar echo occurrences as a function of Te/Ti are similar to the bi-Maxwellian (Maxwellian) population distribution function, respectively.

The results are quantitatively compared with the modern theory of the electron thermal diffusive instability. It is concluded that within the primary cone of the modified FB-waves the ionospheric plasma permanently is in the stage of the termodynamical non-equilibrium.

**GA2.02/W/21-B4** Poster **0930-13**

**DETERMINATION OF TEC OF IONIZATION OVER ARGENTINE WITH DIFFERENTIAL DOPPLER MEASUREMENTS AND COMPARISON WITH IRI**

VICTOR H. RIOS (1) and Cesar Valladares (2), Lab. de Técnicas Satelitales (1), (1) Instituto de Física, Universidad Nacional de Tucumán Av. Independencia 1800, (4000) San Miguel de Tucumán - Argentina (2) Institute for Space Research, Boston College, Newton, MA

Differential Doppler measurements of signals from NNSS Navigational Satellites can be used to give the electron content of the ionosphere. Measurements carried out using data from four stations on Argentina. Differential Doppler data from two station are combined, resulting in considerably more reliable results, particularly when there is strong horizontal structure in the ionosphere, as is often the case in Equatorial and polar regions. Examples of model calculations and experimental measurements are also included. In applications of the trans-ionospheric propagation of radio waves first order range errors are proportional to (slant) electron content of the ionosphere, second order errors to the square of this quantity. The results are compared with the IRI model and typical examples are used to demonstrate the differences between model values and observed values. We have tried to highlight the global nature of such discrepancies aiming at providing an eventual basis for incorporating needed modification the predictive capability of the IRI for the equatorial and low latitude ionosphere. In many applications range differences are more important than range itself and this especially true for all interferometric methods. Range difference measurements are influenced by differences of electron content or "horizontal gradients"

**GA2.02/W/02-B4** Poster **0930-14**

**HF RADAR OBSERVATIONS OF SMALL SCALE PLASMA TURBULENCE PARAMETERS AT THE MAGNETIC EQUATOR**

K.S. VISWANATHAN (Space Physics Laboratory, Vikram Sarabhai Space Centre, Trivandrum 695 022, India, email: spl\_vssc@vssc.org)

The small scale turbulence parameters of electron density irregularity strength, anomalous electron collision frequency, the corrected E-W electron drift velocity and their spatial/temporal changes are derived in the equatorial electrojet location of Trivandrum (dip 0.5 deg. N), using 18 MHz HF radar observations conducted during daytime in the altitude region of 90-115 km mostly on quiet days. The effects of plasma turbulence on the altitude maximum of electron drift velocity and the shape of the profile are presented. The temporal variations of these parameters are examined in the light of the scattered signal power and drift velocity. Specifically the dependence of irregularity strength on power during weak and strong electrojet times is presented and the underlying physical processes are discussed.

**GA2.02/W/12-B4** Poster **0930-15**

**A COMPARATIVE STUDY OF THE COLOCATED HF AND VHF RADAR EASUREMENTS IN THE EQUATORIAL ELECTROJET**

K.S. VISWANATHAN (Space Physics Laboratory, Vikram Sarabhai Space Centre, Trivandrum - 695 022, India, email: spl\_vssc@vssc.org)

A comparative study of the lower order spectral moments, obtained from the electrojet altitudes by means of 18 and 54.95 MHz coherent backscatter radars, operating at Trivandrum (dip 0.5 deg N) is carried out. The advantage of using HF data for specific studies like plasma turbulence parameters, longitudinal variability of electron drift velocity, zonal and vertical drifts during spread F conditions is emphasized. The altitude extent of the signal is larger in HF than that of VHF, in view of HF power aperture being nearly two orders of magnitude greater than VHF system. HF spectral information is obtained as low as 80 km, which is regarded as due to zonal winds and this value, in turn, is used to get the estimates of the winds upto 120 km. Also HF radar is used to study effectively the turbulence parameters and their spatial/temporal variation, in view of the absence of type I irregularities, unlike the VHF case. The HF radar signal presence in a larger altitude region is used by considering higher degree polynomial, even when the velocity profiles are distorted. The diurnal behaviour of electric fields by HF observations is clearly brought out. The derived parameters, by both the systems are compared and the observed similarities/differences are discussed in the light of the structured spectral shapes and the behaviour of the two scale sizes of the irregularities probed.

**GA2.02/W/20-B4** Poster **0930-16**

**QUASI-PERIODIC BEHAVIOUR OF TYPE II IRREGULARITIES IN THE E REGION OFF THE MAGNETIC EQUATOR**

K.S. VISWANATHAN, Sudha Ravindran, K.S.V. Subbarao (Space Physics Laboratory, Vikram Sarabhai Space Centre, Trivandrum - 695 022, India, email: spl\_vssc@vssc.org)

Observations of E region FAI of 2.8 m scale size are made on several days in summer and equinoctial months during nighttime using the Indian MST radar at Gadanki (dip 12.5 deg.N). Observations made at altitude interval of 1.2 km and time interval of mostly five min in the altitude region of 90-120 km are used for the present study. The Doppler spectra are of type II quasi Gaussian, ranging from a narrow single peak to wide multiple peak, showing variability in time and altitude. The drift of the irregularities does not generally exceed 40 m/s. The drifts in the altitude range of 100-115 km are mostly downward at night and upward occasionally. The intensity and drift of the signals are oscillatory in nature showing quasi-periodic behaviour

with periods in the range 25-35 min. The amplitude of the wave is found to increase from lower to higher altitudes with phase propagation downwards, indicating gravity wave activity. This is attributed to the formation of irregularities due to gradient drift instability mechanism in the presence of sporadic E layers with sharp gradients modulated by gravity waves, as discussed by Woodman et al. (1991) for midlatitude observations. The observations are discussed in the light of local treatment of the instability mechanism.

**GA2.02/W/13-B4** Poster **0930-17**

**EQUATORIAL SPREAD-F LONGITUDINAL BEHAVIOUR**

Anna DEPUEVA (IZMIRAN, Troitsk, Moscow Region, 142092, Russia, email: depueva@izmiran.rssi.ru)

Simultaneous bottomside and topside ionograms were analysed for the two different longitudinal positions ( Djibouti and Huancayo) prior to and during equatorial spread-F and non-spread-F conditions. Generalized collisional Rayleigh-Taylor (GRT) instability growth rates were estimated, the term «generalized» being referred to inclusion of electric fields and neutral winds as destabilizing factors, as well as the classic gravitational term. Electron density gradient values were taken from the real experimental N(h)-profiles, neutral ionosphere parameters were calculated by the Kohnlein model. It was shown that the observed spread-F longitudinal behaviour could be hardly explained in frames of GRT instability action. This result should be useful for distinguishing global and local triggering spread-F mechanisms.

**GA2.02/W/16-B4** Poster **0930-18**

**HF AND VHF RADAR OBSERVATIONS OF EQUATORIAL SPREAD F**

R. SEKAR and E.A. Kherani (both at Physical Research Laboratory,Ahmedabad 380 009, India, email: rsekar@prl.ernet.in) A.K. Patra (Department of Physics, K.O. College, Gumla 835 207, India) P.B.Rao (both at National MST Radar Facility, P.O. Box 123,Tirupati 517 502, India, email: nmrf@isro.ernet.in) K.S. Viswanathan, C.V. Devasia and K.S.V. Subbarao (Space Physics Laboratory, Vikram Sarabhai Space Centre, Trivandrum 695 022,India, email: spl\_vssc@vssc.org)

A coordinated observational campaign, involving simultaneous operation of the 18 MHz HF and 53 MHz VHF radars located respectively at Trivandrum (8.5 deg.N, 77 deg.E; dip 0.5 deg.N) and Gadanki (13.5 deg.N, 79.2 deg.E, dip 12.5 deg.N), has been conducted during March-April 1998. The observations are presented in the form of height-time variations of signal intensity, mean Doppler velocity transverse to the magnetic field and velocity spectral width. The Doppler spectra at both HF and VHF are found to be of simple Gaussian to multi-peak complex characteristics. The signal intensity variations at the two frequencies are found to be, in general, well correlated. The topside multiple plume structures observed at VHF on most of the intense ESF events are found to resemble that simulated by Haug and Kelley (J. Geophys. Res., 101, 293, 1996) through gravity wave seeding. The Doppler velocities at 18 MHz are typically less than 50 m/s, while they could be as high as 200 m/s at VHF in the topside, indicating the dispersive nature of ESF irregularities. The velocity spectral widths are found to be as large as or even larger than the mean Doppler velocities observed at the two frequencies.

**GA2.02/E/16-B4** Poster **0930-19**

**PRODUCTION OF ELECTRIC FIELD PERTURBATIONS BY GRAVITY WAVE WINDS IN THE E REGION SUITABLE FOR INITIATING EQUATORIAL SPREAD F IRREGULARITIES**

Satya Prakash and H.S.S. SINHA, Research Laboratory, Navrangpura, Ahmedabad -380 009, INDIA, email: hsinha@prl.ernet.in

We present here a mechanism where the electric field perturbations, which can map up to the F-region base, are produced through the interaction of the electric field perturbations with sporadic-E layers and a thin E layer. The mechanism operates in two steps. In the first step, the thickness of the E layer is reduced due to the downward transport of plasma by the downward electric fields. These downward electric fields, which map down from the F region to the E region, are generated by the eastward winds in the F region through dynamo action. In the second step the electric field perturbations is produced through interaction of the electric field perturbations having vertical wavelengths similar or larger than the thickness of these layers. These electric field perturbations are produced through Hall conductivity and their amplitudes can be much larger than those produced through the mechanisms proposed earlier. These electric field perturbations are very well suited for the growth of seed irregularities in the base of the F region. The characteristics of these seed irregularities are such that they can account for the growth of multiple equatorial spread F plumes, through the Rayleigh Taylor Instability, observed in the equatorial F region during late evening hours. In the mechanism proposed earlier, the electric field perturbations are produced when the wave front of gravity wave in the meridian plane is parallel to B. The proposed mechanism is effective practically at all latitudes as there is no such restriction on the orientation of the wave front of the gravity wave with respect to B.

**GA2.02/E/07-B4** Poster **0930-20**

**OPTICAL IMAGING OF PLASMA DEPLETIONS FROM SHAR**

H.S.S. SINHA, Shikha Raizada and R.N. Misra, Physical Research Laboratory, Navrangpura, Ahmedabad -380 009, INDIA

A multi-wavelength all sky optical imaging instrument developed at PRL was operated from a low latitude station SHAR (13°N, 82°E). The purpose of the experiment was to study the nature of very large-scale irregularities using airglow emissions at 630 nm and 777.4 nm. One of the very interesting features which emerged from this study is the eastward tilt of the depletions which lies between 10 - 15°. This is a significant result as the earlier observations from the American sector showed that the plasma depletions are tilted in westward direction. Our data suggests that these tilts might be associated with the altitudinal increase of nighttime plasma drifts.

The airglow images display multiple depletions, which are characterized with varying degree of depletions. It is observed that the E-W extent of the depletions varies with depletion depth. Shallower depletions appear to be associated with smaller zonal width as compared to deeper depletions. This might be probably the manifestation of the fact that deeper bubbles, characterized by large amplitudes, represent well-developed irregularities.

The distance between adjacent depletions i.e. the inter depletion distance (IDD) is found to vary between 100 km to about 950 km suggesting that gravity waves might be the seeding agency for generating such large scale structures.

**GA2.03** **Wednesday 28 July**

**TOWARD ANSWERING CRITICAL PROBLEMS IN IONOSPHERIC RESEARCH**

Location: Gisbert Kapp, NG15 CRI  
Location of Posters: Gisbert Kapp, Coffee Room

**Wednesday 28 July AM**

Presiding Chairs: B. Thide, (Swedish Institute of Space Physics, Uppsala, Sweden), J.M. Ruohoniemi, (The John Hopkins University, USA)

**TOWARD ANSWERING CRITICAL PROBLEMS IN IONOSPHERIC RESEARCH**

**GA2.03/E/08-B3** **0930**

**SEASONAL AND SEMIANNUAL CHANGES IN THE F2-LAYER**

Henry RISHBETH (Department of Physics and Astronomy, University of Southampton, Southampton SO17 1BJ, UK, email: hr@phys.soton.ac.uk)

The seasonal, annual and semiannual variations of the quiet F2-layer represent a challenging problem in ionospheric physics. It is now becoming possible to construct a unified picture which is closely linked to the global circulation in the thermosphere, which is driven by solar XUV radiation and inputs from the solar wind and magnetosphere. This paper outlines the present understanding and reviews some unsolved questions.

**GA2.03/W/01-B3** **0950**

**IMAGING THE HIGH-LATITUDE IONOSPHERIC COVECTION PATTERN**

Raymond A. GREENWALD, J. M. Ruohoniemi, and R. J. Barnes (all at Johns Hopkins University, Applied Physics Laboratory, Johns Hopkins Rd., Laurel, MD, 20723, USA, email: mike\_ruohoniemi@jhuapl.edu)

Many important advances in ionospheric research have resulted from the advent of spacecraft-borne imagers that effectively take snapshots of the global pattern of auroral luminosity. When connected in temporal sequence, the images dramatically demonstrate the dynamical behavior of auroral processes. With the realization of the SuperDARN concept in the northern and southern hemispheres, it has become possible to similarly 'image' the high-latitude pattern of ionospheric convection velocity. Although the field of view of each radar is limited to about 10% of the high-latitude one, combining the information from all six radars in the northern hemisphere results in coverage of nearly 1/2 of the entire convection pattern. The temporal resolution available is 1-2 minutes. This global, instantaneous view has been needed to elucidate the manner in which the global pattern responds to IMF variations. We outline the technique for deriving snapshots of the convection pattern and present examples of comparison with imager and low-altitude satellite data. With the increasing emphasis on now-casting and fore-casting the state of the ionosphere, we have developed an extensive on-line facility for accessing SuperDARN products. This includes near real-time maps of the global convection pattern and time series of the cross-polar cap potential variation. These products may be thought of as space weather reports and are available to the general community at the Internet address: <http://superdarn.jhuapl.edu/html>. We will discuss the critical science topics that are being addressed with the unique capabilities of SuperDARN, describe the upgrades to the system that are underway, and the availability of SuperDARN products.

**GA2.03/W/02-B3** **1010**

**THE FORENOON IONOSPHERIC ELECTRON DENSITY VARIATIONS OVER THE MU RADAR**

S.-R. ZHANG, S. Fukao, and Y. Otsuka (Radio Atmospheric Science Center, Kyoto University, Japan, email: shunrong@kurasc.kyoto-u.ac.jp; fukao@kurasc.kyoto-u.ac.jp; otsuka@kurasc.kyoto-u.ac.jp)

This paper deals with the diurnal variations of electron density profile measured by the MU radar during 1986-1995 period, nearly a full solar cycle. We focus on the so-called forenoon "bite out" of ionization, which is characterized with a lower electron density occurring around 8-11 LT. The statistic study shows that it appears more clearly in summer than in other seasons and for lower solar activity (LSA) than for higher solar activity (HSA). The density depletion becomes increased with increasing height. To understand the involved physical mechanism, a theoretical model is applied, in corporation with MU radar measurements of the ion drift and plasma temperatures during the period, so that the relative importance of the O/N2 ratio, the neutral wind, the vertical component of electric field induced drift, the plasma temperature, and the topside O+ flux can be analyzed. It is found that (1) in summer at higher solar activity, a higher electron temperature is a necessity to produce a lower forenoon electron density through increasing the plasma diffusion and the O+ loss rate; the poleward neutral wind is favorable to the lower density, but it alone can not significantly deduce the electron density. (2) in summer at lower solar activity, both the poleward neutral wind and the higher electron temperature play significant roles to cause the forenoon bite out. (3) there is no indication for a lower O/N2 ratio to account for the bite out. (4) the effect of the vertical drifts induced by the local eastwest electric field tends to cancel the bite out. (5) the forenoon decrease of O+ flow at 500 km is favorable for a lower density around the F2 peak but its importance is not essential for the bite out.

**GA2.03/W/09-B3** **1030**

**SPACE OBSERVATIONS OF ION CYCLOTRON WAVES EXCITED BY A ULF RADAR**

K. MURSULA, T. Bösinger, and T. Kivisaari (Department of Physical Sciences, University of Oulu, P.O. Box 3000, FIN-90401 Oulu, Finland, email: Kalevi.Mursula@oulu.fi); P. P. Belyaev (Radiophysical Research Institute, Nizhny Novgorod, Russia); Sobchakov and A. B.Vasiliev (Russian Inst. of Powerful Radiostructure, St.Petersburg, Russia); L. Blomberg (Alfvén Laboratory, Royal Institute of Technology, Stockholm, Sweden)

The first ULF radar experiment was carried out in Kola Peninsula in September 1993. During the experiment the current (Imax = 150-200 A) of a 60 km long power line was modulated in a sinusoidal fashion at frequencies between 0.3 and 5.2 Hz. The magnetic signal of this varying line current was recorded in several ground-based magnetometers at variable distances ranging from 300 km to 2000 km. In this paper we discuss the spectral and polarization properties of the signal received by the Finnish chain of pulsation magnetometers. Moreover, we have analyzed the electric field observations made simultaneously by the Freja satellite within and slightly above the ionosphere. Freja observes ion cyclotron waves with the frequency of the radar modulation frequency far away from the footprint of the ULF radar. This



provides direct evidence for the fact that the ULF radar signal can excite a propagating wave in the ionosphere.

**GA2.03/E/02-B3 1120**

**TRAVELING IONOSPHERIC DISTURBANCES OBSERVED IN THE 630NM NIGHTGLOW IMAGES AT MULTI-STATIONS IN JAPAN**

Kazuo SHIOKAWA, Mitsumu Ejiri, and Tadahiko Ogawa (Solar-Terrestrial Environment Laboratory, Nagoya University, 3-13, Honohara, Toyokawa, Aichi 442-8507, Japan, Email: shiokawa@stelab.nagoya-u.ac.jp); Minoru Kubota (Communication Research Laboratory, 4-2-1, Nukuikita, Koganei 184-8795, Japan, Email: mkubota@crf.go.jp); Akinori Saito (Department of Geophysics, Kyoto University, Sakyo-ku, Kyoto 606-8502, Japan, Email: saitoua@kugi.kyoto-u.ac.jp); Shoichiro Fukao (Radio Atmospheric Science Center, Kyoto University, Uji 611-0011, Japan, Email: fukao@kurasc.kyoto-u.ac.jp); Shinichi Miyazaki (Geographical Survey Institute, Kitagou, Tsukuba 305-0811, Japan, Email: miyazaki@gsi-mc.go.jp); Kenichi Nakajima and Takeshi Sakanoi (Graduate School of Science, Tohoku University, Aoba-ku, Sendai 980-8578, Japan, Email: ken@pat.geophys.tohoku.ac.jp)

We have conducted imaging observation of 630nm airglow using five all-sky cooled-CCD cameras in Japan during the F-region Radio and Optical measurement of Nighttime TIDs (FRONT) campaign on May 16-24, 1998. The cameras are located at Moshiri (44N, 142E), Zao (38N, 141E), Kiso (35N, 138E), Shigaraki (35N, 136E), and Bisei (35N, 134E). Traveling ionospheric disturbances (TIDs) have been observed as wave structures in the images on May 19-23. Most of the structures have a wave front with a direction of NW-SE and move toward SW with a velocity of about 100 m/s. Typical wavelength of the structures was 200-400 km. The wavelength tends to decrease with decreasing latitudes from Moshiri to Bisei. Similar wave structures are also seen in the two-dimensional distribution of total electron content (TEC) obtained by more than 900 GPS receivers of the GPS Earth Observation Network (GEONET) in Japan. Based on these observations, we discuss possible production and propagation mechanisms of the mid-latitude TIDs.

**GA2.03/E/03-B3 1140**

**DAY-TO-DAY CHANGES IN THE SQ IONOSPHERIC CURRENT SYSTEM**

Robert STENING (School of Physics, University of New South Wales, Sydney 2052, Australia, email: R.Stening@unsw.edu.au)

During times of magnetic quiet there are still large day-to-day changes in the amplitude and shape of the daily magnetic variations at various observatories. These variations include such large changes as the reverse equatorial electrojet and the "invasion" of the winter current system by the summer system. One presumes that these changes are brought about by changes in the upper atmosphere (tidal) wind systems. In order to confirm this, comparisons need to be made between changes in the global current systems and changes in the global wind systems.

**GA2.03/W/06-B3 1200**

**AN AUTOMATIC PROCEDURE FOR DETECTION OF IONOSPHERIC STORMS**

Lj.R. CANDER (Rutherford Appleton Laboratory, Chilton, Didcot, Oxon, OX11 0QX, UK, email: l.cander@rl.ac.uk) M.M. Milosavljevic (Faculty of Electrical Engineering, Belgrade University, Belgrade, Yugoslavia, email: emilosam@ubbg.etf.bg.ac.yu)

Many space weather applications require knowledge of the ionospheric F region response to the great geomagnetic storms, particularly its commencement and duration. The precise detection of the ionospheric storm periods in off-line mode can be performed using a new so-called modified generalised likelihood ratio (MGLR) algorithm. This algorithm has been applied on the critical frequencies of the ionospheric F2 layer, foF2 time series measured at Slough, Juliusruh, Rome and Belgrade ionospheric stations during the February 1986 storm. It is found that MGLR algorithm enables not only fully automatic detection of abrupt changes in foF2 variations but inspection of different kind of ionospheric variability before and after the storms.

**GA2.03/E/04-B3 1220**

**BISTATIC RADAR OBSERVATIONS OF THE E-REGION IRREGULARITIES DURING TROMSO HEATING EXPERIMENTS**

Nataly BLAGOVESHCHENSKAYA, Tatyana Borisova, Viktor Kornienko (all at Department of Geophysics, Arctic and Antarctic Research Institute, 38 Bering str., St. Petersburg, 199397, Russia, Email: nataly@aari.nw.ru); Michael Rietveld (Max-Planck-Institut fur Aeronomie, D-37191 Katlenburg-Lindau, Germany, Email: rietveld@linmpi.mpg.de)

Results of Tromso heating experiments in the night-side auroral Es region from bistatic radar measurements combined with multi-instrument observations at Tromso are presented. Experiments were carried out during Tromso heating campaign in February 1996 from 20 to 23 UT when the pump wave was reflected from auroral Es-layer. The bistatic HF radar was sensitive to irregularities having spatial dimensions of 12-15 m across the geomagnetic field lines. We show that dynamics of the auroral Es layer as well as the development of some geophysical phenomena in the ionosphere-magnetosphere system are affected by the powerful HF radio waves. The action of the ionospheric heating is found in modifications of the particle precipitation, visible auroral forms, field-aligned currents, and magnetic pulsations around the heated volume. The conclusion is made that the strong positive feedback in the substorm current wedge is set as a result of the heater action. Two general categories of the artificial field-aligned irregularities (AFAls) in the auroral Es region are recognized from heating experiments. The first type of AFAls has the small growth and relaxation times in response to the HF heater action. The velocities of these AFAls are near 0 m/s suggesting that the scattered signals are coming from some stationary bulk feature of the heated plasma. The second type exhibits the large phase velocities up to 800 m/s. Their motion was consistent with the background plasma drift. Possible generation mechanisms of AFAls are discussed.

**GA2.03/L/01-B3 1400**

**FIRST GEOPHYSICAL ULF (0.1-10 HZ) GROUND-BASED FACILITY**

L.A.Sobchakov, A.V.Vasiljev and N.L.Astakhova (Russian Institute of Powerful Radiostructure (RIPR), 68, 11-Line, 199161, St.-Petersburg, Russia); P.P.BELYAEV, S.V.Polyakov, M.N.Yakunin and S.V.Isaev (Radiophysical Research Institute (NIRFI), B.Pecherskaya St., 25, N.Novgorod, 603 600, Russia, e-mail: belyaev@nirfi.sci-nnov.ru); A.G.Litvak and A.I.Smirnov (Institute of Applied Physics of Russian Academy of Science (IAP RAS), Uljanov St., 46, N.Novgorod, 603600, Russia)

After the first successful artificial ULF experiment in September 1993, three Russian Institutes, RIPR, St.-Petersburg, NIRFI and IAP RAS created the easy flexible ULF facility for geophysical applications. The first testing of this facility, located on the Kola Peninsula, Russia, the region with very small conductivity, was carried out during July 1998. The ULF facility consists of 108-km powerline grounded at both ends with using of river power station buildings (Kola peninsula powerline Company). The portable 50 kW amplifier provided a radiation current of 60-100 A in the line. The crust conductivity under powerline achieves the value of 10-4 – 5\*10-5 mho/m. The measurements of far field were carried out at distances 500 (RIPR) and 1500 km (NIRFI) for magnetic and electric field components. The near magnetic field measurements were carried out by Finnish scientific groups from University of Oulu and Sodankjula Laboratory. The good signal/noise ratio allows us to obtain valid characteristics of ULF signals. The measured amplitude-frequency dependence (proportional to f<sup>-1/2</sup>, where f – frequency in Hz), polarization and space distribution (R-2, R-distance in km) of ULF fields were in line with theory predictions for daytime conditions. For the nighttime one, dramatic discrepancy was observed due to the influence of anisotropy of ionosphere and its temporal variations.

**GA2.03/W/07-B3 1420**

**FLEXIBLE PRIOR MODEL, THREE-DIMENSIONAL IONOSPHERIC TOMOGRAPHY**

RICHARD CORNELLY, Walter Kuklinski, (University of Mass. Lowell, Department of Electrical Engineering, One University Avenue, Lowell Mass, 01854)

An ionospheric reconstruction system, that use constraints from knowledge of ionospheric physics, to produce a set of advanced and unique solutions, consistent with available TEC measurement data, to the underdetermined set of equations resulting from the ionospheric density reconstruction problem, will be presented. A major obstacle to implementing wide-scale ionospheric monitoring systems, is caused by the geometry of the ground based underdetermined receiver and orbiting satellite measurement techniques. The resulting TEC data, will contain limited information about variation of electron density with altitude. Recently, a class of iterative algorithms that allow to incorporate additional information, have been successfully used to provide solutions, without a great deal of additional computational complexity. In addition, the nature of the solutions obtained is known to be close to an initial density solution model in the Kullback-Liebler sense. It is also known that, current state of the art prior density models can only simulate a representative ionosphere. As a result, daily and sudden variations in ionospheric electron density will not be represented in these models. This presentation, will focus on a three-dimensional ionospheric density reconstruction system, that uses a set of geometrical transformations to produce updated prior models, containing additional information not well represented in current state of the art ionospheric density models. The updated priors are consequently used as initial solution models to, a specific set of iterative algorithms, which provide a spatially constrained density solution, consistent with the available data and our knowledge of ionospheric physics.

**GA1.03/W/04 1440**

**ANALYSIS OF IONOSPHERIC PLASMA PATCH CHARACTERISTICS OBSERVED BY DGS-256 IN MIDDLE AND SOUTH CHINA DURING SPREAD-F PROCESS**

JIAN-SHAN GUO(Center for Space Science and Applied Research, Chinese Academy of Sciences, P.O.Box 8701, Beijing 100080,P.R.China, Email: guojs@center.casar.ac.cn) Hong Zheng, She-ping Shang, Nana Liu(idem)

This paper describes two processes of spread-F development observed at Hainan(110°E,19°N on Feb.1,1990) and Beijing( 116°E,40°N on Jun.22,1989) Ionospheric Observatories, and shows how the amplitude and status panels of ionogram varies during the periods, and from which the size and drift velocity of the plasma patches can be estimated approximately by making use of the data of Doppler shift, polarization and amplitude on the panels of ionogram. The simulation of the processes has been made for illustrating the method of the estimation . In both cases , the spread-F's develop very similar and quiet as usual: beginning at well known F trace with resolved satellite trace above, then the satellite trace wider more and more so that the normal F trace could be no longer identified, and finally the resolved satellite trace appears again. the status panels on the corresponding ionograms, however, shows wave like motion characteristics. The Doppler shift identified from status value on the satellite trace varies quasi-periodically from plus to minus three times for Hainan and two times for Beijing during the patches passing overhead. the passing period of the patches is about 1.5 hours for the tow cases. The characteristics of the patch in Hainan are as follows: drift velocity is about 50m/s (estimated roughly by the Doppler shift and virtual height from the status value of satellite trace). The horizontal wavelength is about 180-270km. The horizontal size of the patch is about 540-810km. A simulation results of a amplitude and status panels of ionogram and patch structure in spatial and velocity space(assumed weak fluctuation) for the patch with similar average characteristics as measured show very similar manner as appeared in the measurement

**GA2.03/E/07-B3 1500**

**RESPONSE OF GLOBAL ION COMPOSITION IN THE TOPSIDE IONOSPHERE ON THE SOLAR ACTIVITY CHANGES**

V. TRUHLIK, L. Triskova, and J. Smilauer (all at Institute of Atmospheric Physics, 141 31 Praha 4, Czech Republic, email: vtr@ufa.cas.cz)

Mass spectrometer data base resulting from the Active mission for the maximum of solar cycle 22 completed by available data from the Goddard Comprehensive Ionosphere Data Base for the minimum of solar cycle 21 was used to study the solar cycle influence on the behavior of major and minor ions in the topside ionosphere up to 3000 km. Attention is focused on changes in the distribution of O+, H+, He+ as major ions; occurrence of minor NO+, N2+, O2+, N+ ions is considered as well. Experimental and modeled distributions are compared, discrepancies between them are discussed.



**GA2.03/L/02-B3 1520**

**FIRST MEASUREMENTS OF ARTIFICIAL ULF (0.3-5 HZ) SIGNALS FROM GROUND-BASE FACILITY AT THE LONG DISTANCE 1500 KM**

L.A.Sobchakov, A.V.Vasiljev and N.L.Astakhova (Russian Institute of Powerful Radiostructure (RIPR), 68, 11-Line, 199161, St.-Petersburg, Russia) P.P.BELYAEV, S.V.Polyakov and S.V.Isaev (Radiophysical Research Institute (NIRFI), B.Pecherskaya St., 25, N.Novgorod, 603 600, Russia, e-mail: belyaev@nirfi.sci-nnov.ru)

During Sept., 18–19, 1993, RIPR and NIRFI performed the first unique artificial experiment devoted to an excitation of large-scale ULF fields and measurements at the long distance 1500 km from ULF facility. The ULF facility was located at the Kola peninsula, near Murmansk, Russia and consisted of 55-km powerline grounded at both ends and current source with output current of 100-120 A. The crust conductivity in this region achieved the value 10-4 – 5\*10-5 mho/m. The operating frequencies were 0.32, 1.3, 2.6 and 5.2 Hz (20 min "on", 10 min "off") during three cycles over day, night and early morning conditions. The measurements of two horizontal N-S(H) and E-W(D) magnetic components were performed at the distance of 1500 km from facility, near N.Novgorod and were accompanied in Finland by University of Oulu (J.Kangas and T.Bosinger) with using of Finnish pulsation magnetometers chain. The measured amplitude-frequency dependence and polarization of magnetic fields were found to be in line with simple waveguide-cavity theory predictions for daytime conditions and to be in a dramatic discrepancy for nighttime ones. The observed distinctions can be explained by a strong influence of a signal ducted into the slow MHD-ionospheric waveguide and, in the same time, by ionospheric resonance properties in the ULF range (Ionospheric Alfvén Resonator, IAR) for electromagnetic waves excited in the cavity Earth-ionosphere. Simultaneous measurements of natural electromagnetic background confirm this consideration.

**GA2.03/W/05-B3 1600**

**IN SITU MEASUREMENT OF THE PHASE RELATIONSHIPS BETWEEN F-REGION ELECTRON DENSITY AND ELECTRIC FIELD FLUCTUATIONS**

P. MURALIKRISHNA, M.G.S. Aquino and S.M. Soares (all at Instituto Nacional de Pesquisas Espaciais - INPE/MCT, C.P. 515, 12201-970, São José dos Campos - SP, Brazil, email: murali@dae.inpe.br)

In-situ measurement of the height variation of the ionospheric electric field and electron density variations were made with a rocket-borne double probe and two different types of electron density probes, namely a conventional Langmuir Probe and a High Frequency Capacitance probe. A Brazilian made SONDA III rocket launched on 18-th December, 1995 at 2117 hrs (LT) from the equatorial rocket launching station, Alcântara reached an apogee altitude of 557km and covered a horizontal range of 589km. Several ground equipments were operated during the launch campaign with the specific objective of knowing the ionospheric conditions at the time of launch and thereby to launch the rocket into an F-region prone to the presence of plasma bubbles. The rocket in fact passed through several medium scale plasma bubbles and the electric field double probe and the electron density probes detected the presence of a wide spectrum of electric field and electron density irregularities. In the base of the F-region the electric field double probe measurements clearly indicated the presence of large amplitude fluctuations, closely associated with large amplitude electron density irregularities. But in the height region close to the rocket apogee though the electron density profile showed the presence of large scale spatial structures, the electric field measurements did not show fluctuations of similar amplitude. A study of the relationship between the phases of the electron density and electric field fluctuations at different height regions is reported here. The phase relationship between these two parameters is not only an indication of the nature of the electric field fluctuations but also depends on the specific plasma instability mechanism responsible for the generation of the plasma irregularities.

**GA2.03/P/02-B3 1620**

**THE EFFECT OF SOLAR X-RAY FLARES ON EARTH'S IONOSPHERE AND TELE-SERVICES**

M. A. Mosalam SHALTOUT, and S. El-Genedi (National Research Institute of Astronomy and Geophysics, Helwan - Cairo - Egypt Phone (202) 2630833; Fax (202) 5548020 Email: mamshalout@frcu.eun.eg)

Solar x-ray flares causing a sudden ionospheric disturbance (S I D) affecting on telecommunications and Tele-services. Solar x-rays flares measured during the period 1981 - 1995 by GOES x-ray detector and published by Solar - Geophysical Data of NOAA, Boulder, Colorado, USA are analysed. Also, sudden ionospheric disturbances SID'S, which world - wide observed during the same period (1981-1995) and published in Solar - Geophysical Data of NOAA, Boulder, Colorado, USA are analysed. The used technique is the time series analysis for non - equal spaced data for the both solar x-rays flares and SID'S. The analysis shows a short and long term periodicities in the solar x-ray flares similar to that of SID'S.

Also, evaluation for some solar active regions which produced high energetic flares and consequently sudden ionospheric disturbances of high importance during (1981 - 1995) was carried out. The method of cumulative summation curves was made to predict the occurrence of high energetic flares in the solar active region by two or three days before the releasing of the flare energy. It is interested for predicting the sudden disturbances in the telecommunications and Tele-services.

**GA2.03/P/01-B3 1640**

**NEW ELECTRON ENERGY TRANSFER AND COOLING RATES BY ELECTRON IMPACT EXCITATION OF N2 O2 AND O(3P)**

A V PAVLOV (Institute of Terrestrial Magnetism, Ionosphere and Radio Wave Propagation of the Russia Academy of Science, Troitsk, Moscow Region, 142092, Russia)

The electron energy transfer and cooling rates by vibrational excitation of N2 and O2 and cooling rate of thermal electrons by electron impact excitation of fine structure levels of atomic oxygen have been calculated and fitted to new analytical expressions as functions of the electron temperature by use the revised excited cross sections. These new analytical expressions available to the researcher for quick reference and accurate computer modeling with a minimum of calculations. The new O2(v) rates are up to a factor of 5-18 larger than those of Prasad and Furman (J. Geophys. Res., 78, 6701-6707, 1973). The difference between the new electron cooling rate due to N2(v) and those of Stubbe and Varnum (Planet. Space Sci., 20, 1121-1126, 1972) is up to a factor of 1.7. We found that at the F region altitudes of the ionosphere the new fine structure O(3P) cooling rate is less than the currently used fine structure cooling rate of Hoegy (Geophys. Res. Lett., 3, 541-544, 1976) by a factor of 2-4 for 400-700 ≤ Te - Tn ≤ 3000-3080 K and Tn = 800-1200 K where Te is the electron temperature and Tn, is the neutral translation temperature. We have shown that the vibrational levels v=1-4 (O2) and v=1-7 (N2) are enough to calculate the O2 (v) and N2 (v) electron cooling rates. Our results provide sufficient evidence to neglect the effects of the excitation of the a1Dg, and b1Sg+ electronic states of O2 with thermal electrons on the calculation of the electron temperature. It is also shown that the currently accepted rate of electron energy loss associated with rotational transitions in O2 must be decreased by a factor of 13 and electron energy loss associated with rotational transitions in N2 must be multiplied by a factor of 1.255.

**GA2.03/W/08-B3 1700**

**IS IT POSSIBLE TO SOLVE THE PROBLEM WITH INSUFFICIENCY OF THE INPUT PARAMETERS IN THE RE-TIME IONOSPHERIC MODELS**

N.A. KILIFARSKA, D.P. OUZOUNOV (Geophysical Institute, Bulgarian Academy of Sciences, Sofia 1113, Bulgaria)

The great temporal and spatial variability of the ionosphere, especially during the magnetic disturbances, is one of the main reasons for ionospheric modelling failure till this time. Standard statistical methods become helpless because of missing or bad quality of measurements during disturbed periods. The theoretical ionospheric models, on their turns, become more and more sophisticated. However, creation of fully-coupled self-consistent 3-dimensional time dependent models of the ionosphere-thermosphere system, are only partly successful in reproducing the observed irregularities in ionospheric storm reactions, because they rely heavily on a realistic picture of the magnetospheric input (global spatial-temporal variations of the magnetospheric electric fields, particle precipitation, etc.). Its turn out that sophistication of the models can not solve the problem with input parameters and only shift it toward higher levels of dependence. The present study presents an original approach to solve the problem with insufficiency of the input parameters when the spatial real time distribution of foF2 is simulated. A theoretical ionospheric model (TIM) is combined with a special procedure for updating the input parameters (thermospheric constituents and winds) on the base of the currently measured hourly values of foF2 and hmF2 ionospheric parameters. This means auto-correction of the model according to the current ionospheric conditions detected in a meridional chain of ionospheric stations. The accuracy of TIM model in foF2 simulation (presented by spatial relative errors between measured and calculated values) is ±10% during the most hours of the disturbed period.

**GA2.03/L/04-B3 1720**

**INVESTIGATIONS OF SOME CRITICAL PROBLEMS IN IONOSPHERIC RESEARCH BY ACTIVE METHODS**

ROMANOVSKY

Abstract not available at time of going to press

Wednesday 28 July PM

**GA2.03/W/03-B3 Poster 1400-01**

**MODELING OF THE RESONANCE SPECTRAL STRUCTURE OF ATMOSPHERIC NOISE BACKGROUND IN PC-1 FREQUENCY RANGE**

A. G. DEMEKHOV (Institute of Applied Physics, Nizhny Novgorod, Russia; email: andrei@appl.sci-nnov.ru); P. P. Belyaev, S. V. Isaev (both at: Radiophysical Research Institute, Nizhny Novgorod, Russia); J. Manninen, and T. Turunen (both at: Sodankyla Geophysical Observatory, Sodankyla, Finland)

We calculate the frequency spectrum of the electromagnetic background noise in frequency range 0.1-5 Hz based on the model attributing its formation to the ionospheric resonant filtration of the radiation from lightning discharges (Belyaev et al., 1989). Characteristics of the resonance spectral structure (RSS) formed due to the ionospheric Alfvén resonator are obtained and their dependence on ionospheric parameters is considered. RSS variation during a day and during a solar cycle is discussed. The calculations are compared to the ULF ground based observations at Sodankyla and mutual consistency of both is demonstrated. Opportunities to use such data to determine some of ionospheric parameters are discussed.

**GA2.03/W/05-B3 Poster 1400-02**

**IN SITU MEASUREMENT OF THE PHASE RELATIONSHIPS BETWEEN F-REGION ELECTRON DENSITY AND ELECTRIC FIELD FLUCTUATIONS**

P. MURALIKRISHNA, M.G.S. Aquino and S.M. Soares (all at Instituto Nacional de Pesquisas Espaciais - INPE/MCT, C.P. 515, 12201-970, São José dos Campos - SP, Brazil, email: murali@dae.inpe.br)

In-situ measurement of the height variation of the ionospheric electric field and electron density variations were made with a rocket-borne double probe and two different types of electron density probes, namely a conventional Langmuir Probe and a High Frequency Capacitance probe. A Brazilian made SONDA III rocket launched on 18-th December, 1995 at 2117 hrs (LT) from the equatorial rocket launching station, Alcântara reached an apogee altitude of 557km and covered a horizontal range of 589km. Several ground equipments were operated during the launch campaign with the specific objective of knowing the ionospheric conditions at the time of launch and thereby to launch the rocket into an F-region prone to the presence of plasma bubbles. The rocket in fact passed through several medium scale plasma bubbles and the electric field double probe and the electron density probes detected the presence of a wide spectrum of electric field and electron density irregularities. In the base of the F-region the electric field double probe measurements clearly indicated the presence of large amplitude fluctuations, closely associated with large amplitude electron density irregularities. But in the height region close to the rocket apogee though the electron density profile showed the presence of large scale spatial structures, the electric field measurements did not show fluctuations of similar amplitude. A study of the relationship between the phases of the electron density and electric field fluctuations at different height regions is reported here.

The phase relationship between these two parameters is not only an indication of the nature of the electric field fluctuations but also depends on the specific plasma instability mechanism responsible for the generation of the plasma irregularities.

**GA2.03/W/11-B3 Poster 1400-03**

**GEOMAGNETIC STORMS: A STATISTICAL STUDY**

G.I. Gordienko and S.N. Mukasheva (both at Institute of Ionosphere, Academy of Sciences, Almaty 480020, Kazakhstan, email: gord@ionos.alma-ata.su) Lj.R. CANDER (Rutherford Appleton Laboratory, Chilton, Didcot, Oxon, OX11 0QX, UK)

A statistical method is applied to test the efficiency of some geophysical factors for geomagnetic storm forecast. Values of daily 2800 MHz solar flux F10.7, geomagnetic field intensity and Alma-Ata neutron monitor pressure-corrected values in the period 1965-1989 are used to analyze their variations in different frequency ranges, to detect some peculiarities in the variations and to determine a statistical connection degree between the peculiarities and storm probability. It has been obtained that the probability is greater when the first derivative values, for example in F10.7 (t), are more than some thresholds.

**GA2.03/E/01-B3** Poster **1400-04**

**LIMIT ACCURACY OF HF-DIAGNOSTICS OF THE IONOSPHERIC PLASMA**

Natalia V. NASTASYINA, Pavel F. Denisenko and Dmitry A. Noranovich (Institute of Physics, Rostov State University, 194, Stachky Ave., 344090, Rostov-on-Don, Russia, e-mail: denis@iphys.rnd.runnet.ru)

The modern investigations of physic-chemical processes in the ionosphere brings more strong requirements to accuracy of the ionospheric parameters diagnostics. For this aim the new technique of experiment is developed. However, the possibilities of traditional diagnostic methods not always are used to a total degree. In particular, this fact take place in topside ionospheric soundings. In present paper three problems are described: 1) real heights determination under vertical satellite sounding; 2) diagnostics of effective electron collision frequency by method A1; 3) vertical Doppler diagnostics. In all described cases for determination of the ionospheric parameters it is necessary to inverse the Volterra integral equations of first kind. The computer simulation shown that the root-mean-squares errors of determining values depend on signal polarisation, frequency range, geomagnetic latitude of observation point and on radius of frequency correlation of signal fluctuations. Under using waves of ordinary polarisation for experimental measurements the errors in diagnostics of searching ionospheric parameters (vertical velocity of plasma motions, real heights or electron collision frequency) increase from magnetic pole to equator. The applying extraordinary polarising waves for diagnostics gives opposite dependence, i.e. errors are minimal on magnetic equator and maximal in polar ionosphere. On the middle latitudes the root-mean-squares errors of real heights make about 25% from the errors of group paths measurements. Under accuracy of measurements of radio wave absorption 1dB the errors of effective electron collision frequency reach. Under errors of Doppler frequency shift determination in 0,01 Hz the errors of determination of vertical velocity of plasma motion make about 2 m/s. Obtained estimators allow to carry out the optimal choice of polarisation of sounding signals for getting minimal confidential intervals for diagnosing parameters.

**GA2.03/E/05-B3** Poster **1400-05**

**THE DETERMINATION OF NON-MONOTONE N(H)-PROFILES FROM IONOSPHERIC VERTICAL SOUNDING DATA USING REGULARISATION METHOD**

Natalia V. NASTASYINA and Pavel F. Denisenko (Institute of Physics, Rostov State University, 194, Stachky Ave., 344090, Rostov-on-Don, Russia, e-mail: denis@iphys.rnd.runnet.ru)

The main difficulty under research of temporal variations of N(h)-profiles from ground based vertical ionospheric sounding data relates with existence of gaps on the ionograms caused by radio wave absorption in the D-region by existence of valley. Using the radio wave absorption in Beynon-Rangaswamy's method allows to determine the real heights in the E-region with the errors no more than 2E3 km. Under reconstruction of non-monotone N(h)-profiles upper of E-region from the ordinary and extraordinary traces of the ionograms the errors in real heights reach 10E20 km at the F-region beginning. At present paper the method is described for calculation of non-monotone N(h)-profiles based on using regularization algorithm. Under non-monotone N(h)-profiles determination the ionogram traces of both ordinary and extraordinary polarising waves were used. The application of purposed regularisation scheme reveals two interesting peculiarities. Firstly, the regularising solution is weakly depend on random errors of experimental measurements while the Least-Squares-Method-solution is strongly depend on these errors. Secondly, the regularisation method for middle latitudes conditions gives the confidential intervals for real heights in 3 times smaller than Least Squares Method (LSM). Under errors of virtual heights in 1 km the errors in regularising solution make from 1 km to 3 km while errors in LSM-solution make 10 km. These results conform with theoretical estimating errors of monotone N(h)-profile reconstruction. Under determination of non-linear parameter, valley depth, the error makes 2 %. It is shown that due to the regularization method the real heights are determined with errors about 10% of errors in virtual heights.

**GA2.03/E/06-B3** Poster **1400-06**

**Nonequilibrium Processes and Organized Structures in Near Cosmic Space**

Vjacheslav M. Somsikov (Institute of Ionosphere, Kameskoe Plato, 480068 Alma-Ata, Republic of Kazakhstan, email: nes@kaznet.kz); Gennadiy V. KHREBTOV and Ibragim E. Suleimenov (both at Institute of Ionosphere, Kameskoe Plato, 480068 Alma-Ata, Republic of Kazakhstan, email: gn@ionos.alma-ata.su)

Transition processes in Near Cosmic Space during magnetic storms and in sunrise-sunset hours of day has been investigation by the methods of non equilibrium dynamics. By joint processing of experimental records of variations of a magnetic field, cosmic rays and ionosphere of parameters the occurrence of dynamic chaos final Hausdorff dimension in variations of a magnetic field and ionosphere of concentration in transitive periods is established. It was found that at transitive hours in ionosphere parameters the additional oscillatory mode has appeared. The comparative analysis of results of processing of records of cosmic rays and magnetic field, has allowed to assume that the variations, registered on ground, of a magnetic field and variations of cosmic rays in a minute range of frequencies arise on ionosphere heights. Therefore our results testify to presence of the determined chaos in Near Cosmic Space in transitive periods of days.

**GA2.03/E/09-B3** Poster **1700-07**

**LOW LATITUDE IONOSPHERIC SCINTILLATIONS AND THEIR CORRELATION WITH CYCLE SLIPS IN GPS**

REDDY (Indian Institute of Geomagnetism, Dr Nanabhoj Moos Road, Mumbai, India, Email: gvreddy@iig.iigm.res.in)

Abstract not available at time of going to press

**GA2.03/E/10-B3** Poster **1700-08**

**EXTRACTING IONOSPHERIC INFORMATION USING GPS MEASUREMENTS.**

Claudio BRUNINI (Facultad de Ciencias Astronomicas y Geofisicas, Universidad Nacional de La Plata, Buenos Aires, Argentina; e-mail: claudio@fcaglp.fcaglp.unlp.edu.ar); Maria Andrea Van Zele (Facultad de Ciencias Exactas y Naturales, Universidad de Buenos Aires y CONICET, Buenos Aires, Argentina, e-mail: avanzele@tango.gl.fcen.uba.ar); Amalia Meza (Facultad de Ciencias Astronomicas y Geofisicas, Universidad Nacional de La Plata, Buenos Aires, Argentina; e-mail : ameza@fcaglp.fcaglp.unlp.edu.ar) Mauricio Gende (Facultad de Ciencias Astronomicas y Geofisicas, Universidad Nacional de La Plata y Conicet, Buenos Aires, Argentina; e-mail: mgende@fcaglp.fcaglp.unlp.edu.ar)

Signals from GPS satellites received at the surface of the earth have passed through the terrestrial atmosphere and are therefore affected by refraction in the ionosphere and the lower

neutral atmosphere. In Geodesy and in Astrometry these refraction effects are typically seen as a nuisance and are removed from the measurements using appropriate models. The complementary point of view is that the refraction effects in GPS measurements contain useful information accumulated by passing through the atmosphere. In this scenario, the ionospheric and tropospheric delay are seen as remotely sensed data related to atmospheric parameters, with the possibility to recover some or all of these parameters through proper data analysis. The main goal of this kind of ionosphere research is to make use the capability of these observations to continuously and routinely ionosphere monitoring at global scale. In particular, we will focus in the estimation of parameters describing the distribution of free electrons in the ionosphere and their changes along time. We describe the algorithms used to produce ionospheric global maps automatically. We analyse the GPS observations collected in some years by around forty earth stations globally distributed and we discuss the correlation between some estimators obtained from the ionospheric model and the geomagnetic and solar activity.

**GA3.02** **Tuesday 27 – Wednesday 28 July**

**MAGNETOSPHERIC SUBSTORM ONSET: OBSERVATIONS, THEORIES, MODELS**

Location: Gisbert Kapp E203 LT1  
Location of Posters: Gisbert Kapp, Coffee Room

**Tuesday 27 July AM**

Presiding Chair: G Rostoker (STEL, Nagoya Univ, Japan)

**MAGNETOSPHERIC SUBSTORM ONSET: OBSERVATIONS, THEORIES, MODELS-1**

**GA3.02/W/16-B2** Invited **0900**

**TOWARD A REFERENCE TIMEFRAME FOR MAGNETOSPHERIC SUBSTORM ONSET AND DYNAMICS RESEARCH**

Ching-I. MENG and Kan Liou (both at The Johns Hopkins University Applied Physics Laboratory, Laurel, MD 20723-6099, USA, email: Ching.Meng@jhuapl.edu)

Since we first made the report at the ICS-4 meeting a year ago there is a growing awareness that the timing of substorm onset determined from many substorm onset indicators can lead to error. The importance of the onset timing that may adversely affect substorm researches will be reviewed. In addition a summary of our statistical result on calibrating substorm onset signatures will be given to strengthen the need of consensus on unifying the timing of substorm onset. Specifically we used auroral breakups as the substorm onset to compare the timing of onset with other onset signatures: low-latitude Pi 2 pulsations, dispersionless energetic particle injections at the geosynchronous orbit, and auroral kilometric radiations (AKR). Statistically none of the three onset signatures alone can reliably time the substorm onset. This is mainly because substorms are not the only means in producing these signatures. In addition most of the onset signatures are not observed at the initial onset location in the magnetotail. As a result, propagation effects may cause an inevitably inconsistent result from one case to another. This expectation is confirmed by our statistical result even though onset signatures are identified with the use of auroral breakups. It is found that substorm associated Pi 2 pulsations lag behind auroral breakups by 1 - 2 min, on average, depending on the relative location of the ground magnetometer and the onset location. Geosynchronous energetic particle injections were found to lag behind auroral breakups by a various amount (from 0 to more than 10 min). A slightly delay (less than 1 min) of AKR onset relative to auroral breakups is also found, suggesting the most reliable timing tool among the three surveyed onset indicators. Implications of this investigation result will be discussed.

**GA3.02/W/43-B2** **0920**

**SUBSTORM TIMING USING P11 PULSATIONS FROM HIGH LATITUDE MAGNETOMETER ARRAYS**

J.L. POSCH, K N Erickson, and M J Engebretson (Physics Department, Augsburg College, Minneapolis, MN 55454; ph. 612-330-1040; e-mail: posch@augsborg.edu) A T Y Lui (JHU/APL, Laurel, MD 20723), R L Arnoldy (Space Science Center, University of New Hampshire, Durham, NH 03824); H Fukunishi (Faculty of Science, Tohoku University, Sendai, 980-77, Japan)

The accurate timing of onsets continues to be an important issue in substorm studies. Pi2 pulsations (40 - 150 second period) have been widely used to time substorm onsets. This study explores the use of Pi1 pulsations (1-40 second period) as an alternative indicator. The use of high time resolution magnetometer data from numerous high latitude stations, including a search coil magnetometer in Sondrestromfjord, Greenland, and the US and British AGO arrays in Antarctica at 65° - 80° MLAT has made Pi1 activity a viable possibility for such timing. We have examined a set of substorm onsets identified at JHU/APL by visual inspection of global auroral images from the Polar UVI for selected periods from March 1996 through October, 1997. These onsets have been compared to Pi1 activity seen on the ground at high latitudes. Our results indicate that Pi1 onset times often agree with those of the POLAR identified events when the Antarctic ground stations are between 2200 and 0200 MLT. This Pi1 often is simultaneous across all Antarctic stations and is nearly simultaneous with the Pi2 pulsations. Pi1 may be a more accurate way to time the substorm onset since the period is much shorter than that of Pi2 pulsations and allows for less error when determining the start time. In addition, unlike Pi2 pulsations, Pi1 pulsations weaken in amplitude as they propagate away from the footpoint of the source region.

**GA3.02/E/11-B2** **0935**

**ON THE FALLACY IN EXISTING METHODS OF SUBSTORM TIMING**

V.M. MISHIN, T.I. Saifudinova, A.D. Bazarzhapov, L.V. Minenko, and P.A.Sedykh (all at Institute of Solar-Terrestrial Physics, P.O.Box 4026, Irkutsk, 664033, Russia, email: mishin@iszf.irk.ru),

In a classic NENL model of substorms, the commencement of the substorm active phase is called the expansion onset and is identified with the start of the open tail reconnection. The expansion onset time is determined as the time of the first observed substorm onset, and this tradition has persisted to date. However, it has become clear in recent years that first substorm onsets are produced not by the open magnetic flux reconnection but by instabilities in the near (closed) tail. Hence traditional methods of timing have to be supplanted by others. Examples of a misleading timing by traditional methods are given. To ensure a correct timing, we suggest methods based on using the plot of variation, in the course of the substorm, of the open magnetic flux determined by means of MIT2 (Mishin et al., JGR, 1997, p. 19845).

**GA3.02/W/42-B2 0950**

**OBSERVATIONS OF SUBSTORM-LIKE SIGNATURES IN AN NEAR GROUND STATE MAGNETOSPHERE**

Peter R. SUTCLIFFE (Hermanus Magnetic Observatory, P O Box 32, Hermanus 7200, South Africa; E-mail: psutclif@csir.co.za)

Substorm-like signatures have been observed under conditions with which substorms are not normally associated, namely, extremely quiet solar wind conditions when the magnetosphere is in a near ground state. A number of years of data were scanned for extremely quiet intervals on the basis of ap indices and solar wind parameters. During many of these quiet intervals Pi2 pulsations, which had amplitudes similar to those typically observed during substorm expansion phases, were observed at low latitudes. A variety of other ground based and satellite data sets were inspected for the presence of associated substorm signatures. The occurrence, magnitude, and localization of the substorm-like signatures observed are discussed. Studies of these less complex events should facilitate a better understanding of the mechanisms responsible for substorm onsets and intensifications.

**GA3.02/W/15-B2 1005**

**THE ROLE OF SOLAR WIND IN SUBSTORM TRIGGER MECHANISM: A REVISIT WITH POLAR UVI IMAGERY**

K. LIUO, D. G. Sibeck, P. T. Newell, C.-I. Meng (all at The Johns Hopkins University Applied Physics Laboratory, Laurel, MD 20723-6099, USA, email: kan.liuo@jhuapl.edu)

One of the outstanding issues in magnetospheric physics is that of the trigger mechanism(s) of substorm expansion phase onset. Past studies have shown that variations in solar wind magnetic field and/or plasma can trigger substorm onset. In contrast, the occurrence of substorm onsets during steady solar wind conditions has been reported and suggests a triggering mechanism that is internal to the magnetosphere. In a recent study of substorm timing, we found that most of the commonly used substorm onset indicators are subject to delay with respect to auroral breakups. We therefore suspect that this highly controversial issue of a possible solar wind onset trigger may be due to large uncertainties in the onset determination from previous studies. In the present study we re-investigate the influence of sudden changes of the solar wind magnetic fields on substorm onsets by using a list of about 1000 auroral breakups determined from Polar UVI imagery. To further improve the accuracy of our correlative study we use the near Earth solar wind data from IMP-8, GEOTAIL, and INTERBALL-TAIL spacecraft. We will present detailed results and discuss the implications of these findings.

**GA3.02/W/56-B2 1020**

**SUPERIMPOSED EPOCH ANALYSES OF SOLAR WIND CONDITIONS AROUND ONSET FOR VARIOUS DIPOLE TILT ANGLES**

N.J. FLOWERS. (Address not available at time of going to press) A.D. Johnstone

Periods of southward interplanetary magnetic field load the magnetotail with energy that is subsequently unloaded into the magnetosphere by a sequence of processes collectively termed a substorm. The mechanism responsible for this unloading of energy and how this is triggered is a source of ongoing controversy.

Caan et al. [1977, 1978], McPherron et al. [1986], Lyons [1996], and Henderson et al. [1996], debate the possibility that a northward turning of the IMF, or a reduction in the induced electric field, is responsible for the triggering of substorms. This work investigates the possibility that IMF changes may be responsible for triggering onset by using superimposed epoch analyses of solar wind data from around onsets. Identifying nearly 200 substorm onsets with CRRES data, a superimposed epoch analysis of IMP-8 solar wind variables around onset is made. Separating data contributing to the analyses by dipole tilt angle to the Sun results in differing typical IMF component signatures being seen around the grouped onset time. This may indicate the dipole tilt effects the onset mechanism, or the 15 MeV inner radiation belt formed during CRRES's lifetime effected the onset mechanism, or the long-term seasonal changes occurring in the solar wind over CRRES's lifetime were significant (tilt is a selector for season). It is hoped that work using IMP-8 and WIND data from an extended multi-year epoch will be ready to present at the meeting, indicating which conclusion is correct and providing insights into the triggering debate.

For the general, no tilt discrimination case, no significant structure in IMF vectors is seen prior to event onset, other than a Bz reduction. This indicates that although some events are undoubtedly triggered by changes in the IMF, reductions in the solar wind electric field are not mandatory for event occurrence. It is concluded that the substorm onset is an internal process susceptible to external perturbation.

Presiding Chair: J. Samson (Dept of Physics, Uni of Alberta, Canada)

**GA3.02/L/03-B2 1055**

**A STATISTICAL INVESTIGATION OF SUBSTORM TRIGGERING**

Tung-Shin SHU and R L McPherron (IGPP & ESS/UCLA, Los Angeles, CA 90024-1567; 310-825-2441; email: tshu@igpp.ucla.edu; mcpherr@igpp.ucla.edu)

An outstanding problem in magnetospheric physics is deciding whether substorms are always triggered by external changes in the interplanetary magnetic field (IMF) or solar wind plasma, or whether they sometimes occur spontaneously. Over the past decade, arguments have been made on both sides of this issue. In fact, there is considerable evidence that some substorms are triggered. However, equally persuasive examples of substorms with no obvious trigger can also be found. It is evident further works required to determine whether there is a physical relation between IMF triggers and substorm onset. In the work reported here a substorm list was created by using two independent substorm signatures: AL index and Pi 2 pulsations. Possible IMF triggers were determined by ISEE-2 and Imp-8 observations. These lists allow us to consider several questions. First we can assess the frequency of occurrence of potential IMF triggers and calculate the probability that the observed association with substorm onset is due to chance. Second, with the ISEE observations near local noon immediately upstream of the bow shock there can be little question about propagation delay to the magnetopause, or whether a particular IMF feature hits the magnetopause. It thus eliminates the objections that the calculated arrival time is erroneous and that the monitor missed a potential trigger incident at the subsolar point. Finally the joint observations can be used to determine the probability that a signature detected at one spacecraft will be missed by the other.

**GA3.02/W/39-B2 1110**

**CAN PSEUDOBREAKUPS BE PREDICTED?**

ZHOU, X.-Y., B.T. Tsurutani, J.K. Arballo (Jet Propulsion Laboratory, California Institute of Technology, Pasadena, CA 91109) D. Berdichevsky, and R.P. Lepping (Goddard Space Flight Center, Code 695.0, Greenbelt, MD 20771)

We statistically analyze many interplanetary shock events where there are both WIND interplanetary data and POLAR UV imaging data. We find that the shock compression events trigger pseudobreakups (PBs), substorm onsets, or enhance (pre-existing) substorm intensities. Using WIND interplanetary data and ground-based data, it is now believed that we can predict when PBs will occur and when substorm expansion phases will occur.

**GA3.02/L/01-B2 Invited 1125**

**THE SUBSTORM ONSET AS SEEN IN GROUND-BASED OBSERVATION - IMPLICATIONS FOR SUBSTORM MODELS**

Hermann OPGENOORTH (Swedish Inst of Space Physics, Uppsala Division, S-75591 Uppsala Sweden,) and Paul Eglitis (both also at: Finnish Meteorological Institute, Geophysical Division Helsinki, Finland (Tel +46-18-3036661, fax +46-18-403100, E-mail: opg@irfu.se; paul@irfu.se)

The magnetospheric substorm is a large scale instability which converts magnetospheric excess energy stored in current systems and magnetic field deformations into particle energy and heat production in the ionosphere and ring current. In spite of intensive studies during the last 30 years the exact mechanism for the onset of this instability has not exactly been identified. The reason for this is the global character of the observed disturbance pattern, involving a vast region of space. Detailed in situ observations have so far not been able to solve the exact temporal sequence and consequently the causal relation of the different observed processes in the near Earth space plasma.

The only method which can simultaneously monitor processes in the near-Earth and more distant plasma sheet is the observation of aurora, electric field and current systems in the nightside ionosphere, which within a few degrees of latitude is connected to all relevant regions of near-Earth space. Temporal sequences of processes in different latitude regions of the nightside ionosphere are indicative of consecutive processes in the near Earth and distant plasmasheet. Exact timing of ground-based observations in both latitude and longitude, can solve some of the remaining questions of causality in space plasma processes associated with substorms. We will present recent observations from the Scandinavian network of stations, which includes 3 incoherent scatter radars (EISCAT UHF, VHF and ESR), two coherent radar systems (CUTLASS and STARE) and networks of magnetometers and digital all-sky cameras. Our observations around substorm onsets will be discussed on the background of different substorm models.

**GA3.02/W/09-B2 1145**

**JOINT SUPERDARN AND POLAR OBSERVATIONS OF SUBSTORM EXPANSION PHASE ONSET**

M.LESTER (Department of Physics and Astronomy, University of Leicester, Leicester, LE1 7RH, UK, Email: mle@ion.le.ac.uk); and N.J. Fox (Goddard Space Flight Center, mail Code 695, Greenbelt, Maryland 20771, USA).

The global nature of ionospheric convection at expansion phase onset and its relation to the auroral activity remains a topic of much uncertainty. For example, if reconnection in the tail begins at expansion phase onset, signatures are expected in the ionospheric convection. The SuperDARN radars are well placed to image the ionospheric flow over much of the northern hemisphere, while the auroral imagers on the Polar spacecraft can provide simultaneous global images of the aurora. This paper presents observations of ionospheric convection by SuperDARN during 2 expansion phase onsets separated by two hours.

**GA3.02/E/13-B2 1200**

**MODELLING OF SUBSTORM ONSET PROCESSES USING RADIOWAVE ABSORPTION OBSERVATIONS, CONVECTION ANALYSIS AND XRSTED SATELLITE DATA**

Peter STAUNING (Solar-Terrestrial Physics Division, Danish Meteorological Institute, Lyngbyvej 100, DK-2100 Copenhagen X, Denmark. E-mail: pst@dmi.dk)

Substorms are global phenomena controlled by the interactions of the ionospheric and magnetospheric regions separated by distances of several tens to hundreds of thousands of km. In view of the propagation delays involved in the magnetosphere-ionosphere communication the explosive brightening of aurora and the sudden development of magnetic bays may appear contradictory. A possible explanation is offered by theories which invoke the development near the ionosphere of large field-aligned potential structures that could accelerate the magnetospheric plasma particles to generate the sudden and highly variable energetic auroral particle radiation which are characteristic features of ionospheric substorm onsets. We have analyzed the onset processes seen in our high-latitude magnetometer and riometer recordings. The combination of the time-varying AMIE potential patterns to describe the polar convection, and high-resolution, localized observations of substorm activity using, among others, imaging riometer recordings, have been used as the basis for modelling substorm onset processes. We find that field-aligned potential structures can have positive feedback to the ionospheric potentials affected by conductivity changes caused by the accelerated particles. We suggest that such coupled potential systems may provide a general acceleration mechanism. The ground-based observations will be augmented by data from Xrsted and other satellites.

**GA3.02/W/60-B2 1215**

**TO INVESTIGATE THE CONVERGENCE OF THE SUBSTORM ONSET SIGNATURES**

A.G.YAHNIN (Polar Geophysical Institute, Apatity, Russia, E-mail: ahnin@pgi.kolasc.net.ru); V.A.Sergeev, M.V.Kubysheva (Institute of Physics, University of St-Petersburg, Russia, E-mail: sergeev1@snoopy.phys.spbu.ru); N.L.Borodkova (Space Research Institute, Moscow, Russia, E-mail: nbor@afed.iki.rssi.ru); T.Bosinger (Dept of Physical Science, University of Oulu, Oulu, Finland, E-mail: Tilmann.Bosinger@oulu.fi); T.I.Pulkkinen (Finnish Meteorological Institute, Helsinki, Finland, E-mail: Tuija.Pulkkinen@fmi.fi)

To investigate the convergence of the substorm onset signatures and their reliability to describe adequately magnetospheric processes we study the substorm commencing at 2053 UT on Dec 15, 1996. It was observed by a number of ground based instruments and by two ISTP spacecraft Interball-1 and Geotail. Clear auroral breakup has been detected by several TV cameras situated on Kola Peninsula and Scandinavia. Simultaneously several magnetic stations recorded the onset of magnetic bay and Pi2/PiB pulsations. Interball-1 situated in the



tail lobe at X=-10 Re registered sharp decrease of the magnetic field strength, and a little bit later Geotail detected fast tailward flow and bipolar variation of the magnetic field Bz component near the neutral sheet at X=23 Re. The study showed that when the observations are made in appropriate place both auroral and magnetic onset signatures occur at the same time. The observed sequence of magnetotail phenomena agrees with the onset scenario in which the current disruption occurs in the near-Earth plasma sheet in close relation to reconnection process and generation of tailward moving plasmoid. The results are confirmed by consideration of several other substorms selected on the basis of good conjunction between the ground-based network and mid-tail satellite.

**GA3.02/W/12-B2 1230**

**SIMULTANEOUS OBSERVATIONS OF DIPOLARIZATIONS IN THE NEAR TAIL PLASMASHEET/LOBE BOUNDARY AND SUBSTORM ACTIVITY ON THE GROUND**

NAIGUO LIN, C. A. Cattell, (School of Physics and Astronomy, University of Minnesota, Minneapolis, MN 55455, USA Email: lin@waves.space.umn.edu); M. J. Engebretson, (Dept. of Physics, Augsburg College, Minneapolis, MN 55454-1338, USA); R. P. Lepping, (NASA Goddard Space Flight Center, Greenbelt, MD 20771, USA); R. P. Lin (UC Berkeley, SSL-305 (Space Sciences Laboratory), CA 94720, USA)

A sudden dipolarization followed by long period (about 25 minutes) compressional magnetic fluctuations with shorter period waves superimposed on them was observed by the Wind spacecraft in the magnetotail near midnight on Sep 17, 1995, at a position of (-15, 0, 2)Re in GSE coordinates. The spacecraft was near the boundary between the northern tail lobe and the plasmasheet. Signatures of several dipolarizations are observed during the fluctuations. Observations of anticorrelation between the variations of the magnetic field and of the energetic electrons are consistent with alternating plasma sheet thinning and expanding. Ground data from stations located near the footprints of the magnetic field lines crossed by the spacecraft during the event showed negative bays occurring near local midnight, which indicate substorm activity. The onset times of Pi2 on the ground varied for different stations. Simultaneous observations from Geotail, which was near local noon at about 20 Re upstream from the Earth, showed similar fluctuations in IMF Bz, with an amplitude of about 5 nT. It is suggested that the periodic southward-northward turning of the IMF may have caused the periodic plasma sheet thinning and the compressional fluctuations, which carried the disturbance to the near tail and triggered substorms. The relationship between the onset of a substorm on the ground and the dipolarization in space will be discussed.

**Tuesday 27 July PM**

Presiding Chair: Y. Kamide, (STEL, Nagoya University, Toyokawa, Japan)

**MAGNETOSPHERIC SUBSTORM ONSET: OBSERVATIONS, THEORIES, MODELS-2**

**GA3.02/E/14-B2 Invited 1400**

**HOW AND WHERE AURORAL BREAKUP BEGINS**

Y. KAMIDE (Solar-Terrestrial Environment Laboratory, Nagoya University, Toyokawa, Aichi-ken 442-8507, Japan, email: kamide@stelab.nagoya-u.ac.jp)

The auroral substorm is one of the elements of the magnetospheric substorm, and an auroral breakup is the first indicator of substorm expansion onset. It is thus crucial to use auroral breakups to time various substorm phenomena in the magnetosphere. This paper discusses observational constraints on substorm initiation theories by differentiating the necessary and sufficient conditions that lead to the sudden expansion processes that occur in conjunction with auroral breakups. It is important to realize that an auroral breakup begins from a preexisting auroral arc; it does not start from "nothing." The strong statistical dependence of the latitude of auroral breakups and the probability of substorm occurrence on the southward component of the interplanetary magnetic field (IMF) is also discussed. The IMF orientation controls the strength of substorms as well.

**GA3.02/W/62-B2 Invited 1420**

**IMPLICATIONS OF IONOSPHERIC CONVECTION OBSERVATIONS DURING THE 24 NOVEMBER GEM SUBSTORM EVENT**

L. R. LYONS (Department of Atmospheric Sciences, UCLA, Los Angeles, CA 90095-1565, USA, email: larry@atmos.ucla.edu); J. M. Ruohoniemi (Johns Hopkins University, Applied Physics Laboratory, Johns Hopkins Rd., Laurel, MD 20723-6099, USA, email: mike\_ruohoniemi@spacemail.jhuapl.edu)

Here we present data from the GEM substorm interval that provides strong evidence that such convection reductions lead to substorm onset and that substorms do not occur during conditions of steady enhanced convection. This GEM interval has unusually good coverage of global ionospheric convection from the SuperDARN radars, and unusually ideal IMF conditions (sharp southward turning followed first by ~1.25 hr of steady southward IMF and then by a small and a large northward turning). Convection is found to be quite steady during the 1.25 hr interval of steady southward IMF, and substorms are not seen during this interval. This is consistent with earlier observations during convection bays and implies that internal magnetotail instabilities during periods of enhanced convection do not generally lead to substorm onset. Two onsets are clearly identified in auroral zone data during the period of the two IMF northward turnings, each at a time consistent with IMF triggering. The time of magnetopause impact of individual IMF changes cannot be precisely determined from IMF measurements, so that IMF triggering of the onsets cannot be proofed using the IMF measurements alone. However, convection responses to the IMF changes can clearly be identified in the SuperDARN data. It is found that the reductions in global convection associated with the two northward turnings initiate ~1 min prior to each of the two onsets. The first (smaller) northward turning is found to give a small convection reduction and the onset of a small substorm, while the second (much larger) northward turning is found to give a large reduction in global convection and the onset of a large substorm. This implies that substorm triggering by the IMF does not push the magnetotail over an instability threshold. If so, the smaller northward turning, which followed a prolonged growth-phase period with strongly southward IMF, should have led to a large substorm. It suggests that substorms result from an adjustment to conditions of reduced convection, small reductions leading to small substorms and large reductions leading to large substorms.

**GA3.02/E/06-B2 Invited 1440**

**TAIL CURRENT DISRUPTION: OBSERVATIONAL CONSTRAINTS ON SUBSTORM TRIGGER MODELS**

Shin-ichi OHTANI (The Johns Hopkins University Applied Physics Laboratory, Johns Hopkins Road, Laurel, MD20723-6099, USA, Email: ohtani@jhuapl.edu)

The formation of a Near-Earth neutral line (NENL) and the trigger of tail current disruption are two important concepts of substorm physics. The objective of this paper is to address the cause-effect relationship between these two processes from the observational viewpoint of tail current disruption. Such an approach should be a good complement to the recent studies of plasma sheet plasma flow, which tend to place an emphasis on the formation of a NENL. The list of issues to be addressed include (1) the role of tail current disruption in the global substorm dynamics, (2) the relative timing of the NENL formation and tail current disruption, and (3) the temporal and spatial characteristic scales of tail current disruption. A special emphasis will be placed on observations that are difficult to implement in the so-called pile-up model, which explains dipolarization and the apparent reduction of the tail current intensity in terms of the transfer of magnetic flux from the near-Earth reconnection site. The paper seeks to list observational constraints to be considered in modeling the substorm trigger.

**GA3.02/E/09-B2 Invited 1500**

**KINETIC CHARACTERIZATION OF PLASMA SHEET DYNAMICS**

G. K. PARKS, L. J. Chen, M. McCarthy Geophysics Program, University of Washington, Seattle, WA D. Larson and R. P. Lin Space Sciences Laboratory, UC Berkeley, Berkeley, CA H. Reme, CESR, Toulouse, France T. Sanderson, ESTEC, Noordwijk, The Netherlands

The plasma data provided by the Wind 3D instrument are of high quality sufficient to formulate a kinetic picture of the plasma sheet dynamics. This will augment our current understanding which is based primarily on fluid description using the plasma bulk parameters. A kinetic picture is needed because observations clearly show that the plasma distributions consist of more than one population across the central plasma sheet to the lobe regions. Thus describing the dynamics using the bulk parameters alone will be incomplete and can lead to incorrect conclusions. This talk will focus on kinetic properties of both ions and electrons. We will compare, evaluate and discuss new features including possible sources of bursty bulk flows.

**GA3.02/W/21-B2 Invited 1520**

**MODELING OF TIME-EVOLVING MAGNETIC FIELDS DURING SUBSTORMS**

G. LU (High Altitude Observatory, National Center for Atmospheric Research, Boulder, CO 80301; 303-497-1554); N. A.; Tsyganenko (Raytheon STX Corporation, NASA GSFC, Greenbelt, MD); A. T. Y. Lui (Applied Physics Laboratory, Johns Hopkins University, Laurel, MD); H. J. Singer (Space Environment Center, National Oceanic and Atmospheric Administration, Boulder, CO); T. Nagai (Tokyo Institute of Technology, Tokyo, Japan); and S. Kokubun (Solar-Terrestrial Environment Laboratory, Nagoya University, Japan)

An attempt has been made to model the dynamics of the magnetospheric magnetic field during substorms, by modifying the 1996 version of the data-based model by Tsyganenko [1996]. The modified model incorporated an adjustment to the intensity and thickness of the near-tail current sheet and a contribution from the substorm current wedge. These improvements made it possible to use the model to represent the evolution of the magnetic field during the entire substorm sequence of growth, expansion, and recovery. The modeled magnetic fields have been tested against satellite observations during three isolated substorms. According to the model results, during the substorm growth phase, the thickness of the tail current sheet was gradually decreased while the intensity of the tail current was gradually increased; by the end of the growth phase, a thin current sheet of 190-1340 km in half thickness was formed in a narrow region around X ~ -7.5 RE, with a maximum westward current density of 9-23 nA/m<sup>2</sup>. During the substorm expansion phase, an eastward current associated with the substorm current wedge started to develop around X ~ -12 RE, resulting in a collapse of the previously stretched field configuration. At the peak of an intense substorm, the net tail current flow became eastward between X = -11 and X = -13 RE, accompanied by a negative (southward) Bz tailward of -13 RE.

**GA3.02/W/41-B2 1600**

**SIMULATION OF DISPERSIONLESS INJECTIONS OF ENERGETIC PARTICLES ASSOCIATED WITH MAGNETOSPHERIC SUBSTORMS**

XINLIN LI and D. N. Baker (LASP, University of Colorado, 1234 Innovation Drive, Boulder, CO 80303-7814, USA; 303-492-3514, email: lix@kitron.colorado.edu); M. Temerin (SSL, UC Berkeley, CA 94720, USA) G D Reeves and R D Belian (MS D-436, LANL, Los Alamos, NM 87545)

Energetic particle (tens to hundreds of keV) injections into the inner magnetosphere are typical indicators of the onset of expansive phase of magnetospheric substorms. It is generally understood that the expansive phase corresponds to a rapid change of the magnetic field, described as dipolarization, which is associated with a strong inductive electric field predominantly in the dawn-to-dusk direction. We have conducted test particle simulations in order to understand how electric and magnetic fields change during substorm onset and how such changes can produce dispersionless injections of electrons [Li et al., 1998] and ions and other particle features observed in the inner magnetosphere. The dipolarization process was modeled with only one component of the electric field which is westward and a consistent magnetic field. Our simulation results reproduce observed electron and proton injections and subsequent drift echoes. We found that the temporal profile of injected fluxes is determined by the temporal profile of the time-varying magnetic field. Modeling these frequently observed dispersionless injections of energetic particles in the inner magnetosphere will help us to understand the reconfiguration of magnetotail during the expansive phase of magnetospheric substorms.

**GA3.02/W/54-B2 1615**

**OCCURRING IN THE NIGHTSIDE NEAR-EARTH TAIL AFTER SUBSTORM EXPANSION PHASE ONSET**

Z.X. CHEN, A. Korth, C. Mouikis (all at: Max-Planck-Institut fuer Aeronomie, D-37191 Katlenburg-Lindau, Germany, Email: chen@ciscos.mpae.gwdg.de); Z.Y. Pu (Department of Geophysics, Peking University, Beijing 100871, China, Email: zypu@pku.edu.cn)

Inspired by the qualitative picture of earthward expansion of tail current disruption, we propose in the beginning of this paper that there may occur an earthward propagating abnormal magnetic field configuration in the nightside near-Earth tail after substorm expansion phase onset. This abnormal magnetic field configuration is characterized by an earthward declining

**MAGNETOSPHERIC SUBSTORM ONSET: OBSERVATIONS, THEORIES, MODELS-3**

**GA3.02/W/14-B3** Invited **0830**

**SUBSTORM ONSET AT A PREBREAKUP ARC: "MINIMUM-B" MODEL**

Galperin Yuri (Space Research of Institute of RAS, 84/32 Profsoyuznaya St, Moscow, 117810 Russia, Email: ygalperin@iki.rssi.ru)

An excellent example of ground-based monochromatic optical measurements of prebreakup arc and substorm onset as typical for 35 cases was published by J. Deehr (SUBSTORMS 2, 229, 1994). This event and some other evidence are interpreted as showing the existence of an extended magnetic field minimum in the near-Earth plasma sheet at the "root" of the prebreakup arc, and effects of its deepening before the onset.

The "Minimum-B" theory (Galperin et al., GRL, 19, 2163, 1992) for generation of FA double-sheet current loop feeding a stable homogeneous auroral arc predicted a minimum in the radial magnetic field profile in the neutral sheet as a steady double-sheet FA current generator. For a prebreakup arc this generator is located at the inner edge (or at an outward gradient) of the cross-tail linear current density. Such a minimum was deduced by Sergeev et al., Space Sci. Rev., 1996 in a unique case of long duration Stationary Magnetospheric Convection on November 24, 1981.

Simultaneous satellite data from AUREOL-3 and DE-2 have shown the double-sheet FAC/arc at the predicted place.

An extension of the "Minimum-B" theory to substorm onset (Galperin and Bosqued, Cosmic Research, 1998) supposed a deepening of the magnetic field minimum. For a sharp deepening the inferred increase of FA current will lead to auroral activation or onset according to the "M-I coupling?" theory by Kan et al., JGR, 1988. A neutral line can form if the magnetic field in the minimum reverses sign. Or, the deepening can gradually proceed till a "critical" low value at which CCI or other instabilities lead to a local cross-tail "current disruption?". The ground-based optical data mentioned above in many details give strong support for such a scenario.

**GA3.02/E/18-B3** Invited **0850**

**A SYNTHESIS OF THE NEUTRAL LINE AND CURRENT DISRUPTION MODELS FOR SUBSTORM ONSET**

Z.Y. PU, K.B. Kang, S.Y. Fu, and Z.X. Chen (Department of Geophysics, Peking University, Beijing, China, email: zypu@pku.edu.cn); A. Korth, Q.G. Zong, C.G. Mouikis, R.W.H. Friedel (Max-Planck-Institute for Aeronomy, Katlenburg-Lindau, Germany, email: korth@sprotte.mpae.gwdg.de); M. H. Hong (Institute of Geophysics, Academia Sinica, Beijing, China, email: kytang@mail.c-geos.ac.cn); Z. X. Liu (Center for Space Science and Application Research, Academia Sinica, Beijing, China, email: liu@sun20.cssar.ac.cn); T. Pulkkinen (Finnish Meteorological Institute, Helsinki, Finland, email: tuija.pulkkinen@fmi.fi)

It is found that the presence of a decelerated earthward flow destabilizes the drift ballooning mode (DBM) in both equatorial and off-equatorial regions near the inner edge of the plasma sheet (IEPS). The unstable DBM excites coupled Alfvénic slow magnetosonic waves, which carry field-aligned currents into and out of the ionosphere, forming a quasi-periodic current wedge. The total Wedge current may be comparable to the DP 1 current in a large substorm if the azimuthal electric field of the waves is about 5 mV/m. The interplay of the coupled Alfvénic slow magnetosonic waves with the magnetosphere and ionosphere provides the means to the magnetosphere-ionosphere coupling and field line resonance. A synthesis of the near-Earth neutral line model and near-Earth current disruption models for the onset of substorm expansion phase seems to exist. While an earthward flow resulting from reconnection in the midtail is braking near the IEPS, it compresses the plasma populations ahead of its front and pushes them further earthward. This may lead the DBM to explosively grow, causing cross-tail current disruption/diversion and dipolarization of the magnetic field. The expansion onsets would be initiated in the near-Earth tail in the 6 to 13 Re range and preferentially in the premidnight sector. Substorm injection can yield a domino effect in the potentially unstable region. This substorm scenario covers the midtail, the near-Earth tail, and the ionosphere. It integrates current disruption with magnetic reconnection, and might also integrate with the magnetosphere-ionosphere coupling and field line resonance. Decelerated tailward flows may also initiate substorms through generation of the DBM in the near-Earth tail. Instabilities other than the DBM can trigger the substorm expansion phase as well.

**GA3.02/W/38-B3** Invited **0910**

**KINETIC BALLOONING INSTABILITY AS A MECHANISM FOR SUBSTORM ONSET OBSERVED BY AMPTE/CC**

C. Z. CHENG (Princeton Plasma Physics Laboratory, Princeton University, Princeton, NJ 08543; 609-243-2648)

The underlying physical processes of substorm onset which leads to substorm explosive growth phase and subsequent current disruption observed by AMPTE/CC are presented. Toward the end of late growth phase before the onset of current disruption a low frequency global instability with a wave period of \$50-75\$ seconds is excited and grows exponentially to a large amplitude with  $\delta B / B \gtrsim 0.3$  at the onset of current disruption. The plasma  $\beta$  reaches to a high value of  $\beta \approx 50$ . Just before the onset an enhanced duskward ion drift of ion distribution is observed and lasts only about one half of the wave period of the low frequency instability. The enhanced duskward ion drift at the onset is correlated with the excitation of higher frequency instabilities (with wave periods 15 sec, 10, sec, etc.) so that the plasma evolves into a turbulence state. During the current disruption phase plasma transport causes plasma pressure profiles (averaged over the turbulent fluctuation scales) to evolve so that the magnetic field configuration changes from a tail-like to a dipole-like geometry. Thus, to correctly model the substorm onset it is necessary to understand the observed low frequency instability which occurs at high  $\beta$  ( $\approx 50$ ) and the associated duskward ion drift. We have proposed a new theory of kinetic ballooning instability which can explain the observed plasma features before the substorm onset. The kinetic ballooning instability can become unstable due to the free energy associated with nonuniform plasma pressure with gradient in the same direction as the magnetic field curvature. There are other theories of substorm onset based on the ballooning instability, i.e., the MHD ballooning instability theory and the nonlinear MHD ballooning instability theory. In order to improve our modeling of the substorm onset we will assess the strength and weakness among these theories based on the ballooning instability by comparing their prediction with the observed features of plasma and magnetic field.

equatorial curvature radius of the magnetic field lines. In the following parts, we provide an indirect evidence for this abnormal configuration. Since the plasma processes are usually related to magnetic field variations during substorm development, it is expected that there exist some special plasma processes which are subject only to the abnormal magnetic field configuration. The first possible process we can think of is the field-aligned acceleration of energetic ions during substorm expansion phase. We use ions and electrons pitch angle distribution data from the particle spectrometer S321 on board GEOS 2 satellite in this paper. Data analysis shows that there are two kinds of field-aligned distribution variations for energetic ions after substorm onsets: the toward-equator acceleration and off-equator acceleration. By examination of the parallel substorm-period Lorentz equation of ions, we find that magnetic field configuration is the dominant factor in determining the energetic ions field-aligned acceleration directions during the course of the substorm expansion phase. Two kinds of field-aligned distribution variations originate from two kinds of substorm-period magnetic field configurations. The toward-equator field-aligned acceleration of energetic ions results from the normal configuration, while the off-equator field-aligned acceleration of energetic ions can only result from the abnormal configuration.

**GA3.02/W/13-B2** **1630**

**RADIAL EXTENT AND PROPAGATION OF ENERGETIC PARTICLE INJECTIONS AT SUBSTORM ONSET**

R. H. W. FRIEDEL, G. D. Reeves, M. G. Henderson (all at Los Alamos National Laboratory, Los Alamos, NM, USA); J. F. Fennell and J. L. Roeder (both at The Aerospace Corporation, P.O. Box 92957, Los Angeles, CA 90009); A. Korth Max Planck-Institute, Lindau, Germany)

Near-Earth energetic particle injections have become a reliable and widely used indicator of substorm onset. Dispersionless injections indicate onset location; and timing the same injection on two radially separated spacecraft allows the determination of radial propagation. Data from CRRES and LANL have show such injections far off midnight and as close as 4.5 Re. LANL/CRRES studies have established earthward propagation of the injection front with speeds 24 km/s between  $L=6.6$  and  $L=5$ .

Here we intend to extend this study to AMPTE altitudes: this may yield the first direct evidence of "breaking flows". Recent observations and simulations suggest a scenario in which substorm injections are connected to bursty bulk flows originating at a near-Earth neutral line (NENL). The breaking and diversion of the flows may produce a compressional wave which leads to dipolarization and also reverses the local magnetic gradient and allows energetic particles to surf the wave. The resulting transport and acceleration injects particles into the trapping region which they would otherwise not have been able to reach, including regions where there was little or no field stretching during the growth phase. If this connection can be established observationally this would point to the classical NENL model, in which the trigger is equivalent to whatever starts off reconnection at the NENL.

**GA3.02/W/18-B2** **1645**

**GLOBAL MULTISPECTRAL IMAGING OF AN ISOLATED SUBSTORM**

S. A. CUMMER, R. R. Vondrak, R. F. Pfaff (Laboratory for Extraterrestrial Physics, NASA/GSFC, Greenbelt, MD 20771, USA, Email: steve.cummer@gscf.nasa.gov); N. Ostgaard, J. Bjordal, J. Stadsnes (Department of Physics, University of Bergen, Bergen, Norway); D. L. Chenette (Lockheed Martin Advanced Technology Center, Palo Alto, CA 94304, USA); M. J. Brittmacher, G. K. Parks (Geophysics Program, University of Washington, Seattle, WA 98195, USA); J. B. Sigwarth, L. A. Frank (Department of Physics and Astronomy, University of Iowa, Iowa City, IA 52242, USA); C. W. Carlson (Space Sciences Laboratory, University of California, Berkeley, CA 94720, USA)

The suite of global auroral imagers on the Polar satellite offers the first simultaneous view of the aurora at visible (the VIS instrument), ultraviolet (the UVI instrument), and x-ray (the PIXIE instrument) wavelengths. These instruments provide not only an opportunity to study substorm morphology at these wavelengths simultaneously but also provide the capability for quantitative remote sensing of the ionospheric effects of the observed energetic particle precipitation. To utilize and test these capabilities, we searched for a relatively isolated and simple substorm which was viewed fully by the three Polar imagers. Such an event occurred on 25 Jan 98 beginning at approximately 0410 UT. We compare the apparent substorm onset times seen in the various emissions (visible, ultraviolet, 3-12 keV x-rays, and 10-25 keV x-rays), and we examine the spatial and temporal morphology of the observed emissions throughout the substorm to understand the different particle populations responsible for them. We also compare estimates, based on images from the three instruments, of the total ionospheric conductance in a number of regions and compare these to direct calculations of ionospheric conductance from energetic electron measurements.

**INTRODUCTION TO DEBATE** **1700**

**GA3.02/W/52-B2** **1705**

**A DEBATE ON WHICH SUBSTORM MODEL BEST EXPLAINS EXPANSIVE PHASE ONSET**

Wolfgang BAUMJOHANN (Max-Planck-Institut für extraterrestrische Physik, D-85740 Garching, Germany, email: bj@mpe.mpg.de); Gordon ROSTOKER (Department of Physics, University of Alberta, Edmonton, Alberta, Canada T6G 2J1, email: rostoker@space.ualberta.ca)

At the present time, few space scientists doubt that magnetic field line merging in the magnetotail plays an important role in substorm activity. Since the mid 1970's, the near-earth neutral line (NENL) model has provided a framework in which most researchers try to understand their data. However, over the years several other models have been proposed which differ in many ways from the NENL paradigm. In the past decade, these several models have had their better features combined in a framework which differs significantly from the NENL picture in many important ways. At the same time, the NENL model itself has evolved significantly to meet objections based on ground based and satellite observations. There now are two competing frameworks in which substorm activity can be understood and this paper seeks to compare the two in a presentation which takes the form of a debate between the two authors and which will, towards the latter stages, involve participation by the attendees. The debate will focus on which model allows one to best understand the onset of the substorm expansive phase.



**GA3.02/E/01-B3 0930**

**IONOSPHERIC EFFECTS IN THE FORMATION OF AURORAL ARC LINKED TO THE CROSS-TAIL CURRENT DISRUPTION**

MANJU PRAKASH(Department of Physics and Astronomy, Suny at Stony Brook, Stony Brook, New York 11794-3800, USA, email: mprakash@nuclear.physics.sunysb.edu)

Recently Lui and Murphree [1998] have proposed a substorm onset model which combines the field line resonance (FLR) model for arc formation with the cross-field instability for current disruption. The model accounts for the observations that the substorm onset begins by brightening of the pre-existing auroral arc which derives its energy from the current disruption in the near-Earth region. Since the evolution of FLRs (which cause auroral arc) and the threshold for the excitation of cross-field instability (which leads to current disruption) are modified due to the modified ionospheric boundary conditions during substorms, it is worthwhile to examine the role ionosphere plays in the various predictions of this model. The present work will examine the role of feedback instability and the propagation of Alfvén waves (along the dipole field lines) in the development of various components of this model. The initial analytical studies will be extended to numerical calculations. \vskip 5mm \ni Lui, A. T. Y. and J. S. Murphree, A substorm model with onset location tied to an auroral arc, (J Geophys. Res. Lett., 25, ) 1269, 1998.

**GA3.02/W/17-B3 0945**

**LOCALISED RECONNECTION AND THE DISRUPTION OF THE NEAR EARTH PLASMA SHEET**

P L PRITCHETT and F V Coroniti (both at Department of Physics and Astronomy, University of California, Los Angeles, CA 90095-1547, USA, email: pritchet@physics.ucla.edu)

In recent years a number of spacecraft conjunction studies have provided clear evidence for the limited longitudinal extent of activations in and disruptions of the near-Earth plasma sheet. These observations are inconsistent with the traditional view that substorm onset involves a tearing instability along an extended neutral line. The ballooning mode instability in the near-Earth plasma sheet has also been proposed as a trigger mechanism for substorm onset. Previous 3-D electromagnetic particle simulations [Pritchett and Coroniti, 1999] have suggested that this mode saturates at a fairly benign level when the spatial scale of its nonlinear development reaches that of the ion gyroradius. It produces only modest changes in the magnetic topology and plasma distributions and stimulates relatively slow flows. Thus it fails to produce the typical onset signatures of high-speed earthward flows and tailward expulsion of a plasmoid. As an alternative mechanism, we are investigating the possibility that a localized region of weak  $B_z$ , produced by either a peaked convection electric field or by mirrored energetic ions, could lead to isolated reconnection at neutral points and produce the characteristic features of breakup.

**GA3.02/E/05-B3 1000**

**ONSET OF TAIL RECONNECTION IN THE COURSE OF MAGNETOSPHERIC SUBSTORMS: NUMERICAL SIMULATIONS**

JOERG BUECHNER (Max-Planck-Institut fuer Aeronomie, Max-Planck-Str. 2, D-37191 Katlenburg-Lindau, Germany)

Reconnection takes place in the course of magnetospheric substorms. The question is, whether it is a cause or consequence of substorm onsets and current disruptions. While the large scale dynamics of reconnection is well described agnetohydrodynamically with some ad hoc assumptions about a certain plasma non-ideality, MHD cannot explain the reason for the onset of reconnection and its inherent three-dimensional structure. We present current results of numerical simulations of collisionless reconnection through thin current sheets and discuss them in the context of the substorm onset problem.

**GA3.02/W/06-B3 1015**

**EXPLOSION TYPE DYNAMICS OF THE MAGNETOTAIL CURRENT SHEET: SUBSTORM ACTIVATIONS**

A.P.KROPOTKIN, (Skobeltsyn Institute of Nuclear Physics, Moscow State University, Moscow 119899, Russia)

Traditionally, fast substorm processes in the magnetosphere are considered as manifestations of large-scale (tearing-mode) instability of the magnetotail current sheet (CS), with characteristic time scales on the order of minutes. However, this concept is controversial: if the CS equilibrium is unstable, how does it manage to stay quiet for a long time preceding the substorm onset? Inversely, if it stays stable for that time but is only developing towards marginal stability due to quasi-static evolution, how can it become extremely unstable in a short time afterwards?

The clue to the problem lies in the nonlinear dynamics of the system. A catastrophe of equilibrium takes place at the marginal stability point. In a generic situation, the nonlinear dynamics of equilibrium loss is described by a single equation for the amplitude of the marginal mode. The equation involves both nonlinear saturation of the mode and its spontaneous symmetry violation. The latter results in the fact that in the course of quasi-static evolution, in advance of the fast equilibrium loss, the system becomes metastable. The (slowly varying) linear term which would fully determine the process time scale in the standard linear approach, plays a quite different role here. Its balance with the highest-order nonlinear term determines the (slowly-varying) saturation level for the disturbed vector potential amplitude  $A$ . The fast stage of evolution appears to be of "explosion instability" type,  $A \sim 1/(t_0 - t)$ , being independent of the linear growth rate. The moment of the "explosion"  $t_0$  is shifted to later times from the moment  $t_M$  when the system reaches marginal stability. That shift depends on the scale of the initial (fluctuation, seed) disturbance  $A_0$ : for smaller  $A_0$  it is greater, so that the system stays in the metastable state for longer times.

**GA3.02/W/40-B3 1050**

**A GLOBAL SIMULATION STUDY OF THE NOVEMBER 24, 1996, GEM SUBSTORM CHALLENGE EVENT**

J RAEDER (Institute of Geophysics and Planetary Physics, University of California, 405 Hilgard Ave, Los Angeles, CA 90095, USA, email: jraeder@gigpp.ucla.edu); L A Frank and J Sigwarth (The University of Iowa, Iowa City, IA 52242, USA); S Kokubun (STELAB, Nagoya University, 3-13 Honohara, Toyokawa, Aichi 442, Japan); R P Lepping and K W Ogilvie (NASA Goddard Space Flight Center, Greenbelt, MD 20771, USA); H Singer (NOAA R/E/SE, Space Environment Center, 325 Broadway, Boulder CO 80303, USA)

The GEM (Geospace Environment Modeling program) substorm challenge event provides a

unique opportunity to test magnetospheric models and to elucidate what they can tell us about the substorm process. The event in question occurred on November 24, 1996, around 2230 UT, and was observed by a wide variety of instruments, including the Polar-VIS auroral imager, several magnetospheric spacecraft, and ground magnetometers. This substorm is an isolated event that follows several hours of quiet magnetospheric conditions. In this talk we present the results from our global simulation of this event and discuss in detail the timing of the substorm signatures and the possible onset triggers.

**GA3.02/W/32-B3 1105**

**PARTIAL ENERGIZATION AND PRECIPITATION DURING SUBSTORM EXPANSION PHASE IN DUNGEY'S MODEL MAGNETOSPHERE**

Michael SCHULZ (Lockheed Martin Advanced Technology Center, Dept H1-11, Bldg 255, 3251 Hanover Street, Palo Alto, CA 94304, e-mail: schulz@agena.spasci.com)

Dungey's model magnetosphere consists of a dipole field plus uniform southward Delta B parallel to the dipole moment. A magnetospheric substorm can be simulated with this model by making the "tail" field Delta B and the cross-magnetospheric convection electric field suitably time-dependent. A gradual increase in Delta B from 7.8 nT (nominal quiet-time value) to 51 nT (for example) simulates substorm growth phase, during which the boundary between closed and open field lines shifts equatorward from 18° to 25° magnetic colatitude in the ionosphere. (Trapped particles escape into the "tail" during the growth phase of this model substorm.) Expansion phase is simulated by letting Delta B relax quickly back to 7.8 nT. The resulting (induced) electric field energizes charged particles (whether originally present or newly introduced across the neutral line), especially those on field lines that map to colatitudes between 18° and 25° in the ionosphere. This process can supply trapped relativistic electrons (mirroring near the magnetic equator) for radiation belts [as with Birn and Hesse, JGR, 99, 109-119, 1994] and also lower-energy precipitating auroral electrons (modeled here as being in strong pitch-angle diffusion). Particle energy gain is estimated in each case by expressing the Hamiltonian as a function [Schulz and Chen, JGR, 100, 5627-5633, 1995; Schulz, 103, 61-67, 1998] of the respectively conserved (i.e., adiabatically invariant) quantities in the limits of vanishing and strong pitch-angle scattering. Representative results for equatorially mirroring particles barely trapped at expansion-phase onset: 9.4-keV electrons become 640-keV electrons at L = 5.594; 3.2-keV protons become 67-keV protons at L = 5.58. Representative results for particles in strong pitch-angle diffusion, barely trapped at expansion-phase onset: 9.4-keV electrons become 48.6-keV electrons at L = 5.594; 3.2-keV protons become 12-keV protons at L = 5.58, all these results having been deduced from analytical expressions.

**GA3.02/W/34-B3 1120**

**AN INVESTIGATION OF THE PI2 TRAVEL TIME IN THE MAGNETOTAIL DURING THE SUBSTORM ONSET**

Yan SONG, Robert L. Lysak (both at School of Physics and Astronomy, University of Minnesota, 116 Church St. SE, Minneapolis, MN 55455, USA, e-mail: yan@aurora.space.umn.edu & bob@aurora.space.umn.edu), Dong-Hun Lee (Kyung Hee University, Yongin, Kyunggi 449-701, Korea, e-mail: dhlee@nms.kyunghee.ac.kr)

The quantitative calculation of the Pi2 travel time in the tail is important to help to clarify cause and effect during substorm expansion onset. A systematic numerical calculation of the MHD wave travel time of a magnetic perturbation (such as Pi2) from the neutral sheet in the tail to the ionosphere will be presented. For different stretched tail topologies, the travel time of the fast mode and shear mode MHD waves from different tail locations (-5 Re to -30 Re) to the ionosphere will be given. The travel time of fast flows caused by mid-tail (-15-30 Re) reconnection from the reconnection site to the near-Earth region (~ 6-10 Re) and the travel time of the rarefaction wave from the near-Earth region to the mid-tail region are also calculated. The results will be compared with observational facts.

Wave-related and convection-related phenomena must be distinguished. The previous theories of reconnection and the generation of field-aligned current are basically based on a convection picture. Establishment of new theoretical concepts of reconnection and the generation of field-aligned current is necessary to understand the mechanisms of the substorm onset.

**GA3.02/L/07-B3 1135**

**MEASURING THEORIES FOR TRIGGERING SUBSTORM EXPANSION WITH OBSERVATIONAL CONSTRAINTS**

Anthony LUI (The Johns Hopkins University Applied Physics Laboratory, Laurel, MD 20723-6099, USA, email: Tony.Lui@jhuapl.edu)

A number of theories are documented in the literature for the onset of substorm expansion. The prominent plasma instabilities include tearing, ballooning, drift-kink, cross-field current, and Kelvin-Helmholtz. Many of these theories are proposed on the basis of some selective observational indications. In this paper, we shall first identify some essential observational constraints on the substorm expansion onset process. We then evaluate briefly the strength and weaknesses of these theories and assess how well they satisfy the observational constraints identified above.

**GA3.02/W/37-B3 1150**

**ROBUSTNESS OF SANDPILE/AVALANCHE MODELS FOR AGNETOSPHERIC ENERGY STORAGE AND RELEASE**

Nicholas W. WATKINS (British Antarctic Survey, High Cross, Madingley Road, Cambridge, CB3 0ET, UK, Email: NWW@bas.ac.uk); Sandra C. Chapman and George Rowlands (both at Physics Department, University of Warwick, Coventry, CV4 7AL,UK, Email: sandrac@astro.warwick.ac.uk); Richard O. Dendy and Per Helander (EURATOM/UKAEA Fusion, Culham Science Centre, Abingdon, Oxfordshire, OX14 3DB, UK, Email: richard.dendy@ukaea.org.uk)

Most investigations of the substorm problem have focused on single substorm episodes or event groups. An alternative is to analyse the overall statistics of magnetospheric energy release, and thereby constrain the underlying physics. This usually requires definition of a substorm "event" via a thresholding process. In contrast, self-organised criticality (SOC) predicts that certain open dissipative systems will evolve to a critical state where all energy release statistics display both power law frequency spectra and power law distributions for event occurrence, size and duration. The demonstration of such a distribution for a measured geomagnetic index, and the proposal on theoretical grounds that the magnetosphere may be in an SOC state, have motivated cellular automaton ("sandpile") simulations of magnetospheric energy confinement and release ("avalanches"). Previous models have taken the limit where energy inflow ("fueling") is slow relative to dissipation, and either uniform or random. However the magnetospheric system of interest has both slow and fast periods, mixed together in the observed indexes, and its fueling is naturally modulated.



We have developed a sandpile model which accommodates both constant and fluctuating fuelling at a broad range of rates, and have studied the resultant distribution of energy release events. The power law form of the probability distribution is remarkably robust, except under extreme loading.

from the calculated results that power and rate of the open magnetic flux reconnection exceed those for the first active phase, as in the case of solar flares (see Mishin et al. (GA4.02), this issue).

**GA3.02/W/27-B3 1205**

**THE ROLE OF SELF ORGANISED CRITICALITY IN THE SUBSTORM PHENOMENON AND ITS RELATION TO LOCALISED RECONNECTION IN THE PLASMA SHEET**

A J KLIMAS (Laboratory for Extraterrestrial Physics, Code 692, NASA/GSFC, Greenbelt, MD 20771; 301--286--3682; e-mail: alex.klimas@gssc.nasa.gov); D Vassiliadis (USRA; at Code 696, NASA/GSFC, Greenbelt, MD 20771; 301--286--9060; e-mail: vassi@lepgst.gsfc.nasa.gov); J A Valdivia (National Research Council; at NASA/Goddard Space Flight Center, Greenbelt, MD, 20771; 301--286--3545; e-mail: alejo@roselott.gsfc.nasa.gov); D N Baker (Laboratory for Astrophysics and Space Physics, University of Colorado, Boulder, CO 80309; 303--492--4509; e-mail: baker@lynx.colorado.edu)

Recent observations of the magnetotail plasma sheet have shown it to be a dynamic and turbulent region. Borovsky et al. [J. Plasma Phys., 1997] have found strong turbulence in the plasma sheet at ~ 20 RE tailward of Earth; the turbulence is observed at all activity levels. The existence of strong turbulence in the plasma sheet in the region associated with substorm onset might be thought difficult to reconcile with the coherence and repeatability of the substorm cycle. We review a variety of evidence that strongly suggests the magnetotail is driven, through magnetic flux transfer, into a state of "self-organized criticality" (SOC). It is an important property of physical systems that evolve into SOC that they self-organize into a unique local dynamic state. This global state is inevitable, and repeatable. In this state, however, small- spatiotemporal-scale system fluctuations are unpredictable and can be only described statistically. This is the basis, we think, for the global coherence and repeatability of the substorm phenomenon in the turbulent plasma sheet. At, or near, substorm onset the plasma sheet can be described by a global SOC state containing significant small scale turbulence. In several recent studies, "sandpile" models were driven into SOC and then shown to reproduce various measures of substorm activity. We discuss the plasma physical foundation of these sandpile models. The evolution of simple continuum plasma sheet models into SOC-like states will be demonstrated. We view the substorm phenomenon as an avalanche of many small econnection events in the turbulent plasma sheet under the assumption that the plasma sheet is in a SOC state.

**GA3.02/E/08-B3 Poster 0900-03**

**PLASMA SHEET TURBULENCE AND SUBSTORM EXPANSION ONSET**

Elizaveta E. ANTONOVA and Ilya L. Ovchinnikov (both at Skobel'syn Institute of Nuclear Physics, Moscow State University, Moscow, 119899, Russia, email: oi@tasdp.npi.msu.ru)

Plasma sheet experimental observations supported the hypothesis about the existence of the medium scale developed turbulence and quasi-diffusion particle transport. The measured diffusion coefficient is very close to predicted one and is much larger than Bohm diffusion coefficient. The theory of the plasma sheet with medium scale developed turbulence explains the existence of a quite stable plasma sheet and its substorm dynamics, including plasma sheet thinning during substorm growth phase and plasma sheet thickening during substorm expansion phase. Plasma sheet with minimal thickness is formed in the near to Earth plasma sheet regions where dawn-dusk electric field has maximal amplitude. The growth of plasma sheet thickness in the developed approach is connected with the growth of the level of turbulence. The external source of  $B_z < 0$  magnetic field can destroy the plasma sheet stability and lead to the formation of neutral line and plasmoid. The connection of tail processes with the inner magnetosphere processes and the inner magnetosphere substorm onset is discussed.

**GA3.02/W/30-B3 Poster 0900-04**

**PHYSICS-BASED 2D RUNNING CELLULAR AUTOMATA AS MODELS OF MAGNETIC FIELD NEAR NEUTRAL SHEET**

Jouni TAKALO (Department of Physics, Un. of Jyväskylä, P.O.Box 35, FIN-40351, Jyväskylä, Finland, now at GSFC, Code 692, Greenbelt, MD 20771, USA, email: jouni@roselott.gsfc.nasa.gov); Jussi Timonen (Department of Physics, Un. of Jyväskylä, P.O.Box 35, FIN-40351, Jyväskylä, Finland, email: timonen@snafu.phys.jyu.fi); Alex Klimas, Juan Valdivia and Dimitris Vassiliadis (All at GSFC, Code 692, Greenbelt, MD 20771, USA, email: alex@bokeh.gsfc.nasa.gov)

Magnetic field models based on cellular automata (CA) are presented. These models feature self-organized critical behavior with power-law scalings both in durations and sizes of avalanches. The models have also nonlinear energy dissipation. Sometimes a large scale avalanche has external reason, sometimes the avalanche is internal without any external trigger. The present models, isotropic and anisotropic, are two dimensional running CAs, such that the models are fed at every round, not just in the state of relaxation. Both models have full physical interpretation in terms of magnetohydrodynamic equations. The heights of the CA are magnetic flux densities, and the change of the heights are the time derivatives of the flux densities.

**GA3.02/W/10-B3 1220**

**SEPARATION OF THE SCALING PROPERTIES OF THE DIRECTLY DRIVEN AND UNLOADING COMPONENTS OF THE MAGNETOSPHERE**

Mervyn P FREEMAN and Nicholas W Watkins (British Antarctic Survey, High Cross, Madingley Road, Cambridge, CB3 0ET, UK, email: M.P.Freeman@bas.ac.uk)

It has been proposed that the magnetosphere can be naturally driven to a scale invariant state that is insensitive to the driver. This state is known as Self-Organised Criticality (SOC). So far, evidence to support this is mainly based upon scale invariant properties of the Auroral Electrojet (AE) index including the broad power law distribution of energy dissipating burst events. However, it is well known that a component of the AE index is directly related to the solar wind driver which itself has scale invariant properties. Thus, in this paper, we compare the scaling properties of the solar wind driver with those of the AE indices in order to evaluate to what extent the latter provide evidence that the magnetosphere, rather than the solar wind, is an SOC system.

**GA3.02/W/31-B3 Poster 0900-05**

**SUBSTORM AS A GLOBAL MAGNETOSPHERIC INSTABILITY**

I.I.ALEXEEV and S.Yu.Bobrovnikov (Institute of Nuclear Physics, Moscow State University, Moscow, Russia)

The substorm onset was theoretically studied. It was described as a global transition from a metastable magnetospheric state to another stable state with lower energy. In contrary to the usual approach we investigate not local instability in the tail but global magnetospheric instability. Based on paraboloid model the magnetospheric dynamics during substorm growth phase was investigated.

A key role of the Region 1 field-aligned currents was revealed. Critical values of the model parameters depend on intensity of field-aligned currents was calculated. It was shown that at growth phase, when the IMF has southward direction, the Region 1 field-aligned currents serve as a stabilization factor which permits the magnetosphere to go to the metastable configuration. And after IMF turns northward or a sudden pulse in solar wind dynamic pressure this stabilization factor disappears. The criteria of the transition of the magnetosphere from metastable configuration to expansion was presented. On the basis of this criteria the scenario of substorm which take into account an influence of field-aligned currents was constructed. This scenario is based on global magnetospheric model. Parameters of this model have obvious physical sense and can be calculated from the satellites and on-ground measurements. As a results a new explanation of substorm onset was presented.

**Wednesday 28 July AM**

Presiding Chair: G. Lu, (High Altitude Observatory, NCAR, Boulder, USA)

**MAGNETOSPHERIC SUBSTORM ONSET: OBSERVATIONS, THEORIES, MODELS-1**

**GA3.02/E/12-B3 Poster 0900-01**

**RECURRENT SUBSTORMS AT THE EARTH AND HOMOLOGOUS FLARES ON THE SUN**

P.A. SEDYKH, L.V. Minenko, V.I. Sidorov, S.S. Adelkhanov, and V.M. MISHIN (all at Institute of Solar-Terrestrial Physics, P.O.Box 4026, Irkutsk, 664033, Russia, email: mishin@iszf.irk.ru)

For the time interval (00-11) UT, May 3, 1986 (CDAW9C), the MIT2 method (Mishin et al. [JGR, 1997, p.19845]) was used in calculating, at steps of 6 min, the values of the open magnetic flux  $\Psi$ , the magnetospheric tail length  $L$ , and the potential difference  $U_{pc1}$  on the dayside throat of the polar cap boundary. We assumed  $U_{pc1} \sim M$ , where  $M$  is the dayside magnetopause reconnection rate. For the interval considered, the plot of  $M(UT)$  shows a nearly monotonic decrease of  $U_{pc1}$  values, that are the characteristics of the solar wind geoeffectiveness. From this plot, it is obvious that four recurrent substorms were observed in the interval considered, with corresponding changes of the parameters AE,  $U_{pc1}$ ,  $\Psi$ , and  $L$ . Such a recurrence suggests the existence of the external energy source of substorms, which persisted at a supercritical level during ~11 hours. It is pointed out that homologous solar flares in terms of models such as CSHKP leave room for a similar interpretation. In CSHKP models, the flare is produced as a consequence of the reconnection of the open magnetic flux created by the external energy source. Therefore, the homogeneity of the flares presupposes a long persistence of their external energy source. This conclusion is not trivial because it is generally believed that the "opening" of the magnetic flux occurs suddenly due to the rise of a filament.

**GA3.02/W/08-B3 Poster 0900-06**

**ON THE STABILITY OF CHARGED PARTICLE ORBITS IN A SHEARED MAGNETIC REVERSAL MODELLING THE QUIET TIME GEOTAIL.**

M. TSALAS, (Dept of Physics, Uni of Warwick, Coventry, Email: maximost@astro.warwick.ac.uk); S. C. Chapman and G. Rowlands

The motion of charged particles in a simple model for the geotail with a shear component has been investigated. It was found that as the value of  $\beta$  (in GSE) is increased, the position of the integrable region varies accordingly. This variation is analytically predicted using a multiple timescale perturbation technique. It was also observed that for a certain interval of  $\beta$ , the whole of the phase space becomes chaotic via a bifurcation sequence. We investigate this region of global chaos by looking at the stability of the periodic orbits. Since each type of orbit contributes differently to the cross tail current distribution, knowing how the introduction of a shear component influences the topology of the phase space could help in the understanding of the currents observed in the region.

**GA3.02/E/19-B3 Poster 0900-02**

**THE RECONNECTION POWER AND RATE IN THE COURSE OF EACH OF THE TWO ACTIVE PHASES OF MAGNETOSPHERIC SUBSTORMS**

V. MISHIN, T. Saifudinova, A. Bazarzhapov, P. Sedykh (all at Institute of Solar-Terrestrial Physics, P.O.Box 4026, Irkutsk, 664033, Russia, email: mishin@iszf.irk.ru)

Broadly speaking, the "magnetospheric substorms - solar flares" analogy has become public knowledge, without its quantitative characteristics, however. Obtaining such characteristics is one of motivations of this work, which is a continuation of papers of Mishin et al. (a) and (b), (this issue). We are based on existing substorm models (models with Current Disruptions, CDs), assuming a two-stage development: first active phase - reconnection in the near, closed, tail; and second active phase - open magnetic flux reconnection in the middle tail. Mishin et al. [1997] used the magnetogram inversion technique to determine the open magnetic flux  $\Psi$  in the tail lobes. In this paper, time profiles of  $\Psi$  have been used as the main addition to the traditional data base to estimate the Poynting flux to the magnetosphere, and the reconnection power and rate in the course of each of the two active phases of the two magnetospheric substorms being investigated (CDAW6 and CDAW9C events). It is evident

**GA3.02/E/15-B3 Poster 0900-07**

**A POSSIBLE ROLE OF ION DEMAGNETIZATION IN SUBSTORM GENERATION**

Wladislav LYATSKY (Polar Geophysical Institute, Apatity, 184200, Russia, email: lyatsky@pgi-ksc.murmansk.su)

A new model for the substorm generation based on stimulated ion diffusion across magnetic field lines in the magnetotail plasma sheet is studied. The essence of the model is: the ion demagnetization in the plasma sheet produces a radially-directed ion diffusion which leads to a charge separation and the formation of field-aligned currents eliminating these charges. The magnitude of these currents depends on the ionospheric conductivity. The effect of field-aligned currents on the ionospheric conductivity produces the instability of this system consisting in a sharp increase of the ion diffusion, the dipolarization of the magnetic field in the plasma sheet and the substorm beginning. The model includes the following issues: (1) Before the substorm onset, the magnetotail plasma sheet approaches to the Earth and magnetic field lines are stretched from the Earth. (2) Partially demagnetized (because of their large Larmor radius)

ions in the magnetotail plasma sheet move from the Earth. This produces a radially-directed electric field which limits the ion escape and produces a system of field-aligned currents with upward current at the boundary of the ion demagnetization and downward current poleward of this boundary. (3) The magnitude of field-aligned currents is controlled by the ionospheric conductivity. For quiet conditions the ionospheric conductivity is small and field-aligned currents are weak. The increase of the ion diffusion before a substorm leads to increase of field-aligned currents. This stimulates an increase of the ionospheric conductivity which leads to a new increase of the ion diffusion and the substorm beginning.

**GA3.02/E/03-B3** Poster **0900-08**

**HALL-MHD SIMULATIONS OF THE DRIFT KINK INSTABILITY IN THE MAGNETOTAIL**

R. V. REDDY and G. S. Lakhina (both at Indian Institute of Geomagnetism, Dr. Nanabhoj Moos Road, Colaba, Mumbai - 400 005, India, email: vreddy@iig.iigm.res.in)

The stability of the current sheets of the Harris type against the drift kink mode is studied using two dimensional Hall-MHD simulations, in which we include the effects of the electron pressure gradient and the Hall current. These Hall-MHD effects allow the relative electron-ion cross field streaming, which is necessary to obtain the drift kink mode. The simulation experiments are carried out to find the growth rates and the real frequencies for near-Earth magnetotail parameters. The obtained simulation results of the drift kink instability are compared with other cross-field current instabilities in the magnetotail. Implications of these results for the disruption of the near-Earth plasma sheet and the triggering of substorms are discussed.

**GA3.02/W/63-B3** Poster **0900-09**

**CURRENT DISRUPTION AT SUBSTORM ONSET: BREAKDOWN OF THE ALEXANDER-ORBACH CONDITION FOR THE CRITICAL PERCOLATION**

Alexander V. MILOVANOY and Lev M. Zelenyi (both at Space Research Institute, Profsoyuznaya street, 84/32, 117810 Moscow, Russia, e.mail: amilovan@mx.iki.rssi.ru) Pierluigi Veltri and Gaetano Zimbardo (both at University of Calabria, 87036 Arcavacata di Rende, Italy, e.mail: zimbardo@fis.unical.it)

Self-organized critical states of the Earth's magnetotail are analyzed. The local stretching and thinning of the tail is associated with the site of the substorm current disruption just prior to the onset when the critical states are characterized by the metastable magnetic field structures. We show that the self-organized geometry of such structures is that of a critical percolating network exhibiting some universal topological features. We quantify these features in terms of the improved Alexander-Orbach (AO) condition [1] which relates the Hausdorff fractal dimension of the network to its basic topological characteristic, the index of connectivity. Application of the AO condition has led us to prove that the self-organized states can be described by the power-law magnetic energy density spectrum, with the slope close to -7/3; this slope has been earlier recognized in the AMPTE satellite experiments as reported by Ohtani et al. [2]. In our study, the AO relation is treated as the structural stability condition of the critical state. We speculate that the cross-tail current disruption at the substorm onset could be understood as the violation of the AO stability condition followed by the breakdown of the critical (metastable) percolating network.

We analyze the structural properties of the magnetic field and plasma turbulence at the substorm onset with use of such unconventional methods as fractal geometry, percolation theory, fractional differential calculus, and homotopic topology. The specific feature of our study is basically geometric approach which assumes a self-consistent relationship between the topology of the system and main "physical" characteristics of the turbulence. We model numerically the self-organized critical states in the Earth's magnetotail by the so-called fractional Brownian surfaces whose topological properties recover well the main assumptions of our approach. The particle dynamics on the fractional Brownian surfaces with the imposed transversal electric field is simulated. The anomalous heating, diffusion, and acceleration rates of the particles are analyzed in relation with the fractal geometry of the turbulence; we show that these anomalous rates appear in unconventional scaling laws depending on the connectivity properties of the fractal. Some observational manifestations of our study are discussed in view of the recent spacecraft measurements of the magnetotail.

**GA3.02/W/35-B3** Poster **0900-10**

**NON-ADIABATIC PARTICLE DYNAMICS AND MAGNETIC FIELD RECONNECTION BY THE LINEAR MAGNETOSONIC WAVE EXCITATION IN THE CURRENT SHEET OF THE EARTH'S MAGNETOTAIL**

A.P.KROPOTKIN and O.O.Trubachev, (Skobel'syn Institute of Nuclear Physics, Moscow State University, Moscow, 119899, Russia)

In the stability theory of a current sheet (CS) it is usually adopted that plasma is fully confined in the CS. As a result, possible unstable modes are evanescent outside CS. It is argued that since normally there is a uniform cold plasma background outside CS, the specific CS-bound mode may be linearly coupled to spatial modes of that uniform medium. Waves propagating away from the CS may provide a means of energy dissipation being necessary for tearing process in the CS, and this results in magnetic field reconnection. Linear excitation is considered of a fast magnetosonic wave in such a non-uniform medium. That linear excitation has a low threshold, and does not need any preliminary turbulence level. The wave being excited, interacts with particles dynamically, resulting in a non-adiabatic and dissipative force due to the wave-particle momentum exchange. The force does not exist in the Hamiltonian dynamics of test particles but is an important point of self-consistent plasma systems analysis. As a result, the limitations imposed earlier on the tearing-like instabilities are weakened.

**GA3.02/W/49-B3** Poster **0900-11**

**NON LINEAR DYNAMICS OF THE EQUILIBRIUM LOSS IN THE GEOMAGNETOTAIL PLASMA SYSTEM BASED ON A "COMBINED" PLASMA KINETIC EFFECT**

A.P.KROPOTKIN and O.O.Trubachev, Skobel'syn (Institute of Nuclear Physics, Moscow State University, Moscow, 119899, Russia); A.T.Y. Lui, Johns Hopkins University, Applied Physics Lab., Laurel MD 20723-6099 USA

The substorm onset instability combines features of "macro" scale electromagnetic disturbance of the tearing mode type, and the "micro" scale plasma turbulence which is generated by the cross-field current instability (CCI) and modulated in coherence with the large scale disturbance. Both components are involved in a feedback loop. It is assumed that the current sheet (CS) is thin enough for CCI turbulence to already exist. Current density variations of the large scale disturbance result in additional CCI generation; on the other hand, that additional plasma turbulence provides, in quasilinear approximation, a flow of electrons which violates the frozen-in condition for magnetized electrons, and thus destabilizes the tearing mode. The process is nonlinear. However the threshold amplitude diminishes as the CS thins during the substorm growth phase, so that the instability sets in when the threshold gets smaller than the background fluctuations or externally driven disturbances.

**GA3.02/W/22-B3** Poster **0900-12**

**STATISTICAL OBSERVABLES FOR TESTING MAGNETOSPHERIC SANDPILE MODELS**

Nicholas W. WATKINS and Mervyn P. Freeman (both at British Antarctic Survey, High Cross, Madingley Road, Cambridge, CB3 0ET, UK, Email: NWW@bas.ac.uk.) Richard O. Dendy (EURATOM/UKAEA Fusion, Culham Science Centre, Abingdon, OX14 3DB, UK, Email: richard.dendy@ukaea.org.uk)

Earth's magnetosphere is a complex, open, driven, dissipative system. Generically, such systems often display various forms of "simple" behaviour - examples include low dimensional chaos and "sandpile" phenomenology. However, not all observables derived from such systems are independent, and care must be taken to uncover implicit linkage and avoid redundant information. We illustrate this problem with reference to current interest in self-organised criticality (SOC) sandpile models of the magnetosphere, which have been used to interpret geomagnetic index time series. In particular, we evaluate the information contained in power spectra, structure functions, amplitude probability distribution functions (PDFs), burst size PDFs, and inter-burst interval PDFs. We consider recent progress in relating power law slopes to the decade range covered by instabilities, and show how this illuminates which types of substorm data can usefully be compared with the output of SOC sandpile models.

**GA3.02/W/20-B3** Poster **0900-13**

**TIME-SPATIAL CHARACTERISTICS OF AURORAL LUMINOSITY DURING DOUBLE BREAKUPS**

ILIA KORNILOV, Tatyana Kornilova (both at Polar Geophysical Institute, Apatity, Murmansk region, 184200, Russia, E-mail: kornilov@pgi.kolasc.net.ru); Oleg Kornilov (Institute of Physics, St.Petersburg State University, St.Petersburg, Petrodvorets, 198904, Russia)

During strong magnetic disturbances the phenomenon named as double breakups (DB) is sometimes observed in the region of auroral oval. DB represent simultaneous poleward expansion in two regions separated by latitude in the same longitudinal sector. A typical feature of double breakups is correlation of luminosity of the northern and southern breakups. Correlation characteristics were studied on the base of TV auroral data. It was shown that the close interaction of auroras in the region of the north and south breakups exists. In the time of strong magnetic disturbances lasting for several hours the repeated in 30-50 minutes sequences of DB are observed. At the time scale of the order of any sequence duration a correlation between auroral intensity of the northern breakups and southern ones occur. Maximum intensity of the north breakup in average 5 minutes leads the same of the southern breakup. Inside the small time scale of the order of 100-200 s the stable correlation of the luminosity has been registered: fast auroral luminosity variations in the region of north breakup 2-5 s lead ones of the southern breakup.

**GA3.02/W/03-B3** Poster **0900-14**

**MULTI-POINT OBSERVATIONS OF SUBSTORM SERIES UNDER CONTINUOUS SOUTHWARD IMF ON DECEMBER 22-23, 1996**

Yu. I. YERMOLAEV, L. M. Zelenyi, A. A. Petrukovich (Space Research Institute, Moscow 117810, Russia, Email: yermol@afed.iki.rssi.ru), V. A. Sergeev (St.Petersburg University, Russia), T. Mukai (ISAS, Japan), S. Kokubun (STEL, Japan), K. Liou, C.-I. Meng (APL/JHU, USA), G. Parks (Un. of Washington, USA), J.-A. Sauvaud (CESR/CNES, France)

Multi-point observations by ground-based stations and a fleet of ISTP satellites allow us to study plasma processes in different regions of near-Earth space during an interesting interval on December 22-23, 1996 which was characterized by ~ 20 hour southward IMF and almost constant solar wind pressure ~ 1.2 nPa. Five substorm events were observed during this period of continuous external driving. Several global effects of these substorms are described. Our results demonstrate the principle importance of prehistory of magnetotail activity on the development of each of subsequent substorm. In particular, comparison of measurements in the plasma sheet on both flanks showed (1) similar loading/unloading processes in the tail correlated with substorm development, and (2) a strong bursty convection concentrated in a narrow (dY ~ 15 Re) channel.

The work was supported in part by INTAS grant 96-2346.

**GA3.02/W/25-B3** Poster **0900-15**

**AN EIGEN MODE ANALYSIS OF THE AURORAL ELECTROJET**

WEN-YAO XU (Institute of Geophysics, Chinese Academy of Sciences, Beijing 100101, China, email: wyxu@mail.c.geos.ac.cn)

A substorm involves "directly driven" and "loading-unloading" processes, which have different temporal-spatial features and are correlated respectively with the large-scale magnetospheric convection and substorm current wedge. In order to quantitatively separate these two components, a new technique of eigen mode analysis, Method of Natural Orthogonal Components (MNOC) is used to analyze the ionospheric equivalent current systems. The results show that the current pattern of the first eigen mode exhibits a two-cell construction, characterizing the large-scale magnetospheric convection and directly driven process, while the secondeigen mode shows a concentrated westward electrojet at midnight sector, characterizing the substorm current wedge and the loading-unloading process. The first mode consistently exists whenever during quiet periods or at substorms, and its intensity increases from the beginning of the growth phase of substorms, then quickly intensifies in the expansion phase. On the other hand, the intensity of the second mode remains to be near zero during both quiet time and the growth phase of substorms, its rapid enhancement occurs in the expansion phase. These characteristics in the current patterns and the intensity variations coincide with the defined physical processes of the directly driven and loading-unloading components. On the basis of these results a suggestion about a modified AE index is proposed.

**GA3.02/W/33-B3** Poster **0900-16**

**PREDICTION OF SUBSTORMS FOLLOWING SHARP NORTHWARD TURNINGS OF THE IMF**

Gerard BLANCHARD (Department of Chemistry and Physics, Southeastern Louisiana University, SLU 10878, Hammond, LA 70402-0878, Email: gblanchard@selu.edu) Larry Lyons (Department of Atmospheric Sciences, University of California, Los Angeles, CA, 90095-1565, Email: larry@atmos.ucla.edu) James Spann (Space Plasma Physics Branch, Space Science Laboratory, NASA/Marshall Space Flight Center, NASA Mail Code ES83, Huntsville, AL 35812, Email: jim.spann@msfc.nasa.gov)

It has been shown that there is an association between changes of the interplanetary magnetic field (IMF) that are expected to lead to a reduction in magnetospheric convection (northward



turnings, reductions in |By|) and the onset of the expansion phase of substorms. This has been previously demonstrated by analyses of IMF data during time intervals associated with identified substorm onsets. Here we examine whether observations of northward turnings of the IMF can be used to predict the occurrence of substorms. We first identified sharp northward turnings that follow an interval of steady, southward IMF using measurements from the Wind spacecraft during the first 180 days of 1997. We also required that the northward turning be observed by either IMP-8 or GEOTAIL, in addition to Wind, and that one of the observing satellites be sufficiently close to the Earth-Sun line, or that the two observing satellites be sufficiently separated in YGSE, that we are reasonably certain that the northward turning affected the magnetosphere. We also used the dual observations to estimate the arrival of the northward turning at the Earth. Using these criteria, we predicted 17 substorms. We then searched for the following signatures of substorm onset around the time of the predicted onset: auroral brightening followed by auroral bulge expansion observed by Polar UVI, geosynchronous particle injection, geosynchronous magnetic field dipolarization, and an appropriate magnetic disturbance at the surface of the Earth. Of the 17 predictions of substorms, 10 were successful in that a substorm onset was observed within +/- 12 min of the predicted onset, 1 is indeterminate due to a lack of data at the Earth, 1 had unusual activity that we have not been able to identify, and 5 were unsuccessful. The 5 failures fall into two groups that we can eliminate through modification of our selection criteria for northward turnings. Two of the northward turnings that failed to produce substorms were preceded by the lowest average |BzGSM| of the set; The remaining 3 were the only cases in which the northward turning was accompanied by a simultaneous sharp increase in |ByGSM|. The increase in |ByGSM| would be expected to prevent the decrease in convection that would otherwise be expected to be associated with a northward turning. These results indicate that it is an IMF change that leads to a reduction in convection, rather than just a northward turning or reduction in |By| that is associated with substorms, and that at least some substorms can be predicted by measurements of the IMF that affects the magnetosphere.

**GA3.02/E/16-B3** Poster **0900-17**

**THE TRIGGERING MECHANISM OF RANDOM SUBSTORMS**

Chen SHEN (Center for Space Science and Applied Research, Chinese Academy of Sciences, Beijing 100080, China, e-mail: sc@center.casar.ac.cn); Zhenxing Liu (Center for Space Science and Applied Research, Chinese Academy of Sciences, Beijing 100080, China, e-mail: liu@center.casar.ac.cn)

The triggering mechanism of random substorms has been studied by using an equivalent circuit method. It is found that, during the growth phase, if there is an interplanetary discontinuity approaching the dayside magnetopause, the interplanetary and magnetopause current sheets will interact with each other, the magnetic reconnection is enhanced greatly, and the dawn-dust potential drop increases considerably within short time. The simulation shows that, the cross tail current will reach its critical value shortly after the north turning of the IMF, the current disruption occurs, and the expansion phase of substorms takes place.

**GA3.02/E/17-B3** Poster **0900-18**

**DEVELOPMENT OF THE DAYSIDE AURORA DURING MAGNETOSPHERIC SUBSTORMS**

R. P. RIJNBEEK and P. N. Smith (both at Space Science Centre, School of CPES, University of Sussex, Brighton BN1 9QH, UK, email: R.P.Rijnbeek@sussex.ac.uk); M. I. Pudovkin (Institute of Physics, State University, St. Petersburg, 198904 Russia, email: Mikhail.Pudovkin@pobox.spbu.ru); G. V. Starkov (Polar Geophysical Institute, Murmansk Region, Apatity, 184200 Russia, email: starkov@pgi.kolasc.net.ru)

We have analysed optical data obtained from Spitzbergen during the winter periods of 1980-1983. This study has shown that there are three maxima in the intensity of dayside auroral luminosity during the course of a substorm in the nightside magnetosphere: the first maximum is observed during the preliminary/growth phase, the second immediately after the onset of the breakup, and the third during the maximum of the substorm. The poleward motion of the dayside aurora increases after the beginning of the preliminary phase. The intensity of the ionospheric electric field, deduced from the auroral velocity, is in the range 30-50 mV/m (for comparison, during quiet magnetic conditions the value of the electric field is about 10 mV/m). This increase in the electric field coincides with the first maximum of the auroral luminosity. Short-lived fading of the aurora is observed on both the dayside and nightside before substorm onset. A brief intensification of the luminosity in the green line appears after the substorm onset. The intensity of the ionospheric electric field decreases around the time of onset, but the value is still enhanced compared to that observed during quiet conditions. The primary maximum in the luminosity coincides with the maximum of the nightside substorm, and with a renewed increase of the electric field in the dayside ionosphere.

**GA3.02/E/04-B3** Poster **0900-19**

**COUPLING BETWEEN SUBSTORMS AND ULF DISTURBANCES IN THE DAYSIDE CUSP**

Viacheslav PILIPENKO, Natalia Kleimenova, Olga Kozyreva (Institute of the Earth Physics, B.Gruzinskaya, 10, 123810, Moscow, Russia, e-mail: vpilipenko@uiepe-ras.scgis.ru) Mark Engebretson (Augsburg College, Minneapolis, MN55454, USA, e-mail: engebret@augsborg.edu)

The recently deployed magnetometer network MACCS in Arctic Canada and the extension of the "210 Magnetic Meridian" array of stations to Siberia provide an opportunity for the study of a possible coupling between the nighttime substorm activity and the behavior of ULF pulsations in the dayside cusp. Several events with a response of the dayside long-period magnetic pulsations to substorms and to IMF variations have been revealed. An onset of a substorm can result in the suppression of the IPCL/PC5 activity in the dayside cusp. At the recovery phase of a substorm the pulsation activity returns back to the pre-onset level. The essential role of By component of IMF has been elucidated: the effect is revealed only during periods of negative By. Several interpretation of the effect found are possible, among them is that the behavior of pulsation's intensity as the occurrence of an ULF precursor of a substorm.

**GA3.02/E/02-B3** Poster **0900-20**

**PLASMA PRESSURE IN THE HIGH LATITUDE MAGNETOSPHERE AND SUBSTORM EXPANSION PHASE ONSET**

Maria O. RIAZANTSEVA (Skobel'syn Institute of Nuclear Physics, Moscow State University, Moscow, 119899, Russia; email: maria@orearm.msk.ru)

The results of high latitude plasma pressure observations are interpreted as the proof of high latitude quasi-ring current existence. The current carries are mainly the auroral ions of plasma sheet origin. Such ions form the plasma structure surrounding the Earth at all local times. Plasma pressure in the ring is near to isotropic and constitute of the order of 1 nPa. Measured plasma pressure meanings are comparable with the solar wind dynamic pressure. High latitude quasi-ring current growth may lead to real or effective eastward current formation. Such current produce positive magnetic field disturbance near the Earth and negative

magnetic field disturbance in the geomagnetic tail. The simple model is developed giving the possibility to evaluate the contribution of the magnetic field of high latitude ring current in the near Earth and near tail magnetic field. It is shown that eastward ring current can be considered as the course of near tail current disruption and substorm expansion phase inset.

**GA3.02/E/05-B3** Poster **0900-21**

**ENERGETIC PARTICLE INJECTIONS AND MAGNETIC FIELD PERTURBATIONS FROM CRRES DATA**

Kozelova T.V., Lazutin L.L., KOZELOV B.V. (Polar Geophysical Institute, Apatity, Russia, e-mail: kozelov@pgi.kolasc.net.ru) Rasinkangas R. (University of Oulu, Oulu, Finland)

The dynamical variability of particle fluxes, associated with substorm processes, is the subject of intensive study of many years. A key feature of substorm 'dispersionless' injections is that the particle fluxes increase nearly simultaneously over a very broad range of energies (including both electrons and ions). Lezniak and Winckler (1970) showed the correlation of increases in the electron fluxes with increases of local magnetic field. Moore et al (1981) proposed that the injections correspond to some kind of compressional wave that propagates Earthward and may be associated with westward current of perturbation. However, the increase in the magnetic field strength (dipolarization) after substorm onset may indicate, that the total westward current intensity decreases suddenly (i.e. current disruption) or the eastward current of perturbation appears. We investigated changes in the magnetospheric cross-field current during the proton and electron injections on the CRRES spacecraft. The differential vectors of the magnetic field have been used to identify the current perturbations. The line current model have been used to interpret equivalent currents, associated with these magnetic field perturbations. Analysis of current perturbations showed that the current of perturbation in the injection front may be directed both westward and eastward depending on the spacecraft position in respect to the site of active region.

**GA3.02/W/58-B3** Poster **0900-22**

**GROUND AND SPACECRAFT OPTICAL OBSERVATIONS OF SUBSTORMS**

V. TAGIROV (Polar Geophysical Institute, Apatity, 184200, Russia, Email: tagirov@pgi.kolasc.net.ru); V.Arinin (Russian Federal Nuclear Center, Sarov, 607190, Russia, Email: root@gdd.vniief.ru); C.-I.Meng, K. Liou, D. Sibeck, and A.T.Y. Lui (all at the John Hopkins University, Applied Physics Laboratory, Laurel, MD 20723, USA, Email: david.sibeck@jhuapl.edu); L.A.Frank and D.Morgan (both at University of Iowa, Iowa City, IA 52242, USA); G.Parks (University of Washington, Seattle, WA 98195,USA)

In conjunction with NASA's Polar satellite program, we have conducted a campaign of auroral substorm observations using a low-light-level all-sky TV observations at Loparskaya (68.6° N, 33.3° E geographic, 65.0° N, 114.2° E geomagnetic) located at Kola Peninsula, North-West of Russia. The satellite optical observations were made both in UVI and visible ranges of wavelengths. We present substorm activity on December 9, 1996. We used keogram presentation of satellite UVI and ground based TV data to compare the dynamics of auroral display at different ranges of wavelengths in time interval more than three hours. Although TV observations began about an hour later than the satellite ones the rest parts of keograms coinciding in time demonstrated strong similarity in both ranges of emissions. The onsets occurred periodically and duration of each substorm was about 75 minutes. The first onset which was registered only by UVI camera was very weak and took place at 66-68° geom. latitude at 2020 UT, the next one was more intensive and occurred at 64-67° at 21.32 UT and the last one was very strong and started at 63-65° at 2250 UT. The common feature of all onsets was a poleward leap of the aurora and then slow equatorward moving. Such behavior showed that the more closer to the Earth onset takes place the more intensive it is. The first onset was registered only by POLAR UVI camera, there was no any signature of disturbance seen by visual camera or ground based magnetic stations. No disturbance was registered also in IMF or solar wind characteristics prior to this onset. The second onset started just above Loparskaya, where all-sky camera was located. According to WIND satellite data it was probably triggered by a northward turning of the IMF Bz component and an increase of the solar wind dynamic pressure about 8 minutes prior to onset. Ground optical, magnetic and POLAR satellite data show that the onset covered a very limited area and lasted about 15 minutes without further developing to the recovery phase. The third onset did not exhibit any noticeable external triggering factors. The IMF was stable and strongly southward, and the solar wind dynamic pressure did not exhibit any changes. But contrary to the previous onsets this one developed into a very intense substorm expanding from the region located slightly westward from Loparskaya towards both the evening and morning sectors as it widened and finally covered the entire oval.

**GA3.02/W/04-B3** Poster **0900-23**

**MAGNETOSPHERIC ENERGETICS DURING MODERATE SUBSTORMS: IMP8 AND GEOTAIL OBSERVATIONS**

Anna BELEHAKI (Institute of Ionospheric and Space Research, National Observatory of Athens); Ioanna Tzagouri (Nuclear and Particle Physics Section, Physics Department, University of Athens)

The energy budget of the magnetosphere during moderate sunstorms is estimated, using IMP8 observations from the interplanetary medium and GEOTAIL from the deep tail phase of the mission. It is assumed that the energy, that entered the magnetosphere due to electromagnet coupling with the solar wind, is described by the epsilon parameter, proposed by Akasofu. The estimation of the energy input and the energy dissipated in the magnetotail during a substorm process was based on two specific events occurred during 1993. The analysis of energetic particle, magnetic field and plasma data from the EPIC, MGF and CPI experiments on board GEOTAIL gave us the possibility to estimate the position of the Near Earth Neutral Line location, the time of plasmoid release, the size of the plasmoid, its convection velocity and finally the energy dissipated for the plasmoid formation and acceleration downtail. Our results suggest that the energy dissipated in the ionospheric Joule heating is comparable to the energy dissipated in accelerating the plasmoid, and these two are the most prominent modes of dissipation of the input solar wind energy into the Earth's magnetosphere.

**GA3.02/L/02-B3** Poster **0900-24**

**GEOTAIL SPACECRAFT OBSERVATIONS OF ENERGETIC ION SPECTRAL AND COMPOSITIONAL VARIATIONS NEAR SUBSTORM ONSET**

S.P. CHRISTON, G. Gloeckler (Dept. of Physics, Univ. of Maryland, College Park, MD 20742), A.T.Y. Lui, R.W. McEntire, E.C. Roelof, D.J. Williams (JHU/APL, Laurel, MD 20723), T.E. Eastman (Plasmas International, Silver Spring, MD 20910), and S. Kokubun (STEL, Nagoya University, Toyokawa, Japan).

Measurements of energetic hydrogen and oxygen ions in the near-Earth ( $X > -30$  Re) magnetosphere obtained by Geotail during the ISTP interval are used to investigate the energy spectra and relative composition before and after abrupt flux increases associated with



magnetic field dipolarizations (characteristics generally associated with substorm onsets). Measurements of charge state composition from EPIC/STICS at  $\sim 9.4\text{-}210$  keV/e and mass composition from EPIC/ICS at  $>50$  keV to 3 MeV are used. The relative abundance of energetic high-charge state oxygen ions of solar wind origin to low-charge state oxygen ions of ionospheric origin provides a measure of the relative importance of these two plasma sources. Although it has been shown that the relative abundance of ionospheric oxygen generally increases with geomagnetic activity, substorm-related changes in the oxygen spectral shape remain to be determined in a statistically meaningful manner. Such changes in spectral shape can be identified with different acceleration scenarios. We investigate differential flux variations of the energetic ion populations (at a minimum for protons and oxygen) for a large sample of occurrences and compare their relation to other locally and globally determined parameters (noting their association to published tabulations of substorm onsets) with the intent to determine "typical" variations and, if any, classes and ranges of differences from this determined norm.

**GA3.02/L/04-B3** Poster **0900-25**

**QUASI-PERIODIC FIELD AND ENERGETIC PARTICLE STRUCTURES: SIMULTANEOUS OBSERVATIONS BY GEOTAIL AND INTERBALL IN THE NEAR MAGNETOTAIL**

George KARAGEVREKIS\*, D. V. Sarafopoulos and E. T. Sarris (Demokritos University of Thrace 67100 Xanthi, Greece email: postdoc@creator.space.noa.gr); I. A. Daglis and A. Belehaki (national Observatory of Athens, Institute of Ionospheric and Space Research, 15236 Athens, Greece); V. Lutsenko (Space Research Institute, Profsoyuznaya 84/32, Moscow 117810, Russia); S. Kokubun (Solar-Terrestrial Environment Laboratory, Nagoya University, 442 Toyokawa, Japan); \*Also at National Observatory of Athens

On November 1, 1995 a strong negative Bz component of the IMF as recorded on board the Wind spacecraft was followed by recurrent quasi-periodic and intense tailward fluxes of energetic particles in the central plasma sheet (GEOTAIL/EPIC measurements at  $X=-23R_E$ ), as well as by energetic particle fluxes in the plasma sheet boundary layer (INTERBALL/DOCK-2 measurements). Thanks to the location of Interball, which differs only in the Z direction with respect to the location of Geotail, a better understanding of the morphology associated with the near magnetotail during substorm activity is obtained. At the same time the tailward detected bursts of energetic particles were associated with corresponding negative bays of ground-based magnetograms at midnight local time, as well as with energetic particle injections at geosynchronous orbit (LANL 1987-097 spacecraft). We suggest that during this event the energy was not dissipated through the ejection of a single plasmoid/flux rope, but rather through the creation of multiple plasmoids/flux ropes.

**GA3.02/L/05-B3** Poster **0900-26**

**LOCATIONS OF DUSK-TO-DAWN CROSS-TAIL CURRENT DEDUCED FROM THEMAGNETIC VARIATIONS AT GOES-5 AND AMPTE-CCE DURING THE SUBSTORM ONSETS**

Kouta OKADA (Kyushu University, Hakozaki, Fukuoka, 812-8581, Japan, email: okada@geo.kyushu-u.ac.jp)

It has been widely accepted that during substorm expansion onsets Pi 2 pulsations are observed globally at the dipole equator, and magnetic field changes are often detected at the nightside geosynchronous orbit. Using high-time resolution magnetic field data from the geosynchronous satellite GOES 5 during the interval from March 1 to June 20, 1986, we examined the dynamical field changes in the nightside magnetosphere. The first peak in space are found to show a peculiar feature. In order to explain the peculiar feature, we propose that the current disruption region should be set up in the inner magnetosphere than  $6.6R_E$  during the substorm expansion onset. Furthermore, we will show a local time distribution of the events of the magnetic field change at the substorm expansion onset in the nightside magnetosphere.

**GA3.02/L/06-B3** Poster **0900-27**

**FIELD-ALIGNED CURRENTS PRIOR TO A SUBSTORM EXPANSION PHASE ONSET**

V. A. VELICHKO, R. N. Boroyev and D. G. Baishev (Institute of Cosmophysical Research and Aeronomy, 31 Lenin Ave., Yakutsk 677891, Russia, email: lae@sci.yakutia.ru)

We have selected a set of substorms, a center location of which at the moment of an expansion phase has been determined on the magnetogram from the auroral stations. During a substorm growth phase at middle and low latitudes the bays in the geomagnetic field D-component are found: the negative bay was observed westward of the future substorm center, the positive bay - eastward. The magnetograms of mid-latitude stations extended in longitude allowed to rebuild directions and to estimate the longitudinal scale size of the downward and upward field-aligned currents, arising in the expected substorm center a few minutes prior to the expansion phase onset. At the beginning of expansion phase the field-aligned currents reverse their direction on each side from the substorm center.

**GA3.02/L/08-B3** Poster **0900-28**

**IMF CONTROL OF STORM AE ACTIVITY**

Tadanori ONDOH (Space Earth Environment Laboratory, Kitano, Tokorozawa 359-1152, Japan, (email: 77771903@people.or.jp)

Since solar wind parameters simultaneously observed by separate satellites show the same variation on time scales above 30 minutes or more, hourly values of AE and Dst indices during small geomagnetic storms are compared with those of IMF-BZ and solar wind pressure to study the cause of storm AE activity. All storm AE increases occur during Dst decreases for the southward IMF-BZ, and storm AE minima coincide with northward IMF-BZ maxima. At least, two large storm AE increases above 600 nT occur and the first storm AE activity develops together with the Dst, decrease, southward IMF-BZ increase, and solar wind pressure increase. The second larger storm AE activity occurs with a larger southward IMF-BZ, but not with a solar wind pressure increase. The storm AE activity is primarily controlled by the IMF-BZ polarity, and the dayside magnetosphere before the storm AE increase recovers from its distorted state. The storm AE activity explosively begins with the auroral electrojet caused by the tail reconnection. Since closed magnetic field lines in the tail are stretched more tailward with increasing the southward IMF-BZ, curvature drifts of hot ions may produce a partial eastward ring current near the tail equatorial plane beyond  $X=-10 R_E$ . However, gradient drifts of hot ions injected from the tail are dominant within  $X=-8 R_E$  in the equatorial plane and form an westward ring current. This is a favorable condition for generating the reconnection in the near-Earth tail, since the partial eastward ring current locally weakens the westward cross tail current in the near Earth tail.

**GA3.03** **Thursday 29 July**

**DETERMINATION OF POLAR CAP BOUNDARY: IMPLICATIONS FOR MAGNETOSPHERIC ENERGETICS**

Location: Gisbert Kapp, NG15 LR1  
Location of Posters: Gisbert Kapp, Coffee Room

**Thursday 29 July AM**

Presiding Chair: K.Kauristie (Finnish Meteorological Institute, Helsinki, Finland)

**DETERMINATION OF POLAR CAP BOUNDARY: IMPLICATIONS FOR MAGNETOSPHERIC ENERGETICS**

**GA3.03/W/03-B4** Invited **0930**

**MAPPING THE HIGH-LATITUDE, HIGH-ALTITUDE EXTENSION OF THE PLASMA SHEET USING POLAR ENERGETIC PARTICLE OBSERVATIONS**

HARLAN E. SPENCE (Boston University Center for Space Physics, 725 Commonwealth Avenue, Boston, MA 02215, email: spence@bu.edu), J. F. Fennell and J. L. Roeder (both at The Aerospace Corporation, P.O. Box 92957, Los Angeles, CA 90009), R. Friedel (Los Alamos National Lab, Mail Stop D-436, Los Alamos, NM 87545), T. A. Fritz, K. L. Hirsch, and M. Althman (all at BU), M. Grande (Rutherford Appleton Laboratory, Chilton, Didcot, Oxfordshire, OX11 0QX, England), M. Kivelson and J. Green (Institute for Geophysics and Planetary Physics, University of California Los Angeles, CA 90095)

For the past several years, the NASA/POLAR spacecraft has been exploring the high-altitude, high-latitude magnetosphere. This region has not been well-sampled in the past and certainly not with such comprehensive instrumentation. In this review presentation we highlight recent studies using POLAR data that have explored the nature of the open/closed magnetic field boundary at high altitudes. These analyses have focussed on the location of the energetic particle trapping boundary and its control by parameters such as dipole tilt, solar wind dynamic pressure, interplanetary magnetic field orientation, and geomagnetic activity levels. In this study, these analyses will be extended by comparing the observed boundary encounters to simple, parameterized phenomenological models of the expected magnetic field geometry, under a variety of conditions. Finally, the local measurements of particle boundaries will be compared to auroral boundaries deduced from coincident global auroral imaging from the POLAR spacecraft.

**GA3.03/E/05-B4** **1000**

**THE STATISTICAL POLAR CAP BOUNDARY AND DYNAMICS: ENERGETIC PARTICLE RESULTS FROM SAMPEX**

S.G. KANEKAL (Code 696, NASA GSFC and RTISS, Greenbelt Rd, Greenbelt, MD 20904, USA, e-mail:kanekal@lepsam.gsfc.nasa.gov) D.N.Baker (Laboratory for Atmospheric and Solar Physics, University of Colorado, Boulder, CO, 80309) J.B.Blake (The Aerospace Corporation, MS259, Los Angeles, CA 90009) B.Klecker (Max planck Institut für Extraterrestrische Physik, Garching, Germany) G.M. Mason (Dept. of Physics, Univ. of Maryland, College Park, MD 20742) R.A. Mewaldt (California Institute for Technology, Pasadena, CA 91125)

We use instruments aboard SAMPEX to determine energetic particle boundaries in the polar regions. These boundaries are related to the polar cap, namely, the region of open magnetic flux tubes. SAMPEX is in a low earth polar orbit and executes about 15 orbits per day and has almost continuous data coverage from August 92 to present. The energetic particle boundaries are determined from particle measurements of energy thresholds ranging from about 30 keV to 0.50 MeV. We discuss the statistical features of the energetic particle boundaries and study the boundary dynamics under the influence interplanetary parameters such as the Interplanetary magnetic field and the solar wind velocity.

**GA3.03/E/07-B4** Invited **1020**

**DYNAMICS OF THE AURORAL LUMINOSITY BOUNDARY OF THE POLAR CAP DURING SUBSTORMS**

M. BRITTNACHER, D. Chua, M. Fillingim, G. Parks, and R. Wellman (all at Geophysics Program, Box 351650, University of Washington, Seattle, WA 98195, USA, Email: britt@geophys.washington.edu); J. Spann (NASA Marshall Space Flight Center, Huntsville, AL 35812, USA); and G. Germany (Center for Space and Astronomy Research, University of Alabama in Huntsville, Huntsville, AL 35899, USA)

The area of the polar cap during substorms has been measured using images from the Polar Ultraviolet Imager (UVI) for different interplanetary magnetic field (IMF) conditions. Changes in the poleward boundary of auroral luminosity have been analyzed in relation to substorm phase and IMF orientation. Reconnection models of flux transport into the polar cap during the substorm growth phase, and loss from the polar cap during the expansion phase, provide a framework by which these UVI observations can be analyzed. By comparison of the observations with the model predictions we can determine to what extent these models accurately predict the polar cap dynamics, and also where anomalous behavior calls for a new understanding of the dynamics beyond what these models provide. It was found that the polar cap boundary near noon and midnight usually shifted down in latitude by 1-2 degrees and 3-4 degrees respectively, increasing the area of the polar cap during the substorm growth phase as predicted. However, this growth phase phenomenon also unexpectedly occurs independently of the IMF Bz component. The polar cap area also increased due to motion of the dawn and dusk aurora to lower latitudes, although the latitudinal shifts were asymmetric, not always concurrent, and continued well into the substorm expansion phase. What is not explained by the models is that the poleward auroral boundary in the nightside region sometimes reached very high latitudes (greater than 80 degrees MLat) greatly decreasing the polar cap area, independent of the magnitude of the substorm.

**GA3.03/W/05-B4** **1110**

**OPTICAL DETERMINATION OF THE POLAR CAP AREA AND OPEN MAGNETIC FLUX WITH THE VISIBLE IMAGING SYSTEM**

J. B. SIGWARTH and L. A. Frank (Both at: Department of Physics and Astronomy, The University of Iowa, Iowa City, IA 52242, E-mail: sigwarth@iowasp.physics.uiowa.edu).

The Visible Imaging System (VIS) on the Polar spacecraft acquires global images of Earth's northern auroral oval at multiple wavelengths and at a temporal resolution of approximately one minute. The wobble compensated or "despun" images of the VIS Earth Camera have a spatial resolution of approximately 100 km at the apogee altitude of 51,000 km. The VIS Earth Camera is sensitive predominantly to the atomic oxygen emissions at 130.4 nm and 135.6 nm.

The images acquired with the VIS Earth Camera are used to determine the poleward boundary of the auroral oval. From the identified boundary, the polar cap area and total open magnetic flux in the polar cap are calculated. The rate of change of the observed open magnetic flux in the polar cap is the net result of the source of open flux due to merging on the dayside and the loss of open flux to reconnection in the magnetotail. In addition, with knowledge of solar wind parameters it is possible to estimate the magnetic energy stored in the lobe fields of the magnetosphere. Several example sequences of VIS images that show the variation of the polar cap area, total open magnetic flux, and estimated energy stored in the magnetotail lobe fields will be presented. These will include the substorm that occurred on January 12, 1997 where the polar cap area and open magnetic flux continued to increase for 30 minutes after the onset of the substorm at 0725 UT.

**GA3.03/E/06-B4** Invited **1130**

#### DETERMINATION OF POLAR CAP BOUNDARY FROM GUMICS RUNS

Pekka JANHUNEN (Finnish Meteorological Institute, Geophysical Research, POB 503, FIN-00101, Helsinki, Finland, email: Pekka.Janhunen@fmi.fi)

The GUMICS ionosphere-magnetosphere coupling simulation is a global MHD code coupled with an electrostatic ionosphere. Techniques such as adaptive hierarchically refined Cartesian grid and temporal subcycling are used to speed up processing, which would otherwise be too involved for existing computers. The emphasis in GUMICS is a good modeling of the ionosphere and good resolution in the near-Earth region.

An MHD simulation suits well for the determination of the polar cap boundary, since from an MHD simulation, one can determine the open-closed field line boundary by numerically integrating many magnetic field lines starting from the ionosphere and seeing whether they return to the Earth (closed) or hit the boundary of the simulation box (open). This method corresponds directly to the definition of open and closed field lines.

We study the dynamical behavior of the polar cap boundary in GUMICS runs in varying IMF conditions. We also study how the polar cap boundary is related to the Region-1 current system and the ionospheric potential pattern, to see if these can be used as observational proxies of the polar cap boundary.

**GA3.03/W/11-B4** **1200**

#### FAST AND POLAR OBSERVATIONS OF THE POLAR CAP BOUNDARY, FIELD-ALIGNED CURRENTS AND CONVECTION ELECTRIC FIELDS DURING CME EVENTS

CYNTHIA CATTELL, A. Bowser, C. McBrady, K. Sigsbee and J. Wygant (School of Physics and Astronomy, University of Minnesota, Minneapolis, MN 55455, USA, Email: cattell@belka.space.umn.edu); C. Carlson, R. Ergun, J. McFadden, F. Mozer, W. Peria (Space Sciences Lab, University of California, Berkeley, CA 94720, USA); G. Le, C. Russell, R. Strangeway (IGPP, University of California, Los Angeles, CA, USA); R. Elphic (Los Alamos National Lab, Los Alamos, NM 87545, USA); M. Brittacher and G. Parks (Geophysics Program, University of Washington, Seattle, WA 98195, USA)

There have been many CME encounters with the earth's magnetosphere since the launch of FAST in August, 1996. The short orbital period and data coverage for almost every auroral zone crossing allow us to determine the changes in field-aligned currents, convection electric fields and particle boundaries with time to determine the effects of solar wind plasma and magnetic field properties. In this paper, we present observations of the polar cap boundary as determined from four different methods- convection reversal, location of field-aligned currents, particle signatures and optical signatures from the Polar UVI imager. In addition, observations of field-aligned currents and convection electric fields from Polar perigee passes will be used to provide auxiliary observations which, for most events, are at different local times than the FAST observations. The resulting polar cap sizes will be compared to solar wind parameters observed by WIND. This results of this study will enhance our understanding of the coupling of the solar wind and the magnetosphere during CME events. The comparison of multiple techniques to determine the polar cap boundary will aid in estimating the accuracy of these methods for different local times.

**GA3.03/W/10-B4** **1220**

#### THE POLAR CAP BOUNDARY DURING NORTHWARD IMF

J.C. GREEN (University of California, Los Angeles, Department of Earth and Space Sciences, 405 Hilgarde, Los Angeles, CA, 90048, email: jgreen@igpp.ucla.edu); M.G. Kivelson, R.J. Walker, K.K. Khurana (all at the University of California, Los Angeles, Department of Earth and Space Sciences, 405 Hilgarde, Los Angeles, CA, 90048); H.E. Spence (Boston University, Dept of Astronomy and Space Physics, Boston, MA), J.B. Blake (The Aerospace Corporation, Los Angeles, CA)

The configuration of the polar cap during northward IMF is still debated. Both single event studies and large statistical studies have been employed in an attempt to understand how solar wind parameters affect the movement of the polar cap boundary. Xu (1995) and Newell et al (1997) investigated several events of prolonged duration of northward IMF using SAMPEX data. Both found that the polar cap closes with duration of northward IMF but complete closure can be inhibited by a finite By component. Large statistical studies have been less successful at finding correlations. A recent statistical study by Kanekal et al (1998) using SAMPEX data found that the polar cap actually increased with increasing magnitude or northward IMF.

We have investigated the nighttime energetic ion boundary using POLAR CEPPAD energetic ion data. The boundary was determined by noting the drop off in flux of ions corresponding to the high energy tail of the plasma sheet. It's not unambiguous that this is the open/closed field line boundary but changes in this energetic particle boundary give an indication of the configuration and dynamics of the magnetosphere during northward IMF. Our initial results show that, like the Kanekal et al (1998) study, the nighttime energetic ion boundary appears to move equatorward with increasing duration of northward IMF and magnitude of Bz. This may indicate a complete shift of the polar cap towards the nightside during northward IMF. We will further investigate the cause of this finding and also what role the Bx component of the solar wind may have play in controlling the polar cap boundary.

**Thursday 29 July PM**

Presiding Chair: K.Kauristie (Finnish Meteorological Inst, Helsinki, Finland)  
Concurrent Poster Session

**DETERMINATION OF POLAR CAP BOUNDARY: IMPLICATIONS FOR MAGNETOSPHERIC ENERGETICS**

**GA3.03/W/12-B4** Invited **1400**

#### MONITORING THE OPEN-CLOSED BOUNDARY OF THE POLAR CAP USING PARTICLE PRECIPITATION OBSERVATIONS

THOMAS SOTIRELIS, Patrick T. Newell, Joseph P. Skura and Ching-I. Meng (The Johns Hopkins University Applied Physics Laboratory, Laurel, Maryland)

The location of the open-closed boundary of the polar cap varies greatly, as does the quantity of open flux it encloses. The amount of open flux is central to describing the magnetospheric state. Reliably monitoring this boundary would permit an explicit ongoing diagnostic for the amount of energy stored in the lobes of the magnetotail. Observations of precipitating particles by low altitude polar orbiting satellites can be used to identify individual points on the open-closed boundary. A fleet of such spacecraft can provide several nearly simultaneous points. Hence, boundary shapes and the enclosed flux can be estimated. Factors impacting the accuracy of such estimates will be discussed, such as the number of points available and the definition of nearly simultaneous. The status of an ongoing effort to automate such determinations using observations from the fleet of DMSP and NOAA satellites, and so to provide a time history of the open-closed boundary and the open flux starting from 1984, will be presented.

**GA3.03/W/13-B4** **1430**

#### AUTOMATED DETERMINATION OF THE POLAR CAP BOUNDARY FROM POLAR UVI IMAGES

J.B. BAKER, C.R. Clauer, J.M. Daida, V.O. Papitashvili (all at Space Physics Research Laboratory, University of Michigan, Ann Arbor, MI 48109-2143, USA, email: bakerjb@zsu.sprl.umich.edu) A.J. Ridley (Southwest Research Institute, San Antonio, TX 78238-5166, USA, email: ridley@worf.space.swri.edu) M.J. Brittacher (Geophysics Program, University of Washington, Seattle, WA 98195-1650, email: britt@geophys.washington.edu)

The POLAR UVI instrument can instantaneously image the entire auroral distribution at good spatial and temporal resolution. It thus provides a suitable dataset with which to investigate the dynamics of the polar cap on a global scale without the need for extrapolation or statistical fitting. It is important to have good temporal and spatial resolution of polar cap variations in order to better understand the coupling of the magnetosphere to the ionosphere and solar wind. To this end, an automated technique has been developed to obtain polar cap boundaries from POLAR UVI images. The technique has been calibrated against DMSP particle precipitation and ground magnetometer data, and we present the results of this calibration. Relationships between electron precipitation, auroral intensity, and field-aligned currents which emerged during the calibration process are discussed. We also present preliminary results of a study of how the polar cap area behaves during periods of both steady and time-varying IMF conditions.

**GA3.03/W/07-B4** **1450**

#### EFFECTS OF THE ENERGY INPUT DURING SUBSTORM EXPANSION PHASE TO THE SUBSTORM SIZE

E.I.A. KALLIO, T.I. Pulkkinen, H.E.J. Koskinen\*, A. Viljanen (Finnish Meteorological Institute, Geophysical Research, P.O.Box 503, FIN-00101 Helsinki, email: Eija.Kallio@fmi.fi; \* also at University of Helsinki; Department of Physics, P.O.Box 9, FIN-00014 University of Helsinki J. A. Slavin, K. Ogilvie NASA Goddard Space Flight Center, Greenbelt, MD, USA

During the substorm cycle, energy is extracted from the solar wind, stored in the magnetotail, and later explosively dissipated in the magnetosphere-ionosphere system. While the energy input and dissipation must balance over longer time periods, factors that contribute to the exact moment of the onset of the explosive expansion and the size of the substorm are still largely unknown. In this study, we have identified substorms from the local electrojet index created from the IMAGE magnetometer chain in Scandinavia and Finland during the entire year of 1997. Each of the substorms has been tagged with an onset time and start of growth phase time. The WIND magnetic field and plasma measurements are then used to compute the epsilon-parameter, that characterizes energy input to the magnetosphere, and its time integral from the start of the substorm growth phase. These two parameters are compared with ionospheric dissipation, namely the local electrojet index and its time integral, which represent the ionospheric Joule heating. We compare and contrast cases when the energy input stops at or close to the substorm expansion onset with events where the energy input continues to the expansion phase. Our aim is to evaluate to which extent the substorm expansion dissipates previously stored energy and how much of the energy comes directly from the solar wind.

**GA3.03/W/04-B4** **1510**

#### THE LATITUDE OF THE AURORAL ELECTROJET - LONG-TERM VARIATION AND DEPENDENCE ON THE SOLAR WIND VELOCITY

VENNERSTROEM, Susanna (Danish Space Research Inst, Juliane Maries Vg 30, Copenhagen, Denmark, Email: sv@dstri.dk)

By using the H/Z-ratio of the groundbased magnetic observations at high latitudes, it is possible to determine the latitudinal position of the auroral electrojet. For a few high-latitude observatories records of hourly values of H and Z exist back to around 1920. We use these long-time series to investigate the long-term and solar cycle variation of the latitude of primarily the westward auroral electrojet. We find that in the late declining phase of the solar cycle, where the geomagnetic activity is mainly due to high speed streams from coronal holes, the electrojet is located at relatively higher latitudes than during solar maximum for similar geomagnetic activity levels. We compare with satellite measurements of the solar wind, especially the solar wind velocity.

**GA3.03/E/04-B4** **1530**

#### DYNAMICS OF THE POLAR CAP BOUNDARIES AND AREA IN THE COURSE OF SUBSTORMS

V.M. MISHIN, A.D. Bazarzhapov, T.I. Saifudinova, and D.Sh. Shirapov (all at Institute of Solar-Terrestrial Physics, P.O.Box 4026, Irkutsk, 664033, Russia, email: mishin@iszf.irk.ru)

The polar cap can be determined as an area inside the high-latitude boundary of FAC Region 1. Such a method was introduced on the basis of magnetogram inversion technique MIT2, tested through comparison with auroral imagery from the Viking and DE2 spacecrafts, and used in timing and analyzing substorms [Mishin et al., 1997, p.19845; and Ref's therein]. During the past >10 years, data on the dynamics of the polar cap boundaries and area (i.e., on the open magnetic flux dynamics) has been amassed by above authors for >20 substorms including those studied in frames of CDAW6 and CDAW9. This paper summarizes the main results on the entire set of accumulated data. It also presents results derived from comparing the boundaries and area of the northern polar cap by the MIT2 method, with those obtained recently using other methods by Lyons et al., and Baker et al.

**GA3.03/W/01-B4** Invited **1610**

**IONOSPHERIC SIGNATURES OF THE POLAR CAP BOUNDARY AND APPLICATION TO MEASUREMENT OF RECONNECTION**

Gerard BLANCHARD (Department of Chemistry and Physics, Southeastern Louisiana University, SLU 10878, Hammond, LA 70402, Email: gblanchard@selu.edu); Larry Lyons (Department of Atmospheric Sciences, University of California, Los Angeles, CA, 90095-1565, Email: larry@atmos.ucla.edu)

The polar cap boundary corresponds to the surface separating open and closed field lines in the magnetosphere. Magnetospheric reconnection is equivalent to a plasma flow through this surface at altitudes down to the ionospheric F region. It is thus possible to calculate the reconnection rate from measurements of ionospheric flow, provided that the location and velocity of the polar cap boundary are determined. Sharp differences in precipitating electron characteristics across the boundary create detectable ionospheric signatures of the boundary. On the nightside of the Earth, the location of the polar cap boundary in a magnetic meridian can be monitored continuously using a meridian scanning photometer or incoherent scatter radar. With a meridian scanning photometer, we seek the increase in auroral emission at the boundary. The ratio of 6300 Å emission to 5577 Å favors 6300 Å at the poleward edge of the auroral zone. We show that there is a sharp increase in 6300 Å intensity at the polar cap boundary and present criteria for identifying the boundary. The signature of the polar cap boundary observed by incoherent scatter radar is an increase in the E-region electron density, and the polar cap boundary is identifiable by placing a threshold on density. We demonstrate that the boundaries determined by these two methods (radar and photometer) agree to within 0.6 degrees. On the dayside, the increase in electron density is masked by photoionization. We show, however, that by accounting for the photoionization, a threshold on the ionization rate identifies the polar cap boundary. Once the location and velocity of the polar cap boundary in a meridian is known, the reconnection rate in that meridian can be computed from radar measurements of ionospheric flow. We present examples of measurements.

**GA3.03/W/06-B4** **1640**

**THE RELATIONSHIP BETWEEN HF RADAR BACKSCATTER AND THE NIGHTSIDE POLAR CAP BOUNDARY**

M. LESTER, S.E. Milan (both at Department of Physics and Astronomy, University of Leicester, Leicester, LE1 7RH, UK, Email: mle@ion.le.ac.uk), V. Besser and R. Smith (both at Geophysical Institute, University of Alaska, Fairbanks, 903 Koyukuk Drive, Fairbanks, Alaska 99755-7320, USA)

The SuperDARN radars often observe in the nightside scatter a gradient in the spectral width parameter as a function of latitude, with high values at higher latitudes. This gradient has been related in one case to the boundary between the Central Plasma Sheet and the Boundary Plasma Sheet. In this paper we discuss data from the CUTLASS Finland radar which indicates that the gradient is co-located with the poleward boundary of the red line (630.0 nm) emission, which in turn has been suggested as an indicator for the polar cap boundary. We discuss these interpretations of the spectral width gradient in terms of the dynamic behaviour of the magnetotail, demonstrating when the polar cap boundary can be identified by this technique.

**GA3.03/W/08-B4** **1700**

**ON THE USE OF SUPERDARN HF RADAR BACKSCATTER CHARACTERISTICS FOR DETERMINING THE NOON POLAR CAP BOUNDARY**

M PINNOCK, A. S. Rodger British Antarctic Survey, Madingley Road Cambridge CB3 0ET, UK (email: M.Pinnock@bas.ac.uk) SuperDARN PIs.

Previous work has demonstrated a link between the equatorward edge of cusp particle precipitation, detected by satellites and ground based optical measurements, and the occurrence of large Doppler spectral widths in SuperDARN HF radar data sets. The radar Doppler spectral width data, obtained on meridional pointing beams, has been used as a proxy for the location of the polar cap boundary (PCB), and this data used to measure the flow of plasma across the PCB and hence derive the reconnection electric field in the ionosphere. However, the precise cause of the Doppler spectral width enhancement, usually interpreted as the signature of small scale (< 45 km) electric field variations, is not known. The earlier work has also used only single radar data sets with a field of view limited to ~2 of MLT. In a case study using 4 of the SuperDARN radars we examine the Doppler spectral width boundary determined over 6 h of MLT around the noon sector and its relationship to the convection pattern, also determined from the radar data. A clear link between variations in the poleward velocity component and the offset of the Doppler spectral width boundary from the likely location of the PCB is observed for many, but not all, of the radar scan periods. This reinforces the intimate link between cusp particle precipitation and the Doppler spectral width data, in particular when time-of-flight effects on the cusp ions are taken into account. Progress towards calibrating the offset between the Doppler spectral width boundary and the true PCB will be reported. Illustrations of the dynamic behaviour of the boundary will also be shown.

**GA3.03/W/02-B4** **1720**

**STATISTICAL ANALYSIS OF HIGH-LATITUDE IONOSPHERIC FLOWS ASSOCIATED WITH THE ASYMMETRIC EFFECT OF THE Y COMPONENT OF THE INTERPLANETARY MAGNETIC FIELD.**

H. KHAN and S. W. H. Cowley. (University of Leicester, University Road, Leicester, LE1 7RH, UK.)

Ionospheric flow velocities, measured by the EISCAT UHF radar located at Tromsø, Norway, together with solar wind measurements of the interplanetary magnetic field (IMF) By component, have been studied in a statistical manner. It has been suggested that the flow asymmetries on closed field lines ascribed to the effects of the IMF By can be explained using the simplistic 'dipole plus uniform field' model. Previous studies of the ionospheric flow onset after the North-South (BZ) turnings of the IMF revealed the typical twin vortical flow pattern was produced ~5-15 min after perturbations were incident at the ionosphere. Cross correlations between simultaneous ionospheric vector velocities, observed on closed field lines, and the IMF By component were calculated using nominal lags of 0, 5, 10 and 15 min to illustrate the overall asymmetric trends in the data sets. The flow asymmetries observed using the positive northward vector velocity in particular, clearly illustrate flows indicating a shift in the polar cap position as a whole, in the opposite sense to that of the direction of the IMF By. Simultaneously the flow pattern centre is displaced towards increasing local time from noon and midnight for positive IMF By, and conversely for negative By, in the northern hemisphere. Both these features are consistent with the asymmetric shifts proposed by the 'dipole plus uniform field' model, where the first indicates the latitudinal tilt of the ionospheric footprints of field lines that lie in the dawn-dusk meridian, and the second describes the displacement in longitude of those field lines in the noon-midnight meridian.

**GA3.03/W/09-B4** **1740**

**EVIDENCE OF ANTI-SUNWARD FLOW ON CLOSED FIELD LINES IN THE IONOSPHERE: POSSIBLE EXISTENCE OF A VISCOUS CELL**

Adalbjorn THOROLFSSON, Jean-Claude CERISIER (both at Centre d'étude des Environnements Terrestre et Planétaires, 4 avenue de Neptune, 94107 Saint-Maur, France, Email: thorolfs@cetp.ipsl.fr) and Mike Pinnock (British Antarctic Survey, High Cross, Madingley Rd., Cambridge CB3 0ET, UK)

There is still an ongoing debate about whether the low-latitude boundary layer (LLBL) on the flanks of the magnetosphere is open or closed. Using satellite and SuperDARN ionospheric radar data, we carry out a case study of the flow in the afternoon ionosphere with respect to particle boundaries obtained with satellite data. We find evidence for anti-sunward flow near the convection reversal boundary that is associated with closed field lines. This indicates that at least a part of the LLBL is on closed field lines. These results are discussed and the possibility of a viscous cell on the flanks is evoked.

Thursday 29 July PM

**GA3.03/E/03-B4** Poster **1400-01**

**SIZE OF THE AURORAL OVAL AS INFERRED FROM GEOMAGNETIC VARIATIONS AT THE ANTARCTIC LOCATIONS, TRANS-AURORAL ITALIAN STATION TERRA NOVA BAY, AND SUB-AURORAL INDIAN STATION MAITRI**

G.Rajaram, A.N.HANCHINAL, and Tarun (all Indian Institute of Geomagnetism, Dr.Nanabhai moos Road, Colaba, MUMBAI-5,INDIA. E-mail: arun@iig.res.in); M.Candidi(CNR-IFSI, CP 27 FRASCATI, 00044- ITALY. E-mail: candidi@ifsi.rm.cnr.it)

It is generally known that the auroral oval shifts equatorward during magnetically disturbed conditions (high Kp and AE indices). What is less known is the extent of broadening of the auroral oval, which is also known to occur during magnetic disturbance. This work tries to focus on this aspect by examining the X, Y and Z geomagnetic variations at the trans-auroral location Terranova bay (geog.74o 41'S, 164o 07'E, geomag.-77.34o, 279.41o E) and Maitri (geog.70o 46' S, 11o 44' E, geomag.-66.8 S, 56.3oE). Characteristics of the variations indicate whether the location does or does not experience the signature of the auroral electrojet events i.e. whether it is within the auroral oval or not.

Events during Nov-Dec 1994 are chosen for this study; IMF data and AE data are also available for the same periods. An attempt is made to relate information on the size of the auroral oval (inferred as discussed above) to conditions of polarity and intensity of the IMF.

**GA3.03/E/02-B4** Poster **1400-02**

**THE EARTH'S MAGNETOSPHERE AS A NON-LINEAR ELECTRODYNAMIC SYSTEM**

Vladimir SHELOMENTSEV and Sergey Sheshukov (both at Institute of Solar-Terrestrial Physics, 664033, P.O.Box 4026, Irkutsk, Russia, email: vshel@iszf.irk.ru)

Results of the prediction filter technique applied to the solar wind parameters (used as an input data) and the magnetospheric parameters (used as an output data) strongly support a supposition about a non-linearity of the magnetospheric response to changes of the external conditions. Forms of the filters depend on a general level of the magnetospheric disturbance as well as on a disturbance type. Thus, a ratio of the contributions of the fast magnetospheric response (driven processes) and the delayed response (unloading processes) varies from an initial (isolated) substorm to the subsequent (non-isolated) ones. Additional analysis testifies about an importance of the inner state of the magnetosphere for the development and the energetics of a single disturbance. It appears that the magnetospheric-ionospheric electric circuit contains the non-linear elements. The analogue of this circuit gives an insight into the observed regularities of the electric fields, currents, and energetics during a substorm development. This study is supported by the RFBR grants 95-05-14385, 98-05-65120.

**GA3.03/E/01-B4** Poster **1400-03**

**THE NORTHERN POLAR CAP AREA IN THE COURSE OF THE CDAW-9C SUBSTORM AS DEDUCED FROM DE-1 DATA AND UPDATED MIT-2**

D.Sh. Shirapov, A.D. Bazarzhapov, T.I. Saifudinova, and V.M. MISHIN (all at Institute of Solar-Terrestrial Physics, P.O.Box 4026, Irkutsk, 664033, Russia, email: mishin@iszf.irk.ru),

The magnetogram inversion technique-2 (MIT-2) is useful for calculating the density distribution of field-aligned currents in the geomagnetic frame of reference and for determining the polar cap boundaries and area S as the area of the region poleward of Iijima and Potemra's zone 1 currents [Mishin V.M. et al., J.Geophys.Res., 1997, v.102, p.19845]. This paper is based on using a new version of MIT-2 with a nearly twice as high spatial resolution. Assuming that  $F = B_s$  (where F is the open magnetic flux across the area S, and B is the mean value of the geomagnetic field strength in the polar cap) we calculated the values of F at steps of five minutes for the time interval (0000-3000)UT, May 3, 1986 (CDAW-9C substorm) and compared results obtained with similar data from DE-1 reported by Baker D.N. et al. [Geophys. Monogr. Ser., v. 84, ed. By H.Waite, Jr., 1994, p.101]. The difference between the two data does not exceed 13% of the mean value of F.

**GA3.03/L/01-B4** Poster **1400-04**

**A LATITUDINAL DISPLACEMENT OF THE OPTICAL AURORA CONJUGANCY ON THE POLEWARD EDGE OF AN AURORAL BULGE**

V.G. VOROBEV, O.I. Yagodkina (Polar Geophysical Institute, Apatity, Murmansk region, Russia, 184200, Email: vorobjev@pgi.kolasc.net.ru), D. Sibeck, K. Liou, C.-I. Meng (Applied Physics Laboratory, Johns Hopkins University, Laurel, MD 20723-6099 USA, Email: david.sibeck@jhuapl.edu)

Simultaneous optical observations at the Antarctic station Mirny ( $F^o = -77.320$ ) and UVI images of the northern auroral oval from POLAR satellite were used to examine the high-latitude aurora conjugacy during the substorm development. It was found the significant discrepancy between the location of the poleward edge of the auroral bulge in two hemispheres up to 50 of the corrected geomagnetic latitude. A value and direction of the conjugacy displacement are not connected with the tilt angle of the magnetic dipole but rather depend on the interplanetary magnetic field (IMF) orientation in the ecliptic plane. Aurorae were observed at more high latitudes in northern hemisphere when  $B_x < 0$  and  $B_y > 0$  and on the contrary the aurorae were registered at more high latitudes in south hemisphere when  $B_x > 0$  and  $B_y < 0$ . The similar asymmetry was observed as well at the magnetic activity level in the conjugated high latitude areas. The latitude of aurorae in both hemispheres well coincided when the IMF changes the orientation a few times before and during the substorm or when the IMF orientation is differed from the spiral structure. However, actually in these events the local bright auroral forms were often observed only in one of hemispheres and were not registered in the other one. Obtained



results can testify the high efficiency of the interplanetary Bx penetration into the magnetosphere.

**GA3.04 Monday 26 – Tuesday 27 July**

**GROWTH, PROPAGATION AND DAMPING OF ULF WAVES IN MAGNETOSPHERES**

Location: School of Education G33 LT  
Location of Posters: Conference Room

**Monday 26 July AM**

Presiding Chair: Dr C.L. Waters (The University of Newcastle, NSW, Australia)

**GA3.04/L/01-B1 Invited 0830**

**ALFVEN RESONANCES AND ALFVEN EIGEN MODES IN THE MAGNETOSPHERE**

A. GUGLIELMI (Institute of Physics of the Earth, B.Gruzinskaya, 10, Moscow, 123810 Russia, Email: gugi@uipe-ras.scgis.ru)

Thereport is devoted to the theory of Alfvén waves as related to the magnetospheric physics with theoretical results compared against the ground and satellite based data. In the case of Alfvén resonances, attention focuses on the problem of the remote diagnostics of the magnetosphere using the so-called ULF ranger technique. It is based on the known lateral structure of the resonances, and on the additional information which is contained in the impedance relations on the Earth's surface. This allow us to widen the range of diagnostic tools when we use an observation of the waves in Pc 3 - 5 frequency band. The prospects for remote sensing of the plasmopause position are discussed. In the case of Alfvén eigen modes, the linear and nonlinear aspects of the theory are outlined. The emphasis is on the structure induced nonlinearity of the medium. Particular attention has been given to the energy and mass transport in the ionosphere-magnetosphere coupled system.

**GA3.04/E/03-B1 0900**

**PC3S AND DC TRAINS: A CAUSAL CONNECTION?**

Gary D. EGBERT (College of Oceanic and Atmospheric Sciences, Oregon State University, 104 Ocean Admin. Bldg, Corvallis, OR 97331, e-mail: egbert@oce.orst.edu); Markus Eisel (GeoForschungsZentrum Potsdam, Telegrafenberg, 14473 Potsdam, Germany, e-mail: eisel@gfz-potsdam.de); Sierra Boyd and H.F. Morrison (both at Engineering Geoscience, University of California, Berkeley, CA, e-mail: em@seismo.berkeley.edu)

To study possible electromagnetic (EM) precursors to earthquakes, magnetotelluric (MT) stations have recorded EM data almost continuously (at 40 Hz sampling rate) since late 1995 at two sites along the San Andreas fault 150 and 300 km south-east of San Francisco, California. (Geomagnetic dipole latitude: 43 degrees, L approximately 1.8). Using classical and multivariate transfer function (TF) methods we show that the usual MT assumption that external magnetic fields are spatially uniform (over a distance of 150 km) is violated to a significant degree in the period range 10-30 seconds. We furthermore show that inter-station TFs vary significantly in time, with systematic variations due to time of day, and day of week. The overall spatial and temporal pattern of EM field variations implied by the TF estimates and related statistics (for periods from 10 to 300 s) is consistent with a combination of two distinct sources:

Pc3 geomagnetic pulsations, and cultural EM noise due to the San Francisco Bay Area Rapid Transit (BART) DC electric railway. Several aspects of the association between the two sources suggest that at least some of the PC activity may be causally related to the BART signal, but this issue needs further investigation. Our study also highlights some of the advantages of a TF approach (normally used for solid earth EM induction studies to eliminate external source variations) for some aspects of ionospheric studies. In particular we obtain clean estimates of Pc3 resonance frequencies (fundamental, plus the second and third harmonics) with our approach.

**GA3.04/L/02-B1 0920**

**DENSITY DEPENDENCE OF ALFVEN EIGENFREQUENCIES IN THE GLOBAL CORE PLASMA MODEL**

R.E. Denton (Physics and Astronomy Department, Wilder Laboratory, Dartmouth College, Hanover, NH 03755-3528, email: richard.denton@dartmouth.edu)L. Gallagher and Paul D. Craven (NASA Marshall Space Flight Center, Mail Code ES83, Building 4481, 382, Huntsville, Alabama 35812, USA, email: dennis.gallagher@msfc.nasa.gov)

There has been some interest in the possibility of using ULF to diagnose the magnetospheric plasma. One possible application to remotely sense the field line distribution of mass density using measurements of frequencies of toroidal field line resonance(global scale Alfvén waves with magnetic oscillations in the direction). It is of interest, therefore, to know what has been inferred about the magnetospheric density from other. Here we use a simplified version of the Global Core Plasmato examine the effect of parallel density dependence on toroidal line resonance modes. The magnetospheric density dependence is on observations by DE-1; the model couples at low altitudes to International Reference Ionosphere. We find that in the outer, the toroidal field line resonance modes have spacing to that obtained with a density dependence of 1/R along field, where R is the radial distance from the Earth. Closer to the, the effective radial dependence steepens since the steep density dependence is in nearer proximity to all locations the field line.

**GA3.04/L/03-B1 Invited 0940**

**DISPERSIVE FIELD LINE RESONANCES**

R. RANKIN, J. C. Samson, I. Voronkov (all at Department of Physics, University of Alberta, Edmonton, Alberta, Canada T6G 2J1, email: rankin@space.ualberta.ca) V. Tikhonchuk (P. N. Lebedev Physics Institute, Russian Academy of Sciences, Moscow 117924, Russia)

Field line resonances (FLRs) are standing shear Alfvén waves in the dipole-like region of the Earth's magnetosphere. With dispersive effects of electron inertia, electron thermal pressure, and ion gyroradius, FLRs can form intense field aligned currents, parallel and perpendicular electric fields, and deep field aligned density cavities. The low conductivity in cavities can also lead to enhanced electric fields in the low altitude magnetosphere below 1Re, as observed in satellite missions such as FAST. We shall discuss observations of FLRs in satellite and ground data, and present a self-consistent model which describes the interaction between fundamental mode standing shear and density waves. Using specified field aligned variations

of density, magnetic field, electron and ion temperatures, we classify the interaction of the waves as electron dispersive (ED) or ion dispersive (ID). In the ED case, we identify conditions under which enhanced parallel electric fields and density perturbations can be generated, and consider the energies to which auroral electrons might be accelerated. In the ID case, the interaction of the waves evolves through the generation of coupled shear-Alfvén-ion-acoustic solitons. It is found that dispersion and nonlinearity can drive electric fields and density fluctuations that are much larger than in the non-dispersive case, with very short perpendicular scales comparable to the inertial length and ion gyro-radius, respectively. The processes involved may go some way to explaining recent observations of density cavities and strong electric fields by the Freja and FAST spacecraft, and in predicting their temporal and spatial nonlinear evolution.

**GA3.04/E/02-B1 1010**

**EVOLUTION AND TRANSFORMATION OF STRONG MAGNETOHYDRODYNAMIC (MHD) DISTURBANCES IN MAGNETOSPHERIC RESONATOR**

N.A. BARKHATOV (Nizhniy Novgorod State Pedagogical University, 1, Ulyanova str., Nizhniy Novgorod 603005, Russia, e-mail: nikolay@barkh.sci-nnov.ru); N.S. Belliustin (Radiophysical Research Institute, 25, Bolshaya Pecherskaya str., Nizhniy Novgorod, 603600, Russia, e-mail: nick@nbell.sci-nnov.ru); P.G. Khurlopov (Institute of Applied Physics, 46, Ulyanova str., Nizhniy Novgorod, 603600, Russia, e-mail: pasha@sci-nnov.ru)

The peculiarities of developmental dynamics of strong magnetohydrodynamic disturbance in magnetosphere are investigated. The effects of transformation of Alfvén wave propagating along the Earth magnetic field into fast and slow magnetosound waves at collision of opposing impulses are considered. The dependence of effects on angle of Alfvén wave declination to magnetic field and on ratio of sound velocity in plasma to Alfvén velocity is analysed. Non-linear Alfvén wave transformation in a magnetosound ones is also investigated for various inclination angles of Earth magnetic field at the reflecting boundaries of the magnetospheric resonator. The special attention is given to effects, which increase with decreasing of temperature and sound velocity in plasma. The analytical evaluations, matched with considered effects in case of average nonlinearity are made, and peculiarities of limit approach of cold plasma are also studied. The role of near Earth space ionosphere-atmosphere in these phenomena is investigated. It is marked, that strong Alfvén wave can induce the essential plasma concentration redistribution in the Earth ionosphere, dependence of this effect on the ratio of Alfvén velocity to sound one is considered.

**GA3.04/W/20-B1 Invited 1100**

**ELECTROMAGNETIC WAVES FROM 0.1 TO 4 HZ OBSERVED BY POLAR**

B.J. ANDERSON (JHU/APL, Laurel, MD, 20723, USA, e-mail: brian.anderson@jhuapl.edu); C T Russell (IGPP, UCLA, Los Angeles, CA, 90024, USA, e-mail: ctrussell@igpp.ucla.edu); R Pfaff (GSFC, Greenbelt, MD, 20771, USA, e-mail: rob.pfaff@gsfc.nasa.gov); C A Cattell (Department of Physics and Astronomy, University of Minnesota, Minneapolis, MN, 55454, USA, e-mail: cattell@belka.spa.umn.edu); S A Fuselier (Lockheed/Martin Advanced Technology Center, Palo Alto, CA, 94304, USA, e-mail: fuselier@agena.spasci.com)

The Polar orbit is ideal for studies of electromagnetic ion cyclotron (EMIC) waves because it samples magnetic field lines in the magnetosphere over a wide range of latitudes offering the opportunity to study the propagation characteristics as never before. Here we present initial results of analysis of electromagnetic waves recorded by the Polar magnetic and electric fields experiments. Magnetometer data have been processed for 0.1 to 4 Hz fluctuations with <0.1 nT sensitivity from March 1996 through April 1998. Hundreds of instances of electromagnetic waves in this frequency range occur and fall into three categories: (1) EMIC waves in the magnetosphere, (2) broadband fluctuations associated with boundary layers and the cusp, and (3) band-limited EMIC-like fluctuations poleward of the cusp on open field lines. The magnetospheric EMIC waves occur primarily on field lines that map to the afternoon magnetosphere beyond 5 Re, consistent with previous analyses. The broadband fluctuations are most intense in the cusp proper where the magnetic field strength is depressed due to diamagnetic effects. The polar cap EMIC-like waves may be related to the polar cap Pc 1 events reported by Dyrud et al. [1997]. We selected a total of 42 events with strong magnetic signatures for comparison with electric field data. Poynting flux and wave vector determination analyses will be reported for each class of events to identify the direction of energy flow and their wave mode.GA3.04/E/01

**GA3.04/W/11-B1 1130**

**CAN ION CYCLOTRON WAVES PROPAGATE FROM THE EQUATORIAL MAGNETOSPHERE TO THE GROUND?**

J.R. JOHNSON and C. Z. Cheng (Princeton University, Plasma Physics Laboratory, Princeton, NJ 08543, E-mail: jrj@pppl.gov, fcheng@pppl.gov)

Ion cyclotron waves are important for transferring energy from protons to heavy ions, as remote indicators of proton dynamics, and in regulating proton anisotropy. However, for over a decade it has not been understood how these waves could be generated in the equatorial magnetosphere and be observed on the ground so reliably. Theoretical results based on ray-tracing, in fact, predicted that these waves are reflected at the Buchsbaum resonance (ion-ion hybrid resonance due to helium or oxygen) and cannot reach the ground. We present solutions of the coupled full wave equations for ion cyclotron waves propagating along auroral field lines and predict Poynting fluxes, wave amplitudes, and polarizations along a field aligned coordinate. Our results suggest that even for significant concentrations of oxygen and helium substantial wave power can reach low altitudes due to mode conversion and tunnelling. The waves reflect off the ionosphere and are strongly absorbed as they propagate back toward the magnetosphere leading to substantial wave absorption. Reflection and absorption coefficients are presented for waves incident from the equatorial magnetosphere, and windows of wave transmission and absorption can be predicted for ion cyclotron waves in the magnetosphere depending on azimuthal wave number and frequency. The ionosphere can also significantly affect wave propagation because the waves are at relatively high frequency. Significant amounts of wave energy can be dissipated at the ionosphere in addition to the energy that is absorbed at the ion resonances.

**GA3.04/W/08-B1 1150**

**NON-STATIONARY ALFVÉN RESONATOR: NEW RESULTS ON PC1 PEARLS AND IPDP EVENTS**

K. MURSULA, T. Bräysy, J. Kangas, R. Kerttula, P. Pollari, and T. Pikkarainen, (Department of Physical Sciences, University of Oulu, P.O. Box 3000, FIN-90401 Oulu, Finland, e-mail: Kalevi.Mursula@oulu.fi); K. Prikner (Geophysical Institute, 14131 Praha, Czech Republic); F. Z. Feygin, and O. A. Pokhotelov (Institute of Physics of the Earth, Moscow, Russia)

On December 15, 1984, a series of Pc1 pearls was observed by the Finnish search-coil magnetometer network, which subsequently increased in frequency and developed to a structured IPDP after substorm onset. The EISCAT radar was simultaneously monitoring the mid- to high-latitude ionosphere. We have calculated the ionospheric resonator properties during the different phases of the event using EISCAT observations. Contrary to earlier results, we find that the Pc1/IPDP wave frequency observed on ground corresponds to the maximum of the transmission coefficient rather than that of the reflection coefficient. This casts strong doubts on the bouncing wave packet model of Pc1 pearls. Instead, we present evidence for the alternative model of pearl formation by ULF waves modulating the Pc1 growth rate. The wave source was seen to move to lower latitudes during the IPDP event. Also, the properties of the ionospheric resonator could be modified so as to allow the observed increase in wave frequency. Therefore, we propose a new model for the IPDP formation, whereby the ionosphere acts as an active agent in forming the IPDP signal on the ground

**GA3.04/L/04-B1 1210**

**OBSERVATIONAL TEST OF ION CYCLOTRON WAVE PROPERTIES IN THE VICINITY OF THE BI-ION HYBRID RESONANCE FREQUENCY**

R E ERLANDSON (The Johns Hopkins University Applied Physics Laboratory, Laurel, MD 20723 USA, email: erlandson@jhuapl.edu); A J Ukhorsky (Moscow Institute of Physics and Technology, Russia); B L Giles and J A Slavin (NASA/GSFC, Greenbelt, MD 20771 USA)

The purpose of this study is to investigate the propagation of electromagnetic ion cyclotron (EMIC) waves in the vicinity of the bi-ion hybrid resonance frequency. Specifically, evidence of wave reflection, attenuation, and transmission will be sought for EMIC waves generated near the equator in the frequency range above the helium gyrofrequency. Observations using the Dynamics Explorer-1 (DE-1) satellite magnetic field experiment and Retarding Ion Mass Spectrometer (RIMS) will be used in this study. DE-1 was launched on August 3, 1981 and operated for nearly 10 years. DE-1 was placed in an elliptical-polar orbit with an apogee altitude of 4.6 Re. DE-1's orbit is ideally suited to study wave propagation as the satellite orbit follows nearly the same L-shell at low magnetic latitudes. Preliminary results based on observations acquired off the equator near L=4.5 in the dusk sector suggest that there is little change in EMIC wave amplitudes near the bi-ion hybrid frequency. These observations suggest that the waves tunnel through the stop band region or are simply unaffected. The later may occur in cases when the helium ion concentration is low. Observations from RIMS will be used to constrain the possibilities.

**GA3.04/W/47-B1 1230**

**WHAT CONTROLS THE OCCURRENCE OF DAYSIDE PC1-2 PULSATIONS?**

Mark ENGBRETSON and Jennifer Posch (both at Physics Department, Augsburg College, Minneapolis, MN 55454 USA, e-mail: engebret@augsborg.edu); Roger Arnoldy (University of New Hampshire, Durham, NH 03824 USA); Brian Anderson (JHU/APL, Laurel, MD 20723 USA); W. Jeffrey Hughes (Boston University, Boston, MA 02215 USA); Hiroshi Fukunishi (Faculty of Science, Tohoku University, Sendai, 980-77, Japan); Christopher Russell (IGPP, UCLA, Los Angeles, CA 90024 USA)

Magnetic pulsations in the Pc 1 and 2 frequency range (0.1 to ~1 Hz), have been studied both in space and on the ground for decades, and are known to be generated by wave-particle instabilities in the outer magnetosphere. While earlier studies near the plasmapause revealed a temporal association with magnetic storms, increasing evidence suggests that events at higher L shells in the dayside magnetosphere show a quite different dependence. The increasing availability of ground observations from high latitude sites in Antarctica and Arctic Canada, along with the consistent availability of solar wind and interplanetary magnetic field (IMF) data during the ISTEP era, has led to a new appreciation of the significant control of such events by variations in the solar wind and IMF; the most prominent of these is the triggering of intense events, both sustained and transient, by enhancements in solar wind pressure. Comparison of Pc 1-2 events with the Dst geomagnetic activity index during 1996 and 1997 shows a strong correlation between Pc 1-2 activity and positive Dst (or sharp increases in Dst), consistent with the solar wind pressure effect. We also observed a modest anticorrelation between Pc 1-2 occurrence and negative Dst and with geomagnetic storms or their recovery phases. These results are also consistent with earlier unpublished studies of data from the AMPTE CCE satellite. Of the 20 Pc 1-2 events observed during good conjunctions between the elliptically-orbiting POLAR satellite and Antarctic ground stations during these two years, 17 were associated with moderate or large solar wind pressure increases. These observations suggest that the outer magnetosphere is frequently marginally unstable to ion cyclotron wave emissions, regardless of the occurrence of storms. Our continuing investigations of these events will focus on local plasma conditions on the flux tubes where these waves are observed.

**Monday 26 July PM**

Presiding Chair: Prof K. Yumoto (Kyushu University, Japan)

**GA3.04/L/05-B1 Invited 1400**

**GROWTH, PROPAGATION AND DAMPING OF ULF WAVES IN PLANETARY MAGNETOSPHERES**

Carsten OTHMER, Karl-Heinz Glassmeier (Institut fuer Geophysik und Meteorologie, TU Braunschweig, Germany)

Planetary magnetospheres arenatural laboratories for many plasma physical processes one of which are ULF pulsations. Together with magnetic storms and substorms, they constitute the most important signatures of magnetospheric dynamics. Numerous observations of ULF waves in the terrestrial magnetosphere have been reported, and they have also been found in the magnetospheres of Mercury, Jupiter and Saturn. The special environments that the different planetary magnetospheres present us with, have major consequences for the behavior of ULF waves. Possible excitation mechanisms, propagation characteristics and damping processes for ULF waves and their relation to magnetospheric parameters such as size, background magnetic field, plasma sources, properties of the ionosphere, multi-ion effects etc. are discussed. Special emphasis will be paid to a comparative view of ULF waves under these different conditions.

**GA3.04/W/36-B1 1430**

**ULF WAVES IN THE JOVIAN MAGNETOSPHERE**

C. T. RUSSELL, K. K. Khurana and M. G. Kivelson (All at Institute of Geophysics and Planetary Physics, University of California, Los Angeles, CA, USA, e-mail: crussell@igpp.ucla.edu)

The main energy and mass source in the jovian magnetosphere is Io at a radial distance of 5.9 jovian radii. The immediate vicinity of Io contains strong ion cyclotron and mirror mode waves but more than 20 Io radii away the magnetosphere is largely quiet even on field lines

connected to Io. The plasma circulation in the jovian magnetosphere is largely corotational with a radial component that moves outward, slowly at first and then ever more quickly. The wave phenomena seen in the magnetosphere seem to be controlled by this radial transport. The waves increase in amplitude with radial distance in the dipolar magnetosphere and are stronger transverse to the field off the equator and more strongly compressional near the equator. At about 24 RJ the magnetic field switches from being quasi-dipolar to being magnetodisk-like. Near the inner edge of this region the level of wave turbulence is highly variable. In the lobes of the magnetodisk the field is generally quiet, in the current sheet it is more turbulent and the amplitude of this turbulence increases with radial distance. The surface of the magnetodisk itself appears to ring with a period of about 10 minutes. Russia, e-mail: leon@iszf.irk.ru)

Presiding Chair: Dr C.L. Waters (The University of Newcastle, NSW, Australia)

**POSTER REVIEW 1450**

F.W. Meink

**GA3.04/E/08-B1 Poster 1520-01**

**NONLINEAR INTERACTION OF ORDINARY ELECTROMAGNETIC AND ALFVEN WAVES**

Adam Yukhimuk, Lena SIRENKO (both at Department of Space Plasma Physics, Main Astronomical Observatory NASU, Kyiv, 252650, Ukraine); Olga Falko (Department of Astronomy and Space Physics, Kyiv National University, Kyiv, 252022, Ukraine)

The scattering of ordinary electromagnetic wave on the kinetic Alfvén wave in the magnetized plasma with small plasma parameter ( $b=8\pi nT/B0^2$ ) is investigated. Nonlinear dispersion equation and instability growth rates are found on the basis of two-fluid magnetohydrodynamics. It is shown that ordinary electromagnetic wave can decay on the kinetic Alfvén wave and other ordinary electromagnetic wave. Parametric instability considered in the paper could take place in the ionosphere and magnetosphere of Earth, where plasma parameter is small. The analysis of the satellite measurements point out that scattering of ordinary electromagnetic wave on the kinetic Alfvén wave more effective than ion cyclotron wave.

**GA3.04/E/15-B1 Poster 1520-02**

**EXCITATION OF PS6 PULSATIONS AND FORMATION OF AURORAL STRUCTURES STRETCHED ALONG THE MERIDIAN DURING DISTURBANCES**

S.I. SOLOVYEV, D.G. Baishev, N.E. Molochushkin and A.A. Fedorov (all at: Institute of Cosmophysical Research and Aeronomy, 677891 Yakutsk, Russia, E-mail: s.i.solovoyev@sci.yakutia.ru); K. Yumoto (Kyushu University 33, Fukuoka 812-81, Japan, e-mail: yumoto@geo.kyushu-u.ac.jp); M.J. Engebretson (Department of Physics, Augsburg College, Minneapolis, MN 55454, USA, e-mail: engebret@augsborg.edu); W.J. Hughes (Department of Astronomy and Center for Space Physics, Boston, MA 02215, USA, e-mail: hughes@buasta.bu.edu)

This paper reports on the results of statistical study of Ps6 pulsations and their relationship to N-S aurora and omega bands using data of geomagnetic observations from magnetometer networks and optical data for 1994-1998. We investigated main properties of Ps6 pulsations and characteristics of auroral structures, their relationship to types of magnetospheric disturbances, and also the dynamics of ionospheric Ps6 currents. It is found that intense Ps6 pulsations accompanied by N-S aurora and omega bands which are observed in the pre-midnight and morning sectors, respectively, are a fine structure of SMC events or convection bays although they can be observed also in the course of a substorm. Ionospheric Ps6 currents flow predominantly northward (southward) for auroral structures drifting along the azimuth to the west (the east) before (after) the midnight. On Geotail data during N-S aurora the fluctuations of electric field Ey component and BBF-events in the plasma sheet are observed. Possible sources of auroral structures and currents responsible for Ps6 pulsations are discussed.

**GA3.04/E/14-B1 Poster 1520-03**

**GIANT PULSATIONS: A NONLINEAR PHENOMENON**

O.A.Pokhotelov and Yu.G.KHABAZIN (both at Institute of Physics of the Earth, 123810 Moscow, Russia, E-mail: khabazin@uipe-ras.scgis.ru); K.Mursula and J.Kangas (both at Department of Physical Sciences, University Oulu, Linnanmaa, FIN-90570 Oulu, Finland, E-mail: Kalevi.Mursula@oulu.fi); P.K. Shukla (Institut für Theoretische Physik IV, Ruhr-Universität Bochum, D-44780 Bochum, Germany, E-mail: ps@tp4.ruhr-uni-bochum.de); L.Stenflo (Department of Plasma Physics, Umea, University S-90187 Umea, Sweden, E-mail: lennart.stenflo@physics.umu.se); I.Mann and D.Milling (both at Department of Physics, University of York, Heslington, York YO1 5DD, UK)

The theory developed up to the present to account for giant pulsations (Pgs) has been dominated by the linear approximation. Nevertheless, exceptionally high amplitudes and purely monochromatic features of the pulsation wave trains indicate the importance of nonlinear effects. Among a great variety of different nonlinear mechanisms, the nonlinear phase mixing of the resonant particles due to the finiteness of the pulsation amplitude is of great importance. We present a simple approach to this problem and provide a certain experimental background in favour of a nonlinear behaviour of the wave packets. We demonstrate that many intriguing peculiarities, e.g., exceptionally long duration of the giant pulsations, can be explained in terms of monochromatic modes exhibiting strong nonlinear wave-particle interactions in the presence of quasi-stationary injection of resonant particles during magnetic storms.

**GA3.04/W/27-B1 Poster 1520-04**

**GROUND-BASED AND POLAR SPACECRAFT OBSERVATIONS OF A GIANT (PG) PULSATION AND ITS ASSOCIATED SOURCE MECHANISM.**

D.M. WRIGHT, T.K. Yeoman, J. Storey and I.J. Rae (Department of Physics & Astronomy, University of Leicester, University Road, Leicester, UK. LE1 7RH)

A study of a giant pulsation event has been undertaken. The wave was observed at the ground on the Scandinavian IMAGE magnetometer network where the amplitude maximised in the vicinity of Tromsø (TRO), Norway (66.4° N geomagnetic). The ionospheric signature of the wave, which exhibited an azimuthal wave number (m) of about 30, was simultaneously recorded by a high-latitude HF Doppler sounder operating near Tromsø. This was possible due to the high spatial resolution of the sounder measurements. In addition, the CAMMICE instrument on the POLAR spacecraft, located east of Tromsø, detected a dispersed proton population on closed field lines shortly before the ULF wave was observed by the ground-based instrumentation. The role played by these particles, which were injected on the nightside during a substorm several hours earlier, in the generation mechanism of the wave will also be discussed.



GA3.04/E/16-B1 Poster 1520-05

## INFLUENCE OF A DRIFT-BOUNCE INSTABILITY ON THE ALFVEN WAVE STRUCTURE IN THE MAGNETOSPHERE

Dmitri Yu. KLIMUSHKIN (Institute of Solar-Terrestrial Physics, Irkutsk 33, P.O.Box 4026, 664033, Russia; e-mail: klimush@iszf.irk.ru)

This report discusses the influence of a drift-bounce instability on the MHD wave structure in the magnetosphere. It is assumed that the magnetospheric plasma consists of two components: (1) the low-energy core component that determines the structure of the wave, and (2) the high-energy low density component which determines the instability of the wave. The field line curvature, non-zero plasma pressure, and finite resistance of the ionosphere are taken into account. The drift-bounce instability that develops due to the resonance of energetic particles with the electromagnetic field of the hydromagnetic wave, is often treated as the mechanism for generation of geomagnetic pulsations with high azimuthal wave number ( $m > 1$ ) in the magnetosphere. A combined action of finite pressure of the core component and field line curvature leads to the propagation of Alfvén waves across the magnet

GA3.04/E/17-B1 Poster 1520-06

## THE SOLITARY STRUCTURES IN OVERDENSE IONOSPHERIC PLASMA

A.V. KOCHETOV and B.A. Mironov (both at Institute of Applied Physics, N.Novgorod, Russia, e-mail: kochetov@applsci-nnov.ru); G. I. TERINA and V.N. Bubukina (both at Radiophysical Research Institute, N.Novgorod, Russia, e-mail: ter@nirfi.sci-nnov.ru)

The results of the modelling of nonlinear dynamic effects arising in the ionospheric plasma under the action of the powerful radio waves are presented. Numerical solutions of nonlinear Schrödinger equation in the linearly inhomogeneous plasma layer excited by the heating radio wave were obtained. The processes of the formation of the solitary structures of the electric field and disturbances of plasma density and processes of their relaxation for different values of density gradient and the amplitude of the heating wave were analyzed. The spatial evolution of the electric field and disturbances of the plasma density and time dependencies of the reflected signal were obtained. With the heater turn-on the penetration of the solitary structure into the overdense plasma takes place which increases under the heating power increase and the decrease of the plasma density gradient. The decreasing of the scale of the spatial soliton structure, the periodic and chaotic solitons generation during the heater time are observed. When the heater is turned off, the solitons continue to travel into the overdense plasma for some time, increasing in the amplitude, until they reach the turning point. Then they reflect and propagate into the underdense plasma, decreasing in the amplitude, and disappear. The obtained results allow to interpret the appearance of the scattered signal after the heater turn-off - "after effect plasma signal" (AEPS). This work was supported by the Education Department of Russia. (grant N 97-0-5.3-113).

GA3.04/W/46-B1 Poster 1520-07

## FRACTAL DYNAMICS OF HIGH-LATITUDE LONG-PERIOD IRREGULAR PULSATIONS IN A FREQUENCY BAND (2,1-5,5) MHZ

KLAIN, B.I., Kurzhkovskaya, N.A. (both at Geophysical Observatory "Borok" of the United Institute of Physics of the Earth of Academy of Science of Russia, 152742 Borok, Yaroslavl, Nekouz, Russia, e-mail: klain@borok.adm.yar.ru)

The dynamics of fractal dimension (D) of high-latitude long-period irregular pulsations of np-type in a frequency band (2,1-5,5) MHz have been studied. The study was performed based on the data obtained by the observations of magnetic field of high-latitude observatories of Northern and Southern hemispheres of a magnetosphere. It was shown, that the fractal dimension of np-pulsations depends from a degree disturbance of a magnetosphere and geomagnetic latitude of an observatory. The increase of geomagnetic activity lead to magnification of fractal dimension of pulsations. During intense geomagnetic storms the linear relation D from a Dst-variation and duration of an initial phase of storms was discovered. For moderate - perturbed conditions the latitudinal profile of fractal dimension of np-pulsations was constructed. It was revealed, that in a narrow interval of latitudes 69-71° quantities D are less, than in lower and high latitudes. It is supposed that the fractal dimension reflects change structure of pulsations and the chosen interval of latitudes corresponds to a standing of boundary of the magnetospheric resonator. The possibility of application D as the indicator of a degree perturbation of a high-latitude magnetosphere, and also for monitoring its structure is considered.

GA3.04/W/10-B1 Poster 1520-08

## SUNRISE EFFECT ON VERY LOW-LATITUDE PC3 PULSATIONS

Y.M. TANAKA, K. Yumoto, A. Yoshikawa, T.I. Kitamura (Department of Earth and Planetary Sciences, Kyushu University, Fukuoka, 812-8581, Japan, E-mail: tanaka@geo.kyushu-u.ac.jp; E-mail: yumoto@geo.kyushu-u.ac.jp); B.J. Fraser (Department of Physics, University of Newcastle, Newcastle, NSW 2308, Australia, E-mail: pbj@cc.newcastle.edu.au); D. Cole (IPS Radio and Space Services, Learmonth Solar Observatory, Exmouth, W.A. 6707, Australia, E-mail: david@ips.oz.au)

We statistically investigated wave characteristics of Pc 3 pulsations observed at very low-latitude stations, GUA (Mlat=5.6°, Mlong=215.60°), and CR1 (Mlat=3.1°, Mlong=273.50°). When both the two stations were located in the interval from 0800 to 1700 LT, very small phase differences of Pc 3 were found to be observed in the H component, indicating a nearly zero azimuthal wave number. Moreover, a 180° phase shift of Pc 3 across 0730 LT was newly found in the H component, which may be related to the change of the ionospheric conductivity in the sunrise region. The sunrise effect on low-latitude Pc 3 pulsations was also examined by analyzing data from the 2100 magnetic meridian network. At low latitudes ( $L = 1.2-2.1$ ), a 180° phase shift across the sunrise was found in the D component, while no phase shift in the H component. This phase variation is consistent with the previous result, a 90° rotation of polarization major axis around the sunrise. The phase variation of low-latitude Pc 3 pulsations across the sunrise suggests that a secondary electric field built up by the charges at a terminator on the sunrise

GA3.04/W/26-B1 Poster 1520-09

## THE PHASE STRUCTURE OF EQUATORIAL AND VERY LOW LATITUDE ULF WAVES ACROSS DAWN

Colin WATERS, Murray Sciffer, Brian Fraser, Kristie Foulkes (all at Department of Physics, University of Newcastle, Callaghan, 2308, NSW, Australia, e-mail: colin@physics.newcastle.edu.au); Kate Brand (Physics Department, The University of Birmingham, Edgbaston, Birmingham B15 2TT, UK); O. Sakaand, K. Yumoto (Department of Earth and Planetary Sciences, Kyushu University 33 6-10-1 Hakozaki, Fukuoka 812-8581, Japan, e-mail: yumoto@geo.kyushu-u.ac.jp)

Most Pc3 ULF waves observed at low latitudes have been associated with toroidal mode hydromagnetic wave resonances in the plasmasphere. In the near equatorial regions, a band of Pc3-4 ULF wave activity is often seen and usually has enhanced amplitude at the equator. Due to the difficulty in exciting toroidal resonances at very low latitudes, this wave energy has been attributed to fast mode ULF waves. The phase difference between data recorded at longitudinally spaced equatorial magnetometers show a marked change at dawn when one station is in sunlight and the other in darkness. The phase structure with latitude is also seen to show a large phase shift near the equator, in agreement with previous studies. A model of ULF wave propagation through the equatorial ionosphere has been developed. Using IRI data and parameters relevant to the local conditions, the observed phase structures are modelled and compared with the experimental data. It is shown that the phase shifts at dawn and with latitude are probably due to two mechanisms. The first is of ionospheric origin as refilling occurs and the other involves propagation of the waves.

GA3.04/W/41-B1 Poster 1520-10

## GEOMAGNETIC RESPONSE TO THE EARTH'S ARRIVAL OF A SOLAR MASS EJECTION

Stefania LEPIDI, Antonio Meloni (both at Istituto Nazionale di Geofisica, Roma, Italy; E-mail: stefania.lepidi@aquila.infn.it); Patrizia Francia, Umberto Villante (both at Dipartimento di Fisica, Università di L'Aquila, L'Aquila, Italy; E-mail: patrizia.francia@aquila.infn.it); Alan J. Lazarus (Center for Space Research, MIT, Cambridge, USA; E-mail: ajl@space.mit.edu); Ronald P. Lepping (Lab. for Extraterrestrial Physics, NASA/GSFC, Greenbelt, USA; E-mail: rpl@leprl1.gsfc.nasa.gov)

An analysis of the low frequency geomagnetic field fluctuations at an Antarctic (Terra Nova Bay) and a low latitude (L'Aquila, Italy) station during the Earth's passage of a coronal ejection on April 11, 1997 shows that major solar wind pressure variations were followed at both stations by an high fluctuation level. During northward interplanetary magnetic field conditions and when Terra Nova Bay is close to the local geomagnetic noon, coherent fluctuations, at the same frequencies (3.6 mHz) and with a polarization pattern indicating an antisunward propagation, were observed simultaneously at the two stations. The appearance of similar features at a wide latitudinal and longitudinal separation suggests that the observed waves might be interpreted as global magnetospheric modes triggered by an external stimulation.

GA3.04/E/10-B1 Poster 1520-11

## POSSIBLE CONTAMINATION OF GEOMAGNETIC PULSATION DATA BY ELECTROMAGNETIC INDUCTION EFFECT

Baldev R. ARORA (Indian Institute of Geomagnetism, Colaba, Mumbai 400 005, India, e-mail: bra@iig.igm.res.in); Nalin B. Trivedi, Antonio L. Padilha and Icaro Vitorello (all at Instituto Nacional de Pesquisas Espaciais, Sao Jose dos Campos, Brazil, e-mail: trivedi@dge.inpe.br)

The quantification of wave polarization characteristics of ULF waves from the geomagnetic field variations is done under 'a priori' assumption that fields of internal induced currents are in-phase with the external inducing fields. Such approximation is valid only in areas where internal electrical conductivity distribution varies only as a function of depth. Lateral conductivity variations, either in the form of land-ocean contrast or those associated with crustal structures, perturb the flow pattern of induced currents. The amplitude and phase changes that these perturbations produce in the resultant fields recorded at Earth's surface, make the determination of polarization and phase of the oscillating external signals problematic. In this paper, with the help of magnetovariational data from an array of magnetometers in the equatorial belt of Brazil, we present examples of geomagnetic micropulsation events contaminated by anomalous induction effects. These induction effects, if not properly guarded for, lead to highly over estimates of the equatorial enhancement and also suggest changes in the azimuth of ULF waves as they propagate through the equatorial electrojet. Given this observational evidence, guidelines to identify and estimate the extent of induction effects in geomagnetic pulsations data are briefly outlined.

GA3.04/L/06-B1 Poster 1520-12

## A MAGNETOSPHERIC MHD DISTURBANCE, TRIGGERED BY AN IMPULSIVE SOURCE IN THE IONOSPHERE

Anatoly S. LEONOVICH (Institute of Solar-Terrestrial Physics, 664033, Irkutsk, P.O.Box 4026,

A theory has been constructed for standing quasi-Alfvén waves excited in the magnetosphere by a broad-band source localized in the ionosphere. A detailed study is made of the oscillations generated by a narrowly localized (across geomagnetic field lines) impulsive source. It is shown that oscillations from such a source can occur in two different regimes. The initial regime is characterized by the fact that the excited standing wave oscillates throughout the space with the same frequency equal to the frequency of toroidal Alfvénic eigen-oscillations of the magnetosphere on the magnetic shell where the source is localized. In the asymptotic regime, the oscillation field of the standing Alfvén wave occupies a distinctly delineated (across field lines) region. In every point of the region the waves are oscillating with their eigenfrequency.

A numerical calculation is made of the total field of standing quasi-Alfvén waves excited in the magnetosphere by an impulsive source localized in the ionosphere. It is shown that the fundamental harmonic of standing waves reaches an asymptotic regime already after the first oscillation period. All other harmonics oscillate in the initial regime during many oscillation periods of the fundamental harmonic. Such a picture of the oscillations adequately depicts the MHD disturbances recorded as part of active MASS experiments aboard the AUREOLE-3 satellite. The point at which the leading edge of a strong electromagnetic impulse was recorded, is quite well associated with the southern boundary of localization of the fundamental harmonic of standing waves. The form and duration of the impulse recorded aboard the satellite is also adequately described.

GA3.04/W/34-B1 Poster 1520-13

## A MODEL FOR ULF WAVE PROPAGATION THROUGH THE IONOSPHERE

Murray SCIFFER and Colin Waters (both at Physics Department and CRC for Satellite Systems, University of Newcastle, Callaghan, 2308, NSW, Australia, e-mail: colin@physics.newcastle.edu.au)

ULF waves from the magnetosphere interact with the ionosphere and are detected by ground based magnetometers. Furthermore, the role of ULF waves in Doppler data obtained from HF radars is being re-examined with the increasing number of SuperDARN radar studies. Central to these investigations is the understanding of ULF wave structure and particle motion as a function of altitude through the ionosphere. Most studies that look at ULF waves and their interaction with this region, treat the ionosphere as an infinitely thin sheet with height integrated quantities. In this paper we present a more detailed model of ULF wave propagation through the ionosphere that allows the incident wave modes to be specified. The model assumes constant horizontal wave structure with variation in the vertical direction only. Using realistic particle populations with altitude and an anisotropic complex conductivity



tensor, the ULF wave is modelled as an electromagnetic wave so that the electric and magnetic field perturbations may be obtained as a function of height. The incident wave mode mix between the fast and shear Alfvén modes may also be specified and the inclination of the magnetic field or dip angle is a free parameter. Results for various dip angles, ionospheric conditions and incident horizontal wave structure and wave mode mixes are discussed within the context of experimental magnetometer data.

**GA3.04/W/30-B1** Poster **1520-14**

**ULF WAVES AND IONOSPHERE: MULTI-STEP MODE CONVERSION BETWEEN DIVERGENT AND ROTATIONAL ELECTRIC FIELD BY THE IONOSPHERIC HALL EFFECT**

A.YOSHIKAWA and K.Yumoto (both at Department of Earth and Planetary Sciences, Kyushu University, Hakozaki, Fukuoka 812-8581, JAPAN, e-mail: yoshi@geo.kyushu-u.ac.jp)

Natures of reflection and mode conversion of MHD waves at the inductive ionosphere are investigated by using the reflection and mode conversion tensor of MIA system. In the MIA system, 8 wave elements (FAC and rotational current of magnetosonic mode in the magnetosphere, divergent and rotational Hall and Pedersen current in the ionosphere and divergent and rotational displacement current in the neutral atmosphere) are coupled through the ionospheric multi-step Hall effect. To clarify the differences between inductive and electrostatic response of ionosphere for reflection process of shear Alfvén wave, various physical quantities are compared in both treatments. Inductive ionosphere requires the renormalization of rotational electric field to the divergent one, and generates the divergent Hall current, which directly closed via the FAC. The existence of divergent Hall current brings about the redistribution of 8 wave elements are very different from in the electrostatic ionosphere. It is shown that the ionospheric currents associated with the ULF pulsations at high conducting ionosphere are almost borne by Hall current both rotational and divergent parts of ion

**GA3.04/W/15-B1** Poster **1520-15**

**AN IONOSPHERIC MECHANISM OF COMPRESSIONAL-SHEAR ALFVEN WAVE TRANSFORMATION**

P. NENOVSKI, B. Andonov, P. Muhtarov (Geophysical Institute, Bulgarian Academy of Sciences, Sofia, Bulgaria)

The experimental evidence of a compressional-shear wave transformation events recorded simultaneously at geostationary orbit and the foot of the same field lines (Lanzerotti and Tartaglia, 1972) is examined in view of the recent theoretical findings for an elliptization effect produced directly by the ionosphere. It is found that due to the ionosphere dissipation effect compressional waves could be transformed into nearly transverse wave seen at the ground. According to theoretical findings the elliptization effect emerges under certain ionospheric/wave conditions. The Lanzerotti and Tartaglia results for a left-hand elliptization of 0.7 (nearly circular) and a polarization plane rotation of 45 degree could easily be produced in winter conditions and subauroral ionosphere. The effect depends on a wave parameter proportional to the squared horizontal wavenumber, the Hall region thickness and the wave period. Thus the ionosphere dissipation effect is possibly an effective mechanism for an elliptic polarization with left- hand sense (in the northern hemisphere) and a 45 degree rotation angle (when the elliptization effect is maximum) seen by Lanzerotti and Tartaglia's experiment.

**GA3.04/W/17-B1** Poster **1520-16**

**THE SPATIAL STRUCTURE OF HIGH LATITUDE PC5 GEOMAGNETIC PULSATIONS: IMAGING RIOMETER OBSERVATIONS**

Pavlo PONOMARENKO, Brian J Fraser, Michael B Terkildsen, Sean T Ables, and Fred W Menk (all in Department of Physics, CRC for Satellite Systems, University of Newcastle, Callaghan, NSW, 2308 Australia, E-mail: phpp@alinga.newcastle.edu.au); Ray J Morris (Australian Antarctic Division, Channel Hwy, Kingston, TAS, 7050 Australia)

Geomagnetic pulsations observed on the ground indicate the signatures of MHD plasma waves propagating in the magnetosphere and ionosphere. Due to their large field of view, the magnetometers provide relatively low spatial resolution, which in many cases exceeds the characteristic horizontal scale size of the wave. One of the possibilities to improve the resolution is connected with the use of multibeam imaging riometers. These measure cosmic noise absorption (CNA) at low ionospheric altitudes due to the high electron collisional frequency and allow the study of the spatial structure and dynamics of CNA events. Previous magnetometer measurements at high latitudes have shown that resonant Pc5 pulsations sometimes are accompanied by similar variations in CNA. The question about the mechanism of such a correlation is open, and different mechanisms can be considered. The current study attempts to use the imaging riometer SHIRE at the Australian Antarctic cusp station Davis to investigate the spatio-temporal structure of Pc5 pulsations at high latitudes. The CNA events were selected using several steps. Firstly, Pc5 events with a pronounced spectral maximum were identified in the magnetometer data from Davis. Secondly, a co-located broadband riometer was used as a reference to look for the coincident spectral maxima in CNA variations. Thirdly, for the correlated events we used SHIRE data to determine the spatial distribution of the pulsations' intensity and phase for the dominant spectral component. The phase shift between neighbouring beams was used then to restore the vector of the horizontal propagation velocity of the waves.

**GA3.04/W/09-B1** Poster **1520-17**

**POLARIZATION STRUCTURE OF MIDDLE-LATITUDE PC3-4 PULSATIONS DERIVED FROM THEIR ELECTRIC FIELD SIGNATURE**

D. DANOV (1), J.Vero (2), B.Zieger (2), and P. Nenovski (3) ((1) Solar-Terrestrial Influences Laboratory, Sofia, Bulgaria, (2) Geodetic and Geophysical Research Institute, Sopron, Hungary, (3) Geophysical Institute, Sofia, Bulgaria)

We have analyzed one month data of the electric field of Pc3-4 geomagnetic pulsations recorded at middle-latitude station (Nagyecenk, Hungary). In addition to the spectral analysis a polarization study of the geomagnetic pulsations under quiet and disturbed conditions is performed. The purpose of this study is to examine the electric field signature of the well-registered sunrise changes of the polarization plane rotation. The polarization plane rotation change at sunrise has been documented by magnetic field measurements. The electric field signature of Pc3-4 pulsations yields however such sunrise effect occasionally and it does not exist regularly. An explanation of the results is presented provided that the geomagnetic pulsations in selected frequency ranges are of magnetosonic type. The interpretation is based on the electric/magnetic field asymmetry in the polarization changes through the ionosphere-atmosphere system. Influences from the atmosphere- lithosphere system are additionally accounted for.

**GA3.04/E/05-B1** Poster **1520-18**

**THE STUDY OF THE IONOSPHERIC SOURCES OF THE GEOMAGNETIC PULSATIONS BY THE MAGNETIC GRADIENTOMETRIC METHODS**

KOPYTENKO, Yury; Ismagilov, Valery; Kopytenko, Eugene; Zaitsev, Dmitri; Voronov, Pavel; (SPbF IZMIRAN, 191023, Box 188, Muchnoj per.2, St. Petersburg, RUSSIA, E-mail: ek@eak.izmi.ras.spb.ru)

Values of phase velocities of the geomagnetic wave front propagating along the Earth surface were received using data of a magnetic gradientometer during experiment in subauroral zone in autumn of 1997. The gradientometer consists of 3 three component magnetovariation complex MVC-1DG situated in tops of a triangle and spaced at a distance, 6 - 8 km. Original algorithms of the data processing were used. Typical values of the geomagnetic wave fronts velocities are 20 - 60 km/sec, normal to wave front magnetic gradients of geomagnetic pulsations are about 0.01 nT/km and depend from a distance to ionospheric source and amplitude of the geomagnetic pulsations. The directions to the ionospheric sources of the geomagnetic pulsations were calculated during periods of different geomagnetic activity using a method of magnetic location in ULF frequency range.

**GA3.04/W/21-B1** Poster **1520-19**

**MONITORING SPATIAL AND TEMPORAL VARIATIONS OF THE PLASMAPAUSE REGION USING GEOMAGNETIC FIELD LINE RESONANCES**

D.K. MILLING, R.A. Mathie and I.R. Mann (Department of Physics, University of York, York YO10 5DD); F.W. Menk (department of Physics, University of Newcastle, Callaghan, N.S.W., 2308, Australia).

The use of cross-phase and related techniques can yield the field-line resonance frequency between latitudinally spaced pairs of magnetometers. This data can then be used to estimate the temporal and spatial variations in plasma mass density. Such analysis has been applied to the data from a dense array of temporary stations in Fenno-Scandinavia with the aim of studying the plasma density variations across the plasmapause region as a function of geomagnetic activity, LT and UT. An attempt is made to specify the minimum instrumentation which would be required for near real-time monitoring of the plasmasphere and plasmapause.

**GA3.04/W/51-B1** Poster **1520-20**

**MONITORING SPATIAL AND TEMPORAL VARIATIONS IN THE DAYSIDE PLASMASPHERE USING GEOMAGNETIC FIELD LINE RESONANCE**

Fred W. MENK and Colin L. Waters (both at Department of Physics, CRC for Satellite Systems, University of Newcastle, Callaghan, NSW, 2308, Australia, e-mail: physpuls3@cc.newcastle.edu.au); David Orr and David Milling (both at Department of Physics, University of York, Heslington, York, YO10 5DD, UK, e-mail: dave@samsun.york.ac.uk); Mark A. Clilverd and Andy J. Smith (both at British Antarctic Survey, Madingley Road, Cambridge, CB3 0ET, UK, e-mail: MACL@pcmail.nerc-bas.ac.uk)

It is well known that the resonant frequency of geomagnetic field lines is determined by the magnetic field and plasma density. Using ground magnetometer arrays and cross-phase and related methods, the field line resonance frequency was determined across L=2.8-4.5 in the northern hemisphere, and 9-10 hours away in local time at L=2.8 in the southern hemisphere, for several days in October and November 1990. The temporal and spatial variation in plasma density was thus evaluated and compared with VLF whistler measurements of electron densities at similar times and locations. The plasma mass loading was also estimated. Other features that were examined include the plasma mass density power law, diurnal variations in plasma density at low latitudes, substorm refilling effects, and a longitudinal asymmetry in plasma density.

**GA3.04/E/11-B1** Poster **1520-21**

**EXCITATION OF HARMONIC CYCLOTRON WAVES IN THE EARTH'S MAGNETOSPHERE**

Oleg POKHOTELOV, Felix Feygin and Vladimir Gladyshev (all at Institute of Physics of the Earth, 123810 Moscow, Russia, E-mail: pokh@uipe-ras.scgis.ru); Dmitrii Pokhotelov (Thayer School of Engineering, Dartmouth College 800 Cummings Hall, Hanover, NH 03755-8000, USA, E-mail: dmitrii.pokhotelov@dartmouth.edu); Michel Parrot (LPCE/CNRS, 3A, Avenue de la Recherche Scientifique 45071 Orleans Cedex 2, France, e-mail: mparrot@cnrs-orleans.fr); Jorma Kangas and Kalevi Mursula (both at Department of Physical Sciences, University of Oulu, FIN-90570 Oulu, Finland, e-mail: jorma@sgo.fi; kalevi.mursula@oulu.fi)

A theoretical model for the generation of ion cyclotron harmonic waves observed in the deep plasmasphere both during disturbed and quiet conditions is presented. It is shown that during quiet magnetic conditions these waves are generated by a weak kinetic instability involving hot helium ions with a ring like distribution. The existence of such ions in the magnetosphere during quiet magnetic conditions is confirmed by the satellite data. A simple analytical model of this instability accounting for the longitudinal inhomogeneity of the ambient magnetic field is used. During magnetic storms there is a transition to a strong hydrodynamic instability involving the oxygen ions of ionospheric origin. The development of kinetic instability during this time is suppressed by the field aligned inhomogeneity of the dipole magnetic field. Such a scenario of harmonic cyclotron wave excitation is in a good agreement the ULF/ELF wave observations on board the AKEBONO satellite during disturbed and quiet times.

**GA3.04/W/28-B1** Poster **1520-22**

**A MECHANISM OF PC1 PEARL FORMATION BASED ON ALFVEN SWEEP MASER**

A.G. DEMEKHOV, V.Y. Trakhtengerts (both at: Institute of Applied Physics, Nizhny Novgorod, Russia; e-mail: andrei@appl.sci-nnov.ru); S.V. Isaev, S.V. Polyakov, P.P. Belyaev, V.O. Rapoport (all at: Radiophysical Research Institute, Nizhny Novgorod, Russia)

A self-consistent model for the generation of Pc-1 pearl emissions based on the nonlinear magnetosphere/ionosphere coupling is considered. Formation of pearls is attributed to the pulsating regime of the Alfvén sweep maser (ASM) with nonlinear selective mirrors. Such mirrors are formed by the conjugate ionospheres: their reflection coefficient has an oscillatory frequency dependence due to eigenmodes of the ionospheric Alfvén resonator; nonlinear magnetosphere/ionosphere feedback is provided by the dependence of the value and frequency of the reflection maxima on the flux of energetic protons precipitated into the ionospheres in the course of Alfvén wave generation in the magnetosphere. A nonlinear soliton-like solution of the ASM model is found which corresponds to a single wave packet having the positive frequency drift and oscillating between the conjugate ionospheres. Properties of this solution are shown to explain many observational characteristics of Pc1 pearls, such as their morningside predominance, correlation with low magnetic activity, spatio-

temporal and spectral patterns. Results of numerical simulations of the ASM equations are presented.

**GA3.04/E/04-B1** Poster **1520-23**

**THE PONDEROMOTIVE INFLUENCE OF ION CYCLOTRON WAVES ON THE FIELD-ALIGNED DISTRIBUTION AND MOTION OF IONS IN THE EQUATORIAL ZONE OF THE MAGNETOSPHERE**

Anatol GUGLIELMI (United Institute of Physics of the Earth, B. Gruzinskaya, 10, Moscow, 123810 Russia, e-mail: gugl@uipe-ras.scgis.ru); Kanji Hayashi (Department of Earth and Planetary Physics, University of Tokyo, 7-3-1 Hongo, Bunkyo, Tokyo, Japan 113, e-mail: hayashi@sunep1.geoph.s.u-tokyo.ac.jp); Rickard Lundin (Swedish Institute of Space Physics, BOX 812, S-98128 Kiruna, Sweden, e-mail: rickard@irf.se); Alexander Potapov (Institute of Solar-Terrestrial Physics, P.O.B. 4026, Irkutsk, 664033 Russia, e-mail: potapov@iszf.irk.ru)

The effects of ponderomotive forces of ion-cyclotron waves in the near-equatorial region of the magnetosphere have been investigated using hydrodynamic, quasi-hydrodynamic and "test-particle" approaches. Main attention was paid to the application of general theory to the magnetospheric physics. It has been shown that the problem of the ponderomotive impact of the waves upon the plasma density may be formally reduced to a problem of phase transition of the second kind. In such a formalism, the plasma distribution is altered dramatically as the imaging point in the plane of governing parameters crosses some demarcation line. The magnetic equator turns out to be an attractor for a heavy ion. Heavy ions congest near the magnetic equator provided the waves are comparatively strong. This suggests that the ponderomotive effects play a role in formation of structure and dynamics of the magnetosphere.

**GA3.04/W/12-B1** Poster **1520-24**

**THE ION CYCLOTRON RESONATOR**

A. V. GUGLIELMI (Institute of Earth Physics, Moscow, Russia e-mail: gugl@scgis.fisgeos.iitp.ru); C. T. Russell (Institute of Geophysics and Planetary Physics, University of California, Los Angeles, CA, USA, e-mail: ctrussell@igpp.ucla.edu)

Ion cyclotron waves travelling parallel to the magnetic field away from the equator in a planetary magnetosphere may be reflected back toward the equator in a multi-ion plasma restricting the ion cyclotron waves to the near equatorial region. This process occurs because the local gyrofrequency increases away from the equator and the wave frequency that is constant in Hz, approaches the cut-off frequency where it is reflected. Structure in the spectrum of ion cyclotron waves published by Fraser et al. [JGR, 1992] suggests that the ion cyclotron resonator may occur in the magnetosphere at least on occasion. On the other hand if the waves propagate slightly off angle, they can become right handed and propagate into the ionosphere and be lost. We examine more recent POLAR data to determine if frequency structure is present in the ion cyclotron waves near the equatorial plane.

**GA3.04/W/23-B1** Poster **1520-25**

**POYNTING VECTOR MEASUREMENTS OF ELECTROMAGNETIC ION CYCLOTRON WAVES WITH FREQUENCIES ABOVE THE HELIUM CYCLOTRON FREQUENCY: CRRES OBSERVATIONS**

P. Manuasu, and B.J. FRASER, (Physics Department, CRC for Satellite Systems, University of Newcastle, NSW, 2308, Australia, e-mail: phbjf@cc.newcastle.edu.au)

Previous studies of electromagnetic ion cyclotron (EMIC) waves in the equatorial middle magnetosphere using Poynting vector calculations from the CRRES spacecraft dE and dB wave fields have shown that the waves propagate essentially in field-aligned directions. Ray angles are typically less than 30 degrees with respect to the magnetic field direction. This study was only concerned with wave frequencies below the helium cyclotron frequency  $f(\text{He}^+)$ . A new study underway considers the energy propagation characteristics of a number of EMIC wave events from CRRES with  $f > f(\text{He}^+)$ . Included in the study are examples of events showing harmonic structure and an association with cold plasma density cavities or gradients.

**G3.04/W/18-B1** Poster **1520-26**

**RELATION BETWEEN PC1 PEARLS AND ULF WAVES STUDIED BY THE POLAR SATELLITE AND GROUND OBSERVATIONS**

T. BRÄYSSY, K. Mursula, R. Rasinkangas, and P. Tanskanen (Department of Physical Sciences, University of Oulu, P.O. Box 3000, FIN-90401 Oulu, Finland, E-mail: Timo.Brassy@oulu.fi) F. Mozer (Space Science Laboratory, University of California at Berkeley, Berkeley, CA 94720, USA)

The electromagnetic ion cyclotron (EMIC) waves are among the most common wave forms inside the magnetosphere. One special type of EMIC waves, particularly typical for the inner magnetosphere, are the Pc1 pearls consisting of regularly repeating emissions of EMIC waves observed on ground. The standard model of pearls assumes that they are due to a wave packet bouncing along the field line from one ionosphere to another (BWP model). However, there are several facts that are problematic for this model. For example, a recent event study using Viking satellite observations excludes the BWP model as a cause to the observed EMIC burst structure (Mursula et al., JGR 102, 17611, 1997) and verifies that ULF waves modulate EMIC wave growth (Rasinkangas and Mursula, GRL 25, 869, 1998). Also, an earlier case study using simultaneous ground and Polar satellite observations of EMIC and ULF wave activity seems to support the modulation model as a cause for repetitive structure of Pc1 pearl pulsations (Mursula et al., Adv. in Space Res., in print, 1999). Here we look for further evidence for ULF modulation of EMIC wave growth using several pearl events observed on ground by the Finnish magnetometer chain and simultaneously monitored by the electric field instrument (EFI) onboard Polar spacecraft.

**GA3.04/W/33-B1** Poster **1520-27**

**NEW CONSTRAINTS ON THEORIES OF PC1 PEARL FORMATION**

K. Mursula, J. Kangas, R. KERTTULA, T. Pikkarainen (Department of Physical Sciences, University of Oulu, P.O. Box 3000, FIN-90401 Oulu, Finland, E-mail: Raine.Kerttula@oulu.fi); A. Guglielmi and O. Pokhotelov (United Institute of Physics of the Earth, 123810 Moscow, Russia); A. Potapov (Institute of Solar-Terrestrial Physics, Irkutsk, Russia)

We study structured Pc1 pulsations (also called Pc1 pearls) observed on ground, concentrating on the relation between the pearl repetition period  $t$  and the wave frequency  $f$ . Earlier studies suggest that the product  $tf$  is roughly constant. We re-examine this relation and show that a simple inverse law is excluded. Instead, our observations suggest the relation  $t \propto f^{-p}$  with  $p=0.59 \pm 0.06$ , posing a new, strict constraint on theories of Pc1 pearl formation. We

also study the L-dependence of various combinations of  $t$  and  $f$  using a model L-value, and extract additional constraints from these combinations. We discuss these constraints in the bouncing wave packet model of pearl formation, and determine the range of allowed parameter values in this model. We present two models of energetic ions with different L-distributions, and show that one of them can be excluded by the constraints derived. We also discuss how to further improve on these constraints to better test the bouncing wave packet model and other theories of Pc1 pearl formation.

**GA3.04/W/29-B1** Poster **1520-28**

**STORM-TIME PC1 ACTIVITY AT HIGH AND MID-LATITUDES**

R. KERTTULA, K. Mursula, T. Pikkarainen, J. Kangas (Department of Physical Sciences, University of Oulu, P.O. Box 3000, FIN-90401 Oulu, Finland, E-mail: Raine.Kerttula@oulu.fi)

We study Pc1 pulsations observed at a high-latitude station (Sodankylä) and a mid-latitude station (Nurmijärvi) during magnetic storms. We have analyzed altogether 18 storms occurring in low sunspot years (1976-78 and 1984-88). The Dst minimum of the strongest (weakest, respectively) storm was -226 nT (-77 nT), and the mean (median) Dst value was -133 nT (-110 nT). Pc1 activity was studied from the day of sudden storm commencement (denoted by day 0) onwards during six consecutive days. The two main types of Pc1 pulsations, the structured and unstructured Pc1's, were studied separately.

Structured pulsations strongly depend on the evolution of storms. Their activity increases from day 0 to day 4 by a factor of about five, reaching a maximum occurrence on day 4 at both stations. Slightly more events are seen at Sodankylä than at Nurmijärvi. Also the diurnal distribution of structured Pc1's suffers a dramatic change during the storm process. On days 1 and 2 structured pulsations are strongly concentrated in the evening sector. During the later recovery (days 3-5) the activity shifts to the morning sector. On the other hand, unstructured pulsations show only weak dependence on the storm evolution. The daily occurrence of unstructured Pc1's remains nearly constant, reaching weak maxima on day 1 or 2. The diurnal distribution with a noon maximum is nearly unchanged. We also study the changes of Pc1 activity with the intensity of the storm.

**GA3.04/W/24-B1** Poster **1520-29**

**STATISTICAL STUDY OF ION CYCLOTRON WAVES BY FREJA SATELLITE**

T. KIVISAARI, K. Mursula, and T. Bräyssy (Department of Physical Sciences, University of Oulu, P.O. Box 3000, FIN-90401 Oulu, Finland, E-mail: Tarmo.Kivisaari@oulu.fi)

The Swedish Freja satellite was launched in 1992 and it ceased to operate in 1996. The orbital inclination was 63 degrees and period 109 minutes with apogee and perigee heights of 1750 km and 600 km, respectively. The F1 electric field instrument of Freja was a spherical double probe instrument, which measured the two orthogonal components of the electric field in the spin plane.

We have used an automated system to search for and view electromagnetic ion cyclotron (EMIC) waves in Freja F1 instrument data. Using that system, we have analysed one full apogee rotation period of Freja satellite data from August to December, 1993. Based on these observations we have collected statistical information of occurrence and characteristic of EMIC waves. Wave occurrence seems to be organised according to the development of magnetic storms. During the approximately 100 days studied, one major, one intermediate and eight minor storms occurred. The maximum number of waves was found during the major storm. Waves with lowest latitudes (below 50° CGMLat) were only found during the two largest storms. The diurnal distribution of waves also followed the storm development with increase of night-side wave activity during the main phase of largest storms. Waves with largest amplitudes occurred preferentially during the storm main phase. The results suggest that ion cyclotron waves are an important factor in the decay of the ring current after storm onset.

**GA3.04/W/37-B1** Poster **1520-30**

**ACTIVITY OF PC1 GEOMAGNETIC PULSATIONS FOR 1957 - 1992**

Emma T. MATVEYEVA, Vladimir F. Ruban (Geophysical Observatory Borok, Institute of Physics of the Earth RAS, Borok, Nekouz, Yaroslavl, 152742, Russia, e-mail: emma@borok.adm.yar.ru)

The index of Pc1 activity suitable for a computer analysis is suggested on a basis of a detailed catalogue of Pc1 (0.2-5.0 Hz) pulsations obtained as a result of processing of continuous observation from 1957 till 1992 at the observatory Borok (geomagnetic latitude 54.05 degrees N and longitude 113.44). As a unit of activity a 15-minutes interval is accepted during which the pulsations are observed no less than 5 minutes. The index of activity N is a sum of such intervals in each day by UT. The use of the index N is illustrated by the results of the study of seasonal and cyclic Pc1 activity, its relationship with the cases of magnetic storms and sector boundaries of IMF. Along with a geophysics the index can be used for a wide range of disciplines for which the effect of natural electromagnetic field in this frequency range can be of practical or scientific interest.

**GA3.04/W/31-B1** Poster **1520-31**

**A NEW APPROACH ON THE INTERPRETATION OF COMPRESSIONAL MHD WAVES IN THE MAGNETOSPHERE**

Dong-Hun LEE (Dept of Astronomy & Space Science, Kyung Hee University, Yongin, Kyunggi, 449-701, Korea, e-mail: dhlee@nms.kyunghee.ac.kr)

Previous theoretical and numerical studies for cavity/waveguide modes assume perfectly reflecting boundary conditions at the outermost boundary whether the system is 1-D, 2-D or 3-D. The perfect boundary condition mathematically corresponds to the infinite potential wall (or the infinite Alfvén speed), which assumes that the system should lie in the region surrounded by two infinite "walls" both at the inner and outer boundaries. In order to investigate how compressional waves differently behave in the presence of realistic Alfvén speed gradient at the outer boundary, we newly adopt a quantum mechanical approach to obtain the wave solution. By using an analogy with the Schrodinger's equation, dynamics of compressional MHD wave propagation is theoretically studied in the dayside and nightside magnetosphere. The wave solutions are obtained for dayside and nightside Alfvén speed profiles, respectively, without any arbitrary boundary condition at the magnetopause or the bow shock. The result shows that the previous cavity/waveguide models are found to be inappropriate for studying compressional wave properties in the magnetosphere. We introduce the role of virtual resonances which generally represent any possible compressional modes in the magnetosphere.



**GA3.04/W/06-B1** Poster **1520-32**

**THE NATURE OF MAGNETOSONIC RESONANCE**

A.D.M. WALKER (University of Natal, Durban)

The nature of field line resonances in the magnetosphere associated with standing transverse Alfvén waves is well understood. Another type of resonance is associated with the slow magnetosonic wave. It occurs when the plasma  $\beta$  is near unity. The theory of how this resonance is excited is developed. Its possible relevance to storm type pulsations and to long period oscillations observed near the magnetopause is discussed.

**GA3.04/W/02-B1** Poster **1520-33**

**PHASEMIXING AND PHASE MOTION OF ALFVEN WAVES IN THE PLASMA SHEET BOUNDARY LAYER**

A.N. WRIGHT (Mathematical Institute, University of St. Andrews, St. Andrews, Fife KY16 9SS, Scotland, U.K., e-mail: andy@dcs.st-and.ac.uk); W. Allan (NIWA, P. O. Box 14-901, Kilbirnie, Wellington, New Zealand, e-mail: w.allan@niwa.cri.nz); R.D. Elphinstone and L.L. Cogger (both at Department of Physics and Astronomy, University of Calgary, Calgary, AB, Canada T2N 1N4, e-mail: rob@hobbes.phys.ucalgary.ca, cogger@phys.ucalgary.ca)

The time-dependent phase structure of Alfvén waves on tail-like field lines is studied. Alfvén waves generated on field lines threading the PSBL have received little attention compared to those on dipole-like field lines, but may be shown to have an equatorward phase motion. Phasemixing in the magnetotail proves to have a much richer behaviour than that on near-Earth (dipole-like) field lines as not only the Alfvén frequency varies across the background field lines, but the field-aligned wavenumber varies too. The two contributions tend to cancel each other partially for typical tail equilibria. Observations are given of a double oval configuration showing long period pulsations on the poleward portion of this oval. Equatorward phase motion is observed and supports the theory presented here. These observations illustrate that Pc 5 pulsation activity can be more complicated than thought previously, and can occur at locations not in the dipole-like region as is commonly supposed. The concepts presented in this paper provide a powerful framework with which to interpret observations related to auroral arcs, substorms and magnetospheric equilibria.

**GA3.04/W/40-B1** Poster **1520-34**

**EXCITATION OF RESONANT ALFVEN WAVES IN THE MAGNETOSPHERE BY NEGATIVE ENERGY SURFACE WAVES ON THE MAGNETOPAUSE**

M.S. RUDERMAN and A.N. Wright (both at School of Mathematical and Computational Sciences, University of St. Andrews, St Andrews, Fife KY16 9SS, Scotland, U. K.)

The instability of the magnetopause caused by the resonant interaction of a negative energy surface wave with Alfvén waves localised in the vicinity of the resonant magnetic surface is considered. The most important property of this instability is that it takes place for flow velocities in the magnetosheath below the Kelvin-Helmholtz (KH) threshold velocity, i.e., when there is no KH instability of the magnetopause. The magnetopause is modelled by an MHD tangential discontinuity with a magnetic-free plasma on the magnetosheath side and cold plasma on the magnetospheric side. It is shown that one of the two surface waves that propagate along the discontinuity when the shear velocity is smaller than the KH threshold velocity is a negative energy wave when the shear velocity is larger than a critical velocity. This negative energy wave propagates tailward in the magnetospheric frame, although it propagates sunward in the magnetosheath frame. When, in addition, a resonant condition is satisfied, the negative energy surface wave resonantly interacts with localized Alfvén waves. This interaction results in growth of both the surface wave and the Alfvén waves. The resonant condition can only be satisfied when the plasma density increases and, consequently, the Alfvén velocity decreases in the direction toward the magnetopause in its vicinity. The increment of the resonant instability is calculated under the assumption that the plasma density changes only in a slab in the vicinity of the magnetopause with the thickness much smaller than the wavelength. The possible observational signatures of the resonant instability are discussed.

**GA3.04/W/19-B1** Poster **1520-35**

**THREE-DIMENSIONAL SIMULATIONS OF POLOIDAL AND COMPRESSIONAL PC4-5 MAGNETOSPHERIC WAVES**

Richard E. DENTON and Mary K. Hudson (Department of Physics and Astronomy, 6127 Wilder Lab, Dartmouth College, Hanover, NH 03755, USA, e-mail: richard.denton@dartmouth.edu); Elena V. Belova (Princeton Plasma Physics Laboratory, Princeton, NJ 08543, USA, e-mail: ebelova@pppl.gov).

A three-dimensional hybrid MHD/gyrokinetic simulation code has been constructed in order to study the self consistent generation and effects of wave-particle induced poloidal and compressional Pc 4-5 magnetospheric waves. These are global scale Alfvén-like waves with large azimuthal mode number; they are usually thought to be driven by a combination of the drift mirror and drift bounce resonance modes. In the simulation, the high energy ring current is represented as gyrokinetic particles, while the bulk plasma is represented by MHD-like equations. A nonlinear delta  $f$  scheme is used to reduce the numerical noise. Our model uses cylindrical co-ordinates with the magnetic field along the direction of the gradient in the polar angle. This allows inclusion of the radial variation of fields and curvature without the complications of dipole geometry. Results to date will be presented.

**GA3.04/W/05-B1** Poster **1520-36**

**AN EXPLANATION OF THE PC5 PULSATION POLARIZATION PUZZLE OBSERVATION AT SOUTH POLE STATION**

E.A. Bering (1), P. NENOVSKI (2) ((1)Space Physics Department, University of Houston, Houston, (2)Geophysical institute, Bulgarian Academy of Sciences, Sofia)

The Bering et al's experiment during the austral summer 1985-1986 (1995) has revealed a strange opposite handedness in Pc5 pulsation electric and magnetic field polarization. This experimental puzzle proves to be unexplained till now. The main peculiarities comes from the fact that while the magnetic field polarization remains practically unchanged, the electric field changes its polarization when the South Pole station crosses the local noon (1330 UT). This polarization reversal is closely related to the auroral Pc5 pulsation phenomenology seen at dawn and dusk meridians. The Pc5 pulsation magnetic field polarization at cusp latitudes seems to behave differently. Two explanations of this discrepancy are suggested. The first suggests a coexistence of waves of different nature/polarizations and different wavelengths. The second - compressional/magnetosonic waves event. The latter are of left-hand polarization before noon and of right-hand after noon similar to the usual high-latitude Pc5

pulsations. According to the Nenovski's polarization model (1994) the ionosphere in the southern hemisphere should induce a considerable right-hand polarization effect. This polarization effect reduces/increases the initially left/right-hand polarization. A situation exists when the initial Pc5 pulsation left-hand polarization cannot cancel the right-hand effect from the ionosphere. Then the magnetic field polarization at the ground appears to be opposite to the initial. We have examined both the ionosphere/atmosphere and the wave parameter conditions under which such an effect could take place. The ice-ground conditions are also considered.

**GA3.04/W/25-B1** Poster **1520-37**

**POLAR CUSP PC3-5 RANGE GEOMAGNETIC PULSATIONS TRIGGERED BY SSC**

KLEIMENOVA N.G., Kozyreva O.V., Bitterly M., Short J.-J.

The digital 2-second and 1-minute data at antarctic observatory Dumont d'Urville ( $\approx 80.5\theta$ ) for 36 daytime and all night SSC events in quiet geomagnetic activity have been analyzed. It was found that all of the SSC events as usual were accompanied by long period (1-5 mHz) and two narrow bands of Pc4 ( $\approx 8-11$  mHz and  $\approx 18-20$  mHz) geomagnetic pulsations. In daytime Pc3 (25-60 mHz) could be also excited. The SSC occurrence leads to subsequent long lasting (several hours) continue "regime" of these irregular pulsations in which the Pc4 and Pc3 wave packets are noncoherent in time and shape. But the simultaneous Pc4 wave packets near cusp and at subauroral Kerquelen station located about  $120\theta$  to the West have been found. We suppose that Pc4(SSC) pulsations represent the global cavity mode and Pc3's are connected with different local sources at cusp and subauroral latitudes.

**GA3.04/W/42-B1** Poster **1520-38**

**A PC5 ULF WAVE WITH LARGE AZIMUTHAL WAVENUMBER OBSERVED WITHIN THE MORNING SECTOR PLASMASPHERE BY SAMNET**

G.CHISHAM (British Antarctic Survey, Cambridge, UK); I.R.Mann (Department of Physics, University of York, York, UK)

We present details of an unusual Pc5 ULF wave with a large azimuthal wavenumber ( $m$ ) which is observed within the plasmasphere by ground-based magnetometers. In a previous statistical study, 129 Pc5 events were identified at mid-latitudes by the U.K. Sub-Auroral Magnetometer Network (SAMNET), but only three displayed large azimuthal wavenumbers ( $m > 10$ ). Analysis of the variation of wave parameters during one of these events using a novel complex demodulation technique is presented. The technique reveals the temporal variation of wave characteristics including the azimuthal wavenumber and wave frequency, and allows us to study the azimuthal dispersion characteristics of the wave and estimate the azimuthal phase and group speeds. The method used to estimate the azimuthal wavenumbers resolves the ambiguity resulting from aliasing, which can occur for large- $m$  waves observed at stations more than one azimuthal wavelength apart. The drift-bounce resonance mechanism is discussed as a possible wave excitation mechanism for this event, and resonance with H<sup>+</sup> and/or O<sup>+</sup> ions at the inner edge of the ring current is presented as a possible excitation scenario.

**GA3.04 /W/04-B1** Poster **1520-39**

**DAYSIDE MAGNETOPAUSE ULF WAVES OBSERVED BY GEOTAIL**

Tohru SAKURAI, Yutaka Tonegawa, Takuya Kitagawa (Department of Aeronautics and Astronautics, School of Engineering, Tokai University, 1,117 Hiratsuka 259-1292, Japan, e-mail: sakurai@ms.u-tokai.ac.jp); Kiyofumi Yumoto (Department of Earth and Sciences, Kyusyu University, 6-10-1 Hakozaki, Fukuoka 812-8581, Japan, e-mail: yumoto@geo.kyusyu-u.ac.jp); Susumu Kokubun (Solar Terrestrial Environmental Laboratory, Nagoya University, 3-13 Honohara, Toyokawa 442-8507, Japan, e-mail: kokubun@stelab.nagoya-u.ac.jp); Toshifumi Mukai, Koichiro Tsuruda (both at The Institute of Space and Aeronautical Science, 3-1-1 Yoshinodai, Sagami-hara 229-8510, Japan, e-mail:mukai@stp.isas.ac.jp)

The Geotail satellite took the orbits of skimming the dayside low-latitude magnetopause since December 1994. These orbits present a good opportunity for the study of excitation and propagation of ULF waves near the dayside magnetopause. The instrumentation on board Geotail is good for such a task since the satellite measured simultaneous magnetic, electric fields and low-energy plasma. Based on these data we have studied the excitation and propagation characteristics for the ULF waves, Pc3/4 and Pc5. The most interesting study concerns Poynting fluxes for both modes of resonance and propagation of these ULF waves.

**GA3.04/W/01-B1** Poster **1520-40**

**PROPAGATION OF PC3-4 PULSATIONS AT HIGH LATITUDES**

Tim A. Howard and Fred W. MENK (both at Department of Physics, CRC for Satellite Systems, University of Newcastle, Callaghan, NSW, 2308, Australia, e-mail: physpuls3@cc.newcastle.edu.au)

It is well known that at high latitudes field line resonances (FLRs) fall in the Pc5 (<7 mHz) range, and that the Pc3-4 (7-50 mHz) range includes burst-like signals with very short coherence lengths. However, the generation and propagation mechanisms of stable, sinusoidal Pc3-4 pulsations at these latitudes have not yet been established. Using 19 stations of the Arctic IMAGE magnetometer array, we have examined the variation in amplitude, phase and coherence with latitude and longitude for Pc3-4 waves seen across the entire array. Amplitudes decreased exponentially with decreasing latitude and frequency of the pulsations was closely related to the strength of the IMF and the solar wind cone angle. High coherence was observed over large spatial distances. There is no evidence that these Pc3-4 pulsations are harmonics of FLRs. The interstation meridional and azimuthal phases, when mapped into the equatorial plane of the magnetosphere, relate to fast mode waves propagating Earthward and away from the noon meridian. Accordingly, we believe the pulsations are due to forced field line oscillations driven by inward propagating compressional waves generated in the upstream solar wind.

**GA3.04/L/08-B1** Poster **1520-41**

**CHARACTERISTICS OF PI2 MAGNETIC PULSATIONS OBSERVED AT THE CPMN STATIONS: A REVIEW OF THE STEP RESULTS**

Kiyohumi YUMOTO (Department of Earth and Planetary Sciences, Kyushu University 33, Fukuoka 8912-8581, Japan, Email: yumoto@geo.kyushu-u.ac.jp), The CPMN group.

From analyses of magnetic data from the CPMN stations, we can find the following observational results; (1) Pi 2 magnetic pulsations observed on the ground are an ensemble of various hydromagnetic modes excited at high, middle, low and equatorial latitudes. Each mode exhibits its own propagation (timing) and spatial illumination. (2) Although there are



apparent longitudinal propagation and latitudinal time delay of Pi 2's, the difference of the timing of maximum Pi 2 wave energy among the CPMN stations is within 100sec in the latitudinal and longitudinal directions. (3) When a low-latitude single station is located in the sector of 00-24 hr LT, 20-03 hr LT, and 23-01 hr LT, respectively, 62%, 79%, and 100% of auroral breakups identified by the POLAR satellite have associated Pi 2's. 66% of the low-latitude Pi 2's occur within 1 min of the auroral breakups, and 85 Bs (B within 2 min). It is concluded that when a ground single station is located at the midnight sector of 23-01 LT, we can see almost 100% one-to-one correspondence between auroral breakups and low-latitude Pi 2's. But the ground station is located outside the midnight sector, we can expect only 60-80% correspondence of the relation with 1-2 min time delays of Pi 2 onsets to auroral breakups. The Pi 2's is still a good indicator of substorms, however, the use of them should be with care.

**GA3.04/W/14-B1** Poster **1520-42**

**PROPAGATION MECHANISM OF PRELIMINARY REVERSE IMPLUSE OF SC/SI**

Kentarou KITAMURA and Kiyohumi Yumoto (both at Department of Earth and Planetary Sciences, Kyushu University, 6-10-1 Hakozaki, Fukuka, Japan, E-mail: kentaro@geo.kyushu-u.ac.jp); the CPMN Group (E-mail: yumoto@geo.kyushu-u.ac.jp)

A negative impulse just before onset of sc/si main impulse, called PRI (Preliminary Reverse Impulse), is often observed on the ground in daytime. PRI is considered to be caused by a twin-vortex type ionospheric current (DP-field), which is generated by the electric field penetrating into the polar ionosphere, during a compression of the magnetosphere by passage of the interplanetary shock or discontinuity. In this paper, characteristics of sc/si magnetic variations are studied to investigate propagation mechanism of PRI of the DP-field. By analyzing the magnetometer network data along the 210 deg. magnetic meridian, we can get some new aspects of magnetic variations of the DP-field. A good linear relation is found between the peak time when the negative impulse of PRI is maximum and the ratio of negative impulse (PRI range) to the step-like variation (DL-field range). The latitudinal delay of the PRI peak time had been explained by using the signal propagation of sc/si from high latitude to the equatorial region. However, the present result indicates that the latitudinal time delay of PRI apparently appears in the relation of the ratio between.

**GA3.04/L/09-B1** Poster **1520-43**

**LONGITUDINAL PROPOGATION CHARACTERISTICS OF PI2**

UOZUMI, T. (Dept of Earth & Planetary Sciences, Kyushu University, Japan. Email: uozumi@geo.kyushu-u.ac.jp)

To examine longitudinal propagation characteristics of Pi 2 observed in auroral and low-latitude regions, magnetic energy variation defined as  $dH^2 + dD^2 + dZ^2$  were calculated for Pi 2 events occurred during the interval between Feb.11th to Mar.31st 1996. And the time when the variation of energy became maximum and their magnitude were compared among stations. The main results of statistical analysis are summarized as follows (1) In the auroral region, the Pi 2 wave energy shows the maximum at the pre-midnight meridian (PMM). And the eastward and westward propagations are recognized in the dawn and dusk sector, respectively. (2) The longitudinal dependence of amplitude in the auroral region become approximately  $\exp(-x^2)$ , where x is the difference of longitude measured from the PMM. (3) At higher latitude in the auroral region (Kotel'nyy :  $\phi=69.94$ ), Pi 2 wave energy become the maximum earlier than at lower latitude stations (Kotzebue :  $\phi=64.52$ , Chokurdakh :  $\phi=64.67$ ). (4) In low-latitude stations at Kagoshima ( $L=1.22$ ) and Ewa beach ( $L=1.17$ ), it is recognized that eastward Pi 2 propagation in dawn sector, on the other hand, westward propagation is not clear in dusk sector.

**GA3.04/W/45-B1** Poster **1520-44**

**PROPAGATION OF GEOMAGNETIC SUDDEN COMMENCEMENT (SC)**

T. ARAKI (Dept. of Geophysics, Graduate School of Science, Kyoto Univ., Kyoto 606-8502, Japan, e-mail: araki@kugi.kyoto-u.ac.jp); K. Yumoto (Dept. of Earth Science, Faculty of Science, Kyushu Univ., Fukuoka 812-81, Japan); K. Shiohara (STE Lab., Nagoya Univ., Toyokawa 442-8507, Japan); D. Orr and Physics, Univ. of York, York YO1 5DD, UK.)

The geomagnetic sudden commencement (SC) is initiated by an eastward magnetopause current increase due to sudden compression of the dayside magnetosphere. It is transmitted to the day side equatorial ionosphere by a compressional HM wave with an averaged speed of about 600 km/sec. A westward electric current flows in the equatorial ionosphere to shield the magnetic field increase on the ground and initial rise may apparently delay from that of above the ionosphere. The compressional HM wave propagates from day side to night side above the ionosphere with a time delay of 20-40 sec and causes night side SC on the ground. There is another mode of instantaneous transmission from day side to night side in the space between the ionosphere and the ground. This mode is nearly evanescent and does not transmit much energy. If the onset of SC is sufficiently sharp, however, detectable geomagnetic increase is observed almost simultaneously both in day side and night side. These characteristics of SC propagation is described by showing results of data analysis.

**GA3.04/W/35-B1** Poster **1520-45**

**THEORY OF LOCALIZED RESONANT OSCILLATIONS IN THE NIGHTSIDE MAGNETOSPHERE EXCITED BY TIME-DEPENDENT PARALLEL CURRENTS OVER THE AURORAL IONOSPHERE**

A.E. ANTONOVA, Yu. I. Gubar' and A.P. Kropotkin (Skobel'syn Institute of Nuclear Physics, Moscow State University, Moscow, 119899, Russia)

Theory of transverse-small-scale Alfvén resonant waves is modified in order to use it for substorm phenomena modeling. Poloidal disturbances are considered, for which field-aligned currents are of substorm origin (belong to the substorm current wedge system), and polarization corresponds to the effects of magnetic "dipolarization" and increased plasma radial convection. Nonresonant components of the substorm disturbance in the near-Earth portion of the magnetotail plasma sheet are assumed to serve as an external source for Alfvén resonance generation. This occurs in the form of "extraneous" field-aligned currents on the poloidal resonant surfaces (PRS) arising due to spreading over the ionosphere of those disturbances which are brought there from the dipolarization region. Nonresonant constituent of the impulsive disturbance with continuum frequency spectrum excites simultaneously and in a coherent manner a lot of resonances at different PRS. During radial propagation, different resonant waves overlap, and their phase velocity differences result in phase mixing leading to the disturbance amplitude decrease without dissipation in the ionosphere. Results are applied to interpretation of the time-dependent substorm current wedge and Pi 2 pulsations. Another application is related to intense short-term inductive electric field of the resonant disturbance. Such a field may effectively accelerate energetic particles. Analysis of

observational data (Baker and Pulkkinen, 1998) suggests that strong low-frequency (2-20 mHz) waves may be indeed responsible for such acceleration.

**GA3.04/L/10-B1** Poster **1520-46**

**ION CYCLOTRON WAVES IN JUPITER'S MAGNETOSPHERE**

Panagiota PETKAKI and M. K. Dougherty

Magnetometer data from the Ulysses Jupiter flyby is examined, and in particular middle magnetosphere observations near the magnetodisk. Ion cyclotron waves are searched for in the heavy ion gyrofrequency regime ( $\$SO^+_{2\$}$ ,  $\$SO^+_{3\$}$ ,  $\$S^+_{34\$}$ ,  $\$O^+_{46\$}$  and  $\$S^+_{47\$}$ ). Power spectral peaks in the ion cyclotron frequency range in the Ulysses magnetometer data have been found in the past. Here we thoroughly examine the high resolution 1 sec data, with ion cyclotron waves signatures being observed on several occasions both close to the magnetic equator and at some distance from it. Rippling and warping of the magnetodisk, as observed by Ulysses, could be the cause of such ion cyclotron signatures arising some distance from the magnetic equator. Lower mass ions are observed further away from the planet and the heaviest mass ion signatures only appear close to the Io torus. Polarisation analysis of the observations are also presented and theoretical implications of the wave signatures discussed.

**GA3.04/L/01** Poster **1520-47**

**POLAR SPACECRAFT OBSERVATIONS OF ELECTRIC ULF WAVES**

J. H. CLEMMONS, F. S. Mozer, Berkeley, H. Laakso, R. F. Pfaff, P. J. Chi, C. T. Russell,

Fields measurements from the Polar spacecraft of magnetospheric ultra-low frequency (ULF) waves in the Pc3-5 frequency range are analyzed to provide new insights into the properties and evolution of the waves. Polar's high altitude, high-inclination orbit gives a new perspective on the waves, and the combination of electric and magnetic measurements provides a powerful analysis tool for the determination of wave nodal structure, standing wave character, polarization, and energy flow. Results from a survey of more than two years of Polar data are presented. Preliminary analyses indicate that power in the electric component is peaked near noon, with lower frequencies having narrower peaks. In keeping with previous results from geosynchronous orbit, the electric component generally has more power in the azimuthal direction than in the radial direction, indicating the prevalence of poloidal modes. Further analyses and comparison to the magnetic perturbations are discussed.

**GA3.04-B1** Poster **1520-48**

**ULF/VLF/ELF OBSERVATIONS DURING THE SOLAR TOTAL ECLIPSE.**

Keyun TANG, Fenglin Peng, Zuoli Ning and Shaofeng Yang, Y.Tanaka and K.Yumoto

During the period around the total solar eclipse of March 9, 1997, coordinated observations including optical, radio, gravity, acoustic, ionospheric, geomagnetic, ULF/VLF waves observations, as well as Schumann Resonance observation were conducted in Mohe area near the north-east border between China and Russia.

Pi 2 and Pc 4 geomagnetic pulsation were observed. Obvious jumps during the solar eclipse could be found. Polarization analyses were completed, and we found that mirror effects of polarization orientation for Southern Hemisphere and Northern Hemisphere were destroyed. Observations of VLF waves show a clear decreasing on amplitude during the solar eclipse. We had also measured the frequency and amplitude variations of the first Schumann resonance mode. The records and analyses show significant variations away above the usual daily variation. On March 9, 1997, the day of the solar eclipse occurred, the amplitude of the first SR mode dropped dramatically. For the three-quarters just after the first contact, the amplitude dropped 94%, and reached the minimum at the middle eclipse, then gradually recovered to the normal level at the last contact. The amplitude variation of the first SR mode was well consisted with the solar eclipse process. We could conclude that the significant amplitude variation of the first SR mode was caused by the solar eclipse process. The measurements during the total solar eclipse suggest us that the local ionosphere environment is very important to influence the propagation and receiving of SR waves. A model to describe the propagation mechanism of SR waves will be discussed.

**Tuesday 27 July AM**

Presiding Chair: Dr. B.J. Anderson (The University of Newcastle, NSW, Australia)

**GA3.04/L/11-B2** Invited **0900**

**ULF WAVES AND THE INDUCTIVE IONOSPHERE**

Akimasa. YOSHIKAWA (Department of Earth and Planetary Sciences, Kyushu University, Hakozaki, Fukuoka 812-8581, Japan, e-mail: yoshi@geo.kyushu-u.ac.jp)

Natures of reflection and mode conversion of MHD waves at the inductive ionosphere are investigated. The most important view obtained in the course of study was the "divergent Hall current" (DHC), which directly closes the FAC in the ionosphere. It is well known that when a shear Alfvén wave is incident on the ionosphere, the 90 degree rotation of the wave's magnetic field across the ionosphere is caused by the Hall effect. The rotation is a guiding principle in the diagnostics of geomagnetic pulsations at high latitudes. However, such a rotation is only a result of one-step mode conversion. On the other hand, the DHC is an ionospheric divergent current driven by the rotational electric field that is produced as a result of multi-step mode conversion between divergent and rotational electric fields arising from the Hall effect in the ionosphere. The DHC is shown to be a primary source of physical phenomena arising from the multi-step mode conversion. The ionospheric currents associated with the ULF pulsations at the inductive ionosphere are almost borne by Hall current both rotational and divergent parts in quantity, and causes a frequency shift and horizontal dispersion of standing field line oscillation. In this paper, various aspects of the DHC are analyzed and its physical background is elucidated.

**GA3.04/W/22-B2** **0930**

**PHASE STRUCTURE OF DAMPING STANDING ALFVÉN WAVES IN THE MAGNETOSPHERE**

Margaret KIVELSON (Department of Earth and Space Sciences and Institute of Geophysics and Planetary Physics, University of California, Los Angeles, CA 90095-1567, USA, e-mail: mkivelson@igpp.ucla.edu); David J. Southwood (European Space Agency, Headquarters, 8-10 rue Mario-Nikis, F75738 Paris Cedex 15, France, e-mail: dsouthwo@hq.esa.fr)

There are various damping mechanisms for magnetospheric Alfvén waves. The most significant damping mechanism for the waves is usually absorption in the ionospheres at the feet of field lines. We work through a simple model of damped standing waves and use it to

investigate the changing phase relations between electric and magnetic perturbations along the background field. We show how the phase variation relates to the energy flux into the ionosphere. The work not only improves our understanding of the behaviour of magnetospheric waves, but also explicitly characterises key aspects of eigenoscillations of the system. In an era when correlations between ground and space are common and can be critical elements in timing geophysical phenomena, it is important to understand this aspect of the field-aligned structure.

**GA3.04/E/06-B2 0950**

**INFLUENCE OF IONOSPHERIC CONDUCTIVITY ON MIDDLE AND LOW LATITUDE Pc3-4 PULSATIONS**

Nadezhda YAGOVA, Viacheslav Pilipenko, Evgenij Fedorov (Institute of the Physics of the Earth, Moscow 123810, Russia, e-mail: vpilipenko@uipe-ras.scgis.ru); Kiyohumi Yumoto (Kyushu University 33, Fukuoka 812-81, Japan, email: yumoto@geo.kyushu-u.ac.jp)

Longitudinal and latitudinal variations of the parameters of the magnetospheric Alfvén resonator have been calculated using a semi-empirical model of the ionosphere-magnetosphere plasma distribution. The calculated values of damping rates of Alfvén oscillations at mid-latitudes during the dark period are too high for the "free-end" and "quarter-wave" oscillation regimes to be realized. At low latitudes relatively high quality factors are expected both at day and night-time conditions. A drastic change of a field-aligned structure of Alfvén oscillations during the transition from day-side to night-side ionospheric conditions might not happen due to conjugated variations of plasma density in the ionosphere and in the magnetosphere. The analysis of the experimental data recorded at middle and low latitude stations of the "210 Magnetic Meridian" magnetometer network and the station l'Aquila gives the following results: (a) the pulsation amplitude in a frequency band near fundamental harmonic of Alfvén field line resonance has the strongest dependence on the ionospheric conductivity; (b) the influence of day/night ionospheric conditions on the Pc3 amplitudes at low geomagnetic latitudes is weaker in comparison with the one at mid-latitudes; (c) the ionospheric conductivity control of the Pc3 amplitude at middle latitudes weakens with the harmonic number. The experimental observations are in accordance with the predictions of the numerical model.

**GA3.04/W/16-B2 1010**

**HIGH-LATITUDE OBSERVATIONS OF ULF WAVES WITH LARGE AZIMUTHAL WAVENUMBERS**

T. K. YEOMAN, D. M. Wright (Department of Physics and Astronomy, University of Leicester, University Road, Leicester, LE1 7RH, U.K.); A. B. Stockton-Chalk (School of Physics and Astronomy, University of Birmingham, Edgbaston, Birmingham, B15 2TT)

DOPE (The Doppler Pulsation Experiment) is an HF Doppler sounder deployed at Tromsø, Northern Norway for the investigation of the ionospheric signatures of ULF wave phenomena of magnetospheric origin. This high-latitude Doppler sounder has been demonstrated to be a highly sensitive instrument for the investigation of ULF waves of large azimuthal wavenumber. These waves are assumed to be driven by magnetospheric wave-particle interactions, and are difficult to study by other means due to their strong spatial integration between the ionosphere and the ground. The occurrence and characteristics of these waves will be discussed, and their ground and ionospheric characteristics compared for various values of azimuthal wavenumber.

**GA3.04/L/12-B2 Invited 1100**

**PI2 PULSATIONS**

Prof. Margeret KIVELSON

Pi 2 pulsations (impulsive signals with periods of 40-150 seconds) are widely used to time substorms and to track geomagnetic activity. Despite the utility of this type of pulsation for substorm studies, the mechanisms that generate the wave signals is not well established. We present the first detailed observations that directly relate Pi 2 pulsations to flow bursts in the magnetotail. We describe the steps in the generation of mid- and low-latitude Pi 2 pulsations by flow bursts. On the ground, the first indication of activity is a linearly increasing (precursor) perturbation that lasts ~90 seconds, which is due to inward convection from the distant magnetotail. An abrupt change of slope of the analyzed wave amplitude corresponds to the true start of the wave signal. Mid-latitude Pi 2 are generated when the flow reaches the inner magnetosphere, where it is braked by the rapidly rising magnetic pressure. Pulsations arise from the transient response of the ionosphere to currents generated by the braking. The braking also generates compressional waves that directly drive low-latitude (monochromatic) Alfvén oscillations. We show that low-latitude, flank Pi 2s are directly correlated with temporal oscillations of the flow velocity, delay

**GA3.04/W/32-B2 1130**

**PI2 PULSATIONS IN THE THREE-DIMENSIONAL DIPOLE MAGNETOSPHERE**

Dong-Hun LEE (Dept of Astronomy & Space Science, Kyung Hee University, Yongin, Kyunggi, 449-701, Korea, e-mail: dhlee@nms.kyunghee.ac.kr); Robert L. Lysak and Yan Song (School of Physics and Astronomy, University of Minnesota, 116 Church St. SE, Minneapolis, MN55455, USA, e-mail: bob@aurora.space.umn.edu, yan@aurora.space.umn.edu)

Pi2 pulsations have been numerically studied in a new 3-D dipole model, which allows a realistic Alfvén speed profile for the plasmasphere and outer magnetosphere in the tailward region. This model includes a reasonable inner/outer boundary condition, which is differentiated from the previous numerical models. When an impulse associated with the substorm onset is assumed, we investigate how Pi2 modes are developed in time as well as how field-aligned currents are produced and distributed over the whole nightside magnetosphere. The results are compared with current theoretical and observational characteristics. The effects of non-axisymmetric geometry around the tailward magnetosphere have also been examined and discussed in detail.

**GA3.04/E/12-B2 1150**

**UARS OBSERVATION OF A PI2 PULSATION AT 600 KM ALTITUDE**

Kazue TAKAHASHI and Brian J. Anderson (both at Johns Hopkins University Applied Physics Laboratory, Laurel, MD 20723-6099; e-mail: kazue.takahashi@jhuapl.edu); James B. Gary (University of Texas at Dallas, e-mail: gary@utdallas.edu); Kiyohumi Yumoto (Department of Earth and Planetary Sciences, Kyushu University; e-mail: yumoto@geo.kyushu-u.ac.jp)

Satellites in low-altitude orbits provide unique opportunities to study the ionospheric screening

effects on ULF waves propagating from the magnetosphere. This paper reports an observation of a Pi2 pulsation at an altitude of approximately 600 km from the Upper Atmosphere Research Satellite (UARS). The Pi2 pulsation occurred on November 18, 1993 when the satellite was over the western Pacific near the three ground magnetometer sites, Chichijima (L = 1.14, MLT = 23), Ewa Beach (L = 1.17, MLT = 03), and Guam (L = 1.07, MLT = 23). On the ground the Pi2 was visible in the H component from 1337 to 1343 UT at all locations with the same period of 43s but with an amplitude ranging from 3 nT (Guam) to 1 nT (Ewa Beach). At the satellite the same pulsation was detected in the northward component (parallel to the ground H component) of the magnetic field with an amplitude of 3 nT. The phase delay between space and ground was very small. Overall, the wave observed by UARS appear to have reached the ground with little modification in amplitude and polarization. The results support the idea that low-latitude Pi2 pulsations originate from fast mode oscillations in the inner magnetosphere.

**GA3.04/L/13-B2 1210**

**CPMN GROUP, LOCAL TIME DEPENDENCE OF PI2 PULSATIONS; A STATISTICAL STUDY**

Li Yan and Kiyohumi YUMOTO (both at Department of Earth and Planetary Sciences, Kyushu University 33, Fukuoka 8912-8581, Japan, Email: yumoto@geo.kyushu-u.ac.jp), The CPMN group

Local time dependence of Pi 2 pulsations is studied statistically using the 210 MM data at the various latitudes. 249 Pi 2 events are recognized in one month data of February, 1995. 68% Pi 2 events are observed at night time within this month at a low-latitude station MSR. For both occurrence and wave amplitude, there are three maxima at premidnight, slightly post midnight, and prenoon; two minima at late afternoon and just after sunrise. The three maxima decrease at significantly different rate with decreasing latitude. The wave frequency show different contents and different local time dependence at auroral latitude and mid- to low-latitudes. Mid- and low-latitude Pi 2'-have an additional frequency component than auroral-latitude Pi 2's. The local time dependence of the "equatorial enhancement" is also obtained, which agrees with previous studies at most local time except for the large ratio in the few hours after sunrise that has not been reported.

**Tuesday 27 July PM**

Presiding Chair: Dr. R.E. Denton (Dartmouth College, Hanover, Germany)

**GA3.04/L/14-B2 Invited 1400**

**DIAGNOSING Pc5 MAGNETOSPHERIC WAVEGUIDE MODE EXCITATION MECHANISMS**

I.R. MANN (Dept. of Physics, University of York, Heslington, York, YO10 5DD, U.K., email: ian@aurora.york.ac.uk) A.N. Wright (Mathematical Institute, University of St. Andrews, St. Andrews, Fife, Scotland, KY16 9SS, U.K., email: andy@dcs.st-and.ac.uk)

We show how the compressional modes supported by a waveguide with a free magnetopause boundary have characteristics which are strongly local time and solar wind speed dependent, being either leaky, trapped, or energised by magnetopause instabilities. These waveguide modes are believed to excite Pc5 field line resonances (FLRs) in the magnetosphere. We show how the characteristics of the resulting FLRs can be used to probe the energy sources responsible for driving the compressional waveguide modes, and hence be used to determine the pathway for energy transport from the solar wind to the resonances. In particular, the characteristics of multiple harmonic FLRs can be used to diagnose their energy sources and to distinguish between resonances excited by solar wind non-uniformities or through the development of magnetopause instabilities. Using observations previously reported in the literature, we show examples of this diagnostic analysis and conclude that the dawn/dusk asymmetry in Pc5 FLR characteristics may be linked to different excitation mechanisms operating either side of noon. In particular, we suggest that the majority of dawn-side FLRs may be excited by waveguide modes which are amplified through the development of instabilities on, and through the action of over-reflection at, the magnetopause. Wave excitation by this mechanism generates a spectrum displaying preferred azimuthal wavenumbers, similar to that observed, and which is previously unexplained. Moreover, this mechanism is likely to generate quarter-wavelength modes which have lower frequencies than the standard (magnetopause velocity node) half-wavelength modes. This may provide an explanation for the very low (millihertz) eigenfrequency spectrum required to drive the FLRs which are observed at these frequencies by HF radars and ground-based magnetometers, especially on the flanks.

**GA3.04/W/38-B2 1430**

**COUPLING BETWEEN FIELD LINE RESONANCES AND LEAKY CAVITY MODES**

A.D.M. WALKER (University of Natal, Durban)

If a wave is incident on the magnetopause from the solar wind then, if its frequency matches that of a leaky cavity mode, it is captured and causes oscillation of the cavity mode. If its frequency does not match a cavity mode frequency then it is essentially reflected from the magnetopause without penetrating the magnetosphere. Those waves which are captured may excite field line resonances. The mechanism of this process is discussed using WKBJ methods and other analytic techniques. This approach, while only approximate, has the advantage of allowing easy visualisation of the physical processes.

**GA3.04/L/15-B2 1450**

**Pc5 ULF PULSATIONS ASSOCIATED WITH WAVEGUIDE MODES OBSERVED WITH THE IMAGE MAGNETOMETER ARRAY**

R. A. MATHIE, I. R. Mann, Department of Physics, University of York, York YO10 5DD, England, (e-mail: rod@aurora.york.ac.uk; ian@aurora.york.ac.uk); F. W. Menk, Department of Physics, University of Newcastle, Newcastle, NSW 2308, Australia. (email: phypuls3@cc.newcastle.edu.au); D. Orr, Department of Physics, University of York, York YO10 5DD, England, (e-mail: david@aurora.york.ac.uk)

Several recent publications have reported high latitude radar observations of field line resonances (FLRs) displaying discrete and very stable frequencies in the Pc5 range. It is believed that these quantized frequency FLRs may be associated with cavity/waveguide harmonics of the outer magnetosphere but the prevalence and reported stability of the frequencies remain controversial. We examine the statistics of 137 Pc5 pulsation events identified from three months of IMAGE magnetometer data and show that these discrete frequencies are also prominent in ground-based data. We also examine amplitude, phase and polarization characteristics and show that these FLRs have features which are strongly local time dependent.

**GA3.04/W/07-B2 1510**

**HIGH-LATITUDE ULF WAVES OBSERVED BY THE POLAR SPACECRAFT**

P J CHI, C T Russell and G Le (All at Institute of Geophysics and Planetary Physics, University of California, Los Angeles, CA 90095, USA; e-mail: pchi@igpp.ucla.edu); J H Clemmons (Aerospace Corporation, El Segundo, CA; e-mail: James.H.Clemmons@aero.org)

High-latitude ULF waves have been extensively studied by ground-based observations but very few ULF-wave studies have been made at these latitudes in the magnetosphere. The Polar satellite provides such an opportunity. The polar cusp is a region rich in ULF waves coming from the magnetopause and boundary layer. The cusp is also thought to be an entry point for waves generated beyond the magnetopause, at the bow shock or in the magnetosheath. To better understand the characteristics of high-latitude ULF waves, we conduct a statistical survey of the occurrence of ULF waves observed by Polar MFE instrument. Continuous wavelet analysis is applied as an objective tool for selecting wave events in one full year of MFE data. Our results show that transverse Pc3 waves are dominant near the cusp region. However, compressional Pc3 waves are more likely to occur in the subsolar magnetosphere. This is consistent with our previous case study which suggests that, in the region near the cusp, the ULF Poynting flux propagates mainly along the field lines and the wave energy does not appear to propagate directly from the cusp into the magnetosphere across field lines. Transverse waves also occur at different L-shells that are consistent with the field line resonance picture. Compressional Pc5 waves have a high occurrence rate on the tail field lines at high latitudes, and they may be caused by perturbations on the magnetospheric boundaries.

**GA3.04/L/16-B2 Invited 1600**

**LOW FREQUENCY GEOMAGNETIC FIELD FLUCTUATIONS AT A LOW LATITUDE STATION**

U. VILLANTE, P. Francia (both at Dipartimento di Fisica, Università de L'Aquila, Italy, E-mail: umberto.villante@aquila.infn.it) and S. Lepidi (Istituto Nazionale di Geofisica, Roma, Italy)

The power spectral analysis of the geomagnetic field fluctuations at a low latitude station (L'Aquila, Italy, IGRF95 geomagnetic coordinates 36.2N, 87.5E) shows statistical evidence at discrete frequencies for daytime power enhancements which become more clear during periods characterized by higher solar wind speed. These power enhancements occur at frequencies which approximately correspond to those detected at auroral latitudes both in the F-region drift velocities and in the ground geomagnetic field fluctuations and generally interpreted in terms of field line resonances set up by magnetospheric cavity/waveguide compressional modes driven by external stimulations.

Case studies of selected events show that fluctuations at the same discrete frequencies are observed in correspondence to the Earth's arrival of solar wind pressure pulses. A comparison with observations performed at an Antarctic high latitude station shows that on these occasions the discrete modes appear simultaneously at both stations approximately at the same frequencies. The appearance of similar features at a wide latitudinal and longitudinal separation suggests to interpret these events in terms of global oscillations of the whole magnetosphere. Moreover, the polarization pattern is consistent with an antisunward propagation.

**GA3.04/W/43-B2 1630**

**FIELD LINE RESONANCES AND WAVEGUIDE MODES AT LOW LATITUDES: OBSERVATIONS**

Fred W. MENK, Colin L. Waters and Brian J. Fraser (all at Department of Physics, CRC for Satellite Systems, University of Newcastle, Callaghan, NSW, 2308, Australia, e-mail: physpuls3@cc.newcastle.edu.au)

Although Pc 3-4 ULF pulsations are commonly observed at low latitudes, many of their features are poorly understood. A 12-station magnetometer array was operated in eastern Australia specifically to examine these aspects. The following have been investigated and will be discussed: the variation in field line eigenfrequency with latitude, and hence the significance of ionospheric heavy ions; the scale size, Q and damping of the field line resonances; and the propagation characteristics of ULF waves below the local resonance frequency. A remarkable feature of the observed power spectra is the presence of multiple closely spaced peaks across the entire latitude range. The Pc 3-4 pulsations are probably due to field line oscillations driven by incoming compressional mode waves which excite cavity or waveguide modes in the magnetosphere.

**GA3.04/E/09-B2 1650**

**LOW LATITUDE PC3-4 PULSATIONS**

D.R.K. Rao, B.M. PATHAN and R.S. Udare (all at Indian Institute of Geomagnetism Colaba, Mumbai 400 005, India, e-mail: bmpathan@iig.iigm.res.in)

Employing digital data on ULF geomagnetic pulsations from three latitudinal stations in the Indian longitudinal region, few spatial characteristics of Pc3-4 are studied. Different techniques of analysis on the three identified frequency bands of pulsation signals have been used. At the lowest frequency band (102 to 47 sec), the amplitudes of the signal in both NS and EW directions in the horizontal plane, are noticed to be highly subdued at a station far away from the equatorial electrojet influence as well as the Sq focus. The identified cross phase (or time delay) between the latitudes of extreme northern and southern stations has yielded two frequencies at 35 and 50 mHz, by Gradient technique. The validity of 35 mHz cross phase is discussed in terms of excitation by a broad band source and propagation of signal through cavity resonance mode at low and equatorial regions. The latitudinal propagation is found to be highly variable (mx or my lying between 3 and 12) and the propagation is mostly directed away from the equator. Few hodograph results towards polarization are discussed.

**GA3.04/L/17-B2 1710**

**VALIDATION OF THE PHASE GRADIENT TECHNIQUE FOR INFERRING MAGNETOSPHERIC RESONANCES FREQUENCIES**

W. GOEDECKE, Colorado School of Mines Golden Colorado, CO, USA (email: wgoeck@mines.edu); C. T. Russell and P. J. Chi (both at Institute of Geophysics and Planetary Physics, University of California, Los Angeles, CA, 90095-1567, USA)

Simultaneous GPS synchronized one-second triaxial magnetometer data from four stations over a range of 9 degrees in geomagnetic latitude were collected in the Western United States, at Boulder, South Park, the Air Force Academy, Los Alamos, New Mexico and Los Angeles, California. Their equivalent L shells range from 1.7 to 2.3. The ULF horizontal component is nearly unchanged from high to low L shells with the exception of broadband attenuation with

some extra loss of high frequency components. Both phase difference and amplitude ratio dynamic spectra help identify resonances. The resonance was found to accentuate certain frequency bands, but the standing modes do not dominate the observed signal enough to mask the non-resonating frequencies.

The observed signal is complex, comprised of several frequencies over a time interval of several periods. The signal's center frequency shifts, not unlike a drifting frequency modulated wave, allowing resonance of several L shells. Phase skipping was also observed. There appeared to be a merging of wave periods from upper to lower L shells along with the selected attenuation of high frequency components.

Additional data have been collected from the north-south station pair in Srobarova, in the Slovak Republic, and Tihany, Hungary. These reveal times when a propagating mode occurs, that is, when the phase gradient changes proportionally with the frequency. This constant time shift independent of frequency is best revealed by a time difference plot, unlike the phase difference plot. In this case, no or appreciable resonance was found. Observatories of lower L shells generally receive the signal first, but on several days at this European pair the higher L shell observed the signal first.

During most intervals appreciable declination component pulsations were also observed, with very little phase gradient or time shift between station pairs.

**GA3.05 Wednesday 28 July**

**ACCELERATION, TRANSPORT AND LOSSES IN THE INNER MAGNETOSPHERE**

Location: School of Education G33 LT

Location of Posters: School of Education, Conference Room

**Wednesday 28 July AM**

Concurrent Poster Session

**GA3.05/W/28-B3 0830**

**ENERGIZATION OF RING CURRENT IONS AND RELATIVISTIC RADIATION BELT ELECTRONS DURING GEOMAGNETIC STORMS**

J L ROEDER, J F Fennell, R S Selesnick, and J B Blake (The Aerospace Corporation, Los Angeles, CA, 90009, USA, email: James.L.Roeder@aero.org) M. Grande (Rutherford Appleton Lab, Chilton, Didcot Oxon OX11 0QX, UK) S. Livi (Max-Planck-Institute for Aeronomy, 37191 Katlenburg-Lindau, Germany)

Geomagnetic storms are known to cause the energization and transport of ions in the magnetospheric ring current. This process may be described by the change in the total kinetic energy content of the ion populations which is related to the Dst magnetic index through the Dessler-Parker-Sckopke relation. Such events also are related to the energization of relativistic electrons in the radiation belts. The electron acceleration may occur as either a very rapid injection by shock-driven induced electric fields or an increase over several days in the storm recovery phase. The observed storms have a wide range of efficiency for the energization of both ion and electrons. Using data from the Polar CAMMICE and CEPPAD instruments we characterize several storms according to the magnitude of the ion and the electron acceleration. We then compare the energization events with the intensity of the storms according to the magnitude and duration of the Dst variations. The kinetic energy content of the measured fluxes integrated over the inner magnetosphere is used to characterize both the ion and electron acceleration. The CAMMICE MICS instrument provides ion composition data in the energy-per-charge range of 1-200 keV/e. The CEPPAD IPS sensor extends the measured ion energy range with proton fluxes in the range 20-1500 keV. The combination of these two instruments provide excellent energy coverage of the ring current ion populations. The data from the CEPPAD HIST sensor over the energy range 0.7-7 MeV are used to characterize the relativistic electrons in the outer radiation belt. For example, the January 1997 magnetic cloud event caused a exhibited a large enhancement in the high energy electrons, but only a moderate response in Dst (-78 nT), with a corresponding increase in the ring current ions. The May 15, 1997 storm (-115 nT), in contrast, caused a more substantial ring current ion variation, but a smaller electron enhancement. The existence of pre-existing "seed" populations in the magnetosphere may account for some of these differences.

**GA3.05/E/02-B3 0850**

**LONG TERM VARIATION OF THE LOW-ALTITUDE TRAPPED PROTON POPULATION MEASURED BY SAMPEX/PET**

M. KRUGLANSKI, D. Heynderickx and J. Lemaire (BIRA/IASB, Brussels, Belgium) M.D. Looper and J.B. Blake (The Aerospace Corp., Los Angeles, California) E.J. Daly (ESTEC/ESA, Noordwijk, The Netherlands)

It has been firmly established that the low-altitude trapped proton population exhibits strong time variations related to geomagnetic secular variation and neutral atmosphere conditions. The flux measurements of the Proton Electron Telescope (PET) onboard the polar satellite SAMPEX constitute an adequate data set to distinguish different time scales and to characterise the respective variations. We demonstrate the effect of the secular geomagnetic variation by comparing the (I,Bm) distribution of trapped protons measured by SAMPEX/PET with the distribution measured by AZUR satellite in 1969. Using TIROS data spanning two solar cycles, Huston and Pfitzer have studied the variation related to the atmosphere's response to the solar UV flux on a time scale of the solar cycle. The four years (1992-1996) of PET data at our disposal allow us to analyse in more detail the relation between the proton flux variation and solar activity during the most recent descending solar cycle phase. After accounting for the effects described above, the PET data still exhibit a clear systematic variation on a shorter time scale. The residual flux variation, which can be as high as a factor 2, is strongly correlated with the seasonal variation of the MSISE-90 total mass density in the SAA at the altitude of mirroring protons. Our analysis of the SAMPEX data shows that a modern low-altitude proton model must take into account variations on at least three different time scales. This work was funded by ESA's Technology Research Programme, ESA/TOS-EMA, Space Environments and Effects Major Axis.

**GA3.05/W/39-B3 0910**

**SPECTRUM CHARACTERISTICS OF THE RELATIVISTIC ELECTRONS IN THE OUTER RADIATION BELT DURING MAGNETIC STORMS**

Takahiro OBARA (Hiraiso Solar Terrestrial Res. Ctr., 3601, Isozaki, Hitachinaka, Ibaraki, 311-1102 Japan, email: T.Obara@crl.go.jp)

Once a major magnetic storm takes place, the relativistic electrons in the outer radiation belt disappear entirely. After the disappearance of the relativistic electrons which can last as much



as one day, an increase in the flux occurs and sometimes exceeds the pre-storm levels. The return flux is evident at first in a low L-shell (3-4) region, which propagates to higher L shells. Based on Akebono (EXOS-D) observation, an investigation has been made on the spectrum characteristics of the relativistic electrons. Results demonstrate that there is a systematic tendency in the spectrum from 300 keV to 2.5 MeV; i.e. both decay and growth are severer for higher energy and time delay of recover is apparent for higher energy. On the contrary, fast recover is made for lower energy electrons. We have also studied on a correlation of the electron flux increase and the IMF Bz polarity as well as the polar cap index during the storm recovery phase. Results demonstrate that a large flux enhancement occurred when the IMF was southward and the PC index was quite large. Source particles are effectively supplied due to the enhanced magnetic activity and they may be accelerated up to MeV range by some processes within outer radiation belt. We will discuss possible way(s) to increase the outer belt electrons during the storm recovery phase.

**GA3.05/E/07-B3 0930**

**SOLAR CYCLE CHANGES OF ENERGETIC PARTICLE PROPERTIES IN THE INNER MAGNETOSPHERE**

D.N. BAKER and X. Li (Laboratory for Atmospheric and Space Physics, University of Colorado, Campus Box 590, Boulder, Colorado, 80309-0590, USA, e-mail: baker@lynx.colorado.edu); J.B. Blake (The Aerospace Corporation, MS 259, Los Angeles, CA 90009); S.G. Kanekal (Goddard Space Flight Center, Greenbelt, MD 20771)

The near-Earth region responds powerfully to changes on the sun and in the solar wind. The Earth's radiation belts and inner magnetosphere show pronounced differences in their characteristics as the sun's magnetic and solar wind properties change. Solar coronal holes produce regular, recurrent solar wind stream interactions in geospace, often enhancing highly relativistic electrons (HREs) and causing recurrent magnetic storms. These phenomena are characteristic of the approach to solar minimum. On the other hand, major geomagnetic disturbances associated with a periodic coronal mass ejections occur most frequently around solar maximum. We review the observational and modeling results that demonstrate differences throughout the inner part of geospace during the course of the 11-year solar cycle. We place particular emphasis on long-term, homogeneous data sets from SAMPEX and POLAR missions.

**GA3.05/E/16-B3 0950**

**RELATIVISTIC ELECTRON EVENTS IN THE OUTER ZONE DURING AUGUST-SEPTEMBER 1998: SAMPEX AND POLAR MEASUREMENTS**

S.G. KANEKAL (Code 696, NASA GSFC and RTISS, Greenbelt, MD 20904, USA, e-mail: kanekal@lepsam.gsfc.nasa.gov); D.N. Baker (Laboratory for Atmospheric and Solar Physics, University of Colorado, Boulder, CO, 80309); J.B. Blake (The Aerospace Corporation, MS259, Los Angeles, CA 90009); B. Klecker (Max Planck Institut für Extraterrestrische Physik, Garching, Germany); G.M. Mason (Dept. of Physics, Univ. of Maryland, College Park, MD 20742); R.A. Mewaldt (California Institute for Technology, Pasadena, CA 91125)

The dynamics of the radiation belts seen from the perspective of relativistic electron dynamics exhibit both properties common to such events as well as variations amongst them. In this paper, we study the relativistic electron enhancement events in the outer zone during the months of August and September 1998. We use data from multiple satellites to characterize the interplanetary conditions and relativistic electrons in the earth's magnetosphere. For the latter, detectors onboard POLAR and SAMPEX satellites are used to measure electrons over an energy range of several eV to MeV and covering almost all L-shells. Since SAMPEX and POLAR orbit at approximately 800 km and 2-9 Re altitudes respectively, pitch angle and spatial information are also obtained. Sensors on WIND provide information about the interplanetary conditions. Observations and comparisons of particle spectra and fluxes covering a large range of L-shells and energies will be presented. This study will also attempt to compare and contrast these case studies with previous measurements.

**GA3.05/W/01-B3 1010**

**OBSERVATIONS OF THE SHOCK INJECTION OF MAGNETOSPHERIC PARTICLES IN MAY AND AUGUST 1998: COMPARISON WITH THE GREAT EVENT OF 24 MARCH 1991**

J B BLAKE, M D Looper, R S Selesnick (The Aerospace Corporation, Los Angeles, CA, 90009, email: jbernard.blake@aero.org) X Li and D N Baker (LASP, University of Colorado, Boulder, CO, 80303) M K Hudson (Physics and Astronomy Department, Dartmouth College, Hanover, NH 03755)

The very strong SSC event of 24 March 1991 was observed by CRRES to inject large fluxes of electrons with energies exceeding 15 MeV and protons of several tens of MeV deep into the magnetosphere in a time period of a couple of minutes (Blake et al. 1992). The physics underlying this unprecedented observation was described by Li et al. 1993. On 4 May 1998 and 26-28 August 1998 SSC injections were observed by 1997-068 (in HEO orbit) and by SAMPEX. The energy spectra of protons and electrons, the L value of the peak intensity, the relative intensities of these events and the high-L seed population will be compared and contrasted.

J. B. Blake, W. A. Kolasinski, R. W. Fillius, and E. G. Mullen, Injection of Electrons and Protons with Energies of Tens of MeV into L < 3 on 24 March 1991, Geophys. Res. Lett., 21, 1992 Xinlin Li, I. Roth, M. Temerin, J. R. Wygant, M. K. Hudson, and J. B. Blake, Simulation of the Prompt Energization and Transport of Radiation Belt Particles During the March 24, 1991 SSC, Geophys. Res. Lett., 20, 2423, 1993

**GA3.05/W/30-B3 1100**

**OBSERVATIONS OF THE OUTER RELATIVISTIC RADIATION BELT USING GPS SATELLITES**

R. H. W. FRIEDEL, T. Cayton, C. Ingraham, G. D. Reeves (all at Los Alamos National Laboratory, Los Alamos, NM, USA)

Los Alamos has for many years been flying environmental radiation monitors on the GPS (Global Positioning Satellites) series of spacecraft. Currently three GPS spacecraft carry these monitors. The GPS orbit (12 hour, 4 Re, 45 degree inclination) is ideally suited to sampling the outer radiation belt: Each spacecraft covers the range of L=4 to open field lines four times an orbit, giving a time resolution of three hours per pass. Combining the measurements from three spacecraft gives an unprecedented in-situ resolution in the outer relativistic radiation belt. The relativistic electron response can be quite different from the main ring current response as observed by Dst. The past history of the relativistic electron population plays a crucial role: Already elevated flux levels can be quite insensitive to storms, and large changes in relativistic electrons can be observed without any visible signature in Dst. We further present some first observations of relativistic radiation belt asymmetries observed before the May 1997 magnetic storm.

**GA3.05/W/24-B3 1120**

**OCCURRENCE OF ELECTROMAGNETIC ION CYCLOTRON WAVES IN ASSOCIATION WITH GEOMAGNETIC STORMS**

B J ANDERSON and R E Erlanson (both at The Johns Hopkins University Applied Physics Laboratory, Laurel, MD, 20723, USA, email: brian.anderson@jhuapl.edu)

Electromagnetic ion cyclotron waves are thought to provide significant pitch angle scattering of energetic protons, especially during geomagnetic storms. We use observations from the AMPTE/CCE and DE-1 spacecraft to assess whether ion cyclotron wave occurrence has a systematic correlation with storms. Case studies indicate that low L Pc 1 emissions can persist for long periods of time in a given local time sector, primarily during the main and recovery phases of storms. This result is consistent with modeling in that low L Pc 1 are observed, but the occurrence of the waves relative to storm phase and their sustained character are not understood. Statistical analysis of AMPTE/CCE data throughout the five year mission yields data on 72 storms. Superposed epoch analysis of these events shows that even during storms, wave occurrence is dominated by sources in the outer magnetosphere in the afternoon dayside. There does not appear to be a pronounced overall increase in Pc 1 occurrence during storms although the intensity of the events is higher. The most pronounced effect is a decrease in wave normalized frequency below the equatorial He+ gyrofrequency but above the O+ gyrofrequency, that begins just at main phase onset and lasts between 12 to 24 with the longer duration corresponding to more intense storms. This frequency shift is interpreted in terms of downward shift of maximum unstable wave frequency with increased plasma beta.

**GA3.05/E/06-B3 1140**

**THE TEMPORAL EVOLUTION OF INJECTED ELECTRON DISTRIBUTIONS IN THE INNER MAGNETOSPHERE**

Nigel P. MEREDITH and Alan D. Johnstone (both at Mullard Space Science Laboratory, University College London, Holmbury St Mary, Dorking, Surrey, RH5 6NT, UK, Email: npm@mss.lucl.ac.uk); Richard B. Horne (British Antarctic Survey, Natural Environment Research Council, Madingley Road, Cambridge, CB3 0ET, UK, Email: r.horne@bas.ac.uk); Roger R. Anderson (Department of Physics and Astronomy, University of Iowa, Iowa City, Iowa, IA 52242-1479, USA).

The temporal evolution of injected electron distributions in the energy range 0.1 < E < 30 keV are examined using data from the CRRES satellite. Equatorial electron distributions and concomitant wave spectra on the night-side of the Earth in the range 3.8 < L < 6.8 are studied as a function of time since the end of the previous injection event determined from the AE index. Pancake electron distributions, so-called because of their appearance in velocity space where they peak at the 90 degree pitch angle, are seen to develop from injected distributions that are nearly isotropic in velocity space. Outside L = 6.0 the pancakes are seen to develop on a time scale of approximately 5 hours. Strong ECH and whistler mode wave intensities are associated with the injected distributions and exponential fits reveal wave decay constants of 2.15 +/- 0.13 and 2.4 +/- 0.16 hours respectively. Inside L = 6.0 the situation is complicated by the proximity of the plasmapause and inward convection times that increase significantly with decreasing L-value. Outside L = 6.0, in the marginally stable state, the phase space density contours lie approximately along the curves for diffusion by whistler mode waves but inside L = 6.0 the pancakes are more sharply peaked at 90 degrees. These results suggest that whistler mode waves play a dominant role outside L = 6.0, whereas inside L = 6.0 the ECH waves also play a significant role.

**GA3.05/E/09-B3 1200**

**ELECTRON PITCH ANGLE DIFFUSION BY ELECTROSTATIC ELECTRON CYCLOTRON HARMONIC WAVES AS A SOURCE OF PANCAKE DISTRIBUTIONS**

RICHARD B. HORNE (British Antarctic Survey, Madingley Road, Cambridge CB3 0ET, U.K., email: R.Horne@bas.ac.uk); Richard M. Thorne (Department of Atmospheric Sciences, University of California, Los Angeles, U.S.A., email: rmt@atmos.ucla.edu)

It has been suggested that highly anisotropic electron pancake distributions are the result of pitch angle diffusion by electrostatic electron cyclotron (ECH) harmonic and whistler mode waves in the equatorial region. Here we present pitch angle diffusion rates for ECH wave spectra centred at different frequencies corresponding to spacecraft observations. The wave spectra are carefully mapped to the correct resonant electron velocities. We show that previous diffusion calculations of ECH waves at (n+0.5)f<sub>ce</sub>, driven by the loss cone instability, result in large diffusion rates over a small range of pitch angles near the loss cone and therefore cannot account for pancake distributions. However, when the wave spectrum is centred at higher frequencies in the band (1.9f<sub>ce</sub>) the diffusion rate is very small inside the loss cone, but peaks just outside and remains large over a wide range of pitch angles up to 60 degrees or more. Since ECH waves near 2f<sub>ce</sub> are cyclotron damped we suggest that pancake distributions can be formed by pitch angle diffusion as the waves are damped, and not as they grow, after propagation in a non-homogeneous medium. The calculated diffusion rates suggest that ECH waves at amplitudes of the order of 1 mV/m can form pancake distributions on a timescale of a few hours, which is consistent with recent CRRES observations following substorm injections near geostationary orbit.

**GA3.05/W/22-B3 1220**

**EFFECTS OF BETATRON DRIFT ON THE PLASMASPHERIC PLASMA AND RADIATION BELT PARTICLES**

Hiroshi OYA (Department of Geophysics, Graduate School for Science, Tohoku University, Sendai, 980-8578, Japan. email: oya@stpp1.geophys.tohoku.ac.jp)

From the distribution of the plasmaspheric plasma detected from the upper hybrid frequency observed by the plasma wave spectra of PWS experiment on board the Akebono (EXOS-D) satellite, the time variation of the plasmaspheric plasma structure has been studied as the function of the Dst and ASY indices. It has been confirmed that the plasmaspheric plasma is controlled by the drift motion called here the "Betatron drift" that is caused by the induction electric field due to the time variation of the magnetic field associated with the time variation of the ring current. In the period of dB/dt < 0, detected on the earth, the plasma makes exodus towards outside of the plasmapause while the hot magnetospheric plasmas immigrate into the inside region of the plasmasphere, in the period of dB/dt > 0. Formation processes of the plasmapause is also controlled by this betatron drift; the processes then not simply follow the convection and refilling mechanism as has been accepted to be established mechanism of the plasmasphere and plasmapause formation. The mechanism of the betatron drift can also be applicable to understand recently discovered storm time variations of the radiation belt particles.

**GA3.05/W/17-B3 1400**

**SUBSTORM ACCELERATION OF 0.5 MEV ELECTRONS ON THE RECOVERY PHASE OF RECURRENT MAGNETIC STORMS**

A.V. DMITRIEV and Yu.S. Minaeva (Institute of Nuclear Physics, Moscow State University, 119899, Moscow, Russia, email: dalex@srdlan.npi.msu.u)

The dynamics of electrons with energy ~0.5 MeV in the outer radiation belt is studied using CORONAS-1 satellite data obtained in March-May 1994. The strong increases of the electron fluxes are observed on the recovery phase of recurrent magnetic storms when the Earth is crossed by fast solar wind streams from large coronal holes on the Sun. The recovery phases of recurrent magnetic storms are accompanied by substorm activity induced by Alfvénic waves in the fast solar wind. The substorm activity is accompanied by effective acceleration of the electrons in the outer radiation belt.

**GA3.05/W/34-B3 1420**

**OUTER ZONE ELECTRON RADIAL DIFFUSION MODEL OF OCTOBER 1991 MAGNETIC STORM**

D.H. BRAUTIGAM (Air Force Research Laboratory, Hanscom AFB, MA 01731, email: brautigam@plh.af.mil) J.M. Albert (Institute for Scientific Research, Boston College, Boston, MA 02115)

Using Combined Release and Radiation Effects Satellite (CRRES) data, the response of the outer radiation belt electrons to the 9 October 1990 magnetic storm is analyzed in terms of a radial diffusion model. Electron differential flux from the Medium Electron A instrument (MEA) is transformed into phase space density as a function of the three adiabatic invariants. The invariants are determined by magnetic field data from CRRES and the Tsyganenko 1989 Kp driven model. The radial diffusion equation is solved using time dependent radial diffusion coefficients  $D(t)$  and time dependent outer boundary conditions parameterized by data from Los Alamos National Laboratory geosynchronous satellite 1989\_046. The diffusion model accounts for both significant flux decreases and increases throughout the region in the several hundreds keV electrons. However, the results suggest that an internal source is required to account for the gradual increase in the >1 MeV electrons throughout the recovery phase. Whistler chorus waves were observed by CRRES to be greatly enhanced throughout the recovery phase suggesting that energy diffusion via cyclotron resonance may be a potential acceleration mechanism.

**GA3.05/W/08-B3 1440**

**MODELING THE INFLUENCE OF CAPITAL EVENTS ON THE HIGH ENERGY PROTON BELT**

ANGÉLIQUE VACARESSE, Daniel Boscher, and Sébastien Bourdarie (ONERA, Département d'Environnement Spatial, 2 Avenue Edouard Belin, P. O. Box 4025, 31055 Toulouse Cedex 04, France, Email: Angeliq.Vacresse@onecert.fr)

Protons in the 10 MeV 100 MeV range are usually very stable in the radiation belt. Such high energy particles are trapped in the belt for years. Nevertheless, strong active periods can modify this population. First, particles can decrease at the outer edge of the belt, in relationship to magnetospheric modifications, due to changes in the magnetic field itself. These magnetospheric variations, traduced by magnetopause and magnetospheric shielding fluctuations, are parameterized with the help of geomagnetic indexes and solar wind parameters. On another hand, high energy solar protons from eruptions can penetrate deeply in the magnetosphere, giving rise to a second proton belt in the 30 MeV range. That has been seen on CRRES (Combined Release and Radiation Effect Satellite), not only during the March, 1991 major event [Gussenhoven et al., 1993], but also during smaller events [Hudson et al., 1998]. Such changes in the magnetospheric boundary conditions have been modeled by particle fluctuations observed on GOES satellites at geostationary orbit. Results of modeling such physical processes using the Salammbô code [Beutier et al., 1995] will be shown in this study. The influence of such a strong dynamics on the high energy proton belt is analyzed, as well as the effects of worst cases (losses and Solar Proton Events). This work can contribute to a reference proton radiation belt model. It also allows to progress towards Space Weather considerations through the study of a parameter signature and a statistical repartition of main events, the prediction still needing better in-flight measurements and solar activity understanding.

**GA3.05/W/29-B3 1500**

**STOCHASTIC ELECTRON ACCELERATION TO RELATIVISTIC ENERGIES BY SUPERLUMINOUS WAVES**

Richard M. THORNE and F. Xiao (Department of Atmospheric Sciences, UCLA, Los Angeles CA 90095-1565, e-mail: rmt@atmos.ucla.edu) D. Summers (Department of Mathematics and Statistics, Memorial University of Newfoundland, Canada A1C5S7)

Intense superluminous waves (with phase speeds exceeding the velocity of light) are excited in the auroral cavity during disturbed magnetospheric conditions. Previous ray tracing studies have demonstrated that these waves can propagate into the lower L region of closed magnetic field lines. Here we explore the potential resonant interactions with trapped outer-zone electrons. Relativistic resonant diffusion surfaces are constructed for each superluminous wave mode and we identify waves which could contribute to the acceleration of outer-zone electrons to relativistic energies (>1 MeV) during disturbed conditions.

**GA3.05/E/21-B3 1520**

**ENTRY OF HIGH ENERGY PARTICLES INTO THE EARTH'S MAGNETOSPHERE**

Mostafa EL-ALAOUI, Maha Ashour-Abdalla (Both at UCLA-IGPP, Los Angeles, CA 90095-1567, USA, e-mail: mostafa@igpp.ucla.edu)

During the upcoming solar maximum, energetic solar particle events will increase in frequency and severity. Traveling along interplanetary magnetic field (IMF) field lines, they reach the Earth's magnetosphere and enter it, increasing populations of energetic particles and affecting spacecraft operations. We will study the interactions of these particles with the magnetosphere and their access to the inner magnetosphere by using a combination of MHD and large scale kinetic simulations. While we do not expect the particles with the highest energies to be strongly affected by the magnetic fields of the magnetosphere, it is clear that the energetic particle spectrum will be influenced in a complex manner before being trapped by the Earth's field. Starting from the solar wind, we will calculate and follow the orbits of several thousand

H+ ions forward in time until they are lost at the edges of the simulation box, precipitate into the ionosphere or become trapped. In addition, we will determine and evaluate the success these highly energetic particles (> 0.1 MeV) from the solar wind have in reaching and penetrating the Earth's magnetosphere. Any energization and transport processes that these ions undergo inside the Earth's magnetosphere will also be examined.

**GA3.05/W/26-B3 1600**

**MULTIPLE SATELLITE STUDY OF THE ENERGETIC ELECTRON RESPONSE TO THE MAY 1998 MAGNETIC STORM**

J F FENNELL, J L Roeder, J B Blake, R S Selesnick (The Aerospace Corporation, Los Angeles, CA, 90009, USA, email: joseph.f.fennell@aero.org); R H W. Friedel and G D Reeves (Los Alamos National Laboratory, MS: D436, Los Alamos, NM 87545, United States); M Grande and M Carter (Rutherford Appleton Laboratory, Chilton-Didcot, OX110QX, United Kingdom)

We combine the energetic electron observations from Polar and HEO (94-026, 95-034, and 97-068) to the large magnetic storm of May 2-9, 1998. These observations are taken by high-altitude high-inclination satellites at energies > 100 keV. The HEO (94-026, 95-034, and 97-068) satellites are in ~12 hour orbits at different local times while Polar is in an 18 hour orbit. The HEO coverage occurs roughly in the pre-noon/pre-midnight, post-noon/post-midnight and dawn/ dusk regions of the inner magnetosphere. Polar covers the pre-noon/pre-midnight region. HEO 94-026 and 95-034 provide coverage generally for L\* 4 while HEO 97-068 covers L\* 2 and Polar covers L\*3. These data are combined to provide a picture of the evolution of the energetic electrons with time, local time, L and energy. These combined observations will be presented and discussed in terms of the development of the storm from the electron perspective at mid to high latitude. We will also compare these off-equator observations to the observations taken near the equator by LANL geosynchronous and GPS satellites.

**GA3.05/E/11-B3 1620**

**STORM ASSOCIATED HRE (HIGHLY RELATIVISTIC ELECTRON) EVENTS OBSERVED IN LOW EARTH ORBIT**

Richard A. GOLDBERG (NASA Goddard Space Flight Center, Laboratory for Extraterrestrial Physics, Code 690, Greenbelt, MD, USA, email: richard.a.goldberg.2@gsfc.nasa.gov); W. Dean Pesnell (Nomad Research Inc., Bowie, MD 20716, USA, email: pesnell@nomadresearch.com); David L. Chenette, Edward E. Gaines, Michael Schulz (all at Lockheed Martin Advanced Technology Center, Lockheed Martin, Palo Alto, CA 94304, USA, email: chenette@spasci.com) Charles H. Jackman (NASA Goddard Space Flight Center, Laboratory for Atmospheres, Code 916, Greenbelt, MD 20771, USA, email: jackman@assess.gsfc.nasa.gov)

Highly relativistic electrons populate the trapped radiation belts especially during the recovery phases of geomagnetic storms (as indicated by Dst). Their subsequent precipitation can be energetically important for the upper atmosphere and thus needs to be characterized in terms of spectral energy distribution, spatial extent, and frequency of occurrence. We have studied the characteristics of HRE events for E > 0.3 MeV from Oct 1991 through Sept 1994 with data from the High-Energy Particle Spectrometer (HEPS) aboard UARS. Each event has a characteristic signature such that the delay to onset and the event duration seem to increase with particle energy over the indicated range. Energy-time maps of the electron flux have been refined to distinguish between trapped and precipitating electrons and (in this context) to separate measurements by hemisphere (north vs south) in bins of width DL = 1/4. The minimum L at which HRE events could be discerned seemed to increase with time during the 3-year interval studied (i.e., during the declining phase of Solar Cycle 22).

**GA3.05/W/42-B3 1640**

**MULTIPLE DISCRETE-ENERGY ION FEATURES IN THE INNER MAGNETOSPHERE**

Xinlin Li and D.N. Baker (LASP, University of Colorado, 1234\ Innovation Drive, Boulder, CO 80303-7814, USA; 303-492-3514; email: lix@kitron.colorado.edu); M Temerin (SSL, UC Berkeley, CA 94720, USA); W K Peterson (Lockheed Martin, Palo Alto, CA 94304, USA); J Fennell (Aerospace Corporation, Los Angeles, CA 90009-2957, USA);

Recent measurements from the ion composition sensors (CAMMICE/MICS and TIMAS) on board the POLAR satellite often show multiple peaked spectra, which are seen as multiple bands in energy-time plots. Although similar phenomena had also been observed by CRRES satellite around its apogee ( $r=6.3R_E$ ) and were interpreted as a possible drift echo effect [Grande et al., 1992].

POLAR data reveal that these multiple bands of ion fluxes are over a very large range of L (L=2.5-7) and energy (a few keV to hundreds of keV) independent of the charge and mass of the ions. Our test particle simulation shows that these multiple bands are a manifestation of drift echoes of different energy ions. Initial injection of these ions into the inner magnetosphere is caused by earthward propagating time-varying fields associated with a dipolarization process during a substorm onset. Modeling these multiple discrete-energy ion features provides valuable new information about how deep into the magnetosphere impulsive electric fields and changes in magnetic fields can penetrate.

**GA3.05/W/38-B3 1700**

**SIGNATURES OF MAGNETIC FIELD EFFECTS ON RING CURRENT DEVELOPMENT AND DECAY FOR THE JUNE 4-5, 1991 STORM**

M. W. LIEMOHN, J. U. Kozyra (both at: Univ. of Michigan, 2455 Hayward, Ann Arbor, MI 48109, USA, email: liemohn@umich.edu); M. F. Thomsen (Space and Atmospheric Sciences, MS D466, LANL, Los Alamos, NM 87545, USA); J. L. Roeder (The Aerospace Corp., MS: M2/260, P. O. Box 92957, Los Angeles, CA 90009, USA); P. Song (Univ. of Michigan, 2455 Hayward, Ann Arbor, MI 48109, USA); J. E. Borovsky, and T. E. Cayton (both at: Space and Atmospheric Sciences, MS D466, LANL, Los Alamos, NM 87545, USA)

This study investigates the effects of a greatly compressed magnetic field on the development and decay of the ring current during the June 4-5, 1991 geomagnetic storm. Observations from both the LANL geosynchronous orbit satellite 1989-046 and the CRRES satellite show magnetosheath encounters on June 5, indicating that the magnetic field is highly compressed and/or distorted. To study the effects of these distortions on the near-Earth plasma transport, the RAM code is used to simulate the energetic ion motion in the inner magnetosphere, using geosynchronous orbit data for boundary condition inputs. The results are compared with CRRES MICS and LANL MPA data. The effects of various processes on the propagation and precipitation of the particles are examined, including effects of ion demagnetization and non-adiabatic motion, the time-varying geomagnetic field, and dayside compression of the magnetopause. These processes increase the loss rate of the ring current, and their relative importance to ring current dynamics is investigated and discussed.



**GA3.05/W/10-B3** **1720**

**SCATHA OBSERVATIONS OF DISPERSING ION SIGNATURES IN THE INNER MAGNETOSPHERE**

R. J. STRANGEWAY (Institute of Geophysics and Planetary Physics, University of California, Los Angeles, CA 90095, USA, Email: strange@igpp.ucla.edu); H. L. Collin (Lockheed Martin ATC Space Physics Lab., 3251 Hanover St., Palo Alto, CA 94304, USA, Email: collin@spasci.com)

The Spacecraft Charging at High Altitudes (SCATHA) spacecraft was launched in the late 1970's into a near geosynchronous orbit. Included in the instrument complement was an ion composition experiment which could measure ions with energies in the range 0.1 to 32 keV/e, and resolve masses up to and including singly charged Oxygen. In this paper we will review SCATHA ion composition observations, emphasizing the occurrence of dispersing ion signatures. Through comparisons with theoretical predictions of the drift path trajectories we will determine the source location of the dispersing ions. We will further address the question of whether these dispersing ions are injected locally, i.e., injected from the ionosphere, or if they correspond to pre-existing magnetospheric plasma populations that have been accelerated by induction electric fields.

**GA3.05/W/09-B3** **1740**

**THE "MAIN" SUBSTORM AS A MAJOR SOURCE OF STORM-INJECTED RADIATION BELT ENERGETIC ELECTRONS**

Lyudmila V. TVERSKAYA (Skobeltsyn Institute of Nuclear Physics, Moscow State University, Moscow, 119899, Russia, email: tverskaya@taspd.npi.msu.su)

As the author has proposed earlier, the major storm-time injection of energetic radiation belt electrons takes place when west auroral electrojet is shifted to its lowest latitude position during the storm main phase. Particles are injected into the field weakened by the ring current. On the storm recovery phase particle's energy must markedly rise adiabatically. As has been shown recently, an injection of relativistic electrons at L~3 really takes place on a time scale of "main" substorm. That substorm is characterized by the lowest latitude position of auroral electrojets during the storm main phase. The results of coordinated analysis of night-side trapped radiation boundary collapse in the equatorial plane and the ground magnetic data are presented. An appearance of the injected electrons of up to ~5 MeV energy during the "main" substorm was registered on the GLONASS satellite on the several-minutes time scale. Data on several-MeV electrons from RELAY-1 are analysed too. As is shown, position of the intensity maximum of storm-time injected relativistic electrons (Lmax) is in a good consistence with the previously reported formula:  $|Dst|_{max} = 27500/(Lmax)^{4.4}$ . The roles of "main" substorms and sudden impulses in formation of the storm "new" radiation belts are compared. The cases of "fast" collective shift of the outer radiation belt are discussed too. It is shown that both recently registered cases and the observed in 60-s may be well explained in a framework of the theory of particle transport under the influence of sudden impulses.

**Wednesday 28 July AM**

**GA3.05/E/18-B3** **0900-01**

**MODELING FIELD-ALIGNED POTENTIALS PRODUCED BY NON-ADIABATIC ION MOTION IN THE PLASMA SHEET**

Maha ASHOUR-ABDALLA, Vahe Peroomian (Both at UCLA-IGPP, Box 951567, Los Angeles, CA 90095-1567, USA, e-mail: mabdalla@igpp.ucla.edu); Lev M. Zelenyi (Space Research Institute, Academy of Sciences, Moscow, Russia, e-mail: IZelenyi@iki.rssi.ru)

Previous studies of the effects of ion nonadiabaticity on the magnetotail indicate that, even for steady solar wind conditions, the magnetotail evolves into a quasi-steady state with periodic oscillations. In this study, we employ a self-consistent large-scale kinetic model to evaluate the contribution electrons make to the dynamics of the magnetotail. Because of their small inertia, electrons should have an nearly equilibrium Boltzmann distribution along field lines, and thus parallel electric fields should result, which would assure charge neutrality. The parallel potential has a pronounced disturbing influence on ions, accelerating or decelerating them along field lines and causing drifts across field lines. Including in our model the effects of electron heating during convection enhances this tendency. We discuss the self-consistent pattern of parallel potentials in the magnetotail and the inner magnetosphere that result from the motion of non-adiabatic ions and charge-neutralizing Boltzmann electrons.

**GA3.05/W/46-B3** **0900-02**

**SIMULATION OF ION COMPOSITION OF THE EARTH'S RADIATION BELTS**

BASHKIROV

Abstract not available at time of going to press

**GA3.05/W/33-B3** **0900-03**

**CHARGED PARTICLE ACCELERATION BY WEAK AND STRONG ELECTROSTATIC TURBULENCE IN THE INNER AURORAL MAGNETOSPHERE**

Peter BESPALOV (Institute of Applied Physics, Russian Academy of Science, 46 Ulyanov st., Nizhny Novgorod, 603600, Russia, Email: peter@appl.sci-nnov.ru)

Magnetic field-aligned electric currents are typical for the auroral magnetosphere. In our opinion, the regions with field-aligned current can be responsible for effective charged particle acceleration in the high-latitude inner magnetosphere for stationary and nonstationary conditions, especially if a plasma turbulence exists. In this work, we analyze the acceleration processes. Accelerations of charged particles by a quasistatic electric field, by weak or strong plasma turbulence are taken into account. Solutions of stationary kinetic equation are found for acceleration by weak and strong plasma turbulence in an inhomogeneous magnetic field for different correlations between system time and space scales. The estimate of energy input shows the efficiency of the acceleration mechanism in such processes in the chosen parts of the energetic spectrum. This model contributes to understanding both the flux distribution of energetic particle at high latitudes and the global energy budget of the inner magnetosphere.

**GA3.05/E/19-B3** **0900-04**

**SPATIAL DISTRIBUTION OF ELECTRON FLUXES (>0.08 MEV) AT LOW L-SHELLS MEASURED IN THE EXPERIMENT ON BOARD "MIR-SPECTR" ORBITAL COMPLEX.**

A.V.BOGOMOLOV, G.Ya.Kolesov, Yu.I.Logachev, I.N. Myagkova (all at Skobeltsyn Institute of Nuclear Physics, Moscow State University, Vorob'evy Gory, 119899 Moscow, Russia).

Fluxes of electrons with the energies >80 keV were measured in the experiment "GRIF-1" onboard the module "SPECTR" of orbital station "MIR" at altitude ~400 km since October 1995. The complex of instruments "GRIF-1" includes the charged particle detectors with large and small geometrical factor. It permits to measure the variations of electron fluxes both in the Earth's Radiation Belts and in the regions closed to the geomagnetic equator. The higher fluxes of >0.08 MeV electrons were detected near L=1.4, L=1.7 and L=2.2. Maps of electron spatial distribution and L-B diagrams at the altitude 400 km are obtained.

**GA3.05/W/06-B3** **0900-05**

**CASE STUDY OF THE INNER MAGNETOSPHERIC CONVECTION DURING TWO RECENT GEOMAGNETIC STORMS**

A. BOONSIRISETH and R. M. Thorne (both at Dept. of Atmospheric Sciences, UCLA, 405 Hilgard Ave. MS7127, Los Angeles, CA, 90095, email: amyb@atmos.ucla.edu); G. Lu (NCAR/HAO, P.O.Box 3000, Boulder, CO 80307-3000)

Due to the important role that convection plays in particle and energy transport into the inner region of the magnetosphere during a geomagnetic storm, there has been many past and present attempts of modelling the electric field. But to date, the electric field models for the inner magnetosphere have been unable to reproduce the large variations seen during storms. This project will involve a case study of the convective electric field during two recent storms and Jan. 10 and May 15, 1997. The dependence of the electric field on several solar wind parameters (BIMF, Pdyn) will be carefully analyzed using data from WIND and an electric field mapped from ionospheric potentials generated by AMIE with T96 magnetic field model. The region covered by this study ranges from L=2.5Re to L=6.5Re for all local times. Each major feature of the electric field throughout both storms will be studied in relation to solar wind and IMF changes. The conclusions of this study will hopefully provide some basis for future convection modelling efforts.

**GA3.05/W/11-B3** **0900-06**

**PLASMASPHERIC MATERIAL AT THE RECONNECTING MAGNETOPAUSE**

Yi-Jiun SU, JOSEPH E. BOROVSKY, Michelle F. Thomsen, David J. McComas, and Richard C. Elphic (Space and Atmospheric Sciences Group, Los Alamos National Laboratory, Los Alamos, New Mexico 87544, USA, Email: ysu@lanl.gov; jborovsky@lanl.gov; mthomsem@lanl.gov; dmccomas@lanl.gov; relphic@lanl.gov)

During geomagnetic storms, cold and dense plasmaspheric material is observed to drain toward the dayside magnetopause when the solar wind pressure is strong and the IMF is southward. What is the fate of draining plasmaspheric material at the magnetopause? Does the plasmaspheric material participate in the dayside reconnection? In this study, we will present observations from Los Alamos Magnetospheric Plasma Analyzers at geosynchronous orbit during such plasmaspheric drainage events. For a set of events where cold plasmaspheric material is observed immediately adjacent to the magnetopause/ low-latitude boundary layer, we examine the detailed ion distributions, from ~1eV to ~40keV, for evidence that the draining plasmaspheric ions and the entering magnetosheath ions are simultaneously present on the same flux tube, which is a signature that the plasmaspheric flux tubes experience reconnection. In a preliminary examination of 18 such events during 1997-98, four cases were found where the plasmaspheric ions appeared simultaneously with magnetosheath-like plasma. In one of the four cases, the draining plasmaspheric ions appear to be energized by the reconnection process. We will present the results of a more extensive study, extending back to the previous maximum of the solar cycle. The results have significant implications regarding the fate of draining plasmaspheric material at the magnetopause and, indeed, regarding the parameters controlling the operation of dayside reconnection.

**GA3.05/W/47-B3** **0900-07**

**THE JANUARY 1997 STORM AS SEEN WITH THE SALAMMBO 3D CODE**

BOURDARIE

Abstract not available at time of going to press

**GA3.05/E/22-B3** **0900-08**

**THEORY AND MODELING OF RELATIVISTIC ELECTRONS ASSOCIATED WITH SUBSTORM INJECTIONS**

ANTHONY A. CHAN, Hee-Jeong Kim, Richard A. Wolf (all at Department of Space Physics and Astronomy, MS 108, Rice University, Houston, TX 77005, USA, Email: anthony-chan@rice.edu); and Joachim Birn (NIS-1, MS D466, Los Alamos National Laboratory, Los Alamos, NM 87545, USA)

The adverse effects of MeV electrons on technology and on humans in space has brought renewed interest to the problem of understanding the sources and dynamics of these energetic particles. Ongoing measurements, often from multiple spacecraft, are enabling the best characterization yet of the phenomenology of the electron flux variations and of the solar wind and magnetospheric conditions which are correlated with the large, potentially-damaging flux increases, but much work remains in order to fully understand the underlying physical mechanisms. Theory and simulation efforts will be reviewed with emphasis on identifying the physical processes responsible for the transport and acceleration of relativistic electrons in Earth's magnetosphere during magnetic storms. Recent calculations of rapid injection of energetic plasma sheet electrons to an outer trapping region, followed by subsequent slow radial transport to the inner magnetosphere, will be presented.

**GA3.05/E/04-B3** **0900-09**

**CEP EVENTS DURING THE MAY 2-4, 1998 STORM PERIOD**

Jiasheng CHEN, Theodore A. Fritz, and Harlan E. Spence (all at Center for Space Physics, Boston University, 725 Commonwealth Avenue, Boston, MA 02215 USA, http://buspace.bu.edu/EPG/jiasheng/chen.html, email: chen@buasta.bu.edu)

The POLAR spacecraft has observed five large cusp energetic particle (CEP) events in the high altitude dayside polar cusp during the May 2-4, 1998 geomagnetic storm period. Two events were detected on May 2 at about 2:10 and 19:00 UT, two events were detected on May 3 at 13:42 and 17:42 UT, and one event was detected on May 4 at 5:30 UT. They have event durations of about 4.7, 8.4, 3.0, 0.6, and 6.6 hours, in which the time averaged Data values were about -4, -65, -60, -68, and -180 nT, respectively. The second event had the longest CEP event time period since the discovery of the CEP event in 1996 [Chen et al., GRL, 24, 1447, 1997]. It is found that the ion flux in the 5/4/98 CEP event is two to three orders of magnitude larger than that in the 8/27/96 CEP event over the energy range of 20-2000 keV. The simultaneous observations indicated that in the energies of 60-1400 keV the ion fluxes in the



cusps were higher than that in locations including upstream from the bow shock, downstream in the magnetosheath, and magnetopause. These new observations support previous discovery [Chen et al., JGR, 103, p.69, 1998] that the high-altitude dayside cusp is a new acceleration region of the magnetosphere.

**GA3.05/W/03-B3** Poster **0900-10**

**EVOLUTION OF PLASMASPHERIC REFILLING: COMPARISON OF OBSERVATIONS WITH AN INTERHEMISPHERIC PLASMASPHERE MODEL**

R. H. COMFORT, P. G. Richards, J-H Liao, (all at The University of Alabama in Huntsville, CSPAR, TH S101, Huntsville, AL 35899, USA, Email: comfortr@cspar.uah.edu); P. D. Craven (NASA/Marshall Space Flight center, Space Sciences Laboratory, ES 83, Redstone Arsenal, AL, 35812, USA, Email: Paul.Craven@msfc.nasa.gov.)

The evolution of the plasmasphere is closely coupled to processes governing flux tube refilling and transport. In this study we follow this evolution through a series of sequential ion observations made by the Retarding Ion Mass Spectrometer (RIMS) on the Dynamics Explorer 1 (DE1) satellite and with the intervening time intervals filled in by simulations made with the Field Line Interhemispheric Plasma (FLIP) model. The FLIP model solves the continuity and momentum equations for the major ion species as well as the energy equations for ions and electrons along entire flux tubes from 100 km altitude in both hemispheres. Convection has recently been included in the code, driven by a dawn-dusk electric field model. Since the observations are necessarily restricted to two local time passes through the plasmasphere per orbit, the FLIP code will follow the observed flux tubes as they corotate and convect through the other local times. The period of DE1 (~7 hours) is such that nearly the same flux tubes are observed every second day, or every sixth orbit. The intervening observations provide additional information regarding longitudinal variations. Simulations will use the initial plasmasphere observations to define initial conditions of where the plasmopause is located and the extent of filling in the plasma trough. The composite of observations and simulations allows assessment of the degree to which the FLIP simulations accurately describe the processes which govern flux tube refilling over the two-day period between observations on the same flux tubes. To the extent that the convection electric field model in the FLIP code is accurate, this composite also provides a global picture of what is happening in and near the plasmasphere during the period. Of particular interest are changes in plasma composition as refilling proceeds.

**GA3.05/W/37-B3** Poster **0900-11**

**PRECIPITATION OF THE RING CURRENT IONS DUE TO TURBULENT DIFFUSION AT ION-CYCLOTRON WAVES**

A. G. DEMEKHOV, D. L. Pasmanik, and V. Y. Trakhtengerts (all at: Institute of Applied Physics, Russian Academy of Science, 46 Ulyanov st., 603600 Nizhny Novgorod, Russia; e-mail: andrei@appl.sci-nnov.ru)

Results of self-consistent calculations of the pitch angle and energy distribution of the ring current (RC) protons due to the charge-exchange processes and pitch angle diffusion at ion-cyclotron waves are presented. Spatial and temporal dependence of the energetic proton source and background plasma density is taken into account. Energetic ion lifetime is shown to be strongly affected by wave-induced loss processes during both main and recovery phases of a magnetic storm. The important role of the cold plasma evolution for the dynamics of the RC proton precipitation is demonstrated. Relation of the model results to satellite data on trapped and precipitated energetic ion fluxes is discussed.

**GA3.05/W/07-B3** Poster **0900-12**

**RAY TRACING AND THE POLARISATION OF ELECTROMAGNETIC ION CYCLOTRON WAVES IN THE MIDDLE MAGNETOSPHERE**

G. Dowdell, B. J. FRASER, and Y. D. Hu (Physics Department, CRC for Satellite Systems, University of Newcastle, NSW, 2308, Australia, email: pbhjf@cc.newcastle.edu.au)

The proton cyclotron instability generates electromagnetic ion cyclotron (EMIC) waves, which propagate in the left-hand (LH) polarised mode. It is therefore expected that LH polarised waves would predominate in the magnetosphere. However this is not the situation, and linear and right-hand (RH) polarised waves have been frequently observed by the GEOS-1/2, AMPTE/CCE and CRRES spacecraft in the equatorial region of the middle and outer magnetosphere. In a multi-ion plasma the existence of a crossover frequency associated with the presence of He<sup>+</sup> ions in a predominantly H<sup>+</sup> plasma has been invoked in the past to explain these linear and RH polarisations. It is difficult for this mechanism to explain the observation of linear and low ellipticities which are seen over a wide range of geomagnetic latitude. It is shown in this study using ray tracing techniques that the wave normal angle increases rapidly with propagation off the equator in response to the inhomogeneous medium. Polarisation analysis performed in conjunction with ray tracing shows that this model can predict low ellipticities over a wide spatial range of latitude, in general agreement with AMPTE/CCE and CRRES results.

**GA3.05/W/23-B3** Poster **0900-13**

**INJECTED ENERGETIC IONS AT L~3-4 DURING THE EARLY MAIN PHASE OF THE LARGE MAGNETIC STORM ON 24 MARCH, 1991**

S.Y. Fu (Max-Planck-Institut für Aeronomie, D-37191 Katlenburg-Lindau, Germany Email: syfu@linmpi.mpg.de); B. Wilken (Max-Planck-Institut für Aeronomie, D-37191 Katlenburg-Lindau, Germany Email: syfu@linmpi.mpg.de); Q.G. Zong (Max-Planck-Institut für Aeronomie, D-37191 Katlenburg-Lindau, Germany Email: syfu@linmpi.mpg.de); Z.Y. Pu (Department of Geophysics, Peking University, Beijing 100871, China Email: zypu@pku.edu.cn)

Substorm-associated ion flux enhancements in the inner magnetosphere during the early stage of the large storm on 24 March, 1991 are investigated in this paper. The ion composition measurements are made by MICS onboard the CRRES satellite at L=3.2 (±0.3) and local time 1830 to 1900 LT in the time interval of interest. It is found that there are apparently two groups of ions intensified in the event. The low energy group (E/Q < 80 keV/e) of ions have a trapped distribution peaked at 90° (pancake PADs) and exhibit strong energy dispersion effects. In contrast, high energy ions (80 keV/e < E/Q < 140 keV/e) have intense fluxes at small pitch angles (butterfly PADs), and show peaks (E/Q ≈ 100 keV/e) in the energy spectra (flux vs energy per charge) for all four most abundant ion species. The striking differences in the energy and pitch angle distributions between these two groups of ions suggest different energization and transport processes. The first group of ions is possibly energized before they are convected by the gradient B drift to the dusk side and reach the position of the satellite. The second group maybe accelerated directly by the enhanced electric field (estimated magnitude is about 5 mV/m) and the diffusive process at high latitude moves them into the inner region.

**GA3.05/W/16-B3** Poster **0900-14**

**PC1 ULF WAVES...**

Dr Kanji HAYASHI (Department of Earth and Planetary Physics The University of Tokyo, Japan)

PC1 ULF waves are known to be typically enhanced in intensity and in extent of source distribution in the course of major magnetic storms, especially in the recovery phase. This well known fact, however, is a kind of those ingrained in the minds of researchers based on past statistics or on accumulation of impressive events. These after light shows of magnetic storm being appropriate to be named as PC1 storm are interesting to study how storm time plasma in the outer-inner magnetosphere is accommodated with producing free energy for the electromagnetic waves. In this paper results on spatial and temporal characteristics PC1 regions associated with magnetic storms are reported based on comprehensive analyses of data obtained by the semi-global network operated during the STEP period with induction magnetometers. Also we would like to propose that it is worth to devote some effort to achieve global network more plausibly for detecting PC1 waves especially in the plasmopause latitudes by linking established sites on Internet and by adding new sites in blank areas.

**GA3.05/E/12-B3** Poster **0900-15**

**POSSIBLE WAVE MODES FOR RELATIVISTIC ELECTRON SCATTERING AND STOCHASTIC ACCELERATION DURING MAGNETIC STORMS**

RICHARD B. HORNE (British Antarctic Survey, Madingley Road, Cambridge CB3 0ET, U.K., email: R.Horne@bas.ac.uk); Richard M. Thorne (Department of Atmospheric Sciences, University of California, Los Angeles, U.S.A., email: rmt@atmos.ucla.edu)

The possibility of electron stochastic energization to relativistic energies (> 1 MeV) via resonant wave-particle interactions during a magnetic storm is explored. The minimum electron energy Emin for cyclotron resonant interaction with various electromagnetic waves is calculated for conditions representative of storm-times. Since Emin > 1 MeV for resonance with L-mode ion cyclotron waves, intense stormtime EMIC waves could contribute to relativistic electron loss, but not acceleration. Inside the plasmopause whistler mode waves, and highly oblique magnetosonic waves near the lower hybrid frequency, can resonate with electrons over the important energy range from approximately 0.1 to 1 MeV. In low density regions outside the plasmopause, the whistler, RX, LO and Z modes can resonate with electrons over a similar energy range. These waves have the potential to contribute to the stochastic acceleration of electrons up to relativistic energies during magnetic storms.

**GA3.05/W/20-B3** Poster **0900-16**

**ACCELERATION OF ENERGETIC ELECTRONS AND PROTONS ON HIGH-LATITUDE FIELD LINES AT HIGH ALTITUDES**

Tatyana A. IVANOVA, Elmar N. Sosnovets, Lyudmila V. Tverskaya (Skobeltsyn Institute of Nuclear Physics, Moscow State University, Moscow, 119899, Russia, email: ivanova@taspd.npi.msu.ru)

We analyze the particle data from MOLNIYA-1 and GORIZONT satellites. Increases of tens-keV electron fluxes and fluxes of protons of the energies from tens keV to several MeV on the high latitude field lines are studied. Simultaneous data from on-ground geomagnetic observatories are analysed as well. An appearance of particles in the local time sector of dusk-night-early-dawn typically correlates with an increasing of magnetic disturbances on a corresponding field line on the phase of the substorm expansion. Since there are no significant proton fluxes in the interplanetary medium in that periods, the mentioned effect shows that protons of up to ~1 MeV energy are accelerated on high-latitude field lines in the magnetosphere. The possible mechanisms of acceleration are discussed. Variations of the energetic particle intensity with a period of several minutes through ~1 hour, measured in both day and late-dawn sectors of the magnetosphere at 5-7 Re are investigated. As is shown, synchronous variations of both proton and electron intensities are connected with the geomagnetic variations of DP-2 type and sudden impulses.

**GA3.05/W/18-B3** Poster **0900-17**

**ENERGETIC PARTICLES TRAPPED IN THE HIGH-LATITUDE DAYSIDE CUSP: COMPARISON WITH OTHER POPULATIONS AND THE PROBLEM OF ORIGIN**

A. E. Antonova, Yu.I. Gubar' and A. P. KROPOTKIN, (Skobeltsyn Institute of Nuclear Physics, Moscow State University, Moscow, 119899, Russia)

Model concept of energetic particle trapping in the high-latitude outer dayside magnetosphere associated with off-equatorial magnetic field minima, has been proposed long ago (Shabansky, 1972; Shabansky and Antonova, 1968; Antonova and Shabansky, 1975, 1976). Aside from the observational evidence of energetic particle enhancements in the corresponding regions which was obtained on several (mainly Soviet) spacecraft, and was analysed earlier, recent observations of energetic heavy ions, protons, and electrons in the dayside polar cusp, onboard INTERBALL (Savin et al., 1998) and POLAR (Chen et al., 1997, 1998; Sheldon et al., 1998) are shown to support the model (Antonova et al., 1998). A plausible origin mechanism for the dayside high-latitude particle fluxes consists of: (a) particle injection (and possible acceleration) during magnetospheric substorm activity on nightside; (b) drift-shell branching effect bringing near-equatorial (at nightside) particles to dayside high-latitude regions; (c) pitch-angle and cross-drift-shell diffusion of particles which eventually produces the locally trapped population. Comparative analysis of particle fluxes and energetic spectra in the cusp population and in the normal outer radiation belt favors such a scenario.

**GA3.05/W/48-B3** Poster **0900-18**

**INCREASES OF ELECTRON AND DPROTON FLUXES ON THE BOUNDARY OF OUTER RADIATION BELT IN APRIL 1994**

Gotselyuk, KUZNETSOV ( Skobeltsyn Institute of Nuclear Physics, Lomonosov Moscow State University, 119899, Moscow, Russia, e-mail: kuznets@srldan.npi.msu.ru)

Abstract not available at time of going to press

**GA3.05/E/08-B3** Poster **0900-19**

**VARIATIONS OF GEOMAGNETIC DISTURBANCE INDICES, CONTROLLING ENERGETIC PARTICLE TRANSVERSE DIFFUSION IN THE RADIATION BELTS**

A.V.Dmitriev, D.V. Kalinin, S.N.KUZNETSOV and B.Yu.Yushkov (all at Skobeltsyn Institute of Nuclear Physics, Lomonosov Moscow State University, 119899, Moscow, Russia, e-mail: kuznets@srldan.npi.msu.ru)

Energetic particle transverse diffusion is one of the main processes responsible for radiation

belt dynamics. The transverse diffusion coefficient is a function of geomagnetic disturbances. Different types of geomagnetic disturbances are observed: sudden storm commencements, magnetic storms and substorms which are characterized by certain indices such as number of SSC, Dst-variation, AE and Ap indices. We analyse these indices in connection with solar activity and tilt of the geomagnetic dipole to the ecliptic plane. Certain time variation of all these indices connected with solar activity 11-year cycle is obtained. Variation of the number of SSC on a shorter time scale were not found. 6-month and diurnal variation of magnetic storm number and AE and Ap indices was found. This variation is connected quantitatively with the tilt of the geomagnetic dipole to the ecliptic plane.

**GA3.05/W/36-B3** Poster **0900-20**

**TIME SCALES OF THE EARTH'S RADIATION BELTS VARIATION: ANALYSIS OF THE TIROS/NOAA DATA**

Yoshizumi MIYOSHI, Akira Morioka, and Hiroaki Misawa (all at Upper Atmosphere and Space Research Laboratory, Tohoku University, Sendai, 980-8578, Japan, email: miyoshi@stpp2.geophys.tohoku.ac.jp)

Many studies on the static and dynamic behavior of the earth's radiation belts have been performed. However, the response of energetic particles with respect to the external variations with the wide range of time scales has not been well known in detail except for the case of storm and sub-storm. The variability and its time scales of the radiation belts have important information to investigate generation and dissipation process of energetic particles, and driving parameters of the inner magnetosphere.

Using the data set of the TIROS/NOAA satellites during the long period of 1979-1998, we have performed analysis to derive characteristic time scales of the electron flux variation. As the result, the existence of the variation synchronized with the solar cycle in both the inner and outer radiation belts was confirmed. It was also shown that the radiation belts changed in relation to the various variability of the geomagnetic activity; i.e., annual and semi-annual variations, and the recurrent activity. Correlation studies between solar parameters and electron flux variations indicated that there was L-dependent phase lag between the sun spot number and the electron flux, and this phase lag was shorter compared with the diffusion time expected by the traditional radial diffusion.

**GA3.05/W/31-B3** Poster **0900-21**

**SYNCHROTRON RADIATION FROM THE EARTH'S RADIATION BELT: INVESTIGATION OF AKEBONO/PWS DATA**

Akira MORIOKA, Hiroaki Misawa, and Yoshizumi Miyoshi (All at: Upper Atmosphere and Space Research Laboratory, Tohoku University, Sendai, 980-8578, Japan, email: morioka@stpp2.geophys.tohoku.ac.jp.)

The radiation produced by relativistic electrons artificially injected into the earth's magnetosphere had been reported in 1960s. However, the radiation from natural relativistic electrons in the earth's radiation belt has not been detected. The EM waves at 3MHz observed with the Akebono satellite were investigated to search the synchrotron component from the earth's radiation belt. The statistical analysis using the data from 1989 to 1995 showed that the wave activity has a positive correlation with energetic electrons which were detected by the NOAA satellite: the linear relation between the 3MHz EM wave intensities and the flux of relativistic electrons. This result shows the first detection of the natural synchrotron radiation produced in the earth's radiation belt.

**GA3.05/W/02-B3** Poster **0900-22**

**DETERMINATION OF THE EFFECTS OF SUBSTORMS ON THE STORM-TIME RING CURRENT USING NEURAL NETWORKS**

V MUNSAMI (Hermanus Magnetic Observatory, P O Box 32, Hermanus, 7200, South Africa, E-mail: vmunsami@csir.co.za)

A controversy exists as to whether the injection of particles into the ring current is caused by the induced electric fields associated with the expansive phase of substorms or by the enhanced convection electric fields that are driven by the solar wind. In order to investigate the causal storm-substorm relation, an artificial neural network (ANN) is used to examine the relationship between the definitive, high time resolution (1 minute), auroral electrojet index (AL) and ring current index (SYM-H). The network is trained on data taken from the 10-year period between 1984 and 1994 in which substorm onsets are identified by Pi2 geomagnetic pulsations. The performance of the network and its implication to the effects of substorms on the storm-time ring current is discussed.

**GA3.05/E/17-B3** Poster **0900-23**

**A MODEL FOR ENERGY RELEASE DURING BURSTY BULK FLOW**

B P PANDEY (Indian Institute of Geomagnetism, Bombay 400 005, India, email: pandey@iig.iigm.res.in); G.S.Lakhina (Indian Institute of Geomagnetism, Bombay 400 005, India, email: pandey@iig.iigm.res.in)

A simple model for bursty bulk flows (BBFs) in terms of bursty type of driven reconnection is developed. A bursty type reconnection may be induced at the magnetopause boundary due to the solar wind forcing. The magnetic energy release during the current sheet reconnection is calculated. In this model, persistent plasma energization is provided by ongoing external driving. Possible implication of this mechanism on plasma acceleration is briefly discussed.

**GA3.05/W/41-B3** Poster **0900-24**

**SOME THIN EFFECTS IN ELECTRON PLASMA AT GEOSYNCHRONOUS DISTANCES**

Boris V. Marjin, Nikolay N. PAVLOV, Elmar N. Sosnovets, and Michail V. Teltsov (Skobel'tsyn Institute of Nuclear Physics, Moscow State University, Moscow, 119899, Russia, email: nnpavlov@taspp.npi.msu.ru)

We analyze the data from GORIZONT-35 for 1992-1994. Two spectrometers of electron plasma measured fluxes in field-align and field-perpendicular directions in the energy range 0.1-12 keV. Somewhat new approach of fitting the spectra with multi-Maxwellian distribution function is applied. The method allows us to recognize several simultaneously existing plasma populations and to trace their characteristic temperatures along time/orbit. Time resolution of 128 seconds disallows working in storm periods. Although in rather quiet geomagnetic conditions, such effect as entering a new population into the observed energy range and traversing the range by the temperature of this population is sometimes seen. Three populations exist in the 0.1-12 keV interval in those periods. In many cases the time of appearance of a new population coincides with an injection identified by A-indices. And in

many cases the changing of temperature of the injected population looks like cooling. We discuss possible explanation of this effect as either time- or spatial-based one, as well as either convective or injection nature of a new population. Total energy of each Maxwellian ensemble of plasma-electrons is estimated. Some other effects and results of statistical and correlation analysis performed for the measured data are also reported.

**GA3.05/W/32-B3** Poster **0900-25**

**CUSP ENERGETIC PARTICLES OBSERVED BY INTERBALL TAIL PROBE**

N.PISSARENKO, S.Savin, V.Lutsenko, I.Kirpichev, E.Budnik, A.Moszhukhina, E.Morozova (Space Research Institute, 117810, Moscow, Russia I.Sandahl (Swedish Institute of Space Physics, Box 812, 981 28 Kiruna, Sweden)

Observations made by the Interball Tail Probe in the Cusp region have found some events with s.c. Cusp energetic particles (CEP) - protons with energy 1-3 MeV. These increases continued during some tens minutes and went from the distance 1-2 Earth's radius as far as magnetopause. Most probably this population is trapped inside a diamagnetic cavity which was allowed by the origin of different disturbances in the high latitude geomagnetic field. The comparison with other phenomena showed the coincidence of such events with low frequency turbulence in the nearby plasma regions.

**GA3.05/W/19-B3** Poster **0900-26**

**FINE SPATIAL STRUCTURE OF THE OUTER RADIATION BELT IN QUIET AND DISTURBED CONDITION**

George POPOV (Irkutsk State Economics Academy, 11 Lenin str., Irkutsk 664015, Russia, Email: popov@isea.irk.ru); Vitalii Degtjarev, Sergei Sheshukov and Svetlana Chudnenko (all three at Institute of Solar-Terrestrial Physics, P.O.Box 4026,Irkutsk 664033, Russia, Email: shesh@istp.irk.ru); Geoff Reeves (Los Alamos National Laboratory, NIS-2, Mail Stop D-436, Los Alamos, New Mexico, 87545, USA Email: reeves@lanl.gov); Alan Johnstone (Mullard Space Science Laboratory, Hholumbury St.Mary, Dorking, Surrey RH5 6NT, UK, Email: adj@mssl.ucl.ac.uk)

It is well known, that data from simultaneous measurements of radiation on several geostationary spacecrafts distributed in longitude make it possible to reconstruct the spatial distribution (in magnetic coordinate system) of charged particles measured and L-values scanned ranges approximately from 6.6 till 7.0. Electron fluxes data from LANL geostationary spacecrafts were statistically treated and ordered in a special magnetic coordinate system. The data treating procedure allowed to obtain the dynamics of quasi-trapped electrons of different energies on different L-shells. It was found, that a rather permanent fine spatial structure of the quasi-trapped electrons exists with maximum of fluxes near L = 6.78 and MLT=12. This structure looks like asymmetrical "mini-belt". The position of the maximum depends of the electron energy (the more is the energy, the smaller is the L - value) and changes with magnetic activity. Dynamics of this "mini-belt" for both quiet and disturbed periods is illustrated and discussed. During isolated magnetic storms the mini-belt maximum shifts in regular manner outward and inward; a diffusion wave of quasi-trapped particles propagates from outside of the geostationary orbit and serves as a source of new particles for mini-belt. The azimuthal geometry of this diffusion wave extracted from experimental data is illustrated. The possible role of fine spatial structure is discussed in relation with well-known "anomalous" dynamics of the inner radiation belt.

**GA3.05/W/15-B3** Poster **0900-27**

**RESONANT ENHANCEMENT OF RELATIVISTIC ELECTRON FLUXES**

ILAN ROTH AND Mike Temerin (SSL, UC Berkeley, CA 94720, USA, Email: ilan@ssl.berkeley.edu), Mary Hudson (Dartmouth College, NH 03750, USA)

The enhancement in the flux of relativistic electrons during active geomagnetic periods is of major importance as use of the near-earth space environment increases. Enhancement of energetic electron fluxes at L ~ 4-5 were observed during geomagnetic storm intervals, as well as during quieter times following high speed solar wind stream arrival at 1 AU. The HIST instrument on the POLAR satellite measured numerous large enhancements in f(L) at low L shells during active periods, as well as increase at L=4.5 of <1 MeV electrons which precedes increase in the >1 MeV, without significant flux increase initially at higher L values. This observation, and others by HEO spacecraft suggest that a local heating mechanism may be operative. It is suggested that the ubiquitous, obliquely propagating whistler waves interact with electrons which bounce along the geomagnetic field lines. The unducted whistler chorus which is a typical signature of the substorm expansion phase, interacts with the seed of sub-relativistic electrons. For an oblique wave propagation the energetic electrons with large gyroradius (larger than the perpendicular wavelength) can interact resonantly with multiple harmonics of the whistler waves on their bounce trajectories along the inhomogeneous magnetic field. Whistler waves, which propagate obliquely to the magnetic field, can interact with energetic electrons through Landau, cyclotron, and higher harmonic resonant interactions when the Doppler-shifted wave frequency equals any (positive or negative) integer multiple of the local relativistic gyrofrequency. This interaction occurs over large spatial distances when an electron is bouncing in the terrestrial magnetic field. The resulting resonant interaction violates the first and the second adiabatic invariants and results in electron energization at relativistic energies. The analysis of the energization with the help of particle and Hamiltonian simulations of these interactions are presented.

**GA3.05/E/23-B3** Poster **0900-28**

**A PI2 ONSET AS OBSERVED AT GEOSYNCHRONOUS ALTITUDE.**

O. SAKA, (Dept. Phys. Kurume National College of Technology, Kurume, Japan and Dept. Earth and Planetary Sci., Kyushu University, Fukuoka, Japan); D.N. Baker, (Laboratory for Atmospheric and Space Physics, University of Colorado, Boulder, CO, USA)

The initial responses of the magnetic field lines at Pi 2 onset are examined in the midnight sector of geosynchronous altitude (L~6.6). The onset of the Pi 2 disturbances at the satellite altitude is determined by employing the ground magnetometer station at the dip-equator (Huancayo, Peru) located in the meridian of the geosynchronous satellites, Goes 5 and 6. The initial disturbances at L~6.6 are characterized by a decrease of the field magnitude B, an increase of the radial component V, and a nearly equal opportunity of increase/decrease of the northward component H. Based on the model calculation, we infer that the formation of the dusk-to-dawn current in the midnight sector at a L close to the geosynchronous altitude could invoke the initial disturbances outlined above.

**GA3.05/E/05-B3** Poster **0900-29**

**IONIZATION DYNAMICS OF THE F LAYER IN THE DIFFUSE AURORA AND SAR-ARC REGION**



Ievenko I.B., Khalipov V.L., Alexeyev V.N., STEPANOV A.E. (Institute of Cosmophysical Research and Aeronomy, Yakutsk 677891, Russia, email: ikfia@sci.yakutia.ru)

Study results of the subauroral luminosity dynamics and ionisation at heights of F2-layer on the ground-based photometric and ionospheric observation data at the Yakutsk meridian for  $K_p=3-5$  are present. The following features have been related: 1. At the beginning of prolonged magnetic activity (several hours) at latitudes of the brightening SAR-arc the increase of the F2 regular layer height with a velocity up to 30 m/s and the decrease of the electron density by 2-4 times are occurred. 2. Under the repeated increase of activity (the expansion phase of the next substorm) in the aftermidnight sector the polar edge is observed already equatorward of the diffuse precipitation boundary and shifted with the velocity of 20-50 m/s to the sounding station zenith. 3. Results of complex measurements suggest that SAR-arc and sporadic ionization motion equatorward of the diffuse precipitation zone is caused by the penetration of the magnetospheric convection electric field into the plasmasphere.

**GA3.05/W/35-B3** Poster **0900-30**

**SECOND-ORDER INTERACTIONS IN THE PLASMA SHEET**

Elena VILLALON (Northeastern University, Boston Ma 02115, USA, e-mail: villalon@ph.af.mil)

The nearly isotropic fluxes of low energy electrons ( $< 10$  keV), observed above the diffuse aurora can be attributed to interactions between quasi-electrostatic plasma waves and particles in the plasma sheet. Banded electrostatic cyclotron harmonic (ECH) emissions have been detected by the CREES satellite, near equatorial regions at the shells  $L = 3.5$  to 7. The frequency bandwidths of the ECH emissions extend between harmonic intervals of the electron gyrofrequency, and their spectrum can be quite broad. The ECH waves with a sufficiently broad frequency spectrum can satisfy the conditions for second-order resonance interactions with the low energy electrons. Second-order resonance interactions are characterized by variations of the frequencies as waves and electrons propagate along the field lines. The frequency variations along field lines maintain the resonance interactions for extended distances by compensating for magnetic field inhomogeneities. These concepts were originally applied by Villalon and Burke, J. Geophys. Res., 100 (1995), to the interactions of whistler and electrons, and they were proved to be very efficient to precipitate electrons into the atmospheric loss cone. Because the wave amplitudes that are known just outside the plasmasphere are low, it is not possible to explain electron precipitation with coherent interactions for a single frequency wave since they fall out of resonance due to the inhomogeneities. We investigate the effects that second-order interactions have in the coupling of ECH waves and electrons, and compare them to single frequency coherent electrostatic interactions.

**GA3.05/W/12-B3** Poster **0900-31**

**PITCH ANGLE DIFFUSION VIA CHAOS IN THE ELECTRON-WHISTLER MODE WAVE INTERACTION**

W J WYKES and S C Chapman, (University of Warwick, Coventry, UK)

We investigate the interaction between electrons gyrating about a uniform background magnetic field and two anti-parallel whistler mode waves as a mechanism for pitch angle diffusion and subsequent scattering into the loss cones as a source of auroral precipitation. For a single whistler wave (in the Earth's magnetosphere, for example), the wave couples with electrons propagating in an anti-parallel direction. There is no stochasticity and the system is Hamiltonian in form. The second whistler wave introduces chaos into the system. Near resonance with either of the waves, particles are still trapped and execute regular motion. Off resonance the orbits are stochastic. For small wave amplitudes the system is Hamiltonian to first order with two degrees of freedom. Numerically integrating the full system of equations we can investigate the growth of the stochastic regions as the wave amplitude increases. For small wave amplitudes regular KAM surfaces dominate phase space. When the wave amplitudes is increased stochastic orbits appear between the two resonances and as the wave amplitude increases further the stochastic region grows, until stochastic trajectories dominate phase space and regular trajectories are confined to close to the resonances. We calculate the Lyapunov exponents averaged over phase space for the full system of equations to quantify the degree of stochasticity in the system as a function of wave amplitude, wave frequency and particle velocity.

**GA3.05/W/49-B3** Poster **0900-32**

**DYNAMIC MODEL OF THE PROTON EARTH'S RADIATION BELT**

BASHKIROV

Abstract not available at time of going to press

**GA3.05/W/25-B3** Poster **0900-33**

**MULTIPLE SATELLITE STUDY OF THE MAY 1998 MAGNETIC STORM: RING CURRENT RESPONSE**

J F FENNEL, J L Roeder , J B Blake (The Aerospace Corporation, Los Angeles, CA, 90009, USA, email: joseph.f.fennell@aero.org); R. H. W. Friedel, G. D. Reeves and M. Henderson (Los Alamos National Laboratory, MS: D436, Los Alamos, NM 87545, United States); M. Grande (Rutherford Appleton Laboratory, Chilton- Didcot, OX110QX, United Kingdom); T. A. Fritz (Boston University, Boston, MA 02215, United States); S. Livi (Max Planck Institute for Aeronomy, Katlenburg-Lindau, Germany)

One of the problems of performing ring current studies with in-situ data has been the poor spatial/temporal sampling of the inner magnetosphere that has been provided by single satellite studies. Generally, the recent (since 1984) studies of the ring current have relied on single satellites in geotransfer or higher apogee orbits with periods of 10 hours or more. The recent observations taken by the Polar satellite in an 18 hour orbit are representative of this problem. For this study we combine the detailed composition observations from Polar CAMMICE experiment with proton observations by HEO (94-026, 95-034, and 97-068) satellites in ~12 hour orbits at different local times. The HEO coverage occurs roughly in the pre-noon/pre-midnight, post-noon/post-midnight and dawn/ dusk regions of the inner magnetosphere. Polar covers the pre-noon/pre-midnight region. The minimum Dst ~ -216 nT occurred on May 4, 1998 near 0530 UT. Polar was outbound through the near noon ring current region from ~0400 UT until it exited the plasma sheet and entered the magnetosheath (during the shock) near 0615 and again near 0645 UT. It did not resample the ring current until after 1920 UT on May 4. Adding the HEO data provides ring current traversals near 0000, 0500, 0600, 0800, 0830,1100, and 1400 UT on May 4 during the DST minimum and early storm recovery. These data are combined to provide a picture of the evolution of the ring current as a map of its peak position and outer and inner edges as a function of time and local time. The combined observations will be presented and discussed in terms of the development of the storm main phase and its initial recovery.

**GA3.05/W/13-B3** Poster **0900-34**

**SUBSTORM-ASSOCIATED PARTICLE POPULATIONS IN THE INNER MAGNETOSPHERE AS OBSERVED BY POLAR/CAMMICE AND CEPPAD**

N. Y. GANUSHKINA, T. I. Pulkkinen (Finnish Meteorological Institute, Helsinki, Finland); V. A. Sergeev (Institute of Physics, University of St. Petersburg, St. Petersburg, Russia); D. N. Baker, T. E. Turner (Laboratory for Atmospheric and Space Physics, University of Colorado, Boulder, CO, USA); M. Grande, B. Kellett (Rutherford Appleton Laboratory, Chilton, Didcot, UK); J. F. Fennell, J. Roeder (The Aerospace Corporation, Los Angeles, CA, USA); and T. A. Fritz (Boston University, Boston, MA, USA)

The Charge and Mass Magnetospheric Ion Composition Experiment (CAMMICE) and the Comprehensive Energetic Particle and Pitch Angle Distribution (CEPPAD) instruments onboard POLAR probe the substorm-associated composition of particle populations in the Earth's magnetosphere over the range of 6 keV/e to 400 keV/e. The periods when POLAR was near magnetic midnight (2200 - 0200 MLT) are considered. The plasma sheet thickness variations during the different substorm phases are examined in a statistical sense. The results are compared with global auroral images and their mappings to the magnetotail. On many passes a spectacular feature was found such as plasma sheet-like (10-50 keV) and radiation belt-like populations overlapped at L=5-6. It also has a sharp earthward boundary. The relationship of appearance of such events to the magnetic activity was examined. As many of these structures appear after substorm onset they could be the midlatitude prints of substorm-related inward injection of plasma material.

**GA3.05/E/14-B3** Poster **0900-35**

**DYNAMICS OF ANOMALOUS COSMIC RAY IONS STRIPPED IN THE OUTER ATMOSPHERE**

S.N.KUZNETSOV and B.Yu.Yushkov (both at Skobel'syn Institute of Nuclear Physics, Lomonosov Moscow State University, 119899, Moscow, Russia, e-mail: kuznets@srldan.npi.msu.ru)

The main problems in analysing the ACR radiation belt are developing of the model of charged particle nonadiabatic motion and finding the adiabatic motion boundary. We propose to use parameter "chi" for analysing the two different modes of motion. Here "chi" is the ratio of the particle gyration radius to the curvature radius of magnetic field line at the equator. We constructed a Poincare mapping for particle dynamics in a dipole field based on the quasi-adiabatic motion model. This method was applied to motion analysis of particles with variable charge (ions during their stripping). The life-times for particles with different "chi" and the adiabatic motion boundary for different L-shells were found. The probability of trapping for ACR ions stripped in outer atmosphere on different L-shells is analysed.

**GA3.05/E/13-B3** Poster **0900-36**

**PARAMETERS OF PARTICLE POPULATIONS IN THE INNER MAGNETOSPHERE, DETERMINED WITH A HELP OF DIFFUSION WAVES OF ELECTRONS**

MINEEV Yu.V. (Skobel'syn Institute of Nuclear Physics, Moscow State University, 119899, Moscow, Russia, e-mail: mineev@srldan.npi.msu.ru)

Onboard several satellites (Interkosmos and Cosmos series) rapid diffusion waves of energetic electrons were obtained with simultaneous shift of maxima within energy range 0.1-2.0 MeV towards low L-shells. These waves have high velocity, which is more than ring current velocity. They are an effective instrument to study the processes of acceleration, transport and losses of particles in the inner magnetosphere. Determining the diffusion wave velocity permits us to calculate the radial diffusion coefficient for outer radiation belt, that can not be easily obtained by other methods (for example, by solving the diffusion equation). The role of injection and fast radial diffusion during disturbed magnetospheric conditions and during the recovery phase of the storm in creating the electron population of the inner magnetosphere is discussed. The new calculated distribution function was used to estimate the electron's source time value corresponding to the definite radial diffusion coefficients and cross term (pitch-angle scattering and energy loss by Coulomb interaction, wave-particle interaction) for the inner radiation belt electrons during maximum and minimum solar activity. The connection between waves and spectral peculiarities of particles observed onboard several satellites are considered. The data of satellites Interkosmos-19 and Cosmos-1686 about energetic electrons fluxes profiles (L<2.5) are also better described by the diffusion under influence of the electric fields fluctuations.

**GA3.05/W/27-B3** Poster **0900-37**

**NORMALIZED >50 MEV PROTON FLUX MAPS FOR SPACE OPERATIONS**

E.G. MULLEN (Assurance Technology Corporation, Carlisle, MA 01741, email: mullen@assurtech.com); G. Ginot, M.S. Gussenhoven, D.H. Brautigam (Air Force Research Laboratory, Hanscom AFB, MA 01731); D. Madden (Institute for Scientific Research, Boston College, Newton, MA 02159)

Protons in the Earth's inner radiation belt are the source of Single Event Effects (SEEs) on low altitude satellites. Precise knowledge of the position of the belt in geographic coordinates is hampered by temporal variations, two of which are a) fluctuations in the Earth's magnetic moment and b) enhancements and additional peaks in proton fluxes beyond  $L = 1.8$ . The change in position, direction and magnitude of the Earth's magnetic moment has been substantial since the NASA AP8 models were constructed. In addition, a second peak in high energy proton fluxes was created during a very large magnetic storm in March 1991. Data taken on the APEX and CRRES satellites are used to produce three-dimensional contour maps of normalized flux of protons with energies >50 MeV in geographic coordinates. These maps may also be used to give relative probabilities of experiencing Single Event Effects (SEEs) in the Earth's inner radiation belt, and as such, have proven useful to operations on spacecraft such as the Hubble Telescope. To make the maps, the data are averaged in 3 degree by 3 degree bins in geographic latitude and longitude, and in 50 km steps in altitude. All geographic longitudes, and latitudes between +70 degrees and -70 degrees are covered. The altitude range extends from 350 km to 14,000 km. This geographic range includes the complete region of inner belt >50 MeV protons, except in the area of the South Atlantic Anomaly (SAA) below 350 km. The maps easily locate the SAA when ascending in altitude, and an "Indonesian Anomaly" when descending in altitude from above 15,000 km. They also clearly show the second proton peak falling within an envelope determined by the primary peak.

**GA3.05/E/01-B3** Poster **0900-38**

**OBSERVATIONS OF QUASI-TRAPPED ELECTRON FLUXES (>0.5 MEV) UNDER THE INNER RADIATION BELT ON BOARD "CORONAS-I" SATELLITE**

S.N. Kuznetsov, I.N.MYAGKOVA (both at Skobel'syn Institute of Nuclear Physics, Lomonosov Moscow State University, 119899, Moscow, Russia, e-mail: irina@srldan.npi.msu.ru)

Electrons with the energies >0.5 MeV were observed at altitude about of 500 km in the experiment on board 'CORONAS-I' satellite, launched in March 1994. Significant electrons



peaks at L=2.1-2.3, narrow electron peaks at L=1.6 and in the western side of Brazilian Magnetic Anomaly significant electron peaks near L=1.3 were observed during March-May 1994. Dependencies of anomalous electron in peaks on L, local and universal time, parameters of interplanetary medium and geomagnetic activity indexes for Northern and Southern hemispheres were studied. Empirical model of anomalous electron fluxes under radiation belt (for L<2.2) based on these studying results was built.

**GA3.05/E/15-B3** Poster **0900-39**

**ASSESSING THE ROLE THAT GEOCORONAL CHARGE EXCHANGE PLAYS AS A SOURCE FOR THE PLASMASPHERE**

Herbert O. Funsten, Joseph E. BOROVSKY (both at Space and Atmospheric Sciences Group, Los Alamos National Laboratory, Los Alamos, NM 87545, USA, email: jborovsky@lanl.gov), Michael W. Liemohn, and Janet U. Kozyra (both at Space Research Laboratory, University of Michigan, Ann Arbor, MI 48109)

The charge-exchange collisions between plasma-sheet (ring-current) ions and the hydrogen atoms of the geocorona produce cool protons that are trapped in the dipole portions of the Earth's magnetosphere. Theoretical estimates are presented which indicate that the production rate of these cool ions is a few tons per day in the magnetosphere or about 0.5 per cubic centimeter per day at geosynchronous orbit. With the use of computer simulations, the role of these charge-change ions in the refilling of the plasmasphere is studied. It is determined that these ions could be important for early time refilling and consequently could play a role as a catalyst for the late-time refilling.

**GA3.05/W/14-B3** Poster **0900-40**

**SIMULATION OF CME-DRIVEN RADIATION BELT PARTICLE ACCELERATION FOR SOLAR MAXIMUM EVENTS**

M. K. Hudson, S. R. ELKINGTON, and J. G. Lyon (Department of Physics and Astronomy, Dartmouth College, Hanover, NH 03755, email: mary.hudson@dartmouth.edu); J. B. Blake (Aerospace Corporation, Los Angeles, CA 90009)

The first CME-driven interplanetary shock events with radiation belt particle effects comparable to the 1989-1991 solar maximum have now been observed with the new millennium fleet of spacecraft. A 3-D global MHD simulation of the May 1-4 and Aug 27-28, 1998, events has been used to drive guiding center test particle trajectory simulations for both radiation belt electrons and protons. These are the first events to show clear trapping of solar energetic protons deep in the magnetosphere for this solar maximum, comparable for the case of the Aug 27-28 period with the Great Storm of March 24, 1991, in terms of trapping and acceleration mechanism. Effects of ring current buildup and recovery on the nonadiabatic loss and subsequent energization of protons as the background magnetic field dipolarizes are included in the analysis. While it appears that trapping of solar energetic protons is due to the initial shock compression of the magnetopause (Hudson, et al., 1997), dipolarization due to ring current recovery transports them radially inward increasing their energy above detector thresholds.

**GA3.05/W/43-B3** Poster **0900-41**

**VARIATIONS OF IONS O+ AND H+ ENERGY DENSITY IN RING CURRENT DURING MODERATE MAGNETIC STORM**

L. A. Dremukhina, Ya. I. FELDSTEIN, A. E. Levitin (Institute of Terrestrial Magnetism, Ionosphere and Radio Wave Propagation, Troitsk, Moscow Region, 142092, Russia, email: lgromova@izmiran.troitsk.ru) M. Greenspan (Department of Physics, University of Maryland, College Park, MD 20742, USA)

Observations of ions O+ and H+ energy density every 3 minutes in the magnetosphere equatorial plane at  $2 < L < 7$  by AMPTE/CCE satellite are used for analysis of contribution of the ring current and near-Earth plasma sheet to the observed on the ground Dst magnetic field variation in the course of moderate magnetic storm in November 1986. Based on DMS data on auroral plasma precipitations structural boundaries the location of boundary between the ring current and the current in the magnetospheric tail is determined. Relative contribution of ions O+ and H+ to the energetic of the ring current and adjacent plasma sheet region is evaluated. Characteristic times of the ring current decay at various L-shells for ions O+ and H+ are calculated and compared with values of the ring current decay parameter on the basis of ground geomagnetic data. Energy balance equation in the inner magnetosphere is used for modelling of magnetic field variations on the Earth's ground during magnetic storm in dependence on interplanetary medium parameters.

**GA3.05/W/40-B3** Poster **0900-42**

**ASYMMETRIC RESPONSE OF RING CURRENT TO SUDDEN SOUTHWARD TURNING OF IMF**

Kumiko HASHIMOTO (Communications Research Laboratory, Koganei, Tokyo 184, JP, email: hashimoto@crl.go.jp), Yusuke Ebihara (The Graduate University for Advanced Studies, JP), Takashi Kikuchi (CRL, JP) and Masaki Ejiri (NIPR, JP)

We have investigated the development of the ring currents caused by a sudden southward turning of IMF, by using INTERMAGNET magnetometer data in mid and low latitudes and a simulation of the ring current. A sudden southward turning of IMF Bz from +10 to -17 nT was observed by GEOTAIL at 17:19 UT on September 5, 1995. The southward turning was followed by magnetic H-component decreases at low latitudes in 17-23 MLT and by increases in 9-14 MLT, with a time lag of 9 min after the increase of the convection electric field as inferred from the polar cap magnetometer data. The local time asymmetry of the magnetic H component changed drastically after the northward turning of IMF depressed the convection electric field at 17:52 UT. The magnetic field decreased from evening to morning hours, and increased in early morning. We simulated the development of the ring current with a convection electric field calculated from the observed solar wind parameters, by applying the ring current model by Ebihara and Ejiri [1998]. The result of simulation shows that the enhanced convection electric field causes outflow of ring current particles which have been developed before the event. As a result, the ground magnetic field increases in the day-side. Consequently, the ring current condition before the event is crucial for the asymmetric ring current.

**GA3.05/E/10-B3** Poster **0900-43**

**EFFECT OF RADIATION BELT ORIENTATION AND STRENGTH ON GROUND GEOMAGNETIC FIELD VARIATIONS**

James M E, Som Sharma, H Chandra, P S Shah and R G RASTOGI, (Physical Research Laboratory and Gujrat University Ahmedabad 380 009, India, e-mail: parvs@prl.ernet.in)

Using the equatorial Dst(H) index as the indicator of the intensity of ring current, the relationship have been computed between daily means of Dst(H) and daily means of the northward (X) and eastward(Y) components of the geomagnetic field at world wide stations during 1958. Significant longitudinal and regional inequalities have been isolated related to the corresponding regional anomalies in the earths magnetic field. Quantitative explanations are found between the delta X / delta Y and the deviation of dipole meridian with respect to the ground magnetic meridian of the station.

**GA3.05/W/44-B3** Poster **0900-44**

**POST-STORM EVOLUTION OF HIGHLY RELATIVISTIC ELECTRON PITCH-ANGLE DISTRIBUTIONS**

Michael SCHULZ, David L. Chenette, and Edward E. Gaines (all at Lockheed Martin Advanced Technology Center, Palo Alto, CA 94304, USA, email: schulz@agena.spacis.com) Richard A. Goldberg (NASA/GSFC, Laboratory for Extraterrestrial Physics, Code 690, Greenbelt, MD 20771, USA, email: richard.a.goldberg.2@gssc.nasa.gov) W. Dean Pesnell (Nomad Research Inc., Bowie, MD 20716, USA, email: pesnell@nomadresearch.com)

This is a theoretical account of UARS electron observations described by Goldberg et al. (this session). Stormtime radial transport tends to increase phase-space densities of trapped relativistic electrons but typically leads to flux increases at specified energies only as the ring current decays. Flux enhancements at this stage are (for kinematical reasons) greatest for equatorially mirroring electrons, and so pitch-angle anisotropies are large. Subsequent pitch-angle diffusion broadens the flux enhancement to particles that mirror off-equator, thus gradually increasing low-altitude electron intensities on time scales ~ 20% of corresponding lifetimes against diffusion into the loss cone. This is because broadening and loss reflect distinct eigenvalues of the same diffusion operator. Corresponding time scales for post-storm growth and decay of off-equatorial electron intensities thus increase with electron energy above an L-dependent critical energy ( $E^* \sim 300$  keV at L = 3) for which electron lifetimes are shortest.

**GA3.05/W/04-B3** Poster **0900-45**

**MAGNETOSPHERIC ENERGETICS DURING STORMS**

Niescja E TURNER and Dan Baker (LASP, Univ. of CO, Boulder, CO 80309-0590 USA, Email: turner@daria.colorado.edu); Tuija Pulkkinen (Finnish Meteorological Institute, Helsinki, Finland); Vania Jordanova (University of New Hampshire); Gang Lu (HAO/NCAR); Mike Henderson (Los Alamos); Joe Fennell and Jim Roeder (Aerospace Corp.) Ted Fritz (Boston University)

Magnetospheric energy flow is traced through ten storms, with particular focus on the ring current. For each storm, we trace energy input into the magnetosphere, along with ring current energy calculated from POLAR CMMICE data. We calculate the energy density in the ring current using the MICS detector on the POLAR CMMICE experiment. Where available, we use a ring current model to correct for azimuthal asymmetry of the current and then multiply by the volume to estimate the total energy. Consideration is also given to ENA data as a proxy for ring current particle measurements in order to provide a more continuous data set. Energy input is estimated with the epsilon parameter. Additionally, AMIE data are used for several storms to trace the energy flow into the ionosphere through joule heating and auroral electron precipitation. The resulting time series of ring current energy, ionospheric joule heating, and auroral electron precipitation are then compared with the input energy, the measured Dst, and the measured AE in order to trace the evolution of the energetics of the system as a whole.

**GA3.05/W/05-B3** Poster **0900-46**

**MAGNETOSHEATH OXYGEN AND MAGNETOSPHERE PARTICLE TRANSPORT**

B. Wilken, Q.G. Zong, S. Y. Fu, S. Livi, U. Mall (all at Max-Planck-Institut fuer Aeronomie, D-37191 Katlenburg-Lindau, Germany Email: wilken@linmpi.mpg.de); M. Grand (Space Science Division, Rutherford Appleton Laboratory, Chilton, Didcot, Oxon, England) T. A. Fritz (Boston University, Boston, USA)

Particle spectrometer HEP-LD onboard Geotail frequently detected impulsive flux enhancement of energetic oxygen ions in the duskside magnetosheath. These oxygen ions are usually moving in a downstream direction. In all cases the observed events are related to geomagnetic activity such as substorms and magnetic storms. In some favourable cases it was possible to compare the magnetosheath flux level of oxygen ions with the flux level in the adjacent magnetosphere. It was found that the magnetospheric flux was too low to serve as a local source for particle leakage. Occasional observations of anisotropic oxygen ions in the outer magnetosphere during substorm activity may provide a clue for the oxygen transport.

**GA3.08** Saturday 24 – Monday 26 July

**MAGNETOTAIL DYNAMICS AND RELATIONSHIP TO HIGH-LATITUDE IONOSPHERIC PHENOMENA**

Location: School of Education G33 LT (Saturday Only)  
Location: Gisbert Kapp E203 LT1 (Monday)  
Location of Posters: Gisbert Kapp, Coffee Room

**Saturday 24 July AM**

Presiding Chair: T. Nagai, (Tokyo Institute of Technology, Japan)

**GA3.08/W/21-A6** **0900**

**THE RESPONSE OF THE MAGNETOSPHERE TO AN INTERPLANETARY SHOCK: THE MAGNETOSPHERIC COMPRESSION ON SEPTEMBER 24, 1998**

C. T. RUSSELL, P. Chi, Guan Le, J. Raeder and R. J. Strangeway (All at Institute of Geophysics and Planetary Physics, University of California, Los Angeles, CA 90095-1567, USA, email: crussell@igpp.ucla.edu); H. J. Singer (Space Environment Center, NOAA, Boulder, CO, USA); H. Kawano (Kyushu University, Fukuoka, Japan); T. E. Moore (Goddard Space Flight Center, Greenbelt, MD, USA); W. K. Peterson (Lockheed Martin, Palo Alto, CA, USA)

At approximately 2344 UT on September 24, 1998 the nose of the magnetosphere was suddenly compressed by a strong interplanetary shock wave. As evidenced by successive compressions of the magnetic field at GOES 10, POLAR and GOES 8, the compressional wave moved rapidly through the magnetosphere. At POLAR the compression caused the magnetopause to move closer to the spacecraft, causing rapid cross field flows and altering the location of the conjugate point in the ionosphere. The pre-existing flows were heated locally only slightly by betatron acceleration because the flows were mainly field aligned.

Waves also did not lead to much heating because they were small in amplitude. Centrifugal heating may have been a more important local process. Some of the observed change in the plasma observed at POLAR was associated with the motion of the non-uniform polar cap outflow across POLAR. Snapshots of the polar cap by FAST confirm that the outward polar cap flows are non-uniform at this time but also show that strong heating is present and subsequently is very important in determining the outflow of plasma. Ground station recordings, synchronized with GPS signals, enable the disturbance to be followed through the magnetosphere from high latitudes to low. This event teaches us much about how the ionosphere is coupled to the magnetosphere and demonstrates the symbiosis of ground based, ionospheric and magnetospheric observations with modelling in magnetospheric studies.

GA3.08/W/09-A6

0920

## POLAR IONOSPHERIC OUTFLOW RESPONSE TO SOLAR WIND CONDITIONS AT 2-9 RE

Moore, T.E. and B.L. GILES (both at NASA Goddard Space Flight Center, Greenbelt, MD 20771 USA, Email: thomas.e.moore@gsc.nasa.gov), M.O. Chandler (NASA Marshall Space Flight Center, Huntsville, AL 35812 USA), M.R. Collier (NASA Goddard Space Flight Center, Greenbelt, MD 20771 USA), H.L. Collin (Lockheed Martin Advanced Technology Center, Palo Alto, CA, 94304 USA), R. Fitzenteit (NASA Goddard Space Flight Center, Greenbelt, MD 20771 USA), W.K. Peterson (Lockheed Martin Advanced Technology Center, Palo Alto, CA, 94304 USA), C.J. Pollock (Southwest Research Institute, San Antonio, TX 78228 USA), C.T. Russell and R.J. Strangeway (both at University of California, Los Angeles, CA 90024 USA)

We report observations of direct ionospheric plasma outflow response to the incidence of an interplanetary shock and associated coronal mass ejection upon the earth's magnetosphere. Data from the WIND spacecraft, 185 RE upstream of Earth, document the passage of an interplanetary shock at 23:20 UT on 24 Sept. 1998, traveling at 860 km/s. The polar cap plasma environment sampled by the POLAR spacecraft changed abruptly at 23:45 UT, reflecting a displacement of the previously remote plasma mantle to the vicinity of the spacecraft, as the shock propagated through the polar magnetosphere. At about 02:00 UT, POLAR reentered the lobe and polar wind, finding it had changed to a colder, slower, and denser outflow dominated by O<sup>+</sup> plasma. The O<sup>+</sup>-dominated outflow continued as the spacecraft passed through the northern cleft at ~4.5 RE and then the southern cleft at 1.8 RE (geocentric). Such a direct response of the ionosphere to solar wind pressure disturbances is of potential significance to the dynamics of the magnetotail.

GA3.08/W/17-A6

0940

## CENTRIFUGAL ACCELERATION OF IONS OBSERVED ON POLAR SPACECRAFT NEAR 9 RE OVER POLAR CAP UPON ARRIVAL OF CME-DRIVEN SHOCK

John B. CLADIS, Harry L. Collin, and William K. Peterson (all at Lockheed Martin Advanced Tech. Center, 3251 Hanover Street, B 255, Palo Alto, CA 94304, USA, email: cladis@spasci.com) Thomas E. Moore (NASA Goddard SFC, Code 692, Bldg. 2, Greenbelt, MD 20771-1000, USA, email: thomas.e.moore@gsc.nasa.gov) Christopher T. Russell (Inst. of Geophysics and Planetary Physics, UCLA, Los Angeles, CA 90095-1567, USA, email: crussel@igpp.ucla.edu)

A shock driven by a coronal mass ejection struck the magnetosphere about 2344 UT on September 24, 1998. The POLAR spacecraft was near apogee over the northern polar cap, at (X,Y,Z)GSM = (-2.3803, -2.7148, 8.1450) in RE. During the following 144 s, from 2345:18 UT to 2347:42 UT, (1) the magnetic field measured on-board with the UCLA magnetometer increased sharply from 126.16 nT to 182.00 nT; (2) the field components changed from (B<sub>X</sub>,B<sub>Y</sub>,B<sub>Z</sub>)GSM = (84.91, 32.55, -87.45) to (151.11, 50.655, -87.867); (3) the full rotation of B was 19.870; and (iv) the velocity components of both the H<sup>+</sup> and O<sup>+</sup> ions increased by about 75 km/s antiparallel to B. We suggest the ions were flung along -B by the "motion" of the magnetic field, according to the centrifugal-acceleration process first described by Cladis [GRL, 13, 893,1986]. A parallel-velocity increase of 35 km/s was computed by integrating the term  $d\mathbf{v}/dt = \mathbf{v} \times d\mathbf{e}/dt$ , using the local values of  $\mathbf{v}$  (the drift velocity) implied by the ion-velocity components perpendicular to the magnetic field and the measured values of  $\mathbf{e}(t) = \mathbf{B}(t)/B(t)$ . The higher acceleration of the ions was confirmed by a computer simulation of the process along the ion paths.

GA3.08/W/13-A6

0940

## FAST OBSERVATIONS DURING THE SEPTEMBER 24TH AND 25TH 1998 MAGNETIC STORM

R. J. STRANGWAY, C. T. Russell (both at: Institute of Geophysics and Planetary Physics, University of California, Los Angeles, CA 90095, USA, Email: strange@igpp.ucla.edu), D. M. Klumpp (Lockheed Martin Advanced Technology Center, 3251 Hanover St., Palo Alto, CA 94304, USA), C. W. Carlson, J. P. McFadden, R. E. Ergun (all at: Space Sciences Laboratory, University of California, Berkeley, CA 94720, USA), T. E. Moore (NASA Goddard Space Flight Center, Greenbelt, MD 20771, USA), and W. K. Peterson (Lockheed Martin Advanced Technology Center, 3251 Hanover St., Palo Alto, CA 94304, USA)

During September 24th and 25th 1998 the FAST spacecraft acquired data over the Northern Polar Cap in the noon-midnight local time sector. This allowed for detailed observations of the dayside cusp at ~ 4000 km altitude. The spacecraft was therefore ideally suited for monitoring the outflow of ionospheric plasma which was also observed at the higher altitude POLAR spacecraft. The interval around the Sudden Impulse (SI) at 23:45 UT on September 24th is characterized by enhanced field-aligned currents in the cusp region. Because the FAST orbital period is ~ 135 minutes, we can provide snapshots of the cusp region, and FAST passes through the cusp at ~ 00:10 UT on September 25th, some 35 minutes after the SI. The field-aligned currents at this time are significantly larger than on the previous orbit. Large fluxes of 100 eV oxygen ions are also observed to be flowing out of the ionosphere, with decreasing energy for increasing latitude. These ions form a conic in pitch angle, consistent with the "pressure cooker" model of ion acceleration, where transverse heating overcomes a downward electric field. As already noted the field-aligned currents are weaker on the previous orbit, and a weaker oxygen conic is also observed. This suggests that the main effect of the increased solar wind dynamic pressure is to enhance already existing ion outflow through an increase in the field-aligned currents and the associated parallel electric fields and ion heating in the cusp ionosphere.

GA3.08/W/05-A6

1040

## THE RESPONSE OF THE MAGNETOSPHERE TO AN INTERPLANETARY SHOCK: GROUND-BASED OBSERVATIONS OF THE SUDDEN IMPULSE ON SEPTEMBER 24, 1998

P. Chi, Guan Le, J. Raeder, C. T. RUSSELL and E. Zesta (All at Institute of Geophysics and Planetary Physics, University of California, Los Angeles, CA, USA, email: pchi@igpp.ucla.edu); K. Yumoto, H. Kawano and K. Kitamura (All at Kyushu University, Fukuoka, Japan); V. Angelopoulos (University of California, Berkeley, CA, USA); M. Moldwin (Florida Institute of Technology, FL, USA)

The strong interplanetary shock wave that intersected the front of the magnetosphere at about 2344 UT on Sept. 24, 1998, launched a compression of the magnetosphere that was followed around the globe by a new generation of magnetometers with rapid sampling and precise GPS-synchronized timing. Magnetometers of these chains included those in the Circum Pan Pacific Magnetometer Network, those in the IGPP/LANL array, those in the MEASURE array and those in the MACCS array. The event exhibited all the classical signatures of an SI including the preliminary decrease before the main increase in the H-component. The ability to model this event and its induced ionospheric currents using an MHD code allows us to compare the compression as it is seen in the magnetosphere with the response of the ionospheric currents.

GA3.08/W/02-A6

Invited

1100

## RECENT ADVANCES IN MAPPING MAGNETOTAIL BOUNDARIES USING SUPERDARN HF RADARS

Mervyn P. FREEMAN (British Antarctic Survey, High Cross, Madingley Road, Cambridge, CB3 0ET, U.K., email: M.P.Freeman@bas.ac.uk)

We review and discuss recent publications which have shown how HF radars can remotely sense magnetotail boundaries and thereby measure how these boundaries respond to changes in the IMF and to substorms. Specifically, we present the following: (1) Evidence for a relationship between the boundary plasma sheet/central plasma sheet (bps/cps) interface in the magnetotail and the equatorward edge of HF radar backscatter from the ionosphere or a latitudinal gradient in the Doppler spectral width of the backscatter. (2) Examples using this empirical relationship to track both rapid (of order 1 min) and slow (of order 1 h) changes in the ionospheric projection of the bps/cps interface. (3) Comparison of the time-varying location of the bps/cps interface observed in these examples with that predicted by a magnetic reconnection-based magnetospheric model using concurrent solar wind observations.

GA3.08/W/25-A6

1130

## ELECTRON PRECIPITATION AS A FUNCTION OF MAGNETOTAIL STRETCHING

THOMAS SOTIRELIS and Patrick T. Newell, The Johns Hopkins University Applied Physics Laboratory, Laurel, Maryland, 20723

A model for the differential energy flux of precipitating electrons from 32 eV to 30 keV is presented. The model spectra are keyed to the degree of magnetotail stretching as inferred from the precipitation itself. The result is less smeared and more flexible than previous work because a given portion of the oval—such as from the structured/unstructured boundary to the poleward edge of the oval—is averaged only with the appropriate precipitation. Data from twelve years and eight DMSP spacecraft are used. Extensive variations in the energy flux, average energy, and spatial extent of the precipitation are seen for different degrees of magnetotail stretching.

GA3.08/W/31-A6

1150

## AURORAL PRECIPITATION BOUNDARIES AND THE MAGNETOSPHERIC TAIL ENERGETICS FOR VARIOUS LEVEL OF THE MAGNETIC ACTIVITY

YA. I. FELDSTEIN, L. I. Gromova (Institute of Terrestrial Magnetism, Ionosphere and Radio Wave Propagation, Troitsk, Moscow Region, 142092, Russia, email: Igmova@izmiran.troitsk.ru) B. V. Rezhnev, G. V. Starkov, V. G. Vorobjev (Polar Geophysical Institute, Apatity, Murmansk region, 184200, Russia, email: vorobjev@pgi.kolasc.net.ru)

luminosity structure allow to suggest physically substantiated method of the plasma regimes boundaries identification (Newell et al.,1996; Feldstein and Galperin,1996). The interrelationship between these high-latitude plasma regimes in the nightside to dawnside sectors and plasma domains of the distant magnetosphere has been demonstrated. DMSP satellites data have been used for statistical investigation of the plasma regimes boundaries dynamics depending on the magnetic activity level. Boundaries determining the polar cap location (b6) and characteristic break of latitudinal variation of the electron energy (b2e) have been used to define the magnetic flux dynamics and to calculate the magnetic energy in the magnetospheric tail during the transition period from the quiet conditions to the very disturbed ones. P.Newell, Y. Feldstein, Y. Galperin, C.-I. Meng, JGR, 101,A5,10737-10748, 1996; Y. Feldstein, Y. Galperin, Cosmic Research,34, N3, 209-227, 1996.

GA3.08/W/22-A6

1210

## ENERGETIC IONS FROM THE POLAR SATELLITE AS TRACERS FOR PLASMA SHEET CONDITIONS

P. K. Toivanen, D. N. Baker, W. K. Peterson (LASP, University of Colorado at Boulder, Boulder, CO, USA, Email: petri.toivanen@lasp.colorado.edu) T. I. Pulkkinen (Finnish Meteorological Institute,Helsinki, Finland)

Observations from the POLAR satellite obtained by the Toroidal Imaging Mass-Angle Spectrograph (TIMAS) and by the MICS sensor of the Charge and Mass Magnetospheric Ion Composition experiment (CMMICE) frequently show multiple peaked distributions in energetic H<sup>+</sup> and O<sup>+</sup> ions (12–120 keV) in the dusk side magnetosphere. These ions are on open drift paths and thus drift from the tail plasma sheet to the dusk side geostationary region. Our earlier results suggest that, under certain geomagnetic conditions, these observations can be used to determine remotely characteristics of the plasma sheet over a large portion of the tail. In this study, we mainly address the large-scale electric field, which is responsible for the acceleration of these ions during their drift from the plasma sheet. To trace back the observed distributions, we use an ionospheric electric field model mapped to the plasma sheet together with a modified version of the T89 model in our drift model. These traced-back distributions are then linked to GEOTAIL observations, which show frequently pristine field-aligned O<sup>+</sup> beams on energy range up to a few keV originating from the ionosphere. Thus our final aim is to form a coherent picture of O<sup>+</sup> flow from the ionosphere to the plasma sheet and of consequent earthward transport and related acceleration of O<sup>+</sup> ions.

Saturday 26 July PM

Presiding Chair: Mark Lester, (University of Leicester, UK)

GA3.08/W/29-A6

Invited

1400

## OBSERVATIONS PERTAINING TO THE LOCATION OF THE SUBSTORM ONSET INSTABILITY

L. A. FRANK, J. B. Sigwarth and W. R. Paterson (All at: Department of Physics and Astronomy, The University of Iowa, Iowa City, IA, USA, email: frank@iowasp.physics.uiowa.edu) S. Kokubun (Solar-



Terrestrial Environment Laboratory, Nagoya University, 3-13 Honohara, Toyokawa, Aichi 442, Japan)

Recent observations of the initially brightened auroral arc at substorm onset provide considerable evidence that the instability is located at geocentric radial distances in the range of about 6 to 12 Re. These findings are based upon unique, high-resolution images from a camera for visible wavelengths on board the Polar spacecraft. The location of the onset instability is particularly important for theoretical analysis and modelling of magnetospheric substorms in that the plasma and magnetic field parameters are significantly different at the above radial distances compared to those for radial distances in the range of 20 to 30 Re which are used for several current theory efforts. Simultaneous measurements of plasmas and magnetic fields at the relevant radial distances in the equatorial magnetotail are used to search for the position of the onset instability. It is found that the onset instability is initially confined to a narrow range of longitudes (local time) and rapidly expands in longitude and to greater radial distances.

**GA3.08/E/01-A6 1430**

**COMPARISON OF AURORAL ARCS OBSERVED WITH POLAR/VIS MEDIUM-RESOLUTION CAMERA AND FINNISH ALL-SKY CAMERAS AND THEIR MAPPING TO THE MAGNETOTAIL**

T. I. PULKKINEN, K. Kauristie, and M. T. Syrjasuo (Finnish Meteorological Institute, PO Box 503, FIN-00101 Helsinki, Finland, tel. 358-9-19294654, fax 358-9-19294603, e-mail: tuija.pulkkinen@fmi.fi) D. N. Baker, N. E. Turner (Laboratory for Atmospheric and Space Physics, University of Colorado, Boulder, CO 80309-0590) L. A. Frank and J.B. Sigwarth (Department of Physics and Astronomy, University of Iowa, Iowa City, IA 52242) T. Mukai, Institute of Space and Astronautical Science, Sagami-hara, Japan) S. Kokubun (Solar Terrestrial Environment Laboratory, Nagoya University, Toyokawa, Japan) L. Zelenyi (Space Research Institute, Moscow, Russia)

The POLAR/VIS medium-resolution camera can resolve auroral arcs to a scale of a few km. The camera observations show individual arcs embedded within a diffuse band of luminosity, allowing for detailed examination of the auroral breakups and their relation to other substorm onset-associated processes. Observations from the POLAR/VIS medium-resolution camera, Earth camera, Finnish all-sky camera network, and ISTP spacecraft are utilized to examine details of auroral arc breakups and their mapping to the magnetotail during several substorm events in late 1997 and early 1998. In particular, an isolated substorm of about 400-nT intensity occurred on Dec 17, 1997, after almost 20 hours of quiescence. The POLAR/VIS medium resolution camera observed two intensifications in the auroras at 2051 UT and at 2221 UT. The all-sky camera data from Kilpisjärvi showed that auroral activity intensified at 2050 UT, the auroras moved equatorward between 2140 and 2230 UT, after which a strong breakup and poleward motion of auroras followed. Magnetic field modelling techniques are utilized to obtain an accurate mapping between the auroral observations and the magnetotail substorm signatures as observed by GEOTAIL and INTERBALL Tail Probe, both in the nightside magnetotail. The results are used to discuss the processes prior to the global instability onset and their association to the processes creating auroral breakups.

**GA3.08/W/03-A6 1450**

**THE EXPLOSIVE PHASE OF THE SUBSTORM**

John C. SAMSON, R. Rankin, and I. Voronkov (all at Department of Physics, University of Alberta, Edmonton, Alberta, Canada T6G 2J1, email: samson@space.ualberta.ca)

The explosive phase of the substorm, with time scales of 10s of second to minutes, follows the initial brightening of an arc on field lines threading the inner edge of the plasma sheet. Optical data from the Canadian CANOPUS array indicate that the initial brightening is followed within 10s of seconds by enhanced cross tail currents in the inner plasmasheet, and then by dipolarization. Lobe flux reconnection begins within three minutes of the initial arc brightening, indicating an extremely dynamic process with Alfvénic time scales. We argue that the Alfvénic time scales indicate that the explosive phase requires a nonlinear instability. We discuss a hybrid model in which the explosive phase is triggered by shear flow ballooning followed by tearing and reconnection. Ultimately, lobe flux reconnection begins at about 25-30 RE down the magnetotail.

**GA3.08/W/19-A6 1520**

**SHARE RADAR OBSERVATIONS OF INTENSE FLOW BURSTS IN THE MAGNETOTAIL**

A. D. M. WALKER and J P S Rash (University of Natal, Durban) K B Baker (The Johns Hopkins University Applied Physics Laboratory) M Pinnock and J R Dudeney (British Antarctic Survey)

Observations are presented of a very unusual event on March 10 1997. At this time, the solar wind conditions were extremely quiet. On the night side the SHARE and Halley radars observed a succession of flow bursts in the ionosphere with velocities exceeding 2 km per s. The poster presents a variety of observations including data from satellites in the solar wind, low altitude satellites passing over the radar field of view, and ground based instrumentation from unmanned ground instruments under the field of view in Antarctica. The event shows some of the characteristics of a substorm, but occurs in the absence of any external driving mechanism. It may be that this is an observation of a fundamental mode of magnetospheric oscillation, uncontaminated by external driving mechanisms.

**GA3.08/W/32-A6 Invited 1600**

**HF RADAR OBSERVATIONS OF IONOSPHERIC CONVECTION IN THE NIGHTSIDE AURORAL ZONE DURING SUBSTORMS**

T. K. Yeoman (Department of Physics and Astronomy, University of Leicester, University Road, Leicester, LE1 7RH, U.K. )

High time resolution data from HF radars reveal short-lived convection signatures in the auroral ionosphere during the three phases of the magnetospheric substorm. For example, transient modulations of the electrojet currents during the substorm expansion phase have reported in data from HF radars. The features typically show an interval of suppressed electric field, characterised by large equivalent currents deduced from ground magnetometers, presumably as a consequence of enhanced ionospheric conductivity due to energetic particle precipitation. Following this an enhanced electric field causes a vortical flow. Ground magnetometer data has suggested that the flow vortices propagate azimuthally at up to 6 km s<sup>-1</sup>, and are typically characterised by equatorward flow enhancements of order 600 m s<sup>-1</sup>. Recent data from high time resolution HF scans parallel to the L-shell have provided direct measurements of the azimuthal propagation and plasma velocity during such impulsive convection features. The features are not usually accompanied by Pi2 pulsations and in one case study there is some evidence from Geotail spacecraft data of a relationship a dawnward perturbation and dipolarisation of the magnetic field and dawnward plasma flow in the

magnetotail, perhaps related to bursty bulk flows. The possible implications of these observations for the substorm process will be discussed.

**GA3.08/W/07-A6 1630**

**CUTLASS HF RADAR OBSERVATIONS OF HIGH LATITUDE AZIMUTHALLY PROPAGATING CONVECTION FEATURES DURING MAGNETOSPHERIC SUBSTORMS**

J.A. WILD and T.K. Yeoman (both at Radio & Space Plasma Physics Group, Dept. of Physics and Astronomy, Leicester University, University Road, Leicester, UK, LE1 7RH. Email: jaw11@ion.le.ac.uk)

Previous observations have identified transient high latitude convection features in the substorm electrojets associated with the expansion phase which were inferred to propagate azimuthally from ground magnetometer data. In addition, during the substorm recovery phase, high time resolution radar modes have been used to study omega bands propagating in an eastward direction. The high time resolution and multi-point nature of the observations leads to a refinement of the previous models of omega band structure. This study combines new data from the CUTLASS radars with observations from the IMAGE, SAMNET, NIPR and Greenland magnetometer networks and the STARE VHF radar in order to look at the zonal flows within the CUTLASS radar field of view. Intervals have been identified in which regions of pulsed flow propagating eastwards are observed directly by the radar and also demonstrate characteristic magnetic behaviour. By directly combining measurements of magnetic field strength and line of sight velocity it is possible to estimate the height integrated ionospheric conductivities at several points within the fields of view of the radars. The continuous nature of the multi-instrumental observations allows the study of the occurrence of azimuthally propagating convection features with respect to substorm phase as well as yielding information regarding the bulk properties and structure of the features themselves.

**GA3.08/E/09-A6 1650**

**THE ELECTRICAL COUPLING OF MAGNETOSPHERIC FLOW VORTEXES AND FLOW CHANNELS TO THE RESISTIVE IONOSPHERE**

John W. Bonnell and Joseph E. BOROVSKY (both at Space and Atmospheric Sciences Group, Los Alamos National Laboratory, Los Alamos, NM 87545, USA, email: jborovsky@lanl.gov)

Owing to their polarization electric fields, flows in the magnetosphere drive field-aligned currents that electrically couple to the ionosphere. The details of d.c. current systems driven by flow vortexes in the magnetosphere are examined. It is found that the current systems driven by positive (angular velocity antiparallel to B) and negative (angular velocity parallel to B) vortexes differ greatly. Positive vortexes drive stronger current systems, dissipate more power, and spread across B whereas negative vortexes drive weaker currents, dissipate less power, and do not spread across B.

The signatures above the ionosphere of the two types of vortexes also differ. The details of d.c. current systems driven by flow channels in the magnetosphere are examined. A flow channel in the magnetosphere will exhibit an asymmetry when it couples to the ionosphere; this asymmetric coupling is explored. Extrapolating these studies to flow turbulence in the plasma sheet, predictions are made about the statistics of electric-field divergence at low altitudes and flow vorticity at high altitudes.

**GA3.08/W/26-A6 1710**

**PLASMA SHEET VARIATIONS DURING SUBSTORM ACTIVITY: OBSERVATIONS ON 17TH MAY 1996**

J.STOREY, M. Lester (Both at Radio & Space Plasma Physics Group, University of Leicester, Leicester, United Kingdom) T. A. Fritz (Dept. of Astronomy, Boston University, Boston, USA) C. T. Russell (Institute of Geophysics and Planetary Physics / UCLA, Los Angeles, USA) M. Brittner (University of Washington Geophysics Program, Seattle, USA) J. B. Blake (The Aerospace Corporation, Los Angeles, USA) J. Scudder (Department of Physics & Astronomy, University of Iowa, Iowa City, USA)

This presentation details the initial results obtained from a study of an interval of substorm activity observed in the high-latitude plasma sheet by the Polar spacecraft, during a pass over the Scandinavian sector on 17th May 1996. The study makes use of the CAMMICE and MFE instruments on board the Polar spacecraft, specifically to investigate any substorm related plasma flows and associated magnetic field variations. Other Polar instruments from which data have been used include two other particle instruments, Hydra and CEPPAD, and the Ultra-Violet Imager (UVI), which provides images of the auroral zone throughout the interval and hence shows ground signatures of the plasma flows observed in situ. Other instrumentation includes the WIND magnetometer and the IMAGE and SAMNET magnetometer chains. These instruments provide background data sets that are used to confirm the presence of substorm activity and give the timing of the onset of any such activity. The particle instruments observe PSBL signatures twice during this interval. The first entry into the PSBL is due to a slight re-configuration of the field geometry caused by pseudobreakups occurring at 20:48 and 21:00 UT. The continuing growth phase causes the tail field lines to become more tail-like resulting in the spacecraft exiting the plasma sheet, before the expansion phase onset results in the spacecraft observing CPS ions at 21:45UT.

**GA3.08/E/08-A6 Invited 1730**

**ON THE ROLE OF RESONANCES IN THE TRANSPORT IN THE MAGNETOSPHERE**

ENNIO R. SANCHEZ, SRI International, 333 Ravenswood Ave., Menlo Park, CA 94025

The Sun-Earth connection produces magnetospheric boundaries, cavities, and waveguides where ULF resonances and instabilities can be excited. A combination of simultaneous measurements from high-, low-, and ground-altitude instruments has been used to identify how ULF resonances influence transport in the magnetosphere and onset and evolution of substorms. Intervals were selected for which ISTP spacecraft were appropriately positioned in conjugate positions to ground-based magnetometer and radar chains. Spectral analysis of the observations for the first time establishes a direct relationship between Pc-5 pulsations measured on the ground and the periodicity of dipolarizations and particle injections at geosynchronous altitude, discrete westward electrojet intensifications, plasma and magnetic field oscillations of the plasma sheet and lobes, plasma and magnetic field oscillations in the magnetosheath, and plasma density, convection, and magnetic field pulsations in the plasma sheet. These observations strongly suggest a coupling of resonant cavity modes, which involve energy transfer from compressional oscillations propagating from the outer magnetosphere into the near-Earth closed field lines, with other wave modes in different parts of the magnetosphere. Those modes include waveguide modes originated in the high-latitude open field line regions of the magnetosphere, and waveguide modes in the low-latitude closed field line regions of the magnetosphere encompassed by the low-latitude boundary layers and the plasma sheet. The coupled response of different magnetospheric regions to solar wind



input defines a measure of coherence of the magnetosphere-ionosphere system. The coherence of the system defines a correlation between periodicities in reconnection and bursty plasma transport in the magnetotail and periodicities in magnetic flux buildup and particle injection in the near-Earth region.

**Monday 26 July AM**

Presiding Chair: Larry Lyons, (UCLA, Department of Atmospheric Sciences, Los Angeles, USA)  
Concurrent Poster Session

**GA3.08/W/12-B1** Invited **0930**

**THE GLOBAL IONOSPHERIC CONVECTION RESPONSE TO CHANGES IN THE SOLAR WIND AND INTERPLANETARY MAGNETIC FIELD ORIENTATION**

AARON RIDLEY (Southwest Research Institute, San Antonio, TX 78228-0510, USA, email: ridley@zed.space.swri.edu)

It has been shown that the ionospheric convection is closely coupled to the interplanetary magnetic field (IMF) orientation and more loosely coupled to the solar wind speed and density. Most studies of the convection have investigated the statistical steady state conditions. Recently, a number of studies have focused on the how the convection changes in response to IMF reorientations. The first studies of this kind showed localized observations of how the convection changed with time. More recently, studies have focused upon how the global convection changes. One result of the global studies is that the global convection pattern is shown to change as a whole, instead of the change in convection spreading slowly over the polar cap. Examples of such simultaneous changes are shown to occur for both IMF orientation changes and sudden changes in the dynamic pressure of the solar wind. We present arguments on the interpretation of the convection data, showing the simultaneous change in convection in the noon, dawn, and dusk sectors. We present ground-based magnetometer data to verify these arguments. In addition, we discuss the ramifications of these observations on the dynamics of the magnetosphere-ionosphere system.

**GA3.08/E/03-B1** **1000**

**DYNAMICS OF HIGH-LATITUDE IONOSPHERIC CONVECTION AND CURRENT SYSTEM FOLLOWING A SUDDEN SOUTHWARD TURNING OF THE IMF**

Nozomu NISHITANI and Tadahiko Ogawa (Solar-Terrestrial Environment Laboratory, Nagoya University, 3-13 Honohara, Toyokawa, Aichi 442-8507, Japan, e-mail: nisitani@stelab.nagoya-u.ac.jp) Natsuo Sato and Hisao Yamagishi (National Institute of Polar Research, 1-9-10 Kaga, Itabashi, Tokyo 173-8515, Japan) Mike Pinnock (British Antarctic Survey, High Cross, Madingley Road, Cambridge CB3 0ET, England) Jean-Paul Villain (LPCE/CNRS, 3A Av. de la Recherche Scientifique, 45071 Orléans Cedex 2, France) George Sofko (Department of Physics & Engineering Physics, University of Saskatchewan, 116 Science Place, Saskatoon, SK, S7N 5E2 Canada)

One example of the global dynamics of ionospheric convection and current system has been studied by using the SuperDARN radar network and high-latitude magnetograms when the IMF changed stepwise from northward to strongly southward. There were two-step changes in the ionospheric flow pattern. The first change of the convection pattern can be characterized by a sudden formation of a large flow vortex in the afternoon sector. This change propagated from the noon sector to the evening sector within 2 to 4 minutes. The second change, which occurred twenty minutes later, can be characterized by a sudden antisunward shift of the flow vortex. The ionospheric current system observed by the high-latitude magnetograms showed gradual formation of the DP2 current system. The formation began simultaneously with the first response of the convection flow and completed a few minutes after the second response. Distortion of the DP2 current system, that is, antisunward shift of the center of the two vortices, occurred simultaneously with the second response of the ionospheric convection pattern. From these observations, we speculate that the first response is associated with the propagation of magnetosonic waves, and that the second response is due to the configuration change of the magnetosphere after the solar wind discontinuity arrived in the magnetotail region.

**GA3.08/W/27-B1** Invited **1040**

**ION AND ELECTRON HEATING IN MAGNETIC RECONNECTION**

M. Hoshino (The University of Tokyo, Tokyo, 113-0033 Japan, email: hoshino@geophy.s.u-tokyo.ac.jp)

The origin of hot and dense plasma in the Earth's plasma sheet has been a long-standing problem. Observations have established that the ion temperature is the order of several keV, and the ion temperature in the plasma sheet is always about several times larger than the electron temperature. Many microscopic and macroscopic plasma processes are thought to be involved in the plasma heating: magnetic reconnection plays an important role on energy conversion process from magnetic into kinetic energy, and provides the preferential plasma heating of ions. Current-driven instabilities around the plasma sheet boundary layer are believed to be substantial for the electron heating. Strong turbulence of waves in the plasma sheet is probably important for understanding the hot plasmas as well. These effects are undoubtedly important for various stages of magnetotail evolution associated with magnetic reconnection. We have started to investigate the self-consistent plasma heating and acceleration processes in association with the kinetic magnetic reconnection by using a three-dimensional, electromagnetic, particle-in-cell simulation, in which both the current-driven instabilities and the collisionless reconnection process are described. We have studied where and when ions and electrons gain their energy during reconnection evolution. The results are discussed in terms of the GEOTAIL observations.

**GA3.08/E/02-B1** **1110**

**SIGNATURES OF MAGNETOTAIL VARIABILITY IN THE AURORAL ZONE**

VAHE PEROOMIAN, Maha Ashour-Abdalla (Both at UCLA-IGPP, Box 951567, Los Angeles, CA 90095-1567, USA, e-mail: vahe@igpp.ucla.edu) Lev M. Zelenyi (Space Research Institute, Academy of Sciences, Moscow, Russia, e-mail: lzelenyi@iki.rssi.ru)

We use a self-consistent, large-scale kinetic model to investigate the formation of the magnetotail and the auroral manifestations of the complicated temporal dynamics that occur there during quiet periods. In our model, the magnetotail's current is calculated by following ion trajectories in a magnetic field that is made up of ion currents calculated at the previous time step. The model takes into account both the local inductive and global dawn-dusk electric fields. We find that the magnetotail is quite variable: magnetic islands are formed, then decay and merge. This process appears to be quasi-periodic, and results from the cycles of loss and replenishment that current-carrying particles undergo in the current sheet; these cycles are themselves caused by the rapid and non-adiabatic energization of ions in the vicinity of the x-lines that form in the model. Ion inertia determines the characteristic time scale for this periodicity, which is on the order of 5 - 10 minutes. The magnitude of the dawn-dusk electric

field also influences the time scale. In our model, ion acceleration near the temporally variable location of the x-line stimulates the formation of quasi-periodic, velocity-dispersed ion structures in the ion precipitation profile. Many polar-orbiting spacecraft have observed structures such as these. We will compare our results with these observations.

**GA3.08/W/33-B1** **1130**

**WIND OBSERVATIONS OF THE NEAR-EARTH PLASMA SHEET: SOLAR WIND AND GEOMAGNETIC ACTIVITY DEPENDENCE**

M. OIEROSET, T. D. Phan, L. Chan, and R. P. Lin (Space Sciences Laboratory, University of California, Berkeley, CA 94720, E-mail: oieroset@ssl.berkeley.edu)

We have studied 20 WIND perigee passes through the plasma sheet earthward of 24 Re. The plasma sheet observations are sorted according to region, interplanetary magnetic field values, solar wind plasma parameters, and Kp values, in an attempt to increase our understanding for the causes of the variations in the plasma sheet plasma parameters. Preliminary results indicate a cold and dense plasma sheet for low Kp values while the plasma sheet gradually becomes heated and less dense with increasing Kp. Our findings are also in agreement with GEOTAIL observations by Terasawa et al. (GRL, 24, 935-938, 1997), showing a cold and dense plasma sheet for northward IMF when the IMF is averaged over several hours prior to the plasma sheet observations. We also survey the interrelationship between the thermal and flow parameters in the plasma sheet in order to investigate the structure and dynamics of the plasma sheet.

**GA3.08/E/12-B1** **1150**

**IS THE MHD APPROACH VALID IN THE DISTANT PLASMA SHEET?**

Oleg TROSHICHEV (Arctic and Antarctic Research Institute, St.Petersburg, 199397, Russia, email: olegtro@ari.nw.ru); Elizabeth Antonova (Scobeltsin Institute of Nuclear Physics, Moscow State University, Moscow, 119899, Russia, email antonova@orearm.msk.ru); Yohsuke Kamide (Solar Terrestrial Environment Laboratory, Nagoya University, Toyokawa, Aichi, 442, Japan, email: kamide@stelab.nagoya-u.ac.jp)

Measurements of the magnetic field and low energy plasma by the GEOTAIL spacecraft were utilized to study correspondence between the plasma velocity and magnetic oscillations in the distant plasma sheet at X = -(79-200) RE. A total of 14 extremely quiet days from available GEOTAIL data in 1993-1994 (12-s averages of the magnetic field and plasma parameters) were chosen for the analysis, identification of the plasma sheet and estimation of the magnetic activity being realized according to Troshichev et al. [JGR, in press]. Case study of behavior of magnetic field and plasma velocity shows that correspondence between the changes in these parameters often is not carried out. The Fourier analysis also sometimes shows striking discrepancy in the frequent spectra for magnetic and plasma parameters when powerful oscillations of plasma velocity (usually VY or/and VZ components) in range 3-8 min occurs against the almost calm magnetic field and vice versa. These results suggest that MHD approach is often violated in the distant plasma sheet even under the extremely quiet conditions.

**GA3.08/W/24-B1** **1210**

**OBSERVATION OF PROLONGED, STEADY RECONNECTION IN THE MAGNETOTAIL BY THE GEOTAIL SPACECRAFT**

R. T. Mist and C. J. OWEN (Astronomy Unit, Queen Mary and Westfield College, London, UK), T. Mukai (Institute of Space and Astronautical Science, Sagami-hara, Japan), S. Kokubun (Solar Terrestrial Environment Laboratory, Nagoya University, Toyokawa, Japan)

It is relatively unusual for conditions in the distant tail to allow a spacecraft to remain in the central plasma sheet continuously for a prolonged period. However, on October 27, 1994, when the Geotail spacecraft was situated in the deep tail (X=-170 RE, Y=20 RE and Z=0 RE), the spacecraft crossed from the north to the south lobe, and spent about 4 hours continuously in the plasma sheet. The magnetic field and plasma moment data throughout this period are consistent with the plasma sheet being formed by quasi-steady reconnection. The level of geomagnetic activity during this period is steady and moderate, with no obvious enhancements due to substorms. We analyse the two-dimensional ion distributions from the LEP instrument during this interval, and study the plasma populations in the north and south lobes, the PSBL and the plasma sheet. We compare these observed distributions with the predictions of reconnection models based on the balance of magnetic field and plasma stresses at the central, cross-tail current sheet. In these models, the plasma sheet population is formed by both heating and acceleration of the inflowing lobe plasma during its interaction with the current sheet. We show that the observed ion distributions are consistent with the expectations of these reconnection models.

**Monday 26 July PM**

Presiding Chairs: M. Hoshino, (University of Tokyo, Japan)  
M. Fujimoto, (Tokyo Int. Tech, Tokyo, Japan)

**GA3.08/W/14-B1** Invited **1400**

**THE EARTH'S DYNAMIC MAGNETOTAIL**

A. Nishida (Institute of Space and Astronautical Science, Sagami-hara, 229-8510, Japan, email: nishida@gtl.isas.ac.jp)

Following the first comprehensive study of the magnetotail conducted with the IMP 1 satellite, Ness [1969] reviewed the latest findings on the physics of the Earth's magnetotail. It is impressive that most of the fundamental concepts were already established in that review. At the end of the paper he listed outstanding problems which future studies should be directed to resolve. In the present paper we shall summarize the advances made in the physics of the magnetotail with reference to the problems he listed, and discuss the remaining issues. Answers to the problems he enumerated as (1) to (6) are given in the following. (1) The formation of the magnetotail is due to magnetic reconnection on the magnetopause. (2) Coherent, well-ordered tail exists at least to the distance of 200 Re and there is no indications of filamentation. (3) The merging across the neutral sheet is impulsive at the near-Earth neutral line. (4) Accelerations both in the magnetotail and in the solar flare are governed by magnetic reconnection. (5) Accelerations occur at the slow-mode shock and in the neutral sheet including the vicinity of the neutral sheet. (6) Electron islands events correspond to plasmoids and plasma-sheet boundary layer. Remaining important issues include (1) mixing of plasma-sheet and magnetosheath plasmas in the LBL, (2) paucity of the slow-mode shock identification, and (3) trigger of the near-Earth reconnection.

**GA3.08/W/16-B1 1430**

**AURORAL POLEWARD BOUNDARY INTENSIFICATIONS: A FUNDAMENTAL MAGNETOSPHERIC DISTURBANCE COUPLING BURSTY PLASMA SHEET FLOWS TO THE AURORAL IONOSPHERE**

L. R. Lyons (Department of Atmospheric Sciences, UCLA, Los Angeles, CA 90095-1565, USA, email: larry@atmos.ucla.edu); G. T. Blanchard (Department of Chemistry & Physics University of Southeastern Louisiana SLU 10878, Hammond, LA 70402-0878, USA); T. Nagai (Department of Earth and Planetary Sciences, Tokyo Institute of Technology, Tokyo 152, Japan); T. Yamamoto, T. Mukai, A. Nishida (All at: Institute of Space and Astronautical Science, Sagamiyama 229, Japan); J. C. Samson (Department of Physics, University of Alberta, Edmonton, Alberta, T6G 2E9, Canada); S. Kokubun (Solar-Terrestrial Environment Laboratory, Nagoya University, Toyokawa 442, Japan)

Poleward boundary intensifications are nightside geomagnetic disturbances that have an auroral signature that moves equatorward from the poleward boundary of the auroral zone. They occur repetitively, and they appear to be the most intense auroral disturbance at times other than the expansion phase of substorms. They connect to the magnetotail via upward field-aligned currents that are sufficiently intense that a field-aligned potential drop is required. We have used data from nightside conjunctions of the GEOTAIL spacecraft in the magnetotail with the CANOPUS ground-based array in central Canada. During periods with identifiable poleward boundary intensifications, we find that the plasma sheet has considerable structure and bursty flow activity. During periods without such intensifications, the plasma sheet is far more stable with little flows. This is consistent with the intensifications being the result of the mapping to the ionosphere of the electric fields that give rise to bursty flows within the plasma sheet. Two different types of plasma sheet disturbance have been found to be associated with the poleward boundary intensifications. The first is flows that result from Speiser motion of particles in a localized region of thin current sheet. The second, seen preferentially in the near-Earth plasma sheet, consists of energy dispersed ion structures that culminate in bursts of low energy ions and isotropic low-energy electrons. Both are associated with localized regions of enhanced dawn-to-dusk electric fields.

**GA3.08/W/23-B1 1450**

**CHARACTERISTICS OF AURORAL POLEWARD BOUNDARY INTENSIFICATIONS**

Efthya Zesta (Department of Atmospheric Sciences, UCLA, Los Angeles, CA 90095-1565, USA, email: ezesta@atmos.ucla.edu); Larry R. Lyons (Department of Atmospheric Sciences, UCLA, Los Angeles, CA 90095-1565, USA); John C. Samson (Department of Physics, University of Alberta, Edmonton, Alberta, T6G 2E9, Canada); Erick Donovan (Department of Physics and Astronomy, University of Calgary, Calgary, Alberta, T2N 1N4, Canada)

Poleward Boundary Intensifications (PBIs) of the aurora are a frequently occurring auroral-zone disturbance. They consist of auroral enhancements that move equatorward from near the magnetic separatrix and are associated with ground magnetic disturbances of 20-100 nT and P12 pulsations. They are a phenomenon distinct from substorms, occurring both during substorm and non-substorm periods, and are often observed both during enhanced convection intervals and during quiet times. We used meridional scanning photometer data from the CANOPUS stations during the winter of 1996-1997 to identify a number of periods with PBI events. We investigate both the occurrence characteristics and the correlation of PBIs with the IMF direction and magnitude. We find that PBIs are statistically a dusk-to-midnight region phenomenon and are therefore associated with the upward region 1 field-aligned currents. We find that only half of our identified events are associated with substorms. The non-substorm associated PBIs are found to have a clear preference for a radial IMF. However, the radial IMF is a necessary but not sufficient condition for the occurrence of PBI events in the nightside aurora. We also examine all-sky-imager data from the CANOPUS station of Gillam at the time of our PBI events and determine the possible correlation of PBI events, identified in the meridional scanning photometer data, with short-lived, north-south aligned auroral arcs and with equatorward moving east-west aligned auroral arcs.

**GA3.08/W/28-B1 1510**

**LOCAL INTENSIFICATION OF THE TAIL CURRENT AND ASSOCIATED OCCURRENCE OF MAGNETIC RECONNECTION IN THE MAGNETOTAIL**

T. MUKAI, Y. Asano, I. Shinohara, and Y. Saito (Institute of Space and Astronautical Science, Yoshinodai, Sagamiyama 229-8510, Japan, email: mukai@stp.isas.ac.jp); T. Nagai (Department of Earth and Planetary Sciences, Tokyo Institute of Technology, Tokyo 152-8551, Japan, email: nagai@geo.titech.ac.jp)

Recent GEOTAIL observations have clearly demonstrated a crucial role of magnetic reconnection in substorms. There are well-known growth phase signatures in the magnetotail, such as increasing pressure and configuration change to the tail-like magnetic field, representing enhancement of the tail current and thinning of the current sheet. However, these signatures are seen over a wide range of distances down the tail and are not enough to explain a certain location where the reconnection is first initiated. Fortunately we have found a substorm event in which the GEOTAIL spacecraft stayed in the current sheet at a distance of ~17 Re and could clearly observe temporal evolution of the tail current intensification and associated occurrence of magnetic reconnection there. Following the gradual increase in the growth phase, the tail current density increased sharply a few minutes before the onset. The tailward fast flows and increasing plasma temperatures were also observed to start in association with the intensification of the current density. These signatures can be interpreted as the initial occurrence of magnetic reconnection associated with local thinning of the current sheet (because the case is very rare). As time proceeds, the current sheet further thins and the current density is further intensified. This sequence evolves explosively through a few steps in several minutes, expanding the active region.

**GA3.08/W/34-B1 Invited 1550**

**THE HALL TERM EFFECTS IN MAGNETIC RECONNECTION**

Dr Masaki Fujimoto Dept. Earth Planet. Sci., Tokyo Inst. Tech

Geotail observations have shown that there are strong field-aligned currents (FACs) that are very likely to be the Hall current generated in magnetotail reconnection. 2D Hall MHD simulations do show that the FACs due to the Hall term are significant and should not be neglected in considering coupling to the ionosphere. These lead us to make 3D Hall MHD simulations of magnetic reconnection to study the three-dimensional structure of the generated FACs. Details of the results, especially in comparison with those obtained by MHD models, will be discussed.

**GA3.08/W/11-B1 1620**

**SIMULATIONS SHOWING GENERATION OF FILAMENTARY FIELD-ALIGNED CURRENTS ABOVE THE AURORAL IONOSPHERE**

Daniel W. Swift (Geophysical Institute, University of Alaska, Fairbanks, AK 99775-7320, USA, email: swift@gi.alaska.edu) Yu Lin (Physics Department, 206 Allison Laboratory, Auburn University, Auburn, AL 36849-5311, USA, email: ylin@physics.auburn.edu)

A two-dimensional hybrid code is used to simulate the midnight meridian plane of the magnetosphere. The simulation domain extends from the Earth's ionosphere to 35 Earth radii in the antisunward direction and to 11 Earth radii along the polar axes. The simulation is driven by a dawn-to-dusk electric field imposed at the boundaries. The sequence of events follows those associated with the growth and expansive phases of the substorm. Momentum exchange between the plasma being accelerated Earthward in the neutral sheet and the magnetic field results in a stretching of the magnetic field lines and thinning of the plasma sheet. A pair of field-aligned currents develops connecting the inner edge of the plasma sheet to the auroral ionosphere, with the downward current equatorward of the upward current. The breaking of the inward plasma flow drives these currents. Next follows the apparent dipolarization. "Dipolarization" is carried outward by plasma rebounding off the dipole field. Ion-ion two streaming instabilities are excited behind the expanding dipolarization front. The effect of these instabilities is propagated Earthward along magnetic field lines by shear Alfvén waves. These are seen as field-aligned current filaments above the auroral ionosphere. We take the upward field-aligned current filaments as proxies for auroral arcs.

**GA3.08/W/15-B1 1640**

**STUDY OF THREE-DIMENSIONAL HYBRID SIMULATION OF MAGNETOTAIL RECONNECTION**

MASAO NAKAMURA (Solar-Terrestrial Environment Laboratory, Nagoya University, Honohara 3-13, Toyokawa, Aichi 442-8507, Japan, Email: nakamura@stelab.nagoya-u.ac.jp) and Masaki Fujimoto (Department of Earth and Planetary Sciences, Tokyo Institute of Technology, Ookayama 2-12-1, Meguro, Tokyo 152, Japan)

The three-dimensional structure of magnetic reconnection in a thin current sheet (thickness comparable to the relevant ion inertia length), which models the near-Earth tail current sheet just before substorm onsets, are studied by means of 3-D hybrid simulations (ion particle, charge neutralizing massless electron fluid). Magnetic reconnection is initiated by fixing a localized anomalous resistivity in the plasma sheet and generates fast plasma flows in the Earth-tail direction as a result of its explosive growth. On the other hand, the thin plasma sheet is unstable to the tail Kelvin-Helmholtz (K-H) instability, which kinks plasma sheet in the cross-tail plane. For the small resistivity cases, the tail K-H instability is well generated before the explosive growth of reconnection starts. While the kink structure of the plasma sheet modifies the plasma flow, the essential features, such as the dawn-dusk asymmetry of plasma flows and field configuration, still remains unchanged from the large resistivity case where the explosive growth starts before the influence of the tail K-H instability is visible.

**GA3.08/E/04-B1 1700**

**SIGNATURES OF MAGNETOTAIL RECONNECTION DERIVED BY NUMERICAL SIMULATIONS AND VERIFIED IN SPACE**

JOERG BUECHNER AND B. Nikutowski (Max-Planck- Institut fuer Aeronomie, Max-Planck-Str. 2, D-37191 Katlenburg-Lindau, Germany)

The true physics behind magnetic reconnection is still an open question. On the other hand large scale topological considerations have shown that reconnection must take place in the Earth's magnetotail. The magnetotail is, therefore, an appropriate site to test reconnection models. We have developed a kinetic model of three-dimensional reconnection and derived its signatures by kinetic plasma simulations. Here we present current results of numerical plasma simulations of specific signatures of collisionless reconnection through thin current sheets. We illustrate some of them in the context of ISTP spacecraft measurements of INTERBALL-1 and GEOTAIL.

**GA3.08/W/20-B1 1720**

**A TAIL CROSSING AT 200 RE--GEOTAIL/HEP-LD OBSERVATION**

B. Wilken, Q.G. Zong ( both at Max-Planck-Institut fuer Aeronomie, D-37191 Katlenburg-Lindau, Germany, Email: wilken@lindpi.mpg.de) T. Doku (Advanced Research Center for Science and Engineering, Waseda university, Tokyo, Japan) S. Kokubun (Solar-Terrestrial Environment Laboratory, Nagoya University, Toyokawa, Japan)

In April 1994 Geotail was travelling on a deep tail trajectory. Sustained moderate geoactivity was driven by the passage of a corotating interaction region (CIR) which started on 3 April and continued until 20 April. On 17 April a CME impinged on the magnetosphere and caused a major magnetic storm. Geotail observed the CME in the dusk magnetosheath/magnetosphere interface at a GSE position (-200,30,-5 Re). Shortly after the CME Geotail started the dusk-to-dawn tail passage. The general level of activity in the magnetotail was found to be very low which corresponded to rather quiet conditions in the geosynchronous orbit and on the ground. However, quasi-periodic low intensity energetic particle bursts embedded in plasmoid-like structures passed Geotail. In the absence of corresponding near-Earth disturbances it is suggested that the regular structures in the deep tail resulted from large amplitude Alfvén wave in the solar wind.

**GA3.08/E/07-B1 1740**

**NUMERICAL SIMULATION OF PLASMOID DYNAMICS**

B P PANDEY, G.S.Lakhina and M.Roy (Indian Institute of Geomagnetism, Bombay 400 005, India, email: pandey@iig.iigm.res.in, lakhina@iig.iigm.res.in)

The plasmoid dynamics has been studied by a 2-D magnetohydrodynamic simulation code for a magnetotail configuration which takes into account the flaring of the tail. The plasmoid formation and its subsequent motion down the tail is followed for a few hundreds of Alfvén time. Simultaneously, the spatial and temporal evolution of density, pressure, temperature and magnetic field is studied. The results are compared with the Geotail observations.

Monday 26 July AM

Presiding Chair: T. Nagai, Tokyo Int. Tech, Japan

**GA3.08/W/06-B1** Poster **0900-01**

**THE RESPONSE OF THE MAGNETOSPHERE TO AN INTERPLANETARY SHOCK: GLOBAL SIMULATIONS OF THE SEPTEMBER 24, 1998 SUDDEN IMPULSE EVENT**

J RAEDER, C T Russell (both at: Institute of Geophysics and Planetary Physics, University of California, 405 Hilgard Ave, Los Angeles, CA 90095, USA, email: jraeder@igpp.ucla.edu)

A very strong interplanetary shock was observed by the Wind spacecraft on September 24, 1998, 2221 UT. The resulting sudden impulse (SI) was observed by several magnetospheric spacecraft, as well as by ground magnetometers. This event gives us a unique opportunity to study the response of the magnetosphere using our global magnetosphere - ionosphere model, and to compare our results in detail with the observations. Besides providing an assessment of the accuracy and robustness of our model for such an event, we will also present a more complete picture of the magnetospheric response as the observations alone could provide. In particular, we will discuss the propagation of the SI initiated waves through the magnetosphere, SI modifications to the current systems, and the causes of the ground magnetic perturbations.

**GA3.08/W/04-B1** Poster **0900-02**

**TAIL PLASMA FLOWS AND ELECTROJET ACTIVITY**

Tsugunobu Nagai (Earth and Planetary Sciences, Tokyo Institute of Technology, Tokyo 152-8551, Japan, email: nagai@geo.titech.ac.jp) Tuija I. Pulkkinen (Finnish Meteorological Institute, P.O.Box 503 FIN-00101 Helsinki, Finland, email: tuija.pulkkinen@fmi.fi) Peter Stauning, Danish Meteorological Institute, Lyngbyvej 100, DK-2100 Copenhagen, Denmark, email: pst@dmi.dk) Toshifumi Mukai (Institute of Space and Astronautical Science, Sagami-hara 229-8510, Japan, email: mukai@gtl.isas.ac.jp) Susumu Kokubun (Solar-Terrestrial Environment Laboratory, Nagoya University, Toyokawa 442-8507, Japan, email: kokubun@stelab.nagoya-u.ac.jp)

The spacecraft Geotail observes tailward/earthward convection plasma flows in the plasma sheet at radial distances of 10-30 Re in association with substorm activity. The ground magnetometer chains in Scandinavia and Greenland monitor electrojet activity, and the central latitude of the westward electrojet can be determined. In this paper, we examine the relationship between tail plasma flows and ground electrojet activity. Tailward plasma flows observed at 20-30 Re are usually associated with westward electrojets at magnetic latitudes of 64-68 degrees, whereas earthward plasma flows observed around 30 Re re often associated with the westward electrojet near 70 degrees. Unusual tailward plasma flows inside 20 Re are related with the westward electrojet near 60 degrees. We present several event studies and statistical results.

**GA3.08/E/10-B1** Poster **0900-03**

**SUBSTORM ACTIVITY AS A SELF-ORGANIZED CRITICAL PHENOMENON**

Vadim M.URITSKY, Mikhail I.Pudovkin (Department of Geophysics, St.Petersburg State University, Petrodvorets, St.Petersburg 198904, Russia, Email: uritsky@snoopy.phys.spbu.ru, pudovkin@snoopy.phys.spbu.ru)

The effect of self-organized criticality (SOC) is proposed as an internal mechanism of generation of  $1/f^b$ -like fluctuations in Earth's magnetosphere. It was suggested that localized in space current instabilities developing in the magnetospheric tail at the initial substorm phase can be considered as the SOC avalanches - dynamic clusters, superposition of which leads to the  $1/f^b$  fluctuations of macroscopic characteristics of the system. Using sandpile model of SOC, numerical investigation of both spatially localized and global disturbances of magnetospheric current layer was carried out. The dependence of model's sensitivity on the accumulated internal energy was shown to be similar to that characterizing natural geomagnetic activity. The power spectrum of sandpile model fluctuations controlled by real solar wind parameters reproduces all distinctive features of the AE fluctuations spectrum, including presence of two frequency ranges with different spectral slopes, that provides an important evidence for our hypothesis. Furthermore, quantitative and qualitative conformity between disturbed dynamics of self-organized critical state of the model and the main phases of real magnetospheric substorm development is demonstrated.

The results obtained suggest that the application of the theory of SOC and cellular automaton technique creates a new promising approach for modelling substorm activity. This approach seems to be adequate for the describing of fractal stochastic features of geomagnetic variations which are difficult to interpret on the base of traditional methods.

**GA3.08/W/30-B1** Poster **0900-04**

**ONE-DIMENSIONAL KINETIC MODEL OF THE PLASMA SHEET EVOLUTION DURING A SUBSTORM ACTIVATION**

V.I.Domrin and A.P.Kropotkin, Skobel'syn Institute of Nuclear Physics, Moscow State University, Moscow, 119899, Russia

A one-dimensional simulation model is constructed for analysis of the plasma sheet (current sheet, CS) evolution in the near-Earth tail region where an intense CS thinning is known to occur during a substorm activation. Dynamics of the hot plasma in the plasma sheet and of the ambient cold plasma is examined on the kinetic equation basis; a macroparticle code is used for ions to solve the equations while electrons are considered as a massless cold background. Self-consistent electromagnetic fields are calculated as numerical solutions of the Maxwell equations. The plasma sheet evolution takes place under action of an MHD disturbance that is applied on the boundary of the simulation box. That disturbance is assumed to be a consequence of fast tearing process occurring further in the magnetotail.

In the course of the simulated evolution, the electric field of the disturbance penetrates down to the central plane of the CS. That results in acceleration of ions in the CS; accelerated ions then escape CS along the field lines. Eventually the initial CS becomes replaced by an anisotropic one. The current is now carried by initially cold ions which are brought into CS by convection from the tail lobes. Magnetic field "annihilation" is a consequence: electromagnetic energy brought to CS from both sides, is transformed into energy of accelerated ions.

**GA3.08/W/01-B1** Poster **0900-05**

**GENERAL ANALYTICAL THEORY OF SELF-CONSISTENT QUASIADIABATIC CURRENT SHEETS**

Zelenyi Lev (Space Research Institute, Russian academy of sciences, 117810, Moscow, Russia, Email: lzelenyi@iki.rssi.ru); Sitnov Mikhail and MALOVA HELMI (Skobel'syn Institute of Nuclear Physics, 117899, Moscow, Russia, email: sm@dec1.npi.msu.su, mlv@dec1.npi.msu.su)

The basics of unified analytical theory of the structure of self-consistent quasiadiabatic current sheets created by the impinging ion streams are presented. The problem is considered neglecting the jumps of the invariant  $I_z$  of nonmagnetized ions. Nonlocal analogue of the Grad-Shafranov equation for the sources of arbitrary anisotropy is obtained and solved numerically. The universal solutions corresponding to the regimes of strong and weak anisotropies are investigated. Resulting self-consistent current is a sum of the drift cyclotron current and the magnetization currents flowing in the opposite directions. The maximum thickness of the current sheet is achieved in a case of weak anisotropy and equals to the thermal gyroradius of ions outside the sheet. In a case of strong anisotropy the sheet is compressed to minimal thickness. The effects of real nonadiabaticity are considered when the quasiadiabatic approximation is violated. Jumps of quasiadiabatic invariant  $I_z$  result in the gradual suppression of anisotropy and smearing of the current sheet. Influence of electron component creates an additional layer which also effectively broadens the current structure. We also discuss the relevant experimental data from ISEE and modern ISTP spacecraft (Geotail, INTERBALL) about the structure of the current sheets in the distant and near Earth parts of the tail.

**GA3.08/W/10-B1** Poster **0900-06**

**EVIDENCES OF UNMAGNETIZED ELECTRON MOTION WITHIN THE PLASMA SHEET AND ITS POSSIBLE CAUSES**

Marina STEPANOVA (Universidad de Santiago de Chile, Ecuador 3493, Casilla 307, Santiago, Chile, email: mstepano@lauca.usach.cl), Elizavieta Antonova, Ilya Ovchinnikov, Mickail Teltzov, Elena Vikhreva, (all at Skobel'syn Institute of Nuclear Physics, Moscow State University, Moscow 119899, Russia, email: antonova@tasped.npi.msu.su)

We present the results of experimental and theoretical investigation of unmagnetized stochastic motion of electrons and plasma mixing within the plasma sheet. Analysis of electron temperature distributions within the plasma sheet has been made using Intercosmos-Bulgaria-1300 polar orbiting satellite. It was shown, that the temperature, which has been obtained taking into consideration the acceleration of precipitating electrons by field-aligned potential drop, is nearly constant in the meridional direction within upward field-aligned current region and their values do not change for different orbits during a quiet geomagnetic time. Analysis of spatial fluctuations of precipitating electron fluxes at a fixed electron energy has shown, that fluctuation spectra of primary electrons have a power dependence and is close to the spectra of electric field fluctuations observed within the plasma sheet. The results of observations are interpreted as the consequence of stochastic plasma sheet particle motion and intensive plasma sheet plasma mixing. The role of different processes in such stochasticization is analyzed. For the majority of plasma sheet ions, their Larmor radius can be comparable with the radius of curvature of magnetic field line which can be the source of stochasticization. But, in case of electrons such mechanism can be effective only for particles with quite high energy or in the regions of extremely low  $B_z$ . Therefore, it is suggested that the main source of observed electron stochasticization and one of the powerful source of ion stochasticization is their motion in the inhomogeneous electric fields with characteristic scales comparable with particle Larmor radius. Chaotization of particle trajectories may be the part of stochasticization process. Particle motion in the homogeneous magnetic field and regular inhomogeneous electric field having sinusoidal distribution in one direction and homogeneous distribution in perpendicular direction is analyzed as an example of a chaotic motion.

**GA3.08/W/08-B1** Poster **0900-07**

**APPLICATION OF AN INVERSION METHOD BASED ON MID-LATITUDE MAGNETIC DATA TO ESTIMATIONS OF MEANINGS OF PARAMETERS OF THE GEOMAGNETIC TAIL AND THE IONOSPHERE**

Vagina L.I.

On the basis of an inversion method based on mid-latitude magnetic data during the development of 71 substorms we have calculated characteristic temporary and spatial substorm current systems parameters: characteristic times of current increase and decrease, maximal current values, characteristic spatial sizes. The received characteristics were used to find the values of the constants for the homogeneous differential equation of the second order with constant factors. Using the received constants we have made estimations of meanings of parameters of the geomagnetic tail and the ionosphere. The meanings of estimated parameters have appeared within the limits of typical meanings of parameters of a geomagnetic tail and ionosphere, received other methods.

**GA3.08/E/06-B1** Poster **0900-08**

**PECULIARITY OF GEOMAGNETIC FIELD ON GEOSTATIONARY ORBIT, CONSEQUENCE FOR STATIONARY CONVENTION**

KUZNETSOV S.N. (Skobel'syn Institute of Nuclear Physics, Lomonosov Moscow State University, 119899, Moscow, Russia, e-mail: kuznets@srldan.npi.msu.su)

Analysis of GOES data on geomagnetic field during 1993-94 years shown that in time intervals near equinox we observe stationary increasing of the magnetic field near local midnight. This effect was not observed in solstice intervals. We proposed that this effect is projecting to midnight range of unreally position of field-align currents. This effect may be connected with asymmetry in precipitation of cosmic ray electrons in magnetic lines of a plasma tail. The range of quasispherical field near midnight may be foundation of theta-strap in an aurora.

**GA3.08/E/05-B1** Poster **0900-09**

**ON THE KELVIN-HELMHOLTZ HYDROMAGNETIC INSTABILITY**

ANZOR GVELESIANI (Institute of Geophysics, Georgian Academy of Sciences, 1, M. Alexidze Str., Tbilisi 380093, Georgia, email: vazha@excite.com)

An analytical magnetohydrodynamic model of tangential discontinuity stability in the Earth's magnetosphere plasma sheath, magnetopause and plasma and neutral sheets is suggested. The general discussion relations for multilayer plasma flows of plane and cylindrical configuration are received. It is shown the role of the plasma compressibility and geometric parameters - thickness and curvature of layers boundaries - on the Kelvin-Helmholtz hydromagnetic instability. The compressibility of plasma results in destabilisation of plasma layers motion. It is found the parameter (product respectively the relations of plasma densities and magnetic fields squares of the neighbouring layers) from the value of each (more or less than 1) defines the effect of the geometry both of tangential discontinuity surface on the cylindrical and plane form of incompressible plasmatic jets.



**GA3.09 Thursday 29 – Friday 30 July**

**QUANTITATIVE TESTS AND INTERCOMPARISON OF SOLAR-TERRESTRIAL AND GEOMAGNETIC FIELD MODELS (WITH DIVISION II, IV, V)**

Location: Muirhead Tower G08 LT  
Location of Posters: Student Room 1st Floor

**Thursday 29 July AM**

Presiding Chair: Jon Linker, (SAIC, San Diego)  
Concurrent Poster Session

**QUANTITATIVE MODELING 1**

**GA3.09/E/13-B4 0930**

**PROPOSED METRICS FOR THE U.S. NATIONAL SPACE WEATHER PROGRAM**

R A WOLF (Space Physics and Astronomy Dept., Rice University MS108, P.O. Box 1892, Houston, TX 77251, U.S.A.); T J Fuller-Rowell (NOAA Space Environment Center, 325 Broadway, Boulder, CO 80303, U.S.A.)

The U.S. National Space Weather Program (NSWP) has an overarching goal "to achieve an active, synergistic, interagency system to provide timely, accurate, and reliable space weather warnings, observations, specifications, and forecasts within the next 10 years." Among the critical elements contributing to a successful NSWP is the need to establish metrics against which quantitative goals can be defined and progress can be measured. The definition of space-weather metrics departs significantly from the traditional approach to space science, which places little emphasis on quantifying progress toward the long-term goal of understanding. A report prepared for the U. S. National Science Foundation proposes specific metrics that measure ability to specify and forecast various space-weather parameters. The highest priority physical parameters that must be predicted from ionosphere-thermosphere science are the electron density, neutral mass density, and amplitude of electron density irregularities. The corresponding magnetosphere-ionosphere parameters are the high-latitude ionospheric electric field, auroral electron flux, magnetic indices, and geosynchronous electron fluxes. Among the parameters that solar and interplanetary science must predict are solar-wind bulk properties and the fluxes of solar protons, EUV, and X-rays; times at which disturbances leave the Sun must be predicted, as well as solar-wind transit times.

**GA3.09/W/30-B4 0945**

**MODELLING CORONAL MASS EJECTIONS AND PROMINENCE ERUPTIONS**

S. K. ANTIOCHOS (Code 7675, Naval Research Lab, Washington, DC, USA)

The most violent and most energetic manifestations of solar activity are the disruptions of the Sun's magnetic field that give rise to coronal mass ejections (CME) and prominence/filament eruptions. These phenomena are the main drivers of space weather. They are also one of the most interesting of solar phenomena from the viewpoint of basic MHD physics and present a great challenge to MHD theory. In this talk, I will review the major theoretical models for solar magnetic disruptions, and the progress to date on numerical simulations of CMEs/prominence eruptions. In particular, I will focus on the question of the physical requirements, (as predicted by our present understanding), for violent magnetic disruptions on the Sun, and the possibilities for forecasting such events with numerical simulations.

**GA3.09/W/08-B4 1010**

**GLOBAL 3D MHD MODELING OF THE SOLAR CORONA AND SOLAR WIND**

Arcadi V. USMANOV (Institute of Physics, University of St.-Petersburg, St.-Petersburg 198904, Russia, e-mail: usmanov@snoopy.phys.spbu.ru)

A self-consistent 3D MHD model of a steady coronal outflow with a flux of WKB Alfvén waves in a dipolar magnetic field is developed. The results of simulation demonstrate the formation of a bimodal structure consisting of fast and slow wind. The computed parameters are generally consistent with the data from the Ulysses mission and with parameters typically found at the coronal base. It is shown that two processes determine the meridional distribution of solar wind plasma and magnetic field parameters: (i) the primary meridional relaxation and formation of a flat meridional profile of all the flow and magnetic field parameters (outside the equatorial band) in the region where magnetic forces dominate the thermal and wave gradient forces, and (ii) the secondary meridional redistribution due to the poleward thermal pressure gradient that formed as a result of the primary process. A series of successful simulation runs for the three-dimensional solar wind flow in the axial and tilted dipole magnetic field geometry has been carried out. The results of the 3D simulation are consistent with and further extend those obtained previously with an axisymmetric model.

**GA3.09/W/27-B4 1035**

**MAGNETOHYDRODYNAMIC MODELING OF THE SOLAR CORONA FOR SPACE-WEATHER APPLICATIONS**

JON A. LINKER, Zoran Mikic, Roberto Lionello, Pete Riley, Dalton Schnack, and Alfonso Tarditi (Science Applications International Corporation, San Diego, CA 92121)

Solar wind conditions upstream of Earth play a primary role in the initiation of geomagnetic activity. Satellites monitoring solar wind conditions at the L1 point can provide at most a one hour warning of important changes in the solar wind. The prediction of geomagnetic activity days in advance requires the forecasting of solar wind conditions at Earth orbit using remote observations of the Sun. In this talk we will discuss the present status of our magnetohydrodynamic (MHD) computations of the corona and solar wind. We will describe our progress to date in modeling the background solar corona and solar wind, which is essential for predicting the onset of fast solar wind streams at Earth. We will also discuss the elements we believe are necessary for success in modeling CME propagation to 1 A.U. Research supported by NASA and NSF; computations performed at NERSC and SDSC.

**GA3.09/W/05-B4 1110**

**PREDICTING SOLAR WIND SPEEDS**

Y.-M. WANG (Code 7672W, Naval Research Laboratory, Washington, DC 20375-5352, USA, E-mail: ywang@yucca.nrl.navy.mil)

Empirical studies have shown that the solar wind speed is inversely correlated with the divergence rate of magnetic flux tubes near the Sun. We discuss how this relationship can be used to predict the solar wind speed at Earth using photospheric magnetograms. We also discuss the implications of the wind speed - expansion factor correlation for the origin of fast and slow wind, with particular emphasis on the relationship between slow wind, open and closed field regions of the corona, and coronal streamers.

**GA3.09/E/06-B4 1135**

**SEMIPHENOMENOLOGICAL MODEL OF FILAMENT-GENERATED SOLAR WIND**

K.G.IVANOV and A.F.Harshiladze (Institute of Terrestrial Magnetism, Ionosphere and Radio Wave Propagation of Russian Academy of Sciences (IZMIRAN), Troitsk, Moscow Region, 142092 Russia, email: Kivanov@izmiran.troitsk.ru)

A semiphenomenological computer model of the solar wind proton number density and velocity variations at the Earth's orbit during special intervals of high solar filament activity was developed. The model allows to compute the proton number density (one hour averaged) long before (up to four days) arrival of solar prominence plasma at the Earth's orbit. The model suitable to the low speed solar wind (for example, the solar wind during the July 1978 event) and to an isolated coronal mass ejection as well (for example, July 10-11, 1996 ISTP event).

**GA3.09/E/08-B4 1150**

**COMPARISONS OF GLOBAL GUMICS-4 RUNS WITH MESOSCALE GROUND-BASED DATA**

Pekka JANHUNEN and Kirsti Kauristie (both at Finnish Meteorological Institute, Geophysical Research, POB 503, FIN-00101, Helsinki, Finland, email: Pekka.Janhunen@fmi.fi)

The most recent version of the GUMICS ionosphere-magnetosphere coupling simulation code is part of a flexible general MHD software. The new simulation incorporates automatic grid adaptation, which enables one to study cases with nonzero dipole tilt with no loss in accuracy. Apart from adaptive unstructured grid, GUMICS uses temporal subcycling, which provides additional significant speedup because the Alfvén speed is a steeply changing function of position.

To evaluate GUMICS, comparisons with observations are needed. Previous comparisons with older GUMICS versions with global SuperDARN convection patterns showed that higher resolution observations would also be useful. On the other hand, direct comparisons with magnetospheric satellites are plagued by the difficulty of getting a global picture. In this study we apply GUMICS for simulating recent intervals for which solar wind/IMF data and interesting MIRACLE data (a Scandinavian network of all-sky cameras, magnetometers and radars) is available. Within its accuracy limitations, GUMICS predicts the ionospheric conductivities, currents and electric field. Possibilities for intercomparisons with MIRACLE data include comparisons of GUMICS height-integrated Pedersen conductivity patterns with all-sky camera pictures, GUMICS horizontal electric fields with the STARE radar, and comparisons of simulated magnetograms with real ones provided by the by the IMAGE network.

**GA3.09/E/03-B4 1215**

**VALIDATION OF GLOBAL MHD MODELS: GRID CONVERGENCE AND BOUNDARY CONDITIONS**

D. L. DEZEEUW, T. I. Gombosi, C. P. T. Groth, and K. G. Powell (The University of Michigan, Ann Arbor, MI, USA, e-mail: darrens@umich.edu)

With advances in computing technology over the last decade, large-scale global models of the space environment have become increasingly sophisticated and complicated. It is crucial to make sure that these codes are validated as much as possible before they are used as analysis and forecasting tools and simulation results are compared with observations. This talk will concentrate on several important aspects of code validation, including grid convergence and the effects of boundary conditions.

Ideally, all MHD simulation results should be independent of the grid on which they are solved, but that is not always the case. A grid convergence study is useful in determining an acceptable level of grid influence in a solution. Grid convergence studies are not often practical to carry out, since most global models are being used at the limit of the available computing resources and significant increases in resolution are not possible. Grid convergence studies for several global magnetospheric configurations will be shown.

Procedures for prescribing boundary conditions can also play a role in the validity and accuracy of global MHD simulations. The type of boundary condition and boundary location (both inner and outer) can lead to differences in simulation results. Several global magnetospheric configurations illustrating these differences will be presented.

**Thursday 29 July PM**

Presiding Chair: Terry Onsager, (NOAA R/E/SE, Space Environment Centre, Boulder Co, USA)

**QUANTITATIVE MODELING 2**

**GA3.09/W/12-B4 1400**

**QUANTITATIVE COMPARISONS BETWEEN GLOBAL MHD SIMULATIONS OF MAGNETOSPHERE AND IN SITU MEASUREMENTS**

M. WILTBERGER, C. C. Goodrich, R. E. Lopez, K. Papadopoulos (All at Astronomy Department, University of Maryland, College Park, MD 20742; (301) 405-7936; email: wiltbermj@spp.astro.umd.edu); J G Lyon (Department of Physics and Astronomy, Dartmouth College, Hanover, NH 03755); T. I. Pulkkinen (Finnish Meteorological Institute, P.O.Box 503 FIN-00101 Helsinki)

Spacecraft and ground data combined with multiscale computer models developed by the ISTP are providing a new and coherent picture of the magnetospheric substorms and storms. The Lyon-Fedder-Mobarry (LFM) Global MHD code is dynamically driven by solar wind data provided from upstream satellites and includes coupling between the magnetosphere and ionosphere. The simulation output can be directly compared with the field and flow quantities measured by magnetospheric satellites, ground data from CANOPUS, SUPERDARN, and other ground investigations, as well as images from the POLAR satellite.

We have used the LFM to simulate a variety of events including the storms associated with January 10-11, 1997 and May 1-4, 1998 magnetic cloud passages as well as substorms that occurred on March 9, 1995, May 15, 1996 and Dec 10, 1996. While the number of simulated events is still small, in a statistical sense, they provide us with opportunity to make comparisons between the observations and the simulation under a variety of solar wind conditions. Our results show that the LFM is capable of accurately representing the global magnetospheric state. Direct comparison with spacecraft measurements in the magnetotail is

a particularly challenging task due presence of small scale structures. In order to assess the models accuracy as well as examine both the in situ observations and the results in the larger magnetospheric context we conclude with a series of scientific visualizations that present both the satellite observations and the simulation results for the region near the spacecraft.

**GA3.09/W/29-B4 1425**

**COMPARISONS OF EMPIRICAL MAGNETIC FIELD MODELS, MHD SIMULATIONS, AND ISTR OBSERVATIONS**

T I PULKKINEN, (Finnish Meteorological Institute, Helsinki, Finland); M Wiltberger, (University of Maryland, College Park, MD)

Because the magnetospheric research largely depends on a few point measurements from a vast region of space, developing realistic models for the magnetospheric configuration and dynamics is especially important. Empirical models for the magnetospheric magnetic field describe the state of the magnetosphere at a given set of magnetospheric activity parameters, solar wind and IMF parameters. On the other hand, global MHD simulations give a self-consistent description of the temporal evolution of the magnetosphere for a specified solar wind input.

A substorm on Dec 10, 1996, consisted of two onsets, one at 0731 UT and another, larger, at 0800 UT. The early phases of the substorm have been modeled using both empirical models and MHD simulations. Observations indicate that the first onset was localized and did not lead to global reconfiguration. The empirical model results suggest that a thin current sheet was already present during the first onset, and that it persisted throughout the second onset. The MHD simulations do not produce much activity during the first onset, but predict the onset of the second activation within only a few minutes. By comparing the results, the strengths and weaknesses of each of the modeling approaches is discussed.

**GA3.09/W/15-B4 1450**

**WHAT GLOBAL MODELERS NEED TO KNOW ABOUT IONOSPHERE OUTFLOWS**

GILES, B. L. (NASA Goddard Space Flight Center, Greenbelt, MD 20771 USA, Email: barbara.giles@gssc.nasa.gov); D. C. Delcourt (Centre d'Etudes Terrestre et Planetaire, St. EsMaur-des-Fosses, France 94107); D. L. Gallagher (NASA Marshall Space Flight Center, Huntsville, AL 35812 USA); T.E. Moore (NASA Goddard Space Flight Center, Greenbelt, MD 20771 USA); W.K. Peterson (Lockheed Martin Advanced Technology Center, Palo Alto, CA, 94304 USA); G. R. Wilson (Mission Research Corporation, Nashua, NH 03062 USA)

In the 1980's, detectors on S3-3 and Dynamics Explorer observed substantial amounts of ionosphere plasma flowing outward into the magnetosphere. Contemporary observations from Polar, Geotail and ISEE provide evidence that this plasma source substantially contributes to the magnetosphere environment extending at least to the mid-magnetotail region. The exact role of this plasma with regard to magnetosphere dynamics is still highly speculative although the concept enjoys renewed attention within the global modeling community. We present low-energy plasma observations from the POLAR spacecraft to illustrate dependences of the ionosphere source on solar wind and IMF conditions. Emphasis will be given to variations in flux strength, breadth in location, and the global extent of the outflow. Based on these observations, results from previous studies, and particle trajectory code calculations, we will also present initial results of a semi-empirical model of the ionosphere plasma source. Understanding the ionosphere plasma source and its response to solar influences is of significance when seeking to resolve terrestrial versus solar wind participation to the dynamics of the magnetosphere.

**GA3.09/E/02-B4 1505**

**COMPARISON OF THREE QUANTITATIVE MAGNETIC FIELD MODELS OF THE MAGNETOSPHERE**

Jean Claude KOSIK (Division Mathematiques, bpi 1214, CNES, 18 Av. E.Belin, 31401 Toulouse Cedex 4, France, email: jean-claude.kosik@cnes.fr)

A quantitative magnetic field model of the magnetosphere has been developed using poloidal vector fields and a NSSDC data base (Kosik, Annales Geophysicae, 1,1999). The main features of this model are briefly presented: ring current region, distant field, magnetopause current system, neutral sheet. The model, tilt and Kp dependent, can be compared to the Tsyganenko 89c model for different Kp and tilt angles. The difference between the total magnetic field and the magnetic field of internal origin, IGRF, is calculated for different Kp values. The corresponding delta B contours which give a clear signature of the ring current region are plotted and compared to the experimental results of Sugiura and Poros. Another comparison is made with the model Tsyganenko96-V1 which depends on the Dst index. Finally the models are compared to a series of magnetic field data and conclusions are drawn.

**GA3.09/W/11-B4 1520**

**INFLUENCE OF THE REGION 1 FIELD-ALIGNED CURRENTS ON DISTURBED MAGNETOSPHERIC STRUCTURE**

Igor ALEXEEV (Institute of Nuclear Physics, Moscow State University, Russia, 119899, email: alexeev@dec1.npi.msu.su)

Based on dynamic paraboloid model of the magnetosphere the contribution of the Region 1 field-aligned currents (FAC) to the pressure balance at subsolar point was calculated. The influence of the Region 1 FAC on the equilibrium condition at the inner edge of the tail plasma sheet was studied. The two different aspects of the FAC influence on magnetospheric magnetic field was studied. First, the twist of the magnetic field lines caused by FAC was calculated. Second the displacement of the open field lines bundle to the sunward direction was determined. The FAC control of the magnetospheric structure was investigated.

**GA3.09/E/12-B4 1600**

**MODELLING THE EARTH'S TRAPPED RADIATION BELTS: CURRENT STATUS AND FUTURE DEVELOPMENTS**

D. HEYNDRICKX and M. Kruglanski (BIRA/IASB, Brussels, Belgium)

Since their discovery, the Earth's trapped radiation belts have been the subject of several modelling efforts that aim to predict the distribution of the trapped particle population for a given state of the magnetosphere. In general, a trapped radiation belt model uses a coordinate system attached to the geomagnetic field which controls the behaviour of the electron and proton populations. We review the most used geomagnetic coordinate systems and discuss the requirements on the models of the magnetic field on which they are based. Changes in the magnetic field configuration necessitate regular updates of the radiation belt models.

Requirements for new models are presented, as well as the data and developments needed to build them.

**GA3.09/E/05-B4 1625**

**RICE CONVECTION MODEL DATA COMPARISONS**

T W Garner, R A WOLF, and R W Spiro (Space Physics and Astronomy Dept., Rice University MS108, P.O. Box 1892, Houston, TX 77251, U.S.A.); W J Burke (Air Force Research Labs, Hanscom AFB, MA 01731); N C Maynard (Mission Research Corp., 1 Tara Bd., Nashua, NH 03062, U.S.A.)

An extensive series of Rice Convection Model runs has been carried out for the major magnetic storm of June 4-5, 1991, in an effort to clarify the processes involved in injection of the storm-time ring current. Model predictions are compared with electric fields and kilovolt-particle fluxes measured from CRRES and with ion drifts and precipitating-electron measurements from DMSP. The runs have been successful in reproducing the most basic features of the injection, including deep injection of fresh ions into the inner magnetosphere and the penetration of convection fields into the inner magnetosphere. However, there are quantitative disagreements with regard to many details. The implications of the results for overall understanding of ring-current injection will be assessed.

**GA3.09/E/04-B4 1650**

**NONADIABATIC PARTICLE MOTION NEAR TRAPPING BOUNDARY IN TSYGANENKO T89 MODEL**

Prof. S.N.KUZNETSOV and A.Yu.Rybakov (both at Skobel'syn Institute of Nuclear Physics, Lomonosov Moscow State University, 119899 Moscow, Russia)

Energetic charged particle motion at trapping boundary region was calculated with using Tsyganenko T89 model. Calculation based on model of particle nonadiabatic motion in dipole field developed at Skobel'syn Institute of Nuclear Physics. Position of precipitation region of energetic particles was found depending on parameter of adiabatic motion, geomagnetic latitude and geomagnetic local time for different geomagnetic disturbances. Comparison with precipitating and quasi-trapped particle fluxes measured by "CORONAS-I" satellite was performed.

**GA3.09/W/20-B4 1705**

**A MODEL OF THE SPATIAL STRUCTURE OF THE HIGH LATITUDE MAGNETIC PERTURBATIONS (HLMP)**

J. A. VALDIVIA (Code 692, NASA/GSFC, Greenbelt, MD 20771; 301-286-3545; e-mail: alejo@roselott.gsfc.nasa.gov) D Vassiliadis (NASA/GSFC/USRA) A J Klimas (NASA/GSFC)

We have generalized the standard nonlinear dynamical approach devised for the AL-VBs coupling [Vassiliadis et al., J. Geophys. Res., 100, 3495, 1995] to construct a two dimensional dynamical model of the spatial structure of the high latitude magnetic perturbations (HLMP). This model is constructed with the help of nonlinear time series techniques from a discrete set of ground magnetometers measurements and WIND data. Different models are constructed for each of the three magnetometer chains (1) Canopus, (2) IMAGE and (3) MM210, which can then be compared with each other. A two dimensional model of the spatial structure of the HLMP is constructed using the fact that as the Earth rotates, the ground magnetometer chain essentially samples the spatial structure of the HLMP repeatedly and for many levels of activity. Therefore, a novel technique is used to reconstruct a full dynamical model, driven by solar wind data from a suitable two dimensional initial condition, of the two dimensional spatial structure of the HLMP and the related equivalent current system (HLCS). This effort is aimed at generating a two dimensional dynamical model of the spatial structure of the high latitude current systems. These models can be used to visualize and to predict the spatial evolution of the current systems as observed by multiple ground stations. Hence, these models could be also useful as a spaceweather forecasting tool.

**GA3.09/W/14-B4 1720**

**HIGH-LATITUDE GROUND GEOMAGNETIC FIELD MODELS WITH A NONLINEAR COUPLING TO THE SOLAR WIND INPUT**

D. VASSILIADIS (NASA/GSFC/USRA, at: Code 692, NASA/GSFC, Greenbelt, MD 20771; 301-286-9060; email: vassi@lepgst.gsfc.nasa.gov); J. A. Valdivia, A. J. Klimas, D. N. Baker

Many ground geomagnetic field models are data-based, but most of them are independent of activity, or classify activity according to a geomagnetic index. However it appears possible to represent the dependence of the geomagnetic and current spatial distribution on several distinct processes and parametrize the field models more self-consistently. Clearly such processes are primarily the large-scale convection imposed by the recent solar wind electric field, and, to higher order, internal magnetospheric processes. Here we present a new type of ground geomagnetic field model which is parametrized directly by the solar wind E-field and the internal magnetospheric activity level. The internal activity is represented self-consistently in terms of measurements from four high-latitude magnetometer chains from which a spatial-temporal pattern is constructed. A month-long interval in 1995, which is dominated by high-speed streams and in which WIND monitors the interplanetary conditions during its ascent towards L1, is used as the database for model development ("training"). We extend the techniques used in geomagnetic index prediction / modeling, to represent the geomagnetic state and express it as a superposition of basic geomagnetic patterns. Each pattern is associated with an equivalent current system in a way similar to the method of Sun et al. [JGR A6, 1998]. Starting from an initial geomagnetic state the model is stepped in time by finding similar geomagnetic / solar-wind states among the large number of states stored in the database, and interpolating their dynamics. The field model will be tested for its ability to predict the spatiotemporal development of geomagnetic events while driven by the solar wind input or PC index. The amplitude information obtained from the spatiotemporal predictions will then be compared to that of AL/AU index models.

Similarly to other geomagnetic models (e.g. IZMEM) this model can be coupled to the height-integrated conductivity to estimate ionospheric electrodynamic parameters, such as currents and E-fields, and convection patterns.

**GA3.09/E/09-B4 1735**

**CURRENT CONFIGURATION IN THE HIGH LATITUDE MAGNETOSPHERE AND MAGNETOSPHERE MAGNETIC FIELD MODELING**

Elizaveta E ANTONOVA and Natalia Yu. Ganushkina (both at Skobel'syn Institute of Nuclear Physics, Moscow State University, Moscow, 119899, Russia; email: antonova@taspd.npi.msu.su)

Quantitative modeling of the magnetospheric magnetic field require the proper selection of the

inner magnetosphere current systems. Among such systems the inner Earth currents (IGRF field), tail current, inner magnetosphere westward ring current, magnetopause currents and field-aligned currents are ordinarily selected. The analysis of plasma pressure distribution in the magnetosphere and the topology of high latitude magnetosphere show on the existence of one more current system quasi-ring current localized far from equatorial plane near noon. Current lines of this current system have the forms of cut rings. High latitude earthward plasma pressure gradients produce westward currents, anti-earthward plasma pressure gradients produce eastward currents. It is shown that any growth of inner magnetosphere plasma pressure must lead to the appearance of the effective eastward ring current. The role of eastward ring current in the magnetopause motion and near noon field line stretching during substorms is analyzed. The magnetopause pressure balance is discussed.

**Friday 30 July AM**

Presiding Chair: Tim Fuller-Rowell, (NOAA R/E/SE, Space Environment Centre, Boulder Co, USA)

**QUANTITATIVE MODELING 3**

**GA3.09/E/07-B5 0830**

**HIGH-LATITUDE CONVECTION PATTERNS: METRICS**

Y. KAMIDE (Solar-Terrestrial Environment Laboratory, Nagoya University, Toyokawa, Aichi-ken 442-8507, Japan, email: kamide@stelab.nagoya-u.ac.jp)

A number of empirical and semi-empirical models for the large-scale distribution of the electric potential, or convection, in the ionosphere have been proposed. These models, which are sorted according to various solar wind conditions, are the result of satellite and radar observations of electric fields, as well as ground-based magnetometer measurements through so-called magnetometer inversion techniques. To evaluate these models in terms of how well they can predict or reproduce the reality, it is important to realize that ionospheric convection patterns consist of two components. One can be predicted reasonably well by proper solar wind parameters, and the other is caused by some "internal" processes in the magnetosphere-ionosphere system. Thus, for a given condition in the solar wind, the response of the convection patterns in the ionosphere can vary to a significant degree.

**GA3.09/W/18-B5 0855**

**RECONSTRUCTION OF HIGH LATITUDE IONOSPHERIC CONVECTION PATTERNS FROM CROSS-POLAR SATELLITE PASSES**

Peter ISRALEVICH and Alexander Ershkovich (Department of Geophysics and Planetary Sciences, Tel Aviv University, Ramat Aviv 69978, Israel, email: peter@jupiter1.tau.ac.il); Vladimir PAPITASHVILI (Space Physics Research Laboratory, University of Michigan, Ann Arbor, MI 48109, USA, email: papita@umich.edu)

In this study we attempt the reconstruction of ionospheric convection patterns over the entire polar region solely from satellite measurements of the electric fields (or ion drifts) made along the cross-polar pass(es). In a simple case, a single cross-polar pass divides the polar cap in two sub-regions; however, additional near-simultaneous passes increase the number of subdivisions and significantly improve the overall calculations. Both horizontal components of the measured vector are required for calculations; the ionospheric electric potential and its normal derivative are set to zero at the equatorial boundary of the polar region. The stream function method is proposed for solving the boundary value problem. The polar ionosphere is taken as a plane with the constant geomagnetic field over the entire polar region; it is supposed that existing field-aligned currents close at altitudes of 100-150 km. Under these assumptions the field vertical derivative equals to zero at the altitudes of several hundred kilometers (e.g., 300-800), and the problem becomes two-dimensional. Assuming also that the two-dimensional ionospheric plasma flow is incompressible, we reduce the magnetohydrodynamic flow to the hydrodynamic one and introduce the stream function strictly related to the ionospheric electrostatic potential in the polar cap. We tested the method using the modeled convection patterns for various IMF conditions and then validated the results reconstructing the patterns from the simulated cross-polar passes over both the northern and southern polar caps.

**GA3.09/W/25-B5 0910**

**HIGH LATITUDE IONOSPHERIC CONVECTION MODEL DERIVED FROM DMSP DATA AND PARAMETERIZED BY THE IMF STRENGTH AND DIRECTION**

Vladimir PAPITASHVILI (Space Physics Research Laboratory, University of Michigan, Ann Arbor, MI 48109, USA, email: papita@umich.edu); Frederick Rich (Air Force Research Laboratory, Hanscom Air Force Base, Hanscom MA 01731, USA, email: rich@plh.af.mil); Marc Hairston (Center for Space Sciences, University of Texas at Dallas, Richardson, TX 75080, USA, email: hairston@utdallas.edu); Boris BELOV (Institute of Terrestrial Magnetism, Ionosphere and Radio Wave Propagation, IZMIRAN, Troitsk, Moscow Region, 142092, Russia, email: bbelov@adonis.iasnet.ru)

The ionospheric electrostatic potentials obtained from thermal ion drift measurements made by DMSP satellites in 1993&#61485;1996 are binned by every 1 degree CGM latitude and 0.5 hour MLT over both the northern and southern polar regions. Then the linear regression analysis technique is applied to the IMF data and the DMSP potentials in each bin. However, the available satellite orbits provide lesser coverage over the dayside and nightside sectors of the polar region; some bins have no coverage at all. Recently we re-calibrated electric potentials provided by the IZMIRAN Electrodynamic Model (IZMEM) against xperimental DMSP observations. This allowed us to parameterize the DMSP ionospheric potentials by the IMF strength and direction (e.g., 11.5 kV/nT and &#61485;5.0 kV/nT for the southward and northward IMF, respectively). The background" cross-polar potential estimated from DMSP data equals ~33 kV if the IMF is near zero. In this study, we filled the gaps in the DMSP observations over dayside and nightside sectors by the IZMEM potentials and then applied the spherical harmonic analysis to the combined DMSP/IZMEM set of ionospheric potentials for various IMF conditions.

**GA3.09/W/06-B5 0925**

**CORRECTNESS OF COUPLED MODELS OF THE HIGH AND MID-LATITUDE IONOSPHERE**

J. J. SOJKA and R. W. Schunk (Center for Atmospheric and Space Sciences, Utah State University, Logan, Utah 84322-4405, Email: fasojka@sojka.cass.usu.edu)

Theoretical formulations of the ionosphere, thermosphere, and magnetosphere are well established. Their numerical solutions in the form of global models, whether stand alone or coupled, are proliferating due to the continued technological breakthroughs, leading to lower costs of computing. The increasing awareness of the adverse effects of space weather through programs such as the US National Space Weather Program (NSWP), is acting to fuel

this proliferation. Stumbling along at a somewhat slower pace is the process of evaluating the accuracy, correctness, or even usefulness of such developments. This stage involves the use of "ground truth" observations of the geospace system. However, the acquisition of such data is difficult, and casting it into a mathematically sufficient data base so that it can be used to evaluate models is even more challenging. Experimentally, the complete constraint of ionospheric models is far from achievable. Therefore, we present procedures and initial steps that we are taking to evaluate ionospheric models. The philosophy presented involves emphasizing the evaluation of the inputs as well as the ionospheric outputs. The sensitivity of the system to changes in the inputs is used to determine the relative importance of input knowledge. Both stand alone ionospheric and magnetosphere-ionosphere coupled models will be discussed. The presentation will also demonstrate that most present day models are approaching 100% "correctness", but that they also still have approximately zero skill (usefulness)! The old adage "garbage-in implies garbage-out" is very applicable in today's NSWP environment.

**GA3.09/W/03-B5 0950**

**SPACE WEATHER SPECIFICATION AND FORECAST VERIFICATION**

M V CODRESCU, and T J Fuller-Rowell (CIRES-University of Colorado/NOAA - SEL, 325 Broadway, Boulder, CO 80303, USA; e-mail: codrescu@sec.noaa.gov); P Wilkinson (IPS Radio and Space Services, Haymarket, AUSTRALIA)

The increasing use of models for Space Weather specification and forecast and the existence of a variety of competing models with different strengths and weaknesses require continual consideration of validation and verification issues. Consistent approaches based on unified metrics need to be implemented in order to assess progress and to inform potential users about product and service reliability. The evaluation of space weather models is made more difficult by the use of the output of one model as input to another and the sparsity of measurements in the Sun-Earth chain. A number of models have been verified and validated as research tools and are now ready to start verification and validation under operational conditions. We use the Coupled Thermosphere Ionosphere Model (CTIM) to illustrate the verification and validation issues encountered at the Space Environment Center in Boulder, Colorado in the transition of a research model into operations. We will discuss uncertainties due to imprecise knowledge of forcings, initial conditions, subgrid scale processes, and uncertain physical or chemical parameters.

**GA3.09/W/04-B5 1035**

**GLOBAL MODELING OF IONOSPHERIC TOTAL ELECTRON CONTENT DURING GEOMAGNETIC STORMS**

G. LU (HAO/NCAR, Boulder, CO 80301; 303-497-1554, email: ganglu@ncar.ucar.edu); A. D. Richmond (HAO/NCAR, Boulder, CO 80301); R. G. Roble (HAO/NCAR, Boulder, CO 80301); X. Pi (JPL, Pasadena, CA 91109)

During geomagnetic storms, energy inputs from the magnetosphere can have dramatic effects on the upper atmospheric environment. One such effect is the changes in the ionospheric electron density that can perturb communication and navigation systems. In this paper, we show that, by using realistic time-dependent high-latitude ionospheric convection and auroral precipitation derived from the AMIE procedure, the NCAR TIE-GCM is capable to reproduce many observed features of ionospheric disturbances in response to the January 1997 geomagnetic storm. In particular, we compare the model simulated ionospheric electron density variations with those observed from the Global Positioning System (GPS) ground-based and low-earth orbiting receivers.

**GA3.09/W/19-B5 1100**

**COMPARISON BETWEEN SUPIM SIMULATIONS, ISR DATA AND GPS TEC MEASUREMENTS**

B. MACPHERSON, S. A. Gonzalez, M. P. Sulzer (all at Arecibo Observatory, HC3 Box 53395, Arecibo, 00612, Puerto Rico, U.S.A. Email: bmacpher@naic.edu, sixto@naic.edu, sulzer@naic.edu); G. J. Bailey (The Upper Atmosphere Modeling Group, University of Sheffield, England, Email: g.bailey@sheffield.ac.uk); M. C. Kelley (Cornell University, Email: mikek@anise.ee.cornell.edu); C. Wang (USC, Email: cwng@cams-00.usc.edu); G. hajj and X. Pi (JPL, Email: hajj@cobra.jpl.nasa.gov, xqp@maggie.jpl.nasa.gov)

Because of the effects of the Earth's space environment on the applications of advanced technology, forecasting ionospheric daily variations is a crucial goal of the National Space Weather Program. However, no ionospheric model exists that comes close to the predictive power of meteorological models, due mainly to the relative paucity of ionospheric data and several uncertainties in ionospheric modeling. Therefore, improved ionospheric modeling and a comprehensive ionospheric set of measurements are required to be able to reach the goal of space weather forecasting. Total electron content (TEC, the integrated electron density along therapy path) data from the Global Positioning System (GPS) present a potentially powerful tool to monitor the ionosphere due to the continuous data available from hundreds of ground stations. Furthermore, the availability of space-based TEC data from the GPS/MET mission, and several low-Earth orbiters tracking GPS to be launched in the next two-three years, provides a sampling of the ionosphere from a previously unavailable vantage point. We are currently developing an ionospheric model capable of assimilating GPS TEC measurements that is based on the the Sheffield University Plasmasphere Ionosphere Model (SUPIM). The eventual goal is to be able to nowcast and forecast global ionosphere electron densities, along with other parameters, using the model and near realtime TEC observations from GPS. We will discuss results obtained by comparing TEC obtained from GPS with TEC deduced from topside ionosphere data taken at the Arecibo Incoherent Scatter Radar facility. These data will also be compared with results from SUPIM. Data from both quiet and disturbed conditions will be discussed.

**GA3.09/E/10-B5 1115**

**AN ASSESSMENT OF MODELS FOR EQUATORIAL PLASMA BUBBLES**

JOHN M. RETTERER (Air Force Research Lab., Hanscom AFB, MA, 01731, USA, email: retterer@plh.af.mil)

Equatorial plasma bubbles are the structured depletions of plasma density which develop in the ionosphere after sunset, with which Equatorial Spread-F radio scatter and scintillation are associated. Devising tests for a theoretical model of the equatorial plasma bubbles is a challenge because of their sensitive dependence on the structure of the background plasma and the stochastic nature of the unobservable perturbations from which they grow; it is doubtful whether it will ever be possible to predict the exact location and structure of the bubbles that form on a particular evening, but likepredictions of favorable conditions for thunderstorms on a summer afternoon forecasts of a statistical nature are possible. In



preparation for the development of components of a scintillation forecast model, a review of the assumptions and physics built into current models of the formation of equatorial bubbles was carried out. One of the conclusions was that our understanding of bubble formation is mature enough that it is appropriate to replace the simplified models of the characteristics of the ionospheric plasma with detailed, realistic models. Some of the consequences of this quest for detail will be illustrated with the results of a new simulation code. The results will be shown side-by-side with data from both ground-based observations and satellite flythroughs, inviting at least qualitative comparison. Formidable challenges remain, including the description of the three-dimensional character of the plasma depletions, the development of smaller-scale structure, and then a specification of the information needed to characterize the level and nature of the resulting scintillations. Coordinated collection of data of the many aspects of these phenomena will be required to achieve the level of understanding necessary to combine them to develop an reliable scintillation forecast model.

**GA3.09/W/10-B5 1140**

**NEUTRAL DENSITY MODELING AND VALIDATION**

Geoff CROWLEY (Southwest Research Institute, San Antonio, TX 78238-5166; email: crowley@picard.space.swri.edu)

Global 3D first-principles models of the thermosphere and ionosphere are at an advanced stage of development and can potentially make important contributions to Space Weather specification and forecasting. The problem has been in showing that these models can routinely improve on the performance of simple empirical models. Neutral densities are of great interest for predicting satellite orbits, and in this paper, we review the state of the art in global modeling of the neutral density, including techniques currently in operational use. Detailed model/data comparisons are presented and the metrics needed to quantify the performance of current and future models are discussed. We address the likely sources of deviations between the models and data, and ask how these might be mitigated. The implications for use of first principles models in real-time Space Weather applications are explored.

**GA3.09/W/24-B5 1205**

**STUDY OF ASSESSING CURRENT THERMOSPHERE MODELS WITH NEURAL-NETWORK-BASED THERMOSPHERE MODELS**

Jianhua TIAN and Quanfu Fan (both at Center for Space Science and Applied Research, Academia Sinica, 100080, Beijing, China email: jhtian@earth.sepc.ac.cn)

A neural-network-based thermosphere model (NNTM), which has good statistical and generalized capability in modeling total atmospheric density and can provide more data coverage than the current observed data, is used to assessing the accuracy of some current thermosphere models such as MSIS90, MET and CIRA72.

Comparisons are made between the computed values of total atmospheric density between NNTM and other three models. The results show that in the altitude range of 200-400km, MSIS90 is systematically better than MET and CIRA72 in modeling of total density variations under most cases. In 400-600km, MSIS90 is equivalent to MET, while CIRA72 does worse and generates higher total density.

**Thursday 29 July AM**

Presiding Chair: Jimmy Raeder (IGPP/UCLA, Los Angeles)

**QUANTITATIVE MODELLING POSTERS**

**GA3.09/E/11-B4 Poster 0900-01**

**POTENTIAL FIELD APPROXIMATION OF MAGNETIC FIELDS ON THE SUN FROM DAILY MAGNETOGRAMS**

Dmitri I. PONYAVIN (Institute of Physics, University of St.Petersburg, 198904, Russia, e-mail: ponyavin@snoopy.phys.spbu.ru)

Daily full-disk magnetograms measured at Stanford were taken separately to infer a large-scale magnetic field configuration in framework of potential field theory. A regularization technique was applied to resolve spherical harmonics from the data covering only visible solar disk. Sets of daily spherical expansion coefficients collected few days later serve as input entries for extrapolating procedure. This procedure was constructed to resolve trends in large-scale magnetic field evolution. Coefficients were than used to predict large-scale magnetic field configurations just near the solar and source surface - the origin of the heliospheric current sheet and solar wind streams. Results of comparison between actual and predicted magnetic fields were presented and discussed.

**GA3.09/W/23-B4 Poster 0900-02**

**PREDICTABILITY LIMITS FOR LONG-TERM HELIOSPHERIC PLASMA AND MAGNETIC FIELD VARIATIONS**

I.S. VESELOVSKY, A.V. Dmitriev, A.V. Suvorova, M.V. Tarsina, M.O. Riazantseva (Institute of Nuclear Physics, Moscow State University, 119899 Moscow, Russia, Email: veselov@dec1.npi.msu.su)

Solar wind and interplanetary magnetic field are the manifestations of the solar activity that impact on the Earth's magnetosphere most effectively. Correlation functions are calculated for the main average plasma and magnetic field parameters using the data base obtained in 1964-1998 in the heliosphere near the Earth. The flowing time window with a variable width is used for the regression analysis. Characteristic correlation time intervals are found and used for the evaluation of dynamical predictability limits. The role of regular and irregular variations is discussed in attempts of statistical predictions inside and beyond these correlation times under different averaging time intervals and procedures. The prediction of heliospheric parameters by means of Artificial Neural Networks is presented for 1999-2000.

**GA3.09/W/16-B4 Poster 0900-03**

**COMPARISON BETWEEN SATELLITE OBSERVATIONS AND RESULTS FROM THE TSYGANENKO AND TOFFOLETTO-HILL MODELS**

Pieter B KOTZÉ (Hermanus Magnetic Observatory, P O Box 32, Hermanus 7200, South Africa; e-mail: pkozze@csir.co.za)

Magnetic field measurements obtained from Geotail and other satellites during disturbed periods are compared with calculations from both the Tsyganenko 96 and the Toffoletto-Hill 93 magnetospheric field models. Solar wind particle and magnetic field data from the Wind and

IMP8 satellites are used as dynamic input to these models. We investigate disturbances of the Earth's magnetosphere caused by magnetic cloud events resulting in different orientations of the interplanetary magnetic field. The response of the magnetosphere to the passage of the January 10-11, 1997 magnetic cloud event was modelled and compared with data obtained from the Geotail satellite, while using input data from the Wind spacecraft located in an upstream position. Similarly, a magnetic cloud observed by Wind on February 8-9, 1995, located at an upstream distance of 193 Re, resulted in substorm activities being monitored by both the IMP8 and Geotail satellites in different regions of the magnetotail. Modelling results from both the Tsyganenko and Toffoletto-Hill models are compared with observations.

**GA3.09/W/22-B4 Poster 0900-04**

**COMBINING THE RICE CONVECTION MODEL WITH MHD**

F. R. TOFFOLETTO(1), R. A. Wolf(1), J. Birn(2), and M. Hesse(3) (1) Department of Space Physics and Astronomy, MS 108, Rice University, Houston, TX 77251-1892, USA. (email: toffo@rice.edu) (2) MS D466, Group NIS-1, Los Alamos Nat Lab, Los Alamos, NM 87545, USA (email: jbirn@lanl.gov) (3) Electrodynamic Branch, NASA/Goddard Space Flight Center, Greenbelt, MD 20771, USA (email: hesse@gssc.nasa.gov)

We will describe results from a collaborative effort that is aimed at the development of a self-consistent computational model of a substorm, by coupling the physics of the inner magnetosphere and the ionosphere, as represented by the Rice Convection Model (RCM), and the physics of the tail, as represented by the Los-Alamos/Goddard MHD model of tail dynamics. Another essential element is an equilibrium code that has been developed through a Los-Alamos/Goddard/Rice collaboration. We will present results from the fully merged Tail-MHD/RCM model that test substorm ideas for theoretical consistency. This project evolved as part of the NSF Geospace Environment Modeling (GEM) effort to develop a modular Global Geospace General Circulation Model (GGCM) and consists of a prototypical coupling of a Core Module to a Tail/Substorm Module.

**GA3.09/W/26-B4 Poster 0900-05**

**MODELING THE TRAPPING BOUNDARY OF THE RADIATION BELTS AT HIGH AND LOW LATITUDES**

Mohamed J. ALOTHMAN and Theodore A. Fritz (both at Center for Space Physics, Boston University, Boston, MA 02215, Email: alothman@bu.edu and fritz@bu.edu)

A model for the High Latitude Isotropic Boundary (HLIB) was introduced by the authors in previous work. This model is based on the ability of particles to bounce between the mirror points while conserving their first and second adiabatic invariants. However, in the region where the magnetic field departs from dipole-like to tail-like in the nightside, the field line radius of curvature becomes comparable to the particle radius of gyration and the first invariant is violated resulting in pitch angle scattering and the generation of the isotropic fluxes seen at low altitudes equatorward of the trapping boundary. Further modeling revealed that particles with intermediate equatorial pitch angles get scattered into the loss cone while those with angles near 90 degrees are almost unaffected by this scattering process. The observations of ISEE 1 and 2 of pitch angle distributions with a depletion around 90 degrees, or what is known as butterfly distributions in different Magnetic Local Times (MLT) support this result. Previous work done on ISEE data, shows that the butterfly distributions are generated by magnetopause shadowing. Further analysis of ISEE observations of the butterfly distributions suggests that the magnetopause can act as both a sink and a source for particles with energy between 24 keV and 2 MeV. Furthermore, modeling the HLIB 30 keV ion fluxes as measured by the NOAA/TIROS as a function of MLT showed a very significant increase in the flux between 3 and 7 am MLT. These observations suggest a population of energetic particles can enter the nightside magnetosphere with an equatorial pitch angle around 90 degrees from one flank of the magnetopause and exit from the other without getting trapped into the radiation belts through scattering. This hypothesis will be examined by the combination of observations from low latitude by ISEE, high latitude from the NOAA/TIROS satellites, and models of the scattering process.

**GA3.09/E/01-B4 Poster 0900-06**

**A POLOIDAL VECTOR FIELD MODEL OF THE MAGNETOSPHERE WITH FIELD ALIGNED CURRENTS**

Jean Claude KOSIK (Division Mathematiques, bpi 1214, CNES, 18 Av. E.Belin, 31401 Toulouse Cedex 4, France, email: jean-claude.kosik@cnes.fr)

A magnetic field model of the magnetosphere different from the model Kosik99 (Annales geophysicae, 1,99) has been developed. This simplified model has been built using poloidal vector fields only. The magnetic field created by the magnetopause currents is described by one poloidal vector field expressed in cylindrical coordinates. The magnetic field produced by the tail current sheet is described by two poloidal vector fields also expressed in cylindrical coordinates. The curl of these poloidal vector fields can describe the dawn-dusk current flow. The ring current region is described also by a poloidal vector field expressed in spherical coordinates and the generating function adequately describes the depression in the external field. To obtain field aligned currents strictly along the magnetic field lines of the magnetosphere, the J field must be similar to the B field. The J field is also a poloidal vector field and the equations of the J lines are similar to the B field equations. The field aligned current equations can be considered as the degenerate form of the force free equations and the poloidal J field as the curl of a toroidal magnetic field. In our model this toroidal magnetic field is a small perturbation of the poloidal vector field of the magnetosphere and neglected in this first approach.

**GA3.09/W/09-B4 Poster 0900-07**

**INTERCOMPARISON OF MATHEMATICAL MODELS OF SOLAR ACTIVITY, INTERPLANETARY MAGNETIC FIELD AND MAGNETIC FIELD ON THE EARTH**

Tamara KUZNETSOVA, Lev Tsurulnik and Valery Petrov (all at IZMIRAN, Troitsk, Moscow region, 142092, Russia, email: tvkuz@izmiran.rssi.ru)

A method of nonlinear spectral analysis (called the method of global minimum: MGM) has been used to find periodicities in annual Wolf sunspot numbers (W) during the period 1700-1997. Data on interplanetary magnetic field (IMF) measured in solar wind during space era (1963-1997) are used to find periodicities in IMF. The longest set of magnetic observations on the Earth (D-component at Hartland, 1810-1995) is used for calculation of geomagnetic spectrum. We use MGM advantages: self-consistent selection from a data set of a trend, ability to single out periods which are longer than an input data set. The powerest triplet at period T=204 yr. in W testifies to the existence of the slowest non-stationary processes in sunspot formation. Trend in IMF module is described by harmonic at T=198 yr. Our analysis shows that W has the best correlation with IMF module (compared with the other solar wind parameters). These long harmonics in the both spectra show that long-term increase of solar

activity (IMF module) has been finished; decline phase is in progress. Comparative analysis of solar activity and geomagnetic spectra shows that significant spectral peaks of the geomagnetic spectrum are contained in the solar spectrum (periods with error bars coincide: Gleisberg's, Fritz's periods and others). However, harmonics of the solar model that have analog in the geomagnetic spectrum are not the poorest ones. For example, one of the poorest spectral peaks in the solar spectrum at  $T=11.1$  yr. is lower confidence limit in the geomagnetic spectrum. Thus, for supporting of the processes responsible for geomagnetic variations are important defined spectral lines of solar activity spectrum. The common periodicities (their amplitude and phase) in the Sun (W), in the Geospace (IMF module), on the Earth (D-component of the magnetic field) are analyzed

**GA3.09/W/01-B4** Poster **0900-08**

**ASSESSMENT OF IONOSPHERIC MODELS: WEATHER SPECIFICATION**

D.T. DECKER, J.O. Wise, W.S. Borer (All at Air Force Research Laboratory, Hanscom AFB, MA USA 01731-3010, Email: decker@phl.af.mil) P.H. Doherty (Institute for Scientific Research, Boston College, Chestnut Hill MA USA 02167, Email: doherty@phl.af.mil) R.E. Daniell Jr.(Computational Physics Inc., 240 Bear Hill Rd, Waltham, MA USA 02451, Email: daniell@cpiboston.com)

In recent years there has been work towards using day specific observations and ionospheric models to provide a weather specification of the ionosphere. For example the climatological models IRI, PIM and RIBG are three models that have been used in work of this type. In particular, the U.S. Air Force has developed the Parameterized Real-time Ionospheric Specification Model (PRISM) over the last 10 years. This model uses both ground-based and space-based data available in near real-time to modify the Parameterized Ionospheric Model (PIM) and thus provide a near-real time specification of the ionosphere. While there have been a few validation studies of PRISM, they have been fairly limited in scope and do not provide, as complete and comprehensive validation of PRISM as is practical. In this paper, we discuss the data assimilation capabilities of PRISM and our assessment of its ability to provide improved ionospheric specification. We will particularly focus on the interplay between data coverage, the accuracy of the PIM climatology, the observed spatial and temporal correlations in the ionosphere, and the observed day-to-day variations.

**GA3.09/W/02-B4** Poster **0900-09**

**ASSESSMENT OF IONOSPHERIC MODELS: THE CLIMATOLOGY**

P.H. DOHERTY (Institute for Scientific Research, Boston College, Chestnut Hill, MA USA 02167, Email: doherty@phl.af.mil), D.T. Decker, P.J., Sultan, W.S. Borer (All at Air Force Research Laboratory, Hanscom AFB, MA USA 01731-3010, Email: decker@phl.af.mil), R.E. Daniell Jr. (Computational Physics Inc., 240 Bear Hill Rd, Waltham, MA USA 02451, Email: daniell@cpiboston.com)

The growing focus on space weather has generated interest in quantifying the "state of the art". In part, this requires establishing quantitative metrics and assessing the baseline performance of current models. We are presently involved in a comprehensive effort to assess various ionospheric models, which will contribute to establishing an ionospheric baseline. This effort will eventually involve ionospheric models of various types including empirical, semi-empirical, theoretical, specification, and forecast. For this paper, we focus on several available climatological models: Bent, Chiu, FAIM, IRI, PIM, and RIBG. In order to have a comprehensive approach, we are using a variety of ground-based and satellite-based datasets. These include data from incoherent scatter radar, ground-based ionosondes and digisondes, DMSP in-situ measurements, TOPEX TEC measurements, Faraday rotation TEC measurements, ground-based GPS TEC measurements, and satellite-based TEC measurements. Besides providing a complete picture of what aspects of the models are validated, this work will provide the opportunity to quantify the climatology and weather contained in these datasets. This quantification of the observed ionospheric weather will be useful in establishing goals for future space weather models. In this paper, we will discuss the goals, the methodology, and the results to date of this assessment effort.

**GA3.09/W/21-B4** Poster **0900-10**

**ON THE DEFINITION OF THE QUIET IONOSPHERE AT MIDDLE LATITUDES DURING THE 21ST SOLAR CYCLE**

Anna BELEHAKI and George Moraitis (Institute of Ionospheric and Space Research, National Observatory of Athens) Ioanna Tsagouri (Nuclear and Particle Physics Section, Physics Department, University of Athens)

The dependence of the foF2 critical frequency measured in Rome ionospheric station at local noon on the sunspot number Rz, has been examined during the 21st solar cycle (1976-1986). A clear linear response of the F2 layer critical frequency was found for low level of solar activity (Rz up to 85) while for higher values of Rz the ionospheric response turned to be better fitted by an exponential curve. The quiet values of the foF2 in Rome ionospheric station has been reproduced using the multiple regression method, for low and high level of solar activity. The quantity QoF2 obtained from this model was compared with the monthly median values of the foF2 parameter, for intervals of very quiet magnetospheric activity during various phases of the solar cycle. The results show a much better fit of the QoF2 with the observed values of the foF2 parameter than that we get using the monthly median to define the quiet ionosphere.

**GA3.09/W/07-B4** Poster **0900-11**

**STATISTICAL CORRELATION BETWEEN THE FOF2 DISTURBANCES AT MIDDLE LATITUDES AND THE GEOMAGNETIC ACTIVITY**

Ioanna TSAGOURI (Nuclear and Particle Physics Section, Physics Department, University of Athens) Anna Belehaki and George Moraitis (Institute of Ionospheric and Space Research, National Observatory of Athens) Helen Mavromichalaki (Nuclear and Particle Physics Section, Physics Department, University of Athens)

The correlation between the foF2 middle latitude ionospheric disturbances during several great geomagnetic storms has been investigated aiming the forecasting of the geomagnetic structure during geomagnetic storms. The middle latitude ionospheric disturbances have been estimated using the quantity  $dfo=100^{*}(foF2-QoF2)/QoF2$ , where the QoF2 is the quiet value of the foF2 parameter, computed using the method of multiple regression between the observed foF2 parameter at a given ionospheric station at middle latitude and the sunspot number Rz. The quantity dfo was computed using data from a chain of 9 middle latitude stations around the earth for several geomagnetic storms with  $aa>200$ , occurred during the 21st solar cycle, between 1976-1986. The correlation coefficient between dfo parameter in each station and various geomagnetic indices (AE,Dst and Kp) was calculated to determine the dependence of the ionospheric middle latitude disturbances on the intensity of magnetic storms, the storm onset sector and the previous energy state of the magnetosphere.

**GA3.09/W/13-B4** Poster **0900-12**

**IZMEM MODEL AND GROUND-BASED AND SATELLITES OBSERVATIONS OF THE IONOSPHERIC CONVECTION**

L. I. GROMOVA, Ya. I. Feldstein, A. E. Levitin (Institute of Terrestrial Magnetism, Ionosphere and Radio Wave Propagation, Troitsk, Moscow Region, 142092, Russia, email: lgromova@izmiran.troitsk.ru)

The space electromagnetic weather model IZMEM has been utilized to define convection at the ionospheric altitude for different directions and intensity of the interplanetary magnetic field (IMF) components. These modeled results have been compared with the convection observed by Akebono, Viking, and Dynamic Explorer satellites. The comparison results have been used for the mutual calibration of both satellite measurements and ground-based SuperDARN observations of the ionospheric convection. The Viking satellite observations allowed to calibrate existing convection models determining convection dependence on the interplanetary magnetic field for the case of the unstable orientation of the IMF vector.

**GA3.09/W/28-B4** Poster **0900-13**

**INVESTIGATION OF BUILDING NEURAL-NETWORK-BASED THERMOSPHERE MODELS**

Jianhua TIAN and Quanfu Fan (both at Center for Space Science and Applied Research, Academia Sinica, 100080, Beijing, China email: jhtian@earth.sepc.ac.cn)

By using satellite drag density data, the neural-network-based thermosphere models (NNTM) are established to compute the total atmospheric density in the altitude ranges of 200-400km and 400-600km, respectively. Comparisons are made between TMNN and other empirical thermosphere models such as MET, MSIS90 and CIRA72. The results indicate that the overall mean and standard deviations of NNTM are lower than other three models except that MET has a relatively low overall mean deviation in 400-600km. With regard to the distribution of occurrence frequency of the data residuals, NNTM also has a more satisfactory result. In general, with the variation of a specific parameter (F10.7, geomagnetic indices Kp, altitude, latitude, day of year, local solar time etc.), there is a obviously lower value and fluctuation for the mean deviation of NNTM in comparison with that of other models. For the standard deviation, NNTM still has a lower value, however, its curve of standard deviation varying with a specific parameter exhibits a similar shape with the other models. From the results above, it can be seen that NNTM has good statistical and generalized capability in modeling total atmospheric density.

**GA4.03** **Thursday 29 July**

**SOLAR MAGNETIC FIELD: REVERSALS, POLAR FIELD, DYNAMO**

Location: Gisbert Kapp NG16 LR2  
Location of Posters: Gisbert Kapp, Coffee Room

**Thursday 29 July AM**

Presiding Chairs: V N Obridko (IZMIRAN, Moscow Region, Russia), D H Hathaway (NASA/MSFC, Huntsville, USA)

**Introduction** **0830**

V N OBRIDKO

**GA4.03/W/13-B4** Invited **0835**

**POLAR MAGNETIC FIELD REVERSAL OF THE SUN DURING 1880-1999**

Valentine I. MAKAROV (Pulkovo Astronomical Observatory RAS Saint Petersburg, 196140, Russia)

The modern theory of solar activity supposes the generation of the kilogauss magnetic field by the dynamo mechanism at the base of the convection zone. It is generally believed and observations clearly show that the generation and reversal of a poloidal field is the outstanding problem in solar dynamo theories. The special interest are the facts of strong magnetic fields (more than 1500 G) found in polar faculae and connection between strong fluctuation of polar activity and sunspot area in the next sunspot cycle. The non-trivial problem in solar dynamo theories concerns the regeneration of this poloidal field. In this connection we emphasize great importance of H-alpha magnetic charts, as a new method of research of the solar magnetic fields particularly in the period when the magnetic observations of the Sun are not made. Thanks to long-time ground - base and SOHO observations there is the crisis of the modern solar dynamo theory. The old theories did not work and new ones do not exist so far. Two types of large-scale magnetic fields and formation of a zonal magnetic structures of the Sun during 11 cycles, the properties of polarward and equatorward (torsional oscillations) of the magnetic fields in the global magnetic cycle are discussed. Discovery of three-fold magnetic field reversal in 11-yr cycles has been incentive for understanding the nature of the magnetic solar cycle. It are discussed essential conditions for single and three fold magnetic field reversals, dependence of the polarward rate of the sunspot activity and theoretical model for description of the observational data. It is considered the polar drift of the magnetic neutral lines in he current 23-th solar cycle (1995-1999), "quiet" and "active" versions of the polar magnetic field reversal. It is shown that polar drift rate of the latitude zones does not exceed 2 m/sec for a low-power activity. In this case the migration time of the latitude zone lasts about a cycle. Using observational data for 11 solar cycles the polar magnetic field reversals during Maunder minimum will be discussed.

**GA4.03/L/01-B4** Invited **0905**

**THE REFERENCE POINTS OF SOLAR CYCLE**

G.V.KUKLIN (Institute of Solar-Terrestrial Physics PO Box 4026, Irkutsk-33, 664033, Russia)

A conception of turning points of cyclic curve of solar cycle was introduced by Chistyakov in 1966. In 1986 Vitinsky, Kuklin and Obridko linked these points with changes of solar activity regimes and renamed them into the reference points. The solar cycle consists of 4 phases: the minimum epoch min, the ascending branch Asc, the maximum epoch Max and the descending branch Des, separated with the reference points t(mA), t(AM), t(MD) and t(Dm). In addition the moments of minimum t(m) and maximum t(M) are the reference points also. For example t(MD) corresponds to the end of polarity reversal in the solar polar caps. Besides mentioned reference points there are preminima, grandfluctuations etc. still more. The reference points

revealed with the help of relative Wolf numbers need to be defined more accurate using other solar activity indices. A list of pretendants to reference and turning points was published by Kuklin in 1992.

Typical changes of regimes of dreen corona emission linked with the reference points were revealed by Badalyan and Kuklin in 1993. Similar peculiarities for indices of the solar global magnetic field were found by Obridko et al. in 1994. In 1998 Kuklin et al. Discovered significant changes of weak correlation coefficients between the solar activity indices and the indices of interplanetary medium and geoelectromagnetic field at the reference points. There are grounds to consider that the reference points determine the organisation structure of the solar cycle and of the solar-terrestrial relationship mechanisms.

**GA4.03/W/05-B4** Invited **0940**

**DYNAMO PREDICTION FOR SOLAR CYCLE 23 USING POLAR FIELDS**

Kenneth SCHATTEN (AI-Solutions, 10001 Derekwod Lane, suite 215,Lanham MD 20706 USA, email:Kschatten@solar.stanford.edu)

Solar activity prediction methods vary widely. They range from examinations of planetary orbits, to Fourier & power series analyses, to artificial intelligence methods e.g. neural nets, to a variety of statistical methods. We concentrate on "precursor methods." These methods were originally developed by Ohl, Gnevyshev, Brown, Obridko, and others. The geomagnetic precursor methods were surprising in that it was not clear why geomagnetic fluctuations could be used to predict solar activity. It was puzzling as to how the Sun could broadcast its future activity levels to the Earth! We now have developed some understanding for how these methods work and have expanded the prediction methods using "solar dynamo precursor" methods. One notably uses a "SODA" index (Solar Dynamo Amplitude), which attempts to measure the trapped magnetic flux inside the Sun, based upon toroidal an poloidal fields. We explain how these methods work, and update a prediction of solar activity for cycle 23. We suggest cycle 23 will be somewhat smaller than cycle 22 based upon these techniques. Estimates suggest a maximum smoothed International Sunspot Number near ~ 130 +/- 30, or a smoothed 2800 MHz radio flux (F10.7) of ~ 180 +/- 30 Hz.

**GA4.03/E/04-B4** **1045**

**POLAR MAGNETIC FIELD REVERSALS....**

Elena E. BENEVOLENSKAYA (Pulkovo Astronomical Observatory, 196140, St. Petersburg, Russia, email: Elena.Benevolenskaya@pobox.spbu.ru)

The polar magnetic field on the Sun changes its sign during the maxima of solar sunspot cycles. It is known that the phenomenon of three-fold reversals of polar magnetic field occurred in solar cycle 20. Other three-fold reversals of the polar magnetic field took place in the southern hemisphere in solar cycles 12 and 14 and in the northern hemisphere alone in solar cycles 16 and 18 (Makarov and Sivaraman, 1989). I present a model of the polar magnetic field reversals. This model is confirmed by the new analysis of magnetograph data of Mount Wilson Observatory and H-alpha charts, which is also presented.

**GA4.03/E/05-B4** **1100**

**THE EXCITATION OF LINEAR WAVES IN THE POLARITY REVERSAL MAGNETIC FIELD OF THE SUN**

A.D. Pataraya (Department of Theoretical Astrophysics, Abastumani Astrophysical Observatory, 2a Kazbegi Ave., Tbilisi, 380060, Georgia); T.A. PATARAYA (Department of physics, Tbilisi State University, 2 Chavchavadze Ave., Tbilisi, 380028, Georgia. E-mail: cipdd@access.sanet.ge

It is known from the alpha and omega dynamo theory, that toroidal and axial components of magnetic field do not change their sign simultaneously. For the dynamo number close to 1 in linear theory the phase difference between them is about pi/2; for the weakly non-linear dynamo waves pi/4. The linear Rossbi and Alfvén waves are discussed in the paper during the interval of time of 2 years. During this interval the sign for the components of magnetic field is changing when: 1) the toroidal component of the magnetic field is zero and axial components are Constant; 2) the longitudinal component of the magnetic field is zero and the toroidal component is constant. In the former case the toroidal component of the magnetic field is taken into account with the shear to the longitudinal direction and in the later case is considered longitudinal component of the velocity with the shear to the toroidal direction. The first effect shows that the wave with the large amplitude propagates mainly to the equatorial direction, and wave propagated towards wave lines has smaller amplitude. In the second case the wave with larger amplitude propagates towards wave lines. The mentioned effects well explain the existed observational data.

**GA4.03/W/02-B4** **1115**

**STRUCTURE AND DYNAMICS OF THE LARGE SCALE SOLAR MAGNETIC FIELD AT A LONG TIME INTERVAL**

V.N.OBRIDKO and B.D.Shelting (Izmiran, Troitsk, Moscow Region, 142092, Russia, Email: solter@izmiran.troitsk.ru)

The structure of the large-scale solar magnetic field (LSMF) has been analyzed at a long time interval (1915-1998) and has been compared with the IMF to show good correlation between both data series. The study of the zonal structure (g10-coefficients) revealed the Hale cycle in variations of the odd coefficients responsible for the symmetry of the hemispheres. Variations of the even coefficients, responsible for the asymmetry of the hemispheres, display much shorter periods of the order of 2-3 years.

The 2- and 4-sector structures were analyzed to reveal the periods equal to 30 and 40 Carrington rotations. It was shown that the rotation period of the magnetic field of the Sun as a whole, as well as of the 2- and 4-sector structures during 1940-1965 was longer than at the beginning and at the end of the Century. Some rotation characteristics were shown to change sharply at the polarity reversals.

**GA4.03/E/03-B4** **1130**

**SOLAR MAGNETIC FIELD: EXISTENCE OF A PREFERRED LONGITUDE**

E.J.SMITH, M.Neugebauer, A.Ruzmaikin, J.Feynman and A.H.Vaughan (Jet Propulsion Laboratory California Institute of Technology, Pasadena CA 91109, USA, email: esmith@jplsp.jpl.nasa.gov)

Eleven year variations are a fundamental aspect of the sun's magnetic field. An important question is whether or not there are aspects of the field that persist in spite of the obvious solar cycle variations. One way such an invariant feature could be manifested is the existence of a "preferred" longitude at which a structure or a series of events are independent of the solar cycle or its phases. During cycle 20, a preferred longitude was, in fact, identified from which fast solar wind originated (Gosling et al., JGR, p.2371, 1977). Motivated by these

considerations, we investigated the behavior of the solar wind speed and the radial component of the heliospheric magnetic field over the prior and subsequent cycles using all available spacecraft measurements obtained inside 3 AU. It has been found that a preferred longitude corresponding to a source of fast wind and the m=1 component of the solar magnetic field has persisted over the last 35 years (Neugebauer et al., 1999). The solar rotation period associated with this persistent feature is 27.01 to 27.06 days. Magnetic activity on sun-like stars evident in calcium II H and K emissions also provides evidence of preferred longitudes that persist over several activity cycles in some stars (Vaughan, Science, p.793,1984). These combined observations indicate that this aspect of the sun's magnetic field is not anomalous but may be of fundamental importance in understanding solar-stellar magnetic fields and their generation.

**GA4.03/E/01-B4** **1145**

**THE MECHANISM OF THE BIENNIAL SOLAR CYCLE.**

Elena E. BENEVOLENSKAYA (Pulkovo Astronomical Observatory, 196140, St. Petersburg, Russia, email: Elena.Benevolenskaya@pobox.spbu.ru)

In the frame of the Parker's dynamo theory a model of biennial magnetic cycle on the Sun is presented. This model is based on the idea of two dynamo sources separated in space. The first source which gives rise to Hale's cycle may be located at the lower level of the convection zone, and the second source of the biennial cycle may operate in subsurface regions of the Sun. The model is formulated in terms of two couple systems of non-linear differential equations. It is demonstrated that in the case of weak interaction between the two dynamo sources the basic features of the magnetic cycle such as existence of two component and observed temporal variations of biennial cycle can be reproduced.

**GA4.03/W/10-B4** **1200**

**THE NORTH-SOUTH ASYMMETRY OF THE SOLAR AND HELIOSPHERIC MAGNETIC FIELD DURING ACTIVITY MINIMA**

Silvia BRAVO and Americo Gonzalez-Esparza (Instituto de Geofisica, UNAM, Ciudad Universitaria, Mexico D.F. 04510, email: sbravo@tonatihu.igeofcu.unam.mx, americog@fis-esp.igeofcu.unam.mx)

Recent in situ spacecraft observations and the analysis of the galactic cosmic ray intensity at Earth have shown that the heliospheric magnetic field exhibited a north-south asymmetry and that the heliospheric current sheet was inclined with respect to the solar equator during the last sunspot minimum (1996) and probably also during the previous minimum in 1986. In this paper we study the structure of the solar magnetic field at these times to see if this structure can account for the heliospheric asymmetries observed.

**GA4.03/W/04-B4** **1215**

**ZONAL STRUCTURE AND CYCLIC EVOLUTION OF LARGE-SCALE SOLAR MAGNETIC FIELDS**

E.V.IVANOV and V.N.Obridko (IZMIRAN, Troitsk, Moscow Region, 142092, Russia, email: solter@izmiran.troitsk.ru)

The structure and evolution of large-scale solar magnetic fields have been analysed for the time interval of 1969-1996 (Carrington rotations 1543-1916). The radial, meridional, and azimuthal components of the magnetic field vector and their absolute values were calculated from the Stanford magnetic maps for every 10 degree interval in the heliographic region from 70S up to 70N and were averaged over a Carrington rotation. The auto- and cross-correlation analysis have been applied to study the relationship between the time variations of intensity of the radial and meridional components of the magnetic field and their absolute values at the equator and at higher-latitude regions. A pronounced zonal structure and quasi-biennial variations of the large-scale solar magnetic fields have been revealed. The relationship and differences between the cyclic evolution of large-scale solar magnetic fields in the equatorial (below 50 degrees) and polar (above 50 degrees) heliographic zones are discussed.

**GA4.03/W/03-B4** **1230**

**FORMATION AND STRUCTURE OF PROMINENCES**

C. Z. CHENG and G. S. Choe (Princeton Plasma Physics Laboratory, Princeton University, Princeton, NJ 08543)

Based on the 2-1/2D MHD model we have obtained current sheet equilibrium configurations in a quadrupolar field geometry, and we have shown that resistive MHD evolution of these current sheet equilibria can lead to two different prominence field topologies via reconnection processes: one with an X-point and one with a magnetic island hanging in the solar atmosphere. The X-point configuration may occur during solar flares. The field configuration with a magnetic island, where the prominence material resistably, resembles the prominence magnetic field model suggested by Malville. We will illustrate how the Malville type prominence configuration may offer a possibility to understand the 3D prominence chiral structure of barbs by introducing additional localised magnetic poles in the photosphere so that the magnetic island shape can be distorted to form barbs attracted to the magnetic pole locations. We will also discuss possible causes of prominence eruption by considering (1) changes in the magnetic field around the prominence flux tube, (2) rapid growth of instabilities in the prominence flux tube, and (3) drainage of the material downward along the legs.

Thursday 29 July PM

Presiding Chairs: K Schatten (AI Solutions, Lanham MD 20706, USA), L Kitchatinov (ISZF, Institute for Solar-Terrestrial Physics, Irkutsk, Russia)

**GA4.03/W/09-B4** Invited **1400**

**A SURVEY AND SYNTHESIS OF SOLAR CYCLE PREDICTION TECHNIQUES**

David H. HATHAWAY, Robert M. Wilson, and Edwin J. Reichmann (Mail Code ES82, NASA/MSFC, Huntsville, AL 35812 USA, e-mail: david.hathaway@msfc.nasa.gov)

A number of techniques for predicting solar activity on a solar cycle time scale are identified, described, and tested with historical data. Some techniques, e.g. regression and curve-fitting, work well as solar activity approaches maximum and provide a complete description of future activity, while others, e.g. geomagnetic precursors, work well near solar minimum but only provide an estimate of the amplitude of the cycle. A synthesis of different techniques is shown to provide a more accurate and useful forecast of solar cycle activity levels. A combination of two un-correlated geomagnetic precursor techniques provides the most accurate prediction of the amplitude of a solar activity cycle at a time well before activity minimum. A mathematical function dependent upon the time of cycle initiation and the cycle amplitude then describes the



levels of solar activity for the next complete cycle. As the time of cycle maximum approaches better estimates of the cycle amplitude are obtained by fitting previous activity levels to this function. The success of the geomagnetic precursors in predicting future solar activity suggests that solar magnetic phenomena at latitudes above the sunspot activity belts are linked to solar activity which occurs many years later in the lower latitudes.

**GA4.03/W/15-B4 Invited 1435**

**PREDICTION OF SOLAR AND GEOPHYSICAL INDICES...**

Jo Ann JOSELYN (NOAA Space Environment Center, Email: jjoselyn@esc.noaa.gov)

Indices of solar and geomagnetic activity exhibit patterns of cycles approximately 11 years in length. Because both solar and geophysical activity can harm technological systems, predictions of solar and geomagnetic activity are desirable for the purpose of long-range planning especially for satellite operations. At the beginning of Cycle 22, a number of thoughtful but disparate predictions for the cycle amplitude were published. The most successful were generally based on precursor, or, solar dynamo concepts. During the recent solar minimum, there have again been a number of papers published predicting the behavior of Cycle 23. Again, the range in the published predictions is large. In 1996, 1997, and again in 1998, a panel of international scientists met to review forecasts of Solar Cycle 23 solar and geomagnetic activity. The panel examined the techniques used and arrived at a consensus for a cycle of smoothed sunspot number amplitude of 160 (between extremes of 130 and 190) reaching maximum near March 2000 (between extremes of June 1999 and January 2001). Besides producing a consensus forecast of the amplitude of the solar cycle, the panel predicted the approximate total number and annual number of geomagnetic disturbances expected during Cycle 23. For both solar and geomagnetic activity, the consensus forecasts are for cycles similar to Cycle 22: large, but familiar. This talk will review the techniques that have been used for cycle predictions, and will compare them with the progress of Cycle 23 through June, 1999.

**GA4.03/W/12-B4 Invited 1510**

**THE SOLAR DYNAMO**

L.L.KITCHATINOV (Institute for Solar-Terrestrial Physics, P.O. Box 4026, Irkutsk, 664033, Russia, email: kit@iszf.irk.ru)

The problem of constructing a reasonable solar dynamo model is discussed in relation to the new data on the rotation law supplied by the GONG and SOI-MDI observations. The equatorward activity migration is hardly possible to explain by the standard mechanism of the dynamo wave propagation along the isorotational surfaces. Magnetic field advection by the meridional flow and/or anisotropic turbulent transport are the possible alternatives. The field transport mechanisms would have "enough time" to influence the field dynamics over the activity cycle only if the simulated cycle period is not too short compared with the observed period of about 22 yrs. Dynamo models usually produce (roughly) ten-times shorter cycles. The cycle duration is much sensitive to the top boundary conditions. Implementation of new conditions allowing for a non-free escape of the generated fields from the dynamo region increases the simulated cycle period to its observed value. Multi-periodicities in non-linear dynamos are also discussed in relation to the grand cycles of the solar activity.

**GA4.03/L/02-B4 Invited 1615**

**PERIOD OF SOLAR DYNAMO-CYCLE**

Valery N.KRIVODUBSKIY (Kyiv University Astronomical Observatory Observatorna Street 3Kyiv - 53, UA - 254053, Ukraine)

According to mean magnetic field concept, the action of the helical turbulence (alpha-effect) and radial differential rotation (Omega-effect) play main role in the generation of the solar large-scale magnetic fields (alphaOmega-dynamo). According to Parker (Ap.J. 1955, V. 122, 293) the solution of the dynamo equations, describing the evolution of toroidal and poloidal components of the global magnetic fields, can be treated as the displacement of magnetic dynamo-waves on solar surface. The period T of dynamo-waves is determined by parameters of alpha-effect and radial differential rotation in the solar convective zone (SCZ). Youshimura (Ap.J.S. 1975, V.29, 467) had specified that the direction of dynamo-wave displacement (toward equator or pole) depends on the sign (negative or positive respectively) of the product of alpha-effect and radial gradient of angular velocity. The behaviour of the helical turbulence parameter (alpha-parameter) in the SCZ was investigated. The alpha-effect contributions due to radial gradients of plasma density and of turbulent velocities were taken into account. Our calculations for the SCZ model by Stix (1989) have shown that the azimuthal alpha-parameter, which is the most important for the alphaOmega-dynamo, changes its sign from positive to negative near the zone bottom (in northern hemisphere). So-called magnetic quenching (suppression) of the alpha-effect due to feedback of the global magnetism was researched. It is found that the essential magnetic quenching takes place near the base of the SCZ (quenching-function Psi is equal approximately to 0.4). Using the values of quenched alpha-parameter and radial gradient of angular velocity, obtained from the recent helioseismological researches, we determined the direction of migration and estimated the period T of the dynamo-waves excited by alphaOmega-dynamo in the overshoot layer (z=165-180 Mm) of the SCZ. At the latitudes higher 35 degrees dynamo-wave is directed toward the poles, while at lower latitudes it displaces toward the equator. Calculated period T is about 9 years that is in satisfactory agreement with the observed solar cycle duration. Low-latitude dynamo-wave probably is manifest in the sunspot cycle whereas the wave moving toward the poles is apparently responsible for the polar drift of high-latitude background magnetic fields.

**GA4.03/W/14-B4 1630**

**EXTENSION OF CORONAL MAGNETIC FIELDS TO THE SOLAR WIND STREAMS**

N.A.LOTOVA and V.N.Obridko (IZMIRAN, Troitsk, Moscow Region, Russia, email: nlotova@izmiran.troitsk.ru), K.V.Vladimirskii (FIAN, Leninsky Prospekt 53, Moscow, 117924, Russia); V.Rusin (Astronomical Institute, Slovak Academy of Sciences, Tatranska Lomnica 135, 05960, Slovak Republic, Email: vrusin@auriga.ta3.sk)

An investigation of the mechanism of the stream structure formation in the solar wind flow has been carried out. Complex analysis of the observational data for magnetic fields at the photosphere level, the white corona views and the geometry of the solar wind transition region was carried out. It has been shown that the structure of the magnetic field close to the Sun's surface is the basic factor determining the solar wind flow structure in the course of all stages of the following acceleration process up to the supersonic streams far from the Sun. A distinct anti-correlation between the magnetic field intensity at the corona level and the distance of the transition region from the Sun is the crucial argument showing the extension of the solar magnetic fields far in the plasma streams.

**GA4.03/E/02-B4 1645**

**MAGNETIC FLUX EMERGENCE AND GEOMAGNETIC ACTIVITY, A CLOSE CORRELATION**

Blanca MENDOZA, Alejandro Lara, Dolores Maravilla and Jose Valdes-Galicia, (Instituto de Geofisica UNAM, Ciudad Universitaria, 04510, Mexico D.F. Mexico, email: blanca@tonatiuh.igeofcu.unam.mx)

We analyse data of magnetic flux emergence for solar cycles 21 and 22, Helios 1 interplanetary shocks for cycle 21 and sudden storm commencements (SSC's) for cycles 11 to 22. A dominant variation of 3-years periodicity was found for all three phenomena during cycles 21 and 22. This indicates a correlation and a possible influence of the rate of solar magnetic flux emergence to produce the interplanetary phenomena studied in this work; in particular, the suggested role of coronal mass ejections as a means by which magnetic flux and stresses are taken out of the corona seems to be plausible. When taking cycles 11 to 22 in SSC's, the main periodicity changes to around 4 years.

**GA4.03/W/08-B4 1700**

**GENERATION OF LARGE-SCALE MAGNETIC STRUCTURES AND OSCILLATING GLOBAL MAGNETIC FIELD DUE TO DEFORMATIONAL AND SHEAR INSTABILITY**

Evgeniy TIKHOMOLOV and Vladimir Mordvinov (Institute of Solar-Terrestrial Physics, P.O. Box 4026,Irkutsk, 664033 Russia, email: e\_tikh@iszf.irk.ru)

We present a model in which interaction between deformational and shear instability gives rise to generation of the global magnetic field oscillating with 22-year period. Instability takes place in high- and mid-latitudes near the interface between convective and radiative zones. At the background of the oscillating global magnetic field the evolution of the large-scale magnetic structures is considered. These structures are generated in low-latitudes by a set of Rossby vortices. Interaction between Rossby vortices brings about rather complicated behaviour of the magnetic fields. Nevertheless, numerical simulations reproduce some peculiarities in the dynamics of the magnetic field in several solar complexes of activity.

**GA4.03/E/07-B4 Poster 1715-01**

**POLAR MAGNETIC FIELD REVERSALS IN THE 19TH SOLAR CYCLE**

Dmitri I. PONYAVIN (Institute of Physics, University of St.Petersburg, 198904, Russia, e-mail: ponyavin@snoopy.phys.spbu.ru)

H-alpha synoptic charts of large-scale magnetic fields restored by Makarov and Sivaraman have been used to trace a history of magnetic field reversals at the poles of the Sun. A smoothed filtering technique was applied to reveal a large-scale organization and evolution of magnetic fields. It was suggested that actually a single reversal occurred in the Northern Hemisphere during a course of solar cycle 19.

**GA4.03/W/01-B4 Poster 1720-02**

**COMPLEX STRUCTURE OF CYCLIC VARIATIONS OF LARGE-SCALE SOLAR MAGNETIC FIELDS AND SOLAR ACTIVITY**

Yu.R.RIVIN (IZMIRAN, 142092, Troitsk, Moscow Region, Russia, email: solter@izmiran.troitsk.ru)

Variations of solar activity with a period of about 11 years, that are usually attributed to the sunspot dynamics, form merely a part of the general dynamics of the large-scale solar magnetic fields [1-2]. They only reflect the dynamics of the quasi-axial dipole alpha-omega-dynamo at the center of the convection zone. This dynamo mechanism generates the magnetic field, changing with a period of about 22 years and is responsible for more than 90% of sunspots. It also plays a key role in the amplitude modulation of the interplanetary magnetic field (IMF) and cosmic rays. Another (quadrupole) source, that is at the bottom of the convection zone, is likely to play an important role in generation of active regions with peculiar sunspots and the sector structure of the general magnetic field of the Sun and IMF, as well as in the field and activity asymmetry between the two solar hemispheres. This source may also have other manifestations. ReferencesRivin Yu.R. Bulletin of the Russian Academy of Sciences. PHYSICS. 1998. V.62. N9. Rivin Yu.R. Astronomy Letters. 1999 (in press).

**GA4.03/W/07-B4 Poster 1725-03**

**VARIATIONS OF INTERPLANETARY MEDIUM PARAMETERS IN 11YR SOLAR CYCLE**

GROMOVA, Ludmilla (IZMIRAN, Inst of Terrestrial magnetism, Ionosphere and Raditaion, Troitsk, Email: Igromova@izmiran.troitsk.ru)

Abstract missing at time of going to press

**GA4.03/E/06-B4 Poster 1730-04**

**LONGITUDINAL STRUCTURE OF SOLAR MAGNETIC FIELDS DURING THE TRANSITION FROM CYCLE 22 TO CYCLE 23 INFERRED FROM SOHO MDI DATA**

Elena E. BENEVOLENSKAYA (Pulkovo Astronomical Observatory, 196140, St. Petersburg, Russia, email: Elena.Benevolenskaya@pobox.spbu.ru); A. G. Kosovichev (W. W. Hansen Experimental Physics Laboratory, Stanford University, Stanford, CA 94305-4085; email: sasha@quake.stanford.edu); J. T. Hoeksma (W. W. Hansen Experimental Physics Laboratory, Stanford University, Stanford, CA 94305-4085; email: todd@quake.stanford.edu); P. H. Scherrer (W. W. Hansen Experimental Physics Laboratory, Stanford University, Stanford, CA 94305-4085; email: phil@quake.stanford.edu)

We present the results of investigation the latitudinal and longitudinal structure of the solar magnetic field by using full disk SOHO MDI data. It was found that during the transition from cycle 22 to cycle 23 solar activity clustered in fixed longitudinal zones, and that the old magnetic fluxes were replaced by new magnetic fluxes in the same fixed longitudinal regions. The most interesting longitudinal zone was located from 240 deg to 280 deg. From the CR1911 until CR1918, there was a complex of activity of old magnetic fluxes.

This complex of solar activity first emerged in the southern hemisphere and decayed to CR1916. Then, the next old magnetic flux appeared in the same longitudinal zone in the northern hemisphere and existed until CR1919. The same longitudinal zone became active again in CR1923 when a complex of solar activity of new magnetic flux emerged. This longitudinal zone of pronounced activity existed for more than 15 Carrington rotations. Apparently, this zone was the place of reversal of polarity of the toroidal magnetic field during the transition from one cycle to another. We discuss implications of these results for theories of solar cycle.

GA4.03/W/11-B4 Poster 1735-05

## THE AMPLITUDE AND PERIOD OF THE SOLAR CYCLE AS TRACERS OF A NONLINEAR DYNAMO WAVE

Isabella Dmitrieva, Kirill KUZANYAN, and Vladimir Obridko (IZMIRAN, Troitsk, 142092 Moscow region, RUSSIA, email: bella@izmiran.troitsk.ru, email: kuzanyan@dnmtm.ru, email: solter@izmiran.troitsk.ru)

Relation of the solar cycle period and its amplitude is a complex problem as there is no direct correlation between these two quantities. Nevertheless, the period of the cycle make an important influence to the Earth's climate, that has been noted by many authors, e.g., Soon et al., 1996. Friis-Christensen and Lassen (1991) revealed the correlation between the cycle length and the Earth's global temperature variation. This problem has been extensively studied but there is no reasonable explanation of such mechanism given yet. The authors make an attempt to analyse the solar indices data with account of recent developments of asymptotic theory of the solar dynamo. The use of the WKB method enables us the estimates of the amplitude and the period of the cycle versus dynamo wave parameters in the framework of the one-dimensional Parker's migratory dynamo (Meunier et al., 1997; Bassom et al., 1998). These estimates link the period  $T$  and the amplitude  $A$  with dynamo number  $D$  and thickness of the generation layer of the solar convective zone  $h$ . However, we have not revealed any prominent correlation between the above quantities, which is in agreement with previous authors. Instead, we have noted that the maximum amplitude of the cycle and the temporal derivative of the monthly Wolf numbers at the very beginning of the phase of growth of the cycle have high correlation coefficient of order 0.96. The hope is that this dependence may be useful for understanding the mechanism of the solar dynamo wave and prediction of the average maximum amplitude of solar cycles.

GA4.03/L/03-B4 Poster 1740-06

## 2D ASYMPTOTIC SOLAR DYNAMO IN THE LIGHT OF INTERNAL ROTATION

G. Belvedere, L. Paterno' (both at Institute of Astronomy, University of Catania, Viale A. Doria, 6, 95125 Catania, Italy; e-mail: gbelvedere@alpha4.ct.astro.it, e-mail: lpaterno@alpha4.ct.astro.it), and Kirill KUZANYAN (IZMIRAN, Solar-Terrestrial Dept., Troitsk, Moscow Region, 142092, Russia, email: kuzanyan@dnmtm.ru)

The mean field dynamo equations for a two-dimensional (radius-latitude) alpha-omega model are solved in the leading order of asymptotic expansion by the use of the WKB method. The limiting case of short waves (large regeneration rates) is considered. The solution is shown to possess properties of travelling dynamo waves and to obey the so-called Yoshimura theorem. The intrinsic role of the alpha- and omega-factors is discussed. The solution obtained is compared with the one calculated earlier for a one-dimensional model. By using the solar internal differential rotation profile given by a helioseismological inversion, we calculate the location and structure of the different wings of the dynamo wave. Equatorward and poleward branches are found. We compare the solution obtained with available observations of the solar activity cycle.

GA4.03/E/08-B4 Poster 1745-07

## WEAKLY NON-LINEAR DYNAMO WAVES

A.D. PATARAYA (Department of Theoretical Astrophysics, Abastumani, Astrophysical Observatory, 2a Kazbegi Ave., Tbilisi, 380060, Georgia); T.A. PATARAYA (Department of physics, Tbilisi State University, 2 Chavchavadze Ave., Tbilisi, 380028, Georgia. E-mail: cipdd@access.sanet.ge)

Weakly non-linear dynamo waves are investigated with the help of magnetohydrodynamic equations. The solution is given for the amplitude of the weakly non-linear waves and investigated stability for these amplitudes. For alpha omega and alpha in square dynamo waves some conditions of stability are obtained taking into account Coriolis forces in the equation of movement. One of the conditions of stability shows that the wave vector is very close to the normal of the angular velocity of the rotation of Star or Sun.

GA4.03/W/17-B4 Poster 1750-08

## SPACE-TIME ORDER OF SOLAR LARGE-SCALE MAGNETIC FIELD OVER 40N-40S LATITUDINAL INTERVAL

Lyubov PLYUSNINA (Institute of Solar-Terrestrial Physics, Russian Academy of Sciences, Siberian Branch, P.O. Box 4026, Irkutsk, 664033, Russia, email: lplus@iszf.irk.ru)

Simple technique is suggested to distinguish a trace of long-lived components of large-scale magnetic field (LSMF) with a life time compared or exceeded the solar cycle duration. Its principal variation from those being traditionally used for this purpose is to maintain the 10' resolution through the longitude. The synoptic Ha maps over 1955-1990 are used as input data. The analysis of the LSMF trace over 3.5 solar activity cycles shows the LSMF not to include any other long-lived components except those rotated with the periods of 27 (LSMF27) and 28 (LSMF28) days. Rather high resolution through the longitude allows one to distinguish the structure and evolutionary peculiarities of the LSMF components. On the basis of the study carried out it may be assumed that the LSMF28 originates in every even cycle and dominates next uneven and even cycles. Thus, this component exists over 3 cycles (~33 years) and is most pronounced over 2 last cycles (~22 years). There are two LSMF28 with different phases in even cycles: old and new ones. The LSMF27 is much more fragmented through the longitude and appears to originate again in each new cycle.

GA4.03/W/16-B4 Poster 1755-09

## FRACTAL PROPERTIES OF LARGE-SCALE MAGNETIC FIELDS ON THE SUN

Irina I. SALAKHUTDINOVA (Institute of Solar-Terrestrial Physics, Russian Academy of Sciences, P.O. Box 4026, Irkutsk, 664033, Russia, email: isalakh@iszf.irk.ru)

It is common knowledge that the magnetic field on the Sun has a cellular, discrete structure. This paper is concerned with fractal properties of the large-scale magnetic field distribution on the Sun. Synoptic maps from the Mt. Wilson, Kitt Peak and Stanford observatories covering the entire observing period from 1959 to 1976, from 1976 to 1985 and from 1976 to 1998, respectively, were used in the study. Method of fractal analysis were applied on a two-dimensional grid. For each Carrington rotation, the following characteristics were calculated: 1) the fractal dimension of the maps; and 2) statistical characteristics of the magnetic field distribution such as the distribution density function, the kurtosis, and asymmetry. It was found that large-scale magnetic fields have a high fractal dimension of about  $\sim 2.7$  when averaged over all rotations, on scales larger than  $20 \times 25'$ ; on smaller scales, the fractal dimension changes by  $\sim 0.3$  and becomes equal to  $\sim 3.0$  averaged over all rotations. The  $20 \times 25'$  scale corresponds to the size of active regions. It was also found that the fractal dimension changes from rotation to rotation and shows some time dependence with a period  $\sim 30$  years, although this period is on the boundary of the time interval of observation. The distribution density

This page may be copied freely

function of large-scale magnetic fields on the Sun is characterised by an exponential dependence in this grid. The exponential dependence was also found to change at  $20 \times 20'$  scales in this case. The exponent at smaller and larger scales than the indicated one is  $\sim 0.4$  and  $\sim 3.6$ , respectively. The exponent varies with the time with a period  $\sim 11$  years. The obtained statistical characteristics show a strong departure from a normal law. Also, these characteristics vary with solar cycle phases. This study has shown that the fractal character of magnetic fields on the Sun manifests itself also in the spatial distribution of large-scale magnetic fields.

GA4.04

Friday 30 July

## ENERGETIC PARTICLES IN THE HELIOSPHERE: LOCAL AND INTERSTELLAR SOURCES, SOLAR CYCLE DEPENDENCE AND 3D STRUCTURE

Location: Gisbert Knapp NG16 LR2

Location of Posters: Gisbert Kapp, Coffee Room

Friday 30 July AM

Presiding Chair: N.A.Schwadron (University of Michigan, Ann Arbor, USA)  
Concurrent Poster Session

## ENERGETICS PARTICLES IN THE HELIOSPHERE: LOCAL AND INTERSTELLAR SOURCES, SOURCES CYCLE DEPENDENCE AND 3D STRUCTURE-1

GA4.04/E/07-B5 Invited 0830

## PICKUP IONS AS TOOLS FOR PROBING THE COMPOSITION AND PHYSICAL STATE OF THE LOCAL INTERSTELLAR CLOUD

G. GLOECKLER (Department of Physics and IPST, University of Maryland, College Park, MD 20742, USA; e-mail: gg10@umail.umd.edu); L. A. Fisk, N. A. Schwadron and T. H. Zurbuchen (all at Department of Atmospheric, Oceanic and Space Sciences, University of Michigan, Ann Arbor, MI 48109, USA); J. Geiss (International Space Science Institute, Hallerstrasse No. 6, CH-3012 Bern, Switzerland)

Neutral gas and large dust grains from the Local Interstellar Cloud (LIC) surrounding our solar system have easy access to the inner heliosphere. Most interstellar atoms penetrate to roughly 3 AU before they become ionized and are swept away with the solar wind. In situ measurements of pickup ions provide a new powerful tool for deducing important properties of the nearby interstellar medium, including its elemental and isotopic composition, its ionization state and pressure. After the discovery of interstellar pickup helium with the earth-orbiting AMPTE/IRM spacecraft, it was not until Ulysses before most of the other interstellar pickup ions, including the rare Helium-3 isotope, were discovered and studied. We will briefly review some of the latest results of these pioneering studies based on data from the Solar Wind Ion Composition Spectrometer (SWICS) on Ulysses. We will also discuss how measurements in the near future with instruments orders of magnitude more sensitive than those on Ulysses and AMPTE, would address questions on the physical properties and nucleosynthetic status of the present-day galaxy, questions important for understanding the origin of our solar system, the stars, our galaxy, and the nature and destiny of the universe.

GA4.04/W/17-B5 0900

## ENERGETIC ATOMS OF HELIOSPHERIC ORIGIN

M Hilchenbach(1), KC Hsieh(2) and A Czechowski(3) (1)Max-Planck-Institut fuer Aeronomie, 37191 Lindau, Germany (2)Department of Physics, University of Arizona, Tucson, AZ 85721 USA (3)Space Research Centre, Polish Academy of Sciences, PL 00716 Warsaw, Poland

Heliospheric energetic hydrogen atoms have been detected at 1 AU by the suprathermal particle sensor CELIAS on SOHO. These energetic neutrals are seen as result of anomalous cosmic ray (ACR) protons transcharging with the local interstellar medium (LISM) in the outer heliosphere. The resulting neutrals then travel on ballistic trajectories, unaffected by the interplanetary magnetic field (IMF), to the inner heliosphere. In the vicinity of the sun, a fraction of these energetic neutral hydrogen is ionised again via photoionisation or collision with the solar wind protons and electrons. We will discuss the implication of this process on the energetic particle quiet time fluxes.

GA4.04/E/06-B5 0920

## REGARDING THE CORRELATION BETWEEN INTERSTELLAR PICK-UP IONS AND SOLAR WIND PROTONS

Daniel WINTERHALTER (Jet Propulsion Laboratory, California Institute of Technology Pasadena, CA 91109-8099, USA, email: daniel.winterhalter@jpl.nasa.gov) George Gloeckler (University of Maryland College Park, MD 20742-2425, USA) Phillip Isenberg (University of New Hampshire Durham, NH 03824-3525, USA) Edward J. Smith (Jet Propulsion Laboratory, California Institute of Technology Pasadena, CA 91109-8099, USA)

Interstellar hydrogen is primarily ionized by charge exchange with solar wind protons. This directly implies that the pick-up hydrogen density should be linearly correlated with the solar wind proton density. However, it has been reported that this correlation is very poor, probably because of the limited data set used in the previous studies. In this study, we use Ulysses data from 1990 to 1997 with radial coverage ranging from 1 AU to 5 AU, and the heliographic latitude nearly spanning from solar pole to pole. We compare daily averages of the pick-up hydrogen obtained by the SWICS instrument with daily averages of solar wind parameters, primarily the solar wind proton density, obtained by SWOOPS. In addition, measurements by the magnetometer were used to investigate any contribution by the heliospheric magnetic field direction and fluctuation to the solar wind/pickup hydrogen interaction. Preliminarily, we find that the pick-up hydrogen count increases with increasing radial distance as expected. Further, the correlation between solar wind protons and pick-up hydrogen count increases with increasing radial distance, and the correlation decreases at high solar wind speeds ( $> 740$  km/s).

GA4.04/E/05-B5 0940

## DEPENDENCE OF THE HELIUM PICKUP ION DISTRIBUTION ON THE IMF DIRECTION AND VELOCITIES OF THE SOLAR WIND AND INTERSTELLAR GAS



Y.E. LITVINENKO, E. Moebius (both at Space Science Center, University of New Hampshire, Durham, NH 03824, USA, email: yuri.litvinenko@unh.edu), H. Grunwaldt (Max Planck Institut fur Aeronomie, D-37189 Katlenburg-Lindau, Germany), M. Aellig (Center for Space Research, MIT, Cambridge, MA 02139, USA), P. Bochsler (Physikalisches Institut der Universitat Bern, CD-3012 Bern, Switzerland), D. Hovestadt (Max Planck Institut fur Extraterrestrische Physik, D-85740 Garching, Germany), M. Hilchenbach (Max Planck Institut fur Aeronomie, D-37189 Katlenburg-Lindau, Germany), F.M. Ipavich (Department of Physics and Astronomy, University of Maryland, College Park, MD 20742, USA)

We study variations of the Helium pickup ion distribution with the IMF direction and the solar wind and interstellar gas velocities. The pickup Helium data provided by the CELIAS CTOF sensor onboard SOHO are combined with the solar wind data from CELIAS MTOF Proton Monitor and the interplanetary magnetic field data from WIND convectively extrapolated to the SOHO position. We confirm an earlier finding that the pickup Helium flux density in the antisunward direction decreases significantly when the interplanetary magnetic field is parallel to the solar wind velocity. This is most likely due to incomplete pitch angle scattering from the sunward hemisphere in phase space. A new effect identified in the data is a shift of the pickup ion velocity cut-off to values significantly exceeding twice the solar wind speed. The shift is observed by SOHO on the upwind side, with the effect being more pronounced for lower solar wind speeds, whereas no shift was observed by AMPTE SULEICA on the downwind side. The inclusion of the local interstellar gas velocity into the model distribution leads to agreement with observations. Therefore the velocity cut-off depends not only on the solar wind speed but also on the neutral Helium inflow speed and the position of a spacecraft. We study this variation and suggest using it as a diagnostics of the inflow.

**GA4.04/E/02-B5 Invited 1020**

**SOURCES AND ACCELERATION OF ENERGETIC PARTICLES IN THE HELIOSPHERE**

B. KLECKER, A.T. Bogdanov (both at Max-Planck-Institut fuer extraterrestrische Physik, Garching, D-85740, Germany, Email: bek@mpe.mpg.de)

Measurements of energetic particles are now available from a fleet of spacecraft in the inner and outer heliosphere, covering energies from keV to GeV, elements from H to Fe, and radial distances from 1 to ~ 70 AU. These measurements provide new insight into the sources of these particles and the acceleration processes involved. Recent measurements with advanced instrumentation of high sensitivity onboard Ulysses, SAMPEX, Geotail, WIND, SOHO and ACE led to the discovery of interstellar and interplanetary sources of pickup ions, of multiply charged Anomalous Cosmic Rays (ACRs) and of new ACR elements not observed previously. The pickup ions, together with solar wind ions, are the seed population for acceleration processes acting e.g. at interplanetary shocks, at corotating interaction regions, and at the solar wind termination shock. In this paper we review the recent measurements of pickup ions and ACRs, discuss the questions of pre-acceleration in the inner heliosphere and of injection efficiencies of pickup and solar wind ions, summarize the implications of the ACR ion charge measurements for acceleration and loss processes, and discuss open questions.

**GA4.04/W/03-B5 1050**

**A NEW SEED POPULATION FOR ENERGETIC PARTICLES IN THE HELIOSPHERE**

N. A. SCHWADRON, L. A. Fisk, G. Gloeckler\*, and T. H. Zurbuchen (all at Department of Atmospheric, Oceanic, and Space Sciences, University of Michigan, Ann Arbor, MI, USA, 48109-2143, email: nathanas@umich.edu, lafisk@umich.edu, gg10@umail.umd.edu, thomasz@engin.umich.edu); J. Geiss (International Space Science Institute, Bern, Switzerland CH-3012, email: geiss@issi.unibe.ch) \*G. Gloeckler also at Department of Physics and ISTP, University of Maryland, College Park, Maryland, USA, 20742.

A new source of pickup ions has been discovered, the "inner source". The composition is similar to that of the solar wind which suggests the most plausible production mechanism involves the absorption and re-emission of solar wind ions from interplanetary dust grains. Inner source pickup ions may also be a significant seed population for accelerated particles in co-rotating interaction regions (CIRs). Accelerated inner source ions may therefore influence the composition of CIR-accelerated particles which is known to differ from that of interstellar pickup ions. Our present observational knowledge of inner source composition will be discussed and implications for accelerated particles in the heliosphere and the anomalous component will be explored.

**GA4.04/W/13-B5 1110**

**ENERGETIC SOLAR PROTONS FROM DIFFERENT SOURCES**

L.I. MIROSHNICHENKO (1), R. Pérez Enriquez (2), and B. Mendoza (Instituto de Geofísica UNAM, México, D. F., 04510, MEXICO; (1) Permanent address: IZMIRAN, Troitsk, Moscow Region, 142092, RUSSIA; (2) Campus UNAM, Juriquilla, Querétaro

As it is widely accepted now, a significant fraction of the solar energetic particles (SEPs) observed at 1 AU after major solar flares are actually accelerated at a CME-driven shock. Besides, in the emerging new paradigm for SEP acceleration in different sources at or near the Sun, the existence of two types of flares - impulsive and gradual ones - is recognized. Within this concept, it is tempting to separate also SEPs into two groups - interacting and escaping ones, - and to derive their "source spectra" by observational data on different solar emissions (gamma rays, neutrons, protons, etc.). By different techniques, those spectra have been restored for 80 solar proton events (SPE) of 1949-1991. In this paper, all available data on the source spectra of solar cosmic rays (SCR) are summarised and revised. The data are presented in the form of the Catalogue of the source spectra. Then, we separate them depending on the source type and interplanetary conditions of SEP propagation, taking into account existing uncertainties in the derived power-law spectral indexes. It is shown, in particular, that the spectrum indexes in some events (February 23, 1956; January 28, 1967; May 07, 1978; February 16, 1984; June 15, 1991 and others) do not correlate with each other at different energy thresholds (>10 MeV and >500 MeV). Moreover, the source spectra reveal a spectral steepening for high energies, such a peculiarity may be characteristic of large events (e.g., of February 23, 1956 one). It should be emphasized the great importance of the Catalogue data as an initial information for the development of a comprehensive quantitative theory of particle acceleration at the Sun. The theory should explain the spectrum form in the entire range of observed SCR energies (rigidities), from >1 MeV (43.5 MV) to >20 GeV (20.9 GV for protons), by a single model or, at least, by a single scenario, taking into account a possibility of multiple particle acceleration.

**GA4.04/W/02-B5 1130**

**NEW OBSERVATIONS OF THE TRANSPORT OF ENERGETIC PARTICLES FROM IMPULSIVE SOLAR FLARES**

J. E. MAZUR (The Aerospace Corporation, 2350 E. El Segundo Blvd., El Segundo, CA, 90245-4691, USA, email: joseph.mazur@aero.org); G. M. Mason and J. R. Dwyer (both at Department of Physics,

University of Maryland, College Park, MD 20742, USA, email: mason@sampx3.umd.edu, dwyer@umstep.umd.edu); J. Giacalone (Department of Planetary Sciences, University of Arizona, 1629 E. University Blvd., Tucson, AZ 85721-0092, USA, email: giacalon@lpl.arizona.edu)

Interplanetary particle events from impulsive solar flares are enriched in Ne-Fe and in the 3He isotope compared to the solar wind; they also show little scattering in the interplanetary medium. Whereas the details of higher intensity shock-associated particle events depend on the observer's changing connection to a propagating shock, the impulsive events probe the transport in the interplanetary medium from a more localized source at the sun to 1 AU. We have used instrumentation on board the NASA Advanced Composition Explorer (ACE) spacecraft, launched in late 1997, to measure the ionic composition and temporal profiles of dozens of impulsive flares with high sensitivity. These new measurements show that subtle changes in the interplanetary magnetic field can greatly affect the observed event profiles, sometimes disconnecting the observer from one event while another nearly simultaneous particle injection continues unaffected. We will report on these new findings from ACE and their interpretation using a numerical simulation of charged particle transport in a meandering interplanetary magnetic field.

**GA4.04/W/18-B5 1150**

**ENERGY SPECTRA AND ABUNDANCES VARIATIONS OBSERVED BY ACE DURING THE AUGUST 1998 SOLAR ENERGETIC PARTICLE EVENT**

G.C. HO (Applied Physics Laboratory, Johns Hopkins University, Laurel, MD 20723-6099, USA, Email: george.ho@jhuapl.edu); R.B. Decker; R.E. Gold; S. M. Krimigis (all at Applied Physics Laboratory, Johns Hopkins University, Laurel, MD 20723-6099, USA, Email: robert.decker@jhuapl.edu); G.M. Mason; J.R. Dwyer (Department of Physics, University of Maryland, College Park, MD 20742, USA, Email: mason@sampx2.umd.edu); and J.E. Mazur (Aerospace Corporation, El Segundo, CA 90245-4617, USA, Email: joseph.mazur@aero.org)

As we approach the maximum of solar cycle 23, Solar Energetic Particle (SEP) events are occurring with increasing frequency. In contrast to the previous solar maximum, however, in this cycle we have an array of highly sensitive instruments onboard various spacecraft within the heliosphere to observe SEP events. Hence, we are able to study individual SEP over much boarder energy ranges and resolve more ion species than ever before. In this talk, we will present results using the Ultra Low Energy Spectrometer (ULEIS) onboard the ACE spacecraft for a SEP event. On August 24, 1998 a X10/3B flare was reported at N35E09 and its associated Type II radio burst was also seen on WIND. One and a half-days later, an interplanetary shock was observed on ACE. The shock produced large enhancements of particles up to few MeV per nucleon. We will discuss the elemental abundance ratios of C, N, O, Ne, Mg, Si, and Fe both as a function of time and energy from few tens of keV to a few MeV per nucleon. The energy spectra of these ions will be compared with current acceleration models.

**GA4.04/E/01-B5 1210**

**WIND OBSERVATIONS OF ENERGETIC PROTON EVENTS AT TRANSIENT INTERPLANETARY SHOCKS**

M. MAKSIMOVIC(1), D. Lario(1), T.R. Sanderson(1), D. Berdechevsky(2) and A. Szabo(2) (1) Space Science Department of ESA/ESTEC, PO Box 299, 2200 AG Noordwijk, The Netherlands (2)NASA Goddard Space Flight Center, Greenbelt, MD 20771, USA

Between December 1994 and May 1997 the WIND spacecraft observed ~30 transient interplanetary shocks. We analyze the relation between the properties of these interplanetary shocks (local shock speed, Alfvén Mach number, magnetic compression ratio, angle between the normal to the shock and the upstream magnetic field direction) and the energetic proton intensities observed around the shock passage. We compute the energy spectra and the three-dimensional anisotropies of protons in the energy range 20 keV - 10 MeV observed by the solid state detector of the WIND/3DP instrument. We investigate the correlation between shock strengths and proton fluxes as well as the behaviour of the proton anisotropies and spectra around the shock.

**Friday 30 July PM**

Presiding Chair: T.H.Zurbuchen (University of Michigan, Ann Arbor, USA)  
Concurrent Poster Session

**ENERGETICS PARTICLES IN THE HELIOSPHERE: LOCAL AND INTERSTELLAR SOURCES, SOURCES CYCLE DEPENDENCE AND 3D STRUCTURE-2**

**GA4.04/W/06-B5 Invited 1400**

**TRANSPORT OF ENERGETIC PARTICLES IN HELIOGRAPHIC LATITUDE BY DIRECT MAGNETIC CONNECTION: EVOLUTION DURING THE SOLAR CYCLE.**

L. A. FISK, T. H. Zurbuchen, and N. A. Schwadron, (Department of Atmospheric, Oceanic, and Space Sciences University of Michigan)

One of the important results from the Ulysses mission has been the apparent ease with which energetic particles propagate in heliographic latitude. Particles that are accelerated in Co-Rotating Interaction Regions (CIRs) at low latitudes are seen at the highest heliographic latitudes; low latitude CIRs affect the modulation of galactic cosmic rays at high latitudes. These observations have led to new models for the heliospheric magnetic field in which field lines acquire a systematic polar component, and thus can provide for direct magnetic connection from low to high latitudes. The mechanisms for creating these polar components are straightforward at solar minimum, but less obvious as solar activity increases and the well-developed polar coronal hole pattern breaks down. In this paper the new models for the heliospheric magnetic field are reviewed and the likely evolution of the mechanisms which create the systematic polar component of the field during the solar cycle are discussed.

**GA4.04/W/07-B5 1430**

**COMPARISON OF EISCAT IPS RADIAL AND MERIDIONAL SOLAR WIND VELOCITY MEASUREMENTS WITH MEASUREMENTS MADE BY ULYSSES.**

MORAN PJ, Breen AR, Fallows RA, Williams PJS. (Physics Department, UWA, Penglairs Hill, Aberystwyth, Ceredigion. SY23 3BZ)

Observations of interplanetary scintillation (IPS) made using EISCAT allow accurate solar wind velocity measurements to be made at all heliographic latitudes, whilst extended observations enable the large-scale direction of the solar wind flow to be determined. The IPS results show the high latitude wind to be similar in velocity to measurements made by ULYSSES and the data also regularly show there to be a small but significant non-radial component of around 1



or 2 degrees, generally in the meridional direction from the pole to the equator. A comparison of both velocity measurements along a streamline, and large scale non-radial flow are made between the EISCAT and ULYSSES datasets.

**GA4.04/W/15-B5 1450**

**SHOCK EVOLUTION AND THEIR RELATION TO ENERGETIC PARTICLES IN THE OUTER HELIOSPHERE**

J. D. RICHARDSON, A. J. Lazarus, K. I. Paularena (M.I.T., Center for Space Research, 37-655, Cambridge, MA, USA, 02139); R. Decker (Johns Hopkins Applied Physics Lab., Laurel, MD); and F. McDonald (IPST, University of Maryland, MD)

Shocks in the solar wind are important for initial energization of pickup ions in the solar wind. As the solar wind propagates outward, the frequency of shocks and their strength decrease. The timing of energetic particle increases is no longer as closely related to the passage of shocks. We discuss the evolution of shocks observed by Voyager from 1 to 58 AU and their relationship to energetic particle increases.

**GA4.04/E/03-B5 1510**

**THE TERMINATION SHOCK: 1979 - 1995**

Y. C. WHANG and J. Y. Lu (both at Department of Mechanical Engineering, Catholic University of America, Washington, D. C., email: whang@cua.edu) L. F. Burlaga (NASA Goddard Space Flight Center, Greenbelt, Maryland)

We study the varying location, jump condition, and shock speed of the termination shock from 1979 through 1995 taking into account the effects of pickup protons. Pickup protons and neutral hydrogen are calculated using a hot hydrogen model. Plasma and magnetic field data from Voyagers over a 17-year period from 1978 through 1994 are used as input to carry out this study. The full MHD equations are integrated to extrapolate input data from the Voyager trajectory to the upstream of the termination shock. The flow condition across the shock is required to satisfy the jump equations formulated in the moving shock frame of reference, and the solar wind flow immediately downstream of the shock is required to satisfy the condition of constant reverse Riemann invariant. The postshock temperature of pickup protons is calculated using recently obtained empirical formula of Whang and Burlaga.

**GA4.04/W/05-B5 Invited 1530**

**THE PHYSICS OF THE TRANSPORT OF GALACTIC AND ANOMALOUS COSMIC RAYS IN THE HELIOSPHERE**

J. R. JOKIPII and J. Kota, (University of Arizona, Tucson, AZ, 85721 USA Email: Jokipii@lpl.arizona.edu)

Observations of cosmic rays, magnetic fields and plasmas from a variety of spacecraft over the past several years, and associated modelling efforts, have led to a reasonably-complete picture of the quiet heliosphere. Models and computer simulations can account for the major observed features of cosmic rays and their interactions. This will be illustrated by showing the results of simulations and their physical interpretation. The major remaining problem appears to be the precise modes of latitudinal transport of energetic particles.

As we approach the next solar maximum, it is expected that the nature of the heliosphere, and hence its interactions with cosmic rays, will change dramatically. Progress in understanding and modelling these changes will also be discussed.

**GA4.04/W/14-B5 Invited 1620**

**SPATIAL AND TEMPORAL VARIATIONS OF ANOMALOUS COSMIC RAYS IN THE HELIOSPHERE**

R. A. LESKE, A. C. Cummings, R. A. Mewaldt, and E. C. Stone (Space Radiation Laboratory, Mail Code 220-47, California Institute of Technology, Pasadena, CA 91125 USA, email: ral@srl.caltech.edu); E. R. Christian (NASA/Goddard Space Flight Center, Code 661, Greenbelt, MD 20771 USA)

Anomalous cosmic rays (ACRs) provide a sensitive probe of the access of cosmic rays to the inner heliosphere, varying in intensity by more than two orders of magnitude during the course of the solar cycle. Their distribution in the heliosphere, specifically their radial and latitudinal intensity gradients, as well as the variation of these gradients with the magnetic polarity of the solar cycle, provide important constraints on theories of the transport of these particles from their acceleration site at the solar wind termination shock. We review measurements of the ACR intensities and spectra as determined in the outer heliosphere by the Pioneer and Voyager spacecraft, at high latitudes by Ulysses, and at 1 AU by SAMPEX, ACE, and other spacecraft, and compare these measurements to models of the modulation and transport of ACRs. We also discuss new information becoming available from the ACE spacecraft. With its outstanding statistical accuracy, ACE data can provide a detailed record of ACR intensity and spectral changes on short time scales during the approach to solar maximum, and with its excellent mass resolution, the spectra of individual ACR isotopes may be monitored.

**GA4.04/W/04-B5 1650**

**SOLAR CYCLE EFFECTS ON THE SPECTRUM OF ACR OXYGEN**

D.C. HAMILTON, M.E. Hill, and G. Gloeckler (all at Department of Physics, University of Maryland, College Park, MD, 20742, USA, Email: douglas.c.hamilton@umail.umd.edu); R.B. Decker and S.M. Krimigis (both at Johns Hopkins Applied Physics Laboratory, Laurel, MD)

The Voyager 1/2 LECIP instruments have measured the anomalous cosmic ray oxygen spectrum (0.3 - 40 MeV/nuc), mostly in the outer heliosphere, during the two solar cycles since the spacecraft were launched in 1977. Large temporal and spatial variations in intensity have been observed, particularly in the low energy portion of the spectrum. At Voyager 1, the peak ACR oxygen flux was observed at a nearly constant energy of 1.3 MeV/nucleon during the years 1993 to 1998 as V1 travelled from 53 AU to 71 AU. The flux at that energy increased by a factor of about 80 from 1992 to 1998, largely as a result of declining modulation during the approach to solar minimum. In fact the ACR flux at V1 and V2 continued to increase in 1997 and 1998 after the nominal minimum of the 11-year solar activity cycle in 1996. In addition, a comparison of the ACR oxygen spectra at Voyager 1 and Voyager 2 has revealed effects resulting from the 22-year solar magnetic cycle. In the 1997 solar minimum, the flux was higher at V1 than at V2, indicative of less modulation at V1, which was 16 AU farther from the sun. However, during the previous solar minimum in 1987, the ACR oxygen flux was higher at V2 than at V1 even though V1 was about 8 AU farther from the sun. The difference in the data from the two solar minima is apparently explained by the 1990 polarity reversal of the solar magnetic field. Predicted ACR drift patterns in 1987 produce maximum ACR fluxes near the

heliographic equator while those in 1997 produce low fluxes near the equator. V2 was near the equator in 1987 while V1 was at 31° latitude, and the large negative latitudinal gradient dominated the positive radial gradient. In 1997 both gradients would lead to a larger flux at V1. We will discuss these and other solar cycle variations in the ACR oxygen spectrum.

**GA4.04/W/09-B5 1710**

**COMPOSITION OF ANOMALOUS COSMIC RAYS**

A. C. CUMMINGS, C. D. Steenberg, and E. C. Stone (all at Caltech, Mail Code 220-47, Pasadena, CA, USA 91125, email: ace@srl.caltech.edu)

Anomalous cosmic rays (ACRs) originate as interstellar neutral gas which enters the heliosphere, becomes ionized, and then is accelerated at the solar wind termination shock, currently thought to lie within approximately 90 AU from the Sun. The composition of ACRs is important to questions concerning the injection and acceleration process at the solar wind termination shock, as well as to questions about the composition and ionization state of the gas in the local interstellar medium. We present a study of the composition of ACRs using energy spectra acquired during the current solar minimum period with instruments on the Voyager spacecraft. We use a full-drift model to describe the propagation of these particles in the heliosphere. We will compare the results with previous determinations and discuss the implications of the findings. This work was supported by NASA under contract NAS7-918.

**GA4.04/W/16-B5 1730**

**HELIUM FLUXES IN THE HELIOSPHERE**

E. KEPPLER, (Max Planck Institut Fur Aeronomie, Katlenburg-Lindau, D-37101 Germany, Email: Keppler@linmpi.mpg.de); M. Fraenz, B. Heber:

We shall discuss the observation of Helium-ion-fluxes observed in the high latitude Heliosphere as observed by the EPAC instrument on Ulysses. We also shall review observations of the p/He ratio variations observed during encounters with CIR related shocks in the Heliosphere.

**GA4.04/W/12-B5 1750**

**SPECTRAL AND COMPOSITION CHARACTERISTICS OF ENERGETIC IONS UPSTREAM OF THE EARTH'S BOW SHOCK**

M. I. DESAI, J. R. Dwyer, and G. M. Mason (Dept. Of Physics, University of Maryland, College Park, MD 20742); J. E. Mazur (Aerospace Corp., Los Angeles, CA 90009). T. T. von Rosenvinge, and R. P. Lepping (NASA/GSFC, Greenbelt, MD 20771)

Since the launch of the WIND spacecraft in November 1994 until the middle of 1998, the SupraThermal Energetic Particle (STEP) telescope has detected well over a thousand short-duration (lasting typically from a few minutes up to a few hours) ion intensity enhancements originating from the vicinity of the Earth's bow shock. We present here for the first time a detailed statistical analysis of the differential energy spectra of ion species such as H, He, CNO, NeS, and Fe in the 30 keV/nucleon up to a few MeV/nucleon energy range associated with such events. We also survey the abundances of heavy ions such as C, Ne, and Fe relative to O observed during the events. We discuss the implications of the above results for the traditional models that have been proposed to account for the origin and acceleration of these upstream ions.

Friday 30 July AM

Presiding Chair: N.A.Schwadron (University of Michigan, Ann Arbor, USA)

**ENERGETICS PARTICLES IN THE HELIOSPHERE: LOCAL AND INTERSTELLAR SOURCES, SOURCES CYCLE DEPENDENCE AND 3D STRUCTURE-1**

**GA4.04/E/04-B5 Poster 0830-01**

**ANISOTROPY AND SCATTERING MEAN FREE PATH OF INTERSTELLAR PICK-UP IONS**

Z. Nemeth and G. ERDOS (both at KFKI Research Institute for Particle and Nuclear Physics, 1525 Budapest P.O. Box 49, Hungary, Email: erdos@rmki.kfki.hu), A. Balogh (The Blackett Laboratory, Imperial College, London SW7 2BZ, UK, email: a.balogh@ic.ac.uk)

Pitch angle distributions of interstellar pick-up ions at high heliographic latitude have been studied in connection with the scattering mean free path of the particles. Based on high time resolution Ulysses magnetic field measurements, we have determined the pitch angle of pick-up ions at the moment of ionization. We have found that the long time average of the source anisotropy of the pick-up ions is not a ring distribution, due to large deviations of the magnetic field from Parker spiral. We have solved the transport equation of pick-up ions including an anisotropic source term consistent with magnetic field measurements, and we have estimated the value of the scattering mean free path which results in particle distribution matching Ulysses observations. Our conclusion is that the scattering mean free path of pick-up ions is significantly smaller than reported earlier.

**GA4.04/W/01-B5 Poster 0830-02**

**LOW ENERGY PROTONS AS A PROBE OF INTERPLANETARY ENVIRONMENT PERTURBATIONS**

M.F. Bakhareva, A.V. DMITRIEV, I.S. Veselovsky, and M.A. Zeldovich (Institute of Nuclear Physics, Moscow State University, 119899, Moscow, Russia, email: dalex@srdlan.npi.msu.ru)

The main aspects of the relationship between the fluxes of low energy (about 1 MeV) protons and interplanetary medium conditions are discussed in the paper using observational data for more than 100 events in 1972-1994 and theoretical arguments. The effective acceleration (stochastic and magnetic pumping) of the protons at the interplanetary shocks defines the background level and strong variations of particle fluxes. Solar cycle variations of background proton fluxes are associated with acceleration and propagation conditions in the heliosphere. The strong enhancements of the low energy proton fluxes are produced by corotating and CME shocks. These enhancements forestall the perturbations up to tens hours. This property of the low energy proton fluxes permits to consider these particles as a probe of the interplanetary perturbations. Methods of a short-term prediction based on this property are presented and discussed.



**GA4.04/W/10-B5** Poster **0830-03**

**STATISTICS OF PROTON EVENTS MEASURED ON HIGH-ALTITUDE SATELLITE GRANAT IN 1990-1995**

Eugene A. Chuchkov, Elena E. Grigorenko, Sergey I. Ermakov, Nickolay N. Kontor, German P. Lyubimov, Nickolay N. PAVLOV, Vladimir I. Tulupov, and Boris Ya. Scherbovsky (Skobel'syn Institute of Nuclear Physics, Moscow State University, Moscow, 119899, Russia, email: nnpavlov@taspd.npi.msu.su).

We measured fluxes of protons of 1 MeV through tens MeV energy on the GRANAT in 1990-1995. The satellite's orbit is as high as 200 000 km in its initial apogee. Our instrument has two blocks of sensors continuously directed sunward and opposite respectively. Common time resolution is 20 minutes and 2 minutes - for few channels only. A period of the mission falls on the time of high solar activity and many solar events have been recorded in our data collection. This paper presents some results of the statistical analysis performed for the acquired data. In the analysis we try to identify every individual enhancement in proton-flux intensity. For each enhancement, such characteristics as amplitude, duration, fluence, and some others are picked up for the available energy channels. Where is possible and reasonable, the overlapped enhancements are decomposed to the superposition of elementary profiles that could be bound to the individual solar events. Involving of different energy channels allows us to estimate energy spectrum of propagating protons for each event and, further, to assess total energy of accelerated particles for a particular solar flare. All mentioned parameters are gathered into statistical distributions. A dependence of various characteristics of those distributions on the phase of a solar cycle is also studied.

**GA4.04/W/08-B5** Poster **0830-04**

**PARTICLE DIFFUSION IN A GAS OF NON-LINEAR MHD STRUCTURES: AN INELASTIC BILLARD MODEL**

B. LEFEBVRE and V. Krasnoselskikh (LPCE/CNRS, 3A av. De la Recherche Scientifique, F-45071, Orleans, France. Email: lefebvre@cnrs-orleans.fr)

Diffusion and acceleration of particles by "coherent structures" in large-scale plasma turbulence is studied. Our model is inspired from the Lorentz gas, but with inelastic collisions. Its statistical properties such as diffusion, Lyapunov exponents, entropy are studied. The applications we have in mind are:

- a) diffusion and acceleration in the quasi-parallel shock region
- b) particle heating in the solar corona where multiple reconnection sites may occur.

**GA4.04/W/11-B5** Poster **0830-05**

**TWO-COMPONENT STRUCTURE AND BI-DIRECTIONAL ANISOTROPY OF RELATIVISTIC PROTON IN THE SEPTEMBER 29, 1989 EVENT**

E.V. VASHENYUK (1) and L.I. Miroshnichenko (2) (1) Polar Geophysical Institute, Apatity, 184200, RUSSIA; (2) Instituto de Geofísica UNAM, México, D. F., 04510, MEXICO; Permanent address: IZMIRAN, Troitsk, Moscow Region, 142092, RUSSIA

Ground Level Enhancement (GLE) of September 29, 1989 was remarkable, in particular, by strong variations of the energy spectrum and anisotropy direction of relativistic solar cosmic rays (SCR). Although a CME-driven shock has been proposed as the most plausible mechanism to account for the behaviour of relativistic protons during all the event, no generally accepted explanation exists at present. We try to explain these peculiarities relying upon a concept of two SCR components. The first, hard prompt component (PC) was suggested to originate from impulsive behind-the-limb flare, its anisotropy being directed outwards the Sun. The source of the second, soft delayed component (DC) presumably occupied a wide area (as large as a CME), however, it had a pronounced bidirectional anisotropy. It means that the IMF during the GLE might have a shape of giant loop with its both ends rooted into the Sun. Some observational data indicate that such a structure was built-up before the event, due to intensive eruptive activity behind the solar limb. It is argued that the DC acceleration, ejection and propagation have been operating behind the CME-driven shock.

**GA4.04/L/01-B5** Poster **0830-06**

**THE DIMENSION OF MODULATION REGION IN THE HELIOSPHERE AND HIGH RIGIDITY COSMIC RAY-SOLAR ACTIVITY HYSTERESIS PHENOMENON**

LEV DORMAN (IZMIRAN, Technion and Israel Cosmic Ray Center, affiliated to Tel Aviv University; Current address: P.O.Box 2217, Qazrin 12900, ISRAEL; email: lid@physics.technion.ac.il); Irina Dorman (Institute of History of Science and Technology, Russian Academy of Science, Staropansky 1/5, Moscow 103012, RUSSIA); N. Iucci and M. Parisi (Terza Università di Roma, Dipartimento di Fisica "E. Amaldi", Via della Vasca Navale 84, 00146 Rome, Italy); G. Villoresi (IFSI/CNR-Frascati c/o Terza Università di Roma, Dipartimento di Fisica "E. Amaldi", Via della Vasca Navale 84, 00146 Rome, Italy)

On the basis of cosmic ray (CR) neutron monitor and muon telescope data as well as solar activity (SA) data for 5 solar cycles the CR-SA hysteresis phenomenon is investigated. Obtained results show that by high rigidity CR particles it can be determined only the effective dimension of modulation region in the Heliosphere (in dependence of particle rigidity) but not the distance from the Sun to the terminal shock wave. This effective dimension of modulation region decreased with CR rigidity increasing. High rigidity CR particles don't feel the situation out of modulation region up to the terminal shock wave but its global time variation contains an important information on the CR diffusion coefficient distribution in the inner Heliosphere and connection with SA.

**GA4.04/L/02-B5** Poster **0830-07**

**HYSTERESIS PHENOMENON IN LONG-TERM COSMIC RAY-SOLAR ACTIVITY CONNECTION AND COSMIC RAY MODULATION IN THE LAST 250 YEARS**

LEV DORMAN (IZMIRAN, Technion and Israel Cosmic Ray Center, affiliated to Tel Aviv University; Current address: P.O.Box 2217, Qazrin 12900, ISRAEL; email: lid@physics.technion.ac.il); Irina Dorman (Institute of History of Science and Technology, Russian Academy of Science, Staropansky 1/5, Moscow 103012, RUSSIA); N. Iucci and M. Parisi (Terza Università di Roma, Dipartimento di Fisica "E. Amaldi", Via della Vasca Navale 84, 00146 Rome, Italy); G. Villoresi (IFSI/CNR-Frascati c/o Terza Università di Roma, Dipartimento di Fisica "E. Amaldi", Via della Vasca Navale 84, 00146 Rome, Italy)

On the basis of cosmic ray (CR) neutron monitor, muon telescope, and ionization chamber data, as well as solar activity (SA) data for the last 6 solar cycles, the hysteresis phenomenon in the connection between CR and SA is investigated. On the basis of low rigidity CR data we determine the average (for solar cycle) dimension of the Heliosphere and CR propagation parameters. The results, obtained separately for odd and even solar cycles, are compared and

discussed in the frame of CR convection-diffusion propagation model, by taking into account drift effects. Then, on the basis of data for 1965-1998 we determine the expected change of CR propagation parameters and position of terminal shock wave during these solar cycles. We tested the obtained results by using CR and SA monthly data for 1953-1965. Then, by using the available SA data in the past (including the period of Maunder SA minimum), we obtain information on the time variations of solar wind properties and CR modulation versus particle rigidity for the last 250 years.

**GA4.04/L/03-B5** Poster **0830-08**

**THE 27-DAY VARIATION OF COSMIC RAYS IN CONNECTION WITH INHOMOGENEOUS DISTRIBUTION OF SOLAR ACTIVITY AND WITH THE POSITION OF INTERPLANETARY NEUTRAL CURRENT SHEET**

LEV DORMAN (IZMIRAN, Technion and Israel Cosmic Ray Center, affiliated to Tel Aviv University; Current address: P.O.Box 2217, Qazrin 12900, ISRAEL; E-mail: lid@physics.technion.ac.il), J.F. Valdes-Galicia (Instituto de Geofísica UNAM, 04510 Mexico D.F., MEXICO)

Based on daily data of the cosmic ray neutron intensity detected at Deep River we determined the amplitude and phase of cosmic ray 27-day variation for each solar rotation for periods during the ascending (1976-1978, 1986-1988) and descending (1982-1984, 1991-1993) phases of solar cycles 21 and 22. We compare the obtained results with the 27-day variation of solar activity and with the evolution of the interplanetary neutral current sheet tilt-angle. The conclusion of our research is that 27-day cosmic ray variation is caused by at least two mechanisms. The first is rotated inhomogeneous modulation, and the second is caused by the rotation of the inclined interplanetary neutral current sheet and existing of transverse cosmic ray gradients connected with the sheet (which leads to cosmic ray 27-day variation with amplitude to be approximately proportional to the tilt-angle).

**GA4.04/L/04-B5** Poster **0830-09**

**ON THE DEPENDENCE OF SOLAR WIND AND IMF PARAMETERS FROM HELIOLATITUDE AND SOLAR ACTIVITY LEVEL**

LEV I. DORMAN (IZMIRAN, Technion and Israel Cosmic Ray Center, affiliated to Tel Aviv University; Current address: P.O.Box 2217, Qazrin 12900, ISRAEL; email: lid@physics.technion.ac.il), H. Ahluwalia (Dep. of Physics and Astronomy, University of New Mexico, Albuquerque, USA)

The formation and change in time of cosmic ray convection-diffusion and drift anisotropies determined mainly by space-time variations of solar wind speed and interplanetary magnetic field (IMF) parameters in the Hale solar cycle. To determine these variations we used hourly data on OMNI tape available at the National Space Science Data Center (Greenbelt, MD) contained a composite of the multispacecraft observations, obtained over different periods in 1965-1990. We separated all solar wind and IMF data for AWAY and TOWARD directions of IMF in dependence of solar activity level for three zones of the Earth's heliolatitude: NORTH (effective heliolatitude +6 degrees), EQUATORIAL (effective heliolatitude 0 degrees) and SOUTH (effective heliolatitude -6 degrees). Obtained results for 1965-1990 we compare with recent Ulysses data.

**GA4.04/L/05-B5** Poster **0830-10**

**ON THE COSMIC RAY PROPAGATION PARAMETERS CHANGING AND HELIOSPHERE TERMINAL SHOCK WAVE MOVING DURING THE SOLAR CYCLE**

LEV DORMAN (IZMIRAN, Technion and Israel Cosmic Ray Center, affiliated to Tel Aviv University; Current address: P.O.Box 2217, Qazrin 12900, ISRAEL; email: lid@physics.technion.ac.il); Irina Dorman (Institute of History of Science and Technology, Russian Academy of Science, Staropansky 1/5, Moscow 103012, RUSSIA); N. Iucci and M. Parisi (Terza Università di Roma, Dipartimento di Fisica "E. Amaldi", Via della Vasca Navale 84, 00146 Rome, Italy); G. Villoresi (IFSI/CNR-Frascati c/o Terza Università di Roma, Dipartimento di Fisica "E. Amaldi", Via della Vasca Navale 84, 00146 Rome, Italy)

On the basis of investigation of CR-SA hysteresis phenomenon by data of neutron monitor world-wide network, stratospheric and space probe CR measurements as well as SA and SW data for 1965-1990 we determine approximately the expected change of CR propagation parameters and position of terminal shock wave during the solar cycle. The testing of obtained results we made by using CR and SA monthly data for 1954-1965. Here we use the following denotes: CR - cosmic ray intensity (we use monthly average data for neutron monitors with low cut-off rigidity), SA - solar activity (we use monthly average data of sunspot numbers), SW - solar wind (we use monthly average data of total interplanetary magnetic field, of solar wind speed and solar wind plasma density).

**Friday 30 July PM**

Presiding Chair: T.H.Zurbuchen (University of Michigan, Ann Arbor, USA)

**ENERGETICS PARTICLES IN THE HELIOSPHERE: LOCAL AND INTERSTELLAR SOURCES, SOURCES CYCLE DEPENDENCE AND 3D STRUCTURE-2**

**GA4.04/L/06-B5** Poster **1400-01**

**COSMIC RAY HYSTERESIS EFFECTS IN DEPENDENCE OF PARTICLE RIGIDITY AND DIMENSIONS OF EFFECTIVE MODULATION REGION**

LEV DORMAN (IZMIRAN, Technion and Israel Cosmic Ray Center, affiliated to Tel Aviv University; Current address: P.O.Box 2217, Qazrin 12900, ISRAEL; email: lid@physics.technion.ac.il); Irina Dorman (Institute of History of Science and Technology, Russian Academy of Science, Staropansky 1/5, Moscow 103012, RUSSIA); N. Iucci and M. Parisi (Terza Università di Roma, Dipartimento di Fisica "E. Amaldi", Via della Vasca Navale 84, 00146 Rome, Italy); G. Villoresi (IFSI/CNR-Frascati c/o Terza Università di Roma, Dipartimento di Fisica "E. Amaldi", Via della Vasca Navale 84, 00146 Rome, Italy)

Our studies of the neutron component data have made possible to find the hysteresis character of the relationships between the variations in solar activity and in cosmic ray intensity. This effect arises from the delay of the interplanetary processes (responsible for cosmic ray modulation) with respect to the initiating solar processes which correspond to some effective velocity of solar wind and shock waves propagation. We extended these investigations with taking into account data of cosmic ray observations by ionization chambers, muon telescopes and neutron monitors and supermonitors on the stations with different cut-off rigidity as well as data of cosmic ray measurements in stratosphere and on space probes. Obtained results on hysteresis effects for about 4 solar cycles we analyze in the frame of theory of cosmic ray nonlinear modulation and determine the dimension of effective modulation region in dependence from particle rigidity.

**GA4.04/L/07-B5** Poster **1400-02**

**LOW RIGIDITY COSMIC RAY-SOLAR ACTIVITY HYSTERESIS PHENOMENON, PARTICLE PROPAGATION PARAMETERS AND AVERAGE DIMENSION OF THE HELIOSPHERE**

LEV DORMAN (IZMIRAN, Technion and Israel Cosmic Ray Center, affiliated to Tel Aviv University; Current address: P.O.Box 2217, Qazrin 12900, ISRAEL; email: lid@physics.technion.ac.il); Irina Dorman (Institute of History of Science and Technology, Russian Academy of Science, Staropansky 1/5, Moscow 103012, RUSSIA); N. Iucci and M. Parisi (Terza Università di Roma, Dipartimento di Fisica "E. Amaldi", Via della Vasca Navale 84, 00146 Rome, Italy); G. Villoresi (IFI/CNR-Frascati c/o Terza Università di Roma, Dipartimento di Fisica "E. Amaldi", Via della Vasca Navale 84, 00146 Rome, Italy)

On the basis of low rigidity cosmic ray (CR) intensity data obtained for the last several solar cycles by ground-based neutron monitors and by stratospheric and space probe measurements as well as solar activity (SA) and solar wind (SW) data the hysteresis phenomenon is investigated for the several suppositions on CR diffusion coefficient connection with SA and distribution in the Heliosphere. By comparison of expected CR-SA hysteresis with observed one we determine in the first approximation the average for solar cycle dimension of the Heliosphere and CR propagation parameters as well as expected CR intensity out of the Heliosphere in dependence of particle rigidity.

**GA4.04/L/08-B5** Poster **1400-03**

**GAMMA-RAY PRODUCTION IN THE HELIOSPHERE BY GALACTIC AND SOLAR COSMIC RAYS**

LEV DORMAN (IZMIRAN, Technion and Israel Cosmic Ray Center, affiliated to Tel Aviv University; Current address: P.O.Box 2217, Qazrin 12900, ISRAEL; email: lid@physics.technion.ac.il),

The interaction of cosmic ray particles (protons, nucleus and electrons) with matter determines main processes of high-energy gamma ray generation: through neutral pion decay and bremsstrahlung emissivity. From other side, the intensity of these processes depends from the space-time distribution of matter as well as from the space-time distribution of cosmic ray energy spectrum and contents. By solving self-consistent spherical-symmetric problem for the Heliosphere (with taking into account energetic particle pressure influence on solar wind plasma propagation and energetic particle kinetic stream instability influence on the small-scale magnetic structure of plasma) we determine galactic cosmic ray modulation in the interplanetary space in dependence from the level of solar activity, from the radial distance and from the particle energy as well as plasma density space-time distribution. On the basis of these results we calculate approximately an expected gamma-ray emissivity of the Heliosphere from galactic cosmic rays in dependence of direction of view for inside and outside observers. Then we determine approximately expected gamma-ray emissivity of Heliosphere from solar cosmic rays for great solar energetic particle events.

**GA4.04/L/09-B5** Poster **1400-04**

**COSMIC RAY ANISOTROPIES IN THE HELIOSPHERE**

LEV DORMAN (IZMIRAN, Technion and Israel Cosmic Ray Center, affiliated to Tel Aviv University; Current address: P.O.Box 2217, Qazrin 12900, ISRAEL; E-mail: lid@physics.technion.ac.il )

Cosmic ray anisotropy is one of main characteristics of galactic cosmic rays. The observed cosmic ray anisotropy in the interplanetary space consists mainly from two parts with different origin and different dependences from particle rigidity and from interplanetary magnetic field (IMF). One part is produced by cosmic ray convection-diffusion processes and does not depend from the direction of IMF; the other part is produced by cosmic ray drift processes and strongly depends from the direction of IMF. Both parts are connected with cosmic ray gradients and parameters of cosmic ray propagation in the space. This review paper reflects research of 3-dimensional, North- South and ecliptic cosmic ray anisotropies in the Heliosphere, on determination by cosmic ray anisotropy data transport parameters of cosmic ray propagation and distribution of cosmic ray density gradients in the interplanetary space.

**GA4.04/L/10-B5** Poster **1400-05**

**ADDITIONAL CHARGED PARTICLE PROPAGATION IN SPACE PLASMA WITH TWO TYPES OF SCATTERS: APPLICATIONS TO THE HELIOSPHERE**

LEV DORMAN (IZMIRAN, Technion and Israel Cosmic Ray Center, affiliated to Tel Aviv University; Current address: P.O.Box 2217, Qazrin 12900, ISRAEL; E-mail: lid@physics.technion.ac.il); V. Shogenov (Kabardino-Balkar State University, Nalchik, Russia).

We determine the transport parameters for cosmic ray propagation in the Heliosphere in the frame of model [1]. In this model first type of scatterers are magnetic inhomogeneities frozen in solar wind (as a background plasma) moved with some velocity  $w$ . These scatterers are characterized by transport path  $W(R)$ , where  $R$  is the rigidity of charged particles. The second type of scatterers are magnetic clouds, high speed streams, shock waves (considered only as scatterers) moved with some average velocity  $u$  and characterized by transport path  $U(R)$ . From the collisional Boltzmann equation we derive the diffusion approximation and then determine diffusion tensor and effective convection speed which will be characterize cosmic ray propagation and modulation in in the Heliosphere (the additional cosmic ray acceleration we consider in [2]).

References:[1] L.I. Dorman, V.Kh. Shogenov,1985. J. Exp. Theor. Phys., 89, 1624. [2] L. Dorman, V. Shogenov, 1999. Report on GA 4.04 Symposium.

**GA4.04/L/11-B5** Poster **1400-06**

**THE EVENT OF 24 MAY 1990 AND THE PROBLEM OF SOLAR NEUTRON PROPAGATION THROUGH THE EARTH'S ATMOSPHERE: DOES THE "REFRACTION" EFFECT EXIST**

LEV DORMAN (IZMIRAN, Technion and Israel Cosmic Ray Center, affiliated to Tel Aviv University; Current address: P.O.Box 2217, Qazrin 12900, ISRAEL; E-mail: lid@physics.technion.ac.il); V. Shogenov (Kabardino-Balkar State University, Nalchik, Russia).

To obtain absolute values of solar neutron intensity changing in dependence of altitude and zenith angle of the Sun we recalculate all available experimental data with taking into account the type of detector as well as the change of galactic cosmic ray intensity in dependence of altitude and cut-off rigidity (by using analytical approximation for neutron component coupling function). After this procedure the attenuation length of solar neutrons in the assumption of straight-ahead transport from the Sun through the atmosphere reduces from unreasonable great value of 208 g/sq.cm to 149 g/sq.cm. The obtained value still contradicts with data on neutron cross-sections. Then we take into account the "refraction" effect in solar neutron propagation through the atmosphere according to our calculations and the attenuation length reduces to about 110 g/sq.cm) in accordance with neutron cross-section data.

**GA4.04/L/12-B5** Poster **1400-07**

**SIMULATION OF SOLAR NEUTRON SCATTERING AND ATTENUATION IN THE ATMOSPHERE FOR DIFFERENT INITIAL ZENITH ANGLES**

LEV DORMAN (IZMIRAN, Technion and Israel Cosmic Ray Center, affiliated to Tel Aviv University; Current address: P.O.Box 2217, Qazrin 12900, Israel; email: lid@physics.technion.ac.il), I.V. Dorman (Institute of History of Science and Technology RAN, Staropansky 1/5, Moscow 103012, Russia) J.F. Valdes-Galicia (Instituto de Geofisica, UNAM, Mexico)

We test the usually used suggestion that solar neutron propagation through the atmosphere for some initial zenith angle  $T$  of the Sun will be the same as for vertical direction, but for the depth  $h/\cos T$ . Our simulation of multi-scattering of neutrons on small angles with attenuation for different initial zenith angles shows that this suggestion is not correct. The main cause of this is the bigger attenuation of neutrons scattered to the bigger zenith angles which grows asymmetry in the neutron angle distribution. Media zenith angle of solar neutrons decreases during its propagation through the atmosphere.

**GA4.04/L/13-B5** Poster **1400-08**

**DRIFT ANISOTROPY AND TRANSVERSE GRADIENTS OF COSMIC RAYS IN THE INTERPLANETARY SPACE ACCORDING TO GROUND AND UNDERGROUND OBSERVATIONS FOR ABOUT 25 YEARS**

LEV I. DORMAN (IZMIRAN, Technion and Israel Cosmic Ray Center, affiliated to Tel Aviv University; Current address: P.O.Box 2217, Qazrin 12900, ISRAEL; email: lid@physics.technion.ac.il), H. Ahluwalia (Dep. of Physics and Astronomy, University of New Mexico, Albuquerque, USA)

We used 25 years data of underground muon telescopes and ground based neutron supermonitors as well as data of solar wind speed and interplanetary magnetic field (IMF) parameters (mainly for 1965-1990). We separated all data for AWAY and TOWARD directions of IMF in three zones: NORTH (effective heliolatitude of the Earth +6 degrees ), EQUATORIAL (effective heliolatitude 0 degrees) and SOUTH (effective heliolatitude -6 degrees ). We take into account that cosmic ray convection-diffusion anisotropy not depend from the direction of IMF and drift anisotropy changes the sign with the changing of the IMF direction. We separate these two types of cosmic ray anisotropies and determine the dependence of cosmic ray drift anisotropy from particle rigidity as well as transverse gradient in the interval from +6 degrees to -6 degrees.

**GA4.04/L/14-B5** Poster **1400-09**

**COSMIC RAY CONVECTION-DIFFUSION ANISOTROPY IN THE INTERPLANETARY SPACE ACCORDING TO GROUND AND UNDERGROUND OBSERVATIONS**

LEV I. DORMAN (IZMIRAN, Technion and Israel Cosmic Ray Center, affiliated to Tel Aviv University; Current address: P.O.Box 2217, Qazrin 12900, ISRAEL; email: lid@physics.technion.ac.il), H. Ahluwalia (Dep. of Physics and Astronomy, University of New Mexico, Albuquerque, USA)

To determine the clean cosmic ray convection-diffusion anisotropy we used 25 years data of underground muon telescopes and ground based neutron supermonitors as well as space apparatus data of solar wind speed and interplanetary magnetic field (IMF) parameters (mainly for 1965-1990). We separate all data for AWAY and TOWARD directions of IMF in the three zones of the Earth's heliolatitude: NORTH, EQUATORIAL and SOUTH. Since the cosmic ray convection-diffusion anisotropy does not depend from the direction of IMF, but drift anisotropy change the sign with the changing of the IMF direction we excluded the drift anisotropy from observation data and in the first time obtained information on the clean cosmic ray convection-diffusion anisotropy in the interplanetary space in dependence of particle energy in the interval from few GeV to about 300 GeV and in dependence on heliolatitude. We discuss obtained results in the frame of modern theory of cosmic ray anisotropy formation in the Heliosphere.

**GA4.06** **Monday 26 July**

**IAGA DIVISION IV REPORTER REVIEWS**

Location: School of Education 135 LT

**Monday 26 July AM**

Presiding Chair: J.G.Luhmann (Space Sciences Lab., University of California, Berkeley, USA)

**GA4.06/W/04-B1** Invited **0900**

**SOLAR WIND INTERACTIONS WITH MAGNETOSPHERES: A TUTORIAL UPDATE ON PHENOMENOLOGY AND PHYSICS**

C. T. RUSSELL (Institute of Geophysics and Planetary Physics, University of California, Los Angeles, CA 90095-1567, USA, email: ctrussell@igpp.ucla.edu)

The size of a planetary magnetosphere is determined by the balance between the solar wind dynamic pressure and the magnetic and plasma pressure exerted by the planetary magnetosphere. The shape of the magnetosphere is additionally affected by the drag of the solar wind on the obstacle. Increasingly it is found that this drag is predominantly associated with reconnection. It is not yet well understood what controls the rate of reconnection of the interplanetary magnetic field (IMF) to that of the Earth but the ionosphere is believed to be important. If so, then investigation of the magnetosphere of Mercury is a high priority because its weak ionosphere provides an important contrast to Earth's. In fact Luhmann and co-workers have proposed that Mercury does not have substorms but rather the magnetosphere is immediately responsive to the solar wind. The ISTEP program is making significant inroads in understanding both the coupling of the ionosphere and the magnetosphere and the magnetosphere with the solar wind. Current systems, through potential drops and wave particle interactions, heat ions that escape into the magnetosphere while the energy for this process is provided by the solar wind. The solar wind entry into the polar cusp differs from northward to southward IMF populating dayside field lines and the nightside field lines relative to the bifurcation field line in these two situations. The motion of the cusp in local time for different by polarities provides unambiguous evidence for motion of the reconnection site on the magnetopause. Jupiter provides an important contrast to the terrestrial magnetosphere. The Mach number of the solar wind has increased substantially by 5.2 AU, changing the conditions for IMF reconnection with the planetary magnetic field. It supplies much mass, perhaps one ton per second to the magnetosphere. This mass is spun up by the corotational electric field enforced by the ionosphere and a magnetodisk is formed. Radial outward and convection transports the ions to the tail where reconnection separates them from the planetary magnetic field and the emptied closed field lines convect back into the magnetosphere. It is possible that in contrast to the terrestrial magnetosphere, jovian magnetospheric activity is internally, not externally driven.



**GA4.06/W/08-B1** Invited **0940**

**STRUCTURES IN THE CORONA, THE SOLAR WIND, AND THE LARGE-SCALE HELIOSPHERE: NEW RESULTS FROM RECENT ACTIVITY MINIMUM**

Rainer SCHWENN (Max-Planck-Institut fuer Aeronomie, D 37191 Katlenburg-Lindau, Germany, Email: schwenn@linmpi.mpg.de)

The space missions SOHO and Ulysses were lucky to be fully operational during the recent solar activity minimum in 1996. They encountered the sun in exactly the same magnetic configuration as did Skylab and Helios one full Hale cycle ago. Then, many basic features of the 3D heliosphere were discovered. This time, we observed in much more detail, how closely the magnetic topology of the corona is associated with the solar wind stream structure. The boundaries separating fast coronal hole flow from slow solar wind confined to the equatorial streamer belt can be traced all the way down to the sun. For the first time, the slow wind was made visible, and its acceleration profiles was measured. Its release mechanism remains under debate. The fast wind was found to be accelerated much closer to the sun. It reaches its final speed inside 10 Rs. Evidence for strong ion cyclotron heating was also found.

**GA4.06/W/06-B1** Invited **1040**

**AN UPDATE ON UNDERSTANDING THE CORONA**

Ruth ESSER (Harvard Smithsonian Center for Astrophysics, 60 Garden Street, Cambridge MA 02138, USA, email: resser@cfa.harvard.edu)

Observations from the Solar Heliospheric Observatory and from ground based instruments carried out over the past few years have led to results that demand a revision of the physical picture of the inner corona. These results, particularly the ones concerning particle temperatures and flow speeds, have initiated new investigations of possible heating mechanisms operating in the inner corona. The picture of the coronal plasma that emerges from these new observations, as well as recently suggested heating mechanisms will be discussed. The consequences of the new observations and heating mechanisms for solar wind modelling will be addressed. Different approaches to solarwind modelling will be compared.

**GA4.06/W/02-B1** Invited **1120**

**CORONAL MASS EJECTIONS NEAR THE SUN AND IN THE SOLAR WIND: PRESENT UNDERSTANDING**

J. T. GOSLING (Los Alamos National Laboratory, Los Alamos NM 87545, USA, email: jgosing@lanl.gov)

Coronal mass ejections, or CMEs, play a fundamental role in the long-term evolution of the solar corona and are the prime source of transient (as opposed to corotating) solar wind disturbances and large, non-recurrent geomagnetic storms. Recent years have witnessed a virtual explosion of CME-related studies. This interest and emphasis arise both because of an increased awareness of the importance of these events to solar-terrestrial physics and because of superb new observations available from SOHO, YOHKOH, WIND, ACE, and Ulysses. This paper attempts to provide an overview of present understanding of CMEs in both their solar and heliospheric contexts, with emphasis on results from the last ~5 years.

Monday 26 July PM

**GA4.06/W/07-B1** **1400**

**ION COMPOSITION AND SOURCES IN THE HELIOSPHERE**

P. BOCHSLER (Physikalisches Institut, University of Bern, Sidlerstrasse 5 CH 3012 Bern Switzerland Email: Peter.Bochsler@soho.unibe.ch)

Most charged particles in the heliosphere originate either from the solar wind or from interstellar neutrals penetrating deep into the innermost parts of the solar system where they are converted into 'pick-up ions' either by charge exchange with solar particles or by photoionisation, to be swept out again, together with the magnetized solar wind plasma. Minor sources in the heliosphere are cometary dust, and cometary and planetary atmospheres. Each source has its specific features, i.e. velocity distributions, and ionic, elemental, and isotopic abundance pattern. Compositional information of the charged heliospheric medium is often used to identify and disentangle contributions from different sources. On the other hand, compositional data provide valuable information about the sources themselves. This review will concentrate on results from the Ulysses-, WIND-, SOHO- and ACE-missions.

**GA4.06/W/05-B1** **1440**

**OVERVIEW OF FIRST RESULTS FROM THE ADVANCED COMPOSITION EXPLORER**

E. C. STONE (Space Radiation Laboratory, Mail Code 220-47, California Institute of Technology, Pasadena, CA 91125 USA, email: ecs@srl.caltech.edu)

The Advanced Composition Explorer (ACE) is providing high resolution observations of the elemental and isotopic composition of ions and energetic particles of solar, local interstellar, and galactic origin. Studies of these three samples of matter will address the origin of the elements and their subsequent processing, the formation of the corona and the acceleration of the solar wind, and energetic particle acceleration and transport. Six high resolution spectrometers cover an energy interval ranging from the solar wind to galactic cosmic rays with collecting powers 10 to 1000 times greater than previously available. Three other instruments that monitor the interplanetary environment also provide real time data to the NOAA alert system for impending geomagnetic storms. Launched on August 25, 1997, ACE arrived at the L1 libration point 1.5 million kilometers upwind of Earth in December 1997 to begin a mission extending at least five years to the next maximum in solar activity. This talk will provide an overview of some of the first results from ACE, including high time-resolution measurements of the composition of the solar wind and coronal mass ejections, studies of the ionic charge-state and isotopic composition of the first solar particle events of cycle 23, and high-resolution measurements of the isotopic composition of anomalous and galactic cosmic rays.

**GA4.06/W/01-B1** **1540**

**THE 3-D HELIOSPHERE: HOW ULYSSES HAS CHANGED OUR VIEW**

R. J. FORSYTH (The Blackett Laboratory, Imperial College, London SW7 2BZ, UK, email: r.forsyth@ic.ac.uk)

The Ulysses mission, with its aims of establishing how heliospheric phenomena depend on latitude, and to make the first observations of the polar regions of the heliosphere, has now been underway for more than 8 years. The mission is providing a unique data set covering, among others, the solar wind, the heliospheric magnetic field, energetic particles and cosmic rays. The polar orbit of the spacecraft about the Sun brought Ulysses into the high latitude regions of the heliosphere during 1994 and 1995 during a time when solar activity was decreasing and approaching minimum, allowing these phenomena to be studied in perhaps their simplest states. This review focuses on the contributions that Ulysses has made so far to our knowledge of the 3-D heliosphere, both confirming accepted theory, and throwing up new unexpected results. Ulysses is now well on its way to returning to high latitudes in 2000 and 2001. Some of the open questions that Ulysses will address at this time of solar maximum when the structure of the heliosphere is expected to be much more complex will be briefly discussed.

**GA4.06/W/03-B1** **1620**

**AN UPDATE ON GALILEO RESULTS ON JUPITER'S MAGNETOSPHERE**

N. KRUPP (Max-Planck-Institut für Aeronomie, D- 37191 Katlenburg-Lindau, Germany, email: krupp@linmpi.mpg.de)

A new era of outer planets exploration began when the Galileo spacecraft reached Jupiter in December 1995. Galileo is up to now performing in-situ measurements in the Jovian magnetosphere as the first orbiting spacecraft of an outer planet. Measurements along the elliptic orbits cover nearly all local times and distances between 6 and 142 Jovian radii (RJ). In this report the Galileo results on Jupiter's magnetosphere based on energetic particle measurements of the Energetic Particles Detector (EPD) will be summarized in context to results of other instruments onboard Galileo. They will be compared to the perspective derived from the previous flyby missions. Three-dimensional particle anisotropies in the Jovian magnetosphere show that a dawn-dusk asymmetry exists with larger anisotropy amplitudes in the dawn than in the dusk sector at comparable distances. Also larger radial/field-aligned anisotropies in the dusk magnetosphere are found. Particle flow in the corotation direction are observed in the Jovian magnetotail at distances of 142 RJ. These results require a modification of earlier models of the global flow pattern. Another result of Galileo is the evidence for large-scale dynamic processes within the Jovian magnetotail changing the energetic particle intensities and the slope of energy-time spectra periodically. Strong particle bursts occurring in the predawn sector at distances of 100 RJ and over 100 energy-time dispersed particle signatures in the inner magnetosphere document substorm- or storm-like processes in the Jovian magnetosphere. Energetic particle results onboard Galileo also contribute to the study of the interaction between the Jovian magnetosphere and the Galilean satellites. At Io electron beams along the Io flux tube have been discovered, and at Ganymede the ion sputtering rate could be determined. One of the main results of Galileo so far is the discovery of Ganymede's magnetosphere within the Jovian magnetosphere. Important properties of Ganymede's magnetosphere were derived from changes in the flow direction and magnitude of energetic ions and their loss-cone distributions could be used to determine the surface magnetic field of Ganymede.

**DIVISION IV VIDEOFEST** **1700**

**GA4.08** **Wednesday 28 – Thursday 29 July**

**INTERPLANETARY MEDIUM AND GEOPHYSICAL PHENOMENA DURING MAGNETIC STORMS (WITH DIV. II, III, IV)**

Location: School of Education 135 LT  
Location of Posters: School of Education, Conference Room

Wednesday 28 July AM

Concurrent Poster Session

**GA4.08/W/07-B3** Invited **0830**

**SOLAR SOURCE REGIONS OF CORONAL MASS EJECTIONS**

S.P. PLUNKETT (1), B.J. Thompson (2), O.C. St. Cyr(3), R.A. Howard (4) (1) Universities Space Research Association, Naval Research Laboratory, Washington, DC 20375, USA. (2) NASA Goddard Space Flight Center, Greenbelt, MD 20771, USA. (3) Computational Physics Inc., NASA Goddard Space Flight Center, Greenbelt, MD 20771, USA. (4) Naval Research Laboratory, Washington, DC 20375, USA.

It is generally accepted that coronal mass ejections (CMEs) are the major solar drivers of many space weather phenomena, including large, non-recurrent geomagnetic storms and solar energetic particle events. High-quality synoptic observations of the solar corona, as carried out by the EIT and LASCO experiments on SOHO, provide near real-time imaging of CMEs, and can be used to help predict the occurrence of geomagnetic disturbances several days in advance. Extreme-ultraviolet images of the low corona and solar disk, as recorded by EIT, reveal a complex web of CME signatures. These observations, together with visible light observations of the outer corona by LASCO, have provided new insights into the origin and initiation of CMEs, and their subsequent evolution as they propagate outwards into the interplanetary medium. In this paper, we use these observations to address the following questions. What types of quiescent solar structures are most likely to produce a CME? How do the manifestations of CME activity near the solar surface relate to the observed properties of CMEs at larger distances from the Sun? Finally, can our improved understanding of CME origins improve our ability to identify potentially geo-effective solar events?

**GA4.08/W/06-B3** **0905**

**MAGNETIC CLOUD INTERACTION WITH THE SOLAR WIND AND THE RELATION TO MAGNETIC STORMS**

Alisson DAL LAGO, Walter D. Gonzalez, Alicia L. Clua de Gonzalez and Luis E. A. Vieira (National Institute for Space Research, INPE, CP 515, Sao Jose dos Campos 12201-970, Sao Paulo, Brazil, e-mail: dallago@dge.inpe.br)

Magnetic clouds are interplanetary structures with a large rotation in the magnetic field direction, an enhanced field strength (typically >10 nT), a low proton temperature and plasma beta parameter, and a radial extent which takes about 24h to cross the spacecraft, near 1 AU. If the speed of the cloud is larger than the upstream slow solar wind plus the magnetosonic wave's phase velocity, a fast shock wave will form in front of the cloud. Using some previously reported magnetic cloud events we study the role of the static (thermal plus magnetic) pressure in the enhancement of the magnetic field strength inside the cloud, as it interacts with

the sheath region of the fast ejecta. The interaction between these clouds and other streams is also addressed. This reinforces the relation of this type of fast ejecta to intense magnetic storms. We observe that some slow non-shock magnetic clouds can also lead to intense storms if they are compressed by another high-speed stream.

**GA4.08/W/19-B3 0930**

**EXPANSION AND DECELERATION OF ICMES**

T. MULLIGAN and C. T. Russell (Institute of Geophysics and Planetary Physics and the Department of Earth and Space Sciences, University of California Los Angeles, USA, e-mail: tamitha@igpp.ucla.edu)

In order to predict the geomagnetic consequences of an ICME seen in advance of striking the Earth we must understand how it is evolving as it propagates. Observations of ICMEs show unambiguous evidence for expansion in their magnetic profiles. The rate of expansion can be deduced together with the size and orientation of the ICME for rope-like structures. The velocities of ICMEs can be measured twice by a single spacecraft. The velocity of the driven shock can first be estimated by the density comparison and then the velocity of the leading edge of the ICME can be measured. Sometimes the velocity of the trailing edge of the ICME provides a third measurement. These velocities can be used to estimate the deceleration or acceleration of ICMEs if expansion of the ICME is taken into account. We apply this formalism to a set of ICMEs observed by Pioneer Venus including those associated with specific CME events observed in quadrature with coronagraphs.

**GA4.08/W/10-B3 Invited 1030**

**THE INTERPLANETARY ORIGIN OF INTENSE AND SUPERINTENSE GEOMAGNETIC STORMS AND OF INTENSE AND FREQUENT SUBSTORMS**

W. D. GONZALEZ, A. L. Clua de Gonzalez, A. dal Lago and L. E. Vieira (National Institute for Space Research, INPE, CP 515, Sao Jose dos Campos 12201-970, Sao Paulo, Brazil, e-mail: gonzalez@dge.inpe.br)

Around solar maximum, two interplanetary structures are important for the development of storms, involving an intense and long duration Bs component of the IMF: the sheath region behind the forward shock of a fast CME, and the CME ejecta itself. Frequently, these structures lead to the development of intense storms with a two-step growth in their main phases. These structures also lead sometimes to the development of very intense storms, especially when an additional streams involved. The second stream can compress the primary cloud, bringing with it additional Bs structures. Thus, at times very intense storms are associated with three or more Bs structures. We also discuss evidence that magnetic clouds with very intense core magnetic fields tend to have large velocities, thus implying large amplitude interplanetary electric fields that can drive very intense storms.

During solar minimum, high field regions called Corotating Interaction Regions (CIRs) are created by the interaction of fast streams (emanating from coronal holes) with low speed streams associated with the heliospheric current sheath. However, because the Bs component is typically highly fluctuating within the CIRs, the related storms have weaker strengths, although intense substorms can develop. Frequently, high speed streams are accompanied by long-duration and large-amplitude Alfvénic fluctuations, with their Bs component causing intermittent reconnection. The intense, continuous and long duration auroral activity associated with these fluctuations is called High-Intensity Long Duration and Continuous Auroral Activity (HILDCAAs).

**GA4.08/E/17-B3 1105**

**REPLY OF THE GEOMAGNETIC FIELD TO THE SOLAR WIND VARIATION DURING STORM TIME**

Maria Andrea VAN ZELE and Otto Schneider (both at Geofísica, Dto. de Ciencias Geológicas, Ciudad Universitaria, 1428 Buenos Aires, Argentina)

The dependence of the geomagnetic variation due to the symmetrical equatorial ring current during a storm is calculated from the Dst indices and the ram pressure of the solar wind. The dynamical process of the ring evolution is expressed by a linear differential equation; the non homogeneous part can be expressed with good agreement by a linear combination between the dawn-dusk component of a delayed interplanetary electric field Ey(IMF) and its derive Ey'(IMF). The model is tested on the basis of solar parameters recorded each 5 minutes, and magnetograms, for the first months of 1979. The characteristic time T (decay) is calculated for periods when Bz(IMF)0 (homogeneous equation). The term of the non homogeneous part depending of Ey(IMF) acts as a rectifier; if Bz(IMF)>0 the magnetosphere is a closed system and the plasmasphere allows the quick entry of particles or eject them if Ey is varying, as the AE indices show. The delay between the arrival of the solar wind at the magnetospheric nose and their influence on the ring is of some 60 minutes; while the factor accompanying Ey(IMF) is the same for the studied storms, the factor multiplying Ey'(IMF) varies slightly.

Wednesday 28 July PM

**GA4.08/E/07-B3 Invited 1300**

**ENERGETICS AND TOPOLOGY OF THE MAGNETOSPHERE DURING GEOMAGNETIC STORMS**

D.N. BAKER (Laboratory for Atmospheric and Space Physics, University of Colorado, Cam-pus Box 590, Boulder, Colorado, 80309-0590, USA, email: baker@lynx.colorado.edu)

Major geomagnetic storms represent a powerful extraction of energy from the solar wind flow and subsequent dissipation of that energy in many different forms. Ring current injection and decay, ionospheric Joule heating, particle precipitation into the atmosphere, and several other physical processes are exhibited rather clearly in large storm events. The modern-day constellation of operating spacecraft gives an unprecedented opportunity to study magnetic storm processes and energetics. This paper focuses on recent coronal mass ejection (CME) events that have been well-observed near the sun. These disturbances are followed from the sun to their arrival in near-Earth space. The reconfiguration of the magnetosphere under the driving influence of CME/magnetic clouds is examined and the energetics of various forms of input and output are assessed. It is concluded that a good understanding can be obtained of magnetospheric configuration changes and energy flow using space-based and ground-based observations.

**GA4.08/W/05-B3 1335**

**FACTORS AFFECTING THE INTENSITY OF THE STORM-TIME RING CURRENT**

M. F. THOMSEN (Space and Atmospheric Sciences, Los Alamos National Laboratory, Los Alamos, NM 87545, USA, Email: mthomsen@lanl.gov), J. P. Smith (University of Texas, Austin, TX), J. E. Borovsky (Los Alamos National Laboratory, Los Alamos, NM; Email: jborovsky@lanl.gov), and M. R. Collier (Goddard Space Flight Center, Greenbelt, MD)

The relationship between the strength of the storm-time ring current and several potential source-strength parameters is explored for a number of geomagnetic storms that have occurred over the last few years. A good correlation is found between the maximum value of abs(Dst\*) (Dst\* =Dst corrected for magnetopause currents) in each storm and the plasma-sheet density observed at geosynchronous orbit during the 12 hours preceding the storm maximum. A similar comparison of abs(Dst\*) with interplanetary parameters shows that abs(Dst\*) is significantly and independently correlated with the eastward interplanetary electric field and the solar-wind density, with optimal time lags of less than one hour and five hours, respectively. A consistent picture emerges from these results in which the solar wind feeds the near-earth plasma sheet on a time scale of about 5 hours, and that enhanced magnetospheric convection caused by an increased eastward interplanetary electric field leads directly to the injection of this source population into the ring current region.

**GA4.08/W/02-B3 1400**

**A STUDY OF TWO-STEP MAIN PHASE MAGNETIC STORMS**

L. E. VIEIRA, W. D. Gonzalez, A. L. Clua de Gonzalez and A. Dal Lago (National Institute for Space research, INPE, CP 515, Sao Jose dos Campos 12201-970, Sao Paulo, Brazil, e-mail: eduardo@dge.inpe.br)

It has been recently shown that a substantial fraction of intense geomagnetic storms have their main phases with a two-step development, that is, before the ring current has decayed significantly to the prestorm level, a new major particle injection occurs, leading to a further development of the ring current, and making Dst decrease a second time. Also, most of the interplanetary structures that cause these storms have been observed to be magnetic clouds, in which the two-step main phase response corresponds to the two Bs (southward Bz component of the IMF) structures encountered in the sheath region ahead of the cloud and in the cloud itself. In this work we divide the clouds in two groups, concerning the rotation in the Bz component of the cloud. Thus, we investigate the difference in the geomagnetic response (peak Dst value) to the two types of clouds, one with a south-north (SN) rotation and the other with a north-south (NS) rotation. We expect a different response in peak Dst, because in the SN case the Bs field of the cloud comes much closer in time to the Bs field of the sheath region, than in the NS case.

**GA4.08/E/16-B3 Invited 1425**

**INTERPLANETARY AND MAGNETOSPHERIC ELECTRIC FIELDS DURING GEOMAGNETIC STORMS: WHAT IS MORE IMPORTANT, STEADY STATE FIELDS OR FLUCTUATING FIELDS?**

Y. KAMIDE (Solar-Terrestrial Environment Laboratory, Nagoya University, Toyokawa, Aichi-ken 442-8507, Japan, email: kamide@stelab.nagoya-u.ac.jp)

Most of the Dst variance during intense geomagnetic storms can be reproduced by changes in large-scale electric fields in the solar wind. A continuous controversy exists, however, as to whether the successive occurrence of substorms, i.e., magnetospheric electric fields, plays a direct role in the energization of storm-time ring current particles. This talk proposes that, during magnetic storms, the quasi-steady component of the interplanetary electric fields is important in enhancing the ring current, while changes in the solar wind electric fields are responsible for initiating magnetospheric substorms. Thus, in a Gedanken experiment, if we were to control the solar wind, generating purely steady southward IMF (interplanetary magnetic field), we would be able to create a geomagnetic storm during which no substorms occur.

**GA4.08/W/15-B3 1530**

**INTERBALL MULTI-SATELLITE OBSERVATIONS OF MAGNETOSPHERIC RESPONSE TO MAGNETIC CLOUDS**

Yu. I. YERMOLAEV, G. N. Zastenker, N. L. Borodkova, R. A. Kovrazhkin, N. S. Nikolaeva, M. N. Nozdachev, S. P. Savin, L. M. Zelenyi (Space Research Institute, Moscow 117810, Russia, Email: yermol@afed.iki.rssi.ru); Z. Nemecek, J. Safrankova (Charles University, Praga, Czech Republic); J.-A. Sauvaud (CESR/CNES, Toulouse, France)

Several results of statistical studies related to the interaction of interplanetary magnetic clouds with the Earth's magnetosphere as observed on the INTERBALL satellites during 1995-1998 are presented. Magnetosphere response to the clouds is usually the same as its response to the similar changes of solar wind and IMF parameters and the main cause of very strong magnetospheric disturbances is high pressure pulses on leading and trailing edges of clouds. Interactions of clouds with the magnetosphere results in its compression and deformation, large scale motions of the magnetic tail and initiations of storms and substorms. Several important consequences of these processes are (1) observations of magnetospheric regions and boundaries much closer to the Earth than on average; (2) increases of density and temperature in outer regions of magnetosphere; (3) multiple crossings of geomagnetic tail boundaries presumably due to tail flapping, and (4) bursty fluxes of high energy ions and electrons in the auroral region and polar cap. The work was supported in part by INTAS grant 96-2346.

**GA 4.08/E/22-B3 1555**

**ROLE OF HELICON MODES IN THE INJECTION OF OXYGEN IONS IN THE RING CURRENT**

G. S LAKHINA (Indian Institute of Geomagnetism, Colaba, Mumbai-400 005, India, email: lakhina@iig.res.in)

The presence of an ionospheric-origin anisotropic oxygen ion beam can excite a helicon mode instability in the near-Earth plasma sheet region. The helicon mode instability could be excited under the conditions when the usual long wavelength fire-hose modes are stable. The modes are likely to attain saturation as the typical e-folding time of the instability is about a few minutes in the near-Earth plasma sheet region. Therefore, the instability could significantly affect substorm dynamics and lead to enhanced ionosphere-magnetosphere coupling. Low-frequency turbulence produced by these modes could scatter electrons trapped in the inner central plasma sheet region and help excite the ion tearing modes, leading to substorm onset.

As a result the oxygen ions would be injected towards the Earth's nightside magnetosphere. Repeated injection by this process would lead to enhanced oxygen ions in the storm-time ring current.

**GA.08/W/11-B3 1620**

**THE GEOTAIL ORBIT MAY 12 TO 17, 1997 - AN OUTSTANDING EXAMPLE FOR SOLAR-TERRESTRIAL INTERACTION**

B. WILKEN, Q.G. Zong (Max-Planck-Institut fuer Aeronomie, D-37191 Katlenburg-Lindau, Germany, email: wilken@linmpi.mpg.de); T. Doke (Advanced Research Center for Science and Engineering, Waseda university, Tokyo, Japan); T. A. Fritz (Boston University, Boston, USA); M. Grand (Space Science Division, Rutherford Appleton Laboratory, Chilton, Didcot, Oxon, England); S.Livi, U. Mall (Max-Planck-Institut fuer Aeronomie, D-37191 Katlenburg-Lindau, Germany)

In the interval of interest the elliptical 8 x 30 Re Geotail orbit had a apogee in the undisturbed solar wind at about 1500 LT. On the outbound path, the spacecraft crossed the magnetopause at 0900 LT and bowshock 1030 LT. The interplanetary loop of the trajectory (outside the bow shock) started early 13 May and continued until the beginning of May 16 when Geotail passed the bow shock on the inbound leg at a local time position of 1800 LT. The inbound magnetopause crossing occurred at 1930 LT. Throughout the interplanetary segment Geotail observed the arrival of flare particles on April 12, the appearance of a CME on 15-16 May which appears to be intimately connected with a CIR. In addition, an energetic oxygen event was observed when Geotail approached the dusk magnetopause. This paper provides a global perspective of this interest interval.

**GA.08/E/01-B3 1645**

**PROBLEMS OF IONOSPHERIC F-LAYER STORMS**

Henry RISHBETH (Department of Physics and Astronomy, University of Southampton, Southampton SO17 1BJ, UK, email: hr@phys.soton.ac.uk)

The effects of geomagnetic activity on the ionospheric F-layer are complex and difficult to understand in detail. The most striking changes are the large decreases of F-layer electron density during large magnetic storms. The well-catalogued "initial-phase" and "main-phase" effects in F-layer storms are well on the way to being understood, it being widely accepted that changes of neutral air composition play a big part in at least the "main-phase" changes of electron density. Many intriguing problems remain, however, for example how storm effects depend on solar activity, to what extent they might be predictable, and the response of the F-layer to low levels of magnetic activity that cannot be classified as well-defined "storms".

Thursday 29 July AM

**GA.08/W/18-B4 Invited 0830**

**MAGNETOSPHERE-IONOSPHERE COUPLING: HOW DO OXYGEN IONS GET INTO THE STORM-TIME RING CURRENT AND WHY IS THERE A DELAY?**

HARLAN E. SPENCE (Boston University Center for Space Physics, 725 Commonwealth Avenue, Boston, MA 02215, email: spence@bu.edu), J. L. Roeder and J. F. Fennell (The Aerospace Corporation, P.O. Box 92957, Los Angeles, CA 90009), R. Friedel (Los Alamos National Lab, Mail Stop D-436, Los Alamos, NM 87545), T. A. Fritz (BU), and M. Grande (Rutherford Appleton Laboratory, Chilton, Didcot, Oxfordshire, OX11, OXQ, England)

During geomagnetic storms, the composition of magnetospheric ring current ions can change dramatically. The main phase of a storm is accompanied by the appearance of heavy ions, most notably oxygen. The heavy ions during storms can often contribute significantly to the total energy density of the hot magnetospheric ion population. At times it can be the predominant component of the total plasma pressure. Therefore, it plays an important dynamical role in the physical development of magnetic storms. In this presentation, we shall review the latest observations of heavy ions in the magnetosphere from data collected by the NASA/USAF CRRES satellite and most recently by the CAMMICE experiment on the NASA/POLAR satellite. We shall compare the heavy ion composition as a function of magnetic storm strength and prior activity history. One critical parameter, the time delay between magnetic storm onset and the arrival of energetic heavy ions into the ring current will be explored. Finally we shall assess the role of the ionosphere as a source for magnetospheric, energetic heavy ions and the physical mechanisms for ion transport.

**GA.08/W/13-B4 0905**

**ENERGETIC OXYGEN EVENTS IN THE MAGNETOSHEATH CAUSED BY GEOACTIVITY**

Q.G. ZONG, B. Wilken (Max-Planck-Institut fuer Aeronomie, D-37191 Katlenburg-Lindau, Germany, Email: zong@linmpi.mpg.de), T. Doke (Advanced Research Center for Science and Engineering, Waseda university, Tokyo, Japan) T. A. Fritz (Boston University, Boston, USA), M. Grand (Space Science Division, Rutherford Appleton Laboratory, Chilton, Didcot, Oxon, England) S.Livi, U. Mall (Max-Planck-Institut fuer Aeronomie, D-37191 Katlenburg-Lindau, Germany), D. J. Williams (The Johns Hopkins University, Johns Hopkins Road, Maryland, USA)

On 26 January 1994, two energetic oxygen ion bursts were observed in the dayside magnetosheath when the spacecraft was located at (4.3, 16.3, 0.7) R<sub>e</sub>. The oxygen enhancements peaked at energies of about 260 keV. The commencement of the two impulsive flux increases at 1405 and 1440 UT are delayed by about 15 minutes relative to the onset of two substorm injections at 1349 and 1422 UT. On 10 January 1997, the impact of a CME led to a moderate storm (Dst = -84 nT). Throughout the early phase of the storm Geotail was skimming the afternoon magnetopause and observed energetic oxygen intensities persisting for 150 min. The angular distributions of these ions are rather anisotropic. The oxygen events are characterised by strong impulsive increases in the flux whereas energetic protons and helium ions were essentially absent. These observations suggest that heavier energetic ions can leak out of the dayside magnetosphere into the magnetosheath during magnetospheric activity.

**GA.08/W/03-B4 Invited 0930**

**DEVELOPMENTS, POSSIBLE INTERACTIONS, AND DECAY OF THE MAGNETOSPHERIC RING CURRENT AND THE MAGNETOTAIL CURRENTS**

J.U. KOZYRA, C.R. Clauer, T.I. Gombosi, M.W. Liemohn, J. Lande, D.L. DeZeeuw, C.P.T. Groth, K.G. Powell (University of Michigan, Ann Arbor, Michigan 48109-2143 USA, email: jukozyra@engin.umich.edu)

The Dst-index, corrected for the effects of magnetopause currents, has commonly been used to track the development and decay of the ring current during magnetic storms. In-situ observations of energetic ring current ions imply that the Dst index may not always monitor

changes solely in the ring current but may reflect important contributions from other current systems. Recent studies examining the relationship between the symmetric ring current, the partial ring current, and the magnetotail current, and their relative contributions to the Dst-index, are reviewed. To examine the possible advantages of more complete local time magnetic field information, a drift-loss model of the ring current is used to calculate the local-time-dependent depression in the surface magnetic field due solely to the ring current during its development and decay. These model-generated magnetic field signatures are compared to observations from a longitudinal chain of 18-20 mid-latitude magnetometers. Contributions from various current systems are identified in the magnetometer data on the basis of characteristic spatial and temporal signatures. A local-time-averaged magnetic field depression is derived from this data and compared to the modelled and observed Dst-indices. Finally, an investigation of the magnetic signature at the Earth's surface of the partial ring current and tail currents, and their strength relative to the ring current contribution, is made using the BATS-R-US global MHD model. Since there are some events in which the velocity (V) and the number density (N) values in the cloud change substantially with respect to those in the nearby structures, we address the role of the dynamic pressure (1/2NmV<sup>2</sup>) in the overall pressure distribution.

**GA.08/W/14-B4 1035**

**PROPOSAL OF A SET OF DST-AFFILIATED INDICES FOR IMPROVEMENT OF MAGNETIC STORM INTENSITY REPRESENTATION**

Masahisa SUGIURA (Research Institute of Science and Technology, Tokai University, Tokyo 151-0063, Japan, email: sugiura@jspan.kugi.kyoto-u.ac.jp) Toyohisa Kamei (Graduate School of Science, Kyoto University, Kyoto 606-8512, Japan, email: toyo@kugi.kyoto-u.ac.jp)

In the recent years, considerable attention has been paid to the relationship between solar wind parameters and magnetic storms and/or substorms. The relationship between magnetic storms and substorms still remains to be an unsettled problem. In the studies of these subjects and also in the investigations of various disturbance phenomena, the Dst and AE indices are frequently used as numerical parameters representing the intensities of magnetic storms and substorms, respectively. However, by definition, the Dst index expresses only the axially symmetric component in the Fourier expansion of the low latitude disturbance magnetic field on the earth's surface with respect to local time. In the development phase to the maximum phase of magnetic storms, especially in intense magnetic storms, higher harmonic components are generally not negligible. A proposal is made to make a set of parameters affiliated with the conventional Dst index available to the scientific community to improve magnetic storm representation for the studies on various aspects of magnetic storms. Using the proposed parameters, a statistical and case investigation of axially asymmetric magnetic storm fields is made, giving attention to the phases of the higher harmonics. Relations to other disturbance phenomena are also discussed in the context of this set of parameters.

**GA.08/W/09-B4 1105**

**THE GEOTAIL AND RING CURRENT DYNAMICS UNDER DISTURBED CONDITIONS**

V.V. KALEGAEV (Institute of Nuclear Physics, Moscow State University, 119899 Moscow, Russia)

The magnetospheric magnetic field is highly time-dependent and may undergo rapid changes (magnetospheric substorms and geomagnetic storms). These are events during which the most interesting magnetospheric physics phenomena (auroras, precipitations at high latitudes, acceleration of particle beams in the geotail etc.) occur. The dynamics of magnetospheric large-scale current systems was studied for the case of magnetic storm on 23-27 November 1986 using the dynamic paraboloid model and data of on-ground and satellite measurements. A set of "submodels" calculating the magnetospheric current systems response to the changes in solar wind conditions was developed. The magnetic field variations at the Earth's surface as well as on the geostationary orbit are calculated and compared with the Dst and GOES 6 measurements respectively. Comparison of independently obtained magnetopause currents, ring current and geotail currents contributions into Dst shows that they are about one order. The energy stored in geotail is calculated in terms of paraboloid model. It correlates strongly with the energy flow in the magnetosphere generated by solar wind - magnetosphere dynamo. The total energy of ring current particles is calculated using data of AMPTE/CCE measurements. It was shown that this energy increases when auroral activity diminishes. During substorm activity energy stored in the magnetotail transports mainly to the auroral ionosphere.

Thursday 29 July PM

**GA.08/E/18-B4 Invited 1300**

**F-REGION RESPONSE TO GEOMAGNETIC DISTURBANCES**

A.D. DANILOV (Institute of Applied Geophysics, Rostokinskaya 9, Moscow 129 128, Russia)

The F2-region response to geomagnetic disturbances usually called an ionospheric storm is a rather complicated event. It consists of so called positive and negative phases, which have very complicated spatial and temporal behaviour. During the recent decade there was a significant progress in understanding of this behaviour. The principal features of the positive and negative phase distribution and variations have been explained on the basis of the principal concept: during a geomagnetic disturbance there is an input of energy into the polar ionosphere, which changes thermospheric parameters, such as composition, temperature and circulation. Composition changes directly influence the electron concentration in the F2 region. The circulation spreads out the heated gas to lower latitudes. The conflict between the storm-induced circulation and regular one determines spatial distribution of the negative and positive phases in various seasons. There are still problems unsolved. The most acute ones are: the appearance of positive phases before the beginning of a geomagnetic disturbance, occurrence of strong negative phases at the equator, the role of vibrationally excited nitrogen in forming the negative phase, the relation of positive phases to the dayside cusp.

**GA.08/E/06-B4 1335**

**A REVIEW OF THE EFFECTS OF GEOMAGNETIC STORMS ON THE HIGH AND MID-LATITUDE THERMOSPHERE AND IONOSPHERE**

DAVID REES (CASS, Utah State Univ. Utah State University, Logan, UT 84322-4405, USA). Email: walnut1@easy.net.co.uk.)

During geomagnetic storms, the interaction of the solar wind with the magnetosphere generates a large and highly variable, inflow of energy and momentum through the combination of intense Joule and particle heating, and through momentum coupling from the rapidly-motion of ionospheric plasma to the neutral gas via ion drag. At times of very large geomagnetic disturbances, the auroral oval expands equatorward, sometimes penetrating to 45° magnetic latitude, or even lower. The large and complex disturbances generated within



the high-latitude thermosphere may be seen as large increases of temperature, density, major changes of neutral composition, while very rapid wind flows and large amplitude waves are also generated which may subsequently propagate creating truly global effects. Gross disturbances of the global ionosphere usually accompany these thermospheric disturbances. The ionosphere not only reacts to changes thermospheric density, composition and flows, but also to changes of ionisation sources and processes directly exciting ions and electrons. Observations describing the nature and scale of disturbances of the thermosphere and ionosphere during geomagnetic storms will be evaluated, using appropriate numerical simulations by global coupled models, highlighting the distinct roles of energetic, dynamical and chemical coupling between the thermosphere and ionosphere.

GA4.08/E/05-B4

1400

#### HEIGHT PROFILE OF THE EFFECT OF GEOMAGNETIC STORMS BETWEEN THE IONOSPHERE MAXIMUM AND THE TROPOSPHERE

Jan LASTOVICKA (Institute of Atmospheric Physics, Bocni II, 141 31 Prague 4, Czech Republic, email: jla@ufa.cas.cz); Alexei D. Danilov (Institute of Applied Geophysics, Rostokinskaya str. 9, 129226 Moscow, Russia, email: hcicag@sunny.aha.ru)

A geomagnetic storm is a complex process. Its various features act at different heights. In the F2 region, the mid-latitude effect is basically an ionospheric response to storm-induced changes in the neutral atmosphere, which are primarily a consequence of a strong Joule heating of the auroral thermosphere. At lower heights, the role of ionization and photochemistry processes increases due to shorter electron lifetime. At the base of the F1 region ( $h \sim 160-170$  km), the storm effect is almost absent. Further down, the most pronounced feature is the filling in the valley between E and F regions. At E-region maximum a complex action of several factors results in a slight decrease of foE, even though below and above the electron density increases. Further down, in the lower ionosphere, a large increase of electron density is observed as a consequence of a very large increase of particle precipitation. In the neutral upper middle atmosphere, the effects of enhanced particle precipitation weaken with decreasing altitude and become insignificant and/or absent in the stratosphere. The effect of geomagnetic storms re-appears in the lower atmosphere, but as an effect of different morphology and origin. The most promising mechanism seems to be at present Tinsley's hypothesis of "electrofreezing". Thus, we find three height regions of distinctly different processes: (1) F2-region, where the ionospheric effect is basically a response to storm-time changes of the neutral thermosphere, (2) the lower ionosphere and upper middle atmosphere, where the effects are caused by storm-related precipitation of energetic particles, (3) the lower atmosphere, where the effect is possibly related to changes in galactic cosmic rays and atmospheric electricity.

GA4.08/P/02-B4

1425

#### IONOSPHERIC STORM EFFECTS AT MILLSTONE HILL DURING THE GEOMAGNETIC STORMS OF 5-14 JUNE 1991: COMPARISON OF THE IZMIRAN MODEL RESULTS AND DATA

A V PAVLOV (Institute of Terrestrial Magnetism, Ionosphere and Radio Wave Propagation of the Russia Academy of Science, Troitsk, Moscow Region, 142092, Russia)

This study compares measurements of the ionospheric F region at Millstone Hill during the severe geomagnetic disturbances of 5-14 June 1991 with results from the IZMIRAN time-dependent mathematical model of the Earth's ionosphere and plasmasphere. The inclusion of the measured exospheric temperature in the MSIS-86 model and the atomic oxygen correction factors improves the agreement between the modelled and measured NmF2 and electron temperatures. Anomalously low values of the F-peak altitude seen as a "G condition" on ionograms and observed on June 5, 10, and 13 exist in the ionosphere due to wind-induced plasma drift velocities, when a poleward wind forces O<sup>+</sup> ions to lower altitudes where the increased recombination rate decreases [O<sup>+</sup>] and increases [NO<sup>+</sup>] and [O<sub>2</sub><sup>+</sup>]. The increases in the O<sup>+</sup>(4S) + N<sub>2</sub> loss rate due to vibrationally excited N<sub>2</sub>(v) and O<sub>2</sub>(v) lead to the decreases in the daytime F2 peak electron density up to a factor of 2 and 1.4 respectively. The difference between the non-Boltzmann and Boltzmann distribution assumptions of O<sub>2</sub>(v) and between ion and neutral temperature can lead to an increase up to about 7% or a decrease up to about 8% of the calculated NmF2 and to changes of the electron temperature up to 300 K as a result of an increase or a decrease of the loss rate of O<sup>+</sup>(4S) ions and the electron cooling rate. The IZMIRAN model uses the new cooling rate of thermal electrons by electron impact excitation of fine structure levels of atomic oxygen based on the revised excited cross sections (Bell et al., Monthly Notices of the Royal Astronomical Society, 293, L83-L87, 1998). It is found for the first time that this cooling rate is not one of the dominant electron cooling processes in the F region of the ionosphere.

GA4.08/E/03-B4

1520

#### F1 LAYER AT GEOMAGNETICALLY DISTURBED TIME AT LOW SOLAR ACTIVITY AS MEASURED AT PRUHNICE STATION

D. BURESOVA (Institute of Atmospheric Physics, Bocni II, 141 31 Prague Czech Republic, e-mail: buresd@ufa.cas.cz)

This paper attempts to demonstrate the changes of the F1 layer main parameter and structure during geomagnetic storms. To analyse F1 region behaviour we have selected ten periods of rather strong geomagnetic activity (5<Kp<8) with similar course and with at least three 91 quiet 91 days before the event for different seasons from 1994 - 1996. The electron density profiles for these periods, derived from all available hourly ionograms from Pruhonice station (50B0N, 15B0E) were analysed to investigate electron density variability of the F1 layer. Seasonal differences and a diurnal asymmetry of the effects in the F1 layer are presented. The storm negative influence in NmF2 appears to be much stronger in the morning than in the afternoon hours, mainly for spring, geomagnetically disturbed time. We have 921 found a significant effect of geomagnetic storm in electron density in the F1 region in spring while there is a substantial effect in autumn at 180 and 190 km heights. We have compared our results with these obtained from ionograms from some other European ionospheric stations. In general, the F1 layer appears to be much more stable during geomagnetic storms than the F2 layer.

GA4.08/W/01-B4

Invited

1545

#### GEOMAGNETIC FIELD MODELLING FOR MAGNETIC STORMS AND ITS COMPARISON WITH OBSERVATIONS

Igor. ALEXEEV (Institute of Nuclear Physics, Moscow State University, Moscow, 119899, Russia, email: alexeev@dec1.npi.msu.su); Yasha Feldstein (Institute of Terrestrial Magnetism, Ionosphere, and Radio Wave Propagation of the Russian Academy of Science, Troitsk, 142092, Russia, email: gromova@izmiran.rssi.ru)

The main topics which will be discussed: a) the development of the dynamic paraboloid magnetospheric model; b) the usage of this model for calculation of contributions of Chapman-Ferraro current, the ring current, and currents in the tail plasma sheet to the ground magnetic field variations during magnetic storms; and c) investigation of auroral electrojets dynamics, behavior of boundaries of plasma precipitation and usage the paraboloid magnetic field model for revelation of the interrelationship between geomagnetic phenomena at low altitudes and large-scale magnetospheric plasma structure. Key parameters of the model, ground state of the magnetosphere and its energy were determined. Input model parameters were determined by the solar wind velocity and density, IMF strength and direction, tail lobe magnetic flux value of F<sub>10</sub>, and total energy of ring current particles. The characteristic boundaries of the auroral particle precipitation, determined based on DMSP particle measurements, were used to calculate a value of F<sub>10</sub>. The influence of the field-aligned, tail and ring currents on the magnetospheric magnetic field structure was studied. It was found that the polar cap area is strongly controlled by the tail current. The paraboloid model was used for mapping the electrojet center and boundaries into the magnetosphere, and the study of the relationship between electrojets and magnetospheric plasma domains during magnetic storms. Analysis of magnetic field variations during magnetic storms shows that the contribution of the ring current, tail current and magnetopause currents to the Dst variation are roughly equal.

GA4.08/W/16-B4

1610

#### TEMPORAL AND SPATIAL DEVELOPMENT OF THE RING CURRENT DURING MAGNETIC STORMS INFERRED FROM GROUND MAGNETIC DATA

C. R. CLAUER, J. Lande, J. U. Kozyra, M. Liemohn (Space Physics Research Laboratory, University of Michigan, Ann Arbor, MI 48109-2143, USA, email: rclauer@umich.edu)

The Dst-index is traditionally utilized to characterise the development and decay of the ring current during magnetic storms. This index, however, has many shortcomings, which have been discussed by a number of authors in recent meetings and papers. For example, the tail current, partial ring current, and magnetopause boundary currents all make contributions to the disturbance field which do not necessarily cancel, nor which are adequately corrected for in creating Dst. In addition, the ring current development and decay processes are not symmetrically distributed and do not necessarily produce a symmetric ring current. Thus, it is important to undertake the analysis of the low latitude storm-time magnetic disturbance field in both high temporal and spatial resolution. Using data from a longitudinal chain of 18 to 20 middle altitude magnetic observatories, we investigate the world-wide disturbance field during several magnetic storms. We find both symmetric and asymmetric development and decay of the magnetic disturbance field. Comparisons with theory are obtained by comparison with results obtained using the Ring current Atmospheric Interaction Model to compute and track the local time dependent depression of the surface magnetic field through the same events.

GA4.08/W/12-B4

1635

#### INFLUENCE OF SHOCK-INDUCED IONOSPHERIC CONDUCTIVITY ENHANCEMENTS ON STORM MAIN PHASE INTENSITIES

B. TSURUTANI, X.-Y. Zhou, J.K. Arballo, and D. Winterhalter, (Jet Propulsion Laboratory, California Institute of Technology, Pasadena, 91109, email: btsurutani@jplsp.jpl.nasa.gov) T. Araki (Kyoto University, Dept of Geophysics, Kyoto 606, Japan); H. Yang (National Institute of Polar Research, Tokyo, Japan); G. Rostoker (University of Alberta, Edmonton, Alberta, Canada T6G 2J1); T. J. Hughes (Canadian Space Agency, PO BOX 7275, Vanier, ON, Canada K1L 8E3) R. P. Lepping and D. Berdichevsky (Goddard SFC, Code 695.0, Greenbelt, MD 20771) W. D. Gonzalez (INPE - CAIXA Postal 515, 12200 Sao Jose Dos Campos, Sao Paulo, Brazil)

Interplanetary shocks lead to SIs and SSCs (SIs with following magnetic storm main phases). It is well known that the IMF BS within the interplanetary sheaths and magnetic clouds lead to strong magnetic reconnection and the main phases of magnetic storms. However, the shocks themselves can cause enhanced dayside aurora and nightside pseudobreakups (PBs) and substorm expansion phases. Interplanetary shocks compress the outer magnetosphere, lead to adiabatic compression of pre-existing magnetospheric plasma, and loss of particles to the ionosphere by the loss cone instability. The particle loss is associated with the auroral light intensification and also enhanced ionospheric conductivity.

The latter effect, enhanced ionospheric conductivity, may influence the intensity of the magnetic storm main phase, which follows. We examine the WIND 1997 interplanetary shocks to study dayside aurora, nightside PBs and substorms. We will comment on the ionospheric effects on later storm main phase intensities using specific examples.

Wednesday 28 July AM

GA4.08/E/20-B3

Poster

0900-01

#### RELATIONSHIP BETWEEN THE SOLAR SOURCES OF INTERPLANETARY PLASMA STREAMS AND TYPES OF LONG AURORAL DISTURBANCES

M.G.GELBERG, S.Z.Kershengolz, S.V.Sharaeva (Institute of Cosmophysical Research and Aeronomy, 31 Lenin Ave., 677891 Yakutsk, Russia, email: lae@sci.yakutia.ru)

The influence of four solar sources: suddenly disappearing filaments (SDF), coronal holes (CH), heliospheric current sheet (HCS) and solar flares (sf) on the development of four types of long (>10 h) auroral disturbances (HILDCAA) for 51 events are investigated. At the analysis the classifications of interacting streams of interplanetary plasma (by K.G. Ivanov) and HILDCAA (by the authors) are used.

It is shown that SDF streams creates the second type HILDCAA, for CH and HCS stream classes the first type HILDCAA predominate, sf-streams causes the third type HILDCAA. It is found that in interacting of interplanetary plasma streams from a few solar sources, the total intermixing of streams near the Earth's orbit did not occur. It is found that if SDF stream interacted with the streams from other solar sources, then in auroral zone the second type HILDCAA was developed. Sf-streams probably are less dominated in the streams of mixed classes.

The fourth type of HILDCAA coinciding with the stationary convection periods is observed only one time, 16.08.78, when the Earth crossed the SDF+CH streams, but the probability of its appearance is about 0,25. Its absence in the considered events testifies to the non-completeness of classification of interplanetary plasma streams and their solar sources by K.G. Ivanov.

GA4.08/E/11-B3

Poster

0900-02

#### DISTRIBUTION OF HILDCAA OF DIFFERENT TYPES FROM SEASON TO SEASON AND IN A SOLAR ACTIVITY CYCLE

M.G. GELBERG, S.Z. Kershengolz, S.V. Sharaeva (Institute of Cosmophysical Research and Aeronomy, 31 Lenin Ave., 677891 Yakutsk, Russia, email: lae@sci.yakutia.ru)

A possibility to classify the long auroral disturbances (HILDCAA) into four types by using

minute values of auroral indices has been shown. The variations of HILDCAA appearance frequency of each type from season to season and in a solar activity cycle are investigated on data of auroral indices for the period of 1978-1993. It is found that a probability of appearance of the first type HILDCAA has two maxima in spring and in autumn, and minima - in summer and in winter. The distribution of the appearance frequency of the fourth type HILDCAA has a wide maximum in the period from April to August, and for the remaining months of an year it is equal to 1/4 of maximum one. In seasonal distributions for the second and third types a clear minimum in June and growth of the probability of HILDCAA appearance to the winter months are found.

The analysis of distribution of the appearance probability of different type disturbances of HILDCAA in a solar activity cycle shown that appearance frequency of the first and fourth types was maximum in years of maximum solar activity, and for the second and third types - at the minimum solar activity.

**GA4.08/W/22-B3** Poster **0900-03**

**HELIOSPHERIC EVENTS AND DEVELOPMENTS OF GEOMAGNETIC STORMS**

BADRUDDIN

Abstract not available at time of going to press

**GA4.08/P/01-B3** Poster **0900-04**

**PERIODICITIES IN GEOMAGNETIC STORMS AND SOLAR ACTIVITY CYCLE**

Probas RAYCHAUDHURI (Department of Applied Mathematics, Calcutta University, Calcutta 700 009, India email: prc@cucc.ernet.in)

Geomagnetic storms are large disturbances in the Earth's magnetosphere, often sustaining for several days or more. During the period of geomagnetic storms, the magnetic field measured at the surface of the Earth perturbed by strong electric field flowing within both the magnetosphere and ionosphere, the aurora brightness and extends to low magnetic latitudes, and intense fluxes of charged particles are generated within the magnetosphere. Periodicities in geomagnetic storms are of very much interest to us because of their adverse effects on radio communications, satellite systems and power grid etc. In this paper we have studied 173 geomagnetic storms data which are related with the Forbush decreases (FD) for the years 1976-1986 and have found that geomagnetic storms data exhibit periods around 1.5, 2.38, 4.81 and 7.56 years at 99% confidence level (CL). We have studied also FD with solar flare data and major solar proton events (SPE) data ( $E > 10$  MeV) for the years 1976-1986 and have found that FD, solar flare data exhibit periods around 0.95, 2.4 and 4.75 years at 99% CL, while SPE data exhibit periods around 2.6 and 5.0 years at 95% CL. We expect also that coronal mass ejections (CMEs) have the same periodic behaviour as SPE data, geomagnetic storms data etc. are associated with CMEs. Common periodicity around 2.5 years of solar neutrino data, sunspot number data, FD data, major solar proton events data, geomagnetic storms data etc. suggest that they behave similarly and may have a common origin.

**GA4.08W/04-B3** Poster **0900-05**

**THE ENERGY INPUT TO THE AURORAL REGION DURING TWO TYPES OF GEOMAGNETIC STORMS**

L.P.SHADRINA and V.G.Vasilieva (Institute of Cosmophysical Research and Aeronomy SB RAS, 31 Lenin ave., Yakutsk, 677891, Russia email: l.p.shadrina@sci.yakutia.ru)

The geomagnetic storms for the period from 1973 to 1986 was examined. It is shown, that during two types of storms, differs by the numerical parameter  $b = (DDst / SAE)$ , the energy input to the auroral region has an essential distinctions. During first type storms (with  $b > 0.02$ ) the energy enters to the auroral activity by impulsive processes. This display both in auroral oval dynamics and in auroral indices behaviour. Second type of storms (with  $b < 0.01$ ) accompanies by gradual energy input to the auroral zone. It is proposed, that the cause of this difference is a high values of interplanetary magnetic field variability  $sH$  during first type of geomagnetic storms.

**GA4.08/W/17-B3** Poster **0900-06**

**THE DISTRIBUTION OF ENERGETIC OXYGEN EVENTS IN THE MAGNETOSHEATH**

Q.G. ZONG, B. Wilken (Max-Planck-Institut fuer Aeronomie, D-37191 Katlenburg-Lindau, Germany Email: zong@linmpi.mpg.de)

GEOTAIL observations with the HEP-LD spectrometer in the dayside magnetosheath between Jan. 1996 and Dec. 1997 have been examined with respect to the occurrence of bursty oxygen events. The oxygen observed in these events has an energy from 140 to 4000 keV, the origin is thought to be terrestrial. Without exception the bursts are observed in association strong geomagnetic activity (magnetic storms or substorms). The occurrence frequency of oxygen burst events exhibits a strong dawn-dusk (GSE Y axis) symmetry. All oxygen events have been detected in the duskside magnetosheath. Since these oxygen ion events in the magnetosheath are strongly related to magnetic storms, it is thus suggested that the oxygen ions may escape from the ring current via a dayside reconnection or leakage process.

**GA4.08/W/24-B3** Poster **0900-07**

**MAGNETICS FIELD IN THE STORM TIME MAGNETOSPHERE**

FESHCHENKO and Malstev

Abstract not available at the time of going to press

**GA4.08/W/08-B3** Poster **0900-08**

**STORM-SUBSTORM RELATIONSHIP: THE "MAIN" SUBSTORM**

Lyudmila V. TVERSKAYA (Skobeltsyn Institute of Nuclear Physics, Moscow State University, Moscow, 119899, Russia, email: tverskaya@tasped.npi.msu.ru)

Development of the concept of the "main" substorm has a long history. It has started in 70-s as far as was shown the shift of the west electrojet to L-3 at the main phase of a strong magnetic storm. All published cases of direct observations of the ring current asymmetry were analysed. To the day, just one case has been registered on a time scale compared with substorm duration (~1 hour). As appears, in that case the night-day asymmetry of the main-phase ring current measured near the equatorial plane has a sign opposite to that calculated from the low-latitude magnetic stations' data. This effect was explained as a result of distortion

of Dst-variation by the strong polar electrojets and it was observed in several storms. Last year a substorm that is characterised by the lowest latitude position of the auroral electrojets during the main phase of a storm has been called the "main" substorm. As is shown for many storms, electrojets reach their lowest latitude position some hours before  $|Dst|$  reaches its maximum. Various approaches to the study of an empirical dependence of the west electrojet position (Lw) on Dst amplitude are compared. The formula that well describes this dependence in whole range of the storm Dst amplitudes (50 - 600 nT) is:  $|Dst| = 27500 / (Lw)^{1.4}$ . Contribution of "main" and other substorms to the formation of the storm ring current is discussed.

**GA4.08/E/02-B3** Poster **0900-09**

**INTERPLANETARY AND GEOMAGNETIC PRECURSORS OF FORTHCOMING GEOMAGNETIC STORMS**

K.G.IVANOV, E.P.Romashets, and V.G.Petrov (Institute of Terrestrial Magnetism, Ionosphere and Radio Wave Propagation of Russian Academy of Sciences (IZMIRAN); Troitsk, Moscow Region, 142092 Russia, email: romash@izmiran.rssi.ru)

Three phase dynamics of the interplanetary and geomagnetic disturbances is usual during the Earth's voyage through the coronal streamer belt. As a rule, a broad region just ahead of a forward interplanetary shock wave is responsible for the first (growth) phases of such disturbances (heliospheric substorms).

These regions and their geomagnetic effects may be considered as precursors of forthcoming more intensive disturbances. The MHD structure of typical interplanetary precursors (January 4-5 and May 14, 1997 ISTP events) and their geomagnetic effects will be considered.

**GA4.08/E/10-B3** Poster **0900-10**

**LOW-FREQUENCY OSCILLATIONS BEFORE RECURRENT HIGH-SPEED FLOWS - THE POSSIBLE FORERUNNERS OF MAGNETIC STORMS.**

Olga KHABAROVA (Department of Solar-Terrestrial Physics, The Institute of Terrestrial Magnetism, Ionosphere and Radiowaves Propagation, Russia 142092, Moscow region, Troitsk; email: MARYL@izmiran.troitsk.ru)

Steady long-period (from minutes till hours) oscillations of solar wind components before high-speed flows are considered. The conditions of their origin and consequent effect on the magnetic field of the Earth are discussed. 10 high-speed with most precisely exhibited such oscillations are chosen. It is found out, that the oscillations of various periods have a various nature, in the main they appear due to large-scale instabilities. The most low-frequency oscillations are registered in region of orbit of the Earth before recurrent high-speed flows from coronal holes. The calculations show, that they are evoked by gradient instabilities of solar wind plasma near high-speed flow. For the half of selected flows there are data about practically simultaneous registration of magnetic field of the Earth oscillations of close frequencies (range Pc6). Thus, it is possible to assume, that considered long-period oscillation can excite the oscillations of geomagnetic field and to be forerunners of magnetic storms.

**GA4.08/E/09-B3** Poster **0900-11**

**MAGNETIC STORM EFFECTS ON EQUATORIAL ELECTROJET CURRENT**

R.G.RASTOGI, (Department of Physics, Gujarat University and Physical Research Laboratory, Ahmedabad 380 009 India, email: parvs@prl.ernet.in)

It has been shown that every one of the aspects of a magnetic storm i.e. storm sudden commencement (SSC), storm time variation (Dst), and disturbance daily variation (SD) in all the three D, H and Z components of the geomagnetic field at low latitudes has a characteristic special signatures of the equatorial electrojet. Distinct longitudinal inequalities in these storm effects are identified with some non-dipole characteristics of the earth's magnetic field. The preliminary negative impulse in SSC(H) at equatorial latitudes are shown to be related to the IMF changes during the impact of solar plasma with the earth's magnetosphere.

**GA4.08/E/08-B3** Poster **0900-12**

**MAGNETIC DISTURBANCE EFFECTS ON DECLINATION AT LOW AND MIDDLE LATITUDES**

RASTOGI, R.G. and M.E.James (Department of Physics, Gujarat University, Ahmedabad 380 009, India Winch, D.E., School of Mathematics and University of Sydney, Sydney NSW Australia)

The Eastward component (Y) at geomagnetic field at low and middle latitudes are studied for storm time and disturbance daily variations. Storm time (Dst) variations in Y are shown to faithfully follow the corresponding variations of Dst variations of H field at equatorial and low latitudes. Significant longitudinal effects are isolated in the disturbance effects in Y field. Quantitative explanations are given for the observed effects at different longitudes around the earth. It is concluded that the disturbance ring current cannot be considered as axially symmetric for explaining the observed storm time effects on ground magnetic fields.

**GA4.08/E/21-B3** Poster **0900-13**

**FIELD -ALIGNED CURRENTS AS SEEN BY THE POLAR AND INTERBALL -2 DURING 11 JANUARY 1997 EVENT**

A.Z. BOCHEV 1, Guan Le 2, V.G. Petrov 3, D.L. Danov 1, Y.L. Feldstein 3, P.T. Newell 4 1 Solar - Terrestrial Influences Laboratory, BAS, Sofia, Bulgaria 2 Institute of Geophysics and Planetary Physics, Los Angeles, USA 3 Institute of Earth's Magnetism and Radiowave Propagation (IZMIRAN), Moscow, Russia 4 Applied Physics Laboratory, The John Hopkins University, Laurel, USA

In this talk field-aligned currents (FAC) in the north auroral magnetosphere during the CME geomagnetic storm on January 11, 1997 are examined by using data mainly from magnetic field experiments on board of INTERBALL -2 and POLAR satellites. During the event from 0300 to 0600 UT, the spacecrafts crossed the dusk side from low to high latitudes in the altitudinal range 12000 to 40000 km. FAC structures were identified for sure on both magnetograms. The measurements permitted to monitor two unusual FAC systems separated from each other. The equatorward system was a remarkable demonstration of intense oscillating fields during steady Bz IMF  $>> 0$ , immediately after the end of the most dramatic compression of the magnetosphere. In contrast the poleward system appeared as irregular structures probably controlled by a strong unsteady By IMF. Correlations with double -theta aurora are discussed also.

**GA4.08/L/01-B3** Poster **0900-14**

**MAGNETIC EFFECT OF REGION 1 FIELD-ALIGNED CURRENTS IN A COURSE OF MAGNETIC SUBSTORM**

Elena BELENKAYA (Institute of Nuclear Physics, Moscow State University, Moscow, 119899, Russia, Email: Elena@dec1.npi.msu.us)

In a course of magnetic substorm, dynamics of the Region 1 field-aligned currents generated by the solar wind is considered. Based on a simple spherical model, magnetic field of the field-aligned currents is calculated everywhere up to on-ground level. During magnetic storm the polar cap boundary significantly shifts equatorward together with zones where Region 1 field-aligned currents flow into and out of the ionosphere. The magnitude of the Region 1 field-aligned currents increases in a course of substorm. As a consequence, magnetic effect of the Region 1 currents significantly depends on a phase of substorm, and have a maximum in a main phase.

**GA4.08/E/04-B3** Poster **0900-15**

**THE DYNAMICS OF INTERACTION BETWEEN MAGNETIZED SOLAR WIND FLOW AND THE EARTH--MAGNETOSPHERE SYSTEM**

N.A. BARKHATOV (Nizhny Novgorod State Pedagogical University, 1, Ulyanova str., Nizhny Novgorod 603005, Russia, email: nikolay@barkh.sci-nnov.ru); N.S. Belliustin (Radiophysical Research Institute, 25, Bolshaya Pecherskaya str., Nizhny Novgorod, 603600, Russia, email: nick@nbell.sci-nnov.ru); A.E. Levitin (Institute of Terrestrial Magnetism, Ionosphere and Radio Wave Propagation, Troitsk, 142092, Russia, email: Igomova@izmiran.troitsk.ru)

One-dimensional calculating medium for space-time dynamics simulation of interaction between the Solar wind magnetised flow and magnetosphere-Earth system is constructed. Possibility of elementary modelling of quasi-stationary structure like bow shock wave, arising at collision of space plasma flow with Earth magnetic field is investigated. Non-stationary transitional processes, induced by density and velocity inhomogeneities in a solar wind flow are analysed by means of calculating program. It is shown, that the calculating system allows to obtain theoretical graphics of possible magnetic field variations on Earth surface at various inhomogeneities' characteristics for comparisons by the measurements. Thus the numerical calculations allow to adjust a relationship between sharply varying conditions in the Solar wind (concentrations, velocities, components of interplanetary magnetic field) and amplitude and scale of impulse (including SI), registered on the Earth surface. Obtained forms of magnetic field variations can be used for co-interpretation of Earth and Satellite measurements on magnetic field and other medium parameters.

**GA4.08/E/24-B3** Poster **0900-16**

**HELIO GEOPHYSICAL SITUATION DURING TWO SUBSTORMS**

YEVLASHIN

Abstract not available at time of going to press

**GA4.08/E/13-B3** Poster **0900-17**

**EXTERNAL MULTIDIMENSIONAL CLUSTER CLASSIFICATION OF GEOMAGNETOSPHERIC STORMS**

Joseph KOVALEVSKY and Elena Kovalevskaya (Institute of Terrestrial Magnetism? Ionosphere and Radiowave Propagation RAS IZMIRAN 142092 Troitsk, Moscow Region, Russia, email: jkoval@izmiran.rssi.ru)

The external multidimensional cluster classification of 31 geomagnetospheric storms (GMS) by support processes is presented for the purpose of setting of comparatively homogeneous groups (clusters) of such events with rather alike in support processes and inner structures. Every GMS is characterized by inner structure, consisting of 32 measuring and derivate physical processes. The discussion is restricted to the case of four-dimensional classification. These GMS are analyzed from the point of view of the type and scale similarity of four support processes (Bz- and By- components of IMF, Dst- and AE- indices) of their physical core. The core is composed of storm initial and main phases and quick part of recovery phase. It is clearing up what of the greatest importance is for GMS external classification: the scale of changes of support processes or their character independent on the scale. It is demonstrated that for GMS cores two classifications are effective both according to inner processes similarity and according to inner processes correlativity. Two common clusters (with respect to both type and scale similarity) and two specific groups (for type and scale similarity) have been obtained. Obtained clusters and groups are characterized by different variants of inner structure, and hence by different variants of core physical development. Particular emphasis has been placed on the interplanetary- magnetospheric couplings analysis of three intense (Dst-124 #-149 nT) GMS of the scale similarity group. These storms have different complex internal physical structure development of which are impossible to represent by single known interplanetary parameter (say, Bz, Ey, or e).

**GA4.08/E/15-B3** Poster **0900-18**

**AN INVESTIGATION OF INTENSE GEOMAGNETOSPHERIC STORMS USING SEQUENTIAL-CLUSTER ANALYSIS**

Joseph KOVALEVSKY and Elena Kovalevskaya, Institute of Terrestrial Magnetism, Ionosphere and Radiowave Propagation, RAS, IZMIRAN, 142092, Troitsk, Moscow Region, Russia, e-mail: jkoval@izmiran.rssi.ru;

Intense geomagnetospheric storms (GMS) can be thought of as the complex system physical phenomena or as pattern recognition objects. For solution of part of unsolved GMS physical problems we invoke to adequate approach: to pattern recognition methods, including the sequential and cluster analysis. The effectiveness of sequential-cluster analysis of empirical and theoretical data is demonstrated on example of two GMS (27.08 and 28.09, 1978). The distinctive feature of these two GMS is that they have nearly equal minimal, mean value and dispersion of Dst -field and of IMF Bz - component, but rather different athumathal interplanetary electric field (Ey), and Akasofu (e) and Murayama (FM) parameters. The GMS are characterized by interconnected set of 29 plasma processes of which 13 are initial and 16 are 'derivative' processes derived for physical interpretation of phenomenon. The 'geoeffective' parameters search, the most important processes relationships revealing and consideration of processes dynamic on the base of dendrite structure analysis are done. It is shown that none of the known theoretical 'geoeffective' parameters cannot provide an equally adequate interpretation of phases peculiarities of the whole Dst - processes. It has been revealed an important role of IMF Bx- and By- component and proton temperature T in the development of studied GMS. The Dst-AE couplings was weak.

**GA5.08** **Monday 26 July**

**ANALYSIS AND INTERPRETATION OF OERSTED AND OTHER SATELLITE MAGNETIC FIELD SURVEY DATA (WITH DIV. I)**

Location: Muirhead Tower G08 LT  
Location of Posters: Student Room (1st Floor)

**Monday 26 July AM**

Presiding Chairs: John Quinn (US Geological Survey, Federal Center, Denver, USA), Andrew Jackson (School of Earth Sciences, Leeds Uni, UK)

**GA5.08/E/03-B1** **0900**

**THE OERSTED GEOMAGNETIC SATELLITE MISSION. INSTRUMENTATION AND DATA HANDLING. PRESENTATION OF INITIAL RESULTS**

T. NEUBERT (1), P. Stauning (1), E. Friis-Christensen (2), F. Primdahl (2,3), J. Jørgensen (3), I. Laursen (3), T. Risbo (4), and N. Olsen (2) 1. Danish Meteorological Institute, Lyngbyvej 100, DK-2100 Copenhagen, Denmark. Fax: +45 3915 7460. E-mail: neubert@dmi.dk 2. Danish Space Research Institute, DK-2100 Copenhagen, Denmark 3. Dep. Automat., Danish Technical University, DK-2800 Lyngby, Denmark 4. University of Copenhagen, DK-2100 Copenhagen, Denmark

The Xrsted satellite is equipped with instrumentation for high-precision measurements of the Earth's magnetic field. The satellite, furthermore, carries instruments for detection of the high-energy charged-particle radiation environment and for remote sensing of the upper atmosphere. The Xrsted satellite is launched into a near-earth polar orbit in January 1999. The orbit has an inclination of 96 degrees and a height varying between 620 and 850 km. The initial orbit plane is at 15-03 hours local time. At a nodal drift of 0.77 degrees/day the satellite will achieve a noon-midnight orbit in the middle of its planned 14 months mission. The principal aim of the satellite is to accomplish an accurate mapping of the Earth's magnetic field arising from internal sources and the detection of current systems in space. Prime focus will be on high-latitude field-aligned current systems and energetic particle radiation and their coupling to ionospheric convection and polar radiowave absorption features. The presentation will briefly outline the instrumentation of the Xrsted satellite and describe the data handling procedures. The main emphasis will be on the presentation of initial results of the measurements from the satellite and correlated high-latitude ground-based observations.

**GA5.08/E/02-B1** Invited **0920**

**OERSTED INTERNAL FIELD SCIENCE AND INITIAL FIELD MODELS**

Nils OLSEN (Danish Space Research Institute, Juliane Maries Vej 30, DK-2100 Copenhagen, e-mail: nio@dsri.dk), Robert A. Langel (Goddard Space Flight Center (Emeritus), Greenbelt/MD, 20707, USA), Torben Risbo (Geophysical Department, Copenhagen University, Juliane Maries Vej 30, DK-2100 Copenhagen) and Terence J. Sabaka (Hughes STX Corp., Lanham/MD, 20706, USA)

The main objective of the high-precision geomagnetic satellite mission Oersted (launched in January 1999) is to measure the Earth's magnetic field with an accuracy of better than 2 nT. We will present first results about the Oersted internal field research, and especially on the main field modelling effort.

**GA5.08/W/06-B1** **0945**

**COMPARISONS OF MAGNETIC FIELDS MEASURED BY ØRSTED SATELLITE WITH MODELED HIGH-LATITUDE FIELD-ALIGNED CURRENT SYSTEMS**

Vladimir PAPITASHVILI\*, Freddy Christiansen, Torsten Neubert, Ole Rasmussen, and Peter Stauning (Danish Meteorological Institute, Lyngbyvej 100, DK-2100, Copenhagen, Denmark, email vp@dmi.dk; \*also at SPRL, University of Michigan); Lidia Dremukhina and Anatoly Levitin (Institute of Terrestrial Magnetism, Ionosphere and Radio Wave Propagation, Troitsk, Moscow Region, 142092, Russia, email: Igomova@izmiran.troitsk.ru)

An automated technique based on derivation of field-aligned current distributions for various IMF conditions from the IZMIRAN Electrodynamic Model (IZMEM, <http://www.spri.umich.edu/MIST>) is developed and utilised for calculations of the magnetic field disturbances along the Ørsted satellite orbit. The "modelled" satellite magnetograms are compared with Ørsted observations to determine possible contributions to these measurements from the varying 3-D magnetosphere-ionosphere current systems. This allows better interpretation of satellite magnetograms over polar latitudes for case studies, as well as the construction of a new model of field-aligned currents from the Ørsted data. The presentation will focus on detailed comparisons of newly obtained field-aligned current distributions with the Iijima-Potemra Region 1/Region 2 system as well as with the cusp DPY currents for various IMF conditions. These new results and the automated technique could also be utilised for correction of satellite observations from the external field contribution over polar latitudes to better fit the data for the main geomagnetic field modelling.

**GA5.08/W/02-B1** **1005**

**PRELIMINARY RESULTS FROM THE DANISH SATELLITE OERSTED, A REPORT FROM THE IPGP GROUP**

YVES COHEN, Gauthier Hulot, Mioara Manda Alexandrescu, Pascale Ultré-Guéard, Benoit Langlais, Christophe Vernin, Jean-Louis Le Mouel (Institut de Physique du Globe de Paris, 4 Place Jussieu, 75252 Paris Cedex 05, France, email: cohen, ghulot, mioara, ultré, langlais, vernin, lemouel@ipgp.jussieu.fr)

The Danish magnetic satellite Oersted was to be launched on January 16, 1999 at 10:39:52 UTC, from Vandenberg Air Force Base in California, just a few hours after the final deadline for submitting the present abstract. It is therefore not yet clear what the status of the mission will be by the time of the meeting. IPGP being involved through CNES (French Space Agency) in the commissioning of the Overhauser magnetometer, our team nevertheless intends to report on at least some preliminary results concerning the intensity data acquired with this instrument. It is otherwise hoped that in the mean time, more complete data sets, acquired by both the OVH intensity magnetometer and the CSC vectorial magnetometer during the first few months of the flight, will also have been made available to the international community involved in the Oersted program. IPGP being part of this community (through two proposals, "Modelling the Earth's main magnetic field and characterising the equatorial electro-jet through its magnetic effects measured from space", "The variations of the field of internal origin: characterisation and interpretation"), we will hopefully report on our first preliminary results. These will mainly concern main field and secular variation modelling for the beginning of 1999, based on both Oersted data and ground measurements. Tentative comparisons with models derived from the MAGSAT 1980 mission will also be discussed. Outline of our proposals will otherwise be recalled.



**GA5.08/W/05-B1 1055**

**MODELING OF MAGNETIC FIELDS FROM HIGH-LATITUDE CURRENT SYSTEMS ALONG MAGNETIC SURVEY SATELLITE ORBITS**

L. A. DREMUKHINA, Ya. I. Feldstein, A. E. Levitin (Institute of Terrestrial Magnetism, Ionosphere and Radio Wave Propagation, Troitsk, Moscow Region, 142092, Russia, email: lgromova@izmiran.troitsk.ru); V. O. Papatashvili (Space Physics Research Laboratory, University of Michigan, Ann Arbor, MI 48109, USA, email: papita@umich.edu)

The IZMIRAN Electro-dynamic Model (IZMEM, <http://www.spri.umich.edu/MIST>) is utilised to define the distribution of high-latitude field-aligned currents over both the Northern and Southern polar regions dependent on the interplanetary magnetic field (IMF) strength and direction. Then the magnetic field disturbances caused by these currents are calculated along the magnetic survey satellite orbit from the Biot-Savart's law for various IMF conditions. The magnetograms obtained by MAGSAT in 1979-1980 are modeled to show capabilities of the proposed technique. Calculations of the magnetic field contributions from field-aligned currents along the orbits can be performed in both the geographic co-ordinates and the "corrected geomagnetic latitude - magnetic local time" co-ordinates. The obtained modelling results are in good agreement with experimental observations in defining the high-latitude, field-aligned current spatial distribution. However, the offset produced by subtraction of the main magnetic field model (e.g., DGRF-1980) from satellite data causes some discrepancies; more studies are required in fitting the model with data and tuning the technique. Some applications of the proposed technique to the forthcoming magnetic satellite surveys (e.g., Oersted, CHAMP, etc.) are discussed.

**GA5.08/W/09-B1 1115**

**EFFECT OF THE EQUATORIAL ELECTROJET ON INTERNAL MAGNETIC FIELD MODELS COMPUTED FROM SATELLITE DATA PASCALE**

ULTRE-GUERARD and Yves Cohen (Institut de Physique du Globe de Paris, 4 Place Jussieu, 75252 Paris Cedex 05, France, email: ultre, cohen@ipgp.jussieu.fr)

At the beginning of the eighties, 20 years before the Oersted project, Magsat, the first satellite devoted to vectorial measurements of the total Earth magnetic field, has shown how such a dense and homogeneous satellite data set could improve magnetic field models. However, internal field models computed with satellite data include the ionospheric contributions since the horizontal ionospheric currents are located under the satellite orbit. This was a central issue with Magsat data as its orbit was sun-synchronous at 6h and 18h, i.e., local times with significant ionospheric activity. In this study, we focus our attention on the equatorial electrojet current and quantify the error on main magnetic field and also crustal models due to this equatorial current. In doing so, residuals on each component of the magnetic field are computed by subtracting main field models to the data and then averaged in 2 x 2 degree bins. These residuals are then fitted using a current sheet model and the result is referred to as the equatorial electrojet reference model (EERM), estimated at the Magsat altitude. This EERM is then inverted in a Spherical Harmonic Analysis up to degree and order 13. The computed model (EECM) is shown to have significant contribution on main field models and to have the same order of magnitude as the Earth field around degree 13. The EE contribution is also shown to be significant at the CMB. It is now usual to reduce the effect of the horizontal ionospheric current by using simultaneously observatory and space data. In order to test this method we use a synthetic EE current and compute the corresponding synthetic values at Magsat location as well as for about 100 observatories. A new model is then computed extracting the magnetic potential associated to the EE current in order to quantify the improvement on the main field model.

**GA5.08/W/12-B1 Invited 1135**

**INVERTING VECTOR MAGSAT DATA FOR THE CRUSTAL POWER SPECTRUM**

David LOWE (1), R L Parker (1), C G Constable (1), M E Puricker (2) (1) Cecil H and Ida M (Green Institute of Geophysics and Planetary Physics, Scripps Institute of Oceanography, University of California at San Diego, La Jolla, CA 92093-0225, USA) (2) Geodynamics Branch and Raytheon, ITSS, Goddard Space Flight Center, MD 20771, USA)

A model of the crustal Mauersberger-Lowes spectrum (RI) is essential in producing detailed core field models - Rygaard-Hjalsted et al. (1997) demonstrated relationships between RI and the component covariance matrices used in core field inversions. The crustal field is isolated from MAGSAT dawn and dusk data by subtracting the Comprehensive Model (under development at GSFC by Sabaka, Langel, Olsen and Richmond) to account for sources in the ionosphere, magnetosphere and core. The passes are restricted to +/-50j dipole latitude because the Comprehensive Model does not reproduce high latitude features (field aligned currents) particularly well. A high quality subset of this data has been compiled by visually inspecting the crustal residuals for features (gaps, tears) that, in addition to being non-geomagnetic in origin, would contaminate spectral estimates. The power spectral density (PSD) of each flight local component along each "good" great circle path (GCP) is robustly estimated using multitapers. Following O'Brien (1996), the PSDs are then inverted for a smooth RI, at wavelengths down to 800km (l=50). The same techniques will be applied to higher accuracy vector data from RSTED (when available). Resolution limits for crustal field models can be set at the signal-to-noise transition in the spectral domain. This wave-number (kres) varies from pass to pass. It is possible to subdivide these GCPs into continental and oceanic and investigate whether these regions' different compositions and formation processes translate into different kres and RI.

**Monday 26 July PM**

Concurrent Poster Session

**GA5.08/E/07-B1 1330**

**MAGNETIC SUSCEPTIBILITY CONTRASTS OF THE LITHOSPHERE**

J. DYMENT (CNRS UMR "Domaines Océaniques", Institut Universitaire Européen de la Mer, Université de Bretagne Occidentale, Plouzané, France; email: jerome@univ-brest.fr); J. Arkani-Hamed (Earth and Planetary Sciences, McGill University, Montreal, Canada)

Because they mix the fundamentally different physics of the induced and remanent magnetization in the lithosphere, satellite magnetic anomalies are often difficult to interpret in terms of geology. We determine the induced magnetic anomalies of the Earth by removing a model of the magnetic anomalies due to the remanent magnetization of the oceanic lithosphere from the observed satellite anomalies. For consistency with the observed data, the remanent magnetic anomalies are filtered following the processing scheme applied to the Magsat data to remove the external and core field components. The resulting induced magnetic anomalies are inverted to bulk magnetic susceptibility contrasts. The new bulk susceptibility contrast map display relatively simple figures in the oceans, with the exception

of the large and north-south trending anomalies removed by the initial processing of the satellite data. Normal oceanic crust shows a uniformly low bulk susceptibility, whereas oceanic plateaus exhibit higher bulk susceptibilities related to their thicker crust.

Subduction zones display higher bulk susceptibilities due to the magnetization of the colder subducted slabs. Passive margins present a consistent signature, with a higher bulk susceptibility over the continents, a lower one over the oceans, and a representative bulk susceptibility contrast of about 0.65 to 0.70 SI km across the ocean-continent boundary. Variations of the bulk susceptibility contrast across the ocean-continent boundary depends on the nature of the continental lithosphere and the type of continental margin.

**GA5.08/W/08-B1 Invited 1350**

**RECOGNITION OF LITHOSPHERIC REMANENT MAGNETIZATION IN THE SOUTH ATLANTIC FROM SATELLITE**

M PURUCKER (Geodynamics Branch, Goddard Space Flt Ct, Greenbelt, MD 20771 USA, email: purucker@geomag.gsfc.nasa.gov); J Dyment and N Grammatica (Universite de Bretagne Occidentale, Plouzane, France, email: jerome@catamaran-gw.univ-brest.fr)

In order to enhance our knowledge of the oceanic lithosphere, especially in poorly studied areas like the South Atlantic, we have compared Magsat observations with a new model of the remanent magnetization of the world's oceans developed by Dyment and Arkani-Hamed. The South Atlantic region is characterised by high levels of external magnetic fields and a north-south magnetic grain, both of which pose problems for the polar-orbiting Magsat magnetic field satellite. The Magsat observations that we use are those of Cain et al (JGG, 1990), who solved simultaneously for both core and lithospheric fields up to degree and order 49. A comparison between model and observations permits recognition, for the first time from satellite, of 1) the Cretaceous quiet zones, 2) the period of more rapid field change in the early Tertiary, and 3) the enhanced signal over the spreading ridge. The observations also show other, previously recognised features of the satellite field in the South Atlantic, including Walvis ridge and the Cretaceous quiet zone north of the South Sandwich islands. The observations of Cain et al appear to be superior to the observations of Arkani-Hamed et al in recovering north-south trending signals. However, the Arkani-Hamed et al observations appear to be superior in recovering east-west trending signals. The greater amplitude in the Cain et al observations confirm the results of Dyment and Arkani-Hamed that deeper oceanic sources are required and that the basaltic layer is inadequate to produce the observed signal.

**GA5.08/W/10-B1 1415**

**USING QUALITY SATELLITE MAGNETIC DATA IN MODELS OF THE MAIN GEOMAGNETIC FIELD**

Alan THOMSON (Global Seismology and Geomagnetism Group, British Geological Survey, West Mains Road, Edinburgh, EH9 3LA, Scotland. e-mail: a.thomson@bgs.ac.uk)

The Oersted satellite mission should provide a magnetic data-set of comparable quality to that of Magsat. In this paper we examine the characteristics of models of the core-generated field based, at least in part, on such satellite data (possibly using early Oersted data, if available). Comparisons will be made with main-field models derived solely from ground-based measurements.

**POSTER VIEWING 1435**

**GA5.08/W/13-B1 1545**

**FINE TUNING GLOBAL FIELD MODELS BASED ON SATELLITE MAGNETIC OBSERVATIONS**

Joseph CAIN and D Mozzoni (Geophysical Fluid Dynamics Institute, Florida State University, Tallahassee, Florida 32306-4360, USA)

In past analyses of the data from projects such as Vanguard 3, Cosmos49, POGO and Magsat, it was clear that in all instances the separation of sources has not been carried out completely. The integration of the vertical component of Magsat data to obtain internal spherical harmonic coefficients to degree 65 (M07AV6) resulted in a curious double hump in the residual diagrams, with no obvious relation to a separation of the data in local time or any other parameter that could be envisioned. Although the model differed only slightly from those derived later using all components and least squares adjustment so as to produce a near Gaussian error distribution, the difficulty remained a mystery without satisfactory explanation. In the least squares adjustments of all the components to produce such models as M102189 a prior "reduction" was made of each component by fitting residual curves separately for the dawn and dusk portions of the orbits with polynomials. This reduction significantly reduced the overall residuals of fit to the data, but left unanswered the nature of the variations. Attempts to statistically evaluate the nature of the residuals by season and altitude or other geophysical parameters, also produced no obvious pattern. Lastly, determinations of the variational field from surface magnetic observatories for each 24 hour period and computation of the estimated field at satellite altitude on the assumption of E-layer horizontal electrical current sheets could not be related to residual patterns in the Magsat data. The generally accurate internal field models that resulted in spite of such uncertainties was due to the fact that the internal field is mostly vertical, and the vertical current components have no effect on the scalar potential. During the dawn and dusk periods of Magsat data there were enough intervals where the imbedded horizontal currents were small that their effects were equally negligible in the resulting models. Likewise, for POGO, the large volume of data allowed a selection of the quietest intervals during early morning hours when such currents were very low. Even so, the fact that POGO models could achieve residual distributions near 1 nT, whereas even with many more terms, the best Magsat models were in the range of 5-10 nT implied the need for better reductions. These issues are discussed and evaluated for the more recent data from Ørsted and Astrid-2 projects.

**GA5.08/E/01-B1 1605**

**BACKUS EFFECT AND PERPENDICULAR ERRORS IN HARMONIC MODELS OF REAL VS. SYNTHETIC DATA**

C.V. VOORHIES, J. Santana and T. Sabaka (Geodynamics Branch, Code 921, NASA's Goddard Space Flight Center, Greenbelt, MD 20771 USA; email: voorhies@geomag.gsfc.nasa.gov)

Measurements of geomagnetic scalar intensity on a thin spherical shell alone are not enough to separate internal from external source fields; moreover, such scalar data are not enough for accurate modelling of the vector field from internal sources because of un-modelled fields and small data errors. Spherical harmonic models of the geomagnetic potential fitted to scalar data alone therefore suffer from well-understood Backus effect and perpendicular errors. Curiously, errors in some models of simulated 'data' are very much less than those in models of real data. We analyse select Magsat vector and scalar measurements separately to illustrate Backus

effect and perpendicular errors in models of real scalar data. By using a model to synthesise 'data' at the observation points, and by adding various types of 'noise', we illustrate such errors in models of synthetic 'data'. Perpendicular errors prove quite sensitive to the maximum degree in the spherical harmonic expansion of the potential field model fitted to the scalar data. Small errors in models of synthetic 'data' are found to be an artefact of matched truncation levels. For example, consider scalar synthetic 'data' computed from a degree 14 model. A degree 14 model fitted to such synthetic 'data' yields negligible error, but amplifies 4 nT (rms) added noise into a 60 nT error (rmss); however, a degree 12 model fitted to the noisy 'data' suffers a 492 nT error (rmss through degree 12). Geomagnetic measurements remain unaware of model truncation, so the small errors indicated by some simulations cannot be realised in practice. Errors in models fitted to scalar data alone approach 1,000 nT (rmss) and several thousand nT (maximum).

Monday 26 July PM

**GA5.08/E/06-B1** Poster **1400-01**

**THE INTERMEDIATE ANOMALIES AT THE TERRITORY OF RUSSIA AND SURROUNDING AREA**

Valentina I. KOLESOVA, Victor I. Pochtarev and Maria A. Effendieva (St.-Petersburg filial, Institute of Terrestrial Magnetism, Ionosphere and Radiowave Propagation, Muchnoy per.2, box 188, 191023, St.-Petersburg, Russia, email: kmp@telecom.lek.ru)

For the first, the intermediate anomalies were detected by V.I.Pochtarev at the territory of USSR using the generalized airborne magnetic data in 1965. Later M.A.Vasilyeva carried out the new generalisation of the relative airborne magnetic data with the help of the total force data measured at base net. The space spectral analysis of the obtained chart gave the opportunity to detect the long-wave components having the periods 200-350, 500-700 and 1100-1300 km. The first two components are the more intensive at the Russian and East Siberian Platforms, they reached 700 nT; the intensity of the third component everywhere is equal 150-200 nT. It was shown, that the regions having the large particularities in the lithosphere of the ancient shields and platforms near the Moho's boundary are marked by the stationary 200-350 km magnetic and gravitational components. The zones of the high seismic velocities placed under Moho's boundary are detected by 500-700 km magnetic and gravitational anomalies. The chart of the intermediate anomalies was compiled at the base of M.A.Vasilyeva's total force map. The detected space spectral characteristics were taking into account. The obtained intermediate anomalies were interpreted with the help of the original author's method at the base of the magnetic, gravitational and seismic data. All intermediate anomalies are placed in the regions of the ancient shields and platforms with the high thickness of the Earth's crust. The same intermediate anomalies are detected in the POGO magnetic data.

**GA5.08/E/05-B1** Poster **1400-02**

**PECULIARITIES OF A SUBSTORM DEVELOPMENT WITH THE SHARP BEGINNING OF AN EXPANSION PHASE**

R.N.BOROYEV (Institute of Cosmophysical Research and Aeronomy, 31 Lenin Ave., 677891 Yakutsk, Russia, email: lae@sci.yakutia.ru)

On AE-indices the sub-storms with the sharp beginning of an expansion phase have been selected. A moment of expansion and the longitude localisation of the sub-storm center was determined as on ae and on data of ground magnetovariation stations. By using data satellite measurements of the geomagnetic field in the geostationary orbit a study of the magnetospheric current system in period of such sub-storms has been carried out. In all considered events the satellites the GEOS-5 and GEOS-6 were either in the midnight or morning sector. It is found that before the expansion phase onset for the sub-storms with a sudden beginning the field-aligned currents are not observed in-like the sub-storms with a gradual beginning of the expansion phase [1]. It is apparently explained by the narrow longitudinal localisation of a sub-storm center before the expansion phase onset as compared with a distance between the satellites.

**GA5.08/W/04-B1** Poster **1400-03**

**PROFILES OF THE MAGNETIC ANOMALIES ON THE NEAR SURFACE, STRATOSPHERICAL AND SATELLITE ALTITUDES**

Yu. P. Tsvetkov, N. M. ROTANOVA, and V. I. Odintsov, Institute of Terrestrial Magnetism, Ionosphere and Radio Wave Propagation, Russian Academy of Sciences, IZMIRAN, Troitsk, Moscow Region, 142092, Russia, email: golovkov@izmiran.rssi.ru

Profiles of the anomaly crustal field to the extent of 6000 km having one and the same route have been constructed. Crustal fields on the near-surface altitudes were obtained from a map of magnetic anomalies of territory USSR (1974), on the satellite and on the stratospherical altitudes data of the MAGSAT and of the balloon surveys were used. The spectral analysis and comparison of amplitude-frequent characteristics for each of profiles were done. As the standard for the comparison the results of spectral analyses of the balloon surveys were chosen. The present researches have shown: firstly, the agreement (except for two sites of ~200 km) of the balloon and near-surface profiles, high identity of the profile spectra in range of wavelengths of 200-2200 km, and also reliable correlation of the crustal fields on satellite and stratospheric altitudes in frequency domain of 500-3000 km, secondly, the agreement of the spatial distribution of spectral harmonics of investigated profiles upto wavelengths of ~2000 km.

Conclusion is made, data of the balloon surveys may be used for an estimation of accuracy of the regional maps.

**GA5.08/W/11-B1** Poster **1400-04**

**SPATIAL-TEMPORAL AND SPECTRAL ANALYSIS OF THE GEOMAGNETIC DATA FROM MAGSAT NINA**

Nina Rotanova, Vadim Golovkov, Andrei Kharitonov (Institute of Terrestrial Magnetism, Ionosphere and Radio Wave Propagation, Russian Academy of Sciences, IZMIRAN, Troitsk, Moscow Region, 142092, Russia, email: golovkov@izmiran.rssi.ru)

The method of natural orthogonal components (NOC) was applied to the satellite data from MAGSAT. It was used to solve the following satellite survey problems: - revelation and extraction of the spurious data; - separation of the residual field obtained after removing of the main field from observed ones, on parts originated by the crustal magnetisation and the ionospheric current systems. A conclusion is made that the technique of NOC analysis allows to find a solution of the above-mentioned tasks and should be included into the scheme of the satellite data processing to prepare both the vector and scalar magnetic anomaly maps. Spectral analysis was applied to the geomagnetic field data from MAGSAT. Spectra were

computed by the maximum entropy method. It is shown that a set of three spectral peaks within about 500 km, 1000 km and 3000 km are singled out on the satellite altitudes, connected with anomaly fields. Reality of the obtained spectral peaks is confirmed by results of the spectral analysis of the gravity field. The spectral estimations of the anomaly field were used for determination of the depths of the magnetic sources.

**GA5.08/W/07-B1** Poster **1400-05**

**CRUSTAL MAGNETIC ANOMALIES FROM SATELLITE: THEIR RELATIONSHIPS WITH LITHOSPHERE**

Sergei D. ODINTSOV (Institute of Terrestrial Magnetism, Ionosphere and Radio Wave Propagation, Troitsk, Moscow reg., 142092, Russia, Email: odintsov@izmiran.rssi.ru)

The simple method ("SIMP") of construction maps of the anomaly magnetic field for middle latitudes by using the Magsat satellite data is suggested. Anomaly maps were constructed by SIMP for a series of regions (for territory of Western and Eastern Europe, of the Pakistan and of the most part of territory of Russia). The comparison of such maps was made with other maps received by the classical method. The comparison showed some disagreements between these maps for same regions. The careful analysis of our maps (the comparison with near-surface, airborne and balloon's surveys) showed the some advantage over received maps by classical method. Using the interpolated data of anomalies we created models of anomalies by the method of Spherical Cap Harmonic Analysis. These models are compared with the ones of gravitational anomaly maps. Also anomalies maps were directly compared with tectonic and geologic maps. The results obtained in the present study are discussed.

**GA5.08/E/08-B1** Poster **1400-06**

**HOW DOWNWARD FIELD CONTINUATION CAN CONTRIBUTE TO MAGNETIC FIELD ANALYSIS AND INTERPRETATION**

Wigor A. WEBERS, (GeoForschungsZentrum Potsdam, Telegrafenberg, D-14473 Potsdam, Germany)

The well-known spherical harmonic analysis (SHA) as adequate global internal magnetic field model is an infinite power series expansion from the mathematical point of view. Consequently, ground-based and satellite altitude SHA field models show different convergence quality that reflects different physical contents of the SHA terms of both field data sets. The practical calculations use finite SHA partial sums truncated at a definite index. The downward field continuation procedure WIGCONT uses the invariant characteristic of functional behaviour of the contributions of the SHA terms, i.e. of the functional system of the SHA expansion to the volume of a parallelepiped in a mathematical functional space as regularising criterion. Applying this procedure enables to evaluate the physical content of the satellite SHA model in comparison to the simultaneous ground-based one. This relates to the spatial characteristics of the SHA terms and to its different time structure when the behaviour of the SHA field models in time is investigated. Moreover, when the downward continued satellite altitude SHA model is referred to the simultaneous ground-based one and compared with model calculations then the different contributions of the external field to both data sets can be studied.

**GA5.08/W/01-B1** Poster **1400-07**

**MONITORING THE EQUATORIAL ELECTROJET ACTIVITY USING GROUND STATIONS DURING THE OERSTED MISSION**

YVES COHEN, (IPGP, Observatoire de St Maur, 4 avenue Neptune, 94107 St Maur des Fossés, France, email: cohen@ipgp.jussieu.fr); Vafi Doumouya, (Univ. Côte d'Ivoire, FAST Dépt de Physique, 22 BP 582 Abidjan 22, Côte d'Ivoire, email: doumouv@syfed.ci.refer.org); Pascale Ultré-Guéard, (IPGP, 4 place Jussieu, 75252 PARIS Cedex 05, France, email: ultré@ipgp.jussieu.fr); and Jacques Vassal, IRD, 32 avenue H. Varagnat, 93143 Bondy Cedex, France, email: jacques.vassal@bondy.orstom.fr

The Equatorial Electrojet is an ionospheric current that regularly flows along the geomagnetic equator. Its amplitude is a combination of diurnal and seasonal variations. Its magnetic activity can be measured by any magnetic station around the geomagnetic equator. It is also measured by any low altitude polar orbiting satellite. It has been shown that the large-scale magnetic field created by this current affect the description of both crustal and main magnetic fields deduced from polar orbiting satellite measurements.

In order to reduce this effect, an independent estimate of this current based on ground stations is necessary. A chain of 3 ground magnetic stations was installed perpendicularly to the geomagnetic equator, just before the launching of the Oersted satellite. These data will be collected during the whole mission, and will be used to remove the effect of this current from the satellite profiles. We propose here a method that can be used to isolate the Equatorial Electrojet effect from satellite data.

**GA6.02** Monday 26 July

**400 YEARS OF GEOMAGNETISM**  
Location: Gisbert Kapp NG15 LR1

Monday 26 July PM

Presiding Chair: A.L. Orozco, (Geophysics Institute, National University of Mexico)

**GA6.02/E/01-B1** Invited **1400**

**400 YEARS OF GEOMAGNETIC FIELD CHARTING AND MODELLING**

David R BARRACLOUGH (British Geological Survey, Murchison House, West Mains Road, Edinburgh EH9 3LA, UK)

William Gilbert's assertion, in 1600, that the Earth is a great magnet can be regarded as presenting the first model of the geomagnetic field. Edmond Halley's Atlantic and World Charts of about 100 years later were the first magnetic charts to be published - and were also the first charts to use contour lines. The development of geomagnetic field models during the 400 years since Gilbert and of geomagnetic charts in the 300 years since Halley will be described. Emphasis will be on global models and charts, and on mathematical models. The close relationship between charts and mathematical models will be explored.



GA6.02/E/09-B1

1420

## FORTY OR FOUR CENTURIES REMOTE PAST HISTORY AND SUPERSTITION SCIENCE

Luz M.Barreto (Observatorio Nacional, Rua General Bruce, 586, 20921-400, Rio de Janeiro, RJ, Brasil e-mail: barreto@on.br)

In spite of its prominent place in the History of Science, for a long time Geomagnetism was a kind of myth. A "South-Directing Chart" in China (2634 b.C.) is the oldest notice, but the first quotation about the compass use was made by Shen Kua (1088 b.C.), also in China. The first European reference to a compass was made in 1190 a.D. by Nehkham and it is probable that Marco Polo's descriptions about the Chinese Technology could be the reason for European curiosity. There are no clear written documents about that natural phenomena. The period of forty centuries could be called the "Prehistoric Geomagnetism". The important role of the compass for the Great Navigation success was not a source of scientific activities. There were two reasons for this : to maintain the nautical techniques in secret, and the mystic Middle Age thinking. The birth of Galileo's Scientific Method was the greatest scientific historical landmark, and it had provoked in Geomagnetism a bright spot, the publication of Gilbert's "De Magnete" (1600). It could be considered as the first ever published scientific book. Hundred years later, Halley presented his Magnetic Atlantic Charts. The "Prehistoric Period" had finished. However, the real meaning of the Geomagnetic Field was not established, since only the value of two angles, a mere qualitative concept, had been achieved. In 1832, Gauss created his measuring instruments and methods, to describe completely the vector "Geomagnetic Field". The Science of Geomagnetism was born.

GA6.02/E/16-B1

1435

## REMARKS ON LIFE AND WORK OF -JULIUS BARTELS

Hannelore and KARL-HEINZ BERNHARDT (Platz der Vereinten Nationen 3, D-10249 Berlin, Germany)

J. Bartels (1899-1964), who was president of IAGA (1954-57) and, later, vice-president of IUGG (1957-63), worked at the beginning of his academic career at the university of Berlin and at the forestry college of Eberswalde from 1927 to 1944. Bartels' activities during this period of his life as well as his relation to the Prussian Academy of Sciences are characterized based on archival records. Also most of his significant contributions to mathematical statistics in meteorology and geophysics, which are considered in some details as an important part of his versatile lifework, have been written in this time.

Following the doctor thesis (Göttingen, 1923), Bartels started in the fields of statistics with the study of cyclic variations of meteorological and geomagnetic parameters which are superimposed by strong non-cyclic components. The application of the synchronization method in this connection required to eliminate carefully the selection or curvature effect, which had often been misinterpreted formerly. Further, Bartels improved the methods of periodogram analysis and the statistical testing of their results on the basis of the contemporary theory of probability. Special attention was paid by him to problems of statistical testing in case of auto-correlated data as connected with the phenomena of persistence and quasi-persistence in meteorological and geophysical time series. Finally, he introduced special Monte Carlo like methods, as the shaking test, to test the significance and the reliability of phenomena observed in time series. His rigorous criticism and the numerous remarks to avoid misleading conclusions from incorrect statistical data interpretation should be considered as exemplary also nowadays.

GA6.02/E/17-B1

1450

## HISTORICAL NOTES ON GEOMAGNETIC MEASUREMENTS IN AND AROUND ICELAND

KRISTJANSSON (University of Iceland, Geophysics Division, Sciences Institute, Hungi-Hofsvallagata 53, Reyjavik 107, Iceland Email: leo@raunvis.hi.is)

Abstract not available at time of going to press

GA6.02/E/08-B1

1505

## EARLY HISTORY OF GEOMAGNETIC RESEARCH IN INDIA

R.G.RASTOGI, (Department of Physics, Gujarat University and Physical Research Laboratory, Ahmedabad 380 009 India, e-mail: parvs@prl.ernet.in)

India has a long standing of geomagnetic research since as early as 1792 when regular magnetic observations were started at Madras. Later Simla, Madras and Trivandrum formed part of the global network of observatories organised by Gottingen Magnetic Union in 1835. The development of geomagnetic and ionospheric observatories in India are discussed with thirteen geomagnetic observatories operating today between the latitudes of electrojet center and Sq focus. On the scientific research side, the publications by Prof.J.A. Broun (1874) "Observations of magnetic declination made at Trivandrum and Augustia Malley" and by N.A.F. Moos (1910) "Magnetic observations made at the Government Observatory Bombay for the period 1846 to 1905" forms the classical monumental works on Geomagnetism. Some of pioneering research on solar, lunar and storm time variations of the magnetic field at low latitudes are described.

GA6.02/W/01-B1

1520

## DECLINATION AND LONGITUDE: FRENCH THEORY AND OBSERVATION IN THE EARLY 17TH'S CENTURY

Pascale ULTRE-GUERARD and Mioara Manda Alexandrescu (Institut de Physique du Globe de Paris, 4 Place Jussieu, 75252 Paris Cedex 05, France, email: ultre, mioara@ipgp.jussieu.fr)

Using archive materials held in libraries at Paris and Dieppe, we pay tribute to some of our French ancestors who made notable advances in both the theoretical and observational development of geomagnetism during the early 17th century. About two years after "De Magnete", a French cartographer, Guillaume de Nautonnier, published his monumental "Mecométrie de l'eymant cest a dire la manière de mesurer les longitudes par le moyen de l'eymant". Nautonnier claimed, by considering observed values of declination, that all magnetic meridians converge in a regular fashion to the magnetic poles, one located near Greenland and the other near Georges V land. This would lead to a method of determining longitude at sea, which was perhaps the most important scientific problem at the time. In 1611, Didier Dounot's "Confutation" showed that the values of declination do not support Nautonnier's hypothesis. The subsequent debate on this subject during the first half of XVIIth century proved to be extremely important in the development of geomagnetism. Another important French contribution at that time was by Jean Guérard, a hydrographer, described by Fournier, as: "one of the most precise observer he had ever known, who wanted to have the most exact magnetic compass...". In one the Captain Guérard's maps the

declination of the magnetic compass is indicated in order to show navigators where the compass is more or less declining (1631). This map is centered on the Atlantic Ocean and predates Edmond Halley's well-known chart of declination in the Atlantic by 70 years. However, the declination values are plotted in 17 distinct locations, and so the chart cannot really be compared with Halley's isogonic representation of declination. The declination values measured by Guérard are presented and compared with an existing historical model.

GA6.02/E/03-B1

1535

## WILLIAM GILBERT AND "THE MAGNET" A VISIONARY WORK

A. OROZCO (Instituto de Geofísica, Ciudad Universitaria, 04510, Mexico, D.F., Mexico; email: adolfo@tonatiuh.igeofcu.unam.mx:)

In 1600 The Magnet by William Gilbert came out from the press. This book is considered as the beginning of the scientific studies about geomagnetism. This masterpiece of work was not only a complete study about the known facts about the magnetic needle, compasses, magnetic materials, and properties of the magnetic stone, but also it contains a very imaginative and clever set of theories and hypothesis about the origin, characteristics and evolution of the magnetic field of the earth. At a distance of 400 years it is very interesting and enlightening to study the visionary proposals of Gilbert, his life, the support he received from the Royal Authorities and the impact of this scientific work. The aim of this paper is to present only some outlines of the work and the impact of the book of Gilbert with the idea to promote a more complete and insightful work on the history of geomagnetism along this four centuries.

GA6.02/E/04-B1

Invited

1610

## GEOMAGNETISM AND FUNDAMENTAL SCIENCE

Giovanni P. GREGORI (IFA-CNR, via Fosso del Cavaliere 100, 00133 Roma, Italy; e-mail: gregori@atmos.ifa.rm.cnr.it)

The history of geomagnetism can be conceived from different viewpoints, such as e.g. dealing (1) with the discovery of the time- and space-morphology of the field, or (2) with the ideas about its prime cause, or (3) with instruments, or (4) with the heuristic potential of the geomagnetic record for studying Earth's history, etc. The present contribution is mainly concerned with the impact of geomagnetism on fundamental science, and the related feedback. The early investigations by Descartes culminated with Gilbert's De Magnete, while Kepler attempted at explaining the planetary orbits by means of the magnetic force, until Newton formulated the law of universal gravitation (thus starting the still surviving dichotomy between gravitation and e.m.-weak forces). In 1820 Ampere discovered the magnetic effects of an electric current, while Gauss was developing potential theory up to a stage of excellence, and he did not afford in setting order into electrostatics, a target that was later achieved by Maxwe l l. The interaction between geomagnetism and fundamental physics later implied on one side the unsuccessful search for the generation of the magnetic field by rotating an electrically neutral object. On the other hand, two basic aspects are as yet inadequate a tely exploited. (1) The approximation of steady flow of a plasma is inadequate, and there is need for applying, rather, the Hamilton/Jacobi (instead of Newton/Maxwell's) formulation e.g. for explaining the magnetosphere, its substorms and storms, etc. or for investigating the average skin depth of penetration of a time varying external field into an approximately spherical heterogeneous Earth. (2) The interaction between the gravitational (tidal) force and the dynamo is a basic process that appears like l y to be an ubiquitous feature in the universe, suited also for explaining planetary and lunar magnetic fields. The events in history of science, concerned with the viewpoint here considered, seem to be still in progress.

GA6.02/E/07-B1

1630

## J.J. NERVANDER AND HELSINKI GEOMAGNETIC OBSERVATORY (1838-1912)

H. NEVANLINNA (Finnish Meteorological Institute, P.O.Box 503, FI-00101 Helsinki, Finland, email: heikki.nevanlinna@fmi.fi)

J.J. Nervander (1805-1848), Physics Professor at Helsinki University, was the first geomagnetician in Finland. He introduced electromagnetism and geomagnetism to Finnish scientific community in the 1820's and 1830's. Nervander designed one of the first galvanometers applying Ørsted's invention of electric and magnetic interaction. He was the central figure in establishing a full-scale geomagnetic observatory in Helsinki in 1838. Under Nervander's ambitious leadership the observatory routines and instrumentations were on high international level. Magnetic and meteorological observations started in 1844. Nervander's premature death interrupted the data treatment and publication of observation material. However, observations were continued after him almost 70 years. The observation frequency was 6 times per hour (H, D and Z) until 1857, and one hour after that. At the Finnish Meteorological Institute, the successor of Nervander's magnetic observatory, all magnetic observations made at the observatory have been transformed into electronic form. There are altogether 1,000,000 observations of H and D which form a rather homogeneous and continuous series of magnetic field observations 1844-1910. The quality of Z data is poor. Using H and D we have derived local geomagnetic activity indices K and Ak. The correlation between Helsinki activity indices with global aa-index since 1868 is good: on monthly basis the correlation coefficient is 0.95 and even on daily level 0.8. Helsinki activity index series can be thus used for analyzing magnetic activity for two solar cycles 1844-1868 from which time not much other magnetic data is available.

GA6.02/E/06-B1

1645

## TANAKADATE'S STUDY ON VERTICAL CURRENTS

HARUYO YOSHIDA (Graduate School of Science, Department of Physics (history of science), Hokkaido University, Kita-10, Nishi-8, Kita-Ku, Sapporo, 060, Japan, e-mail: hyoshida@hps.sci.hokudai.ac.jp)

Vertical currents are assumed as an interesting topic in history of geomagnetic study. However, little attention has been paid to the early development of this study which Tanakadate(1856-1952), Japanese physicist, was actively engaged in. A hypothesis of vertical currents was proposed by Schmidt in 1895. He claimed that a small part of geomagnetic force was caused by electric currents traversing the earth's surface and had no corresponding potential. This led to a heated controversy between two groups over the existence of vertical currents. One group(Schmidt, Bauer) drew a conclusion from the magnetic state of the earth as a whole that vertical currents did exist. The other (Rucker, Carlheim-Gyllenskiöld, van Rijkvorsel, and Liznar) got the negative results based on minute and accurate magnetic surveys on their own countries. Tanakadate, a man of deep insight into this difficult problem, joined neither of the groups and approached it from an independent point of view. Successfully accomplishing a magnetic survey of Japan(1893-96) as complete as those of European countries, he improved the method employed by the latter group and deduced a detailed distribution of vertical currents in Japan. Current distributions for Austria and the UK were also



calculated in order to compare them with that for Japan. By drawing lines of equal vertical currents, Tanakadate found that these calculations for different countries gave a line of no current running through the middle of each country, while magnetic distributions display different patterns. Tanakadate thus doubted rather the effectiveness of the method to examine the existence of currents than the reality of the hypothetical currents as some predecessors had done.

**GA6.02/E/10-B1****1700****A CENTURY OF GEOMAGNETIC OBSERVING IN NEW ZEALAND**

Don MCKNIGHT (Institute of Geological & Nuclear Sciences, PO Box 30-368, Lower Hutt, New Zealand, email: d.mcknight@gns.cri.nz)

1999 marks the centenary of New Zealand's geomagnetic observing programme. It was in February 1899 that the first comprehensive survey of the magnetic field in New Zealand and its outlying islands commenced, and in November 1901 that continuous recording of the field commenced in Christchurch. At the time this was only the fourth permanent observatory in the Southern Hemisphere.

The first magnetic observations were made in New Zealand in 1642 by Abel Tasman.

Further observations were made over the next 250 years by Cook, Stokes, Drury and numerous other navigators and surveyors. It was the practical need for reliable geomagnetic information together with the scientific need for more data from the Southern Hemisphere that led to the establishment of the observatory programme in 1899. The observatory opened in time to provide calibration facilities for Scott's first Antarctic expedition, and went on to host numerous other Antarctic expeditions and survey vessels.

The Christchurch observatory was forced to vacate its site in a city park due to the installation of an electric tram system in 1905. The new site at Amberley, 40 km to the north, eventually became disturbed as well and in 1978 the observatory was shifted again, this time 40 km to the southwest to its present site in the Eyrewell Forest. During its near-century of continuous operation the observatory has gone through a number of upgrades, the most recent being a change to digital instrumentation in 1990.

Eyrewell observatory serves as the reference station for repeat station survey work in the New Zealand region and is a member of INTERMAGNET. Examination of its history reveals lessons concerning the siting and value of such a facility, and also the importance of the prompt measurement and publication of results.

**GA6.02/W/06-B1****1715****ONE HUNDRED YEARS OF GEOMAGNETIC MEASUREMENTS AT THE LA PLATA ASTRONOMICIA OBSERVATORY AND MAGNETIC SATATIONS**

Julio Cesar GIANIBELLI and Iris Rosalia (Cabassi, Observatorio Astronomico De La Plata Paso Del Bosque email: jcg@fcaglp.fcaglp.unlp.edu.ar, rosy@fcaglp.fcaglp.unlp.edu.ar)

When the Astronomical Observatory at La Plata, Argentina, was created in 1882, a pavilion was building for magnetic observations. The first observations were carried-out in 1889. The development of investigations, surveys and instalations of two permanent magnetic observatories (Las Acacias and Trelew) was carried out to the present. An historical review of the geomagnetism evolution and the present state of the discipline in Argentina, are present.

**GA6.02/E/11-B1****1730****JOHANN VON LAMONT - FIRST YEARS OF GEOMAGNETIC RESEARCH IN MUNICH, 1836 - 1845**

Martin BEBLO and Heinrich Soffel (both at Geophysical Observatory Fuerstenfeldbruck, University of Munich, Ludwigshoeh 8, D-82256 Fuerstenfeldbruck, Germany, Email: magnetic@fur.observatory.uni-muenchen.de).

Johann von Lamont started with sporadic geomagnetic observations in Munich in 1836. Since 6 o'clock in the morning on August 1st, 1840, he run regular observations with variometers built by Gauss and Meyerstein in Goettingen. In May and June 1841 Lamont replaced the Gauss variometers (suspended magnets with a weight of 25 lb - 11.4 kg) by instruments of his own design using very small and light magnets. These instruments improved significantly accuracy and sensitivity of geomagnetic measurements and made geomagnetic surveys possible. Some years later Lamont developed his travel thodolite and distributed 45 instruments of this type for scientific work worldwide. His instruments became international standard for geomagnetic instruments for more than 50 years.

**GA6.02/W/04-B1****1745****EDMOND HALLEY'S VOYAGES IN THE "PARAMORE" (1698-1700) AND THE FIRST ISOSONIC CHART OF THE EARTH'S MAGNETIC FIELD**

Toby D G CLARK (British Geological Survey, West Mains Rd., Edinburgh, EH9 3LA, Scotland, UK; e-mail: t.clark@bgs.ac.uk)

As well as marking the 400th anniversary of Gilbert's "de Magnete", it is also 300 years since the astronomer Edmond Halley was given command of the "Paramore" which he sailed around the Atlantic recording measurements of magnetic declination. His motivation was a combination of his wish to collect data to improve his theory of the Earth's magnetic field, published in 1692, and his interest in improving navigation methods. His two voyages, made in the years 1698-1700, were not without adventure, and on his return he compiled a chart of magnetic declination, which is reputed to be the first on which contour lines were used to depict a physical quantity. Halley's measurements remain an important dataset for modern geophysicists studying the secular variation of the geomagnetic field over the last few centuries. In this paper we will outline Halley's theory of the Earth's magnetic field, examine his voyages with reference to the log of the "Paramore", and finally compare the 17th century voyages with a modern expedition being planned to commemorate this anniversary.

**A**



G6

Monday 26 – Wednesday 28 July

**GEODSY BEYOND 2000 - THE CHALLENGE OF THE FIRST DECADE**  
Location: Haworth Building 101LT

Monday 26 July AM

Presiding Chair: G. Beutler. (Astronomical Institute of Bern Switzerland)

**REFERENCE FRAME DEFINITION AND IMPLEMENTATION**

G6/E/04-B1

0830

**THE INTERNATIONAL TERRESTRIAL REFERENCE SYSTEM AND ITS ROLE INTO A GLOBAL EARTH OBSERVATION SYSTEM**

Claude BOUCHER, Zuheir Altamimi and Patrick Sillard (all at IGN/ENSG/LAREG, 6-8 Avenue Blaise Pascal, 77455 Marne-la-Vallée, France, email: boucher@ensg.ign.fr)

A terrestrial reference system is a key element of an integrated Earth observation system. This paper reviews the basic concepts and illustrates this fact with several examples: links with GPS and IGS, geophysical and oceanographic applications. Then a short summary of what is currently done by the International Earth Rotation Service, including new developments on time series and reference solutions presented. A focus on the ITRF2000 program is given in this paper.

G6/W/05-B1

0850

**CORE: CONTINUOUS, HIGH ACCURACY EARTH ORIENTATION MEASUREMENTS FOR THE NEW MILLENNIUM**

NANCY R. VANDENBERG and C. C. Thomas (both at NVI, Inc./Goddard Space Flight Center, Greenbelt, MD 20771 USA, Email: nrv@gemini.gsfc.nasa.gov), J. Bosworth, B. Chao, T. Clark, C. Ma (all at NASA/GSFC, Laboratory for Terrestrial Physics, Greenbelt, MD 20771 USA)

The international geodetic VLBI community will inaugurate during 1999 a new phase of the program called CORE: Continuous Observations of the Rotation of the Earth. The capabilities of the new Mark IV correlators, available as of mid-1999, will enable greater sensitivity, more frequent observing sessions and improved system throughput.

The CORE program, begun in 1996 with the CONT96 campaign, has gradually increased the number of observing sessions per week. As of early 1999 the average is 2.5 24-hour sessions per week (including the NEOS sessions). This will expand to 3.5 sessions per week in the second half of 1999, with the goal being continuous sessions by 2001.

More than 20 global VLBI stations are participating in geodetic data acquisition sessions in 1999. These sessions will add nearly 300,000 individual observations to the geodetic VLBI data base. Accuracy goals for each 24-hour session are 3.5  $\mu$ sec for UT1 and 100 milli-arcsec for pole position.

The CORE program's scientific goals are focused on the needs of Earth system science in the new millennium, concentrating on areas that include the solid Earth core (libration, core modes, free core nutation), variations in sub-daily and long-term ocean tides, and episodic signals (earthquakes, geomagnetic jerks). These science areas can be effectively addressed with the high accuracy, continuous Earth orientation measurements provided by the CORE data.

G6/E/03-B1

0910

**EARTH SCALE BELOW A PART PER BILLION FROM SATELLITE LASER RANGING**

D. E. SMITH and R. Kolenkiewicz (Laboratory for Terrestrial Physics, NASA GSFC Code 920, Greenbelt, MD 20771, USA, e-mail: dsmith@tharsis.gsfc.nasa.gov) P. J. Dunn and M. H. Torrence (Raytheon Corp., 7701 Greenbelt Rd., Greenbelt, MD 20770, USA)

Since the LAGEOS I satellite was launched in 1976, the systematic instrument error of the best satellite laser ranging observatories has been steadily reduced to the current level of only a few millimeters. Advances in overall system accuracy, in conjunction with improved satellite, Earth, orbit perturbation and relativity modeling, now allows us to determine the value of the geocentric gravitational coefficient (GM) to less than a part per billion (ppb). This precision has been confirmed by observations of the LAGEOS II satellite, and is supported by results from Starlette, albeit at a lower level of precision. When we consider observations from other geodetic satellites orbiting at a variety of altitudes and carrying somewhat more complex retro-reflector arrays, we obtain consistent measures of scale, which however must be based upon empirically determined, satellite-dependent detector characteristics. We will present the most recent estimate of GM, which lies within the two ppb uncertainty of the current standard, but differs from it by more than the error of the new estimate. Both the current standard and our recommended value fall comfortably within the ten ppb uncertainty of that determined from the most accurate alternative: from lunar laser ranging observations. The precision of the estimate of GM from satellite laser ranging has improved by an order of magnitude in each of the last two decades, and we will discuss projected advances which will result in further refinements in this measure of Earth scale.

G6/C/G5/W/06-B1

0930

**LONG-TERM STABILITY OF ALTIMETRIC DATA WITH APPLICATIONS TO MEAN SEA-LEVEL CHANGE**

P MOORE, M D Reynolds and P Sterlini Aston Geodesy Group, Division of Civil Engineering, Aston University, Birmingham, B4 7ET, UK, email: moorep@aston.ac.uk

The oceanographic community has access to near 14 years of altimetric data ranging from GEOSAT in 1985-1989 to the current TOPEX/Poseidon and ERS-2 missions. For sea-level rise studies careful validation is required to avoid contamination of the results by spurious non-oceanographic effects. In this study we first utilise in situ tide gauge data to monitor stability of the TOPEX/Poseidon data base. This series is then linked to both ERS satellites by dual satellite crossovers. The analysis is then extended to incorporate GEOSAT ERM data through tide gauge enhanced dual satellite crossovers with TOPEX. Results of the stability analysis are utilised to extract global mean sea-level change over the period 1986-1999.

G6/L/02-B1

0950

**MEASURING THE EARTH CENTRE WITH PART-PER-BILLION RELATIVE POSITIONING TECHNIQUES**

FENG

Abstract not available at time of going to press

G6/E/01-B1

1010

**GEODETTIC MODEL TECTONIC PLATE MOTIONS**

Mikhail PRILEPIN (United Institute of Physics of the Earth, B.Gruzinskaya Str., 10, 123810 Moscow, Russia, email: prilepin@uipe-ras.scgis.ru) Vladimir Shevchenko (United Institute of Physics of the Earth, B.Gruzinskaya Str., 10, 123810 Moscow, Russia)

Geodetic data for velocity movements of the main tectonic plates are one of the most valuable contributions of geodesy to Earth science in the last 15 years. These data verify in general the results obtained by geology, paleomagnetism and seismology and make the fact of tectonic plate movements much more convincing. The good agreement on average of the rates for global plates in different time scales - quasi-real time for geodetic rates and 3 millions years for geology-geophysical rates - shows that the evolutionary transformation of upper geospheres of the Earth are going at rate at the level 10<sup>-9</sup> R, where R - radius of the Earth. This can also serve as evidence that there was no extantion of the Earth for at least the last three millions years. In report the analysis and evaluation of the data for rate movements obtained by SLR, VLBI and GPS are carried out and the geodetic model of annual rates for main plate together with an averaged interplate deformation feature is developed, taking into account the data from regional projects in California, Caribbean Sea, South America, Mediterranean Sea, Caucasus, Tian-Shan, Himalay, Tibet, Japan and Kurily-Kamchatka. Using the geodetic model the, boundaries of some small plates are specified, the real rates of subduction and collision of some plates are determined. Significant differences in the rates between NUVEL-1 and geodetic data in some places and the problem of stability in time of the global geodetic reference frames are discussed.

Presiding Chair: M.G.Sideris University of Calgary (Canada)

**HIGH-RESOLUTION GRAVITY FIELD MODELING**

G6/C/G3/E/43-B1

1100

**GFZ-1 IMPACTS ON GLOBAL GRAVITY FIELD SOLUTIONS**

BODE, A., König, R., Massmann, F.-H., Raimondo, J.-C., Reigber, C., Schwintzer, P.

Nearly three years of GFZ-1 data are evaluated for use in global gravity field satellite-only solutions. GFZ-1 is the lowest geodetic mission ever flown for the pure purpose of gravity field recovery. GFZ-1 provides at its altitude a so far unknown piece of knowledge of the gravity field at high degrees and orders. It is therefore also a good test object for precise orbit determination in view of the upcoming missions CHAMP and GRACE. As GFZ-1 data are of type SLR, the known uneven distribution of the data in time and space limits the use for gravity field recovery. The problems of assimilating GFZ-1 data into gravity field solutions and the benefits are discussed.

G6/C/G3/W/32-B1

1120

**IMPROVEMENTS IN GLOBAL GRAVITY FIELD MODELS FOR OCEAN CIRCULATION STUDIES**

D. P. CHAMBERS, M. C. Kim, S. Poole, J. C. Ries, and B. D. Tapley (University of Texas at Austin, Center for Space Research, R1000, Austin, TX, 78712, USA, Email: chambers@csr.utexas.edu)

Current global marine geoid models based on satellite tracking data are inadequate for resolving the long-wavelength ocean circulation to better than 5 cm/sec, especially in the tropics. Studies have been conducted to improve geoid models by combining information from ocean general circulation models with satellite altimetry data to determine the marine geoid signal. The solutions also include satellite tracking data and surface gravity measurements. The data have been combined with various weights, and the effect of relative data weighting on the solution is discussed. The result of the study is a new high resolution gravity field that improves the determination of the general ocean circulation from satellite altimetry while maintaining comparable satellite orbits with older models.

G6/C/G3/E/09-B1

1140

**ON THE MODELING OF LONG WAVELENGTH SYSTEMATIC ERRORS IN SURFACE GRAVIMETRIC DATA**

Nikolaos K. PAVLIS (Raytheon ITSS Corporation, 7701 Greenbelt Rd., Greenbelt, MD 20770, USA, email: npavlis@geodesy2.gsfc.nasa.gov)

Long wavelength systematic errors in (near) global gravity anomaly data bases have been identified as a major limitation of these data for several years now. The specific origin of these systematic errors is not clearly understood, although several possible causes have been identified [Heck, 1990]. To minimize their effects, down weighting (sometimes rather arbitrary) of surface gravimetry, and elimination of its very long wavelength contribution is employed in current global geopotential solutions. Pavlis [1998] proposed an alternative approach for the treatment of these effects, whereby one attempts to separate the long wavelength systematic errors (in the form of low degree surface spherical harmonic models), from the valid gravitational signal present in the data. He demonstrated that this could be done in a combination solution environment where satellite tracking information and surface gravimetric data are simultaneously adjusted.

On the basis of the preliminary results mentioned above, further analyses will be reported here. These aim specifically to address the question of highest degree up to which the separation between systematic errors and gravitational signal can be accomplished reliably, given the currently available satellite tracking and surface gravimetric data. The feature applicability of this technique, in anticipation of various geopotential mapping missions (e.g., CHAMP, GRACE and GOCE) will also be addressed. In addition, the identification of the specific cause(s) for the observed systematic errors in the gravimetric data will be attempted.



**G6/C/G3/E/23-B1****1200****INVESTIGATION OF DIFFERENT METHODS FOR THE COMBINATION OF GRAVITY AND GPS/LEVELLING DATA**

Heiner DENKER 1 (email: denker@ife.uni-hannover.de) Johannes Ihde 2 (email: ihde@leipzig.ifag.de) Uwe Schirmer 2 (email: schirmer@leipzig.ifag.de) Wolfgang Torge 2 (email: torge@ife.uni-hannover.de) Hans-Georg Wenzel 1 (email: wenzel@ife.uni-hannover.de) 1 (Institut fuer Erdmessung, Uni Hannover, Schneiderberg 50, D-30167 Hannover), Germany 2 (Bundesamt fuer Kartographie und Geodäsie, Aussenstelle Leipzig, Karl-Rothe-Strasse 10-14, D-04105 Leipzig, Germany)

Two different methods for the combined computation of the quasigeoid are compared in a test area in Germany. Both methods are based on the remove-restore technique and use the global geopotential model EGM96, point gravity data with a spacing of a few km, a digital terrain model and GPS/levelling control points (with a spacing of about 25 km).

In method 1 the global model is combined first with the gravity and terrain data using the least squares spectral combination technique with integral formulas. The resulting height anomalies are given in a 1.0' x 1.5' grid. Then a smooth corrector surface is developed from the GPS/levelling data by least squares collocation, including a signal and a trend component. The second method is based on a common adjustment of the EGM96 reduced gravity and height anomaly observations using point masses and appropriate weight relations. The point masses are arranged at a depth of 10 km, 30 km and 200 km, and in hilly areas also at a depth of 5 km.

Both techniques are compared from the methodological and numerical point of view. The results are discussed and show an agreement at the cm level.

**G6/W/01-B1****1220****WORLD GEODETIC DATUM 2000**

ERIK W. GRAFAREND and Alireza Azmoudeh-Ardalan, (Geodetic Institute, Stuttgart University Geschwister-Scholl-Str. 24D D-70174 Stuttgart, Germany Tel: +49+711+1213390 Fax: +49 711 121 3285, email: grafarend@gis.uni-stuttgart.de)

Based on current best estimates of fundamental geodetic parameters, i.e., (Grafarend and Ardalan, Journal of Geodesy 71 (1997) 673-679), GM (Ries et al., Geophys. Res. Letters 19 (1992) 529-531), (Lemoine et al., GRAGEOMAR 1996, International Association of Geodesy Symposia 117, (1996) 461-469) and the form parameters of a Somigliana-Pizzetti level ellipsoid, namely the semi-major axis  $a$  and semi-minor axis  $b$  (or equivalently the linear eccentricity) are computed. There are six parameters namely the four fundamental geodetic parameters and the two form parameters ( $a$ ,  $b$ ) or which determine the ellipsoidal reference gravity field of Somigliana-Pizzetti type constraint to two non-linear condition equations. Their iterative solution leads to best estimates, for the tide-free geoid of reference and for the zero-frequency tide geoid of reference. The best estimates of the form parameters of a Somigliana-Pizzetti level ellipsoid, ( $a$ ,  $b$ ), differ significantly by -0.398m, -0.454m, respectively, from the data of the Geodetic Reference System 1980.

**Monday 26 July PM**

Presiding Chair: P.J. de Jonge, (Mathematical Geodesy and Positioning The Netherlands)

**SATELLITE POSITIONING FOR HIGH-PRECISION APPLICATIONS****G6/C/G1/E/32-B1****1400****COMPUTATION OF PRECISE GLONASS ORBITS FOR IGEX**

Daniel INEICHEN, Markus Rothacher, Tim Springer, and Gerhard Beutler (Astronomical Institute, University of Berne, Sidlerstrasse 5, CH-3012 Berne, Switzerland, email: daniel.ineichen@aiub.unibe.ch)

On October 19, 1998, the beginning of the International GLONASS Experiment (IGEX), the Center for Orbit Determination in Europe (CODE) has started to compute precise orbits for all active GLONASS satellites. The duration of the campaign was initially arranged for three months, but was prolonged for at least three additional months. One of the main reasons for this extension was the launch of three new GLONASS satellites at the end of the year 1998. The processing of the IGEX network is done on a routine basis at CODE and precise ephemerides are made available through the global IGEX data centers. The improved GLONASS orbits are referred to the International Terrestrial Reference System (ITRF96) and to GPS system time. They are therefore fully compatible with GPS orbits and allow a combined processing of both satellite systems. All GLONASS satellites are equipped with a laser reflector array and the SLR ground network is tracking most of the GLONASS satellites. First comparisons of the GLONASS orbits computed by CODE with the SLR measurements show that the orbit accuracy is in the order of 20cm. The experiences made with the processing of the IGEX network and the benefits of improved GLONASS orbits for regional network processing will be the main topics of the presentation.

**G6/C/G1/L/16-B1****1420****IMPACT OF A THIRD NAVIGATIONAL FREQUENCY ON GPS AND GNSS-2 AMBIGUITY RESOLUTION**

P.J.G TEUNISSEN, N.F. Jonkman, P. Joosten, D. Odijk (department of Mathematical Geodesy and Positioning, Faculty of Civil Engineering and Geosciences, Delft University of Technology, Thijsseweg 11, 2629 JA Delft, The Netherlands, email: p.j.g.teunissen@geo.tudelft.nl)

Wide ranging design studies are currently conducted for both the Global Positioning System (GPS) as well as the European second generation Global Navigation Satellite System (GNSS-2). Although the studies are carried out within different frameworks - for the GPS within the framework of modernizing the current systems' architecture, for the GNSS-2 within the framework of overall system design - some of the options under consideration are the same. Amongst these is the implementation of a third navigational frequency in order to enhance ambiguity resolution performance for real-time high-precision position determination. In this contribution the ambiguity resolution performance will be compared and analyzed for some of the triple frequency scenarios discussed in the literature, i.e. a third civil GPS frequency, the GPS C/A code split spectrum or dual signal scenario and a GNSS-2 triple frequency set-up. The merit of each of these scenarios will be judged by means of ambiguity resolution success rates, being the probability of estimating ambiguities at their correct integer values. The success rates are evaluated for the basic single-epoch geometry-free observation model using both the bootstrapped as well as the integer least squares estimator. In addition, the optimal choice for the parametrization of the ambiguities will also be identified.

**G6/W/04-B1****1440****FOUR-DIMENSIONAL GEODESY: TIME DEPENDENT INVERSION FOR EARTHQUAKE AND VOLCANIC SOURCES**

Paul SEGALL (Geophysics Department, Stanford University, Stanford CA, 94305 email: segall@stanford.edu)

The past five years has witnessed a tremendous expansion in the number of permanent Global Positioning System (GPS) receivers. There are now GPS networks in Japan, California, and Hawaii that provide crustal deformation data that are dense in both space and time. These data, combined with tilt and borehole strain measurements, can be used to invert for spatial and temporal variations in fault slip and magma chamber dilation. Previously, space-time inversions had been hampered by poor signal to noise in the data, contaminating non-tectonic motions near the instrument (benchmark wobble), and our lack of knowledge of the temporal character of aseismic motions. The recently introduced Network Inversion Filter (Segall and Matthews, J.G.R., 1997) yields estimates of quasi-static fault slip as a function of space and time using data from dense continuous geodetic networks. The NIF employs time domain, Kalman filtering, and allows for non-parametric descriptions of slip velocity, local benchmark motion, and measurement error. A state-space model for the full geodetic network is adopted, so that all data from a given epoch are analyzed together. This allows the filter to distinguish between non-steady fault slip and local surficial effects like benchmark wobble. We have used the Network Inversion Filter to analyze the time-dependence of post-seismic slip following the 1989 Loma Prieta earthquake, to image rift-zone deformation opening and aseismic fault slip following the January 30, 1997 eruption at Kilauea volcano, Hawaii, and to image a propagating dike off the Izu Peninsula in Japan. In situations where the geometry of the causative geologic structures is unknown it is advantageous to use filtering techniques to image the strain-rate fields in space and time.

**G6/C/G1/W/36-B1****1500****SOUTHERN CALIFORNIA CRUSTAL DEFORMATION AND ITS TECTONIC IMPLICATIONS**

Zheng-Kang SHEN and David D. Jackson (both at Department of Earth & Space Sciences, UCLA, Los Angeles, CA 90095-1567, USA; email: zshen@ess.ucla.edu)

The Crustal Deformation Working Group of the Southern California Earthquake Center has recently released its Southern California Crustal Deformation Velocity Map 2.0 ([http://www.scecdc.scec.org/group\\_e/release.v2](http://www.scecdc.scec.org/group_e/release.v2)). We analyzed the geodetic data used in the release and derived station velocities before and after the 1992 Landers earthquake. Significant velocity changes were found for sites located within about 60 km of the earthquake epicenter. The average strain rate in the region increased from  $-0.10$  to  $-0.30$  micro-radian/yr. We also estimated fault slip rates in southern California using the pre-Landers geodetic velocities and elastic dislocation theory. We used a modified fault model, defined by the California Department of Mine and Geology (USGS Open-file Report 96-706) and derived mainly from geological information, to lay out the fault geometry. We adopted the CDMG fault slip rates and uncertainties as a priori data to constrain the least-squares inversion of geodetic data for fault slip rates. Generally the geodetic and geologic estimates are quite consistent, except for a few places. For example, the geodetic rates are significantly lower than the geologic rates along the Mojave, San Bernardino, and Coachella Valley sections of the San Andreas, but the other way round at the Brawley seismic zone and the Imperial fault. These discrepancies suggest that the current fault slip rate beneath the locking depth along the San Andreas is lower than its long-term average. This may reflect the fact that the San Andreas has experienced no large earthquake since 1857, and the fault has passed the time period of rapid post-seismic deformation and entered one of slow deformation. On the other hand, the Landers and Imperial faults are still being affected by post-seismic deformation caused by the 1992 Landers and the 1940 and 1971 Imperial Valley earthquakes respectively. A second inversion of the geodetic velocities derived from the post-Landers data reveals a substantial reduction of the fault slip rate along the Mojave section of the San Andreas and a significant increase of the fault slip rate along the San Bernardino section of the San Andreas respectively. These results suggest a decrease of the earthquake probability along the Mojave section and an increase of the probability along the San Bernardino section of the San Andreas, independently conforming previous estimates obtained by analyzing Coulomb stress change along faults caused by the Landers earthquake.

**G6/C/G1/L/24-B1****1520****A CONTINUOUSLY OPERATING GPS-BASED VOLCANO DEFORMATION MONITORING IN INDONESIA: CHALLENGES AND PRELIMINARY RESULTS**

Chris RIZOS, Shaowei Han, Craig Roberts & Xitujiao Han (at School of Geomatic Engineering The University of New South Wales, Sydney, Australia, email: c.rizos@unsw.edu.au, s.han@unsw.edu.au, z218371@student.unsw.edu.au, xj.han@unsw.edu.au) Hasaunudin Abidin (at Department of Geodetic Engineering, Institute of Technology Bandung Bandung, Indonesia, email: hzabidin@indo.net.id) R. Sukyhar (at Vulcanological Survey of Indonesia, Bandung, Indonesia)

In the past decade or so there has been increasing interest in the use of permanent, continuously operated GPS networks, and a small number of continuous networks have been deployed in the USA, Japan, Canada and several other developed countries for large scale crustal motion studies. However, only in Japan has it been possible to establish a country-wide continuous GPS network to support seismic research, and ultimately contribute to hazard mitigation through the implementation of an earthquake warning system. Even with such a dense network of high quality dual-frequency GPS receivers as established by Japan's Geographical Survey Institute, the station separation is of the order of 20km or more. There are, however, applications of GPS deformation systems which require receiver densities of the order of just a few kilometres. Furthermore, the high cost of such GPS systems means that most countries cannot possibly afford to establish such systems. Applications of dense permanent GPS arrays include monitoring of volcano flanks, micro-faults, ground subsidence due to underground mining or fluid extraction, slope stability, and even engineering structures such as dams, bridges, etc. This paper describes the design of an automatic GPS-based volcano deformation system that is being deployed by the authors on an Indonesian volcano in early 1999. The basis of the design is the use of a number of low-cost GPS receivers across the area of interest, each costing less than US\$2000 each. The critical technical problems that had to be overcome, and preliminary results obtained to date, will be described.

**G6/C/G1/W/19-B1****1540****GPS DATA COLLECTION STRATEGIES FOR THE QUASI-CONTINUOUS MONITORING OF DEFORMATION IN REGIONS OF HIGH SEISMIC RISK**

MIKAEL LILJE (Geodetic Research Division, National Land Survey, 801 82 Gavle, Sweden, email: mikael.lilje@lm.se) Paul Cross and Paul Cruddle (both at Department Geomatic Engineering, University College London, WC1E 6BT, London, UK, email: paul.cross@ge.ucl.ac.uk, paul.cruddle@ge.ucl.ac.uk).

The research described in this paper is part of the EC funded project GPS Seismic Hazard in Greece (SING), one of the objectives of which is to optimize GPS data collection strategies for the monitoring of the crustal strain. As part of this work the concept of a quasi-continuous approach has been developed in which small numbers of receivers are moved from station to station when they (and logistical support) are available. In this way large numbers of stations can be monitored in a flexible way without the need for dense arrays of permanently located receivers and without the need to plan campaigns involving large groups of people and the associated complex logistics. The practical implementation of a quasi-continuous procedure involves the establishment of temporary base stations whilst other receivers are moved in the local regions. The efficiency is then a function of the time spent on each station and the distance between the stations, and this paper specifically addresses these issues. The particular observation system that we describe consists of two permanent observing receivers at ITRF sites within Greece, a limited number semi-permanent stations and a small number of mobile GPS receivers moving from point to point in a quasi-continuous manner. Data collected during part of the 1998 SING fieldwork in Greece has been processed using a variety of subsets of the data available to answer the specific questions raised and detailed conclusions are drawn which lead to practical guidelines for optimum observation strategies to be used for future data collection within the SING project.

Presiding Chair: B.Heck, (Universitat Karlsruhe, Germany)

## ADVANCES IN THEORY AND NUMERICAL TECHNIQUES

G6/W/07-B1

1620

### THE MACCULLAGH REPRESENTATION OF THE TIME-VARYING GRAVITY FIELD

GRAFAREND, E.W. (Geodetic Institute, Stuttgart University Geschwister-Scholl-Str. 24D D-70174 Stuttgart, Germany Tel: +49+711+1213390 Fax: +49 711 121 3285, email: grafarend@gis.uni-stuttgart.de; Engels, J.; Varga, P.

The Cartesian moments of the mass density of a gravitating body and the spherical coefficients of its external gravity field are related in a peculiar way. In particular the products of inertia can be expressed by the gravitational coefficients (MacCullagh-formulae). Here we focus on the small variations of the Cartesian moments due to tidal displacement, loading displacement, displacements generated by incremental centrifugal forces or transverse surface stresses, respectively. Accepting the Love-Shida-hypotheses, which are valid in spherical approximation, the mass conservation law allows a representation of the incremental mass density by the respective excitation function. A representation of an arbitrary Cartesian monome is always possible by sums of solid spherical harmonics multiplied by powers of the radius. Introducing these representations into the definition of the Cartesian moments we arrive at an extension of the MacCullagh formulae. In particular, for excitation functions with a vanishing harmonic coefficient of degree zero also the (diagonal) incremental moments of inertia can be represented by the excitation coefficients. An application of these relations consists in model computations of the length of day, which depends on the polar moment of inertia of the earth.

G6/C/G4/L/01-B1

1640

### DIRECT METHODS IN PHYSICAL GEODESY

Petr HOLOTA (Research Institute of Geodesy, Topography and Cartography, 250 66 Zdiyb 98, Praha-vechod, Czech Republic, email: gope@asu.cas.cz)

In this paper an approach is applied to the recovery of the gravity potential from boundary data that can be ranged under non-classical methods in the solution of boundary value problems. Two interpretations are shown with a particular view to the nature of Stokes', Molodensky's and other boundary value problems in physical geodesy. First the approach is discussed in terms of calculus of variations and the determination of the disturbing potential is treated as a minimization problem for a quadratic functional. The role of the respective Euler's conditions is explained. Then an interpretation based on Lax-Milgram's lemma is demonstrated that exhibits a broader flexibility. The paper contains a discussion concerning bilinear forms that define the problems under consideration and treats also the related functional-analytic aspects. Subsequently, an interpretation of the solution in terms of various function bases is approached with the particular view to the construction of the respective Galerkin's system. Finally, appropriate estimates of the accuracy are discussed.

G6/C/G4/E/04-B1

1700

### WAVELETS AND COLLOCATION: AN INTERESTING SIMILARITY

Christopher KOTSAKIS (Dept. of Geomatics Engineering, University of Calgary, 2500 University Drive N.W., Calgary, Alberta, Canada T2N 1N4 email: ckotsaki@ucalgary.ca)

A rigorous theoretical connection between the statistical (non-stochastic) collocation principle and the multiresolution(MR)/wavelet framework of signal approximation is made in this paper. The rapid developments in MR and wavelet theory over the past few years have provided very efficient tools for spectral studies of irregular gravity field signals, which are often, however, thought as competitive with the already applied concepts and techniques in gravity field modeling. It is the aim of this paper to demonstrate that the wavelet formalism indeed lies at the very core of the mathematical foundations of Physical Geodesy and it fits perfectly into the concept of the statistical approximation of the gravity field. In particular, it will be shown how the use of the minimum mean square error criterion always gives rise to a MR Analysis Approximation in the Hilbert space  $L_2(\mathbb{R})$ , under some very mild constraints on the behavior of the (deterministic) covariance function of the unknown field. In this way, the so-called stationarity restriction problem in operational gravity field modeling becomes just a 'pseudo-problem'. Some other practical issues, such as the selection of data referencing models for spectral analysis purposes, as well as other computational and modelling considerations, are also explained and finally some conclusions are given at the end of the paper.

G6/C/G4/W/18-B1

1720

### COORDINATE SYSTEMS IN FOUR-DIMENSIONAL SPACE-TIME GEODESY

Volker SCHWARZE (Uni of Stuttgart, Dept of Geodetic Science, Geschwister Scholl-Strass, Stuttgart, 70174, Germany, Email: schwarze@gis.uni.de)

In mathematical geodesy coordinate systems of spatially isotropic type or parallel type are pretty well known in the two-dimensional case. These concepts can also be applied to define four-dimensional space-time coordinate systems. It can also be shown that the concept of holonomy and the construction of appropriate coordinate systems are closely related. Numerical examples demonstrating the application in geodesy are widely discussed.

G6/C/G3/E/35-B1

1740

### RECOVERING THE GLOBAL GRAVITY FIELD FROM SATELLITE MEASUREMENTS OF THE FULL GRAVITY GRADIENT

Margarita PETROVSKAYA (Main Astronomical Observatory of Russian Academy of Sciences, Pulkovskoe Shosse 65, Pulkovo, St. Petersburg, 196140, Russia, email: petrovsk@gao.spb.ru) Janusz Zielinski (Polish Space Research Center, Barticka 18A, 00-716, Warsaw, Poland, email: jbz@cbk.waw.pl)

Earlier, main aspects of the spaceborne boundary value (BV) problem were discussed for the most optimal case, when the global Earth potential is approximated from the full magnitude G of the gravity gradient. The expression for G was derived which depends on both the second and first order partial derivatives of the disturbing potential. In the present paper the unique BV equation  $G(\text{obs})=G(\text{Cnm})$  is compiled where  $G(\text{Cnm})$  is the spherical harmonic series, depending on the unknown potential coefficients Cnm, and the observable Gobs is expressed in terms of the local orbital coordinates. This equation is solved with respect to Cnm in form of a simple quadrature formula. By means of simultaneous exclusion of the first order potential derivatives from both sides of the BV equation, its reduced version is derived and the corresponding solution for the potential coefficients is found which depends only on the components of the gravity gradient tensor. The above BV relation is also transformed to the form which is appropriate for applying the least squares procedure in simultaneous processing of satellite and surface observations.

Tuesday 27 July AM

Presiding Chair: R. Rummel (Technische Universität München, Germany)

## A STRATEGY FOR MEETING THE CHALLENGE

PANEL DISCUSSION

0930

G. Beutler, (Astronomical Institute of Bern), M.G Sideris (Uni of Calgary), P.J de Jonge (Delft Uni of Technology, Mathematical Geodesy and Positioning), B. Heck (Universitat Karlsruhe)

Presiding Chair: K.H.Ilk Bonn University (Germany)

## SEAMLESS GRAVITY-DEVELOPMENT IN SATELLITE AND AIRBOURNE GRAVIMETRY

G6/C/G2/E/12

1100

### DIRECT AND LOCAL COMPARISON BETWEEN DIFFERENT SATELLITE MISSIONS FOR THE GRAVITY FIELD ON THE FLIGHT

Alberta Albertella, Federica MIGLIACCIO and Fernando Sanso' (all at Politecnico di Milano, Dip. IAR, Sez. Rilevamento, Piazza Leonardo da Vinci 32, 20133 Milano, Italy, e-mail: fsanso@ipmtf4.topo.polimi.it)

Many different satellite missions are in project at this moment to estimate the global gravity field of the earth and its time variations. The principles of measurement are basically three, namely the measurement of accurate orbit anomalies and of non-gravitational forces acting on the satellite; the measurement of the differential orbit anomalies and of their time variations along the line of sight of two twin satellites; the measurement of the gradiometer tensor. In all three cases it is interesting to be able to compare the observations of one and the same mission at different times at points close in space, as well as observations from different missions approximately on the same area. This in fact can produce an on the flight calibration or cross-calibration procedure. To reach this goal an interesting procedure is to try to "localize" the observations so that the problem is reduced to the comparison of different functionals of T in the same zone of space. The equations for this purpose are analyzed and a few simulations are performed.

G6/C/G3/W/08-B2

1120

### SIMULATION OF GOCE ORBIT DETERMINATION AND GRAVITY FIELD RECOVERY

J. Van Den IJSEL, R. Koop and P. Visser (Delft Institute for Earth-Oriented Space Research, Delft, The Netherlands, email: jose.vandenijsel@lr.tudelft.nl) A. Selig, P. Hoyng and M. Smit (SRON, Utrecht, The Netherlands) N. Sneeuw, J. Mueller and R. Rummel (IAPG, München, Germany)

The Gravity field and steady-state Ocean Circulation Explorer (GOCE) is one of 4 ESA candidate missions in the Earth Explorer Mission program. Its main mission objective is a high-resolution, high-accuracy and homogeneous determination of the static Earth's global gravity field. To this aim GOCE will be equipped with a gradiometer providing Satellite Gravity Gradiometry (SGG) measurements, a GPS/GLONASS (GRAS) receiver providing Satellite-to-Satellite Tracking (STT) measurements and a Drag Free Control (DFC) to compensate non-conservative forces. The gravity field recovery of the GOCE mission will be based on both SST and SGG measurements. The gradiometer is particularly sensitive to the medium and high frequency gravity field information and the GRAS receiver will be used for the long and medium wavelengths. In the framework of the preparations for this mission and parallel to the phase A development a simulator facility is being developed. The main purpose of this simulator is to show how all system aspects of the satellite affect both the SGG and SST measurement accuracy and hence the final achievable gravity field recovery accuracy. To this end orbit recovery simulations are conducted to determine realistic values for the achievable orbit accuracy in the presence of error sources like e.g. measurement noise, dynamic modeling errors for the gravity and tides model and tropospheric correction errors. Furthermore, software is developed for the least-squares estimation of geopotential coefficients from SGG and SST data from GOCE. The procedure is based on an iterative, semi-analytical approach with a block-diagonal normal matrix. Recent progress in the development of the simulator will be shown.

G6/E/02-B2

1140

### AIRBORNE GRAVITY FIELD SURVEYING FOR OCEANOGRAPHY, GEOLOGY AND GEODESY - THE EXPERIENCES FROM AGMASCO

LUDGER TIMMEN (GeoForschungsZentrum Potsdam, Telegrafenberg, D-14473 Potsdam, Germany, email: timmen@gfz-potsdam.de) Luisa Bastos (Univ. of Porto, Obs. Astronomico, Monte da Virgem, P-4430 V. N. Gaia, Portugal, email: lcbastos@oa.fc.up.pt) Rene Forsberg (National Survey and Cadastre, Rentemestervej 8, DK-2400 Copenhagen NV, Denmark, email: rf@kms.min.dk) Arne Gidskehaug (University of Bergen, Inst. of Solid Earth Physics, Allegaten 41, N-5007 Bergen, Norway, email: arneg@ifj.uib.no) Uwe Meyer (Alfred-Wegener-Institut, Columbusstr., D-27568 Bremerhaven, Germany, email: umeyer@awi-bremerhaven.de)

Within the European AGMASCO project (Airborne Geoid Mapping System for Coastal

Oceanography), cooperations with user groups from Oceanography, Geology and Geodesy have been arisen. The airplane based gravimetry/altimetry system provides a rapid surveying procedure which is specially employed in not easily available marine and land areas (e.g. coastal/shelf areas, polar regions). In Geodesy, it serves for the improvement and refinement of already existing geoids and of future satellite-only models. The availability of precise regional geoids allow the monitoring of the dynamic sea-surface topography by satellite altimetry. For applications in geology and geotechnics, gravimetry is a pre-surveying method for exploration of energy resources. Exemplary the AGMASCOC products such as gravity anomalies, sea-surface heights and improved regional geoids (Skagerrak/1996, Fram Strait/1997, Azores/1997) will be discussed. The accuracies correspond to the state-of-the-art of airborne gravimetry/altimetry.

**G6/E/05-B2**

**1200**

**A COMPARISON OF STABLE PLATFORM AND STRAPDOWN AIRBORNE GRAVITY**

C.L. Glennie, K.P. Schwarz, A.M. BRUTON (Department of Geomatics Engineering, The University of Calgary, 2500 University Drive N.W. Calgary, Alberta, Canada T2N 1N4 R). Forsberg, A.V. Olesen, K.R. Kellner, (KMS, National Survey and Cadastre, Rentemestervej 8, DK-2400 Copenhagen NV, Denmark)

To date, most operational airborne gravity results have been obtained using damped two-axes stable platform gravimeter systems such as the LaCoste and Romberg (LCR) S-model marine gravimeter. However, successful flight tests have also been flown using a strapdown inertial navigation system (INS), showing accuracy comparable to that obtained with the LCR gravimeter.

In June of 1998 three flight tests were undertaken which tested the LCR gravimeter and a strapdown INS gravity system side by side. To our knowledge this was the first time such a comparison flight was undertaken. The flights occurred in Disko Bay, off the west coast of Greenland. Several of the flight lines were flown along existing shipborne gravity profiles to allow for an independent source of comparison of the results.

This paper will present the results and analysis of these flight tests. The measurement method and error models for both the stable platform and strapdown INS gravity systems will be presented and contrasted. An inter-comparison of gravity estimates from both systems will be given, along with a comparison of the individual estimates with existing shipborne gravity profiles. The platform gravimeter and strapdown system have very different error behaviour, and therefore, combining the two estimates could give an overall increase in the performance and stability of airborne gravity

**G6/C/G3/W/21-B2**

**1220**

**CALIBRATION/VALIDATION METHODS FOR GRACE**

Christopher JEKELI (Department of Civil and Environmental Engineering and Geodetic Science, Ohio State University, 2070 Neil Ave., Columbus, OH 433210, USA, e-mail: jekeli.1@osu.edu).

The upcoming GRACE (Gravity Recovery and Climate Experiment) satellite mission is expected to map Earth's global gravitational field with unprecedented accuracy, especially at the long wavelengths. The measurements are line-of-sight range rates between two co-orbiting, low-altitude satellites that can be transformed into geopotential differences. One method to attempt the calibration and validation of GRACE data is to compare the long-wavelength field constructed from these data to a long-wavelength field obtained from terrestrial measurements. To achieve useful validation, the terrestrial standard must be based on extremely accurate data that are globally distributed. Moreover, if the terrestrial data distribution is not uniform and sufficiently dense, their long-wavelength constituents are difficult to ascertain. On the other hand, however, since in situ geopotential differences are derived from GRACE data, calibration and validation can be conducted at the local level. That is, using very accurate local terrestrial gravity fields that are upward continued to satellite altitude, one can calibrate GRACE data without requiring the construction of a global field. This paper compares the different calibration schemes, from the theoretical view (downward versus upward continuation, frequency versus space domain), the practical view (types of terrestrial data bases; e.g., global absolute gravity nets versus local, high-accuracy geoids and other models), and the science view (gravity mapping, as well as temporal changes).

**Tuesday 27 July PM**

Presiding Chair: C. Rizos, (University of New South Wales, Australia)

**THE CHALLENGE OF KINEMATIC POSITIONING AND ATTITUDE DETERMINATION**

**G6/W/06-B2**

**1400**

**THE MUTUAL IMPACT OF MODERN KINEMATIC METHODS AND AIRBORNE GEOSCIENCES**

Alain GEIGER, Marc Cocard, Maurizio Scaramuzza, Hans-Gert Kahle and Etienne Favey (Institute of Geodesy and Geodynamics, Swiss Federal Institute of Technology, ETH-Hoenggerberg, CH-8093 Zurich, Switzerland, email: geiger@geod.ethz.ch)

Satellite methods open new fields of expertise for geodetic sciences. Especially kinematic methods are of growing interest for a large variety of applications. Airborne surveying in geosciences call for precise trajectory. Examples are aero-photogrammetry, Laser scanning for terrain elevation determination or airborne geophysics (gravimetry, magnetics). To document these developments, projects are presented which show the mutual impact of kinematic applications and geodesy. An integrated Laser-Profilier system, including DGPS and attitude sensors, was implemented on an aircraft to determine profiles of sea surface heights, and to monitor glacial fluctuations at the decimeter-level. On the fly ambiguity resolution algorithms were developed to constrain the position of the aircraft below the 10-cm level. Extensive campaigns were carried out in the Ionian and Aegean Seas. This area includes one of the steepest gradients of the geoid coincident with the Hellenic subduction zone.

The satellite geodetic methods can also be used to verify and validate new procedures in civil aviation. Geodetic methods may even be integrated into operational systems (blunder detection or RAIM algorithms, on the fly carrier phase solutions). An example is given of a project for analyzing and testing the feasibility of GPS-aided approaches for civil aviation in the Swiss Alps. During several test flights and dedicated ground missions various problems, such as satellite visibility, multipathing, GPS signal interference and the influence of the topography on the navigation and the GPS system were addressed. The tests showed the potential of satellite based systems for approaches, in particular for use in rugged terrain.

**G6/C/G3/W/45-B2**

**1420**

**ABSOLUTE KINEMATIC GPS POSITIONING**

Jay Kwon, Christopher JEKELI, and Shin-Can Han (all at Department of Civil and Environmental Engineering and Geodetic Science, Ohio State University, 2070 Neil Ave., Columbus, OH 433210, USA, e-mail: jekeli.1@osu.edu).

The Global Positioning System (GPS) has proved invaluable for precise positioning of moving-base platforms, such as aerial photogrammetric systems and ocean buoys that are used to study ocean circulation and sea level changes. To achieve sub-decimeter accuracy in position requires differential data processing with respect to a fixed base station in order to cancel the large GPS satellite clock errors (due primarily to Selective Availability). However, differential GPS methods introduce some additional errors, such as higher noise and unmodeled tropospheric delay differences for longer baselines (> 100 km). Also without a direct data link between the two receivers, these methods restrict the amount of data processing that can be done on board the moving platform. We have developed a method to estimate the GPS satellite clock errors to an accuracy as good as ±0.3 ns (±0.3 cm) and arbitrary resolution using OSU's GPS orbit determination software. With these estimates it is possible to conduct accurate absolute positioning of any moving base, unfettered by base station support requirements. This paper presents the clock estimation results and discusses applications to remote kinematic positioning.

**G6/E/06-B2**

**1440**

**A GPS/INS/IMAGING SYSTEM FOR KINEMATIC MAPPING IN FULLY DIGITAL MODE**

Mohamed M.R. Mostafa (Department of Geomatics Engineering, The University of Calgary, 2500 University Dr. N.W., Calgary, Alberta, Canada T2N 1N4, E-mail: mmmmosta@acs.ucalgary.ca); Klaus-Peter SCHWARZ (Department of Geomatics Engineering, The University of Calgary, 2500 University Dr. N.W., Calgary, Alberta, Canada T2N 1N4, E-mail: schwarz@ensu.ucalgary.ca)

This paper describes the development and testing of a fully digital multi-sensor system for aerial image capture and georeferencing for applications in remote sensing, mapping, and GIS. This system has been developed at The University of Calgary. The main objective of developing such a system is to acquire and georeference digital imagery in remote areas where ground control is neither available nor needed. The system incorporates a navigation grade strapdown Inertial Navigation System, GPS receivers, and two high resolution digital cameras. The two digital cameras capture strips of overlapping nadir and oblique images. They are configured in such a way as to overcome the geometric limitation of their small format size. Image exposure time and INS digital records are time-tagged in real time by the GPS. The INS/GPS-derived trajectory allows for the determination of the six independent parameters describing the motion of the carrier aircraft. Those trajectory parameters are directly related to the problem of exterior orientation. During postprocessing, image exterior orientation information is extracted from the INS/GPS-derived trajectory. This approach eliminates the need for ground control to provide 3D position of objects that appear in the field of view of the system imaging component. Test flights were conducted over the campus of The University of Calgary. In this paper, the multi-sensor system configuration and calibration is briefly reviewed and results of the test flights are discussed in some detail. First results indicate that major applications of such a system in the future are in mapping of utility lines, roads, pipelines (at mapping scales of 1:1000 and smaller), and the generation of digital elevation models for engineering applications.

**G6/C/G3/E/11-B2**

**1500**

**GPS BASED ATTITUDE AND POSITION DETERMINATION FOR AIRBORNE REMOTE SENSING**

Kevin SHERIDAN and Paul Cross (both at Department of Geomatic Engineering, University College London, Gower Street, London WC1E 6BT, UK, email: sheridan@ge.ucl.ac.uk and pcross@ge.ucl.ac.uk)

The design and testing of a GPS based position and attitude determination system for the direct georeferencing of airborne imagery is discussed. By combining dual frequency, high data rate GPS receivers with a relatively simple gyroscopic attitude and heading reference system, position and orientation data can be collected at a rate which matches that of a typical airborne scanner, with an accuracy adequate for georeferencing any imaged features.

Data collected in two flight trials in October 1998 have been processed using software developed at University College London and the University of Newcastle Upon Tyne, to determine a best estimate of the aircraft trajectory. The software employs single epoch ambiguity resolution, a modified double differencing algorithm for direct determination of attitude parameters, and a Kalman filter for data integration. The performance of this system is compared to that of a commercially available GPS multi-antenna attitude determination unit (Ashtech ADU2). Position and attitude are also calibrated using classical photogrammetric techniques with ground control.

Details of the computation methods are presented, and results are shown with an analysis of the possible applications.

**G6/W/03-B2**

**1520**

**ADAPTIVE KALMAN FILTERING FOR INS/GPS/GLONASS INTEGRATION**

Jinling WANG, Mike Stewart and (Maria Tsakiri School of Spatial Sciences Curtin University of Technology GPO Box, U1987, Perth, WA 6845 Australia Email: Wang@vesta.curtin.edu.au)

Inertial Navigation System (INS) and satellite based positioning systems (GPS and GLONASS) are widely used autonomous positioning and attitude determination techniques. Either system has its own features. In the GPS/GLONASS systems, carrier phase measurements are superior in accuracy as long as integer carrier phase ambiguities are correctly resolved and no cycle-slips occur. The NS provides self-contained and high-rate accurate measurements within short time periods. However, systematic errors in the INS measurements may grow over time without bounds. Integration of GPS/GLONASS and INS can overcome shortcomings of each system. For integrated INS/GPS/GLONASS positioning, the high accuracy of INS measurements over short time periods is useful for cycle-slip correction and ambiguity resolution, whereas the precise carrier phase measurements are ideally suitable for continuous INS calibration.

Tightly-coupled INS/GPS/GLONASS integration is commonly implemented using a Kalman filter combining disparate raw measurements from INS and GPS/GLONASS sensors. Reliable Kalman filtering results, however, are highly dependent on the correct definition of stochastic models used in the filtering process. Stochastic modeling for INS and GPS/GLONASS measurements is not trivial, however. In this paper, a newly developed adaptive Kalman filtering algorithm is employed to estimate stochastic model for the measurements. Testing results from some experiments will be presented.

Presiding Chair: K. Kahmen (Technical University of Vienna, Austria)

**PRECISION ENGINEERING-NEW CONCEPTS AND SYSTEMS**

**G6/L/01-B2**

**1620**

**GEOTECHNICAL EXPLORATION - WIDER FIELDS OF ACTIVITY FOR GEODESISTS AND GEOPHYSICISTS**

Ewald BRUECKL (Institute of Geodesy and Geophysics, Vienna University of Technology, A-1040 Wien, Gusshausstrasse 27-29, Austria, email: brueckl@luna.tuwien.ac.at)



In April 1998 the Symposium on Geodesy for Geotechnical and Structural Engineering was held in Eisenstadt, Austria, by the IAG, SC4. During one working session, titled "Geotechnical Exploration Strategy", experts from the fields of geotechnical exploration gave a view over tasks, methodology, results, and significance of geotechnical exploration based on a multidisciplinary approach combining the individual geoscientific methods. The geodetic community has a traditional position within geotechnical exploration, however, it turns out geodesists are rarely included into the planning and decision making team and new fields of activities are not occupied by geodesists adequately to their knowledge and expertise.

Based on an operational model of a multidisciplinary exploration team a strategy is drafted to improve the situation described above. Essential impulses could come from the universities by combining a universal education in Geodesy with a good geophysical training. This can diversify the methods to be offered and improve the ability to develop geoscientific models. The construction and maintenance of databases including visualization and data exchange, as well as the global optimization of complex systems is fundamental to geodetic and geophysical work and additional geoscientific applications of these techniques should be emphasized. Further, a basic understanding of Geology and related geosciences is important to promote the integration into a geotechnical exploration team.

**G6/L/02-B2****1640****BUILDING STRUCTURES AS KINEMATIC SYSTEMS**

Rainer FLESCH (Civil Engineering Research Unit \_FPZ P Arsenal, Faradaygasse 3, A-1030 Vienna, email: flesch@arsenal.ac.at); Dr.-Ing. Heribert Kahmen, (University of Technology Vienna, Institute of Geodesy and Geophysics, Dept. of Applied and Engineering Geodesy, Gusshausstrasse 27 - 29/E128/3, A-1040 Vienna, email: Heribert.Kahmen@tuwien.ac.at)

At the end of the 20th century, builders all around the world are pushing the limit in their quest for structural height and length. The competition for building bigger and taller is as old as civilization. Opening a new area in building the first skyscrapers began rising in Chicago and New York toward the end of the nineteenth century. Meanwhile, a new group of tall structures enters the picture: radio and TV broadcasting masts, towers, and industrial chimneys. The worlds' tallest structure is the KTHI TV mast (629 m) in Fargo, USA. At the same time the span lengths of bridges are increasing. In the near future main spans of more than 2000 m will be possible. For safety inspection of civil engineering structures dynamic methods have to be developed. The described method is a combination of dynamic insitu testing and Finite Element Modelling. For testing of the models a great variety of geodetic measurement systems and other sensor systems is available. It will be shown, how different types of sensor systems can be used for the different inspection tasks.

**G6/C/G1/E/55-B2****1700****MONITORING THE HEIGHT DEFLECTIONS OF THE HUMBER BRIDGE BY GPS AND GLONASS**

Gethin ROBERTS, Vidal Ashkenazi and Alan Dodson (IESSG, University of Nottingham, Nottingham, NG7 2RD, UK, Email: gethin.roberts@nottingham.ac.uk)

This presentation details trials recently conducted by the IESSG whereby kinematic GPS and the Russian equivalent to GPS, Global'naya Navigatsionnaya Sputnikovaya Sistema (GLONASS), were used to monitor the deflection of the Humber Bridge, UK, under a loading of 160 tons, moved across the bridge by five articulated lorries. The trial consisted of placing four dual frequency GPS receivers and a GPS/GLONASS receiver on the bridge deck, a dual frequency GPS receiver upon one of the lorries and reference receivers placed on land. The data, gathered at 5 Hz, was then processed in an On the Fly manner resulting in a precision of the order of a few millimetres. Finite element modelling of such structures can take advantage of similar trials and results. The results were compared to a Finite Element Model by the Department of Mechanical Engineering at the University of Brunel, UK, and showed remarkable comparisons. Further trials were conducted in order to assess the use of single frequency carrier phase GPS receivers to position strategic locations upon the bridge at a rate of 10Hz. These trials demonstrated that a fast data capture rate would enable such GPS positioning to be used to monitor the deflection of smaller structures with a higher rate of movement.

**G6/L/03-B2****1720****MOBILE MULTI-SENSOR SYSTEMS: THE NEW TREND IN MAPPING AND GIS APPLICATIONS**

Naser EL-SHEIMY (Assistant Professor, Department of Geomatics Engineering, The University of Calgary, 2500 University Dr., N.W., Calgary, Alberta, Canada, Tel: (403) 220 7587, Fax: (403) 284 1980, E-mail: naser@ensu.ucalgary.ca)

Multi-sensor systems have become an emerging trend in mapping and GIS applications because they allow a task-oriented implementation of geodetic concepts at the measurement level. Examples of such systems can be found in airborne remote sensing, airborne laser scanning and mobile mapping from vans and trains. All of them have in common that the sensors necessary to solve a specific problem are mounted on a common platform. By synchronizing the data streams accurately, the solution of a specific problem is possible by using data from one integrated measurement process only. The post-mission integration of results from a number of disjointed measurements processes and the unavoidable errors inherent in this process are avoided. This results in greater conceptual clarity, task-oriented system design and data flow optimization, and also offers in most cases the potential for real-time solutions, which are becoming more important in many applications.

The presentation will cover both, the concept of multi-sensor integration and implementation aspects. Based on experience with a number of different systems, features common to most systems will be identified and a unified model for multi-sensor integration will be formulated. Suitable observables for these models will be assessed, and factors affecting system performance will be discussed. All major features will be illustrated by examples. Finally, data-flow optimization and the potential for automation of the data acquisition and feature extraction process will be reviewed with a view to future systems.

**G6/L/04-B2****1740****TRAFFIC GUIDANCE AND CONTROL -TECHNOLOGICAL CHALLENGES FOR GEODESY AND GEOMATICS**

Wolfgang MOHLENBRINK (Institute for Applications of Geodesy to Engineering), University of Stuttgart, Geschwister-Scholl-Str. 24D, D-70174 Stuttgart, Germany  
Email: wolfgang.moehlenbrink@iagb.uni-stuttgart.de

Land vehicle navigation units for mono- and multimodal traffic systems based on digital rail and road maps are seen as booming markets for future geo-information services. Especially car navigation systems based on standardized digital road maps provide key technology for

traffic guidance and control. The emerging border crossing market require standardized metric and topological reference systems. Due to the changing professional cernel competences of geodesists - the classical scenario of expertise in accuracy for local, regional and global geometric networks will be changed to the picture of an information service provider for accurate complete up-to-date and in time available information with precise geometrical attributes. Therefore a special working group \_Traffic Guidance and Control with members of industry, traffic authorities and IAG-experts with the following tasks: development of topological information structures for intermodal traffic guidance systems definition of information quality requirements for traffic information services research work on information and data quality procedures for safety relevant traffic systems operations has been proposed and founded at SC 4(IAG) at Eisenstadt, Austria, hold on April 20-22, 1998.

These technological challenges could be a future market for all members of IAG.

**Wednesday 28 July AM**

Presiding Chair: C.C. Tscherning, (University of Copenhagen, Denmark)

**ADVANTAGES AND DRAWBACKS OF THE CURRENT IAG STRUCTURE****G6/L/05-B3****0830****AN ANALYSIS OF THE CURRENT IAG STRUCTURE**

SCHWARZ, K.P

**G6/L/06-B3****0855****THE PROS AND CONS OF HAVING SECTIONS**

SANSO

**G6/L/07-B3****0920****IAG SERVICES IN THE CURRENT FRAMEWORK**

MUELLER

**G6/L/08-B3****0945****COULD THE COMMISSIONS DO WITHOUT SECTIONS?**

WENZEL

**G6/L/09-B3****1010****THE ROLE OF IAG SPECIAL STUDY GROUPS**

WOLF

Presiding Chair: M. Feissel, Observatoire de Paris (France)

**THE ROLE OF IAG SERVICES IN SUPPORT OF RESEARCH IN GEODESY AND GEODYNAMICS****G6/L/10-B3****1100****IGS INTERNATIONAL GPS SERVICE FOR GEODYNAMICS****G6/L/11-B3****1115****BGI INTERNATIONAL GRAVIMETRIC BUREAU****G6/L/12-B3****1130****IGeS - INTERNATIONAL GEOID SERVICE****G6/L/13-B3****1145****IERS - INTERNATIONAL EARTH ROTATION SERVICE****G6/L/14-B3****1200****ICET - INTERNATIONAL CENTRE OF EARTH TIDES****G6/L/15-B3****1215****PSMSL - PERMANENT SERVICE FOR MEAN SEA LEVEL****G6/L/16-B3****1230****BIMP/TIME - BUREAU INTERNATIONAL DES POIDS ET MESURES**

index

The IUGG 99 Office has made every effort to list Surnames and first names in the correct order in this index. We apologise for errors and suggest that if in doubt, you check both names as entries in the index. *Thank you*

# a

- Aaro Sven**  
(G3/E/19-A5 1610-25)  
(GA5.12/E/06-A2 1600-03)
- Aas Eyvind**  
(P15/E/05-B4 1445)
- Abam Kingdon**  
(HW2/W/11-B1 1640)
- Abam T K S**  
(HS5/W/47-A3 1545-03)
- Abaseev Sergey S.**  
(ST5/W/28-B4 0930-05)
- Abbad S.**  
(ST1/E/87-A2 0930-12)
- Abbas H.**  
(G1/L/13-A3 1620-89)
- Abbs Deborah J.**  
(JWM08/W/08-A3 1200)  
(MC04/W/11-B2 1400)
- Abdalla Mohamed**  
(JSA19/L/06-A4 1400-03)
- Abdallah Mdaghri**  
(HS3/W/22-A2 1135)
- Abdel-Latif Ayman**  
(JSA19/L/04-A4 1400-01)
- Abdel Razek Mohamed H.**  
(GA1.04/P/01-A6 1200)
- Abdel-Hafez Tarek**  
(JSA19/L/01-A4 0915)
- Abdeldayem Abdelaziz L.**  
(GA1.05/W/13-A5 1730)
- Abdelhaq Dr**  
(GA4.09/W/13-A6 1220)
- Abd-Elmotaal Hussein**  
(G3/W/55-A5 1610-65)  
(G4/E/01-A3 1620-30)
- Abdrakhimov M. Z.**  
(ST4/E/54-B1 1400-13)
- Abdrakhmatov Kanatbek E.**  
(ST2/E/25-A5 1400-12)
- Abdu M. A.**  
(JSA20/C/GA2.02/W/20-A5 1200-12)  
(JSA20/W/24-A5 1200-07)  
(JSA20/W/47-A5 1110)  
(GA2.02/E/08-B5 1100)  
(GA2.02/W/08-B5 0920)
- Abdulla A.**  
(GA1.02/E/30-A20930)
- Abdullabekov K. N.**  
(G5/E/43-A4 1230-11)
- Abe Kuniaki**  
(JSS42/P/02-B5 0910)
- Abella Rafael**  
(JSV47/E/10-B5 1400-07)  
(JSP23/E/06-B2 1600)
- Abidin H.Z.**  
(G5/L/01-A4 1145)
- Abidin Hasanuddin Z.**  
(JSP23/E/27-B2 1700)  
(G6/C/G1/L/24-B1 1520)  
(JSV36/E/01-B3 1610)
- Ables Sean T.**  
(GA3.04/W/17-B1 1520-16)
- Ablitt B.**  
(P15/L/22-B3 1135)
- Abo M.**  
(JSA20/W/09-A4 1200-11)
- Abolghasem M.**  
(G4/C/G5/W/01-A3 1620-27)
- Abou Elenean K.**  
(ST2/E/07-A4 1700)  
(ST2/E/51-A4 1715)
- Abou-Dina Mostafa S.**  
(GA1.02/P/04-A1 1400)
- Abrahamson Niels**  
(GA1.04/W/08-A4 0930-05)
- Abrahamsson Katarina**  
(JSP21/W/02-A4 1150)
- Abrahamyan Hrachya**  
(JSP23/E/11-A5 0830-10)
- Abramova L.**  
(GA1.02/L/03-A2 0930)
- Abrams Mark**  
(MI06/L/04-B1 0950)
- Abrikosov A.**  
(G4/W/09-A3 1620-25)
- Abril M.**  
(ST5/W/56-B3 0900-01)
- Abtout A.**  
(JSS44/E/07-B4 0930-16)  
(G5/E/27-A4 1230-05)  
(G5/P/03-A4 1230-04)  
(GA5.01/E/28 A1 0900-01)
- Abu-Ashour Nasser M.**  
(GA5.12/P/01-A2 1600-09)
- Abu-El-Ata Ahmed**  
(JSA19/W/04-A4 1400-05)
- Abuel-Atta Ahmed**  
(ST3/W/42-B4 1030)
- Aburjania George D**  
(GA4.09/P/01-A5 1600-01)
- Achauer Uli**  
(JSS46/E/03-B4 1420)
- Achauer Ulrich**  
(JSS46/W/02-B4 1500)  
(ST4/E/10-B3 0940)
- Ackerman T. P.**  
(MI10/W/25-B1 0930)
- Ackerman Thomas P.**  
(MI10/W/18-B2 1735)
- Ackerman Tomas P.**  
(MI10/W/15-B1 1000)
- Ackley S. F.**  
(JSA09/W/17-A2 1715)
- Acosta J.**  
(GA5.12/E/04 A2 0930)
- Acosta Jose**  
(JSA40/E/07-B5 0950)
- Acre Mario Fernandez**  
(JSS42/E/18-B5 1010)
- Across development team**  
(JSV47/E/02-B5 1230)
- Acuna G.**  
(G3/E/44-A5 1610-66)
- Acuña M.**  
(GA2.02/L/01-B4 1000)
- Acuna M. H.**  
(GA4.10/W/13-A4 0930)  
(GA4.01/W/11-A2 1100)
- Acuna P.**  
(GA4.10/W/13-A4 0930)
- Adachi Yuuya**  
(JSM24/E/11-B1 1205)
- Adám Antal**  
(GA6.01/P/05-A5 1715)  
(GA6.01/P/05-A5 1715)
- Adam J.**  
(G1/E/31-A3 1620-65)  
(G1/E/46-A3 0930)
- Adam Jozsef**  
(G3/E/41-A5 1610-84)
- Adamenko V. N.**  
(MC02/P/03-B2 1710)
- Adamova Albina**  
(ST5/E27-B1 0830-13)
- Adams John**  
(ST5/W/01-B3 0900-05)  
(ST1/E/06-A4 0930-39)  
(ST1/E/58-A2 1400-18)
- Adekugbe-Joseph A. O.**  
(G4/E/07-A3 1620-32)  
(JSG14/L/02-A3 1218-27)
- Adelina Iren**  
(JSP23/E/53-A5 0830-08)
- Adelkhanov S. S.**  
(GA3.02/E/12-B3 0900-01)
- Adler Mary-Jeanne**  
(HS1/W/48-B4 1005)  
(HS4/W/09-A4 1510)
- Adler Robert**  
(JSM41/E/01-B3 1620)  
(MW02/E/06-B3 1720)  
(JSM41/W/01-B3 1705)
- Adrian Hitchman**  
(GA1.02/E/01-A2 0930)
- Adriani A**  
(JSM01/W/08-A4 1450)
- Adriani Alberto**  
(JSA09/W/12-A2 1630)
- Aellig M.**  
(GA4.04/E/05-B5 0940)
- Afilhado Alexandra**  
(U7/E/03-B1 0830-17)
- Afonso Germano B.**  
(G2/W/11-A2 1630-05)
- Agarwal A. K.**  
(GA1.02/W/12-A1 1050)  
(GA1.02/W/23-A1 1400)
- Ageev Vladimir V.**  
(GA1.02/E/37-A1 1605)
- Agnihotri R.**  
(P07/E/03-A3 1430)
- Agrawal P. K.**  
(JSA37/E/02-B3 1715)  
(ST4/E/16-B1 1200)
- Aguilar A.**  
(JSP23/C/U5/W/14-B2 1210)
- Agustine Eleonora**  
(GA 1.05/E/12-A5 0850)
- Ahern Tim**  
(JWS33/W/22-B2 1635-01)  
(JWS33/W/22-B3 0900-01)  
(U7/W/18-B1 0830-19)
- Ahluwalia H.**  
(GA4.04/L/04-B5 0830-09)  
(GA4.04/L/13-B5 1400-08)  
(GA4.04/L/14-B5 1400-09)
- Ahmad-Berger Zarina**  
(G1/W/08-A3 1620-35)
- Ahmed A Amar**  
(GA5.12/P/01-A2 1600-09)
- Ahmed Fathy Mohamed**  
(GA5.01/P/01 0900-02)  
(GA5.01/P/03 1300-01)  
(GA5.01/P/04 1615)
- Ahrens Thomas J**  
(JSS02/E/18-A1 1145)  
(ST6/W/06-A1 0830-08)
- Ai-Chen Zhang**  
(JSM43/E/08-B5 0920)  
(JSM43/E/11-B5 0940)
- Aiguo Ruan**  
(JSS07/P/01-A2 1105)
- Aiken Jim**  
(P15/E/03-B3 1440)  
(P15/E/04-B4 1135)  
(P15/L/29-B3 1550)  
(P15/L/26-B3 1110)
- Aikio A.**  
(GA3.06/W/30-A2 0930-17)
- Aiming Cao**  
(SW1/W/04-B5 1200)
- Airaksinen Paavo J.**  
(JSG28/E/22-B1 1400-01)
- Airo Meri-Lisa**  
(GA5.11/L/04 A3 1430-05)
- Ajith J. J.**  
(P09/E/02-A2 0950)
- Ajith K. J.**  
(P14/E/07-A4 1400-01)
- Aka Akpa**  
(HS1/W/50-B5 1640)
- Akacem N.**  
(GA5.01/E/19 A1 1730)
- Akagi Kazuaki**  
(JSM01/W/23-A4 1620-06)
- Akahori Koji**  
(JSM26/W/25-B2 1700-11)
- Akaku Kouhei**  
(ST4/W/23-B1 1400-10)
- Akamatsu J.**  
(ST3/W/39-B4 1400-08)
- Akamatsu Junpei**  
(ST3/E/30-B4 0930-13)  
(ST3/E/31-B3 1000)  
(ST3/E/35-B4 0930-14)
- Akasheh B.**  
(ST2/E/09-A4 1130)
- Akhmetzanov Albina**  
(GA1.01/W/37-A5 1715)
- Akihidekasai**  
(P09/W/04-A1 1440)
- Akins J. A.**  
(ST6/W/06-A1 0830-08)
- Akio Kitoh**  
(MC01/E/13-A1 1130)
- Akio Suzuki**  
(ST6/E/11-A2 1530)
- Akira Morioka**  
(GA2.02/E/04-B4 0930-10)
- Akira Yoneda**  
(JSS02/E/11-A1 0830-08)
- Akitomo Kazunori**  
(P12/W/08-A1 1600)
- Akitomo Kazunori**  
(P13/W/01-B1 1150)  
(P13/W/02-B2 1050)
- Akiyoshi H**  
(MI02/W/15-A5 1100)
- Akiyoshi Hideharu**  
(JSM01/W/116-A5 1000)  
(JSM01/W/29-A5 0940)  
(MI02/E/03-A5 1240)
- Akkargan Sahin**  
(ST4/W/37-B1 0830-03)
- Akmaev R. A.**  
(JSA20/W/39-A4 1200-03)
- Aksenov V. V.**  
(ST1/E/47-A2 1400-35)
- Aktar Mustafa**  
(G5/E/23-A4 1230-08)
- Akulov Vadim M.**  
(JSA15/W/20-A5 1400-14)
- Al Aasm I. S.**  
(GA1.04/W/03-A4 0930-15)
- Al Naimi Latifa Sh.**  
(JSA19/W/06-A4 0900)
- Al Saadi J.**  
(JSM26/W/11-B1 0940)
- Alan Linde**  
(JSV47/E/01-B5 1400-05)
- Alapaty Kiran**  
(MI07/W/05-A2 1140)
- Albarede F.**  
(JSV29/E/02-B1 1440)
- Albarelo Dario**  
(ST3/W/15-B5 1500)  
(ST7/L/03-A2 1430)
- Alberoni Pier Paolo**  
(JSP05/E/03-A1 1130)
- Albers Frank**  
(MI08/W/18-A4 1150)
- Albers Michael**  
(ST4/W/10-B3 1650)
- Albert J. M.**  
(GA3.05/W/34-B3 1420)
- Albert Ramses**  
(ST3/W/42-B4 1030)
- Albertella Alberta**  
(G6/C/G2/E/12 1100)
- Alberto Cirella**  
(JSV47/E/01-B5 1400-05)
- Alberto Cominguez**  
(JSS44/W/19-B4 0930-01)
- Albrecht Franz M.**  
(JWM08/E/01-A2 1400)
- Alcamo Joseph**  
(HW1/L/10-A4 0930)
- Alcantar-Israde I.**  
(GA1.05/W/27-A5 0900-03)
- Alcantar F.**  
(JSP23/C/U5/W/14-B2 1210)
- Aldridge Keith**  
(JSA17/W/13-A4 1430)
- Alejandra Salles**  
(JSM01/E/37-A4 1000)  
(JSM01/E/36-A4 1620-10)
- Alekseev G V**  
(JSM18/W/11-A5 1020)
- Alekseev Vladimir**  
(JSP23/W/22-B1 010)  
(ST1/E/15-A2 0930-09)
- Alekseev Vladimir A.**  
(JSM41/E/05-B5 1530)
- Alekseyev G V**  
(JSM18/W/07-A5 0940)
- Alexander Joan**  
(MW01/W/05-A5 0930)
- Alexander M J**  
(JSM01/W/53-A3 1400)  
(MW07/E/08-A4 1450)  
(MW07/W/02-A4 0940)  
(JSA20/W/07-A5 0930)
- Alexander Michael**  
(JSP25/E/32-B3 1400)  
(JSP25/W/57-B4 1640)
- Alexander S. Shelton**  
(JWS33/W/02-B3 0900-20)
- Alexandr V**  
(MI09/E/09-A5 1145-05)
- Alexandrescu M.**  
(JSA10/E/06-A2 0945)
- Alexandrescu Mioara**  
(JSS13/W/04-A5 1630)  
(JWA34/W/09-B2 1150)
- Alexandrescu Mioara Mandea**  
(GA5.09/W/07 A2 1400-01)  
(JSA17/C/GA1.19/W/09-A4 0950)  
(JSA17/W/06-A4 1130)  
(JSA17/W/15-A4 1410)  
(GA1.07/W/04-B2 1100)  
(GA5.08/W/02-B1 1005)



## INDEX

- (GA6.02/W/01-B1 1520)
- Alexandrov E. B.**  
(GA5.01/E/08-A1 1045)  
(GA5.01/E/13-A1 1115)
- Alexandrova Olga**  
(JSP49W/07-B5 1210-12)
- Alexeev Igor**  
(GA3.07/W/31-A4 0930-01)  
(GA3.07/W/25-A3 0900-01)  
(GA3.02/W/31-B3 0900-05)  
(GA3.09/W/11-B4 1520)  
(GA4.08/W/01-B4 1545)
- Alexeev V. A.**  
(U3/W/16-A31200)
- Alexeev Vladimir**  
(JSP23/C/U5/W/05-B1 0830-14)
- Alexeyev V. N.**  
(JSA20/W/43-A4 1200-23)  
(JSA20/W/31-A4 1200-19)  
(GA3.05/E/05-B3 0900-29)
- Aleynik D. L.**  
(JSP25/C/U2/E/02-B1 0830-03)
- Ali M.**  
(GA1.05/W/01-A6 1515)
- Alf Kirkevåg**  
(MI01/W/16-A3 1010)
- Alfe Dario**  
(JSS02/W/10-A1 0830-11)
- Alfier R**  
(JSM01/W/02-A5 1210)  
(JSM01/W/37-A5 1400)
- Alfonsi Laura**  
(ST7/W/01-A2 1145)
- Alfonso Lester**  
(M104/E/17-B1 0900-13)  
(M104/E/23-B4 1005)
- Alfredsen Knut**  
(HW3/W/05-B4 1115)
- Alguacil G**  
(JSV47/W/20-B5 1400-13)  
(JSV47/W/01-B5 1045)  
(JSV47/W/17-B5 1400-14)  
(JSV47/W/29-B5 1400-22)  
(JSV47/W/30-B5 1400-23)  
(ST5/W/55-B5 1225)  
(ST5/W/56-B3 0900-01)  
(ST5/W/66-B4 1400-06)  
(ST5/E/11-B4 1420)
- Al-Hajjah Aiman**  
(JSA16/E/19-A3 0830-22)
- Ali Mohammad**  
(GA1.03/W/17-B2 1500)  
(GA1.03/W/25-B2 1440)
- Ali T.**  
(JSS31/L/04-B2 0830-17)
- Al-Ibiary Mohammad G.**  
(ST3/W/42-B4 1030)
- Alisse J.-R.**  
(JSM26/W/20-B1 1520)  
(JSP49/W/21-B5 1620)
- Alkaz Vasile**  
(ST3/E/40-B5 0845)  
(ST3/E/45-B4 1745)
- Alkemade Frans J. M.**  
(JSM01/W/39-A4 1020)  
(JSM01/W/15-A5 1720)
- Allaart M**  
(JSM01/W/37-A5 1400)
- Allain Serge**  
(JSG11/W/13-A4 1400-09)  
(U7/W/14-B1 0830-12)
- Allan Richard P**  
(MC08/E/01-A4 1045)
- Allan Robert J.**  
(JSP23/W/04-A5 0910)
- Allan R. J.**  
(JSP25/W/61-B4 0930)  
(JSP25/E/26-B5 1600)  
(JSP25/W/22-B1 1400)
- Allan W**  
(MI02/W/07-A4 1600)  
(GA3.07/W/10-A5 0930)  
(GA3.04/W/02-B1 1520-33)
- Allard R.**  
(P13/E/08-B2 1600-02)
- Allègre Claude**  
(ST1/W/35-A2 1400-21)
- Allen H**  
(JSA06/E/09-A1 1155-01)
- Allen J T**  
(JSP05/W/18-A1 1520)  
(P11/W/19-B4 1500)  
(P11/W/28-B4 1400)
- Allen J. H.**  
(GA4.01/E/08-A2 1600)
- Allen M. R.**  
(MC02/W/13-B2 1430)  
(MI11/W/07-B5 0915)
- Allen Myles**  
(JSA16/E/01-A3 0830-19)
- Allen R. M.**  
(ST4/W/03-B3 1630)
- Allison Ian**  
(P13/W/05-B1 1640)
- Alloway Brent**  
(JSV36/E/19-B3 0900-18)
- Almar Ivan**  
(GA2.02/E/11-B5 1600)
- Almarza R. Torres**  
(P10/W/09-A3 1050)
- Almeida Eugenio**  
(GA1.02/W/15-A2 0930)  
(GA1.02/W/38-A2 0930)
- Almendros J.**  
(JSV47/W/01-B5 1045)  
(JSV47/W/20-B5 1400-13)  
(JSV47/W/29-B5 1400-22)  
(JSV47/W/30-B5 1400-23)  
(ST5/W/56-B3 0900-01)
- Alonso S**  
(MI07/W/02-A2 1210)  
(MI07/W/03-A2 1420)
- Allothman M.**  
(GA3.03/W/03-B4 0930)
- Allothman Mohamed J.**  
(GA3.09/W/26-B4 0900-05)
- Alp Osman**  
(G3/E/14-A5 1610-67)
- Alperovich Leonid**  
(GA2.02/W/32-B4 1620)
- Alpers M**  
(JSM01/W/37-A5 1400)
- Alpert Pinhas**  
(MI05/E/05-A5 1020)  
(MI09/E/02-A5 0937)  
(JSM24/E/08-B1 1500)  
(JSP25/E/23-B1 1440)
- Alphonse C**  
(GA4.02/W/07-A4 1100)
- Al-Saadi Jassim**  
(JSM01/L/30-A5 1640)
- Al-Yamani Faiza**  
(PW1/E/07-A61500)
- Alsono Del Rosario**  
(P11/E/28-B5 0950)
- Altadill David**  
(JSA35/E/01-B1 1420)  
(JSA20/W/34-A4 1204)
- Altamimi Zuheir**  
(G1/C/G5/E/02-A3 1620-101)
- Altamimi Zuheir**  
(G6/E/04-B1 0830)
- Althausen Dietrich**  
(MI09/W/08-A5 1542)
- Altiner Y.**  
(JSS31/L/04-B2 0830-17)
- Altiner Yüksel**  
(G1/E/04-A3 1620-50)
- Altinok Yildiz**  
(JWS33/C/ST2/W/02-B2 1635-20)  
(JWS33/W/02-B3 0900-20)
- Altshuler E**  
(MC01/E/02-A4 1430)
- Altyntsev A.**  
(GA4.02/E/06-A4 1400-09)  
(GA4.02/E/13-A4 1400-08)
- Alva-Valdivia L.**  
(GA1.05/W/16-A6 0900-07)
- Alvarado Alexandra**  
(JSP23/C/U5/E/05-A6 0830-06)
- Alvarado Guillermo**  
(JSV47/W/02-B5 1400-17)
- Alvarez Garcia Francisco**  
(JSP25/E/11-B2 0930-02)
- Alvarez R.**  
(GA5.12/E/04 A2 0930)
- Alvarez Rosa**  
(GA5.01/L/01 A1 0900-03)  
(JSA40/E/05-B5 1400-17)
- Alves Sonia Maria**  
(G1/E/45-A3 1620-74)
- Amagai J.**  
(G2/E/01-A2 1630-12)  
(G2/W/01-A2 1630-01)
- Amagai Jun**  
(G2/E/04-A2 1630-13)  
(G2/E/08-A2 1630-11)
- Amalvict Martine**  
(JSA09/W/16-A2 0930-01)  
(JSG14/W/02-A3 1700-15)
- Ambaum Marten H. P**  
(MI05/E/30-A1 1120)
- Amblard Pierre-Olivier**  
(ST5/W/05-B3 1440)
- Ambraseys N.**  
(JSP23/C/U5/W/06-A6 1010)
- Ambrizzi Tércio**  
(MC10/E/04-B1 1715)
- Ambrosius B. A. C.**  
(JSG28/E/01-B1 1040)  
(G5/L/01-A4 1145)
- Ambrosius Boudewijn**  
(G5/E/36-A4 1215)
- Amelynck C.**  
(JSM26/W/29-B2 1700-09)
- Amenna Mohamed**  
(GA1.04/W/31-A4 1220)
- Ametistova L. E.**  
(JSP25/W/93-B3 0830-02)
- Amiranashvili Avtandil**  
(MI10/E/11-B1 0900-01)  
(MI102/E/04-A4 0950)  
(MI103/E/03-A3 1040)
- Amiranashvili Vazha**  
(MI03/E/03-A3 1040)  
(MI09/W/05-A5 1145-08)  
(MI110/E/07-B3 1505)  
(MI110/E/11-B1 0900-01)
- Amiri Saeed**  
(ST6/P/01-A1 0830-01)
- Amita K.**  
(JSA15/W/14-A4 1400-16)
- Amm Olaf**  
(GA1.02/W/33-A2 0930)  
(JSA06/W/07-A11155-05)  
(GA3.06/W/23-A2 1740)  
(GA3.07/W/66-A5 0900-01)
- Ammar Ahmed A.**  
(JSA27/P/02-B1 1400-03)  
(JSA27/W/01-B1 1000)
- Ammosov P P**  
(JSM01/W/108-A2 1600-25)
- Amoruso Antonella**  
(JSV47/E/01-B5 1400-05)
- Amory-Mazaudier C.**  
(JSA20/P/01-A5 1501)
- An Soon-Il**  
(JSP25/W/66-B1 1150)
- Anabtawi Aseel**  
(GA4.10/W/19-A4 1710)
- Anad F.**  
(GA5.01/E/19 A1 1730)
- Anagnostou Emmanouil**  
(JSM41/W/01-B3 1705)
- Anand M. B**  
(ST2/W/33-A5 1400-08)
- Anand S. P.**  
(JSS44/E/15-B4 0930-15)  
(JSS44/E/16-B4 0930-14)
- Ananda M B**  
(ST2/W/20-A3 1515)
- Ananicheva Maria**  
(U2/E/13-A2 1400)
- Ananthakrishnan A.**  
(GA4.02/E/07-A4 1400-02)
- Anatoly Pereskokov**  
(JSP49/W/20-B5 1210-17)
- ANCELLET Gerard**  
(JSM26/L/04-B2 1700-16)
- Andersen O**  
(G3/L/05-A5 1610-01)  
(G3/W/15-A5 1610-12)  
(G3/W/30-A5 1610-06)  
(JSP25/W/32-B3 0830-03)  
(JSS31/W/05-B3 0830-05)
- Andersen Ole B.**  
(P10/W/13-A4 1110)  
(JSG11/W/15-A4 1400-11)  
(P15/W/07-B3 1650)  
(JSP25/W/34-B3 0830-04)
- Andersen Per Helge**  
(JSG14/E/22-A3 1106-03)
- Anderson B. J.**  
(GA4.01/W/11-A2 1100)  
(GA3.04/W/20-B1 1100)  
(GA3.05/W/24-B3 1120)  
(GA3.04/W/47-B1 1230)  
(GA3.04/E/12-B2 1150)
- Anderson C.**  
(ST6/W/02-A1 0830-04)
- Anderson David**  
(MI05/W/28-A1 1440)  
(JSG28/W/01-B2 1400-16)
- Anderson Kenneth D.**  
(JSG28/E/10-B1 1400-13)
- Anderson Mark**  
(HS2/W/07-B1 1120)
- Anderson Ole B.**  
(JSP49/W/06-B5 1210-04)
- Anderson P. S.**  
(JSM04/E/09-A2 1140)  
(JSM04/E/0-A2 1240)
- Anderson Robert G.**  
(JSP30/C/JSV22/E/01-B1 1400-19)
- Anderson Roger R.**  
(GA3.05/E/06-B3 1140)
- Andersson**  
(JSA06/L/06 0935)
- Andersson L.**  
(HW2/W/23-B1 0900-05)
- Ando Masataka**  
(ST1/E/01-A4 0930-12)  
(ST1/W/44-A3 1420)  
(JWA34/E/08-B2 1230)
- Andonov B.**  
(GA3.04/W/15-B1 1520-15)
- Andrade Daniel**  
(JSP23/C/U5/E/05-A6 0830-06)
- Andreea M. O.**  
(P15/L/17-B4 1550)
- Andreas E. L.**  
(JSM04/W/02-A2 0930)
- Andreastuti Supriyati**  
(JSV30/E/01-B1 0920)  
(JSV30/E/01-B1 1400-10)  
(JSV36/E/19-B3 0900-18)
- Andrescu Maria**  
(ST4/E/43-B1 1400-09)
- Andreson O. B.**  
(G2/W/03-A2 1630-18)
- Andrew Smith Renshaw**  
(MI06/E/07-B1 1400-09)
- Andrews Michael D.**  
(GA4.02/W/25-A4 1400-23)
- Andre Raphael**  
(GA3.07/E/18-A6 0900)
- Andrianov Nicolay S.**  
(GA2.02/L/04-B4 0930-07)
- Andritsanos V. D.**  
(G3/W/22-A5 1610-07)
- Angel Miguel**  
(MC01/E/32-A2 1620)
- Angel Ortiz Miguel**  
(G1/E/15-A3 1620-55)
- Angell James K.**  
(JSP25/W/27-B5 1500)
- Angelopoulos V**  
(GA3.08/W/05-A6 1040)
- Angermann D. Michel**  
(JSS31/W/12-B2 1420)
- Angermann Detlef**  
(JSS31/E/07-B2 1210)  
(JSS44/E/41-B4 0930-35)  
(G1/E/49-A3 0910)
- Anghel Marius**  
(ST1/E/02-A1 1400)
- Angrilli A.**  
(MC09/W/07-B2 01)
- Angrilli F.**  
(JSA10/W/03-A2 0930)
- Angus Douglas**  
(ST1/W/21-A4 0930-01)
- Anisimov Vladimirovich Mikhail**  
(P07/W/16-A3 0900-05)
- Anisimov M. V.**  
(P12/E/01-A1 1030-04)  
(P12/W/06-A1 1030-10)
- Anklin M**  
(JSA16/W/15-A3 0830-41)  
(JSA16/W/20-A3 0830-53)
- Annan James D.**  
(GA2.01/W/01-A1 1150)
- Anna Giuseppe D.**  
(JSS42/E/19-B5 1700-14)
- Annaka T.**  
(ST3/E/56-B4 1400-20)  
(JSP23/C/U5/E/16-A5 1620)
- Anner Thomas C.**  
(HW3/W/07-B4 1205)
- Annegarn H J**  
(MI02/L/18-A5 1430)
- Ansal A.**  
(JSP23/W/17-A6 0830)
- Ansal Atilla**  
(JSP23/W/20-A6 1130)
- Ansari I. A.**  
(GA1.02/P/05-A1 1050)
- Ansher J. A.**  
(GA4.10/W/08-A5 1020)
- Anshu Jin**

- (ST1/W/69-A1 1640)
- Anthes Richard**  
(JSG28/W/25-B2 1400-11)  
(JSG28/W/27-B2 1110)  
(JSG28/W/04-B2 1400-13)
- Anthony Steven**  
(HS3/W/31-A2 1705)
- Antiochos S. K.**  
(GA3.09/W/30-B4 0945)
- Antoine David**  
(P15/L/30-B40950)
- Antonio Pazos**  
(GA5.01/E/26-A1 1500)
- Antonova A. E.**  
(GA3.04/W/35-B1 1520-46)  
(GA3.05/W/18-B3 0900-17)
- Antonova Elizabeth**  
(GA3.08/E/12-B1 1150)  
(GA3.02/E/08-B3 0900-03)
- Antonova Elizaveta E.**  
(GA3.09/E/09-B4 1735)  
(GA3.10/E/01-A6 1425)  
(GA3.10/E/03-A6 1700-15)
- Antonova Elizavieta**  
(GA3.08/W/10-B1 0900-06)
- Antsiferov A. V**  
(JSA27/L/01-B1 1400-02)
- Anufriev A.**  
(GA1.01/E/09-A5 0900-01)
- Anufriev Alexander**  
(GA1.01/W/22-A5 1115)  
(GA1.01/W/32-A5 1100)
- Anujee T. K.**  
(P09/E/02-A2 0950)
- Anzenhofer M**  
(JSH12/W/06-A5 1130)
- Anzenhofer Michael**  
(JSG11/E/10-A3 1400)  
(G3/E/43-A5 1610-17)  
(G3/W/07-A5 1610-15)
- Anzidel Marco**  
(G5/W/20-A4 1230-03)
- Aoi Shin**  
(ST3/W/24-B4 0930-07)
- Aonashi Kazumasa**  
(JSG28/W/07-B1 1400-07)  
(JSG28/E/26-B1 1400-11)
- Aotani T.**  
(JSV36/W/01-B3 0900-12)
- Aoudia Abdelkrim**  
(ST2/W/34-A4 1515)
- Aoyama Hiroshi**  
(ST5/W/32-B4 1400-05)
- Aoyama Yuichi**  
(JSG14/W/13-A3 1700-06)  
(JSG14/W/14-A3 1124-09)  
(JSG14/W/20-A3 1700-11)
- Aparin V. P.**  
(GA1.03/W/34-B3 1100)
- Apel John R.**  
(P10/E/10-A3 1210)
- Apostolov Emil M.**  
(JSA20/W/34-A4 1204)
- Appourchoux Thierry**  
(JSA16/W/25-A3 0830-46)
- prea Claudia Maria**  
(JSS46/W/10-B4 1600)
- Aptikaev F. F.**  
(ST3/E/01-B5 1400)
- Aquino M. G. S.**  
(GA2.02/E/08-B5 1100)  
(GA2.03/W/05-B3 1400-02)  
(GA2.03/W/05-B3 1600)
- Aquino Marcio**  
(G1/E/51-A3 1620-76)
- Arabelos D.**  
(G3/L/06-A5 0925)  
(ST1/W/49-A3 0900-02)
- Aragus-Aragus L.**  
(HW1/L/00-A4 0930)
- Arai Masazumi**  
(U7/E/02-B1 0830-10)
- Arain Muhammed Altaf**  
(MC01/W/13-A3 1635)
- Araki T.**  
(GA3.04/W/45-B1 1520-45)  
(GA4.08/W/12-B4 1635)
- Araki Tohru**  
(JWS33/W/37-B2 1430)  
(GA5.06/W/09-A3 1000)  
(JSA06/W/26-A2 1230)
- Aramaki Shigeo**  
(JSV36/E/17-B3 1400-09)
- Araña V.**  
(JSV47/W/30-B5 1400-23)
- Arana Vicente**  
(JSP23/E/02-B1 1210)  
(JSP23/E/26-B2 1050)
- Araneo Diego C.**  
(JSM01/E/38-A4 1620-09)
- Arango Hernan**  
(MC01/E/16-A2 1230)
- Araújo Pereira José de**  
(HS3/W/12-A1 1515)
- Arballo J. K.**  
(GA4.09/W/11-A6 0920)
- Arballo J. K.**  
(GA3.02/W/39-B2 1110)  
(GA4.08/W/12-B4 1635)
- Arber T. D.**  
(GA3.07/E/15-A4 1130)  
(GA6.01/E/06-A6 0920)
- Arbetter Todd**  
(P13/W/06-B2 1600-04)
- Arbogast Philippe**  
(MI05/W/46-A3 0940)
- Arbor Ann**  
(JSA35/W/06-B1 1400)
- Arbor Spakman**  
(JSS13/W/01-A4 1720)
- Archer David**  
(HS1/W/09-B5 0940)
- Archer S D**  
(JSP21/L/03-A4 1720)
- Arculus Richard**  
(JSV30/W/09-B1 1000)
- Ardeleanu Luminita**  
(ST1/E/11-A4 0930-21)
- Ardisson Marie Hanne**  
(JSA15/E/10-A3 1640)
- Aref A.**  
(JSS44/P/06-B4 0930-17)
- Arefiev Vladimir N.**  
(MI06/W/08-B1 1400-01)  
(MI06/W/08-B2 1400-01)
- Arefiev Sergej**  
(ST3/E/52-B3 1445)
- Arendt Anthony**  
(HS2/W/18-B2 1000)
- Arendt Steve**  
(U8/W/05-B3 1640-02)
- Arfeuille Gilles**  
(P13/W/25-B1 1110)
- Argo P E**  
(MI03/W/05-A3 1140)
- Argo Paul**  
(MI05/W/33-A5 1130)
- Arheimer Berit**  
(HS3/W/24-A2 1225)
- Aric Kay**  
(JSA19/W/12-A4 1000)
- Arijs E.**  
(JSM26/W/29-B2 1700-09)
- Arinin V.**  
(GA3.02/W/58-B3 0900-22)
- Ariyibi E. A.**  
(GA1.02/L/02-A2 0930)
- Arizou Madani**  
(G3/P/06-A5 1610-71)
- Arkani-Hamed J.**  
(GA5.08/E/07-B1 1330)
- Arkhipkin A. V.**  
(P12/W/12-A1 1030-03)
- Arkhipkin V. S.**  
(P11/W/14-B5 1150-08)
- Armante R**  
(MI05/W/30-A3 1220)
- Armi Laurence**  
(JSP49/E/07-B5 1050)  
(JSP49/L/01-B5 1110)  
(JSP49/W/12-B5 1130)
- Armienta M. A.**  
(HW2/W/21-B1 0900-03)
- Armienta Maria Aurora**  
(JSV36/C/U6/W/08-B3 1400-21)
- Armigliato Alberto**  
(JSS42/W/21-B5 0950)
- Armstrong Phillip A.**  
(JSS44/W/10-B4 1110)  
(JSS44/W/17-B4 0930-31)
- Armstrong R.**  
(JSM41/E/19-B4 1750)  
(JSM41/E/09-B4 1635)
- Arnarson Halldor**  
(JSS42/W/06-B5 1400)
- Arnold N. F.**  
(JSA20/W/04-A4 1200-02)  
(JSA20/W/29-A4 1200-13)
- Arnold Neil**  
(JSA45/W/16-B5 0950)
- Arnoldy R. L.**  
(GA3.02/W/43-B2 0920)
- Arnoldy Roger**  
(GA3.04/W/47-B1 1230)
- Arnoso J.**  
(G5/W/26-A4 1550-06)
- Arora B. R.**  
(GA1.07/E/01-B2 1020)  
(GA3.04/E/10-B1 1520-11)
- Arpa Ma. Carmencita B.**  
(VS2/E/07-B3 1230)
- Arriaga Arlindo**  
(JSM41/W/28-B4 0930)
- Arritt Raymond W**  
(MC01/W/08-A4 0950)  
(MC01/E/17-A5 0930)
- Arsadi E.M.**  
(JSA15/E/17-A3 1440)  
(GA1.02/E/29-A2 0930)  
(JSA15/E/02-A5 0830-05)
- Artale Vincenzo**  
(P11/L/04-B5 0930)  
(P11/L/03-B5 0910)
- Artamonov Jurij**  
(P07/E/02-A3 0900-06)
- Aruliah Anasuya L.**  
(GA2.07/W/27-A1 1510)
- Arun T.**  
(GA3.03/E/03-B4 1400-01)
- Arvelius Johan**  
(JSM26/W/26-B2 1700-10)
- Arvidsson R.**  
(ST2/E/51-A4 1715)
- Aryan Graham**  
(VS2/W/02-B3 1400-02)
- Arzhakova Svetlana**  
(HS1/W/12-B4 1745-02)
- Arzoumanian Valery**  
(ST3/E/52-B3 1445)
- Asabina Elena**  
(HS1/W/08-B5 0830-01)
- Asada T.**  
(JSA15/W/30-A4 0940)
- Asai Michiru**  
(ST1/W/24-A3 1130)
- Asano Y.**  
(GA3.08/W/28-B1 1510)
- Asano Yuko**  
(HW5/E/05-A3 1100)
- Asanuma Jun**  
(JSM24/W/04-B1 0930)
- Ascher Uri**  
(GA1.02/W/30-A1 1415)
- Asharaf T. T. M.**  
(P09/E/02-A2 0950)
- Ashby C. Travis**  
(MC04/W/08-B1 1425)
- Ashchepkov I. V.**  
(JSV30/C/U6/E/10-B1 1400-24)  
(JSV30/C/U6/E/11-B1 1400-25)  
(JSV36/C/U6/E/09-B3 1400-22)  
(JSV22/C/U6/L/02-A5 0900-04)
- Ashjaee Javad**  
(G1/E/09-A3 1620-22)
- Ashkenazi Vidal**  
(G1/C/G5/E/04-A3 1620-100)  
(G1/E/42-A3 1620-72)  
(G1/E/51-A3 1620-76)  
(G1/E/52-A3 1620-77)  
(G1/E/56-A3 1620-80)  
(G1/L/09-A3 1640-87)  
(G6/C/G1/E/55-B2 1700)
- Ashour Attia A.**  
(GA1.02/P/04-A1 1400)  
(GA6.01/E/10-A5 0930)
- Ashour-Abdalla M.**  
(GA4.10/E/04-A5 1420)
- Ashour-Abdalla Maha**  
(GA3.05/E/18-B3 0900-01)  
(GA3.05/E/21-B3 1520)  
(GA3.08/E/02-B1 1110)
- Ashtiany M. G.**  
(ST3/E/56-B4 1400-20)  
(JSP23/C/U5/E/16-A5 1620)
- Assinovskaya Bela**  
(ST2/E/32-A5 1145)  
(ST3/E/43-B4 1130)
- Assumpcao M.**  
(ST4/E/05-B1 1520)  
(ST4/E/65-B2 1520)
- Assunção Marcelo**  
(ST1/W/20-A4 0930-04)
- Astafurova E. G.**  
(JSS44/L/04-B4 1640)
- Astakhova Elena D.**  
(MI04/E/07-B1 0900-14)
- Astakhova N. L.**  
(GA2.03/L/01-B3 1400)  
(GA2.03/L/02-B3 1520).
- Aster Richard**  
(ST5/W/04-B5 1145)
- Asteriadis G.**  
(ST1/W/49-A3 0900-02)
- Astiz Luciana**  
(ST5/W/63/B3 0900-11)
- Astiz Mar**  
(JSV47/E/06-B5 1400-03)  
(JSP23/E/02-B1 1210)  
(JSP23/E/26-B2 1050)
- Astling Elford**  
(JSM43/W/08-B4 1110)
- Astraldi Mario**  
(P11/W/12-B4 1640)
- Aswathanarayana U.**  
(U7/C/U1/E/05-B1 0830-06)
- Aswatharayana U.**  
(PW1/E/01-A61220)
- Ata Abou El**  
(ST2/E/07-A4 1700)
- Atakan K.**  
(JSP23/C/U5/E/16-A5 1620)  
(ST3/E/56-B4 1400-20)
- Atakan Kuvvet**  
(JSS42/E/18-B5 1010)  
(ST4/W/54-B1 1620)
- Atalay Ayele**  
(ST2/W/09-A4 1745)
- Atanasiu Ligia Narciza**  
(JSA40/P/01-B5 1400-05)  
(JSS44/P/07-B4 0930-20)
- Athanassiadou Maria**  
(JSM43/E/09-B4 1150)
- Atlas E**  
(MI02/L/19-A4 1410)  
(JSP21/W/11-A4 1050)
- Atlas Elliot L.**  
(JSM26/W/04-B2 1130)
- Atreya Sushil**  
(MC09/W/08-B2 1400)
- Atsumu**  
(MC01/W/31-A1 1400)
- Attya El-Sayed**  
(JSS42/W/18-B4 1620)
- Audad Guillermo**  
(JSP25/W/88-B5 0930)
- Aubry Marie-Pierre**  
(JSV22/E/02-A5 1130)
- Auer Ingeborg**  
(JWM08/W/13-A2 1500)  
(MC02/W/11-B2 1210)
- Augath W.**  
(G1/E/31-A3 1620-65)  
(G1/E/46-A3 0930)
- Auger Emmanuel**  
(JSS46/E/05-B4 1440)  
(JSS46/W/08-B4 0930-03)
- Augusto Márcio**  
(HS5/W/09-A1 1710)
- Aulanier Guillaume**  
(GA4.01/L/01-A2 1220)  
(GA4.02/W/14-A4 0925)
- Aumont Olivier**  
(MC01/W/58-A5 1620)
- Aung Than H.**  
(P09/E/08-A1 1130)
- Aushev V. M**  
(JSM01/W/112-A2 1600-19)  
(GA4.01/W/14-A2 1400-08)
- Austin G. L.**  
(JWM08/L/02-A3 1400)
- Austin Geoff**  
(JWM08/W/04-A2 1020)
- Austin John**  
(MW 07/E/06-A4 1700)  
(MW01/E/03-A5 1650)  
(MW01/E/02-A5 1150-05)
- Austin Philip H.**  
(MI10/W/20-B2 1635)
- Austin R. T.**  
(MI104/E/25-B4 0930)
- Avagimov A. A.**  
(ST1/E/62-A4 0930-40)  
(ST1/E/70-A3 1700)
- Avakyan S. V.**  
(JSA16/C/GA4.07/E/25-A3 0830-21)
- Avanessian Ashot**  
(ST1/W/67-A1 1050)
- Avdeev Dmitry**  
(GA1.02/L/04-A1 1605)  
(GA1.02/W/26-A1 1605)

# INDEX

- Avdev Stoyan**  
(G3/E/33-A5 1610-47)
- Averbuch Olivier**  
(GA1.04/W/35-A4 0930-11)
- Avissar Roni**  
(MC01/W/34-A5 0945)  
(JSM43/W/09-B5 1140)  
(JSM43/W/11-B4 1700)  
(MI04/W/20-B1 1450)
- Avoird Ernst Van Der**  
(MW06/W/06-A3 1620)
- Avrett Eugene H.**  
(JSA16/E/09-A3 1100)
- Awaji Toshiyuki**  
(P12/W/08-A1 1600)  
(P12/W/20-A1 1030-09)
- Axford W.I.**  
(GA4.05/L/01-A1 1400)
- Awaji Toshiyuki**  
(P13/W/01-B1 1150)
- Ayadi Abdelhakim**  
(JSA46/W/14-B4 0950)  
(ST2/W/30-A5 1400-18)
- Ayers Greg**  
(MI01/W/19-A2 1720)
- Ayhan Emin**  
(G5/E/23-A4 1230-08)
- Ayhan Mehmet Emin**  
(JSS31/L/04-B2 0830-17)  
(JSS31/L/05-B2 1600)
- Aylward A. D.**  
(JSA20/W/04-A4 1200-02)
- Ayouaz A.**  
(G1/L/13-A3 1620-89)
- Ayrault Franck**  
(MI05/E/23-A3 1400)
- Azeem S I**  
(JSM01/W/107-A1 1510)
- Azeem S. M. I.**  
(JSA20/W/17-A6 1031)
- Aziz H. Abdul**  
(GA1.15/W/09-B4 1400)
- Azmoudeh-Ardalan Alireza**  
(G6/W/01-B1 1220)  
(G3/W/08-A5 1610-08)  
(G3/W/08-A5 1610-09)
- Azpilicueta Francisco**  
(JSG11/W/01-A4 1050)
- Azzali S.**  
(JSM41/E/03-B5 1105)
- (GA1.05/W/40-A6 0900-03)**
- Backhaus J. O.**  
(P09/E/06-A1 1110)  
(P14/W/16-A4 1700)
- Bacmeister Julio T.**  
(MI04/E/27-B1 1705)
- Baci Günruh**  
(ST2/W/22-A5 1400-13)
- Badger Jake**  
(MI05/E/27-A2 1140)
- Badiali L.**  
(JWS33/E/03-B2)  
(JWS33/E/03-B3 0900-06)  
(JWS33/E/05-B2 1635-03)  
(JWS33/E/05-B3 0900-03)
- Badruddin**  
(GA4.08/W/22-B3 0900-03)
- Baduev Alfred B.**  
(JSA15/W/20-A5 1400-14)
- Bae Seok-Hee**  
(JSA06/W/28-A1 1155-13)
- Baehr Christophe**  
(MI05/E/23-A3 1400)
- Baer Ferdinand**  
(MW03/W/12-B4 1430)
- Baer Gideon**  
(G1/W/16-A3 1620-06)
- Baer M.**  
(ST5/L/02-B3 0900-02)
- Báez A.**  
(JSP21/C/U4/W/03-A4 0910)  
(JSP23/W/72/C/U4/W/03-A6 0830-18)
- Bagala L. G.**  
(GA4.02/E/08-A4 1400-05)  
(GA4.02/E/10-A4 1400-03)
- Baggaley W J**  
(JSM01/E/39-A1 0940)
- Bahls Susanne**  
(HS4/W/12-A4 1630)
- Bai Denghai**  
(JSV36/E/08-B3 0900-06)
- Baik Jong-Jin**  
(MW07/W/07-A4 1640)
- Bailey David A**  
(MC01/W/12-A2 1650)
- Bailey G. J.**  
(JSA20/W/48-A4 1200-31)  
(GA3.09/W/19-B5 1100)
- Bailey Rick**  
(JSM41/W/14-B4 1500)
- Bailey S. M.**  
(JSA45/E/10-B4 1125)
- Bailey Scott M.**  
(JSA16/E/12-A3 0830-14)
- Baimoldaeva A.**  
(ST4/E/71-B2 0930-25)
- Baines K. H.**  
(MC09/W/10-B2 1515)  
(MC09/W/06-B2 1630)
- Baines Peter G.**  
(JSP39/E/11-B4 1400)  
(JSP49/L/02-B5 1500)  
(MW06/E/06-A3 1200)
- Baird D. T.**  
(GA4.10/W/14-A4 0900)
- Baisheng Ye**  
(HS2/W/14-B1 1620)  
(HS2/W/19-B2 1020)  
(HS2/W/24-B2 1220)
- Baishev D. G.**  
(GA3.02/L/05-B3 0900-26)  
(GA3.04/E/15-B1 1520-02)
- Bajc Jure**  
(ST2/E/03-A5 1400-26)
- Baker Calum**  
(ST1/W/61-A1 1500)
- Baker D. N.**  
(GA4.01/E/08-A2 1600)  
(GA3.08/E/01-A6 1430)  
(GA3.02/W/27-B3 1205)  
(GA3.02/W/41-B2 1600)  
(GA3.03/E/05-B4 1000)  
(GA3.05/E/07-B3 0930)  
(GA3.05/E/16-B3 0950)  
(GA3.05/E/23-B3 0900-28)  
(GA3.05/W/13-B3 0900-34)  
(GA3.08/W/22-A6 1210)  
(GA3.09/W/14-B4 1720)  
(GA4.08/E/07-B3 1300)  
(JSA45/E/10-B4 1125)
- Baker Dan**  
(GA3.05/W/04-B3 0900-45)
- Baker Haydar**  
(GA5.12/E/02-A2 1600-07)
- Baker Helen**  
(JSG28/E/16-B1 1400-14)  
(JSG28/W/06-B1 1400-06)  
(JSG28/E/07-B1 0950)
- Baker J. B.**  
(GA3.03/W/13-B4 1430)
- Baker K. B.**  
(GA3.08/W/19-A6 1520)
- Baker Karen**  
(P15/L/01-B4 1205)
- Baker Kile B**  
(GA3.10/W/11-A6 1700-12)
- Baker Trevor F.**  
(JSG14/L/11-A3 1430)
- Baker Vidal Trevor**  
(JSG11/E/15-A4 1010)
- Bakhareva M. F.**  
(GA4.04/W/01-B5 0830-02)
- Bakhmeteva N. V.**  
(JSA20/W/42-A4 1200-22)  
(JSA20/W/46-A4 1200-20)
- Bakhsoliani Muraz**  
(MI10/E/11-B1 0900-01)
- Bakirov Apas B.**  
(ST2/E/25-A5 1400-12)
- Bakkehoi Steinar**  
(JSP23/C/U5/E/08-B1 1700)
- Bakun W. H.**  
(ST3/W/10-B4 1515)
- Bala Andrei**  
(JSS 44/E/08-B4 0930-21)  
(JSS 44/E/23-B4 0930-22)
- Balabas M. V.**  
(GA5.01/E/13 A1 1115)
- Balachandran Nambath**  
(MW08/W/06-A2 1730)  
(MW08/W/01-A2 1530)
- Balandina Svetlana E.**  
(JSA15/E/58-A5 0830-13)
- Balasis G.**  
(GA1.02/E/30-A20930)
- Balassanian S.**  
(JSP23/C/U5/E/16-A5 1620)  
(JSP23/W/38-B2 1720)  
(ST3/E/56-B4 1400-20)
- Balassanian Serguei**  
(ST1/W/67-A1 1050)
- Balassubramoniam G.**  
(JSS44/E/04-B4 1010)
- Balch C**  
(JSA06/W/10-A1 1400)
- Balchand A N.**  
(PW1/E/06-A6 1440)  
(P09/E/04-A1 1050)  
(P14/E/07-A4 1400-01)  
(P09/E/02-A2 0950)
- Baldi P.**  
(JSV36/W/17-B3 1500)
- Baldi Paolo**  
(G5/W/17-A4 1415-04)  
(G5/W/20-A4 1230-03)
- Baldrige W. Scott**  
(JSS46/W/10-B4 1600)
- Baldwin Mark P.**  
(MI12/W/02-B4 1630)  
(MW08/W/04-A2 1630)  
(MC06/W/05-A1 1020)
- Baldwin Michael**  
(MC04/E/04-B2 1625)
- Balestri Stefano**  
(JSM26/W/16-B2 1210)
- Balis D**  
(JSM01/W/37-A5 1400)  
(JSP21/W/09-A4 1130)
- Baliunas Sallie**  
(GA6.01/W/18-A5 1455)
- Balland A**  
(G3/E/40-A5 1610-05)
- Ballani L.**  
(JSA40/W/03-B5 1400-07)
- Ballard J**  
(JSM01/W/08-A4 1450)
- Balloomeil Leila Saado**  
(P11/P/05-B5 1150-05)
- Balme M. R.**  
(JSA10/W/07-A2 1415)
- Balmino G.**  
(G3/E/27-A5 1610-02)
- Balogh A.**  
(GA4.01/W/13-A2 1420)  
(GA4.02/W/20-A4 1400-18)  
(GA4.04/E/04-B5 0830-01)
- Balogh Andre**  
(GA4.09/E/06-A6 1500)  
(GA4.09/E/12-A6 1520)
- Balsley Ben B.**  
(JSM32/E/03-B3 0930)
- Bamandas Basu**  
(GA2.02/W/27-B5 1140)
- Banasik Kazimierz**  
(HS3/W/02-A1 0925)
- Bandyopadhyay G**  
(GA1.04/P/02-A4 1710)
- Banerdt B.**  
(JSA10/W/03-A2 0930)
- Banfield Colin E.**  
(JWM08/W/06-A3 1500)
- Banglin Zhang**  
(MC01/W/62-A1 1430)
- Banic C M**  
(MI01/W/03-A1 0900-03)
- Banic Cathy**  
(MI01/W/04-A1 1640)
- Banks R. J.**  
(GA1.02/E/16-A2 0930)
- Banola S.**  
(GA 2.02/E/14-B5 1040)
- Bansemir Aaron R**  
(MI03/W/06-A3 1000)
- Bantges R. J.**  
(MI06/W/31-B2 1210)
- Banzon V F**  
(MI09/L/03-A5 0830)
- Baokun Li**  
(ST3/E/29-B3 1530)
- Baoli Li**  
(G1/E/33-A3 1620-66)
- Baoxiang Xu**  
(G1/L/10-A3 1620-30)
- Baptista António M.**  
(JSS42/W/25-B4 1600)
- Baptista M. A.**  
(JSS42/E/03-B5 1700-12)
- Baptista Paulo**  
(G5/W/03-A4 1230-01)
- Barabanova E.**  
(HW1/L/08-A4 1130)
- Barabash S.**  
(GA4.10/W/24-A4 1125)
- Baran A. J.**  
(MI06/E/10-B2 1150)
- Baran Anthony J.**  
(MI04/E/26-B2 0950)
- Baran Lubomir W.**  
(JSG28/E/28-B2 1400-01)
- Baranov V.**  
(ST3/W/52-B4 0930-20)
- Baranyi Tunde**  
(GA6.01/P/08-A5 0900)
- Barberi Franco**  
(UL3-B2)  
(VS2/E/02-B3 1110)
- Barberi Graziella**  
(JSV47/W/09-B5 1200)
- Barbosa André**  
(JSM43/W/03-B4 1400)
- Barcilon Albert**  
(MI11/E/12-B5 1000)
- Barclay J.**  
(JSV30/W/14-B1 1120)
- Bard Pierre-Yves**  
(ST3/W/20-B3 0945)  
(JSP23/E/01-A6 1110)
- Bárdossy A.**  
(HS1/W/49-B4 0925)
- Barka Aykut**  
(JSS31/L/04-B2 0830-17)  
(G5/E/23-A4 1230-08)
- Barker Andrew P**  
(HS5/W/34-A3 1000)
- Barker H. W.**  
(MI10/W/16-B2 1435)
- Barker Rod A.**  
(JSM26/E/10-B2 1000)
- Barkhatov N. A.**  
(GA3.04/E/02-B1 1010)  
(GA4.08/E/04-B3 0900-15)
- Barlage Mike**  
(HS3/W/28-A2 1515)
- Barlier F**  
(G3/E/27-A5 1610-02)  
(G5/E/29-A4 1015)
- Barmin M.**  
(U8/E/09-B3 1155)
- Barmin Michael**  
(JSA09/E/05-A3 0900)
- Barnard S**  
(MC01/L/07-A2 1430)
- Barnes R. J.**  
(GA2.03/W/01-B3 0950)
- Barnes Rob**



- (JWS33/W/27-B2 1635-22)  
(JWS33/W/27-B3 0900-22)
- Barnett T. P.**  
(MC02/W/01-B2 1100)
- Barnier Bernard**  
(P12/E/05-A1 1520)
- Barnola J M**  
(JSP21/W/11-A4 1050)
- Barraclough D.**  
(GA1.01/W/31-A5 1645)
- Barraclough David R.**  
(GA6.02/E/01-B1 1400)
- Barray Jean-Luc**  
(JSM26/L/04-B2 1700-16)
- Barreto L.M.**  
(GA5.06/E/06 A3 1600)
- Barreto Luiz M.**  
(GA6.02/E/09-B1 1420)
- Barrett Eric**  
(JSM41/E/260-B3 1635)
- Barrett Michael H.**  
(HS5/W/34-A3 1000)
- Barrett Mike H.**  
(HS5/W/31-A3 0900)
- Barrie L A**  
(MI01/L/04 1055)
- Barrie Len**  
(MI01/W/12-A1 0945)
- Barrientos Sergio**  
(U8/W/03-B3 1425)
- Barriot Jean-Pierre**  
(JSA10/W/03-A2 0930)  
(JSA10/W/11-A2 1000)  
(JSA10/W/14-A3 1430-02)  
(JSA10/W/12-A2 1615)
- Barros Inocencio J. M.**  
(JSP23/E/27-B2 0830-14)
- Barros J. M.**  
(JSP23/E/23-B2 0830-09)
- Barros Lucas**  
(ST1/W/20-A4 0930-04)
- Barroso Carla S. F.**  
(JSM43/W/03-B4 1400)
- Bartolozzi Federico**  
(JSP23/P/03-A5 0830-19)
- Barry Leon**  
(MI05/W/20-A1 1500)
- Barry Roger G.**  
(JWS33/W/34-B2 1635-02)
- Barszczus Hans G.**  
(GA1.03/L/01-B1 0940)
- Bar-Sever Yoaz**  
(JSG28/E/14-B1 1400-21)  
(JSG28/L/01-B1 1400-03)
- Barsugli Joseph J.**  
(JSP25/W/24-B1 0850)
- Barsukov P.**  
(GA1.02/L/03-A2 0930)
- Barthelmes Franz**  
(JSG14/E/10-A3 1700-17)
- Barth C. A.**  
(JSA45/E/10-B4 1125)
- Barth John A.**  
(P10/W/04-A5 1600-05)
- Bartle G A**  
(HW5/W/11-A3 0940)
- Bartnicki Jerzy**  
(MI01/L/01-A1 1210)
- Bartolozzi Federico**  
(JSP23/P/04-A5 0830-05)  
(JSP23/P/05-A5 0830-04)  
(JSP23/W/90-B1 0830-13)
- Barton Charles**  
(GA1.02/E/05-A1 1015)  
(GA5.01/E/07 A1 1445)  
(GA5.01/E/19 A1 1730)
- Barton E. D.**  
(P10/W/09-A3 1050)
- Barton Ian**  
(JSM41/W/30-B3 1220)
- Barulin Boris S.**  
(JSA40/W/15-B5 1400-02)
- Barzaghi Riccardo**  
(JSS46/E/06-B4 0930-02)  
(G3/E/18-A5 1610-68)
- Baschek Burkard**  
(P11/E/05-B4 1440)
- Basham P.**  
(ST3/E/56-B4 1400-20)  
(JSP23/C/U5/E/16-A5 1620)
- Basham Peter**  
(U8/W/03-B3 1425)
- Bashkirov**  
(GA3.05/W/46-B3 0900-02)  
(GA3.05/W/49-B3 0900-32)
- Bashkov Viktor**  
(G5/E/46-A4 1115-09)
- Bashkuev Yury B.**  
(JSA15/W/20-A5 1400-14)
- Basili A.**  
(JWS33/E/03-B2)  
(JWS33/E/03-B3 0900-06)  
(JWS33/E/05-B2 1635-03)  
(JWS33/E/05-B3 0900-03)
- Bass J D**  
(ST6/C/JSS02/W/08-A2 1720)
- Bassinot Franck**  
(JSV22/E/02-A5 1130)
- Bastani M.**  
(GA1.02/W/41-A1 0830)
- Bastidas Luis**  
(HW4/W/01-B2 1200)
- Bastos Luisa**  
(G1/E/37-A3 1620-69)  
(G1/W/39-A3 1620-45)  
(G3/E/01-A5 1610-26)  
(G5/W/03-A4 1230-01)  
(G6/E/02-B2 1140)
- Batalev Vlad**  
(GA1.02/E/22-A2 0930)
- Bates I.**  
(GA3.07/W/49-A3 0900-02)
- Bates J. R.**  
(U3/W/16-A31200)
- Bates John**  
(MC01/L/03-A1 1415)  
(MC08/W/08-A3 1400)
- Bates M. P.**  
(GA1.04/E/11-A4 1610)
- Bates T S**  
(MI09/W/14-A5 1030)  
(MI09/W/14-A5 1145-21)
- Batista I. S.**  
(JSA20/W/24-A5 1200-07)  
(GA2.02/W/08-B5 0920)
- Batista P P**  
(JSM01/W/94-A3 1220)
- Batista P**  
(JSM01/W/45-A2 1600-06)
- Batillo Josep**  
(ST7/L/01-A2 1230)  
(JSA35/E/01-B1 1420)  
(ST5/W/15-B4 1400)
- Battelli P.**  
(JWS33/E/03-B2)  
(JWS33/E/03-B3 0900-06)
- Bauch D.**  
(P07/L/02-A3 1125)
- Bauer Hans-Stefan**  
(MW02/W/10-B3 0950)
- Bauer O.**  
(GA4.02/E/08-A4 1400-05)  
(GA4.02/E/10-A4 1400-03)
- Bauer Peter**  
(JSM41/L/02-B3 1550)  
(MI06/W/10-B1 1500)
- Bauer Siegfried J.**  
(GA4.10/L/03-A4 1110)  
(JSA10/W/13-A3 1000)
- Bauguitte S**  
(MI02/L/19-A4 1410)
- Bauguitte Stéphane**  
(U2/E/14-A2 1420)
- Baumann Robert**  
(MI01/E/03-A1 1700)
- Baumert Helmut**  
(P09/W/02-A1 09100)  
(JSP49/W/19-B5 1210-08)
- Baumgardner D.**  
(JSP21/C/U4/W/03-A4 0910)  
(JSP23/W/72/C/U4/W/03-A6 0830-18)
- Baumgardner Darrel**  
(MI08/W/09-A4 1515)
- Baumgardner J.**  
(JSA20/E/27-A4 1200-21)
- Baumgarten Gerd**  
(JSM01/E/47-A1 1000)
- Baumgartner Michael F.**  
(HS2/W/05-B1 1020)  
(HS2/W/10-B1 1400)
- Baumjohann Wolfgang**  
(GA3.02/W/52-B2 1705)
- Baur Michael**  
(JSP23/W/26-A5 1150)
- Bautista A.**  
(GA1.05/W/07-A6 0900-06)
- Bautista Bartolome C.**  
(ST2/W/21-A5 1400-02)  
(ST3/E/51-B4 1400-09)
- Bautista Leonila P.**  
(ST3/E/51-B4 1400-09)  
(ST2/W/21-A5 1400-02)
- Bava K. Abdulla**  
(P08/W/05-A2 1640)
- Bawden G.**  
(JSS31/E/11-B2 1010)
- Bay F.**  
(JSP23/E/03-A6 0930)
- Bay Francesca**  
(ST3/E/04-B4 1400-12)
- Baydulov Vasilij G.**  
(JSP39/W/01-B3 1442-15)  
(JSP39/W/30-B3 1436-13)
- Bayer Reinhold**  
(P07/W/12-A3 0900-03)
- Bayou Boualem**  
(GA1.04/W/31-A4 1220)
- Bayraktutan M. Salih**  
(ST4/L/03-B1 0830-04)
- Bayuk Irina O.**  
(ST5/W/27-B4 0930-07)  
(ST5/W/50-B5 0930-04)
- Bazaciu Olivia**  
(ST 5/E/06-B5 0930-13)  
(ST1/E/02-A1 1400)
- Bazanova Lilia I.**  
(JSV30/C/JSV22/E/04-B1 1400-18)
- Bazarzhapov A.**  
(GA3.02/E/19-B3 0900-02)
- Bazarzhapov A. D.**  
(GA3.02/E/11-B2 0935)  
(GA3.03/E/01-B4 1400-03)  
(GA3.03/E/04-B4 1530)
- Beagley S R**  
(JSM01/W/10-A3 1650)  
(MW01/W/04-A5 1500)
- Beagley Stephen**  
(MW05/W/04-A2 1200)
- Beal Lisa M.**  
(P11/W/16-B3 0950)  
(P12/E/06-A1 1030-05)
- Beamish David**  
(JSA06/W/27-A1 1035)
- Bean Chris**  
(ST1/W/09-A4 0930-13)  
(ST4/W/52-B1 1740)
- Beard A G**  
(JSM01/W/11-A2 1210)  
(JSM01/W/72-A2 1600-02)  
(MW04/W/01-A1 0950)  
(JSA20/W/32-A4 1025)  
(JSA20/W/22-A4 1146)  
(JSA20/W/30-A4 1526)
- Beard G**  
(JSM01/W/98-A2 1600-05)
- Beard Kenneth V.**  
(JSA16/W/08-A3 0830-40)
- Beasley William H**  
(MI03/W/03-A3 1620)  
(MI03/W/04-A3 1700)  
(MI03/W/06-A3 1000)
- Beattie L.**  
(HS3/W/27-A2 1450)
- Beavan J.**  
(G5/E/39-A4 1200)
- Beavan John**  
(G1/E/18-A3 1620-56)  
(JWM08/E/07-A2 1040)  
(JSG28/W/28-B1 1220)  
(JSS31/L/01-B2 1150)
- Beblo Martin**  
(GA6.01/E/18-A5 0900-01)  
(GA6.01/E/18-A5 0900-02)  
(GA6.02/E/11-B1 1730)
- Bechtold P**  
(MI05/L/03-A4 1140)
- Beck A**  
(JSM01/W/37-A5 1400)
- Becker Alfred**  
(HS3/W/25-A2 1400)  
(HS4/W/32-A5 1710)
- Becker Keir**  
(JWA34/E/06-B2 1600)
- Becker Matthias**  
(JSG28/W/21-B1 1400-02)
- Becker-Ross Helmut**  
(MI06/W/18-B2 1400-04)  
(MI06/W/18-B1 1400-04)
- Beckman Olof**  
(GA 6.01/E/11-A5 1615)  
(GA 6.01/E/11-A5 1615)
- Beckmann Aike**  
(P13/W/03-B1 1720)
- Bednarova Emilia**  
(HS4/W/24-A5 1200)
- Beer Juerg**  
(JSA16/E/37-A3 0830-07)  
(JSA16/W/21-A3 1600)
- Beer Tom**  
(JSP23/W/09-B1 1050)  
(JSP23/W/19-A5 1050)
- Begalishvili Nodar**  
(MI10/E/11-B1 0900-01)
- Beghoul Noureddine**  
(ST5/W/12-B3 1500)
- Begovic Milena**  
(P08/E/04-A2 1500)
- Behar Marcelo**  
(JSM26/E/19-B2 1700-02)
- Behrend Dirk**  
(G1/E/16-A3 1620-24)  
(G3/E/31-A5 1610-48)
- Behrendt John**  
(JSA09/W/05-A3 0930)  
(JSA09/W/07-A2 0930-02)
- Behzad Alaei**  
(ST2/P/09-A4 1145)
- Beiying Wu**  
(MI09/E/03-A5 1145-02)
- Beketova Lena**  
(ST5/E/39-B3 1125)
- Bekryaev Roman**  
(MI11/W/08-B5 1500)
- Bekryaev R V**  
(JSM18/W/07-A5 0940)
- Bela Assinovskaya**  
(ST2/E/46-A5 1400-33)
- Belayev A.**  
(JSP23/W/38-B2 1720)
- Belcher Stephen E**  
(JSP49/W/01-B51640)
- Belehaki A.**  
(GA3.02/L/04-B3 0900-25)  
(GA3.08/L/02-B1 0900-11)
- Belehaki Anna**  
(GA3.02/W/04-B3 0900-23)  
(GA3.09/W/07-B4 0900-11)  
(GA3.09/W/21-B4 0900-10)
- Belenkaya Elena**  
(GA4.08/L/01-B3 0900-14)  
(GA3.07/E/11-A4 0930-02)
- Beles Michael**  
(MI05/L/02-A2 0950)
- Beletsky A. B.**  
(JSA20/W/11-A4 1200-10)  
(JSM26/W/35-B2 1700-12)
- Beliaeva E. A.**  
(SW1/E/08-B5 1030-03)
- Belian R. D.**  
(GA3.02/W/41-B2 1600)
- Belikovich V. V.**  
(GA2.01/W/02-A1 0900-01)  
(JSA20/W/42-A4 1200-22)  
(JSA20/W/46-A4 1200-20)
- Belin E.**  
(G2/E/06-A2 1630-03)
- Belinskaya A. Yu.**  
(JSA45/W/01-B5 1110-04)
- Beljaars Anton**  
(MI10/W/11-B3 1615)
- Belkryaev Roman**  
(MC02/W/04-B1 1600-06)
- Bella Francesco**  
(ST1/E/48-A2 0930-10)
- Bellecci C.**  
(JSA15/E/60-A4 1400-13)  
(JSA45/E/17-B5 1110-01)
- Bellecci Carlo**  
(JWS36/E/25-B3 1710)
- Bellia Carmelo**  
(JSV47/E/03-B5 1400-02)
- Belliustin N. S.**  
(GA3.04/E/02-B1 1010)  
(GA4.08/E/04-B3 0900-15)  
(GA4.08/E/04-B3 0900-15)
- Belokopytov Vladimir**  
(P11/E/23-B5 1420)  
(P11/W/07-B4 1520)
- Belousov Alexander**  
(JSS42/W/28-B5 1700-01)  
(VS2/C/U6/W/13-B3 1400-33)  
(VS2/C/U6/W/14-B3 1400-34)
- Belousova Anna**  
(HS5/W/30-A2 1735)
- Belousova Marina**  
(JSS42/W/28-B5 1700-01)  
(VS2/C/U6/W/13-B3 1400-33)  
(VS2/C/U6/W/14-B3 1400-34)
- Belov Boris**  
(GA3.09/W/25-B5 0910)

## INDEX

- (GA5.09/W/13 A2 1210)
- Belova Elena V.**  
(GA3.04/W/19-B1 1520-35)
- Belova Evgenia**  
(JSA35/E/08-B1 1210)
- Beltaos S.**  
(HW3/W/01-B4 0915)
- Belvedere G.**  
(GA4.03/L/03-B4 1740-05)
- Belyaev**  
(JSA35/L/01-B1 1650)  
(JSA35/L/02-B1 1720)
- Belyaev A.**  
(JSM26/W/14-B2 1700-14)  
(JSM01/C/MW07/W/10-A2 1600-27)
- Belyaev P P**  
(JSM03/L/03-A1 1400)  
(GA2.03/L/01-B3 1400)  
(GA2.03/L/02-B3 1520)  
(GA2.03/W/03-B3 1400-01)  
(GA2.03/W/09-B3 1030)  
(GA3.04/W/28-B1 1520-22)
- Belza Carmelo**  
(G1/W/10-A3 1620-37)
- Ben Sari D.**  
(JSS31/E/13-B3 0830-14)
- Benahmed Daho S.**  
(G1/L/13-A3 1620-89)
- Benahmed S.**  
(G3/P/02-A5 1610-76)  
(G3/P/04-A5 1610-75)
- Benahwd S.**  
(G3/P/05-A5 1610-74)
- Benciolini Battista**  
(G4/W/06-A3 1125)
- Bencze Pál**  
(GA6.01/P/05-A5 1715)  
(GA2.02/E/11-B5 1600)
- Bende-Michl Ulrike**  
(HS3/W/30-A2 1640)
- Bendimerad Fouad**  
(JSP23/E/19-A6 1440)
- Bendjoudi Hocine**  
(HS4/W/10-A4 1530)
- Benedetti Angela**  
(MI04/W/11-B1 0900-02)
- Benediktov E. A.**  
(JSA20/W/42-A4 1200-22)  
(JSA20/W/46-A4 1200-20)
- Benedito Baptista**  
(HS5/W/09-A1 1710)  
(HS5/W/18-A2 1140)
- Benevolenskaya Elena E.**  
(GA4.03/E/01-B4 1145)  
(GA4.03/E/04-B4 1045)  
(GA4.03/E/06-B4 1730-03)
- Benfield Greig**  
(JSP23/E/23-B2 0830-09)
- Ben-Gai Tehilla**  
(MC02/E/04-B2 1510)
- Bengtsson L.**  
(JSP25/E/27-B2 0930)
- Bengtsson Lennart**  
(JSM41/W/13-B3 1400)  
(MW02/W/10-B3 0950)
- Benhallou Hadj**  
(ST2/E/04-A5 1400-25)
- Benjamin Stan**  
(MC04/E/01-B2 1400)  
(MC04/E/06-B2 1450)  
(MC04/E/07-B2 1425)  
(MC05/E/03-B4 1210)
- Benjamin Stanley G**  
(MC01/W/05-A3 1430)
- Benkevich Leonid**  
(GA3.07/W/53-A6 0900-01)
- Bennett R.**  
(JSS31/E/13-B3 0830-14)
- Bennett R A**  
(JSG11/W/05-A3 1440)  
(JSG11/W/09-A3 1500)
- Bennett R G T**  
(JSM01/E/39-A1 0940)
- Bennett Richard A.**  
(JSS31/E/08-B2 0950)
- Bennie S. L.**  
(GA1.02/W/18-A2 0930)
- Bennett V. L.**  
(MI06/W/11-B1 1400-03)  
(MI06/W/11-B2 1400-03)
- Benny N. Peter**  
(P12/E/02-A1 1030-06)
- Benoit R.**  
(JWM08/E/06-A2 1120)
- Benouar Djillali**  
(ST2/E/04-A5 1400-25)
- Bentley C R**  
(JSH12/W/09-A4 1400-03)
- Bentley Charles**  
(JSG14/E/23-A3 1500)
- Bentley Charles R.**  
(JSA09/L/03-A2 1445)
- Bentley R.D**  
(GA4.02/W/08-A4 1215)
- Benxing Zheng**  
(HS2/W/24  
(JSG28/W/23-B2 1130)
- Benzon H.-H**  
(JSG28/W/23-B2 1130)
- Berarducci A. M**  
(GA5.01/E/05 A1 1645)  
(GA5.01/E/11 A1 1300-02)
- Berberan Antonio**  
(JSP23/E/23-B2 0830-09)
- Berbery Ernesto H**  
(MC01/W/30-A4 1615)
- Berchem Jean**  
(GA3.07/W/72-A4 1030)
- Berdeklis Peter**  
(MI03/L/02-A3 1220)
- Berdichevsky D.**  
(GA3.02/W/39-B2 1110)  
(GA4.04/E/01-B5 1210)  
(GA4.08/W/12-B4 1635)
- Berdichevsky Mark**  
(GA1. 02/E/17-A2 0930)  
(GA1.02/E/28-A1 1605)
- Berdunov N. V.**  
(JSA45/E/11-B5 1030)
- Berenguer Jean-Luc**  
(ST7/W/03-A2 1605-01)
- Berge E**  
(MI01/L/01-A1 1210)
- Berger A.**  
(GA6.01/E/02-A5 1120)
- Berger Andre**  
(MI07/E/03-A2 1400)  
(MC11/E/17-B3 1010)  
(MC11/E/18-B3 0850)
- Berger C.**  
(G2/E/06-A2 1630-03)
- Berger Franz H.**  
(MI06/W/06-B1 1400-14)  
(MI06/W/06-B2 1400-14)
- Berger Jonathan**  
(U7/W/16-B1 0830-16)
- Bergerat F.**  
(GA1.04/W/13-A6 1100)
- Berge-Thierry Catherine**  
(ST5/W/39-B5 0910)
- Bergin Michael H**  
(MI09/L/05-A5 1620)
- Bergman Eric**  
(ST5/E/07-B5 0930-09)
- Bergman John W.**  
(MC10/W/07-B1 1100)
- Bergman Michael**  
(JSS07/W/03-A2 1720)
- Bergmann H.**  
(HS1/W/38-B5 0830-05)
- Bergot T.**  
(MI05/W/44-A3 1120)
- Bergsson B. H.**  
(ST4/W/03-B3 1630)
- Bergstrom Robert W**  
(MI09/W/13-A5 1145-18)  
(MI09/W/15-A5 1500)
- Bergstrom Sten**  
(HS3/W/24-A2 1225)
- Bergwerff J B**  
(JSM01/W/55-A5 1510)
- Berhardt**  
(GA3.01/LL/01-A2 1445)
- Bering E. A.**  
(GA3.04/W/05-B1 1520-37)
- Berkeley Lawrence**  
(MI01/W/02-A30900)
- Berkman Rikhard**  
(GA5.01/E/06 A1 1215)
- Bernaerts Arnd**  
(ST3/E/17-B5 0945)
- Bernard A. Chouet**  
(JSV47/W/16-B5 1000)
- Bernard E. N.**  
(JSS42/W/24-B4 1120)  
(JSS42/W/25-B4 1140)  
(JSS42/W/26-B5 1440)  
(JSS42/W/27-B4 0940)
- Bernard P.**  
(ST1/E/87-A2 0930-12)
- Bernard Philippe**  
(GA5.12/W/09-A2 1600-10)
- Bernd Zolitschka**  
(VS3/E/05-B3 0900-04)
- Berndt Hauke**  
(JSM04/W/11-A2 1735)
- Bernhardt**  
(GA6.02/E/16-B1 1435)
- Bernhardt Karl-Heinz**  
(GA6.01/P/06-A5 1700)
- Bernhardt P.**  
(JSA20/E/27-A4 1200-21)
- Berrilli F.**  
(JSA16/E/44-A3 0830-33)
- Berrino Giovanna**  
(JSS46/W/02-B4 1500)
- Berrisford Paul**  
(MW02/E/03-B3 1010)  
(MW02/W/06-B3 1600)
- Berry P. A. M.**  
(JSM41/W/22-B5 1015)  
(G3/W/01-A5 1610-46)  
(G3/W/12-A5 1610-44)  
(G3/W/48-A5 1610-43)
- Berseneva G. P.**  
(P11/E/12-B5 1640)
- Bertaux J. L.**  
(JSA10/W/03-A2 0930)
- Berthelie J. J.**  
(JSA10/E/06-A2 0945)  
(JSA10/W/03-A2 0930)
- Berthomier M**  
(GA4.09/L/01-A5 1600-06)
- Bertrand Cedric**  
(GA6.01/W/11-A5 1425)
- Bertrand E.**  
(JSS46/E/07-B4 0930-04)
- Bertrand N.**  
(HS2/W/26-B2 1400)
- Bertucco Libero**  
(G2/E/09-A2 1630-25)
- Berz G**  
(JSP23/C/U5/W/13-A5 1440)
- Bessat Frederic**  
(MC02/W/10-B1 1600-01)
- Besser V.**  
(GA3.03/W/06-B4 1640)
- Besutiu Georgeta**  
(GA5.12/L/02-A2 1600-06)
- Besutiu Lucian**  
(GA5.12/L/02-A2 1600-06)
- Beswick K**  
(MI02/W/13-A5 1510)
- Beswick Karl M**  
(MI02/W/01-A5 1450)
- Beth Stefan**  
(G4/W/02-A3 1500)
- Bettadpur S. V.**  
(JSA37/W/09-B3 1100)
- Betts Richard**  
(MC01/E/33-A1 1730)  
(MC07/E/04-A2 1215)
- Benediktov E.A.**  
(GA2.01/W/02-A1 0900-01)
- Beutler G.**  
(G2/L/02-A2 0945)
- Beucler Eric**  
(ST4/L/06-B2 0930-29)
- Beulen M.**  
(MI12/W/11-B5 0945)
- Beutler Gerhard**  
(G6/C/G1/E/32-B1 1400)  
(JSG28/E/24-B2 1010)  
(U7/W/07-B1 0830-01)  
(G2/L/08-A2 1145)
- Beven Keith**  
(HW4/E/04-B2 1100)  
(HW4/E/06-B2 1500)
- Bevilacqua Richard M.**  
(JSM26/W/31-B2 1150)  
(JSM26/W/08-B2 1700-15)  
(JSM01/W/04-A4 1510)
- Bevis Michael**  
(JSG28/E/21-B2 1400-14)  
(JSG28/L/01-B1 1400-03)  
(JSS31/E/04-B2 1400)  
(JSG28/W/06-B1 1400-06)  
(MC08/L/09-A3 1545)  
(MC08/L/14-A4 0945)
- Beyerle G**  
(JSM01/W/08-A4 1450)
- Bezgrshnov A. M.**  
(P10/W/11-A5 1600-03)
- Bezzeghoud M.**  
(ST2/E/47-A4 1630)
- Bezzeghoud Mourad**  
(JSS46/W/14-B4 0950)
- Bhardwaj Anil**  
(MC09/P/02-B2 1045)  
(GA4.10/P/03-A4 1200)  
(GA4.10/W/25-A5 1200)  
(GA4.10/W/27-A4 1725)  
(GA4.10/W/28-A4 1655)
- Bharti Lokesh**  
(JSA16/W/14-A3 0830-38)
- Bhat B. C**  
(ST2/W/33-A5 1400-08)
- Bhatia S. C.**  
(ST3/E/18-B4 1145)
- Bhatt Kandarp**  
(JSA16/W/14-A3 0830-38)
- Bhattacharya S. N.**  
(ST1/P/02-A4 0930-03)  
(ST2/L/01-A3 1715)  
(SW1/P/01-B5 0915)
- Bhattacharyya R. K.**  
(ST4/E/20-B1 0830-26)  
(ST4/E/34-B1 0830-27)  
(ST4/E/40-B1 0830-28)
- Bhushan R.**  
(P07/E/03-A3 1430)
- Bi Daohua**  
(JSM24/W/11-B2 0930)
- Bi Dave**  
(MC03/W/04-B4 1110)
- Biagi L**  
(G3/L/19-A5 1610-69)  
(G3/W/47-A5 1610-45)  
(G3/W/25-A5 1610-81)
- Biagi P. F.**  
(JSA15/W/15-A3 0950)  
(ST1/W/14-A1 1150)
- Bian Shaofeng**  
(G3/W/51-A5 1610-49)
- Bian Sun Jianchun**  
(MI06/E/04-B1 1630)
- Biancale R**  
(G3/E/40-A5 1610-05)  
(G3/E/27-A5 1610-02)
- Bianchi C.**  
(JSA45/E/17-B5 1110-01)
- Bianco F.**  
(JSV47/W/15-B5 1400-08)  
(ST5/W/56-B3 0900-01)
- Bianco G.**  
(JSG14/W/19-A3 1600)
- Bibby H. M.**  
(GA1.02/W/11-A2 0930)  
(GA1.02/W/18-A2 0930)
- Bibikova Tamara N.**  
(ST1/E/15-A2 0930-09)
- Bibilashvili Tamar**  
(MI01/W/15-A1 0900-01)
- Bidigare R.**  
(P15/L/26-B3 1110)
- Bidoae Razvan**  
(JSS42/E/19-B4 1020)  
(JSS42/W/06-B5 1400)
- Bidokhti A. A.**  
(JSP49/P01-B5 1210-01)  
(P11/P/01-B5 1150-01)
- Bielik Miroslav**  
(JSS 44/E/02-B4 1440)
- Biella Giancarlo**  
(JSS46/E/04-B4 1400)  
(JSS46/E/06-B4 0930-02)
- Bierl Reinhard**  
(HS5/W/01-A1 1405)
- Biernat H K**  
(GA4.02/W/24-A4 1400-22)
- Biesecker D. A.**  
(GA4.02/W/03-A4 1705)
- Bigg Grant**  
(P07/W/13-A3 0900-04)  
(P07/W/11-A3 1225)  
(JSP25/L/02-B2 1700)
- Bijaksana Satria**  
(GA1.05/E/14-A5 1710)  
(GA1.05/E/12-A5 0850)
- Bijwaard Harmen**  
(JSS13/W/01-A4 1720)  
(JSS13/W/06-A4 1430)
- Bilhalva Saraiva Jaci Maria**  
(MI05/W/26-A4 1400-05)  
(MI05/W/16-A4 1400-11)
- Bilham Roger**  
(JSS31/E/06-B2 1500)
- Bilin Xu**  
(G1/C/G2/E/02-A3 1620-105)
- Billiris Haris**

- (G5/E/36-A4 1215)  
(JSS31/W/11-B2 1620)
- Bin Guo**  
(GA1.03/W/18-B3 1600)
- Binder P.**  
(JWM08/E/06-A2 1120)
- Bindoff N. L.**  
(JSP25/W/32-B3 0830-03)
- Bindoff Nathaniel L.**  
(P12/W/10-A1 1150)
- Bingel Ferit**  
(P11/L/07-B5 1745)
- Bingham Frederick**  
(P12/W/02-A1 0930)
- Binghua Zheng**  
(ST1/W/49-A3 0900-02)
- Bingley Richard**  
(G1/C/G5/E/04-A3 1620-100)  
(JSG11/E/15-A4 1010)  
(G1/E/38-A3 0950)  
(G1/E/52-A3 1620-77)  
(G1/L/09-A3 1640-87)
- Binh Nguyen Xuan**  
(ST1/E/80-A2 1400-11)
- Bintanja Richard**  
(JSM04/E/01-A2 1010)
- Birn J.**  
(GA3.09/W/22-B4 0900-04)
- Birn Joachim**  
(GA3.05/E/22-B3 0900-08)
- Bishop Craig**  
(JSP39/W/32-B3 1130)
- Bishop J.**  
(JSA20/W/27-A4 1200-17)
- Biswas Dipak Kumar**  
(GA1.03/W/11-B2 1400)  
(GA1.15/W/02-B4 1700)
- Bitan Arie**  
(MC02/E/04-B2 1510)
- Biter Mircea**  
(JSS 44/E/23-B4 0930-22)
- Bittencourt J. A.**  
(JSA20/W/05-A5 1200-05)
- Bitterly J.**  
(GA1.02/W/21-A2 0930)
- Bitterly M.**  
(GA3.04/W/25-B1 1520-38)
- Bjardal J.**  
(GA3.02/W/18-B2 1645)
- Bjornsson Axel**  
(ST5/W/14-B3 0900-06)
- Bjornsson H.**  
(MC11/W/04-B3 1740)  
(P13/W/27-B1 1210)
- Black Robert X**  
(MWO6/W/02-A3 1500)
- Black T**  
(MC01/L/18-A4 1715)  
(U3/W/14-A3 0900-15)
- Black Thomas L.**  
(MI04/E/08-B1 1650)
- Blackburn Mike**  
(MI05/E/27-A2 1140)  
(MI05/E/19-A1 0950)
- Blackford Michael**  
(JSS42/E/02-B4 1040)
- Blade Ileana**  
(P13/W/10-B1 1700)
- Blagoveshchenskaya Nataly**  
(GA2.03/E/04-B3 1220)
- Blagoveshchensky Donat V**  
(JSA06/E/03-A11155-10)
- Blaht John**  
(JSM41/W/34-B4 1530)
- Blain Cheryl Ann**  
(P10/E/02-A4 1010)  
(P10/E/16-A4 1400)
- Blake**  
(GA3.05/W/01-B3 1010)
- Blake Donald R.**  
(JSM26/W/04-B2 1130)
- Blake J. B.**  
(GA3.03/E/05-B4 1000)  
(GA3.03/W/10-B4 1220)  
(GA3.05/E/02-B3 0850)  
(GA3.05/E/07-B3 0930)  
(GA3.05/E/16-B3 0950)  
(GA3.05/W/14-B3 0900-40)  
(GA3.05/W/25-B3 0900-33)  
(GA3.05/W/26-B3 1600)  
(GA3.05/W/28-B3 0830)  
(GA3.08/W/26-A6 1710)  
(GA4.01/E/08-A2 1600)
- Blake Stephen**  
(JSP23/E/18-B2 0930)
- Blakely Richard**  
(JSA40/E/08-B5 1005)
- Blanchard G. T.**  
(GA3.08/W/16-B1 1430)
- Blanchard Gerard**  
(GA3.02/W/33-B3 0900-16)  
(GA3.03/W/01-B4 1610)
- Blanchet J P**  
(MI01/L/04 1055)
- Blanco M. J.**  
(JSV47/W/30-B5 1400-23)
- Blanco-Cano X.**  
(GA4.10/W/05-A5 1655)
- Blank Lev**  
(G2/E/16-A2 1630-08)
- Blanck Bruno**  
(P11/L/03-B5 0910)
- Blatter L.**  
(JSV30/E/03-B1 1100)
- Blazev Krsto**  
(ST1/P/03-A4 0930-18)  
(U3/P/02-A3 0900-08)
- Blecki J.**  
(GA3.07/L/06-A5 0900-02)  
(GA4.09/W/04-A5 1600-02)
- Blick Graeme**  
(G1/E/18-A3 1620-56)
- Blitzkow Denizar**  
(G3/E/04-A5 1610-90)  
(G3/W/19-A5 1610-96)  
(G3/W/26-A5 1610-70)
- Blix Dr. Tom Arild**  
(JSM32/W/12-B2 1100)
- Block Arthur**  
(U3/W/05-A30900-11)
- Bloemink H. R.**  
(MI06/W/14-B2 1010)
- Bloom Cornelis**  
(JSA09/W/12-A2 1630)
- Blomberg L G**  
(GA3.10/W/10-A6 1700-03)  
(GA3.10/W/13-A6 1050)
- Blomberg L.**  
(GA2.03/W/09-B3 1030)
- Blower Jon**  
(VS2/W/11-B3 1400-08)
- Bloxham Jeremy**  
(U3 /W/02-A31700)  
(GA1.01/W/23-A6 0900)  
(JSA17/W/04-A4 1650)
- Blumetti A. M.**  
(ST2/W/17-A5 1400-19)
- Bluth G. J. S.**  
(VS2/W/10-B3 1400-07)
- Bluth Gregg**  
(JSM41/W/23-B4 1630-07)  
(VS2/W/05-B3 1400-04)  
(MI01/C/JSV36/E/06-A1 0900-14)
- Blyth E. M.**  
(HW4/W/05-B2 1420)
- Bobbio Antonella**  
(ST7/W/03-A2 1605-01)
- Bobrovnikov S. Yu.**  
(GA3.02/W/31-B3 0900-05)
- Bochev A. Z.**  
(GA4.08/E/21-B3 0900-13)  
(GA3.06/L/06-A2 1050)
- Bochsler P.**  
(GA4.04/E/05-B5 0940)
- Bock Erik**  
(JSM41/W/07-B4 1620-05)
- Bock Juliane M.**  
(GA1.05/W/34-A6 1430)
- Bock Yehuda**  
(JSG28/L/01-B1 1400-03)  
(JSS31/W/01-B3 0830-02)  
(G1/E/08-A3 1620-21)  
(G1/L/05-A3 0830)  
(G1/W/16-A3 1620-06)
- Bockman L. L.**  
(ST2/E/43-A5 1400-31)
- Bodaghjamali Javad**  
(MI04/W/25-B1 0900-03)  
(MI10/W/14-B1 0900-05)  
(MI10/W/22-B1 0900-04)
- Bode A.**  
(G6/C/G3/E/43-B1 1100)  
(G3/E/27-A5 1610-02)
- Bodeker Gregory E.**  
(MI12/E/02-B5 1115)  
(MI12/E/05-B5 1135)
- Bodhaine Barry**  
(MI08/E/08-A4 1750)
- Bodri L.**  
(MC02/E/10-B1 0950)
- Bodvarsson Reynir**  
(ST5/W/13-B3 1640)  
(ST5/W/14-B3 0900-06)  
(ST1/W/29-A4 0930-34)  
(ST1/W/57-A3 1110)
- Boeder Volker**  
(G1/W/32-A3 1620-15)
- Boehler Reinhard**  
(JSS02/W/02-A1 1620)
- Boehm Johannes**  
(G1/E/35-A3 1620-67)
- Boehm M. T.**  
(MI10/W/04-B4 0950)
- Boening Claus**  
(MC01/W/52-W2 1135)
- Boerner D. E.**  
(P15/W/09-B4 1115)
- Boers Paul**  
(HS3/W/29-A2 1615)
- Bof Marcel**  
(JSA15/E/08-A3 1600)
- Bógalo Mari Fe**  
(GA1.05/W/33-A6 1730)
- Bogart Richard**  
(JSA16/W/20-A3 0830-53)
- Bogdanov A**  
(GA4.02/W/28-A4 1720)  
(GA4.02/E/02-A4 1400-06)
- Bogdanov A. T.**  
(GA4.04/E/02-B5 1020)
- Bogdanova Svetlana P.**  
(GA4.02/W/27-A4 1400-24)
- Bogdanova Yulia**  
(GA3/06/L/09-A3 1740)
- Bogomolov A. V.**  
(GA3.05/E/19-B3 0900-04)
- Bogomolov Leonid**  
(ST4/E/08-B1 0830-24)
- Bogorodsky Pjotr**  
(P13/W/23-B2 1600-13)
- Bogoyavlenskaya G. E.**  
(JSV30/E/10-B1 1400-03)
- Bogris N.**  
(GA1.02/E/30-A20930)
- Bogusch E. B.**  
(GA4.09/W/15-A6 0900)
- Bogusz Janusz**  
(G1/E/26-A3 1620-60)  
(G5/E/44-A4 1558-10)  
(G5/E/45-A4 1115-03)  
(JSG 28/E/23-B2 1400-02)
- Bohlke Johnkari F**  
(HS3/W/15-A1 1705)
- Böhm Reinhard**  
(MC02/W/11-B2 1210)
- Bojan Uran**  
(JWS33/E/12-B3 0900-30)
- Bojkov B. R.**  
(JSM01/W/37-A5 1400)
- Bokelmann Goetz H R**  
(JSS07/E/11-A2 1155)
- Bol'shakov P. V.**  
(MC02/E/05-B1 1600-08)
- Bol'shakov V. A.**  
(MC02/E/05-B1 1600-08)  
(MC02/E/06-B1 1600-05)  
(GA1.05/E/04-A6 0900-05)
- Boldyrev Sergey A.**  
(ST4/W/11-B2 0930-04)
- Bolgov Mikhail V.**  
(HS1/W/03-B5 0920)
- Bolt Bruce A.**  
(ST3/E/33-B3 0830)  
(U5/E/03-A4 1430)
- Bolton Edward W.**  
(JSV47/W/25-B5 1400-18)
- Bolton H**  
(JSS02/W/03-A2 1000)
- Bolton S. J.**  
(GA4.10/W/34 1620)
- Bolton S.**  
(GA4.10/W/32-A4 1635)
- Bolvin David**  
(JSM41/E/01-B3 1620)
- Bomin Sun**  
(HS2/W/03-B1 0940)
- Bond Gerard**  
(MC03/E/02-B4 0930)
- Bondar Istvan**  
(U8/L/01-B3 1640-03)
- Bondar Tatiana N**  
(GA5.09/W/08 A2 1130)  
(GA1.01/W/33-A5 1630)
- Bondarenko V.**  
(G3/E/26-A5 1610-36)
- Böning C.**  
(P08/W/07-A2 1400)
- Bonforte A.**  
(JSV36/W/23-B3 1515)
- Bonforte Alessandro**  
(JSG28/E/25-B1 1400-15)
- Bongartz K.**  
(HW4/E/16-B2 1520)
- Bonino G.**  
(JSA16/W/43-A3 1630)
- Bonnefond P.**  
(G2/E/06-A2 1630-03)
- Bonnell John W.**  
(GA3.08/E/09-A6 1650)
- Bonnin J.**  
(ST5/E/02-B3 1400)
- Bonomi Tullia**  
(HS5/W/38-A3 1145)
- Bonvalot S.**  
(JSV36/W/17-B3 1500)
- Bony Sandrine**  
(MWO2/E/05-B3 1100)
- Booker John**  
(JSS44/W/02-B5 0930)  
(GA1.02/W/07-A1 1605)  
(GA1.02/W/39-A2 0930)
- Boon S.A.**  
(ST6/W/11-A1 0830-11)
- Boonsiriseth A.**  
(GA3.05/W/06-B3 0900-05)
- Booth David**  
(U8/E/02-B3 1640-05)
- Booth Simon**  
(G1/L/09-A3 1640-87)
- Bopp Laurent**  
(MC01/W/55-A5 1715)
- Bordonaro Osvaldo**  
(GA1.04/L/07-A4 1500)
- Borer W. S.**  
(GA3.09/W/01-B4 0900-08)  
(GA3.09/W/02-B4 0900-09)
- Borevsky L. V.**  
(ST4/E/52-B1 1400-03)
- Borg Kjell**  
(GA5.01/E/32 A1 0900-09)
- Borges Fernando**  
(ST2/E/48-A5 1400-22)
- Borges J. F.**  
(ST2/E/47-A4 1630)
- Borges José F.**  
(ST4/E/27-B1 1400-17)
- Borghini Alessandra**  
(G3/E/18-A5 1610-68)
- Borghini Mireno**  
(P11/W/06-B4 0930)
- Boris Ladanivsky**  
(GA1.02/E/15-A1 1605)
- Boris S**  
(GA1.02/E/36-A1 1605)  
(GA1.02/E/37-A1 1605)
- Borisov Nikolay**  
(JSA15/W/22-A5 1400-18)
- Borisova Tatyana**  
(GA2.03/E/04-B3 1220)
- Bormann Niels**  
(MI06/E/05-B1 1140)  
(JWM08/E/02-A2 1140)  
(JWM08/E/07-A2 1040)  
(JWM08/W/04-A2 1020)
- Bormann Peter**  
(ST7/E/03-A2 0930)  
(ST7/E/04-A2 0950)
- Bornhold Brian D.**  
(JSS42/E/12-B4 1500)  
(JSS42/E/12-B5 1700-07)
- Borodkova N. L.**  
(GA3.02/W/60-B2 1215)  
(GA4.08/W/15-B3 1530)  
(GA3.07/W/56-A4 0930-03)
- Borovsky Joseph E.**  
(GA3.07/E/08-A4 1000)  
(GA4.09/E/01-A6 1700)  
(GA3.05/E/15-B3 0900-39)  
(GA3.05/W/11-B3 0900-06)  
(GA3.08/E/09-A6 1650)  
(GA3.05/W/38-B3 1700)  
(GA4.08/W/05-B3 1335)
- Boroyev R. N.**  
(GA3.02/L/05-B3 0900-26)  
(GA5.08/E/05-B1 1400-02)
- Borque M. J.**  
(G5/W/19-A4 1230-02)
- Borradaile Dr. Graham**  
(JSS13/W/07-A5 1650)
- Borre Kai**



# INDEX

- (G1/L/17-A3 1100)
- Borrman Stephan**  
(JSM26/W/37-B2 1100)  
(JSM26/W/16-B2 1210)
- Borrman Stephan**  
(JSA09/W/12-A2 1630)
- Bosart Brian**  
(MI05/W/35-A4 0930)
- Bosch Ernest**  
(G1/E/15-A3 1620-55)
- Bosch Wolfgang**  
(JSG11/W/01-A4 1050)  
(G1/W/26-A3 1620-42)  
(G1/W/41-A3 1620-46)  
(JSG14/W/03-A3 1700-09)
- Boscher Daniel**  
(GA3.05/W/08-B3 1440)
- Boschi E.**  
(ST2/E/21-A5 1400-24)
- Boschi Lapo**  
(ST4/E/22-B3 1140)
- Bösinger T.**  
(GA2.03/W/09-B3 1030)  
(GA3.02/W/60-B2 1215)
- Boska Josef**  
(JSA20/E/03-A4 1200-24)  
(JSA20/E/21-A4 1000)  
(JSA20/E/07-A4 1200-30)
- Boskova Jaroslava**  
(JSM01/E/21-A2 1600-16)
- Bostock Michael**  
(ST4/W/40-B2 1140)  
(ST4/W/19-B2 0930-15)
- Boswell Stephen**  
(JSP21/W/03-A4 1420)
- Bosworth J.**  
(G6/W/05-B1 0850)
- Bosworth John**  
(U7/W/07-B1 0830-01)
- Bosy Jarosaw**  
(G5/W/07-A4 1516-09)
- Boteler David**  
(JSA06/W/04-A1 1155-04)  
(JSA06/W/06-A1 1135)  
(JSA06/W/14-A1 1700)  
(JSA06/W/17-A1 1155-14)  
(JSA06/E/10-A1 1155-03)  
(JSA06/E/13-A1 1155-02)  
(JSA06/E/09-A1 1155-01)  
(JSA06-A1 0830)  
(JSP23/L/05-B1 950)
- Boterhoven M.**  
(JSM41/W/36-B4 1110)
- Bothmer Volker**  
(GA4.01/E/09-A2 1200)
- Bott Andreas**  
(MI08/E/03-A3 1400)
- Bottrell Simon H.**  
(HS5/W/34-A3 1000)
- Botvinovsky Vsevolod V.**  
(JSA09/C/GA5.01/W/20-A3 1200)  
(JSS07/W/08-A2 0930-03)
- Botzet Michael**  
(HW1/E/03-A4 1430)  
(MC01/E/34-A4 1020)
- Bouabdallah H.**  
(GA1.05/W/37-A5 1420)  
(GA1.04/W/22-A4 1420)
- Boubnov Boris M.**  
(JSP39/W/23-B3 1427-10)
- Boucher Claude**  
(G6/E/04-B1 0830)  
(U7/W/07-B1 0830-01)  
(U7/W/14-B1 0830-12)  
(JSG11/W/13-A4 1400-09)
- Boucher C.**  
(G1/E/46-A3 0930)  
(G2/E/06-A2 1630-03)  
(G1/C/G5/E/02-A3 1620-101)  
(G1/L/06-A3 0850)
- Boudewijn Ambrosius**  
(JSS31/W/11-B2 1620)
- Boudon Y**  
(G3/E/27-A5 1610-02)  
(G2/E/06-A2 1630-03)  
(G5/E/29-A4 1015)
- Bougeault Philippe**  
(JWM08/W/03-A2 0940)
- Bougher S. W.**  
(GA4.10/L/05-A4 1040)  
(GA4.10/W/14-A4 0900)
- Bouhadad Youcef**  
(ST2/P/02-A4 1645)
- Bouhadad Youcef**  
(ST3/P/5-B4 1200)
- Boulgeault P.**  
(JSP39/E/16-B3 0830)
- Bounama Christine**  
(U3/W/05-A30900-11)
- Bounds S.**  
(GA2.02/L/01-B4 1000)
- Bouniol D.**  
(MI05/W/42-A4 1010)
- Bourdarie Sébastien**  
(GA3.05/W/08-B3 1440)  
(GA3.05/W/47-B3 0900-07)
- Bourdillon A.**  
(JSA20/E/26-A4 1200-14)
- Bourdillon Alain**  
(GA2.02/W/17-B4 0930-01)
- Bourenas Nasreddine**  
(GA5.12/E/02-A2 1600-08)
- Bourouis S.**  
(G5/E/27-A4 1230-05)
- Bourouis Seid**  
(ST2/W/30-A5 1400-18)
- Bourqui Michael**  
(JSM26/W/03-B3 0950)
- Bouruet-Aubertot P.**  
(JSP39/E/19-B2 1050)  
(JSP49/E/08-B5 1420)
- Bousquet P.**  
(MC01/W/07-A5 1145)
- Bousquet Philippe**  
(MC01/W/43-A5 1130)
- Bouziane Mustapha**  
(G3/P/06-A5 1610-71)
- Boville Byron A.**  
(MC01/L/11-A2 1725)  
(U3/W/01-A3. 1100)
- Bower K N**  
(MI02/W/13-A5 1510)  
(M104/E/16-B4 1220)
- Bower Keith N**  
(MI01/E/05-A1 1430)
- Bowers D.**  
(U8/E/01-B3 1640-08)  
(U8/E/07-B3 1640-07)
- Bowers David**  
(U8/E/11-B3 1520)
- Bowser A.**  
(GA3.03/W/11-B4 1200)
- Box Gail**  
(MI09/E/01-A5 1145-01)  
(MI01/W/10-A2 1740)  
(MI01/W/19-A2 1720)
- Boy Jean-Paul**  
(JSG14/W/02-A3 1700-15)
- Boyarchuk K. A.**  
(JSA15/E/53-A4 1400-01)
- Boyarchuk S. A.**  
(U3/E/03-A3 0900-02)
- Boyd P.**  
(P08/W/01-A2 1440)
- Boyd Sierra**  
(GA3.04/E/03-B1 0900)
- Boyd T. M.**  
(ST5/E/10-B5 0930-08)
- Boyd Tim**  
(P13/W/15-B2 1600-10)
- Boyden John**  
(JSA16/E/11-A3 0830-15)  
(JSA16/W/38-A3 0830-54)
- Boyer Don L.**  
(JSP39/E/02-B4 1520)
- Boyle James**  
(MW02/E/09-B3 1520)  
(MC01/L/04-A1 1615)
- Boyou Zhang**  
(JSV22/E/03-A5 0900-02)
- Bozo Laszlo**  
(MI01/W/21-A1 0900-10)
- Bozzo Emanuele**  
(JSA09/E/09-A3 1015)  
(JSA09/W/07-A2 0930-02)
- Braathen G. O**  
(JSM01/W/37-A5 1400)
- Braconnot Pascale**  
(MC01/E/11-A3 0845)
- Bradford M. S.**  
(GA4.10/W/14-A4 0900)
- Bradley Alexander S**  
(ST1/L/01-A2 1400-24)
- Bradley C. R.**  
(ST5/W/38-B3 1740)
- Bradley Chris**  
(HS4/W/17-A5 0930)
- Bradley Pierce**  
(JSM01/L/30-A5 1640)
- Bradley Raymond S.**  
(HS2/W/03-B1 0940)  
(MC02/E/23-B1 1450)  
(MC02/W/07-B1 1510)
- Braesicke P**  
(JSM01/W/05-A1 1700)
- Braganza Karl**  
(MC02/W/02-B2 1130)
- Bragato P. L.**  
(ST3/W/18-B3 1500)
- Bragin Oleg A.**  
(ST1/W/73-A3 0900-10)
- Bragin Vasily Yu.**  
(ST1/W/73-A3 0900-10)
- Bragin Vitaly**  
(G5/E/34-A4 1230-12)  
(ST4/E/08-B1 0830-24)
- Bragin Yury A.**  
(ST1/W/73-A3 0900-10)
- Braginsky Stanislav I.**  
(JSA17/C/GA1.19/W/10-A4 1610)
- Braisby John D.J.**  
(GA1.05/E/08-A6 1545)
- Braitenberg Carla**  
(JSS44/E/40-B4 0930-13)
- Braitseva Olga**  
(JSP23/E/04-B1 0830-08)
- Brand Kate**  
(GA3.04/W/26-B1 1520-09)
- Brandon Mark**  
(ST4/W/14-B2 1700)  
(ST4/W/15-B3 1500)
- Brandt Alan**  
(JSP39/W/29-B2 1130)
- Brandt Peter**  
(JSA16/W/12-A3 0830-52)  
(P12/W/19-A1 1030-08)  
(P14/W/07-A4 1400-10)  
(P14/W/14-A4 1140)
- Brandt Ute**  
(GA1.05/E/09-A5 0900-02)  
(GA1.05/E/15-A5 0900-01)  
(GA1.03/E/03-B2 1620)  
(GA1.03/E/05-B2 1640)
- Branney Michael J.**  
(VS2/E/06-B3 1400-21)
- Brasseur G**  
(JSM01/W/41-A4 1150)
- Brasseur Guy**  
(MI02/E/02-A4 1120)
- Brasseur Guy P.**  
(JSA45/W/05-B4 1055)  
(JSM26/W/08-B2 1700-15)
- Brasseur O.**  
(MW03/W/11-B4 1725)
- Bratseth Arne M**  
(MI05/E/09-A1 1400)
- Brauer Achim**  
(GA1.05/E/09-A5 0900-02)
- Braun Alexander**  
(G3/W/07-A5 1610-15)
- Braun Scott A.**  
(MI04/W/06-B3 1105)
- Braunger R. M.**  
(GA4.09/W/15-A6 0900)
- Brautigam D H**  
(GA3.10/W/03-A6 0950)  
(GA3.10/W/12-A6 1700-09)  
(JSA06/W/11-A1 0955)  
(GA3.05/W/27-B3 0900-37)  
(GA3.05/W/34-B3 1420)
- Bravo S**  
(GA4.01/W/02-A2 1400-06)
- Bravo Silvia**  
(GA4.03/W/10-B4 1200)
- Bräysy T.**  
(GA3.04/W/08-B1 1150)  
(GA3.04/W/24-B1 1520-29)  
(G3.04/W/18-B1 1520-26)
- Brecht S. H.**  
(GA4.10/W/33-A4 1400)
- Breed A. M.**  
(JSA20/E/04-A6 1136)  
(GA2.02/E/02-B4 1740)
- Breen A. R.**  
(GA4.04/W/07-B5 1430)  
(GA4.02/E/07-A4 1400-02)  
(GA4.05/E/02-A1 1010)
- Breen R.**  
(GA4.01/W/09-A2 1140)
- Breger Ludovic**  
(JSS02/W/11-A1 1700)  
(ST4/W/08-B3 1120)
- Breil Pascal**  
(HW2/W/03-B1 1100)
- Bremen Lueder V.**  
(MI10/W/06-B2 1005)
- Brenner Andrew J.**  
(HS3/W/28-A2 1515)
- Brenner Stephen**  
(P11/E/17-B4 1600)
- Bresch David N**  
(MW06/W/01-A3 1140)
- Brestensky J.**  
(GA1.01/E/15-A6 1145)
- Bretherton Francis**  
(U7/L/01-B1 1725)
- Breung M.**  
(JWS33/W/08-B2 1635-26)  
(JWS33/W/08-B3 0900-26)
- Breus T.**  
(GA6.01/E/04-A5 0900-07)
- Brian Baptie**  
(JSV47/E/05-B5 0845)
- Brick N. V.**  
(JSA45/W/02-B5 1110-09)
- Briegleb Bruce P**  
(MC07/W/22-A2 1620)
- Brimich Ladislav**  
(JSV36/E/16-B3 1640)
- Brimley Bill**  
(HW3/W/02-B4 0940)
- Bringfelt Björn**  
(MC01/W/17-A4 1125)
- Brinkman D. G.**  
(MC09/W/02-B2 1215)
- Brinksma E**  
(JSM01/W/55-A5 1510)
- Brinton Eric W.**  
(G5/E/38-A4 1415-02)
- Briole P.**  
(JSV36/W/17-B3 1500)
- Briole Pierre**  
(JSS31/W/11-B2 1620)  
(G5/E/36-A4 1215)  
(G2/E/09-A2 1630-25)  
(JSP23/C/US/W/07-B2 0950)
- Brisbourne Alex**  
(JSS07/E/07-A2 1225)
- Brito D.**  
(GA1.01/W/09-A5 0900-03)  
(GA1.01/W/30-A5 1215)
- Brittnacher M.**  
(GA3.03/E/07-B4 1020)  
(GA3.03/W/11-B4 1200)  
(GA3.08/W/26-A6 1710)
- Brittnacher M. J.**  
(GA3.02/W/18-B2 1645)
- Brix Holger**  
(JSM18/W/06-A4 1500)
- Broccoli Anthony J**  
(JSM 18/E/06-A4 1700)  
(MC02/E/09-B2 0900)
- Brocher T. M.**  
(ST4/L/01-B1 0830-02)
- Brockmann Elmar**  
(G1/W/05-A3 1620-34)
- Brockmann Uwe H.**  
(P10/E/07-A5 1130)  
(P10/E/09-A5 1110)
- Brodholt John**  
(ST6/E/10-A2 1700)
- Brodtscholl Arnold**  
(JSV36/W/11-B3 1400-06)
- Brognez G.**  
(MI06/E/10-B2 1150)
- Bromley Chris**  
(JSV36/W/02-B3 0930)
- Bromwich David**  
(JSM18/W/15-A4 1140)  
(JSM04/W/03-A2 1030)
- Bromwich David H**  
(MI08/W/04-A4 1050)
- Brondeel Marijke**  
(G1/E/43-A3 1620-73)
- Bronster Axel**  
(HW4/E/32-B2 0900-13)  
(HW4/E/33-B2 0900-15)
- Brook M**  
(MI03/W/05-A3 1140)
- Brook Marx**  
(JSM03/W/02-A1 1650)
- Brooke John**  
(GA6.01/E/21-A5 1645)
- Brosnahan J W**  
(JSM01/E/26-A2 1020)
- Broutman Dave**  
(MW07/E/07-A4 1210)
- Brouwer F.**  
(G1/E/31-A3 1620-65)
- Brovar B.V**

- (G3/E/28-A5 1610-03)  
**Brovelli M. A.**  
 (G3/W/47-A5 1610-45)  
**Brovkin Victor**  
 MC11/E/19-B4 1145)  
**Brown A. R.**  
 (MI04/E/18-B3 1505)  
**Brown Amy**  
 (ST2/E/23-A3 1600)  
**Brown I. A.**  
 (JSM41/LL/01-B4 1625-06)  
**Brown John M.**  
 (MC01/W/05-A3 1430)  
 (MC04/E/01-B2 1400)  
 (MC04/E/07-B2 1425)  
**Brown J. Michael**  
 (ST6/W/13-A2 1630)  
 (ST4/W/21-B2 1120)  
**Brown Laurie**  
 (GA1.15/E/06-B4 1645)  
 (JSV36/W/07-B3 1400)  
**Brown Laurie L.**  
 (GA5.11/W/01 A3 0930)  
**Brown P D**  
 (MC07/W/17-A3 1115)  
**Brown P. A.**  
 (MI06/W/30-B1 1400-11)  
 (MI06/W/30-B2 1400-12)  
**Brown Patrick D**  
 (MC08/L/09-A3 1545)  
**Brown Philip R. A.**  
 (MI10/E/08-B3 0920)  
**Brown Ross**  
 (JSM41/W/21-B4 1735)  
 (JSM41/W/12-B4 1720)  
**Brown S**  
 (HS5/W/19-A2 1200)  
**Brown Timothy J.**  
 (JSP25/W/55-B2 0950)  
**Browne David R.**  
 (P10/W/29-A3 1720)  
**Browning K A**  
 (MI05/E/06-A1 1630)  
 (MI05/W/27-A4 1400-08)  
 (MI05/L/05-A5 0920)  
 (MI05/E/02-A3 1620)  
 (MI05/W/32-A4 1400-04)  
**Brozina John M.**  
 (G3/L/22-A5 1220)  
**Brubaker John**  
 (P10/W/05-A3 1150)  
**Bruce Terry**  
 (MC04/W/09-B2 1600)  
**Bueckl Ewald**  
 (G6/L/01-B2 1620)  
 (G3/E/22-A5 1610-32)  
 (JSP23/W/02-A5 1110)  
**Brugge R.**  
 (JSP25/E/05-B1 1110)  
**Bruhwieler L**  
 (JSM01/W/53-A3 1400)  
**Bruhwieler Lori**  
 (JSM26/W/12-B1 1000)  
 (MC06/C/JSM01/W/43-A1 1625)  
**Bruinsma S.**  
 (G5/E/29-A4 1015)  
**Brun Eric**  
 (MC01/L/05-A2 1100)  
**Brundell James**  
 (JSA15/W/31-A4 1120)  
**Brune W.**  
 (JSM26/W/18-B2 1550)  
**Brunetti M.**  
 (GA6.01/E/14-A5 1600)  
**Brunini C.**  
 (JSG28/W/1-B2 1140)  
**Brunini Claudio**  
 (GA2.03/E/10-B3 1700-08)  
 (JSG11/W/01-A4 1050)  
 (G1/E/40-A3 1620-27)  
 (G1/W/41-A3 1620-46)  
**Brunner Fritz K.**  
 (G1/E/01-A3 1620-19)  
 (G1/E/17-A3 1620-104)  
 (G1/E/27-A3 1620-61)  
 (G1/L/03-A3 1540)  
**Bruno Coppi**  
 (GA2.02/W/27-B5 1140)  
**Bruno Roberto**  
 (GA4.09/W/03-A6 1600)  
**Brunton A M**  
 (G3/E/12-A5 1610-18)  
 (GA4/E/11-A3 1620-14)  
**Brunton A. M.**  
 (G6/E/05-B2 1200)
- Bruyas Anne-Marie**  
 (ST7/W/03-A2 1605-01)  
**Bruyninx C.**  
 (G1/E/46-A3 0930)  
**Bryan Frank O**  
 (MC01/E/12-A2 1215)  
**Bryan George**  
 (MC04/W/15-B1 0915)  
**Bryden Harry L.**  
 (P14/W/11-A4 1500)  
**Brzezinski Aleksander**  
 (JSG14/W/23-A3 1127-10)  
**Bubukina V. N.**  
 (GA2.01/W/02-A1 0900-01)  
 (GA4.09/W/06-A5 1600-03)  
 (GA4.02/W/35-A4 1400-27)  
 (GA3.04/E/17-B1 1520-06)  
**Buch E.**  
 (G2/W/03-A2 1630-18)  
**Bucha Václav**  
 (GA6.01/P/13-A5 0900-04)  
**Buchert S.C.**  
 (JSA20/E/10-A4 1200-04)  
 (JSA20/E/13-A4 1508)  
**Bucholtz A**  
 (MI08/W/08-A4 1545)  
**Bucholtz Anthony**  
 (MI04/W/35-B2 1450)  
 (MI10/W/23-B2 1420)  
**Buchtele Josef**  
 (HW4/E/31-B2 0900-12)  
**Buckley Henry**  
 (MC01/E/05-A1 1030)  
 (MC01/E/28-A1 1600)  
**Budd William F.**  
 (MC03/W/04-B4 1110)  
 (JSM04/W/05-A2 1445)  
**Budi E. N.**  
 (JSV47/W/03-B5 1400-12)  
**Budnick Elena**  
 (GA3.07/W/04-A5 0900-03)  
 (GA3.07/W/15-A5 0900-07)  
**Budnik E.**  
 (GA3.05/W/32-B3 0900-25)  
**Buechner Joerg**  
 (GA3.02/E/05-B3 1000)  
 GA3.08/E/04-B1 1700)  
 (GA3.07/E/24-A4 0930-04)  
 (GA4.09/W/04-A5 1600-02)  
 (GA4.02/E/01-A4 1600)  
 (GA4.10/E/03-A5 1640)  
**Buerki Beat**  
 (JSG28/W/06-B1 1400-06)  
**Buesseler Ken. O.**  
 (P07/W/14-A3 1035)  
**Buettner Ralf**  
 (VS2/E/14-B3 1400-25)  
 (VS2/W/01-B3 1400-01)  
 (VS2/W/18-B3 0930)  
**Buffagni Andrea**  
 (HW2/W/09-B1 1600)  
**Buffett B. A.**  
 (JSG14/L/09-A3 1000)  
 (JSA17/E/02-A4 1710)  
 (JSS02/E/06-A1 1600)  
 (JSS07/E/01-A2 1650)  
**Bufoen E.**  
 (ST2/W/06-A4 1600)  
**Buizza Roberto**  
 (JWM08/W/11-A3 1220)  
**Bukreeva E.**  
 (ST4/E/71-B2 0930-25)  
**Bullister J**  
 (MC01/W/36-A5 1700)  
**Bulychev A**  
 (G3/W/52-A5 1610-14)  
**Bulychev A. A.**  
 (JSA37/W/01-B3 1745-01)  
**Bunce E. J.**  
 (GA4.10/W/02-A5 1005)  
**Bunge H.-P.**  
 (JSS13/L/01-A5 1710)  
 (ST4/E/23-B3 1200)  
**Bunge Hans-Peter**  
 (JSS13/W/14-A5 1010)  
**Bungum H.**  
 (ST2/E/11-A5 1215)  
 (ST2/E/12-A5 1400-32)  
 (ST2/E/31-A5 1200)  
 (ST2/E/43-A5 1400-31)  
 (ST3/E/13-B4 1400-15)  
 (ST3/E/14-B5 1130)  
**Bungum Hilmar**  
 (ST1/E/06-A4 0930-39)  
**Burakhovich Tatjana**
- (GA1.02/E/14-A2 0930)  
**Burchfiel Clark**  
 (JSS31/W/08-B2 1640)  
**Burde Georgy I.**  
 (JSP39/W/10-B3 1150)  
**Burdelhaya Irina A.**  
 (GA1.07/W/07-B2 1220)  
 (GA1.01/W/33-A5 1630)  
 (GA5.09/W/05 A2 1400-02)  
 (GA5.09/W/01 A2 1400-04)  
**Buresova D.**  
 (GA4.08/E/03-B4 1520)  
**Burgess David**  
 (GA4.09/W/14-A6 1720)  
**Burgess Margo M.**  
 (HS2/W/09-B1 1200)  
**Burgess R.**  
 (VS3/E/01-B3 0900-03)  
**Burgess William**  
 (HS5/W/29-A2 1715)  
**Buriez Jean-Claude.**  
 (MI06/E/10-B2 1150)  
 (MI06/W/05-B1 1400-06)  
 (MI06/W/05-B2 1400-06)  
**Buriti R A**  
 (JSM01/W/104-A2 1150)  
 (JSM01/W/94-A3 1220)  
**Burkart Michael**  
 (HS3/W/14-A1 1640)  
**Burke Eleanor J**  
 (MC01/W/13-A3 1635)  
**Burke K.**  
 (JSV22/W/06-A5 1000)  
**Burke W. J.**  
 (GA3.09/E/05-B4 1625)  
**Burkhardt Ulrike**  
 (MI05/E/16-A1 1200)  
**Bürki Beat**  
 (MI06/W/18-B1 1400-04)  
 (MI06/W/18-B2 1400-04)  
**Burkill P H**  
 (JSP21/L/03-A4 1720)  
**Burla L F**  
 (GA4.02/W/24-A4 1400-22)  
**Burlaga L. F.**  
 (GA4.04/E/03-B5 1510)  
**Burlacu V.**  
 (ST1/W/60-A3 0900-07)  
**Burlando Paolo**  
 (HS4/W/30-A5 1510)  
**Burnett William**  
 (HW5/E/04-A3 1500)  
 (HW5/E/06-A3 1620)  
**Burns A. G.**  
 (U3/W/17-A3 0900)  
**Burns G B**  
 (JSM01/E/43-A2 1600-10)  
 (JSM32/L/01-B3 1125)  
**Burns Gary**  
 (JSA35/W/06-B1 1400)  
**Burr G. S.**  
 (P07/E/03-A3 1430)  
**Burrage Mark**  
 (MW04/W/11-A1 0925)  
**Burrows John P.**  
 (MI06/E/13-B1 1100)  
 (MI09/E/08-A5 1645)  
**Burt T. P.**  
 (HS3/W/19-A2 0950)  
**Burton R. R**  
 (MI05/W/15-A5 0940)  
**Burtsev A. A.**  
 (ST3/E/39-B3 1200)  
 (ST5/E/02-B3 1400)  
**Burwell David**  
 (JSP23/W/01-B2 1500)  
**Busalacchi Antonio J**  
 JSP05/W/09-A2 10)  
**Bush BC**  
 (MI08/W/08-A4 1545)  
**Bush Brett**  
 (MI10/W/23-B2 1420)  
**Bush M.**  
 (MI04/E/18-B3 1505)  
**Bushati S.**  
 (JSP23/W/38-B2 1720)  
**Bushell Andrew C.**  
 (MI04/E/12-B3 1420)  
**Businger Steven**  
 (JSG28/L/01-B1 1400-03)  
**Businger Steve**  
 (MC08/L/09-A3 1545)  
 (MC08/L/14-A4 0945)  
**Busse F. H.**  
 (JSP39/W/34-B2 1500)
- Bussièeres Normand**  
 (MI06/E/16-B1 1400-17)  
 (MI06/E/16-B2 1400-17)  
**Busslinger Andreas**  
 (ST4/W/13-B1 0840)  
**Butchart Neal**  
 (MI02/W/15-A5 1100)  
 (MW 07/E/06-A4 1700)  
 (MW01/E/03-A5 1650)  
**Butler James**  
 (JSP21/W/05-A4 1520)  
 (JSP21/L/04-A5 0930)  
 (JSP21/W/12-A4 1110)  
 (JSP21/W/15-A4 1600)  
 (JSP21/W/17-A4 1500)  
**Butler John**  
 (JSA16/W/07-A3 0830-34)  
**Butler R.**  
 (JWA34/W/08-B2 1500)  
**Butler Rhett**  
 (U7/W/16-B1 0830-16)  
**Butler S L**  
 (JSS13/W/09-A5 0950)  
**Buzzi Andrea**  
 (JWM08/W/16-A3 1010)  
**Bye John A. T.**  
 (JSP25/W/37-B1 1600)  
 JSP39/W/31-B4 1010)  
 (JSH12/W/01-A5 1200)  
**Byerlee J.D.**  
 (JSA15/W/06-A3 1030)  
**Byers Loren W.**  
 (ST6/E/01-A2 1730)  
**Byrne Paul**  
 (JSA20/W/29-A4 1200-13)  
**Byshev V. I.**  
 (JSP25/C/U2/E/02-B1 0830-03)  
**Bystricky Erik**  
 (ST3/W/44-B3 0930)  
**Bystrom Soren**  
 (GA5.12/E/03-A2 1600-05)

## C

- Caballero Cecilia**  
 (GA1.04/W/15-A6 1520)  
**Caballero Margarita**  
 (GA1.05/W/28-A5 0900-04)  
**Caballero-Miranda C.**  
 (GA1.05/W/07-A6 0900-06)  
 (GA1.05/W/16-A6 0900-07)  
**Cabassi Iris R.**  
 (GA5.01/W/17 A1 1300-05)  
 (GA5.06/W/06 A3 1640)  
**Cable Jaye E.**  
 (HW5/E/06-A3 1620)  
 (P09/W/09-A2 1050)  
**Cabosnarvaez William**  
 (JSP25/E/11-B2 0930-02)  
**Cabral Enrique**  
 (JSV36/E/13-B3 1445)  
**Cacciani A.**  
 (MC09/W/04-B2 1030)  
**Cacciani Marco**  
 (JSM26/W/16-B2 1210)  
**Cacoñ Stefan**  
 (G5/W/07-A4 1516-09)  
**Cafarella Lili**  
 (GA1.01/W/29-A5 1700)  
 (GA5.01/W/03 A1 0920)  
**Cafaro F.**  
 (JSP23/C/U5/W/01-B2 0830-15)  
**Caffier Ines**  
 (VS2/W/18-B3 0930)  
**Cahalan Roberts F.**  
 (MI10/E/03-B2 0930)  
**Cai Weixin**  
 (G5/W/26-A4 1550-06)  
**Caielli Grazia**  
 (JSS46/E/04-B4 1400)  
 (JSS46/E/05-B4 1440)  
 (JSS46/E/06-B4 0930-02)  
**Cain Joseph**  
 (GA5.09/W/09 A2 1030)  
 (GA5.12/W/06 A2 1440)  
 (GA5.08/W/13-B1 1545)  
**Cakir Recep**  
 (ST2/W/19-A4 1215)  
 (JWS33/W/02-B3 0900-20)  
**Calahorrano Acinno**  
 (JSP23/C/U5/E/05-A6 0830-06)

# INDEX

- Calais E.**  
(G2/E/06-A2 1630-03)
- Calcagnile Gildo**  
(JSA40/W/01-B5 1205)
- Calcutt S.**  
(JSA10/W/03-A2 0930)  
(MC09/W/07-B2 01)  
(MC09/W/10-B2 1515)
- Calcutt Simon**  
(MC09/W/11-B2 1500)
- Caldeira K**  
(MC01/W/36-A5 1700)
- Caldwell T. G.**  
(GA1.02/W/11-A2 0930)  
(GA1.02/W/18-A2 0930)
- Calkins D. J.**  
(HW3/W/09-B4 1455)
- Callander Peter**  
(HS5/W/14-A2 1000)  
(HW5/W/15-A3 1540)
- Callewier L.**  
(HS3/W/33-A2 200)
- Callis Linwood B**  
(JSM01/E/15-A5 1700)  
(JSA 45/E/13-B4 1005)
- Calov Reinhard**  
(MC11/E/12-B3 1220)
- Calvo J. P.**  
(GA1.15/W/09-B4 1400)
- Calvo Manuel**  
(GA1.04/W/02-A5 1640)  
(GA1.03/W/24-B1 1440)
- Calzadilla Alexander**  
(GA3.07/E/13-A4 0930-05)
- Camacho J. T.**  
(G5/W/26-A4 1550-06)
- Camelbeeck Thierry**  
(ST3/W/53-B4 1400)  
(ST4/P/6-B1 0830-11)
- Cammas Jean-Pierre**  
(MI05/W/23-A4 0950)  
(MI05/W/08-A4 1400-07)  
(MI05/W/07-A3 1440)  
(MI05/L/03-A4 1140)
- Campana Ken**  
(MC01/W/02-A1 1445)
- Campana Kenneth A.**  
(MC04/E/04-B2 1625)
- Campbell G. Garrett**  
(MW02/W/09-B3 1400)
- Campbell J.**  
(G2/L/09-A2 1200)
- Campbell James**  
(JSG11/E/06-A4 1400-03)  
(JSG11/E/07-A4 1400-04)
- Campbell Kenneth W.**  
(ST3/W/46-B3 1730)
- Campbell Wallace H.**  
(JSA09/W/20-A3 1130)  
(JSP23/L/04-A5 1130)
- Campbell-Smith P.**  
(MC09/W/10-B2 1515)
- Campin Jean-Michel**  
(MC01/E/01-A5 1730)  
(MC01/L/06-A2 1415)  
(P07/E/04-A3 1205)
- Campin J-M**  
(MC01/W/36-A5 1700)
- Camps P.**  
(GA1.03/W/01-B1 1000)
- Canavate M Ruiz**  
(P11/E/28-B5 0950)
- Cander L R**  
(JSA06/W/15-A2 1010)  
(JSA06/W/13-A1 1155-08)
- Cander L. J. R.**  
(GA2.03/W/06-B3 1200)  
(GA2.03/W/11-B3 1400-03)
- Candidi M.**  
(GA3.03/E/03-B4 1400-01)
- Caniaux G**  
(MI05/W/08-A4 1400-07)
- Caniaux Guy**  
(MI05/W/29-A3 1200)
- Cannon M. Elizabeth**  
(G1/E/48-A3 1620-01)
- Cannon P S**  
(JSA06/W/32-A1 1155-11)
- Canziani Pablo O**  
(JSM01/E/37-A4 1000)  
(JSM01/E/38-A4 1620-09)  
(JSM01/E/36-A4 1620-10)  
(JSM26/E/19-B2 1700-02)
- Cao**  
(MC08/L/10-A3 1005)
- Cao Dinh Trieu**  
(ST2/E/08-A3 1115)
- Cao Jamin**  
(JSS44/E/24-B5 1010)
- Cao Zuohao**  
(MC08/L/10-A3 1045)
- Capelli Giuseppe**  
(HS5/W/39-A3 1205)
- Capra Alessandro**  
(G3/E/21-A5 1610-22)
- Capuano Paolo**  
(JSS46/E/07-B4 0930-04)  
(JSS46/W/02-B4 1500)
- Caputo M.**  
(ST1/W/45-A2 1400-39)
- Caputo Riccardo**  
(ST3/E/07-B4 1000)
- Car Marjeta**  
(JWS33/E/12-B2 1635-30)
- Carabin Guy**  
(HW5/W/01-A3 0900)
- Carballo Dácil**  
(JSV36/W/20-B3 0900-09)
- Carbary J. F.**  
(JSM32/W/07-B3 1100)
- Carbone R. E.**  
(MC04/E/10-B1 1035)
- Carbone Vincenzo**  
(GA4.09/W/03-A6 1600)
- Cardenas Martin**  
(JSP23/E/01-A6 1110)
- Cárdenes Lourdes**  
(JSV36/C/U6/W/01-B3 1400-20)
- Cardin Philippe**  
(GA1.01/W/28-A5 0900-06)  
(JSA17/C/GA1.19/W/11-A4 1450)  
(GA1.01/W/09-A5 0900-03)
- Cardin Vanessa**  
(P11/W/22-B4 1620)
- Cardoso Carla**  
(JSM43/W/13-B4 1420)
- Cardoso Rita Margarida**  
(JSM01/C/MW07/W/01-A2 1600-28)
- Cardwell J**  
(M104/E/14-B1 0900-06)  
(M104/E/16-B4 1220)
- Cargill P. J.**  
(GA3.07/W/23-A5 1400)
- Carl Peter**  
(U3/P/01-A3 0900-07)  
(JSP25/P/01-B2 0930-06)  
(MC02/P/02-B2 1730)  
(MI11/E/07-B5 1200)  
(VS3/P/02-B3 0900-06)
- Carleer M**  
(MC08/E/02-A3 1130)
- Carli Bruno**  
(JSA09/W/12-A2 1630)
- Carlsen N. F.**  
(P15/W/07-B3 1650)
- Carlson C. W.**  
(GA4.09/W/02-A6 1000)  
(GA4.09/W/07-A6 0940)  
(GA3.06/W/19-A2 0930)  
(GA3.08/W/13-A6 0940)  
(GA3.02/W/18-B2 1645)
- Carlson C.**  
(GA3.03/W/11-B4 1200)
- Carlson Robert W.**  
(MC09/W/10-B2 1515)  
(MC09/W/06-B2 1630)
- Carlut J.**  
(GA1.03/W/22-B3 0900)  
(GA1.03/W/27-B1 1600)
- Carmichael Ian S E**  
(JSV30/E/03-B1 1100)
- Carmichael Ise**  
(JSV30/W/14-B1 1120)
- Carmon Naomi**  
(HS5/W/17-A2 1120)
- Carmona E.**  
(JSV47/W/01-B5 1045)  
(JSV47/W/15-B5 1400-08)  
(JSV47/W/20-B5 1400-13)  
(ST5/W/55-B5 1225)  
(ST5/W/56-B3 0900-01)  
(ST5/W/66-B4 1400-06)
- Carmona I**  
(MI09/E/02-A5 0937)
- Carmona Yitzhak**  
(JSP25/E/23-B1 1440)
- Carney J.**  
(GA1.04/L/06-A4 0930-03)
- Carnochan S.**  
(G4/W/15-A3 1620-23)
- Caro M.A.**  
(G5/W/19-A4 1230-02)
- Carosio Alessandro**  
(G4/W/01-A3 1620-05)
- Carozzi**  
(JSA06/L/06 0935)
- Carpenter Lucy**  
(U2/E/14-A2 1420)
- Carpenter Scott J**  
(MI05/W/09-A4 1400-10)  
(MI04/L/02-B3 0905)
- Carracedo J. C.**  
(VS3/E/03-B3 0900-02)  
(VS3/E/07-B3 1450)
- Carrasco-Nunez Gerardo**  
(VS2/E/06-B3 1400-21)
- Carrigan Jim**  
(GA5.01/W/11 A1 0900-05)
- Carrilho F.**  
(ST2/E/47-A4 1630)  
(ST2/E/48-A5 1400-22)
- Carrillo A.**  
(GA4.01/W/02-A2 1400-06)
- Carrupt Machado Wagner**  
(G1/E/44-A3 1620-28)
- Carslaw Ken**  
(JSM26/W/16-B2 1210)
- Carslaw Kenneth S.**  
(MI06/W/26-B2 1110)
- Carswell Allan I**  
(JSM01/W/40-A2 1520)
- Carter M.**  
(GA3.05/W/26-B3 1600)
- Carvalho Alexandra**  
(G5/E/46-A4 1548-05)  
(G5/E/47-A4 1546-04)
- Carvalho dos Santos Marcelo**  
(G1/E/54-A3 1620-79)
- Carvalho Juraci**  
(ST1/W/20-A4 0930-04)
- Carver G.**  
(JSM26/E/16-B3 1130)
- Cary Frand**  
(GA4.10/W/11-A5 1450)
- Casamitjana Xavier**  
(JSP39/W/38-B4 1150)
- Casas B.**  
(JSP23/W/07-B1 930)
- Casey Rob**  
(JWS33/W/22-B2 1635-01)  
(JWS33/W/22-B3 0900-01)
- Casey T.**  
(JSP25/W/95-B5 1620)
- Casott Norbert**  
(G4/W/02-A3 1500)
- Cassidy John**  
(JSV36/E/01-B3 1610)
- Cassou Christophe**  
(JSP25/E/19-B3 1720)
- Castelain Gabriel**  
(MW07/W/18-A4 1510)
- Castellano Mario**  
(JSV47/E/01-B5 1400-05)  
(JSV47/W/15-B5 1400-08)  
(ST5/W/56-B3 0900-01)
- Castiglione B.**  
(GA1.02/L/01-A2 0930)
- Castro Belmiro M.**  
(P10/E/08-A4 1700)
- Castro Manuel De**  
(MC01/E/27-A4 1645)  
(MC01/E/35-A4 1415)
- Castro Rita**  
(JSA19/W/03-A4 1400-06)
- Casula Giuseppe**  
(G5/W/17-A4 1415-04)  
(G5/W/20-A4 1230-03)
- Catalan M.**  
(GA5.12/E/04 A2 0930)
- Catalan-Morollon M.**  
(P11/E/28-B5 0950)
- Catalao J C**  
(G3/E/38-A5 1610-72)
- Catane Sandra G.**  
(VS2/E/07-B3 1230)
- Catoire V.**  
(JSM26/W/29-B2 1700-09)
- Cattell C. A.**  
(GA3.02/W/12-B2 1230)  
(GA3.04/W/20-B1 1100)
- Caulfield C. P.**  
(JSP49/W/02-B5 1520)
- Cautenet Guy**  
(MI01/E/22-A2 1700)
- Cayan Daniel R.**  
(GA6.01/W/12-A6 1020)
- Cayton T.**  
(GA3.05/W/30-B3 1100)  
(GA3.05/W/38-B3 1700)
- Cazenave A.**  
(JSG14/E/02-A3 1700-05)  
(JSG11/E/04-A3 0910)  
(JSG11/E/16-A4 1030)  
(JSM41/E/31-B5 1415)
- Cebula Richard. P.**  
(JSA16/W/14-A3 0830-38)
- Cecchini S.**  
(GA6.01/W/03-A5 1525)
- Cecic Ina**  
(ST3/E/19-B4 1400-03)
- Cecil H.**  
(GA5.08/W/12-B1 1135)
- Cejkowska Vera**  
(ST2/E/38-A5 1400-23)
- Celik Cahit Tagi**  
(G1/C/G5/E/04-A3 1620-100)
- Centrone M.**  
(JSA16/E/43-A3 0830-01)
- Cerisier J. C.**  
(JSA10/W/03-A2 0930)  
(JSA10/W/11-A2 1000)
- Cerisier Jean -Claude**  
(GA3.03/W/09-B4 1740)
- Cermak V.**  
(MC02/E/10-B1 0950)
- Cernadas Daniel**  
(ST1/W/59-A4 0930-36)
- Cerniar M.**  
(JSA37/W/04-B3 1200)
- Cerniglia M. C.**  
(JSM26/E/22-B1 1210)
- Cernih Dragana**  
(ST5/E/36-B5 0930-14)  
(ST2/E/38-A5 1400-23)
- Cerv V.**  
(GA1.02/W/13-A2 0930)  
(GA1.02/W/19-A2 0930)  
(GA1.02/W/28-A2 0930)
- Cesar Moya**  
(ST1/W/69-A1 1640)
- Cess D.**  
(MI10/W/23-B2 1420)
- Cess Robert D.**  
(MI04/W/17-B1 1635)
- Chaboureau Jean-Pierre**  
(MI05/W/23-A4 0950)  
(MI05/L/03-A4 1140)  
(MI05/W/36-A4 1400-03)
- Chacho E.**  
(HW3/W/08-B4 1430)
- Chadha R K**  
(ST1/E/67-A3 1010)
- Chai Goh Pong**  
(G1/L/22-A3 1640-95)
- Chakrabarti S.**  
(JSA20/E/27-A4 1200-21)
- Chakrabarty D.**  
(JSA20/W/20-A5 1135)
- Chamberland S.**  
(JWM08/E/06-A2 1120)
- Chambers D. P.**  
(G6/C/G3/W/32-B1 1120)  
(JSM41/W/09-B4 1515)
- Chambers P. A.**  
(HW3/W/04-B4 1050)
- Chandramohan P.**  
(PW1/P/01-A6 0940)
- Chan Anthony A.**  
(GA3.05/E/22-B3 0900-08)
- Chan Johnny C. L.**  
(JSP25/C/MI05/W/01-B2 1150)  
(JSP25/C/MI05/W/34-B1 0830-04)
- Chan K L**  
(MW04/W/16/C/JSM01/E/14-A1 1135)
- Chan L.**  
(GA3.08/W/33-B1 1130)
- Chan Shaowei**  
(G1/L/08-A3 1620-86)
- Chandler M O**  
(GA3.10/W/01-A6 1630)  
(GA3.08/W/09-A6 0920)
- Chandra H.**  
(JSA20/W/20-A5 1135)  
(GA3.05/E/10-B3 0900-43)
- Chandra Sekhar M**  
(HS5/W/50-A3 1630-01)
- Chandra Suresh**  
(JSP39/E/25-B3 1439-14)
- Chandrasekhar E.**  
(GA1.02/E/27-A2 0930)



- Chang C.-P.**  
(MC10/P/02-B1 1625)
- Chang Chia-Chyang**  
(G1/W/03-A3 1620-33)  
(G1/W/38-A3 1620-44)  
(G3/W/45-A5 1610-73)
- Chang P. C. Y.**  
(P15/L/22-B3 1135)
- Chang Prof. Tom**  
(GA4.09/W/16-A6 1400)
- Chang Ruey-Gang**  
(G3/W/45-A5 1610-73)
- Chang S**  
(MC01/L/13-A3 1135)
- Chang Y. S.**  
(JSA20/W/28-A5 1200-10)
- Changrong He**  
(ST1/E/55-A2 1400-08)
- Chanin Marie-Lise**  
(U2/L/02-A2 1500)
- Chanton Jeffrey**  
(HW5/E/04-A3 1500)  
(HW5/E/06-A3 1620)
- Chanut J P**  
(JSG11/E/13-A4 1400-05)
- Chanut Jean-Pierre**  
(P15/L/05-B4 1610)
- Chao B.**  
(G6/W/05-B1 0850)  
(JSG14/E/09-A3 1700-01)  
(JSG14/W/05-A3 1100-01)
- Chao B. F.**  
(U7/E/05-B1 0900)
- Chao Benjamin F.**  
(JSG14/E/11-A3 1212-25)  
(JSG14/W/10-A3 1151-18)  
(JSG14/E/04-A3 1109-04)
- Chao C. K.**  
(JSA20/W/28-A5 1200-10)
- Chao C.H. Jason**  
(G1/E/20-A3 1620-26)
- Chao Dingbo**  
(G2/W/16-A2 1630-20)  
(G3/L/11-A5 1610-13)  
(G3/L/18-A5 1610-10)  
(G3/W/27-A5 1610-86)  
(G3/W/50-A5 1610-55)
- Chao Jih**  
(JSA06/W/14-A1 1700)
- Chao Y.**  
(U3/W/08-A30900-13)
- ChaoDingbo**  
(G5/W/09-A4 1445)
- Chaparro Marcos A.**  
(GA1.05/W/26-A6 1200)
- Chapellaz J**  
(MI02/L/19-A4 1410)
- Chapman David S.**  
(JSS44/W/10-B4 1110)  
(JSS44/W/17-B4 0930-31)  
(MC02/E/19-B1 1130)
- Chapman P. J.**  
(HS3/W/03-A1 0950)
- Chapman Peter**  
(JSA20/W/29-A4 1200-13)
- Chapman Sandra**  
(GA4.10/W/04-A4 1505)  
(GA3.02/W/08-B3 0900-06)  
(GA3.05/W/12-B3 0900-31)  
(GA3.02/W/37-B3 1150)
- Chappellaz J**  
(JSP21/W/11-A4 1050)
- Charlock Thomas P**  
(MI08/E/05-A3 0940)  
(M106/E/09-B1 1400-13)  
(M106/E/09-B2 1400-13)
- Chartier Jean-Marie**  
(G3/E/16-A5 1610-40)
- Chartrand D J**  
(MW01/W/04-A5 1500)
- Chashechkin Yuli D.**  
(JWM08/W/07-A3 1120)  
(JSP39/W/01-B3 1442-15)  
(JSP39/W/07-B2 1720)  
(JSP39/W/09-B3 1445-16)  
(JSP39/W/22-B3 1448-17)  
(JSP39/W/30-B3 1436-13)  
(JSP49/W/05-B5 1210-02)  
(JSP49/W/13-B5 1210-03)
- Chasiev I. S.**  
(GA5.01/E/29 A1 1100)
- Chatfield Robert B**  
(JSM26/E/05-B2 1430)
- Chatila Khaled**  
(P15/L/05-B4 1610)
- Chatterjee Soma**  
(ST1/P/09-A2 1400-19)
- Chattopadhyay Gayatri**  
(ST4/E/34-B1 0830-27)  
(ST4/E/40-B1 0830-28)
- Chau H D**  
(GA5.01/E/25 A1 1530)
- Chave Alan**  
(JWA34/W/07-B2 0910)  
(JWA34/W/08-B2 1500)  
(P16/W/03-B5 1110)  
(JWA34/E/07-B2 1420)
- Chave Alan D.**  
(GA1.02/W/05-A2 0930)
- Chaves Dias**  
(G1/L/02-A3 1620-840)
- Chavez-Garcia Francisco**  
(JSP23/E/01-A6 1110)
- Chavez J.**  
(ST3/E/41-B5 1000)
- Chebchoub Assia**  
(HS1/W/45-B41720)
- Chebrov Victor**  
(ST4/W/14-B2 1700)  
(ST4/W/15-B3 1500)  
(ST2/W/13-A3 0845)
- Chedin Alain**  
(JSM41/L/05-B3 1120)
- Chekhmir Anatoly**  
(VS2/W/06-B3 0830)
- Chelidze Tamaz**  
(ST1/E/10-A4 0930-20)  
(ST1/E/12-A4 0930-22)  
(ST1/E/18-A4.0930-05)
- Chemaa B.**  
(G3/P/02-A5 1610-76)  
(G3/P/05-A5 1610-74)
- Chembarisov E I**  
(HS5/W/49-A3 1545-05)
- Chembarisova E I**  
(HS5/W/49-A3 1545-05)
- Cheminee Jean Louis**  
(JSA15/E/10-A3 1640)
- Chen Chang-Hwa**  
(JSV30/C/JSV22/E/11-B1 1400-17)
- Chen Chen Ling**  
(JSP23/E/50-B2 0830-10)
- Chen Cheng-Hong**  
(JSV30/E/09-B1 1400-02)
- Chen Cheng-Ta**  
(MW02/W/04-B3 0910)
- Chen Chih-Chieh**  
(MI05/E/14-A2 1120)
- Chen Chow-Son**  
(GA1.02/W/24-A2 0930)
- Chen Chun-Sung**  
(G1/E/34-A3 1420)
- Chen G C**  
(JSS02/E/04-A1 0830-06)
- Chen Ganglin**  
(ST6/JSS02/W/19- A1 0830-18)
- Chen Hong**  
(ST1/P/06-A3 0900-15)
- Chen Hongbin**  
(MI06/E/04-B1 1630)
- Chen Hung-Chih**  
(G1/W/38-A3 1620-44)
- Chen J. L.**  
(G5/W/25-A4 1100)  
(JSG14/W/07-A3 1154-19)  
(JSG14/W/24-A3 1700-04)
- Chen Jiasheng**  
(GA3.07/E/05-A4 1400)  
(GA3.05/E/04-B3 0900-09)
- Chen Kongzhe**  
(G1/W/30-A3 1620-13)
- Chen L. J.**  
(GA3.02/E/09-B2 1500)
- Chen Ling**  
(ST3/E/42-B5 1415)  
(JSP23/C/U5/E/15-A6 1500)
- Chen Margaret W**  
(GA3.06/W/03-A2 1220)
- Chen Minghang**  
(MC08/W/03-A3 1650)
- Chen Mingxiang**  
(MW02/E/04-B3 1140)
- Chen Mingyue**  
(MI12/W/12-B4 1135)
- Chen Ping**  
(MC10/W/08-B1 1155)
- Chen Q. Y.**  
(ST2/E/05-A3 1000)
- Chen Qi-Fu**  
(JSP23/C/U5/E/15-A6 1500)
- (JSP23/E/50-B2 0830-10)  
(ST1/E/60-A2 0930-01)  
(ST3/E/42-B5 1415)
- Chen Qiu-shi**  
(MI05/W/47-A2 1400)  
(MI07L/04-A2 1230)
- Chen Shyh**  
(MC01/W/44-A4 1110)
- Chen Sung-An**  
(JSG11/E/09-A3 0930)
- Chen Ting**  
(G5/W/09-A4 1445)
- Chen Tsing-Chang**  
(MW06/W/08-A3 1020)
- Chen Wu**  
(G1/C/G5/E/04-A3 1620-100)  
(G1/E/52-A3 1620-77)  
(JSG28/E/07-B1 0950)
- Chen Xiaofei**  
(ST3/E/26-B3 1100)  
(ST5/E/01-B4 1205)  
(ST1/E/83-A3 1520)
- Chen Xin**  
(JSA09/W/13-A2 1215)
- Chen Y.**  
(JSG28/W/02-B1 1400-09)
- Chen Y. C.**  
(P10/E/14-A3 1500)
- Chen Y Q**  
(JSG11/W/22-A3 1150)  
(G5/W/27-A4 1512-07)
- Chen Y. L.**  
(ST5/E/32-B5 0850)
- Chen Yi-Jau**  
(G1/E/34-A3 1420)
- Chen Yong**  
(JSP23/C/U5/E/15-A6 1500)  
(ST3/E/34-B4 1400-04)  
(ST3/E/42-B5 1415)
- Chen Yongqi**  
(G3/W/31-A5 1610-56)  
(G4/P/05-A3 1620-07)  
(G1/W/01-A3 1620-02)
- Chen Yuchun**  
(JSP25/E/21-B3 1420)  
(P11/E/14-B3 1110)
- Chen Yun-Tai**  
(ST 5/E/37-B4 1520)  
(U4/E/04-A41145)
- Chen Yun-Tai Chen**  
(ST1/E/54-A2 1400-07)
- Chen Z. X.**  
(GA3.02/E/18-B3 0850)  
(GA3.02/W/54-B2 1615)
- Chenette David L.**  
(GA3.02/W/18-B2 1645)  
(GA3.05/E/11-B3 1620)  
(GA3.05/W/44-B3 0900-44)  
(JSA45/E/16-B4 1510)
- Cheney Robert**  
(JSM41/E/27-B4 1430)
- Cheng C. Z.**  
(GA3.02/W/38-B3 0910)  
(GA3.04/W/11-B1 1130)  
(GA4.03/W/03-B4 1230)  
(GA4.02/W/05-A4 1020)  
(GA4.20/W/05-A4 1400-14)
- Cheng H. X.**  
(ST4/E/55-B2 1620)
- Cheng K**  
(JSG11/W/17-A4 1150)
- Cheng M. K.**  
(JSG14/W/11-A3 1700-02)  
(JSM41/W/06-B4 1545)
- Cheng Zhaohui**  
(MI10/W/08-B2 1220)
- Cheng-Cheng Liu**  
(P15/W/02-B3 1400)
- Cherhych A. A.**  
(JSS44/L/04-B4 1640)
- Cherniavski V.**  
(JSP39/E/20-B2 1540)  
(JSS44/E/26-B4 0930-38)  
(JSS44/E/28-B4 0930-37)
- Chernigovskaya M. A.**  
(JSM26/W/35-B2 1700-12)
- Chernobay I.**  
(U8/W/12-B3 1640-04)
- Chernous Pavel**  
(ST3/E/48-B5 1100)
- Chernous Pavel**  
(JSP23/C/U5/E/08-B1 1700)  
(JSP23/C/U5/E/18-B1 0830-11)
- Chernouss S.**  
(GA3.06/W/09-A2 0930-15)
- Chernov Yury**  
(ST3/E/11-B4 1400-17)  
(ST3/E/12-B4 1400-16)
- Chernova L. P.**  
(HS2/W/15-B2 0900)
- Chernyshev Sergei D.**  
(ST1/E/42-A3 0900-14)
- Chertok Iliia**  
(GA4.01/W/10-A2 1400-01)  
(GA4.02/W/11-A4 1750)
- Cherubini C.**  
(JSP23/C/U5/W/01-B2 0830-15)
- Cheshire L.**  
(JWS33/W/33-B2 1635-32)  
(JWS33/W/33-B3 0900-32)
- Chesnokov Evgenii M.**  
(ST5/W/02-B4 0930-06)
- Chesnokov Evgenii M.**  
(ST5/W/08-B4 1145)  
(ST5/W/27-B4 0930-07)  
(ST5/W/28-B4 0930-05)  
(ST5/W/50-B5 0930-04)
- Chevrel S.**  
(JSA10/E/01-A2 1515)
- Chevrot Sebastien**  
(JSS13/W/15-A4 1500)  
(ST4/E/10-B3 0940)  
(ST4/L/06-B2 0930-29)
- Chi P.**  
(GA3.08/W/05-A6 1040)  
(GA3.08/W/21-A6 0900)
- Chi P. J.**  
(GA3.04/L/17-B2 1710)  
(GA3.04/W/07-B2 1510)
- Chiaki Kobayashi**  
(MC01/E/13-A1 1130)
- Chiang Chung-Jung**  
(HS5/W/25-A2 1525)
- Chiang W. L.**  
(JSA20/W/28-A5 1200-10)
- Chiappini Massimo**  
(JSA09/E/09-A3 1015)  
(JSA09/W/05-A3 0930)  
(JSA09/W/07-A2 0930-02)
- Chiarabba C.**  
(JSS46/E/07-B4 0930-04)
- Chiarabba Claudio**  
(JSS46/E/03-B4 1420)  
(JSS46/E/04-B4 1400)  
(JSS46/W/02-B4 1500)  
(JSS46/W/11-B4 1540)
- Chiavettieri Cinzia**  
(JSS42/W/03-B4 1420)
- Chiba Hitoshi**  
(P16/L/01-B5 0910)
- Chiba Tatsuro**  
(JSV36/E/17-B3 1400-09)
- Chie-Song Shieh**  
(ST3/W/35-B3 0900)
- Chikmachev V. I.**  
(MC09/E/06-B2 1730)
- Childers Vicki A.**  
(G3/L/22-A5 1220)
- Chilingarashvili Stephan**  
(JSA20/I/01-A4 1200-16)
- Chilson Phil**  
(JSM26/W/26-B2 1700-10)
- Chilton P J**  
(HS5/W/21-A2 1405)
- Chinnery M. A.**  
(ST 5/E/22-B4 1700)
- Chio G. S.**  
(GA4.02/W/05-A4 1020)  
(GA4.20/W/05-A4 1400-14)
- Chiodini Giovanni**  
(JSV36/W/04-B3 1115)
- Chipperfield Martyn**  
(JSM26/W/07-B1 1500)  
(JSM26/W/09-B3 0830)  
(JSM26/W/21-B2 1700-07)  
(JSA09/W/12-A2 1630)  
(JSM01/E/40-A5 1450)  
(JSM01/W/32-A5 1040)  
(JSM01/W/37-A5 1400)
- Chirkov Yeugeny**  
(JSA15/W/16-A5 0830-12)  
(JSP23/W/10-B1 1150)  
(ST1/E/74-A2 1400-04)  
(SW1/W/02-B5 1000)
- Chisham G.**  
(GA3.04/W/42-B1 1520-39)  
(GA3.07/W/67-A6 0900-02)  
(GA3.10/W/26-A5 1225)
- Chistyakova L.V.**  
(JSA20/W/44-A4 1200-33)

## INDEX

- Chiswell Stephen M.**  
(P11W/20-B3 0850)
- Chitaladze A.**  
(ST4W/53-B1 0830-31)
- Chiu Hung-Chie**  
(ST3E/26-B3 1100)  
(ST1E/83-A3 1520)
- Chmyrev Vitaly**  
(JSA15W/22-A5 1400-18)  
(GA2.02W/29-B4 0930-03)
- Cho Akio**  
(ST1E/56-A2 1400-37)
- Cho Ha-Man**  
(MI01E/18-A1 0900-11)
- Cho Han-Ru**  
(M104E/12-B1 1115)
- Chobotok Igor**  
(JSA15E/16-A5 1400-03)
- Choe G. S.**  
(GA4.03W/03-B4 1230)
- Choi Jae-Chon**  
(MI01E/18-A1 0900-11)
- Choi K. H.**  
(JSP23C/U5E/20-B2 1110)
- Choi S. G.**  
(JSA27E/06-B1 1130)
- Choi S. W.**  
(JSA27E/06-B1 1130)
- Chol Wookap**  
(JSM01P/02-A4 1210)
- Chojnicki Tadeusz**  
(G5E/13-A4 1115-02)
- Chome Frederic**  
(MC01E/15-A5 0845)
- Chomette Olivier**  
(MI01E/22-A2 1700)
- Chongyin Li**  
(MW06P/04-A3 1400)  
(JSP25P/02-B1 0830-10)  
(JSP25P/04-B1 1740)  
(MC10W/06-B1 1450)
- Chopp M. A.**  
(JSS31W/03-B2 0930)
- Chou Chia**  
(JSP25W/26-B1 1050)  
(MI04L/13-B1 0945)
- Chou Joyce**  
(MI06W/19-B2 1230)  
(MI09W/16-A5 1710)
- Choudhury B. J.**  
(U7E/01-B1 1135)
- Chouet B.**  
(JSV47W/17-B5 1400-14)
- Chouet B. A.**  
(JSS46W/05-B4 1150)
- Chouet Bernard**  
(JSV29W/07-B1 1400)  
(JSV47E/04-B5 0830)  
(JSV47W/18-B5 1100)  
(U6W/03-B2 1005)  
(JSV47W/24-B5 0945)
- Choularton T. W.**  
(M104E/14-B1 0900-06)  
(M104E/16-B4 1220)  
(MI02W/13-A5 1510)
- Choularton Thomas W**  
(MI01E/05-A1 1430)
- Choularton Tom W**  
(MI02W/01-A5 1450)
- Chouliaras G.**  
(ST1E/28-A3 0900-17)
- Chouliaras N. G.**  
(ST1E/46-A3 1620)
- Chourasia L.P**  
(JSA19P/02-A4 1145)
- Chouteau Michel**  
(JSA27W/02-B1 0920)
- Choux C.**  
(VS2E/10-B3 1400-23)
- Christensen Andrew**  
(JWS33W/27-B3 0900-22)
- Christensen Gordon**  
(P07L/03-A3 0900-08)
- Christensen Jens H**  
(MC01E/03-A4 1445)  
(MC01W/35-A4 1630)  
(MC01W/21-A4 1400)
- Christensen O. B.**  
(MC01W/35-A4 1630)
- Christensen Tina**  
(GA2.01E/13-A1 0900-02)
- Christensen Ulrich**  
(GA1.01E/03-A6 1215)  
(GA1.01E/04-A6 0945)  
(ST4E/64-B3 1710)
- (ST4W/10-B3 1650)  
(ST4W/17-B3 0830-06)
- Christian E. R.**  
(GA4.04W/14-B5 1620)
- Christiansen B**  
(MC07W/02-A2 1015)
- Christiansen Freddy**  
(GA2.01E/13-A1 0900-02)  
(GA3.10W/18-A5 1155)  
(GA5.08W/06-B1 0945)
- Christie Douglas**  
(U8E/08-B3 0940)
- Christos P.**  
(GA3.02L/02-B3 0900-24)
- Christoph M.**  
(JSP25E/27-B2 0930)  
(JSP25W/53-B3 0850)
- Christoph Reigber**  
(JSS44E/41-B4 0930-35)
- Christova Cenka**  
(ST2E/45-A3 0900)  
(ST2L/02-A4 1500)  
(ST2E/07-A4 1700)
- Chu Peter C.**  
(P10E/14-A3 1500)  
(P12E/04-A1 1110)  
(JSP25E/21-B3 1420)  
(M111E/05-B5 1630)  
(P11E/13-B3 1050)  
(P11E/14-B3 1110)  
(P11E/15-B3 1130)
- Chua D.**  
(GA3.03E/07-B4 1020)
- Chuangding Zhang**  
(G2E/01-A2 1630-23)
- Chuang Catherine C**  
(MI01W/17-A3 0950)
- Chuangzhen Zhu**  
(ST1P/05-A3 0900-08)
- Chub Victor E**  
(HS5W/48-A3 1545-04)
- Chubarenko Boris V.**  
(P10E/19-A5 1600-08)
- Chubarenko Irina P**  
(U3E/02-A30900-01)
- Chuchkov Eugene A.**  
(GA4.04W/10-B5 0830-03)
- Chuda Takashi**  
(MI04E/03-B1 0900-07)
- Chudnenko Svetlana**  
(GA3.05W/19-B3 0900-26)
- Chujkova Nadejda A.**  
(U3W/06-A3 0900-12)
- Chullat Arnaud**  
(GA1.01W/17-A5 1615)
- Chumakov Mikhail**  
(JSP23W/28-B1 0830-01)
- Chumburidze Zurab**  
(M103E/03-A3 1040)
- Chun Hye-Yeong**  
(MW07W/07-A4 1640)
- Chun Young-Sin**  
(MI01E/18-A1 0900-11)
- Chunduru R.**  
(ST4W/33-B1 0830-29)
- Chung C.-H.**  
(JSS44W/14-B4 0930-12)
- Chung Jen-Kuang**  
(JSP23C/U3W/21-B2 1740)  
(U3W/21-A30900-17)
- Chun-Kai Teng**  
(ST1E/50-A2 1400-36)
- Church John A.**  
(P12W/10-A1 1150)  
(JSP49W/06-B5 1210-04)
- Church M. J.**  
(GA1.05W/20-A5 0900-06)
- Churikov V. A.**  
(JSP23C/U5W/16-A5 0830-17)  
(ST1W/62-A2 1400-16)
- Churikova T. G.**  
(JSV30W/11-B1 0900)
- Churilova T. I.**  
(P11E/12-B5 1640)
- Chursin Alexander**  
(JSS44W/20-B4 0930-23)
- Chylek P**  
(MI01L/04-A1 1055)
- Ciais P**  
(MC01W/07-A5 1145)  
(MC01W/43-A5 1130)
- Ciais Philippe**  
(MC01W/15-A2 1740)
- Cianetti Spina**  
(ST4W/60-B3 0830-01)
- Ciddor Philip E.**  
(G5P/02-A4 1130-02)
- Cierpka K.**  
(JSA20W/08-A4 1200-27)
- Ciesielski Paul E.**  
(MI04W/09-B3 0850)  
(MI04W/18-B3 1600)
- Cifelli Francesca**  
(ST3W/33-B4 1400-01)  
(ST7E/09-A2 1605-05)
- Cifuentes G.**  
(JSV36E/11-B3 0900-15)
- Cifuentes O.**  
(JSS31W/12-B2 1420)
- Cifuentes Oscar**  
(JSS31E/04-B2 1400)
- Cihlar Josef**  
(JSM41W/26-B3 0900)  
(HW1E/02-A4 0930)
- Cimini G.**  
(JSS46E/07-B4 0930-04)
- Cimini Giovanni B.**  
(JSS46E/04-B4 1400)
- Cimini Giovanni Battista**  
(ST4W/35-B2 0930-03)
- Cini Castagnoli G.**  
(JSA16W/43-A3 1630)
- Ciocciu Nadejda**  
(GA1.02E/39-A1 1050)
- Cioppa M. T.**  
(GA1.04W/05-A4 0930-14)
- Cirillo A.**  
(JSV47E/08-B5 1400-04)
- Cisak J.**  
(JSA40L/01-B5 1400-21)
- Cisneros J**  
(JSM01W/37-A5 1400)
- Civetta Lucia**  
(JSP23E/42-B2 1010)  
(JSV36C/U6W/02-B3 1400-19)
- Civitaresse Giuseppe**  
(P11E/19-B4 1150)  
(P11E/20-B4 1720)  
(P11E/21-B4 1700)
- Cladis John B.**  
(GA3.08W/17-A6 0940)
- Clainche Yvonnick Le**  
(MC01E/11-A3 0845)
- Clappier A**  
(MI07L/02-A2 1620)
- Clara de Lacy M.**  
(G3W/25-A5 1610-81)  
(G5W/19-A4 1230-02)
- Clark David A.**  
(GA1.04W/06-A4 0930)  
(GA5.11W/07-A3 1100)  
(GA5.11W/04-A3 1010)  
(GA1.07W/05-B2 0920)
- Clark Martyn P.**  
(HS2W/06-B1 1120)
- Clark P A.**  
(MI05E/20-A3 1700)
- Clark R R**  
(JSM01W/64-A2 1600-22)
- Clark Richard**  
(JSG28W/01-B2 1400-16)
- Clark T.**  
(G6W/05-B1 0850)  
(G2L/09-A2 1200)
- Clark T. A.**  
(G2C/G5W/23-A2 1515)
- Clark Thomas A.**  
(G1W/23-A3 1620-09)  
(JSG14W/05-A3 1100-01)
- Clark Toby**  
(JSA06W/27-A1 1035)
- Clark Toby D G**  
(GA5.01W/04-A1 1700)  
(GA6.02W/04-B1 1745)
- Clarke A D**  
(MI01L/05-A1 0900-09)  
(MI09L/01-A5 1145-22)  
(MI09L/01-A5 1744)
- Clarke A. B.**  
(VS2W/21-B3 1400-14)
- Clarke Ellen**  
(JWS33W/26-B2 1635-04)  
(JWS33W/26-B3 0900-04)  
(JSA06W/27-A1 1035)
- Clarke James**  
(MC08W/07-A3 1210)
- Clarke P.**  
(GA1.04L/06-A4 0930-03)
- Clarke Peter**  
(G5E/36-A4 1215)
- (JSS31W/11-B2 1620)
- Clarke J. T.**  
(GA4.10W/32-A4 1635)
- Classen Sabine**  
(JSP39W/33-B3 1424-09)
- Claud C**  
(MI05W/30-A3 1220)
- Claude H**  
(JSM01W/37-A5 1400)
- Claudia Troise**  
(JSV47E/01-B5 1400-05)
- Clauer C. R.**  
(GA3.03W/13-B4 1430)  
(GA4.08W/03-B4 0930)  
(GA4.08W/16-B4 1610)  
(GA3.07W/14-A6 0900-03)
- Clausen Bente**  
(HS3W/16-A1 1730)
- Clauer Christoph**  
(ST6E/03-A1 0830-14)  
(JSA19W/07-A4 1115)  
(ST4W/64-B1 1400-12)  
(ST4W/49-B1 1640)
- Claussen Martin**  
(U2L/01-A2 0930)
- Clayton R.**  
(ST5W/L/04-B3 0900-13)
- Clayton R. W.**  
(JWS33E/08-B2 1635-10)  
(JWS33E/08-B3 0900-10)
- Clement A.**  
(MC03W/05-B4 0950)
- Clement Brad**  
(GA1.03W/05-B2 1040)
- Clemesha Barclay**  
(JSM01W/19-A2 1600-07)  
(JSM01W/45-A2 1600-06)
- Clemmons J.**  
(GA2.02L/01-B4 1000)
- Clemmons J. H.**  
(GA3.04W/07-B2 1510)
- Clerbaux Cathy**  
(MC08E/02-A3 1130)
- Cliilverd Mark A.**  
(JSA15W/17-A4 1100)  
(GA3.04W/51-B1 1520-20)
- Clint O. C.**  
(JSA15W/18-A4 1400-02)
- Close Gareth**  
(G1E/56-A3 1620-80)
- Clothiaux E. E**  
(MI10W/25-B1 0930)
- Clough P T**  
(MC08E/02-A3 1130)
- Clough S A**  
(MC01W/33-A1 1515)  
(MC07W/17-A3 1115)  
(MC08E/08-A3 1445)
- Clough Shepard A**  
(MC08W/06-A3 1505)  
(MC08L/09-A3 1545)  
(MC08W/04-A4 1130)  
(MC08L/09-A3 1545)  
(MC08L/09-A3 1545)
- Clow Gary D.**  
(MC02E/08-B1 1100)
- Clowes Ron M.**  
(JSS44L/01-B4 1210)
- Clua de Gonzalez A. L.**  
(GA4.08W/02-B3 1400)  
(GA4.08W/10-B3 1030)  
(GA4.08W/06-B3 0905)
- Cluckie I**  
(JWM08L/02-A3 1400)
- Coals A V**  
(JWM08W/16-A3 1010)
- Cobas José A.**  
(JSV36C/U6W/01-B3 1400-20)
- Cobb Mark**  
(P10E/16-A4 1400)
- Cobby David**  
(P14E/01-A4 1400-02)
- Cocard M.**  
(JSA37W/04-B3 1200)
- Cocard Marc**  
(G6W/06-B2 1400)  
(G5E/36-A4 1215)
- Cocina Ornella**  
(JSV47W/09-B5 1200)  
(JSV47W/12-B5 1400-10)
- Codrescu M. V.**  
(GA3.09W/03-B5 0950)  
(JSA20W/41-A5 1200)
- Coë H.**  
(MI02W/13-A5 1510)

- Coe Hugh**  
(MI02/W/01-A5 1450)
- Coe Robert R. S.**  
(GA1.03/W/28-B2 1140)
- Coe Robert S.**  
(GA1.03/W/04-B1 1140)
- Coffey Helen**  
(JSA16/C/GA.07/W/30-A3 0830-59)
- Coffey Helen E.**  
(GA5.06/W/07 A3 1100)
- Coffin Millard F.**  
(JSV22/L/05-A5 1420)  
(U6/NW/04-B2 1035)
- Cogger L. L.**  
(GA3.04/NW/02-B1 1520-33)
- Cohen C. M. S.**  
(GA4.10/W/16-A5 1145)
- Cohen Judah**  
(HS2/W/02-B1 0920)
- Cohen Steven**  
(JSS31/W/09-B2 1130)
- Cohen Yves**  
(GA5.08/W/01-B1 1400-07)  
(GA5.08/W/02-B1 1005)  
(GA5.08/W/09-B1 1115)  
(JSA37/W/08-B3 1430)
- Coira Beatriz**  
(GA1.04/W/32-A5 1510)
- Colacino M.**  
(GA6.01/E/22-A5 0900-06)  
(GA6.01/E/23-A5 0900-05)
- Colacino Michele**  
(GA6.01/L/03-A5 1730)
- Colarco Peter R**  
(MI01/L/06-A1 1110)
- Cole D**  
(JSA06/W/17-A1 1155-14)  
(GA3.04/W/10-B1 1520-08)
- Cole J**  
(MC01/W/42-A1 1015)
- Cole P. D.**  
(VS2/W/12-B3 1400-09)  
(VS2/W/14-B3 1150)
- Coleman I J**  
(GA3.07/L/01-A6 0900-04)
- Coleman R.**  
(JSP25/W/32-B3 0830-03)
- Coleman Richard**  
(JSM41/W/14-B4 1500)  
(JSP49/W/06-B5 1210-04)
- Coles G.**  
(GA1.05/W/20-A5 0900-06)
- Coles Richard**  
(JSA06/W/08-A1 1520)  
(JSA06/W/17-A1 1155-14)  
(U7/L/01-B1 0950)
- Coley R**  
(GA3.10/W/10-A6 1700-03)
- Colic Kresimir**  
(G3/E/41-A5 1610-84)
- Colin R**  
(MC08/E/02-A3 1130)
- Collard Andrew**  
(MI06/E/07-B1 1400-09)  
(MI06/E/07-B2 1400-10)
- Collatz G James**  
(MC01/W/54-A3 1705)
- Collier Jonathan**  
(ST4/E/04-B3 1550)  
(ST4/E/32-B3 1610)
- Collier M. R.**  
(GA3.08/W/09-A6 0920)  
(GA4.08/W/05-B3 1335)
- Collier Michael R.**  
(GA3.07/P/01-A3 0900)
- Collin Fabienne**  
(JSS44/E/19-B4 0930-25)
- Collin Harry L.**  
(GA3.05/W/10-B3 1720)  
(GA3.08/L/01-B2 0900-10)  
(GA3.08/L/01-B2 900-10)  
(GA3.08/W/09-A6 0920)  
(GA3.08/W/17-A6 0940)
- Collin H L**  
(GA3.06/L/03-A2 0930-03)  
(GA3.06/L/02-A2 0930-02)
- Colling David J.**  
(JSM26/E/10-B2 1000)
- Collins D**  
(MI09/W/14-A5 1030)
- Collins Dave**  
(ST1/W/51-A3 0930)
- Collins J M D**  
(MI09/W/14-A5 1145-21)
- Collins Richard**  
(JSM01/E/42-A2 1600-09)
- Collins William**  
(MI02/E/10-A4 1100)
- Collins Dave**  
(ST1/W/61-A1 1500)
- Colman A.**  
(JSP25/W/95-B5 1620)
- Colomer Jordi**  
(JSP39/W/23-B3 1427-10)  
(JSP39/W/38-B4 1150)
- Colony R.**  
(P07/L/02-A3 1125)
- Cotelli M.**  
(JSV36/W/17-B3 1500)  
(JSV36/W/23-B3 1515)
- Cotlice Nicolas**  
(JSS13/W/18-A5 1420)
- Comfort R H**  
(GA3.10/W/01-A6 1630)  
(GA3.05/W/03-B3 0900-10)
- Comiso Josefino C.**  
(JSM41/W/10-B3 1500)  
(P13/E/02-B2 1400)
- Comppagnucci Rosa H**  
(JSM01/E/36-A4 1620-10)  
(JSM01/E/37-A4 1000)  
(JSM01/E/38-A4 1620-09)
- Conant W C**  
(MI01/E/07-A2 0930)
- Conde M.**  
(JSA20/E/17-A6 1154)
- Conde M. G.**  
(JSA20/E/04-A6 1136)
- Congli Zhao**  
(JAS15/P/02-A5 0830-08)
- Congwei Hu**  
(G5/W/14-A4 1510-06)
- Conkright M. E.**  
(P15/W/08-B3 1710)
- Connerney J.**  
(GA4.10/W/32-A4 1635)
- Connolley W M**  
(MC01/E/19-A2 1635)
- Connor B C**  
(MI02/E/06-A5 0910)
- Connor Brian J.**  
(MI12/E/05-B5 1135)  
(MI12/E/02-B5 1115)
- Connor Charles**  
(JSP23/W/08-A5 0830-03)  
(JSP23/W/27-B2 0830-08)  
(VS2/W/15-B3 1400-10)
- Connor Chuck**  
(VS2/W/08-B3 1400-06)
- Conrad C.**  
(HW1/L/10-A4 1130)
- Console R.**  
(ST1/W/42-A1 1110)  
(ST1/W/45-A2 1400-39)  
(ST1/W/53-A2 1600)
- Console Rodolfo**  
(ST1/W/13-A3 1740)
- Consolini Giuseppe**  
(GA1.01/W/20-A5 0900-05)
- Constable C. G.**  
(GA5.08/W/12-B1 1135)
- Constable Steven**  
(GA1.02/L/AW1-A2 0930)  
(GA1.02/L/AW2-A2 0930)
- Constantin A.P.**  
(JSA15/P/05-A5 0830-03)
- Constantin Ionescu Frank**  
(JSP23/W/26-A5 1150)
- Contadakis M.**  
(ST1/W/49-A3 0900-02)
- Conte Aida M.**  
(VS2/W/22-B3 1400-15)
- Coticelli Sandro**  
(JSV30/E/11-B1 1400-14)  
(JSV30/W/06-B1 1400-13)  
(JSV30/W/08-B1 1040)
- Conversano Fabio**  
(P11/E/21-B4 1700)  
(P11/W/12-B4 1640)
- Conversano Roberto**  
(P11/L/04-B5 0930)
- Cook**  
(JSA06/L/06 0935)
- Cook Alan**  
(GA6.01/E/03-A5 0900)
- Cook Edward**  
(JSP25/E/14-B4 1720)
- Cook J. W.**  
(JSA16/W/13-A3 0830-47)
- Cook T.**  
(JSA20/E/27-A4 1200-21)
- Cooke Richard A. C.**  
(HSA3/W/05-A1 1110)
- Cooper Andrew**  
(MC04/E/05-B2 1715)
- Cooper Claire**  
(JSP25/E/12-B3 0830)
- Cooper Reid F**  
(ST6/C/JSS02/W/04-A2 1620)
- Copeland Jeff**  
(JWM08/E/07-A2 1040)  
(JWM08/W/04-A2 1020)  
(JWM08/W/01-A2 1630)
- Copin-Montégut Claire**  
(P08/E/04-A2 1500)
- Coradini M.**  
(JSA10/W/06-A2 1430)
- Corbett Reide**  
(HW5/E/04-A3 1500)
- Cordero Eugene C.**  
(JSM26/W/02-B1 1650)
- Cordery Ian**  
(HS1/W/07-B4 1140)  
(HS5/W/11-A2 0900)  
(HW1/L/06-A4 1630)
- Cord-Hinrich Jahn**  
(G1/W/29-A3 1620-12)
- Cordini Jucilei**  
(G1/E/03-A3 1620-49)
- Cordoba Gustavo**  
(VS2/W/26-B3 1400-29)
- Corela C.**  
(JSS42/E/07-B5 1700-13)
- Cornelissen G.**  
(GA6.01/E/04-A5 0900-07)
- Corner B.**  
(GA1.04/E/11-A4 1610)
- Cornford Dan**  
(JSP05/W/12-A1 1620)  
(MI06/W/27-B1 1400-11)  
(MI06/W/27-B2 1400-11)
- Cornley Richard**  
(GA2.03/W/07-B3 1420)
- Coroniti F. V.**  
(GA3.02/W/17-B3 0945)  
(GA4.10/W/09 A5 1710)
- Corrigan C**  
(MI01/W/02-A3 0900)
- Cortes Abel**  
(JSV36/C/U6/W/08-B3 1400-21)
- Cortesi Ugo**  
(JSA09/W/12-A2 1630)
- Corti S.**  
(MI11/W/01-B5 0830)
- Coskun Ali Kilicoglu**  
(JSS31/L/05-B2 1600)
- Coskun Demir Ali Turkezer**  
(JSS31/L/03-B3 0830-16)
- Cossart Goertz von**  
(JSM32/W/05-B2 0930)
- Costa A.**  
(GA4.02/E/09-A4 1400-04)
- Costa Giovanni**  
(ST1/W/71-A4 0930-29)  
(ST3/W/49-B3 0915)  
(ST5/W/31-B4 1640)
- Costa Maria João**  
(ST4/E/27-B1 1400-17)
- Cotton D.**  
(JSA20/E/27-A4 1200-21)
- Cotton Michael G.**  
(G5/P/02-A4 1130-02)
- Cotton Richard**  
(MI04/E/11-B4 1120)
- Cotton W R**  
(MI08/W/01-A4 1205)
- Cotton William R.**  
(MC04/W/08-B1 1425)  
(MI04/W/12-B3 1630)
- Courtillot V.**  
(GA1.03/W/22-B3 0900)
- Coustenis Athena**  
(MC09/W/12-B2 0930)
- Couvert Pierre**  
(MI06/W/05-B1 1400-06)  
(MI06/W/05-B2 1400-06)
- Couture Mark**  
(MI01/W/04-A1 1640)
- Covey Curt**  
(MC01/W/18-A2 1705)
- Coward David A.**  
(GA1.07/W/05-B2 0920)
- Cowley S. W. H.**  
(GA3.03/W/02-B4 1720)  
(GA4.10/W/02-A5 1005)
- Cowling S. A.**  
(MC11/E/13-B3 1640)
- Cox C.**  
(JSG14/E/09-A3 1700-01)
- Cox Christopher M.**  
(G3/E/05-A5 1200)
- Cox Michelle**  
(JSP21/L/01-A4 1010)
- Cox Peter**  
(MC01/E/33-A1 1730)  
(MC01/E/36-A3 1605)
- Cox R. A.**  
(JSM26/L/02-B2 1400)
- Cox S. J. D.**  
(JSS31/W/15-B3 0830-09)
- Coy Larry**  
(MW01/W/06-A5 1400)
- Cragin J. H.**  
(HW3/W/19-B4 1015)
- Craig George**  
(MI05/W/20-A1 1500)
- Craig George C.**  
(JSM26/W/22-B1 1130)  
(MI04/W/22-B3 1135)
- Cramer W**  
(MC01/L/22-A55 1505)
- Crampin Stuart**  
(JSP23/E/29-B2 1440)  
(JSS07/E/02-A2 1005)  
(ST1/E/57-A2 1620)
- Crane Patrick**  
(JSA16/W/11-A3 0830-25)
- Craven J. A.**  
(JSA44/L/03-B4 1150)
- Craven P. D.**  
(GA3.04/L/02-B1 0920)  
(GA3.05/W/03-B3 0900-10)  
(GA3.10/W/01-A6 1630)
- Cravens T. E.**  
(GA4.10/W/18-A5 1230)  
(GA4.01/W/08-A2 1710)  
(GA4.10/W/21-A4 1620)
- Crawford Wayne**  
(JWA34/W/06-B2 1010)
- Creager K C**  
(JSS07/E/04-A2 1620)  
(ST4/L/01-B1 0830-02)
- Cremers A. B.**  
(JWS33/W/08-B2 1635-26)  
(JWS33/W/08-B3 0900-26)
- Crespi Mattia**  
(G5/W/19-A4 1230-02)
- Cresswell Doug**  
(P13/E/09-B2 0950)
- Crétaux Jean-Francois**  
(G2/E/06-A2 1630-03)  
(JSG14/E/02-A3 1700-05)  
(JSG11/E/04-A3 0910)  
(JSG11/E/16-A4 1030)
- Criag George C.**  
(MI04/L/04-B1 0840)
- Cribb M. C.**  
(MI10/W/16-B2 1435)
- Cridler M. D.**  
(GA4.10/W/13-A4 0930)
- Crisci Alfonso**  
(HS1/W/21-B4 1120)
- Crisci G. M.**  
(JSA45/E/17-B5 1110-01)  
(JSA15/E/60-A4 1400-13)  
(JSP23/E/57-B1 0830-09)
- Crisci Gino M.**  
(JSV36/E/25-B3 1710)
- Crise Alessandro**  
(P11/E/20-B4 1720)  
(P11/E/21-B4 1700)
- Crisp D.**  
(MC09/W/07-B2 01)  
(JSA10/W/03-A2 0930)
- Crisp N.**  
(P11/W/19-B4 1500)
- Cristallini Ernesto**  
(JSS44/W/19-B4 0930-01)
- Cristina Maria**  
(G3/W/26-A5 1610-70)
- Cristina Pacino Maria**  
(G3/E/39-A5 1610-93)  
(G3/W/19-A5 1610-96)
- Croley D.**  
(GA4.09/W/11-A6 0920)
- Crommelynck D**  
(JSA16/W/15-A3 0830-41)
- Cronan David**  
(JSV36/P/01-B3 1130)
- Crook Andrew**



## INDEX

(MC04/E/09-B1 1130)  
(MI04/E/28-B3 0935)

**Crosby Norma**  
(JSA06/W/18-A1 1155-12)

**Cross Matthew**  
(JWS33/W/34-B2 1635-02)

**Cross Matthew D.**  
(HW1/E/01-A4 1130)

**Cross Paul**  
(G1/E/11-A3 1620-52)  
(G5/E/36-A4 1215)  
(G6/C/G1/W/19-B1 1540)  
(G6/C/G3/E/11-B2 1500)  
(JSS31/W/11-B2 1620)

**Crossley David**  
(JSP39/E/10-B2 1430)  
(JSG14/E/18-A3 1700-14)

**Crosson R. S.**  
(ST4/L/01-B1 0830-02)

**Crowe Allan S.**  
(HW5/W/10-A3 0920)

**Crowley G.**  
(JSA20/W/40-A6 0948)

**Crowley Geoff**  
(GA3.09/W/10-B5 1140)

**Crucifix M Berger**  
(MC01/W/11-A3 0945)

**Cruddace Paul**  
(G5/E/36-A4 1215)  
(G6/C/G1/W/19-B1 1540)  
(JSS31/W/11-B2 1620)

**Cserepes Laszlo**  
(ST4/E/64-B3 1710)

**Cserreze M**  
(MC01/W/14-A4 1155)

**Csiszar Ivan**  
(JSM41/E/07-B4 1705)  
(JSM41/E/30-B5 1400)

**Csontos Andras**  
(GA5.01/W/16-A1 1145)

**Cuadrado Diana G.**  
(P09/W/07-A1 0950)

**Cubasch Ulrich**  
(JSA16/E/07-A3 1400)

**Cuevas E.**  
(JSM26/W/27-B1 1440)

**Cuevas Jose Luis**  
(JSA40/E/05-B5 1400-17)

**Cuevas Julia**  
(GA1.04/W/02-A5 1640)

**Cullather R I**  
(MC01/W/14-A4 1155)

**Cullen Heidi**  
(JSP25/E/14-B4 1720)

**Cullen John J.**  
(P15/L/18-B41400)

**Cummer S. A.**  
(GA3.02/W/18-B2 1645)

**Cummer Steven A.**  
(JSA34/W/07-B1 1440)

**Cummings A. C.**  
(GA4.04/W/09-B5 1710)  
(GA4.04/W/14-B5 1620)

**Cummins Phil R.**  
(JSS31/W/16-B2 1110)

**Cumnock J A**  
(GA3.10/W/10-A6 1700-03)  
(GA3.10/W/13-A6 1050)

**Cunde Zhang**  
(ST1/W/49-A3 0900-02)

**Cunha Sérgio**  
(G1/W/39-A3 1620-45)

**Cunha Telmo**  
(G1/W/39-A3 1620-45)

**Cunnold D**  
(JSM01/W/12-A2 1600-15)  
(JSP21/E/04-A5 1110)

**Cupal Ivan**  
(GA1.01/W/22-A5 1115)  
(GA1.01/W/27-A5 0900-04)

**Curic Mladjen**  
(MI01/W/13-A1 0900-13)  
(MI03/W/10-A3 1400-02)  
(MI04/W/03-B3 1050)

**Curran Mark A J**  
(JSM18/W/08-A5 1100)  
(JSM18/W/13-A5 1140)

**Currie B.**  
(MI06/W/20-B1 1400-07)  
(MI06/W/20-B2 1400-07)

**Curry Judy**  
(P13/W/06-B2 1600-04)

**Curtis Scott**  
(JSM41/E/01-B3 1620)  
(MW02/E/06-B3 1720)

**Curto Juan Jose**  
(JSA35/E/01-B1 1420)

**Cusack Stephen**  
(MI04/E/04-B4 1035)

**Cuvelier C**  
(MI07/L/01-A2 1120)

**Cynthia Cattell**  
(GA3.03/W/11-B4 1200)

**Cyr O. C.**  
(GA4.01/E/03-A2 1010)

**Czechowski A.**  
(GA4.04/W/17-B5 0900)

**Czerwinski Tomasz**  
(JSA15/E/33-A3 1050)

## d

**Da Costa Jose M.**  
(GA5.06/W/08-A4 1140)

**Dach R.**  
(G1/L/04-A3 1620-85)  
(JSA09/L/02-A2 1230)

**Daehler Mark**  
(JSM01/W/04-A4 1510)

**Dag Solheim Skilbrei**  
(G3/E/19-A5 1610-25)

**Daglis I. A**  
(GA3.02/L/04-B3 0900-25)  
(GA3.08/L/02-B1 0900-11)

**Daglis Ioannis A**  
(GA2.07/W/26-A1 1425)

**D'Agrella-Filho Manoel**  
(GA1.05/E/16-A5 1520)  
(GA1.04/E/09-A4 0930-07)  
(GA1.04/E/15-A4 1630)  
(GA1.04/E/16-A4 1650)

**Dahlback Arne**  
(MI08/W/10-A4 1805)

**Dahle A.**  
(ST3/E/13-B4 1400-15)

**Daho A.**  
(G3/P/02-A5 1610-76)  
(G3/P/04-A5 1610-75)  
(G3/P/05-A5 1610-74)

**Dai Liwen**  
(G1/W/30-A3 1620-13)

**Daida J. M.**  
(GA3.03/W/13-B4 1430)

**Daignieres Marc**  
(ST7/W/03-A2 1605-01)

**Daihong Yan**  
(ST1/E/41-A3 0900-09)

**Dal Lago Alisson**  
(GA4.08/W/02-B3 1400)  
(GA4.08/W/10-B3 1030)  
(GA4.08/W/06-B3 0905)

**Dale Andrew C.**  
(P10/W/04-A5 1600-05)

**Dalin P A**  
(JSA06/W/01-A1 1500)

**Dall J**  
(JSH12/W/05-A5 0900)

**Daly C**  
(MC01/E/20-A5 1405)

**Daly Christopher**  
(JWM08/W/05-A2 1540)

**Daly E. J.**  
(GA3.05/E/02-B3 0850)

**Dalyuk I. V.**  
(JSM41/W/05-B5 1515)

**Dalziel S. B.**  
(JSP39/L/02-B2 1010)

**Damaske Detlef**  
(JSA09/W/07-A2 0930-02)

**Dameris Martin**  
(MC08/E/05-A3 0900-02)  
(MI02/W/03-A5 1200)  
(MI02/W/17-A5 1220)

**Daminelli R.**  
(JSP23/E/08-A6 0950)

**Damon Paul E.**  
(JSA16/E/15-A3 0830-23)

**Dani K K**  
(MI01/P/02-A31145)  
(MI04/P/01-B3 1220)

**Daniel Elena**  
(JWS33/E/10-B2 1635-05)  
(JWS33/E/10-B3 0900-05)  
(JSA09/E/10-A2 0930-06)

**Daniel Güntner**  
(HS4/W/32-A5 1710)

**Daniel John**  
(MI04/W/14-B2 1120)

**Daniel Loic**  
(U7/W/14-B1 0830-12)

**Daniel R.**  
(JSP25/W/49-B4 0950)

**Daniel Stich**  
(ST5/E/11-B4 1420)

**Daniel Vincent**  
(JSM26/L/04-B2 1700-16)

**Daniell R. E.**  
(GA3.09/W/01-B4 0900-08)  
(GA3.09/W/02-B4 0900-09)

**Danilov A. D.**  
(GA4.08/E/18-B4 1300)  
(GA4.08/E/05-B4 1400)  
(GA2.01/E/06-A1 1440)

**Dann Scott**  
(JSA20/E/06-A5 1200-08)

**Danov D.**  
(GA3.04/W/09-B1 1520-17)

**Danov D. L.**  
(GA4.08/E/21-B3 0900-13)

**Daoyi Xu**  
(ST1/W/49-A3 0900-02)

**Darby Desmond**  
(JSS31/W/09-B2 1130)  
(JSS31/L/01-B2 1150)

**Dare Peter**  
(G1/C/G5/W/18-A3 1620-103)  
(G1/L/26-A3 1640-97)  
(G1/W/17-A3 1620-39)

**Daren Lu**  
(MI01/E/13-A3 1125)

**D'Argenio B.**  
(GA1.03/E/06-B2 0900)  
(GA1.15/E/05-B4 1530-01)

**D'Arrigo Rosanne**  
(JSP25/E/14-B4 1720)

**Das A. K.**  
(GA1.04/P/02-A4 1710)

**Das L. K.**  
(ST4/W/33-B1 0830-29)

**Das S**  
(JSS13/W/11-A4 1520)

**Das Shamita**  
(ST3/W/09-B3 1415)

**Dash S. K.**  
(JSP25/L/04-B2 0930-08)

**Dashevskii Yili**  
(JSA15/W/13-A5 0830-15)

**Dassargues Alain**  
(HW5/W/01-A3 0900)  
(HS1/W/02-B4 1740-01)

**Dater David T**  
(G3/W/20-A5 1610-24)

**D'Attellis Carlos**  
(JSA16/C/GA4.07/W/34-A3 0830-55)

**D'Auria L**  
(ST5/W/60-B5 1125)

**Davaille Anne**  
(ST4/W/36-B3 1440)

**Davey M. K.**  
(JSP25/E/05-B1 1110)  
(JSP25/E/22-B1 0830-06)

**Davey Mike**  
(MC01/E/14-A3 1000)

**David C**  
(JSM01/W/08-A4 1450)

**David J.**  
(GA3.04/W/22-B2 0930)

**David L Roberts**  
(MC07/E/05-A2 1135)

**David Rhoades**  
(ST1/W/23-A1 1130)

**David W. Reynolds**  
(MC04/W/09-B2 1600)

**Davidovich Natalia**  
(U2/E/13-A2 1400)

**Davidson Jim**  
(JSS42/E/16-B4 1220)

**Davidson Jon**  
(JSV30/W/05-B1 1400-12)  
(U6/W/07-B2 1135)

**Davidson Jon P.**  
(JSV30/W/06-B1 1400-13)  
(JSV30/W/08-B1 1040)

**Davidson Russell**  
(JSP21/W/03-A4 1420)

**Davies H C**  
(MI05/E/24-A1 1650)  
(JWM08/E/06-A2 1120)

**Davies Huw C**  
(MI05/E/04-A1 1420)  
(MW06/W/01-A3 1140)

**Davies J**  
(JSM01/W/37-A5 1400)  
(MI09/W/01-A5 1145-19)

**Davies J. Huw**  
(JSV30/E/07-B1 0840)  
(ST4/E/23-B3 1200)

**Davies J. A.**  
(GA2.02/W/04-B4 1700)

**Davies James E.**  
(P15/W/05-B3 1630)

**Davies Robert**  
(JSS31/W/11-B2 1620)

**Davila J. M.**  
(JSS31/E/13-B3 0830-14)

**Davis C. A.**  
(MC04/L/01-B1 1100)

**Davis Chris**  
(JSM43/W/08-B4 1110)

**Davis D.**  
(JSM26/W/18-B2 1550)

**Davis Earl**  
(JWA34/E/06-B2 1600)

**Davis J L**  
(JSG11/W/05-A3 1440)  
(JSG11/W/09-A3 1500)  
(JSG11/E/05-A3 1520)  
(JSS31/E/13-B3 0830-14)

**Davis James L.**  
(JSS31/E/08-B2 0950)

**Davis Peter J.**  
(U7/W/18-B1 0830-19)

**Davis Richard F.**  
(P15/L/18-B4 1400)

**Dawes G.**  
(GA1.02/E/16-A2 0930)

**Dawson P. B.**  
(JSS46/W/05-B4 1150)

**Dawson Phillip**  
(JSV47/E/04-B5 0830)  
(JSV47/W/18-B5 1100)  
(JSV47/W/16-B5 1000)

**Day S. J.**  
(JSV36/E/20-B3 1400-12)  
(VS3/E/01-B3 0900-03)  
(VS3/E/03-B3 0900-02)  
(VS3/E/07-B3 1450)

**Day Simon J.**  
(JSP23/E/23-B2 0830-09)

**Day Steven M.**  
(ST1/W/68-A1 1420)

**Daydou Y.**  
(JSA10/E/01-A2 1515)

**De Backer H**  
(JSM01/W/37-A5 1400)

**De Campos Cláudia Jacodino**  
(MI05/W/16-A4 1400-11)  
(MI05/W/26-A4 1400-05)  
(JSP49/W/14-B5 1210-09)

**De Crook Theo**  
(ST3/W/26-B4 0930-03)

**De Cuevas Beverly**  
(JSM18/W/04-A4 1520)

**De Franceschi G.**  
(JSA45/E/17-B5 1110-01)

**De Franco Roberto**  
(JSS46/E/03-B4 1420)  
(JSS46/E/04-B4 1400)  
(JSS46/E/05-B4 1440)  
(JSS46/E/06-B4 0930-02)

**De Freitas Correia**  
(G5/E/07-A4 1554-08)  
(G5/E/08-A4 1556-09)

**De Freitas Silvio R.C.**  
(G1/E/03-A3 1620-49)  
(JSS44/E/12-B4 0930-03)

**De Geer Lars-Erik**  
(U8/W/08-B3 1005)

**De Gori P.**  
(JSS46/E/07-B4 0930-04)

**De Groot-Hedin Catherine**  
(U8/W/02-B3 1640-01)

**De Heus Henk**  
(G1/L/11-A3 1200)

**De Hka Schenková Z.**  
(ST3/W/13-B5 0915)

**De Jong Kees**  
(G4/E/05-A3 1620-09)

**De Jonge Paul**  
(G1/E/08-A3 1620-21)

**De La Beaujardiere O**  
(GA3.07/W/12-A6 0900-05)

**De Lugao Patricia P.**  
(GA1.02/W/35-A2 0930)

**De Matteis R**  
(ST5/W/60-B5 1125)

- De Matteis Raffaella**  
(JSS46/E/04-B4 1400)
- De Mazière M**  
(JSM01/E/44-A4 1620-14)
- De Michelis Paola**  
(GA1.01/W/20-A5 0900-05)  
(GA1.01/W/29-A5 1700)
- De Natale G.**  
(JSS46/E/07-B4 0930-04)
- De Natale Giuseppe**  
(JSS46/E/03-B4 1420)  
(JSS46/E/05-B4 1440)  
(JSS46/W/11-B4 1540)  
(JSV36/E/25-B3 1710)  
(JSS46/W/02-B4 1500)  
(MC11/E/07-B4 1125)
- De Paula E. R.**  
(GA2.02/W/08-B5 0920)
- De Rita D.**  
(VS3/E/02-B3 1550)
- De Saint Ours Patrice**  
(JSV36/W/03-B3 0900-13)
- De Santis A.**  
(GA1.01/W/31-A5 1645)  
(GA1.02/W/13-A2 0930)  
(GA1.02/W/19-A2 0930)
- De Toma Giuliana**  
(SA16/E/22-A3 0830-16)  
(JSA45/E/03-B5 1110-11)
- De Verdieri Alain C.**  
(JSP39/E/18-B4 0930)  
(JSP39/W/20-B4 1740)  
(JSP25/E/35-B4 1150)  
(JSP25/W/03-B4 1520)
- De Villiers G. du T.**  
(HS5/W/10-A1 1730)
- De Villiers M. P.**  
(M105/E/28-A5 1000)
- De Viron O**  
(G5/L/05-A4 1000)
- De Vita Sandro**  
(JSP23/C/U4/W/01-A6 0830-17)
- Dean W.**  
(JSA45/E/16-B4 1510)
- Deboudt Karine**  
(MI01/E/02-A1 0900-07)
- Decker D. T.**  
(GA3.09/W/01-B4 0900-08)  
(GA3.09/W/02-B4 0900-09)
- Decker Kurt**  
(JSA19/W/12-A4 1000)
- Decker R.**  
(GA4.04/W/15-B5 1450)
- Decker R. B.**  
(GA4.04/W/04-B5 1650)  
(GA4.04/W/18-B5 1150)
- Deese Heather E.**  
(P14/W/05-A4 1420)
- Degnan**  
(G2/L/10-A2 1215)
- Degobbi Danilo**  
(PW1/E/02-A6 1140)
- Degrazia Gervásio Annes**  
(JSP49/W/14-B5 1210-09)
- Degtjarev Vitalii**  
(GA3.05/W/19-B3 0900-26)
- Dehairs Frank**  
(PW1/P/01-A6 0940)
- Dehant V**  
(G5/L/05-A4 1000)  
(G5/L/04-A4 1115-14)  
(JSA10/W/03-A2 0930)  
(JSG14/E/04-A3 1109-04)
- Dehant Veronique**  
(JSA10/W/11-A2 1000)
- DeHka Schenková Z.**  
(ST3/W/38-B5 1445)
- Dehls J.**  
(ST2/E/43-A5 1400-31)
- Dehui Lu**  
(JSS44/p/04-B5 1050)
- Deif Ahmed**  
(ST3/W/42-B4 1030)
- Dejan Janc**  
(MI04/W/03-B3 1050)
- Dekkers M. J.**  
(GA1.15/W/01-B4 1415)  
(GA1.03/W/15-B3 1540)
- Dekusar Olga**  
(JWA34/W/02-B2 1620)  
(GA5.01/W/01 A1 1300-03)  
(GA5.01/W/06 A1 1300-14)  
(JSP23/E/38-A6 0830-09)
- Del Gaudio Vincenzo**  
(JSA40/W/01-B5 1205)
- Del Negro Ciro**  
(JSA15/W/02-A4 1400-18)
- Del Pezzo E.**  
(JSS46/W/09-B4 0930-05)  
(JSV47/W/17-B5 1400-14)  
(JSV47/W/20-B5 1400-13)  
(JSV47/W/29-B5 1400-22)  
(JSV47/W/30-B5 1400-23)  
(ST5/W/56-B3 0900-01)  
(ST5/W/66-B4 1400-06)
- Del Valle Venencio Maria**  
(JSP23/E/46-B1 0830-07)  
(JSP23/W/37-A5 0830-07)
- Delaboudiniere J. P.**  
(GA4.02/W/29-A4 1545)
- Delamere Jennifer**  
(MI08/E/06-A4 1235)
- Delaney J. R.**  
(P16/W/03-B5 1110)
- Delannee C**  
(GA4.02/W/29-A4 1545)
- Delano Gobbi Maria P.**  
(JSM01/W/45-A2 1600-06)
- Delarue Jean-Francois**  
(JSA15/E/27-A4 1400-04)
- Delcourt D. C.**  
(GA3.09/W/15-B4 1450)
- Delgenio Anthony D.**  
(MI04/E/24-B1 0900-17)  
(MI10/E/09-B4 1205)
- Delipetrov Todor**  
(ST1/P/03-A4 0930-18)  
(U3/P/02-A3 0900-08)
- Della Rose D.**  
(GA5.06/W/05 A3 1520)
- Dellino Pierfrancesco**  
(VS2/E/08-B3 1010)
- Delloue J**  
(JSM01/P/03-A2 1600-18)  
(JSM01/P/03-A2 1540-18)
- Delloue Jean**  
(GA2.02/W/17-B4 0930-01)
- Delor C.**  
(JSS44/L/05-B-4 0930-04)
- Delworth Thomas L.**  
(MC02/E/09-B2 0900)
- Delworth Tom**  
(JSP25/E/16-B4 1500)
- Dembelov Mikhail G.**  
(JSA15/W/20-A5 1400-14)
- Demehenko R.**  
(P09/W/05-A1 1640)
- Demekhov A. G.**  
(GA2.07/W/31-A2 0930-09)  
(GA2.03/W/03-B3 1400-01)  
(GA3.04/W/28-B1 1520-22)  
(GA3.05/W/37-B3 0900-11)
- Demers Serge**  
(P15/L/05-B4 1610)
- Demetrescu Crisan**  
(MC02/E/15-B1 1600-13)  
(ST4/E/43-B1 1400-09)  
(GA1.02/E/39-A1 1050)
- Demets Chuck**  
(JSS31/E/06-B2 1500)
- Demezhko Dmitry**  
(MC02/E/21-B1 1600-10)
- Demianov G V**  
(G3/E/28-A5 1610-03)  
(G3/W/02-A5 1140)
- Demianov Gleb**  
(G1/E/09-A3 1620-22)
- Demidova Tatiana**  
(JSP25/E/37-B3 0830-08)  
(JSP39/E/05-B4 1640)  
(JSP39/E/23-B3 1409-04)
- Demir Coskun**  
(JSS31/L/04-B2 0830-17)
- Demmel J.**  
(U3/W/08-A30900-13)
- Demott Paul J.**  
(MI04/W/08-B4 1435)
- Demoulin P**  
(JSM01/E/44-A4 1620-14)  
(GA4.02/E/03-A4. 1400-01)
- Demoulin Pascal**  
(GA4.01/L/01-A2 1220)
- Dendy Richard O.**  
(GA3.02/W/22-B3 0900-12)  
(GA3.02/W/37-B3 1150)
- Deng Ganjin**  
(ST1/P/12 0930-37)
- Deng Qianhui**  
(JSA15/E/52-A5 0830-09)
- Deng Xiaoli**  
(G2/W/16-A2 1630-20)  
(G3/L/18-A5 1610-10)
- Denis Nicolas**  
(ST5/W/57-B5 1400-01)
- Denisenko Pavel F.**  
(GA2.03/E/01-B3 1400-04)  
(GA2.03/E/05-B3 1400-05)
- Denisov Alex**  
(JWA34/W/02-B2 1620)  
(GA5.01/W/01 A1 1300-03)  
(GA5.01/W/06 A1 1300-14)
- Denisov Alexey**  
(JSM24/W/03-B1 1030-02)
- Denker Heiner**  
(G6/C/G3/E/23-B1 1200)
- Denning S**  
(MC01/L/19-A5 1045)
- Dennis P. F.**  
(P07/W/17-A3 0955)
- Dennis Paul**  
(HS5/W/37-A3 1125)
- Dennis Paul F.**  
(P07/W/03-A3 1640)
- Dentith Michael C.**  
(GA5.11/L/02 A3 1430-03)
- Denton R. E.**  
(GA3.04/L/02-B1 0920)
- Denton Richard E.**  
(GA3.04/W/19-B1 1520-35)  
(GA3.07/W/71-A5 0900)
- Depuev V. Kh.**  
(JSA15/E/31-A5 1400-15)  
(JSA15/E/55-A5 1400-16)
- Depueva Anna**  
(JSA15/W/21-A5 1400-05)  
(JSP23/W/39-B1 1520)  
(GA2.02/W/13-B4 0930-17)
- Deque Michel**  
(JSP25/E/08-B3 1150)
- Dera Jerzy**  
(P15/W/04-B4 1055)
- Derder M. E. M.**  
(JSS44/E/07-B4 0930-16)
- Derder Mohamed El-Messaoud**  
(GA1.04/W/31-A4 1220)
- Dere K. P.**  
(GA4.02/W/33-A4 1400-26)
- Dere Kenneth**  
(GA4.02/W/30-A4 0900)
- Dergachev Valentin**  
(JSA16/E/21-A3 0830-08)  
(JSA16/E/16-A3 0830-09)
- Derks H.**  
(JSG28/E/01-B1 1040)
- Der-Ru Song**  
(ST6/E/05-A1 0830-15)
- Derwent Richard**  
(M102/E/10-A4 1100)
- Dery Stephen**  
(JSM04/E/01-A2 1010)
- Desai M. I.**  
(GA4.04/W/12-B5 1750)
- Desai Shailen**  
(JSG28/E/14-B1 1400-21)
- Desai Shailen D.**  
(JSG14/E/15-A3 1115-06)
- Desaulniers-Soucy N.**  
(MI10/E/10-B2 1705)
- Desborough Carl**  
(MC01/E/21-A3 1445)
- Deschamps Anne**  
(ST7/W/03-A2 1605-01)  
(JSS46/E/07-B4 0930-04)  
(JSS46/W/02-B4 1500)  
(JSS46/W/11-B4 1540)
- Descherevsky A. V.**  
(ST1/E/53-A2 0930-11)
- Deser Clara**  
(JSP25/W/57-B4 1640)
- Desgagné M.**  
(JWM08/E/06-A2 1120)
- Despa A.**  
(GA4.09/W/12-A6 1620)
- Despotashvili Marina**  
(ST1/C/GA4.10/E/01-A4 0930-43)  
(JSA45/E/15-B5 1110-06)
- Desroziers G.**  
(MI05/W/45-A3 1140)
- Dessler A E**  
(JSM01/W/12-A2 1600-15)
- Dessoky Mohamed**  
(ST4/E/51-B1 1400-20)
- Dethloff Klaus**  
(JSP25/W/33-B4 0930-03)  
(JSP25/W/38-B4 0930-04)
- Dethof Antje**  
(JSM26/E/02-B2 1020)
- Dettinger Michael D.**  
(GA6.01/W/12-A6 1020)
- Dettinger Kleusberg D.**  
(JSG28/W/1-B2 1140)
- Deussen Bertold Dierk**  
(G4/W/02-A3 1500)
- Deutsch K A**  
(JSM01/E/39-A1 0940)
- Deuzé J. L.**  
(MI09/L/02-A5 0855)
- Devara P C S**  
(MI01/P/02-A31145)  
(MI04/P/01-B3 1220)
- Devasia C. V.**  
(GA2.02/W/05-B5 0900)  
(GA2.02/W/07-B5 1620)  
(GA2.02/W/16-B4 0930-18)
- Devaux Wedge J.P.**  
(ST6/W/02-A1 0830-04)
- Deveson Abigail C. L.**  
(MI05/W/32-A4 1400-04)
- Devine Joseph M.**  
(JSP23/W/24-B2 1150)
- Devoti R.**  
(G1/W/27-A3 1620-40)  
(JSG14/W/19-A3 1600)
- Dewey Ken**  
(U2/E/14-A2 1420)
- Dewitte S.**  
(JSA16/W/15-A3 0830-41)
- Dezeeuw D. L.**  
(GA3.09/E/03-B4 1215)  
(GA4.08/W/03-B4 0930)
- DeZeeuw D L**  
(GA3.10/E/09-A6 1600)  
(GA4.01/E/01-A2 1220)  
(GA4.10/E/07-A5 1525)  
(GA4.10/W/10-A4 1215)
- Dhar R. L.**  
(HS5/W/40-A3 1225)
- Di Donato G**  
(JSG11/W/02-A3 1540)  
(JSG14/W/19-A3 1600)
- Di Francia A.**  
(JSP23/E/57-B1 0830-09)
- Di Gregorio S.**  
(JSP23/E/57-B1 0830-09)
- Di Mauro D**  
(GA1.02/W/13-A2 0930)  
(GA1.02/W/19-A2 0930)
- Di Mauro Domenico**  
(JSA15/W/25-A5 0830-14)
- Di Stefano G.**  
(JSA45/E/17-B5 1110-01)
- Di Stefano Raffaele**  
(JSS46/E/04-B4 1400)
- Diab Ain Shams**  
(JSA19/W/06-A4 0900)
- Diagortas D.**  
(ST3/E/36-B3 1615)
- Dial R M**  
(JSM03/W/05-A1 1630)
- Dianski Nikolai A**  
(MWO6/W/07-A3 1100)
- Diasamidze Mzia**  
(JSP49/E/06-B5 1210-10)  
(JSP49/E/10-B5 1210-11)
- Diasamidze Zhuzhuna**  
(JSP49/E/06-B5 1210-10)
- Diaz Lazaro**  
(JSA40/E/05-B5 1400-17)
- Dibben Paul**  
(MI06/E/07-B1 1400-09)  
(MI06/E/07-B2 1400-10)
- Dick Galina**  
(JSG 28/E/11-B1 1120)
- Dick M I**  
(JSA06/W/15-A2 1010)
- Dickey J. O.**  
(JSG14/E/13-A3 1700-07)  
(JSG14/L/08-A3 1145-16)
- Dickey Jean**  
(JSG28/L/01-B1 1400-03)
- Dickey Jean O**  
(MC01/E/06-A2 1015)
- Dickey T.**  
(P15/E/02-B3 0915)
- Dickinson E**  
(MC01/W/32-A2 0930)
- Dickinson Robert**  
(U3/E/05-A3 0900-04)

# INDEX

- Dickman S. R.**  
(JSA17/W/12-A4 0930)  
(JSG14/L/03-A3 1130-11)  
(JSG14/L/04-A3 1133-12)
- Dicks E M**  
(MI05/E/06-A1 1630)
- Didenko Alexey**  
(GA1.04/E/12-A5 0900)
- Didesbulidze Goderdzi**  
(JSA20/I/01-A4 1200-16)
- Diego Mercerat**  
(JSS44/W/19-B4 0930-01)
- Dier H**  
(JSM01/W/37-A5 1400)
- Dierness Heidi**  
(P15/L/01-B4 1205)
- Dieter Andre**  
(GA2.02/W/17-B4 0930-01)
- Dieterich CH.**  
(P08/W/07-A2 1400)
- Dietrich D.**  
(P13/E/08-B2 1600-02)
- Dietrich David E.**  
(P10/W/20-A3 1700)
- Dietrich Michel**  
(JSS46/E/03-B4 1420)
- Dietrich R**  
(JSG11/E/13-A4 1400-05)  
(JSH12/W/07-A4 1400-02)  
(G1/L/04-A3 1620-85)  
(JSA09/L/02-A2 1230)
- Dietrich Volker J.**  
(JSV36/E/04-B3 1230)
- Dijkstra Tom**  
(JSP23/C/U5/W/03-B1 1420)
- Dileep Kumar**  
(ST2/W/20-A3 1515)
- Dill R.**  
(JSG14/W/16-A3 1203-22)
- Dillon Kevin**  
(HW5/E/04-A3 1500)
- Dils R. M.**  
(HS3/W/06-A1 1135)  
(HS3/W/08-A1 1225)
- Dimate C.**  
(JSP23/C/U5/E/16-A5 1620)  
(ST3/E/56-B4 1400-20)
- DiMego Geoffrey J.**  
(MC04/E/04-B2 1625)
- Dimitrios A.**  
(HS4/L/02-A4 0930)
- Dimmer Claudia H.**  
(JSP21/W/13-A4 0950)
- Dimov D.**  
(GA1.04/W/13-A6 1100)  
(JSA40/W/09-B5 1400-11)
- Dinardini Clezio M.**  
(GA2.02/W/08-B5 0920)
- Dineva S.**  
(ST5/W/15-B4 1400)
- Dineva Savka**  
(ST3/E/53-B4 1230)  
(ST2/W/10-A5 1400-16)
- Dingenen Rita Van**  
(MI01/L/03-A1 1400)
- Dingwell Donald B.**  
(U6/W/09-B2 1530)
- Dinter Georg**  
(JSP23/E/44-A6 1210)
- Dintrans Boris**  
(JSP39/W/44-B3 1451-18)
- Dipteris Eva C.**  
(ST5/E/18-B1 0830-12)
- Dipti Raut**  
(PW1/P/01-A6 0940)
- Dirksen Oleg V.**  
(JSV30/C/JSV22/E/04-B1 1400-18)
- Disse Markus**  
(JSP23/W/31-A5 0950)
- Dittfeld Hans-Juergen**  
(JSG14/E/10-A3 1700-17)
- Divins D.**  
(JSS42/L/01 1700-21)
- Dixon Jacqueline E.**  
(JSV36/E/31-B3 1400-14)
- Dixon M. A. G.**  
(MI05/E/08-A3 1600)  
(MI05/E/02-A3 1620)
- Dixon R S**  
(MI05/W/27-A4 1400-08)
- Dixon Timothy**  
(JSV36/E/13-B3 1445)
- Dixon Timothy H.**  
(JSV36/E/31-B3 1400-14)  
(U7/L/07-B1 1700)
- Djakov Pyotr**  
(JSA15/W/32-A5 0830-16)  
(ST1/W/33-A4 0930-10)  
(ST2/W/01-A3 1400)  
(JWS33/W/05-B2 1635-19)  
(JWS33/W/05-B3 0900-19)
- Djaja Rochman**  
(JSP23/E/27-B2 1700)
- Djatieva Zalina**  
(GA1.02/W/27-A1 1605)
- Jedi S. W.**  
(JSA15/W/14-A4 1400-16)
- Djellit Hamou**  
(GA1.04/W/31-A4 1220)
- Djuth F.**  
(JSA20/W/48-A4 1200-31)
- Dmitriev A. V.**  
(GA3.07/W/60-A4 0930-06)  
(GA3.05/E/08-B3 0900-19)  
(GA3.05/W/17-B3 1400)  
(GA3.09/W/23-B4 0900-02)  
(GA4.04/W/01-B5 0830-02)
- Dmitrieva Isabella**  
(GA4.03/W/11-B4 1735-04)
- Dmitriev Vladimir**  
(GA1.02/E/23-A1 1605)
- Dmitrieva I V**  
(JSA06/W/21-A1 1155-25)
- Dobes P.**  
(ST4/E/06-B1 1400-18)
- Doblas-Reyes**  
(MW03/E/02-B4 0950)
- Doblas-Reyes Francisco Javier**  
(JSP25/E/08-B3 1150)
- Dobran Flavio**  
(JSP23/E/31-A5 1210)  
(ST7/L/02-A2 1605-07)
- Dobrica Venera**  
(GA1.02/E/39-A1 1050)
- Dobrollubov S. A**  
(P12/W/16-A1 1030-02)  
(P12/W/15-A1 1030-01)  
(JSP25/W/93-B3 0830-02)
- Dodson Alan**  
(G6/C/G1/E/55-B2 1700)  
(JSG28/E/07-B1 0950)  
(JSG28/E/16-B1 1400-14)  
(JSG28/W/06-B1 1400-06)  
(JSG11/E/15-A4 1010)  
(G1/E/38-A3 0950)
- Doell Petra**  
(HW1/L/10-A4 0930)
- Doerenbecher Alex**  
(MI05/W/21-A3 1100)  
(MI05/W/44-A3 1120)
- Doerflinger Erik**  
(ST7/W/03-A2 1605-01)
- Dogliani Ciorciari C.**  
(G5/W/22-A4 1540-01)
- Doherty P. H.**  
(GA3.09/W/02-B4 0900-09)
- Doi Koichiro**  
(JSH12/W/04-A4 1400-01)
- Doi Nobuo**  
(ST4/W/23-B1 1400-10)
- Doin M. P.**  
(ST4/W/43-B2 0930-02)
- Dojcinovski Dragi**  
(ST3/W/53-B4 1400)
- Doke T.**  
(GA3.08/E/04-B1 1700)  
(GA4.08/W/11-B3 1620)  
(GA4.08/W/13-B4 0905)
- Dokukin Vladimir**  
(JSP23/W/22-B1 010)
- Dolan James F.**  
(ST3/W/19-B4 1630)
- Dolce Mauro**  
(JSP23/L/06-A6 1400)
- Dolenc David**  
(ST3/E/19-B4 1400-03)
- Dolguikh Grigoriy I.**  
(ST5/W/58-B5 1500)
- Döll Petra**  
(HS1/W/04-B4 1640)
- Domburg P.**  
(HS3/W/17-A2 0900)
- Dominey-Howes Dale**  
(JSS42/W/01-B5 0850)  
(JSS42/W/28-B5 1700-09)
- Domingo Vicente**  
(JSA16/W/25-A3 0830-46)
- Dominh K**  
(JSG11/E/04-A3 0910)
- Domrin V. I.**  
(GA3.08/W/30-B1 0900-04)
- Donald A.**  
(GA4.09/W/11-A6 0920)
- Donati Stefano**  
(ST7/E/09-A2 1605-05)  
(ST3/W/33-B4 1400-01)
- Doney S**  
(MC01/W/36-A5 1700)
- Dong D.**  
(JSG14/E/13-A3 1700-07)
- Dong Wen Jie**  
(GA1.01/E/12-A5 0900-08)  
(JSV22/E/14-A5 1050)
- Dong Wenjie**  
(MC04/E/08-B2 1205)
- Dong Ye Min**  
(MC01/W/40-A1 1115)
- Donnadille D.**  
(MI05/W/07-A3 1440)
- Donnadille J**  
(MI05/L/03-A4 1140)  
(MI05/W/08-A4 1400-07)  
(MI05/W/30-A3 1220)
- Donohue Robert**  
(HS3/W/11-A1 1450)
- Donovan David P.**  
(MI06/W/14-B2 1010)  
(MI10/W/17-B2 1620)
- Donovan E. F**  
(GA2.07/W/11-A1 0940)
- Donovan Erick**  
(GA3.08/W/23-B1 1450)
- Dontsov O. V.**  
(ST3/W/17-B4 0930-17)
- Dorbath Catherine**  
(JSS46/W/14-B4 0950)
- D'Oreye Nicolas**  
(JSP23/E/27-B2 0830-14)
- Dorman**  
(GA4.09/L/03-A5 1600-09)  
(GA4.09/L/04-A5 1600-10)
- Dorman Clive**  
(P10/W/17-A3 1640)  
(JSP39/W/27-B3 0950)
- Dorman I. V.**  
(GA4.04/L/12-B5 1400-07)
- Dorman Irina**  
(GA4.04/L/01-B5 0830-06)  
(GA4.04/L/02-B5 0830-07)  
(GA4.04/L/05-B5 0830-10)  
(GA4.04/L/06-B5 1400-01)  
(GA4.04/L/07-B5 1400-02)
- Dorman Lev**  
(JSA06/L/01-A1 1155-21)  
(JSM03/L/01-A1 0900)  
(JSM03/L/02-A1 0920)  
(JSA06/L/07-A1 1155-22)  
(JSA06/L/08-A1 1155-23)  
(GA4.04/L/01-B5 0830-06)  
(GA4.04/L/02-B5 0830-07)  
(GA4.04/L/03-B5 0830-08)  
(GA4.04/L/04-B5 0830-09)  
(GA4.04/L/05-B5 0830-10)  
(GA4.04/L/06-B5 1400-01)  
(GA4.04/L/07-B5 1400-02)  
(GA4.04/L/08-B5 1400-03)  
(GA4.04/L/09-B5 1400-04)  
(GA4.04/L/10-B5 1400-05)  
(GA4.04/L/11-B5 1400-06)  
(GA4.04/L/12-B5 1400-07)  
(GA4.04/L/13-B5 1400-08)  
(GA4.04/L/14-B5 1400-09)
- Dormolenko Tatiana A.**  
(P10/E/19-A5 1600-08)
- Dormy Emmanuel**  
(GA1.01/W/28-A5 0900-06)  
(GA1.01/W/34-A5 1000)
- Dorokhov V**  
(JSM01/W/37-A5 1400)
- Dorostian Arezou**  
(JSP23/C/U5/E/19-A6 0830-04)
- D'Ortenzio Fabrizio**  
(P11/L/02-B5 0850)
- Dos Santos Carvalho**  
(G1/E/45-A3 1620-74)
- Dozzo H. W.**  
(GA1.02/W/23-A1 1400)
- Dost Bernard**  
(ST1/W/58-A3 0850)  
(ST7/W/03-A2 1605-01)  
(JWS33/W/22-B3 0900-01)  
(ST3/W/04-B4 0945)  
(ST5/W/35-B3 0900-08)
- Dotsenko Igor**  
(JSA15/E/16-A5 1400-03)
- Dottridge Jane**  
(HS5/W/29-A2 1715)
- Dou Suqin**  
(ST2/E/57-A3 1430)
- Doubik Philip**  
(VS2/W/15-B3 1400-10)
- Doufexopoulou M. G.**  
(ST4/W/57-B1 0830-01)
- Douglas A.**  
(ST 5/E/22-B4 1700)  
(U8/E/01-B3 1640-08)  
(U8/E/07-B3 1640-07)  
(U8/P/02-B3 0900)
- Douglas Alan**  
(U8/E/11-B3 1520)
- Douglas G C**  
(MI08/L/02-A4 1220)
- Douglass A. R.**  
(JSM26/E/22-B1 1210)
- Douglass Anne**  
(MW01/W/06-A5 1400)
- Doumouya Vafi**  
(GA5.08/W/01-B1 1400-07)
- Doutriaux C.**  
(MC02/W/01-B2 1100)
- Doutriaux Charles**  
(MC01/E/30-A1 0945)
- Doutriaux-Boucher M.**  
(MI06/E/10-B2 1150)
- Doutriaux-Boucher Marie**  
(MW02/E/02-B3 1640)
- Douville Herve**  
(MC01/E/36-A3 1605)  
(MC01/L/05-A2 1100)  
(HS2/W/01-B1 0900)
- Dovbnya B. V.**  
(GA3.07/W/47-A6 0900-06)
- Dovgyallo**  
(JWS33/E/09-B2 1115)
- Dowdell G.**  
(GA3.05/W/07-B3 0900-12)
- Dowden Prof. Richard**  
(JSM03/W/04-A1 1100)
- Dowden Richard**  
(JSA15/W/31-A4 1120)
- Dowdeswell Julian**  
(JSH12/E/02-A5 1100)
- Downes Hilary**  
(JSV30/C/U6/E/05-B1 1400-26)  
(JSV30/W/13-B1 1400-05)
- Downes Malcolm T.**  
(HS3/W/16-A1 1730)
- Downing T.**  
(JSP23/W/12-B2 1400)
- Dowson M**  
(G3/W/01-A5 1610-46)
- Dozier Jeff**  
(HS2/W/08-B1 1140)
- Draeger Ulrike**  
(GA1.03/W/08-B1 1400)
- Dragomir Gospodinov**  
(ST2/W/32-A5 1400-15)
- Drakatos G.**  
(ST1/E/28-A3 0900-17)  
(ST1/E/46-A3 1620)
- Drange H**  
(MC01/W/36-A5 1700)
- Drapek R**  
(MC01/W/04-A5 1425)
- Drdla K.**  
(JSM26/W/31-B2 1150)
- Dremukhina L A**  
(GA3.10/W/17-A6 1700-07)
- Dremukhina Lidia**  
(GA3.05/W/43-B3 0900-41)  
(GA5.08/W/05-B1 1055)  
(GA5.08/W/06-B1 0945)
- Dreschhoff Gisela A. M.**  
(JSA45/E/04-B4 0830)
- Drevillon Marie**  
(MW06/E/07-A3 1000)
- Drewes**  
(G2/L/11-A2 1230)
- Drewes H.**  
(JSG14/W/16-A3 1203-22)
- Drewes Hermann**  
(JSG11/W/01-A4 1050)  
(G1/E/29-A3 1620-63)  
(G1/E/41-A3 1620-71)  
(G1/W/12-A3 1620-38)  
(G1/W/26-A3 1620-42)  
(G1/W/41-A3 1620-46)  
(G2/L/08-A2 1145)  
(JSS31/W/07-B3 0830-07)  
(U7/W/07-B1 0830-01)



- Dricker I. G.**  
(JSS07/W/04-A2 0930-01)
- Drijfhout Sybren**  
(JSP25/W/43-B3 1620)
- Drinkwater Mark R.**  
(P13/E/16-B2 1440)
- Driscoll M L.**  
(G3/W/30-A5 1610-06)
- Dritschel D. G.**  
(JSM26/E/17-B3 0910)
- Drobot Sheldon**  
(HS2/W/07-B1 1120)
- Droegemeier Kelvin**  
(JSG28/W/01-B2 1400-16)
- Droogers Peter**  
(JSM41/W/20-B5 1220)
- Drori Ron**  
(MI09/W/04-A5 0954)
- Drosdowsky Wasyl**  
(JSP25/W/65-B1 1420)
- Drossart P.**  
(MC09/W/10-B2 1515)
- Druitt T.**  
(VS2/E/10-B3 1400-23)  
(VS2/E/13-B3 1130)  
(VS2/W/21-B3 1400-14)
- Drumea Anatol**  
(ST3/E/40-B5 0845)  
(ST2/E/53-A5 1400-21)
- Drummond B. J.**  
(JSS44/L/08-B4 0930-43)
- Drummond L. A.**  
(U3/W/08-A30900-13)
- Dryn E. A.**  
(GA 4.01/W/14-A2 1400-08)
- Drysdale Euain**  
(MI12/E/03-B4 1520)  
(MI12/W/04-B4 1440)  
(MI12/W/05-B4 1115)
- Du Z. J.**  
(ST4/W/12-B1 1440)  
(ST4/W/61-B1 1500)
- Duan Mingzhen**  
(JSM41/E/17-B3 1750)  
(MI06/E/04-B1 1630)
- Duan Q.**  
(HW4/E/12-B2 0930)
- Duba A. G.**  
(GA1.02/E/18-A1 0945)
- Dubinsky Z.**  
(P15/L/19-B3 1500)
- Dubrov Mstislav N.**  
(G5/E/32-A4 1415-06)  
(ST1/E/04 0930-38)
- Dubrovin Pavel V.**  
(GA1.05/W/15-A6 0900-09)
- Ducarme B.**  
(ST1/E/87-A2 0930-12)
- Ducarme Bernard**  
(JSS02/E/01-A1 0830-03)
- Duck Thomas J.**  
(JSM01/W/40-A2 1520)
- Ducklow Hugh W.**  
(P08/E/03-A2 1520)  
(P11/E/29-B5 1050)
- Dudkin Fedir**  
(JSA15/E/15-A4 1400-09)
- Dufresne Jean-Louis**  
(MC01/W/15-A2 1740)
- Duda S. J.**  
(ST1/E/08-A2 1400-26)
- Dudeny J. R.**  
(GA3.08/W/19-A6 1520)
- Dudhia A.**  
(MI06/W/11-B1 1400-03)  
(MI06/W/11-B2 1400-03)
- Dudkin Fedir**  
(JWA34/E/10-B2 1640)
- Duennelier F. K.**  
(JWA34/W/08-B2 1500)
- Duguay Claude R.**  
(JSM41/W/12-B4 1720)
- Duha Jánia**  
(G2/W/11-A2 1630-05)
- Duka Bejo**  
(GA1.01/E/01-A5 0900-07)
- Dulac Francois**  
(MI01/W/22-A1 1150)
- Duma Gerald**  
(JSA15/E/54-A3 1420)
- Dumenil Lydia**  
(HW1/E/03-A4 1430)  
(MC01/W/46-A3 1620)
- Dumoulin C.**  
(ST4/W/43-B2 0930-02)
- Dumville Mark**  
(G1/E/56-A3 1620-80)
- Dunbar Nelia**  
(JSV30/E/05-B1 0940)
- Dunbar Paula K.**  
(G3/W/33-A5 1420)  
(ST7/W/05-A2 1605-03)
- Duncan Fairlie T.**  
(JSM01/L/30-A5 1640)
- Dundas R. M.**  
(MI10/E/01-B2 1535)
- Dungan Michael**  
(JSV30/W/07-B1 1200)  
(VS2/W/13-B3 1050)  
(VS3/W/25-B3 1620)
- Dunkerton Timothy J.**  
(MI12/W/02-B4 1630)
- Dunkley P.**  
(G1/E/46-A3 0930)
- Dunlop David J**  
(GA1.05/W/02-A5 1100)  
(GA1.05/W/04-A5 0950)  
(GA1.05/W/08-A5 0910)  
(GA1.05/W/36-A6 0830)  
(GA1.05/W/38-A5 0830)
- Dunlop M. W.**  
(GA3.07/W/22-A4 0930-07)  
(GA3.07/W/63-A4 0930-08)
- Dunn Michael**  
(JSV36/W/07-B3 1400)
- Dunn P. J.**  
(G6/E/03-B1 0910)  
(G5/E/10-A4 1522-12)
- Dunn S. M.**  
(HS3/W/17-A2 0900)
- Dunn Tim**  
(P09/E/03-A2 1010)
- Duque M R**  
(ST2/E/48-A5 1400-22)
- Duque M. Rosa**  
(ST4/E/25-B1 1400-06)  
(ST4/E/27-B1 1400-17)
- Durkee P A**  
(MI09/W/14-A5 1030)  
(MI09/W/14-A5 1145-21)
- Durukal Eser**  
(JSP23/W/18-A6 1050)
- Dutay J-CI**  
(MC01/W/36-A5 1700)
- Dutkiewicz Stephanie**  
(P08/W/06-A2 0950)
- Dutra Severino L. G.**  
(GA5.06/W/08 A4 1140)
- Dutrieux A**  
(MI07/E/03-A2 1400)
- Dutta K.**  
(P07/E/03-A3 1430)
- Dutton Ellsworth**  
(MI08/E/08-A4 1750)
- Dutton G S**  
(JSM01/W/56-A4 1620-07)
- Dutton Geoffrey S.**  
(JSM26/W/05-B1 0920)
- Duykerke Peter G.**  
(MI04/L/06-B3 1400)
- Dvoretzkaya L. G.**  
(JWS33/E/06 -B2 1635-12)  
(JWS33/E/06-B2 1230)  
(JWS33/E/06-B3 0900-12)
- Dvortsov Victor L.**  
(JSM26/W/04-B2 1130)
- Dwyer J. R.**  
(GA4.04/W/02-B5 1130)  
(GA4.04/W/12-B5 1750)  
(GA4.04/W/18-B5 1150)  
(GA5.08/E/07-B1 1330)  
(GA5.08/W/08-B1 1350)  
(P16/E/03-B5 0930)
- Dychenko Anatoly**  
(ST1/E/27-A2 1400-01)  
(ST1/E/29-A2 0930-04)  
(ST1/E/31-A2 1400-25)  
(ST1/E/34-A2 1400-02)
- Dyment J**  
(GA5.08/E/07-B1 1330)  
(GA5.08/W/08-B1 1350)  
(P16/E/03-B5 0930)
- Dyer C S**  
(JSA06/E/11-A1 0835)
- Dymnikov V.**  
(MI11/W/03-B5 1230)
- Dyson P L**  
(GA3.10/E/06-A6 1700-10)  
(JSA06/E/06-A1 1155-19)  
(JSM01/E/43-A2 1600-10)
- (JSA20/E/04-A6 1136)  
(JSA20/E/17-A6 1154)  
(GA2.02/E/02-B4 1740)
- Dzhola Anatoly**  
(MI02/W/08-A4 1510)
- Dziak Robert P.**  
(ST2/W/08-A5 0845)  
(P16/W/05-B5 0830)
- Dziewonski A.**  
(ST2/E/21-A5 1400-24)
- Dziewonski Adam M.**  
(ST4/E/22-B3 1140)
- (JSP49/E/11-B5 1210-05)
- Egeland A.**  
(GA6.01/L/01-A5 1240)
- Egeland Alv**  
(GA3.10/W/20-A6 0920)
- Eglitis Paul**  
(GA3.02/L/01-B2 1125)
- Egorin A. V.**  
(JSS44/E/32-B4 1740)
- Egorov I. B.**  
(GA2.02/W/23-B5 1640)
- Egorov O. N.**  
(ST3/W/17-B4 0930-17)
- Egorov Victor**  
(GA5.01/L/04 A1 1300-12)
- Egorova Larisa**  
(JSA45/W/18-B4 1450)
- Egozcue Juan José**  
(ST3/E/04-B4 1400-12)
- Eguchi Takao**  
(JSS13/E/01-A5 1210)
- Ehlers Todd A.**  
(JSS44/W/10-B4 1110)  
(JSS44/W/17-B4 0930-31)
- Ehrlicher S**  
(JSP23/C/US/W/13-A5 1440)
- Eicken H.**  
(P07/L/02-A3 1125)  
(P07/W/08-A3 1015)
- Eicken Hajo**  
(P13/W/26-B1 1010)
- Eidmann Gunnar**  
(JSM01/E/28-A4 1430)  
(JSM01/E/19-A5 0900)
- Eiges Pavel**  
(GA3.07/W/39-A3 1100)
- Eiji Ohtani**  
(ST 6/E/11-A2 1530)
- Eikenberg Jost**  
(HW5/W/14-A3 1440)
- Einescu B.D.**  
(JSA15/P/01-A5 0830-04)
- Eisel Markus**  
(GA1.02/E/13-A1 0845)  
(GA3.04/E/03-B1 0900)
- Eisen O.**  
(JSM04/W/12-A2 1535)
- Eiswirth Matthias**  
(HS5/W/41-A3 1400)
- Ejiri M**  
(JSM01/W/01-A3 1140)  
(GA2.02/W/09-B4 0900)
- Ejiri Mitsumu**  
(GA2.03/E/02-B3 1120)  
(JSM01/E/30-A2 1600-24)
- Ekdahl Anja**  
(JSP21/W/02-A4 1150)
- Eker Zeki**  
(JSA16/W/12-A3 0830-52)
- Ekman Martin**  
(JSP25/E/24-B3 0910)
- Ekstrom G.**  
(ST2/E/21-A5 1400-24)
- Ekstrom Goran**  
(JSS13/W/15-A4 1500)
- Ekwurzel Brenda**  
(P07/W/19-A3 1550)
- El-Alaoui Mostafa**  
(GA3.05/E/21-B3 1520)
- Elansky Nikolay F.**  
(MI06/E/13-B1 1100)
- Elberskirch Jochen**  
(JSG14/L/05-A3 1142-15)
- Eldholm O.**  
(ST2/E/31-A5 1200)
- Eldholm Olav**  
(U6/W/04-B2 1035)
- Eldin Alaa**  
(JSS44/P/06-B4 0930-17)
- Elena V.**  
(GA1.05/W/39-A6 0900-02)
- El-Foul Djamel**  
(ST2/P/02-A4 1645)  
(ST3/P/5-B4 1200)
- El-Genedi S.**  
(GA2.03/P/02-B3 1620)  
(GA6.01/P/08-A5 0900-20)
- Elgered G**  
(JSG11/W/05-A3 1440)  
(JSG28/W/05-B1 1010)
- El-Hady Sherif**  
(ST4/E/51-B1 1400-20)
- Eliseev Alexey V.**  
(MW02/E/02-B3 1640)
- Elisrafy Abouelhoda M.**

## e

## Eack Kenneth B

(MI03/W/03-A3 1620)  
(MI03/W/05-A3 1140)  
(MI03/W/04-A3 1700)

## Eagles G

(GA1.04/L/01 0930-18)

## Eanes R. J

(G5/W/25-A4 1100)  
(JSG14/W/24-A3 1700-04)  
(JSA37/W/09-B3 1100)

## Eanes Richard

(G2/W/07-A2 1430)

## Earle G.

(GA2.02/L/01-B4 1000)

## Eastman T. E.

(GA3.02/L/02-B3 0900-24)

## Ebel Adolf

(JSM01/E/33-A1 1050)

## Ebel John E.

(ST2/W/28-A5 1115)

## Ebert E.

(MC04/W/13-B2 1050)

## Ebihara Yusuke

(GA3.05/W/40-B3 0900-42)

## Eccles Dr. Vince

(JSA06/W/31-A11155-09)

## Eckermann E. O.

(JSM01/W/22-A2 1600-21)

## Eckermann Stephen

(MW07/E/07-A4 1210)

(MW07/E/03-A4 1400)

(MW07/W/19-A4 1420)

## Ecklund Warner L.

(MI04/W/26-B3 0830)

## Eckman R.

(JSM26/W/11-B1 0940)

## Edel Jean-Bernard

(GA1.04/W/16-A4 1140)

## Eden Carsten

(JSP25/W/20-B4 1620)

## Ederle Eliana

(G1/L/02-A3 1620-840)

## Ediger Dilek

(P11/E/25-B4 1010)

## Edmonson C

(JSM01/W/107-A1 1510)

## Edoardo Del Pezzo

(JSV47/E/01-B5 1400-05)

## Eduard Ghent D.

(JSS07/E/10-A2 0930-04)

## Eduard Sulstarova

(ST1/E/69-A4 0930-13)

## Eduard Vashenyuk

(JSA45/L/03-B4 1205)

## Edwards A. C.

(HS3/W/17-A2 0900)

(HS3/W/03-A1 0950)

## Edwards David P

(MW05/E/01-A2 1115)

## Edwards John

(MI04/E/09-B1 1420)

## Effendieva Maria A.

(GA5.08/E/06-B1 1400-01)

(JWS 33/E/01-B2 1635-13)

(JWS 33/E/01-B3 0900-13)

## Efimova G. A.

(ST6/W/05-A1 0830-07)

(ST6/W/08-A1 0830-10)

## Efremova Ludmila

(HS5/W/05-A1 1525)

## Eftaxias K.

(GA1.02/E/30-A20930)

## Egbert Gary D.

(GA1.07/E/02-B2 1000)

(GA1.07/E/03-B2 1140)

(GA3.04/E/03-B1 0900)

## INDEX

- (JSS44/P/06-B4 0930-17)
- Elizabeth Lucek**  
(GA4.09/E/12-A6 1520)
- Elken Jüri**  
(P11/W/13-B3 1640)
- Elkington S. R.**  
(GA3.05/W/14-B3 0900-40)
- Elkins James W.**  
(JSM26/W/05-B1 0920)  
(JSP21/L/04-A5 0930)  
(JSM01/W/56-A4 1620-07)  
(JSP21/W/12-A4 1110)  
(JSP21/W/15-A4 1600)  
(JSP21/W/17-A4 1500)
- Ellingson Robert G**  
(MC07/W/09-A2 1500)  
(MI06/W/12-B2 1500)  
(MI10/W/08-B2 1220)
- Elliott C. R. N**  
(HW2/W/05-B1 1140)
- Elliott H A**  
(GA3.10/W/01-A6 1630)
- Ellis J Bryan**  
(HS5/W/13-A2 0940)
- Elmas Ali**  
(ST2/W/19-A4 1215)
- Elmore R. D.**  
(GA1.04/W/40-A4 1010)
- Elo Seppo**  
(JSS44/E/11-B4 0930-29)
- Elokhov Aleksandr S.**  
(MI06/E/13-B1 1100)
- Elosegui P.**  
(JSS31/E/13-B3 0830-14)
- Elphic R.**  
(GA3.03/W/11-B4 1200)
- Elphic Richard C.**  
(GA3.05/W/11-B3 0900-06)  
(GA4.09/E/01-A6 1700)
- Elphinstone R. D.**  
(GA3.04/W/02-B1 1520-33)
- El-Sabh Mohammed**  
(JSG11/E/13-A4 1400-05)  
(P09/E/07-A1 1620)  
(P09/E/06-A1 1110)  
(P09/E/08-A1 1130)
- Elsadek Mohamed A.**  
(JSA27/P/02-B1 1400-03)
- El-Sayed El-Said**  
(JSA19/L/05-A4 1400-02)
- Elsberry Russell L.**  
(MC05/E/05-B4 1110)
- El-Sheimy Naser**  
(G6/L/03-B2 1720)
- Elsirafy Aboulhoda M.**  
(JSA27/P/01-B1 1050)
- Elsworth D.**  
(VS3/E/07-B3 1450)
- Eltayeb I.A**  
(GA1.01/W/04-A5 0930)
- Emery B.A.**  
(JSA20/W/40-A6 0948)
- Emery W. J.**  
(P10/W/26-A3 1440)  
(P13/W/14-B2 1520)
- Emilenko Aleksander S**  
(MI01/E/20-A2 1450)
- Emmanouloudis Dimitrios A.**  
(HS4/L/02-A4 0930)
- Emmons Louisa**  
(MI02/E/02-A4 1120)
- Emmons L.**  
(JSP21/E/04-A5 1110)
- Emori Seita**  
(MW03/W/05-B4 1530)
- Encrenaz T.**  
(MC09/W/10-B2 1515)
- Endo Nobuhiko**  
(JSM24/W/07-B1 1030-03)
- Ene Mirel**  
(ST4/E/43-B1 1400-09)
- Enescu B. D.**  
(JSA15/P/05-A5 0830-03)
- Enescu Bogdan**  
(ST1/W/66-A3 0900-16)
- Enescu D.**  
(JSA15/P/05-A5 0830-03)  
(JSA15/P/01-A5 0830-04)
- Engdahl E. R.**  
(ST5/E/07-B5 0930-09)  
(ST5/E/10-B5 0930-08)  
(U8/E/09-B3 1155)
- Engebretson M. J.**  
(GA3.02/W/12-B2 1230)  
(GA3.02/W/43-B2 0920)
- (GA3.04/E/15-B1 1520-02)  
(GA3.02/E/04-B3 0900-19)  
(GA3.04/W/47-B1 1230)
- Engel A.**  
(JSM26/W/06-B1 0900)
- Engel Heinz**  
(JSP23/W/31-A5 0950)
- Engelen Richard**  
(MC01/L/03-A1 1415)
- Engelhardt G.**  
(G1/E/31-A3 1620-65)  
(JSA09/L/02-A2 1230)
- Engels J.**  
(G4/C/G5/W/01-A3 1620-27)
- Engels U.**  
(JSA37/W/03-B3 1630)
- England Matthew H.**  
(P12/W/23-A1 1400)  
(MC01/L/08-A2 1445)  
(P07/W/06-A3 0935)
- England Philip**  
(G5/E/36-A4 1215)  
(JSS31/W/11-B2 1620)
- English Steve**  
(MI06/E/07-B1 1400-09)  
(MI06/E/07-B2 1400-10)
- Engman Edwin T.**  
(JSM41/W/02-B5 0945)
- Enomoto Takeshi**  
(MC10/E/07-B1 1400)
- Enomoto Y.**  
(JSA15/E/19-A3 1500)
- Enomoto Yuji**  
(JSA15/W/08-A4 1040)
- Enric Palle**  
(JSA16/W/17-A3 0830-36)
- Entekhabi Dara**  
(HS2/W/02-B1 0920)
- Eojin Kim**  
(GA4.10/L/01-A4 1145)  
(GA4.10/W/29-A4 1520)
- Eparvier Frank**  
(JSA16/E/12-A3 0830-14)
- Ephishov Ivan I.**  
(JSG28/E/28-B2 1400-01)
- Eppelbaurn**  
(JSP23/W/00-B1 0910)
- Erdik M.**  
(JSP23/C/U5/E/16-A5 1620)  
(ST3/E/56-B4 1400-20)
- Erdik Mustafa**  
(JSP23/W/18-A6 1050)
- Erdos G.**  
(GA3.07/E/06-A3 0900-03)  
(GA4.04/E/04-B5 0830-01)
- Ereditato Davide**  
(JSV47/E/03-B5 1400-02)
- Ergintav Semih**  
(G5/E/23-A4 1230-08)
- Ergun R.**  
(GA3.03/W/11-B4 1200)
- Ergun R. E.**  
(GA3.08/W/13-A6 0940)  
(GA4.09/W/02-A6 1000)  
(GA4.09/W/07-A6 0940)
- Ergünd Mustafa**  
(G1/E/04-A3 1620-50)
- Erickson G M**  
(GA3.10/W/02-A6 1615)
- Eriksson**  
(JSA06/L/06 0935)
- Eriksson A.**  
(GA4.09/W/05-A6 1140)
- Erickson K. N.**  
(GA3.02/W/43-B2 0920)
- Erincheck Yuriy**  
(JSS44/W/21-B4 1700)
- Erker E**  
(G3/E/11-A5 1610-31)
- Erlandson R. E.**  
(GA3.04/L/04-B1 1210)  
(GA3.05/W/24-B3 1120)
- Erlendsson P.**  
(ST4/W/03-B3 1630)
- Ermakov Sergey I.**  
(GA4.04/W/10-B5 0830-03)
- Ermini A.**  
(JSA15/W/15-A3 0950)
- Ermini A. A.**  
(ST1/W/14-A1 1150)
- Ermolli I.**  
(JSA16/E/43-A3 0830-01)  
(JSA16/E/44-A3 0830-33)
- Ernest Hildner**  
(GA4.01/W/03-A2 1650)
- Ernesto Marcia**  
(GA1.04/E/17-A4 0930-01)
- Ernst Tomasz**  
(JSA15/W/25-A5 0830-14)
- Erram Vinit C.**  
(JSS44/E/15-B4 0930-15)  
(JSS44/E/16-B4 0930-14)
- Errera Q.**  
(JSM26/W/01-B3 1210)
- Ershkovich Alexander**  
(GA3.09/W/18-B5 0855)
- Ershov Sergey**  
(JSA15/E/36-A4 1400-10)  
(JSS02/E/17-A1 0830-10)
- Erwin Edward H.**  
(GA5.06/W/07 A3 1100)
- Erzinger Joerg**  
(JSV36/E/02-B3 1100)
- Esau Igor**  
(MC04/E/03-B2 1140)
- Esparza Gonzales**  
(GA4.01/W/06-A2 1400-07)
- Espinosa Aranda J. M.**  
(JSP23/C/U5/W/14-B2 1210)
- Espindola Juan Manuel**  
(JSV29/W/02-B1 1540)
- Espy Patrick**  
(JSA20/W/13-A4 1200-06)
- Essery R.**  
(HS2/W/32-B2 1440)  
(HS2/W/11-B1 1420)  
(JSM43/W/12-B5 1120)
- Essery Richard**  
(MC01/L/05-A2 1100)
- Essery Richard L H**  
(MC07/E/05-A2 1135)
- Ester M.**  
(GA3.02/W/09-B2 1145)
- Etchevers Pierre**  
(HS2/W/01-B1 0900)
- Etling Dieter**  
(JSP39/E/08-B3 1010)
- Eugeny Afonin**  
(P15/W/03-B3 1025)
- Evangelos Emmanouloudis**  
(HS4/L/02-A4 0930)
- Evans Andy**  
(G1/E/42-A3 1620-72)
- Evans Frank**  
(MI04/L/21-B2 1720)
- Evans Hugh**  
(JSA06/W/18-A1 1155-12)
- Evans J D**  
(G3/W/54-A5 1610-50)
- Evans Jenni L.**  
(JSP23/E/20-A5 1400)  
(MC05/E/04-B4 0930)
- Evans Katherine J**  
(MW06/W/02-A3 1500)
- Evans Mathew**  
(U2/E/14-A2 1420)
- Evans R H**  
(MI09/L/03-A5 0830)
- Evans Russ**  
(U8/E/02-B3 1640-05)
- Evans Scott**  
(JSA20/W/49-A6 0930)
- Evans T.**  
(P09/W/11-A1 1010)  
(P07/W/20-A3 0900-07)
- Evans W F J**  
(MC07/W/15-A2 1440)  
(MC07/W/16-A2 1600)
- Evers Laslo**  
(ST3/W/04-B4 0945)  
(ST5/W/35-B3 0900-08)
- Evison Frank**  
(ST1/W/28-A3 1400)
- Exertier P.**  
(G2/E/06-A2 1630-03)  
(G3/E/27-A5 1610-02)
- Exertier Pierre**  
(G5/E/29-A4 1015)
- Extence Chris**  
(HW2/W/16-B2 1100)
- Eyido Haluk**  
(G5/E/23-A4 1230-08)
- (VS3/E/02-B3 1550)
- Fabian Karl**  
(GA1.05/W/11-A5 1120)
- Fabre A**  
(JSP21/W/11-A4 1050)
- Faccenna Claudio**  
(ST4/E/48-B3 1420)
- Faeh Donat**  
(ST3/E/04-B4 1400-12)
- Faeh D.**  
(JSP23/E/03-A6 0930)
- Fagundes P. R.**  
(JSA20/W/05-A5 1200-05)  
(JSA20/W/50-A5 1200-09)
- Fahey D W**  
(JSM01/W/56-A4 1620-07)  
(JSM26/W/33-B1 1620)  
(JSM26/W/05-B1 0920)
- Fahrbach Eberhard**  
(P13/P/01-B2 1130)
- Fahrutdinova A. N.**  
(JSA20/W/05-A5 1030)
- Fahrutdinova Antonina**  
(JSM01/E/04-A2 1130)  
(MW04/W/01-A1 0950)
- Fainberg Ed.**  
(GA1.02/L/03-A2 0930)
- Fairall C. W.**  
(JSM04/W/02-A2 0930)  
(MI08/L/05-A3 1705)  
(MI08/W/16-A4 1600)
- Fairbanks Rick G.**  
(P07/W/04-A3 0900-02)  
(P07/W/19-A3 1550)
- Fairhead J. Derek**  
(G3/W/26-A5 1610-70)  
(GA5.12/E/08 A2 1140)  
(JSA27/E/07-B1 0940)
- Fairlie D.**  
(JSM26/W/11-B1 0940)
- Fairlie T. Duncan**  
(JSM01/L/30-A5 1640)
- Fako Pavol**  
(HS3/W/22-A2 1135)
- Fakultat P. K. Shukla**  
(GA4.09/E/02-A6 1100)
- Falk R.**  
(JSG14/E/21-A3 1700-18)
- Falko Olga**  
(GA3.04/E/08-B1 1520-01)
- Fall Gregory M**  
(JSM01/E/23-A3 1200)
- Fallows A**  
(GA4.01/W/09-A2 1140)
- Fallows R.A**  
(GA4.02/E/07-A4 1400-02)  
(GA4.05/E/02-A1 1010)  
(GA4.04/W/07-B5 1430)
- Faloon I.**  
(JSM26/W/18-B2 1550)
- Falthammar C G.**  
(GA4.02/E/06-A4 1400-09)  
(GA4.02/E/13-A4 1400-08)
- Falvey Mark**  
(JWM08/E/07-A2 1040)  
(JSG28/W/28-B1 1220)  
(MI06/E/03-B1 1120)
- Fan C. W.**  
(P11/E/15-B3 1130)
- Fan Chenwu**  
(P12/E/04-A1 1110)
- Fan Quanfu**  
(GA3.09/W/24-B5 1205)
- Fan Xingzhao.**  
(GA1.15/W/05-B4 1730)
- Fang Ming**  
(G4/W/13-A3 1620-24)
- Fang Peng**  
(JSG28/L/01-B1 1400-03)
- Fang X. M.**  
(GA1.05/E/17-A6 1630)
- Fang Zheng**  
(MI11/E/12-B5 1000)
- Fanrong Chen**  
(JSV30/C/JSV22/P/02-B1 1400-23)
- Fantini Dr. MARRIZIO**  
(MC05/W/42-A1 0930)
- Farag Karam S.**  
(GA1.04/P/01-A6 1200)
- Farges T H**  
(JSM01/P/03-A2 1600-18)  
(JSA20/E/26-A4 1200-14)  
(JSM01/P/03-A2 1540-18)
- Faria H H**  
(MI03/W/08-A3 1400-01)

f

Fabbri M

- Farmer David**  
(JSP49/E/07-B5 1050)  
(JSP49/L/01-B5 1110)
- Farnell Les**  
(GA1.01/W/36-A5 0900-09)
- Farquharson F. A. K.**  
(JSM24/L/01-B2 1010)
- Farrara J. D.**  
(MI12/W/12-B4 1135)  
(U3/W/08-A30900-13)
- Farrugia C J**  
(GA3.07/W/41-A3 0900-04)  
(GA4.02/W/24-A4 1400-22)
- Fassnacht S. R.**  
(HS2/W/12-B1 1540)
- Fast H**  
(JSM01/W/37-A5 1400)
- Fast I.**  
(JSM26/E/13-B3 0850)
- Faul U**  
(ST6/C/JSS02/W/15-A2 1640)
- Faulkner Duncan S.**  
(HS1/W/68-B5 1400)
- Favetto Alicia**  
(JSS44/W/02-B5 0930)  
(GA1.02/W/39-A2 0930)
- Favey Etienne**  
(G6/W/06-B2 1400)
- Fearn D. R.**  
(GA1.01/W/06-A6 1015)
- Fearn Peter R C S**  
(P15/W/05-B3 1630)
- Featherstone W E**  
(G3/W/54-A5 1610-50)  
(G3/W/49-A5 1610-78)  
(G3/W/44-A5 1025)
- Featherstone Will**  
(G3/E/03-A5 1610-64)  
(G3/W/43-A5 1610-52)
- Fedorenko Yu**  
(JSA06/W/22-A2 0930)
- Fedorenko Yura**  
(ST3/E/48-B5 1100)  
(ST5/E/39-B3 1125)  
(U8/E/06-B3 1215)
- Fedorov A. A.**  
(GA3.04/E/15-B1 1520-02)
- Fedorov Andrei**  
(GA3.07/W/08-A5 0900-05)  
(GA3.07/W/28-A4 0930-09)
- Fedorov A. N.**  
(GA5.01/W/15 A1 1300-06)  
(JSA15/L/01-A5 0830-10)  
(ST1/W/04-A2 1400-14)
- Fedorov D. V.**  
(JSA45/E/11-B5 1030)
- Fedorov Evgenij**  
(GA3.04/E/06-B2 0950)  
(JSA15/E/06-A4 1400-08)
- Fedorova Natalia**  
(GA5.11/W/02 A3 1430-06)  
(JSA40/W/13-B5 1400-14)  
(JSS44/W/20-B4 0930-23)
- Fedotov Sergei A.**  
(JSV36/E/05-B3 1400-08)  
(ST1/E/42-A3 0900-14)
- Fedotova O. I.**  
(GA5.01/W/15 A1 1300-06)
- Fehler Michael**  
(JSS46/W/10-B4 1600)  
(ST5/W/04-B5 1145)
- Fehler Mike**  
(ST5/W/24-B4 0930)
- Fehlmann Rene**  
(MI05/E/04-A1 1420)  
(MW06/W/01-A3 1140)
- Fei Li**  
(G3/L/40-A5 1610-98)  
(G3/L/40-A5 1610-98)
- Fei Z. L.**  
(G4/W/22-A3 1620-18)
- Feichter J**  
(JSM01/W/25-A4 1130)
- Feichter Johann**  
(MI01/W/18-A1 1510)  
(MI01/W/20-A2 1640)
- Feigin A. M.**  
(JSM26/E/01-B2 1700-03)  
(JSM26/E/04-B2 1700-05)
- Feigin Alexander**  
(JSM26/E/03-B2 1700-08)  
(MI11/E/03-B5 1745)
- Feignier Bruno**  
(ST5/E/33-B5 1205)
- Feijt A.**  
(MI06/W/14-B2 1010)  
(MI10/W/17-B2 1620)
- Feijt Arnout**  
(JSG28/E/09-B1 1200)
- Feingold G**  
(MI08/W/01-A4 1205)
- Feizabadi B. A**  
(ST6/P/02-A2 0830-02)
- Fejer B. G.**  
(JSA20/W/16-A5 1443)
- Fekete Balazs**  
(HW1/L/11-A4 1430)
- Feldman Konstantin**  
(P10/E/13-A5 1440)
- Feldman W. C.**  
(GA4.01/W/05-A2 1450)
- Feldstein Y. I.**  
(GA4.08/E/21-B3 0900-13)
- Feldstein Ya. I.**  
(GA3.08/W/31-A6 1150)  
(GA3.05/W/43-B3 0900-41)  
(GA3.09/W/13-B4 0900-12)  
(GA5.08/W/05-B1 1055)  
(GA3.10/W/17-A6 1700-07)
- Feldstein Yasha**  
(GA4.08/W/01-B4 1545)
- Felpeto Alicia**  
(JSP23/E/02-B1 1210)  
(JSP23/E/26-B2 1050)
- Feltz W F**  
(MC08/L/01-A3 1045)
- Feng**  
(G6/L/02-B1 0950)
- Feng Dasheng**  
(JSG28/E/27-B2 1400-04)  
(MI06/W/29-B1 1010)
- Feng Guozhang**  
(JSP23/W/35-A5 0830-02)
- Feng Lanying**  
(JSP23/C/U5/E/20-B2 1110)
- Feng Shizuo**  
(P10/W/02-A4 1210)
- Fennell J. F.**  
(GA4.08/W/18-B4 0830)  
(GA3.02/W/13-B2 1630)  
(GA3.03/W/03-B4 0930)  
(GA3.05/W/13-B3 0900-34)  
(GA3.05/W/25-B3 0900-33)  
(GA3.05/W/26-B3 1600)  
(GA3.05/W/28-B3 0830)  
(GA3.05/W/04-B3 0900-45)
- Fennessy M J**  
(MC01/E/02-A4 1430)
- Ferdinand Richard W.**  
(ST4/P/6-B1 0830-11)
- Ferguson I. J.**  
(JSS44/L/03-B4 1150)
- Ferland R.**  
(G1/C/G5/E/15-A3 1620-102)
- Fernandes M. J.**  
(G3/L/8-A5 1400)
- Fernandes Noomen Rui**  
(G5/W/03-A4 1230-01)
- Fernández Alberto**  
(MC01/L/05-A2 1100)
- Fernandez Jose**  
(JSV36/E/15-B3 1655)  
(JSV36/W/21-B3 1400-01)
- Fernandez R.**  
(GA4.02/E/08-A4 1400-05)  
(GA4.02/E/10-A4 1400-03)
- Fernando H. J. S.**  
(JSP39/W/42-B2 0930)  
(JSP39/W/23-B3 1427-10)
- Fernetti Lopez**  
(G4/E/09-A3 1620-03)
- Fernsler F**  
(JSM03/W/03-A1 1420)
- Ferraccioli Fausto**  
(JSA09/E/09-A3 1015)  
(JSA09/W/05-A3 0930)  
(JSA09/W/07-A2 0930-02)
- Ferrandiz Jose M.**  
(G1/W/10-A3 1620-37)
- Ferrante O.**  
(GA6.01/E/22-A5 0900-06)
- Ferrari Graziano**  
(ST7/E/05-A2 1200)  
(ST7/L/03-A2 1430)  
(ST7/E/07-A2 1215)
- Ferrari L.**  
(JSV30/E/11-B1 1400-14)
- Ferraro C.**  
(JSG28/W/15-B1 1400-04)
- Ferreira Costa Moises**  
(G1/E/54-A3 1620-79)
- Ferrick M. G.**  
(HW3/W/09-B4 1455)  
(HW3/W/19-B4 1015)
- Ferrier Bradley S.**  
(MI04/W/06-B3 1105)
- Ferrier R. C.**  
(HS3/W/17-A2 0900)  
(HS4/W/15-A4 1730)
- Ferris Julie**  
(JSA09/W/05-A3 0930)
- Ferrucci Fabrizio**  
(JSA15/W/02-A4 1400-18)
- Fesen C.**  
(JSA20/W/40-A6 0948)
- Feshchenko**  
(GA4.08/W/24-B3 0900-07)
- Feygin F. Z.**  
(GA3.04/W/08-B1 1150)
- Feygin Felix**  
(GA3.04/E/11-B1 1520-21)
- Feynman J.**  
(GA4.03/E/03-B4 1130)
- Feynman Joan**  
(JSA45/W/11-B4 1430)  
(JSA06/W/09-A1 1600)
- Ficek Dariusz**  
(P15/W/04-B4 1055)
- Fichetef T.**  
(P13/E/05-B1 1520)
- Fichetef Th**  
(MC01/W/26-A3 0915)
- Fichetef Thierry**  
(MC01/E/32-A2 1620)
- Fiedrich Frank**  
(JSP23/C/U5/E/14-A5 1420)
- Field A.**  
(P11/W/16-B3 0950)
- Field Amy**  
(P12/E/06-A1 1030-05)
- Field Edward H.**  
(ST3/W/19-B4 1630)
- Field P. R.**  
(MI04/E/14-B1 0900-06)  
(MI04/E/01-B4 1450)  
(MI04/E/04-B4 1035)
- Fielding S.**  
(P11/W/19-B4 1500)
- Figari Eduardo**  
(GA1.04/L/05-A6 1500)
- Figueras S.**  
(ST5/E/34-B3 0830)
- Figurski Mariusz**  
(JSG 28/E/23-B2 1400-02)  
(G5/E/44-A4 1558-10)
- Filippidis Evangelos I.**  
(HS4/L/02-A4 0930)
- Filippidis I**  
(HS4/L/02-A4 0930)
- Filippov Sergey V.**  
(GA5.09/W/05 A2 1400-02)
- Filling Holger**  
(GA6.01/P/04-A5 0900-08)
- Fillingim M.**  
(GA3.03/E/07-B4 1020)
- Fine Isaac V.**  
(JSS42/E/12-B4 1500)  
(JSS42/E/12-B5 1700-07)
- Finenko Zosim Z.**  
(P11/L/06-B5 1730)
- Fink H.-P.**  
(JSM26/W/29-B2 1700-09)
- Fink Jonathan H.**  
(VS3/W/26-B3 0900-01)  
(VS3/W/26-B3 1630)
- Finkele Klara**  
(MI05/W/31-A4 1120)
- Finlayson D. M.**  
(JSS44/L/08-B4 0930-43)  
(JSS46/W/07-B4 1030)  
(JSS44/L/07-B4 0930-44)
- Finnigan Timothy D.**  
(P14/W/01-A4 1400-03)
- Fiocco Giorgio**  
(JSA09/W/12-A2 1630)
- Fiorini Francesca**  
(JSS42/W/21-B5 0950)
- Firbas Peter**  
(U8/L/01-B3 1640-03)
- Fischer J**  
(MI09/W/10-A5 1145-12)
- Fisher G M**  
(JSM01/W/106-A2 1600-01)
- Fisher H H**  
(MC01/E/20-A5 1405)
- Fisher M. A.**  
(ST4/L/01-B1 0830-02)
- Fisk Len**  
(GA4.02/W/18-A4 1735)
- Fisk L. A.**  
(GA4.05/W/07-A1 1000)  
(GA4.04/E/07-B5 0830)  
(GA4.04/W/03-B5 1050)  
(GA4.04/W/06-B5 1400)
- Fitas J. S.**  
(ST2/E/47-A4 1630)
- Fitriani Dini**  
(GA 1.05/E/12-A5 0850)
- Fitz Gerald J. D**  
(ST6/C/JSS02/W/15-A2 1640)  
(ST6/W/04-A1 0830-06)
- Fitzenreiter R.**  
(GA3.08/W/09-A6 0920)
- Fitzpatrick Melanie**  
(MI08/E/13-A3 1100)
- Flagan R C**  
(MI09/W/14-A5 1030)  
(MI09/W/14-A5 1145-21)
- Flament Pascal**  
(MI01/E/02-A1 0900-07)
- Flanagan Megan P.**  
(ST4/W/20-B3 0840)
- Flato Gregory M.**  
(JSM41/W/12-B4 1720)  
(MC01/L/10-A2 1550)
- Fleischmann Uli**  
(P07/W/12-A3 0900-03)  
(P08/W/09-A2 1110)
- Fleitout L.**  
(ST6/W/02-A1 0830-04)  
(ST4/W/43-B2 0930-02)
- Fleitout Luce**  
(JSS13/W/03-A5 1130)
- Fleming Eric L.**  
(JSA45/E/12-B4 0915)
- Flesch Rainer**  
(G6/L/02-B2 1640)
- Fleta J.**  
(ST3/E/41-B5 1000)  
(ST5/E/34-B3 0830)
- Fletcher Hilary J.**  
(JSS31/W/14-B2 1440)
- Fligge M.**  
(JSA16/W/36-A3 0930)
- Flittner David**  
(JSG28/E/27-B2 1400-04)
- Florek Stefan V.**  
(JSG28/W/06-B1 1400-06)  
(MI06/W/18-B1 1400-04)  
(MI06/W/18-B2 1400-04)
- Flores A.**  
(JSG28/E/20-B1 1400-16)
- Florez Juan**  
(G1/E/29-A3 1620-63)  
(G1/E/36-A3 1620-68)  
(G3/E/02-A5 1610-94)
- Flosadottir Agusta**  
(P16/E/07-B5 1400)
- Flowers N. J.**  
(GA3.02/W/56-B2 1020)
- Floyd L. E.**  
(JSA16/W/13-A3 0830-47)
- Floyd Linton**  
(JSA16/E/11-A3 0830-15)  
(JSA16/W/11-A3 0830-25)  
(JSA16/W/20-A3 0830-53)  
(JSA16/W/38-A3 0830-54)
- Fluche Bernhard**  
(GA1.02/W/02-A2 0930)  
(GA1.02/W/04-A2 0930)
- Flück Paul**  
(JSS42/W/25-B4 1600)
- Flugel W.-A.**  
(HW4/E/16-B2 1520)
- Flügel Wolfgang-Albert**  
(HS4/W/08-A4 1450)  
(HW5/W/12-A3 1040)
- Flynn Luke**  
(JSP23/E/40-A5 1740)
- Flynn Michael J**  
(MI01/E/05-A1 1430)
- Fofi M.**  
(JSA16/E/43-A3 0830-01)
- Folco Pingue**  
(JSV47/E/01-B5 1400-05)
- Foldvary Lorant**  
(JSG14/W/20-A3 1700-11)
- Foley Jonathan A**  
(MC07/E/04-A2 1215)
- Folland C.**



# INDEX

- (JSP25/W/95-B5 1620)
- Folland Chris**  
(JSP25/E/10-B4 1600)  
(JSP25/W/61-B4 0930)
- Follows M**  
(MC01/W/36-A5 1700)
- Follows Michael J.**  
(P08/E/07-A2 1050)  
(P08/W/06-A2 0950)
- Fomenko Alexander**  
(MC01/E/07-A4 1700)
- Fomenko Elena**  
(GA1.02/E/03-A1 1605)  
(GA1.02/E/33-A1 1605)  
(GA1.02/E/34-A1 1500)
- Fomichev V I**  
(JSM01/W/10-A3 1650)
- Fomichev Victor**  
(MW05/W/04-A2 1200)  
(MW05/W/05-A2 0940)
- Fonseca Joao F B D**  
(JSP23/E/23-B2 0830-09)  
(JSP23/E/27-B2 0830-14)
- Fonseca J. F. B. D.**  
(VS3/E/01-B3 0900-03)  
(JSV36/E/26-B3 1400-10)  
(ST3/E/09-B4 1400-14)
- Font Graciela**  
(G3/E/04-A5 1610-90)  
(G3/W/14-A5 1610-79)  
(G3/W/19-A5 1610-96)
- Font J.**  
(JSM41/W/27-B5 0930)
- Fontenla J. M.**  
(GA4.02/E/09-A4 1400-04)
- Fontenla Juan**  
(JSA16/E/09-A3 1100)
- Fontes Sergio L.**  
(GA1.02/W/35-A2 0930)
- Fonteyn D**  
(JSM01/W/08-A4 1450)  
(JSM26/W/01-B3 1210)
- Foot John S.**  
(JSM26/E/10-B2 1000)
- Forbes J M**  
(JSM01/W/67-A1 1110)  
(MW04/E/01-A1 1400)  
(JSA20/W/37-A5 1200-01)
- Forbes R. M**  
(M104/E/27-B4 1135)
- Forbes Terry**  
(GA4.02/W/09-A4 1125)  
(GA4.02/W/17-A4 1400-16)
- Foreman M. G. G.**  
(P10/E/06-A5 1050)
- Forget F.**  
(MC09/W/07-B2 01)
- Formisano V.**  
(MC09/W/07-B2 01)
- Forrai Yosef**  
(G1/W/16-A3 1620-06)
- Forsberg N Nielsen**  
(JSH12/W/05-A5 0900)
- Forsberg R.**  
(G1/E/37-A3 1620-69)  
(G3/L/8-A5 1400)  
(G3/W/49-A5 1610-78)
- Forsberg Rene**  
(G3/L/04-A5 1610-19)  
(G3/W/46-A5 1610-91)  
(JSA09/W/08-A2 1045)  
(G6/E/02-B2 1140)
- Forster F**  
(MC07/W/08-A2 1420)
- Förster M.**  
(JSA37/W/03-B3 1630)
- Forster P M de F**  
(MC07/W/04-A2 1115)
- Forster Piers**  
(MW01/E/01-A5 1620)
- Forsyth R. J.**  
(GA4.01/W/13-A2 1420)  
(GA4.02/W/20-A4 1400-18)
- Forté A M**  
(JSS02/E/09-A2 1030)
- Forward Troy**  
(G1/W/13-A3 1620-05)
- Foster James**  
(JSG28/E/21-B2 1400-14)  
(JSG28/L/01-B1 1400-03)
- Foster S S D**  
(HS5/W/21-A2 1405)
- Fotheringham Paul**  
(GA1.01/W/16-A6 1200)
- Fouad Kadry M.**  
(JSA27/P/04-B1 1210)
- Foulger G.**  
(JSS31/E/11-B2 1010)
- Foulger G. R.**  
(JSS46/W/04-B4 1130)  
(JSS46/W/06-B4 1110)  
(JSS46/W/12-B4 1210)  
(JSV47/W/08-B5 1400-19)  
(JSV47/W/13-B5 1145)  
(ST4/W/03-B3 1630)  
(ST4/W/12-B1 1440)  
(ST4/W/61-B1 1500)
- Foulkes Kristie**  
(GA3.04/W/26-B1 1520-09)
- Fourrie N**  
(MI05/W/30-A3 1220)
- Fowler C.**  
(P13/W/14-B2 1520)
- Fowler Catherine**  
(JSM01/E/27-A5 1150)
- Fowler Laura D.**  
(M110/W/21-B1 1620)
- Fox Alan**  
(JSP05/W/08-A2 0930)
- Fox Christopher G.**  
(ST2/W/08-A5 0845)  
(P16/W/05-B5 0830)
- Fox Geoffrey**  
(ST1/E/59-A1 1230)
- Fox N. J.**  
(GA3.02/W/09-B2 1145)
- Fox Nicola J.**  
(GA4.01/W/07-A2 1620)
- Fox Peter A.**  
(JSA16/E/09-A3 1100)
- Fox-Rabinovitz Michael**  
(JSP05/W/15-A1 1440)  
(MC01/E/17-A5 0930)  
(MC01/W/06-A5 0830)  
(MI07/W/01-A2 1100)
- Foyn Lars**  
(P07/L/03-A3 0900-08)
- Fraedrich Klaus**  
(MC11/W/01-B4 1205)
- Fraenz M.**  
(GA4.04/W/16-B5 1730)
- Fragner Elisabeth**  
(G2/L/12-A20 1630-06)
- Francalanci Lorella**  
(JSV30/E/11-B1 1400-14)  
(JSV30/W/08-B1 1040)
- Franceschina G.**  
(JSP23/E/08-A6 0950)
- Francesco Giuliano**  
(ST5/W/31-B4 1640)
- Francia P.**  
(GA3.04/L/16-B2 1600)  
(GA3.04/W/41-B1 1520-10)
- Francia Patrizia**  
(GA3.10/W/22-A6 1700-14)
- Francile C.**  
(GA4.02/E/10-A4 1400-03)
- Francis J**  
(MI08/W/11-A3 1720)
- Francis Jennifer**  
(MI08/W/06-A4 0900)  
(JSM04/W/01-A2 1620)
- Francis N M**  
(JSA06/W/32-A1 1155-11)
- Francis O.**  
(G1/W/22-A3 1620-41)
- Francis Peter**  
(U6/W/12-B2 1500)
- Francis Peter N**  
(MI09/E/07-A5 1525)
- Francisco Joco**  
(G1/E/28-A3 1620-62)  
(G1/E/44-A3 1620-28)
- Franck Siegfried**  
(U3/W/05-A30900-11)
- Francofonte S.**  
(ST1/E/17-A3 1050)
- Francois Louis**  
(MC11/E/04-B3 1620)
- Frank Evison**  
(ST1/W/23-A1 1130)
- Frank L A**  
(GA4.10/W/09 A5 1710)  
(GA4.10/W/05-A5 1655)  
(GA4.10/W/17-A5 1400)  
(GA3.02/W/18-B2 1645)  
(GA3.02/W/40-B3 1050)  
(GA3.02/W/58-B3 0900-22)  
(GA3.03/W/05-B4 1110)  
(GA3.08/E/01-A6 1430)
- (GA3.08/W/29-A6 1400)
- Franké B**  
(MI02/W/05-A5 0950)
- Franké Peter**  
(JSG28/W/21-B1 1400-02)
- Franké S.**  
(GA2.02/L/01-B4 1000)
- Franké Steve**  
(JSM01/W/62-A2 1110)  
(MW04/W/11-A1 0925)
- Frank-Kamenetsky Alexander**  
(JSA35/W/06-B1 1400)
- Franks Stewart W.**  
(HW4/E/06-B2 1500)
- Franssens Ghislain**  
(MI01/W/26-A2 1140)
- Fraser B. J.**  
(GA3.06/W/06-A3 1150)  
(GA3.04/W/10-B1 1520-08)  
(GA3.04/W/23-B1 1520-25)  
(GA3.05/W/07-B3 0900-12)  
(GA3.04/W/26-B1 1520-09)  
(GA3.04/W/17-B1 1520-16)  
(GA3.04/W/43-B2 1630)
- Fraser G**  
(JSM01/W/67-A1 1110)
- Fraser G J**  
(JSM01/E/39-A1 0940)
- Fraser P.**  
(JSP21/E/04-A5 1110)
- Fraser P. J.**  
(JSM26/W/06-B1 0900)
- Fraser Paul**  
(JSP21/E/02-A4 0930)  
(JSP21/L/01-A4 1010)
- Fraser Paul J**  
(MI02/W/12-A4 1430)
- Fratini Maria Rosaria**  
(JSS46/E/05-B4 1440)
- Frawley James J.**  
(JSA37/W/06-B3 1645)  
(JSA09/E/11-A3 1000)
- Freda Carmela**  
(VS2/W/22-B3 1400-15)
- Frederiksen Andrew W.**  
(ST4/W/19-B2 0930-15)
- Frederiksen Carsten**  
(MW02/L/01-B3 1220)
- Frederiksen Carsten S**  
(MW06/W/05-A3 1430)
- Frederiksen Jorgen S**  
(MI05/E/07-A1 1140)  
(MW06/W/05-A3 1430)  
(MI11/E/01-B5 0930)
- Freeden Willi**  
(G4/W/02-A3 1500)
- Freeman M P**  
(GA3.10/W/26-A5 1225)
- Freeman Mervyn P**  
(GA3.08/W/02-A6 1100)  
(GA3.02/W/10-B3 1220)  
(GA3.02/W/22-B3 0900-12)
- Freese Dietmar**  
(MI08/W/05-A3 1515)  
(MI04/W/04-B1 0900-08)
- Frehmann Torsten**  
(HS5/W/20-A2 1220)
- Frei Christoph**  
(JWM08/E/08-A2 1520)  
(JWM08/W/05-A2 1540)  
(MC01/E/38-A5 1000)
- Freidenreich S M**  
(MC07/W/12-A2 1155)
- Freiman M T**  
(MI02/L/01-A5 1140)  
(MI02/L/18-A5 1430)
- Freistühler Elke**  
(HW2/W/18-B2 1140)
- Freitag J.**  
(P07/W/08-A3 1015)
- French W J R**  
(JSM01/E/43-A2 1600-10)  
(JSM32/L/01-B3 1125)
- Freudenreich H.**  
(GA2.02/L/01-B4 1000)
- Freund Friedemann**  
(ST1/L/01-A2 1400-24)
- Frevert Volker**  
(G1/E/06-A3 1620-20)
- Frew Nelson**  
(JSM41/W/07-B4 1620-05)
- Frew R. D.**  
(P07/W/17-A3 0955)
- Frey Fred**  
(JSV22/L/05-A5 1420)
- Freybourger Marion**  
(ST4/E/10-B3 0940)
- Freymueller Jeffrey T.**  
(JSS31/W/14-B2 1440)
- Frez Jose**  
(JSA40/E/07-B5 0950)
- Fridman Alexey**  
(ST5/E/38-B4 1740)
- Friedel R.**  
(GA3.03/W/03-B4 0930)  
(GA4.08/W/18-B4 0830)
- Friedel R. H. W.**  
(GA3.02/W/13-B2 1630)  
(GA3.05/W/25-B3 0900-33)  
(GA3.05/W/26-B3 1600)  
(GA3.05/W/30-B3 1100)  
(GA3.02/E/18-B3 0850)
- Friedel S.**  
(JSV36/W/25-B3 0900-04)
- Friedlingstein Pierre**  
(MC01/W/15-A2 1740)
- Friedrich Martin**  
(GA2.01/W/04-A1 1415)
- Fris-Christensen Eigil**  
(GA3.10/E/07-A6 1700-08)  
(JSA16/E/34-A3 1500)  
(GA5.08/E/03-B1 0900)  
(JSA37/L/02-B3 0900)
- Fritts D C**  
(JSM01/P/03-A2 1600-18)  
(JSM01/W/36-A1 1400)  
(MW04/W/04-A1 0900)  
(JSM01/E/05-A1 1210)  
(JSM01/W/67-A1 1110)  
(JSM01/P/03-A2 1540-18)
- Fritts Dave**  
(JSM01/W/62-A2 1110)  
(MW04/W/11-A1 0925)
- Fritts David C**  
(MW07/W/14-A4 1110)  
(JSM32/W/06-B2 1135)  
(JSP39/W/36-B2 1700)  
(JSP49/W/18-B5 1600)  
(U8/W/05-B3 1640-02)
- Fritz T. A.**  
(GA3.03/W/03-B4 0930)  
(GA3.05/W/05-B3 0900-46)  
(GA3.05/W/13-B3 0900-34)  
(GA3.05/W/25-B3 0900-33)  
(GA3.08/W/26-A6 1710)  
(GA4.08/W/11-B3 1620)  
(GA4.08/W/13-B4 0905)  
(GA4.08/W/18-B4 0830)  
(GA3.05/W/04-B3 0900-45)  
(GA3.05/E/04-B3 0900-09)  
(GA3.09/W/26-B4 0900-05)
- Froger Jean-Luc**  
(G2/E/09-A2 1630-25)
- Frohlich C.**  
(MC02/E/12-B1 1600-11)
- Frohlich Claus**  
(JSA16/W/18-A3 0900)  
(JSA16/W/25-A3 0830-46)  
(JSA16/W/20-A3 0830-53)  
(JSA16/W/38-A3 0830-54)  
(JSA16/W/15-A3 0830-41)  
(MI09/W/09-A5 1145-11)  
(JSA16/W/36-A3 0930)
- Frolkis V A**  
(MC07/W/13-A2 1640)  
(JSA16/W/09 A3 0830-50)
- Frolova Aleksandra**  
(ST3/E/06-B4 0930-11)  
(ST3/E/49-B5 1045)
- Frolova N. I.**  
(ST3/E/01-B5 1400)  
(ST3/E/05-B5 0930)  
(ST3/E/15-B4 1400-05)  
(JSP23/E/33-A5 1640)  
(JSP23/E/55-A5 0830-16)
- Fromm Michael D.**  
(JSM26/W/08-B2 1700-15)
- Fromm Mike D.**  
(JSM01/W/04-A4 1510)
- Frost Dan**  
(JSS07/E/05-A2 1540)
- Frost Gina**  
(GA1.04/E/04-A6 1400)
- Fryer Gerard J.**  
(JSS42/W/13-B5 1700-02)
- Fu Chao**  
(MW05/W/04-A2 1200)
- Fu G Y**  
(G3/W/09-A5 1610-27)  
(G5/W/16-A4 1542-02)

- Fu Guang-yu**  
(G5/E/42-A4 1544-03)
- Fu Qiang**  
(MC07/W/11-A3 1015)  
(MI10/W/16-B2 1435)
- Fu Rong**  
(MC01/W/32-A2 0930)  
(MW02/E/04-B3 1140)
- Fu Rongshan**  
(ST4/W/55-B2 1420)  
(JSS02/E/02-A1 0830-04)
- Fu S. Y.**  
(GA3.02/E/18-B3 0850)  
(GA3.05/W/05-B3 0900-46)  
(GA3.05/W/23-B3 0900-13)
- Fuchs Dr. E.**  
(HW2/W/15-B2 0950)
- Fudeyasu Hironori**  
(JSM24/W/04-B1 0930)
- Fujie Gou**  
(ST4/W/34-B1 1400)
- Fujii Hideyuki**  
(JSM24/E/02-B1 1440)
- Fujii Masahiko**  
(U2/E/08-A2 1200)  
(P08/E/02-A2 0930)
- Fujii Naoyuki**  
(G5/E/33-A4 1504-03)
- Fujii Ryoichi**  
(JSA20/E/18-A6 1118)
- Fujii Yoichiro**  
(JSS31/E/12-B3 0830-13)  
(JSS31/W/06-B3 0830-06)
- Fujima Koji**  
(JSS42/E/20-B5 1700-20)  
(JSS42/E/21-B5 1700-19)  
(JSS42/P/01-B5 1210)
- Fujimori Hidetoshi**  
(P16/E/06-B5 1500)  
(P16/E/11-B5 1440)
- Fujimoto Masaki**  
(GA3.08/W/15-B1 1640)  
(GA3.08/W/34-B1 1550)
- Fujinawa Y**  
(GA1.02/W/08-A2 0930)  
(JSA15/E/19-A3 1500)
- Fujinawa Yukio**  
(JSA15/W/08-A4 1040)
- Fujinuma Y.**  
(U7/L/03-B1 0830-07)
- Fujioka Kantaro**  
(P16/L/01-B5 0910)
- Fujita Eisuke**  
(JSV47/W/31-B5 0930)
- Fujita Shigeru**  
(GA2.07/W/17-A2 0930-01)
- Fujiwara Hiroyuki**  
(ST3/W/24-B4 0930-07)
- Fujiwara Satoshi**  
(GA5.09/W/05-A2 1400-02)
- Fujiwara Tateki**  
(P09/W/04-A1 1440)  
(P09/W/12-A2 0910)  
(P09/W/13-A2 0930)  
(P09/W/14-A1 1520)
- Fujiwara Toshiya**  
(JSV30/W/10-B1 1400-08)  
(JSV36/C/U6/W/06-B3 1400-23)  
(MI04/E/22-B4 1150)
- Fukao S.**  
(GA2.02/W/09-B4 0900)  
(GA2.03/W/02-B3 1010)  
(MI06/W/02-B1 1400-18)  
(MI06/W/02-B2 1400-18)  
(GA2.02/L/06-B4 0940)  
(U7/E/07-B1 1045)
- Fukao Shoichiro**  
(JSA20/W/15-A5 0905)  
(JSA20/W/25-A4 0935)  
(JSM01/W/38-A2 1600-26)
- Fukao Yoshio**  
(JWA34/W/01-B2 0930)  
(ST5/W/54-B3 0900-10)  
(U7/W/13-B1 0830-15)
- Fukasawa Masao**  
(JSP25/W/64-B3 0830-01)
- Fukuda Yoich**  
(JSG14/W/13-A3 1700-06)
- Fukuda Yoichi**  
(G3/L/09 1610-23)  
(JSG14/W/20-A3 1700-11)  
(ST4/W/31-B1 0830-23)
- Fukui Yasuo**  
(JSM01/W/48-A4 1620-02)  
(JSM01/W/68-A4 1620-11)
- Fukuma K.**  
(GA1.05/W/04-A5 0950)  
(GA1.05/W/22-A6 1700)  
(GA1.05/W/32-A6 1645)
- Fukumoto Masaaki**  
(GA 2.02/E/12-B4 1640)
- Fukunishi H.**  
(GA3.02/W/43-B2 0920)
- Fukunishi Hiroshi**  
(GA3.04/W/47-B1 1230)  
(GA3.07/L/07-A6 0900-07)
- Fukuoka Kouichiro**  
(GA1.02/E/20-A1 1605)
- Fukusawa H.**  
(GA1.05/E/17-A6 1630)  
(GA1.05/W/01-A6 1515)  
(GA1.05/W/32-A6 1645)
- Fukushima Hajime**  
(MI09/E/04-A5 1145-03)  
(P15/L/21-B4 0925)
- Fukushima Naoshi**  
(GA5.09/P/01-A2 1230)  
(JSA09/P/01-A3 1145)
- Fukushima Yoshihiro**  
(HS2/W/21-B2 1120)
- Fukuta Norihiko**  
(MI10/W/14-B1 0900-05)
- Fulchignoni M.**  
(MC09/W/07-B2 01)
- Fulker Dave**  
(JSG28/W/01-B2 1400-16)
- Fuller M. P.**  
(HS3/W/27-A2 1450)
- Fuller Mike**  
(GA1.01/E/06-A5 1445  
(GA1.04/E/04-A6 1400)
- Fuller-Rowell T. J.**  
(JSA20/W/26-A5 1425)  
(JSA20/W/41-A5 1200)  
(GA3.06/W/18-A3 1450)  
(GA3.09/E/13-B4 0930)  
(GA3.09/W/03-B5 0950)
- Fulton John**  
(JSP39/W/14-B3 1050)
- Funakoshi Kenichi**  
(JSS02/E/14-A1 1740)  
(ST6/E/09-A2 1430)
- Funck Thomas**  
(JSS44/W/03-B4 1400)
- Funiello Francesca**  
(ST7/E/09-A2 605-05)  
(ST3/W/33-B4 1400-01)  
(ST4/E/48-B3 1420)
- Funiello Renato**  
(HS5/W/39-A3 1205)
- Funsten Herbert O.**  
(GA4.09/E/01-A6 1700)  
(GA3.05/E/15-B3 0900-39)
- Fuqing Peng**  
(G4/P/03-A3 1620-16)
- Furnari Mario Mango**  
(JSS46/E/03-B4 1420)
- Furue Ryo**  
(JSP49/W/16-B5 1210-06)
- Furukawa Kinji**  
(MI06/E/17-B1 1650)
- Furumura Takashi**  
(ST3/W/11-B4 0930-02)  
(ST5/W/14-B4 0930-02)
- Furuya M.**  
(G2/W/01-A2 1630-01)
- Furuya Masato**  
(G2/E/08-A2 1630-11)  
(G5/E/21-A4 1115-04)
- Fuselier S. A.**  
(GA3.04/W/20-B1 1100)
- Fusina Robert A.**  
(P10/W/16-A4 1420)
- Futaana Yoshifumi**  
(JWS33/W/37-B2 1430)
- G**
- Gabillet Celine**  
(JSP39/E/18-B4 0930)
- Gabriel Axel**  
(MI02/W/02-A4 1200)
- Gabriel G.**  
(JSA40/W/06-B5 1400-09)
- Gabrielov Andrei**  
(ST4/W/50-B2 1220)
- (ST1/W/43-A2 1440)
- Gacic Miroslav**  
(P11/W/22-B4 1620)
- Gaertner Miguel A**  
(MC01/E/27-A4 1645)  
(MC01/E/35-A4 1415)
- Gaetano De Luca**  
(JSV47/E/01-B5 1400-05)
- Gage Kenneth**  
(JSM26/W/34-B2 1510)
- Gage Kenneth S.**  
(MI04/W/26-B3 0830)
- Gaidash Sergey P.**  
(JWA34/E/01-B2 1740)
- Gaina Carmen**  
(ST4/W/04-B3 0830-02)
- Gainanov A. G.**  
(JSA37/W/01-B3 1745-01)
- Gaines Edward E.**  
(GA3.05/E/11-B3 1620)  
(GA3.05/W/44-B3 0900-44)  
(JSA45/E/16-B4 1510)
- Gaivornoskaya T. V.**  
(JSA15/E/31-A5 1400-15)
- Galal A. A**  
(GA4.01/E/07-A2 1730)
- Galanis Jordan**  
(G5/E/36-A4 1215)  
(JSS31/W/11-B2 1620)
- Galban Fernando**  
(JSS31/E/04-B2 1400)
- Galdeano A.**  
(JSS44/L/05-B-4 0930-04)
- Galiev**  
(JSP23/W/87-B1 1740)
- Gallii Ehud**  
(JSG11/W/06-A3 1720)
- Galitchanina Larisa**  
(GA 5.11/E/02-A3 1430-09)
- Galkin Yuri S.**  
(G5/P/02-A4 1130-02)
- Galkin Yuriy**  
(G1/C/G5/E/26-A3 1620-106)  
(G2/E/16-A2 1630-08)  
(G2/E/22-A2 1630-07)
- Gallagher D. L.**  
(GA3.09/W/15-B4 1450)
- Gallagher M W**  
(MI02/W/13-A5 1510)
- Gallagher P. D.**  
(GA3.04/L/02-B1 0920)
- Gallagher W**  
(MI02/W/01-A5 1450)
- Gallardo Clemente**  
(MC01/E/35-A4 1415)
- Gallart Francesc**  
(HS4/W/12-A4 1630)
- Galliev**  
(JSP23/W/88-B1 0830-05)  
(JSP23/W/89-B1 0830-10)
- Gallino Stefano**  
(JSM43/E/02-B4 1440)
- Gallipoli Maria Rosaria**  
(ST3/E/07-B4 1000)  
(ST3/E/22-B5 1515)
- Galloway David**  
(GA1.01/W/36-A5 0900-09)
- Gallus William A.**  
(MC04/W/16-B1 1620)
- Galluzzo D.**  
(JSV47/W/15-B5 1400-08)
- Galperin Yuri**  
(GA3.07/W/17-A5 0900-04)  
(GA3.02/W/14-B3 0830)
- Galvani Alessandro**  
(G5/W/20-A4 1230-03)
- Galvão Carlos Oliveira**  
(HS1/W/20-B5 1700)
- Galvin A. B.**  
(GA4.02/E/02-A4 1400-06)
- Galvin D A B**  
(GA4.02/W/28-A4 1720)
- Gamble John**  
(JSV30/E/05-B1 0940)
- Gamma A**  
(JSM01/W/37-A5 1400)
- Gandolfi Stefano**  
(G3/E/21-A5 1610-22)
- Ganguli Supriya B.**  
(GA2.07/L/01-A1 1400)
- Ganguly Jibamitra**  
(JSS44/E/39-B4 0930)
- Ganopolski Andrey**  
(MC01/W/38-A3 0930)  
(U2/L/01-A2 0930)
- Ganushkina N. Y.**  
(GA3.05/W/13-B3 0900-34)
- Gao Lianmei**  
(P10/L/06-A3 1500)  
(P11/E/06-B3 1010)
- Gao Xiao Qing**  
(GA1.01/E/12-A5 0900-08)
- Gao Xiaoqing**  
(GA6.01/E/19-A5 0900-09)  
(MC02/E/13-B1 1600-02)  
(ST4/E/21-B1 1400-04)  
(ST4/E/62-B1 1400-22)  
(SW1/E/04-B5 0845)  
(SW1/E/09-B5 0830)
- Gao Yuan**  
(ST1/W/06-A2 1400-17)
- Garashi Kiyoshi I.**  
(GA2.02/E/13-B4 1100)
- Garate J.**  
(JSS31/E/13-B3 0830-14)
- Garate Jorge**  
(G1/W/10-A3 1620-37)
- Garcia A.**  
(JSV47/W/29-B5 1400-22)
- Garcia Alberto A.**  
(MI04/E/23-B4 1005)
- Garcia Alicia**  
(JSV47/E/06-B5 1400-03)  
(JSV47/E/10-B5 1400-07)  
(JSP23/E/02-B1 1210)  
(JSP23/E/06-B2 1600)  
(JSP23/E/26-B2 1050)
- Garcia E.**  
(JSV36/E/11-B3 0900-15)
- Garcia M.**  
(ST3/E/56-B4 1400-20)  
(JSP23/C/U5/E/16-A5 1620)
- Garcia Marc A.**  
(P13/W/10-B1 1700)
- Garcia Norberto O.**  
(JSP23/E/46-B1 0830-07)  
(JSP23/W/37-A5 0830-07)
- Garcia Raphael**  
(JSA17/E/05-A4 1210)
- Garcia-Fernandez Mariano**  
(ST3/W/08-B4 0930-08)
- Garcon V.**  
(P08/W/04-A2 1010)
- Garduño-Monroy V. H.**  
(GA1.05/W/27-A5 0900-03)
- Garjel J.-C.**  
(ST1/E/87-A2 0930-12)
- Garmier Romain**  
(JSA10/W/12-A2 1615)
- Garner T. W.**  
(GA3.09/E/05-B4 1625)
- Garnero E. J.**  
(JSA17/E/01-A4 1150)  
(JSS02/W/01-A1 1425)
- Garratt J. R.**  
(MC01/E/37-A1 1700)  
(MW02/E/01-B3 1700)
- Garratt L D**  
(MC01/E/37-A1 1700)
- Garric G**  
(MI05/E/26-A1 1100)
- Garzman Boris**  
(HW4/E/24-B2 0900-02)
- Gartsman Boris**  
(HS1/W/76-B5 1725-02)
- Gary D. Egbert**  
(GA1.02/E/13-A1 0845)
- Gary James B.**  
(GA3.04/E/12-B2 1150)
- Gasiewski Al**  
(MI08/E/10-A3 1735)
- Gasparik Tibor**  
(JSS02/W/17-A1 0830-11)
- Gasparini Gian Pietro**  
(P11/W/12-B4 1640)
- Gasparini Paolo**  
(JSS46/E/03-B4 1420)  
(JSS46/E/05-B4 1440)  
(JSS46/W/02-B4 1500)  
(ST4/W/60-B3 0830-01)
- Gassó S**  
(MI09/W/14-A5 1030)  
(MI09/W/14-A5 1145-21)
- Gauld Jonathan K.**  
(GA2.01/W/06-A1 1135)
- Gaur V. K**  
(ST2/W/33-A5 1400-08)
- Gavarini Carlo**  
(JSP23/L/07-A6 1420)
- Gavilanes Juan Carlos**

## INDEX

- (JVS36/C/U6/W/08-B3 1400-21)
- Gavrilov Nikolai M**  
(JSM01/W/38-A2 1600-26)  
(JSA20/W/25-A4 0935)  
(JSM01/C/GA2.15/W/80-A3 1100)
- Gavriilyeva G A**  
(JSM01/W/108-A2 1600-25)
- Gawa T. O.**  
(GA2.02/W/09-B4 0900)  
(GA 2.02/E/12-B4 1640)  
(GA2.02/L/06-B4 0940)
- Gaya-Pique Lluis**  
(GA1.03/E/01-B3 1120)
- Gayet J P**  
(MI08/L/03-A3 1010)
- Gayet Jean-Francois**  
(MI01/E/03-A1 1700)
- Gbuyiro S.**  
(JSP25/L/03-B2 0930-04)
- Gedney Nicola**  
(MC01/E/36-A3 1605)
- Gee J.**  
(GA1.05/W/14-A5 1650)
- Gegout P.**  
(JSG14/E/13-A3 1700-07)  
(JSG14/L/08-A3 1145-16)
- Gegout Pascal**  
(JSG14/W/02-A3 1700-15)
- Gehbauer Fritz**  
(JSP23/C/U5/E/14-A5 1420)
- Geiger A.**  
(JSA37/W/04-B3 1200)  
(G6/W/06-B2 1400)
- Geiger Alain**  
(G1/W/12-A3 1620-38)
- Geiping Liu**  
(ST11/W/40-A4 0930-11)  
(ST11/W/64-A3 0900-03)
- Geiss J.**  
(GA6.01/W/19-A6 1210)  
(GA4.04/E/07-B5 0830)  
(GA4.04/W/03-B5 1050)
- Geladze George**  
(MC08/E/06-A3 0900-01)
- Gelaro Ron**  
(M105/E/25-A2 1100)
- Gelberg M. G.**  
(GA4.08/E/11-B3 0900-02)  
(GA4.08/E/20-B3 0900-01)
- Gelety Vladimir F.**  
(JSA16/W/33-A3 0830-28)
- Geller Marvin A**  
(MW04/W/09-A1 1650)  
(MW04/W/10-A1 1630)  
(JSM26/W/04-B2 1130)
- Gelo S.**  
(G1/W/02-A3 1620-32)
- Gemael Camil**  
(G1/E/45-A3 1620-74)
- Gende Mauricio**  
(G1/E/40-A3 1620-27)  
(GA2.03/E/10-B3 1700-08)
- Gendt Gerd**  
(JSG 28/E/11-B1 1120)
- Gengxu Wang**  
(HS5/W/46-A3 1545-02)
- Genikhovich Eugene L.**  
(HS2/W/03-B1 0940)
- Genna Antonin**  
(GA5.12/W/09-A2 1600-10)
- Gennai Naomi**  
(ST2/E/20-A3 0930)
- Gensane Olivier**  
(JSA15/W/23-A3 0930)
- Gente P.**  
(P16/E/03-B5 0930)
- Genthon C**  
(MC01/E/19-A2 1635)
- Genthon Christophe**  
(MC11/L/03-B3 1200)
- George S. E.**  
(JSP25/E/33-B3 1130)
- Georgiadis Teo**  
(JSM26/W/16-B2 1210)
- Georgieva Katya**  
(JSA16/C/GA4.07/W/32-A3 0830-60)
- Georgieva L. V.**  
(P11/E/12-B5 1640)
- Gerard; J.-C.**  
(GA4.10/W/32-A4 1635)
- Gerdas Ruediger**  
(JSM18/W/06-A4 1500)
- Gerding Michael**  
(JSM01/W/44-A3 1730)
- Gergely T.**  
(JWS33/E/09-B2 1115)
- Germann Peter F.**  
(HS3/W/22-A2 1135)
- Germany G.**  
(GA3.03/E/07-B4 1020)
- Gernandt H**  
(JSM01/W/37-A5 1400)
- Gernik Vladislav**  
(GA1.05/E/02-A5 1400)
- Gero Michel**  
(JSS31/E/07-B2 1210)
- Geronimo Nardo**  
(G4/E/09-A3 1620-03)
- Gerova Gergana**  
(MI05/W/12-A4 1400-12)
- Gerstbach Gottfried**  
(G3/C/G6/W/02/-A5 1610-51)  
(G3/W/41-A5 1610-80)
- Gerstenecker C.**  
(JVS36/W/06-B3 1400-02)  
(JVS36/W/10-B3 1400-03)  
(JVS36/W/24-B3 1400-05)
- Gert Kahle Hans-**  
(G6/W/06-B2 1400)
- Gerten Dieter**  
(HS3/W/25-A2 1400)
- Gertisser Ralf**  
(JVS36/W/08-B3 0900-14)
- Gessmann C. K**  
(JSS02/W/18-A1 1640)
- Gethin Roberts**  
(G1/E/56-A3 1620-80)
- Getko Ryszarda**  
(GA6.01/P/07-A5 0900-10)
- Gettelman Andrew**  
(JSM26/W/32-B1 1150)
- Gettings Mark**  
(GA5.11/W/08 A4 1430-08)
- Geuna Silvana**  
(GA1.04/L/05-A6 1500)
- Geyer J.**  
(HW4/E/30-B2 0900-10)
- Ghan S. J.**  
(JWM08/W/10-A2 1650)
- Ghandriche H.**  
(JSS44/E/07-B4 0930-16)
- Gharibi M.**  
(GA1.02/W/41-A1 0830)
- Gheitanchi M. R**  
(ST5/E/04-B4 1440)  
(ST5/E/03-B4 1400-01)  
(ST5/E/05-B4 1400-02)
- Gheitanchi Mohammad Reza**  
(JSS07/P/03-A2 1205)  
(JSP23/C/U5/E/19-A6 0830-04)  
(ST2/E/09-A4 1130)  
(ST2/E/17-A4 1000)  
(ST2/E/29-A4 1200)
- Gheitanchi R.**  
(ST3/E/25-B3 1130)
- Gheonjian L.**  
(GA6.01/E/04-A5 0900-07)
- Ghezali B**  
(G4/P/02-A3 1620-17)  
(G1/L/25-A3 1640-96)  
(G5/P/03-A4 1230-04)
- Ghil Michael**  
(P14/L/01-A4 1400-04)
- Ghosh S**  
(MI01/W/14-A1 1450)
- Ghosh Suchita**  
(MC09/L/01-B2 1000)
- Giacalone J.**  
(GA4.04/W/02-B5 1130)
- Gialanella Paola**  
(GA1.15/W/03-B4 1530-06)  
(GA1.15/W/07-B4 1530-05)
- Gialanella Paola Romana**  
(GA1.04/W/20-A6 1000)
- Giampiccolo E.**  
(ST2/W/07-A5 0900)
- Gianibelli Julio C**  
(GA5.06/W/06 A3 1640)  
(GA5.01/W/17 A1 1300-05)  
(JSA17/W/05-A4 1010)
- Gianibelli Julio Cesar**  
(GA6.02/W/06-B1 1715)
- Giannitsis Constantine**  
(MC02/E/17-B1 1400)
- Giardini D.**  
(JSA10/W/03-A2 0930)  
(JSP23/C/U5/E/16-A5 1620)  
(JSP23/E/03-A6 0930)  
(ST3/E/56-B4 1400-20)  
(ST5/L/02-B3 0900-02)
- (ST3/E/04-B4 1400-12)  
(ST4/E/48-B3 1420)
- Gibbons Steven John**  
(JSP39/W/13-B3 1400-01)
- Gibert D.**  
(JSS44/L/05-B-4 0930-04)
- Gibert Dominique**  
(JSS46/E/03-B4 1420)  
(JSA17/C/GA1.19/W/09-A4 0950)
- Gibson Gary**  
(JSP23/E/54-A5 1520)  
(ST2/E/23-A3 1600)  
(ST3/E/02-B3 1515)
- Gibson J. J.**  
(HW3/W/10-B4 1520)
- Gidaspow Dimitri**  
(VS2/E/02-B3 1110)
- Gidroingeo**  
(JSA19/L/07-A4 1400-10)
- Gidskehaug Arne**  
(G6/E/02-B2 1140)
- Giese B. S.**  
(JSM41/W/09-B4 1515)
- Giesecke**  
(JSP23/C/U5/E/16-A5 1620)
- Giesecke M.**  
(ST3/E/56-B4 1400-20)
- Gigola Silvia**  
(JSA16/C/GA4.07/W/34-A3 0830-55)
- Gil Antonio J.**  
(G3/W/25-A5 1610-81)  
(G5/W/19-A4 1230-02)
- Gilbert Dean**  
(MI01/W/04-A1 1640)
- Gilbert F.**  
(ST5/W/42-B5 1400)
- Gilberto Saccorotti**  
(JSAV7/E/01-B5 1400-05)
- Giles B. L.**  
(GA3.04/L/04-B1 1210)  
(GA3.08/W/09-A6 0920)  
(GA3.09/W/15-B4 1450)
- Gill J.**  
(JVS30/W/04-B1 1400-07)
- Gillam S.**  
(MC09/W/04-B2 1030)
- Gillan Mike**  
(JSS02/W/10-A1 0830-11)
- Gille J C**  
(JSM01/W/12-A2 1600-15)
- Gillen K. P.**  
(GA1.04/W/03-A4 0930-15)
- Gillet Philippe**  
(JSS02/W/16-A2 0930)  
(JSS13/W/18-A5 1420)  
(JSS02/W/06-A2 1215)
- Gilliland W. J.R.**  
(G3/W/49-A5 1610-78)
- Gil-Pacca Igor I.**  
(GA1.04/E/15-A4 1630)  
(GA1.04/E/16-A4 1650)
- Gimeno Yurima**  
(JVS36/W/12-B3 0900-08)
- Gin R B B**  
(MI03/W/08-A3 1400-01)
- Ginet G.**  
(GA3.05/W/27-B3 0900-37)
- Ginis Isaac**  
(MC05/W/01-B4 1150)
- Ginsari Victoria**  
(ST3/E/08-B4 1400-13)
- Ginzel G**  
(HS4/W/05-A4 1225)
- Giordani H.**  
(MI06/W/07-B1 1220)
- Giordani Hervé**  
(MI05/W/29-A3 1200)
- Giordanni H.**  
(MI04/L/10-B3 1520)
- Giordano G.**  
(VS3/E/02-B3 1550)
- Giorgetta M. A.**  
(MC06/W/02-A1 1715)
- Giovambattista R. D**  
(JWS33/E/05-B3 0900-03)  
(JWS33/E/03-B2 1635-06)  
(JWS33/E/03-B3 0900-06)  
(JWS33/E/05-B2 1635-03)
- Giovambattista R. Di**  
(ST11/W/38-A2 0930-02)
- Giovanelli Giorgio**  
(JSA09/W/12-A2 1630)
- Giovanelli Giorgio**  
(JSM26/W/16-B2 1210)
- Giovani L.**  
(JWS33/E/03-B2)  
(JWS33/E/03-B3 0900-06)
- Gitis V.**  
(JWS33/E/09-B2 1115)  
(SW1/E/06-B5 1215)
- Gitis V. G.**  
(SW1/W/04-B5 1200)
- Gitterman Yefim**  
(U8/E/04-B3 1640-09)  
(U8/W/15-B3 1640-10)
- Giunchi Carlo**  
(ST4/W/24-B1 0830-22)  
(ST4/W/60-B3 0830-01)
- Given D.**  
(ST5/W/L/04-B3 0900-13)
- Gizzi Fabrizio T.**  
(GA1.01/E/12-A5 0900-08)
- Gladman Graham**  
(JSP25/W/07-B4 1420)
- Gladstone G. R.**  
(GA4.10/W/21-A4 1620)  
(GA4.10/W/32-A4 1635)
- Gladstone Randall G.**  
(GA4.10/W/25-A5 1200)
- Gladychhev Vladimir**  
(GA3.04/E/11-B1 1520-21)
- Glangeaud Francois**  
(JSAV7/W/19-B5 1400-16)
- Glassmeier K.-H.**  
(GA3.04/L/05-B1 1400)
- Glassmeier K. H.**  
(JSA10/E/06-A2 0945)
- Glatzmaier Gary**  
(JSA17/E/02-A4 1710)  
(JSA10/W/09-A3 1115)
- Glazman Roman**  
(JSP39/W/25-B4 0910)
- Glazovsky Andrey**  
(JSH12/E/02-A5 1100)
- Glazunov A V**  
(MW06/W/07-A3 1100)
- Glebovsky V. Yu**  
(GA5.12/L/01 A2 1010)  
(JSS44/L/04-B4 1640)
- Glebovsky Vladimir**  
(GA5.11/W/06 A3 1200)
- Gleckler Peter**  
(MC01/L/01-A1 0930)  
(MC01/E/30-A1 0945)
- Glen Dick**  
(JSS44/L/07-B4 0930-44)
- Glen Jonathan M. G.**  
(GA1.03/W/04-B1 1140)  
(GA1.03/W/28-B2 1140)  
(GA1.01/W/15-A5 1500)
- Glennie C L**  
(G3/E/12-A5 1610-18)  
(G6/E/05-B2 1200)
- Gloeckler G.**  
(GA3.02/L/02-B3 0900-24)  
(GA4.04/E/07-B5 0830)  
(GA4.04/W/03-B5 1050)  
(GA4.04/W/04-B5 1650)  
(GA4.05/W/07-A1 1000)  
(GA6.01/W/19-A6 1210)
- Gloeckler George**  
(GA4.02/W/18-A4 1735)
- Gloeckler George**  
(GA4.04/E/06-B5 0920)
- Glonti Vladimir**  
(JSP49/E/06-B5 1210-10)  
(JSP49/E/10-B5 1210-11)
- Glover David**  
(JSM41/W/07-B4 1620-05)
- Glover Robin**  
(U3/L/01-A3 1500)
- Gnibidenko Z. N.**  
(GA1.15/W/10-B4 1745)
- Gobbi D**  
(JSM01/W/104-A2 1150)  
(JSM01/W/94-A3 1220)
- Godic Matjaz**  
(ST3/E/19-B4 1400-03)
- Godin S**  
(JSM01/W/37-A5 1400)
- Goedecke W.**  
(GA3.04/L/17-B2 1710)
- Goerres Barbara**  
(JSG11/E/07-A4 1400-04)
- Goetz Hans-Jorgen**  
(JSS44/W/08-B5 0850)  
(JWS33/W/08-B2 1635-26)  
(JWS33/W/08-B3 0900-26)  
(JWS33/W/23 -B2 1635-07)



- (JWS33/W/23-B3 0900-07)  
(JSS44/E/27-B5 0910)
- Gogorza Claudia S.G.**  
(GA1.05/W/26-A6 1200)  
(GA1.03/W/12-B2 1520)
- Gohda Noriaki**  
(U7/E/02-B1 0830-10)
- Gokarn S. G.**  
(GA1.02/E/06-A2 0930)
- Gokhberg Michail**  
(JSA15/E/44-A4 1220)  
(JSA15/E/49-A4 1000)  
(JSA15/E/39-A4 1140)
- Golaz Jean-Christophe**  
(MI04/W/12-B3 1630)
- Gold R. E.**  
(GA4.04/W/18-B5 1150)
- Goldberg Richard A.**  
(GA3.05/E/11-B3 1620)  
(GA3.05/W/44-B3 0900-44)  
(JSA45/E/16-B4 1510)
- Golenko Nikolay**  
(P11/E/09-B3 1620)
- Golinko Vladimir**  
(JSS42/E/13-B5 1700-06)
- Golitsyn G. S.**  
(JSP23/E/48-A5 0830-09)
- Golovkov Vadim**  
(GA5.08/W/11-B1 1400-04)
- Golovkov Vadim P.**  
(JSA37/W/02-B3 1445)  
(GA5.09/W/08-A2 1130)  
(GA5.09/W/01-A2 1400-04)  
(GA5.09/W/05-A2 1400-02)  
(GA1.01/W/33-A5 1630)
- Golovkov Vladimir**  
(GA1.07/W/07-B2 1220)
- Goltz J.**  
(ST5/W/L/04-B3 0900-13)
- Golubtsova Nina**  
(GA1.02/E/28-A1 1605)
- Goluchowska Beata**  
(GA1.05/E/10-A6 1115)
- Golynsky Alexander V.**  
(GA5.12/W/05-A2 1600-01)  
(JSA09/W/19-A2 0930-07)
- Golyshv Sergei**  
(GA1.02/L/04-A1 1605)
- Goma Willy S.**  
(MI06/E/12-B2 1400-09)
- Gombosi T. I.**  
(GA3.09/E/03-B4 1215)  
(GA4.08/W/03-B4 0930)  
(GA3.10/E/09-A6 1600)  
(GA4.10/E/07-A5 1525)  
(GA4.10/W/10-A4 1215)
- Gombosi Tamas**  
(GA4.10/W/19-A4 1710)
- Gombosil.**  
(GA4.01/E/01-A2 1220)
- Gomez A J**  
(MI02/W/07-A4 1600)
- Gómez Antonio Pérez**  
(JSA20/W/45-A4 1200-32)
- Gomez Francisca**  
(JSP23/E/02-B1 1210)  
(JSP23/E/26-B2 1050)
- Gonzales S.**  
(GA2.02/L/01-B4 1000)
- Goncharenko L P**  
(JSM01/W/64-A2 1600-22)  
(JSA20/W/17-A6 1031)
- Goncharenko Larisa**  
(JSA20/W/53-A6 1013)
- Goncharova Marina**  
(GA3.10/E/08-A6 1700-11)
- Gong S L**  
(MI01/L/04 1055)  
(MI01/W/03-A1 0900-03)
- Gong W**  
(MC01/E/23-A4 1035)
- Gonzalez A.**  
(U7/E/03-B1 0830-17)
- Gonzalez Alicia C. de**  
(JSA20/C/GA2.02/W/20-A5 1200-12)
- Gonzalez Carrie A.**  
(JWS33/W/09-B2 1635-08)  
(JWS33/W/09-B3 0900-08)  
(JWS33/W/30-B2 1515)
- Gonzalez F. I.**  
(JSS42/L/01 1700-21)  
(JSS42/W/05-B5 1700-11)  
(JSS42/W/07-B5 1500)  
(JSS42/W/25-B4 1140)  
(JSS42/W/26-B5 1440)
- Gonzalez Frank**  
(JSS42/W/10-B4 1640)
- Gonzalez S. A.**  
(GA3.09/W/19-B5 1100)  
(JSA20/W/48-A4 1200-31)
- Gonzalez W. D.**  
(JSA20/C/GA2.02/W/20-A5 1200-12)  
(GA4.08/W/02-B3 1400)  
(GA4.08/W/10-B3 1030)  
(GA4.08/W/06-B3 0905)
- Gonzalez-Esparza Americo**  
(GA4.03/W/10-B4 1200)
- Goodison Barry**  
(JSM41/W/21-B4 1735)
- Goodison Barry E.**  
(JSM41/W/12-B4 1720)
- Goodrich C. C.**  
(GA3.09/W/12-B4 1400)
- Gooldsby Donald**  
(HS3/W/14-A1 1640)
- Goosse H.**  
(P13/E/05-B1 1520)
- Goosse Hugues**  
(MC01/E/01-A5 1730)  
(P07/E/04-A3 1205)
- Goozovat Stephen**  
(JSA17/W/12-A4 0930)
- Gopalakrishnan S. G.**  
(JSM43/W/09-B5 1140)  
(JSM43/W/11-B4 1700)
- Gopalswamy N.**  
(GA4.01/W/17-A2 0900)
- Gorbatikov Andrei V.**  
(ST1/W/37-A4 0930-01)
- Gorbunov Vladimir**  
(G5/L/02-A4 1115-06)  
(ST5/E/08-B5 1520)
- Gorbuz Cemil**  
(G5/E/23-A4 1230-08)
- Gordeev E. I.**  
(ST1/W/14-A1 1150)
- Gordeev Evgenii**  
(ST2/W/13-A3 0845)  
(JSV47/W/04-B5 0900)  
(ST4/W/14-B2 1700)  
(ST4/W/15-B3 1500)
- Gordienko Vadim**  
(JSS44/E/36-B4 0930-34)
- Gordon Chris**  
(JSP25/E/12-B3 0830)
- Gordon David**  
(JSS31/W/03-B2 0930)
- Gordon H R**  
(MI09/L/03-A5 0830)
- Gorkan Onur**  
(G5/E/23-A4 1230-08)
- Gor'kavii Nikolay**  
(ST5/E/38-B4 1740)
- Gorman Michael**  
(JSH12/E/02-A5 1100)
- Gorodetskaya Irina**  
(MI12/E/01-B4 1610)
- Gorodisky J.**  
(JSA15/E/18-A5 1400-01)
- Gorodyski Yuriy**  
(JSA15/E/16-A5 1400-03)
- Gosar Andrej**  
(ST3/W/14-B4 0930-01)  
(ST3/W/32-B4 1400-02)
- Gosling J. T.**  
(GA4.01/W/05-A2 1450)  
(GA4.01/W/13-A2 1420)  
(GA4.02/W/20-A4 1400-18)  
(GA4.01/W/11-A2 1100)
- Gosling T.**  
(GA4.01/E/09-A2 1200)
- Gossler J.**  
(JSV47/W/03-B5 1400-12)
- Goswami B. N.**  
(JSP25/W/89-B2 1400)
- Goto Chiaki**  
(JSS42/E/20-B5 1700-20)
- Goto T.**  
(GA1.02/L/05-A2 0930)  
(JSA15/W/07-3 1740)
- Goto Tadanori**  
(JSA15/E/38-A4 1400-03)
- Gotoh Tadanori**  
(JSA15/E/27-A4 1400-04)
- Gouda Magdy A.**  
(GA5.12/P/01-A2 1600-09)  
(JSA27/W/01-B1 1000)
- Goula X.**  
(ST3/E/41-B5 1000)  
(ST5/E/34-B3 0830)
- Gourine B.**  
(G5/P/03-A4 1230-04)
- Govaerts Yves M.**  
(JSM41/W/28-B4 0930)
- Govier Anna**  
(HS5/W/16-A2 1100)
- Govoni A.**  
(ST3/W/18-B3 1500)
- Goyet Catherine**  
(JSM41/W/07-B4 1620-05)
- Goyette Stephane**  
(MW03/W/02-B4 1710)
- Gradinarsky L. P.**  
(JSG28/W/05-B1 1010)
- Gradinarsky Lubomir P.**  
(G1/E/16-A3 1620-24)
- Graf Hans-F**  
(MI01/W/07-A2 1510)  
(MI01/W/20-A2 1640)  
(JSM26/L/03-B2 1450)  
(JSP25/P/05-B5 1520)
- Grafarend E. W.**  
(G6/W/07-B1 1620)  
(G6/W/01-B1 1220)  
(G4/C/G5/W/04-A3 1620-28)  
(G2/W/04-A2 1630-04)  
(G4/C/G5/W/01-A3 1620-27)  
(G3/W/08-A5 1610-08)  
(G3/W/08-A5 1610-09)  
(G4/W/17-A3 1400)
- Grafodatsky Oleg S**  
(JSA06/W/16-A1 0915)
- Graham A.**  
(P10/E/12-A4 1050)
- Graham A. Ryan**  
(JSV47/W/16-B5 1000)
- Graham Gerhard**  
(SW1/W/06-B5 0930)
- Graham Phil**  
(MC01/W/17-A4 1125)
- Grainger R G**  
(JSM01/W/08-A4 1450)  
(JSM01/W/12-A2 1600-15)  
(MI09/W/02-A5 1145-07)
- Grainger Simon**  
(JSM26/W/10-B3 1010)
- Gramblichkova Danka**  
(HS4/W/24-A5 1200)
- Grammatica N.**  
(GA5.08/W/08-B1 1350)
- Grammatika Nafsika**  
(GA1.07/W/06-B2 1200)  
(JSA10/W/10-A2 1600)
- Grand Stephen**  
(JSS13/W/02-A4 1400)
- Grande M.**  
(GA3.05/W/05-B3 0900-46)  
(GA4.08/W/11-B3 1620)  
(GA4.08/W/13-B4 0905)  
(GA3.03/W/03-B4 0930)  
(GA3.05/W/13-B3 0900-34)  
(GA3.05/W/25-B3 0900-33)  
(GA3.05/W/26-B3 1600)  
(GA3.05/W/28-B3 0830)  
(GA4.08/W/18-B4 0830)
- Grandpre Jean De**  
(MW01/W/04-A5 1500)  
(MW05/W/04-A2 1200)
- Granger Ken**  
(JSP23/E/43-A5 0930)  
(MC05/E/06-B4 1230)
- Grant A. L. M.**  
(MI04/E/18-B3 1505)
- Grant Don**  
(G1/E/18-A3 1620-56)
- Grant Keith E**  
(MI01/W/17-A3 0950)
- Gras John**  
(MI01/W/19-A2 1720)
- Gratton Yves**  
(P09/E/01-A2 1145)  
(P11/E/16-B4 1420)
- Gravestock P.**  
(VS3/E/03-B3 0900-02)
- Gray**  
(JSM24/E/14-B1 1010)
- Gray D. M.**  
(HS2/W/11-B1 1420)
- Gray Lesley**  
(JSM01/E/13-A4 1620-08)  
(JWS33/W/35-B2 1635-33)  
(JWS33/W/35-B3 0900-33)  
(MI12/E/03-B4 1520)  
(MI12/W/04-B4 1440)  
(MI12/W/05-B4 1115)
- Gray Mike**  
(MI04/E/09-B1 1420)
- Gray Suzanne**  
(MI05/W/25-A3 1640)  
(P07/W/02-A3 1620)
- Gray Warren**  
(JWM08/W/04-A2 1020)  
(JWM08/W/12-A3 1440)  
(MI05/E/13-A2 1650)  
(MI05/E/21-A2 1420)  
(JSM41/W/11-B3 1430)  
(MI06/E/01-B1 1610)
- Greatbatch R. J**  
(JSP25/W/10-B4 1440)
- Grechko Evgeny**  
(MI02/W/08-A4 1510)
- Green Aidan**  
(JSM01/W/109-A4 1620-15)
- Green Arthur W.**  
(JWA34/E/03-B2 1720)  
(JWA34/E/04-B2 1700)  
(JWA34/E/05-B2 1130)  
(JWA34/E/07-B2 1420)
- Green C. M.**  
(GA 5.12/E/10 A2 1120)
- Green J.**  
(GA3.03/W/03-B4 0930)
- Green J. C.**  
(GA3.03/W/10-B4 1220)
- Green Pamela**  
(HW1/L/11-A4 1430)
- Green Tim**  
(U2/E/14-A2 1420)
- Greenfield J.**  
(P09/W/05-A1 1640)
- Greenspan M.**  
(GA3.05/W/43-B3 0900-41)
- Greenwald Raymond A.**  
(GA2.03/W/01-B3 0950)  
(GA3.07/W/58-A6 0900-18)  
(GA3.10/W/06-A6 1210)
- Greer Anthony**  
(JSA40/W/12-B5 0920)
- Greet P. A.**  
(JSM32/L/01-B3 1125)  
(JSM01/E/43-A2 1600-10)  
(JSA20/E/17-A6 1154)  
(JSA20/E/04-A6 1136)
- Greff-Lefftz Marianne**  
(JSA17/W/01-A4 1510)  
(JSG14/E/16-A3 1700-12)  
(JSS13/W/14-A5 1010)
- Gregg Michael**  
(P14/E/05-A4 1640)  
(P14/W/16-A4 1700)  
(P14/W/02-A4 1400-12)
- Gregg Watson W.**  
(P08/W/06-A2 0950)
- Gregori G.**  
(JSA15/E/60-A4 1400-13)
- Gregori Giovanni P**  
(GA6.01/E/19-A5 0900-09)  
(GA1.01/E/12-A5 0900-08)  
(GA6.01/L/03-A5 1730)  
(JSP23/E/16-B1 0830-04)  
(JSV22/E/14-A5 1050)  
(SW1/E/09-B5 0830)  
(GA6.02/E/04-B1 1610)  
(JSV29/E/04-B1 1400-03)  
(JSV36/E/25-B3 1710)  
(ST4/E/21-B1 1400-04)  
(ST4/E/39-B2 0930-26)  
(JSA45/E/17-B5 1110-01)
- Gregorova Dagmar**  
(GA1.04/L/02-A5 1600)
- Grekhov O. E.**  
(ST1/W/04-A2 1400-14)
- Grekhov O. M.**  
(JSA15/L/01-A5 0830-10)
- Gregory**  
(MI10/W/07-B3 1435)
- Gregory Andrew**  
(MI12/W/15-B4 1215)
- Gregory D.**  
(MC04/W/14-B2 1115)  
(MI04/W/01-B1 1505)
- Gregory Jonathan**  
(P13/E/09-B2 0950)
- Greiner-Mai H.**  
(JSA40/W/03-B5 1400-07)
- Grell Georg**  
(MC04/E/01-B2 1400)
- Grenfell J Lee**  
(MI02/W/09-A4 1220)
- Gresta S.**

## INDEX

- (ST2/W/07-A5 0900)  
**Grewé Volker**  
(MC08/E/05-A3 0900-02)  
(MI02/W/03-A5 1200)
- Grezio A.**  
(P13/E/14-B1 1500)
- Gribb Tye T**  
(ST16/C/JSS02/W/04-A2 1620)
- Grieger Norbert**  
(JSM01/E/01-A1 1720)
- Griesshaber Erika**  
(ST4/W/49-B1 1640)
- Griffin W. L.**  
(JSS44/E/20-B4 1720)  
(JSS44/W/21-B4 1700)
- Griffiths M**  
(MI05/E/06-A1 1630)
- Griffiths Morwenna**  
(MI05/L/05-A5 0920)
- Grigorenko Elena E.**  
(GA4.04/W/10-B5 0830-03)
- Grigorian A.G.**  
(JSA15/E/21-A5 1400-02)
- Grigoryuk A. P.**  
(JWS33/E/06 -B2 1635-12)  
(JWS33/E/06-B2 1230)  
(JWS33/E/06-B3 0900-12)
- Grimm Th.**  
(JSP49/E/09-B5 1400)
- Grimmond C S**  
(HS5/W/06-A1 1610)
- Grinko B. N.**  
(ST4/E/31-B1 0830-06)
- Griot Daphne-Anne**  
(JSS02/W/06-A2 1215)  
(JSS07/W/07-A2 1400)
- Gritsoun A.**  
(MI11/W/03-B5 1230)
- Grodent D.**  
(GA4.10/W/32-A4 1635)
- Groenendijk Piet**  
(HS3/W/29-A2 1615)
- Groetzner A.**  
(JSP25/W/19-B5 1720)
- Groisman Pavel Ya.**  
(HS2/W/03-B1 0940)  
(MC02/E/23-B1 1450)
- Gromova L. I.**  
(GA3.08/W/31-A6 1150)  
(GA3.09/W/13-B4 0900-12)
- Gromova Ludmilla**  
(GA4.03/W/07-B4 1725-02)
- Gronskaya Tatiana**  
(HS5/W/05-A1 1525)
- Grose W.**  
(JSM26/W/11-B1 0940)
- Grose William**  
(JSM01/L/30-A5 1640)
- Gross Richard**  
(JSG14/W/18-A3 1112-05)  
(JSG14/E/15-A3 1115-06)  
(JSG14/E/04-A3 1109-04)
- Gross S. J.**  
(ST1/W/26-A3 1210)
- Gross T**  
(JSH12/C/JSS31/E/05-A5 0930)
- Grossi P**  
(MI07/L/01-A2 1120)  
(MI07/L/02-A2 1620)
- Grossman Allen S.**  
(MC01/L/04-A1 1615)
- Grossman Klaus U**  
(MW05/W/09-A2 1020)
- Grote E**  
(JSS02/W/14-A1 1115)
- Groten Erwin**  
(G5/L/07-A4 1130-01)
- Groth C P T**  
(GA3.10/E/09-A6 1600)  
(GA4.01/E/01-A2 1220)  
(GA4.10/E/07-A5 1525)  
(GA4.10/W/10-A4 1215)  
(GA3.09/E/03-B4 1215)  
(GA4.08/W/03-B4 0930)
- Grove-Rasmussen J.**  
(JSG28/W/17-B2 1400-05)  
(JSG28/W/23-B2 1130)
- Groves Keith M**  
(JSA06/W/05-A2 0950)
- Gruber N**  
(MC01/W/36-A5 1700)
- Gruber Sabine**  
(MI01/E/12-A1 1005)
- Gruber Th.**  
(G3/W/39-A5 1100)
- Gruen Eberhard**  
(JSA10/W/16-A3 1130)
- Gruenthal Gottfried**  
(ST3/E/16-B4 1400-19)
- Grunthal G.**  
(ST3/E/56-B4 1400-20)
- Grunthal G.**  
(JSP23/C/U5/E/16-A5 1620)
- Grunwaldt H.**  
(GA4.04/E/05-B5 0940)
- Grushinsky Andrej N.**  
(JSA09/W/04-A2 0930-08)
- Gruzdev Alexandr M.**  
(MI06/E/13-B1 1100)
- Gruzinskaya B.**  
(GA3.04/L/01-B1 0830)
- Grzesiak M**  
(GA4.09/W/01-A6 1440)
- Gu So**  
(ST4/E/29-B1 0830-14)
- Gu Zhifang**  
(MI01/E/20-A2 1450)
- Gualtieri Lyn**  
(GA1.15/E/06-B4 1645)
- Guangding Liu**  
(JSS44/P/03-B5 0950)
- Guangqing Zhou**  
(JSP25/P/02-B1 0830-10)
- Guangyao**  
(P10/W/21-A5 1600-02)
- Gubar Yu. I.**  
(GA3.04/W/35-B1 1520-46)  
(GA3.05/W/18-B3 0900-17)
- Gubatenko Valeriy P.**  
(GA1.02/E/36-A1 1605)
- Gubbins David**  
(GA1.01/W/08-A5 1130)
- Gubby Robin**  
(JSA06/W/03-A1 0855)
- Gubler E.**  
(G1/E/46-A3 0930)
- Gudmundsson Agust**  
(GA1.15/E/03-B4 1430)  
(GA1.15/P/01-B4 1630)
- Gudmundsson Magnus T.**  
(JSV36/W/13-B3 1400-04)  
(JSA09/W/14-A2 1000)
- Gudmundsson O.**  
(JSS46/W/07-B4 1030)
- Gudmundsson Oli**  
(ST5/W/26-B5 0930-10)
- Gueguen Philippe**  
(JSP23/E/01-A6 1110)
- Guendel Federico**  
(ST2/W/18-A5 1015)  
(ST3/E/34-B4 1400-04)
- Guest P. S.**  
(JSM04/W/02-A2 0930)
- Guerin Roger**  
(HS4/W/10-A4 1530)
- Guglielmi A.**  
(JSA15/E/13-A4 1400-07)  
(GA3.04/L/01-B1 0830)  
(GA3.04/W/33-B1 1520-27)  
(GA3.04/W/12-B1 1520-24)  
(GA3.04/E/04-B1 1520-23)
- Guglielmi Anatoly**  
(GA3.07/E/01-A6 0900-08)
- Guichong Ouyang**  
(G4/E/02-A3 1620-11)
- Guiderson T. P.**  
(P07/W/10-A3 1510)
- Guillot Laurent**  
(JSS02/W/06-A2 1215)
- Guillou H.**  
(VS3/E/03-B3 0900-02)  
(VS3/E/07-B3 1450)
- Guillou Hervi**  
(GA1.15/E/06-B4 1645)
- Guinasso N**  
(JSG11/W/17-A4 1150)
- Guixi Yi**  
(SW1/W/09-B5 1100)
- Guiying Yang**  
(MC01/W/01-A2 1000)
- Guldberg A.**  
(MW02/W/07-B3 1500)
- Gulev S. K.**  
(JSP25/W/93-B3 0830-02)
- Gultepe I.**  
(MI04/W/07-B4 1400)  
(MI06/W/16-B2 1030)
- Gummow R**  
(JSA06/E/13-A11155-02)
- Gunasekera R. C.**  
(JSS46/W/04-B4 1130)
- Gunawan Dodo**  
(JSP25/W/15-B2 1010)
- Gundestrup C C**  
(JSH12/W/05-A5 0900)
- Gundogdu Oguz**  
(ST2/W/27-A4 1230)  
(JWS33/C/ST2/W/02-B2 1635-20)  
(JWS33/W/02-B3 0900-20)
- Gunn John T.**  
(P13/W/15-B2 1600-10)
- Gunter Andrea**  
(HW4/E/33-B2 0900-15)
- Güntner Andreas**  
(HS4/W/32-A5 1710)
- Guo**  
(JSP23/W/00-A6 1740)
- Guo Jian-Shan**  
(U7/W/12-B1 0830-02)
- Guo Mingzhu**  
(ST3/E/10-B3 1045)
- Guo Wanwu**  
(GA5.11/L/02-A3 1430-03)  
(GA5.11/L/03-A3)
- Guo Zitian**  
(JSM26/E/05-B2 1430)
- Guocai Zhu**  
(HS2/W/22-B2 1140)
- Guodong Cheng**  
(HS5/W/46-A3 1545-02)
- Guojie Meng**  
(SW1/W/04-B5 1200)
- Guojun Zhai**  
(G3/W/38-A5 1610-42)  
(G4/W/07-A3 1620-12)
- Guomin Zhang**  
(ST2/W/03-A3 1215)
- Guoze Zhao**  
(JSS44/E/41-B4 0930-10)
- Gupalo T A.**  
(ST6/P/03-A2 0830-03)
- Gupta H.**  
(JSP23/C/U5/E/16-A5 1620)  
(ST3/E/56-B4 1400-20)
- Gupta H. K.**  
(ST3/E/18-B4 1145)  
(ST1/E/67-A3 1010)
- Gupta Harsh K**  
(ST1/E/43)
- Gupta Hoshin**  
(HW4/W/01-B2 1200)
- Gupta M.**  
(U3/W/08-A30900-13)
- Gupta S K**  
(HS5/W/43-A3 1440)
- Gürer Aysan**  
(GA1.02/E/35-A2 0930)
- Gurfinkel Yuri**  
(JSA06/C/U4/E/02-A1 1155-26)
- Gurhathakurta. E. U. M.**  
(GA4.02/E/07-A4 1400-02)
- Gurk Marcus**  
(GA1.02/W/10-A2 0930)
- Gurman J. B.**  
(GA4.01/W/01-A2 1400-04)
- Gurnell Angela M.**  
(HS2/W/17-B2 0940)
- Gurnett D. A.**  
(GA4.09/W/15-A6 0900)  
(GA4.10/W/05-A5 1655)  
(GA4.10/W/08-A5 1020)  
(GA4.10/W/34 1620)
- Gurney**  
(MC01/L/21-A5 1200)
- Gurnis M**  
(JSS02/C/ST6/W/01-A1 1515)
- Gurnis Michael**  
(JSS13/W/05-A5 0900)  
(ST4/W/01-B3 1100)  
(ST4/W/04-B3 0830-02)
- Gurrola H.**  
(ST4/W/30-B2 1400)
- Gursoy Halil**  
(GA1.04/W/37-A4 0930-17)
- Gurtner W.**  
(G1/E/31-A3 1620-65)  
(G1/E/46-A3 0930)
- Gurtz Joachim**  
(HS4/W/29-A5 1450)
- Gurubaran S**  
(JSM01/E/10-A2 1600-12)  
(JSA20/W/10-A5 1200-02)
- Gurunadha Rao V V S**  
(HS5/W/43-A3 1440)  
(HS5/W/40-A3 1225)
- Guryanov V. V.**  
(JSA45/E/11-B5 1030)
- Gusel'nikov Vladimir I**  
(JSA06/W/16-A1 0915)
- Gusev Alexander**  
(G5/E/46-A4 1115-09)  
(ST4/L/02-B3 0830-05)  
(ST4/L/10-B3 0830-07)
- Gusev Oleg**  
(MC09/E/01-B2 1545)
- Gusev Yeugeny**  
(HW4/E/05-B2 1645)  
(HW4/E/20-B2 1700)  
(MC01/E/04-A3 1415)  
(MC01/E/10-A3 1150)
- Gusev Yeugeny M.**  
(U7/E/04-B1 0830-05)
- Guseva T. V**  
(JSA19/E/02-A41400-09)
- Gusiakov V. K.**  
(JSS42/W/02-B5 1110)  
(JSS42/W/22-B4 1520)  
(JWS33/W/06-B2 1045)
- Gusinsky**  
(JWA34/L/01-B2 1400)
- Gusman A. Jake**  
(HS5/W/27-A2 1635)
- Gussenhoven M S**  
(GA3.10/W/03-A6 0950)  
(GA3.05/W/27-B3 0900-37)
- Gustafsson Nils**  
(MC01/W/47-A4 1005)
- Gutdeutsch Rolf**  
(ST3/W/43-B5 0900)
- Gutdeutsch Rudolf**  
(ST3/P/02-B4 1015)
- Gutierrez R**  
(JSG11/W/17-A4 1150)
- Gutman Garik**  
(JSM41/E/07-B4 1705)  
(JSM41/E/18-B5 1135)  
(JSM41/E/30-B5 1400)
- Gutman Seth**  
(JSG28/E/13-B1 1400-05)  
(MC05/E/03-B4 1210)  
(MI06/E/11-B1 1400-02)  
(MI06/E/11-B2 1400-02)
- Gutowski Jr. William J**  
(MC01/W/08-A4 0950)
- Guya Naser H.**  
(GA5.12/E/09-A2 1600-11)
- Guyot Francois**  
(JSS02/W/16-A2 0930)
- Guymer T. H.**  
(JSM41/E/06-B3 1720)
- Gvelesiani Anzor**  
(GA4.09/E/03-A5 1600-07)  
(GA4.09/E/05-A5 1600-08)  
(JSA20/W/52-A4 1200-01)  
(MI09/E/10-A5 1145-06)  
(ST7/E/02-A2 1605-04)  
(JSA20/W/51-A4 1128)  
(GA3.08/E/05-B1 0900-09)  
(JSP49/E/06-B5 1210-10)  
(JSP49/E/10-B5 1210-11)
- Gvishiani A. D.**  
(ST3/E/39-B3 1200)  
(ST5/E/02-B3 1400)
- Gvran Marklund**  
(GA3.06/P/02-A2 1000)
- Gwanmesia Gabriel**  
(ST6/JSS02/W/19-A1 0830-18)
- Gwinner K.**  
(JSV36/W/17-B3 1500)
- Gyodakia Eduard**  
(ST1/E/52-A3 1640)
- Gyodakyan Naira**  
(ST1/E/52-A3 1640)
- Gzrlishvili Tengiz**  
(M103/E/03-A3 1040)  
(M110/E/07-B3 1505)

## h

- Ha Kim Kim**  
(GA4.10/L/01-A4 1145)
- Ha Kim Yong**  
(GA4.10/L/01-A4 1145)  
(GA4.10/W/29-A4 1520)  
(JSM01/W/110-A4 1620-03)
- Ha Kim Yu Yi**

- (GA4.10/W/29-A4 1520)
- Haag Maja**  
(GA1.03/W/06-B2 0940)
- Haak Hein**  
(ST1/W/58-A3 0850)
- Haak V.**  
(GA1.02/W/06-A2 0930)
- Haamer Joel**  
(P11/W/26-B5 1150-10)
- Haapala Jari**  
(P13/E/06-B2 1010)
- Haas Christian**  
(P13/W/26-B1 1010)
- Haas Dirk**  
(JSG11/E/06-A4 1400-03)
- Haas R.**  
(G5/W/13-A4 1115-01)
- Haas Ruediger**  
(G1/E/16-A3 1620-24)
- Haase J.**  
(G2/E/06-A2 1630-03)
- Haber Eldad**  
(GA1.02/W/30-A1 1415)
- Haberle R. M.**  
(MC09/W/07-B2 01)
- Hacker J. N.**  
(JSP39/L/02-B2 1010)
- Haddad Ziad**  
(MI06/W/03-B1 1400-16)  
(MI06/W/03-B2 1400-16)
- Haddadj Fawzia Asfirane**  
(GA5.12/W/09-A2 1600-10)
- Haddon R. A.W.**  
(ST1/E/06-A4 0930-39)  
(ST1/E/58-A2 1400-18)
- Hadi Samsul**  
(JSP23/E/27-B2 1700)
- Haerendel G.**  
(GA4.02/E/10-A4 1400-03)
- Hafner K.**  
(JWS33/E/08-B3 0900-10)  
(ST5/W/L/04-B3 0900-13)  
(JWS33/E/08-B2 1635-10)
- Hagan M E**  
(MW04/E/01-A1 1400)  
(JSA20/W/37-A5 1200-01)
- Hagan Maura**  
(JSM01/W/62-A2 1110)  
(MW04/W/11-A1 0925)
- Hagan Maura E.**  
(JSM01/W/31-A3 0900)
- Hagemann S**  
(MC01/W/35-A4 1630)
- Hagemann Stefan**  
(HW1/E/03-A4 1430)
- Hager Bradford H.**  
(G4/W/13-A3 1620-24)
- Hagfors T.**  
(GA2.01/W/07-A1 1055)  
(JSA20/W/08-A4 1200-27)
- Hahmann Andrea N**  
(MC01/W/32-A2 0930)
- Hahn D**  
(MC01/L/13-A3 1135)
- Haider S. A.**  
(GA4.10/P/03-A4 1200)  
(GA4.10/W/27-A4 1725)  
(MC09/P/02-B2 1045)
- Haidu Calin**  
(HW4/E/11-B2 1715)
- Haidu Ionel**  
(HW4/E/03-B2 0900-08)  
(HW4/E/11-B2 1715)  
(MC02/E/24-B1 1600-09)
- Haidvogel Dale**  
(JSP39/E/02-B4 1520)
- Haidvogel Dale B**  
(MC01/E/16-A2 1230)  
(MC01/E/24-A2 1155)
- Haigh J. D.**  
(MI06/W/31-B2 1210)
- Haigh Joanna D**  
(MC08/W/07-A3 1210)  
(MW01/W/10-A5 1150-06)  
(JSA16/W/03-A3 1430)
- Haine T. W. N.**  
(JSP25/W/75-B4 0930-02)
- Haines Bruce**  
(JSG28/E/14-B1 1400-21)  
(JSG28/L/01-B1 1400-03)
- Haines Keith**  
(P11/W/23-B4 0950)  
(P14/E/01-A4 1400-02)  
(P14/E/06-A4 1440)  
(JSP05/W/07-A2 0950)
- Haines Meredith**  
(JSP23/W/01-B2 1500)
- HaineThomas**  
(P07/W/02-A3 1620)
- Hairston Marc**  
(GA3.09/W/25-B5 0910)
- Haji Abu D. A.**  
(G5/L/01-A4 1145)
- Hajj G.**  
(GA3.09/W/19-B5 1100)
- Hajj George**  
(JSG28/W/12-B2 1030)
- Hakansson Bertil**  
(P11/E/26-B3 1600)
- Halberg F.**  
(GA6.01/E/04-A5 0900-07)
- Halberg Franz**  
(GA6.01/E/05-A5 0900-11)
- Haldoupis Christos**  
(GA2.02/W/03-B4 0930-02)  
(GA2.02/W/06-B4 1120)  
(GA2.02/W/10-B4 0920)  
(GA2.02/W/17-B4 0930-01)
- Hale Robert A.**  
(P10/W/20-A3 1700)
- Haley Pat**  
(P12/W/17-A1 1720)
- Hall C M**  
(JSM01/W/67-A1 1110)
- Hall Chris**  
(JSM01/W/62-A2 1110)  
(MW04/W/11-A1 0925)
- Hall Jeremy**  
(JSS44/W/03-B4 1400)
- Hall Joanne**  
(MC05/W/02-B4 1130)
- Hall Minard**  
(JSV47/W/05-B5 1400-15)
- Hall Minard L.**  
(JSP23/C/U5/E/05-A6 0830-06)
- Hall Tim**  
(MW01/W/06-A5 1400)
- Haller Larske**  
(JSS44/E/11-B4 0930-29)
- Halliday M.**  
(JSA37/W/04-B3 1200)
- Hallinan Tom**  
(GA 2.01/E/07-A1 0900)
- Halliwell George**  
(JSP25/W/47-B4 1400)
- Halpern David**  
(JSM41/E/29-B3 1735)
- Hamada Misuzu**  
(HW5/E/05-A3 1100)
- Hamaguchi H.**  
(JSS46/W/03-B4 1010)  
(JSV36/E/18-B3 1400-13)  
(JSV36/W/09-B3 1430)  
(JSV47/W/22-B5 1130)  
(JSV47/W/26-B5 1400-09)
- Hamano Yozo**  
(GA1.03/W/09-B3 1520)  
(U7/L/02-B1 1515)
- Hambach Ulrich**  
(GA1.03/W/14-B3 1440)  
(GA1.03/W/20-B3 1420)
- Hamed Khaled H.**  
(HS1/W/42-B4 1625-02)
- Hamid Zandifar**  
(st2/p/12-a4 1015)
- Hamid R. H**  
(GA4.01/E/07-A2 1730)
- Hamilton Kevin**  
(JSM26/W/12-B1 1000)  
(MC06/C/JSM01/W/43-A1 1625)
- Hamilton A. S.**  
(HW3/W/17-B4 0925)
- Hamilton D. C.**  
(GA4.04/W/04-B5 1650)
- Hamilton K**  
(JSM01/W/53-A3 1400)
- Hamilton Kevin**  
(MC06/W/03-A1 1145)  
(MW01/W/09-A5 0900)  
(MW04/W/06-A1 1425)  
(MW03/W/08-B4 1035)
- Hamilton Robert M.**  
(ST3/W/25-B5 0830)
- Hamill T**  
(MI05/L/04-A3 0900)
- Hamlin Timothy**  
(MI03/W/01-A3 1520)
- Hammerl Christa**  
(ST3/P/4-B5 1115)  
(ST3/P/6-B5 1230)
- (ST3/W/43-B5 0900)
- Hamoudi Mohamed**  
(GA5.12/E/02-A2 1600-08)
- Hamza Abdelhaq M.**  
(GA2.02/W/33-B4 1520)
- Hamza M.**  
(GA4.09/W/13-A6 1220)
- Hamza Valiya M.**  
(ST4/W/84-B1 0940)
- Han Dejiang**  
(MI10/W/08-B2 1220)
- Han Guoqi**  
(P10/W/22-A4 1130)
- Han In-Seong**  
(JSP49/W/08-B5 1010)
- Han Lijie**  
(ST4/W/04-B3 0830-02)
- Han Qingyuan**  
(MI06/W/19-B2 1230)
- Han Seh-Sub**  
(JSS42/P/01-B5 1210)
- Han Shaowei**  
(JSG11/W/23-A4 1210)  
(G1/L/22-A3 1640-95)  
(G1/L/23-A3 1010)  
(G1/W/07-A3 1620-04)  
(G6/C/G1/L/24-B1 1520)
- Han Shin-Can**  
(G6/C/G3/W/45-B2 1420)
- Han Uk**  
(G5/P/06-A4 1415-05)
- Han Xiujiao**  
(G6/C/G1/L/24-B1 1520)
- Han Yan-Ben**  
(GA 6.01/E/12-A5 0900-12)  
(GA 6.01/E/12-A5 0900-12)
- Han Yong**  
(MI08/E/10-A3 1735)
- Han Ziguang**  
(MI01/W/06-A2 1200)
- Hanada H**  
(G3/E/15-A5 1610-39)  
(G2/W/05-A2 1500)
- Hanado Hiroshi**  
(JSG28/W/07-B1 1400-07)
- Hanawa Kimio**  
(P12/C/JSP21/E/01-A1 0950)  
(P12/W/02-A1 0930)
- Hanchinal A. N.**  
(GA3.03/E/03-B4 1400-01)
- Handa S.**  
(JSA15/W/14-A4 1400-16)
- Handler R. A.**  
(P09/W/11-A1 1010)  
(P07/W/20-A3 0900-07)
- Handley Chris D**  
(HS5/W/33-A3 0940)
- Handoh Itsuki C.**  
(JSP25/L/02-B2 1700)
- Handorf Dörthe**  
(JSP25/W/33-B4 0930-03)  
(JSP25/W/38-B4 0930-04)  
(JSP25/W/68-B4 0930-01)
- Haney Robert L.**  
(P10/W/20-A3 1700)
- Hang Y. H.**  
(MI10/W/19-B3 1715)
- Hankin S.**  
(JSS42/W/26-B5 1440)
- Hanna Edward**  
(GA6.01/E/16-A6 1005)
- Hanna Pawlowska**  
(MI01/W/05 1740)
- Hannachi A.**  
(JSP25/E/34-B1 0830-05)
- Hannah David M.**  
(HS2/W/17-B2 0940)
- Hannelore**  
(GA6.01/P/06-A5 1700)
- Hans Muhlhaus**  
(ST4/W/62-B3 0830-04)
- Hans Nilsson**  
(GA2.02/W/01-B4 1500)
- Hansen G**  
(JSM01/W/37-A5 1400)
- Hansen G M**  
(MI09/W/07-A5 1145-10)
- Hansen J A**  
(JSP05/W/01-A1 0950)  
(MI11/W/07-B5 0915)
- Hansen K. C.**  
(GA4.10/E/07-A5 1525)
- Hansen M**  
(MC01/W/60-A2 0945)
- Hansen Roger**  
(JSS42/W/11-B5 1700-15)
- Hans-Gert Kahle**  
(JSS31/W/11-B2 1620)
- Hans-Joachim Linthe**  
(GA5.01/E/16 A1 1430)
- Hansmeier Arnold**  
(JSA16/W/12-A3 0830-52)
- Hanson William B**  
(GA3.10/W/10-A6 1700-03)  
(GA3.10/W/13-A6 1050)
- Hanssen Ramon**  
(JSG28/E/09-B1 1200)
- Hansson Ulf**  
(MC01/W/17-A4 1125)
- Hanus Vaclav**  
(ST2/E/33-A3 1130)  
(ST2/E/37-A5 1400-07)
- Hao Ping**  
(SW1/E/03-B5 1015)
- Hao Quang Truong**  
(GA1.02/E/26-A2 0930)
- Hao T Q**  
(GA5.01/E/25 A1 1530)
- Happgood Mike**  
(GA3.07/W/61-A4 0930-10)  
(JSA06/W/18-A1 1155-12)  
(JWS33/W/16-B2 1130)
- Happell James D.**  
(JSP21/W/01-A4 1640)
- Hara Hirohisa**  
(GA6.01/W/17-A6 0830)
- Hara Tatsuhiko**  
(ST5/E/17-B4 1400-04)
- Harabaglia P.**  
(JSS46/E/07-B4 0930-04)
- Harabaglac. P.**  
(G5/W/22-A4 1540-01)
- Harada Satoshi**  
(ST2/E/58-A5 1400-04)
- Haraguchi Satoru**  
(JSV30/C/JSV22/W/01-B1 1400-22)
- Haran Terry**  
(HW1/W/01-A4 1130)
- Harangi Szabolcs**  
(JSV30/W/13-B1 1400-05)
- Harangozo Steve**  
(JSM18/P/01-A4 1200)
- Harbi Assia**  
(ST2/E/04-A5 1400-25)
- Hardarson Björn S.**  
(GA1.15/P/01-B4 1630)  
(GA1.15/E/03-B4 1430)
- Hardebeck J.**  
(ST2/W/10-A5 0930)
- Harder Markus**  
(JSM04/E/03-A2 1510)  
(JSM04/W/11-A2 1735)  
(JSA09/E/07-A2 1645)  
(MC01/L/10-A2 1550)
- Hardi Peter**  
(GA4.05/L/04-A1 1615)
- Hardy Rolland L.**  
(JSA40/L/02-B5 1400-20)
- Hardy Thomas B.**  
(HW2/W/02-B1 0940)
- Harding Karen**  
(JSA06/W/17-A1 1155-14)
- Hare S**  
(MI05/E/15-A1 1610)
- Harford C.**  
(VS2/E/13-B3 1130)
- Harford Chloe L.**  
(JSV36/C/JSA15/W/34-B3 1415)
- Hargreaves John K.**  
(GA2.01/W/01-A1 1150)
- Harikrishnan M.**  
(P10/W/08-A3 0950)
- Harinarayana T.**  
(GA1.02/E/3A2 0930)
- Harlin Jeremiah**  
(MI03/W/01-A3 1520)
- Harms Sabine**  
(P13/P/01-B2 1130)
- Harnisch Guenter**  
(G3/E/42-A5 1520)  
(G3/E/42-A5 1520)
- Harnisch Martina**  
(G3/E/42-A5 1520)  
(G3/E/42-A5 1520)
- Haro Barbás Blas F. de**  
(JSA20/W/45-A4 1200-32)
- Harper David**  
(HW2/W/01-B1 0920)
- Harri A.-M.**  
(MC09/W/07-B2 0930-01)



# INDEX

- (JSA10/W/03-A2 0930)  
**Harri Ari-Matti**  
(MC09/E/04-B2 1015)  
**Harries J. E.**  
(MI04/C/MC07/W/21)  
(JSM26/E/10-B2 1000)  
**Harrington J Y**  
(MI08/W/15-A3 1430)  
**Harris Andrew**  
(JSP23/E/40-A5 1740)  
**Harris M. J.**  
(JSA20/W/04-A4 1200-02)  
**Harris N. R. P.**  
(JSM01/W/37-A5 1400)  
**Harris Robert N.**  
(MC02/E/19-B1 1130)  
**Harris Ruth A.**  
(ST1/W/68-A1 1420)  
**Harrison Dr. Richard A.**  
(GA4.02/W/22-A4 1400-20)  
**Harrison L**  
(MC07/W/17-A3 1115)  
**Harrison Richard**  
(GA4.01/W/12-A2 1400-02)  
**Harrop P.**  
(VS3/E/01-B3 0900-03)  
**Harry L. Bryden**  
(U2-E/11-A2 1100)  
**Harsh K Gupta**  
(ST1/E/43-A2 1400)  
**Harshiladze A. F.**  
(GA3.09/E/06-B4 1135)  
**Harsson B. G.**  
(G1/E/31-A3 1620-65)  
**Hart C. J. R.**  
(GA1.04/W/19-A4 0930-12)  
**Hart Robert**  
(MC05/E/04-B4 0930)  
**Hartinger H.**  
(G1/E/01-A3 1620-19)  
(G1/E/27-A3 1620-61)  
**Hartle R. E.**  
(GA4.10/W/30-A4 1450)  
**Hartmann Gernot**  
(JWS33/W/12-B2 1635-09)  
(JWS33/W/12-B3 0900-09)  
**Hartmann Joerg**  
(MI04/W/04-B1 0900-08)  
**Haruhisa Nakamichi**  
(JSV47/W/26-B5 1400-09)  
**Harvey Chris**  
(JWS33/W/16-B2 1130)  
**Harvey Danny J.**  
(JWS33/E/17-B2 1400)  
**Harvey Karen L.**  
(JSA16/C/GA4.07/W/31-A3 0830-61)  
**Harvey Mark**  
(JSM01/W/28-A1 1640)  
(JSM01/W/47-A1 1620)  
(JSM26/W/10-B3 1010)  
**Harwood R S**  
(JSM01/E/16-A5 0920)  
(MW01/W/03-A5 1150-03)  
**Hasager Charlotte B.**  
(JSM43/E/12-B4 1620)  
**Hase H.**  
(JSA15/W/14-A4 1400-16)  
**Hase Hideaki**  
(JSA15/E/41-A4 1400-14)  
**Hasebe Fumio**  
(MC06/C/JSM01/E/35-A1 1600)  
(MC06/W/04-A1 1400)  
(JSM26/W/34-B2 1510)  
**Hasegawa Akira**  
(JSS44/W/09-B4 0930-08)  
**Hasegawa Hiroshi**  
(G3/L/15-A5 1610-21)  
**Hasemi A.**  
(JSS44/W/01-B4 0930-06)  
**Hashi Kazumasa**  
(JSS42/W/08-B4 1400)  
**Hashimoto Kumiko**  
(GA3.05/W/40-B3 0900-42)  
**Hashimoto M.**  
(U7/L/03-B1 0830-07)  
**Hashimoto T.**  
(JSA15/W/14-A4 1400-16)  
**Hashimoto Takeshi**  
(JSA15/E/41-A4 1400-14)  
**Hashino Michio**  
(HS3/W/18-A2 0925)  
**Hasnain S. I.**  
(HW3/W/18-B4 0950)  
**Hasnain Syed I.**  
(HW5/W/13-A3 1140)  
**Hass C.**  
(P07/W/08-A3 1015)  
**Hassan Ahmed Ramadan**  
(P11/P/05-B5 1150-05)  
**Hassan Nasser**  
(JSA27/W/01-B1 1000)  
**Hassan Nasser M.**  
(JSA19/W/06-A4 0900)  
(ST2/W/15-A5 1400-28)  
**Hassancen Abddel-Rady**  
(JSA19/L/04-A4 1400-01)  
(JSA19/L/01-A4 0915)  
(JSA19/L/05-A4 1400-02)  
(JSA19/L/06-A4 1400-03)  
**Hassanzadeh Jamshid**  
(ST4/E/61-B1 1400-05)  
**Hasselmann K.**  
(MC02/W/01-B2 1100)  
**Hastings David A.**  
(G3/W/33-A5 1420)  
**Hasumi Hiroyasu**  
(MC01/W/41-A2 1400)  
**Hata M.**  
(JSA15/E/19-A3 1500)  
**Hata Masayasu**  
(JSA15/E/59-A4 1400-19)  
**Hatakeyama Tadahiro**  
(GA1.03/W/09-B3 1520)  
**Hatam-Chavari Y.**  
(G3/E/30-A5 1610-30)  
**Hatanaka Yuki**  
(JSG28/W/07-B1 1400-07)  
**Hatayama Takaki**  
(P12/W/08-A1 1600)  
**Hathaway David H.**  
(GA4.03/W/09-B4 1400)  
**Hattori Katsumi**  
(JSP23/C/U5/E/04-B1 1440)  
(ST1/W/37-A4 0930-01)  
**Hatzfeld D.**  
(ST4/E/66-B2 0930-06)  
(ST4/E/68-B2 1500)  
**Hau L. N.**  
(GA3.07/W/54-A4 0930-11)  
**Hauchecorne Alain**  
(MW07/W/04-A4 1130)  
(MW07/W/13-A4 1720)  
**Hauglustaine Didier**  
(MI02/E/02-A4 1120)  
**Haukssson E**  
(ST2/W/10-A5 0930)  
(ST5/W/L/04-B3 0900-13)  
**Hauser R.**  
(JWS33/W/33-B2 1635-32)  
(JWS33/W/33-B3 0900-32)  
**Hautot Sophie**  
(JSA19/W/08-A4 1130)  
**Havnes Ove**  
(JSA35/E/04-B1 1010)  
**Havskov Jens**  
(JSS42/E/18-B5 1010)  
(ST4/W/54-B1 1620)  
**Hay Lauren**  
(HW4/W/02-B2 1000)  
**Hayakawa H**  
(GA4.10/L/02-A4 1055)  
(GA4.10/W/34-A5 1620)  
**Hayakawa M**  
(JSA15/E/19-A3 1500)  
**Hayakawa Masashi**  
(JSP23/C/U5/E/04-B1 1440)  
(JSP23/W/32-B1 1130)  
(JSP23/W/33-B1 0830-02)  
(JSP23/W/34-B1 0830-15)  
(ST1/W/37-A4 0930-01)  
**Hayasaka Tadahiro**  
(MI01/E/09-A1 0900-02)  
**Hayashi K.**  
(GA5.06/W/04 A3 1440)  
**Hayashi Kanji**  
(GA3.04/E/04-B1 1520-23)  
(GA3.05/W/16-B3 0900-14)  
**Hayashi Shintaro**  
(JSV36/E/17-B3 1400-09)  
**Hayashi Taiichi**  
(JSM24/W/04-B1 0930)  
(JSM24/W/10-B1 1420)  
**Hayashida Akira**  
(GA1.05/W/01-A6 1515)  
(GA1.03/W/17-B2 1500)  
(GA1.03/E/09-B2 1100)  
(GA1.03/W/31-B2 1120)  
**Haygarth Phil**  
(HS3/W/01-A1 0900)  
**Haynes P.**  
(JSM26/W/20-B1 1520)  
**Haynes Peter**  
(JSM26/E/08-B1 1040)  
(JSM26/E/21-B3 1050)  
(MC06/E/02-A1 0940)  
**Hays Paul B.**  
(JSM01/E/23-A3 1200)  
**Hayward Nathan**  
(JSA19/L/02-A4 1015)  
**Haywood James M**  
(MI09/E/07-A5 1525)  
**Hazeleger Wilco**  
(JSP25/W/43-B3 1620)  
**Hazzard James**  
(ST1/W/51-A3 0930)  
(ST1/W/61-A1 1500)  
**He Changrong**  
(ST1/E/07-A2 1400-32)  
**He Ruiqing**  
(JSA19/W/09-A4 0930)  
**Head James W.**  
(U6/W/04-B2 1035)  
**Heal Kate**  
(HS5/W/03-A1 1445)  
**Healy John**  
(JSP23/W/03-B2 1520)  
**Healy Richard**  
(JSM41/W/07-B4 1620-05)  
**Healy S. B.**  
(MI06/E/08-B2 1630)  
**Hearnshaw Charlotte**  
(MI05/W/18-A2 1010)  
**Heathwaite A. L.**  
(HS3/W/08-A1 1225)  
**Heathwaite Louise**  
(HS3/W/01-A1 0900)  
**Heaton T.**  
(ST5/W/L/04-B3 0900-13)  
**Hebenstreit Gerald T.**  
(JSS42/W/15-B5 1230)  
**Heber B.**  
(GA4.04/W/16-B5 1730)  
**Heber Bernd**  
(GA4.01/E/09-A2 1200)  
**Hecai Niu**  
(JSV30/C/JSV22/P/02-B1 1400-23)  
**Hecht Matthew W**  
(MC01/E/12-A2 1215)  
**Heck Bernard**  
(G4/W/20-A3 1225)  
(JSA09/W/11-A2 0930-04)  
**Hedlin Michael A H**  
(JSS13/W/19-A4 1620)  
**Hedling G**  
(JSG11/W/05-A3 1440)  
**Hedling Gunnar**  
(G1/E/14-A3 1620-54)  
**Hedstrom D. M.**  
(JSM24/E/14-B1 1010)  
**Heelis R.**  
(GA2.02/L/01-B4 1000)  
**Heelis R. A.**  
(JSA20/W/21-A5 1519)  
(JSA20/W/28-A5 1200-10)  
(GA2.02/W/18-B5 1440)  
(GA2.02/W/34-B5 1420)  
**Hefti S.**  
(GA4.05/W/07-A1 1000)  
**Hefti Simon**  
(GA4.02/W/18-A4 1735)  
**Hegai V. V.**  
(JSA15/E/31-A5 1400-15)  
(JSA15/E/55-A5 1400-16)  
(U3/E/03-A3 0900-02)  
**Hegai Valeri**  
(JSA15/W/09-A5 1400-07)  
(JSA20/W/08-A4 1200-28)  
**Hegerl G. C.**  
(MC02/W/01-B2 1100)  
**Hegg D**  
(MI09/W/14-A5 1030)  
(MI09/W/14-A5 1145-21)  
**Hegymegi Laszlo**  
(GA5.01/W/16 A1 1145)  
**Heider F.**  
(GA1.05/E/19-A5 1200)  
**Heider Franz**  
(GA1.05/W/34-A6 1430)  
(GA1.03/E/09-B2 1100)  
(GA1.03/W/31-B2 1120)  
**Heifetz Eyal**  
(JSP39/W/32-B3 1130)  
**Heiken Grant**  
(U4/W/06-A4 1015)  
**Heikes B.**  
(JSM26/W/18-B2 1550)  
**Heikkinen Pekka**  
(JSS44/W/13-B4 1420)  
**Heil Petra**  
(P13/W/05-B1 1640)  
**Heilig Balazs**  
(GA5.01/W/16 A1 1145)  
**Heimann Martin**  
(MC01/W/39-A5 1215)  
(JSM24/E/01-B1 1145)  
**Heimpel Moritz**  
(JSP39/W/33-B3 1424-09)  
**Hein Gunter**  
(G3/E/01-A5 1610-26)  
**Hein Ralf**  
(MC08/E/05-A3 0900-02)  
(MI02/W/03-A5 1200)  
**Hein Ron Gunter**  
(G5/W/03-A4 1230-01)  
**Heinemann Guenther**  
(JSM 04/E/06-A2 1120)  
**Heinemann T H**  
(MI09/W/10-A5 1145-12)  
**Heinrich Roswitha**  
(ST3/W/48-B4 1400-10)  
**Heinson Graham**  
(GA1.02/L/AW1-A2 0930)  
**Heinz I. L. K. Karl**  
(G2/L/04-A2 1015)  
**Heinz Vos**  
(VS3/E/05-B3 0900-04)  
**Heitzler D.**  
(GA4.02/E/02-A4 1400-06)  
**Heitzler J R**  
(JSA06/E/02-A2 1110)  
**Hejda Pavel**  
(GA5.01/L/02 A1 0900-04)  
**Heki Kosuke**  
(G2/W/05-A2 1500)  
(JSG28/E/29-B1 1400-18)  
**Helaly Sobhy**  
(JSA19/W/04-A4 1400-05)  
**Helander Per**  
(GA3.02/W/37-B3 1150)  
**Helas G**  
(MI02/L/18-A5 1430)  
**Helbig Klaus**  
(JSS07/L/04-A2 0935)  
**Heldal Hilde Elise**  
(P07/L/03-A3 0900-08)  
**Helena Silvia**  
(G5/E/07-A4 1554-08)  
(G5/E/08-A4 1556-09)  
**Heleno da Silva S. I. N.**  
(VS3/E/01-B3 0900-03)  
**Heleno Sandra I N**  
(JSP23/E/23-B2 0830-09)  
(JSP23/E/27-B2 0830-14)  
(JSV36/E/26-B3 1400-10)  
**Helffrich G**  
(JSS13/E/04-A4 1700)  
**Helffrich George**  
(JSA09/W/15-A3 0830)  
(JSS13/E/02-A5 1610)  
(ST4/E/04-B3 1550)  
(ST4/E/15-B3 1000)  
(ST4/E/32-B3 1610)  
**Heller Friedrich**  
(GA1.15/W/07-B4 1530-05)  
(GA1.05/E/05-A6 1215)  
(GA1.05/W/33-A6 1730)  
(GA1.04/W/20-A6 1000)  
**Helliwell R C**  
(HS4/W/15-A4 1730)  
**Hellmer H. H.**  
(P13/W/08-B1 1620)  
**Hello Gwennelle**  
(MI05/W/22-A3 1000)  
**Hellweg Peggy**  
(JSP23/E/27-B2 0830-14)  
**Helmberger D V**  
(JSS02/C/ST6/W/01-A1 1515)  
**Helmberger Donald V.**  
(ST4/W/01-B3 1100)  
**Helmi Malova**  
(GA3.08/W/01-B1 0900-05)  
**Henry B.**  
(GA1.05/W/37-A5 1420)  
**Hendel Roland**  
(JSS13/E/06-A5 1400)  
**Henderson Gary**  
(JSA17/W/13-A4 1430)  
**Henderson M.**  
(GA3.05/W/25-B3 0900-33)  
(GA3.05/W/04-B3 0900-45)

- Henderson M. G.**  
(GA3.02/W/13-B2 1630)
- Henderson Roddy**  
(JWM08/W/01-A2 1630)  
(JWM08/W/04-A2 1020)
- Henderson-Sellers Ann**  
(MC01/E/09-A3 1550)  
(MC01/E/31-A3 1100)  
(MW02/L/01-B3 1220)
- Hendy Ingrid**  
(GA1.05/W/34-A6 1430)
- Henger Manfred**  
(U8/W/06-B3 1505)
- Henk A Dijkstra**  
(MW06/W/06-A3 1620)
- Hennen O**  
(JSM01/E/44-A4 1620-14)
- Henry B.**  
(GA1.04/L/04-A6 0900)  
(GA1.04/W/10-A6 0940)  
(GA1.04/W/13-A6 1100)  
(GA1.04/W/21-A4 1400)  
(GA1.04/W/22-A4 1420)  
(GA1.03/W/01-B1 1000)
- Henry Bernard**  
(GA1.04/W/31-A4 1220)
- Hense Andreas**  
(JSG14/L/05-A3 1142-15)
- Hense I.**  
(P08/W/07-A2 1400)
- Herd R.**  
(VS2/E/13-B3 1130)
- Heribert Kahmen**  
(G6/L/02-B2 1640)
- Herman Benjamin**  
(JSG28/E/27-B2 1400-04)  
(MI06/W/29-B1 1010)
- Herman Jay**  
(MI01/W/25-A2 1430)  
(MI08/E/08-A4 1750)  
(MI09/E/02-A5 0937)
- Herman M**  
(MI09/L/02-A5 0855)
- Hernandez**  
(JSM01/E/39-A1 0940)
- Hernandez E.**  
(GA5.01/E/04 A1 1400)
- Hernández Francisco J.**  
(JSV36/W/14-B3 0900-11)
- Hernández J**  
(G3/E/44-A5 1610-66)
- Hernandez Napoleon**  
(G1/W/12-A3 1620-38)  
(G1/W/26-A3 1620-42)
- Hernández Pedro A.**  
(JSP21/W/10-A5 1150)  
(JSV36/C/U6/W/01-B3 1400-20)  
(JSV36/W/01-B3 0900-12)  
(JSV36/W/04-B3 1115)  
(JSV36/W/12-B3 0900-08)  
(JSV36/W/14-B3 0900-11)  
(JSV36/W/16-B3 0900-10)  
(JSV36/W/20-B3 0900-09)  
(JSV36/W/26-B3 1215)
- Herne David**  
(HW5/W/16-A3 1600)
- Herraiz Miguel**  
(JSA20/E/07-A4 1200-30)
- Herranz P.**  
(GA5.12/E/04 A2 0930)
- Herrero Andre**  
(ST7/W/03-A2 1605-01)  
(JSS46/E/04-B4 1400)  
(JSS46/W/15-B4 0930-01)
- Herrero-Bervera E.**  
(GA1.15/E/04-B4 1515)  
(GA1.03/W/07-B1 1500)  
(GA1.03/W/13-B1 0920)  
(GA1.15/C/U6/W/05-B4 1530-07)
- Herrero-Bervera Emilio**  
(GA1.01/W/18-A5 1430)  
(GA1.04/W/39-A5 1620)
- Herring Lynn**  
(JSA16/W/11-A3 0830-25)
- Herring T. A.**  
(JSG14/L/09-A3 1000)
- Herring Thomas**  
(JSS31/E/04-B2 1400)
- Herring Thomas A.**  
(JSG28/E/26-B1 1400-11)
- Herring Tom**  
(U7/W/07-B1 0830-01)
- Herrmann Andreas**  
(HS4/W/12-A4 1630)
- Herrmann P**  
(MC01/L/07-A2 1430)
- Hertzog Albert**  
(MW07/W/04-A4 1130)  
(MW07/W/13-A4 1720)
- Hertzog D. C.**  
(GA5.01/W/12 A1 1300-04)  
(JWS33/W/25-B2 1415)
- Heslop David**  
(GA1.03/W/20-B3 1420)
- Hesse M.**  
(GA3.09/W/22-B4 0900-04)
- Hestnes Erik**  
(JSP23/C/U5/E/08-B1 1700)
- Hewson Tim D.**  
(MI05/W/32-A4 1400-04)
- Heynderickx D**  
(JSA06/E/07-A1 1620)
- Heyderickx D.**  
(GA3.09/E/12-B4 1600)
- Heyman Ofer**  
(MI10/E/05-B3 1745)
- Heynderickx D.**  
(GA3.05/E/02-B3 0850)
- Heywood K. J**  
(P07/W/17-A3 0955)
- Heywood Karen J.**  
(P12/W/11-A1 1130)  
(P07/W/03-A3 1640)
- Hibbard Kathy A**  
(MC01/L/22-A55 1505)
- Hickey Michael P.**  
(MC09/E/02-B2 1715)
- Hicks E.**  
(ST2/E/31-A5 1200)  
(ST2/E/43-A5 1400-31)
- Hicks E. C.**  
(ST2/E/11-A5 1215)  
(ST2/E/12-A5 1400-32)
- Hideaki Hase**  
(JSA15/E/02-A5 0830-05)
- Hideki Nagashima**  
(JSP49/W/24-B5 1210-16)
- Higareda R.**  
(JSP23/C/U5/W/14-B2 1210)
- Higashi Takahiro**  
(GA1.05/W/05-A5 1500)
- Higashikawa A**  
(JSM01/W/01-A3 1140)
- Higgins J**  
(MC07/W/11-A3 1015)
- Higgins Mark**  
(JSG28/E/16-B1 1400-14)
- Highwood Eleanor**  
(MI01/W/08-A2 1120)
- Higuchi Hiroyuki**  
(HS5/W/35-A3 1045)
- Higuchi Tomoyuki**  
(GA3.10/E/04-A6 1115)
- Higurashi Akiko**  
(MI09/E/06-A5 0920)  
(MI09/E/06-A5 1145-20)
- Higutsh Riko**  
(P15/L/21-B4 0925)
- Hiitola Pekka**  
(GA2.01/W/09-A1 1400)
- Hilaire Legros**  
(G5/W/15-A4 0930)
- Hilchenbach M.**  
(GA4.02/E/02-A4 1400-06)  
(GA4.04/E/05-B5 0940)  
(GA4.04/W/17-B5 0900)
- Hildebrand Steven**  
(JSS46/W/10-B4 1600)
- Hilgen F. J.**  
(GA1.15/W/08-B4 1445)  
(GA1.15/W/09-B4 1400)
- Hilgen Frits**  
(GA1.15/W/11-B4 1530-03)
- Hilger K. B.**  
(P15/W/07-B3 1650)  
(G2/W/03-A2 1630-18)
- Hilgers**  
(JSA06/L/06 0935)
- Hilgers Alain**  
(JSA06/W/18-A1 1155-12)
- Hill A. E.**  
(P10/E/06-A5 1050)  
(P10/W/06-A4 1640)
- Hill Brittain**  
(JSP23/W/27-B2 0830-08)  
(JSP23/W/08-A5 0830-03)  
(VS2/W/08-B3 1400-06)  
(VS2/W/15-B3 1400-10)
- Hill Chris**  
(G1/E/52-A3 1620-77)
- Hill D. C.**  
(MC02/W/13-B2 1430)
- Hill D. P.**  
(JSS46/W/12-B4 1210)
- Hill Edward**  
(P09/W/04-A1 1440)
- Hill M. E.**  
(GA4.04/W/04-B5 1650)
- Hill Mimii J.**  
(GA1.03/W/07-B1 1500)
- Hill Reginald J.**  
(G5/P/02-A4 1130-02)
- Hillgren Valerie**  
(JSS02/W/02-A1 1620)
- Hilmer Michael**  
(JSA09/E/07-A2 1645)  
(JSM04/W/11-A2 1735)
- Hilmi Karim**  
(JSG11/E/13-A4 1400-05)
- Hilton D R**  
(JSS13/E/03-A5 1500)
- Hinderer J.**  
(G2/E/06-A2 1630-03)
- Hinderer Jacques**  
(JSA09/W/16-A2 0930-01)  
(JSG14/E/18-A3 1700-14)  
(JSG14/W/02-A3 1700-15)
- Hindmarsh C A**  
(JSH12/W/11-A5 1700)
- Hindmarsh Richard**  
(JSH12/W/09-A4 1400-03)
- Hindmarsh Richard C A**  
(JSP05/W/14-A1 1420)
- Hines Keith M.**  
(JSM04/W/03-A2 1030)  
(MI08/W/04-A4 1050)
- Hino Ryota**  
(ST4/W/34-B1 1400)
- Hipkin Roger**  
(JSA37/E/03-B3 1215)
- Hiragara Kazuro**  
(G5/E/33-A4 1504-03)
- Hirahara Kazuro**  
(JSG28/E/02-B1 1400-20)  
(JSG28/E/03-B2 1400-15)
- Hirahara M.**  
(GA2.07/W/28-A1 0830)
- Hirano Satoshi**  
(JSS31/W/16-B2 1110)
- Hirasawa Naohiko**  
(MI08/E/01-A4 1015)  
(MI08/E/04-A4 0930)
- Hirata K.**  
(GA1.03/W/29-B1 0900)  
(U7/L/10-B1 0830-20)
- Hirata Naoshi**  
(JSS44/W/04-B4 0930-05)  
(JSS44/W/09-B4 0930-08)  
(JSS46/W/18-B4 0930-07)  
(ST5/W/32-B4 1400-05)
- Hirayama Ken-ichi**  
(HW3/W/16-B4 0900)
- Hirn Alfred**  
(U7/E/03-B1 0830-17)
- Hiroaki Misawa**  
(GA2.02/E/04-B4 0930-10)
- Hirooka T.**  
(MI12/W/10-B4 1650)  
(JSM01/W/20-A1 0900)
- Hirose Takashi**  
(HS4/W/03-A4 1045)
- Hiroshi Fukunishi**  
(JSM03/E/06-A1 1600)
- Hiroshi Niino**  
(JSP39/E/06-B3 1415-06)  
(JSP39/E/01-B3 1500-21)  
(MI04/E/03-B1 0900-07)
- Hiroshi Oya**  
(GA2.02/E/04-B4 0930-10)
- Hirota Isamu**  
(MI12/E/04-B5 1155)
- Hiroyuki Ozawa**  
(G5/L/06-A4 1400)
- Hirsch K. L.**  
(GA3.03/W/03-B4 0930)
- Hirschi Michael C.**  
(HSA3/W/05-A1 1110)
- Hirst Anthony C.**  
(JSP25/W/46-B5 0830)  
(MC03/W/04-B4 1110)
- Hirst Tony**  
(MC02/W/02-B2 1130)
- Hisarli M.**  
(GA1.04/W/27-A6 1140)
- Hisarli Mümtaz**  
(JSA40/W/04-B5 1400-08)
- Hisashi Kato**  
(JSM01/W/23-A4 1620-06)
- Hisayoshi Shimizu**  
(GA1.02/W/22-A2 0930)
- Hiscock Kevin**  
(HS5/W/37-A3 1125)
- Hitchman Adrian**  
(GA1.02/W/31 1000)
- Hitoshi Kawakatsu**  
(JSV47/W/11-B5 1115)
- Hittelman Allen M.**  
(JWS33/W/10 -B2 1635-11)  
(JWS33/W/10-B2 0945)  
(JWS33/W/10-B3 0900-11)  
(G3/W/20-A5 1610-24)  
(G3/W/33-A5 1420)  
(ST7/W/05-A2 1605-03)
- Hittelman Allen M.**  
(JSP23/W/30-A5 830-01)
- Hiyama Tetsuya**  
(HS2/W/21-B2 1120)
- Hjelt Sven-Erik**  
(JSA40/E/10-B5 1025)
- Hnilo J. J.**  
(MC02/W/01-B2 1100)
- Hnilo Justin J**  
(MC01/L/04-A1 1615)  
(MC01/W/31-A1 1400)
- Ho G. C.**  
(GA4.04/W/18-B5 1150)
- Hobbs B. E.**  
(JSS31/W/15-B3 0830-09)
- Hobe M. V.**  
(P15/L/17-B4 1550)
- Hobson Mike**  
(JSM43/E/10-B4 1640)
- Hochschild Gerd**  
(MI02/W/06-A5 1010)
- Hochstaedter A. G.**  
(JSV30/W/04-B1 1400-07)
- Hocke K.**  
(JSG28/W/10-B2 1400-06)
- Hocking W K**  
(JSM01/W/67-A1 1110)
- Hocking Wayne**  
(JSM01/W/62-A2 1110)  
(MW04/W/11-A1 0925)
- Hodges Alan**  
(JSP23/E/36-B2 0830-13)
- Hodges K**  
(MW02/E/03-B3 1010)
- Hodges Kevin I.**  
(MI05/W/19-A1 0910)
- Hodgkinson G.**  
(GA1.04/E/11-A4 1610)
- Hodgkinson R. A.**  
(HS3/W/06-A1 1135)
- Hodgson Katy**  
(JSP23/E/49-B2 0830-07)
- Hodson A. J.**  
(HS2/W/29-B2 1540)
- Hoeg Per**  
(JSG28/W/17-B2 1400-05)  
(JSG28/W/23-B2 1130)  
(JSG28/W/12-B2 1030)
- Hoeggerl Norbert**  
(G3/E/22-A5 1610-32)  
(G5/E/11-A4 1230-09)
- Hoehn Eduard**  
(HS4/W/23-A5 1140)
- Hoejerslev Niels K.**  
(P15/E/05-B4 1445)
- Hoeksema J. T.**  
(GA4.03/E/06-B4 1730-03)  
(GA4.02/W/13-A4 1005)
- Hoeksema Todd**  
(JSA16/W/25-A3 0830-46)
- Hoepfner Joachim**  
(MC11/P/02-B3 0950)
- Hoernle K. A**  
(JSV30/W/02-B1 1400-06)  
(JSV30/W/04-B1 1400-07)
- Hoff R.**  
(MI06/W/16-B2 1030)  
(MI01/L/04 1055)
- Hoff Ray**  
(MI01/W/04-A1 1640)
- Hoffmann G.**  
(MC11/P/02-B3 0950)
- Hoffmann Kenneth A.**  
(GA1.01/W/10-A5 1400)
- Hoffmann P**  
(MW04/W/01-A1 0950)
- Hoffmann Peter**

## INDEX

- (JSM01/C/MW07/W/09-A2 1600-34)  
(JSM01/E/04-A2 1130)
- Hoffmann Viktor**  
(GA1.05/W/41-A5 0900-09)  
(GA1.05/W/42-A6 1100)
- Hofmann-Wellenhof Bernhard**  
(G3/E/41-A5 1610-84)
- Hofstetter Rami**  
(U8/W/15-B3 1640-10)
- Hogan Robin**  
(MI06/W/23-B2 0930)
- Hogervorst W**  
(JSM01/W/55-A5 1510)
- Hognadottir Thordis**  
(JSV36/W/13-B3 1400-04)
- Hohmann R.**  
(P07/W/15-A3 1145)
- Hohmann Roland**  
(P07/W/18-A3 1720)
- Høgerslev N. K.**  
(G2/W/03-A2 1630-18)
- Holback**  
(JSA06/L/06 0935)
- Holben Brent**  
(MI09/W/03-A5 1145-17)
- Holhsneider Mathias**  
(ST1/W/35-A2 1400-21)
- Holland Katleen G**  
(JSS02/E/18-A1 1145)
- Hollandt Jörg**  
(JSA16/W/06-A3 0830-48)
- Hollerbach Rainer**  
(GA1.01/E/16-A5 0900)
- Hollingsworth A.**  
(MW03/L/01-B4 1020)
- Hollingsworth J. L**  
(GA4.10/L/05-A4 1040)  
(GA4.10/W/14-A4 0900)
- Holloway Peter E.**  
(JSP39/W/17-B4 1050)
- Hollweg Joseph V**  
(GA4.05/W/05-A1 1050)
- Holman Ian**  
(HS5/W/32-A3 0920)
- Holme J.**  
(ST3/E/13-B4 1400-15)
- Holmes Rob**  
(JSM41/E/28-B3 1515)
- Holmes Simon**  
(G3/W/43-A5 1610-52)
- Holmgren Karin**  
(MC03/E/09-B4 1010)  
(MC09/E/09-B2 1700)
- Holota Peter**  
(G6/C/G4/L/01-B1 1640)
- Holt B. J.**  
(JSA20/W/28-A5 1200-10)
- Holt Teddy**  
(JSP39/W/27-B3 0950)
- Holtet Jan A**  
(GA2.01/E/05-A1 0950)
- Holub Kirk**  
(MI06/E/11-B1 1400-02)  
(MI06/E/11-B2 1400-02)
- Holzbecher E**  
(HS4/W/05-A4 1225)
- Holzer Thomas E.**  
(GA4.05/L/02-A1 0830)
- Holzmann Hubert**  
(HW5/E/07-A3 1420)  
(HW4/E/08-B2 1400)
- Holzworth Robert H.**  
(JSA35/E/01-B1 1420)  
(GA2.01/W/08-A1 1640)
- Homar V**  
(MI07/W/02-A2 1210)  
(MI07/W/03-A2 1420)
- Honary F.**  
(GA2.01/E/11-A1 1205)  
(GA2.01/E/12-A1 1220)  
(GA2.01/W/06-A1 1135)  
(GA2.01/W/07-A1 1055)
- Honda Meiji**  
(JSM18/W/10-A5 1000)  
(JSP25/W/59-B3 0950)
- Hong H**  
(PW1/E/04-A6 0900)
- Hong Jing-Shan**  
(MI05/W/24-A4 1400-06)
- Hong M. H.**  
(GA3.02/E/18-B3 0850)
- Hong S Y**  
(MC01/W/60-A2 0945)
- Hong Song-You**  
(MI04/E/08-B1 1650)
- Hongli Zhang**  
(JAS15/P/02-A5 0830-08)
- Hongmei Wang**  
(JSA27/P/05-B1 0900)
- Hongre Lionel**  
(GA1.01/W/15-A5 1500)
- Hong-Shen Zhang**  
(JSM43/E/11-B5 0940)
- Honjo S.**  
(GA1.03/W/29-B1 0900)
- Honkura Y**  
(GA1.02/W/08-A2 0930)  
(GA1.01/W/05-A5 0900-10)  
(GA1.02/L/05-A2 0930)  
(JSA15/E/57-A4 1400-15)  
(JSA15/W/07-3 1740)
- Honkura Yoshimori**  
(JSA15/W/12-A5 0830-01)
- Honsho C.**  
(P16/E/03-B5 0930)
- Hood Lon**  
(JSA45/L/01-B4 1710)  
(MI12/W/11-B5 0945)  
(MW08/W/02-A2 1405)
- Hoogerboord J E**  
(G3/W/01-A5 1610-46)  
(G3/W/12-A5 1610-44)  
(G3/W/48-A5 1610-43)  
(JSM41/W/22-B5 1015)
- Hooper Dave**  
(JSM26/W/26-B2 1700-10)
- Hooten Jason**  
(VS2/W/09-B3 0950)
- Hopcraft K. I.**  
(P15/L/22-B3 1135)
- Hopcroft M.**  
(GA4.10/W/04-A4 1505)
- Hope Pandora**  
(JSM24/W/11-B2 0930)  
(JSM24/W/12-B2 0950)
- Hoppel K.**  
(JSM26/W/31-B2 1150)
- Hoppel Karl**  
(JSM01/W/04-A4 1510)
- Horacek Josef**  
(GA5.01/L/02 A1 0900-04)
- Horanyi M.**  
(JSA10/W/16-A3 1130)
- Horanyi Mihaly**  
(GA4.10/W/22-A4 1600)
- Horbury Tim**  
(GA4.09/E/06-A6 1500)  
(GA4.09/E/12-A6 1520)
- Horen H.**  
(P16/E/03-B5 0930)
- Hori T. M. Kameda**  
(JSS31/W/04-B3 0830-04)
- Horinouchi T.**  
(JSM26/W/30-B1 1110)
- Horinouchi Takeshi**  
(MW01/W/14-A5 1035)
- Horne Richard B.**  
(GA3.05/E/06-B3 1140)  
(GA3.05/E/09-B3 1200)  
(GA3.05/E/12-B3 0900-15)
- Hornig C S**  
(GA1.05/W/30-A6 0950)
- Hornig Gunnar**  
(GA4.02/W/23-A4 1400-21)
- Hornik H.**  
(G1/E/46-A3 0930)
- Hornsby David**  
(HS3/W/15-A1 1705)
- Horsburgh K. J.**  
(P10/W/06-A4 1640)
- Horwood G. R**  
(ST6/C/JSS02/W/15-A2 1640)
- Hörz Herbert**  
(GA6.01/P/09-A5 0900-13)
- Hoshiba Mitsuyuki**  
(ST3/W/11-B4 0930-02)
- Hoshino M.**  
(GA3.08/W/27-B1 1040)
- Hoskins B. J.**  
(MC10/P/03-B1 0930)
- Hoskins Brian**  
(JSP25/W/08-B2 1110)  
(JSP39/W/32-B3 1130)  
(MC10/E/01-B1 0950)  
(UL4-B4)  
(MI05/E/27-A2 1140)  
(MI05/W/19-A1 0910)  
(MI05/W/28-A1 1440)
- Hoskins Brian J.**  
(MC10/W/04-B1 1425)
- Hoskins Brian V**  
(MC01/W/51-A2 1045)
- Hoskins Prof. Brian J.**  
(JSP25/W/73-B2 1440)
- Hosney Hassan**  
(JSS44/E/29-B4 0930-18)
- Hosono Kohji**  
(ST1/E/89-A2 1720)
- Hossain Lail S.**  
(MC05/W/03-B4 1030)
- Hotin Sergey V.**  
(JWS 33/E/01-B2 1635-13)  
(JWS 33/E/01-B3 0900-13)
- Hou Junsheng**  
(JSA40/W/02-B5 1400-06)
- Hou Yu-Tai**  
(MC01/W/02-A1 1445)
- Houa Václav**  
(GA1.15/E/02-B4 1530-02)
- Houtze Hsu**  
(JSS44/W/06-B5 1130)
- Hove Teresa Van**  
(MC08/W/02-A4 1005)
- Hovenier J W**  
(JSM01/W/55-A5 1510)
- Hovde Susan**  
(MI10/W/01-B2 1035)  
(MI12/W/17-B5 1055)
- Hovestadt D.**  
(GA4.04/E/05-B5 0940)  
(GA4.02/W/28-A4 1720)  
(GA4.02/E/02-A4 1400-06)
- Howard R. A.**  
(GA4.02/W/33-A4 1400-26)  
(GA4.08/W/07-B3 0830)
- Howard Russell A.**  
(GA4.02A/W/25-A4 1400-23)
- Howard Tim A.**  
(GA3.04/W/01-B1 1520-41)
- Howarth John**  
(P10/E/05-A4 1600)  
(P10/E/20-A5 1600-04)  
(P10/E/21-A4 1620)
- Howe Bruce**  
(P16/E/06-B5 1500)  
(P16/E/11-B5 1440)
- Howells V. St.C.**  
(JSA20/W/32-A4 1025)
- Hoyer M.**  
(G3/E/44-A5 1610-66)
- Hoyer Melvin**  
(G1/W/12-A3 1620-38)  
(G1/W/26-A3 1620-42)
- Hoynig P.**  
(G2/W/08-A2 1630-22)  
(G6/C/G3/W/08-B2 1120)
- Hoyningen-Huene Wolfgang von**  
(MI09/E/08-A5 1645)
- Hoyos M.**  
(GA1.15/W/09-B4 1400)
- Hramushin Vasily**  
(JSS42/E/09-B5 1640)
- Hrouda Frantisek**  
(GA1.04/E/14-A5 1400)  
(GA1.04/L/02-A5 1600)
- Hsu Christina**  
(MI01/W/25-A2 1430)
- Hsieh K. C.**  
(GA4.04/W/17-B5 0900)
- Hsu H. T.**  
(JSA40/E/12-B5 1400-01)  
(JSP25/E/29-B1 0830-02)  
(G3/L/10-A5 1610-11)  
(G3/W/42-A5 1120)
- Hsu Houtze**  
(ST4/W/55-B2 1420)
- Hsu Hou-Tze**  
(JSA37/P/01-B3 1145)
- Hsu Hsiao-Ming**  
(JSM43/W/08-B4 1110)
- Hsu Kenneth J.**  
(JSV30/C/JSV22/E/11-B1 1400-17)
- Hsueh Y.**  
(JSP39/E/12-B4 1110)
- Hu Hui**  
(G5/E/42-A4 1544-03)
- Hu Jianguo**  
(JSG11/E/11-A4 0950)
- Hu Shengbiao**  
(ST4/W/46-B1 1000)
- Hu Y. D.**  
(GA3.05/W/07-B3 0900-12)
- Hu Yong-X**  
(MI08/L/04-A3 1750)
- Hu Yuxian**  
(ST3/E/50-B4 0930-19)
- Hu Z.-Z.**  
(JSP25/E/27-B2 0930)
- Hu Zeyong**  
(JSM24/W/04-B1 0930)
- Huaman Mercedes**  
(JSM32/E/03-B3 0930)
- Huang Baochun**  
(GA1.04/W/12-A5 1120)  
(GA1.04/W/28-A5 1140)
- Huang C Y**  
(GA3.10/W/03-A6 0950)
- Huang Jianliang**  
(G3/L/01-A5 1610-61)
- Huang Jingsong**  
(G1/W/01-A3 1620-02)
- Huang L.-Y.**  
(JSS44/W/14-B4 0930-12)
- Huang N. E.**  
(MC04/L/03-B1 1205)
- Huang Shaopeng**  
(MC02/W/12-B1 0900)  
(MC02/W/14-B1 0930)
- Huang Tai-Yin**  
(JSA20/W/55-A4 1200-09)
- Hubert Daniel**  
(GA3.07/E/14-A3 0900-05)
- Hubert Wayne**  
(HW3/W/07-B4 1205)
- Huck Thierry**  
(JSP25/E/35-B4 1150)  
(JSP25/W/03-B4 1520)
- Hudak D.**  
(MI06/W/20-B1 1400-07)  
(MI06/W/20-B2 1400-07)
- Hudak David R**  
(MI08/L/08-A4 1430)  
(JWM08/W/06-A3 1500)
- Huddleston D. E.**  
(GA4.10/W/05-A5 1655)  
(GA4.10/W/07-A5 1655)  
(GA4.10/W/08-A5 1020)
- Huddleston Mark P.**  
(GA1.07/W/05-B2 0920)
- Huddleston Matt**  
(MC01/E/14-A3.1000)
- Hudson H. S.**  
(GA4.01/W/01-A2 1400-04)
- Hudson James G**  
(MC07/W/07-A3 0915)
- Hudson M. K.**  
(GA3.05/W/14-B3 0900-40)  
(GA3.04/W/19-B1 1520-35)
- Hudson Mary**  
(GA3.05/W/15-B3 0900-27)
- Huerre Gael**  
(JSP39/E/24-B4 1700)
- Hues V.**  
(G2/W/03-A2 1630-18)
- Huess Viebeke**  
(P10/W/13-A4 1110)
- Huey-Chu Huang**  
(ST3/W/35-B3 0900)
- Huffman George**  
(JSM41/E/01-B3 1620)  
(MW02/E/06-B3 1720)
- Hug René**  
(G1/W/21-A3 1620-08)
- Huggenberger P.**  
(JSP23/E/03-A6 0930)
- Hughes Anwen J.**  
(HS5/W/34-A3 1000)
- Hughes C. W.**  
(P16/W/01-B5 1620)
- Hughes Chris W.**  
(JSG14/L/11-A3 1430)  
(JSM18/W/04-A4 1520)  
(GA3.10/W/23-A6 0935)
- Hughes Jeffrey**  
(GA3.04/W/47-B1 1230)
- Hughes T. J.**  
(GA4.08/W/12-B4 1635)
- Hughes W. J.**  
(GA3.04/E/15-B1 1520-02)  
(GA3.07/W/62-A5 0900-06)
- Hugo A.**  
(JSP23/C/U5/E/05-A6 0830-06)
- Hui Hu**  
(G3/E/32-A5 1610-53)  
(JSP23/C/U5/E/13-B1 0830-03)
- Hui Li**  
(G1/E/33-A3 1620-66)
- Huijun Yang**  
(JSP23/W/01-B2 1500)
- Hulburt E O**



- (MW07/W/19-A4 1420)  
(MW08/W/01-A2 1530)
- Hulla Jozef**  
(HS4/W/24-A5 1200)
- Hulot G.**  
(GA1.03/W/22-B3 0900)
- Hulot Gauthier**  
(GA5.08/W/02-B1 1005)  
(JSA37/W/08-B3 1430)  
(GA1.01/W/17-A5 1615)  
(JSA17/C/GA1.19/W/09-A4 0950)  
(JSA17/W/06-A4 1130)  
(JSA17/W/15-A4 1410)  
(JSG14/L/08-A3 0930)
- Hunegnaw Addisu**  
(G3/W/13-A5 1610-82)
- Hung-Chie Chiu**  
(ST3/W/35-B3 0900)
- Hunt B. G.**  
(MC03/E/03 1130)
- Hunt Doug**  
(JSG28/W/25-B2 1400-11)
- Hunt Dr. Bruce**  
(HW5/W/15-A3 1540)
- Hunt J. C. R.**  
(JSP39/E/16-B3 0830)
- Huppert Amit**  
(JSP25/E/23-B1 1440)
- Hurk B. V. D.**  
(U7/E/01-B1 1135)
- Hurley M D**  
(MC07/W/22-A2 1620)
- Hurrell Jim**  
(JSP25/W/71-B4 1050)
- Hursan Gabor**  
(GA1.02/E/21-A1 1445)  
(GA1.02/E/23-A1 1605)
- Hurst D F**  
(JSM01/W/56-A4 1620-07)
- Hurter S.**  
(ST4/W/65-B1 0900)
- Hus J.**  
(GA1.05/W/17-A6 1715)
- Husebye Eystein S.**  
(ST3/E/48-B5 1100)  
(ST5/E/39-B3 1125)  
(U8/E/06-B3 1215)
- Hussey Glenn**  
(GA2.02/W/17-B4 0930-01)
- Hutchison D.**  
(G1/C/G5/E/15-A3 1620-102)
- Huthance John**  
(P10/E/23-A3 0910)
- Hutt Charles R.**  
(U7/W/16-B1 0830-16)
- Hutton K.**  
(ST5/W/L/04-B3 0900-13)
- Huuskonen Asko**  
(GA2.01/W/09-A1 1400)
- Hwan Park Jung**  
(G5/P/06-A4 1415-05)
- Hwang Cheinway**  
(JSG11/E/09-A3 0930)  
(G3/E/43-A5 1610-17)
- Hyndman David W**  
(JSA19/W/09-A4 0930)
- Hyndman R. D.**  
(JSS44/E/31-B4 1130)
- Hyodo Masayuki**  
(GA1.03/W/10-B2 1420)  
(GA1.03/W/11-B2 1400)  
(GA1.15/W/02-B4 1700)
- Iacono Michael J**  
(MC08/W/04-A4 1130)  
(MC08/L/09-A3 1545)  
(MC01/W/33-A1 1515)  
(MC08/E/08-A3 1445)
- Iacono R.**  
(MW03/W/04-B4 1415)
- Iancu Viorica**  
(JSS44/E/18-B4 1500)
- Iannaccone Giovanni**  
(JSS46/E/05-B4 1440)
- Ibanez J.**  
(JSS46/W/09-B4 0930-05)  
(JSV47/W/01-B5 1045)
- Ibáñez J. M.**  
(JSV47/W/17-B5 1400-14)
- (JSV47/W/20-B5 1400-13)  
(JSV47/W/29-B5 1400-22)  
(JSV47/W/30-B5 1400-23)  
(ST5/W/55-B5 1225)  
(ST5/W/56-B3 0900-01)  
(ST5/W/66-B4 1400-06)
- Ibarrola G.**  
(JSP23/C/U5/W/14-B2 1210)
- Ibbitt Richard**  
(JWM08/W/01-A2 1630)  
(JWM08/W/04-A2 1020)
- Ibragimova Valentine I**  
(JWS33/W/21-B2 1605)  
(JWS33/W/21-B2 1620)
- Ibrahim E.**  
(ST2/E/07-A4 1700)
- Ibrahim E. M.**  
(ST2/E/49-A4 1730)
- Ibrayev Rashit A.**  
(P11/E/07-B3 0910)
- Ice George**  
(HS3/W/32-A2 1730)
- Ichikawa Masatake**  
(ST3/W/22-B4 0930-04)
- Ichikawa R.**  
(G2/E/01-A2 1630-12)  
(G2/W/01-A2 1630-01)
- Ichikawa Ryuichi**  
(G2/E/08-A2 1630-11)  
(G2/W/12-A2 1630-02)  
(JSG28/E/21-B2 1400-14)  
(JSG28/W/07-B1 1400-07)
- Ichikawa Tomomichi**  
(GA1.05/W/05-A5 1500)
- Ichiki M.**  
(GA1.02/L/05-A2 0930)  
(JSA15/W/07-3 1740)
- Ichinose Takumi**  
(JSA45/E/05-B5 1110-02)
- Ichiyagagi Kimpel**  
(MW02/E/07-B3 1440)
- Ida M.**  
(GA5.08/W/12-B1 1135)
- Ida Yoshiaki**  
(JSV47/W/27-B5 0915)  
(JSV47/W/31-B5 0930)
- Ide Satoshi**  
(ST5/W/32-B4 1400-05)  
(ST1/W/27-A2 1400-22)
- Ivenko I. B.**  
(GA3.05/E/05-B3 0900-29)
- Iga Shinichi**  
(MC09/E/05-B2 03)
- Igarashi George**  
(JSV36/W/14-B3 0900-11)  
(ST1/W/30-A2 0930-07)
- Igarashi K.**  
(GA 2.01/E/07-A1 0900)  
(JSA20/W/02-A4 1200-05)  
(JSM01/E/42-A2 1600-09)
- Igarashi Kiyoshi**  
(JSM01/E/34-A2 1600-14)
- Ignatyev Sergey**  
(P10/E/18-A5 1500)
- Ignatyev V. M.**  
(JSA20/W/31-A4 1200-19)  
(JSA20/W/43-A4 1200-23)
- Igumnov Valerie**  
(ST1/W/67-A1 1050)
- Ihde J.**  
(G1/E/31-A3 1620-65)  
(JSA09/L/02-A2 1230)
- Ihde Johannes**  
(G6/C/G3/E/23-B1 1200)
- Iida Masatora**  
(P12/W/08-A1 1600)
- Iidaka Takashi**  
(ST4/W/51-B2 1740)
- Iinuma Yoshiteru**  
(MI01/W/19-A2 1720)
- Iitaka Hiroshi**  
(JSA15/W/08-A4 1040)
- Iizuka S.**  
(JSA15/W/30-A4 0940)
- Iizuka Satoshi**  
(JSP25/P/07-B1 1620)
- Ijssel J. Van Den**  
(G6/C/G3/W/08-B2 1120)
- Ikedo M.**  
(JSP25/W/82-B5 1440)  
(JSP25/W/18-B4 0930-05)  
(JSP05/W/04-A1 0910)
- Ikedo Motoyoshi**  
(P08/E/02-A2 0930)  
(P13/W/24-B1 1130)
- Ikehara Ken**  
(P08/W/05-A2 1640)
- Ikehata Yoshito**  
(JSP39/W/48-B2 1110)
- Ikeya Motoji**  
(SW1/W/03-B5 1115)  
(JSA15/E/01-A4 1400-05)  
(JSA15/E/04-A3 1130)
- Ikoma Y.**  
(JSA15/W/14-A4 1400-16)
- Ilhan Sanli**  
(JSS31/L/05-B2 1600)
- Ilinski D. A.**  
(JSS44/W/15-B4 0930-19)
- Ilk Karl Heinz**  
(JSA37/E/05-B3 1130)  
(JSA37/E/04-B3 1015)
- Ilkiskis O. Metin**  
(GA1.02/E/35-A2 0930)
- Illes-Almar Erzebet**  
(GA2.02/E/11-B5 1600)
- Illingworth Anthony**  
(MI06/W/23-B2 0930)  
(MC04/E/02-B2 0950)
- Iluz D.**  
(P15/L/19-B3 1500)
- Ilyinykh Yuri S.**  
(JSP49/W/05-B5 1210-02)
- Imada Yukihito**  
(ST1/W/24-A3 1130)
- Imamura Fumihiko**  
(JSS42/E/21-B5 1420)  
(JSS42/P/01-B5 1210)  
(JSS42/W/08-B4 1400)
- Imanishi Kazutoshi**  
(ST1/W/50-A2 1400-23)
- Imanishi Yuichi**  
(G3/W/28-A5 1610-34)
- Imaoka Keiji**  
(JSM41/E/08-B4 1210)
- Imasaka Naoto**  
(JSA15/W/12-A5 0830-01)
- Imasato Norihisa**  
(JSP25/W/94-B3 1500)
- Imawaki Shiro**  
(JSP25/W/64-B3 0830-01)
- Immel T.**  
(JSA20/W/40-A6 0948)
- Imoto Masajiro**  
(ST3/W/27-B4 1530)
- Imparato Alberto**  
(ST5/W/34-B4 0930-01)
- In Teiji**  
(P12/W/08-A1 1600)
- Inall Mark E.**  
(JSP49/W/17-B5 1210-07)
- Inan Umran S**  
(JSM03/E/03-A1 1010)
- Ineichen D.**  
(G1/E/31-A3 1620-65)
- Ineichen Daniel**  
(G6/C/G1/E/32-B1 1400)
- Ineson S.**  
(JSP25/E/05-B1 1110)  
(JSP25/E/22-B1 0830-06)
- Ingham Malcom**  
(GA1.02/E/11-A2 0930)  
(GA1.02/E/31-A2 0930)
- Ingraham C.**  
(GA3.05/W/30-B3 1100)
- Ingram William**  
(JSA16/E/01-A3 0830-19)  
(MC07/E/02-A2 1400)
- Innis J. L.**  
(JSA20/E/04-A6 1136)  
(JSA20/E/17-A6 1154)
- Inniss L. V.**  
(P09/W/09-A2 1050)
- Inostroza M.**  
(JSP23/C/U5/W/14-B2 1210)
- Inouchi Kunimitsu**  
(HS4/W/25-A5 1220)
- Inoue J**  
(GA1.02/W/08-A2 0930)
- Inoue Takahiro**  
(MW03/W/03-B4 1230)
- Inoue Toru**  
(JSS02/E/14-A1 1740)
- Inoue Toshiro**  
(JSM41/L/04-B3 1445)
- Intrieri J**  
(MI08/L/09-A4 1615)
- Intrieri J M**  
(MI08/L/05-A3 1705)  
(MI08/W/16-A4 1600)
- Ioane Dumitru**  
(JSS44/E/18-B4 1500)  
(JSS44/P/07-B4 0930-20)
- Iodis Viktor**  
(G1/E/09-A3 1620-22)
- Ionica Florin**  
(JSA27/W/03-B11400-01)
- Ionov Dmitriy V.**  
(MI06/E/13-B1 1100)  
(MI06/E/13-B1 1100)
- Iorio Daniela Di**  
(P14/W/16-A4 1700)
- Iorio Daniela**  
(HS5/W/39-A3 1205)
- Iorio M.**  
(GA1.03/E/06-B2 0900)  
(GA1.15/E/05-B4 1530-01)
- Ioseliani Z.**  
(JSA20/W/52-A4 1200-01)
- Ioseliani Zurab**  
(GA4.09/E/03-A5 1600-07)
- Ioshpa Boris**  
(GA4.01/W/19-A2 1400-03)
- Ipavich F. M.**  
(GA4.04/E/05-B5 0940)
- Irifune Tetsuo**  
(JSS02/E/14-A1 1740)
- Irikura Kojiro**  
(ST3/W/01-B3 1645)  
(ST3/W/06-B4 0930-05)  
(ST3/W/16-B4 0930-06)  
(ST3/W/50-B3 1700)
- Irons Sarah L.**  
(MI04/E/20-B1 0900-09)
- Irwin P.**  
(MC09/W/10-B2 1515)
- Isaac G. A.**  
(MI04/W/07-B4 1400)  
(MI06/W/16-B2 1030)
- Isaac G. R.**  
(GA6.01/E/20-A5 1030)
- Isaev N V**  
(GA3.10/E/10-A6 1700-02)  
(JSA15/L/02-A5 1400-06)
- Isaev S V**  
(JSM03/L/03-A1 1400)  
(GA2.03/L/01-B3 1400)  
(GA2.03/L/02-B3 1520)  
(GA2.03/W/03-B3 1400-01)  
(GA3.04/W/28-B1 1520-22)
- Isaia Roberto**  
(VS2/E/08-B3 1010)
- Isakov Vlad**  
(P10/L/01-A4 0930)
- Isenberg Phillip**  
(GA4.04/E/06-B5 0920)
- Isezaki Nobuhiro**  
(GA5.12/W/01 A5 0950)
- Ishibashi H.**  
(GA5.06/W/04 A3 1440)
- Ishida Mitsuo**  
(JSV36/C/U6/W/06-B3 1400-23)  
(JSV36/C/U6/W/11-B3 1400-17)  
(ST5/E/15-B3 0900-04)  
(ST5/E/21-B3 0950)
- Ishido Tsuneo**  
(JSA15/W/05-A3 0910)
- Ishido Tuneo**  
(JSV36/E/28-B3 0900-03)  
(JSHV36/W/02-B3 0930)
- Ishihara Hiroya**  
(JSS42/W/01-B5 1620)
- Ishihara Takemi**  
(G3/L/15-A5 1610-21)  
(GA5.12/W/01 A5 0950)
- Ishihara Yasushi**  
(ST3/E/38-B4 0930-12)
- Ishii M.**  
(GA2.02/W/09-B4 0900)
- Ishii Mamoru**  
(JSA20/E/18-A6 1118)
- Ishii Teruaki**  
(JSV30/C/JSV22/W/01-B1 1400-22)
- Ishikawa Hirohiko**  
(JSM24/W/04-B1 0930)
- Ishikawa Hiroyuki**  
(ST3/W/22-B4 0930-04)
- Ishikawa N.**  
(GA1.05/W/22-A6 1700)
- Ishikawa Y.**  
(JSA15/E/57-A4 1400-15)
- Ishikawa Yoichi**  
(JSP05/E/02-A1 0850)  
(P12/W/08-A1 1600)
- Ishizaka Joji**

## INDEX

(JSM41/E/13-B4 1400)  
**Ishizaki Hiroshi**  
(MC01/E/26-A2 1500)  
**Ishmuratov R A**  
(MW04/W/01-A1 0950)  
**Isichko Eugene**  
(ST3/E/40-B5 0845)  
(ST3/E/45-B4 1745)  
**Iskandarani Mohamed**  
(MC01/E/16-A2 1230)  
**Ismagilov Yury**  
(GA3.04/E/05-B1 1520-18)  
**Ismail-Zadeh Alik**  
(ST4/E/53-B1 0830-05)  
(ST2/E/41-A4 1445)  
**Isoda F.**  
(GA2.02/W/09-B4 0900)  
**Israelevich Peter**  
(GA3.09/W/18-B5 0855)  
**Isseven T.**  
(GA1.04/W/27-A6 1140)  
**Istratov V. A.**  
(JSA27/E/05-B1 1400-08)  
**Istvan Laszlo**  
(MC01/W/62-A1 1430)  
**Italiano F.**  
(ST1/E/17-A3 1050)  
(JSS44/E/21-B4 1540)  
(JSV36/E/03-B3 0900-19)  
**Itano Toshihisa**  
(MC05/E/07-B4 0950)  
**Itikarai**  
(JSS46/W/07-B4 1030)  
**Ito Ester Regina Kazuko**  
(MC10/E/04-B1 1715)  
**Ito Kiyoshi**  
(ST1/W/66-A3 0900-16)  
(ST2/E/22-A5 1400-06)  
(ST2/E/30-A5 1400-05)  
**Ito Shin-ichi**  
(JSP25/W/25-B3 0830-06)  
**Ito Shinobu**  
(ST4/W/34-B1 1400)  
**Ito Tetsuya**  
(JSP23/W/33-B1 0830-02)  
**Itota Chizu**  
(GA1.03/W/02-B3 0920)  
**Iucci G**  
(JSA06/L/07-A1 1155-22)  
(JSA06/L/08-A1 1155-23)  
**Iucci N.**  
(GA4.04/L/01-B5 0830-06)  
(GA4.04/L/05-B5 0830-10)  
(GA4.04/L/06-B5 1400-01)  
(GA4.04/L/07-B5 1400-02)  
(GA4.04/L/02-B5 0830-07)  
**Iudicone Daniele**  
(P11/L/03-B5 0910)  
**Ivan Moroz**  
(GA1.02/E/15-A1 1605)  
**Ivankina T.I.**  
(ST6/W/05-A1 0830-07)  
**Ivanov E. V.**  
(GA4.02/W/31-A4 1400-25)  
(GA4.01/E/06-A21400-05)  
(GA4.03/W/04-B4 1215)  
**Ivanov K. G.**  
(GA3.09/E/06-B4 1135)  
(GA4.08/E/02-B3 0900-09)  
(GA4.01/E/05-A2 0950)  
**Ivanov Kirill**  
(GA5.11/W/02 A3 1430-06)  
**Ivanov Leonid**  
(P11/E/01-B5 1440)  
(P11/E/08-B5 1500)  
(P11/E/23-B5 1420)  
(P11/W/07-B4 1520)  
**Ivanov S. I.**  
(MC09/E/06-B2 1730)  
**Ivanov V. V.**  
(P13/E/03-B2 1600-03)  
(MI05/E/11-A4 1400-14)  
**Ivanov Vitaliy**  
(P11/E/18-B5 1520)  
**Ivanov Yu. A.**  
(P12/W/06-A1 1030-10)  
(P12/E/01-A1 1030-04)  
**Ivanova Dorothea**  
(JSP25/W/55-B2 0950)  
**Ivanova E.V.**  
(MI05/E/11-A4 1400-14)  
**Ivanova Pavlina K.**  
(JSA20/E/02-A6 1212)  
**Ivanova Tatyana A.**  
(GA3.05/W/20-B3 0900-16)

**Ivchenko M**  
(GA4.09/L/01-A51600-06)  
**Ivchenko V O**  
(JSM18/E/07-A4 1440)  
**Ivchenko Vladimir**  
(JSA09/W/02-A2 1745)  
(P13/W/18-B2 1600-06)  
**Ivetskaya Tatyana**  
(JSS42/E/04-B5 1700-17)  
(JSS42/E/09-B5 1640)  
**Ivers David**  
(GA1.01/L/01-A5 0900-12)  
(GA1.01/W/35-A5 1200)  
(GA1.01/W/36-A5 0900-09)  
**Iversen Trond**  
(MI01/W/09-A1 1025)  
(MI01/W/11-A2 1100)  
**Ivey Greg**  
(JSP39/W/47-B4 1430)  
**Ivey Gregory N.**  
(P14/W/01-A4 1400-03)  
**Ivins Erik**  
(JSH12/W/14-A5 1630)  
**Iwabuchi Hironobu**  
(MI01/E/09-A1 0900-02)  
**Iwabuchi Tetsuya**  
(JSG14/W/04-A3 1200-21)  
(JSG28/E/29-B1 1400-18)  
(JSG28/W/08-B1 1030)  
(JSG28/W/11-B1 1400-08)  
**Iwasa Koji**  
(ST1/E/44-A1 1720)  
**Iwasaka Yasunobu**  
(JSM01/W/68-A4 1620-11)  
**Iwasaki S. I.**  
(JSS42/E/06-B4 1440)  
**Iwasaki Shin'ichi**  
(JSS42/E/17-B5 1030)  
(JSS42/E/17-B5 1700-22)  
**Iwasaki Takaya**  
(JSS44/W/01-B4 0930-06)  
(JSS44/W/07-B4 0930-07)  
(JSS44/W/09-B4 0930-08)  
(MW03/E/09-B4 1130)  
**Iwasaki Toshiki**  
(JSM01/W/23-A4 1620-06)  
(MI01/E/17-A1 1720)  
**Iwase Ryoichi**  
(JWA34/W/11-B2 1110)  
(P16/E/13-B5 0950)  
(U7/L/10-B1 0830-20)  
**Iwata T.**  
(G2/W/05-A2 1500)  
**Iwata Tomotaka**  
(ST3/W/01-B3 1645)  
(ST3/W/06-B4 0930-05)  
(ST3/W/16-B4 0930-06)  
(ST3/W/24-B4 0930-07)  
**Iwi A.**  
(JSM26/W/28-B3 1110)  
**Iyemori Toshihiko**  
(GA2.07/W/30-A1 1530 )  
(JWS33/W/37-B2 1430)  
**Iyengar R. V.**  
(GA1.02/W/20-A2 0930)  
**Iz H. B.**  
(JSG28/W/02-B1 1400-09)  
**Izmiran Ruzhin Yu. Ya**  
(JSA15/E/25-A5 1400-08)  
**Izumi Takuya**  
(JSP25/W/40-B2 0930-07)

## J

**Jackman Charles H.**  
(GA3.05/E/11-B3 1620)  
(JSA45/E/12-B4 0915)  
(JSA45/E/16-B4 1510)  
**Jackson A.**  
(JSA37/E/08-B3 1500)  
(GA1.01/E/11-A5 0900-16)  
**Jackson Andrew**  
(GA5.09/E/01 A2 1150)  
(GA5.09/W/07 A2 1400-01)  
**Jackson Charles**  
(MC11/W/03-B3 0930)  
**Jackson D. R.**  
(JSM26/E/14-B1 1540)  
(MW01/E/02-A5 1150-05)  
**Jackson Darren**  
(MC01/L/03-A1 1415)

**Jackson David**  
(ST4/W/50-B2 1220)  
**Jackson David D.**  
(G6/C/G1/W/36-B1 1500)  
(JSS31/W/10-B2 1030)  
(ST3/W/19-B4 1630)  
(ST1/W/63-A2 1520)  
**Jackson Ian**  
(ST6/C/JSS02/W/15-A2 1640)  
(ST6/W/04-A1 0830-06)  
**Jackson R.**  
(JSS31/L/02-B2 1520)  
**Jackson Thomas**  
(HW4/E/25-B2 0900-03)  
**Jackson Thomas J.**  
(JSM41/W/19-B5 0900)  
**Jacob D.**  
(JSM26/W/18-B2 1550)  
(MI02/W/09-A4 1220)  
**Jacob Daniela**  
(MC01/W/28-A4 1140)  
(MC01/W/47-A4 1005)  
**Jacob Jossy P.**  
(JSP49/W/19-B5 1210-08)  
**Jacobi C H**  
(JSM01/W/69-A1 1130)  
(JSM01/W/72-A2 1600-02)  
**Jacobi Ch**  
(MW04/W/01-A1 0950)  
(JSA20/W/02-A4 1200-05)  
**Jacobi Christoph**  
(JSA20/E/14-A4 1110)  
(JSM01/E/04-A2 1130)  
(MW06/W/03-A3 1520)  
(JSA45/W/10-B5 0900)  
**Jacobi H-W.**  
(JSM04/E/04-A2 1240)  
**Jacobowitz Herbert**  
(JSM41/E/04-B3 1150)  
**Jacobs F.**  
(JSV36/W/25-B3 0900-04)  
**Jacobson A**  
(MI03/W/09-A3 1640)  
**Jacobson A R**  
(MI03/W/05-A3 1140)  
**Jacobson Abram**  
(MI05/W/33-A5 1130)  
**Jacobson Mark Z**  
(MI01/E/08-A2 1020)  
**Jaeger Anne**  
(HW4/E/32-B2 0900-13)  
**Jaeger Jill.**  
(U2/E/16-A21640)  
**Jaegle L.**  
(JSM26/W/18-B2 1550)  
**Jaenicke Ruprecht**  
(MI01/E/12-A1 1005)  
**Jafari Mohammad Ashtari**  
(ST2/E/06-A5 1400-14)  
**Jagovkina Svetlana**  
(JSP21/W/14-A5 1210)  
**Jahr Thomas**  
(G5/W/08-A4 1415-03)  
(ST4/W/67-B1 1700)  
**Jain Atul K**  
(MC07/W/22-A2 1620)  
**Jain Rajmal**  
(GA5.06/W/02 A4 1620)  
(JSA16/W/10-A3 0830-39)  
(JSA16/W/14-A3 0830-38)  
**Jakacki Jaromir**  
(P11/W/02-B3 1700)  
**Jakeman E.**  
(P15/L/22-B3 1135)  
**Jakob Christian**  
(MI04/W/24-B1 1400)  
(MI06/W/23-B2 0930)  
(MI10/W/11-B3 1615)  
(MW02/W/05-B3 0930)  
**Jakobsdottir S.**  
(ST4/W/03-B3 1630)  
**Jakobsdottir Steinunn S.**  
(ST5/W/21-B3 0910)  
**Jakowski N.**  
(JSG28/W/10-B2 1400-06)  
**Jakowski Norbert**  
(G1/W/27-A3 1620-11)  
**James D.**  
(ST4/E/05-B1 1520)  
**James I N**  
(MI05/E/26-A1 1100)  
(MI05/E/15-A1 1610)  
**James Ian N**  
(MW07/W/06-A4 1230)  
**James M. E.**

(GA3.05/E/10-B3 0900-43)  
(GA4.08/E/08-B3 0900-12)  
**James R**  
(JSH12/W/14-A5 1630)  
**James Ron**  
(GA1.01/W/36-A5 0900-09)  
**Jamin Cao**  
(ST4/P/10-B1 0830-08)  
**Jan Sileny**  
(ST1/E/05-A2 1400-30)  
**Jandiere Vachtang**  
(GA4.09/P/01-A5 1600-01)  
**Jandieri George**  
(JSP49/E/06-B5 1210-10)  
(JSP49/E/10-B5 1210-11)  
**Janhunnen Pekka**  
(GA3.06/E/04-A2 0930-04)  
(GA3.03/E/06-B4 1130)  
(GA3.09/E/08-B4 1150)  
**Janjic Z**  
(MC01/L/18-A4 1715)  
(U3/W/14-A3 0900-15)  
**Janoo L.**  
(GA4.02/W/24-A4 1400-22)  
**Jan-Peter**  
(JSM24/E/01-B1 1145)  
**Jansen L**  
(JSA06/E/09-A1 1155-01)  
**Jansma Pamela**  
(JSS31/E/06-B2 1500)  
**Janssen Frank**  
(P11/W/18-B3 1440)  
**Janssen Volker**  
(G1/W/07-A3 1620-04)  
**Jarisch Michael**  
(MW04/E/02-A1 1010)  
**Javaherian Abdolrahim**  
(U8/E/05-B3 1640-11)  
**Jarvis G T**  
(JSS13/C/ST2/W/25-A4 1740)  
**Jarvis Martin**  
(JSA20/E/22-A4 1200-07)  
**Jault Dominique**  
(GA1.01/W/28-A5 0900-06)  
(JSA17/C/GA1.19/W/11-A4 1450)  
**Jault J.**  
(GA1.01/W/30-A5 1215)  
**Jaumann R.**  
(JSA10/W/03-A2 0930)  
**Javadi Farhad**  
(ST1/E/36-A40930-24)  
**Javaherian Abdolrahim**  
(ST1/E/36-A40930-24)  
(ST1/E/40-A4 0930-07)  
**Javakhishvili Zurab**  
(ST1/E/10-A4 0930-20)  
(ST1/E/12-A4 0930-22)  
(ST1/E/18-A4.0930-05)  
**Javakhishvili Zurab**  
(ST3/E/52-B3 1445)  
**Javanmard Sohaila**  
(MI04/W/25-B1 0900-03)  
(MI10/W/14-B1 0900-05)  
(MI10/W/22-B1 0900-04)  
**Javelle Pierre**  
(HW4/E/27-B2 0900-05)  
**Jaworski L.**  
(G1/W/02-A3 1620-32)  
**Jaya Rao Y.**  
(MI04/P/01-B3 1220)  
**Jayappa K S.**  
(PW1/P/03-A6 1120)  
(P09/P/02-A1 1150)  
(JSG11/W/17-A4 1150)  
(ST6/W/10-A2 1500)  
**Jayawardena A. W.**  
(HS1/W/74-B4 1600)  
**Jdanova Liudmila**  
(G3/E/19-A5 1610-25)  
(GA 5.11/E/02 A3 1430-09)  
(GA5.12/E/06-A2 1600-03)  
**Jean-Louis Brenguier**  
(MI01/W/05 1740)  
**Jeanloz Raymond**  
(JSS02/W/01-A1 1425)  
(JSS02/W/20-A1 1035)  
**Jefferies Chris**  
(HS5/W/16-A2 1100)  
**Jekell Christopher**  
(G3/W/17-A5 1610-20)  
(G6/C/G3/W/21-B2 1220)  
(G6/C/G3/W/45-B2 1420)  
**Jeker Dominique**  
(JSM01/W/70-A4 1620-13)  
**Jelenska Maria**

- (GA1.04/W/34-A4 0930-10)  
**Jenkins A**  
 (HS4/W/15-A4 1730)  
**Jenne R.**  
 (HW1/L/00-A4 0930)  
**Jenouvrier A**  
 (MC08/E/02-A3 1130)  
**Jens Mingram**  
 (VS3/E/05-B3 0900-04)  
**Jensen C. O.**  
 (JSG28/W/23-B2 1130)  
**Jensen Jorgen**  
 (JWM08/W/04-A2 1020)  
**Jensen Niels**  
 Otto (JSM43/E/12-B4 1620)  
**Jentsch Gerhard**  
 (JSV36/E/15-B3 1655)  
 (JSV36/W/24-B3 1400-05)  
 (JSA09/E/04-A2 1200)  
**Jenzer U.**  
 (JSM26/W/29-B2 1700-09)  
**Jeong Son Su**  
 (JSM01/W/110-A4 1620-03)  
**Jeremy C.**  
 Phillips (JSV47/W/16-B5 1000)  
**Jerram Dougal**  
 (JSV22/W/08-A5 0900)  
**Jewitt G. P. W.**  
 (HW2/W/17-B2 1120)  
**Jewson S. P.**  
 (JSP25/W/17-B2 1620)  
**Jewson Stephen**  
 (JSP25/W/30-B1 0930)  
**Jhoon Kim**  
 (GA4.10/W/29-A4 1520)  
**Jhoon Yu Yi**  
 (GA4.10/L/01-A4 1145)  
**Ji Fei**  
 (MI06/E/02-B2 1520)  
**Ji Tang**  
 (JSS44/E/41-B4 0930-10)  
**Ji Y**  
 (MC01/L/18-A4 1715)  
 (U3/W/14-A3 0900-15)  
**Jia M Y**  
 (G3/W/23-A5 1610-28)  
**Jia Minghai**  
 (G1/L/12-A3 1620-88)  
 (G1/W/28-A3 1440)  
**Jiafeng Wang**  
 (MI11/E/10-B5 1645)  
**Jiahong Wen**  
 (HS2/W/22-B2 1140)  
**Jian Liu Shi**  
 (GA1.03/W/10-B2 1420)  
**Jian Pei-Ru**  
 (ST5/W/23-B5 0930-03)  
**Jian Wang**  
 (HS2/W/13-B1 1600)  
**Jian Zhang**  
 (ST4/W/39-B1 1400-07)  
**Jiancheng Kang**  
 (HS2/W/22-B2 1140)  
**Jiang F. Z**  
 (G3/W/42-A5 1120)  
**Jiang H**  
 (MI08/W/01-A4 1205)  
**Jiang Jun**  
 (G5/E/30-A4 1115-05)  
 (G5/W/26-A4 1550-06)  
**Jiang L.**  
 (ST3/W/39-B4 1400-08)  
**Jiang Lequn**  
 (ST3/E/31-B3 1000)  
**Jiang Lili**  
 (ST4/W/38-B1 1100)  
**Jiang Qingfang**  
 (JWM08/W/14-A3 1140)  
**Jiang W. W.**  
 (JSA27/E/06-B1 1130)  
**Jiang Weiping**  
 (G1/W/30-A3 1620-13)  
**Jiang Yuehua**  
 (JSV36/C/U6/E/08-B3 1400-25)  
**Jiang Z.**  
 (G2/E/10-A2 1630-14)  
**Jiang Zhao**  
 (JSA15/E/52-A5 0830-09)  
 (JSV36/E/08-B3 0900-06)  
**Jianjun Zhang**  
 (G4/P/07-A3 1620-08)  
**Jiankang Han**  
 (HS2/W/22-B2 1140)  
**Jianping Li**  
 (MI11/W/02-B5 1530)  
 (MI05/W/03-A4 1400-13)  
**Jie Liu**  
 (JSP23/C/U5/E/15-A6 1500)  
 (ST1/W/31-A4 0930-35)  
 (ST2/W/03-A3 1215)  
**Jieshou Zhu**  
 (JSS44/E/24-B5 1010)  
**Jifong Xu**  
 (JSV30/C/JSV22/P/02-B1 1400-23)  
**Jihua Sun**  
 (JSP25/P/04-B1 1740)  
**Jimenez A.**  
 (JSP23/C/U5/W/14-B2 1210)  
**Jimenez Maria-Jose**  
 (ST3/W/08-B4 0930-08)  
**Jin Fei-Fei**  
 (JSP25/W/66-B1 1150)  
 (JSP25/W/91-B5 0850)  
**Jin Guangwen**  
 (JSV36/E/08-B3 0900-06)  
 (GA1.02/E/25-A2 0930)  
**Jin Qing-Min**  
 (JSV30/C/JSV22/E/16-B1 1400-20)  
**Jingnan Liu**  
 (G1/C/G5/E/09-A3 1620-99)  
**Jingshi Liu**  
 (HS1/W/64-B4 1440)  
 (HS2/W/21-B2 1120)  
**Jinhai Chen**  
 (JSS44/C/U4/W/07-B4 0930-42)  
**Jinhai Yu**  
 (G4/P/03-A3 1620-16)  
**Jintian Gao**  
 (JAS15/P/02-A5 0830-08)  
**Jirong Mao**  
 (G3/E/32-A5 1610-53)  
**Jiseok Song**  
 (ST2/E/39-A3 0900)  
**Jiuxin Shi**  
 (P13/W/16-B1 1600)  
**Ji-yang Wang**  
 (ST4/W/41-B1 1400-01)  
**Jo Ieng**  
 (MI04/E/17-B1 0900-13)  
**Jochmann Horst**  
 (JSG14/P/01-A3 1206-23)  
**Joerin C**  
 (HS4/W/13-A4 1650)  
**Johannessen Sophia**  
 (P15/L/18-B4 1400)  
**Johannesson Haukur**  
 (GA1.15/E/03-B4 1430)  
**Johansson J. M.**  
 (JSG28/W/05-B1 1010)  
 (JSG11/W/05-A3 1440)  
 (JSG11/W/09-A3 1500)  
 (JSG11/E/05-A3 1520)  
 (G5/W/11-A4 0945)  
**Johansson Jan**  
 (MI04/E/20-B1 0900-09)  
**Johansson Jan M.**  
 (G1/E/16-A3 1620-24)  
**Johansson Jussi**  
 (JSG28/E/22-B1 1400-01)  
**Johansson M.**  
 (JSM41/L/01-B4 1625-06)  
**John L**  
 (MC01/W/45-A4 1500)  
**John Paul**  
 (ST2/W/20-A3 1515)  
**John Robert J.**  
 (GA4.01/E/09-A2 1200)  
**Johns William**  
 (P14/W/05-A4 1420)  
**Johnson Colin**  
 (MI02/E/10-A4 1100)  
**Johnson Alan**  
 (JSV36/P/01-B3 1130)  
**Johnson D. W.**  
 (MI04/E/21-B3 1645)  
**Johnson Doug**  
 (MI04/E/01-B4 1450)  
 (MI04/E/04-B4 1035)  
 (MI04/E/11-B4 1120)  
 (MI01/L/03-A1 1400)  
**Johnson Douglas W**  
 (MI01/E/11-A3 1205)  
**Johnson J. R.**  
 (GA3.04/W/11-B1 1130)  
**Johnson Jay R.**  
 (GA3.07/W/52-A4 0930-12 )  
**Johnson John**  
 (P10/W/12-A3 1130)  
**Johnson L. R.**  
 (ST4/E/67-B2 0930-17)  
 (ST1/E/86-A2 0930-06)  
**Johnson Lane**  
 (ST5/W/06-B3 1400-03)  
**Johnson Paul A.**  
 (ST6/E/01-A2 1730)  
**Johnson R. E.**  
 (GA4.10/W/33-A4 1400)  
**Johnson R M**  
 (JSM01/W/107-A1 1510)  
 (JSA20/W/17-A6 1031)  
**Johnson R. W.**  
 (JSS46/W/07-B4 1030)  
**Johnson Richard H.**  
 (MI04/W/09-B3 0850)  
 (MI04/W/18-B3 1600)  
**Johnson Tammy**  
 (HS2/W/08-B1 1140)  
**Johnson Ted**  
 (JSP39/W/28-B4 1540)  
**Johnson Thomas J.**  
 (JSG14/W/10-A3 1151-18)  
**Johnson Torrence V.**  
 (JSA10/W/04-A3 1145)  
**Johnston G. M.**  
 (G3/W/49-A5 1610-78)  
**Johnston Malcolm**  
 (JSA15/E/27-A4 1400-04)  
**Johnston Malcolm J.S.**  
 (JSA15/E/38-A4 1400-03)  
 (JSA15/W/06-A3 1030)  
 (JSA15/W/29-A3 1540)  
**Johnston Paul V.**  
 (MI12/E/02-B5 1115)  
**Johnstone Alan**  
 (GA3.05/W/19-B3 0900-26)  
**Johnstone Alan D.**  
 (GA3.05/E/06-B3 1140)  
**Johnstone D. W.**  
 (JSS44/L/08-B4 0930-43)  
**Johnstone David**  
 (JSS44/L/07-B4 0930-44)  
**Jokela Jorma**  
 (G1/E/25-A3 1620-59)  
**Jokinen Jarkko**  
 (ST4/E/13-B1 1140)  
**Jokipii J. R.**  
 (GA4.04/W/05-B5 1530)  
**Jolla La**  
 (MI04/W/35-B2 1450)  
**Joly A**  
 (MI05/W/30-A3 1220)  
**Joly Alain**  
 (MI05/E/23-A3 1400)  
 (MI05/W/46-A3 0940)  
**Jón Egill Kristjánsson**  
 (MI01/W/16-A3 1010)  
**Jonas P R**  
 (MI01/W/14-A1 1450)  
**Jonas Peter R.**  
 (MI04/E/20-B1 0900-09)  
**Jonathan Shanklin**  
 (JSM01/E/27-A5 1150)  
**Jones A**  
 (MI02/L/19-A4 1410)  
**Jones A. E.**  
 (JSM04/E/04-A2 1240)  
**Jones Anna E.**  
 (JSM04/W/06-A2 1220)  
**Jones C**  
 (MC01/W/42-A1 1015)  
 (MI05/E/18-A2 1450)  
 (MI05/E/03-A4 1400-02)  
 (JSP25/W/17-B2 1620)  
 (JSP39/W/41-B3 1210)  
**Jones C. A.**  
 (GA1.01/W/11-A6 0930)  
 (GA1.01/W/13-A5 1145)  
**Jones Chris**  
 (GA1.01/E/02-A6 1130)  
 (MC01/E/33-A1 1730)  
**Jones Colin**  
 (MC01/W/17-A4 1125)  
**Jones Colin G.**  
 (MI04/W/10-B1 1200)  
**Jones D. L.**  
 (GA1.04/E/11-A4 1610)  
**Jones David**  
 (MI08/E/10-A3 1735)  
**Jones David A.**  
 (JSP25/W/72-B3 1700)  
**Jones David C.**  
 (MI10/E/08-B3 0920)  
**Jones G O L**  
 (JSM01/E/05-A1 1210)  
**Jones Gareth S.**  
 (MC02/E/02-B2 1400)  
 (MC02/E/14-B2 1450)  
**Jones H. G.**  
 (HS2/W/26-B2 1400)  
**Jones Harrison P.**  
 (JSA16/C/GA4.07/W/31-A3 0830-61)  
**Jones I. W.**  
 (HS2/W/30-B2 1600)  
**Jones J. L.**  
 (ST2/W/10-A5 0930)  
**Jones L. E.**  
 (ST5/W/38-B3 1740)  
**Jones L. M.**  
 (ST5/W/L/04-B3 0900-13)  
**Jones P. D.**  
 (MC02/W/01-B2 1100)  
**Jones Richard**  
 (MC01/L/16-A4 0930)  
**Jones Robert Davie**  
 (MI04/W/02-B3 1205)  
**Jones Roderic**  
 (JSM01/W/97 1610)  
**Jones Xu Li-**  
 (MI01/E/07-A2 0930)  
**JonesGareth**  
 (JSA16/E/01-A3 0830-19)  
**Jonker H. J.**  
 (MI10/W/07-B3 1435)  
**Jonker Harm J. J.**  
 (MI04/L/06-B3 1400)  
**Jonkman N. F.**  
 (G6/C/G1/L/16-B1 1420)  
**Jonson Jan Eiof**  
 (MI01/L/01-A1 1210)  
**Jonsson Bo**  
 (G1/E/14-A3 1620-54)  
**Jonsson B**  
 (JSG11/W/05-A3 1440)  
**Joosten P.**  
 (G6/C/G1/L/16-B1 1420)  
**Jordan D. L.**  
 (P15/L/22-B3 1135)  
**Jordanova D.**  
 (GA1.04/W/13-A6 1100)  
**Jordanova Diana**  
 (GA1.05/W/17-A6 1715)  
**Jordanova N.**  
 (GA1.04/W/13-A6 1100)  
 (GA1.03/W/30-B3 1400)  
**Jordanova Neili**  
 (GA1.05/W/21-A6 1130)  
 (GA1.05/W/31-A5 0900-05)  
**Jordanova Vania**  
 (GA3.05/W/04-B3 0900-45)  
**Jörg F. W. Negendank**  
 (VS3/E/05-B3 0900-04)  
**Jorge P M**  
 (JSM01/W/45-A2 1600-06)  
**Joselyn Jo Ann**  
 (GA4.03/W/15-B4 1435)  
**Joseph B.**  
 (JSM26/E/17-B3 0910)  
 (JSM26/E/18-B2 1700-06)  
**Joseph E. John**  
 (GA1.02/W/20-A2 0930)  
**Joseph Joachim H.**  
 (MI07/L/03-A2 1600)  
 (MI10/E/05-B3 1745)  
 (MI10/E/06-B2 1400)  
**Joseph P. V.**  
 (JSP25/E/18-B2 1420)  
 (MI04/E/19-B1 1130)  
**Jossia J. K.**  
 (PO9/E/02-A2 0950)  
**Jost Volker**  
 (JSM41/L/02-B3 1550)  
**Jou Ben J-D**  
 (MI05/W/24-A4 1400-06)  
**Jou Ben Jong-Dao**  
 (MC04/W/17-B1 0940)  
**Joussaume Sylvie**  
 (MC01/E/11-A3 0845)  
**Juang H H**  
 (MC01/W/60-A2 0945)  
**Juchniewicz J**  
 (GA4.09/W/04-A5 1600-02)  
**Judge D.L.**  
 (JSA16/W/11-A3 0830-25)  
**Juergen Klotz**  
 (JSS44/E/41-B4 0930-35)  
**Juhani Kakkuri**  
 (G5/E/31-A4 1430)  
**Juhász Arpad**  
 (JWS33/W/24-B2 1635-31)  
 (JWS33/W/24-B3 0900-31)



# INDEX

**Juhnilo Stin J.**  
(MW02/E/09-B3 1520)  
**Jules Hill**  
(JSM01/E/27-A5 1150)  
**Julia Slingo**  
(MC01/W/01-A2 1000)  
(JSP25/W/36-B1 1210)  
**Julian B. R.**  
(JSS31/E/11-B2 1010)  
(JSS46/W/04-B4 1130)  
(JSS46/W/06-B4 1110)  
(JSS46/W/12-B4 1210)  
(JSV47/W/08-B5 1400-19)  
(JSV47/W/13-B5 1145)  
(ST4/W/03-B3 1630)  
**Juliane Tscherning**  
(JSH12/W/05-A5 0900)  
**Jull A. J. T.**  
(P07/E/03-A3 1430)  
**Jun Jiang**  
(ST1/E/41-A3 0900-09)  
**Jun Lin**  
(G4.02/W/17-A4 1400-16)  
**Jungao Song**  
(JSP23/C/U5/W/09-A6 1620)  
**Junge M.**  
(JSP25/W/75-B4 0930-02)  
**Junichi Fujiwara Jun Ito**  
(HS4/W/19-A5 1010)  
**Junlai Liu**  
(ST6/E/06-A1 0830-16)  
**Jurdy Donna**  
(JSA10/W/05-A2 1400)  
**Jürgen Fischer**  
(MI01/W/05 1740)  
**Jurgen Neuberg**  
(JSV47/E/05-B5 0845)  
**Jürrens Rolf**  
(JSM04/W/11-A2 1735)  
**Jussila J.**  
(GA3.06/W/32-A2 0930-14)  
**Jxrgensen J.**  
(GA5.08/E/03-B1 0900)  
**Jyoti G.**  
(ST6/W/06-A1 0830-08)  
**Jyoti N.**  
(GA2.02/W/07-B5 1620)

# K

**Kaas E.**  
(MW02/W/07-B3 1500)  
**Kaban M. K.**  
(JSS44/E/32-B4 1740)  
**Kabashi Ismail**  
(G1/E/53-A3 1620-78)  
**Kabin K.**  
(GA4.10/E/07-A5 1525)  
**Kachi Misako**  
(JSM41/E/08-B4 1210)  
(MI06/E/17-B1 1650)  
**Kaczmarek Slawomir**  
(P15/W/04-B4 1055)  
**Kaczorowski Marek**  
(G5/E/28-A4 1415-07)  
**Kadirov Azer**  
(ST4/L/03-B1 0830-04)  
**Kadzialko-Hofmoki Magdalena**  
(GA1.04/W/34-A4 0930-10)  
**Kafka Lidis J**  
(JSM01/E/23-A3 1200)  
**Kaftan Vladimir**  
(G1/E/09-A3 1620-22)  
(ST1/E/71-A4 0930-14)  
**Kagan Boris A.**  
(JSP49/E/03-B5 0850)  
**Kagiyama T.**  
(JSA15/W/14-A4 1400-16)  
**Kagiyama Tsuneomi**  
(JSA15/E/07-A5 0830-02)  
(JSV36/W/15-B3 0900-01)  
**Kahar J.**  
(JSV36/E/01-B3 1610)  
(G3/L/13-A5 1610-92)  
(G5/L/01-A4 1145)  
(JSP23/E/27-B2 1700)  
**Kahle H.-G.**  
(JSG28/W/06-B1 1400-06)  
(MI06/W/18-B1 1400-04)  
(MI06/W/18-B2 1400-04)  
**Kahle Hans-Gert**

(G1/W/12-A3 1620-38)  
(G5/E/36-A4 1215)  
**Kahlouche S**  
(G5/P/03-A4 1230-04)  
(G1/L/13-A3 1620-89)  
(G3/P/02-A5 1610-76)  
(G3/P/04-A5 1610-75)  
(G3/P/05-A5 1610-74)  
(G4/P/02-A3 1620-17)  
**Kahmen Ing Heribert**  
(G1/L/07-A3 1140)  
**Kahveci Muzaffer**  
(JSS31/L/04-B2 0830-17)  
**Kainuma S.**  
(GA 2.01/E/07-A1 0900)  
**Kainyek G.**  
(HS2/W/23-B2 1200)  
**Kaiser Diethelm**  
(ST3/W/43-B5 0900)  
**Kaistrenko Victor**  
(JSS42/E/23-B5 1700-05)  
**Kajiwara Tatsuya**  
(GA1.02/E/33-A1 1605)  
(GA1.02/E/34-A1 1500)  
**Kakehi Shigeo**  
(P09/W/14-A1 1520)  
**Kalachnikov A**  
(JSS02/E/08-A1 0830-07)  
**Kaladze Tamaz**  
(GA4.09/E/04-A6 1740)  
(GA4.09/E/05-A5 1600-08)  
**Kalegaev V. V.**  
(GA3.07/W/36-A3 0900-06)  
(GA4.08/W/09-B4 1105)  
**Kalinin D. V.**  
(GA3.05/E/08-B3 0900-19)  
**Kalitin V. T.**  
(HW3/W/12-B4 1635)  
**Källberg Per Cullather**  
(JSM18/W/15-A4 1140)  
**Kallenrode May-Britt**  
(GA4.01/E/09-A2 1200)  
**Kallio E. I. A.**  
(GA3.03/W/07-B4 1450)  
**Kallio Esa J**  
(GA3.10/W/11-A6 1700-12)  
**Kallos G**  
(MI05/L/06-A4 1400-09)  
**Kalmychov Gennady V.**  
(JSA16/W/33-A3 0830-28)  
**Kaloumaira Atu**  
(JSP23/E/37-A5 1010)  
(JSS42/E/08-B5 1700-10)  
**Kalscheuer Thomas**  
(JSA37/E/03-B3 1215)  
**Kamachi Masafumi**  
(JSP05/E/07-A1 1110)  
**Kamae Katsuhiko**  
(ST3/W/50-B3 1700)  
**Kamalabadi F.**  
(JSA20/E/27-A4 1200-21)  
**Kamali Golamali**  
(MI04/W/25-B1 0900-03)  
(MI10/W/14-B1 0900-05)  
(MI10/W/22-B1 0900-04)  
**Kame Nobuki**  
(ST1/E/09-A2 1400-31)  
**Kamburelis Anastasios**  
(GA2.02/W/10-B4 0920)  
**Kamei Toyohisa**  
(GA4.08/W/14-B4 1035)  
(JWS33/W/37-B2 1430)  
(GA5.01/W/05 A1 0835)  
(GA5.06/W/01 A3 0940)  
(GA5.06/W/09 A3 1000)  
(JSA06/W/26-A2 1230)  
**Kamenkovich Vladimir**  
(JSA09/W/02-A2 1745)  
**Kamenogradsky Nikita Ye.**  
(MI06/W/08-B1 1400-01)  
(MI06/W/08-B2 1400-01)  
**Kamide Y.**  
(GA3.02/E/14-B2 1400)  
(GA3.09/E/07-B5 0830)  
(GA4.08/E/16-B3 1425)  
(GA 3.08/E/12-B1 1150)  
**Kamide Yohsuke**  
(GA3.10/W/09-A6 1700-13)  
(JSA06/W/23-A1 1440)  
**Kaminski Thomas**  
(MC01/W/39-A5 1215)  
**Kaminskis J.**  
(G3/W/06-A5 1610-83)  
**Kamp Peter J. J.**  
(JSS44/W/10-B4 1110)

**Kamphaus R. A.**  
(JSS42/L/01 1700-21)  
**Kampunzu A. B.**  
(JSV22/E/10-A5 0900-03)  
**Kamrul Hasan M**  
(HS5/W/29-A2 1715)  
**Kana Masaki**  
(ST2/W/31-A5 1400-34)  
**Kanae Shinjiro**  
(JSM24/W/14-B1 1520)  
**Kanaizumi Tomoyuki**  
(P16/E/06-B5 1500)  
**Kanamatsu Toshiya**  
(GA1.15/C/U6/W/05-B4 1530-07)  
(GA1.04/W/39-A5 1620)  
**Kanamitzu M**  
(MC01/W/60-A2 0945)  
**Kanamori H.**  
(ST5/W/L/04-B3 0900-13)  
**Kanani Entela**  
(G4/W/01-A3 1620-05)  
**Kanda W.**  
(JSA15/W/14-A4 1400-16)  
**Kandalgaonkar S S**  
(MI03/E/04-A3 1020)  
(MI03/E/05-A3 1120)  
**Kandell Stephen J**  
(HS5/W/04-A1 1505)  
**Kane Tim**  
(JSA35/W/08-B1 0900)  
**Kaneda Yoshiyuki**  
(JSS31/W/16-B2 1110)  
(JWA34/W/04-B2 1440)  
(JSA19/W/02-A4 1400-07)  
**Kanekal S. G**  
(GA4.01/E/08-A2 1600)  
(GA3.03/E/05-B4 1000)  
(GA3.05/E/07-B3 0930)  
(GA3.05/E/16-B3 0950)  
(JSA45/E/10-B4 1125)  
**Kaneko Akihiro**  
(G2/E/08-A2 1630-11)  
**Kaneko Arata**  
(P10/P/01-A4 1520)  
(U7/E/02-B1 0830-10)  
**Kaneko Katsuya**  
(JSV30/W/12-B1 1400-09)  
**Kaneshima Satoshi**  
(JSS13/E/02-A5 1610)  
**Kaneta Shi'ichi**  
(MI09/W/03-A5 1145-17)  
**Kaneyama Shinji**  
(JSV30/C/JSV22/W/01-B1 1400-22)  
**Kang Hee Sook**  
(P11/E/06-B3 1010)  
(P10/L/06-A3 1500)  
**Kang Z**  
(G3/E/27-A5 1610-02)  
**Kang K. B.**  
(GA3.02/E/18-B3 0850)  
**Kangas J.**  
(GA2.02/W/15-B4 0930-12)  
(GA2.02/W/19-B4 1600)  
(GA2.02/W/25-B4 0930-11)  
(GA3.04/E/14-B1 1520-03)  
(GA3.04/W/08-B1 1150)  
(GA3.04/W/29-B1 1520-28)  
(GA3.04/W/33-B1 1520-27)  
**Kangas Jorma**  
(GA3.04/E/11-B1 1520-21)  
**Kaniuth Klaus**  
(JSG11/W/01-A4 1050)  
(G1/E/29-A3 1620-63)  
(G1/W/04-A3 1620-03)  
(G1/W/12-A3 1620-38)  
(G1/W/18-A3 1620-07)  
(G1/W/26-A3 1620-42)  
(G1/W/41-A3 1620-46)  
**Kanjorski Nancy**  
(ST2/L/03-A5 1030)  
**Kanonidi Kharlampy**  
(JSA16/W/24-A3 0830-45)  
(JSA06/W/29-A11155-07)  
(JSA16/W/02-A3 0830-49)  
**Kanonidi Konstantin**  
(JSA16/W/24-A3 0830-45)  
**Kao C. Y. J**  
(MI10/W/19-B3 1715)  
**Kapicka Ales**  
(GA1.05/W/21-A6 1130)  
(GA1.05/W/31-A5 0900-05)  
**Kaplan Jed O.**  
(MC11/E/11-B4 1400)  
**Kaplunenko Dmitry**  
(JSP25/W/06-B1 0830-07)

**Kapur Nipun**  
(ST1/E/30-A2 1400-06)  
**Kapustin V N**  
(MI01/L/05-A1 0900-09)  
(MI09/L/01-A5 1145-22)  
(MI09/L/01-A5 1744)  
**Kapustina O. V.**  
(JSA15/E/48-A5 1400-09)  
**Karaca Mehmet**  
(P14/L/01-A4 1400-04)  
**Karagevrekis George**  
(GA3.02/L/04-B3 0900-25)  
(GA3.08/L/02-B1 0900-11)  
**Karakasev Deljo**  
(U3/P/02-A3 0900-08)  
**Karato Shun-ichiro**  
(JSS02/E/07-A2 1145)  
(JSS07/E/03-A2 1740)  
(JSS07/E/05-A2 1540)  
(JSS07/L/03-A2 1500)  
**Karátson D.**  
(JSV30/W/01-B1 1400-04)  
(VS2/W/03-B3 1210)  
**Karcher Fernand**  
(JSM41/W/04-B4 1015-04)  
**Karczewski Jean-Francois**  
(JWA34/W/06-B2 1010)  
(ST5/W/33-B3 0900-07)  
(U7/W/01-B1 0830-14)  
(ST7/W/03-A2 1605-01)  
**Karelsky K. V.**  
(JSM43/E/03-B5 1200)  
(JSM43/E/05-B5 1220)  
**Kariyappa R.**  
(JSA16/E/32-A3 0830-27)  
**Karl Wibjorn**  
(MC09/E/09-B2 1700)  
**Karlén Wibjorn**  
(MC03/E/09-B4 1010)  
**Karner Olavi**  
(JSM41/W/31-B4 1005-02)  
**Karner Stephen**  
(ST1/W/16-A2 1400-29)  
**Karol Igor**  
(JSA16/W/09-A3 0830-50)  
(JSP21/W/14-A5 1210)  
(MC07/W/13-A2 1640)  
**Karol Igor L.**  
(MI06/E/13-B1 1100)  
**Karoly David**  
(MC02/W/02-B2 1130)  
**Karoly David J.**  
(JSM26/W/02-B1 1650)  
**Karoly Prof. David**  
(JSM26/W/10-B3 1010)  
**Karstens Ute**  
(JSM24/W/01-B1 1400)  
**Karuna Kumar K.**  
(HS5/W/50-A3 1630-01)  
**Karvonen Tuomo**  
(HS3/W/20-A2 1015)  
(HS3-W/21-A2 1110)  
**Kasahara Junzo**  
(JWA34/W/11-B2 1110)  
(JWA34/W/12-B2 1050)  
(ST4/W/34-B1 1400)  
**Kasatkina Elena**  
(JSA45/L/03-B4 1205)  
**Kasaya T.**  
(GA1.02/L/05-A2 0930)  
(JSA15/W/07-3 1740)  
**Kashaev Viktor**  
(G1/E/09-A3 1620-22)  
**Kashcheyev B L**  
(JSM01/W/72-A2 1600-02)  
(JSM01/W/69-A1 1130)  
(JSA45/E/19-B5 1110-03)  
**Kashgarian M.**  
(P07/W/10-A3 1510)  
**Kashima Motohiko**  
(JSP25/W/64-B3 0830-01)  
**Kashin Felix V.**  
(MI06/W/08-B1 1400-01)  
(MI06/W/08-B2 1400-01)  
**Kashiwaya Kenji**  
(GA1.03/W/10-B2 1420)  
**Kastensen J.**  
(P12/W/07-A1 0850)  
**Kassabov Martin**  
(MI04/W/05-B1 0900-10)  
**Kassabova Tzveta**  
(MI04/W/05-B1 0900-10)  
**Kassarar I.**  
(ST4/E/66-B2 0930-06)  
(ST4/E/68-B2 1500)

- Katagiri Shuichiro**  
(MI08/L/06-A3 1605)
- Katao Hiroshi**  
(JWA34/E/08-B2 1230)
- Katayama J. S.**  
(GA1.01/W/05-A5 0900-10)
- Kato Aitaro**  
(ST1/W/47-A2 1400-12)
- Kato K.**  
(GA 2.01/E/07-A1 0900)
- Kato Naoyuki**  
(ST1/E/81-A2 1640)
- Kato Norifumi**  
(JSS42/W/09-B5 1520)
- Kato Osamu**  
(JSP25/W/25-B3 0830-06)
- Kato T.**  
(JSS31/W/04-B3 0830-04)  
(G5/E/39-A4 1200)
- Kato W.**  
(JSS44/W/01-B4 0930-06)
- Katsube John**  
(JSA27/E/02-B1 1150)
- Katsumoto M.**  
(U7/L/03-B1 0830-07)
- Katsuo F.**  
(G2/W/01-A2 1630-01)
- Katsuyama Masanori**  
(HW5/E/05-A3 1100)
- Katz Brian G. H.**  
(HS3/W/15-A1 1705)
- Katzfey Jack J**  
(MC01/W/45-A4 1500)  
(MC01/W/49-A5 0900)
- Kauark-Leite**  
(HS5/W/09-A1 1710)  
(HS5/W/18-A2 1140)
- Kaufman Yoram**  
(MI09/E/02-A5 0937)  
(MI09/L/07-A5 1145-16)
- Kauker Frank**  
(MC01/L/09-A2 1515)
- Kauristie K.**  
(GA3.06/W/28-A3 1540)  
(GA3.08/E/01-A6 1430)  
(GA3.09/E/08-B4 1150)
- Kaviris G.**  
(ST4/E/66-B2 0930-06)  
(ST5/E/35-B5 0830)
- Kawaguchi Katsuyoshi**  
(P16/E/13-B5 0950)  
(U7/L/10-B1 0830-20)  
(JWA34/W/11-B2 1110)
- Kawahara Jun**  
(ST5/W/11-B4 1225)
- Kawahara Midori**  
(ST3/W/22-B4 0930-04)
- Kawahara T. D.**  
(JSA20/W/09-A4 1200-11)
- Kawahata Hodaka**  
(GA1.05/W/29-A6 1445)
- Kawakami N**  
(GA1.02/W/08-A2 0930)
- Kawakata Hironori**  
(ST1/E/56-A2 1400-37)
- Kawamoto Kazuaki**  
(MI08/L/06-A3 1605)  
(MI10/W/02-B1 0900-11)
- Kawamoto Nozomi**  
(JSM01/E/02-A5 1130)
- Kawamura Hiroshi**  
(JSM41/E/20-B4 1140)  
(JSM41/E/23-B3 1415)
- Kawamura R.**  
(JSG14/W/09-A3 1121-08)
- Kawanabe Yoshihisa**  
(HS4/W/22-A5 1120)
- Kawano H.**  
(GA3.08/W/05-A6 1040)  
(GA3.08/W/21-A6 0900)
- Kawano Hideaki**  
(GA5.01/E/32 A1 0900-09)
- Kawano N.**  
(G2/W/05-A2 1500)  
(MI06/W/02-B1 1400-18)  
(MI06/W/02-B2 1400-18)
- Kawasaki Ichiro**  
(JSS46/W/18-B4 0930-07)
- Kawase Kazushige**  
(ST3/W/27-B4 1530)
- Kawata Yoshiaki**  
(JSP23/E/15-A6 1640)  
(JSS42/P/01-B5 1210)  
(JSS42/W/01-B5 1620)
- Kawazoe M.**  
(JSA15/W/30-A4 0940)
- Kaye Andrew**  
(U2/E/14-A2 1420)
- Kayaalp Ahmet S**  
(JSP25/W/37-B1 1600)
- Kayahara Takahiro**  
(MW02/E/07-B3 1440)
- Kaymaz Zerefsan**  
(GA3.07/W/70-A3 0930)
- Kazahaya Kohei**  
(HS5/W/35-A3 1045)  
(JSV36/E/12-B3 0900-17)
- Kazansky A.Yu.**  
(GA1.04/L/03-A5 0920)
- Kazansky Alex**  
(GA1.05/W/31-A5 0900-05)
- Kazaryan Susanna A.**  
(U3/W/06-A3 0900-12)
- Kazimirovsky E S**  
(JSM03/W/01-A1 1720)  
(JSA20/W/11-A4 1200-10)  
(JSA20/W/44-A4 1200-33)  
(JSA20/E/07-A4 1200-30)  
(JSM01/W/50-A2 1600-11)  
(JSM26/W/35-B2 1700-12)
- Kazimirovsky Ed.**  
(JSA45/W/01-B5 1110-04)
- Kazmin Alexander**  
(JSM41/W/15-B4 1125)
- Kazmin Alexander S.**  
(JSP25/W/48-B5 1130)
- Kazunari Shibata**  
(GA4.02/W/01-A4 1200)
- Kazuo Kobayashi**  
(ST4/E/35-B1 1420)
- Kazurova Anastasia**  
(GA1. 02/E/17-A2 0930)
- Kazushige Obara**  
(ST5/W/30-B5 0930-01)
- Ke Haller Lars**  
(G3/E/19-A5 1610-25)
- Keable Murray**  
(MI05/W/05-A1 1010)
- Keady J. P.**  
(GA3.06/W/41-A2 0930-22)
- Kearsley A. H. W.**  
(G1/W/08-A3 1620-35)  
(JSG11/W/23-A4 1210)  
(G3/W/49-A5 1610-79)
- Kearsly**  
(G1/L/21-A3 1640-94)
- Keating G. M.**  
(GA4.10/L/05-A4 1040)  
(GA4.10/W/14-A4 0900)
- Keating Pierre**  
(JSA27/E/02-B1 1150)
- Keay Kevin**  
(JSM18/W/01-A4 1640)  
(JSM18/W/12-A4 1600)
- Kebeasy Rashad M.**  
(U8/W/11-B3 0925)
- Kebeasy T.**  
(G5/E/48-A4 1230-06)
- Kechra Frédéric**  
(GA1.04/E/02-A6 0920)
- Kecskemety K.**  
(GA4.10/W/18-A5 1230)
- Keenan Douglas J.**  
(JSP25/E/31-B4 0930-06)
- Keers Henk**  
(ST5/W/06-B3 1400-03)
- Keevallik Sirje**  
(MC02/E/03-B1 1600-03)
- Kefei Zhang**  
(G1/E/56-A3 1620-80)
- Keidron P**  
(MC07/W/17-A3 1115)
- Keihm Stephen J.**  
(G1/E/16-A3 1620-24)
- Keiji Takemura**  
(ST4/W/26-B1 0830-18)
- Keil Andreas**  
(MC07/W/10-A3 0955)  
(MI09/W/08-A5 1542)
- Keiling A.**  
(GA3.06/W/42-A2 1110)
- Keilis-Borok Vladimir**  
(JSP23/W/03-B2 1520)  
(ST1/W/43-A2 1440)  
(ST2/E/41-A4 1445)  
(ST2/W/12-A5 0830)  
(U4/W/04-A4 0945)  
(ST4/W/50-B2 1220)
- Keimig Frank**  
(MC02/E/23-B1 1450)
- Keller Jörg**  
(JSV36/W/08-B3 0900-14)
- Keller K**  
(G3/L/04-A5 1610-19)
- Keller K R C S**  
(JSH12/W/05-A5 0900)
- Keller Kristi**  
(GA2.07/W/08-A2 0930-02)
- Keller Linda**  
(JSM18/E/03-A4 1420)
- Keller Wolfgang**  
(G2/E/02-A2 1545)  
(G4/E/10-A3 1105)
- Kellett B.**  
(GA3.05/W/13-B3 0900-34)
- Kelley M. C.**  
(GA3.09/W/19-B5 1100)
- Kelley Michael**  
(GA2.02/L/07-B4 0930-08)
- Kellogg P. J.**  
(GA4.02/W/20-A4 1400-18)
- Kelly F**  
(JSG11/W/17-A4 1150)
- Kelsch Matthew**  
(MC04/W/07-B1 1700)
- Kendall C.**  
(HW3/W/09-B4 1455)
- Kendall J-Michael**  
(JSS07/E/07-A2 1225)
- Kendrick Eric**  
(JSS31/E/04-B2 1400)
- Kennedy K.**  
(JSA19/W/13-A4 0945)
- Kennedy Todd M.**  
(P09/W/06-A2 0850)
- Kenneth Wohletz**  
(VS2/W/20-B3 1400-13)
- Kennett B. L. N.**  
(ST4/E/55-B2 1620)  
(ST5/W/43-B3 1520)  
(UL2 Thursday 22 July 0830)
- Kennett James P.**  
(GA1.05/W/34-A6 1430)
- Kennewell J**  
(JSA06/W/17-A1 1155-14)
- Kent G S**  
(MI09/W/07-A5 1145-10)
- Kent Joss**  
(U2/E/14-A2 1420)
- Kentang Le**  
(JSP23/C/U5/W/17-B1 1640)  
(P11/W/25-B3 1400)  
(P13/W/16-B1 1600)
- Kenyon Steve**  
(JSA09/W/08-A2 1045)
- Kepler E.**  
(GA4.04/W/16-B5 1730)
- Keramitsoglou Iphigenia**  
(JSM26/E/10-B2 1000)
- Kerr Y. H.**  
(JSM41/W/27-B5 0930)
- Kerridge Brian**  
(JSM26/W/19-B2 1700-13)
- Kerridge Brian J**  
(MW05/W/08-A2 1130)
- Kersely L.**  
(JSA20/W/18-A6 0905)
- Kershaw Peter**  
(P07/L/03-A3 0900-08)
- Kershaw Roy**  
(MI04/E/04-B4 1035)
- Kershengolz S. Z**  
(GA4.08/E/11-B3 0900-02)  
(GA4.08/E/20-B3 0900-01)
- Kerttula R.**  
(GA3.04/W/08-B1 1150)  
(GA3.04/W/29-B1 1520-28)  
(GA3.04/W/33-B1 1520-27)
- Kerzenmacher Tobias**  
(MW07/W/21-A4 1000)
- Kessel R. L.**  
(GA3.07/W/48-A3 1400)
- Kestin Tahl**  
(JSP25/W/65-B1 1420)
- Kettle J.**  
(P15/L/17-B4 1550)
- Kettleborough J A**  
(JSM01/W/51-A4 1620-04)
- Key J**  
(MI08/W/11-A3 1720)
- Key R M**  
(MC01/L/23-A5 1640)  
(P07/W/05-A3 1700)
- Keys J. G.**  
(MI12/E/05-B5 1135)
- Keyword Melita**  
(MI01/W/19-A2 1720)
- Kezys V.**  
(MI06/W/20-B1 1400-07)  
(MI06/W/20-B2 1400-07)
- Khavarova O V**  
(JSA06/W/21-A1 1155-25)
- Khavarova Olga**  
(GA4.09/E/11-A5 1600-05)  
(JSA06/C/U4/E/02-A1 1155-26)  
(GA4.08/E/10-B3 0900-10)
- Khazazin Yu. G.**  
(GA3.04/E/14-B1 1520-03)
- Khairtdinov M. S.**  
(JWS33/E/06 -B2 1635-12)  
(JWS33/E/06-B2 1230)  
(JWS33/E/06-B3 0900-12)
- Khalifov A.**  
(G5/P/03-A4 1230-04)
- Khalil H.**  
(G5/E/41-A4 1230-07)  
(G5/E/48-A4 1230-06)
- Khalipov V. L.**  
(GA3.05/E/05-B3 0900-29)
- Khan H.**  
(GA3.03/W/02-B4 1720)
- Khan Valentina M.**  
(MI11/E/06-B5 1715)
- Khanderkar Madhav L.**  
(JSP23/C/U5/P/01-A5 0830)
- Khantadze**  
(JSA20/W/52-A4 1200-01)
- Khantadze Archil**  
(GA4.09/E/03-A5 1600-07)
- Kharchenko Victor**  
(G2/E/22-A2 1630-07)
- Kharchilava Jumber**  
(MI02/E/04-A4 0950)
- Kharonov Andrei**  
(GA5.08/W/11-B1 1400-04)
- Kharkov B. V. Kalchenko**  
(JSA45/E/19-B5 1110-03)
- Kharlanenkova N Ye**  
(JSM18/W/07-A5 0940)
- Kharousy A. L.**  
(P11/P/02-B5 1150-02)
- Khatiwala Samar P.**  
(P07/W/04-A3 0900-02)
- Khatkevich Y. M.**  
(ST1/W/14-A1 1150)
- Khattatov Vyacheslav**  
(JSM26/W/16-B2 1210)
- Khavroshkin Oleg**  
(ST3/E/54-B4 1400-11)  
(ST1/W/16-A3 0900-19)
- Khaydarova Lev**  
(HW5/E/08-A3 1120)
- Khaydarova Valentina A.**  
(U7/E/04-B1 0830-05)
- Khazai E**  
(HS5/W/51-A3 1630-02)
- Khazan Ya. M.**  
(JSS44/E/35-B4 0930-33)  
(JSS44/E/43-B4 0930-24)
- Khazaradze Nodar**  
(ST1/C/GA4.10/E/01-A4 0930-43)
- Khelaia N. V.**  
(MI04/E/02-B1 0900-12)
- Khelaia Nodia E. I.**  
(MI04/E/02-B1 0900-12)
- Kherani E. A.**  
(GA 2.02/E/01-B5 1400)  
(GA2.02/W/16-B4 0930-18)
- Kherroubi A.**  
(GA1.04/W/21-A4 1400)
- Kheshgi Haroon S.**  
(MC02/W/09-B2 1600)
- Khokhlov A.**  
(GA1.03/W/22-B3 0900)
- Khomutov S.Y.**  
(GA5.01/W/07 A1 1300-07)  
(GA5.01/W/15 A1 1300-06)  
(JSA15/L/01-A5 0830-10)  
(ST1/W/04-A2 1400-14)
- Khon Jaqueline**  
(GA5.01/W/17 A1 1300-05)
- Khotyaintsev Y**  
(GA4.09/L/01-A5 1600-06)  
(GA4.09/L/02-A6 0840)
- Khrebtov Gennadiy V.**  
(GA2.02/L/02-B4 0930-05)  
(GA2.03/E/06-B3 1400-06)
- Khrometskaya Ye. A.**  
(ST5/E/26-B5 0930-12)
- Khrometskaya Yelena**

## INDEX

- (ST1/E/74-A2 1400-04)  
**Khromova T. E.**  
 (HS2/W/15-B2 0900)  
**Khudukon B. Z.**  
 (GA2.02/W/22-B4 1720)  
**Khurana K. K.**  
 (GA3.03/W/10-B4 1220)  
 (GA3.04/W/36-B1 1430)  
 (GA4.10/W/15-A5 0930)  
 (GA4.10/W/05-A5 1655)  
 (GA4.10/W/08-A5 1020)  
 (GA4.10/W/23-A5 1725)  
 (GA4.10/W/20-A5 1545)  
 (GA4.10/W/26-A5 1035)  
**Khurlapov P. G.**  
 (GA3.04/E/02-B1 1010)  
**Khutorova**  
 (GA4.09/L/05-A5 1600-11)  
**Khutorova Olga G.**  
 (GA2.02/L/03-B4 0930-06)  
 (JSA45/L/05-B5 1110-05)  
**Khvedelidze**  
 (MI05/W/41-A4 1400-01)  
**Khvedelidze Z.**  
 (ST4/W/53-B1 0830-31)  
**Kida Hideji**  
 (MW03/E/04-B4 1610)  
**Kideys Ahmet E.**  
 (P11/L/07-B5 1745)  
**Kidson John**  
 (MW06/E/05-A3 1600)  
**Kijko Andrzej**  
 (SW1/W/06-B5 0930)  
**Kikuchi Masayuki**  
 (ST3/E/38-B4 0930-12)  
 (ST1/W/73 0930-31)  
 (ST2/W/31-A5 1400-34)  
 (JSM41/E/23-B3 1415)  
**Kikuchi T.**  
 (P15/L/16-B4 1505)  
**Kikuchi Takashi**  
 (GA3.07/W/03-A6 0900-09)  
 (JSA20/W/33-A5 1200-11)  
**Kiladis George**  
 (MW06/E/05-A3 1600)  
**Kiladis George N.**  
 (MI12/W/14-B5 1005)  
**Kilbane-Dawe I**  
 (JSM01/W/37-A5 1400)  
**Kilburn C.**  
 (JSV29/W/01-B1 1620)  
**Kilburn C. R. J.**  
 (JSV36/E/21-B3 1400-11)  
**Kilburn M**  
 (JSS02/W/18-A1 1640)  
**Kilicoglu Ali**  
 (JSS31/L/04-B2 0830-17)  
**Kilifarska N. A.**  
 (GA2.02/W/26-B4 1140)  
 (GA2.03/W/08-B3 1700)  
**Killeen L.**  
 (U3/W/17-A3 0900)  
**Killeen T L**  
 (JSM01/W/106-A2 1600-01)  
 (JSM01/W/107-A1 1510)  
**Kim Chang S.**  
 (P10/W/01-A5 1420)  
**Kim Dongsoo**  
 (MC04/E/07-B2 1425)  
**Kim Duk Jin**  
 (JSP23/C/U5/E/20-B2 1110)  
**Kim Ed**  
 (MI08/E/10-A3 1735)  
**Kim Hee-Jeong**  
 (GA3.05/E/22-B3 0900-08)  
**Kim Hyung Rae**  
 (JSA09/W/18-A3 1100)  
**Kim Jeong-Woo**  
 (MW07/W/07-A4 1640)  
**Kim Jhoon**  
 (JSM01/W/110-A4 1620-03)  
**Kim Ji-Young**  
 (MI01/E/18-A1 0900-11)  
**Kim Kee-Hyun**  
 (P07/W/01-A3 0900-01)  
**Kim Kuh**  
 (P11/E/22-B3 1150)  
**Kim Kyung-Ryul**  
 (P11/E/22-B3 1150)  
**Kim M. C.**  
 (G6/C/G3/W/32-B1 1120)  
**Kim S. A. B.**  
 (JSP25/E/17-B3 1520)  
**Kim Sumi**  
 (JSM01/P/02-A4 1210)
- Kim V.P.**  
 (JSA15/E/55-A5 1400-16)  
**Kim Vitali**  
 (JSA15/W/09-A5 1400-07)  
 (JSA20/W/08-A4 1200-28)  
**Kim Wonsik**  
 (JSM24/W/02-B1 1030-01)  
**Kimata Fumiaki**  
 (G5/E/33-A4 1504-03)  
 (JSG28/E/18-B1 1400-10)  
**Kimoto Masahide**  
 (JSP24/W/45-B2 1640)  
 (JSP25/W/91-B5 0850)  
**Kimura Ryuji**  
 (MI04/E/03-B1 0900-07)  
**Kind F.**  
 (JSP23/E/03-A6 0930)  
**King Brian A.**  
 (P14/W/11-A4 1500)  
**King Daniel**  
 (JSP21/W/05-A4 1520)  
**King Daniel B.**  
 (JSP21/W/15-A4 1600)  
 (JSP21/W/17-A4 1500)  
**King J. C.**  
 (JSM04/W/04-A2 1645)  
 (JSM04/E/09-A2 1140)  
 (JSA09/E/06-A2 1600)  
 (MI08/E/02-A4 0945)  
**King J. G.**  
 (GA1.05/W/12-A5 930)  
**King P**  
 (MI01/W/03-A1 0900-03)  
**King Robert W.**  
 (JSG28/E/26-B1 1400-11)  
**Kingsley S.**  
 (JSA15/W/15-A3 0950)  
**Kingsley S.P**  
 (ST1/W/14-A1 1150)  
**Kingston Mona**  
 (JSA27/W/03-B11400-01)  
**Kinoshita Atsuya**  
 (JSM01/W/23-A4 1620-06)  
**Kinoshita Hajimu**  
 (JSA19/W/02-A4 1400-07)  
 (JWA34/W/12-B2 1050)  
 (U7/L/10-B1 0830-20)  
**Kinter J L**  
 (MC01/E/02-A4 1430)  
 (MC01/L/02-A1 1145)  
**Kipfer Rolf**  
 (JSV36/E/04-B3 1230)  
**Kiratzki A**  
 (ST4/E/68-B2 1500)  
 (ST4/E/66-B2 0930-06)  
 (ST2/W/14-A4 1400)  
**Kirbani S.**  
 (JSV36/W/10-B3 1400-03)  
**Kirby F.**  
 (G3/W/49-A5 1610-78)  
**Kirchengast Gottfried**  
 (JSM41/W/13-B3 1400)  
**Kirchner A.**  
 (JSS44/W/08-B5 0850)  
**Kirchstetter T**  
 (MI01/W/02-A30900)  
**Kireenkova S. M.**  
 (ST6/W/05-A1 0830-07)  
 (ST6/W/14-A1 0830-13)  
**Kirkevåg Alf**  
 (MI01/W/11-A2 1100)  
**Kirkwood Sheila**  
 (JSM01/W/18-A3 0940)  
 (JSM26/W/26-B2 1700-10)  
 (JSA35/E/08-B1 1210)  
 (JSA35/W/01-B1 1120)  
 (JSM32/W/03-B2 1435)  
**Kirling J. L.**  
 (P11/E/15-B3 1130)  
**Kirov Boyan**  
 (JSA16/C/GA4.07/W/32-A3 0830-60)  
**Kirpichev I.**  
 (GA3.05/W/32-B3 0900-25)  
**Kiryushin Alexei**  
 (ST2/W/34-A4 1515)  
**Kis Károly**  
 (GA5.12/W/04 A2 1420)  
**Kiselev A A**  
 (MC07/W/13-A2 1640)  
 (JSA16/W/09-A3 0830-50)  
**Kiselev M. V.**  
 (GA1.03/W/34-B3 1100)  
**Kiselev Sergey**  
 (JWA34/W/02-B2 1620)  
 (GA5.01/W/06 A1 1300-14)
- (GA5.01/W/01 A1 1300-03)  
**Kissling Edi**  
 (JSS46/W/11-B4 1540)  
**Kissling Eduard**  
 (JSS46/E/03-B4 1420)  
**Kistler L. M.**  
 (GA4.02/E/02-A4 1400-06)  
 (GA4.02/W/28-A4 1720)  
**Kistovich Anatoliy V.**  
 (JSP39/W/22-B3 1448-17)  
**Kistovich Yuri V.**  
 (JSP49/W/05-B5 1210-02)  
 (JSP49/W/13-B5 1210-03)  
**Kita H.**  
 (GA1.03/W/17-B2 1500)  
 (GA1.03/W/25-B2 1440)  
**Kitada K.**  
 (ST1/E/33-A1 1600)  
**Kitae L.**  
 (HW1/L/08-A4 1130)  
**Kitae L. M.**  
 (HS2/W/04-B1 1000)  
**Kitagawa H.**  
 (GA1.05/W/01-A6 1515)  
**Kitagawa Hiroto**  
 (MI01/E/17-A1 1720)  
**Kitagawa Takuya**  
 (GA3.04 /W/04-B1 1520-40)  
**Kitahara T.**  
 (JSA20/W/09-A4 1200-11)  
**Kitamura K.**  
 (GA3.08/W/05-A6 1040)  
 (GA3.04/W/14-B1 1520-43)  
**Kitamura T. I.**  
 (GA3.04/W/10-B1 1520-08)  
 (JSA20/E/16-A5 1200-06)  
**Kitamura Tai-Ichi**  
 (JSA20/W/33-A5 1200-11)  
**Kitashirakawa-Oiwake Sakyo**  
 (JSP25/W/94-B3 1500)  
**Kitchatinov L. L.**  
 (GA4.03/W/12-B4 1510)  
**Kite Geoff**  
 (JSM41/W/20-B5 1220)  
**Kittel G F**  
 (MC01/E/20-A5 1405)  
**Kiuchi H.**  
 (G2/W/01-A2 1630-01)  
**Kiuchi Hitoshi**  
 (G2/E/08-A2 1630-11)  
**Kivanc O.**  
 (JSA20/W/40-A6 0948)  
**Kivekas Maija Paasonen**  
 (HS3-W/21-A2 1110)  
**Kivelson M.**  
 (GA3.03/W/03-B4 0930)  
**Kivelson M. G.**  
 (GA3.03/W/10-B4 1220)  
 (GA3.04/L/12-B2 1100)  
 (GA3.04/W/36-B1 1430)  
 (GA4.10/W/05-A5 1655)  
 (GA4.10/W/07-A5 1740)  
 (GA4.10/W/08-A5 1020)  
 (GA4.10/W/23-A5 1725)  
 (GA4.10/W/20-A5 1545)  
 (GA4.10/W/26-A5 1035)  
 (GA4.10/W/31-A5 1510)  
**Kivelson Margaret**  
 (GA3.04/W/22-B2 0930)  
**Kivisaari T.**  
 (GA2.03/W/09-B3 1030)  
 (GA3.04/W/24-B1 1520-29)  
**Kiyoharu Takano**  
 (MC01/E/13-A1 1130)  
**Kiyoshi Fujino**  
 (ST 6/E/11-A2 1530)  
**Kjeldsen Thomas R.**  
 (HS1/W/17-B4 1700)  
**Kjus S. H.**  
 (GA4.09/W/05-A6 1140)  
**Klaassen G P**  
 (MW07/W/05-A4 1740)  
**Klain B. I.**  
 (JSA16/C/GA4.07/W/37-A3 0830-56)  
 (GA3.04/W/46-B1 1520-07)  
**Klatt Olaf**  
 (P07/W/07-A3 1740)  
**Klawe Mattius**  
 (JSP23/E/10-B2 1420)  
**Kleb Mary**  
 (JSM01/L/30-A5 1640)  
**Klecker B**  
 (GA4.02/W/28-A4 1720)  
 (GA4.02/E/02-A4 1400-06)  
 (GA3.03/E/05-B4 1000)
- (GA3.05/E/16-B3 0950)  
 (GA4.04/E/02-B5 1020)  
**Kleeman Richard**  
 (JSP25/W/58-B1 1130)  
**Klees Roland**  
 (G2/L/05-A2 1100)  
 (G4/W/12-A3 1420)  
 (JSG28/E/09-B1 1200)  
**Kleijer F.**  
 (JSG28/E/01-B1 1040)  
**Kleimenova N. G.**  
 (GA3.04/W/25-B1 1520-38)  
**Kleimenova Natalia**  
 (GA3.02/E/04-B3 0900-19)  
**Klein Baltink H.**  
 (JSG28/E/01-B1 1040)  
**Klein Birgit**  
 (P11/W/24-B4 1130)  
 (P07/W/07-A3 1740)  
**Klein Stephen A.**  
 (MI04/W/24-B1 1400)  
**Klein Thomas**  
 (JSM 04/E/06-A2 1120)  
 (MI05/W/43-A2 0930)  
**Klein U**  
 (MI02/W/05-A5 0950)  
**Klein W.**  
 (ST1/W/26-A3 1210)  
**Klein William**  
 (ST1/E/59-A1 1230)  
**Kleindienst Hannes**  
 (HS2/W/10-B1 1400)  
**Klenke M.**  
 (HW4/E/16-B2 1520)  
**Kleinn Jan**  
 (MC01/E/38-A5 1000)  
**Kletetschka Gunther**  
 (GA5.11/W/02 A3 0910)  
 (GA5.11/W/03 A3 1430-02)  
**Kley Dieter**  
 (JSM26/L/01-B2 0930)  
**Klimas A J**  
 (GA3.02/W/27-B3 1205)  
 (GA3.09/W/14-B4 1720)  
 (GA3.09/W/20-B4 1705)  
 (GA3.02/W/30-B3 0900-04)  
**Klimov S**  
 (GA4.09/W/04-A5 1600-02)  
**Klimushkin Dmitri Yu.**  
 (GA3.04/E/16-B1 1520-05)  
**Klingelé E.**  
 (JSA37/W/04-B3 1200)  
**Kliore Arvydas J.**  
 (GA4.10/W/19-A4 1710)  
 (JSA10/W/01-A3 0930)  
**Klochek Nikolai**  
 (JSA16/E/03-A3 0830-31)  
**Klöcking Beate**  
 (HS3/W/25-A2 1400)  
**Klosko S.**  
 (JSG14/E/09-A3 1700-01)  
**Klostermeyer J.**  
 (JSP32/E/02-B2 1500)  
**Klotz J.**  
 (JSS31/W/12-B2 1420)  
 (JSS31/E/07-B2 1210)  
**Klotz Juergen**  
 (G1/E/49-A3 0910)  
**Klumpar D M**  
 (GA3.06/W/22-A2 1620)  
 (GA3.08/W/13-A6 0940)  
**Kluse Zygmunt**  
 (P11/W/02-B3 1700)  
**Klymak Jody M.**  
 (P14/W/02-A4 1400-12)  
**Klymovych Yevhen**  
 (JSP23/C/U5/E/04-B1 1440)  
**Knab Mathis**  
 (GA1.05/W/41-A5 0900-09)  
 (GA1.05/W/42-A6 1100)  
**Knapp Barry**  
 (SA16/E/22-A3 0830-16)  
**Knight Jeffrey**  
 (MI02/W/15-A5 1100)  
 (MW01/E/03-A5 1650)  
**Knight K.S.**  
 (ST6/W/11-A1 0830-11)  
**Kniveton Dominic**  
 (MI06/E/14-B1 1520)  
**Knorr Wolfgang**  
 (JSM24/E/01-B1 1145)  
 (JSM41/E/18-B5 1135)  
**Knox Steven**  
 (MI05/W/33-A5 1130)  
**Knudsen J.M.**



- (JSA10/E/06-A2 0945)
- Knudsen P**  
(G3/W/15-A5 1610-12)  
(G3/W/30-A5 1610-06)  
(G2/E/05-A2 1630-21)  
(G2/W/03-A2 1630-18)  
(G3/L/05-A5 1610-01)  
(JSA09/E/04-A2 1200)  
(JSG11/W/15-A4 1400-11)  
(JSS31/W/05-B3 0830-05)  
(P15/W/07-B3 1650)  
(JSP25/W/34-B3 0830-04)
- Knudsen T.**  
(P15/W/07-B3 1650)  
(G2/W/03-A2 1630-18)
- Knuteson R O**  
(MC08/L/01-A3 1045)  
(MI06/W/22-B1 1200)
- Ko Malcolm**  
(JSP21/W/05-A4 1520)
- Kobaladze Z.**  
(JSA20/W/52-A4 1200-01)
- Kobayashi K.**  
(JSA20/W/09-A4 1200-11)
- Kobayashi Kazuo**  
(JSS07/E/09-A2 1025)
- Kobayashi Taiyo**  
(JSP25/W/94-B3 1500)  
(JSV47/W/22-B5 1130)
- Kobea A.T.**  
(JSA20/P/01-A5 1501)
- Koblentz-Mishke Olga J.**  
(P15/W/04-B4 1055)  
(P15/W/09-B4 1115)
- Kobolev Vladimir**  
(ST4/E/42-B1 1400-19)
- Koch D**  
(MI02/W/09-A4 1220)
- Koch Michael**  
(HS2/W/05-B1 1020)
- Kochetov A. V.**  
(GA3.04/E/17-B1 1520-06)  
(GA4.09/W/06-A5 1600-03)  
(GA4.02/W/35-A4 1400-27)
- Kociu Siasi**  
(JSP23/E/45-A6 0830-10)
- Kodama Yuji**  
(JSM24/E/09-B1 0910)
- Koehler Ines**  
(MI02/W/03-A5 1200)
- Koenig-Langlo G.**  
(JSM04/E/04-A2 1240)
- Koepken Christina**  
(JSG28/W/21-B1 1400-02)
- Koerner Alexander**  
(JSV36/W/11-B3 1400-06)
- Koerner Roy M.**  
(JSM41/W/12-B4 1720)
- Koesters M.**  
(JSS44/W/08-B5 0850)
- Koeve W.**  
(P08/W/04-A2 1010)
- Koff G. L.**  
(JSP23/E/55-A5 0830-16)  
(ST3/E/15-B4 1400-05)
- Kofman Wlodek**  
(JSA10/W/14-A3 1430-02)
- Koganemaru Ken-ichi**  
(JSP23/C/U5/W/19-A6 1720)
- Kogiso Tetsu**  
(GA1.03/L/01-B1 0940)
- Kohl John L.**  
(GA4.05/W/02-A1 0910)
- Kohl Thomas**  
(ST4/W/13-B1 0840)  
(JSS44/W/17-B4 0930-31)
- Kohler D. D.**  
(P15/L/24-B31730)
- Kohlstedt David L.**  
(JSS07/L/03-A2 1500)
- Kohno Tadashi**  
(HS4/W/22-A5 1120)
- Kohnová Silvia**  
(HS1/W/37-B5 1505-02)
- Koike Toshio**  
(JSM24/W/13-B2 1115)  
(JSM41/W/16-B5 1000)
- Koistinen Tapio**  
(JSS44/E/11-B4 0930-29)
- Koivula H**  
(JSG11/W/05-A3 1440)  
(G5/E/48-A4 1230-06)
- Koivula Hannu**  
(G1/E/10-A3 1620-23)  
(G1/E/21-A3 1620-57)
- (G5/E/12-A4 1518-10)  
(JSG28/E/22-B1 1400-01)
- Koivusalo Harri**  
(HS3/W/20-A2 1015)  
(HS3-W/21-A2 1110)
- Koizumi Kin-ichiro**  
(G3/W/28-A5 1610-34)
- Kojima M.**  
(GA4.02/E/07-A4 1400-02)
- Kojima Masayoshi**  
(GA4.01/W/04-A2 1520)
- Kojiri Toshiharu**  
(HS1/W/06-B4 1100)
- Kok G. L.**  
(JSP21/C/U4/W/03-A4 0910)  
(JSP23/W/72/C/U4/W/03-A6 0830-18)
- Kokhanovsky Alex A**  
(MI09/W/11-A5 1145-13)
- Kokkonen H**  
(ST6/C/JSS02/W/15-A2 1640)
- Kokubun S**  
(GA3.10/W/04-A6 1450)  
(GA3.10/W/21-A6 1700-17)  
(GA3.10/W/09-A6 1700-13)  
(GA3.02/L/02-B3 0900-24)  
(GA3.02/L/04-B3 0900-25)  
(GA3.02/W/03-B3 0900-14)  
(GA3.02/W/21-B2 1520)  
(GA3.02/W/40-B3 1050)  
(GA3.04/W/04-B1 1520-40)  
(GA3.08/E/01-A6 1430)  
(GA3.08/E/04-B1 1700)  
(GA3.08/L/02-B1 0900-11)  
(GA3.08/W/16-B1 1430)  
(GA3.08/W/24-B1 1210)  
(GA3.08/W/29-A6 1400)  
(GA3.08/W/04-B1 0900-02)
- Kolcak Demir**  
(ST2/W/19-A4 1215)  
(JWS33/C/ST2/W/02-B2 1635-20)  
(JWS33/W/02-B3 0900-20)
- Kolenkiewicz R.**  
(G5/E/10-A4 1522-12)  
(G6/E/03-B1 0910)
- Kolesov G. Ya.**  
(GA3.05/E/19-B3 0900-04)
- Kolesova Valentina I.**  
(GA5.08/E/06-B1 1400-01)  
(JWS 33/E/01-B2 1635-13)  
(JWS 33/E/01-B3 0900-13)
- Kolev Staycho**  
(JSM01/E/06-A2 1600-13)  
(MI03/P/01-A3 1600)
- Kolomiitsev O. P.**  
(GA2.02/W/23-B5 1640)
- Koloskov A. A.**  
(JSV30/W/11-B1 0900)
- Kolpin Dana**  
(HS3/W/14-A1 1640)
- Komarov Igor I.**  
(ST5/L/01-B3 0900-14)
- Komazawa M.**  
(ST3/W/39-B4 1400-08)  
(ST3/E/55-B4 1400-18)
- Konda Masanori**  
(JSP25/W/94-B3 1500)
- Kondo T.**  
(G2/W/01-A2 1630-01)
- Kondo Tetsuro**  
(G2/E/01-A2 1630-12)  
(G2/E/04-A2 1630-13)  
(G2/E/08-A2 1630-11)
- Kondo Y.**  
(JSM26/W/18-B2 1550)  
(JSM26/E/05-B2 1430)
- Kondorskaya Nadezhda**  
(ST1/E/74-A2 1400-04)  
(ST2/P/10-A4 0945)
- Kondratyev K Ya**  
(MI01/P/01-A3 1225)  
(MC02/P/03-B2 1710)
- Kondratyev Sergei**  
(HS5/W/05-A1 1525)
- Kondratyuk Vladimir**  
(U7/W/05-B1 0830-09)
- Kong Qinxin**  
(MI01/E/20-A2 1450)
- Kong Xiangru**  
(GA1.02/E/17-A2 0930)
- König R**  
(G6/C/G3/E/43-B1 1100)
- Kono Masaru**  
(GA1.03/W/16-B3 0940)  
(GA1.01/W/19-A5 1600)  
(GA1.01/W/25-A5 1515)
- Kono Yoshiteru**  
(ST2/E/20-A3 0930)
- Kononovich Edward**  
(JSA16/W/05-A3 0830-43)  
(JSA16/W/19-A3 0830-44)  
(JSA16/W/23-A3 0830-42)
- Konovalov Igor**  
(JSM26/E/01-B2 1700-03)  
(JSM26/E/03-B2 1700-08)  
(MI12/E/06-B4 1500)
- Konovalov Sergey**  
(P11/E/01-B5 1440)  
(P11/E/08-B5 1500)
- Konovalov Sergey K.**  
(P08/E/01-A2 1600)
- Konovalov V. G.**  
(HW4/E/29-B2 0900-09)
- Kontny Bernard**  
(G5/W/07-A4 1516-09)
- Kontor Nikolay N.**  
(JSA09/W/22-A3 1230)  
(GA4.04/W/10-B5 0830-03)  
(JWS33/W/20-B2 1635-21)  
(JWS33/W/20-B3 0900-21)
- Konyukhov Boris**  
(JSA15/W/11-A3 1110)  
(JSA15/W/23-A3 0930)
- Koop R.**  
(G6/C/G3/W/08-B2 1120)
- Koop Radboud**  
(G2/E/11-A2 1630-24)  
(G2/W/08-A2 1630-22)
- Kopaev A.**  
(ST4/E/36-B1 1400-23)  
(ST4/E/37-B2 0930-22)
- Kopnichev Yuri**  
(ST5/E/23-B5 0930-02)  
(ST1/E/21-A4 0930-06)
- Kopp E.**  
(JSM26/W/29-B2 1700-09)
- Kopp Ernest**  
(JSA35/E/03-B1 0930)
- Kopteva Rimma**  
(GA1.05/W/24-A6 1145)
- Kopytenko**  
(GA3.04/E/05-B1 1520-18)
- Kopytenko Eugene**  
(JWS33/W/28-B2 1635-14)  
(JWS33/W/28-B3 0900-14)  
(GA5.01/W/21-A1 1415)
- Kopytenko Valery**  
(GA3.04/E/05-B1 1520-18)
- Kopytenko Yuri**  
(JWA34/E/03-B2 1720)  
(JWA34/E/04-B2 1700)  
(JWS33/W/28-B2 1635-14)  
(JWS33/W/28-B3 0900-14)
- Kopytenko Yuri**  
(GA5.01/W/21 A1 1415)  
(JSP23/W/32-B1 1130)  
(JSP23/W/34-B1 0830-15)
- Korablev A.**  
(JSP25/W/42-B3 0830-05)
- Korablev A. A.**  
(P13/E/03-B2 1600-03)
- Koracin Darko**  
(P10/L/01-A4 0930)
- Korago Evgeniy**  
(GA5.11/W/06 A3 1200)
- Korchagin Nikolai**  
(JSP39/E/23-B3 1409-04)
- Korchagin Nikolay**  
(JSP39/E/21-B3 1412-05)  
(JSP39/E/21-B3 1454-19)
- KorcZ Miroslaw**  
(G1/E/26-A3 1620-60)
- Koren Ilan**  
(MI07/L/03-A2 1600)
- Koren V.**  
(HW4/E/12-B2 0930)
- Korepanov Valery**  
(JWA34/E/10-B2 1640)  
(GA5.01/E/06 A1 1215)  
(GA5.01/E/15 A1 1300-10)  
(GA5.01/E/15 A1 1300-10)  
(GA5.01/E/16 A1 1430)  
(JSA15/E/15-A4 1400-09)  
(JSP23/C/U5/E/04-B1 1440)
- Korhonen Juha V.**  
(G3/E/19-A5 1610-25)  
(GA 5.11/E/01 A3 0950)  
(GA 5.11/E/01 A3 1430-01)  
(GA5.11/E/03 A3 1430-10)  
(GA5.11/L/01 A3 1140)  
(GA5.12/E/03-A2 1600-05)
- (GA5.12/E/06-A2 1600-03)  
(GA5.12/L/03-A2 1600-04)  
(JSS44/E/11-B4 0930-29)
- Korja Annakaisa**  
(JSS44/W/13-B4 1420)
- Korja Toivo**  
(GA5.12/L/03-A2 1600-04)
- Kormendi Alpar**  
(GA5.01/E/01 A1 1300-11)  
(GA5.01/E/02 A1 1715)  
(GA5.01/W/16 A1 1145)
- Kormiltsev Valery**  
(JSA40/W/14-B5 1400-15)
- Kornblueh Luis**  
(JSM41/W/13-B3 1400)
- Kornienko Victor**  
(GA2.07/E/05-A1 1200)
- Kornienko Viktor**  
(GA2.03/E/04-B3 1220)
- Kornilov Ilia**  
(GA3.06/L/04-A2 0930)  
(GA3.02/W/20-B3 0900-13)
- Kornilov Oleg**  
(GA3.02/W/20-B3 0900-13)  
(GA3.06/L/05-A3 1720)
- Kornilova Tatyana**  
(GA3.02/W/20-B3 0900-13)
- Korolyov Yuri**  
(JSP23/C/U5/E/12-A6 0830-07)
- Korono Nickolai V.**  
(VS2/C/U6/E/07-B3 1400-36)
- Koronovsky Nickolai V.**  
(ST7/E/10-A2 1445)
- Korotova G.I.**  
(GA3.07/W/06-A4 0930-14 )
- Korsch Russell**  
(JSS44/L/07-B4 0930-44)
- Korsnes Reinert**  
(JSM04/E/05-A2 1420)
- Korte Monika**  
(GA5.01/E/10 A1 1630)
- Korth A.**  
(GA3.02/E/18-B3 0850)  
(GA3.02/W/13-B2 1630)  
(GA3.02/W/54-B2 1615)
- Korth W**  
(JSH12/W/07-A4 1400-02)
- Koryakin Eugenij D.**  
(JSA09/W/04-A2 0930-08)
- Kosa Laszlo**  
(JSV30/W/13-B1 1400-05)
- Kosarian Minoo**  
(ST6/P/01-A1 0830-01)
- Kosch M.**  
(GA2.01/E/11-A1 1205)  
(JSA20/W/08-A4 1200-27)
- Kosch M. J.**  
(GA2.01/W/07-A1 1055)  
(GA3.06/W/25-A3 1520)
- Kosek Wieslaw**  
(JSP25/W/02-B2 0930-05)
- Koshel Konstantin**  
(JSP39/W/24-B3 1457-20)  
(JSP49/W/07-B5 1210-12)
- Koshchug Dmitry**  
(ST7/W/04-A2 1605-02)
- Koshimura Shun-ichi**  
(JSS42/E/21-B5 1420)
- Koshravi Rashid**  
(JSA45/W/05-B4 1055)
- Koshyk J N**  
(JSM01/W/63-A3 1500)
- Koshyk John**  
(MW03/W/07-B4 1115)
- Koshyk John N**  
(MW01/W/13-A5 0830)
- Koskinen Hannu**  
(JSA06/W/14-A1 1700)
- Koskinen Hannu E. J.**  
(GA3.07/W/18-A4 0930-13)  
(GA3.10/W/11-A6 1700-12)
- Kosik Jean Claude**  
(GA3.09/E/01-B4 0900-06)  
(GA3.09/E/02-B4 1505)
- Koskinen H. E. J.**  
(GA3.03/W/07-B4 1450)
- Kosovichev A. G.**  
(GA4.03/E/06-B4 1730-03)
- Kossobokov Vladimir**  
(JSA15/W/10-A4 0900)  
(JSP23/W/03-B2 1520)  
(ST1/W/34-A3 0900-06)  
(ST1/W/43-A2 1440)  
(ST1/W/54-A2 1700)
- Kostov Vladimir**

## INDEX

- (MW05/W/07-A2 1215)
- Kostecki Maciej**  
(GA1.05/E/05-A6 1215)
- Kostelevy Jan**  
(G1/E/57-A3 1620-81)
- Kosterov Andrei A**  
(GA1.05/W/39-A6 0900-02)  
(GA1.05/W/03-A6 0900-01)  
(GA1.05/W/40-A6 0900-03)
- Kosters A. J. M.**  
(JSG28/E/01-B1 1040)
- Kostin Vlalimir**  
(U8/W/02-B3 1030)
- Kostrov Nick**  
(JSA40/W/14-B5 1400-15)
- Kostyanev Simeon**  
(G3/E/33-A5 1610-47)  
(JSP23/E/30-A5 0830-14)
- Kosuga Masahiro**  
(ST5/W/30-B5 0930-01)  
(ST2/W/26-A5 1400-01)
- Kota J.**  
(GA4.04/W/05-B5 1530)
- Kotake Y.**  
(G5/E/39-A4 1200)
- Kothari U. C.**  
(HS1/W/62-B5 0830-07)
- Kotroni V**  
(MI05/L/06-A4 1400-09)
- Kotsakis Christopher**  
(G6/C/G4/E/04-B1 1700)
- Kotthoff Holger**  
(JSG11/E/07-A4 1400-04)
- Kottmeier C.**  
(JSM04/W/12-A2 1535)
- Koitnauer Pavel**  
(G5/W/07-A4 1516-09)  
(JSP23/W/29-A6 1600)  
(ST3/W/13-B5 0915)  
(ST3/W/38-B5 1445)
- Kotzé Pieter B**  
(GA5.09/W/11 A2 1400-05)  
(GA3.09/W/16-B4 0900-03)
- Kotzev Valentin**  
(JSS31/W/08-B2 1640)
- Kouba D.**  
(ST4/E/46-B2 0930-07)
- Kouba J.**  
(G2/L/02-A2 0945)
- Kouba Jan**  
(G1/E/60-A3 1620-82)
- Koudella C.**  
(JSP49/E/08-B5 1420)
- Kouker Wolfgang**  
(MI12/W/16-B5 1215)
- Kourafalou Vassiliki**  
(P10/L/01-A4 0930)
- Kournossenko Alexei.**  
(JSM01/W/116-A5 1000)
- Kourtidis K.**  
(JSP21/W/09-A4 1130)
- Kouskouna Vicki**  
(JSP23/E/56-A6 0830-08)
- Kousuke Shono**  
(JSS02/E/11-A1 0830-08)
- Koutoulaki Katerina**  
(MW05/W/08-A2 1130)
- Kouts Tarmo**  
(P11/W/13-B3 1640)
- Kouwen N.**  
(HS2/W/12-B1 1540)
- Kovacs Peter**  
(JWS33/W/24-B2 1635-31)  
(JWS33/W/24-B3 0900-31)
- Kovalam S**  
(JSM01/W/36-A1 1400)  
(MW04/W/04-A1 0900)
- Kovalenko V. A.**  
(GA4.05/W/04-A1 0950)
- Kovalenko Vladimir**  
(JSA16/E/28-A3 0830-11)
- Kovalevskaya Elena**  
(GA4.08/E/13-B3 0900-17)  
(GA4.08/E/15-B3 0900-18)
- Kovalevsky Joseph**  
(GA4.08/E/13-B3 0900-17)  
(GA4.08/E/15-B3 0900-18)
- Kovba V.**  
(P09/W/05-A1 1640)
- Kovrazhkin R. A.**  
(GA4.08/W/15-B3 1530)
- Kovshov S.**  
(ST3/P/9-B4 1400-22)
- Kowalczyk Eva A**  
(MC01/W/50-A5 1230)
- Koyaguchi Takehiro**  
(GA1.03/W/23-B1 1040)  
(JSV30/W/12-B1 1400-09)  
(VS2/E/01-B3 1400-18)
- Koyama Masato**  
(VS3/E/04 1650)
- Koyama T.**  
(JSA15/W/14-A4 1400-16)
- Koyama Takao**  
(GA1.02/W/05-A2 0930)
- Koyama Yasuhiro**  
(G2/E/04-A2 1630-13)  
(G2/E/08-A2 1630-11)  
(G2/W/12-A2 1630-02)  
(G2/E/01-A2 1630-12)  
(G2/W/01-A2 1630-01)
- Kozak J.**  
(ST1/E/47-A2 1400-35)
- Kozelov B. V.**  
(GA3.06/W/07-A2 0930-21)  
(GA3.02/E/05-B3 0900-21)
- Kozelova T. V.**  
(GA3.02/E/05-B3 0900-21)
- Kozly Liudmila**  
(P13/W/13-B2 1600-11)
- Kozlov Eugene**  
(JWS33/W/13-B2 1100)
- Kozlov Vadimir**  
(JSP39/W/24-B3 1457-20)
- Kozlova M. O.**  
(GA2.02/W/22-B4 1720)
- Kozlova Olga**  
(MI12/E/01-B4 1610)
- Kozlovskaya Elena**  
(JSS44/W/11-B4 0930-28)  
(ST6/W/03-A1 0830-05)
- Kozlovsky Alexander**  
(GA3.06/W/12-A2 0930-08)  
(GA3.06/W/13-A2 0930-09)
- Kozyra J. U.**  
(GA3.01/W/02-A2.1030)
- Kozyra Janet U.**  
(GA3.05/W/38-B3 1700)  
(GA4.08/W/03-B4 0930)  
(GA4.08/W/16-B4 1610)  
(GA3.05/E/15-B3 0900-39)
- Kozyreva O. V.**  
(GA3.04/W/25-B1 1520-38)
- Kozyreva Olga**  
(GA3.02/E/04-B3 0900-19)
- Krabill W**  
(JSH12/C/JSS31/E/05-A5 0930)
- Kracke Dieter**  
(ST3/W/48-B4 1400-10)
- Kradolfer U.**  
(ST5/L/02-B3 0900-02)
- Krall Evelyn**  
(HS1/W/27-B5 1500-01)
- Krankowski A.**  
(G1/E/13-A3 1620-53)
- Krasakopoulou Evangelia**  
(P11/E/28-B5 0950)
- Krasnopolsky Vladimir**  
(MI06/W/32-B2 1610)
- Krasnoselskikh V.**  
(GA4.04/W/08-B5 0830-04)  
(GA4.05/W/01-A1 1220)
- Krasnova Maria A.**  
(ST5/W/50-B5 0930-04)
- Krasovskaia Irina**  
(HS1/W/39-B4 1400)
- Krauklis Ian**  
(GA3.07/W/27-A5 0900-08)
- Kravanja Stefano**  
(ST5/W/31-B4 1640)
- Kravchenko N.**  
(ST3/P/10-B4 1400-23)
- Kravetz Roman O.**  
(JSA20/E/11-A4 1200-29)
- Kreen L.**  
(GA5.01/E/18 A1 0900-07)
- Krehbiel P R**  
(MI03/W/05-A3 1140)
- Krehbiel Paul**  
(JSM03/W/02-A1 1650)  
(MI03/W/01-A3 1520)
- Kreher Karin**  
(MI12/E/02-B5 1115)
- Krein Andreas**  
(HS5/W/01-A1 1405)
- Krenke A.**  
(HW1/L/08-A4 1130)
- Krenke A. N.**  
(HS2/W/04-B1 1000)  
(HS2/W/15-B2 0900)
- Kress Nurit**  
(P11/E/17-B4 1600)
- Kreutz Karl J**  
(JSM18/W/15-A4 1140)
- Kreyscher Martin**  
(MC01/L/10-A2 1550)
- Kriainen Jussi**  
(G3/E/19-A5 1610-25)  
(JSS44/E/11-B4 0930-29)
- Krichak Simon**  
(MI05/E/05-A5 1020)  
(MI07/E/02-A2 1510)
- Krijgsman W.**  
(GA1.15/W/01-B4 1415)  
(GA1.15/W/08-B4 1445)  
(GA1.15/W/09-B4 1400)
- Krijgsman Wout**  
(GA1.15/W/11-B4 1530-03)
- Krimigis S. M.**  
(GA4.04/W/04-B5 1650)  
(GA4.04/W/18-B5 1150)
- Kripalani R. H.**  
(JSP26/P/03-B2 1500)
- Krishna K. S.**  
(ST4/E/31-B1 0830-06)
- Krishnamurthy V.**  
(JSP25/W/89-B2 1400)  
(MC01/L/02-A1 1145)
- Kristek Jozef**  
(ST3/W/01-B3 1645)  
(ST3/W/20-B3 0945)  
(ST3/W/44-B3 0930)
- Kristiansen Jorn**  
(MC02/W/05-B1 1430)
- Kristjansson**  
(GA6.02/E/17-B1 1450)
- Kristjansson Egill Jon**  
(MI01/W/11-A2 1100)
- Kristjánsson Jon Egill**  
(MC02/W/05-B1 1430)
- Kristjansson Leo**  
(GA1.03/P/01-B1 1100)  
(GA1.15/E/03-B4 1430)  
(GA1.15/P/01-B4 1630)  
(GA6.01/L/02-A5 1630)
- Kriviliiov V**  
(GA3.10/E/08-A6 1700-11)
- Krivodubskij Valery N.**  
(GA4.03/L/02-B4 1615)
- Krivolutsky Alexei**  
(JSA45/E/09-B5 1010)  
(JSA16/E/10-A3 0830-20)  
(JSM01/E/33-A1 1050)
- Krol Martin**  
(HW4/E/32-B2 0900-13)
- Krom Michael D.**  
(P11/E/17-B4 1600)
- Kroner Corinna**  
(G5/W/08-A4 1415-03)
- Kropotkin A. P.**  
(GA3.02/W/06-B3 1015)  
(GA3.02/W/35-B3 0900-10)  
(GA3.02/W/49-B3 0900-11)  
(GA3.04/W/35-B1 1520-46)  
(GA3.05/W/18-B3 0900-17)  
(GA3.08/W/30-B1 0900-04)
- Krotkov Nickolay**  
(P15/L/27-B4 1630)
- Krotoff Oleg L.**  
(GA1.02/W/25-A1 1605)
- Krs Miroslav**  
(GA1.04/L/07-A4 1200)
- Kruczyk Micha**  
(G5/E/44-A4 1558-10)
- Krueger A. J.**  
(U7/W/06-B1 1635)
- Krueger Arlin**  
(JSM41/W/23-B4 1630-07)
- Krueger Cláudia Pereira**  
(G1/W/09-A3 1620-36)
- Krueger Frank**  
(ST4/E/10-B3 0940)
- Krueger Kirstin**  
(MI12/W/07-B4 1030)
- Kruger A. C.**  
(JSP25/E/30-B1 0830-01)
- Kruglanski M.**  
(GA3.05/E/02-B3 0850)  
(GA3.09/E/12-B4 1600)  
(JSA06/E/07-A1 1620)
- Kruiver P. P.**  
(GA1.03/W/15-B3 1540)  
(GA1.15/W/01-B4 1415)
- Kruizinga G. L. H.**  
(G1/E/47-A3 1620-75)
- Krummel P B**  
(MC01/E/37-A1 1700)
- Krupchatnikoff Vladimir**  
(MC01/E/22-A5 1525)  
(MC01/E/07-A4 1700)
- Krupitsky Alexander**  
(JSA09/W/02-A2 1745)
- Krupp N.**  
(GA4.10/W/26-A5 1035)
- Kruse Lars**  
(MI06/W/18-B1 1400-04)  
(MI06/W/18-B2 1400-04)
- Kruse Lars Peter**  
(JSG28/W/06-B1 1400-06)
- Kryakunova O.N.**  
(GA 4.01/W/14-A2 1400-08)
- Kryokova A V**  
(G3/E/28-A5 1610-03)
- Krysanova Valentina**  
(HS3/W/25-A2 1400)
- Krywkwow J.**  
(HW4/E/32-B2 0900-13)
- Kryza Ryszard**  
(GA1.04/W/08-A4 0930-05)
- Ksenofontov Alexander**  
(JSP39/W/11-B4 0950)
- Kuang Weijia**  
(JSG14/E/11-A3 1212-25)
- Kuba Naomi**  
(MI01/E/09-A1 0900-02)  
(MI04/E/22-B4 1150)
- Kubilay Nilgun**  
(MI01/W/22-A1 1150)
- Kubo Tomoaki**  
(ST 6/E/11-A2 1530)
- Kubota M.**  
(GA2.02/W/09-B4 0900)  
(GA2.03/E/02-B3 1120)
- Kubota Sanae**  
(JWS33/W/27-B2 1635-22)  
(JWS33/W/27-B3 0900-22)
- Kubyskin I**  
(GA4.02/W/24-A4 1400-22)
- Kubyskhina M. V.**  
(GA3.02/W/60-B2 1215)
- Kucharski Fred**  
(MI05/E/01-A3 1420)
- Kucheruk N. V.**  
(P11/W/27-B5 1150-11)  
(P11/W/01-B5 1620)  
(P11/W/03-B5 1150-06)
- Kuchmin O. A.**  
(HW3/W/11-B4 1610)  
(HW3/W/12-B4 1635)
- Kudeki E.**  
(GA2.02/L/01-B4 1000)
- Kudela K.**  
(GA3.08/L/02-B1 0900-11)
- Kudriashov**  
(JWS33/L/1-B2 1635-14)  
(JWS33/L/1-B3 0900-15)
- Kuechenhoff Helmut**  
(JSS44/E/14-B4 0930-30)
- Kuehtreiber Norbert**  
(G3/E/34-A5 1610-85)  
(G3/W/55-A5 1610-65)  
(G3/E/41-A5 1610-84)
- Kuell V**  
(JSM01/W/41-A4 1150)
- Kuempel Hans-Joachim**  
(JSV36/W/11-B3 1400-06)
- Kuge Keiko**  
(ST3/W/06-B4 0930-05)  
(ST5/E/17-B4 1400-04)
- Kuhn Michael**  
(G3/W/18-A5 1610-54)
- Kuhnke F.**  
(JSA10/E/06-A2 0945)
- Kuiper Klaudia**  
(GA1.15/W/11-B4 1530-03)
- Kujawa Lech**  
(G1/E/26-A3 1620-60)
- Kukharenko Peter Yu.**  
(ST5/W/02-B4 0930-06)  
(ST5/W/08-B4 1145)
- Kukharenko Yuri A.**  
(ST5/W/02-B4 0930-06)  
(ST5/W/08-B4 1145)
- Kukkonen Ilmo T.**  
(ST4/E/13-B1 1140)
- Kuklin G. V.**  
(GA4.03/L/01-B4 0905)
- Kuklin Georgy V.**  
(GA6.01/W/15-A5 0900-14)
- Kuklinski Walter**

- (GA2.03/W/07-B3 1420)
- Kuksa Yu.**  
(GA1.02/L/03-A2 0930)
- Kulhanek O.**  
(ST2/E/51-A4 1715)
- Kulhánek Ota**  
(ST3/E/34-B4 1400-04)
- Kulik Sergey**  
(GA1.02/E/14-A2 0930)
- Kulikov Evgueni A.**  
(JSS42/E/12-B4 1500)  
(JSS42/E/12-B5 1700-07)
- Kulikov M. Y.**  
(JSM26/E/01-B2 1700-03)  
(JSM26/E/04-B2 1700-05)
- Kulinich Anatoli**  
(JSS44/E/11-B4 0930-29)  
(G3/E/19-A5 1610-25)
- Kulkarni Ashwini**  
(JSP26/P/03-B2 1500)
- Kultima J.**  
(GA5.01/E/17 A1 1300-08)
- Kuma Ken-Ichi**  
(JSP05/E/10-A1 10)
- Kumagi Hiroyuki**  
(JSV47/W/24-B5 0945)
- Kumamoto Takashi**  
(ST3/W/27-B4 1530)
- Kumar B. K.**  
(ST4/W/32-B1 0830-30)
- Kumar Bishm**  
(HS4/L/01-A4 0930)  
(HS4/L/01-A4 0930)
- Kumar M. Ravi**  
(ST1/E/08-A2 1400-26)  
(ST2/E/60-A3 1145)
- Kumar Muneendra**  
(G1/E/60-A3 1620-82)
- Kumar Vimal**  
(P12/E/02-A1 1030-06)
- Kumazawa Mineo**  
(JSV47/E/02-B5 1230)
- Kuminov Aleksand**  
(JSA45/E/09-B5 1010)
- Kump Lee**  
(HW5/E/04-A3 1500)
- Kumpel H J**  
(ST1/E/67-A3 1010)
- Kunag Weijia**  
(GA1.01/E/13-A6 1100)
- Kungurtsev L.V.**  
(GA1.04/L/03-A5 0920)
- Kuniko Y.**  
(GA1.05/W/01-A6 1515)  
(GA1.03/W/25-B2 1440)
- Kunimori H.**  
(G2/W/01-A2 1630-01)
- Kunitake M.**  
(GA5.06/W/04 A3 1440)  
(JSA20/E/10-A4 1200-04)  
(JSA20/E/13-A4 1508)
- Kunitake Manabu**  
(JSA20/E/08-A4 1200-18)  
(JSA20/E/08-A4 1200-25)
- Kunitomo Takahiro**  
(JSV47/E/02-B5 1230)
- Kunjumon Ignatius**  
(MC01/W/59-A1 1645)
- Kunow Horst**  
(GA4.01/E/09-A2 1200)
- Künzi K F**  
(MI02/W/05-A5 0950)
- Kunzmann Thomas**  
(GA1.05/W/06-A5 1630)
- Kuo B.Y.**  
(JSA17/E/01-A4 1150)
- Kuo Ban-Yan**  
(ST5/W/23-B5 0930-03)
- Kuo Chaincy**  
(JSS13/W/16-A4 1540)
- Kuo K.-S.**  
(MI06/W/13-B1 1400-08)  
(MI06/W/13-B2 1400-08)
- Kuo Long-Chen**  
(G5/W/02-A4 1502-02)
- Kuo Ying-Hwa**  
(JSG28/W/20-B2 1400-07)  
(JSG28/W/25-B2 1400-11)  
(JSG28/W/27-B2 1110)
- Kuo-Fong Ma**  
(ST6/E/05-A1 0830-15)
- Kupko VI.**  
(ST3/P/10-B4 1400-23)  
(ST3/P/8-B4 1400-21)  
(ST3/P/9-B4 1400-22)
- Kuramoto Chieko**  
(G3/W/28-A5 1610-34)
- Kurashima A.**  
(G5/E/39-A4 1200)
- Kurazhkovskaya N. A.**  
(JSA16/C/GA4.07/W/37-A3 0830-56)  
(GA3.04/W/46-B1 1520-07)
- Kurazhkovsky A.Yu.**  
(JSA16/C/GA4.07/W/37-A3 0830-56)
- Kurgansky Mikhail V.**  
(JSP25/W/38-B4 0930-04)
- Kurihara N.**  
(G2/E/01-A2 1630-12)
- Kurihara Noriyuki**  
(G2/E/08-A2 1630-11)
- Kurihara Yoshio**  
(MW03/E/07-B4 1200)
- Kurihara Takaji**  
(GA5.01/W/05 A1 0835)
- Kurimo Maija**  
(GA5.12/E/03-A2 1600-05)  
(GA5.12/L/03-A2 1600-04)
- Kuroda Koji**  
(JSS02/E/14-A1 1740)
- Kuroda Shunsuke**  
(MI08/L/06-A3 1605)
- Kuroishi Yuki**  
(G3/W/11-A5 1500)
- Kurschner D**  
(JSM01/W/72-A2 1600-02)  
(MW04/W/01-A1 0950)
- Kursinski E. Robert**  
(JSG28/E/27-B2 1400-04)  
(JSG28/W/12-B2 1030)  
(MI06/W/29-B1 1010)
- Kurt Mustafa**  
(JSS31/L/04-B2 0830-17)
- Kurth W. S.**  
(GA4.09/W/15-A6 0900)  
(GA4.10/W/05-A5 1655)  
(GA4.10/W/08-A5 1020)  
(GA4.10/W/34 1620)
- Kurucz Robert L.**  
(JSA16/E/09-A3 1100)
- Kurtz R. D.**  
(JSS44/L/03-B4 1150)
- Kurz Manfred**  
(MI05/E/12-A1 1550)
- Kusaba Keiji**  
(ST6/E/09-A2 1430)
- Kusche Juergen**  
(G4/E/17-A3 1620-13)  
(JSA37/E/04-B3 1015)  
(JSA37/E/05-B3 1130)
- Kushiday T.**  
(JSA15/E/19-A3 1500)
- Kushnir Yochanan**  
(JSP25/W/09-B4 1110)
- Kushwaha Subhash**  
(ST1/E/67-A3 1010)
- Kusinski Oleg**  
(JSP23/E/38-A6 0830-09)
- Kustas William P.**  
(JSM41/W/18-B5 1205)
- Kusuma M. A.**  
(JSV36/E/01-B3 1610)  
(JSP23/E/27-B2 1700)
- Kusumoto Shigekazu**  
(ST4/W/26-B1 0830-18)  
(ST4/W/31-B1 0830-23)
- Kutas Roman**  
(ST4/E/42-B1 1400-19)
- Kutepov Alexander**  
(MC09/E/01-B2 1545)
- Kutiev I**  
(JSA06/W/15-A2 1010)
- Kutterer Hansjoerg**  
(G1/W/42-A3 1120)  
(G4/W/21-A3 1620-01)  
(JSA09/W/11-A2 0930-04)  
(JSA09/L/02-A2 1230)
- Kutuzova Ekaterina**  
(MI12/E/01-B4 1610)
- Kutzner Carsten**  
(GA1.01/E/04-A6 0945)
- Kuvshinov Alexei**  
(GA1.02/L/04-A1 1605)  
(GA1.02/W/26-A1 1605)
- Kuwahara V. S.**  
(P15/L/16-B4 1505)
- Kuzanyan K.**  
(GA1.01/W/26-A5 1015)
- Kuzanyan Kirill**  
(GA4.03/L/03-B4 1740-05)  
(GA4.03/W/11-B4 1735-04)
- Kuzhevskij B. M.**  
(SW1/E/08-B5 1030-03)
- Kuzmin Yu. O.**  
(JSP23/C/U5/W/16-A5 0830-17)  
(ST1/W/62-A2 1400-16)
- Kuznetsov Alexey**  
(GA1.02/W/27-A1 1605)  
(GA3.06/W/04-A2 0930-20)
- Kuznetsov Gotselyuk**  
(GA3.05/W/48-B3 0900-18)
- Kuznetsov Jurly**  
(ST1/E/71-A4 0930-14)
- Kuznetsov S. N.**  
(GA3.07/E/25-A4 0930-15)  
(GA3.05/E/01-B3 0900-38)  
(GA3.05/E/08-B3 0900-19)  
(GA3.05/E/14-B3 0900-35)  
(GA3.08/E/06-B1 0900-08)  
(GA3.09/E/04-B4 1650)
- Kuznetsov V. V.**  
(GA5.01/W/15 A1 1300-06)  
(GA5.01/W/15 A1 1300-06)  
(JSA15/L/01-A5 0830-10)  
(ST1/W/04-A2 1400-14)
- Kuznetsov Vladimir V.**  
(GA1.01/W/07-A5 0900-11)  
(JSA09/C/GA5.01/W/20-A3 1200)  
(JSA17/C/GA1.19/W/07-A4 1530)  
(JSS07/W/08-A2 0930-03)
- Kuznetsova Ludmila**  
(JWS33/W/17-B2 1635-17)  
(JWS33/W/17-B3 0900-17)
- Kuznetsova M**  
(JSA06/W/22-A2 0930)
- Kuznetsova Tamara**  
(GA3.07/W/35-A4 0930-16)  
(GA6.01/W/15-A5 0900-14)  
(JSA06/W/29-A11155-07)  
(JSA16/W/35-A3 0830-57)  
(GA3.09/W/09-B4 0900-07)
- Kuznetsova Valentina**  
(JSA15/E/16-A5 1400-03)
- Kværna Tormod**  
(U8/W/04-B3 1450)  
(U8/W/16-B3 1640-12)
- Kwin Kozyra Janet**  
(JSA06/W/14-A1 1700)
- Kwon Jay**  
(G3/W/17-A5 1610-20)  
(G6/C/G3/W/45-B2 1420)
- Kwon Young Oh**  
(P11/E/22-B3 1150)
- Kylikilanti Antti**  
(G1/E/10-A3 1620-23)
- Kylling Arve**  
(MI08/W/10-A4 1805)
- Kyrö E**  
(JSM01/W/37-A5 1400)
- Kyrölä Erkki**  
(JSA45/W/04-B5 1110-10)  
(JSA45/W/12-B4 1620)
- Kyzyrov Yuriy**  
(JSA20/C/JSM01/E/32-A4 1200-15)
- (**
- La Rocca M.**  
(JSS46/W/09-B4 0930-05)  
(JSV47/W/15-B5 1400-08)  
(JSV47/W/29-B5 1400-22)  
(JSV47/W/30-B5 1400-23)  
(ST5/W/56-B3 0900-01)
- Laakso**  
(JSA06/L/06 0935)
- Labak Peter**  
(ST3/P/4-B5 1115)  
(ST3/P/6-B5 1230)
- LaBelle J.**  
(GA2.02/E/08-B5 1100)
- Labendz Daniel**  
(GA1.02/W/16-A1 1050)
- Labitzke Karin**  
(MW08/E/02-A2 1500)  
(MW08/E/03-A2 1430)
- Labonnette D.**  
(JSM26/W/29-B2 1700-09)
- Labonnote L. C.**  
(MI06/E/10-B2 1150)
- Lacasse Christian**  
(VS3/W/27-B3 0900-05)
- Lacassin Robin**  
(ST2/E/01-A3 1100)
- Lachlan-Cope Tom**  
(MI08/E/07-A3 1115)  
(MI08/W/19-A3 1130)  
(MI04/W/29-B4 1505)
- Lackie Mark A.**  
(GA1.04/W/06-A4 0930)
- Ladkin Russ**  
(MI08/E/07-A3 1115)  
(MI08/W/19-A3 1130)
- Ladkin Russell**  
(MI04/W/29-B4 1505)
- Laeufer G.**  
(JSV36/W/06-B3 1400-02)  
(JSV36/W/24-B3 1400-05)
- Lafleur Caroline**  
(P11/E/16-B4 1420)
- Lagerloef G. S. E.**  
(JSM41/W/27-B5 0930)
- Lagerloef Gary**  
(JSP25/W/67-B5 1150)
- Lagg A.**  
(GA4.10/W/26-A5 1035)
- Lagios E.**  
(JSP23/W/38-B2 1720)
- Lagmay Alfredo**  
(VS2/C/U6/W/12-B3 1400-32)
- Lagouvardos K**  
(MI05/L/06-A4 1400-09)
- Lagova Natalia**  
(ST1/E/74-A2 1400-04)
- Lagun Victor**  
(JSP21/W/14-A5 1210)  
(JSM18/W/09-A4 1620)  
(MI05/W/10-A5 1110)
- Lahav Rohen**  
(MI09/W/12-A5 1145-14)
- Lahoz W A**  
(MW01/W/12-A5 1150-01)  
(MI12/W/01-B4 1420)
- Lakhina G. S.**  
(GA 4.08/E/22-B3 1555)  
(GA3.02/E/03-B3 0900-08)  
(GA3.05/E/17-B3 0900-23)  
(GA3.08/E/07-B1 1740)  
(GA4.05/E/01-A1 1210)
- Lal Manohar**  
(JSM01/W/101-A5 1740)
- Lal Shyam**  
(MI02/E/08-A4 0930)
- Laliam M. S.**  
(HS1/W/75-B5 0830-09)
- Lam Hing-Lan**  
(JSA06/W/17-A1 1155-14)
- Lam M. M.**  
(P 14/E/09-A4 1400-11)
- Lamarche Juliette**  
(GA1.04/W/35-A4 0930-11)
- Lamarque Jean-François**  
(JSM26/W/13-B1 1420)
- Lamash B. E.**  
(GA1.05/E/21-A5 1220)
- Lambeck Kurt**  
(JSS31/L/02-B2 1520)  
(JSG11/W/06-A3 1720)  
(JSH12/E/04-A5 1400)
- Lambert D**  
(MI05/L/03-A4 1140)  
(MI05/W/08-A4 1400-07)
- Lambin Eric**  
(U2/E/17-A2 1600)
- Lammer Helmut**  
(GA4.10/L/03-A4 1110)  
(JSA10/W/13-A3 1000)
- Lammers Richard**  
(HW1/L/11-A4 1430)
- Lamontagne M.**  
(ST2/E/50-A5 1130)
- Lamy P.**  
(GA4.02/W/29-A4 1545)
- Lan L. T. P.**  
(GA1.04/W/24-A5 1100)
- Lanari R.**  
(JSV36/W/23-B3 1515)
- Lancelot Ch.**  
(P11/W/08-B5 1600)
- Lande J.**  
(GA4.08/W/03-B4 0930)  
(GA4.08/W/16-B4 1610)
- Lander J. F.**  
(JSS42/W/02-B5 1110)
- Landgraf M.**  
(JSA10/W/16-A3 1130)
- Landini A. M**  
(JSA19/W/11-A4 1400-04)



# INDEX

- Landis Robert**  
(U7/L/06-B1 1200)
- Landwehr Jurate**  
(HW1/E/02-A4 0930)
- Lane Stephen J.**  
(VS2/W/02-B3 1400-02)
- Lane Todd P**  
(MW07/E/04-A4 0900)
- Lane-Serff Gregory**  
(P14/W/03-A4 1400-05)
- Lanfear Kenneth J.**  
(HW1/W/02-A4 1130)
- Lang H.**  
(G1/E/31-A3 1620-65)
- Lang Herbert**  
(HS4/W/29-A5 1450)
- Lang K.**  
(JSP23/E/03-A6 0930)
- Lang Stephen E.**  
(MI04/W/06-B3 1105)
- Langbein Irmgard**  
(MI12/W/16-B5 1215)
- Langbein John**  
(JSV36/W/21-B3 1400-01)
- Lange Jens**  
(HS4/W/28-A5 1430)
- Lange M**  
(MW04/W/01-A1 0950)
- Lange Martin**  
(JSA45/W/10-B5 0900)
- Langel Robert A.**  
(GA5.08/E/02-B1 0920)
- Langematz U**  
(JSM01/W/05-A1 1700)  
(JSM01/W/16-A5 1110)
- Langematz Ulrike**  
(MW01/W/11-A5 1550)  
(MI12/W/07-B4 1030)
- Langer J**  
(MI02/W/05-A5 0950)
- Langereis C. G.**  
(GA1.03/W/15-B3 1540)  
(GA1.15/W/01-B4 1415)  
(GA1.15/W/04-B4 1500)
- Langevin Y.**  
(JSA10/W/03-A2 0930)
- Langford Andrew O.**  
(JSM26/W/13-B1 1420)
- Langlais Alexandrescu**  
(GA5.09/W/02 A2 0950)
- Langlais Benoit**  
(GA5.09/W/02 A2 0950)  
(GA1.07/W/04-B2 1100)  
(GA5.08/W/02-B1 1005)  
(JSA37/W/08-B3 1430)
- Langland Rolf**  
(MI05/E/25-A2 1100)
- Langley R. B.**  
(JSG28/E/05-B2 0950)
- Langmuir C. H.**  
(JSV30/W/04-B1 1400-07)
- Langston C. A.**  
(ST4/W/30-B2 1400)
- Lankreijer Anco**  
(JSS 44/E/02-B4 1440)
- Lannuzel Serge**  
(JSG11/W/13-A4 1400-09)
- Lanzerotti L. J.**  
(JWA34/W/07-B2 0910)
- Lapenna P. V.**  
(JSA15/E/60-A4 1400-13)
- Lappen Cara-Lyn**  
(MI08/L/02-A4 1220)
- Laqnder James F.**  
(JSP23/W/30-A5 830-01)
- Lara Alejandro**  
(GA4.03/E/02-B4 1645)
- Larchevêque M.**  
(MI10/E/14-B2 1520)  
(MI11/E/04-B5 1430)
- Lario D.**  
(GA4.04/E/01-B5 1210)
- Larionov V. I.**  
(ST3/E/01-B5 1400)  
(ST3/E/05-B5 0930)  
(JSP23/E/33-A5 1640)
- Larkin Alice**  
(JSA16/W/03-A3 1430)
- Larkina V. I**  
(ST1/E/03-A4 0930-26)  
(ST1/E/03-A4 0930-25)  
(JSA15/E/25-A5 1400-08)
- Larkina Vera**  
(JSP23/W/39-B1 1520)
- Larry J.**  
(JSA20/W/49-A6 0930)
- Larsen G. B.**  
(JSG28/W/23-B2 1130)
- Larsen Howard**  
(JSM41/W/11-B3 1430)  
(JWM08/W/04-A2 1020)
- Larsen N**  
(JSM01/W/08-A4 1450)
- Larsen S.**  
(MC09/W/07-B2 01)
- Larsen Tine B**  
(JSS13/W/13-A5 1150)
- Larson D.**  
(GA4.05/W/07-A1 1000)
- Larson K**  
(JSH12/C/JSS31/E/05-A5 0930)
- Larson W. A. D.**  
(GA3.02/E/09-B2 1500)
- Larter R. D.**  
(JSV30/L/01-B1 1400-15)
- Lary David**  
(MI02/W/20-A5 1640)
- Lascareo Delfino**  
(JSP23/L/01-A6 0830-05)
- Laske G.**  
(ST5/W/42-B5 1400)  
(ST5/W/L/03-B3 0900-12)
- Laske Gabi**  
(JSS02/W/03-A2 1000)
- Laskownicka Anna**  
(ST1/W/25-A4 0930-02)
- Lasocki Stanislaw.**  
(ST1/W/25-A4 0930-02)
- Lastovicka Jan**  
(JSM01/E/21-A2 1600-16)  
(GA4.08/E/05-B4 1400)  
(JSA45/E/02-B4 1640)
- Latchman Joan L.**  
(JSP23/W/24-B2 1150)
- Laterra Emanuele F.**  
(GA1.02/W/35-A2 0930)
- Lathuillere C**  
(JSM01/P/03-A2 1600-18)  
(JSM01/P/03-A2 1540-18)
- Latif M**  
(MC01/L/12-A3 1020)  
(JSP25/W/13-B5 0950)  
(JSP25/W/19-B5 1720)
- Latif Mojib**  
(JSP25/W/11-B1 1640)
- Latron Jerome**  
(HS4/W/12-A4 1630)
- Latteck Ralph**  
(JSM01/C/MW07/W/09-A2 1600-34)
- Latynina Ludmila**  
(JWS33/E/16 -B2 1635-16)  
(JWS33/E/16-B3 0900-16)
- Lau K.-M.**  
(MI04/W/27-B1 0900-20)
- Laudenbach Nils**  
(ST4/W/17-B3 0830-06)
- Laurain O**  
(G3/E/27-A5 1610-02)
- Laursen I.**  
(GA5.08/E/03-B1 0900)
- Lavender Samantha**  
(P15/E/01-B4 0900)
- Laver Jon**  
(JSA06/L/02-A1 1055)
- Lavielle M.**  
(GA1.02/E/38-A1 1605)
- Lavoie Diane**  
(P09/E/07-A1 1620)
- Law C.**  
(GA4.10/W/13-A4 0930)
- Law Cliff**  
(P08/W/01-A2 1440)
- Law Kathy**  
(MI01/W/12-A1 0945)  
(U3/E/07-A3 1000)  
(U2/E/14-A2 1420)  
(JSM26/W/07-B1 1500)
- Law Rachel**  
(MC01/L/20-A5 1115)
- Lawlis Jeff**  
(JSS07/E/05-A2 1540)
- Lawrence Bryan N.**  
(JSM01/E/31-A3 1430)  
(JSM01/E/39-A1 0940)
- Lawrence Martin**  
(U8/W/03-B3 1425)
- Lawson R. Paul**  
(MI04/W/15-B4 1420)  
(MI08/W/03-A4 1500)
- Lawton R. O.**  
(MI06/W/15-B1 0910)
- Laxon Seymour**  
(P13/E/15-B2 1500)  
(JSA09/W/01-A2 1145)
- Lay T.**  
(JSA17/E/01-A4 1150)
- Layne G. D.**  
(JSV30/W/02-B1 1400-06)
- Lazare M**  
(MI01/L/04 1055)
- Lazaro Clara**  
(G3/E/01-A5 1610-26)  
(JSV36/E/26-B3 1400-10)
- Lazarus A. J.**  
(GA4.04/W/15-B5 1450)  
(GA3.04/W/41-B1 1520-10)
- Lazarus Alan J**  
(GA3.10/W/22-A6 1700-14)  
(GA4.01/E/09-A2 1200)
- Lazic Lazar**  
(MI05/W/06-A5 1150)
- Lazo Bienvenido**  
(GA2.07/E/04-A2 0930-05)
- Lazutin L. L.**  
(GA3.02/E/05-B3 0900-21)
- Lazzara Matthew**  
(JSM41/E/28-B3 1515)  
(JSM41/E/22-B4 0945)
- Le Cocq Catherine M.**  
(G1/W/44-A3 1620-48)
- Le G.**  
(GA3.03/W/11-B4 1200)
- Le Goff M.**  
(GA1.04/L/04-A6 0900)  
(GA1.04/W/10-A6 0940)
- Le Guan**  
(GA3.08/W/05-A6 1040)  
(GA3.08/W/21-A6 0900)  
(GA4.08/E/21-B3 0900-13)
- Le Huy Minh**  
(JSA17/W/15-A4 1410)
- Le Masurier Wesley E.**  
(JSA09/E/12-A2 0930)
- Le Meur Emmanuel**  
(JSH12/W/09-A4 1400-03)
- Le Mouel Jean-Louis**  
(JSA15/E/10-A3 1640)  
(JSA15/W/10-A4 0900)  
(GA5.01/W/18 A1 0950)  
(JSA15/W/23-A3 0930)  
(JSA17/C/GA1.19/W/09-A4 0950)  
(JSA17/W/03-A4 1230)  
(JSA17/W/15-A4 1410)  
(ST1/W/35-A2 1400-21)  
(GA5.08/W/02-B1 1005)
- Le Provost C.**  
(P13/W/12-B2 1110)  
(U7/W/02-B1 0830-11)
- Le Treut Herve**  
(MW02/E/02-B3 1640)  
(MW02/E/05-B3 1100)
- Leach D.**  
(GA1.04/L/04-A6 0900)
- Leaitch R**  
(MI01/L/04 1055)
- Leaitch Richard**  
(MI01/W/04-A1 1640)  
(MI01/W/12-A1 0945)
- Leaitch W R**  
(MI01/W/03-A1 0900-03)
- Lean H W**  
(MI05/E/20-A3 1700)
- Lean Judith**  
(JSA16/E/12-A3 0830-14)  
(MW08/W/01-A2 1530)
- Learner R C M**  
(MC08/W/07-A3 1210)
- Leary Dr. Colleen A.**  
(MI05/W/09-A4 1400-10)
- Leat P. T.**  
(JSV30/L/01-B1 1400-15)
- Leat Philip**  
(JSV22/W/05-A5 1630)
- Leavesley George**  
(HW4/W/02-B2 1000)
- Lebedev K.V.**  
(P12/E/01-A1 1030-04)  
(P12/W/06-A1 1030-10)
- Lebedev Igor**  
(JWS33/W/17-B2 1635-17)  
(JWS33/W/17-B3 0900-17)
- Lebedev M. M.**  
(JSP25/C/U2/E/02-B1 0830-03)
- Lebedev S. A.**  
(JWS33/W/03-B2 1145)
- Lebreton J. P.**  
(JSA10/L/01-A3 0900)  
(JSA10/W/06-A2 1430)
- Lecointre Jerome**  
(JSP23/E/49-B2 0830-07)
- Leder S.**  
(JSM26/E/13-B3 0850)
- Ledrew Ellsworth F.**  
(JSM41/W/12-B4 1720)
- Ledvina S. A.**  
(GA4.10/W/18-A5 1230)
- Lee C.W.**  
(JSP23/C/U5/E/20-B2 1110)
- Lee Chi-Yu**  
(JSV30/E/09-B1 1400-02)
- Lee Dong-Hun**  
(GA3.02/W/34-B3 1120)  
(GA3.04/W/31-B1 1520-31)  
(GA3.04/W/32-B2)
- Lee G.**  
(GA3.04/W/07-B2 1510)
- Lee Guenho**  
(JSA06/W/28-A1 1155-13)
- Lee Jae-Young**  
(P10/W/23-A5 0930)
- Lee Jenn-Taur**  
(G5/W/21-A4 1506-04)
- Lee Kyung-Ho**  
(JSS07/E/05-A2 1540)
- Lee Lou**  
(JSG28/W/20-B2 1400-07)
- Lee III Robert B.**  
(JSA16/E/19-A3 0830-22)  
(JSA16/W/15-A3 0830-41)
- Lee Sunhee**  
(JWM08/W/04-A2 1020)
- Lee T. O.**  
(GA1.05/W/19-A6 1500)  
(GA1.05/W/22-A6 1700)
- Lee William H. K**  
(U3/W/21-A30900-17)
- Leena P**  
(MI05/E/17-A5 1230)
- Lees Jonathan**  
(ST4/W/14-B2 1700)  
(ST4/W/15-B3 1500)
- Lees Jonathan M.**  
(JSS46/W/01-B4 1230)  
(JSV30/W/11-B1 0900)  
(JSV47/W/25-B5 1400-18)  
(ST4/W/36-B3 1440)  
(JSV47/W/04-B5 0900)  
(ST2/W/13-A3 0845)
- Lees Matthew**  
(HW4/E/04-B2 1100)
- Leeuwenburgh O.**  
(G2/W/03-A2 1630-18)
- Lefebvr B.**  
(GA4.05/W/01-A1 1220)
- Lefebvre B.**  
(GA4.04/W/08-B5 0830-04)
- Lefevre F.**  
(JSM26/E/18-B2 1700-06)  
(P13/W/12-B2 1110)  
(U7/W/02-B1 0830-11)
- Lefevre Franck**  
(MW01/W/02-A5 1150-04)
- Legen'ka A.D.**  
(JSA15/E/31-A5 1400-15)
- Legrand Michel**  
(MI01/E/22-A2 1700)
- Legras B.**  
(JSM26/E/17-B3 0910)  
(JSM26/E/18-B2 1700-06)  
(JSM26/L/04-B2 1700-16)
- Legresy Benoit**  
(JSH12/W/03-A5 0830)
- Legros Hilaire**  
(JSA17/W/01-A4 1510)
- Leguizamon S.**  
(JSM41/E/03-B5 1105)
- Legutke Stefanie**  
(JSP25/W/11-B1 1640)
- Lehmacher G**  
(JSM01/W/41-A4 1150)
- Lehtinin Markku**  
(GA2.01/W/09-A1 1400)
- Lei X**  
(G3/W/09-A5 1610-27)
- Leibundgut Chris**  
(HS4/L/03-A4 0930)
- Leibundgut Christian**  
(HS4/W/11-A4 1600)  
(HS4/W/14-A4 1710)
- (JSP39/W/16-B4 1210)**

- (HS4/W/28-A5 1430)  
**Leighton H**  
 (MI01/L/04 1055)  
**Leighton Henry**  
 (MI01/W/04-A1 1640)  
**Leinen Stefan**  
 (G1/W/25-A3 1620-10)  
**Leite F**  
 (G3/L/8-A5 1400)  
**Leitinger R**  
 (JSA06/W/15-A2 1010)  
**Lellouch E.**  
 (MC09/W/10-B2 1515)  
**Leloup Phillipe Herve**  
 (ST2/E/01-A3 1100)  
**Lemaire J.**  
 (GA3.05/E/02-B3 0850)  
**Lemaire Philippe**  
 (JSA16/W/06-A3 0830-48)  
**Lemaitre Y**  
 (MI05/L/06-A4 1400-09)  
**Lemke Peter**  
 (JSA09/E/07-A2 1645)  
 (JSM04/E/03-A2 1510)  
 (JSM04/W/11-A2 1735)  
 (MC01/L/10-A2 1550)  
**Lemoine F G**  
 (G3/E/07-A5 1610-04)  
**Lemoine Frank G.**  
 (G3/E/05-A5 1200)  
**Lemoine Jean-Michel**  
 (G3/E/27-A5 1610-02)  
**Lemos C.**  
 (JSS42/E/03-B5 1700-12)  
**Lenardic Adrian**  
 (ST4/W/06-B2 1200)  
**Lenihan J M**  
 (MC01/W/04-A5 1425)  
**Lenk Onur**  
 (G5/E/23-A4 1230-08)  
 (JSS31/L/04-B2 0830-17)  
**Lennartsson O. W.**  
 (GA3.08/L/01-B2 0900-10)  
 (GA3.08/L/01-B2 900-10)  
**Lenschow Donald**  
 (JSM43/E/01-B4 1050)  
**Lensky Itamar M.**  
 (MI06/W/04-B1 1710)  
**Lensky Nadav**  
 (VS2/W/06-B3 0830)  
**Leon G Byerley**  
 (MI03/W/06-A3 1000)  
**Leonard Kins**  
 (P07/L/03-A3 0900-08)  
**Leonard Mark**  
 (ST5/E/19-B3 1205)  
 (ST5/E/28-B3 1400-04)  
**Leonard S R**  
 (MI08/E/02-A4 0945)  
**Leonard Steven**  
 (MI08/W/19-A3 1130)  
 (MI04/W/29-B4 1505)  
**Leonardi V.**  
 (ST1/E/26-A2 1400-05)  
**Leonhardt Roman**  
 (GA1.03/E/09-B2 1100)  
 (GA1.03/W/31-B2 1120)  
**Leonovich Anatoly S.**  
 (GA3.04/L/06-B1 1520-12)  
**Lepidi S.**  
 (GA3.04/L/16-B2 1600)  
 (GA3.04/W/41-B1 1520-10)  
**Lepidi Stefania**  
 (GA3.10/W/22-A6 1700-14)  
**Lepping G A**  
 (GA4.02/W/24-A4 1400-22)  
**Lepping R P**  
 (GA4.02/W/24-A4 1400-22)  
 (GA4.01/W/11-A2 1100)  
 (GA3.02/W/12-B2 1230)  
 (GA3.02/W/39-B2 1110)  
 (GA3.02/W/40-B3 1050)  
 (GA4.04/W/12-B5 1750)  
 (GA4.08/W/12-B4 1635)  
 (GA3.04/W/41-B1 1520-10)  
**Lerner David N.**  
 (HS5/W/31-A3 0900)  
**Lesack L.**  
 (HW3/W/06-B4 1140)  
**Lesage Philippe**  
 (JSV47/W/02-B5 1400-17)  
 (JSV47/W/19-B5 1400-16)  
**Lescinsky David T.**  
 (VS3/W/26-B3 0900-01)  
 (VS3/W/26-B3 1630)  
**Lesht Barry**  
 (MC08/W/02-A4 1005)  
**Lesik Oksana**  
 (ST2/E/28-A5 1400-10)  
 (ST2/E/25-A5 1400-12)  
 (ST5/E27-B1 0830-13)  
**Lesins G**  
 (MC07/W/11-A3 1015)  
 (MI01/L/04 1055)  
**Leslie Lance**  
 (MW07/E/07-A4 1210)  
**Leslie Wayne**  
 (P12/W/17-A1 1720)  
**Leske R. A.**  
 (GA4.04/W/14-B5 1620)  
**Lesquer Alain**  
 (JSS46/W/14-B4 0950)  
**Lester M.**  
 (GA2.02/W/04-B4 1700)  
 (GA2.02/W/14-B4 0930-09)  
 (GA3.03/W/06-B4 1640)  
 (GA3.08/W/26-A6 1710)  
**Lester Mark**  
 (GA2.01/E/05-A1 0950)  
 (JSA20/W/29-A4 1200-13)  
**Lesur Vincent**  
 (GA5.09/E/01 A2 1150)  
**Leszczynski Wojciech**  
 (G1/E/26-A3 1620-60)  
**Letreut Herve**  
 (MC01/W/15-A2 1740)  
**Leuliette E. W.**  
 (JSM41/W/09-B4 1515)  
**Leuliette Eric W.**  
 (JSG14/E/20-A3 1700-08)  
**Leung L R**  
 (MC01/E/23-A4 1035)  
 (JWM08/W/10-A2 1650)  
**Lev Zelenyi**  
 (GA3.08/W/01-B1 0900-05)  
**Levchenko I.**  
 (ST4/E/71-B2 0930-25)  
**Leven Carsten**  
 (GA1.05/W/41-A5 0900-09)  
 (GA1.05/W/42-A6 1100)  
**Leven J. H.**  
 (JSS44/L/08-B4 0930-43)  
**Levin B. W**  
 (JSP49/W/09-B5 1720)  
 (SW1/W/02-B5 1000)  
**Levin Boris W**  
 (ST1/E/88-A4 0930-17)  
 (JSP23/E/12-B2 0830-05)  
 (JSP23/W/10-B1 1150)  
**Levin Vadim**  
 (ST2/W/13-A3 0845)  
 (ST4/W/14-B2 1700)  
 (ST4/W/15-B3 1500)  
**Levis Samuel**  
 (MC11/E/05-B3 1440)  
**Levitin A. E.**  
 (GA3.05/W/43-B3 0900-41)  
 (GA3.09/W/13-B4 0900-12)  
 (GA4.08/E/04-B3 0900-15)  
 (GA5.08/W/05-B1 1055)  
 (GA3.06/W/17-A3 1700)  
 (GA3.10/W/17-A6 1700-07)  
**Levitin Anatoly**  
 (GA5.08/W/06-B1 0945)  
**Levitskiy Vladimir V.**  
 (JSP39/W/22-B3 1448-17)  
**Levitte Dov**  
 (G1/W/16-A3 1620-06)  
**Levitus Sydney**  
 (JSP25/E/02-B4 1010)  
**Levshin A.**  
 (U8/E/09-B3 1155)  
**Levshin Anatoli**  
 (JSA09/E/05-A3 0900)  
**Levy M. A.**  
 (JSP39/W/42-B2 0930)  
**Levy M F**  
 (JSA06/W/15-A2 1010)  
**Lewandowski Marek**  
 (GA1.04/W/08-A4 0930-05)  
 (GA1.04/W/35-A4 0930-11)  
**Lewchuk M.T.**  
 (GA1.04/L/04-A6 0900)  
 (GA1.04/W/03-A4 0930-15)  
 (GA1.04/W/05-A4 0930-14)  
**Lewis Andrew**  
 (GA5.01/E/07 A1 1445)  
**Lewis C.**  
 (JSP39/W/40-B2 1620)  
**Lewis G. D.**  
 (P15/L/22-B3 1135)  
**Lewis Gregory M.**  
 (JSP39/W/02-B3 1421-08)  
 (MI10/W/20-B2 1635)  
**Lewis J. Patrick**  
 (GA2.02/E/10-B5 1700)  
**Lewis Trevor**  
 (JSS44/E/31-B4 1130)  
 (MC02/E/11-B1 1150)  
**Lfcthi Daniel**  
 (MC01/E/38-A5 1000)  
**Lhasuren Erdenedalai**  
 (ST2/E/39-A3 0900)  
**Li**  
 (GA3.05/W/42-B3 1640)  
 (MI04/L/08-B1 1720)  
**Li Baosheng**  
 (ST6/C/JSS02/W/19-A1 0830-18)  
**Li Chongyin**  
 (JSP25/P/06-B1 1520)  
**Li Fang**  
 (MI09/E/05-A5 1145-04)  
**Li G Wolf D**  
 (JSH12/W/13-A5 1430)  
**Li Hui**  
 (G3/W/09-A5 1610-27)  
 (G3/W/23-A5 1610-28)  
 (G5/W/16-A4 1542-02)  
 (G5/E/42-A4 1544-03)  
**Li J.-J.**  
 (GA1.05/E/17-A6 1630)  
**Li J.T. Hoeksema**  
 (GA4.02/W/10-A4 1650)  
**Li Jiancheng**  
 (G3/L/11-A5 1610-13)  
 (G3/W/24-A5 1610-29)  
 (G3/W/27-A5 1610-86)  
 (G3/W/50-A5 1610-55)  
**Li Jiren**  
 (JSM41/W/17 -B5 1430)  
**Li Juan**  
 (JSP23/C/U5/E/15-A6 1500)  
**Li Jun**  
 (JSM18/W/08-A5 1100)  
**Li K.**  
 (ST3/W/39-B4 1400-08)  
**Li Li**  
 (U3/P/03-A3 0900-09)  
**Li Lin**  
 (JSM04/W/03-A2 1030)  
**Li Long**  
 (JSM43/W/12-B5 1120)  
**Li Man**  
 (MC08/W/03-A3 1650)  
**Li Mian**  
 (P10/W/24-A5 1520)  
**Li Qinghe**  
 (JSS07/P/01-A2 1105)  
 (ST4/E/29-B1 0830-14)  
**Li Shenghui**  
 (JSS44/W/02-B5 0930)  
 (GA1.02/W/39-A2 0930)  
**Li Shengle**  
 (G5/E/30-A4 1115-05)  
**Li Shian-Jiann**  
 (MW01/W/01-A5 1105)  
**Li Shi-Yu**  
 (ST1/W/06-A2 1400-17)  
**Li Shuhua**  
 (JSM01/W/101-A5 1650-01)  
 (JSM26/W/02-B1 1650)  
**Li Tie-Jun**  
 (ST4/W/80-B1 0830-07)  
**Li Tim**  
 (MC10/P/02-B1 1625)  
**Li Weiping**  
 (MC10/W/02-B1 1650)  
**Li X.**  
 (GA3.05/E/07-B3 0930)  
**Li X. S.**  
 (GA6.01/E/02-A5 1120)  
**Li Xiang**  
 (MI09/W/16-A5 1710)  
**Li Xinlin**  
 (GA3.02/W/41-B2 1600)  
**Li Y. X**  
 (G5/W/27-A4 1512-07)  
**Li Yuguo**  
 (GA1.02/P/02-A1 1605)  
**Li Z. X.**  
 (G5/W/16-A4 1542-02)  
**Li Zhanqing**  
 (MC01/W/22-A1 1500)  
 (MC07/W/14-A3 1055)  
**Li Zhenghang**  
 (G1/W/30-A3 1620-13)  
**Li Zhengxiang**  
 (GA5.11/L/02 A3 1430-03)  
**Li Zheng-xin**  
 (G5/E/18-A4 1525)  
 (G5/E/42-A4 1544-03)  
 (JSG14/E/01-A3 1700-13)  
**Liang Guoping**  
 (ST4/E/24-B2 0930-24)  
**Liangping Xiong**  
 (ST4/W/39-B1 1400-07)  
**Liao J-H**  
 (GA3.05/W/03-B3 0900-10)  
**Lichner Lubomir**  
 (HS3/W/22-A2 1135)  
**Lidberg Martin**  
 (G1/W/43-A3 1620-47)  
**Liddicoat Joseph C.**  
 (GA1.03/W/28-B2 1140)  
**Lide Tian**  
 (HS2/W/27-B2 1420)  
**Lidia Demoulin Pascal**  
 (GA4.02/W/14-A4 0925)  
**Liebermann Robert C.**  
 (ST6/JSS02/W/19- A1 0830-18)  
**Liebsch G**  
 (JSG11/E/13-A4 1400-05)  
**Liemohn M.**  
 (GA4.08/W/16-B4 1610)  
 (GA3.05/W/38-B3 1700)  
 (GA4.08/W/03-B4 0930)  
 (GA3.05/E/15-B3 0900-39)  
**Lienert Barry**  
 (MC08/L/09-A3 1545)  
 (MC08/L/14-A4 0945)  
**Lifeng Luo**  
 (MC01/W/19-A1 1715)  
**Li-Juan He**  
 (JSS44/W/12-B4 0930-40)  
 (ST4/W/41-B1 1400-01)  
**Lilienberg Dmitri A**  
 (JSG11/E/17-A3 1700)  
**Lilje Mikael**  
 (G5/E/36-A4 1215)  
 (G6/C/G1/W/19-B1 1540)  
**Liljegren James**  
 (MC08/W/02-A4 1005)  
 (MI08/W/13-A4 1530)  
**Lilley Ted**  
 (GA1.02/L/AW1-A2 0930-25)  
 (GA1.02/W/31 1000)  
 (GA1.02/E/01-A2 0930-22)  
**Lima J. Nuno**  
 (JSV36/E/26-B3 1400-10)  
**Lima Jos N.P.**  
 (JSP23/E/23-B2 0830-09)  
**Lima Noemi**  
 (JSP21/W/10-A5 1150)  
**Lin Ching I**  
 (MC08/W/03-A3 1650)  
**Lin H**  
 (MI01/L/04 1055)  
 (MI01/W/03-A1 0900-03)  
**Lin Jau-Yi**  
 (ST3/W/30-B3 1115)  
**Lin Jun**  
 (GA4.02/W/09-A4 1125)  
**Lin Lin**  
 (ST4/W/42-B3 1220)  
**Lin Naiguo**  
 (Ga3.02/W/12-B2 1230)  
**Lin R. P.**  
 (GA3.02/E/09-B2 1500)  
 (GA3.02/W/12-B2 1230)  
 (GA3.08/W/33-B1 1130)  
 (GA4.05/W/07-A1 1000)  
 (GA4.10/W/13-A4 0930)  
**Lin Wayne**  
 (JSV30/E/09-B1 1400-02)  
**Lin Ying**  
 (MC04/E/04-B2 1625)  
**Lin Yu**  
 (GA3.08/W/11-B1 1620)  
**Lin Zhonghui**  
 (HW4/E/07-B2 0900-06)  
**Linden Anders H.**  
 (GA5.12/E/03-A2 1600-05)  
**Linden P. F.**  
 (JSP39/E/19-B2 1050)  
 (JSP39/L/02-B2 1010)  
**Linden Prof. Paul**  
 (JSP39/W/43-B2 0900)  
**Linderfelt W R**  
 (HW5/W/11-A3 0940)  
**Lindholm C.**

# INDEX

- (ST2/E/31-A5 1200)  
(ST2/E/43-A5 1400-31)
- Lindholm C. D.**  
(ST2/E/11-A5 1215)  
(ST2/E/12-A5 1400-32 )  
(ST3/E/13-B4 1400-15)  
(ST3/E/14-B5 1130)
- Lindner K**  
(MI02/NW/05-A5 0950)  
(G1/L/04-A3 1620-85)  
(JSA09/L/02-A2 1230)  
(JSA09/W/11-A2 0930-04)
- Lindsay Cara**  
(G1/C/G5/W/18-A3 1620-103)
- Lindsay Jan**  
(VS2/W/19-B3 1400-12)
- Lindsey R**  
(MI08/W/11-A3 1720)
- Lindström Göran**  
(HS1/W/44-B4 1420)
- Lindzen Richard S.**  
(MC02/E/17-B1 1400)
- Lingenfelter G.**  
(JSM26/W/11-B1 0940)
- Lin-Gun Liu**  
(ST6/E/05-A1 0830-15)  
(ST6/W/07-A1 0830-09)
- Linker Jon A.**  
(GA3.09/W/27-B4 1035)
- Linkin V.**  
(MC09/W/07-B2 01)
- Linkwitz Klaus**  
(G1/E/22-A3 1620-58)
- Linthead Conor**  
(HW2/W/04-B1 1120)
- Linthe Hans-Joachim**  
(JWS33/E/13-B2 1500)  
(GA5.06/E/02 A3 0920)
- Linying Wang**  
(ST1/P/05-A3 0900-08)
- Lionello Roberto**  
(GA3.09/W/27-B4 1035)
- Liou Chi-Sann**  
(MC04/W/05-B2 1515)
- Liou Kan.**  
(GA3.02/W/03-B3 0900-14)  
(GA3.02/W/15-B2 1005)  
(GA3.02/W/58-B3 0900-22)  
(GA3.03/L/01-B4 1400-04)  
(GA3.02/W/16-B2 0900)
- Lioudmila Jdanova**  
(JSS44/E/11-B4 0930-29)
- Lipman Peter**  
(VS2/W/13-B3 1050)
- Lippincott C. R.**  
(JSA20/W/28-A5 1200-10)
- Lirio Juan M.**  
(GA1.03/W/12-B2 1520)
- Lischeid Gunnar**  
(JSA19/W/10-A4 1100)
- Lisov M. G.**  
(JSA27/E/05-B1 1400-08)
- Lisowski Michael**  
(JVS36/W/19-B3 1400-07)
- Lisowsky Mike**  
(JSG28/W/06-B1 1400-06)
- Liss P S.**  
(JSP21/L/03-A4 1720)
- List Roland**  
(MI03/L/02-A3 1220)
- Listanco Eddie L.**  
(JSV30/E/08-B1 1400-01)
- Lister John**  
(JSA17/C/GA1.19/W/02-A4 1630)
- Litasov Konstantin**  
(JSS02/W/05-A1 0830-01)  
(JSS02/W/09-A1 0830-02)
- Litasov Yury**  
(JSS02/W/05-A1 0830-01)
- Lithgow-Bertelloni Carolina**  
(JSS13/W/10-A5 1100)
- Lithoprobe Scientists**  
(JSS44/L/01-B4 1210)
- Little R.**  
(JSS31/L/02-B2 1520)
- Littlewood I.G.**  
(HW1/L/01-A4 1130)
- Litvak A. G.**  
(GA2.03/L/01-B3 1400)
- Litvin Yuriy**  
(JSS02/E/03-A1 0830-05)
- Litvinenko Oleg A.**  
(JSA20/E/11-A4 1200-29)
- Litvinenko Y. E.**  
(GA4.04/E/05-B5 0940)
- Litynska Z**  
(JSM01/W/37-A5 1400)
- Liu Bin**  
(JSS02/E/02-A1 0830-04)
- Liu Chongbing**  
(G3/L/40-A5 1610-98)  
(G3/L/40-A5 1610-98)  
(ST4/L/40-B1 0830-32)
- Liu D Z**  
(G3/W/09-A5 1610-27)
- Liu Dajie**  
(G5/W/14-A4 1510-06)
- Liu Futian**  
(ST2/E/52-A3 1200)  
(JSS44/W/16-B5 1150)  
(ST4/E/12-B1 0830-15)
- Liu Gerald**  
(JSG28/W/20-B2 1400-07)
- Liu Guangren**  
(MI01/E/20-A2 1450)
- Liu Guodong**  
(JSA15/E/52-A5 0830-09)
- Liu Guowei**  
(HS1/W/65-B4 1500)
- Liu H.**  
(JSG28/W/04-B2 1400-13)
- Liu Han-Li**  
(JSM01/W/31-A3 0900)
- Liu Hongbing**  
(ST4/L/05-B2 0930-12)
- Liu Hui .**  
(P12/E/04-A1 1110)
- Liu Huixin**  
(JSA45/W/13-B4 1145)
- Liu Jianhua**  
(JSS44/W/16-B5 1150)  
(ST4/E/12-B1 0830-15)
- Liu Jinli**  
(MI06/E/04-B1 1630)
- Liu Jinzhao**  
(ST4/E/24-B2 0930-24)
- Liu Jun**  
(ST6/JSS02/W/19- A1 0830-18)
- Liu J.Y.**  
(JSA15/E/31-A5 1400-15)
- Liu Jie**  
(JSP23/C/U5/E/21-B2 0830-11)
- Liu Jingnan**  
(G1/W/30-A3 1620-13)  
(G3/W/27-A5 1610-86)  
(G5/W/09-A4 1445)
- Liu Jinli**  
(MI09/E/05-A5 1145-04)
- Liu Kuanhou**  
(JSA40/W/02-B5 1400-06)
- Liu Lintao**  
(JSA40/E/12-B5 1400-01)  
(JSP25/E/29-B1 0830-02)
- Liu Liping**  
(JSM24/E/02-B1 1440)
- Liu Nana**  
(U7/W/12-B1 0830-02)
- Liu Ping**  
(MC10/E/03-B1 1515)  
(MC10/W/03-B1 1220)
- Liu Q W**  
(JSG11/W/22-A3 1150)  
(G5/W/27-A4 1512-07)
- Liu Qinyu**  
(JSP25/E/03-B2 1130)
- Liu S.**  
(HS1/W/19-B4 1620-01)
- Liu Saijun**  
(JSS44/C/U4/W/07-B4 0930-42)
- Liu Suxia**  
(HS1/W/28-B5 0830-04)  
(HW4/E/07-B2 0900-06)  
(JSM24/E/12-B1 1710)  
(JSM43/E/06-B4 1130)
- Liu W. Timothy**  
(JSM41/W/24-B4 1155)  
(JSP25/E/21-B3 1420)  
(JWS33/W/19-B2 1635-29)  
(JWS33/W/19-B3 0900-29)
- Liu Wen-Cheh**  
(HS5/W/25-A2 1525)
- Liu Xiang**  
(P13/E/16-B2 1440)
- Liu Xu**  
(G4/W/10-A3 1620-26)
- Liu Y.**  
(JSG28/W/02-B1 1400-09)
- Liu Yang P.**  
(P09/E/03-A2 1010)
- Liu Yimin**  
(MC10/E/03-B1 1515)  
(MC10/W/01-B1 1125)  
(MC10/W/03-B1 1220)
- Liu Yonggang**  
(P10/P/01-A4 1520)
- Liu Yongqiang**  
(MI04/W/20-B1 1450)
- Liu Yuyan**  
(GA1.04/W/11-A6 1440)
- Liu Yifan**  
(GA4.10/W/10-A4 1215)
- Liu Z. X.**  
(GA3.02/E/18-B3 0850)
- Liu Zhenxing**  
(GA3.02/E/16-B3 0900-17)  
(GA3.07/E/12-A4 0930-17)
- Livermore R. A.**  
(JSV30/L/01-B1 1400-15)
- Livermore Roy A.**  
(GA1.04/L/01 0930-18)
- Livi S.**  
(GA4.10/W/26-A5 1035)  
(GA3.05/W/05-B3 0900-46)  
(GA3.05/W/25-B3 0900-33)  
(GA3.05/W/28-B3 0830)  
(GA4.08/W/11-B3 1620)  
(GA4.08/W/13-B4 0905)
- Livingston Hugh D.**  
(P07/W/14-A3 1035)
- Livingston J M**  
(MI09/W/14-A5 1030)  
(MI09/W/15-A5 1500)
- Liyan Xinxing**  
(JSA40/W/16-B5 1400-03)
- Lizeca J. L.**  
(JSP23/C/U5/E/20-B2 1110)
- Lizeca Jose Luis**  
(JSV36/L/02-B3 1400-16)
- Ljubushin Aleksei**  
(JWS33/E/16 -B2 1635-16)  
(JWS33/E/16-B3 0900-16)
- Llewelin Ed**  
(VS2/W/17-B3 1400-11)
- Libangoh R.-U.**  
(GA1.04/P/03-A4 1730)
- Lloyd Geoffrey E.**  
(JSS07/W/06-A2 1520)
- Lloyd John W.**  
(HS5/W/34-A3 1000)
- Lloyd Nick**  
(JSM01/E/47-A1 1000)
- Loarn P.**  
(GA4.10/W/26-A5 1035)
- Lobanchenko Alexander**  
(ST1/E/24-A3 0900-04)
- Lobatskaya R.M.**  
(JSP23/E/55-A5 0830-16)
- Loberth Jürgen**  
(JSP21/W/05-A4 1520)  
(JSP21/W/15-A4 1600)  
(JSP21/W/17-A4 1500)
- Lobianco B**  
(G3/W/26-A5 1610-70)
- Lock A. P.**  
(MI04/E/18-B3 1505)
- Locke Corinne A.**  
(JSV36/E/01-B3 1610)
- Lockner D.**  
(JSA15/W/06-A3 1030)
- Loder John W.**  
(P10/W/22-A4 1130)
- Loehnert Ulrich**  
(MI06/W/28-B2 0950)
- Loeng Harald**  
(P14/E/08-A4 1400-07)
- Loewenthal Dan**  
(JWS33/P/2-B2 1550)  
(ST5/L/02-B4 0930-08)
- Lofgren B M**  
(MC01/W/38-A4 1210)
- Logachev Yu. I.**  
(GA3.05/E/19-B3 0900-04)
- Lognonne P.**  
(JSA10/W/03-A2 0930)
- Lognonné Ph.**  
(JSA10/W/06-A2 1430)
- Lohmann U**  
(MI01/L/04-A3 1055)
- Lohmann Ulrike**  
(MI01/W/12-A1 0945)  
(MI01/W/18-A1 1510)  
(MW02/W/01-B3 1620)  
(MW02/W/05-B3 0930)
- Lokhorst B. A.**  
(ST3/W/04-B4 0945)
- Lokshin Yu.**  
(G3/E/26-A5 1610-36)
- Lokshyn Yu.**  
(ST3/W/52-B4 0930-20)
- Lolok David**  
(JVS36/W/03-B3 0900-13)
- Lomakin Pavel**  
(P07/E/02-A3 0900-06)
- Lomax Anthony**  
(ST5/W/39-B5 0910)
- Lomax Antony**  
(JSS46/E/04-B4 1400)  
(ST7/W/03-A2 1605-01)
- London Julius**  
(SA16/E/22-A3 0830-16)  
(JSA45/E/03-B5 1110-11)
- London Steven D.**  
(JSP39/E/17-B2 1520)
- Lonerang Patrick**  
(MW08/W/06-A2 1730)  
(MW08/W/01-A2 1530)
- Long Charles N.**  
(MI10/W/15-B1 1000)  
(MI10/W/18-B2 1735)
- Looper M. D.**  
(GA3.05/E/02-B3 0850)
- Lopanthuk A. A.**  
(G5/P/4-A4 1508-05)
- Lopez Marcelo**  
(GA4.02/W/14-A4 0925)
- Lopez-Loera H.**  
(JSA15/W/24-A4 1400-17)
- Lopez Philippe**  
(MI05/E/29-A4 1100)
- Lopez R. E.**  
(GA3.09/W/12-B4 1400)
- Lopez-Puertas Manuel**  
(MW05/E/01-A2 1115)  
(MW05/W/08-A2 1130)
- Lorén Anders**  
(JSP21/W/02-A4 1150)
- Lorenz Frank**  
(ST2/W/11-A4 1430)
- Lorenz Frank P.**  
(ST5/W/19-B3 1145)
- Lorenz S. J.**  
(MC11/E/06-B4 0900)
- Loskutov Eugene M.**  
(MI11/E/03-B5 1745)
- Loster T.**  
(JSP23/C/U5/W/13-A5 1440)
- Lothar Schüller**  
(MI01/W/05 1740)
- Lotova N. A.**  
(GA4.03/W/14-B4 1630)
- Lott F**  
(MW05/W/17-A4 1530)
- Lott J. E.**  
(HS3/W/27-A2 1450)
- Louden Keith**  
(JSS44/W/03-B4 1400)
- Loughe Andy**  
(JSP25/W/24-B1 0850)
- Loughlin S. C.**  
(VS2/W/14-B3 1150)
- Louis Moresi**  
(ST4/W/62-B3 0830-04)
- Loutre M F**  
(MI07/E/03-A2 1400)  
(MC01/W/11-A3 0945)  
(GA6.01/E/02-A5 1120)
- Louvari E.**  
(ST2/W/14-A4 1400)
- Lovejoy S.**  
(JSP23/W/13-B1 1110)  
(MI10/E/14-B2 1520)  
(JSM43/W/01-B5 1000)  
(JSP39/W/15-B3 1110)  
(MI10/E/10-B2 1705)  
(MI11/E/02-B5 1400)  
(MI11/E/04-B5 1430)
- Lowe D C**  
(MI02/W/07-A4 1600)
- Lowe David**  
(GA5.08/W/12-B1 1135)
- Lowe R P**  
(MW05/W/01-A2 1145)
- Lowe Robert**  
(GA3.07/W/26-A3 0900-08)
- Loves Frank**  
(GA5.09/W/10 A2 0930)  
(GA1.07/W/03-B2 0900)
- Lowman J P**  
(JSS13/C/ST2/W/25-A4 1740)
- Loyer Sylvain**



- (G3/E/40-A5 1610-05)  
**Lozano C. J.**  
 (P11/E/15-B3 1130)  
**Lozano Carl**  
 (P12/W/17-A1 1720)  
**Lozano Socorro**  
 (GA1.05/W/28-A5 0900-04)  
**Lozovatsky Iossif**  
 (JSP39/W/11-B4 0950)  
 (JSP49/W/04-B5 0910)  
 (P11/W/10-B5 1715)  
**Lu Daren**  
 (MI09/E/05-A5 1145-04)  
 (JSM41/E/17-B3 1750)  
**Lu G.**  
 (GA3.02/W/21-B2 1520)  
 (GA3.05/W/06-B3 0900-05)  
 (GA3.09/W/04-B5 1035)  
**Lu Gang**  
 (GA3.05/W/04-B3 0900-45)  
**Lu H. I.**  
 (MW02/W/03-B3 1200)  
**Lu Haibing Daren**  
 (MI06/E/04-B1 1630)  
**Lu J. Y.**  
 (GA4.04/E/03-B5 1510)  
**Lu Riyu**  
 (MC10/W/04-B1 1425)  
**Lu S. L.**  
 (P10/E/14-A3 1500)  
**Lu Shihua**  
 (JSP25/E/21-B3 1420)  
 (P11/E/14-B3 1110)  
**Lu Xinyou**  
 (GA1.02/W/07-A1 1605)  
**Lu Yang**  
 (G3/L/10-A5 1610-11)  
**Lu Yang**  
 (G3/W/42-A5 1120)  
**Lubchich A. A.**  
 (GA3.07/W/16-A4 0930-18.)  
**Lubimov Vladimir**  
 (JSA06/C/U4/E/02-A1 1155-26)  
**Lubin Dan**  
 (MI08/W/04-A4 1050)  
 (MI08/W/14-A3 1635)  
**Lubnina Natalia**  
 (GA1.04/E/12-A5 0900)  
**Luca Crescentini**  
 (JSA47/E/01-B5 1400-05)  
**Luca Gaetano De**  
 (JSA47/W/18-B5 1100)  
**Luceri V.**  
 (G1/W/27-A3 1620-40)  
 (JSG14/W/19-A3 1600)  
**Luckett R.**  
 (VS2/E/13-B3 1130)  
 (VS2/W/14-B3 1150)  
**Luckhurst R**  
 (JSA06/W/17-A1 1155-14)  
**Ludin Andrea**  
 (P07/W/15-A3 1145)  
**Ludmany Andras**  
 (GA6.01/P/08-A5 0900-20)  
**Ludmila Kagan**  
 (GA2.02/L/07-B4 0930-08)  
**Ludmila M. Ka**  
 (GA2.02/L/06-B4 0940)  
**Ludwig Wolfgang**  
 (MC01/W/58-A5 1620)  
**Luebken F.-J.**  
 (JSM32/W/01-B2 1600)  
 (JSM32/W/08-B3 1005)  
**Luehr Birger-G.**  
 (ST1/W/10-A3 0910)  
**Luehr H.**  
 (JSA37/W/03-B3 1630)  
**Luehr Hermann**  
 (JSA20/W/33-A5 1200-11)  
**Luethi Daniel**  
 (MC01/E/25-A5 0915)  
**Lugovenko Igor V.**  
 (JSA40/W/15-B5 1400-02)  
**Lugovenko Vladislav N.**  
 (JSA40/W/15-B5 1400-02)  
**Luhmann J. G.**  
 (GA4.01/W/11-A2 1100)  
 (GA4.02/W/10-A4 1650)  
 (GA4.10/W/33-A4 1400)  
**Lühr Birger-G.**  
 (JSV36/E/07-B3 0900)  
**Lühr H.**  
 (JSA37/W/05-B3 0945)  
 (JSA20/P/01-A5 1501)  
**Lui A. T. Y.**  
 (GA3.02/L/02-B3 0900-24)  
 (GA3.02/W/21-B2 1520)  
 (GA3.02/W/43-B2 0920)  
 (GA3.02/W/49-B3 0900-11)  
 (GA3.02/W/58-B3 0900-22)  
**Lui Anthony**  
 (GA3.02/L/07-B3 1135)  
**Lui Zhenxing**  
 (GA3.10/E/02-A6 1645)  
**Luigi La Volpe**  
 (VS2/E/14-B3 1400-25)  
**Luis Joaquim**  
 (G5/E/46-A4 1548-05)  
**Luthardt W.**  
 (JSM26/W/29-B2 1700-09)  
**Luiz Augusto**  
 (HS5/W/18-A2 1140)  
**Luizar Oswaldo**  
 (GA3.06/L/07-A2 0930-12)  
**Lukianova R. Yu.**  
 (GA3.07/W/68-A5 0900-09 )  
 (GA3.10/W/05-A6 1700-05)  
 (GA 5.06/E/05 A3 1400)  
**Lukin I.**  
 (ST3/P/9-B4 1400-22)  
**Lukk Albert**  
 (ST5/W/22-B4 1400-03)  
**Lukyanov Alexander**  
 (JSM01/W/116-A5 1000)  
**Lulo Arben**  
 (JSA27/E/10-B1 1400-09)  
**Luminita Ardeleanu**  
 (ST1/E/05-A2 1400-30)  
**Lund Björn**  
 (ST1/W/29-A4 0930-34)  
 (ST1/W/57-A3 1110)  
 (ST2/W/24-A5 1400-30)  
**Lund E. J.**  
 (GA4.02/E/02-A4 1400-06)  
**Lund Steve**  
 (GA1.03/W/05-B2 1040)  
**Lundgren P.**  
 (JSV36/W/23-B3 1515)  
**Lundin R**  
 (GA3.06/W/37-A2 1640)  
 (GA2.07/W/16-A1 0855)  
 (GA4.10/W/24-A4 1125)  
**Lundin Rickard**  
 (GA3.04/E/04-B1 1520-23)  
**Lundstedt H**  
 (JSA06/W/19-A2 1130)  
**Lunine Jonathan I.**  
 (JSA10/E/02-A3 0830)  
**Luo B. P.**  
 (MI06/W/26-B2 1110)  
**Luo Lifeng**  
 (MC01/W/29-A3 1205)  
**Luo Q.**  
 (ST3/W/39-B4 1400-08)  
**Luo Xiao-rong**  
 (ST4/W/80-B1 0830-07)  
**Luo Y**  
 (JSM01/W/67-A1 1110)  
 (MC01/E/23-A4 1035)  
 (JSA20/W/02-A4 1200-05)  
**Luo Yiyong**  
 (P10/W/21-A5 1600-02)  
**Luo Yong**  
 (MC01/P/01-A4 1155)  
**Luo Zhicai**  
 (G3/W/31-A5 1610-56)  
**Luthardt J.**  
 (G1/E/31-A3 1620-65)  
**Luthcke Scott B.**  
 (G3/E/05-A5 1200)  
**Luther Mark E.**  
 (JSP23/W/01-B2 1500)  
**Lüthi D.**  
 (JWM08/E/06-A2 1120)  
**Lutikov Alexander**  
 (ST1/W/36-A4 0930-28)  
**Lutsenko E. I.**  
 (MI05/W/10-A5 1110)  
**Lutsenko V.**  
 (GA3.02/L/04-B3 0900-25)  
 (GA3.05/W/32-B3 0900-25)  
**Lutsenko V. N.**  
 (GA3.08/L/02-B1 0900-11)  
**Luttazzi Costante**  
 (P11/W/06-B4 0930)  
**Lyakho Vladimir**  
 (VS2/W/06-B3 0830)  
**Lyard F.**  
 (P13/W/12-B2 1110)  
 (U7/W/02-B1 0830-11)  
 (JSG11/W/03-A3 1010)  
 (JSP05/W/10-A1 1150)  
**Lyatskaya Alla M.**  
 (GA2.07/W/20-A2 0930-06)  
**Lyatsky W**  
 (GA3.10/E/08-A6 1700-11)  
**Lyatsky Wladislav**  
 (GA3.06/E/01-A2 1450)  
 (GA3.06/E/05-A2 0930-06)  
 (GA3.02/E/15-B3 0900-07)  
**Lybekk B.**  
 (GA4.09/W/05-A6 1140)  
**Lykov V. I.**  
 (ST1/W/39-A3 1150)  
**Lynch A H**  
 (MC01/W/14-A4 1155)  
**Lynch Amanda H**  
 (MC01/W/12-A2 1650)  
 (JSA09/L/04-A2 1515)  
**Lynch Lloyd L.**  
 (JSP23/C/U5/W/02-B2 1130)  
 (JSP23/C/U5/W/04-B2 0830-06)  
 (JSP23/W/24-B2 1150)  
**Lynch M**  
 (MI09/W/01-A5 1145-19)  
**Lynch M. J.**  
 (JSM41/W/36-B4 1110)  
 (MI06/W/22-B1 1200)  
**Lynch Mervyn J.**  
 (P15/W/05-B3 1630)  
**Lynch Peter**  
 (MI05/W/31-A4 1120)  
**Lynn Harvey V**  
 (JSM01/L/30-A5 1640)  
**Lynn O. Ma.**  
 (JSV29/W/04-B1 1700)  
**Lyon J. G.**  
 (GA3.05/W/14-B3 0900-40)  
 (GA3.09/W/12-B4 1400)  
**Lyon-Caen Helene**  
 (G5/E/36-A4 1215)  
 (ST4/E/66-B2 0930-06)  
 (ST4/E/68-B2 1500)  
 (JSS31/W/11-B2 1620)  
**Lyons Jim**  
 (ST5/W/01-B3 0900-05)  
**Lyons L. R.**  
 (GA3.02/W/62-B2 1420)  
 (GA3.08/W/16-B1 1430)  
**Lyons Larry**  
 (GA3.02/W/33-B3 0900-16)  
 (GA3.03/W/01-B4 1610)  
 (GA3.08/W/23-B1 1450)  
**Lyons Timothy W.**  
 (P09/W/06-A2 0850)  
**Lysak Robert L.**  
 (GA3.06/W/27-A2 1430)  
 (GA2.07/W/25-A1 1100)  
 (GA3.02/W/34-B3 1120)  
 (GA3.04/W/32-B2)  
**Lytle Victoria I.**  
 (JSM04/W/05-A2 1445)  
**Lyubimov German P.**  
 (GA4.04/W/10-B5 0830-03)  
**Lyubovtseva Yulia**  
 (MI01/E/06-A1 0900-04)  
 (MI01/E/15-A1 0900-05)  
 (JSP39/W/06-B2 0950)  
**MacDonald William**  
 (GA1.04/W/26-A4 1520)  
**MacDougall John**  
 (JSM01/W/62-A2 1110)  
 (JSM01/W/67-A1 1110)  
 (MW04/W/11-A1 0925)  
**MacDowall R. J.**  
 (GA4.02/W/20-A4 1400-18)  
**Mace Gerald G.**  
 (MI10/W/25-B1 0930)  
**Macedonio Giovanni**  
 (VS2/W/21-B3 1400-14)  
 (VS2/E/02-B3 1110)  
**Macedônio da Silva Reginaldo**  
 (G1/L/02-A3 1620-84)  
**Machenhauer Bennert**  
 (MC01/E/34-A4 1020)  
 (MC01/W/35-A4 1630)  
 (HW1/E/03-A4 1430)  
**Macheret Yuri**  
 (JSH12/E/02-A5 1100)  
**Machida Isao**  
 (HS4/W/21-A5 1100)  
 (HS4/W/18-A5 0950)  
**Macke A.**  
 (MI06/W/16-B2 1030)  
 (MI06/W/28-B2 0950)  
 (MI10/W/06-B2 1005)  
**Mackensen A.**  
 (P07/W/08-A3 1015)  
**MacKenzie I A**  
 (JSM01/E/16-A5 0920)  
**MacKenzie Rob**  
 (JSM26/W/16-B2 1210)  
**Mackiv Bogdan**  
 (JSA30/C/U6/E/05-B1 1400-26)  
**MacMillan D.S.**  
 (G1/W/24-A3 1520)  
 (G2/C/G5/W/23-A2 1515)  
**MacMillan Daniel**  
 (JSS31/W/03-B2 0930)  
**MacMillan Susan**  
 (JSA40/W/08-B3 0900)  
 (GA5.01/W/11 A1 0900-05)  
 (GA5.09/W/06 A2 1010)  
**MacNiocail Conall**  
 (GA1.04/W/31-A4 0900)  
**MacPherson B.**  
 (JSA20/W/48-A4 1200-31)  
 (GA3.09/W/19-B5 1100)  
**MacPherson C G**  
 (JSS13/E/03-A5 1500)  
**Macropoulos Kostas**  
 (JSP23/E/56-A6 0830-08)  
**Maddern T. M.**  
 (GA2.02/E/02-B4 1740)  
**Madec Gurvan**  
 (U2/E/07-A21140)  
**Mader G**  
 (JSG11/W/17-A4 1150)  
**Mader Heidi**  
 (VS2/W/17-B3 1400-11)  
**Maderich V.**  
 (P09/W/05-A1 1640)  
**Maderich Vladimir**  
 (P14/W/04-A4 1400-06)  
 (P11/W/15-B4 1740)  
 (P13/W/13-B2 1600-11)  
**Madhusoodanan M. S.**  
 (P09/E/02-A2 0950)  
**Madsen S N**  
 (JSH12/W/05-A5 0900)  
**Maechling P.**  
 (ST5/W/L/04-B3 0900-13)  
**Maeda K.**  
 (JSA15/E/19-A3 1500)  
**Maeda Kenji**  
 (ST1/E/89-A2 1720)  
 (ST1/W/13-A3 1740)  
**Maeda Shin**  
 (JSS02/E/16-A1 1720)  
**Maekawa R**  
 (JSM01/W/01-A3 1140)  
**Maffione Robert**  
 (P15/L/28-B3 1200)  
 (P15/W/01-B3 1000)  
**Magiera Tadeusz**  
 (GA1.05/E/05-A6 1215)  
**Magnuson J. J.**  
 (HW3/W/03-B4 1005)  
**Magson V. Auster**  
 (GA5.01/P/02 1230)  
**Mahadevan T. M.**  
 (ST2/E/18-A3 1730)



- Ma C.**  
 (G1/W/24-A3 1520)  
 (G2/C/G5/W/23-A2 1515)  
 (G6/W/05-B1 0850)  
**Ma Chopo**  
 (JSG14/W/05-A3 1100-01)  
**Ma Kuo-Fong**  
 (ST5/W/23-B5 0930-03)  
**Ma Qingzhong**  
 (GA1.02/E/07-A1 1605)  
**Ma Shengli**  
 (ST1/E/07-A2 1400-32)  
**Ma Xinghua**  
 (GA1.04/W/12-A5 1120)  
**Ma Yaoming**  
 (JSM24/W/04-B1 0930)  
**Ma Zhuang-Shi**  
 (GA1.01/W/13-A5 1145)  
**Maas Leo**  
 (JSP39/E/14-B4 1500)  
**MacCready Parker**

## INDEX

- Mahaja Swadesh**  
(GA4.05/E/03-A1 1440)
- Mahar Francisco**  
(VS2/C/U6/W/12-B3 1400-32)
- Maharaj-Sharma Rawatee**  
(JSA16/W/01-A3 0830-51)
- Maher Barbara A.**  
(GA1.05/W/25-A5 0900-08)
- Maheskumar R S**  
(MI01/P/02-A31145)  
(MI04/P/01-B3 1220)
- Mahieu E**  
(JSM01/E/44-A4 1620-14)
- Mahmoud S**  
(G5/E/41-A4 1230-07)  
(G5/E/48-A4 1230-06)
- Mahmoud Salah**  
(JSS31/E/12-B3 0830-13)
- Mahongo Shigalla B.**  
(PW1/W/01-A61520)
- Mahowald Natalie**  
(MC11/E/16-B3 1700)
- MaHuilan Zhou Yanlu**  
(SW1/W/01-B5 0945)
- Maier-Reimer E**  
(MC01/W/36-A5 1700)  
(MC01/W/58-A5 1620)
- Maillard Didier**  
(JSG11/W/13-A4 1400-09)
- Maiorov Andrey**  
(G1/E/09-A3 1620-22)
- Maiwald Ulrike**  
(ST1/W/67-A1 1050)
- Maixner Uwe**  
(MI08/W/18-A4 1150)
- Maiyza Ibrahim A. A.**  
(P11/P/05-B5 1150-05)
- Majchrowski Roman**  
(P15/W/04-B4 1055)
- Majeed T.**  
(GA4.10/W/32-A4 1635)
- Majorov A N**  
(G3/E/28-A5 1610-03)
- Mak Mankin**  
(MW06/E/08-A3 0930)
- Makarenko Nikolay**  
(G1/E/09-A3 1620-22)
- Makarov Valentine I.**  
(GA4.03/W/13-B4 0835)
- Makarova Ludmila**  
(JSA45/W/17-B5 1110-07)  
(JSA45/W/19-B4 1550)  
(JSA16/E/05-A3 0830-04)
- Makarova M V**  
(MI02/W/14-A4 1450)
- Mäkelä J. S**  
(GA3.06/W/11-A2 0930-10)
- Makeyeva L. I.**  
(JSS07/W/04-A2 0930-01)
- Maki Norio**  
(JSS42/P/01-B5 1210)
- Makin Zinoviy**  
(G5/L/03-A4 1115-13)
- Makinen J**  
(G3/E/11-A5 1610-31)
- Makinen Jaakko**  
(G3/E/01-A5 1610-26)
- Mäkinen T.**  
(MC09/W/07-B2 01)
- Makino Masahiko**  
(JSP23/W/06-B2 1640)  
(JSA40/W/07-B5 1400-10)
- Makropoulos B. K.**  
(ST1/E/14-A3 1500)
- Makropoulos K.**  
(ST1/E/87-A2 0930-12)  
(ST3/E/36-B3 1615)  
(ST4/E/66-B2 0930-06)  
(ST4/E/68-B2 1500)  
(ST5/E/35-B5 0830)
- Makshatas Alexander**  
(P13/E/13-B2 1600-01)
- Makshatas Alexander P.**  
(JSM04/E/05-A2 1420)
- Maksimovic M.**  
(GA4.04/E/01-B5 1210)
- Maksimovskikh Sergei**  
(JSA40/W/13-B5 1400-14)
- Maksudov S. Kh.**  
(G5/E/43-A4 1230-11)
- Maksymchuk Valentyn**  
(JSA15/E/16-A5 1400-03)  
(GA5.01/E/09-A1 0900-06)
- Makukhin Vladimir**  
(MI02/E/07-A5 1620)
- Malacic Vlado**  
(PW1/W/02-A6 1000)  
(JSP49/W/23-B5 1210-14)
- Malanotte-Rizzoli**  
(P08/E/03-A2 1520)
- Malanotte-Rizzoli Paola**  
(P11/E/11-B4 1050)  
(P11/E/29-B5 1050)
- Malarkey J.**  
(P10/W/08-A3 0950)
- Malcolm R.**  
(HS4/W/15-A4 1730)
- Maldonado S.**  
(JSP23/C/U5/W/14-B2 1210)
- Malin G**  
(JSP21/L/03-A4 1720)
- Malischewsky P. G.**  
(ST5/W/L/05-B3 1400-06)
- Malita Zina**  
(JSS 44/E/23-B4 0930-22)
- Malkin Zinoviy**  
(G2/C/G5/L/13-A2 1630-17)  
(JSA15/E/14-A5 1400-04)
- Malkki Anssi M**  
(GA3.10/W/11-A6 1700-12)
- Malkovets Vladimir**  
(JSS02/W/05-A1 0830-01)
- Mall U.**  
(GA3.05/W/05-B3 0900-46)  
(GA4.08/W/11-B3 1620)  
(GA4.08/W/13-B4 0905)
- Mallet I**  
(MI05/L/03-A4 1140)
- Mallet Isabelle**  
(MI05/W/23-A4 0950)
- Mallik S. B.**  
(GA1.04/P/02-A4 1710)
- Malone S. D.**  
(ST2/W/07-A5 0900)
- Maltrud Matthew E**  
(MC01/E/12-A2 1215)
- Malstev**  
(GA4.08/W/24-B3 0900-07)
- Maltsev Paul**  
(ST1/W/37-A4 0930-01)
- Maltsev Pavlo**  
(JSP23/C/U5/E/04-B1 1440)
- Maluski Henri**  
(JSS07/E/10 A2 0930-04)
- Malyshev Alexander**  
(ST1/C/Jsa10/W/15-A3 0900-12)  
(ST1/E/76-A4 0930-15)  
(JSA10/W/08-A2 1045)  
(JSP23/E/24-B1 0830-16)
- Malyshev Alexander I.**  
(JSV47/W/10-B5 1400-21)  
(VS2/W/04-B3 1400-03)  
(VS2/W/07-B3 1400-05)
- Malysheva Lidiya K.**  
(JSA10/W/08-A2 1045)
- Mamani M.**  
(GA1.02/L/01-A2 0930)
- Man Otaker**  
(GA1.04/L/07-A4 1200)
- Manabu Hashimoto**  
(ST1/W/01-A1 1740)
- Manamohan Rao N**  
(HS5/W/43-A3 1500)
- Manca Beniamino Bruno**  
(P11/E/19-B4 1150)  
(P11/E/20-B4 1720)
- Manchev Atanas**  
(MI03/W/07-A3 1400-03)
- Mancini Marco**  
(HW4/W/04-B2 0900-07)
- Mandea Mioara**  
(JSA37/W/08-B3 1430)
- Mandea Miora**  
(GA5.09/W/02 A2 0950)
- Mandelbaum M. M.**  
(JSA15/E/43-A5 0830-17)
- Mandrescu N.**  
(ST3/W/05-B4 1615)
- Mandrini Cristina H.**  
(GA4.01/L/01-A2 1220)  
(GA4.02/W/14-A4 0925)  
(GA4.02/E/03-A4. 1400-01)
- Manes Alexander**  
(MC02/E/04-B2 1510)
- Manglik Ajay**  
(ST4/E/26-B1 1220)
- Mango Furnari Mario**  
(ST5/W/34-B4 0930-01)
- Manizade S**  
(JSH12/C/JSS31/E/05-A5 0930)
- Man'kovsky Viktor I.**  
(P11/W/17-B5 1400)
- Mann Graham**  
(JSM04/E/01-A2 1010)
- Mann I.**  
(GA3.04/E/14-B1 1520-03)  
(GA3.04/L/14-B2 1400)  
(GA3.04/W/21-B1 1520-19)
- Mann I. R.**  
(GA3.07/W/32-A5 1000)  
(GA3.10/W/26-A5 1225)
- Mann Michael**  
(JSP25/E/14-B4 1720)
- Mann Michael E.**  
(JSP25/W/61-B4 0930)  
(MC02/W/07-B1 1510)
- Mannik Aarne**  
(JSM01/C/MW07/W/11-A2 1600-30)
- Manninen J.**  
(GA2.03/W/03-B3 1400-01)
- Manning D**  
(G3/W/30-A5 1610-06)
- Manning M R**  
(MI02/W/07-A4 1600)
- Mannoji Nobutaka**  
(JSP05/W/17-A1 10)  
(JSG28/E/21-B2 1400-14)  
(JSG28/W/18-B1 1140)
- Manohar G K**  
(MI03/E/04-A3 1020)  
(MI03/E/05-A3 1120)
- Manson A H**  
(JSM01/W/67-A1 1110)  
(MW04/W/01-A1 0950)
- Manson Alan**  
(JSM01/E/04-A2 1130)  
(JSM01/E/25-A3 1020)  
(JSM01/W/62-A2 1110)  
(MW04/W/11-A1 0925)
- Mansy Jean-Louis**  
(GA1.04/W/35-A4 0930-11)
- Manton M. J.**  
(JSM41/W/25-B3 0930)
- Mantovani Maria**  
(G5/E/08-A4 1556-09)
- Mantovani Marta S. M.**  
(JSS44/E/12-B4 0930-03)  
(JSS44/E/45-B4 0930-41)
- Mantua Nathan**  
(JSP25/W/56-B5 1700)
- Mantyniemi Paivi**  
(ST3/E/44-B3 1215)
- Manuel Catalán**  
(GA5.01/E/26 A1 1500)
- Manuel Davila Quijano**  
(G1/W/10-A3 1620-37)
- Manurung Parluhutan**  
(MI06/E/05-B1 1140)  
(G5/E/06-A4 1500-01)  
(JSG28/W/13-B1 1400-17)
- Manusiu P.**  
(GA3.04/W/23-B1 1520-25)
- Manzella A.**  
(GA1.02/W/19-A2 0930)
- Manzini Dr. Elisa**  
(JSM01/W/28-A1 1640)
- Manzini E**  
(JSM01/W/25-A4 1130)
- Manzini Elisa**  
(JSM41/W/13-B3 1400)
- Mao Jian-Ren**  
(JSV22/E/15-A5 1550)  
(JSV22/E/18-A5 1610)
- Mao Jietai**  
(MI06/E/02-B2 1520)
- Mao Xianjin**  
(GA1.02/E/07-A1 1605)
- Maouche S.**  
(GA1.05/W/37-A5 1420)  
(GA1.04/W/21-A4 1400)  
(GA1.04/W/22-A4 1420)
- Maouche Said**  
(ST2/E/04-A5 1400-25)
- Mapes Brian**  
(JSP39/W/46-B3 0930)  
(MI04/W/34-B1 1045)
- Maqueda M. M.**  
(HS2/W/23-B2 1200)
- Maqueda Morales**  
(MC01/E/32-A2 1620)
- Marabini**  
(JSP23/W/00-A5 0830-06)
- Maramai Alessandra**  
(JSS42/E/19-B5 1700-14)
- Maravilla Dolores**  
(GA4.03/E/02-B4 1645)
- Marcellini A.**  
(JSP23/E/08-A6 0950)
- Marcello Martini**  
(JSV47/E/01-B5 1400-05)
- Marcelo Assumpcao**  
(JSS 31/E/01-B3 0830-10)
- Marcelo Costa**  
(G1/E/45-A3 1620-74)
- Marchand A**  
(MI09/L/02-A5 0855)
- Marchand P Goloub**  
(MI09/L/02-A5 0855)
- Marchenko Alexander**  
(G4/W/09-A3 1620-25)
- Marchetti A.**  
(JWS33/E/03-B2 1635-06)  
(JWS33/E/03-B3 0900-06)
- Marcuello Alex**  
(GA1.02/W/38-A2 0930)
- Marcus S.L.**  
(JSG14/L/08-A3 1145-16)
- Marcus Steven L**  
(MC01/E/06-A2 1015)
- Mare Yamamoto**  
(JSV47/W/11-B5 1115)
- Mares Alleana**  
(JSP25/W/35-B3 1440)
- Mares C.**  
(JSP25/W/12-B1 0830-09)  
(JSP25/W/35-B3 1440)
- Mares Ileana**  
(JSP25/W/12-B1 0830-09)
- Maresca R.**  
(JSS44/W/09-B4 0930-05)  
(JSV47/E/08-B5 1400-04)
- Margvelashvili Nugzar**  
(P13/W/13-B2 1600-11)
- Margvelashvily N.**  
(P09/W/05-A1 1640)
- Marianne Greff-L**  
(G5/W/15-A4 0930)
- Marin Diego**  
(JSA20/E/07-A4 1200-30)
- Marin J. A.**  
(GA5.12/E/04 A2 0930)
- Marino Miguel A.**  
(HS15/W/27-A2 1635)
- Mariotti A.**  
(JSM26/E/17-B3 0910)
- Mariotto Giovanni**  
(HW4/W/04-B2 0900-07)
- Marjeta Car**  
(JWS33/E/12-B3 0900-30)
- Marjin Boris V.**  
(GA3.05/W/41-B3 0900-24)
- Marks Crispin J.**  
(MI06/E/05-B1 1140)  
(JWM08/E/02-A2 1140)
- Marks Pip**  
(JSP23/E/36-B2 0830-13)
- Markus Franecz**  
(GA4.09/W/14-A6 1720)
- Marlar J.**  
(P09/W/05-A1 1640)
- Marone Chris**  
(ST1/W/16-A2 1400-29)
- Marone Eduardo**  
(G1/E/03-A3 1620-49)
- Marquardt C**  
(MW08/E/01-A2 1700)  
(JSM26/E/13-B3 0850)
- Marques D.**  
(GA1.02/E/38-A1 1605)
- Marquis M.**  
(JWS33/W/33-B2 1635-32)  
(JWS33/W/33-B3 0900-32)
- Marr Gregory C.**  
(G3/E/05-A5 1200)
- Marra J.**  
(P15/L/26-B3 1110)
- Marrara Francesco**  
(ST3/W/14-B4 0930-01)  
(ST3/W/49-B3 0915)
- Mars Jérôme**  
(JSV47/W/19-B5 1400-16)  
(ST5/W/05-B3 1440)
- Marsal O.**  
(JSA10/W/03-A2 0930)
- Marsan David**  
(ST1/W/09-A4 0930-13)  
(ST4/W/52-B1 1740)
- Marsden R. J.**  
(GA4.01/E/09-A2 1200)
- Marsh J. S.**  
(JSV22/W/02-A5 0920)

- Marsh P.**  
(HS2/W/11-B1 1420)  
(HS2/W/32-B2 1440)  
(HW3/W/06-B4 1140)
- Marsh Phillip**  
(HS4/W/31-A5 1630)
- Marsh S M**  
(JSM01/E/39-A1 0940)
- Marshall John C.**  
(P08/W/06-A2 0950)
- Marshall P. D.**  
(U8/P/02-B3 0900)
- Marshall Susan**  
(JSM24/W/05-B2 1135)  
(JSP25/W/04-B3 1110)
- Marshall Thomas C**  
(MI03/W/03-A3 1620)
- Marsiat Isabelle**  
(MC11/L/02-B3 1720)
- Marsigli Chiara**  
(JVM08/W/11-A3 1220)
- Marsland S. J.**  
(P13/E/10-B1 1400)
- Marson I**  
(G3/E/11-A5 1610-31)  
(JSA15/E/60-A4 1400-13)
- Marson Iginio**  
(JSV36/E/25-B3 1710)
- Martelli M.**  
(JSS44/E/21-B4 1540)
- Martens Marcel**  
(G1/L/11-A3 1200)
- Marti Olivier**  
(M0c1/E/11-A3 0845)  
(MC11/E/09-B4 1520)
- Marti Urs**  
(G3/W/53-A5 1610-88)
- Martilli A**  
(MI07/L/02-A2 1620)
- Martin Ana Lillian**  
(JSV36/E/11-B3 0900-15)
- Martin C.**  
(M104/E/25-B4 0930)
- Martin D**  
(JSG11/W/17-A4 1150)
- Martin Douglas M.**  
(JSS42/W/23-B4 1200)
- Martin Eric**  
(HS2/W/01-B1 0900)  
(MC01/L/05-A2 1100)
- Martin Francisco**  
(JSV36/W/20-B3 0900-09)
- Martin Francisco J**  
(MW05/W/08-A2 1130)
- Martin G. M.**  
(MI04/E/18-B3 1505)
- Martin Gill**  
(MI04/E/04-B4 1035)
- Martin J.**  
(GA5.12/E/04 A2 0930)
- Martin J. E**  
(MI05/W/41-A1 1710)
- Martin Jose**  
(G1/W/10-A3 1620-37)
- Martin Keith**  
(MI02/W/01-A5 1450)
- Martin M.**  
(ST5/W/19-B3 1145)
- Martin P**  
(HW1/L/12-A4 1630)  
(JSA10/E/01-A2 1515)
- Martin Ulrike**  
(VS2/E/11-B3 1400-24)  
(VS2/E/15-B3 1400-26)  
(VS2/E/17-B3 1400-27)
- Martinec Jaroslav**  
(HS4/W/06-A4 1400)
- Martinelli G.**  
(ST1/E/17-A3 1050)  
(JSS44/E/21-B4 1540)
- Martinelli Giovanni**  
(ST7/L/02-A2 1415)  
(ST7/L/03-A2 1430)
- Martinelli Patricia**  
(GA1.02/W/01-A1 1050)
- Martinez-Benjamin J. J.**  
(G1/E/47-A3 1620-75)
- Martinez Daniel**  
(M104/E/17-B1 0900-13)  
(M104/E/23-B4 1005)
- Martinez William**  
(G1/E/29-A3 1620-63)  
(G1/E/36-A3 1620-68)  
(G3/E/02-A5 1610-94)
- Martinez-Garcia M.**  
(G1/E/47-A3 1620-75)
- Martinez-Zubieta Ana**  
(JSP21/W/10-A5 1150)
- Martini Marcello**  
(JSS46/E/05-B4 1440)  
(JSV47/W/18-B5 1100)
- Martini Marino**  
(JSV36/E/27-B3 1040)
- Martinson Douglas**  
(P13/W/22-B1 1050)
- Martinuzzi J.-M.**  
(JSM41/W/27-B5 0930)
- Marty Bernard**  
(JSV36/C/U6/W/10-B3 1400-18)  
(U6/W/10-B2 1430)
- Marty Ch.**  
(MC02/E/12-B1 1600-11)
- Marty J. C.**  
(G3/E/27-A5 1610-02)
- Martyshko A. L.**  
(GA1.02/E/19-A1 1515)
- Marubashi Katsuhide**  
(JSA06/W/20-A1 1420)
- Marui Atsunao**  
(HS4/W/22-A5 1120)
- Marullo Salvatore**  
(P11/L/01-B5 0830)
- Maruyama Kenichi**  
(MI04/E/22-B4 1150)  
(MI01/E/09-A1 0900-02)
- Marx L**  
(MC01/L/02-A1 1145)
- Marykutty Michael**  
(GA4.10/W/28-A4 1655)
- Marza V.**  
(ST1/W/60-A3 0900-07)
- Marza Vasile**  
(ST1/W/20-A4 0930-04)
- Marzocchi W.**  
(ST1/W/17-A3 1600)
- Marzouk Imam**  
(ST4/E/51-B1 1400-20)
- Masataka Ando**  
(ST1/W/64-A3 0900-03)  
(ST1/W/69-A1 1640)
- Masato Sugi**  
(MC01/E/13-A1 1130)
- Masamura Kenji**  
(JSS42/E/20-B5 1700-20)
- Masayuki Kikuchi**  
(ST5/E/16-B4 1500)  
(ST5/E/17-B4 1400-04)  
(ST5/W/18-B3 1700)
- Mascart Patrick**  
(MI05/W/08-A4 1400-07)  
(MI05/L/03-A4 1140)  
(MI05/W/07-A3 1440)  
(MI05/W/23-A4 0950)
- Maschenkov S.P.**  
(GA5.12/L/01 A2 1010)  
(JSS44/L/04-B4 1640)
- Maschenkov Sergei**  
(GA5.11/W/06 A3 1200)
- Mascia Umberto**  
(JSA40/W/01-B5 1205)
- Mashhadi-Hossain-Ali M**  
(G3/E/30-A5 1610-30)
- Maskaoui K**  
(PW1/E/04-A6 0900)
- Maslanik James**  
(MC01/W/14-A4 1155)  
(P13/W/14-B2 1520)  
(P13/W/17-B2 1600-07)
- Maslowski Wieslaw**  
(P13/W/22-B1 1050)
- Masolov V. N.**  
(GA5.12/W/05-A2 1600-01)
- Mason G. M.**  
(GA3.03/E/05-B4 1000)  
(GA3.05/E/16-B3 0950)  
(GA4.04/W/02-B5 1130)  
(GA4.04/W/12-B5 1750)  
(GA4.04/W/18-B5 1150)
- Masri U.**  
(G1/L/14-A3 1620-90)
- Massie Steven T.**  
(JSM26/W/08-B2 1700-15)
- Massey R S**  
(MI03/W/05-A3 1140)
- Massmann F H**  
(G3/E/27-A5 1610-02)  
(G6/C/G3/E/43-B1 1100)
- Massom Robert A.**  
(JSM04/W/05-A2 1445)
- Masson Ph.**  
(JSA10/W/06-A2 1430)
- Masson Valery**  
(JSM43/E/07-B4 1720)
- Masters G**  
(JSS02/W/03-A2 1000)  
(ST5/W/42-B5 1400)
- Masuda Akira**  
(JSP39/E/13-B4 1720)
- Masuda H.**  
(JSA15/W/14-A4 1400-16)
- Masuda Harue**  
(P16/L/01-B5 0910)
- Masuda Yoshio**  
(JSP25/W/18-B4 0930-05)
- Masutani F.**  
(JSA15/W/14-A4 1400-16)
- Masutani Fumio**  
(JSV36/W/15-B3 0900-01)
- Masuzawa Toshiyuki**  
(GA1.03/W/10-B2 1420)
- Mata E.**  
(G5/W/19-A4 1230-02)
- Matafonov G. K.**  
(JSA45/W/01-B5 1110-04)
- Matas Jan**  
(JSS02/W/16-A2 0930)
- Matasova Galina**  
(GA1.05/W/31-A5 0900-05)
- Matcharashvili Teimuraz**  
(ST1/E/10-A4 0930-20)  
(ST1/E/12-A4 0930-22)  
(ST1/E/18-A4.0930-05)
- Matear R**  
(MC01/W/36-A5 1700)
- Mateus Antonio**  
(GA1.02/W/15-A2 0930)
- Mather James**  
(MI10/W/15-B1 1000)
- Mathers Lucy**  
(P16/W/02-B5 1640)
- Mathews P. M.**  
(JSG14/L/09-A3 1000)
- Mathie R. A.**  
(GA3.04/L/15-B2 1450)  
(GA3.04/W/21-B1 1520-19)
- Mathieu A.**  
(MI04/L/10-B3 1520)  
(MI06/W/07-B1 1220)
- Matias Luis**  
(U7/E/03-B1 0830-17)
- Matonse Adao Henrique**  
(U2/E/05-A21620)
- Matos Joao L.**  
(JSV36/E/26-B3 1400-10)  
(JSP23/E/23-B2 0830-09)
- Matos Liliana**  
(GA1.02/W/15-A2 0930)
- Matsomotu Takeshi**  
(JSS42/E/20-B5 1150)
- Matson D. L.**  
(JSA10/L/01-A3 0900)
- Matsubara Makoto**  
(JSS44/W/04-B4 0930-05)  
(JSS46/W/18-B4 0930-07)
- Matsuda Tokiyoshi**  
(SW1/W/03-B5 1115)
- Matsuda Tomonori**  
(JSA15/E/04-A3 1130)
- Matsuda Yoshihisa**  
(MC09/E/03-B2 02)  
(MC09/E/05-B2 03)  
(MC10/E/07-B1 1400)
- Matsumi Yutaka**  
(JSM01/W/60-A4 1550)
- Matsumoto H.**  
(GA4.09/W/10-A6 1200)
- Matsumoto Hirokazu**  
(G5/P/02-A4 1130-02)
- Matsumoto Hiroshi**  
(JSA15/E/01-A4 1400-05)  
(SW1/W/03-B5 1115)
- Matsumoto Takeshi**  
(JSP23/C/U5/E/23-A6 1700)
- Matsumoto Takumi**  
(JSA15/W/08-A4 1040)
- Matsumura Shouichi**  
(GA5.01/W/05 A1 0835)
- Matsumura Shozo**  
(ST1/E/81-A2 1640)  
(ST1/E/89-A2 1720)
- Matsumura T.**  
(JSS42/W/08-B4 1400)  
(JSG28/W/04-B2 1400-13)
- Matsumo Takeshi**  
(JSP49/W/08-B5 1010)
- Matsuno Taroh**  
(JSP25/W/28-B5 1010)  
(MW03/E/05-B4 1145)
- Matsushima Masaki**  
(GA1.01/W/21-A5 0945)  
(GA1.01/W/05-A5 0900-10)
- Matsushima N.**  
(GA1.02/W/18-A2 0930)
- Matsushima T.**  
(G5/E/39-A4 1200)  
(JSS44/W/01-B4 0930-06)
- Matsutomi Hideo**  
(JSS42/P/01-B5 1210)
- Matsuura Tomonori**  
(JSP25/P/07-B1 1620)
- Matsuyama Masafumi**  
(JSS42/W/17-B5 1600)
- Matsuyama Masashi**  
(JSS42/P/01-B5 1210)
- Matthews Rachel**  
(HS3/W/01-A1 0900)
- Matthias-Maser Sabine**  
(MI01/E/12-A1 1005)
- Matthiense Stephan**  
(P14/E/06-A4 1440)  
(P14/E/01-A4 1400-02)
- Mattioli Glen**  
(JSS31/E/06-B2 1500)  
(JSV36/E/13-B3 1445)
- Matveev Rostislav F**  
(G5/E/32-A4 1415-06)  
(ST1/E/04 0930-38)
- Matveyeva Emma T.**  
(GA3.04/W/37-B1 1520-30)
- Matvienko Jury D.**  
(ST1/E/42-A3 0900-14)
- Matzander U.**  
(GA1.02/W/41-A1 0830)
- Matzka Juergen**  
(GA1.05/W/06-A5 1630)  
(GA1.05/W/25-A5 0900-08)  
(GA1.05/W/34-A6 1430)
- Maugeri M.**  
(GA6.01/W/03-A5 1525)
- Mauk B.**  
(GA4.10/W/01-A5 1130)  
(GA4.10/W/06-A5 1435)  
(GA4.10/W/32-A4 1635)
- Mauk B. H.**  
(GA4.10/W/03-A5 1110)
- Maul George A.**  
(JSS42/W/23-B4 1200)
- Maupin Valerie**  
(ST4/W/28-B2 0930-09)
- Maura Hagan**  
(JSM01/W/30-A4 1000)
- Maurellis Ahilleas N**  
(GA4.10/W/21-A4 1620)
- Mauro Di Vito**  
(JSV47/E/01-B5 1400-05)
- Mavromichalaki Helen**  
(GA3.09/W/07-B4 0900-11)
- Mawtari Hideo**  
(G3/L/09 1610-23)
- Maximiva Tatiana G.**  
(U3/W/06-A3 0900-12)
- Maximenko Nikolai A.**  
(P12/E/03-A1 1010)
- Maximova Olga V.**  
(P11/W/01-B5 1620)
- Max-Planck**  
(MC01/12-A3 1020)
- Maxworthy T.**  
(JSP49/E/09-B5 1400)
- May W.**  
(MW02/W/07-B3 1500)
- Mayberry Gari C.**  
(VS2/W/05-B3 1400-04)  
(MI01/C/JSV36/E/06-A1 0900-14)
- Mayer Bernhard**  
(MI08/W/10-A4 1805)
- Mayer M.**  
(G1/L/04-A3 1620-85)  
(JSA09/L/02-A2 1230)
- Mayer Michael**  
(JSA09/W/11-A2 0930-04)
- Mayer-Rosa D.**  
(JSP23/C/U5/E/16-A5 1620)  
(JSP23/E/03-A6 0930)  
(ST3/E/56-B4 1400-20)
- Maynard N C**  
(GA3.10/W/02-A6 1615)  
(GA3.09/E/05-B4 1625)
- Mayr H G**  
(MC06/C/JSM01/E/22-A1 1505)



## INDEX

- (MW04/W/16/C/JSM01/E/14-A1 1135)  
(GA4.10/W/30-A4 1450)
- Mazur J. E.**  
(GA4.04/W/02-B5 1130)  
(GA4.04/W/12-B5 1750)  
(GA4.04/W/18-B5 1150)
- Mazur Stanislaw**  
(GA1.04/W/34-A4 0930-10)
- Mazza S.**  
(ST2/E/21-A5 1400-24)
- Mazzella A. A.**  
(GA2.02/W/24-B5 1500)
- Mazzinghi Piero**  
(JSM26/W/16-B2 1210)
- Mazzini I.**  
(VS3/E/02-B3 1550)
- Mbius E**  
(GA4.02/W/28-A4 1720)
- McAdoo David**  
(JSA09/W/01-A2 1145)
- Mcatee B. K.**  
(JSM41/W/36-B4 1110)
- McBrady C.**  
(GA3.03/W/11-B4 1200)
- McBride John L.**  
(JSP25/W/15-B2 1010)  
(MC04/W/13-B2 1050)
- McCarthy M.**  
(GA3.02/E/09-B2 1500)
- McCaul Eugene W.**  
(MW02/W/03-B3 1200)
- McCausland P. J. A.**  
(GA1.04/W/19-A4 0930-12)
- McCloskey John**  
(ST1/W/09-A4 0930-13)
- McComas D. J.**  
(GA4.01/W/05-A2 1450)  
(GA4.02/W/20-A4 1400-18)
- McComas David**  
(GA4.09/E/12-A6 1520)
- McComas David J.**  
(GA3.05/W/11-B3 0900-06)
- McConnell J C**  
(JSM01/W/10-A3 1650)  
(MW01/W/04-A5 1500)
- McConnell John**  
(MW05/W/04-A2 1200)
- McCormack David**  
(ST5/W/01-B3 0900-05)  
(ST5/W/61-B3 1225)
- McCormack John**  
(JSM26/E/11-B3 0930)  
(MW02/E/04-B3 1140)
- McCracken K. G.**  
(JSA45/E/04-B4 0830)
- McCrea I.**  
(GA 2.01/E/12-A1 1220)
- McCue K.**  
(JSP23/C/U5/E/16-A5 1620)  
(ST3/E/56-B4 1400-20)
- McCue Scott**  
(JSM41/W/07-B4 1620-05)
- McCulloch Archie**  
(JSP21/W/13-A4 0950)
- McDade Ian C.**  
(MW05/W/01-A2 1145)
- McDonnell Jeff**  
(HS4/W/01-A4 0945)
- McEachern Ben**  
(JSP39/W/12-B3 1430-11)  
(JSP39/W/35-B3 1433-12)
- McEntire R. W.**  
(GA3.02/L/02-B3 0900-24)
- McEnroe Suzanne A.**  
(GA5.11/W/01 A3 0930)  
(GA5.11/W/05 A3 1120)
- McEntire R. W.**  
(GA4.10/W/01-A5 1130)
- McFadden J.**  
(GA3.03/W/11-B4 1200)
- McFadden J. P.**  
(GA3.08/W/13-A6 0940)  
(GA4.09/W/02-A6 1000)  
(GA4.09/W/07-A6 0940)
- McFarlane N**  
(MI01/L/04 1055)
- McFarlane N A**  
(JSM01/W/10-A3 1650)
- McFarlane Norm**  
(MW07/W/20-A4 1620)
- McFiggans Gordon**  
(MI02/W/01-A5 1450)  
(MI02/W/13-A5 1510)
- McGowan Hamish**  
(JSM43/W/06-B4 1030)
- McGregor Glenn R.**  
(HS2/W/17-B2 0940)
- McGregor J L**  
(MC01/W/49-A5 0900)
- McGregor James**  
(JWM08/E/07-A2 1040)  
(MI05/E/21-A2 1420)  
(MI06/E/03-B1 1120)
- McGregor John L.**  
(MW03/W/06-B4 1400)  
(MC01/W/50-A5 1230)
- McGuffie Kendal**  
(MC05/W/02-B4 1130)
- McGuire R.**  
(ST3/E/56-B4 1400-20)  
(JSP23/C/U5/E/16-A5 1620)
- McGuire Robin K.**  
(JSP23/E/34-A6 0850)  
(ST3/E/47-B5 1145)
- McGuire W. J.**  
(JSV36/E/20-B3 1400-12)  
(JSV36/E/21-B3 1400-11)  
(VS3/E/06-B3 1430)  
(VS3/E/07-B3 1450)
- McIntosh William**  
(JSV30/E/05-B1 0940)
- McIntyre H P**  
(MI02/L/19-A4 1410)
- McIntyre H**  
(JSP21/W/11-A4 1050)
- McIntyre Michael E**  
(JSM01/E/17-A3 0830)  
(GA6.01/E/01-A5 1210)  
(JSP39/L/01-B2 0830)
- McKenzie J. F.**  
(GA4.05/L/01-A1 1400)
- McKnight Don**  
(GA1.02/E/11-A2 0930)  
(GA6.02/E/10-B1 1700)
- McLandress Charles**  
(MW04/E/03-A1 1100)  
(MW07/E/08-A4 1450)
- McLaren Alison J.**  
(P08/E/07-A2 1050)
- McLaughlin K. L.**  
(U8/W/01-B3 1400)
- McLean Peter**  
(JSP05/E/05-A2 1130)
- McLean S. J.**  
(GA5.12/W/08 A2 1220)
- McLean Susan**  
(JWS33/W/36-B2 1635-18)  
(JWS33/W/36-B3 0900-18)  
(JWS33/W/10 -B2 1635-11)  
(JWS33/W/10-B2 0945)  
(JWS33/W/10-B3 0900-11)
- McMurtry Gary**  
(GA1.15/C/U6/W/05-B4 1530-07)
- McNeave Christopher K.**  
(HW1/E/01-A4 1130)
- McNutt Stephen R**  
(JSA15/P/06-A3 1720)  
(JSV36/P/02-B3 1400-15)  
(JSV47/P/01-B5 1400-24)  
(VS3/P/01-B3 1510)
- McPhaden Michael J.**  
(U2/E/12-A2 1120)
- McPherron R. L.**  
(GA3.02/L/03-B2 1055)
- McPherron Robert**  
(JSA06/W/24-A2 1210)
- McPherron Robert L.**  
(GA5.06/W/03 A3 1120)
- McPherson J. Ian**  
(MI106/E/16-B1 1400-17)  
(MI106/E/16-B2 1400-17)
- McPowell C.A.**  
(GA1.04/E/11-A4 1610)
- McQueen Claire**  
(JSP23/C/U5/L/01-B1 1500)  
(ST3/E/57-B4 1400-24)  
(ST3/W/41-B4 1400-07)
- McQueen Herbert**  
(JSS31/L/02-B2 1520)
- McWilliams K. A.**  
(GA3.07/W/19-A6 0900-11)
- Meacham Stephen P.**  
(JSP25/W/31-B4 1130)
- Meagher Jonathan**  
(MI06/W/03-B1 1400-16)  
(MI06/W/03-B2 1400-16)
- Mechoso Carlos R.**  
(MI12/W/12-B4 1135)  
(MW03/W/10-B4 1215)  
(U3/W/08-A30900-13)
- Medina Sofia**  
(JSV36/W/12-B3 0900-08)
- Medaris Jr. Gordon**  
(JSS07/E/10-A2 0930-04)
- Medeiros A. F.**  
(JSA20/W/24-A5 1200-07)
- Medvedev A S**  
(MW07/W/05-A4 1740)
- Medvedev P**  
(G3/W/52-A5 1610-14)  
(G3/W/02-A5 1140)
- Medvedev P. P.**  
(JWS33/W/03-B2 1145)
- Medvedeva I.V.**  
(JSA20/W/11-A4 1200-10)
- Medzhitov Renat Renat**  
(GA1.02/W/22-A2 0930)
- Meek C E**  
(JSM01/W/67-A1 1110)  
(MW04/W/01-A1 0950)  
(JSA20/W/02-A4 1200-05)
- Meek Chris**  
(JSM01/W/62-A2 1110)  
(MW04/W/11-A1 0925)
- Meerkötter Ralf**  
(MI01/E/03-A1 1700)
- Meertens C.**  
(U7/L/07-B1 1700)
- Megnin Charles**  
(ST4/W/08-B3 1120)
- Mehlhorn Jens**  
(HS4/W/14-A4 1710)  
(JSP23/C/U5/E/14-A5 1420)
- Mehra A.**  
(P13/E/08-B2 1600-02)
- Mehta Amita**  
(JSM41/E/10-B3 1205)
- Mehta V.**  
(JSP25/W/95-B5 1620)
- Mehta Vikram M.**  
(JSP25/E/15-B5 1640)  
(JSP25/E/16-B4 1500)
- Mei Shirong**  
(ST1/E/32-A4 0930-07)  
(ST1/E/37-A4 0930-08)  
(ST1/E/37-A4 0930-08)
- Meier T.**  
(ST5/W/L/05-B3 1400-06)
- Meigh J. R.**  
(JSM24/L/01-B2 1010)
- Meilano I.**  
(JSV36/E/01-B3 1610)
- Meissner Katrin**  
(JSM18/W/06-A4 1500)
- Meilano I.**  
(JSP23/E/27-B2 1700)
- Meixner H**  
(G3/E/27-A5 1610-02)
- Meijas M. Bruno**  
(P11/E/28-B5 0950)
- Mekhonoshin Alexey**  
(JSS02/W/05-A1 0830-01)
- Mele F.**  
(JWS33/E/03-B2 1635-06)  
(JWS33/E/03-B3 0900-06)  
(JWS33/E/05-B2 1635-03)  
(JWS33/E/05-B3 0900-03)
- Mele Giuliana**  
(ST4/W/56-B2 0930-11)  
(JSA15/W/25-A5 0830-14)  
(JSS07/W/05-A2 0930-02)
- Meleik Magdy L.**  
(JSS44/P/06-B4 0930-17)
- Melekestev I. V.**  
(ST3/W/17-B4 0930-17)  
(JSV30/C/JSV22/E/04-B1 1400-18)
- Melekestev Ivan**  
(JSP23/E/04-B1 0830-08)
- Melhman Bob**  
(JSA40/E/07-B5 0950)
- Melián Gladys**  
(JSV36/C/U6/W/01-B3 1400-20)
- Melka K.**  
(ST4/E/06-B1 1400-18)
- Melnik Oleg**  
(VS2/W/16-B3 0910)
- Melnikova Valentina**  
(ST2/W/01-A3 1400)
- Melo L**  
(MW05/W/01-A2 1145)
- Meloni Antonio**  
(GA1.01/W/20-A5 0900-05)  
(GA1.01/W/29-A5 1700)  
(GA5.01/W/03 A1 0920)  
(JSA15/W/25-A5 0830-14)
- (GA3.04/W/41-B1 1520-10)
- Melzer Yosef**  
(G1/W/16-A3 1620-06)
- Mena Mabel**  
(GA1.03/W/21-B3 1000)
- Mende S. B.**  
(GA3.06/L/08-A3 1130)
- Mende Werner**  
(JSA16/E/37-A3 0830-07)  
(JSA16/E/42-A3 0830-02)
- Mendes V.**  
(JSS31/E/13-B3 0830-14)
- Mendes Virgilio B.**  
(JSS31/E/09-B3 0830-11)
- Mendes-Victor L.**  
(U7/E/03-B1 0830-17)  
(JSS42/E/07-B5 1700-13)
- Mendes-Victor Luis**  
(GA1.02/W/15-A2 0930-11)  
(GA1.02/W/38-A2 0930-10)  
(GA1.02/W/40-A2 0930-12)  
(JSA19/W/03-A4 1400-06)
- Méndez Carolina**  
(JSV36/W/20-B3 0900-09)
- Mendillo M.**  
(JSA20/E/27-A4 1200-21)
- Mendoza B.**  
(GA4.04/W/13-B5 1110)
- Mendoza Blanca**  
(GA4.03/E/02-B4 1645)  
(JSA16/E/17-A3 0830-05)
- Meneguzzo Francesco**  
(HS1/W/22-B4 0905)
- Menenti Massimo**  
(JSM41/E/03-B5 1105)
- Meneses Belen**  
(JSV36/W/16-B3 0900-10)
- Meneti Massimo**  
(U7/E/01-B1 1135)
- Meng Ching I.**  
(JSA20/W/49-A6 0930)  
(GA3.02/W/03-B3 0900-14)  
(GA3.02/W/15-B2 1005)  
(GA3.02/W/58-B3 0900-22)  
(GA3.03/L/01-B4 1400-04)  
(JSM32/W/07-B3 1100)  
(GA3.02/W/16-B2 0900)  
(GA3.03/W/12-B4 1400)  
(JWS33/W/27-B3 0900-22)
- Meng Wen**  
(JSP25/W/76-B1 0830-08)
- Menge F.**  
(G1/L/04-A3 1620-85)  
(JSA09/L/02-A2 1230)
- Menge Falko**  
(G1/W/32-A3 1620-15)  
(JSA09/W/13-A2 1215)
- Mengel J G**  
(MW04/W/16/C/JSM01/E/14-A1 1135)
- Mengsha Yoseph**  
(JSM43/E/01-B4 1050)
- Meniatti J. D.**  
(GA4.09/W/15-A6 0900)
- Menk F. W.**  
(GA3.07/W/44-A6 0900-20)
- Menk Fred W.**  
(GA2.07/W/10-A1 1730)  
(GA3.04/L/15-B2 1450)  
(GA3.04/W/21-B1 1520-19)  
(GA3.04/W/17-B1 1520-16)  
(GA3.04/W/01-B1 1520-41)  
(GA3.04/W/43-B2 1630)  
(GA3.04/W/51-B1 1520-20)
- Mentese Hüseyin**  
(GA6.01/W/16-A6 1250)
- Menviel Michel**  
(GA1.02/E/09-A1 1530)
- Menvielle M.**  
(GA1.02/E/38-A1 1605)  
(GA1.02/W/28-A2 0930)  
(GA5.06/E/01 A3 0900)  
(GA5.06/W/09 A3 1000)  
(JSA10/E/06-A2 0945)  
(JSA10/W/03-A2 0930)  
(JSA10/W/10-A2 1600)  
(GA1.02/E/10-A1 0915)
- Menzel Lucas**  
(HW4/E/01-B2 1630)
- Menzel W Paul**  
(MC08/L/12-A3 1630)
- Merabet N.**  
(GA1.05/W/37-A5 1420)  
(GA1.04/W/21-A4 1400)  
(GA1.04/W/22-A4 1420)
- Merchant C. J.**

- (MC05/E/02-B4 1010)
- Mercier Franck**  
(JSM41/E/31-B5 1415)
- Meredith Michael P.**  
(P07/W/03-A3 1640)  
(P07/W/17-A3 0955)
- Meredith Nigel P.**  
(GA3.05/E/06-B3 1140)
- Meredith P.**  
(JSV29/W/01-B1 1620)
- Meredith P. G.**  
(ST6/W/11-A1 0830-11)
- Merienne M F**  
(MC08/E/02-A3 1130)
- Meriwether J. W.**  
(GA2.02/W/24-B5 1500)
- Merka J.**  
(GA 3.07/E/03-A5 0900-10)
- Merkuriev S. A.**  
(GA5.12/L/01 A2 1010)
- Merry Charles**  
(G3/W/34-A5 1610-89)
- Mertikas Stelios**  
(JSG11/E/03-A4 1400-02)
- Merveilleux Du Vignaux Nicolas**  
(JSS13/W/03-A5 1130)
- Merz R.**  
(HS1/W/61-B5 1515-04)
- Merzlyakov E M**  
(JSM01/W/69-A1 1130)  
(JSM01/W/72-A2 1600-02)
- Merzlyakov Eugeny**  
(JSM01/E/04-A2 1130)
- Mesbah Maher A.**  
(JSP23/E/35-B2 0830-12)  
(JSA40/L/01-B5 1400-19)
- Meshek M.**  
(JWS33/W/33-B2 1635-32)  
(JWS33/W/33-B3 0900-32)
- Mészáros Ivan**  
(HS3/W/22-A2 1135)
- Métaxian Jean-Philippe**  
(JSV47/W/02-B5 1400-17)  
(JSV47/W/05-B5 1400-15)
- Metcalfe Sarah E.**  
(GA1.05/E/08-A6 1545)
- Mete Nakiboglu S.**  
(JSS31/L/05-B2 1600)
- Methven J.**  
(JSM26/E/14-B1 1540)
- Methven John**  
(U2/E/14-A2 1420)  
(JSP39/W/32-B3 1130)
- Métris G.**  
(G5/E/29-A4 1015)
- Metris Gilles**  
(G4/W/08-A3 1620-21)
- Metwally Mohamed**  
(JSA19/L/05-A4 1400-02)
- Metzger Kurt**  
(P16/E/06-B5 1500)
- Metzig R**  
(JSH12/W/07-A4 1400-02)
- Meurers Bruno**  
(G3/E/22-A5 1610-32)
- Mewaldt R. A.**  
(GA3.03/E/05-B4 1000)  
(GA3.05/E/16-B3 0950)  
(GA4.04/W/14-B5 1620)
- Meybeck Michel**  
(HW1/L/09-A4 0930)
- Meyer C K**  
(JSM01/W/67-A1 1110)
- Meyer Christian**  
(JSM01/W/100-A1 1450)
- Meyer Uwe**  
(G6/E/02-B2 1140)
- Meywerk J**  
(MI01/W/22 1000)
- Meza A.**  
(JSG28/W/1-B2 1140)
- Meza Amalia**  
(GA2.03/E/10-B3 1700-08)  
(G1/E/40-A3 1620-27)
- Mezcua Julio**  
(ST2/E/36-A4 1615)
- Mezenina Zifa**  
(GA1.04/E/06-A4 0930-08)
- Mi Take**  
(MI04/L/16-B3 0950)
- Mian Lin**  
(GA1.03/W/18-B3 1600)
- Michaelsen Joel**  
(HS2/W/08-B1 1140)
- Michalsky J**  
(MC07/W/17-A3 1115)
- Michel Claude**  
(HW4/E/11-B2 1130)
- Michell D. L.**  
(MI06/W/16-B2 1030)
- Michl C.**  
(HW4/E/16-B2 1520)
- Mickiewicz Al.**  
(JSA15/E/33-A3 1050)
- Mickle L**  
(MI02/W/09-A4 1220)
- Middleton Jason H.**  
(P10/E/22-A3 1600)
- Middleton John**  
(P10/W/18-A3 1400)
- Mickler Dave**  
(JSM41/W/14-B4 1500)
- Micolau**  
(JSA35/E/01-B1 1420)
- Midgley Rik**  
(P14/E/10-A4 1540)
- Midzi Vunganai**  
(ST4/W/54-B1 1620)
- Mied R. P.**  
(P07/W/20-A3 0900-07)  
(P09/W/11-A1 1010)
- Mieding Birgit**  
(P10/E/09-A5 1110)
- Miehe Jean-Marc**  
(GA5.12/W/09-A2 1600-10)
- Migliaccio Federica**  
(G6/C/G2/E/12 1100)
- Miglietta Mario**  
(JWM08/W/16-A3 1010)
- Migulin V. V.**  
(ST1/E/03-A4 0930-26)  
(ST1/E/03-A40930-25)
- Migunov N. I.**  
(JSA15/W/01-A5 0830-07)
- Mihalescu Mihaela**  
(JSP25/W/35-B3 1440)
- Mihailov Vladimir**  
(ST3/W/53-B4 1400)
- Mihaylov D.**  
(ST5/W/15-B4 1400)
- Mihaylov Dimitar**  
(ST2/W/10-A5 1400-16)
- Mikhail Sitnov**  
(GA3.08/W/01-B1 0900-05)
- Mikhailov Dmitry N.**  
(ST5/W/40-B4 0930-04)
- Mikhailov Yu. M.**  
(JSA15/E/48-A5 1400-09)
- Mikhailov Yury**  
(JSP23/C/U5/W/05-B1 0830-14)
- Mikhailova G. A.**  
(JSA15/E/48-A5 1400-09)
- Mikhailova Natalia N.**  
(ST5/L/01-B3 0900-14)
- Mikhalev A. V.**  
(JSM26/W/35-B2 1700-12)  
(JSM03/W/01-A1 1720)  
(JSA20/W/11-A4 1200-10)
- Mikhalevsky Peter N.**  
(P16/E/02-B5 1600)
- Mikhaltsov N. E.**  
(GA1.04/L/03-A5 0920)
- Mikhaylovskaya Irina**  
(JSA15/E/36-A4 1400-10)  
(JSS02/E/17-A1 0830-10)
- Mikhaylovskaya Sergey Irina**  
(ST1/C/JSS02/E/17-A2 0930-13)
- Mikheev Oleg**  
(JSA15/W/32-A5 0830-16)  
(JWS33/W/05-B2 1635-19)  
(JWS33/W/05-B3 0900-19)
- Mikic Zoran**  
(GA3.09/W/27-B4 1035)
- Mikio Tobita**  
(G5/L/06-A4 1400)
- Mikkelsen I. S**  
(JSM01/W/37-A5 1400)
- Miklaszewski Riczard**  
(GA4.05/E/03-A1 1440)
- Miklius Asta**  
(JSV36/W/19-B3 1400-07)
- Mikolaichuk Alexander**  
(G5/E/34-A4 1230-12)  
(ST2/E/28-A5 1400-10)
- Mikolajewicz U.**  
(MC02/W/01-B2 1100)
- Mikolajewicz Uwe**  
(MC11/E/10-B4 1500)
- Milan S E**  
(GA3.07/W/42-A6 0900-12)
- (GA2.02/W/04-B4 1700)  
(GA2.02/W/14-B4 0930-09)  
(GA3.03/W/06-B4 1640)
- Milana Giuliani**  
(JSV47/W/18-B5 1100)
- Milanovsky Svet**  
(HW3/W/11-B4 1610)  
(HW3/W/12-B4 1635)  
(JSS44/E/32-B4 1740)  
(ST4/E/52-B1 1400-03)  
(ST4/E/54-B1 1400-13)
- Milburn H. B.**  
(JSS42/W/25-B4 1140)
- Milenkova Lubka**  
(JSM01/E/06-A2 1600-13)
- Miles Osmaston**  
(MC09/L/03-B2 1530)
- Milkereit Bernd**  
(JSA27/E/09-B1 1110)
- Milkereit Claus**  
(ST1/W/67-A1 1050)
- Millar I. L.**  
(JSV30/L/01-B1 1400-15)
- Mille Alban**  
(JSA15/E/27-A4 1400-04)
- Miller A J**  
(JSA16/C/GA4.07/W/28-A3 0830-58)  
(MC01/W/02-A1 1445)
- Miller Arthur J.**  
(JSP25/W/05-B5 1050)
- Miller Ben**  
(JSP21/E/02-A4 0930)
- Miller Benjamin R.**  
(JSP21/L/02-A4 1440)
- Miller Gerald S.**  
(P10/L/02-A5 1600-09)  
(P11/E/04-B3 0930)
- Miller H.**  
(JSA09/L/02-A2 1230)
- Miller Jennifer**  
(JSP25/W/09-B4 1110)
- Miller L. J.**  
(MC04/E/10-B1 1035)
- Miller M.**  
(MI04/W/01-B1 1505)
- Miller Richard Gordon**  
(HW3/W/20-B4 0900-01)
- Miller Richard L.**  
(MC05/W/03-B4 1030)
- Miller Ron L.**  
(MC02/W/03-B2 0930)
- Miller William L.**  
(P15/L/18-B4 1400)
- Milligan Peter**  
(GA1.02/L/AW1-A2 0930)
- Milligan Peter R.**  
(GA1.02/E/01-A2 0930)  
(GA1.02/W/31 1000)
- Milling D.**  
(GA3.04/E/14-B1 1520-03)
- Milling D. K.**  
(GA3.04/W/21-B1 1520-19)  
(GA3.04/W/51-B1 1520-20)
- Mills Franklin**  
(MI09/L/06-A5 1145-15)
- Mills Michael J**  
(MI02/W/11-A5 1410)
- Millward G.**  
(JSA20/W/41-A5 1200)
- Millward G. H.**  
(JSA20/W/26-A5 1425)
- Milly P. C. D.**  
(HW4/E/17-B2 1610)  
(JSM24/W/08-B2 1155)
- Milne G A**  
(JSG11/W/09-A3 1500)  
(JSG11/E/05-A3 1520)
- Milner Simon C.**  
(GA1.03/W/04-B1 1140)
- Miloslav Alaoui**  
(HS3/W/22-A2 1135)
- Milosavljevic M. M.**  
(GA2.03/W/06-B3 1200)
- Milovanov Alexander V.**  
(GA3.02/W/63-B3 0900-09)
- Milsom John**  
(ST2/E/33-A3 1130)
- Min Wang**  
(G1/L/10-A3 1620-30)
- Min Wen**  
(MW06/P/1-A3 1700)
- Min Wu Yih**  
(U3/W/21-A3 0900-17)
- Minaeva Yu. S.**  
(GA3.05/W/17-B3 1400)
- Mineev Yu. V.**  
(GA3.05/E/13-B3 0900-36)
- Minenko L. V.**  
(GA3.02/E/11-B2 0935)  
(GA3.02/E/12-B3 0900-01)
- Ming Wei**  
(G3/E/42-A5 0940)
- Ming Zha**  
(G1/C/G2/E/02-A3 1620-105)  
(G4/E/02-A3 1620-11)
- Mingquan Mu**  
(JSP25/P/02-B1 0830-10)
- Mingram Jens**  
(VS2/C/U6/E/01-B3 1400-35)  
(GA1.05/E/09-A5 0900-02)
- Mingruo Jiao**  
(ST2/W/03-A3 1215)
- Mingzhi Ma**  
(JSS44/E/41-B4 0930-10)
- Minnis Patrick**  
(MI04/W/35-B2 1450)
- Minobe Shoshiro**  
(JSP25/W/56-B5 1700)  
(JSP25/W/70-B5 1110)
- Minomaru Mariko**  
(JSM01/W/48-A4 1620-02)
- Minoo Kosarian**  
(ST4/E/61-B1 1400-05)
- Minschwaner K**  
(MC07/W/22-A2 1620)
- Miranashvili Avtandil A.**  
(M110/E/07-B3 1505)
- Miranda J. M.**  
(JSS42/E/03-B5 1700-12)  
(G5/E/46-A4 1548-05)  
(G5/E/47-A4 1546-04)
- Miranda Jorge**  
(GA1.02/W/40-A2 0930)
- Miranda Luiz B.**  
(P10/E/08-A4 1700)
- Miranda Pedro A M**  
(JSP05/W/13-A2 1150)  
(JSM01/C/MW07/W/01-A2 1600-28)
- Miranda Pedro M. A.**  
(JSM43/W/03-B4 1400)  
(JSM43/W/13-B4 1420)
- Mircea Radulian**  
(ST1/E/05-A2 1400-30)
- Mireault Y.**  
(G1/C/G5/E/15-A3 1620-102)
- Miro Gloria**  
(JSA20/E/07-A4 1200-30)
- Mironov B A**  
(GA4.09/W/06-A5 1600-03)  
(GA4.02/W/35-A4 1400-27)  
(GA3.04/E/17-B1 1520-06)
- Mironyuk S. V.**  
(JSS42/W/12-B5 1700-16)
- Miroshnichenko L. I.**  
(GA4.04/W/11-B5 0830-05)  
(GA4.04/W/13-B5 1110)  
(GA4.02/W/21-A4 1400-19)  
(GA4.02/E/07-A4 1400-02)
- Miroslav K. R. S.**  
(GA1.15/E/02-B4 1530-02)
- Miroslawa Ostrowska**  
(P15/W/09-B4 1115)
- Mirzaei Noorbakhsh**  
(ST2/E/29-A4 1200)
- Mirzoev Kamil**  
(ST5/W/22-B4 1400-03)
- Misawa Hiroaki**  
(GA3.05/W/31-B3 0900-21)  
(GA3.05/W/36-B3 0900-20)
- Mishima Toshiaki**  
(GA1.05/E/17-A6 1630)
- Mishin A.V.**  
(JSA19/E/02-A41400-09)
- Mishin E. V**  
(GA2.07/W/14-A1 1000)
- Mishin V**  
(GA4.02/E/06-A4 1400-09)  
(GA4.02/E/13-A4 1400-08)  
(GA3.02/E/19-B3 0900-02)
- Mishin V. M.**  
(GA3.02/E/11-B2 0935)  
(GA3.02/E/12-B3 0900-01)  
(GA3.03/E/01-B4 1400-03)  
(GA3.03/E/04-B4 1530)
- Mishina M.**  
(GA1.02/L/05-A2 0930)  
(JSA15/W/07-3 1740)
- Mishonov Alexey**  
(P15/W/03-B3 1025)
- Mishonov Alexey V.**

# INDEX

- (P11/W/17-B5 1400)
- Mishra D. C.**  
(JVS22/E/09-A5 1110)
- Mishra N. C.**  
(JSP23/W/99-B2 0830-03)
- Misra R. N.**  
(GA 2.02/E/07-B4 0930-20)  
(GA2.02/E/05-B5 1120)
- Mist R. T.**  
(GA3.07/W/07-A5 0900-11)  
(GA3.10/W/21-A6 1700-17)  
(GA3.08/W/24-B1 1210)
- Mital G. S.**  
(JSA09/E/03-A3 1215)
- Mitchell D. L.**  
(GA4.10/W/13-A4 0930)  
(M104/E/25-B4 0930)  
(M104/W/21-B4 1020)  
(M110/W/13-B2 1650)  
(HW4/E/02-B2 0900-14)  
(JSP25/W/55-B2 0950)
- Mitchell Kenneth**  
(JSM24/E/05-B1 1650)
- Mitchell J. Kent**  
(HS3/W/02-A1 0925)  
(HSA3/W/05-A1 1110)
- Mitchell John**  
(JSA16/E/01-A3 0830-19)
- Mitchell Kenneth E**  
(MC01/W/30-A4 1615)  
(MC01/L/18-A4 1715)
- Mitchell Moncrief W.**  
(M104/L/02-B3 0905)
- Mitchell N J**  
(JSM01/W/11-A2 1210)  
(JSM01/W/72-A2 1600-02)  
(MW04/W/01-A1 0950)  
(JSA20/W/22-A4 1146)  
(JSA20/W/30-A4 1526)  
(JSA20/W/32-A4 1025)
- Mitchell Nicholas**  
(JSM01/E/04-A2 1130)
- Mitchell Todd**  
(JSP25/W/87-B1 1700)
- Mitchum G. T.**  
(JSM41/W/09-B4 1515)
- Mitev Valentin**  
(JSM26/W/16-B2 1210)  
(JSA09/W/12-A2 1630)
- Mitkin Vladimir V.**  
(JSP39/W/01-B3 1442-15)  
(JSP39/W/07-B2 1720)  
(JSP39/W/09-B3 1445-16)
- Mitomi Yasushi**  
(P15/L/21-B4 0925)
- Mitrovica J X**  
(JSS02/E/09-A2 1030)  
(JSG11/W/02-A3 1540)  
(JSG11/W/09-A3 1500)  
(JSG11/E/05-A3 1520)  
(JSG11/W/10-A3 1620)
- Mitsuzawa Kyohiko**  
(P16/E/13-B5 0950)
- Mittermaier M P**  
(M102/L/01-A5 1140)
- Mitzeva Rumjana**  
(M103/W/07-A3 1400-03)  
(M105/W/12-A4 1400-12)
- Miura Akira**  
(GA3.07/L/04-A4 0930-19)
- Miura Daisuke**  
(JVS29/W/03-B1 1400-01)  
(JVS29/W/05-B1 1400-02)
- Miura S.**  
(JVS36/E/18-B3 1400-13)
- Miwa Atsushi**  
(JSG28/E/18-B1 1400-10)
- Mix A. C.**  
(P07/W/05-A3 1700)
- Miyabuchi Y**  
(HW2/W/19-B1 0900)
- Miyagawa H.**  
(JSA20/W/09-A4 1200-11)
- Miyahara S.**  
(M112/W/10-B4 1650)
- Miyahara Saburo**  
(JSA20/W/54-A5 1020)  
(JSM01/L/01-A2 0930)  
(MW04/W/05-A1 1545)
- Miyaji Naomichi**  
(JSS42/E/14-B5 1700-04)
- Miyakawa Koji**  
(JYS47/E/02-B5 1230)
- Miyake Hiroe**  
(ST3/W/16-B4 0930-06)
- Miyake T.**  
(GA4.09/W/10-A6 1200)
- Miyako Naya**  
(JSP49/W/24-B5 1210-16)
- Miyaoka Kunihide**  
(HS4/W/03-A4 1045)
- Miyashita K.**  
(JSS44/W/01-B4 0930-06)
- Miyazaki S.**  
(GA2.02/W/09-B4 0900)
- Miyazaki Shim**  
(JSM24/W/04-B1 0930)
- Miyazaki Shinichi**  
(GA2.02/E/13-B4 1100)  
(GA2.03/E/02-B3 1120)  
(JSG28/E/29-B1 1400-18)
- Miyoshi Y**  
(JSM01/W/20-A1 0900)
- Miyoshi Yasunobu**  
(M112/W/03-B4 1400)  
(MW04/W/05-A1 1545)
- Miyoshi Yoshizumi**  
(GA3.05/W/31-B3 0900-21)  
(GA3.05/W/36-B3 0900-20)
- Mizogami T.**  
(JSS44/W/01-B4 0930-06)
- Mizuta Ryo**  
(JSM26/W/23-B1 1730)
- Mizutani K**  
(JSM01/E/42-A2 1600-09)
- Mlawer E J**  
(MC01/W/33-A1 1515)  
(MC08/E/08-A3 1445)  
(MC07/W/17-A3 1115)  
(MC08/L/09-A3 1545)  
(MC08/W/04-A4 1130)  
(MC08/W/06-A3 1505)  
(M108/E/06-A4 1235)
- Mlynczak Marty**  
(JSA20/W/06-A4 1425)
- Mo Xinguo**  
(HW4/E/07-B2 0900-06)  
(JSM24/E/12-B1 1710)
- Mo Xinguo**  
(JSM43/E/06-B4 1130)
- Mobbs S D**  
(JWM08/W/16-A3 1010)
- Mobbs Stephen**  
(MW07/W/08-A4 0920)
- Möbius E**  
(GA3.06/W/29-A2 1720)
- Mocanu Victor**  
(ST2/W/11-A4 1430)
- Mochizuki Hiromine**  
(ST1/W/47-A2 1400-12)
- Moczso Peter**  
(ST3/W/01-B3 1645)  
(ST3/W/20-B3 0945)  
(ST3/W/44-B3 0930)
- Modica G.**  
(JWS33/E/03-B2)  
(JWS33/E/03-B3 0900-06)
- Moebius E.**  
(GA4.02/E/02-A4 1400-06)  
(GA4.04/E/05-B5 0940)
- Moen J.**  
(GA3.07/W/01-A6 1130)
- Moerner Nils-Axel**  
(GA6.01/W/14-A5 1145)
- Mofjeld H. O.**  
(JSS42/W/05-B5 1700-11)  
(JSS42/W/07-B5 1500)  
(JSS42/W/25-B4 1140)
- Mogi T.**  
(JSA15/E/17-A3 1440)  
(JSA15/W/14-A4 1400-16)
- Mogi Toru**  
(GA1.02/E/20-A1 1605)  
(GA1.02/E/29-A2 0930)  
(GA1.02/E/33-A1 1605)  
(GA1.02/E/34-A1 1500)  
(JSA15/E/02-A5 0830-05)
- Mogilatov V.**  
(GA1.02/W/03-A1 1050)
- Mohamed A. S**  
(G5/E/41-A4 1230-07)
- Mohamed Ahmed**  
(JSA19/W/04-A4 1400-05)
- Mohamed S.**  
(JSP23/C/U5/E/10-A6 0830-03)
- Mohammad Reza Gheitanchi**  
(ST2/P/09-A4 1145)  
(ST2/P/12-A4 1015)
- Mohankumar S. V.**  
(M106/W/25-B2 1130)
- Mohanty P. K.**  
(JSP25/L/04-B2 0930-08)
- Mohlenbrink Wolfgang**  
(G6/L/04-B2 1740)
- Mohr J**  
(JSH12/W/05-A5 0900)
- Mohr S.**  
(JWS33/W/23 -B2 1635-07)  
(JWS33/W/23-B3 0900-07)
- Moirano Juan**  
(JSG11/W/01-A4 1050)  
(G1/W/18-A3 1620-07)  
(G1/W/41-A3 1620-46)
- Mokhov Igor I.**  
(M111/E/08-B5 0900)  
(MW02/E/02-B3 1640)
- Mokrik Robert**  
(JSG14/W/06-A3 1215-26)
- Mokrov Evgeny**  
(JSP23/C/U5/E/18-B1 0830-11)
- Mokrov Evgeny**  
(ST3/E/48-B5 1100)
- Molchanov Oleg**  
(ST1/W/37-A4 0930-01)
- Moldovan Iren-Adelina**  
(JSP23/E/52-B1 0830)
- Moldovan Ivan**  
(JSP23/E/53-A5 0830-08)
- Moldoveanu C. L.**  
(ST3/W/03-B3 1630)  
(ST3/W/05-B4 1615)
- Moldwin M.**  
(GA3.08/W/05-A6 1040)
- Molina Enrique**  
(JSS42/E/18-B5 1010)
- Molinari R. L.**  
(P11/W/16-B3 0950)
- Molines J-M**  
(MC01/L/07-A2 1430)
- Molkov Yaroslav I.**  
(M111/E/03-B5 1745)
- Moller Jr. O**  
(P10/E/11-A5 1600-01)  
(P10/E/15-A4 1720)
- Molnar P.**  
(U8/E/09-B3 1155)
- Molochushkin N. E.**  
(GA3.04/E/15-B1 1520-02)
- Molteni F.**  
(M111/W/01-B5 0830)
- Molteni Franco**  
(JWM08/W/11-A3 1220)
- Molyneux M. G**  
(JSM01/W/37-A5 1400)
- Molz F. J.**  
(JSA19/W/01-A4 1400-08)
- Momar Working Group**  
(P16/E/04-B5 1050)
- Momma Hiroyasu**  
(P16/E/10-B5 1010)  
(P16/E/13-B5 0950)
- Monachesi Giancarlo**  
(ST3/E/22-B5 1515)
- Moncrief W. Mitchell**  
(M104/L/11-B1 1520)  
(M104/W/13-B1 0915)
- Moncrieff Mitch**  
(M104/L/12-B1 1145)
- Monem Abdel**  
(JSP23/C/U5/E/10-A6 0830-03)
- Monfort Patrick**  
(P15/L/05-B4 1610)
- Monfray Patrick**  
(MC01/W/15-A2 1740)  
(MC01/W/55-A5 1715)  
(MC01/W/58-A5 1620)
- Monico Galera**  
(G1/E/28-A3 1620-62)  
(G1/E/44-A3 1620-28)
- Monks Paul**  
(U2/E/14-A2 1420)
- Monserat S.**  
(JSP23/W/07-B1 930)
- Monserat Sebastian**  
(JSS42/E/25-B5 1700-08)
- Monson H. H.**  
(JSA20/W/02-A4 1200-05)
- Montagner Jean-Paul**  
(JSS02/W/06-A2 1215)  
(JSS07/W/07-A2 1400)  
(JSS13/W/15-A4 1500)  
(JWA34/W/06-B2 1010)  
(ST4/L/06-B2 0930-29)  
(ST4/W/25-B2 1720)  
(ST5/W/33-B3 0900-07)
- (U7/W/01-B1 0830-14)
- Montague Derek C**  
(M101/W/06-A2 1200)
- Montaldo Nicola**  
(HW4/W/04-B2 0900-07)
- Montani A**  
(M105/E/06-A1 1630)
- Montani Andrea**  
(JWM08/W/11-A3 1220)  
(M105/W/14-A3 0920)
- Montelli Raffaella**  
(JSS46/E/04-B4 1400)
- Montesions F.**  
(JSA40/W/10-B5 1400-12)
- Monti Guarnieri A.**  
(G3/W/47-A5 1610-45)
- Montuori C.**  
(ST1/W/42-A1 1110)
- Montzka Stephen**  
(JSP21/W/05-A4 1520)  
(JSP21/W/12-A4 1110)  
(JSP21/W/15-A4 1600)  
(JSP21/W/17-A4 1500)
- Moore Christopher N. K.**  
(P10/L/06-A3 1500)  
(JSP39/W/04-B4 1130)  
(P11/E/06-B3 1010)
- Moon Deok-Soo**  
(P07/W/01-A3 0900-01)
- Moon Woil M.**  
(JSA27/E/06-B1 1130)  
(JVS36/L/02-B3 1400-16)
- Moon Woil M.**  
(JSP23/C/U5/E/20-B2 1110)  
(JSP23/C/U5/E/20-B2 1110)
- Mooney W.**  
(U8/E/09-B3 1155)
- Mooney Walter**  
(JSA40/E/08-B5 1005)
- Moore Blake**  
(P13/W/09-B2 1600-05)
- Moore Charles**  
(JSM03/W/02-A1 1650)
- Moore F L**  
(JSM01/W/56-A4 1620-07)
- Moore Fred L.**  
(JSM26/W/05-B1 0920)
- Moore Gerald**  
(P15/E/01-B40900)  
(P15/E/03-B3 1440)  
(P15/E/04-B4 1135)
- Moore John**  
(JSA09/W/06-A2 0930-03)
- Moore K G**  
(M101/L/05-A1 0900-09)
- Moore P.**  
(G4/W/15-A3 1620-23)  
(G6/C/G5/W/06-B1 0930)
- Moore R. D.**  
(HW3/W/17-B4 0925)
- Moore Robert J.**  
(U5/L/02-A4 1700)
- Moore Robert M.**  
(JSP21/W/08-A4 1400)
- Moore Roger**  
(G1/E/56-A3 1620-80)
- Moore Sean**  
(M110/W/03-B2 1205)
- Moore T E**  
(GA3.10/W/01-A6 1630)
- Moore Terry**  
(G1/E/51-A3 1620-76)  
(G1/E/52-A3 1620-77)  
(G1/E/54-A3 1620-79)
- Moore Thomas E.**  
(GA3.08/W/09-A6 0920)  
(GA3.08/W/13-A6 0940)  
(GA3.08/W/21-A6 0900)  
(GA3.09/W/15-B4 1450)  
(GA3.08/W/17-A6 0940)
- Mora Mauricio**  
(JVS47/W/02-B5 1400-17)
- Moraitis George**  
(GA3.09/W/07-B4 0900-11)  
(GA3.09/W/21-B4 0900-10)
- Morales J.**  
(JVS47/W/30-B5 1400-23)  
(ST5/W/56-B3 0900-01)  
(ST5/W/66-B4 1400-06)
- Morales Miquel M.**  
(P13/E/12-B1 0910)  
(P13/W/27-B1 1210)
- Moran P. J.**  
(GA4.04/W/07-B5 1430)  
(GA4.01/W/09-A2 1140)



- (GA4.02/E/07-A4 1400-02)  
(GA4.05/E/02-A1 1010)
- Morat Pierre**  
(JSA15/W/23-A3 0930)
- Morcrette J -J**  
(MC08/E/08-A3 1445)
- Morcrette Jean-Jacques**  
(M106/E/09-B1 1400-13)  
(M106/E/09-B2 1400-13)  
(MW02/E/05-B3 1100)
- Mordvinov Alexander V.**  
(GA6.01/W/05-A5 0900-15)  
(JSA16/W/26-A3 0830-29)  
(JSA16/W/33-A3 0830-28)
- Mordvinov Vladimir**  
(GA4.03/W/08-B4 1700)
- Moreau F.**  
(JSS44/L/05-B-4 0930-04)
- Moreaux G.**  
(G2/W/03-A2 1630-18)
- Moreaux Guilhem**  
(G4/W/19-A3 1520)
- Morel André**  
(P15/L/30-B4 0950)
- Morelli A.**  
(ST4/W/18-B2 1440)  
(ST2/E/21-A5 1400-24)
- Morena Benito A de la**  
(JSA20/E/07-A4 1200-30)  
(JSA35/E/01-B1 1420)
- Moresi Louis**  
(ST4/W/06-B2 0930-01)  
(ST4/W/06-B2 1200)  
(JSS13/W/05-A5 0900)
- Moretto Therese**  
(GA3.10/E/07-A6 1700-08)
- Morgachev V. I.**  
(ST4/E/52-B1 1400-03)
- Morgan D.**  
(GA3.02/W/58-B3 0900-22)
- Morgan Michael C.**  
(MI05/E/14-A2 1120)  
(MI05/E/22-A2 1550)
- Morgan P.**  
(JSS31/W/15-B3 0830-09)
- Morgan Peter**  
(G1/E/18-A3 1620-56)  
(G1/W/08-A3 1620-35)
- Morgan S. P.**  
(G5/L/01-A4 1145)
- Morgan Vin**  
(JSM18/W/08-A5 1100)  
(JSM18/W/13-A5 1140)
- Morgan W. J.**  
(ST4/W/03-B3 1630)
- Morgenstern O.**  
(JSM26/E/16-B3 1130)
- Morgenstern Olaf**  
(JSM26/E/15-B2 1700-04)
- Morgounov Vitali A.**  
(JSA15/E/37-A5 1400-10)  
(JSP23/C/U5/E/11-B2 0830-02)  
(ST1/E/22-A2 1400-27)
- Mori Atsushi**  
(JSP39/E/01-B3 1500-21)
- Mori H.**  
(GA 2.01/E/07-A1 0900)
- Mori Toshiya**  
(JSV36/W/01-B3 0900-12)  
(JSV36/W/26-B3 1215)
- Morikawa H**  
(ST3/W/39-B4 1400-08)  
(ST3/E/30-B4 0930-13)  
(ST3/E/35-B4 0930-14)
- Morioka Akira**  
(GA3.05/W/31-B3 0900-21)  
(GA3.05/W/36-B3 0900-20)
- Moritz R E**  
(MI08/L/05-A3 1705)
- Mork Martin**  
(P11/W/09-B3 1500)
- Mörner Nils-Axel**  
(JSS42/W/16-B5 1700-03)  
(MC03/W/02-B4 1210)  
(JSG11/W/12-A3 1740)  
(JSG14/W/08-A3 1157-20)  
(JSP23/C/U5/W/10-B1 1600)
- Moroz Yu. F.**  
(JSA15/E/43-A5 0830-17)  
(JSA15/E/51-A5 1400-11)  
(ST4/E/60-B1 0830-10)
- Morozov Alexander A.**  
(ST6/E/08-A1 0830-17)
- Morozov Eugene**  
(JSP 49/E/01-B5 1210-15)
- (JSP39/E/05-B4 1640)  
(JSP49/E/02-B5 0830)
- Morozov Sergey**  
(ST3/E/48-B5 1100)
- Morozov V. N.**  
(G5/P/4-A4 1508-05)
- Morozova E.**  
(GA3.05/W/32-B3 0900-25)
- Morris B. L.**  
(HS5/W/21-A2 1405)
- Morris C. Jon**  
(MC02/W/06-B2 1630)
- Morris D.**  
(GA4.02/W/28-A4 1720)
- Morris J**  
(JSA06/E/09-A1 1155-01)
- Morris P.**  
(GA5.12/W/02 A2 1100)
- Morris R J**  
(JSA06/E/06-A1 1155-19)  
(GA3.10/E/06-A6 1700-10)
- Morris Ray J.**  
(GA2.02/E/02-B4 1740)  
(GA3.04/W/17-B1 1520-16)
- Morrison D.**  
(JSM32/W/07-B3 1100)
- Morrison Graeme**  
(GA1.01/W/06-A6 1015)
- Morrison H. F.**  
(GA3.04/E/03-B1 0900)
- Morshchikhin Sergei I.**  
(GA1.05/W/40-A6 0900-03)
- Morss R**  
(MI05/L/04-A3 0900)
- Mortensen M. D.**  
(JSG28/W/23-B2 1130)  
(JSG28/W/26-B2 1400-08)
- Mortera-Gutierrez Carlos A.**  
(ST2/E/44-A5 0945)
- Mortlock Richard**  
(P07/W/04-A3 0900-02)  
(P07/L/02-A3 1125)  
(P07/W/19-A3 1550)
- Moruffdeen A. Adabanija**  
(JSA19/L/08-A4 1400-11)
- Moses J. D.**  
(JSA16/W/13-A3 0830-47)
- Moshanov Anatoly V.**  
(JSA15/W/20-A5 1400-14)
- Moshchenko Alexander**  
(P10/E/13-A5 1440)
- Moskvin Igor**  
(JSA45/W/17-B5 1110-07)
- Mostafa Mohamed M. R.**  
(G6/E/06-B2 1440)
- Mostajir Behzad**  
(P15/L/05-B4 1610)
- Mostovoi Gueorgui V.**  
(MI04/E/07-B1 0900-14)  
(MI10/E/04-B1 0900-15)
- Mostryukov A. O.**  
(ST1/W/39-A3 1150)
- Mosugu Mary**  
(HS4/W/17-A5 0930)
- Moszukhina A.**  
(GA3.05/W/32-B3 0900-25)
- Motao Huang**  
(G3/W/38-A5 1610-42)  
(G4/W/07-A3 1620-12)
- Motell Craig**  
(MC08/L/09-A3 1545)  
(MC08/L/14-A4 0945)
- Mothes Patricia**  
(JSP23/C/U5/E/05-A6 0830-06)
- Motoi Tatsuo**  
(MC01/E/26-A2 1500)
- Motovilov Edward A.**  
(ST6/E/08-A1 0830-17)
- Motschmann U.**  
(JSA10/E/06-A2 0945)
- Mouchet Anne**  
(MC01/L/06-A2 1415)
- Mouheb H.**  
(G1/L/13-A3 1620-89)
- Moukikis C.**  
(GA3.02/W/54-B2 1615)
- Moukikis C. G.**  
(GA3.02/E/18-B3 0850)
- Moulin C**  
(MI09/L/03-A5 0830)
- Mountney Nigel**  
(JSV22/W/08-A5 0900)
- Mourtada-Bonnefoi C. C.**  
(JSV29/E/02-B1 1440)
- Mousa Ashraf**  
(JSG 28/E/04-B1 1400-12)
- Mousa Salah A.**  
(GA1.04/P/01-A6 1200)
- Mouzaia H.**  
(G5/P/03-A4 1230-04)
- Moynot B.**  
(G3/E/27-A5 1610-02)
- Mozer F.**  
(GA3.03/W/11-B4 1200)  
(G3.04/W/18-B1 1520-26)
- Mozheng Wei**  
(MI05/E/07-A1 1140)
- Mozzoni D.**  
(GA5.08/W/13-B1 1545)
- Mozzoni David**  
(GA5.09/W/09 A2 1030)  
(GA5.12/W/06 A2 1440)
- Mravlag Erhard**  
(GA2.01/W/10-A1 1505)
- Mshra Nrusingha C.**  
(JSM41/P/01-B3 1235)
- Mu Mingquan**  
(JSP25/P/06-B1 1520)
- Mu Mu**  
(MI11/E/10-B5 1645)
- Mucciarelli Marco**  
(ST3/E/07-B4 1000)  
(ST3/E/22-B5 1515)
- Muco Betim**  
(ST1/E/82-A4 0930-16)  
(ST2/E/56-A5 1400-20)
- Mueller**  
(G6/L/07-B3 0920)
- Mueller Andreas**  
(JSA15/E/30-A3 1620)
- Mueller Doerthe**  
(MI09/W/08-A5 1542)
- Mueller Ivan**  
(U7/W/07-B1 0830-01)
- Mueller J.**  
(G2/W/08-A2 1630-22)
- Mueller Juergen**  
(G2/E/11-A2 1630-24)
- Mueller R Dietmar**  
(JSS13/W/05-A5 0900)  
(ST4/W/04-B3 0830-02)
- Mueller R. J.**  
(JSA15/W/29-A3 1540)
- Mueller-Mellin Reinhold**  
(GA4.01/E/09-A2 1200)
- Mueller-Wodarg I. C. F.**  
(JSA20/W/12-A4 1544)
- Muench Robin**  
(P14/E/08-A4 1400-07)  
(P13/E/17-B1 0950)  
(P13/E/01-B1 0830)  
(P13/W/15-B2 1600-10)
- Muhtarov P.**  
(GA3.04/W/15-B1 1520-15)  
(JSA06/W/15-A2 1010)
- Mukai Sonoyo**  
(MI09/W/06-A5 1145-09)
- Mukai Toshifumi**  
(GA3.02/W/03-B3 0900-14)  
(GA3.08/E/01-A6 1430)  
(GA3.08/W/16-B1 1430)  
(GA3.08/W/24-B1 1210)  
(GA3.08/W/28-B1 1510)  
(GA3.04 /W/04-B1 1520-40)  
(GA3.08/W/04-B1 0900-02)  
(GA3.10/W/09-A6 1700-13)  
(GA3.10/W/04-A6 1450)  
(GA3.10/W/21-A6 1700-17)
- Mukherjee K. K.**  
(ST4/W/33-B1 0830-29)
- Mukhin Dmitry N.**  
(MI11/E/03-B5 1745)  
(MI11/W/09-B5 1730)
- Mukhina A. Y.**  
(JSM26/E/01-B2 1700-03)
- Mukhina Anna**  
(JSM26/E/03-B2 1700-08)
- Mukhtarov Pl.**  
(JSA20/W/30-A4 1526)
- Mukhtarov Plamen**  
(JSM01/W/99-A1 1130)
- Mulei Kithia Shadrack**  
(HS5/W/45-A3 1545-01)
- Mullen E. G.**  
(GA3.05/W/27-B3 0900-37)
- Mullen R.**  
(GA1.04/L/06-A4 0930-03)
- Muller Achim**  
(G1/E/60-A3 1620-82)
- Muller G.**  
(JSA20/W/32-A4 1025)
- Muller H G**  
(MW04/W/01-A1 0950)  
(JSM01/W/11-A2 1210)  
(JSA20/W/22-A4 1146)  
(JSA20/W/30-A4 1526)
- Muller Heinz**  
(JSM01/E/04-A2 1130)
- Müller I.**  
(JSA19/W/13-A4 0945)
- Muller J. P.**  
(MI10/E/01-B2 1535)
- Mulligan T.**  
(GA4.01/W/11-A2 1100)  
(GA4.08/W/19-B3 0930)
- Muloshi**  
(MI06/L/02-B1 1400-15)  
(MI06/L/02-B2 1400-15)
- Mulvaney R**  
(JSP21/W/11-A4 1050)  
(MI02/L/19-A4 1410)
- Munekane Hiroshi**  
(JSV36/W/27-B3 0900-05)
- Munhoven Guy**  
(HS2/W/30-B2 1600)  
(HS2/W/31-B2 1620)
- Munirova Lira**  
(ST2/E/40-A3 1415)
- Muniz Luiz**  
(GA5.01/E/24 A1 1515)
- Munot A.**  
(JSP23/W/25-B2 0830-01)
- Munro Philip**  
(ST5/W/01-B3 0900-05)
- Munsami V.**  
(GA3.05/W/02-B3 0900-22)
- Muradymov Genady**  
(GA 5.11/E/02 A3 1430-09)
- Murakam Makoto**  
(G5/L/06-A4 1400)
- Murakami**  
(G2/L/14-A2 1630-26)
- Murakami Fumitoshi**  
(JSV36/C/U6/W/06-B3 1400-23)
- Murakami H.**  
(GA1.02/L/05-A2 0930)  
(JSA15/W/07-3 1740)
- Murakami Hiroshi**  
(JSM41/E/08-B4 1210)
- Muralikrishna P.**  
(GA2.02/E/08-B5 1100)  
(GA2.02/W/08-B5 0920)  
(GA2.03/W/05-B3 1400-02)  
(GA2.03/W/05-B3 1600)
- Murata Yasuaki**  
(JSA40/W/07-B5 1400-10)
- Murayama Yasuhiro**  
(JSM01/E/34-A2 1600-14)  
(JSM01/E/42-A2 1600-09)  
(GA2.01/E/07-A1 0900)
- Murcay F**  
(MC07/W/17-A3 1115)
- Murnane Richard**  
(MC01/W/58-A5 1620)
- Muro Andrea di**  
(JSV29/E/01-B1 1720)  
(JSV29/W/04-B1 1700)
- Murphy D. J.**  
(JSM32/L/01-B3 1125)  
(JSM01/E/43-A2 1600-10)  
(JSA20/E/17-A6 1154)  
(JSA20/E/04-A6 1136)
- Murphy G**  
(JSM01/W/37-A5 1400)
- Murphy J. R.**  
(GA4.10/L/05-A4 1040)
- Murphy N.**  
(GA4.10/W/16-A5 1145)  
(MC09/W/04-B2 1030)
- Murr D L**  
(GA3.10/W/23-A6 0935)
- Murr David**  
(GA3.07/W/24-A6 1000)
- Murrat Steve**  
(P14/W/05-A4 1420)
- Murray Anne**  
(GA5.09/W/07 A2 1400-01)
- Murray James W**  
(P08/E/01-A2 1600)  
(P08/E/03-A2 1520)
- Murray John B.**  
(JSV36/E/01-B3 1610)
- Murray Stephen P.**  
(P14/E/04-A4 1040)
- Murru M.**

## INDEX

(ST1/W/42-A1 1110)  
(ST1/W/53-A2 1600)

**Mursula K.**  
(GA6.01/W/03-A5 1525)  
(GA2.03/W/09-B3 1030)  
(GA3.04/E/14-B1 1520-03)  
(GA3.04/W/08-B1 1150)  
(GA3.04/W/24-B1 1520-29)  
(GA3.04/W/29-B1 1520-28)  
(GA3.04/W/33-B1 1520-27)  
(G3.04/W/18-B1 1520-26)

**Mursula Kalevi**  
(GA3.04/E/11-B1 1520-21)

**Murthy N. S. R.**  
(ST4/W/32-B1 0830-30)

**Murthy N. V. S. S.**  
(PW1/P/01-A6 0940)

**Murty K. P. R. Vittal**  
(JSP49/W/03-B5 1700)  
(JSP49/W/15-B5 1210-18)

**Murty K. S.**  
(JSP23/W/100-B2 0830-04)  
(ST7/P/01-A2 1500)

**Murty T. S.**  
(P09/E/06-A1 1110)  
(P09/E/08-A1 1130)

**Muschen Bettina**  
(HS4/W/08-A4 1450)

**Muschietti L.**  
(GA4.09/W/07-A6 0940)

**Mushayandebvu M. F.**  
(GA5.12/E/10 A2 1120)

**Mushayandebvu Martin F.**  
(JSA27/E/07-B1 0940)

**Mushtak Vadim**  
(JSA35/E/05-B1 1630)

**Musiaka Katumi**  
(JSM24/W/02-B1 1030-01)  
(JSM24/W/14-B1 1520)  
(JSM24/W/15-B1 1610)  
(HW1/L/07-A4 1430)

**Music Biljana**  
(MI01/W/13-A1 0900-13)

**Musienko Elena**  
(ST11/E/24-A3 0900-04)  
(ST2/E/26-A5 1400-11)  
(SW1/E/07-B5 1030-02)

**Musingi John Kioko**  
(HS5/W/45-A3 1545-01)

**Musmann G.**  
(JSA10/E/06-A2 0945)  
(JSA10/W/03-A2 0930)

**Musson R.**  
(JSP23/C/U5/E/16-A5 1620)  
(ST3/E/56-B4 1400-20)  
(ST3/E/21-B4 1715)  
(ST3/E/23-B5 1200)

**Musson R. M. W.**  
(JSP23/C/ST3/E/21-A5 0910)

**Musumeci C.**  
(ST2/W/07-A5 0900)

**Musy A**  
(HS4/W/13-A4 1650)

**Muzik Ivan**  
(HS1/W/73-B5 1730-03)

**Mwami James**  
(JSM24/C/U1/P/03-B1 1030-04)

**Myachkin V. V.**  
(JSV47/E/07-B5 1400-01)  
(ST4/W/11-B2 0930-04)

**Myachkin Victor V.**  
(ST1/W/32-A2 0930-08)

**Myagkov Sergey V**  
(HS5/W/48-A3 1545-04)

**Myagkova I. N.**  
(GA3.05/E/01-B3 0900-38)  
(GA3.05/E/19-B3 0900-04)

**Myakoshin O I**  
(JSM18/W/11-A5 1020)

**Myers Edward**  
(JSS42/W/25-B4 1600)

**Myers Paul**  
(P11/W/23-B4 0950)

**Myhre Gunnar**  
(MC07/W/20-A3 0935)

**Mysak L. A.**  
(P13/W/27-B1 1210)  
(JSP25/W/44-B5 1400)  
(MC11/W/05-B3 1140)  
(P13/W/25-B1 1110)

**Mysak Lawrence A**  
(JSM18/W/02-A5 0900)

**Mysatov Evgeiny**  
(GA5.11/W/06 A3 1200)

## n

**Nabed N.**  
(G1/L/25-A3 1640-96)

**Nabi-Bidhendi M.**  
(ST6/P/02-A2 0830-02)  
(ST6/P/01-A1 0830-01)

**Nabney Ian T.**  
(MI06/W/27-B1 1400-11)  
(MI06/W/27-B2 1400-11)

**Nacer Laouami**  
(ST3/P/5-B4 1200)

**Nachiappan Rm. P.**  
(HS4/L/01-A4 0930)  
(HS4/L/01-A4 0930)

**Nachkebia Nugzar**  
(ST1/C/GA4.10/E/01-A4 0930-43)  
(JSA45/E/15-B5 1110-06)

**Nachtnebel Hans Peter**  
(HW4/E/08-B2 1400)  
(HW5/E/07-A3 1420)

**Nadeau R. M.**  
(ST1/E/86-A2 0930-06)

**Nadejda A. Chujkova**  
(JSS31/W/02-B3 0830-03)

**Nadim F.**  
(ST3/E/13-B4 1400-15)  
(ST3/E/14-B5 1130)

**Naef Felix**  
(HS4/W/30-A5 1510)

**Nagahama Hideaki**  
(JSM01/W/68-A4 1620-11)

**Nagahama Hiroyuki**  
(ST1/E/51-A4 0930-10)

**Nagahama Tomoo**  
(JSM01/W/48-A4 1620-02)  
(JSM01/W/68-A4 1620-11)

**Nagai T.**  
(GA3.02/W/21-B2 1520)  
(GA3.08/W/16-B1 1430)  
(GA3.08/W/28-B1 1510)

**Nagai Tsugunobu**  
(GA3.08/W/04-B1 0900-02)

**Nagamine Koichiro**  
(JSV47/W/07-B5 1215)

**Naganjaneyulu K.**  
(GA1.02/E/3A2 0930)

**Nagao T.**  
(JSA15/E/17-A3 1440)  
(JSA15/E/19-A3 1500)

**Nagao Toshiyasu**  
(JSA15/E/02-A5 0830-05)  
(ST1/W/37-A4 0930-01)

**Nagasaka Moh**  
(JSP49/W/10-B5 0950)

**Nagasawa C.**  
(JSA20/W/09-A4 1200-11)

**Nagashima Hideki**  
(JSP49/W/10-B5 0950)

**Nagashima Tatsuya**  
(MC06/C/JSM01/E/35-A1 1600)  
(MC06/W/04-A1 1400)  
(MI02/E/03-A5 1240)

**Nagata Wayne**  
(JSP39/W/02-B3 1421-08)

**Nagata Yutaka**  
(P12/C/JSP21/E/01-A1 0950)

**Nagatsuma Tsutomu**  
(GA5.06/W/04 A3 1440)

**Nagaya Yoshiharu**  
(GA5.01/W/05 A1 0835)  
(JSA15/E/40-A3 1700)

**Nagy A. F.**  
(GA4.10/W/10-A4 1215)

**Nagy Andrew F.**  
(GA4.10/W/12-A4 0950)

**Nahed E. El Arabi**  
(HS5/W/24-A2 1505)

**Nair U. S.**  
(MI06/W/15-B1 0910)  
(MI10/W/10-B2 1150)

**Naiguo Lin**  
(GA4.02/W/20-A4 1400-18)

**Nailya Bagmanova**  
(ST1/E/64-A4 0930-02)

**Naito Isao**  
(JSG14/W/04-A3 1200-21)  
(JSG14/W/09-A3 1121-08)  
(JSG14/W/14-A3 1124-09)  
(JSG28/E/29-B1 1400-18)  
(JSG28/W/08-B1 1030)

(JSG28/W/11-B1 1400-08)  
(JSG28/W/14-B2 0930)  
(JSG28/W/16-B1 1400-19)

**Naito Yoko**  
(MI12/E/04-B5 1155)

**Naja Manish**  
(MI02/E/08-A4 0930)

**Najafi-Alamdari Mehdi**  
(G3/E/30-A5 1610-30)

**Najjar R G**  
(MC01/W/36-A5 1700)

**Nakada Setsuya**  
(JSV29/W/06-B1 1500)

**Nakaegawa Toshiyuki**  
(JSM24/W/15-B1 1610)

**Nakagawa Tobita**  
(G5/L/06-A4 1400)

**Nakai Nobuyuki**  
(JSA45/E/05-B5 1110-02)

**Nakai Sun'ichi**  
(ST1/W/30-A2 0930-07)

**Nakajima Hideo**  
(U7/E/02-B1 0830-10)

**Nakajima K.**  
(GA2.02/W/09-B4 0900)

**Nakajima Kenichi**  
(GA2.03/E/02-B3 1120)

**Nakajima Takahiro**  
(GA1.01/W/21-A5 0945)

**Nakajima Teruyuki**  
(MI08/L/06-A3 1605)  
(MI09/E/06-A5 0920)  
(MI09/E/06-A5 1145-20)  
(MI09/E/08-A5 1645)  
(MI10/W/02-B1 0900-11)  
(U7/L/04-B1 1400)

**Nakamichi Haruhisa**  
(JSV47/W/22-B5 1130)

**Nakamra Kozo**  
(MI04/W/23-B3 1035)

**Nakamura Hisashi**  
(JSP25/W/40-B2 0930-07)  
(JSP25/W/48-B5 1130)  
(JSP25/W/59-B3 0950)

**Nakamura M.**  
(ST3/W/39-B4 1400-08)

**Nakamura Masaki**  
(ST5/W/69-B5 0930-11)

**Nakamura Masao**  
(GA3.08/W/15-B1 1640)

**Nakamura Misao**  
(ST5/E/16-B4 1500)

**Nakamura Dr. Norihiro**  
(GA5.11/W/09 A3 1430-07)

**Nakamura Mamoru**  
(ST2/W/04-A5 1400-03)

**Nakamura Ryosuke**  
(MI04/E/22-B4 1150)

**Nakamura Shuichi**  
(ST2/E/22-A5 1400-06)

**Nakamura Shigehisa**  
(JSG11/P/01-A3 1420)

**Nakamura T**  
(JSM01/W/01-A3 1140)  
(MW04/W/04-A1 0900)  
(JSM01/W/36-A1 1400)  
(JSA20/W/09-A4 1200-11)

**Nakamura Tadas K.**  
(GA3.06/W/35-A2 1510)

**Nakamura Takuji**  
(JSM01/E/30-A2 1600-24)  
(JSM01/W/38-A2 1600-26)

**Nakamura Toshiaki**  
(P16/E/06-B5 1500)  
(P16/E/11-B5 1440)

**Nakamura Tomohiro**  
(P12/W/08-A1 1600)  
(P12/W/20-A1 1030-09)  
(P14/W/12-A4 1520)

**Nakamura Yasuyuki**  
(ST4/W/48-B2 0930-14)

**Nakamura Yutaka**  
(JSP23/C/U5/E/06-B2 1620)

**Nakane H**  
(JSM01/W/37-A5 1400)  
(MI02/W/15-A5 1100)

**Nakane Hideaki**  
(JSM01/W/116-A5 1000)  
(JSM01/W/48-A4 1620-02)  
(JSG28/E/12-B2 1200)

**Nakanishi Asami**  
(HW5/E/05-A3 1100)

**Nakanishi Masao**  
(JSS07/E/09-A2 1025)

**Nakano Iwao**

(P16/E/06-B5 1500)  
(P16/E/11-B5 1440)

**Nakao S.**  
(G5/E/39-A4 1200)

**Nakata Akifumi**  
(P11/W/21-B5 1150-09)

**Nakatani I.**  
(GA4.10/L/02-A4 1055)  
(GA4.10/W/34-A5 1620)

**Nakatsuka Tadashi**  
(JSP23/W/06-B2 1640)  
(JSA40/W/07-B5 1400-10)

**Nakayama Takeshi**  
(JSA15/W/08-A4 1040)

**Nakayama Wataru**  
(JSP23/C/U5/W/19-A6 1720)

**Nakazawa Tetsuo**  
(JSP25/W/14-B1 1010)

**Nam V. H.**  
(GA1.04/W/24-A5 1100)

**Namboothiri Parameswaran S.**  
(JSG28/E/12-B2 1200)

**Namiki N.**  
(G2/W/05-A2 1500)

**Nanayama Futoshi**  
(JSS42/W/14-B5 0830)

**Nanjing Douke Xie**  
(JSV36/C/U6/E/08-B3 1400-25)

**Nanjo Kazuyoshi**  
(ST1/E/51-A4 0930-10)

**Nanni T.**  
(GA6.01/W/03-A5 1525)

**Napoli Rosalba**  
(JSA15/W/02-A4 1400-18)

**Narayanan R.**  
(JSA20/W/20-A5 1135)

**Nardelli Bruno Buongiorno**  
(P11/L/01-B5 0830)  
(P11/L/02-B5 0850)

**Nardi A.**  
(JSG28/W/15-B1 1400-04)

**Narteau Clement**  
(JSA17/W/03-A4 1230)  
(ST1/W/35-A2 1400-21)

**Naruoka Tomohiro**  
(HS3/W/13-A1 1615)

**Nascimento Nilo Oliveira**  
(HS5/W/09-A1 1710)  
(HS5/W/18-A2 1140)

**Nasonova Olga**  
(MC01/E/04-A3 1415)  
(MC01/E/10-A3 1150)  
(HW4/E/05-B2 1645)  
(HW4/E/20-B2 1700)

**Nastasyina Natalia V.**  
(GA2.03/E/01-B3 1400-04)  
(GA2.03/E/05-B3 1400-05)

**Nastula Jolanta**  
(JSG14/E/08-A3 1136-13)

**Nasuno Tomoe**  
(MI04/E/15-B1 1435)

**Nataf H-C**  
(GA1.01/W/09-A5 0900-03)  
(GA1.01/W/30-A5 1215)

**Natali Maria Paula**  
(G1/W/41-A3 1620-46)

**Natapov Lev M.**  
(JSS44/W/21-B4 1700)

**Natasha Petrova**  
(ST4/L/10-B3 0830-07)

**Naud C.**  
(MI04/C/MC07/W/21)  
(MI06/W/31-B2 1210)  
(MI10/E/14-B2 1520)

**Naumov A. P.**  
(ST1/E/16-A3 0900-11)  
(GA1.02/E/36-A1 1050)  
(GA5.01/E/29 A1 1100)  
(JSA15/E/20-A5 1400-12)

**Naumov V. B.**  
(JSV30/E/10-B1 1400-03)

**Nava B**  
(JSA06/W/15-A2 1010)

**Navarro J. M.**  
(JSV36/W/04-B3 1115)  
(JSV36/W/12-B3 0900-08)

**Naveau Philippe**  
(MI04/L/12-B1 1145)

**Navrotsky Vadim V.**  
(PW1/W/03-A6 1200)  
(ST5/W/58-B5 1500)  
(U7/C/U3/W/11-B1 0830-08)

**Nazaretian S.**  
(JSA15/E/21-A5 1400-02)

**Nazarova Margarita**

- (JSA16/E/10-A3 0830-20)  
(JSA45/E/09-B5 1010)
- Nazarova N G**  
(G3/E/28-A5 1610-03)
- Neaga Vasile**  
(GA5.12/L/02-A2 1600-06)
- Neagu Elena**  
(GA4.09/E/01-A6 1700)
- Neal C.**  
(HS3/W/03-A1 0950)
- Neale Richard**  
(MC01/W/51-A2 1045)  
(JSP25/W/36-B1 1210)
- Neall Vincent**  
(JSP23/E/49-B2 0830-07)
- Nechaev O. Yu.**  
(SW1/E/08-B5 1030-03)
- Nechaev Stanislav**  
(GA5.01/L/04-A1 1300-12)
- Nechitailenko Vitaly**  
(JWS 33/E/14-B2 1620)
- Nedoluha Gerald E.**  
(JSM01/W/04-A4 1510)
- Neefs E.**  
(JSM26/W/29-B2 1700-09)
- Neelin David**  
(MI04/L/13-B1 0945)  
(U3/W/13-A3 1400)  
(MC01/L/15/-A3 1500)
- Neelin J. David**  
(JSP25/W/26-B1 1050)
- Neganova Olena**  
(GA1.02/E/40-A1 1050)
- Negendank Jörg F.W.**  
(GA1.05/E/09-A5 0900-02)  
(GA1.05/E/15-A5 0900-01)  
(GA1.03/E/03-B2 1620)  
(GA1.03/E/05-B2 1640)  
(VS2/C/U/6/E/01-B3 1400-35)
- Neggers Roel**  
(MI03/W/02-A3 1500)  
(MI04/W/33-B1 1535)
- Negishi Hiroaki**  
(ST4/L/09-B2 0930-18)
- Negredo A M**  
(JSG11/W/02-A3 1540)  
(ST2/W/06-A4 1600)
- Negri Andrew J.**  
(JSM41/W/01-B3 1705)
- Nehlig Pierre**  
(GA5.12/W/09-A2 1600-10)
- Nehybka Vladimir**  
(ST2/L/05-A5 1400-17)
- Neilan R.**  
(G2/L/02-A2 0945)
- Neilson R P**  
(MC01/W/04-A5 1425)
- Neiman V. G.**  
(JSP25/C/U2/E/02-B1 0830-03)
- Neki Maroka**  
(JSV36/W/15-B3 0900-01)  
(JSA15/E/07-A5 0830-02)
- Nelkin Eric**  
(JSM41/E/01-B3 1620)
- Nelly Bagmanova**  
(ST2/E/26-A5 1400-11)
- Nelson Grenville**  
(P10/L/04-A5 1600-06)
- Nemecek Z.**  
(GA 3.07/E/16-A3 0900-09)  
(GA4.08/W/15-B3 1530)
- Nemeth Karoly**  
(VS2/E/05-B3 1400-20)  
(VS2/E/11-B3 1400-24)  
(VS2/E/17-B3 1400-27)
- Nemeth Z.**  
(GA4.04/E/04-B5 0830-01)
- Nenovski P.**  
(GA3.04/W/05-B1 1520-37)  
(GA3.04/W/09-B1 1520-17)  
(GA3.04/W/15-B1 1520-15)  
(GA3.07/W/57-A4 0930-20)  
(GA2.07/W/18-A1 1450)
- Nepomnyaschaya E.V.**  
(GA4.02/W/31-A4 1400-25)
- Neprochnov Yu. P.**  
(ST4/E/31-B1 0830-06)
- Neprochnov Yuri**  
(JSS44/P/03-B5 0950)
- Nerem R. S.**  
(JSA37/W/09-B3 1100)  
(JSM41/W/09-B4 1515)
- Nerem R. Steve**  
(JSG14/E/20-A3 1700-08)  
(JSG14/W/24-A3 1700-04)
- Nerozzi Fabrizio**  
(JWM08/W/11-A3 1220)
- Neri Augusto**  
(VS2/W/21-B3 1400-14)  
(JSV29/E/01-B1 1720)  
(VS2/E/02-B3 1110)  
(VS2/E/03-B3 1400-19)
- Neri Giancarlo**  
(JSV47/W/09-B5 1200)
- Neto D. Urbano**  
(P10/E/11-A5 1600-01)
- Neuberg**  
(JSV47/L/01-B5 1400-25)
- Neuberg Jurgen**  
(JSV29/W/09-B1 1600)  
(ST4/E/49-B3 0920)
- Neuberg Jurgen W.**  
(VS3/W/28-B3 1400)
- Neubert Torsten**  
(GA5.08/E/03-B1 0900)  
(GA5.08/W/06-B1 0945)  
(GA2.01/E/13-A1 0900-02)
- Neudegg D A G**  
(A3.07/W/37-A6 0900-13)
- Neugebauer Horst J.**  
(ST4/W/49-B1 1640)
- Neugebauer M.**  
(GA4.03/E/03-B4 1130)
- Neuhauser Doug**  
(JWS33/W/22-B2 1635-01)  
(JWS33/W/22-B3 0900-01)
- Neuman N.**  
(HS2/W/32-B2 1440)
- Neumeyer Juergen**  
(JSG14/E/10-A3 1700-17)
- Nevanlinna H**  
(JSA06/E/09-A1 1155-01)  
(GA5.01/E/17-A1 1300-08)  
(GA5.01/E/18-A1 0900-07)  
(GA6.02/E/07-B1 1630)
- Nevedrova Nina**  
(JSA15/W/13-A5 0830-15)
- Nevejans D.**  
(JSM26/W/29-B2 1700-09)
- New L**  
(MC01/L/07-A2 1430)
- Newell P. T.**  
(GA3.02/W/15-B2 1005)  
(GA4.08/E/21-B3 0900-13)
- Newall Patrick**  
(GA3.10/W/24-A6 1400)
- Newell Patrick T.**  
(GA3.03/W/12-B4 1400)  
(GA3.08/W/25-A6 1130)
- Newbury J. A.**  
(GA3.07/E/04-A3 0900-10)
- Newell Patrick T.**  
(GA3.01/W/05-A2.1315)
- Newitt Larri R.**  
(GA5.09/W/01 A2 1400-04)
- Newman Andrew V.**  
(JSV36/E/31-B3 1400-14)
- Newman Gregory**  
(GA1.02/W/26-A1 1605)
- Newman J. C.**  
(JSS42/W/05-B5 1700-11)  
(JSS42/W/07-B5 1500)
- Newman Matthew**  
(MW06/W/04-A3 1640)
- Newmark J. S.**  
(JSA16/W/13-A3 0830-47)
- Newton Bob**  
(P13/W/22-B1 1050)
- Nezlin N. P.**  
(P11/W/05-B5 1700)
- Ngan K**  
(JSM01/W/63-A3 1500)
- Nguyen Dinh Xuyen**  
(ST1/E/49-A3 0900-13)
- Nguyen Ngoc Thuy**  
(ST1/E/73-A3 0900-18)
- Nguyen Xuan Binh**  
(ST2/E/08-A3 1115)
- Ni S**  
(JSS02/C/ST6/W/01-A1 1515)
- Nicholls Neville**  
(U5/W/22-A4 1600)  
(JSP25/W/65-B1 1420)
- Nicholson R. A.**  
(JSP23/W/38-B2 1720)
- Nicholson S**  
(MC01/W/60-A2 0945)
- Nicholson Todd**  
(ST5/W/26-B5 0930-10)
- Niciejewski R J**  
(JSM01/W/107-A1 1510)  
(JSM01/W/106-A2 1600-01)
- NicklessGraham**  
(JSP21/W/13-A4 0950)
- Nickovic Slobodan**  
(MI01/W/22-A1 1150)
- Nicolas Joelle**  
(G2/E/06-A2 1630-03)
- Nicoletta F.**  
(JSP23/E/57-B1 0830-09)
- Nieke Barbara**  
(P15/L/18-B41400)
- Nielsen A. A.**  
(P15/W/07-B3 1650)  
(G2/W/03-A2 1630-18)
- Nielsen E.**  
(GA2.01/W/07-A1 1055)  
(GA2.02/W/15-B4 0930-12)  
(GA2.02/W/19-B4 1600)  
(GA2.02/W/25-B4 0930-11)
- Nielsen Hans**  
(GA2.01/E/07-A1 0900)
- Nielsen J. E.**  
(JSM26/E/22-B1 1210)
- Nielsen K E**  
(MI09/W/14-A5 1030)  
(MI09/W/14-A5 1145-21)
- Nielsen Otto**  
(GA5.01/W/08 A1 1200)
- Nielsen Soren Bom**  
(MC02/E/15-B1 1600-13)  
(ST4/E/43-B1 1400-09)
- Nielsen-Gammon John**  
(JSP39/W/14-B3 1050)  
(MC04/W/06-B1 1450)  
(MC04/W/10-B1 1515)  
(MI05/W/02-A5 0900)
- Niemeier W.**  
(G1/L/04-A3 1620-85)  
(JSA09/L/02-A2 1230)
- Nightingale Phil**  
(P08/W/01-A2 1440)
- Nigmatov G. M.**  
(JSP23/E/33-A5 1640)
- Nikiforov Valerian**  
(GA1.02/W/22-A2 0930)
- Nikitin A. N.**  
(ST6/W/05-A1 0830-07)
- Nikitina Lidia**  
(JWA34/E/03-B2 1720)  
(JWA34/E/04-B2 1700)
- Nikolaev Alexei**  
(ST1/E/16-A4 0930-05)  
(ST1/E/63-A3 0830)
- Nikolaev Alexei V.**  
(JSS46/E/01-B4 0930-06)
- Nikolaev Vsevolod**  
(ST1/E/16-A4 0930-05)
- Nikolaeva N. S.**  
(GA4.08/W/15-B3 1530)
- Nikolai Tarasov**  
(ST1/E/63-A3 0830)
- Nikolashkin S. V.**  
(JSA20/W/31-A4 1200-19)  
(JSA20/W/43-A4 1200-23)
- Nikol'skaya; Kommunela**  
(GA4.05/E/03-A1 1440)
- Nikonova Marina**  
(JSA16/E/03-A3 0830-31)
- Nikutowski B**  
(GA4.09/W/04-A5 1600-02)  
(GA3.08/E/04-B1 1700)
- Nila Stepanenko**  
(ST2/E/53-A5 1400-21)
- Nils-Axel**  
(ST2/W/23-A5 1230)
- Nilsson**  
(JSA35/W/05-B1 1140)
- Nilsson Hans**  
(JSM26/W/26-B2 1700-10)  
(GA2.07/W/07-A1 1140)
- Ning Jinsheng**  
(G3/W/27-A5 1610-86)  
(G3/W/31-A5 1610-56)  
(ST4/L/40-B1 0830-32)
- Ning Zeng**  
(MC11/E/01-B4 1225)
- Ninglian Wang**  
(HS2/W/16-B2 0920)  
(HS2/W/20-B2 1040)
- Ninomiyama M**  
(JSM01/W/116-A5 1000)
- Nishi Noriyuki**  
(JSM26/W/34-B2 1510)
- Nishi Y.**  
(GA1.02/W/18-A2 0930)
- Nishi Yuji**  
(JSV36/W/02-B3 0930)  
(JSV47/E/03-B5 1400-02)
- Nishida A.**  
(GA3.08/W/14-B1 1400)  
(GA3.08/W/16-B1 1430)  
(GA3.10/W/04-A6 1450)
- Nishida Masahiro**  
(JSM01/E/03-A2 1430)  
(JSG28/E/12-B2 1200)  
(JSM26/E/09-B1 1400)
- Nishida Ryohei**  
(ST1/W/24-A3 1130)
- Nishida Yasunori**  
(JSA15/E/40-A3 1700)  
(JSA15/E/56-A3 0850)  
(JSV36/E/23-B3 0900-07)  
(JSV36/E/24-B3 0900-02)
- Nishigami Kin'ya**  
(ST1/E/01-A4 0930-12)  
(ST2/E/34-A5 0915)
- Nishimura I. Y.**  
(JSS46/W/07-B4 1030)
- Nishimura K.**  
(ST3/W/39-B4 1400-08)
- Nishimura Keiichi**  
(ST3/E/55-B4 1400-18)
- Nishimura Kouichi**  
(JSP39/W/21-B3 0900)
- Nishimura M.**  
(GA2.02/W/09-B4 0900)
- Nishimura Sou**  
(ST1/W/44-A3 1420)
- Nishimura Susumu**  
(GA1.02/E/29-A2 0930)
- Nishimura Takeshi**  
(JSV29/W/07-B1 1400)
- Nishimura Yuichi**  
(JSS42/E/14-B5 1700-04)
- Nishino Masanori**  
(GA2.01/E/01-A1 1110)  
(GA2.01/E/05-A1 0950)
- Nishitani Nozomu**  
(GA2.01/E/05-A1 0950)  
(GA 2.02/E/12-B4 1640)  
(GA3.08/E/03-B1 1000)
- Nishitani T.**  
(GA1.02/L/05-A2 0930)  
(JSA15/W/07-3 1740)
- Nishiyama Nobumasa**  
(JSS02/E/14-A1 1740)
- Nishiyoshi T.**  
(MI12/W/10-B4 1650)
- Nishimura Takeshi**  
(JSV47/W/22-B5 1130)  
(JSV47/L/02-B5 1400-26)
- Nisia Krusche**  
(JSP49/W/11-B5 1210-13)
- Niu Fenglin**  
(ST4/W/51-B2 1740)
- Niu Guo-Yue**  
(MC01/E/08-A1 1745)
- Niwan Masanori**  
(MC06/W/01-A1 1650)  
(MC06/W/04-A1 1400)
- Niyogi Devdutta S**  
(MI107/W/05-A2 1140)  
(MI07/W/04-A2 1440)
- Nkagawa Yoshimichi**  
(GA4.02/W/04-A4 1400-13)
- Noack T.**  
(JSP23/E/03-A6 0930)
- Noblet Nathalie de**  
(U3 W/07-A3 1130)
- Nobumasa Komori**  
(P12/W/08-A1 1600)
- Nobuo Matsushima**  
(JSV47/E/03-B5 1400-02)
- Noci G.**  
(GA6.01/W/13-A6 1150)
- Noguchi Hideyuki**  
(JSP25/W/28-B5 1010)
- Noguchi Shin-Ichi**  
(ST1/E/81-A2 1640)  
(ST1/E/89-A2 1720)
- Noir Jérôme**  
(JSA17/C/GA1.19/W/11-A4 1450)
- Nolasco Rita**  
(JSA19/W/03-A4 1400-06)
- Nolet G.**  
(ST4/W/03-B3 1630)
- Noll S. N.**



## INDEX

(GA4.10/W/14-A4 0900)  
**Nombela M**  
 (GA1.05/W/23-A6 1230)  
**Nomicos Costas**  
 (JSP23/W/23-B1 1720)  
**Nomura A.**  
 (JSA20/W/09-A4 1200-11)  
**Nomura Ryotaro**  
 (GA1.03/W/10-B2 1420)  
**Nonaka Masami**  
 (P12/W/21-A1 1620)  
**Noone K J**  
 (MI09/W/14-A5 1030)  
 (MI09/W/14-A5 1145-21)  
**Noone Kevin**  
 (JSM26/W/16-B2 1210)  
**Norabuena Edmundo**  
 (JSV36/E/13-B3 1445)  
**Norandovich Dmitry A.**  
 (GA2.03/E/01-B3 1400-04)  
**Norberg O.**  
 (GA4.10/W/24-A4 1125)  
**Norihito Mayama**  
 (JSS02/E/11-A1 0830-08)  
**Normandeau James E.**  
 (JSS31/E/08-B2 0950)  
**Norquist D.**  
 (MC01/L/13-A3 1135)  
**Norquist Donald C.**  
 (MI10/W/05-B2 1020)  
**Norris Peter**  
 (JSM41/W/11-B3 1430)  
**North Robert**  
 (U8/E/10-B3 1135)  
**Northrop Paul J.**  
 (HS1/W/59-B5 1140)  
**Norton W.**  
 (JSM26/W/28-B3 1110)  
 (JSM01/W/42-A1 0830)  
 (JSM01/W/46-A3 1710)  
 (MW04/W/08-A1 1450)  
**Norton Warwick**  
 (JSM01/W/07-A1 1430)  
 (MW01/W/10-A5 1150-06)  
**Nosov M. A.**  
 (JSS42/W/12-B5 1700-16)  
 (JSS42/W/20-B4 1700)  
**Nosov M. V. M. A.**  
 (JSP49/W/09-B5 1720)  
**Nossal S.**  
 (JSA20/W/27-A4 1200-17)  
**Noto Masayuki**  
 (JSP25/E/01-B3 1640)  
 (JSP25/E/01-B5 1210)  
**Nothnagel Axel**  
 (JSG11/E/06-A4 1400-03)  
**Notsu Kenji**  
 (JSV36/W/01-B3 0900-12)  
 (JSV36/W/14-B3 0900-11)  
 (JSV36/W/26-B3 1215)  
**Novakov T**  
 (MI01/W/02-A30900)  
**Novelo-Casanova D. A.**  
 (ST2/W/05-A5 1000)  
 (ST5/W/17-B3 0850)  
**Novik Oleg**  
 (JSA15/E/36-A4 1400-10)  
 (JSS02/E/17-A1 0830-10)  
 (ST1/C/Jss02/E/17-A2 0930-13)  
**Novikova Nina M.**  
 (U7/E/04-B1 0830-05)  
**Novikova Olga**  
 (ST1/W/54-A2 1700)  
**Novotna Dagmar**  
 (JSA16/E/23-A3 0830-17)  
 (JSA16/E/39-A3 0830-18)  
**Novotryasov Vadim V.**  
 (ST5/W/58-B5 1500)  
**Nowaczyk Norbert R.**  
 (GA1.05/E/09-A5 0900-02)  
 (GA1.05/E/15-A5 0900-01)  
 (GA1.15/E/01-B4 1715)  
 (GA1.03/E/03-B2 1620)  
 (GA1.03/E/04-B2 1600)  
 (GA1.03/E/05-B2 1640)  
**Nowak Ilona**  
 (G3/E/42-A5 1520)  
 (G3/E/42-A5 1520)  
 (G5/E/37-A4 1415-01)  
**Nozawa Satonori**  
 (JSA20/E/18-A6 1118)  
**Nozrdachev M**  
 (GA4.09/W/04-A5 1600-02)  
**Nozdrachev M. N.**  
 (GA4.08/W/15-B3 1530)

**Nuccio P. M.**  
 (JSV36/W/05-B3 1145)  
 (JSS44/E/21-B4 1540)  
**Nulman Alla**  
 (GA1.05/W/24-A6 1145)  
**Nuñez Héctor**  
 (GA1.03/W/12-B2 1520)  
**Nunez Juan I.**  
 (GA1.03/E/01-B3 1120)  
**Nunnari Giuseppe**  
 (G2/E/09-A2 1630-25)  
**Nuth V.**  
 (JSM41/W/06-B4 1545)  
**Nurtaev B.S.**  
 (ST1/E/20-A4 0930-06)  
**Nützmann G**  
 (HS3/W/26-A2 1425)  
 (HS4/W/05-A4 1225)  
**Nwilo Dr. P C**  
 (JSG11/E/14-A4 1400-06)  
**Nyblade A. A.**  
 (ST4/W/30-B2 1400)  
**Nygren T.**  
 (GA2.02/W/22-B4 1720)  
**Nyu P.**  
 (JSA15/E/21-A5 1400-02)  
**Nzuve Wambua Boniface**  
 (HS5/W/45-A3 1545-01)

## O

**Obana Koichiro**  
 (JWA34/E/08-B2 1230)  
**Obara T.**  
 (GA5.06/W/04 A3 1440)  
**Obara Takahiro**  
 (JSA06/W/02-A1 1640)  
 (GA3.05/W/39-B3 0910)  
**Oberheide Jens**  
 (MW04/E/02-A1 1010)  
**Oberhuber J. M.**  
 (JSP25/E/27-B2 0930)  
**Oberndorfer Helmut**  
 (G2/E/11-A2 1630-24)  
**Obridko V. N.**  
 (JSA16/E/13-A3 0830)  
 (GA4.02/W/31-A4 1400-25)  
 (JSA06/W/21-A1 1155-25)  
**Obridko Vladimir**  
 (GA4.01/W/19-A2 1400-03)  
 (GA4.03/W/02-B4 1115)  
 (GA4.03/W/04-B4 1215)  
 (GA4.03/W/14-B4 1630)  
 (GA4.03/W/11-B4 1735-04)  
**O'Brien K.**  
 (JSA45/L/02-B5 0920)  
 (JSA06/L/09-A1 1155-20)  
 (GA6.01/L/05-A5 0900-03)  
**O'Brien Paul**  
 (JSA06/W/24-A2 1210)  
**Obukhov A. M.**  
 (JSP39/W/23-B3 1427-10)  
**Ocak Mustafa**  
 (JSS31/L/04-B2 0830-17)  
 (G1/E/04-A3 1620-50)  
**Oceano Woods Hole**  
 (P14/E/02-A4 1210)  
**O'Connell Rick**  
 (JSS31/E/04-B2 1400)  
**O'Connor F**  
 (JSM01/W/37-A5 1400)  
**Oda H.**  
 (GA1.03/W/17-B2 1500)  
**Oda Hirokuni**  
 (GA1.05/W/22-A6 1700)  
 (GA1.05/W/13-A5 1730)  
**Odedra A.**  
 (ST1/E/90-A 11620)  
**Odah Hatem**  
 (GA1.03/W/19-B1 1420)  
**Odegard Mark**  
 (JSA27/E/07-B1 0940)  
**Odijk D.**  
 (G6/C/G1/L/16-B1 1420)  
**Odijk Dennis**  
 (G1/E/62-A3 1220)  
**Odintsov Sergei D.**  
 (GA5.08/W/07-B1 1400-05)  
**Odintsov V. I.**  
 (GA5.08/W/04-B1 1400-03)  
**Odintsov Vladimir**  
 (JWS33/W/01-B2 1445)  
**O'Doherty Simon**  
 (JSP21/E/02-A4 0930)  
**O'Dowd Colin**  
 (MI01/L/03-A1 1400)  
**Oey Lie Yauw**  
 (P10/L/03-A3 1010)  
**O'Farrell Siobhan P.**  
 (P12/W/05-A1 1420)  
 (P13/W/19-B2 0930)  
**Offermann Dirk**  
 (JSM01/E/19-A5 0900)  
 (JSM01/W/41-A4 1150)  
 (JSM01/E/28-A4 1430)  
 (MW 07/E/03-A4 1400)  
 (MW04/E/02-A1 1010)  
 (MW07/W/19-A4 1420)  
**Offiler David**  
 (JSG28/E/16-B1 1400-14)  
**Offutt Dr.**  
 (MI10/W/05-B2 1020)  
**Ofman L.**  
 (GA4.05/W/03-A1 1500)  
**Ogata Yoshihiko**  
 (ST3/W/27-B4 1530)  
**Ogawa H.**  
 (P15/L/16-B4 1505)  
**Ogawa H. S.**  
 (JSA16/W/11-A3 0830-25)  
**Ogawa Hideo**  
 (JSM01/W/48-A4 1620-02)  
 (JSM01/W/68-A4 1620-11)  
**Ogawa T**  
 (JSM01/W/01-A3 1140)  
 (JSA15/W/14-A4 1400-16)  
**Ogawa Tadahiko**  
 (JSM01/E/30-A2 1600-24)  
 (GA2.03/E/02-B3 1120)  
 (GA3.08/E/03-B1 1000)  
 (GA2.02/E/13-B4 1100)  
**Ogawa Toru**  
 (JSA45/E/05-B5 1110-02)  
**Ogawa Toshihiro**  
 (JSM26/W/34-B2 1510)  
**Ogawa Y.**  
 (GA1.02/L/05-A2 0930)  
 (GA1.02/W/18-A2 0930)  
 (JSA15/W/07-3 1740)  
**Ogawa Yasuo**  
 (GA1.02/E/06-A2 0930)  
 (JSV36/W/02-B3 0930)  
**Ogibalov V P**  
 (MW05/E/03-A2 1230)  
 (MW05/W/03-A2 1040-01)  
 (MW05/W/06-A2 1040-02)  
**Ogibalov Vladimir**  
 (MW05/W/07-A2 1215)  
**Ogilvie K.**  
 (GA3.03/W/07-B4 1450)  
**Ogilvie K. W.**  
 (GA3.02/W/40-B3 1050)  
 (GA4.02/W/24-A4 1400-22)  
**Ogino Shin-Ya**  
 (MC06/C/JSM01/W/58-A1 1120)  
**Ogino T.**  
 (GA4.10/E/04-A5 1420)  
**Oglesby Bob**  
 (JSM24/W/05-B2 1135)  
 (JSP25/W/04-B3 1110)  
**Ogren John A**  
 (MI09/L/05-A5 1620)  
**Oguma Sachiko**  
 (P12/C/JSP21/E/01-A1 0950)  
**Ogunade S O**  
 (JSA06/L/03-A1 1115)  
**Oguz Temel**  
 (P08/E/03-A2 1520)  
 (P11/E/29-B5 1050)  
**Ohata Tetsuo**  
 (HW3/W/14-B4 1725)  
 (JSM24/E/06-B1 0950)  
 (JSM24/E/09-B1 0910)  
**Ohi K.**  
 (GA1.05/E/17-A6 1630)  
**Ohlenbusch Renke**  
 (HS5/W/41-A3 1400)  
**Ohminato Takao**  
 (ST4/W/23-B1 1400-10)  
 (JSV47/E/03-B5 1400-02)  
**Ohmura A.**  
 (MC02/E/12-B1 1600-11)  
**Ohmura Atsumu**  
 (JSH12/W/12-A5 1000)  
**Ohnaka M.**  
 (ST1/E/90-A1 1620)

**Ohnaka Mitiyasu**  
 (ST1/W/47-A2 1400-12)  
**Ohno Hideo**  
 (ST6/E/09-A2 1430)  
**Ohno Hiroyuki**  
 (JSM24/E/06-B1 0950)  
**Ohring George**  
 (JSM41/E/04-B3 1150)  
**Ohrnberger M.**  
 (JSV47/W/06-B5 1400-11)  
**Ohsaki Shotaro**  
 (JSP49/W/08-B5 1010)  
**Ohshima Kay I.**  
 (P13/E/11-B1 1440)  
**Ohta Takeshi**  
 (JSM24/E/09-B1 0910)  
**Ohta Tatehisa**  
 (JSA45/E/05-B5 1110-02)  
**Ohtake Masakazu**  
 (JSV47/W/22-B5 1130)  
**Ohtake Masakazu**  
 (ST1/W/22-A3 1440)  
**Ohtani Eiji**  
 (JSS02/E/16-A1 1720)  
**Ohtani Ryu**  
 (JSG28/W/14-B2 0930)  
 (JSG28/W/16-B1 1400-19)  
**Ohtani Shinichi**  
 (GA3.02/E/06-B2 1440)  
 (GA3.10/E/04-A6 1115)  
**Ohte Nobuhito**  
 (HW5/E/05-A3 1100)  
**Ohyama Masamitsu**  
 (GA4.02/W/01-A4 1200)  
**Oieroset M.**  
 (GA3.08/W/33-B1 1130)  
**Oikawa Jun**  
 (JSV47/W/27-B5 0915)  
**Oike Kazuo**  
 (ST3/E/51-B4 1400-09)  
 (ST2/W/21-A5 1400-02)  
**Oike Okamoto.**  
 (JSA15/E/19-A3 1500)  
**Ojo O.**  
 (JSP25/L/03-B2 0930-04)  
**Ojo Simon O.**  
 (JSM41/L/01-B5 1500)  
**Okada Hiromi**  
 (JSV36/W/26-B3 1215)  
**Okada Kouta**  
 (GA3.02/L/05-B3 0900-26)  
**Okada T.**  
 (JSS44/W/01-B4 0930-06)  
**Okada Yasuhiko**  
 (MI09/W/06-A5 1145-09)  
**Okal Emile A.**  
 (U8/E/03-B1 1110)  
**Okano S**  
 (JSM01/W/01-A3 1140)  
**Okasha A.**  
 (GA6.01/P/12-A5 0900-19)  
**Oke B T. R.**  
 (HS5/W/06-A1 1610)  
**Oki Riko**  
 (MI06/E/17-B1 1650)  
**Oki Taikan**  
 (JSM24/W/02-B1 1030-01)  
 (JSM24/W/14-B1 1520)  
 (JSM24/W/15-B1 1610)  
 (HW1/L/07-A4 1430)  
**Okten Adnan**  
 (GA6.01/W/16-A6 1250)  
**Okimura Takashi**  
 (GA1.03/W/10-B2 1420)  
**Okubo Shuhei**  
 (G3/L/09 1610-23)  
 (G5/E/21-A4 1115-04)  
**Okubo Yasukuni**  
 (ST4/E/45-B1 1400-11)  
 (ST4/W/23-B1 1400-10)  
**Okuma Shigeo**  
 (JSP23/W/06-B2 1640)  
 (JSA40/W/07-B5 1400-10)  
**Okunishi Kazuo**  
 (JSP23/C/U5/W/11-A5 1500)  
**Olafsdottir Birna**  
 (GA5.01/W/10 A1 1300-09)  
**Olafsson H.**  
 (JSP39/E/16-B3 0830)  
**Olaleye J. B.**  
 (G4/E/23-A3 1620-20)  
 (JWS33/E/15-B2 1635-28)  
 (JWS33/E/15-B3 0900-28)  
**Oldenbourg Doug**  
 (GA1.02/W/30-A1 1415)

- Oldfield F.**  
(U2/E/10-A2 1010)
- Oleg N.**  
(G4/W/09-A3 1620-25)
- Oleg Shumilov**  
(JSA45/L/03-B4 1205)
- Olendrzynski Krzysztof**  
(MI01/L/01-A1 1210)
- Olesen A.**  
(G3/L/8-A5 1400)
- Olesen Arne V**  
(G3/L/04-A5 1610-19)
- Olesen O.**  
(ST2/E/43-A5 1400-31)
- Oleynikov**  
(JSM01/W/69-A1 1130)
- Oleynikov A N**  
(JSM01/W/69-A1 1130)  
(JSM01/W/72-A2 1600-02)
- Olijnyk Helmut**  
(ST6/W/10-A2 1500)
- Oliveira Carlos A. S.**  
(ST3/E/09-B4 1400-14)
- Oliveira Galvão Carlos de**  
(HS3/W/12-A1 1515)
- Oliver Sophia**  
(MW04/W/03-A1 1610)
- Oliver Tony**  
(HS5/W/14-A2 1000)
- Oliver W.**  
(JSA20/E/27-A4 1200-21)
- Olivera C.**  
(ST5/E/34-B3 0830)
- Olivieri M.**  
(ST4/W/18-B2 1440)
- Ollagney Frédéric**  
(GA1.04/E/02-A6 0920)
- Ollikainen Matti**  
(G1/E/21-A3 1620-57)
- Ollitraul Michel**  
(JSP39/E/18-B4 0930)
- Olmedillas J. C.**  
(ST5/E/34-B3 0830)
- Olroriz Federico**  
(GA1.15/E/02-B4 1530-02)
- Olsen H.**  
(G2/E/05-A2 1630-21)
- Olsen Niils**  
(GA5.08/E/03-B1 0900)  
(GA5.08/E/02-B1 0920)  
(JSA37/E/06-B3 1400)  
(GA3.10/E/07-A6 1700-08)
- Olson B**  
(MI08/L/09-A4 1615)
- Olsson P Q.**  
(MI08/W/15-A3 1430)
- Olsson Sverker**  
(ST1/W/29-A4 0930-34)
- Oltmans Samuel**  
(JSM26/W/34-B2 1510)  
(JSM26/W/05-B1 0920)
- Olunloyo V. O. S.**  
(G4/E/23-A3 1620-20)
- Olunloyo V. O. S. B.**  
(JWS33/E/15-B3 0900-28)  
(JWS33/E/15-B2 1635-28)
- O'Mongain Aoife**  
(ST4/E/49-B3 0920)  
(U8/E/02-B3 1640-05)
- Omstedt Anders**  
(MC01/W/17-A4 1125)
- Omur Demirkol E.**  
(G3/L/07-A5 1610-77)
- Omura Y.**  
(GA4.09/W/10-A6 1200)
- Omura Yoshiharu**  
(GA3.01/W/03-A2 1400)
- Oncescu Mihnea C**  
(JSP23/W/26-A5 1150)
- Onda Yuichi**  
(HS4/W/19-A5 1010)
- Ondoh Tadanori**  
(JSA15/P/03-A4 0920)
- Ondoh Tadanori**  
(GA3.02/L/08-B3 0900-28)
- O'Neill A**  
(MW01/W/12-A5 1150-01)
- O'Neill Alan**  
(MI12/W/01-B4 1420)  
(JSM26/E/02-B2 1020)  
(MI12/W/15-B4 1215)  
(MW02/W/06-B3 1600)
- O'Neill N**  
(MI01/L/04 1055)
- O'Neill W A**  
(MC01/W/42-A1 1015)
- Onera Véronique Achard**  
(MW07/W/18-A4 1510)
- Ongaro Tomaso Esposti**  
(VS2/E/03-B3 1400-19)
- Oni Eburn Adefunmilayo**  
(JSA40/E/04-B5 1225)
- Ono Y.**  
(GA1.05/E/17-A6 1630)
- Onodera Shinichi**  
(HS3/W/13-A1 1615)  
(HS4/W/03-A4 1045)
- Onoue K.**  
(ST3/W/39-B4 1400-08)
- Onsager T.G.**  
(GA3.01/W/04-A2 0830)
- Onur Tan**  
(ST2/E/13-A5 1400-29)  
(ST2/E/14-A4 1115)
- Ooe M.**  
(G2/W/05-A2 1500)
- Ooe Masatusgu**  
(JSG14/W/13-A3 1700-06)
- Ononincx Patrick J.**  
(ST5/W/03-B3 1420)
- Openshaw Steve**  
(GA1.03/W/13-B1 0920)  
(GA1.03/W/20-B3 1420)
- Opgenoorth Hermann**  
(GA3.02/L/01-B2 1125)
- Oraevsky Victor N.**  
(JSA37/W/02-B3 1445)  
(JSM41/E/05-B5 1530)
- Oraevsky Viktor**  
(JSP23/W/22-B1 010)  
(GA6.01/W/15-A5 0900-14)
- Oram D. E.**  
(JSM26/W/06-B1 0900)
- Oram David**  
(JSP21/E/02-A4 0930)  
(MI02/W/12-A4 1430)  
(JSP21/W/11-A4 1050)
- Orbay N.**  
(GA1.04/W/27-A6 1140)
- Orbay Naci**  
(JSA40/W/04-B5 1400-08)  
(GA6.01/W/16-A6 1250)
- Orcutt Igpp John A.**  
(P16/W/04-B5 1130)
- Orcutt J.**  
(ST5/W/L/03-B3 0900-12)
- Orcutt John**  
(U8/W/02-B3 1640-01)  
(U8/W/13-B3 1600)
- Ord A.**  
(JSS31/W/15-B3 0830-09)
- O'Reilly Suzanne Y.**  
(JSS44/E/20-B4 1720)  
(JSS44/W/21-B4 1700)
- Orihara Y.**  
(JSA15/E/17-A3 1440)
- Orlando Salvatore**  
(GA4.01/L/01-A2 1220)
- Orlic Mirko**  
(P10/L/01-A4 0930)
- Orlic Nastjenjka**  
(PW1/E/02-A6 1140)
- Orlov V. N.**  
(ST4/E/52-B1 1400-03)
- Orlova Irina**  
(P07/E/02-A3 0900-06)
- Orlova L. A.**  
(GA1.15/W/10-B4 1745)
- Orlyuk M. I.**  
(JSS44/W/18-B5 0930)
- Orlyuk Mikhail**  
(GA5.12/L/02-A2 1600-06)
- Ortega Beatriz**  
(GA1.05/W/28-A5 0900-04)
- Orozco A.**  
(GA5.01/E/04 A1 1400)  
(GA6.02/E/03-B1 1535)
- Orr David**  
(GA3.04/L/15-B2 1450)  
(GA3.04/W/45-B1 1520-45)  
(GA3.04/W/51-B1 1520-20)
- Orr James C**  
(MC01/W/55-A5 1715)  
(MC01/W/56-A5 1600)  
(MC01/W/36-A5 1700)  
(MC01/W/58-A5 1620)  
(MC01/L/23-A5 1640)
- Orris R L**  
(MW04/W/02-A1 1710)
- Orsi Giovanni**  
(JSP23/C/U4/W/01-A6 0830-17)  
(JSV36/C/U6/W/02-B3 1400-19)  
(VS2/E/08-B3 1010)
- Orsolini Yvan J.**  
(JSM26/W/09-B3 0830)  
(JSM41/W/04-B4 1015-04)
- Ort Michael**  
(VS2/W/09-B3 0950)
- Ortiz Ada**  
(JSA16/W/25-A3 0830-46)
- Ortiz J. D.**  
(P07/W/05-A3 1700)
- Ortiz R.**  
(JSV47/W/17-B5 1400-14)  
(JSV47/W/29-B5 1400-22)  
(JSV47/W/30-B5 1400-23)  
(ST5/W/56-B3 0900-01)
- Ortiz Ramon**  
(JSV47/E/06-B5 1400-03)  
(JSV47/E/10-B5 1400-07)  
(JSP23/E/02-B1 1210)  
(JSP23/E/06-B2 1600)  
(JSP23/E/26-B2 1050)
- OrtizBevia Maria Jose**  
(JSP25/E/11-B2 0930-02)  
(JSP25/E/25-B2 0930-01)
- Orton G.**  
(MC09/W/10-B2 1515)
- Orvik Kjell Arild**  
(P11/W/09-B3 1500)
- Osadchuk A.**  
(U7/W/11-B1 0830-18)
- Osborne B**  
(MI09/W/01-A5 1145-19)
- Osborne B. J.**  
(MI06/W/22-B1 1200)
- Osborne S**  
(MI04/E/21-B3 1645).
- Osborne Simon R**  
(MI01/E/11-A3 1205)
- Oschillies A.**  
(P08/W/04-A2 1010)
- Osella Ana**  
(GA1.02/W/01-A1 1050)  
(GA1.02/W/39-A2 0930)  
(JSS44/W/02-B5 0930)  
(JSS44/W/05-B4 0930-02)
- Osella Ana M**  
(ST1/W/59-A4 0930-36)
- Osete C.**  
(GA1.15/W/06-B4 1530-04)
- Osete Cristina**  
(GA1.04/W/20-A6 1000)  
(GA1.05/W/33-A6 1730)
- Osete M. L.**  
(GA1.15/W/06-B4 1530-04)  
(GA1.03/E/01-B3 1120)  
(GA1.15/W/03-B4 1530-06)  
(GA1.15/W/07-B4 1530-05)
- Osete Maria Luisa**  
(GA1.04/W/20-A6 1000)  
(GA1.04/W/15-A6 1520)
- Osher B.**  
(JWS33/E/09-B2 1115)
- Osher B. V.**  
(SW1/E/06-B5 1215)
- Oshiman N.**  
(GA1.02/L/05-A2 0930)  
(JSA15/W/07-A3 1740)
- Oshiman Naoto**  
(JSA15/E/57-A4 1400-15)
- Osipenko Nataly**  
(JSS42/E/13-B5 1700-06)
- Osman Salah**  
(JSA19/L/01-A4 0915)
- Osmaston Miles**  
(JSV30/L/02-B1 1400-16)  
(JSV22/L/01-A5 1150)  
(ST2/L/04-A3 0830)
- Osorio Isabel**  
(G4/P/01-A3 1620-22)  
(JSG28/E/08-B2 1400-09)
- Osorio J. P.**  
(JSP23/E/23-B2 0830-09)
- Osorio J. Pereira**  
(JSG28/E/08-B2 1400-09)  
(JSV36/E/26-B3 1400-10)
- Osorio Jose**  
(G5/W/03-A4 1230-01)
- Ostgaard N.**  
(GA3.02/W/18-B2 1645)
- Oström E**  
(MI09/W/14-A5 1145-21)  
(MI09/W/14-A5 1030)
- Ostrovskii Alexander G.**  
(P11/E/03-B3 1420)
- Ostrowska Mirosława**  
(P15/W/04-B4 1055)
- Otakar Man**  
(GA1.15/E/02-B4 1530-02)
- Otava Jiri**  
(GA1.04/E/14-A5 1400)
- Othman Tarek**  
(P11/P/02-B5 1150-02)
- Othmer C.**  
(GA3.04/L/05-B1 1400)
- Otofujii Yo-ichiro**  
(GA1.05/W/05-A5 1500)  
(GA1.04/W/11-A6 1440)  
(GA1.04/W/28-A5 1140)
- Otruba Wolfgang**  
(JSA16/W/12-A3 0830-52)
- Otsubo Toshimichi**  
(G2/W/12-A2 1630-02)  
(G2/W/01-A2 1630-01)
- Otsuka Y.**  
(GA2.02/W/09-B4 0900)  
(GA2.03/W/02-B3 1010)
- Otto A**  
(GA4.09/W/04-A5 1600-02)
- Otto-Bliesner Bette L.**  
(MC11/E/08-B4 1540)
- Ouali R. Ait**  
(JSS44/E/07-B4 0930-16)
- Ouzar D.**  
(JSS31/E/13-B3 0830-14)
- Ouédraogo M.**  
(HS1/W/51-B4 1750-03)
- Ousadou Farida**  
(ST2/W/30-A5 1400-18)
- Ouzounov D. P.**  
(GA2.03/W/08-B3 1700)
- Ovchinnikov Ilya**  
(GA3.08/W/10-B1 0900-06)  
(GA3.02/E/08-B3 0900-03)
- Ovchinnikov Ilya L**  
(GA3.10/E/03-A6 1700-15)
- Overpeck Scott**  
(MI05/W/02-A5 0900)
- Owen A. J.**  
(JSS44/L/08-B4 0930-43)
- Owen C. J.**  
(GA3.08/W/24-B1 1210)  
(GA3.10/W/21-A6 1700-17)
- Owen Susan**  
(JSV36/W/19-B3 1400-07)
- Owen Tobias**  
(JSA10/W/13-A3 1000)
- Owen Toby**  
(MC09/W/08-B2 1400)
- Owens T. J.**  
(ST4/W/30-B2 1400)
- Owens W. H.**  
(GA1.04/L01-A5 1450)
- Oya Hiroshi**  
(GA3.05/W/22-B3 1220)
- Oyama Shinichiro**  
(JSA20/E/18-A6 1118)
- Oyebande Lekan**  
(HW2/W/12-B2 0910)
- Oyvind Seland**  
(MI01/W/16-A3 1010)
- Ozaki Junichi**  
(ST1/W/24-A3 1130)
- Ozawa Taku**  
(JSH12/W/04-A4 1400-01)
- Ozcep F.**  
(GA1.04/W/27-A6 1140)
- Ozcep Ferhat**  
(GA6.01/W/16-A6 1250)
- Ozdemir Ozden**  
(GA1.05/W/02-A5 1100)  
(GA1.05/W/08-A5 0910)  
(GA1.05/W/38-A5 0830)
- Ozer Naside**  
(ST2/W/19-A4 1215)  
(ST2/W/27-A4 1230)  
(JWS33/C/ST2/W/02-B2 1635-20)  
(JWS33/W/02-B3 0900-20)
- Ozerov Alexei**  
(ST4/W/14-B2 1700)  
(ST4/W/15-B3 1500)  
(ST2/W/13-A3 0845)
- Ozsoy Emin**  
(P14/W/16-A4 1700)  
(P11/E/07-B3 0910)  
(P11/E/23-B5 1420)  
(P11/W/07-B4 1520)

## P

- Paasonen-Kivekäs Maija**  
(HS3/W/20-A2 1015)
- Paatashvili T.**  
(GA6.01/E/04-A5 0900-07)
- Pacca I. G.**  
(GA1.04/P/03-A4 1730)
- Paccagnella Tiziana**  
(JWM08/W/11-A3 1220)
- Paccara P.**  
(VS3/E/02-B3 1550)
- Pacheco J.**  
(ST5/W/17-B3 0850)
- Pacheco Javier**  
(JSS42/W/19-B5 1700-18)
- Pacino Maria Cristina**  
(G3/E/04-A5 1610-90)  
(G4/E/08-A3 1620-31)
- Pacione R.**  
(JSG28/W/15-B1 1400-04)
- Paden Jack**  
(JSA16/E/19-A3 0830-22)
- Padgett Alex**  
(JSA09/E/05-A3 0900)
- Padilha Antonio L.**  
(GA3.04/E/10-B1 1520-11)
- Pagani M.**  
(JSP23/E/08-A6 0950)
- Pagarete Joaquim**  
(JSS31/E/13-B3 0830-14)  
(JSS31/E/09-B3 0830-11)
- Pagounis V. N.**  
(ST4/W/57-B1 0830-01)
- Pais Alexandra**  
(JSA17/W/06-A4 1130)  
(JSA17/W/15-A4 1410)
- Pajunp Arja**  
(GA3.06/E/13-A2 0930-13)
- Pajunpää Kari**  
(GA5.01/E/18-A1 0900-07)  
(JSA10/E/06-A2 0945)  
(GA5.01/E/15-A1 1300-10)  
(GA5.01/E/15-A1 1300-11)  
(JSA06/W/04-A1 1155-04)
- Paka Vadim**  
(P11/E/09-B3 1620)
- Paklar Gordona Beg**  
(P10/L/01-A4 0930)
- Paladio-Melosantos**  
(JSV29/W/04-B1 1700)
- Palchik Nadezhda**  
(JSP23/E/32-A5 0830-11)
- Palamarchuk V. K.**  
(GA5.01/W/15-A1 1300-06)
- Palangio Paolo**  
(GA5.01/W/03-A1 0920)  
(JSA15/W/25-A5 0830-14)
- Palladino Danilo M.**  
(VS2/W/22-B3 1400-15)
- Pälli Anja**  
(JSA09/W/06-A2 0930-03)
- Palma Angela**  
(ST7/W/03-A2 1605-01)
- Palma Elbio D.**  
(P09/L/01-A2 1130)  
(P09/L/02-A2 1135)  
(P09/L/03-A2 1140)
- Palmer Anne**  
(JSM18/W/13-A5 1140)
- Palmer Robert**  
(HS5/W/32-A3 0920)
- Palmer T. N.**  
(M11/W/01-B5 0830)
- Palmer Teresa L.**  
(JSP39/W/36-B2 1700)
- Palomo C.**  
(GA5.12/E/04-A2 0930)
- Paishin Nick**  
(GA1.02/W/22-A2 0930)
- Paltridge Garth**  
(MI08/-A3 0830)  
(MI08/-A3 0930)
- Palus Milan**  
(JSA16/E/23-A3 0830-17)  
(JSA16/E/39-A3 0830-18)
- Pan B. T.**  
(GA1.05/E/17-A6 1630)
- Pan Yongxi**  
(GA1.03/L/04-B1 1520)
- Pan Zaitao**  
(HS1/W/36-B4 1025-01)
- (MC01/W/08-A4 0950)
- Panagi P**  
(MI05/E/06-A1 1630)
- Pancheva D**  
(JSM01/W/98-A2 1600-05)  
(JSA20/W/30-A4 1526)
- Pancheva Dora**  
(JSM01/E/33-A1 1050)  
(JSM01/W/99-A1 1130)
- Pandey B. P.**  
(GA3.05/E/17-B3 0900-23)  
(GA3.08/E/07-B1 1740)  
(GA4.05/E/01-A1 1210)
- Pandey Dharendra K.**  
(JSA16/E/19-A3 0830-22)
- Pandey O. P.**  
(JSA37/E/02-B3 1715)  
(ST4/E/16-B1 1200)
- Pandithurai G**  
(MI09/W/03-A5 1145-17)
- Pandolfo Lionel**  
(MC02/W/03-B2 0930)
- Panfilov Andrey I.**  
(JWA34/E/01-B2 1740)
- Panishko Svetlana K.**  
(JSA20/E/11-A4 1200-29)
- Pankhurst Bob**  
(JSV22/W/05-A5 1630)
- Pankov V**  
(JSS02/E/08-A1 0830-07)
- Pankratov Oleg**  
(GA1.02/L/04-A1 1605)  
(GA1.02/W/26-A1 1605)
- Pankratz Leroy W.**  
(GA5.01/E/01-A1 1300-11)  
(GA5.01/E/14-A1 1130)
- Pant Tarun Kumar**  
(JSA20/E/24-A5 1200-04)  
(JSA20/W/56-A4 1200-26)
- Pantea Aurelian**  
(JSP23/E/52-B1 0830)  
(JSP23/E/53-A5 0830-08)
- Pantea H. A.**  
(ST1/W/60-A3 0900-07)
- Panza G. F.**  
(JSS44/L/02-B4 1520)  
(ST3/W/03-B3 1630)  
(ST3/W/05-B4 1615)
- Panza Giuliano F.**  
(JSS42/W/18-B4 1620)  
(JSV47/W/12-B5 1400-10)  
(ST3/W/02-B4 1645)  
(ST3/W/07-B3 0845)  
(ST3/W/12-B5 1430)  
(SW1/W/07-B5 1130)  
(ST3/W/51-B4 1415)  
(ST1/W/71-A4 0930-29)  
(ST1/E/05-A2 1400-30)
- Paonita Antonio**  
(JSV36/W/05-B3 1145)
- Pap Judit**  
(GA6.01/W/09-A6 0945)  
(JSA16/E/11-A3 0830-15)  
(JSA16/W/20-A3 0830-53)  
(JSA16/W/38-A3 0830-54)  
(JSA16/W/36-A3 0930)
- Papadimitriou P.**  
(ST4/E/66-B2 0930-06)  
(ST4/E/68-B2 1500)  
(ST5/E/35-B5 0830)
- Papadopoulos G.**  
(SW1/E/06-B5 1215)
- Papadopoulos G. A.**  
(JSS42/E/18-B5 1130)  
(ST1/E/77-A4 0930-09)
- Papadopoulos K.**  
(GA3.09/W/12-B4 1400)
- Papaioannou Ch. A.**  
(ST3/L/01-B4 1400-25)
- Papale Paolo**  
(JSV29/W/08-B1 1640)  
(VS2/W/29-B3 1400-31)
- Paparo G**  
(JSA15/E/60-A4 1400-13)
- Paparo I. G.**  
(JSA45/E/17-B5 1110-01)
- Papazachos B.**  
(ST2/W/14-A4 1400)
- Papazachos B. C.**  
(ST3/L/01-B4 1400-25)
- Papazachos C. B.**  
(ST3/L/01-B4 1400-25)
- Papazachos Costas**  
(ST2/E/61-A4 1415)
- Pape Hansgeorg**  
(JSA19/W/07-A4 1115)
- Papitashvili Natalia**  
(GA5.09/W/13-A2 1210)
- Papitashvili V. O**  
(GA5.06/E/05-A3 1400)  
(GA3.03/W/13-B4 1430)  
(GA5.08/W/05-B1 1055)
- Papitashvili Vladimir**  
(GA3.09/W/18-B5 0855)  
(GA3.09/W/25-B5 0910)  
(GA5.08/W/06-B1 0945)  
(GA1.07/W/07-B2 1220)  
(GA2.01/E/13-A1 0900-02)  
(GA2.07/W/21-A2 0930-08)  
(GA3.10/W/08-A6 1700-06)  
(GA3.10/W/18-A5 1155)  
(GA5.09/W/13-A2 1210)  
(JSA06/W/23-A1 1440)
- Papitashvili Volodya**  
(JSA35/W/06-B1 1400)
- Papkov V. V.**  
(JSM43/E/03-B5 1200)  
(JSM43/E/05-B5 1220)
- Paponov Dmitry V.**  
(GA2.02/L/03-B4 0930-06)
- Papoula Joanna**  
(JSP23/C/U5/P/04-A6 0830-15)
- Paradissis Demitris**  
(JSS31/W/11-B2 1620)
- Paradissis Dimitris**  
(G5/E/36-A4 1215)
- Parareda Carme**  
(G1/E/15-A3 1620-55)
- Pardo M.**  
(GA5.12/E/04-A2 0930)
- Paris J.**  
(GA5.06/E/01-A3 0900)  
(GA5.06/E/04-A33 1020)
- Parisi M.**  
(GA4.04/L/01-B5 0830-06)  
(GA4.04/L/02-B5 0830-07)  
(GA4.04/L/05-B5 0830-10)  
(GA4.04/L/06-B5 1400-01)  
(GA4.04/L/07-B5 1400-02)
- Park Jeffrey**  
(ST4/W/14-B2 1700)  
(ST4/W/15-B3 1500)  
(ST2/W/13-A3 0845)
- Park Ki-Joon**  
(MI01/E/18-A1 0900-11)
- Parke M**  
(JSG11/W/17-A4 1150)
- Parker D. J**  
(MI05/W/15-A5 0940)
- Parker Daryl**  
(JSA16/E/11-A3 0830-15)  
(JSA16/W/38-A3 0830-54)
- Parker Doug**  
(MI05/W/18-A2 1010)
- Parker Douglas J.**  
(MI05/W/17-A2 1630)
- Parker Eleanor**  
(JSP23/C/U5/W/03-B1 1420)
- Parker R. L.**  
(GA5.08/W/12-B1 1135)
- Parkinson Dudley**  
(GA5.01/E/19-A1 1730)
- Parkinson M L**  
(JSA06/E/06-A1 1155-19)
- Parkinson R. J.**  
(HS3/W/27-A2 1450)
- Parks G.**  
(GA3.02/W/03-B3 0900-14)  
(GA3.02/W/58-B3 0900-22)  
(GA3.03/E/07-B4 1020)  
(GA3.03/W/11-B4 1200)  
(GA3.02/E/09-B2 1500)  
(GA3.02/W/18-B2 1645)
- Parmet Bart**  
(HS1/W/54-B5 1510-03)
- Parol Frederic**  
(MI06/W/05-B1 1400-06)  
(MI06/W/05-B2 1400-06)
- Parphenuk Olga**  
(ST4/E/57-B1 0830-19)
- Parrish A**  
(MI02/E/06-A5 0910)
- Parrish David F.**  
(MC04/E/04-B2 1625)
- Parronodo C**  
(JSM01/W/37-A5 1400)
- Parrot Michel**  
(JSA15/E/10-A3 1640)  
(JSA15/E/45-A5 1400-13)  
(GA3.04/E/11-B1 1520-21)
- Parseliunas Eimuntas**  
(G3/W/46-A5 1610-91)
- Parsons Barry**  
(G5/E/36-A4 1215)  
(JSS31/W/11-B2 1620)
- Parsons D**  
(MI05/E/06-A1 1630)
- Parsons T.**  
(ST4/L/01-B1 0830-02)
- Parvez Imtiyaz A.**  
(ST1/W/55-A2 1400-13)  
(SW1/W/05-B5 0900)
- Parviainen N.**  
(JSM24/E/14-B1 1010)
- Pascal B.**  
(GA1.01/W/09-A5 0900-03)
- Pascal Bernard**  
(ST1/E/85-A1 1210)
- Pashina N N**  
(G3/E/28-A5 1610-03)
- Pashkevich Inna**  
(GA5.12/L/02-A2 1600-06)
- Pasmanik D. L.**  
(GA3.05/W/37-B3 0900-11)
- Pasternak Andrew**  
(JSM03/E/04-A1 1730)
- Pasynok Sergey**  
(G5/W/05-A4 1115-07)  
(G5/W/24-A4 1115-08)
- Pataraya Avtandil**  
(JSA20/I/01-A4 1200-16)
- Patane Giuseppe**  
(JSV47/E/03-B5 1400-02)
- Pataraya A.**  
(ST4/W/53-B1 0830-31)
- Pataraya A. D.**  
(GA4.03/E/05-B4 1100)  
(GA4.03/E/08-B4 1745-06)
- Pataraya T. A**  
(GA4.03/E/05-B4 1100)  
(GA4.03/E/08-B4 1745-06)
- Patel Pati**  
(ST4/P/01-B2 0930-10)
- Patella Domenico**  
(JSV36/E/25-B3 1710)  
(JSV36/E/35-B3 0830)
- Paterno L.**  
(GA4.03/L/03-B4 1740-05)  
(GA6.01/W/07-A6 1100)
- Paterson W R**  
(GA4.10/W/09-A5 1710)  
(GA4.10/W/05-A5 1655)  
(GA4.10/W/17-A5 1400)  
(GA3.08/W/29-A6 1400)
- Pathan B. M.**  
(GA2.02/E/14-B5 1040)  
(GA3.04/E/09-B2 1650)
- Patra A. K.**  
(GA2.02/E/01-B5 1400)  
(GA2.02/W/16-B4 0930-18)  
(GA2.02/W/28-B5 1000)
- Patrick D. Brown**  
(MC08/L/09-A3 1545)
- Patrino Paolo**  
(JWM08/W/11-A3 1220)
- Patsourakos S.**  
(GA4.02/E/09-A4 1400-04)
- Patterson G**  
(JSA06/W/17-A1 1155-14)
- Paul H.**  
(GA1.01/W/21-A5 0945)
- Paul J.**  
(U3/W/04-A3 1630)  
(JSA10/W/09-A3 1115)
- Paula Alexandra**  
(ST3/E/09-B4 1400-14)
- Paula E. R. de**  
(JSA20/W/24-A5 1200-07)  
(JSA20/W/50-A5 1200-09)
- Paularena K. I.**  
(GA4.04/W/15-B5 1450)
- Paulo S**  
(JSM01/W/45-A2 1600-06)
- Pauluhn Anuschka**  
(JSA16/W/06-A3 0830-48)
- Pauly Bruce**  
(JSP23/E/27-B2 0830-14)
- Pauly Steve**  
(JSP23/E/27-B2 0830-14)
- Pavan Valentina**  
(MC01/W/64-A3 0900)  
(JSP25/E/06-B3 0930)
- Pavel Dmitri Voronov**  
(GA3.04/E/05-B1 1520-18)
- Pavel Hejda**



- (GA1.01/W/27-A5 0900-04)  
**Pavelin E. G.**  
 (JSM26/E/07-B2 1700-01)  
**Paveljev A.**  
 (JSG28/W/10-B2 1400-06)  
**Pavlenko Olga**  
 (ST3/W/23-B4 0930-18)  
 (ST3/W/28-B4 0930-16)  
**Pavlenkova Galina**  
 (JSV22/E/07-A5 0940)  
**Pavlenkova Nina**  
 (JSV22/E/07-A5 0940)  
 (JSS44/E/01-B4 1620)  
 (ST4/E/17-B2 0930-19)  
**Pavlis Ericos C**  
 (JSG11/E/03-A4 1400-02)  
 (JSG14/E/05-A3 1706-03)  
**Pavlis Dr. Nikolaos K.**  
 (G3/E/45-A5 0955)  
 (G4/E/16-A3 1440)  
**Pavlis Nikolaos K.**  
 (G6/C/G3/E/09-B1 1140)  
**Pavlov A. F.**  
 (GA5.01/W/15 A1 1300-06)  
 (JSA15/L/01-A5 0830-10)  
 (ST1/W/04-A2 1400-14)  
**Pavlov A. V.**  
 (GA2.03/P/01-B3 1640)  
 (GA4.08/P/02-B4 1425)  
**Pavlov Nickolay N.**  
 (GA3.05/W/41-B3 0900-24)  
 (GA4.04/W/10-B5 0830-03)  
 (JWS33/W/20-B2 1635-21)  
 (JWS33/W/20-B3 0900-21)  
 (GA3.10/W/14-A6 1700-16)  
 (JSA09/W/22-A3 1230)  
**Pavlov Vladimir**  
 (GA1.03/E/02-B3 1140)  
**Pawlak Geno**  
 (JSP39/W/06-B2 0950)  
 (JSP49/W/12-B5 1130)  
**Pawson Steven**  
 (JSM26/W/36-B1 1710)  
 (MI12/W/07-B4 1030)  
 (MW01/W/07-A5 1150-02)  
 (JSM01/W/02-A5 1210)  
 (MW01/W/12-A5 1150-01)  
**Paxton L. J.**  
 (JSM32/W/07-B3 1100)  
 (JWS33/W/27-B2 1635-22)  
 (JWS33/W/27-B3 0900-22)  
**Pchelkin Aleksandr V.**  
 (JSA40/W/15-B5 1400-02)  
**Pduovkin Mikhail I.**  
 (GA4.02/W/27-A4 1400-24)  
**Peacock Neil**  
 (JSA09/W/01-A2 1145)  
 (P13/E/15-B2 1500)  
**Peacock Sheila**  
 (JSA19/L/02-A4 1015)  
**Pearce A. F.**  
 (JSM41/W/36-B4 1110)  
 (P15/W/05-B3 1630)  
**Pearse Merrin**  
 (G1/E/18-A3 1620-56)  
**Pearson Charles P.**  
 (HS3/W/16-A1 1730)  
**Pearl Mervyn**  
 (HS5/W/08-A1 1650)  
**Peccerillo A.**  
 (JSS44/L/02-B4 1520)  
**Pecherskaya B.**  
 (GA2.03/L/01-B3 1400)  
 (GA2.03/L/02-B3 1520)  
**Pechersky D. M.**  
 (JSA17/E/04-A4 1110)  
**Peci Veronika**  
 (ST1/E/69-A4 0930-13)  
**Peckett Cristina F.**  
 (JSP21/E/03-A4 1700)  
**Pecseli H. L.**  
 (GA4.09/W/05-A6 1140)  
**Pecskay Zoltan**  
 (JSV30/C/U6/E/05-B1 1400-26)  
**Pedersen H.**  
 (ST4/E/68-B2 1500)  
 (ST5/W/05-B3 1440)  
**Pedersen L. B**  
 (GA1.02/W/41-A1 0830)  
**Pedersen Lef Toudal**  
 (P13/E/02-B2 1400)  
**Peiling Lu**  
 (JSP23/C/U5/P/01-A6 0830-14)  
**Peishan Chen**  
 (ST3/E/29-B3 1530)
- Pei-yu Zhang**  
 (G5/E/25-A4 1115-10)  
**Pek Josef**  
 (GA1.02/P/02-A1 1605)  
**Pekdeger Asaf**  
 (ST1/W/67-A1 1050)  
**Pekevski Lazo**  
 (ST2/E/38-A5 1400-23)  
 (ST 5/E/36-B5 0930-14)  
**Pelgrum H.**  
 (U7/E/01-B1 1135)  
**Pelinovsky Efim**  
 (JSP39/E/07-B3 1418-07)  
 (JSS42/E/05-B5 0930)  
 (JSS42/E/13-B5 1700-06)  
**Pelt Jaan**  
 (GA6.01/E/21-A5 1645)  
**Peltier Richard**  
 (U3/E/01-A3 1600)  
 (JSH12/W/10-A5 1600)  
 (ST4/W/42-B3 1220)  
**Peltier W. R.**  
 (JSM26/L/05-B2 1700-17)  
 (JSP49/W/02-B5 1520)  
 (JSS13/W/09-A5 0950)  
 (JSH12/E/03-A5 1500)  
 (JSG14/E/14-A3 1630)  
**Peña J. A.**  
 (JSV47/W/20-B5 1400-13)  
**Peña Javier**  
 (JSP23/E/06-B2 1600)  
 (JSV47/E/06-B5 1400-03)  
**Pendlebury D**  
 (JSM01/W/09-A4 1620-05)  
**Pendleton W R J R**  
 (JSM01/W/105-A3 1120)  
**Penduff Thierry**  
 (P12/E/05-A1 1520)  
**Peneva Elissaveta**  
 (P14/E/03-A4 1620)  
**Peng Gongbing**  
 (JSM18/W/05-A4 1020)  
**Peng Han-Yih**  
 (ST3/E/37-B3 1145)  
**Peng Tsung-Ren**  
 (HS5/W/25-A2 1525)  
**Penkett Stuart**  
 (U2/E/14-A2 1420)  
 (MI02/W/12-A4 1430)  
 (MI02/L/19-A4 1410)  
 (JSP21/W/11-A4 1050)  
 (JSM26/W/06-B1 0900)  
**Penkov George S.**  
 (JSM24/L/02-B1 1730)  
**Penkova Natalia V.**  
 (JSM24/L/02-B1 1730)  
 (U7/E/04-B1 0830-05)  
**Penna Nigel**  
 (JSG28/E/07-B1 0950)  
 (JSG28/E/16-B1 1400-14)  
 (JSG11/E/15-A4 1010)  
 (G1/E/38-A3 0950)  
 (G1/L/09-A3 1640-87)  
**Penner Joyce E**  
 (MI01/E/01-A1 0900-08)  
 (MI01/L/02-A1 0905)  
 (MI01/W/17-A3 0950)  
**Perdigón Candelaria**  
 (JSP21/W/10-A5 1150)  
**Perdomo R.**  
 (JSS31/W/12-B2 1420)  
**Pereira Osorio J.**  
 (G3/E/01-A5 1610-26)  
 (G4/P/01-A3 1620-22)  
**Perejaslova Nina**  
 (JSA16/E/10-A3 0830-20)  
 (JSA45/E/09-B5 1010)  
**Perenne Nicolas**  
 (JSP39/E/02-B4 1520)  
**Peresan Antonella**  
 (SW1/W/07-B5 1130)  
 (ST1/W/71-A4 0930-29)  
**Pereskokov Anatoly**  
 (P13/W/21-B2 1600-12)  
**Pérez Carlos A.**  
 (MI04/E/23-B4 1005)  
**Perez E. Navarro**  
 (P10/W/09-A3 1050)  
**Perez Eduardo**  
 (JSA40/E/05-B5 1400-17)  
**Pérez Enriquez R.**  
 (GA4.04/W/13-B5 1110)  
 (GA4.02/W/21-A4 1400-19)  
**Pérez-González Alfredo**  
 (GA1.05/W/33-A6 1730)
- Perez Nemesio**  
 (JSV36/W/03-B3 0900-13)  
 (JSV36/W/04-B3 1115)  
 (JSV36/W/16-B3 0900-10)  
 (JSV36/W/26-B3 1215)  
 (JSV36/C/U6/W/01-B3 1400-20)  
 (JSV36/W/01-B3 0900-12)  
 (JSV36/W/12-B3 0900-08)  
 (JSV36/W/14-B3 0900-11)  
 (JSV36/W/20-B3 0900-09)  
 (JSP21/W/10-A5 1150)  
**Pérez Nemesio M.**  
 (ST1/W/30-A2 0930-07)  
**Perez Omar J**  
 (ST1/E/45-A3 1230)  
**Perez P**  
 (JSA06/W/30-A2 1150)  
**Perez-Urquioloa J. J. Catalan**  
 (P11/E/28-B5 0950)  
**Peria W.**  
 (GA3.03/W/11-B4 1200)  
**Perini Giulia**  
 (JSV30/W/06-B1 1400-13)  
 (JSV30/W/08-B1 1040)  
**Peristikh Alexei N.**  
 (JSA16/E/15-A3 0830-23)  
**Perlikov Alexander**  
 (JSP23/C/U5/E/18-B1 0830-11)  
**Perillo Gerardo M. E.**  
 (P09/W/01-A1 1420)  
 (P09/W/07-A1 0950)  
 (P09/W/08-A1 1600)  
 (P09/L/03-A2 1140)  
**Perit J**  
 (JSH12/W/07-A4 1400-02)  
 (G1/L/04-A3 1620-85)  
 (JSA09/L/02-A2 1230)  
**Perlwith Judith**  
 (JSM26/L/03-B2 1450)  
 (JSP25/P/05-B5 1520)  
**Peroomian Vahe**  
 (GA3.08/E/02-B1 1110)  
 (GA3.05/E/18-B3 0900-01)  
**Perosanz F**  
 (G3/E/40-A5 1610-05)  
**Perovich Donald K.**  
 (JSA09/L/01-A2 1415)  
**Perraut S.**  
 (GA4.10/W/26-A5 1035)  
**Perraut Sylvaine**  
 (GA3.06/P/01-A3 0900)  
**Perrin Charles**  
 (HW4/E/11-B2 1130)  
**Perrin M.**  
 (P16/E/03-B5 0930)  
**Perrin Mireille**  
 (GA1.03/W/24-B1 1440)  
**Perron N. M.**  
 (HW3/W/09-B4 1455)  
**Perry G**  
 (MI09/L/02-A5 0855)  
**Persson P. O. G.**  
 (JSM04/W/02-A2 0930)  
 (MI08/W/16-A4 1600)  
**Pertel Mikhail**  
 (JSA15/E/14-A5 1400-04)  
 (JSA15/E/39-A4 1140)  
**Peruzza L.**  
 (JSP23/W/16-A6 1520)  
**Peschke Gerd**  
 (HS4/W/02-A4 1015)  
**Pesci Arianna**  
 (G5/W/20-A4 1230-03)  
**Pesek Ivan**  
 (G3/E/08-A5 1610-95)  
**Pesnelli**  
 (JSA45/E/16-B4 1510)  
**Pesnelli Dean W.**  
 (GA3.05/E/11-B3 1620)  
 (GA3.05/W/44-B3 0900-44)  
**Pesonen Lauri J.**  
 (GA5.11/L/01 A3 1140)  
**Petch Jon**  
 (MI04/E/ 09-B1 1420)  
**Peter Benny N.**  
 (P13/E/07-B1 1420)  
**Peter Bespalov**  
 (GA3.05/W/33-B3 0900-03)  
**Peter Th.**  
 (MI06/W/26-B2 1110)  
**Peter Thomas**  
 (JSM26/W/16-B2 1210)  
 (JSM01/W/21-A4 1400)  
**Peters C.**  
 (GA1.05/W/20-A5 0900-06)
- (GA1.05/W/35-A6 1010)  
**Peters Dieter H. W.**  
 (MI12/C/MW08/W/08-B5 1235)  
**Peters Hartmut**  
 (JSP49/W/19-B5 1210-08)  
**Peters Hartmut**  
 (P09/W/02-A1 09100)  
**Peters Norman E**  
 (HS4/W/26-A5 1240)  
 (HS3/W/11-A1 1450)  
**Petersen Nikolai**  
 (GA1.05/W/06-A5 1630)  
**Peterson Curt D.**  
 (JSS42/W/25-B4 1600)  
**Peterson Ray**  
 (JSM18/W/03-A4 1400)  
**Peterson Thomas**  
 (JSP23/W/32-B1 1130)  
 (JSP23/W/34-B1 0830-15)  
**Peterson William K**  
 (GA3.10/W/11-A6 1700-12)  
 (GA3.08/W/13-A6 0940)  
 (GA3.08/L/01-B2 0900-10)  
 (GA3.08/L/01-B2 900-10)  
 (GA3.08/W/09-A6 0920)  
 (GA3.08/W/21-A6 0900)  
 (GA3.08/W/22-A6 1210)  
 (GA3.09/W/15-B4 1450)  
 (GA3.08/W/17-A6 0940)  
**Petit G.**  
 (G2/E/10-A2 1630-14)  
**Petoukhov Vladimir K.**  
 (JSP25/W/68-B4 0930-01)  
**Petrinec S. M.**  
 (GA3.06/W/21-A2 0930-05)  
**Petroff Catherine**  
 (JSS42/W/06-B5 1400)  
**Petrone C. M.**  
 (JSV30/E/11-B1 1400-14)  
**Petropoulos Basil**  
 (JSA16/E/14-A3 0830-03)  
**Petrosino S.**  
 (JSS46/W/09-B4 0930-05)  
 (JSV47/E/08-B5 1400-04)  
 (JSV47/W/01-B5 1045)  
 (JSV47/W/15-B5 1400-08)  
 (ST5/W/56-B3 0900-01)  
**Petroski Thomas**  
 (MC04/W/06-B1 1450)  
**Petrosyan A.**  
 (MC09/W/07-B2 01)  
**Petrosyan A. S.**  
 (JSM43/E/03-B5 1200)  
 (JSM43/E/05-B5 1220)  
**Petrosyan Arakel**  
 (MC09/E/04-B2 1015)  
**Petrov Alexei**  
 (P10/E/18-A5 1500)  
**Petrova L N**  
 (JSM01/C/MW07/E/01-A2 1540-31)  
 (JSM01/C/MW07/E/02-A2 1600-32)  
**Petrov N.**  
 (ST3/W/52-B4 0930-20)  
**Petrov V. G.**  
 (GA4.08/E/02-B3 0900-09)  
 (GA4.08/E/21-B3 0900-13)  
**Petrov Valery**  
 (GA3.09/W/09-B4 0900-07)  
**Petrova Natasha**  
 (ST4/L/02-B3 0830-05)  
 (G5/E/46-A4 1115-09)  
**Petrova T.**  
 (JSA40/W/09-B5 1400-11)  
 (JSA40/W/10-B5 1400-12)  
 (JSA40/W/11-B5 1400-13)  
**Petrovskaya Margarita**  
 (G6/C/G3/E/35-B1 1740)  
 (G4/E/16-A3 1440)  
 (G4/E/16-A3 1440)  
 (G4/E/21-A3 1620-19)  
**Petrovsky Eduard**  
 (GA1.05/W/21-A6 1130)  
 (GA1.05/W/31-A5 0900-05)  
**Petrns Norman E.**  
 (HS5/W/04-A1 1505)  
**Petrukhin V. F.**  
 (GA2.02/W/30-B4 0930-04)  
**Petrukovich A. A.**  
 (GA3.02/W/03-B3 0900-14)  
**Pettit Will**  
 (ST1/W/51-A3 0930)  
**Petts G. E.**  
 (HW2/W/06-B1 1410)  
**Petukhin A. G.**  
 (ST3/W/17-B4 0930-17)

# INDEX

- Pevzner Lev**  
(ST4/E/18-B1 1400-14)
- Peylin P**  
(MC01/W/07-A5 1145)  
(MC01/W/43-A5 1130)
- Peymirat C.**  
(JSA20/P/01-A5 1501)
- Peyton Valerie**  
(ST4/W/14-B2 1700)  
(ST4/W/15-B3 1500)
- Pezzo E. Del**  
(JSV47/W/01-B5 1045)  
(JSV47/W/15-B5 1400-08)  
(JSV47/W/21-B5 1400-20)  
(JSV47/E/08-B5 1400-04)
- Pfaff R. F.**  
(GA3.04/W/20-B1 1100)  
(GA3.07/L/03-A4 1430)  
(GA3.07/L/02-A5 0900-12)  
(GA2.02/L/01-B4 1000)  
(GA3.02/W/18-B2 1645)
- Pfirman S.**  
(P07/L/02-A3 1125)  
(P07/W/08-A3 1015)
- Pfister Leonhard**  
(MW07/W/15-A4 0830)
- Pfister Markus**  
(HS2/W/10-B1 1400)
- Pflug Bringfried**  
(MI09/E/08-A5 1645)
- Pham Dinh Nguyen**  
(ST1/E/49-A3 0900-13)
- Pham Quang Hung**  
(ST1/E/49-A3 0900-13)  
(ST1/E/73-A3 0900-18)
- Pham Rosalyn**  
(JWS33/W/27-B2 1635-22)  
(JWS33/W/27-B3 0900-22)
- Phanikumar M. S.**  
(JSA19/W/09-A4 0930)
- Phan T. D.**  
(GA3.08/W/33-B1 1130)
- Phan Tai**  
(GA3.07/W/13-A4 1200)
- Phan-trong Trinh**  
(ST2/E/01-A3 1100)  
(ST7/E/11-A2 1530)
- Philippa R.**  
(MC02/E/12-B1 1600-11)
- Philippov Nikolai**  
(GA 5.11/E/02 A3 1430-09)
- Phillips Collin**  
(GA1.01/L/01-A5 0900-12)  
(GA1.01/W/35-A5 1200)
- Phillips Jeremy**  
(VS2/W/11-B3 1400-08)  
(VS2/W/02-B3 1400-02)
- Phillips Katrina L.**  
(JSM18/W/13-A5 1140)
- Phillips Thomas J**  
(MC01/E/18-A3 1535)
- Phillips W. Scott**  
(ST5/W/04-B5 1145)
- Philpot W. D.**  
(P15/L/24-B31730)
- Phipp Morgan J.**  
(ST5/W/L/03-B3 0900-12)
- Pi X.**  
(GA3.09/W/04-B5 1035)  
(GA3.09/W/19-B5 1100)
- Piacsek S.**  
(P13/E/08-B2 1600-02)
- Piacsek Steve**  
(P12/W/17-A1 1720)
- Piatti A.**  
(G2/W/15-A2 1630-19)
- Piccolini L.**  
(JWS33/E/03-B2)  
(JWS33/E/03-B3 0900-06)
- Piccolo M. Cintia**  
(P09/W/01-A1 1420)  
(P09/W/08-A1 1600)
- Pickens Jim**  
(JSV36/W/07-B3 1400)
- Pickett J. S.**  
(GA3.07/W/46-A5 0900-13)  
(GA4.09/W/15-A6 0900)
- Pickett Jolene**  
(GA4.09/W/11-A6 0920)
- Piera Jaume**  
(JSP39/W/38-B4 1150)
- Pierce Clive**  
(MC04/E/05-B2 1715)
- Pierce R.**  
(JSM26/W/11-B1 0940)
- Pierini S.**  
(P14/W/06-A4 1400-09)
- Piero Dellino**  
(VS2/E/14-B3 1400-25)
- Pierr Pierpaolo**  
(JSA40/W/01-B5 1205)
- Pierson Thomas C**  
(JSP23/E/14-B1 1620)
- Pietrafesa L. J.**  
(MC04/L/03-B1 1205)
- Pietroniro A.**  
(HW3/W/04-B4 1050)
- Pike Christopher R.**  
(GA1.05/E/01-A6 0910)
- Piketh S J**  
(MI02/L/01-A5 1140)  
(MI02/L/18-A5 1430)
- Pikkarainen T.**  
(GA3.04/W/08-B1 1150)  
(GA3.04/W/29-B1 1520-28)  
(GA3.04/W/33-B1 1520-27)
- Pilipenko Viacheslav**  
(GA3.02/E/04-B3 0900-19)  
(GA3.04/E/06-B2 0950)  
(GA3.07/E/19-A6 0900-14)  
(JSA15/E/06-A4 1400-08)  
(JSA15/E/09-A4 1200)  
(JSA15/E/45-A5 1400-13)
- Pilkington M.**  
(GA5.12/E/07 A2 1520)
- Pillai J. S.**  
(JSM43/W/10-B5 0900)
- Pimenta A. A.**  
(JSA20/W/05-A5 1200-05)
- Pincon J. L.**  
(JSA10/E/06-A2 0945)
- Pinet Celine**  
(HS4/W/10-A4 1530)
- Pinet P. C.**  
(JSA10/E/01-A2 1515)
- Pinhas Alpert**  
(MI07/E/01-A2 1700)  
(MI07/E/02-A2 1510)  
(MI07/E/04-A2 1640)  
(MI07/W/02-A2 1210)  
(MC02/E/04-B2 1510)
- Pinker Rachel T**  
(MC01/W/30-A4 1615)  
(MC01/W/62-A1 1430)  
(MI09/W/03-A5 1145-17)
- Pinnock M**  
(GA3.03/W/08-B4 1700)  
(GA3.08/W/19-A6 1520)  
(GA3.03/W/09-B4 1740)  
(GA3.08/E/03-B1 1000)
- Pinnock R. A.**  
(JSM41/W/22-B5 1015)  
(G3/W/12-A5 1610-44)  
(G3/W/48-A5 1610-43)
- Pinot Sophie**  
(MC11/L/01-B3 1440)
- Pinsky Vladimir**  
(U8/W/07-B3 1625)  
(U8/W/15-B3 1640-10)
- Pinto I R C A**  
(MI03/W/08-A3 1400-01)
- Pinto Jorge**  
(G1/E/59-A3 1620-29)  
(JSS31/E/09-B3 0830-11)
- Pinto Jr. O**  
(MI03/W/08-A3 1400-01)
- Pinty Bernard**  
(JSM24/E/01-B1 1145)
- Piochi Monica**  
(JSV36/C/U6/W/02-B3 1400-19)
- Piper J. D. A.**  
(GA1.04/P/02-A4 1710)
- Piper John**  
(GA1.04/W/37-A4 0930-17)
- Pires Carlos A. L**  
(JSP05/W/13-A2 1150)
- Pirjola Risto**  
(GA1.02/W/33-A2 0930)  
(JSA06/W/04-A1 1155-04)  
(JSA06/W/06-A1 1135)  
(JSA06/E/09-A1 1155-01)  
(JSA06/W/07-A11155-05)
- Pirog O. M.**  
(JSA20/W/44-A4 1200-33)
- Piromallo C.**  
(ST2/E/21-A5 1400-24)  
(ST4/W/18-B2 1440)
- Pirro F.**  
(JWS33/E/03-B2)  
(JWS33/E/03-B3 0900-06)
- Pirro M.**  
(JWS33/E/03-B2)  
(JWS33/E/03-B3 0900-06)
- Pirttijarvi Markku**  
(JSA40/E/10-B5 1025)
- Pirttilä Juha**  
(GA2.01/W/09-A1 1400)
- Pirzola Risto**  
(GA1.02/W/37-A1 0930)
- Pisacane G.**  
(JWM08/W/02-A2 1220)
- Pisanko Dr. Yuri**  
(GA4.05/L/03-A1 1450)
- Pisarenko V. F**  
(JSP23/E/48-A5 0830-09)  
(JSP23/E/47-A6 0830-12)
- Pisarev S. V.**  
(P13/E/03-B2 1600-03)  
(P13/E/04-B1 0930)
- Pisarevskaya Lyudmila**  
(P13/L/02-B1 1740)
- Piscini Alessandro**  
(JSS42/E/19-B5 1700-14)
- Pishchalnik V. M.**  
(P11/W/14-B5 1150-08)
- Pissarenko N.**  
(GA3.05/W/32-B3 0900-25)
- Piterbarg Leonid I**  
(JSP05/E/09-A1 1640)
- Pitt A. M.**  
(JSS46/W/12-B4 1210)
- Pitts Michael C.**  
(JSG28/W/03-B2 1400-10)  
(JSM41/W/08-B4 1000-01)
- Pizzino Luca**  
(JSV36/E/22-B3 0900-16)
- Plag Hans-Peter**  
(G2/L/03-A2 1000)  
(JSS44/E/11-B4 0930-29)
- Plagmann M**  
(JSM01/E/39-A1 0940)
- Planck Max**  
(GA4.05/E/02-A1 1010)
- Plane John**  
(JSM01/W/44-A3 1730)  
(JSM32/W/04-B2 1625)
- Plank G E**  
(JSM01/E/39-A1 0940)
- Plantevin Paul-Henri**  
(JSM26/W/07-B1 1500)
- Plastino Wolfango.**  
(ST1/E/48-A2 0930-10)
- Plate Erich J.**  
(U4/L/02-A41115)
- Platt R.**  
(M104/E/25-B4 0930)
- Pletchov Pavel**  
(JWS33/W/13-B2 1100)
- Pleshacov D**  
(G3/W/52-A5 1610-14)
- Pletchov Pavel**  
(ST7/W/04-A2 1605-02)
- Plomerova J.**  
(JSS44/E/13-B4 0930-27)  
(ST4/E/46-B2 0930-07)
- Plotkin V. V.**  
(JSA35/W/04-B1 1550)  
(JSA15/L/01-A5 0830-10)  
(ST1/W/04-A2 1400-14)
- Plotnikov Vladimir**  
(JSP25/W/06-B1 0830-07)
- Plotnikova L. M**  
(ST1/E/20-A4 0930-06)
- Plumb Alan**  
(JSM01/E/40-A5 1450)
- Plumb R. Alan**  
(JSM26/E/20-B1 0830)
- Plunkett S. P**  
(GA4.08/W/07-B3 0830)  
(GA4.02/W/34-A4 1525)  
(GA4.01/W/01-A2 1400-04)  
(GA4.02/W/03-A4 1705)
- Plunkett Simon**  
(GA4.01/L/01-A2 1220)
- Plyusnina Lyubov**  
(GA4.03/W/17-B4 1750-07)
- Poberejsky Valentina**  
(HW5/E/08-A3 1120)
- Poberovsky A V**  
(MI02/W/14-A4 1450)
- Pochtarev Victor I.**  
(GA5.08/E/06-B1 1400-01)
- Pociask-Karteczka J.**  
(HW2/W/24-B1 0900-06)
- Podgorny A. I.**  
(GA4.02/L/02 1400-11)  
(GA4.02/L/03 1400-12)
- Podgorny I A**  
(MI01/E/07-A2 0930)
- Podgorny I. M**  
(GA4.02/L/02 1400-11)
- Podladchikova O.V.**  
(GA4.05/W/01-A1 1220)
- Poezzhalova George**  
(JSG11/E/02-A4 1400-01)
- Poezzhalova Olga**  
(JSG11/E/02-A4 1400-01)
- Pogoreltsev A I**  
(JSM01/W/102-A2 1600-03)  
(JSM01/W/103-A1 0920)  
(JSM01/W/112-A2 1600-19)
- Pohl Jean**  
(ST4/E/14-B1 0920)
- Pohl M.**  
(JSA09/L/02-A2 1230)
- Poidras Thierry**  
(GA1.03/W/08-B1 1400)
- Pointet F**  
(HS4/W/13-A4 1650)
- Poirier Jean-Paul**  
(JSA17/W/03-A4 1230)
- Pokhotelov Dmitrii**  
(GA3.04/E/11-B1 1520-21)
- Pokhotelov O.**  
(GA3.04/W/33-B1 1520-27)  
(GA3.07/W/02-A3 0900-11)
- Pokhotelov O. A.**  
(GA3.04/E/14-B1 1520-03)  
(GA3.04/W/08-B1 1150)
- Pokhotelov Oleg**  
(GA3.04/E/11-B1 1520-21)  
(GA4.09/E/08-A6 1120)  
(JSA15/E/45-A5 1400-13)  
(JSA15/E/49-A4 1000)  
(MW03/W/01 B4 1445)  
(JSP05/W/05-A1 1700)  
(MI05/W/11-A5 1210)
- Pokrovsky O. M.**  
(JSM41/W/05-B5 1515)
- Pokrovsky Oleg**  
(MI04/W/28-B2 1135)  
(MW03/W/01-B4 1445)  
(U7/W/05-B1 0830-09)
- Polcher Jan**  
(MC01/W/46-A3 1620)
- Polekh N. M.**  
(JSA20/W/44-A4 1200-33)
- Polkko J.**  
(MC09/W/07-B2 01)
- Pollack Henry N.**  
(MC02/W/12-B1 0900)  
(MC02/W/14-B1 0930)
- Pollari P.**  
(GA2.02/W/15-B4 0930-12)  
(GA2.02/W/19-B4 1600)  
(GA2.02/W/25-B4 0930-11)  
(GA3.04/W/08-B1 1150)
- Pollock C. J.**  
(GA3.08/W/09-A6 0920)
- Polonic Gabriela**  
(ST4/E/43-B1 1400-09)
- Polyakov S. V.**  
(GA2.03/L/01-B3 1400)  
(GA2.03/L/02-B3 1520)  
(GA3.04/W/28-B1 1520-22)
- Polyakova O S**  
(JSM01/C/MW07/E/02-A2 1600-32)
- Pomeroy J.**  
(HS2/W/32-B2 1440)  
(JSM24/E/14-B1 1010)  
(JSM43/W/12-B5 1120)
- Pomeroy J. W.**  
(HS2/W/11-B1 1420)
- Pommereau J. P.**  
(MC09/W/07-B2 01)  
(JSA10/W/03-A2 0930)
- Pomposiello M. Cristina**  
(GA1.02/W/39-A2 0930)  
(JSA19/W/11-A4 1400-04)  
(JSS44/W/02-B5 0930)
- Pomroy H R**  
(MI05/W/36-A4 1400-03)  
(MI05/W/37-A3 1500)
- Ponater Michael**  
(MC07/E/01-A2 1035)  
(MC08/E/05-A3 0900-02)  
(MI02/W/03-A5 1200)
- Ponchaut F**  
(JSG11/W/03-A3 1010)  
(U7/W/02-B1 0830-11)

- Poncín Ch**  
(MC01/W/26-A3 0915)
- Pondrelli S.**  
(ST2/E/21-A5 1400-24)
- Pongetti Francesco**  
(JSV36/E/22-B3 0900-16)
- Ponomarenko Pavlo**  
(GA3.04/W/17-B1 1520-16)  
(GA3.07/W/50-A6 0900-15)
- Ponomarev A.**  
(JSP23/W/38-B2 1720)
- Ponomarev A. V.**  
(ST1/W/11-A2 1400-28)  
(ST1/W/07-A3 0900-05)  
(SW1/W/04-B5 1200)
- Ponomarev E. A.**  
(GA2.02/W/30-B4 0930-04)
- Ponomarev Vladimir**  
(JSP25/W/06-B1 0830-07)  
(P10/E/17-A3 1520)
- Ponomareva Vera**  
(JSP23/E/04-B1 0830-08)
- Ponomarjov Maxim G.**  
(JSP39/E/04-B3 1403-02)
- Ponte Rui M.**  
(JSG14/E/12-A3 0900)
- Ponyavin Dmitri I**  
(GA4.02/E/12-A4 1400-10)  
(JSA16/E/35-A3 0830-06)  
(GA3.09/E/11-B4 0900-01)  
(GA4.03/E/07-B4 1715)
- Pook Michael**  
(MI08/L/01-A4 1120)
- Poole S.**  
(G6/C/G3/W/32-B1 1120)
- Pop Aurel**  
(ST4/E/43-B1 1400-09)
- Popa Mihaela**  
(ST1/E/61-A2 1400-09)
- Pope S K**  
(MI08/W/08-A4 1545)
- Pope Shelly K.**  
(MI04/W/35-B2 1450)  
(MI10/W/23-B2 1420)
- Pope V. D.**  
(JSM26/E/14-B1 1540)
- Pope Vicky**  
(MC01/E/05-A1 1030)  
(MC01/E/28-A1 1600)
- Popecki M. A.**  
(GA4.02/E/02-A4 1400-06)  
(GA4.02/W/28-A4 1720)
- Popescu Emilia**  
(ST1/E/78-A2 1400-15)  
(ST1/E/79-A2 1400-10)
- Popinski Waldemar**  
(JSG11/W/14-A4 1400-10)
- Poplavsky Alexander**  
(JSP23/C/U5/E/12-A6 0830-07)
- Popov Anatoly M.**  
(JSA15/W/20-A5 1400-14)  
(JSA16/W/33-A3 0830-28)
- Popov A. M.**  
(ST4/W/45-B1 0830-09)
- Popov George**  
(GA3.05/W/19-B3 0900-26)
- Popov Jurij**  
(P07/E/02-A3 0900-06)
- Popov Sergei**  
(JSP23/W/11-A5 1720)  
(JSP23/W/28-B1 0830-01)
- Popov Yuri**  
(ST6/E/03-A1 0830-14)  
(ST4/E/14-B1 0920)  
(ST4/E/18-B1 1400-14)
- Popov Yuri**  
(GA1.02/W/27-A1 1605)
- Popova Irina**  
(GA1.02/E/20-A1 1605)
- Popova Valeria**  
(U2/E/15-A2 1440)
- Popova Valeria V.**  
(JSM24/W/09-B2 1215)
- Porter**  
(MC08/L/14-A4 0945)
- Porter H S**  
(MC06/C/JSM01/E/22-A1 1505)  
(MW04/W/16/C/JSM01/E/14-A1 1135)
- Porter John**  
(MC08/L/09-A3 1545)  
(MC08/L/14-A4 0945)  
(MI09/L/04-A5 1055)
- Portmann Robert**  
(MI04/W/14-B2 1120)
- Portnyagin Yuri**  
(JSM01/W/69-A1 1130)  
(JSM01/W/72-A2 1600-02)  
(MW04/W/01-A1 0950)  
(JSM01/E/04-A2 1130)  
(JSM01/E/07-A2 1000)
- Posadas A. M.**  
(ST5/W/66-B4 1400-06)
- Posch J. L.**  
(GA3.02/W/43-B2 0920)
- Posch Jennifer**  
(GA3.04/W/47-B1 1230)
- Posmentier Eric**  
(GA6.01/W/18-A5 1455)
- Posner Arik**  
(GA4.01/E/09-A2 1200)
- Pospisil Jiri**  
(ST3/P/4-B5 1115)
- Postlylyakov Oleg V.**  
(MI06/E/13-B1 1100)
- Potapov Alexander**  
(GA3.04/E/04-B1 1520-23)  
(GA5.01/L/04-A1 1300-12)
- Potemkin V.**  
(MC03/E/01 1150)
- Potemkin Vladimir**  
(MI02/E/07-A5 1620)
- Pottelette Raymond**  
(GA3.06/W/40-A3 0830)
- Potter Gerald L**  
(MC01/L/04-A1 1615)  
(MC01/W/31-A1 1400)
- Poudjoun Djomani Yvette H.**  
(JSS44/W/21-B4 1700)
- Poulet G.**  
(JSM26/W/29-B2 1700-09)
- Poulos Gregory S.**  
(U8/W/05-B3 1640-02)
- Poulsen Caroline**  
(MI06/E/07-B1 1400-09)  
(MI06/E/07-B2 1400-10)
- Pous Jaume**  
(GA1.02/W/38-A2 0930)
- Poutanen M**  
(JSG11/W/05-A3 1440)
- Poutanen Markku**  
(G1/E/10-A3 1620-23)  
(G1/E/21-A3 1620-57)  
(G5/E/12-A4 1518-10)  
(G5/E/31-A4 1430)
- Powell Christopher McA**  
(GA5.11/L/02-A3 1430-03)
- Powell K G**  
(GA3.10/E/09-A6 1600)  
(GA4.10/W/10-A4 1215)  
(GA4.01/E/01-A2 1220)  
(GA4.10/E/07-A5 1525)  
(GA3.09/E/03-B4 1215)  
(GA4.08/W/03-B4 0930)
- Powell Kathleen A.**  
(MI01/W/24-B1 1400-05)  
(MI01/W/24-B1 1730)  
(MI06/W/24-B2 400-05)  
(MI10/W/09-B1 0900-16)
- Power R. A.**  
(JSA20/W/28-A5 1200-10)
- Power S.**  
(JSP25/W/95-B5 1620)
- Power Scott**  
(MC02/W/02-B2 1130)
- Power Scott B.**  
(JSP25/W/46-B5 0830)  
(JSP25/W/61-B4 0930)
- Powers Darnell**  
(MI08/W/09-A4 1515)
- Pozo C. F. El**  
(GA 2.01/E/11-A1 1205)  
(GA 2.01/E/12-A1 1220)
- Pradelle Frediric**  
(MI01/E/22-A2 1700)
- Prakasam K. S.**  
(ST2/E/10-A3 1645)  
(ST4/E/03-B2 0930-20)
- Prakash Manju**  
(GA3.02/E/01-B3 0930)
- Prakash Satya**  
(GA2.02/E/16-B4 0930-19)
- Prasad Gajendra**  
(JSS42/E/08-B5 1700-10)
- Prasad Sheo S.**  
(JSP21/L/05-A5 1010)
- Prather Michael**  
(MI02/L/20-A4 1640)  
(MW01/W/06-A5 1400)  
(MI02/W/09-A4 1220)
- Praticelli N.**  
(GA1.02/W/19-A2 0930)
- Pratomosunu Bambang S**  
(JSG11/E/12-A3 0950)
- Pratomosunu Mujiana**  
(JSG11/E/12-A3 0950)
- Pratt Larry**  
(P14/W/10-A4 1000)  
(P14/W/05-A4 1420)
- Pratt T. L.**  
(ST4/L/01-B1 0830-02)
- Praus J. Pek**  
(GA1.02/W/13-A2 0930)  
(GA1.02/W/19-A2 0930)  
(GA1.02/W/28-A2 0930)
- Prawirosoehardjo Boedijanti**  
(JSA20/W/13-A4 1200-06)
- Prech L.**  
(GA3.07/E/02-A5 0900-14)
- Preedy Neil**  
(HS3/W/01-A1 0900)
- Prego Juan A**  
(MC01/E/27-A4 1645)  
(MC01/E/35-A4 1415)
- Presennakumar B.**  
(MI06/W/25-B2 1130)
- Preston L. A.**  
(ST4/L/01-B1 0830-02)
- Pretorius E**  
(HS5/W/10-A1 1730)
- Preuss Jane**  
(JSS42/E/19-B4 1020)
- Preusse Peter**  
(MW 07/E/03-A4 1400)  
(MW07/W/19-A4 1420)
- Prévot M.**  
(GA1.03/W/01-B1 1000)  
(GA1.03/W/08-B1 1400)  
(GA1.03/W/24-B1 1440)
- Prezzi Claudia**  
(GA1.04/W/07-A4 0930-02)
- Pribnow D.**  
(ST4/W/64-B1 1400-12)  
(ST4/W/65-B1 0900)
- Price C**  
(MI02/W/09-A4 1220)
- Price Colin**  
(JSA35/E/05-B1 1630)  
(JSP25/E/23-B1 1440)  
(U7/E/09-B1 0830-04)
- Price David**  
(JSS02/W/10-A1 0830-11)
- Price J. D.**  
(MI04/E/05-B3 1700)
- Price James F.**  
(P14/E/02-A4 1210)
- Price Richard**  
(JSV30/E/05-B1 0940)  
(JSV30/W/09-B1 1000)  
(JSV30/E/01-B1 0920)  
(JSV30/E/01-B1 1400-10)
- Priest George R.**  
(JSS42/W/25-B4 1600)
- Priest Prof. E. R.**  
(GA4.05/W/06-A1 1130)
- Prieur Louis**  
(P11/E/16-B4 1420)
- Prigancova Alina**  
(JSA16/E/14-A3 0830-03)
- Prijatna Kosasih**  
(G3/L/13-A5 1610-92)
- Prikner K.**  
(GA3.04/W/08-B1 1150)
- Prikryl P.**  
(GA3.07/W/40-A6 0900-16)
- Prilepin Mikhail**  
(JSP23/E/51-A6 0830-13)  
(G6/E/01-B1 1010)  
(JSS31/E/03-B2 1700)
- Primdahl F.**  
(GA5.08/E/03-B1 0900)  
(JSA10/E/06-A2 0945)
- Pringle Malcolm S.**  
(GA1.15/E/03-B4 1430)  
(GA1.15/P/01-B4 1630)  
(JSV36/C/JSA15/W/34-B3 1415)
- Prinn Ron**  
(JSP21/E/02-A4 0930)  
(JSP21/E/04-A5 1110)
- Prinz Dianne**  
(JSA16/W/11-A3 0830-25)
- Prishepo V. A.**  
(GA1.02/E/36-A1 1050)
- Pritchard M. J.**  
(ST4/W/03-B3 1630)
- Pritchett P. L.**  
(GA3.02/W/17-B3 0945)  
(GA3.06/W/14-A3 0940)  
(GA4.10/W/09-A5 1710)
- Privitera Eugenio**  
(JSV47/W/09-B5 1200)  
(JSV47/W/12-B5 1400-10)
- Probst Jean-Luc**  
(MC01/W/58-A5 1620)
- Proctor Michael**  
(GA1.01/E/02-A6 1115)
- Proffitt Michael**  
(MI12/W/17-B5 1055)
- Prokoviev Yury M**  
(JSA06/W/16-A1 0915)
- Pronin A.**  
(JSP23/W/38-B2 1720)
- Proshutinsky Andrey**  
(JSP25/W/63-B5 1420)  
(P13/W/17-B2 1600-07)
- Proshutinsky Tatiana**  
(P13/W/17-B2 1600-07)
- Proskuryakova Tamara A.**  
(ST1/E/15-A2 0930-09)
- Protat Y. Lemaitrea**  
(MI05/W/42-A4 1010)
- Provan G**  
(GA3.10/W/15-A6 1700-04)
- Provost A.**  
(JSV29/E/02-B1 1440)
- Prowse T. D.**  
(HW3/W/10-B4 1520)  
(HW3/W/15-B4 0835)
- Pruner Petr**  
(GA1.15/E/02-B4 1530-02)  
(GA1.04/L/07-A4 1200)
- Prychodko Michail**  
(JSV30/C/U6/E/05-B1 1400-26)
- Pryse S E**  
(GA3.10/W/19-A6 1005)
- Ptacek Carol J.**  
(HW5/W/10-A3 0920)
- Pu Z. Y.**  
(GA3.02/E/18-B3 0850)  
(GA3.02/W/54-B2 1615)  
(GA3.05/W/23-B3 0900-13)
- Pucher R.**  
(JSA40/W/06-B5 1400-09)
- Pucher Rudolf**  
(GA1.03/E/08-B2 0920)
- Puckrin E**  
(MC07/W/15-A2 1440)  
(MC07/W/16-A2 1600)
- Pudenz S.**  
(HS3/W/26-A2 1425)
- Pudovkin M. I.**  
(GA3.02/E/17-B3 0900-18)  
(GA3.08/E/10-B1 0900-03)
- Pudovkin Mikhail**  
(GA4.09/E/11-A5 1600-05)  
(JSA16/C/GA4.07/E/26-A3 0830-13)  
(JSA16/E/27-A3 0830-12)
- Puga Larry**  
(JSA16/W/38-A3 0830-54)
- Pugacheva S. G.**  
(JSM41/E/32-B4 1010-03)
- Puglisi G.**  
(JSV36/W/17-B3 1500)  
(JSV36/W/23-B3 1515)
- Puglisi Giuseppe**  
(G2/E/09-A2 1630-25)  
(JSG28/E/25-B1 1400-15)
- Pulinets S.A.**  
(JSA15/E/31-A5 1400-15)  
(JSA15/E/53-A4 1400-01)  
(JSA15/E/55-A5 1400-16)  
(JSA15/W/28-A5 1400-17)
- Pulkkinen Anitti**  
(JSA06/W/06-A1 1135)
- Pulkkinen Pentti J.**  
(GA6.01/E/21-A5 1645)
- Pulkkinen T. I.**  
(GA3.01/W/01-A2 0915)  
(GA3.02/E/18-B3 0850)  
(GA3.08/E/01-A6 1430)  
(GA3.02/W/60-B2 1215)  
(GA3.03/W/07-B4 1450)  
(GA3.05/W/13-B3 0900-34)  
(GA3.08/W/22-A6 1210)  
(GA3.09/W/12-B4 1400)  
(GA3.09/W/29-B4 1425)  
(GA3.05/W/04-B3 0900-45)  
(GA3.08/W/04-B1 0900-02)
- Pulkkinen Tuija I**  
(GA3.10/W/11-A6 1700-12)
- Pumphrey H C**



## INDEX

(JSM01/W/12-A2 1600-15)  
**Purbawinata Mas Atje**  
(JSV36/E/07-B3 0900)  
**Purdie Duncan A.**  
(JSP21/E/03-A4 1700)  
**Purdy J.**  
(JWM08/L/02-A3 1400)  
**Puri K.**  
(MC04/W/13-B2 1050)  
**Purucker M.**  
(GA5.08/W/12-B1 1135)  
(GA5.08/W/08-B1 1350)  
(JSA40/W/05-B5 1120)  
(GA5.12/W/07 A2 1200)  
(GA5.12/E/07 A2 1520)  
**Purucker Michael**  
(GA5.11/E/01 A3 0950)  
(GA5.11/E/01 A3 1430-01)  
**Purucker Mike**  
(GA5.11/W/02 A3 0910)  
(GA5.11/W/03 A3 1430-02)  
**Pushkarlov G.**  
(ST3/P/9-B4 1400-22)  
**Putis Marian**  
(GA1.04/L/02-A5 1600)  
**Putnam Scott N.**  
(MC02/E/19-B1 1130)  
**Putzka Alfred**  
(P08/W/09-A2 1110)  
(P07/W/12-A3 0900-03)  
**Pyle D. M.**  
(VS2/W/14-B3 1150)  
**Pyo Kyung**  
(JSA06/W/28-A1 1155-13)

## q

**Qi Yunquiao**  
(JSM24/W/04-B1 0930)  
**Qian Jiadong**  
(SW1/W/04-B5 1200)  
**Qian Jiadong**  
(GA1.02/E/07-A1 1605)  
**Qi-Liang Liu**  
(ST1/E/50-A2 1400-36)  
**Qing Liu Su**  
(GA1.03/W/10-B2 1420)  
**Qing Zheng**  
(MC01/W/40-A1 1115)  
**Qingcun Zeng**  
(MI05/W/03-A4 1400-13)  
**Qinghe Li**  
(JSS44/p/04-B5 1050)  
**Qingming Gui**  
(G4/P/07-A3 1620-08)  
**Qiu Bo**  
(P12/W/08-A1 1600)  
**Quadfasel D.**  
(P12/W/07-A1 0850)  
**Quanfu Fan**  
(GA3.09/W/28-B4 0900-13)  
**Quartly G. D.**  
(JSM41/E/06-B3 1720)  
**Quattrocchi Fedora**  
(JSV36/E/22-B3 0900-16)  
**Queen John**  
(ST5/W/02-B4 0930-06)  
(ST5/W/08-B4 1145)  
**Queral Pillar**  
(GA1.02/W/38-A2 0930)  
**Quere Corinne Le**  
(MC01/W/55-A5 1715)  
**Quidelleur X.**  
(GA1.03/W/27-B1 1600)  
**Quiel Friedrich**  
(HS4/W/08-A4 1450)  
**Quilty E.**  
(JSS31/E/11-B2 1010)  
**Quingyun D Miaoyue**  
(JSA27/L/02-B1 1400-05)  
**Quinn P K**  
(MI09/W/14-A5 1030)  
(MI09/W/14-A5 1145-21)  
**Quinn Paul**  
(HS3/W/31-A2 1705)  
**Quinn Paul T.**  
(JSM26/W/19-B2 1700-13)  
**Quinnell K. J.**  
(JSM32/L/01-B3 1125)  
**Quintanar Arturo**  
(JSA16/E/17-A3 0830-05)

**Quintero Ronnie**  
(ST2/W/18-A5 1015)  
**Quirnbach Markus**  
(HS5/W/20-A2 1220)  
**Quniton William L.**  
(HS4/W/31-A5 1630)

## R

**Raabe Thomas**  
(P10/E/07-A5 1130)  
**Raad Peter**  
(JSS42/W/06-B5 1400)  
(JSS42/E/19-B4 1020)  
**Raban Avner**  
(JSG11/W/06-A3 1720)  
**Rabassa Jorge**  
(GA1.15/E/06-B4 1645)  
**Rabie Said I.**  
(GA5.12/P/01-A2 1600-09)  
(JSA27/W/01-B1 1000)  
**Rabinovich A. B.**  
(JSP23/W/07-B1 930)  
**Rabinovich Alexander B.**  
(JSS42/E/12-B4 1500)  
(JSS42/E/12-B5 1700-07)  
(JSS42/E/25-B5 1700-08)  
**Racette Paul**  
(MI08/E/10-A3 1735)  
**Radchenko Anton**  
(GA 5.11/E/02 A3 1430-09)  
**Radej Karel**  
(G1/E/60-A3 1620-82)  
**Rademacher Horst**  
(JSP23/E/27-B2 0830-14)  
**Radhakrishna I.**  
(ST1/E/67-A3 1010)  
**Radhakrishna T.**  
(JSS44/E/04-B4 1010)  
**Radicella S M**  
(JSA06/W/15-A2 1010)  
(JSA15/E/55-A5 1400-16)  
**Radick Richard R.**  
(JSA16/W/39-A3 1200)  
**Radilov Andrej**  
(GA5.01/W/21 A1 1415)  
(JWS33/W/28-B2 1635-14)  
(JWS33/W/28-B3 0900-14)  
**Raducu Cristina**  
(HS4/W/09-A4 1510)  
**Radulian M.**  
(ST3/W/05-B4 1615)  
(JSS 44/E/23-B4 0930-22)  
(ST 5/E/06-B5 0930-13)  
**Radulian Mircea**  
(ST1/E/61-A2 1400-09)  
(ST1/E/78-A2 1400-15)  
(ST1/E/79-A2 1400-10)  
**Radygin R. V.**  
(JWS33/E/06 -B2 1635-12)  
(JWS33/E/06-B2 1230)  
(JWS33/E/06-B3 0900-12)  
**Radziwill Nicole**  
(MC05/E/03-B4 1210)  
(MI06/E/11-B1 1400-02)  
(MI06/E/11-B2 1400-02)  
**Rady M. A.**  
(P09/E/06-A1 1110)  
**Rae Cho Gwang**  
(JSM01/W/110-A4 1620-03)  
**Rae J.**  
(GA3.07/W/59-A5 0900-15)  
**Rae I. J.**  
(GA3.04/W/27-B1 1520-04)  
**Raeder J.**  
(GA3.02/W/40-B3 1050)  
(GA3.08/W/05-A6 1040)  
(GA3.08/W/06-B1 0900-01)  
(GA3.08/W/21-A6 0900)  
**Raeder Joachim**  
(GA3.06/W/01-A2 1150)  
(GA3.10/W/16-A6 1515)  
**Raeesi M.**  
(JSS07/P/03-A2 1205)  
(ST2/E/17-A4 1000)  
(ST 5/E/03-B4 1400-01)  
(ST 5/E/04-B4 1440)  
**Raes Frank**  
(MI01/L/03-A1 1400)  
(MI01/W/01-A1 0900-06)  
(MI01/W/18-A1 1510)

**Raffalski Uwe**  
(MI02/W/06-A5 1010)  
**Raffi I.**  
(GA1.15/W/08-B4 1445)  
**Raga G. B.**  
(JSP21/C/U4/W/03-A4 0910)  
(JSP23/W/72/C/U4/W/03-A6 0830-18)  
**Ragnar Stefansson**  
(ST1/W/52-A2 1500)  
**Ragnarsson S.**  
(ST4/W/03-B3 1630)  
**Ragoulskaia M V**  
(JSA06/W/21-A1 1155-25)  
**Ragouskaia Maria**  
(JSA06/C/U4/E/02-A1 1155-62)  
**Rahmstorf Stefan**  
(MC01/W/38-A3 0930)  
**Rai S. S.**  
(ST2/E/24-A3 1700)  
(ST4/E/03-B2 0930-20)  
**Raileanu Victor**  
(JSS 44/E/08-B4 0930-21)  
**Raimondo J. C.**  
(G6/C/G3/E/43-B1 1100)  
(G3/E/27-A5 1610-02)  
**Raina K. S.**  
(GA2.02/W/28-B5 1000)  
**Rainer Singer**  
(JSA06/W/14-A1 1700)  
**Räisänen Jouni**  
(MC01/W/17-A4 1125)  
**Raizada Shikha**  
(GA 2.02/E/07-B4 0930-20)  
(GA2.02/E/05-B5 1120)  
**Raj P. E.**  
(MI04/P/01-B3 1220)  
(MI01/P/02-A31145)  
**Rajagopalan Balaji**  
(JSP25/E/23-B1 1440)  
(JSP25/W/09-B4 1110)  
**Rajaram G.**  
(GA3.03/E/03-B4 1400-01)  
**Rajaram Girija**  
(GA3.06/E/12-A3 1640)  
**Rajaram Mita**  
(JSA37/L/01-B3 1730)  
(JSS44/E/15-B4 0930-15)  
(JSS44/E/16-B4 0930-14)  
**Rajaram R**  
(JSM01/E/10-A2 1600-12)  
(JSM01/W/101-A5 1740)  
(JSA20/W/10-A5 1200-02)  
**Rajeev K**  
(MI01/E/07-A2 0930)  
**Rajendran C. P.**  
(ST2/E/55-A3 1745)  
**Rajendran Kusala**  
(ST2/E/55-A3 1745)  
**Rakhlin Leonid**  
(GA5.01/E/16 A1 1430)  
**Ram Avadh**  
(ST3/P/7-B4 1500)  
(ST4/P/01-B2 0930-10)  
(SW1/W/05-B5 0900)  
(ST1/P/09-A2 1400-19)  
(ST1/W/55-A2 1400-13)  
**Ramachandran S**  
(MC07/W/12-A2 1155)  
**Ramakrishna Rao D.**  
(MI06/W/25-B2 1130)  
**Raman A. V.**  
(PW1/P/01-A6 0940)  
**Raman Sethu**  
(MI07/W/05-A2 1140)  
(MI07/W/04-A2 1440)  
**Ramanathan V**  
(MI01/E/07-A2 0930)  
**Ramankutty Navin**  
(MC07/E/04-A2 1215)  
**Ramaprasad J**  
(MI09/L/07-A5 1145-16)  
**Ramaraju H K**  
(HS5/W/43-A3 1500)  
**Ramaswamy M**  
(MC07/W/01-A2 0930)  
**Ramaswamy V**  
(MC07/W/12-A2 1155)  
**Ramatschi Markus**  
(JSA09/E/04-A2 1200)  
**Rambabu H. V.**  
(JSA09/E/03-A3 1215)  
**Ramesh D. S.**  
(ST4/E/19-B2 0930-16)  
**Ramesh K. B.**  
(JSA20/E/12-A5 1400)

**Ramesh R**  
(HS5/W/26-A2 1545)  
(P07/E/03-A3 1430)  
**Ramirez Juan**  
(JSA16/E/17-A3 0830-05)  
**Ramis C**  
(MI07/W/02-A2 1210)  
(MI07/W/03-A2 1420)  
**Ramkumar T. K.**  
(JSA20/W/10-A5 1200-02)  
**Ramón Torres-Hernández J.**  
(GA1.05/W/16-A6 0900-07)  
**Ramonet M**  
(MC01/L/21-A5 1200)  
**Ramrath Antje**  
(GA1.05/E/15-A5 0900-01)  
(GA1.03/E/03-B2 1620)  
**Ramsingh Chandradath**  
(JSP23/C/U5/W/04-B2 0830-06)  
**Ranalli G.**  
(ST2/E/50-A5 1130)  
**Randall D. A.**  
(MI04/W/27-B1 0900-20)  
(MI10/W/21-B1 1620)  
**Randall David A**  
(MI08/L/02-A4 1220)  
**Randel W J**  
(JSM01/W/12-A2 1600-15)  
(JSM01/W/52-A4 0930)  
**Randel William J**  
(JSM01/W/14-A4 1620-12)  
(MI12/W/09-B4 0945)  
**Ranganna G**  
(HS5/W/43-A3 1500)  
**Rangarajan G K**  
(GA3.10/L/02-A6 1700-18)  
(GA5.06/E/06 A3 1600)  
**Rango Albert**  
(HS4/W/06-A4 1400)  
(JSM41/W/18-B5 1205)  
**Rangelov**  
(ST1/E/74-A4 0930-41)  
(ST1/E/74-A4 0930-42)  
**Rangelov B.**  
(ST3/E/05-B5 0930)  
(ST3/E/17-B5 0945)  
**Rankin Andrew M.**  
(JSM04/W/06-A2 1220)  
**Rankin R.**  
(GA3.04/L/03-B1 0940)  
(GA3.08/W/03-A6 1450)  
**Ranta Aarne**  
(GA2.01/W/01-A1 1150)  
**Ranvir Singh Dhillon**  
(GA2.02/W/31-B4 1400)  
**Rao C. K.**  
(GA1.02/E/06-A2 0930)  
**Rao D. Goapala**  
(ST4/E/31-B1 0830-06)  
**Rao D. R. K.**  
(GA2.02/E/14-B5 1040)  
(GA3.04/E/09-B2 1650)  
**Rao G V**  
(ST2/E/42-A3 1630)  
**Rao H. N. R.**  
(JSA20/E/12-A5 1400)  
**Rao J. V. S. V.**  
(JSA20/E/12-A5 1400)  
(JSA20/E/16-A5 1200-06)  
**Rao N. Purnachandra**  
(ST2/E/60-A3 1145)  
**Rao P. B.**  
(GA 2.02/E/01-B5 1400)  
(GA2.02/W/28-B5 1000)  
**Rao R. U. M**  
(ST4/E/38-B1 1400-02)  
(JSS44/E/09-B4 0950)  
(MC02/E/07-B1 1010)  
(ST2/E/42-A3 1630)  
**Rapalini Augusto E.**  
(GA1.04/L/07-A4 1500)  
(GA1.04/W/32-A4 1440)  
**Rapela Carlos W.**  
(GA1.04/W/32-A4 1440)  
**Rapoport V. O.**  
(GA3.04/W/28-B1 1520-22)  
**Raposo Maria Irene B**  
(GA1.04/E/17-A4 0930-01)  
(GA1.04/E/09-A4 0930-07)  
**Rapp M.**  
(JSM32/W/01-B2 1600)  
**Rasch Phil**  
(MW01/W/06-A5 1400)  
**Rash J. P. S.**  
(GA3.08/W/19-A6 1520)

- Rasheed K.**  
(P09/E/02-A2 0950)  
(P09/E/04-A1 1050)
- Raschke Erhard**  
(MI08/W/18-A4 1150)
- Rasinkangas R.**  
(GA3.02/E/05-B3 0900-21)  
(G3.04/W/18-B1 1520-26)
- Rasmussen O.**  
(GA1.07/W/07-B2 1220)
- Rasmussen Ole**  
(GA5.08/W/06-B1 0945)  
(GA3.10/W/18-A5 1155)  
(GA5.01/W/08-A1 1200)
- Raspopov Oleg**  
(JSA16/E/21-A3 0830-08)  
(JSA16/E/16-A3 0830-09)
- Rasson Jean L.**  
(GA5.01/E/23-A1 0900-08)  
(GA5.01/E/30-A1 1300-13)  
(JWA34/E/02-B2 1210)
- Rastogi R. G.**  
(GA2.02/E/09-B5 0940)  
(GA3.05/E/10-B3 0900-43)  
(GA4.08/E/08-B3 0900-12)  
(GA4.08/E/09-B3 0900-11)  
(GA6.02/E/08-B1 1505)  
(GA1.02/E/0A2 0930)  
(GA5.01/E/12-A1 0905)
- Rasulov D. K.**  
(GA1.01/E/08-A5 0900-13)  
(U3/E/04-A3 0900-03)  
(JSA40/E/06-B5 1400-18)
- Rasulov D. Kh.**  
(JSA27/E/08-B1 1400-07)  
(JSA37/E/07-B3 1745-02)
- Ratag Mezak A.**  
(JSA16/E/04-A3 0830-32)  
(JSA16/E/20-A3 0830-30)
- Ratcliff J. Todd**  
(JSA10/W/09-A3 1115)
- Rau Steffen**  
(GA1.01/E/03-A6 1215)
- Rauch E.**  
(JSP23/C/U5/W/13-A5 1440)
- Raudsepp Urmas**  
(P11/W/13-B3 1640)
- Raval U.**  
(JSV22/E/13-A5 1440)  
(ST2/E/27-A3 1615)  
(JSS44/E/42-B4 0930-32)  
(ST4/E/72-B2 0930-23)
- Ravat D.**  
(JSA37/W/06-B3 1645)  
(GA5.12/W/03-A2 1500)  
(GA5.12/E/07-A2 1520)
- Ravat Dhananjay**  
(GA5.11/W/02-A3 0910)  
(GA5.11/W/03-A3 1430-02)
- Ravegnani F**  
(JSM01/W/37-A5 1400)
- Raveo Poasa**  
(JSP23/E/37-A5 1010)
- Ravi Govindaraju**  
(MC01/W/06-A5 0830)
- Ravilly M.**  
(P16/E/03-B5 0930)
- Ravindran Sudha**  
(GA2.02/W/05-B5 0900)  
(GA2.02/W/20-B4 0930-16)
- Rawls Walter**  
(HW4/E/19-B2 1440)
- Ray E A**  
(JSM01/W/56-A4 1620-07)
- Ray Eric A.**  
(JSM26/W/05-B1 0920)
- Ray R. D.**  
(ST4/E/69-B2 0930-21)  
(JSP49/E/11-B5 1210-05)  
(JSG14/E/04-A3 1109-04)
- Rayan Ali**  
(JSS31/E/12-B3 0830-13)
- Raychaudhuri Probhas**  
(GA4.08/P/01-B3 0900-04)  
(JSA10/C/GA4.15/P/02-A2 1630)
- Raynaud Stephane**  
(U2/E/07-A21140)
- Rayner Peter**  
(MC01/L/20-A5 1115)  
(MC01/W/39-A5 1215)  
(MI06/E/07-B2 1400-10)
- Ré Guillermo H.**  
(GA1.04/W/33-A6 1540)
- Reading Anya M.**  
(ST2/W/37-A5 1400-35)
- Reason Chris J. C.**  
(JSP25/E/26-B5 1600)  
(JSP25/W/22-B1 1400)
- Reay Anthony**  
(JSV30/W/09-B1 1000)
- Rebetsky Jury**  
(JSS 44/E/27-B5 0910)
- Rebez A.**  
(JSP23/W/16-A6 1520)
- Rebez Alessandro**  
(ST3/W/29-B4 1700)
- Rebolledo-Vieyra M.**  
(GA1.05/W/07-A6 0900-06)
- Rebordão J. M.**  
(G4/P/01-A3 1620-22)
- Rebordo J. M.**  
(JSG28/E/08-B2 1400-09)
- Rebscher Dorothee**  
(JSV36/W/11-B3 1400-06)
- Réchou A.**  
(JSM32/W/03-B2 1435)
- Reddy**  
(GA2.03/E/09-B3 1700-07)
- Reddy B. M.**  
(GA2.02/W/23-B5 1640)
- Reddy G K**  
(ST2/E/42-A3 1630)
- Reddy R. V.**  
(GA3.06/E/10-A3 1000)  
(GA3.02/E/03-B3 0900-08)
- Reddy Remata S.**  
(MC05/W/03-B4 1030)
- Redler R.**  
(P08/W/07-A2 1400)
- Redler Rene**  
(JSP25/W/20-B4 1620)
- Redondo J. M.**  
(JSP39/W/39-B4 1620)
- Reed Duncan W.**  
(HS1/W/67-B5 1200)
- Reeder Michael J.**  
(MW07/E/04-A4 0900)
- Rees David**  
(GA3.06/E/06-A3 1430)  
(JSM01/E/47-A1 1000)  
(GA4.08/E/06-B4 1335)
- Reeves Claire**  
(U2/E/14-A2 1420)
- Reeves Colin**  
(GA 5.12/E/10-A2 1120)  
(JSV22/E/05-A5 1400)
- Reeves G. D.**  
(GA4.01/E/08-A2 1600)  
(GA3.02/W/13-B2 1630)  
(GA3.02/W/41-B2 1600)  
(GA3.05/W/25-B3 0900-33)  
(GA3.05/W/26-B3 1600)  
(GA3.05/W/30-B3 1100)
- Reeves Geoff**  
(GA3.05/W/19-B3 0900-26)
- Refson Keith**  
(ST6/E/10-A2 1700)
- Reichmann Edwin J.**  
(GA4.03/W/09-B4 1400)
- Reid**  
(JSA27/E/07-B1 0940)
- Reid I M**  
(JSM01/W/36-A1 1400)  
(MW04/W/04-A1 0900)
- Reid Ian**  
(JSS44/W/03-B4 1400)
- Reid S. J**  
(JSM01/W/37-A5 1400)
- Reid Stephen J.**  
(JSM26/W/13-B1 1420)  
(MI12/W/14-B5 1005)
- Reidar Jan**  
(G3/E/19-A5 1610-25)
- Reidar Løvlie**  
(GA1.15/W/05-B4 1730)
- Reigber C.**  
(G6/C/G3/E/43-B1 1100)
- Reigber C. H.**  
(G2/L/02-A2 0945)
- Reigber Ch.**  
(G3/E/27-A5 1610-02)  
(G3/W/39-A5 1100)  
(JSA37/W/05-B3 0945)
- Reigber Christoph**  
(JSG28/E/11-B1 1120)  
(JSS31/E/07-B2 1210)
- Reigber G. W.**  
(JSS31/W/12-B2 1420)
- Reilinger R**  
(JSS31/W/08-B2 1640)  
(JSS31/L/04-B2 0830-17)  
(JSS31/E/03-B2 1700)
- Reilinger Robert**  
(G5/E/23-A4 1230-08)
- Reimer E**  
(JSM01/W/37-A5 1400)
- Reinders Jan**  
(GA1.03/W/14-B3 1440)
- Reineman Richard C.**  
(G5/E/38-A4 1415-02)
- Reiner M. J.**  
(GA4.01/E/04-A2 1120)
- Reiner Rummel**  
(G4/W/11-A3 1145)
- Reinhart E**  
(G3/E/11-A5 1610-31)
- Reisner J. M.**  
(MI10/W/19-B3 1715)
- Relinger R.**  
(JSS31/E/13-B3 0830-14)
- Reme H.**  
(GA3.02/E/09-B2 1500)
- Remedios J J**  
(JSM01/W/08-A4 1450)  
(JSM01/W/12-A2 1600-15)
- Remedios John**  
(MC09/W/11-B2 1500)
- Remer L**  
(MI09/L/07-A5 1145-16)
- Remer Lorraine**  
(MI07/L/03-A2 1600)
- Remy Frederique**  
(JSH12/W/03-A5 0830)
- René Preusker**  
(MI01/W/05 1740)
- Renee Tatusko**  
(MI08/E/08-A4 1750)
- Renfrew I. A.**  
(JSM04/W/0-A2 1645)
- Renger W.**  
(MI06/W/26-B2 1110)  
(JSM26/W/16-B2 1210)
- Renja Alma**  
(JSA27/E/10-B1 1400-09)
- Renne Paul R.**  
(GA1.03/W/04-B1 1140)
- Renssen Hans**  
(JSA16/E/21-A3 0830-08)
- Renshaw Richard**  
(MI06/E/07-B2 1400-10)
- Rentsch Matthias**  
(G3/E/43-A5 1610-17)  
(G3/W/07-A5 1610-15)
- Renwick James**  
(MW06/E/03-A3 1120)
- Renwick James A.**  
(MI06/E/05-B1 1140)
- Renyova Svetlana**  
(MI12/E/01-B4 1610)
- Repnev Alexandr**  
(JSA45/E/09-B5 1010)
- Reshetnyak Maxim**  
(GA1.03/E/02-B3 1140)
- Reshetnyak Maxim**  
(GA1.01/W/27-A5 0900-04)  
(GA1.01/E/09-A5 0900-01)  
(GA1.01/W/26-A5 1015)
- Resovsky Joseph**  
(ST5/E/12-B5 1420)  
(JSS13/E/05-A4 1640)
- Retdcher Günther**  
(G1/E/20-A3 1620-26)  
(G1/E/53-A3 1620-78)
- Retterer John M.**  
(GA3.09/E/10-B5 1115)
- Reuter Andreas**  
(MI08/W/12-A3 1145)  
(MI08/W/18-A4 1150)
- Revell Michael**  
(JWM08/W/04-A2 1020)  
(MI05/E/13-A2 1650)  
(MI05/E/21-A2 1420)  
(MW06/E/03-A3 1120)  
(MW06/E/05-A3 1600)
- Revercomb H E**  
(MC08/L/01-A3 1045)
- Revitt Michael**  
(HS5/W/12-A2 0920)
- Rey Daniel**  
(GA1.05/W/23-A6 1230)  
(GA1.04/W/15-A6 1520)  
(GA1.15/W/03-B4 1530-06)
- Reyes M.**  
(JSV36/E/11-B3 0900-15)
- Reynir Bodvarsson**  
(ST1/W/52-A2 1500)
- Reynolds B**  
(HS3/W/03-A1 0950)
- Reynolds Curt**  
(HW4/E/19-B2 1440)
- Reynolds M. D.**  
(G6/C/G5/W/06-B1 0930)
- Reynolds R. J.**  
(JSA20/W/27-A4 1200-17)
- Rezhenov B. V**  
(GA3.08/W/31-A6 1150)
- Reznikov A E**  
(JSA06/W/25-A1 1155-25)
- Rhee Hwang-Jae**  
(JSA06/W/28-A1 1155-13)
- Rhee T. S.**  
(P15/L/17-B4 1550)
- Rhew Robert C.**  
(JSP21/L/02-A4 1440)
- Rhoades David**  
(ST1/W/28-A3 1400)
- Riad S.**  
(JSP23/C/U5/E/16-A5 1620)  
(ST3/E/56-B4 1400-20)
- Riazantseva M. O.**  
(GA3.09/W/23-B4 0900-02)  
(GA3.02/E/02-B3 0900-20)
- Ribe Neil**  
(ST4/E/64-B3 1710)
- Ribeiro Helena**  
(JSS31/E/09-B3 0830-11)
- Ribeiro Helena**  
(G1/E/59-A3 1620-29)
- Ribera d'Alcala' Maurizio**  
(P11/E/19-B4 1150)  
(P11/E/20-B4 1720)  
(P11/E/21-B4 1700)  
(P11/W/12-B4 1640)
- Ribes André**  
(JSA10/W/11-A2 1000)
- Ricard Yanick**  
(JSS02/W/16-A2 0930)  
(JSS13/W/18-A5 1420)  
(ST4/W/24-B1 0830-22)
- Riccardo Leoni**  
(JSV29/W/04-B1 1700)
- Rich F J**  
(GA3.10/W/03-A6 0950)  
(GA3.10/W/10-A6 1700-03)
- Rich Frederick**  
(GA3.09/W/25-B5 0910)
- Rich Frederick J.**  
(GA2.02/E/13-B4 1100)
- Richard Arculus J.**  
(JSV30/E/13-B1 1220)
- Richard Eugene D**  
(GA1.01/W/12-A5 0900-14)
- Richard I**  
(JSM18/W/15-A4 1140)
- Richard Luckett**  
(JSV47/E/05-B5 0845)
- Richard Peter Rayer**  
(MI06/E/07-B1 1400-09)
- Richard R. L**  
(GA4.10/E/04-A5 1420)
- Richards K. J.**  
(P 14/E/09-A4 1400-11)
- Richards P. G.**  
(GA3.05/W/03-B3 0900-10)
- Richards Paul L**  
(HS3/W/28-A2 1515)
- Richardson J. D.**  
(GA3.07/W/11-A4 0930)  
(JSA06/W/01-A1 1500)  
(GA4.10/W/35-A5 1215)  
(GA4.04/W/15-B5 1450)
- Richer Hannah**  
(U2/E/14-A2 1420)
- Richmond A.**  
(JSA20/P/01-A5 1501)
- Richmond A. D.**  
(JSA20/W/40-A6 0948)
- Richmond Arthur D.**  
(GA3.06/W/05-A3 1100)  
(JSA37/W/07-B3 1600)
- Richmond D.**  
(GA3.09/W/04-B5 1035)
- Richter B**  
(G3/E/11-A5 1610-31)  
(JSG14/W/16-A3 1203-22)
- Richter Bernd**  
(G2/L/03-A2 1000)  
(G3/E/42-A5 1520)

# INDEX

- G3/E/42-A5 1520)  
(G5/E/37-A4 1415-01)  
(G5/E/38-A4 1415-02)  
(JSG14/E/21-A3 1700-18)
- Rico J.**  
(GA5.12/E/04 A2 0930)
- Riddick John C.**  
(GA5.01/E/03 A1 0935)
- Ridgway Ken**  
(JSM41/W/14-B4 1500)
- Ridley A.**  
(JSA20/W/40-A6 0948)
- Ridley A. J.**  
(GA3.03/W/13-B4 1430)
- Ridley Aaron**  
(GA3.08/W/12-B1 0930)  
(GA3.07/W/30-A6 0930)  
(GA3.10/W/08-A6 1700-06)
- Rieger E.**  
(GA4.02/E/10-A4 1400-03)
- Riemann U**  
(HS5/W/07-A1 1630)
- Rienecker Michele**  
(JSP25/W/60-B1 0950)
- Rientjes T.**  
(HW4/E/W/03-B2 1730)
- Riepl-Thomas Judith**  
(ST3/W/20-B3 0945)
- Ries J. C.**  
(G6/C/G3/W/32-B1 1120)
- Ries John C**  
(JSG11/W/19-A3 1130)
- Riese M**  
(JSM01/W/41-A4 1150)
- Riese Martin**  
(MW 07/E/03-A4 1400)  
(MW04/E/02-A1 1010)
- Rietveld M.**  
(GA2.01/W/07-A1 1055)  
(JSA20/W/08-A4 1200-27)
- Rietveld Michael**  
(GA2.03/E/04-B3 1220)
- Riggin D**  
(JSM01/W/36-A1 1400)  
(JSM01/W/67-A1 1110)  
(MW04/W/04-A1 0900)  
(JSM01/E/05-A1 1210)
- Riggin Dennis**  
(JSM01/W/62-A2 1110)  
(MW04/W/11-A1 0925)
- Riggin Dennis M**  
(JSM01/C/MW07/W/23-A2 1600-33)
- Rigi M G**  
(HS5/W/51-A3 1630-02)
- Rigor I.**  
(P07/L/02-A3 1125)
- Rigozo Nivaor Rodolfo**  
(JSA16/W/07A3 0830-34)
- Riguzzi Federica**  
(G5/W/20-A4 1230-03)
- Riis F.**  
(ST2/E/43-A5 1400-31)
- Rijnbeek R. P.**  
(GA3.02/E/17-B3 0900-18)
- Rijsberman Michiel**  
(HS5/W/22-A2 1425)
- Rikiishi Kunio**  
(JSA15/E/40-A3 1700)
- Riley C.**  
(VS2/W/25-B3 1400-28)
- Riley C. M.**  
(VS2/W/10-B3 1400-07)
- Riley Pete**  
(GA3.09/W/27-B4 1035)
- Riley S J**  
(HS5/W/19-A2 1200)
- Riley T. R.**  
(JSV30/L/01-B1 1400-15)
- Riley Teal**  
(JSV22/W/05-A5 1630)
- Rim Hyung-Jin**  
(G2/W/10-A2 1445)
- Rinaldi Carlos**  
(GA1.04/L/05-A6 1500)
- Rind D**  
(MI02/W/09-A4 1220)
- Rind David**  
(MW08/W/01-A2 1530)  
(MW08/W/06-A2 1730)
- Ringdal Frode**  
(U8/W/04-B3 1450)  
(U8/W/16-B3 1640-12)
- Ringer Mark**  
(MI06/E/15-B2 1730)
- Rinke Annette**  
(JSP25/W/38-B4 0930-04)  
(MC01/E/03-A4 1445)
- Rintoul Stephen**  
(P12/W/09-A1 1700)  
(P12/W/22-A1 0910)
- Rios Victor H.**  
(JSA20/W/45-A4 1200-32)  
(G1/W/27-A3 1620-11)  
(GA2.02/W/21-B4 930-13 )
- Rippeth T. P.**  
(P10/E/04-A5 1600-07)  
(P10/E/05-A4 1600)  
(P10/L/05-A4 1150)
- Rippeth Tom P.**  
(JSP49/W/17-B5 1210-07)
- Risad Samir**  
(JSP23/E/45-A5 0830-15)
- Risbo T.**  
(GA5.08/E/03-B1 0900)
- Rise M.**  
(JSM26/W/01-B3 1210)
- Rishbeth Henry**  
(GA2.03/E/08-B3 0930)  
(GA4.08/E/01-B3 1645)
- Risk G. F.**  
(GA1.02/W/11-A2 0930)
- Rison W**  
(MI03/W/05-A3 1140)
- Rison William**  
(JSM03/W/02-A1 1650)  
(MI03/W/01-A3 1520)
- Ritchie Jerry C.**  
(JSM41/W/18-B5 1205)
- Ritchie L. J.**  
(VS2/W/12-B3 1400-09)
- Ritschel Bernd**  
(JWS33/E/02-B2 1635-23)  
(JWS33/E/02-B3 0900-23)
- Ritsemma J.**  
(ST4/W/30-B2 1400)  
(JSS02/C/ST6/W/01-A1 1515)
- Ritter O.**  
(GA1.02/E/16-A2 0930)  
(GA1.02/W/06-A2 0930)
- Ritter P.**  
(GA1.02/W/06-A2 0930)
- Ritzwoller M.**  
(U8/E/09-B3 1155)
- Ritzwoller Michael**  
(ST5/E/12-B5 1420)  
(JSA09/E/05-A3 0900)  
(JSS13/E/05-A4 1640)
- Rius A.**  
(JSG28/E/20-B1 1400-16)  
(JSS31/E/13-B3 0830-14)
- Rius Antonio**  
(G1/E/16-A3 1620-24)
- Rivett Michael**  
(HS5/W/36-A3 1105)
- Rivin Yu. R.**  
(GA4.03/W/01-B4 1720-01)
- Rizikova Snezina**  
(ST1/W/72-A3 0900-20)  
(ST1/W/72-A4 0930-32)
- Rizos Chris**  
(G1/L/08-A3 1620-86)  
(G1/L/22-A3 1640-95)  
(G1/L/23-A3 1010)  
(G1/W/07-A3 1620-04)  
(G1/W/08-A3 1620-35)  
(JSG11/W/23-A4 1210)  
(G6/C/G1/L/24-B1 1520)
- Rizzoli Paola Malanotte**  
(P11/L/01-B5 0830)
- Roadnight Carol**  
(MW07/W/08-A4 0920)
- Roads John**  
(MC01/W/44-A4 1110)  
(JSM24/W/05-B2 1135)  
(JSP25/W/04-B3 1110)  
(MW02/W/03-B3 1200)
- Rob Wim**  
(JSS13/W/01-A4 1720)
- Robert Mueller**  
(JSA15/E/38-A4 1400-03)
- Robert Stopar**  
(JWS33/E/12-B3 0900-30)
- Robert Weisberg**  
(JSP23/W/01-B2 1500)
- Roberts Andrew P.**  
(GA1.05/E/01-A6 0910)
- Roberts Brian**  
(JSA27/E/09-B1 1110)
- Roberts Clive**  
(JSV36/C/U6/E/04-B3 1400-24)
- (JSV36/E/01-B3 1610)
- Roberts Craig**  
(G6/C/G1/L/24-B1 1520)
- Roberts David L**  
(MI01/E/04-A1 1130)  
(MI01/E/14-A2 1400)
- Roberts F. P.**  
(MC05/E/01-B4 0910)
- Roberts Gethin**  
(G6/C/G1/E/55-B2 1700)  
(G1/E/42-A3 1620-72)
- Roberts Nigel M.**  
(MI05/E/20-A3 1700)  
(MI05/E/08-A3 1600)  
(MI05/E/02-A3 1620)
- Roberts Paul**  
(GA1.01/W/34-A5 1000)  
(GA6.01/W/04-A6 0850)  
(JSS02/W/07-A1 1215)  
(JSP39/W/37-B2 1400)
- Roberts Peter**  
(JSS46/W/10-B4 1600)
- Robertson D. M.**  
(HW3/W/03-B4 1005)
- Robertson Douglas**  
(G3/L/14-A5 1610-58)
- Robertson Franklin**  
(MC08/W/05-A30945)  
(JSM24/W/05-B2 1135)  
(JSP25/W/04-B3 1110)
- Robertson Franklin R.**  
(MW02/W/03-B3 1200)
- Robertson Stacey D.**  
(JSA09/W/15-A3 0830)
- Robinson Allan R.**  
(JSP39/W/18-B4 0830)
- Robinson David**  
(MC02/E/18-B2 1150)
- Robinson H. B.**  
(U3/W/08-A30900-13)
- Robinson Ian S.**  
(JSM41/L/03-B4 1040)
- Robinson Luke M**  
(MC07/E/05-A2 1135)
- Robinson T. R.**  
(GA2.02/L/8-B4 1440)
- Robinson Terry**  
(JSA45/W/16-B5 0950)  
(JSA20/W/29-A4 1200-13)
- Roble R. G.**  
(JSA20/P/01-A5 1501)  
(JSA20/W/40-A6 0948)
- Roble Raymond**  
(JSA16/E/12-A3 0830-14)
- Roble Raymond G.**  
(JSM01/W/31-A3 0900)
- Robock Alan**  
(MC01/W/19-A1 1715)  
(MC01/W/29-A3 1205)  
(MW01/L/01 1430)  
(JSM24/W/06-B1 1105)  
(MC02/E/18-B2 1150)
- Robunson Allan**  
(P12/W/17-A1 1720)
- Roca A.**  
(ST3/E/41-B5 1000)  
(ST5/E/34-B3 0830)
- Rocca M. La**  
(JSV47/W/01-B5 1045)
- Rocchi V.**  
(JSV29/W/01-B1 1620)  
(JSV36/E/21-B3 1400-11)
- Rochette Pierre**  
(GA1.03/E/07-B1 1120)  
(GA1.04/E/02-A6 0920)  
(JSV22/E/02-A5 1130)  
(MI03/E/01-A3 1200)
- Rock Donald R.**  
(GA2.02/E/10-B5 1700)
- Rockel Burkhard**  
(MC01/W/47-A4 1005)
- Rockel Burkhardt**  
(JSM24/W/01-B1 1400)
- Rocken Chris**  
(JSG28/W/20-B2 1400-07)
- Rocken Christian**  
(JSG28/E/12-B2 1200)  
(JSG28/W/25-B2 1400-11)  
(JSM26/E/09-B1 1400)  
(JSG28/W/27-B2 1110)  
(G2/L/06-A2 1115)  
(JSM01/E/03-A2 1430)  
(MC08/W/02-A4 1005)
- Rodda Harvey J. E.**  
(HS3/W/10-A1 1425)
- Rodda John C.**  
(U7/P/01-B1 1110)
- Roderic Jones**  
(JSM01/W/97 1610)
- Rodger A.**  
(JSM41/W/36-B4 1110)
- Rodger A. S.**  
(GA3.03/W/08-B4 1700)  
(GA3.07/E/20-A6 0900-17)
- Rodger Craig J.**  
(JSA15/W/17-A4 1100)
- Rodgers C. D.**  
(MI06/W/11-B1 1400-03)  
(MI06/W/11-B2 1400-03)
- Rodgers D J**  
(JSA06/E/11-A1 0835)
- Rodgers Keith**  
(JSP25/W/11-B1 1640)
- Rodgers W.**  
(MC09/W/04-B2 1030)
- Rodhe Johan**  
(P11/W/26-B5 1150-10)
- Rodionov Yu. I.**  
(JWS33/E/06 -B2 1635-12)  
(JWS33/E/06-B2 1230)  
(JWS33/E/06-B3 0900-12)
- Rodkin M. V.**  
(JWS33/W/04-B2 1635-24)  
(JWS33/W/04-B3 0900-24)  
(JSP23/E/47-A6 0830-12)  
(JSP23/E/48-A5 0830-09)  
(ST1/E/23-A2 1400-33)
- Rodnikov A. G.**  
(JSV22/P/01-A5 1650)  
(JWS33/W/04-B2 1635-24)  
(JWS33/W/04-B3 0900-24)
- Rodolfi Giuliano**  
(HS4/W/08-A4 1450)
- Rodriguez Jose**  
(JSP21/W/05-A4 1520)
- Rodriguez L B**  
(HW5/W/14-A3 1400)
- Rodriguez Lizzette**  
(JSV36/E/13-B3 1445)
- Rodriguez Maria E.**  
(GA1.03/W/12-B2 1520)
- Rodriguez Paqui**  
(JSV36/W/16-B3 0900-10)
- Rodriguez R.**  
(JSA20/W/48-A4 1200-31)
- Rodriguez Rubén**  
(G3/E/39-A5 1610-93)
- Rodriguez-Caderot Gracia**  
(G3/W/25-A5 1610-81)  
(G5/W/19-A4 1230-02)
- Rodwell Mark**  
(JSP25/E/10-B4 1600)  
(MC10/E/01-B1 0950)
- Roe H. S.**  
(P11/W/19-B4 1500)
- Roeker S. W.**  
(JSS07/W/04-A2 0930-01)
- Roeckner E.**  
(JSP25/E/27-B2 0930)  
(MC02/W/01-B2 1100)
- Roekner Erich**  
(MW02/W/04-B3 0910)
- Roeder Helmut**  
(VS2/W/01-B3 1400-01)
- Roeder J. L.**  
(GA3.05/W/13-B3 0900-34)  
(GA3.02/W/13-B2 1630)  
(GA3.03/W/03-B4 0930)  
(GA3.05/W/25-B3 0900-33)  
(GA3.05/W/26-B3 1600)  
(GA3.05/W/28-B3 0830)  
(GA3.05/W/38-B3 1700)  
(GA4.08/W/18-B4 0830)  
(GA3.05/W/04-B3 0900-45)
- Roelandt Caroline**  
(MC11/E/02-B3 1540)
- Roelof E. C.**  
(GA3.02/L/02-B3 0900-24)
- Roemer Alexander**  
(JSA19/W/12-A4 1000)
- Roemmich Dean**  
(U7/E/06-B1 1450)
- Roerink G.**  
(JSM41/E/03-B5 1105)  
(U7/E/01-B1 1135)
- Roesler F. L.**  
(JSA20/W/27-A4 1200-17)
- Roether Wolfgang**  
(P11/W/24-B4 1130)
- Roettger Juergen**



- (GA2.01/E/09-A1 1540)  
**Roettger Jurgen**  
 (U7/E/07-B1 1045)  
**Roff Dr. Gregory**  
 (JSM01/W/28-A1 1640)  
**Roff G**  
 (MW01/W/12-A5 1150-01)  
**Rogel Philippe**  
 (MW06/E/07-A3 1000)  
**Roger Daniel Jean**  
 (JSA16/W/07-A3 0830-34)  
**Roger E**  
 (MC01/L/18-A4 1715)  
 (U3/W/14-A3 0900-15)  
**Rogers David**  
 (JSP39/W/27-B3 0950)  
**Rogers Eric**  
 (MC04/E/04-B2 1625)  
**Rogers H**  
 (JSM18/W/15-A4 1140)  
**Rogério Silvio**  
 (G5/E/07-A4 1554-08)  
 (G5/E/08-A4 1556-09)  
**Rogers Neil**  
 (JSA27/E/02-B1 1150)  
**Roget Elena**  
 (JSP39/W/38-B4 1150)  
**Rognvaldsson Sigurdur Th**  
 (ST5/W/13-B3 1640)  
**Rogowski Jerzy B.**  
 (G1/E/26-A3 1620-60)  
**Rogozhin Evgeny**  
 (ST2/W/16-A 0930)  
**Rogozhin Ye. A.**  
 (JSS07/W/04-A2 0930-01)  
**Rohling Eelco J.**  
 (P07/W/11-A3 1225)  
 (P07/E/01-A3 1400)  
**Rohini T**  
 (PW1/P/01-A6 0940)  
**Rojas Maisa**  
 (JSM01/W/07-A1 1430)  
**Rokityansky Igor I.**  
 (JSA15/E/23-A4 1400-11)  
 (JSA15/E/24-A4 1400-12)  
**Rollason Rosemary**  
 (JSM01/W/44-A3 1730)  
**Roman Anatol**  
 (ST3/E/45-B4 1745)  
**Roman Daniel R.**  
 (JSA09/E/11-A3 1000)  
**Romanelli Fabio**  
 (JSS42/W/18-B4 1620)  
 (ST3/W/07-B3 0845)  
 (ST3/W/12-B5 1430)  
**Romanjuk Oleg**  
 (GA1.02/E/40-A1 1050)  
**Romanov Peter**  
 (JSM41/E/07-B4 1705)  
 (JSM41/E/30-B5 1400)  
**Romanov S**  
 (GA4.09/W/04-A5 1600-02)  
**Romanov V**  
 (GA4.09/W/04-A5 1600-02)  
**Romanova N. Y.**  
 (GA1.03/W/34-B3 1100)  
**Romanovsky**  
 (GA2.03/L/04-B3 1720)  
**Romanovsky Yury**  
 (U8/W/02-B3 1030)  
 (JSA06/L/05-A2 1030)  
**Romanowicz Barbara**  
 (JSS02/W/11-A1 1700)  
 (JSS13/W/16-A4 1540)  
 (JWA34/W/06-B2 1010)  
 (ST4/W/08-B3 1120)  
 (U7/W/10-B1 1610)  
**Romanyuk Tanya**  
 (JSA40/E/08-B5 1005)  
 (JSS 44/E/27-B5 0910)  
**Romashets E**  
 (GA4.02/E/05-A4 1400-07)  
 (GA4.01/E/06-A21400-05)  
 (GA4.01/E/05-A2 0950)  
**Romashets E. P.**  
 (GA4.08/E/02-B3 0900-09)  
**Romashkin P A**  
 (JSM01/W/56-A4 1620-07)  
**Romashkova Leontina**  
 (ST1/W/34-A3 0900-06)  
 (ST1/W/54-A2 1700)  
**Romeo G.**  
 (JSA45/E/17-B5 1110-01)  
**Romeo Gianni**  
 (JVS36/E/22-B3 0900-16)
- Romero R**  
 (MI07/W/02-A2 1210)  
 (MI07/W/03-A2 1420)  
**Romick G. J.**  
 (GA3.06/W/10-A3 1620)  
 (JSM32/W/07-B3 1100)  
**Romick Gerald J.**  
 (JSA20/W/49-A6 0930)  
**Romushkevich Raissa**  
 (ST6/E/03-A1 0830-14)  
 (ST4/E/14-B1 0920)  
**Ronghui Lin**  
 (JSP23/C/U5/E/07-A6 0830-02)  
 (JSP23/C/U5/E/09-A6 0830-01)  
**Rongo R.**  
 (JSP23/E/57-B1 0830-09)  
**Rongshan Fu**  
 (JSS44/W/06-B5 1130)  
**Rongsheng Zeng**  
 (ST2/E/35-A3 1500)  
**Ronkko A**  
 (JSA06/W/21-A1 1155-24)  
**Ronkin Yuri L.**  
 (JVS22/W/03-A5 0900-01)  
**Rood R. B.**  
 (JSM26/E/22-B1 1210)  
**Rood Richard**  
 (JSM26/W/36-B1 1710)  
**Rood Richard B**  
 (MW01/W/01-A5 1105)  
**Rööm Rein**  
 (JSM01/C/MW07/W/11-A2 1600-30)  
**Rooney Gabriel**  
 (JSM24/E/03-B1 1125)  
**Roos-Serote M.**  
 (MC09/W/10-B2 1515)  
**Roper R G**  
 (JSM01/E/26-A2 1020)  
**Rosa B.**  
 (JSS46/E/07-B4 0930-04)  
**Rosa Maria L.**  
 (JSS44/W/05-B4 0930-02)  
**Rosa Robert**  
 (JSS31/L/02-B2 1520)  
**Rosalia Iris**  
 (GA6.02/W/06-B1 1715)  
**Rosanov N. I.**  
 (JSA15/W/01-A5 0830-07)  
**Rosanova Juliya B.**  
 (GA1.05/W/10-A6 0900-08)  
**Rosario Arlindo**  
 (JSP23/E/23-B2 0830-09)  
 (JSP23/E/27-B2 0830-14)  
**Rosas I.**  
 (JSP21/C/U4/W/03-A4 0910)  
 (JSP23/W/72/C/U4/W/03-A6 0830-18)  
**Roscoe H. K.**  
 (JSM04/E/04-A2 1240)  
**Roscoe Howard**  
 (JSM01/E/27-A5 1150)  
 (JSP23/E/07-A6 0830-11)  
**Rose Bill I.**  
 (VS2/W/05-B3 1400-04)  
**Rose Fred G.**  
 (M106/E/09-B1 1400-13)  
 (M106/E/09-B2 1400-13)  
**Rose W. I.**  
 (U7/W/06-B1 1635)  
 (VS2/W/10-B3 1400-07)  
 (U4/W/05-A41215)  
 (JSP23/C/U4/W/05-A6 0830-19)  
**Roseand Bill I.**  
 (MI01/C/JVS36/E/06-A1 0900-14)  
**Rosen O. M.**  
 (JSS44/E/32-B4 1740)  
**Rosen P.**  
 (JVS36/W/23-B3 1515)  
**Rosen Richard D**  
 (MC01/E/06-A2 1015)  
 (JSG14/E/12-A3 0900)  
**Rosenberg T. J.**  
 (GA2.01/W/05-A1 1705)  
 (GA2.01/W/03-A1 0925)  
**Rosenberg Ted**  
 (JSA09/W/10-A3 1115)  
**Rosenbloom N A**  
 (MC01/E/20-A5 1405)  
**Rosenfeld Daniel**  
 (MI09/W/04-A5 0954)  
 (MI09/W/12-A5 1145-14)  
 (MI04/C/MI06/W/10-B3 1150)  
 (MI06/W/04-B1 1710)  
**Rosenlof Karen H.**  
 (JSM26/W/05-B1 0920)  
 (JSM01/W/34-A3 1750)
- Rosi Mauro**  
 (JSV29/E/01-B1 1720)  
 (JSV29/W/04-B1 1700)  
**Rosier Suzanne**  
 (MW01/E/01-A5 1620)  
**Rosier Suzanne M.**  
 (MI12/W/05-B4 1115)  
**Rosner R.**  
 (MC09/W/04-B2 1030)  
**Rossa A M**  
 (MI05/E/24-A1 1650)  
**Rossi S.**  
 (MI12/W/11-B5 0945)  
**Rosso Renzo**  
 (HW4/W/04-B2 0900-07)  
**Rossov William B.**  
 (MI06/W/19-B2 1230)  
 (MW02/E/08-B3 0840)  
**Rostoker G.**  
 (GA4.08/W/12-B4 1635)  
**Rostoker Gordon**  
 (GA3.02/W/52-B2 1705)  
 (GA6.01/W/08-A5 0835)  
 (JSP23/C/U5/W/18-B1 0830)  
**Rotanova N**  
 (GA5.12/W/07 A2 1200)  
 (GA5.08/W/04-B1 1400-03)  
 (GA5.08/W/11-B1 1400-04)  
**Rotanova Nina**  
 (JSA15/W/21-A5 1400-05)  
**Roth Frank**  
 (JSP23/W/80-B1 1400)  
**Roth Ilan**  
 (GA3.05/W/15-B3 0900-27)  
**Rothacher Markus**  
 (G6/C/G1/E/32-B1 1400)  
 (JSG28/E/24-B2 1010)  
 (G1/E/58-A3 1500)  
 (JSG14/E/03-A3 1103-02)  
**Rother M.**  
 (JSA37/W/03-B3 1630)  
**Rothery David**  
 (JSP23/E/18-B2 0930)  
**Rothkaehl H.**  
 (GA3.07/W/33-A5 0900-16)  
 (GA2.07/W/24-A2 0930-07)  
**Rotondi Renata**  
 (ST3/E/53-B4 1230)  
**Rottman Gary**  
 (JSA16/E/06-A3 1030)  
 (JSA16/E/22-A3 0830-16)  
 (JSA16/E/12-A3 0830-14)  
**Rottman Gary J.**  
 (JSA45/E/03-B5 1110-11)  
**Rotwain Irina**  
 (ST1/W/43-A2 1440)  
 (ST1/W/54-A2 1700)  
 (ST2/W/12-A5 0830)  
 (ST1/W/71-A4 0930-29)  
**Rouland D**  
 (ST5/E/02-B3 1400)  
**Rouleau Pierre**  
 (JSA40/E/07-B5 0950)  
 (ST5/E/29-B4 1030)  
**Roult Genevieve**  
 (ST5/W/63/B3 0900-11)  
 (JWA34/W/06-B2 1010)  
 (JWS33/W/22-B2 1635-01)  
 (JWS33/W/22-B3 0900-01)  
 (ST5/W/33-B3 0900-07)  
 (ST5/W/57-B5 1400-01)  
 (U7/W/01-B1 0830-14)  
**Rountree M. W.**  
 (HW2/W/07-B1 1430)  
**Roussignol M.**  
 (GA1.02/E/38-A1 1605)  
**Routh P. S.**  
 (ST4/W/33-B1 0830-29)  
**Routhier Michael**  
 (HW1/L/11-A4 1430)  
**Rouvier H.**  
 (GA1.04/L/04-A6 0900)  
 (GA1.04/W/10-A6 0940)  
**Roux A.**  
 (GA4.10/W/26-A5 1035)  
 (GA4.10/W/34 1620)  
**Rovira L M G**  
 (GA4.02/E/03-A4. 1400-01)  
**Rovira M**  
 (GA4.02/E/09-A4 1400-04)  
 (GA4.02/E/08-A4 1400-05)  
 (GA4.02/E/10-A4 1400-03)  
**Rowe Charlotte**  
 (ST5/W/04-B5 1145)  
**Rowe Lindsay**
- (HS4/W/01-A4 0945)  
**Rowell David**  
 (JSP25/E/10-B4 1600)  
**Rowland H L**  
 (JSM03/W/03-A1 1420)  
**Rowlands Dave**  
 (G1/W/10-A3 1620-37)  
**Rowlands David D.**  
 (G3/E/05-A5 1200)  
**Rowlands G.**  
 (GA3.02/W/08-B3 0900-06)  
 (GA3.02/W/37-B3 1150)  
**Rowley Clark**  
 (MC05/W/01-B4 1150)  
**Roy A.**  
 (ST4/E/20-B1 0830-26)  
**Roy K. K**  
 (ST4/W/33-B1 0830-29)  
 (ST4/W/32-B1 0830-30)  
 (GA1.02/W/32-A2 0930)  
 (GA1.02/W/34-A1 1050)  
**Roy M.**  
 (GA3.08/E/07-B1 1740)  
**Roy Somnath Baidya**  
 (JSM43/W/11-B4 1700)  
**Roy Sudipa**  
 (JSP23/W/99-B2 0830-03)  
**Roy Sukanta**  
 (JSS44/E/09-B4 0950)  
 (ST4/E/38-B1 1400-02)  
**Royer A**  
 (MI01/L/04 1055)  
**Royer Thomas C.**  
 (JSP25/W/39-B1 1500)  
**Royle J A**  
 (MC01/E/20-A5 1405)  
**Rozanov Eugene**  
 (MI06/E/13-B1 1100)  
**Rozanov Evgeny**  
 (JSP21/W/14-A5 1210)  
**Rozelot Jean**  
 (JSA16/W/41-A3 0830-26)  
**Rozluski Cezary**  
 (JSA15/W/04-A5 0830-11)  
**Ru Rong**  
 (JSM26/E/11-B3 0930)  
**Ruban V. F.**  
 (ST1/W/39-A3 1150)  
**Ruban Vladimir F.**  
 (GA3.04/W/37-B1 1520-30)  
**Rubie D. C**  
 (JSS02/W/18-A1 1640)  
**Rubie Dave C.**  
 (JSS07/E/05-A2 1540)  
**Rubino Angelo**  
 (P12/W/19-A1 1030-08)  
 (P14/W/07-A4 1400-10)  
 (P14/W/14-A4 1140)  
 (P14/W/06-A4 1400-09)  
**Rubio Belen**  
 (GA1.05/W/23-A6 1230)  
**Rucol Vladimir**  
 (JWA34/E/01-B2 1740)  
**Rudajev V.**  
 (ST1/E/47-A2 1400-35)  
**Rudakov Vladimir**  
 (JSM26/W/16-B2 1210)  
**Rudder Anne De**  
 (MW01/W/02-A5 1150-04)  
**Rudels Bert**  
 (P13/W/17-B1 0950)  
**Rudenko Sergei**  
 (G2/E/35-A2 1630-16)  
**Ruderman M. S.**  
 (GA3.04/W/40-B1 1520-34)  
**Rudolf Bruno**  
 (MW02/W/08-B3 1420)  
 (JWM08/E/0-A2 1400)  
**Rudolph J.**  
 (JSP21/W/06-A5 1050)  
**Rudolph Stephan**  
 (G4/E/17-A3 1620-13)  
 (JSA37/E/04-B3 1015)  
 (JSA37/E/05-B3 1130)  
**Rudower Chaussee**  
 (GA5.01/P/02 1230)  
**Rudzka Elzbieta**  
 (HS3/W/02-A1 0925)  
**Rueda Juan**  
 (ST2/E/36-A4 1615)  
**Ruediger Klaus Paolo**  
 (JSG11/E/06-A4 1400-03)  
**Ruedilsabelle**  
 (JSA16/W/06-A3 0830-48)  
**Rüeger Jean M.**

# INDEX

- (G5/P/02-A4 1130-02)  
**Ruess Diethard**  
 (G3/E/22-A5 1610-32)  
 (G5/E/11-A4 1230-09)  
**Ruester R.**  
 (GA2.02/E/06-B4 1420)  
**Ruethi Max**  
 (HW5/W/14-A3 1440)  
**Ruffini G.**  
 (JSG28/E/20-B1 1400-16)  
**Rui Hualan**  
 (JSW33/W/32-B2 1635-25)  
 (JSW33/W/32-B3 0900-25)  
**Rui Wang**  
 (G3/E/32-A5 1610-53)  
 (G4/W/07-A3 1620-12)  
**Ruifeng Liu**  
 (ST4/E/11-B4 1400-07)  
**Ruiyuan Liu**  
 (GA2.01/E/01-A1 1110)  
 (GA3.06/W/08-A3 1210)  
**Ruiz A. M.**  
 (G5/W/19-A4 1230-02)  
**Ruiz Andres G.**  
 (JSP23/C/U5/E/05-A6 0830-06)  
**Ruiz Carlos V.**  
 (GA1.04/W/15-A6 1520)  
**Ruiz Joaquin**  
 (JSV30/L/03-B1 1140)  
**Ruiz Mario**  
 (JSV47/W/05-B5 1400-15)  
**Ruiz Mario C.**  
 (JSP23/C/U5/E/05-A6 0830-06)  
**Ruiz Mario M.**  
 (G5/W/19-A4 1230-02)  
**Ruiz-Martinez Vicente Carlos**  
 (GA1.15/W/03-B4 1530-06)  
**Rummel R.**  
 (G2/W/08-A2 1630-22)  
**Rummel Reiner**  
 (G2/L/01-A2 0930)  
 (JSA37/E/01-B3 0915)  
 (U7/E/08-B1 0925)  
**Rummukainen M.**  
 (JSM01/W/37-A5 1400)  
**Rummukainen Markku**  
 (MC01/W/17-A4 1125)  
 (MI04/W/10-B1 1200)  
**Rundkvist Dmitry**  
 (ST2/W/12-A5 0830)  
**Rundle J. B.**  
 (ST1/W/26-A3 1210)  
 (JSV36/W/21-B3 1400-01)  
 (JSV36/E/15-B3 1655)  
**Rundle John B.**  
 (ST1/E/59-A1 1230)  
**Ruohoniemi J. M.**  
 (GA2.03/W/01-B3 0950)  
 (GA3.02/W/62-B2 1420)  
**Ruohoniemi J Michael**  
 (GA3.10/W/06-A6 1210)  
 (GA2.07/W/29-A1 1650)  
**Ruomei Sun**  
 (ST1/W/31-A4 0930-35)  
**Rupolo Volfango**  
 (P11/L/03-B5 0910)  
**Russell L M**  
 (MI09/W/14-A5 1030)  
**Russell C. T.**  
 (GA3.07/W/74-A5 0900-17)  
 (GA4.09/W/04-A5 1600-02)  
 (JSA10/W/02-A3 1045)  
 (MI03/W/09-A3 1640)  
 (GA4.01/W/11-A2 1100)  
 (GA4.10/W/08-A5 1020)  
 (GA3.03/W/11-B4 1200)  
 (GA3.04/L/17-B2 1710)  
 (GA3.04/W/07-B2 1510)  
 (GA3.04/W/12-B1 1520-24)  
 (GA3.04/W/20-B1 1100)  
 (GA3.04/W/36-B1 1430)  
 (GA3.08/W/05-A6 1040)  
 (GA3.08/W/09-A6 0920)  
 (GA3.08/W/13-A6 0940)  
 (GA3.08/W/21-A6 0900)  
 (GA3.08/W/26-A6 1710)  
 (GA4.08/W/19-B3 0930)  
 (GA3.08/W/06-B1 0900-01)  
**Russell Christopher**  
 (GA3.04/W/47-B1 1230)  
**Russell Christopher T.**  
 (GA3.08/W/17-A6 0940)  
**Russell Cindy**  
 (SA16/E/22-A3 0830-16)  
**Russell Gary L.**  
 (JSG14/E/20-A3 1700-08)  
**Russell J. E.**  
 (MI04/C/MC07/W/21)  
 (MI06/W/31-B2 1210)  
**Russell L M**  
 (MI09/W/14-A5 1145-21)  
**Russell Philip B**  
 (MI09/W/13-A5 1145-18)  
 (MI09/W/15-A5 1500)  
 (MI09/W/14-A5 1030)  
 (MI09/W/14-A5 1145-21)  
**Russell C. T.**  
 (GA4.10/W/07-A5 1740)  
 (GA4.10/W/05-A5 1655)  
**Russo Guido**  
 (ST5/W/34-B4 0930-01)  
**Russo R.**  
 (JSS07/W/01-A2 1125)  
**Rust W David**  
 (MI03/W/03-A3 1620)  
**Rusticucci Matilde**  
 (MC02/E/20-B1 1600-07)  
**Rutenberg Eckhard**  
 (HS4/L/03-A4 0930)  
**Rutenko Alexander N.**  
 (PW1/W/03-A61200)  
**Rutger Wahlstrom**  
 (ST3/E/16-B4 1400-19)  
**Ruti P. M.**  
 (JWM08/W/02-A2 1220)  
**Rutigliano P.**  
 (JSG14/W/19-A3 1600)  
 (JSP23/C/U5/W/01-B2 0830-15)  
**Rutledge J. T.**  
 (ST1/E/72-A4 0930-08)  
**Rutledge Steven A.**  
 (MI04/L/02-B3 0905)  
**Rutschmann Peter**  
 (VS2/W/26-B3 1400-29)  
**Ruttener Erik**  
 (ST3/W/40-B3 1430)  
**Ruzhin Yury**  
 (JSP23/W/23-B1 1720)  
 (JSP23/W/39-B1 1520)  
 (JSP23/W/22-B1 010)  
**Ruzmaikin A.**  
 (GA4.03/E/03-B4 1130)  
 (JSA45/W/11-B4 1430)  
**Ryabov Igor**  
 (JSS42/E/05-B5 0930)  
**Ryan Brian F.**  
 (JWM08/W/08-A3 1200)  
**Ryan C. G.**  
 (JSS44/E/20-B4 1720)  
**Rybach Ladislaus**  
 (ST4/W/13-B1 0840)  
**Rybakov A. Yu.**  
 (GA3.09/E/04-B4 1650)  
**Rybin Anatoly**  
 (GA1.02/E/22-A2 0930)  
**Rybinkov Pavel V.**  
 (P11/W/03-B5 1150-06)  
**Rycroft Michael**  
 (JSA35/E/01-B1 1510)  
**Rycroft Michael J**  
 (JSM03/E/07-A1 1450)  
 (JSM03/E/02-A1 0940)  
**Rymer Hazel**  
 (JSV36/C/U6/E/04-B3 1400-24)  
 (JSV36/E/01-B3 1610)  
**Rynn Jack**  
 (JSS42/E/08-B5 1700-10)  
 (JSS42/E/16-B4 1220)  
 (JSP23/E/36-B2 0830-13)  
 (JSP23/E/37-A5 1010)  
 (JSP23/E/39-A5 1700)  
**Rytisk Alexandr**  
 (GA1.05/W/24-A6 1145)  
**Ryuji Kimura**  
 (JSP39/E/06-B3 1415-06)  
**Rzhevsky Yu. S.**  
 (JSS44/E/05-B4 0930-11)  
 (GA1.05/E/07-A5 1440)  
 (GA1.04/E/08-A4 0930-13)  
 (GA1.04/E/03-A5 0940)  
 (GA1.04/E/07-A5 1000)  
**Saadini R**  
 (JSG11/W/02-A3 1540)  
 (JSG14/W/12-A3 1209-24)  
 (JSG14/W/19-A3 1600)  
**Sabaka T.**  
 (GA5.08/E/01-B1 1605)  
 (GA5.08/E/02-B1 0920)  
**Sabaka T. J.**  
 (GA5.09/W/03 A2 1110)  
**Sabanin Anton**  
 (JSM24/W/03-B1 1030-02)  
**Sabatino Sofia**  
 (GA6.01/W/02-A5 1055)  
**Sabbione Nora C.**  
 (ST1/W/59-A4 0930-36)  
 (JSS44/W/05-B4 0930-02)  
**Sabine C L**  
 (MC01/L/23-A5 1640)  
**Sabitova Tamara**  
 (ST5/E27-B1 0830-13)  
**Sabri Ahmed M.**  
 (JSA27/P/02-B1 1400-03)  
 (JSS44/P/06-B4 0930-17)  
**Saccorotti G.**  
 (JSV47/E/08-B5 1400-04)  
 (JSV47/W/01-B5 1045)  
 (JSV47/W/20-B5 1400-13)  
 (ST5/W/56-B3 0900-01)  
 (ST5/W/65-B3 1400-01)  
 (ST5/W/66-B4 1400-06)  
**Saccorotti Gilberto**  
 (JSV47/E/04-B5 0830)  
 (JSV47/W/18-B5 1100)  
 (JSV47/W/21-B5 1400-20)  
**Sacher M.**  
 (G1/E/31-A3 1620-65)  
**Sackler Beverly**  
 (ST5/L/02-B4 0930-08)  
**Sackler Raymond**  
 (ST5/L/02-B4 0930-08)  
**Sackler Raymond & Beverly**  
 (JWS33/P/2-B2 1550)  
**Sackler Raymond & Beverly**  
 (MI07/E/04-A2 1640)  
**Sacks I. Selwyn**  
 (ST1/E/68-A4 0930-12)  
 (JSV47/E/01-B5 1400-05)  
**Sadashivaiah C**  
 (HS5/W/43-A3 1500)  
**Sadidkhai Ahmad**  
 (ST1/E/40-A4 0930-07)  
 (U8/E/05-B3 1640-11)  
**Sadouh Sylvian**  
 (JSP39/W/19-B2 1210)  
**Sadykov D.**  
 (ST4/E/71-B2 0930-25)  
**Saemundsson Thorsteinn**  
 (GA6.01/L/02-A5 1630)  
**Safak Erdal**  
 (JSP23/E/05-A6 1150)  
**Safanda J.**  
 (MC02/E/10-B1 0950)  
 (ST4/E/06-B1 1400-18)  
**Safrankova J.**  
 (GA4.08/W/15-B3 1530)  
 (GA 3.07/E/10-A3 1130)  
**Safronov Guennady**  
 (JSP23/W/11-A5 1720)  
 (JSP23/W/28-B1 0830-01)  
**Saghafi M**  
 (JSP49/P01-B5 1210-01)  
 (P11/P/01-B5 1150-01)  
**Sagiya Takeshi**  
 (ST1/E/81-A2 1640)  
 (ST1/W/73 0930-31)  
 (ST2/W/35-A3 0945)  
**Sagnotti Leonardo**  
 (GA1.04/W/36-A5 1430)  
**Sahai Y.**  
 (JSA20/W/05-A5 1200-05)  
 (JSA20/W/50-A5 1200-09)  
**Sahu B. K.**  
 (GA 5.12/E/10 A2 1120)  
 (JSV22/E/05-A5 1400)  
**Sailor R V**  
 (G3/W/30-A5 1610-06)  
**Saifudinova T.**  
 (GA3.02/E/19-B3 0900-02)  
 (GA3.02/E/11-B2 0935)  
 (GA3.03/E/01-B4 1400-03)  
 (GA3.03/E/04-B4 1530)  
**Sailhac P.**  
 (JSS44/L/05-B4 0930-04)  
**Sainato Claudia**  
 (JSS44/W/02-B5 0930)  
 (GA1.02/W/39-A2 0930)  
 (JSA19/W/11-A4 1400-04)  
**Saito A.**  
 (GA2.02/W/09-B4 0900)  
**Saito Akinori**  
 (GA2.02/E/13-B4 1100)  
 (GA2.03/E/02-B3 1120)  
 (JWS33/W/37-B2 1430)  
**Saito Masanori**  
 (ST3/E/38-B4 0930-12)  
**Saito Tomomi**  
 (ST5/W/30-B5 0930-01)  
**Saito Y.**  
 (GA3.08/W/28-B1 1510)  
**Saito Genji**  
 (JSV36/E/12-B3 0900-17)  
**Saka O.**  
 (GA3.05/E/23-B3 0900-28)  
**Sakaand O.**  
 (GA3.04/W/26-B1 1520-09)  
**Sakai Hideo**  
 (JSA15/W/08-A4 1040)  
**Sakai Shinichi**  
 (JSP05/E/04-A1 0830)  
 (JSS44/W/04-B4 0930-05)  
 (JSS44/W/07-B4 0930-07)  
 (JSS46/W/18-B4 0930-07)  
**Sakamoto Izumi**  
 (JSA19/W/02-A4 1400-07)  
 (JSV30/W/10-B1 1400-08)  
 (JSV36/C/U6/W/06-B3 1400-23)  
 (JSV36/C/U6/W/11-B3 1400-17)  
**Sakanaka Shinya**  
 (GA1.02/L/05-A2 0930)  
 (JSA15/W/07-3 1740)  
 (JSA15/W/14-A4 1400-16)  
 (JSA15/E/12-A3 0830)  
 (JSA15/E/41-A4 1400-14)  
**Sakanoi T.**  
 (GA2.02/W/09-B4 0900)  
 (GA2.03/E/02-B3 1120)  
**Sakata S.**  
 (JSS42/E/06-B4 1440)  
 (JSS42/E/17-B5 1030)  
 (JSS42/E/17-B5 1700-22)  
 (GA3.04 W/04-B1 1520-40)  
**Sakoi Hisayuki**  
 ST2/W/26-A5 1400-01)  
**Sakr K.**  
 (G5/E/41-A4 1230-07)  
**Sakuma Sadaomi**  
 (G3/L/15-A5 1610-21)  
**Sakura Yosuo**  
 (HS4/W/18-A5 0950)  
**Sakuraba Ataru**  
 (GA1.01/W/14-A6 1130)  
**Salah Joseph E**  
 (JSM01/W/64-A2 1600-22)  
 (JSA20/W/17-A6 1031)  
 (JSA20/W/53-A6 1013)  
**Salah Lobna Mohammed**  
 (P11/P/05-B5 1150-05)  
**Salakhutdinova Irina I.**  
 (GA4.03/W/16-B4 1755-08)  
**Salazar José M. L**  
 (JSV36/W/12-B3 0900-08)  
 (JSV36/W/14-B3 0900-11)  
 (JSV36/C/U6/W/01-B3 1400-20)  
 (JSV36/W/01-B3 0900-12)  
 (JSV36/W/04-B3 1115)  
 (JSV36/W/16-B3 0900-10)  
 (JSV36/W/20-B3 0900-09)  
 (JSP21/W/10-A5 1150)  
 (ST1/W/30-A2 0930-07)  
**Salbach H.**  
 (G1/L/04-A3 1620-85)  
 (JSA09/L/02-A2 1230)  
**Salah Hussain**  
 (G1/W/17-A3 1620-39)  
**Salgado Rui**  
 (JSM43/W/13-B4 1420)  
**Salihoglu Ilkay**  
 (P11/E/25-B4 1010)  
 (P11/E/27-B5 1130)  
**Saliy Konstantin**  
 (G1/E/09-A3 1620-22)  
**Salk Mujgan**  
 (G1/E/04-A3 1620-50)  
**Salstein David A.**  
 (JSG14/E/08-A3 1136-13)  
 (JSG14/E/04-A3 1109-04)  
 (JSG14/E/12-A3 0900)  
 (MC01/E/06-A2 1015)  
**Saltzman Eric**  
 (JSP21/W/07-A4 1620)

# S

- Saavuori Heikki**  
 (GA5.11/E/03 A3 1430-10)

- Salukvadze T. G.**  
(M104/E/02-B1 0900-12)
- Salvati Roberto**  
(HS5/W/39-A3 1205)
- Salyor James**  
(P10/L/02-A5 1600-09)
- Salzen K Von**  
(M101/L/04 1055)
- Sambale Christoph**  
(HS4/W/02-A4 1015)
- Sambridge Malcolm**  
(ST5/E/24-B3 1720)  
(ST5/W/26-B5 0930-10)
- Samir Riad**  
(JSS44/E/29-B4 0930-18)
- Sammonds P.**  
(JSV29/W/01-B1 1620)  
(JSA10/W/07-A2 1415)
- Sammonds P. R.**  
(JSA15/W/18-A4 1400-02)
- Samodurov Anatoliy**  
(P11/E/01-B5 1440)  
(P11/E/08-B5 1500)
- Samra M. I.**  
(P11/P/02-B5 1150-02)  
(P11/P/03-B5 1150-03)
- Samson J. C.**  
(GA3.04/L/03-B1 0940)  
(GA3.08/W/16-B1 1430)
- Samson John C.**  
(GA3.08/W/03-A6 1450)  
(GA3.08/W/23-B1 1450)  
(GA3.06/W/15-A2 1400)
- Samsonov A. A.**  
(GA3.07/W/34-A3 0900-12)
- Samsonov Igor V.**  
(GA1.05/W/39-A6 0900-02)
- Sanahuja Blai**  
(JSA16/W/25-A3 0830-46)
- Sanchez Ennio R.**  
(GA3.08/E/08-A6 1730)
- Sanchez G.**  
(JSV36/E/11-B3 0900-15)
- Sanchez Laura**  
(G1/E/29-A3 1620-63)  
(G1/E/36-A3 1620-68)  
(G1/E/41-A3 1620-71)  
(G3/E/02-A5 1610-94)
- Sanchez Luis**  
(JSA16/W/25-A3 0830-46)
- Sanchez M. A.**  
(JSP39/W/39-B4 1620)
- Sanchez-Vila X.**  
(HS5/W/28-A2 1655)
- Sanchezgomez Emilia**  
(JSP25/E/25-B2 0930-01)
- Sandahl I.**  
(GA3.05/W/32-B3 0900-25)
- Sandahl Ingrid**  
(GA3.10/W/11-A6 1700-12)
- Sanders Ryan**  
(M104/W/14-B2 1120)
- Sanderson T.**  
(GA3.02/E/09-B2 1500)
- Sanderson T. R.**  
(GA4.04/E/01-B5 1210)  
(GA4.01/E/09-A2 1200)
- Sandholt Per Even**  
(GA3.10/W/20-A6 0920)
- Sandi H.**  
(ST1/W/60-A3 0900-07)
- Sangode S. J.**  
(GA1.04/E/05-A4 0930-16)
- Sankey D.**  
(JSM01/W/61-A5 1430)
- Sankov Vladimir**  
(ST2/W/01-A3 1400)
- Sannino Gianmaria**  
(P11/L/04-B5 0930)
- Sano Itaru**  
(M109/W/06-A5 1145-09)
- Sansivero Fabio**  
(JSP23/C/U4/W/01-A6 0830-17)
- Sanso**  
(G6/L/06-B3 0855)
- Sansó F**  
(G4/W/03-A3 1205)
- Sanso Fernando**  
(G6/C/G2/E/12 1100)
- Santana J.**  
(GA5.08/E/01-B1 1605)
- Santee Michelle**  
(JSM01/W/26-A5 0830)
- Santee Michelle L.**  
(JSM26/W/08-B2 1700-15)
- Santer B. D.**  
(MC02/W/01-B2 1100)  
(MW02/E/09-B3 1520)
- Santer Benjamin D**  
(MC01/L/04-A1 1615)
- Santer Richard**  
(M101/E/02-A1 0900-07)
- Santerre Rock**  
(G1/E/30-A3 1620-64)
- Santich N**  
(M109/W/01-A5 1145-19)
- Santillán Marcelo**  
(JSA20/W/45-A4 1200-32)
- Santimay Basu**  
(JSA06/W/05-A2 0950)
- Santis Angelo De**  
(GA1.03/E/01-B3 1120)
- Santoleri Rosalia**  
(P11/L/01-B5 0830)  
(P11/L/02-B5 0850)  
(P11/L/03-B5 0910)
- Santolik O.**  
(GA3.07/E/09-A5 0900-18)
- Santos Fernando**  
(GA1.02/W/15-A2 0930)  
(GA1.02/W/38-A2 0930)  
(GA1.02/W/40-A2 0930)  
(JSA19/W/03-A4 1400-06)
- Sanver M.**  
(GA1.04/W/27-A6 1140)
- Sanz E.**  
(GA1.15/W/09-B4 1400)
- Sanz J. L.**  
(GA5.12/E/04 A2 0930)
- Sapoznikov Filipp V.**  
(P11/W/03-B5 1150-06)
- Sapozhnikov V. V.**  
(P08/E/05-A2 1620)
- Sapunov Vladimir**  
(GA5.01/W/01 A1 1300-03)  
(GA5.01/W/06 A1 1300-14)  
(JSP23/E/38-A6 0830-09)  
(JSM24/W/03-B1 1030-02)  
(JWA34/W/02-B2 1620)
- Sapuzhak Oleg**  
(GA1.02/E/40-A1 1050)
- Sapuzhak Yaroslav**  
(GA1.02/E/40-A1 1050)
- Sar Johannes P. Ristau**  
(JSS31/E/14-B3 0830-15)
- Saracco Ginette**  
(JSA17/C/GA1.19/W/09-A4 0950)
- Saraev Alexander**  
(JSA15/E/14-A5 1400-04)  
(JSA15/E/39-A4 1140)
- Sarafopoulos D. V.**  
(GA3.02/L/04-B3 0900-25)
- Sarao Angela**  
(JSV47/W/12-B5 1400-10)  
(ST3/W/09-B3 1415)  
(ST3/W/34-B3 1400)
- Sardeshmukh Prashant D.**  
(JSP25/W/24-B1 0850)  
(MW06/W/04-A3 1640)
- Saritha P. R.**  
(P09/E/02-A2 0950)
- Sarkar N. D.**  
(ST1/E/08-A2 1400-26)
- Sarkar A.**  
(P07/E/03-A3 1430)
- Sarkisyan Artem S.**  
(P11/E/07-B3 0910)
- Sarma A. A. L. N.**  
(HS1/W/14-B4 1200)
- Sarmiento J. L.**  
(P08/W/02-A2 1130)  
(JSP21/W/04-A5 0950)  
(MC01/W/58-A5 1620)
- Sarnocchia Sefania**  
(P11/L/02-B5 0850)
- Sarrailh Michel**  
(G3/W/24-A5 1610-33)  
(G3/W/24-A5 1610-29)
- Sarris E. T.**  
(GA3.02/L/04-B3 0900-25)  
(GA3.08/L/02-B1 0900-11)
- Sarson Graeme R.**  
(GA1.01/W/24-A6 1000)  
(GA1.01/W/11-A6 0930)
- Sarychev V. T.**  
(GA1.03/W/34-B3 1100)
- Sas A.**  
(G3/E/26-A5 1610-36)
- Sasai Yochi**  
(JSA15/E/57-A4 1400-15)
- (JSA15/E/27-A4 1400-04)  
(JSA15/E/38-A4 1400-03)  
(JSA15/E/40-A3 1700)  
(JSV36/E/23-B3 0900-07)
- Sasaki T.**  
(GA1.05/E/17-A6 1630)
- Sasaki Toru**  
(JSM01/W/23-A4 1620-06)
- Sasaoka Hideki**  
(JSA15/E/04-A3 1130)
- Sassorova Elena V**  
(ST1/E/88-A4 0930-17)  
(JSP23/E/12-B2 0830-05)  
(SW1/E/10-B5 1145)
- Sastri J. Hanumath**  
(JSA20/E/12-A5 1400)  
(JSA20/E/16-A5 1200-06)
- Sas-Uhrynowski A.**  
(G3/E/26-A5 1610-36)  
(JSG14/E/19-A3 1745-16)
- Satake Kenji**  
(JSS42/W/14-B5 0830)  
(ST3/W/27-B4 1530)
- Satheesh S K**  
(M101/E/07-A2 0930)
- Sato Haruo**  
(ST1/W/22-A3 1440)  
(JSS46/E/01-B4 0930-06)  
(JSV47/W/22-B5 1130)  
(ST4/W/59-B1 0830-17)  
(ST5/W/24-B4 0930)
- Sato Hiroshi**  
(JSS44/W/07-B4 0930-07)  
(JSS44/W/09-B4 0930-08)  
(JSV30/C/JSV22/W/01-B1 1400-22)
- Sato Kaoru**  
(JSM01/E/09-A1 1550)  
(JSM01/E/12-A2 1500)
- Sato Ken**  
(GA1.04/W/11-A6 1440)
- Sato Minemori**  
(JSV36/W/09-B3 1430)  
(JSV47/W/22-B5 1130)
- Sato N.**  
(JSG14/W/09-A3 1121-08)
- Sato Natsuo**  
(GA 2.02/E/12-B4 1640)  
(GA3.08/E/03-B1 1000)
- Sato Natuo**  
(GA2.01/E/05-A1 0950)
- Sato Nji**  
(JSS42/W/09-B5 1520)
- Sato Satoshi**  
(P09/W/14-A1 1520)
- Sato T.**  
(JSV36/E/18-B3 1400-13)
- Sato Tadahiro**  
(JSG14/W/13-A3 1700-06)  
(JSG14/W/20-A3 1700-11)
- Sato Toshinori**  
(JWA34/W/12-B2 1050)
- Sato Yasuo**  
(MW03/E/03-B4 1625)
- Satoh H.**  
(GA1.02/L/05-A2 0930)  
(JSA15/W/07-3 1740)
- Satoh Yoshinori**  
(HS4/W/22-A5 1120)
- Satomura Mikio**  
(G3/W/28-A5 1610-34)
- Satori Gabriella**  
(JSA35/E/07-B1 1610)
- Satoru Urakawa**  
(ST 6/E/11-A2 1530)
- Satoshi I**  
(G5/L/06-A4 1400)
- Satoshi Kaneshima**  
(JSV47/W/11-B5 1115)
- Satyanarayalia B**  
(PW1/P/01-A6 0940)
- Satyanarayana M.**  
(M106/W/25-B2 1130)
- Sauer Herbert H.**  
(JSA45/L/02-B5 0920)  
(GA6.01/L/05-A5 0900-03)  
(JSA06/L/09-A1 1155-20)
- Sauli Petra**  
(JSA20/E/03-A4 1200-24)  
(JSA20/E/21-A4 1000)
- Saunders Clive**  
(M103/W/07-A3 1400-03)
- Saunders M. A.**  
(JSP25/E/33-B3 1130)  
(MC05/E/01-B4 0910)  
(MC05/E/02-B5 1010)
- Sausen Robert**  
(MC07/E/01-A2 1035)
- Sauter Edward A.**  
(GA5.01/E/14 A1 1130)
- Sauvaud J. A.**  
(GA3.02/W/03-B3 0900-14)
- Savaidis A. A.**  
(ST3/L/01-B4 1400-25)
- Saveliev Dmitry**  
(JWA34/W/02-B2 1620)
- Saveliev Dmitry**  
(GA5.01/W/01 A1 1300-03)  
(GA5.01/W/06 A1 1300-14)
- Saveliev Vladimir L.**  
(GA1.02/W/25-A1 1605)
- Savjärvi H.**  
(MC09/W/07-B2 01)
- Savin S.**  
(GA3.05/W/32-B3 0900-25)  
(GA4.08/W/15-B3 1530)  
(GA4.09/W/04-A5 1600-02)
- Savina Olga**  
(JSM01/W/96-A3 0920)
- Savrov Lev**  
(G3/E/06-A5 1610-59)
- Sawada Toyoaki**  
(JSA15/W/08-A4 1040)
- Saxena D. P.**  
(HW2/W/20-B1 0900-02)
- Saxena V K**  
(M101/P/03-A3 0930)
- Saxena Vinod**  
(JSM18/P/02-A5 1120)
- Sayed Ahmed**  
(JSA19/W/04-A4 1400-05)
- Saylor James H.**  
(P11/E/04-B3 0930)
- Scaife Adam**  
(MW01/E/03-A5 1650)  
(MW07/E/06-A4 1700)
- Scalera Giancarlo**  
(GA6.01/W/06-A6 1235)  
(ST4/P/02-B2 0930-27)
- Scambos Ted A.**  
(HW1/W/01-A4 1130)
- Scaramuzza Maurizio**  
(G6/W/06-B2 1400)
- Scarlato Piergiorgio**  
(JSV36/E/22-B3 0900-16)  
(VS2/W/22-B3 1400-15)
- Scarpa Roberto**  
(JSS46/E/03-B4 1420)  
(JSS46/E/05-B4 1440)  
(JSV47/E/01-B5 1400-05)  
(JSV47/W/18-B5 1100)
- Schaake J.**  
(HW4/E/12-B2 0930)
- Schaake John**  
(JSM24/E/05-B1 1650)
- Schaefer C. H.**  
(G2/W/04-A2 1630-04)
- Schaefer N U.**  
(G3/E/17-A5 1610-62)
- Schaefer U.**  
(G4/E/18-A3 1540)
- Schaefer Bernd**  
(MW 07/E/03-A4 1400)  
(MW07/W/19-A4 1420)
- Schaer Christoph**  
(MC01/E/25-A5 0915)
- Schaer Stefan**  
(G1/E/58-A3 1500)  
(JSG28/E/24-B2 1010)
- Schanz Lars**  
(JSM41/L/02-B3 1550)
- Schär C.**  
(JWM08/E/06-A2 1120)
- Scharfen Gregory**  
(JWS33/W/34-B2 1635-02)
- Scharroo**  
(G2/L/07-A2 1130)
- Schätz M.**  
(GA1.04/W/30-A4 1100)
- Schatten Kenneth**  
(GA4.03/W/05-B4 0940)
- Schauer Ursula**  
(P14/E/08-A4 1400-07)  
(P13/E/17-B1 0950)
- Schauffler Sue M.**  
(JSM26/W/04-B2 1130)
- Scheer Christoph**  
(MC01/E/38-A5 1000)
- Scheer Juergen**  
(JSM01/E/11-A2 1600-08)  
(JSM01/E/25-A3 1020)



# INDEX

- Scheibner E.**  
(JSS31/W/15-B3 0830-09)
- Scheinert Mirko**  
(JSA09/W/03-A2 0930-05)
- Scheiner Ronald**  
(MI10/W/06-B2 1005)
- Schelle Holger**  
(JSS31/E/07-B2 1210)
- Schellenberg T. J.**  
(GA4.10/W/14-A4 0900)
- Schellnhuber Hans-Joachim**  
(U3/W/05-A3 0900-11)
- Schenewerk M. S.**  
(G1/W/22-A3 1620-41)  
(G1/E/43-A3 1620-73)
- Schenk Vladimir**  
(ST3/W/13-B5 0915)  
(ST3/W/38-B5 1445)  
(G5/W/07-A4 1516-09)  
(JSP23/W/29-A6 1600)
- Schenke Hans Werner**  
(JSA09/W/13-A2 1215)  
(G1/L/04-A3 1620-85)  
(JSA09/L/02-A2 1230)
- Schenkova Zdeoka**  
(JSP23/W/29-A6 1600)  
(G5/W/07-A4 1516-09)
- Scherbaum F.**  
(ST1/E/87-A2 0930-12)  
(JSV47/W/06-B5 1400-11)
- Scherbovsky Boris Ya.**  
(GA4.04/W/10-B5 0830-03)
- Scherliess L.**  
(JSA20/W/16-A5 1443)
- Scherneck H. G.**  
(G5/W/11-A4 0945)  
(G5/W/13-A4 1115-01)  
(JSG11/W/05-A3 1440)  
(JSG11/W/09-A3 1500)  
(JSG11/E/05-A3 1520)
- Scherrer P. H.**  
(GA4.03/E/06-B4 1730-03)
- Scherrer Simon**  
(HS4/W/30-A5 1510)
- Schertzer D.**  
(JSP23/W/13-B1 1110)  
(JSM43/W/01-B5 1000)  
(JSP39/W/15-B3 1110)  
(MI10/E/10-B2 1705)  
(MI10/E/14-B2 1520)  
(MI11/E/02-B5 1400)  
(MI11/E/04-B5 1430)
- Schiano Maria Elisabetta**  
(P11/W/06-B4 0930)
- Schick Asher P.**  
(HS4/W/28-A5 1430)
- Schiebe Frank R.**  
(JSM41/W/18-B5 1205)
- Schimmel David S**  
(MC01/W/09-A5 1445)  
(MC01/E/20-A5 1405)
- Schimetschek J.**  
(JSP23/C/U5/W/13-A5 1440)
- Schimmel M.**  
(ST4/E/65-B2 1520)
- Schirmer Uwe**  
(G6/C/G3/E/23-B1 1200)
- Schlager H.**  
(JSM26/W/18-B2 1550)
- Schlatter A.**  
(G1/L/14-A3 1620-90)
- Schlegel K.**  
(JSA20/W/08-A4 1200-27)  
(GA2.02/E/06-B4 1420)  
(GA2.02/L/8-B4 1440)
- Schlegel Kristian**  
(GA2.02/W/03-B4 0930-02)  
(GA2.02/W/06-B4 1120)  
(GA2.02/W/10-B4 0920)
- Schlesinger M.**  
(MI06/E/13-B1 1100)
- Sch lindwein V.**  
(ST4/W/12-B1 1440)
- Schlitzer Reiner**  
(MC01/W/24-A5 1745)
- Schlösser A**  
(MC01/L/14-A3 1400)
- Schlösser C Adam**  
(MC01/L/02-A1 1145)
- Schlösser P.**  
(P07/L/02-A3 1125)
- Schlösser Peter**  
(P07/W/04-A3 0900-02)  
(P07/W/18-A3 1720)  
(P07/W/19-A3 1550)
- (P07/W/15-A3 1145)  
(P13/W/22-B1 1050)
- Schlueter W.**  
(G2/L/09-A2 1200)
- Schlueter Wolfgang**  
(JSG28/W/21-B1 1400-02)
- Schlüter W.**  
(G1/E/31-A3 1620-65)  
(G1/E/46-A3 0930)
- Schlüssel Peter**  
(JSM41/L/02-B3 1550)
- Schmann A. H.**  
(HW4/E/30-B2 0900-10)
- Schmeling Harro**  
(JSS13/W/17-A5 0930)
- Schmetz Johannes**  
(JSM41/W/28-B4 0930)
- Schmid B**  
(MI09/W/14-A5 1030)  
(MI09/W/14-A5 1145-21)
- Schmid Beat**  
(MI09/W/15-A5 1500)
- Schmidli J.**  
(JWM08/E/06-A2 1120)
- Schmidli Juerg**  
(MI05/L/01-A2 1200)
- Schmidt A**  
(JSV30/W/02-B1 1400-06)  
(JSV30/W/04-B1 1400-07)
- Schmidt Gavin**  
(MC02/W/03-B2 0930)  
(P07/W/09-A3 1450)
- Schmidt Karin**  
(G3/W/10-A5 1610-35)
- Schmidt Nan**  
(JSP23/W/01-B2 1500)
- Schmidt Phillip W.**  
(GA1.04/W/06-A4 0930)  
(GA5.11/W/04 A3 1010)  
(GA1.07/W/05-B2 0920)
- Schmidt S.**  
(JWS33/W/08-B2 1635-26)  
(JWS33/W/08-B3 0900-26)
- Schmidt Tanya**  
(JSM43/W/11-B4 1700)
- Schmidt Torsten**  
(MI09/E/08-A5 1645)
- Schmidt William**  
(MC02/W/08-B1 1600-04)
- Schmieder B**  
(GA4.02-A4 0845)
- Schmieder Brigitte**  
(GA4.02/W/14-A4 0925)
- Schmieder J.**  
(JSP23/C/U5/W/13-A5 1440)
- Schmincke Hans-Ulrich**  
(VS3/W/27-B3 0900-05)
- Schmitgen Sandra**  
(U2/E/14-A2 1420)
- Schmitt Axel**  
(VS2/W/19-B3 1400-12)
- Schmitt Guenter**  
(JSP23/E/44-A6 1210)
- Schmitz Gerhard**  
(JSM01/E/01-A1 1720)  
(MI02/W/02-A4 1200)
- Schmitz Martin**  
(G1/W/32-A3 1620-15)
- Schmucker Ulrich**  
(GA1.02/P/02-A1 1605)  
(GA1.07/P/01-B2 1120)
- Schmugge Thomas J.**  
(JSM41/W/18-B5 1205)
- Schmus William R. Van**  
(GA1.05/E/16-A5 1520)
- Schnack Dalton**  
(GA3.09/W/27-B4 1035)
- Schnadt Christina**  
(MI02/W/03-A5 1200)  
(MI02/W/17-A5 1220)
- Schneider Dieter**  
(G1/W/05-A3 1620-34)
- Schneider E.**  
(GA1.02/W/14-A2 0930)
- Schneider Niklas**  
(JSP25/W/13-B5 0950)  
(JSP25/W/51-B5 0910)
- Schneider Otto**  
(GA4.08/E/17-B3 1105)
- Schneider Tapio**  
(MC02/W/16-B2 0950)
- Schnell Klaus**  
(HS5/W/41-A3 1400)
- Schnepp Elisabeth**  
(GA1.03/E/08-B2 0920)
- Schodlok M. P.**  
(P13/W/08-B1 1620)
- Schoeffel H -J**  
(JSS13/W/11-A4 1520)
- Schoene Tilo**  
(JSA09/W/13-A2 1215)
- Scholes Lian**  
(HS5/W/12-A2 0920)
- Schöne T.**  
(G1/L/04-A3 1620-85)  
(JSA09/L/02-A2 1230)
- Schoon N.**  
(JSM26/W/29-B2 1700-09)
- Schopf Paul S.**  
(JSP25/E/36-B2 1520)
- Schorlemmer D.**  
(ST3/W/45-B4 1430)
- Schott J.-J.**  
(GA1.02/W/21-A2 0930)
- Schramm Julie**  
(P13/W/06-B2 1600-04)
- Schreiner Bill**  
(JSG28/W/25-B2 1400-11)
- Schröder Franz**  
(MI01/E/03-A1 1700)
- Schröder Wilfried**  
(GA6.01/P/01-A5 0900-17)  
(GA6.01/P/02-A5 0900-16)  
(GA6.01/E/04-A5 0900-07)  
(GA6.01/E/05-A5 0900-11)
- Schroeter Jens**  
(SP05/W/03-A2 10)
- Schrum Corinna**  
(P11/E/07-B3 0910)  
(P11/W/18-B3 1440)
- Schubert G.**  
(MC09/W/02-B2 1215)  
(ST6/W/02-A1 0830-04)
- Schubert Gerald**  
(JSA10/W/09-A3 1115)  
(MC09/E/02-B2 1715)
- Schubert Siegfried**  
(MC08/W/03-A3 1650)
- Schubert Wayne H.**  
(MI04/W/18-B3 1600)
- Schuh H.**  
(JSG14/W/16-A3 1203-22)
- Schuh Harald**  
(G2/W/06-A2 1630-09)  
(G2/W/14-A2 1630-10)
- Schühle Udo**  
(JSA16/W/06-A3 0830-48)
- Schultz Gert A.**  
(HS4/W/27-A5 1400)  
(HS5/W/20-A2 1220)
- Schulz A**  
(JSM01/W/37-A5 1400)
- Schultz Adam**  
(P16/W/04-B5 1130)
- Schulz Jan-Peter**  
(MC01/W/46-A3 1620)
- Schulz Jörg**  
(JSM41/L/02-B3 1550)
- Schulz Michael**  
(GA3.02/W/32-B3 1105)  
(GA3.05/E/11-B3 1620)  
(GA3.05/W/44-B3 0900-44)  
(MC11/E/14-B4 0920)
- Schulz R.**  
(JSA40/W/06-B5 1400-09)
- Schulze Joachim**  
(U8/W/03-B3 1425)
- Schulz-Schoellhammer Kathrin**  
(JSM01/C/MW07/W/09-A2 1600-34)
- Schunk R. W.**  
(GA5.06/W/05 A3 1520)  
(GA3.09/W/06-B5 0925)
- Schüpbach Evi**  
(U2/E/14-A2 1420)
- Schupler Bruce R.**  
(G1/W/23-A3 1620-09)
- Schuster Sandra**  
(JSM04/E/03-A2 1510)
- Schutt D.**  
(ST5/L/01-B5 0930-05)
- Schutz B**  
(JSG11/W/17-A4 1150)
- Schutz B E**  
(JSH12/W/09-A4 1400-03)
- Schutz Bob E.**  
(G2/W/10-A2 1445)
- Schuurmans Cornelius J. E.**  
(GA6.01/E/13-A5 1440)  
(GA6.01/E/13-A5 1440)
- Schwab Fred**  
(JSA40/E/07-B5 0950)
- Schwab Soares**  
(G5/E/08-A4 1556-09)  
(G5/E/07-A4 1554-08)
- Schwadron N. A.**  
(GA4.05/W/07-A1 1000)  
(GA4.04/E/07-B5 0830)  
(GA4.04/W/03-B5 1050)  
(GA4.04/W/06-B5 1400)
- Schwadron Nathan**  
(GA4.02/W/18-A4 1735)
- Schwahn W.**  
(JSG14/E/21-A3 1700-18)
- Schwandner Florian M.**  
(JSV36/E/04-B3 1230)
- Schwarb Manfred**  
(JWM08/E/08-A2 1520)  
(JWM08/W/05-A2 1540)
- Schwartz Barry**  
(MC04/E/06-B2 1450)
- Schwartz Stephen E**  
(MC07/W/05-A3 0830)  
(MI09/L/05-A5 1620)
- Schwartz Steven J.**  
(GA3.07/E/04-B3 1000)  
(GA3.07/E/21-A3 0900-13)
- Schwarz**  
(G6/L/05-B3 0830)
- Schwarz Gerhard**  
(GA5.01/E/32 A1 0900-09)  
(GA5.12/E/03-A2 1600-05)
- Schwarz K P**  
(G3/E/12-A5 1610-18)  
(G4/E/11-A3 1620-14)
- Schwarz Klaus-Peter**  
(G6/E/05-B2 1200)  
(G6/E/06-B2 1440)
- Schwarze**  
(G1/L/15-A3 1640-91)
- Schwarze Volker**  
(G6/C/G4/W/18-B1 1720)
- Schwarzkopf M D**  
(MC07/W/12-A2 1155)
- Schwegmann Wolfgang**  
(G2/W/06-A2 1630-09)
- Schweiger Axel J**  
(MI08/W/15-A3 1430)  
(MI08/W/11-A3 1720)
- Schweitzer Johannes**  
(ST5/W/48-B5 0950)  
(U8/W/04-B3 1450)  
(U8/W/10-B3 1640-06)  
(U8/W/16-B3 1640-12)
- Schwenn Howard**  
(JSA06/W/14-A1 1700)
- Schwenn R.**  
(GA4.02/E/08-A4 1400-05)  
(GA4.05/E/02-A1 1010)
- Schwierz Cornelia**  
(MI05/E/04-A1 1420)
- Schwingsenschuh K.**  
(JSA10/E/06-A2 0945)
- Schwintzer P**  
(G3/E/27-A5 1610-02)  
(G3/W/39-A5 1100)  
(G6/C/G3/E/43-B1 1100)  
(JSA37/W/05-B3 0945)
- Sciaccia Umberto**  
(JSV36/E/22-B3 0900-16)
- Sciarretta C.**  
(JSG28/W/15-B1 1400-04)  
(G3/L/19-A5 1610-69)  
(JSG14/W/19-A3 1600)
- Scibek J.**  
(HW3/W/17-B4 0925)
- Sciffer Murray**  
(GA3.04/W/26-B1 1520-09)  
(GA3.04/W/34-B1 1520-13)
- Scoffield Rod A.**  
(MC04/W/12-B2 0925)
- Scinocca John**  
(MW07/W/20-A4 1620)
- Sconcia Brett**  
(JSP25/W/73-B2 1440)
- Scoon G.**  
(JSA10/W/06-A2 1430)
- Scot Robert B.**  
(JSP49/W/22-B5 0930)
- Scott Bradley J.**  
(JSV36/W/02-B3 0930)
- Scott James**  
(JSP25/E/32-B3 1400)
- Scott Robert B.**  
(JSP39/W/28-B4 1540)
- Scotto C.**

- (JSA45/E/17-B5 1110-01)  
**Scudder J.**  
 (GA3.08/W/26-A6 1710)  
**Scudder Jack D**  
 (GA3.07/L/09-A5 0900-19)  
 (GA4.02/W/24-A4 1400-22)  
 (GA4.09/W/15-A6 0900)  
 (GA4.09/E/10-A6 1640)  
**Sebai Amal**  
 (JWA34/W/06-B2 1010)  
**Sebata Kouichi**  
 (G2/E/01-A2 1630-12)  
 (G2/W/01-A2 1630-01)  
 (G2/E/04-A2 1630-13)  
 (G2/E/08-A2 1630-11)  
**Secanell R.**  
 (ST3/E/41-B5 1000)  
**Secco Richard**  
 (ST6/C/JSS02/W/19-A2 1740)  
**Seckmeyer Gunther**  
 (MI08/L/07-A4 1720)  
**Sedaeva Valentina**  
 (JSS42/E/23-B5 1700-05)  
**Sedov Boris**  
 (JSA09/E/01-A2 1700)  
**Sedukhina G. F.**  
 (JWS33/E/06 -B2 1635-12)  
 (JWS33/E/06-B2 1230)  
 (JWS33/E/06-B3 0900-12)  
**Sedykh P.**  
 (GA3.02/E/19-B3 0900-02)  
**Sedykh P. A.**  
 (GA3.02/E/11-B2 0935)  
 (GA3.02/E/12-B3 0900-01)  
**Seeber Guenter**  
 (G1/W/32-A3 1620-15)  
 (JSA09/W/13-A2 1215)  
 (G1/L/04-A3 1620-85)  
 (JSA09/L/02-A2 1230)  
**Seed A. W**  
 (JWM08/L/02-A3 1400)  
**Seeger H.**  
 (G1/E/46-A3 0930)  
**Seeger Hermann**  
 (JSS31/L/04-B2 0830-17)  
 (G1/E/04-A3 1620-50)  
**Seegraef Christian**  
 (JWS33/W/18-B2 1635-27)  
 (JWS33/W/18-B3 0900-27)  
**Seevuori Heikki**  
 (JSS44/E/11-B4 0930-29)  
**Segall Paul**  
 (G6/W/04-B1 1440)  
 (JSV36/W/19-B3 1400-07)  
**Segantine Paulo C. L.**  
 (G1/L/01 1620-83)  
 (G1/L/02-A3 1620-840)  
**Segawa J.**  
 (GA1.02/W/20-A2 0930)  
**Segawa Jiro**  
 (G3/L/15-A5 1610-21)  
 (G3/W/28-A5 1610-34)  
**Seghedi Antoneta**  
 (JSS44/E/18-B4 1500)  
**Seghedi Ioan**  
 (JSV30/C/U/6/E/05-B1 1400-26)  
**Segovia Monica**  
 (JSP23/C/U/5/E/05-A6 0830-06)  
**Segschneider J**  
 (JSP05/W/16-A1 1400)  
**Seidemann R.**  
 (JWS33/W/08-B2 1635-26)  
 (JWS33/W/08-B3 0900-26)  
**Seinfeld J H**  
 (MI09/W/14-A5 1145-21)  
 (MI09/W/14-A5 1030)  
**Seipold Ulf**  
 (ST4/E/13-B1 1140)  
**Seitz Kurt**  
 (G3/L/20-A5 1610-60)  
**Sekar R.**  
 (GA 2.02/E/01-B5 1400)  
 (GA2.02/W/16-B4 0930-18)  
**Sekelsky Stephen M.**  
 (M104/E/25-B4 0930)  
**Sekido Mamoru**  
 (G2/E/01-A2 1630-12)  
 (G2/E/08-A2 1630-11)  
**Sekiguchi Haruko**  
 (ST3/W/01-B3 1645)  
 (ST3/W/24-B4 0930-07)  
**Sekiguchi Wataru**  
 (JSA15/E/40-A3 1700)  
**Sekine S.**  
 (JSS44/W/01-B4 0930-06)  
**Sekine Yoshihiko**  
 (P14/W/09-A4 1400-08)  
**Sekse Magnar**  
 (HS5/W/15-A2 1020)  
**Seland Øyvind**  
 (MI01/W/09-A1 1025)  
**Selemenov Konstantin**  
 (JSP25/W/21-B3 0830-07)  
**Selesnick R. S.**  
 (GA3.05/W/26-B3 1600)  
 (GA3.05/W/28-B3 0830)  
**Selig A.**  
 (G6/C/G3/W/08-B2 1120)  
 (G2/W/08-A2 1630-22)  
**Sellami S.**  
 (JSP23/C/U/5/E/16-A5 1620)  
 (JSP23/E/03-A6 0930)  
**Sellami Souad**  
 (ST3/E/56-B4 1400-20)  
 (ST3/E/04-B4 1400-12)  
**Sellschopp Jurgen**  
 (P12/W/17-A1 1720)  
**Semakov N.N.**  
 (GA5.01/W/15 A1 1300-06)  
**Semblat Jean-Francois**  
 (JSP23/E/01-A6 1110)  
**Semeniuk Kirill**  
 (JSM01/W/24-A3 1630)  
**Semenov A. I.**  
 (JSA45/L/04-B4 1225)  
**Semenov Gennady**  
 (JSS44/P/03-B5 0950)  
**Semenov V S**  
 GA4.02/W/24-A4 1400-22)  
**Semet M. P.**  
 (JSV30/E/10-B1 1400-03)  
**Semovski Sergei V.**  
 (P11/E/10-B3 0830)  
**Semtner Albert**  
 (P13/W/22-B1 1050)  
**Semyonov G. A.**  
 (P13/W/20-B2 1600-08)  
 (P10/W/11-A5 1600-03)  
**Semyonov Igor V.**  
 (JSV22/W/03-A5 0900-01)  
**Semyonov Vladimir K.**  
 (MI06/W/08-B2 1400-01)  
 (MI06/W/08-B1 1400-01)  
**Sen M. K.**  
 (ST4/W/33-B1 0830-29)  
**Sen Omer L**  
 (MC01/W/53-A3 1650)  
**Send Uwe**  
 (P11/E/05-B4 1440)  
**Senda Yoshimichi**  
 (ST2/W/26-A5 1400-01)  
**Sengoku Arata**  
 (GA5.01/W/05 A1 0835)  
**Senin B.V.**  
 (ST1/E/03-A4 0930-26)  
 (ST1/E/03-A4 0930-25)  
**Senior Catherine**  
 (MW02/E/05-B3 1100)  
**Sennikov N.V.**  
 (GA1.04/L/03-A5 0920)  
**Seno Tetsuzo**  
 (ST4/W/81-B1 0830-25)  
**Senos L.**  
 (ST2/E/47-A4 1630)  
**Seok Cho**  
 (JSA06/W/28-A1 1155-13)  
**Seoung Kyu Lee**  
 (ST2/E/39-A3 0900)  
**Seppo Elo**  
 (G3/E/19-A5 1610-25)  
**Serban Delia Zemira**  
 (MC02/E/15-B1 1600-13)  
 (ST4/E/43-B1 1400-09)  
**Serebryakova O. N.**  
 (JSA15/L/02-A5 1400-06)  
**Serebryanaya Polina**  
 (G5/L/02-A4 1115-06)  
 (JWA34/E/03-B2 1720)  
 (JWA34/E/04-B2 1700)  
 (ST5/E/08-B5 1520)  
**Serebryany Andrey**  
 (P10/E/01-A4 1440)  
**Serenko V.**  
 (P09/W/05-A1 1640)  
**Sergeev V. A.**  
 (GA3.02/W/60-B2 1215)  
 (GA3.05/W/13-B3 0900-34)  
**Sergeeva N. A**  
 (JWS33/W/04-B2 1635-24)  
 (JWS33/W/04-B3 0900-24)  
**Sergeeva N. G**  
 (ST1/E/03-A4 0930-25)  
 (ST1/E/03-A4 0930-26)  
**Sergeyev Konstantin A.**  
 (JSM24/L/02-B1 1730)  
**Sergievsky V. V.**  
 (HW3/W/12-B4 1635)  
**Serra Teresa**  
 (JSP39/W/38-B4 1150)  
**Serreze Mark C.**  
 (HS2/W/06-B1 1120)  
**Seth Anji**  
 (MC01/W/23-A4 1515)  
**Seth S. P.**  
 (GA4.10/P/03-A4 1200)  
 (MC09/P/02-B2 1045)  
**Seto N.**  
 (ST3/W/39-B4 1400-08)  
**Setyadj B.**  
 (JSV36/E/01-B3 1610)  
**Sevastianov M. S.**  
 (JWS33/E/06 -B2 1635-12)  
 (JWS33/E/06-B2 1230)  
 (JWS33/E/06-B3 0900-12)  
**Sevcik S.**  
 (GA1.01 /E/15-A6 1145)  
**Sevilla M. J.**  
 (G3/E/38-A5 1610-72)  
**Sevruck Boris**  
 (JWM08/E/03-A2 1440)  
**Seyed-Mahmoud Behnam**  
 (JSA17/W/13-A4 1430)  
**Seze G.**  
 (MI04/L/10-B3 1520)  
 (MI06/W/07-B1 1220)  
 (MI06/W/05-B1 1400-06)  
 (MI06/W/05-B2 1400-06)  
**Sguerso Domenico**  
 (G1/W/31-A3 1620-14)  
 (G1/W/35-A3 1620-17)  
**Shabalova Marina V.**  
 (JSP25/W/90-B4 1740)  
**Shadrina L. P.**  
 (GA4.08/W/04-B3 0900-05)  
**Shaffer D. Lynn**  
 (GA2.02/E/10-B5 1700)  
**Shaffery L**  
 (MW02/E/03-B3 1010)  
 (MI05/E/18-A2 1450)  
 (MI05/E/03-A4 1400-02)  
**Shagimuratov Irk I.**  
 (JSG28/E/28-B2 1400-01)  
**Shah P. S.**  
 (GA3.05/E/10-B3 0900-43)  
**Shaikh A. A.**  
 (GA3.06/E/02-A3 1020)  
**Shakhramanjan M. A.**  
 (JSP23/E/33-A5 1640)  
**Shalaby Mahmoud H.**  
 (JSA27/P/01-B1 1050)  
**Shalamyansky Arkadiy M.**  
 (MI06/E/13-B1 1100)  
**Shalimov Sergei**  
 (GA2.02/W/03-B4 0930-02)  
 (JSA15/E/49-A4 1000)  
**Shalin A. Y.**  
 (JSM26/W/35-B2 1700-12)  
**Shaltout M. A. Mosalam**  
 (GA2.03/P/02-B3 1620)  
 (GA6.01/P/08-A5 0900-20)  
 (GA6.01/P/10-A5 0900-18)  
 (GA6.01/P/12-A5 0900-19)  
 (JSA10/C/GA4.15/P/01-A2 1100)  
 (JSA10/C/GA4.15/P/03-A3 1400-01)  
**Shalyapin Vladimir**  
 (P10/E/18-A5 1500)  
**Shamir Uri**  
 (HS5/W/17-A2 1120)  
**Shan Jiazeng**  
 (JSS44/C/JSS07/P/02-B4 0930-39)  
**Shang She-ping**  
 (U7/W/12-B1 0830-02)  
**Shang-Ping Xie**  
 (JSP25/W/16-B4 1700)  
**Shanker D.**  
 (ST3/E/46-B4 0930)  
**Shankar Ude**  
 (HS3/W/10-A1 1425)  
**Shankland Thomas J.**  
 (ST6/E/01-A2 1730)  
 (GA1.02/E/18-A1 0945)  
**Shanov Stefan**  
 (ST2/E/59-A5 1400-27)  
**Shao Ji-Cheng**  
 (GA1.01/E/06-A5 1445)  
**Shapiro Melvyn**  
 (MI05/E/25-A2 1100)  
 (MI05/L/01-A2 1200)  
**Shapiro Nikolai M.**  
 (JSS42/W/19-B5 1700-18)  
**Shapiro V. D.**  
 (GA4.09/E/13-A6 1020)  
**Shapiro Vsevolod**  
 (JSS44/W/20-B4 0930-23)  
 (GA1.01/W/37-A5 1715)  
 (JSA15/W/33-A3 1400)  
**Shapovalov Sergei**  
 (P11/W/10-B5 1715)  
**Sharada M. K.**  
 (P08/W/08-A2 1420)  
**Sharaeva S. V**  
 (GA4.08/E/11-B3 0900-02)  
 (GA4.08/E/20-B3 0900-01)  
**Sharaf El Din S. H**  
 (PW1/P/02-A61420)  
**Sharif Koorosh**  
 (ST3/E/25-B3 1130)  
**Sharma Shashi P.**  
 (JSA40/E/10-B5 1025)  
**Sharma Shiv**  
 (MC08/L/09-A3 1545)  
 (MC08/L/14-A4 0945)  
**Sharma Som**  
 (GA3.05/E/10-B3 0900-43)  
**Sharma Som Kumar**  
 (JSA20/W/20-A5 1135)  
**Sharma U. C.**  
 (HSA3/W/05-A1 1015)  
**Sharp Martin**  
 (HS2/W/18-B2 1000)  
**Sharp William E.**  
 (MI06/L/04-B1 0950)  
**Sharples Jonathan**  
 (P10/W/28-A5 1010)  
**Shashkanov Vladimir A**  
 (GA1.05/W/40-A6 0900-03)  
 (GA1.05/W/03-A6 0900-01)  
 (GA1.05/W/10-A6 0900-08)  
 (GA1.05/W/15-A6 0900-09)  
 (GA1.05/W/39-A6 0900-02)  
**Shatashvili Luli**  
 (ST1/C/GA4.10/E/01-A4 0930-43)  
 (JSA45/E/15-B5 1110-06)  
**Shatashvili Nana**  
 (GA4.05/E/03-A1 1440)  
**Shatwell Tom**  
 (HS5/W/11-A2 0900)  
**Shaw John**  
 (GA1.03/W/07-B1 1500)  
 (GA1.03/W/13-B1 0920)  
 (GA1.03/W/19-B1 1420)  
 (GA1.03/W/20-B3 1420)  
**Shay Lynn K.**  
 (P10/W/16-A4 1420)  
**Shcherbakova V. P.**  
 (GA1.05/E/19-A5 1200)  
 (GA1.05/E/20-A5 1140)  
 (GA1.05/E/21-A5 1220)  
**Shcherbakova V. V.**  
 (GA1.05/E/19-A5 1200)  
**Shea M. A.**  
 (GA 6.01/E/15-A5 1510)  
 (JA 45/E/07-B4 0945)  
 (JSA45/E/04-B4 0830)  
**Shearer Peter M.**  
 (ST4/W/20-B3 0840)  
 (ST4/W/44-B21640)  
 JSS13/W/19-A4 1620)  
**Shebalin Peter**  
 (ST1/W/03-A4 0930-27)  
 (ST1/W/35-A2 1400-21)  
**Shedlock K.**  
 (JSP23/C/U/5/E/16-A5 1620)  
 (ST3/E/56-B4 1400-20)  
 (ST5/E/10-B5 0930-08)  
**Sheehan R.**  
 (GA2.02/W/24-B5 1500)  
**Shefov**  
 (GA6.01/P11-A5 0900-22)  
**Shefov Nikolaj**  
 (JSA16/W/19-A3 0830-44)  
**Sheinin Vladimir I.**  
 (ST6/E/08-A1 0830-17)  
**Shelomentsev Vladimir**  
 (GA 5.06/E/03 A3 1500)  
 (GA3.03/E/02-B4 1400-02)  
**Shelting B. D.**  
 (GA4.03/W/02-B4 1115)  
**Shelton Alexander S.**  
 (ST2/W/19-A4 1215)

# INDEX

- Shen Chen**  
(GA3.10/E/02-A6 1645)  
(GA3.02/E/16-B3 0900-17)
- Shen Colin Y.**  
(P10/W/16-A4 1420)
- Shen Hung Tao**  
(HW3/W/16-B4 0900)
- Shen Jason Jiun-San**  
(JSV30/C/JSV22/E/11-B1 1400-17)
- Shen Jia-Lin**  
(JSV30/C/JSV22/E/17-B1 1400-21)
- Shen L.-F.**  
(ST1/E/90-A 11620)
- Shen Po Yu**  
(MC02/W/12-B1 0900)
- Shen Wei-Zhou**  
(JSV30/C/JSV22/E/16-B1 1400-20)  
(JSV30/C/JSV22/E/17-B1 1400-21)
- Shen Zheng-Kang**  
(G6/C/G1/W/36-B1 1500)  
(JSS31/W/10-B2 1030)
- Shengle Li**  
(ST1/E/41-A3 0900-09)
- Shengli Ma**  
(ST1/E/55-A2 1400-08)
- Shennan Ian**  
(JSG11/E/08-A3 1640)
- Shepard A Clough**  
(MI08/E/06-A4 1235)
- Shepherd G G**  
(JSM01/W/112-A2 1600-19)
- Shepherd Gordon**  
(JSA16/W/01-A3 0830-51)  
(JSA20/W/13-A4 1200-06)  
(JSA20/W/19-A4 1450)  
(JSM01/W/30-A4 1000)
- Shepherd John**  
(JSP23/C/U5/W/04-B2 0830-06)
- Shepherd John B.**  
(JSP23/W/24-B2 1150)
- Shepherd Marianna**  
(JSA20/W/13-A4 1200-06)
- Shepherd T G**  
(JSM01/W/61-A5 1430)  
(JSM01/W/09-A4 1620-05)  
(JSM01/W/63-A3 1500)  
(JSM01/W/24-A3 1630)  
(U3/W/10-A3 0930)
- Sherburn Steven**  
(JSV36/W/02-B3 0930)
- Sheremet V. I.**  
(GA1.02/E/36-A1 1050)
- Sheridan Kevin**  
(G1/E/11-A3 1620-52)  
(G6/C/G3/E/11-B2 1500)
- Sherman David M**  
(JSS02/C/ST6/W/09-A1 1400)
- Shermatov E**  
(HS1/W/26-B5 0830-03)
- Sherstukov Boris G.**  
(JSA16/W/04-A3 0830-37)
- Sherstyukov Boris**  
(JSA16/E/40-A3 0830-24)
- Sherwin T.**  
(P11/W/30-B5 1150-12)
- Sheshukov Sergei**  
(GA3.05/W/19-B3 0900-26)  
(GA3.03/E/02-B4 1400-02)
- Shettle Eric P.**  
(JSM01/W/04-A4 1510)
- Sheu Rong-Shyang**  
(JSM43/W/07-B5 1100)
- Shevchenko George**  
(JSS42/E/04-B5 1700-17)
- Shevchenko V. V.**  
(JSM41/E/32-B4 1010-03)  
(MC09/E/06-B2 1730)  
(JSA10/E/04-A2 1500)  
(JSA10/E/05-A3 1500-03)
- Shevchenko Vladimir**  
(G6/E/01-B1 1010)
- Shibata Akira**  
(JSM41/E/08-B4 1210)  
(JSP25/W/94-B3 1500)
- Shibuya H.**  
(GA1.03/W/29-B1 0900)
- Shi Che**  
(ST2/W/03-A3 1215)
- Shi Shunying**  
(ST1/P/13-A3 1720)
- Shi Yaolin**  
(JSP23/C/U5/E/21-B2 0830-11)
- Shibasaki Kazuo**  
(JSM01/W/74-A2 1600-17)
- Shibuya Kazuo**  
(JSG14/W/13-A3 1700-06)  
(JSH12/W/04-A4 1400-01)
- Shigeno K.**  
(JSS42/W/14-B5 0830)
- Shikaze Steven G.**  
(HW5/W/10-A3 0920)
- Shimada Jun**  
(HS4/W/04-A4 1105)  
(HS4/W/25-A5 1220)
- Shimada Mitsuhiko**  
(ST6/E/06-A1 0830-16)  
(ST1/E/56-A2 1400-37)  
(ST4/E/30-B1 0830-16)
- Shimada Seiichi**  
(JSG28/E/26-B1 1400-11)  
(JSG28/W/07-B1 1400-07)  
(JSS31/W/06-B3 0830-06)
- Shimamura H.**  
(JSS46/W/07-B4 1030)
- Shimazaki Kunihiko**  
(ST3/W/27-B4 1530)
- Shimizu Atsushi**  
(JSM01/W/91-A2 1600-23)
- Shimizu H.**  
(JWA34/W/07-B2 0910)
- Shimizu Hisayoshi**  
(GA1.02/W/05-A2 0930)
- Shimizu Shuji**  
(JSM24/E/02-B1 1440)
- Shimizu Yoshihisa**  
(JSP23/C/U5/W/19-A6 1720)
- Shimizu Yugo**  
(JSP25/W/25-B3 0830-06)
- Shimoizumi M.**  
(JSA15/W/14-A4 1400-16)
- Shimoike Yoichi**  
(JSV36/W/01-B3 0900-12)
- Shimokawa Koichi**  
(JSS42/W/14-B5 0830)
- Shimomura Osamu**  
(ST6/E/09-A2 1430)
- Shimura Koichiro**  
(GA1.03/L/01-B1 0940)
- Shin Tzay-Chyn**  
(JSP23/C/U3/W/21-B2 1740)  
(U3/W/21-A30900-17)
- Shina Hiroyuki**  
(GA4.10/E/05-A4 1005)
- Shinagawa Hiroyuki**  
(JSA20/E/18-A6 1118)
- Shindell D T**  
(MI02/W/09-A4 1220)
- Shindell Drew**  
(MW08/W/01-A2 1530)  
(MW08/W/06-A2 1730)  
(MC02/W/03-B2 0930)
- Shindo Shizuo**  
(HS4/W/18-A5 0950)  
(HS4/W/21-A5 1100)
- Shine K P**  
(MC07/W/04-A2 1115)  
(MC07/W/08-A2 1420)  
(MC07/W/19-A2 1520)  
(MW01/E/01-A5 1620)
- Shinkai Hitoshi**  
(P13/W/24-B1 1130)
- Shinohara Hiroshi**  
(JSV36/E/12-B3 0900-17)
- Shinohara I.**  
(GA3.08/W/28-B1 1510)
- Shinohara Manabu**  
(GA5.01/E/32 A1 0900-09)  
(JSA20/W/33-A5 1200-11)
- Shinohara Masanao**  
(JSS44/W/09-B4 0930-08)  
(ST4/W/34-B1 1400)
- Shinzaburo Fujiwara**  
(G5/L/06-A4 1400)
- Shiokawa K**  
(JSM01/W/01-A3 1140)  
(GA2.02/W/09-B4 0900)  
(GA3.04/W/45-B1 1520-45)
- Shiokawa Kazuo**  
(GA3.06/E/11-A2 1700)  
(GA3.10/E/05-A6 0830)  
(JSM01/E/30-A2 1600-24)  
(GA2.02/E/13-B4 1100)  
(GA2.03/E/02-B3 1120)
- Shiotani Masato**  
(JSM01/E/02-A5 1130)  
(MC06/W/01-A1 1650)  
(JSM26/W/34-B2 1510)
- Shirapov D. Sh.**  
(GA3.03/E/01-B4 1400-03)  
(GA3.03/E/04-B4 1530)
- Shirasaki Yuichi**  
(JWA34/W/11-B2 1110)
- Shirman Boris**  
(GA5.01/W/19 A1 1600)
- Shirman Mikael**  
(JSA17/W/03-A4 1230)
- Shirochkov Alexander**  
(JSA16/E/05-A3 0830-04)  
(JSA45/W/17-B5 1110-07)  
(JSA45/W/19-B4 1550)
- Shirooka Ryuichi**  
(JSM24/E/02-B1 1440)
- Shirshov P. P.**  
(P12/E/01-A1 1030-04)  
(P12/W/06-A1 1030-10)
- Shishikura Shin**  
(JSV36/E/17-B3 1400-09)
- Shishkina Olga**  
(JSP39/L/04-B3 1503-22)  
(JSP39/L/05-B2 1740)  
(P13/L/02-B1 1740)
- Shiyin Liu**  
(HS2/W/16-B2 0920)  
(HS2/W/19-B2 1020)  
(HS2/W/20-B2 1040)  
(HS2/W/14-B1 1620)
- Shi-Yu Li**  
(ST1/E/50-A2 1400-36)
- Shi-Zhuang Ma**  
(GA1.02/W/36-A1 1430)  
(JSA17/W/08-A4 1030)
- Shkyar D. R.**  
(U3/E/03-A3 0900-02)
- Shmakin A. B.**  
(HW4/E/17-B2 1610)  
(JSM24/W/08-B2 1155)  
(JSM24/W/09-B2 1215)
- Shneyer Vitaly S.**  
(JWA34/E/01-B2 1740)
- Shogenov V.**  
(GA4.04/L/10-B5 1400-05)  
(GA4.04/L/11-B5 1400-06)
- Shogenova Alla**  
(GA1.05/W/09-A5 1540)  
(ST6/W/12-A1 0830-12)
- Shoichiro Fukao**  
(GA2.03/E/02-B3 1120)
- Shoji Kusunoki**  
(MC01/E/13-A1 1130)
- Shook K. R.**  
(HS2/W/11-B1 1420)
- Short J.-J.**  
(GA3.04/W/25-B1 1520-38)
- Shorter J A**  
(G3/W/30-A5 1610-06)
- Shoshany M.**  
(P15/L/19-B3 1500)
- Shounian Guo**  
(JSS44/p/04-B5 1050)
- Shoutilin Sergey**  
(P13/E/13-B2 1600-01)
- Showail Abdallah Ahmed**  
(GA5.12/W/09-A2 1600-10)
- Shrestha S**  
(HS5/W/19-A2 1200)
- Shu Saibing**  
(ST2/E/57-A3 1430)
- Shu Tung-Shin**  
(GA3.02/L/03-B2 1055)
- Shuai Ping**  
(ST1/P/13-A3 1720)
- Shuckburgh Emily**  
(JSM26/E/21-B3 1050)
- Shufen Sun**  
(JSM04/W/07-A2 1200)
- Shukla J**  
(MC01/E/02-A4 1430)  
(MC01/L/02-A1 1145)
- Shukla P. K.**  
(GA3.04/E/14-B1 1520-03)
- Shukowsky Vladimir**  
(G5/E/07-A4 1554-08)  
(G5/E/08-A4 1556-09)  
(JSS44/E/12-B4 0930-03)  
(JSS44/E/45-B4 0930-41)
- Shulman Georgy E.**  
(P11/L/07-B5 1745)
- Shum C. K.**  
(JSM41/W/06-B4 1545)  
(JSG11/E/10-A3 1400)  
(JSG11/W/17-A4 1150)  
(G3/E/43-A5 1610-17)  
(JSA09/E/02-A2 1115)
- Shuman Vladimir**  
(GA1.02/E/08-A1 1050)
- Shumila V.**  
(ST1/E/72-A4 0930-08)  
(ST1/E/75-A3 0950)  
(ST1/W/21-A4 0930-01)
- Shumilov Oleg**  
(JSA16/E/21-A3 0830-08)
- Shumilov S.**  
(JWS33/W/08-B2 1635-26)  
(JWS33/W/08-B3 0900-26)
- Shuoyu Zhou**  
(ST1/W/56-A1 1700)
- Shutes Brian**  
(HS5/W/12-A2 0920)
- Shuto Nobuo**  
(JSS42/E/15-B4 1000)  
(JSS42/E/21-B5 1420)  
(JSS42/P/01-B5 1210)  
(JSS42/W/08-B4 1400)
- Shuttleworth James W.**  
(HW4/W/01-B2 1200)  
(MI06/W/01-B2 1710)  
(MC01/W/13-A3 1635)  
(MC01/W/53-A3 1650)
- Shutts G J**  
(MI05/W/27-A4 1400-08)
- Shuvaeva Natalia L.**  
(JSM24/W/09-B2 1215)
- Shuzo Takemoto**  
(ST4/W/26-B1 0830-18)
- Shved G M**  
(JSM01/C/MW07/E/01-A2 1540-31)  
(JSM01/C/MW07/E/02-A2 1600-32)  
(MW05/E/03-A2 1230)  
(MW05/W/06-A2 1040-02)
- Shyllon E. A.**  
(G4/E/23-A3 1620-20)  
(JWS33/E/15-B2 1635-28)  
(JWS33/E/15-B3 0900-28)
- Sibeck D.**  
(GA3.02/W/58-B3 0900-22)  
(GA3.03/L/01-B4 1400-04)  
(GA3.02/W/15-B2 1005)
- Sibeck D. G.**  
(GA3.07/W/65-A3 0900-14)
- Sichingabula Henry M.**  
(HS1/W/31-B5 1720-01)
- Siddans Richard**  
(JSM26/W/19-B2 1700-13)
- Sideris G.**  
(JSP23/W/38-B2 1720)
- Sideris Michael**  
(G3/L/01-A5 1610-61)  
(G3/W/22-A5 1610-07)  
(G3/W/49-A5 1610-78)  
(G4/W/22-A3 1620-18)
- Sidi C.**  
(JSP49/W/21-B5 1620)
- Sidorenko G.**  
(G3/E/26-A5 1610-36)
- Sidorin A.Ya.**  
(ST1/E/53-A2 0930-11)
- Sidorin Igor**  
(ST4/W/01-B3 1100)
- Sidorin I**  
(JSS02/C/ST6/W/01-A1 1515)
- Sidorov V. I.**  
(GA3.02/E/12-B3 0900-01)
- Sidorova Larissa**  
(GA2.07/W/06-A1 1610)  
(GA2.07/W/09-A2 0930-03)
- Siebert A.**  
(JSP23/C/U5/W/13-A5 1440)
- Siebert K D**  
(GA3.10/W/02-A6 1615)
- Siebesma A. P**  
(MI04/W/33-B1 1535)  
(MI10/W/07-B3 1435)
- Siebesma Pier**  
(MI10/W/11-B3 1615)  
(MI03/W/02-A3 1500)
- Siedler Gerold**  
(P12/W/04-A1 1500)
- Siefring C L**  
(JSM03/W/03-A1 1420)
- Siehl A.**  
(JWS33/W/08-B2 1635-26)  
(JWS33/W/08-B3 0900-26)
- Siems Steve**  
(JSP21/L/01-A4 1010)
- Sierk Bernd**  
(JSG28/W/06-B1 1400-06)  
(MI06/W/18-B1 1400-04)  
(MI06/W/18-B2 1400-04)
- Siero F. J.**  
(GA1.15/W/08-B4 1445)



- Sigmundsson Freysteinn**  
(ST5/W/14-B3 0900-06)
- Signer Thomas**  
(G1/W/05-A3 1620-34)  
(G1/W/21-A3 1620-08)
- Sigsbee K.**  
(GA3.03/W/11-B4 1200)  
(GA3.02/W/40-B3 1050)
- Sigwarth J. B.**  
(GA3.08/E/01-A6 1430)  
(GA3.02/W/18-B2 1645)  
(GA3.03/W/05-B4 1110)  
(GA3.08/W/29-A6 1400)
- Sihra Kamaljit**  
(MC09/W/11-B2 1500)  
(MC07/W/19-A2 1520)
- Siili T.**  
(MC09/W/07-B2 01)  
(MC09/W/01-B2 04)  
(MC09/W/01-B2 1200)
- Sikharulidze David**  
(ST1/C/GA4.10/E/01-A4 0930-43)
- Silbergleit Virginia**  
(JSA16/C/GA4.07/W/34-A3 0830-55)  
(JSA16/W/22--A3 0830-35)  
(MI02/W/04-A5 0930)
- Sililo Oliver T. N.**  
(HS5/W/23-A2 1445)
- Sillard Patrick**  
(G1/C/G5/E/02-A3 1620-101)  
(G6/E/04-B1 0830)
- Silva Agenor Cunha da**  
(PW1/W/06-A6 1400)
- Silva Ana-Maria**  
(MI09/E/08-A5 1645)
- Silva Luis Felipe Alberca**  
(JSA35/E/01-B1 1420)
- Silveira Graca**  
(ST4/W/25-B2 1720)
- Silver Paul**  
(ST4/E/15-B3 1000)
- Silver Paul G.**  
(JSS07/E/11-A2 1155)  
(JSS07/W/01-A2 1125)
- Silvia Marta**  
(G5/E/08-A4 1556-09)
- Simberova S.**  
(GA4.02/W/34-A4 1525)
- Simek Jaroslav**  
(G1/E/57-A3 1620-81)  
(G3/E/08-A5 1610-95)
- Simeonov Petio**  
(JSM01/E/06-A2 1600-13)
- Simkanin J.**  
(GA1.01/E/15-A6 1145)
- Simmonds Ian**  
(JSM18/W/01-A4 1640)  
(JSM18/W/12-A4 1600)  
(MI05/W/05-A1 1010)  
(JSM24/W/11-B2 0930)  
(JSM24/W/12-B2 0950)  
(JSP25/W/72-B3 1700)  
(MC02/W/06-B2 1630)
- Simmonds P.**  
(JSP21/E/04-A5 1110)
- Simmonds Peter**  
(JSP21/E/02-A4 0930)  
(JSP21/W/13-A4 0950)
- Simnett George**  
(GA4.02/W/16-A4 0945)
- Simon Bernard**  
(JSG11/W/13-A4 1400-09)  
(U7/W/14-B1 0830-12)
- Simon D.**  
(JSG14/E/21-A3 1700-18)
- Simon Pascal**  
(MW01/W/02-A5 1150-04)
- Simoneau Pierre**  
(MW07/W/18-A4 1510)
- Simonich Dale**  
(JSM01/W/19-A2 1600-07)
- Simonovic S. P.**  
(HS1/W/77-B5 1600)
- Simons W. J. F.**  
(G5/L/01-A4 1145)
- Simonyan Anahit**  
(GA1.01/E/07-A5 0900-15)
- Simpson J. H.**  
(P10/E/04-A5 1600-07)  
(P10/E/05-A4 1600)  
(P09/W/04-A1 1440)  
(P10/L/05-A4 1150)  
(P14/E/10-A4 1540)  
(P10/W/08-A3 0950)  
(PW1/W/05-A6 0920)
- Singer Brad**  
(JSV36/W/07-B3 1400)
- Singer Bradley**  
(GA1.15/E/06-B4 1645)  
(VS3/W/25-B3 1620)
- Singer H. J.**  
(GA3.08/W/21-A6 0900)  
(GA3.02/W/40-B3 1050)  
(GA3.02/W/21-B2 1520)
- Singer Silvia**  
(GA1.04/W/07-A4 0930-02)  
(GA1.04/W/32-A5 1510)
- Singer W**  
(MW04/W/01-A1 0950)  
(JSM 32/E/04-B2 1005)
- Singer Werner**  
(JSM01/C/MW07/W/09-A2 1600-34)  
(JSM01/E/04-A2 1130)
- Singh A. K.**  
(GA1.02/W/32-A2 0930)  
(GA1.02/W/34-A1 1050)
- Singh A. K.**  
(HW3/W/18-B4 0950)
- Singh B. P.**  
(JSA37/L/01-B3 1730)
- Singh D. D.**  
(ST4/W/54-B1 1620)
- Singh H.**  
(JSM26/W/18-B2 1550)
- Singh Harsh**  
(ST3/P/7-B4 1500)
- Singh Khalsa Siri Jodha**  
(JWS33/W/33-B3 0900-32)
- Singh Kumar Abhay**  
(HW5/W/13-A3 1140)
- Singh R**  
(JSV29/P/01-B1 1400-04)  
(JSM41/P/01-B3 1235)
- Singh R. B.**  
(HS5/W/52-A3 1630-03)  
(HW1/L/12-A4 1430)  
(HS1/W/72-B5 0830-08)
- Singh R. N.**  
(JSS44/E/39-B4 0930)  
(ST4/E/26-B1 1220)
- Singh Ramesh P.**  
(JSP23/W/99-B2 0830-03)
- Singh S. K.**  
(ST2/E/24-A3 1700)  
(ST5/W/17-B3 0850)
- Singh Satish**  
(JSS46/E/03-B4 1420)
- Singh Shri Krishna**  
(JSS42/W/19-B5 1700-18)
- Singh Vijay P.**  
(U7/E/04-B1 0830-05)
- Sinha H. S. S**  
(GA 2.02/E/16-B4 0930-19)  
(GA 2.02/E/07-B4 0930-20)  
(GA2.02/E/05-B5 1120)
- Sinha Martin**  
(JSA40/W/12-B5 0920)
- Sinito Ana M.**  
(GA1.03/W/12-B2 1520)  
(GA1.03/W/21-B3 1000)  
(GA1.05/W/26-A6 1200)
- Sinityn V. I.**  
(ST3/W/17-B4 0930-17)
- Sinkula Bruce**  
(JSM41/E/28-B3 1515)
- Sinogeikin S V**  
(ST6/C/JSS02/W/08-A2 1720)
- Sinyakov Valery P.**  
(MI06/W/08-B1 1400-01)  
(MI06/W/08-B2 1400-01)
- Sinyova Zlata I.**  
(ST5/L/01-B3 0900-14)
- Siporski L.**  
(G3/E/26-A5 1610-36)
- Siren C.**  
(GA4.02/W/28-A4 1720)
- Sirenko Lena**  
(GA3.04/E/08-B1 1520-01)
- Sirne Ricardo**  
(JSA16/C/GA4.07/W/34-A3 0830-55)
- Siscoe G L Siscoe**  
(GA3.10/W/02-A6 1615)
- Sitar R. J.**  
(GA3.07/W/43-A6 0900-19)
- Sivan Dorit**  
(JSG11/W/06-A3 1720)
- Sivaramkrishnan S.**  
(JSM43/W/10-B5 0900)
- Sizov Yury**  
(JSA16/W/02-A3 0830-49)
- (JSA16/W/24-A3 0830-45)
- Sizova Lilia**  
(GA3.06/W/33-A2 0930-23)
- Sjoberg Lars E**  
(G4/E/03-A3 1620-29)  
(G1/C/G5/E/05-A3 1620-98)  
(G5/E/03-A4 1552-07)
- Skacelov Zuzana**  
(ST2/L/05-A5 1400-17)
- Skachko S. N.**  
(JSP49/W/09-B5 1720)
- Skagseth Oystein**  
(P11/W/09-B3 1500)
- Skaloud J**  
(G4/E/11-A3 1620-14)
- Skalsky Alexander**  
(GA3.07/W/29-A3 0900-15)
- Skamarock W. C.**  
(MC04/L/01-B1 1100)
- Skiba Yuri**  
(JSP39/W/26-B3 1506-23)
- Skilbrei Jan Reidar**  
(JSS44/E/11-B4 0930-29)  
(GA5.12/E/06-A2 1600-03)  
(JSA09/W/21-A3 1045)
- Skilling Ian**  
(VS2/W/23-B3 1400-16)  
(VS2/W/24-B3 1400-17)
- Skinner W**  
(JSM01/W/107-A1 1510)
- Sklower K.**  
(U3/W/14-A3 0900-15)
- Skobeleva T. P.**  
(JSA10/E/04-A2 1500)
- Skobeltsyn**  
(GA3.02/W/49-B3 0900-11)
- Skone Susan**  
(G1/E/48-A3 1620-01)  
(JSA06/E/04-A1 1155-06)
- Skoug R. M.**  
(GA4.01/W/05-A2 1450)
- Skovorodkin Yu. P**  
(JSA19/E/02-A4 1400-09)
- Skrivankova P**  
(JSM01/W/37-A5 1400)
- Skura Joseph P.**  
(GA3.03/W/12-B4 1400)
- Slavin J. A.**  
(GA3.03/W/07-B4 1450)  
(GA3.04/L/04-B1 1210)
- Slavina Lidia B.**  
(ST1/W/32-A2 0930-08)
- Slavov Slavey**  
(ST3/W/51-B4 1415)
- Slawomir Kaczmarek**  
(P15/W/09-B4 1115)
- Sledzinski J**  
(G3/E/11-A5 1610-31)
- Sledzinski Janusz**  
(G5/E/17-A4 1520-11)
- Sleeman Reinoud**  
(ST5/W/03-B3 1420)  
(ST5/W/35-B3 0900-08)
- Slejko D.**  
(ST3/E/56-B4 1400-20)  
(ST3/W/18-B3 1500)  
(JSP23/C/U5/E/16-A5 1620)  
(JSP23/W/16-A6 1520)  
(JSP23/W/17-A6 0830)
- Slingo Anthony**  
(MC08/E/07-A3 0900)
- Slingo J.**  
(JSP25/W/17-B2 1620)
- Slingo J. M.**  
(JSP25/E/05-B1 1110)
- Slingo Julia**  
(JSM26/E/02-B2 1020)  
(JSP25/W/08-B2 1110)  
(MW02/W/02-B3 1120)
- Slingo Lahoz J**  
(MC01/W/42-A1 1015)
- Slobodan P. Simonovic**  
(JWS33/W/14-B2 1200)
- Sloyan Bernadette**  
(P12/W/13-A1 1440)
- Slunga Ragnar**  
(ST1/W/29-A4 0930-34)  
(ST1/W/57-A3 1110)  
(ST2/W/24-A5 1400-30)  
(ST5/W/13-B3 1640)
- Slunyaev Alexey**  
(JSP39/E/07-B3 1418-07)
- Smalley Robert**  
(JSS31/E/04-B2 1400)
- Smart D. F.**  
(JSA 45/E/07-B4 0945)  
(JSA45/E/04-B4 0830)  
(GA 6.01/E/15-A5 1510)
- Smeed D. A.**  
(P11/W/19-B4 1500)  
(P11/W/28-B4 1400)
- Smellie J. L.**  
(JSV30/L/01-B1 1400-15)
- Smethurst Mark**  
(GA1.04/W/01-A4 0950)
- Smirnov Ruslan**  
(JSA16/W/05-A3 0830-43)
- Smilauer J.**  
(GA2.03/E/07-B3 1500)
- Smirnov A. I.**  
(GA2.03/L/01-B3 1400)
- Smirnov E. Ya.**  
(ST4/W/58-B2 0930-28)
- Smirnov V. F**  
(GA2.07/E/01-A2 0930-10)
- Smirnova Natalia**  
(JSP23/W/32-B1 1130)  
(JSP23/W/33-B1 0830-02)  
(JSP23/W/34-B1 0830-15)
- Smirnova Tanya**  
(MC04/E/07-B2 1425)
- Smirnova Tatiana G**  
(MC01/W/05-A3 1430)
- Smit M.**  
(G6/C/G3/W/08-B2 1120)
- Smit Martijn**  
(G2/E/11-A2 1630-24)  
(G2/W/08-A2 1630-22)
- Smit Patrick**  
(ST3/E/52-B3 1445)  
(ST3/W/40-B3 1430)
- Smith**  
(GA4.01/E/02-A2 1400)
- Smith A.**  
(JSP39/W/40-B2 1620)
- Smith A. D.**  
(JSS44/W/14-B4 0930-12)  
(JSS13/W/12-A5 1520)
- Smith A M**  
(GA3.10/W/19-A6 1005)
- Smith Alan**  
(JSV36/E/13-B3 1445)
- Smith Andrew**  
(MI06/E/07-B2 1400-10)
- Smith Andy J.**  
(GA3.04/W/51-B1 1520-20)
- Smith Anne K**  
(JSM01/W/17-A3 1540)
- Smith C. L.**  
(P10/E/06-A5 1050)
- Smith D A**  
(MI03/W/05-A3 1140)
- Smith D. E.**  
(G5/E/10-A4 1522-12)  
(G6/E/03-B1 0910)
- Smith David**  
(MI05/W/33-A5 1130)  
(JSP39/E/02-B4 1520)
- Smith Dr. Dru**  
(G3/W/56-A5 1440)
- Smith E. J.**  
(GA4.01/W/13-A2 1420)  
(GA4.03/E/03-B4 1130)  
(MC09/W/04-B2 1030)
- Smith Edward J.**  
(GA4.04/E/06-B5 0920)
- Smith Eric**  
(ST6/E/01-A2 1730)
- Smith Gideon P.**  
(JSA09/W/15-A3 0830)
- Smith Ian**  
(JSV30/E/05-B1 0940)  
(JSV36/E/19-B3 0900-18)
- Smith Ian E. M.**  
(JSV30/E/01-B1 0920)  
(JSV30/E/01-B1 1400-10)  
(JSV30/E/04-B1 1400-11)
- Smith Ian N.**  
(JSP25/W/22-B1 1400)  
(JSP23/W/04-A5 0910)
- Smith J.**  
(JSM41/E/19-B4 1750)
- Smith J. P.**  
(GA4.08/W/05-B3 1335)
- Smith John N.**  
(P07/L/01-A3 0905)
- Smith Leonard A.**  
(MI11/W/04-B5 1515)
- Smith Neville**  
(JSM41/W/33-B3 1000)

## INDEX

- (JSP25/W/58-B1 1130)  
(U7/W/17-B1 1425)
- Smith P. N.**  
(GA3.02/E/17-B3 0900-18)
- Smith P R**  
(JSA06/E/06-A1 1155-19)  
(GA3.10/E/06-A6 1700-10)
- Smith R.**  
(GA3.03/W/06-B4 1640)
- Smith R. N. B**  
(MI04/E/18-B3 1505)
- Smith R W**  
(JSM01/E/39-A1 0940)
- Smith Raymond**  
(P15/L/01-B4 1205)
- Smith Richard D**  
(MC01/E/12-A2 1215)
- Smith Roderick**  
(MC01/W/47-A4 1005)
- Smith Ronald**  
(JWM08/W/14-A3 1140)  
(JWM08/E/04-A3 0930)
- Smith Samantha**  
(MI04/E/24-B1 0900-17)  
(MI10/E/09-B4 1205)
- Smith Sharon L.**  
(HS2/W/09-B1 1200)
- Smith Tracy**  
(MC05/E/03-B4 1210)
- Smith W. A. Nimmo**  
(P10/E/12-A4 1050)
- Smith W. S.**  
(MI10/W/19-B3 1715)
- Smith William L.**  
(MI06/W/09-B1 0930)
- Smithers Jeffrey**  
(HS1/W/34-B5 1120)
- Smithson M.**  
(P16/W/01-B5 1620)
- Smithson M. J.**  
(P13/W/04-B2 1600-09)
- Smolka A.**  
(JSP23/C/U5/W/13-A5 1440)
- Smriglio Guiseppe**  
(JWA34/W/10-B2 0950)
- Smyshlyayev Sergei P.**  
(MI12/W/08-B4 1710)
- Smythe David K**  
(JSA19/W/12-A4 1000)
- Smythe-Wright Denise**  
(JSP21/E/03-A4 1700)  
(JSP21/W/03-A4 1420)
- Snee L. W.**  
(JSV30/W/01-B1 1400-04)
- Sneeuw Nico**  
(G2/E/11-A2 1630-24)  
(G2/W/08-A2 1630-22)
- Snegirev A. M.**  
(HW3/W/11-B4 1610)  
(HW3/W/12-B4 1635)
- Sneyers Raymond**  
(GA6.01/P/03-A5 1400)
- Snider Jefferson R**  
(MI01/W/06-A2 1200)
- Snitil B.**  
(JSV36/W/24-B3 1400-05)
- Snoke Arthur**  
(ST4/E/05-B1 1520)
- Snow K**  
(JSG11/W/17-A4 1150)
- Snow Marty**  
(SA16/E/22-A3 0830-16)
- Snowden C. B.**  
(U8/E/07-B3 1640-07)
- Snyder C**  
(MI05/L/04-A3 0900)
- So Gu Kim**  
(ST2/E/39-A3 0900)
- Soares Antonio**  
(GA1.02/W/40-A2 0930)
- Soares Carlos Roberto**  
(G1/W/09-A3 1620-36)
- Soares Jose Eduardo**  
(ST1/W/20-A4 0930-04)
- Soares Pedro M. M.**  
(JSM43/W/03-B4 1400)  
(JSM43/W/13-B4 1420)
- Soares S. M.**  
(GA2.03/W/05-B3 1400-02)  
(GA2.03/W/05-B3 1600)
- Sobchakov**  
(GA2.03/W/09-B3 1030)
- Sobchakov L. A.**  
(GA2.03/L/01-B3 1400)  
(GA2.03/L/02-B3 1520).
- Sobel Adam H.**  
(JSM26/W/32-B1 1150)
- Sobisevich Alexey L.**  
(ST1/W/18-A4 0930-19)  
(ST1/W/19-A4 0930-03)
- Sobisevich Leonid E.**  
(ST1/W/18-A4 0930-19)  
(ST1/W/19-A4 0930-03)
- Sobol V.**  
(ST3/P/9-B4 1400-22)
- Sobolev G.**  
(JSP23/W/38-B2 1720)
- Sobolev G. A.**  
(ST6/W/05-A1 0830-07)  
(JSA15/W/01-A5 0830-07)  
(ST1/W/07-A3 0900-05)  
(ST1/W/08-A1 1440)  
(ST1/W/11-A2 1400-28)  
(ST1/W/38-A2 0930-02)  
(SW1/W/04-B5 1200)
- Sobolev Yakov**  
(U8//02-B3 1030)
- Sobral J. H. A.**  
(GA2.02/W/08-B5 0920)  
(JSA20/C/GA2.02/w/20-A5 1200-12)  
(JSA20/W/24-A5 1200-07)
- Sochevanova N. A.**  
(GA5.12/L/01 A2 1010)
- Soffel H.**  
(GA1.04/W/18-A4 1120)
- Soffel Heinrich**  
(GA6.01/E/18-A5 0900-01)  
(GA6.01/E/18-A5 0900-02)  
(GA6.02/E/11-B1 1730)  
(ST4/E/14-B1 0920)
- Soffel Heinrich C.**  
(JSS44/E/14-B4 0930-30)
- Sofia Sabatino**  
(JSA16/W/16-A3 1130)
- Sofield D J**  
(U4/W/05-A41215)  
(JSP23/C/U4/W/05-A6 0830-19)
- Sofko George**  
(GA3.08/E/03-B1 1000)
- Sohn Byung-Ju**  
(MI09/E/04-A5 1145-03)
- Sojka J. J.**  
(GA2.07/W/12-A1 1120)  
(GA5.06/W/05 A3 1520)  
(GA3.09/W/06-B5 0925)
- Sokolik Irina N**  
(MI01/L/06-A1 1110)
- Sokoloff D.**  
(GA1.01/E/09-A5 0900-01)  
(GA1.01/W/26-A5 1015)
- Sokolov Serguei**  
(P12/W/09-A1 1700)  
(P12/W/22-A1 0910)
- Sokolov Vladimir**  
(ST3/E/11-B4 1400-17)  
(ST3/E/12-B4 1400-16)  
(ST3/E/20-B4 0930-10)  
(ST3/E/32-B4 0930-09)
- Sokolova Inna**  
(ST1/E/21-A4.0930-06)
- Sokolovskiy Sergey**  
(JSG28/W/25-B2 1400-11)
- Sokov A. V.**  
(P12/W/15-A1 1030-01)  
(P12/W/16-A1 1030-02)
- Sol Jose German**  
(JSA35/E/01-B1 1420)
- Solanki Sami**  
(JSA16/W/06-A3 0830-48)  
(JSA16/W/36-A3 0930)
- Solarino S.**  
(ST5/E/18-B1 0830-12)
- Soler-Arechalde A. M.**  
(GA1.05/W/07-A6 0900-06)
- Soliman Nagy**  
(JSA19/L/04-A4 1400-01)
- Solodilov Leonid**  
(ST2/P/10-A4 0945)
- Solomon Philip M.**  
(MI12/E/02-B5 1115)
- Solomon S. C.**  
(JSA45/E/10-B4 1125)
- Solomon Stanley C.**  
(JSA16/E/12-A3 0830-14)
- Solomon Susan**  
(MI02/W/11-A5 1410)  
(JSM26/W/04-B2 1130)  
(MI04/W/14-B2 1120)  
(U6/E/02-B2 1400)
- Solov'ev Mark V.**  
(P11/W/17-B5 1400)
- Soloviev Alexandre**  
(ST2/E/41-A4 1445)  
(ST1/E/35-A2 1400-34)  
(ST1/W/43-A2 1440)
- Solovieva Maria S.**  
(ST4/W/11-B2 0930-04)
- Solovjova T V**  
(JSM01/W/72-A2 1600-02)  
(MW04/W/01-A1 0950)  
(JSM01/W/69-A1 1130)
- Solovyev S.I.**  
(GA3.07/E/17-A6 0900-10)  
(GA3.04/E/15-B1 1520-02)
- Solovyova Tatyana**  
(JSM01/E/07-A2 1000)
- Somayajulu B. L. K.**  
(P07/E/03-A3 1430)
- Somayajulu V. V.**  
(JSA20/E/12-A5 1400)
- Somoza Ruben**  
(GA1.04/L/05-A6 1500)  
(GA1.04/W/07-A4 0930-02)  
(GA1.04/W/32-A5 1510)
- Somsikov Vjacheslav M.**  
(GA2.02/L/02-B4 0930-05)  
(GA2.03/E/06-B3 1400-06)
- Son V T**  
(GA5.01/E/25 A1 1530)
- Sona Giovanna**  
(G3/E/18-A5 1610-68)
- Song Inseong**  
(G1/L/18-A3 1620-31)
- Song Myung-Duk**  
(MW07/W/07-A4 1640)
- Song P**  
(GA3.10/E/09-A6 1600)  
(GA3.05/W/38-B3 1700)
- Song Yan**  
(GA3.02/W/34-B3 1120)  
(GA3.04/W/32-B2)  
(GA2.07/W/23-A1 1220)
- Song-You Hong**  
(MW03/E/01-B4 1655)
- Sonnerup Buo**  
(GA3.10/W/02-A6 1615)
- Sookoletsy L.**  
(P15/L/19-B3 1500)
- Soon Willie**  
(GA6.01/W/18-A5 1455)
- Sopeña Alfonso**  
(GA1.15/W/03-B4 1530-06)
- Sorensen M. B.**  
(JSG28/W/17-B2 1400-05)  
(JSG28/W/23-B2 1130)
- Sorenson S. A.**  
(JSP39/W/28-B4 1540)
- Sorokin Valery**  
(GA2.02/W/29-B4 0930-03)  
(JSA15/W/22-A5 1400-18)
- Sorooshian Soroosh**  
(HW4/W/01-B2 1200)  
(JSG28/W/01-B2 1400-16)
- Sosnovets Elmar N.**  
(GA3.05/W/20-B3 0900-16)  
(GA3.05/W/41-B3 0900-24)  
(JWS33/W/20-B2 1635-21)  
(JWS33/W/20-B3 0900-21)  
(GA3.10/W/14-A6 1700-16)  
(JSA09/W/22-A3 1230)
- Sothern R. B.**  
(GA6.01/E/04-A5 0900-07)
- Sotirelis Thomas**  
(GA3.03/W/12-B4 1400)  
(GA3.08/W/25-A6 1130)
- Soudarin L**  
(JSG11/E/04-A3 0910)  
(JSG11/E/16-A4 1030)  
(JSG14/E/02-A3 1700-05)
- Soufflet Veronique**  
(MI01/E/02-A1 0900-07)
- Soulsby C**  
(HS4/W/15-A4 1730)
- Soukharev Boris**  
(JSA 45/E/01-B4 1740)  
(JSA45/E/06-B5 1110-08)  
(MI12/E/01-B4 1610)
- Soulis E. D.**  
(HS2/W/12-B1 1540)
- Souprayen Claude**  
(MW07/W/13-A4 1720)  
(MW07/W/04-A4 1130)
- Souriau Annie**  
(JSA17/E/05-A4 1210)
- Sousounis Peter**  
(HS3/W/28-A2 1515)
- Southon J.**  
(P07/W/10-A3 1510)
- Souvermezoglou Ekaterini**  
(P11/E/28-B5 0950)
- Souza Alejandro J.**  
(PW1/W/05-A6 0920)  
(P10/W/08-A3 0950)
- Soward Andrew**  
(GA1.01/E/16-A5 0900)
- Sowle Dave**  
(MI10/W/03-B2 1205)
- Spacek L**  
(MI01/L/04 1055)  
(MI01/W/03-A1 0900-03)
- Spahr J. A**  
(U3/W/08-A30900-13)
- Spakman W.**  
(U8/E/09-B3 1155)
- Spallarossa D. Eva E.**  
(ST5/E/18-B1 0830-12)
- Spampinato Salvatore**  
(JSV47/W/09-B5 1200)
- Spang Reinhold**  
(JSM01/E/19-A5 0900)  
(JSM01/E/28-A4 1430)
- Spann J.**  
(GA3.03/E/07-B4 1020)  
(GA3.02/W/33-B3 0900-16)
- Spann J F**  
(GA3.10/W/10-A6 1700-03)
- Spano Massimo**  
(JSA09/E/09-A3 1015)
- Sparks J.**  
(JSV36/C/JSA15/W/34-B3 1415)
- Sparks R. S. J.**  
(U6/E/06-B2 1105)  
(VS2/W/12-B3 1400-09)  
(VS2/W/14-B3 1150)
- Sparks Stephen**  
(VS2/W/16-B3 0910)
- Sparks Steve**  
(VS2/W/08-B3 1400-06)  
(JSP23/W/08-A5 0830-03)
- Spirling L. C.**  
(JSM26/E/22-B1 1210)
- Spirling Lynn**  
(MW01/W/06-A5 1400)
- Spataro W.**  
(JSP23/E/57-B1 0830-09)
- Spatharas V.**  
(GA1.03/W/30-B3 1400)
- Speich Sabrina**  
(P11/L/03-B5 0910)
- Spence Harlan E.**  
(GA3.03/W/03-B4 0930)  
(GA3.05/E/04-B3 0900-09)  
(GA4.08/W/18-B4 0830)
- Speranza F. Fattori**  
(ST1/W/45-A2 1400-39)
- Sperber Ken**  
(MC01/E/14-A3.1000)  
(MC01/L/12-A3 1020)
- Sperner Blanka**  
(ST2/W/11-A4 1430)
- Spicak Ales**  
(ST2/E/33-A3 1130)  
(ST2/E/37-A5 1400-07)
- Spichak Vjacheslav**  
(GA1.02/E/09-A1 1530)  
(GA1.02/E/20-A1 1605)  
(JSV36/E/14-B3 0945)
- Spiro R. W.**  
(GA3.09/E/05-B4 1625)
- Spitzer Klaus**  
(JSA27/W/02-B1 0920)  
(GA1.02/W/02-A2 0930)  
(GA1.02/W/04-A2 0930)  
(GA1.02/W/29-A1 0900)
- Spohn T.**  
(JSA10/W/03-A2 0930)
- Sposato A.**  
(VS3/E/02-B3 1550)
- Sprenger M.**  
(JWM08/E/06-A2 1120)
- Springer T.**  
(G1/E/31-A3 1620-65)  
(G2/L/02-A2 0945)
- Springer Tim**  
(G6/C/G1/E/32-B1 1400)
- Spuehler E.**  
(ST5/L/02-B3 0900-02)
- Sreedevi M. G.**  
(P09/E/02-A2 0950)
- Sreelatha. P.**

- (MI06/W/25-B2 1130)  
**Srefanov Petar**  
 (JSP23/E/30-A5 0830-14)  
**Sridevi Jade**  
 (ST2/W/33-A5 1400-08)  
**Sridharan R.**  
 (JSA20/E/24-A5 1200-04)  
 (JSA20/W/20-A5 1135)  
 (JSA20/W/23-A5 1200-03)  
 (JSA20/W/56-A4 1200-26)  
**Sridharan S.**  
 (JSA20/W/10-A5 1200-02)  
**Srinagesh D.**  
 (ST2/E/10-A3 1645)  
 (ST2/E/24-A3 1700)  
**Srinivasan G**  
 (MC01/W/19-A1 1715)  
 (MC01/W/29-A3 1205)  
**Srinivasan R**  
 (ST2/E/42-A3 1630)  
**Srinivasan Vajapeyam S.**  
 (HS3/W/12-A1 1515)  
**Srivastava H N**  
 (MI02/P/01-A5 1600)  
 (JSA15/P/04-A4 1400-06)  
 (JSP23/L/08-A5 0830-18)  
 (ST1/P/02-A4 0930-03)  
 (ST7/P/02-A2 1515)  
 (U3/P/04-A3 0900-10)  
 (MC02/P/01-B2 1010)  
 (MI11/P/02-B5 0945)  
 (ST5/P/04-B4 1720)  
 (SW1/P/01-B5 0915)  
 (U8/P/01-B3 1640-13)  
**Srivastava N.**  
 (GA4.05/E/02-A1 1010)  
**Srivastava S.**  
 (GA1.02/W/32-A2 0930)  
 (GA1.02/W/34-A1 1050)  
**Srivastava Sanjay**  
 (SW1/P/01-B5 0915)  
**Srokosz M. A.**  
 (JSM41/E/06-B3 1720)  
**Ssosti E.**  
 (JSV36/W/23-B3 1515)  
**St. Cyr O. C.**  
 (GA4.08/W/07-B3 0830)  
**Staal Cees Van**  
 (JSA27/E/02-B1 1150)  
**Stacey Michael W.**  
 (P09/E/01-A2 1145)  
**Stadsnes J.**  
 (GA3.02/W/18-B2 1645)  
**Stahelin Johannes**  
 (JSM01/W/27-A5 1530)  
 (JSM01/W/70-A4 1620-13)  
**Stagg Kim A.**  
 (HS5/W/34-A3 1000)  
**Stahl Kerstin**  
 (HS1/W/29-B4 0945)  
**Stainforth D**  
 (JSM01/W/46-A3 1710)  
**Stakes Debra**  
 (JWA34/W/06-B2 1010)  
**Stamatiou N.**  
 (GA2.01/E/11-A1 1205)  
 (GA2.01/W/07-A1 1055)  
**Stambler N.**  
 (P15/L/19-B3 1500)  
**Stammer Detlef**  
 (JSG14/E/12-A3 0900)  
**Stamnes Knut**  
 (MI08/-A3 0830)  
 (MI08/-A3 0930)  
 (MI08/E/06-A4 1235)  
 (MI08/E/08-A4 1750)  
**Stamper Richard**  
 (JSA06/W/18-A1 1155-12)  
**Stancalie George**  
 (HS4/W/09-A4 1510)  
**Stanchev V. L.**  
 (JSA40/W/09-B5 1400-11)  
**Stanev E.**  
 (P11/W/08-B5 1600)  
**Stanev E. V.**  
 (P07/W/14-A3 1035)  
**Stanev Emil**  
 (P14/E/03-A4 1620)  
**Staneva J.**  
 (P11/W/08-B5 1600)  
**Staneva J. V.**  
 (P07/W/14-A3 1035)  
**Stanica D.**  
 (JSA15/P/01-A5 0830-04)  
**Stanica Dumitru**  
 (GA1.02/E/04-A2 0930)  
**Stanichny S. V.**  
 (P11/E/12-B5 1640)  
**Stanley Mark**  
 (JSM03/W/02-A1 1650)  
**Stanway J. D**  
 (MI10/E/10-B2 1705)  
**Staquet Chantal**  
 (JSP39/E/24-B4 1700)  
 (JSP49/E/05-B5 1440)  
**Staquet Damtp C.**  
 (JSP49/E/08-B5 1420)  
**Starke Andreas**  
 (P10/E/07-A5 1130)  
**Starkov G.**  
 (GA3.06/W/31-A2 0930-16)  
**Starkov G. V.**  
 (GA3.02/E/17-B3 0900-18)  
 (GA3.08/W/31-A6 1150)  
**Starostenko Vitaly I.**  
 (JSA40/E/02-B5 1045)  
**Starovoi Oleg**  
 (U7/W/03-B1 0830-03)  
**Starovoi Yuri**  
 (ST5/W/36-B3 0900-03)  
**Stashchuk Natalia**  
 (P11/E/09-B3 1620)  
 (P11/E/18-B5 1520)  
**Stasiewicz K**  
 (GA4.09/L/01-A5 1600-06)  
 (GA4.09/W/04-A5 1600-02)  
 (GA4.09/L/02-A6 0840)  
**Stasiuk Mark**  
 (JSP23/W/24-B2 1150)  
**Staudacher Thomas**  
 (JSA15/E/10-A3 1640)  
**Staudenrausch H.**  
 (HW4/E/16-B2 1520)  
**Staudinger Michael**  
 (MI02/E/01-A4 1010)  
**Stauning P.**  
 (GA2.01/E/01-A1 1110)  
 (GA2.01/E/08-A1 1005)  
 (GA2.01/W/05-A1 1705)  
 (GA2.01/E/13-A1 0900-02)  
 (GA3.07/W/20-A5 0900-20)  
 (GA5.06/E/05-A3 1400)  
 (GA1.07/W/07-B2 1220)  
 (GA5.08/E/03-B1 0900)  
**Stauning Peter**  
 (GA3.02/E/13-B2 1200)  
 (GA3.08/W/04-B1 0900-02)  
 (GA5.08/W/06-B1 0945)  
 (GA3.10/W/18-A5 1155)  
**Stavrakakis G.**  
 (ST1/E/87-A2 0930-12)  
**Stavrakakis G. N.**  
 (ST1/E/46-A3 1620)  
**Stavrakakis George**  
 (G5/E/36-A4 1215)  
 (ST1/E/28-A3 0900-17)  
**Stacy Sandy**  
 (ST1/W/09-A4 0930-13)  
**Stearns Charles**  
 (JSM18/E/01-A4 1220)  
 (JSM18/E/03-A4 1420)  
 (MI05/L/02-A2 0950)  
 (JSM41/E/22-B4 0945)  
 (JSM41/E/28-B3 1515)  
**Stebel K**  
 (JSM01/W/18-A3 0940)  
 (JSM32/W/03-B2 1435)  
**Steck Lee**  
 (JSS46/W/10-B4 1600)  
**Steel Michael E.**  
 (HS1/W/32-B5 1100)  
**Steele H. M.**  
 (JSM26/W/31-B2 1150)  
**Steele P.**  
 (JSP21/E/04-A5 1110)  
**Steen Ake**  
 (GA3.06/W/34-A3 1400)  
 (MI02/W/06-A5 1010)  
**Steenberg C. D.**  
 (GA4.04/W/09-B5 1710)  
**Steenbrink Joris**  
 (GA1.15/W/04-B4 1500)  
 (GA1.15/W/11-B4 1530-03)  
**Stefanov**  
 (ST1/E/84-A2 0930-05)  
**Stefaniuk Michal**  
 (JSA15/E/33-A3 1050)  
**Stefano Guiseppe Di**  
 (MI03/L/01-A3 1400-04)  
**Stefansson R.**  
 (ST4/W/03-B3 1630)  
**Stefansson Ragnar**  
 (ST5/W/14-B3 0900-06)  
 (ST5/W/21-B3 0910)  
 (ST1/E/57-A2 1620)  
**Stefanutti Leopoldo**  
 (JSM26/W/16-B2 1210)  
**Steffen Konrad**  
 (MI08/W/02-A4 1000)  
**Steffen W.**  
 (U2-E/09-A2 0950)  
**Steffensen Jorgen Peder**  
 (JSM18/W/08-A5 1100)  
**Steger J**  
 (JSM01/W/37-A5 1400)  
**Steil Benedikt**  
 (MC08/E/05-A3 0900-02)  
**Stein Seth**  
 (JSG28/W/01-B2 1400-16)  
**Stein Uri**  
 (MC01/W/06-A5 0830)  
 (MI07/W/01-A2 1100)  
**Steinberger Bernhard**  
 (JSS13/W/17-A5 0930)  
**Steinegger Michael**  
 (JSA16/W/12-A3 0830-52)  
**Steiner Andrea K.**  
 (JSM41/W/13-B3 1400)  
**Steiner Nadja**  
 (JSM04/E/03-A2 1510)  
**Stein M**  
 (JSP21/L/03-A4 1720)  
**Stejskal M.**  
 (ST4/E/06-B1 1400-18)  
**Stekauerova Vlasta**  
 (HW4/E/23-B2 0900-01)  
**Stelfox C E**  
 (JSP21/L/03-A4 1720)  
**Stella M**  
 (MW05/W/01-A2 1145)  
**Stellmacher Rita**  
 (JSA16/E/37-A3 0830-07)  
**Stenborg G.**  
 (GA4.02/E/08-A4 1400-05)  
**Stenichkov Georgiy**  
 (MC01/W/34-A5 0945)  
 (MW01/L/01 1430)  
**Stenflo L.**  
 (GA3.04/E/14-B1 1520-03)  
**Stening Robert**  
 (GA2.03/E/03-B3 1140)  
 (JSA20/E/06-A5 1200-08)  
 (JSA20/E/14-A4 1110)  
**Stepanov A. E.**  
 (GA2.07/E/02-A2 0930-04)  
 (GA3.05/E/05-B3 0900-29)  
**Stepanova M. V.**  
 (GA3.06/W/26-A2 1130)  
**Stepanova Marina**  
 (JSA06/W/30-A2 1150)  
 (GA3.08/W/10-B1 0900-06)  
**Stephan A.**  
 (JSA20/E/27-A4 1200-21)  
**Stephan S.**  
 (JSA20/E/27-A4 1200-21)  
**Stephen D**  
 (JSM01/W/22-A2 1600-21)  
**Stephen J. Lane**  
 (JSV47/W/16-B5 1000)  
**Stephen R.**  
 (JSV36/C/JSA15/W/34-B3 1415)  
**Stephens Graeme**  
 (MC01/L/03-A1 1415)  
 (MC08/L/02-A4 0900)  
**Stephens Graeme L.**  
 (JSM41/L/02-B3 1050)  
 (MI04/W/11-B1 0900-02)  
**Stephens R. L.**  
 (GA4.10/W/14-A4 0900)  
**Stephenson David B.**  
 (JSP25/E/06-B3 0930)  
**Stépien C.**  
 (JSM26/W/29-B2 1700-09)  
**Stappeler J.**  
 (JWM08/E/05-A2 1200)  
**Sterlini P.**  
 (G6/C/G5/W/06-B1 0930)  
**Stevens Bjorn**  
 (MI04/W/31-B3 1450)  
**Stevens David P.**  
 (P12/W/11-A1 1130)  
**Stevens Duane**  
 (MC08/L/09-A3 1545)  
 (MC08/L/14-A4 0945)  
**Stevens Ian**  
 (P10/W/12-A3 1130)  
**Stevenson David**  
 (MI02/W/19-A4 1620)  
 (MI02/E/10-A4 1100)  
**Stewart Adrian**  
 (JSP23/C/US/L/01-B1 1500)  
 (ST3/E/57-B4 1400-24)  
**Stewart Bob**  
 (JSV30/E/01-B1 0920)  
 (JSV30/E/01-B1 1400-10)  
**Stewart Mike**  
 (G6/W/03-B2 1520)  
 (G1/L/12-A3 1620-88)  
 (G1/W/13-A3 1620-05)  
 (G1/W/28-A3 1440)  
 (G1/W/33-A3 1620-16)  
 (G1/W/40-A3 1620-18)  
 (HS4/W/01-A4 0945)  
**Stewart P. J.**  
 (JSG28/E/05-B2 0950)  
**Stewart R**  
 (MI06/W/20-B1 1400-07)  
 (MI06/W/20-B2 1400-07)  
**Stewart Robert**  
 (JSV30/E/05-B1 0940)  
**Stewart Ronald E.**  
 (JSM24/E/07-B2 1055)  
 (MC08/L/10-A3 1045)  
 (MI08/L/08-A4 1430)  
**Stichler Willibald**  
 (HS4/W/12-A4 1630)  
**Stiller**  
 (MI04/L/15-B1 0900-18)  
**Stiller Olaf**  
 (MI04/W/22-B3 1135)  
**Stixrud Lars**  
 (JSS02/E/05-A1 1045)  
 (JSS07/E/08-A2 1430)  
**Stocks B**  
 (MI01/W/03-A1 0900-03)  
**Stockton-Chalk A. B.**  
 (G3.04/W/16-B2 1010)  
**Stoddard Paul**  
 (JSA10/W/05-A2 1400)  
**Stoeva Peshka**  
 (JSP23/E/30-A5 0830-14)  
**Stoew B. G.**  
 (JSG28/W/05-B1 1010)  
**Stoker P. H**  
 (GA2.01/E/02-A1 0900-04)  
 (GA2.01/E/04-A1 0900-03)  
 (GA2.01/E/03-A1 1040)  
**Stoll J. B.**  
 (GA1.02/W/14-A2 0930)  
**Stollhofen Harald**  
 (JSV22/W/08-A5 0900)  
**Stolzenburg Maribeth**  
 (MI03/W/03-A3 1620)  
**Stone E.C.**  
 (GA4.10/W/16-A5 1145)  
 (GA4.04/W/09-B5 1710)  
 (GA4.04/W/14-B5 1620)  
**Stone Edward C.**  
 (UL1 Tuesday 20 July 0830)  
**Stone Lewi**  
 (JSP25/E/23-B1 1440)  
**Stopar Robert**  
 (JWS33/E/12-B2 1635-30)  
**Storchak Dmitry**  
 (ST5/W/52-B3 0930)  
 (ST5/W/12-B3 1500)  
 (ST5/W/46-B5 0930)  
**Storey J.**  
 (GA3.04/W/27-B1 1520-04)  
 (GA3.08/W/26-A6 1710)  
**Storey Michael**  
 (JSS13/W/13-A5 1150)  
**Storz Wolfgang**  
 (GA1.02/W/02-A2 0930)  
**Stott Peter**  
 (JSA16/E/01-A3 0830-19)  
 (MC02/E/14-B2 1450)  
 (MC02/E/02-B2 1400)  
**Stouffer Ronald J.**  
 (MC02/E/18-B2 1150)  
**Stowe Larry**  
 (JSM41/E/30-B5 1400)  
**St-Pierre Claude**  
 (G1/E/30-A3 1620-64)  
**Strack John**  
 (MC04/W/10-B1 1515)  
**Strahan Susan**  
 (MW01/W/06-A5 1400)  
**Strakhov A V**  
 (G3/E/17-A5 1610-62)



## INDEX

- (G4/E/18-A3 1540)
- Strakhov V**  
(G3/E/17-A5 1610-62)
- Strakhov V N**  
(G4/E/18-A3 1540)
- Strangeway R**  
(MI03/W/09-A3 1640)  
(GA3.03/W/11-B4 1200)  
(GA3.05/W/10-B3 1720)  
(GA3.08/W/09-A6 0920)  
(GA3.08/W/13-A6 0940)  
(GA3.08/W/21-A6 0900)
- Strangeway R. J.**  
(GA3.06/W/20-A3 0920)  
(GA4.10/W/05-A5 1655)  
(GA4.10/W/07-A5 1740)
- Strass Volker H.**  
(P13/P/01-B2 1130)
- Strasse Wagramer**  
(HS4/W/20-A5 1030)
- Stratton Rachel**  
(MW03/E/06-B4 0935)
- Straub S. M.**  
(JSV30/W/02-B1 1400-06)  
(JSV30/W/04-B1 1400-07)
- Straub Susanne**  
(JSV36/E/11-B3 0900-15)
- Straus D**  
(MC01/L/02-A1 1145)
- Strawbridge K.**  
(MI06/W/16-B2 1030)
- Strawbridge Kevin**  
(MI01/W/04-A1 1640)
- Strelets V.**  
(ST3/P/8-B4 1400-21)
- Strickland Douglas J.**  
(JSA20/W/49-A6 0930)
- Strobel Darrell F.**  
(JSM01/W/33-A3 1610)  
(MC09/L/02-B2 1430)
- Stroeve Pavel A.**  
(JSA09/W/04-A2 0930-08)
- Ström Johan**  
(JSM26/W/16-B2 1210)
- Stromeyer D.**  
(JSA40/W/03-B5 1400-07)
- Strong Kimberly**  
(MC09/W/11-B2 1500)
- Stroud V**  
(JSP21/W/11-A4 1050)  
(MI02/L/19-A4 1410)
- Strykowski Gabriel**  
(JSA40/E/03-B5 1140)
- Strzyszcz Zygmunt**  
(GA1.05/E/05-A6 1215)  
(GA1.05/E/10-A6 1115)
- Stuart Graham**  
(JSS07/E/07-A2 1225)
- Stuber Klaus**  
(G1/W/04-A3 1620-03)  
(G1/W/12-A3 1620-38)
- Stuber Nicola**  
(MC07/E/01-A2 1035)  
(MC08/E/05-A3 0900-02)
- Stucchi Massimiliano**  
(ST3/W/29-B4 1700)
- Stumptner Willibald**  
(JSA10/W/13-A3 1000)  
(GA4.10/L/03-A4 1110)
- Sturges W. T.**  
(JSM26/W/06-B1 0900)
- Sturges William T**  
(MI02/L/19-A4 1410)  
(MI02/W/12-A4 1430)  
(JSP21/W/11-A4 1050)
- Sturman Andrew**  
(JSM43/W/06-B4 1030)
- Sturrock Georgina**  
(JSP21/E/02-A4 0930)  
(JSP21/L/01-A4 1010)
- Stutzmann Eleonore**  
(JSS13/W/15-A4 1500)  
(JWA34/W/06-B2 1010)  
(ST4/W/25-B2 1720)  
(ST5/W/33-B3 0900-07)  
(ST5/W/63/B3 0900-11)  
(U7/W/01-B1 0830-14)
- Su Hui**  
(JSP25/W/26-B1 1050)
- Su Jilan**  
(P10/P/01-A4 1520)
- Su Pu.**  
(GA1.15/W/05-B4 1730)
- Su S. Y.**  
(JSA20/W/21-A5 1519)
- (JSA20/W/28-A5 1200-10)  
(GA2.02/W/18-B5 1440)  
(GA2.02/W/34-B5 1420)
- Su Wenying**  
(MI06/E/02-B2 1520)  
(MI01/E/10-A1 0900-12)
- Su Yi-Jiun**  
(GA3.05/W/11-B3 0900-06)
- Su Z. B.**  
(U7/E/01-B1 1135)
- Suarez Max**  
(MC01/W/06-A5 0830)
- Suarez Max J.**  
(MI04/E/27-B1 1705)
- Subandriyo**  
(JSV36/W/11-B3 1400-06)
- Subba Rao C.**  
(HS5/W/42-A3 1420)
- Subba Rao D V**  
(G3/E/20-A5 1610-57)
- Subba Rao N. V.**  
(HS5/W/42-A3 1420)
- Subbarao K. S. V.**  
(GA2.02/W/05-B5 0900)  
(GA2.02/W/16-B4 0930-18)  
(GA2.02/W/20-B4 0930-16)
- Subbarao K. V.**  
(JSV22/E/06-A5 1500)  
(ST2/E/18-A3 1730)
- Subbotina M. M.**  
(P12/E/01-A1 1030-04)  
(P12/W/06-A1 1030-10)
- Subrahmanyam K**  
(HS5/W/40-A3 1225)
- Subramanian P**  
(GA4.02/W/33-A4 1400-26)
- Suchzhev S. P.**  
(JSP23/E/33-A5 1640)
- Suchy V.**  
(ST4/E/06-B1 1400-18)
- Sud Y. C.**  
(MI04/W/27-B1 0900-20)
- Sudman Yonadav**  
(JSS31/W/01-B3 0830-02)
- Suendermann Juergen**  
(P10/E/03-A5 1400)  
(JSG14/E/06-A3 1148-17)
- Suenkel H**  
(JSG11/E/01-A3 0850)  
(G4/E/15-A3 1620-15)
- Suetnova E.**  
(JSP39/E/20-B2 1540)  
(JSS44/E/26-B4 0930-38)  
(JSS44/E/28-B4 0930-37)
- Suga Toshio**  
(P12/C/JSP21/E/01-A1 0950)  
(P12/W/02-A1 0930)
- Suganda Oni K.**  
(JSV36/E/01-B3 1610)
- Sugata S**  
(MI02/W/15-A5 1100)
- Sugi M.**  
(JSG14/W/09-A3 1121-08)
- Sugi Masato**  
(MW03/E/10-B4 1005)
- Sugi Noriko**  
(ST7/W/06-A2 1110)
- Sugihara Mituhiko**  
(JSV36/E/28-B3 0900-03)  
(JSV36/W/02-B3 0930)
- Sugimoto Nobuo**  
(JSG28/E/12-B2 1200)
- Sugimoto Takashige**  
(U7/E/02-B1 0830-10)
- Suginohara Nobuo**  
(MC01/W/41-A2 1400)
- Sugjura M.**  
(JSA15/W/30-A4 0940)
- Sugjura Masahisa**  
(GA5.01/W/05 A1 0835)  
(GA5.06/W/01 A3 0940)  
(GA5.06/W/09 A3 1000)  
(JSA06/W/26-A2 1230)  
(GA4.08/W/14-B4 1035)
- Suhadolc Panza Peter**  
(ST5/W/31-B4 1640)
- Suhadolc Peter**  
(ST3/W/09-B3 1415)  
(ST3/W/14-B4 0930-01)  
(ST3/W/34-B3 1400)  
(ST3/W/49-B3 0915)  
(ST2/E/03-A5 1400-26)  
(ST2/W/34-A4 1515)
- Suhanto Edi**  
(JSV36/E/01-B3 1610)
- Sukanta Roy**  
(MC02/E/07-B1 1010)
- Sukhorukov A I**  
(JSM03/E/05-A1 1130)
- Sukhyar R.**  
(JSV36/E/01-B3 1610)  
(JSV36/E/07-B3 0900)  
(G6/C/G1/L/24-B1 1520)
- Suleimani Elena N.**  
(JSS42/W/11-B5 1700-15)
- Suleimenov Ibragim**  
(JSA16/E/24-A3 0830-10)
- Suleimenov Ibragim E.**  
(GA2.02/L/02-B4 0930-05)  
(GA2.03/E/06-B3 1400-06)
- Sulerzhitsky Leopold**  
(JSP23/E/04-B1 0830-08)
- Sulistiyo Yustinus**  
(JSV36/E/02-B3 1100)
- Sultan P. J.**  
(GA3.09/W/02-B4 0900-09)
- Sulzer M. P.**  
(GA3.09/W/19-B5 1100)  
(JSA20/W/48-A4 1200-31)
- Sumita Ikuro**  
(GA1.03/W/09-B3 1520)
- Summers D.**  
(GA3.05/W/29-B3 1500)
- Summerson R. M. V.**  
(P16/W/01-B5 1620)
- Sun Bomim**  
(MC02/E/23-B1 1450)
- Sun He-Ping**  
(JSA37/P/01-B3 1145)
- Sun Juazhen**  
(MC04/E/09-B1 1130)
- Sun Ruomei**  
(JSS44/W/16-B5 1150)  
(ST4/E/12-B1 0830-15)  
(ST2/E/52-A3 1200)
- Sun S A**  
(G3/W/09-A5 1610-27)  
(G3/W/23-A5 1610-28)
- Sun Wenke**  
(G1/C/G5/E/05-A3 1620-98)  
(G4/E/03-A3 1620-29)  
(G5/E/03-A4 1552-07)
- Sun Xunying**  
(ST4/E/24-B2 0930-24)
- Sun Yuezhi**  
(ST4/E/24-B2 0930-24)
- Sun Zhiming**  
(GA1.04/W/12-A5 1120)
- Sunanda Basu**  
(JSA06/W/05-A2 0950)
- Sundar Christopher**  
(MI09/W/16-A5 1710)
- Suntharalingam P.**  
(JSP21/W/04-A5 0950)  
(P08/W/02-A2 1130)
- Supic Mirko**  
(PW1/E/02-A6 1140)
- Sur Halil I.**  
(P11/E/07-B3 0910)
- Surguy Anna**  
(ST5/W/45-B3 0900-09)
- Surkov Vadim**  
(JSA15/E/06-A4 1400-08)
- Surn Yoo**  
(JSA06/W/28-A1 1155-13)
- Surotkin V. A.**  
(GA2.02/W/23-B5 1640)
- Susagna T.**  
(ST3/E/41-B5 1000)  
(ST5/E/34-B3 0830)
- Susskind Joel**  
(JSM41/E/10-B3 1205)
- Suzcynsky David M**  
(MI03/W/04-A3 1700)
- Sutcliffe John**  
(HW2/W/14-B2 0930)
- Sutcliffe Peter R.**  
(GA3.02/W/42-B2 0950)  
(GA5.09/W/11 A2 1400-05)
- Sutherland B R**  
(MW07/W/03-A4 1040)
- Sutherland Ross A.**  
(HS5/W/02-A1 1425)
- Sutisna Sobar**  
(JSG11/E/12-A3 0950)  
(G5/E/06-A4 1500-01)
- Sutor Julius**  
(HW4/E/23-B2 0900-01)
- Sutton R. T.**  
(JSP25/W/17-B2 1620)
- Sutton Rowan**  
(JSP25/W/07-B4 1420)  
(JSP25/W/30-B1 0930)
- Sutyryn N. A.**  
(GA2.02/W/30-B4 0930-04)
- Suvorova A. V.**  
(GA3.09/W/23-B4 0900-02)
- Suwa Hiroshi**  
(JSP23/C/US/W/11-A5 1500)
- Suxia Liu**  
(JSM24/E/04-B1 1225)
- Suyanto I.**  
(JSV36/W/10-B3 1400-03)  
(JSV36/W/24-B3 1400-05)
- Suyehiro Kiyoshi**  
(ST4/W/34-B1 1400)
- Suzuki Akihiro**  
(ST1/E/44-A1 1720)
- Suzuki Akio**  
(JSS02/E/16-A1 1720)
- Suzuki Isao**  
(JSS02/E/11-A1 0830-08)
- Suzuki Masakazu**  
(HW4/E/09-B2 0900-11)
- Suzuki Rikie**  
(JSM41/E/14-B5 1150)
- Suzuki Shin-ichi**  
(JSP39/E/06-B3 1415-06)
- Suzuki Yasuhiro**  
(ST3/W/27-B4 1530)
- Suzuki Yoshinori**  
(MI10/W/14-B1 0900-05)
- Svancara Jan**  
(ST2/L/05-A5 1400-17)
- Svarc J. E.**  
(JSS31/E/11-B2 1010)
- Svedhem H.**  
(JSA10/W/16-A3 1130)
- Svehla Drazen**  
(G3/E/41-A5 1610-84)
- Sven Aaro**  
(JSS44/E/11-B4 0930-29)
- Svensson**  
(JSA06/L/06 0935)
- Svetov Boris S.**  
(JSA15/E/58-A5 0830-13)
- Svirezhev Yuri**  
(U3/W/05-A3 0900-11)
- Svirko Yu. P.**  
(JSA15/E/53-A4 1400-01)
- Svitlov S**  
(G3/E/25-A5 1610-38)  
(G3/E/15-A5 1610-39)  
(G3/E/24-A5 1610-37)  
(G3/E/26-A5 1610-36)
- SVO science team**  
(JSP23/C/US/W/07-B2 0950)
- Svyazhina Ideya**  
(GA1.04/E/06-A4 0930-08)
- Swart D P J**  
(JSM01/W/55-A5 1510)
- Swartz W.**  
(GA2.02/L/01-B4 1000)
- Swathi P. S.**  
(P08/W/08-A2 1420)
- Swenson E. M.**  
(P09/W/09-A2 1050)
- Swift Daniel W.**  
(GA3.08/W/11-B1 1620)
- Swift Jim**  
(P14/E/08-A4 1400-07)
- Swinbank R**  
(JSP05/W/13-A1 1600)  
(MW01/W/12-A5 1150-01)  
(MW04/W/02-A1 1710)
- Sy Alexander**  
(P08/W/09-A2 1110)
- Syheva N. K.**  
(GA1.05/E/21-A5 1220)
- Sykorova I.**  
(ST4/E/06-B1 1400-18)
- Symons D. T. A.**  
(GA1.04/W/03-A4 0930-15)  
(GA1.04/W/05-A4 0930-14)  
(GA1.04/W/19-A4 0930-12)
- Symons Leighton**  
(G1/E/38-A3 0950)
- Syndergaard S.**  
(JSG28/W/17-B2 1400-05)  
(JSG28/W/23-B2 1130)
- Syrjasuo M. T.**  
(GA3.08/E/01-A6 1430)
- Szabo A.**  
(GA4.04/E/01-B5 1210)
- Szabo Adam**

- (GA4.01/E/09-A2 1200)  
(GA3.07/W/09-A3 1430)
- Szabo Csaba**  
(JSV30/W/13-B1 1400-05)
- Szaniawski Rafal**  
(GA1.04/W/35-A4 0930-11)
- Szaraniec Edward**  
(JSS07/L/04-A2 0935)
- Szarka Laszlo**  
(GA1.02/E/10-A1 0915)
- Szarka L.**  
(JSA10/E/06-A2 0945)
- Szeidovitz Gyoza**  
(ST3/P/2-B4 1015)
- Szeto Kit K**  
(MI08/L/08-A4 1430)
- Szoucha Marcin**  
(G1/E/26-A3 1620-60)
- Szتانو O.**  
(VS2/W/03-B3 1210)
- (JSM01/W/29-A5 0940)  
(MC06/C/JSM01/E/35-A1 1600)  
(MC06/W/04-A1 1400)  
(MI02/E/03-A5 1240)
- Takahashi Masaki**  
(JSV36/E/17-B3 1400-09)
- Takahashi Narumi**  
(JSA19/W/02-A4 1400-07)
- Takahashi Tetsuya**  
(P09/W/12-A2 0910)  
(P09/W/13-A2 0930)
- Takahashi Tomoyuki**  
(JSS42/P/01-B5 1210)  
(JSS42/W/01-B5 1620)
- Takahashi Y.**  
(G2/W/01-A2 1630-01)  
(GA1.02/L/05-A2 0930)  
(GA1.02/L/05-A2 0930)  
(JSA15/W/07-3 1740)  
(JSA15/W/07-3 1740)  
(G2/E/08-A2 1630-11)
- Takakai Synji**  
(JSA15/E/01-A4 1400-05)
- Takakura S.**  
(GA1.02/W/18-A2 0930)
- Takalo Jouni**  
(GA3.02/W/30-B3 0900-04)
- Takamura Tamio**  
(JSG28/W/07-B1 1400-07)  
(P15/L/21-B4 0925)  
(MI09/W/03-A5 1145-17)
- Takanami Tetsuo**  
(ST1/E/68-A4 0930-12)
- Takayama Tomomi**  
(JSP25/W/25-B3 0830-06)
- Takayuki Usui**  
(MI09/E/06-A5 0920)
- Takeda Hiroyuki**  
(JSM41/E/23-B3 1415)
- Takeda Masahiko**  
(GA1.07/W/08-B2 0900-02)  
(JWS33/W/37-B2 1430)
- Takeda T.**  
(JSS44/W/01-B4 0930-06)
- Takeda Tetsuya**  
(JSS44/W/07-B4 0930-07)
- Takeda Tokao**  
(MI04/W/23-B3 1035)  
(MI04/E/22-B4 1150)  
(MI01/E/09-A1 0900-02)
- Takeda Tomoyoshi**  
(ST3/W/22-B4 0930-04)
- Takehiko Mori**  
(JSV47/W/11-B5 1115)
- Takematsu Masaki**  
(P11/E/03-B3 1420)
- Takemoto Shuzo**  
(ST4/W/31-B1 0830-23)
- Takemura K.**  
(GA1.03/W/17-B2 1500)  
(GA1.05/W/01-A6 1515)
- Takemura Keiji**  
(ST4/W/31-B1 0830-23)
- Takenaka Hiroshi**  
(ST5/W/14-B4 0930-02)  
(ST5/W/16-B4 0930-03)
- Takeo Minoru**  
(ST5/W/32-B4 1400-05)  
(ST1/W/46-A1 1520)  
(ST1/W/50-A2 1400-23)
- Takeuchi Kensuke**  
(P12/W/21-A1 1620)  
(JSP25/W/25-B3 0830-06)
- Takigawa Masayuki**  
(JSM01/W/29-A5 0940)  
(MI02/E/03-A5 1240)
- Takiguchi H.**  
(G5/E/39-A4 1200)
- Takle Eugene S**  
(MC01/W/08-A4 0950)
- Takumi Kato**  
(ST 6/E/11-A2 1530)
- Takumi Ichi**  
(JSA15/E/59-A4 1400-19)
- Takuo Shibusaki**  
(ST4/W/48-B2 0930-14)
- Talahashi H.**  
(JSA20/W/24-A5 1200-07)
- Talai Ben**  
(JSV36/W/03-B3 0900-13)
- Talaya J.**  
(JSS31/E/13-B3 0830-14)
- Talaya Julia**  
(G1/E/15-A3 1620-55)
- Talbot Christopher**  
(ST4/E/53-B1 0830-05)
- Talipova Tatjana**  
(JSP39/E/03-B2 1640)  
(JSP39/E/07-B3 1418-07)
- Tamagawa Ichiro**  
(JSM24/W/04-B1 0930)
- Tamisiea Mark**  
(JSG14/W/01-A3 1700-10)
- Tammet Hannes**  
(JSA35/E/08-B1 1210)
- Tamura Takao**  
(HS3/W/18-A2 0925)
- Tan B. H**  
(ST6/C/JSS02/W/15-A2 1640)
- Tan Czhe-Min**  
(MI05/W/13-A2 1610)
- Tan D.**  
(JSM26/W/18-B2 1550)
- Tan Kwok-Aun**  
(MW07/E/07-A4 1210)
- Tan Shiling**  
(G5/W/26-A4 1550-06)
- Tan Zhe-Min**  
(MI04/W/23-B3 1035)
- Tanabe Tadashi**  
(GA5.09/W/05 A2 1400-02)
- Tanada Toshikazu**  
(ST1/E/89-A2 1720)
- Tanaka Akiko**  
(ST4/E/45-B1 1400-11)
- Tanaka Hidefumi**  
(GA1.03/W/26-B3 1040)  
(GA1.01/W/19-A5 1600)
- Tanaka Katsunori**  
(HW4/E/09-B2 0900-11)
- Tanaka S.**  
(JSS46/W/03-B4 1010)  
(JSV36/W/09-B3 1430)  
(JSV47/W/22-B5 1130)  
(JSV47/W/26-B5 1400-09)  
(GA1.03/W/10-B2 1420)
- Tanaka Tadashi**  
(HS4/W/16-A5 0900)  
(JSA06/W/14-A1 1700)
- Tanaka Torao**  
(JSS31/W/06-B3 0830-06)  
(JSV36/E/01-B3 1610)
- Tanaka Y.**  
(JSA15/E/17-A3 1440)  
(JSA15/W/14-A4 1400-16)
- Tanaka Y. M.**  
(GA3.04/W/10-B1 1520-08)
- Tanaka Yao**  
(JSS31/E/12-B3 0830-13)
- Tanaka Yoshikazu**  
(GA1.02/E/29-A2 0930)  
(GA1.02/W/22-A2 0930)  
(JSA15/E/02-A5 0830-05)  
(JSA15/E/27-A4 1400-04)  
(JSA15/E/38-A4 1400-03)  
(JSA15/E/41-A4 1400-14)
- Tandong Yao**  
(HS2/W/25-B2 1240)  
(HS2/W/27-B2 1420)  
(HS2/W/28-B2 1440)
- Tang Changyuan**  
(HS4/W/18-A5 0950)
- Tang Conrad**  
(G4/P/05-A3 1620-07)
- Tang Ji**  
(GA1.02/E/25-A2 0930)  
(JSA15/E/52-A5 0830-09)
- Tang Maocang**  
(MC02/E/13-B1 1600-02)  
(ST4/E/62-B1 1400-22)  
(SW1/E/04-B5 0845)
- Tang Wenqing**  
(JSM41/W/24-B4 1155)  
(JWS33/W/19-B3 0900-29)
- Tangtham Nipon**  
(HW4/E/09-B2 0900-11)
- Taniguchi Hidetsugu**  
(JSV30/C/JSV22/W/01-B1 1400-22)
- Taniguchi Keisuke**  
(ST4/W/02-B1 0830-20)
- Taniguchi Makoto**  
(HS3/W/09-A1 1400)  
(HS4/W/25-A5 1220)  
(HW5/E/06-A3 1620)
- Tanimoto Junji**  
(G3/W/28-A5 1610-34)
- Tanimoto Youichi**  
(JSP25/W/16-B4 1700)  
(JSP25/W/28-B5 1010)
- Tanré D**  
(MI09/L/02-A5 0855)
- Tanskanen P.**  
(G3.04/W/18-B1 1520-26)
- Tao Guo-Qing**  
(JSA37/P/01-B3 1145)
- Tao H.**  
(GA 2.01/E/12-A1 1220)
- Tao Kui-Yuan**  
(JSV22/E/15-A5 1550)  
(JSV22/E/18-A5 1610)  
(JSV30/C/JSV22/E/17-B1 1400-21)
- Tao Wei-Kuo**  
(MI04/W/06-B3 1105)
- Taori Alok**  
(JSA20/W/20-A5 1135)  
(JSA20/W/23-A5 1200-03)
- Taoyuan Fan**  
(JSS44/E/30-B5 1110)
- Tapirdamaz C.**  
(GA1.04/W/27-A6 1140)
- Tapley B. D.**  
(G5/W/25-A4 1100)  
(JSG14/W/11-A3 1700-02)  
(G6/C/G3/W/32-B1 1120)  
(JSA37/W/09-B3 1100)
- Tapley Byron**  
(JSG11/E/10-A3 1400)  
(JSG11/W/19-A3 1130)  
(JSG14/L/10-A3 1400)
- Tappin David**  
(JSP23/C/U5/E/23-A6 1700)
- Tappin David R.**  
(JSS42/E/20-B5 1150)
- Tapponnier Paul**  
(ST2/E/01-A3 1100)
- Tara L. Jensen**  
(MI08/W/03-A4 1500)
- Taran Yuri**  
(JSV36/C/U6/W/08-B3 1400-21)
- Taranov V. A.**  
(G3/E/28-A5 1610-03)
- Tarassenko Yury**  
(SW1/E/07-B5 1030-02)
- Tarasov N. T.**  
(ST1/E/70-A3 1700)
- Tarasov Nikolay T.**  
(ST5/L/06-B4 1400-08)
- Tarasova N. V.**  
(ST1/E/70-A3 1700)
- Tarasova Nadezhda V.**  
(ST5/L/06-B4 1400-08)
- Tarassov Viktor**  
(GA5.01/E/15 A1 1300-10)  
(GA5.01/E/15 A1 1300-10)
- Tarbeyev Yu. V.**  
(GA5.01/E/29 A1 1100)
- Taricco C.**  
(JSA16/W/43-A3 1630)
- Tardini R.**  
(JWS33/E/03-B2)  
(JWS33/E/03-B3 0900-06)
- Tarditi Alfonso**  
(GA3.09/W/27-B4 1035)
- Tarek O. T.**  
(P11/P/03-B5 1150-03)
- Tarek Othman**  
(P11/P/04-B5 1150-04)
- Tarits P.**  
(JSA10/W/10-A2 1600)
- Tarits Pascal**  
(JSA19/W/08-A4 1130)  
(JSS13/W/04-A5 1630)  
(JWA34/W/06-B2 1010)  
(JWA34/W/09-B2 1150)  
(P16/E/04-B5 1050)
- Tarling D. H.**  
(GA1.03/E/06-B2 0900)  
(GA1.15/E/04-B4 1515)  
(GA1.15/E/05-B4 1530-01)
- Tarraga Marta**  
(JSV47/E/10-B5 1400-07)  
(JSP23/E/06-B2 1600)
- Tarsina M. V.**  
(GA3.09/W/23-B4 0900-02)
- Tartaglione N.**  
(JWM08/W/02-A2 1220)
- Tashiro K.**  
(JSS44/W/01-B4 0930-06)
- Tase Norio**  
(HS3/W/09-A1 1400)  
(HS4/W/25-A5 1220)
- Tasenko Sergey**  
(JSA06/L/05-A2 1030)
- Tashchilin A. V.**  
(GA2.07/W/02-A1 1630)

## INDEX

- Tashkhojaev D. A.**  
(G5/E/19-A4 1230-10)
- Tatar Orhan**  
(GA1.04/W/37-A4 0930-17)
- Tatarinov V. N.**  
(ST6/P/03-A2 0830-03)  
(G5/P/4-A4 1508-05)
- Tatevian Ruben**  
(G2/E/16-A2 1630-08)  
(G5/P/02-A4 1130-02)
- Tatevian Suria**  
(U7/W/03-B1 0830-03)
- Tatevossian Ruben**  
(ST3/W/29-B4 1700)
- Tatiana G. Maximova**  
(JSS31/W/02-B3 0830-03)
- Tauber S.**  
(GA1.02/E/16-A2 0930)
- Tavakkoli F**  
(G3/E/30-A5 1610-30)
- Tavartkiladze Kukuri**  
(M110/E/07-B3 1505)  
(M110/E/11-B1 0900-01)
- Tavera José M.**  
(GA1.15/E/02-B4 1530-02)
- Taxeidis Kostas**  
(JSP23/E/56-A6 0830-08)
- Taylor F. W.**  
(JSA10/W/06-A2 1430)  
(MC09/W/10-B2 1515)
- Taylor Frederic**  
(MC09/W/11-B2 1500)
- Taylor K. E.**  
(MC02/W/01-B2 1100)
- Taylor Jonathan**  
(MC08/E/04-A4 1150)
- Taylor Karl E**  
(MC01/E/30-A1 0945)
- Taylor Lyla**  
(U8/W/04-B3 1450)  
(U8/W/16-B3 1640-12)
- Taylor Lynda**  
(HS5/W/36-A3 1105)
- Taylor M J**  
(JSM03/W/05-A1 1630)  
(JSM01/W/105-A3 1120)  
(JSM01/C/GA2.15/W/80-A3 1100)
- Taylor Mark A. J.**  
(JSS46/W/19-B4 0930)
- Taylor Patrick**  
(GA5.11/W/02 A3 0910)  
(GA5.11/W/03 A3 1430-02)  
(JSA09/E/11-A3 1000)  
(JSA09/W/18-A3 1100)
- Taylor Patrick T.**  
(JSA37/W/06-B3 1645)
- Taylor Peter A.**  
(JSM43/E/01-B4 1050)  
(JSM43/E/02-B4 1440)  
(JSM43/E/04-B4 1500)  
(JSM43/W/04-B4 1600)  
(JSM04/E/01-A2 1010)
- Taylor V.**  
(JSA20/E/27-A4 1200-21)
- Taymaz Tuncay**  
(ST2/E/13-A5 1400-29)  
(ST2/E/15-A4 1100)
- Tchebotareva Irina J.**  
(JSS46/E/01-B4 0930-06)  
(ST4/W/59-B1 0830-17)  
(ST5/W/53-B5 0930-07)
- Tchepik Anatoli**  
(JSS44/E/11-B4 0930-29)  
(G3/E/19-A5 1610-25)  
(GA 5.11/E/02 A3 1430-09)  
(GA5.12/E/05-A2 1600-02)  
(GA5.12/E/06-A2 1600-03)
- Tcherning C C**  
(G4/W/03-A3 1205)
- Tchiguirinskaia I**  
(JSA19/W/01-A4 1400-08)  
(JSP23/W/13-B1 1110)  
(JSM43/W/01-B5 1000)  
(JSP39/W/15-B3 1110)
- Tealeb A**  
(G5/E/41-A4 1230-07)
- Tealeb Ali**  
(JSS31/E/10-B3 0830-12)  
(JSS31/E/12-B3 0830-13)
- Techine P.**  
(U7/W/02-B1 0830-11)
- Teisseyre Roman**  
(JSA15/W/25-A5 0830-14)
- Teixeira Joao**  
(M110/W/11-B3 1615)
- Teixeira Miguel A. C.**  
(JSP49/W/01-B5 1640)
- Telbisz T.**  
(VS2/W/03-B3 1210)
- Tellam John H**  
(HS5/W/31-A3 0900)  
(HS5/W/34-A3 1000)
- Telpukhovskiy Nikolay A.**  
(JSA15/W/20-A5 1400-14)
- Telitsov M.**  
(GA3.05/W/41-B3 0900-24)  
(GA3.08/W/10-B1 0900-06)
- Telitsov Michail V**  
(GA3.10/W/14-A6 1700-16)
- Temerin M.**  
(GA3.02/W/41-B2 1600)  
(GA3.05/W/15-B3 0900-27)
- Tencate James A.**  
(ST6/E/01-A2 1730)
- Teng Ta-Liang**  
(ST1/E/83-A3 1520)  
(ST3/E/26-B3 1100)
- Tennyson J**  
(MC08/E/02-A3 1130)
- Tepley C.**  
(GA2.02/L/01-B4 1000)
- Tepley III Frank J.**  
(JSV30/W/06-B1 1400-13)
- Teptin Guerman M.**  
(GA2.02/L/04-B4 0930-07)  
(JSA45/L/05-B5 1110-05)
- Terecito Bacolcol**  
(JSV29/W/04-B1 1700)
- Tereshchenko E. D.**  
(GA2.02/W/22-B4 1720)
- Tereschenkov V. P.**  
(P12/W/12-A1 1030-03)  
(P12/W/15-A1 1030-01)  
(P12/W/16-A1 1030-02)
- Terina G I**  
(GA4.09/W/06-A5 1600-03)  
(GA4.02/W/35-A4 1400-27)  
(GA4.09/W/09-A5 1600-04)
- Terina G. I.**  
(GA3.04/E/17-B1 1520-06)
- Terkiltsen Michael B.**  
(GA3.04/W/17-B1 1520-16)
- Terray Laurent**  
(JSP25/E/19-B3 1720)  
(MW06/E/07-A3 1000)
- Tertulliani Andrea**  
(ST7/E/09-A2 1605-05)  
(ST3/W/33-B4 1400-01)
- Teruo Yamashita**  
(ST1/E/09-A2 1400-31)
- Tesaker Einar**  
(HW3/W/05-B4 1115)
- Tesauro M.**  
(JSV36/W/23-B3 1515)
- Tesmer Volker**  
(G2/W/14-A2 1630-10)
- Tett P**  
(P10/W/03-A5 0850)  
(P10/W/23-A5 0930)
- Tett Simon**  
(JSA16/E/01-A3 0830-19)
- Tett Simon. F. B.**  
(MC02/W/13-B2 1430)  
(MC02/E/14-B2 1450)  
(MC02/E/02-B2 1400)
- Teunissen P. J. G.**  
(G6/C/G1/L/16-B1 1420)
- Teyssevre Hubert**  
(JSM26/W/07-B1 1500)  
(JSM26/W/21-B2 1700-07)  
(MW01/W/02-A5 1150-04)
- Teyssier Christian**  
(JSA40/E/01-B5 1400-16)
- Teyssoneyre Valerie**  
(ST5/E/33-B5 1205)
- Tezkan Bülent**  
(JSA27/P/04-B1 1210)
- Thatcher Wayne**  
(JSS31/E/11-B2 1010)
- Thayer Jeffrey P.**  
(JSM32/W/05-B2 0930)
- Thieman Jim**  
(JWS33/W/16-B2 1130)
- Thejll Peter**  
(JSA16/W/42-A3 0830-62)
- Thirot Jean-Louis**  
(JWA34/W/06-B2 1010)
- Thoa N. T. K.**  
(GA1.04/W/24-A5 1100)  
(GA1.04/E/13-A4 0930-09)
- Thomas**  
(GA1.03/L/02-B1 1640)  
(GA1.03/L/03-B1 1620)
- Thomas Bridget**  
(HW3/W/02-B4 0940)
- Thomas C.**  
(G2/E/10-A2 1630-14)
- Thomas C. C.**  
(G6/W/05-B1 0850)
- Thomas Gary E.**  
(JSM32/W/11-B2 1400)  
(MI02/W/11-A5 1410)
- Thomas Maik**  
(JSG14/E/06-A3 1148-17)
- Thomas Michael**  
(JSA27/E/02-B1 1150)
- Thomas Percival**  
(JSP21/W/16-A5 1130)
- Thomas R**  
(JSH12/C/JSS31/E/05-A5 0930)  
(JSH12/W/09-A4 1400-03)
- Thomas R J**  
(MI03/W/05-A3 1140)
- Thomas Ronald**  
(MI03/W/01-A3 1520)
- Thomas S**  
(JSH12/W/14-A5 1630)
- Thomas Susan**  
(JSA16/E/19-A3 0830-22)
- Thomason Larry W.**  
(JSG28/W/03-B2 1400-10)  
(JSM41/W/08-B4 1000-01)
- Thompson B. J**  
(GA4.08/W/07-B3 0830)  
(GA4.01/W/01-A2 1400-04)  
(GA4.02/W/03-A4 1705)
- Thompson Barbara**  
(GA4.01/L/01-A2 1220)  
(GA4.01/E/09-A2 1200)
- Thompson Greig**  
(JSM18/E/01-A4 1220)
- Thompson P. F.**  
(JSG14/W/24-A3 1700-04)
- Thompson R**  
(JSA06/W/17-A1 1155-14)
- Thompson Ren**  
(JSV36/W/07-B3 1400)  
(VS3/W/25-B3 1620)
- Thompson Richard**  
(JSA06/E/12-A1 1155-16)
- Thompson Roy**  
(GA1.05/E/08-A6 1545)  
(GA1.05/E/13-A6 0850)
- Thompson Thayne M.**  
(JSP21/L/04-A5 0930)
- Thomsen M. F.**  
(GA3.05/W/38-B3 1700)  
(GA4.08/W/05-B3 1335)  
(GA3.05/W/11-B3 0900-06)
- Thomson Alan**  
(GA5.08/W/10-B1 1415)  
(JSA06/W/27-A1 1035)  
(JWM08/W/06-A3 1500)
- Thomson C. J**  
(ST5/W/25-B4 0950)
- Thomson Neil**  
(JSA15/W/31-A4 1120)  
(JSA15/W/17-A4 1100)
- Thomson Richard E.**  
(JSS42/E/12-B4 1500)  
(JSS42/E/12-B5 1700-07)
- Thorne R. M.**  
(GA4.10/W/06-A5 1435)
- Thorne Richard M.**  
(GA3.05/W/06-B3 0900-05)  
(GA3.05/E/09-B3 1200)  
(GA3.05/E/12-B3 0900-15)  
(GA3.05/W/29-B3 1500)
- Thornton P E**  
(MC01/E/20-A5 1405)  
(MC01/W/09-A5 1445)
- Thorolfsson Adalbjorn**  
(GA3.03/W/09-B4 1740)
- Thorolfsson Sveinn T.**  
(HS5/W/15-A2 1020)
- Thorpe Alan J**  
(MI05/E/06-A1 1630)  
(MI05/W/36-A4 1400-03)  
(MI05/W/37-A3 1500)  
(MI05/E/01-A3 1420)  
(MI05/L/05-A5 0920)  
(MI05/W/25-A3 1640)  
(MI05/W/14-A3 0920)
- Thorpe S. A.**  
(P10/E/12-A4 1050)
- Thorrold Bruce S.**  
(HS3/W/10-A1 1425)
- Thuburn J**  
(JSM01/W/42-A1 0830)
- Thuburn John**  
(JSM26/W/22-B1 1130)  
(MI12/W/15-B4 1215)  
(MI05/W/20-A1 1500)
- Thuillier G**  
(JSM01/P/03-A2 1600-18)  
(JSM01/P/03-A2 1540-18)
- Thunis P**  
(MI07/L/01-A2 1120)  
(MI07/L/02-A2 1620)
- Thurber C.**  
(U8/E/09-B3 1155)
- Thurnherr A. M.**  
(P 14/E/09-A4 1400-11)
- Tiampo K. F.**  
(ST1/W/26-A3 1210)  
(JSV36/W/21-B3 1400-01)
- Tiampo Kristy F.**  
(JSV36/E/15-B3 1655)
- Tian Jianhua**  
(GA3.09/W/24-B5 1205)  
(GA3.09/W/28-B4 0900-13)
- Tian Shao-Fen**  
(JSM24/E/11-B1 1205)
- Tianfeng Wan**  
(ST4/C/GA1.01/E/17-B2 0930-30)
- Tianyao Hao**  
(JSA27/P/05-B1 0900)  
(JSS44/P/03-B5 0950)
- Tianzeng**  
(P16/E/01-B5 1520)
- Tiberius Christian**  
(G1/L/17-A3 1100)
- Tie X**  
(JSM01/W/41-A4 1150)
- Tie Xue Xi**  
(JSM26/W/08-B2 1700-15)
- Tiing Yang**  
(JSP23/C/U5/W/08-A5 1600)
- Tikhomolov Evgeniy**  
(GA4.03/W/08-B4 1700)
- Tikhonchuk V.**  
(GA3.04/L/03-B1 0940)
- Tikhonov Ivan**  
(ST1/C/Jsa10/W/15-A3 0900-12)  
(ST1/E/76-A4 0930-15)
- Tikhonov V. N.**  
(JSA45/W/02-B5 1110-09)
- Tikhonova Olga**  
(JSP23/W/11-A5 1720)
- Tikku Anahita**  
(JSA09/W/01-A2 1145)
- Tikoff Basil**  
(JSA40/E/01-B5 1400-16)
- Tilgner A**  
(JSS02/W/14-A1 1115)  
(JSP39/W/34-B2 1500)
- Tillman. J. E.**  
(MC09/W/07-B2 01)
- Timiovska Lenka S.**  
(ST3/E/03-B4 0930-15)
- Timlin Michael**  
(JSP25/W/57-B4 1640)
- Timmen L.**  
(G1/E/37-A3 1620-69)
- Timmen Ludger**  
(G6/E/02-B2 1140)
- Timmermann Ralph**  
(P13/W/03-B1 1720)
- Timmis C.**  
(JSM26/W/27-B1 1440)
- Timmreck Claudia**  
(MI01/W/07-A2 1510)  
(MI01/W/20-A2 1640)
- Timofeev E.**  
(GA3.06/W/24-A2 0930-24)
- Timofeev E. E.**  
(GA2.02/W/15-B4 0930-12)  
(GA2.02/W/19-B4 1600)  
(GA2.02/W/25-B4 0930-11)
- Timofeev Vladimir**  
(JSS02/E/01-A1 0830-03)  
(ST2/W/01-A3 1400)
- Timofeev Yu M**  
(MI02/W/14-A4 1450)  
(MI09/E/09-A5 1145-05)
- Timofeyev Yuri**  
(MW05/W/07-A2 1215)
- Timofeyev Yuriy M.**  
(MI06/E/13-B1 1100)
- Timonen Jussi**



- (GA3.02/W/30-B3 0900-04)
- Ting Mingfang**  
(MC10/E/02-B1 1600)
- Ting Yang**  
(JSP23/C/U5/W/09-A6 1620)
- Tinmaker**  
(MI04/L/18-B1 0900-19)
- Tinmaker M I**  
(MI03/E/05-A3 1120)  
(MI03/E/04-A3 1020)
- Tinsley Brian A.**  
(JSA16/W/08-A3 0830-40)  
(JSA45/W/03-B4 1400)
- Tinti Stefano**  
(JSS42/W/03-B4 1420)  
(JSS42/W/21-B5 0950)
- Tintoré J.**  
(P11/W/28-B4 1400)
- Tischner T.**  
(HS3/W/07 1200)
- Titov Oleg**  
(JSG11/W/08-A4 1130)  
(G2/W/09-A2 1630-15)  
(G2/W/13-A2 1530)  
(JSG14/L/01-A3 1118-07)
- Titov V. V.**  
(JSS42/W/05-B5 1700-11)  
(JSS42/W/07-B5 1500)
- Titov Vasily**  
(JSS42/W/10-B4 1640)
- Titov Vyacheslav.S.**  
(GA4.02/W/23-A4 1400-21)
- Titz Helmut**  
(G1/E/35-A3 1620-67)
- Tkalcic Hroveje**  
(JSS02/W/11-A1 1700)
- Tobin D C**  
(MC08/L/01-A3 1045)  
(MC08/W/06-A3 1505)
- Tobiska W. Kent**  
(JSA16/E/12-A3 0830-14)
- Tocho Claudia**  
(G3/E/04-A5 1610-90)  
(G3/W/14-A5 1610-79)  
(G3/W/19-A5 1610-96)
- Toda T.**  
(P15/L/16-B4 1505)
- Todd Martin**  
(JSP25/E/36-B2 0930-03)  
(JSP25/L/01-B2 1210)  
(MI06/E/14-B1 1520)
- Toffoletto F. R.**  
(GA3.09/W/22-B4 0900-04)
- Tokuchi Naoko**  
(HW5/E/05-A3 1100)
- Toh H.**  
(GA1.02/W/20-A2 0930)
- Toivanen P. K**  
(GA3.08/W/22-A6 1210)
- Tokarczyk Ryszard**  
(JSP21/W/07-A4 1620)
- Toksoz Nafi**  
(G5/E/23-A4 1230-08)  
(JSS31/L/04-B2 0830-17)
- Tokuchi Naoko**  
(HW5/E/05-A3 1100)
- Tokumar Munetoshi**  
(GA4.01/W/04-A2 1520)
- Tolkachev Pavel**  
(G1/E/09-A3 1620-22)
- Tolmacheva A. V.**  
(JSA20/W/42-A4 1200-22)  
(JSA20/W/46-A4 1200-20)
- Toloshinov A. V.**  
(HW3/W/11-B4 1610)
- Tolson R. H.**  
(GA4.10/W/14-A4 0900)
- Tolstykh M. L.**  
(JSV30/E/10-B1 1400-03)
- Tolstykh Mikhail**  
(MC04/E/03-B2 1140)
- Tomasi Behrend**  
(JSG11/E/06-A4 1400-03)
- Tomasso M.**  
(GA1.04/L/06-A4 0930-03)
- Tomé Phillip**  
(G1/W/39-A3 1620-45)
- Tomezzoli Renata N.**  
(GA1.04/W/26-A4 1520)
- Tomczack Matthias**  
(P12/W/01-A1 1030-11)  
(P12/W/03-A1 0830)
- Tomoki Tsutsui**  
(JSV47/W/11-B5 1115)
- Tomoo Katsura**  
(JSS02/E/11-A1 0830-08)
- Tomoki Tsutsui**  
(JSV47/W/11-B5 1115)
- Tompkins Adrian**  
(M104/W/32-B1 0900)  
(M104/W/32-B1 0900)
- Tondi Rosaria**  
(JSS46/E/04-B4 1400)  
(JSS46/E/06-B4 0930-02)  
(JSS46/E/04-B4 1400)  
(JSS46/E/06-B4 0930-02)
- Tonegawa Yutaka**  
(GA3.04/W/04-B1 1520-40)  
(GA3.04/W/04-B1 1520-40)
- Tongxia Bai**  
(ST3/E/29-B3 1530)  
(ST3/E/29-B3 1530)
- Tooman Tim**  
(MI10/W/03-B2 1205)
- Toon Owen B**  
(MI01/L/06-A1 1110)  
(MI02/W/11-A5 1410)
- Topcu Dile H.**  
(P10/E/09-A5 1110)
- Tor Tam Khoon**  
(G1/L/22-A3 1640-95)
- Tor Working Group**  
(JSS44/E/38-B4 0930-26)
- Toramaru Atsushi**  
(VS2/W/27-B3 0850)
- Torbert R B**  
(GA4.02/W/24-A4 1400-22)
- Torge Wolfgang**  
(G6/C/G3/E/23-B1 1200)
- Torii M.**  
(GA1.03/W/17-B2 1500)  
(GA1.05/E/17-A6 1630)  
(GA1.05/W/01-A6 1515)  
(GA1.05/W/22-A6 1700)  
(GA1.05/W/30-A6 0950)  
(GA1.05/W/32-A6 1645)  
(GA1.05/W/08-A5 0910)  
(GA1.05/W/38-A5 0830)
- Tornatore Vincenza**  
(G3/E/18-A5 1610-68)
- Torrence Christopher**  
(JSP25/W/01-B4 1210)
- Torrence M. H.**  
(G6/E/03-B1 0910)  
(G5/E/10-A4 1522-12)
- Torsvik Trond**  
(GA1.04/W/01-A4 0950)
- Torta J. Miquel**  
(GA5.01/E/03-A1 0935)  
(GA1.03/E/01-B3 1120)
- Tosha T.**  
(GA1.02/W/18-A2 0930)
- Tosha Toshiyuki**  
(JSV36/W/02-B3 0930)
- Toshifumi Mukai**  
(GA2.02/E/04-B4 0930-10)
- Toshiyuki Awaji**  
(P14/W/12-A4 1520)
- Tosic Ivana**  
(MI05/W/06-A5 1150)
- Toteva Tatiana**  
(ST1/W/72-A3 0900-20)  
(ST1/W/72-A4 0930-32)
- Toth B.**  
(HS2/W/11-B1 1420)
- Toth Gyula**  
(G3/E/41-A5 1610-84)
- Toth James**  
(MI06/W/01-B2 1710)
- Toth Zoltan**  
(JSP25/W/24-B1 0850)
- Totterdell Ian**  
(MC01/E/33-A1 1730)
- Touam S**  
(G5/P/03-A4 1230-04)  
(G1/L/13-A3 1620-89)  
(G1/L/25-A3 1640-96)
- Touchard Y.**  
(GA1.03/E/07-B1 1120)
- Touchard Yannick**  
(JSV22/E/02-A5 1130)
- Tourpali C.**  
(JSP21/W/09-A4 1130)
- Tourre Yves**  
(JSP25/W/09-B4 1110)
- Tovmassian A.**  
(ST1/E/26-A2 1400-05)
- Townley L R**  
(HW5/W/11-A3 0940)
- Toya Yozo**  
(ST1/W/41-A2 1420)
- Toyoda Miho**  
(JSP25/W/94-B3 1500)
- Tozzi R.**  
(GA1.01/W/31-A5 1645)
- Trad D.**  
(GA1.02/L/01-A2 0930)
- Trakhtengerts V. Y.**  
(GA3.04/W/28-B1 1520-22)  
(GA3.05/W/37-B3 0900-11)
- Trampert J.**  
(U8/E/09-B3 1155)
- Tranter M.**  
(HS2/W/29-B2 1540)  
(HS2/W/30-B2 1600)
- Trapeznikov Yuri**  
(ST4/E/08-B1 0830-24)  
(ST5/E/38-B4 1740)
- Trapeznikov Yuriy**  
(G5/E/34-A4 1230-12)
- Traskin M. Z.**  
(ST4/E/54-B1 1400-13)
- Trattner K. J.**  
(GA3.08/L/01-B2 0900-10)  
(GA3.08/L/01-B2 900-10)  
(GA3.07/W/51-A5 0900-21)
- Trautmann T.**  
(MI06/W/26-B2 1110)
- Treder Hans-Jürgen**  
(GA6.01/P/01-A5 0900-17)
- Trees C. C.**  
(P15/L/26-B3 1110)
- Tregoning Paul**  
(JSS31/L/02-B2 1520)
- Tregubenko Victor**  
(JSP23/C/U5/E/04-B1 1440)
- Tremam**  
(MI11/L/01-B5 1130)
- Tremblay Bruno**  
(P13/L/01-B2 1150)
- Tremblay Louis-Bruno**  
(P13/W/25-B1 1110)
- Tremel Herbert**  
(G1/E/29-A3 1620-63)  
(G1/E/41-A3 1620-71)  
(G1/W/12-A3 1620-38)
- Trepte C R**  
(MI09/W/07-A5 1145-10)
- Tricca Aude**  
(HW5/W/14-A3 1440)
- Trichtchenko L**  
(JSA06/E/10-A1 1155-03)
- Trier S.**  
(MC04/E/10-B1 1035)  
(MC04/L/01-B1 1100)
- Trieu Cao Dinh**  
(JSS 44/E/34-B4 0930-09)  
(ST1/E/80-A2 1400-11)
- Trifu C.-I.**  
(ST1/W/21-A4 0930-01)  
(ST1/E/72-A4 0930-08)  
(ST1/E/75-A3 0950)
- Trigari A.**  
(VS3/E/02-B3 1550)
- Trigila Raffaello**  
(VS2/W/22-B3 1400-15)
- Trimmer R**  
(G3/W/30-A5 1610-06)
- Trindade Ricardo**  
(GA1.04/E/17-A4 0930-01)  
(GA1.05/E/16-A5 1520)
- Trinh Phan-Trong**  
(ST3/E/27-B4 1730)
- Tripathy S. C.**  
(JSA16/W/10-A3 0830-39)
- Trishchenko Alexander**  
(MC01/W/22-A1 1500)  
(MC07/W/14-A3 1055)
- Triskova L.**  
(GA2.03/E/07-B3 1500)
- Trivedi N. B.**  
(JSA20/W/24-A5 1200-07)
- Trivedi Nalin B.**  
(GA5.06/W/08 A4 1140)  
(GA3.04/E/10-B1 1520-11)
- Troccoli Alberto**  
(JSP05/W/11-A1 1500)
- Troch P. A.**  
(HS3/W/33-A2 200)
- Troch Peter A.**  
(HW4/W/04-B2 0900-07)
- Trofimov Igor L.**  
(JWA34/E/01-B2 1740)
- Troise C.**  
(JSS46/E/07-B4 0930-04)
- Trond Iversen**  
(MI01/W/16-A3 1010)
- Troshichev O. A.**  
(GA5.06/E/05 A3 1400)
- Troshichev Oleg**  
(GA3.10/W/09-A6 1700-13)  
(JSA06/W/14-A1 1700)  
(GA3.08/E/12-B1 1150)  
(JSA35/W/06-B1 1400)  
(JSA45/W/18-B4 1450)
- Troshina Elena**  
(JSS42/E/13-B5 1700-06)
- Trousenkov Serge**  
(JSP25/W/06-B1 0830-07)
- Troyan Vladimir**  
(JSP23/W/32-B1 1130)  
(JSP23/W/34-B1 0830-15)
- Trubachev O. O.**  
(GA3.02/W/35-B3 0900-10)  
(GA3.02/W/49-B3 0900-11)
- True Scott A.**  
(G1/E/60-A3 1620-82)
- Truhlik V.**  
(GA2.03/E/07-B3 1500)
- Trulsen J.**  
(GA4.09/W/05-A6 1140)
- Trupin Andy**  
(JSA09/E/02-A2 1115)
- Trujillo Ancor**  
(JSV36/W/12-B3 0900-08)
- Trumbull Robert**  
(VS2/W/19-B3 1400-12)
- Trusenkova Olga**  
(JSA09/W/06-B1 0830-07)  
(P10/E/17-A3 1520)
- Tsagouri Ioanna**  
(GA3.02/W/04-B3 0900-23)  
(GA3.09/W/07-B4 0900-11)  
(GA3.09/W/21-B4 0900-10)
- Tsai Yi-Ben**  
(ST3/W/30-B3 1115)  
(JSP23/C/U3/W/21-B2 1740)  
(U3/W/21-A30900-17)
- Tsakiri Maria**  
(G1/L/12-A3 1620-88)  
(G1/W/13-A3 1620-05)  
(G1/W/28-A3 1440)  
(G1/W/33-A3 1620-16)  
(G6/W/03-B2 1520)
- Tsalas M.**  
(GA3.02/W/08-B3 0900-06)
- Tsapanos Heodoros**  
(ST2/E/45-A3 0900)
- Tscherning C.C.**  
(G2/W/03-A2 1630-18)
- Tselioudis George**  
(MW02/W/05-B3 0930)
- Tseng Ching-Liang**  
(G1/W/34-A3 1620-43)
- Tseng Hong-Zeng**  
(JSG11/E/10-A3 1400)  
(G3/E/43-A5 1610-17)
- Tsias A.**  
(MI06/W/26-B2 1110)
- Tsidulko Marina**  
(MI07/E/04-A2 1640)
- Tsirulnik Lev**  
(GA6.01/W/15-A5 0900-14)  
(JSA16/W/35-A3 0830-57)  
(GA3.09/W/09-B4 0900-07)
- Tsitverblit Naftali**  
(JSP39/W/03-B3 1509-24)
- Tsou J J**  
(MI02/E/06-A5 0910)
- Tsuboi Seiji**  
(ST2/W/31-A5 1400-34)  
(ST5/W/54-B3 0900-10)  
(U7/W/13-B1 0830-15)
- Tsubokawa T**  
(G3/E/15-A5 1610-39)  
(G2/W/05-A2 1500)
- Tsuda T**  
(JSM01/W/01-A3 1140)  
(JSM01/W/36-A1 1400)  
(MW04/W/04-A1 0900)  
(JSA20/W/09-A4 1200-11)
- Tsuda Toshitaka**  
(JSM01/C/MW07/W/23-A2 1600-33)  
(JSM01/E/03-A2 1430)  
(JSM01/E/30-A2 1600-24)  
(JSG28/E/02-B1 1400-20)  
(JSG28/E/03-B2 1400-15)  
(JSG28/E/12-B2 1200)  
(JSM26/E/09-B1 1400)
- Tsuei Gwo-Chyang**

## INDEX

- (G3/W/40-A5 1610-97)  
**Tsakamoto S.**  
 (GA1.05/E/17-A6 1630)  
**Tsuji Daijuro**  
 (G5/E/21-A4 1115-04)  
**Tsuji Hiroshi**  
 (JSV47/W/27-B5 0915)  
**Tsuji Yoshinobu**  
 (JSS42/P/01-B5 1210)  
**Tsujimura Maki**  
 (HS4/W/16-A5 0900)  
 (HS4/W/19-A5 1010)  
**Tsakamoto Osamu**  
 (JSM24/W/04-B1 0930)  
**Tsumura Noriko**  
 (ST5/W/30-B5 0930-01)  
**Tsunakawa Hideo**  
 (GA1.03/L/01-B1 0940)  
 (GA1.01/W/19-A5 1600)  
**Tsunami Sakhalin**  
 (JSS42/E/09-B5 1640)  
**Tsuneomi Kagiyama**  
 (JSV36/W/27-B3 0900-05)  
**Tsunomura Satoru**  
 (GA5.01/W/05 A1 0835)  
**Tsurud A. K.**  
 (GA4.10/W/34-A5 1620)  
 (GA4.10/L/02-A4 1055)  
**Tsuruda Koichiro**  
 (GA3.04/W/04-B1 1520-40)  
**Tsuruta S**  
 (G3/E/15-A5 1610-39)  
**Tsurutani B.**  
 (GA4.08/W/12-B4 1635)  
 (GA3.02/W/39-B2 1110)  
**Tsurutani B T.**  
 (GA4.09/W/15-A6 0900)  
 (JSA20/C/GA2.02/W/20-A5 1200-12)  
**Tsurutani Bruce**  
 (GA4.09/W/11-A6 0920)  
**Tsutsui Kazuo**  
 (JSG14/W/20-A3 1700-11)  
**Tsutsui Tomoki**  
 (ST3/E/55-B4 1400-18)  
**Tsvetkov Yu**  
 (GA5.12/W/07 A2 1200)  
**Tsvetkov Yu. P.**  
 (GA5.08/W/04-B1 1400-03)  
**Tsvyaschenko Vladimir**  
 (ST4/E/42-B1 1400-19)  
**Tsybine Nikolay**  
 (ST1/W/03-A4 0930-27)  
**Tsyganenko N. A.**  
 (GA3.02/W/21-B2 1520)  
 (ST3/E/54-B4 1400-11)  
**Tsyplakov Vladislav**  
 (ST1/W/16-A3 0900-19)  
**Tsyro Svetlana**  
 (MI01/L/01-A1 1210)  
**Tubia José María**  
 (GA1.04/W/02-A5 1640)  
**Tuck Adrian**  
 (MI10/W/01-B2 1035)  
 (MI12/W/17-B5 1055)  
 (MI12/W/14-B5 1005)  
**Tugrul Suleyman**  
 (P11/E/25-B4 1010)  
 (P11/E/27-B5 1130)  
**Tulkens P**  
 (MC01/W/11-A3 0945)  
**Tulkens Philippe**  
 (MC11/W/02-B4 1650)  
**Tulupov Vladimir I.**  
 (GA4.04/W/10-B5 0830-03)  
**Tumarkin Alexei**  
 (ST3/W/37-B3 1715)  
**Tumwikirize Isaiah**  
 (ST7/L/04-A2 1605-07)  
**Tuncay Taymaz**  
 (ST2/E/14-A4 1115)  
**Tung K.-A.**  
 (JSS44/W/14-B4 0930-12)  
**Tuomi Tapio**  
 (JSA35/E/08-B1 1210)  
**Tuominen Ilkka**  
 (GA6.01/E/21-A5 1645)  
**Turbitt Chris**  
 (GA5.01/E/03 A1 0935)  
 (GA5.01/W/04 A1 1700)  
**Turco R. P.**  
 (U3/W/08-A30900-13)  
 (JSM26/W/31-B2 1150)  
**Turcotte Donald**  
 (JSP23/W/03-B2 1520)  
**Türkez Ali**  
 (G1/E/04-A3 1620-50)  
**Turmon Michael**  
 (JSA16/W/20-A3 0830-53)  
**Turner Dave**  
 (MC08/L/01-A3 1045)  
**Turner J. V.**  
 (HW5/W/11-A3 0940)  
**Turner John**  
 (JSM18/L/01-A4 1720)  
**Turner N. E.**  
 (GA3.08/E/01-A6 1430)  
 (GA3.05/W/04-B3 0900-45)  
**Turner P.**  
 (GA1.04/L/06-A4 0930-03)  
**Turner R. E.**  
 (P09/W/09-A2 1050)  
**Turner T. E.**  
 (GA3.05/W/13-B3 0900-34)  
**Tursunmetov Gidroingeo R.**  
 (JSA27/E/01-B1 1400-06)  
**Tursunmetov R.**  
 (JSA19/L/07-A4 1400-10)  
**Turunen Esa**  
 (GA2.01/W/11-A1 1605)  
 (JSA45/W/04-B5 1110-10)  
 (JSA45/W/12-B4 1620)  
**Turunen T.**  
 (GA2.03/W/03-B3 1400-01)  
**Tuttle J.**  
 (MC04/E/10-B1 1035)  
 (MC04/L/01-B1 1100)  
**Tverskaya Lyudmila V.**  
 (GA3.05/W/09-B3 1740)  
 (GA3.05/W/20-B3 0900-16)  
 (GA4.08/W/08-B3 0900-08)  
**Tyapkina Olga**  
 (JSP23/C/U5/E/08-B1 1700)  
**Tyson P D**  
 (MI02/L/01-A5 1140)  
 (MI02/L/18-A5 1430)  
**Tyson Peter**  
 (MC03/E/09-B4 1010)  
 (MC09/E/09-B2 1700)  
**Tyupkin Yu.**  
 (JWS33/W/29-B2 0930)  
 (JWS33/W/03-B2 1145)  
**Tyupkin Yu. S.**  
 (ST1/W/38-A2 0930-02)  
 (ST1/W/07-A3 0900-05)  
**Tzanis A**  
 (ST1/E/13-A4 0930-23)  
 (ST1/E/14-A3 1500)  
**Tziavos I. N**  
 (G3/W/22-A5 1610-07)  
 (G3/W/05-A5 1010)
- ## U
- Uberoi C**  
 (GA4.05/E/01-A1 1210)  
**Uchida Akito**  
 (ST3/E/30-B4 0930-13)  
 (ST3/E/35-B4 0930-14)  
**Uchida Hiroshi**  
 (JSP25/W/64-B3 0830-01)  
**Uchida T.**  
 (GA1.02/W/18-A2 0930)  
**Uda Saneyuki**  
 (GA1.03/W/23-B1 1040)  
**Udare R. S.**  
 (GA3.04/E/09-B2 1650)  
**Uddstrom Michael**  
 (MI06/E/01-B1 1610)  
**Udias A.**  
 (ST2/W/06-A4 1600)  
**Ueda Hideki**  
 (ST1/W/22-A3 1440)  
**Ueda Seiya**  
 (ST1/W/37-A4 0930-01)  
**Ueda Toshifumi**  
 (HS5/W/35-A3 1045)  
**Uehara Katsuto**  
 (JSG11/W/07-A4 1400-07)  
**Ueki S.**  
 (JSS46/W/03-B4 1010)  
 (JSV36/E/18-B3 1400-13)  
 (JSV36/W/09-B3 1430)  
 (JSV47/W/22-B5 1130)  
 (JSV47/W/26-B5 1400-09)  
**Uemda Yasuhiro**  
 (ST1/E/33-A1 1600)  
**Ueno Kenichi**  
 (JSM24/E/02-B1 1440)  
**Ueno Naoko**  
 (GA1.05/E/06-A6 0900-04)  
**Ueno Tuyoshi**  
 (GA1.05/W/05-A5 1500)  
**Uetake Teppei**  
 (MC06/C/JSM01/E/35-A1 1600)  
 (MC06/W/04-A1 1400)  
**Ufimtsev Gennady F.**  
 (U3/W/09-A3 0900-14)  
**Ugarov A. N.**  
 (JSP23/E/33-A5 1640)  
 (ST3/E/01-B5 1400)  
 (ST3/E/05-B5 0930)  
**Uhan J.**  
 (HW2/W/22-B1 0900-04)  
**Uhlenbrook Stefan**  
 (HS4/L/03-A4 0930)  
 (HS4/L/03-A4 0930)  
 (HS4/W/11-A4 1600)  
**Ui Tadahide**  
 (JSV36/E/17-B3 1400-09)  
**Uji Gokanoshō**  
 (JSP23/C/U5/W/11-A5 1500)  
**Ukhorsky A. J.**  
 (GA3.04/L/04-B1 1210)  
**Ukita Jinro**  
 (JSP25/W/59-B3 0950)  
**Ukrainsky Vladimir**  
 (P07/E/02-A3 0900-06)  
**Ulaanbaatar Tarzadin**  
 (JSM18/E/04-A4 1740)  
 (G5/E/20-A4 1115-12)  
 (MC07/E/03-A3 1135)  
 (MC08/E/03-A4 1210)  
 (ST7/E/01-A2 1605-06)  
 (U3/E/08-A3 0900-06)  
 (JSA27/E/04-B1 1400-04)  
 (MC02/E/01-B1 1600-12)  
 (MW03/E/08-B4 1500)  
**Ulbrich U.**  
 (JSP25/W/53-B3 0850)  
**Ulbrich Uwe**  
 (JSP23/E/10-B2 1420)  
**Ulrich Thomas**  
 (GA2.01/W/11-A1 1605)  
 (JSA45/W/04-B5 1110-10)  
 (JSA45/W/12-B4 1620)  
**Uljev Valery**  
 (JSA45/W/17-B5 1110-07)  
**Ullerstig Anders**  
 (MI04/W/10-B1 1200)  
 (MC01/W/17-A4 1125)  
**Ulomov V.**  
 (JSP23/C/U5/E/16-A5 1620)  
 (ST3/E/56-B4 1400-20)  
**Ulomov Valentin I.**  
 (ST3/W/21-B4 1115)  
**Ulrich Roger**  
 (JSA16/E/11-A3 0830-15)  
 (JSA16/W/38-A3 0830-54)  
**Ultras-Guerard P.**  
 (GA5.08/W/09-B1 1115)  
 (GA1.07/W/04-B2 1100)  
 (GA5.08/W/01-B1 1400-07)  
 (GA5.08/W/02-B1 1005)  
 (GA6.02/W/01-B1 1520)  
 (JSA37/W/08-B3 1430)  
**Umatani Shin-ichiro**  
 (JSP25/W/64-B3 0830-01)  
**Umeda Koji**  
 (JSV36/E/17-B3 1400-09)  
**Umino Norihito**  
 (JSS44/W/01-B4 0930-06)  
 (JSS44/W/09-B4 0930-08)  
**Uno Koji**  
 (GA1.04/W/17-A6 1420)  
 (GA1.05/W/05-A5 1500)  
**Uno Natsuko**  
 (P09/W/13-A2 0930)  
**Unsworth Martyn**  
 (GA1.02/W/07-A1 1605)  
**Untch Agathe**  
 (MC06/E/01-A1 1440)  
**Uozumi T.**  
 (GA3.04/L/09-B1 1520-44)  
**Urakawa Satoru**  
 (ST6/E/09-A2 14:30)  
**Uran Bojan**  
 (JWS33/E/12-B2 1635-30)  
 (ST5/E/30-B3 1400-05)  
**Uranova Svetlana**  
 (ST3/E/49-B5 1045)  
**Urban Tim**  
 (JSG11/E/10-A3 1400)  
 (JSG11/W/19-A3 1130)  
**Urbanic T. I.**  
 (ST1/E/72-A4 0930-08)  
 (ST1/E/75-A3 0950)  
**Urbini Giuseppe**  
 (JSV36/E/22-B3 0900-16)  
**Urdukanov Rufet**  
 (ST3/W/23-B4 0930-18)  
**Uri Stein**  
 (MC01/E/17-A5 0930)  
**Urtsky Vadim M.**  
 (GA3.08/E/10-B1 0900-03)  
**Urrutia-Fucugauchi J.**  
 (GA1.05/W/07-A6 0900-06)  
 (GA1.05/W/27-A5 0900-03)  
 (JSA15/W/24-A4 1400-17)  
**Usmanov Arcadi V.**  
 (GA3.09/W/08-B4 1010)  
**Usoskin I.**  
 GA6.01/W/03-A5 1525)  
**Ustjak Sergej**  
 (GA1.05/W/21-A6 1130)  
**Usui Takayuki**  
 (MI09/E/06-A5 1145-20)  
**Utada Hisashi**  
 (GA1.02/W/20-A2 0930)  
 (GA1.02/W/05-A2 0930)  
 (GA1.02/W/22-A2 0930)  
 (JSA15/E/07-A5 0830-02)  
 (JSS44/E/41-B4 0930-10)  
 (JSV36/W/27-B3 0900-05)  
 (JWA34/W/12-B2 1050)  
 (U7/L/02-B1 1515)  
**Utale Ana**  
 (ST1/E/78-A2 1400-15)  
**Utkin Iona S.**  
 (JSV36/E/05-B3 1400-08)  
**Utkin Konstantin B.**  
 (JSP49/E/03-B5 0850)  
**Utkina Ludmila I.**  
 (JSV36/E/05-B3 1400-08)  
**Utsugi Mitsuru**  
 (JSA15/E/56-A3 0850)  
**Utsumi Wataru**  
 (JSS02/E/14-A1 1740)  
**Uttal T**  
 (MI08/L/09-A4 1615)  
 (MI08/L/11-A4 1400)  
 (MI08/W/16-A4 1600)  
**Uyeda S.**  
 (JSA15/E/17-A3 1440)  
 (JSA15/E/19-A3 1500)  
**Uyeda Seiya**  
 (JSA15/E/02-A5 0830-05)  
**Uyeshima Makoto**  
 (GA1.02/L/05-A2 0930)  
 (JSA15/W/07-A3 1740)  
 (JSA15/E/40-A3 1700)  
 (JSS44/E/41-B4 0930-10)  
 (JSV36/E/23-B3 0900-07)
- ## V
- Vacaflor Jose Luis**  
 (G4/E/09-A3 1620-03)  
 (G4/E/13-A3 1620-02)  
**Vacaresse Angélique**  
 (GA3.05/W/08-B3 1440)  
**Vaccari F.**  
 (ST3/W/05-B4 1615)  
**Vaccari Fabio**  
 (ST3/W/12-B5 1430)  
**Vaccari Franco**  
 (ST3/W/02-B4 1645)  
 (ST3/W/07-B3 0845)  
 (ST3/W/51-B4 1415)  
**Vadas Sharon L**  
 (MW07/W/14-A4 1110)  
**Vadkovsky Vsevolod N.**  
 (GA1.04/E/10-A4 0930-04)  
**Vagina L. I.**  
 (GA3.08/W/08-B1 0900-07)  
**Vaher Rein**  
 (JSS44/E/11-B4 0930-29)  
 (GA5.11/E/03 A3 1430-10)  
**Vakkilainen Pertti**  
 (HS3/W/20-A2 1015)  
 (HS3-W/21-A2 1110)  
**Valcke Sophie**  
 (JSP25/E/19-B3 1720)

- Valdes Jan Paul**  
(MC01/E/36-A3 1605)
- Valdes Paul**  
(MI05/E/27-A2 1140)
- Valdes Paul J**  
(U3/L/01-A3 1500)  
(MC11/E/15-B4 1045)
- Valdes-Galicia J. F.**  
(GA4.04/L/03-B5 0830-08)  
(GA6.01/L/01-A6 1130)
- Valdes-Galicia Jose**  
(GA4.03/E/02-B4 1645)
- Valdes-Gonzalez C.**  
(ST2/W/05-A5 1000)
- Valdivia J. A.**  
(GA3.02/W/27-B3 1205)  
(GA3.09/W/14-B4 1720)  
(GA3.09/W/20-B4 1705)
- Valdivia Juan**  
(GA3.02/W/30-B3 0900-04)
- Valdivieso Da Costa Maria**  
(JSP39/W/20-B4 1740)
- Valensise Gianluca**  
(ST3/E/07-B4 1000)
- Valensise M. R.**  
(GA6.01/E/22-A5 0900-06)
- Valente Maria Antonia**  
(MW07/W/06-A4 1230)
- Valentina Kobbzova**  
(GA1.02/E/15-A1 1605)
- Valentine Greg**  
(U4/W/06-A4 1015)  
(VS2/W/26-B3 1400-29)
- Valerie**  
(ST2/W/13-A3 0845)
- Valero F P J**  
(MI08/W/08-A4 1545)
- Valero Francisco P. J**  
(MI10/W/23-B2 1420)  
(MI04/W/35-B2 1450)
- Vales Dina**  
(U7/E/03-B1 0830-17)
- Valet Jean-Pierre**  
(GA1.01/W/18-A5 1430)
- Valiente Marcos**  
(JSV36/W/16-B3 0900-10)
- Valiya Hamza M.**  
(ST7/W/02-A2 1400)
- Valladares C E**  
(GA3.10/W/07-A6 0855)  
(GA2.02/W/24-B5 1500)
- Valladares Cesar**  
(GA2.02/W/21-B4 930-13 )
- Vallance J W**  
(U4/W/05-A4 1215)  
(JSP23/C/U4/W/05-A6 0830-19)
- Valle-Levinson Arnold**  
(P09/W/10-A1 1500)
- Vallianatos F.**  
(ST1/E/13-A4 0930-23)  
(ST1/E/14-A3 1500)
- Vallianatos Filippos**  
(JSP23/W/23-B1 1720)
- Vallinkoski M. K.**  
(GA2.02/W/15-B4 0930-12)  
(GA2.02/W/19-B4 1600)  
(GA2.02/W/25-B4 0930-11)
- Vallis Geoffrey**  
(JSP25/W/03-B4 1520)
- Van Bavel A.-M.**  
(JSM26/W/29-B2 1700-09)
- Van Beek G**  
(JSA06/E/09-A1 1155-01)
- Van Bochove E.**  
(HS2/W/26-B2 1400)
- Van Dam S**  
(JSH12/C/JSS31/E/05-A5 0930)
- Van Dam T. M.**  
(G1/W/22-A3 1620-41)  
(G1/E/43-A3 1620-73)
- Van De Ven Frans**  
(HS5/W/22-A2 1425)
- Van Decar J.**  
(ST4/E/65-B2 1520)
- Van Den Akker C.**  
(HW4/E/W/03-B2 1730)
- Van Den Berg Meindert W.**  
(ST3/W/04-B4 0945)
- Van Den Ijssel J.**  
(G2/W/08-A2 1630-22)
- Van Der Hoeven A. G. A.**  
(JSG28/E/01-B1 1040)
- Van Der Marel H.**  
(JSG28/E/01-B1 1040)
- Van Der Marel Hans**  
(G1/E/46-A3 0930)  
(G1/L/18-A3 1620-31)  
(G1/L/11-A3 1200)
- Van Der Plicht Johannes**  
(JSA16/E/21-A3 0830-08)
- Van Der Pluijm Ben**  
(GA1.04/W/31-A4 0900)
- Van Der Veer P.**  
(HW4/E/W/03-B2 1730)
- Van Der Voo Ann**  
(JSS13/W/01-A4 1720)
- Van Der Voo Rob**  
(GA1.04/W/31-A4 0900)
- Van Driel-Gesztelyi Lidia**  
(GA4.01/L/01-A2 1220)  
(GA4.02/W/14-A4 0925)
- Van Eck T.**  
(ST5/W/15-B4 1400)
- Van Eck Torild**  
(ST3/E/53-B4 1230)  
(ST5/W/03-B3 1420)  
(ST5/W/35-B3 0900-08)  
(ST2/W/10-A5 1400-16)
- Van Gelderen Martin**  
(G4/W/11-A3 1145)  
(G4/W/12-A3 1420)
- Van Heijst Hendrik**  
(ST4/W/04-B3 0830-02)
- Van Herpe Y.**  
(HS3/W/33-A2 200)
- Van Hoolst T**  
(G5/L/05-A4 1000)
- Van Loon D.**  
(G5/L/01-A4 1145)
- Van Lammeren A. C. A. P.**  
(JSG28/E/01-B1 1040)  
(MI06/W/14-B2 1010)  
(MI10/W/17-B2 1620)
- Van Loon Harry**  
(MW08/E/02-A2 1500)  
(MW08/E/03-A2 1430)
- Van Ommen Tas D**  
(JSM18/W/13-A5 1140)
- Van Onselen Kyra**  
(JSG11/W/21-A3 1210)
- Van Roozendaal M**  
(JSM01/E/44-A4 1620-14)
- Van Vugt Nicole**  
(GA1.15/W/04-B4 1500)
- Van Ypersele Jean-Pascal**  
(GA6.01/W/11-A5 1425)
- Van Zele Maria Andrea**  
(G1/E/40-A3 1620-27)  
(GA2.03/E/10-B3 1700-08)  
(GA4.08/E/17-B3 1105)
- Vanbauce Claudine**  
(MI06/W/05-B1 1400-06)  
(MI06/W/05-B2 1400-06)
- Vandaele A C**  
(MC08/E/02-A3 1130)
- Vandamme Didier**  
(GA1.04/E/02-A6 0920)  
(GA1.03/E/07-B1 1120)
- Vandemeulebrouck J.**  
(ST1/E/87-A2 0930-12)
- Vandenberg N.**  
(G2/L/09-A2 1200)
- Vandenberg Nancy R.**  
(G6/W/05-B1 0850)
- Vanek Jiri**  
(ST2/E/33-A3 1130)  
(ST2/E/37-A5 1400-07)
- Vanicek Michael**  
(P12/W/04-A1 1500)
- Vanicek Petr**  
(G3/W/54-A5 1610-50)  
(G3/L/01-A5 1610-61)
- Vanin Nikolay**  
(P10/E/13-A5 1440)
- Vanneste J.**  
(JSM26/W/20-B1 1520)
- Vanneste Jacques**  
(MW07/W/13-A4 1720)
- Vannitsem S.**  
(MI11/E/09-B5 1215)
- Vanruymbecke M.**  
(ST1/E/87-A2 0930-12)
- Vanyan Leonid**  
(GA1.02/E/17-A2 0930)  
(GA1.02/W/22-A2 0930)  
(GA1.02/W/27-A1 1605)
- Vanyan Leonid L.**  
(JWA34/E/01-B2 1740)
- Varadi Ferenc**  
(JSA16/W/20-A3 0830-53)
- (JSA16/W/38-A3 0830-54)
- Varanasi Prasad**  
(MC08/W/01-A3 1150)
- Varani A.**  
(JWS33/W/33-B2 1635-32)  
(JWS33/W/33-B3 0900-32)
- Vardavas Ilias**  
(MC09/W/09-B2 1130)
- Varfolomeeva Irina**  
(HS5/W/05-A1 1525)
- Varga Peter**  
(ST3/P/2-B4 1015)
- Vargas Walter**  
(MC02/E/20-B1 1600-07)
- Vargin Pavel**  
(JSM01/E/33-A1 1050)
- Varley C. A**  
(GA4.01/W/09-A2 1140)
- Varley Nick**  
(JSV36/W/18-B3 1200)
- Varotsos C**  
(JSM01/W/37-A5 1400)
- Varshalomidze Guram**  
(JSP49/E/10-B5 1210-11)
- Varskog Per**  
(P07/L/03-A3 0900-08)
- Vasco D. W.**  
(ST4/E/67-B2 0930-17)
- Vasco Don**  
(ST5/W/06-B3 1400-03)
- Vashenyuk E. V.**  
(GA4.04/W/11-B5 0830-05)  
(GA4.02/W/19-A4 1400-17)
- Vasiliev Sergey S.**  
(JSA16/E/16-A3 0830-09)
- Vasilieva T.**  
(GA1.02/L/03-A2 0930)
- Vasiliev A. B.**  
(GA2.03/W/09-B3 1030)
- Vasilieva V. G.**  
(GA4.08/W/04-B3 0900-05)  
(JSA06/E/05-A1 1155-17)
- Vasilieva Valeriya**  
(P13/L/02-B1 1740)
- Vasiljev A. V.**  
(GA2.03/L/01-B3 1400)  
(GA2.03/L/02-B3 1520).
- Vasiljevic I M**  
(JSA06/W/13-A1 1155-08)
- Vasilkov Alexander**  
(P15/L/27-B4 1630)
- Vasilyev V. I.**  
(JSA45/W/02-B5 1110-09)
- Vasilyeva-Vashakmadze Nonna S.**  
(ST7/E/02-A2 1605-04)
- Vassal J.**  
(JSA20/P/01-A5 1501)
- Vassal Jacques**  
(GA5.08/W/01-B1 1400-07)
- Vassie J. M.**  
(P16/W/01-B5 1620)
- Vassiliadis Dimitris**  
(GA3.02/W/27-B3 1205)  
(GA3.09/W/14-B4 1720)  
(GA3.09/W/20-B4 1705)  
(GA3.02/W/30-B3 0900-04)
- Vassily Lykosssov**  
(MC01/E/22-A5 1525)
- Vassova**  
(JSP23/W/60-A5 0830-12)
- Vasilyunas Vytenis M.**  
(GA3.01/E/01-A2.1645)  
(GA4.10/W/27-A4 1725)
- Vatrr William**  
(G1/E/60-A3 1620-82)
- Vaughan A. H.**  
(GA4.03/E/03-B4 1130)
- Vaughan G.**  
(JSM26/W/24-B3 1150)  
(JSM26/W/27-B1 1440)
- Vaughn Geraint**  
(JSM01/W/109-A4 1620-15)
- Vavilov S. I.**  
(GA5.01/E/08 A1 1045)
- Vázquez-Suñé E.**  
(HS5/W/28-A2 1655)
- Vdovichev A. O.**  
(GA4.02/E/07-A4 1400-02)
- Vecsey L.**  
(ST4/E/46-B2 0930-07)
- Vedernikov Vladimir I.**  
(P11/L/06-B5 1730)
- Veerabuthiran. S.**  
(MI06/W/25-B2 1130)
- Veerawamy K.**  
(JSS44/E/42-B4 0930-32)  
(ST4/E/72-B2 0930-23)
- Veerawamy K.**  
(JSV22/E/13-A5 1440)
- Vegener T. N.**  
(HS2/W/04-B1 1000)
- Veis G.**  
(ST1/E/87-A2 0930-12)
- Veis George**  
(G5/E/36-A4 1215)  
(JSS31/W/11-B2 1620)
- Veit A.**  
(JSA09/L/02-A2 1230)
- Vej Maries**  
(JSH12/W/05-A5 0900)
- Velden Christopher**  
(MI06/W/17-B2 1650)
- Velders Guus J. M.**  
(JSM01/W/39-A4 1020)  
(JSM01/W/15-A5 1720)
- Velez E.**  
(G5/W/26-A4 1550-06)
- Velez P.**  
(P11/W/19-B4 1500)
- Velichko V. A.**  
(GA3.02/L/06-B3 0900-27)
- Veliciu Serban**  
(MC02/E/22-B1 1210)  
(ST4/E/41-B1 1400-21)
- Velikin S. A.**  
(HW3/W/11-B4 1610)  
(HW3/W/12-B4 1635)
- Veloso Alberto**  
(U8/W/03-B3 1425)
- Veltri Pierluigi**  
(GA4.09/W/03-A6 1600)  
(GA3.02/W/63-B3 0900-09)
- Venegas Silvia A.**  
(JSP25/W/44-B5 1400)  
(JSM18/W/02-A5 0900)
- Vener Galin**  
(MC01/E/22-A5 1525)
- Veneziano Joseph**  
(P11/E/13-B3 1050)
- Venhodová Daniela**  
(GA1.15/E/02-B4 1530-02)
- Venkatachalappa M.**  
(HS5/W/43-A3 1500)
- Vennerstroem Susanna**  
(GA3.03/W/04-B4 1510)
- Venugopalan**  
(P10/E/09-A5 1110)
- Venuti G.**  
(G2/W/15-A2 1630-19)  
(G4/W/03-A3 1205)
- Venzke S.**  
(JSP25/W/13-B5 0950)
- Vera Emilio**  
(JSA09/W/15-A3 0830)
- Verbeiren Roland**  
(ST3/W/53-B4 1400)
- Verdiere Alain Colin De**  
(P12/E/05-A1 1520)
- Verdun J.**  
(JSA37/W/04-B3 1200)
- Vereshchaka Alexander L.**  
(P16/L/02-B5 1150)
- Veretenenko Svetlana**  
(JSA16/C/GA4.07/E/26-A3 0830-13)  
(JSA16/E/27-A3 0830-12)
- Vergasova Galina**  
(JSM01/W/50-A2 1600-11)
- Vergniolle Sylvie**  
(JSV29/E/03-B1 1740)
- Verhoef W.**  
(JSM41/E/03-B5 1105)
- Verma Saurabh K.**  
(JSA40/E/10-B5 1025)  
(JSS44/E/10-B4 1030)  
(JSA09/E/03-A3 1215)
- Vermeer M.**  
(G1/E/46-A3 0930)
- Vermeer Martin**  
(JSG11/E/05-A3 1520)  
(JSG28/E/22-B1 1400-01)
- Vermeersen L L A**  
(JSG11/W/02-A3 1540)  
(JSG14/W/12-A3 1209-24)  
(JSG14/W/19-A3 1600)
- Vernet Maria**  
(P15/L/01-B4 1205)
- Vernin C.**  
(GA5.06/W/09 A3 1000)
- Vernin Christophe**  
(GA5.08/W/02-B1 1005)



# INDEX

- Vernon Frank L.**  
(JWS33/E/17-B2 1400)
- Vero J.**  
(GA3.04/W/09-B1 1520-17)
- Vero József**  
(GA6.01/P/05-A5 1715)
- Veronez Mauricio Roberto**  
(G1/L/02-A3 1620-840)
- Veronneau Marc**  
(G3/E/13-A5 1610-63)
- Verosub Kenneth L.**  
(GA1.03/W/31-B2 1120)  
(GA1.05/E/01-A6 0910)
- Verrier Violaine**  
(MI03/E/01-A3 1200)
- Verrieres S A**  
(JSM01/P/03-A2 1600-18)  
(JSM01/P/03-A2 1540-18)
- Verronen Pekka**  
(JSA45/W/04-B5 1110-10)  
(JSA45/W/12-B4 1620)
- Vershkov Andrey**  
(G4/E/16-A3 1440)  
(G4/E/16-A3 1440)
- Vershovskii A. K.**  
(GA5.01/E/13-A1 1115)
- Versiani Bruno Rabelo**  
(HS1/W/23-B5 1000)
- Verstraete Michel**  
(JSM24/E/01-B1 1145)
- Veselovskii Igor**  
(JSM01/W/45-A2 1600-06)
- Veselovsky I. S.**  
(GA3.09/W/23-B4 0900-02)  
(GA4.04/W/01-B5 0830-02)  
(GA4.02/W/06-A4 1400-15)
- Vespe F.**  
(G1/W/27-A3 1620-40)  
(JSP23/C/U5/W/01-B2 0830-15)  
(JSG28/W/15-B1 1400-04)
- Vetrano Anna**  
(P11/W/12-B4 1640)
- Vettoretti G**  
(MC11/W/08-B3 1120)
- Vezzu Guido**  
(HW5/W/14-A3 1440)
- Vialle C**  
(JSM01/W/37-A5 1400)
- Viatte P**  
(JSM01/W/37-A5 1400)
- Vicente Gilberto A.**  
(MC04/W/12-B2 0925)
- Vickers J.**  
(JSA20/E/27-A4 1200-21)
- Victor Luis Mendes**  
(ST4/W/25-B2 1720)
- Victor Ramos**  
(JSS44/W/19-B4 0930-01)
- Vidmont Natalia**  
(ST3/E/54-B4 1400-11)  
(ST1/W/16-A3 0900-19)
- Vieira L. E.**  
(GA4.08/W/02-B3 1400)  
(GA4.08/W/10-B3 1030)
- Vieira Luis E. A.**  
(GA4.08/W/06-B3 0905)
- Vieira R.**  
(G5/W/26-A4 1550-06)
- Viereck Rodney**  
(JSA16/W/38-A3 0830-54)
- Viezzoli Dino**  
(P11/W/22-B4 1620)
- Viger Roland**  
(HW4/W/02-B2 1000)
- Vignudelli Stefano**  
(P11/W/12-B4 1640)
- Vigo-Aguiar Isabel**  
(G1/W/10-A3 1620-37)
- Vikhorev Alexander A.**  
(ST5/W/27-B4 0930-07)  
(ST5/W/28-B4 0930-05)  
(ST5/W/50-B5 0930-04)
- Vikhreva Elena**  
(GA3.08/W/10-B1 0900-06)
- Vila P.**  
(JSA20/E/26-A4 1200-14)
- Vila P. M.**  
(JSM01/P/03-A2 1540-18)  
(JSM01/P/03-A2 1600-18)
- Vilanova Susana P.**  
(ST3/E/09-B4 1400-14)
- Vilas Juan**  
(GA1.04/W/07-A4 0930-02)
- Vilas Juan F.**  
(GA1.04/W/32-A5 1510)
- (GA1.04/W/33-A6 1540)  
(GA1.03/W/12-B2 1520)
- Vilas F**  
(GA1.05/W/23-A6 1230)
- Vilibric Ivica**  
(P10/W/27-A4 0950)
- Vililov V. V.**  
(GA1.03/W/34-B3 1100)
- Viljanen A.**  
(GA3.03/W/07-B4 1450)
- Viljanen Ari**  
(GA1.02/W/33-A2 0930)  
(GA1.02/W/37-A1 0930)  
(GA5.01/W/13-A1 0900-11)  
(JSA06/W/04-A1 1155-04)  
(JSA06/W/06-A1 1135)  
(JSA06/W/07-A1 1155-05)
- Villagomez Darwin**  
(JSP23/C/U5/E/05-A6 0830-06)
- Villain J. P.**  
(JSA20/E/26-A4 1200-14)
- Villain Jean-Paul**  
(GA3.08/E/03-B1 1000)
- Villalain Juan Jose**  
(GA1.15/W/03-B4 1530-06)  
(GA1.15/W/07-B4 1530-05)  
(GA1.04/W/15-A6 1520)  
(GA1.04/W/20-A6 1000)
- Villalon Elena**  
(GA3.05/W/35-B3 0900-30)
- Villante U.**  
(GA3.04/L/16-B2 1600)
- Villante Umberto**  
(GA3.04/W/41-B1 1520-10)  
(GA3.10/W/22-A6 1700-14)
- Villares-Duran A.**  
(P11/E/28-B5 0950)
- Villasenor A.**  
(ST5/E/10-B5 0930-08)  
(U8/E/09-B3 1155)
- Villoresi G.**  
(GA4.04/L/01-B5 0830-06)  
(GA4.04/L/02-B5 0830-07)  
(GA4.04/L/05-B5 0830-10)  
(GA4.04/L/06-B5 1400-01)  
(GA4.04/L/07-B5 1400-02)
- Villoresi N**  
(JSA06/L/07-A1 1155-22)  
(JSA06/L/08-A1 1155-23)
- Vincent Bob**  
(JSM01/W/62-A2 1110)  
(MW04/W/11-A1 0925)
- Vincent Mark**  
(JSP23/W/01-B2 1500)
- Vincent Patrick**  
(JSH12/W/03-A5 0830)
- Vincent R A**  
(JSM01/E/43-A2 1600-10)  
(JSM01/W/36-A1 1400)  
(MW04/W/04-A1 0900)
- Vincent Robert A**  
(MW07/W/02-A4 0940)  
(JSA20/W/01-A5 0955)  
(MI12/W/06-B5 0900)
- Vincent Wilma J.**  
(P15/W/05-B3 1630)
- Vinciguerra S.**  
(JSV36/E/20-B3 1400-12)  
(JSV36/E/21-B3 1400-11)
- Vinnichuk Natalia**  
(JSA40/W/13-B5 1400-14)
- Vinnik L.**  
(ST4/E/66-B2 0930-06)
- Vinnik L. P.**  
(JSS07/W/04-A2 0930-01)
- Vinnik Lev**  
(JSS13/W/15-A4 1500)
- Vinnikov Konstantin Y**  
(MC01/W/19-A1 1715)  
(MC01/W/29-A3 1205)  
(JSM24/W/06-B1 1105)  
(MC02/E/18-B2 1150)
- Vinod Gaur**  
(ST2/W/20-A3 1515)
- Vinogradov**  
(JSP23/W/61-A5 0830-13)
- Vinzce. Yann**  
(VS3/W/25-B3 1620)
- Vionnet C A**  
(HW5/W/14-A3 1400)
- Viorica Iancu**  
(JSS07/E/10-A2 0930-04)
- Viracucha Diego**  
(JSP23/C/U5/E/05-A6 0830-06)
- Virdi T.**  
(GA2.02/W/15-B4 0930-12)  
(GA2.02/W/19-B4 1600)  
(GA2.02/W/25-B4 0930-11)
- Virieux J**  
(ST5/W/60-B5 1125)  
(JSS46/W/08-B4 0930-03)
- Virieux Jean**  
(JSS46/E/03-B4 1420)  
(JSS46/E/04-B4 1400)  
(JSS46/E/05-B4 1440)  
(ST5/W/39-B5 0910)  
(ST7/W/03-A2 1605-01)
- Virtanen Heikki**  
(ST5/E/13-B5 1440)
- Virtanen Johanna**  
(HS3-W/21-A2 1110)
- Visarion Marius**  
(JSS44/P/07-B4 0930-20)
- Visconti Guido**  
(JSM26/W/16-B2 1210)  
(JSA09/W/12-A2 1630)
- Visheratin Konstantin N.**  
(JSA16/W/04-A3 0830-37)
- Visheratin Konstantin K.**  
(MI06/W/08-B1 1400-01)  
(MI06/W/08-B2 1400-01)
- Visser P.**  
(G6/C/G3/W/08-B2 1120)
- Visser Pieter**  
(G2/W/08-A2 1630-22)  
(G2/E/11-A2 1630-24)
- Viswanathan K. S.**  
(GA2.02/W/02-B4 0930-14)  
(GA2.02/W/05-B5 0900)  
(GA2.02/W/12-B4 0930-15)  
(GA2.02/W/16-B4 0930-18)  
(GA2.02/W/20-B4 0930-16)  
(GA2.02/W/28-B5 1000)
- Vita-Finzi C.**  
(JSA10/W/07-A2 1415)
- Vitko Jr. John**  
(MI10/W/23-B2 1420)
- Vitorello Icaro**  
(GA3.04/E/10-B1 1520-11)
- Vitushkin Leonid F**  
(G3/E/16-A5 1610-40)
- Vitvar Tomas**  
(HS4/W/29-A5 1450)
- Vizan H.**  
(GA1.04/L/06-A4 0930-03)
- Vizan Haroldo**  
(GA1.04/L/05-A6 1500)
- Vlasenko Vasily**  
(P11/E/09-B3 1620)  
(P11/E/18-B5 1520)
- Vlasova Nataliya A**  
(GA3.10/W/14-A6 1700-16)
- Vlassova E**  
(JSA06/W/22-A2 0930)  
(JSA06/W/21-A1 1155-24)
- Vlastou Georgia**  
(MC09/W/09-B2 1130)
- Vodjannikov V V**  
(JSM01/W/112-A2 1600-19)
- Voelksen Christof**  
(JSA09/W/13-A2 1215)
- Voemel Holger**  
(JSM26/W/34-B2 1510)
- Vogel Richard**  
(HW4/E/26-B2 0900-04)
- Vogt C.**  
(MI10/E/01-B2 1535)
- Vojtiskova Marie**  
(G1/E/60-A3 1620-82)
- Voiculescu Mirela**  
(GA2.02/W/10-B4 0920)  
(GA2.02/W/06-B4 1120)
- Voight B.**  
(VS2/E/13-B3 1130)  
(JSS42/W/28-B5 1700-01)  
(VS2/C/U6/W/14-B3 1400-34)
- Voigt Stefan**  
(HS2/W/05-B1 1020)
- Voitenok Alexander**  
(ST4/L/04-B2 0930-05)
- Volant Philippe**  
(ST5/W/39-B5 0910)
- Volk M C**  
(JSM01/W/56-A4 1620-07)
- Volk Michael**  
(JSA09/W/12-A2 1630)  
(JSM26/W/16-B2 1210)
- Volker Haak**  
(GA5.01/E/10-A1 1630)
- Volker Schwarze**  
(G2/W/02-A2 1415)
- Volker Lorenz**  
(VS2/E/14-B3 1400-25)
- Volkov Viktor A.**  
(ST1/E/04 0930-38)
- Völkken C.**  
(G1/L/04-A3 1620-85)
- Völkken Ch.**  
(JSA09/L/02-A2 1230)
- Volozh Yuri**  
(ST4/E/53-B1 0830-05)
- Volpi G**  
(GA1.02/W/19-A2 0930)
- Volpe Luigi La**  
(VS2/E/08-B3 1010)
- Volti Theodora**  
(ST1/E/57-A2 1620)
- Volwerk M**  
(GA4.10/W/20-A5 1545)
- Vömel Holger**  
(JSM26/W/05-B1 0920)
- Von Bloh Werner**  
(U3/W/05-A30900-11)
- Von Der Gathen P**  
(JSM01/W/37-A5 1400)
- Von Frese R. B**  
(GA5.12/W/02-A2 1100)
- Von Frese Ralph**  
(JSA09/E/11-A3 1000)  
(JSA09/W/18-A3 1100)
- Von Rosenvinge T. T.**  
(GA4.04/W/12-B5 1750)
- Von Steiger R.**  
(GA6.01/W/19-A6 1210)
- Vondrak R. R.**  
(GA3.02/W/18-B2 1645)
- Voorhies C V**  
(JSS02/E/13-A1 0830-09)  
(GA5.08/E/01-B1 1605)
- Voosoghi B.**  
(G4/C/G5/W/04-A3 1620-88)
- Vorobeva Inessa**  
(ST1/E/35-A2 1400-34)
- Vorobieva Inna**  
(ST1/W/54-A2 1700)
- Vorobjev V. G.**  
(GA3.07/L/08-A6 0900-21)  
(GA3.10/L/01-A6 1700-01)  
(GA3.03/L/01-B4 1400-04)  
(GA3.08/W/31-A6 1150)
- Voronkov I.**  
(GA3.04/L/03-B1 0940)  
(GA3.08/W/03-A6 1450)
- Voropayev Sergey**  
(JSP39/W/08-B2 1150)  
(JSP39/W/12-B3 1430-11)  
(JSP39/W/35-B3 1433-12)
- Voros Zoltan**  
(JWS33/W/24-B2 1635-31)  
(JWS33/W/24-B3 0900-31)
- Vörösmarty Charles**  
(HW1/L/09-A4 0930)  
(HW1/L/11-A4 1430)
- Voss Reinhard**  
(JSA16/E/07-A3 1400)
- Vourlidas Angelos**  
(GA4.02/W/33-A4 1400-26)  
(GA4.02/W/34-A4 1525)  
(GA4.02/W/25-A4 1400-23)
- Vovk Valery**  
(JSA45/W/18-B4 1450)
- Vsevolod V. V.**  
(GA1.01/W/02-A5 0900-02)
- Vuckovic Vladan**  
(MI04/W/03-B3 1050)
- Vuglinsky V. S.**  
(HW3/W/13-B4 1700)
- Vujovic Dragana**  
(MI01/W/13-A1 0900-13)
- Vukovic Zlatko**  
(MI03/W/10-A3 1400-02)
- Vvedensky Denis**  
(JWS33/E/16-B2 1635-16)  
(JWS33/E/16-B3 0900-16)
- Vyakhirev V. D.**  
(GA2.01/W/02-A1 0900-01)
- Vyazilov Evgeny D.**  
(JWS33/W/21-B2 1605)  
(JWS33/W/21-B2 1620)
- Vyazilova Nataly A.**  
(JSP25/W/41-B1 1720)
- Vyushkova Tatyana**  
(JSM01/E/33-A1 1050)

## W

- Wada Hiroo**  
(ST2/E/30-A5 1400-05)
- Wada Yutaka**  
(VS2/W/28-B3 1400-30)
- Waddington Edwin D.**  
(MC02/E/08-B1 1100)
- Wadhams Peter**  
(P13/E/02-B2 1400)  
(JSM18/E/05-A4 0940)
- Wadley Martin**  
(P07/W/13-A3 0900-04)
- Wagener Thorsten**  
(HW4/E/04-B2 1100)
- Wahr J.**  
(JSA37/W/09-B3 1100)  
(JSH12/C/JSS31/E/05-A5 0930)
- Wahr John**  
(JSG14/E/23-A3 1500)  
(JSG14/W/01-A3 1700-10)  
(JSH12/E/03-A5 1500)  
(JSG14/E/15-A3 1115-06)
- Waite Jr. J. H.**  
(GA4.10/W/21-A4 1620)  
(GA4.10/W/32-A4 1635)
- Wajsowicz Roxana C.**  
(JSP25/E/36-B2 1520)
- Wakimizu Kenji**  
(MI10/W/14-B1 0900-05)
- Wakimoto Roger M.**  
(MI05/W/35-A4 0930)
- Wakita Hiroshi**  
(ST11/W/30-A2 0930-07)
- Walch J. J.**  
(G2/E/06-A2 1630-03)
- Wald D.**  
(ST5/W/L/04-B3 0900-13)
- Waldteufel P.**  
(JSM41/W/27-B5 0930)
- Walker A. D. M.**  
(GA3.04/W/06-B1 1520-32)  
(GA3.04/W/38-B2 1430)  
(GA3.08/W/19-A6 1520)  
(GA3.07/L/05-A5 1100)
- Walker Anne**  
(JSM41/W/21-B4 1735)  
(JSM41/W/12-B4 1720)
- Walker G. K.**  
(MI04/W/27-B1 0900-20)
- Walker J. G.**  
(P15/L/22-B3 1135)
- Walker M.**  
(JSA37/E/08-B3 1500)  
(GA1.01/E/11-A5 0900-16)
- Walker P.**  
(GA4.10/W/13-A4 0930)
- Walker R.**  
(GA4.10/W/32-A4 1635)
- Walker R. J.**  
(GA3.03/W/10-B4 1220)
- Walker Raymond J**  
(GA4.10/E/06-A5 0945)  
(GA4.10/E/04-A5 1420)
- Walker S.**  
(GA3.07/W/05-A3 0900-16)
- Walker Sharyl E.**  
(HS3/W/02-A1 0925)  
(HSA3/W/05-A1 1110)
- Wallace Douglas W. R.**  
(JSP21/W/01-A4 1640)
- Wallace Paul**  
(JSV22/L/05-A5 1420)
- Walland David**  
(JSP25/W/46-B5 0830)
- Walmsley R. J.**  
(G4/W/15-A3 1620-23)
- Walsh Dr. R. W**  
(GA4.05/W/06-A1 1130)
- Walsh John**  
(JSP25/W/57-B4 1640)  
(MC02/E/18-B2 1150)
- Walter Bernard**  
(P11/W/29-B3 1520)
- Walterscheid R. L.**  
(MC09/W/02-B2 1215)  
(MC09/E/02-B2 1715)
- Walterscheid R L**  
(JSM01/W/03-A2 1400)  
(JSM01/W/66-A2 1600-20)
- Walton Derek**  
(GA1.05/E/11-A5 1040)
- Walzer U.**  
(ST5/W/L/05-B3 1400-06)
- Waizer Uwe**  
(JSS13/E/06-A5 1400)
- Wan Tianfeng**  
(JSA40/E/01-B5 1400-16)
- Wandinger Ulla**  
(MI09/W/08-A5 1542)
- Wang**  
(MI04/L/19-B1 1215)  
(MI04/L/20-B1 0900-21)
- Wang B.**  
(JSG28/W/04-B2 1400-13)
- Wang Bin**  
(MI11/E/12-B5 1000)
- Wang Chung-Ho**  
(HS5/W/25-A2 1525)
- Wang Chunzai**  
(JSP25/W/29-B1 0910)
- Wang De-Zi**  
(JSV30/C/JSV22/E/16-B1 1400-20)
- Wang Gengchen**  
(MI01/E/20-A2 1450)
- Wang Guomin**  
(JSP25/W/58-B1 1130)
- Wang H G**  
(JSM01/W/12-A2 1600-15)
- Wang Hailan**  
(MC10/E/02-B1 1600)
- Wang Hui**  
(P10/W/02-A4 1210)
- Wang J.**  
(JSP25/W/82-B5 1440)
- Wang Jiemin**  
(JSM24/W/04-B1 0930)  
(JSM24/W/13-B2 1115)
- Wang Jijun**  
(JSV36/E/08-B3 0900-06)  
(JSA15/E/52-A5 0830-09)
- Wang Jin**  
(G3/W/17-A5 1610-20)
- Wang Jinglin**  
(G1/W/40-A3 1620-18)  
(G1/W/13-A3 1620-05)  
(G4/W/16-A3 1620-04)  
(G6/W/03-B2 1520)
- Wang Jiyang**  
(JSS44/W/12-B4 0930-40)
- Wang Ji-Yang**  
(ST4/W/22-B1 1120)  
(ST4/W/46-B1 1000)
- Wang Julian X. L.**  
(JSP25/W/27-B5 1500)
- Wang Kai**  
(P10/W/02-A4 1210)
- Wang Kelin**  
(JSS42/W/25-B4 1600)
- Wang Ling**  
(MW04/W/09-A1 1650)  
(MW04/W/10-A1 1630)
- Wang Miaoyue**  
(JSA19/L/03-A4 1200)
- Wang Rongjiang**  
(ST1/W/67-A1 1050)
- Wang Shejiao**  
(ST4/W/07-B1 1400-08)
- Wang Shouhong**  
(MI11/W/06-B5 1100)  
(MI04/E/29-B3 1730)
- Wang Shouping**  
(MI08/E/11-A3 1530)  
(MI-08/E/12-A3 1500)
- Wang Suyun**  
(ST3/E/50-B4 0930-19)
- Wang W.**  
(U3/W/17-A3 0900)
- Wang W-C**  
(MC01/E/23-A4 1035)
- Wang Xialong**  
(JSA20/W/19-A4 1450)
- Wang Xiao-Chun**  
(JSP25/W/91-B5 0850)
- Wang Y.**  
(ST3/W/39-B4 1400-08)
- Wang Y.-M.**  
(GA3.09/W/05-B4 1110)  
(G3/L/21-A5 1610-16)
- Wang Yanbin**  
(JSS02/W/12-A2 1115)  
(ST5/W/14-B4 0930-02)  
(ST5/W/16-B4 0930-03)
- Wang Yang**  
(GA1.07/W/02-B2 0900-01)  
(JSA40/W/17-B5 1400-04)  
(MC03/W/03 1030)
- (ST4/W/29-B1 1400-16)  
(ST4/W/68-B1 1400-15)  
(JSS13/W/08-A5 1440)
- Wang Yongguang**  
(JSP25/C/MI05/W/01-B2 1150)
- Wang Yue-Jin**  
(JSG 28/E/17-B2 1400-03)
- Wang Zhaomin**  
(MC11/W/06-B3 1100)
- Wanke H.**  
(JSA10/W/06-A2 1430)
- Wanliss J A**  
(GA3.10/W/26-A5 1225)
- Wanninger Lambert**  
(G1/E/06-A3 1620-20)
- Waple Anne M.**  
(MC02/W/07-B1 1510)
- Warburton R. J.**  
(G5/E/38-A4 1415-02)
- Ward William E**  
(JSM01/W/10-A3 1650)  
(JSA20/W/03-A4 1200-12)  
(MW04/E/02-A1 1010)
- Wardle Dick**  
(JSS44/W/03-B4 1400)
- Ware Randolph**  
(JSG28/W/01-B2 1400-16)  
(JSG28/W/25-B2 1400-11)  
(JSG28/E/12-B2 1200)  
(JSM26/E/09-B1 1400)
- Ware Randolph H.**  
(JSM01/E/03-A2 1430)
- Warner Christopher D**  
(JSM01/E/17-A3 0830)  
(MW 07/E/06-A4 1700)
- Warner Thomas**  
(JSM43/W/08-B4 1110)  
(JSM43/W/07-B5 1100)
- Warner Tom**  
(MC04/E/09-B1 1130)
- Warn-Varnas A.**  
(P13/E/08-B2 1600-02)
- Warn-Varnas Alex**  
(P12/W/17-A1 1720)
- Warren B**  
(JSM18/W/03-A4 1400)
- Warren Linda M.**  
(ST4/W/44-B21640)
- Warren Stephen G**  
(MI08/E/09-A4 0830)  
(MI08/E/13-A3 1100)
- Warshaw Stephen I.**  
(GA2.02/E/10-B5 1700)
- Washington Richard**  
(JSP25/E/36-B2 0930-03)  
(JSP25/L/01-B2 1210)
- Wasilewski Peter**  
(GA5.11/W/02 A3 0910)  
(GA5.11/W/03 A3 1430-02)
- Wassermann J.**  
(JSV47/W/03-B5 1400-12)  
(JSV47/W/06-B5 1400-11)
- Watada Shingo**  
(ST5/W/54-B3 0900-10)  
(U7/W/13-B1 0830-15)
- Watanabe Hidefumi**  
(JSV36/W/22-B3 0915)
- Watanabe Kazutoshi**  
(ST2/W/26-A5 1400-01)
- Watanabe Kunihiko**  
(ST1/W/24-A3 1130)
- Watanabe Masahiro**  
(JSP24/W/45-B2 1640)
- Watanabe Masakazu**  
(GA3.07/E/07-A5 1430)
- Watanabe S.**  
(MI12/W/10-B4 1650)
- Watanabe Shigeto**  
(GA2.07/W/13-A1 0920)
- Watanabe Takashi**  
(GA4.01/W/04-A2 1520)  
(GA4.02/W/04-A4 1400-13)  
(GA4.02/W/15-A4 1145)
- Watanabe Tatsuro**  
(P11/W/21-B5 1150-09)  
(P13/W/24-B1 1130)
- Watanabe Y.**  
(GA6.01/E/04-A5 0900-07)
- Watar Shinichi**  
(GA4.02/W/15-A4 1145)
- Waters C. L.**  
(GA2.07/W/15-A1 1710)
- Waters Colin**  
(GA3.04/W/26-B1 1520-09)  
(GA3.04/W/34-B1 1520-13)
- (GA3.04/W/43-B2 1630)  
(GA3.04/W/51-B1 1520-20)
- Watkins B. J.**  
(GA2.01/W/05-A1 1705)
- Watkins Brenton J**  
(JSM01/E/34-A2 1600-14)
- Watkins M.**  
(JSG14/E/04-A3 1109-04)
- Watkins Nicholas W.**  
(GA3.02/W/10-B3 1220)  
(GA3.02/W/22-B3 0900-12)  
(GA3.02/W/37-B3 1150)
- Watanabe Tatsuro**  
(JSM18/W/10-A5 1000)
- Watson A.**  
(P08/W/01-A2 1440)
- Watson G D**  
(HW5/W/11-A3 0940)
- Watts Philip D.**  
(MI04/E/26-B2 0950)
- Watts Robert**  
(HS5/W/14-A2 1000)
- Watts Sarah K.**  
(MI04/E/26-B2 0950)
- Waugh Darryn**  
(JSM01/E/40-A5 1450)  
(JSM01/W/06-A4 1100)  
(JSM01/W/101-A5 1650-01)  
(JSM01/W/14-A4 1620-12)
- Wdowinski Shimon**  
(JSG11/W/06-A3 1720)  
(G1/W/16-A3 1620-06)
- Wdowinski Shimon**  
(JSS31/W/01-B3 0830-02)
- Weatherhead Elizabeth**  
(MI08/E/08-A4 1750)  
(MI08/L/10-A4 1650)
- Weatherwax A T**  
(GA3.06/W/39-A2 0930-18)  
(GA2.01/W/05-A1 1705)  
(GA2.01/W/03-A1 0925)
- Weaver Andrew J**  
(U3/W/12-A3 1430)
- Weaver C.**  
(ST4/L/01-B1 0830-02)
- Weaver Chris**  
(MI04/W/20-B1 1450)
- Weaver J. T.**  
(GA1.02/W/12-A1 1050)
- Weaver Ronald L. S.**  
(JWS33/W/11-B2 1000)  
(JWS33/W/33-B2 1635-32)  
(JWS33/W/33-B3 0900-32)  
(JWS33/W/34-B2 1635-02)
- Webb Charles**  
(G2/W/10-A2 1445)
- Webb David F.**  
(GA4.02/W/02-A4 1500)  
(GA4.01/W/18-A2 0930)
- Webb F.**  
(JSV36/W/23-B3 1515)
- Webb F. H.**  
(G5/W/11-A4 0945)
- Webb Mark**  
(MI04/E/04-B4 1035)  
(MW02/E/05-B3 1100)
- Webb Mark J.**  
(MI04/E/26-B2 0950)
- Webb Sharon**  
(ST6/W/04-A1 0830-06)
- Webb Spahr C.**  
(JWA34/W/05-B2 1540)
- Weber Georg**  
(JSG28/W/21-B1 1400-02)
- Weber N.**  
(MC11/W/07-B4 1630)
- Weber Robert**  
(G2/L/12-A20 1630-06)  
(JSG14/E/03-A3 1103-02)
- Weber Zoltán**  
(ST5/W/62-B5 0930-06)
- Webers Wigor A.**  
(GA5.08/E/08-B1 1400-06)
- Webers Wigor A.**  
(GA5.12/E/01 A2 1400)
- Webster F.**  
(HW1/L/13-A4 1630)
- Webster Paul.**  
(HS1/W/24-B5 1420)
- Wedin**  
(JSA06/L/06 0935)
- Wefers Johannes**  
(JSP23/E/10-B2 1420)
- Wegner Alfred**  
(P12/W/13-A1 1440)

# INDEX

- Wehner Michael**  
(MC01/W/10-A2 10300)
- Wehrli C H**  
(MI09/W/09-A5 1145-11)
- Wehrli Christoph**  
(JSA16/W/20-A3 0830-53)  
(JSA16/W/36-A3 0930)
- Wei Dongping**  
(ST4/W/81-B1 0830-25)
- Wei Luo**  
(ST3/P/1-B4 1400-06)
- Wei Mozheng**  
(MI11/E/01-B5 0930)
- Wei Zi-Gang**  
(GA5.09/W/04 A2 1400-03)
- Wei Ziqing**  
(G1/E/07-A3 1620-51)  
(G4/E/12-A3 1620-10)
- Weibin Han**  
(SW1/W/09-B5 1100)
- Weichman Peter B.**  
(JSP39/W/25-B4 0910)
- Wei-Chyung Wang**  
(MW03/W/09-B4 1515)
- Weidner Donald J**  
(JSS02/W/12-A2 1115)
- Weidner George**  
(JSM18/E/03-A4 1420)  
(JSM41/E/22-B4 0945)
- Weigle Rainer**  
(P12/W/19-A1 1030-08)  
(P14/W/07-A4 1400-10)
- Weiler Markus**  
(HS4/W/30-A5 1510)
- Weiliang Li**  
(MI01/E/13-A3 1125)
- Weill A.**  
(MI04/L/10-B3 1520)  
(MI06/W/07-B1 1220)  
(MC09/W/10-B2 1515)
- Weimer D R**  
(GA3.10/W/02-A6 1615)
- Weimer Daniel**  
(GA3.10/W/25-A6 1140)
- Weirig Marie-France**  
(MC01/W/24-A5 1745)
- Weirig M-F**  
(MC01/W/36-A5 1700)
- Weisberg Robert H.**  
(JSP25/W/29-B1 0910)
- Weise A.**  
(JSV36/W/24-B3 1400-05)
- Weisheimer Antje**  
(JSP25/W/33-B4 0930-03)  
(JSP25/W/38-B4 0930-04)  
(JSP25/W/68-B4 0930-01)
- Weisheimer Antje**  
(MC01/E/03-A4 1445)
- Weiss Andrea K.**  
(JSM01/W/27-A5 1530)
- Weiss Michele**  
(JWS33/W/27-B2 1635-22)  
(JWS33/W/27-B3 0900-22)
- Weiss R.**  
(JSP21/E/04-A5 1110)
- Weiss Ray**  
(JSP21/E/02-A4 0930)  
(JSP21/L/02-A4 1440)
- Weith Heiko**  
(ST1/W/67-A1 1050)
- Weich R. M.**  
(MI06/W/13-B1 1400-08)  
(MI06/W/13-B2 1400-08)  
(MI06/W/15-B1 0910)  
(MI06/W/19-B2 1230)  
(MI10/W/10-B2 1150)
- Welch Ronald M**  
(MI09/W/16-A5 1710)
- Welle Wolfgang**  
(JSV36/W/11-B3 1400-06)
- Weller R.**  
(JSM04/E/04-A2 1240)
- Wellman R.**  
(GA3.03/E/07-B4 1020)
- Wells N. C.**  
(P13/E/14-B1 1500)  
(JSM18/E/07-A4 1440)
- Wells Neil**  
(JSA09/W/02-A2 1745)
- Wen D.-J.**  
(JSS44/W/14-B4 0930-12)
- Wen Hanjiang**  
(JSG11/E/01-A3 0850)  
(G4/E/15-A3 1620-15)
- Wen Kuo-Liang**  
(ST3/E/37-B3 1145)
- Wen L**  
(JSS02/C/ST6/W/01-A1 1515)  
(JSS02/W/01-A1 1425)
- Wendicsh Manfred**  
(MC07/W/10-A3 0955)  
(MI09/W/08-A5 1542)
- Wendler Gerd**  
(P13/W/09-B2 1600-05)
- Wendling Peter**  
(MI01/E/03-A1 1700)
- Weng Wensong**  
(JSM43/E/02-B4 1440)  
(JSM43/E/04-B4 1500)  
(JSM43/W/04-B4 1600)
- Wenger J**  
(JSM01/W/37-A5 1400)
- Wenjuan Zhou**  
(HS2/W/19-B2 1020)
- Wenjun Li**  
(HS2/W/13-B1 1600)
- Wenk T.**  
(JSP23/E/03-A6 0930)
- Wen-ling Fan**  
(U3/E/06-A3 0900-05)
- Wenqing Tang**  
(JWS33/W/19-B2 1635-29)
- Wenyng Su**  
(MI09/E/03-A5 1145-02)
- Wenzel**  
(G6/L/08-B3 0945)
- Wenzel F.**  
(ST5/W/19-B3 1145)
- Wenzel Friedemann**  
(JSP23/W/26-A5 1150)  
(ST2/W/11-A4 1430)
- Wenzel Hans-Georg**  
(G6/C/G3/E/23-B1 1200)
- Wenzhi Shen**  
(JAS15/P/02-A5 0830-08)
- Wepperning Ralf**  
(P07/W/15-A3 1145)
- Wergen Werner**  
(MC01/W/47-A4 1005)
- Werne Joseph A.**  
(JSM32/W/06-B2 1135)  
(JSP39/W/36-B2 1700)  
(JSP49/W/18-B5 1600)
- Werner Tomasz**  
(GA1.04/W/09-A4 0930-06)  
(GA1.04/W/34-A4 0930-10)
- Wernicke Brian P.**  
(JSS31/E/08-B2 0950)
- Wernik W.**  
(GA4.09/W/01-A6 1440)
- Wernli H**  
(MI05/E/24-A1 1650)
- Wernli Heini**  
(M105/E/25-A2 1100)  
(MI05/L/01-A2 1200)
- Wernli Henry**  
(JSM26/W/03-B3 0950)
- West V**  
(MW01/W/03-A5 1150-03)
- Westbrook Graham K**  
(JSA19/L/02-A4 1015)
- Westerhaus Malte**  
(ST1/W/10-A3 0910)  
(JSV36/E/07-B3 0900)  
(JSV36/W/11-B3 1400-06)
- Weston**  
(G1/L/19-A3 1640-92)
- Westwater Ed**  
(MI08/E/10-A3 1735)
- Wex Heike**  
(MI09/W/08-A5 1542)
- Wgorionova V. B.**  
(P08/E/05-A2 1620)
- Whale Kathy**  
(GA1.02/E/11-A2 0930)
- Whaler K A**  
(GA5.12/W/03 A2 1500)  
(GA5.12/E/07 A2 1520)
- Whang Y. C.**  
(GA4.04/E/03-B5 1510)
- Wheater Howard**  
(HW4/E/04-B2 1100)
- Wheaton S M**  
(JSM01/W/12-A2 1600-15)  
(MI09/W/02-A5 1145-07)
- Wheeler Matthew**  
(JSP39/W/46-B3 0930)
- Wheeler P.**  
(P07/W/05-A3 1700)
- Whitaker Jeffrey S.**  
(JSP25/W/24-B1 0850)
- White Antony**  
(GA1.02/L/AW1-A2 0930)  
(GA1.02/L/AW2-A2 0930)
- White Benjamin S.**  
(MC02/W/09-B2 1600)
- White Dick**  
(JSA45/E/03-B5 1110-11)
- White James C**  
(JSM18/W/15-A4 1140)
- White G**  
(JSM18/W/03-A4 1400)
- White Neil J.**  
(JSP49/W/06-B5 1210-04)
- White Oran. R.**  
(JSA16/E/12-A3 0830-14)  
(JSA16/E/09-A3 1100)  
(SA16/E/22-A3 0830-16)
- White Pamela**  
(JWS33/W/26-B2 1635-04)  
(JWS33/W/26-B3 0900-04)
- White Warren B.**  
(JSP25/W/49-B4 0950)  
(GA6.01/W/12-A6 1020)
- White W W**  
(GA3.10/W/02-A6 1615)
- Whitehead Emily**  
(HS5/W/37-A3 1125)
- Whiteside Lowell S.**  
(JSP23/W/30-A5 830-01)
- Whiteway J. A.**  
(JSM26/E/07-B2 1700-01)
- Whiteway James A**  
(MW07/E/05-A4 1150)  
(JSM01/W/40-A2 1520)
- Whittaker A. G.**  
(GA1.05/W/35-A6 1010)
- Whittemore Ray**  
(HS3/W/32-A2 1730)
- Whitworth T.**  
(P16/W/01-B5 1620)
- Wicht Johannes**  
(GA1.01/E/03-A6 1215)  
(JSP39/W/41-B3 1210)
- Wicki Fridolin**  
(G4/W/01-A3 1620-05)
- Widarto D.S.**  
(JSA15/E/17-A3 1440)
- Widarto Djedi S.**  
(GA1.02/E/29-A2 0930)  
(JSA15/E/02-A5 0830-05)
- Wieczerkowski Karin**  
(JSG11/W/10-A3 1620)  
(JSS02/E/09-A2 1030)
- Wiederhold H.**  
(JSA40/W/06-B5 1400-09)
- Wiederkehr Karl Heinrich**  
(GA6.01/P/02-A5 0900-16)
- Wiemer S.**  
(ST1/E/28-A3 0900-17)  
(ST3/W/45-B4 1430)
- Wiemer Stefan**  
(JSV36/P/02-B3 1400-15)  
(JSV47/E/09-B5 1400-06)  
(JSV47/W/07-B5 1215)  
(ST3/E/24-B4 1445)  
(ST1/E/81-A2 1640)  
(ST1/W/41-A2 1420)  
(ST1/E/89-A2 1720)
- Wienholz Kerstin**  
(G1/L/20-A3 1640-93)
- Wiens D**  
(JSS13/E/04-A4 1700)
- Wiens Douglas A.**  
(JSA09/W/15-A3 0830)
- Wiens K C**  
(MI03/W/05-A3 1140)
- Wiens Rudolph H**  
(JSM01/W/112-A2 1600-19)  
(JSM01/E/30-A2 1600-24)
- Wiera R.**  
(JSA40/W/10-B5 1400-12)
- Wieser A.**  
(G1/E/01-A3 1620-19)
- Wieser Andreas**  
(G1/E/17-A3 1620-104)
- Wiget Adrian**  
(G1/E/58-A3 1500)  
(G1/W/05-A3 1620-34)  
(G1/W/21-A3 1620-08)
- Wigley T. M. L.**  
(MC02/W/01-B2 1100)
- Wigmosta M. S.**  
(JWM08/W/10-A2 1650)
- Wigner J.-P.**  
(JSM41/W/27-B5 0930)
- Wijbrans Jan**  
(GA1.15/W/11-B4 1530-03)
- Wilcock Robert J.**  
(HS3/W/10-A1 1425)
- Wild-Allen K.**  
(P10/W/03-A5 0850)  
(P10/W/15-A5 0950)
- Wild J. A.**  
(GA3.08/W/07-A6 1630)
- Wild Martin**  
(MC01/W/31-A1 1400)
- Wild Matthew**  
(JSA06/W/18-A1 1155-12)
- Wild O J**  
(MI02/W/09-A4 1220)
- Wild Oliver**  
(MI02/L/20-A4 1640)
- Wild Urs**  
(G1/E/58-A3 1500)  
(G1/W/21-A3 1620-08)
- Wild W.**  
(MC09/W/04-B2 1030)
- Wildermann E**  
(G3/E/44-A5 1610-66)
- Wildermann Eugen**  
(G1/W/12-A3 1620-38)  
(G1/W/26-A3 1620-42)
- Wildner Manfred**  
(GA1.05/W/42-A6 1100)
- Wildt Steffen**  
(G1/E/06-A3 1620-20)
- Wilhelm Klaus**  
(JSA16/W/06-A3 0830-48)
- Wilken B.**  
(GA4.10/W/26-A5 1035)  
(GA3.05/W/05-B3 0900-46)  
(GA3.05/W/23-B3 0900-13)  
(GA3.08/W/20-B1 1720)  
(GA4.08/W/11-B3 1620)  
(GA4.08/W/13-B4 0905)  
(GA4.08/W/17-B3 0900-06)
- Wilkin J.**  
(P10/W/26-A3 1440)
- Wilkinson P.**  
(JSA06/W/17-A1 1155-14)  
(GA3.09/W/03-B5 0950)
- Wilkinson Phil**  
(JSA06/W/14-A1 1700)
- Will Pettitt**  
(ST1/W/61-A1 1500)
- Willebrand Juergen**  
(JSP25/W/20-B4 1620)
- Willemann Raymond J.**  
(ST5/W/12-B3 1500)  
(ST5/W/45-B3 0900-09)  
(ST5/W/52-B3 0930)
- Willen Ulrika**  
(MI04/W/10-B1 1200)  
(MC01/W/17-A4 1125)
- Willgalis Stefan**  
(G1/W/29-A3 1620-12)
- William Arias**  
(GA5.01/E/21 A1 1005)
- Williams Bob**  
(P15/W/03-B3 1025)
- Williams C. A.**  
(GA5.12/W/08 A2 1220)
- Williams Christopher R.**  
(MI04/W/26-B3 0830)
- Williams D. J.**  
(GA3.02/L/02-B3 0900-24)  
(GA4.08/W/13-B4 0905)  
(GA4.10/W/06-A5 1435)  
(GA4.10/W/08-A5 1020)  
(GA4.10/W/01-A5 1130)  
(GA4.10/W/26-A5 1035)
- Williams Earle**  
(JSM03/E/01-A1 1510)  
(U7/E/09-B1 0830-04)
- Williams P. J.**  
(GA2.02/W/15-B4 0930-12)  
(GA2.02/W/19-B4 1600)  
(GA2.02/W/25-B4 0930-11)
- Williams P. J. S.**  
(GA4.04/W/07-B5 1430)  
(GA4.05/E/02-A1 1010)  
(GA4.02/E/07-A4 1400-02)  
(JSA20/E/10-A4 1200-04)  
(JSA20/E/13-A4 1508)  
(JSA20/W/22-A4 1146)  
(JSA20/W/30-A4 1526)  
(JSM01/W/11-A2 1210)  
(GA4.01/W/09-A2 1140)
- Williams Paul I**



- (MI02/W/01-A5 1450)  
(MI02/W/13-A5 1510)  
**Williams Richard G.**  
(P08/E/07-A2 1050)  
**Williams Simon**  
(JWS33/W/35-B2 1635-33)  
(JWS33/W/35-B3 0900-33)  
**Willms Trevor**  
(GA1.03/W/05-B2 1040)  
**Williamson Paul**  
(JSA40/W/08-B3 0900)  
**Willis**  
(G2/L/11-A2 1400)  
**Willis Bill**  
(JSA06/W/03-A1 0855)  
**Willmot A. J.**  
(HS2/W/23-B2 1200)  
(P13/E/12-B1 0910)  
**Willmott Andrew J.**  
(P13/W/27-B1 1210)  
**Willson Richard C.**  
(JSA16/W/15-A3 0830-41)  
(JSA16/W/26-A3 0830-29)  
**Wilmes H**  
(G3/E/11-A5 1610-31)  
(JSG14/E/21-A3 1700-18)  
**Wilmes Herbert**  
(G5/E/37-A4 1415-01)  
**Wilson A.**  
(GA2.01/E/04-A1 0900-03)  
(GA2.01/E/02-A1 0900-04)  
(GA2.01/E/03-A1 1040)  
**Wilson C. R.**  
(G5/W/25-A4 1100)  
(JSG14/W/07-A3 1154-19)  
(JSG14/W/10-A3 1151-18)  
(JSM41/W/06-B4 1545)  
**Wilson D. S.**  
(GA1.15/W/08-B4 1445)  
**Wilson Damian**  
(MI04/E/04-B4 1035)  
**Wilson G. R.**  
(GA3.09/W/15-B4 1450)  
**Wilson H.**  
(P10/W/03-A5 0850)  
**Wilson Julian**  
(MI01/W/01-A1 0900-06)  
(MI01/W/18-A1 1510)  
**Wilson Quintero**  
(GA5.01/E/21 A1 1005)  
**Wilson R. S**  
(JSA16/W/15-A3 0830-41)  
(JSA16/E/19-A3 0830-22)  
**Wilson W. D.**  
(P11/W/16-B3 0950)  
**Wilson Robert M.**  
(GA4.03/W/09-B4 1400)  
**Wiltberger M.**  
(GA3.09/W/12-B4 1400)  
**Winant C. D.**  
(P09/W/03-A1 0930)  
(P10/W/19-A3 1620)  
**Winarso Paulus**  
(JSP25/W/15-B2 1010)  
**Winch Denis**  
(GA5.09/E/01 A2 1150)  
**Windelband Martin**  
(MC01/E/34-A4 1020)  
**Wingham Duncan**  
(JSG14/E/23-A3 1500)  
**Winker David M.**  
(MI01/W/24-B1 1400-05)  
(MI01/W/24-B1 1730)  
(MI06/W/24-B2 400-05)  
(MI10/W/09-B1 0900-16)  
**Winkler Aldo**  
(GA1.04/W/36-A5 1430)  
**Winkler Christopher R**  
(MW06/W/04-A3 1640)  
**Winsor Peter**  
(P11/W/11-B5 1150-07)  
**Winter Helmuth**  
(JSS44/E/14-B4 0930-30)  
**Winter Thierry**  
(ST3/E/27-B4 1730)  
**Winterhalter D.**  
(GA4.08/W/12-B4 1635)  
**Winterhalter Daniel**  
(GA4.04/E/06-B5 0920)  
**Winters Timothy A.**  
(P07/W/03-A3 1640)  
**Wiratmo Joko**  
(MC04/L/02-B2 1650)  
**Wirth Achim**  
(P14/L/01-A4 1400-04)  
**Wirth M**  
(JSM01/W/08-A4 1450)  
(MI06/W/26-B2 1110)  
**Wirtz A.**  
(JSP23/C/U5/W/13-A5 1440)  
**Wise J. O.**  
(GA3.09/W/01-B4 0900-08)  
**Witchayangkoon S**  
(G1/L/01 1620-83)  
**Withers P. J. A.**  
(HS3/W/06-A1 1135)  
**Wittmann Géza**  
(GA5.12/W/04 A2 1420)  
**Woch J.**  
(GA4.10/W/26-A5 1035)  
**Wohletz Kenneth**  
(VS2/W/18-B3 0930)  
**Wohltmann I**  
(MI02/W/05-A5 0950)  
**Wolf**  
(G6/L/09-B3 1010)  
**Wolf Detlef**  
(JSG11/W/10-A3 1620)  
**Wolf Peter**  
(G3/E/42-A5 1520)  
(G3/E/42-A5 1520)  
**Wolf R. A.**  
(GA3.01/E/03-A2.1115)  
(GA3.09/E/05-B4 1625)  
(GA3.09/E/13-B4 0930)  
(GA3.09/W/22-B4 0900-04)  
(GA3.05/E/22-B3 0900-08)  
**Wolff Eric W.**  
(JSM04/W/06-A2 1220)  
**Wolff J.-O.**  
(P13/E/10-B1 1400)  
(JSP39/W/31-B4 1010)  
**Wong Annie P. S.**  
(P12/W/10-A1 1150)  
**Wong Ann-Marie M.**  
(P10/E/22-A3 1600)  
**Wonik T.**  
(JSA40/W/06-B5 1400-09)  
**Woo G.**  
(ST3/E/13-B4 1400-15)  
**Wood B. J**  
(JSS02/W/18-A1 1640)  
**Wood E.**  
(HW1/L/14-A4 1630)  
**Wood I. G.**  
(ST6/W/11-A1 0830-11)  
**Wood Nigel**  
(JSM43/E/10-B4 1640)  
**Wood Paul**  
(HW2/W/08-B1 1450)  
**Wood Peter**  
(JSV30/E/05-B1 0940)  
**Wood R.**  
(MI04/E/21-B3 1645).  
(MI04/E/04-B4 1035)  
**Wood Robert**  
(MI01/E/11-A3 1205)  
**Wood Stephen W.**  
(MI12/E/02-B5 1115)  
**Woodage Margaret J**  
(MI01/E/14-A2 1400)  
**Woodley William L.**  
(MI04/C/MI06/W/10-B3 1150)  
**Woodman Ronald**  
(JSM32/E/03-B3 0930)  
**Woods Andrew**  
(VS2/W/08-B3 1400-06)  
(JSP23/W/08-A5 0830-03)  
**Woods John**  
(P15/W/02-B3 1400)  
(U7/W/09-B1 0835)  
**Woods Thomas**  
(JSA16/E/0-A3 1030)  
(SA16/E/22-A3 0830-16)  
(JSA16/E/12-A3 0830-14)  
**Woods Thomas N.**  
(JSA45/E/03-B5 1110-11)  
**Woodward Robert**  
(JWS33/W/15-B2 1015)  
(U7/W/18-B1 0830-19)  
**Woodward Stephanie**  
(MC07/E/02-A2 1400)  
(MI01/E/04-A1 1130)  
**Woodward T. I.**  
(GA3.07/W/21-A3 0900-17)  
**Woodworth Phil**  
(JSG11/A3 0830)  
(JSG11/E/10-A3 1400)  
**Woodworth Philip**  
(P16/W/01-B5 1620)  
(P16/W/02-B5 1640)  
(U7/W/04-B1 0830-13)  
**Woolnough Steven**  
(JSP25/W/08-B2 1110)  
**Wooff David**  
(P08/W/03-A2 1150)  
**Wooster Martin**  
(JSP23/E/18-B2 0930)  
**Wöppelmann G.**  
(G1/E/31-A3 1620-65)  
**Wöppelmann Guy**  
(JSG11/W/13-A4 1400-09)  
(U7/W/14-B1 0830-12)  
**Worm Horst-Ulrich**  
(GA1.05/W/14-A5 1650)  
(GA1.05/L/01 0930)  
**Worrall F.**  
(HS3/W/19-A2 0950)  
**Worthington E. W.**  
(GA5.01/E/32 A1 0900-09)  
**Worthington R M**  
(JSM01/C/MW07/W/16-A2 1600-29)  
(JSM26/W/24-B3 1150)  
**Worthington Tim J.**  
(JSV30/E/04-B1 1400-11)  
**Wozniak Bogdan**  
(P15/W/04-B4 1055)  
**Wozniak Slawomir B.**  
(P15/W/06-B3 1420)  
**Wratt David**  
(JWM08/E/07-A2 1040)  
(JWM08/W/01-A2 1630)  
(JWM08/W/04-A2 1020)  
**Wright A. N.**  
(GA3.04/L/14-B2 1400)  
(GA3.04/W/02-B1 1520-33)  
(GA3.04/W/40-B1 1520-34)  
**Wright Andrew N.**  
(GA3.07/W/38-A5 1130)  
**Wright D. M.**  
(GA3.04/W/16-B2 1010)  
(GA3.04/W/27-B1 1520-04)  
**Wright Rob**  
(JSP23/E/18-B2 0930)  
**Wrobel B.**  
(JSV36/W/06-B3 1400-02)  
**Wronowski R**  
(GA4.09/W/04-A5 1600-02)  
**Wu Beiyang**  
(MI02/E/09-A4 1140)  
(MI01/E/10-A1 0900-12)  
**Wu C**  
(MC08/W/03-A3 1650)  
**Wu Charles T.**  
(JSV30/C/JSV22/E/11-B1 1400-17)  
**Wu D L**  
(MW04/W/02-A1 1710)  
**Wu Dexing**  
(P10/W/02-A4 1210)  
**Wu Dong L**  
(MW07/E/08-A4 1450)  
**Wu Dr. S T**  
(GA4.02/W/32-A4 1635)  
**Wu Guoxiong**  
(JSP25/W/76-B1 0830-08)  
(MC10/W/01-B1 1125)  
(MC10/W/02-B1 1650)  
(MC10/W/03-B1 1220)  
**Wu Huatao**  
(JSS46/W/01-B4 1230)  
**Wu J. M**  
(GA2.02/W/18-B5 1440)  
(GA2.02/W/34-B5 1420)  
(JSA20/W/28-A5 1200-10)  
**Wu Jian-Guo**  
(GA2.01/E/13-A1 0900-02)  
**Wu Jicang**  
(G5/W/14-A4 1510-06)  
**Wu Patrick**  
(JSH12/E/03-A5 1500)  
**Wu Q**  
(JSM01/W/107-A1 1510)  
(JSM01/W/106-A2 1600-01)  
**Wu Ru-Shan**  
(ST5/W/47-B4 1010)  
**Wu S. T.**  
(JSA16/E/13-A3 0830)  
**Wu Shiguo**  
(JSA19/W/02-A4 1400-07)  
**Wu X**  
(JSH12/C/JSS31/E/05-A5 0930)  
**Wu Xiaoping**  
(MI04/L/02-B3 0905)  
(MI04/W/13-B1 0915)  
**Wu Xingren**  
(MC03/W/04-B4 1110)  
(P13/W/05-B1 1640)  
(JSM04/W/05-A2 1445)  
**Wu Yih-Min**  
(JSP23/C/U3/W/21-B2 1740)  
(ST3/W/30-B3 1115)  
**Wu Yun**  
(ST1/P/12 0930-37)  
**Wuebbena Gerhard**  
(G1/W/32-A3 1620-15)  
**Wuebbles Donald J**  
(MC07/W/22-A2 1620)  
**Wulf Sabine**  
(VS2/C/U6/E/01-B3 1400-35)  
(VS3/E/05-B3 0900-04)  
**Wulff Andrew**  
(JSV36/W/07-B3 1400)  
**Wuxing Duan**  
(G1/C/G2/E/02-A3 1620-105)  
(G1/E/07-A3 1620-51)  
**Wygant J.**  
(GA3.03/W/11-B4 1200)  
**Wykes W. J.**  
(GA3.05/W/12-B3 0900-31)  
**Wylie Donald P**  
(MC08/L/12-A3 1630)  
**Wynne R. H.**  
(HW3/W/03-B4 1005)  
**Wyss M.**  
(ST3/W/45-B4 1430)  
(JSV36/P/02-B3 1400-15)  
(JSV47/W/07-B5 1215)  
(ST1/E/28-A3 0900-17)  
**Wyss Max**  
(ST1/W/41-A2 1420)

## X

- Xia Jun**  
(HW2/W/10-B1 1620)  
**Xiang A M**  
(G3/W/09-A5 1610-27)  
(G3/W/23-A5 1610-28)  
**Xiang-Chu Yin**  
(ST1/E/50-A2 1400-36)  
**Xiangdong Z.**  
(JSM26/W/27-B1 1440)  
**Xiangru Kong**  
(ST4/L/05-B2 0930-12)  
**Xiao F.**  
(GA3.05/W/29-B3 1500)  
**Xiao Jingbing**  
(JSM04/E/01-A2 1010)  
**Xiao D Kecheng**  
(JSM01/W/68-A4 1620-11)  
**Xiaolin Cao**  
(ST4/P/10-B1 0830-08)  
**Xiaolin Xiong**  
(JSV22/E/03-A5 0900-02)  
**Xiaoming Li**  
(JSP23/E/22-B1 0830-06)  
**Xiaoping Jin**  
(HS2/W/22-B2 1140)  
**Xiaoping Wu**  
(G2/E/01-A2 1630-23)  
**Xiaoxia Huang**  
(JSA27/P/05-B1 0900)  
**Xiaoxin Zhang**  
(GA3.07/W/64-A3 0900-18)  
**Xie Fang-Gui**  
(JSV30/C/JSV22/E/17-B1 1400-21)  
**Xie Furen**  
(ST2/E/57-A3 1430)  
**Xie L.**  
(MC04/L/03-B1 1205)  
**Xie Li-Li**  
(ST3/E/10-B3 1045)  
**Xie Shang-Ping**  
(JSP25/W/28-B5 1010)  
**Xie Xiao-Bi**  
(ST5/W/47-B4 1010)  
**Xinkang Hu**  
(G1/L/10-A3 1620-30)  
**Xing C F**  
(G3/W/09-A5 1610-27)  
(G3/W/23-A5 1610-28)  
**Xing Guang-Fu**  
(JSV22/E/15-A5 1550)  
(JSV22/E/18-A5 1610)  
(JSV30/C/JSV22/E/16-B1 1400-20)  
**Xing Ruying**

# INDEX

- (ST1/E/37-A4 0930-08)  
(ST1/E/37-A4 0930-08)
- Xing Tang Bang**  
(GA1.03/W/10-B2 1420)
- Xinping Zhang**  
(HS2/W/27-B2 1420)  
(HS2/W/28-B2 1440)
- Xinsheng Gao**  
(HS2/W/22-B2 1140)
- Xiong Liang-Ping**  
(JSS44/W/12-B4 0930-40)  
(ST4/W/41-B1 1400-01)
- Xiong Xiong**  
(JSS44/W/06-B5 1130)  
(ST4/W/55-B2 1420)
- Xiongang Huang**  
(ST1/P/07 0930-30)
- Xiuji Zhou**  
(MI01/E/13-A3 1125)
- Xu Caijun**  
(G1/W/01-A3 1620-02)  
(G5/W/09-A4 1445)
- Xu Hehua**  
(ST4/W/39-B1 1400-07)
- Xu Guochang**  
(G1/E/37-A3 1620-69)  
(G2/E/05-A2 1630-21)  
(G1/E/19-A3 1620-25)
- Xu Jianjun**  
(JSP25/C/MI05/W/01-B2 1150)  
(JSP25/C/MI05/W/34-B1 0830-04)
- Xu Jian-Qiao**  
(JSA37/P/01-B3 1145)
- Xu Jusheng**  
(G5/W/09-A4 1445)
- Xu Li-Sheng**  
(ST 5/E/37-B4 1520)
- Xu Ming**  
(MC10/P/01-B1 1015)
- Xu Peifen**  
(JSS44/W/16-B5 1150)  
(ST4/E/12-B1 0830-15)
- Xu Peiliang**  
(JSS31/W/06-B3 0830-06)
- Xu Peiliang**  
(G4/W/14-A3 1045)
- Xu Qing**  
(ST4/W/27-B2 0930-08)  
(ST4/W/47-B2 0930-13)
- Xu Shaoquan**  
(G1/W/30-A3 1620-13)
- Xu Wen-Yao**  
(GA5.09/W/04 A2 1400-03)
- Xu Yousheng**  
(GA1.02/E/18-A1 0945)
- Xue Huai-Min**  
(JSV22/E/18-A5 1610)
- Xue Yongkang**  
(JSM04/W/07-A2 1200)  
(MI07/W/05-A2 1140)  
(MC01/L/18-A4 1715)  
(MC01/W/54-A3 1705)  
(MI07/W/04-A2 1440)
- Xuecheng Yuan**  
(JSS44/p/02-B5 1210)
- Xuemi Zhang**  
(ST4/P/10-B1 0830-08)
- Xueyuan Yu**  
(JSV30/C/JSV22/P/02-B1 1400-23)
- Xuhui Shen**  
(ST2/E/19-A3 1445)
- Xuwen-Yao**  
(GA3.02/W/25-B3 0900-15)
- (JSA15/E/05-A3 1150)  
(JSA15/E/09-A4 1200)
- Yagova Southwood Nadezhda**  
(GA3.04/E/06-B2 0950)
- Yahnin A. G.**  
(GA3.06/W/16-A2 0930-11)  
(GA3.02/W/60-B2 1215)
- Yaibin Zhang**  
(ST1/E/41-A3 0900-09)
- Yajnik K. S.**  
(P08/W/08-A2 1420)
- Yakovlev O.**  
(JSG28/W/10-B2 1400-06)
- Yakunin M. N.**  
(GA2.03/L/01-B3 1400)  
(JSM03/L/03-A1 1400)
- Yakutsk A T**  
(JSM01/W/108-A2 1600-25)
- Yaln Namk**  
(G5/E/23-A4 1230-08)
- Yamada Hiroyuki**  
(JSM24/E/02-B1 1440)
- Yamada K.**  
(GA1.05/W/01-A6 1515)
- Yamada Makoto**  
(ST5/E/16-B4 1500)
- Yamada Yoshikazu**  
(JSA15/E/59-A4 1400-19)
- Yamaga Takashi**  
(MI12/W/13-B4 1155)
- Yamagishi H.**  
(GA2.02/E/12-B4 1640)
- Yamagishi Hisao**  
(GA2.01/E/01-A1 1110)  
(GA2.01/E/05-A1 0950)  
(GA3.08/E/03-B1 1000)
- Yamaguchi T.**  
(JSA15/E/17-A3 1440)
- Yamamoto Kiyohiko**  
(ST1/W/12-A2 1400-03)
- Yamamoto Joeta**  
(JSG28/W/07-B1 1400-07)
- Yamamoto M.**  
(GA2.02/W/09-B4 0900)  
(MI06/W/02-B1 1400-18)  
(MI06/W/02-B2 1400-18)  
(GA2.02/L/06-B4 0940)
- Yamamoto T.**  
(GA3.08/W/16-B1 1430)
- Yamamoto Tatsundo**  
(GA3.10/W/09-A6 1700-13)
- Yamanaka Chihiro**  
(JSA15/E/04-A3 1130)
- Yamanaka Goro**  
(P12/C/JSP21/E/01-A1 0950)
- Yamanaka Manabu D.**  
(MC06/C/JSM01/W/58-A1 1120)
- Yamanaka Y**  
(MCc01/W/36-A5 1700)
- Yamanaka Yasuhiro**  
(P08/E/02-A2 0930)  
(ST5/E/17-B4 1400-04)  
(ST5/W/18-B3 1700)
- Yamanaka Yoshiko**  
(ST2/W/31-A5 1400-34)
- Yamane Shigeru**  
(JSA15/W/08-A4 1040)
- Yamanouchi Takashi**  
(MI08/E/01-A4 1015)  
(MI08/E/04-A4 0930)  
(MI08/E/05-A3 0940)
- Yamaoka Koshun**  
(JSV47/E/02-B5 1230)
- Yamashita Futoshi**  
(JSA15/E/28-A5 0830-06)
- Yamashita Teruo**  
(ST1/E/66-A2 1400-38)
- Yamasaki Masanori**  
(MI04/E/15-B1 1435)
- Yamasaki T.**  
(GA1.03/W/29-B1 0900)  
(JSS46/W/03-B4 1010)
- Yamazaki Daisuke**  
(JSS07/E/05-A2 1540)
- Yamazaki Fumio**  
(JSP23/C/U5/W/19-A6 1720)
- Yamazaki Kuniko M.**  
(JSP39/E/13-B4 1720)
- Yamazaki Makoto**  
(HW3/W/16-B4 0900)
- Yamazaki Toshitsugu**  
(GA1.05/W/22-A6 1700)  
(GA1.05/W/29-A6 1445)
- Yamazaki Y. H.**  
(JSM26/L/05-B2 1700-17)
- Yamazki Toshitsugu**  
(GA1.03/W/03-B2 1000)
- Yan L.**  
(GA3.04/L/13-B2 1210)
- Yan Feng**  
(MI01/E/01-A1 0900-08)
- Yan Kagan**  
(ST1/W/63-A2 1520)
- Yan Xing Li**  
(G1/L/10-A3 1620-30)
- Yan Zhongqiong**  
(JSS44/E/24-B5 1010)
- Yan Zhongwei**  
(MC02/W/15-B2 1650)  
(GA6.01/W/10-A5 0900-21)
- Yanagidani Takashi**  
(JSA15/E/28-A5 0830-06)  
(ST1/E/56-A2 1400-37)
- Yananaka Chihiro**  
(JSA15/E/01-A4 1400-05)
- Yan-Ben Han**  
(G5/E/24-A4 1115-11)  
(G5/E/25-A4 1115-10)  
(ST1/E/65-A4 0930-11)
- Yang C-H**  
(MC01/L/13-A3 1135)
- Yang Chi**  
(MC02/W/15-B2 1650)
- Yang Daqing**  
(HW3/W/14-B4 1725)
- Yang Guiying**  
(MWO2/W/02-B3 1120)
- Yang H.**  
(GA4.08/W/12-B4 1635)
- Yang Haijun**  
(JSP25/E/03-B2 1130)
- Yang Hongmei He Ping**  
(G1/L/10-A3 1620-30)
- Yang Jiayan**  
(JSP25/W/83-B2 1720)
- Yang Ming**  
(JSG28/W/09-B2 1400-12)  
(JSG28/W/22-B2 1220)  
(G1/W/34-A3 1620-43)
- Yang Shanlin**  
(GA1.03/W/19-B1 1420)
- Yang Shi-Keng**  
(MC01/W/02-A1 1445)
- Yang Xiaohua**  
(MC01/W/47-A4 1005)
- Yang Yuanxi Xi'an**  
(G1/E/39-A3 1620-70)
- Yang Yuesuo**  
(HS5/W/31-A3 0900)
- Yang Zhenyu**  
(GA1.04/W/11-A6 1440)  
(GA1.04/W/12-A5 1120)  
(GA1.04/W/28-A5 1140)
- Yang Zhi-xian**  
(ST3/E/28-B5 1215)
- Yang Zhong**  
(GA1.03/W/05-B2 1040)
- Yang Zhu-Liang**  
(JSV30/C/JSV22/E/17-B1 1400-21)  
(JSV22/E/15-A5 1550)  
(JSV22/E/18-A5 1610)
- Yang Zong-Liang**  
(MC01/E/08-A1 1745)  
(MC01/W/13-A3 1635)  
(MC01/W/53-A3 1650)
- Yanhong Yin**  
(ST4/c/GA1.01/E/17-B2 0930-30)
- Yannick Peter**  
(G5/E/36-A4 1215)
- Yano Yusaku**  
(ST4/E/45-B1 1400-11)
- Yanovskaya Tatyana**  
(ST2/E/40-A3 1415)
- Yanqing Zhu**  
(G4/W/10-A3 1620-26)
- Yao Changli**  
(JSA40/E/01-B5 1400-16)
- Yao Huaxia**  
(HS1/W/13-B5 0830-02)
- Yao Tnadong**  
(JSM24/W/13-B2 1115)
- Yaolin Shi**  
(JSS 31/E/01-B3 0830-10)  
(JSS44/E/30-B5 1110)  
(ST4/W/09-B3 0830-03)  
(ST1/W/31-A4 0930-35)
- Yaremchuk Maxim**  
(P12/W/18-A1 1640)
- Yarmukhamedov A. R.**  
(G5/E/19-A4 1230-10)
- (G5/E/43-A4 1230-11)  
(ST2/E/54-A5 1400-09)
- Yaron Ofer**  
(MI10/E/06-B2 1400)
- Yaroshevich M. I.**  
(JSP23/E/48-A5 0830-09)
- Yasuaki Sudo**  
(JSV47/W/11-B5 1115)
- Yasuda Ichiro**  
(JSP25/E/01-B3 1640)  
(JSP25/E/01-B5 1210)  
(JSP25/W/25-B3 0830-06)
- Yasuda Y.**  
(GA1.05/W/32-A6 1645)
- Yasuhara Masaya**  
(HS4/W/22-A5 1120)  
(HS5/W/35-A3 1045)  
(JSV36/E/12-B3 0900-17)
- Yasui Maya**  
(VS2/E/01-B3 1400-18)
- Yasunari Tetsuzo**  
(JSM24/E/11-B1 1205)  
(JSM24/W/07-B1 1030-03)  
(JSM24/W/13-B2 1115)
- Yasyuki Sato**  
(GA2.02/E/04-B4 0930-10)
- Yau Andrew W**  
(GA3.06/E/07-A2 1550)
- Yau M K**  
(MC08/L/10-A3 1045)  
(MI10/W/12-B1 1100)
- Yayla Mehmet**  
(P11/E/25-B4 1010)  
(P11/E/27-B5 1130)
- Yee J. H.**  
(JSA20/L/03-A4 1400)
- Yee Jeng-Hwa**  
(JSM01/W/33-A3 1610)
- Yegani F.**  
(ST6/P/02-A2 0830-02)
- Yegorova Tamara P.**  
(JSA40/E/02-B5 1045)
- Yeh H. C.**  
(GA2.02/W/18-B5 1440)  
(GA2.02/W/34-B5 1420)  
(JSA20/W/21-A5 1519)  
(JSA20/W/28-A5 1200-10)
- Yeh Harry**  
(JSS42/W/06-B5 1400)  
(JSS42/W/09-B5 1520)
- Yeh Y. C.**  
(GA2.02/W/18-B5 1440)  
(GA2.02/W/34-B5 1420)  
(JSA20/W/28-A5 1200-10)
- Yeh Yeong-Tein**  
(ST3/E/37-B3 1145)
- Yelles-Chaouche A. K.**  
(JSS44/E/07-B4 0930-16)  
(G5/E/27-A4 1230-05)
- Yen Chin-Hsiang**  
(G5/W/02-A4 1502-02)
- Yeoman**  
(GA3.10/W/26-A5 1225)
- Yeoman T. K.**  
(GA2.01/W/06-A1 1135)  
(GA3.07/W/69-A6 1100)  
(GA3.10/W/15-A6 1700-04)  
(GA3.04/W/16-B2 1010)  
(GA3.04/W/27-B1 1520-04)  
(GA3.08/W/07-A6 1630)  
(GA3.08/W/32-A6 1600)
- Yepes Hugo A.**  
(JSP23/C/U4/E/03-A6 0830-16)
- Yermolaev Yu**  
(GA4.09/W/04-A5 1600-02)
- Yermolaev Yu. I.**  
(GA3.02/W/03-B3 0900-14)  
(GA4.08/W/15-B3 1530)
- Yevlashin**  
(GA4.08/E/24-B3 0900-16)
- Yi Dingrong**  
(JSP25/W/44-B5 1400)
- Yi Yuchan**  
(G3/E/43-A5 1610-17)
- Yi Yuhong**  
(MI01/W/12-A1 0945)
- Yigitbas Erdinc**  
(ST2/W/19-A4 1215)
- Yildiz Yesim Coban**  
(P11/E/25-B4 1010)  
(P11/E/27-B5 1130)
- Yilmaz Aysen**  
(P11/E/25-B4 1010)  
(P11/E/27-B5 1130)

- (P11/L/06-B5 1730)  
**Yilmaz Y.**  
 (GA1.04/W/27-A6 1140)  
**Yin Jing-Yuan**  
 (ST1/E/32-A4 0930-07)  
**Yin L.**  
 (GA4.10/W/09 A5 1710)  
**Yin Y.-H.**  
 (GA1.05/W/32-A6 1645)  
**Yingzhe Tang**  
 (G1/C/G2/E/02-A3 1620-105)  
**Yipeng Wang**  
 (ST2/E/19-A3 1445)  
**Yliniemi Jukka**  
 (ST6/W/03-A1 0830-05)  
 (JSS44/W/11-B4 0930-28)  
**Yoden Shigeo**  
 (JSM26/W/23-B1 1730)  
 (JSM26/W/25-B2 1700-11)  
 (MI12/W/13-B4 1155)  
**Yogodzinski Gene M.**  
 (JSV30/W/11-B1 0900)  
**Yoichi Fukuda**  
 (ST4/W/26-B1 0830-18)  
**Yokoyama I.**  
 (ST2/E/49-A4 1730)  
**Yonemitsu T**  
 (JSM01/W/20-A1 0900)  
**Yonesaka Takashi**  
 (HS4/W/04-A4 1105)  
**Yong Qing Lu**  
 (P08/P/01-A2 1700)  
**Yong Jie Liu**  
 (JSP23/E/50-B2 0830-10)  
**Yonghui Wu**  
 (MI11/E/10-B5 1645)  
**Yongjian Ding**  
 (HS2/W/14-B1 1620)  
 (HS2/W/16-B2 0920)  
 (HS2/W/19-B2 1020)  
 (HS2/W/20-B2 1040)  
 (HS2/W/24-B2 1220)  
**Yongkang Xue**  
 (MC01/W/60-A2 0945)  
 (U3/W/14-A3 0900-15)  
**Yongli Yan**  
 (ST4/L/05-B2 0930-12)  
**Yongming Liu**  
 (MI11/E/10-B5 1645)  
**Yongsheng Li**  
 (JSP23/C/U5/E/13-B1 0830-03)  
**Yongzhong Ouyang**  
 (G3/W/38-A5 1610-42)  
 (G4/W/07-A3 1620-12)  
**Yool A**  
 (MC01/W/36-A5 1700)  
**Yoon Jin-ho**  
 (MW06/W/08-A3 1020)  
**Yoon P H**  
 (GA3.06/W/38-A2 0930-19)  
**Yorke Thomas H.**  
 (HW1/W/02-A4 1130)  
**Yoshiaki I. D. A.**  
 (JSV29/E/05-B1 1420)  
**Yoshida Akio**  
 (ST1/E/81-A2 1640)  
 (ST1/E/89-A2 1720)  
 (ST2/E/58-A5 1400-04)  
**Yoshida Haruyo**  
 (GA6.02/E/06-B1 1645)  
**Yoshida Hiromu**  
 (HS3/W/18-A2 0925)  
**Yoshida Jiro**  
 (JSP49/W/10-B5 0950)  
**Yoshida Mario**  
 (VS2/E/09-B3 1400-22)  
**Yoshida S.**  
 (JSA15/W/18-A4 1400-02)  
**Yoshida Shingo**  
 (JSA15/E/46-A3 1210)  
 (ST1/W/73 0930-31)  
**Yoshida Shuji**  
 (JSM01/W/93-A2 1600-04)  
**Yoshida Yasuhiro**  
 (ST1/W/13-A3 1740)  
**Yoshihara Arata**  
 (GA1.03/W/10-B2 1420)  
**Yoshihara Takayuki**  
 (JSG28/E/02-B1 1400-20)  
 (JSG28/E/03-B2 1400-15)  
**Yoshikawa A.**  
 (GA3.04/L/11-B2 0900)  
 (GA3.04/W/10-B1 1520-08)  
 (GA3.04/W/30-B1 1520-14)  
**Yoshikawa Yutaka**  
 (P13/W/01-B1 1150)  
**Yoshiki Motoyoshi**  
 (JSM01/E/12-A2 1500)  
**Yoshinari Hiroshi**  
 (JSP25/W/25-B3 0830-06)  
**Yoshino T.**  
 (G2/E/01-A2 1630-12)  
**Yoshino Taizoh**  
 (G2/E/08-A2 1630-11)  
 (G2/W/01-A2 1630-01)  
**Yoshioka Naoto**  
 (ST1/E/44-A1 1720)  
**Youichi Sugiyama**  
 (P09/W/14-A1 1520)  
**Young Chang-Chi**  
 (ST3/W/30-B3 1115)  
**Young J. B.**  
 (ST 5/E/22-B4 1700)  
 (U8/E/01-B3 1640-08)  
**Young J. T.**  
 (JSM41/E/22-B4 0945)  
 (JSM41/E/28-B3 1515)  
**Young R. Paul**  
 (ST1/W/51-A3 0930)  
 (ST1/W/61-A1 1500)  
**Young S. A.**  
 (MI04/E/25-B4 0930)  
**Yszkovicza L**  
 (G3/W/29-A5 1610-87)  
**Yu Jyh-Yih**  
 (G1/W/34-A3 1620-43)  
**Yu Li Shi-**  
 (ST1/E/54-A2 1400-07)  
**Yu Lisan**  
 (JSP25/W/60-B1 0950)  
**Yu Natalia**  
 (GA3.09/E/09-B4 1735)  
**Yu Shui-Bei**  
 (ST3/E/37-B3 1145)  
**Yu Shui-Beih**  
 (G5/W/02-A4 1502-02)  
**Yu Ting-To**  
 (JSG28/W/22-B2 1220)  
**Yu V Mineev**  
 (JSA06/E/01-A1 1155-18)  
**Yu.V Nikitin.**  
 (ST1/W/02-A4 0930-33)  
**Yu Yanxiang**  
 (ST3/E/50-B4 0930-19)  
**Yuan Dongliang**  
 (JSP05/E/08-A1 0930)  
**Yuan Xiaojun**  
 (JSM04/W/1-A2 1710)  
 (JSM18/W/17-A4 1120)  
**Yuan Yaochu**  
 (P10/P/01-A4 1520)  
**Yuan Zhu**  
 (U7/E/02-B1 0830-10)  
**Yuanqing Zhu**  
 (JSP23/C/U5/W/08-A5 1600)  
 (JSP23/C/U5/W/09-A6 1620)  
**Yucel Ismail**  
 (MI06/W/01-B2 1710)  
**Yudin Valery A**  
 (MW04/W/09-A1 1650)  
 (MW04/W/10-A1 1630)  
**Yuen David A**  
 (JSS13/W/13-A5 1150)  
**Yueqing Zhu**  
 (JWS 33/E/04-B2 1215)  
**Yugov V. A .**  
 (JSA20/W/43-A4 1200-23)  
 (JSA20/W/31-A4 1200-19)  
**Yuichi Nishimura**  
 (VS2/E/09-B3 1400-22)  
**Yukhimuk Adam**  
 (GA3.04/E/08-B1 1520-01)  
**Yukimatu A. S.**  
 (GA 2.02/E/12-B4 1640)  
**Yulianti Ian**  
 (GA1.05/E/12-A5 0850)  
**Yum Seongsoo**  
 (MC07/W/07-A3 0915)  
**Yumoto K.**  
 (GA3.04/E/15-B1 1520-02)  
 (GA3.04/L/08-B1 1520-42)  
 (GA3.04/L/13-B2 1210)  
 (GA3.04/W/10-B1 1520-08)  
 (GA3.04/W/26-B1 1520-09)  
 (GA3.04/W/30-B1 1520-14)  
 (GA3.04/W/45-B1 1520-45)  
 (GA3.08/W/05-A6 1040)  
**Yumoto Kiyofumi**  
 (GA3.04/W/04-B1 1520-40)  
 (GA2.02/E/13-B4 1100)  
 (GA3.04/E/06-B2 0950)  
 (GA3.04/E/12-B2 1150)  
 (GA3.04/W/14-B1 1520-43)  
 (GA1.02/W/22-A2 0930)  
**Yumoto Kiyohumi**  
 (GA5.01/E/32 A1 0900-09)  
 (JSA15/E/09-A4 1200)  
 (JSA20/E/08-A4 1200-18)  
 (JSA20/E/08-A4 1200-25)  
**Yun L. P.**  
 (G5/E/19-A4 1230-10)  
**Yun Wu**  
 (ST1/W/56-A1 1700)  
**Yunck Thomas**  
 (MI06/W/29-B1 1010)  
**Yunck Thomas P.**  
 (JSG28/E/27-B2 1400-04)  
**Yunev Oleg**  
 (P15/W/03-B3 1025)  
**Yunev Oleg A.**  
 (P11/L/06-B5 1730)  
 (P11/L/07-B5 1745)  
**Yuneva Tatyana V.**  
 (P11/L/07-B5 1745)  
**Yunez Miguel**  
 (GA4.01/W/06-A2 1400-07)  
**Yunfeng Luo**  
 (MI01/E/13-A3 1125)  
**Yunga S.**  
 (ST1/W/15-A2 1400-20)  
 (ST1/W/48-A2 0930-03)  
**Yunga Sergei**  
 (ST2/W/16-A 0930)  
 (ST4/W/63-B1 1720)  
 (ST5/W/22-B4 1400-03)  
**Yurasov Gennady**  
 (P10/E/13-A5 1440)  
 (P12/E/07-A1 1030-07)  
**Yurganov Leonid**  
 (MI02/W/08-A4 1510)  
**Yurkov E.**  
 (SW1/E/02-B5 1030-01)  
**Yurtsever Yuecel**  
 (HS4/W/20-A5 1030)  
**Yusa Yuki**  
 (G3/L/09 1610-23)  
**Yushak M.**  
 (HW3/W/19-B4 1015)  
**Yushkin V.**  
 (ST4/E/36-B1 1400-23)  
**Yushkov B. Yu.**  
 (GA3.05/E/08-B3 0900-19)  
 (GA3.05/E/14-B3 0900-35)  
**Yushkov V**  
 (JSM01/W/37-A5 1400)  
**Yushkov Vladimir**  
 (JSM26/W/16-B2 1210)  
**Yuval Shay-El**  
 (JSM24/E/08-B1 1500)  
**Yuwei Chen**  
 (ST1/P/07 0930-30)  
**Yu-zhuo Qiu**  
 (U3/E/06-A3 0900-05)  
**Yvetot Paul**  
 (JSA15/E/08-A3 1600)  
 (JSA15/E/10-A3 1640)  
 (JSA15/E/40-A3 1700)  
 (JSV36/E/23-B3 0900-07)  
**Yvon-Lewis Shari**  
 (JSP21/W/05-A4 1520)  
 (JSP21/W/17-A4 1500)  
 (JWS33/W/01-B2 1445)  
 (U7/W/03-B1 0830-03)  
**Zaitseva Svetlana A.**  
 (GA4.02/W/27-A4 1400-24)  
**Zaitsev Alexander**  
 (GA3.07/W/45-A6 0900-22)  
**Zaja A.**  
 (GA1.02/W/19-A2 0930)  
**Zakharov Daniil**  
 (G2/E/22-A2 1630-07)  
**Zakharov V F**  
 (JSM18/W/11-A5 1020)  
**Zakharov Vladimir S.**  
 (ST4/E/58-B1 0830-21)  
**Zamani A.**  
 (ST 5/E/04-B4 1440)  
**Zang Deyan**  
 (G4/P/05-A3 1620-07)  
**Zang Shaoxian**  
 (JSS02/E/04-A1 0830-06)  
 (ST2/E/05-A3 1000)  
 (ST4/E/02-B3 0900)  
 (ST5/E/32-B5 0850)  
**Zanimonska A.**  
 (JSA40/L/01-B5 1400-21)  
**Zanimonskiy Y.**  
 (JSA40/L/01-B5 1400-21)  
 (JSG14/E/19-A3 1745-16)  
**Zanis Prodrimos**  
 (U2/E/14-A2 1420)  
**Zanutta Antonio**  
 (G5/W/20-A4 1230-03)  
**Zanyomski E**  
 (G3/E/26-A5 1610-36)  
**Zaretsky N S**  
 (JSA06/E/05-A1 1155-17)  
**Zarifi (Raeesi) Z.**  
 (ST2/E/17-A4 1000)  
**Zarifi Z.**  
 (JSS07/P/03-A2 1205)  
 (ST 5/E/04-B4 1440)  
**Zaripov R. B.**  
 (MI04/E/13-B3 1120)  
**Zastenker G. N.**  
 (GA4.08/W/15-B3 1530)  
 (JSA06/W/01-A1 1500)  
**Zatelli Paolo**  
 (G1/W/31-A3 1620-14)  
 (G1/W/35-A3 1620-17)  
 (G4/W/06-A3 1125)  
**Zatman Stephen**  
 (JSS02/W/13-A1 1450)  
**Zavialov P.**  
 (P10/E/11-A5 1600-01)  
 (P10/E/15-A4 1720)  
**Zavyalov A.D**  
 (ST1/W/02-A4 0930-33)  
 (ST1/W/07-A3 0900-05)  
 (ST1/W/65-A3 0900-01)  
**Zayonchek A. V.**  
 (JSS44/L/04-B4 1640)  
**Zayonchek Andrew**  
 (G3/W/04-A5 1610-41)  
 (GA5.11/W/06 A3 1200)  
**Zdorov Alexander G.**  
 (JSA15/E/37-A5 1400-10)  
**Zdunek Ryszard**  
 (G5/W/10-A4 1514-08)  
**Zeggai A.**  
 (G1/L/13-A3 1620-89)  
 (G1/L/25-A3 1640-96)  
**Zeigarnik V. A.**  
 (ST1/E/70-A3 1700)  
**Zeitlin Vladimir**  
 (JSP39/W/45-B3 1406-03)  
**Zeldovich M. A.**  
 (GA4.04/W/01-B5 0830-02)  
**Zelensky Nikita P.**  
 (G3/E/05-A5 1200)  
**Zelenyi L.**  
 (GA3.08/E/01-A6 1430)  
**Zelenyi L. M.**  
 (GA3.02/W/03-B3 0900-14)  
 (GA4.08/W/15-B3 1530)  
 (GA3.02/W/63-B3 0900-09)  
 (GA3.05/E/18-B3 0900-01)  
 (GA3.08/E/02-B1 1110)  
**Zemtsov Victor**  
 (GA1.05/W/18-A6 0900-10)  
 (GA1.05/W/38-A5 0900-07)  
**Zender Charles S.**  
 (MI10/W/23-B2 1420)  
**Zeng Hualin**  
 (JSA40/L/01-B5 1400-16)  
**Zeng Ning**

## Z

- Zabarinskaya L. P.**  
 (JWS33/W/04-B2 1635-24)  
 (JWS33/W/04-B3 0900-24)  
**Zadorozhny Alexander M.**  
 (JSA35/W/02-B1 1050)  
 (JSM32/W/02-B2 1210)  
**Zadro Maria**  
 (JSS44/E/40-B4 0930-13)  
**Zahn Ulf Von**  
 (JSM32/W/05-B2 0930)  
 (JSM01/W/44-A3 1730)  
**Zaitcev A. V.**  
 (JSA45/E/11-B5 1030)  
 (JSA37/W/02-B3 1445)  
**Zaitsev Eugene**  
 (GA3.04/E/05-B1 1520-18)  
**Zaitzev Alexander**



## INDEX

- (JSM24/W/16-B1 1630)  
(JSP25/W/26-B1 1050)  
(MC01/L/15/-A3 1500)
- Zentrum Geo Forschungs**  
(JSV36/E/02-B3 1100)
- Zenwen An**  
(ST1/P/05-A3 0900-08)
- Zerbini Susanna**  
(G2/L/03-A2 1000)
- Zerefos C**  
(JSM01/W/37-A5 1400)  
(JSP21/W/09-A4 1130)
- Zervos F.**  
(JSP23/W/38-B2 1720)
- Zesta E.**  
(GA3.08/W/05-A6 1040)
- Zesta Eftyhia**  
(GA3.08/W/23-B1 1450)
- Zeyen Hermann**  
(JSS 44/E/02-B4 1440)
- Zezilak Jioi**  
(HW4/E/31-B2 0900-12)
- Zhan Xiwu**  
(MC01/W/54-A3 1705)
- Zhan Yan**  
(GA1.02/E/25-A2 0930)  
(JSA15/E/52-A5 0830-09)  
(JSV36/E/08-B3 0900-06)
- Zhang Changyou**  
(JSA27/E/07-B1 0940)
- Zhang Guomin**  
(JSP23/C/U5/E/21-B2 0830-11)  
(ST1/E/37-A4 0930-08)  
(ST1/E/37-A4 0930-08)  
(U3/P/03-A3 0900-09)
- Zhang Huai**  
(ST4/E/24-B2 0930-24)
- Zhang Huqiang**  
(MW02/L/01-B3 1220)  
(MC01/E/09-A3 1550)
- Zhang Ivhai Yan**  
(P08/P/01-A2 1700)
- Zhang Jiahua**  
(JSM41/E/11-B5 1445)  
(JSM41/E/24-B5 1030)
- Zhang Jian**  
(ST4/W/09-B3 0830-03)
- Zhang K.**  
(GA1.01/W/13-A5 1145)
- Zhang K. F.**  
(G3/W/49-A5 1610-78)
- Zhang Kefei**  
(G3/E/03-A5 1610-64)
- Zhang Keke**  
(GA1.01/W/08-A5 1130)  
(JSP39/W/41-B3 1210)
- Zhang L. D.**  
(GA4.09/W/11-A6 0920)
- Zhang Lin**  
(JSM18/W/14-A4 1040)
- Zhang Minghua**  
(JSA40/W/02-B5 1400-06)  
(JSA40/W/16-B5 1400-03)  
(MI10/W/23-B2 1420)
- Zhang P.**  
(JSP23/C/U5/E/16-A5 1620)  
(ST3/E/56-B4 1400-20)
- Zhang Pei-zhen**  
(ST3/E/28-B5 1215)
- Zhang Qing Lu**  
(P08/P/01-A2 1700)
- Zhang QingYun**  
(MW06/P/2-A3 1220)
- Zhang Qunshan**  
(JSS02/E/02-A1 0830-04)
- Zhang S.-R.**  
(GA2.03/W/02-B3 1010)
- Zhang Shengpan**  
(JSA20/W/13-A4 1200-06)
- Zhang Shimin**  
(ST2/E/57-A3 1430)
- Zhang T.**  
(JSM41/E/19-B4 1750)
- Zhang Y.**  
(JSS31/W/15-B3 0830-09)
- Zhang Y J**  
(G3/W/09-A5 1610-27)
- Zhang Yanbin**  
(G5/E/30-A4 1115-05)
- Zhang Yongsheng**  
(MC10/P/02-B1 1625)
- Zhang Yushen**  
(ST4/L/40-B1 0830-32)
- Zhang Z**  
(PW1/E/04-A6 0900)
- Zhao Dapeng**  
(ST4/E/01-B3 1400)
- Zhao Guoze**  
(JSV36/E/08-B3 0900-06)  
(GA1.02/E/25-A2 0930)  
(JSA15/E/52-A5 0830-09)
- Zhao J-P.**  
(JSP25/W/82-B5 1440)
- Zhao Juan**  
(GA 6.01/E/12-A5 0900-12)
- Zhao Junmeng**  
(GA1.02/E/25-A2 0930)
- Zhao Qingyun**  
(MC04/E/04-B2 1625)  
(MI04/E/08-B1 1650)
- Zhao Weimin**  
(HW4/E/07-B2 0900-06)
- Zhao X P**  
(GA4.02/W/13-A4 1005)  
(GA4.02/W/10-A4 1650)
- Zhao Y.**  
(GA4.02/W/10-A4 1650)
- Zhao Yu**  
(JSV22/E/15-A5 1550)  
(JSV22/E/18-A5 1610)
- Zhao Z-C**  
(MC01/E/23-A4 1035)
- Zhao Zongci**  
(MC01/P/01-A4 1155)  
(MW03/P/01-B4 1640)
- Zhaoyong Xu**  
(ST1/W/56-A1 1700)
- Zharinov Nikolai A.**  
(ST1/E/42-A3 0900-14)
- Zhdanov Michael**  
(GA1.02/E/21-A1 1445)  
(GA1.02/E/23-A1 1605)
- Zhelev Z. H.**  
(JSA40/W/09-B5 1400-11)  
(JSA40/W/10-B5 1400-12)  
(JSA40/W/11-B5 1400-13)
- Zhelevsky A. I.**  
(GA5.01/W/15 A1 1300-06)
- Zheleznyak M.**  
(P09/W/05-A1 1640)
- Zheleznyak Mark**  
(P13/W/13-B2 1600-11)
- Zheng Guan**  
(G3/W/38-A5 1610-42)  
(G4/W/07-A3 620-12)
- Zheng Hong**  
(U7/E/02-B1 0830-10)  
(U7/W/12-B1 0830-02)
- Zheng Yi**  
(JSS44/E/33-B4 0930-36)
- Zhengfang Wang**  
(P08/P/01-A2 1700)
- Zhengxiang Fu**  
(ST1/W/40-A4 0930-11)  
(ST1/W/64-A3 0900-03)
- Zhengyuan Li**  
(ST1/W/56-A1 1700)
- Zhenhai Zhu**  
(JSA27/P/05-B1 0900)
- Zhenua Zhao**  
(JSV22/E/03-A5 0900-02)
- Zhenxia Long**  
(MC10/W/06-B1 1450)
- Zherebtsov Gely**  
(JSA16/E/28-A3 0830-11)
- Zhigang Wei**  
(MC04/E/08-B2 1205)
- Zhijia Li**  
(HS1/W/53-B5 0830-06)
- Zhijia Zhan**  
(JAS15/P/02-A5 0830-08)
- Zhiping Lu**  
(G1/C/G5/E/09-A3 1620-99)  
(G1/E/33-A3 1620-66)
- Zhiwei Bao**  
(JSV22/E/03-A5 0900-02)
- Zhizhin M. N.**  
(ST3/E/39-B3 1200)  
(ST5/E/02-B3 1400)
- Zhizhko G. O.**  
(GA2.07/W/22-A1 1020)
- Zhong Qing**  
(MC01/W/25-A1 1630)  
(U3/W/15-A30900-16)  
(MI11/W/05-B5 1545)
- Zhong Wenyi**  
(MC08/W/07-A3 1210)  
(MW01/W/10-A5 1150-06)
- Zhongliang Wu**  
(ST 7/E/06-A2 1130)
- (ST1/E/19-A4.0930-04)
- Zhongqun Yan**  
(ST4/P/10-B1 0830-08)
- Zhou**  
(JSS31/P/01-B3 0830-01)
- Zhou Huilan**  
(ST5/W/43-B3 1520)
- Zhou Hui-Lan**  
(ST1/W/06-A2 1400-17)
- Zhou J L**  
(PW1/E/04-A6 0900)
- Zhou Jingnan**  
(JSM43/E/04-B4 1500)
- Zhou Jun L**  
(P09/E/03-A2 1010)
- Zhou Qi You**  
(HS4/W/04-A4 1105)
- Zhou Shijian**  
(G4/P/05-A3 1620-07)
- Zhou Shinjian**  
(G4/P/04-A3 1620-06)
- Zhou Shuntai**  
(JSA16/C/GA4.07/W/28-A3 0830-58)
- Zhou Shuoyu**  
(ST1/P/12 0930-37)  
(ST1/P/13-A3 1720)
- Zhou X.-Y.**  
(GA3.02/W/39-B2 1110)  
(GA4.08/W/12-B4 1635)
- Zhou Y.-H.**  
(JSG14/W/09-A3 1121-08)
- Zhou Yuanze**  
(ST4/E/02-B3 0900)  
(ST5/E/32-B5 0850)
- Zhu Jieshou**  
(ST4/P/10-B1 0830-08)
- Zhu L.**  
(GA5.06/W/05 A3 1520)
- Zhu Liangbao**  
(ST4/W/27-B2 0930-08)  
(ST4/W/47-B2 0930-13)
- Zhu Lie**  
(GA3.06/E/03-A2 0930-01)
- Zhu Rixiang**  
(GA1.03/L/04-B1 1520)
- Zhu S**  
(G3/E/27-A5 1610-02)
- Zhu Xun**  
(MW05/W/10-A2 1000)  
(JSM01/W/33-A3 1610)
- Zhu Y.-J.**  
(JSG28/W/04-B2 1400-13)
- Zhu Yueqing**  
(ST1/E/37-A4 0930-08)  
(SW1/E/03-B5 1015)
- Zhu Zhicheng**  
(GA1.04/W/11-A6 1440)
- Zhukov Vladimir A.**  
(JWA34/E/01-B2 1740)
- Zichu Xie**  
(HS2/W/16-B2 0920)  
(HS2/W/20-B2 1040)  
(HS2/W/28-B2 1440)
- Zichu Xie**  
(HS2/W/22-B2 1140)
- Ziebart Marek**  
(G1/L/26-A3 1640-97)
- Zieger B.**  
(GA3.04/W/09-B1 1520-17)
- Ziehlann Christine**  
(MI11/W/04-B5 1515)
- Zielinski J. B.**  
(G1/E/46-A3 0930)  
(G1/W/02-A3 1620-32)
- Zielinski Janusz**  
(G6/C/G3/E/35-B1 1740)
- Zieliński Janusz B.**  
(G5/W/10-A4 1514-08)
- Zilberstein Oleg**  
(JSP23/W/11-A5 1720)  
(JSP23/W/28-B1 0830-01)
- Zilitinkevich Sergej**  
(JSM04/W/08-A2 0950)
- Zimanowski Bernd**  
(VS2/E/14-B3 1400-25)  
(VS2/W/01-B3 1400-01)  
(VS2/W/18-B3 0930)
- Zimbardo Gaetano**  
(GA3.02/W/63-B3 0900-09)
- Zimmer C.**  
(GA4.10/W/23-A5 1725)
- Zimmer Martin**  
(JSV36/E/02-B3 1100)
- Zimmerman Mark E.**  
(JSS07/L/03-A2 1500)
- Ziniu Xiao**  
(MW06/P/1-A31700)  
(JSP25/P/04-B1 1740)
- Zinno R. J.**  
(ST1/E/72-A4 0930-08)
- Zioutas G.**  
(ST1/W/49-A3 0900-02)
- Zirizzotti Achille**  
(GA5.01/W/03 A1 0920)
- Zivic Mladen**  
(ST2/E/03-A5 1400-26)  
(ST3/W/14-B4 0930-01)
- Zlotnicki Jacques**  
(JSA15/E/08-A3 1600)  
(JSA15/E/10-A3 1640)  
(JSA15/E/27-A4 1400-04)  
(JSA15/E/38-A4 1400-03)  
(JSA15/W/10-A4 0900)  
(JSA15/E/40-A3 1700)  
(JSV36/E/23-B3 0900-07)  
(JSV36/E/24-B3 0900-02)
- Zohary Tamar**  
(P11/E/17-B4 1600)
- Zolesi B.**  
(JSA45/E/17-B5 1110-01)
- Zolitschka Bernd**  
(VS2/C/U6/E/01-B3 1400-35)
- Zollo Aldo**  
(ST7/W/03-A2 1605-01)  
(ST5/W/60-B5 1125)  
(JSS46/W/08-B4 0930-03)  
(JSS46/E/03-B4 1420)  
(JSS46/E/04-B4 1400)  
(JSS46/E/05-B4 1440)  
(JSS46/W/15-B4 0930-01)  
(ST5/W/34-B4 0930-01)
- Zong Q. G.**  
(GA3.02/E/18-B3 0850)  
(GA3.05/W/05-B3 0900-46)  
(GA3.05/W/23-B3 0900-13)  
(GA3.08/E/04-B1 1700)  
(GA4.08/W/11-B3 1620)  
(GA4.08/W/13-B4 0905)  
(GA4.08/W/17-B3 0900-06)
- Zong Yongqiang**  
(JSG11/E/08-A3 1640)
- Zonno Gaetano**  
(ST3/W/08-B4 0930-08)
- Zou X.**  
(JSG28/W/04-B2 1400-13)
- Zoya Kalmetieva**  
(ST2/E/26-A5 1400-11)
- Zschau Jochen**  
(ST1/W/10-A3 0910)  
(ST1/W/67-A1 1050)  
(JSV36/E/07-B3 0900)  
(JSV36/W/11-B3 1400-06)
- Zubinsky Vladimir**  
(G1/E/09-A3 1620-22)
- Zubov Vladimir**  
(JSP21/W/14-A5 1210)  
(MI06/E/13-B1 1100)
- Zubovich Alexander**  
(G5/E/34-A4 1230-12)
- Zuelsdorf R S**  
(MI03/W/09-A3 1640)
- Zuenko Yury**  
(P12/E/07-A1 1030-07)
- Zuidema Paquita**  
(MI04/L/21-B2 1720)
- Zulaikah Siti**  
(GA1.05/E/14-A5 1710)
- Zuohao Cao**  
(MC08/L/10-A31045)
- Zuoping Zheng**  
(JSP30/C/JSV22/P/02-B1 1400-23)
- Zupancic Polona**  
(ST3/E/19-B4 1400-03)  
(ST3/W/32-B4 1400-02)
- Zurbuchen T. H.**  
(GA4.04/E/07-B5 0830)  
(GA4.04/W/03-B5 1050)  
(GA4.04/W/06-B5 1400)  
(GA4.05/W/07-A1 1000)
- Zurbuchen Thomas**  
(GA4.02/W/18-A4 1735)
- Zuzlewski Stephane**  
(JWS33/W/22-B2 1635-01)  
(JWS33/W/22-B3 0900-01)
- Zverev L. A.**  
(ST3/E/15-B4 1400-05)
- Zverev S. M.**  
(JSS44/W/15-B4 0930-19)
- Zvereva Tatjana I.**  
(GA1.07/W/01-B2 0940)

(GA1.07/W/07-B2 1220)  
**Zverev V L**  
(GA3.10/L/01-A6 1700-01)  
**Zveryaev Igor**  
(JSP25/W/21-B3 0830-07)  
(JSP25/W/52-B3 1010)  
**Zwally J**  
(JSH12/W/09-A4 1400-03)  
**Zweifel P.**  
(ST5/L/02-B3 0900-02)  
**Zwing A.**  
(GA1.04/W/18-A4 1120)  
(GA1.04/W/30-A4 1100)  
**Zykina Valentina**  
(GA1.05/W/31-A5 0900-05)  
**Zykov Mihail**  
(GA5.11/W/06 A3 1200)  
**Zyrkis Ilya**  
(ST1/E/74-A2 1400-04)  
**Zyryanova Olga**  
(JSA16/E/24-A3 0830-10)